革新的低侵襲アプローチによる次世代医療法の開発と難治性疾患治療への応用

平成 27 年度～平成 31 年度
私立大学戦略的研究基盤形成支援事業
研究成果報告書

令和２年５月

学校法人名　聖マリアンナ医科大学
大　学　名　聖マリアンナ医科大学
研究組織名　難病治療研究センター
研究代表者　遊道　和雄

目　次

1. 研究成果概要　1

2. 論文・学会報告等リスト　49

はじめに

聖マリアンナ医科大学難病治療研究センター　遊道 和雄

平素より、聖マリアンナ医科大学大学院ならびに難病治療研究センターの活動・運営に御高配をたまわり、誠に有り難うございます。皆様がたの御助力のおかげ様をもちまして、平成 27 年度～平成 31 年度「私立大学戦略的研究基盤形成支援事業」（研究プロジェクト名：革新的低侵襲アプローチによる次世代医療法の開発と難治性疾患治療への応用）を無事終了することができました。皆様方の御厚情に感謝申し上げます。

急速な高齢化社会を迎えつつある我が国において、難治性疾患を取り巻く現状は厳しく、患者お一人おひとりにより良い医療を提供し、ひいては社会的損失を軽減させていく弛まぬ努力が求められています。我々は、難病治療研究センターに求められる主題・使命は「難治性疾患の克服・制圧」にあるという信念のもと、当センターがこれまでに蓄積してきた「知」と「人」の資源を基盤に、研究施設の財産であるサイエンスに関するあらゆるノウハウ、科学研究費、知的財産や人的資源を集約して難治性疾患克服に取り組んでまいりました。

もちろん、研究資源の集約は本センター内の既存のフレームワークを基盤としつつも、有機的かつ横断的に連携し進められていくべきであり、研究者、研究グループとしての連携は難病治療研究センターや大学内に留まらず、国内外の研究機関と建設的な関係を構築し、かつ、可能な限り早急に医療の現場で貢献できるよう、文科省、厚労省をはじめとする公的機関や企業を包括した産官学連携を世界的視野で展開していく段階にあります。

こうした産官学の充実した連携機構を構築していくには、地道な研究活動に加えて、目的意識に裏づけされた強い意志と努力を要し、なによりも組織に活力を与える若い力が求められます。これからの難病治療研究センターは、中・長期的展望に立った研究計画の推進に加えて、医学生、大学院生をはじめ次世代を担う研究者、後進の育成に重きをおいていくことが肝要と心得ます。本事業の研究プロジェクトについては、研究段階から公的研究助成を受けて創薬や新規医療技術創製の具体的な検証段階、すなわち製品化や工業化に向けた諸問題の検討・解決ステージへと上がり、いくつかの研究成果は国内外の大学や産業界（企業）との共同研究が進捗し、臨床の場での実用化に向けて着実に歩を進めております。

今後も難治性疾患の克服・制圧に向けて何を、そして如何になすべきかについて考え、大学院教育と研究に邁進してまいります。今後とも皆様の御指導御鞭撻の程、宜しくお願い申し上げます。

平成 27 年度～平成 31 年度「私立大学戦略的研究基盤形成支援事業」
研究成果報告書概要

１ 学校法人名　聖マリアンナ医科大学　　２ 大学名　聖マリアンナ医科大学

３ 研究組織名　難病治療研究センター

４ プロジェクト所在地　神奈川県川崎市宮前区菅生２－１６－１

５ 研究プロジェクト名　革新的低侵襲アプローチによる次世代医療法の開発と難治性疾患治療への応用

６ 研究観点　研究拠点を形成する研究

７ 研究代表者

研究代表者名	所属部局名	職名
遊道　和雄	難病治療研究センター	センター長・大学院教授

８ プロジェクト参加研究者数　15　名

９ 該当審査区分　理工・情報　　(生物・医歯)　　人文・社会

１０ 研究プロジェクトに参加する主な研究者

研究者名	所属・職名	プロジェクトでの研究課題	プロジェクトでの役割
遊道　和雄	難病治療研究センター センター長 教授	低侵襲アプローチ（新規ナノカプセル・DDS・経皮吸収・光温熱刺激）技術の向上	薬剤ナノカプセル、経皮吸収・DDS、光・温熱刺激による細胞活性制御技術を開発
唐澤　里江	難病治療研究センター 講師	低侵襲アプローチ（新規ナノカプセル・DDS・経皮吸収・光温熱刺激）技術の向上	薬剤ナノカプセル、経皮吸収・DDS、光・温熱刺激による細胞活性制御技術を開発
鈴木　越	難病治療研究センター 講師	低侵襲アプローチ（新規ナノカプセル・DDS・経皮吸収・光温熱刺激）技術の向上	薬剤ナノカプセル、経皮吸収・DDS、光・温熱刺激による細胞活性制御技術を開発
藤井　亮爾	難病治療研究センター 講師	低侵襲アプローチ（新規ナノカプセル・DDS・経皮吸収・光温熱刺激）技術の向上	薬剤ナノカプセル、経皮吸収・DDS、光・温熱刺激による細胞活性制御技術を開発
武永　美津子	先端創薬科学研究部門・特任教授	低侵襲アプローチ（新規ナノカプセル・DDS・経皮吸収・光温熱刺激）技術の向上	薬剤ナノカプセル、経皮吸収・DDS、光・温熱刺激による細胞活性制御技術を開発
黒川　真奈絵	疾患プロテオーム・分子病態治療	低侵襲アプローチに応答する新規細胞受容分子の同定	各種細胞における低侵襲アプローチに応答する細胞内応答分子を同定

	学大学院教授		
有戸　光美	疾患プロテオーム・分子病態治療学・講師	低侵襲アプローチに応答する細胞受容分子に関する蛋白質翻訳後修飾の網羅的解析	低侵襲アプローチに応答する細胞内応答蛋白の翻訳後修飾を網羅的解析
佐藤　利行	疾患プロテオーム・分子病態治療学・助教	低侵襲アプローチに応答する新規細胞受容分子の同定	各種細胞における低侵襲アプローチに応答する細胞内応答分子を同定
加藤　智啓	疾患プロテオーム・分子病態治療学・教授	低侵襲アプローチに応答する細胞受容分子に関する蛋白質翻訳後修飾の網羅的解析	低侵襲アプローチに応答する細胞内応答蛋白の翻訳後修飾を網羅的解析
戸澤　晃子	難病治療研究センター准教授	低侵襲アプローチの具体的方法の検証	治療法開発に向けた低侵襲アプローチ法の開発
山野　嘉久	難病治療研究センター大学院教授	低侵襲アプローチの具体的方法の検証	治療法開発に向けた低侵襲アプローチ法の開発
佐藤　知雄	難病治療研究センター准教授	低侵襲アプローチの具体的方法の検証	治療法開発に向けた低侵襲アプローチ法の開発
八木下　尚子	難病治療研究センター講師	細胞内応答分子を介する抗炎症・抗腫瘍効果の検証	低侵襲アプローチによる抗炎症、抗腫瘍効果の検討
新谷　奈津美	難病治療研究センター助教	細胞内応答分子を介する抗炎症・抗腫瘍効果の検証	低侵襲アプローチによる抗炎症、抗腫瘍効果の検討
山口　葉子	難病治療研究センター・客員教授	低侵襲アプローチの具体的方法の検証	治療法開発に向けた低侵襲アプローチ法の開発
（共同研究機関等）			

＜研究者の変更状況（研究代表者を含む）＞

旧

プロジェクトでの研究課題	所属・職名	研究者氏名	プロジェクトでの役割
低侵襲アプローチに応答する細胞受容分子に関する蛋白質翻訳後修飾の網羅的解析	疾患プロテオーム・分子病態治療学・准教授	岡本　一起	低侵襲アプローチに応答する細胞内応答蛋白の翻訳後修飾を網羅的解析

（変更の時期：平成 29 年　4 月　1 日）

新

変更前の所属・職名	変更(就任)後の所属・職名	研究者氏名	プロジェクトでの役割
疾患プロテオーム・分子病態治療学・教授	疾患プロテオーム・分子病態治療学・教授	加藤　智啓	低侵襲アプローチに応答する細胞内応答蛋白の翻訳後修飾を網羅的解析

旧

プロジェクトでの研究課題	所属・職名	研究者氏名	プロジェクトでの役割
低侵襲アプローチの具体的方法の検証	難病治療研究センター・准教授	山口　葉子	治療法開発に向けた低侵襲アプローチ法の開発・研究テーマ３研究代表者

（変更の時期:平成 28 年 7 月 1 日）

新

変更前の所属・職名	変更(就任)後の所属・職名	研究者氏名	プロジェクトでの役割
難病治療研究センター・准教授	難病治療研究センター・大学院教授	山野　嘉久	治療法開発に向けた低侵襲アプローチ法の開発・研究テーマ３研究代表者

旧

プロジェクトでの研究課題	所属・職名	研究者氏名	プロジェクトでの役割
低侵襲アプローチの具体的方法の検証	難病治療研究センター・准教授	山口　葉子	治療法開発に向けた低侵襲アプローチ法の開発

（変更の時期:平成 28 年 7 月 1 日）

新

変更前の所属・職名	変更(就任)後の所属・職名	研究者氏名	プロジェクトでの役割
難病治療研究センター・准教授	難病治療研究センター・客員教授	山口　葉子	治療法開発に向けた低侵襲アプローチ法の開発

旧

プロジェクトでの研究課題	所属・職名	研究者氏名	プロジェクトでの役割
－	－	－	－

（変更の時期:平成 29 年 4 月 1 日）

新

変更前の所属・職名	変更(就任)後の所属・職名	研究者氏名	プロジェクトでの役割
難病治療研究センター・准教授	難病治療研究センター・准教授	戸澤　晃子	治療法開発に向けた低侵襲アプローチ法の開発

11　研究の概要（※　項目全体を10枚以内で作成）

（1）研究プロジェクトの目的・意義及び計画の概要

急速な高齢化に伴い、2025 年には我が国の 65 歳以上の高齢者人口は 30%を超え、寝たきり人口も 450 万人強になると予想されており、2025 年の年間医療費は 59 兆円、介護費を加えると 94 兆円にも上るという試算もある。超高齢化社会においては、医療費負担の激増はいうに及ばず、労働・生産人口の減少によって社会基盤そのものの脆弱化が危惧され、その対策が社会的急務とされている。これに対して、最新医学・医療の研究・教育・実践を担う大学にも問題解決のために求められるものは大きい。

様々な制約 (経済的負担、副作用等) のため、これまで手術や薬物療法を受けられなかった高齢者や患者にも制約なく、身体的・経済的負担の少ない医療が受けられ、寝たきりにならずに能力に応じて社会貢献できる社会を実現するため、**大学には次世代の新規医薬・医療技術の研究開発と、その実践に向けた人材育成と研究基盤の構築が求められている。**

本研究プロジェクトは、「革新的 DDS 技術・低侵襲アプローチによる細胞活性の制御法」に関する研究成果を基盤に、**薬剤ナノカプセル技術、経皮吸収 DDS および特定波長条件の光刺激・メカニカルストレス・温熱刺激に応答する細胞内ストレス応答因子を介した細胞活性の制御技術を開発し、様々な疾患の基盤病態である炎症や細胞増殖・老化・変性を低侵襲アプローチによってコントロールして治療に結び付けようとするもの**で、①「低侵襲アプローチ技術の向上」、②「細胞内応答蛋白・遺伝子を活性化する低侵襲的アプローチ条件の検証」、③「低侵襲的アプローチによる治療効果の検証（動物・臨床試験）」を進め、光感受・応答機構の解明を通じて、「光感受・操作技術による骨粗鬆症・関節軟骨変性の予防と治療を目的とする新規医療技術の開発に結実した。

この研究成果に基づき**「切らない」、「刺さない」で治療する低侵襲的医療システムの研究拠点を構築してきた。**これにより、**手術療法や薬物療法（薬の内服、注射、経皮吸収）を中心とする治療体系とは次元の異なる医療システムを創出**し、地域格差なく、これまでリスクがあり手術や薬物療法を受けられなかった患者や高齢者にも**負担の少ない最新医療を提供できるように、大学の研究・教育基盤の充実と若手研究者の育成を今後とも進めていく。**

（2）研究組織

本研究プロジェクトの遂行のため、以下の役割分担体制を組織して研究を行なった。

①　研究代表者（プロジェクトリーダー・遊道）

- 研究拠点運営・マネジメントを統括・研究拠点運営委員会を適宜開催した。
- 本プロジェクトを構成する３つの研究テーマの研究開発活動を統括した。

・ 拠点の研究開発活動の基本的な研究戦略・企画等の策定ならびに進捗に合わせた軽微な変更や調整を行なった。

② 研究チームサブリーダー（遊道、黒川、山野）

・ プロジェクトリーダーの指揮の下で、研究開発を遂行・研究開発活動の進捗管理を行なった。
・ 本研究に必要な機器･装置の研究者利用の調整、研究チーム間の連携管理会議（月1回）を行なった。

テーマ１：低侵襲アプローチ技術の向上
（サブリーダー・遊道，研究分担者・唐澤，鈴木，藤井，武永）
テーマ２：低侵襲アプローチに応答する新規細胞内応答分子の同定
（サブリーダー・黒川，研究分担者・加藤，佐藤利行，有戸）
テーマ３：低侵襲アプローチの具体的方法の検証
（サブリーダー・山野，研究分担者・山口，佐藤知雄，八木下，新谷，戸澤）

③ 研究プロジェクトの戦略支援統括　（責任者：研究代表者・サブリーダー3名）

・ 研究拠点の運営支援、産業化を見据えた研究開発活動の研究戦略や企画等のサポートを行なった。
・ ワークショップ、シンポジウムの開催等による研究者間のネットワーク構築、若手研究者及び大学院学生等の人材育成を図るように努めた。

④ 知財戦略統括（責任者：研究代表者・サブリーダー3名，知財事業推進センター）

・ 聖マリアンナ医科大学・知財事業推進センターと連携して、研究成果を基にした知財戦略を検討し、得られた研究成果の知的財産権獲得に努めた。

⑤ 学外組織（他大学、研究機関、企業、自治体等）、学内既存組織（各部局等）との連携・調整窓口機能　（責任者：研究代表者・サブリーダー3名）

難病治療研究センター内に、オープンラボ・研究者ラウンジ（研究者が交流しながら研究を実施できるスペース）を設け、大学院生（当該研究テーマ担当・10 名）、研究員・研究技術者（各研究テーマ担当・約 20 名）の活用を促してきた。本研究支援事業終了もオープンラボの活用を継続していく予定である。

これにより本研究試験事業の終了後も、研究フェーズの異なる研究者・研究技術者の結集・融合により革新的なイノベーションの創出を目指し、研究開発成果の統合化を推進していく。

（3）研究施設･設備等

難病治療研究センター

難病の病因・病態の解明と治療法開発を目的として 1990 年にアイソトープ研究施設と実験動物研究施設を併設する地下１階地上３階、使用総面積約 6,195 ㎡の独立棟として

設立され、本研究プロジェクト遂行のための実験解析・観察機器・装置： フローサイトメーター(4~5 時間/日)、フランツセル機器(2~6 時間/日)、共焦点レーザー顕微鏡(2~4 時間/日)、ナノテクノロジー実験機器(4~6 時間/日)、蛍光検出器(6~8 時間/日)、HPLC(4~5 時間/日)、LC-MS(6~8 時間/日)等の分析機器が整備されている（機器利用時間：各時間/日×平均月 25 日)。当該センターは 10 名の専任教員が運用を担当し、センター所属研究員・共同研究機関登録研究員約 25 名、大学院生 5～10 名が研究施設・機器を使用して研究活動を行なっている。

<u>大学院先端医学研究施設</u>

当該研究施設（261 m^2）には分子生物学部門、培養研究部門、プロテオミクス研究部門、再生医学研究部門の４部門が設置され、共同利用の大型研究設備や各種研究用機器が整備されている。これらの研究施設・研究機器は、基礎、臨床講座並びに大学院の教育・研究に、さらに学生の実験実習等に幅広く利用されている（10～15 名/日)。

実験解析・観察装置： 共焦点レーザー顕微鏡類(2~4 時間/日)、プロテオミクス解析機器・質量分析器(4~8 時間/日)、DNA 解析・次世代シーケンス(4~8 時間/日)等の解析機器（機器利用時間：各時間/日×平均月 25 日)

(4)研究成果の概要 ※下記、13及び14に対応する成果には下線及び＊を付すこと。

近年、**物理的刺激（力学的ストレス、熱、光、音、電磁波等）がどのように感知され、細胞内情報伝達路を経て、最終的な生理的応答や病態的応答を導くかの具体的な仕組み(メカノバイオロジー機構)** の解明と、これらを応用した革新的医療機器・医療技術の創出に向けた新研究領域に注目が集まっている（2015 年度：AMED CREST, 2016 年度：JST 戦略的創造研究推進事業・さきがけ)。

我々は、非薬物・低侵襲的アプローチとして注目されている**メカノバイオロジー機構のうち、光刺激に対する細胞応答(光操作技術)**に注目し、特定波長条件の光を骨粗鬆症や関節症の患部へ照射し、**骨・軟骨細胞の光感受・応答を介して、疾患患部の細胞活性を制御する研究**を進めた。

これにより、**高齢者に多い骨粗鬆症、骨折、軟骨変性を「薬によらず」、「切らない」、刺さない」で予防・治療する非薬物・低侵襲的な低侵襲性医療機器**開発に繋がった。

本研究支援事業の間に、光操作技術・光治療効果発現のメカニズム解明に向けた光感受機構の解析を進め、基礎実験成果・動物試験結果を基に、「骨粗鬆症、骨量・骨質低下に起因する骨折」と「関節軟骨変性・変形性関節症」を対象とする光医療器の原理検証機を作製して、治療効果の科学的根拠実証の試験をなうことができた。

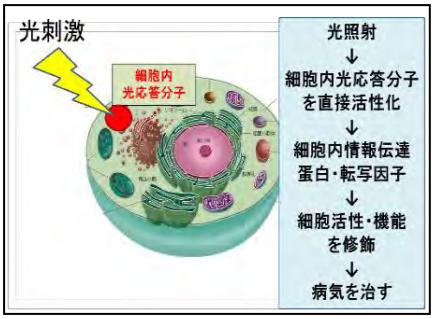

以下に、革新的低侵襲的アプローチによる細胞活性制御技術の確立と医療応用を目指

した研究成果を概説する。

研究テーマ１： 低侵襲アプローチ(ナノカプセル化製剤・DDS・経皮吸収・光温熱刺激）の向上・細胞活性変化の解析

平成 27～28 年度： 末梢血単核細胞、関節滑膜・骨・軟骨、腫瘍、血管および末梢神経組織由来の細胞を用いた in vitro 実験系において、各種条件の新規ナノカプセル化製剤・DDS・経皮吸収・光温熱刺激の存在下・非存在下に上記の細胞を培養し、それぞれの細胞に特異的な細胞活性（細胞増殖能、基質合成能、炎症性サイトカイン等の産生能、基質分解酵素産生能など）を in vitro において解析し、各細胞において低侵襲アプローチ条件ごとの細胞応答能を評価した。

さらに、これまでに同定した細胞内応答蛋白の siRNA を用いて当該蛋白発現を抑制した細胞株を作製し、各条件下の細胞活性の変化を評価し、低侵襲アプローチ条件下に応答する細胞内応答蛋白の機能および細胞活性変化の解析を進めた。

平成 29 年度： 平成 27～28 年度および研究テーマ２で同定した低侵襲アプローチに応答した細胞内応答蛋白の siRNA を用いて当該蛋白の発現抑制細胞株を作製し、各種条件の低侵襲アプローチ下に細胞を培養し、各細胞に特異的な細胞活性を解析して、各種の低侵襲アプローチ条件ごとに、細胞応答能・活性変化を評価した。

平成 30 年－31 年度： 平成 30 年度と最終年度は、特に光感受因子・応答機構の解明について有望な知見が得られ、骨粗鬆症・軟骨変性の予防ならびに治療法開発につながる研究を展開した（研究成果は＜優れた成果が上がった点＞欄に後述した）。

研究テーマ２： 低侵襲アプローチに応答する新規細胞内受容分子の同定/蛋白質翻訳後修飾の網羅的解析

平成 27～28 年度： 末梢血単核細胞、関節滑膜・骨・軟骨、腫瘍、血管および末梢神経組織由来の細胞を用いた in vitro 実験系において、各種条件の新規ナノカプセル化製剤・DDS・経皮吸収・光温熱刺激の存在下・非存在下に上記の細胞を培養し、プロテオーム解析（網羅的解析）を行ない、低侵襲アプローチ条件ごとに応答する蛋白質を解析した。既存の細胞内応答蛋白の各非薬物性刺激条件下における発現についても、各細胞において検証した。

上記実験系において同定した細胞内応答蛋白の機能解析に向けて、同定蛋白発現を抑制した細胞株を作製し、各種の低侵襲アプローチ条件下の細胞活性と、細胞内応答蛋白発現抑制細胞の網羅的解析を行ない、低侵襲アプローチに対応する細胞内応答蛋白の機能・活性化のメカニズムの解析を進め、研究成果を研究テーマ１・３にフィードバックした。

平成 29 年度： 平成 27～28 年度の実験を継続し、各種の低侵襲アプローチ（新規ナノカプセル化製剤・DDS・経皮吸収・光温熱刺激）条件下に各種細胞を培養し、各種低侵襲アプローチごとに、応答する蛋白質の翻訳後修飾異常の網羅的検出と解析を進め、研究テーマ１・３へフィードバックした。

平成 30 年－31 年度：　各種の低侵襲アプローチ（新規ナノカプセル化製剤・DDS・経皮吸収・光温熱刺激）条件のうち、顕著な効果が期待できそうな知見が得られた光刺激に対する各種細胞の光刺激応答蛋白質の翻訳後修飾異常の網羅的検出と解析を進め、研究テーマ１・３へフィードバックした（研究成果は＜優れた成果が上がった点＞欄に後述した）。

研究テーマ３：　細胞活性変化を誘導する最適な低侵襲アプローチ(新規ナノカプセル化製剤・DDS・経皮吸収・光温熱刺激)条件の検証

平成 27～28 年度：　各種の低侵襲アプローチ（新規ナノカプセル化製剤・DDS・経皮吸収・光温熱刺激）条件下で細胞を培養し、上記の各細胞に特異的な細胞活性（細胞増殖能、基質合成能、炎症性サイトカイン等の産生能、基質分解酵素産生能など）を in vitro 実験系において解析し、各細胞毎に各種低侵襲アプローチによる細胞活性変化の差異を検証して、細胞活性変化を誘導する最適な低侵襲アプローチおよび刺激条件を検証した。

さらに、動物試験用の低侵襲アプローチ（新規ナノカプセル化製剤・DDS・経皮吸収・光温熱刺激）や刺激装置（プローブ等）を試作し、改良した。

平成 29 年度：　骨関節症・関節炎、自己免疫疾患および癌性疾患の各疾患モデル動物に対して、平成 27～28 年で改良した動物試験用の低侵襲アプローチ用製剤・装置（プローブ等）を用いた治療効果判定の動物実験を継続中である（病理組織学的検討、血液生化学的解析）。また、臨床試験用の低侵襲アプローチ方法の具体的検証に向けて装置の仕様検討（刺激因子ごとの照射装置作成・プローブ改良等）を行ない、関節炎疾患、骨関節症疾患、自己免疫疾患、心血管炎、動脈硬化、癌性疾患を対象とする臨床試験の実施に向けた準備（試験機作製、安全性試験、プロトコール作成）を行なった（平成 30 年度以降も計画継続）。

平成 30 年－31 年度：　各種の低侵襲アプローチ（新規ナノカプセル化製剤・DDS・経皮吸収・光温熱刺激）条件のうち、臨床応用・医療機器開発が期待できる知見が得られた光刺激について、動物試験用の低侵襲アプローチ用製剤・装置（プローブ等）を用いた治療効果判定の動物実験予察を施行した。

また、臨床試験用の低侵襲アプローチ方法の具体的検証に向けて装置の仕様検討（刺激因子ごとの照射装置作成・プローブ改良等）に基づいた試験機を作製し、骨粗鬆症および変形性関節症(関節軟骨変性)を対象とする臨床試験の実施に向けた準備（試験機作製、安全性試験、プロトコール作成を行なった（平成 30 年度計画　から継続し、研究成果は＜優れた成果が上がった点＞欄に後述した）。

全体計画の研究成果・達成サマリー（研究テーマ１・２・３）

上記のように、本研究支援事業の期間内に骨・軟骨細胞、皮膚、血管内皮細胞等を用いて、低侵襲的アプローチとしてナノカプセル化製剤、経皮 DDS 技術、光刺激、メカニカルストレス、温熱刺激による細胞活性制御法を解析し、低侵襲的アプローチに

よる疾患患部の細胞活性の修飾を介した治療効果を in vitro および in vivo (疾患モデル動物)実験系において検討した。

平成 30 年度と令和元年度は、低侵襲アプローチのうちメカニカルストレスと光刺激について注力し、**両刺激に応答する因子・機構の解析と、病態ならびに治療効果発現のメカニズムを詳解し、臨床試験に向けたプロトコールと治療試作機の仕様を検討**した。

＜優れた成果が上がった点＞

特に成果がみられたのは、以下に概説する① 外因性刺激のうち、メカニカルストレスに応答する DNA 損傷修復酵素 (Ogg1, APEX2)の活性化の機序ならびに② 外因性刺激(メカニカルストレス)に応答する細胞エネルギー(ATP)産生の調節機構としての 5'-AMP-activated protein kinase (AMPK)と sirtuin (NAD 依存性脱アルキル化酵素)の役割と相互作用に関する解析結果である。

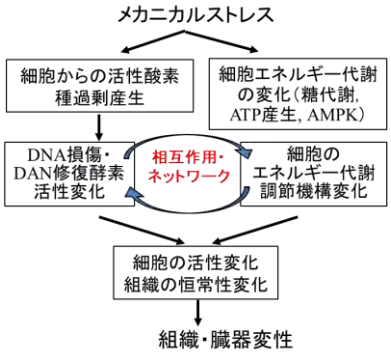

① メカニカルストレスに応答する DNA 損傷修復酵素(Ogg1, APEX2)の活性化の機序

DNA 損傷に対する防御機構として、DNA 修復酵素 AP エンドヌクレアーゼ (APEX2)や 8-oxoguanine DNA glycosylase (Ogg1)の発現変化が様々な疾患の病因・病態に関与することが指摘されており、我々はメカニカルストレス評価系の関節軟骨モデルにおいて、DNA 損傷の発現度は正常軟骨に比べて変性軟骨で高く、逆に DNA 修復酵素（Ogg1, APEX2）の発現度は軟骨組織変性度と相関して低下していることを見出した（図 1, *33, 国際学会*6, *12）。

本研究プロジェクトから、過度なメカニカルストレス刺激によって惹起される活性酸素種や炎症性サイトカインによる DNA 損傷が高発現する一方、DNA 修復酵素(APEX2, Ogg1)活性は低下することが明らかとなった。我々は DNA 損傷の程度が DNA 修復酵素による修復能を上回った場合には、DNA 損傷が蓄積し、その結果として細胞死、組織の恒常性低下や組織変性を誘導されると考え、細胞・組織・臓器にとって適切なメカニカルストレス刺激条件を明らかにする解析が進んだ（図 1, 論文*16,*26, *33）。

図1A. メカニカルストレスが誘導するDNA酸化損傷と修復酵素活性低下

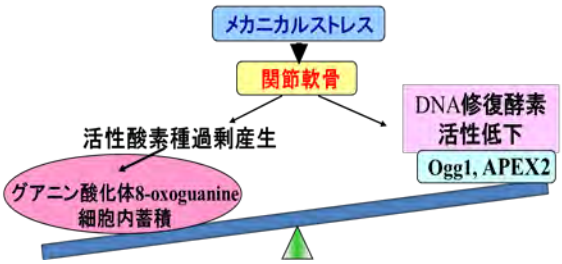

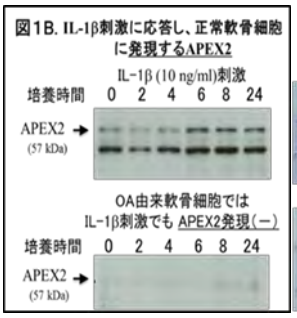

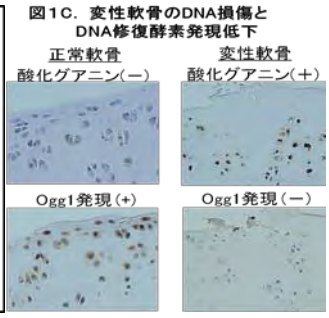

② 外因性刺激（メカニカルストレス）に応答する細胞エネルギー産生の調節機構

メカニカルストレスおよび炎症刺激を特に受けやすい研究評価組織モデルとして関節軟骨を解析し、荷重等のストレスに応答し、軟骨細胞のエネルギー代謝（グルコース取り込み、アデノシン三リン酸 ATP 産生）は一過性に亢進し、ミトコンドリア内のクエン酸回路－電子伝達系の亢進により過剰のフリーラジカル・活性酸素が発生して漏出すること、これが前述の DNA 酸化損傷の一因となること、さらに ATP 産生量を制御する細胞内エネルギーセンサーとしての役割を担う 5'-AMP-activated protein kinase (AMPK)活性も、メカニカルストレスに応答して変化することを見出した。

また、軟骨細胞核内に発現する NAD 依存性脱アセチル化酵素活性を持つ sirtuin 1 (Sirt-1)もエネルギーセンサーとして働き、AMPK 活性と相互に制御し合うフィードバックネットワークのあることを初めて見出した（論文*16, 26、国際学会*6, *12）。

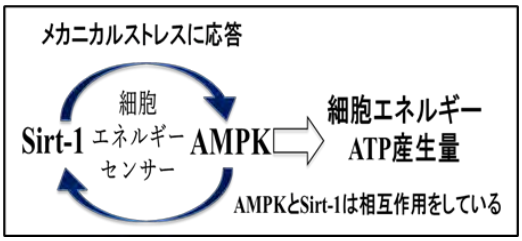

さらに我々は、メカニカルストレスに応答して軟骨細胞が過剰な活性酸素種 (フリーラジカル) を産生するメカニズムおよび DNA 損傷には、細胞エネルギー代謝（ATP 産生・細胞呼吸鎖; 解糖系- クエン酸回路-電子伝達系）が密接に関与すること、すなわち過度のメカニカルストレスに応答して、i) 軟骨細胞内へのグルコース取り込み、ATP 産生が一過性に亢進すること、ii) ATP 産生亢進の過程でミトコンドリア内のクエン酸回路－電子伝達系の作用が亢進し、過剰のフリーラジカルが産生されて漏出すること（これが酸素分子と結合し活性酸素種となる）、iii) グルコース取込み・ATP 産生の亢進に伴い、エネルギーセンサーAMPK–Sirt-1 活性は低下、iv) この脱アセチル化活性を持つ Sirt‐1 活性低下が、DNA 損傷修復酵素（Ogg1, APEX 2）の活性低下の一因となることを示す予備実験結果を得ている（下図）。

メカニカルストレスに対して、細胞・組織がどのように応答するか、特に「メカニカルストレス応答調節機構」(細胞内のストレス応答蛋白, 細胞応答情報伝達路)、「DNA 修復酵素の活性変化」及び「細胞エネルギー代謝調節機構」について、研究を継続していく。

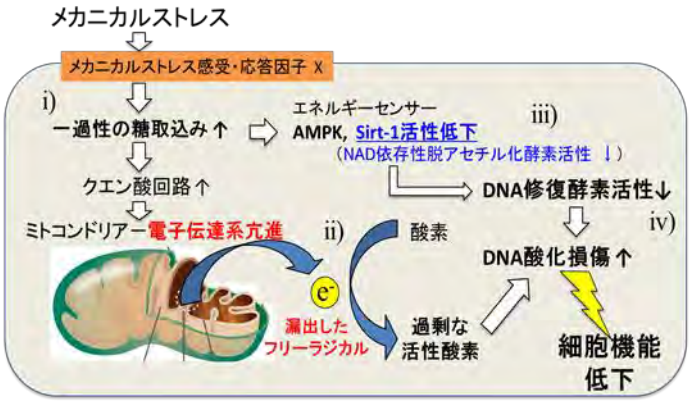

さらに特筆すべき研究結果として、

③ 特定波長条件の光刺激に応答する光感受・応答因子の同定、光刺激刺激受容後の細胞情報伝達経路および最終応答としての細胞活性変化の機序の解析が進んだ点が挙げられる。

我々は、低侵襲的アプローチとして「光刺激に対する細胞応答」に注目し、特定波長条件の光照射によって細胞内光応答蛋白･細胞内情報伝達因子の活性を修飾(スイッチをオン/オフ)させ、疾患組織の細胞活性・機能を制御して治療に結び付ける光治療技術の研究を進めた。

平成 27～29 年度は、先ず関節軟骨と骨組織を中心に実験を進め、光照射による

① 滑膜線維芽細胞の炎症性サイトカイン産生の抑制（抗炎症）、

② 骨芽細胞の骨形成能の増強、③ 破骨細胞の分化成熟の抑制、

④ 破骨細胞による骨吸収能の抑制の効果を確認した（論文投稿・出願準備中）。

さらに、特定波長条件の光照射によって骨芽細胞では転写因子 CLOCK-Bmal, 軟骨細胞では PER-CRY 複合体の発現が増強することを確認し、これらを光刺激感受因子の候補蛋白と考えて、さらに光刺激に応答する細胞活性の変化の解析を継続し、

平成 30 年～令和元年度には

⑤ 特定条件の光照射によって、骨芽細胞活性は増強すること、

⑥ Bmal を抑制した骨芽細胞では、光照射による骨形成増強効果はみられないことを確認、光照射による骨形成能増強効果は CLOCK-Bmal 複合体を介すると考察

⑦ 動物実験および臨床試験用の低侵襲アプローチ方法の具体的検証に向けた装置の仕様検討（照射装置作成・プローブ改良等）を行ない、関節炎および骨関節疾患を対象とする臨床試験の実施に向けた準備（試験機作製、プロトコール作成）を行なった。

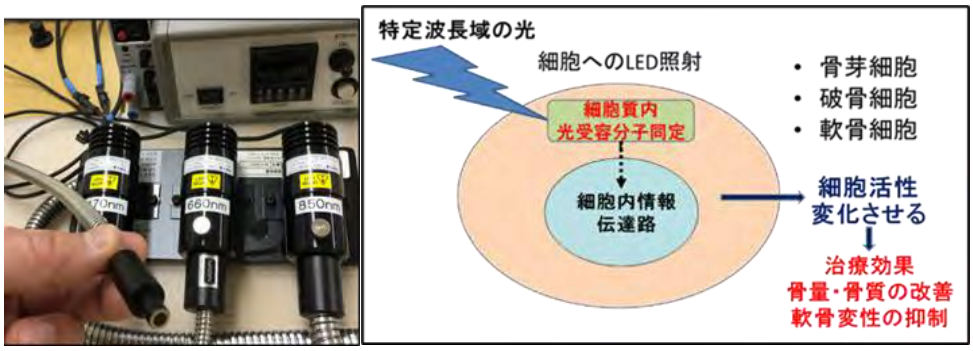

これらの研究成果を基に、特定波長条件の光刺激を感受する機構（細胞内応答蛋白の同定)、光刺激受容後の細胞内変化･情報伝達経路および最終応答としての細胞活性変化の機序を解明し、低侵襲的アプローチとして光照射によって、細胞内応答蛋白ならびに細胞内情報伝達因子の活性を修飾(スイッチをオン/オフ)させ､疾患部組織の細胞活性・機能を制御して治療に結び付ける低侵襲的な光治療技術の研究を進めていく（論文投稿・新規特許出願準備中)。

＜課題となった点＞

研究進捗で明らかとなった問題点とその克服法の検討:　研究の基幹である各種の低侵襲的アプローチに対する細胞応答機構は、ターゲットとする組織・臓器・細胞によって、それぞれにおいて特徴があり、細胞活性を修飾しうる刺激条件も異なる可能性がある。本研究プロジェクトにおいても、低侵襲的アプローチ（例えば温熱刺激、光刺激、ナノ

カプセル化製剤等）の最適条件において、ある細胞・組織に対しては有効であるが、近傍の他の組織・細胞に対しては無効または別の作用が発現する可能性もあり得ることが明らかとなった。

そこで、今後の検討課題として細胞・組織毎に有効な低侵襲的アプローチ条件を詳らかにして、各々個別に対応できるように実験系および医療技術開発に組み込むことを検討して行く予定である。

＜自己評価の実施結果と対応状況＞

本研究支援事業の期間は、研究者全員参加の研究会議（月1回）に加えて、難病治療研究センター主催のセミナー・難病研修会（前述）を、医学・医療領域に限定せず異分野領域の研究者、看護師、薬剤師、理学療法士、患者（患者の会・家族）を対象に開催し、以下の取り組みを行ない、以下の点に留意して検討を進めてきた。

- 研究会議において、研究テーマごとの進捗度・問題点などを全員で公開討論し、研究遂行のための人員・研究費配分の妥当性や調整を協議した。
- 対話型ワークショップの実施により、研究過程において得られる効果・課題・改善点等について検証し、研究活動へフィードバックするように努めた。

拠点のビジョン・イメージ、拠点の研究開発活動から派生する研究開発課題に関連する新たなシーズ・ニーズを、連携の範囲を広げた多様な異分野・異業種・異領域の参加者（医療統計家、知財事業企画部門等）によるワークショップを今後とも企画し、新しい研究シーズ・ニーズの発掘するように努める。

＜外部（第三者）評価の実施結果と対応状況＞

外部評価実施に関しては、以下の 3 点で対応してきた。

① 前述の研究会議、セミナー・研修会に、外部評価者として学外研究者、医学・医療専門家（会によっては非専門領域の外部評価者・弁理士・弁護士）を参加招聘し、研究内容からの逸脱の有無、進捗度、動物試験や生命倫理上の問題点の有無等の評価を依頼、研究活動に反映している。

② 年に一回の学外研究者を対象とした公開研究会・シンポジウムにおいて、研究成果を公開して研究部外者（専門領域）の意見・評価をその後の研究活動に反映するようにしている。

③ 本研究支援事業終了後も、これまでに得られた研究成果を、国内外の学会および査読のある国際学術専門誌に論文として発表して評価を得ていく。研究業績は、研究代表者所属の難病治療研究センターのホームページ（http://nanchiken.jp/）に掲載していく。

＜研究期間終了後の展望＞

研究成果によって期待される医療の革新、社会への貢献について検討

本研究支援事業の期間中に得られた成果を基にした医療技術の開発は、これまでの研究成果と既存技術の応用によって十分に達成可能であり、さらに LED 等の光源、光ファイ

バープローブなど最先端光工学のイノベーションと医療応用によるバリューチェーンに大いに寄与し、国際競争力のある新産業創出が期待できるものを考える。

本研究支援事業の研究プロジェクトを今後とも推進することにより、これまでの手術療法や薬物療法（薬の内服、注射、経皮吸収）のいずれにもよらず、疾患患部に選択的に光照射して細胞活性を変化させることで治療に結び付ける非薬物・低侵襲医療技術を完成させ、これを基盤とする在宅医療機器を医療情報・地域医療インフラと連携させることが期待される。これにより、医療機関への 通院回数や入院日数を抑制し、医療現場の過度な負担を軽減させることで限られた医療　資源を弾力的に運用することができるようになる。

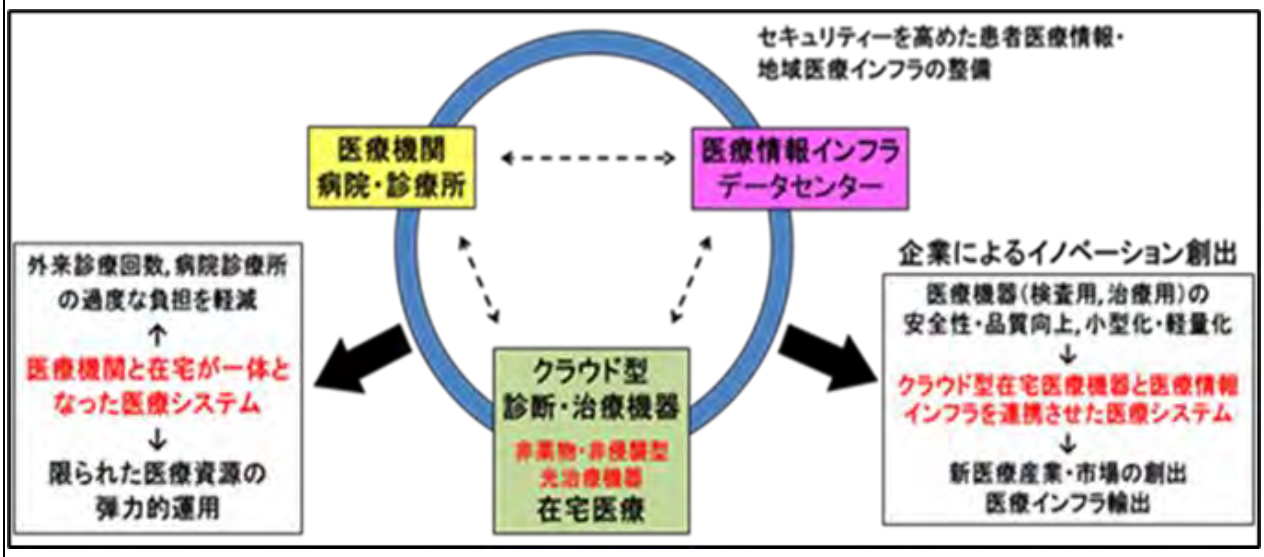

＜研究成果の副次的効果＞

本研究プロジェクトの基盤となる先行知財・基礎特許を補強する知見が得られているので、国際特許出願や新規知財としての出願を準備中である。また、研究支援事業の間に得られた「光刺激に対する細胞応答・細胞活性修飾」の成果を医療機器として実用化に向けて展開するため、医療機器開発企業・オージー技研株式会社と共同研究契約を結び、動物試験および臨床試験に向けて医療機器試作機を作製し、産学連携の研究を継続している。

12　キーワード（当該研究内容をよく表していると思われるものを8項目以内で記載してください。）

（1）低侵襲アプローチ　（2）Drug delivery system (DDS)　（3）物理的刺激
（4）光刺激感受因子　（5）メカニカルストレス　（6）温熱刺激
（7）薬剤ナノカプセル技術　（8）難治性疾患

13 研究発表の状況（研究論文等公表状況。印刷中も含む。）
上記、11(4)に記載した研究成果に対応するものには＊を付すこと。

＜雑誌論文＞

研究テーマ1関連 主要論文.

2019 年度

1. Kumai T, Yui N, Yatabe K, Sasaki C, Fujii R, Takenaga M, Fujiya H, Niki H, Yudoh K. A novel, self-assembled artificial cartilage–hydroxyapatite conjugate for combined articular cartilage and subchondral bone repair: histopathological analysis of cartilage tissue engineering in rat knee joints. International Journal of Nanomedicine, 2019;14：1283-1298.
2. Kaiyu Jiang, Rie Karasawa, Zihua Hu, Yanmin Chen, Lucy Holmes, Kathleen M. O'Neil, James N. Jarvis. Plasma Exosomes From Children With Juvenile Dermatomyositis Are Taken Up By Human Aortic Endothelial Cells and Are Associated With Altered Gene Expression in Those Cells. Pediatr Rheumatol Online J. 2019;17(1)：41-doi: 10.1186/s12969-019-0347-0.
3. Rie Karasawa, James N. Jarvis. Using the Tools of Proteomics to Understand the Pathogenesis of Idiopathic Inflammatory Myopathies. Current Opinion in Rheumatology, 2019;doi：10.1097/BOR.0000000000000643.

2018 年度

4. Kazuo Yudoh, Rie Karasawa. Effects of low-level laser therapy on clinical characteristics and laboratory profiles in synovitis in patients with rheumatoid arthritis. Nov Tech Arthritis Bone Res , 2018;2(5)：1-8.
5. Takenaga Mitsuko, Niimi Jun, Hamaguchi Akemi, Asano Teita, Tsuchiya Reiko, Ohta Yuki, Yudoh Kazuo, Inoue Hajime. Protective effect of boiogito extract with glucosamine HCL against adjuvant-induced arthritis in rats. Traditional & Kampo Medicine , 2018;5(1)：38-44.
6. Karawsawa R, Tamaki M, Sato T, Tanaka M, Nawa M, Yudoh K, Jarvis JN..Multiple Target Autoantigens on Endothelial Cells Identified in Juvenile Dermatomyositis Using Proteomics. Rheumatology (Oxford), 2018;57(4)：671-676.
7. Fujii R, Komatsu R, Sato T, Seki I, Konomi K, Aono H, Niki H, Yudoh K, Nishioka K, Nakajima T. SPACIA1/SAAL1 deletion results in a moderate delay in collagen-induced arthritis activity, along with mRNA decay of cyclin-dependent kinase 6 gene. International Journal of Molecular Sciences , 2018;19(12)：E3828.
8. Ohta Yuki, Takenaga Mitsuko, Hamaguchi Akemi, Ootaki Masanori, Takeba Yuko, Kobayashi Tsukasa, Watanabe Minoru, Iiri Taroh, Matsumoto Naoki. Isolation of adipose-derived stem/stromal cells from cryopreserved fat tissue and transplantation into rats with spinal cord injury. International jornal of molecular sciences, 2018;19(7)：1963.
9. 遊道和雄、藤井亮爾. 免疫、全身性疾患における診断・治療の現状と求める医薬品・医療機器・再生医療像　第 8 節全身性エリテマトーデス　希少疾患用医薬品の適応拡大と事業性評価 2018:388-392.
10. 唐澤里江. 血管炎動物モデル. 炎症と免疫 , 2018;26(5)：75-80.
11. 遊道和雄、藤井亮爾. 健康長寿マーカーとしての長寿遺伝子関連たんぱく濃度測定. FOOD STYLE 21 , 2018;22(12)：37-41.
12. 藤井亮爾，小松梨恵，仁木久照，遊道和雄. 関節リウマチ由来滑膜線維芽細胞において炎症性サイトカインで誘導される細胞周期因子 cyclin-dependent kinase 6. 聖マリアンナ医科大学雑誌 ,

2019;46(4)：239-247.

2017 年度

13. Suzuki E, Fujita D, Takahashi M, Oba S, Nishimatsu H. Therapeutic effects of mesenchymal stem cell-derived exosomes in cardiovascular disease. Adv Exp Med Biol , 2017;998：179-185.
14. Suzuki E, Imuta H, Fujita D, Takahashi M, Oba S, Kiyosue A, Nishimatsu H. Endogenous interleukin-1beta is implicated in intraplaque hemorrhage in apolipoprotein E gene null mice. Circ J , 2018;82：1130-1138.
15. Yudoh Kazuo, Yoshioka Hirotaka, Yui Naoko, Karasawa Rie. Therapeutic Potential of Nanocarbon C60 Fullerene in Osteoarthritis. International Journal of Development Research , 2017;7(4)：12450-12453.

*16. Kobayashi Hajime, Terauchi Koh, Yui Naoko, Yatabe Kanaka, Kamada Toshikazu, Fujiya Hiroto, Niki Hisateru, Musha Haruki, Yudoh Kazuo. The Nicotinamide Adenine Dinucleotide (NAD)-Dependent eacetylase Sirtuin-1 Regulates Chondrocyte Energy Metabolism through the Modulation of Adenosine Monophosphate-Activated Protein Kinase (AMPK) in Osteoarthritis (OA). Journal of Arthritis, 2017;6(2)：1-8.

17. Yudoh Kazuo, Yui Naoko, Kumai Takanori, Karasawa Rie. Cell-to-Cell Interactions of Activated T Cells with Adjacent Cells in Inflamed Tissue in Inflammatory Diseases. Nov Tech Arthritis Bone Res , 2017;2(3)：1-6.
18. Karasawa R, Tamaki M, Sato T, Tanaka M, Nawa M, Yudoh K, Jarvis JN. Multiple Target Autoantigens on Endothelial Cells Identified in Juvenile Dermatomyositis Using Proteomics. Rheumatology (Oxford), 2018; in press.
19. Shinagawa S, Okazaki T, Ikeda M, Yudoh K, Kisanuki Y, Yanagisawa M, Kawahata K, Ozaki S. T cells upon activation promote endothelin 1 production monocytes via INF-γ and TNF-α. SCIENTIFIC REPORTS , 2017;7(14500)：1-8.
20. Yudoh Kazuo, Kumai Takanori, Fujiya Hiroto, Yui Naoko, Karasawa Rie. Cartilage Tissue Engineering-A Novel Biomaterial for Cartilage Repair Generated by Self- Assembly: Creation of a Self-Organized Articular Cartilage-like Tissue. Novel Techniques in Arthritis & Bone Research , 2017;1(2)：1-3.
21. 遊道和雄. 関節リウマチと変形性関節症. アレルギーの臨床 , 2017;37(5)：69-73.
22. 鈴木弘子、箕輪千佳、木下瞳、有馬里佳、川島康裕、片山富雄、唐澤里江. 難病相談における「アロマとリラクゼーションの会」の取り組み. 聖マリアンナ医科大学雑誌 , 2017;45：25-29.

2016 年度

23. Suzuki E, Nishimatsu H, Homma Y. Erectile dysfunction and chronic kidney disease and renal transplantation International book of erectile dysfunction 2016;341-360.
24. Wu Y, Nakagawa S, Takahashi H, Kawabata Y, Suzuki E, Uehara Y. The angiotensin II receptor antagonist, losartan, enhances regulator of G protein signaling 2 mRNA expression in vascular smooth muscle cells of Wistar rats. Hypertens Res, 2016;39：295-301.
25. Wu Y, Takahashi H, Suzuki E, Kruzliak P, Soucek M, Uehara Y. Impaired response of regulator of Galphaq signaling-2 mRNA to angiotensin II and hypertensive renal injury in Dahl salt-sensitive rats. Hypertens Res, 2016;39：210-216.

*26. Terauchi K, Kobayashi H, Yatabe K, Yui N, Fujiya H, Niki H, Musha H, Yudoh K. The NAD-Dependent Deacetylase Sirtuin-1 Regulates the Expression of Osteogenic Transcriptional Activator Runt-Related Transcription Factor 2 (Runx2) and Production of Matrix Metalloproteinase (MMP)-13 in Chondrocytes in Osteoarthritis. Int. J. Mol. Sci, 2016;17(7)：1019.

27. Yoshioka H, Yui N, Yatabe K, Fujiya H, Musha H, Niki H, Karasawa R, Yudoh K. Polyhydroxylated C60

Fullerenes Prevent Chondrocyte Catabolic Activity at Nanomolar Concentrations in Osteoarthritis. Int.J.Clin.Rheumatol, 2016;11(5):70-76.

28. Arito Mitsumi, Mitsui Hiroyuki, Kurokawa-Suzuki Manae, Yudoh Kazuo, Kamada Toshikazu, Niki Hisateru, Kato Tomohiro. Effects of soy peptides on IL-1β-induced matrix-degrading enzymes in human articular chondrocytes. Integrative molecular medicine , 2016;3(3):661-665.
29. Suzuki E, Fujita D, Takahashi M, Oba S, Nishimatsu H. Stem cell-derived exosomes as a therapeutic tool for cardiovascular disease. World journal of stem cells , 2016;8:297-305.

2015 年度

30. Takenaga M, Yamamoto Y, Takeuchi T, Ohta Y, Tokura Y, Hamaguchi A, Asai D, Nakashima H, Oishi S, Fujii N. Potential new chemotherapy strategy for human ovarian carcinoma with a novel KSP inhibitor. Biochemical and Biophysical Research Communications , 2015;463(3):222-228.
31. Jun Shimizu, Hiroshi Oka, Yoshihisa Yamano, Kazuo Yudoh, Noboru Suzuki. Cutaneous manifestations of patients with relapsing polychondritis: an association with extracutaneous complications. Clin. Rheumatol, 2016;35:781-783.
32. Yudoh K, Karasawa R, Ishikawa J. Age-related decrease of sirtuin 2 in peripheral blood mononuclear cells in human. Curr Aging Sci , 2015;8(3):256-258.

*33. Yui Naoko, Yudoh Kazuo, Fujiya Hiroto, Musha Haruki. Mechanical and oxidative stress in osteoarthritis. Journal of Physical Fitness and Sports Medicine , 2016;5(1):81-86.

34. Nishimatsu H, Suzuki E, Saito Y, Niimi A, Nomiya A, Yamada D, Homma Y. Neuromedin B restores erectile function by protecting the cavernous body and the nitrergic nerves from injury in a diabetic rat model. PLoS One , 2015;10:e0133874.
35. Nishimatsu H, Suzuki E, Saito Y, Niimi A, Nomiya A, Fukuhara H, Kume H, Homma Y. Senescent cells impair erectile function through induction of endothelial dysfunction and nerve injury in mice. PLoS One , 2015;10:e0124129.
36. Jun Shimizu, Hiroshi Oka, Yoshihisa Yamano, Kazuo Yudoh, Noboru Suzuki. Cardiac involvement in relapsing polychondritis in Japan. Rheumatology(Oxford) , 2016;55(3):583-584.
37. Suzuki E, Fujita D, Takahashi M, Oba S, Nishimatsu H. Adult stem cells as a tool for kidney regeneration. World J Nephrol , 2016;5:43-52.
38. Karasawa R, Jarvis N. Using proteomic and genomic methods to understand JDM. Japanese Journal of clinical Immunology , 2015;38(3):150-156.
39. Suzuki E, Fujita D, Takahashi M, Oba S, Nishimatsu H. Adipose tissue-derived stem cells as a therapeutic tool for cardiovascular disease. World journal of cardiology, 2015;7:454-465.
40. 吉岡広孝, 油井直子, 前川敬祐, 河野光登, 武者春樹, 遊道和雄. 関節リウマチ患者の関節症状に対する大豆ペプチド摂取の有効性評価. 応用薬理 , 2015;88：39-46.
41. 遊道和雄. 慢性疲労症候群最新調査. NHK　今日の健康 , 2015;(330)：90-93.
42. 遊道和雄. 慢性疲労症候群（筋痛性脳脊髄炎）-「日常生活困難度調査」から見えてきたもの- いつでも元気, 2015;(286)：18-21.

研究テーマ2関連　主要論文

2019 年度

43. Kaji T, Arito M, Tsutiya A, Sase T, Onodera H, Sato T, Omoteyama K, Sato M, Suematsu N, Kurokawa MS, Tanaka Y, Kato T. Layilin enhances the invasive ability of malignant glioma cells via SNAI1 signaling. Brain

Res. 2019 Sep 15;1719:140-147. doi: 10.1016/j.brainres.2019.05.034.

44. Omoteyama K, Sato T, Arito M, Sato M, Suematsu N, Kurokawa MS, Kato T. Effects of salazosulfapyridine on the profile of cell surface proteins, revealed by biotinylation of cell surface proteins and 2-dimentional electrophoresis. Biochim Biophys Acta Proteins Proteom. 2019 Jan;1867(1):47-56. doi: 10.1016/j.bbapap.2018.05.007.

2018 年度

45. Tsuno H, Arito M, Suematsu N, Sato T, Hashimoto A, Matsui T, Omoteyama K, Sato M, Okamoto K, Tohma S, Kurokawa MS, Kato T. A proteomic analysis of serum-derived exosomes in rheumatoid arthritis. BMC Rheumatol. 2018 Nov 27;2:35. doi: 10.1186/s41927-018-0041-8.
46. Imanishi Hiroharu, Igarashi Suguru, Yamaguchi Yoko, Suzuki Nao. Anti-aging Effect on Skin of Autologous Transplantation of Tissue Fragments from Thawed Cryopreserved Ovaries. Journal of St. Marianna University , 2018;9(1)：7-14.
47. Sekiguchi Kiyoshi, Sato Masaaki, Yokoyama K. Michiyo, Sato Toshiyuki, Tsutiya Atsuhiro, Omoteyama Kazuki, Arito Mitsumi, Suematsu Naoya, Kato Tomohiro, Kurokawa S. Manae. Effects of memantine on the growth and protein profiles of neuroblastoma cells. Integrative Molecular Medicine, 2018;51(1):1-8. DOI: 10.15761/IMM.1000317

2017 年度

48. Shimazaki K, Arito M, Sato T, Omoteyama K, Sato M, Kurokowa MS, Suematsu N, Niki H, Kato T. Roles of layilin in human synovial fibroblasts revealed by proteomic analysis. Integrative Molecular Medicine. 4(6): 2017, doi: 10.15761/IMM.1000316, 2017
49. Ooka S, Kurokawa MS, Yokoyama M, Arito M, Sato T, Sato M, Takakuwa Y, Omoteyama K, Suematsu N, Kawahata K, Kato T. Effects of iguratimod on protein profiles of chondrosarcoma cells. Integrative Molecular Medicine. 4(6): doi: 10.15761/IMM.1000315, 2017
50. Matsuura T. Sato M, Nagai K, Sato T, Arito M, Omoteyama K, Suematsu N, Okamoto K, Kato T, Soma Y, Kurokawa MS. Serum peptides as putative modulators of inflammation in psoriasis. Journal of dermatological science. 87(1):36-49. 2017
51. Katano M. Kurokawa MS, Matsuo K, Suematsu N, Okamoto K, Kamada T, Nakamura H, Kato T. Phosphoproteome analysis of synoviocytes from patients with rheumatoid arthritis. International Journal of Rheumatic Diseases. 20(6):708-721. 2017
52. Kato M, Hamada-Tsutsumi S, Okuse C, Sakai A, Matsumoto N, Sato M, Sato T, Arito M, Omoteyama K, Suematsu N, Okamoto K, Itoh F, Sumazaki R, Tanaka Y, Yotsuyanagi H, Kato T, Kurokawa MS. Effects of vaccine-acquired polyclonal anti-HBs antibodies on the prevention of HBV infection of non-vaccine genotypes. Journal of gastroenterology. 52（9）:1051–1063. 2017
53. Sase T, Arito M, Onodera H, Omoteyama K, Kurokawa MS, Kagami Y, Ishigami A, Tanaka Y, Kato T. Hypoxia-induced production of peptidylarginine deiminases and citrullinated proteins in malignant glioma cells. Biochemical and biophysical research communications. 482(1):50-56. 2017

2016 年度

54. Nozawa Y, Arito M, Omoteyama K, Sato M, Takakuwa Y, Ooka S, Kurokawa MS, Kato T. Comprehensive analysis of surface proteins of peripheral mononuclear blood cells in patients with systemic lupus erythematosus. Integrative Molecular Medicine. 3(6): 1-5. 2016
55. Furukawa H, Chikada M, Yokoyama MK, Arito M, Kurokawa MS, Sato T, Sato M, Omoteyama K, Suematsu

N, Kobayashi T, Sagane M, Suzuki H, Ando T, Kato T, Miyairi T. Characterrization of small leucine-rich proteoglycans in aortic valves of paitients with aortic valve stenosis. Integrative Molecular Medicine. 3(5):796-801. 2016

56. Okamoto K, Hirata-Tsuchiya S, Kitamura C, Omoteyama K, Sato T, Arito M, Kurokawa MS, Suematsu N, Kato T. A Small Nuclear Acidic Protein (MTI-II, Zn2+-binding protein, parathymosin) that Inhibits Transcriptional Activity of NF-κB and its Potential Application to Anti-Inflammatory Drugs. Endocrinology. 157(12):4973–4986. 2016.
57. Arito M, Mitsui H, Kurokawa MS, Yudoh K, Kamada T, Niki H, Kato T. Effects of soy peptides on IL-1β-induced matrix-degrading enzymes in human articular chondrocytes. Integrative molecular medicine. 3(3): 661-665. 2016
58. Sase T, Arito M, Onodera H, Kurokawa MS, Tanaka Y, Kato T. Effects of edaravone on hypoxic human astrocytes revealed by a proteomic approach. Biomedical Research. 27 (4): 1064-1070. 2016
59. Tsuno H, Suematsu N, Sato T, Arito M, Matsui T, Iizuka N, Omoteyama K, Okamoto K, Tohma S, Kurokawa MS, Kato T. Effects of methotrexate and salazosulfapyridine on protein profiles of exosomes derived from a human synovial sarcoma cell line of SW982. Proteomics. Clinical applications. 10(2):164-71. 2016
60. Suzuki H, Chikada M, Yokoyama MK, Kurokawa MS, Ando T, Furukawa H, Arito M, Miyairi T, Kato T. Aberrant glycosylation of lumican in aortic valve stenosis revealed by a proteomic analysis. International heart journal. 57(1):104-111. 2016.

2015 年度

61. Adachi T, Arito M, Suematsu N, Kamijo-Ikemori A, Omoteyama K, Sato T, Kurokawa MK, Okamoto K, Kimura K, Shibagaki Y, Kato T. Roles of layilin in TNF-alpha-induced epithelial-mesenchymal transformation of renal tubular epithelial cells. Biochemical and biophysical research communications. 467(1):63-69. 2015
62. Arito M, Nagai K, Ooka S, Sato T, Takakuwa Y, Kurokawa MS, Sase T, Okamoto K, Suematsu N, Kato T. Altered acetylation of proteins in patients with rheumatoid arthritis, revealed by acetyl-proteomics. Clinical and experimental rheumatology. 2015. 33(6):877-86.
63. Koizumi H, Arito M, Endo W, Kurokawa MS, Okamoto K, Omoteyama K, Suematsu N, Beppu M, Kato T. Effects of tofacitinib on nucleic acid metabolism in human articular chondrocytes. Modern rheumatology / the Japan Rheumatism Association. 25(4): 30:1195-1206.522-527. 2015.
64. Suzuki I, Noguchi M, Arito M, Sato T, Omoteyama K, Maedomari M, Hasegawa H, Suematsu N, Okamoto K, Kato T, Yamaguchi N, Kurokawa MS. Serum peptides as candidate bio- markers for dementia with Lewy bodies. International Journal of Geriatric Psychiatry. 30:1195-1206. 2015.

研究テーマ3関連　主要論文

2019 年度

65. Nagasaka M, Yamagishi M, Yagishita N, Araya N, Kobayashi S, Makiyama J, Kubokawa M, Yamauchi J, Hasegawa D, Coler-Reilly ALG, Tsutsumi S, Uemura Y, Arai A, Takata A, Inoue E, Hasegawa Y, Watanabe T, Suzuki Y, Uchimaru K, Sato T, Yamano Y. Mortality and risk of progression to adult T-cell leukemia/lymphoma in HTLV-1-associated myelopathy/tropical spastic paraparesis. Proc Natl Acad Sci U S A, 2020 in press.
66. Araujo A, Bangham CRM, Casseb J, Gotuzzo E, Jacobson S, Martin F, Penalva A, Puccioni-Sohler M, Taylor GP, Yamano Y. Management of HAM/TSP. systematic review and consensus-based recommendations 2019.

Neurology Clinical Practice, 2020 in press.

67. Yamauchi J, Sato T, Yagishita N, Araya N, Hasegawa D, Tsutsumi S, Nagasaka M, Coler-Reilly A, Inoue E, Takata A, Hasegawa Y, Yamano Y. Use of cerebrospinal fluid CXCL10 and neopterin as biomarkers in HTLV-1-associated myelopathy/tropical spastic paraparesis treated with steroids. J Neurol Neurosurg Psychiatry, 91(3):321-323, 2020.
68. Takeda R, Ishigaki T, Ohno N, Yokoyama K, Kawamata T, Fukuyama T, Araya N, Yamano Y, Uchimaru K, Tojo A. Immunophenotypic analysis of cerebrospinal fluid reveals concurrent development of ATL in the CNS of a HAM/TSP patient. Int J Hematol. 2020 in press.
69. 八木下尚子、山野嘉久. 患者レジストリの分類. 脳神経内科, 92(3):271-275, 2020.
70. Katsuya H, Islam S, Tan BJY, Ito J, Miyazato P, Matsuo M, Inada Y, Iwase SC, Uchiyama Y, Hata H, Sato T, Yagishita N, Araya N, Ueno T, Nosaka K, Tokunaga M, Yamagishi M, Watanabe T, Uchimaru K, Fujisawa JI, Utsunomiya A, Yamano Y, Satou Y. The Nature of the HTLV-1 Provirus in Naturally Infected Individuals Analyzed by the Viral DNA-Capture-Seq Approach. Cell Rep, 29(3):724-735, 2019.
71. Yamaguchi I, Furusawa Y, Kawaguchi T, Yagishita N, Tanzawa K, Yamano Y, Matsuda F. Establishment of a Comprehensive Information Infrastructure and a Support Organization for Rare Disease Research in Japan (RADDAR-J). Stud Health Technol Inform, 264:1080-1083, 2019.
72. Tsutsumi S, Sato T, Yagishita N, Yamauchi J, Araya N, Hasegawa D, Nagasaka M, Coler-Reilly A, Inoue E, Takata A, Yamano Y. Real-World Clinical Course of HTLV-1-Associated Myelopathy/Tropical Spastic Paraparesis (HAM/TSP) in Japan. Orphanet Journal of Rare Diseases, 14(1):227, 2019.
73. Tamaki K, Sato T, Tsugawa J, Fujioka S, Yagishita N, Araya N, Yamauchi J, Coler-Reilly A, Nagasaka M, Hasegawa Y, Yamano Y, Tsuboi Y. Cerebrospinal Fluid CXCL10 as a Candidate Surrogate Marker for HTLV-1-Associated Myelopathy/Tropical Spastic Paraparesis. Front Microbiol, 10:2110, 2019.
74. Yamauchi J, Yamano Y, Yuzawa K. Risk of Human T-cell Leukemia Virus Type 1 Infection in Kidney Transplantation. N Engl J Med, 380(3):296-298, 2019.
75. Morio Y, Izawa KP, Omori Y, Katata H, Ishiyama D, Koyama S, Yamano Y. The Relationship between Walking Speed and Step Length in Older Aged Patients. Diseases, 7(1), 2019.
76. Furusawa Y, Yamaguchi I, Yagishita N, Tanzawa K, Matsuda F, Yamano Y, RADDAR‐J Research and Development Group. National platform for Rare Diseases Data Registry of Japan. Learn Health Sys, e10080, 2019.
77. 山内淳司、山野嘉久. HAM の病態と HTLV-1 感染細胞の異常. 細胞, 51(10):20-23, 2019.
78. 山野嘉久. HTLV-1 関連脊髄症. 内科学書　改訂第 9 版. 総編集：南学　正臣, 386-387, 2019 年 8 月 30 日, 中山書店.
79. 山野嘉久, 他：「HTLV-1 関連脊髄症（HAM）診療ガイドライン 2019」作成委員会. HTLV-1 関連脊髄症（HAM）診療ガイドライン 2019. 編集：「HTLV-1 関連脊髄症（HAM）診療ガイドライン 2019」作成委員会, 監修：日本神経学会, 日本神経治療学会, 日本神経免疫学会, 日本神経感染症学会, 日本 HTLV-1 学会, 日本移植学会. 1-181, 2019 年 6 月 5 日, 南江堂.
80. 山野嘉久. HTLV-1 関連脊髄症 [指定難病 26]. 指定難病ペディア 2019、水澤英洋、五十嵐　隆、北川泰久、高橋和久、弓倉　整　監修・編集. 95-97、日本医師会、東京、2019.
81. 山野嘉久. HTLV-1 関連脊髄症（HAM）に対する新規治療法. Annual Review 神経 2019, 149-154, 2019.

2018 年度

82. Yodo Sugishita, Naoki Okamoto, Atsushi Uekawa, Takayuki Yamochi, Mariko Nakajima, Chie Namba, Suguru Igarashi, Takumi Sato, Sei Ohta, Makoto Takenoshita, Shu Hashimoto, Akiko Tozawa, Yoshiharu

Morimoto, Nao Suzuki. Oocyte retrieval after heterotopic transplantation of ovarian tissue cryopreserved by closed vitrification protocol. Journal of assisted reproduction and genetics , 2018;35(11) : 2037-2048.

83. Sato T, Coler-Reilly ALG, Yagishita N, Araya N, Inoue E, Furuta R, Watanabe T, Uchimaru K, Matsuoka M, Matsumoto N, Hasegawa Y, Yamano Y. Mogamulizumab (Anti-CCR4) in HTLV-1-Associated Myelopathy. N Engl J Med, 378(6):529-538, 2018.
84. Shimizu, J, Yamano Y, Kawahata K, Suzuki N. Relapsing polychondritis patients were divided into three subgroups: patients with respiratory involvement (R subgroup), patients with auricular involvement (A subgroup), and overlapping patients with both involvements (O subgroup), and each group had distinctive clinical characteristics. Medicine, 97:42(e12837), 2018.
85. Oka T, Mizuno H, Sakata M, Fujita H, Yoshino T, Yamano Y, Utsumi K, Masujima T, Utsunomiya A. Metabolic abnormalities in adult T-cell leukemia/lymphoma and induction of specific leukemic cell death using photodynamic therapy. Scientific Reports, 8:14979, 2018.
86. Kuramitsu M, Okuma K, Nakashima M, Sato T, Sasaki D, Hasegawa H, Umeki K, Kubota R, Sasada K, Sobata R, Matsumoto C, Kaneko N, Tezuka K, Matsuoka S, Utsunomiya A, Koh KR, Ogata M, Ishitsuka K, Taki M, Nosaka K, Uchimaru K, Iwanaga M, Sagara Y, Yamano Y, Okayama A, Miura K, Satake M, Saito S, Watanabe T, Hamaguchi I. Development of reference material with assigned value for human T-cell leukemia virus type 1 quantitative PCR in Japan. Microbiol Immunol, 62:673-676, 2018.
87. Sato T, Yamano Y. Targeting human T-lymphotropic virus type 1-infected cells with an anti-C-C chemokine receptor 4 antibody in T-lymphotropic virus type 1-associated myelopathy. Clinical and Experimental Neuroimmunology, 9(3):153-154, 2018.
88. Kawano N, Yoshida S, Kawano S, Kuriyama T, Tahara Y, Toyofuku A, Manabe T, Doi A, Terasaka S, Yamashita K, Ueda Y, Ochiai H, Marutsuka K, Yamano Y, Shimoda K, Kikuchi I. The clinical impact of human T-lymphotrophic virus type 1 (HTLV-1) infection on the development of adult T-cell leukemia-lymphoma (ATL) or HTLV-1-associated myelopathy (HAM) / atypical HAM after allogeneic hematopoietic stem cell transplantation (allo-HSCT) and renal transplantation. J Clin Exp Hematop, 107-121, 2018.
89. Sato T, Yagishita N, Tamaki K, Inoue E, Hasegawa D, Nagasaka M, Suzuki H, Araya N, Coler-Reilly A, Hasegawa Y, Tsuboi Y, Takata A, Yamano Y. Proposal of Classification Criteria for HTLV-1-Associated Myelopathy/Tropical Spastic Paraparesis Disease Activity. Front Microbiol, 9:1651, 2018.
90. Hirano M, Jimbo K, Ogawa M, Ochi K, Makiyama J, Kawamata T, Yokoyama K, Tanaka T, Inamoto Y, Yamano Y, Fukuda T, Uchimaru K, Imai Y, Tojo A. Chronic inflammatory demyelinating polyneuropathy in adult T-cell leukemia-lymphoma patients following allogeneic stem cell transplantation Bone Marrow Transplantation. Bone Marrow Transplantation, Published online, 2018.DOI: https://doi.org/10.1038/s41409-018-0202-9
91. Shimizu J, Yamano Y, Yudoh K, Suzuki N. Organ Involvement Pattern Suggests Subgroups within Relapsing Polychondritis. Arthritis Rheumatol, 70(1):148-149, 2018.
92. 山野嘉久. HTLV-1 関連脊髄症. 感染症, 48(6):25-28,2018.
93. 山野嘉久.「特集　HTLV-1 関連脊髄症—病態解明と治療の最新情報」はじめに 医学のあゆみ, 267(10):735, 2018.
94. 八木下尚子. HAM の臨床情報基盤—患者レジストリ“HAM ねっと”. 医学のあゆみ, 267(10):746-750, 2018.
95. 佐藤知雄. HAM の疾患活動性分類と治療. 医学のあゆみ, 267(10):756-760, 2018.
96. 山野嘉久、山内淳司、新谷奈津美、八木下尚子、佐藤知雄. HTLV-1 関連脊髄症（HAM）の病態・診断・治

療.神経内科, 89(3):297-303, 2018.

97. 八木下尚子、山野嘉久. 希少難病 HAM の患者レジストリを活用した治療薬開発への取り組みと展望 Jpn Pharmacol Ther (薬理と治療), 46(7):1113-1116, 2018.

2017 年度

98. Futagami M, Yokoyama Y, Sato S, Miyagi E, Tozawa-ono A, Suzuki N, Fujimura M, Aoki Y, Sagae S, Sugiyama T. Contributions of the japanese gynecologic oncology group (jgog)in lmproving the quality of life in women with gynecological malignancies. Springer Link, 2018; in press.
99. Yoshioka Norihito, Hasegawa Junichi, Tozawa Akiko, Nakamura Kentaro, Kawahara Tai, Maeda Ichiro, Suzuki Nao. Sonohysterography in a suspected case of uterine perforation after dilatation and curettage for retained placenta. Case Report in Perinatal Medicine, 2017; DOI-10.1515/crpm-2017-0011.
100. Akiko Tozawa-Ono, Manabu Kubota, Chika Honma, Yuko Nakagawa, Noriyuki Yokomichi, Norihito Yoshioka, Chiharu Tsuda, Tatsuru Ohara, Hirotaka Koizumi, Nao Suzuki. Glycan profiling using formalin-fixed, paraffin-embedded tissues: Hippeastrum hybrid lectin is a sensitive biomarker for squamous cell carcinoma of the uterine cervix. The Journal of Obstetrics and Gynaecology Research , 2017;43(8)：1326-1334.
101. Kawano Noriaki, Kuriyama Takuro, Yoshida Shuro, Kawano Sayaka, Yamano Yoshihisa, Marutsuka Kousuke, Minato Seiichirou, Yamashita Kiyoshi, Ochiai Hidenobu, Shimoda Kazuya, Ishikawa Fumihiko, Kikuchi Ikuo. The Impact of a Humanized CCR4 Antibody (Mogamulizumab)on Patients with Aggressive-Type Adult T-Cell Leukemia-Lymphoma Treated with Allogeneic Hematopoietic Stem Cell Transplantation. Journal of Clinical and Experimental Hematopathology , 2017;56(3)：135-144.
102. Kuramitsu Madoka, Sekizuka Tsuyoshi, Yamochi Tadanori, Firouzi Sanaz, Sato Tomoo, Umeki Kazumi, Sasaki Daisuke, Hasegawa Hiroo, Kubota Ryuji, Sobata Rieko, Matsumoto Chieko, Kaneko Noriaki, Momose Haruka, Araki Kumiko, Saito Masumichi, Nosaka Kisato, Utsunomiya Atae, Koh Kiryang, Ogata Masao, Uchimaru Kaoru, Iwanaga Masako, Sagara Yasuko, Yamano Yoshihisa, Okayama Akihiko, Miura Kiyonori, Satake Masahiro, Saito Shigeru, Itabashi Kazuo, Yamaguchi Kazunari, Kuroda Makoto, Watanabe Toshiki, Okuma Kazu, Hamaguchi Isao. Proviral features of human T cell leukemia virus type 1 in carriers with indeterminate western blot analysis results. Journal of clinical microbiology , 2017;55(9)：2838-2849.
103. Sato Tomoo, Ariella L.G.Coler-Reilly, Yagishita Naoko, Araya Natsumi, Inoue Eisuke, Furuta Rie, Watanabe Toshiki, Uchimaru Kaoru, Matsuda Masao, Matsumoto Naoki, Hasegawa Yasuhiro, Yamano Yoshihisa. Mogamulizumab(Anti-CCR4) in HTLV-1 Associated Myelopathy. The NEW ENGLAND JOURNAL of MEDICINE , 2018;378(6)：529-538.
104. Ariella L.G.Coller-Reilly, Sato Tomoo, Matsuzaki Toshio, Nakagawa Masanori, Niino Masaaki, Nagai Masahiro, Nakamura Tatsufumi, Takenouchi Norihiro, Araya Natsumi, Yagishita Naoko, Inoue Eisuke, Yamano Yoshihisa. Effectiveness of Daily Prednisolone to Slow Progression of Human T-Lymphotropic Virus Type 1-Associated Myelopathy/Tropical Spastic Paraparesis: A Multicenter Retrospective Cohort Study. Neurotherapeutics : the journal of the American Society for Experimental Neuro Therapeutics , 2017; : DOI-10.1007/s13311-017-0533-z.
105. Sawada L, Nagano Y, Hasegawa A, Kanai H, Nogami K, Ito S, Sato T, Yamano Y, Tanaka Y, Masuda T, Kannagi M. IL-10-mediated signals act as a switch for lymphoproliferation in Human T-cell leukemia virus type-1 infection by activating the STAT3 and IRF4 pathways. PLoS pathogens , 2017;13(9)：e1006597.
106. Terada Y, Kamoi K, Ohno-Matsui K, Miyata K, Yamano C, Coler-Reilly A, Yamano Y. Treatment of rheumatoid arthritis with biologics may exacerbate HTLV-1-associated conditions: A case report. Medicine ,

2017;96(6)：e6021.

107. 戸澤晃子, 吉岡範人, 大原樹, 鈴木直. 婦人科手術周術期の静脈決戦塞栓症の予防と治療に関する最近の話題. 産婦人科の実際 , 2017;66(6)：773-780.
108. 八木下尚子, 中島利博. 関節リウマチ発症因子シノビオリン. アレルギーの臨床, 2017;37(9):72-78.
109. 山野嘉久. HTLV-1 関連脊髄症の診断と治療. 日本内科学会雑誌 , 2017;106(7)：1404-1409.
110. 山野嘉久. HTLV-1 関連脊髄症に対するヒト化抗 CCR4 抗体療法開発の背景. 神経治療学, 2017;34(4)：453-457.
111. 八木下尚子, 山野嘉久. HAM 患者レジストリ「HAM ねっと」によるリアルワールドデータの活用. PHARMSTAGE , 2017;17(6)：19-22.
112. 山野嘉久. HTLV-1 関連脊髄症[HAM：HTLV-1-associated myelopathy]. CareNet 希少疾病ライブラリ, 2017.

2016 年度

113. Yagishita N, Aratani S, Fujita H, Yamano Y, Nishioka K, Nakajima T. Synoviolin is a Novel Pathogenic Factor of Arthropathy and Chronic Inflammation. New Developments in the Pathogenesis of Rheumatoid Arthritis 2017;123-135.
114. Gallo RC, Willems L, Hasegawa H; Global Virus Network's Task Force on HTLV-1: Accolla R, Bangham C, Bazarbachi A, Bertazzoni U, Anna B, Cheng H, Chieco-Bianchi L, Ciminale V, Gessain A, Gotuzzo E, Hall W, Hermine O, Jacobson S, Macchi B, Mahieux R, Matsuoka M, McSweegan E, Murphy EL, Reis J, Simon V, Tagaya Y, Taylor GP, Watanabe T, Yamano Y. Screening transplant donors for HTLV-1 and-2. Blood , 2016;128(26):3029-3031.
115. Fujita H, Aratani S, Fujii R, Yamano Y, Yagishita N, Araya N, Izumi T, Azakami K, Hasegawa D, Nishioka K, Nakajima T. Mitochondrial ubiquitin ligase activator of NF-kB regulates NF-kB signaling in cells subjected to ER stress. Int J Mol Med , 2016;37:1611-1618.
116. Yamano Y, Coler-Reilly A. HTLV-1 induces a Th1-like state in CD4+ CCR4+ T cells that produces an inflammatory positive feedback loop via astrocytes in HAM/TSP. Journal of neuroimmunology, 2016: DOI-10.1016.
117. Coler-Reilly ALG, Yagishita N, Suzuki H, Sato T, Araya N, Inoue E, Takata A, Yamano Y. Nation-wide epidemiological study of Japanese patients with rare viral myelopathy using novel registration system (HAM-net). Orphanet Journal of Rare Diseases , 2016;11(1):69.
118. Terao C, Yoshifuji H, Yamano Y, Kojima H, Yurugi K, Miura Y, Maekawa T, Handa H, Ohmura K, Saji H, Mimori T, Matsuda F. Genotyping of relapsing polychondritis identified novel susceptibility HLA alleles and distinct genetic characteristics from other rheumatic diseases. Rheumatology , 2016;55(9):1686-1692.
119. 八木下尚子, 中島利博. 関節リウマチ発症因子シノビオリン. 別冊　BIO Clinica　慢性炎症と疾患 , 2016;5(3)：137-143.
120. 新谷奈津美, 佐藤知雄, アリエラ・コラライリー, 八木下尚子, 山野嘉久. HTLV-1 関連脊髄症（HAM）の分子病態解明による治療薬開発の新展開. Japanese Journal of Clinical Immunology , 2016;39(3)：207-212.
121. 山野嘉久. HTLV-1 関連脊髄症の病態に基づいた疾患修飾薬の開発. Modern Physician , 2016;36(7)：682-687.
122. 八木下尚子, 中島利博.　関節リウマチ発症因子シノビオリン. アレルギーの臨床 , 2017;37(2)：94-100.
123. 八木下尚子, 中島利博.　関節リウマチ発症因子シノビオリン. アレルギーの臨床 , 2016;36(13)：84-90.

124. 山野嘉久, 齋藤滋. HTLV-1. 産科と婦人科 , 2016;83(9)：1021-1026.
125. 新谷奈津美, 山野嘉久. HTLV-1 関連脊髄症（HAM）の分子病態と治療. 血液内科 , 2017;74(3)：373-379.

2015 年度

126. Fujita H, Yagishita N, Aratani S, Saito-Fujita T, Morota S, Yamano Y, Hansson MJ, Inazu M, Kokuba H, Sudo K, Sato E, Kawahara KI, Nakajima F, Hasegawa D, Higuchi I, Sato T, Araya N, Usui C, Nishioka K, Nakatani Y, Maruyama I, Usui M, Hara N, Uchino H, Elmer E, Nishioka K, Nakajima T. The E3 ligase synoviolin controls body weight and mitochondrial biogenesis through negative regulation of PGC-1β. The EMBO journal , 2015;34(8)：1042-1055.
127. Usuba Ayano, Handa Hiroshi, Inoue Teppei, Azagami Shinya, Yamano Yoshihisa, Mineshita Masamichi, Miyazawa Teruomi, Baumbach Jorg Ingo. Breath Analysis for Relapsing Polychondritis Assessed by Ion Mobility Spectrometry. International Journal for Ion Mobility Spectrometry , 2015;(18)：177-183.
128. Kuramitsu M, Okuma K, Yamochi T, Sato T, Sasaki D, Hasegawa H, Umeki K, Kubota R, Sobata R, Matsumoto C, Kaneko N, Naruse I, Yamagishi M, Nakashima M, Momose H, Araki K, Mizukami T, Mizusawa S, Okada Y, Ochiai M, Utsunomiya A, Koh KR, Ogata M, Nosaka K, Uchimaru K, Iwanaga M, Sagara Y, Yamano Y, Satake M, Okayama A, Mochizuki M, Izumo S, Saito S, Itabashi K, Kamihira S, Yamaguchi K, Watanabe T, Hamaguchi I.. Standardization of Quantitative PCR for Human T-cell Leukemia Virus Type 1 in Japan: A Collaborative Study. Journal of Clinical Microbiology , 2015;53(11)：3485-3491.
129. Martin F, Inoue E, Cortese ICM, de Almeida Kruschewsky R, Adonis A, Grassi MFR, Galvo-Castro B, Jacobson S, Yamano Y, Taylor GP, Bland M. Timed walk as primary outcome measure of treatment response in clinical trials for HTLV-1-associated myelopathy: a feasibility study. Pilot and Feasibility Studies, 2015;1：35.
130. Usuba Ayano, Yamashiro Tsuneo, Handa Hiroshi, Matsuoka Shin, Yamano Yoshihisa, Mineshita Masamichi, Miyazawa Teruomi. Quantitative Computed Tomography Measurement of Tracheal Cross-Sectional Areas in Relapsing Polychondritis: Correlations with Spirometric Values. Respiration , 2015;90(6)：468-473.
131. Yamano Y. How does human T-lymphotropic virus type 1 cause central nervous system disease? The importance of cross-talk between infected T cells and astrocytes. Clinical and Experimental Neuroimmunology , 2015;6(4)：395-401.
132. Bangham C, Araujo A, Yamano Y, Taylor G. HTLV-I-Associated Myelopathy/Tropical Spastic Paraparesis. Nature Reviews Disease Primers, 2015; Published online.
133. 石塚賢治, 山野嘉久, 宇都宮與, 内丸薫. HTLV-1 キャリア外来の実態調査. 臨床血液 , 2015;56(6)：666-672.
134. 山野嘉久. HTLV-1 関連脊髄症（HAM）－分子病態解明による治療薬開発の新展開. 医学のあゆみ , 2015;255(5)：485-490."
135. 山野嘉久, 新谷奈津美, 八木下尚子, 佐藤知雄. 免疫性神経疾患－基礎・臨床研究の最新知見－. 日本臨牀 , 2015;73(7)：546-553.
136. 山野嘉久. HAM に対するヒト化 CCR4 抗体の医師主導治験. 臨床評価 , 2016;43(2)：418-421.

＜図書＞

研究テーマ1関連.

1. 遊道和雄. 治療に関するシステマティックレビュー 筋痛性脳脊髄炎/慢性疲労症候群(ME/CFS)診療の手引き 2019:159-169.
2. 遊道和雄、清水孝恒. 骨・関節疾患 やさしい臨床医学テキスト 第４版 2018;363-370.

3. 遊道和雄. 第 7 章　自己免疫疾患領域での診断のあり方と求める診断技術　第 1 節　全身性エリテマトーデスの診断の現状と求める診断技術 疾患・病態検査・診断法の開発 2017;323-326.
4. 武永美津子, 五十嵐理慧, 水島徹. リピッドマイクロスフェア DDS キャリア作製プロトコール集 2015:213-224.
5. 遊道和雄. 変形性関節症(Osteoarthritis:OA)治療法の今後の展開 : OA 治療を目的をとする自己注射薬の可能性について 自己注射 2016:32-37.

研究テーマ2関連.

研究テーマ3関連.

5. 山野嘉久. 15 HTLV-1 関連脊髄症 [指定難病 26] 指定難病ペディア 2019:95-97.
6. 山野嘉久, 他 :「HTLV-1 関連脊髄症（HAM）診療ガイドライン 2019」作成委員会. HTLV-1 関連脊髄症（HAM）診療ガイドライン 2019. 2019:1-181.
7. 山野嘉久. HTLV-1 関連脊髄症 内科学書　改訂第 9 版 2019:386-387.
8. 山野嘉久. 痙性対麻痺（HAM を含む） 今日の治療指針 2016 2016:964-965.
9. 山野嘉久. HTLV-1 関連脊髄症（HAM） 難病事典 2015:2-5.

＜学会発表＞

研究テーマ1関連.

【国際学会】

1. Rie Karasawa, James N. Jarvis, Toshiko Sato, Megumi Tanaka, Mark Hicar, Kazuo Yudoh, Terrance P O'Hanlon, Payam Noroozi-Farhadi, Lisa G. Rider. Clinical Correlations of Autoantibodies Against Heat Shock Cognate 71 kDa Protein in Patients with Juvenile Dermatomyositis. The American College of Rheumatology/Association of Rheumatology Professionals Annual Meeting, 2019.
2. Rie Karasawa, Paul A. Monach, Toshiko Sato, Megumi Tanaka, David Cuthbertson, Simon Carette, Nader A. Khalidi, Curry L. Koening, Carol Langford, Carol A. McAlear, Larry W. Moreland, Christian Pagnoux, Philip Seo, Antoine G. Sreih, Kenneth J. Warrington, Steven R. Ytterberg, Kazuo Yudoh, James N. Jarvis, Peter A. Merkel.. Identification of Target Antigens for Anti-Endothelial Cell Antibodies in Patients with Takayasu's Arteritis Using Proteomics. The 19th International Vasculitis & ANCA Workshop, 2019.
3. Rie Karasawa, Toshiko Sato, Megumi Tanaka, Mayumi Tamaki, Kazuo Yudoh, James N. Jarvis. Anti-Endothelial Cell Antibodies in Pediatric Rheumatic Diseases. The American College of Rheumatology Annual Meeting 2018, 2018.

*6. Yudoh Kazuo, Terauchi Koh, Kobayashi Hajime, Yui Naoko, Fujiya Hiroto, Niki Hisateru, Musha Haruki. Impact of NAD-Dependent Deacetylase Sirtuin-1 in the Osteophyte Formation and the Degradation of Articular Cartilage in Osteoarthritis(OA). 2017 World Congress on Osteoarthritis, 2017.

7. Karasawa Rie, Tamaki Mayumi, Sato Toshiko, Tanaka, Megumi, Yudoh Kazuo, James N. Jarvis. Anti-endothelial cell antibodies in juvenile dermatomyositis. 2017 Pediatric Rheumatology Symposium, 2017.
8. Kaiyu Jiang, Zihua Hu, Rie Karasawa, Yanmin Chen, James Jarvis. Plasma exosomes from children with juvenile dermatomyositis are taken up by human aortic endothelial cells and are associated with altered gene expression in those cells. 2017 American College of Rheumatology Annual Meeting, 2017.
9. Karasawa Rie, Tamaki Mayumi, Sato Toshiko, Tanaka Megumi, Yudoh Kazuo, James Javis. Anti-endothelial cell antibodies in juvenile dermatomyositis: A proteomics-based approach. 2017 American College of Rheumatology Annual Meeting, 2017.

10. Rie Karasawa, Paul A. Monach, Toshiko Sato, Mayumi Tamaki, Megumi Tanaka, Takahiro Okazaki, Masamichi Oh-Ishi, Kazuo Yudoh, James N. Jarvis, Peter A. Merkel. Zyxin is a novel autoantigen for anti-endothelial cell antibodies in giant cell arteritis. The 18th International Vasculitis & ANCA Workshop 2017, 2017.
11. Rie Karasawa, Mayumi Tamaki, Megumi Tanaka, Toshiko Sato, Kazuo Yudoh, James N. Jarvis. Identification of target antigens for anti-endothelial cell antibodies in patients with juvenile dermatomyositis using proteomics. The 18th International Vasculitis & ANCA Workshop 2017, 2017.

*12. Yui N, Musya H, Fujiya H, Yatabe K, Yoshioka H, Terauchi K, Yudoh K. The Role of ATP-Activeted Protein Kinase (AMPK) in the Chondrocyte Energy Balance and IL-β-induced Production of MMP-13 in Osteoarthritis(OA). The OARSI 2016 World Congress, 2016.

13. Karasawa R, Tamaki M, Tanaka M, Sato T, Yudoh K, James N. Javis. Novel autoantigens for endotheliol cell antibodies in pediatric rheumatic diseases indentified by proteomics. 2016 CARRA Scientific Meeting, 2016.
14. Rie Karasawa, Mayumi Tamaki, Megumi Tanaka, Toshiko Sato, Kazuo Yudoh, James N. Jarvis. Novel autoantigens for anti-endothelial cell antibodies in pediatric rheumatic diseases indentified by proteomics. American College of Rheumatology Annual Meeting 2016, 2016.
15. Ohta Yuki, Takenaga Mitsuko, Hamaguchi Akemi, Niimi Jun, Ootaki Masanori, Watanabe Minoru, Takeba Yuko, Iiri Taro, Matsumoto Naoki. Transplantation of adipose-derived stem/stromal cells is useful in regenerative medicine. 第 18 回国際ヒトレトロウィルス HTLV 会議, 2017.
16. Rie Karasawa, Toshiko Sato, Mayumi Tamaki, Mikiya Fujieda, Ohta Hidekazu, Kazuo Yudoh. Roles of Peroxiredoxin 2 in Patients With Kawasaki Disease. Pediatric Academic Societies' Annual Meeting, 2015.
17. Rie Karasawa, Mayumi Tamaki, Alisa Li, Kaiyu Jiang, Kazuo Yudoh, James N. Jarvis. Identification of Target Antigens for Anti-Endothelial Cell Antibodies in Patients With Juvenile Dermatomyositis Using Proteomics. Pediatric Academic Societies' Annual Meeting, 2015.
18. N Yui, H Yoshioka, H Fujiya, H Musha, R Karasawa, K Yudoh. WATER-SOLUBLE C60-(OH)24 FULLERENE HYDROXIDE AS ATHERAPEUTIC AGENT THE DEGENERATION OF ARTICULAR CARTILAGE IN OSTEOARTHRITIS. 2015 OARSI World Congress on Osteoarthritis, 2015.
19. Yui N, Musha H, Fujiya H, Yatabe K, Yoshioka H, Terauchi k, Yudoh K. Significance of Defense Mechanism for Oxidative DNA Damage in Osteoarthritis(OA): DNA Repair Enzyme, Apurinic/Apyrimidinic Endonuclease(APEX2), Protects Against the Catabolysis of Articular Cartilage in OA. 15th International Conference on ISANH Antioxidants, 2015.
20. Rie Karasawa, Mayumi Tamaki, Yanmin Chen, Kaiyu Jiang, Kazuo Yudoh, James N. Jarvis. Identification of target antigens for anti-endothelial cell antibodies in patients with pediatric rheumatic diseases using proteomics. American College of Rheumatology, 2015.
21. Ryoji Fujii, Iwao Seki, Rie Komatsu, Miwa Takai, Tomomi Kohara, Tomoo Sato, Kohji Konomi, Hiroyuki Aono, Kazuo Yudoh, Kusuki Nishioka, Toshihiro Nakajima. SPACIA1/SAAL1-Deficient Mice Show Reduced Disease Progression in Collagen-Induced Arthritis. American College of Rheumatology, 2015.

【国内学会】

22. 熊井隆智, 遊道和雄, 小谷貴史, 谷田部かなか, 油井直子, 仁木久照, 藤谷博人. 自己組織化技術による人工軟骨-人工骨複合バイオマテリアルの創製－ラット膝関節における軟骨組織の組織学的分析－. 第 34 回日本整形外科学会基礎学術集会, 2019.
23. 遊道和雄. 自己組織化技術による人工軟骨－人工骨複合バイオマテリアルの創製. 2019 年度明治大学・聖マリアンナ医科大学共同研究会, 2019.

24. 小松梨恵, 關巖, 佐藤知雄, 許斐康嗣, 青野浩之, 遊道和雄, 仁木久照, 西岡久寿樹, 中島利博, 藤井亮爾. SPACIA1/SAAL1 の遺伝子欠損は CDK6 の mRNA 分解に関与し、CIA モデルにおける関節炎の進展を軽減する. 第 34 回日本整形外科学会基礎学術集会, 2019.
25. 藤井亮爾, 小松梨恵, 中島利博, 仁木久照, 遊道和雄.. 関節リウマチ滑膜細胞において TNF α は cdk4 ではなく cdk6 遺伝子を発現誘導する. 第 34 回日本整形外科学会基礎学術集会, 2019.
26. 熊井隆智, 遊道和雄, 小谷貴史, 谷田部かなか, 油井直子, 仁木久照, 藤谷博人. 三次元培養下における骨芽細胞および破骨細胞の力学的ストレス応答能の解析. 第34回日本整形外科学会基礎学術集会, 2019.
27. 小松梨恵, 關巖, 佐藤知雄, 許斐康嗣, 青野浩之, 遊道和雄, 仁木久照, 西岡久寿樹, 中島利博, 藤井亮爾. マウスコラーゲン誘導関節炎の重症度の違いにおける SPACIA1/Saal1 遺伝子欠損の影響. 第 63 回日本リウマチ学会, 2019.
28. 藤井亮爾, 小松梨恵, 遊道和雄, 仁木久照, 西岡久寿樹, 中島利博. 滑膜細胞における SPACIA1/SAAL1 は TNF-α誘導性の CDK6 発現を部分的に制御する. 第 62 回日本リウマチ学会総会・学術集会, 2018.
29. 遊道和雄. ME/CFS 治療に関するシステマティックレビュー. 第 14 回日本疲労学会総会・学術集会, 2018.
30. 寺内昂, 遊道和雄, 小林創, 熊井隆智, 油井直子, 藤谷博人, 仁木久照. NAD 依存性脱アセチル化酵素 Sirtuin1 は軟骨細胞で骨形成転写因子 Runx2 と蛋白分解酵素 MMP-13 を制御する. 第 33 回日本整形外科学会基礎学術集会, 2018.
31. 熊井隆智, 遊道和雄, 小谷貴史, 谷田部かなか, 油井直子, 仁木久照, 藤谷博人. 軟骨再生医療に向けた自己組織化技術を用いた人工軟骨-人工骨複合体バイオマテリアルの創製. 第 33 回日本整形外科学会基礎学術集会, 2018.
32. 遊道和雄. 光刺激の感受・細胞応答機構の解明と骨関節疾患に対する光医療器開発への応用. 2017 年度　明治大学・聖マリアンナ医科大学共同研究会, 2017.
33. 小松梨恵, 遊道和雄, 仁木久照, 西岡久寿樹, 中島利博, 藤井亮爾. SPACIA1/SAAL1 が制御する CDK6 発現量の減少は RA 滑膜細胞の増殖を抑制する. 第 61 回日本リウマチ学会総会・学術集会, 2017.
34. 小林創, 遊道和雄, 寺内昂, 谷田部かなか, 油井直子, 仁木久照, 藤谷博人. 変形性膝関節症において sirt-1 は軟骨細胞のエネルギー代謝を制御する. 第 32 回日本整形外科学会基礎学術集会, 2017.
35. 小松梨恵, 關巖, 佐藤知雄, 青野浩之, 山野嘉久, 遊道和雄, 仁木久照, 西岡久寿樹, 中島利博, 藤井亮爾. SPACIA/SAAL1 の遺伝子欠損はコラーゲン誘導関節炎モデルにおける関節炎の進展を軽減する. 第 60 回日本リウマチ学会総会・学術集会, 2016.
36. 品川尚志, 岡崎貴裕, 池田真理, 遊道和雄, 山田秀裕, 尾崎承一. 活性化Ｔ細胞によるエンドセリン産生誘導機構の解析～ヒトとマウスの相同性の検討～. 第 60 回日本リウマチ学会総会・学術集会, 2016.
37. 清水潤、鈴木登、岡寛、山野嘉久、遊道和雄. 再発性多発軟骨炎（RP)における皮膚病変と皮膚外合併症との関連検討（多施設アンケート調査）. 第 60 回日本リウマチ学会総会・学術集会, 2016.
38. 遊道和雄. ME/CFS 治療ガイドラインの作成に向けて. 第 12 回日本疲労学会総会・学術集会, 2016.
39. 土屋聖子, 太田有紀, 武永美津子, 大滝正訓, 新美純, 大石真也, 藤井信孝, 松本直樹, 津川浩一郎. 新規合成 KSP(Kinesin spindle protein)阻害剤のヒト乳癌細胞に対する抗腫瘍効果に関する研究. 第 24 回日本乳癌学会学術総会, 2016.
40. 寺内昂, 遊道和雄, 小林創, 油井直子, 藤谷博人, 仁木久照, 武者春樹. NAD 依存性脱アセチル化酵素 Sirtuin1 と骨形成転写因子 Runx2 の変性軟骨細胞における役割. 第 31 回日本整形外科学会基礎学

術集会, 2016.

41. 小林創, 油井直子, 寺内昂, 藤谷博人, 遊道和雄, 仁木久照, 武者春樹. 変形性関節症の軟骨細胞におけるエネルギー代謝と Sirtuin1 との関連について. 第 31 回日本整形外科学会基礎学術集会, 2016.
42. 太田有紀, 土屋聖子, 武永美津子, 角田智志, 大滝正訓, 新美純, 大石真也, 藤井信孝, 渡辺実, 武半優子, 飯利太朗, 松本直樹. ヒト乳癌細胞に対する新規 KSP(kinesin spindle protein)阻害薬の効果. 第 37 回日本臨床薬理学会, 2016.
43. 太田有紀, 新美純, 濱口明美, 大滝正訓, 渡辺実, 武半優子, 飯利太朗, 松本直樹, 武永美津子. 下肢筋委縮に対する脂肪組織由来幹細胞移植の効果. 第 16 回日本再生医療学会総会, 2017.
44. 吉岡広孝, 藤谷博人, 油井直子, 谷田部かなか, 寺内昂, 小林創, 工藤貴章, 大野真弘, 武者春樹, 遊道和雄. 関節リウマチの関節症状に対する大豆ペプチド摂取の有効性評価. 第 53 回九州リウマチ学会, 2017.
45. 小松梨恵, 佐藤知雄, 山野嘉久, 遊道和雄, 別府諸兄, 西岡久寿樹, 中島利博, 藤井亮爾. コラーゲン誘導関節炎における CDK6 阻害剤の効果. 第 59 回日本リウマチ学会総会・学術集会, 2015.
46. 伊東宏, 山田秀裕, 品川尚志, 御影秀徳, 松下広美, 水島万智子, 山崎宜興, 尾崎承一, 遊道和雄, 山野嘉久. 治療抵抗性気管軟化症に対しトシリズマブが有効であった再発性多発軟骨炎の 1 例. 第 59 回日本リウマチ学会総会・学術集会, 2015.
47. 鈴木登, 清水潤, 岡寛, 山野嘉久, 遊道和雄. 再発性多発軟骨炎（RP)の血管病変（多施設アンケート調査）. 第 59 回日本リウマチ学会総会・学術集会, 2015.
48. Takahashi M, Sato T, Fujita D, Myojo M, Kiyosue A, Suzuki E. Adipose-Derived Stem Cells Stimulate Reendothelialization and Inhibit Neointimal Formation in Stented Rat Abdominal Aorta. 日本循環器学会学術総会, 2015.
49. 武永美津子, 石原務, 新美純, 濱口明美, 太田有紀, 水島徹. Nano PGE1 の慢性炎症に対する作用. 第 31 回日本 DDS 学会学術集会, 2015.
50. 武永美津子, 石原務, 新美純, 濱口明美, 太田有紀, 水島徹. PGE1 含有徐放製剤（Nano PGE1）のアジュバント関節炎に対する作用. 第 36 回日本炎症・再生医学会, 2015.
51. 西松寛明、鈴木 越. 脂肪幹細胞の antiaging の意義. 第 11 回日本抗加齢医学会, 2015.
52. 品川尚志、岡崎貴裕、池田真理、遊道和雄、柳沢正史、木佐貫泰、山田秀裕、尾崎承一. 活性化 T 細胞により誘導される血管内皮細胞非依存性エンドセリン産生機構の解析. 第43回日本臨床免疫学会総会, 2015.
53. 淺井大輔, 金本大成, 寺久保繁美, Ashutosh Chilkoti, 武永美津子,中島秀喜. インジェクタブル人工エラスチンゲルによる抗 HIV ペプチドのデポ製剤化. 第 37 回バイオマテリアル学会大会, 2015.
54. 太田有紀, 土屋聖子, 武永美津子, 大滝正訓, 渡辺実, 武半優子, 飯利太朗, 松本直樹. 癌細胞に対する新規 KSP 阻害薬の効果. 第 36 回日本臨床薬理学会学術総会, 2015.
55. 太田有紀, 武永美津子, 大滝正訓, 渡辺実, 武半優子, 飯利太朗, 松本直樹. 凍結脂肪組織からの組織幹細胞の単離と研究利用の試み. 第 15 回日本再生医療学会総会, 2016.
56. Okamoto K, Sato M, Omoteyama K, Sato T, Arito M, Kurokaw MS, Suematsu N, Yudo K, Kato T. In vivo anti? inflammatory action of the inhibitory sequence in the NFκB comrepressor a new peptidepharmaceutical. BMB2015 (第 38 回日本分子生物学会年会、第 88 回日本生化学会大会), 2015.
57. 武永美津子, 竹内智起, 山本有貴, 都倉享恵, 新美純, 濱口明美, 太田有紀, 淺井大輔, 大石真也, 中島秀喜, 藤井信孝. 新規合成 KSP 阻害剤のヒト卵巣がんに対する抗腫瘍効果. 日本薬学会第 136 年会, 2016.

研究テーマ2関連.

【国際学会】

58. Kurokawa S Manae. Development of Novel Serum Peptide Biomarkers - Toward Clinical Application -. 32nd International Synposium on Pediatric Surgery Research. 2019.
59. Kurokawa MS, Nagai K, Sato T, Sato M, Takakuwa Y, Ooka S, Arito M, Kato T. Oxidative modification of myeloperoxidase in anti-neutrophil cytoplasmic antibody (ANCA)-associated vasculitides. The 18th International Vasculitis & ANCA Workshop. 2017/3/25-28. Tokyo.
60. Suzuki H, Chikada M, Yokoyama M, Kurokawa M, Furukawa H, Arito M, Miyairi T, Kato T. Aberrant Glycosylation of Lumican in Aortic Valve Stenosis Revealed by a Proteomic Analysis. 23th ASCVTS 2015. 2015/5 Hong Kong.

【国内学会】

61. 佐藤政秋、佐藤利行、表山和樹、土屋貴大、有戸光美、末松直也、加藤智啓、黒川真奈絵. 顕微鏡的多発血管炎の新規血清ペプチドバイオマーカー候補 AC13 の MALDI-TOF/MS による定量. 第 92 回日本生化学会大会. 2019.
62. 佐々木 琳子、永井 宏平、西端 智也、佐藤 政秋、佐藤 利行、黒川 真奈絵、加藤 智啓. ANCA 関連血管炎患者における自己抗原 Myeloperoxidase の翻訳後修飾の解析. 日本プロテオーム学会 2019 年大会. 2019.
63. 黒川真奈絵. 新規血清ペプチドバイオマーカーの臨床応用を目指してー内部標準を用いた質量分析による定量法の開発ー. 日本プロテオーム学会 2019 年大会. 2019.
64. 表山和樹、佐藤利行、佐藤政秋、土屋貴大、有戸光美、末松直也、黒川真奈絵、加藤智啓. A Distintegrin And Metalloprotease 17 (ADAM17) 新規基質の探索. 第 15 回日本臨床プロテオゲノミクス研究会. 2019.
65. 有戸光美、佐藤利行、表山和樹、佐藤政秋、黒川真奈絵、加藤智啓. 滑膜繊維芽細胞におけるライリンの役割. 第 63 回日本リウマチ学会総会・学術集会. 2019.
66. 表山和樹、佐藤利行、土屋貴大、佐藤政秋、有戸光美、末松直也、黒川真奈絵、加藤智啓. HeLa 細胞におけるエクトドメインシェディングの網羅的解析. 第 91 回日本生化学会大会. 2018.
67. 佐藤政秋、関口潔、佐藤利行、土屋貴大、表山和樹、有戸光美、末松直也、加藤智啓、黒川真奈絵. 神経細胞の蛋白質プロファイルに与えるメマチンの影響. 第 91 回日本生化学会大会. 2018.
68. 有戸光美、梶友紘、土屋貴大、佐藤政秋、佐藤利行、表山和樹、黒川真奈絵、末松直也、田中雄一郎、加藤智啓. 悪性神経膠腫細胞におけるライリンの役割. 第 91 回日本生化学会大会. 2018.
69. 佐藤利行、佐藤政秋、横山倫代、高桑由希子、大岡正道、表山和樹、有戸光美、末松直也、川畑仁人、加藤智啓、黒川真奈絵. イグラチモドが軟骨肉腫細胞の蛋白質プロファイルに与える影響. 第 91 回日本生化学会大会. 2018.
70. 黒川真奈絵. 2D-DIGE を用いた自己免疫疾患のバイオマーカーおよび薬剤の新規作用の探索. 第 69 回日本電気泳動学会総会. 2018.
71. 嶋﨑孝輔、有戸光美、佐藤利行、表山和樹、佐藤政秋、黒川真奈絵、末松直也、仁木久照、加藤智啓. プロテオミクス法を用いた、ヒト滑膜繊維芽細胞株におけるライリンの機能解析. 日本質量分析学会・日本プロテオーム学会　2018 年合同大会. 2018.
72. 佐藤政秋、関口潔、佐藤利行、土屋貴大、表山和樹、有戸光美、末松直也、加藤智啓、黒川真奈絵. 神経細胞の蛋白質プロファイルに与えるメマチンの影響. 日本質量分析学会・日本プロテオーム学会　2018 年合同大会. 2018.
73. 黒川真奈絵、大岡正道、横山倫代、有戸光美、佐藤利行、佐藤政秋、高桑由希子、表山和樹、末松

直也、川畑仁人、加藤智啓．イグラチモドが軟骨肉腫細胞の蛋白質プロファイルに与える影響．日本質量分析学会・日本プロテオーム学会　2018 年合同大会．2018.

74. 表山和樹、佐藤利行、土屋貴大、佐藤政秋、有戸光美、末松直也、黒川真奈絵、加藤智啓．2D-DIGE 法によるエクトドメインシェディングの解析．日本質量分析学会・日本プロテオーム学会　2018 年合同大会．2018.

75. 大岡正道、佐藤利行、佐藤政秋、高桑由希子、表山和樹、有戸光美、黒川真奈絵、加藤智啓．軟骨細胞の蛋白質プロファイルに対するイグラチモドの影響. 第 62 回日本リウマチ学会総会･学術集会．2018.

76. 橋本茜、尾上裕太郎、浄弘由紀子、西野芽玖、黒川真奈絵、加藤智啓、永井宏平．　好中球 Myeloperoxidase の等電点を変化させる酸化修飾の同定と定量. 2017 年度生命科学系学会合同年次大会（ConBio2017）日本分子生物学会/日本生化学会．2017/12/6～8．兵庫県

77. 佐藤利行、長島義斉、佐藤政秋、表山和樹、有戸光美、末松直也、加藤智啓、黒川真奈絵．再発性多発軟骨炎における血清ペプチドファイルの解析．2017 年度生命科学系学会合同年次大会（ConBio2017）日本分子生物学会/日本生化学会．2017/12/6～8．兵庫県

78. 佐藤政秋、松浦哲彦、永井宏平、佐藤利行、有戸光美、表山和樹、末松直也、加藤智啓、相馬良直、黒川真奈絵．尋常性乾癬の病態に関与する血清ペプチドの同定．2017 年度生命科学系学会合同年次大会（ConBio2017）日本分子生物学会/日本生化学会．2017/12/6～8．兵庫県

79. 黒川真奈絵、関口潔、佐藤政秋、佐藤利行、土屋貴大、表山和樹、有戸光美、末松直也、加藤智啓．神経細胞の蛋白質プロファイルに与えるメマンチンの影響．2017 年度生命科学系学会合同年次大会（ConBio2017）日本分子生物学会/日本生化学会．2017/12/6～8．兵庫県

80. 黒川真奈絵、加藤智啓．関節リウマチ滑膜細胞のリン酸化プロテオーム解析—Phosphoproteome analysis of synoviocytes from patients with rheumatoid arthritis. 日本プロテオーム学会 2017 年大会（JHUPO 第 16 回大会）．2017/7/26～28．大阪府.

81. 表山和樹、佐藤利行、佐藤政秋、有戸光美、末松直也、黒川真奈絵、加藤智啓．二次元電気泳動によるシェディングの解析. An analysis of shidding by two-dimensional polyacrylamide gel electrophoresis. 日本プロテオーム学会 2017 年大会（JHUPO 第 16 回大会）．2017/7/26～28．大阪府.

82. 黒川真奈絵、佐藤政秋, 永井宏平, 佐藤利行, 有戸光美, 表山和樹, 加藤智啓．乾癬性関節炎における血清ペプチドプロファイルの解析．第 61 回日本リウマチ学会総会・学術集会．2017/4/20～4/22．福岡県

83. 大岡正道、高桑由希子, 有戸光美, 黒川（鈴木）真奈絵, 加藤智啓．イグラチモドの軟骨肉腫細胞（OUMS27）タンパク質に対する作用の網羅的検出．第 61 回日本リウマチ学会総会・学術集会．2017/4/20～4/22．福岡県

84. 表山和樹、佐藤政秋, 佐藤利行, 有戸光美, 末松直也, 黒川真奈絵, 加藤智啓．シェディングを受けたタンパク質の網羅的検出方法．第 61 回日本リウマチ学会総会・学術集会．2017/4/20～4/22．福岡県

85. 有戸光美、嶋﨑孝輔, 黒川真奈絵, 佐藤利行, 表山和樹, 加藤智啓．滑膜細胞における Layilin の機能探索．第 61 回日本リウマチ学会総会・学術集会．2017/4/20～4/22．福岡県

86. 佐瀬泰玄、有戸光美, 小野寺英孝, 加藤智啓, 田中雄一郎．ヒト神経膠腫細胞株における PAD の発見およびシトルリン化タンパク質の産生．日本脳神経外科学会第 75 回学術総会．2016/9/29～10/1．福岡県

87. 岡本一起、佐藤政秋、表山和樹、佐藤利行、有戸光美、末松直也、黒川真奈絵、遊道和雄、加藤智啓．NF-κB コリプレッサー（MTI-II）の作用部位をさらに短くしたペプチド．第 89 回日本生化学会大会．2016/9/25～9/27．宮城県

88. 有戸光美、安達崇之、末松直也、池森敦子、表山和樹、佐藤利行、黒川真奈絵、岡本一起、木村健二郎、柴垣有吾、加藤智啓. 腎尿細管上皮細胞の TNF-α 誘導性上皮間葉移行に対する layilin の役割. 第 89 回日本生化学会大会．2016/9/25～9/27．宮城県
89. Kurokawa MS, Arito M, Sato T, Suematsu N, Okamoto K, Kato T. Serum peptides as candidate biomarkers for dementia with Lewy bodies. 第 89 回日本生化学会大会．2016/9/25～9/27．宮城県
90. 表山和樹、佐藤利行、佐藤政秋、有戸光美、岡本一起、末松直也、黒川真奈絵、加藤智啓．シェディングによって放出される細胞表面タンパク質の網羅的な検出. 日本プロテオーム学会 2016 年大会（JHUPO 第 14 回大会）．2016/7/28～7/29．東京都
91. 長島義斉、佐藤利行、表山和樹、有戸光美、加藤智啓、黒川真奈絵．再発性多発軟骨炎における血清ペプチドファイルの解析．日本プロテオーム学会 2016 年大会（JHUPO 第 14 回大会）．2016/7/28～7/29．東京都
92. 岡本一起、佐藤政秋、表山和樹、佐藤利行、有戸光美、黒川真奈絵、末松直也、遊道和雄、礒橋文秀、加藤智啓. 炎症性転写因子 NF-κB のコリプレッサー MTI-II を利用した短いペプチド抗炎症剤. (ア) 第 68 回日本ビタミン学会．2016/6/17～6/18．富山県
93. 永井宏平、有戸光美、黒川真奈絵、大岡正道、表山和樹、加藤智啓．ANCA 関連血管炎における好中球ミエロペルオキシダーゼの酸化修飾．第 60 回日本リウマチ学会総会・学術集会．2016/4/21～4/23．神奈川県
94. 野澤洋平、有戸光美、黒川真奈絵、佐藤政秋、大岡正道、表山和樹、加藤智啓．SLE 患者末梢血単核球の表面蛋白質プロファイルの解析. 第 60 回日本リウマチ学会総会・学術集会. 2016/4/21～4/23. 神奈川県
95. 長島義斉、佐藤利行、佐藤政秋、表山和樹、有戸光美、加藤智啓、黒川真奈絵．再発性多発軟骨炎における血清ペプチドファイルの解析. 第 60 回日本リウマチ学会総会・学術集会. 2016/4/21～4/23. 神奈川県
96. 津野宏隆、有戸光美、末松直也、佐藤利行、表山和樹、佐藤政秋、橋本篤、松井利浩、當間重人、黒川真奈絵、加藤智啓．関節リウマチ患者血清中 exosome のプロテオーム解析．第 60 回日本リウマチ学会総会・学術集会．2016/4/21～4/23．神奈川県
97. 表山和樹、佐藤利行、有戸光美、末松直也、黒川真奈絵、加藤智啓．シェディングに特化した新規分析方法の確立に関する研究．第 60 回日本リウマチ学会総会・学術集会．2016/4/21～4/23．神奈川県
98. 岡本一起、佐藤政秋、表山和樹、佐藤利行、有戸光美、黒川真奈絵、末松直也、遊道 和雄、加藤 智啓．NF–κB コリプレッサー（MTI–II）の作用部位を利用した短鎖ペプチド抗炎症薬の In vivo 試験（In vivo anti–inflammatory action of the inhibitory sequence in the NF–κB co–repressor (MTI–II) – a new peptide pharmaceutical）BMB2015（第 38 回日本分子生物学会年会・第 88 回日本生化学会大会）．2015/12/1～12/4．兵庫県
99. 黒川真奈絵、有戸光美、加藤智啓．プロテオミクスを用いた RA の病態解析．第 43 回日本関節病学会．2015/11/5～11/6．北海道
100. 永井宏平、内田貞輔、浄弘由紀子、西野芽玖、佐藤利行、大岡正道、有戸光美、黒川真奈絵、加藤智啓．好中球 Myeloperoxidase の等電点をアルカリ側にシフトさせる酸化修飾の解析．日本プロテオーム学会 2015 年会．2015/7/23～7/24．熊本県
101. 表山和樹、有戸光美、佐藤利行、岡本一起、末松直也、黒川真奈絵、加藤智啓．シェドミクス法の確立に関する研究．日本プロテオーム学会 2015 年会．2015/7/23～7/24．熊本県
102. 黒川真奈絵、有戸光美、佐藤利行、表山和樹、末松直也、岡本一起、加藤智啓．レビー小体型認知症における血清ペプチドバイオマーカーの探索. 日本プロテオーム学会 2015 年会. 2015/7/23～7/24.

熊本県

103. 有戸光美、黒川真奈絵、大岡正道、表山和樹、加藤智啓．SLE 患者末梢血単核球の表面蛋白質プロファイルの解析．日本プロテオーム学会 2015 年会．2015/7/23～7/24．熊本県

104. 岡本一起、表山和樹、佐藤利行、有戸光美、黒川真奈絵、末松直也、遊道和雄、礒橋文秀、加藤智啓．炎症性転写因子 NF-κB のコリプレッサーMTI-II を利用した抗炎症剤の in vivo 抗炎症効果と副作用．日本ビタミン学会第 67 回大会．2015/6/5～6/6．奈良県

105. Kurokawa MS, Suzuki I, Noguchi M, Arito M, Sato T, Omoteyama K, Maedomari M, Hasegawa H, Suematsu N, Okamoto K, Kato T, Yamaguchi N. Serum peptides as candidate biomarkers for dementia with Lewy bodies. 第 11 回日本臨床プロテオーム研究会．2015/5/23．東京都

106. 野澤洋平、有戸光美、黒川真奈絵、大岡正道、表山和樹、加藤智啓．SLE 患者末梢血単核球の表面蛋白質プロファイルの解析．第 59 回日本リウマチ学会総会・学術集会．2015/4/23～4/25．愛知県

107. 内田貞輔、永井宏平、佐藤利行、大岡正道、有戸光美、尾崎承一、黒川真奈絵、加藤智啓．ANCA 関連血管炎における好中球ミエロペルオキシダーゼの酸化修飾．第 59 回日本リウマチ学会総会・学術集会．2015/4/23～4/25．愛知県

108. 有戸光美、小泉英樹、遠藤渉、黒川真奈絵、表山和樹、別府諸兄、加藤智啓．ヒト関節軟骨細胞における tofacitinib の核酸代謝に対する影響．第 59 回日本リウマチ学会総会・学術集会．2015/4/23～4/25．愛知県

109. 有戸光美、黒川真奈絵、表山和樹、遊道和雄、中村洋、別府諸兄、加藤智啓．ヒト関節軟骨細胞における Layilin を介したシグナルによる炎症因子の誘導．第 59 回日本リウマチ学会総会・学術集会．2015/4/23～4/25．愛知県

110. 表山和樹、佐藤利行、有戸光美、末松直也、黒川真奈絵、加藤智啓．サーフェスオミックスを利用したサラゾスルファピリジンの作用の解析．第 59 回日本リウマチ学会総会・学術集会．2015/4/23～4/25．愛知県

研究テーマ3関連.

【国際学会】

111. Yamauchi J, Yamano Y, Matsuoka M, Ichimaru N, Nishikido M, Shibagaki Y, Sugitani A, Nakamura N, Mieno M, Yuzawa K. High risk of HAM/TSP after HTLV-1 infection via kidney transplantation: A nationwide survey in Japan. The 19th International Conference on Human Retrovirology: HTLV and Related Viruses, 24-26 April 2019, Lima, Peru.

112. Sato T, Yagishita N, Araya N, Yamauchi J, Inoue E, Matsumoto N, Hasegawa Y, Yamano Y. Progress report on a long-term study of anti-CCR4 antibody (mogamulizumab) in patients with HAM/TSP. The 19th International Conference on Human Retrovirology: HTLV and Related Viruses, 24-26 April 2019, Lima, Peru.

113. Yamano Y. Treatment of HAM/TSP. The 19th International Conference on Human Retrovirology: HTLV and Related Viruses, 24-26 April 2019, Lima, Peru.

114. Yamano Y. Anti-C-C chemokine receptor 4 monoclonal antibody therapy in human T-lymphotropic virus type 1-associated myelopathy (HAM/TSP). 11th Pan-Asian Committee on Treatment and Research in Multiple Sclerosis (PACTRIMS CONGRESS 2018), 1-3 November 2018, Sydney, Australia.

115. Yamano Y. Current situation of patient centered medicines development in Japan. The 19th International Conference on Pharmaceutical Medicine (ICPM2018), 27-29 September 2018（27）, Tokyo, Japan.

116. Yamano Y. Recent progress of therapeutic strategy for HTLV-1-associated myelopathy (HAM/TSP). The 14th

International Congress of Neuroimmunology (ISNI 2018), 27-31st August, 2018, Brisbane Australia.

117. Yamano Y. Treatment of HAM/TSP. IRVA Tokyo Conference 2018 & International Symposium, 12 July 2018, Tokyo, Japan.
118. Akiko Tozawa, Hiraku Endo, Tze Fang Wong, Yuko Nagasawa, Hiroyuki Yamanaka, Noriyuki Yokomichi, Shinji Hosonuma, Norihito Yoshioka, Shiho Kuji, Imari Deura, Tatsuru Ohara, Yoshiaki Okuma, Kazushige Kiguchi, Nao Suzuki. EFFICACY EVALUATION OF HYBRID CAPTURE II WITH ASC-US IN PREGNANT WOMEN: A SINGLEINSTITUTE REVIEW OF 84 PATIENTS. 17th Biennial Meeting of the International Gynecologic Cancer Society (IGCS 2018), 2018.
119. Shiho Kuji, Tze Fang Wong, Hiroyuki Yamanaka, Yuko Nagasawa, Noriyuki Yokomichi, Ayako Miura, Ami Kondo, Shinji Hosonuma, Norihito Yoshioka, Imari Deura, Tatsuru Ohara, Akiko Tozawa, Haruhiro Kondo, Hiromichi Gomi, Nao Suzuki. FIGO STAGE IIIB AND IVA, TREATMENT AND PROGNOSIS OF THE BULKY CERVICAL CANCER. 17th Biennial Meeting of the International Gynecologic Cancer Society (IGCS 2018), 2018.
120. Yamano Y. Establishment of a platform to accelerate rare disease data registries in Japan. The Office of Rare Disease Research (ORDR) of the National Center for Advancing. National Institutes of Health (NIH), 2017.
121. Yamano Y, Sato T, A. Coler-Reilly, Yagishita N, Araya N, Inoue E, Furuta R, Watanabe T, Uchimaru K, Matsuoka M, Matsumoto N, Hasegawa Y. Phase 1/2 Study of Mogamulizumab, an anti-CCR4 Monoclonal antibody, in Patients with HTLV-1-associated myelopathy(HAM/TSP). XXIII World Congress of Neurology, 2017.
122. Aratani S, Fujita H, Yagishita N, Yokota M, Nishioka K, Nakajima T. E3 Ubiquitin ligase synoviolin inhibitors has effects on obesity. International Conference on Obesity and Chronic Diseases (ICOCD-2016), 2016.
123. Yamano Yoshihisa. Viruses in neuroimmunological disorders. 13th International Congress of Neuroimmunology (ISNI 2016), 2016.
124. Tada Mayako, Yamano Yoshihisa, Sato Tomoo, Sasaki Mitsuho, Sakate Ryuichi, Hinomura Akiko, Hirata Makoto, Tanaka Hidenori, Kojima Hiroto, Kohara Arihiro, Matsuyama Akifumi. Investigation of Human Leukocyte Antigen on Human T-Lymphotropic Virus Type-1 Associated Myelopathy(HAM)by the Rare Disease Bank. 18th International Conference on Human Retrovirology: HTLV and Related Viruses, 2017.
125. Sawada Leila, Nagano Yoshiko, Hasegawa Atsuhiko, Ito Sayaka, Sato Tomoo, Yamano Yoshihisa, Tanaka Yuetsu, Masuda Takao, Kannagi Mari. IL-10-mediated Signals as a Switch to Proliferation in HTLV-1-infected T Cells. 18th International Conference on Human Retrovirology: HTLV and Related Viruses, 2017.
126. Yamakawa Natsuko, Amano Saaya, Kawakami Hitomi, Yamashita Hitomi, Yagishita Naoko, Araya Natsumi, Sato Tomoo, Takata Ayako, Matsuo Tomohiro, Yamano Yoshihisa. A New Index Describing Urinary Dysfunction in Patients with Human T-lymphotropic Virus Type 1-associated Myelopathy. 18th International Conference on Human Retrovirology: HTLV and Related Viruses, 2017.
127. Matsuzaki Toshio, Saito Mineki, Yamano Yoshihisa, Nagai Masahiro, Takashima Hiroshi, Izumihara Tomomaro, Yoshitama Tamami, Kubota Ryuji. Effect of Biologic Agents on HAM/TSP with Rheumatoid Arthritis. 18th International Conference on Human Retrovirology: HTLV and Related Viruses, 2017.
128. Yamano Yoshihisa. The New Phase of HAM/TSP Research. 18th International Conference on Human Retrovirology: HTLV and Related Viruses, 2017.
129. Yuzawa Kenji, Matsuoka Masao, Yamano Yoshihisa, Ichimaru Naotsugu, Nishikido Masaharu, Shibagaki Yugo, Sugitani Atsushi, Nakamura Nobuyuki, Mieno Makiko, Yamauchi Junji. High Risk with Human T-cell

Leukemia Virus Type 1 for HTLV-1 Associated Myelopathy after Living Kidney Transplantation in Japan. The 18th International Conference on Human Retrovirology: HTLV and Related Viruses, 2017.

130. Yamagishi Makoto, Nakano Kazumi, Fujikawa Dai, Kobayashi Seiichiro, Araya Natsumi, Sato Tomoo, Yagishita Naoko, Iwanaga Masako, Utsunomiya Atae, Tanaka Yuetsu, Yamano Yoshihisa, Watanabe Toshiki, Uchimaru Kaoru. Comparative Transcriptome Analysis of HTLV-1-infected Cells and ATL Cells. The 18th International Conference on Human Retrovirology: HTLV and Related Viruses, 2017.
131. Mayako Tada, Yoshihisa Yamano, Tomoo Sato, Mitsuho Sasaki, Ryuichi Sakate, Akiko Hinomura, Makoto Hirata, Hidenori Tanaka, Hiroto Kojima, Arihiro Kohara, Akifumi Matsuyama. Investigation of Human Leukocyte Antigen on Human T-Lymphotropic Virus Type-1 Associated Myelopathy (HAM) by the Rare Disease Bank. The 18th International Conference on Human Retrovirology: HTLV and Related Viruses, 2017.
132. Leila Sawada, Yoshiko Nagano, Atsuhiko Hasegawa, Sayaka Ito, Tomoo Sato, Yoshihisa Yamano, Yuetsu Tanaka, Takao Masuda, Mari Kannagi. IL-10-mediated Signals as a Switch to Proliferation in HTLV-1-infected T Cells. The 18th International Conference on Human Retrovirology: HTLV and Related Viruses, 2017.
133. Toshio Matsuzaki, Mineki Saito, Yoshihisa Yamano, Masahiro Nagai, Hiroshi Takashima, Tomomaro Izumihara, Tamami Yoshitama, Ryuji Kubota. Effect of Biologic Agents on HAM/TSP with Rheumatoid Arthritis. The 18th International Conference on Human Retrovirology: HTLV and Related Viruses, 2017.
134. Higashikuse Yuta, Nagai Go, Araya Natsumi, Yagishita Naoko, Sato Tomoo, Yamano Yoshihisa. Development of a New Assay for Quantification of HTLV-1 Proviral DNA. The 18th International Conference on Human Retrovirology: HTLV and Related Viruses, 2017.
135. Ariella L. G. Coler-Reilly, Sato Tomoo, Matsuzaki Toshio, Nakagawa Masanori, Niino Masaaki, Nagai Masahiro, Nakamura Tatsufumi, Takenouchi Norihiro, Araya Natsumi, Yagishita Naoko, Yamano Yoshihisa. Daily Prednisolone Slows the Progression of HAM/TSP. The 18th International Conference on Human Retrovirology: HTLV and Related Viruses, 2017.
136. Tamaki Keiko, Sato Tomoo, Ariella Coler-Reilly, Inoue Eisuke, Tsugawa Jun, Yamano Yoshihisa, Tsuboi Yoshio. Biomarkers for Predicting Treatment Response in Patients with HTLV-1-Associated Myelopathy/Tropical Spastic Paraparesis (HAM/TSP). The 18th International Conference on Human Retrovirology: HTLV and Related Viruses, 2017.
137. Araya Natsumi, Sato Tomoo, Yagishita Naoko, Ariella Coler-Reilly, Uchimaru Kaoru, Yamano Yoshihisa. Prevalence, Incidence, and Evidence of High ATL Risk among HAM/TSP Patients. The 18th International Conference on Human Retrovirology: HTLV and Related Viruses, 2017.
138. Yamakawa Natsuko, Amano Saaya, Kawakami Hitomi, Yamashita Hitomi, Yagishita Naoko, Araya Natsumi, Sato Tomoo, Takata Ayako, Matsuo Tomohiro, Yamano Yoshihisa. A New Index Describing Urinary Dysfunction in Patients with Human T-lymphotropic Virus Type 1-associated Myelopathy. The 18th International Conference on Human Retrovirology: HTLV and Related Viruses, 2017.
139. Sato Tomoo, Inoue Eisuke, Yagishita Naoko, Araya Natsumi, Takata Ayako, Yamano Yoshihisa. Effectiveness of Low-Dose Oral Prednisolone to Treat and Slow Progression of HAM/TSP: A Nationwide Prospective Cohort Study. The 18th International Conference on Human Retrovirology: HTLV and Related Viruses, 2017.
140. Suzuki Hiroko, Sato Kentaro, Kikuchi Takayuki, Kimura Miyuna, Arifuku Hirotaka, Komita Midori, Shimada Kanade, Seki Kurumi, Tachibana Marika, Yagishita Naoko, Ariella Coler-Reilly, Sato Tomoo, Araya Natsumi, Ishikawa Miho, Koike Mikako, Saito Yumi, Takata Ayako, Yamano Yoshihisa. Patient Satisfaction Survey for HAM-net Registrants. The 18th International Conference on Human Retrovirology:

HTLV and Related Viruses, 2017.

141. Kawano Noriaki, Yamano Yoshihisa, Kawano Sayaka, Kawamata Toyotaka, Yoshida Shuro, Kuriyama Takuro, Uchimaru Kaoru, Marutsuka Kousuke, Minato Seiichirou, Yamashita Kiyoshi, Ochiai Hidenobu, Shimoda Kazuya, Ishikawa Fumihiko, Kikuchi Ikuo. The Development of Human T-cell Leukemia Virus Type 1 (HTLV-1)-Associated Myelopathy (HAM)-Mimicking Myelitis Following Allogeneic Hematopoietic Stem Cell Transplantation for Acute Type Adult T-cell Leukemia-lymphoma (ATL). The 18th International Conference on Human Retrovirology: HTLV and Related Viruses, 2017.
142. Inoue Eisuke, Ariella Coler-Reilly, Araya Natsumi, Yagishita Naoko, Sato Tomoo, Takata Ayako, Yamano Yoshihisa. Progression Patterns of Osame's Motor Disability Score for HAM/TSP Patients. The 18th International Conference on Human Retrovirology: HTLV and Related Viruses, 2017.
143. Yamano Y. HTLV-1 induces a Th1-like state in CD4+CCR4+ T cells that produces an inflammatory positive feedback loop via astrocytes in HAM/TSP. 40Years of Neuroimmunology, 2015.
144. Yamauchi J, Sato T, Yagishita N, Araya N, Chikaraishi T, Shibagaki Y, Yamano Y. HTLV-1-Associated Myelopathy in Preoperatively HTLV-1 Negative Recipients after Kidney Transplantation from HTLV-1 Positive Donors. 52nd ERA-EDTA Congress, 2015.
145. Araya N, Sato T, Tomaru U, Coler-Reilly A, Yagishita N, Yamauchi J, Hasegawa A, Kannagi M, Akiyama H, Hasegawa Y, Takahashi K, Kunitomo Y, Tanaka Y, Utsunomiya A, Jacobson S, Yamano Y. HTLV-1 Tax induces Th1 master regulator T-bet and thus IFN-γ in CD4+CCR4+ T-cells of virus-associated myelopathy patients. 17th International Conference on Human Retrovirology: HTLV and Related Viruses, 2015.
146. Kikuchi T, Sawabe A, Negishi Y, Noda A, Hirai Y, Inoue E, Kimura M, Sato K, Araya N, Yagishita N, Sato T, Yamano Y. Evaluation of clinical outcome measures for HAM/TSP. 17th International Conference on Human Retrovirology: HTLV and Related Viruses, 2015.
147. Sato K, Kikuchi T, Kimura M, Komita M, Shimada K, Seki K, Tachibana M, Yagishita N, Coler-Reilly A, Sato T, Arayta N, Ishikawa M, Koike M, Saito Y, Suzuki H, Takata A, Yamano Y. Patient Satisfaction Survey for HAM-net Registrants. 17th International Conference on Human Retrovirology: HTLV and Related Viruses, 2015.
148. Coler-Reilly A, Yagishita N, Sato T, Araya N, Ishikawa M, Koike M, Saito Y, Suzuki H, Yamano Y, Takata A. HAM-net national patient registration system reveals details of how Japanese patients with HTLV-1-associated myelopathy/tropical spastic paraparesis progress over time. 17th International Conference on Human Retrovirology: HTLV and Related Viruses, 2015.

149. Yamano Y, Yamauchi J, Coler-Reilly A, Sato T, Araya N, Yagishita N, Kunitomo Y, Takahashi K, Tanaka Y, Akiyama H, Hasegawa Y, Utsunomiya A.. Humanized anti-CCR4 antibody KW0761 targets HTLV-1-infected CD4+CCR4+ and CD8+CCR4+ T-cells to treat HAM/TSP. 17th International Conference on Human Retrovirology: HTLV and Related Viruses, 2015.
150. Ishihara M, Araya N, Sato T, Saichi N, Fujii R, Yamano Y, Ueda K. A three-factor plasma diagnostic model of human T -cell leukemia virus-1 associated myelopathy. 17th International Conference on Human Retrovirology: HTLV and Related Viruses, 2015.
151. Kimura M, Yamauchi J, Taisho H, Sato T, Yagishita N, Araya N, Sato K, Kikuchi T, Hasegawa Y, Chikaraishi T, Shibagaki Y, Yamano Y. Characteristics of HAM/TSP after kidney transplantation from HTLV-1 positive living donors. 17th International Conference on Human Retrovirology: HTLV and Related Viruses, 2015.
152. Ishihara M, Araya N, Sato T, Saichi N, Fujii R, Yamano Y, Ueda K. Membrane Proteome Profiling to Discover Therapeutic Targets for HTLV-1 Associated Myelopathy. 14th Human Proteome Organization,

2015.

【国内学会】

153. 山野嘉久. 希少難病 HTLV-1 関連脊髄症（HAM）の患者参加型の研究と創薬. 第 26 回 HAB 研究機構学術年会, 2019 年 6 月 20 日～22 日〔21 日〕, 東京（品川区旗の台）
154. Nakamura H, Takeuchi F, Furusawa Y, Yamaguchi I, Yamano Y, Matsuda F. The current situation and needs of rare disease registries in Japan. 第 60 回日本神経学会学術大会（60th ANNUAL MEETING OF THE JAPANESE SOCIETY OF NEUROLOGY）, 2019 年 5 月 22 日～25 日〔22 日〕, 大阪（大阪府大阪市北区中之島）
155. Furusawa Y, Yamaguchi I, Yagishita N, Tanzawa K, Kamatani Y, Natsukawa M, Takahashi Y, Kosugi S, Yamano Y, Matsuda F. An Integarative Platform for Rare Diseases Research of Japan. 第 60 回日本神経学会学術大会, 2019 年 5 月 22 日～25 日〔23 日〕, 大阪（大阪府大阪市北区中之島）
156. 山野嘉久. HAM の病態と治療. 第 60 回日本神経学会学術大会, 2019 年 5 月 22 日～25 日〔23 日〕, 大阪（大阪府大阪市北区中之島）
157. 山野嘉久. HAM を対象としたマルチオミクス解析による ATL 発症リスク因子の同定・新規標的分子をターゲットとした HAM 治療法の開発. AMED 感染症実用化研究事業（新興・再興感染症に対する革新的医薬品等開発推進研究事業）「ATL/HAM の発症基盤の解明と発症ハイリスクグループの同定」研究班　平成 30 年度第 2 回班会議, 2019 年 3 月 26 日, 東京（東京都港区白金台）
158. 山野嘉久. 神経難病 HTLV-1 関連脊髄症(HAM)の患者が支える研究と創薬. 第 92 回日本薬理学会年会, 2019 年 3 月 14~16 日〔16 日〕, 大阪（大阪府大阪市北区中之島）
159. 山野嘉久. HAM の革新的治療となる抗 CCR4 抗体製剤のコンパッショネートユースによる長期投与試験. 平成 30 年度厚生労働省&AMED 支援課題「HTLV-1 関連疾患研究領域」研究班合同発表会, 2019 年 2 月 9 日, 東京（港区白金台）
160. 山野嘉久. HAM ならびに HTLV-1 陽性難治性疾患に関する国際的な総意形成を踏まえた診療ガイドラインの作成. 平成 30 年度厚生労働省&AMED 支援課題「HTLV-1 関連疾患研究領域」研究班合同発表会, 2019 年 2 月 9 日, 東京（港区白金台）
161. 山野嘉久. HAM・HTLV-1 陽性難治性疾患の診療ガイドラインに資する統合的レジストリの構築によるエビデンスの創出. 平成 30 年度厚生労働省&AMED 支援課題「HTLV-1 関連疾患研究領域」研究班合同発表会, 2019 年 2 月 9 日, 東京（港区白金台）
162. 山野嘉久. HAM の治療薬開発を促進する代替エンドポイントとしてのバイオマーカーの実用化研究. 平成 30 年度厚生労働省&AMED 支援課題「HTLV-1 関連疾患研究領域」研究班合同発表会, 2019 年 2 月 9 日, 東京（港区白金台）
163. 山野嘉久. HAM の治療薬開発を促進する代替エンドポイントとしてのバイオマーカーの実用化研究. 2018 年度 AMED6 事業合同成果報告会, 2019 年 2 月 7・8 日〔8 日〕, 東京（千代田区丸の内）
164. 山野嘉久. HAM の革新的治療となる抗 CCR4 抗体製剤のコンパッショネートユースによる長期投与試験. 2018 年度 AMED6 事業合同成果報告会, 2019 年 2 月 7・8 日, 東京（千代田区丸の内）
165. 山岸誠, 鈴木穣, 新谷奈津美, 佐藤知雄, 八木下尚子, 山内淳司, 中村龍文, 渡邉俊樹, 山野嘉久, 内丸薫. HTLV-1 感染細胞の多層オミクスデータから見る HAM の分子病態解析. 厚生労働省難治性疾患（神経免疫疾患）政策および実用化研究班平成 30 年度合同班会議, 2019 年 1 月 17・18 日〔18 日〕, 東京（千代田区平河町）
166. 佐藤賢文, 宮里パオラ, 勝屋弘雄, 宇都宮與, 山岸誠, 内丸薫, 新谷奈津美, 山内淳司, 八木下尚子, 佐藤知雄, 山野嘉久. HTLV-1 感染者末梢血中プロウイルス配列の網羅的解析. 厚生労働省難治性疾患（神経免疫疾患）政策および実用化研究班平成 30 年度合同班会議, 2019 年 1 月 17・18 日〔18 日〕,

東京（千代田区平河町）

167. 八木下尚子, 佐藤知雄, 山内淳司, 高田礼子, 山野嘉久. HAM 患者レジストリ「HAM ねっと」を用いた HAM の疫学的解析. 厚生労働省難治性疾患（神経免疫疾患）政策および実用化研究班平成 30 年度合同班会議, 2019 年 1 月 17・18 日〔18 日〕, 東京（千代田区平河町）

168. 佐藤知雄, 八木下尚子, 新谷奈津美, 井上永介, 松本直樹, 長谷川泰弘, 山野嘉久. HAM 患者に対する抗 CCR4 抗体長期投与試験の中間報告. 厚生労働省難治性疾患（神経免疫疾患）政策および実用化研究班平成 30 年度合同班会議, 2019 年 1 月 17・18 日〔18 日〕, 東京（千代田区平河町）

169. 山内淳司, 山野嘉久, 湯沢賢治. 腎移植における HTLV-1 感染リスクに関する全国疫学調査. 厚生労働省難治性疾患（神経免疫疾患）政策および実用化研究班平成 30 年度合同班会議, 2019 年 1 月 17・18 日〔18 日〕, 東京（千代田区平河町）

170. 山野嘉久. HAM 関連研究班合同班会議, 2018 年 12 月 2 日, 東京（千代田区）≪山野班 CCR4・山野班エビデンス・HTLV ガイドライン班≫

171. 佐藤知雄、八木下尚子、新谷奈津美、井上永介、古田梨愛、渡邉俊樹、内丸薫、松岡雅雄、松本直樹、長谷川泰弘、山野嘉久. HAM 治療薬としての抗 CCR4 抗体製剤（モガムリズマブ）. 第 23 回日本神経感染症学会総会・学術大会, 2018 年 10 月 19 日～20 日,東京（東京都江戸川区）

172. 山内淳司、山野嘉久、佐藤知雄、八木下尚子、新谷奈津美、松岡雅雄、市丸直嗣、錦戸雅春、柴垣有吾、杉谷 篤、中村信之、三重野牧子、湯沢賢治. 腎移植患者の HTLV-1 関連疾患発症に関する全国調査. 第 23 回日本神経感染症学会総会・学術大会, 2018 年 10 月 19 日～20 日,東京（東京都江戸川区）

173. 山内淳司、山野嘉久、佐藤知雄、八木下尚子、新谷奈津美、松岡雅雄、市丸直嗣、錦戸雅春、柴垣有吾、杉谷 篤、中村信之、三重野牧子、湯沢賢治. HTLV-1 陽性臓器移植患者レジストリの構築. 第 54 回日本移植学会, 2018 年 10 月 3 日～5 日, 東京都(東京都港区)

174. 佐藤知雄、八木下尚子、新谷奈津美、井上永介、古田梨愛、渡邉俊樹、内丸薫、松岡雅雄、松本直樹、長谷川 泰弘、山野 嘉久. HTLV-1 関連脊髄症に対する抗 CCR4 抗体製剤（モガムリズマブ）の医師主導治験. 第 30 回日本神経免疫学会, 2018 年 9 月 20 日～21 日, 福島（福島県郡山市）

175. 八木下尚子、山内淳司、佐藤知雄、山野嘉久. 希少疾患 HAM に対する患者レジストリの活用. 第 30 回日本神経免疫学会, 2018 年 9 月 20 日～21 日, 福島（福島県郡山市）

176. 山内淳司、山野嘉久、佐藤知雄、八木下尚子、新谷奈津美、松岡雅雄、市丸直嗣、錦戸雅春、柴垣有吾、杉谷 篤、中村信之、三重野牧子、湯沢賢治. 腎移植後 HTLV-1 関連疾患の発症に関する全国調査. 第 30 回日本神経免疫学会, 2018 年 9 月 20 日～21 日, 福島（福島県郡山市）

177. 佐藤知雄、八木下尚子、新谷奈津美、井上永介、古田梨愛、渡邉俊樹、内丸薫、松岡雅雄、松本直樹、長谷川泰弘、山野嘉久. HAM 患者に対する抗 CCR4 抗体製剤（モガムリズマブ）の安全性と有効性. 第 5 回日本 HTLV-1 学会学術集会, 2018 年 8 月 31 日～9 月 2 日, 東京(東京都千代田区)

178. 八木下尚子、高橋克典、山内淳司、佐藤知雄、山野嘉久. HAM 患者レジストリ「HAM ねっと」の運営. 第 5 回日本 HTLV-1 学会学術集会, 2018 年 8 月 31 日～9 月 2 日, 東京(東京都千代田区)

179. 山内淳司、山野嘉久、佐藤知雄、八木下尚子、新谷奈津美、松岡雅雄、市丸直嗣、錦戸雅春、柴垣有吾、杉谷 篤、中村信之、三重野牧子、湯沢賢治. 腎移植における HTLV-1 感染症の危険性. 第 5 回日本 HTLV-1 学会学術集会, 2018 年 8 月 31 日～9 月 2 日, 東京(東京都千代田区)

180. 山野嘉久. 希少難病 HAM に対する新規治療薬の開発. 第 75 回聖マリアンナ医科大学医学会学術集会, 2018 年 7 月 14 日, 川崎市（神奈川県川崎市宮前区菅生）

181. 山野嘉久. 本研究班の概要について・難病プラットフォームについて AMED 平成 30 年度 日本医療研究開発機構研究費（難治性疾患実用化研究事業）「HAM・HTLV-1 陽性難治性疾患の診療ガイドラインに資する統合的レジストリの構築によるエビデンスの創出」（山野班エビデンス）平成 30 年度

第 1 回班会議, 2018 年 6 月 17 日, 鹿児島（鹿児島県姶良市蒲生町久末）

182. 山野嘉久. 患者レジストリが支える HTLV-1 関連脊髄症（HAM）研究の最近の進歩 Recent Progress in the research for HTLV-1-associated Myelopathy (HAM) brought by patient registry. 第 59 回日本神経学会学術大会, 2018 年 5 月 23 日～26 日, 札幌（北海道札幌市中央区）

183. 山野嘉久. HAM 患者悉皆登録システムと連動した臨床ゲノム情報基盤の構築. ＨＡＭ＆ＨＴＬＶ－１診療ガイドライン班（山野班）・「ヒトとウイルスのゲノム情報と臨床情報の統合による HTLV-1 関連疾患の診療支援全国ネットワークの確立」班（松田班）平成 29 年度合同班会議. 2018 年 2 月 27 日, 京都（京都府京都市上京区河原町）

184. 山野嘉久. HAM ならびに HTLV-1 陽性難治性疾患に関する国際的な総意形成を踏まえた診療ガイドラインの作成. 平成２９年度厚生労働省&AMED 委託研究開発費「HTLV-1 関連疾患研究領域」研究班合同発表会. 2018 年 2 月 24 日, 東京（港区白金台）

185. 山野嘉久. HAM に対する日本発の革新的治療となる抗 CCR4 抗体の実用化研究. 平成２９年度厚生労働省&AMED 委託研究開発費「HTLV-1 関連疾患研究領域」研究班合同発表会. 2018 年 2 月 24 日, 東京（港区白金台）

186. 山野嘉久. HAM に対する日本発の革新的治療となる抗 CCR4 抗体の実用化研究. 難治性疾患実用化研究事業及び免疫アレルギー疾患等実用化研究事業（免疫アレルギー疾患実用化研究分野）2017 年度合同成果報告会, 2018 年 2 月 9 日, 神奈川（神奈川県横浜市西区）

187. 山岸誠、新谷奈津美、石崎伊純、佐藤知雄、八木下尚子、中村龍文、渡邉俊樹、山野嘉久、内丸薫. HAM 発症に至る遺伝子発現異常の推移と ATL 発症リスク因子の同定の試み. 厚生労働省難治性疾患（神経免疫疾患）政策および実用化研究班平成 29 年度合同班会議, 2018 年 1 月 18・19 日〔19 日〕, 東京（千代田区平河町）

188. 佐藤賢文、宮里パオラ、勝屋弘雄、稲田優紀、宇都宮與、佐藤和雄、山野嘉久. HTLV-1 感染者末梢血中プロウイルス配列の網羅的解析. 厚生労働省難治性疾患（神経免疫疾患）政策および実用化研究班平成 29 年度合同班会議, 2018 年 1 月 18・19 日〔19 日〕, 東京（千代田区平河町）

189. 佐藤知雄、八木下尚子、玉木慶子、井上永介、長谷川大輔、新谷奈津美、長谷川泰弘、坪井義夫、高田礼子、山野嘉久. HAM の新しい疾患活動性分類基準の提案. 厚生労働省難治性疾患（神経免疫疾患）政策および実用化研究班平成 29 年度合同班会議, 2018 年 1 月 18・19 日〔19 日〕, 東京（千代田区平河町）

190. 山野嘉久、佐藤知雄、八木下尚子、新谷奈津美、井上永介、古田梨愛、渡邉俊樹、内丸薫、松岡雅雄、松本直樹、長谷川泰弘. HAM 患者に対するヒト化抗 CCR4 抗体の第 1/2a 相試験. 厚生労働省難治性疾患（神経免疫疾患）政策および実用化研究班平成 29 年度合同班会議, 2018 年 1 月 18・19 日〔19 日〕, 東京（千代田区平河町横道憲幸,

191. 戸澤晃子, 吉岡範人, 大原樹, 大熊克彰, 大川千絵, 小泉宏隆, 高木正之, 木口一成, 鈴木直. 腹水播種がサルコイド反応のみであった卵管類内膜腺癌の一例. 第 58 回日本臨床細胞学会総会, 2017.

192. 蔦幸児, 富永英一郎, 戸澤晃子, 赤羽智子, 大原樹, 小林佑介, 平沢晃, 阪埜浩司, 鈴木直, 青木大輔. 腹水卵巣細胞の CD44 各アイソフォーム発現量と化学療法の効果と関連性の検討. 第 58 回日本臨床細胞学会総会, 2017.

193. 戸澤晃子, 永澤侑子, 横道憲幸, 細沼信示, 吉岡範人, 大原樹, 大熊克彰, 前田一郎, 木口一成, 鈴木直. ASC-US における HPV-DNA 検査の有用性と臨床上の留意点. 第 58 回日本臨床細胞学会総会, 2017.

194. 戸澤晃子, 佐藤匠, 竹内淳, 永澤侑子, 近藤亜未, 三浦彩子、横道憲幸, 吉岡範人, 大原樹, 近藤春裕, 鈴木直. 腹腔鏡下手術後早期に再発した卵巣明細胞癌 I 期の 2 例. 日本婦人科腫瘍学会第 59 回学術講演会, 2017.

195. 永澤 侑子, 吉岡 伸人, 赤間 孝洋, 今井 悠, 清水 拓哉, 横道 憲幸, 吉岡 範人, 久慈 志保, 出浦伊万里, 津田 千春, 大原 樹, 近藤 春裕, 戸澤 晃子, 鈴木 直. IVF 周期中に着床遅延が疑われた一例. 第 57 回日本産科婦人科内視鏡学会学術講演会, 2017.
196. 戸澤晃子, 鈴木由妃, 永澤侑子, 横道憲幸, 吉岡範人, 杉下陽堂, 久慈志保, 近藤春裕, 出浦伊万里, 大原樹, 根津あや, 富永果林, 右田王介, 鈴木直. 遺伝性卵巣癌症候群患者へのリスク低減卵巣癌管摘出術の後方視的検討. 第 3 回日本産科婦人科遺伝診療学会学術講演会, 2017.
197. 本間千夏, 吉岡範人, 山下敦己, 大原樹, 長江千愛, 戸澤晃子, 瀧　正志, 鈴木直. 婦人科手術の周術期管理を安全に施行することが可能であった先天性無フィブリノゲン血症. 第72回聖マリアンナ医科大学医学会学術集会, 2017.
198. 宮地恵子, 東久世裕太, 小野達也, 永井豪, 篠田達也, 関野久邦, 井上恵, 三浦清徳, 小林誠一郎, 内丸薫, 山野嘉久. ＨＴＬＶ－１　プロウイルスＤＮＡ検出キットの臨床的有用性の検討. 第４回日本ＨＴＬＶ－１学会　学術集会, 2017.
199. 長谷川大輔, 八木下尚子, 井上永介, 新谷奈津美, 髙田礼子, 長谷川泰弘, 佐藤知雄, 山野嘉久. 臨床経過とバイオマーカーに基づくＨＡＭの疾患活動性分類基準の提案. 第４回日本ＨＴＬＶ－１学会学術集会, 2017.
200. Leila Sawada, Yoshiko Nagano, Atsuhiko Hasegawa, Sayaka Ito, Tomoo Sato, Yoshihisa Yamano, Yuetsu Tanaka, Takao Masuda, Mari Kannagi. Potential contribution of IL-10-mediated STAT3 signals to push HTLV-1-infected cells towards proliferation by enhancing survivin and IRF4 expression. 第４回日本ＨＴＬＶ－１学会学術集会, 2017.
201. 平野光人, 今井陽一, 神保光児, 小川弥穂, 越智清純, 川俣豊隆, 横山和明, 大野伸広, 山野嘉久, 福田隆浩, 内丸薫, 東條有伸. ＡＴＬ患者の同種造血幹細胞移植後に慢性炎症性脱髄性多発ニューロパチーを発症した３症例の解析. 第４回日本ＨＴＬＶ－１学会　各術集会, 2017.
202. 佐藤知雄, 井上永介, 八木下尚子, 新谷奈津美, 長谷川大輔, 高田礼子, 山野嘉久. ＨＡＭ患者レジストリを活用した低用量経口プレドニゾロン維持療法の有効性と安全性に関する検討. 第４回日本ＨＴＬＶ－１学会　学術集会, 2017.
203. 八木下尚子, 佐藤知雄, 長谷川大輔, 新谷奈津美, 井上永介, 高田礼子, 山野嘉久. ＨＴＬＶ－１関連脊髄症（ＨＡＭ）の新たな運動障害重症度評価指標の提案. 第４回日本ＨＴＬＶ－１学会　学術集会, 2017.
204. 山野嘉久. HAM の患者レジストリによるリアルワールドデータを活用した治療薬開発の展望. 第４回日本ＨＴＬＶ－１学会学術集会, 2017.
205. 山野嘉久. ＨＡＭに対する新規治療薬の開発. 第２２回日本神経感染症学会, 2017.
206. 山野嘉久. HAM の患者レジストリによるリアルワールドデータを活用した治療薬開発の展望. 第 35 回日本神経治療学会総会, 2017.
207. 玉木慶子、佐藤知雄、津川潤、山野嘉久、坪井義夫. HAM 患者における治療効果を予測するバイオマーカーの検討. 第 3 回日本 HTLV-1 学会学術集会, 2016.
208. 新谷奈津美、佐藤知雄、八木下尚子、高橋克典、内丸薫、山野嘉久. HTLV-1 関連脊髄症（HAM）における HAS-Flow 法を用いた ATL 発症高危険度患者の予測. 第 3 回日本 HTLV-1 学会学術集会, 2016.
209. 山野嘉久. HAM の分子病態解明による治療薬開発の新展開. 第 3 回日本 HTLV-1 学会学術集会, 2016.
210. 井上永介、Ariella Coler-Reilly、新谷奈津美、八木下尚子、佐藤知雄、高田礼子、山野嘉久. HAM 発症から診断までの期間における納の運動障害重症度の経時推移の解析. 第 3 回日本 HTLV-1 学会学術集会, 2016.
211. 佐藤知雄、Ariella Coler-Reilly、新谷奈津美、八木下尚子、中村龍文、永井将弘、新野正明、竹ノ内徳博、中川正法、松崎敏男、山野嘉久. HAM 患者に対する経口ステロイド維持療法の長期的効果. 第

3 回日本 HTLV-1 学会学術集会, 2016.

212. 津川浩一郎、山野嘉久、中島貴子、上野隆彦、牛谷真由美、桑原理恵、藤原佐百合、小林理々子. 聖マリアンナ医科大学臨床研究データセンターの現状. 第 1 回日本臨床薬理学会関東・甲信越地方会, 2016.

213. 山野嘉久. 希少難病 HAM の分子病態解明による治療薬開発の新展開. 第 1 回日本臨床薬理学会関東・甲信越地方会, 2016.

214. Sawada L, 永野佳子, 長谷川温彦, 金井光, 佐藤知雄, 山野嘉久, 田中勇悦, 神奈木真理.. IL-10 は survivin と IRF4 の誘導を介して HTLV-1 感染細胞の増殖を促進する. 第 75 回日本癌学会学術総会, 2016.

215. 山野嘉久. HAM の CCR4 モノクローナル抗体療法. 第 34 回日本神経治療学会総会, 2016.

216. 山野嘉久. 生体腎移植における HTLV-1 感染リスクについて. 第 53 回大阪腎移植病理組織研究会, 2016.

217. 山野嘉久. HAM について. 第 1 回 HTLV-1 治療研究講演会・第 1 回スマイルリボン全国大会, 2017.

218. 沢辺愛加, 根岸由衣, 野田和里, 平井祐士, 井上永介, 新谷奈津美, 八木下尚子, 佐藤知雄, 山野嘉久. 希少難病 HAM の臨床的有効性評価指標の検討. 第 56 回日本神経学会学術大会, 2015.

219. 野妻 智嗣, 松浦 英治, 久保田 龍二, 児玉 大介 松崎 敏男, 渡邊 修, 三井 純, 石浦 浩之, 山野嘉久, 辻 省次, 出雲 周二, 髙嶋 博. エクソーム関連解析による HAM 疾患感受性遺伝子の探索. 第 56 回日本神経学会学術大会, 2015.

220. 佐藤健太郎, 菊池崇之, 木村未祐奈, 込田みどり, 島田奏, 関来未, 橘茉莉花, 八木下尚子, 佐藤知雄, 新谷奈津美, 石川美穂, 小池美佳子, 齋藤祐美, 鈴木弘子, 高田礼子, 山野嘉久. 患者レジストリへの介入方法と患者満足度の変化. 第 56 回日本神経学会学術大会, 2015.

221. 木村未祐奈, 佐藤健太郎, 菊池崇之, 八木下尚子, 新谷奈津美, 石川美穂, 小池美佳子, 齋藤祐美, 佐藤知雄, 鈴木弘子, 木村美也子, 高田礼子, 山野嘉久. HAM 患者レジストリ「HAM ねっと」を活用した経年的前向き調査. 第 56 回日本神経学会学術大会, 2015.

222. 山野嘉久, 山内淳司, 大勝秀樹, 佐藤知雄, 八木下尚子, 新谷奈津美, 長谷川泰弘, 力石辰也, 柴垣有吾. HTLV-1 陽性ドナーからの生体腎移植による HAM の発症率と特徴. 第 56 回日本神経学会学術大会, 2015.

223. 山内淳司, 柴垣有吾, 佐藤知雄, 八木下尚子, 新谷奈津美, 山野嘉久, 力石辰也. HTLV-1 陽性ドナーからの生体腎移植によりレシピエントに発症する HAM の特徴. 第 60 回日本透析医学会学術集会・総会, 2015.

224. 石原誠人, 新谷奈津美, 佐藤知雄, 藤井理沙, 最知直美, 宇都宮與, 山野嘉久, 植田幸嗣. 定量膜プロテオーム解析によるヒト T 細胞性白血病ウイルス 1 型（HTLV-1）関連疾患に対する新規治療標的の探索. 日本プロテオーム学会 2015 年会, 2015.

225. 山野嘉久.希少難病を知る－再発性多発軟骨炎の病態－. 第 20 回日本難病看護学会学術集会, 2015.

226. 山内淳司, 佐藤知雄, 八木下尚子, 新谷奈津美, 大勝秀樹, 長谷川泰弘, 力石辰也, 柴垣有吾, 湯沢賢治, 山野嘉久. HTLV-1 陽性ドナーから陰性レシピエントへの生体腎移植による HAM の特徴. 第 2 回日本 HTLV-1 学会学術集会, 2015.

227. 佐藤知雄, 安藤仁, 高橋克典, 國友康夫, Ariella Coler-Reilly, 新谷奈津美, 八木下尚子, 山野嘉久. HTLV-1 関連脊髄症(HAM)における髄液細胞のケモカイン受容体解析. 第 2 回日本 HTLV-1 学会学術集会, 2015.

228. 石原誠人, 新谷奈津美, 佐藤知雄, 藤井理沙, 最知直美, 宇都宮與, 山野嘉久, 植田幸嗣.末梢血 CD4 陽性 T 細胞を用いた膜プロテオーム解析による HTLV-1 関連疾患に対する新規治療標的の探索. 第 2 回日本 HTLV-1 学会学術集会, 2015.

229. 鈴木弘子, 石川美穂, 小池美佳子, 齊藤祐美, 八木下尚子, 山野嘉久. HAM 患者の思いを知る? SEIQoL-DW（個人の生活の質評価法）を用いた関わりを通して? 第 2 回日本 HTLV-1 学会学術集会, 2015.
230. 八木下尚子, 鈴木弘子, 石川美穂, 小池美佳子, 齊藤祐美, 新谷奈津美, 佐藤知雄, 高田礼子, 山野嘉久. HAM 患者レジストリ「HAM ねっと」の経年的患者満足度調査. 第 2 回日本 HTLV-1 学会学術集会, 2015.
231. 倉光球, 大隈和, 矢持忠徳, 山野嘉久, 長谷川寛雄, 上平憲, 岡山昭彦, 久保田龍二, 出雲周二, 成瀬功, 相良康子, 佐竹正博, 渡邉俊樹, 山口一成, 浜口功. HTLV-1 核酸検査の標準化および検出感度の検討：多施設共同研究. 第 2 回日本 HTLV-1 学会学術集会, 2015.
232. 夛田まや子, 佐々木光穂, 平田誠, 樋野村亜希子, 坂手龍一, 西下直希, 山野嘉久, 吉良潤一, 小原有弘, 松山晃文.難病バンクにおける HLA タイピング導入による難病研究推進. 第 24 回日本組織適合性学会, 2015.
233. 山野嘉久.HAM の治療展望. 第 27 回日本神経免疫学会学術集会, 2015.
234. 石原誠人, 新谷奈津美, 佐藤知雄, 藤井理沙, 最知直美, 宇都宮與, 山野嘉久, 植田幸嗣. 定量膜プロテオーム解析による成人 T 細胞性白血病に対する治療標的の探索. 第 74 回日本癌学会学術集会, 2015.
235. 山野嘉久. HTLV-1 関連脊髄症（HAM）に対する抗 CCR4 抗体療法の開発. 第 43 回日本臨床免疫学会総会, 2015.
236. 山野嘉久. 腎移植患者の HTLV-1 感染と HAM 発症. 第 49 回日本臨床腎移植学会, 2016.

＜研究成果の公開状況＞（上記以外）

シンポジウム・学会等の実施状況、インターネットでの公開状況等

ホームページで公開している場合には、URL を記載してください。

＜既に実施しているもの＞

難病治療研究センター研究活動・業績公開： http://nanchiken.jp/

知財事業推進センター活動公開： http://www.marianna-u.ac.jp/chizai/index.html

基礎と臨床を結ぶ分子病態研究会（第 8 回：2015 年, 第 9 回：2016 年, 第 10 回：2017 年）

＜これから実施する予定のもの＞

聖マリアンナ医科大学難病治療研究センター主催・難治研セミナー（年 3～4 回開催）

聖マリアンナ医科大学難病治療研究センター主催・私立大学戦略的研究基盤形成支援事業・研究成果報告シンポジウム（令和 2 年年 3 月に予定していたが、新型コロナ感染拡大のため 9 月以降に延期予定）

14 その他の研究成果等

「12 研究発表の状況」で記述した論文、学会発表等以外の研究成果及び企業との連携実績があれば具体的に記入してください。 また、上記11(4)に記載した研究成果に対応するものには＊を付してください。

当該研究プロジェクト関連の企業との共同研究契約:

オージー技研株式会社（光刺激応答機構の解明と、光刺激を応用する医療機器開発、平成 28 年度～）

論文、学会発表以外の研究成果報告

1. 遊道和雄. Tietse 症候群について. 難治性疾患等政策研究事業(難治性疾患政策研究事業)軟骨炎症性疾患の診断と治療体系の確立班第 3 回班会議, 2020.
2. 遊道和雄.「老化のメカニズム」最新研究から分かった健康長寿を伸ばす生活習慣について. ２０１９年度後期かわさき市民アカデミー・地域協働講座, 2019.
3. 遊道和雄. 健康寿命の延伸に向けて―細胞寿命・老化の発生機序と疾患との関連―. かわさき市民アカデミー2018 年度前期・地域協働講座 A, 2018.
4. 遊道和雄. 医療現場から産業界に望むこと～共に歩み医療向上にむけて～. 文京区・大田区・川崎市連携事業　医工連携展示フェア, 2018.
5. 遊道和雄. EBM に基づいた評価による CFS 治療ガイドライン作成に向けて. 平成 29 年度日本医療研究開発機構委託研究開発費　障害者対策総合研究事業「慢性疲労症候群に対する治療評価と治療ガイドラインの作成」研究班　第 1 回班会議, 2017.
6. 遊道和雄. ME/CFS の治療ガイドライン草案について. 平成 29 年度日本医療研究開発機構委託研究開発費　障害者対策総合研究事業「慢性疲労症候群に対する治療評価と治療ガイドラインの作成」研究班　最終班会議, 2018
7. 山野嘉久. HAM の診療ガイドライン 2019 を踏まえた診断と治療. Takeda Web Seminar, 2019 年 7 月 29 日, 東京（品川区）
8. 山野嘉久. 私が鹿児島市立病院で学んだこと・その後に私が歩んだ道. 鹿児島市立病院研修医・若手医師向けセミナー by 神経内科, 2019 年 4 月 19 日, 鹿児島（鹿児島市上荒田町）
9. 山野嘉久. HTLV-1 関連脊髄症（HAM）の診断と新薬の研究. 平成 30 年度実践薬学セミナー, 2019 年 3 月 24 日, 鹿児島（鹿児島市宇宿）
10. 山野嘉久. HTLV-1 母子感染の予防と対策. 平成 30 年度不妊・不育・HTLV-1 相談に関する研修, 2019 年 2 月 12 日, 神奈川（大和市中央）

11. 山野嘉久. HTLV-1 母子感染予防対策について. 平成 30 年度神奈川県母子保健対策検討委員会, 2019 年 2 月 7 日, 神奈川（横浜市中区海岸通）
12. 山野嘉久. HTLV-1 の基礎知識とキャリア妊産婦・患者への支援. 平成 30 年度山梨県母子感染予防対策研修会, 2019 年 1 月 22 日, 山梨県（甲府市丸の内）
13. 山野嘉久. How to develop novel therapy for rare diseases. 京都大学ゲノム医学講座特別講義, 2018 年 12 月 13 日, 京都（京都市左京区聖護院川原町）
14. 山野嘉久. HTLV-1 母子感染の予防と対策. 神奈川県母子学術研修会, 2018 年 11 月 21 日, 神奈川（横須賀市小川町）
15. 山野嘉久. ～治療、そして予防まで～医師主導治験によるマリアンナ発の医療イノベーションへの挑戦. 第 9 回オールマリアンナ・ナレッジフェア講演会. 2018 年 11 月 12 日, 神奈川（川崎市宮前区菅生）
16. 山野嘉久. 難病 HAM 患者さんの笑顔を目指して. 第 43 回宮崎大学医学部第二内科開講記念講演会. 2018 年 11 月 10 日, 宮崎県（宮崎市松山）
17. 山野嘉久. HTLV-1 関連難病の新たな治療戦略.「世界 HTLV デー」制定記念講演会. 2018 年 11 月 10 日, 東京（港区白金台）
18. 山野嘉久. HAM について. 第２回ＨＴＬＶ－１治療研究講演会. 2018 年 2 月 28 日, 京都（京都府京都市上京区河原町）
19. 山野嘉久. HTLV-1 母子感染の予防と対策. 平成 29 年度不妊・不育・HTLV-1 相談に関する研修. 2018 年 2 月 14 日, 神奈川県（大和市中央）
20. 山野嘉久. HTLV-1 母子感染予防対策について. 平成 29 年度神奈川県母子保健対策検討委員会. 2018 年 1 月 29 日, 神奈川県（横浜市中区海岸通）
21. 山野嘉久. HTLV-1 の基礎知識とキャリア妊産婦・患者への支援. 平成 29 年度 HTLV-1 母子保健感染予防対策研修会. 2018 年 1 月 23 日, 山梨（甲府市）
22. 山野嘉久. 患者レジストリを活用した難病医療の充実と新薬開発の促進. 医療ビッグデータコンソーシアム　第 1 回ライフサイエンス部会, 2017.
23. 山野嘉久. 患者レジストリがもたらす難病医療の充実と新薬開発について. 中枢性尿崩症(CDI)の会総会・勉強会　難病医療の充実とネットワーク　-患者登録サイト HAM ねっと-, 2017.
24. 山野嘉久. 患者レジストリがもたらす難病医療の充実と新薬開発について. 難病医療の充実とネットワーク　-患者登録サイト HAM ねっと-, 2017.
25. 山野嘉久. 難病患者さんの笑顔を目指して　～臨床と基礎の研究成果を活かした医師主導治験の軌跡～. 京都府立医科大学特別講義, 2017.
26. 山野嘉久. 希少難病 HAM の患者レジストリを活用した治療薬開発への取り組みと展望. 第 17 回 CRC と臨床試験のあり方を考える会議 2017, 2017.
27. 山野嘉久. HTLV-1 関連脊髄症（HAM）の病態・疫学の特徴と KW-0761 の可能性. 協和発酵キリン社内セミナー, 2017.
28. 増原直子, 森下真千子, 仲井暎子, 小池典子, 山崎顕, 太田有紀, 松本直樹, 平山佑三子, 高橋まりも, 山野嘉久. 患者レジストリを活用した希少難病 HTLV-1 関連脊髄症患者対象の医師主導治験を支援して-CRC に求められる臨床試験マネジメントとは. 第 17 回 CRC と臨床試験のあり方を考える会議 2017 in 名古屋, 2017.
29. 山野嘉久. HAM に対するＣＣＲ４抗体の第 1/2 a 相試験の結果ならびに開発進捗報告, HAM に対するステロイドの医師主導治験の背景と進捗報告, 難病プラットフォーム（RADDAR-J)研究班の活動内容について, 診療ガイドラインの作成方針と役割分担、進捗状況について, HAM 患者の生命予後, ATL 発症リスクについて. HAM 関連研究班合同班会議, 2017.

30. 遊道和雄. ME/CFS の治療ガイドライン草案について. 平成 29 年度日本医療研究開発機構委託研究開発費　障害者対策総合研究事業「慢性疲労症候群に対する治療評価と治療ガイドラインの作成」研究班　第 2 回班会議, 2017.
31. 佐藤知雄，八木下尚子，玉木慶子，井上永介，長谷川大輔，新谷奈津美，長谷川泰弘，坪井義夫，高田礼子，山野嘉久. HAM の新しい疾患活動性分類基準の提案. 厚生労働省難治性疾患（神経免疫疾患）政策および実用化研究班平成 29 年度合同班会議, 2018.
32. 山野嘉久，佐藤知雄，八木下尚子，新谷奈津美，井上永介，古田梨愛，渡邉俊樹，内丸薫，松岡雅雄，松本直樹，長谷川泰弘. HAM 患者に対するヒト化抗 CCR4 抗体の第 1/2a 相試験. 厚生労働省難治性疾患（神経免疫疾患）政策および実用化研究班平成 29 年度合同班会議, 2018.
33. 山岸誠，新谷奈津美，石崎伊純，佐藤知雄，八木下尚子，中村龍文，渡邉俊樹，山野嘉久，内丸薫. HAM 発症に至る遺伝子発現異常の推移と ATL 発症リスク因子の同定の試み. 厚生労働省難治性疾患（神経免疫疾患）政策および実用化研究班平成 29 年度合同班会議, 2018.
34. 佐藤賢文，宮里パオラ，勝屋弘雄，稲田優紀，宇都宮興，佐藤知雄，山野嘉久. HTLV-1 感染者末梢血液中プロウイルス配列の網羅的解析. 厚生労働省難治性疾患（神経免疫疾患）政策および実用化研究班平成 29 年度合同班会議, 2018.
35. 山野嘉久. HAM に対する日本発の革新的治療となる化抗 CCR4 抗体の実用化研究. 難治性疾患実用化研究事業及びアレルギー疾患等実用化研究事業（免疫アレルギー疾患実用化研究分野）2017 年度合同成果報告会, 2018.
36. 山野嘉久. HAM に対する日本発の革新的治療となる抗 CCR4 抗体の実用化研究. 平成 29 年度厚生労働省＆ＡＭＥＤ委託研究開発費「ＨＴＬＶ-1 関連疾患研究領域」研究班合同発表会, 2018.
37. 山野嘉久. ＨＡＭならびにＨＴＬＶ-1 陽性難治性疾患に関する国際的な総意形成を踏まえた診療ガイドラインの作成. 平成 29 年度厚生労働省＆ＡＭＥＤ委託研究開発費「ＨＴＬＶ-1 関連疾患研究領域」研究班合同発表会, 2018.
38. 山野嘉久. ＨＡＭ患者悉皆登録システムと連動した臨床ゲノム情報基盤の構築. ＨＡＭ＆ＨＴＬＶ-1 診療ガイドライン班（山野班）・「ヒトとウイルスのゲノム情報と臨床情報の統合によるＨＴＬＶ-1 関連疾患の診療支援全国ネットワークの確立」班（松田班）平成 29 年度合同班会議., 2018.
39. 荒谷聡子、藤田英俊、八木下尚子、中島若巳、西岡久寿樹、中島利博. シノビオリン阻害剤の実用化に向けて.　第 5 回医薬工 3 大学包括連携推進シンポジウム, 2016.
40. 遊道和雄. 日本における CFS 治療ガイドラインの作成・CFS に対する治療効果の文献的評価. 平成 28 年度日本医療研究開発機構委託研究開発費　障害者対策総合研究事業「慢性疲労症候群に対する治療評価と治療ガイドラインの作成」研究班第 1 回班会議, 2016.
41. 荒谷聡子、藤田英俊、八木下尚子、山野嘉久、西岡久寿樹、中島利博. 関節リウマチにおける転写後修飾による多重化シグナル調節機構の解析。. 第 3 回 JCR ベーシックリサーチカンファレンス, 2016.
42. 藤田英俊、荒谷聡子、八木下尚子、山野嘉久、須藤カツ子、内野博之、西岡久寿樹、中島利博. リウマチ発症因子シノビオリンによる新規エネルギー代謝機構の解明。. 第 3 回 JCR ベーシックリサーチカンファレンス, 2016.
43. 山野嘉久. HAM における ATL 発症リスクの頻度と HAS-Flow 法を用いた予測. 平成 28 年度厚生労働科学研究費「HAM ならびに HTLV-1 陽性難治性疾患に関する国際的な総意形成を踏まえた診療ガイドラインの作成」「HTLV-1 陽性難治性疾患の診療の質を高めるためのエビデンス構築」合同班会議, 2016.
44. 山野嘉久. ガイドラインのスコープについて. 平成 28 年度厚生労働科学研究費「HAM ならびに HTLV-1 陽性難治性疾患に関する国際的な総意形成を踏まえた診療ガイドラインの作成」「HTLV-1

陽性難治性疾患の診療の質を高めるためのエビデンス構築」合同班会議, 2016.

45. 山野嘉久. HAM における ATL の発症率および高リスク群の解析. 日本医療研究開発機構難治性疾患実用化研究事業「神経筋疾患の原因究明および革新的治療法開発に関する研究」平成２８年度研究班会議, 2016.
46. 山野嘉久. ＨＡＭについて～より良い治療を目指して～. 平成２８年度ＨＴＬＶ-１対策講演会「知りましょう！ＨＴＬＶ-１のこと～ヒトＴ細胞白血病ウィルスとは～」, 2016.
47. 山野嘉久. HAM 患者レジストリ「HAM ねっと」による難病医療の向上を目指して. AMED 連携シンポジウム, 2017.
48. 山野嘉久. 医師主導の開発：市販薬の追加適応獲得. 平成２８年度大阪大学ＭＥＩプロフェッショナルコース, 2017.
49. 遊道和雄. ME/CFS 治療ガイドラインの作成に向けて. 平成 28 年度日本医療研究開発機構委託研究開発費　障害者対策総合研究事業「慢性疲労症候群に対する治療評価と治療ガイドラインの作成」研究班　第 2 回班会議, 2017.
50. 新谷奈津美, 佐藤知雄, 八木下尚子, 渡邉俊樹, 内丸薫, 山野嘉久. HAM における ATL の合併率、発症率および高リスク群に関する解析. 厚生労働省難治性疾患（神経免疫疾患）政策および実用化研究班平成 28 年度合同班会議, 2017.
51. 山岸誠, 新谷奈津美, 中野和民, 佐藤知雄, 八木下尚子, 渡邉俊樹, 山野嘉久, 内丸薫. HAM と ATL の発症機構と病態の解明に向けた遺伝子発現の網羅的比較解析. 厚生労働省難治性疾患（神経免疫疾患）政策および実用化研究班平成 28 年度合同班会議, 2017.
52. 山川奈津子, 天野佐亜哉, 川上仁美, 山下瞳, 八木下尚子, 新谷奈津美, 佐藤知雄, 松尾朋博, 山野嘉久. HAM の新しい排尿障害重症度評価指標の提案. 厚生労働省難治性疾患（神経免疫疾患）政策および実用化研究班平成 28 年度合同班会議, 2017.
53. 佐藤賢文, 宮里パオラ, 山野嘉久. DNA プローブと次世代シークエンスを活用した高精度 HTLV-1 プロウイルス解析法の開発. 厚生労働省難治性疾患（神経免疫疾患）政策および実用化研究班平成 28 年度合同班会議, 2017.
54. 山野嘉久. 重要臨床課題と CQ、HAM ねっとの概要とその疫学情報の活用、スコープ案について. 平成 28 年度第 3 回 HTLV ガイドライン班班会議, 2017.
55. 山野嘉久. HTLV-1 って何？ 第 40 回聖マリアンナ医科大学公開講座, 2017.
56. 山野嘉久. HAM に対する日本発の革新的治療となる抗 CCR4 抗体の実用化研究. HTLV-1 関連疾患研究領域　研究班合同発表会, 2017.
57. 山野嘉久. HAM の革新的な医薬品等の開発促進に関する研究. HTLV-1 関連疾患研究領域　研究班合同発表会, 2017.
58. 山野嘉久. HAM ならびに HTLV-1 陽性難治性疾患に関する国際的な総意形成を踏まえた診療ガイドラインの作成. HTLV-1 関連疾患研究領域　研究班合同発表会, 2017.
59. 山野嘉久. HAM の革新的な医薬品等の開発促進に関する研究. 難治性疾患実用化研究事業　免疫アレルギー疾患等実用化研究事業　2016 年度合同成果報告会, 2017.
60. 山野嘉久. HAM に対する日本発の革新的治療となる抗 CCR4 抗体の実用化研究. 難治性疾患実用化研究事業　免疫アレルギー疾患等実用化研究事業　2016 年度合同成果報告会, 2017.
61. 遊道和雄. 健康寿命延長に向けて一老化研究最前線一. 第 40 回聖マリアンナ医科大学公開講座「最新医学講義」, 2017.
62. 山野嘉久. HTLV-1 母子感染の予防. 平成 28 年度不妊・不育・HTLV-1 相談に関する研修, 2017.
63. 山野嘉久. HAM の革新的な医薬品等の開発促進に関する研究、HAM に対する日本発の革新的治療となる抗 CCR4 抗体の実用化研究. HAM 関連研究班合同班会議　平成 28 年度活動報告, 2017.

64. 山野嘉久. 重要臨床課題と CQ、HAM ねっとの概要とその疫学情報の活用、スコープ案について. 平成 28 年度 HAM 関連研究班合同班会議, 2017.
65. 山野嘉久. HTLV-1 の基礎知識と最新情報について、キャリア妊産婦・患者への支援について. 平成 28 年度山梨県 HTLV-1 母子感染予防対策研修会, 2017.
66. 夛田まや子、佐々木光穂、平田誠、樋野村亜希子、坂手龍一、山野嘉久、吉良潤一、小島裕人、小原有弘、松山晃文. 難病バンクにおける遺伝子探索導入による難病研究推進. 日本薬学会第 137 年会, 2017.
67. 遊道和雄. 慢性疲労症候群患者の日常生活困難度調査事業・実態調査の報告. 平成 26 年度厚生労働省「慢性疲労症候群患者の日常生活困難度調査事業」報告会, 2015.
68. 山野嘉久. 希少難病 HAM 患者レジストリー「HAM ねっと」の臨床研究・治験への応用　～運営事務局の立場から～. 第 15 回 CRC と臨床試験のあり方を考える会議 2015 inKOBE, 2015.
69. 山野嘉久. 臓器移植後に伴うＨＴＬＶ－１関連疾患発症の実態について. 第 9 回 HTLV-1 対策推進協議会, 2015.
70. 山野嘉久. HAM に対する日本発の革新的治療となる抗 CCR4 抗体の実用化研究. 革新的医療技術創出拠点プロジェクト統合戦略会議, 2015.
71. 山野嘉久. HTLV-1 の基礎知識とＨＡＭについて. 鹿児島県 HTLV-1 対策講演会, 2015.
72. 山野嘉久. 医師主導の開発 : 市販薬の追加適応獲得. 大阪大学臨床医工学・情報学スキルアップ講座, 2015.
73. 山野嘉久. HTLV-1 陽性ドナーから陰性レシピエントへの生体腎移植による HAM の特徴について. 日本医療研究開発機構研究費（難治性疾患実用化研究事業）「神経筋疾患の原因究明および革新的治療法開発に関する研究」平成 27 年度班会議, 2015.
74. 山野嘉久. ここまで進んでいます！HAM 革新的な新薬開発の最新情報. HTLV-1 講演会, 2015.
75. 山野嘉久. HTLV-1 関連脊髄症（HAM）について. GHRCC 研究室セミナー, 2016.
76. 山野嘉久. HTLV-1 母子感染の予防. 平成 27 年度母子保健関連研修, 2016.
77. 山野嘉久. HTLV-1 母子感染予防対策について～現況と展望～. 平成 27 年度神奈川県母子保健対策検討委員会, 2016.
78. 山野嘉久、山内淳司、佐藤知雄、八木下尚子、新谷奈津美、大勝秀樹、長谷川泰弘、湯沢賢治. HTLV-1 陽性ドナーから陰性レシピエントへの生体腎移植による HAM の特徴. 厚生労働省難治性疾患（神経免疫疾患）政策および実用化研究班平成 27 年度合同班会議, 2016.
79. 佐藤知雄、新谷奈津美、八木下尚子、山野嘉久. HAM の進行度の特徴と関連バイオマーカーの検討. 厚生労働省難治性疾患（神経免疫疾患）政策および実用化研究班平成 27 年度合同班会議, 2016.
80. 玉木慶子, 津川潤, 佐藤知雄, 山野嘉久, 坪井義夫. HAM における治療効果を予想するバイオマーカーの検討. 厚生労働省難治性疾患（神経免疫疾患）政策および実用化研究班平成 27 年度合同班会議, 2016.
81. 遊道和雄. CFS 治療ガイドラインの作成に向けたＣＦＳ治療効果の文献的評価. 平成 27 年度第 2 回厚生労働省「慢性疲労症候群に対する治療評価と治療ガイドラインの作成」研究班班会議, 2016.
82. 山野嘉久. HAM の革新的な医薬品の開発促進に関する研究. 平成 27 年度厚生労働科学研究費&日本医療研究開発機構(AMED)委託研究開発費　HTLV-1 関連疾患研究領域研究班合同発表会, 2016.
83. 山野嘉久. HAM に対する日本発の革新的治療となる抗 CCR4 抗体の実用化研究. 平成 27 年度厚生労働科学研究費&日本医療研究開発機構(AMED)委託研究開発費　HTLV-1 関連疾患研究領域研究班合同発表会, 2016.
84. 山野嘉久, 長谷川泰弘, 松本直樹, 井上永介、松岡雅雄、内丸薫, 髙田礼子, 中島孝, 森豊隆志. HAM に対するヒト化抗 CCR4 抗体の医師主導治験. 2015 年度 AMED 6 事業合同成果報告会, 2016.

85. 山野嘉久, 長谷川泰弘, 新野正明, 藤原一男, 中川正法, 竹之内徳博, 永井将弘, 吉良潤一, 中村龍文, 髙嶋博, 渡嘉敷崇, 米澤久司, 坪井義夫, 髙田礼子, 齊藤峰輝, 外丸詩野, 植田幸嗣、松田文彦, 井上永介. HAM の革新的な医薬品等の開発促進に関する研究. 2015 年度 AMED 6 事業合同成果報告会, 2016.
86. 山野嘉久. HTLV-1 ウイルスを知ってください。母子感染予防から, 相談ができる地域づくりをめざして. HTLV-1 感染予防対策研修会, 2016.
87. 山野嘉久. HTLV-1 の基礎知識と最新情報について.キャリア妊産婦・患者への支援について. 平成 27 年度山梨県 HTLV-1 母子感染予防対策研修会, 2016.
88. 山野嘉久. HAM の分子病態解明による治療薬開発の新展開. 長崎大学病院自己免疫・炎症性疾患勉強会, 2016.
89. 山野嘉久. HAM の病態機序に基づいた疾患修飾薬の開発. 日沼頼夫先生メモリアルシンポジウム HTLV-1 研究の現況と展望, 2016.
90. Yamano Y. How does HTLV-1 cause CNS disease? - The importance of cross-talk between infected T-cells and astrocytes. The Inaugural Asia-Pacific School of Neuroimmunology Meeting, 2015.

15 「選定時」及び「中間評価時」に付された留意事項及び対応

＜「選定時」に付された留意事項＞

- メインは siRNA のように見えるが、siRNA は低侵襲とは言い切れない、物理的刺激による応答蛋白活性法の研究深化を期待する。
- 若手研究者の育成と外部評価の導入を具体化してほしい。

＜「選定時」に付された留意事項への対応＞

- 本研究プロジェクトは、上記留意事項に御指摘いただいたように物理的刺激として「特定波長条件の光刺激・メカニカルストレス・温熱刺激」を選定し、これら物理的刺激に応答する細胞内因子を介する細胞活性の制御技術を開発して治療に応用しようとするものである。これら物理的刺激に対して、どのような細胞内の因子が応答するか、その因子が物理的刺激に対する応答蛋白として、どのような細胞情報伝達経路で細胞活性の変化に関与するかを検証する実験法（細胞内因子の阻害実験）の手段・ツールの一つとして siRNA を利用した基礎実験を計画したもので、siRNA は研究の主軸である低侵襲アプローチの手段ではないことを全研究者に周知徹底して実験を行なった。

- 大学院生(当該研究テーマ担当・約 10 名)、若手研究員・研究技術者（各研究テーマ担当・約 20 名）が研究プロジェクトへ参加し、実験に積極的に取り組むような計画・体制を整えた。若手研究者は必ず研究者全員参加の研究会議（月 1 回）に加えて、難病治療研究センター主催のセミナー・難病研修会に参加して、課題・改善点等について情報を共有し、個々の研究活動へフィードバックするように指導した。

- 外部評価実施に関しては、以下の 3 点で対応した。

  ① 研究会議、セミナー・研修会に、外部評価者として学外研究者、医学・医療専門家（会によっては非専門領域の外部評価者・弁理士・弁護士）を参加招聘し、研究内容からの逸脱の有無、進捗度、動物試験や生命倫理上の問題点の有無等の評価を依頼、研究活動に反映するように努めた。

  ② 年に一回の学外研究者を対象とした公開研究会・シンポジウムにおいて、研究成果を公開して研究部外者(専門領域)の意見・評価をその後の研究活動に反映するようにした。

  ③ 研究成果は査読のある国際学術専門誌に論文として投稿し、評価を得るようにした。

＜「中間評価時」に付された留意事項＞

該当なし

＜「中間評価時」に付された留意事項への対応＞

該当なし

論文・学会報告等リスト

平成 27 年度～平成 31 年度

2015. 4

PubMed

Abstract

Full text links

BenthamScience Full-Text Article

Curr Aging Sci. 2015.8(3) 256-8

Age-related Decrease of Sirtuin 2 Protein in Human Peripheral Blood Mononuclear Cells.

Yudoh K[1]. Karasawa R. Ishikawa J.

Author information

Abstract

Sirtuin 2, which is mainly present in cytoplasm, plays an important role in mammalian development, caloric restriction, metabolic regulation cellular antioxidant potential and the regulation of aging. We found that the protein level of sirtuin 2 in human peripheral blood mononuclear cells (PBMCs) decreases with an advance in donor age in men and women. Our data suggest that sirtuin 2 level in PBMCs decreases with age in both men and women and may have a potential as a useful biomarker monitoring health conditions and aging.

PMID: 25643068 [PubMed - in process]

LinkOut - more resources

PubMed Commons

PubMed Commons home

0 comments

How to join PubMed Commons

Age-related decrease of sirtuin 2 protein in human peripheral blood mononuclear cells.

Kazuo Yudoh[1], Rie Karasawa[1], Junji Ishikawa[2]

1. Department of Frontier Medicine, Institute of Medical Science, St. Marianna University School of Medicine. 2-16-1 Sugao, Miyamae-ku, Kawasaki, Kanagawa 216-8512, Japan.
2. Translational Health Science Group, Preventive Healthcare Research Center, FANCL Research Institute, 12-13 Kamishinano, Totsuka-ku, Yokohama, Kanagawa 244-0806, Japan.

Key-words: sirtuins, aging, peripheral blood mononuclear cells, biomarker, physical activity, sirtuin 2, age-related disease, healthy condition

Summary

Sirtuin 2, which is mainly present in cytoplasm, plays an important role in mammalian development, caloric restriction, metabolic regulation cellular antioxidant potential and the regulation of aging. We found that the protein level of sirtuin 2 in human peripheral blood mononuclear cells (PBMCs) decreases with advance of donor age in men and women. Our data suggest that sirtuin 2 level in PBMCs decreases with age in both men and women and may have a potential as a useful biomarker monitoring health conditions and aging

Introduction.

Sirtuins are nicotinamide adenine dinucleotide (NAD)-dependent protein deacetylases that are associated with protein acetylation, metabolism, and age-related diseases [1]. Sirtuins were initially found to decelerate aging in Nematoda. More recently, it has been reported that sirtuins may participate in the caloric restriction on metabolism and longevity in mammals [1,2]. Human has seven sirtuins (sirtuin 1~7) which are functionally nonredundant. Sirtuins conduct their functions via deacetylation of target proteins in the different cellular compartment [2]. Roles of sirtuin family may be classified into two categories – the regulation of metabolism and the response to stresses, such as oxidative stress and heat shock stress.

Previous reports have clearly indicated that sirtuin 2 (SIRT2), which is mainly present in cytoplasm, participates in stress responses by regulating cell cycle mitotic checkpoint and cell death (apoptosis) through the deacetylation of target proteins [3,4]. Furthermore, recent studies clearly revealed different characteristics of SIRT2 function, in addition to effects of SIRT2 on cell cycle function and stress-induced apoptotic pathway. Several transcription factors, including a homeobox transcription factor (HoxA10) and a forkhead box O transcription factor (FOXO), physically interact with SIRT2 [5,6]. Also, it has been demonstrated that SIRT2 reduces levels of reactive oxygen species (oxidative stress) into the cells and deacetylates transcription factors in response to caloric restriction [6]. These findings indicate that SIRT2 has an important role in caloric restriction, metabolic regulation and cellular antioxidant potential and is involved in the regulation of aging.

More recently, North BJ et al. clearly demonstrated that the SIRT2 activation participates in the regulation of aging in mice [7]. They found that the activation of SIRT2 induces the overexpression of the mitotic checkpoint of kinase gene BubR1 and increases median lifespan in mice. BubR1 is known to be a component of the spindle assembly checkpoint that has emerged as a key regulator of aging and longevity in mice. Their

findings clearly indicate that SIRT2 activity counteract the aging and age-related diseases. Kumar R et al. also reported that lower serum sirtuins (sirtuin1, sirtuin2, sirtuin3) levels significantly associated with frailty in older age groups [8]. Their findings demonstrated that serum level of sirtuin has a potential as a distinctive marker for frailty in elder people.

Here, for the first time in humans, we report that the protein level of SIRT2 in human peripheral blood mononuclear cells (PBMCs) decreases with donor age in men and women.

Methods.

We analyzed the protein level of SIRT2 in PBMCs in healthy controls, after written informed consent. The protocol was approved by the ethics committee of St. Marianna University School of Medicine. The healthy control group consisted of 91 volunteers (aged 26 to 66 years old, male: 44 cases, female: 47 cases). Exclusion criteria were immune disorders, diabetes, metabolic diseases or malignant diseases.

PBMCs were isolated by Ficoll gradient centrifugation method. Peripheral blood from a healthy donor was diluted with equal amounts of phosphate buffer saline, overlaid on Ficoll medium (GE Healthcare UK Ltd. Buckinghamshire, UK) and centrifuged at 1200 rpm for 30 minute at 22°C. After the centrifugation, PBMC pellets were collected. Protein levels of SIRT2 in PBMCs were analyzed by the western blot analysis and the enzyme-linked immunosorbent assay (ELISA) using a human specific antibody for SIRT2 (Abcam plc. Cambridge, UK).

Results.

Our western blot analysis revealed that the protein level of SIRT2 in PBMC's was significantly decreased with donor age. An inverse correlation between the SIRT2 level and donor age was observed (Figure 1, r^2= 0.3475, P<0.01). Noteworthy, concentrations of SIRT2 in PBMC's, which were analyzed by ELISA, also showed an inverse correlation with donor age (Figure 2, r^2= 0.2734, P<0.01).

Discussion.

Our data clearly show for the first time in humans that the SIRT2 level in PBMCs decreases with age in both men and women. Although further studies are needed to clarify whether or not sirtuin activity is a function of age and can be altered through medical condition, medicines, foods, supplements, smoking, or physical exercise, SIRT2 levels in PBMC's may have a potential as a useful biomarker monitoring health conditions and aging that are widely and transversely influenced by the inflammation, senescence

(cellular aging), or degeneration of organs and tissues as a result of change of the cellular activity.

Previous report demonstrated that serum sirtuins have great potential to be diagnostic protein marker for frailty in older age groups of 60's or above [8]. Serum levels of sirtuin1, 2, and 3 were significantly lower in patients with frail compared with the non-frail. Also, it has been suggested that SIRT2 induces the checkpoint kinase of BubR1, a key regulator of aging and longevity, to increase lifespan in mice [7]. These findings suggest that sirtuin activity is associated with aging and age-related diseases.

Sirtuin has generated considerable interest as an important player in aging biology and age-related diseases. Recent study indicated that some types of exercise influence the activity of sirtuins in several tissues including PBMC's [9]. This suggests that exercise induces the activition of sirtuin and has a potential to prevent age-related diseases. Oxidative stress is also well known to induce the cellular lifespan and to be implicated with aging and age-related diseases. Antioxidants such as beta-carotene, alpha-tocopherol and ascorbic acid exert an antioxidant effect and a pro-oxidant effect according to their concentration [10]. Since SIRT2 reduces levels of reactive oxygen species (oxidative stress) into the cells, antioxidants as well as exercise may also influence the activity of SIRT2. Antioxidant may affect the activity of SIRT2 as well as a cellular oxidative condition. Further studies are needed to clarify the involvement of SIRT2 pathway in the aging biology. SIRT2 may have a role of regulator and biomarker of aging and longevity. We would like to conclude that SIRT2 will be novel targets to treat the common diseases of aging.

Acknowledgement

Corresponding Author: Yudoh K, MD, PhD. Department of Frontier Medicine, Institute of Medical Science, St. Marianna University School of Medicine. 2-16-1 Sugao, Miyamae-ku, Kawasaki, Kanagawa 216-8512, Japan (yudo@marianna-u.ac.jp).

Author Contributions: Dr. Yudoh, Dr. Karasawa and Dr. Ishikawa had full access to all of the data in the study and take responsibility for the integrity of the data and the accuracy of the data analysis.

Study concept and design: Yudoh, Karasawa, Ishikawa.

Acquisition of data: Yudoh, Karasawa.

Analysis and interpretation of data: Yudoh, Karasawa, Ishikawa.

Drafting of the manuscript: Yudoh, Karasawa.

Critical revision of the manuscript for important intellectual content: Yudoh, Karasawa, Ishikawa.

Statistical analysis: Yudoh, Karasawa.

Administrative, technical, and material support: Yudoh, Karasawa, Ishikawa.

Study supervision: Ishikawa.

Conflict of Interest Disclosures: The authors have completed and submitted the ICMJE Form for Disclosure of Potential Conflicts of Interest and none were reported. The authors declare that they have no competing interests.

Funding/Support: This study was supported by KENKOIN Medical Corporation Foundation.

Role of the Sponsor: KENKOIN Medical Corporation Foundation had no role in the design and conduct of the study; collection, management, analysis, and interpretation of the data; preparation, review, or approval of the manuscript; and decision to submit the manuscript for publication.

Disclaimer: The opinions expressed are those of the authors and do not reflect the position or policy of the Institute of Medical Science, St. Marianna University School of Medicine, or the FANCL Research Institute.

Additional Contributions: We thank our colleagues in the Department of Frontier Medicine at St. Marianna University School of Medicine for their thoughtful comments and advice during the early stages of this project. They were not compensated for their contributions.

References.

1. Guarente L.. Sirtuins, Aging, and Metabolism. *Cold Spring Harb Symp Quant Biol.* 2011;76: 81-90.
2. Guarente L. Sirtuins, aging, and medicine. *New Engl J Med.* 2011;364: 2235–2244.
3. Inoue T, Hiratsuka M, Osaki M, Oshimura M. The molecular biology of mammalian SIRT proteins: SIRT2 in cell cycle regulation. *Cell Cycle.* 2007; 6(9):1011-1018.
4. Dryden SC, Nahhas FA, Nowak JE, Goustin AS, Tainsky MA. Role for human SIRT2 NAD-dependent deacetylase activity in control of mitotic exit in the cell cycle. *Mol Cell Biol.* 2003;23:3173-3185.
5. Bae NS, Swanson MJ, Vassilev A, Howard BH. Human histone deacetylase SIRT2 interacts with the homeobox transcription factor HOXA10. *J Biochem (Tokyo).* 2004; 135:695-700.
6. Wang F, Nguyen M, Qin XF, Tong Q. SIRT2 deacetylates FOXO3a in response to oxidative stress and caloric restriction. *Aging Cell.* 2007;6(4):505-14.
7. North BJ, Rosenberg MA, Jeganathan KB, Hafner AV, Michan S, Dai J, Baker DJ, Cen Y, Wu LE, Sauve AA, van Deursen JM, Rosenzweig A, Sinclair DA. SIRT2 induces the checkpoint kinase BubR1 to increase lifespan. EMBO J. 2014;33:1438-1453.
8. Kumar R, Mohan N, Upadhyay AD, Singh AP, Sahu V, Dwivedi S, Dey AB, Dey S. Identification of serum sirtuins as novel noninvasive protein markers for frailty. Aging Cell 2014:975-980.
9. Suwa M, Sakuma K. The potential role of sirtuins regarding the effects of exercise on aging-related diseases. Curr Aging Sci. 2013;6(2):178-88.
10. de Oliveira BF, Veloso CA, Nogueira-Machado JA, Martins Chaves M. High doses of in vitro beta-carotene, alpha-tocopherol and ascorbic acid induceoxidative stress and secretion of IL-6 in peripheral blood mononuclear cellsfrom healthy donors. Curr Aging Sci. 2012 Jul;5(2):148-56.

Figure legends.

Figure 1. Inverse correlation between SIRT2 level in PBMCs and donor age. (data from western blot analysis)

Figure 2. Inverse correlation between SIRT2 concentration in PBMCs and donor age. (data from ELISA)

Revised Figure 1

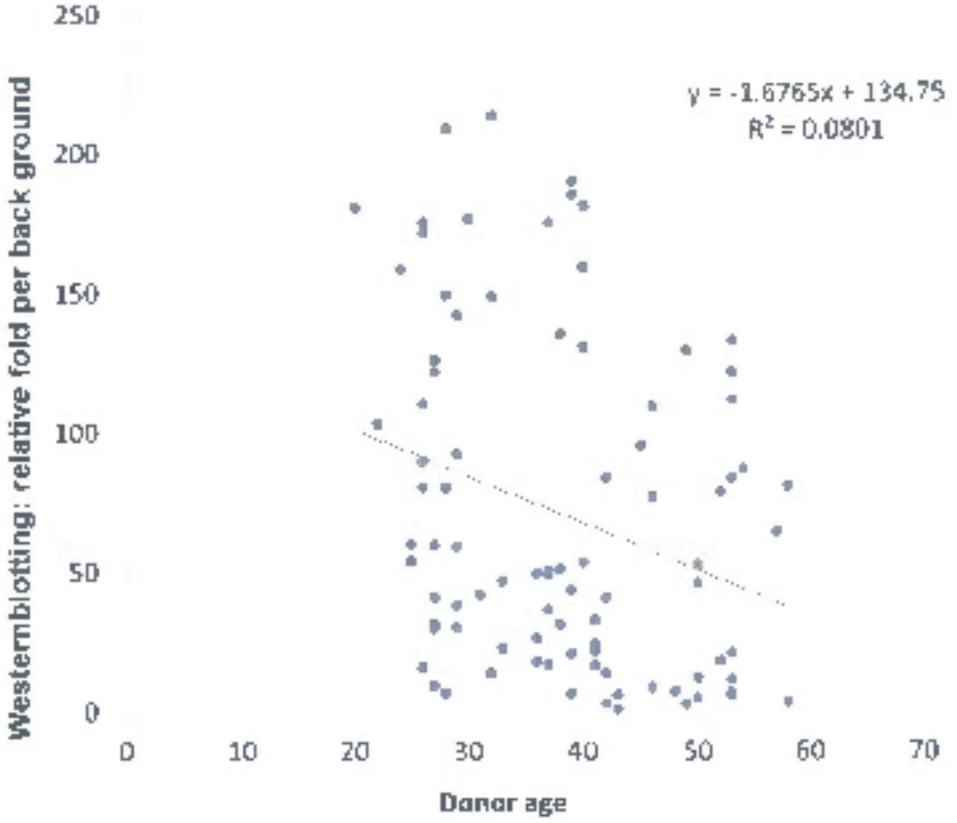

Revised Figure 2

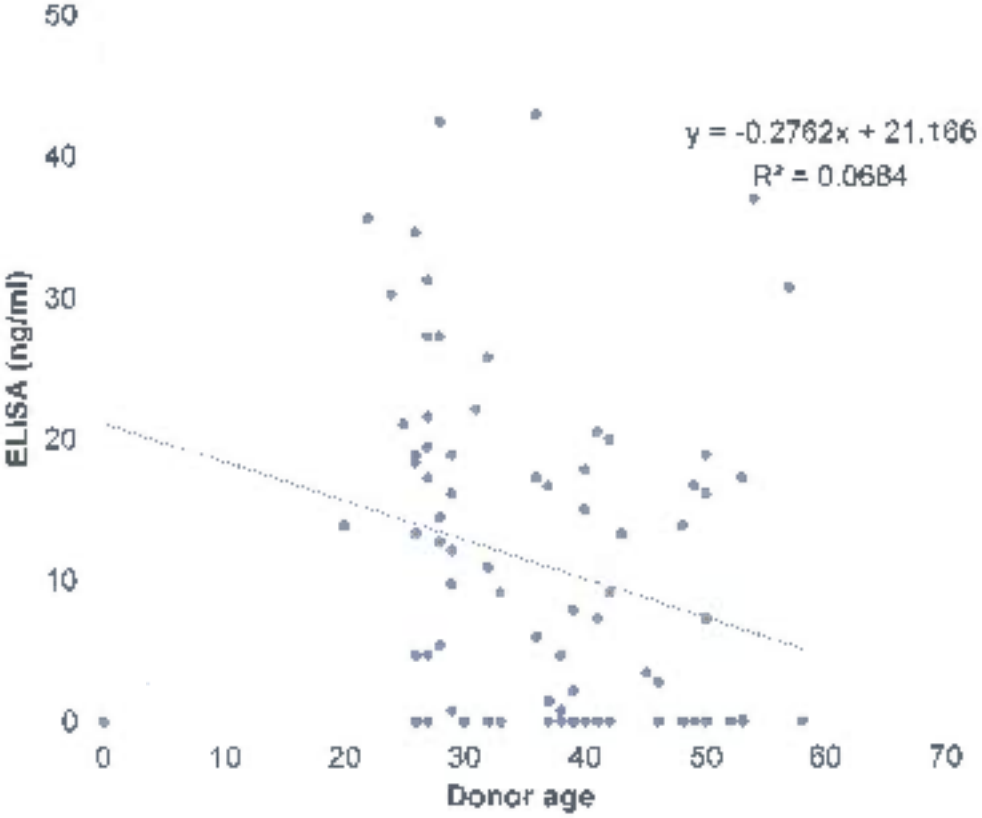

応用薬理 Oyo Yakuri
Pharmacometrics 88 (3-4) 39-45 (2015) 南江堂

関節リウマチ患者の関節症状に対する大豆ペプチド摂取の有効性評価

吉岡 宏孝[1], 山口 直郎[1,*], 前川 敬祐[2], 河野 光雅[3], 武者 春樹[3], 湯浅 和雄[3,*]

[1]〒216-8512 神奈川県川崎市宮前区菅生2-16-1 聖マリアンナ医科大学スポーツ医学講座
[2]〒216-8511 神奈川県川崎市宮前区菅生2-16-1 聖マリアンナ医科大学 臨床治験研究センター
[3]〒402-0102 茨城県つくば郡[illegible]町[illegible]
不二製油株式会社 つくば[illegible]研究センター 基盤研究所

Assessment of the Effect of Soy Peptide in Joint Symptoms of Rheumatoid Arthritis Patients

Hirotaka Yoshioka[1], Naoto Yu[1,*], Keisuke Maegawa[2], Mitsumasa Kohno[3], Haruki Musya[3] and Kazuo Yudoh[3,*]

[1]*Department of Sports Medicine, St. Marianna University School of Medicine, 2-16-1 Sugao, Miyamae-ku, Kawasaki, Kanagawa, 216-8512, Japan*
[2]*Clinic Research Department, Fuji Oil Co., Ltd., 1-3 Kiyomidai, Tsukuba-gun, Ibaraki, 400-0107, Japan*
[3]*Institute of Medical Science, St. Marianna University School of Medicine, 2-16-1 Sugao, Miyamae-ku, Kawasaki, Kanagawa, 216-8512, Japan*

Received January 8, 2014; Accepted March 20, 2015

We evaluated the efficacy of a powder containing soy peptide for improving rheumatoid arthritis symptoms and mitigating joint pain in comparison with a placebo group using a double-blind method. Sixteen outpatients being prescribed therapeutic agents for rheumatoid arthritis were randomly divided into two groups (placebo group and soy peptide group). Subjects took 30 g of a powder containing the test item, which contained either 8 g of soy peptide or not (placebo group), for 8 weeks. Treatment outcomes as measured by inflammatory marker levels and objective and subjective evidence of anti-inflammatory effects were compared between the soy peptide and the placebo groups using the Student-t test. No adverse effects or clinically severe problems were observed in any of the subjects during the entire 8-weeks period. The present report indicates that continued soy peptide intake for alleviating rheumatoid arthritis symptoms may have value as a complement to the usual therapy for rheumatoid arthritis.

Keywords: Soy peptide, Rheumatoid Arthritis, DAS28 (Disease Activity Score (DAS) 28), Clinical Disease Activity Index (CDAI)

緒 言

[illegible]

[illegible]

[illegible]
[illegible]
[illegible]
[illegible]

[illegible]

[illegible]

疾患で，多くの患者が関与している（Capuron et al. 2010）．この人工的に作る酵素活性による人工ペプチド，及び同物質に対する抗ヒトマクロファージ・ケモカイン（macrophage chemotactic factor）TNFα やインターロイキン（IL）6 の分泌を抑制するペプチドの産生を誘導することが報告されている．また活性酸化種を含むことが上記 in vitro 実験系において確認されている（de Mejia et al. 2009, Chakrabarti et al. 2011）．一方，in vivo 実験系においては，ヒトリンパ球を移植したNOD/SCID マウスモデル（Kovacs-Nolan et al. 2012, Yang et al. 2012），ヒトTNFα 遺伝子トランスジェニックマウスモデル（Mohammad et al. 2012），[illegible]

[illegible]

方　法

1）被験者の選定

[illegible]

2）試験方法

本試験は，被験者（16 名）を[illegible]

[illegible]

試験は，イ）～ヘ）の[illegible]

3）試験食品

[illegible]

Table 1 Composition of test formulation

(grams per pack or a day)

	Peptide group	Placebo group
Powdered Soy peptide*	9.15	0.00
Dextrin	5.84	14.99
Maltitol	13.21	13.21
Sweetener	0.01	0.01
Citric acid	1.35	1.35
Flavoring	0.50	0.50
Gelatine	0.03	0.03
Total	30.00	30.00

*: Soy peptide purity of powdered soy peptide is 87.4%

4）評価方法

試験期間は，[illegible]

[illegible]

DAS28 は，28 か所の関節について痛みや腫脹があるか調査し，各関節の程度を点数化（0～3 段階），患者自身による GA マークド VAS（0～100），血液検査データ（血沈や CRP，[illegible]）を用いて，下記の計算式により算出する．Disease Activity Score (DAS) 28 は，[illegible] 活動性の指標である Clinical disease activity index (CDAI) の代わりとなるものである．

DAS28 は，28 か所の関節について痛みや腫脹があるか調査し，各関節の程度を点数化（0～3 段階），患者自身による GA マークド VAS（0～100），

[illegible]

DAS28 = 0.56 × √TJC + 0.28 × √SJC + 0.70 × LN + 0.36 × LnCRP + 0.014 × VAS + 0.96

（TJC：腫脹関節数，SJC：圧痛関節数，LN：圧痛関節数，CRP：患者のVAS）．CDAI は，下記関節数（28関節）＋ 医師評価（0～10cm）＋ 患者評価（0～10cm）の VAS）．DAS28 スコアの関値ならびに，それぞれ活動期，寛解の中間値を用いて，グループ分けを行い，ロジスティック回帰および一変量および多変量ロジスティック回帰分析によって，関値のよく当てはまるかどうかを検討した．[illegible]

5）統計解析方法

[illegible] 群間では Student-t 検定を用いて行った．有意水準は 5% ($p<0.05$)，有意傾向を 10% ($p<0.1$) とした．

結　果

1）検査者の背景

本研究対象は，男性1,350人，女性1,950人の合計3,300人（男性40%，女性60%）の，初診時年齢61.5歳（53～69歳），発症年齢中央値18.5年（14～18年）であった．ベースライン時点でのグループ間の検査結果の患者背景は下記の通りであった．[illegible]

[illegible]

[illegible]

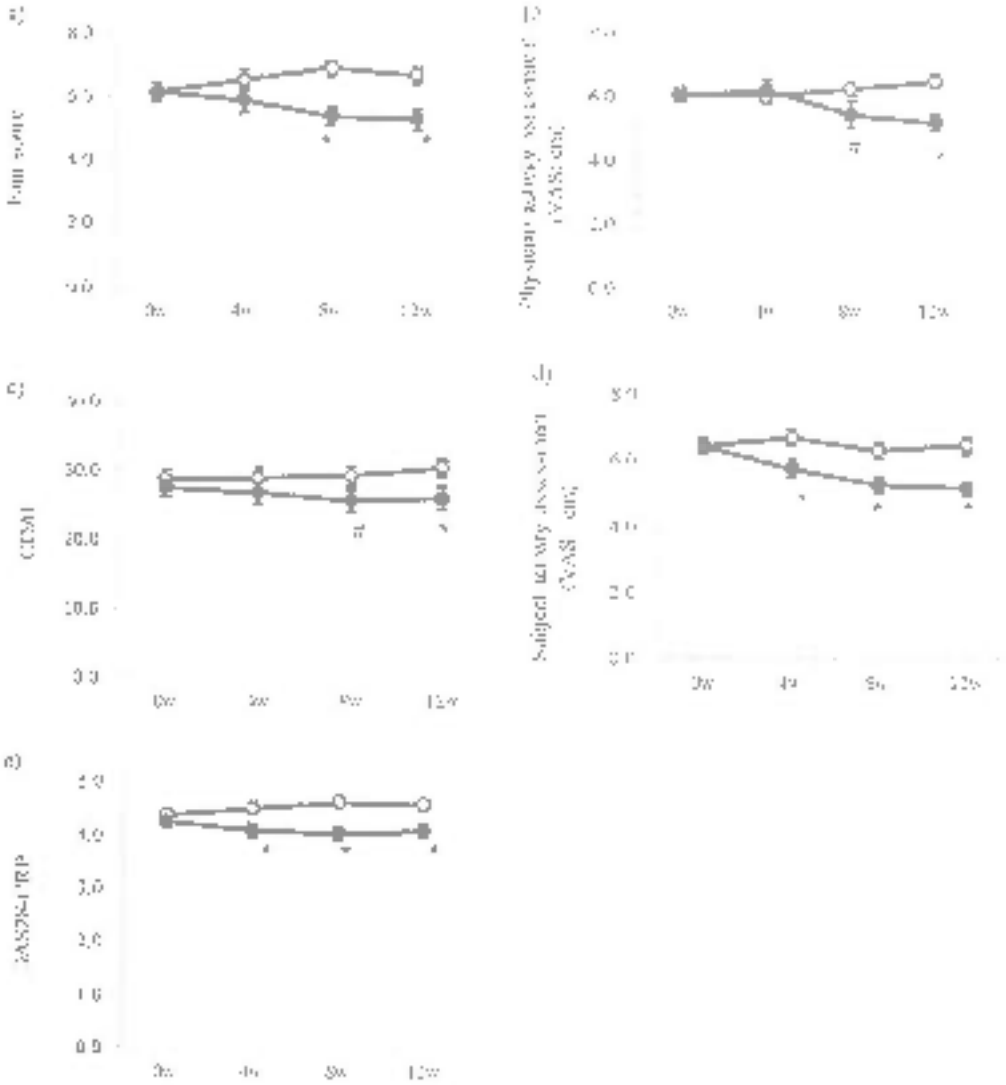

Figure 1 Evaluation of objective and subjective anti-rheumatic effect: a) pain score, b) physician activity assessment, c) CDAI, d) subject activity assessment, and e) DAS28-CRP
●: peptide group and ○: placebo group
CDAI (Clinical disease activity index): Index of severity of daily living improved.
DAS28-CRP (Disease Activity Score 28- C-reactive protein): Score of degree of rheumatoid arthritis symptoms and inflammation calculated from joint pain with pain and swelling for 28 joints or inflammation, and evaluation of symptoms by the patient (VAS)
*: significantly different from placebo group ($p < 0.05$)
#: significantly difference tendency from placebo group ($p < 0.1$)

[illegible] (p<0.05, Figure 1d).

3) 血液検査データ

[illegible] 0.1 ng/ml [illegible] (p<0.05). [illegible] 0.7 ± 0.6 ng/ml [illegible] 0.8 ng/ml [illegible] 5.6 ± 1.7 ng/ml [illegible] (p<0.1). [illegible] (p<0.05, Figure 2a) [illegible] 0.6 ng/ml. [illegible] 0.7 ± 0.5 ng/ml [illegible] (p<0.05, Figure 2b) [illegible] TNF-α [illegible] 0.8 ng/ml [illegible] 5.6 ± 1.7 ng/ml [illegible] (p<0.1, Figure 2c) [illegible]

[illegible]

[illegible]

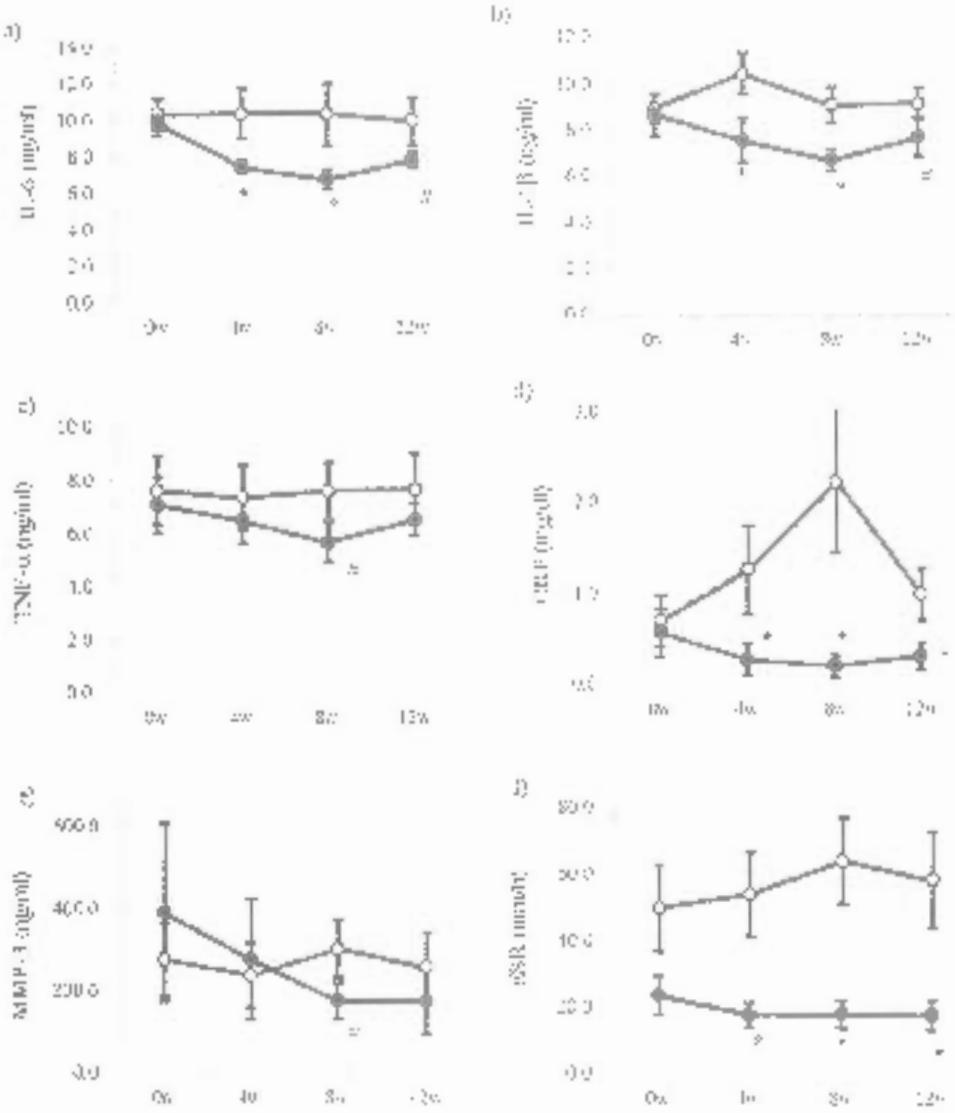

Figure 2 Changes of inflammatory marker levels. a) IL-6, b) IL-1β, c) TNF-α, d) CRP, e) MMP-3 and f) ESR.

● peptide group and ○ placebo group.

IL-6: Interleukin-6, IL-1β: Interleukin-1 beta, TNF-α: Tumor necrosis factor alpha, CRP: C-reactive protein, MMP-3: matrix metalloproteinase 3, and ESR: erythrocyte sedimentation rate.

* significantly different from placebo group ($p < 0.05$)

significantly difference tendency from placebo group ($p < 0.1$).

考　察

関節リウマチの治療は薬物療法が中心であり，疾患の進行を抑止するために早期に適切な薬剤を用いることが重要．NSAIDs，副腎皮質ホルモン，メトトレキサート（以下，MTX）などの疾患修飾性抗リウマチ薬（DMARDs）などが用いられている（Scholes et al. 2012）．しかしこれらの NSAIDs 及び MTX，胃腸障害や上部消化管潰瘍などの重篤な副作用が問題となっており，その問題となっている副作用は，発生頻度が高く，数十～数千万人単位，そして近年，高齢者に多い傾向にある．また，COX2 阻害薬が中枢性の COX2 選択的阻害薬の服用では，心血管系の障害が起こるリスクがあり，その服用中止の時期も問題となっており，薬剤の安全な使用と管理が求められている（Scholes et al. 2012）．一方，関節リウマチの病態に関する研究は，多くの分子レベルでサイトカインが重要な役割を果たしていることが，発症機構を解明する研究，MTX に代表される免疫抑制剤などの薬剤開発，DMARDs（disease-modifying anti-rheumatic drugs）による標的サイトカイン阻害薬の開発などの臨床的に進展している（Kaneko et al. 2014，Gibofsky 2014）．しかしながら，これらの新規治療法では，non-responder が存在し，responder であっても長期使用によって薬剤に効果が減弱することがあることから，安全性と有効性の観点から問題となっている（Mergin et al. 2003）．また，抗リウマチ薬（免疫学的製剤・分子標的薬）による炎症サイトカインの生体内利用は，長期安全性，発癌性，感染症，中枢性・末梢性除去，骨髄抑制等の様々な問題点から問題となっ，その使用の際には十分な注意が必要とされている（van Nies et al. 2014）．

本研究の結果結果から，様々な薬剤による治療を受けているにもかかわらず，関節及び骨の破壊修復および関節痛を訴えている重症リウマチ患者に対して，ヒアルロナン（HA）を単独投与することにより，疼痛リウマチにおける炎症（腫脹・関節変形）を抑制する効果を有することが，患者本人の自覚的評価（患者活動性評価：VAS）（図3）による身体的疼痛自覚（医師活動性評価：VAS, CDAI）による医師の評価（VAS, Pain score）との比較した．その結果，HA，VAS が生理的に有（Pain score）患者 VAS のリウマチ，ヒアルロナン投与で改善が…の大きく…．近年，医師と患者による評価の乖離が報告され，その原因として患者は多部位の…を訴えるのに対し，医師は関節の腫脹・変形を主の重症度の判断基準とされ，HA が患者の痛みを…している点が挙げられている（Studenic et al. 2012）．また，医師リウマチ専門…，患者とのコミュニケーション…，患者と…の…，評価は…の患者…，…，…（Dangadee et al. 2013）．このような…，最近…変形…患者…，…．…，…．

…，…，…，…リウマチ患者…，…．…，…．

…，…，…，…．…，…．…，…．

[illegible] (Asamoto et al. 2012, Tachibana N et al. 2005 and Yamazaki et al. 2012). [illegible] 結果は、[illegible] (Takuchi et al. 2010)。今回の結果は、大豆成分が関節リウマチに対して、疾患活動性の抑制に寄与していることを示唆しており、[illegible] 除外されるべきではなく、同様にリウマチ治療に応用されるべきであることを示唆する。

本試験において、[illegible] ESR は [illegible] 値が [illegible] 大きく、89 mm/h を示した。[illegible] 値は [illegible] 値を示した。一方、ESR 以外の急性期マーカーである CRP では [illegible] 値を示した。[illegible] 値は [illegible] 値を示した。[illegible] 値は [illegible] 値を示した。[illegible] 値は

(8): 2407-14

Morgan C, Gau M, Brignavel D, Bradbury P, Gallow W, Lis M, Siroua A, Bruce IN. Contribution of patient related differences in multidrug resistance to disease and its [illegible]. Ann Rheum Dis. 2013;62:1:e15-9.

Scholes M, Smolen JS. Treating rheumatoid arthritis to target: evidence-based recommendations for enhanced disease management. Rheumatol Clin. 2012;8:1-2.

Stalnacke P, Radner H, Smolen JS, Aletaha D. Discrepancies between patients and physicians in their perceptions of rheumatoid arthritis disease activity. Arthritis Rheum. 2012 Sep;64(9):2814-23.

Tachibana N, Matsumoto I, Fukui K, Aoki S, Nato H, Abe K, Takematsu K. Intake of Soy Protein Isolate Alters Hepatic Gene Expression in Rats. J Agric Food Chem. 2005;53:11:4251-4257.

Taku K, McCay MK, Kurzer MS, Mizuno S, Watanabe S, Ishimi Y. Effects of soy isoflavone supplements on bone turnover markers in menopausal women: systematic review and meta-analysis of randomized controlled trials. Bone. 2010 Aug;47(2):113-23.

Torres N, Tovar-Palacio C, Tovar AR. Regulation of lipid metabolism by soy protein and its implication in diseases mediated by lipid disorders. J Nutr Biochem. 2006 Jan;17 (1):365-75.

van Nies JA, Krabbe A, Schoones JW, Huizinga TW, Kloppenburg M, van der Helm-van Mil AH. What is the evidence for the presence of a therapeutic window of opportunity in rheumatoid arthritis? A systematic literature review. Ann Rheum Dis. 2014;73:861-870.

Watari T, Hoshi M, Nakamoto T, Tsai M, Muto Y. Soy-derived di- and tripeptides alleviate colon and ileum inflammation in piglets with dextran sulfate sodium sulfate-induced colitis. J Nutr. 2012;142(2):363-8.

Yamazaki T, Shimano K, Miura S, Ezaki O. Dietary β-conglycinin prevents fatty liver induced by a high-fat diet by a decrease in PPARγ2 protein. J Nutr Biochem. 2012;23(2):123-132.

Review article

Using proteomic and genomic methods to understand JDM

Ric Kawasaki[1,2] and James N. Jarvis[1]

[1] Department of Pediatrics and Genetics, Genomics & Bioinformatics Program, University at Buffalo, Buffalo NY, USA
[2] Department of Frontier Medicine, St. Marianna University School of Medicine, Kawasaki, Japan

(Accepted April 9, 2015)

summary

Juvenile dermatomyositis is a complex illness characterized by vascular/perivascular inflammation, primarily in the skin and muscles. In this review, we discuss how proteomic and genomic technologies have expanded our understanding of the immune pathogenesis of this disease. We will also discuss further directions that the field may take to use existing and developing technologies to further our understanding of this often-perplexing disease.

Key words: juvenile dermatomyositis; proteomics; anti-endothelial cell antibodies (AECA); genomics; gene expression profiling

Introduction

Juvenile dermatomyositis (JDM) is the most common clinical phenotype of myositis in children and accounts for approximately 85% of the juvenile idiopathic inflammatory myopathies (JIIM)[1-4]. While classified as a "myopathy," JDM, is also considered a systemic autoimmune vasculopathy that includes muscle tissue but can also involve other organ systems. We are increasingly recognizing that the spectrum of clinicopathologic groups and serologic phenotypes in pediatric myopathies, including JDM, is quite heterogeneous. Among other things, we are finding the these different groups can be defined by the presence of myositis-specific or myositis-associated autoantibodies, each with differing demographics, clinical manifestations, laboratory findings, and prognoses. However, the etiology of JDM is unknown, and we lack biomarkers in patients with JDM for diagnosis.

This paper, we will discuss how new approaches and technologies are broadening our understanding of the heterogeneity of autoantibody expression in JDM and discuss how unbiased proteomics approaches may further advance understanding. In addition, we discuss the new insights that genomics approaches, and gene expression profiling in particular, have added new insights into disease pathogenesis.

1. The clinical spectrum of JDM

As noted above, JDM is a systemic, inflammatory, idiopathic disease of affecting the skin, the muscles and other organs. In the USA, the incidence rate of JDM is estimated to be 3.2 per 1 million children per year, with the median age at onset between 5.9 and 7.5 years. There is a slight female preponderance in new cases, with male:female ratios varying between 1:2.2 to 1:2.7[1,4]. In Japan, the prevalence of JDM is estimated to be 17.4 per 1 million children, with male:female ratios 1:2.3[5]. While it is difficult to compare incidence statistics in one country with prevalence data from another, it is reasonable to conclude that JDM is one of the rarer childhood-onset rheumatic diseases in both Japan and North America. At the same time, older data suggests that, if anything, the disease in more common in Japanese children than in North American[5,6].

The clinical feature at presentation include Gottron's papules, heliotrope rash, proximal muscle weakness, myalgia, arthralgia and/or arthritis and described as "dermatomyositis" exist in both children and adults, there are differences between in children and in adults that suggest that the entity we designate "JDM" may be pathologically distinct. Vascular and perivascular inflammation in the skin, gastrointestinal tract, lungs, kidneys, eyes and heart are prominent pathological features of JDM not encountered to the same degree in the adult form of the disease. Furthermore subcutaneous and intramuscular calcinosis, which is often refractory to treatment, remains a vexing clinical problem for anywhere from 15-50% of JDM patients[1,7-11]. A retrospective review of sch-

Saharan African children with JDM found a cumulative frequency of calcinosis in 71% of the affected children[17]. In addition, there are cases in children where rash is prominent but muscle involvement either absent or minimal. These entities are sometimes referred to as clinically amyopathic dermatomyositis (CADM) or hypomyopathic dermatomyositis. Despite the absence of prominent muscle symptoms, these children are at risk for rapidly progressive interstitial lung disease (RP-ILD), which can be fatal. It is reported that CADM occurs with a frequency of 1%[11].

2. Autoantibodies in JDM

Previous studies showed there are significant correlations between clinical phenotype and the presence and/or the type of autoantibodies in patients with JDM. For example, antinuclear antibodies (ANA) are detected in 27% to 72% of children with JDM (vs. 10–30% of healthy children)[1,2,3], and anti-TIF1 (anti-p155/140) and anti-NXP2 (anti-p140/anti-MJ), myositis-specific autoantibodies (MSAs) that are detected frequently in 23% to 38% and 18% to 28% of JDM patients, respectively[12,13]. Shah et al.[14] reported that anti-Ro (5% of patients), anti-U1-RNP (2% of patients) and anti-PM-Scl (3% of patients) can rarely be detected in JDM patients; these antibodies are sometimes referred to as myositis-associated autoantibodies (MAAs). It is useful to note that these antibodies are far from a universal phenomenon in JDM. Shah et al.[14] reported that 28% of the patients they studied with JDM had no myositis autoantibody. Anti-Jo-1 were negative in almost all of patients with JDM (< 5%)[3].

Expression of specific autoantibodies often correlates with specific clinical features. For example, in patients with anti-TIF1, clinical features include cutaneous ulceration and edema, severe photosensitive rashes, lower creatine kinase levels, and a chronic course[15]. In patients expressing anti-NXP2, dysphagia, muscle cramps, and increased calcinosis are distinguishing clinical features, although these patients typically pursue a monocyclic course[13]. Patients expressing MAAs as well as MSAs, have extra-muscular involvement, for example, Raynaud's phenomenon, sclerodactyly and arthritis seen in patients with anti-U1-RNP, and Raynaud's phenomenon, arthritis, dysphagia and interstitial lung disease in patients with anti-PM-Scl, anti-Ro antibodies, are common in patients with overlap myositis (i.e., patients expressing complex phenotypes that may include clinical features of scleroderma, systemic lupus, or rheumatoid arthritis). However, little has been reported on the relationship between these autoantibodies and specific clinical features[3]. Although the number of JDM patients expressing anti-Jo-1 antibody is very small, these patients frequently have ILD, arthritis, Raynaud's phenomenon, fevers, and mechanic's hands[19].

Furthermore there are significant differences between JDM and juvenile polymyositis (JPM) in presence of autoantibodies such as anti-p155/140, anti-Jo-1, anti-Mi-2, anti-SRP and anti-U1-RNP[3]. As well as JPM, there are significant differences between JDM and JDM overlapping with another autoimmune or connective tissue disease in median ANA titer and in presence of autoantibodies such as anti-p155/140, anti-aminoacyl tRNA synthetase, anti-Jo-1, anti-Ro, anti-U1-RNP, anti-PM-Scl, anti-Sm and anti-La[3].

As noted above, ILD, including RP-ILD, is a well-described feature of CADM. This complication is associated with the presence of anti-melanoma differentiation-associated gene 5 (MDA5) antibodies in patients with PM, DM and JDM. Kobayashi et al.[20] showed that anti-MDA5 antibodies were detected in all eight patients with RP-ILD and in 71% of the patients with chronic ILD, but in no JDM patients without ILD. In addition serum levels of anti-MDA5 antibody were also significantly higher in the JDM patients with RP-ILD than in those with chronic ILD or non-ILD. Tansley et al.[21] investigated relationship between the presence of anti-MDA5 autoantibodies and clinical phenotype of the patients with JDM. They showed that anti-MDA5 antibodies were closely related to clinical phenotypes, including skin and oral ulcerations and milder muscle disease. In addition, 21% of JDM patients with anti-MDA5 had ILD, but none of those had RP-ILD[21]. It should be noted that ILD is still rare in JDM, affecting only 2–5% of patients compared with DM[1,4]. At the same time, it must be noted that RP-ILD is one of the fatal complication of JDM.

3. Anti-endothelial cell antibodies (AECA)

Anti-endothelial cell antibodies (AECA) are autoantibodies against antigens on endothelial cell (EC) surfaces.

AECA have been detected in patients with connective tissue diseases, inflammatory diseases, and primary and secondary vasculitis[22-26]. There are many reports that AECA may be involved in EC activation and vascular disorders via increased expression of adhesion molecules, complement activation, increased levels of pro-inflammatory cytokines and chemokines and induction of apoptosis and thrombosis[1,24-26]. Furthermore it is reported the titers of AECA are associated with disease activity and the presence of AECA may be reliable biomarkers for vasculitis[27-29].

JDM is an autoimmune vasculopathy that may involve multiple organ systems in addition to skin and muscle. Intestinal ischemia due to vessel inflammation and thrombotic occlusion, for example, is a rare but serious, sometimes lethal event. Thus AECA are attractive candidates for biomarkers in patients with JDM. Yu et al.[12] reported that IgG AECA were detected in 76.0% of 25 JDM patients with active disease and in 29.4% of 17 control patients by ELISA, when using human umbilical vein endothelial cell lysates as a means of detection. On the other hand, anti-p155/140 antibodies and anti-p140 antibodies were detected in 36% and 28% of the patients with JDM and in none of the control patients[12].

To understand mechanistic roles of AECA in the pathophysiology of diseases, it is useful to identify the specific antigens targeted by these antibodies. This is best done with an unbiased and comprehensive proteomic analysis. Karasawa et al.[30] identified target antigens for AECA in patients with primary systemic vasculitis such as Takayasu's arteritis and with secondary systemic vasculitis such as systemic lupus erythematosus using proteomic approaches. Protein extracted from human umbilical vein endothelial cells (HUVEC) were used as an antigen source for this research. To select autoantigens expressed specifically in ECs, protein extracted from HeLa cells were used as a control. Extracted proteins were separated by two-dimensional electrophoresis, and transferred them into membranes. Western blotting using sera samples from patients with systemic vasculitis was used to select the autoantigens candidates by choosing only positive blots in HUVEC samples but not in HeLa samples. By peptide mass finger printing, the sequence of them was identified. One of identified proteins was peroxiredoxin2 (Prx2), an antioxidant enzyme. IgG antibodies to recombinant Prx2 were detected in 69% of the patients with systemic vasculitis and in 7% of the patients with collagen diseases without vasculitis but not in the healthy donors. The titers of anti-Prx2 antibodies were correlated with disease activity and the presence of anti-Prx2 antibodies was closely related to increased level of both D-dimer and thrombin-antithrombin complex. Furthermore anti-Prx2 antibodies induced increased inflammatory cytokines and chemokines secretion from HUVEC including IL-6, growth regulated oncogene (GRO)-α and IL-1β[30].

Fujieda et al.[31] reported that IgG antibodies to recombinant Prx2 were detected in 43.3% of the patients with Kawasaki disease (KD) and in 10% of the patients with sepsis but not in the healthy donors. Furthermore, the anti-Prx2-positive group showed a longer period of fever, decreased responses to high-dose γ-globulin therapy and increased excretion of urinary 8-isoprostaglandin as compared with anti-Prx2-negative group.

Although there are several reports about pathogenic roles of AECA in vascular disorders, the pathogenic roles of AECA remain incompletely understood. We believe, however, that such a comprehensive, unbiased approach to the identification of target antigens on/within AECA in patients with JDM will significantly expand the repertoire of known JDM-associated antibodies in the same way that this approach has expanded our knowledge of the autoantibody repertoire in other forms of vasculitis.

4. Detection of biomarkers in patients with JDM using proteomic techniques

Proteomic techniques make it possible to identify specific proteins, modification of proteins, and protein expression levels[32-34]. Proteomic techniques may also be helpful for analyzing the differences in time-course, such as between pre- and post-treatment patients. These same approaches may also characterize subtly different disease phenotypes. An additional advantage to this approach is its suitability for many kinds of samples, including sera, plasma, urine, saliva, cerebrospinal fluid and synovial fluid[34]. An example of the utility of an unbiased proteomic approach can be found in the recent work of O'Hanlon et al.[35]. These authors reported results from proteomic analysis of plasma samples from monozygotic (MZ) twin pairs discordant for systemic autoimmune dis-

eases (SAID), their sample included 2 patients with JDM as well as juvenile arthritis and systemic lupus) as well as matched healthy controls. Proteomic approaches consisted of examination of patterns of protein expression using differential quantitative proteomic analysis (one-dimensional reverse-phase liquid chromatography-mass spectrometry). Affected twins expressed higher levels of retinoblastoma-binding protein 1 and leucine-rich α2-glycoprotein 1 compared to either unaffected twins or unrelated controls. In addition, decreased plasma levels of paraoxonase 1 were detected in affected twins compared to same groups. Random Forest multivariate analysis identified seven proteins that crisply segregated affected and unaffected twins by their expression levels. Four of these were already identified on the univariate analysis. Thus, using a combination of both wet lab and computational approaches, as is done in genomics, is likely to yield the best means for identifying useful biomarkers for JDM.

5. Genetic basis of JDM

In many ways, the field of genomics as applied to JDM is still in its infancy. For example, while we have some understanding of the genetic contribution to JDM[52], those studies have been largely undertaken using "candidate gene" approaches. For example, increased risk for JDM has been reported in individuals carrying an HLA B8-DR3 haplotype[53]. However, the best-documented genetic associations for JDM are with the class II HLA antigen, DQA1*0501, associations that appear to be common for multiple ethnic groups[37]. In addition to being a risk factor for disease per se[16], affected children expressing the DQA1*0501 allele may be at higher risk for pursuing a chronic or persistent disease course than are children with JDM who do not express this allele.

Alleles within the TNFA gene have also shown associations with JDM. At position −308 within the TNFA promoter, a G → A substitution occurs in approximately 20% of healthy Caucasians. In *in vitro* models, the "A" allele is associated with more robust TNFα production to specific stimuli than is the more common −308 "G" allele. It was therefore of great interest when Pachman and colleagues reported a strong association between the −308 "A" allele and JDM in Caucasian children. Furthermore, this allele was strongly associated with a more severe clinical course (including calcifications) in children with this disease[54,55]. Because TNFα is a critical initiator and regulator of both innate and adaptive immune responses, these findings support the hypothesis that JDM, like other childhood rheumatic diseases[31], involves complex interactions between innate and adaptive immunity.

While these observations provide some useful insight, we are largely in the dark as to whether there are other genetic loci that contribute to disease susceptibility. Conspicuously absent from the literature is a genome-wide association study (GWAS), such as the one recently completed for juvenile idiopathic arthritis (JIA)[42]. Even that study was small by GWAS standards (1,800 subjects), and, given the rarity of JDM relative to JIA, gathering a sufficient number of subjects to perform a meaningful GWAS would be extraordinarily difficult. However, continuing with candidate gene approaches alone is unlikely to significantly advance the field. Among other things, most genetic risk for complex traits doesn't reside within the canonical coding regions of genes. In the Hinks study of JIA, for example, 22 of the 24 risk-associated single nucleotide polymorphisms (SNPs) were located within intronic or intergenic regions of the genome. This finding is consistent with almost every other GWAS for complex traits[56] and has naturally led to the question, "What's in those regions?" For JIA, we have some answers, as we have recently demonstrated that all of the JIA-associated SNPs that are not within the coding genome are located within linkage disequilibrium (LD) blocks that contain H3K4me1/H3K27ac-marked enhancers in either T cells or neutrophils[29].

Given that a GWAS approach to understanding genetic risk in JIA impractical, what alternatives are there for us to derive a better understanding of this disease? There are two approaches that might be taken. One approach would be exome sequencing, which queries only the coding parts of the genome. While this approach has been typically applied to Mendelian traits, there is emerging interest in using this approach to identify rare variants that may be associated with complex human diseases[57]. An advantage to this approach is that meaningful information could be acquired with hundreds of patients, rather than the thousands or tens of thousands required to obtain meaningful information from GWAS. The disadvantage,

of course, is that this approach provides no information about non-coding parts of the genome, where disease risk for most complex traits is typically located, as noted previously[6]. Alternatively, deep sequencing of whole genomes is becoming increasingly attractive as costs of next-generation sequencing continue to fall and new platforms continue to evolve.

6. Transcription profiling

Transcription profiling using hybridization based microarrays is an attractive approach for both understanding disease pathogenesis and to develop clinically relevant biomarkers[6]. Despite their limitations[7], this technology has provided some useful insights into JDM pathogenesis. For example, in 2002, Tezak et al reported a distinct type I interferon "signature" in muscle biopsies of a select group of patients with JDM[8]. Specifically, muscle biopsies in children with JDM were distinguished from children with non-inflammatory myopathies as well as healthy controls by the expression of genes know to be induced by type I interferons. Disease duration was subsequently shown to have a significant impact on muscle expression profiles in JDM[9]. The type I interferon signature has also been demonstrated on whole blood expression profiling in treated patients with JDM (this study included both adult and pediatric JDM subjects)[10]. In this study, the signature was not as strong as in the Tezak study but was clearly associated with active disease. Each of these studies is limited by the number of samples or patients studied (for example, in the Chen study, only 3 samples were studied in the short disease duration group; in the Baechler study, only 2 of the subjects were children, and all subjects were already on medication). These small numbers are therefore prone to high false discovery rates that can't be completely eliminated with any bioinformatics approach. A larger patient population of untreated patients (9 girls and 8 boys) was described by Frank et al in a study aimed at discovering gene expression network structures in both JIA and JDM[11]. These authors demonstrated that, like physiologic systems, gene co-expression networks in childhood rheumatic diseases like JDM display the same hub-and-node structures as physiologic systems[12,13]. Furthermore, such networks could be identified in both peripheral blood mononuclear cells and neutrophils. These findings are consistent with the increasingly-accepted theory that complex human diseases are associated with cellular "rewiring" that must be corrected in order to achieve therapeutic response[14,15]. At the same time, achieving this rewiring may be challenging, as network structures that display hub-and-node configurations are particularly resistant to external impingement[16].

In summary, preliminary studies using genomic approaches have added some valuable insights into JDM that have simultaneously added more questions. Future work will likely be aimed at: (1) a better understanding of the genetic contribution to JDM; (2) understanding the origins of the type I interferon signature; and (3) understanding the biology of therapeutic response, as it currently under way for JIA[17].

Conclusion

In conclusion, both proteomic and genomic approaches have provided both useful insights into disease pathogenesis and provided direction for biomarker development. A focused effort to compare Japanese and North American patients with JDM would likely provide new and valuable information regarding the genetics and epigenetics of this disease.

References

1) Ernste, F.C., Reed, A.M.: Recent advances in juvenile idiopathic inflammatory myopathies. *Curr Opin Rheumatol* **26**: 671–678, 2014.

2) Rider, L.G., et al.: Developments in the classification and treatment of the juvenile idiopathic inflammatory myopathies. *Rheum Dis Clin North Am.* **39**: 877–904, 2013.

3) Shah, M., et al.: The clinical phenotypes of the juvenile idiopathic inflammatory myopathies. *Medicine* (Baltimore) **92**: 25–41, 2013.

4) McCann, L.J., et al.: The Juvenile Dermatomyositis National Registry and Repository (UK and Ireland): clinical characteristics of children recruited within the first 5 yr. *Rheumatology* (Oxford) **45**: 1255–1260, 2006.

5) Robinson, A.B., et al.: Clinical characteristics of children with juvenile dermatomyositis: the Childhood Arthritis and Rheumatology Research Alliance Registry. *Arthritis Care Res* (Hoboken) **66**: 404–410, 2014.

6) Mendez, E.P., et al.: US incidence of juvenile dermatomyositis, 1995-1998: results from the National Institute of Arthritis and Musculoskeletal and Skin Diseases Registry. *Arthritis Rheum* **49**: 300–305, 2003.

7) Kobayashi, S., et al.: Characteristics of juvenile dermatomyositis in Japan. *Acta Paediatr Jpn*. **39**: 257–262, 1997.

8) Rider, L.G., et al.: Textbook of Pediatric Rheumatology. 6th ed. Elsevier Saunders, Philadelphia. 375–413, 2011.

9) Ravelli, A., et al.: Long-term outcome and prognostic factors of juvenile dermatomyositis: a multinational, multicenter study of 490 patients. *Arthritis Care Res* (Hoboken) **62**: 63–72, 2010.

10) Christen-Zaech, S., et al.: Persistent association of nailfold capillaroscopy changes and skin involvement over thirty-six months with duration of untreated disease in patients with juvenile dermatomyositis. *Arthritis Rheum*. **58**: 571–576, 2008.

11) Fuller, G., et al.: Juvenile dermatomyositis in South African children is characterised by frequent dystropic calcification: a cross sectional study. *Pediatr Rheumatol Online J*. **12**: 2017.

12) Yu, H.H., et al.: Detection of anti-p155/140, anti-p140, and antiendothelial cells autoantibodies in patients with juvenile dermatomyositis. *J Microbiol Immunol Infect*. **14**: S1:84–1182, 2014.

13) Targoff, I.N., et al.: A novel autoantibody to a 155-kd protein is associated with dermatomyositis. *Arthritis Rheum*. **54**: 3682–3689, 2006.

14) Fujimoto, M., et al.: Myositis-specific anti-155/140 autoantibodies target transcription intermediary factor 1 family proteins. *Arthritis Rheum*. **64**: 513–522, 2012.

15) Gunawardena, H., et al.: Clinical associations of autoantibodies to a p155/140 kDa doublet protein in juvenile dermatomyositis. *Rheumatology* (Oxford) **47**: 324–328, 2008.

16) Ichimura, Y., et al.: Anti NXP2 autoantibodies in adult patients with idiopathic inflammatory myopathies: possible association with malignancy. *Ann Rheum Dis*. **71**: 710–713, 2012.

17) Gunawardena, H., et al.: Autoantibodies to a 140-kd protein in juvenile dermatomyositis are associated with calcinosis. *Arthritis Rheum*. **60**: 1807–1814, 2009.

18) Hoshino, K., et al.: Anti MDA5 and anti-TIF1-gamma antibodies have clinical significance for patients with dermatomyositis. *Rheumatology* (Oxford) **49**: 1726–1733, 2010.

19) Rider, L.G., et al.: The myositis autoantibody phenotypes of the juvenile idiopathic inflammatory myopathies. *Medicine* (Baltimore) **92**: 223–243, 2013.

20) Kobayashi, N., et al.: Clinical and laboratory features of fatal rapidly progressive interstitial lung disease associated with juvenile dermatomyositis. *Rheumatology* (Oxford). 2014 Oct 6. pii. ken385. [epub ahead of print].

21) Tansley, S.L., et al.: UK Juvenile Dermatomyositis Research Group.Anti-MDA5 autoantibodies in juvenile dermatomyositis identify a distinct clinical phenotype: a prospective cohort study. *Arthritis Res Ther*. **16**: R138, 2014.

22) Belizna, C., et al.: Antiendothelial cell antibodies in vasculitis and connective tissue disease. *Ann Rheum Dis*. **12**: 1545–1550, 2006.

23) Kurasawa, R., et al.: Peroxiredoxin 2 is a novel autoantigen for anti-endothelial cell antibodies in systemic vasculitis. *Clin Exp Immunol*. **161**: 459–470, 2010.

24) Donicianso, D.S., et al.: Pathogenic role of anti-endothelial cell antibodies in autoimmune rheumatic diseases. *Lupus*. **18**: 1233–1238, 2009.

25) Yang, Y.H., et al.: The immunobiology of Henoch-Schönlein purpura. *Autoimmun Rev*. **7**: 179–184, 2008.

26) Wedderburn, L.R., Rider, L.G.: Juvenile dermatomyositis: new developments in pathogenesis, assessment and treatment. *Best Pract Res Clin Rheumatol*. **23**: 665–678, 2009.

27) Navarro, M., et al.: Anti-endothelial cell antibodies in systemic autoimmune diseases: prevalence and clinical significance. *Lupus*. **6**: 521–526, 1997.

28) Aydintug, A.O., et al.: Antibodies to endothelial cells in patients with Behçet's disease. *Clin Immunol Immunopathol*. **67**: 157–162, 1993.

29) Yang, Y.H., et al.: The level of IgA antibodies to human umbilical vein endothelial cells can be enhanced by TNF alpha treatment in children with Henoch-Schönlein purpura. *Clin Exp Immunol*. **130**: 352–357, 2002.

30) Park, M.C., et al.: Anti-endothelial cell antibodies and antiphospholipid antibodies in Takayasu's arteritis: correlations of their titers and isotype distributions with disease activity. *Clin Exp Rheumatol*. **24**: S10–6, 2006.

31) Fujieda, M., et al.: A novel anti-peroxiredoxin autoantibody in patients with Kawasaki disease. *Microbiol Immunol*. **56**: 56–61, 2012.

32) Karasawa, R.: Progress and Clinical Applications in Proteomics. *Journal of Data Mining in Genomics & Proteomics* 81: 1–6, 2012.

33) Karasawa, R., et al.: Anti-endothelial cell antibodies (AECA) in patients with systemic vasculitis: our research using proteomics. *Expert Opin Biol Ther.* 11: 77–87, 2011.

34) De Franceschi, L., et al.: Proteomic analysis of biological fluids from autoimmune-rheumatological disorders. *Proteomics Clin Appl.* 5: 78–89, 2011.

35) O'Hanlon, T.P., et al.: Plasma proteomic profiles from disease-discordant monozygotic twins suggest that molecular pathways are shared in multiple systemic autoimmune diseases. *Arthritis Res Ther* 13: R181, 2011.

36) Reed, A.M.: Myositis in children. *Curr Op Rheumatol.* 13: 428–433, 2001.

37) Reed, A.M., Sterling, J.: The HLA-DQA1*0501 allele in juvenile dermatomyositis as seen in multiple racial groups. *Hum Immunol.* 44: 131–135, 1995.

38) Reed, A.M., et al.: Immunogenetic studies in families of children with juvenile dermatomyositis. *J Rheumatol.* 25: 1000–1002, 1998.

39) Pachman, L.M., et al.: TNFalpha-308A allele in juvenile dermatomyositis: association with increased production of tumor necrosis factor alpha, disease duration, and pathologic calcifications. *Arthritis Rheum.* 43: 2368–2377, 2000.

40) Pachman, L.M., et al.: Juvenile dermatomyositis: the association of the TNF alpha-308 allele and disease chronicity. *Curr Rheumatol Reports.* 3: 379–386, 2001.

41) Jarvis, J.N.: Mechanisms of pathogenesis and inflammation in the pediatric rheumatic diseases. *Curr Opin Rheumatol.* 10: 459–467, 1998.

42) Hinks, A., et al.: Dense genotyping of immune-related disease regions identifies 14 new susceptibility loci for juvenile idiopathic arthritis. *Nature Genet.* 45: 664–669, 2013.

43) Maurano, M., et al.: Systematic localization of common disease-associated variation in regulatory DNA. *Science.* 337: 1190–1195, 2012.

44) Jiang, K.*, et al.: Disease associated SNPs from non coding regions in juvenile idiopathic arthritis are located within or adjacent to functional genomic elements of human neutrophils and CD4+ T cells. *Arthritis Rheum.* 2015; In press.

* These authors contributed equally to this work.

45) Kiezun, A., et al.: Exome sequencing and the genetic basis of complex traits. *Nature Genet.* 44: 623–630, 2012.

46) Jarvis, J.N., et al.: Gene expression profiling in pediatric rheumatic disease: What have we learned? What can we learn? *Curr Prob Rheum.* 17: 602–611, 2005.

47) Rosenfeld, S.: Do DNA microarrays tell the story of gene expression? *Gene Regul Syst Bio.* 4: 61–73, 2010.

48) Tezak, Z., et al.: Gene expression profiling in DQA1*0501+ children with untreated dermatomyositis: a novel model of pathogenesis. *J Immunol.* 168: 4154–4163, 2002.

49) Chen, Y.-W., et al.: Duration of chronic inflammation alters gene expression in muscle from untreated girls with juvenile dermatomyositis. *BMC Immunol.* 9: 43, 2008.

50) Baechler, E.C., et al.: An interferon signature in the peripheral blood of dermatomyositis patients is associated with disease activity. *Mol Med.* 13: 59–68, 2007.

51) Frank, M.B., et al.: Disease associated pathophysiologic structures in pediatric rheumatic diseases show characteristics of scalle-free networks seen in physiologic systems.implications for psathogenesis and treatment. *BMC Med Genomics.* 2: 9, 2009.

52) Ravasz, E., et al.: Hierarchical organization of modularity of networks. *Science.* 297: 1551–1555, 2002.

53) Jeong, H., et al.: The large-scale organization of metabolic networks. *Nature.* 407: 651–654, 2000.

54) Barabási, A.-L., et al.: Network medicine: a network-based approach to human illness. *Nature Rev Genet.* 12: 56–68, 2011.

55) Carlucci, A.: Rewiring makes the difference. *Mol Systems Biol.* 7: 463, 2011.

56) Albert, R., et al.: Error and attack tolerance of complex networks. *Nature.* 406: 378–382, 2000.

57) Jiang, K., et al.: Genomic characterization of remission in juvenile idiopathic arthritis. *Arthritis Res Therapy.* 15: R100, 2013.

2016. Mar. 35(3): 781-3

Clin Rheumatol
DOI 10.1007/s10067-016-3185-3

BRIEF REPORT

Cutaneous manifestations of patients with relapsing polychondritis: an association with extracutaneous complications

Jun Shimizu[1] · Hiroshi Oka[2] · Yoshihisa Yamano[2] · Kazuo Yudoh[1] · Noboru Suzuki[1]

Received: 5 December 2015 / Accepted: 21 December 2015
© International League of Associations for Rheumatology (ILAR) 2016

Abstract The aim of this study was to determine the prognostic characteristics of patients with relapsing polychondritis (RP) accompanying cutaneous manifestations in Japan. We analyzed a cohort of 239 patients with RP in view of cutaneous and extracutaneous complications. Thirty three cases (14%) developed cutaneous manifestations and 23 cases had both cutaneous and extracutaneous manifestations. Five RP patients developed myelodysplastic syndrome (MDS) and all of the five patients had cutaneous manifestations, including Sweet's syndrome. Only one patient died of MDS among the five patients, suggesting rather better prognosis as compared with ordinary MDS. Five RP patients developed Behcet's disease and all the five patients had cutaneous manifestations. Death rate of the RP patients with cutaneous manifestations (15%) was slightly higher than that of whole Japanese RP patient cohort (9.2%). RP patients with cutaneous manifestations had a slightly higher death rate, than those without cutaneous manifestations. MDS of RP patients had a rather better prognostic impact in Japan. Further studies are needed to elucidate the pathophysiology of RP, which brings about development of extracutaneous manifestations, especially MDS and Behcet's disease.

Keywords Behcet's disease · Cutaneous manifestations · Epidemiology · Myelodysplastic syndrome · Relapsing polychondritis

✉ Noboru Suzuki
n-suzuki@juntendo.ac.jp

[1] Institute of Medical Science and Departments of Immunology and Medicine, St. Marianna University School of Medicine, Kawasaki 216-8511, Japan

[2] Rheumatic Diseases Center, Tokyo Medical University Hachioji Medical Center, Hachioji, Tokyo 193-0998, Japan

Relapsing polychondritis (RP) is characterized by recurrent inflammation and degeneration of cartilaginous tissue [1]. Cutaneous manifestations were not rare in RP patients [2]. RP patients with cutaneous manifestations frequently had extracutaneous complications [2, 3]. Thus, we reanalyzed a cohort of 239 patients with RP of our original multi-institutional survey of Japanese major medical facilities [4–6].

We obtained responses from 121 facilities and clinical information of 239 RP patients was accumulated. The average age of onset diagnosis was 52.7 years old (range 3–97) and the male-to-female ratio was 1.1:1 (127 males and 112 females) [4]. Biopsies were performed in 228 patients (95 %) and histological confirmation of RP was obtained in 138 patients (58 %).

Auricular and nasal chondritis were shown in 187 patients (78 %) and 94 patients (39 %), respectively, during follow-up. One hundred and twenty patients (50 %) showed airway involvement. Neurological (12 %) and cardiac involvements (7.1 %) were less frequent than airway involvement but suggested to be major determinants of disease severity [5, 6].

Thirty three cases (14 % of 239 cases) developed cutaneous manifestations. Their mean age of onset was 54. The male-to-female ratio was 1 to 1.1. The cutaneous manifestations included oral aphthous in 5 patients, genital ulcer in 1 patient, purpura in 2 patients, urticarial papules in 4 patients, bluish-red papules in 2 patients, erythema elevatum diutinum in 2 patients, nodules on the limbs in 11 patients, superficial phlebitis in 3 patients, sterile pustules in 1 patient, and ulcer lesions on the limbs in 2 patients.

In the literatures, cutaneous manifestations developed 11 to 53 % of patients with RP [2, 3, 7, 8]. Thus, RP patients with cutaneous manifestations were less frequent in Japan.

Twenty three cases (70 % of 33 cases) of RP patients with cutaneous manifestations developed their extracutaneous complications (Table 1).

Published online: 16 January 2016

Table 1 Major complications in 239 patients with RP and percentages of their cutaneous manifestations

	Number of patients without the 239[a] patients	Number of patients with cutaneous complications (%)	M/F ratio	Mean age of disease onset (yr)
Hematologic disorders				
Myelodysplastic syndrome	5	5 (100)	3:2	58.8
Connective tissue diseases				
Behcet's Disease	5	5 (100)	3:2	32.5
Systemic vasculitis	1	1 (100)	0:1	42
Sjogren Syndrome	2	1 (50)	2:1	30.0
Systemic lupus erythematosus	3	1 (33)	0:1	55.0
Dermatologic diseases				
Psoriasis	1	1	1:0	11
Atopic dermatitis	1	1	0:1	25
Pyoderma gangrenosum	1	1	0:1	36
Drug-induced hypersensitivity syndrome[b]	1	1	1:0	54
Cardiovascular diseases				
Deep vein thrombosis	2	2 (100)	2:0	67.5
Myocardial infarction	3	1 (33)	1:0	73.0
Valvular disease	5	1 (20)	1:0	56.0
Neurological diseases				
Cerebral vascular disease	5	3 (60)	3:2	74.0
encephalitis/meningitis	12	1 (8.3)	0:1	26.0

[a] In total, 33 patients with RP had cutaneous manifestations, and 23 patients of them had minor complications. Two patients had two complications

[b] Percentages of RP patients with cutaneous manifestation in the subgroup of patients with such complication

[c] The patient's drug-induced hypersensitivity syndrome was caused by sulfamethoxazole

Five RP patients developed MDS (5/239, 2.1 %). All the 5 RP patients with MDS had cutaneous manifestations [9, 10].

One patient with MDS suffered from erythema nodosum-like lesion of lower extremities. Three and two RP patients with MDS exhibited nodule on the limbs and blanchable papules (similar to those typically seen in patients with Sweet's syndrome), respectively. Accordingly, two RP patients with MDS were diagnosed as having Sweet's syndrome.

One RP patient with MDS died with an unidentified cause in our survey. Thus, survival rate in RP patients with MDS (80 %, during the mean follow-up period of 2.8 years) looked better than those of ordinary MDS patients (3-year survival rates were 63 and 4 % in low- and high-risk groups, respectively, by an MDS conference report in 2014 of Japan's Ministry of Health, Labor and Welfare).

RP patients developed several connective tissue diseases (11 cases out of 239 cases, 4.6 %), including five patients with Behcet's disease (Table 1). All of the five RP patients with Behcet's disease had cutaneous manifestations.

In contrast, cutaneous manifestations have rarely developed in RP patients with encephalitis/meningitis (1 case out of 12 cases, 8.3 %).

A 79-year-old male patient with psoriasis and a 69-year-old female patient with systemic vasculitis and erythema nodosum-like lesions died of cerebral vascular diseases. A 58-year-old male patient with MDS and Sweet's syndrome, a 77-year-old female patient with erythema nodosum-like lesions and a 84-year-old female patient with diabetes mellitus and purpura died of unidentified causes.

We reported that RP death rate in Japan was 9.2 % [4]. Within RP patients with cutaneous manifestations, 4 cases had died out of 33 cases; accordingly, death rate was 12.5 %, slightly higher than those without cutaneous manifestations. Simple RP without any complications may have better prognosis than RP with any forms of cutaneous complications.

In conclusion, 14 % of patients with RP developed cutaneous manifestations and this subpopulation exhibited high complication rate, consistent with a previous report [2]. Even though, MDS of RP patients seemed to be milder than the ordinary MDS.

Compliance with ethical standards

Disclosures None.

Source of funding This work and the original epidemiological study [1] were supported in part by Grants-in-Aid from the Research Committee of Rare Diseases, the Ministry of Health, Labor and Welfare of Japan.

References

1. Lakhi K, Zervakis E, Kalfakis N, Voudouris A, Livir-Rallatos C, Fessas C (2002) Relapsing polychondritis: a clinical review. Semin Arthritis Rheum 31:384–395
2. Kumar C, Rasi R, Lapuente JL, Rybord M, Papo T, Piette JC (2011) Dermatologic manifestations of relapsing polychondritis: A study of 300 cases at a single center. Medicine (Baltimore) 90:103–109
3. Delaporta M, Karmaniolis K, Matsouka A, Magkasis A, Papadaveli E (2018) Cutaneous manifestations in relation to rheumatologic parameters in a cohort of primary myelodysplastic syndrome patients. Int J Anal Pathol Cytol 22:243–248
4. Oda H, Yamano Y, Shimizu J, Yudoh K, Suzuki N (2014) A large-scale survey of patients with relapsing polychondritis in Japan. Intl Conf Regen 34:149–156
5. Shimizu J, Oda H, Yamano Y, Yudoh K, Suzuki N (2015) Cardiac involvement in relapsing polychondritis in Japan. Rheumatology (Oxford) [Epub ahead of print]
6. Suzuki N, Shimizu J, Oda H, Yamano Y, Yudoh K (2014) Neurological involvement of relapsing polychondritis in Japan: an epidemiological study. Intl Conf Regen 34:206–208

7. Hergeck P J, Pirie G (2001) Relapsing polychondritis. Aust Fam Phys J Int Rheumatol 18:773–778
8. Watkins S, Magil JM Jr, Barrow-Gaul EA (2000) An unusual nasopharyngeal relapsing polychondritis case report and review of the literature. Int J Pediatr Otorhinolaryngol 48:59–67. doi:10.1016/s0165-5876(99)00223-8
9. Voigt H, Miller W (1993) Autoimmune phenomena in patients with hypersplenism. Leukemia Lymphoma 24:455–489
10. Schaeverbeke T, Mathieu L, Mathieu L, Bonnet C, Lefebvre T, Lavalle C (2002) [Chronic cutaneous mucocutaneous and relapsing polychondritis]. Ann Dermatol Venereol 129:1299–1302 [Article in French]

© Springer

J Phys Fitness Sports Med, 5 (1): 81-86 (2016)
DOI: 10.7600/jpfsm.5.81

JPFSM: *Short Review Article*

Mechanical and oxidative stress in osteoarthritis

Naoko Yui[1*], Kazuo Yudoh[2], Hiroto Fujiya[1] and Haruki Mushi[1]

[1] *Department of Sports Medicine, St. Marianna University School of Medicine, 2-16-1 Sugao, Miyamae-ku, Kawasaki, Kanagawa 216-8511, Japan*

[2] *Department of Frontier Medicine, Institute of Medical Science, St. Marianna University School of Medicine, 2-16-1 Sugao, Miyamae-ku, Kawasaki, Kanagawa 216-8512, Japan*

Received: January 5, 2016 / Accepted: February 9, 2016

Abstract Osteoarthritis (OA) is one of the most common age-related degenerative joint disorders. In addition to aging, various life-style related factors, such as obesity and overuse of joints, have been recognized as major risk factors for OA. It has been revealed that mechanical force acting on articular cartilage induces chondrocytes to produce excess amounts of reactive oxygen species (ROS), which are known to be an OA-related catabolic factor. In addition, it has been reported that mechanical stress-induced ROS directly damage chondrocyte DNA, resulting in the downregulation of cellular activity and induction of apoptosis in osteoarthritic chondrocytes. Notably, molecular events associated with DNA oxidative damage influence the regulation of chondrocyte activity and cellular viability, supporting the notion that mechanical stress-induced oxidization of chondrocyte DNA participates in the pathogenesis of OA. Here, we review accumulating evidence supporting the involvement of mechanical and oxidative stresses in cartilage homeostasis and the pathogenesis of OA.

Keywords : osteoarthritis, DNA repair enzyme, oxidative stress, chondrocytes, articular cartilage

Introduction

The ratio of elderly persons aged 75 or older will increase; it is expected to exceed 25% in 2055[1]. Since Japan currently has an aging population, we need to adapt to cope with this changing demographic. To maintain physical condition, independent living and social participation, even in elderly people, it is necessary to develop preventive and therapeutic strategies for age-related musculoskeletal diseases.

In this review article, we aim to contribute to the extension of healthy life expectancy, by focusing on one of the most common age-related joint musculoskeletal diseases, osteoarthritis (OA), and discussing the pathogenesis of joint degeneration in OA.

In patients with OA, joint destruction and related symptoms become aggravated with disease progression as well as aging[2,3]. Tissue damage increases with time after onset. Articular cartilage has no nervous or vascular structure and minimal capacity for self-repair, so that it is necessary to establish preventive measures as well as early treatment strategies against articular cartilage degeneration[4,5] (Fig. 1).

However, the search for effective therapy for cartilage degeneration is still ongoing. It is therefore a matter of urgency to find new therapeutic agents and strategies that are clinically effective in treating age-associated musculoskeletal diseases, especially OA, in order to preserve high levels of activity of daily living in elderly people[3].

During the development of OA, mechanical and chemical stresses exerted on articular cartilage downregulate the stable cellular activities of chondrocytes and induce the production of catabolic factors, such as proinflammatory cytokines and chemokines[6-10]. In addition, in response to mechanical and chemical stresses, it is well known that articular chondrocytes produce excess amounts of reactive oxygen species (ROS) as well as proinflammatory cytokines and chemokines[11,12]. These catabolic factors are thought to accelerate the progression of bone and joint degeneration with aging. However, the mechanism of cartilage degeneration in OA still remains unclear. The aim of this review is to discuss the pathogenesis of cartilage degeneration from the point of view of cartilage and chondrocyte biology in OA.

What happens in articular cartilage under mechanical stress?

Mechanical force applied to articular cartilage directly downregulates chondrocyte activity such as production of cartilage matrix components (proteoglycan and type II collagen) and induces chondrocyte apoptosis. In addition to its direct effects causing the degeneration/destruction of articular cartilage structure (surface fibrillation and development of cartilage clefts)[13-16]. These catabolic changes may affect the homeostasis/maintenance potential of

*Correspondence: aburaimsuke@marianna-u.ac.jp

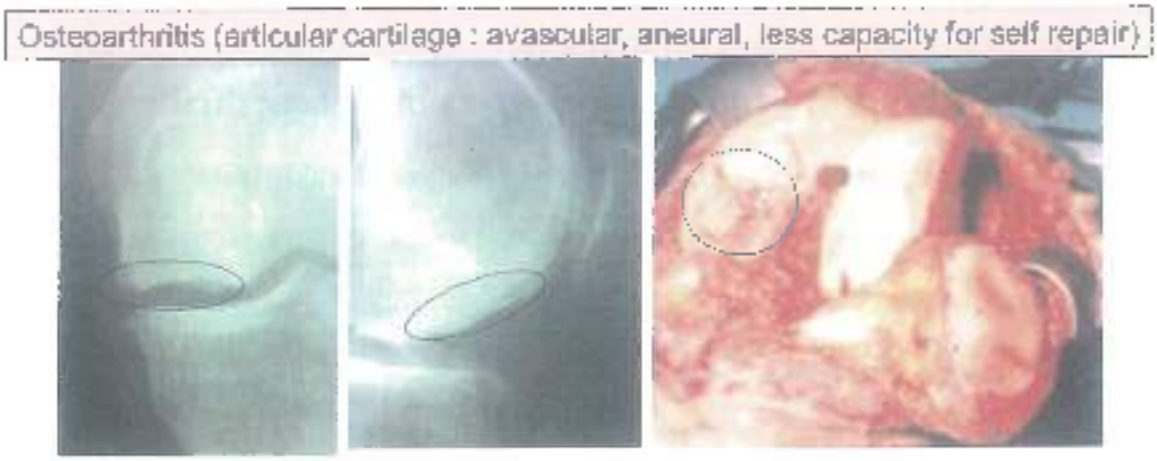

Fig. 1 The age-related bone and joint disease, osteoarthritis.

articular cartilage.

Further, it has been reported that the effect of mechanical stress on articular cartilage increases production of excess amounts of ROS (superoxide, nitric oxide, hydrogen peroxide and peroxynitrite) as OA-related catabolic factors[1,12,13,15]. Previous studies have provided ample confirmation of the generation of ROS in degenerated articular cartilage[18-20]. These findings suggest that mechanical stress applied to articular cartilage may induce oxidative stress in OA cartilage tissue. Interestingly, previous reports demonstrated that treatment with C60 fullerene, a strong free radical scavenger, prevented such catabolic responses in osteoarthritic chondrocytes *in vitro* and the degeneration of articular cartilage *in vivo* in an OA rat model, suggesting the involvement of oxidative stress in the progression of cartilage degeneration in OA[20].

In the next section, we will discuss the implication of oxidative stress in the pathogenesis of OA.

Oxidative stress in degenerated articular cartilage: oxidative damage vs. cellular antioxidants

Previous studies have already demonstrated that degeneration of articular cartilage is partially mediated by oxygen free radicals[7-9]. Kurz et al. showed that application of mechanical force to articular cartilage is sufficient to stimulate the production of ROS by chondrocytes, leading to depolymerisation of hyaluronic acid and chondrocyte death[6,21]. Green et al. demonstrated that chondrocyte death is induced by adherence of inflammatory leukocytes to chondrocytes, and by induction of ROS production from chondrocytes in response to mechanical stress on cartilage[22]. These findings clearly indicate that chronic excess ROS production by chondrocytes, which is induced by the effect of mechanical force on cartilage, plays an important role in the cartilage degeneration that occurs after mechanical injury to cartilage (Fig. 2).

Indeed, it has already been reported that the presence of oxidative damage was histologically confirmed in OA cartilage[23]. Our previous studies also demonstrated the presence of DNA oxidative damage in osteoarthritic chondrocytes[24], with osteoarthritic chondrocytes, but not normal chondrocytes, expressing high levels of oxidized forms of tyrosine (nitrotyrosine).

The oxidized nucleotide 8-oxoguanine (8-oxo-7,8-dihydroxyguanine) is produced by ROS in large amounts in both DNA and nucleotides[25]. As an oxidized form of guanine, 8-oxoguanine is a major causative factor involved in ROS-induced mutagenesis, since it can form a stable base pair with adenine (A) or cytosine (C) during DNA replication[26], resulting in A:T (thymine) to C:G (guanine) and G:C to T:A point mutations. These mutations are thought to be involved in the pathogenesis of a variety of malignant and degenerative diseases[26,27]. Oxidation of guanine to 8-oxoguanine is repaired by 8-oxoguanine DNA glycosylase (Ogg1), an enzyme that recognizes and hydrolyses the aberrant base in the DNA backbone[27]. Ogg1 is thought to protect against activation of the intrinsic apoptotic pathway in response to oxidative stress by augmenting DNA repair in a variety of cells[27,28]. Kikuchi et al. demonstrated that 8-oxoguanine levels in large motor neurons of the spinal cord were increased in patients with amyotrophic lateral sclerosis (ALS) and subarachnoid haemorrhage (SAH), together with a lower mitochondrial expression of the DNA repair enzyme Ogg1[29]. Their finding indicates that oxidative damage may accumulate in the mitochondria of motor neurons in ALS and SAH and that Ogg1 may not repair the damage efficiently, which may lead to a loss of motor neurons in these diseases. These findings further suggest that impairment of the ability of the DNA repair enzyme Ogg1 to protect against the accumulation of 8-oxoguanine is involved in the pathogenesis of oxidative stress-induced diseases including neural degenerative diseases and musculoskeletal diseases.

We also observed depletion of the cellular antioxidant, Ogg1, in degenerated articular cartilage participates, at least in part, in the development of cartilage degeneration

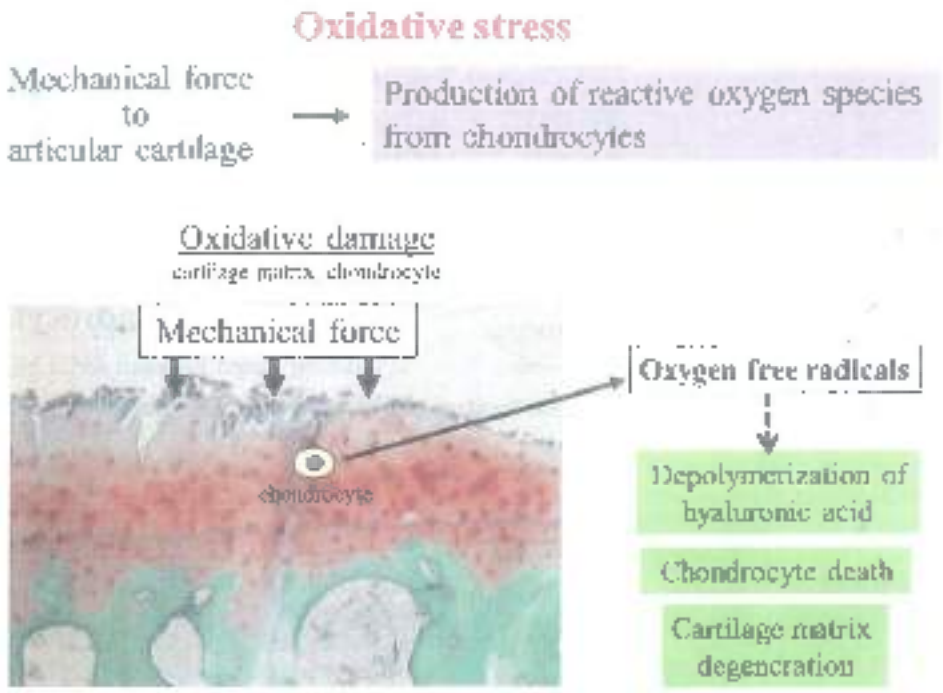

Fig. 2 Mechanical stress-induced oxidative damage in OA cartilage.

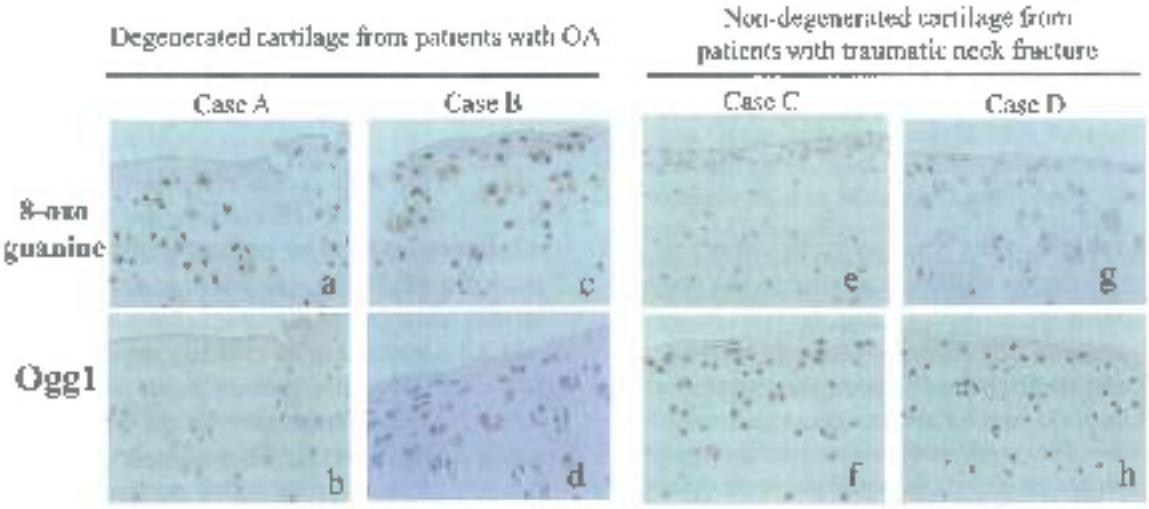

Fig. 3 **Oxidative damage in OA cartilage: impairment of the ability of DNA repair enzyme (Ogg1) to against the accumulation of an oxidized form of guanine (8-oxoguanine).**
A higher expression pattern of 8-oxoguanine was observed in the degenerated cartilage regions (a, c) from patients with OA. In contrast to the degenerated cartilage, almost all of the non-degenerated regions isolated from traumatic articular cartilage samples were negative for 8-oxoguanine immunostaining (e, g). Immunopositivity for Ogg1 was predominant in the non-degenerated cartilages compared with the degenerated cartilages (f, h). In contrast, chondrocytes were more weakly stained in the degenerated cartilages (b, d). (Unpublished data, Institute of Medical Science, St. Marianna University)

in OA.

Recently, we observed increased levels of 8-oxoguanine and decreased levels of its repair enzyme Ogg1 in OA chondrocytes, but not in normal chondrocytes, in OA model rabbits and patients with OA (Fig. 3, unpublished data). Our data suggest that Ogg1 may play an important role in protecting against ROS-induced DNA damage (resulting in the downregulation of chondrocyte activity and augmentation of apoptosis) and cartilage degeneration in OA (Fig. 4).

These findings provide a novel pathogenic mechanism linking oxidant-mediated DNA damage and OA chondrocytes.

In OA, mechanical stress induced generation of ROS may cause direct damage to chondrocytes and cartilage matrix components, resulting in the degeneration of ar-

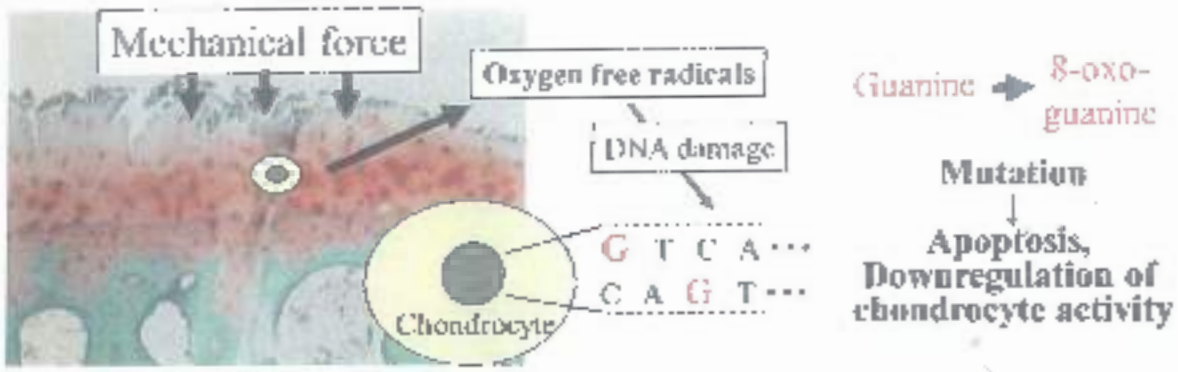

Fig. 4 Mechanical force exerted on articular cartilage induces DNA oxidative damage in chondrocytes and leads to cartilage degeneration.

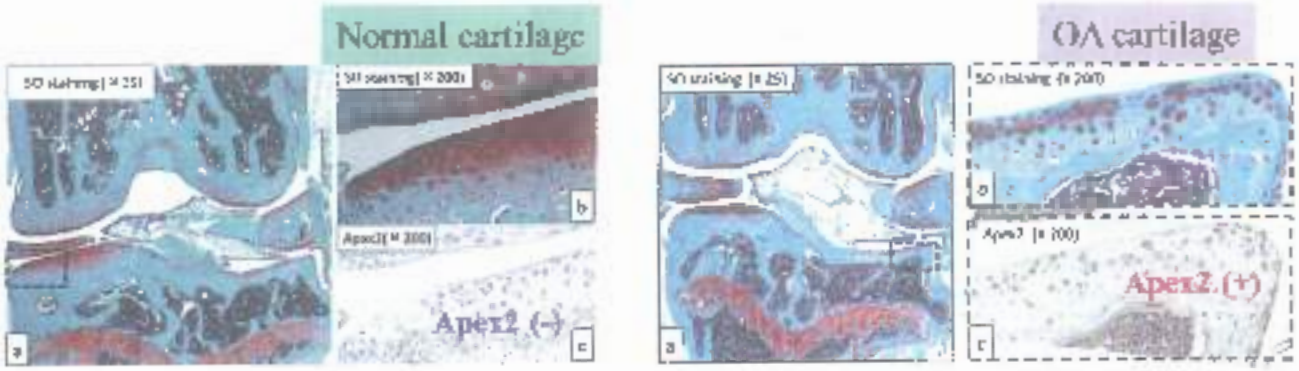

Fig. 5 Expression of the DNA repair enzyme APEX2 in an OA mouse model.
(Data from Yui N., et al. IJMS, 2014)

ticular cartilage. While previous studies have provided ample confirmation of ROS generation in OA cartilage, further studies are needed to clarify the exact mechanism of ROS-mediated degeneration of articular cartilage.

In the next section, we will review the protective mechanism against OA in articular cartilage.

DNA damage repair enzymes in articular cartilage

Although ROS mediate various cellular signalling pathways, higher levels of ROS can induce oxidative DNA damage and the resultant cellular apoptosis that contribute to aging, malignancy and degenerative diseases[8,31]. Oxidative DNA lesions accumulate in nuclear and mitochondrial genomes during aging, and this can increase dramatically in age-related neurodegenerative diseases such as Parkinson's disease[32-34]. Regarding musculoskeletal diseases, we previously reported that oxidative DNA damage in chondrocytes accumulates in the degenerated articular cartilage in OA, reducing its maintenance potential[35].

Oxidative damage to nucleic acids is counteracted by the activity of several DNA repair enzymes such as apurinic/apyrimidinic (AP) endonuclease 2 (APEX2). AP sites occur in DNA following spontaneous hydrolysis, exposure to DNA damaging agents, or treatment with DNA glycosylases that remove specific abnormal bases[36]. AP expression sites are pre-mutagenic lesions that can prevent normal DNA replication, so cellular mechanisms identify and repair such sites[8,37]. It has been reported that APEX2 is involved in the critically important DNA repair pathway[38]. This base excision repair pathway involving APEX2 is largely responsible for the repair of DNA oxidative damage by ROS. A Recent report clearly indicated that APEX2 was required for the generation of replication protein and the recruitment of a checkpoint protein complex to DNA oxidative damage sites[39].

More recently, we provided evidence that the change in chondrocyte anti-oxidative activity that occurs through the APEX2-associated DNA repair pathway may be involved in the progression of articular cartilage degeneration in OA. We observed that APEX2 expression in chondrocytes was induced by OA-related catabolic factors *in vitro*, and was associated with the degeneration of articular cartilage in an *in vivo* OA mouse model (Fig. 5)[35].

Furthermore, downregulation of APEX2 using small interfering RNA decreased chondrocyte activity *in vitro*[35]. These findings indicate that APEX2 may prevent the oxidative stress-induced downregulation of chondrocyte activity in OA.

Mitochondria are a major source of intracellular free radicals, which are closely involved in oxidative damage and may cause degeneration of various tissues including

articular cartilage[19]. In mitochondria, the base excision repair pathway is primarily responsible for removing oxidized nucleic acid from DNA. In humans, oxidized nucleic acids in DNA are repaired by DNA repair enzymes (such as Ogg1 and APEX2) that recognize and hydrolyze aberrant bases in the DNA backbone[20].

Such impaired DNA repair function in osteoarthritic chondrocytes may result in mitochondrial dysfunction and chronic oxidative damage to chondrocytes and cartilage tissue in OA. These observations suggest that downregulation of the oxidized DNA excision repair pathway is closely involved in the pathogenesis of articular cartilage degeneration. This may indicate a protective mechanism against mechanical stress mediated DNA oxidative damage in OA chondrocytes.

Conclusion

In conclusion, previous reports clearly demonstrated that mechanical stress to articular cartilage induces generation of ROS from chondrocytes, causing oxidative stress, and that the related oxidative damage to chondrocyte DNA accumulates in the degenerated articular cartilage in OA. In addition, the DNA repair enzyme does not repair the damage efficiently, which may lead to downregulation of chondrocyte activity and reduced maintenance potential of articular cartilage in OA. Although further studies are needed to clarify the exact involvement of mechanical and oxidative stresses in the pathogenesis of OA, previous findings establish an innovative role for DNA repair enzymes in protecting articular cartilage and chondrocytes against mechanical stress-induced oxidative damage of chondrocytes and articular cartilage.

Conflict of Interests

The authors declare that there is no conflict of interests regarding the publication of this article.

Acknowledgments

We would like to thank M. Tamaki, M. Tanaka and T. Sato for excellent technical assistance.

References

1) Policy information. 2011. The current situation and the future direction of the Long-term Care Insurance System in Japan: with a focus on the housing for the elderly. *Ministry of Health, Labour and Welfare*. http://www.mhlw.go.jp/english/policy/care-welfare/care-we'fare-elder'y/index.html

2) Greene MA and Loeser RF. 2015. Aging-related inflammation in osteoarthritis. *Osteoarthritis Cartilage* 23: 1966-1971. doi: 10.1016/j.joca.2015.01.008.

3) Leong DJ and Sun HB. 2011. Events in articular chondrocytes with aging. *Curr Osteoporosis Rep* 9: 196-201. doi: 10.1007/s11914-011-0070-3.

4) Germanier J, Guilak F, Weinberg JB, Piscitsky DS and Bernor R. 2002. Influence of hypoxia and reoxygenation on cytokine induced production of proinflammatory mediators in articular cartilage. *Arthritis Rheum* 46: 968-975.

5) Teoliati PS and McCarty DJ. 1971. Synovial fluid pH, lactate, oxygen and carbon dioxide partial pressure in various joint diseases. *Arthritis Rheum* 14: 475-484.

6) Loeser RF. 2006. Molecular mechanisms of cartilage destruction: mechanics, inflammatory mediators, and aging collide. *Arthritis Rheum* 54: 1357-1360. doi: 10.1002/art.21815.

7) Pelletier JP, Martel-Pelletier J and Raynauld JP. 2006. Most recent developments in strategies to reduce the progression of structural changes in osteoarthritis: today and tomorrow. *Arthritis Rev Ther* 8: 206. doi: 10.1186/ar1932.

8) Loeser RF, Chubinskaya S, Del Carlo M and Grande A. 2002. Detection of nitrotyrosine in aging and osteoarthritic cartilage: correlation of oxidative damage with the presence of interleukin-1beta and with chondrocyte resistance to insulin-like growth factor 1. *Arthritis Rheum* 46: 2349-2357. doi: 10.1002/art.10496.

9) Agarwal S, Deschner J, Long P, Verma A, Hofman C, Evans CH and Piesco N. 2004. Role of NF-κB transcription factors in anti-inflammatory and pro-inflammatory actions of mechanical signals. *Arthritis Rheum* 50: 3541-3548. doi: 10.1002/art.20601.

10) Guilak F, Fermor B, Keefe FJ, Kraus VB, Olson SA, Pisetsky DS, Setton LA and Weinberg JB. 2004. The role of biomechanics and inflammation in cartilage injury and repair. *Clin Orthop Relat Res* 423: 17-26.

11) Evans CH and Stefanovic-Racic M. 1996. Nitric oxide in arthritis. *Method* 10: 38-42. doi: 10.1006/meth.1996.0076.

12) Abramson SB, Attur M, Amin AR and Clancy R. 2001. Nitric oxide and inflammatory mediators in the perpetuation of osteoarthritis. *Curr Rheumatol Rep* 3: 535-541.

13) Del Carlo M Jr and Loeser RF. 2002. Nitric oxide-mediated chondrocyte cell death requires the generation of additional reactive oxygen species. *Arthritis Rheum* 46: 394-403.

14) Aigner T, Hemmel M, Neureiter D, Gebhard PM, Zeller G, Kirchner T and McKenna L. 2001. Apoptotic cell death is not a widespread phenomenon in normal aging and osteoarthritis human articular knee cartilage: a study of proliferation, programmed cell death (apoptosis), and viability of chondrocytes in normal and osteoarthritic human knee cartilage. *Arthritis Rheum* 44: 1304-1312. doi: 10.1002/1529-0131(200106)44:6<1304::AID-ART222>3.0.CO;2-T.

15) Horton WE Jr, Feng L and Adam C. 1998. Chondrocyte apoptosis in development, aging and disease. *Matrix Biol* 17: 107-115.

16) Kurz B, Lemke A, Kehl M, Domm C, Patwari P, Frank EH, Grodzinsky AJ and Schünke M. 2004. Influence of tissue maturation and antioxidants on the apoptotic response of articular cartilage after injurious compression. *Arthritis Rheum* 50: 123-130. doi: 10.1002/art.11428.

17) Henrotin YE, Bruckner P and Pujol JP. 2003. The role of reactive oxygen species in homeostasis and degradation of cartilage. *Osteoarthr Cartil* 11: 747-755. doi: 10.1016/S1063-4584(03)00150-X.

18) Chen AF, Davies CM, De Lin M and Fermor B. 2009. Oxidative DNA damage in osteoarthritic porcine articular cartilage. *J Cell Physiol* 217: 828-833. doi: 10.1002/jcp.21562.

19) Afonin V, Chumpy R, Matrovic D, Collin P and Lemer A.

2007. Reactive oxygen species and superoxide dismutases: role in joint disease. *Joint Bone Spin* 74: 324-329. doi: 10.1016/j.jbspin.2007.02.002.

20) Yudoh K, Shishido K, Murayama H, Yano M, Matsubayashi K, Takada H, Nakamura H, Masuko K, Kato T and Nishioka K. 2007. Water soluble C60 fullerene prevents degeneration of articular cartilage in osteoarthritis via down regulation of chondrocyte catabolic activity and inhibition of cartilage degeneration during disease development. *Arthritis Rheum* 56: 3307-3318. doi: 10.1002/art.22917.

21) Kurz B, Lemke AK, Fay J, Pufe T, Grodzinsky AJ and Schunke M. 2005. Pathomechanisms of cartilage destruction by mechanical injury. *Ann Anat* 187: 473-485. doi: 10.1016/j.aanat.2005.07.003.

22) Green DM, Noble PC, Ahuero JS and Birdsall HH. 2006. Cellular events leading to chondrocyte death after cartilage impact injury. *Arthritis Rheum* 54: 1509-1517. doi: 10.1002/art.21812.

23) Carlo MD Jr and Loeser RF. 2003. Increased oxidative stress with aging reduces chondrocyte survival: correlation with intracellular glutathione levels. *Arthritis Rheum* 48: 3419-3430. doi: 10.1002/art.11338.

24) Yudoh K, Nguyen T, Nakamura H, Hongo-Masuko K, Kato T and Nishioka K. 2005. Potential involvement of oxidative stress in cartilage senescence and development of osteoarthritis: oxidative stress induces chondrocyte telomere instability and down regulation of chondrocyte function. *Arthritis Res Ther* 7: 380-391. doi: 10.1186/ar1499.

25) Tornaletti S, Maeda LS, Kornberg RD and Hanawalt PC. 2004. Effect of 8-oxoguanine on transcription elongation by T7 RNA polymerase and mammalian RNA polymerase II. *DNA Repair (Amst)* 3: 483-494. doi: 10.1016/j.dnarep.2004.01.003.

26) Darzynkiewicz GE and Crainer F. 2009. Molecular basis of transcriptional mutagenesis at 8-oxoguanine. *J Biol Chem* 284: 31658-31667. doi: 10.1074/jbc.M109.027764.

27) Park MT, Park JH, Halim SH, Ko SI, Lee YR, Chung JH, Sohn SY, Cho Y, Kang LW and Han YS. 2009. Repair activities of human 8-oxoguanine DNA glycosylase are stimulated by the interaction with human checkpoint sensor Rad9-Rad1-Hus1 complex. *DNA Repair (Amst)* 8: 1190-1200. doi: 10.1016/j.dnarep.2009.06.004.

28) Yoon CK, Song PI, Kim MH, Kim JS, Hyun JW, Choi SS, Yoon SP, Chung MH, Chang IY and Yao HD. 2007. Human 8-oxoguanine DNA glycosylase suppresses the oxidative stress induced apoptosis through a p53-mediated signaling pathway in human fibroblasts. *Mol Cancer Res* 5: 1083-1098. doi: 10.1158/1541-7786.MCR-06-0432.

29) Kikuchi H, Furuta A, Nishioka K, Suzuki SO, Nakabeppu Y and Iwaki T. 2002. Impairment of mitochondrial DNA repair enzymes against accumulation of 8-oxo-guanine in the spinal motor neurons of amyotrophic lateral sclerosis. *Acta Neuropathol* 103: 408-414. doi: 10.1007/s00401-001-0480-x.

30) Gackowski D, Speina E, Zielinska M, Kowalewski J, Rozalski R, Siomek A, Paliszek T, Tabek H and Olinski R. 2003. Products of oxidative DNA damage and repair as possible biomarkers of susceptibility to lung cancer. *Cancer Res* 63: 4699-4702.

31) Nunomura A, Perry G, Aliev G, Hirai K, Takeda A, Balraj EK, Jones PK, Ghanbari H, Wataya T, Shimohama S, Chiba S, Atwood CS, Petersen RB and Smith MA. 2001. Oxidative damage is the earliest event in Alzheimer disease. *J Neuropathol Exp Neurol* 60: 759-767. doi: 10.1093/jnen/60.8.759.

32) Zhang J, Perry G, Smith MA, Robertson D, Olsen SJ, Graham DG and Montine TJ. 1999. Parkinson's disease is associated with oxidative damage to cytoplasmic DNA and RNA in substantia nigra neurons. *Am J Pathol* 154: 1423-1429. doi: 10.1016/S0002-9440(10)65396-5.

33) Nakabeppu Y, Tsuchimoto D, Yamaguchi H and Sakumi K. 2007. Oxidative damage in nucleic acids and Parkinson's disease. *J Neurosci Res* 85: 919-934.

34) Venkateshappa C, Harish G, Mythri RB, Mahalaxmi A, Bharath MM and Shankar SK. 2012. Increased oxidative damage and decreased antioxidant function in aging human substantia nigra compared to striatum: implications for Parkinson's disease. *Neurochem Res* 37: 358-369. doi: 10.1007/s11064-011-0619-7.

35) Yu N, Yoshioka H, Fujiya H, Maeda H, Beppu M, Kanasawa R and Yudoh K. 2014. The DNA repair enzyme apurinic/apyrimidinic endonuclease (Apex nuclease) 2 has the potential to protect against down regulation of chondrocyte activity in osteoarthritis. *Int J Mol Sci* 15: 14921-14934. doi: 10.3390/ijms150914921.

36) Georgiadis MM, Luo M, Gaur RK, Delaplane S, Li X and Kelley MR. 2008. Evolution of the redox function in mammalian apurinic/apyrimidinic endonuclease. *Mutat Res* 643: 54-63. doi: 10.1016/j.mrfmmm.2008.04.008.

37) Tsuchi M, and Kelley MR. 2007. The DNA base excision repair protein Ape1/Ref-1 as a therapeutic and chemopreventive target. *Mol Aspects Med* 28: 375-395. doi:10.1016/j.mam.2007.04.005.

38) Willis J, Patel Y, Lentz BL and Yan S. 2013. APE2 is required for ATR-Chk1 checkpoint activation in response to oxidative stress. *Proc Natl Acad Sci USA* 110: 10592-10597. doi: 10.1073/pnas.1301445110.

39) Rusal KN, Wilson G, Pearsall A and Grishko VI. 2014. The role of mitochondrial reactive oxygen species in cartilage matrix destruction. *Mol Cell Biochem* 397: 195-201. doi: 10.1007/s11010-014-2187-z.

40) Kamenisch Y, Fousteri M, Knoch J, von Thaler AK, Fehrenbacher B, Kato H, Becker T, Dolle MF, Kuiper R, Majewski M, Schaller M, van der Horst GT, van Steeg H, Rocken M, Rapaport D, Krutmann J, Mullenders LH and Berneburg M. 2010. Proteins of nucleotide and base excision repair pathways interact in mitochondria to protect from loss of subcutaneous fat, a hallmark of aging. *J Exp Med* 207: 379-390. doi: 10.1084/jem.20091864.

第１章　疾病別で学ぶ自己注射使用の現状と使いやすさの向上

第４節　変形性関節症（Osteoarthritis: OA）治療法の今後の展開：OA 治療を目的とする自己注射薬の可能性について

遊道和雄
聖マリアンナ医科大学　難病治療研究センター　センター長・大学院　教授（医学博士）

（株）技術情報協会
2016 年 3 月発刊「自己注射に対する医師・患者ニーズと製品開発への落とし込み」
抜刷

第４節　変形性関節症（Osteoarthritis: OA）治療法の今後の展開：OA 治療を目的とする自己注射薬の可能性について

１　変形性関節症の疫学・病因病態

変形性関節症（osteoarthritis, OA）は「関節軟骨の変性・摩耗と，その後の二次性滑膜炎および軟骨・骨の新生増殖などに基づく進行性の変性関節疾患」と定義され，病期の進行にしたがって痛みは漸次増悪化していく．関節軟骨変性に伴い，滑膜の炎症・増殖による二次性滑膜炎が起こると関節水腫を生じ，腫脹・圧痛感，関節疼痛を訴えるようになる．さらに OA では，軟骨変性に加えて，骨の増殖性変化（骨棘，軟骨下骨硬化の硬化）が特徴である（図１）[1]．

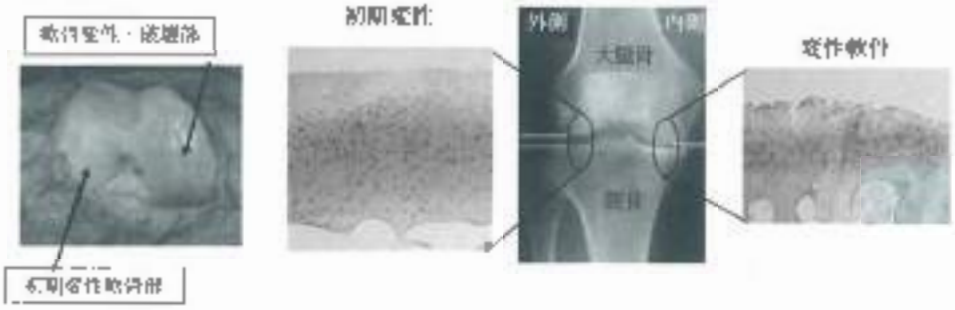

図１　変形性関節症の対象・X 線像・病理組織像

本邦では，50 歳以上でX 線学的に関節変形がみられる画像診断学的 OA 患者は 2500 万人，実際に関節痛を有する OA 患者は 800 万人もおり，有病率に関節リウマチ（RA）の約 10 ～ 20 倍とされている．少子社会の我が国においては毎年 90 万人以上もの新たな OA 発症者がおり，経済的損失は国民総生産の 1%に及ぶとされ，今後高齢化社会が進むに従って患者数の増加が懸念されている[2]．

OA の発症には，機械的ストレス（荷重，肥満，overuse），炎症・免疫反応等，酸化ストレスおよび遺伝的因子等がそれぞれの重みをもって関与し，軟骨基質（細胞外マトリックス）の変性，経胞と細胞外マトリックスの相互関係の破綻や細胞死が直接的または間接的に組織としての恒常性を低下させ，終局的に軟骨変性が進行していくと考えられている（図２）[3]．

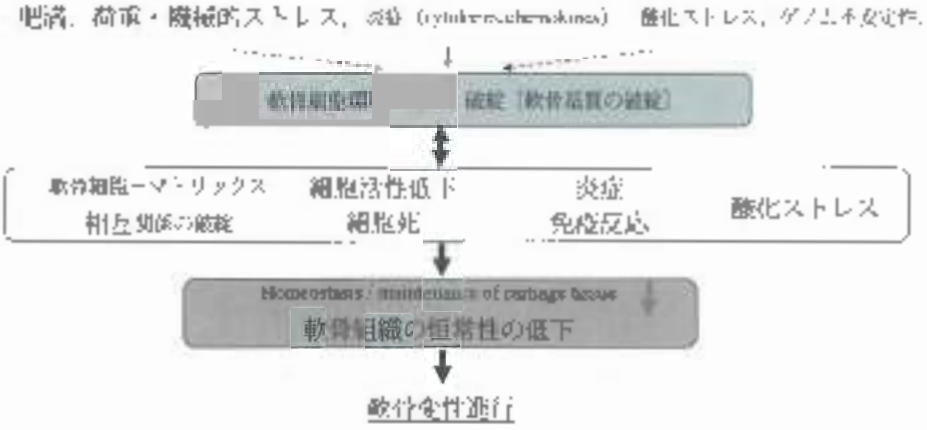

図２　変形性関節症の病因

OA の治療には，骨・軟骨，関節周囲の関節支持組織が発症後早期に障害されること，関節軟骨が極めて無血管であること，骨関節障害による支持性や可動性の低下が日常生活の活動性（activity of daily living, ADL）に大きく影響することを考慮しなければならない．高齢化社会においてADL を維持するためには，より有効な予防法，ならびに病早期からの疾患対策，さらには形骨の治療よりも有効な新規の治療薬や治療戦略の確立が緊急に必要である．

2. 変形性関節症に求められる治療法について

これまでのOA の治療は，1）日常生活動作の変更指導（歩行訓練，サポーター・装具等），消炎鎮痛剤による疼痛の緩和といった対症療法がほとんどである．加齢とともに関節症状の増悪がみられ，病状進行・増悪においては関節痛と関節変形による可動性ならびに支持性の低下から，日常生活動作が大きく障害され，人工関節置換術等の手術療法の適応となることも多い[1]．しかし，外科的治療には，入院加療による時間的ロス，多額なコスト，感染や人工物の破損等の問題に加え，超高齢化社会であるがゆえに数年～数十年後に挿入した人工物の経年的劣化や破損のため，人工関節の再置換を迫られる症例も多く，医療経済学的観点からみても社会的損失は大きく，解決すべき問題点はあり[2]

OA 薬物治療の現状は，「非ステロイド性消炎鎮痛剤の内服」と「ヒアルロン酸製剤の関節内注入」の対症療法で痛みを抑える治療が中心で，根治療法に資する有効な薬剤は未だ存在していない[3]．これまで，OA の病因・病態を基盤とした様々な抗サイトカイン抗体療法や低分子化合物等の治療薬の開発が行なわれきたが，本症が多因子疾患であることから，一因子を標的とするagent（薬剤）のみでは病態の進行や病勢を抑制することは困難かもしれない．本疾患の病態に関連する複数の病因に共通の経路，または因子を同定することができれば，より有効な薬剤開発に資するものと考える．こうした現状を踏まえ，OA において求められる治療薬のプロファイルは，疼痛などの症状を緩和させることに主眼を置いた対症修飾型治療薬（symptom modifying drug）から，対症緩和効に加えて更に，骨・軟骨変性進行に対して直接的に関節構造と機能を維持しうる構築・機能修飾型治療薬（structure & function modifying drug）へと移行していく段階を迎えたといえよう．

現状の対症療法（消炎鎮痛剤・ヒアルロン酸製剤） -> 次世代の新規 OA 治療薬開発へ

これから求められる OA 治療薬 （DMOADs）

症状（関節痛・炎症）修飾型治療薬： Symptom modifying drug

+

組織構築・機能修飾型治療薬： Structure & function modifying drug

近年，関節リウマチについては，病態に関する詳細な研究により標的分子が次々に明らかになり，加えて細胞工学・遺伝子工学の進歩により，抗体医薬の臨床応用が可能となってきた．関節リウマチにおける病理学的なサイトカインや受容体をターゲットとした生物学的製剤（抗体医薬）投与によって全身性の炎症抑制，関節炎（滑膜炎）ばかりでなく，関節・骨破壊を抑える効果が実証され，QOL の向上に大いに寄与するようになってきた[4]．

一方，これまでOA については，未だ期待される治療効果を満たす治療薬は開発されていない．なぜ，OA では RA のような治療薬がまだ開発されていないかを考察するため，次項において関節・軟骨組織の解剖・組織の特性を詳解した．

3. 治療薬開発のための関節軟骨の組織学的特徴の理解

関節軟骨組織は血管および神経分布のない組織で，関節軟骨層（表層，中間層，深層），その下層の石灰化層（石灰化軟骨・軟骨下骨）の層状構造からなり，その境界 tidemark である（図3）．関節液（滑液）との相互作用により，摩擦係数は高度の潤滑性と表面平滑性を示し，かつ軟骨特有の弾性変形効果，潤滑特性に寄与する．この関節軟骨層

と骨との間の石灰化層においては，軟骨組織の周辺に石灰沈着がみられ，コラーゲン線維間には骨構成成分であるハイドロキシアパタイトが沈着しており，軟骨と石灰化層が関節運動によって乖離されないような構造になっている。

17～19歳で成長軟骨板が閉じた後，成長期以降の20歳以降の関節軟骨は永久軟骨と呼ばれる。軟骨組織には，再生のポテンシャルを持つ未分化幹細胞は存在しないため，骨組織のようにリモデリング・修復・再生することはない。また，軟骨組織は無血管で，栄養と酸素は関節液から受動的に供給されるのみ。

関節軟骨層は軟性下骨を介して骨組織に移行するが，OA変性が高度に進み，関節軟骨層ばかりでなく石灰化軟骨層や軟骨下骨も崩壊すれば，石灰化層と骨との境界が不明瞭になり，石灰化層は石灰化が進行し骨化していく（軟骨下骨の硬化）。この変性ステージには，骨髄からの血管進入が石灰化層に及ぶこともあるが，tidemarkを超えて関節軟骨層への侵入は観察されない（図3）。軟骨変性に伴って，もし骨髄側から血管が軟骨層に侵入するとするならば，骨髄側からMSC幹細胞が遊走・進入し，そこで軟骨基質（II型コラーゲンやプロテオグリカン等の軟骨組織を構成する細胞外マトリックス）を再生しうる成熟軟骨細胞に分化する，すなわち，変性軟骨は自然修復・再生のポテンシャルを持つこととなるが，実際には骨髄側から軟骨層へのMSC幹細胞や軟骨前駆細胞の侵入はみられず，軟骨に自己修復能はみられない。

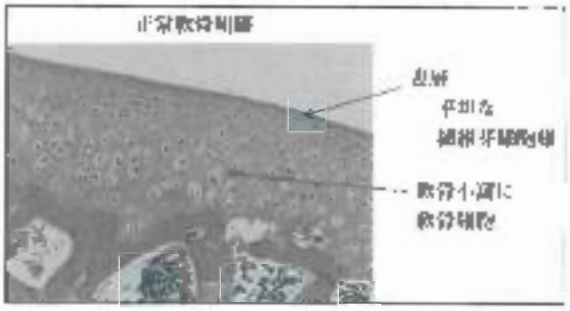

図3　変形性関節症の病理組織像

4.　変形性関節症治療薬の現状と，自己注射薬開発の可能性について

OAは関節が変性する疾患であり，その診断に求められる機能・要素は，柔軟性（関節は痛みなく動かなければならない），可動性（関節は構造上，決められた可動域の範囲で動かなければならない），支持性（関節は安定した支持性がなければならない）の3つであるが，関節軟骨の変性の進行により疼痛を伴って可動性および支持性は障害されていく。軟骨組織には血管がないこと（無血管組織），かつ神経分布もないことを考えると，軟骨破壊・変性が進んでも軟骨組織自体で痛みを知覚することはないはずだが，実際のOA患者の主訴は関節痛である。では，なぜ，どこが関節の痛みを出しているのか？

変形性関節症の痛みの原因は以下の2点である。

① 軟骨変性の進行に伴い可動性や支持性が障害されると，関節を構成する滑膜（関節液産生の場），支持靭帯および関節包に2次的な障害が及び，これらの組織に分布する感覚神経が刺激される。

② 変性が進行して軟骨破壊が高度になれば関節軟骨下骨層などの組織も変性・変形をきたし，その結果，関節は著しく可動性と支持性を失い，骨膜刺激や疼痛が悪化する。

このように，OAにおける関節痛の原因は，関節構成要素のうち軟骨以外の組織に分布する感覚神経が，炎症などにより刺激されるためであり，①は発症早期～中期，②は中期後半～終期に相当し，軟骨変性に伴う関節構成組織への2次的障害の程度によって疼痛レベルも異なると考えられる。

そこで，OAにみられる関節症状について，主に臨床現場で用いられている治療薬について概説し，各々の自己注射への応用展開の価値について考察した。

4.1 OA治療薬としての消炎鎮痛剤

前述のように，OAにおける疼痛発生の主座は，軟骨組織自体にあるのではなく，二次的変化を生じた滑膜炎および軟骨下骨髄の微小骨折にある。OA初期においては二次性滑膜炎を抑制し，炎症症状を抑えることで関節痛をコントロールすることで，引き続く関節軟骨変性や関節変形を抑制することが重要であることから，消炎鎮痛剤は重要な臨床において重要な位置を占める。

4.1.1 非ステロイド性消炎鎮痛薬（Non-steroidal anti-inflammatory drug）

既存の消炎鎮痛剤で問題となる消化管潰瘍などの副作用（鎮痛剤多用による胃潰瘍等）が比較的に少ないとされる選択的シクロオキシゲナーゼ2（COX-2）阻害薬が上市され，関節リウマチやOAにおける関節痛・機能の改善に寄与している。一方，胃潰瘍や心血管系の既往患者において重篤な副作用の報告もあり，適切な投与にならないように薬剤の慎重な服用指導と管理が求められる。また，オピオイド系鎮痛剤（中枢神経系作用薬）のOA疼患における鎮痛効果も期待される[5]。

これらの消炎鎮痛剤は，軟骨変性を向上させる効果よりも，組織学的変化に伴う二次的な炎症症状と，それに起因する疼痛を緩和させることに主眼が置かれており，関節組織の変性を直接的に修復するだけのポテンシャルを有するか否かは今後の評価を待たなければならない。

4.1.2 ステロイド製剤（副腎皮質ホルモン製剤）

ステロイドは強力な消炎鎮痛剤であり，OAにおいても鎮痛効果が期待されるが，ステロイドの乱用・多用は骨粗鬆症や易感染性などの副作用の誘因となるため，その使用には十分注意しなければならない。

4.1.3 消炎鎮痛剤の自己注射の意義

OAの症状である痛みが二次性滑膜炎に起因すると考えると，抗炎症剤（消炎鎮痛剤）を関節腔内に直接注射する臨床的意義は大きい。現在の消炎鎮痛剤は，内服することで消化管から吸収され，または湿布や軟膏・クリーム製剤として経皮吸収され，血液循環により患部（関節滑膜）に運ばれ，抗炎症効果を発揮する。そのため，患部において薬効発現を担保するに必要な薬物濃度を獲得するため，必要な用量の薬剤を内服または経皮吸収させる必要がある。一方，薬剤は全身性に血液循環するため，患部以外の正常組織においても薬効発現濃度で作用し，様々な副作用の一因となる。それ故，関節患部への消炎鎮痛剤の直接投与，できれば患者本人が関節痛の程度に応じて，患部の関節に適宜，直接的に注射投与することが可能になれば，内服薬や経皮吸収剤の用量よりもはるかに低用量の注射投与で薬効が期待でき，関節患部以外の正常組織への副作用も軽減することができると考える。

そこで，どうすれば関節に直接消炎鎮痛剤を投与することができるかを考察すると，前述したように内服にしても経皮吸収剤（湿布，軟膏・クリーム）にしても，末梢血液循環を介して患部の関節組織に薬剤が運搬される過程を必要とするため，患部以外の正常組織に影響せずに薬剤を投与するには関節組織に直接投与するしかなく，関節腔に薬剤を投与する，すなわち関節内注射（注入）することになる。

もし，関節腔へ薬剤を自己注射投与することができれば，医療機関への外来診療回数を減らし，病院・診療所の混雑を緩和させ，限られた医療資源を効率的に運用することができるようになる。しかし，患者自身の関節腔内への注射にはいくつかのハードルが存在するため，関節腔内への自己注射の問題点については後述する。

4.2 関節機能改善剤（ヒアルロン酸製剤）の自己注射の意義

関節機能改善効果（関節軟骨潤滑面の保護作用，関節軟骨摩擦動圧の潤滑性，低摩擦性の維持）をもつ薬剤としてヒアルロン酸製剤が用いられている。ヒアルロン酸は，関節液の主成分で，関節包の内面を覆っている滑膜細胞から産生され，軟骨の抗炎症作用および関節滑動面保護・潤滑作用を持つ[6]。

ヒアルロン酸製剤の関節内注入（注射）療法によって，関節機能の改善が図られ，実際に広く臨床応用されている。ヒアルロン酸製剤の関節機能改善効果によって，関節機能（可動性，支持性）が損なわれることなく維持されると，滑膜への二次性炎症（滑膜炎）は惹起されることはなく，末梢神経への刺激因子（侵害物質やメディエーター，炎症性サ

イトカイン等）の産生も抑止され，関節痛は軽減されるものと考えられる[1]。

現在，臨床の現場では医療機関において，ヒアルロン酸製剤は最低1週間の間隔で関節腔内に直接注射剤として投与される。もし，このヒアルロン酸製剤を自己注射することができれば，患者自身の受診負担ならびに医療機関の過重な負担の軽減に寄与する効果は非常に大きいと考える。一方，消炎鎮痛剤同様，ヒアルロン製剤の患者自身による関節腔内への注射には問題点もある。

4.3 OA治療薬の自己注射の問題点

OA治療薬の自己注射は，前述のように患部の関節腔に薬剤を投与する，すなわち注射針を関節腔内に挿入することを必要としている。もし，この自己注射が皮下注射，筋肉注射であれば，たとえ関節患部近傍への注射であっても，注入された薬剤は皮下または筋肉内の血管から吸収されて全身性の血液循環によって患部の関節組織に到達されるわけであるから，内服薬や経皮吸収剤（湿布，軟膏・クリーム類）の効行動態，全身性副作用リスクとなんら変わらず，むしろ注射針刺入という侵襲リスク（出血，関節腔内，感染）がある分だけデメリットが大きいと言わざるを得ない。

関節腔内への注射の一番の問題点は感染リスクである。皮下への自己注射と異なり，関節腔内に注射針を刺入して薬剤投与しなければOA治療薬自己注射療法の本来の目的を達しないのは前述のごとくであるが，皮膚表面の消毒殺菌を完璧におこなわなければ注射針の刺入に伴って，関節腔内に細菌・ウイルスによる感染症が生じる危険性が極めて高い。医療現場においても，症状のある関節の解剖学的特徴を考慮した安全な刺入部位（皮膚）を手術の際に用いる消毒液で恒重に消毒してヒアルロン酸製剤等を注射しており，これを患者本人が自己注射として行なうことは現状の在宅医療システムでは極めて困難と言わざるを得ない。

そこで，OA治療薬の自己注射療法を開発するために，最低限以下の3つの問題点を克服しなければならないと考える。

① OA関節の解剖学的特徴を考慮した，患者にわかりやすい安全な注射刺入部位（皮膚）の同定

② OA関節症状のある患部の皮膚を患者自身が完璧に殺菌消毒する方法の確立

③ 自己注射薬の注射針の工夫（なるべく細く，痛みを軽減できる形状）・使用後の廃棄管理法

さらに，自己注射する薬剤の性状についても工夫することが望ましい。関節腔内に直接投与された消炎鎮痛剤は，関節包の内面を覆っている滑膜の炎症，すなわち滑膜炎を鎮静化することを目的としていることから，関節滑膜層への移行性を改良した製剤化が期待される。また，関節改善効果のあるヒアルロン酸製剤についても，同製剤は粘度が高いため水溶性薬剤に比べて注入しづらいことを改良した製剤化ができると，注射の際に有用である。

以上のように，OA関節症状の緩和を目的とする自己注射製剤の開発は，患者の受診負担の軽減に結びつき，かつ在宅医療が普及することによって医療現場の過重の負担を軽減できれば，本来の限られた医療資源の有効活用に寄与するものと考える。しかし，OA治療薬の自己注射治療法を開発するためには克服すべき問題点が多く，注射部位（患部皮膚）の殺菌消毒法や注射器・注射針，製剤化について新規医療システムの開発が期待される。

文　　献

1) Yoshimura N. Clin Calcium. Epidemiology of osteoarthritis in Japan: the ROAD study. Clinical Calcium,21 (6): 821-4, 2011

2) de Lange-Brokaar BJ, Ioan-Facsinay A, van Osch GJ, Zuurmond AM, Schoones J, Toes RE, Huizinga TW, Kloppenburg M. Synovial inflammation, immune cells and their cytokines in osteoarthritis: a review. Osteoarthritis Cartilage. 20 (12): 1484-99, 2012

3) 明田整形外科 42 2-6, 2002, 南江堂

4) Zhang W, Moskowitz RW, Nuki G, Abramson S, Altman RD, Arden N, Bierma-Zeinstra S, Brandt KD, Croft P, Doherty M, Dougados M, Hochberg M, Hunter DJ, Kwoh K, Lohmander LS, Tugwell P. OARSI recommendations for the management of hip and knee osteoarthritis, Part II: OARSI evidence-based, expert consensus guidelines. Osteoarthritis and Cartilage. 16, 137-62, 2008

5) Zhang W, Nuki G, Moskowitz RW, Abramson S, Altman RD, Arden NK, Bierma-Zeinstra S, Brandt KD, Croft P, Doherty M,

Dougados M, Hochberg M, Hunter DJ, Kwoh K, Lohmander LS, Tugwell P. OARSI recommendations for the management of hip and knee osteoarthritis, Part III: changes in evidence following systematic cumulative update of research published through January 2009. Osteoarthritis Cartilage. 18 (4): 476-99, 2010.

6) Codreanu C, Damjanov N. Safety of biologics in rheumatoid arthritis: data from randomized controlled trials and registries. Biologics. 27.9.1-6, 2015.

7) Furst DE, Emery P. Rheumatoid arthritis pathophysiology: update on emerging cytokine and cytokine-associated cell targets. Rheumatology (Oxford). 53 (9): 1550-9, 2014.

8) Leung GNL, Rainsford KD, Kean WF. Osteoarthritis of the hand II: chemistry, pharmacokinetics and pharmacodynamics of naproxen, and clinical outcome studies. J Pharm Pharmacol. 66 (3): 347-57, 2014.

9) Masuko K, Murata M, Yudoh K, Kato T, Nakamura H. Anti-inflammatory effects of hyaluronan in arthritis therapy: Not just for viscosity. Int J Gen Med. 2(1,2 77-81, 2009.

2016_5.

Integrative Molecular Medicine

Research Article ISSN: 2056-6360

Effects of soy peptides on IL-1β-induced matrix-degrading enzymes in human articular chondrocytes

Minomi Arito[1], Hiroyuki Murai[2], Masao S Kurokawa[3], Kazuo Yudoh[4], Toshikazu Kamada[5], Eiisaburo Niki[5] and Tomohiro Kato[1]

[1]Clinical Proteomics and Molecular Medicine, St. Marianna University Graduate School of Medicine, 2-16-1, Sugao, Miyamae, Kawasaki, Kanagawa, 216-8512, Japan

[2]Department of Orthopaedic Surgery, St. Marianna University School of Medicine, 2-16-1, Sugao, Miyamae, Kawasaki, Kanagawa 216-8512, Japan

[3]Disease Biomarker Analysis and Molecular Regulation, St. Marianna University Graduate School of Medicine, 2-16-1, Sugao, Miyamae, Kawasaki, Kanagawa, 216-8512, Japan

[4]Institute of Medical Science, St. Marianna University Graduate School of Medicine, 2-16-1, Sugao, Miyamae, Kawasaki, Kanagawa, 216-8512, Japan

[5]Department of Orthopedic Surgery and Rheumatology, Hara Orthopedic Hospital, 3-36-25, Nishi-ikebukuro, Toshima-ku, Tokyo, 171-0021 Japan

Abstract

Background: In osteoarthritis (OA) of the most common joint disease, inflammation is deeply involved in the cartilage degradation. Specifically, inflammatory cytokines like IL-1β are known to enhance production of matrix-degrading enzymes like matrix metalloproteinase (MMP) and a disintegrin and metalloproteinase with thrombospondin motifs (ADAMTS). Recently, soy peptides, generated by hydrolysis enzymatic digestion of soy proteins, have been found to show anti-inflammatory activity. Thereby we investigated whether soy peptides affected IL-1β-induced expression of matrix-degrading enzymes in human articular chondrocytes. Methods: Articular chondrocytes derived from 4 patients with bone fracture and 11 patients with OA were cultured with 0.10, or 100 μM soy peptides for 4 hours. Then, the cells were stimulated with IL-1β for 24 hours. Non-stimulated cells were used as a control. RNA extracted from the cells was subjected to quantitative real time-PCR to assess amounts of mRNA for MMP-3 and ADAMTS-4. Results: Treatment with 100 μM soy peptides significantly suppressed mRNA levels of MMP-3 and ADAMTS-4 induced by the IL-1β stimulation (p=0.038 and p=0.004, respectively), although the treatment with 10 μM soy peptides did not show significant suppression (p=0.92 and p=0.41, respectively). In the 100 μM soy peptides treatment, the suppression of MMP-3 mRNA levels was correlated with that of ADAMTS-4 mRNA levels (R=0.914). Conclusion: Soy peptides suppressed the IL-1β-induced expression of matrix-degrading enzymes in human articular chondrocytes. Soy peptides may have potential to ameliorate cartilage degradation in OA.

Introduction

Osteoarthritis (OA), the most common joint disease, is histologically characterized by degeneration of cartilage and formation of osteophytes, which lead to destruction of joints [1]. Many patients with OA suffer from pain and disability [1]. Thus, to suppress the symptoms of OA and prevent the progress of OA, novel agents should be developed.

Articular chondrocytes maintain the cartilage matrix by producing and degrading matrix proteins such as type II collagen and proteoglycans [2]. In OA, imbalance between production and degradation of the matrix protein leads to cartilage degradation [3]. Inflammation is deeply involved in the cartilage degradation in OA [1]. Inflammatory cytokines like IL-1β are known to be increased in synovial fluid of patients with OA [3]. In particular, IL-1β was reported to enhance secretion of matrix metalloproteinase (MMP) 1, 3, and 13 from chondrocytes that digest multiple types of collagens [4]. Furthermore, IL-1β was reported to enhance secretion of a disintegrin and metalloproteinase with thrombospondin motifs (ADAMTS)-4 and -5 from chondrocytes that digest aggrecan, of a representative proteoglycan [5].

Soybeans contain a large amount of nutrients such as proteins, fats, and carbohydrates. Recently, novel biological roles of soybeans have been highlighted in addition to the roles as nutrients. Specifically, so-called soy peptides, generated by hydrolytic enzymatic digestion of soy proteins, have been reported to show various functions beneficial to health such as cholesterol lowering properties, cognitive impairment prevention, antiviral effects, and anti-inflammatory effects [6-12]. As to the anti-inflammatory effects, soy peptides were reported to suppress lipopolysaccharide (LPS) induced production of cyclooxygenase 2 and prostaglandin E2 in a murine macrophage cell line [10]. Furthermore, soy peptides were reported to suppress LPS-induced production of pro-inflammatory cytokines such as IL-6 and IL-8 in human umbilical vein endothelial cells [11]. In vivo, soy-derived di- and tri-rich peptides were reported to alleviate colon and ileum inflammation in pigs with dextran sodium sulfate induced colitis [12]. Therefore, soy peptides are expected to show anti-inflammatory effects also in human articular chondrocytes, which may lead to suppression of cartilage degradation in OA. However, effects of soy peptides on human articular chondrocytes have not been investigated to our knowledge. We here investigated whether soy peptides suppressed IL-1β-induced expression of matrix-degrading enzymes in human articular chondrocytes.

Correspondence to: Minomi Arito, Clinical Proteomics and Molecular Medicine, St. Marianna University Graduate School of Medicine, 2-16-1, Sugao, Miyamae, Kawasaki, Kanagawa, 216-8511, Japan, Tel: +81-44-977-8111 (ext. 3-238); Fax: +81-44-976-9-6; E-mail: m-arito@marianna-u.ac.jp

Key words: A disintegrin and metalloproteinase with thrombospondin motifs 4 (ADAMTS-4), Chondrocytes, IL-1β, Matrix metalloproteinase 3 (MMP-3), Osteoarthritis, Soy peptides

Received: May 08, 2016, Accepted: May 23, 2016, Published: May 26, 2016

Materials and methods

Clinical samples and preparation of chondrocytes

Human articular cartilage samples were obtained from 4 patients with bone fracture (Normal, N1-4, 1 male, age 58 years, 3 female; mean age 78.0 years [range56-86]) at therapeutic surgery of total hip arthroplasty. Cartilage samples were also obtained from 11 patients with OA (OA1-11, 1 male, age 82 years, 10 female; mean age 78.7 years [range 66-86 years]) at therapeutic surgery of total knee arthroplasty.

The diagnosis of OA was made according to the Kellgren and Lawrence criteria [14]. Written informed consent was obtained from each of the patients and this study protocol was approved by the ethics committee of St. Marianna University School of Medicine. The study was performed in compliance with the World Medical Association Declaration of Helsinki.

For chondrocyte preparation, after careful removal of synovial tissue from cartilage samples, the cartilage was minced, washed, and treated with collagenase (Wako Pure Chemical Industries, Osaka, Japan). Isolated chondrocytes (Passage 0, P0) were washed and grown in monolayer culture in Dulbecco's modified Eagle's medium (DMEM, GIBCO, Carlsbad, CA) supplemented with 10% fetal calf serum (Wako), 100 units/ml penicillin, and 1000 μg/ml streptomycin (Sigma-Aldrich, St. Louis, MO, USA) on type I collagen-coated culture dishes.

Treatment of chondrocytes with IL-1β and soy peptides

Soy peptides (Hinute-AM, FUJI OIL Co. Ltd., Osaka, Japan), which were mainly composed of di- and tri-peptides, were used [15].

The prepared chondrocytes (P1-P3, 1.0×10^5 cells/φ100mm dish) were cultured with 0, 10, and 100 μM soy peptides for 4 hours. Then, the cells were treated with 1 μg/ml IL-1β alone (R&D, Minneapolis, MN, USA), 1 μg/ml IL-1β and 10 μM soy peptides, and 1 μg/ml IL-1β and 100 μM soy peptides for 24 hours. Non-treated cells were used as a control.

Evaluation of cell viability

Cell viability was evaluated by trypan blue staining. Chondrocytes, cultured with 0, 10, or 100 μM soy peptides for 24 hours, were harvested by treatment with 0.1% trypsin-EDTA (Sigma-Aldrich). The cell pellet, collected by centrifugation for 10 min at 1000×g, was stained with 0.4% trypan blue (Sigma-Aldrich). The number of the blue-stained (dead) cells and the total number of cells were counted using a hemocytometer under a microscopy.

Extraction and reverse transcription (RT) of RNA

Extraction of RNA from the chondrocyte samples and reverse transcription of the RNA samples were performed using RNeasy® (Qiagen, Venlo, the Netherlands) and High Capacity cDNA Reverse Transcription Kit® (Life Technologies, Rockville, MD, USA), respectively.

Quantitative real time PCR

Real time PCR was performed using ABI Prism 7900HT Sequence Detection System (Applied Biosystems, Foster City, CA, USA), according to the manufacturer's instructions. To measure mRNA levels for MMP-3 and ADAMTS-4, 1 μg of total RNA-derived cDNA was mixed with TaqMan® Gene Expression Assays (Hs00968305_m1 and Hs00192708_m1, respectively, Applied Biosystems) and TaqMan® Gene Expression Master Mix (Applied Biosystems). Then the mixture was subjected to real time PCR. The thermal cycle conditions was as follows. 50°C for 10 min, followed by 40 cycles of 95°C for 15 s and 60°C for 60 s. To measure mRNA levels for GAPDH, 1 μg of total RNA-derived cDNA was mixed with 300 nM each of the forward and reverse primers and Power SYBR® Master Mix (Applied Biosystems). Nucleotide sequences of the primers for amplification of a 64-bp DNA fragment are as follows. For GAPDH: 5'-TGTTCATTGTTGGAAGGACTCA and 5'-ATGCCAGTGAGCTTCCCGTT. Real time PCR was performed under the same condition as above.

Statistical analysis

Statistical analysis was performed by IBM SPSS Statistics (Ver.22.0). Effects of soy peptides on IL-1β-induced matrix-degrading enzymes were analyzed by Wilcoxon signed-rank test ($p<0.05$).

Results

Effects of soy peptides on IL-1β-induced matrix-degrading enzymes in human articular chondrocytes

Firstly, we tested whether the concentrations of soy peptides used here showed cytotoxicity against human articular chondrocytes. As a result, we confirmed that up to 100 μM soy peptides did not affect viability of the chondrocytes (Figure 1A). We then investigated effects of the soy peptides on IL-1β-induced expression of MMP-3 and ADAMTS-4 in the chondrocytes. We cultured chondrocytes with or without the soy peptides for 4 hours and then stimulated with IL-1β. We then assessed mRNA levels of MMP-3 and ADAMTS-4.

In the assessment of mRNA levels of MMP-3, we first confirmed that mRNA levels of MMP-3 were significantly increased by the IL-1β stimulation ($p<0.01$, Table 1 and Figure 1B, left panel). Of note, in each of the stimulated chondrocyte sample, the mRNA levels of MMP-3 were increased by the IL-1β stimulation. We then evaluated effects of the soy peptides on the IL-1β-induced expression of MMP-3 in chondrocytes. As a result, the treatment with 100 μM soy peptides significantly

Table 1. Effects of soy peptides on IL-1β-induced MMP-3 mRNA levels in human chondrocytes

Sample no	Control	IL-1β	IL-1β +10μM HN-AM	IL-1β +100μM HN-AM
N1	0.003	12.2	16.2	15.9
N2	1.49	53.6	33.3	54.4
N3	3.15	7.2	13.0	11.9
N4	1.45	20.1	10.1	9.27
OA1	1.05	4.52	4.19	2.58
OA2	2.93	1.68	6.08	6.62
OA3	0.73	2.17	2.83	2.49
OA4	0.91	6.50	4.60	3.32
OA5	0.82	47.5	30.2	5.32
OA6	0.37	15.9	20.7	25.7
OA7	0.02	15.9	16.5	5.3
OA8	1.58	12.1	7.98	4.04
OA9	0.22	10.9	10.9	7.15
OA10	1.02	13.0	16.2	6.11
OA11	0.22	5.35	3.91	3.50
Average	1.35	15.5	15.9	11.6
STDEV	0.87	15.3	12.1	15.2
p value	-	<0.01 vs Control	0.9 vs IL-1β	0.035 vs IL-1β

HN: soy peptides

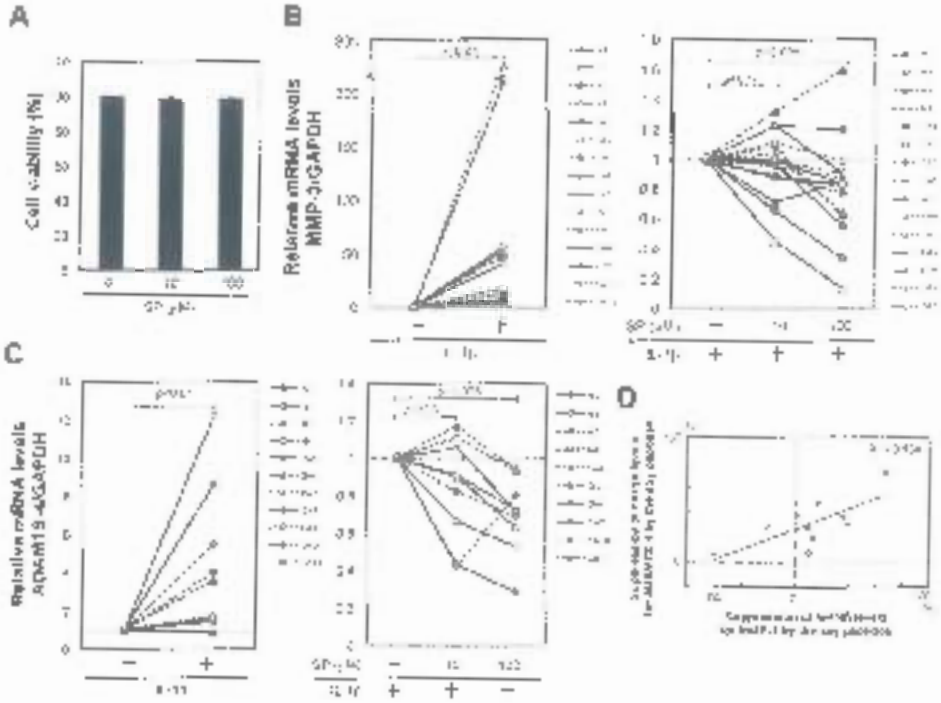

Figure 1. Effects of soy peptides on IL-1β-induced expression of MMP-3 and ADAMTS-4 in human articular chondrocytes. (A) Articular chondrocytes from 3 patients with OA (OA1-3) were cultured with 0, 10, and 100 μM soy peptides for 24 hours. The cells were subjected to trypan blue staining. The cell viability (%) was calculated using the following formula: the number of unstained cells/the total number of cells×100. SP, soy peptides. (B) Articular chondrocytes from 4 patients with bone fracture (N1-4) and 12 patients with OA (OA1-12) were cultured with 0, 10, and 100 μM soy peptides for 4 hours. Then, the cells were stimulated with IL-1β for 24 hours. Non-stimulated cells were used as control. The mRNA levels of MMP-3 and GAPDH were assessed by RT-qPCR. The mRNA levels of MMP-3 were corrected using those of GAPDH. Left: The corrected mRNA levels of MMP-3 were calculated as 1.0 in each of the non-treated samples. Right: The corrected mRNA level of MMP-3 was refitted as 1.0 in each of the 10-μM-treated samples. *p-values were calculated by Wilcoxon signed-rank test using the values listed in Table 1. (C) Articular chondrocytes from 4 patients with bone fracture (N1-4) and 7 patients with OA (OA5-11) were treated similarly as described in (A). The mRNA levels of ADAMTS-4 were corrected using those of GAPDH. Left: The corrected mRNA level of ADAMTS-4 was defined as 1.0 in each of the non-treated samples. Right: The corrected mRNA level of ADAMTS-4 was defined as 1.0 in each of the 10-μM-treated samples. *p-values were calculated by Wilcoxon signed-rank test using the values listed in Table 2. SP, soy peptides. (D) Scatterplot and 95% of mRNA levels for MMP-3 and ADAMTS-4 in each of the chondrocyte samples (4 patients with bone fracture (N1-4) and 6 patients with OA (OA6-11)) were calculated by using the values listed in Table 1 and 2, respectively. A correlation diagram between the expression of mRNA levels for MMP-3 and ADAMTS-4 in the treatment with 100 μM soy peptides is shown. Coefficient of determination (R^2) was calculated by regression analysis.

suppressed mRNA levels of MMP-3 enhanced by the IL-1β stimulation (p=0.056, Table 1 and Figure 1B, right panel), although the treatment with 10 μM soy peptides did not show significant suppression (p=0.91, Table 1 and Figure 1B, right panel).

In the assessment of ADAMTS-4, we first confirmed that mRNA levels of ADAMTS-4 were significantly increased by IL-1β stimulation (p<0.01, Table 2 and Figure 1C, left panel). Ten out of the 12 chondrocyte samples up-regulated the mRNA levels of ADAMTS-4 by the IL-1β stimulation. We thus evaluated effects of the soy peptides on the IL-1β-induced expression of ADAMTS-4 using the 10 chondrocyte samples that positively responded to IL-1β. As a result, the treatment with 100 μM soy peptides significantly suppressed mRNA levels of ADAMTS-4 enhanced by the IL-1β stimulation (p=0.005, Table 2 and Figure 1C, right panel). Although the treatment with 10 μM soy peptides did not show significant suppression (p=0.20, Table 2 and Figure 1C, right panel).

Finally, we investigated correlation of the suppressing effect of the soy peptides on the MMP-3 expression to that of ADAMTS-4 expression. As a result, in the treatment with 100 μM soy peptides, the suppression of MMP-3 mRNA levels was correlated with that of ADAMTS-4 mRNA levels (R^2=0.554, Figure 1D). In addition, the suppressive effect of the soy peptides on the expression of MMP-3 and ADAMTS-4 tended to be higher in patients with OA than in those with bone fracture (Figure 1D).

Discussion

We have found that soy peptides suppressed IL-1β-induced production of MMP-3 and ADAMTS-4 in human articular chondrocytes.

The possible mechanisms for the actions of soy peptides are as follows: 1) soy peptides inhibit the input of IL-1β signal transduction by binding to IL-1β or IL-1β receptors, 2) soy peptides, taken up into chondrocytes, inhibit the intracellular IL-1β signal transduction, and 3) soy peptides bind to their unknown receptors and then block the IL-1β signal transduction.

On the first possible mechanism, IL-1β activates the signal transduction system by specific binding to IL-1β receptors. In the majority of the tested chondrocytes samples, the mRNA levels of MMP-3 of the IL-1β-stimulated chondrocytes group were suppressed by the treatment with 100 μM soy peptides (Figure 1B). However, in a small part of the tested chondrocytes samples, the mRNA levels of MMP-3 were increased by the soy peptides treatment (Figure 1B). If soy peptides bound to IL-1β or IL-1β receptors, the mRNA levels of MMP

Table 2: Effects of soy peptides on IL-1β-induced ADAMTS-4 mRNA levels in human chondrocytes

Sample no	Control	IL-1β	IL-1β +10μM HN-AM	IL-1β +100μM HN-AM
N1	0.16	1.37	1.25	1.00
N2	1.21	2.79	2.94	2.03
N3	2.12	2.74	1.21	2.56
N4	0.96	1.49	1.05	1.38
OA1	2.06	1.72	-	-
OA6	1.98	4.77	5.31	2.43
OA7	1.73	2.06	2.66	1.83
OA8	1.32	1.51	2.56	0.47
OA9	1.47	2.20	1.46	1.16
OA10	0.91	3.64	2.98	2.53
OA11	1.11	1.82	1.65	1.14
Average	1.01	2.23	2.17	1.65
STDEV	0.67	1.16	1.50	1.11
p value	-	<0.01 (vs. Control)	2.20 (vs. IL-1β)	0.005 (vs. IL-1β)

HN: soy peptides

3 would have been suppressed in all the tested chondrocytes samples. Thus, it would be unlikely that soy peptides inhibit the binding between IL-1β and IL-1β receptors.

On the second possible mechanism, we showed that suppression of mRNA levels for MMP-3 were well correlated with that of mRNA levels for ADAMTS-4 in the soy peptides treated chondrocyte samples (R=0.5343, Figure 1D). Thus, we thought that soy peptides suppressed the IL-1β-induced production of MMP-3 and ADAMTS-4 by inhibiting their common pathway. IL-1β activates the signal transduction systems through the activation of multiple protein kinases such as p38 mitogen-activated protein kinase (MAPK), c-Jun N-terminal kinase (JNK), and Akt [15-18]. The activated MAPK, JNK, and Akt enhance production of various inflammatory cytokines and matrix degrading proteins activating transcription factors such as AP-1 and NF-κB [19]. Akt, phosphorylated by activated phosphoinositol 3-kinase (PI3K), leads to activation of NF-κB [20]. NF-κB activates transcription of pro-inflammatory cytokines and matrix-degrading enzymes including MMP-3 and ADAMTS-4 [4,5]. Peptides derived from β-conglycinin of a representative soy protein have been reported to inactivate NF-κB by suppressing phosphorylation of Akt in liver and aorta of LPS induced inflammatory model mice [21]. Thus, we speculate that soy peptides suppress the IL-1β induced production of MMP-3 and ADAMTS-4, probably by inhibiting their PI3K-Akt-NF-κB signaling, by suppressing the phosphorylation of Akt.

On the third possible mechanism, although receptors for soy peptides have not yet been identified, such receptors may exist and deliver signals. For example, M. Chiarugi et al. reported that PEPITEM a peptide proteolytically derived from 14-3-3 zeta delta protein, used cadherin-15 as a receptor and lead to release of sphingosine-1-phosphate from endothelial cells [22]. Like the case of PEPITEM, receptors for soy peptides may exist, which should be investigated. Including these 3 possible mechanisms, the mechanisms for the action of soy peptides should be investigated in the near future.

We have found that soy peptides significantly suppressed the IL-1β-induced production of MMP-3 and ADAMTS-4 in human articular chondrocytes. In the majority of the tested chondrocytes samples, both the mRNA levels of MMP-3 and those of ADAMTS-4 were suppressed by the treatment with 100 μM soy peptides (Figure 1C). However, in a small part of the tested chondrocytes samples, neither the mRNA levels of MMP-3 nor those of ADAMTS-4 were suppressed by the soy peptides treatment (Figure 1C). Thus, the effect of soy peptides would be influenced by the individual genetic backgrounds. There might be subpopulations that show different sensitivity to soy peptides.

It is interesting that the suppressive effect of the soy peptides on the expression of MMP-3 and ADAMTS-4 tended to be higher in the patients with OA than in those with bone fracture (Figure 1D). OA chondrocytes might show higher sensitivity to soy peptides than normal chondrocytes.

Soy peptides used in this study are mainly composed of di- and tri-peptides [14]. However, specific peptides that suppressed the IL-1β induced production of MMP-3 and ADAMTS-4 have not been identified yet. Recently, a tri-peptide of Val-Pro-Tyr, derived from glycinin of a major soy protein, has been reported to down regulate the expression of pro inflammatory cytokines in intestinal epithelial cells and macrophages [22]. The soy peptides used in this study are expected to contain glycinin and thus would contain Val-Pro-Tyr. A tri-peptide of Val-Pro-Tyr might be one of the soy peptides that suppressed the effects of IL-1β in this study. On this point, further investigation is required.

Our data showed that soy peptides suppressed the IL-1β induced production of MMP-3 and ADAMTS-4 in human articular chondrocytes *in vitro*. Our data indicate that soy peptides may be useful to prevent or suppress cartilage degradation in OA.

Acknowledgements

We thank Ms. Sawada Y., Ms. Tamaki M., Ms. Mugi T. and Ms. Suzuki M. for their technical assistance. This work was supported by FUJI OIL CO., LTD.

Conflict of interest statement

Arito M, Matsui F, Kawakawa MS, Niki H, Yudoh K. and Kato T report grants and non-financial support from FUJI OIL Co., Ltd., during the conduct of the study. Kato T reports grants and non-financial support from Chugai Pharmaceutical Co. Ltd., outside the submitted work. Yudoh K reports non-financial support from a Vitamin D3 BioResearch Corporation, outside the submitted work. Kurosaka D has nothing to disclose.

References

1. Lorenz HP, Goldring SR, Sandell LJ, Ilic MZ, Hong SJ (2014) Osteoarthritis and bone: a tale of the joint as an organ. Arthritis Rheum 66: 1797-1807. [Crossref]
2. Goldring MB, Marcu KB (2009) Cartilage homeostasis in health and rheumatic diseases. Arthritis Res Ther 11: 224. [Crossref]
3. Kanemoto K, Sugioka N, Nakamura M, Suzuki T, Aono Y (2012) Inhibitory effect of pro-inflammatory cytokines on cytokine-induced human MMP-13 promoter activity in human chondrocytes. Int J Biol Macromol 51: 419-423. [Crossref]
4. Wuertzner DK, Oyejide AO (2002) Effects of interleukin-1beta and tumor necrosis factor-alpha on expression of matrix-related genes by cultured equine articular chondrocytes. Am J Vet Res 63: 828-837. [Crossref]
5. Ilas E, Geldwert HM, Haag J, Kurz T, Gabriel E, et al. (2004) Relative microarray RNA expression of proteases and aggrecanases in immortalized chondrocytes treated with interleukin-1beta. Arthritis Res 6: 248-257. [Crossref]

5. Inoue N, Nagata K, Sakata K, Yamamoto N. Hypocholesterolemic Peptides in Soybean Protein Hydrolysate. J Agric Food Chem 59: 10: 85. [Crossref]

6. Mochizuki M, Kishi Y, Kishioka T, Fujiwara Y (2011) Soy Peptide Intake Supplementation Improves Serum Dynamic Level and Improves Cognitive Dysfunction in Subjects with Mild Cognitive Impairment. Gen Gerontol 11: 69-73.

8. Kitano-Okada S, Ito R, Sugiyama H, Nakamura S (2014) Oral Administration of Soy Peptides Suppresses Cognitive Decline by Inhibition of Neuroinflammation Induced in SAMP8 Mice. J Agric Food Chem 62: 3563-3569. [Crossref]

9. Matsumoto AO, Nakamura K, Kayama H, Murakami H, Kataoka S, et al. (2011) Enhancer activity of soybean β-conglycinin-derived peptides by acetylation with citraconic anhydride. J Agric Food Chem 59: 9299-9306. [Crossref]

10. Martinez-Villaluenga C, Dia VP, Berhow M, Gonzalez de Mejia E (2009) Protein hydrolysates from beta-conglycinin and glycinin soybean genotypes inhibit lipid accumulation and inflammation in adipocytes. Mol Nutr Food Res 53: 1007-1018. [Crossref]

11. Burns RL, Ng HR, Nguyen S (2014) Soy protein inhibits chemokine-induced VCAM-1 gene expression and monocyte adhesion by inhibiting the NF-κB and AKT signaling pathways in apolipoprotein E-deficient mice. J Nutr 144: 115-121. [Crossref]

12. Young D, Ando M, Sakamoto T, Fan M, Mine Y (2012) Soy-derived dipeptide and tripeptide alleviate colon and ileum inflammation in pigs with acute colitis. J Agric Food Chem 60: 362-368. [Crossref]

13. Kellgren JH, Lawrence JS (1957) Radiological assessment of osteo-arthritis. Ann Rheum Dis 16: 494-502. [Crossref]

14. Nakamori T (2010) Soy peptides as functional food materials. In: Bioactive peptides and peptides as functional foods and nutraceuticals. (Mine Y, Li-Chan ECY, Jiang B, eds.) Wiley-Blackwell Publishing, Hoboken. pp. 265-271.

15. Ding GS, Pfeilschifter J, Siegrist W (1994) Activation of protein kinases and the induction of protein phosphatase 2A in human mesangial cells by interleukin-1 beta. Eur J Biochem 225: 929-941. [Crossref]

16. Barkett M, Gilmore TD (1999) Control of apoptosis by Rel/NF-κB transcription factors. Oncogene 18: 6910-6924. [Crossref]

17. Li X, Tepper JC, Brunetiere H, Arian RK, Kunder CT, et al. (2004) Phosphoinositide 3-kinase mediates T-lymphocyte receptor-induced activation of NF-kappa B in epithelial cells. Infect Immun 72: 4414-4420. [Crossref]

18. Vincenti MP, Coburn CG, Barrett W, Attkinson JM, Herzog W, et al. (2003) IL-1 beta induces IκBζ, MMP-3 and -13, ADAMTS-4, IL-1 beta and TLR-4 in articular cartilage. J Orthop Res 21: 256-264. [Crossref]

19. Williams DM, Jeffery L, Murray JC (1992) Agonist-induced inhibition of NF-κB and AP-1 activity by acting as an IκB functional antagonist. Biochem Biophys Acta 1180: 9-14. [Crossref]

20. Van Tay L, Garcia MD, Wilson W, Raynaud F, de Bono JS, et al. (2008) Targeting the PI3K-AKT-mTOR pathway: progress, pitfalls and promises. Curr Opin Pharmacol 8: 393-412. [Crossref]

21. Clemens W, McCormick HM, Aida P, Karas SL, Yeo EM, et al. (2015) Extracellular regulation of T cell trafficking by a B cell-derived peptide is required in autoimmune and chronic inflammatory disease. Adv Med Sci 7: 457-475. [Crossref]

22. Kawase-Nolan J, Zhang L, Ando M, Nakamori T, Yoshida K, et al. (2012) The PepT1-transportable soy tripeptide VPY reduces intestinal inflammation. Biochem Biophys Acta 1820: 1755-1761. [Crossref]

Copyright: ©2016 Arno M. This is an open-access article distributed under the terms of the Creative Commons Attribution License, which permits unrestricted use, distribution, and reproduction in any medium, provided the original author and source are credited.

2016. 6.

International Journal of
Molecular Sciences

MDPI

Article

The NAD-Dependent Deacetylase Sirtuin-1 Regulates the Expression of Osteogenic Transcriptional Activator Runt-Related Transcription Factor 2 (Runx2) and Production of Matrix Metalloproteinase (MMP)-13 in Chondrocytes in Osteoarthritis

Koh Terauchi [1], Hajime Kobayashi [1], Kanaka Yatabe [1], Naoko Yui [1], Hiroko Fujiya [1], Hisateru Niki [2], Haruki Musha [1] and Kazuo Yudoh [3,*]

1 Department of Sports Medicine, St. Marianna University School of Medicine, Sugao 2-16-1, Miyamae-ku, Kawasaki 216-8511, Japan; koh-sakai@marianna-u.ac.jp (K.T.); hdkobayashi@marianna-u.ac.jp (H.K.); kanaka@marianna-u.ac.jp (K.Y.); aburaimisaki@marianna-u.ac.jp (N.Y.); fujiya-2487@marianna-u.ac.jp (H.F.); musha@marianna-u.ac.jp (H.M.)

2 Department of Orthopaedic Surgery, St. Marianna University School of Medicine, Sugao 2-16-1, Miyamae-ku, Kawasaki 216-8512, Japan; h2niki@marianna-u.ac.jp

3 Department of Frontier Medicine, Institute of Medical Science, St. Marianna University School of Medicine, Sugao 2-16-1, Miyamae-ku, Kawasaki 216-8512, Japan

* Correspondence: yudo@marianna-u.ac.jp; Tel.: +81-44-977-8111 (ext. 4029); Fax: +81-44-979-5056

Academic Editor: Walter Herzog
Received: 22 April 2016; Accepted: 23 June 2016; Published: 28 June 2016

Abstract: Aging is one of the major pathologic factors associated with osteoarthritis (OA). Recently, numerous reports have demonstrated the impact of sirtuin-1 (Sirt1), which is the NAD-dependent deacetylase, on human aging. It has been demonstrated that Sirt1 induces osteogenic and chondrogenic differentiation of mesenchymal stem cells. However, the role of Sirt1 in the OA chondrocytes still remains unknown. We postulated that Sirt1 regulates a hypertrophic chondrocyte lineage and degeneration of articular cartilage through the activation of osteogenic transcriptional activator Runx2 and matrix metalloproteinase (MMP)-13 in OA chondrocytes. To verify whether sirtuin-1 (Sirt1) regulates chondrocyte activity in OA, we studied expressions of Sirt1, Runx2 and production of MMP-13, and their associations in human OA chondrocytes. The expression of Sirt1 was ubiquitously observed in osteoarthritic chondrocytes; in contrast, Runx2 expressed in the osteophyte region in patients with OA and OA model mice. OA related catabolic factor IL-1β increased the expression of Runx2 in OA chondrocytes. OA chondrocytes, which were pretreated with Sirt1 inhibitor, inhibited the IL-1β-induced expression of Runx2 compared to the control. Since the Runx2 is a promotor of MMP-13 expression, Sirt1 inactivation may inhibit the Runx2 expression and the resultant down regulation of MMP-13 production in chondrocytes. Our findings suggest that Sirt1 may regulate the expression of Runx2, which is the osteogenic transcription factor, and the production of MMP-13 from chondrocytes in OA. Since Sirt1 activity is known to be affected by several stresses, including inflammation and oxidative stress, as well as aging, Sirt1 may be involved in the development of OA.

Keywords: osteoarthritis; NAD-dependent deacetylase; sirtuin; Runx2; chondrocytes

1. Introduction

In osteoarthritis (OA), mechanical and chemical stresses to articular cartilage downregulate chondrocyte activities and induce secretion of catabolic factors, such as proinflammatory cytokines and

cartilage degrading enzymes, by chondrocytes [1–4]. In addition to mechanical and chemical stresses, chondrocyte aging is one of the major pathologic factors associated with OA. Indeed, Martin et al reported that aging decreases the chondrocyte activity to maintain the homeostasis of articular cartilage tissue [5–7]. They examined different biomarkers of cellular aging in human articular cartilage tissues and found that chondrocyte senescence correlated with donor aging. Their findings clearly demonstrate that the association between OA and aging is due, at least in part, to the age-related decrease of chondrocytes and cartilage matrix function with aging. Aged chondrocytes may show an insufficient response to anabolic and catabolic factors, such as inflammation and oxidative stress, resulting in cartilage matrix degradation from unbalanced catabolic and anabolic activities [5,8–14].

Recently, numerous reports have demonstrated the impact of the NAD-dependent deacetylase sirtuin-1 (Sirt1) on human aging and age-related diseases [15]. It is well known that Sirt1, when adjusting the pattern of cellular metabolism to nutrient availability, can regulate many metabolic functions including DNA repair, genome stability, inflammatory response, apoptosis, cell cycle, and mitochondrial functions [15]. It has been demonstrated that Sirt1 insufficiency may induce the calcification and atherosclerosis in cardiovascular tissues, through a mechanism involving upregulation of Runt-related transcription factor 2 (Runx2), which is the osteogenic transcriptional activator [16]. This suggests that Sirt1 may protect against the vascular calcification and maintain the vascular function with aging. In contrast to this finding, several reports suggested that Sirt1 promotes the expression of Runx2, and the resultant osteogenic transcription and chondrogenic differentiation of mesenchymal stem cells [17,18]. There are still some conflicting opinions concerning the association between Sirt1 and Runx2 expression. In addition, although there is a general consensus regarding the involvement of Runx2, which is required for chondrocyte hypertrophy and osteophyte formation, in the pathogenesis of OA [19], the role of Sirt1 in the Runx2 in OA chondrocytes remains unknown.

We postulated that the NAD-dependent deacetylase Sirt1 regulates the development of chondrocyte hypertrophic lineage and the progression of cartilage degeneration through activation of Runx2 and production of matrix metalloproteinase (MMP)-13 by chondrocytes in OA. Runx2 is well known to be a promotor of the activation of MMP-13 in chondrocytes [20,21]. If Sirt1 influences Runx2 expression, MMP-13 production could also be mediated by Sirt1 in OA chondrocytes.

To verify whether or not Sirt1 regulates chondrocyte activity in OA, we examined expressions of Sirt1 and Runx2 and production of MMP-13, and their correlations in human chondrocytes.

2. Results and Discussion

2.1. Expression of Runx2 in Human Chondrocytes from Patients with OA

The clinical features of patients we studied are summarized in Table 1. The pre-operative X-ray features of patients are shown in Figure 1. Runx2 was expressed by osteoarthritic chondrocytes from patients with severe OA. As shown in Figure 2A, the Runx2 protein was strongly expressed in osteoarthritic chondrocytes from "Patient 1", "Patient 2" and "Patient 3". These three patients with OA had severe cartilage degeneration and osteophyte formations (Table 1, Figure 1).

The expression of Runx2 in chondrocytes from "Patient 5" with a moderate degree of cartilage degeneration and osteophyte formation was lower than those from other patients with severe OA and osteophyte formation (Figure 1). In contrast to OA patients, the level of expression of Runx2 was very weak in chondrocytes from patient "Patient 4" who had bone necrosis of the femoral condyle (Figure 2A). The degree of Runx2 expression in chondrocytes was associated with the severity of cartilage degeneration and osteophyte formation in articular cartilage tissues. Previous reports demonstrated that induction of an osteogenic transcription factor Runx2 in chondrocytes contributed to the progression of OA through the acceleration of chondrocyte hypertrophy [19,21]. The association of Runx2 expression with the severity of OA including osteophyte formation found in our study is consistent with the results of these reports.

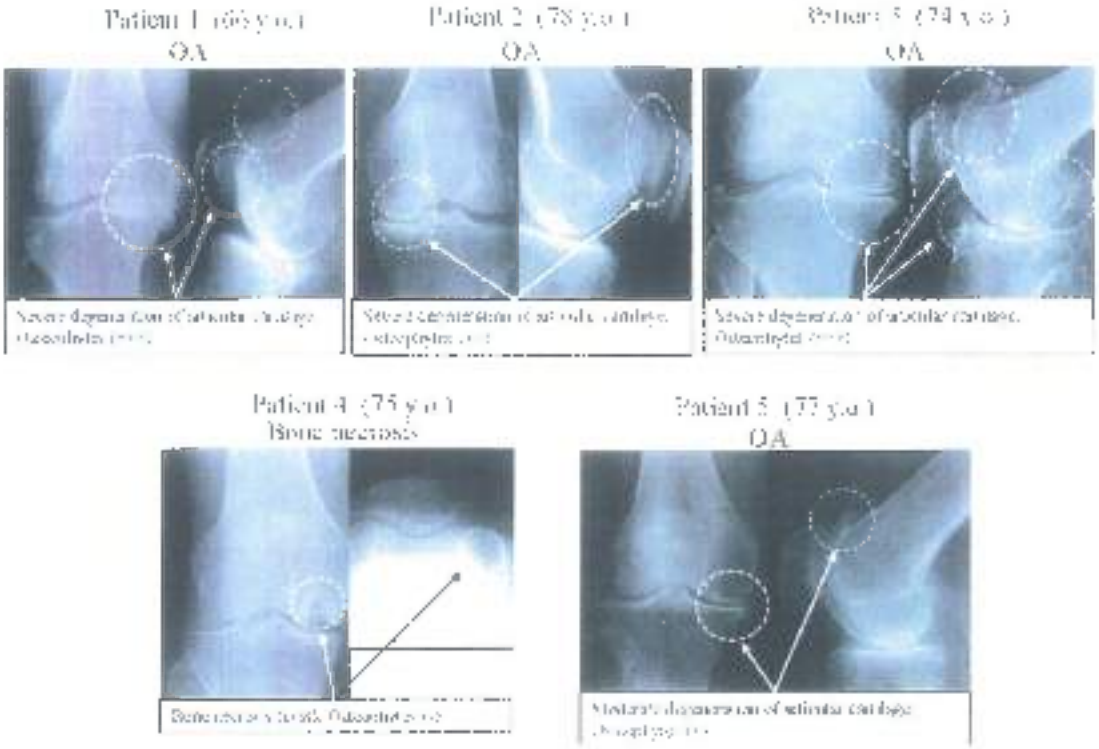

Figure 1. X-ray images of knee joints of donor patients. Patient 1, female, 66 years of age, Patient 2, female, 78 years of age, Patient 3, male, 74 years of age, Patient 4, female, 75 years of age, Patient 5, female, 77 years of age. Patient 1, 2, 3 had severe knee OA with severe cartilage degeneration and osteophyte formation. Patient 4 had idiopathic osteonecrosis of femoral condyle. Patient 5 had moderate knee OA with cartilage degeneration and osteophyte formation. OA: osteoarthritis, y.o., years old.

Table 1. The clinical characteristics of patients.

Patients Number	Age/Gender	Grade of Cartilage Degeneration	Duration of Disease	Symptoms	Osteophyte Formation	Deformation of Joint	Treatment
(1) OA	66 y.o. female	severe OA	[illegible] years		+ + +	severe	NSAIDs HA injection
(2) OA	74 y.o. male	severe OA	[illegible] years	+	+ + +	severe	NSAIDs HA injection
(3) OA	74 y.o. female	severe OA	>20 years		+ + +	severe	NSAIDs HA injection
(4) Bone necrosis	75 y.o. female	moderate OA	>12 years		+	moderate	NSAIDs
(5) OA	77 y.o. female	moderate OA	>20 years		+	moderate	NSAIDs HA injection

y.o.: years old, NSAIDs: nonsteroidal anti-inflammatory drugs; HA: hyaluronic acid

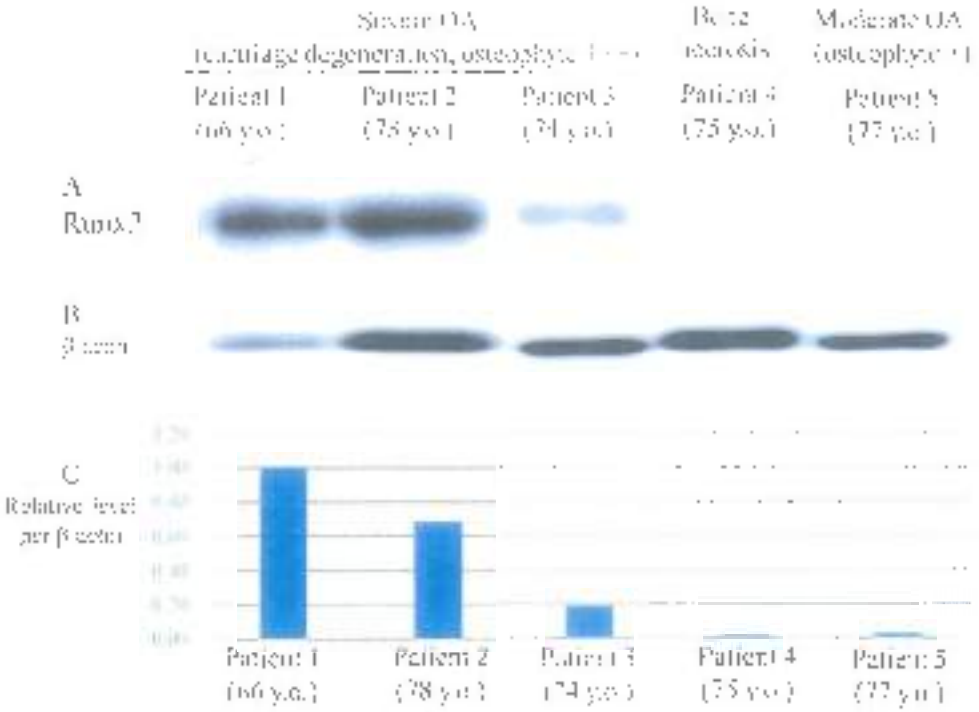

Figure 2. Expression of Runx2 in osteoarthritic chondrocytes from donors. (A) Expression of Runx2 in chondrocytes from patients with OA (Patient 1, 2, 3, 5) and from patient with idiopathic osteonecrosis of femoral condyle (Patient 4); (B) Expression of β-actin; (C) Relative ratio against the level of expression of β-actin. The level of Runx2 expression was analyzed as a relative ratio against the level of expression of β-actin. Runx2 protein was strongly expressed in osteoarthritic chondrocytes from "Patient 1", "Patient 2" and "Patient 3" in comparison with "Patient 4" and "Patient 5".

2.2. OA-Related Factor IL-1β Induces Runx2 Expression in Human Osteoarthritic Chondrocytes

Osteoarthritic chondrocytes from patients with severe OA (Patients 1–3) expressed Runx2 protein during the initial phase (Figure 3a,c,e). These three patients with OA all exhibited severe cartilage degeneration and osteophyte formation (Table 1, Figure 1). The expression of Runx2 in chondrocytes from a patient with moderate OA (Patient 5) and, from a patient with bone necrosis of the femoral condyle (Patient 4) were lower than those from other patients with severe OA (cartilage degeneration and osteophyte formation) at the initial phase (Figure 3g,i). This expression pattern of Runx2 in chondrocytes coincided with the finding shown in Figure 2A. These findings indicate that the Runx2 is implicated with the OA progression, and especially osteophyte formation, in OA cartilage.

After a 24 h incubation period, the expression level of Runx2 increased in the presence of the OA-related factor (IL-1β, 10 ng/mL), in chondrocytes from Patients 2, 3, and 5 (Figure 3d,f,j) but not Patient 1 (Figure 3b), although its expression levels decreased transiently at the 6 and 12 h time-points. The evidence for an IL-1β-induced increase in Runx2 in OA chondrocytes also indicates the role of Runx2 in the development of OA. However, in the present study, there was donor variation of clinical features from the point of view of osteoarthritic degeneration of articular cartilage, especially osteophyte formation, even though all patients underwent arthroplastic surgery. The variation of clinical features was summarized in Table 1.

In addition, the time course of Runx2 expression in the IL-1β-treated chondrocytes was varied in OA patients. There is a general consensus that proinflammatory cytokine, IL-1β, is an OA-related factor. Treatment with IL-1β may affect the chondrocyte microenvironment, viability and several cellular activities including the Runx2 transcription. Further studies are needed to verify why the time courses of Runx2 expression were different in OA patients. IL-1β-induced change of chondrocyte

microenvironment or different responsibility to IL-1β in each patient might be implicated in donor variation. The donor variation may affect the expression patterns of Runx2 in Figures 2 and 3.

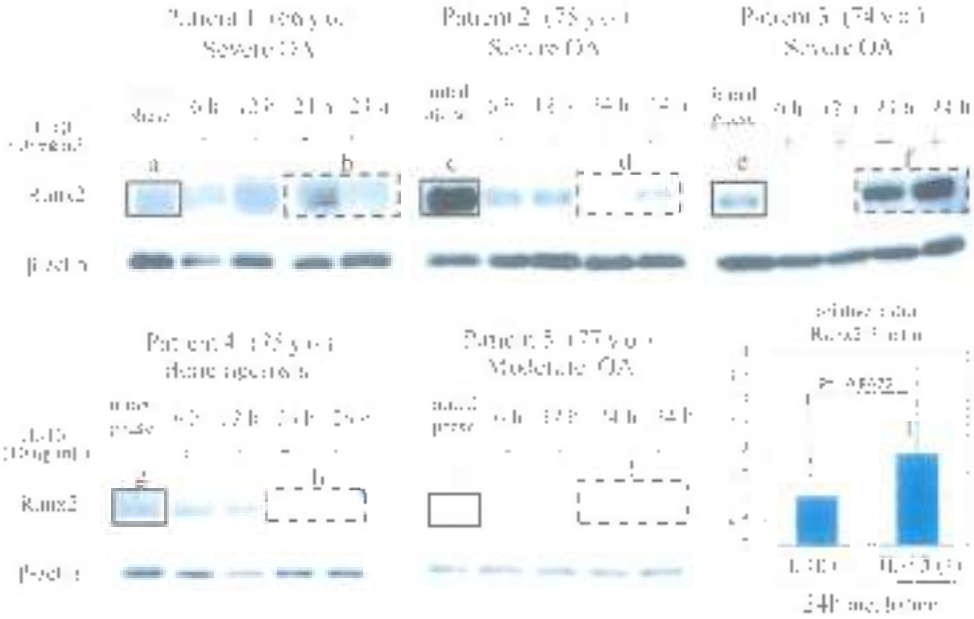

Figure 3. Effects of IL-1β on Runx2 expression in osteoarthritic chondrocytes from donor patients. Time course of Runx2 expression in chondrocytes in the presence of IL-1β (10 ng/mL). At the initial phase, the level of Runx2 expression in chondrocytes was higher in patients with severe OA (Patient 1 (a), Patient 2 (c), and Patient 3 (e)) than in patient with bone necrosis (Patient 4 (g)) and patient with moderate OA (Patient 5 (i)). After 24 h-incubation period, the expression level of Runx2 increased in the presence of the IL-1β (10 ng/mL) in chondrocytes from Patient 2 (d), Patient 3 (f), Patient 5 (j) but not Patient 1 (b) and Patient 4 (h), although the expression levels decreased transiently at 6 and 12 h incubation periods. Solid box indicates the expression of Runx2 at the initial phase. The dash line box indicates the expression of Runx2 at 6 and 12 h incubation periods. The treatment with IL-1β tended to induce the expression of Runx2, although no significant difference was observed between the IL-1β-treated group and the control group.

2.3. Immunopositivity of Runx2 and Sirt1 in the Articular Cartilage in OA Model Mouse

To clarify whether the expression of Runx2 and Sirt1 was correlated with degeneration of articular cartilage in OA, the immunopositivity for Runx2 and Sirt1 was examined in the degenerated articular cartilage sections from a spontaneous OA model mouse, which develops an osteoarthritic process (STR/Ort(Crj) mouse). For immunohistochemical analysis, we got whole knee joint tissues (juxta-articular bone, subchondral bone, meniscus, ligaments, and cartilage tissues) from the OA mouse model. Using the OA mouse model, we can observe the progression or degeneration of OA joint tissues, not only cartilage but also juxta-articular bone and subchondral bone. In elder mice, osteophytes were expressed at the juxta-articular lesion in OA joints, and grow gradually with advance of mouse aging. Interestingly, the expression of Runx2 was localized at the osteophyte lesion in OA mice. In contrast, not only osteophytes but also Runx2 were undetectable in younger mice.

Figure 4 shows representative images of articular cartilages (Safranin-O staining) and immunohistologic staining of Runx2 and Sirt1 in articular cartilages of OA mice. The level of cartilage degeneration (modified Mankin score) and the immunopositivity of Runx2 and Sirt1 in samples of OA mouse articular cartilage are summarized in Table 2.

Severe degeneration of articular cartilage, such as decreased level of Safranin-O staining, chondrocyte loss, surface irregularities, superficial clefts and osteophyte formation were observed in

degenerated articular cartilage from 24-week old mice (representative image in Figure 4A; modified Mankin score 10, Table 2). Interestingly, many strongly Runx2-immunopositive chondrocytes were detected in the osteophyte regions of degenerated articular cartilage from older 24-week-old mice (representative image in Figure 4A, Table 2). In contrast, only faint staining of Runx2 was observed in both normal articular cartilage and slightly degenerated articular cartilage with no osteophyte formation in 12-old mice (Figure 4B, Table 2). In 20-week-old mice, osteophytes were observed at the attachment region of the anterior cruciate ligament (ACL) (data not shown). Around the ACL, we also observed Runx2 protein expression in chondrocytes. Twelve-week old mice showed moderate cartilage degeneration with no osteophyte formation (Figure 4, modified Mankin score 4B, Table 2).

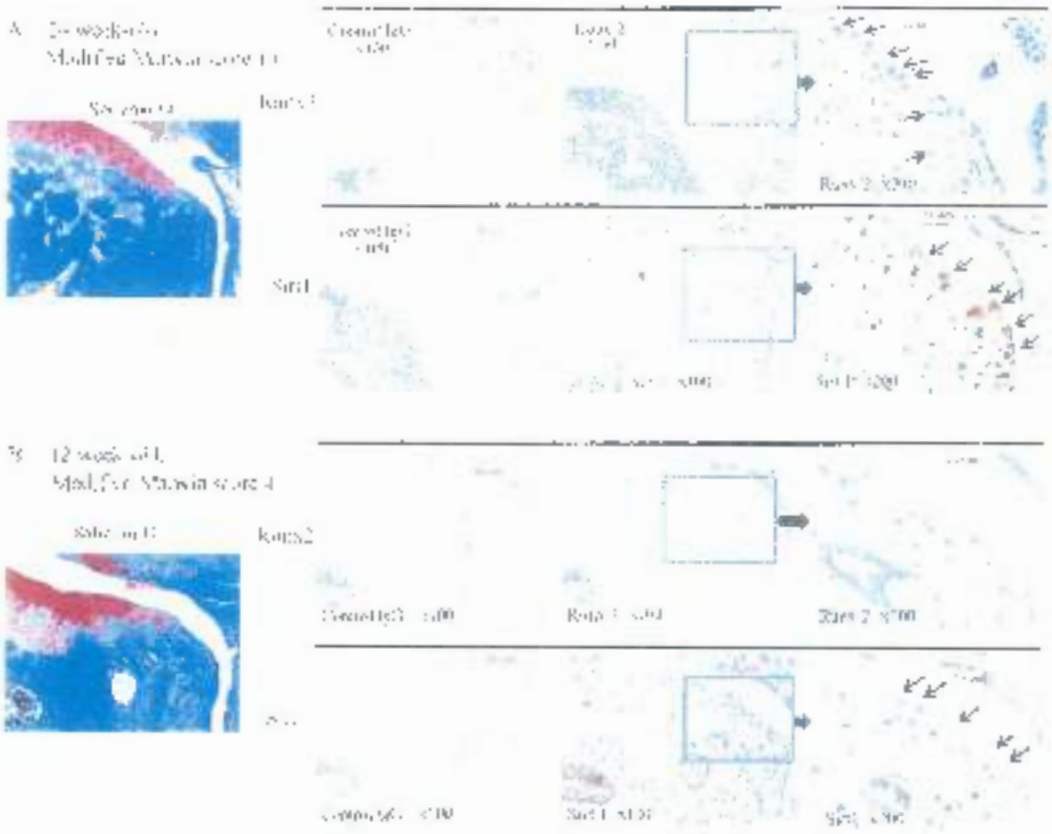

Figure 4. Representative images for Runx2- and Sirt1-immunostaining in mouse OA articular cartilage. (**A**) Representative images of Safranin O staining and Runx2- and Sirt1-immunohistologic staining in severe OA articular cartilage from 24-week old STR/OrtCrlj mice. Safranin O staining (×100). Runx2 immunostaining (×100, ×200); Sirt1 immunostaining (×100, ×200). A higher expression pattern of Runx2 was observed at the osteophyte region in the severely degenerated cartilages. Arrows indicate the Runx2- or Sirt1-immunopositive chondrocytes; (**B**) Representative images of Safranin O staining and Runx2- and Sirt1-immunohistologic staining in moderate OA articular cartilage from 12-week old STR/OrtCrlj mice; Safranin O staining (×100). Runx2 immunostaining (×100, ×200). Sirt1 immunostaining (×100, ×200). Almost all the mildly degenerated cartilages were negative for Runx2 immunostaining in 12-year old mice. Sirt1 was ubiquitously detected in chondrocytes of both normal articular cartilages and degenerated articular cartilages, regardless with or without osteophyte formation. Arrows indicate the Runx2- or Sirt1-immunopositive chondrocytes.

We found that articular cartilage, which had no osteophytes, showed no immunopositivity for Runx2 in chondrocytes (5 osteophyte regions per mouse, 3 mice). These findings indicate that

expression of Runx2 in chondrocytes is correlated with osteophyte formation in OA. Our histologic findings indicate that the expression of Runx2 is correlated with osteophyte formation.

In contrast to the expression pattern of Runx2 in articular cartilage, Sirt1 was ubiquitously detected in chondrocytes of both normal and degenerated articular cartilage, regardless of whether or not osteophyte formation was present (Figure 4A,B, Table 2). At the osteophyte region in degenerated articular cartilage, most Sirt1 positive chondrocytes expressed the Runx2 protein (mean percentage of immunopositivity for Runx2 in Sirt1 positive cells: 92%), although chondrocytes in degenerated cartilage with no osteophytes expressed only Sirt1, but not Runx2 (Figure 4A). These findings suggest that Runx2 expression is associated with Sirt1, at least in part, at the osteophyte region. Recently, several reports demonstrated that Sirt1 plays an important part in chondrocyte activity and cartilage metabolism [22–24]. Dvir-Ginzberg et al. demonstrated that Sirt1 regulated the expression of cartilage-specific gene in human chondrocytes [22]. Takayama et al. reported the role of Sirt1 in the regulation of human chondrocyte apoptosis [23]. In addition, it has been reported that Sirt1 may promote the chondrogenic differentiation of mesenchymal stem cells [18], suggesting the potential involvement of Sirt1 in the chondrocyte differentiation and pathogenesis of OA.

Table 2. Summary of immunohistologic analysis in OA mouse articular cartilages.

	24-Week Old Osteophyte−	24-Week Old Osteophyte+	28 Week Old Osteophyte	30-Week Old Osteophyte+	16-Week Old Osteophyte	32 Week Old Osteophyte
Modified Mankin score	1	9	10	5	4	4
Runx2 positive (% per total cells)	13.2 ± 2.7	14.2 ± 1.9	N.A.	13.4 ± 5.1	5.4 ± 1.0	2.1 ± 0.6
Sirt1 Positive (% per total cells)	43.2 ± 21.2	N.A.	91.1 ± 5.5	85.5 ± 16.3	28.7 ± 7.3	32.3 ± 11.2

N.A.: not available

Thus, we postulated that Sirt1 might have the potential to regulate Runx2 expression in chondrocytes in OA. Since Runx2 regulates the expression of MMP-13 in chondrocytes [19,20], Sirt1 may also regulate the MMP-13 production by chondrocytes through the modulation of Runx2 in OA.

2.4. Sirt1 Regulates Runx2 Expression and MMP-13 Production in OA Chondrocytes

To address whether Sirt1 modulates the expression of Runx2 and MMP-13 in chondrocytes, chondrocytes from four OA patients were pre-treated with Sirt1 inhibitor and their cellular activities were examined in vitro (Figure 5).

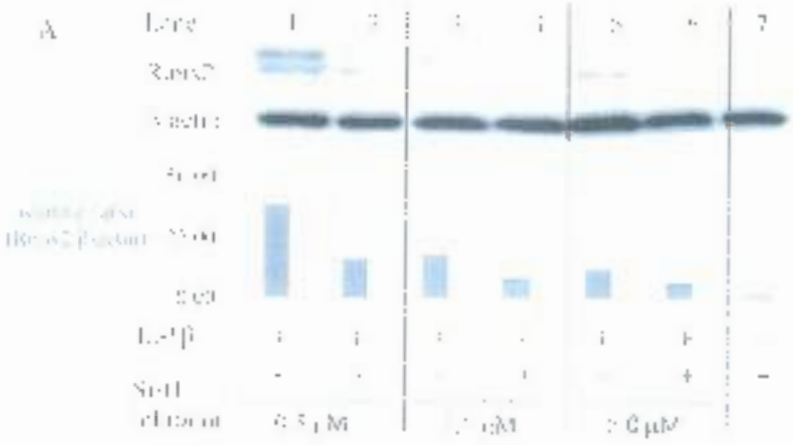

Figure 5. Cont.

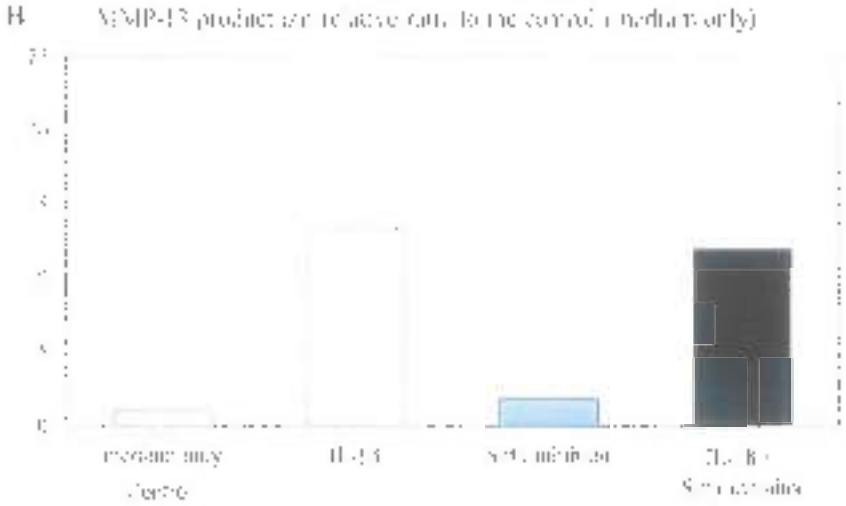

Figure 5. Sirt1 regulates Runx2 expression and MMP-13 production in osteoarthritic chondrocytes. To address whether Sirt1 is necessary to express the Runx2 protein in chondrocyte, OA chondrocytes were preincubated with Sirt1 inhibitor (S)-35 (0.5, 1.0, 5.0 μM). (A) In OA chondrocytes, treatment with IL-1β stimulated the expression of Runx2 (lane 1, 3, 5) compared to the control (lane 7). Sirt1 inhibitor inhibited the IL-1β-induced acceleration of Runx2 expression in chondrocytes (lane 2, 4, 6). (B) Treatment with IL-1β significantly accelerated MMP-13 production from chondrocytes in comparison with the control (medium only) ($p = 0.037$). Treatment with Sirt1 inhibitor only did not influence the MMP-13 production from chondrocytes in comparison with the control. The inhibition of Sirt1 with Sirt1 inhibitor tended to inhibit the IL-1β-accelerated production of MMP-13 in chondrocytes, although no significant difference was observed between the Sirt1 inhibitor-treated IL-1β treated chondrocytes and the Sirt1 inhibitor + IL-1β-treated chondrocytes ($p = 0.832$). The levels of MMP-13 production in both Sirt1 inhibitor-treated group and control group were lower than in those IL-1β-treated groups.

In the absence of IL-1β, the level of Runx2 expression in chondrocytes was very weak (Figure 5A, lane 7). In contrast, treatment with IL-1β stimulated the Runx2 expression in chondrocytes (Figure 5A, lane 1, 3, 5). Interestingly, pre-treatment with Sirt1 inhibitor (S)-35 (0.5, 1.0, 5.0 μM) inhibited the IL-1β-induced increased in Runx2 expression in chondrocytes (Figure 5A, lane 2, 4, 6). Our data clearly indicated that osteoarthritic chondrocytes, which were pre-treated with Sirt1 inhibitor, expressed the decreased level of Runx2 even in the presence of IL-1β (Figure 5A). Buhrmann et al. demonstrated that the Sirt1 activator, resveratrol, induced expression of cartilage-specific genes including Runx2 in mesenchymal stem cells [18]. From their results, they concluded that Sirt1 promotes chondrogenic differentiation of mesenchymal stem cells through the modulation of Runx2 [18]. Kim et al. also indicated that treatment with resveratrol significantly upregulates Sirt1 gene expression in normal and osteoarthritic chondrocytes and induces chondrocytes to differentiate into a hypertrophic state through upregulation of collagen type I, collagen type X and Runx2 [25]. It has been reported that Runx2 regulates the expression of MMP-13 in chondrocytes [19,20]. These data lead to our hypothesis that Sirt1 might activate Runx2 in osteoarthritic chondrocytes, resulting in the upregulation of MMP-13.

As shown in Figure 5B, treatment with IL-1β significantly increased the MMP-13 production from chondrocytes in comparison with controls (medium only) ($p = 0.037$). Pre-treatment with the Sirt1 inhibitor (S)-35 tended to reduce the IL-1β-accelerated production of MMP-13 in chondrocytes, although no significant difference was observed between the IL-1β-treated chondrocytes and the Sirt1 inhibitor + IL-1β-treated chondrocytes ($p = 0.832$, Figure 5B). NAD-dependent deacetylase Sirt1 can act on cell activation and many cellular metabolisms as an important regulator: cell cycle, DNA repair, genome instability, mitochondrial functions, cell differentiation, inflammatory response, and anti-apoptotic pathways, etc., in a variety of cells [15]. Generally, it has been demonstrated that Sirt1

is ubiquitously expressed human somatic cells and controls many cellular activities. In addition, it is well known that many stresses to the cells, such as oxidative stress, inflammation, or aging, affect the Sirtuin1 activity [15,17,18]. The stress-induced inactivation of Sirt1 may reveal the cell in activation and downregulation of cellular metabolism. Since mechanical and chemical stresses to articular cartilage and chondrocytes are known to induce the development of OA, these extrinsic stresses to chondrocytes may influence the Sirt1 activity in chondrocytes and resultant dysfunction of chondrocytes. Thus, we postulated that the OA-related factor induced change of Sirt1 activity may be involved in some changes of chondrocyte activity and metabolism during the progression of OA. In the current study, Sirt1 inactivation with Sirtuin1 inhibitor reduced the IL-1β-accelerated expression of Runx2 in OA chondrocytes, suggesting that the NAD-dependent deacetylase Sirtuin1 may regulate the osteogenic transcriptional activator Runx2 in chondrocytes. Osteogenic transcription factor Runx2 in chondrocytes is known to be closely involved in the endochondral ossification in articular cartilage tissue. Previously, several reports demonstrated that Sirt1 promotes the expression of Runx2 and the resultant osteogenic and chondrogenic differentiation in a variety of cells [16–18]. Iijima suggested that Sirt1 promotes the Runx2 activity via a P53/P21 pathway in vascular endothelial cells [16]. Iijima concluded that Sirtuin1 promotes the vascular calcification via the Runx2 pathway. There may be some common mediators (such as P53 or P21) in the Sirt1-associated pathway for expressions of Runx2 in vascular endothelial cells. In addition, in human chondrocytes, Sirt1 is one of important mediators to regulate the expression of Runx2 through the mechanism involving the acceleration or reduction of signal transduction pathways. There may be some common mediators in the Sirt1-associated pathways for expressions of MMP-13 and Runx2 in OA chondrocytes.

Our data suggest that Sirt1 inactivation may inhibit the expression of Runx2 in OA chondrocytes. Since there is a general consensus that the Runx2 is a promotor of the activation of MMP-13 in chondrocytes [20,21], therefore, we would like to conclude that the Sirtuin1 may, at least in part, have a potential to regulate the expression of MMP-13 through the mechanism involving the Sirtuin1-regulated Runx2 expression in chondrocytes, although further studies are required to clarify the exact effect of Sirtuin1 on Runx2 and MMP-13 expressions.

In contrast to our findings, several other reports demonstrated that Sirt1 downregulated chondrocyte gene expression in OA [23,24]. Dupont et al reported that overexpression of Sirt1 by gene transfection in chondrocytes inhibited expression of osteoarthritic genes such as MMP-13 [24]. They also demonstrated that reduction of Sirt1 by small-interfering RNA caused an increase in MMP-13 production from chondrocytes, suggesting the down-regulatory effect of Sirt1 on the production of MMP-13 in chondrocytes. These findings suggest that Sirt1 plays a protective part to suppress IL-1β induced expression of cartilage degrading enzyme, MMP-13, partially through the NF-kB pathway. However, they did not mention whether or not Sirt1 modulates the expression of Runx2, which is a key regulator of MMP-13 expression in chondrocytes. In the current study, our findings provided evidence that Sirt1 inactivation inhibits the expression of Runx2 and IL-1β-stimulated MMP-13 in OA chondrocytes. Buhrmann et al. and Kim et al. also indicated that Sirt1 activation induced expression of cartilage specific genes including Runx2 in mesenchymal stem cells and chondrocytes, respectively, suggesting the correlation between the Sirt1 activity and the Runx2 activity [18,25]. Although further studies are needed to verify the association between Runx2 and Sirt1 in chondrocytes, Sirt1 may play important roles in chondrocyte hypertrophy/osteophyte formation and MMP-13 expression through activation of Runx2 in chondrocytes (Figure 6).

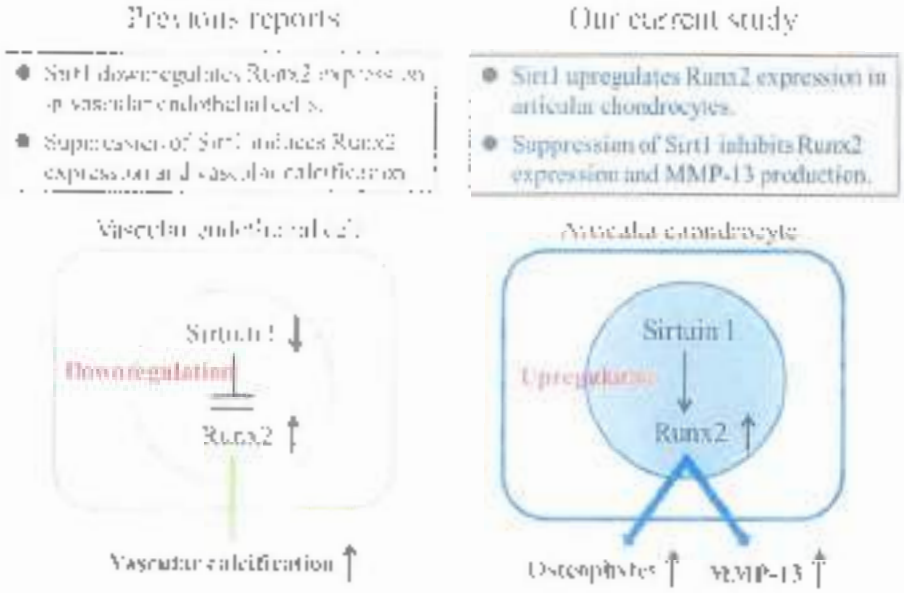

Figure 6. Summary of our current study. The NAD-dependent deacetylase Sirt1 may regulate the osteogenic transcription and chondrocyte hypertrophic factor Runx2 and matrix degrading enzyme MMP-13 in chondrocytes in OA. Arrow "↑" indicates upregulation, Arrow "↓" indicates downregulation.

3. Experimental Section

3.1. Chondrocyte Isolation and Cell Culture

Human articular cartilage tissues of the knee joints were obtained from five patients who underwent arthroplastic knee surgery, after obtaining informed consent. Four of the patients were treated for OA (3 females aged 66, 75, and 77 years, and 1 male aged 74 years) and one for idiopathic osteonecrosis of the femoral condyle (female aged 75 years). The protocol of this study was accepted by our University ethical committee in St. Marianna University School of Medicine (permission code: No.1315, date: 7 January 2006). The clinical features of patients are summarized in Table 1. The pre-operative X-ray features of patients are shown in Figure 1.

At the surgery, degenerated bone and articular cartilage tissues were widely resected for prosthetic joint replacement. Articular cartilage tissues were carefully collected from the resected bone and cartilages (circled areas in each patient, Figure 1). Cartilage samples were cut into small pieces and then, washed with phosphate-buffered saline (PBS). Cartilage pieces were digested with 1.5 mg/mL collagenase B (Sigma, St. Louis, MO, USA) in Dulbecco's modified Eagle's medium (DMEM) (Sigma) at 37 °C overnight on a shaking platform. The isolated chondrocytes were centrifuged and washed three times with PBS. In addition, chondrocytes were cultured in DMEM supplemented with 10% heat-inactivated fetal calf serum, 2 mM L-glutamine, 25 mM HEPES (2-[4-(2-hydroxyethyl)-1-piperazinyl] ethanesulfonic acid), and 100 U/mL penicillin and streptomycin at 37 °C in a humidified atmosphere of 95% air and 5% CO_2 [26].

3.2. Immunohistochemistry for Runx2 and Sirt1 in Mouse OA Articular Cartilages

To clarify the involvement of Runx2 and Sirt1 in the development of cartilage degeneration, we used immunohistochemical analysis to investigate levels of expression of Runx2 and Sirt1 in chondrocytes from an OA mouse model (STR/OrtCrlj mouse). Twenty-four STR/OrtCrlj mice (male, 12 weeks of age) were purchased from Charles River Japan (Yokohama, Japan) [27]. The mice were euthanized with diethyl ether at 4, 8, 12, or 16 weeks from the start of the study ($n = 6$/time-point).

Articular cartilage samples with the subchondral bone were fixed with 4% paraformaldehyde solution for 2 days, and then decalcified in 4% paraformaldehyde containing 0.85% sodium chloride and 10% acetic acid. The tissues were dehydrated in a series of ethanol solutions, infiltrated with xylene and embedded in paraffin. The samples were cut into 6-μm sections. For histological examination of the degree of degeneration in the articular cartilage tissues, some sections were stained with Safranin O-fast green to determine the level of proteoglycan expression. Each cartilage sample was evaluated histologically for the degree of degeneration according to the modified Mankin score (Table 3) [26,28]. To determine the mean damage score, two to three regions were examined from the each animal. Three independent observers examined cartilage damage in a blinded manner.

For immunostaining of articular cartilage, serial sections of paraffin-embedded bone and cartilage tissues were immunostained with antibodies for Runx2 or Sirt1. The 6-μm sections were treated with 3% H_2O_2, followed by blocking of nonspecific protein binding using a blocking agent (Protein Block, Dako, Carpinteria, CA, USA). The sections were incubated with polyclonal antibodies against Runx2 (#12556, 1:50 dilution; Cell Signaling Technology, Danvers, MA, USA) or Sirt1 (#SAB2501994, 1:200 dilution; Sigma) for 1 h at room temperature. The sections were then followed by incubation with biotinylated anti-mouse IgG (Dako, rabbit IgG X0936 for anti-Runx2 antibody (1:3000 dilution), or goat serum X0907 for anti-Sirt1 antibody (1:100 dilution)) for 30 min at room temperature. The sections were then incubated with a streptavidin-horseradish peroxidase complex (LSAB2 Kit; Dako) for 30 min at room temperature. Diaminobenzidine (Sigma) was used as a visible peroxidase reaction product. Finally, the sections were counterstained with Mayer's haematoxylin (Sigma).

Table 3. Modified Mankin Score (criteria for histological evaluation).

Safranin O-fast green staining	
0	uniform staining throughout articular cartilage
1	loss of staining in the superficial zone for less than one half of the length of the plateau
2	loss of staining in the superficial zone one half
3	loss of staining in the superficial and middle zones for less than one half of the length of the plateau
4	loss of staining in the superficial and middle zones for one half or more of the length of the plateau
5	loss of staining in all 3 zones for less than one half of the length of the plateau
6	loss of staining in all 3 zones for one half or more of the plateau
Structure	
0	normal
1	surface irregularities
2	1–3 superficial clefts
4	1–3 clefts extending into the middle zone
5	>3 clefts extending into the middle zones
6	1–3 clefts extending into the deep zones
7	>3 clefts extending into the deep zones
8	clefts extending to calcified cartilage
Chondrocyte loss	
0	no decrease in cell
1	minimal decrease in cells
2	moderate decrease in cells
3	marked decrease in cells
4	very extensive decrease in cells

The number of Runx2- or Sirt1-positive cells was counted in degenerated articular cartilage and osteophyte regions under high-power magnification (×100) for each case [26].

1.3. Effects of IL-1β on Expression of Runx2 and Sirt1 Expressions in Chondrocytes

To study the effects of the OA-related catabolic factor, IL-1β, on the Runx2 and Sirt1 expressions in chondrocytes, chondrocytes were incubated in the presence or absence of IL-1β (10.0 ng/mL) for 6, 12, or 24 h at 37 °C in a humidified atmosphere of 95% air and 5% CO_2. After harvesting, protein was isolated from the cultured cells for immunoblotting analyses as previously described.

Expression levels of Runx2 and Sirt1 in OA chondrocytes were analyzed by western blotting. The antibodies used in the current study were polyclonal antibody against human Runx2 (#FA2006, 1:500 dilution; R&D Systems Inc., Minneapolis, MN, USA), polyclonal antibody against human Sirt1 (1:2000 dilution; Abcam Inc., Cambridge, UK), β-tubulin (1:1000 dilution; Santa Cruz Biotechnology, Santa Cruz, CA, USA) and the corresponding secondary antibodies conjugated with horseradish peroxidase (Dako, goat IgG #p0449 for anti-Runx2 antibody (1:10,000 dilution), or rabbit IgG p04 for anti-Sirt1 antibody (1:10,000 dilution)). The western blotting was replicated using same donor samples. The antibody bound protein bands were visualized by an extended cavity laser system (GE Healthcare Bio-sciences KK, Tokyo, Japan). Densitometry of the signal bands was analyzed as described previously [26].

3.4. Effects of Sirt1 Inactivation on Runx2 Expression and MMP-13 Production in OA Chondrocytes

To verify the effects of Sirt1 inactivation on chondrocyte activity, we examined levels of the cartilage degrading enzyme MMP-13 and the osteogenic transcription factor Runx2 in Sirt1 inhibitor-treated chondrocytes in vitro. OA chondrocytes were obtained from OA patients who had undergone arthroplastic knee surgery (n = 4; all females, aged 72, 74, 75, 75 years).

Cultured chondrocytes were divided into 4 groups: control (medium only), IL-1β-treated group, Sirt1 inhibitor-treated group, and IL-1β + Sirt1 inhibitor-treated group. In the Sirt1 inhibitor-treated group and IL-1β + Sirt1 inhibitor-treated group, chondrocytes were pre-treated with Sirt1 inhibitor (S)-35 (#sc-204279, 0.5, 1.0, 5.0 μM, Santa Cruz Biotechnology Inc.) for 6 h at 37 °C in a humidified atmosphere of 95% air and 5% CO_2. Then IL-1β (10.0 ng/mL) was added into the cell culture. The cells were returned to the incubator for a further 18 h. After the incubation period, the conditioned culture medium was collected and stored at −80 °C until analysis.

The levels of MMP-13 produced by chondrocytes were analyzed using an ELISA kit (MMP-13 assay kit; Amersham Biosciences, Little Chalfont, UK). The level of Runx2 expression in chondrocytes was examined by western blotting analysis as described above.

3.5. Statistical Analysis

The results for each experiment were determined from the mean of triplicated experiments. Data were expressed as mean ± standard deviation. For parametric data, the t-test was used to study the significance of differences between two groups. Non-parametric data were analyzed by Mann–Whitney U test. Probability values of <0.05 were considered statistically significant.

4. Conclusions

In conclusion, our data suggest that the NAD-dependent deacetylase Sirt1 may regulate the osteogenic transcription and chondrocyte hypertrophic factor Runx2 and cartilage matrix degrading enzyme MMP-13 in chondrocytes in OA. Since it has been already demonstrated that Sirt1 activity is influenced by several stresses, including inflammation and oxidative stress, as well as aging, SIRT may participate in the progression of OA. Our study may reveal a novel pathogenic mechanism linking the NAD-dependent deacetylase Sirt1 and its modulation of Runx2 in OA.

Acknowledgments: We would like to thank Megumi Suzuki, S. Mogi, Mayumi Tamaki, Junko Tanaka and Ro Karasawa for excellent technical assistance.

Author Contributions: All authors were involved in drafting the article or revising it critically for important intellectual content, and all authors approved the final version to be published. Koh Terauchi had full access to all of the data in the study and takes responsibility for the integrity of the data and the accuracy of the data analysis. Study conception and design: Koh Terauchi, Hiroto Fujiya, Hisatera Niki, Hiroko Mesha, Kazuo Yudoh, Naoko Yui; Acquisition of data: Koh Terauchi, Hajime Kobayashi, Kazuo Yudoh, Naoko Yui; Analysis and interpretation of data: Kanaka Yatabe, Koh Terauchi, Kazuo Yudoh, Naoko Yui.

Conflicts of Interest: The authors declare no conflict of interest.

Abbreviation

OA	Osteoarthritis
ROS	Reactive oxygen species
PBS	Phosphate-buffered saline
DMEM	Dulbecco's modified Eagle's medium
HEPES	2-[4-(2-hydroxyethyl)-1-piperazine]-ethanesulfonic acid
IL-1β	Interleukin-1β
Runx2	Runt-related transcription factor 2
MMP-13	Matrix metalloproteinase-13

References

1. Loeser, R.F. Molecular mechanisms of cartilage destruction. Mechanics, inflammatory mediators, and aging collide. *Arthritis Rheum.* **2006**, *54*, 1357–1361. [CrossRef] [PubMed]
2. Pelletier, J.P.; Martel-Pelletier, J.; Raynauld, J.P. Most recent developments in strategies to reduce the progression of structural changes in osteoarthritis: Today and tomorrow. *Arthritis Res. Ther.* **2006**, *8*, 206. [CrossRef] [PubMed]
3. Zhang, W.; Nuki, G.; Moskowitz, R.W.; Abramson, S.; Altman, R.D.; Arden, N.K.; Bierma-Zeinstra, S.; Brandt, K.D.; Croft, P.; Doherty, M.; et al. OARSI recommendations for the management of hip and knee osteoarthritis, Part III: Changes in evidence following systematic cumulative update of research published through January 2009. *Osteoarthr. Cartil.* **2010**, *18*, 476–499. [CrossRef] [PubMed]
4. Loeser, R.F.; Carlson, C.S.; Del Carlo, M.; Cole, A. Detection of nitrotyrosine in aging and osteoarthritic cartilage. Correlation of oxidative damage with the presence of interleukin-1β and with chondrocyte resistance to insulin-like growth factor 1. *Arthritis Rheum.* **2002**, *46*, 2349–2357. [CrossRef] [PubMed]
5. Martin, J.A.; Buckwalter, J.A. Aging, articular cartilage chondrocyte senescence and osteoarthritis. *Biogerontology* **2002**, *3*, 257–264. [CrossRef] [PubMed]
6. Martin, J.A.; Buckwalter, J.A. Telomere erosion and senescence in human articular cartilage chondrocytes. *J. Gerontol. A Biol. Sci. Med. Sci.* **2001**, *56*, 172–179. [CrossRef]
7. Martin, J.A.; Buckwalter, J.A. Roles of articular cartilage aging and chondrocyte senescence in the pathogenesis of osteoarthritis. *Iowa Orthop. J.* **2001**, *21*, 1–7. [PubMed]
8. Carlo, M.D., Jr.; Loeser, R.F. Increased oxidative stress with aging reduces chondrocyte survival. Correlation with intracellular glutathione levels. *Arthritis Rheum.* **2003**, *48*, 3419–3430. [CrossRef] [PubMed]
9. Yudoh, K.; Shishido, K.; Murayama, H.; Yano, M.; Matsubayashi, K.; Takeda, H.; Nakamura, H.; Masuko, K.; Kato, T.; Nishioka, K. Water-soluble C60 fullerene prevents degeneration of articular cartilage in osteoarthritis via down-regulation of chondrocyte catabolic activity and inhibition of cartilage degeneration during disease development. *Arthritis Rheum.* **2007**, *56*, 3018–3030. [CrossRef] [PubMed]
10. Kurz, B.; Lemke, A.; Kehn, M.; Domm, C.; Patwari, P.; Frank, E.H.; Grodzinsky, A.J.; Schunke, M. Influence of tissue maturation and antioxidants on the apoptotic response of articular after injurious compression. *Arthritis Rheum.* **2004**, *50*, 123–130. [CrossRef] [PubMed]
11. Kurz, B.; Lemke, A.K.; Fay, J.; Pufe, T.; Grodzinsky, A.J.; Schunke, M. Pathomechanisms of cartilage destruction by mechanical injury. *Ann. Anat.* **2005**, *187*, 473–485. [CrossRef] [PubMed]
12. Chow, D.M.; Nobile, P.C.; Ahuero, J.S.; Birnsali, H.H. Cellular events leading to chondrocyte death after cartilage impact injury. *Arthritis Rheum.* **2006**, *54*, 1509–1517. [CrossRef] [PubMed]
13. Gavrieli, Y.; Sherman, Y.; Ben-Sasson, S.A. Identification of programmed cell death in situ via specific labeling of nuclear DNA fragmentation. *J. Cell Biol.* **1992**, *119*, 493–501. [CrossRef] [PubMed]
14. Sanz, A.; Stefanatos, R.K. The mitochondrial free radical theory of aging: A critical view. *Curr. Aging Sci.* **2008**, *1*, 10–21. [CrossRef] [PubMed]
15. Wątroba, M.; Szukiewicz, D. The role of sirtuins in aging and age-related disease. *Adv. Med. Sci.* **2015**, *61*, 52–62. [CrossRef] [PubMed]
16. Ijima, K. Bone and calcium update: diagnosis and therapy of bone related sin disease update. Regulatory mechanism of mineralization situation (MC) in vascular calcification: impact of vascular smooth muscle cell senescence. *Clin. Calcium* **2011**, *21*, 55–60. [PubMed]

17. Shakibaei, M.; Shayan, P.; Busch, F.; Aldinger, C.; Buhrmann, C.; Lueders, C.; Mobasheri, A. Resveratrol mediated modulation of Sirt-1/Runx2 promotes osteogenic differentiation of mesenchymal stem cells. Potential role of Runx2 deacetylation. *PLoS ONE* 2012, 7, e35712. [CrossRef] [PubMed]
18. Buhrmann, C.; Busch, F.; Shayan, P.; Shakibaei, M. Sirtuin-1 (SIRT1) is required for promoting chondrogenic differentiation of mesenchymal stem cells. *J. Biol. Chem.* 2014, 289, 22048–22062. [CrossRef] [PubMed]
19. Kamekura, S.; Kawasaki, Y.; Hoshi, K.; Shimoaka, T.; Chikuda, H.; Maruyama, Z.; Komori, T.; Sato, S.; Takeda, S.; Karsenty, G.; et al. Contribution of Runx-related transcription factor 2 to the pathogenesis of osteoarthritis in mouse induction of knee joint instability. *Arthritis Rheum.* 2012, 64, 2462–2473. [CrossRef] [PubMed]
20. Wang, X.; Manner, P.A.; Horner, A.; Shum, L.; Tuan, R.S.; Nuckolls, G.H. Regulation of MMP-13 expression by RUNX2 and FGF2 in osteoarthritic cartilage. *Osteoarthr. Cartil.* 2004, 12, 963–973. [CrossRef] [PubMed]
21. Kawaguchi, H. Endochondral ossification signals in cartilage degradation during osteoarthritis progression in experimental mouse models. *Mol. Cells* 2008, 25, 1–6. [PubMed]
22. Dvir-Ginzberg, M.; Gagarina, V.; Lee, E.J.; Hall, D.J. Regulation of cartilage-specific gene expression in human chondrocytes by SirT1 and Nicotinamide Phosphoribosyltransferase. *J. Biol. Chem.* 2008, 283, 36300–36310. [CrossRef] [PubMed]
23. Takayama, K.; Ishida, K.; Matsushita, T.; Fujita, N.; Hayashi, S.; Sasaki, K.; Tei, K.; Kubo, S.; Matsumoto, T.; Fujioka, H.; et al. SirT1 regulation of apoptosis of human chondrocytes. *Arthritis Rheum.* 2009, 60, 2731–2740. [CrossRef] [PubMed]
24. Fujita, N.; Matsushita, T.; Ishida, K.; Kubo, S.; Matsumoto, T.; Takayama, K.; Kurosaka, M.; Kuroda, R. Potential involvement of SIRT1 in the pathogenesis of osteoarthritis through the modulation of chondrocyte gene expressions. *J. Orthop. Res.* 2011, 29, 511–515. [CrossRef] [PubMed]
25. Kur, I.M.J.; Braun, H.J.; Dragoo, J.L. The effect of resveratrol on normal and osteoarthritic chondrocyte metabolism. *Bone Joint Res.* 2014, 10, 51–59. [CrossRef] [PubMed]
26. Yao, N.; Yoshinaka, Y.; Fujiya, H.; Mueller, R.; Beppu, M.; Katesawa, R.; Yudoh, K. The DNA repair enzyme apurinic/apyrimidinic endonuclease (Apex nuclease) 2 has the potential to protect against down-regulation of chondrocyte activity in osteoarthritis. *Int. J. Mol. Sci.* 2014, 15, 14921–14934. [CrossRef] [PubMed]
27. Das-Gupta, E.P.; Lyons, T.J.; Hoyland, J.A.; Lawton, D.M.; Freemont, A.J. New histological observations in spontaneously developing osteoarthritis in the STR/ORT mouse questioning its acceptability as a model of human osteoarthritis. *Int. J. Exp. Pathol.* 1993, 74, 627–634. [PubMed]
28. Mankin, H.J.; Dorfman, H.; Lippiello, L.; Zarins, A. Biochemical and metabolic abnormalities in articular cartilage from osteoarthritis human hips. II. Correlation of morphology with biochemical and metabolic data. *J. Bone Joint Surg. Am.* 1971, 53, 523–537.

© 2016 by the authors; licensee MDPI, Basel, Switzerland. This article is an open access article distributed under the terms and conditions of the Creative Commons Attribution (CC BY) license (http://creativecommons.org/licenses/by/4.0/).

Research Article

International Journal of Clinical Rheumatology

Polyhydroxylated C60 fullerenes prevent chondrocytecatabolicactivityatnanomolar concentrations in osteoarthritis

Aim: Recently, numerous reports have demonstrated that oxidative stress and related chondrocyte aging may participate in the development of osteoarthritis (OA). To further understand the pathogenesis and degenerative process of OA, we have studied water-soluble polyhydroxylated C60 fullerene, a strong free radical scavenger as an anti-oxidant.

Method: We examine the therapeutic effects of five types of water-soluble polyhydroxylated C60 fullerenes (C60(OH)10, C60(OH)24, C60(OH)26, C60(OH)36, C60(OH)44) on OA-related factor-induced catabolic responses in osteoarthritic chondrocytes. In the presence or absence of polyhydroxylated C60 fullerenes (C60(OH)10, C60(OH)24, C60(OH)26, C60(OH)36, C60(OH)44) (0, 10.0 or 100 nM), human osteoarthritic chondrocytes were treated with IL-1β (10.0 ng/ml). After 24 hours incubation, chondrocyte activities were examined.

Results: Water-soluble polyhydroxylated C60 fullerenes inhibited OA-related catabolic responses (IL-1β-upregulation of cartilage-degrading enzyme production and downregulation of proteoglycan production) in OA chondrocytes. C60(OH)10 (C60(OH)24 and C60(OH)26 showed a stronger chondroprotective effect than C60(OH)36 or C60(OH)44.

Conclusion: Our findings indicate that polyhydroxylated C60 fullerenes, especially C60(OH)10, C60(OH)24 and C60(OH)26, may have a part to protect against OA-related factor-induced downregulation of osteoarthritic chondrocyte activities. These data may reveal a novel pathologic mechanism linking oxidative stress-induced development of OA.

Hirotaka Yoshioka[1], Naoko Yui[1], Kanaka Yatabe[1], Hiroto Fujiya[1], Haruki Musha[1], Hisateru Niki[1], Rie Karasawa[1] & Kazuo Yudoh[1*]

[1]Department of Sports Medicine, Kanazawa University School of Medicine, Sugae 2-16-1, Kanazawa, Kanazawa 216-8511, Japan

[2]Department of Orthopaedic Surgery, Shimane University School of Medicine, Sugae 2-16-1, Kanazawa, Kanazawa 216-8511, Japan

[3]Department of Functional Morphology, Institute of Medical Science, Shimane University School of Medicine, Sugae 2-16-1, Kanazawa, Kanazawa 216-8511, Japan

*Author for correspondence
yudoh@med.shimane-u.ac.jp

Keywords osteoarthritis • C60 fullerene • oxidative stress • chondrocytes

Abbreviation: OA: Osteoarthritis; ROS: Reactive Oxygen Species; PBS: Phosphate-Buffered Saline; DMEM: Dulbecco's Modified Eagles Medium; FCS: Fetal Calf Serum; HEPES: 2-[4-(2-hydroxyethyl)-1-piperazinyl] ethanesulfonic acid; IL: Interleukin; MMP-13: Matrix Metalloproteinase-13; ELISA: Enzyme-Linked Immunosorbent Assay

Introduction

Mechanical stress on articular cartilage down-regulates chondrocyte activity and cartilage matrix (review in [1]). Also, it has been reported that mechanical force on articular cartilage stimulates the secretion of matrix degrading enzymes and proinflammatory cytokines from chondrocytes [1,2]. It has been demonstrated that catabolically stressed chondrocytes secrete large amounts of reactive oxygen species (ROS) as well as proinflammatory cytokines (Figure 1) [3-5].

The relation between the production of ROS and the depletion of cellular antioxidants in degenerated articular cartilage tissue has been confirmed by multiple studies. Several reports have already indicated that the cartilage degeneration in osteoarthritis (OA) is mediated by ROS (Figure 1) [1,6,7]. Kurz et al. reported that mechanical force on articular cartilage stimulates excess production of ROS by chondrocytes, facilitating to the degeneration of hyaluronic acid and chondrocyte apoptosis [8]. Green et al. also mentioned that chondrocyte mechanosensitivity is at least partly involved in inducing excess amount of ROS production by chondrocytes in response to mechanical force on cartilage [9]. These studies suggest that mechanical stress-induced ROS produced by chondrocytes may lead to direct damage to chondrocytes and cartilage matrix in OA.

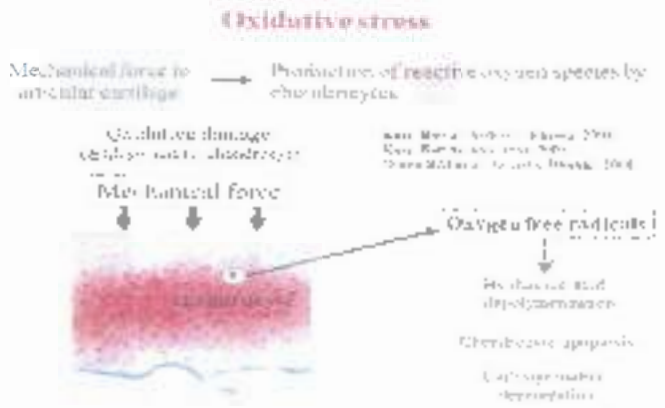

Figure 1: Oxidative stress in osteoarthritis. Numerous reports have demonstrated that chronic excess ROS production by chondrocytes, which is induced by mechanical force on cartilage, plays an important role in the hyaluronic acid depolymerization, chondrocyte apoptotic death and cartilage degeneration that occurs after mechanical injury to cartilage.

Recently, attention has been drawn to the theory that aging reduces the maintenance and homeostatic potential of chondrocytes and articular cartilage matrix [3,10]. Martin et al. examined different surrogate biomarkers of aging in human chondrocytes and demonstrated that chondrocyte aging correlates with the age of the donor [10,11]. They concluded that aged chondrocytes cause an inadequate response to anabolic factors, leading to degradation of the cartilage matrix caused by the imbalance of anabolic and catabolic chondrocyte activities. Chondrocyte aging is thought to mainly participate in oxidative damage in OA articular cartilage. Recent studies also indicated that ROS directly damage repeats of guanines in the telomeric DNA, resulting in ROS-induced telomere shortening [12]. This finding reveals that oxidative stress may cause cellular senescence due to shortening of telomeric DNA. Chondrocyte senescence caused by oxygen free radicals may implicate the oxidative damage in the progression of OA.

Previously, we have already demonstrated that fullerene (C60), an anti-oxidant, can function as a chondroprotective agent against the progression of OA [13]. C60 is a molecule composed entirely of carbon in a unique spherical structure with 30 conjugated double carbon-carbon bonds (Figure 2A) [14,15]. It is known that one C60 molecule can react with at least 34 hydroxyl radicals or 34 methyl radicals to form stable cyclic or non-cyclic adducts and react with oxygen free radicals without being consumed [16]. C60 is known to be the strongest radical scavenger [14-16]. It has been reported that the anti-oxidative potential of C60 is several hundred-fold higher than that of other anti-oxidative agents [13,14,16]. Recently, C60 was shown to inhibit cellular apoptosis by scavenging ROS and to inhibit the degeneration of vertebral disc and articular cartilage, suggesting that C60 has a potential as therapeutic agent to protect against oxidative stress associated pathological features in a variety of diseases. In OA, C60 may be a novel therapeutic agent to prevent both chondrocyte senescence and cartilage matrix degeneration. We have previously confirmed that microconcentrations of C60 in the pM range level (10-100 pM) inhibit the OA related factor-induced production of matrix degrading enzymes and downregulation of cartilage matrix production, as well as chondrocyte aging and apoptosis in vitro. Since C60 is a water soluble factor, we utilized cyclodextrin inclusion C60 [13].

In this study, we examined the therapeutic effects of two types of water soluble polyhydroxylated C60 fullerenes ($C_{60}(OH)_{12}$, $C_{60}(OH)_{24}$, $C_{60}(OH)_{36}$, $C_{60}(OH)_{44}$) on OA related factor-induced catabolic responses in osteoarthritic chondrocytes (Figure 2B). We have demonstrated that water soluble polyhydroxylated C60 fullerenes inhibit the OA-related catabolic reactions (upregulated production of matrix metalloproteinase (MMP)-13, downregulated production of proteoglycan) in chondrocytes at 1000-fold lower concentrations (nM order) than those of other C60 fullerenes (μM order) that had previously been reported to have a protective effect [13]. Our study indicates that polyhydroxylated C60 may have a role in protecting against the

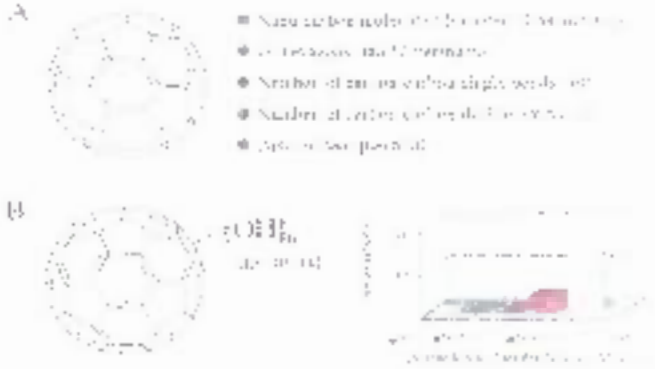

Figure 2: Polyhydroxylated C60. A. The C60 surface consists of 20 hexagons and 12 pentagons, and has 60 carbon–carbon single bonds and 30 carbon–carbon double bonds. The molecule's redox dual property is based on the fact that fullerene possesses a large number of conjugated carbon–carbon double bonds. B. The water solubility of polyhydroxylated C60 depends on the number of hydroxyl groups, such as $C_{60}(OH)_{24}$ (Yamakoshi [17])

OA-related tissue-accelerated development of articular cartilage degradation.

Materials & methods

Chondrocyte isolation and cell culture

Human articular cartilage samples were obtained from bone and cartilage tissues during arthroplasty knee surgery (n=21: 1 female, 81 years of age; 1 male, 84 years of age) after obtaining informed consent from the patients with OA. Chondrocytes were isolated and cultured in Dulbecco's modified Eagle's medium (DMEM, Sigma, St. Louis, MO, USA) with 10% heat-inactivated fetal calf serum (FCS), 2 mM L-glutamine, 25 mM HEPES (2,4-(2-hydroxyethyl) piperazinyl) ethane sulfonic acid), and 100 U/ml penicillin and streptomycin at 37°C in a humidified atmosphere of 95% air and 5% CO_2 as previously reported [18].

Measurement of anabolic and catabolic activities of chondrocytes

Cultured chondrocytes were seeded and cultured into 10 cm culture dishes (BD Biosciences, Franklin Lakes, NJ, USA) at approximately 2.0×10^6 cells per dish and incubated in DMEM with 10% FCS in the presence or absence of IL-1β (0.5 ng/ml, R&D Systems Inc., Minneapolis, MN, USA) or $C_{60}(OH)_{24}$, $C_{60}(OH)_{18}$, $C_{60}(OH)_{12}$, $C_{60}(OH)_{6}$ or $C_{60}(OH)_{0}$ (0.1, 2.0, 10.0 or 100.0 μM, from Vitamin C60 Inc., Tokyo, Japan). We obtained two types of $C_{60}(OH)_{24}$ in this study (a) 37°C in a humidified atmosphere of 95% air and 5% CO_2. After 24-hour incubation period, the culture conditioned medium was collected from each dish and stored at -80°C until analysis.

To study the effect of water-soluble polyhydroxylated C60 on anabolic activity of chondrocytes, the levels of proteoglycan production by chondrocytes were analyzed using an enzyme-linked immunosorbent assay (ELISA) kit in accordance with the manufacturer's protocol (GAG Assay Kit, Chondrex Assays S.A., Nivelles, Belgium). To analyze the catabolic activity of chondrocytes, levels of MMP-13 production from chondrocytes were measured using an ELISA kit (R&D Systems Inc., Minneapolis, MN, USA). Results from each experiment were determined from the mean of triplicate wells.

Statistical analysis

Data are expressed as means ± standard deviation. A two-tailed Student's t-test was used to examine the statistical significant differences between two groups. Analysis of variance was used for comparisons of more than two groups, and differences between two groups within the set were analyzed by a Fisher's protected least significant difference test. Probability values of <0.05 were considered statistically significant.

Results

Inhibitory effects of polyhydroxylated C60 on the IL-1β-mediated production of the cartilage matrix degrading enzyme, MMP-13, in chondrocytes

In Figure 3, production of MMP-13 by human microvascular chondrocytes showed

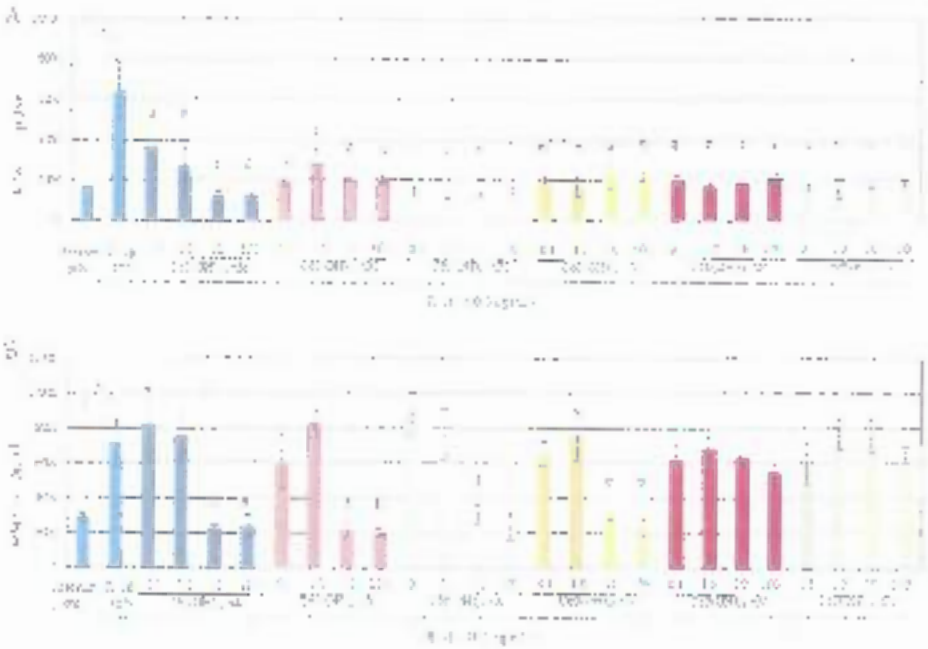

Figure 3: Effects of polyhydroxylated C60 on the production of MMP-13 in chondrocytes. Mean concentration of MMP-13 produced by chondrocytes was significantly higher in the IL-1β-treated group than in the control group (81 years old female: P=0.029, 84 years old male: P=0.037, 0.181 years old female). Even in the presence of IL-1β, treatment with polyhydroxylated C60 tended to decrease the mean concentration of MMP-13 produced by chondrocytes (statistical significances to the IL-1β-treated group: a P=0.066, b P=0.0281, c P=0.023, d P=0.025, e P=0.029, f P=0.046, g P=0.034, h P=0.0350, i P=0.025, j P=0.024, k P=0.034, l P=0.023, m P=0.021, n P=0.0206, o P=0.021, p P=0.033, q P=0.0251, r P=0.0275, s P=0.0350, t P=0.0291, u P=0.025, v P=0.018, w P=0.0281, x P=0.0301). (84 years old male) Treatment with C60(OH)10, C60(OH)24 and C60(OH)36 significantly inhibited the IL-1β-induced production of MMP-13 at the concentration of 10.0 and 100.0 nM, whereas C60(OH)36 and C60(OH)44 did not show the inhibitory effect on the IL-1β-accelerated production of MMP-13 in OA chondrocytes (statistical significances to the IL-1β-treated group: a P=0.021, b P=0.013, c P=0.014, d P=0.016, e P=0.022, f P=0.010, g P=0.030, h P=0.015).

higher in the IL-1β-treated group (IL-1β 10.0 ng/mL) than in the control. IL-1β significantly stimulated MMP-13 production by chondrocytes (81 years old female: P=0.012, 84 years old male: P=0.027). IL-1β is considered to an OA-induced catabolic cytokine that closely participate in the progression of OA, for example, in the acceleration of cartilage degrading enzyme production from chondrocytes [14–16]. Our data were consistent with previous reports.

Interestingly, there was a tendency to decrease the production of MMP-13 by chondrocytes that were treated with polyhydroxylated C60 even in the presence of IL-1β (10.0 ng/mL). In OA chondrocytes from 81 years old female, treatment with each polyhydroxylated C60 ($C_{60}(OH)_{10}$, $C_{60}(OH)_{24}$, $C_{60}(OH)_{36}$, $C_{60}(OH)_{44}$, $C_{60}(OH)_{52}$) significantly inhibited the IL-1β-accelerated production of MMP-13 in the same concentration region (Figure 3A). In OA chondrocytes from 84 years old male, $C_{60}(OH)_{10}$, $C_{60}(OH)_{24}$ and $C_{60}(OH)_{52}$ significantly inhibited the IL-1β-induced production of MMP-13 at the concentration of 10.0 and 100.0 nM, whereas treatment with $C_{60}(OH)_{36}$ and $C_{60}(OH)_{44}$ did not show their inhibitory effect on the IL-1β induced MMP-13 production by OA chondrocytes (Figure 3B). These findings indicate that $C_{60}(OH)_{10}$, $C_{60}(OH)_{24}$ and $C_{60}(OH)_{52}$ but not $C_{60}(OH)_{36}$ or $C_{60}(OH)_{44}$ have the IL-1β stimulated production of MMP-13 in OA chondrocytes.

Effect of polyhydroxylated C60 on chondrocyte production of articular proteoglycan

Figure 4 shows the production levels of proteoglycan, which is the articular cartilage matrix component, by chondrocytes tended to increase in the presence of IL-1β (10.0 ng/mL) compared to the control (81 years old female: P=0.0018, 84 years old male: P=0.0162). In contrast, in OA chondrocytes from

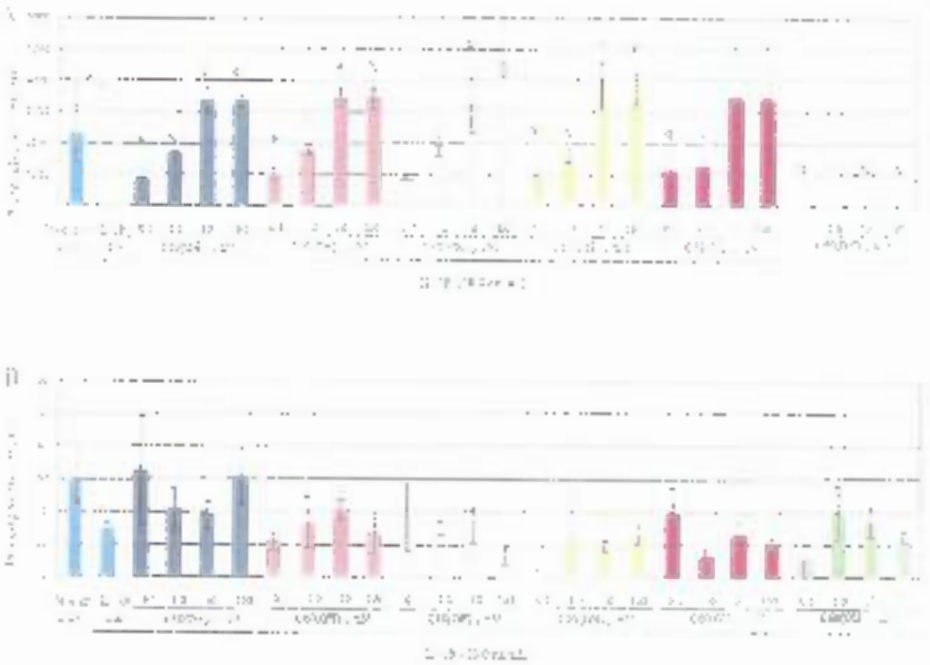

Figure 4: Effect of polyhydroxylated C60 on chondrocyte production of articular proteoglycan. IL-1β lowered the production of proteoglycan from chondrocytes (81 years old female, *P=0.048; 84 years old male, P=0.[illegible]). However, treatment with polyhydroxylated C60, but not C60(OH)44, tended to maintain the proteoglycan production from chondrocytes. At 81 years old female, even in the presence of IL-1β, treatment with polyhydroxylated C60 [illegible] the production of proteoglycan by chondrocytes (statistical significances versus IL-1β treated group: a (P=0.0[illegible]), b (P=0.015), c (P=0.050), d (P=0.0[illegible]), e (P=0.014), f (P=0.043), g (P=0.022), h (P=0.033), i (P=0.017), j (P=0.041), k (P=0.024), l (P=0.011), m (P=0.035), n (P=0.033), o (P=0.015), p (P=0.03[illegible]), q (P=0.011), r (P=0.038), s (P=0.038), t (P=0.038), u (P=0.22[illegible]), v (P=0.036), w (P=0.900), x (P=0.056). In 84 years old male, treatment with polyhydroxylated C60 did not show the protective effect on the IL-1β-decreased production of proteoglycan by chondrocytes.

81 years old female, treatment with $C_{60}(OH)_{18}$, $C_{60}(OH)_{24}$, $C_{60}(OH)_{44}$ and $C_{60}(OH)_{18}$, but not $C_{60}(OH)_{44}$, significantly increased the proteoglycan production from chondrocytes even in the presence of IL-1β (Figure 4A). These findings indicate that polyhydroxylated C60 may have a part to protect against the IL-1β-induced downregulation of proteoglycan production in OA. In OA chondrocytes from 84 years old male, treatment with polyhydroxylated C60 did not show the protective effect on the production of proteoglycan by chondrocytes (Figure 4B).

Discussion

In the present study, our findings indicate that C60 hydroxides inhibit OA-induced catabolic responses (IL-1β-induced production of MMP-13, IL-1β-induced downregulation of proteoglycan production by OA chondrocytes). $C_{60}(OH)_{18}$, $C_{60}(OH)_{24}$ and $C_{60}(OH)_{18}$ showed a stronger chondroprotective effect than $C_{60}(OH)_{44}$ or $C_{60}(OH)_{54}$. These findings suggest that C60 fullerene hydroxides, especially $C_{60}(OH)_{18}$, $C_{60}(OH)_{24}$, and $C_{60}(OH)_{18}$, may have the potential to inhibit the catabolic factor-induced downregulation of chondrocyte activity in OA. These data shed light on novel pathological mechanisms explaining the oxidant-mediated degeneration of articular cartilage.

The C60 surface consists of 20 hexagons and 12 pentagons, and has 60 carbon–carbon single bonds and 30 carbon–carbon double bonds (Figure 2A) [16]. All carbon–carbon double bonds are conjugated. The molecule's antioxidant property is based on the fact that fullerenes possess a large number of conjugated carbon–carbon double bonds which can readily take up an electron, making an attack on radical species highly possible [14-16]. It has been reported that up to 34 radical radicals have been added onto a single C60 molecule [16]. The antioxidant potential is thought to depend on the number of carbon–carbon double bonds in a C60 fullerene [16]. Reducing the number of carbon–carbon double bonds with a concurrent increase of hydroxyl groups such as $C_{60}(OH)_n$ may lead to a reduction

of the antioxidant potential of polyhydroxylated C60 fullerene. Our data also lend support that the chondroprotective potential would be a reflection of the antioxidant potential of $C_{60}(OH)_{24}$ and $C_{60}(OH)_{22}$ were lower than that of $C_{60}(OH)_{18}$, $C_{60}(OH)_{20}$, and $C_{60}(OH)_{16}$.

The water solubility of polyhydroxylated C60 fullerenes is also thought to depend on the number of hydroxyl groups (such as $-ONa$) they contain (figure 1B) [17,19]. A previous report demonstrated that, in contrast to antioxidant potency, an increase in the number of hydroxyl groups of polyhydroxylated C60 fullerenes can improve their water solubility [17]. We also investigated the actual state of dissolved, powdered polyhydroxylated C60. The hydrophilic potential of C60 was lower in $C_{60}(OH)_{18}$ and $C_{60}(OH)_{20}$ than in $C_{60}(OH)_{16}$, or $C_{60}(OH)_{22}$ (data not shown). In addition, we have also found that $C_{60}(OH)_{16}$ helped more readily in comparison with $C_{60}(OH)_{18}$. It has been suggested that fullerenes with fewer than 12 hydroxyl groups have poor water solubility [20-22]. When C60 is derivatized to polyhydroxylated C60, they become water soluble enabling them to cross the cell membrane and reside in the mitochondria, generating oxygen free radicals [23,24].

It is well known that C60 can react with many superoxides without being consumed. It is now thought that C60 may react with ROS as a catalytic substrate without metabolic degradation. C60 has been considered as an anti-oxidant and C60 was shown to inhibit cellular apoptosis by scavenging ROS, suggesting that C60 is a useful agent to protect against oxygen free radical-induced pathological features in a variety of diseases [25-27]. These findings suggest that C60, as a strong anti-oxidant, may influence the cellular microenvironment as a cytoprotectant. The intracellular amounts of C60 may be quantified by high performance liquid chromatography (HPLC). Recently, Asai et al. demonstrated that the C60 amounts in fibroblasts cell line, HT1080 cells, gradually increased and reached the peak after 6 hours of incubation [15]. The C60 fullerene amounts in normal fibroblasts reached the peak after 6 hours of incubation. However, in other cell lines and human somatic cells, the level of intracellular uptake of C60 still remains unknown. We are now planning to analyse the level of intracellular uptake of C60 from chondrocytes by HPLC method.

We think that further studies are required to verify the different mechanisms in chondrocytes originating from osteoarthritic cartilage underlying the biological response to various OA-related catabolic factors (such as mechanical stress and proinflammatory cytokines) as compared with chondrocytes from normal cartilage. Thus, we have been studying some experiments using isolated chondrocytes isolated from degenerated articular cartilages from OA patients who underwent the arthroplasty surgery. In the present study, we have used human osteoarthritic chondrocytes from OA patients and have analyzed the effect of polyhydroxylated C60 fullerenes on chondrocyte activities in vitro. However, during the pre-treatment and culture to gain efficient chondrocyte population for experiments, chondrocytes easily lose the chondrocyte phenotype and hypertrophic differentiation. Thus, in the current study, we made a rule to use primary chondrocytes within 3 passages from the point of view of cell source, since it is difficult to obtain efficient chondrocyte population, we think that primary cultured chondrocytes are useful for experiments requiring numerous number of chondrocytes. Therefore, we are now planning the study using the immortalized chondrocytes.

Conclusion

Further studies are needed to verify the precise effects of polyhydroxylated C60 on chondrocyte activities in OA. Our results reported here demonstrate that water soluble polyhydroxylated C60 can function as a chondroprotective agent against the OA-related catabolic factor mediated developments of OA.

Acknowledgements

We would like to thank M. Suzuki, S. Mogi, M. Tatsuki and T. Tatsuki for excellent technical assistance.

References

1. Hunter T.F., Fridovich I., Pizzo S.V. The role of reactive oxygen species in the degeneration of articular cartilage. Osteoarthritis Cartilage 11, 56-65 (2003).
2. Del Carlo M., Loeser R.F. Increased oxidative stress mediated by nitric oxide in response to fibronectin fragments: involvement of PKC beta and JNK. J. Biochem. Cell. Biol. 35, 1565-1573 (2003).
3. Loeser R.F., Carlson C.S., Del Carlo M., Cole A. Detection of nitrotyrosine in aging and osteoarthritis cartilage. Correlation of oxidation and nitration with chronological age and severity of disease. Arthritis Rheum. 46, 2349-2357 (2002).
4. Del Carlo M.R., Loeser R.F. Nitric oxide-induced chondrocyte death requires the generation of additional reactive oxygen species. Arthritis Rheum. 46, [illegible]

[illegible]

[illegible]

[illegible]

Available online at http://www.journalijdr.com

IJDR

International Journal of DEVELOPMENT RESEARCH

ISSN: 2230-9926

International Journal of Development Research
Vol. 07, Issue, 04, pp.12450-12454, April, 2017

Full Length Research Article

THERAPEUTIC POTENTIAL OF NANOCARBON C60 FULLERENE IN OSTEOARTHRITIS

[1,*]Kazuo Yudoh, [2]Hirotaka Yoshinka, [2]Naoko Yui and [1]Rie Karasawa

[1]Department of Frontier medicine, Institute of Medical Science, St. Marianna University School of Medicine, Japan
[2]Department of Sports Medicine, St. Marianna University School of Medicine, Japan

ARTICLE INFO

Article History:

Received 13th January, 2017
Received in revised form
24th February, 2017
Accepted 22nd March, 2017
Published online 30th April, 2017

Key Words:

Fullerene, Reactive oxygen species,
Oxidative stress,
DNA oxidative damage,
DNA repair enzyme,
Osteoarthritis

ABSTRACT

In osteoarthritis (OA), mechanical stress on articular cartilage stimulates to produce excess amounts of reactive oxygen species (ROS). Studies have provided ample confirmation of the generation of ROS and the depletion of cellular antioxidants in degenerated articular cartilage. 8-Oxoguanine, an oxidized form of guanine, is produced by ROS in DNA. 8-oxoguanine is thought to be a major causative lesion for mutagenesis by ROS, since it can form a stable base pair with adenine as well as with cytosine during DNA replication. 8-Oxoguanine causes A:T to C:G and G:C to T:A transversion mutations. 8-Oxoguanine DNA glycosylase (Ogg1) repairs 8-oxoguanine. In the mitochondria, Ogg1 can protect against activation of the intrinsic apoptotic pathway in response to oxidative stress by augmenting DNA repair in a variety of cells. However, it still remains unclear whether the accumulation of 8-oxoguanine in the cells participates in the pathogenesis of oxidative stress-induced diseases such as OA. Recent reports demonstrated that an increase in 8-oxoguanine and a decrease in Ogg1 were observed in degenerated neural cells compared with normal neural cells in neurodegenerative diseases. We also observed that OA-related catabolic factor induced over expression of 8-oxoguanine and down regulation of Ogg1 in chondrocytes. In the previous studies, we have focused on nanocarbon molecule, fullerene (C60), which acts a strong free radical scavenger, as an anti-oxidant, to prevent the degeneration of articular cartilage. We have demonstrated that C60 has a potential as a protective agent against the degeneration of articular cartilage both in vitro and in vivo OA models. We also found that C60 increased the expressions of DNA repair enzyme Ogg1 in OA chondrocytes. From the results of previous reports, C60 may have a therapeutic potential, as a nanomedicine, to protect against the oxidative stress-induced diseases, through the mechanism involving the acceleration of expression of DNA repair enzyme Ogg1.

Copyright©2017, Kazuo Yudoh et al. This is an open access article distributed under the Creative Commons Attribution License, which permits unrestricted use, distribution, and reproduction in any medium, provided the original work is properly cited.

INTRODUCTION

In osteoarthritis (OA), mechanical and chemical stresses to articular cartilage change the chondrocyte activity and induce the production of OA-related catabolic factors such as proinflammatory cytokines (DelCarlo, 2006; Loeser, 2006; Vaamonde-Garcia *et al.*, 2012). There is a general consensus that chondrocytes produce excess amounts of reactive oxygen species (ROS), comprising superoxide, nitric oxide, hydrogen peroxide and peroxynitrite in response to mechanical force to articular cartilage (Figure 1). Numerous studies have already demonstrated that the degeneration of articular cartilage is partially mediated by oxygen free radicals (Kurz *et al.*, 2004; Kurz *et al.*, 2005; Green *et al.*, 2006).

It has been demonstrated that mechanical force on articular cartilage is sufficient to induce the ROS production by chondrocytes, leading to depolymerization of hyaluronic acid and and chondrocyte apoptotic death (Kurz *et al.*, 2004; Kurz *et al.*, 2005). Other report indicated that chondrocyte death is accelerated by the induction of ROS production by chondrocytes during the mechanical stress to cartilage (Green *et al.*, 2006). These findings clearly indicate that chronic excess ROS production by chondrocytes, which is induced by mechanical force to cartilage, plays an important role in the articular cartilage degeneration. In OA, mechanical stress-induced production of ROS may cause the direct damage to chondrocytes and the cartilage matrix, resulting in the articular cartilage degeneration. The aim of this review is to discuss the pathogenesis of oxidative stress-induced disease and the therapeutic potential of nanocarbon molecule, fullerene, as an anti-oxidative agent in OA (Figure 1).

*Corresponding author: Kazuo Yudoh,
[1]Department of Frontier medicine, Institute of Medical Science, St. Marianna University School of Medicine, Japan

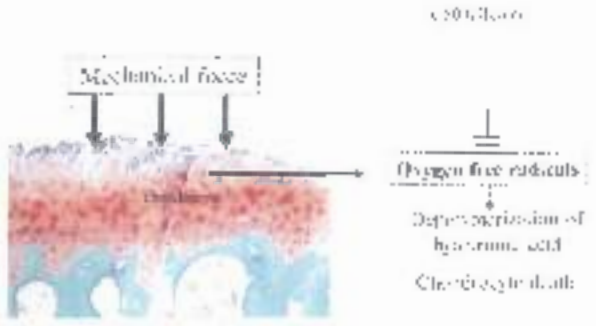

Figure 1. Mechanical stress and oxidative stress in osteoarthritis

DISCUSSION

Fullerene (C60) is known as carbon molecules with a unique cage structure, which is characterized as a strong radical sponge (Krusic *et al.*, 1991). The fullerene's antioxidant property is based on the fact that C60 possesses a large number of conjugated carbon carbon double bonds that can hold an electron, as a free radical scavenger (Krusic *et al.*, 1991, Barky *et al.*, 2007). It has been reported that the antioxidant level of C60 is several hundred-fold higher than that of other antioxidants, such as vitamin C, catalase, and super oxidase dismutase (Liu *et al.*, 2014). Recently, it is suggested that C60 is a therapeutically useful agent to protect against the oxygen free radical-induced pathological features in a variety of diseases. We postulated that C60 fullerene could lead to the development of novel therapeutic strategies in the prevention of cartilage degeneration. We previously demonstrated that water soluble fullerene can function as a protective agent against catabolic stress-induced degeneration of articular cartilage in vitro and in vivo (Yudoh *et al.*, 2007). We confirm that C60 inhibits articular cartilage degeneration in the OA rabbit model (Figure 2).

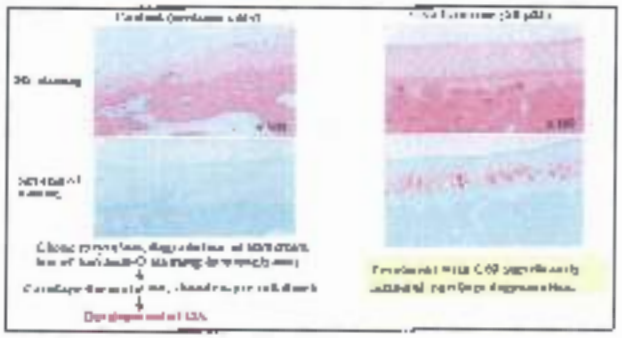

Figure 2. Therapeutic effect of C60 on cartilage degeneration in OA model rabbits

We also compared the therapeutic effect of C60 on cartilage degeneration with that of hyaluronic acid, which is widely used for OA treatment and shows high viscosity and retains moisture, and has lubricating, sealing, and joint protecting functions, in the OA rabbit model (unpublished data). In vitro study, we also examined the effect of C60 on production of cartilage matrix degrading enzymes and production of cartilage matrix components, proteoglycan and type II collagen, in chondrocytes. In addition to the anti-OA effect, we confirmed the anti-inflammatory and anti-bone destructive effects by C60 in our previous studies (Yudoh *et al.*, 2009; Yudoh *et al.*, 2009) (Figure 3).

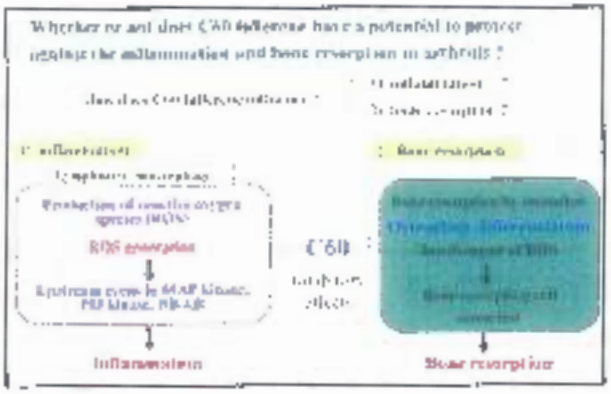

Figure 3. Inhibitory effects of C60 on inflammation and bone resorption

It has been demonstrated that ROS may play a crucial role in inflammation and osteoclast differentiation as a signaling messenger. Therefore, we confirmed that C60 may inhibit the inflammation and differentiation of osteoclasts, resulting in the reduction of inflammatory arthritis and bone destruction in arthritis (Yudoh *et al.*, 2009; Yudoh *et al.*, 2009). While previous studies have provided ample confirmation of ROS generation in OA cartilage, the depletion of cellular antioxidants in degenerated articular cartilage still remains unclear (Figure 4).

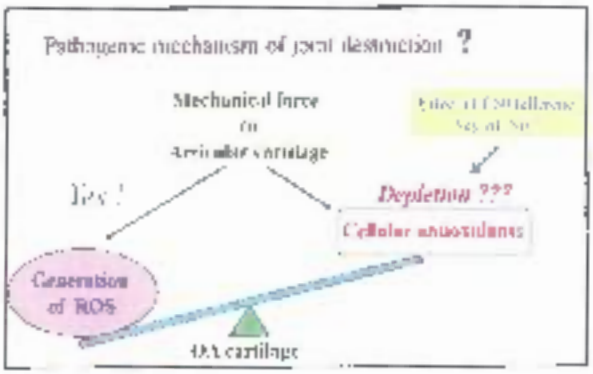

Figure 4. Depletion of cellular antioxidants in osteoarthritic chondrocytes

We have been studying the molecular mechanism of anti-OA effect by C60 from the point of view of DNA oxidative damage and its repair enzyme. It has been reported that large amounts of an oxidized form of guanine, 8-oxo-7,8-dihydroxyguanine (8-oxoguanine), are produced by ROS in DNA (13). This oxidized form of guanine is a causative lesion for mutagenesis by ROS, since it can form a stable base pair with adenine as well as cytosine during DNA replication. 8-Oxoguanine can cause A:T to C:G and G:C to T:A transversion mutations (Figure 5).

These mutations are thought to be involved in the pathogenesis of a variety of malignant diseases and degenerative diseases (Damsma, 2009; Park *et al.*, 2009). 8-Oxoguanine is reported to be repaired by 8-oxoguanine DNA glycosylase (Ogg1), an enzyme that recognises and hydrolyses the aberrant base in the DNA backbone (Yoon *et al.*, 2007). In mitochondria, Ogg1 can protect against activation of the intrinsic apoptotic pathway in response to oxidative stress by augmenting DNA repair in a variety of cells. Kikuchi *et al.* demonstrated that the 8-oxoguanine levels in large motor neurons in the spinal cord were increased in patients with amyotrophic lateral sclerosis.

and subarachnoid haemorrhage, accompanied by lower expression of Ogg1 as the DNA repair enzyme for 8-oxoguanine (Kikuchi *et al.*, 2002). These findings further suggest that impairment of mitochondrial DNA repair enzymes against the accumulation of 8-oxoguanine is involved in the pathogenesis of oxidative stress-induced diseases, such as neural degenerative diseases (Figure 5).

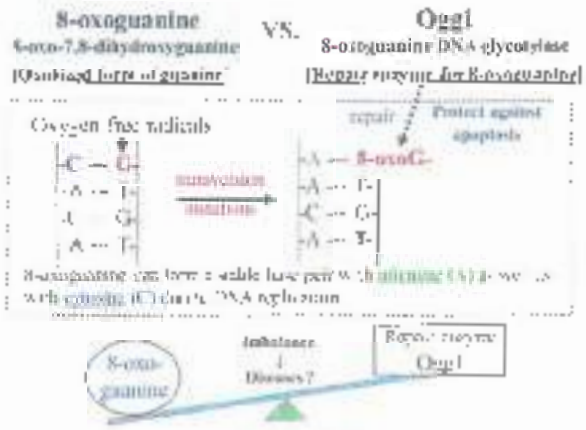

Figure 5. 8-Oxoguanine and 8-oxoguanine DNA glycosylase (Ogg1) in oxidative stress-induced diseases

Our recent study histologically identified that an increase in 8-oxoguanine and a decrease in Ogg1 were observed in OA chondrocytes compared with normal chondrocytes in human articular cartilage (unpublished data, Figure 6) Naoko Yui *et al.*, 2016)

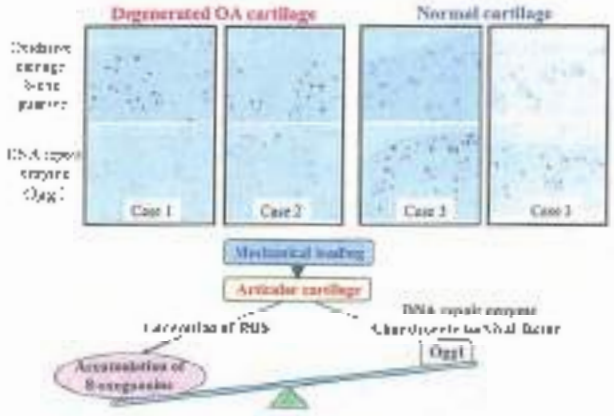

Figure 6. Impairment of the DNA repair enzyme (Ogg1) against the accumulation of oxidized guanine (8-oxoguanine) in human articular cartilage

In addition, OA cartilage showed the impairment of DNA repair enzyme Ogg1 against the accumulation of DNA oxidative damage (8-oxoguanine) in chondrocytes. These findings suggest that Ogg1 may not repair the damage effectively, which may lead to a loss of normal chondrocytes in OA. Interestingly, we have found that OA-related catabolic factor [interleukin-1beta] induced down-regulation of Ogg1 in chondrocytes. Interestingly, even in the presence of catabolic pressure, expression of Ogg1 was maintained by treatment with C60. Furthermore, our study reveals that Ogg1 silencing using small interfering RNA can reduce chondrocyte activity (production of cartilage matrix: proteoglycan and type II collagen from cells) in OA chondrocytes. In contrast, C60 maintained the chondrocyte activity even in Ogg1 deficient chondrocytes.

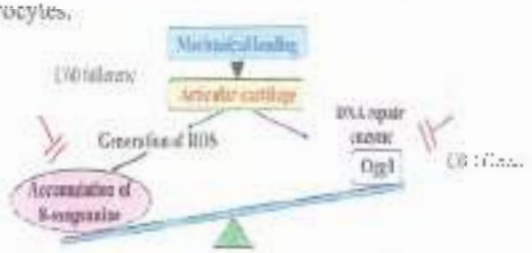

These findings suggest that the induction of Ogg1 by C60 may protect cellular activity and cell death against the catabolic factor in OA (unpublished data, paper preparing).

Conclusion

- Our recent study suggests that the impairment of DNA repair enzyme Ogg1 against the accumulation of DNA oxidative damage (8-oxoguanine) in OA chondrocytes may be involved in the pathogenesis of OA.
- C60 fullerene may have a potential to activate the expression of DNA repair enzyme Ogg1 against the OA-related catabolic factors in OA chondrocytes in addition to the potential of anti-oxidant (oxygen free radical scavenger).

Acknowledgements

We would like to thank M.Tanaka, M Suzuki, and T.Mogi for excellent technical assistance.

Conflict of Interest

All authors declare that they have no competing interests

REFERENCES

Bakry, R., Vallant, R.M., Najam-ul-Haq, M., Rainer, M., Szabo, Z. *et al.* 2007. Medicinal applications of fullerenes. Int J Nanomed. 2: 639–649.

Dantsma, G.E., Cramer, P. 2009. Molecular basis of transcriptional mutagenesis at 8-oxoguanine. J Biol Chem. 284(46):31658-31667.

DelCasto, M., Loeser, R.F. 2006. Chondrocyte cell death mediated by reactive oxygen species-dependent activation of PKC-beta. Am J Physiol Cell Physiol. 290: 802-811.

Green, D.M., Noble, P.C., Ahuero, J.S., Birdsall, H.H. 2006. Cellular events leading to chondrocyte death after cartilage impact injury. Arthritis Rheum. 54:1509-1517.

Kikuchi, H., Furuta, A., Nishioka, K., Suzuki, S.O., Nakabeppu, Y. *et al.* 2002. Impairment of mitochondrial DNA repair enzymes against accumulation of 8-oxoguanine in the spinal motor neurons of amyotrophic lateral sclerosis. Acta Neuropathol. 103(4):408-414.

Krusic, P.J., Wasserman, E., Keizer, P.N., Morton, J.R., Preston, K.F. 1991. Radical reactions of C60. Science. 254: 1183–1185.

Kurz, B., Lemke, A., Kehn, M., Domm, C., Patwari, P. *et al.* 2004. Influence of tissue maturation and antioxidants on the apoptotic response of articular after injurious compression. Arthritis Rheum. 50(1):123-130.

Kurz, B., Lemke, A.K., Fay, J., Pufe, T., Grodzinsky, A.J. *et al.* 2005. Pathomechanisms of cartilage destruction by mechanical injury. Ann Anat. 187:473–485.

Liu, Q., Cui, Q., Li, X.J., Jin, L. 2014. The applications of buckminsterfullerene C60 and derivatives in orthopaedic research. Connect Tissue Res. 55(2): 71-79.

Loeser, R.F. 2006. Molecular mechanisms of cartilage destruction: mechanics, inflammatory mediators, and aging collide. Arthritis Rheum. 54:1357-1360.

Naoko Yui, Kazuo Yudoh, Hiroto Figiya, Haruki Mosha. 2014. Mechanical and Oxidative stress in osteoarthritis. *J Phys Fitness Sports Med.*, 5(1):81-86.

Park, M.J., Park, J.H., Hahn, S.H., Ko, S.L., Lee, Y.R. *et al.* 2009. Repair activities of human 8-oxoguanine DNA glycosylase are stimulated by the interaction with human checkpoint sensor Rad9-Rad1-Hus1 complex. DNA Repair (Amst) 8(10):1190-200.

Vasamonde-Garcia, C., Riveiro-Naveira, R.R., Valcárcel-Ares M.N., Hermida-Carballo, L., Blanco, F.J. *et al.* 2012. Mitochondrial dysfunction increases inflammatory responsiveness to cytokines in normal human chondrocytes. Arthritis Rheum. 64(9): 2927-2936.

Yeon, C.K., Song, P.I., Kim, M.H., Kim, J.S., Hyun, J.W. *et al.* 2007. Human 8-oxoguanine DNA glycosylase suppresses the oxidative stress induced apoptosis through a p53-mediated signaling pathway in human fibroblasts. *Mol Cancer Res.* 5(10):1053-98.

Yudoh, K., Karasawa, R., Masuko, K., Kato, T. 2009. Water-soluble fullerene (C60) inhibits the development of arthritis in the rat model of arthritis. Int J Nanomed. 4:217-225.

Yudoh, K., Karasawa, R., Masuko, K., Kato, T. 2009. Water-soluble fullerene(C60) inhibits the osteoclast differentiation and bone destruction in arthritis. Int J Nanomed. 4:233-239.

Yudoh, K., Shishido, K., Murayama, H., Yano, M., Matsubayashi, K. *et al.* 2007. Water-soluble C60 fullerene prevents degeneration of articular cartilage in osteoarthritis via down-regulation of chondrocyte catabolic activity and inhibition of cartilage degeneration during disease development. Arthritis Rheum. 56(10): 3307-3318.

****

Journal of Arthritis

Kobayashi et al., J Arthritis 2017, 6:2
DOI: 10.4172/2167-7921.1000238

Research Article OMICS International

The Nicotinamide Adenine Dinucleotide (NAD)-Dependent Deacetylase Sirtuin-1 Regulates Chondrocyte Energy Metabolism through the Modulation of Adenosine Monophosphate-Activated Protein Kinase (AMPK) in Osteoarthritis (OA)

Hajime Kobayashi[1], Koh Terauchi[1], Naoko Yui[1], Kanako Yatabe[1], Toshikazu Kamada[2], Hiroto Fujiya[3], Hisakeru Niki[3], Haruki Nisha[4] and Kazuo Yudoh[5]*

[1]Department of Sports Medicine, St. Marianna University School of Medicine, Kawasaki, Japan

[2]Department of Orthopedic Surgery and Rheumatology, Hara Orthopedic Hospital, Tokyo, Japan

[3]Department of Orthopedic Surgery, St. Marianna University School of Medicine, Kawasaki, Japan

[4]Department of Practice Medicine, Institute of Medical Science, St. Marianna University School of Medicine, Kawasaki, Japan

*Corresponding author: Kazuo Yudoh, MD, PhD, Department of Practice Medicine, Institute of Medical Science, St. Marianna University School of Medicine, Sugao 2-16-1, Miyamae-ku, Kawasaki City 216-8511, Japan, Tel: +81-44-977-8111 (ext. 4029); Fax: +81-44-978-3006, E-mail: yudo@marianna-u.ac.jp

Received date: April 11, 2017, Accepted date: April 24, 2017, Published date: April 26, 2017

Copyright: © 2017 Kobayashi H, et al. This is an open-access article distributed under the terms of the Creative Commons Attribution License, which permits unrestricted use, distribution, and reproduction in any medium, provided the original author and source are credited.

Abstract

To clarify how the osteoarthritis (OA)-induced catabolic factor interleukin (IL)-1β affects chondrocyte energy metabolism, and especially to define the downstream pathway linking nicotinamide adenine dinucleotide (NAD)-dependent deacetylase Sirtuin-1 (Sirt-1) to energy metabolism in OA chondrocytes. Human chondrocytes were isolated from articular cartilage samples of patients with OA. The level of energy metabolism of OA chondrocytes was evaluated by monitoring the activity of the energy metabolic sensor, adenosine monophosphate-activated protein kinase (AMPK) and the level of production of adenosine triphosphate (ATP) in chondrocytes in the presence or absence of IL-1β (10 ng/mL). Effects of IL-1β on anabolic and catabolic activities of chondrocytes were analyzed by the levels of production of proteoglycan and matrix metalloproteinase (MMP)-13, respectively. Experiments involving pre-treatment with Sirt-1 inhibitor were also performed to investigate the underlying regulatory mechanism linking Sirt-1 in chondrocyte energy metabolism. IL-1β significantly inhibited the activity of AMPK and production of ATP in OA chondrocytes. The energy metabolism disruption mediated by IL-1β was further decreased by pre-treatment with Sirt-1 inhibitor in OA chondrocytes. Treatment with IL-1β significantly decreased the level of proteoglycan production and significantly increased the level of MMP-13 secretion by chondrocytes. These chondrocyte activities were also reduced by pre-treatment with the Sirt-1 inhibitor in OA chondrocytes. IL-1β inhibits the AMPK - ATP energy metabolic pathway in OA chondrocytes. Our findings also suggest that Sirt-1 activity is involved in anabolic and catabolic cellular activities and that Sirt-1 modulates ATP production through functional regulation of the energy sensor AMPK in chondrocytes.

Keywords: Energy metabolism; Adenosine monophosphate-activated protein kinase; Adenosine triphosphate; Chondrocyte; Sirtuin; Osteoarthritis

Abbreviations: OA: Osteoarthritis; ATP: Adenosine Triphosphate; AMPK: Adenosine Monophosphate-activated Protein Kinase; Sirt: Sirtuin; Runx2: Runt-related Transcription Factor; MMP: Matrix Metalloproteinase; IL: Interleukin; NAD: Nicotinamide Adenine Dinucleotide; NADH: Nicotinamide Adenine Dinucleotide; PBS: Phosphate-buffered Saline; DMEM: Dulbecco's Modified Eagle's Medium; HEPES: 2-[4-(2-hydroxyethyl)-1-piperazinyl]-Ethane Sulfonic Acid

Introduction

Articular cartilage comprises an avascular extracellular matrix containing a sparse population of chondrocytes that are essential for producing, assembling and turning over the articular cartilage matrix components [1,2]. Progressive degeneration of articular cartilage is a common feature of osteoarthritis (OA) [3,4]. OA is the most prevalent joint disease and has a complex pathogenesis and pathophysiology [5-6]. The effects of mechanical force acting on articular cartilage, obesity, inflammation and aging are among the major catabolic factors in OA, suggesting that both extrinsic and intrinsic stresses acting on articular cartilage matrix and chondrocytes are both causal and contributory factors to the catabolic process in OA [7-8].

Sirtuins are nicotinamide adenine dinucleotide (NAD) dependent protein deacetylases that control the protein acetylation and cellular metabolism [9-11]. Sirtuins play important roles as key regulators of numerous functions including regulation of the cytoskeleton, cellular differentiation, cell growth, stress tolerance, cellular metabolism, DNA repair, apoptosis, anti-inflammation, as well as control of cellular senescence in a variety of cells [9,12,13]. The sirtuin family members (sirtuin 1-7) execute their functions by deacetylation of target proteins in the different cellular localizations [9,10]. Several reports indicate that sirtuins may have two important roles - "regulation of cellular metabolism" and "response to cellular stresses (stress tolerance)", which are closely involved in the pathogenesis and pathology of a variety of diseases including stress-induced degenerative diseases such as OA [11-13]. Various cellular stresses such as mechanical stress, oxidative stress, inflammation and aging have been recognized as major risk factors for OA, and all sources of stress could affect the regulation of chondrocyte metabolism [3,8,14-17]. Altered

chondrocyte metabolism and changes in their responses to OA-related stresses are implicated in the creation of an imbalance between catabolic and anabolic reactions, leading to osteoarthritic degeneration of articular cartilage [3,5,12]. We postulated that the level of a key regulator of cellular stresses, sirtuin, in chondrocytes could participate in the pathophysiology of OA.

We and other groups have already demonstrated that sirtuin-1 (Sirt-1) has a functional role and is a key regulator of many molecules in both catabolic and anabolic pathways in OA chondrocytes [18-23]. Sirt-1 has been reported to participate in stress responses by regulating cell death and cellular metabolism through the deacetylation of target proteins in chondrocytes [19,20,22]. It has also been shown to promote the expression of cartilage-specific genes in chondrocytes [22,24,25]. In addition, it has been demonstrated that Sirt-1 inhibits chondrocyte apoptosis by suppressing protein tyrosine phosphatase 1B, caspase and mitochondria-related apoptotic signaling proteins or activating the insulin-like growth factor receptor pathway [26,27]. These findings suggest that the downregulation of Sirt-1 in chondrocytes is responsible for their increased apoptosis and the suppression of chondrocyte anabolism in OA. Recent reports reveal that Sirt-1 in chondrocytes may be involved in the pathophysiology of OA.

More recently, we have demonstrated that Sirt-1 regulates the expression of the osteogenic transcription factor Runt-related transcription factor 2 (Runx2) and production of the cartilage matrix-degrading enzyme, matrix metalloproteinase (MMP)-13, in osteoarthritic chondrocytes [18]. It is well known that MMP-13 contributes to OA cartilage degradation [1-5]. The expression level of MMP-13 is significantly higher in the chondrocytes of advanced stage OA cartilage in comparison with early OA or normal knee cartilage [28]. Furthermore, transgenic mice over-expressing MMP-13 in their articular chondrocytes experience joint degeneration similar to human OA, suggesting that recognition of the regulatory mechanism of MMP-13 expression in chondrocytes may contribute to an understanding of the molecular pathophysiology of enzymatic degradation of articular cartilage [29]. There is a general consensus that Runx2 is required for chondrocyte hypertrophy and osteophyte formation in the joint [30,31]. In addition, Runx2 is known to promote activation of the cartilage degrading enzyme MMP-13 in chondrocytes [32]. Interestingly, our previous study demonstrated that Sirt-1 inactivation inhibited both Runx2 expression and the IL-1β-accelerated production of MMP-13 in chondrocytes [18]. These findings indicate that Sirt-1 activity, which is downregulated by several cellular stresses, may directly influence the expression of Runx2 in chondrocytes, affecting the enzymatic degeneration of articular cartilage and osteophyte formation in OA. We concluded that Sirt-1-regulated Runx2 expression could control the production of MMP-13 and osteophyte formation by OA chondrocytes [18]. We postulate that Sirt1 activity in chondrocytes could be an important contributing factor in the pathogenesis and pathophysiology of OA. However, it still remains unclear how Sirt-1 regulates chondrocyte anabolic and catabolic metabolic processes during OA progression.

The OA-related catabolic factor IL-1β alters chondrocyte activity and induces chondrocyte apoptosis [4-8]. However, few studies have examined how the catabolic cytokine impacts chondrocyte energy metabolism in articular cartilage. Given the change of chondrocyte energy metabolism during the progression of OA, we hypothesized that the build-up of OA-related catabolic factors may disrupt cellular energy metabolism in cartilage, which then compromises chondrocyte activity, cartilage homeostasis and predisposes cartilage to damage. Disturbance in the maintenance of chondrocyte energy metabolism may result in cellular catabolic stress, facilitating the degeneration of articular cartilage.

In this study, we tested our hypothesis using human osteoarthritic chondrocytes stimulated with an OA-related catabolic factor (IL-1β) and revealed that IL-1β profoundly disrupted chondrocyte energy metabolism. This effect may involve interactions between adenosine triphosphate (ATP) production and the energy metabolic sensor, adenosine monophosphate-activated protein kinase (AMPK). Interestingly, we also found that Sirt-1 regulated both the activity of AMPK and the production of ATP in chondrocytes. AMPK and Sirt-1 are thought to be two critical energy sensors that regulate cellular energy balance. Reduced activities of Sirt-1 and AMPK in chondrocytes may limit energy availability for chondrocyte/cartilage maintenance and homeostasis in OA. We discuss the effect of Sirt-1 on energy metabolism through the regulation of the AMPK-ATP energy metabolic pathway.

Materials and Methods

Human chondrocyte cultures

Human articular cartilage tissue samples were obtained from patients' joints during arthroplastic surgery after obtaining informed consent from 11 patients with OA [mean age 72 years (range 58-90 years), 9 knee joints; 2 hip joints]. The protocol of this study was approved by the ethical committee of St. Marianna University School of Medicine (permission number: 1311). The clinical features of patients involved in the current study are summarized in Table 1. Representative pre-operative X-ray features of patients are shown in Figure 1. The severity of knee OA was evaluated by the Kellgren and Lawrence classification [33,34]. The severity of hip OA was also evaluated by the score according to the Kellgren and Lawrence classification for knee OA.

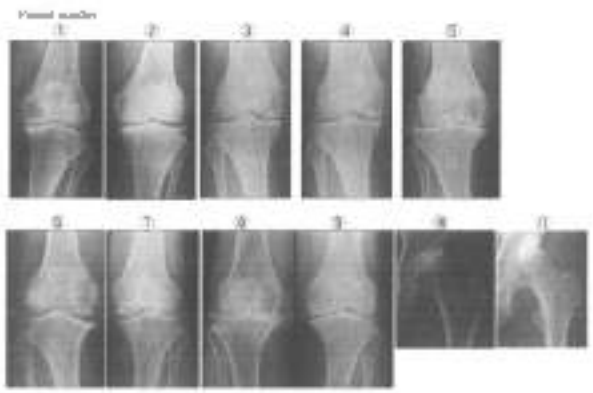

Figure 1: X-ray images of knee and hip joints of patients with OA. All 11 patients with OA had multiple osteophytes, definite joint space narrowing, sclerosis and bony deformity in the joints.

Articular cartilage explants were cut into small pieces, washed with phosphate-buffered saline (PBS) and digested with 0.5 mg/ml collagenase B (Sigma, St. Louis, MO, USA) in Dulbecco's modified Eagle's medium (DMEM) (Sigma) overnight on a shaking platform at

37°C. Isolated chondrocytes were collected following centrifugation, washed three times with PBS, resuspended and cultured in DMEM supplemented with 10% heat-inactivated fetal calf serum (FCS), 2 mM L-glutamine, 25 mM HEPES (2,4-(2-hydroxyethyl)-1-piperazinyl) ethane sulfonic acid), and 100 U/mL penicillin and streptomycin at 37°C in a humidified atmosphere of 95% air and 5% CO_2 as previously reported [18].

Patient Number	Age and Gender	Disease	Severity of OA
1	79 years old, male	Lt knee OA	Grade 3
2	74 years old, male	Lt knee OA	Grade 3
3	72 years old, female	Rt knee OA	Grade 3
4	70 years old, female	Rt knee OA	Grade 3
5	75 years old, female	Rt knee OA	Grade 3
6	69 years old, female	Rt knee OA	Grade 3
7	75 years old, female	Lt knee OA	Grade 3
8	79 years old, female	Rt knee OA	Grade 4
9	80 years old, female	Lt knee OA	Grade 3
10	68 years old, female	Rt hip OA	Grade 4
11	65 years old, male	Lt hip OA	Grade 4

OA: osteoarthritis, Lt: Left, Rt: Right, Severity of OA: Grade 0 (No feature of osteoarthritis), Grade 1 (possible narrowing of joint space and possible osteophytic lipping), Grade 2 (moderate multiple osteophytes, definite narrowing of joint space), Grade 3 (moderate multiple osteophytes, definite narrowing of joint space, and some sclerosis and possible deformity of bones end), Grade 4 (large osteophytes, marked narrowing of joint space, severe sclerosis and definite deformity of bone ends)

Table 1: The Clinical characteristics of patients.

Effects of the OA-related catabolic factor, interleukin (IL)-1β, on Sirt1 expression in chondrocytes

To study the effect of the OA-related catabolic factor, IL-1β, on the expression of Sirt-1 in chondrocytes, chondrocytes were incubated in the presence or absence of IL-1β (10.0 ng/mL) for 24 hours at 37°C in a humidified atmosphere of 95% air and 5% CO_2. After harvesting the cultured cells, cellular proteins were collected for immunoblotting analyses as previously described [18]. The level of Sirt-1 expression in chondrocytes was analyzed by western blotting (Image Quant LAS 4000, GE imagination at work). The antibodies used for western blot analysis were polyclonal against human Sirt-1 (1:1000 dilution, Abcam Inc., Cambridge, UK) and β-tubulin (1:2000 dilution; Santa Cruz Biotechnology, Santa Cruz, CA, USA) and the corresponding secondary antibody conjugated with horseradish peroxidase (Dako rabbit IgG P304 for anti Sirt-1 antibody (1:10000 dilution)). The antibody bound protein bands were visualized using the enhanced cavity laser system (GE Healthcare Bio-sciences KK, Tokyo, Japan).

Effects of Sirt-1 inactivation on energy metabolism in OA chondrocytes

To study the effects of Sirt-1 inactivation on energy metabolism, we examined levels of AMPK and ATP production in the Sirt-1 inhibitor-treated chondrocytes *in vitro*. Cultured chondrocytes were divided into 4 groups, control (medium only), IL-1β treated group, Sirt-1 inhibitor-treated group, and IL-1β + Sirt-1 inhibitor-treated group. In the IL-1β + Sirt-1 inhibitor-treated group, chondrocytes were pre-treated with the Sirt-1 inhibitor (S1 35 Inc 2842179, 1.0 μM, Santa Cruz Biotechnology Inc.) for 6 hours at 37°C in a humidified atmosphere of 95% air and 5% CO_2. Then, IL-1β (10.0 ng/mL) was added and the cells were returned to the incubator for a further 18 hours under the same conditions. In the IL-1β-treated group or the Sirt-1 inhibitor-treated group, chondrocytes were treated with IL-1β (10.0 ng/mL) or the Sirt-1 inhibitor (S1 35 (1.0 μM) for 24 hours at 37°C in a humidified atmosphere of 95% air and 5% CO_2. At the end of the culture period, the conditioned culture medium was collected and stored at −80°C until analysis. The levels of AMPK in chondrocytes were measured using an AMPK assay kit (Thermo Fisher Scientific K.K., Kanagawa, Japan). The level of ATP production by chondrocytes was examined by the intracellular ATP assay kit (Toyo B-NET Co., LTD., Tokyo, Japan).

Effects of Sirt-1 inactivation on proteoglycan and MMP-13 production in OA chondrocytes

To study the effects of Sirt-1 inactivation on chondrocyte activity, we examined levels of production of the articular cartilage matrix component, proteoglycan, and the cartilage degrading enzyme, matrix metalloproteinase (MMP)-13, in the Sirt-1 inhibitor-treated chondrocytes *in vitro*. As described above, cultured chondrocytes were divided into 4 treatment groups. The levels of MMP-13 produced by chondrocytes were measured using an ELISA kit (MMP-13 assay kit; Amersham Biosciences, Little Chalfont, UK). The level of proteoglycan in chondrocytes was examined by ELISA (DIA source PG-EASIA kit, KAP1461, DIA source Immuno Assays S.A.).

Statistical analysis

Data were evaluated using Student's t test. Results are presented as mean ± 95% confidence interval from three independent experiments. Analysis of variance was used for comparisons of more than two groups, and differences between two groups within the set were analysed by a Fisher's protected least significant difference test. Probability values of <0.05 were considered statistically significant.

Results

Severity of knee or hip OA

The clinical features of patients studied are summarized in Table 1. As shown in Figure 1, all 11 patients with OA had multiple osteophytes, definite joint space narrowing, sclerosis and bony deformity in the joints. According to the Kellgren and Lawrence classification, 8 patients with OA were classified as grade 3 and 3 OA patients as grade 4 (Table 1 and Figure 1).

OA-related catabolic factor IL-1β inhibits the expression of Sirtuin-1 in chondrocytes

Sirt-1 protein was ubiquitously expressed in chondrocytes from patients with OA. As shown in the representative image in Figure 2A, treatment with IL-1β inhibited the expression of Sirt-1 in OA chondrocytes. There was a tendency to inhibit the expression of Sirt-1 in OA chondrocytes which were stimulated by IL-1β, although no

significant difference was observed between control group and IL-1β-treated group (Figure 2B).

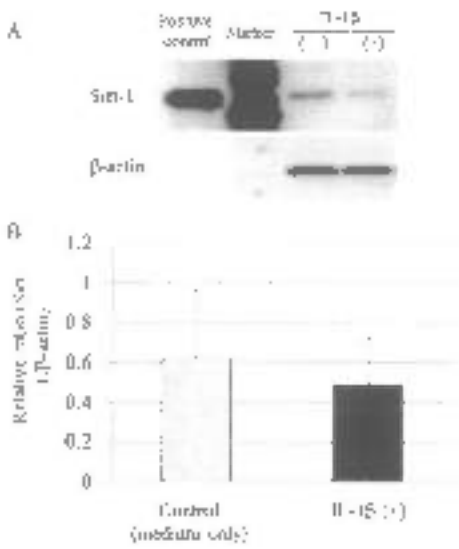

Figure 2: Effect of IL-1β on Sirt-1 expression in OA chondrocytes from donors. A: Representative image of the expression of Sirt-1 in chondrocytes from a patient with OA. Sirt-1 protein was ubiquitously expressed in osteoarthritic chondrocytes from OA patients. Treatment with IL-1β (10.0 ng/mL) inhibited Sirt-1 expression in OA chondrocytes. B: Relative ratio against the level of expression of β-actin. The level of Sirt-1 expression was analyzed as a relative ratio against the level of expression of β-actin. IL-1β tended to inhibit the expression of Sirt-1 protein in OA chondrocytes.

Sirt-1 regulates activity of the energy metabolic sensor AMPK and the production of ATP in human chondrocytes from patients with OA

As shown in Figure 3A, the level of AMPK in chondrocytes was significantly reduced by IL-1β stimulation in comparison with the control group (P=0.009). In addition, treatment with IL-1β significantly reduced the level of ATP production by chondrocytes (P=0.033) compared to control, Figure 3B). These findings indicate that the OA-related catabolic factor IL-1β inhibits levels of the energy sensor AMPK as well as ATP production in chondrocytes, suggesting that energy metabolism is downregulated in osteoarthritic chondrocytes.

To address whether Sirt-1 regulates the levels of AMPK and ATP production in chondrocytes, osteoarthritic chondrocytes from OA patients were pre-treated with Sirt-1 inhibitor and then cellular activities were examined *in vitro*. Pre-treatment with the Sirt-1 inhibitor (S)-35 (1.0 μM) showed a tendency to further inhibit the IL-1β downregulated AMPK in chondrocytes, although no significant difference in the AMPK level was observed between the IL-1β-treated group and the IL-1β + Sirt-1 inhibitor-treated group (Figure 3A). The group treated with Sirt-1 inhibitor alone showed no significant difference in AMPK level in comparison with the control, although there was a tendency to decrease the mean level of AMPK activity in the Sirt-1-treated group.

ATP production by osteoarthritic chondrocytes significantly decreased following treatment with Sirt-1 inhibitor (P=0.002; control group vs. Sirt-1 inhibitor treated group, Figure 3B). Moreover, pre-treatment with Sirt-1 inhibitor further decreased the IL-1β-induced reduction of ATP production in osteoarthritic chondrocytes (P=0.004; IL-1β treated group vs. IL-1β + Sirt-1 inhibitor treated group, Figure 3B). These data led to our hypothesis that Sirt-1 may modulate the level of the energy sensor AMPK in chondrocytes, resulting in the positive regulation of ATP production in OA.

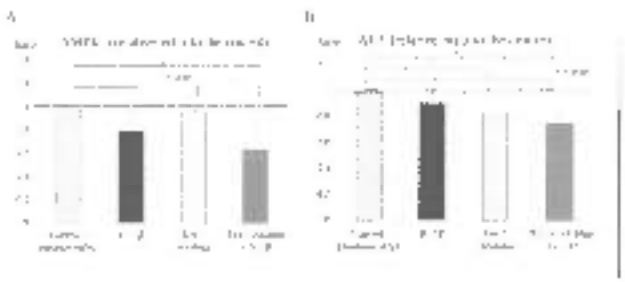

Figure 3: Effects of IL-1β and Sirt-1 inhibitor on AMPK and ATP activity in chondrocytes. A: To address whether Sirt-1 influences AMPK activity in chondrocytes, OA chondrocytes were pre-incubated with the Sirt-1 inhibitor (S)-35 (1.0 μM) for 6 hours. Then, the cells were incubated in the presence or absence of IL-1β (10.0 ng/mL) for 15 hours. Treatment with IL-1β significantly reduced AMPK activity in chondrocytes in comparison with the control (P=0.009). The inhibition of Sirt-1 activity by Sirt-1 inhibitor tended to inhibit IL-1β downregulated AMPK in chondrocytes, although no significant difference was observed between the IL-1β-treated chondrocytes and the Sirt-1 inhibitor + IL-1β-treated chondrocytes. B: Treatment with IL-1β significantly decreased ATP production by chondrocytes in comparison with the control (P=0.033). ATP production by chondrocytes was significantly increased by pre-treatment with Sirt-1 inhibitor in comparison with the control group (P=0.002). The inhibition of Sirt-1 activity by Sirt-1 inhibitor significantly inhibited IL-1β downregulated ATP production in chondrocytes (P=0.004, IL-1β treated group vs. IL-1β + Sirt-1 inhibitor-treated group).

Effects of IL-1β and Sirt-1 inhibitor on the production of MMP-13 and proteoglycan by human chondrocytes from patients with OA

To address whether Sirt-1 regulates the production of MMP-13 and proteoglycan by chondrocytes, osteoarthritic chondrocytes from OA patients were pre-treated with Sirt-1 inhibitor and then cellular activities were examined *in vitro*.

The production of MMP-13 by chondrocytes was significantly increased by IL-1β stimulation in comparison with the control group (Figure 4A, P=0.002). The group treated with Sirt-1 inhibitor alone showed no significant difference in MMP-13 production in comparison with the control. Pre-treatment with Sirt-1 inhibitor showed a tendency to decrease the IL-1β-induced production of MMP-13 by chondrocytes, although no significant difference in

MMP-13 production was observed between the IL-1β-treated group and the IL-13 + Sirt-1 inhibitor treated group (Figure 4A).

Proteoglycan production by osteoarthritis chondrocytes was significantly decreased by treatment with IL-1β (P=0.035, control group vs. IL-1β treated group, Figure 4B). Pre-treatment with Sirt-1 inhibitor tended to further inhibit the IL-13-decreased production of proteoglycan by chondrocytes, although no significant difference was observed in proteoglycan production between the IL-1β-treated group and the IL-1β + Sirt-1 inhibitor-treated groups (Figure 4B).

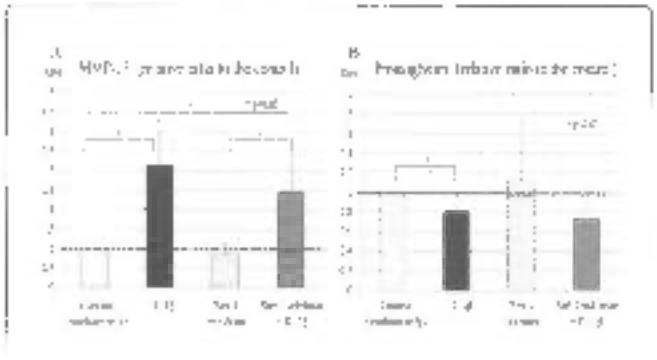

Figure 4: Effects of IL-1β and Sirt-1 inhibitor on MMP-13 and proteoglycan productions in chondrocytes. A: Treatment with IL-1β significantly increased MMP-13 production chondrocytes in comparison with the control (P=0.001). Pre-treatment with Sirt-1 inhibitor showed a tendency to decrease the IL-13 induced production of MMP-13 by chondrocytes, although no significant difference in MMP-13 production was observed between the IL-1β-treated group and the IL-1β + Sirt-1 inhibitor-treated group. B: Proteoglycan production by osteoarthritis chondrocytes significantly decreased with IL-13 treatment (P=0.035, control group vs. IL-1β treated group). Pre-treatment with Sirt-1 inhibitor tended to further inhibit the IL-1β-decreased production of proteoglycan by chondrocytes, although no significant difference was observed between the IL-1β treated group and the IL-1β + Sirt-1 inhibitor-treated group.

Discussion

OA is characterized by structural damage and functional deficit of articular cartilage [1,3]. The normal structure and function of articular cartilage is maintained by articular chondrocytes. As an anabolic process, normal chondrocytes produce essential components of articular cartilage, chiefly type II collagen and proteoglycan [1]. In contrast, OA chondrocytes express matrix-degrading enzymes such as matrix metalloproteinase (MMP) 1, -3 and -13, eventually resulting in osteoarthritic cartilage degeneration and destruction. OA chondrocytes are characterized by stimulated catabolic responses as well as reduced anabolic responses to OA-induced stresses [3-5]. In both cases, chondrocytes use cellular energy to produce cartilage matrix components or cartilage-degrading enzymes (MMPs). The status of chondrocyte energy metabolism could influence cartilage homeostasis as well as chondrocyte activity.

To further understand the pathogenesis and pathophysiology of OA, in the current study, we focused on chondrocyte energy metabolism and its related regulatory mechanism. AMPK is known to be the energy sensor that regulates cellular energy metabolism [35,36]. Once activated, AMPK responds by phosphorylating downstream targets which allow activation of pathways to produce ATP [36,37]. It has been demonstrated that AMPK is activated by several cellular stresses such as nutrient deprivation, heat shock, hypoxia and exercise [35,37-47]. We postulated that the activity of AMPK and its regulated energy metabolism in chondrocytes may be influenced by OA related catabolic stresses, such as mechanical and chemical stresses. In the present study, our data reveal that the OA-related catabolic factor IL-13 inhibits both activity of AMPK and ATP production in OA chondrocytes, suggesting that energy metabolism in chondrocytes is downregulated by OA-related factors during the progression of articular cartilage degeneration. Indeed, previous reports demonstrated that the activity of AMPK is decreased in chondrocytes in aged human and mouse OA cartilage [38,39]. Our findings of the downregulation of the AMPK-ATP energy metabolic pathway in OA chondrocytes are consistent with their findings. From the results of our present study, we conclude that OA induced catabolic stresses could lead to the downregulation of AMPK and its related energy production (ATP) in chondrocytes, resulting in an imbalance between anabolic and catabolic responses to OA related catabolic stresses. AMPK, as an energy sensor, plays a critically-important role in maintaining a healthy chondrocytes and consequently cartilage.

The NAD-dependent protein deacetylase, Sirt-1, is also recognized as another regulator of energy metabolism [37,40-42]. Sirt-1 has critically-important roles in regulating cellular metabolism and controlling responses to cellular stresses via the regulation of target proteins, and is closely involved in the pathophysiology of stress induced degenerative diseases including OA [9,13,20,21]. We postulated that cellular stresses could affect cellular energy metabolism through the regulatory mechanism regulated by Sirt-1 as well as AMPK. Several cellular stresses such as mechanical stress, oxidative stress, inflammation and aging, all of which are OA risk factors, induce osteoarthritic cartilage degeneration [3-8]. These OA related stresses may affect the activity of Sirt-1 as well as AMPK in chondrocytes, consequently facilitating the downregulation of chondrocyte energy metabolism and cartilage matrix homeostasis. Indeed, previous studies demonstrated that decreased expression of Sirt-1 was observed in mouse and human OA cartilages [21,43]. Furthermore, Platas et al. demonstrated that the OA-related catabolic factor, IL-1β, reduced the expression of both Sirt-1 mRNA and Sirt-1 protein in chondrocytes [21]. We also found that IL-1β tended to inhibit the expression of Sirt-1 in chondrocytes. Our current study indicates that Sirt-1 insufficiency leads to further reduction in the IL-1β induced decrease of ATP production by OA chondrocytes. This suggests that Sirt-1, as well as AMPK, is a regulator of energy homeostasis in chondrocytes.

In our current study, Sirt-1 inactivation was shown to decrease both the level of AMPK activity and the production of ATP in OA chondrocytes. This suggests that Sirt-1 activity may positively regulate the activity of AMPK and its resultant ATP production in chondrocytes (Figure 5A). In contrast, previous reports demonstrated that activation of AMPK stimulated Sirt-1 activity in a variety of cell types [44-46]. These findings suggest the existence of a positive feedback loop between Sirt-1 and AMPK in chondrocytes (Figure 5B). This Sirt-1-AMPK feedback loop may control the AMPK-ATP energy metabolic pathway and the energy balance in chondrocytes. In addition, it has been reported that Sirt-1 promotes stress tolerance in chondrocytes [24-27]. Therefore, disruption of the Sirt-1-AMPK feedback loop may not only disrupt chondrocyte energy metabolism but may also decrease chondrocyte stress resistance in OA.

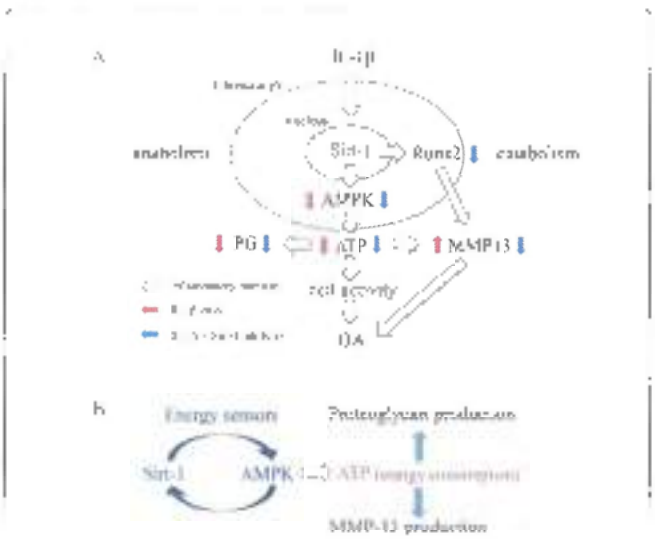

Figure 5: Summary of our current study. A: Sirt-1 regulates chondrocyte energy metabolism (ATP production) through the modulation of AMPK activity in OA chondrocytes. The OA-related catabolic factor IL-1β downregulates Sirt-1 activity and its target AMPK, facilitating the decrease of cellular energy (ATP) and cellular activity in chondrocytes. Since chondrocytes use cellular energy (ATP) production to produce both cartilage matrix components such as proteoglycan and cartilage-matrix degrading enzymes such as MMP-13, Sirt-1 inactivation may downregulate chondrocyte energy metabolism, resulting in a decrease of proteoglycan and MMP-13 production by OA chondrocytes. B: Sirt-1 may regulate cellular energy metabolism through the Sirt-1-AMPK energy sensor loop. Sirt-1 activity may affect energy metabolism, facilitating the regulation of both MMP-13 and proteoglycan production by OA chondrocytes.

This study indicates that Sirt-1 may regulate the stress response of chondrocytes to OA-related catabolic stresses as well as regulating chondrocyte energy metabolism through the modulation of AMPK activity. Both these changes are implicated in creating an imbalance between catabolic and anabolic pathways, leading to osteoarthritic degeneration of articular cartilage. In the present study, Sirt-1 inactivation induced both a further decrease of IL-1β-reduced production of proteoglycan and a decrease in the IL-1β accelerated MMP-13 production by OA chondrocytes. Since chondrocytes require cellular energy (ATP) production to produce both cartilage matrix components such as proteoglycan and cartilage matrix degrading enzymes such as MMP-13, Sirt-1 inactivation may downregulate chondrocyte energy metabolism, resulting in decreases of both proteoglycan and MMP-13 productions by OA chondrocytes (Figure 5A). In contrast to our findings, it has been reported that Sirt-1 insufficiency induces further acceleration of IL-1β-induced MMP-13 production by chondrocytes [47]. Regarding the relationship between Sirt-1 and MMP-13, our previous study indicated that Sirt-1 positively regulates the expression of Runx2, positive transcription factor for MMP-13, in OA chondrocytes [18]. We think that Sirt-1 activity may influence MMP-13 expression via Sirt-1 mediated Runx2 expression in OA chondrocytes [18]. Indeed, some studies demonstrated that Sirt-1 activator induces the expression of Runx2 (promotor for MMP-13 expression) in chondrocytes and mesenchymal stem cells [48,49]. Moreover, it has been reported that IL-1β increases MMP-13 expression and requires Runx2 for this effect in chondrocytes [50]. These findings also support our hypothesis that the Sirt-1-Runx2 interaction may affect expression of the cartilage-degrading enzyme MMP-13 in OA chondrocytes. Although further studies are needed to clarify the exact correlation between Sirt-1 and MMP-13 in chondrocytes, we conclude that Sirt-1 insufficiency may induce the downregulation of Runx2 expression, consequently leading to the decrease of Runx2-promoted MMP-13 expression in OA chondrocytes (Figure 5A). In addition, since Sirt-1 may regulate cellular energy metabolism through the Sirt-1-AMPK energy sensor loop, Sirt-1 insufficiency may affect energy metabolism, facilitating the downregulation of MMP-13 and proteoglycan production by OA chondrocytes (Figure 5B).

In conclusion, our present study indicates that the OA-related catabolic factor, IL-1β, inhibits the AMPK-ATP energy metabolic pathway in OA chondrocytes. Our findings also implicate Sirt-1 activity in anabolic and catabolic cellular activities and suggest it may modulate ATP production through functional regulation of the energy sensor AMPK in chondrocytes. Reduced activities of Sirt-1 and AMPK in chondrocytes may limit energy availability for chondrocyte/cartilage maintenance in OA. Disturbance of the Sirt-1-AMPK positive feedback loop in chondrocytes could affect energy balance and homeostasis in chondrocytes/cartilages, resulting in the progression of OA. Although further studies are needed to clarify the regulatory mechanism of chondrocyte energy metabolism, Sirt-1 and AMPK may be therapeutic targets for OA.

Acknowledgements

This study was supported by JSPS KAKENHI Grant Number 26463133 from the Japan Society for the Promotion of Science (JSPS). We would like to thank M. Suzuki, S. Magi, M. Tamaki, I. Tanate and R. Karasawa for excellent technical assistance.

Competing Interests

The authors declare no conflict of interest.

Authors' Contributions

All authors read and approved the final version to be published. All authors had full access to all of the data in the study and take responsibility for the integrity of the data and the accuracy of the data analysis.

- The conception and design the study, or acquisition of data, or analysis and interpretation; Hajime Kobayashi, Kazuo Yudoh, Kamada Toshikazu, Koh Terauchi, Naoko Yui, Kanaka Yatabe, Hiroto Fujiya, Hisateru Niki, Haruki Musha
- Drafting the article or revising it critically for important intellectuall content; Hajime Kobayashi, Kazuo Yudoh, Naoko Yui, Koh Terauchi.
- Final approval of the version to be submitted, Hajime Kobayashi, Kazuo Yudoh, Hisateru Niki, Haruki Musha

References

1. Goldring MB, Goldring SR (2010) Articular cartilage and subchondral bone in the pathogenesis of osteoarthritis. Ann NY Acad Sci 1192: 230-237.

2. Sellam J, Berenbaum F (2010) The role of synovitis in pathophysiology and clinical symptoms of osteoarthritis. Nat Rev Rheumatol 6: 625-635.
3. Loeser RF, Goldring SR, Scanzello CR, Goldring MB (2012) Osteoarthritis: a disease of the joint as an organ. Arthritis Rheum 64: 1697-1707.
4. Lin-Bryan R (2015) Inflammation and intracellular metabolism: new targets in OA. Osteoarthritis Cartilage 23: 1835-1842.
5. Loeser RF (2006) Molecular mechanisms of cartilage destruction: mechanics, inflammatory mediators, and aging collide. Arthritis Rheum 54: 1357-1360.
6. Pelletier JP, Martel-Pelletier, Raynauld JP (2016) Most recent developments in strategies to reduce the progression of structural changes in osteoarthritis: today and tomorrow. Arthritis Res Ther 4: 206.
7. Jung RK, Lin-Bryan R, Long F, Grubb TM (2016) Emerging role of metabolic signaling in synovial joint remodeling and osteoarthritis. J Orthop Res 34: 2048-2058.
8. Berenbaum F, Griffin TM, Lin-Bryan R (2017) Metabolic Regulation of Inflammation in Osteoarthritis. Arthritis Rheum 69: 9-21.
9. Haigis MC, Sinclair DA (2010) Mammalian Sirtuins: Biological Insights and Disease Relevance. Annu Rev Pathol 5: 253-295.
10. Saiah A, Stein L, Jun S (2011) The Role of Mammalian Sirtuins in the Regulation of Metabolism, Aging, and Longevity. Handb Exp Pharmacol 206: 125-162.
11. Guarente L (2011) Sirtuins, aging, and metabolism. Cold Spring Harb Symp Quant Biol 76: 81-90.
12. Mouchiroud L, Houtkooper RH, Moullan N, Katsyuba E, Ryu D, et al. (2013) The NAD(+)/Sirtuin pathway modulates longevity through activation of mitochondrial UPR and FOXO signaling. Cell 154: 430-441.
13. Jun S, Guarente L (2014) NAD+ and Sirtuins in Aging and Disease. Trends Cell Biol 24: 464-471.
14. Martin JA, Buckwalter JA (2002) Aging, articular cartilage chondrocyte senescence and osteoarthritis. Biogerontology 3: 257-264.
15. Green DM, Noble PC, Ahuero JS, Birdsall HH (2006) Cellular events leading to chondrocyte death after cartilage impact injury. Arthritis Rheum 54: 1506-1517.
16. Nakata K, Shinkai H, Nanjo Y, Yano M, Matsuyoshi K, et al. (2007) Water-soluble CD3 inhibitor prevents degeneration of articular cartilage in osteoarthritis via down-regulation of chondrocyte catabolic activity and inhibition of cartilage degeneration during disease development. Arthritis Rheum 56: 2028-2038.
17. Martel-Pelletier J, Barr AJ, Cicuttini FM, Conaghan PG, Cooper C, et al. (2016) Osteoarthritis. Nat Rev Dis Primers 15: 16072.
18. Terauchi K, Kobayashi H, Yatabe K, Yui N, Fujiya H, et al. (2015) The NAD-Dependent Deacetylase Sirtuin-1 Regulates the Expression of Osteogenic Transcriptional Activator Runt-Related Transcription Factor 2 (Runx2) and Production of Matrix Metalloproteinase (MMP)-13 in Chondrocytes in Osteoarthritis. Int J Mol Sci 16: 8119.
19. D'Adamio S, Cetrullo S, Guidotti S, Borzi RM, Flamigni F (2016) Hydroxytyrosol modulates the levels of microRNA-9 and its target sirtuin 1 thereby counteracting oxidative stress-induced chondrocyte death. Osteoarthritis Cartilage 25: 610-616.
20. Platas J, Guillen MI, Perez Del Caz MD, Gomar I, Gegundez MA, et al. (2016) Paracrine effects of human adipose derived mesenchymal stem cells in inflammatory stress induced senescence features of osteoarthritic chondrocytes. Aging (Albany NY) 8: 1703-1717.
21. Dvir-Ginzberg M, Mobasseri A, Kumar A (2016) The Role of Sirtuins in Cartilage Homeostasis and Osteoarthritis. Curr Rheumatol Rep 18: 45.
22. Yang W, Kang X, Liu J, Li H, Ma Z, et al. (2016) Class Gene Brm/Brg1 Modulates Human Cartilage Gene Expression by Crosstalk With Sirt1. Endocrinology 157: 3096-3107.
23. Matsuzaki T, Matsushita T, Takayama K, Matsumoto T, Nishida K, et al. (2014) Disruption of Sirt1 in chondrocytes causes accelerated progression of osteoarthritis under mechanical stress and during ageing in mice. Ann Rheum Dis 73: 1392-1404.
24. Dvir-Ginzberg M, Gagarina V, Lee EJ, Hall DJ (2008) Regulation of cartilage-specific gene expression in human chondrocytes by SirT1 and nicotinamide phosphoribosyltransferase. J Biol Chem 283: 36300-36310.
25. Fujita N, Matsushita T, Ishida K, Kubo S, Matsumoto T, et al. (2011) Potential involvement of SIRT1 in the pathogenesis of osteoarthritis through the modulation of chondrocyte gene expressions. J Orthop Res 29: 511-515.
26. Takayama K, Ishida K, Matsushita T, Fujita N, Hayashi S, et al. (2009) SIRT1 regulation of apoptosis of human chondrocytes. Arthritis Rheum 60: 2731-2740.
27. Gagarina V, Gabay O, Dvir-Ginzberg M, Lee EJ, Brady JK, et al. (2010) Sirt1 enhances survival of human osteoarthritis chondrocytes by repressing protein tyrosine phosphatase 1B and activating the insulin-like growth factor receptor pathway. Arthritis Rheum 62: 1381-1392.
28. Rao S, Geblard PM, Haag J, Knorr T, Bartnik E, et al. (2002) Relative messenger RNA expression profiling of collagenases and aggrecanases in human articular chondrocytes in vivo and in vitro. Arthritis Rheum 46: 2648-2657.
29. Neuhold LA, Killar L, Zhao W, Sung ML, Warner L, et al. (2001) Postnatal expression in hyaline cartilage of constitutively active human collagenase-3 (MMP-13) induces osteoarthritis in mice. J Clin Invest 107: 35-44.
30. Kamekura S, Kawasaki Y, Hoshi K, Shimoaka T, Chikuda H, et al. (2012) Contribution of runt-related transcription factor 2 to the pathogenesis of osteoarthritis in mice after induction of knee joint instability. Arthritis Rheum 54: 2462-2470.
31. Kawaguchi H (2008) Endochondral ossification signals in cartilage degradation during osteoarthritis progression in experimental mouse models. Mol Cells 25: 1-6.
32. Wang X, Manner PA, Horner A, Shum L, Tuan RS, et al. (2004) Regulation of MMP-13 expression by RUNX2 and FGF2 in osteoarthritic cartilage. Osteoarthritis Cartilage 12: 963-973.
33. Lawrence JS (1977) Osteoarthritis. In: Lawrence JS (editor) Rheumatism in populations. London. William Heinemann Medical Books.
34. Brandt KD, Fife RS, Braunstein EM, Katz B (1991) Radiographic grading of the severity of knee osteoarthritis: relation of the Kellgren and Lawrence grade to a grade based on joint space narrowing, and correlation with arthroscopic evidence of articular cartilage degeneration. Arthritis Rheum 34: 1381-1386.
35. Steinberg GR, Kemp BE (2009) AMPK in health and disease. Physiol Rev 89: 1025-1078.
36. Witczak CA, Sharoff CG, Goodyear LJ (2008) AMP-activated protein kinase in skeletal muscle, from structure and localization to its role as a master regulator of cellular metabolism. Cell Mol Life Sci 65: 3737-3755.
37. Salminen A, Kaarniranta K (2012) AMP-activated protein kinase (AMPK) controls the aging process via an integrated signaling network. Ageing Res Rev 11: 230-241.
38. Terkeltaub R, Yang B, Lotz M, Liu-Bryan R (2011) Chondrocyte AMP-activated protein kinase activity suppresses matrix degradation responses to inflammatory cytokines IL-1β and TNFα. Arthritis Rheum 63: 1928-1937.
39. Petursson F, Husa M, June R, Lotz M, Terkeltaub R, et al. (2013) Linked decreases in liver kinase B1 and AMP-activated protein kinase activity modulate matrix catabolic responses to biomechanical injury in chondrocytes. Arthritis Res Ther 24: R77.
40. Li X (2013) SIRT1 and energy metabolism. Acta Biochim Biophys Sin (Shanghai) 45: 51-60.
41. Chang HC, Guarente L (2014) SIRT1 and other sirtuins in metabolism. Trends Endocrinol Metab 25: 138-145.
42. Finkel T (2015) The metabolic regulation of aging. Nat Med 21: 1416-1423.
43. Dvir-Ginzberg M, Steinmeyer J (2013) Towards elucidating the role of Sirt1 in osteoarthritis. Front Biosci (Elite Ed) 5: 343-355.
44. Fulco M, Cen Y, Zhao P, Hoffman EP, McBurney MW, et al. (2008) Glucose restriction inhibits skeletal myoblast differentiation by activating

SIRT1 through AMPK mediated regulation of Nampt. Dev Cell 14: 661-673.

45. Canto C, Auwerx J (2009) PGC-1alpha, SIRT1 and AMPK, an energy sensing network that controls energy expenditure. Curr Opin Lipidol 20: 98-105.

46. Canto C1, Gerrard-Hines Z, Lenge IN, Lagouge M, Kunega L, et al. (2009) AMPK regulates energy expenditure by modulating NAD+ metabolism and SIRT1 activity. Nature 458: 1056-1060.

47. Matsushita T, Sasaki H, Takayama K, Ishida S, Matsumoto T, et al. (2013) The overexpression of SIRT1 inhibits osteoarthritic gene expression changes induced by interleukin-1β in human chondrocytes. J Orthop Res 31: 531-537.

48. Sirin HH, Braun HH, Dragoi JI. (2011) The effect of resveratrol on normal and osteoarthritic chondrocyte metabolism. Bone Joint Res 3: 51-59.

49. Shakibaei M, Shayan P, Busch F, Aldinger C, Buhrmann C, et al. (2012) Resveratrol mediated modulation of Sirt-1/Runx2 promotes osteogenic differentiation of mesenchymal stem cells: potential role of Runx2 deacetylation. PLOS One 7: e35744.

50. Mengshol JA, Vincenti MP, Brinckerhoff CE. (2001) IL-1 induces collagenase-3 (MMP-13) promoter activity in stably transfected chondrocytic cells: requirement for Runx-2 and activation by p38 MAPK and JNK pathways. Nucleic Acids Res 29: 4361-4372.

関節リウマチと変形性関節症

Rheumatoid arthritis and Osteoarthritis

聖マリアンナ医科大学難病治療研究センター
Institute of Medical Science
St.Marianna University School of Medicine

遊道 和雄（ゆうどう かずお）
Kazuo Yudo

受付 [illegible]
[illegible]
[illegible]
[illegible]
[illegible]

Key words : rheumatoid arthritis, osteoarthritis, synovitis, subchondral bone, articular cartilage

Abstract

著しい関節痛や関節変形をきたす関節リウマチと変形性関節症の病因・病態の相違点特に骨吸収・骨増殖性変化，滑膜炎および関節軟骨の組織特性の関節症状発現における意義の理解を通じて，今後求められる治療法について概説する。

はじめに

関節変性疾患として代表的な関節リウマチ（rheumatoid arthritis, RA）患者は 70～80 万人，変形性関節症（osteoarthritis, OA）患者は 800 万人弱にのぼるとされており，日常生活動作（ADL：activity of daily living）の障害を有する対象患者は年々増加傾向にある。こうした関節疾患の治療に伴う医療費の急増，ならびに運動能力・活動性低下に伴う社会的損失は莫大であり，有効な対策の立案と実行が社会的急務とされている。

本稿では，とくに著しい関節痛や関節変形をきたす RA と OA の病因・病態を相違点の理解を通じて，今後求められる治療法について概説する。

1. 関節リウマチ（RA）と変形性関節症（OA）の疫学的背景，診療の現状

RA は関節滑膜を炎症の主座とする自己免疫疾患であり，病勢の進行により関節破壊の進行とともに，慢性炎症に起因する重度の多臓器障害や全身性消耗症状を呈することもあり，このような重篤な状態にまで至らずとも，外来診療において多くの RA 患者が多関節炎による疼痛・腫脹，これによる歩行・起居，炊飯，洗髪の困難などの ADL 障害を訴えており，症状緩和による ADL 改善が望まれている。

RA については，病因や病態に関する治療学的分子（炎症性サイトカイン）が次々に明らかになり，免疫異常を是正する免疫調整薬，Methotrexate（MTX）薬剤に代表される免疫抑制薬などの抗リウマチ薬（disease-modifying anti-rheumatic drugs）および抗サイトカイン抗体医薬の臨床応用が飛躍的に進展した。しかしながら，これらの抗リウマチ薬にも non-responder が存在し，responder であっても長期使用によって徐々に効果が減弱することがあることから，薬剤の変更や用量増加を余儀なくされることも多い。また，抗リウマチ薬（生

薬学的製剤によるサイトカイン作用の抑制は、見逃せない、骨髄抑制、肝機能障害、骨髄抑制等の様々な副作用の原因となるリスクもあり、その使用と薬剤調整には十分な注意が喚起されている。

変形性関節症（OA）の患者数は、米国において3000万人強、欧州では3,500万人強と推定され、有病者は関節リウマチ（RA）の約10～20倍とされている。OAについても、病態進行に伴う疼痛と関節軟骨変性を、ともに抑制する薬効を持つ新しいOA治療薬 disease Modifying Osteoarthritis Drugs（DMOADs）の臨床応用が望まれているが、大きな期待される治療効果を満たすDMOADsは開発されていない。OAは、本邦でも数十数万人もの新たな発症者がいるとの報告もあり、今後高齢化社会が進むに従って、その関連疾患の増加が懸念されている。

OAの治療は、日常生活動作の改善指導（筋力訓練、ウォーキング、装具等）、消炎鎮痛剤による疼痛の緩和、関節内へのヒアルロン酸製剤の注入といった対症療法がほとんどであり、RAのような病因・病態解析に基づく有効な新規治療法の開発が待たれている。また、正常ヒトにも関節症状の悪化がみられ、骨関節破壊やアライメントの変化を呈する症例には外科的療法（人工関節置換術等）も行われるが、しかし、外科的治療には、入院加療による時間的ロス、苦痛などロス、感染や人工物の破損等の問題に加え、数年～十数年後に挿入した人工物の経年的変化や破損のため、人工関節の再置換を迫られる症例もあり、医療経済学的観点からみても社会的損失は大きく、解決すべき問題点も多くある。

RA、OAともに、骨・軟骨、靭帯等の関節支持組織が発症後早期に破壊されること、関節軟骨が極めて修復能に乏しいこと、骨関節間による支持性や可動性の低下が、患者自の活動性に大きく影響することを考慮して、薬剤療法に加えて理学療法等も含めた総合的な治療計画が必要である。

図1 関節リウマチ症状評価X線像

2. RAとOAにみる関節変形・変形の病態の違い

両疾患の違いを理解するには、まず其々の疾患の特徴を明確にする必要がある。RAは、前述のように滑膜を炎症の主座とする（滑膜炎、血管増生）、関節変性と骨吸収・破壊を伴う自己免疫疾患（免疫異常）であるのに対して、OAは関節軟骨の変性・摩耗とその後の二次性骨硬変、なんらかの骨の新生増殖に基づく進行性の変性関節疾患である。

2-1 RAにおける骨増殖性変化

RAでは免疫異常・炎症による破骨細胞分化・

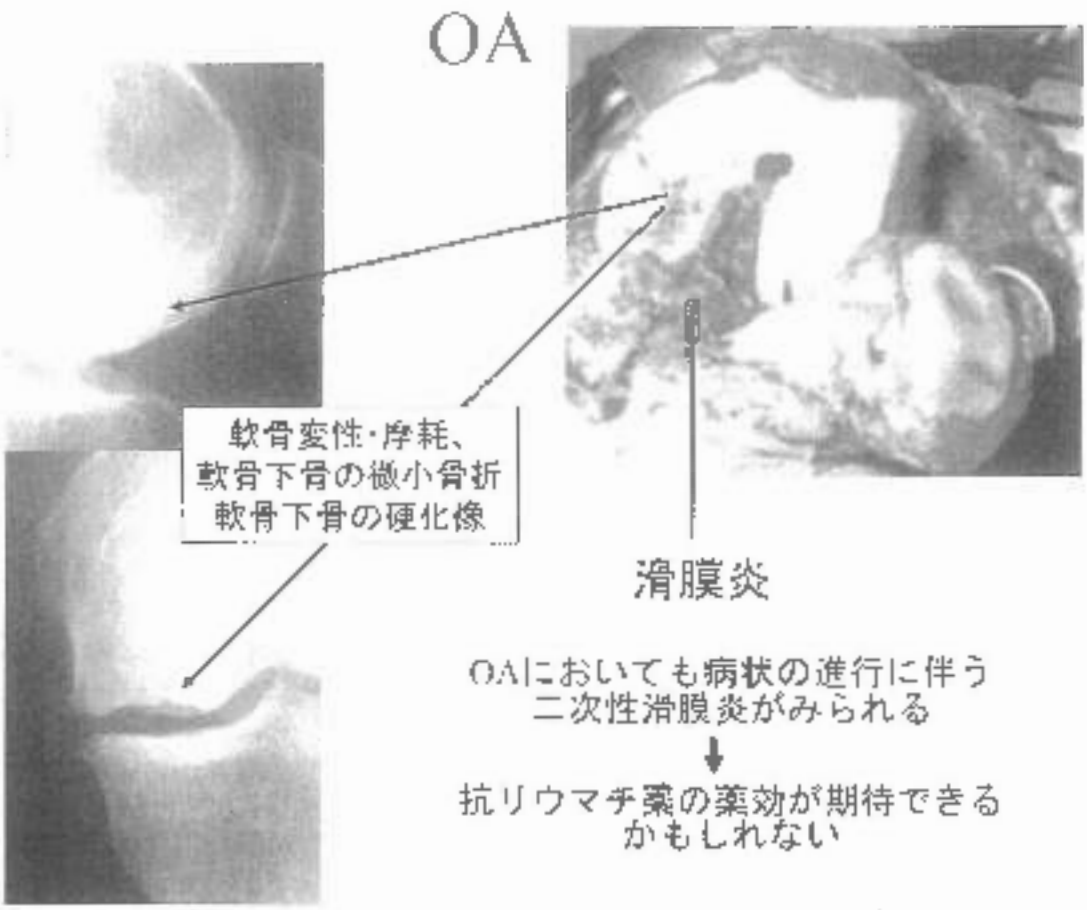

図2　OAにおける滑膜炎の病態との関連

活性化の亢進のため，骨吸収・破壊像が特徴である。これに対して，OAでは軟骨変性に加えて，骨の増殖性変化（骨棘，軟骨下骨層の硬化）が特徴である。すなわち，画像による鑑別診断には，骨関節の単純レントゲン像をていねいに観察し，骨萎縮変化があるか，骨吸収陰影像があるかをみることが第一であり，単純レントゲン像だけでもOAとRAの関節変性・変形の基本的な鑑別は可能である。しかし，RAにおいても骨吸収像だけでなく，二次的な骨硬化像・骨棘が観察されることがあり，とくに第3RA関節炎像に同時的にOAの骨増殖性変化や関節軟骨変性を併発する症例も多い。図1は関節リウマチ患者の膝関節のX線像である。両骨内側関節上にRAに特徴的な骨吸収・陥凹像がみられることに加えて，

OAの初期像である軟骨下骨の肥厚や嚢胞の形成、骨棘も観察される。

2-2 OAにおける滑膜炎

前項の疫学調査にあるように、病因・病態は異なるがRAの特徴である「滑膜炎」が、OAにおいても「二次性滑膜炎」として観察されることもある（図2）。OAにも滑膜炎があるならば、抗リウマチ薬がOAの「二次性滑膜炎」を治療するポテンシャルを持つかもしれない。

そこで、OAの二次性滑膜炎に伴う症状について考察する。

RAにおいても、OAにおいても、朝節に求められる機能は可動性、支持性および無痛性であるが、関節組織の変性・変形の進行によって、可動性・支持性は障害を伴って障害されていく。関節構成組織のうち、特に関節軟骨は、関節液（滑液）上の極低摩擦により高度の低摩擦性・可動性を示し、関節機能を制御している。

関節軟骨の組織特性上の観点からOAにおける関節痛の成因を考えると、軟骨組織には血管がないこと（無血管組織）、かつ神経分布もないことから、仮性・変性が進んでも軟骨組織自体が痛みを誘発することはないということである。

すなわち、OAの痛みの原因は、以下の3点にあると考えられる。

1）軟骨変性の進行に伴う可動性および支持性の障害により、関節を構成する滑膜（関節滑膜の場）、支持靭帯、関節気に二次的な障害が及び、これらの組織に分布する感覚神経が刺激されること。

2）変性が進行して軟骨破壊が高度になれば関節軟骨下骨層など骨組織も変性・変形をきたし、その結果、関節は著しく可動性と支持性を失い、痛覚刺激や変形を惹起していくこと。

このように、OAの痛みは関節組織構成要素の各組織（たとえば、軟骨以外）に分布する感覚神経が各種なことにより組成されるものであると考えられる。また、OAの重症度を考えると、上記2）に発症早期・中期（2）は中期後半・晩期に相当し、疾患変性に伴う関節構成組織への二次的変化の程度によって症状レベルも異なると考えられる。

変形性関節症における変性発生の主座は、軟骨組織自体にあるのではなく、二次的変化を生じた滑膜および軟骨下骨層の微小骨折にある。そのため、特にOA初期においては、二次性滑膜炎のコントロールは極めて重要である。加えて、OAにおいても関節の炎症、特に二次性滑膜炎をコントロールすることで関節痛ばかりでなく、引き続く関節機能性変性や関節変形を抑制することが期待される。

3. 今後の関節疾患治療法に求められるプロファイル

RAとOAは基本的に病因・病態は異なるが、発症後の関節変性・変形には機械的ストレス（荷重、記録 overuse）、炎症／免疫反応、酸化ストレスおよび遺伝的因子等がそれぞれの重みをもって関与し、軟骨基質（細胞外マトリックス）の変性、細胞と細胞外マトリックスの相互関係の破綻や細胞死が直接的または間接的に組織としての生命性を低下させ、経時的に軟骨変性が進行していくと考えられる。

これまで、RA、OAともに病因・病態を基礎とした治療薬・治療法の開発が行なわれきたが、両関節疾患が多因子に影響を受ける点であることから、一因子を修飾するagent（薬剤）のみでは病期の進行や病勢を抑制することは困難かもしれない。変形性の病理に関連する複数の病因に共通の経路、または因子を同定することができれば、より有効な治療戦略に資するものと考える。

このような状況を踏まえ、RA、OAともに今後求められる治療薬のプロファイルは、疼痛や変形などの症状を改善させることに主眼を置いた症状修飾型治療薬（symptom modifying

drug）から、その後初期に加えて早期に「骨・軟骨変性を抑止」または「骨に強靭に関節機能を保持しうる構造・機能修飾型治療（structure/function modifying drug）」へと移行していく図式を考えたいと思います。

おわりに

高齢化社会において、いつまでも歩行などの活動性を維持するためには、加齢にともなう運動器疾患（RA, OA）に対して現状の治療法よりもさらに臨床的可塑性を示す新規の治療法を治療時期の特定が急がれている。

文献

1) Deane KD, El-Gabalawy H. Pathogenesis and prevention of rheumatic disease: focus on preclinical RA and SLE. Nat Rev Rheumatol. 2014; 10(4): 212-28.
2) Kaneko Y, Takeuchi T. A paradigm shift in rheumatoid arthritis over the past decade. Intern Med. 2014;53 (17): 1895-904.
3) 厚生労働省 42:2-6.2002 [閲覧日：
4) Zhang W, Nuki G, Moskowitz RW, et al. OARSI recommendations for the management of hip and knee osteoarthritis. Part III: changes in evidence following systematic cumulative update of research published through January 2009. Osteoarthritis Cartilage. 2010;18 (4): 476-499.

☆ ☆ ☆

Novel Techniques in Arthritis & Bone Research

Juniper Publishers

Short Communication

Volume 2 Issue 2 - May 2017

New Tech Arthritis Bone Res

Copyright © All rights reserved by Kazuo Yudoh

Cartilage Tissue Engineering-A Novel Biomaterial for Cartilage Repair Generated by Self- Assembly: Creation of a Self-Organized Articular Cartilage-like Tissue

Kazuo Yudoh[1*], Noritaka Kumai[2], Naoko Yui[1] and Rie Karasawa[1]

[1]Department of Frontier Medicine, St. Marianna University School of Medicine, Japan

[2]Department of Sports Medicine, St. Marianna University School of Medicine, Japan

Submission: April 25, 2017; **Published:** June 02, 2017

***Corresponding author:** Kazuo Yudoh, Department of Frontier Medicine, Institute of Medical Science, St. Marianna University School of Medicine, Sugao 2-16-1, Miyamae-ku, Kawasaki City 216-8511, Japan, Tel: +81-44-977-8111 (ext. 4029); fax: +81-44-978-2036; Email: yudoh@marianna-u.ac.jp

Summary

For successful articular cartilage tissue engineering, three-dimensional biomaterials created in vitro by cultivation of autologous chondrocytes or mesenchymal stem cells with a collagen gel have been implanted to replace defective or degenerative parts of the articular cartilage in limited cases with local trauma or arthritis. However, several passages of chondrocyte culture are required to obtain a sufficient number of cells for tissue engineering. Several other problems arise including dedifferentiation of chondrocytes during cell culture.

The purpose of our study is to create a novel biomaterial possessing functions and structures comparable to native hyaline articular cartilage by utilizing the physicochemical properties of the cartilage matrix components themselves, in other words, employing a self-assembly technique instead of using chondrocytes to produce cartilage matrices eventually leading to articular cartilage tissue formation. We demonstrate that self-assembly of cartilage components including type II collagen, proteoglycan and hyaluronic acid could construct self-organized cartilage-like material which is characterized by nano-composite structure comparable to articular cartilage and high elasticity and low friction coefficient as small as those of native cartilage.

Introduction

For the treatment of advanced joint destruction and degeneration, reconstruction of joints using new technologies such as tissue engineering are now attracting attention. Biomimetic hydroxyapatite scaffolds for bone tissue engineering have already been so well devised that they have sufficiently high affinity to the bone and enough rigidity similar to bone to be usable for the treatment of bone defects [1]. Since bone itself has growth ability of remodeling, grafted bone is replaced by the host bone tissue through self-organization over a period of several weeks to months. In contrast, materials suitable for cartilage repair still remain to be created which have perfectly cartilage-specific tissue qualities represented by properties of high elasticity and high lubrication [2,3].

Problems of Cartilage Tissue Engineering-Limitation of Cell Source

For the cartilage tissue engineering, chondrocytes are cultured in vitro in collagen or agarose gel to obtain a three dimensional material that can be implanted in a limited number of cases where subjects have a small posttraumatic cartilage defect of less than 3cm3 in volume [3]. Some researchers are trying to obtain cell resources for cartilage tissue engineering by induction of differentiated chondrocytes from mesenchymal stem cells derived from the bone marrow. However, using current technologies, 2~5x106 mature chondrocytes are supposed to be required to fill a 1cm3 cartilage deficit with cartilage-like tissue [3,4]. This requires continuous cell culture over several passages to obtain enough cell resources (number of cartilage cells).

Many problems therefore remain to be solved from the viewpoint of cell-based resources, since cultured cells may lose properties specific to the chondrocyte and may dedifferentiate during passages in culture. Moreover, it takes several months for the tissue-engineered cartilage-like tissue to survive and become organized even when grafted in the defect site, because articular cartilage has less capacity for repair.

Our Novel Biomaterial for Cartilage Repair Generated by Self Assembly-Creation of a Self Organized Articular Cartilage-like Tissue

For the purpose of creating the articular cartilage like tissue applicable to clinical use and overcoming the problem about "cell resource" in cartilage repair, we have been focusing on a novel biomaterial formed by self-assembly [5]. Recently, new materials and devices have been developed through self-assembling materials molecules at the nanometer scale by manipulating the intermolecular relations [6].

Theory of self assembly

Molecules move randomly (Brownian motion) according to thermal motion and they may form a self organized structure based on certain rules depending on the conditions of physicochemical properties such as inter-molecular avidity, surface modification, directions of covalent bonds, and ion arrangements.

Self assembled biomaterial for cartilage tissue engineering

Figure 1: A self-assembled cartilage like complex from hyaluronic acid (HA), aggrecan (AG) and type II collagen.

We demonstrated that it is possible to create a novel biomaterial for cartilage repair with high performance as well as microstructures comparable to hyaline articular cartilage (Figure 1). The analysis by transmission electron microscopy showed that the self-organized collagen polysaccharide complex had a nano-composite structure in which the fibrous collagen was bound to AG binding to HA (arrow head), resembling cartilage tissue. This figure was modified from our previous study [4]. We have developed a technology for creation of cartilage-like tissue not by cultivating chondrocytes to produce cartilage tissue via cartilage matrices, but by self-assembly of the cartilage matrix components, without using cells (Figure 2). Our self-assembled cartilage tissue showed high elasticity (8.5~11 MPa).

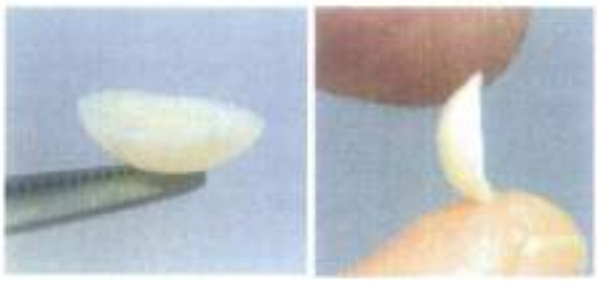

Figure 2: Self assembled cartilage like tissue with high elasticity.

Transplantation of the self-assembled cartilage like tissue into the knee joints of experimental animals

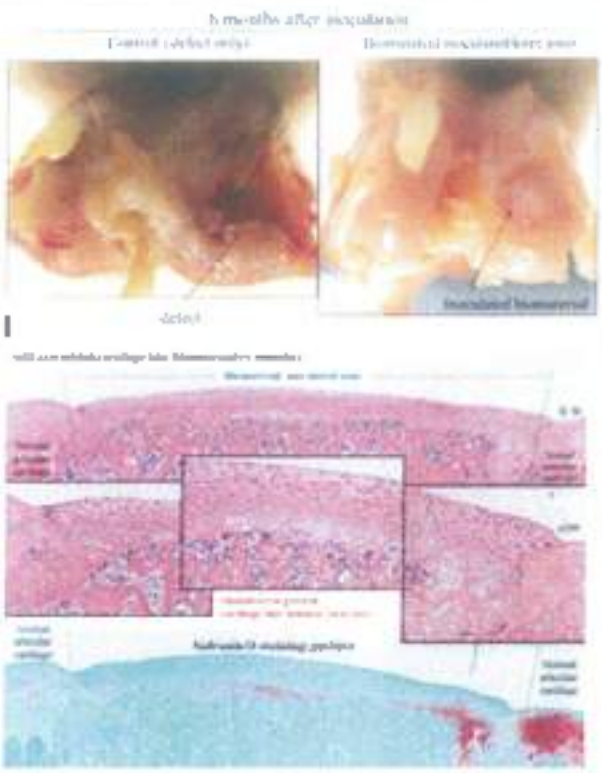

Figure 3: Representative images: transplantation of the self-assembled cartilage like tissue into the knee joints of experimental animals

We transplanted the self-assembled cartilage-like tissue into the OA model animal, partially defecting the articular cartilage tissue of the joint, and examined histologically the transplanted tissue over time (6 weeks after transplantation). The self-organized complex was found even at 6 months to maintain the same tissue structure as was initially observed. In cartilage tissue engineering, an environment suitable for the long-term

How to cite this article: Kawai Y, Nakata S, Yamato Y, Sato K. Cartilage Tissue Engineering-A Novel Biomaterial for Cartilage Repair Generated by Self Assembly-Creation of a Self-Organized Articular Cartilage-like Tissue. Novel Tech. Arthritis Bone Res. 2017; 1-2: 000-007.

survival of chondrocytes is avoided (Figure 3). We prepared the site of articular cartilage defect in each knee joint by drilling the surface of lateral condyle. The self assembled biomaterial was then transplanted into the pit. As a control group, one defect was not treated. Even after 24 weeks, the transplanted self assembled cartilage tissues were maintained in the joint.

Conclusion

The self-organized cartilage-like tissue has a nano-composite structure and is composed of components equivalent to native articular cartilage. It can, moreover, be manufactured in a short time of only a few hours. Our final goal is to develop a biomaterial most suitable for cartilage production. We emphasize the originality of this study, in which we do not need cellular resources like chondrocytes but only cartilage matrix components in order to produce cartilage-like tissue by the self-organization process.

References

1. Tang PF, Li G, Wang B, Chen QJ, Wang Y (2009) Biodynamic Construction and Validation of Porous Carbonated Hydroxyapatite Bone Cement. J Biomed Mater Res B Appl Biomater 90(2): 906-915.
2. Archer CT, Lee AJ, Spector M (2006) Cartilage repair: Synthetic and Stem Cells. Basic Science, Surgical Techniques, and Clinical Outcomes. Sports Med Arthrosc 14(4): 208-216.
3. Jiang CJ, Porter BR (2006) Repair of Injured Articular and Growth Plate Cartilage Using Mesenchymal Stem Cells and Chondrogenic Gene Therapy. Curr Stem Cell Res Ther 1(2): 213-229.
4. Yoshioka K, Tamura R (2012) A novel biomaterial for cartilage repair generated by cell-free molecular creation of a self-organized articular cartilage-like tissue. Journal of Biomechanics and Nanobiotechnology 4: 123-129.
5. Ghosh G (2007) Upstream Efficient Nanomedicine: A Call for Research Commercialization 2(4): 511-521.
6. Shivesh K, Jensen TG (2006) Nanomedicine: Techniques, Pitfalls and Ethical Challenges. J Biomed Biotechnol 2008(5): 51516.

This work is licensed under Creative Commons Attribution 4.0 License

Your next submission with Juniper Publishers will reach you the below assets

- Quality Editorial service
- Swift Peer Review
- Reprints availability
- E-prints Service
- Manuscript Podcast for convenient understanding
- Global attainment for your research
- Manuscript accessibility in different formats (Pdf, E-pub, Full Text, Audio)
- Unending customer service

Track the below URL for one-step submission

https://juniperpublishers.com/online-submission.php

第７章　自己免疫疾患領域での診断のあり方と求める診断技術

第１節　全身性エリテマトーデスの診断の現状と求める診断技術

遊道　和雄
聖マリアンナ医科大学　難病治療研究センター　大学院教授　博士（医学）

株式会社 技術情報協会　発刊書籍
No.1912「疾患・病態検査・診断法の開発」（2017年9月）

第1節　全身性エリテマトーデスの診断の現状と求める診断技術

緒言

SLE（Systemic Lupus Erythematosus）は，自己抗体や DNA 抗 DNA 抗体等の免疫複合体が組織に沈着することで起こる全身性炎症性病変を病態の主座とする自己免疫疾患である。SLE の生命予後は年々改善し，5 年生存率は 90% 以上とされているが，治療抵抗性や再発が多く，重篤な組織・臓器障害を伴う難治性病態の解明と早期診断・治療法の確立が急がれている。

SLE における難治性病態には狼瘡腎炎（ループス腎炎），中枢神経ループス，びまん性肺胞出血，溶血性貧血，血小板減少症，抗リン脂質抗体症候群等があり，病型別では治療抵抗例や予後不良例もみられることから，新規治療法の開発とともに早期診断技術の開発が求められている。本稿では SLE の難治性病態に基づいて，診断技術高度化の必要性を概説する。

1.　SLE の疫学的背景と病因病態について

本邦において，難病認定を受けた SLE 患者数は現在 5 万数千人とされ，好発年齢は 20 ～ 40 歳，男女比は 1：9 で，若い女性可妊年齢の女性が多く，以前から女性ホルモンと病因病態との関連が示唆されてきた。SLE においては，抗核抗体，抗 2 本鎖 DNA 抗体，抗 Sm 抗体，血清補体低，免疫複合体など様々な自己抗体や免疫複合体が検出されることから，これらは SLE 診断のバイオマーカーとして活用され，診断基準にも規定されている。

本邦の病因病態の主座は，抗 2 本鎖 DNA 抗体による免疫複合体の形成と補体による組織・臓器障害とされ，腎臓，肺，皮膚，血液など様々な臓器や組織に障害が認められる。

2　SLE の組織・臓器障害，主症状

SLE 患者でみられる臓器障害や主症状を以下に概説する。

2.1　全身症状

全身倦怠感，易疲労感，発熱が一般的症状としてみられる。

2.2　皮膚・粘膜・関節炎

蝶形紅斑とディスコイド疹が特徴的で，日光曝露で増悪傾向を呈する。皮膚生検で，真皮表皮結合部に IgG 沈着（ループスバンドテスト陽性）が見られることがある。ディスコイド疹は顔面，耳介，頭部，関節背面によくみられ，紅斑は硬結，角化，瘢痕，脱毛をきたすことがある。筋肉痛，関節痛は全経過にわたり，腱鞘炎もみられるが骨破壊を伴うことは稀とされている。

2.3　腎症状

糸球体腎炎（ループス腎炎）は約半数の症例で出現し，急性期では血尿，赤血球円柱，白血球円柱などが尿沈渣で観察される。

2.4　神経症状

中枢神経症状を呈する症例がみられる（CNS ループス），失見当識，妄想，譫などの精神症状，痙攣および脳血管障害を認めることもあり，髄膜炎，脳炎，脳神経障害も稀にみられる。

2.5　心血管症状

心膜炎，心筋炎，大動脈炎症，僧帽弁不全，僧帽弁不全が見られることがある。まれに疣贅が形成されて心内膜炎を呈することもある。反復する血栓性静脈炎や閉塞性血栓症を認めた場合には，抗リン脂質抗体症候群の合併が疑われる。

2.6　血液・造血器症状

溶血性貧血が特徴的である。直接クームス試験陽性で，網状赤血球の増加とハプトグロビンの低下が認められる。抗リン脂質抗体症候群合併例では，血栓症，血小板減少に基づく出血症状や閉塞性血栓がみられることがある。

2.7　泌尿器症状

腎間質性腎炎やループス腎炎によって，腎炎が稀にみられる。

2.8　筋症状

筋炎，間質性肺炎が認められることがあり，稀に血圧低下の合併は予後不良の病態とされている。

3.　SLE の難治性病態

SLE 患者でみられる難治性病態について，診断指標および治療法開発への応用の観点，上掲の問題点を踏まえて以下に概説する。

3.1　難治性ループス腎炎

ステロイド抵抗性のことが多く，増悪増悪や再燃を繰り返しながら腎不全に進行していく難治性腎炎を呈する。本症に対してはシクロホスファミド・パルス療法が導入され，腎機能悪化や腎炎症状寛解の維持が可能となってきたが，15 ～ 20%の症例は腎不全に移行するとされている。

3.2　中枢神経ループス

血清中の抗リボソーム P 抗体と髄液中抗神経細胞抗体や cytokine 6 の上昇がみられ，病態診断として有用であることが示唆されている。

抗リボソーム P 抗体は，大脳血管内皮からの TNF-α 産生を増強させる作用を持つ。さらに，この自己抗体は TNF-α を介して血液脳関門（blood-brain barrier）の透過性を亢進させることで，免疫複合体の中枢神経系への流入と沈着を亢進させることが示唆されており，抗リボソーム P 抗体をターゲットにする治療戦略も進められているという。

また，ループス神経病患者の髄液中に，神経細胞表面のグルタミン酸受容体に対する自己抗体が増加していることや，抗リボソーム P 抗体が認識する神経細胞表面蛋白質の NMDA の存在が報告されている。また，抗カルジオリピン抗体やループスアンチコアグラントが血清中にみられる抗リン脂質抗体症候群症例では多発脳梗塞を示すこともあるとされており，診断の補助因子として活用できることが示唆される。

3.3　抗リン脂質抗体症候群

抗リン脂質抗体症候群の病因として，対象蛋白 β2 グリコプロテイン I に，抗リン脂質抗体による β2-グリコプロテイン I 産生の増加が報告されている。さらに，血栓発症の病態には β2-グリコプロテイン I そのものよりも，β2 グリコプロテイン I を介した自己抗体の補足への利用も指摘されている。また，抗リン脂質抗体症候群の主症状のひとつである妊娠合併症の病因として胎盤活性化の関与が示唆されている。

3.4　SLE の難治性血液・造血器障害

SLE における難治性血液障害として最も注意を要するのは血小板減少であり，血栓性血小板減少性紫斑病，血球貪食

[illegible]および溶血性貧血もみられる。その治療薬はステロイドや免疫抑制薬が主であるが、抗抗核抗体陽性[illegible]による血栓症や、血球貪食症候群における抗サイトカイン療法も効果が期待されている。

4. 現行の診断基準

(主に Systemic Lupus International Collaborating Clinics 分類基準 2012 年について)

SLE の診断基準はアメリカリウマチ学会（ACR）の 1997 年改訂基準が主に用いられてきたが、2012 年に Systemic Lupus International Collaborating Clinics（SLICC）分類基準が公表され、臨床症状項目と血液・免疫学的検査項目を各々に検討することとなり、免疫学的項目には疾患活動性を反映する補体値の項目が追加されている。

以下に SLICC 分類基準を概説する。

4-1 臨床症状項目（11 項目）

(1) 急性皮膚ループス

ループス顔面皮疹、水疱性ループス、中毒性表皮壊死症、表皮直接型ループス皮疹、光線過敏ループス皮疹がみられる。これらの皮膚病変が皮膚筋炎による場合は SLE との鑑別を要する。

(2) 慢性皮膚ループス

円板状皮疹、疣贅状ループス、深在性ループス、円板状ループス、ループス皆脂腺炎、粘膜ループスや瘢痕脱毛がみられる。

(3) 口腔潰瘍

口腔内、舌、鼻腔内に粘膜潰瘍がみられる。鑑別疾患として血管炎、ベーチェット病、ヘルペス感染症、炎症性腸疾患などでみられる口腔潰瘍がある。

(4) 非瘢痕性脱毛

円形脱毛症、梅毒性、鉄欠乏、男性ホルモンによる脱毛症等は鑑別疾患とするが、まばらで細くなった毛髪（薄い毛）がみられる。

(5) 滑膜炎

2 カ所以上の関節腫脹・滑膜炎を伴う滑膜炎症状や関節痛症、または 2 カ所以上の関節痛と 30 分以上の morning stiffness がみられる。

(6) 漿膜炎

一日以上続く典型的な胸膜炎、胸水、病歴等聴きがみられる。一日以上続く心外膜炎、心嚢液貯留、心外膜摩擦音、心外膜炎をいう。

(7) 腎症

尿蛋白クレアチニン比や 24 時間尿蛋白で一日 500mg 以上尿蛋白が検出される。

(8) 神経症状

痙攣、大脳神経障害、血管炎、感染症、脳梗塞、多発性神経炎、骨髄炎などの他の疾患・原因を除く脳神経障害ならびに急性錯乱状態がみられる。

(9) 溶血性貧血

(10) 白血球減少、リンパ球減少

複数回の検査において、少なくとも一回は白血球数 4000/mm³ 未満、または少なくとも一回はリンパ球数 1000/mm³ 未満がみられる（薬剤性、門脈圧亢進、フェルティ症候群、ステロイドに起因する症状、薬剤性、感染症などは除外する）。

(11) 血小板減少

複数回の検査において、少なくとも一回は血小板数 100,000/mm³ 未満である（血栓性血小板減少性紫斑病、薬剤性、門脈圧亢進症などは鑑別疾患として注意を要する）。

4.2　免疫学的検査項目（5項目）

(7) 抗核抗体陽性

(8) 抗2本鎖DNA抗体陽性（ラジオ法1陽性）

(9) 抗Sm抗体陽性

(10) ループス抗凝固因子陽性，梅毒血清反応生物学的偽陽性，カルジオリピン抗体価陽性（2倍以上）または抗β2glycoprotein I陽性

(11) 補体減少

(12) 溶血性貧血がなく直接クームス陽性

これら臨床症状項目11項目，免疫学的検査項目5項目のうち，それぞれ1項目以上，合計4項目を満たす場合はSLEと診断される（SLICC分類基準，2012年）。SLICC分類基準は1997年ACR分類基準よりも，多様な急性・慢性の皮膚病変，胸膜炎・心外膜炎などの漿膜症状や神経病変が含まれ，かつ，免疫学的検査項目を必ず一つ満たすことを基準としている。

5.　SLE診断における補体，自己抗体，免疫複合体の価値

疾患活動性を反映するとされる血清補体価（CH50，C3，C4，CH50感度）の項目が基準に含まれることになった。SLEにおいて，免疫複合体が細胞・臓器に沈着すると，補体が動員・消費されるため補体値が低下するとされており，診断における価値が示されている。

自己抗体のうち抗2本鎖DNA抗体は一般的に疾患特異性が高いとされているが，抗カルジオリピン抗体，ループスアンチコアグラント，抗Sm抗体，抗SSA抗体，抗U1RNP抗体および抗β2グリコプロテインIも陽性のことがあることから，免疫学的検査項目として明記され，診断基準において重要である。

生検による病理所見として，皮膚と腎臓組織の所見は診断上重要である。皮膚生検の組織の免疫染色において，表皮真皮境界部に顆粒状の免疫グロブリンの沈着が観察され，ループスバンドと呼ばれている。ループス腎炎の合併を疑う時には腎生検を行なう。SLEに比較的特異的とされる補体CH50や免疫複合体の沈着を確認することが可能である。これにより，国際腎臓学会によるループス腎炎の病理組織分類に基づいて治療方針を決定することができる。

SCIENTIFIC REPORTS

T cells upon activation promote endothelin 1 production in monocytes via IFN-γ and TNF-α

Received: 16 May 2017
Accepted: 6 October 2017
Published online: 03 November 2017

Shoshi Shinagawa[1], Takahiro Okazaki[2], Mari Ikeda[1], Kazuo Yudoh[2], Yuzi Y. Kisanuki[3], Masashi Yanagisawa[4], Kimito Kawahata[1] & Shoichi Ozaki[2]

Endothelin 1 (ET-1), mainly produced from vascular endothelial cells, induces vasoconstriction in physiological conditions. The endothelin receptor antagonist is among the most effective agents for pulmonary hypertension. However, little is known about the production source of ET-1 in inflammation and immunity. Here, we studied whether T cell-mediated ET-1 production system exists and operates independent of the production system in vascular endothelial cells. ET-1 production was readily detectable in the culture supernatant of human PBMCs and murine spleen cells stimulated with anti-CD3 antibody. Immunocytostaining showed that ET-1-producing cells emerged only in PBMCs stimulated with anti-CD3 antibody. Using the Transwell system, both murine and human monocytes sorted with magnetic beads in the inner chamber produced ET-1 when T cells were activated with antigen or anti-CD3 antibody in the outer chamber. This ET-1 production was inhibited by anti-IFN-γ and/or TNF-α antibody. Furthermore, monocytes purified from ET$^{flx/flx}$;Tie2-Cre(+) mice, which conditionally lack ET-1 in hematopoietic stem cells and vascular endothelial cells, did not produce ET-1 even when stimulated by antigen-specific T cell activation. This study demonstrates the existence of an immune-mediated ET-1 production induced by T cells upon activation through IFN-γ and TNF-α.

A prominent role for the endothelin (ET) system in the physiological regulation of blood pressure has been long recognized[1]. Endothelin 1 (ET-1) is a major factor that induces vasoconstriction and is mainly produced by vascular endothelial cells, the primary source of ET-1 in physiological conditions[2]. Binding of ET-1 to the endothelin type A receptor (ETA) results in vasoconstriction, growth, and remodeling effects[3]. Focusing on this mechanism, endothelin receptor antagonists were developed and have proven to be among the most effective therapeutic agents, especially for controlling pulmonary hypertension[1,4].

Recently, in addition to regulation of the circulatory system through ET-1 from vascular endothelial cells, an increasing body of evidence suggests that the ET-1 system may play a role in some experimental models of inflammation[5–11]. Although the ET-1 production system has been well investigated in normal physiology in vascular endothelial cells, whether a specific ET-1 production system works in inflammatory conditions remains to be determined. Some investigators have suggested that immune cells such as macrophages[12,13] and dendritic cells synthesize ET-1[14]. Production of ET-1 from these cells may occur via lipopolysaccharide stimulations[14] or an autocrine loop mechanism[15]. However, immune-mediated ET-1 producing system other than LPS-triggering ET-1 production remains to be determined.

For this reason, we postulate the possible relationship between T cells and ET-1 producing cells in an immune-mediated ET-1 production system. In our current study, we explored the existence of an ET-1 production and induction system that is related to the immune system, and demonstrate a newly discovered T cell-mediated vascular endothelial cell independent ET-1 production system by using human and murine immune cells.

[1]Division of Rheumatology and Allergology, Department of Internal Medicine, St. Marianna University School of Medicine, Kawasaki, Japan. [2]Department of Frontier Medicine, Institute of Medical Science, St. Marianna University School of Medicine, Kawasaki, Japan. [3]Department of Neurology, Division of Neurogenetics, The Ohio State University Wexner Medical Center, Columbus, Ohio, USA. [4]International Institute for Integrative Sleep Medicine (WPI-IIIS), University of Tsukuba, Tsukuba, Japan. Correspondence and requests for materials should be addressed to T.O. (email: okazaki@marianna-u.ac.jp)

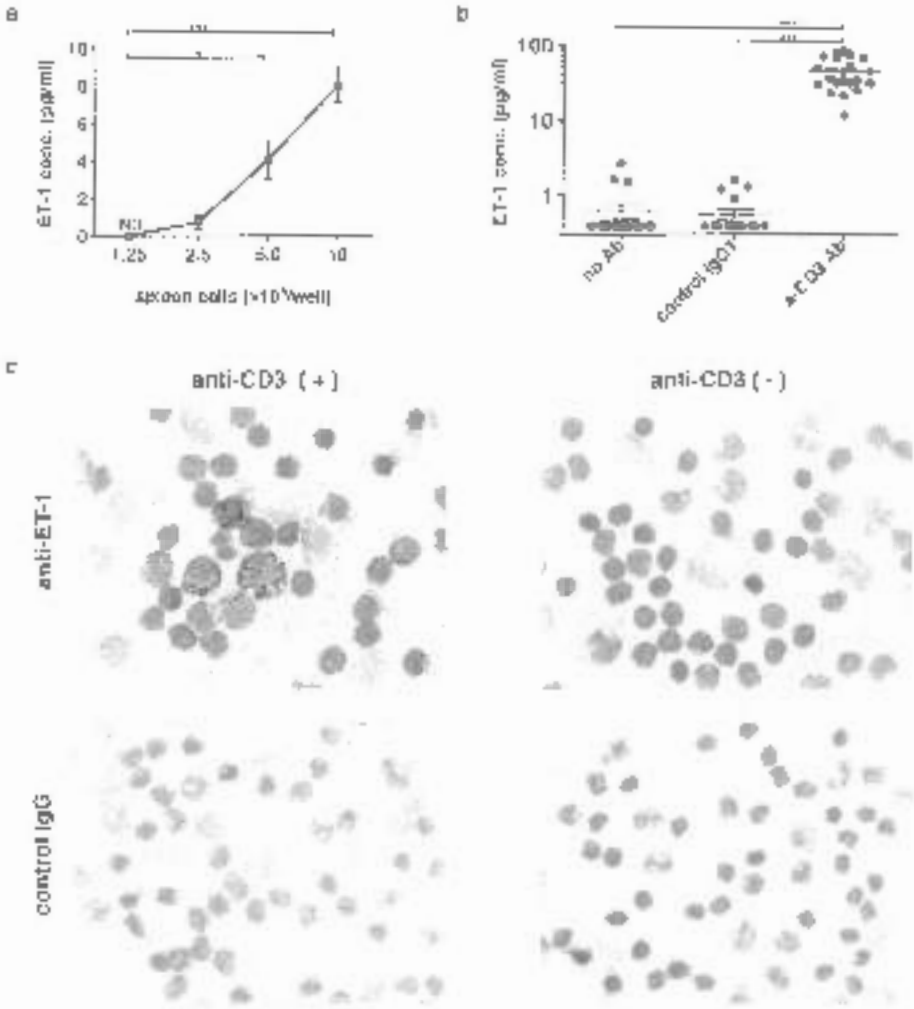

Figure 1. ET-1 production by immune cells following anti-CD3 Ab-mediated activation of T cells in murine spleen cells and human PBMCs. ET-1 production in the culture supernatant of 1×10^6 cells/well of (a) murine spleen cells (b) human PBMCs from 20 healthy donors cultured for 24 h with or without stimulation with 30 μg/ml immobilized anti-human CD3 Ab or control IgG1. The value under the limit of detection (0.39 pg/ml) with ET-1 ELISA assay was defined as 0.39 pg/ml. The assays were performed in triplicate wells. Data are expressed as the mean + SEM. *$p < 0.05$, **$p < 0.001$ as compared with negative control by (a) one-way ANOVA followed by post hoc Tukey's multiple comparison test and (b) Kruskal-Wallis followed by post-hoc Dunn's multiple comparison test. (c) Representative images of immunocytochemical staining of human PBMCs with anti-human ET-1 mAb. PBMCs were cultured in the presence or absence of immobilized anti-human CD3 Ab for 24 h. Brefeldin A (10 μg/ml) was added to the culture for the last 4 h. After fixation with 4% paraformaldehyde and methanol, DAB staining was performed using anti-ET-1 Ab (TR.ET.49.5) or control IgG1. Scale bar represents 20 μm. Similar results (a) and images (c) were obtained in 3 different experiments.

Results

ET-1 production by human PBMCs and murine spleen cells following activation of T cells. T cells express receptors for some vasoconstriction factors such as angiotensin and 5-hydroxytryptamine[21]. Some investigators have used RT-PCR and flow cytometric analysis, and reported that endothelin receptors are expressed in human peripheral T cells[22,23]. Considering that ET-1 may work in an autocrine or paracrine manner, the T cells themselves or adjacent immunocompetent cells could produce ET-1 and stimulate endothelin receptors on activated T cells during inflammation. We investigated whether murine immune spleen cells stimulated with immobilized anti-CD3 Ab can produce ET-1 and observed that such cells produced ET-1 in a cell number dependent manner (Fig. 1a). Based on this fact, we also tested whether T cell activation could promote PBMCs from 20 healthy donors to produce ET-1. This human in vitro study also clearly showed that PBMCs, independent of vascular endothelial cells, produced ET-1 in a manner that was dependent only on the activation of T cells (Fig. 1b). Furthermore, immunocytochemistry showed that cells that produced ET-1 were present among PBMCs activated by immobilized anti-CD3 Ab (Fig. 1c).

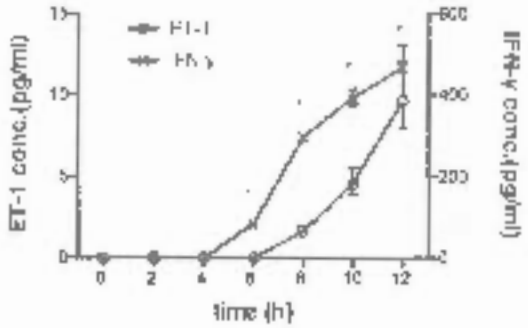

Figure 2. Comparison of the production kinetics between IFN-γ and ET-1 in the culture supernatant of PBMCs stimulated with immobilized anti-CD3 Ab. ET-1 production in the culture supernatant of 1×10^6 cells/well of human PBMCs from a healthy donor cultured with 10 μg/ml immobilized anti-human CD3 Ab. The culture supernatants at appropriate times were collected and measured by ET-1 or IFN-γ ELISA. Assays were performed in triplicate wells, and data represent means ± SEM. ND = not detected. *$P < 0.001$ as calculated compared with negative control (Time 0) by two-way ANOVA followed by post-hoc Sidak's multiple comparison test. Similar results were obtained in 3 different experiments.

ET-1 production from monocytes induced by activated T cells via IFN-γ and TNF-α. To investigate how ET-1 is produced from PBMCs induced by activated T cells, we compared the production kinetics of IFN-γ and ET-1 from activated T cell-induced PBMCs. The kinetics of ET-1 production was clearly later than that of IFN-γ for activation of T cells, suggesting that T cells may induce other immune cells to produce ET-1 in PBMCs (Fig. 2).

Based on previous reports showing that ET-1 is synthesized by macrophages and dendritic cells[7,8], we focused on monocytes as candidates for the source of ET-1 production. T cells and monocytes were purified from PBMCs with magnetic beads and separated with a porous membrane (0.4 μm) using the Transwell system. Purified monocytes in the inner chamber did not produce ET-1 without activated T cells induced by immobilized anti-CD3 Ab in the outer chamber (see Supplementary Fig. S1). Activation of T cells with immobilized anti-CD3 Ab in the outer chamber induced ET-1 production only by monocytes, and not by T cells, in the inner chamber (Fig. 3a). Furthermore, ET-1 production was strongly detected in purified monocytes separated with a porous membrane in the inner chamber by immunofluorescent staining only when T cells were activated with immobilized anti-CD3 Ab in the outer chamber (Fig. 3c). These results indicated that T cells induced monocytes to produce ET-1, possibly via soluble factors released by T cells upon activation. TNF-α is a key cytokine that induces ET-1 production from vascular endothelial cells[27,28]. On the other hands, the cytokines produced by T cells that give rise to macrophages with a phenotype that is distinct from monocytes are IFN-γ, TNF-α, IL-4, and IL-10[29,30]. We next examined the effect of blocking Abs for these cytokines on this T cell-mediated ET-1 production system from monocytes. In the inhibition assay using the double chamber system, Abs against TNF-α and IFN-γ partially inhibited ET-1 production from monocytes, whereas Abs against IL-4 and IL-10 did not (Fig. 3b). Moreover, addition of both Abs blocking IFN-γ and TNF-α completely abolished this ET-1 production from monocytes (Fig. 3c). These findings demonstrated that IFN-γ and TNF-α released from activated T cells induced monocytes to produce ET-1 in human PBMCs.

ET-1 production from monocytes induced by murine antigen-specific CTL activation. Stimulation by immobilized anti-CD3 Ab induces canonical T cell receptor signaling, which may not reflect natural T cell activation. Therefore, we next examined whether antigen-specific T cell activation could induce ET-1 production from monocytes in mice. The Tax-specific CTL line we developed recognizes a specific antigen, Tax11-19 peptide of HTLV-1 restricted with HLA-A2, upon activation in HLA-A2 transgenic HHD mice[31]. Tax-specific CTLs and mitomycin C-treated syngeneic spleen cells from HHD mice were used as antigen-specific T cells and antigen-presenting cells, respectively. Using magnetic beads, murine monocytes were purified from bone marrow cells in HHD mice. Bone marrow-derived monocytes in the inner chamber produced ET-1 only in the presence of antigen-specific activation of CTLs in the outer chamber (Fig. 4a). Furthermore, ET-1 production from monocytes induced by antigen-specific activation of CTLs was also inhibited by anti-IFN-γ and anti-TNF-α Abs (Fig. 4b). Furthermore, from another point of view, to determine whether monocytes can produce ET-1, we used cells from Tie2-Cre;$ET^{flox/flox}$ mice that allow conditional deletion of ET-1 using the Cre-loxP system[32]. Because Tie2 is expressed in endothelial cells and hematopoietic stem cells[33], bone marrow-derived monocytes purified from Tie2-Cre(+);$ET^{flox/flox}$ mice should not be able to produce ET-1. Antigen-specific activation of murine CTLs in the outer chamber induced the bone marrow-derived monocytes purified from Tie2-Cre(−);$ET^{flox/flox}$ mice, which do not harbor the Tie2 promoter, to produce ET-1 in the upper chamber. However, ET-1 production was abolished when using cells from Tie2-Cre(+);$ET^{flox/flox}$ mice in the inner chamber (Fig. 4c). All these findings clearly demonstrated that T cells, upon activation in an antigen-specific manner, promoted monocytes to produce ET-1 via the soluble factors of IFN-γ and TNF-α.

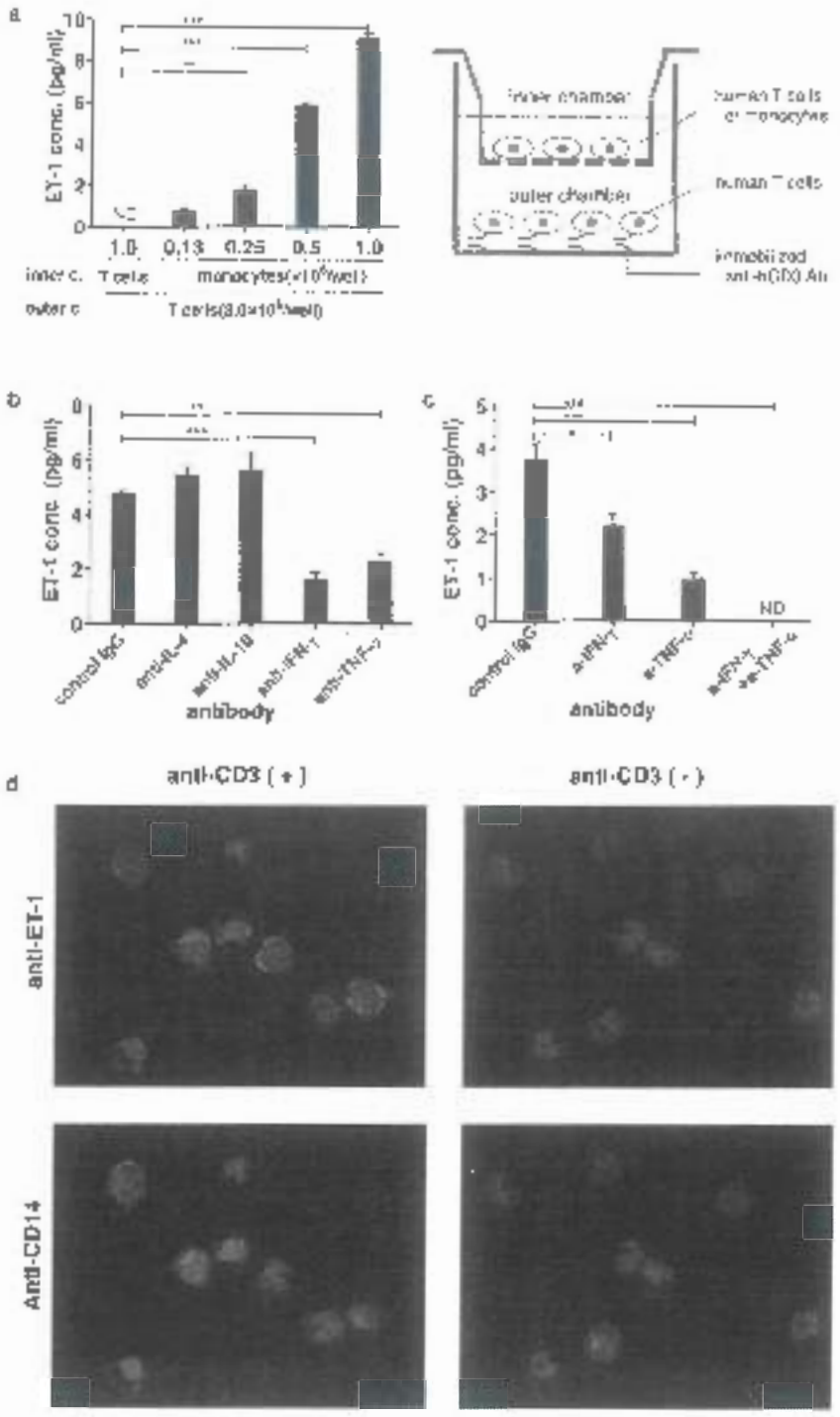

Figure 3. The relationship between T cells and monocytes in ET-1 induction with the double chamber system using human cells. After PBMCs were prepared from 100 ml of whole blood of a volunteer, T cells and monocytes were purified from human PBMCs with Miltenyi MACS, respectively. Three million T cells were stimulated with immobilized anti-CD3 Ab in the outer chamber of the Transwell system (See the schema on the right of Fig. 3a.) In the inner chamber (a), the number of purified T cells or monocytes with magnetic beads is shown on the x axis. For panels (b) and (c), 1.5×10^6 purified human monocytes were cultured for 24 h. The ET-1 concentration in the supernatant of each culture was measured by ng ELISA. The concentration of each blocking Ab used was 30 ug/ml. ND = not detected. The assays were performed in triplicate wells. Data are expressed as the mean + SEM. *p < 0.05, **p < 0.01, ***p < 0.001 as compared with negative control with T cells in the inner chamber (a) or positive control (b,c) by one-way ANOVA followed by post-hoc Tukey's multiple comparison test. (d) Images of the detection of ET-1 production from monocytes purified from PBMCs in the inner chamber. The monocytes in the inner chamber were cultured with T cells in the

outer chamber in the presence or absence of immobilized anti-human CD3 Ab for 24 h. Brefeldin A (10 μg/ml) was added to the culture for the last 4 h. After fixation with 4% paraformaldehyde and 0.5% Triton X-100, immunofluorescent staining was performed using anti-ET-1 Ab (TR ET 48.5) with anti polyclonal mouse IgG(H + L) conjugated with Alexa Fluor 594 (Red) and anti-human CD34 (1:25 dilution) conjugated with Alexa Fluor 488 (Green). Nuclei were visualized with DAPI (Blue). Similar results and images were obtained in at least 3 different experiments (n = 4).

Discussion

ET-1 is a vasoconstriction factor producing powerful contraction of a range of mammalian blood vessel in vitro, including human arteries and veins[1]. In physiological condition, ET-1 synthesized in vascular endothelial cells plays a role in regulating vascular tones by affecting vascular smooth muscles. On the other hand, with the implementation of endothelin receptor antagonist in experimental studies, the blockade of ET-1 mediated signaling with endothelin receptor antagonists reduces the level of inflammation in some animal models of LPS-induced lung inflammation[2], allograft rejection[3], antigen-induced arthritis[4], antigen induced allergic rhinitis[5] and monocrotaline-induced pulmonary artery hypertension[6]. However, how ET-1 is produced and works in such inflammation models other than LPS-induced inflammation remains unknown. Especially in allograft rejection, antigen-induced inflammation and monocrotaline-induced pulmonary artery hypertension models, T cells play a pivotal role in initiating the adaptive immune response[7–9]. In clinical studies, immunosuppressive therapy is effective in some cases of connective tissue disease related pulmonary artery hypertension (PAH), and ET-1 could play a key role in its pathogenesis[10–12]. In idiopathic and connective tissue disease-associated PAH, the existence of perivascular infiltrates and lymphoid follicles that include adaptive immune cells around pulmonary arteries is a pathological finding of pulmonary hypertension[13,14]. Although these experimental, clinical and pathological studies suggest that the ET-1 production system may be modulated by immune cells, the results are conflicting, and evidence for such actions is largely indirect. Thus, we hypothesized that T cells might induce ET-1 production in immune cells. The present study provides clear evidence regarding a potential role for activated T cells to induce the production of ET-1 as a pressor factor from monocytes in both humans and mice.

Endothelin receptors were expressed in T cells[15]. Because ET-1 is considered to act in an autocrine/paracrine manner, endothelin receptors on T cells could be affected by T cells themselves or adjacent immune cells. ET-1 was not detected in the culture supernatant of immobilized anti-CD3 Ab-stimulated T cells (Fig. 3a), whereas both human PBMCs and murine spleen cells stimulated with immobilized anti-CD3 Ab produced significant levels of ET-1 (Fig. 1a,b). Using immunocytochemistry, we also confirmed the existence of ET-1 producing cells among PBMCs stimulated with immobilized anti-CD3 Ab (Fig. 1c). These results indicated that a vascular endothelial cell-independent ET-1 production system can emerge following activation of T cells in human PBMCs and murine spleen cells. Although the primary source of ET-1 synthesis is regarded as vascular endothelial cells, the peptide is produced by other cell types including epithelial cells in the lung, kidney, and colon[16,17] and the choroid plexus and reactive glial cells in the brain[18,19]. Among immune cells, ET-1 synthesis is detected in macrophages[20,21] and dendritic cells[22]. However, little is known about the induction mechanism of ET-1 production by immune cells other than the lipopolysaccharides-activation system of macrophages[23] and the putative autocrine loop mechanism in dendritic cells[24]. To determine how activated T cells could induce immune cells to produce ET-1, we focused on monocytes as a candidate cell type for ET-1 producing immune cells and purified each population of T cells and monocytes with magnetic beads from human PBMCs or murine bone marrow cells. Using the Transwell system, purified T cells, upon activation with immobilized anti-CD3 Ab in the outer chamber, induced monocytes in the inner chamber to produce ET-1 (Fig. 3a, Supplementary Figure S1). Induction of ET-1 production in this non-contact system indicates the existence of soluble mediator molecules between T cells and monocytes. Monocytes/macrophages are highly plastic cells that adopt a variety of activation states. They are broadly divided into classically activated, wound healing, and regulatory macrophages. The important inducers are IFN-γ and TNF-α, IL-4 and IL-10, respectively[25]. Assays using Abs that inhibit these cytokines demonstrated that IFN-γ and TNF-α may be key cytokines for directing monocytes to produce ET-1 as well as induction of classically activated macrophages (Fig. 3b,c, Fig. 4a). Furthermore, in addition to artificial stimulation with immobilized anti-CD3 Ab, antigen-specific activation of cytotoxic T cells led to induction of ET-1 production from bone marrow-derived monocytes in mice, and this induction was blocked by anti-IFN-γ and anti-TNF-α Abs in the Transwell system (Fig. 4b). Since IFN-γ and TNF-α are cytokines produced from CTLs or Th1 cells, we suggest that ET-1 is usually produced during Th1 inflammation and adaptive immunity.

Tie2 is a critical molecule in the development of endothelial cells and hematopoietic stem cells[26]. ET1$^{flox/flox}$;Tie2-Cre mice, which harbor the Tie2 promoter, are conditionally deficient in ET-1 production in endothelial cells and immune cells derived from hematopoietic stem cells[27]. The monocytes purified from bone marrow cells in ET1$^{flox/flox}$;Tie2-Cre mice lost the ability to produce ET-1, but this was not seen in ET1$^{flox/+}$;Tie2-Cre and ET1$^{flox/flox}$;Tie2-Cre(−/+) mice (Fig. 4c). These results also provide evidence for the existence of an ET-1 production system in monocytes induced by T cells upon activation.

The current study suggests that not only acquired immunity may have a potential to directly affect the circulatory system with the newly discovered T cell-mediated ET-1 production mechanism, but also the signal transduction of IFN-γ and TNF-α from T cells to monocytes could play a key role in the regulation of such an immune-mediated ET-1 production system.

In the first part of our study, we focused on the relationship between T cell activation and ET-1 in humans and mice. However, the details of how and where ET-1 is released from monocytes in the immune system are unclear. Further studies will be needed to clarify the physiological and pathological role of the T cell-induced ET-1 production system within the immune system.

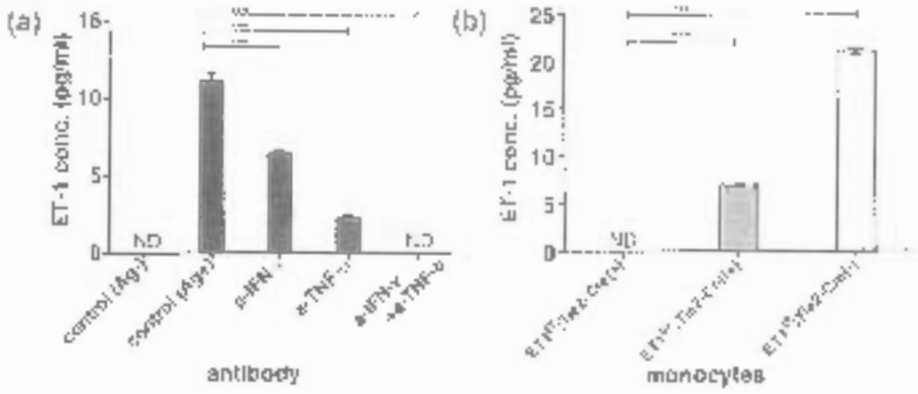

Figure 4. Effect of antigen-specific activation of T cells on monocytes in mice. Three million Tax11-19-specific CTLs were stimulated with 4×10^6 mitomycin C-treated syngeneic spleen cells from HHD mice in the presence or absence of 0.1 μM Tax11-19 peptide as an antigen (Ag) in the outer chamber. In the inner chamber, after bone marrow cells were prepared from 4 mice of femurs in each strain, 1.5×10^6/well of monocytes purified with Mini MACS from bone marrow cells of (a) HHD mice and (b) ET1$^{flox/flox}$;Tie2-Cre(+), ET1$^{flox/+}$;Tie2-Cre(−), and ET1$^{flox/+}$;Tie2-Cre(+) mice were cultured for 24 h. The concentration of each blocking Ab used was 30 μg/ml. ND, not detected. The assays were performed in triplicate wells. Data are expressed as the mean ± SEM. $^{***}p < 0.001$ as compared with positive (a) or negative (b) control by one-way ANOVA followed by post-hoc Tukey's multiple comparison test. Similar results were obtained in two experiments (a,b).

Materials and Methods

Mice. Transgenic HHD-2 mice (gift from Dr. François Lemonnier, Institute Pasteur, Paris, France) were bred in our colony at the Institute of Experimental Animals at St. Marianna University. HHD-2 mice are characterized by knock-out of the murine β2-microglobulin gene, as well as of mouse H-2D^b, plus transgenic expression of human HLA-A2.1 with covalently linked human β2-microglobulin and a murine D^b-derived α3 domain to allow interaction with mouse CD8^N. A tax-specific cytotoxic T lymphocyte (CTL) line was developed from HHD mice. Antigen-specific CTLs recognize the specific antigen of the Tax11-19 peptide of HTLV-1, LLFGYPVYV[17].

Generation of tyrosine kinase with immunoglobulin and epidermal growth factor homology domains-2 (Tie2)-Cre(−);ET$^{flox/flox}$ mice. B6.Cg-Fcrn1$^{-/-}$ tm1 Ywa > (ET$^{flox/flox}$ transgenic) mice harbor a transgene with loxP sites flanking exon 2 of the ET1 gene[18]. B6.Cg-Tg(Tek-cre)1 Ywa (Tie2-Cre transgenic) mice express the Cre recombinase gene under the control of the mouse Tek(Tie2) promoter[19]. Both mouse strains were provided by RIKEN Bioresource Center (Tsukuba, Japan). Tie2-Cre(+)ET$^{flox/flox}$ mice were obtained from crossbreeding these two transgenic lines. To confirm establishment of Tie2-Cre(−).ET$^{flox/flox}$ mice, genomic DNA was prepared from ear lobe biopsies from postnatal day 21 mice and used for genotyping with PCR analysis[20].

Murine spleen cells and bone marrow cells. All animal studies were approved by the Institute of Experimental Animals Committee at St. Marianna University and the methods in these studies were carried out in accordance with the approved guidelines. The murine spleen was removed, the tissue was disrupted, red blood cells were lysed with osmotic lysis, and the single cell suspension was passed through a 70-μm sterile cell strainer. Murine bone marrow cells were obtained from the femur by flushing the shaft with buffer using a syringe with a 25G needle. After obtaining a single-cell suspension by gently pipetting several times, the cells were passed through a cell strainer to remove cell clumps that may clog the column. Cells were washed with PBS (300 × g for 10 minutes) three times.

Human peripheral blood mononuclear cells (PBMCs). Peripheral blood samples from 20 healthy volunteers who provided informed and written consent following permission from the institutional review board at St. Marianna University were used for preparation of PBMCs, which were isolated using Lymphocyte-H (CEDARLANE, Canada). All methods using PBMCs in human studies were carried out in accordance with the approved guidelines.

Cell separation. Immune cells including both human and murine total T cells and monocytes were sorted by negative selection on a Mini-MACS with a cell isolation kit (Miltenyi Biotec, Bergisch Gladbach, Germany) according to the manufacturer's instructions. The efficiency of cell purification was > 95% confirmed by flow-cytometric analysis in each cell purification kit.

IFN-γ and ET-1 ELISA. IFN-γ and ET-1 in the culture supernatant that was harvested at appropriate times were determined using an ELISA Kit (R&D, Minneapolis, MN) according to the manufacturer's instructions. Values of all samples were expressed as means ± SEM of triplicate measurements.

Antibodies. Anti-human cytokine blocking Abs were purchased as follows: IFN-γ and tumor necrosis factor-alpha (TNF-α) from eBioscience Inc. (San Diego, CA), interleukin (IL)-4 from U-cytech (Utrecht, Netherland), and IL-23 from R-Biopharm (Besançon Cedex, France). Anti-murine IFN-γ and TNF-α blocking Abs were purchased from Thermo Scientific (Waltham, MA) and R&D Systems, respectively.

Immunocytochemistry. ET-1 expression was assessed with immunocytochemistry. PBMCs collected from the cultures were prepared on cytospin slides. After fixation with 4% paraformaldehyde and methanol, immunocytochemistry staining was carried out. After blocking with 10% human serum in Block Ace (DS Pharma Biomedical, Osaka, Japan), PBMCs were incubated with diluted primary Abs (anti-ET-1 mAb (TR.ET.48.5) 1:200) overnight at 4 °C. Immunodetection was performed using diluted secondary anti-mouse IgG1 Ab conjugated to horseradish peroxidase (1:1,000, Bethyl Laboratories, Montgomery, TX). Visualization was carried out with the Liquid DAB + Substrate Chromogen System (DAKO, Santa Clara, CA). Images were taken using a BZ-9000 fluorescence microscope (KEYENCE, Osaka, Japan).

In the study using Transwell system, after co-cultured with T cells with or without immobilized anti-CD3 Ab in the outer chamber, monocytes collected from the inner chamber were prepared on cytospin slide. After fixation with 4% paraformaldehyde and 0.5% Triton X-100, immunofluorescence was performed using the following antibodies: anti-ET-1 mAb (TR.ET.48.5, 1:400 dilution) and Alexa Fluor 594-conjugated anti-mouse IgG(H + L) (1:500 diluted) (Jackson ImmunoResearch Inc., West Grove, PA). Cells were incubated in primary antibody diluted in Can Get Signal immunostain (TOYOBO, Osaka, Japan) at 4 °C overnight. After rinsing thrice with PBS(−), Alexa Fluor 594-conjugated secondary antibody was used for detection. Alexa Fluor 488-conjugated anti-human CD14 (1:25 dilution) (BioLegend, San Diego, CA) was subsequently used for double staining. After four additional PBS washes, cells were stained with 4′,6-diamidino-2-phenylindole (DAPI) (Sigma-Aldrich, St. Louis, MO). Images were taken using a BZ-9000 fluorescence microscope (KEYENCE, Osaka, Japan).

Statistical analysis. All of the detection experiments using ELISA were performed in triplicate, and the data were expressed as the mean ± SEM and were analyzed using Graph Pad Prism V6.0 (San Diego, CA). We used one-way ANOVA followed by *post hoc* Tukey's multiple comparison test in Figs 1a, 3a,b, 4a and b. In Fig. 1b, based on the result by D'Agostino & Pearson omnibus normality test, we used Kruskal–Wallis followed by *post-hoc* Dunn's multiple comparison test. Two-way ANOVA was performed in Fig. 2. Significance was accepted as $p < 0.05$.

References

1. Davenport, A. P. *et al.* Endothelin. *Pharmacological reviews* 68, 357–418, https://doi.org/10.1124/pr.115.011544 (2016).
2. Yanagisawa, M. *et al.* A novel potent vasoconstrictor peptide produced by vascular endothelial cells. *Nature* 332, 411–415 (1988).
3. Kedzierski, R. M. & Yanagisawa, M. Endothelin system: the double-edged sword in health and disease. *Annu. Rev. Pharmacol. Toxicol.* 41, 851–876 (2001).
4. Maguire, J. J. & Davenport, A. P. Endothelin receptors and their antagonists. *Seminars in nephrology* 35, 123–136, https://doi.org/10.1016/j.semnephrol.2015.02.002 (2015).
5. Sangaletti, A. L., Rae, G. A. & Henrique, R. Effects of endothelin ETA receptor antagonism on granulocyte and lymphocyte accumulation in LPS-induced inflammation. *J. Cardiov. Res.* 76, 210–216 (2001).
6. Lawrence, T. *et al.* Activation of pro-inflammatory and anti-inflammatory cytokines in heart organs during chronic allograft rejection: roles of endothelin receptor signaling. *Am. J. Transplants.* 1, 242–249 (2001).
7. Imhof, A. K. *et al.* Potent anti-inflammatory and antinociceptive activity of the endothelin receptor antagonist bosentan in monoarthritic mice. *Arthritis Res. Ther.* 13, R97 (2011).
8. Dynase, P. B. *et al.* Bosentan, an endothelin receptor antagonist, ameliorates collagen-induced arthritis: the role of TNF-alpha in the induction of endothelin system genes. *Inflammation research: official journal of the European Histamine Research Society [et al.]* 58, 337–348, https://doi.org/10.1007/s00011-009-0103-5 (2010).
9. Guo, Y. *et al.* Endothelin-1 overexpression exacerbates experimental allergic encephalomyelitis. *Journal of neuroimmunology* 276, 64–73, https://doi.org/10.1016/j.jneuroim.2014.06.016 (2014).
10. Tatar, A. *et al.* The role of endothelin-1 and endothelin receptor antagonists in allergic chronic inflammation: ovalbumin-induced rat model. *Allergology, https://doi.org/10.5167/uzh-115529* (2015).
11. Bonnet, D. *et al.* Myocardial and non-inflammatory effects of chronic bosentan therapy in patients with idiopathic pulmonary hypertension. *Revista portuguesa de cardiologia: orgao oficial da Sociedade Portuguesa de Cardiologia = Portuguese journal of cardiology: an official journal of the Portuguese Society of Cardiology* 33, 211–212, https://doi.org/10.1016/j.repc.2013.10.016 (2014).
12. Elhmouzi-Younes, J. *et al.* Endothelins, peptides with potent vasoactive properties, are produced by human macrophages. *The Journal of experimental medicine* 172, 1741–1744 (1990).
13. Wahl, L. B. *et al.* Murine macrophages produce endothelin-1 after microbial stimulation. *Experimental biology and medicine (Maywood, N.J.)* 230, 692–698 (2005).
14. McKenna, S. *et al.* Endothelin-1 Induces Cappathetin/NF-kappaB-Dependent Endothelin-1 Expression in Hepatic Macrophages. *J. Immunol.* 195, 3596–3609, https://doi.org/10.4049/jimmunol.1500112 (2015).
15. Sun, C. *et al.* Functional analysis of the preproendothelin-1 gene promoter in pulmonary epithelial cells and monocytes. *Biochemical and biophysical research communications* 221, 647–652, https://doi.org/10.1006/bbrc.1996.0651 (1996).
16. Gerfen, G. *et al.* Tumor-induced survival of dendritic cells depends on endothelin-1 and endothelin receptor-mediated beclin-1 induction. *Blood* 118, 3107–3116, https://doi.org/10.1182/blood-2010-10-313-1 (2011).
17. Marala, A. *et al.* Immunosuppressive effect of angiotensin receptor blockers on stimulation of mouse CTLs by angiotensin II. *Int. immunopharmacol.* 9, 1189–1196 (2009).
18. Inoue, M. *et al.* Regulation of antigen-specific CD4+ and CD8+ T cell activation through 5-Hydroxytryptamine 2A receptor. *Int. immunopharmacol.* 11, 64–71 (2011).
19. Gunther, J. *et al.* Angiotensin receptor type 1 and endothelin receptor type A on immune cells mediate migration and the expression of IL-8 and CCL18 when stimulated by autoantibodies from systemic sclerosis patients. *Arthritis Res. Ther.* 16, 505, https://doi.org/10.1186/s13075-014-0505-1 (2014).
20. Khan, I. *et al.* Endothelin Receptors Expressed by Immune Cells Are Involved in Modulation of Inflammation and in Fibrosis. Relevance to The Pathogenesis of Systemic Sclerosis. *Journal of immunology research* 2015, 147615, https://doi.org/10.1155/2015/147615 (2015).
21. Corder, R., Carter, M., Khan, N., Kramm, P. & Vane, J. R. Cytokine regulation of endothelin-1 release from porcine endothelial cells. *Journal of cardiovascular pharmacology* 26 Suppl 3, S96–8 (1995).
22. Kataoka, M. R. & Fan, F. S. Effect of cytokines on the production of endothelin by endothelial cells. *Clinical and experimental rheumatology* 15, 153–157 (1997).
23. Mosser, D. M. & Edwards, J. P. Exploring the full spectrum of macrophage activation. *Nature reviews. Immunology* 8, 958–969, https://doi.org/10.1038/nri2448 (2008).
24. Wynn, T. A., Chawla, A. & Pollard, J. W. Macrophage biology in development, homeostasis and disease. *Nature* 496, 445–455, https://doi.org/10.1038/nature12034 (2013).

26. Kawano, T. et al. Advantage of higher avidity CTL specific for Tax against human T lymphotropic virus 1-infected cell and tumor cell mutants. 773, 11–17 (2011).
27. Pascolo, S. et al. HLA-A2.1-restricted education and cytolytic activity of CD8+ T lymphocytes from beta2-microglobulin (beta2m) HLA-A2.1 monochain transgenic H-2Db beta2m double knockout mice. The Journal of experimental medicine 185, 2043–2051 (1997).
28. Kisanuki, Y. Y. et al. Low blood pressure in endothelial cell-specific endothelin 1 knockout mice. Hypertension 56, 777–783, http://dx.doi.org/10.1161/HYPERTENSIONAHA.109.138701 (2010).
29. Takakura, N. et al. Critical role of the TIE2 endothelial cell receptor in the development of definitive hematopoiesis. Immunity 9, 677–686 (1998).
30. Marino, J., Paster, J. & Benichou, G. Allorecognition by T lymphocytes and Allograft Rejection. Frontiers in immunology 7, 582, https://doi.org/10.3389/fimmu.2016.00582 (2016).
31. Andersson, S. E., Lennmyr, K., Alving, K. & Ekstrom, G. M. Pertussis toxin-induced levels of cytokine- and endothelin-1-like immunoreactivity during the course of carrageenan-induced arthritis in the rat. Inflammation research: official journal of the European Histamine Research Society ... [et al.] 48, 451–456, https://doi.org/10.1007/s000110050492 (1999).
32. Guo, C., Chen, G. & Liu, R. IL-33, rather than IL-25, is crucial for the development of ovalbumin-induced allergic thinks. Molecular Immunology 67, 436–445, https://doi.org/10.1016/j.molimm.2015.07.024 (2015).
33. Cuttica, M. J. et al. Perivascular T-cell infiltration leads to sustained pulmonary artery remodeling after endothelial cell damage. American journal of respiratory cell and molecular biology 45, 62–71, http://dx.doi.org/10.1165/rcmb.2009-0340OC (2011).
34. Giaid, A. et al. Expression of endothelin-1 in the lungs of patients with pulmonary hypertension. The New England journal of medicine 328, 1732–1739 (1993).
35. Sanchez, O., Sitbon, O., Jais, X., Simonneau, G. & Humbert, M. Immunosuppressive therapy in connective tissue disease-associated pulmonary arterial hypertension. Chest 130, 182–189, https://doi.org/10.1378/chest.130.1.182 (2006).
36. Jais, X. et al. Immunosuppressive therapy in lupus and mixed connective tissue disease associated pulmonary arterial hypertension: a retrospective analysis of twenty-three cases. Arthritis Rheum 58, 545–554, http://doi.org/10.1002/art.23203 (2008).
37. Miyamoto-Yamamoto, S. et al. Intensive immunosuppressive therapy improves pulmonary hemodynamics and long-term prognosis in patients with pulmonary arterial hypertension associated with connective tissue disease. Circulation journal: official journal of the Japanese Circulation Society 75, 2068–2074 (2011).
38. Stacher, E. et al. Modern age pathology of pulmonary arterial hypertension. Am J Respir Crit Care Med 186, 261–272, https://doi.org/10.1164/rccm.201201-0077OC (2012).
39. Rabinovitch, M., Guignabert, C., Humbert, M. & Nicolls, M. R. Inflammation and immunity in the pathogenesis of pulmonary arterial hypertension. Circ Res 115, 165–175, https://doi.org/10.1161/CIRCRESAHA.113.301141 (2014).
40. Perros, F. et al. Pulmonary lymphoid neogenesis in idiopathic pulmonary arterial hypertension. Am J Respir Crit Care Med 185, 311–321, https://doi.org/10.1164/rccm.201108-1396OC (2012).
41. Rosenquist, N., Springall, D. R. & Polak, J. M. Localization of endothelin-like immunoreactivity in airway epithelium of rats and mice. The journal of pathology 160, 5–8, https://doi.org/10.1002/path.1711600103 (1990).
42. Zmuda, M. L., Brady, H. R., Kunz, R. C., Gullans, S. R. & Brenner, B. M. Endothelin, a peptide inhibitor of Na+/K+ ATPase in intact proximal tubule epithelial cells. The American journal of physiology 257, C1101–1107 (1989).
43. Takahashi, K. et al. Endothelin in the gastrointestinal tract. Presence of endothelin-like immunoreactivity, endothelin-1 messenger RNA, endothelin receptors, and pharmacological effect. Gastroenterology 99, 1660–1667 (1990).
44. Jang, M. H., Erickson, L. B. & Olson, Y. Brain neurochemical evidence of endothelin-1 in human choroid plexus. Acta neuropathologica 84, 457–461 (1992).
45. Maccarrone, M. M., Ross, C. A. & Snyder, S. H. Endothelin in brain: receptors, mitogenesis, and biosynthesis in glial cells. Proc Natl Acad Sci U S A 87, 2359–2363 (1990).
46. Sechet, R. V. et al. Mice with cardiomyocyte-specific transgenic of the endothelin-1 gene are resistant to hypertrophy and cardiac hypertrophy. Proc Natl Acad Sci USA 108, 2089–2093, https://doi.org/10.1073/pnas.1007510108 (2011).
47. Kisanuki, Y. Y. et al. Tie2-Cre transgenic mice: a new model for endothelial cell-lineage analysis in vivo. Developmental biology 230, 230–242, https://doi.org/10.1006/dbio.2000.9995 (2001).

Acknowledgements

This study was supported in part by a grant-in-aid from the Ministry of Health, Labor, and Welfare of Japan. We would like to thank Toshiko Sato and Mayumi Tamaki for technical assistance provided during the study.

Author Contributions

S.S. and M.I. performed data analysis and prepared manuscript. T.O. helped prepare the manuscript, managed data collection. K.Y. assisted in analysis and interpretation. Y.Y.K. and M.Y. assisted the development of conditional knockout mice. T.O., K.K., and S.O. conceived of and designed the study. All authors reviewed and contributed to the manuscript.

Additional Information

Supplementary information accompanies this paper at http://www.nature.com/scientificreports/srep/srep14590-s1.pdf.

Competing Interests: The authors declare that they have no competing interests.

Publisher's note: Springer Nature remains neutral with regard to jurisdictional claims in published maps and institutional affiliations.

Open Access This article is licensed under a Creative Commons Attribution 4.0 International License, which permits use, sharing, adaptation, distribution and reproduction in any medium or format, as long as you give appropriate credit to the original author(s) and the source, provide a link to the Creative Commons license, and indicate if changes were made. The images or other third party material in this article are included in the article's Creative Commons license, unless indicated otherwise in a credit line to the material. If material is not included in the article's Creative Commons license and your intended use is not permitted by statutory regulation or exceeds the permitted use, you will need to obtain permission directly from the copyright holder. To view a copy of this license, visit http://creativecommons.org/licenses/by/4.0/.

© The Author(s) 2017

Novel Techniques in Arthritis & Bone Research
ISSN: 2575-8888

Juniper Publishers
key to the Researchers

Mini Review
Volume 2 Issue 3 – December 2017
DOI: 10.19080/NTAB.2017.02.555588

Nov Tech Arthritis Bone Res
Copyright © All rights are reserved by Kazuo Yudoh

Cell-to-Cell Interactions of Activated T Cells with Adjacent Cells in Inflamed Tissue in Inflammatory Diseases

Kazuo Yudoh[1*], Naoko Yui[2], Takaneri Kumai[2] and Rie Karasawa[1]

[1]Department of Frontier Medicine, St. Marianna University School of Medicine, Japan

[2]Department of Sports Medicine, St. Marianna University School of Medicine, Japan

Submission: November 29, 2017; **Published:** December 12, 2017

***Corresponding author:** Kazuo Yudoh, Department of Frontier Medicine, Institute of Medical Science, St. Marianna University School of Medicine, Kawasaki, Japan, Tel: 044-977-8111; email: yudoh@marianna.ac.jp

Abstract

Importance of inflammatory cytokine cascade has been pointed out in the pathogenesis of arthritis. Recent clinical studies have already shown the benefit in suppressing proinflammatory cytokines in arthritis, including the central role of those cytokines, particularly tumor necrosis factor (TNF)-α and interleukin (IL)-6, in the progression of bone and joint deterioration. Several candidate pathways are currently being investigated in the pathogenesis of joint deterioration. In consequence, considerable interest has arisen in these pathways that in turn regulate proinflammatory cytokine productions, because they may offer further possible clinical trial against bone and joint diseases.

Recently the attention has been alerted the cell-to-cell interaction may drive proinflammatory cytokine productions, metalloproteinase secretions and the differentiation of bone resorbing osteoclasts. The cell-to-cell membrane contact may have a crucial important role in the progression of inflammation/arthritis, synovial hyperplasia, infiltration of inflammatory cells into the tissue, bone resorption and cartilage degeneration.

It has been reported that the direct cell membrane contact between synovial T cells adjacent macrophages and synovial fibroblasts induces the production of proinflammatory cytokines from macrophages and synovial fibroblasts. Also recent reports indicating the role of receptor activator of NF-κB (RANK) signaling pathway through T cell-osteoclast precursor cell contact in the maturation of osteoclast have revealed the mechanism of bone and joint destruction in arthritis. More recently, we have demonstrated that the cell-cell interactions between activated T cells and chondrocytes may induce articular cartilage destruction through the mechanism involving the acceleration of proteolytic enzyme secretion, suggesting the T cell mediated destruction of articular cartilage through pathways independent on cell contact.

Recent advances in our understanding of the events ongoing in inflamed joint tissues, synovial membrane, bone and cartilage tissue, have shed a light to the elucidation of mechanisms of joint destruction in arthritis. We here reviewed the potential implication of cell-to-cell interactions in the joint deterioration in arthritis. These novel pathways may represent exciting potential therapeutic targets.

Abbreviation: TNF-α: Tumor Necrosis Factor-α; IL: Interleukin; PI-3 kinase: Phosphatidylinositol-3 kinase; NF-κB: Nuclear Factor κB; MMPs: Metalloproteinases; IFN: Interferon; RANK: Receptor Activator of NF-κB

Opinion

Inflammatory arthritis such as rheumatoid arthritis (RA) is characterized by the synovial hyperplasia, neoangiogenesis, the infiltrating lymphocytes and macrophages, and bone and articular destruction [1,2]. A variety of cytokines and chemokines that are mostly produced from synovial infiltrating T cells, macrophages and synovial fibroblasts form a network and deeply participate in the pathogenesis of arthritis. Recent clinical and basic intervention studies have shown the therapeutic effectiveness of the agents, which specifically inhibit the activity of proinflammatory cytokines [3,4]. The predominance of macrophage-derived cytokines, particularly TNF-α, interleukin (IL)-6 and IL-1β in the hierarchy of synovial inflammation has been clearly demonstrated in several recent clinical studies, indicating that those inflammatory cytokines are closely involved in the development of arthritis [4,5].

It has been also revealed that macrophage derived cytokines are closely involved in the osteoclastogenesis and degeneration of articular cartilage, indicating its implication in the articular degeneration in arthritis [3-6]. The factors that promote such macrophage activation could represent effective therapeutic targets, however the mechanisms whereby macrophages participate in the proinflammatory cytokine productions remain still unknown in arthritis.

It becomes clear that not only the relationship between individual cytokines and their target cells but also the cellular cross talk may be involved in the cytokine networks and the pathogenesis of inflammatory arthritis [2,5,7]. In inflamed synovial tissue, numerous numbers of lymphocytes and macrophages are infiltrated and form cellular aggregates [8,9]. The aggregates have a part as a germinal center in the synovial tissue. Mclennan et al. demonstrated that RA synovial fibroblasts show enhanced production of proinflammatory cytokines in response to the direct cell membrane contact between T cells and synovial fibroblasts through specific adhesion molecules suggesting the importance of "cell contact induced inflammation" in synovitis/arthritis [3,6,10]. We have also elucidated the regulatory mechanism whereby the direct cell contact contributes to the production of macrophage-derived cytokines, TNF-α and IL-1 [11]. IL-15 has a stimulatory effect on the cell contact-induced production of proinflammatory cytokines by macrophages [10,12]. Our findings clearly demonstrated that IL-18 also accelerates the macrophage-derived cytokines productions through the direct cell membrane contact [11]. Also, we have studied the synovial infiltrating T cell derived destructions of bone and articular cartilage tissues through the mechanism involving cell-cell contact pathway.

Recent advances in our understanding of the events ongoing in inflamed synovial membrane have revealed that synovial infiltrating T cells may drive inflammation, osteoclastogenesis and destruction of articular cartilage through pathways dependent on cell-to-cell contact [1,3,4,5,10-13]. We have reviewed the mechanism of tissue deterioration in inflammatory diseases from the point of view of the cell-to-cell interactions and the resultant deterioration of inflamed tissue/organ in arthritis (Figure 1).

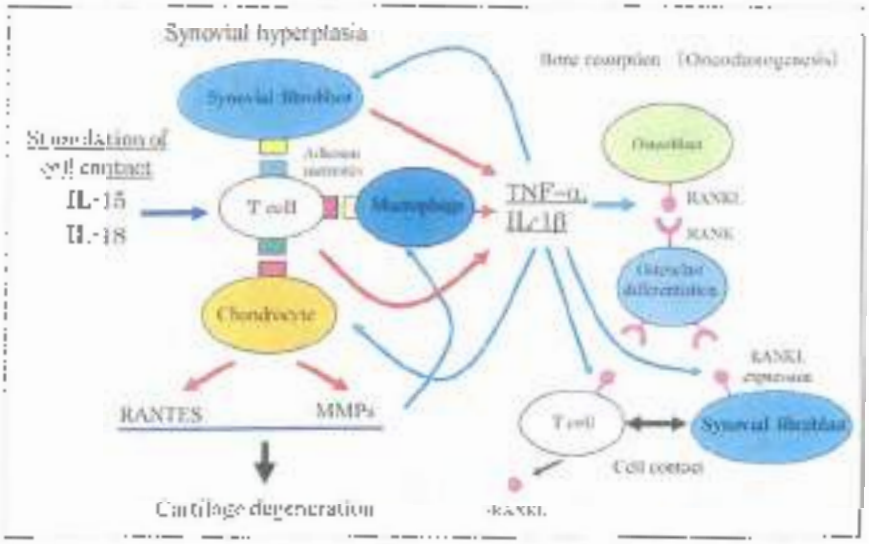

Figure 1: Cell contact-induced inflammation/deformation

Characteristics of Inflamed Synovial Membrane

Inflammatory synovial membrane is characterized by hyperplasia of synovial cells, especially synovial fibroblasts type B cells, neoangiogenesis, and infiltration of T cells and macrophages in the synovium [1-3]. It is well known that the synovitis is mainly regulated by cooperation of various cytokines and chemokines [1-5]. Inflamed synovial membrane has higher levels of proinflammatory cytokines, TNF-α, IL-1, IL-15, IL-18 and IL-21, and lower level of inhibitory cytokines, IL-4 and IL-10 expressions [1-3,6-10-13]. Compatible with these observations, higher rate of NFκB translocation is evident in RA than in osteoarthritis arthritis synovitis. Further descriptions on the neoangiogenesis and the expression of matrix degrading proteolytic enzymes have also been described [14,15]. These studies are important, because they may prove information as to disease mediator pathways in synovial membrane that represent common pathways to articular destruction as opposed to those that more closely reflect and/or may potentially direct causes.

Cytokines and proteases are mainly produced from synovial infiltrating macrophages and synovial fibroblasts [1,2,3,5]. TNF-α and IL-1 act on macrophages and T cells as autocrine/paracrine factors and can induce their secretions each other. Thus, recent studies have paid attention to the mechanism whereby macrophages and synovial fibroblasts are activated for productions of secretory factors.

In inflamed synovial tissue, infiltrating T cells and macrophages lie in juxtaposition within and adjacent to cellular aggregates in the synovial tissue in arthritis, providing for reciprocal cellular cross talk [5]. It has attracted attention that the cell-to-cell contact of T cells with macrophages or synovial fibroblasts induces the production of proinflammatory cytokines with no requirement of other cytokine stimulation [10,11]. Since there is a variety number of infiltrating T cells, macrophages as well as synovial fibroblasts in the synovial tissue, direct cell contact-induced cytokine productions could have a critical

important role in the progression of synovitis. The observation indicated that a fundamental property of synovial infiltrating T cells may be the activation of adjacent cells mediated by cell membrane contact.

We have postulated that the cell-to-cell interaction may modulate not only inflammation but also bone and cartilage destruction through the osteoclastogenesis and proteolytic enzyme production that are induced by the cell membrane contact between T cells and osteoclast precursors or between T cells and chondrocytes.

Interaction of T Cells and Macrophages with Endothelial Cells and Inflammation

Numerous reports have already demonstrated that interactions of T cells and macrophages with vascular endothelial cells play an important role in the pathogenesis of inflammation [16-18]. Circulating macrophages and T cells can attach the vascular endothelial cells and migrate from the circulatory system to an extravascular compartment such as inflammatory organs. T cell or macrophage attachment, invasion, and subsequent degradation of the subendothelial extracellular matrix are crucial important steps to develop the inflammation. It is thought that the ability of activated T cells/macrophages of the immune system to attach and invade the vascular endothelium and to degrade extracellular matrix are very similar to that reported for highly metastatic tumor cells.

cell-macrophage contact and proinflammatory cytokines

Proinflammatory cytokines, especially TNF-α and IL-1, are mainly produced from macrophages. The levels of cytokine production are lesser from T cells than from macrophages. It is very important to elucidate the mechanism whereby infiltrating T cells induce cytokine productions from macrophages in arthritis.

Mitchell et al. [9] demonstrated that the cell membrane contact of T cells with macrophages or synovial fibroblasts induce the progression of proinflammatory cytokines [3,5,10]. The cell contact is thought to induce the production of proinflammatory cytokines with no stimulation by other cytokines and growth factors. These findings indicate that the direct cell contact of the synovial infiltrating T cells with adjacent macrophages in the synovial tissue accelerates the inflammation of synovitis. Furthermore, it has been reported that the cell contact-mediated inflammation is enhanced by IL-15 [12,13,19]. IL-15 stimulated the expression of CD69 or CAM-1 on the cell surface of activated T cells and their adhesion molecules-mediated membrane contact between T cells and macrophages accelerate the production of proinflammatory cytokines by macrophages [13,19]. Based on the properties of the cell contact induced inflammation, to date, it has been evidenced the inhibitory effect of neutralizing antibody for IL-15 against spondyloarthritis [19].

It has been reported that IL-17 or IL-18 with NF κ B activity is closely involved in the pathogenesis of arthritis [11,20,21]. We observed the high levels of these cytokines in the synovial fluid of patient with RA. It has been also reported that IL-18 induces the production of IFN-γ from activated T cells and differentiation of T-helper type 1 cells, suggesting the potential implication of the cytokines in the pathogenesis of arthritis [21,22]. Our findings suggest that IL-18 has a potential to modulate the direct cellular contact induced production of proinflammatory cytokines, TNF-α and IL-1, from macrophages in synovitis. T cell-macrophage contact also accelerates the expression of IL-18 receptor and IL-18 itself in macrophages, suggesting that IL-18 acts as an autocrine factor for the cell membrane contact-mediated inflammation [11]. In arthritis, cell contact of synovial infiltrating T cells with macrophages may induce the secretion of proinflammatory cytokines, IL-6, IL-8, IL-15, IL-17 and IL-18 as well as TNF-α and IL-1, in the synovial tissue. These cytokines secretions through the cell contact form the cytokine network and participate in the pathogenesis of arthritis. We have found that the cell contact-induced inflammation is mediated by the activation of NF κ B and PI-3 kinase of macrophages [11]. Specific inhibitors of both signal transductions completely inhibited the cell contact-mediated production of proinflammatory cytokines in vitro. Based on the properties of cell-to-cell interactions in arthritis, we have demonstrated the inhibitory effects of IL-18 neutralizing antibody on the cell contact-mediated inflammation in arthritis. Inhibition of the cell contact may have a potential to develop a novel therapeutic strategy to arthritis.

Regarding the inhibition of T cell monocyte contact induced production of inflammatory cytokines, it has been reported that serum factor displays an inhibitory effect on the cell contact-mediated activation of monocytes as a homeostatic system. Hyka N. et al. [23] demonstrated that high density lipoprotein-associated apolipoprotein A-I inhibits contact-mediated activation of monocytes by binding activated T cells, inhibiting production of TNF-α and IL-1β. These findings suggest that anti-inflammatory effect of serum factor, apolipoprotein A-I, may lead to therapeutic approaches in inflammatory diseases.

T cell-synovial fibroblast contact and arthritis

It has been demonstrated that T cells can modulate the activity of a variety of cell types through cell contact [1,6,11-13]. Interactions between T cells and synovial fibroblasts result in reduced synthesis of collagen type II and increased production of MMPs, suggesting that the cell contact may be a crucial means of promoting articular cartilage degeneration. Identification of these signals mediating T cell-synovial fibroblast interactions is of crucial importance. We have also found that accelerated productions of proinflammatory cytokines from activated synovial fibroblasts through the direct contact with T cells (unpublished data). These findings provide evidence to support that interactions of synovial fibroblasts with T cells could contribute significantly to the development of arthritis.

How to cite this article: Kasai Y, Nagata Y, Iikuni N, Ito K. Cell-to-Cell Interactions of Activated T Cells and Adjacent Cells in Chronic Inflammatory Diseases. Novel Tech Arthritis Bone Res. 2017; 2(2): 555588. DOI: 10.19080/NTAB.2017.02.555588

Adhesion molecules have been implicated in a number of interactions between T cells and synovial fibroblasts. Intercellular adhesion molecule (ICAM) 1, leukocyte function antigen-1, CD40L, or CD69 have been proposed as adhesion molecules promoting the cell contact [1,4,11,23]. Since the adhesion molecule can mediate the cell-cell interactions, such molecules represent legitimate therapeutic targets has been proposed. Previous reports demonstrated that IL-18 enhanced the expression of VCAM-1, ICAM-1 and E-selectin on the cell surface of synovial fibroblasts [24-26]. We also found that the blocking antibodies to the ligands of VCAM-1 or ICAM-1 inhibited the stimulatory effects of IL-18 on the T cell-synovial fibroblast contact as well as T cell-macrophage contact [11]. These results suggest that VCAM-1 and ICAM-1 may mediate the stimulatory effects of IL-18 on the cell contact of T cells with macrophages or synovial fibroblasts.

Miranda-Carus M.E. et al. demonstrated that RA synovial fibroblasts induces the upregulation of proinflammatory cytokines TNF-α, IFN-γ, IL-6, IL-8, IL-17, CD25 and CD69 expression through a cell contact-dependent system [26]. They found that these proinflammatory cytokines stimulate the further production of IL-6, IL-8, and IL-15 in synovial fibroblasts, thereby, creating a feedback loop that favors persistent synovial inflammation. Especially, the induction of IL-17 in cell contact is an important contributor to the feedback loop. A blocking antibody to IL-17 significantly inhibited T cell contact-dependent expression of IL-6, IL-8, IL-15 and CD54 by synovial fibroblasts. It is well known that IL-17 is a crucial important cytokine in pathogenesis of RA. Elevated levels of IL-17 have been described in synovial fluids in patients with RA but not OA [27,28]. Other report also revealed that methotrexate may disrupt this loop by inhibiting cell contact between T cell-to-synovial fibroblasts [26].

T cell- skin fibroblast contact and systemic sclerosis

In systemic sclerosis, it is well known that T cells infiltrate fibrotic tissues or organs and may be involved with dysregulated production of collagen by fibroblasts. It has been reported that T cell-skin fibroblast contact has a role in the pathogenesis of systemic sclerosis. Chizzolini et al. [29] demonstrated that T cell-fibroblast contact significantly inhibits collagen production by fibroblasts via membrane-associated TNF-α [29]. Their findings revealed that T cells infiltrating the skin of patients with systemic sclerosis deliver inhibitory signals to skin fibroblasts via direct cell-to-cell contact. Also, they mentioned that the cell contact dependent inhibition of collagen production by skin fibroblasts is a powerful characteristic of Th2 cells and is mediated by membrane-bound TNF-α. These findings suggest that therapeutic strategies based on TNF-α blockade could be controlling fibrosis in systemic sclerosis.

T cell-chondrocyte interactions and articular cartilage deterioration

Recently, we examined whether T cell-chondrocyte interactions influence the articular deterioration. We postulated that chondrocytes, as well as infiltrating macrophages and synovial fibroblasts, can act in the joint destruction in response to the cell-cell contact with infiltrating lymphocytes. Our findings of the cell immune response to chondrocytes clearly demonstrated the autologous T cell stimulating properties of OA chondrocytes [30,31]. Co-culture of T cells with irradiated autologous chondrocytes induced the acceleration of T-cell proliferation in vitro, suggesting the presence of immune reaction to articular cartilage. The direct contact between infiltrating T cells and articular chondrocytes may participate in the immune mediated mechanisms of OA. Interestingly, this response was partially blocked by antibodies for HLA class I and II, CD4 and CD8. These findings provide evidence to support that immune response occurs in response to chondrocytes that are exposed during the progression of OA.

Furthermore, we have found that cell contact of activated T cells with chondrocytes induces the secretion of MMP-1, -3, and -13, suggesting the effect of the cell contact on articular cartilage deterioration [31]. The direct T cell-chondrocyte contact via specific adhesion molecules may result in the accelerated secretions of matrix degrading enzymes from chondrocytes consequently leading to the cartilage degeneration.

Indeed, it is rare occurrence that infiltrating T cells directly contact to chondrocytes in normal articular cartilage. However, in the degenerated cartilage during the progression of OA, articular chondrocytes may be exposed to synovial fluid with numerous number of infiltrating T cells. Nakamura et al. observed the presence of degenerated cartilage fragment with articular chondrocytes in the joint fluid of patient with osteoarthritis [32]. It has been demonstrated the CD3 positive mononuclear cells and chondrocyte-like cells in synovial fluid of patients with OA. Destructed cartilage fragments (cartilage matrix component) with articular chondrocytes may be shaved off and be floating in the joint fluid with advance of degeneration of articular cartilage. Thus, articular chondrocytes that are attached on fragmented articular cartilage tissue may contact with the infiltrating lymphocytes in the joint fluid. Also chondrocytes in degenerated cartilage zone may be exposed out and be influenced by several factors in the joint fluid.

Although further studies are needed to clarify the exact implication of T cell-chondrocyte contact in the pathogenesis of OA, the direct contact between activated T cells and chondrocytes may induce the immune response and cartilage matrix degradation.

Osteoclast Differentiation Through Cell Contact-Induced Rank/Rankl System

A number of cytokines and factors produced by RA synovial membrane and by patients tissue are known to have the ability to induce the differentiation of monocyte/macrophage lineage cells into functional osteoclasts [1,33]. These factors are either directly on osteoclast precursor cells or on osteoclasts for example macrophage colony stimulating factor (M-CSF), TNF-α

and IL-1 act indirectly on bone along/osteoblast lineage cells IL-1, IL-11, IL-17 and TNF-α, which in turn contribute to the differentiation of osteoclast precursors [35-38]. The essential and direct acting factor for osteoclast differentiation has been cloned and identified as receptor activator of NF-κB ligand (RANKL) [36-39].

RANKL is a member of the TNF ligand superfamily of cytokines that binds to its signal transducing receptor, RANK [36]. In addition to its required role in the differentiation of osteoclasts from their precursor cells, RANKL also augments osteoclast activity and survival. Synovial membrane provides a source of RANKL that could influence osteoclastogenesis [35]. Synovial fibroblasts from patients with RA produce mRNA and protein for RANKL [40]. RANKL is also expressed by infiltrating T cells in RA synovial membrane. Activated T cells expressing RANKL induce osteoclasts from autologous infiltrating macrophages [41-43]. Synovial tissues may also provide a source of osteoclast precursor cells, as macrophages cultured from RA synovial tissues differentiate into osteoclasts in the presence of M-CSF plus RANKL. Taken together, cell contact between T cells and osteoclast precursors or between synovial fibroblasts and osteoclast precursors through the pathway depending on the RANK/RANKL binding is a crucial important for osteoclastic bone resorption in arthritis.

Conclusion

We reviewed the potential involvement of cell-to-cell interactions of activated T cells with adjacent cells in inflamed articular tissue in the joint destruction (Figure 1). These novel pathways may represent exciting potential therapeutic targets in arthritis.

Acknowledgement

This study was supported by grants from the Ministry of Education, Culture, Sports, Science and Technology of Japan, the Ministry of Health, Labour and Welfare of Japan, and the Japan Rheumatism Foundation.

References

1. Angelotti F, Parma A, Cafaro G, Capecchi R, Alunno A, et al. (2017) One year in review 2017: pathogenesis of rheumatoid arthritis. Clin Exp Rheumatol 35(3): 368-378.

2. Berger T, Dayer JM (2002) Cytokines, accessory proteins, and hormones: IL-1 and TNF-alpha production in contact-mediated activation of monocytes by T lymphocytes. Ann N Y Acad Sci 966: 461-473.

3. Firestein GS, McInnes IB (2017) Immunopathogenesis of Rheumatoid Arthritis. Immunity 46(2): 183-196.

4. Shao M, Hashimoto M, Matsuo T, Fujii T, Furu M, et al. (2013) Cell-cell contact-dependent activation of CD4+ T cells by adhesion molecules on synovial fibroblasts. Mol Med Rep 8(2): 448-453.

5. Mellor-Pita S, Lecoq-Bi P, Low PY (2003) Cell-cell interactions between synovial fibroblasts and T lymphocytes in rheumatoid arthritis. Arthritis Res 5(1): 174-178.

6. Bernardini G, Sponga G, Ferro F, Velasco G, Santoni A (2017) The Multifunctional Role of the Chemokine System in Arthritogenic Processes. Curr Rheumatol Rev 13(3): 11.

7. Nurse DW, Brazier R, Mohlundin E, Palomino-Funne F, Bernasconi GA (2010) Matrix Gaps in rheumatoid arthritis. Arthritis Res 12(1): 109-112.

8. Brennan FM, Hayes AL, Chilvers ER, Green P, Howell JM, et al. (2002) Evidence that rheumatoid arthritis synovial T cells are similar to cytokine-activated T cells: involvement of phosphatidylinositol 3-kinase and nuclear factor kappa B pathways in tumour necrosis factor alpha production in rheumatoid arthritis. Arthritis Rheum 46(1): 31-41.

9. van de Sande MG, Baeten DL (2016) Immunopathology of synovitis: from histology to molecular pathways. Rheumatology (Oxford) 55(4): 599-606.

10. McInnes IB, Leung BP, Sturrock RD, Field M, Liew FY (1997) Interleukin 15 mediates T cell-dependent regulation of tumor necrosis factor alpha production in rheumatoic arthritis. Nat Med 3(2): 189-195.

11. Ito SM, Matsuno H, Nakamura H, Yoshioka K, Yudoh K (2004) Interleukin-18 enhances monocyte tumor necrosis factor alpha and interleukin-1beta production induced by direct contact with T lymphocytes: implications in rheumatoid arthritis. Arthritis Rheum 50(2): 432-443.

12. McInnes IB, Gracie JA (2004) Interleukin-15: a new cytokine target for the treatment of inflammatory diseases. Curr Opin Pharmacol 4(4): 392-397.

13. Muñoz-Valle JF, Valle A, Segura-Mujica M, Perez de Ayala C, Martinez-Maza J. (2004) IL-15 and the interaction of cell contact-dependent synovial fibroblast-T lymphocyte cross-talk in rheumatoid arthritis: effect of methotrexate. Clin Immunol 112(2): 1468-1476.

14. Martel-Pelletier J, McCollum R, Fujimoto N, Obata K, Cloutier JM, et al. (1994) Excess of metalloproteases over tissue inhibitor of metalloproteases may contribute to cartilage degradation in osteoarthritis and rheumatoid arthritis. Lab Invest 70(6): 807-815.

15. Arend WP, Dayer JM (1995) Inhibition of the production and effects of interleukin-1 and tumor necrosis factor alpha in rheumatoid arthritis. Arthritis Rheum 38(2): 151-160.

16. Saveria R, Vladavsky I, Ferrara N (1981) Interaction of T lymphocytes and macrophages with cultured vascular endothelial cells: attachment, ingestion, and subsequent degradation of the subendothelial extracellular matrix. J Gen Physiol 110(2): 169-178.

17. Junge F, Dayer JM, Modoux C, Hyka N, Burger D (2001) IFN-beta inhibits the ability of T lymphocytes to induce TNF-alpha and IL-1 beta production in monocytes upon direct cell-cell contact. Cytokine 14(5): 272-282.

18. Elshabrawy HA, Chen Z, Volin MV, Ravella S, Virupannavar S, et al. (2015) The pathogenic role of angiogenesis in rheumatoid arthritis. Angiogenesis 18(4): 433-448.

19. Kasayama S, Storey CL, Davis WC, Carr DW (1995) Regulation of IL-1-stimulated IFN-gamma production by rolipram. J Immunol 154(5): 2336-2342.

20. Jovanovic DV, Di Battista JA, Martel-Pelletier J, Jolicoeur FC, He Y, et al. (1998) IL-17 stimulates the production and expression of proinflammatory cytokines, IL-beta and TNF-alpha, by human macrophages. J Immunol 160(2): 1643-1651.

21. Yokomizo T, Yoshimoto T, Noguchi E, Okamura H, Iwamoto I (2001) Interleukin-18 regulates both Th1 and Th2 responses. Allergy Asthma Rev Immunol 30: 421-174.

22. Moore JL, Park CC, Zhu Z, Kamoi B, Kato Y, et al. (2002) Signal transduction pathways involved in rheumatoid arthritis synovial fibroblast interleukin-6 and chemokine ligand 11 induction by leukocyte-endothelial cell adhesion. J Biol Chem 277(38): 34661-34667.

23. Boki K, Sayer BM, Mohler E, Kohno T, Edwards CK, et al. (2001) Antirheumatic drugs inhibit the production of interleukin-1beta and human tumor necrosis factor-alpha by lipopolysaccharide-induced activation of human monocytes/T lymphocytes. Blood 97(11): 2801-2809.

24. Murel JC, Park CC, Woods JM, Koch AE. (2001) A novel role for intercellular adhesion molecule 1 in chemokine induction. Cytogen. NF-κB and phosphatidylinositol 3[PI]-kinase-dependent signal transduction pathways. J Biol Chem 276(46): 37070-37075.

25. Yoshida A, Takahashi HE, Nakamura M, Tsugane H, Sorbetto V, Morohashi T, et al. (2001) IL-1β-induced expression of intercellular adhesion molecule-1 in human monocytes: involvement of IL-12 and IFN-gamma production in PBMC. Exp Immunol 110(2): 326-333.

26. Marinelli-Casey ME, Bonta IL, Bugel M, Chones MA, Bazan A, Martinez-Molina E. (2006) Human T cells constitutively express IL-17 that promotes ex vivo T cell homeostatic proliferation through autocrine/autocrine loops. Immunol 176(6): 3656-3662.

27. Kotulska M, Kot A, Lewandowska G, Rzeszotarska B, Czerniak K, Kuwana E, et al. (2000) High levels of IL-17 in rheumatoid arthritis patients: IL-15 triggers in vitro IL-17 production via cytokine-dependent mechanism. Immunol 164(5): 2832-2838.

28. Kotake S, Udagawa N, Takahashi N, Matsuzaki K, Itoh K, et al. (1999) IL-17 in synovial fluids from patients with rheumatoid arthritis is a potent stimulator of osteoclastogenesis. J Clin Invest 103(9): 1345-1352.

29. Chizzolini C, Parel Y, De Seze C, Tyndall A, Avouac A, et al. (2008) Systemic sclerosis Th2 cells inhibit collagen production by dermal fibroblasts via macrophage-associated human interleukin-13 activity. Rheum 46(9): 2594-2604.

30. Sakata M, Maruoka-Hango K, Nakamura H, Onuma H, Tsukuna H, et al. (2003) Osteoclastogenesis in articular chondrocytes stimulate osteoclastogenesis in vitro. Clin Exp Rheumatol 21(5): 564-570.

31. Nakamura I, Pilkey N, Maruoka-Hango K, Y, Ish K, Kim T, et al. (2006) Enhanced production of MMP-1, MMP-3, MMP-13 and RANTES by interaction of chondrocytes and autologous T cells. Rheumatol Int 26(11): 984-990.

32. Gravallese EM, Manning C, Tsay A, Naito A, Pan C, et al. (2000) Synovial tissue in rheumatoid arthritis is a source of osteoclast differentiation factor. Arthritis Rheum 43(12): 250-258.

33. Murphy S, Lopatell L, Lee R, Yamamoto N, Boone T, et al. (1999) A chimeric form of osteoprotegerin inhibits hypercalcemia and bone resorption induced by IL-1, TNF-α, PTH, PTHrP and 1,25(OH)2D3. J Bone Miner Res 14(9): 1479-1485.

34. Nakagawa T, Kobayashi Y, Yamaguchi S, Kawakami A, Eguchi K, et al. (2010) Protein sumoylation and functional difference of nuclear and cytoplasmic isoforms of NF-κB ligand: modulation of the expression by osteotropic factors and cytokines. Biochem Biophys Res Commun 392(1): 7-11.

35. Gravellese EM, Manning C, Wang JT, Goldring SR, Thornhill TS, et al. (1998) Identification of cell types responsible for bone resorption in rheumatoid arthritis and juvenile rheumatoid arthritis. Am J Pathol 152(4): 943-951.

36. Yasuda H, Shima N, Nakagawa N, Yamaguchi K, Kinosaki M, et al. (1998) Osteoclast differentiation factor is a ligand for osteoprotegerin/osteoclastogenesis-inhibitory factor and is identical to TRANCE/RANKL. Proc Natl Acad Sci U S A 95(7): 3597-3602.

37. Lacey DL, Timms E, Tan HL, Kelley MJ, Dunstan CR, et al. (1998) Osteoprotegerin ligand is a cytokine that regulates osteoclast differentiation and activation. Cell 93(2): 165-176.

38. Wong BR, Rho J, Arron J, Robinson E, Orlinick J, et al. (1997) TRANCE is a novel ligand of the tumor necrosis factor receptor family that activates c-Jun N-terminal kinase in T cells. J Biol Chem 272(40): 25190-25194.

39. Kotake S, Udagawa N, Hakoda M, Mogi M, Yano K, Tsuda E, et al. (2001) Activated human T cells directly induce osteoclastogenesis from human monocytes: possible role of T cells in bone destruction in rheumatoid arthritis patients. Arthritis Rheum 44(5): 1003-1012.

40. Ohara T, Hara Y, Kato I. (1996) Effects of T cell adoptive transfer into nude rats on alveolar bone resorption induced by endotoxin. J Periodontol Res 31(6): 414-422.

41. Lahn V, Jacobs JM, Stern JL, Kasebrink AL, Galvin KI. (1996) A role for CD8+ T lymphocytes in osteoclast differentiation in vitro. Endocrinology 137(6): 2457-2465.

42. Kong YY, Feige U, Sarosi I, Bolon B, Tafuri A, et al. Activated T cells regulate bone loss and joint destruction in adjuvant arthritis through osteoprotegerin ligand. Nature 402(6759): 304-309.

43. Horwood NJ, Kartsogiannis V, Quinn JM, Romas E, Martin TJ, et al. (1999) Activated T lymphocytes support osteoclast formation in vitro. Biochem Biophys Res Commun 265(1): 144-150.

This work is licensed under Creative Commons Attribution 4.0 License.
DOI: 10.19080/NTAB.2017.02.555588

Your next submission with Juniper Publishers will reach you the below assets

- Quality Editorial service
- Swift Peer Review
- Reprints as per UKBA
- Extensive Service
- Manuscript hosted for unlimited time period
- Global attractiveness of your research
- Manuscript accessibility in different formats
  (Pdf, E-pub, Full Text, Audio)
- Unleashing customer service

Track the below URL for one-step submission
https://juniperpublishers.com/online-submission.php

How to cite this article: Ozawa Y, Sawada Y, Takano K, Ito K. Type-II-Dependent Interactions of Intended Osteocytes Adjacent Cells in Internal Tissue of Inflammatory Diseases. Nov Tech Arthritis Bone Res. 2017; 2(3): 555588. DOI: 10.19080/NTAB.2017.02.555588

RHEUMATOLOGY

Concise report

doi:10.1093/rheumatology/kex478

Multiple target autoantigens on endothelial cells identified in juvenile dermatomyositis using proteomics

Rie Karasawa[1], Mayumi Tamaki[1], Toshiko Sato[1], Megumi Tanaka[1], Makiko Nawa[2], Kazuo Yudoh[1] and James N. Jarvis[3,4]

Abstract

Objective. Although generally classified within the group of inflammatory myopathies, JDM displays many pathological features of vasculitis. Previous work has shown that AECA are abundant in other forms of vasculitis. We therefore investigated whether such antibodies might also be detected in JDM.

Methods. We screened plasma from children with JDM for the presence of AECA by western blotting and 2D gel electrophoresis (2DE) using proteins extracted from human aortic endothelial cells as the substrate. We performed mass spectrometry to identify candidate antigens from 2DE gels and used ELISA to confirm the presence of specific antibodies.

Results. We identified 22 candidate target autoantigens for AECA probed with JDM plasma. Interestingly, 17 of these 22 target antigens were proteins associated with antigen processing and protein trafficking. ELISA confirmed the presence of antibodies to heat shock cognate 71 kDa protein in JDM plasma, particularly in children with active, untreated disease.

Conclusion. Children with JDM express antibodies to autoantigens in endothelial cells. The clinical and pathological significance of such autoantibodies require further investigation.

Key words: juvenile dermatomyositis, autoantibodies, anti-endothelial cell antibodies, heat shock cognate 71 kDa protein, endothelium, chaperone proteins, proteomics

CLINICAL SCIENCE

Rheumatology key messages

- Anti-endothelial cell antibodies are present in plasma of children with JDM.
- Antibodies to heat shock cognate 71 kDa protein may serve as useful biomarkers in JDM.

Introduction

JDM is the most common form of inflammatory myopathy in children [1]. Although classified as a myopathy, involved tissues in JDM are characterized by prominent vascular and perivascular inflammation that contributes directly to the clinical features of the disease [2]. Indeed, one of the earliest descriptions of JDM in the English language, the classic paper by Banker and Victor, described JDM as '. . . systemic angiopathy . . . of childhood' [3]. Thus, JDM can also be regarded as a form of vasculitis.

Autoantibody expression involving a broad spectrum of autoantigens is a well-documented feature of JDM [1, 4]. These autoantibodies have specific clinical associations, but their relationship to disease pathology remains unclear. These autoantibodies are typically identified by immunoprecipitating protein or DNA from radiolabelled HeLa or K562 cell extracts and double immunodiffusion [1], and thus the actual in vivo cellular targets of these autoantibodies remain unclear. We have recently demonstrated that several forms of vasculitis are associated with autoantibody responses to endothelial cells [5, 6] and the

[1]Department of Pediatric Medicine, St Marianna University School of Medicine, Kawasaki, [2]Institute of Human Genetics and BCC, Tokyo Medical and Dental University, Tokyo, Japan, [3]Department of Pediatrics and Genetics, Genomics & Bioinformatics Program and Genetics, Genomics & Bioinformatics Program, Tulane School of Medicine and Biomedical Sciences University at Buffalo, Buffalo, NY, USA.

Submitted 10 August 2017; revised version accepted 11 October 2017.

Correspondence to: Rie Karasawa, Department of Pediatric Medicine, St Marianna University School of Medicine, 2-16-1 Sugao, Miyamae-ku, Kawasaki 216-8511, Japan.
E-mail: rkarasawa@marianna-u.ac.jp

© The Author(s) 2018. Published by Oxford University Press on behalf of the British Society for Rheumatology. All rights reserved. For permissions, please email: journals.permissions@oup.com

Downloaded from https://academic.oup.com/rheumatology/advance-article/doi/10.1093/rheumatology/kex478/4781431
by guest on 20 January 2018

presence or titre of these autoantibodies may serve as biomarkers of disease or to monitor disease activity. The studies described here were undertaken to determine whether the endothelium in JDM might similarly be targeted by autoantibodies.

Methods

Patients

Plasma of patients with JDM (n = 39) were collected from the University of Oklahoma Pediatric Rheumatology clinic between 2007 and 2011. The mean (s.d.) age of the patients with JDM (28 females and 11 males) was 8 (4) years, with a range of 3–16. Children with active JDM had disease durations ranging from 4 months to 8 years, and were being treated with weekly injectable MTX (25 mg/m^2 body surface area), daily oral steroids (1.0 mg/kg/day) and pulse methylprednisolone given at a dose of 500 mg/m^2 body surface area for intervals ranging from once a week to once a month. Children with inactive disease who were on maintenance therapy with weekly injectable MTX were 11–49 months post-diagnosis. Active disease was defined as the presence of any of the following: JDM-associated rash, periungual capillary abnormalities (dilatation, drop-out) or elevations in serum levels of creatine phosphokinase or aldolase. Deviations of aspartate aminotransferase or alanine amino transferase were considered signs of active disease if MTX-associated hepatic injury was excluded based on clinical grounds and normal serum levels of gamma glutamyl transferase. Plasma of patients with JIA (n = 15, 12 females and 2 males) and healthy children (n = 20, 11 females and 9 males) were collected from the University of Oklahoma and the General Pediatrics clinic at the Women and Children's Hospital of Buffalo. Healthy children with the mean age of 12 (4) years (range, 4–17 years) and JIA with the mean age of 9 (4) years (range, 4–14 years) were included in this study. The patients with JIA included five children with untreated, active disease, five children with active disease on therapy with weekly MTX (NSAIDs (disease duration 2–9 months) and five children on MTX + etanercept who at criteria for clinical remission on medication [7]). Informed consent, and, where appropriate, assent, was obtained from all participants prior to obtaining samples. This study was approved by the ethics committee of St Mariam's University School of Medicine (No.1710) and by the University of Oklahoma (#12134) and University at Buffalo (RB # MOD 08100155) Institutional Review Boards.

Cell culture

Normal human aortic endothelial cells (HAECs), human aortic adventitial fibroblasts (AoAF) and human skeletal muscle cells (SkMCs), and culture media and supplements for HAEC, AoAF and SkMC were obtained from Lonza (Walkersville, MD, USA). Normal human dermal microvascular endothelial cells (HMVEC-D) were obtained from Thermo Fisher Scientific (Waltham, MA, USA). Culture media and supplements for HMVEC-D were obtained from Kurabo Industries (Osaka, Japan). Normal human aortic smooth muscle cells (HAoSMCs) was obtained from Lifeline Cell Technology (Frederick, MD, USA). Culture media and supplements for HAoSMC were obtained from Kurabo Industries (Osaka, Japan). All cells were cultured in the media and supplements as described previously [5]. Cells at passages 3–4 were harvested and stored at −80°C and use for 2D gel electrophoresis (2DE) or SDS–PAGE.

2D gel electrophoresis

2DE was conducted as described previously [5] with the following modifications. Protein (400 μg) from the harvested HAEC was applied onto immobline DryStrip gels (pH3.0–10.0; GE Healthcare, Uppsala, Sweden). After electrophoresis, one gel was used for Coomassie Brilliant Blue R-250 staining and the other gel was used for transfer of the separated proteins onto a nitrocellulose membrane for western blotting (WB).

SDS–PAGE

SDS–PAGE was conducted as described previously [5]. To detect AECA, proteins extracted from HAEC, HMVEC-D, AoAF, HAoSMC and SkMC were used for SDS–PAGE and WB. 20 μg of extracted proteins were applied to 12.5% SDS–PAGE gels, after which the separated proteins on the gels were transferred onto nitrocellulose membranes for WB.

Western blotting

WB after SDS–PAGE or 2DE was performed as described previously [5]. Plasma from patients with JDM were used for SDS–PAGE (five samples) or 2DE (three samples) at a final dilution of 1:100 (1:500 for each donor in SDS–PAGE) or that of 1:100 (1:300 for each donor in 2DE). Then the bound antibodies were reacted with horseradish peroxidase-conjugated goat anti-human IgG (diluted 1:2000). Finally the bound IgG antibodies were visualized using diaminobenzidine.

Protein identification

In-gel digestion was performed as described previously [5]. Analysis of peptides was carried out using an liquid chromatography/tandem mass spectrometry (LC–MS/MS) system, which consisted of a nanoultra high performance liquid chromatography-electrospray ionization-quadrupole time-of-flight system (maXis-II G-CPR, Bruker Daltonics, Billerica, MA, USA). A L-column octadecylsilane-bonded silica (L-column ODS), 0.075 × 150 mm, 3 μm particle size, (Chemical Evaluation Research Institute (CERI), Tokyo, Japan) was used. The eluted peptides were directly electro-sprayed into the spectrometer, with MS/MS spectra acquired in a data-dependent mode. Database searches in the SwissProt database were performed using the Mascot 2.5.1 (Matrix Science, Boston, MA, USA) incorporated into ProteinScapes 1.1 (Bruker Daltonics, Billerica, MA).

ELISA

ELISA was conducted as described previously [5]. To detect antibodies to heat shock cognate 71 kDa protein (HSC70) in plasma, each well of an ELISA plate was

Downloaded from https://academic.oup.com/rheumatology/advance-article/doi/10.1093/rheumatology/kew243/2615411
by guest on 21 June 2022

coated with 0.125 μg of HSC70 (StressMarq Biosciences, Victoria, BC, Canada) in a carbonate buffer (50 mM sodium carbonate, pH 9.6). The plasma diluted 1:200 with 10% Block Ace were reacted with the coated recombinant proteins. Optical density at 490 nm was measured by a microplate reader. The average plus 2 s.d. among the group of healthy donors was defined as 100 arbitrary binding units and was used as a cut-off point for determining reactivity to HSC70.

Statistics

Fisher's exact test was used to compare the frequency of each antibodies between each of the phenotypes and JDM disease states.

Results

Detection of antibodies in patients with JDM

To select the best antigen source, we first detected autoantibodies in plasma from patients with JDM, both active patients without treatment and inactive patients off medication, using proteins extracted from five different cells by WB (Fig. 1A (a) and (b)). Multiple antigens were detected in each cell line, in particular HAEC. Among three types of cells derived from aorta (HAEC, AoAF and HAoSMC), staining patterns appeared to differ most between the HAEC and the other cell lines. We also noted distinct differences in the staining patterns between patients with active JDM and patients with inactive JDM. In plasma from patients with inactive JDM, differences in staining patterns between each cell line were not significant. Based on these results, HAEC were used for 2DE to facilitate identification of specific antigens. We limited 2DE studies to plasma samples from active patients without treatment.

Candidate antigens for AECA detected in JDM by 2DE-WB

To detect JDM-specific antigens on HAEC, results of 2DE-WB using plasma from untreated JDM patients with active disease (Fig. 1B (a)) were compared with results from plasma from healthy children (Fig. 1B (b)). Five candidate protein spots were detected in 2DE-WB (arrows, Fig. 1B (a) and C). Twenty-two proteins from five protein spots recognized by 2DE gels were identified using mass spectrometry (Table 1).

Antibodies against chaperone or co-chaperone proteins identified in patients with JDM

Using pathway analysis, 17 of the 22 candidate target antigens for AECA in JDM were predicted to interact with chaperone proteins involved in antigen processing and presentation. Among the seven chaperone or co-chaperone proteins were HSC70, HSP 90 beta (HS90B) and stress-induced-phosphoprotein 1, a protein that mediates the association of HSC70 and HSP90. IgG autoantibodies to HSC70 were detected by ELISA in 23% of the patients with JDM (n = 50; Fig. 1D). However, 50% of the untreated JDM patients with active disease (n = 10) had anti-HSC70 antibodies, in contrast to 7% (P < 0.05) of the patients with JIA (n = 15) and 6% (P < 0.01) of control children (n = 20). Among treated patients with active disease (n = 15), 13% had detectable anti-HSC70 antibodies, while 14% of the patients with inactive disease (n = 14) had detectable anti-HSC70 antibodies. The frequency of anti-HSC70 antibodies shown was not significantly different with regard to age or sex. On the other hand, IgG autoantibodies to HS90B were detected in 6% of the patients with JDM (n = 31) and IgG autoantibodies to stress-induced-phosphoprotein 1 were not detected (patients with JDM (data not shown).

Discussion

Despite the prominence of the vascular features in JDM, few investigations have focused on this aspect of the pathophysiology of the disease. Thus, the question of how and why blood vessels within the skin and musculature (and other sites) of patients with JDM become targets of immune attack remains unanswered.

In the current paper, we used a proteomic approach to address this question. Specifically, we asked whether endothelial cells might be targets of autoantibodies, a plausible hypothesis given that at least one study has demonstrated the presence of both IgG and complement proteins within the vessel walls of children with JDM [8], although a recent study has not duplicated the finding [9]. We found that a broad spectrum of AECA could be identified in plasma samples from children with JDM (Table 1). These antibodies were more commonly found in children with active, untreated JDM and were rare in children with polyarticular-onset JIA.

These antibodies were not randomly directed toward cell-surface proteins, but seemed to be directed toward proteins involved in antigen processing and stress response (e.g. HSC70). This finding suggests that at least some AECA may play a regulatory role, modifying the processing of antigens, long recognized as an important function of endothelium [10]. In support of a regulatory role for the autoantibodies are the findings of Dr Poep et al. [11], who reported that, in inflammatory myopathies in adults, HSP70 (a homologous protein) is expressed in injured muscle fibers and may be involved in muscle repair and regeneration. This finding is consistent with the report by Mitsunova et al. [12] demonstrating increased levels of HSP70 proteins in serum of adult patients with inflammatory myopathies. Thus, it is possible that the presence of HSC70 antibodies is a response to damaged muscle fibers rather than a primary mechanism of injury. A growing body of evidence supports the idea that type-1 IFN-induced muscle damage may be the primary mechanism of JDM [13, 14].

Rider et al. have shown that specific autoantibodies in childhood inflammatory myopathies are associated with distinct clinical phenotypes, disease complications and/or clinical outcomes. Our patient numbers are too small to determine whether such associations exist for AECA in JDM, and our patient population was homogeneous compared with the broad clinical spectrum of childhood inflammatory myopathies [1]. Studies of a larger, clinically heterogeneous population will be required to determine

Downloaded from http://rheumatology.oxfordjournals.com/ at Universitaetsbibliothek Giessen on February 13, 2012

Fig. 1 Detection of AECA in JDM

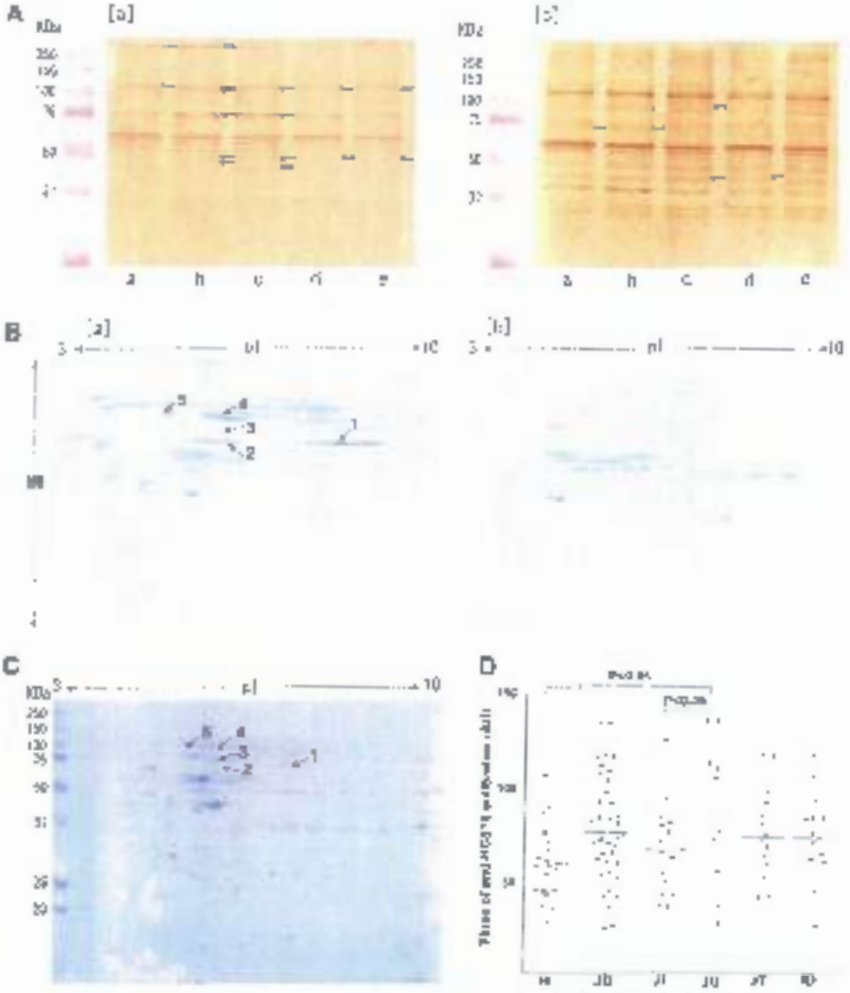

(A) Protein extracted from normal human dermal microvascular endothelial cells (HMVEC-D) (a), normal human aortic endothelial cells (HAEC) (b), human aortic adventitial fibroblasts (AoAF) (c), normal human aortic smooth muscle cells (HAoSMC) (d) and human skeletal muscle cells (SkMC) (e) were separated by SDS-PAGE. Proteins reactive to plasma from patients with active JDM (untreated: a; or patients with inactive JDM off therapy: b) were detected by western blotting (WB). (B) Proteins extracted from HAEC separated by 2D gel electrophoresis (2DE), and antigens detected by WB using plasma from patients with active JDM (untreated (a) or healthy (b) children). Protein spots in AECA recognized predominantly in JDM compared with control plasma are indicated by arrows and spot ID numbers in (a). (C) Locations of the five protein spots analysed by MS are indicated in a Coomassie Brilliant Blue R-250-stained 2DE gel using HAEC extracts. (D) Results of ELISA assays for anti-HSC70 antibodies. H: healthy children; JD: JDM; JA: untreated JDM, active disease; JT: treated JDM, active disease; JI: inactive JDM.

whether there are associations between AECA and specific clinical phenotypes or outcomes.

Our data suggest that antibodies against HSC70, which was one of the antigens identified by mass spectrometry, might be a useful diagnostic biomarker. The autoantigens we identified in JDM did not overlap with what we have seen in systemic vasculitis using a similar approach [5]. There are also reports of autoantigens for AECA in patients with SLE [15-17]. Autoantibodies against HSP family proteins such as HSP60 [15] and HSP90 [16], but not HSP70 [18], were detected by ELISA in SLE. Using ELISA assays, we identified anti-HSC70 in 5 of the 13 samples of children with newly diagnosed, untreated JDM and in fewer than 5% of children with polyarticular JIA. If these findings are corroborated in a larger cohort of patients, anti-HSC70 would have significantly better

Downloaded from rheumatology.oxfordjournals.org at Keio University on February 14, 2011

Table 1 Identification of candidate antigens for AECA in patients with JDM

Spot no.	Protein name	Accession no.	Accession ID	MW (kDa)/pI		MS/MS analysis	
				Observed	Theoretical	Coverage (%)	No. of matched peptides
1	Prelamin-A/C	P02545	LMNA_HUMAN	69/8.5	74/6.57	36.40	27
	Dihydropyrimidinase-related protein 2	Q16555	DPYL2_HUMAN	65/6.5	62/5.96	5.30	3
	Stress-induced-phosphoprotein 1	P31948	STI1_HUMAN	66/6.5	63/6.40	4.30	3
	T-complex protein 1 subunit zeta	P40227	TCPZ_HUMAN	58/6.5	53/5.84	5.60	2
	Cytoskeleton-associated protein 4	Q07065	CKAP4_HUMAN	63/6.5	66/5.63	6.80	2
2	Heterogeneous nuclear ribonucleoprotein K	P61978	HNRPK_HUMAN	69/5.2	51/5.59	33.50	25
	Cytoskeleton-associated protein 4	Q07065	CKAP4_HUMAN	68/5.2	66/5.63	20.40	13
	Prelamin-A/C	P02545	LMNA_HUMAN	69/5.2	74/6.57	11.80	5
	T-complex protein 1 subunit theta	P50990	TCPQ_HUMAN	69/5.2	60/5.41	13.30	5
	Tubulin alpha-1A chain	Q71U36	TBA1A_HUMAN	50/5.2	50/4.94	8.10	2
	Dihydropyrimidinase-related protein 2	P16555	DPYL2_HUMAN	59/5.2	62/5.95	2.10	2
3	Heat shock cognate 71 kDa protein	P11142	HSP7C_HUMAN	75/5.4	71/5.37	42.70	41
	Heat shock 70 kDa protein 1-like	P34931	HS71L_HUMAN	75/5.4	70/5.76	14.50	9
	Stress-70 protein, mitochondrial	P38646	GRP75_HUMAN	75/5.4	74/5.87	12.70	7
	Annexin A6	P08133	ANXA6_HUMAN	75/5.4	76/5.41	6.40	4
	Lamin-B1	P20700	LMNB1_HUMAN	75/5.4	66/5.11	13.50	5
	V-type proton ATPase catalytic subunit A	P38606	VATA_HUMAN	75/5.4	68/5.34	5.00	2
4	Protein-glutamine gamma-glutamyltransferase 2	P21980	TGM2_HUMAN	90/5.1	77/5.11	34.10	23
	HSP 90-beta	P08238	HS90B_HUMAN	90/5.1	83/4.96	16.70	12
	Protein Hook homolog 3	O95067	HOOK3_HUMAN	90/5.1	83/5.12	9.70	5
	Src substrate cortactin	Q14247	SRC8_HUMAN	90/5.1	62/5.24	7.60	4
	Rac GTPase-activating protein 1	P46940	RAGP1_HUMAN	90/5.1	64/4.63	6.60	3
	Fibulin-2	P13796	FBLN2_HUMAN	90/5.1	70/5.29	2.10	2
5	Hematopoietic lineage cell-specific protein	P14317	HCLS1_HUMAN	93/4.5	54/4.73	16.70	11
	HSP 90-beta	P08238	HS90B_HUMAN	93/4.5	83/4.96	14.60	10
	Protein-glutamine gamma-glutamyltransferase 2	P21980	TGM2_HUMAN	93/4.5	77/5.11	11.60	8
	Protein CS-2	Q13439	CSN8_HUMAN	93/4.5	77/4.80	6.40	3

The five protein spots (Fig.1B (a) and C) identified as being JDM-specific were individually digested with trypsin and were subjected to mass spectrometry. Twenty-six proteins from five protein spots were identified.
MS/MS: tandem mass spectrometry; MW: molecular weight

specificity than other screening tests commonly used in primary care settings, for example ANA [18].

In conclusion, we have demonstrated the presence of a broad spectrum of previously unrecognized AECA in children with JDM. Larger studies are needed to determine the clinical significance of these antibodies and their utility and diagnostic or prognostic biomarkers.

Funding: This work was supported by Japan Society for the Promotion of Science KAKENHI Grant Number JP16K10045. This work was also supported by R01-AR050604 from the National Institutes of Health.

Disclosure statement: The authors have declared no conflicts of interest.

Downloaded from https://academic.oup.com/rheumatology/advance-article/doi/10.1093/rheumatology/kex384/4614164
by guest on 20 January 2018

References

1. Shah M, Mamyrova G, Targoff IN, et al. The clinical phenotypes of idiopathic inflammatory myopathies. Medicine 2010;89:205–41.
2. Crowe WE, Bove KE, Lovchik JC, Hilyard EK. Clinical and pathogenetic implications of histopathology in childhood polydermatomyositis. Arthritis Rheum 1982;25:126–39.
3. Danner BC, Victor M. Dermatomyositis, systemic angiopathy in childhood. Medicine 1985;64:261–86.
4. Rider LG, Shah M, Mamyrova G, et al. The myositis autoantibody phenotypes of juvenile idiopathic inflammatory myopathies. Medicine (Baltimore) 2013;92:223–43.
5. Kanekawa H, Kurokawa MS, Yudoh K, et al. Peroxiredoxin 2 is a novel autoantigen for anti-endothelial cell antibodies in systemic vasculitis. Clin Exp Immunol 2010;161:658–70.
6. Kanekawa R, Fujeda M, Ohta K, Yudoh K. Validation of a new biomarker in patients with Kawasaki Disease identified by proteomics. J Data Mining Genomics Proteomics 2013;4:1.
7. Wallace CA, Huang D, Duncelis M, Sawoll A, Giannini EH. Patterns of clinical remission in selected categories of juvenile idiopathic arthritis. Arthritis Rheum 2005;52:3554–62.
8. Whitaker JN, Engle WA. Vascular deposits of immunoglobulin and complement in idiopathic inflammatory myopathy. N Engl J Med 1972;286:333–8.
9. Tanoue A, Selcen D, Engel AG. Microvascular alterations and the role of complement in dermatomyositis. Brain 2010;133:1991–93.
10. Marelli-Berg FM, Jarmin SJ. Antigen presentation by the endothelium: a green light for antigen-specific T cell trafficking? Immunol Lett 2004;93:109–13.
11. Paepe DC, Crowe AK, Weis J, Gieseler JL. Heat shock protein family 70 and 90 in Duchenne muscular dystrophy and inflammatory myopathy: balancing muscle production and destruction. Neuromuscul Disord 2012;22:20–32.
12. Mikulova M, Statkova T, Pleštilova L, et al. Molecular markers of systemic autoimmune disorders: the expression of MHC-located HSP70 genes is significantly associated with autoimmunity development. Clin Exp Rheumatol 2017;35:33–42.
13. Dastmalchi M, Baker JW, Gallay CA, et al. An interferon signature in the peripheral blood of dermatomyositis patients is associated with disease activity. Mol Med 2007;13:56–58.
14. Baechler EC, Bilge H, Reed AM. Type I interferon pathway in adult and juvenile dermatomyositis. Arthritis Res Ther 2011;13:249.
15. Dranoff M, Senécal JL, Raymond Y. Induction of endothelial apoptosis by heat-shock protein 60-reactive antibodies from anti-endothelial cell autoantibody positive systemic lupus erythematosus patients. Arthritis Rheum 2004;50:3221–31.
16. Conroy SE, Faulds GR, Williams W, Latchman DS, Isenberg DA. Detection of autoantibodies to the 90 kDa heat shock protein in systemic lupus erythematosus and other autoimmune diseases. Br J Rheumatol 1994;33:925–6.
17. Sato T, Fujii H, Ono M, et al. A novel autoantibody against fibronectin leucine-rich transmembrane protein 2 expressed on the endothelial cell surface identified by retrovirial vector system in systemic lupus erythematosus. Arthritis Res Ther 2012;14:R197.
18. McGhee JL, Kickingbird LY, Janis JN. Clinical utility of anticuclear antibody testing in children. BMC Pediatr 2004;4:13.

Downloaded from http://rheumatologyadvances.oxfordjournals.org/ by guest on January 2018

TRADITIONAL & KAMPO MEDICINE

ORIGINAL ARTICLE

Protective effect of boiogito extract with glucosamine HCl against adjuvant-induced arthritis in rats

Mitsuko Takenaga,[1,*] Juri Niimi,[1] Akemi Hamaguchi,[1] Teita Asano,[1] Reiko Tsuchiya,[1] Yuki Ohta,[4] Kazuo Yudoh[1] & Hajime Inoue[3,4]

1 Institute of Medical Science, St Marianna University School of Medicine, Kawasaki, Japan
2 Department of Pharmacology, St Marianna University School of Medicine, Kawasaki, Japan
3 Department of Plastic and Reconstructive Surgery, St Marianna University School of Medicine, Kawasaki, Japan
4 Department of Stem Cell Therapy, St Marianna University School of Medicine, Kawasaki, Japan

ABSTRACT

Aim: The effect of boiogito extract combined with glucosamine HCl was assessed in adjuvant-induced arthritis (AIA) rats.

Methods: Rats received a daily oral mixture of boiogito extract (125 mg/kg) and glucosamine HCl (80 mg/kg) before and after complete adjuvant injection. Treatment was continued up to the day when blood and/or tissue were collected (day 12 or day 21). Paw swelling, arthritis score, and inflammatory mediators were assessed.

Results: Combined treatment was more effective for AIA than either agent alone. Both serum nitric oxide (NO) and tissue NO were significantly suppressed in the adjuvant-injected hind paw on day 12. Boiogito extract significantly reduced the tissue level of matrix metalloproteinase (MMP)-13. In addition, interleukin (IL)-1β-induced MMP-13 by SW1353 chondrocytes was dose-dependently suppressed by boiogito extract, while glucosamine HCl had little effect. IL-1β-induced phosphorylation of extracellular signal-related kinase (ERK) was inhibited by the combination of boiogito extract and glucosamine HCl, but was most strongly suppressed by glucosamine HCl alone.

Conclusion: Combined treatment with boiogito extract and glucosamine HCl had a protective effect against AIA in rats. This effect was related to strong suppression of MMP-13 production (mainly by boiogito extract) and inhibition of inflammatory mediator production via ERK signaling (mainly by glucosamine HCl).

KEY WORDS: boiogito, glucosamine HCl, matrix metalloproteinase-13, osteoarthritis

INTRODUCTION

Osteoarthritis (OA) is one of the most common chronic diseases and is a major cause of disability in the elderly. Its incidence is increasing rapidly as the world's population ages. OA is characterized by cellular loss in articular cartilage, an important factor in progressive cartilage deterioration, given that apoptosis of chondrocytes leads to degradation of the extracellular matrix (ECM) in the joint cartilage of OA patients [1]. Matrix metalloproteinases (MMP) play a critical role in the initiation and progression of cartilage destruction together with various cytokines [2,3].

Boiogito is a traditional Japanese herbal medicine containing bo (stem or rhizome of *Sinomenium acutum* (Thunb.) Rehder & E.H. Wilson), ogi (root of *Astragalus membranaceus* Bunge), sojutsu (rhizome of *Atractylodes lancea* DC.), taiso (fruit of *Zizyphus jujuba* Miller var. *inermis* Rehder), kanzo (root of *Glycyrrhiza uralensis* Fisch. ex DC.), and shinkyo (rhizome of *Zingiber officinale* Roscoe). In Japan, boiogito has been used clinically for the treatment of edema, arthritic pain, and nephritic syndrome. Koguro *et al.* reported that treatment with boiogito improved both the Harris hip score and clinical criteria in OA patients [4]. In addition, boiogito has been shown to have a cardioprotective effect in the isolated blood-perfused canine heart [5], to inhibit obesity in ovariectomized rats [6], and to increase fatty acid metabolism by cells of the proximal renal tubules [7]. Furthermore, boiogito has been reported to improve hydrarthrosis in a rat model of knee OA [8].

Glucosamine has been shown to be effective for adjuvant arthritis in rats [9–11]. In addition, Nakamura *et al.* showed that glucosamine significantly improved pain and swelling of arthritis joints compared with placebo in patients with rheumatoid arthritis (RA) [12]. Matsuno *et al.*, however,

*Correspondence: Mitsuko Takenaga
Tel: (+81-44-977-8111)
Fax: (+81-44-976-4947)
Email: m-takenaga@marianna-u.ac.jp
DOI: 10.1111/ctim.12194
Received 9 June 2017, revised 7 December 2017, accepted 7 December 2017

© 2018 The Authors. Traditional & Kampo Medicine published by John Wiley & Sons Australia, Ltd on behalf of Japan Society for Oriental Medicine and Japan Pharmaceutical Society for Wakan-Yaku.
This is an open access article under the terms of the Creative Commons Attribution-NonCommercial-NoDerivs License, which permits use and distribution in any medium, provided the original work is properly cited, the use is non-commercial and no modifications or adaptations are made.

Table 1 Components of boiogito

Original plant	Plant parts	Family name	Japanese name
Scrophularia scorpio (Tanii) Rehder & E.H. Wilson	Stem, rhizome	Menispermaceae	Bo
Astragalus membranaceus Bunge	Root	Leguminosae	Oo
Atractylodes lancea DC	Rhizome	Compositae	Sojutsu
Zanthoxylum piperitum Miliarcer, nipponense Rehder	Fruit	Rutaceae	Taiso
Glycyrrhiza uralensis Fisch ex DC	Root	Leguminosae	Kanzo
Zingiber officinale Roscoe	Rhizome	Zingiberaceae	Shoyo

concluded that glucosamine was more effective for OA than RA [13], and Kulkarni *et al.* reported that glucosamine HCl improved pain in 59 patients with knee OA [14]. Recently, a randomized, double-blind, placebo-controlled trial by Stecza *et al.* showed that glucosamine HCl combined with chondroitin sulfate and bio curcumin was effective for knee OA [15].

Locoiit GI.[®] (Ohta's Isan, Tokyo, Japan) contains boiogito extract and glucosamine HCl and has been used to treat hyperhidrosis or arthritic joint swelling and pain associated with obesity in Japan. The efficacy of this combination of boiogito extract and glucosamine HCl, however, has not been evaluated. The aim of this study was therefore to assessed the effect of this combined product in rats with adjuvant induced arthritis (AIA), and compare it with the effects of boiogito extract or glucosamine HCl alone.

METHODS

Reagents

Boiogito extract (boiogito dried extract-O, Lot No. 10 K176) was provided by Alps Pharmaceutical Industries (Gifu, Japan). Boiogito extract was prepared as follows. The following materials were extracted with 20 volumes of distilled water for 30 min at 95–100°C: bo (X3F138), oo (E3J176), sojutsu (E3U81), taiso (E4C52), kanzo (S15F119), and shoyo (S15G131) (5.0/5.0/3.0/3.0/1.5/1.0; w/w; Table 1). The solution was filtered and concentrated at 60°C in vacuo, followed by spray drying (yield: 17.2%). The extract thus obtained contained 0.77% glycyrrhizic acid and 0.59% sinomenine (Figure S1 and S2).

Glucosamine HCl was purchased from Sigma-Aldrich (St Louis, MO, USA).

Cell lines

Chondrosarcoma cell line (SW1353) was purchased from ATCC (Salisbury, UK). Cells were cultured in D-MEM (Sigma Aldrich) with 10% fetal bovine serum (Invitrogen, Carlsbad, CA, USA) and 1% antibiotic/antimycotic (Thermo Fisher Scientific, Waltham, MD, USA).

Animals

Wistar rats were purchased from Charles River Laboratories Japan (Yokohama, Japan). The rats were housed in an animal room at a constant temperature (22–24°C) and humidity (50–60%) with a 12 h light/dark cycle, and were allowed free access to a standard diet and water. The animal experiments were performed in accordance with the Guidelines for Animal Experimentation of St Marianna University Graduate School of Medicine (approval no. 1901010).

AIA model

Seven-week old female rats (215.7 ± 11.5 g) were randomly divided into the following groups (n = 5 each): (i) saline-treated AIA control group; (ii) combined therapy (boiogito extract 125 mg/kg and glucosamine HCl 80 mg/kg) AIA group; (iii) boiogito extract (125 mg/kg)-treated AIA group; (iv) glucosamine HCl (80 mg/kg)-treated AIA group; and (v) a normal control group. Complete Freund's adjuvant (0.5 mg/0.05 mL, Chondrex, Redmond, WA, USA) was injected once, intradermally, into the right hind foot pad. Test compounds suspended in saline (1 mL/kg) were given orally at 1 h before the adjuvant injection, followed by daily treatment up to day 12 or day 21. Although the daily dose of Locoiit GI.[®] is 3.6 g in humans (approx. 60 mg/kg), a five-fold higher dose was used in this study, corresponding to 125 mg/kg for boiogito extract and 80 mg/kg for glucosamine HCl.

Paw volume was determined every 3 or 4 days with a plethysmometer (TK-101CMP; Unicom, Chiba, Japan). Paw erythema and swelling were then graded as per the following 5-points scale, and arthritis score [16] calculated: 0, no inflammation; 1, swelling and erythema of the digits; 2, moderate swelling and erythema of the paw; 3, severe swelling and erythema of the limb; and 4, severe swelling, erythema, gross deformity, and difficulty using the limb.

Serum measurements and uninjected paw

After in vivo observation, a blood sample was collected under anesthesia, and serum was stored. On day 12, the adjuvant-uninjected hind paw was resected at the ankle under deep anesthesia. Paw tissue samples were homogenized in 20 mmol/L Tris-HCl (pH 7.5), 2 mol/L NaCl, 0.1% Tween-80, 1 mmol/L phenylmethylsulfonylfluoride (PMSF),

and 1 mmol/L ethylenediaminetetra acetic acid (EDTA), followed by centrifugation.

Hyaluronic acid (HA), nitric oxide (NO), prostaglandin (PG)E_2, and MMP-13 were measured with an HA assay kit (Seikagaku, Tokyo, Japan), nitrate/nitrite assay kit, PGE_2 EIA kit (Cayman Chemical, Ann Arbor, MI, USA) and MMP-13 ELISA kit (R&D Systems, Minneapolis, MN, USA), respectively.

Chondrocyte activity

SW1353 cells (3×10^5) were cultured for 24 h in serum-free medium, incubated for 2 h with bologito extract and/or glucosamine HCl, and then cultured in fresh medium containing IL-1β (10 ng/mL) for a further 24 h. Culture supernatants were used for measurement of MMP-13 and tissue inhibitor of matrix metalloproteinase (TIMP)-1 (R&D systems). In addition, cells (2×10^5) incubated for 2 h with reagents were exposed to IL-1β for 15 min, after which phosphorylation of extracellular signal related kinase (ERK) and p38 was assessed.

Bologito extract and glucosamine HCl were dissolved in phosphate-buffered saline and sterilized by passage through a 0.45 μm membrane filter.

Western blotting

Lysates were prepared with 20 mmol/L Tris–HCl (pH 7.5), 150 mmol/L NaCl, 1 (v/v)% Triton X-100, 5 mmol/L EDTA, 1 mmol/L PMSF, 5 μg/mL aprotinin, 5 μg/mL leupeptin, 2 mmol/L imidazole, 1 mmol/L sodium fluoride, 1.15 mmol/L sodium molybdate, 1 mmol/L sodium orthovanadate, and 4 mmol/L sodium tartrate dihydrate.

After centrifugation, the lysates (20 μg) were separated by electrophoresis on 10% sodium dodecylsulfate polyacrylamide gels and proteins were transferred to polyvinylidene difluoride membranes. The membranes were incubated with antibodies targeting p44/42 mitogen-activated protein kinase (MAPK; ERK, rabbit; Cell Signaling Technology, Danvers, MA, USA), phosphor-p44/42 MAP kinase (p-ERK, rabbit; Cell Signaling Technology), phosphor p38 (mouse; Abcam, Cambridge, UK), or p38 (rabbit; Cell Signaling Technology), followed by incubation with electrochemiluminescence (ECL) horseradish peroxidase (HRP) labeled anti-mouse IgG or HRP-labeled anti-rabbit IgG (GE Healthcare Japan, Tokyo, Japan). Then the membranes were incubated with the ECL Prime Western blotting detection system (GE Healthcare Japan) and signals were quantified by densitometry.

Statistical analysis

Data are given as mean ± SEM. One-way analysis of variance followed by Tukey test or Dunnett's test was used to evaluate differences, which were considered to be significant for $P < 0.05$.

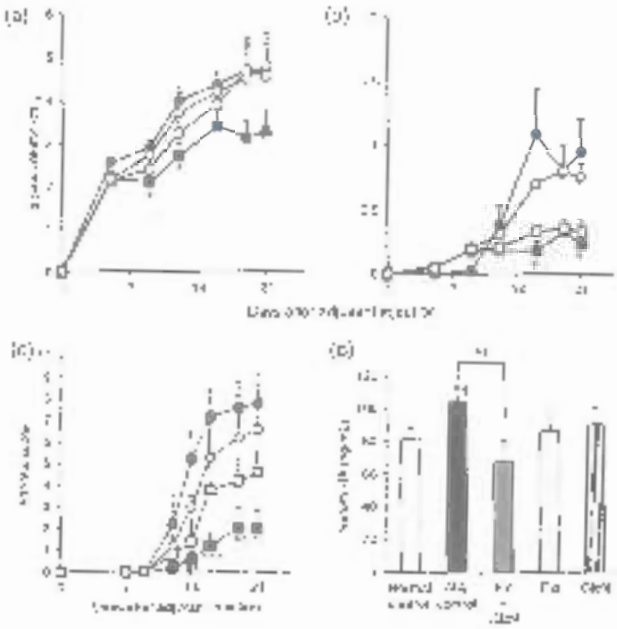

Figure 1 | Effect of intraoral administration of bologito extract with glucosamine HCl (Ext + GlcN), bologito extract alone (Ext), and glucosamine HCl alone (GlcN) on (a,b) change in paw volume (a, adjuvant-injected paw; b, uninjected paw) and (c) arthritis score up to day 21 in rats with adjuvant-induced arthritis (AIA; ● AIA control). (d) Serum hyaluronic acid (HA) on day 21. *$P < 0.05$, **$P < 0.01$ †vs AIA control, ‡vs normal control.

RESULTS

Hind paw swelling and arthritis score

In saline treated AIA control rats, rapid swelling of the right hind paw was noted after adjuvant injection and there was a subsequent steady increase of paw swelling until day 21 (Fig. 1a). In the combined bologito extract and glucosamine HCl (Ext + GlcN)-treated AIA group, however, significant reduction of hind paw swelling was achieved during the observation period.

In the AIA control group, swelling of the adjuvant uninjected left hind paw was detected on day 12 and increased until day 21 (Fig. 1b). In the AIA control, the mean increase of paw volume was >1.0 mL. In the Ext + GlcN AIA group, however, the increase in paw volume was significantly suppressed.

In the AIA control, the arthritis score increased to 7.80 ± 1.08 by day 21 (Fig. 1c), while in the Ext + GlcN AIA group, arthritis score was significantly reduced. Bologito extract alone also reduced the score, but it was not significant; and glucosamine HCl alone had little effect. Thus, combined treatment (Ext + GlcN) was more effective than either agent alone for alleviating the signs and symptoms of AIA.

© 2018 The Authors. Traditional & Kampo Medicine published by John Wiley & Sons Australia, Ltd on behalf of Japan Society for Oriental Medicine and Japan Association for Oriental Medicine

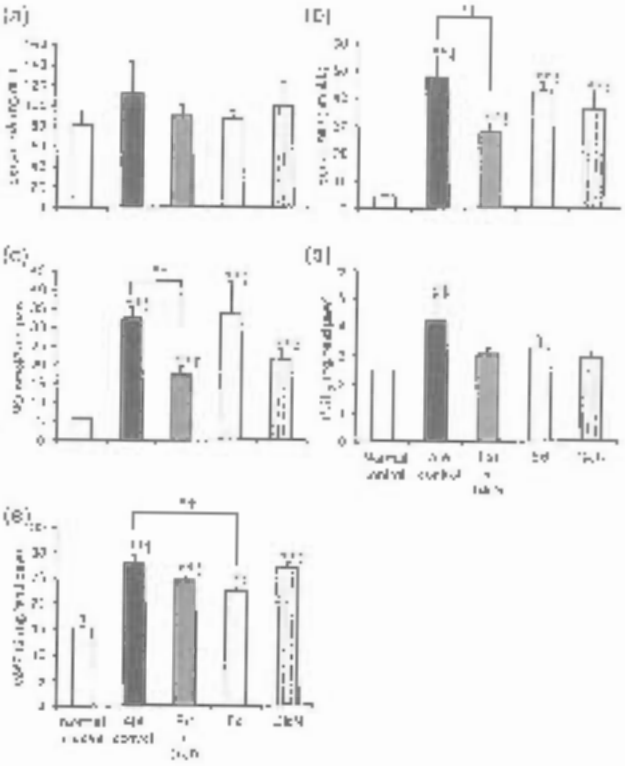

Figure 2 | Effect of boiogito extract (Ext), glucosamine HCl (GlcN) and their combination (Ext + GlcN) in adjuvant-induced arthritis (AIA) rats on day 12. (a,b) Serum (a) hyaluronic acid (HA) and (b) nitric oxide (NO). (c–e) Tissue (c) NO, (d) prostaglandin (PGE_2), and (e) matrix metalloproteinase (MMP)-13 in the adjuvant-uninjected hind paw. *P < 0.05, **P < 0.01 vs AIA control, #vs normal control.

Serum HA was significantly elevated in the AIA control compared with the normal control (Fig. 1d), while in the combined treatment group the increase was significantly suppressed.

Serum HA and NO on day 12

Next, we focused on day 12, which was when the volume of the adjuvant uninjected hind paw began to increase.

Serum HA was slightly elevated in the AIA control. The increase was suppressed in all other treatment groups, but the effect was not significant (Fig. 2a).

In the AIA control, serum NO was dramatically elevated to 48.7 ± 7.5 μmol/L on day 12 (Fig. 2b). In the combined treatment AIA group, serum NO was reduced to 27.7 ± 5.1 μmol/L. Both boiogito extract alone and glucosamine HCl alone suppressed serum NO, but neither agent had a significant effect.

Adjuvant-uninjected hind paw on day 12

Tissue NO was significantly higher in the AIA control compared with the normal control (33.3 ± 3.1 nmol vs 5.9 ± 0.5 nmol per hind paw). Combined treatment lowered the increase (Fig. 2c). Glucosamine HCl suppressed the NO, but the boiogito extract had little effect.

Tissue PGE_2 was significantly higher in the AIA control than in the normal control group (4.21 ± 0.90 ng vs 1.64 ± 0.28 ng per hind paw). PGE_2 was lowered in all treatment groups, but this was not significant (Fig. 2d).

Tissue MMP-13 was significantly increased in the AIA control than in the normal control group (27.9 ± 1.4 ng vs 16.6 ± 2.1 ng per hind paw; Fig. 2e). It was significantly lower in the boiogito extract treated group.

SW1353 chondrocyte MMP-13 and TIMP-1 production *in vitro*

When chondrocytes were exposed to IL-1β, there was a significant increase in MMP-13, while boiogito extract caused

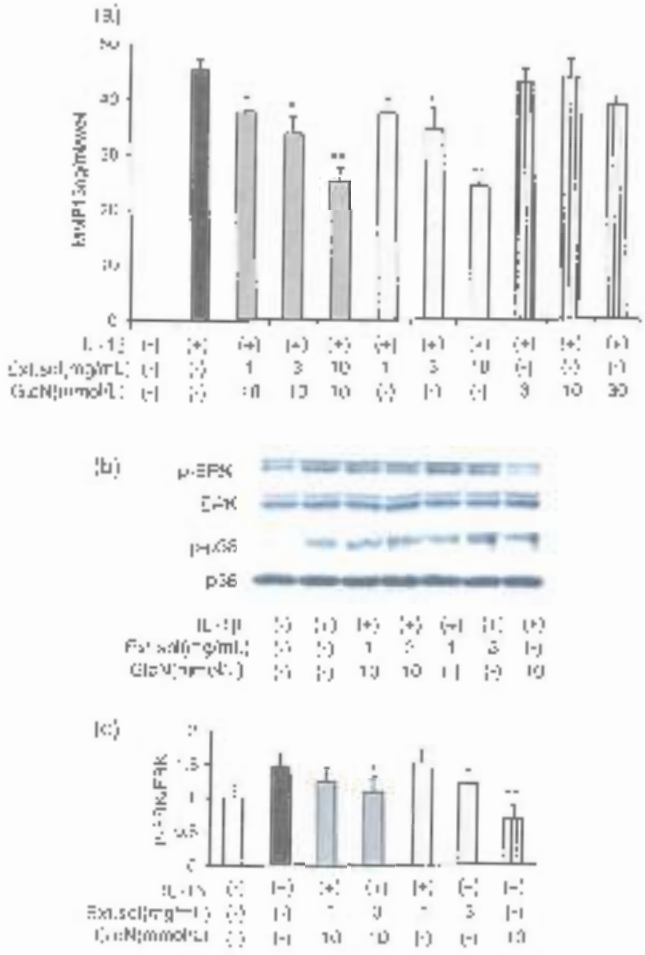

Figure 3 | (a) Effect of boiogito extract (Ext) and/or glucosamine HCl (GlcN) on interleukin (IL)-1β stimulated SW1353 cell matrix metalloproteinase (MMP)-13 production in vitro and on (b,c) phosphorylation of extracellular signal-regulated kinase (ERK) and p38. **P < 0.05, ***P < 0.01 vs control (IL-1β alone).

Table 2 Effect of boiogito and/or glucosamine on IL-1β-induced MMP-13 and TIMP-1 SW1353 cell production

Boiogito extract	Glucosamine HCl	IL-1β	MMP-13 (ng/mL) Mean ± SEM	TIMP-1 (ng/mL) Mean ± SEM	MMP-13/TIMP-1 ratio
(−)	(−)	(−)	−0.05 ± 0.02	19.5 ± 0.31	(−)
(−)	(−)	(+)	4.58 ± 1.05	27.4 ± 0.62	3.16 ± 2.09
(+)	(−)	(+)	4.29 ± 0.46*†	28.3 ± 1.23*†	1.62 ± 0.07**†
(−)	(+)	(+)	4.12 ± 0.77*†	26.8 ± 1.45*†	1.73 ± 0.14**†
(+)	(+)	(+)	4.54 ± 1.10	34.1 ± 1.43	1.46 ± 0.08

*$P < 0.05$;
**$P < 0.01$;
†vs control (IL-1β alone).
Final concentration was 5 mg/mL for boiogito extract and 10 mmol/L for glucosamine HCl.
IL, interleukin; MMP, matrix metalloproteinase; TIMP-1, tissue inhibitor of matrix metalloproteinase.

dose dependent suppression (Fig. 3a). The response to combined treatment was similar to the effect of boiogito extract alone, while glucosamine HCl alone had little influence. Cell viability was similar under all culture conditions.

Boiogito extract increased TIMP-1, and decreased the MMP-13/TIMP-1 ratio, regardless of the presence or absence of glucosamine HCl (Table 2).

Phosphorylation of ERK and p38 by chondrocytes *in vitro*

Exposure of cells to IL-1β increased phosphorylation of ERK by 1.5-fold, while this was dose dependently decreased by boiogito extract and/or glucosamine HCl. The maximum decrease was noted after addition of glucosamine HCl alone (Fig. 3b,c).

In contrast, a 1.8-fold increase of p38 phosphorylation following exposure to IL-1β was not suppressed by either boiogito extract or glucosamine HCl.

DISCUSSION

In the present study, combined treatment with boiogito extract and glucosamine HCl significantly reduced paw edema and the arthritis score in AIA rats. Boiogito extract alone was less potent, indicating that combined therapy may be more effective for joint inflammation in diseases such as OA.

Hyaluronic acid is an inflammatory mediator [17], and its level was significantly decreased by boiogito extract. Both serum and tissue (adjuvant-uninjected hind paw) NO were also significantly suppressed by boiogito extract. Furthermore, tissue PGE_2 was reduced by boiogito extract, although not significant. This suggests that suppression of inflammatory mediators contributes to the anti-arthritic activity of boiogito extract.

Glucosamine has already been reported to be effective in AIA rats [9–11]. Following oral treatment, glucosamine is absorbed and metabolized, after which it may be incorporated into arthritic joints and support chondrocyte function [18]. Nakamura *et al.* reported that glucosamine reduced joint pain and swelling in RA patients [12], while Matsuno *et al.* concluded that glucosamine was more effective for OA than RA [13]. A recent randomized, double-blind, placebo-controlled study showed that glucosamine HCl combined with chondroitin sulfate and bio-curcumin was effective for knee OA [15]. The equivalent dose of glucosamine HCl alone, however, had little influence on AIA in the present rat model. Therefore, it seems that glucosamine HCl itself was not effective against AIA in the present study, but acted to promote the pharmacological effects of boiogito extract.

The TIMP regulate tissue breakdown by blocking the activity of MMP, and the balance between these enzymes is assumed to be a critical determinant of ECM turnover, especially during progression of OA. Boiogito extract significantly reduced tissue MMP-13 in the adjuvant-uninjected hind paw. Boiogito extract also suppressed IL-1β induced MMP-13 production by SW1353 chondrocytes, while increasing TIMP-1, suggesting that not only a decrease of MMP-13 but also reduction of the MMP-13/TIMP-1 ratio may play an important role in suppressing paw edema in vivo. Glucosamine HCl had little effect on MMP-13 and TIMP-1 by chondrocytes.

The MAPK participate in inflammation and joint destruction in both RA and OA, and MAPK inhibitors have been reported to decrease synovial inflammation and cartilage damage in an animal model of arthritis [19]. MAPK are also activated by treating cultured chondrocytes with IL-1β [20]. Liu *et al.* found that MMP-13 was suppressed by inhibiting the phosphorylation of MAPK such as ERK and p38 [21]. In the present study, boiogito extract suppressed ERK phosphorylation in association with a decrease of MMP-13, while glucosamine HCl markedly suppressed ERK phosphorylation with little effect on MMP-13. Scotto d'Abusco *et al.* reported that glucosamine HCl suppressed MMP-13 production by inhibiting the phosphorylation of p38, but not ERK [22], which is inconsistent with the present results. Although further investigation of this issue is required, the present results

© 2018 The Authors. Traditional & Kampo Medicine published by John Wiley & Sons Australia, Ltd on behalf of Japan Society for Oriental Medicine and Wakan-Yaku, International Society for Wakan-Yaku

suggest that ERK signaling might be involved in MMP-13 production by chondrocytes, but glucosamine HCl seems to have little influence on MMP-13 despite suppressing the ERK pathway. Kim *et al.* and Jang *et al.* reported that suppression of ERK had an anti-inflammatory effect [23,24], and glucosamine has been reported to alleviate oxidative stress by inhibition of MAPK signaling [25]. In the present study, both serum and tissue NO were lower on day 12 in rats treated with glucosamine HCl, although the differences were not significant. Therefore, although glucosamine HCl had little influence on MMP-13, it may have had an anti-inflammatory effect via the ERK pathway that contributed to greater *in vivo* reduction of NO.

In conclusion, the combination of boiogito extract and glucosamine-HCl could be an effective treatment for joint inflammation in diseases such as OA. In addition to strong suppression of MMP-13 production by boiogito extract, the anti-inflammatory effect of glucosamine HCl mediated via ERK signaling suggests the more potent anti-arthritic activity of this combination.

It is also important to determine which component of boiogito extract has the most potent anti-arthritic activity. Sinomenine, a major component of boi, has been reported to ameliorate arthritis by acting on MMP [26,27]. The doses of sinomenine tested in this study were equivalent to 0.48 mg/kg (125 mg/kg *in vivo*) and 32 μmol/L (1 mg/mL *in vitro*), being much lower than in previous reports. Although the data are not shown, 50 μmol/L sinomenine alone had a weak inhibitory effect, but a high dose (250 μmol/L) had similar efficacy to that of boiogito extract (Table 2). Therefore, other components of boiogito extract must have contributed to its activity in addition to sinomenine.

ACKNOWLEDGMENTS

This work was partly supported by a grant from the Ministry of Education, Culture, Sports, Science and Technology of Japan under the Academic Frontier project for Private Universities (S1391006). We thank K. Baba, T. Yamazaki and T. Yoshie (Ohta's Isan) for their contribution to the analysis of boiogito extract.

CONFLICT OF INTEREST

The authors declare no conflicts of interest.

REFERENCES

1. Johnson EO, Bates GC, Soucacos PN, Lumbroso P. Neuroanatomy of proprioception. *J Surg Orthop Adv* 2008; **17**: 154–164.
2. Kato AB, Kongerud J, Neustruev O *et al.* TAK1 down-regulation reduces IL-1beta induced expression of MMP13, MMP1 and TNF alpha. *Biomed. Pharmacother.* 2006; **60**: 55–6.
3. Pujol P, Chaubet-Bonnet C, Legendre F *et al.* Interleukin-1 and transforming growth factor-beta 1 as crucial factors in osteoarthritic cartilage metabolism. *Connect. Tissue Res.* 2008; **49**: 293–294.
4. Kobune T, Tatsumi T, Shigeta T, Fujinaga H, Sato T, Nirasawa A. Effect of kampo medicine on pain and range of motion of osteoarthritis of the hip accompanied by acetabular dysplasia: Case report and literature review. *Yonago Med. Bridges* 2011; **6**: 13–17.
5. Yamakawa J, Morigo T, Takeuchi K, Nakatani M, Matano Y, Kobayashi H. Kampo medicine, bofutsushosan, improves obesity in overfed rats. *Evid. Based Complement. Alternat. Med.* 2010; **7**: 87–95.
6. Sugiyama A, Tasahara A, Satoh Y, Yoneyama M, Saegusa Y, Hashimoto K. Cardiac effects of clinically available kampo medicine observed with coronary-isolated, blood-perfused heart preparations. *Jpn. J. Pharmacol.* 2002; **88**: 307–313.
7. Kotsuyashiki K, Matsuyama W, Arai Y *et al.* Boiogito increases the metabolism of fatty acids in proximal tubular cells through peroxisome proliferator activated receptor (PPAR) alpha agonistic activity. *Biol. Pharm. Bull.* 2016; **39**: 143–147.
8. Fujitsuka N, Tamai M, Tsuchiya K *et al.* Boiogito, a kampo medicine, improves hydrarthrosis in a rat model of knee osteoarthritis. *BMC Complement. Altern. Med.* 2015; **15**: 451.
9. Aghazadeh-Habashi A, Karim MH, Asgari W, Jamali F. Glucosamine dose/concentration-effect correlation in the rat with adjuvant arthritis. *J. Pharm. Sci.* 2014; **103**: 765–767.
10. Bonet L, Hill SL, Dieppe-West M, Rose NR. Effect of pre-loading and glucosamine HCl/chondroitin sulfate/manganese ascorbate combination on experimental arthritis in rats. *Exp. Biol. Med.* 2003; **226**: 144–151.
11. Ohta T, Sugano S, Ikeda S, Sakamoto K, Nagaoka I. Preventive actions of a high dose of glucosamine on adjuvant arthritis in rats. *Inflamm. Res.* 2005; **54**: 147–152.
12. Nakamura H, Masuko K, Yudoh K, Kato T, Kamada T, Kawabata T. Effects of glucosamine administration on patients with rheumatoid arthritis. *Rheumatol. Int.* 2007; **27**: 215–219.
13. Matsuno H, Nakamura H, Katayama K *et al.* Effects of an oral administration of glucosamine-chondroitin-quercetin glucoside on the synovial fluid properties in patients with osteoarthritis and rheumatoid arthritis. *Biosci. Biotechnol. Biochem.* 2009; **73**: 288–292.
14. Kalkman C, Leena A, Lohir K, Mishra O, Sai M.A. Randomized comparative study of safety and efficacy of immediate release glucosamine HCl and glucosamine HCl sustained release formulations in the treatment of knee osteoarthritis: A proof of concept study. *J. Pharmacol. Pharmacother.* 2012; **3**: 49–54.

© 2016 The Authors. Traditional Kampo Medicine published by John Wiley & Sons Australia, Ltd
On behalf of Japan Society for Oriental Medicine and Australasian Society for Traditional Medicine. WINGAS-PAID

16. Sterz S, Giordani Morache M et al. The efficacy and safety of a combination of glucosamine hydrochloride, chondroitin sulfate and bio-curcumin with exercise in the treatment of knee osteoarthritis: A randomized double-blind, placebo-controlled study. Eur. J. Phys Rehabil. Med. 2016; **52**: 321–330.
16. Chen H, Kitamura S, Emura R, Ikuno H. Tibetan medicated bath therapy may improve adjuvant arthritis in rat. Evid Based Complement Alternat Med. 2013; **6**: 211–217.
17. Goldberg RL, Huff IP, Lenz ME, Glickman P, Katz R, Thomas EJ. Elevated plasma levels of hydroxyproline in patients with osteoarthritis and rheumatoid arthritis. Arthritis Rheum. 1991; **34**: 799–807.
18. Lavery S, Sandy JD, Colette C, Vachon P, Marier JF, Plaas AH. Synovial fluid levels and serum pharmacokinetics in a large animal model following treatment with oral glucosamine at clinically relevant doses. Arthritis Rheum. 2009; **52**: 181–191.
19. Zheng Y, Li X, Qian X et al. Secreted and O-GlcNAc-Acylated MIF binds to the human EGF receptor and promotes its activation. Mol Cell Biol. 2015; **17**: 1346–1355.
20. Geng Y, Valbracht J, Lotz M. Selective activation of the mitogen-activated protein kinase subgroups c-Jun NH2 terminal kinase and p38 by IL-1 and TNF-in human articular chondrocytes. J Clin Invest. 1996; **98**: 2425–2430.
21. Lu S, Xiao X, Cheng M. Marine inhibit IL-1beta-induced expression of matrix metalloproteinases by suppressing the activation of MAPK and NF-κB in human chondrocytes in vitro. Int. J. Clin. Exp. Pathol. 2015; **8**: 4764–4772.
22. Scotto d'Abusco A, Calamia V, Cicione C, Grigolo B, Politi L, Scandurra R. Glucosamine affects intracellular signalling through inhibition of mitogen-activated protein kinase phosphorylation in human chondrocytes. Arthres Res. Ther. 2007; **9**: R104.
23. Kim DH, Jung WS, Kim MK et al. Genistein inhibits proinflammatory cytokines in human mast cell activation through the inhibition of the ERK pathway. Int. J. Mol Med. 2014; **34**: 1669–1674.
24. Jang BC, Sung SH, Park JG et al. Glucosamine myo-inositol specifically inhibits COX-2 by preventing COX-2 N-glycosylation and by increasing COX-2 protein turnover in a proteasome-dependent manner. J Biol Chem. 2007; **282**: 27623–27637.
25. Yi W, Lin AH, Chen CH et al. Glucosamine attenuates cigarette smoke-induced lung inflammation by inhibiting ROS-sensitive inflammatory signaling. Free Radic. Biol. Med. 2014; **69**: 208–219.
26. Zhou H, Wang YX, Wang J, Cai X, Liu L. Sinomenine ameliorates arthritis via MMPs, TIMPs, and cytokines in rats. Biochem. Biophys. Res. Commun. 2008; **376**: 352–357.
27. Lan Z, Wei M, Chen L, Xie G, Liu X, Zhang X. Role of sinomenine on complete Freund's adjuvant-induced arthritis in rats. IUBMB Life. 2016; **68**: 429–435.

SUPPORTING INFORMATION

Additional Supporting Information may be found in the online version of this article:

Appendix S1 Supplementary Material.
Figure S1 Glycyrrhizic acid.
Figure S2 sinomenine in botogito extract.

© 2016 The Author. Traditional & Kampo Medicine published by John Wiley & Sons Australia, Ltd on behalf of Japan Society for Oriental Medicine and Australian Pharmaceutical Sciences Association

Novel Techniques in Arthritis & Bone Research
ISSN: 2575-8888

Juniper Publishers
Key to the Research

Review Article
Volume Three - Issue 5 - April 2018
DOI: 10.19080/NTABR.2018.03.555616

Nov Tech Arthritis Bone Res
Copyright © All rights are reserved by Kazuo Yudoh

Effects of Low-Level Laser Therapy on Clinical Characteristics and Laboratory Profiles in Synovitis in patients with Rheumatoid Arthritis

Kazuo Yudoh* and Rie Karasawa

Department of Frontier Medicine, Institute of Medical Science, St. Marianna University School of Medicine, Japan

Submission: March 20, 2018; **Published:** April 04, 2018

***Corresponding author:** Kazuo Yudoh, Institute of Medical Science, St. Marianna University School of Medicine, Kawasaki City, Japan
Tel: 81 44-977-8111; Email: yudoh@marianna-u.ac.jp

Abstract

Rheumatoid arthritis (RA) is a chronic disease that requires long-term administration of immunomodulatory drugs, resulting in a greater risk of side effects such as serious infections, malignancies, hepatic or renal dysfunction and cardiovascular diseases. The main treatment for RA is drug therapy and its therapeutic effect has steadily improved. However, problems including side effects such as infection, due to suppression of the immune system and off-target effects at other locations such as the liver, still exist because it is a systemic rather than a topical therapy.

Despite the effectiveness of anti-rheumatic drugs, further studies are needed to reduce the risk of side effects. It has been revealed that light therapy by laser irradiation may accelerate wound healing and tissue repair, as well as provide relief of pain and inflammation. The purpose of this study was to clarify whether laser irradiation treatment has a therapeutic potential as an adjunctive therapy against RA synovitis. We recruited 15 patients with RA (mean age: 64.0 years old, mean duration of follow-up: 8.5 years). A laser therapy device (Pulse 10, Panasonic Healthcare Inc.) was used for diode laser treatment. The laser was applied at one point over the swollen or tender joins for 5 minutes, once a week for a total of 5 sessions. Outcome measures included arthralgia, patients' global assessment, physician's global assessment, the levels of swelling and tenderness of arthritic joints and disability. Also, in addition to laboratory blood tests, such as concentrations of pro-inflammatory cytokines were measured.

A total of 26 joints were treated. After the third or 4th treatment with laser irradiation, there was a tendency for the number of swollen and tender joints to decrease. After the 4th treatment, the ADL and VAS scores showed a tendency to decrease significantly. Although no significant difference was observed in the C-reactive protein value, serum concentrations of a matrix degrading enzyme (metalloprotease-3) and a pro-inflammatory cytokine (interleukin-6) were significantly reduced after the 5th laser irradiation treatment session. Our results indicate that treatment with laser irradiation may have therapeutic potential as an adjunctive therapy against RA synovitis.

Keywords: Laser Therapy; Rheumatoid Arthritis; Arthralgia; Tumor Necrosis Factor-α; Interleukin-1β; Interleukin-6

Introduction

Rheumatoid arthritis (RA) is characterized by synovial hyperplasia, neovascularization and infiltration of lymphocytes and macrophages into the RA synovium [1-3]. Numerous studies have already demonstrated that synovitis is closely involved in the pathogenesis of RA [4-6]. In RA synovium, large numbers of infiltrating T cells, macrophages, osteoclast precursor cells and synovial fibroblasts can be seen. It has been demonstrated that infiltrating lymphocytes and macrophages in RA synovial tissue produce excessive levels of pro-inflammatory cytokines, such as tumor necrosis factor (TNF)-α, interleukin (IL)-1 and IL-6 [4-13]. These cytokines form a network and are key participants in the pathogenesis of arthritis. An imbalance of pro-inflammatory and inhibitory cytokines may, at least in part, participate in the development of arthritis [13]. In addition, periarticular osteopenia can be observed in the early stage of the disease before the erosion of bone becomes evident [14-18]. Previously, we have demonstrated that infiltrating inflammatory cells in RA synovium may modulate not only inflammation but also bone and cartilage destruction [11]. A therapeutic strategy against synovitis may have the potential to inhibit inflammation, joint pain (arthralgia), and the degeneration of bone and cartilage tissues [9-10]. In this study we focused on the synovitis to develop a new therapeutic strategy for RA.

In general, currently-available anti-rheumatic drugs to inhibit RA synovitis include non-steroidal anti-inflammatory drugs (NSAIDs), steroids, disease modifying anti-rheumatic

drugs (DMARDs), immune suppressants, or antibiotics. Anti-rheumatic drugs, such as DMARDs, immune suppressants, and biologics, exert their therapeutic effects via cellular and molecular responses of target cells, such as T cells, B cells, macrophages and synovial fibroblasts [19-22]. In addition to therapeutic drug responses, these anti-RA drugs are likely to induce a variety of side effects, such as anemia, vasculitis, pneumonitis, infection, or liver disorders. Consequently, it is important to consider the balance between therapeutic effects and side effects in anti-rheumatic drugs [21,22]. Novel low-invasive therapies are required to further improve the symptoms and clinical outcomes of RA.

Numerous reports and systematic reviews with meta-analysis have already demonstrated that laser therapy exhibits an anti-inflammatory effect in a variety of diseases [23-28]. It is suggested that laser therapy showed an anti-inflammatory effect through the mechanism involving the control of pro-inflammatory cytokine secretion [23-27]. In RA, synovitis induces joint destructions as well as acute and chronic arthralgia. Treatment with laser illumination may be expected as an adjunctive therapy for RA synovitis, although further studies are needed to clarify possible mechanisms for the therapeutic effect of laser therapy on synovitis.

Based on the results of our previous *in vitro* and *in vivo* studies, we postulated that light therapy may have potential as an adjunctive and low-invasive therapy for RA. The purpose of our clinical study was to clarify whether or not treatment with laser irradiation has therapeutic potential as an adjunctive therapy against RA synovitis. We hypothesized that laser irradiation would have anti-inflammatory and anti-pain effects against the synovitis in RA. If the light therapy proves effective, it would enable the doses of NSAIDs, steroids or immune suppressants to be reduced, resulting in a greatly decreased risk of side effects such as gastric ulcers, osteoporosis or infection.

Patients

Fifteen patients with RA were recruited and received light therapy by laser irradiation against rheumatoid arthritic joints. The protocol of this study was approved by the ethical committee of St. Marianna University School of Medicine (permission number: 1678) and was conducted in accordance with the 2013 Helsinki declaration and its later amendments or comparable ethical standards. Informed consent was obtained from all individual participants included in the study. Table 1 shows the criteria of patient selection for this study. The mean patient age was 64.9 years old, with a range from 48 to 78 years. The mean duration of follow-up was 8.5 years. Six patients showed lower disease activity as defined by a disease activity score (DAS) score of less than 2.7 [29]. Nine patients had active disease as defined by a DAS score of more than 2.7. Table 2 shows patients' profiles in this clinical study. All patients had to have been receiving a stable dose of NSAIDs, steroids, immune suppressants or antibiotics for at least 6 months to participate in the study (Table 3).

Table 1: Criteria of the patient selection.

1	History/clinical of treatments with anti-rheumatic drugs: At least more than 6 months, Stable clinical features.
2	No patient with changes of therapeutic strategies such as anti-rheumatic drugs, rehabilitation, surgery, or other therapies.
3	Frequency of laser illumination therapy: Patients that can be received the illumination therapy at least in once per 2 weeks and total 5 times at most during 8 weeks.
4	No complications such as a heart failure, infection, cancer, diabetes mellitus.

Table 2: Patients' profiles.

Number of RA patients.	15 (male 2, female 13)
Mean age	64.9 years (range, 49 - 78 years)
Duration of follow-up.	8.5 years (3 - 10 years)
DAS28 [29] disease activity	
DAS < 2.7 (slight)	6 patients
DAS 2.7 – 4.1 (moderate)	7 patients
DAS > 4.1 (severe)	2 patients

DAS (disease activity score).

Table 3: Profile of treatment with anti-rheumatic drugs.

Only steroid.	2 patients
Only methotrexate (MTX)	3 patients
Steroid + MTX.	9 patients
Antibiotics (anti-TNF α) + MTX	1 patient

*All patients in the present study had been treated with non-steroidal anti-inflammatory drugs.

TNF (tumor necrosis factor).

Laser Irradiation

All laser irradiation treatments were applied over a period of 4 weeks, once a week for a total of five sessions. A laser therapy device (Pulse 10, Panasonic Healthcare Inc., Japan) was used for treatment with a diode laser [30]. The wave length of this machine was 830 nm, peak output power was 10 W, and power density was 6-7W/cm². The product used in the current study can produce the pulsed laser light with peak output power of 10W (20 milliseconds, irradiation energy 1J/second) by intervals of 180 seconds, which enables to suppress the strong thermal effect and to transmit the laser light into the deeper tissue at the same time. The laser was applied at one points over the swollen or tender joint for 5 minutes. Outcome measures included arthralgia, patients global assessment, physicians global assessment, the levels of swelling and tenderness of arthritic joints and disability. The level of joint pain was evaluated by visual analog scale (VAS). The VAS is a standard 10 cm horizontal scale. The patient indicates the severity of pain by placing a mark between terminal points designated "No pain" and "Pain as bad as it could be". The VAS is scored from 0 (no pain) to 10 (pain as bad as it could be).

How to cite this article: Kazuo Y, Ryo K. Effects of Low-Level Laser Therapy on Clinical Characteristics and Laboratory Proteins in Synovitis in patients with Rheumatoid Arthritis. Nov Tech Arthritis Bone Res. 2018; 2(5): 555595. DOI: 10.19080/NTAB.2018.02.555595

In general, it is well known that the VAS found in the Stanford Health Assessment Questionnaire was found to be the most useful available measure for routine clinical use. However, some patients could not complete this scale without assistance. Therefore, it has been developed a brief pain scale for regular use, based on the frequency of pain in the same 8 activities of daily living (ADL) used to assess difficulty, dissatisfaction, and change in status [31].

The patient was asked: "How often is it painful for you to ..." for each of the 8 ADL (a, b, c, d, e, f, g, h) described below.

a) Dress yourself (including tying shoelaces)?

b) Get in and out of bed?

c) Lift a full cup or glass to your mouth?

d) Walk outdoors on flat ground?

e) Wash and dry your entire body?

f) Bend down to pick up clothing from the floor?

g) Turn regular faucets on and off?

h) Get in and out of a car?

And then, four response options were presented and were scored as follows: never = 0, sometimes = 1, most of the time = 2, and always = 3. The total ADL pain score was the mean score for the 8 responses [31,32].

In addition to laboratory blood tests, serum concentrations of biomarkers for inflammation (C-reactive protein (CRP), pro inflammatory cytokines (TNF-α, IL-1, IL-6)) and matrix degrading enzyme (matrix metalloproteinase (MMP)-3) were measured. The schedule of analysis is summarized in (Table 4).

Table 4: Schedule of analysis

		0 week	4 weeks	5 weeks	6 weeks	7 weeks	8 weeks
Check of patient profile		○					
Laser irradiation			△	△	△	△	△
Objective analysis of arthritis		○	○●	○●	○●	○●	○●
Subjective analysis of arthritis		○	○●	○●	○●	○●	○●
Check of side effects		○	○●	○●	○●	○●	○●
Laboratory tests	Blood test	○	○				●
	CRP	○	○				●
	ESR	○	○				●
	MMP-3	○	○				●
Cytokines (blood samples)	IL-1β	○	○				●
	TNF-α	○	○				●
	IL-6	○	○				●
Diagnostic imaging		△	△				▲
DAS28		○	○				●

○Before irradiation ● After irradiation △ Before irradiation as necessary ▲ After irradiation as necessary CRP (C reactive protein) ESR (erythrocyte sedimentation rate), MMP (matrix metalloproteinase-3) IL (interleukin) TNF (tumor necrosis factor)

Results

Table 5: Laser irradiated joints

Finger joints	3 patients	8 joints
thumb CM joint		2 joints
index finger PIP joint		3 joints
middle finger PIP joint		3 joints
Wrist joints	3 patients	7 joints
Elbow joints	1 patient	1 joint
Shoulder joint	1 patient	1 joint
Knee joints	3 patients	3 joints
Ankle joints	2 patients	4 joints
Total	15 patients	26 joints

CM (carpometacarpal)

PIP (proximal interphalangeal)

A total of 26 joints were treated (Table 5). Relatively more PIP finger and wrist joints were involved in comparison to large joints.

After the 3rd or 4th treatment with laser irradiation, there was a tendency for the number of swollen and tender joints to decrease (Figures 2A & 2B). Regarding ADL (pain) score and VAS of pain, after the 4th treatment, the scores showed a tendency to decrease significantly, suggesting a therapeutic effect of laser irradiation on the rheumatoid synovitis (Figures 2A & 2B). Although no significant difference was observed in the CRP value, serum concentration of matrix metalloproteinase MMP-3 was significantly decreased after the 5th laser irradiation treatment (Figures 3A & 3B).

We observed that serum concentrations of pro inflammatory cytokines (TNF-α and IL-6, but not IL-1β), were decreased after the 5th laser irradiation (Figures 4A-4C). These pro inflammatory

cytokines are mainly produced by synovial fibroblasts, infiltrating T cells and macrophages. We conclude that the laser irradiation against the arthritic joints directly inhibits the production of pro inflammatory cytokines from synovial tissue.

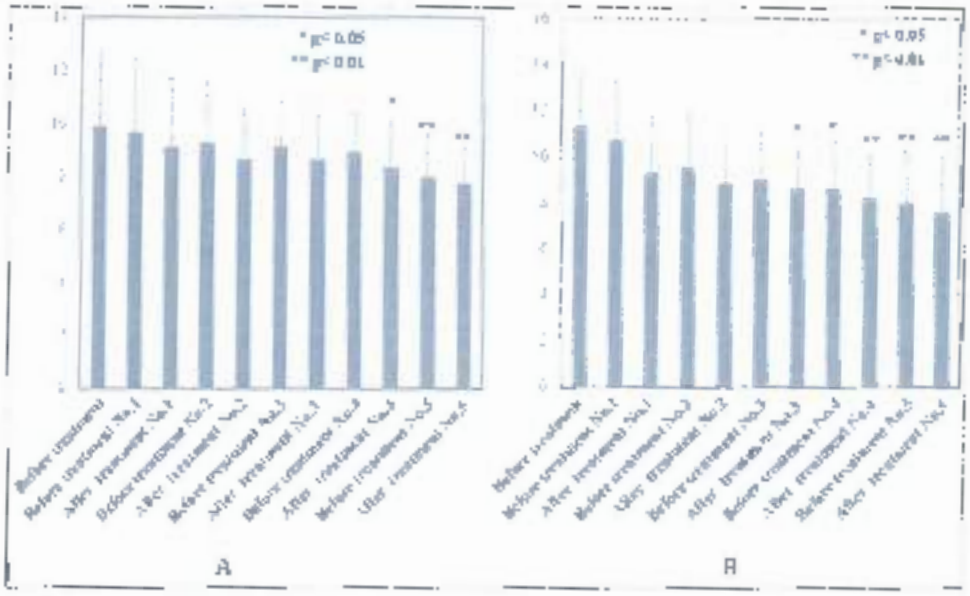

Figure 1: Number of swollen and tender joints.
A: number of swollen joints that received laser irradiation
B: number of tender joints that received laser irradiation.
After the treatment with laser therapy, there was a tendency to decrease number of swollen and tender joints. Number of swollen and tender joints were significantly decreased after the 3rd –4th treatment with laser irradiation (* P<0.05 compared to the initial phase, **P<0.01 compared to the initial phase)

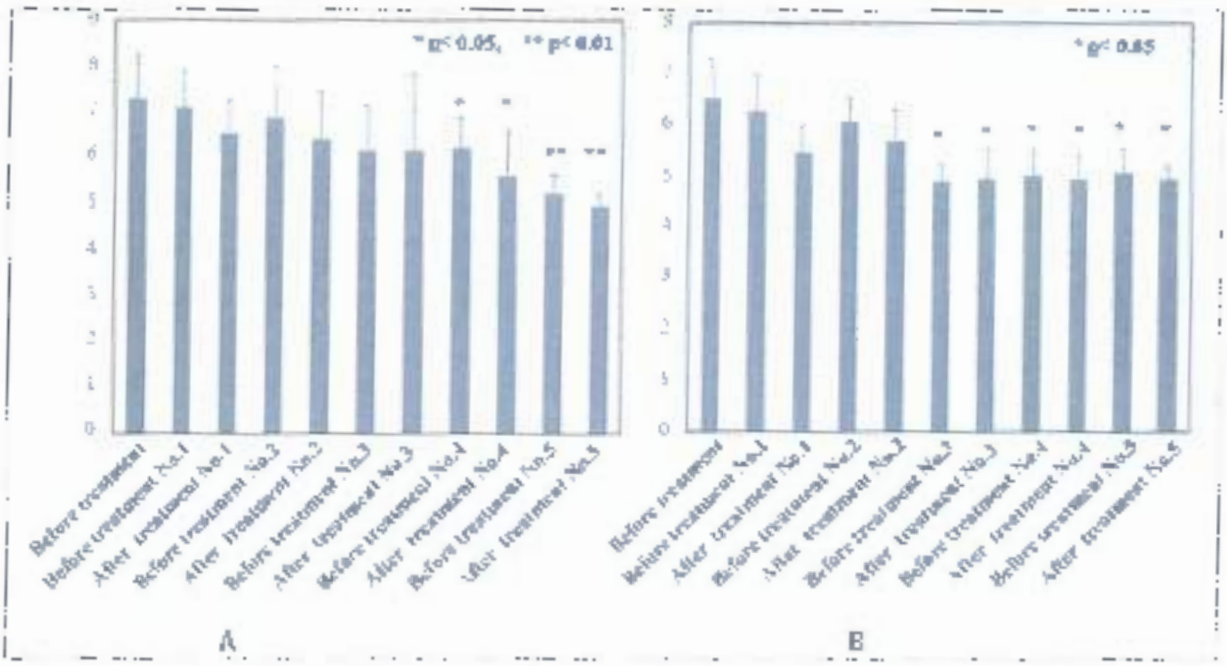

Figure 2 : Pain score and visual analog scale.
A: pain score (ADL score)
B: visual analog scale (VAS) After the treatment with laser therapy, arthralgia was improved. Both pain score and VAS were significantly decreased after the 3rd –4th treatment with laser irradiation (* P<0.05 compared to the initial phase, **P<0.01 compared to the initial phase)

How to cite this article: Kazun Y, Ro K. Effects of Low-Level Laser Therapy on Clinical Characteristics and Laboratory Profiles in Synovitis in Patients with Rheumatoid Arthritis. Novel Tech Arthritis Bone Res. 2018; 2(1): 555596. DOI: 10.19080/NTAB.2018.02.555596

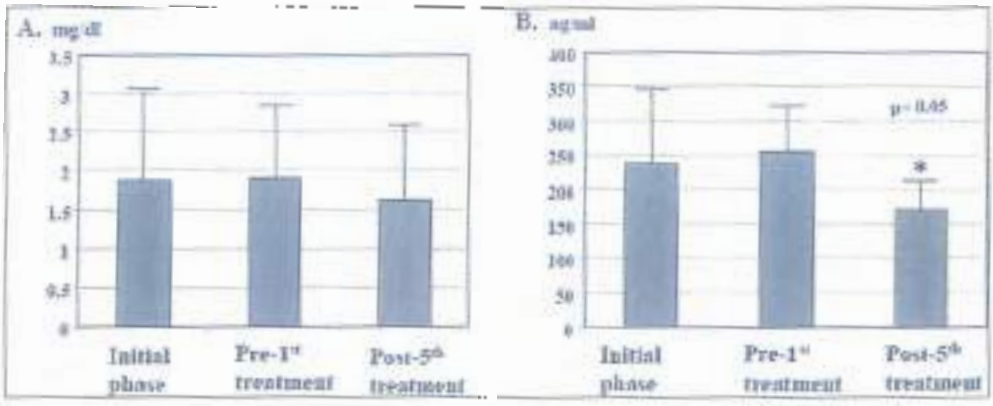

Figure 3 : Serum levels of C-reactive protein and matrix metalloproteinase
A: serum level of biomarker of acute inflammation, C-reactive protein (CRP);
B: serum level of biomarker of joint degeneration/destruction, matrix metalloproteinase (MMP) 3. There was a tendency to decrease the serum level of CRP after laser irradiation, although no significant difference was observed in comparison with the initial phase. The serum level of MMP-3 was significantly decreased after the 5th treatment with laser therapy ($P<0.05$ compared to the initial phase).

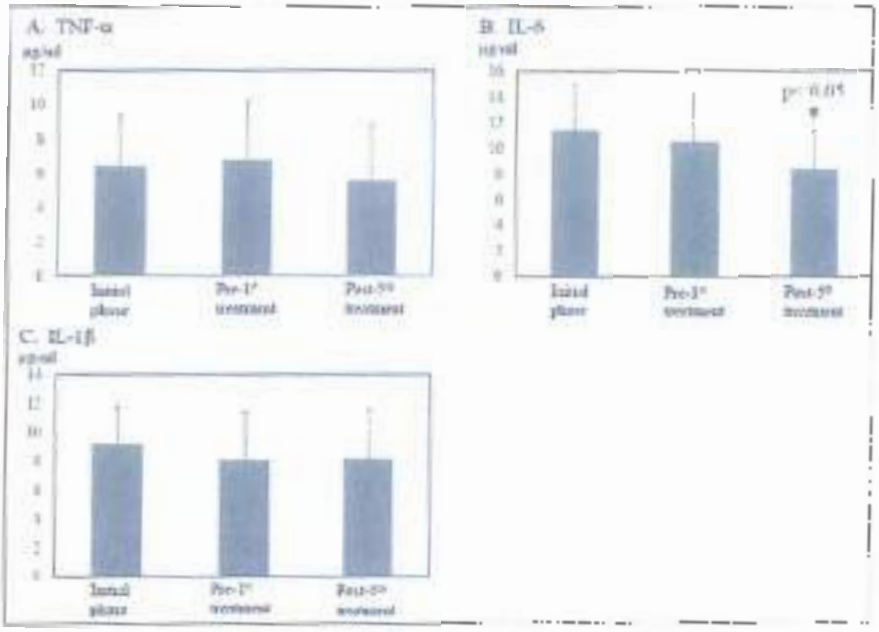

Figure 4 : Serum levels of proinflammatory cytokines, tumor necrosis factor α, interleukin-1β, interleukin-6
A: serum levels of proinflammatory cytokine, tumor necrosis factor (TNF)-α
B: serum levels of proinflammatory cytokine, interleukin (IL)-1β.

Discussion

In this present study, we carried out a clinical trial with a device for laser therapy to clarify whether or not treatment with laser irradiation has therapeutic potential for RA patients. Our present study indicates that there is a tendency for the number of swollen and tender joints to decrease after laser irradiation treatment. The arthralgia was also improved by the treatment. Interestingly, we observed that the laser therapy was more effective in fingers and wrist joints than in other large joints such as shoulder, elbow and knee joints (Table 6), although it still unknown why there was difference in therapeutic effects between small joint and large joints.

Table 6: Therapeutic effects (after the 1st treatment).

	Change for the better			
	Illuminated site	Swelling	Tenderness	VAS
Finger	8 joints	4/6	3/6	7/8
Wrist	2 joints	4/7	5/7	5/7
Elbow	1 joint	0/1	0/1	1/1
Shoulder	1 joint	0/1	0/1	0/1
Knee	5 joints	1/5	2/5	2/5
Ankle	4 joints	2/4	3/4	3/4

VAS (visual analog scale)

How to cite this article: Kawai Y, Ris K. Effects of Low-Level Laser Therapy on Clinical Characteristics and Laboratory Profiles in Patients with Rheumatoid Arthritis. Nov Tech Arthritis Bone Res. 2018; 2(5): 555586. DOI: 10.19080/NTAB.2018.02.555586

In the current study, we used two different pain scales, the VAS and ADL pain score. In general, it is well known that the visual analog pain scale found in the Stanford Health Assessment Questionnaire was found to be the most useful available measure for routine clinical use. However some patients could not complete this scale without assistance. Therefore, it has been developed a brief pain scale for regular use based on the frequency of pain in the same 8 ADL used to assess difficulty, dissatisfaction, and change in status [31]. Previous study demonstrated that the ADL pain scale met psychometric criteria for validity and reliability. Scores on the 2 pain scales were correlated significantly with one another and with other measures of disease status, including tender count, grip strength, walking time, button test, morning stiffness, erythrocyte sedimentation rate, global self-assessment, ADL difficulty, and ADL dissatisfaction scales [32]. They mentioned that the ADL pain scale was more sensitive to problems in ADL than were the ADL scales for difficulty and dissatisfaction. It has been reported that the ADL and visual analog pain scales appear to provide useful data for quantitative assessment of pain in the routine care of rheumatoid arthritis patients [32].

It is well known that laser irradiation has anti-inflammatory effect through the mechanism involving the inhibition of pro-inflammatory cytokine secretion [23-26,28]. Also, laser therapy shows an anti-pain effect via the suppression of the exited sensory nerve and sympathetic nerves and the improvement of blood flow due to vasodilating action in a feedback system of pain [33,34]. The laser therapy also shows an anti-pain effect via the suppression of the exited sensory nerve and sympathetic nerves and the improvement of blood flow due to vasodilating action in a feedback system of pain [35,36]. Generally, there is a feedback system of pain, consisting of the excitation of sensory and sympathetic nerves and narrowing of blood vessels [36,37]. Previous reports revealed that light therapy could suppress these three factors forming the negative spiral of pain [33,34]. In addition, cellular responsiveness against light therapy had been also been evaluated. Previous studies have revealed that light irradiation can induce activation of the cellular respiratory chain, resulting in an increase of cellular energy [production of adenosine triphosphate (ATP)] and a variety of cellular responses such as gene expression, protein synthesis, collagen synthesis, cell proliferation, cell-cell communication, activation of immune cells and intracellular signal transductions [38-40]. As a photobiological response, light irradiation is thought to accelerate wound healing, tissue repair, and the relief of pain and tissue edema [23,41]. As these photobiological responses, the light irradiation is thought to accelerate the wound healing, tissue repair, tissue edema and the relief of pain.

In our study, scores of joint symptoms (number of swollen joints and tender joints), pain score, and VAS gradually decreased with the advance of laser treatment and showed a tendency to decrease significantly after the 4th treatment. This suggests that the laser irradiation in the arthritic joint may reduce the local of synovitis, such as synovial hyperplasia and infiltration of inflammatory cells into synovial tissue, in rheumatoid arthritic joint. The laser treatment may have a potential to decrease the level of inflammation in RA joints. Anti-inflammatory effect of laser irradiation may accumulate according to increase in the laser irradiation number of times, and their joint symptoms may show a tendency to decrease significantly after the 4th treatment. Although further studies are needed to clarify the issue, we would like to conclude that the laser irradiation have an anti-inflammatory effect against rheumatoid synovitis.

Because the laser light spreads rapidly within the human body, a greater output of laser light is required in order to deliver the light to deeper biological tissue. For laser therapy, the device (Gallium-Aluminum-Arsenide Diode) we used in the current study can produce pulsed laser light with a peak output power of 10 W, which simultaneously reduces the strong thermal effect and allows transmission of the laser light into deeper tissue. The device can deliver the laser light more deeply while maintaining average irradiation energy of 1 W which is equivalent to that of conventional laser devices [38]. In deep parts of the body, the intensity of the laser light becomes very low due to diffusion. Sufficient laser light intensity and irradiation energy are achieved by fast switching of the 10 W high-power laser element. By irradiating the high-power laser light periodically, it is possible to transmit laser light into deeper tissue while providing enough cooling time to suppress unnecessary heat generation. Therefore, we believe that the device we used for laser therapy can be safely used to treat synovitis in RA.

Our results showed that the serum concentration of MMP-3, but not CRP, was significantly decreased after the laser irradiation treatments. CRP is produced by the liver in response to inflammation/immune reaction. MMP-3, that is a highly-sensitive marker of joint destruction, is mainly produced by synovial tissue. Laser irradiation against the arthritis joint may directly influence the production of MMP-3 from the inflammatory synovium, but not the production of CRP from liver tissue. We believe this is the reason why the decrease caused by light irradiation was observed in the serum level of MMP-3, but not the CRP value.

Our study also showed that the serum level of pro-inflammatory cytokine IL-6 was significantly decreased after the 5th treatment with laser therapy. In addition, the serum level of pro-inflammatory cytokine TNF-α tended to decrease after laser irradiation, although no significant difference was observed in comparison with the initial phase. These findings suggest that the laser irradiation may have an anti-inflammatory effect in RA synovitis. In RA, it is well known that infiltrating lymphocytes and macrophages in RA synovial tissue produce excessive levels of pro-inflammatory cytokines, such as TNF-α, IL-1 and IL-6. These cytokines form a network and are key participants in the pathogenesis of arthritis. The laser irradiation may influence the production of pro-inflammatory cytokines from infiltrating lymphocytes and macrophages. In contrast, no significant

difference in the serum level of IL-1β was observed by laser irradiation in our present study. Among these pro-inflammatory cytokines, TNF-α and IL-6 seems to be stronger in participation as a pathogenic factor than IL-1β in RA. Indeed, biologics targeting TNF-α and IL-6 are widely used to treat in patients with RA.

In conclusion, from the results of the current study, we conclude that treatment with laser irradiation may have therapeutic potential as an adjunctive therapy against RA synovitis. Future developments in light therapy may be able to provide a new therapeutic choice to a patient with RA. This method may show promise as an adjunctive therapy with no side effects over the short term in inpatients and which could allow new outpatients to carry out treatment at home. Further studies are needed to clarify the exact therapeutic effect of laser irradiation on rheumatoid synovitis. We are now trying to prepare for a new double-blind randomized controlled trial to analyze the effect of light irradiation therapy on synovitis in patients with rheumatoid arthritis.

Acknowledgement

We would like to thank M. Suzuki, S. Mogi, M. Tamaki, and J. Tamate for excellent technical assistance.

Compliance with ethical standards

a. Ethical approval

This study was independently reviewed and approved by the ethics board of St. Marianna University School of Medicine and was conducted in accordance with the 2011 Helsinki declaration and its later amendments or comparable ethical standards.

Informed consent was obtained from all individual participants included in the study.

Conflict of Interest / Funding

This study was supported by Panasonic Healthcare co. ltd. Japan. The sponsor had no control over the interpretation, writing, or publication of this work. The corresponding author had full access to all the data in the study and had final responsibility for the decision to submit for publication.

References

1. Angelotti F, Parma A, Cafaro G, Capecchi R, Alunno A, et al. (2017) pathogenesis of rheumatoid arthritis. Clin Exp Rheumatol 35(31): 350-376.

2. Elshabrawy HA, Chen Z, Volin MV, Ravella S, Virupannavar S, et al. (2015) The pathogenic role of angiogenesis in rheumatoid arthritis. Angiogenesis 18(4): 433-48.

3. van Steenbergen HW, Aletaha D, Beauit-van de Yande LJ, Brouwer E, Castrikum S, et al. (2017) ELIAS: early rheumatoid arthritis suspicious for progression to rheumatoid arthritis. Ann Rheum Dis 76(3): 491-496.

4. Firestein GS, McInnes IB (2017) Immunopathogenesis of Rheumatoid Arthritis. Immunity 46(2): 183-196.

5. van de Sande MG, Baeten DL (2015) Immunopathology of synovitis: from histology to molecular pathways. Rheumatology 55(4): 599-606.

6. Hunter T, Mahle A, Pinard M, Burr A, Krug S, et al. (2017) The Relationship Between Synovial Pathohistology and Magnetic Resonance Imaging Abnormalities in Rheumatoid Arthritis: A Systematic Review. J Rheumatol 44(9): 1311-1324.

7. Bernardini G, Bongio G, Sorice R, Wilson G, Scarceriu A (2017) The Multifunctional Role of the Chemokine System in Arthrogenic Processes. Curr Rheumatol Rep 19(3): 13.

8. Yoon M, Hashimoto M, Mimura T, Pope T, Fujii M, et al. (2017) Cell-contact-dependent activation of CD4+ T cells by adhesion molecules on synovial fibroblasts. Mod Rheumatol. 27(3): 448-456.

9. Koch MH, Brown EM, Krook G, Freeston JE, Middleton G, et al. (2017) Abatacept reduces disease activity and ultrasound power Doppler in ACPA-negative undifferentiated arthritis: a pilot-of-concept clinical and imaging study. Rheumatology 56(1): 58-67.

10. Savarese A, van Vollenhoven R, Fleischmann RM, Emery P, Salmoury I, et al. (2017) Testing treat-to-target outcomes with initial methotrexate monotherapy compared with initial tumour necrosis factor inhibitor (adalimumab) plus methotrexate in early rheumatoid arthritis. Ann Rheum Dis pii: annrheumdis-p. 1-4.

11. Cai YM, Matsuno H, Nakamura H, Nishioka K, Yudoh K (2004) Interleukin-16 enhances monocyte tumor necrosis factor alpha and interleukin-1beta production induced by direct contact with T lymphocytes: implications in rheumatoid arthritis. Arthritis Rheum 50(2): 432-443.

12. McInnes IB, Gravallese EM (2004) Immunopathogenesis of rheumatoid arthritis: a new cytokine target for the treatment of inflammatory diseases. Curr Opin Pharmacol 4(4): 392-399.

13. Miranda-Carus ME, Balsa A, Benito-Miguel M, Perez de Ayala C, Martin M, Cabero E (2004) IL-15 and the initiation of cell contact dependent synovial fibroblast-T lymphocyte cross-talk in rheumatoid arthritis: effect of methotrexate. J Immunol. 15 173(2): 1463-1476.

14. Gravallese EM, Manning C, Tsay A, Naito A, Pan C, et al. (2000) Synovial tissue in rheumatoid arthritis is a source of osteoclast differentiation factor. Arthritis Rheum 43: 250-258.

15. Murphy G, Cappadoni C, Lee R, Shimomura G, Moore T, Lacey DL, et al. (1999) A chimeric form of osteoprotegerin inhibits hypercalcemia and bone resorption induced by IL-1/TNF-α, PTH, PTHrP and 1,25(OH)2D3. J Bone Miner Res 14(9): 1478-1486.

16. Nakashima T, Kobayashi Y, Yamasaki S, Kawakami A, Eguchi K, et al. (2000) Protein expression and functional difference of membrane-bound and soluble receptor activator of NF-κB ligand: modulation of the expression by osteotropic factors and cytokines. Biochem Biophys Res Commun 275: 768-775.

17. Gravallese EM, Harada Y, Wang JT, Gorn AH, Thornhill TS, et al. (1998) Identification of cell types responsible for bone resorption in rheumatoid arthritis and juvenile rheumatoid arthritis. Am J Pathol 152(4): 943-951.

18. Yasuda H, Shima N, Nakagawa N, Yamaguchi K, Kinosaki M, et al. (1998) Osteoclast differentiation factor is a ligand for osteoprotegerin/osteoclastogenesis-inhibitory factor and is identical to TRANCE/RANKL. Proc Natl Acad Sci USA 95(7): 3597-3602.

19. Tanaka Y, Saito K (2014) Intensive intervention followed by treatment holiday from biological DMARDs in patients with rheumatoid arthritis. Drugs 74(18): 2129-2139.

20. Niwa Y, Sato M, Furuya H, Yano B, Iwata Y, et al. (2013) Clinical Characteristics of Rheumatoid Arthritis Patients Achieving Sustained Remission after Six Months of Tumor Necrosis Factor Biological Disease-Modifying Antirheumatic Drugs (DMARDs) Treatment. Intern Med 52(17): 2271-2275.

21. Singh JA, Hossain A, Tanjong Ghogomu E, Mudano AS, Maxwell L, Buchbinder R, et al. (2017) Biologics or tofacitinib for people with rheumatoid arthritis unsuccessfully treated with biologics: a

systematic review and network meta-analysis. Cochrane Database Syst Rev 3.

22. Singh JA, Hossain A, Tanjong Ghogomu E, Mudano AS, Tugwell P, et al. (2016) Biologic or tofacitinib monotherapy for rheumatoid arthritis in people with traditional disease-modifying antirheumatic drug (DMARD) failure: a Cochrane Systematic Review and network meta-analysis (NMA). Cochrane Database Syst Rev 11.

23. Santinoni CD, Oliveira HF, Batista VT, Lemos DA, Verri FR (2017) Influence of low-level laser therapy on the healing of bone tissue in bone defects: A systematic review. J Photochem Photobiol B 169: 83-89.

24. Lee JH, Chiang MH, Chen PH, Ho ML, Lee HE, et al. (2017) Anti-inflammatory effects of low-level laser therapy on human periodontal ligament cells: in vitro study. Lasers Med Sci. 23(3): 469-477.

25. Alayat MS, Aly TH, Elsayed AE, Fadil AS (2017) Efficacy of pulsed N:YAG laser in the treatment of patients with knee osteoarthritis: a randomized controlled trial. Lasers Med Sci. 32(3): 503-511.

26. Alves AN, Fernandes KP, Deana AM, Bussadori SK, Mesquita-Ferrari RA (2014) Effects of low-level laser therapy on skeletal muscle repair: a systematic review. Am J Phys Med Rehabil 93(12): 1077-86.

27. Huang Z, Ma J, Chen J, Shen B, Pei F, et al. (2015) The effectiveness of low-level laser therapy for nonspecific chronic low back pain: a systematic review and meta-analysis. Arthritis Res Ther 17: 360.

28. Huang Z, Chen J, Ma J, Shen B, Pei F, et al. (2015) Effectiveness of low-level laser therapy in patients with knee osteoarthritis: a systematic review and meta-analysis. Osteoarthritis Cartilage 23(10): 1837-1849.

29. http://www.das-score.nl/das28en/

30. Markovich S, Sutto A, Tsakadze Y (2015) Low level laser therapy for sports injuries. Laser Ther 24(1): 17-26.

31. Pincus T, Summey JA, Soraci SA Jr, Wallston KA, Hummon NP (1983) Assessment of patient satisfaction in activities of daily living using a modified Stanford Health Assessment Questionnaire. Arthritis Rheum 26(11): 1346-1353.

32. Gallagher LE, Brooks RH, Summey JA, Pincus T (1987) Quantitative pain assessment for routine care of rheumatoid arthritis patients, using a pain scale based on activities of daily living and a visual analog pain scale. Arthritis Rheum 30(6): 630-636.

33. Bicanova CM, Chavantes MC, Wu X, Anders JJ (2017) The mechanism of photobiomodulation therapy of neuropathic pain by near infrared laser light. Lasers Surg Med 49(5): 516-524.

34. Anders JJ, Moges H, Wu X, Erbguth FJ, Alberico SL, et al. (2014) In vitro and in vivo generation of neurotrophic factors by near infrared laser treatment for injured peripheral nerves. Lasers Surg Med 46(1): 54-65.

35. Benzinger M, Merrow E (2014) Virtual feedback for motor and pain rehabilitation after spinal cord injury. Spinal Cord 201 52(12): 0nf-9on.

36. Hill RL, Roberts TT, Papanicolas DN, Mulligan MT, Tolan AR (2014) Management of chronic musculoskeletal pain. J Am Acad Orthop Surg 22(2): 101-110.

37. Arslan H, Doganay E, Kucukcakir E, Colak MA, Ahmed HMA (2017) Effects of Low-level Laser Therapy on Postoperative Pain after Root Canal Retreatment: A Prelim-nary Placebo-controlled, Double-blind, Randomized Clinical Trial. J Endod 43(11): 1765-1766.

38. Spotti G, De Luca V, Pezzin M, Fiori V, Di Gregorio L, et al. (2015) Effect of low energy light irradiation by light emitting diode on MG63 cells. J Biol Regul Homeost Agents 30(4): 997-1007.

39. de Oliveira LSS, de Araujo AA, de Araujo JMG, Rocha RF, Barbosa CAG, Borges BCJ, et al. (2017) Low-level laser therapy (780 nm) combined with collagen sponge scaffold promotes repair of rat cranial critical-size defects and increases TGF-β, VEGF-A, OPG/RANK and osteocalcin expression. Int J Exp Pathol 98(2): 75-83.

40. Constantin A, Dumitrescu M, Mihai Gurzehi MC, Jeson D, Simionescu M (2017) GD2 laser increases the regenerative capacity of human adipose-derived stem cells by a mechanism involving the redox state and enhanced secretion of pro-angiogenic molecules. Lasers Med Sci 32(1): 117-127.

41. Franco CM, de Lucena Santana C, Takeshishi CB, Alves AN, De Souza Menezes AP, et al. (2013) Effect of laser therapy on skeletal muscle repair process in diabetic rats. Lasers Med Sci 28(5): 1231-1330.

This work is licensed under Creative Commons Attribution 4.0 License
DOI: 10.19080/NTAB.2018.02.555586

Your next submission with Juniper Publishers will reach you the below assets

- Quality Editorial service
- Swift Peer Review
- Reprints availability
- E-prints Service
- Manuscript Podcast for convenient understanding
- Global attainment for your research
- Manuscript accessibility in different formats
  (Pdf, E-pub, Full Text, Audio)
- Unlimited content, stimulating services

Visit the below URL and your manuscript submission on

https://juniperpublishers.com/online-submission.php

8章　免疫、全身性疾患における診断・治療の現状と求める医薬品・医療機器・再生医療像

第8節　全身性エリテマトーデス

遊道和雄
聖マリアンナ医科大学大学院　難病治療研究センター　教授　医学博士
藤井克爾
聖マリアンナ医科大学大学院　難病治療研究センター　准教授　医学博士

株式会社 技術情報協会　発行書籍
No.1060「希少疾患用医薬品の適応拡大と事業性評価」（2018年11月）

第8節　全身性エリテマトーデス

緒言

SLE(Systemic Lupus Erythematosus)は，全身性の炎症，免疫異常を病態とする自己免疫疾患である。抗DNA抗体や，自己抗体群を前駆とする自己抗体などの免疫複合体が全身の臓器・組織に沈着することで生じる様々な障害が，様々なSLE症状に結実となる。近年，SLEの生命予後は大幅改善し，5年生存率などは大幅に延びてきているものの，腎臓・神経系の重症障害を伴う症例や治療抵抗性をみる症例では死亡率も低くなく，早期診断，難治性病態の解明と治療法の確立が急がれている。

SLEにおける特徴性病態には重症ループス腎炎，びまん性肺胞出血，溶血性貧血，血小板減少，抗リン脂質抗体症候群，中枢神経ループス等がある。SLE患者の多くは治療抵抗性や手術後不良例も多いことから，疾患特異的バイオマーカー開発，早期診断技術の開発とともに，さらに新規治療法の開発が必要である。本稿では特に，SLEの難治性病態を対象として，診断技術および治療法の問題点，新規治療法開発動向について概説する。

1.　SLEの疫学・病因病態

SLE患者数（難病認定を受けた症例数）は約5万数千人とされ，好発年齢は20～40歳で，男女比は1:8～9と妊娠可能年齢の女性に多いとされている。SLEの発症は，抗2本鎖DNA抗体，抗Sm抗体，血清補体価，抗核抗体等の免疫複合体など，様々な自己抗体や免疫複合体が全身性の臓器や組織に沈着することで生じる多臓器障害に起因する。

2.　SLEの主症状

SLEの病態形成の主座は，抗DNA抗体等の免疫複合体の形成と補体による全身性の臓器・組織障害と考えられており，皮膚，関，肺，腎などの障害される臓器によって特徴的な症状が認められる。以下に，SLEの主症状や臓器・組織障害を概説する。

2.1　全身症状

発熱，倦�怠感・易疲労感が全身症状として認められることがある。

2.2　皮膚・粘膜部症状

特徴的な蝶形紅斑およびディスコイド疹がみられ，日光過敏や紫外線曝露では増悪することがある。ディスコイド疹は顔面，頭部（頭皮），耳介，四肢，躯幹部に発生，紅斑，鱗屑，萎縮を伴うことがある。通常，強い瘙痒を伴わず，皮膚癌をみることがあり，軟性潰瘍を伴う病変は比較的に多いとされている。

2.3　中枢神経系（central nervous system）ループス

中枢神経症状を伴う患者では，見当識，記憶，精神などの様々な精神神経症状，発熱により，脳血管障害を発症することもある。痙攣発作・昏迷，中枢神経障害がみられることもある。

2.4　心血管症状

心筋炎および心膜炎が生じることがあり，心外膜炎，心嚢炎，心筋炎，心膜肥厚，心嚢液貯留，心不全症状を呈することもある。また，血栓性血管炎，特発性心筋症，冠動脈疾患などがみられる症例では抗リン脂質抗体症候群の合併が疑われる。

⑦ 神経学的

中枢神経障害や末梢神経障害の臨床症状がみられる。痙攣、[illegible]、[illegible]、[illegible]、[illegible]、[illegible]、[illegible]、[illegible]、[illegible]との鑑別が必要である。

⑧ 溶血性貧血

⑨ 白血球減少、リンパ球減少

複数回の検査において、少なくとも一回は白血球数4000/mm³未満、または少なくとも一回はリンパ球数1000/mm³未満がみられる。薬剤性、門脈圧亢進、フェルティ症候群、スプレノメガリー症、感染症との鑑別が必要である。

⑩ 血小板減少

少なくとも一回は血小板数100,000/mm³未満である。血栓性血小板減少性紫斑病、溶血性、門脈圧亢進症との鑑別が必要である。

免疫学的検査項目（6項目）：免疫学的項目には、疾患活動性を反映する補体値の項目が追加された。

① 抗核抗体陽性

② 抗ｄｓ本鎖DNA抗体陽性（ELISA法陽性）

③ 抗Sm抗体陽性

④ 抗リン脂質抗体陽性：ループス抗凝固因子陽性、梅毒血清反応生物学的偽陽性、カルジオリピン抗体価陽性（ＩｇＧ値又はＩｇＭ）およびβ2glycoprotein I陽性

⑤ 補体減少

⑥ 溶血性貧血がなく直接クームス陽性

これら臨床症状項目（11項目）、免疫学的検査項目（6項目）のうち、それぞれ1項目以上、合計4項目を満たす場合はSLEと診断される。これまでのSLE診断基準に比べて、多臓器急性・慢性の皮膚症状、中枢神経症状、および腎機能・心外膜症等の多臓器症状が含まれ、さらに免疫学的検査項目を必ず一つ満たすことを基準としていることから、SLEの病型病態に基づく、より向上した診断および疾患活動性の評価が期待される。

4. SLEの診断および治療法開発に資する自己抗体・補体・免疫複合体

SLEにおいては、免疫複合体が臓器・組織に沈着し、これらの臓器・組織の機能や構造が障害されるとされている。この病態における免疫複合体の沈着に伴って、補体が消費・活性されるため補体価低下（C3, C4, CH50等値）を来すとされており、疾患活動性評価の指標に用いられる。今後の新規治療法開発の観点としての価値も期待される。

自己抗体のうち前述のdsDNA抗体、抗カルジオリピン抗体、ループスアンチコアグラント、抗Sm抗体、抗SS-A抗体、抗U1-RNP抗体およびβ2-グリコプロテインIはSLEにおいて陽性率が高いことがあるため、免疫学的検査項目として診断基準に記載されており、疾患活動性評価の指標の一つとなっている。

ループス腎炎の合併が疑われる場合には腎生検を行ない、SLEに特徴的とされる補体C1qや免疫複合体の沈着を確認することが重要であり、今後これらの因子がループス腎炎の治療ターゲットとなりうるかもしれない。また、腎生検の病理組織結果に基づいて、国際腎臓学会によるループス腎炎の病理組織分類・治療方針を決定することができる。

5. SLE難治性病態と診断技術および治療法開発への展望

5.1 難治性ループス腎炎

寛解増悪や再燃を繰り返しながら腎不全に陥っていく悪性腫瘍類似の腎炎である。本症はステロイド抵抗性のことが多く、シクロホスファミドパルス療法を導入することで腎機能改善や腎炎の進行が可能となってきたが、数年で末期腎不全に移行することもあり、新規治療法の導入による治療成績の向上が望まれる。

5.2 ループス結晶

天然由来成分からのDNAを分子を調整させる作用を持つ抗ループス抗体（抗DNA）と動物モデルの抗神経細胞抗体がintracellularに存在が認められ、診断や治療法が検討されている。ヒストンを介して抗核酸門Histone-DNA bindingの活性化させ、免疫複合体の中枢神経系への侵入と炎症を誘導することが考えられている。抗ループス抗体をターゲットにする治療法開発が期待されている。

ループス結晶に有効性が証明されている、神経毒性抗血清のグルタミン酸受容体に対する自己抗体や、抗リボソーム抗体が認識する神経細胞表面抗原のNSPA発現が報告されている。また、抗カルジオリピン抗体やループスアンチコアグラントが認められるボリン脂質抗体症候群（APS）では、多発脳梗塞をおこすこともあるとされており、病態の一部となることに加えて、これらの因子を目標とする治療戦略・治療手段の効能が期待される。

5.3 SLEの難治性血球・血小板減少

SLEにおける難治性血球減少として自身性血小板減少性紫斑病、血球貪食症候群および溶血性貧血等がみられることもあることから、血小板減少には特に注意が必要である。SLEの薬物療法はステロイド免疫抑制剤が主であるが、血小板減少に伴う血栓性血小板減少性紫斑病に対する血漿交換、血球貪食症候群におけるインターフェロンガンマ抗体療法の治験が検討されている。

5.4 ボリン脂質抗体症候群

抗ボリン脂質抗体症候群の病因として、対象抗原β2-グリコプロテインⅠと、抗ボリン脂質IgGによるβ2-グリコプロテインⅠ複合体の関与が報告されていたが、最近本邦前向き試験にはβ2-グリコプロテインⅠそのものよりも、β2-グリコプロテインⅠを介した自己抗体の産生への作用が指摘されており、病態機構に基づいた新規治療法開発のためにも今後の研究進展が待たれる。

6. SLEの治療のパラダイムシフトに向けて

SLEは多臓器障害（全身性炎症）を特徴とする自己免疫性疾患である。SLEにみられる様々な全身性症状の発現には免疫複合体の組織・臓器沈着が重要な機序であることは前述のとおりであることから、免疫グロブリンや自己抗体を産生する活性化B細胞がSLEの病態形成に中心的な役割を担う。そのため、B細胞そのものや、B細胞への抗原提示を担うT細胞表面抗原を標的とすることでB細胞活性化やT細胞とB細胞間相互作用を制御しうる時代から既存治療薬の適応拡大に期待が集まり、高い安全性と有効性に注目が集まっている。

B細胞は免疫グロブリン、自己抗体、B細胞サイトカイン（BAFF/BLyS）、IL-1、TNF-alpha等の炎症性サイトカインを産生し、獲得免疫に重要な役割を担うだけでなく、SLEの病態にも関与することが知られている。B細胞にはCD19、CD20、CD21、CD22、CD37、CD57等のB細胞グロブリンが発現しているが、なかでもCD20抗原は正常B細胞と90%以上のB細胞型リンパ腫細胞に発現し、ヒト体内のその他の組織には発現しないことから、B細胞上のCD20をターゲットとする抗CD20抗体製剤が難治性SLEの新規治療法として期待され、いくつかの臨床試験が実行されてきた（各々の抗CD20抗体製剤の臨床試験成績については本稿では割愛した）。

また、抗原提示細胞上に発現するCD80/86をリガンドとする共刺激分子CTLA-4は、T細胞に発現するCD28と同じリガンドを介してT細胞にOFFのシグナルを伝達し、T細胞のアポトーシスを誘導することが知られている。そこで、CTLA-4と免疫グロブリンの融合蛋白製剤（アバタセプト）が、T細胞表面上のCD80/86からの共刺激シグナルを阻害することでT細胞選択的共刺激調節剤として働くため、関節リウマチだけでなくSLEの治療薬としての可能性も検討されてきた（SLEを対象としたアバタセプトの臨床試験成績については本稿では割愛した）。

SLE患者では血中B細胞刺激因子B cell activating factor belonging to the tumor necrosis factor family（BAFF）濃度が高値をとし、疾患活動性と自己抗体価が有意に相関しており、BAFFの過剰産生がB細胞の自己寛容破綻に深く関わっている。この知見を基盤として、完全ヒト型BAFF抗体ベリムマブが2011年FDA承認され、56週ごとのSLE治

現時点で除外されている。また、I型IFNの生存に必要な低濃度PAFEを利用する可溶性受容体の組換蛋白「ヒトTACI-Ig融合蛋白エタンセプト」が、SLE治療薬としての有用性が期待されている。

このように、SLEの病態解析を基礎とした新規治療法の開発により、特に難治性SLEの治療のパラダイムシフトが進むことが期待される。

健康寿命・未病の程度をモニターする"健康状態の見える化"の指標としての長寿遺伝子関連脱アセチル化酵素sirtuin

聖マリアンナ医科大学 難病治療研究センター　遊道（ゆうどう） 和雄（かずお）、藤井（ふじい） 亮爾（りょうじ）

FOOD Style 21 2018年12月号（Vol.22 No.12）別冊

健康寿命・未病の程度をモニターする"健康状態の見える化"の指標としての長寿遺伝子関連脱アセチル化酵素sirtuin

聖マリアンナ医科大学 難病治療研究センター　遊道 和雄、藤井 亮爾

はじめに

これまでに、がん、生活習慣病や加齢に伴う疾病に関するさまざまな疾患特異的なバイオマーカーが開発されてきているものの、病気の有無にかかわらず組織・臓器を横断的に、健康や未病の状態を全般的に評価する指標は未だ確立されていない。

われわれは、健康寿命の指標として脱アセチル化・アデノシン二リン酸リボシル転写酵素活性を持つ長寿遺伝子関連タンパクsirtuinに注目した[1,2]。Sirtuinが活性化すると、細胞増殖、細胞成熟や細胞老化に関連するタンパクが翻訳後修飾され、さまざまな組織や臓器の細胞活性・ホメオスタシス代謝が変化し、老化の遅延や寿命延長に影響すると報告されている[1,3]。Sirtuin発現度を測定することで、特定の組織・臓器や疾患に特異的バイオマーカーでは解析できない組織・臓器横断的な加齢・老化・疾病による組織・臓器障害の状態を予測し、全身的な健康や未病の状態のシフトをモニターできると考え、研究を進めてきた。

本稿では、予防医学、ヘルスケアの充実に向けて健康寿命・未病の程度を評価モニターする"健康状態の見える化"の指標としてsirtuinの活用法について概説する。

1．セルフヘルスケアの充実に向けて

1）わが国の高齢化社会の現状

急速な高齢化に伴い、2025年にはわが国の65歳以上の高齢者人口は30%を超え、寝たきり人口も450万人強になると予想されており、2025年の年間医療費は59兆円、介護費を加えると国家予算にも上るという試算もある。また、外出や社会生活を楽しめる健康寿命は実際の寿命より男性では9年、女性では12年も短縮している（図1）。

少子高齢化社会の持続性を確保するためには、高齢者が寝たきりにならずに、能力に応じて社会貢献できる社会となる必要があり、「医療機関への過度な負担」や「膨大な医療費」を軽減するためにも、健康または未病状

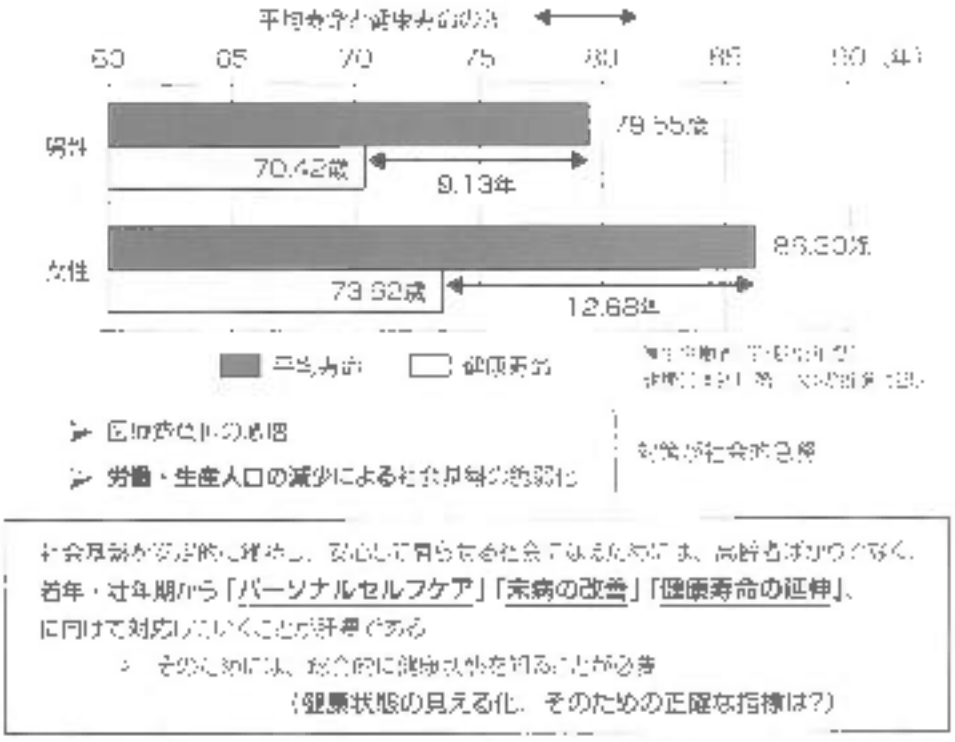

図1　高齢化社会における健康寿命・未病改善における"健康度の見える化"の重要性

態の段階から健康の自己管理、パーソナルセルフケアの充実が重要である。

2）予防医学・セルフケア・セルフメディケーションの充実に向けて解決すべき課題

社会基盤を安定的に維持し、全国民が安心して暮らせる社会になるためには、高齢者ばかりでなく、壮年期、若年期から「健康寿命の延伸」「セルフケア」「セルフメディケーション」に向けて結束していくことが必要であり、そのためには、われわれ一人ひとりが総合的に、かつ客観的に自らの健康状態を知ることが必要である。

しかし、健康意識が高まりつつある最近でも、1年に1回以上定期的に健康診断を受診している生活者は全体の53.5%に過ぎず、30代以下の女性では40%を下回り、20代では男女とも1/3%に満たないといわれている[1]。

こうした現状を踏まえ、セルフケア・セルフメディケーションの充実のためには、健康や未病の状態・時期から客観的に健康状態を把握できるようになることが課題である。この課題の解決のためには科学的エビデンスに基づく「健康度の正確な指標」を、簡便で安価に判定するシステムを開発し、広く活用していくことが重要であると考えている[2,3]。

3）組織・臓器横断的に健康寿命をモニターするバイオマーカー："健康状態の見える化"の指標としての長寿遺伝子関連脱アセチル化酵素 sirtuin

これまでに、がん、生活習慣病や加齢に伴う疾病に関するさまざまな疾患特異的バイオマーカーが開発されているものの、病気の有無にかかわらず臓器・組織・臓器を横断的に、健康や未病の状態を全般的に評価する指標は未だ確立されていない。

そこでわれわれは、長寿遺伝子関連脱アセチル化酵素sirtuinに注目して研究を進め、ヒト検体のsirtuinタンパク発現度を測定することによって、「特定の組織・臓器や疾患に特異的バイオマーカーでは解析できない組織・臓器横断的な加齢・老化・疾病による組織・臓器障害の予測」、または「全身的な健康・未病状態のレベルをモニター」できることを確認してきた。

現在セチル化・アデノシン二リン酸リボシル転写酵素活性を持つsirtuinについては、活性化すると100近くの細胞増殖、細胞周期、細胞老化などの関連細胞内タンパクが翻訳後修飾され、その結果として皮膚、血管、脳、筋などさまざまな組織・臓器の細胞活性・エネルギー代謝が変化し、組織・臓器の老化の速度や寿命にも影響することが明らかになっている[4,5]。われわれは、sirtuinの活性レベルを知ることで、さまざまな組織・臓器の生体応答・変化を横断的に知ることができる「健康状態の見える化」、健康レベルの指標・バイオマーカー」として利用できると考え、検討を進めている（図2）。

2. 長寿遺伝子関連タンパクsirtuinと加齢との関連

近年、国内外の長寿科学に注目が集まり、細胞・組織・臓器の老化のメカニズム、ならびに老化克服・寿命延長の具体的方法や薬剤開発に熱い視線が注がれている。われわれは、NAD依存性脱アセチル化酵素活性を持つsirtuinには、DNA修復酵素の活性化、生命維持

細胞内での役割

脱アセチル化 NAD+レベル転写活性をもつSirtuin
↓
可逆的アセチル化 ― 脱アセチル化サイクル活性化
↓
多くの細胞内タンパクの機能を翻訳後修飾
↓
組織・臓器の細胞活性変化 ⇒ 生体応答に影響

Sirtuins活性化の役割

炎症、酸化ストレスなど外因性ストレスに応答
「DNA損傷修復、タンパク安定性、生体内時計、遺伝子(アポトーシス)細胞死の発現に関与
↓
炎症、細胞老化・細胞死に制御を通じて
組織・臓器のホメオスタシス(平衡)維持に関与

ヒト検体におけるSirtuin活性は、
さまざまな組織・臓器の変性、加齢・老化や炎症の状態が、細胞活性変化の総和として反映した、
組織・臓器横断的にモニターする健康度のマーカー（健康・未病状態の見える化）となりうる。

図2　ヒトの検体でSirtuinタンパクを測定することの意義・科学的根拠

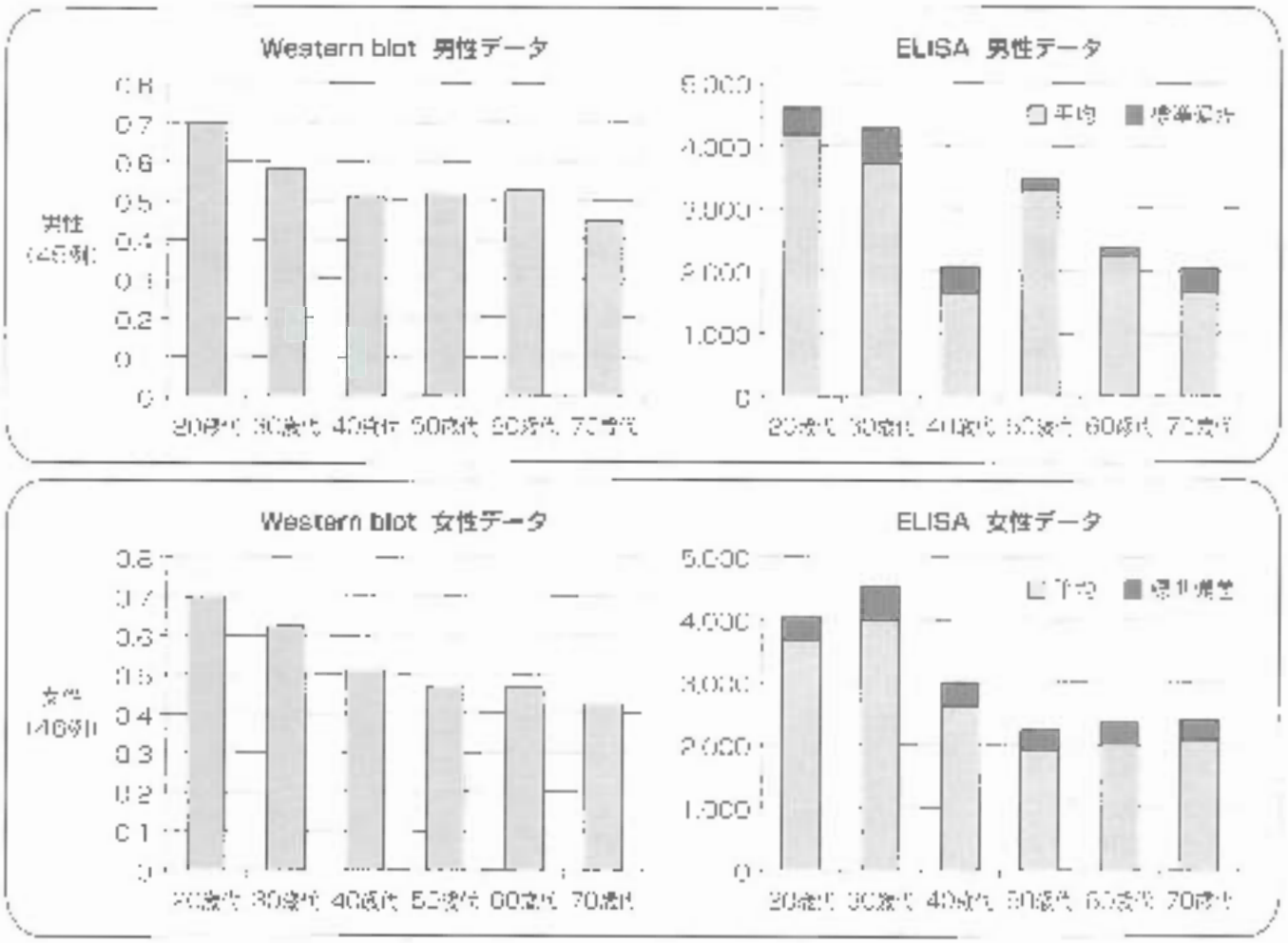

図3　末梢血単核細胞のsirtuin 2発現度の加齢変化（予備実験結果）

に必要な細胞エネルギー（ATP）産生量の調整能、染色体DNA保護作用があることが報告されていることから、老化・長寿科学を研究するうえで最も重要な因子の一つであると考え、「sirtuin活性と老化のメカニズム解析、老化遅延・克服への応用」ならびに「老化・健康評価のバイオマーカーとしてのsirtuin発現度の有用性」について研究してきた。

以下に、血液検体におけるsirtuin 2発現度の加齢に伴う変化について概説する。

これまでにわれわれは、加齢に伴うsirtuin 2発現度の変化を解析するため、臨床試験（予察試験）において健常者91名の末梢血単核細胞におけるsirtuin 2の発現度を解析し、sirtuin 2は加齢に伴って減少することを2種類のタンパク量発現度検査法（western blotting、ELISA法）において確認、この因子がプロテオエイジングや老化・変性に伴う疾患のバイオマーカーになり得ることを示唆する知見を得てきた（投稿準備中、図3）。

また、60歳～70歳代について、変形性関節症患者と非罹患健常者の血液検体を解析したsirtuin 2発現度は、男女ともに加齢に伴って減少する傾向に加えて、加齢関連疾患（変形性関節症）のある場合には、さらに低下傾向があることを確認したので（data not shown）、現在症例数を増やしてこのエビデンスを検証する試験を計画中である。

3. 長寿遺伝子関連タンパクsirtuinのバイオマーカーとしての活用、期待される波及効果

ヒト検体（血液等）におけるsirtuin 2タンパクの発現度を測定することで、特定の組織・臓器の疾患非侵襲的バイオマーカーでは解析できない組織・臓器横断的に、全身的健康および未病の状態のレベルを、客観的簡便にモニターすることが可能となると考える。

この未病や健康寿命の指標として最適なバイオマーカー・sirtuin 2測定システムの確立によって、セルフケア・セルフメディケーションを主とした以下の事業化が期待できると考えている（図4）。

細胞質内に存在し、他のSirtuin familyに比べて簡易に検出可能なSirtuin 2タンパク

↓

特定の病気や臓器に限定されず、組織・臓器横断的に変性・老化の健康状態をモニターする「健康寿命」の指標として最適なバイオマーカーとなり得る。

臨床応用例

- 血液、口腔粘膜由来タンパクのSirtuin 2発現レベルを測定：
  同年代のSirtuin 2発現レベルと比較 ＝ 健康管理・目標設定の具体的指標
- 診察時毎に、経時的Sirtuin 2発現度を測定・モニター：健康管理・評価の指標
- 新規候補物質（食品、医薬品、サプリメント等）のスクリーニング・効果判定の指標

例　老化に伴う品質低下・不調等による変化のモニター
　　運動器疾患のリハビリ・リハビリ・ケアの予防・治療効果のモニター
　　中枢神経系、感覚器機能の加齢変化のモニター

図4　長寿遺伝子関連タンパクsirtuinのバイオマーカーとしての活用法

1）健康診断の検査項目として実用化（健康管理・目標設定の具体的指標として活用）

血液および口腔粘膜検体におけるsirtuin 2発現レベルを測定し、同年代のsirtuin 2発現レベルと比較、または経時的にsirtuin 2発現度をモニターすることで、パーソナルヘルスケア・セルフメディケーションの実現に向けた健康管理・評価の指標として活用できると考えている。

市場・事業規模：健康診断事業については、2015年度、2016年度の国内の健診・人間ドック市場は年9,100億円と推定。本病検査の市場は450億円（診断薬市場6,000億円）と推定。

2）健康食品・医薬品・サプリメントの効果判定、研究開発スクリーニングの指標として活用

健康維持を目的とする食品・医薬品・サプリメント類の効果判定の指標として活用することで、販売促進に寄与することができる。また、新規候補物質開発において、健康改善効果のスクリーニングに応用が可能であり、科学的根拠のある健康関連商品の開発に貢献することができる。さらに、以下のような臓器・組織の加齢に伴う変化を、組織特異的または疾患特異的バイオマーカーと本因子マーカーを組み合わせることにより簡便にモニターすることが可能であり、セルフヘルスケアのための新規事業展開が期待できる。

- 皮膚・毛髪の健康度・老化度評価
- 泌尿器機能（心血管機能・呼吸機能）の加齢変化のサロゲートモニター
- 運動器機能のロコモティブシンドロームの予防・治療の評価
- 中枢神経系・感覚器機能の加齢変化のサロゲートモニター

市場・事業規模：2017年度の日本の健康食品・サプリメント市場規模は1兆5,624億円、健康食品・サプリメント利用者数は5,641万人、1人当たり平均購入金額は27万6,615円と推定されており、年々増加傾向にある。

おわりに（社会的・経済的波及効果について）

社会基盤を安定的に維持し、全国民が安心して暮らせる社会になるためには、高齢者ばかりでなく、壮年期、青年期から「健康寿命の延伸」「セルフメディケーション」に向けて対応していくことが肝要であり、そのためには総合的に健康状態を知ることが必要である。

しかし、健康寿命や健康意識が高まりつつある最近でも、1年に1回以上人間ドックなどで定期的に健康診断を受診している生活者は全体の53%に過ぎず、30代以下の女性は40%を下回り、20代は男女ともに30%に満たないといわれている。ヒト検体におけるSirtuin 2タンパクの発現度を測定することで、特定の組織・臓器の疾患特異的バイオマーカーでは解析できない組織・臓器横断的な変性、老化、寿命による組織・臓器障害の状態を予測し、全身的な健康・未病の状態のレベルをモニターすることができるようになる。

これにより、以下の社会的・経済的波及効果および貢献が期待できる。

1）健康状態を正しく把握することが可能となり、生活習慣の改善努力の動機付けとして活用できる。

2）健康の自己管理手段として普及することにより、健康レベルや未病状態を自己観察することが可能となり、疾病の予防・早期発見を通して生活者の健康寿命を延ばし、医療費削減に寄与できる。

《《《《《参考文献》》》》》

1) Guarente L: Sirtuins, Aging, and Metabolism. *Cold Spring Harb Symp Quant Biol* 2011, 76: 81-90: 2011.
2) Guarente L: Sirtuins, aging, and medicine. *New Engl J Med*, 2011, 364: 2235-2244: 2011.
3) Inoue T, Hiratsuka M, Osaki M, Oshimura M: The mammalian NAD-dependent SIRT protein, SIRT2, in cell cycle regulation. *Cell Cycle*, 2007, 6: 965-1014-1018: 2007.
4) Wang F, Nguyen M, Qin XF, Tong Q: SIRT2 deacetylates FOXO3a in response to oxidative stress and caloric restriction. *Aging Cell*, 2007, 6(4): 505-514: 2007.
5) North BJ, Rosenberg MA, Jeganathan KB, Hafner AV, Michan S, Dai J, Baker DJ, Cen Y, Wu LE, Sauve AA, van Deursen JM, Rosenzweig A, Sinclair DA: SIRT2 induces the checkpoint kinase BubR1 to increase lifespan. *EMBO J*, 2014, 33, 1448-1463: 2014.
6) 健康日本21推進（第二次）, http://www.kenkounippon21.gr.jp/, 厚生労働省
7) 平成23年 臨薬協 OTC薬協 web調査「一般用（OTC）検査薬に関する調査結果について」 http://www.kizai.go.jp/kisei-kaikaku/kaigi-meeting/2013/wg2/kenko-140109/item1_1.pdf.

ゆうとう・かずお：Kazuo Yudo
聖マリアンナ医科大学 難病治療研究センター センター長
1988年3月 鹿児島大学医学部卒業、1990年4月 杏林大学医学部大学院博士課程入学、1991年3月 富士宮市立病院 研修医、1993年8月 米国ベイラー医科大学放射線腫瘍学教室留学、1996年4月 富山医科薬科大学大学院修了・医学博士号取得、1998年8月 米国ベイラー医科大学放射線腫瘍学教室留学、2002年1月 英国グラスゴー大学ウォルフセンター留学、2003年1月 聖マリアンナ医科大学 難病治療研究センター講師、2007年4月 聖マリアンナ医科大学 難病治療研究センター准教授、2010年4月 聖マリアンナ医科大学 難病治療研究センター 難治性疾患病態制御学 大学院教授、2011年4月 聖マリアンナ医科大学 難病治療研究センター センター長、現在に至る

Sirtuin関連論文：

1. The NAD-Dependent deacetylase sirtuin-1 regulates the expression of osteogenic transcriptional activator runx-related transcription factor 2 (Runx2) and production of matrix metalloproteinase (MMP)-13 in chondrocytes in osteoarthritis. *Int J Molecular Science*, 2016, 17: 7: 2016.
2. The Nicotinamide Adenine Dinucleotide (NAD)-Dependent Deacetylase Sirtuin-1 Regulates Chondrocyte energy Metabolism through the Modulation of Adenosine Monophosphate-Activated Protein Kinase (AMPK) in Osteoarthritis (OA). *Journal of Arthritis*, 2017, 6: 238: 2017.

ふじい・りょうじ：Ryuji Fujii
聖マリアンナ医科大学 難病治療研究センター

糖アルコールの新知識 改訂増補版
食品新素材協議会事務局長　早川幸男編著

本書は、食品新素材協議会・早川幸男事務局長の監修のもと、1996年に発刊された「糖アルコールの新知識」の改訂増補版として再編集されたものです。改訂増補版は、各糖アルコールの沿革をはじめ現状や製法、種類と規格、生理的特性、理化学的な利用上の特性と注意事項、利用例とその結果の特徴などを分かりやすく解説しています。また今回は、糖アルコールの総括ともいえる「適正摂取」を追加。この1冊で糖アルコールのすべてが分かる食品関連技術者必見の書となっております。　●A5判　192頁　定価2625円（税込）

お問い合わせ・お申込み ▶ 食品化学新聞社　〒101-0051 東京都千代田区神田神保町3-2 瑞穂文教ビル TEL: 03-3238-7918 FAX.03-3239-7898

International Journal of
Molecular Sciences

MDPI

Article

SPACIA1/SAAL1 Deletion Results in a Moderate Delay in Collagen-Induced Arthritis Activity, along with mRNA Decay of *Cyclin-dependent Kinase 6* Gene

Ryuji Fujii [1,4,*], Rie Komatsu [1,†], Tomio Satu [1], Iwao Seki [2], Koji Konomi [3], Hiroyuki Aono [2], Hisateru Niki [4], Kazuo Yudoh [1], Kosuke Nishioka [5] and Toshihiro Nakajima [1,6,7]

1 Institute of Medical Science, St. Marianna University School of Medicine, Kanagawa 216-8512, Japan; komatsu@marianna-u.ac.jp (R.K.); tomio@marianna-u.ac.jp (T.S.); yudo@marianna-u.ac.jp (K.Y.); marlin@tokyo-med.ac.jp (T.N.)
2 AYUMI Pharmaceutical Corporation, Kyoto 612-8374, Japan; iwao.seki@ayumi-pharma.com (I.S.); hiroyuki.aono@ayumi-pharma.com (H.A.)
3 Santen Pharmaceutical Co., Ltd., Osaka 533-8651, Japan; koji.konomi@santen.com
4 Department of Orthopedic Surgery, St. Marianna University School of Medicine, Kanagawa 216-8511, Japan; h2niki@marianna-u.ac.jp
5 Global Health Innovation Policy Program (GHIPP), National Graduate Institute for Policy Studies (GRIPS), Tokyo 106-8677, Japan; kosuke-nishioka@hz04.plala.or.jp
6 Institute of Medical Science, Tokyo Medical University, Tokyo 160-8402, Japan
7 Misato Marine Hospital, Kochi 781-0112, Japan
* Correspondence: ryuji@marianna-u.ac.jp; Tel.: +81-44-977-8111 (ext. 4213)
† These authors contributed equally to this work.

Received: 31 October 2018; Accepted: 29 November 2018; Published: 30 November 2018

check for updates

Abstract: This study was performed to elucidate the molecular function of the synoviocyte proliferation-associated in collagen-induced arthritis (CIA) 1/serum amyloid A-like 1 (SPACIA1/SAAL1) in mice CIA, an animal model of rheumatoid arthritis (RA), and human RA-synovial fibroblasts (RASFs). *SPACIA1/SAAL1*-deficient mice were generated and used to create mouse models of CIA in mild or severe disease conditions. Cell cycle-related genes, whose expression levels were affected by *SPACIA1/SAAL1* small interfering RNA (siRNA), were screened. Transcriptional and post-transcriptional effects of *SPACIA1/SAAL1* siRNA on cyclin dependent kinase (cdk) 6 gene expression were investigated in human RASFs. *SPACIA1/SAAL1*-deficient mice showed later onset and slower progression of CIA than wild-type mice in severe disease conditions, but not in mild conditions. Expression levels of *cdk6*, but not *cdk4*, which are D type cyclin partners, were downregulated by *SPACIA1/SAAL1* siRNA at the post-transcriptional level. The exacerbation of CIA depends on SPACIA1/SAAL1 expression, although CIA also progresses slowly in the absence of SPACIA1/SAAL1. The CDK6, expression of which is up-regulated by the SPACIA1/SAAL1 expression, might be a critical factor in the exacerbation of CIA.

Keywords: cell cycle; collagen-induced arthritis; cyclin-dependent kinase; proliferation; rheumatoid arthritis; synovitis

1. Introduction

Rheumatoid arthritis (RA) is a chronic autoimmune disease characterized by synovial inflammation and hyperplasia [1,2]. Activated synovial fibroblasts, a major component of the hyperplasic synovial lining, are important in the pathogenesis of synovitis because they secrete cytokines and chemokines, leading to exacerbation of inflammation. Immuno-suppressive biologics

such as tumor necrosis factor (TNF) inhibitors with methotrexate (MTX) have become an important part of the standard care for RA [3]. Folate antagonism by MTX is well known to exert anti-proliferative effects, but the administration of folic or folinic acid with MTX does not diminish the anti-inflammatory potential. Therefore, it is assumed that the anti-proliferative effects of MTX may not work in RA [4]. On the contrary, other studies have shown the potential of an anti-proliferative strategy using a kinase inhibitor of both cyclin dependent kinase (CDK) 4 and CDK6, cyclin D partners in the cell cycle, in some mouse models of RA [5,6]. We believe that the abnormal synovial proliferation in RA should be a crucial target for drug discovery.

In our previous study, we identified synoviocyte proliferation-associated in collagen-induced arthritis (CIA) 1/serum amyloid A-like 1 (*SPACIA1/SAAL1*) as an overexpressed gene in the joint tissue of mice with CIA and indicated that the gene was associated with abnormal synovial proliferation in human RA [7]. We also showed that *SPACIA1/SAAL1* small interfering RNA (siRNA) inhibited the proliferation of RA synovial fibroblasts (RASFs) in vitro and that *SPACIA1/SAAL1* transgenic mice exhibited early onset and rapid progression of CIA. These findings suggested that SPACIA1/SAAL1 could be involved in the progression of synovitis. In the present study, we generated *SPACIA1/SAAL1* deficient mice and observed the molecular function of SPACIA1/SAAL1 in mice CIA and human RASFs.

2. Results

2.1. Generation of SPACIA1-Deficient Mice

A schematic representation of the *SPACIA1/SAAL1* targeted locus to generate *SPACIA1*-deficient mice is shown in Figure 1. The deletion of exon 4 in the *SPACIA1*-deficient mice was confirmed by polymerase chain reaction (PCR) analysis (Figure 1). Heterozygous mice (*SPACIA1*$^{+/-}$) and even homozygous (*SPACIA1*$^{-/-}$) lacking SPACIA1 systemically developed normally and did not show obvious abnormalities.

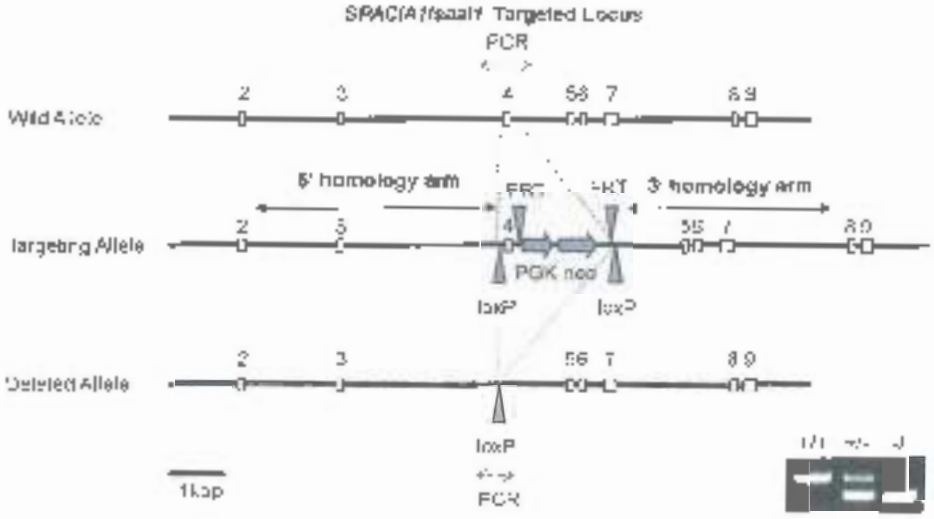

Figure 1. Schematic depiction of the *SPACIA1/SAAL1* gene-targeting strategy. Homologous recombination resulted in exon 4 being flanked by loxP sites, deletion was achieved by Cre recombinase-mediated excision. The *+/+*, *+/−* and *−/−* indicate wild-type (wt), heterozygous and homozygous mice for the *SPACIA1/SAAL1* gene.

2.2. Progression of CIA in SPACIA1-Deficient Mice

In the previous study using SPACIA1 overexpressing mice, we reported that SPACIA1 is a synovitis modifying factor [7]. In this study, to confirm whether SPACIA1 is essential in the

progression of synovitis, arthritis was induced using collagen in the *SPACIA1* deficient mice (Figure 2). In CIA, different effects on the incidence and arthritis score are usually observed among the different production lots of bovine type II collagen (CII). We administered highly- or moderately effective lots of CII to *SPACIA1*-deficient and wild-type (wt) mice. The highly effective lot of CII (labeled "Severe" in Figure 2) eventually caused an arthritis incidence of 100% (Figure 2A) and a high arthritis severity in the wt mice (Figure 2B). On day 30 after the 1st injection, the arthritis incidence of the *SPACIA1*-deficient mice was significantly reduced compared with that of the wt mice (Figure 2A). On days 30 to 35 after the 1st injection, the arthritis severity of the *SPACIA1*-deficient mice was also significantly reduced (Figure 2B). However, no significant differences in arthritis incidence, arthritis severity, antibody titers against bovine CII or histological score were observed on day 42 (Figure 2A,B,E,F). On the other hand, the moderately-effective lot of CII (labeled "Mild" in Figure 2) ultimately resulted in an arthritis incidence of 71% and 56% in *SPACIA1*-deficient and wt mice, respectively (Figure 2C). The arthritis severity was also moderate (Figure 2D). Under these conditions, no significant differences were observed in arthritis incidence, arthritis severity, antibody titers against bovine CII or histological score between *SPACIA1*-deficient and wt mice (Figure 2C–F). SPACIA1 was therefore not essential in the progression of synovitis.

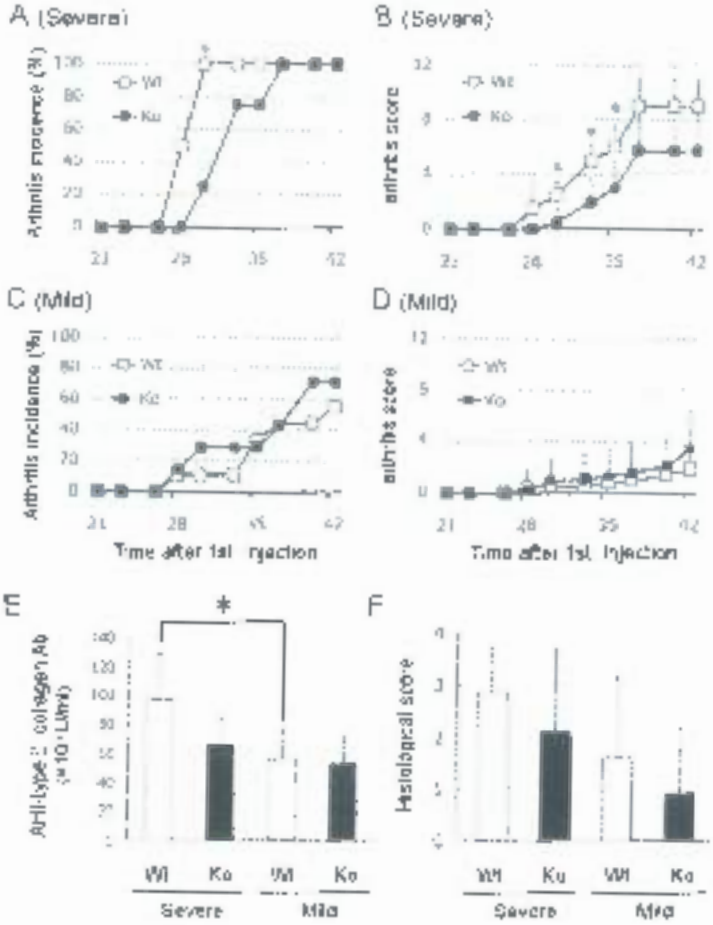

Figure 2. Incidence of arthritis (A,C) and mean arthritis score (B,D) in *SPACIA1* deficient (ko) or wt mice injected with "Severe" or "Mild" collagen II (CII) are shown (wt; n = 4, ko; n = 5 (A,B), wt; n = 9, ko; n = 7 (C,D)). Data points and error bars correspond to the mean and SD, respectively. * $p < 0.05$. (E,F) Anti-CII antibody levels (E) and histopathological scores of the knee joints (F) in *SPACIA1*-deficient or wt mice treated with the "Severe" or "Mild" effective lot of CII. The presented data are from a representative experiment that was repeated three times with similar results. * $p < 0.05$.

2.3. Identification of Cell Cycle Regulators Altered at the mRNA Expression Level by *SPACIA1*

In our previous study, we reported that SPACIA1 is highly expressed in the hyperplastic synovial lining from patients with RA, and could relate RA synovial fibroblast proliferation at the first growth (G1) phase of cell cycle [7]. To identify the cell cycle regulators that are affected by the SPACIA1 expression, we measured the mRNA expression of G1 phase-related genes in RASFs transfected with *SPACIA1* siRNA, compared with mock siRNA. *SPACIA1* siRNA effectively reduced *SPACIA1* mRNA expression in RASFs (Figure 3A). Only the expression of *cdk6* gene was altered two-fold or more by *SPACIA1* siRNA in the G1 phase-related genes that we picked up. The log2 ratio of *cdk6* was −1.6 (Table 1). These results were confirmed by quantitative real time-PCR (qRT-PCR). The mRNA expression of *cdk6* was reduced to half by SPACIA siRNA in RASFs, while that of CDK4, CCN (cyclin) D1, CCNE2 and CDK2 were not significantly altered (Figure 3A). *SPACIA1* siRNA also reduced the expression of CDK6 at the protein level (Figure 3B).

Table 1. Log2 ratio of G1-phase related-genes in human rheumatoid arthritis-synovial fibroblasts treated with siRNA for *SPACIA1*.

G1-phase Related-Genes	Accession Numbers	Log2 Ratio
cyclin-dependent kinase 6 (CDK6)	NM_001259	−1.6
cyclin-dependent kinase 4 (CDK4)	NM_000075	0.04
cyclin-dependent kinase 2 (CDK2)	NM_001798	−0.81
cyclin D1 (CCND1)	NM_053056	−0.07
cyclin D2 (CCND2)	NM_001759	0.29
cyclin D3 (CCND3)	NM_001760	−0.08
cyclin E1 (CCNE1)	NM_001238	0.31
cyclin E2 (CCNE2)	NM_057749	−0.86
p16 Ink4a (CDKN2A)	NM_058197	−0.11
p15 Ink4b (CDKN2B)	NM_004936	0.29
p18 Ink4c (CDKN2C)	NM_078626	−0.75
p19 Ink4d (CDKN2D)	NM_001800	0.27
p21 Cip1 (CDKN1A)	NM_078467	−0.27
p27 Kip1 (CDKN1B)	NM_004064	0.01
p57 Kip2 (CDKN1C)	NM_000076	0.17
Chk1 (CHEK1)	NM_001114121	−0.1
Chk2 (CHEK2)	NM_001005735	−0.04
cdc25A (CDC25A)	NM_001789	0.79

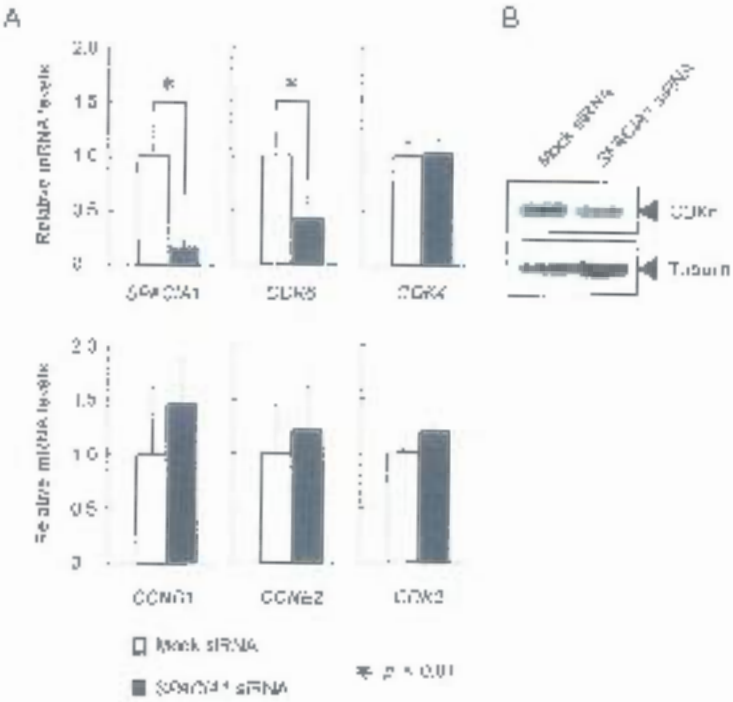

Figure 3. (**A**) The mRNA levels of G1 phase related genes in human rheumatoid arthritis (RA)-synovial fibroblasts (RASFs) with *SPACIA1*-siRNA or mock siRNA. All experiments were performed in triplicate. (**B**) The protein expression levels of CDK6 in RASFs with *SPACIA1*-siRNA or mock siRNA. The alpha tubulin expression levels are shown as the internal control. (**A**,**B**) The presented data are from a representative experiment that was repeated three times with similar results.

2.4. Expression of CDK6 Protein in Human RA-Synovial Tissue

To confirm the expression of the CDK6 protein in human RA-synovitis tissues in vivo, we performed immunohistochemistry, using synovitis tissues from RA patients. Anti CDK6 antibody-specific signals were observed in RA-synovitis tissues, compared with the control of rabbit immunoglobulin G (IgG) (Figure 4A). More intense staining with the anti-CDK6 antibody was observed in multiple (>5) layers of synovial tissue (Figure 4B).

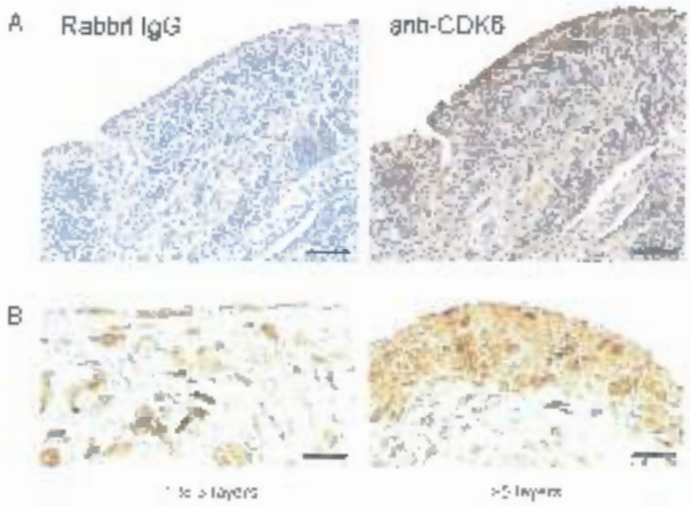

Figure 4. (**A**) Expression of CDK6 in human synovium. CDK6-positive cells (brown) are stained with 3,3′-diaminobenzidine.

Mayer's hematoxylin was used as a counterstain. Normal rabbit immunoglobulin G (IgG) was used as the negative control. Scale bar = 100 μm. (B) Expression of CDK6 in human synovium with (>5 layers) or without (1 to 3 layers) hyperplasia of the synovial lining. Scale bar = 20 μm. (Original magnification is 50× (A) and 200× (B). The presented images are from a RA patient. Similar results were obtained from two different RA patients.

2.5. SPACIA1 Expression Affected cdk6-mRNA Stability, but Not Proximal Promoter Activity of cdk6 Gene

To identify the step in *cdk6* gene-expression that is affected by the SPACIA1 expression, we first performed reporter assays, using the proximal promoter of the *cdk6* gene in RASFs. The *cdk6* promoters (Figure 5A) that we tested (2.5, 1.6 and 0.9 kb DNA fragments upstream of the *cdk6*-start codon) showed almost equal promoter activities in RASFs, and these activities showed an approximately 8-fold increase compared with the control vector (pGV-C52). However, no alterations caused by *SPACIA1*-siRNA were observed, at least in these promoters (Figure 5B). Second, we performed mRNA stability assays. *SPACIA1* siRNA significantly reduced *cdk6* mRNA stability compared with mock siRNA. Sixty minutes after Actinomycin-D treatment, the amount of *cdk6*-mRNA with *SPACIA1* siRNA was reduced to approximately 60%, compared with mock siRNA (Figure 5C). SPACIA1 related to *cdk6*-mRNA expression at the post-transcriptional level.

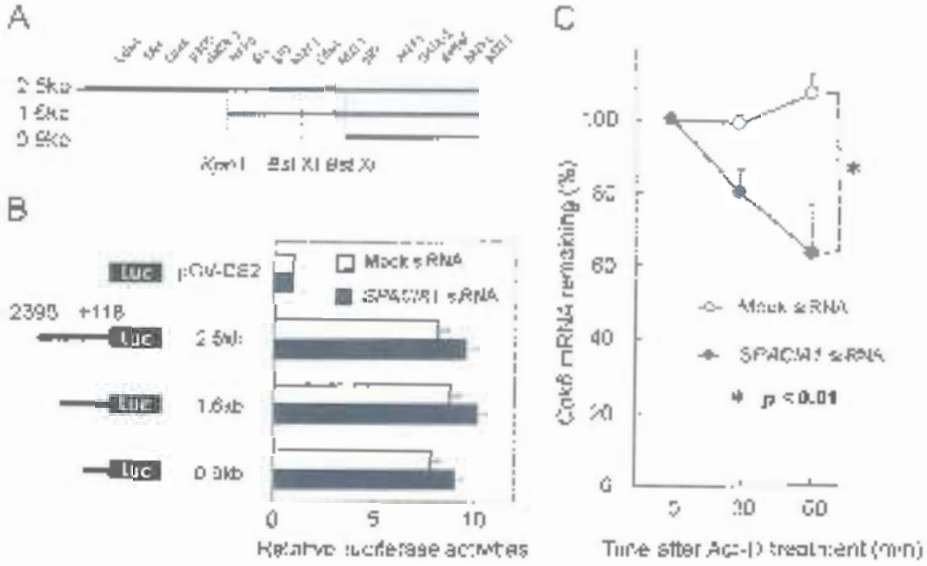

Figure 5. (A) Schematic representation of the *cdk6* proximal promoter region with restriction enzyme and putative transcription factor binding sites. The dots indicate the putative NF-kappa B binding site. (B) The proximal promoter activities of each construction in RASFs with SAPCIA1- or mock siRNA. RASFs were transfected with SPACIA1- or mock siRNA for 72 h. Subsequently, 24 h after transfection of each reporter vector, the promoter activity was measured using the Luciferase Assay System. (C) Messenger RNA stability analysis of the cdk6 gene. RASFs were transfected with SPACIA1- or mock siRNA for 72 h. The cells were harvested 0, 0.5, and 1 h after the addition of Actinomycin D (Act-D). The mRNA levels were measured by quantitative real time-polymerase chain reaction (qRT PCR). (B,C) All experiments were performed in triplicate. The presented data are from a representative experiment that was repeated three times with similar results.

3. Discussion

In our previous study, we employed the mild (modified) form of CIA, using half the amount of CII for the 2nd injection, in transgenic mice overexpressing SPACIA1, because no significant alterations were observed in the severe (general) form of CIA, compared with wt mice [7]. In mild CIA,

SPACIA1-overexpressing mice showed early onset and rapid progression of CIA. These results indicate that endogenous SPACIA1 expression in wt mice reached a plateau at severe CIA, but not in mild CIA. We, therefore, concluded that overexpression of SPACIA1 accelerates the progression of synovitis. In this study, we also employed both severe and mild forms of CIA in *SPACIA*-deficient mice. In severe CIA, *SPACIA1*-deficient mice showed later onset and slower progression of CIA than wt mice, indicating that the rapid progression of CIA in wt mice depends on SPACIA1 expression. Meanwhile, in the mild CIA, *SPACIA1*-deficient mice did not show any significant alterations compared to wt mice (Figure 2C–F). This suggests that CIA might progress independently of the SPACIA1 expression, even in wt mice. Summarizing the above, we reconfirmed that SPACIA1 is an exacerbation factor of CIA, although CIA also progresses slowly in the absence of SPACIA1. Some exacerbation factors that are induced by the SPACIA1 expression, such as CDK6, should be also induced by the other mechanism without SPACIA1. For instance, TNFα signaling induces *cdk6* gene expression in Michigan Cancer Foundation 7 (MCF7) cells, a human breast cancer cell line [8]. Therefore, we have explored such factors that are induced by SPACIA1, not SPACIA1 itself, as drug targets in RA.

As we previously reported [7], SPACIA1 was screened as a factor suspected of showing altered expression in mouse CIA and affecting proliferation of cultured RASFs and was confirmed to be implicated in the G1 phase progression of RASFs. In this study, we screened for G1 phase-related genes, the expression of which was affected by the SPACIA1 expression and identified the *cdk6* gene (Table 1 and Figure 3). SPACIA1 was implicated in the decay of *cdk6* mRNA (Figure 5C) but did not affect proximal promoter activity (Figure 5E). SPACIA1 might thus be a factor regulating the mRNA stability of some inflammation-related genes. In future work, we intend to identify the SPACIA1-responsible element on *cdk6* mRNA.

Synovial proliferation is important in the pathology of RA, as well as abnormal immune responses and inflammation, and therefore constitutes a suitable drug target. However, almost no anti-proliferative agents have been developed to treat RA, while there are many immunosuppressive and anti-inflammatory therapies. Folate antagonism is well known as the antiproliferative effect of MTX. However, other groups have shown that administration of folic or folinic acid with MTX does not diminish the anti-inflammatory potential. This result suggests that the anti-proliferative effect of MTX might not be a major mechanism in RA treatment [4]. Furthermore, Thomas S. et al. reported MTX is a JAK/STAT inhibitor [9], not an inhibitor of AP1 and NF-κB pathways that activate proliferation. Kobsaka et al. also focused on anti-proliferative agents in RA treatment [5,6]. Their anti-CDK 4/6 agent is effective and has a synergistic effect with anti-TNF agents in some animal models of RA. Incidentally, double deficiency of both *cdk4* and *cdk6* results in either late embryonic or postnatal lethality, while single deficiency of *cdk4* or *cdk6* does not [10]. In fact, administration of an overdose of anti-CDK 4/6 agent causes cytopenia as previously described [6]. In this study, *SPACIA1* siRNA down-regulated CDK6, but not CDK4, in RASFs. Single inhibition of CDK6, but not CDK4, may have the potential for the treatment of RA, without causing side effects such as cytopenia. In future work, we aim to validate the potential of anti-CDK6 agents in mouse RA models.

4. Materials and Methods

4.1. Animals

Mice were raised under conventional conditions at our own facilities. Tap water and food were provided ad libitum.

4.2. Gene Targeting in ES Cells and Generation of the SPACIA1-Deficient Mouse Line

Generation of the *SPACIA1*-deficient mouse line was carried out by Ozgene Pty Ltd. (Bentley, Australia). Briefly, to ablate the functional mouse *SPACIA1/SAA3.1* locus, we targeted its exon 4 for deletion using both the flippase/flippase recognition target (FLP/frt) and causes recombinase/locus of crossover (x) in P1 (CRE/loxP) systems to cause a frame shift mutation (Figure 1). The mouse *SPACIA1/SAA3.1*

locus was generated by PCR from C57BL/6 mouse genomic DNA and its sequence was confirmed. The targeting construct was linearized and transfected into embryonic stem (ES) cells by electroporation. Recombinant ES cell clones were selected using G418 and injected into C57BL/6 mouse-derived blastocysts. The exon 4 and neomycin selection cassette was flanked by loxP recombination sites and excised in vivo by crossing with the Cre-Cre deleter strain (Ozgene). Finally, the *SPACIA1*-deficient mice were backcrossed onto the DBA/1J, a DBA/1 mouse strain distributed from The Jackson Laboratory, for 10 or more generations.

4.3. Induction and Assessment of CIA

To induce CIA in *SPACIA1*-deficient mice, two different production lots of CII were used. One lot of the collagen caused severe arthritis (Figure 2A,B), while the other caused mild arthritis (Figure 2C,D). Mice were injected into the base of the tail with 100 μg CII (highly- or moderately effective lot) per mouse for both 1st and 2nd injection. Then, the arthritis score was assessed three times per week using Hughes's scoring system [11]. All of the mice were sacrificed by decapitation, and then samples of their blood were collected to measure the antibody titers against bovine CII and the knee joints were harvested for histological analysis.

4.4. Gene Expression Analysis

To analyze the effect of *SPACIA1* siRNA on mRNA expression of cell cycle-related genes in RASFs, *SPACIA1*- and mock siRNA were transfected into RASFs as described in our previous report [7]. Seventy-two hours after transfection, the cells were harvested and total RNA was extracted using ISOGEN (Nippon Gene, Tokyo, Japan). DNA array analysis using the total RNA and Agilent SurePrint G3 human GE 8×60 K microarray was carried out by TaKaRa Bio Inc., Shiga, Japan. For qRT-PCR assay, cDNA was prepared from the total RNA above, using reverse transcriptase (Toyobo, Osaka, Japan) according to the manufacturer's instructions. Target genes were amplified using an ABI 7500 Real Time PCR System (Thermo Fisher Scientific, Waltham, MA, USA) with the following specific primers: hCDK2, 5′-cctggatgaagatggacggagc-3′ (forward) and 5′-ggcttcaagaaggctatcagagtc-3′ (reverse) (product length, 151 bp); hCDK4, 5′-tgcagtcggtgggtacctgagatg-3′ (forward) and 5′-gctcacrggattaccttcatcc-3′ (reverse) (product length, 144 bp); hCDK6, 5′-gctgtctcactctagcaaccatcc-3′ (forward) and 5′-tcagagcattctgaagacagtagcc-3′ (reverse) (product length, 113 bp), hCCND1, 5′-gtacctgtaggactctcattcggg-3′ (forward) and 5′-cagcactgtgagctggcttcattg-3′ (reverse) (product length, 173 bp), hCCNE2, 5′-aggcattatgacaccacccgaaga-3′ (forward) and 5′-gaatcggctagggcaatcaatcac-3′ (reverse) (product length, 165 bp), human glyceraldehyde-3-phosphate dehydrogenase (hGAPDH), 5′-gcaccgtcaaggctgagaac-3′ (forward) and 5′-atggtggtgaagacgccagt-3′ (reverse) (product length, 141 bp); hSPACIA1, 5′-ggcgtactggcaagtccaagtg-3′ (forward) and 5′-ccagcagagtagggtgggtctgaa-3′ (reverse) (product length, 165 bp). Human GAPDH was utilized for normalization. Each sample was tested in triplicate, and the relative gene expression levels were normalized using the $2^{-\Delta\Delta Ct}$ method.

4.5. Western Blotting

To investigate CDK6 protein expression in RASFs with *SPACIA1*- or mock siRNA, Western blotting assay was performed as previously described [7], using anti-human CDK6 antibody sc-177 (Santa Cruz Biotechnology, Santa Cruz, CA, USA) and anti-human alpha-tubulin antibody T5168 (Sigma-Aldrich, St Louis, MO, USA) as the internal control.

4.6. Immunohistochemistry

Immunohistochemistry was performed as described in our previous report [7]. All of the synovial tissue specimens that were used in this study are from patients to undergo artificial knee joint replacement. The specimen, shown in Figure 4, is from a RA patient who treated with MTX + certolizumab pegol + prednisolone before the joint replacement. The duration of disease was 8 years. Briefly, the tissue specimens were fixed in 10% formalin and then embedded in paraffin. Deparaffinized tissue

sections (5-μm thick) were antigen-retrieved by pressure cooker in 10 mM Tris-HCl (pH 9.0) and 1 mM ethylenediaminetetraacetic acid buffer for 3 min, and then incubated with anti human CDK6 antibody sc-177 (Santa Cruz Biotechnology, Santa Cruz, CA, USA) (2 μg/mL), or normal rabbit IgG (2 μg/mL). Afterwards, the sections were rinsed and visualized by immunoperoxidase staining with the Vectastain Elite ABC kit (Vector Laboratories Ltd., Peterborough, UK) and 3,3′-diaminobenzidine tetrahydrochloride substrate. Mayer's hematoxylin was used as a counterstain. Normal rabbit IgG and normal mouse IgG were used as negative controls.

4.7. Promoter Assay

To find the SPACIA1-responsible element in the proximal promoter region of the *cdk6* gene, reporter assays were performed in RASFs [12]. DNA fragments upstream of the start codon of the *cdk6* gene were amplified by PCR using the following primer sets: 5′-cgcaagcttattggagttaaacaaagcc-3′ (forward), 5′-gctccatggtcggtctagctactgc (reverse) (product length, 2.5 kbp). The fragment was cloned into the pGV-CS2 reporter vector (Nippon Gene) containing the luciferase gene without a promoter. Deletion constructs of 1.6 kbp and 0.9 kbp (Figure 5A,B) were obtained using internal *Kpn* I and *Bst* XI restriction enzyme sites in the 2.5 kbp fragments. Twenty four hours after transfection of each reporter vector into RASFs, promoter activity was measured using the Luciferase Assay System (Promega, Madison, WI, USA).

4.8. Messenger-RNA Stability Assay

RASFs were transfected with *SPACIA1*- or mock siRNA for 72 h and treated with Actinomycin D (Sigma-Aldrich) at 1 μg/mL. The cells were harvested 0, 3.5, and 1 h after the addition of Actinomycin D. The *cdk6* mRNA levels were measured by qRT-PCR.

4.9. Statistical Analyses

The chi-square test (or Fisher's exact test) was used to compare the incidence of arthritis between *SPACIA1*-deficient and wt mice (Figure 2A,C). The Mann-Whitney U test was used to compare the arthritis scores (Figure 2E,D) and the histopathological scores (Figure 2F) between *SPACIA1*-deficient and wt mice. All other statistical analyses were performed using unpaired Student's *t*-test. The criterion for statistically significant differences was $p < 0.05$.

4.10. Ethical Considerations

All human (No. 1315, 7 January 2008) and animal (No. AMI0912T2, 26 December 2009) experimental protocols in this study were approved by the Ethics Review Committee of St. Marianna University School of Medicine. This study was conducted in accordance with the Declaration of Helsinki. We obtained signed consent forms from all of the patients in the study before collecting joint tissue samples from them.

Author Contributions: R.F., T.S., K.K., H.A., K.N. and T.N. were involved in the planning of the study conception and design. H.N. and K.Y. were involved in the recruitment of patients. R.F., R.K., T.S. and I.S. contributed substantially to analysis and interpretation of data. All authors were involved in drafting the article and revising it critically for important content, and all authors read and approved the final manuscript.

Funding: This research was funded by Santen Pharmaceutical Co., Ltd., the Japanese Ministry of Education, Culture, Sports, Science, and Technology (JP25461490, JP22591086, JP24791009); the Japanese Ministry of Health, Labor, and Welfare; MEXT-Supported Program for the Strategic Research Foundation at Private Universities (PS1507086).

Acknowledgments: We would like to thank Nao Watanabe-Asaoka, Katsunori Takahashi, Natsue Yamamoto, Ayaka Une, Yuriko Furuya, Sanae Shinkawa, Yukari Nakagawa, Reshiko Sato-Mogi, Ami Tanaka, Hiroko Ogasawara, Yuko Sato, Yoshiko Urbanczyk, Masumi Yoshimishi and Mika Ishikawa for excellent technical assistance.

Conflicts of Interest: The funders had no role in the design of the study; in the collection, analyses, or interpretation of data; in the writing of the manuscript, or in the decision to publish the results.

Abbreviations

CII	bovine type II collagen
CCN	cyclin
cdk (or CDK)	cyclin-dependent kinase
CIA	collagen-induced arthritis
CRE/loxP	cause's recombinase/locus of crossover (x) in P1
ES	embryonic stem
FLP/frt	flippase/flippase recognition target
GJ	first growth
IgG	immunoglobulin G
hGAPDH	human glyceraldehyde-3-phosphate dehydrogenase
MCF7	Michigan Cancer Foundation-7
MTX	methotrexate
PCR	polymerase chain reaction
qRT-PCR	quantitative real time polymerase chain reaction
RA	rheumatoid arthritis
RASFs	rheumatoid arthritis-synovial fibroblasts
SAAL1	serum amyloid A-like 1
siRNA	small interfering RNA
SPACIA1	synoviocyte proliferation associated in collagen- induced arthritis 1
TNF	tumor necrosis factor
wt	wild-type

References

1. Harris, E.D. Jr. Rheumatoid arthritis. Pathophysiology and implications for therapy. *N. Engl. J. Med.* **1990**, *322*, 1277–1289. [CrossRef] [PubMed]
2. Tanaka, Y.; Yamaoka, K. JAK inhibitor tofacitinib for treating rheumatoid arthritis: From basic to clinical. *Mod. Rheumatol.* **2013**, *23*, 415–424. [CrossRef] [PubMed]
3. Kedlaya, F.M. The role of concomitant methotrexate in biologic therapy for rheumatoid arthritis. *Bull. Hosp. Jt. Dis.* **2013**, *71*, S29–S32.
4. Chan, E.S.; Cronstein, B.N. Methotrexate—how does it really work? *Nat. Rev. Rheumatol.* **2010**, *6*, 175–178. [CrossRef] [PubMed]
5. Sekine, C.; Sugihara, T.; Miyake, S.; Hirai, H.; Yoshida, M.; Miyasaka, N.; Kohsaka, H. Successful treatment of animal models of rheumatoid arthritis with small-molecule cyclin-dependent kinase inhibitors. *J. Immunol.* **2008**, *180*, 1954–1961. [CrossRef] [PubMed]
6. Hosaya, T.; Iwai, H.; Yamaguchi, Y.; Kawahata, K.; Miyasaka, N.; Kohsaka, H. Cell cycle regulation therapy combined with cytokine blockade enhances anti-arthritic effects without increasing immune suppression. *Ann. Rheum. Dis.* **2016**, *75*, 253–259. [CrossRef] [PubMed]
7. Sato, T.; Fujii, R.; Komoto, K.; Yoshida, N.; Arataki, S.; Araya, N.; Asao, H.; Yudoh, K.; Suzuki, N.; Beppu, M.; et al. Overexpression of SPACIA1/SAAL1, a newly identified gene that is involved in synoviocyte proliferation, accelerates the progression of synovitis in mice and humans. *Arthritis Rheumatol.* **2011**, *63*, 3933–3942. [CrossRef] [PubMed]
8. Wu, X.; Wu, M.Y.; Jiang, M.; Zhu, Q.; Bian, X.; Yu, M.D.; Gong, F.R.; Hou, J.; Tao, M.; Shou, C.M.; et al. TNFα sensitizes chemotherapy and radiotherapy against breast cancer cells. *Cancer Cell Int.* **2017**, *17*, 13. [CrossRef] [PubMed]
9. Thomas, S.; Fisher, K.H.; Snowden, J.A.; Danson, S.J.; Brown, S.; Zeidler, M.P. Methotrexate is a JAK/STAT Pathway Inhibitor. *PLoS ONE* **2015**, *10*, e0130778. [CrossRef] [PubMed]
10. Malumbres, M.; Sotillo, R.; Santamaría, D.; Galán, J.; Cerzo, A.; Ortega, S.; Dubus, P.; Barbacid, M. Mammalian cell cycle without the D-type cyclin-dependent kinases Cdk4 and Cdk6. *Cell* **2004**, *118*, 493–504. [CrossRef] [PubMed]

11. Hughes, C.; Wolos, J.A.; Gianniotis, E.H.; Thresh, R. Induction of T helper cell hyporesponsiveness in an experimental model of autoimmunity by using nonmitogenic anti-CD3 monoclonal antibody. *J. Immunol.* 1994, 153, 3319–3325. [PubMed]
12. Fujii, R.; Okamoto, M.; Aratani, S.; Oishi, T.; Ohshima, T.; Taira, K.; Baba, M.; Fukamizu, A.; Nakajima, T. A Role of RNA Helicase A in cis-Acting Transactivation Response Element-mediated Transcriptional Regulation of Human Immunodeficiency Virus Type 1. *J. Biol. Chem.* 2001, 276, 5445–5451. [CrossRef] [PubMed]

© 2008 by the authors. Licensed MDPI, Basel, Switzerland. This article is an open access article distributed under the terms and conditions of the Creative Commons Attribution (CC BY) license (http://creativecommons.org/licenses/by/4.0/).

International Journal of Nanomedicine Dove

ORIGINAL RESEARCH

A novel, self-assembled artificial cartilage–hydroxyapatite conjugate for combined articular cartilage and subchondral bone repair: histopathological analysis of cartilage tissue engineering in rat knee joints

This article was published in the following Dove Medical Press journal:
International Journal of Nanomedicine

Takanori Kumai[1]
Naoko Yui[1]
Kenaka Yatabe[1]
Chizuko Sasaki[2]
Ryoji Fujii[1]
Misuko Takenaga[3]
Hiroto Fujiya[1]
Hisateru Niki[4]
Kazuo Yudoh[1]

[1]Department of Sports Medicine, St Marianna University School of Medicine, Miyamae-ku, Kawasaki 216-8511, Japan; [2]Institute for Ultrastructure Morphology, St Marianna University Graduate School of Medicine, Miyamae-ku, Kawasaki 216-0512, Japan; [3]Department of Frontier Medicine, Institute of Medical Science, St Marianna University School of Medicine, Miyamae-ku, Kawasaki 216-8512, Japan; [4]Department of Orthopaedic Surgery, St Marianna University School of Medicine, Miyamae-ku, Kawasaki 216-8512, Japan

Purpose: We previously created a self-assembled human age-like complex in vitro from only three cartilage components, hyaluronic acid (HA), aggrecan (Acan) and type II collagen, without other materials such as cross-linking agents. Based on this so-designed ACan/HA/collagen complex, we have created three novel types of biphasic cartilage and bone-like scaffolds combined with hydroxyapatite (HAP) for osteochondral tissue engineering. These scaffolds have been developed from self-assembled cartilage component molecules and HAP at the nanometer scale by manipulating the intermolecular relations.

Patients and methods: The surface structure of each self-organized biphasic cartilage and bone-like scaffold was evaluated by scanning electron microscopy, whereas the viscoelasticity was also analyzed in vitro. Three types of artificial cartilage–HAP conjugates were implanted into an osteochondral defect in rat knee joints, and bone and cartilage tissues of the implanted site were examined 4 and 8 weeks after implantation. The tissues were examined histopathologically to evaluate the effects of the implantation on the articular cartilage and subchondral bone tissues.

Results: Qualitative and in vivo data reveal that the self-organized biphasic cartilage and bone-like scaffold conjugated with HAP are superior to the scaffold with no HAP in both cartilage regeneration and subchondral bone regeneration.

Conclusion: Our present study suggests that the self-organized biphasic cartilage and bone-like scaffold, which is conjugated with an HAP layer, may have potential not only to repair articular cartilage defects but also to ameliorate the degeneration of subchondral bone in the diseases with osteochondral defect.

Keywords: cartilage tissue engineering, subchondral bone, articular cartilage, osteoarthritis, self-assembly, hydroxyapatite

Introduction

New technologies such as tissue engineering are now attracting attention for the reconstruction of joint tissues in cases of advanced stage joint degeneration and destruction, such as in traumatic injury and arthritis, including rheumatoid arthritis and osteoarthritis (OA).[1–5] In bone tissue engineering, scaffolds made from the biomaterial hydroxyapatite (HAP) have already been so well developed that they have sufficiently high affinity and enough rigidity similar to bone to be usable for the repair of bone defects.[6]

Correspondence: Kazuo Yudoh
Department of Frontier Medicine, Institute of Medical Science, St Marianna University School of Medicine, Suite 2-16-1, Miyamae-ku, Kawasaki 216-8512, Japan
Tel +81 44 977 8111 ext 4029
Fax +81 44 978 3036
Email yudoh@marianna-u.ac.jp

International Journal of Nanomedicine downloaded from https://www.dovepress.com/ by 202.209.68.3 on 22-Feb-2019
For personal use only.

International Journal of Nanomedicine downloaded from https://www.dovepress.com/ by 202.209.68.3 on 22-Feb-2019
For personal use only.

It is well known that autologous and allografts forms show good osteoconductive power and mechanical properties for the treatment of healing bone defect due to stable structure, little immunogenicity and osteogenic capacity. Also, it has been demonstrated that application of scaffolds, such as HAP, shows a good ability to facilitate bone repair and an osteogenic potential.[]

In contrast to bone tissue, a suitable biomaterial for cartilage repair still remains to be developed. Such a material requires perfect cartilage-specific tissue qualities represented by properties such as high elasticity and high lubrication.[] Articular cartilage is a highly organized tissue composed primarily of proteoglycan aggrecan [AG], type II collagen, and hyaluronic acid (HA) with a small amount of other proteins including elastin, type IX and type X collagen, which has poor spontaneous self-healing capacity.[] Cartilage tissue engineering using autologous chondrocyte implantation, scaffolds, growth factors or their combinations has been tried as a therapeutic strategy for cartilage repair.[] However, there are still several problems to be addressed in developing a strategy for cartilage regeneration.

The first problem to be overcome is the cell source limitation. Symptomatic full-thickness cartilage defects have been treated with autologous chondrocyte implantation.[] This strategy requires a two-stage process whereby the patient's chondrocytes are culture expanded in vitro to obtain a sufficient number and then implanted into the defect.[] In general, for autologous chondrocyte transplantation, a patient's chondrocytes are cultured in a collagen or agarose gel to form a three-dimensional biomaterial. To obtain enough chondrocytes, continuous cell culture over several passages is required.[] During passages in culture, chondrocytes are known to dedifferentiate and to lose chondrocyte-specific properties.[] To improve the availability of chondrocyte resources for cartilage tissue engineering, it has recently been demonstrated that differentiated chondrocytes can be induced from mesenchymal stem cells or induced pluripotent stem (iPS) cells.[] However, the risk of oncogenesis, such as teratoma, still remains during the differentiation of human somatic cells, including chondrocytes, from mesenchymal stem cells or iPS cells.[] Moreover, it takes several months for the tissue engineered cartilage-like tissue to grow and become organized into mature cartilage even when grafted in the defect site.[] Further studies are needed to clarify whether mesenchymal stem cells and iPS cells are suitable as a cell source for cartilage tissue engineering.

The next problem to be considered is how to prevent the leakage of transplanted chondrocytes from the cartilage defect site. To contain cells at the defect site, it is necessary to patch over the defect with a membrane.[] Generally, autologous periosteum has been used as a covering membrane. However, periosteum may be inappropriate for this use, since it has the osteogenic capacity to promote ossification/calcification of covering membranes.[] To create an articular cartilage-like tissue applicable to clinical use in cartilage repair while overcoming the problems of cell supply and covering membranes, various kinds of biomaterials have been created as a scaffold for chondrocyte growth and cartilage regeneration.[]

The third problem of cartilage tissue engineering is the regeneration of subchondral bone in OA. OA is nowadays one of the most frequent chronic diseases and, with the increase in life expectancy, both its prevalence and incidence are expected to rise. This condition is progressive and leads to functional decline and loss in quality of life, with important health care and society costs. Thus, it is important to develop the novel therapeutic strategy for osteoarthritic lesions.

OA has been considered to primarily involve degeneration of articular cartilage. However, recently, subchondral bone deterioration has been widely recognized as a hallmark of OA.[] OA subchondral bone is known to be hypomineralized and to show abnormal bone metabolism, resulting in histopathological degeneration of subchondral bone (Figure 1).[] A functional joint unit comprising articular cartilage and subchondral bone may regulate the homeostasis and maintenance potential of articular cartilage against the progression of OA.[] Thus, histopathological changes of subchondral bone may be involved in the pathogenesis and pathophysiology of cartilage degeneration. Consequently, for cartilage repair in OA, regeneration of subchondral bone as well as articular cartilage is necessary. Although numerous reports have already demonstrated that novel technology, involving autologous chondrocyte implantation, tissue engineering using mesenchymal stem cells or iPS cells and biomaterials, may have therapeutic potential for cartilage repair, it still remains unclear whether implantation of autologous chondrocytes or recently developed biomaterials can repair the histopathological changes of subchondral bone in OA. If the biomaterial may have the potential to repair the osteochondral defect (chondrogenic and osteogenic potential), it may be a useful tool for severe OA with subchondral bone degeneration as well as cartilage degeneration.

We have recently created three types of self-organized biphasic cartilage and bone-like scaffolds combined with HAP, for use in osteochondral tissue engineering, which were developed through self-assembled cartilage component

International Journal of Nanomedicine downloaded from https://www.dovepress.com/ by 202.209.168.3 on 22-Feb-2012
For personal use only

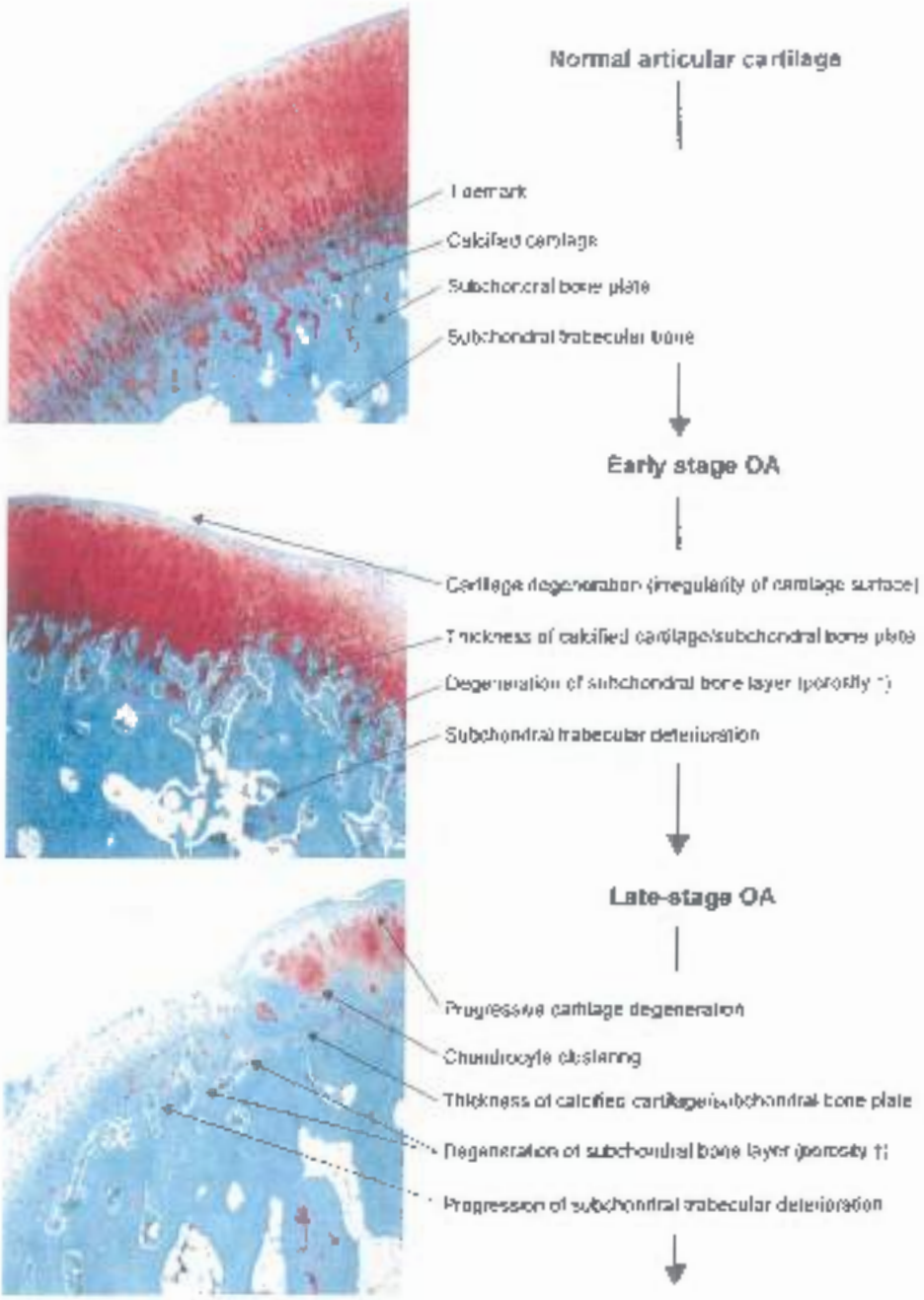

Figure 1 Osteochondral damage during the progression of OA.
Notes: OA subjects allude to a lower tone specimen and to show abnormal bone metabolism, resulting in a corresponding degeneration of calcified bone as well as cartilage damage. During progression of OA, the subchondral bone is also damaged as well as the articular cartilage layer. This severe damage severely affect the mechanical properties of articular tissue, leading to the pain and disability associated with OA.
Abbreviation: OA, osteoarthritis.

molecules and HAP at the nanometer scale by manipulating intermolecular relations. In the current study, we demonstrate that it is possible to create a novel self-organized biphasic cartilage and bone like scaffold combined with an HAP layer for osteochondral tissue repair with high performance as well as microstructures comparable to hyaline articular cartilage and subchondral bone in vitro and in an in vivo rat model.

International Journal of Nanomedicine downloaded from dovepress.com by 202.208.60.4 on 22-Feb-2016
For personal use only

Patients and methods

Scaffolds for osteochondral tissue engineering

In the present study, we prepared three types of self-assembled artificial cartilage scaffolds: 1) self-organized cartilage-like scaffold; 2) self-organized biphasic cartilage and bone-like scaffold combined with an HAP bone block; and 3) self-organized biphasic cartilage and bone-like scaffold coated with HAP powder.

Self-organized cartilage-like scaffold formed from HA, proteoglycan and type II collagen

Solutions were generated by mixing proteoglycan (AG; Sigma-Aldrich Co., St Louis, MO, USA) at a final concentration of 1.0 mg/mL and HA (molecular weight: 280 × 10⁶ Da; Chugai Pharmaceutical, Inc., Tokyo, Japan) at a final concentration of 15% in distilled-deionized water (DDW) at room temperature. Human type II collagen (Collagen Research Center, Inc., Tokyo, Japan) was dissolved in DDW at a final concentration of 0.6 mg/mL at room temperature. The AG + HA solution and the collagen solution were adjusted to pH 9.0. Then, equal volumes of the AG + HA and the collagen solutions were mixed at pH 9.0 and incubated at 37°C in a humidified 95% air and 5% CO_2 atmosphere for 5 hours. After incubation, the mixture was centrifuged for 30 minutes at 50,000 × *g* and then specimens of the self-organized AG/HA/collagen complex were prepared for each experiment.

Formation of the self-organized biphasic cartilage and bone-like scaffold combined with an HAP bone block

We have newly created the self-organized biphasic cartilage and bone-like scaffold combined with an HAP bone block. The self-organized AG/HA/collagen complex was formed by the method described earlier, and then the complex was placed onto an HAP block (homogeneous HAP, porous disk-like block; pore size 100–300 μm, diameter 4 mm × height 2 mm; HOYA Technosurgical, Corp., Tokyo, Japan) and centrifuged at 50,000 × *g* for 30 minutes. Specimens of the self-organized AG/HA/collagen complex combined with the HAP block were then prepared for each experiment.

Formation of the self-organized biphasic cartilage and bone-like scaffold coated with HAP powder

We prepared two types of self-organized biphasic cartilage and bone-like scaffold coated with HAP powder (particle size: 45 μm and 5 μm). It has been reported that natural components with hydroxyl groups connect to HAP powders by dehydration condensation between each hydroxyl group.[11] HAP powders were kindly donated by Sofsera Co. Ltd., Osaka, Japan, and suspended in DDW (1.0 mg/mL). The self-organized AG/HA/collagen complex was formed by the method described earlier, then carefully poured a 1.0 mg/mL suspension of one of the HAP powders and incubated at 4°C overnight. Only the bottom surface of the complex was coated with the HAP solution. Specimens of the self-organized AG/HA/collagen complex coated with HAP powder were then prepared for each experiment.

After the formation of each self-assembled complex, the complex was adjusted by PBS for the adaptation of the in vitro biomaterial to the in vivo microenvironment. The complex was incubated at 37°C in a humidified 95% air and 5% CO_2 atmosphere, to adapt itself to in vivo condition.

Viscoelasticity of the self-organized biphasic cartilage and bone-like scaffold

The viscoelasticity (compression modulus) of the self-assembled scaffolds described earlier was measured using an elasticity measuring device (Rheogel-E1500, UBM Ltd., Kyoto, Japan; experimental conditions: temperature 37°C [35°C–40°C], 10 Hz, equipment configuration [parallel plate]). The scaffold was air-dried overnight using a drying chamber. After complete drying of the complex, the viscoelasticity (compression modulus) of the dried complex was also evaluated using an elasticity measuring device. The dried scaffold was rehydrated with sterilized saline. Then, the viscoelasticity (compression modulus) of the rehydrated complex was again analyzed in the same manner.

Chondrocyte culture in the self-organized scaffold

Human articular cartilage tissue samples were obtained from the knee joint of a patient with OA during arthroplastic knee surgery after obtaining informed consent (male, 79 years). The study protocol was reviewed and approved by the local ethics committee of St Marianna University School of Medicine (permission number: 1355). The procedures followed were in accordance with the ethical standards of the ethics committee and with the Declaration of Helsinki, 1975, as revised in 2008. The patient gave written informed consent before participating in the study. The severity of knee OA was evaluated by the Kellgren and Lawrence classification and was classified as grade 4.[12] Articular cartilage explants were cut into small pieces, washed with PBS and digested with 1.0 mg/mL collagenase II (Sigma-Aldrich Co.) in DMEM (Dako Denmark A/S, Glostrup, Denmark) overnight on a shaking platform at 37°C. Isolated chondrocytes were

International Journal of Nanomedicine downloaded from https://www.dovepress.com/ by 202.208.66.3 on 22-Feb-2019
For personal use only.

collected following centrifugation, washed three times with PBS, resuspended and cultured in DMEM supplemented with 10% heat-inactivated fetal calf serum, 2 mM L-glutamine, 15 mM 2[4-(2-hydroxyethyl)-1-piperazinyl] ethane sulfonic acid (HEPES) and 100 U/mL penicillin and streptomycin at 37°C in a humidified atmosphere of 95% air and 5% CO_2, as previously reported.[2]

The self-organized AG/HA-collagen complex was formed by the method described earlier. Each complex was washed three times with PBS and then the complex was transferred into DMEM. Human chondrocytes were suspended in the DMEM with each self-organized complex at a cell density of 5×10^5/cm^2, followed by slight shaking, and the complex was incubated at 37°C in a humidified 95% air and 5% CO_2 atmosphere. After incubation for 1 or 2 weeks, some of the complexes were fixed for 2 days in 4% paraformaldehyde solution. Specimens of self-assembled complexes conjugated with chondrocytes were prepared for scanning electron microscopy (SEM) study.

Scanning electron microscopy

SEM analysis was performed to verify the surface structure of scaffolds. After serial fixations of scaffold samples with 2% glutaraldehyde, 1% osmium tetroxide and 1% tannic acid aqueous solution, the surface morphology of the scaffolds was observed under a scanning electron microscope (S-4800, Hitachi Ltd., Tokyo, Japan).

Implantation of the self-organized scaffolds for cartilage repair

The animal study protocol was reviewed and approved by the Animal Care and Use Committee of St Marianna University School of Medicine (permission number: 1308019). The procedures followed were in accordance with the Japanese official guidelines for proper conduct of animal experiments and related activities in academic research institutions under the jurisdiction of the Ministry of Education, Culture, Sports, Science and Technology in Japan. Healthy, 9–11-week-old male Sprague Dawley (SD) rats (n=18) were used (Clea Japan Inc., Tokyo, Japan). Hair on the knee joints of bilateral hind limbs was shaved under anesthesia, and the skin surface was disinfected with 70% ethanol (Wako Pure Chemical Industries, Ltd., Osaka, Japan). After disinfection, a skin incision was made in the surgical site over the knee joint. The articular capsule was incised using an external juxta-articular approach (medial approach), and the knee joint was exposed by overturning the patella. A hole (2 mm in diameter and 2 mm deep) was made in the surface of the distal end of the left femoral condyle using a 2 mm diameter drill, and a piece of the new scaffold was implanted in the operated animals of 4- and 8-week observation groups (the self-organized AG/HA/collagen complex alone-implanted group n=5, each self-organized AG/HA/collagen complex-HAP group n=4). After implantation, the surgical site was rinsed with physiological saline (Otsuka Pharmaceutical Factory Inc., Tokyo, Japan), and the incised skin was sutured. In each animal, the contralateral side was also subjected to the same surgical manipulation, but no test material was implanted as a control.

The general condition of all rats was observed once a day during the experimental period. Rats were sacrificed by exsanguination from bilateral femoral arteries under anesthesia in a painless manner at 4 or 8 weeks after surgery. After euthanasia, the tissues including the implanted material were sampled and macroscopically observed. Tissues were fixed with 10% neutral-buffered formalin, then decalcified with EDTA, embedded in paraffin by a routine procedure and cut into 6 µm sections. The sections were stained with H&E for histological assessment of the general morphology of the repair tissue, or Safranin O/fast green (SO/FG) and toluidine blue, to indicate glycosaminoglycan content as per standard protocols.[11]

Histological assessment

Sections were analyzed under light microscopy to examine collagen fiber orientation and to distinguish between hyaline cartilage and fibrocartilage. The histological quality of the repair tissue was assessed and scored using the International Cartilage Repair Society (ICRS) II VAS (each of 14 parameters scored 0%–100%),[12] assessing the parameters listed in Table 1. It has been demonstrated that ICRS II may be most adequate for analysis of tissue engineered and repaired cartilage and that ICRS II represents an improvement over the earlier histological cartilage repair scoring system, although various histologic scoring systems exist for tissue-engineered, repaired and osteoarthritic cartilage.[13]

Results

A self-organized cartilage-like complex formed from HA, proteoglycan (AG) and type II collagen

Our previous study of the self-organized AG/HA/collagen complex revealed that it has a nanocomposite structure in which the fibrous collagen fibrous is bound to AG linking to HA, resembling cartilage tissue, although the original collagen gel was merely a gel form of collagen fibrils having no solid tissue structure.[2,7] In a similar manner, we created

Table 1 International Cartilage Repair Society II scoring system for cartilage repair

Histological parameters	Scores
1. Tissue morphology	0% full-thickness collagen fibers, 100% normal cartilage
2. Matrix staining (metachromasia)	0% no staining, 100% full metachromasia
3. Cell morphology	0% no round cells, 100% mostly round cells
4. Chondrocyte clustering (fibrous or hypertrophied cells)	0% present, 100% absent
5. Surface architecture	0% delamination, or major irregularity, 100% smooth surface
6. Basal integration	No integration, 100% complete integration
7. Formation of a tidemark	0% no calcification front, 100% calcification
8. Subchondral zone (bone/marrow/fibrosis)	0% abnormal, 100% normal marrow
9. Inflammation	0% present, 100% absent
10. Abnormal calcification/ossification	Present, 100% absent
11. Vascularization (within the repaired tissue)	Present, 100% absent
12. Surface/superficial assessment	0% total loss or complete disruption, 100% resembles intact articular cartilage
13. Full-depth core assessment	0% fibrous tissue, 100% normal hyaline cartilage
14. Overall assessment	0% bad (fibrous tissue), 100% good (hyaline cartilage)

a self-assembled cartilage-like complex from only three cartilage components, HA, AG and type II collagen in vitro, without any other materials such as cross-linking agents (Figure 2A). Analysis with SEM revealed a fibrous and three-dimensional reticular structure (Figure 2B).

Observation of the self-organized complex implanted with chondrocytes

After incubation of the self-organized AG-HA-collagen complex with chondrocytes for 1 or 2 weeks, the complex remained dense and the chondrocytes were homogeneously present on the scaffold of fibers forming the complex. Cytoplasmatic extensions denominated the chytopodia, on the surface of the self-organized scaffolds, indicating that chondrocytes were alive within the tissue after the 2-week incubation (Figure 2C).

Self-organized biphasic cartilage and bone-like scaffold combined with an HAP bone block

A self-organized biphasic cartilage and bone-like scaffold combined with an HAP bone block was obtained by

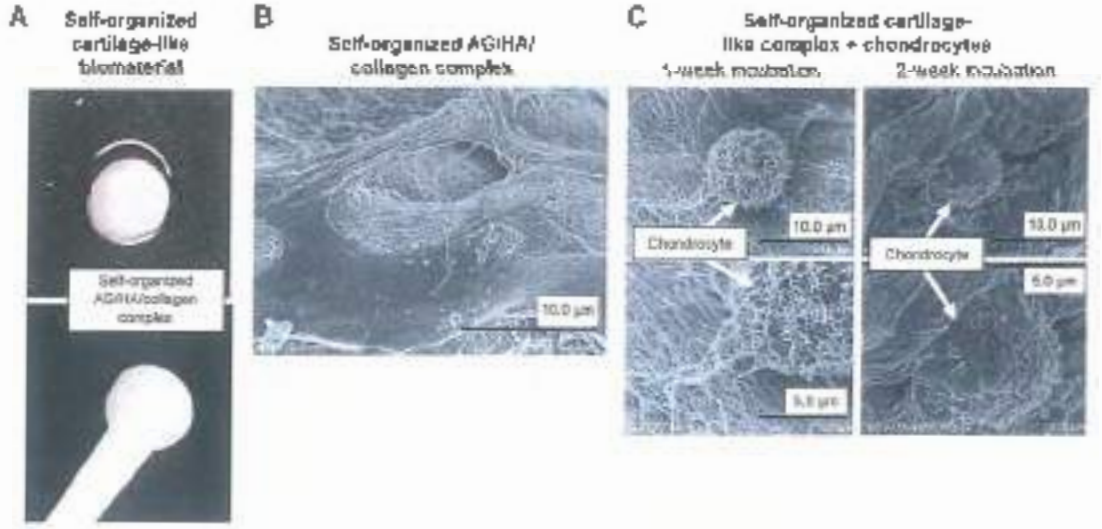

Figure 2 Self-organized cartilage-like scaffold formed from HA, AG and type II collagen in vitro without cartilage-like growth.
Notes: (A) Macroscopic image of self-organized cartilage-like scaffold. (B) The structure of the self-organized AG-HA-collagen complex was observed by SEM. The histological structure of the complex had a fibrous appearance. (C) After 1- and 2-week incubation of chondrocytes with the self-organized AG-HA-collagen complex, chondrocytes were present on the surface of fibers forming the complex.
Abbreviations: AG, agarose; HA, hyaluronic acid; SEM, scanning electron microscopy.

International Journal of Nanomedicine downloaded from https://www.dovepress.com/ by 202.209.68.3 on 22-Feb-2019
For personal use only

International Journal of Nanomedicine downloaded from nijn.dovepress.com by 202.209.58.3 on 22-Feb-2019
For personal use only.

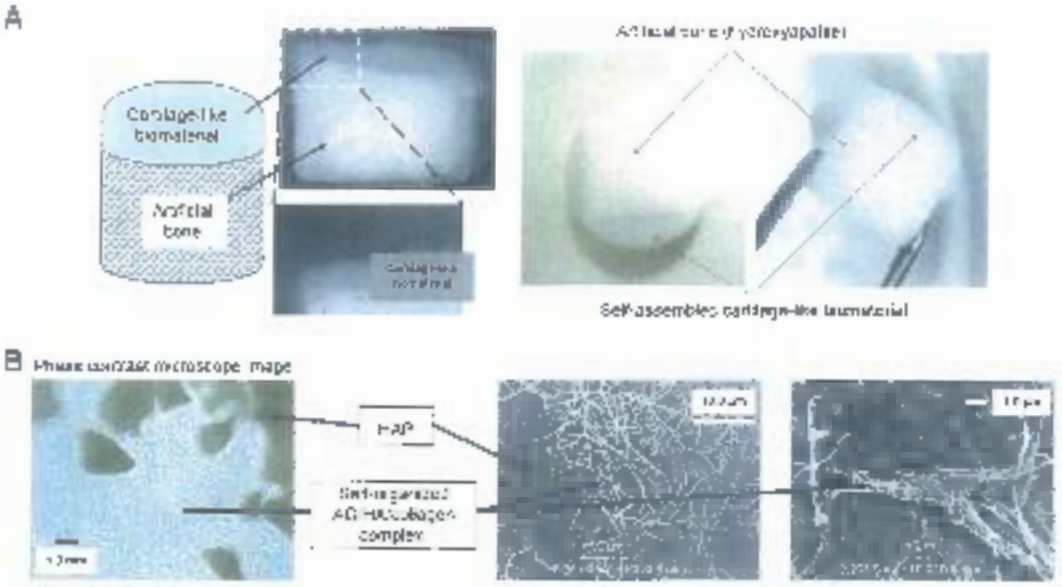

Figure 3 Self-organized bipha s cartilage and bone-like tissue combined with an HAP block.
Notes: (A) Microscopic image of our self-organized cartilage-like tissue combined with an HAP block. (B) The structure of the self-organized cartilage-like tissue combined with an HAP block was observed by SEM.
Abbreviations: HAP, hydroxyapatite; SEM, scanning electron microscopy.

self-organization of the AG/HA/collagen complex on the HAP block in vitro (Figure 1). The self-organized AG/HA/collagen complex bound to the HAP porous block strongly. SEM analysis revealed that fibers of the AG/HA/collagen complex penetrated the interior of multiple pores of the HAP block.

Self-assembled artificial cartilage–HAP powder conjugate

One side of the self-organized AG/HA/collagen complex was coated with an HAP powder of either 40 nm or 5 μm particle size (Figure 4A). We confirmed by SEM that both

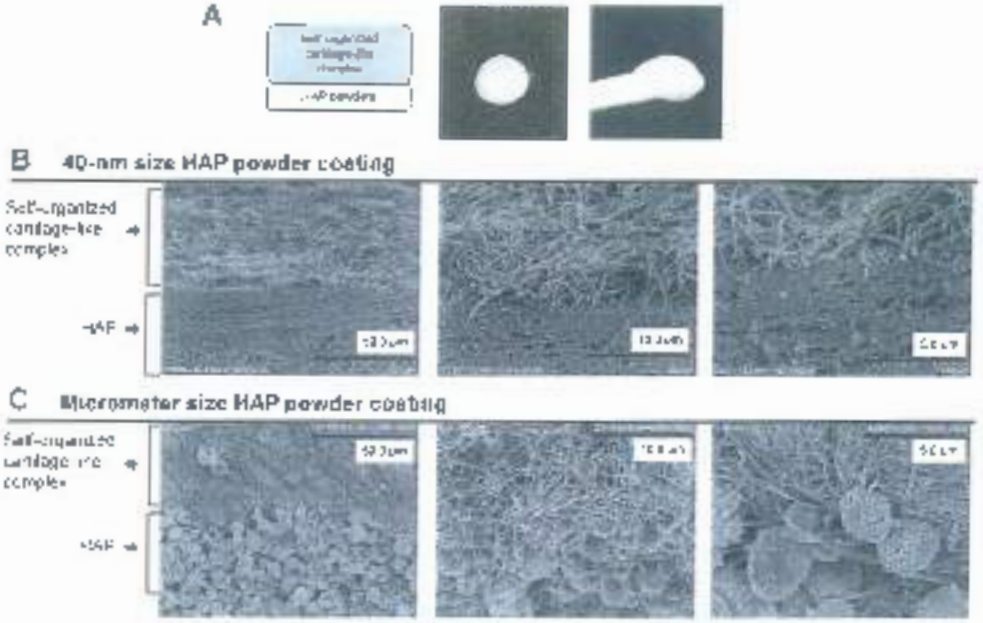

Figure 4 Self-assembled artificial cartilage–HAP powder conjugate.
Notes: (A) Conjugation between the self-organized artificial cartilage–HAP powder conjugate and its microscopic image. (B) The structure of the 40-nm size HAP powder coating complex was observed by SEM. (C) The structure of the 5-μm size HAP powder coating complex was observed by SEM.
Abbreviations: HAP, hydroxyapatite; SEM, scanning electron microscopy.

International Journal of Nanomedicine downloaded from https://www.dovepress.com/ by 202.192.62.3 on 22-Feb-2019
For personal use only.

areas of HAP powder were regularly bonded to self-organized cartilage-like complexes in the form of laminae (Figure 4B: 40-nm powder size coating group, Figure 4C: 5-nm powder size coating group).

Viscoelasticity of self-organized biphasic cartilage and bone-like scaffolds

Nondried scaffolds

Viscoelasticity (compressive modulus) of the nondried (wet) self-organized AG/HA/collagen complex and the nondried self-assembled complex–HAP powder conjugate was 0.275 and 0.347 MPa, respectively. Although no significant difference in the viscoelasticity was observed between the self-organized AG/HA/collagen complex and the self-assembled complex–HAP powder conjugate, the mean viscoelasticity (compressive modulus) was higher in the self-assembled complex–HAP powder conjugate (Figure 5, b: 0.347 MPa) than in the self-organized AG/HA/collagen complex (Figure 5, a: 0.275 MPa).

Dried scaffolds

The viscoelasticity (compressive modulus) of both dried scaffolds (dried self-organized AG/HA/collagen complex and dried self-assembled complex–HAP powder conjugate) was significantly higher than that of their respective nondried original scaffolds (nondried self-organized AG/HA/collagen complex and nondried self-assembled complex–HAP powder conjugate) (Figure 5, a vs c: $P<0.001$, b vs d: $P<0.001$). Although no significant difference in viscoelasticity was observed between the dried self-organized AG/HA/collagen complex and the dried self-assembled complex–HAP powder conjugate, the viscoelasticity of the dried self-assembled complex–HAP powder conjugate tended to increase (Figure 5, d: 0.862 MPa) in comparison with the dried self-organized AG/HA/collagen complex (Figure 5, c: 0.747 MPa).

Rehydrated scaffolds

The mean viscoelasticity (compressive modulus) of the rehydrated self-assembled complex–HAP powder conjugate (Figure 5, e: 0.563 MPa) was significantly higher than that of the rehydrated self-organized AG/HA/collagen complex (Figure 5, f: 0.4 MPa) ($P=0.0147$). Interestingly, viscoelasticity of both rehydrated scaffolds (rehydrated self-organized AG/HA/collagen complex and rehydrated self-assembled complex–HAP powder conjugate) was significantly higher than that of the respective nondried original scaffolds (nondried self-organized AG/HA/collagen complex and nondried self-assembled complex–HAP powder conjugate) (Figure 5, a vs e: $P<0.05$, b vs f: $P<0.01$).

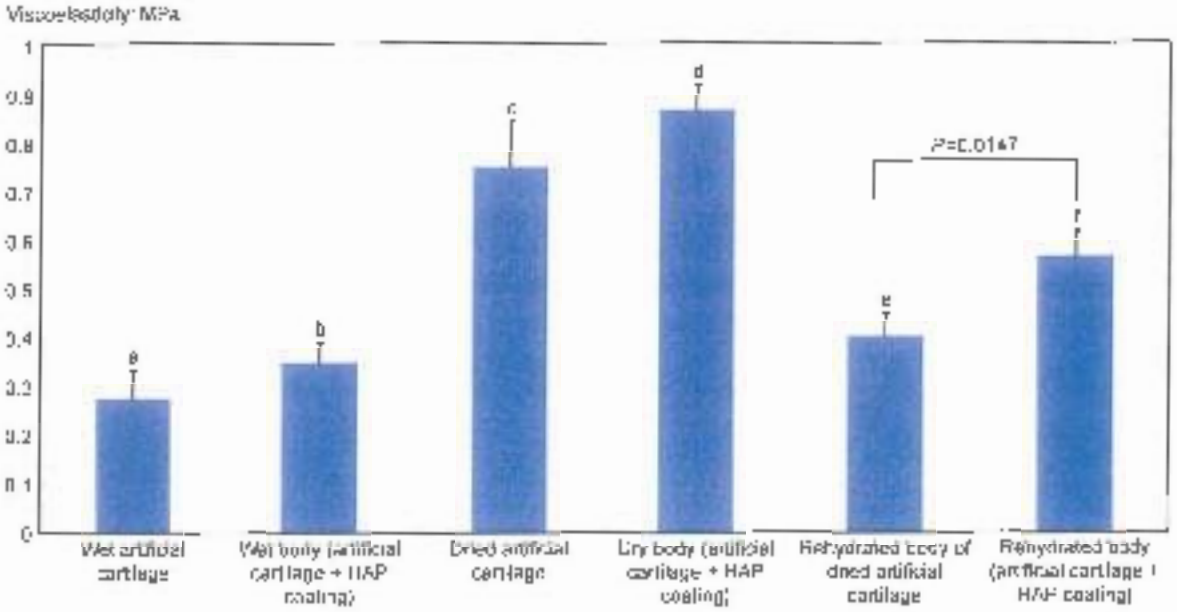

Figure 5 Viscoelasticity of self-organized biphasic cartilage and bone-like scaffolds.
Notes: Only the artificial cartilage and the HAP-coated cartilage were examined and compared in terms of viscoelasticity by applying a load. The groups of wet, dried and rehydrated. A significant difference between the two groups was observed also in rehydrated. Errors were significant. Differences in the viscoelasticity between two groups as following: a vs c: $P<0.05$, b vs d: $P<0.01$, a vs e: $P<0.05$, and b vs f: $P<0.01$.
Abbreviation: HAP, hydroxyapatite.

International Journal of Nanomedicine downloaded from https://www.dovepress.com/ by 202.219.58.3 on 22-Feb-2019
For personal use only.

Scaffold implantation into knee cartilage defects

In the preliminary experiments for the present study, we recognized the chondrogenic potential of self-organized cartilage-like scaffolds that were inoculated into the osteochondral defect of animals. The findings of SO-positive cytoplasmic staining in cells with rounded/spherodial morphology and typical cartilage lacuna formation indicated the chondrogenic activity of the scaffold in vivo (supplemental preliminary data). Based on these preliminary findings, we have designed the present in vivo study to evaluate the repair of osteochondral defect by the self-organized scaffold.

Life span of rats used for in vivo experiments is about 2–4 years. If converted to human life span, 1 year of rats' life span would be equivalent to 20–40 years in human. Therefore, it is thought that 4 and 8 weeks of rats may be equivalent to about 1.6–3 years and 4–6 years in human, respectively. From the point of view of clinical and physiological relevance, to evaluate whether the scaffold may have a useful tool for osteochondral tissue engineering, we think that 4 and 8 weeks as time points for the in vivo experiment are suitable for period of observation.

In every right knee joints, defects were filled with scar tissue and there were clefts between the scar tissue and the healthy surrounding cartilage tissue in both the 4- and 8-week observation groups. In contrast, in the left knee joints, the defect was filled with repair tissue that was similar to the surrounding cartilage tissue.

Sham-operated right knee joints (without implantation of scaffold)

In most sham-operated right knee joints, only fibrous scar tissue with hyperplasia of spindle-shaped fibroblastic cells was observed in the defect, with no regeneration of the cartilage tissue in either the 4- or the 8-week observation group (Figure 6A and B).

Scaffold-implanted left knee joints (4-week observation groups)

As shown in the representative images in Figure 6A, in the 4-week observation group, a stratiform cartilage-like structure with formation of cartilage cavities and the growth of chondrocytes was observed in the scaffold implantation hole, indicating initiation of cartilage regeneration induced by the implanted scaffold. In some implantation sites, there was a depression of the surface layer in the center of the drilled hole. Around this depressed surface layer, poor different stain of chondrocytes and a low level of SO-stained tissue, indicating the low level of proteoglycan production by chondrocytes, were observed.

The success rates of osteochondral tissue regeneration were 33% (1 of 3 knees) in the self-organized AG/HA/collagen complex-inoculated group, 50% (2 of 4 knees) in the self-assembled AG/HA/collagen complex–HAP powder (40 nm size) conjugate-inoculated group, 75% (3 of 4 knees) in the self-assembled AG/HA/collagen complex–HAP powder (5 μm size) conjugate-inoculated group and 100% (3 of 3 knees). 1 sample was broken in the self-assembled AG/HA/collagen complex–HAP block conjugate-implanted group.

Scaffold-implanted left knee joints (8-week observation groups)

As shown in the representative images in Figure 6B, in the 8-week observation group, the growth of chondrocytes, the formation of cartilage cavities and a stratiform cartilage-like structure were observed in the scaffold implantation hole, indicating initiation of osteochondral tissue regeneration induced by the implanted biomaterial.

The success rates of osteochondral tissue regeneration were 33% (1 of 3 knees) in the self-organized AG/HA/collagen complex-inoculated group, 75% (3 of 4 knees) in the self-assembled AG/HA/collagen complex–HAP powder (40 nm size) conjugate-inoculated group and 75% (3 of 4 knees) in the self-assembled AG/HA/collagen complex–HAP powder (5 μm size) conjugate-inoculated group. Unfortunately, when the tissue was cut into 6 μm sections, most of the HAP block parts were broken in the self-assembled AG/HA/collagen complex–HAP block conjugate-implanted group.

Histological assessment of osteochondral tissue regeneration

The histological quality of osteochondral tissue regeneration by scaffolds was evaluated by the ICRS II scoring system (Table 1). The ICRS II scoring system has the potential to evaluate both levels of ossification/calcification and subchondral abnormality as well as articular cartilage abnormality. A higher score in the ICRS II scoring system represents tissue better resembling healthy articular cartilage.

The 4-week observation groups

There was no significant difference in the ICRS II score between the control right knee group and the self-organized AG/HA/collagen complex-inoculated group (Figure 7A, a-b; $P>0.05$). In contrast, the scores of the self-assembled

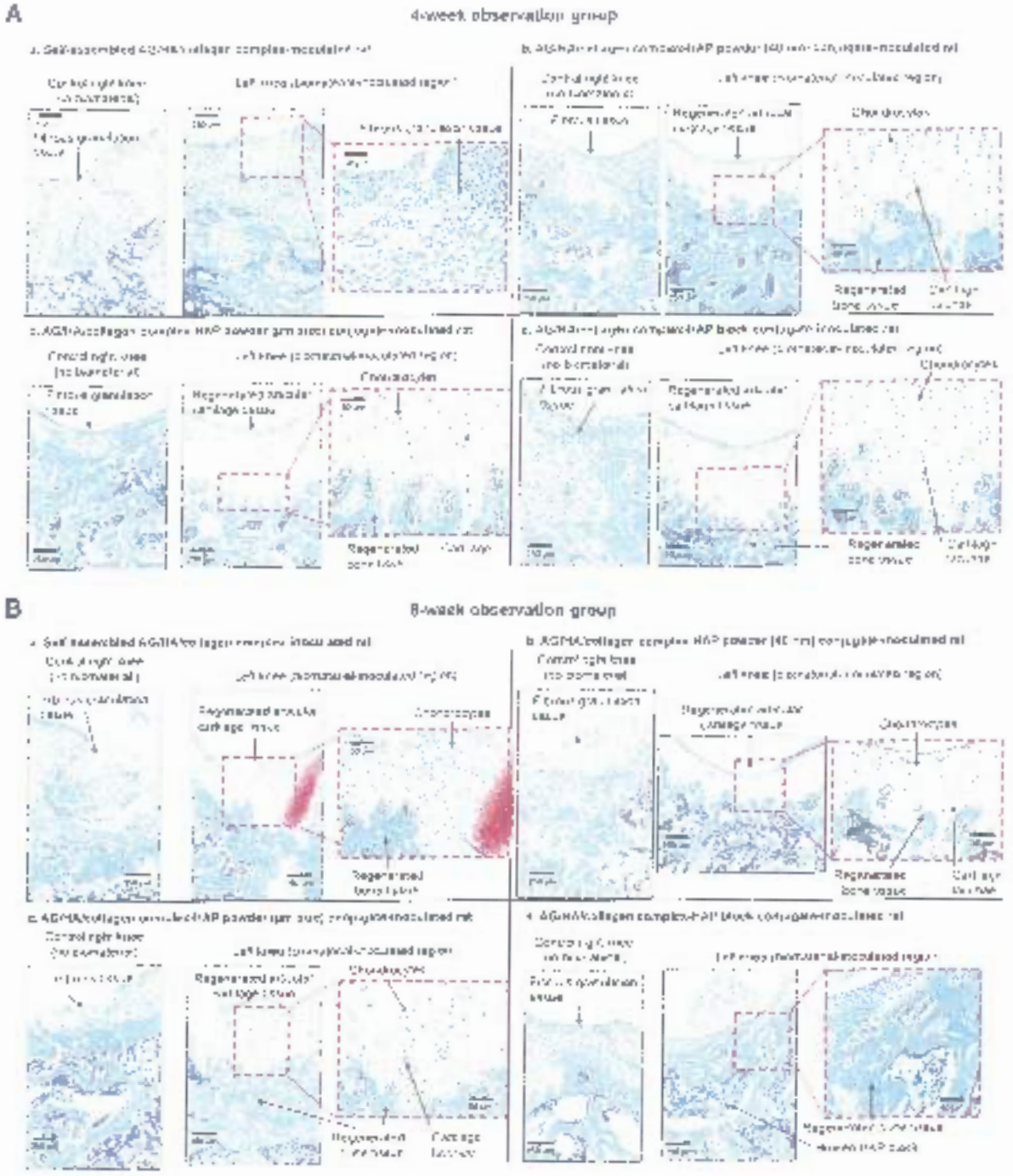

Figure 6 Sa[illegible] showing [illegible] of regenerated cartilage and [illegible] of bone [illegible] at 4 and 8 weeks after implant [illegible]
Note: (A) Representative images of [illegible] right knee joints of rabbits implanted [illegible] 4-week after implantation (control group, n = 3, and self-assembled group, n = 4). (B) Representative images of [illegible] right knee joints of rabbits implanted [illegible] 8-week after implantation (control group, n = 3, and self-assembled group, n = 4).
Abbreviations: AG, agarose; HA, hyaluronic acid; HAP, hydroxyapatite.

AG/HA/collagen complex-HAP powder (5 μm size) conjugate-inoculated group was significantly higher than that of the control right knee group (Figure 7A, [illegible] $P = 0.029$). There was a tendency to increase the mean IHKS II score of the self-assembled AG/HA/collagen complex-HAP powder (40 μm size) conjugate-inoculated group and the self-assembled AG/HA/collagen complex-HAP block conjugate-inoculated group in comparison with each control.

International Journal of Nanomedicine www.dovepress.com by 202.209.58.3 on 22-Feb-2019
For personal use only.

International Journal of Nanomedicine downloaded from https://www.dovepress.com/ by 202.209.61.3 on 22-Feb-2019
For personal use only

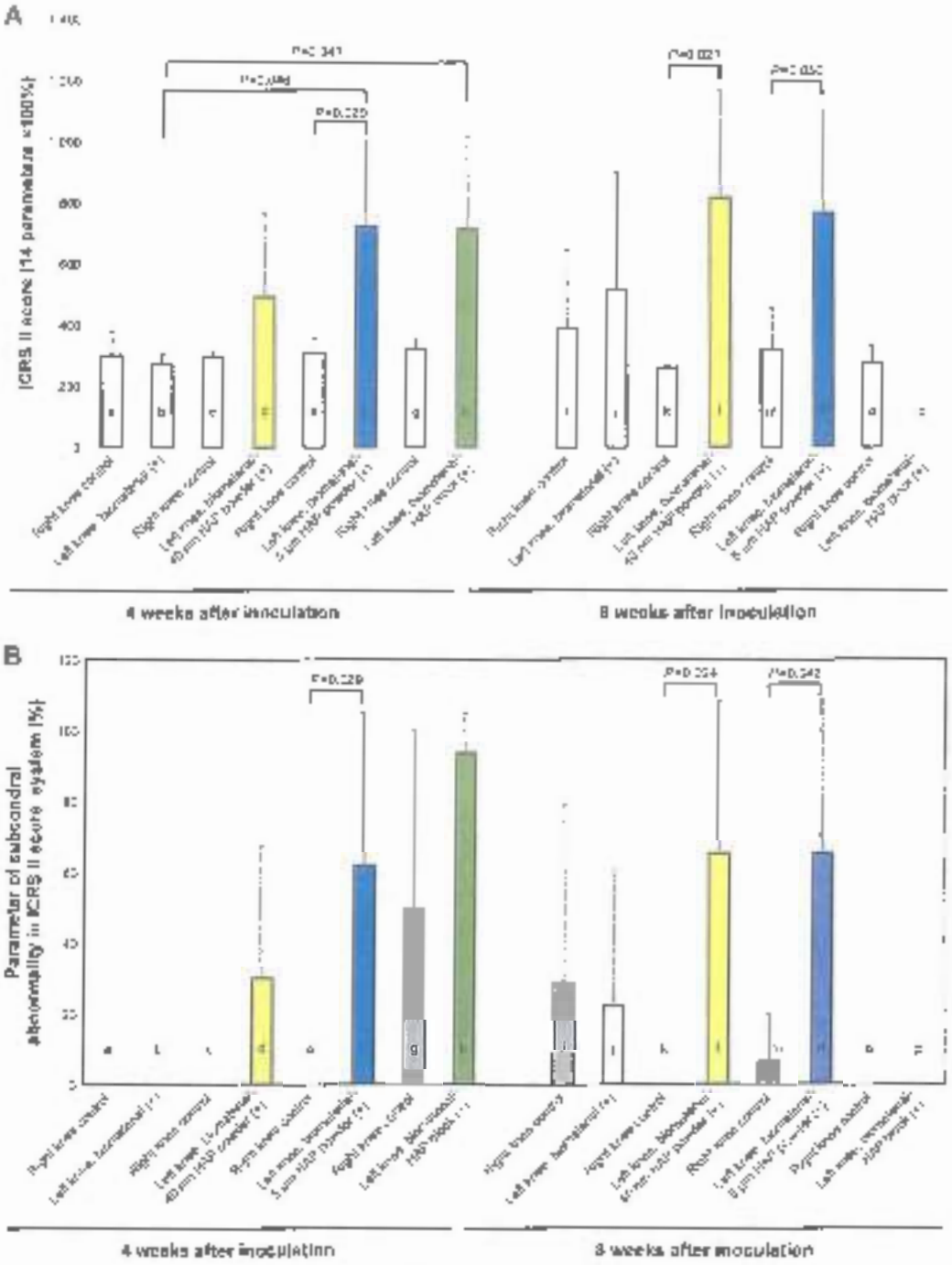

Figure 7 Histological assessment of cartilage regeneration by ICRS II scoring system.
Notes: (A) The histological quality of cartilage regeneration by scaffold was evaluated by the ICRS II scoring system (Table 1). A higher score in the ICRS II scoring system represents a more healthy articular cartilage (normal group = 3, scaffolds-inoculated group, n = 4) (B) Histological assessment of subchondral bone regeneration was evaluated using the subchondral abnormality of the ICRS II scoring system (normal group = 3, scaffolds-inoculated group, n = 4).
Abbreviations: HAP, hydroxyapatite; ICRS, International Cartilage Repair Society.

although no significant difference was found in the score between the scaffold-inoculated group and the control.

Among the four types of iron scaffolds, the self-assembled AG/HA-collagen complex HAP powder (5 μm size) conjugate-inoculated group and the self-assembled AG/HA-collagen complex HAP block conjugate-inoculated group were superior to the only self-assembled AG/HA-collagen complex-inoculated group in terms of the ICRS II score

International Journal of Nanomedicine downloaded from https://www.dovepress.com/ by 202.200.88.2 on 22-Feb-2019
For personal use only.

(Figure 7A, b vs f, $P=0.0046$, b vs n, $P=0.041$). The score of the self-assembled complex–HAP powder (40 nm size) conjugate-inoculated group was higher than that of the only self-assembled complex-inoculated group, although no significant difference was observed between the two groups (Figure 7A, b vs d, $P=0.252$).

The 8-week observation groups

There were significant differences in ICRS II score between the control right knee group and the self-organized AG/HA/collagen complex–HAP powder (40 nm size) conjugate-inoculated group (Figure 7A, k vs f, $P=0.021$). There was a tendency to increase the mean ICRS II score of the self-assembled AG/HA/collagen complex–HAP powder (5 μm size) conjugate-inoculated group in comparison with their respective controls (Figure 7A, m vs n, $P=0.051$). In contrast, no significant difference was observed in the score between the self-assembled AG/HA/collagen complex-inoculated group and the control (Figure 7A, l vs p, $P=0.645$). Regarding the self-organized AG/HA/collagen complex–HAP block, most of the HAP block parts were broken, while the scaffold-inoculated tissue was cut in 6 μm sections. Therefore, histological analysis by ICRSII score was not impossible in the self-organized AG/HA/collagen complex–HAP block (Figure 7B, p).

Among the three types of scaffolds (except for the self-organized AG/HA/collagen complex–HAP block), the mean ICRS II score of both self-assembled AG/HA/collagen complex–HAP powder conjugate-inoculated groups (40 nm and 5 μm powder sizes) was superior to the only self-assembled AG/HA/collagen complex-inoculated group, although no significant differences were observed between each scaffold-inoculated group and their respective control group (Figure 7A, j vs f, $P=0.330$, j vs n, $P=0.4856$).

Histological assessment of subchondral bone regeneration (using the parameter for subchondral abnormality in the ICRS II scoring system)

The histological quality of subchondral bone abnormality (bone marrow lesions in tissue regenerated by scaffolds was assessed using the parameter for evaluation of subchondral bone abnormalities in the ICRS II scoring system (Table 1, Histological parameter number 8). A higher score in this system indicates tissue resembling healthy subchondral bone.

In both the 4- and 8-week observation groups, most sham-operated right knee joints had a very low ICRS II mean score (Figure 7B, a, c, e, k and o; mean score 0%, g, i and m; mean score <30%, h; mean score 50%, l), indicating that the subchondral bone was not regenerated in control knees with no scaffolds.

Most of the knees implanted with the self-assembled AG/HA/collagen complex alone showed no regeneration of subchondral bone at either 4 or 8 weeks (Figure 7B, b and j). In contrast, the groups implanted with both self-organized AG/HA/collagen complex–HAP powder conjugates (both 40 nm and 5 μm powder size) showed significantly higher ICRS II scores in comparison with their respective controls at both 4 and 8 weeks (Figure 7B, e vs f, $P=0.029$, k vs l, $P=0.024$, m vs n, $P=0.042$, but not significant, o vs d, $P=0.158$).

The mean score of the self-assembled AG/HA/collagen complex–HAP block conjugate-inoculated group did show a tendency to increase in comparison with their respective controls, although no significant differences were observed between the self-assembled AG/HA/collagen complex–HAP block-implanted group and the control (Figure 7B, g vs h, $P=0.217$). Histological analysis by ICRSII score was not impossible in the self-organized AG/HA/collagen complex–HAP block, because of the breaking down of the inoculated tissue (Figure 7B, p).

Among the four types of scaffolds, both the self-assembled AG/HA/collagen complex–HAP powder conjugates (40 nm and 5 μm powder sizes) were superior to the self-assembled AG/HA/collagen complex alone in the mean score of parameter for subchondral abnormality at both 4 and 8 weeks (Figure 7B).

Discussion

OA is a common age-related disease with complex pathophysiology, in which the articular cartilage, the underlying bone and other joint tissues are altered.[34,35] Recently, the role of subchondral bone has attracted increasing interest for the pathogenic processes of osteoarticular joint damage in OA.[36–38] Subchondral bone is a complex structure with a subchondral plate and underlying trabeculae, which is biomechanically and biochemically connected to overlying cartilage.[39,40] The functional consistency of articular cartilage and subchondral bone are tightly connected.[41,42] During progression of OA, the subchondral bone is also damaged as well as the articular cartilage layer. Injuries of either tissue adversely affect the mechanical environment as well as the homeostatic balance of the entire joint, resulting in the development of OA (Figure 1).[43] Strong evidence has demonstrated that subchondral bone degeneration is associated with damage of articular cartilage in OA.[44,45] Therefore, tissue engineering approaches

for articular cartilage repair should be accompanied by an adequate restoration of the underlying subchondral bone.

In the present study, to clarify the chondrogenic and osteogenic potential of our scaffolds, we studied it using the osteochondral defect model of rat knee joints. Indeed, this animal model is not representative of osteoarthritic lesions (degenerations of articular cartilage and subchondral bone tissues). Further studies are needed to clarify whether our scaffolds may have the potential to treat the osteoarthritic lesion. Based on our results in the present study, we would like to expand the study for the potential application of the self-assembled scaffold for OA with subchondral bone degeneration as well as cartilage degeneration. If the scaffold may have the potential to repair the osteochondral defect (chondrogenic and osteogenic potentials), it might be a useful tool for osteochondral defect lesions, including severe OA with subchondral bone degeneration in addition to cartilage degeneration (supplemental preliminary data). We will study the potential of our scaffold using the OA animal model. In the present study, we demonstrate for the first time that it is possible to create a self-organized biphasic cartilage and bone-like scaffold combined with HAP to repair both the articular cartilage and the subchondral bone, with high performance as well as microstructures comparable to hyaline articular cartilage and subchondral bone.

Previously, we observed that the HA–AG/type II collagen self-organized complex consisted of 10–500 μm long (2–50 nm diameter) collagen fibers stabilized by HA. HA retains AG molecule in the matrix through specific protein–HA interactions. It is thought that HA forms a scaffold for binding large chondroitin sulfate proteoglycans (AG) in the articular cartilage tissue. HA with superior water-holding ability (2–6 L/g HA) keeps water in the articular cartilage (60%–70% of the wet weight of cartilage tissue).[26–28] Thus, in our study, we used HA as a component for the self-organized cartilage-like complex as well as AG and type II collagen. Our previous in vivo data revealed that the self-assembled AG/HA/collagen complex was able to induce regeneration of articular cartilage tissue by acting as a scaffold to maintain chondrocyte characteristics in the cartilage defect model.[1]

In the present study, we inoculated the self-organized complex with rat nasal cells (chondrocytes). The aim of our in vivo study was to clarify whether the self-organized complex without cell source can repair the degeneration of articular cartilage and subchondral bone (osteochondral defect). The results indicated that our self-organized biphasic cartilage and bone-like scaffold can induce cartilage and subchondral tissue regeneration in an in vivo osteochondral defect rat model (Figures 6–8). Of course, in this in vivo study, we analyzed whether chondrocytes can survive and maintain in the complex or not. As shown in Figure 2C, after incubation of our self-organized AG/HA/collagen complex with chondrocytes for 2 weeks, the chondrocytes, with cytoplasmatic extensions denominated the phylopodia, were homogeneously present on the scaffold of fibers forming the complex. The result from in vitro experiment showed that the complex was environment suitable for growth and survival of chondrocytes.

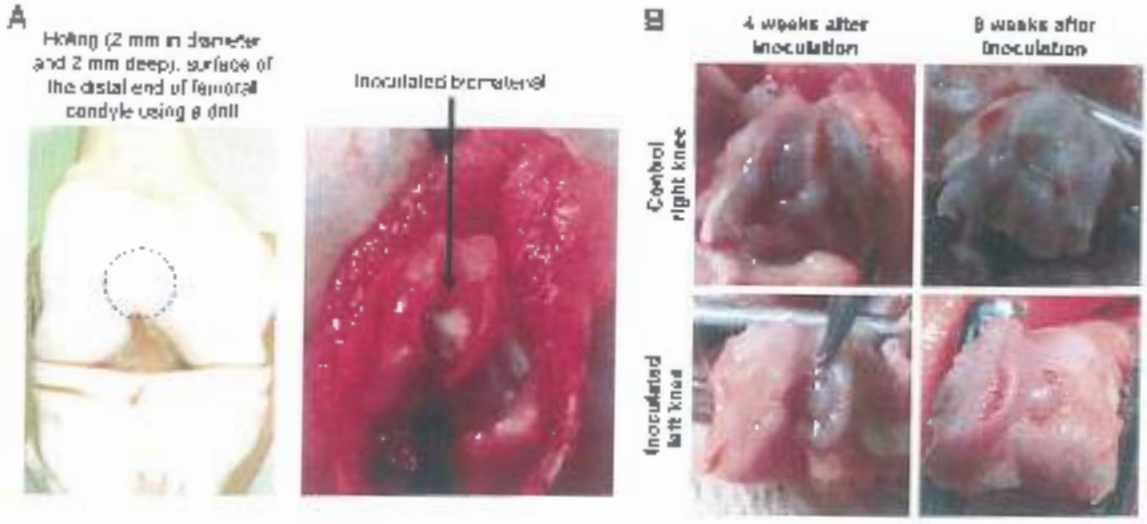

Figure 8 Implantation of self-organized scaffold for cartilage and subchondral bone tissue repair.
Notes: (A) Scanning electron images: creation of the defect (1 mm in diameter and 2 mm deep) in the center of the distal end of femoral condyle using a drill. Implantation of the scaffold for osteochondral tissue repair. (B) Histologic images of the other 4 and 8 weeks after implantation were compared between control and inoculated groups.

International Journal of Nanomedicine downloaded from https://www.dovepress.com/ by 202.208.48.3 on 22-Feb-2019
For personal use only.

International Journal of Nanomedicine downloaded from https://www.dovepress.com/ by 202.209.00.3 on 22-Feb-2013
For personal use only.

Numerous reports have already demonstrated that cartilage tissue engineering, which involves optimized combination of novel scaffolds, cell sources (mesenchymal stem cells, iPS cells) and growth factors, is a suitable therapeutic strategy for cartilage repair.[2,3,4] However, it remains unclear whether these self-organized scaffolds for cartilage repair have the potential to repair the degenerated subchondral bone in OA. In addition, our previous study did not test whether our previous scaffolds were able to induce regeneration of the subchondral bone layer in OA.[1]

In the current study, we have created three types of cartilage-like scaffolds combined with HAP, for osteochondral tissue engineering, which have been developed by combining self-assembled cartilage component molecules (AG/HA and type II collagen) and HAPs (40-nm powder size HAP [Figure 4B], 5 μm powder size HAP [Figure 4C] or an HAP block [Figure 2]) at the nanometer scale by non-polar interfacial interactions. As shown in Figure 3, both HAP powders with 40 nm and 5 μm diameter size were regularly bound to the self-organized AG/HA/collagen complex in the form of lamellae. We postulated that layered HAP on the self-organized scaffolds may induce not only cartilage tissue regeneration but also regeneration of the subchondral bone layer in a degenerated osteochondral lesion in the diseases with osteochondral defect. In the present study, histological evaluation, using a cartilage repair scoring system (ICRS II) indicates that the self-organized cartilage-like scaffolds conjugated with an HAP layer are superior to the self-organized cartilage-like scaffolds with no HAP in terms of cartilage regeneration, with new cartilage tissue resembling normal cartilage morphology with a healthy surface and mid-deep architecture and healthy chondrocyte morphology. In addition, evaluation of parameters of subchondral abnormality using the ICRS II scoring system revealed that the self-organized cartilage-like scaffolds conjugated to an HAP layer, but not the self-organized cartilage-like scaffolds without HAP, can induce regeneration of the subchondral bone layer comparable to normal subchondral bone tissue.

Our present study clearly provides evidence that the cartilage-like scaffold without conjugated HAP, is not enough to regenerate damaged subchondral bone tissue, which is functionally connected with articular cartilage. As mentioned earlier, our cartilage-like scaffold without HAP may have only weak potential to induce complete osteochondral tissue regeneration. Indeed, although the self-organized cartilage-like AG/HA/collagen complex alone (without HAP) showed a tendency to induce articular cartilage regeneration in vivo, even at 8 weeks after implantation, no significant difference in the ICRS II score for cartilage repair was observed between the groups implanted with the self-organized AG/HA/collagen complex and its control (Figure 7A). In contrast, the self-organized AG/HA/collagen complexes with an HAP layer were superior to the self-organized AG/HA/collagen complex alone without an HAP layer in terms of articular cartilage regeneration as well as subchondral bone regeneration (Figure 7A and 8). Unfortunately, when the tissue was cut into 6 μm sections, most of the HAP block parts were broken in the self-assembled AG/HA/collagen complex–HAP block conjugate-implanted group. Histological analysis by ICRS II score was not possible in the self-organized AG/HA/collagen complex–HAP block. Therefore, it still remains unknown which is superior in the scaffold with HAP powders and the scaffold with HAP block. Also, we have studied the level of osteoarthritis-calcification (parameter no. 10 in Table 1) of the scaffold-inoculated knee joints and the control knee joints. The level of the ossification-calcification was significantly lower in the scaffold-inoculated group than in each control (data not shown). Numerous reports and reviews have already demonstrated that biomaterials for cartilage repair are very usable for the intervention against cartilage defects.[1,6,7,8] However, there are few reports concerning whether biomaterials can induce regeneration following subchondral bone degeneration or not. Further studies are needed to verify the exact mechanism and process of cartilage regeneration by biomaterials. We would like to conclude that an HAP layer may be necessary for scaffolds to repair the degeneration of articular cartilage and subchondral bone tissues in OA.

The viscoelasticity of mature articular cartilage is known to be 1.0–3.0 MPa.[9] Regarding the viscoelasticity of our self-organized scaffold, the viscoelasticity of the complete dried scaffold (about 0.8–0.9 MPa) was higher than that of the original (~0.2 MPa). Interestingly, the viscoelasticity of rehydrated scaffold (~0.5–0.6 MPa) was significantly higher than that of the original, but its viscoelasticity was lower than that of the dried scaffold. We assumed a dried scaffold to be control of a wet scaffold. At a clinical place, it may be easy to sterilize a dried material in comparison with a wet material. We supposed that we could use the rehydrated complex from the sterilized and dried complex in clinic. Therefore, we analyzed three types of the self-organized complex (wet, dried and rehydrated complex) to obtain basic data of scaffolds. Although further studies are needed to clarify the usefulness of the rehydrated complex from dried one, a rehydrated complex may be useful as a scaffold for tissue engineering.

Since our self-organized scaffolds showed lower viscoelasticity in comparison with mature articular cartilage,

International Journal of Nanomedicine downloaded from https://www.dovepress.com/ by 202.208.68.3 on 22-Feb-2016
For personal use only.

Further studies are needed to improve the viscoelasticity of the self-organized cartilage-like scaffold. In the present study, viscoelasticity of the rehydrated self-assembled composite HAP powder conjugate was significantly higher than that of the original self-organized AG/HA/collagen complex. As shown in Figure 4, the viscoelasticity of the HAP-coated scaffold tended to increase in comparison with the original (HAP-uncoated) scaffold. This suggests that conjugation of the HAP with the self-organized cartilage-like material may induce improvements of its viscoelasticity. We have been investigating the development of scaffolds for cartilage repair, which can induce perfectly cartilage-specific tissue qualities represented by properties of high elasticity and high lubrication.

Conclusion

In the present study, we have newly created three types of self-organized biphasic cartilage and bone-like scaffolds combined with HAP, for cartilage tissue engineering, which have been developed through self-assembly of cartilage component molecules (HA, AG and type II collagen) and HAP alone, without other materials, such as cross-linking agents, at the nanometer scale by manipulating the intermolecular relations. Our *in vitro* and *in vivo* data reveal that self-organized biphasic cartilage and bone-like scaffolds conjugated to HAP are superior to the self-organized cartilage-like scaffold with no HAP in both cartilage regeneration and subchondral bone defects. Our present study indicates that the self-organized cartilage-like biomaterial, which is conjugated with an HAP layer, may have the potential to repair not only articular cartilage defects but also the degenerated subchondral bone in diseases with osteochondral defect.

Acknowledgments

This study was supported by JSPS KAKENHI Grant Number 26462125 from the Japan Society for the Promotion of Science (JSPS). We would like to thank M Suzuki, S Mogi, M Tanaka, J Tamate and J Niimi, R Kamisawa for excellent technical assistance.

Author contributions

All authors contributed to data analysis, drafting and revising the article, gave final approval of the version to be published, and agree to be accountable for all aspects of the work.

Disclosure

The authors report no conflicts of interest in this work.

References

1. Foster RL, Golding SR, Jenkins SCB, Gunning MB. Osteoarthritis: a disease of the joint as an organ. *Lancet*. 2012;64(6):1597–1599.
2. Mizuno K, Kamisawa R. A novel biomaterial for cartilage regeneration by self-assembly: preparation of a self-organized 3D cartilage-like tissue. *J Biomater Nanobiotechnol*. 2012;3(2):125–128.
3. Ludwigsen R. Tissue engineered osteochondral constructs in vivo models in cartilage repair. *Osteoarthritis Cartilage*. 2010;18(12):1635–1642.
4. Liu S, Qin L, Lin S, et al. PLGA-PEG-PLGA blm materials: cartilage tissue engineering in vivo. *Biomaterials*. 2011;32(31):7729–7739.
5. Sun Z, Li J, Cabe LR, Thomson M, Mikos AG. Effect of osteoblast attachment and proliferation on porous hydroxyapatite scaffolds fabricated with nanophase powder. *Int J Nanomedicine*. 2006;1(2):185–194.
6. Tang G, Liu Z, Wang J, Zhang Q, Wang Y. Development, characterization, and evaluation of porous carbonated hydroxyapatite bone cement. *J Biomed Mater Res B Appl Biomater*. 2009;90B(2):886–893.
7. Yang SR, Yang G, Singh P, Bhatnagar A. Ceramic and non-ceramic hydroxyapatite as a bone graft material: a brief review. *J Pak Med Sci*. 2015;31(1):201–206.
8. Fouad H, Al-Eshaer R, Abdo mah G, et al. Porous polyethylene coated with nanocomposite hydroxyapatite particles as a bone replacement material. *Materials*. 2015;8(6):3[illegible].
9. Newman AP. Articular cartilage repair. *Am J Sports Med*. 1998;26(2):309–324.
10. Gatt C, Sugaya K, Grigolo B. Review on the physical and chemical factors involved in tissue engineering of cartilage. *Biomed Eng Online*. 2005;4:65–67.
11. Correa CR, Rios RC, Mano JF. Multilayered, multicompartmental and hierarchical strategies for cartilage regeneration. *Adv Exp Med Biol*. 2015;881:145–160.
12. Kroksen G, Tingemann I, Lindegaard TC, et al. Autologous chondrocyte transplantation compared with microfracture in the knee. A randomized trial. *J Bone Joint Surg Br*. 2009;86-A(1):455–464.
13. Knutsen G, Drogset JO, Engebretsen L, et al. A randomized multicenter study comparing autologous chondrocyte implantation with microfracture: long-term follow-up at 14 to 15 years. *J Bone Joint Surg Am*. 2016;98(16):1332–1339.
14. Rai V, Dilisio MF, Dietz SE, Agrawal DK. Recent strategies in cartilage repair: a systematic review of the scaffold development and tissue engineering. *J Biomed Mater Res A*. 2017;105(8):2343–2354.
15. Grande DA, Pitman MI, Peterson L, Menche D, Klein M. The repair of experimentally produced defects in rabbit articular cartilage by autologous chondrocyte transplantation. *J Orthop Res*. 1989;7(1):18–28.
16. Brittberg M, Lindahl A, Nilsson A, Ohlsen C, Isaksson O, Peterson L. Treatment of deep cartilage defects in the knee with autologous chondrocyte transplantation. *N Engl J Med*. 1994;331(14):889–895.
17. Kawada K, Ochi M, Uchio Y, et al. Repair of articular cartilage defects with cultured chondrocytes in atelocollagen gel. Comparison with chondrocytes in suspension. *Arch Orthop Trauma Surg*. 2006;126(2):121–128.
18. Sato S, Ito K. Mesenchymal stem cell transplantation improves osteochondrogenesis. *J Bone Joint Surg Br*. 2011;93(4):406–410.
19. Yoshie T, Shimizu T, Cooper N, et al. Chondrogenic induction of intervertebral disc derivative cells from Wharton's jelly embedded in a gelatin hydrogel and without added growth factor: an alternative stem cell source for cartilage tissue engineering. *Stem Cell Rev Rep*. 2015;11(2):260.
20. Ueda K, Matsumura Y, Sato Y, et al. A novel cultured method for gastric investigation-fibroblasts. *Biosci Biotechnol Biochem*. 2011;75(4):409–412.
21. Gropp M, Sela S, Vainer G, et al. Standardization of the teratoma assay for analysis of pluripotency of human ES cells and biology of their differentiated progeny. *PLoS One*. 2012;7(8):e45332.
22. Gaude N, Kikuchi J, Gunchin G, et al. Lysine-specific demethylase 1 inhibition prevents teratoma development from induced pluripotent stem cells. *Oncotarget*. 2013;4(9):1456–1462.

23. [illegible] Zhang X, Kaufer Tsur M, [illegible] M K. [illegible] in the [illegible] of the pervasive [illegible] of [illegible] approaches. *J Orthop Res*. 2012;30(12):1969–1974.
24. [illegible] R, [illegible] A. Compositional [illegible] of [illegible] cartilage of human [illegible] joint: effects of [illegible] defects. *J Biomech*. 2009;42(15):2498–2504.
25. Gansell AP, Madry H, Kramer [illegible]. The subchondral bone in articular cartilage repair: current problems in the surgical management. *Knee Surg Sports Traumatol Arthrosc*. 2010;18(4):456–467.
26. Li G, Yin J, Gao J, et al. Subchondral bone in osteoarthritis: insight into risk factors and microstructural changes. *Arthritis Res Ther*. 2013;15(1):223.
27. Grynpas MD, Alpert B, Katz I, Lenmann I, Pritzker KP. Subchondral bone in osteoarthritis. *Calif Tissue Int*. 1991;49(1):20–26.
28. Sim S, Walsh DA. Osteochondral alterations in osteoarthritis. *Bone*. 2012;51(2):204–211.
29. Castañeda S, Abasolo I, Martínez-Calatrava MJ, Rodríguez-Merchán EC, Schwartz S. Subchondral bone as a key target for osteoarthritis treatment. *Biochem Pharmacol*. 2012;83(3):314–323.
30. Hatakeyama W, Taira M, Chosa N, Kihara H, Ishizaki A, Kondo H. Effects of apatite particle size in nanocrystalline collagen composites on the osteogenic differentiation ability of osteoblastic cells. *Int J Mol Med*. 2011;27(6):1255–1261.
31. Ikada K, Tabata M, Niwata I, Hattori M, Ishisaki A, Kondo H. Effects of addition of nano-hydroxyapatite to highly-purified collagen on osteogenic differentiation in osteoblastic SaOS-2 cells. *Nano Biomed*. 2016;8(2):91–106.
32. Lawrence JS. Osteoarthritis. In: Lawrence JS, editor. Rheumatism in Populations. London, UK: William Heinemann Medical Books; 1977. p. 154.
33. Brandt KD, Fife RS, Braunstein EM, Katz B. Radiographic grading of the severity of knee osteoarthritis: relation of the Kellgren and Lawrence grade to a grade based on joint space narrowing, and correlation with arthroscopic evidence of articular cartilage degeneration. *Arthritis Rheum*. 1991;34(11):1381–1386.
34. Yu N, Yeshua T, Gupta H, et al. The DNA transcriptome of the human osteoarthritic cartilage (APIX microarray) reveals the potential to recognize genes involved in cell and tissue growth, differentiation and chondrocyte aging in osteoarthritis. *J Rheumatol Res*. 2014;3(5):1921–1934.
35. Mainil-Varlet P, Aigner T, Durrer M, Nesic D, Knutsen G, Sandell D, Roberts S. A new histology scoring system for the assessment of the quality of human articular cartilage repair. *ICRS II*. *Osteoarthritis Cartilage*. 2010;18(5):689–698.
36. Rutgers M, van Pel MJ, Dhert WJ, Creemers LB, Saris DB. Evaluation of histological scoring systems for tissue-engineered, repaired and osteoarthritic cartilage. *Osteoarthritis Cartilage*. 2010;18(12):1–6.
37. Yudin K, Kurtz I, Yui N, Kawanishi K. Cartilage tissue engineering: a novel bioactive [illegible] for cartilage repair formulated by self-assembly [illegible] of self-organized artificial cartilage-like [illegible]. *Mol Tissue Engineering Mater Appl*. 2012;1(2):55–62.
38. Johnson VL, Hunter DJ. The epidemiology of osteoarthritis. *Best Pract Res Clin Rheumatol*. 2014;28(1):5–15.
39. Guilgenty YM, Allen KD, Jordan JM. Defining the burden of osteoarthritis in population-based surveys. *Arthritis Care Res*. 2016;68(12):1771–1779.
40. Hunter DJ, Bierma-Zeinstra SMA. Bone remodeling in osteoarthritis. *Nat Rev Rheumatol*. 2011;7(8):445–456.
41. Henrotin Y, Pesesse L, Sanchez C. Subchondral bone and osteoarthritis: biological and cellular aspects. *Osteoporosis Int*. 2012;23(Suppl 8):841–851.
42. Sharma AR, Jagga S, Lee SS, Nam JS. Interplay between cartilage and subchondral bone contributing to pathogenesis of osteoarthritis. *Int J Med Sci*. 2013;4(10):19563–19580.
43. Ciardelli G, Chiellini E, Vozzi G, Bonfiglio M, Giusti P, editors. Biomedical Materials and Tissue Engineering Applications of Polymer Composites. Boca Raton, FL: CRC Press LLC; 2011. p. 243–274.

International Journal of Nanomedicine Dove

Publish your work in this journal

The International Journal of Nanomedicine is an international, peer-reviewed journal focusing on the application of nanotechnology in diagnostics, therapeutics, and drug delivery systems throughout the biomedical field. This journal is indexed on PubMed Central, MedLine, CAS, SciSearch®, Current Contents®/Clinical Medicine, Journal Citation Reports/Science Edition, EMBase, Scopus and the Elsevier Bibliographic databases. The manuscript management system is completely online and includes a very quick and fair peer-review system, which is all easy to use. Visit http://www.dovepress.com/testimonials.php to read real quotes from published authors.

Submit your manuscript here: http://www.dovepress.com/international-journal-of-nanomedicine-journal

International Journal of Nanomedicine downloaded from https://www.dovepress.com/ by 202.209.09.3 on 22-Feb-2019
For personal use only.

原　著

関節リウマチ誌
Vol. 46, pp. 239-247, 2019

関節リウマチ由来滑膜線維芽細胞において炎症性サイトカインで誘導される細胞周期因子 Cyclin-Dependent Kinase 6

藤井 孝徳　　小松 架亜　　千本 久暁　　遠藤 宏樹

（受付：平成30年11月26日）

抄　録

滑膜細胞の異常増殖は関節リウマチ（RA）病態の本質の1つであるにもかかわらず，そのメカニズムには不明な点が多い．本研究ではRA滑膜線維芽細胞において炎症性サイトカインで誘導される細胞周期因子を同定するため，定量的リアルタイムPCR法を用いて遺伝子発現解析を行った．その結果，関節リウマチまたは変形性関節症患者由来の滑膜線維芽細胞においてインターロイキン（IL）-6ではなく，tumor necrosis factor（TNF）-αやIL-1βがG1期の細胞周期調節因子である cyclin-dependent kinase（CDK）-6の遺伝子発現を増強した．TNFα刺激によるCDK6遺伝子発現は，NFκBやAP1経路を介して誘導された．さらにTNFα で刺激したRA滑膜線維芽細胞の増殖は，サイクリンDのパートナーであるCDK6やCDK4をsiRNAにより抑制された．RA滑膜線維芽細胞においてCDK6の遺伝子発現は，TNFαによりNFκBやAP1経路を介して誘導される．CDK6の分子標的薬は，RA滑膜増殖を抑制し，炎症を慢性化する可能性が期待される．

索引用語
関節リウマチ，滑膜，TNFα，CDK6，サイトカイン

緒　言

炎症性サイトカインのTNFα，IL-1βやIL-6などは，生体内において様々な炎症症状をひき起こす因子として知られる[1]．特にTNFαやIL-6に対する抗体製剤は関節リウマチ（RA）を含む様々な慢性炎症の治療において著効をもたらしている[2]．しかしながら，これらの製剤でも臨床的改善が認められない患者も一定数存在し，そのような患者に対する新たな治療法が望まれている．

TNFαは二面性のあるサイトカインであり，その刺激により細胞死が誘導される場合と細胞増殖が誘導される場合があり，TNFαによる細胞増殖の誘導では，細胞内シグナル伝達経路としてAP1経路とNFκB経路が知られている．様々な種類の炎症刺激においてNFκBの活性が増強することが知られているが，少なくともその細胞増殖の一部においてTNFαの細胞増殖誘導作用が関与していることが報告されている[3]．例えば，一部のがん細胞ではTNFαがそのがん細胞増殖に関わり，細胞内ではその刺激によりcyclin-dependent kinase（CDK）4や CDK6の遺伝子発現が誘導されることが報告されている[4]．一方RA滑膜細胞ではTNFαがNFκB経路を介して細胞増殖を誘導することが報告されている[5]．ここで細胞周期のG1期因子，サイクリンDのパートナー

1 聖マリアンナ医科大学　難病治療研究センター
2 聖マリアンナ医科大学　整形外科学

であるキナーゼ，CDK4とCDK6はお互いに非常によく似た機能と構造を持つ因子である。それぞれ単独に欠損させたマウスはお互いに機能を補償するらしく正常に発育する。一方で，CDK4とCDK6の両方を欠損したマウスには骨髄発育が出産後まもなく停止し，血球減少がその原因の1つと考えられている。

我々はRAにおける滑膜細胞の異常増殖に着目し，その増殖に関与する新規因子synoviocyte proliferation-associated in collagen-induced arthritis (serum amyloid A-like 1 (SPACIA1/SAAL1)) を発掘した。そしてSPACIA1過剰発現マウスがRAの動物モデルであるコラーゲン誘導関節炎を増悪化し，滑膜細胞増殖のG1期の進行に関与することを報告した。またSPACIA1がG1期細胞周期因子であるCDK6の遺伝子発現に翻訳レベルで関与していることも報告した。SPACIA1はRA滑膜線維芽細胞において，TNFαなど炎症性サイトカインに誘導されることなく強発現し滑膜細胞増殖を促進している。このサイトカイン非依存的な滑膜細胞増殖を抑制することのRA治療における可能性を検証するためには，TNFαによる滑膜細胞増殖機構の分子機序との区別が重要であると考えるが，その分子機序についてまだ不明な点が多い。本研究では，RA滑膜細胞において炎症性サイトカインが遺伝子発現誘導する細胞周期因子を同定し，その細胞内シグナル伝達経路についても検証した。

実験対料および方法

1. 細胞・培養方法

東京女子医科大学倫理委員会の承認を受け（承認番号：1315），患者に説明して文書同意を受けた関節リウマチ（RA），および変形性関節症（OA）患者（各3名）から採取した滑膜組織をコラゲナーゼ処理した後，滑膜線維芽細胞を分離培養し継代3回以降8週までの細胞を用いた。ダルベッコ変法イーグル培地（シグマ・アルドリッチ，USA）に10%ウシ胎児血清（FBS）（Corning，USA），ペニシリン・ストレプトマイシン（ナカライテスク，京都）を加えた培地を用い，10cmディッシュ（コーニング，Germany）あたり1x10⁶細胞を播種して37℃で培養した。サイトカイン刺激実験（Figure 1）では細胞24時間前に培地交換し，1%FBS存在下で培養した。また炎症性サイトカインとしてTNFα（終濃度10ng/ml），IL-1β（終濃度10ng/ml），IL-6（終濃度5ng/ml）（共に

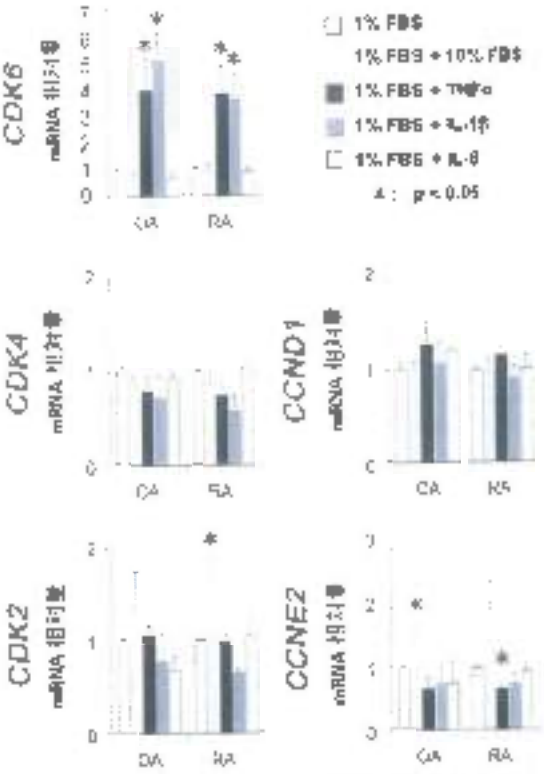

Figure 1.　炎症性サイトカインで刺激した滑膜線維芽細胞における G1 期細胞周期因子の遺伝子発現解析．関節リウマチ（RA）患者3例，変形性関節症（OA）患者3例から得た滑膜線維芽細胞を 1%FBS 存在下 24 時間培養した後，図示したサイトカインなどで 6 時間刺激し，cyclin-dependent kinase (CDK) 2，CDK4，CDK6，cyclin (CCN) D1，CCNE2 の各遺伝子発現量を定量的リアルタイム PCR 法にて定量した。RA，OA 各 3 例の平均値の無刺激対照（1%FBS）に対する相対量を棒グラフにした。＊は，無刺激対照に対する有意差（$p < 0.05$）を示す。1 項の実験を 3 回繰り返し同様の結果を得た。

ともシグマ・アルドリッチ，USA）を，シグナル伝達阻害剤として，NFκB 経路の IKK 阻害剤（BAY11-7082，メルク，Germany），AP1 経路の MEK 阻害剤（PD98059，和光純薬，大阪）と p38 MAPK 阻害剤（SB203580，メルク，Germany）を添加した。

2. 遺伝子発現解析

関節リウマチ，または変形性関節症患者由来の滑膜線維芽細胞を 1%FBS 存在下で 24 時間培養し各

受容性サイトカインを添加して37℃，5%培養培養した後，またはシグナル伝達阻害剤添加30分後にTNFαで刺激し，37℃，3時間培養した後，ISOGEN（ニッポンジーン，東京）を用いて全RNAを抽出した．全RNAから逆転写酵素（TOYOBO，大阪）を用いてcDNAを調整し，下記プライマーとABI 7500 Real-Time PCR System（Thermo Fisher Scientific，USA）を用いて定量的リアルタイムPCRを行った．ヒトGAPDH遺伝子は内部コントロールとして用いた．それぞれ2連で測定し，発現レベルは2$^{-\Delta\Delta Ct}$法で補正した．hCDK2, 5'-cuggagaagugggacggaac-3' (forward) and 5'-ggcucauguuggcuucugaga-3' (reverse) (151 bp), hCDK4, 5' (gcaagucggauguccugaguug-3' (forward) and 5'-gcucauggguucucucaac-3' (reverse) (144 bp), hCDK6, 5'-gcgucucaccugcaaaaac-3' (forward) and 5'-ccaugaccaucgaagacgugcc-3' (reverse) (117 bp), hCCND1, 5'-gcacctgtgcgaacatcatggg-3' (forward) and 5'-cagcacttcgacttcctcatg-3' (reverse) (173 bp), hCCND2, 5'-aggcaugugcacaccagaaga-3' (forward) and 5' gaaugggcagggcaucaucac-3' (reverse) (165 bp), hGAPDH, 5'-gcaccgtcaaggctgagaac-3' (forward) and 5' uggtggtgaagacgccagt-3' (reverse) (141 bp).

3. 組織免疫染色

関節リウマチ患者由来の滑膜線維芽細胞を10%ホルマリンで固定しパラフィン包埋した．5 μm厚の切パラフィン切片を10 mM Tris-HCl（pH 9.0），1 mMエチレンジアミン四酢酸緩衝液中，圧力鍋で3分間抗原賦活化を行った．賦活化した組織切片を5% goat serumで1時間ブロッキングした後，抗ヒトCDK6抗体（sc-177 ラビットポリクローナルIgG，Santa Cruz Biotechnology，USA）（2 μg/mL）または陰性対照としてウサギIgG（Santa Cruz Biotechnology，USA）（2 μg/mL）の溶液に1時間浸漬．洗浄後，Vectastain Elite ABC kit（Vector Laboratories Ltd，UK）とdiaminobenzidine（DAB）（シグマ・アルドリッチ，USA）で可視化した．比較対照としてヘマトキシリン・エオジン染色を行った．

4. siRNAを用いた遺伝子発現抑制実験

CDK6やCDK4に対するsiRNAを用いて各遺伝子の発現抑制実験を行った．RA滑膜線維芽細胞にCDK6 siRNA（Hs_CDK6_8290，シグマ・アルドリッチ，USA）または CDK4 siRNA（Hs_CDK4_2430，シグマ・アルドリッチ，USA），陰性対照としてmock siRNA（5'_UAACGCUAUGAAGAGAUAC_3'）をそれぞれOligofectamine（Invitrogen，USA）を用いてトランスフェクション後，72時間後に総タンパク質を抽出した．タンパク質抽出液を10%ポリアクリルアミドゲル電気泳動後，polyvinylidene difluoride（PVDF）膜へ転写し，10% スキムミルク（シグマ・アルドリッチ，USA）で30分ブロッキングした．抗ヒトCDK6抗体（sc-177 ラビットポリクローナルIgG，Santa Cruz Biotechnology，USA），抗ヒトCDK4抗体（C-8238 マウスモノクローナルIgG，シグマ・アルドリッチ，USA）と内部コントロールとして抗ヒトα-tubulin抗体（T-5168 マウスモノクローナルIgG，シグマ・アルドリッチ，USA）を用いてウエスタンブロッティングを行った．ホースラディッシュペルオキシダーゼを結合した二次抗体（シグマ・アルドリッチ，USA），イモビロン化学発光基質（メルクミリポア，Germany）と検出器（ImageQuant LAS 4000（GE ヘルスケア，USA））を用いた．検出された各タンパク質のバンド強度はNIH 画像解析ソフトImageJ 1.52aにて定量した．

5. 細胞増殖アッセイ

RA滑膜線維芽細胞増殖におけるCDK6の影響を調べるために，CDK6 siRNAと比較対照としてCDK4 siRNAとmock siRNAをRA滑膜線維芽細胞にそれぞれ2回トランスフェクションした．1回目のトランスフェクション後48時間後の各細胞を96well プレートに播種し，TNFα存在下または非存在下で1回目と同様のsiRNAを再びトランスフェクションした．その後72時間培養し，テトラゾリウム塩WST-8を発色基質とする細胞増殖アッセイキット Cell Counting Kit-8（同仁化学研究所，熊本）と吸光度計（バイオラッド，USA）を用い，450 nmの吸光度を細胞増殖活性として測定した．

6. 統計

患者間の個々の値を表す場合は，平均値±標準偏差で，同一検体の測定値を表す場合は平均値±標準誤差で表した．統計処理にはWilcoxon's signed-rank testを用い，p値は0.05以下を有意とみなした．統計ソフトには JMP 12（SAS Institute Inc.，USA）を用いた．

結　果

1. 炎症性サイトカインにより発現誘導される G1 期細胞周期因子

変形性ひざ関節症患者と変形性関節症患者，それぞれ 3 例から得た滑膜線維芽細胞を 1%FBS 存在下 24 時間培養し，炎症性サイトカインとして TNFα，IL-1β，IL-6 と比較対照として 10% FBS をそれぞれ添加して 6 時間刺激し，Figure 1 に示した G1 期の細胞周期因子について遺伝子発現誘導を観察した．各患者から得た細胞間で結果に大きな違いはなく，OA と RA に分けて刺激（1%FBS 培養）の mRNA 量に対する生成量を各 3 例の平均値としてグラフに示した（Figure 1）．刺激に対してサイクリン D のパートナーであるキナーゼ CDK6 の mRNA 相対量は 10%FBS や IL-6 刺激では変化が認められなかったが，TNFα 刺激では OA で 3.9 倍，RA で 2.8 倍，IL-1β 刺激では OA で 5.0 倍，RA で 5.6 倍と，有意に増加した．一方，サイクリン D1（CCND1）や CDK4 ではいずれの刺激でも mRNA 量に有意な変化は認められなかった．CDK2 mRNA 相対量は RA 滑膜線維芽細胞においてのみ，比較対照の 10%FBS 刺激で 1.7 倍に有意に増加した．サイクリン E2（CCNE2）mRNA 相対量は，OA 滑膜線維芽細胞において 10%FBS 刺激により 1.5 倍に増加し，RA 滑膜線維芽細胞においては TNFα 刺激で 34% 有意に減少した．炎症性サイトカイン刺激で mRNA 発現量が有意に増加したのは CDK6 のみであった．また，TNFα と IL-1β の刺激による CDK6 の発現増強において RA と OA 滑膜線維芽細胞間で差異は認められなかった．そのため以後の実験では RA 滑膜線維芽細胞のみを用いた．

2. RA 滑膜線維芽細胞における TNFα 刺激の細胞内シグナル伝達経路

TNFα 刺激の下流細胞内シグナル伝達経路である NFκB 経路と AP1 経路について，それぞれに関する阻害剤の作用を RA 滑膜線維芽細胞の CDK6 遺伝子発現において観察した．NFκB 経路では，1 または 10 μM の IKK 阻害剤（BAY11-7082），AP1 経路では 10 または 50 μM の MEK 阻害剤（PD98059）を 1 または 10 μM の p38 MAPK 阻害剤（SB203580）を用いた（Figure 2）．その結果，10 μM の IKK 阻害剤により NFκB 経路が阻害されると TNFα で誘導された CDK6 mRNA 発現量は 50% 減少し，TNFα 誘導前の状態（無刺激状態）近くまで減少した．また 50 μM の MEK 阻害剤により AP1 経路が阻害され，TNFα で誘導された CDK6 mRNA 発現量は 30% 減少した．

一方，p38 MAPK 阻害剤では CDK6 mRNA 発現に対して抑制効果は認められなかった．p38 MAPK 阻害剤の有効性については，今回試した濃度において TNFα 刺激に対する IL-8 mRNA 発現誘導を十分に阻害することを RA 滑膜線維芽細胞で確認した（データ掲載）．TNFα 刺激による CDK6 遺伝子発現誘導は，RA 滑膜線維芽細胞において NFκB 経路と，部分的に MEK を介した AP1 経路が関与していると考えられたが，p38 MAPK 経路の関与は認められなかった．

3. RA 滑膜組織における CDK6 の発現

RA 滑膜線維芽細胞において TNFα 刺激による

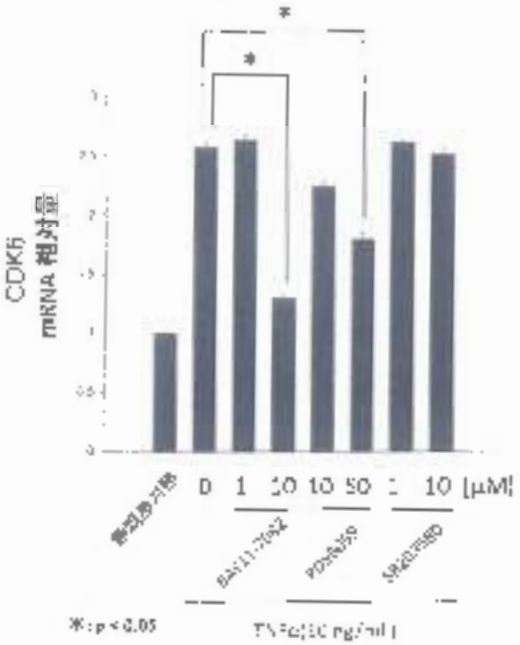

Figure 2. RA 滑膜線維芽細胞における TNFα 誘導性 CDK6 遺伝子発現のシグナル伝達経路．
RA 滑膜線維芽細胞を NFκB 経路阻害剤 "BAY11-7082"，2 種の AP1 経路阻害剤 "PD98059" MEK 阻害剤，"SB203580" p38 MAPK 阻害剤を添加 30 分後に TNFα で 3 時間刺激し，CDK6 mRNA 量を定量した．各群 2 検体測定し，その平均値の無刺激対照に対する相対量を縦軸にとりグラフにした．"*" は，有意差（p < 0.05）を示す．同様の実験を 3 回繰り返し，同様の結果を得た．

CDK5 遺伝子発現誘導に用いられなかったため，実験にヒトの RA 滑膜組織において CDK6 タンパク質の発現を確認した．RA 滑膜組織の連続切片を用いて，抗 CDK6 抗体（anti-CDK6）と陰性対照としてラビット IgG（rabbit IgG）による免疫染色後，またヘマトキシリン・エオジン染色像（HE）を Figure 3 に示した．その結果，細胞表層の滑膜過形成部位において，CDK6 タンパク質の存在を示す陽性が観察され，RA 滑膜組織における CDK6 タンパク質の発現が示された．

4. RA 滑膜線維芽細胞の増殖における CDK6 と CDK4 の発現抑制

CDK6 の RA 滑膜線維芽細胞増殖における関与を調べるため，CDK6 に対する siRNA を用いて増殖アッセイを行った．比較対照として mock siRNA と，CDK6 とよく似た機能と構造を持つ CDK4 の siRNA を用いた．CDK6 に対する siRNA も CDK4 に対する siRNA もそれぞれ特異的に各因子のタンパク質発現量を抑制することをウエスタンブロッティング法により確認した（Figure 4A）．mRNA 発現レベルでは，それぞれの siRNA により CDK6 mRNA が 35%，CDK4 mRNA が 67% 発現抑制されたが，コントロールに対し，タンパク発現レベルでは CDK6 タンパクが 2 割，CDK4 タンパク質が 5 割発現抑制された．10% FBS を含む通常の培養条件下では mock siRNA に対して CDK6 siRNA で 9.5%，CDK4 siRNA で 24% の増殖抑制傾向をみたが有意差は認

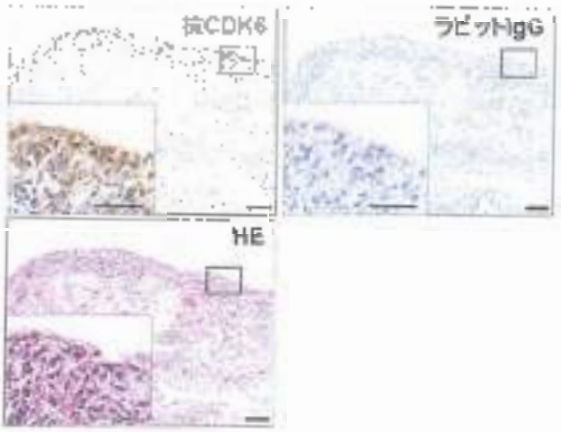

Figure 3.　ヒト RA 滑膜における CDK6 の発現
マウス抗ヒト CDK6 抗体（anti-CDK6）を用いて RA 滑膜組織の免疫染色をおこなった．CDK6 陽性細胞は茶色に染色されている．連続切片を用いた比較対照としてラビット IgG とヘマトキシリン・エオジン染色（HE）を示す．倍率は 40 倍とし角の部分を 200 倍で拡大表示した．スケールバーはそれぞれ 100 μm と 50 μm を示す．実験はヒト滑膜 3 例を用いて独立した実験の結果が得られた．その内の 1 例を示した．

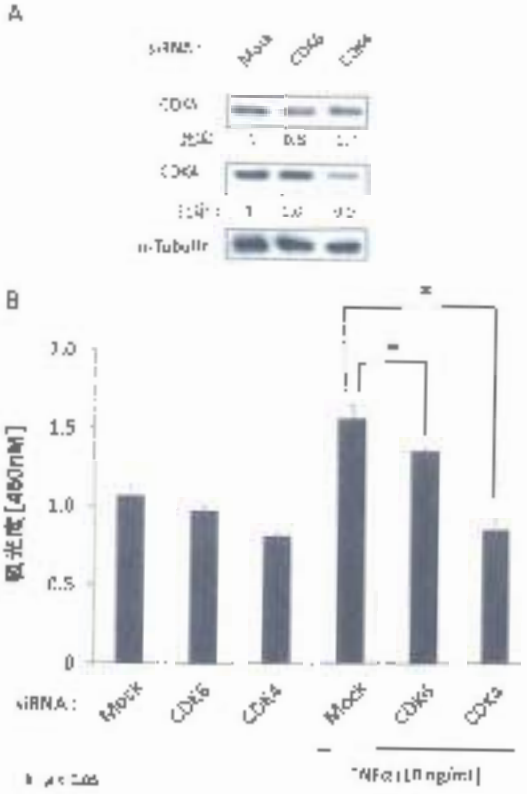

Figure 4.　RA 滑膜線維芽細胞増殖における CDK6，CDK4 発現抑制の影響．
A: CDK6 と CDK4 に対する siRNA の効果をウエスタンブロッティング法により調べた．内部対照として α-Tubulin を用いた．Mock siRNA のバンド強度を 1 として，α-Tubulin のバンド強度で補正した比率をその下に示した．B: TNFα 非存在下，上段は平均 ± SD，CDK6 または CDK4 に対する siRNA を用いて各遺伝子の発現抑制が RA 滑膜線維芽細胞の増殖に及ぼす影響を調べた．細胞増殖活性は市販のキットを用いて 450 nM の吸光度として測定した．各群 6 回で測定し，その平均値 ± 標準誤差をグラフに示した．*は，図示した 2 群間の有意差 $P < 0.05$ を示す．実験を 3 回繰り返した同様の結果を得た．

められなかった。一方，TNFα刺激下の細胞増殖では CDK6 siRNA で 15%，CDK4 siRNA で 46%の有意な増殖抑制を示した（Figure 4B）。CDK6 が TNFα 刺激下の RA 滑膜線維芽細胞増殖に寄与していることが示された。また CDK4 も同増殖に寄与していた。

考　察

本研究の結果，関節リウマチを慢性炎症患者由来の滑膜線維芽細胞において TNFα や IL-1β といった NFκB 経路や AP1 経路を活性化する炎症性サイトカインが G1 期の細胞周期因子である CDK6 の遺伝子発現を増進すること，また CDK6 が TNFα 刺激下の RA 滑膜線維芽細胞増殖に寄与していることが明らかとなった。一方，主に Janus kinase/Signal transducers and activators of transcription（JAK/STAT）経路を活性化する IL-6 の刺激によって，今回調べた G1 期細胞周期因子の中に遺伝子発現を増強するものは認められなかった。これらの結果からはリウマチ薬である TNFα 阻害薬と IL-6 阻害薬は異なる炎症経路を標的としていることが考えられた。

RT-PCR 実験（Figure 2）より，TNFα 刺激による CDK6 遺伝子発現誘導は，RA 滑膜線維芽細胞においてさらに NFκB 経路と一部 MEK を介した AP1 経路の両経路を経由していると考えられた。ところで p38 MAPK 阻害剤は炎症反応として強力な効果が期待されながら奏効していないが，本研究で TNFα 刺激した RA 滑膜線維芽細胞の CDK6 遺伝子発現誘導においても，p38 MAPK を介した AP1 経路は関与を示さなかった。p38 MAPK 選択的抗炎症作用を十分に発揮できない一面を反映した結果であるかもしれない。

我々は RA 滑膜線維芽細胞において sPACIA1 が CDK6 遺伝子発現に転写レベルで関わっていることを既に報告しているが，TNFα 刺激による誘導された CDK6 遺伝子発現においても SPACIA1 の siRNA により CDK6 mRNA 発現量は有意に減少した（データ不掲載）。SPACIA1 は TNFα など炎症性サイトカインで誘導されないため，TNFα は転写レベルで，SPACIA1 は翻訳レベルで，異なる経路から CDK6 の遺伝子発現を制御している可能性が考えられた。

一連のがん結果，例えば乳がんの MCF7 細胞では，炎症性サイトカインである TNFα の刺激により CDK6 と CDK4 の両者を強力に遺伝子発現誘導し，がん細胞増殖を実現する。CDK4 と CDK6 は非常によく似た機能と構造を有する分子であり，おそらくお互いを補償する関係にある。それぞれの欠損マウスは非常に活発，発育するが，両者を同時に欠損したマウスは胚性致死か出産後まもなく死亡する。死因は造血機能の低下によるものと考えられている。また CDK4 と CDK6 の両者を標的とするキナーゼ阻害剤は抗リウマチ薬として期待されているが，これを実験に用いるとマウスにおいて血球数減少をもたらすことが報告されている[illegible]。本研究の結果より，滑膜線維芽細胞は乳がんの MCF7 細胞とは異なり，TNFα の刺激により CDK6 のみ遺伝子発現誘導され CDK4 は誘導されない。炎症により促進される滑膜線維芽細胞の増殖は，がん細胞の増殖とは異なる重要な点であるかもしれない。一方，培養条件下での RA 滑膜線維芽細胞増殖において CDK6，CDK4 の遺伝子発現をそれぞれ抑制したところ，両者で細胞増殖抑制が観察された。CDK6 と CDK4 に対する siRNA はどちらも mRNA レベルで 7 割程度の遺伝子発現抑制効果を示したが，タンパク質レベルでは CDK4 タンパク質が 50%減少したのに対して，CDK6 タンパク質は 20%しか減少しなかった。結果的に CDK4 siRNA の方がより強く細胞増殖を抑制したが，これは単に両遺伝子のタンパク質レベルの減少量の差を反映しているだけかもしれない。少なくとも培養条件下の RA 滑膜線維芽細胞では CDK4 は炎症性サイトカインで誘導されずに恒常的に発現しているのかもしれない。一方，CDK6 は誘導的な因子であり両者とも細胞増殖に寄与していることが示された。

実際リウマチ患者由来の滑膜組織に CDK4 が発現していることが報告されており，また本研究により，同じく CDK6 の発現も示された。RA をはじめとする炎症において重要なサイトカインである TNFα の刺激により滑膜線維芽細胞では CDK4 ではなく CDK6 が遺伝子発現誘導されることが明らかとなった。また本研究の CDK6 の発現は TNFα とは異なる経路と考えられる SPACIA1 によっても転写されている。よって TNFα 阻害薬のみでは十分に抑制できない可能性がある。選択的に CDK4 と CDK6 の両者を標的としてしまうキナーゼ阻害剤ではなく，CDK6 のみを標的とした阻害薬が滑膜線維芽細胞の増殖を抑えることができれば，RA 治療において血球減少などの

[illegible]

謝　辞

本研究は JSPS 科研費基盤研究 (C)(JP25461490, JP22591088), 若手研究 (B)(JP24791069), MEXT 科研費基盤研究戦略的研究基盤形成支援事業 JPS15P12060 の助成を受けたものです。本研究に尽力して下さった，佐藤雅子氏，田中愛美氏，上手純子氏をはじめとする皆様に深謝いたします。

文　献

1) 香月裕，炎症性疾患に関わる腫瘍壊死因子 (TNF) の産生・受容，日本薬理学雑誌 2006; 127: 163–175.

2) 石野清剛夫，インターロイキン 1：細胞消滅制御から慢性炎症性疾患まで，YAKUGAKU ZASSHI 2013; 133: 645–660.

3) 山人豊，リウマチ性疾患における生物学的製剤の進歩，臨床リウマチ 2016; 28: 97–105.

4) 今村孔子，西本憲弘，生物学的製剤の使い分け，臨床リウマチ 2008; 20: 13–18.

5) van Horssen R1, Ten Hagen TL, Eggermont AM. TNFa-pha in cancer treatment: molecular insights, antitumor effects, and clinical utility. Oncologist 2006; 11: 397–408.

6) 河野新弘，佐野・アトピー性皮膚炎と炎症 受容体をミナリウム 第66回 皮膚と炎症 2010; 120: 2175–2180.

7) Wu X, Wu MY, Jiang M, Zhi Q, Bian X, Xu MD, Gong FR, Hou J, Tao M, Shen LM, Duan W, Chen K, Shen M, Li W. TNFa sensitizes chemotherapy and radiotherapy against breast cancer cells. Cancer Cell Int 2017; 17: 13.

8) Yoon J, Kim HY, Park IH, Hwang SH, Lee SY, Cho CS, Lee SK. Regulation of TNF-alpha-mediated hyperplasia through TNF receptors, TRAFs, and NF kappaB in synoviocytes obtained from patients with rheumatoid arthritis. Immunol Lett 2007; 83: 85–93.

9) Malumbres M, Sotillo R, Santamaria D, Galán J, Cerezo A, Ortega S, Dubus P, Barbacid M. Mammalian cells cycle without the D-type cyclin-dependent kinases Cdk4 and Cdk6. Cell 2004; 118: 493–504.

10) Sato T, Fujii R, Kenoye K, Yagishita N, Aratani S, Araya N, Aono H, Yudoh K, Suzuki N, Beppu M, Yamano Y, Nishioka K, Nakajima T. Overexpression of SPACIA1/SAAL1, a newly identified gene that is involved in synoviocyte proliferation, accelerates the progression of synovitis in mice and humans. Arthritis Rheum 2011; 63: 3833–3842.

11) Fujii R, Kouatsu R, Sato T, Seki T, Koromi K, Aono H, Nita H, Yudoh K, Nishioka K, Nakajima T. SPACIA1/SAAL1 Deletion Results in a Moderate Delay in Collagen-Induced Arthritis Activity, along with mRNA Decay of Cyclin-dependent Kinase 6 Gene. Int J Mol Sci 2018; 19: 3928.

12) Izumi T, Fujii R, Izumi T, Nakazawa M, Yagishita N, Tsuchimochi K, Yamano Y, Sato T, Iputa H, Aratani S, Araya N, Azokami K, Hasegawa D, Kasaoka S, Tsuruta R, Yokouti M, Iori K, Beppu M, Maruyama I, Nishioka K, Maekawa T, Koeniya S, Nakajima T. Activation of synoviolin promoter in rheumatoid synovial cells by a novel transcription complex of interleukin enhancer binding factor 3 and GA binding protein alpha. Arthritis Rheum 2008; 60: 63–72.

13) Sweeney SE. The as-yet unfulfilled promise of p38 MAPK inhibitors. Nature Reviews Rheumatology 2009; 5: 475–477.

14) Hosoya T, Iwai H, Yamaguchi Y, Kawakata K, Miyasaka N, Kohsaka H. Cell cycle regulation therapy combined with cytokine blockade enhances antiarthritic effects without increasing immune suppression. Ann Rheum Dis 2016; 75: 254–259.

15) Sekine C, Sugihara T, Miyake S, Hirai H, Yoshida M, Miyazaki N, Kohsaka H. Successful treatment of animal models of rheumatoid arthritis with small-molecule cyclin-dependent kinase inhibitors. J Immunol 2008; 180: 1954–1961.

16) Nozumura YI, Kohsaka H, Nagasaka K, Miyasaka N. Gene transfer of a cell cycle modulator exerts anti-inflammatory effects in the treatment

of arteries. J Immunol 2003; 171: 4913–4919.

Abstract

Pro-inflammatory Cytokines Elicit the Expression of Cell Cycle Regulator Cyclin-Dependent Kinase 6 in Rheumatoid Arthritis Synovial Fibroblasts

Ryoji Fujii[1], Rie Komatsu[1], Hisateru Niki[2], and Kazuo Yudoh[1]

Abnormal synovial proliferation is one of the major characteristics of rheumatoid arthritis (RA). However, the molecular mechanisms behind this process are still unclear. In this study, analysis of gene expression by quantitative real time-PCR was performed to identify cell cycle regulators whose expression is induced by pro-inflammatory cytokines in RA and osteoarthritis synovial fibroblasts. Stimulation with tumor necrosis factor (TNF) α or interleukin (IL) 1β, but not IL-6, induced gene expression of the cell cycle regulator cyclin-dependent kinase (CDK) 6 in RA and osteoarthritis synovial fibroblasts. TNFα mediated CDK6 gene expression through both the NFκB and AP1 pathways. Furthermore, TNFα-stimulated proliferation of cultured RA synovial fibroblasts was inhibited by siRNA for CDK6 or CDK4, both of which are D-type cyclin partners. The expression of CDK6 is induced by TNFα through both the NFκB and AP1 pathways in RA synovial fibroblasts, suggesting that anti-CDK6 drugs might exert therapeutic benefits in RA.

1 Institute of Medical Science, St. Marianna University School of Medicine
2 Department of Orthopedic Surgery, St. Marianna University School of Medicine

2015年度
平成27年度

難治性疾患病態制御学

著書

1) 遠藤和雄　変形性関節症(Osteoarthritis)は[illegible]症状の[illegible]の解釈　[illegible]日医学[illegible]　[illegible]　2016.02 27.

学術論文[和文]

(1) 原著

1) 古見[illegible]　[illegible]　[illegible]　[illegible]　[illegible]　遠藤和雄　関節リウマチ患者の関節炎に対するトシリズマブ[illegible]の有効性評価　[illegible]　2015.04 44

(2) [illegible]

1) 遠藤和雄　[illegible]　[illegible]　[illegible]　2015.(Feb)　13 31

2) 遠藤和雄　[illegible]　SBO　[illegible]　2015.(SPO)　93 95

学術論文[英文]

(1) 原著

1) Yuki K, Kawasaki H, Ishikawa J.. Age related increase of tiptoe 7 in peripheral blood mononuclear cells in human. Curr Aging Sci. 2015.4(3). 236 238.

2) Yui Sawa, Yoshiaki Hirotaka, Fujiya Hirata, Masha Hatoki, Kawasaki Rio, Yudch Kazuo. WATER SOLUBLE CEO COMPLEX FULLERENE AMINOSIDE AS A THERAPEUTIC AGENT AGAINST THE DEGENERATION OF ARTICULAR CARTILAGE IN OSTEOARTHRITIS. Osteoarthritis and Cartilage. 2017.12(2). 164 165.

3) Jun Shimizu, Hiroshi Oka, Yoshiaki Tanaka, Kazuo Sudoh, Nobuo Suzuki. Outcomes and complications of patients with collapsing polyarthritis associated with extraarticular complications. Clin. Rheumatol. . 2015.35(7). 781 786.

4) Yui Sawa, Yudch Sada. Tomiya Hirota, Masha Hatoki. Mechanical and oxidative stress in osteoarthritis. Journal of Physical Fitness and Sports Medicine. 2016.5(1). 51 56.

5) Jun Shimizu, Hiroshi Oka, Yoshiaki Tanaka, Kazuo Sudoh, Nobuo Suzuki. Earlier development in collapsing polychondritis in Japan. Rheumatology International. 2016.37(3). 395 404.

学会発表

(1) 国内学会

1) 金子[illegible]　[illegible]　[illegible]　遠藤和雄　[illegible]　[illegible]　[illegible]　[illegible]　[illegible]　遠藤和雄　[illegible]　[illegible]　[illegible]　[illegible]　[illegible]

48 [illegible] S. Musha P. [illegible] H. [illegible] E. [illegible] H. [illegible] K. [illegible] K. [illegible] Signification of Defective Mechanisms for Oxidative DNA Damage [illegible] Oxidative Stress [illegible] DNA Repair Enzyme. [illegible] Enzymologia [illegible] Fisetin Against the Catabolism of Articular Cartilage [illegible] 15th International Conference on [illegible] Antioxidants. 2016.

49 [illegible] Kaneko, Yuyumi Tanaka, [illegible] Chen, [illegible] Zhang, Kenko Yudai, [illegible] S. [illegible] Identification of target antigens for anti-endothelial cell antibodies in patients with pediatric rheumatic diseases using proteomics. American College of Rheumatology, 2013.

50 [illegible] Ryoji [illegible], Ikuo Sato, Kiyo Komatsu, [illegible], [illegible] Schaya, Tomo Sato, Seiji Kawai, Hiroyuki Sano, Sayuri Tsuchi, Kazuki Shirotoki, Tadashi Saegusa. SPECIAL AAMI Delivery More Slow Reduced Disease Progression in Collagen Induced Arthritis. American College of Rheumatology, 2 16

3. その他

51 [illegible]基盤加藤、[illegible]研究者の[illegible]支援事業・[illegible]の場合、平成26年度厚生労働省・[illegible]研究者の[illegible]法[illegible]支援事業 報告会 2016

52 [illegible]基盤加藤 [illegible]平成26年度補正補助、平成26年度文科省[illegible]事業[illegible]ビジョン[illegible]プログラム 事業報告会、2015

53 [illegible]基盤[illegible] [illegible]年S年度ガイドラインの[illegible]に向けた[illegible]年S治療法[illegible]の[illegible]。[illegible]26年度厚生労働省・[illegible]研究[illegible]における治療[illegible]ガイドラインの作成、研究班公開、2016

		和文	英文
著　書		1	
論　文	原著	1	5
	解説又は総説		
	症例報告		
	その他	2	
学会発表	国内学会	6	1
	国際学会		6
	その他	3	

平成29年度
(2016年度)

難治性疾患病態制御学

学術論文[英文]

1. 執筆

1) Tsuchiki K, Kobayashi H, Yasuno K, Sai S, Fujiya H, Niki H, Moriishi K, Sudo K. The MAP-Dependent Dephosphorylation Domain I Suppresses the Expression of Osteopontin Transcriptional Activation and Related Transcription Factor 2 Binding and Production of Matrix Metalloproteinase 9(MMP-9) in Osteoarthritis. Int J Mol Sci 2016;17(7):1124.

2) Arito Mizoguchi, Mitsuo Hiranuki, Xiaoyang Liu, Masaki Matsuo, Yuko Kado, Kosuke Tomikawa, Naki Shiraiwa, Sato Tsumbaza. Effects of ios peptide on IL-1β-induced matrix degrading enzyme in human articular chondrocytes. Inflammation molecular medicine. 2016;8:331-338.

3) Yoshioka H, Yui S, Yasuno K, Fujiya H, Moriishi K, Niki H, Kawasumi M, Yudoh K. Polyvinylpyrrolidone (PVP) Fullerenes Prevent Chondrocyte Catabolic Activity of Synovial Fibroblasts in Osteoarthritis. Int J Clin Rheumatol. 2016;11(1):70-75.

学会発表

2. 国内学会

1) 長谷 知之, 安藤 朝章, 金井 良祐, 高橋 和俊, 山下 光俊, 宮崎 承, 安田 直人, 佐藤 和俊 ヒトMAP-Dependent Dephosphorylase-1 (MDP-1)の変異型の機能解析. 第60回日本リウマチ学会総会・学術集会. 2016.

2) 佐藤 和俊, 関根 秀隆, 佐藤 紀隆, 青野 佑介, 上野 義久, 高橋 和俊, 上田 孝文, 西岡 久寿樹, 山口 昌博, 藤井 隆夫 分泌型Frizzled-related protein 1(sFRP1)の遺伝子欠損はコラーゲン関節炎およびマウスにおける関節炎の増悪を軽減する. 第60回日本リウマチ学会総会・学術集会. 2016.

3) 佐藤 和俊, 鈴木 俊, 関根 秀隆, 上野 義久, 高橋 和俊, 山崎 哲夫 骨肉腫 [illegible] 第60回日本リウマチ学会総会・学術集会. 2016.

4) 千葉 慎一郎, 吉田 俊司, 中村 耕三, 宍戸 孝明, 高橋 和俊, 中村 [illegible] 第37回日本骨代謝学会総会・学術集会. 2016.

5) 宮城 [illegible], 佐藤 [illegible], 加藤 [illegible], 佐藤 [illegible], 白子 [illegible], 大松 [illegible], 鳴川 [illegible], 高橋 和俊, 川崎 [illegible]. [illegible] 第60回日本リウマチ学会総会. 2016.

6) [illegible], 高橋 和俊, 小林 [illegible], 金井 [illegible], 藤井 [illegible], [illegible] 武者 [illegible] SAOS患者血液中の「[illegible]」の骨形成マーカーP1NPが閉塞性睡眠時無呼吸に及ぼす影響. 第60回日本リウマチ学会総会・学術集会. 2016.

7) [illegible] 青木 [illegible], 金井 [illegible], 藤谷 [illegible], 高橋 和俊, 山下 [illegible], 武者 [illegible] 関節リウマチ患者の骨粗鬆症におけるヒトMAP-Dependent Dephosphorylase-1(MDP-1)の関連について. 第30回日本骨形態学会基礎学術集会. 2016.

8) [illegible] 藤谷 [illegible], 加藤 [illegible], [illegible], [illegible], 小林 [illegible], 小林 [illegible], 山崎 [illegible], 上野 [illegible], 武者 [illegible], 高橋 和俊 関節リウマチ関節炎におけるMAP-Dependent Dephosphorylase-1の有効性評価. 第60回日本リウマチ学会. 2016.

3. 海外学会

1) Zhou S, Moriishi K, Fujiya H, Sakurai K, Yoshioka H, Tsuchiki H, Takeuchi S, Sudoh K. The Role of MAP-Dependent Protein Kinase(MPK)-1 in the Chondrocyte Energy Balance and IL-1β-Induced Production of MMP-13 in Osteoarthritis(OA). The OARSI 2016 World Congress. 2016.

2) Sakurai A, Iwaki M, Tamura M, Sato [illegible], Yudoh K, Jarvis S, Jarvis [illegible]. Novel autoantigens for endothelial cell antibodies in pediatric rheumatic diseases identified by proteomics. 2016 ACR/ARHP Scientific Meeting. 2016.

3) Shirle Kawasaki, Miyuki Tanaka, Miyuki Tanaka, Tadashi Sato, Gaku Tsuji, James N. Jarvis. Novel autoantigens for anti endothelial cell antibodies in pediatric rheumatic diseases identified by proteomics. American College of Rheumatology Annual Meeting. 2016. 2016.

4) Sakiko Kawasaki, Miyuki Tanaka, Mizuki Tanaka, Tadashi Sato, Kazuyo Yudoh, James N. Jarvis. Identification of Japanese autoantigens for anti endothelial cell antibodies in patients with juvenile dermatomyositis using proteomics. The 13th International Vasculitis & ANCA Workshop 2017. 2017.

5) Shiho Kawasaki, Paul A. Monach, Tadashi Sato, Mizuki Tanaka, Megumi Tanaka, Takahiro Okazaki, Masayoshi Ishii, Gaku Tsuji, James N. Jarvis, Peter A. Merkel. Zyxin is a novel autoantigen for anti endothelial cell antibodies in ANCA-associated vasculitis. The 13th International Vasculitis & ANCA Workshop 2017. 2017.

5. その他

1) 高橋 和俊 日本における関節リウマチ患者のライフスタイルの特徴とRAに対する治療効果との関連の評価. 平成28年度日本医療研究開発機構委託研究開発費 難治性疾患克服研究事業 難治性疾患克服のための新しい医療技術と治療ガイドラインの作成 研究班 第1回班会議. 2016.

2) 高橋 和俊 関節炎治療ガイドラインの国際比較について. 平成28年度日本医療研究開発機構委託研究開発費 難治性疾患克服研究事業 難治性疾患克服のための新しい医療技術と治療ガイドラインの作成 研究班 第2回班会議. 2017.

3) 高橋 和俊 関節炎治療ガイドラインについて. 第2回関節リウマチ患者の生活調査 最新治療調査. 2017.

		和文	英文
著書			
論文	原著		3
	解説又は総説		
	症例報告		
	その他		

2

学会発表	国内学会	8	
	国際学会		5
	その他	3	

平成29年度
(2017年度)

1

難治性疾患病態制御学

著書

1. 長澤丰雄 第1章 [illegible] 第1節 [illegible] 第4項 [illegible] 2017. 223-225

2. 長澤丰雄 [illegible] 第4項 2016. 369-370

学術論文[和文]

1) 総説・解説

1. 長澤丰雄. 関節リウマチ患者の関節破壊. [illegible] 2017; 67(5): 69-73

学術論文[英文]

1) 原著

1. Yudai Endo, Toshikazu Kirichekko, Yui Sasaki. Expression Site Therapeutic Potential of Sarcoglycan (SG) Subtypes in Osteoarthritis. International Journal of Development Research. 2017; 7(4): 12659-12663.

2. Kobayashi H, Terauchi S, Yui N, Yatabe K, Kusada I, Fujiwa D, Niki H, Hirata H, Yudai K. The Nicotinamide Adenine Dinucleotide (NAD) Dependent Deacetylase Sirtuin 1 Regulates Chondrocyte Energy Metabolism through the Modulation of Adenosine Monophosphate Activated Protein Kinase (AMPK) in Osteoarthritis OA. Journal of Arthritis. 2017; 6(2): 1-8.

3. Sumagawa S, Okazaki T, Iseki M, Yudai K, Kusunoki Y, Yamagiwa M, Sawahata K, Ozaki S. Toll-like receptor activation promotes osteoblast differentiation through the IKK-γ and TSF 6. SCIENTIFIC REPORTS. 2017; 7(1): 1-6.

4. Yudai Endo, Yui Sasaki, Kazuki Takahashi. Sarcoglycan Site Cell to Cell Interaction of Activated T Cells with Adjacent Cells in Inflamed Tissue in Inflammatory Diseases. Sci Int Arthritis Rheum Res. 2017; 2(3): 1-6.

2) 総説・解説

1. Yudai Endo, Kazuki Takahashi, Fujiwa Hirata, Yui Sasaki. Sakamoto Rio. Cartilage Tissue Engineering A Novel Bioreactor set for Cartilage Repair Generated by Cell Assembly Creation of a Self Organized Articular Cartilage Like Tissue. Novel Techniques in Arthritis & Bone Research. 2017; 1(2): 1-2.

2. Sakamoto Jun, Tarama Yoshihisa, Ishida Naoto, Suzuki Takao, Braun in-volvement pattern suggests sarcoma within relapsing polychondritis: comment on the article by Dion et al. ARTHRITIS & RHEUMATOLOGY. 2017; 69(1): 146-148.

学会発表

1) 国内学会

1. 小林大輔, 長澤丰雄, [illegible], 佐藤久仁, 佐藤久和宏, 田島利恵, 藤井秀樹. SIRT1遺伝子とDNA修復遺伝子の軟骨細胞への機能を検討する. 第61回日本リウマチ学会総会・学術集会. 2017.

2. 小林大輔, 長澤丰雄, [illegible], 佐藤[illegible], 佐藤[illegible], 佐藤[illegible], 藤井秀樹. 関節リウマチ患者における[illegible]の軟骨細胞への影響を検討する. 第32回日本臨床免疫学会総会講演抄録集. 2017.

2) 国際学会

1. ○Kinoch Kaoru, Terauchi Seiki, Kobayashi Hajime, Yui Sasaki, Fujiwa Hirata, Saki Hirata, Hecha Atsushi. Impact of NAD Dependent Deacetylase Sirtuin 1 in the Osteoporotic Formation and the Degeneration of Articular Cartilage in Osteoarthritis (OA). 2017 World Congress on Osteoarthritis. 2017.

2. ○Kawasaki Rio, Tatsuki Hayashi, Sato Toshiko, Tanaka Hiroyuki, Yudai Kazuo, James S. Jarvis. Anti vasoactive-intestinal peptide receptor 2 autoantibodies in juvenile dermatomyositis. 2017 Pediatric Rheumatology Symposium. 2017.

3. ○Kawasaki Rio, Tatsuki Hayashi, Sato Toshiko, Tanaka Hiroyuki, Yudai Kazuo, James Jarvis. Anti vasoactive-intestinal peptide receptor 2 autoantibodies in juvenile dermatomyositis: A proteomics based approach. 2017 American College of Rheumatology Annual Meeting. 2017.

3) 学内講演

1. ○長澤丰雄. 2016年度第[illegible]回学生による[illegible]の[illegible]について. 平成29年度日本大学研究費発表機構委託研究費 関西学院大学総合研究所事業「[illegible]」における治療法・治療薬のシーズの探索. 研究会. 第1回研究会. 2017.

2. ○長澤丰雄. 関節リウマチ・変形性関節症の病態・[illegible]. 2017年度 [illegible]大学・[illegible]医科大学共同研究会. 2017.

3. ○長澤丰雄. [illegible]について. 平成29年度日本大学研究費発表機構委託研究費 関西学院大学総合研究所事業「[illegible]」における治療法・治療薬のシーズの探索. 研究会. 第1回研究会. 2017.

4. ○長澤丰雄. [illegible]について. 大阪[illegible]. 2016.

5. ○長澤丰雄. [illegible]について. 平成29年度日本大学研究費発表機構委託研究費 関西学院大学総合研究所事業「[illegible]」における治療法・治療薬のシーズの探索. 研究会. 第[illegible]回研究会. 2018.

		和文	英文
著　書		2	

2

論　　文	原著		4
	解説又は総説	1	2
	症例報告		
	その他		
学会発表	国内学会	2	
	国際学会		3
	その他	5	

平成30年度
（2018年度）

1

難治性疾患病態制御学

著書

1) 遠藤[illegible]、藤田[illegible]、[illegible]、[illegible]、[illegible]・[illegible]・[illegible]・

平成31年度 令和元年度
(2019年度)

難治性疾患病態制御学

著書

1) 遠藤彰郎 [illegible] 2019:1[illegible]-69

学会発表

1) 国内学会

1) 小松弘恵, 関根, 佐藤知峰, 吉田亜紀, 青野裕介, 遠藤彰郎, 仁木久恵, 永田久紀, 中島円博, 春日雅士 [illegible] 第[illegible]回日本リウマチ学会, 2019

2) 宮崎年隆哲, 遠藤彰郎, 中谷義宏, 谷口彰一郎, 池田直子, 仁木久恵, 倉谷滋人 [illegible] 第[illegible]回日本整形外科学会基礎学術集会, 2019

3) 藤井彩香, 上杉裕恵, 小島丈博, 仁木久恵, 遠藤彰郎 [illegible] 第[illegible]回日本整形外科学会基礎学術集会, 2019

4) 小松弘恵, 関根, 佐藤知峰, 吉田亜紀, 青野裕介, 遠藤彰郎, 仁木久恵, 永田久紀, 中島円博, 春日雅士. [illegible] 第[illegible]回日本整形外科学会基礎学術集会, 2019.

5) 宮崎年隆哲, 遠藤彰郎, 中谷義宏, 谷口彰一郎, 池田直子, 仁木久恵, 倉谷滋人. [illegible] 第[illegible]回日本整形外科学会基礎学術集会, 2019.

2) 国際学会

1) Rie Katsuyama, Paul A. Monach, Toshiko Sato, Megumi Tanaka, David Cuthbertson, [illegible], Sadet A. Jeffrey, Kathy L. Sloan-Lancaster, Carol Langford, Carol A. Mockel, Larry A. Moreland, Christian Pagnoux, Philip Seo, Antoine G. Sreih, Kenneth J. Warrington, Steven R. Ytterberg, Kazuo Arsh, James S. Jakobs, [illegible] A. Merkel. Identification of Target Antigens for Anti Endothelial Cell Antibodies in Patients with Takayasu's Arteritis using Proteomics. The 2019 International Vasculitis & ANCA Workshop, 2019.

2) Rie Katsuyama, James S. Jakobs, Toshiko Sato, Megumi Tanaka, Mary Hunter, Kenji Soda, Lorenzo P. O'Donnell, Payam Nossent-Dehkordi, [illegible] Kobori. Clinical correlations of Autoantibodies Against Heat Shock Cognate 71 kDa Protein in Patients with Juvenile Dermatomyositis. The American College of Rheumatology/Association of Rheumatology Professionals Annual Meeting, 2019

3) その他

1) 大藤彰郎, 自己組織化技術による人工軟骨 人工骨膜付人工関節 [illegible] 第[illegible]回日本関節鏡学会・関節外科学会共同研究会, 2019

2) 宮崎年隆哲, 医工学メカニズムによる関節疾患の[illegible]に関する生活習慣について. [illegible] 対談講演講演, 2019

3) 宮崎年隆哲, Tissue修復[illegible]について. 難治性疾患[illegible]体系の確立[illegible]第3回[illegible]講, 2019.

		和文	英文
著書		1	
論文	原著		
	解説又は総説		
	症例報告		
	その他		
学会発表	国内学会	5	
	国際学会		2
	その他	3	

Journal of Controlled Release 197 (2015) 97–104

Contents lists available at ScienceDirect

Journal of Controlled Release

journal homepage: www.elsevier.com/locate/jconrel

Encapsulation of beraprost sodium in nanoparticles: Analysis of sustained release properties, targeting abilities and pharmacological activities in animal models of pulmonary arterial hypertension

Tomoaki Ishihara [a], Erika Hayashi [a], Shuhei Yamamoto [b], Chisa Kobayashi [b], Yuichi Tamura [c], Ryoichi Sawazaki [a], Fumiya Tamura [a], Kayoko Tahara [a], Tadashi Kasahara [a], Tsutomu Ishihara [d], Mitsuko Takenaga [e], Keiichi Fukuda [c], Tohru Mizushima [a,*]

[a] Faculty of Pharmacy, Keio University, Tokyo 105-8512, Japan
[b] Graduate School of Pharmaceutical Sciences, Kumamoto University, Kumamoto 862-0973, Japan
[c] Department of Cardiology, Keio University School of Medicine, Tokyo 160-8582, Japan
[d] Department of Chemical Biology and Applied Chemistry, College of Engineering, Nihon University, Fukushima 963-8642, Japan
[e] Division of Drug Delivery System, Institute of Medical Science, St. Marianna University, Kawasaki 216-8512, Japan

ARTICLE INFO

Article history:
Received 10 June 2014
Accepted 27 October 2014
Available online 6 November 2014

Keywords:
Prostaglandin I_2
Encapsulation
Biodegradable nanoparticle
Beraprost sodium
Pulmonary arterial hypertension

ABSTRACT

Prostaglandin I_2 (PGI_2) and its analogues (such as beraprost sodium, BPS) are beneficial for the treatment of pulmonary arterial hypertension (PAH). The encapsulation of BPS in nanoparticles to provide sustained release and targeting abilities would improve both the therapeutic effect of BPS on PAH and the quality of life of patients treated with this drug.

BPS was encapsulated into nanoparticles prepared from a poly(lactic acid) homopolymer and monomethoxy poly(ethyleneglycol)–poly(lactide) block copolymer. The accumulation of nanoparticles in damaged pulmonary arteries was examined using fluorescence-emitting rhodamine S-encapsulated nanoparticles. The monocrotaline-induced PAH rat model and the hypoxia-induced mouse model were used to examine the pharmacological activity of BPS-encapsulated nanoparticles.

A nanoparticle, named BPS-NP, was selected among various types of BPS-encapsulated nanoparticles tested; this was based on the sustained release profile *in vitro* and blood clearance profile *in vivo*. Fluorescence-emitting rhodamine S-encapsulated nanoparticles were prepared in a similar manner to that of BPS-NP, and showed accumulation and prolonged residence in monocrotaline-damaged pulmonary peripheral arteries. Intravenous administration of BPS-NP (once per week, 20 μg/kg) protected against monocrotaline-induced pulmonary arterial remodeling and right ventricular hypertrophy. The extent of this protection was similar to that observed with oral administration (once per day, 100 μg/kg) of BPS alone. The once per week intravenous administration of BPS-NP (20 μg/kg) also exhibited an ameliorative effect on hypoxia-induced pulmonary arterial remodeling and right ventricular hypertrophy.

The beneficial effects of BPS-NP on PAH animal models seem to be mediated by its sustained release and tissue targeting profiles. BPS-NP may be useful for the treatment of PAH patients due to reduced dosages and frequency of BPS administration.

© 2014 Elsevier B.V. All rights reserved.

1. Introduction

Pulmonary arterial hypertension (PAH) is a rare but life-threatening disease characterized by progressive increases in pulmonary vascular resistance, vasoconstriction and arterial pressure, which lead to right ventricular (RV) hypertrophy and failure, and subsequently to death [1–3]. Although several classes of drugs have been approved for the treatment of PAH (such as endothelin receptor antagonists and phosphodiesterase-5 inhibitors), the prognosis for this disease remains poor (median survival, 2.8 years) [4,5]. While the primary cause of PAH is unclear, it is believed that pulmonary vasoconstriction, endothelial cell proliferation, inflammation, smooth muscle cell proliferation, and thrombosis play key roles in the pathogenesis of PAH [1,2,6].

The progression of PAH is associated with a reduced production of prostaglandin I_2 (PGI_2) [7,8], a potent vasodilator produced in the vascular endothelium, which also has antithrombotic effects and inhibitory effects on smooth muscle cell proliferation [5,9]. Thus, PGI_2 and its analogues

* Corresponding author at: Department of Drug Discovery and Development, Faculty of Pharmacy, Keio University, 1-5-30, Shibakoen, Minato-ku, Tokyo 105-8512, Japan. Tel./fax: +81 3 5400 2628.
E-mail address: mizushima-th@pha.keio.ac.jp (T. Mizushima).

http://dx.doi.org/10.1016/j.jconrel.2014.10.029
0168-3659/© 2014 Elsevier B.V. All rights reserved.

could be therapeutically beneficial for the treatment of PAH in affected patients [5,10–16]. In fact, the intravenous administration of epoprostenol (PGI_2) is currently the most effective approach for the treatment of PAH, not only because it can ameliorate symptoms of severe PAH, but because it also prolongs life expectancy [16,17]. One major drawback of PGI_2 is that it is very unstable in blood [18,19], meaning that epoprostenol must be intravenously infused on a continuous basis, thereby drastically decreasing the quality of life (QOL) of patients due to problems associated with cosmetic appearance, transportation of an infusion pump and risk of infection [14,20]. For these reasons, stable PGI_2 analogues such as beraprost sodium (BPS) formulated for various routes of administration (oral, subcutaneous and inhalation) have been developed [5,18]. However, the half-life of these PGI_2 analogues in the blood remains short and their therapeutic efficacy in PAH patients is inferior to that of continuously infused epoprostenol [18,21]. For example, the half-life of BPS in the blood is less than 40 min following its oral administration, and it is not effective in the treatment of patients with severe PAH, even with frequent administration [5,22,23]. Therefore, a drug delivery system (DDS) that enables the sustained release of intravenously administered PGI_2 or its analogues would be clinically beneficial. On the other hand, various physiological activities of PGI_2 are related to adverse effects (such as hypotension) due to its whole-body distribution when administered systemically [24]. Furthermore, adverse events, such as headache, jaw pain, vasodilation, nausea, diarrhea, leg pain, and foot pain were observed in patients treated with BPS [23,25]. Therefore, a DDS that enables the specific targeting of PGI_2 or its analogues to the damaged pulmonary arteries is also important.

We recently established a new DDS that enables both the sustained release and specific targeting of encapsulated drugs [26–30]. By employing a nanotechnology approach, drugs are encapsulated in solid nanoparticles prepared from biodegradable and biocompatible poly(lactide) homopolymer (PLA) [31,32]. This type of nanoparticle can be used to achieve the sustained release of encapsulated drug, which takes place concomitantly with the degradation of PLA [28,31,32]. To avoid the uptake of these nanoparticles by the mononuclear phagocyte system [32,33], a monomethoxy poly(ethyleneglycol)–poly(lactide) block copolymer (PEG–PLA) was used in combination with PLA. Furthermore, the encapsulation of drug compounds in small-diameter nanoparticles (50–150 nm) would enhance the selective delivery of the drug to damaged blood vessels due to the enhanced permeability and retention (EPR) effect [34].

In the present study, we succeeded in encapsulating BPS into this type of nanoparticle (BPS-NP). BPS-NP showed a sustained release profile *in vitro* and a prolonged residence in the blood and accumulation in damaged pulmonary peripheral arteries *in vivo*. Compared to the oral administration of BPS alone, the intravenous administration of BPS-NP in animal models of PAH showed ameliorative effects even at lower doses and frequencies of administration. These results suggest that BPS-NP could serve as a useful option for the treatment of PAH patients.

2. Materials and methods

2.1. Materials and animals

BPS, monocrotaline, pentobarbital, fluorescein isothiocyanate (FITC)-labeled albumin and fetal bovine serum (FBS) were obtained from Sigma (St. Louis, MO). D,L-PLA (MW = 5000 or 20,000), 1,4-dioxane, iron chloride and rhodamine S (RS) were from Wako Pure Chemical Industries, Ltd. (Osaka, Japan). L-PLA (MW = 5000 or 20,000) was from Taki Chemical Co., Ltd. (Kakogawa, Japan). PEG–D,L-PLA (average molecular weight of PEG and PLA are 5600 and 9200, respectively) or PEG–L-PLA (average molecular weight of PEG and PLA are 5600 and 9400, respectively) was synthesized and evaluated as described previously [28,35]. Diethanolamine (DEA) was from Tokyo Chemical Industry Co., Ltd. (Tokyo, Japan). Wistar rats (5 weeks old, male) and C57/BL6 mice (8 weeks old, male) were from Kyudo Co., Ltd. (Kumamoto, Japan) or Charles River Laboratories Inc. (Yokohama, Japan). The experiments and procedures described here were carried out in accordance with the Guide for the Care and Use of Laboratory Animals as adopted and promulgated by the National Institutes of Health, and were approved by the Animal Care Committee of Kumamoto University and Keio University.

2.2. Determination of BPS and RS levels in samples

BPS and RS levels in samples were determined by analytical high-performance liquid chromatography (HPLC) with a reverse-phase column (L-column ODS (150 × 4.6 mm, 5 μm, Chemicals evaluation research institute, Tokyo, Japan) or Eclipse XDB-C18 column (150 × 2.1 mm, 5 μm, Agilent Technologies, Santa Clara, CA)). A Waters 2695 Alliance separation module, a Waters 2996 photodiode array detector, and a Waters Alliance system running Empower software (Waters, Milford, MA) were used for HPLC analysis.

For detection of BPS, solvent A (0.1% acetic acid in Methanol) and solvent B (0.1% acetic acid in Milli-Q water) were used at a flow rate of 0.5 ml/min. After injection of the sample (0 min), the mobile phase was changed as follows; 70% solvent A (20 min), a linear gradient of 70–100% solvent A (2 min), 100% solvent A (11 min) and a linear gradient of 100–70% solvent A (2 min). Detection was performed at an optical density of 285 nm.

For detection of RS, solvent A (0.1% acetic acid in acetonitrile) and solvent B (0.1% acetic acid in Milli-Q water) were used at a flow rate of 0.05 ml/min. After injection of the sample, 80% solvent A was used as a mobile phase in isocratic elution mode for 30 min. Detection was performed at an optical density of 530 nm.

2.3. Analysis of solubility of BPS and RS

BPS or RS (0.56 mM) was mixed with DEA (various concentrations) and iron chloride (10 mM) in ethanol. After incubation for 30 min at 25 °C, the pH value of the solutions/suspensions was measured and they were then centrifuged at 13,000 rpm for 10 min to precipitate insoluble BPS or RS. The amount of BPS or RS in the supernatant was determined by analytical HPLC as mentioned above.

2.4. Preparation and characterization of nanoparticles

Nanoparticles were prepared by using the oil-in-water solvent diffusion method as described previously [27,28]. We named nanoparticle types based on the chirality (L or DL) of PLA and PEG–PLA and the molecular weight of PLA (Table 1).

For preparation of L-L20, L-DL20, DL-L20 or DL-DL20, 26 mg of L-PLA or D,L-PLA in 300 μl of 1,4-dioxane, 24 mg of PEG–L-PLA in 300 μl of

Table 1
Characterization of BPS- or RS-encapsulated nanoparticles.
Nanoparticles encapsulated with BPS (A) or RS (B) were prepared by an oil-in-water solvent diffusion method. Particle size and BPS (A) or RS (B) content in the particles were determined by the dynamic light scattering method and HPLC, respectively. Values are mean ± S.E.M. ($n = 3$).

A

NP code	PLA–PEG	PLA $_{(Mw, kDa)}$	Diameter (nm)	BPS content (%)
L-L20	L-PLA–PEG	L-PLA $_{(20)}$	121 ± 2	1.23 ± 0.02
L-DL20 $_{(BPS-NP)}$	L-PLA–PEG	DL-PLA $_{(20)}$	128 ± 3	1.08 ± 0.04
L-L5	L-PLA–PEG	L-PLA $_{(5)}$	109 ± 2	0.86 ± 0.03
L-DL5	L-PLA–PEG	DL-PLA $_{(5)}$	112 ± 1	0.88 ± 0.02
DL-L20	DL-PLA–PEG	L-PLA $_{(20)}$	112 ± 3	1.15 ± 0.08
DL-DL20	DL-PLA–PEG	DL-PLA $_{(20)}$	125 ± 3	0.86 ± 0.06
DL-L5	DL-PLA–PEG	L-PLA $_{(5)}$	108 ± 2	2.39 ± 0.09
DL-DL5	DL-PLA–PEG	DL-PLA $_{(5)}$	107 ± 1	2.16 ± 0.05

B

NP code	PLA–PEG	PLA $_{(Mw, kDa)}$	Diameter (nm)	RS content (%)
RS-NP	L-PLA–PEG	DL-PLA $_{(20)}$	107 ± 1	1.65 ± 0.04

1,4-dioxane or PEG–D,L-PLA in 300 μl of acetone, 2.5 mg of BPS in a mixture of 50 μl of methanol, 150 μl of acetone and 500 μl of 1,4-dioxane, DEA (4.75 mg) in 200 μl of acetone and iron chloride (2.43 mg) in 30 μl of acetone were mixed.

For preparation of L-L5, L-DL5, DL-L5 or DL-DL5, 26 mg of L-PLA or D, L-PLA in 300 μl of 1,4-dioxane, 24 mg of PEG–L-PLA in 300 μl of 1,4-dioxane or PEG–D,L-PLA in 300 μl of acetone, 2.5 mg of BPS in a mixture of 50 μl of methanol and 150 μl of acetone, DEA (4.75 mg) in 200 μl of acetone and iron chloride (2.43 mg) in 30 μl of acetone were mixed.

For preparation of RS-NP, 26 mg of D,L-PLA in 300 μl of 1,4-dioxane, 24 mg of PEG–L-PLA in 300 μl of 1,4-dioxane, 2.5 mg of RS in 500 μl of ethanol, DEA (9.5 mg) in 200 μl of acetone and iron chloride (2.43 mg) in 30 μl of acetone were mixed.

Samples described above were incubated for 10 min at room temperature and added to 25 ml of Milli-Q water stirred at 1000 rpm. After addition of 2.5 ml of 0.5 M EDTA (pH 7.0) and 12.5 μl of 200 mg/ml Tween 80, nanoparticles were purified and concentrated by centriprep YM-50 (Merck Millipore, Billerica, MA).

For determination of the BPS or RS content in nanoparticles, the nanoparticles were degraded by incubation with 50 mM EDTA (pH 7.0) and 1,4-dioxane (final concentration, 80%). After centrifugation, the amount of BPS or RS in the supernatant was determined by analytical HPLC as mentioned above. The drug content was defined as the ratio of BPS or RS weight to the total weight of nanoparticles.

Particle size distribution was determined by the dynamic light scattering method (ZETASIZER Nano-ZS, Malvern Instruments Ltd., Malvern, UK) and the average diameter was calculated by Marquadt's method.

2.5. BPS release from nanoparticles in vitro

BPS-encapsulated nanoparticles were dispersed in a 50% (v/v) solution of FBS in phosphate-buffered saline (PBS). After incubation at 37 °C for the specified period, each suspension (100 μl) was diluted with 900 μl of 50 mM EDTA solution (pH 7.0) and centrifuged at 35,000 rpm for 30 min. The BPS content in the precipitate was determined as described above.

2.6. Determination of BPS- or RS-encapsulated PLA-nanoparticles in blood

BPS-encapsulated nanoparticles were intravenously administered to animals via the tail vein (2 ml/kg). Blood samples were periodically collected from the tail vein into heparin-treated capillary tubes. Each sample (50 μl) was mixed with 150 μl of 1,4-dioxane. After centrifugation (13,000 rpm for 30 min), the BPS content of the supernatant was determined by analytical HPLC as described above.

2.7. Accumulation of BPS- or RS-encapsulated nanoparticles in vivo

Wistar rats anesthetized with pentobarbital were subcutaneously administered either monocrotaline (30 or 60 mg/kg) or saline once only. Two to three weeks after the administration, BPS, BPS-encapsulated nanoparticles, and RS or RS-encapsulated nanoparticles were intravenously administered into the tail vein (2 ml/kg).

For determination of RS, lung homogenates were prepared and mixed with 1,4-dioxane (4 ml/g tissue). After centrifugation (13,000 rpm for 30 min), RS fluorescence intensity of the supernatant was determined by fluorescence spectrophotometry (Infinite 200 PRO, Tecan Group Ltd., Männedorf, Switzerland) at emission and excitation wavelengths of 550 nm and 580 nm, respectively.

For determination of BPS, lung homogenates were prepared in PBS (1 ml/g tissue) and mixed with 1,4-dioxane (4 ml/g tissue) and PBS (3 ml/g tissue). After centrifugation (15,000 rpm for 10 min), the BPS content of the supernatant was determined by analytical HPLC as described above.

For detection of RS, 24 h after the administration of RS or RS-encapsulated nanoparticles, lung sections were prepared and stained with Mayer's hematoxylin followed by 1% eosin alcohol solution (H & E staining). Samples were mounted with malinol and inspected with the aid of an Olympus BX51 microscope.

2.8. Assessment of vascular permeability in animal models of PAH

Vascular permeability assay was performed as described previously [36] with some modifications.

For rats, 3 weeks after the monocrotaline (60 mg/kg) administration, FITC-labeled albumin (10 mg/kg) was intravenously administered into the tail vein (2 ml/kg). Three hours after the administration, rats were killed and perfused with PBS. Lung homogenates were prepared in PBS (5 ml/g tissue).

For mice, after the hypoxia exposure (6 weeks), FITC-labeled albumin (50 mg/kg) was intravenously administered into the tail vein (10 ml/kg). Three hours after the administration, mice were killed and perfused with PBS. Lung homogenates were prepared in 500 μl of PBS.

After centrifugation (15,000 rpm for 10 min), FITC fluorescence intensity of the supernatant was determined by fluorescence spectrophotometry (Infinite 200 PRO) at emission and excitation wavelengths of 488 nm and 530 nm, respectively.

2.9. Development of animal models of PAH

Wistar rats anesthetized with pentobarbital were subcutaneously administered either monocrotaline (60 mg/kg) or saline once only at day 0. BPS-encapsulated nanoparticles or BPS alone were intravenously administered via the tail vein (2 ml/kg) once per week or orally administered (2 ml/kg) once per day, respectively. Pulmonary arterial remodeling and RV hypertrophy were assessed at day 21 as described below.

C57/BL6 mice were kept in a tightly sealed chamber under hypoxic (10% O_2) or normal (20% O_2) conditions for 7 weeks. The status of the hypoxia chamber was maintained using a hypoxic air generator (TEIJIN, Tokyo, Japan) and monitored with an O_2 analyser (JIKO-25SIIR, Jikco Ltd., Tokyo, Japan) as described previously [37]. BPS-encapsulated nanoparticles were intravenously administered once per week via the tail vein (2 ml/kg). Pulmonary arterial remodeling and RV hypertrophy were assessed at week 7 as described below.

2.10. Assessment of pulmonary arterial remodeling and RV hypertrophy

Pulmonary arterial remodeling was assessed based on the wall thickness of the pulmonary peripheral arteries as described previously [38]. Lung tissue samples were fixed in 10% formalin neutral buffer solution for 24 h and embedded in paraffin before being cut into 4 μm-thick sections. Sections were subjected to Elastica van Gieson staining and inspected with the aid of an Olympus BX51 microscope (Olympus, Tokyo, Japan). The external diameter and medial wall thickness were measured for 10 peripheral arteries (rat, 50–200 μm external diameter; mouse, 25–100 μm external diameter) for each lung section and the average value was calculated. The relative medial wall thickness (% wall thickness) was calculated as follows: [medial wall thickness × 2] / [external diameter × 100].

RV hypertrophy was assessed by the relative weight of the RV [38]. After animals had been sacrificed, RV was separated from the left ventricle (LV) and ventricular septum (S), and each of them was weighed. RV hypertrophy was calculated as follows: [RV / (LV + S)].

2.11. Statistical analysis

All values are expressed as the mean ± standard error of the mean (S.E.M.). One-way ANOVA followed by the Tukey's test or the Student's *t*-test for unpaired results was used to evaluate differences between three or more groups or between two groups, respectively, which were considered to be significant for values of $P < 0.05$.

3. Results

3.1. Preparation of BPS-encapsulated PLA-nanoparticles

We recently reported that both the molecular weight and chirality (racemic or optically active) of PLA are important factors for determining the stability of PLA-nanoparticles [28]. In order to obtain an appropriate sustained release profile for BPS and a prolonged residence time in the blood, we prepared various types of BPS-encapsulated nanoparticles by using different combinations of PLA (L-PLA (MW = 20,000), L-PLA (MW = 5000), D,L-PLA (MW = 20,000) or D,L-PLA (MW = 5,000)) and PEG–PLA (PEG–L-PLA or PEG–D,L-PLA) (Table 1). In relation to PGE_1, which has a carboxyl group, we recently reported that insolubilization of PGE_1 by iron chloride under appropriate pH conditions is essential for its encapsulation in PLA-nanoparticles [26, 28]. Since BPS also has a carboxyl group, we used this strategy to encapsulate BPS in PLA-nanoparticles. Fig. 1A shows the solubility of BPS in aqueous solutions with or without iron chloride under various conditions of pH, which was adjusted by the addition of DEA. In the presence of iron chloride, the residual amount of BPS in the supernatant after centrifugation varied with changing pH values (Fig. 1A). On the other hand, in the absence of iron chloride, the residual amount of BPS was not affected by the pH value (Fig. 1A). We used conditions that achieved maximum insolubilization of BPS (30 mM DEA and 10 mM iron chloride) for the encapsulation of BPS in PLA-nanoparticles.

We prepared the BPS-encapsulated nanoparticles from PLA and PEG–PLA by the solvent diffusion method [27,28]. We confirmed that the conditions of 30 mM DEA that achieved the lowest solubility of BPS (Fig. 1A) is the optimum condition for efficient encapsulation of BPS in nanoparticles (Supplemental Fig. S1). Fig. 2A shows the size distributions of representative BPS-encapsulated PLA-nanoparticles (BPS-NP). The average particle size was similar between different types of BPS-encapsulated PLA-nanoparticles (Table 1). The efficiency of encapsulation (BPS content in nanoparticles) was also determined (Table 1).

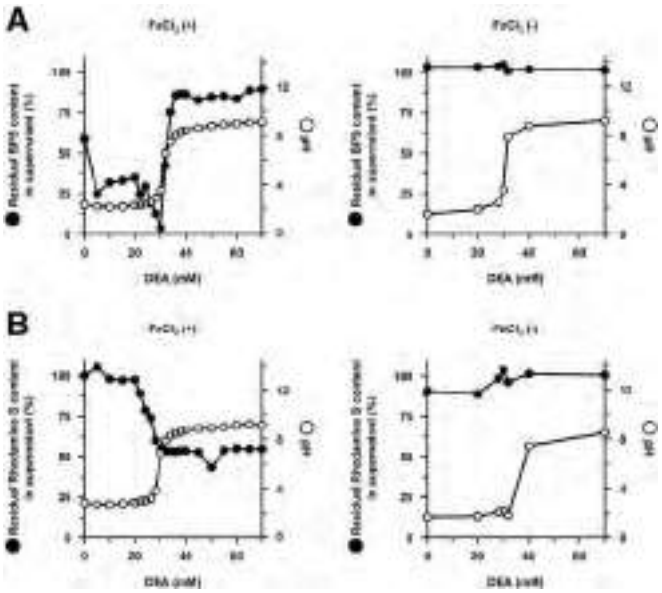

Fig. 1. Solubility of BPS and RS in aqueous solution. An ethanol solution of BPS (A) or RS (B) was added to a 9-fold excess volume of solution containing 10 mM iron chloride (+$FeCl_3$) or 10 mM hydrochloride (−$FeCl_3$) at different pH values obtained by the addition of DEA. After centrifugation, residual BPS (A) or RS (B) in the supernatant was determined by analytical HPLC.

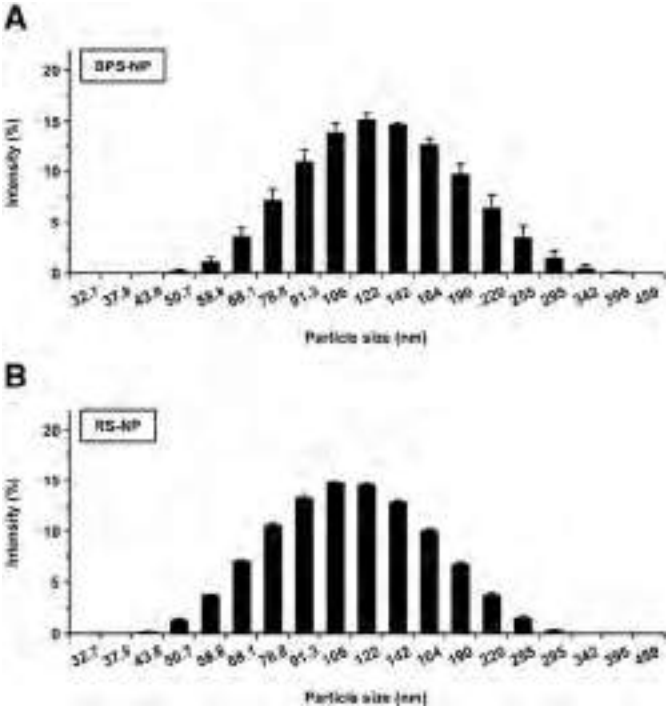

Fig. 2. Size distribution of BPS-NP and RS-NP. BPS-NP (A) and RS-NP (B) particle sizes were determined by the dynamic light scattering method. Values are mean ± S.E.M. ($n = 3$).

3.2. Stability of BPS-encapsulated nanoparticles in vitro and in vivo

The *in vitro* release profile of BPS from each PLA-nanoparticle type was examined in a 50% v/v solution of FBS in PBS at 37 °C, with release determined by measuring the amount of BPS remaining in the nanoparticles. When PEG–D,L-PLA was used (left panel in Fig. 3), a faster release profile of BPS was observed in nanoparticles prepared from lower molecular weight PLA. Furthermore, nanoparticles prepared from D,L-PLA showed the fastest release profile of BPS with respect to those prepared from L-PLA (left panel in Fig. 3). These phenomena are consistent with what was observed for PGE_1-encapsulated nanoparticles in our previous studies [28,29]. We also found here that similar phenomena are observed for nanoparticles prepared from PEG–L-PLA (right panel in Fig. 3), and that the use of PEG–L-PLA instead of PEG–D,L-PLA stimulates or suppresses the release, depending on the PLA species used (Fig. 3).

We next examined the residence time of BPS in the blood (blood clearance profile) for each type of BPS-encapsulated PLA-nanoparticles; rats were intravenously administered nanoparticles of each type and the blood clearance profile was investigated by measuring the change in plasma concentration of BPS. To begin with, we confirmed that intravenously administered BPS alone was rapidly cleared from the blood (Fig. 4A), as reported previously [39]. For nanoparticles prepared from

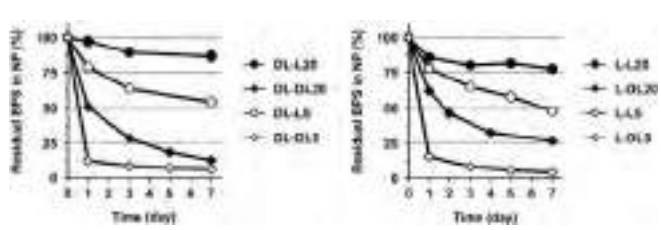

Fig. 3. *In vitro* release profile of BPS from nanoparticles. Each type of BPS-encapsulated nanoparticles was dispersed in 50% FBS in PBS and incubated at 37 °C for the indicated number of days. The amount of BPS remaining in nanoparticles (NP) was determined by analytical HPLC. Values are mean ± S.E.M. ($n = 3$).

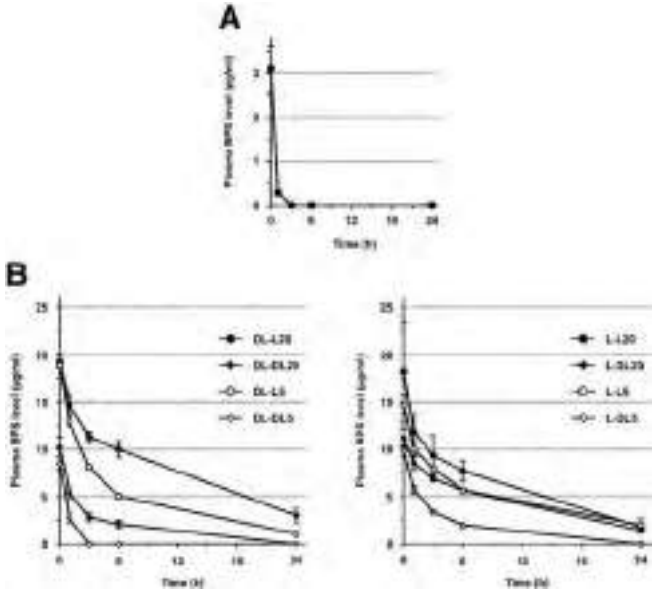

Fig. 4. *In vivo* blood clearance profile of BPS alone and BPS-encapsulated nanoparticles. BPS alone (A) or each type of BPS-encapsulated nanoparticles (B) was administered intravenously at the dose of 1.25 mg BPS/kg. BPS-encapsulated nanoparticles were degraded by 1,4-dioxane (B) and the amount of BPS in plasma was determined by analytical HPLC. Values are mean ± S.E.M. ($n = 3$).

PEG–D,L-PLA (left panel in Fig. 4B), the clearance of BPS became faster as the molecular weight of the PLA used in the nanoparticles was reduced. Moreover, nanoparticles prepared from D,L-PLA exhibited faster BPS clearance times than those prepared from L-PLA (left panel in Fig. 4B). The use of PEG–L-PLA instead of PEG–D,L-PLA stimulates or suppresses the BPS release, depending on the PLA species used (Fig. 4B). Based on these results, we used BPS-encapsulated nanoparticles prepared from a combination of D,L-PLA (Mw = 20,000) and PEG–L-PLA (i.e., L-DL20) and subsequently refer to this type of BPS-encapsulated PLA-nanoparticles as "BPS-NP".

3.3. Accumulation of BPS-NP-like nanoparticles in monocrotaline-damaged pulmonary peripheral arteries

To examine the distribution of BPS-NP in the PAH rat model (monocrotaline-administered rats), we prepared BPS-NP-like fluorescent RS-encapsulated nanoparticles. As shown in Fig. 1B, the solubility of RS decreased in a pH-dependent manner in the presence of iron chloride. In this way, we prepared RS-encapsulated nanoparticles from D,L-PLA (MW = 20,000) and PEG–L-PLA under similar conditions to those used in the preparation of BPS-NP and named the BPS-NP-like RS-encapsulated PLA-nanoparticles as "RS-NP". The size distribution and efficiency of encapsulation of RS-NP were roughly similar to those of BPS-NP (Fig. 2 and Table 1).

We next compared the accumulation of RS in the pulmonary peripheral arteries after administration of RS-NP or RS alone in control and monocrotaline-administered rats. RS-NP or RS alone was intravenously administered 21 days after the administration of monocrotaline and the level of RS in the lung was monitored 1 day later by histopathological analysis (H & E staining). Pulmonary arterial remodeling (hypertrophy of pulmonary peripheral arterial walls) was clearly evident in monocrotaline-administered rats compared with control (Fig. 5A). Analysis of fluorescence patterns in micrographs showed RS accumulation in the pulmonary peripheral arteries of monocrotaline-treated rats administered RS-NP but not in other samples (Fig. 5A).

We also compared the amount of RS in the lung between monocrotaline-administered rats and control rats after the intravenous administration of RS-NP. As shown in Fig. 5B, compared to control rats, a higher level of RS in the lungs of monocrotaline-treated rats was detected from 1 to 5 days after the administration of RS-NP. These results suggest that RS-NP accumulates more efficiently and remains longer in monocrotaline-damaged pulmonary peripheral arteries compared with that seen in those in control.

To test the idea that the accumulation of RS-NP shown in Fig. 5A and B is mediated through EPR effect, we compared the vascular permeability between monocrotaline-treated and control rats using FITC-labeled albumin. As shown in Fig. 5C, the level of FITC-labeled albumin at the lung of monocrotaline-treated rats was about 10 times higher than that in normal rats and the extent of accumulation is comparable to that seen in tumors in previous papers [40]. Such accumulation at the lung was also observed in mice exposed to hypoxia, however, the extent of accumulation was not so apparent as that seen in monocrotaline-treated rats (Fig. 5D). We also examined the accumulation of BPS at the lung of monocrotaline-treated rats after intravenous administration of BPS-NP or free BPS. As shown in Fig. 5E, the higher level of BPS at the lung of monocrotaline-treated rats, compared to control rats, was observed after administration of BPS-NP. On the other hand, we could not detect BPS at the lung after administration of free BPS even in monocrotaline-treated rats (Fig. 5E). Results in Fig. 5 suggest that BPS-NP accumulates more efficiently in monocrotaline-damaged pulmonary peripheral arteries compared with that seen in those in control rats through the EPR effect.

3.4. Pharmacological activity of BPS-NP in PAH animal models

We subsequently examined the effect of BPS-NP on monocrotaline-induced pulmonary arterial remodeling and RV hypertrophy. To begin with, we confirmed the ameliorative effect of the oral administration of BPS in this model. Rats were treated with monocrotaline once only at day 0 and BPS was orally administered once per day for 21 days.

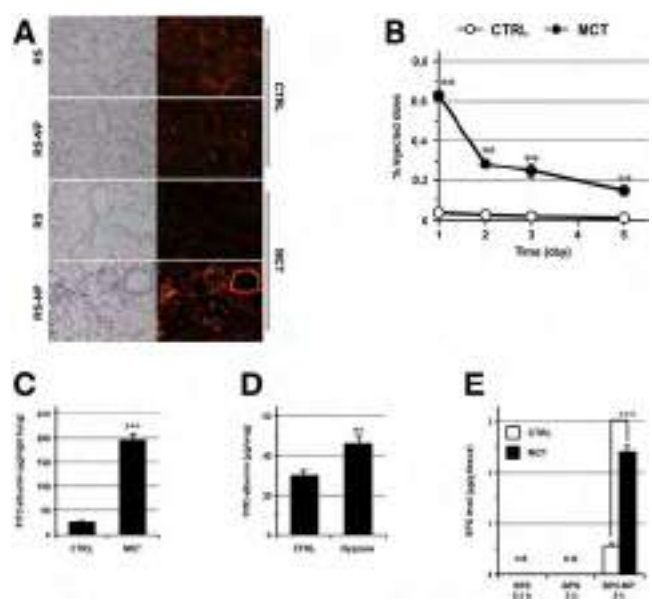

Fig. 5. Accumulation and prolonged residence of RS-NP and BPS-NP in the lung. Rats were treated with monocrotaline (MCT; 30 mg/kg (A, B) or 60 mg/kg (C, E)) or saline (CTRL) once only on day 0. Mice were maintained in a hypoxic chamber (10% O_2, Hypoxia) or under normal conditions (CTRL) (D). On day 21 (A) or 14 (B), RS-NP (A, B) or RS (A) was injected intravenously at a dose of 0.6 mg RS/kg. On day 21 (C) or 45 (D), FITC-labeled albumin was injected intravenously at a dose of 10 (C) or 50 (D) mg/kg. On day 18, BPS alone or BPS-NP was injected intravenously at a dose of 0.9 mg BPS/kg (E). Lung sections were prepared 1 day after the injection of RS-NP or RS and subjected to histopathological examination (H & E staining and fluorescence microscopy) (A). The amounts of RS (B) or FITC (C, D) in the lung homogenates were determined by measuring the emission fluorescence intensity at 580 nm (excitation at 550 nm) (B) or at 530 nm (excitation at 488 nm) (C, D), respectively. The amount of BPS in the lung was determined by analytical HPLC (E). Values are mean ± S.E.M. ($n = 3$–11) ***$P < 0.001$; **$P < 0.01$; versus CTRL; n.d., not detected (<0.66 μg/g tissue).

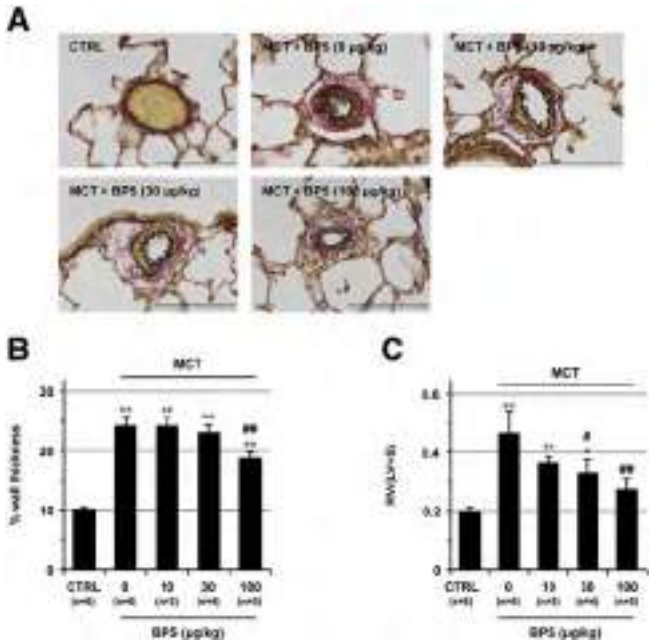

Fig. 6. Effects of BPS alone on monocrotaline-induced pulmonary arterial remodeling and RV hypertrophy. Rats were treated with monocrotaline (MCT; 60 mg/kg) or saline (CTRL) once only on day 0. Indicated doses of BPS alone were orally administered once per day for 21 days (A–C). Sections of pulmonary tissue were prepared on day 21 and subjected to histopathological examination (Elastica van Gieson staining) (A). Pulmonary arterial remodeling (hypertrophy of the pulmonary arterial wall (% wall thickness)) was measured (B). RV hypertrophy (RV / (LV + S)) was measured on day 21 (C). Values are mean ± S.E.M. $^{*}P < 0.05$; $^{**}P < 0.01$; versus CTRL. $\#P < 0.05$; $\#\#P < 0.01$; versus MCT alone. Scale bar, 100 μm.

The pulmonary peripheral arteries were analyzed on day 21. As shown in Fig. 6A, representative photomicrographs demonstrate that the monocrotaline-induced hypertrophy of arterial walls was suppressed by the BPS administration (100 μg/kg). Quantitative analysis revealed that the monocrotaline administration increased the arterial wall thickness and that this change was suppressed by the oral administration of BPS (100 μg/kg) (Fig. 6B).

Monocrotaline-induced RV hypertrophy can be measured by weighing the RV, LV and S as previously described [41]. As shown in Fig. 6C, the administration of monocrotaline increased the ratio of the RV to (LV + S) weight, thus demonstrating RV hypertrophy; the simultaneous oral administration of BPS (30 or 100 μg/kg) suppressed this increase. We confirmed that once per week oral administration of BPS (up to 100 μg/kg) did not affect the monocrotaline-induced pulmonary arterial remodeling and RV hypertrophy (data not shown). These results are all consistent with previously reported findings [42].

We subsequently examined the effect of the intravenous administration of BPS-NP on monocrotaline-induced pulmonary arterial remodeling and RV hypertrophy in a similar way. As shown in Fig. 7, the intravenous administration of BPS-NP (20 or 200 μg BPS/kg) reduced the extent of monocrotaline-induced pulmonary arterial remodeling and RV hypertrophy even when the administration frequency was restricted to once per week. Intravenous administration of BPS-NP (once per week, 2 μg/kg) could not protect against monocrotaline-induced pulmonary arterial remodeling and right ventricular hypertrophy (Supplemental Fig. S2). These results suggest that the encapsulation of BPS into PLA-nanoparticles can permit a reduction in the dose and frequency of BPS required to exert ameliorative effects against monocrotaline-induced disorders.

Hypoxia-induced pulmonary arterial remodeling and RV hypertrophy in mice form the basis of another animal model of PAH, which we also used here to examine the effects of BPS-NP. As shown in Fig. 8, maintaining mice under hypoxic conditions (10% O_2) for 7 weeks induced hypertrophy of the pulmonary peripheral arterial wall and RV hypertrophy, as described previously [37]. The intravenous administration of BPS-NP (20 or 200 μg BPS/kg, once per week) exerted ameliorative effects against these hypoxia-induced disorders (Fig. 8).

4. Discussion

The underlying basis of DDS can be separated into three categories; targeting of lesioned tissues, sustained release, and increasing the efficiency of gastrointestinal absorption. Although a number of DDS carriers have been developed, most of those are developed to satisfy only one of these objectives. In contrast, we recently developed a new type of DDS, PEG-modified PLA-nanoparticles, that provides both sustained release and targeting abilities [26–30]. On the other hand,

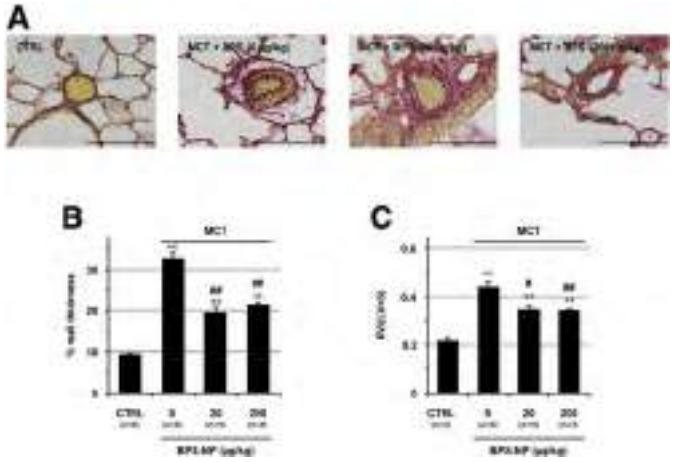

Fig. 7. Effects of BPS-NP on monocrotaline-induced pulmonary arterial remodeling and RV hypertrophy. Rats were treated with monocrotaline (MCT; 60 mg/kg) or saline (CTRL) once only on day 0. Indicated doses of BPS-NP were administered intravenously via the tail vein (2 ml/kg) once per week for 21 days (A–C). Sections of pulmonary tissue were prepared on day 21 and subjected to histopathological examination (Elastica van Gieson staining) (A). Pulmonary arterial remodeling (hypertrophy of the pulmonary arterial wall (% wall thickness)) was measured (B). RV hypertrophy (RV / (LV + S)) was measured on day 21 (C). Values are mean ± S.E.M. $^{**}P < 0.01$ versus CTRL. $\#P < 0.05$; $\#\#P < 0.01$; versus MCT alone. Scale bar, 100 μm.

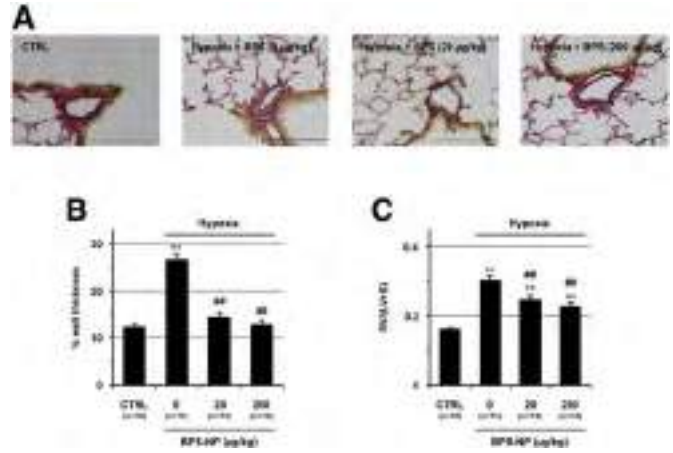

Fig. 8. Effects of BPS-NP on hypoxia-induced pulmonary arterial remodeling and RV hypertrophy. Mice were maintained in a hypoxic chamber (10% O_2, Hypoxia) or under normal conditions (CTRL) for 7 weeks. Indicated doses of BPS-NP were administered intravenously via the tail vein (5 ml/kg) once per week for 7 weeks (A–C). Sections of pulmonary tissue were prepared at week 7 and subjected to histopathological examination (Elastica van Gieson staining) (A). Pulmonary arterial remodeling (hypertrophy of the pulmonary arterial wall (% wall thickness)) was measured (B). RV hypertrophy (RV/(LV + S)) was measured at week 7 (C). Values are mean ± S.E.M. $^{**}P < 0.01$ versus CTRL. $\#\#P < 0.01$ versus hypoxia alone. Scale bar, 100 μm.

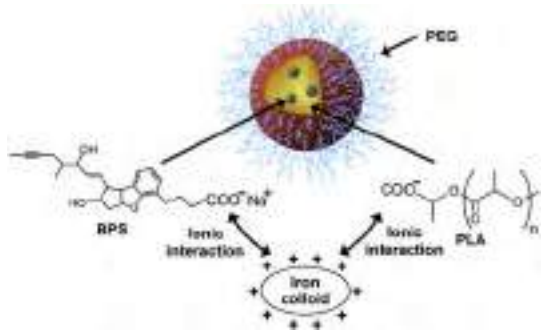

Fig. 9. Schematic illustration of BPS-encapsulated nanoparticles.

DDS carriers for the intravenous administration of PGI_2 and its analogues require both sustained release and targeting abilities, because frequent intravenous administration reduces the QOL of patients and the whole-body distribution of PGI_2 following its systemic administration results in adverse effects (see Introduction section). Thus, we postulated that encapsulation of BPS in PEG-modified PLA-nanoparticles would provide a beneficial treatment option for PAH patients, for which reason we tested this idea here using two animal models.

A major obstacle to preparing drug-encapsulated PLA-nanoparticles is that relatively hydrophilic drugs, such as PGE_1 and BPS, are very hard to encapsulate in hydrophobic PLA-nanoparticles [43]. For PGE_1, we overcame this obstacle by taking advantage of its insolubilization in the presence of iron chloride under appropriate pH conditions [28,29]. We used this same strategy here to insolubilize BPS and succeeded in encapsulating it into PLA-nanoparticles. This finding suggests that BPS is insolubilized by the formation of electrostatic complexes between the carboxyl group in the BPS and iron chloride, along with deprotonation of the carboxyl group and that ionic interaction through a metal bridge is a driving force to encapsulate ionizable BPS in solid PLA nanoparticles, in other words, iron colloid acted as an ionic bridge between the terminal carboxyl group of the PLA chain and the carboxyl group of BPS (Fig. 9).

Various combinations of PEG–PLA and PLA were tested to optimize the sustained release profiles of BPS *in vitro* and its residence period in blood *in vivo*. The results obtained suggested that a faster release profile and a faster clearance from blood could be achieved with nanoparticles prepared from low molecular weight PLA. Furthermore, nanoparticles prepared from D,L-PLA showed a faster release profile and clearance from the blood than those prepared from L-PLA. These observations were similar to those reported for PGE_1-encapsulated PLA-nanoparticles [28,29]. The mechanism by which nanoparticles containing D,L-PLA show a faster release profile and clearance from blood than those prepared only from L-PLA is unclear at present, because the release rate of drugs is regulated by complicated factors such as the thermodynamic stability, kinetic stability and degradation rate of the nanoparticles. Racemic D,L-PLA and isotactic L-PLA have different physicochemical properties [44]. For example, D,L-PLA is an amorphous polymer, but L-PLA is semi-crystalline [44]. The glass-transition temperature of L-PLA is higher than that of D,L-PLA, and hydrolysis of L-PLA is slower than D,L-PLA [44]. We consider that these differences may be involved in the mechanism by which nanoparticles containing D,L-PLA show a faster release profile and clearance from the blood than those prepared only from L-PLA.

We also found here that, following monocrotaline treatment, accumulation of RS in the monocrotaline-damaged pulmonary peripheral arteries was observed in rats administered RS-NP, but not in those administered RS alone. We also observed the higher level of accumulation of FITC-labeled albumin at the lung in monocrotaline-treated rats, compared to control rats. These results suggest that RS-NP is selectively delivered to monocrotaline-damaged arteries, probably as a consequence of the EPR effect. It was reported that inflammation was induced in pulmonary peripheral arteries not only in monocrotaline- or hypoxia-induced PAH animal models, but also in PAH patients [45]. Thus, the results of this study suggest that intravenously administered BPS-NP is likely to be selectively delivered to damaged arteries in PAH patients. This treatment approach would enable potent therapeutic effects to be obtained with a low associated risk of adverse effects.

Based on the ameliorative effects of BPS on monocrotaline-induced pulmonary arterial remodeling and RV hypertrophy, we compared the pharmacological activity of intravenously administered BPS-NP and orally administered BPS alone. The extent of amelioration with a once-weekly intravenous administration of BPS-NP (20 μg BPS/kg) was roughly similar to that obtained with daily oral administration of BPS alone (100 μg/kg). These results suggest that encapsulation of BPS into PLA-nanoparticles enables the effective dose of BPS to be decreased and a lower frequency of administration to be used. This lower targeted dose of BPS would be highly advantageous because it would avoid the adverse effects associated with the systemic administration of PGI_2 analogues. Since PAH has various causes, it is important to determine the effects of the candidate drug in numerous animal models. As such, the observed ameliorative effects of BPS-NP in the hypoxia-induced PAH mouse model add further value to its therapeutic potential in PAH patients.

Although various types of orally administered PGI_2 analogues are available, their efficacy in PAH patients is inferior to that obtained with continuous intravenous infusion of PGI_2. This would appear to be due to the fact that maintenance of a high concentration of PGI_2 around damaged pulmonary arteries is important to achieve its ameliorative effect. The findings of the present study suggest that BPS-NP is targeted to damaged pulmonary arteries and remains there for at least 5 days. Thus, if a similar scenario can be achieved in PAH patients, intravenously administered BPS-NP could be used to maintain high concentrations of BPS around damaged arteries and thus achieve therapeutic efficacy and improved QOL in PAH patients based on a lower frequency of administration.

5. Conclusion

Based on the results of this study, we propose that that improved sustained release properties and targeting abilities achieved with BPS-NP may be therapeutically beneficial for PAH patients as a consequence of the decreased BPS dose and frequency of administration that can be employed.

Supplementary data to this article can be found online at http://dx.doi.org/10.1016/j.jconrel.2014.10.029.

Acknowledgments

This work was supported by Grants-in-Aid for Scientific Research from the Ministry of Health, Labour, and Welfare of Japan (201307008A and 201208005B), as well as Center of Innovation Program from Japan Science and Technology Agency, Scientific Technique Research Promotion Program for Agriculture, Forestry and Food Industry (26048A), and Grants-in-Aid for Scientific Research from the Ministry of Education, Culture, Sports, Science and Technology, Japan (22117515).

References

[1] H.W. Farber, J. Loscalzo, Pulmonary arterial hypertension, N. Engl. J. Med. 351 (2004) 1655–1665.
[2] V.V. McLaughlin, M.D. McGoon, Pulmonary arterial hypertension, Circulation 114 (2006) 1417–1431.
[3] M. Humbert, O. Sitbon, A. Chaouat, M. Bertocchi, G. Habib, V. Gressin, A. Yaici, E. Weitzenblum, J.F. Cordier, F. Chabot, C. Dromer, C. Pison, M. Reynaud-Gaubert, A. Haloun, M. Laurent, E. Hachulla, G. Simonneau, Pulmonary arterial hypertension in France: results from a national registry, Am. J. Respir. Crit. Care Med. 173 (2006) 1023–1030.
[4] G.E. D'Alonzo, R.J. Barst, S.M. Ayres, E.H. Bergofsky, B.H. Brundage, K.M. Detre, A.P. Fishman, R.M. Goldring, B.M. Groves, J.T. Kernis, et al., Survival in patients with

primary pulmonary hypertension. Results from a national prospective registry, Ann. Intern. Med. 115 (1991) 343–349.
[5] D. Montani, M.C. Chaumais, C. Guignabert, S. Gunther, B. Girerd, X. Jais, V. Algalarrondo, L.C. Price, L. Savale, O. Sitbon, G. Simonneau, M. Humbert, Targeted therapies in pulmonary arterial hypertension, Pharmacol. Ther. 141 (2014) 172–191.
[6] S. Sakao, K. Tatsumi, N.F. Voelkel, Reversible or irreversible remodeling in pulmonary arterial hypertension, Am. J. Respir. Cell Mol. Biol. 43 (2010) 629–634.
[7] B.W. Christman, C.D. McPherson, J.H. Newman, G.A. King, G.R. Bernard, B.M. Groves, J.E. Loyd, An imbalance between the excretion of thromboxane and prostacyclin metabolites in pulmonary hypertension, N. Engl. J. Med. 327 (1992) 70–75.
[8] R.M. Tuder, C.D. Cool, M.W. Geraci, J. Wang, S.H. Abman, L. Wright, D. Badesch, N.F. Voelkel, Prostacyclin synthase expression is decreased in lungs from patients with severe pulmonary hypertension, Am. J. Respir. Crit. Care Med. 159 (1999) 1925–1932.
[9] L.H. Clapp, P. Finney, S. Turcato, S. Tran, L.J. Rubin, A. Tinker, Differential effects of stable prostacyclin analogs on smooth muscle proliferation and cyclic AMP generation in human pulmonary artery, Am. J. Respir. Cell Mol. Biol. 26 (2002) 194–201.
[10] M.C. Chaumais, M. Jobard, A. Huertas, C. Vignand-Courtin, M. Humbert, O. Sitbon, A. Rieutord, D. Montani, Pharmacokinetic evaluation of continuous intravenous epoprostenol, Expert Opin. Drug Metab. Toxicol. 6 (2010) 1587–1598.
[11] J.A. Saleh, Role of iloprost and bosentan in pulmonary arterial hypertension, Niger. J. Med. 17 (2008) 13–19.
[12] L.J. Rubin, J. Mendoza, M. Hood, M. McGoon, R. Barst, W.B. Williams, J.H. Diehl, J. Crow, W. Long, Treatment of primary pulmonary hypertension with continuous intravenous prostacyclin (epoprostenol). Results of a randomized trial, Ann. Intern. Med. 112 (1990) 485–491.
[13] S. Rich, J. Pogoriler, A.N. Husain, P.T. Toth, M. Gomberg-Maitland, S.L. Archer, Long-term effects of epoprostenol on the pulmonary vasculature in idiopathic pulmonary arterial hypertension, Chest 138 (2010) 1234–1239.
[14] R. Barst, How has epoprostenol changed the outcome for patients with pulmonary arterial hypertension? Int. J. Clin. Pract. Suppl. (2010) 23–32.
[15] F. Reichenberger, A. Mainwood, N.W. Morrell, J. Parameshwar, J.P. Zaba, Intravenous epoprostenol versus high dose inhaled iloprost for long-term treatment of pulmonary hypertension, Pulm. Pharmacol. Ther. 24 (2010) 169–173.
[16] R.J. Barst, L.J. Rubin, W.A. Long, M.D. McGoon, S. Rich, D.B. Badesch, B.M. Groves, V.F. Tapson, R.C. Bourge, B.H. Brundage, S.K. Koerner, D. Langleben, C.A. Keller, S. Murali, B.F. Uretsky, L.M. Clayton, M.M. Jobsis, S.D. Blackburn, D. Shortino, J.W. Crow, A comparison of continuous intravenous epoprostenol (prostacyclin) with conventional therapy for primary pulmonary hypertension, N. Engl. J. Med. 334 (1996) 296–301.
[17] V.V. McLaughlin, A. Shillington, S. Rich, Survival in primary pulmonary hypertension: the impact of epoprostenol therapy, Circulation 106 (2002) 1477–1482.
[18] K.K. Mubarak, A review of prostaglandin analogs in the management of patients with pulmonary arterial hypertension, Respir. Med. 104 (2010) 9–21.
[19] S.T. Nadler, J.D. Edelman, Inhaled treprostinil and pulmonary arterial hypertension, Vasc. Health Risk Manag. 6 (2010) 1115–1124.
[20] M.G. Dickinson, E.H. Scholvinck, A. Boonstra, A. Vonk-Noordegraaf, R.J. Snijder, R.M. Berger, Low complication rates with totally implantable access port use in epoprostenol treatment of pulmonary hypertension, J. Heart Lung Transplant. 28 (2009) 273–279.
[21] N. Galie, A. Torbicki, R. Barst, P. Dartevelle, S. Haworth, T. Higenbottam, H. Olschewski, A. Peacock, G. Pietra, L.J. Rubin, G. Simonneau, S.G. Priori, M.A. Garcia, J.J. Blanc, A. Budaj, M. Cowie, V. Dean, J. Deckers, E.F. Burgos, J. Lekakis, B. Lindahl, G. Mazzotta, K. McGregor, J. Morais, A. Oto, O.A. Smiseth, J.A. Barbera, S. Gibbs, M. Hoeper, M. Humbert, R. Naeije, J. Pepke-Zaba, Guidelines on diagnosis and treatment of pulmonary arterial hypertension. The Task Force on Diagnosis and Treatment of Pulmonary Arterial Hypertension of the European Society of Cardiology, Eur. Heart J. 25 (2004) 2243–2278.
[22] R.J. Barst, J.S. Gibbs, H.A. Ghofrani, M.M. Hoeper, V.V. McLaughlin, L.J. Rubin, O. Sitbon, V.F. Tapson, N. Galie, Updated evidence-based treatment algorithm in pulmonary arterial hypertension, J. Am. Coll. Cardiol. 54 (2009) S78–S84.
[23] R.J. Barst, M. McGoon, V. McLaughlin, V. Tapson, S. Rich, L. Rubin, K. Wasserman, R. Oudiz, S. Shapiro, I.M. Robbins, R. Channick, D. Badesch, B.K. Rayburn, R. Flinchbaugh, J. Sigman, C. Arneson, R. Jeffs, Beraprost therapy for pulmonary arterial hypertension, J. Am. Coll. Cardiol. 41 (2003) 2119–2125.
[24] M.S. Buckley, J.P. Feldman, Inhaled epoprostenol for the treatment of pulmonary arterial hypertension in critically ill adults, Pharmacotherapy 30 (2010) 728–740.
[25] N. Nagaya, M. Uematsu, Y. Okano, T. Satoh, S. Kyotani, F. Sakamaki, N. Nakanishi, K. Miyatake, T. Kunieda, Effect of orally active prostacyclin analogue on survival of outpatients with primary pulmonary hypertension, J. Am. Coll. Cardiol. 34 (1999) 1188–1192.
[26] T. Ishihara, N. Izumo, M. Higaki, E. Shimada, T. Hagi, L. Mine, Y. Ogawa, Y. Mizushima, Role of zinc in formulation of PLGA/PLA nanoparticles encapsulating betamethasone phosphate and its release profile, J. Control. Release 105 (2005) 68–76.
[27] T. Ishihara, M. Takahashi, M. Higaki, Y. Mizushima, Efficient encapsulation of a water-soluble corticosteroid in biodegradable nanoparticles, Int. J. Pharm. 365 (2009) 200–205.
[28] T. Ishihara, M. Takahashi, M. Higaki, M. Takenaga, T. Mizushima, Y. Mizushima, Prolonging the *in vivo* residence time of prostaglandin E(1) with biodegradable nanoparticles, Pharm. Res. 25 (2008) 1686–1695.
[29] T. Ishihara, Y. Yamashita, N. Takasaki, S. Yamamoto, E. Hayashi, K. Tahara, M. Takenaga, N. Yamakawa, T. Kasahara, T. Mizushima, Prostaglandin E1-containing nanoparticles improve walking activity in an experimental rat model of intermittent claudication, J. Pharm. Pharmacol. 65 (2013) 1187–1194.
[30] M. Takeda, T. Maeda, T. Ishihara, H. Sakamoto, K. Yuki, N. Takasaki, F. Nishimura, T. Yamashita, K. Tanaka, M. Takenaga, R. Igarashi, M. Higaki, N. Yamakawa, Y. Okamoto, H. Ogawa, M. Otsuka, Y. Mizushima, T. Mizushima, Synthesis of prostaglandin E(1) phosphate derivatives and their encapsulation in biodegradable nanoparticles, Pharm. Res. 26 (2009) 1792–1800.
[31] M.S. Shive, J.M. Anderson, Biodegradation and biocompatibility of PLA and PLGA microspheres, Adv. Drug Deliv. Rev. 28 (1997) 5–24.
[32] R. Gref, Y. Minamitake, M.T. Peracchia, V. Trubetskoy, V. Torchilin, R. Langer, Biodegradable long-circulating polymeric nanospheres, Science 263 (1994) 1600–1603.
[33] S. Stolnik, S.E. Dunn, M.C. Garnett, M.C. Davies, A.G. Coombes, D.C. Taylor, M.P. Irving, S.C. Purkiss, T.F. Tadros, S.S. Davis, et al., Surface modification of poly(lactide-co-glycolide) nanospheres by biodegradable poly(lactide)–poly(ethylene glycol) copolymers, Pharm. Res. 11 (1994) 1800–1808.
[34] H. Maeda, J. Wu, T. Sawa, Y. Matsumura, K. Hori, Tumor vascular permeability and the EPR effect in macromolecular therapeutics: a review, J. Control. Release 65 (2000) 271–284.
[35] Piskin, X. Kaitian, E.B. Denkbas, Z. Kucukyavuz, Novel PDLLA/PEG copolymer micelles as drug carriers, J. Biomater. Sci. Polym. Ed. 7 (1995) 359–373.
[36] K. Yamaki, Y. Takano-Ishikawa, M. Goto, M. Kobori, T. Tsushida, An improved method for measuring vascular permeability in rat and mouse skin, J. Pharmacol. Toxicol. Methods 48 (2002) 81–86.
[37] T. Kawakami, H. Kanazawa, T. Satoh, M. Ieda, Y. Ieda, K. Kimura, H. Mochizuki, T. Shimada, C. Yokoyama, S. Ogawa, T. Tanabe, K. Fukuda, AAV–PGIS gene transfer improves hypoxia-induced pulmonary hypertension in mice, Biochem. Biophys. Res. Commun. 363 (2007) 656–661.
[38] H. Obata, Y. Sakai, S. Ohnishi, S. Takeshita, H. Mori, M. Kodama, K. Kangawa, Y. Aizawa, N. Nagaya, Single injection of a sustained-release prostacyclin analog improves pulmonary hypertension in rats, Am. J. Respir. Crit. Care Med. 177 (2008) 195–201.
[39] K. Matsumoto, A. Tajima, Y. Hirano, K. Ohno, T. Yuge, T. Hamasaki, T. Hase, M. Horiba, Pharmacokinetics and Biotransformation of Beraprost Sodium I: Plasma Level Profile of Beraprost Sodium in Rat, Drug Metab. Pharmacokinet. 4 (1989) 713–725.
[40] N.Z. Wu, B. Klitzman, G. Rosner, D. Needham, M.W. Dewhirst, Measurement of material extravasation in microvascular networks using fluorescence videomicroscopy, Microvasc. Res. 46 (1993) 231–253.
[41] T. Itoh, N. Nagaya, T. Fujii, T. Iwase, N. Nakanishi, K. Hamada, K. Kangawa, H. Kimura, A combination of oral sildenafil and beraprost ameliorates pulmonary hypertension in rats, Am. J. Respir. Crit. Care Med. 169 (2004) 34–38.
[42] M. Ueno, T. Miyauchi, S. Sakai, R. Yamauchi-Kohno, K. Goto, I. Yamaguchi, A combination of oral endothelin—a receptor antagonist and oral prostacyclin analogue is superior to each drug alone in ameliorating pulmonary hypertension in rats, J. Am. Coll. Cardiol. 40 (2002) 175–181.
[43] U. Bilati, E. Allemann, E. Doelker, Development of a nanoprecipitation method intended for the entrapment of hydrophilic drugs into nanoparticles, Eur. J. Pharm. Sci. 24 (2005) 67–75.
[44] R. Jalil, J.R. Nixon, Biodegradable poly(lactic acid) and poly(lactide-co-glycolide) microcapsules: problems associated with preparative techniques and release properties, J. Microencapsul. 7 (1990) 297–325.
[45] L.C. Price, S.J. Wort, F. Perros, P. Dorfmuller, A. Huertas, D. Montani, S. Cohen-Kaminsky, M. Humbert, Inflammation in pulmonary arterial hypertension, Chest 141 (2012) 210–221.

Biochemical and Biophysical Research Communications 463 (2015) 222–228

Contents lists available at ScienceDirect

Biochemical and Biophysical Research Communications

journal homepage: www.elsevier.com/locate/ybbrc

Potential new chemotherapy strategy for human ovarian carcinoma with a novel KSP inhibitor

Mitsuko Takenaga [a, *], Yuki Yamamoto [a], Tomoki Takeuchi [b], Yuki Ohta [c], Yukie Tokura [a], Akemi Hamaguchi [a], Daisuke Asai [d], Hideki Nakashima [d], Shinya Oishi [b], Nobutaka Fujii [b]

[a] Institute of Medical Science, St. Marianna University School of Medicine, Miyamae-ku, Kawasaki, Kanagawa 216-8512, Japan
[b] Graduate School of Pharmaceutical Science, Kyoto University, Sakyo-ku, Kyoto 606-8501, Japan
[c] Department of Pharmacology, St. Marianna University School of Medicine, Miyamae-ku, Kawasaki, Kanagawa 216-8512, Japan
[d] Department of Microbiology, St. Marianna University School of Medicine, Miyamae-ku, Kawasaki, Kanagawa 216-8512, Japan

ARTICLE INFO

Article history:
Received 8 May 2015
Available online 19 May 2015

Keywords:
Apoptosis
Kinesin spindle protein
Human ovarian cancer
Neurotoxicity
Securin

ABSTRACT

Among synthetic kinesin spindle protein (KSP) inhibitor compounds, KPYB10602, a six-member lactam-fused carbazole derivative was the most potent *in vitro* against cell growth of human ovarian cancer, A2780. KPYB10602 caused dose-dependent suppression of tumor growth *in vivo*. Mitotic arrest due to KPYB10602 was confirmed *in vitro*, and was characterized by inhibition of securin degradation. Apoptosis after mitotic arrest was associated with an increase in the ratio of pro-apoptotic Bax to anti-apoptotic Bcl-2. Increase of reactive oxygen species (ROS) and caspase pathway were also involved. Furthermore, KPYB10602 caused little neurotoxicity in *vivo*. Therefore, KPYB10602 could be a promising candidate as an anti-tumor agent with reduced adverse events for treating human ovarian cancer.

© 2015 Elsevier Inc. All rights reserved.

1. Introduction

Ovarian cancer is a major cause of death among gynecological malignancies. Significant improvement of the survival time has been achieved since platinum derivatives (cisplatin and carboplatin) and paclitaxel were introduced as standard postoperative chemotherapy [1]. However, the success rate of treatment for advanced, recurrent, or persistent ovarian cancer has remained largely unchanged for several decades, which means that there is a need to consider second-line chemotherapy for this cancer.

Anti-microtubule drugs such as taxanes (including paclitaxel) and vinca alkaloids [2] bind to tubulin and block cell cycle progression through disruption of microtubule dynamics and activation of the spindle checkpoint, leading to cell death [3]. These anti-microtubule agents are used extensively for chemotherapy, however, often cause adverse events such as peripheral neuropathy [4]. This is because tubulin is an essential cytoskeletal protein that is involved in not only cell division but also cell morphology, motility, and intracellular transport. Therefore, there is an urgent need for new anti-tumor agents that do not affect microtubule dynamics.

A potentially attractive target is kinesin spindle protein (KSP), which is also known as Eg5 and KIF11 [5]. It plays a critical role in bipolar spindle formation and separation of duplicated chromosomes during early mitosis by driving the antiparallel sliding of microtubules with energy obtained from ATP hydrolysis. KSP inhibitors cause mitotic arrest in which condensed chromosomes form a ring around unseparated spindle poles, commonly referred to as a monaster spindle with DNA rosette. Thus, inhibition of KSP arrests dividing cells in mitosis and leads to death without affecting microtubule function.

The first specific KSP inhibitor, monastrol [6], was reported in 1999 as a compound that induced monoastral spindle formation. Subsequent inhibitors of the ATPase activity of KSP that have been reported include the dihydropyrimidine-2-thione derivative dimethylenastron [7,8], the quinazolinone derivatives ispinesib [9] and SB-743921 [10], the dihydropyrrole derivative MK-0731 [11], the tetrahydroquinoline derivative EMD-534085 [12], the cysteine derivative S-trityl-L-cysteine [13], and a biphenyl derivative [14].

* Corresponding author. Institute of Medical Science, St. Marianna University School of Medicine, 2-16-1 Sugao, Miyamae-ku, Kawasaki, Kanagawa 216-8512, Japan. Fax: +81 44 976 3747.

E-mail addresses: mitake@marianna-u.ac.jp (M. Takenaga), yukiyma@diary.ocn.ne.jp (Y. Yamamoto), takeuchi.tomoki.32s@st.kyoto-u.ac.jp (T. Takeuchi), yuki-o@marianna-u.ac.jp (Y. Ohta), yukie-t@marianna-u.ac.jp (Y. Tokura), hamaguchi@marianna-u.ac.jp (A. Hamaguchi), asai@marianna-u.ac.jp (D. Asai), hidekin@marianna-u.ac.jp (H. Nakashima), soishi@pharm.kyoto-u.ac.jp (S. Oishi), nfujii@pharm.kyoto-u.ac.jp (N. Fujii).

http://dx.doi.org/10.1016/j.bbrc.2015.05.028
0006-291X/© 2015 Elsevier Inc. All rights reserved.

Some of these KSP inhibitors have undergone clinical trials [10,15–21].

We have also designed a variety of KSP inhibitors [22–24], and have demonstrated that carbazole derivatives exhibit strong anti-tumor activity *in vitro* [25]. Our present study was aimed to evaluate the *in vivo* activity against human ovarian cancer of the most potent KSP inhibitor that we have identified, and investigate the underlying mechanisms *in vitro* and neurotoxicity *in vivo*.

2. Materials & methods

2.1. Reagents

KSP inhibitors were synthesized according to the method by previously reported [25]. The inhibitors tested in this study were KPYB10602 (a six-member lactam-fused carbazole derivative), KPYC12688 (a five-member lactam-fused carbazole derivative), and KPYC12687 (a pyrrole-fused carbazole derivative) (Fig. 1(A)). Paclitaxel and carboplatin were purchased from Sigma–Aldrich Inc. (St. Louis, MO).

2.2. Cells

The human ovarian carcinoma cell line A2780 (Health Protection Agency Culture Collections, Salisbury, UK) was used. Culture was done in RPMI 1640 medium (Sigma–Aldrich) with 10% fetal bovine serum (FBS) (Invitrogen, Carlsbad, CA) and 1% antibiotic-antimycotic (Invitrogen), and cells after two passages were used in this study.

2.3. Animals

Animal experiments were performed in accordance with the Guidelines for Animal Experimentation of St. Marianna University Graduate School of Medicine. Pathogen-free female BALB/c-nu mice (Charles River Laboratories Japan, Yokohama) were housed in an isolated animal room at a constant temperature (23 ± 1 °C) and humidity (50–60%) with a 12-h light/dark cycle, and were allowed free access to 30 kGy CL-2 diet (Clea Japan, Tokyo) and sterilized water. Female BALB/c mice were also housed under similar conditions.

2.4. Cell proliferation assay

Cells (1×10^4) were cultured with inhibitors for 48 h, and the 3-(4,5-dimethylthiazol-2-yl)-2,5-diphenyltetrazolium bromide (MTT) (Sigma–Aldrich) assay and the [^{3}H]-thymidine ([methyl, 1′, 2′-^{3}H]thymidine) (PerkinElmer Japan, Yokohama) incorporation assay were carried out.

2.5. Immuno-staining

Cells (2×10^4) in a Lab-Tek® Chamber Slide (Nalge Nunc International, NY) were cultured with inhibitors for 24 h. Fixed cells were incubated with anti-α/β tubulin (rabbit, Cell Signaling), and reacted with Alexa Fluor® 594 anti-rabbit IgG (Invitrogen). Nuclei were counterstained with 4′,6-diamidino-2-phenylindole (DAPI) (Invitrogen).

2.6. Tumor xenograft study

Seven days after cells (5×10^6) were subcutaneously inoculated into female BALB/c-nu mice, and drug treatments were started (day 0). The KSP inhibitor, KPYB10602 (8 or 80 mg/kg) in olive oil was administered subcutaneously on days 0–4 and day 8. The doses and the administration schedule were determined from the results of preliminary studies on tolerability. Paclitaxel (25 mg/kg) was subcutaneously administered on day 0.

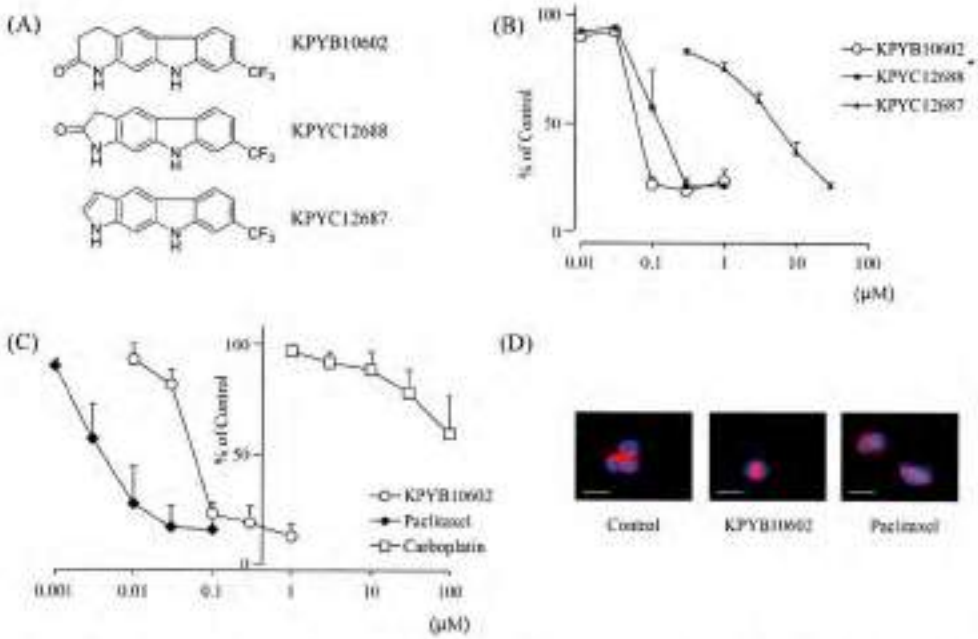

Fig. 1. KSP inhibitors, and their effect on cell growth *in vitro*. (A) Chemical structures of the KSP inhibitors. (B, C) Cells (1×10^4) were cultured with KSP inhibitors, paclitaxel, or carboplatin for 48 h, and MTT assay was performed. Mean ± SD, n = 6. (D) Medium alone (Control), KPYB10602 (1 μM), paclitaxel (0.1 μM). α/β tubulin (red). Nuclei (blue). Scale bars = 25 μm.

Tumor volumes (mm^3) were calculated with the standard formula: length × width^2 × 0.5 [26]. Evaluation was stopped on day 18, since the vehicle control (Control) group, the mean tumor volume reached over 5000 mm^3 and some of them died. After *in vivo* evaluation, tumor specimens were used for hematoxylin–eosin (HE) staining.

2.7. Rota-rod test

Female Balb/c mice was subcutaneously treated with KPYB10602 (80 mg/kg) on days 0–4, or with paclitaxel (25 mg/kg) on day 0. Rota-rod test (MK-610A, Muromachi Kikai Co., Ltd. Tokyo) was carried out at a constant speed (6 rpm). The time being placed on the rod was measured during a period of 300 s, and the total time was calculated.

2.8. Cell cycle

Adherent cells (2×10^6) were replaced with serum-free fresh medium and cultured for 15 h. After further incubation with inhibitors, cells were harvested, fixed with ice-cold 70% ethanol, and kept at −20 °C overnight. Then, cells treated with 20 μg/ml propidium iodide (PI) and 0.1 mg/ml RNase were subjected to flow cytometer (BD LSR II, BD Biosciences, San Diego, CA). At least 30,000 cells were analyzed in each assay.

2.9. Apoptosis assay

Cells were cultured with KPYB10602 as described above, and stained with an FITC annexin V/dead cell apoptosis kit (Invitrogen). Cells with early apoptosis (only stained by FITC) or late apoptosis (stained by both FITC and PI) were analyzed with FlowJo software (Tree Star, Ashland, OH).

2.10. Intracellular reactive oxygen species (ROS)

KPYB10602-treated cells were reacted with 100 μM dichlorofluorescein diacetate (DCFH-DA, Sigma–Aldrich) for 10 min at 37 °C. ROS levels were quantified by determining the mean fluorescence intensity (MFI).

2.11. Western blot analysis

Cell lysates (20 μg) were subjected to electrophoresis on 5–20% SDS polyacrylamide gels. After transferred to PVDF membranes (Clearblot P™, Atto Corporation, Tokyo), anti-securin antibody (clone 19H16L48) (rabbit, Invitrogen), anti-Mad2 antibody (mouse, BD Transduction Laboratories), anti-Bax antibody (rabbit, Cell Signaling) anti-Bcl-2 antibody (rabbit, Cell Signaling), anti-caspase 9 antibody (rabbit, Cell Signaling), anti-caspase 3 antibody (rabbit, Cell Signaling), or anti-β-actin antibody (mouse, Sigma–Aldrich) was applied. Then the membranes were incubated with ECL HRP-labeled anti-mouse IgG or HRP-labeled anti-rabbit IgG (GE Healthcare Japan).

2.12. Statistical analysis

Data are expressed as the mean ± SD (or SE). Mean values were compared by one-way analysis of variance. Statistical analysis was performed by using the Mann–Whitney U-test (*in vivo*) or the unpaired Student's *t*-test (*in vitro*), and significance was accepted at $P < 0.05$.

3. Results

3.1. In vitro anti-tumor activity of KSP inhibitors

All of the KSP inhibitors suppressed the cell growth in a concentration-dependent manner (Fig. 1(B)). KPYC12687 was far less potent than the others. The concentration required to reduce cell growth by 50% (IC_{50}) was 0.078 μM for KPYB10602, 0.105 μM for KPYC12688, and 8.325 μM for KPYC12687 (Table 1). Similar results were obtained in the thymidine uptake assay. Since KPYB10602 was the most potent, it was selected for evaluation of *in vivo* anti-tumor activity.

3.2. In vitro potency of KPYB10602 compared with that of paclitaxel and carboplatin

Prior to *in vivo* evaluation, the *in vitro* effect of KPYB10602 was compared with that of paclitaxel and carboplatin. Cell growth was dose-dependently suppressed (Fig. 1(C)). Based on these IC_{50} values (Table 1), KPYB10602 was 10-fold less potent than paclitaxel, but over 1600-fold more potent than carboplatin. Different from paclitaxel-treated cells, KPYB10602-treated ones were characterized to form a monaster spindle with DNA rosette (Fig. 1(D)).

3.3. In vivo effect of KPYB10602 in A2780 tumor-bearing BALB/c-nu mice

Seven days after cell inoculation, the tumor volume reached around 50 mm^3 (day 0). Tumor volume increased in the vehicle-treated group (Control), reaching about 5000 mm^3 on day 18. KPYB10602 (80 mg/kg) achieved significant suppression compared with the Control (Fig. 2(A)), and complete tumor regression occurred in 3 animals. While KPYB10602 (8 mg/kg) was less effective, the V/V_0 ratio was similar to that in the high dose group up to day 11 (Table 2). Anti-tumor activity diminished after treatment was stopped, however, the high dose of KPYB10602 was able to eradicate some tumors.

The body weight was a little higher in both KPYB10602-treated groups than in the Control (Fig. 2(B)), where solid tumors weighed 3.92 ± 0.90 g (day 18). Extensive nuclear condensation was observed in KPYB10602-treated tumors, suggesting that mitotic arrest was caused (Fig. 2(C)).

Paclitaxel suppressed tumor growth until day 8, after which tumor growth was similar to that in the low-dose KPYB10602 group (Table 2).

3.4. In vivo effect of KPYB10602 on motor coordination in BALB/c mice

Rota-rod test was performed to examine whether KPYB10602 showed neurotoxicity. Paclitaxel induced significant impairment of

Table 1
IC_{50} (μM) of KSP inhibitors, paclitaxel, and carboplatin.

KSP inhibitors	MTT assay	Thymidine incorporation assay
KPYB10602	0.0783 ± 0.0094	0.0405 ± 0.0076
KPYC12688	0.105 ± 0.036	0.0570 ± 0.0072
KPYC12687	8.33 ± 1.40	2.35 ± 0.684
Agents	**MTT assay**	**Thymidine incorporation assay**
KPYB10602	0.056 ± 0.0048	0.035 ± 0.0160
Paclitaxel	0.0051 ± 0.0003	0.001 ± 0.0006
Carboplatin	93.0 ± 15.6	16.8 ± 2.29

A2780 cells were cultured with KSP inhibitors, paclitaxel, or carboplatin for 48 h. Three separate experiments were repeated, and the respective IC_{50} was obtained. Data are expressed as the mean ± SD.

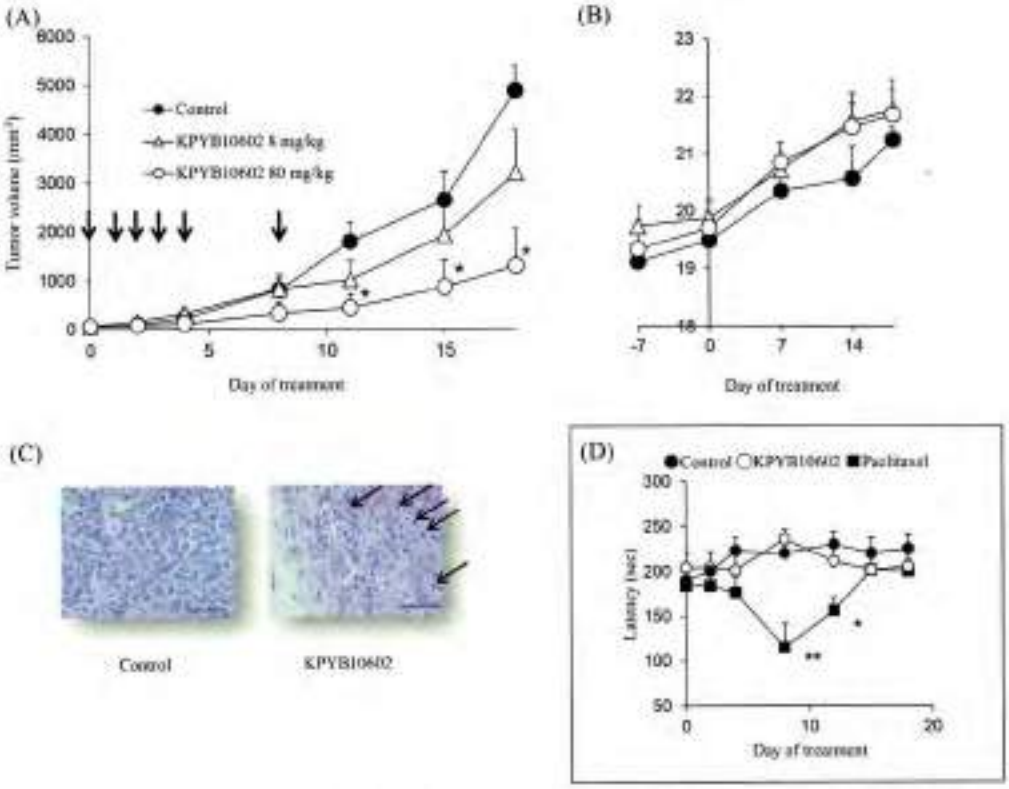

Fig. 2. *In vivo* effect of KPYB10602 on tumor-bearing BALB/c-nu mice (A, B, C), and on motor coordination in BALB/c mice (D). Seven days after cells (5×10^6) inoculation to BALB/c-nu mice, treatment was started (day 0). Subcutaneous treatments were done on days 0–4 and day 8 (arrows). Mean ± SE, n = 7. (A) Tumor volume, (B) Body weight, (C) HE staining. Nuclear condensations (arrows). Scale bars = 50 μm. (D) Balb/c mice received KPYB10602 (80 mg/kg) on days 0–4, or paclitaxel (25 mg/kg) on day 0. Rota-rod test was performed twice a week. Mean ± SE, n = 5. *p < 0.05, **p < 0.01 vs. Control.

coordination on days 8 and 12 (Fig. 2(D)). In contrast, there was no significant difference in performance between mice treated with KPYB10602 and the Control group.

3.5. *In vitro effect of KPYB10602 on cell cycle, ROS production, and expression of cell cycle- or apoptosis-related proteins*

Since nuclear condensation was prominent in KPYB10602-treated tumors (Fig. 2(C)), the *in vitro* effect was focused.

In the absence of drugs, the proportion of 4 N cells in G_2/M phase was relatively constant at around 15–16% (Table 3). KPYB10602 (10 μM) increased the proportion of G_2/M phase cells at 15 h (35.0%), indicating mitotic arrest (Fig. 3(A)). Paclitaxel (2.5 μM) also caused accumulation of G_2/M phase cells, which reached 32.9% In contrast, carboplatin (100 μM) had little effect on G_2/M phase cells (15.2%). The proportion of >4 N cells was also assessed, but there was little difference compared with the Control.

Apoptotic cells (subG$_1$) gradually increased after exposure to the drugs. KPYB10602 (10 μM) increased apoptotic cells from 4.55% to 22.3%. The increase was both time- and concentration-dependent. Also, the proportion of early apoptotic cells was 0.21% in the Control, while it increased to 17.8% in KPYB10602-treated cells (Fig. 3(B)).

Securin degradation is essential for the progress from metaphase to anaphase. The securin/mitotic arrest defective 2 (Mad2) ratio was increased over 2-fold by addition of KPYB10602 (Fig. 3(C)). Concentration-dependent suppression was also observed after 6 h and 24 h of culture (data not shown). Similar results were obtained with paclitaxel, but not with carboplatin (data not shown).

Table 2
V/V_0 ratio in each group.

	Dose (mg/kg)	Day of treatment					
		2	4	8	11	15	18
Control	0	1.82 ± 0.40	4.86 ± 0.47	24.0 ± 8.17	63.4 ± 21.5	138.4 ± 26.9	259.9 ± 18.8
KPYB10602	8	1.98 ± 0.52	4.71 ± 1.49	14.1 ± 6.01	21.8 ± 8.39	62.6 ± 22.4	115.6 ± 39.1
KPYB10602	80	1.42 ± 0.26	1.54 ± 0.66*	15.6 ± 10.4	21.1 ± 12.5	42.1 ± 25.2*	63.9 ± 35.0*
Paclitaxel	25	1.40 ± 0.85	1.64 ± 0.73*	7.64 ± 2.89	22.4 ± 7.30	70.7 ± 24.3	100.1 ± 34.0

The V/V_0 ratio = V (tumor volume on the day of evaluation)/V_0 (tumor volume on the first day of treatment).
Data are expressed as the mean ± SE (n = 7). *p < 0.05 vs. Control.

Table 3
Effects of KPYB10602, paclitaxel, and carboplatin on cell cycle.

(a)	Treatment	(μM)	SubG$_1$	G$_1$	S	G$_2$/M	>4N
	Control	0	2.42	29.6	10	15.4	42.4
	KPYB10602	1	2.25	16.0	7.0	31.3	43.0
		10	2.83	15.3	6.9	31.8	44.6
	Paclitaxel	0.25	2.5	22.8	7.8	24.9	41.8
		2.5	2.15	17.2	7.2	29.3	41.9
	Carboplatin	10	2.72	30.1	6.6	16.9	43.7
		100	2.0	32.2	7.3	15.9	42.6
(b)	Treatment	(μM)	SubG$_1$	G$_1$	S	G$_2$/M	>4N
	Control	0	4.55	44.1	6.1	16.7	28.6
	KPYB10602	1	7.83	27.3	3.3	31.0	31.0
		10	22.3	16.5	3.6	35.0	23.5
	Paclitaxel	0.25	11.4	22.1	4.2	32.3	29.5
		2.5	13.3	26.4	4.1	32.0	24.6
	Carboplatin	10	6.7	42.5	6.8	16.7	26.7
		100	7.2	44.3	8.9	15.2	25.2

A2780 cells were incubated with KPYB10602, paclitaxel, or carboplatin for 6 h (a) or 15 h (b). Each assay was performed three times, and the data obtained from one representative experiment were shown. Each value was expressed as %.

Pro-apoptotic Bax protein increased, and anti-apoptotic Bcl-2 protein decreased slightly (Fig. 3(D)). After 3 h of culture with KPYB10602 (10 μM), the Bax/Bcl-2 ratio showed an almost 2-fold increase, and a concentration-dependent increase of this ratio was also observed after 6, 15, and 24 h of culture. In addition, ROS level increased during incubation with KPYB10602 in a concentration-dependent and time-dependent manner (Fig. 3(E)). Western blot analysis revealed that the levels of cleaved caspase-3 and caspase-9 increased in a concentration-dependent manner (Fig. 3(F)).

4. Discussion

The present study demonstrated that a carbazole-derivative KSP inhibitor, KPYB10602, which was the most potent of the KSP inhibitors tested *in vitro*, had *in vivo* anti-tumor activity in an A2780 human ovarian cancer xenograft model.

It was noted that tumor growth was significantly suppressed with KPYB10602, and there were even some animals with diminished tumors. Furthermore, extensive nuclear condensation was observed in KPYB10602-treated tumors. These findings indicate that KPYB10602 could have induced mitotic arrest, leading to tumor cell death.

It should be noted that KPYB10602-treated animals showed little neurotoxicity. Paclitaxel-treated animals showed impairment of motor coordination during the first 8–12 days, although this subsequently recovered. No such incoordination was observed in animals treated with KPYB10602. These results indicate that KPYB10602 primarily acts on mitotic cells, but does not have much influence on microtubule functions, different from paclitaxel.

Cell cycle analysis confirmed that KPYB10602 induced mitotic arrest, similar to anti-microtubule drugs such as paclitaxel. In addition, subG$_1$ (apoptotic) cells were increased in a dose-dependent manner.

KSP is required for bipolar spindle formation in the mitotic phase, so inhibition of KSP generates monopolar spindle, resulting in unaligned condensed chromosomes and activation of the spindle assembly checkpoint (SAC). This activation finally blocks the degradation of securin through activation of Mad2. Therefore,

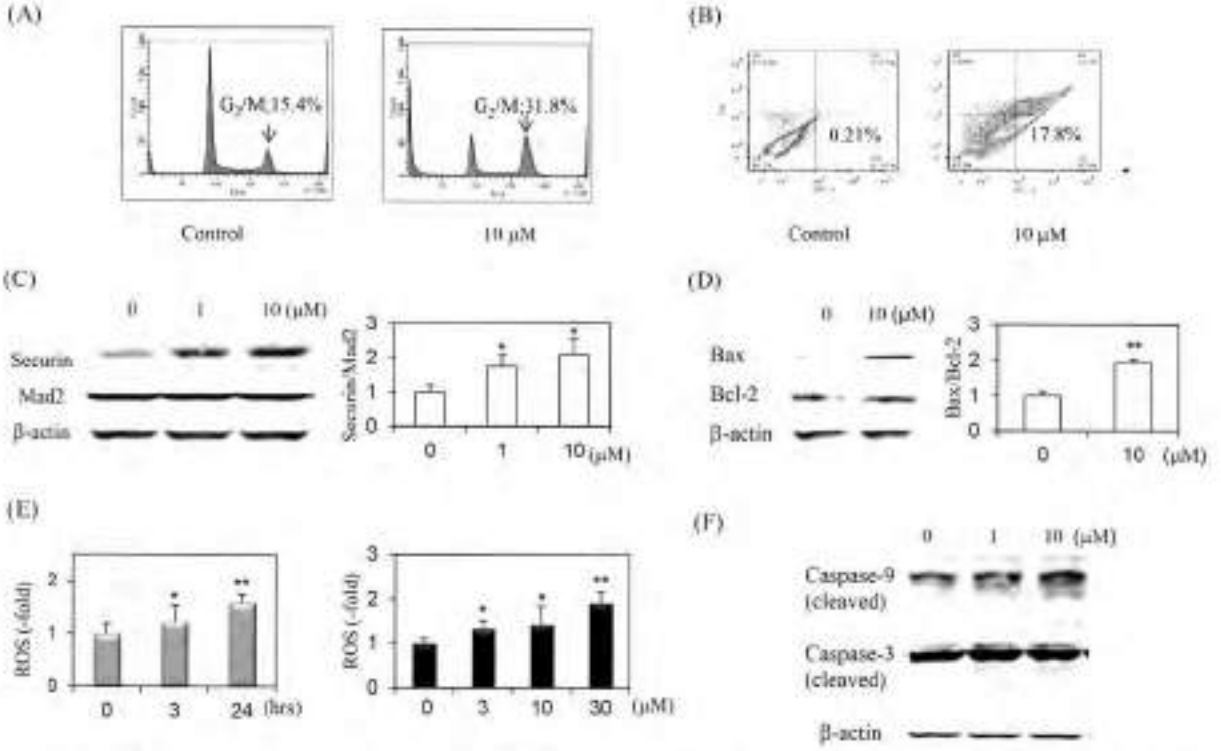

Fig. 3. *In vitro* effect of KPYB10602 on cell cycle (A), apoptosis (B), ROS production (E), and the expression of related proteins (C, D, F). Cells (2×10^6) were cultured with KPYB10602 for 15 h or indicated times. ROS levels (E) were presented as the fold change of MFI. Relative intensity was expressed as securin to Mad2 (C) or Bax to Bcl-2 (D). $^*p < 0.05$, $^{**}p < 0.01$ vs. Control.

securin degradation is essential for the separation of duplicated chromosomes after completion of alignment [27]. KPYB10602 suppressed securin degradation in a concentration-dependent manner, which must have prevented the progression from metaphase to anaphase. Metaphase arrest must have led to apoptotic cell death without affecting microtubules dynamics.

Mitotic arrest can result in cell death through mitotic slippage, which is characterized by development of multinucleated (>4 N) cells [28]. Some KSP inhibitors [26] have been reported to induce mitotic slippage, however, it was not observed under our experimental conditions.

ROS production was induced in a time-dependent and concentration-dependent manner. ROS are generated during mitotic arrest mainly via cytochrome c release in the mitochondria. Bax is a pro-apoptotic protein that increases the leakage of apoptotic factors from the mitochondria, while Bcl-2 is an anti-apoptotic protein that negatively regulates this leakage. KPYB10602 enhanced the expression of Bax and slightly decreased that of Bcl-2, resulting in a marked increase of the Bax/Bcl-2 ratio. This would have contributed to ROS production via promotion of cytochrome c release. In addition, cleaved caspase-9 and -3 were observed. Therefore, not only increased Bax/Bcl-2 but also ROS production would have been involved in caspase activation and apoptosis.

Mitotic arrest can cause the accumulation of P53 [29], and in particular P53 phosphorylated at serine 15 has been reported to induce apoptosis partly via activation of Bax [30]. While P53 expression was increased by carboplatin, KPYB10602 caused little increase of P53 in the present study (data not shown). This might suggest that KPYB10602-induced apoptosis was independent of P53-mediated pathways.

Among KSP inhibitors that we tested *in vitro*, KPYB10602 was the most potent against A2780 human ovarian cancer cells. This potency was reflected by the IC_{50} for KSP ATPase (0.031 μM for KPYB10602, 0.037 μM for KPYC12688, and 0.17 μM for KPYC12687). It should be noted that these compounds are much specific for KSP and do not target other kinesin motor proteins such as CENP-E, Kid, MKLP-1, or KIF-4 [23].

Some KSP inhibitors have already been investigated in preclinical studies [10,15–21]. Some KSP inhibitors have been reported to show inhibitory activity even against drug-resistant ovarian cancer [24], suggesting that these compounds could become a new treatment option for ovarian cancer with less toxicity. Therefore, in the next study, KPYB10602 would have to be examined against drug-resistant ovarian cancer. In parallel, the distribution of a drug can affect its efficacy as well as potency. If *in vivo* drug delivery systems to target tumor cells can be developed, the anti-tumor effect of KPYB10602 could be augmented further.

The specific KSP inhibitor, KPYB10602 showed anti-tumor activity in A2780 tumor-bearing mice. KPYB10602 was proved to suppress securin degradation, leading to mitotic arrest. Mitotic arrest by KPYB10602 must have led to apoptotic cell death without affecting microtubules dynamics, different from paclitaxel. This was supported by the fact that KPYB10602 showed little *in vivo* neurotoxicity. Taken together, KPYB10602 could be a promising candidate as an anti-tumor agent with reduced adverse events for treating human ovarian cancer.

Conflict of interest

The authors declare that there are no conflicts of interest.

Acknowledgments

This work was supported by a Grant-in-Aid for Scientific Research (25462618); Platform for Drug Discovery, Informatics, and Structural Life Science from MEXT, Japan. T.T. is grateful for JSPS Research Fellowships for Young Scientists.

References

[1] I.A. Boere, M.E. van der Burg, Review of dose-intense platinum and/or paclitaxel containing chemotherapy in advanced and recurrent epithelial ovarian cancer, Curr. Pharm. Des. 18 (2012) 3741–3753.
[2] P. Cheetham, D.P. Petrylak, Tubulin-targeted agents including docetaxel and cabazitaxel, Cancer J. 19 (2013) 59–65.
[3] J. Seligmann, C. Twelves, Tubulin: an example of targeted chemotherapy, Future Med. Chem. 5 (2013) 339–352.
[4] R. Oishi, N. Egashira, Peripheral neuropathy induced by anticancer drugs, Fukuoka Igaku Zasshi 104 (2013) 71–80.
[5] E.J. Wojcik, R.S. Buckley, J. Richard, L. Liu, T.M. Huckaba, S. Kim, Kinesin-5: cross-bridging mechanism to targeted clinical therapy, Gene 531 (2013) 133–149.
[6] T.U. Mayer, T.M. Kapoor, S.J. Haggarty, R.W. King, S.L. Schreiber, T.J. Mitchison, Small molecule inhibitor of mitotic spindle bipolarity identified in a phenotype-based screen, Science 286 (1999) 971–974.
[7] M. Gartner, N. Sunder-Plassmann, J. Seiler, M. Utz, I. Vernos, T. Surrey, A. Giannis, Development and biological evaluation of potent and specific inhibitors of mitotic kinesin Eg5, Chembiochem 8 (2006) 1173–1177.
[8] C. Muller, D. Gross, V. Sarli, M. Gartner, A. Giannis, G. Bernhardt, A. Buschauer, Inhibitors of kinesin Eg5: antiproliferative activity of monastrol analogues against human glioblastoma cells, Cancer Chemother. Pharmacol. 59 (2007) 157–164.
[9] D.A. Davis, S.H. Sarkar, M. Hussain, Y. Li, F.H. Sarkar, Increased therapeutic potential of an experimental anti-mitotic inhibitor S8715992 by genistein in PC-3 human prostate cancer cell line, BMC Cancer 6 (2006) 22.
[10] K.D. Holen, C.P. Belani, G. Wilding, S. Ramalingam, J.L. Volkman, R.K. Ramanathan, L.S. Varnit, C.J. Bowen, J.P. Hodge, M.M. Dar, P.T. Ho, A first in human study of SB-743921, a kinesin spindle protein inhibitor, to determine pharmacokinetics, biologic effects and establish a recommended phase II dose, Cancer Chemother. Pharmacol. 67 (2011) 447–454.
[11] C.D. Cox, P.J. Coleman, M.J. Breslin, D.B. Whitman, R.M. Garbaccio, M.E. Fraley, C.A. Buser, E.S. Walsh, K. Hamilton, M.D. Schaber, R.B. Lobell, W. Tao, J.P. Davide, R.E. Diehl, M.T. Abrams, V.J. South, H.E. Huber, M. Torrent, T. Prueksaritanont, C. Li, D.E. Slaughter, E. Mahan, C. Fernandez-Metzler, Y. Yan, L.C. Kuo, N.E. Kohl, G.D. Hartman, Kinesin spindle protein (KSP) inhibitors. 9. discovery of (2S)-4-(2,5-difluorophenyl)-n-[(3R,4S)-3-fluoro-1-methylpiperidin-4-yl]-2-(hydroxymethyl)-N-methyl-2-phenyl-2,5-dihydro-1H-pyrrole-1-carboxamide (MK-0731) for the treatment of taxane-refractory cancer, J. Med. Chem. 51 (2008) 4239–4252.
[12] J.D. Orth, A. Loewer, G. Lahav, T.J. Mitchison, Prolonged mitotic arrest triggers partial activation of apoptosis, resulting in DNA damage and p53 induction, Mol. Biol. Cell. 23 (2012) 567–576.
[13] J.A. Good, T. Wang, O. Rath, H.Y. Kim, S.K. Talapatra, D. Podgorski, S.P. MacKay, F. Kozielski, Optimized S-trityl-L-cysteine-based inhibitors of kinesin spindle protein with potent in vivo antitumor activity in lung cancer xenograft models, J. Med. Chem. 56 (2013) 1878–1893.
[14] C.A. Parrish, N.D. Adams, K.R. Auger, J.L. Burgess, J.D. Carson, A.M. Chaudhari, R.A. Copeland, M.A. Diamond, C.A. Donatelli, K.J. Duffy, L.F. Faucette, J.T. Finer, W.F. Huffman, E.D. Hugger, J.R. Jackson, S.D. Knight, L. Lan, M.L. Moore, K.A. Newlander, L.H. Ridgers, R. Sakowicz, A.N. Shaw, C.M. Sung, D. Sutton, K.W. Wood, S.Y. Zhang, M.N. Zimmerman, D. Dhanak, Novel ATP-competitive kinesin spindle protein inhibitors, J. Med. Chem. 50 (2007) 4939–4952.
[15] A.K. Sould, R.L. Dubowy, A.M. Ingle, M.G. Conlan, J. Sun, S.M. Blaney, P.C. Adamson, A pediatric phase I trial and pharmacokinetic study of ispinesib: A children's oncology group phase I consortium study, Pediatr. Blood Cancer 55 (2010) 1323–1328.
[16] H.L. Gomez, M. Pilico, P. Pimentel, M. Kiyas, M.L. Monsalve, M.C. Conlan, K.G. Sakali, M.M. Chen, J.J. Serogy, A.A. Wolff, R.D. Escandon, Phase I dose-escalation and pharmacokinetic study of ispinesib, a kinesin spindle protein inhibitor, administered on days 1 and 15 of a 28-day schedule in patients with no prior treatment for advanced breast cancer, Anticancer Drugs 23 (2012) 335–341.
[17] K.H. Kim, Y. Xie, E.M. Tytler, R. Woessner, G. Mor, A.B. Alvero, KSP inhibitor ARRY-520 as a substitute for paclitaxel in type I ovarian cancer cells, J. Transl. Med. 7 (2009), 63-5876-7-63.
[18] B.Z. Carter, D.H. Mak, R. Woessner, S. Gross, W.D. Schober, Z. Estrov, H. Kantarjian, M. Andreeff, Inhibition of KSP by ARRY-520 induces cell cycle block and cell death via the mitochondrial pathway in AML cells, Leukemia 23 (2009) 1755–1762.
[19] R. Woessner, B. Tunquist, C. Lemieux, E. Chipala, S. Jackinsky, W. Dewolf Jr., W. Voegtli, A. Cox, S. Rana, P. Lee, D. Walker, ARRY-520, a novel KSP inhibitor with potent activity in hematological and taxane-resistant tumor models, Anticancer Res. 29 (2009) 4373–4380.
[20] H.J. Khoury, G. Garcia-Manero, G. Borthakur, T. Kadia, M.C. Foudray, M. Arellano, A. Langston, B. Bethelmie-Bryon, S. Rush, K. Linwler, S. Karan, H. Simmons, A.I. Marcus, M. Pusuyniski, H. Kantarjian, A phase 1 dose-escalation study of ARRY-520, a kinesin spindle protein inhibitor, in patients with advanced myeloid leukemias, Cancer 118 (2012) 3556–3564.

[21] S.R. Talapatra, N.G. Anthony, S.P. Mackay, F. Kozielski, Mitotic kinesin Eg5 overcomes inhibition to the phase I/II clinical candidate SB743921 by an allosteric resistance mechanism, J. Med. Chem. 56 (2013) 6317–6329.
[22] S. Oishi, T. Watanabe, J. Sawada, A. Asai, H. Ohno, N. Fujii, Kinesin spindle protein (KSP) inhibitors with 2,3-fused indole scaffolds, J. Med. Chem. 53 (2010) 5064–5068.
[23] T. Takeuchi, S. Oishi, M. Kaneda, R. Miu, H. Ohno, J. Sawada, A. Asai, S. Nakamura, I. Nakanishi, N. Fujii, Optimization of diaryl amine derivatives as kinesin spindle protein inhibitors, Bioorg. Med. Chem. 22 (2014) 3171–3179.
[24] T. Takeuchi, S. Oishi, M. Kaneda, H. Ohno, S. Nakamura, I. Nakanishi, M. Yamane, J. Sawada, A. Asai, N. Fujii, Kinesin spindle protein inhibitors with diaryl amine scaffolds: crystal packing analysis for improved aqueous solubility, ACS Med. Chem. Lett. 5 (2014) 566–571.
[25] T. Takeuchi, S. Oishi, T. Watanabe, H. Ohno, J. Sawada, K. Matsuno, A. Asai, N. Asada, K. Kitaura, N. Fujii, Structure–activity relationships of carboline and carbazole derivatives as a novel class of ATP-competitive kinesin spindle protein inhibitors, J. Med. Chem. 54 (2011) 4839–4846.
[26] R. Nakai, S. Iida, T. Takahashi, T. Tsujita, S. Okamoto, C. Takada, K. Akasaka, S. Ichikawa, H. Ishida, H. Kusaka, S. Akinaga, C. Murakata, S. Honda, M. Nitta, H. Saya, Y. Yamashita, ilS58, a novel inhibitor of mitotic kinesin Eg5 and antitumor agent, induces cell death in cancer cells, Cancer Res. 69 (2009) 3901–3908.
[27] R.A. McCloy, S. Rogers, C.E. Caldon, T. Lorca, A. Castro, A. Burgess, Partial inhibition of Cdk1 in G 2 phase overrides the SAC and decouples mitotic events, Cell Cycle 13 (2014) 1400–1412.
[28] C.H. Topham, S.S. Taylor, Mitosis and apoptosis: how is the balance set? Curr. Opin. Cell. Biol. 25 (2013) 780–785.
[29] F. Louwen, J. Yuan, Battle of the eternal rivals: restoring functional p53 and inhibiting polo-like kinase 1 as cancer therapy, Oncotarget 4 (2013) 958–971.
[30] Y.C. Chang, L.C. Lu, M.H. Tsai, Y.J. Chen, Y.Y. Chen, S.P. Yao, C.P. Hsu, The inhibitory effect of ellagic acid on cell growth of ovarian carcinoma cells, Evid. Based Compl. Altern. Med. 2013 (2013) 306705.

Original Article

J. St. Marianna Univ.
Vol. 7, pp. 105–116, 2016

A Novel KSP Inhibitor, KPYB10602, Induces Mitotic Arrest and Cell Death in Breast Cancer Cells

Seiko Kojima-Tsuchiya[1], Yuki Ohta[2], Mitsuko Takenaga[3], Jun Niimi[3], Daiki Watanabe[2], Satoshi Tsunoda[2], Masanori Ootaki[2], Shinya Oishi[4], Nobutaka Fujii[4], Naoki Matsumoto[2], and Koichiro Tsugawa[1]

(Received for Publication: August 25, 2016)

Abstract

Purpose: Taxane-based combination chemotherapy remains the predominant treatment for breast cancer. However, taxane-related drug resistance and neurotoxicity have prompted us to develop substitute treatment strategies. Kinesin spindle protein (KSP), which is essential for formation of the bipolar mitotic spindle and cell cycle progression through mitosis, has been identified as an attractive target for cancer chemotherapy. We investigated, both in vitro and in vivo, the anti-cancer effect of KPYB10602, a novel KSP inhibitor, in breast cancer.

Materials and Methods: Anti-proliferative activity of KPYB10602 in breast cancer cells was assessed by cell viability assay. The anti-cancer effect and inhibitory mechanism of KPYB10602 in breast cancer cells was further explored by immunofluorescence microscopy, flow cytometry, ELISA, and western blotting. In addition, the anti-tumor effect of KPYB10602 was evaluated in subcutaneous xenograft models.

Results: KPYB10602 showed anti-cancer activity in breast cancer cells. The KPYB10602 treatment was shown to result in induction of mitotic arrest with monopolar spindle formation and then apoptotic cell death. This might occurred via a mitochondria-mediated pathway. KPYB10602 also effectively suppressed tumor growth in a subcutaneous xenograft model.

Conclusion: KSP is a good target for breast cancer chemotherapy, and KPYB10602 has a potential as a novel anti-cancer agent for breast cancer.

Key words

kinesin spindle protein, KPYB10602, breast cancer, chemotherapy, anti-microtubule agent

Introduction

Breast cancer is the most commonly diagnosed cancer in women, with 1 in 12 women in Japan developing breast cancer during the course of a lifetime[1)]. In addition, breast cancer mortality in Japan has increased annually[1)]. A multidisciplinary approach to breast cancer treatment, combining surgical oncology, radiation oncology, and medical oncology, has been shown to improve both disease-free survival and overall survival, and this approach was linked, in a large, registry-based study in Scotland, to a reduction in breast cancer mortality[2)].

At present, taxane-containing chemotherapy, administered either as neo-adjuvant or adjuvant therapy in patients with breast cancer, is the standard of care worldwide[3)]. Taxanes bind microtubules directly, resulting in potent suppression of microtubule dynamics, increased microtubule stability, and interphase microtubule bundling; consequently, cells undergo

1 Division of Breast and Endocrine Surgery, Department of Surgery, St. Marianna University School of Medicine
2 Department of Pharmacology, St. Marianna University School of Medicine
3 Institute of Medical Science, St. Marianna University School of Medicine
4 Faculty of Pharmaceutical Sciences, Kyoto University

mitotic arrest and subsequent apoptotic cell death[4]. Microtubule-targeting agents such as taxanes are effective against a variety of cancers including breast cancer[4)5]. However, microtubules are not only essential for mitosis; they are required for other critical physiological functions, such as intracellular transport and organelle positioning[4)6]. Therefore, anti-microtubule agents can cause peripheral neuropathy by interfering with microtubule-based axonal transport[7]. In fact in breast cancer treatment, chemotherapy including the taxanes, especially paclitaxel, causes peripheral neuropathy high frequently[5]. Peripheral neuropathy can be very painful, and thus the patient's quality of life is decreased, and it becomes necessary to modify the drug dosage or even discontinue the drug altogether. Neurotoxicity is one of several dose limiting toxicities of the taxanes[5)7]. Therefore, there is an urgent need for new anti-tumor agents that will not affect microtubule dynamics.

Kinesin spindle protein (KSP), a member of the mitotic kinesin family, is involved in the early stages of mitosis. KSP is responsible for centrosome separation, which is required for formation and maintenance of the bipolar spindle[8]. Inhibition of KSP activity blocks cells in mitosis, and this results in the formation of a monopolar spindle[8)9]. Inhibition of KSP activity is an attractive, candidate chemotherapeutic approach because KSP is expressed predominantly in proliferating cells and is absent from post-mitotic neurons. Therefore, KSP inhibitors are expected not to induce peripheral neuropathy usually observed with traditional microtubule disrupting agents such as paclitaxel[9].

We evaluated, both in vitro and in vivo, the anti-cancer effect of a novel KSP inhibitor that we have identified for possible application to human breast cancer, and we investigated the mechanism explaining its effect.

Materials and Methods

Agents

Five anti-tumor agents were used in the study: KSP inhibitors KPYB10602, KPYC12688, and KPYC12687 were synthesized according to a previously described method[10], and *S*-(methoxytrityl)-L-cysteine was purchased from Watanabe Chemical Industries, LTD (Hiroshima, Japan). Paclitaxel was purchased from Sigma-Aldrich Inc. (St. Louis, MO, USA).

Cell lines and cell culture

Three breast cancer cell lines were used in the study: MCF-7 (luminal A type), MDA-MB-231 (claudin-low type), and HCC1937 (basal like type). Cells were purchased from American Type Culture Collection (ATCC, Rockville, MD, USA). The MCF-7 cells were cultured in Dulbecco's modified Eagle's medium (Wako Pure Chemical Industries, Osaka, Japan) supplemented with 10% fetal bovine serum (FBS, Thermo Fisher Scientific, Waltham, MA, USA) and 1% antibiotic-antimycotic solution (Thermo Fisher Scientific). MDA-MB-231 cells were grown in Leibovitz L15 medium (Sigma-Aldrich Inc.) supplemented with 15% FBS, 2 mM L-glutamine (Thermo Fisher Scientific), 1% $NaHCO_3$ (Thermo Fisher Scientific), and 1% antibiotic-antimycotic solution. HCC1937 cells were grown in RPMI-1640 (ATCC) supplemented with 10% FBS and 1% antibiotic-antimycotic solution. Cells were incubated at 37°C in a humidified atmosphere of 5% CO_2 and 95% room air.

Animals

Animal experiments were performed in accordance with the Guidelines for Animal Experimentation of St. Marianna University Graduate School of Medicine. Thirty-two female BALB/c-nu mice were purchased from Charles Liver Laboratories (Yokohama, Japan). The mice were housed in an isolated animal room that was maintained at a constant temperature (23±1°C) and 50-60% humidity under a 12-hour light/dark cycle and were allowed free access to 30 kGy CL-2 diet (Clea Japan, Tokyo, Japan) and sterilized water. The experimental protocol was approved by the Animal Research Committee, Institute for Animal Experimentation, St. Marianna University Graduate School of Medicine (approval number 1506012).

Cell viability assay

Cells (3×10^3) were seeded on 96-well plates and then incubated for 24 hours to allow cell attachment. The cells were then treated with various concentrations of the KSP inhibitors or paclitaxel for 48 hours or 72 hours. For control, cells were exposed to medium alone. After incubation, 5 mg/mL of 3-(4,5-dimethylthiazol-2-yl)-2,5-diphenylterazolium bromide (MTT, Sigma-Aldrich Inc.) was added to each well, and the plates were incubated for 4 hours. The formazan crystals that formed were dissolved with a stop solution (20% sodium dodecyl sulfate in 0.01N HCl). Absorbance was measured at 570 nm and ref-

erence wavelength of 630 nm with the use of a microplate reader (vient nano, DS Pharma Biomedical Co., Ltd, Osaka, Japan)

Immunofluorescence imaging

Cells (1×10^5) were seeded on glass bottom dishes. Twenty-four hours after seeding, the cells were treated with 1 μM KPYB10602 for 24 hours and then fixed with 4% paraformaldehyde, permeabilized in phosphate-buffered saline (PBS) containing 0.1% Triton X-100, and blocked in 1% bovine serum albumin (BSA) in PBS. The cells were incubated with anti-α-tubulin antibody (diluted 1:500 in 1% BSA-PBS; T6199, Sigma-Aldrich Inc.) in combination with goat anti-mouse secondary antibody conjugated with Alexa Fluor 488 (diluted 1:1000 in 1% BSA-PBS; A21202, Thermo Fisher Scientific). Nuclei were counterstained with 2 μg/mL Hoechst 33342 (Dojindo, Kumamoto, Japan). Fluorescent images were captured with a KEYENCE BZ-9000 fluorescence microscope (KEYENCE Corp., Osaka, Japan).

Cell cycle analysis

Cells (1×10^5) were seeded on 6-well plates, incubated for 24 hours, and treated with 1 μM KPYB10602 for 12, 24, or 48 hours. After incubation, cells were harvested and fixed with ice cold 70% ethanol at −20°C, then treated with 10 μg/mL propidium iodide (PI, Sigma-Aldrich Inc.) and 0.1 mg/mL RNase (Sigma-Aldrich Inc.) for 10 minutes. The DNA content of at least 8,000 cells was analyzed by using a LSR II flow cytometer (BD Biosciences, San Jose, CA, USA) and FACSDiva software (BD Biosciences).

Enzyme-linked immunosorbent assay (ELISA)

Expression levels of securin (MBS947752 Human Securin ELISA kit, MyBioSource, San Diego, CA USA), Bax (ab199080 Human Bax ELISA Kit, Abcam plc, Cambridge, UK) and survivin (7169C PathScan Total Survivin Sandwich ELISA Kit, Cell Signaling Technology, Danvers, MA, USA) were determined according to the kit manufacturer's instructions. Briefly, cells (1×10^5) were seeded on 6-cm dishes, incubated for 24 hours, and treated with 1 μM KPYB10602 for 12, 24, or 48 hours. Following incubation, the floating and adherent cells were harvested for analysis. The total protein concentration was measured (23227 BCA protein assay kit (Thermo Fisher Scientific). Samples containing 25 μg total proteins were used for each aasays.

Quantitation of DNA fragmentation

DNA fragmentation, as a marker of apoptosis, was measured with The Cell Death Detection ELISA^{Plus} kit (Roche Applied Science, Mannheim, Germany) according to the manufacturer's instructions. Briefly, cells (3×10^3) were seeded on 96-well plates and incubated for 24 hours. The cells were then treated with 1 μM KPYB10602 and grown for an additional 12, 24, 48, or 72 hours. After incubation, the cytoplasmic fraction was used for assay.

Western blot analysis

Cells ($1 \times e10^5$) were seeded on 6-cm dishes, incubated for 24 hours, and treated with 1 μM KPYB10602 for 12, 24, or 48 hours. Protein extraction and quantification were performed as described above. Samples containing 30 μg total proteins were separated by electrophoresis on 12% SDS-polyacrylamid gels and transferred to nitrocellulose membranes. Primary antibodies for caspase-3 (sc7272, Santa Cruz Biotechnology Inc., Dallas, TX, USA) (diluted 1:500) and β-actin (Sigma-Aldrich Inc.) (diluted 1:1500) were applied, followed by incubation with horseradish peroxidase-conjugated secondary antibody (MP Biomedicals, Santa Ana, CA, USA). The blots were developed under enhanced chemiluminescence (ImmunoStar Basic, Wako Pure Chemical Industries), and the protein bands were detected with an LAS-3000 medical imager (Fujifilm, Tokyo, Japan).

Breast cancer tumor xenograft studies

Thirty-two mice were injected subcutaneously in the flank with 1×10^7 MDA-MB-231 cells in 100 μL PBS. Seven days after inoculation, the mice were arbitrarily divided into 3 groups. KPYB10602 (20 mg/kg) dissolved in dimethyl sulfoxide (DMSO) diluted with olive oil, was administered intraperitoneally on 3 consecutive days and then twice per week. The dose and the administration schedule were determined on the basis of data obtained in previous studies[11)12)]. Paclitaxel (25 mg/kg), dissolved in DMSO diluted with olive oil, was administered intraperitoneally once a week. As a control, vehicle, DMSO in olive oil, was administered to tumor-bearing mice in a manner like that of the KPYB10602 administration. Tumor volume and animal weight were determined twice a week. Tumor volume (mm^3) was calculated with a standard formula: length × width^2 ×

1/2. All mice were sacrificed on day 24 after initial treatment.

Statistical analysis

All values are expressed as mean + SE. Dunnett's control-comparison test was used to examine differences in securin, DNA fragmentation, Bax, and survivin levels and in tumor volume and body weight, and analysis of covariance (ANCOVA) was used to examine differences in tumor growth rate. All statistical analyses were performed with JMP 12 (SAS Institute Inc., Cary, NC, USA), and $P < 0.05$ was accepted as statistically significant.

Results

Anti-proliferative activity of KSP inhibitors in breast cancer cells

The anti-proliferative activity of the novel synthesized KSP inhibitors (KPYB10602, KPYC12687, and KPYC12688) was evaluated in breast cancer cells. Cell growth was suppressed, no matter which KSP inhibitor was applied; the most efficient anti-proliferative activity was seen with KPYB10602 (**Figure 1a, b**). Therefore, KPYB10602 was used for

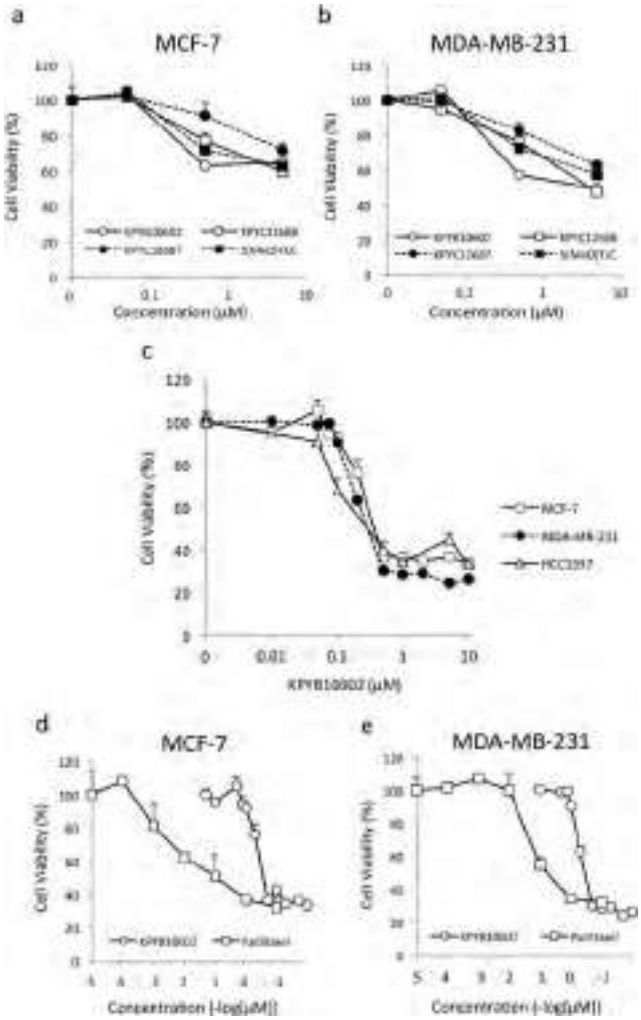

Figure 1. Effects of KSP inhibitors on breast cancer cell growth.

MCF-7 cells (**a**) and MDA-MB-231 cells (**b**) were treated with varying concentrations of KSP inhibitors for 48 hours, and MTT cell proliferation assay was performed. Values are shown as mean + SE (n = 12). (**c**) MCF-7, MDA-MB-231, and HCC1937 cells were treated with KPYB10602 for 72 hours, and MTT cell proliferation assay was performed. MCF-7 cells (**d**) and MDA-MB-231 cells (**e**) were treated with KPYB10602 or paclitaxel for 72 hours, and MTT assay was performed. Values are shown as mean + SE (n = 12).

subsequent experiments. To assess the effects of KPYB10602 on breast cancer cell lines MCF-7, MDA-MB-231, and HCC1937, the cells were treated with varying concentrations of KPYB10602 for 72 h. KPYB10602 suppressed the proliferation of these cells in a concentration-dependent manner (**Figure 1c**) and at the same potency as paclitaxel (**Figure 1d, e**).

Induction of apoptosis by KPYB10602 in breast cancer cell lines via mitotic arrest

We performed immunofluorescence analysis to understand the mechanism underlying the anti-proliferative effect of KPYB10602 in the breast cancer cell lines. Untreated cells showed normal microtubule spread during interphase and a typical bipolar spindle at the metaphase plate during mitosis (**Figure 2**, white arrow). In contrast, the spindle that developed in cells treated with KPYB10602 was monopolar (**Figure 2**, red arrow), and DNA staining was observed as an outer ring surrounding the microtubule staining, a pattern commonly referred to a rosette formation (**Figure 2**, yellow arrow), indicating suppression of centrosome separation.

The mitotic arrest associated with KPYB10602 was further characterized by means of flow cytometric cell cycle distribution analysis. With KPYB10602 treatment, the number of G_2/M phase cells was significantly increased in comparison to the number seen in the control condition (**Figure 3a**), indicating mitotic arrest. The portion of mitotic cells peaked at 24 hours after treatment (G_2/M phase cells: 77.3% of

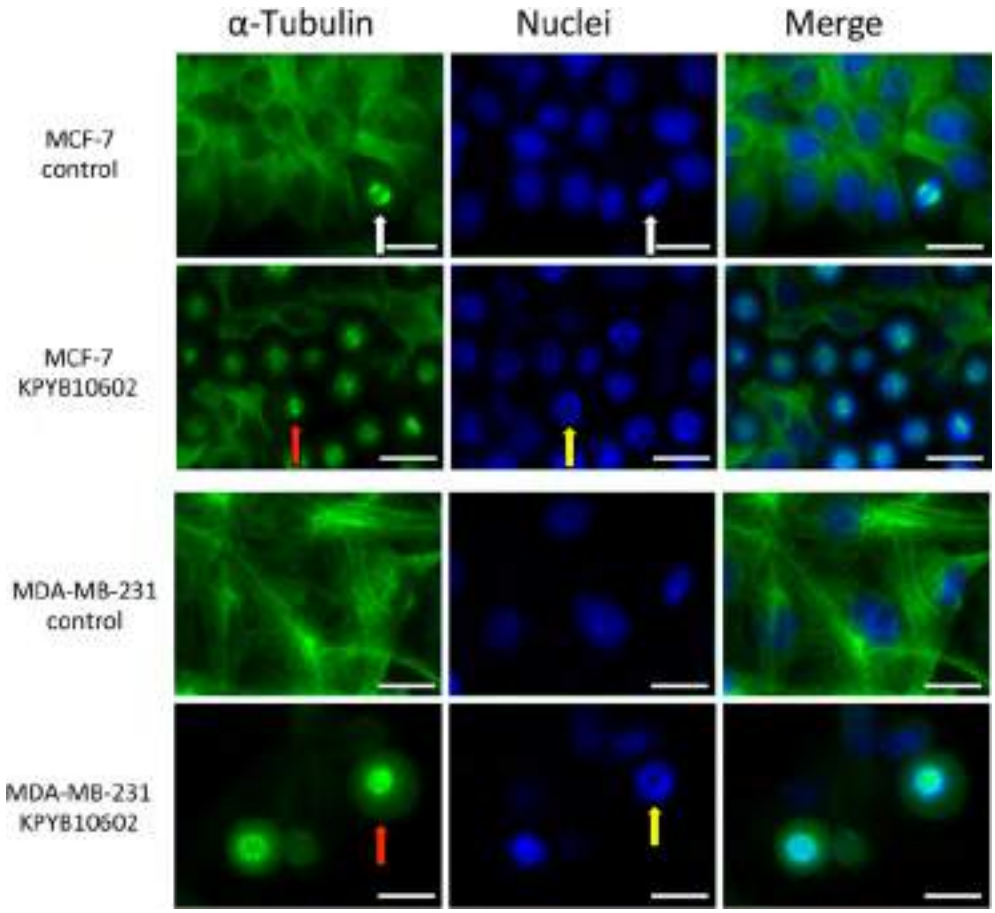

Figure 2. Immunofluorescence staining of breast cancer cells treated with KPYB10602.

After exposure of MCF-7 and MDA-MB-231 cells to 1 μM KPYB10602 for 24 hours, the cells were stained with anti-tubulin antibody (green) and Hoechst 33342 (nuclei, blue). Scale bars represent 20 μm. The experiment was performed in triplicate, and similar results were obtained each time.

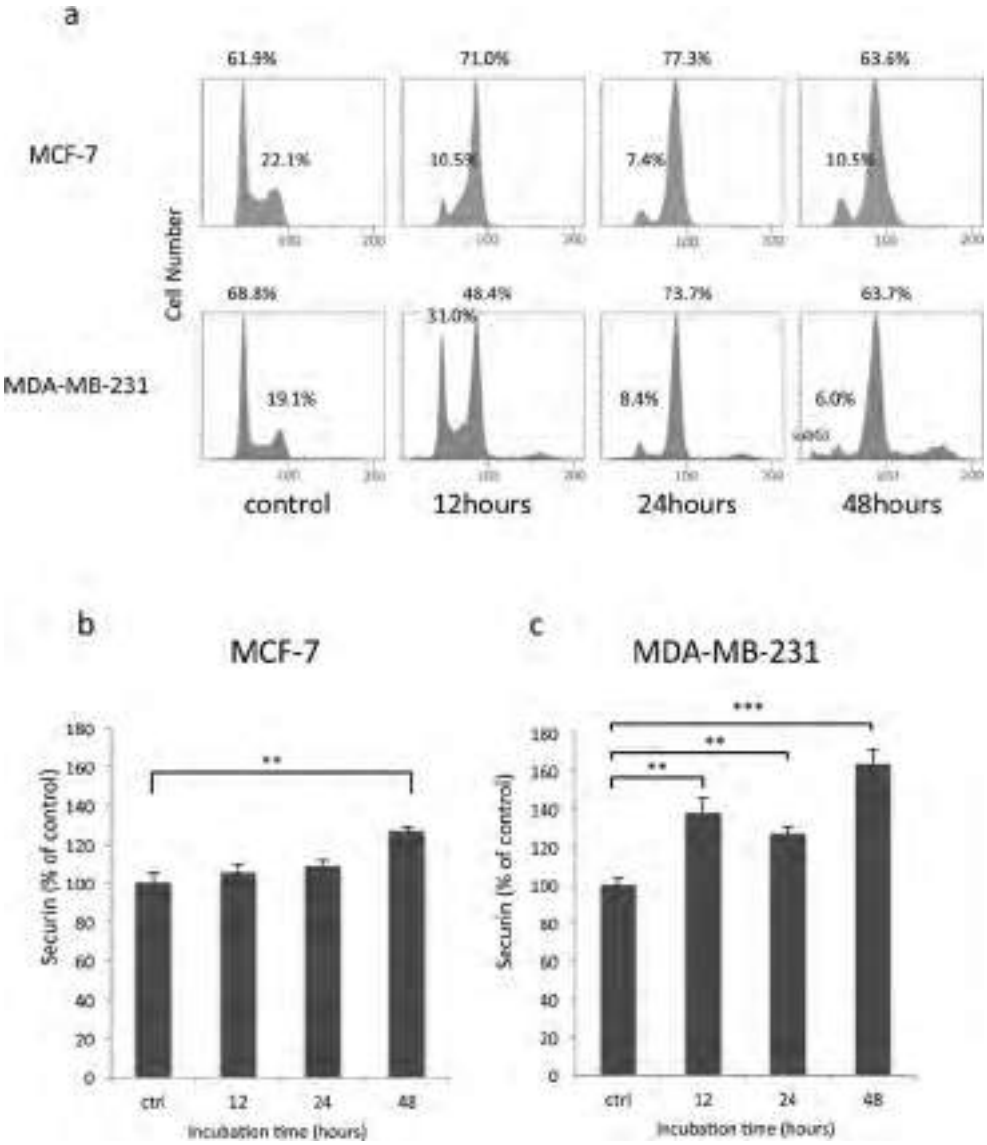

Figure 3. Effects of KPYB10602 on cell cycle.

MCF-7 and MDA-MB-231 cells were treated with 1 μM KPYB10602 for 12, 24, or 48 hours. (**a**) Flow cytometric analysis was performed for evaluation of cell cycle distribution. The experiment was done in triplicate. (**b, c**) The protein levels of securin were evaluated by ELISA. Values are shown as mean + SE (n = 4). **P < 0.01 and ***P < 0.001 vs. control.

MCF-7 cells, 73.7% of MDA-MB-231 cells). The $subG_1$ cells appeared after 48 hours of treatment in MDA-MB-231 cells (3.0 %). In addition, expression of securin, which plays important role in cell cycle progression, increased with the addition of KPYB10602 (**Figure 3b**).

As shown in **Figure 4**, DNA fragmentation was markedly enhanced with KPYB10602 treatment, and this enhancement indicated increased apoptosis of the breast cancer cells. Furthermore, expression of pro-apoptotic protein Bax was increased, and expression of anti-apoptotic protein survivin was significantly decreased (**Figure 5a, b**).

Western blotting revealed absence of caspase-3 expression in MCF-7 cells. MDA-MB-231 cells expressed procaspase-3, but its cleaved forms were not

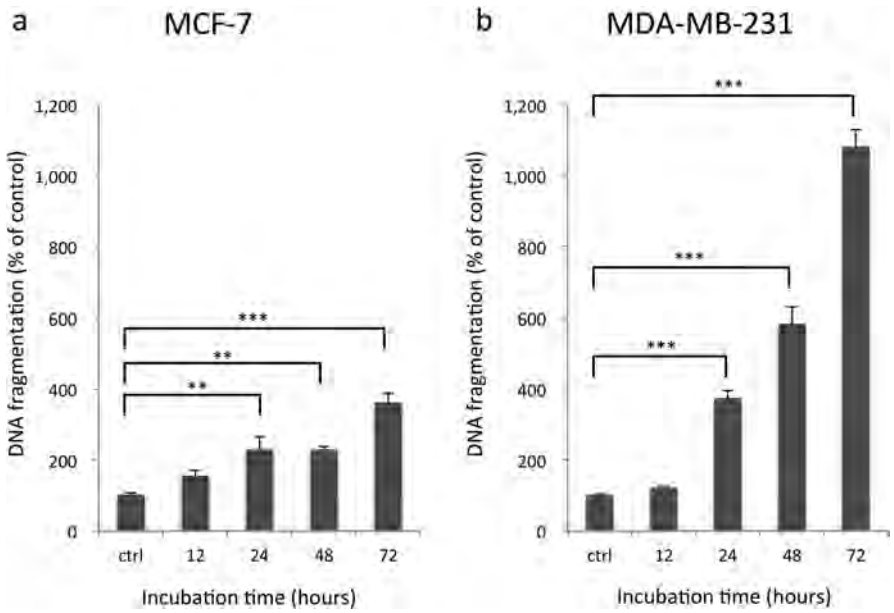

Figure 4. Induction of DNA fragmentation by KPYB10602.

MCF-7 and MDA-MB-231 cells were treated with 1 μM KPYB10602 for 12, 24, 48, or 72 hours. DNA fragmentation was detected by ELISA. Values are shown as mean + SE (n = 8). **P<0.01 and ***P<0.001 vs. control.

detected (**Figure 5c**).

Effect KPYB10602 in the MDA-MB-231 cell xenograft model

By day 7 after injection of the cancer cells into the BALB/c-nu mice, tumor volume reached approximately 120 mm^3 (day 0), and KPYB10602 (20 mg/kg), paclitaxel (25 mg/kg), or vehicle at an equal amount was administered. Although the tumor volume increased in all groups, the growth rate was significantly inhibited with the KPYB10602 treatment and with the paclitaxel treatment ($P < 0.001$) (**Figure 6a**). No significant weight loss or toxicity was observed in either of these 3 groups of mice (**Figure 6b**).

Discussion

This study demonstrated that a novel synthesized KSP inhibitor, KPYB10602, had anti-tumor activity in human breast cancer cell lines and xenograft tumor model.

The taxanes, such as paclitaxel and docetaxel, are microtubule-stabilizing agents that have been widely applied as active chemotherapy agents in the treatment of breast cancer[13]. They inhibit spindle microtubule dynamics, which causes cell cycle arrest and apoptosis[14)15]. However, taxane as an anti-microtubule drug is of limited clinical utility because resistance to the drug develops and patients suffer side effects caused by a mutation of the drug-binding site on β-tubulin[16], overexpression of P-glycoprotein[17], and neurotoxicity[5)6)7].

In contrast to taxanes, KSP inhibitors do not directly interfere with the intracellular function of microtubules[18]. KSP inhibitors are seen as candidate chemotherapeutic agents, the use of which would avoid toxicity in post-mitotic neurons. KPYB10602 has been shown to selectively inhibit KSP ATPase activity with an IC50 of 0.031 μM in human cervical cancer cell lines[10]. In our study, the anti-proliferative effect of KPYB10602 in breast cancer cells was more efficient than that of the other inhibitors. Furthermore, KPYB10602 suppressed tumor growth without apparent toxicity in the subcutaneous xenograft tumor model. In a previously reported study, mice treated with KPYB10602 did not exhibit significantly impaired in motor coordination[19].

KSP is responsible for centrosome separation, which is required for formation and maintenance of the bipolar spindle[8)18]. Inhibition of KSP function by KPYB10602 resulted in a characteristic monoastral spindle phenotype. Like taxanes, KSP inhibitor leads

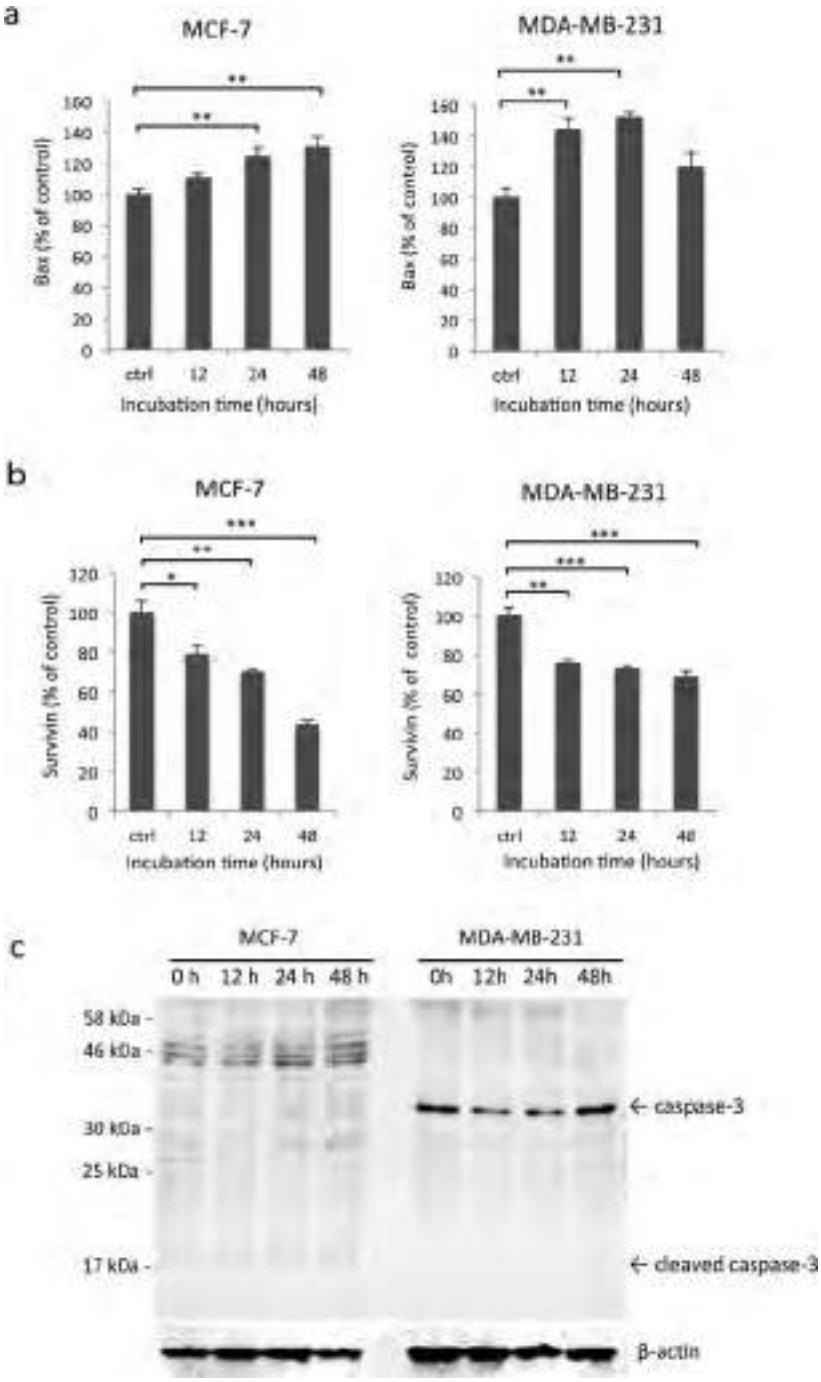

Figure 5. Expression of apoptosis-related factors.

MCF-7 and MDA-MB-231 cells were treated with 1 μM KPYB10602 for 12, 24, or 48 hours. The protein levels of Bax (**a**) and survivin (**b**) were measured by ELISA. Values are shown as mean + SE (n = 4). *P<0.05, **P<0.01 and ***P<0.001 vs. control. Caspase-3 (**c**) was determined by Western blotting, and β-actin was used as a loading control.

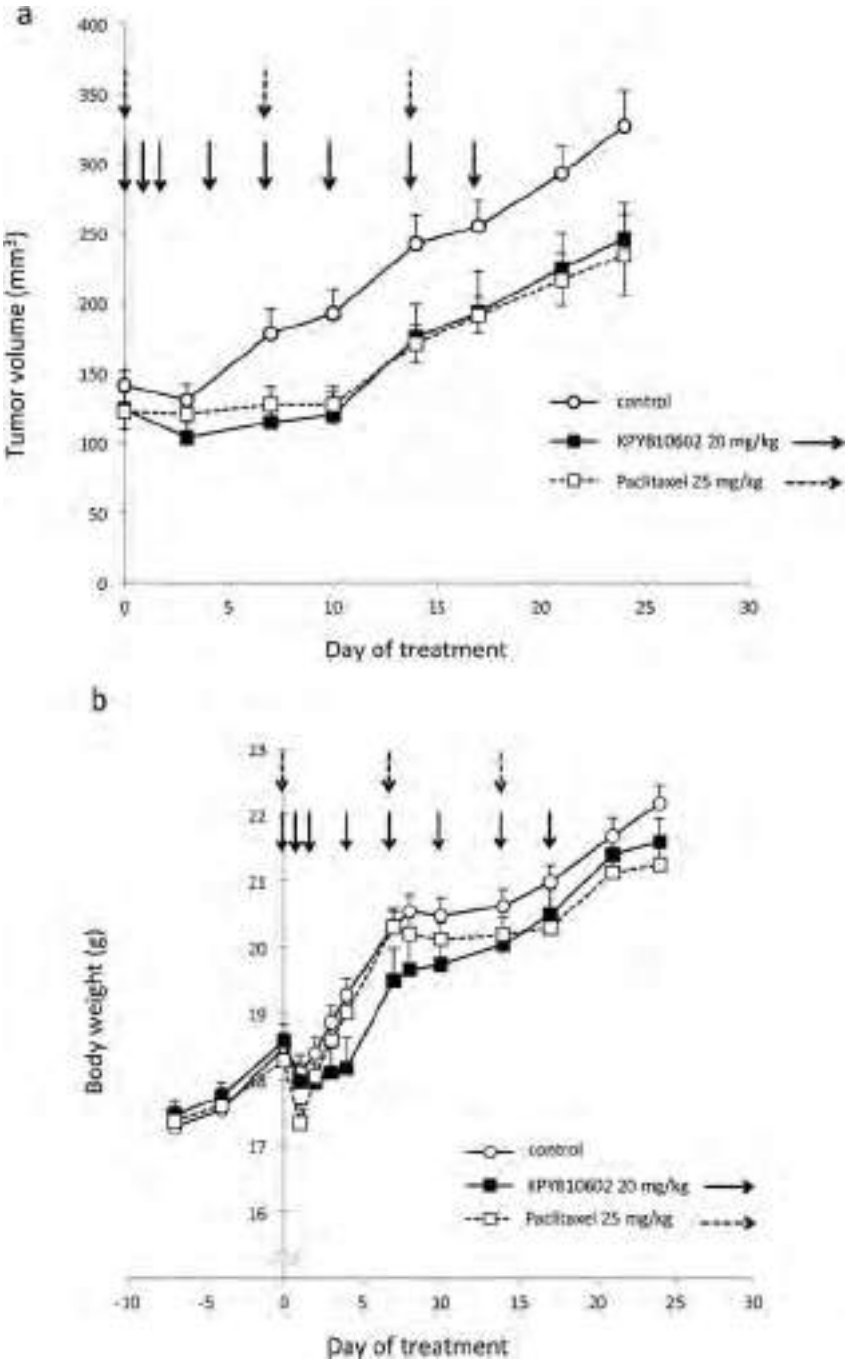

Figure 6. In vivo effect of KPYB10602 on tumor-bearing BALB/c-nu mice.

Mice bearing subcutaneously implanted MDA-MB-231 cells were treated with KPYB10602 (20 mg/kg, n = 10), paclitaxel (5 mg/kg, n = 10), or vehicle (control, n = 12). Tumor volume (**a**) and body weight (**b**) were measured twice a week. Values are shown as mean + SE.

to mitotic arrest and apoptosis. We observed an increase in the number of G2/M phase and sub-G1 cells with KPYB10602 treatment, suggesting that apoptotic cell death resulted after mitotic arrest. At the onset of anaphase, securin is ubiquitinated, leading to its destruction and to the liberation of separase, which results in segregation of the chromosomes[20)21)]. Securin, called an anaphase inhibitor, blocks separase function, preventing segregation of the chromosomes[20)]. KPYB10602 treatment resulted in an increase in securin, indicating the arrest of cell cycle progression from metaphase to anaphase.

Although cell death after prolonged mitosis seems to be a common phenomenon in cells treated with KSP inhibitor, the underlying apoptotic mechanism is not clearly understood. Microtubule-targeting agents are known to induce mitochondrial membrane permeabilization and subsequent induction of apoptosis by modulating Bcl-2 family proteins, including Bax[22)23)]. Bax is a proapoptotic protein, and previous reports have described the induction of apoptosis through elevated Bax expression resulting from KSP inhibition[24–26)]. In addition, survivin, a member of the family of inhibitor of apoptosis proteins (IAPs), seems to be selectively expressed in transformed cells and in most human cancers, including breast cancer[27)28)]. Survivn is released from the mitochondria in the cytosol and inhibits apoptosis by suppression of active caspase-9[27)29)]. In this study, the elevated Bax expression and decreased survivin expression were consistent with an increase in DNA fragmentation following KPYB10602 treatment. Our study data suggest that KPYB10602 induced mitotic arrest, followed by cell death mediated via the mitochondrial pathway.

In this study, MDA-MB-231 cells showed higher level of DNA fragmentation and sub-G1 population than MCF-7 cells did. These differences between the cell lines might be due to its molecular biology. In fact, MCF-7 cells lack caspase-3[30)], and MDA-MB-231 cells have mutant p53[31)]. These 2 proteins are responsible for the induction of apoptosis. In addition to the MCF-7 cells, MDA-MB-231 cells expressed inactive caspase-3, and this expression was independent of the exposure to KPYB10602. Thus we assume that KPYB100602 can induce apoptosis without the activity of caspase-3 and/or p53.

Another advantage of KSP inhibitors is that they can overcome resistance to taxanes caused by overexpression of P-glycoprotein; KSP is not transported out of cells by P-glycoprotein[17)]. Furthermore, KPYB10602 does not affect microtubules dynamics[18)], and it avoids the taxane resistance that results from mutation at the drug-binding site on β-tubulin.

In summary, our in vitro and in vivo experiments showed a novel KSP inhibitor, KPYB10602, to have a potent anti-cancer effect on breast cancer cells. To the best of our knowledge, this is the first study to identify this novel KSP inhibitor as a promising treatment for breast cancer. Further evaluation is needed to elucidate of the apoptotic pathways by which KPYB10602 acts in breast cancer cells.

Acknowledgments

This study was supported by Japan Society for the Promotion of Science Grant-in-Aid for Scientific Research (C) Grant Number JP 15K10074. We would like to thank Prof. Tomohiko Ohta, Department of Translational Oncology, St. Marianna University Graduate School of Medicine, and Dr. Ko Sato, Departmanet of Genomics, St. Marianna University Graduate School of Medicine, for kindly providing breast cancer cell lines, and thank Teita Asano, Institute of Medical Science, St. Marianna University School of Medicine, for his help in the xenograft study. We also would like to thank Tina Tajima for her editorial review of the manuscript.

References

1) Hori M, Matsuda T, Shibata A, Katanoda K, Sobue T, Nishimoto H. Cancer incidence and incidence rates in Japan in 2009: a study of 32 population-based cancer registries for the Monitoring of Cancer Incidence in Japan (MCIJ) project. Jpn J Clin Oncol 2015; 45: 884–891.
2) Kesson EM, Allardice GM, George WD, Burns HJG, Morrison DS. Effects of multidisciplinary team working on breast cancer survival: retrospective, comparative, interventional cohort study of 13 722 women. BMJ 2012; 344: e2718.
3) Denduluri N, Somerfield MR, Eisen A, Holloway JN, Hurria A, King TA, Lyman GH, Partridge AH, Telli ML, Trudeau ME, Wolff AC. Selection of optimal adjuvant chemotherapy regimens for early breast cancer and adjuvant targeted therapy for human epidermal growth factor receptor 2-positive breast cancers: an American Society of Clinical Oncology Guideline Adaptation of the Cancer Care. J Clin Oncol 2016; 67. 0182.
4) Singh P, Rathinasamy K, Mohan R, Panda D.

Microtubule assembly dynamics: an attractive target for anticancer drugs. IUBMB Life 2008; 60: 368–375.
5) Velasco R, Bruna J. Taxane-induced peripheral neurotoxicity. Toxics 2015; 3: 152–169.
6) Scripture CD, Figg WD, Sparreboom A. Peripheral neuropathy induced by paclitaxel: recent insights and future perspectives. Curr Neuropharmacol 2006; 4: 165–172.
7) Arakawa K, Torigoe K, Kuzumaki N, Suzuki T, Narita M. Chemotherapy-induced peripheral neuropathy: clinical symptoms, management and mechanism, Jpn J Pharm Palliat Care Sci 2011; 4: 1–13.
8) Sarli V, Giannis A. Targeting the kinesin spindle protein: basic principles and clinical implications. Clin Cancer Res 2008; 14: 7583–7587.
9) Woessner R, Tunquist B, Lemieux C, Chlipala E, Jackinsky S, Dewolf W, Voegtli W, Cox A, Rana S, Lee P, Walker Det. ARRY-520, a novel KSP inhibitor with potent activity in hematological and taxane-resistant tumor models. Anticancer Res 2009; 29: 4373–4380.
10) Takeuchi T, Oishi S, Watanabe T, Ohno H, Sawada J, Matsuno K, Asai A, Asada N, Kitaura K, Fujii N. Structure-activity relationships of carboline and carbazole derivatives as a novel class of ATP-competitive kinesin spindle protein inhibitors. J Med Chem 2011; 54; 4839–4846.
11) Xing N, Ding S, Saito R, Nishizawa K, Kobayashi T, Inoue T, Oishi S, Fujii N, Lv J, Ogawa O, Nishiyama H. A potent chemotherapeutic strategy in prostate cancer: *S*-(methoxy-trityl)- L-cystein, a novel Eg5 inhibitor. Asian J Androl 2011; 13: 236–241.
12) Ding S, Nishizawa K, Kobayashi T, Oishi S, Lv J, Fujii N, Ogawa O, Nishiyama H. A potent chemotherapeutic strategy for bladder cancer: (S)-methoxy-trityl- L-cystein, a novel Eg5 inhibitor. J Urol 2010; 184: 1175–1181.
13) Ring AE, Ellis PA. Taxanes in the treatment of early breast cancer. Cancer Treat Rev 2005; 31: 618–627.
14) Schmidt M, Bastians H. Mitotic drug targets and the development of novel anti-mitotic anticancer drugs. Drug Resist Updates 2007; 10: 162–181.
15) Jackson JR, Patrick DR, Dar MM, Huang PS. Targeted anti-mitotic therapies: can we improve on tubulin agents? Nat Rev Cancer 2007; 7: 107–117.
16) Giannakakou P, Gussio R, Nogales E, Downing KH, Zaharevitz D, Bollbuck B, Poy G, Sackett D, Nicolaou NC, Fojo T. A common pharmacophore for epothilone and taxanes: molecular basis for drug resistance conferred by tubulin mutations in human cancer cells. Proc Natl Acad Sci USA 2000; 97: 2904–2909.
17) Marcus AI, Peters U, Thomas SL, Garrett S, Zelnak A, Kapoor TM, Giannakakou P. Mitotic kinesin inhibitors induce mitotic arrest and cell death in taxol-resistant and -sensitive cancer cells. J Biol Chem 2005; 280: 11569–11577.
18) Sakowicz R, Finer JT, Beraud C, Crompton A, Lewis E, Fritsch A, Lee Y, Mak J, Moody R, Turincio R, Chabala JC, Gonzales P, Roth S, Weitman S, Wood KW. Antitumor activity of a kinesin inhibitor antitumor activity of a kinesin inhibitor. Cancer Res 2004; 2: 3276–3280.
19) Takenaga M, Yamamoto Y, Takeuchi T, Ohta Y, Tokura Y, Hamaguchi A, Asai D, Nakashima H, Oishi S, Fujii N. Potential new chemotherapy strategy for human ovarian carcinoma with a novel KSP inhibitor. Biochem Biophys Res Commun 2015; 463: 222–228.
20) Zhou J, Yao J, Joshi HC. Attachment and tension in the spindle assembly checkpoint. J Cell Sci 2002; 115: 3547–3555.
21) Jallepalli PV, Waizenegger IC, Bunz F, Langer S, Speicher MR, Peters J, Kinzler KW, Vogelstein B, Lengauer C. Securin is required for chromosomal stability in human cells. Cell 2001; 105: 445–457.
22) Yamaguchi H, Chen J, Bhalla K, Wang HG. Regulation of Bax activation and apoptotic response to microtubule damaging agents by p53 transcription-dependent and -independent pathways. J Biol Chem 2004; 279: 39431–39437.
23) Carter BZ, Mak DH, Woessner R, Gross S, Schober WD, Estrov Z, Kantarjian H, Andreeff M. Inhibition of KSP by ARRY-520 induces cell cycle block and cell death via the mitochondrial pathway in AML cells. Leukemia 2009; 23: 1755–1762.
24) Tao W, South VJ, Diehl RE, Davide JP, Sepp-Lorenzino L, Fraley ME, Arrington KL, Lobell RB. An inhibitor of the kinesin spindle protein activates the intrinsic apoptotic pathway independently of p53 and de novo protein synthesis. Mol Cell Biol 2007; 27: 689–698.
25) Tao W, South VJ, Zhang Y, Davide JP, Farrell L, Kohl NE, Lorensino LS, Lobell RB. Induction of apoptosis by an inhibitor of the mitotic

kinesin KSP requires both activation of the spindle assembly checkpoint and mitotic slippage. Cancer Cell 2005; 8: 49–59.

26) Purcell JW, Davis J, Reddy M, Martin S, Samayoa K, Vo H, Thomsen K, Bean P, Kuo WL, Ziyad S, Billig J, Feiler HS, Gray JW, Wood KW, Cases S. Activity of the kinesin spindle protein inhibitor ispinesib (SB-715992) in models of breast cancer. Clin Cancer Res 2010; 16: 566–576.

27) Mita AC, Mita MM, Nawrocki ST, Giles FJ. Survivin: key regulator of mitosis and apoptosis and novel target for cancer therapeutics. Clin Cancer Res 2008; 14: 5000–5005.

28) Tanaka K, Iwamoto S, Gon G, Nohara T, Iwamoto M, Tanigawa N. Expression of survivin and its relationship to loss of apoptosis in breast carcinomas. Clin Cancer Res 2000; 6: 127–134.

29) Altieri DC. Survivin, versatile modulation of cell division and apoptosis in cancer. Oncogene 2003; 22: 8581–8589.

30) Liang Y, Yan C, Schor NF. Apoptosis in the absence of caspase 3. Oncogene 2001; 20: 6570–6578.

31) Huovinen M, Loikkanen J, Myllynen P, Vähäkangas KH. Characterization of human breast cancer cell lines for the studies on p53 in chemical carcinogenesis. Toxicol In Vitro 2011; 25: 1007–1017.

SCIENTIFIC REPORTS

OPEN

Aminophylline suppresses stress-induced visceral hypersensitivity and defecation in irritable bowel syndrome

Received: 05 July 2016
Accepted: 05 December 2016
Published: 05 January 2017

Teita Asano[1], Ken-ichiro Tanaka[2], Arisa Tada[3], Hikaru Shimamura[3], Rikako Tanaka[3], Hiroki Maruoka[3], Mitsuko Takenaga[1] & Tohru Mizushima[4]

Pharmacological therapy for irritable bowel syndrome (IBS) has not been established. In order to find candidate drugs for IBS with diarrhea (IBS-D), we screened a compound library of drugs clinically used for their ability to prevent stress-induced defecation and visceral hypersensitivity in rats. We selected the bronchodilator aminophylline from this library. Using a specific inhibitor for each subtype of adenosine receptors (ARs) and phosphodiesterases (PDEs), we found that both A_{2B}ARs and PDE4 are probably mediated the inhibitory effect of aminophylline on wrap restraint stress (WRS)-induced defecation. Aminophylline suppressed maternal separation- and acetic acid administration-induced visceral hypersensitivity to colorectal distension (CRD), which was mediated by both A_{2A}ARs and A_{2B}ARs. We propose that aminophylline is a candidate drug for IBS-D because of its efficacy in both of stress-induced defecation and visceral hypersensitivity, as we observed here, and because it is clinically safe.

Irritable bowel syndrome (IBS) is characterized by chronic, recurrent abdominal pain and altered bowel habits (diarrhea or constipation) and is defined by symptom criteria and the absence of detectable organic disease[1]. The prevalence of IBS in the general population is remarkably high (approximately 11% of the world's population), with the young displaying greater susceptibility[1]. Thus, although IBS is not life-threatening, it creates a large burden on global healthcare and causes a serious reduction in the quality of life[2]. However, a therapeutic protocol for the disease, including pharmacological therapy, has not been established. Four subtypes of IBS are recognized, depending on the predominant stool pattern: IBS with constipation (IBS-C), IBS with diarrhea (IBS-D), mixed IBS (IBS-M) and un-subtyped IBS[3].

Although the mechanism underlying the pathogenesis of IBS is not completely understood, several contributory factors have been proposed, including brain-gut axis dysregulation, enhanced visceral perception, altered intestinal microbiota, post-infectious changes in gastrointestinal function and enhanced immunologic reactivity[4–8]. Given that no single causal trigger for IBS has been identified, a combination of physiologic, genetic, environmental and psychological factors seems to be responsible for the visceral hypersensitivity and altered bowel conditions observed in IBS patients. In particular, mental stress in early childhood (such as the loss of a parent, neglect or abuse) is known to induce IBS-related phenotypes in both humans and animals[9,10].

Previously, the pharmacological treatment of IBS-D involved classic anti-diarrheal agents, such as loperamide and anticholinergic drugs. Some clinical studies have also suggested the effectiveness of antidepressants, although others reported contradictory results[11]. Recently, alosetron and ramosetron, two serotonin 3 (5-HT_3) receptor antagonists, were approved for patients with IBS-D[12,13]. This is based on the fact that inhibition of 5-HT_3 receptors in the intestine is associated with the suppression of its motility and fluid secretion[12]. Rifaximin, an antibacterial drug, and eluxadoline, which has both μ-opioid receptor agonist and δ-opioid receptor antagonist activity, were

[1]Institute of Medical Science, St. Marianna University School of Medicine, 2-16-1, Sugao, Miyamae-ku, Kawasaki 216-8512, Japan. [2]Laboratory of Bio-Analytical Chemistry, Research Institute of Pharmaceutical Sciences, Musashino University, 1-1-2αhinmachi, Nishitokyo-shi, 202-8585, Japan. [3]Faculty of Pharmacy, Keio University, 1-5-30, Shibakoen, Minato-ku, Tokyo 105-8512, Japan. [4]LTT Bio-Pharma Co., Ltd, Shiodome Building 3F, 1-2-20 Kaigan, Minato-ku, Tokyo 105-0022, Japan. Correspondence and requests for materials should be addressed to T.A. (email: asano-ti@marianna-u.ac.jp)

also recently approved for IBS-D[14,15]. However, thus far, the outcomes of pharmacological therapy for IBS-D are unsatisfactory[16]. Furthermore, as the 5-HT_3 receptor also regulates other physiological functions, the use of 5-HT_3 receptor antagonists is clinically restricted due to adverse effects, such as ischemic colitis[17]. In fact, the use of alosetron for IBS-D patients is permitted only when no alternative therapies are available[17]. Thus, new target proteins for IBS-D drugs, which enable long-term treatment without serious adverse effects, need to be identified[16,18]. One potential approach is to phenotypically screen compounds for their ability to reduce visceral hypersensitivity and stress-induced defecation in animals.

The number of drugs reaching the marketplace each year is decreasing, mainly due to the fact that unexpected adverse effects of potential drugs are revealed in clinical trials. Thus, we have proposed a new strategy for drug discovery and development (drug re-positioning), which focuses on the use of existing medicines for alternative indications[19]. This strategy screens compounds with clinically beneficial pharmacological activity from a library of medicines that are already in clinical use to develop them for new indications. The advantage of this strategy is the decreased risk of unexpected adverse effects in humans because the safety aspects of these drugs have already been well characterized[19]. Furthermore, as the library size of approved medicines is relatively small, the phenotypic screening of compounds in animals is much easier to implement using a drug re-positioning strategy rather than a general drug discovery approach.

Aminophylline (a mixture of theophylline and ethylenediamine in a 2:1 molecular ratio) is traditionally used as a bronchodilator[20,21]. Although the molecular mechanism governing its efficacy has not been fully defined, aminophylline (theophylline) has been reported to have both antagonizing activity for adenosine receptors (ARs) and inhibitory activity on phosphodiesterases (PDEs), both of which are believed to mediate the bronchodilatory activity of aminophylline[22,23]. Among the four major subtypes of AR (A_1ARs, A_{2A}ARs, A_{2B}ARs and A_3ARs), aminophylline (theophylline) is an antagonist of A_1ARs, A_{2A}ARs and A_{2B}ARs but not of A_3ARs[24,25]. A_1ARs are mainly expressed in the brain and spinal cord, while A_{2A}ARs are expressed in the brain, spinal cord and peripheral tissues/cells (such as the spleen, thymus, leucocytes, small intestine, and colon)[26,27]. A_{2B}ARs are mainly expressed in the peripheral tissues, such as the large intestine[28]. Various pathophysiological roles of ARs have been reported, and agonists and antagonists for these receptors have attracted considerable attention as drugs for various diseases[26]. PDE inhibitors also have various pharmacological activities, and some have already been approved for clinical use[29].

Although previous studies have reported both positive and negative effects of adenosine on intestinal motility and nociception[30–32], the role of each AR subtype in IBS-D remains unknown. In an animal model of acute somatic pain (hot-plate test), an antagonist of A_{2B}ARs but not of A_1ARs or A_{2A}ARs showed an analgesic effect[31], whereas in another animal model of somatic pain (formalin test), an A_{2A}AR antagonist acted as an analgesic[30,33]. A_{2B}AR-knockout mice have been reported to exhibit decreased stool frequency[32] whereas an A_{2B}AR antagonist enhanced colonic contraction in rats[30]. Further, activation of A_1ARs in the spinal cord has an analgesic effect[34]. On the other hand, it has been reported that inhibition of PDE4 suppresses stress-induced defecation[35]. These results suggest that aminophylline (theophylline) may affect visceral hypersensitivity and stress-induced defecation in IBS-D patients and animal models either positively or negatively; however, no study to date has investigated these effects.

In the present study, we used an *in vivo* phenotype screening and drug re-positioning strategy to search for candidate drugs for IBS-D. We screened a compound library consisting of clinically available drugs for the ability of the drugs to prevent stress-induced defecation and visceral pain, and identified aminophylline as a potential candidate. Analysis with a specific inhibitor for each subtype of PDE and AR suggested that PDE4 and A_{2B}ARs probably mediated the inhibitory effect of aminophylline on stress-induced defecation. On the other hand, A_{2A}ARs and A_{2B}ARs appear to be involved in its inhibitory effect on visceral hypersensitivity. On the basis of these results, we propose that aminophylline may be a candidate drug for IBS-D.

Results

Effect of aminophylline on wrap restraint stress (WRS)-induced fecal pellet output. We selected 209 clinically used drugs, including bronchodilators, anticonvulsants, antibiotics, anti-hypertensives and anti-allergy drugs. We did not select anti-cancer drugs. The drugs were screened for their ability to suppress both the visceral pain response to repeated colorectal distension (CRD), and WRS-induced fecal pellet output in rats. Then, aminophylline was identified on the basis of its inhibition of both the visceromotor response (VMR) to CRD and WRS-induced fecal pellet output, as well as the available clinical data of its tolerability. We excluded positive drugs that are positive hits in the screening assay but had severe side effects, such as hypotension and hypoglycemia.

We first examined the effect of oral administration of aminophylline on WRS-induced fecal pellet output. As shown in Fig. 1a, rats subjected to WRS displayed an increase in the number and wet weight of fecal pellets compared to that in unrestrained control rats, as described previously[36]. Oral pre-administration of aminophylline (18 or 60 $mg\,kg^{-1}$) significantly decreased both these indices in a dose-dependent manner (Fig. 1a). Oral pre-administration of ramosetron produced a similar effect (Fig. 1a).

Aminophylline is a complex of theophylline and ethylenediamine, and we found that oral pre-administration of theophylline also significantly decreased the fecal pellet output in rats subjected to WRS (Fig. 1b) at a dose equivalent to that of aminophylline (with respect to the molecular weight of theophylline). In contrast, as shown in Fig. 1c, aminophylline did not affect the fecal pellet output in rats that were not subjected to WRS, even at the higher dose of 180 $mg\,kg^{-1}$. These results suggest that aminophylline can suppress WRS-induced defecation without affecting normal defecation.

It has been reported that neonatal rats subjected to maternal separation show higher sensitivity to a novel stress stimulus, which can be monitored by an increase in fecal pellet output[10]. We therefore examined the

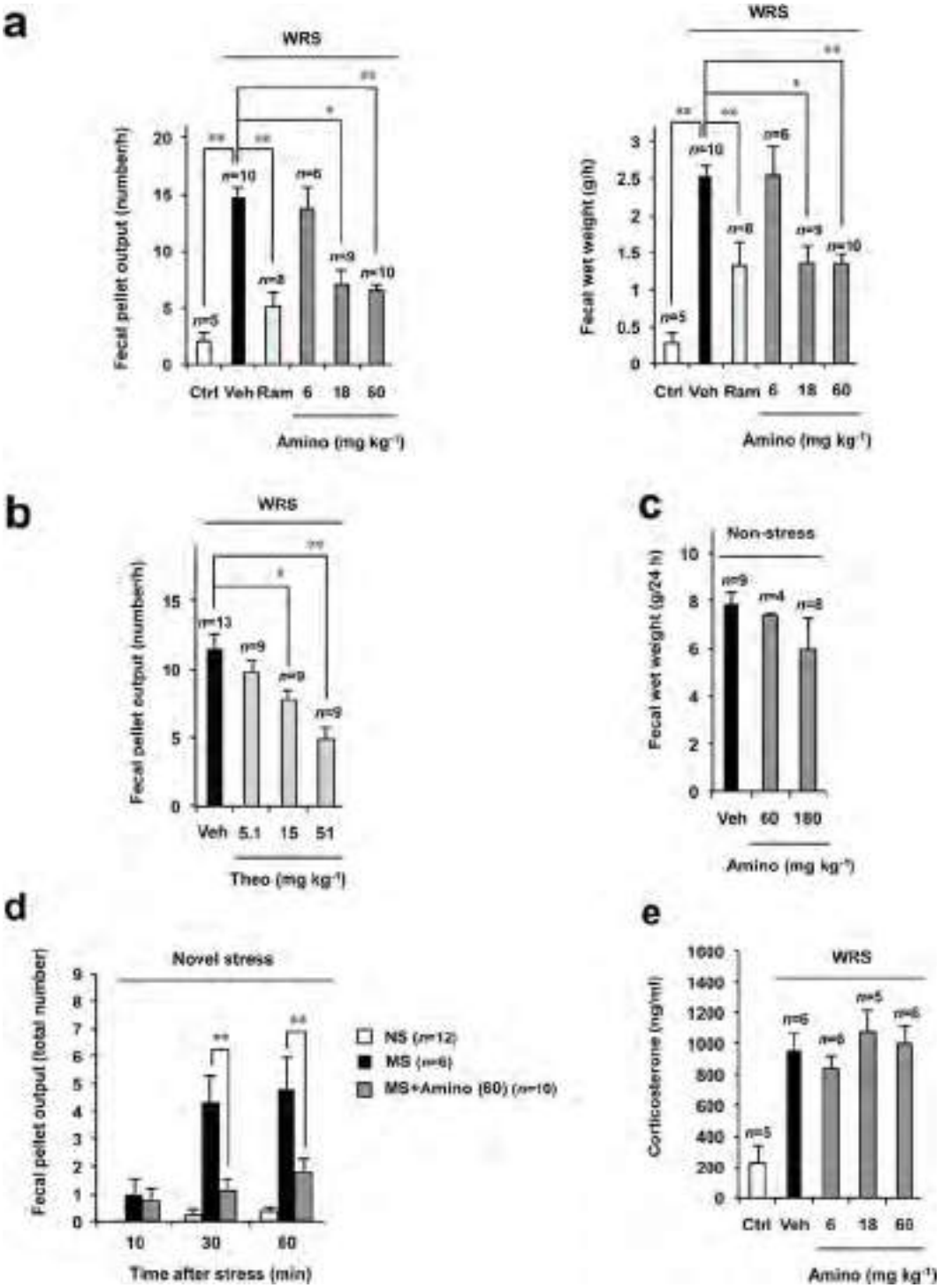

Figure 1. Effects of aminophylline on WRS- and novel stress-induced defecation in rats. Rats were subjected to maternal separation (MS) or non-maternal separation (NS) as described in the Materials and Methods (**d**). The rats received the indicated oral dose of aminophylline (Amino) (mg kg^{-1}) (**a**,**c**–**e**), ramosetron (Ram) (0.03 mg kg^{-1}) (**a**), theophylline (Theo) (mg kg^{-1}) (**b**) or vehicle (Veh: saline) (**a**–**e**). Two hours after the administration, rats were exposed to WRS for 1 h (**a**,**b**,**e**), or novel stress (transfer to a new cage) (**d**) or remained undisturbed for 24 h (**c**). The number (**a**,**b**,**d**) and wet weight (**a**,**c**) of the fecal pellets excreted in 1 h (**a**,**b**), 24 h (**c**) or until the indicated time period (**d**) were determined. After the WRS, the plasma level of corticosterone was measured by ELISA (**e**). The values are the mean ± s.e.m. $^{*}P < 0.05$; $^{**}P < 0.01$ (Tukey test).

effect of aminophylline in this animal model. Indeed, as shown in Fig. 1d, maternal separation stimulated novel stress-induced fecal pellet output, a response that was suppressed by aminophylline.

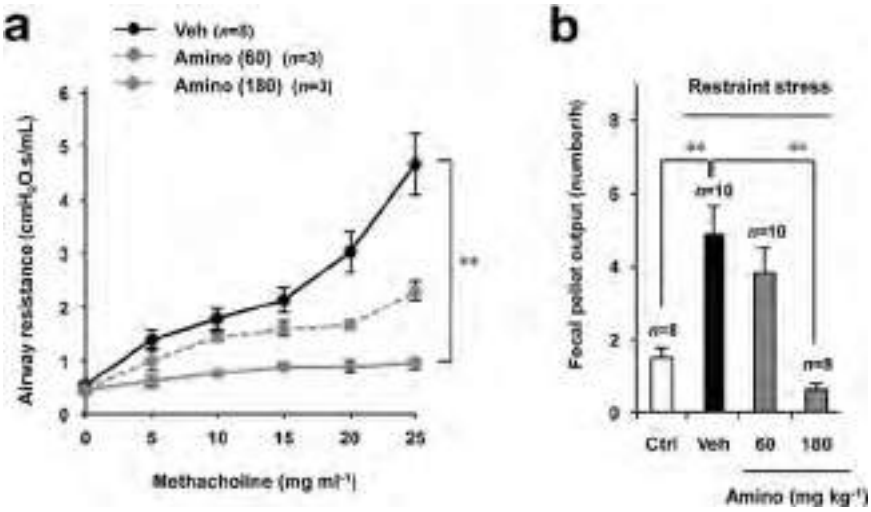

Figure 2. The relationship between the inhibitory effect of aminophylline on defecation and the bronchodilatory effect of aminophylline in mice. The indicated dose (mg kg^{-1}) of aminophylline (Amino) (mg kg^{-1}) or vehicle (Veh: saline) was orally administered to mice (**a**,**b**). After 1 h, the mice were exposed to nebulized methacholine for 5 times, and the airway resistance was determined after each methacholine challenge (**a**). Two hours after aminophylline administration, the mice were subjected to RS for 1 h and the number of fecal pellets excreted during the RS period (1 h) was determined (**b**). Control mice (Ctrl) were left to move freely in their cage. The values are the mean ± s.e.m. $^{*}P < 0.05$; $^{**}P < 0.01$ (Tukey test).

We then examined the effect of aminophylline on the serum level of corticosterone after exposure to WRS. As shown in Fig. 1e, rats subjected to WRS exhibited a significant increase in their serum corticosterone level, an effect that was not ameliorated by pre-administration of aminophylline. This suggests that aminophylline affects WRS-induced fecal pellet output independent of the serum level of corticosterone.

The mechanism undelying aminophylline-dependent suppression of WRS-induced fecal pellet output. For both the clinical application of aminophylline for IBS-D patients and the identification of the molecular mechanism underlying aminophylline-dependent suppression of WRS-induced fecal pellet output, it is important to examine whether this novel pharmacological effect of aminophylline (suppression of defecation) is achieved at a dose similar to that required for its original pharmacological activity (bronchodilation). We therefore compared the dose-response profiles of aminophylline in terms of its inhibitory effect on defecation and its bronchodilatory effect. Given that we had already established the assay system for bronchodilation in mice[37], we used mice for this comparative analysis. Significant inhibition of methacholine-induced bronchoconstriction (an increase in airway resistance; Fig. 2a) and significant inhibition of restraint stress (RS)-induced fecal pellet output (Fig. 2b) were observed after oral administration of 180 mg kg^{-1} aminophylline. The dose of aminophylline required for its bronchodilation also inhibited stress-induced defecation.

Therefore, we focused on the inhibitory effect of aminophylline on both PDEs and ARs. We first examined the effect of a specific antagonist of each AR subtype on WRS-induced defecation. Pre-administration of MRS-1754 (a subtype-specific antagonist of A_{2B}ARs) significantly suppressed fecal pellet output in rats subjected to WRS in a dose-dependent manner (Fig. 3a). However, DPCPX and istradefylline (subtype-specific antagonists of A_1ARs and A_{2A}ARs, respectively) had no significant effect hereon (Fig. 3a).

We also examined the effect of PDE inhibitors on WRS-induced defecation. As shown in Fig. 3b, ibudilast (a subtype non-specific inhibitor of PDEs) significantly suppressed fecal pellet output in rats subjected to WRS. We then used a specific inhibitor of each subtype of PDE. As shown in Fig. 3c, rolipram (a subtype-specific inhibitor of PDE4) but not cilostazol (a subtype-specific inhibitor of PDE3) suppressed the WRS-induced fecal pellet output in rats. These results suggest that the inhibitory effect of aminophylline on WRS-induced defecation is probably mediated by its inhibitory effect on both A_{2B}ARs and PDE4.

Effect of aminophylline on visceral hypersensitivity to CRD. To assess the effect of aminophylline on visceral hypersensitivity, we used a rat model of maternal separation-induced visceral hypersensitivity to CRD, one of the animal models of IBS[10]. As shown in Fig. 4a, the VMR evoked by CRD (EMG amplitude) increased according to the increase in balloon pressure, an effect that was stimulated in rats subjected to early maternal separation as described previously[10]. However, oral pre-administration of aminophylline (60 mg kg^{-1}) significantly suppressed the VMR to a level similar to that observed in non-maternally separated rats (control rats) (Fig. 4a). Oral pre-administration of ramosetron produced a similar effect (Fig. 4a). On the other hand, pre-administration of aminophylline did not affect the VMR to CRD in control rats (without maternal separation) even at the higher dose of 180 mg kg^{-1} (Fig. 4b). We also found that administration of theophylline suppressed the VMR to CRD in rats subjected to maternal separation at a dose equivalent to that of aminophylline (with respect to the molecular weight of theophylline) (Fig. 4c). These results suggest that aminophylline and theophylline suppress the maternal separation-induced visceral hypersensitivity to CRD.

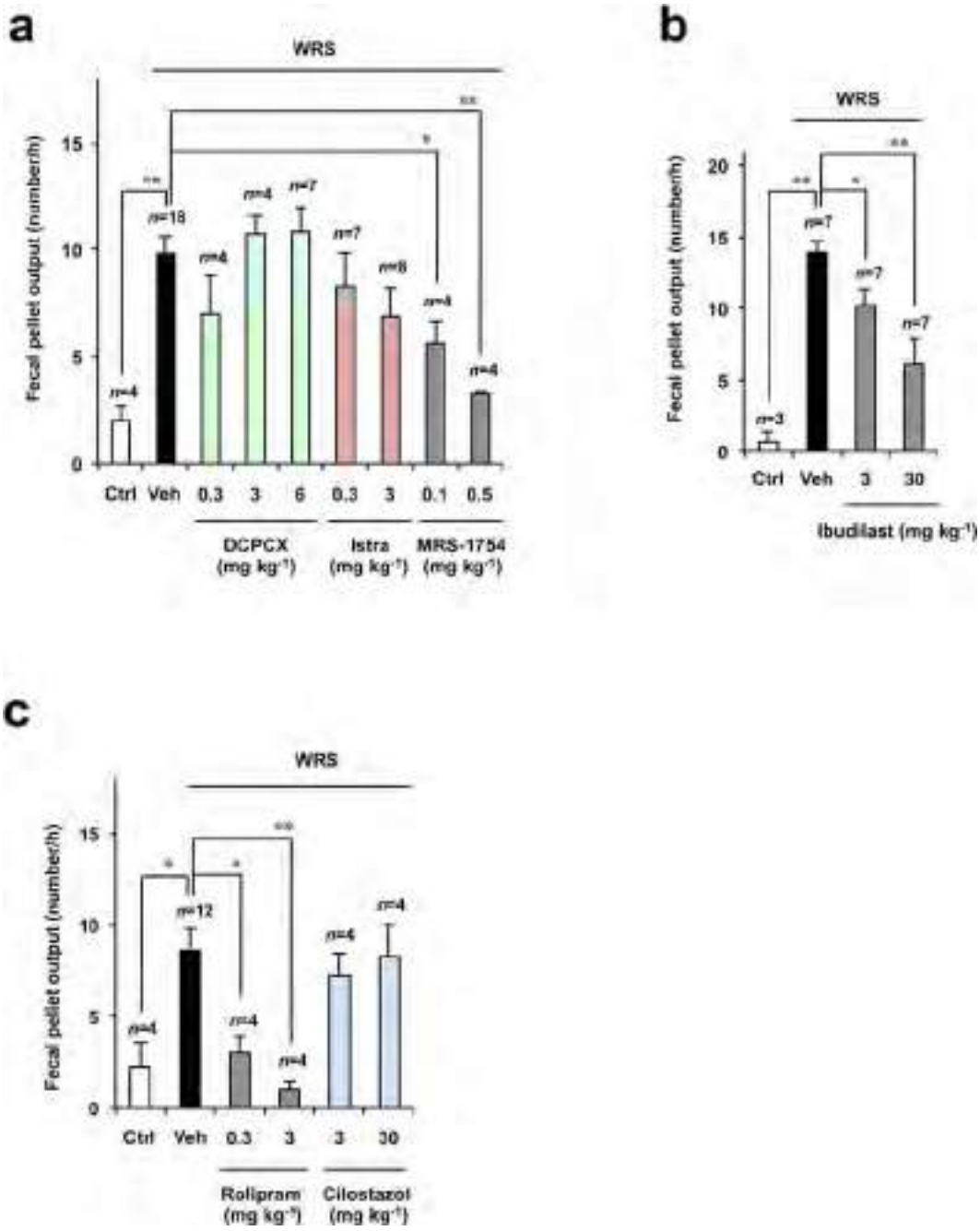

Figure 3. Effects of AR antagonists and PDE inhibitors on WRS-induced defecation in rats. Rats were intraperitoneally administered the indicated dose of DCPCX (a selective A_1AR antagonist) (**a**), istradefylline (Istra) (a selective A_{2A}AR antagonist) (**a**), MRS-1754 (a selective A_{2B}AR antagonist) (**a**), ibudilast (a subtype non-selective PDE inhibitor) (**b**), rolipram (a selective PDE4 inhibitor) (**c**), cilostazol (a selective PDE3 inhibitor) (**c**) or vehicle (Veh: 1% methylcellulose) (**a**–**c**). Fifteen minutes after the administration, rats were subjected to WRS for 1 h. Control rats (Ctrl) were left to move freely in their cage. The number of fecal pellets excreted during this period (1 h) was counted. The values are the mean ± s.e.m. $^{*}P < 0.05$; $^{**}P < 0.01$ (Tukey test).

We then evaluated the therapeutic potential of aminophylline in an acetic acid-induced visceral hypersensitivity. In this model, rat pups received intracolonic administration of acetic acid at 10 days of age and visceral hypersensitivity to CRD was assessed at 5–6 weeks of age. As shown in Fig. 4d, rats subjected to the acetic acid treatment showed visceral hypersensitivity to CRD. However, pre-administration of aminophylline returned the sensitivity to the level observed in control rats.

The mechanism underlying aminophylline-dependent suppression of visceral hypersensitivity to CRD. As shown in Fig. 5a, ibudilast did not significantly affect the VMR to CRD in rats subjected to maternal separation, suggesting that the inhibitory effect of aminophylline on visceral hypersensitivity to CRD

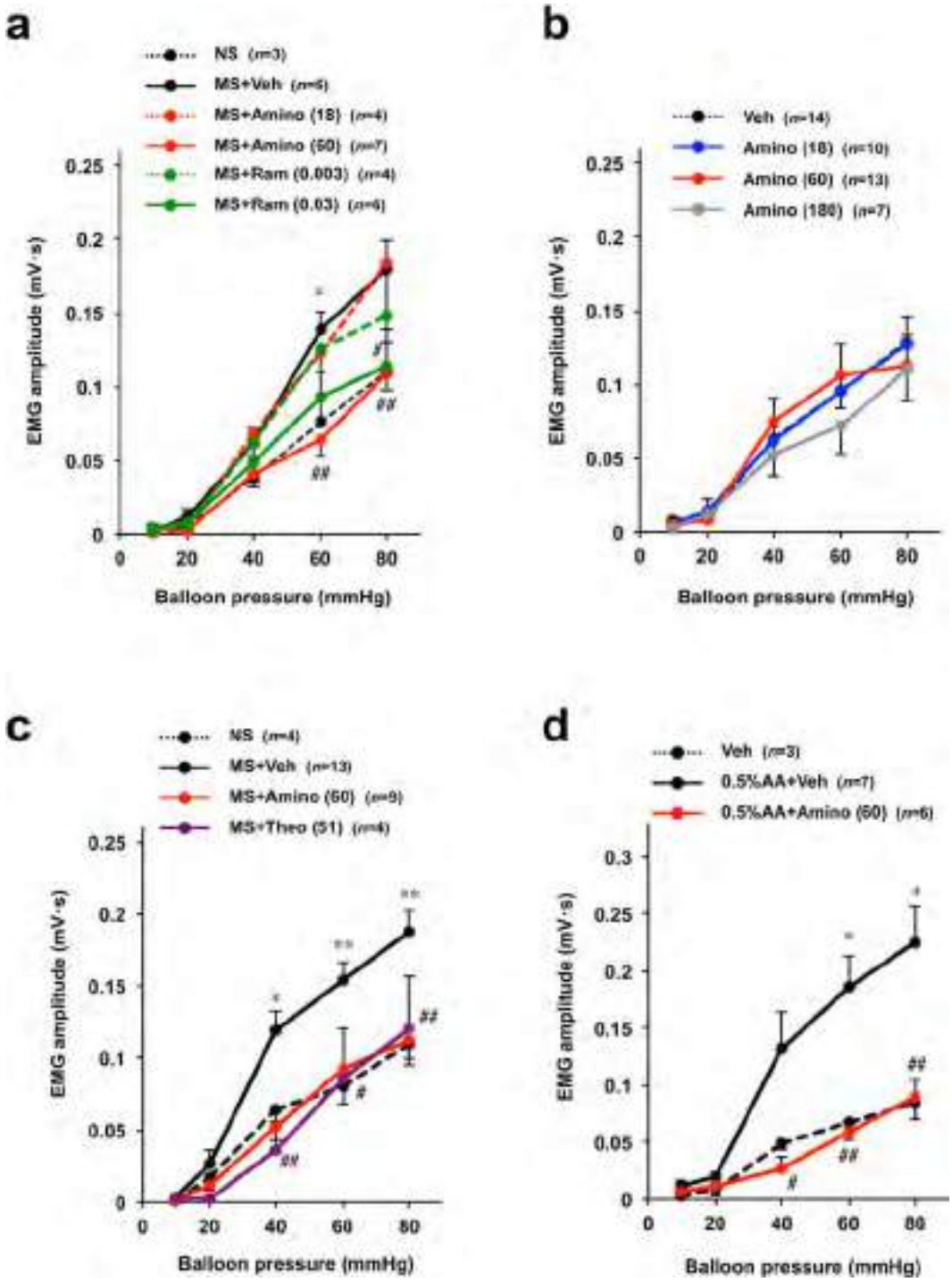

Figure 4. Effects of aminophylline on maternal separation- and acetic acid administration-induced visceral hypersensitivity to CRD in rats. Rats were subjected to maternal separation (MS) or administration of 0.5% acetic acid (AA) as described in the Materials and Methods. The MS and non-maternally separated (NS) rats were orally administered the indicated dose of aminophylline (Amino) (mg kg^{-1}) (**a**,**b**), ramosetron (Ram) (mg kg^{-1}) (**a**), theophylline (Theo) (mg kg^{-1}) (**b**) or vehicle (Veh: saline) (**a**–**c**). Two hours later, the VMR to CRD was monitored by measuring the EMG. The values are the mean ± s.e.m. * or $^{\#}P < 0.05$; ** or $^{\#\#}P < 0.01$ (*, vs NS; $^{\#}$, vs Veh) (Tukey test).

is not mediated by inhibition of PDEs. Thus, we focused on ARs. Pre-administration of istradefylline or MRS-1754 significantly suppressed the VMR to CRD in rats subjected to maternal separation to an extent similar to that observed with aminophylline (Fig. 5b). In contrast, DPCPX did not suppress the VMR to CRD, and indeed a higher dose of this drug had a stimulatory effect (Fig. 5b). These results suggest that the inhibitory effect of

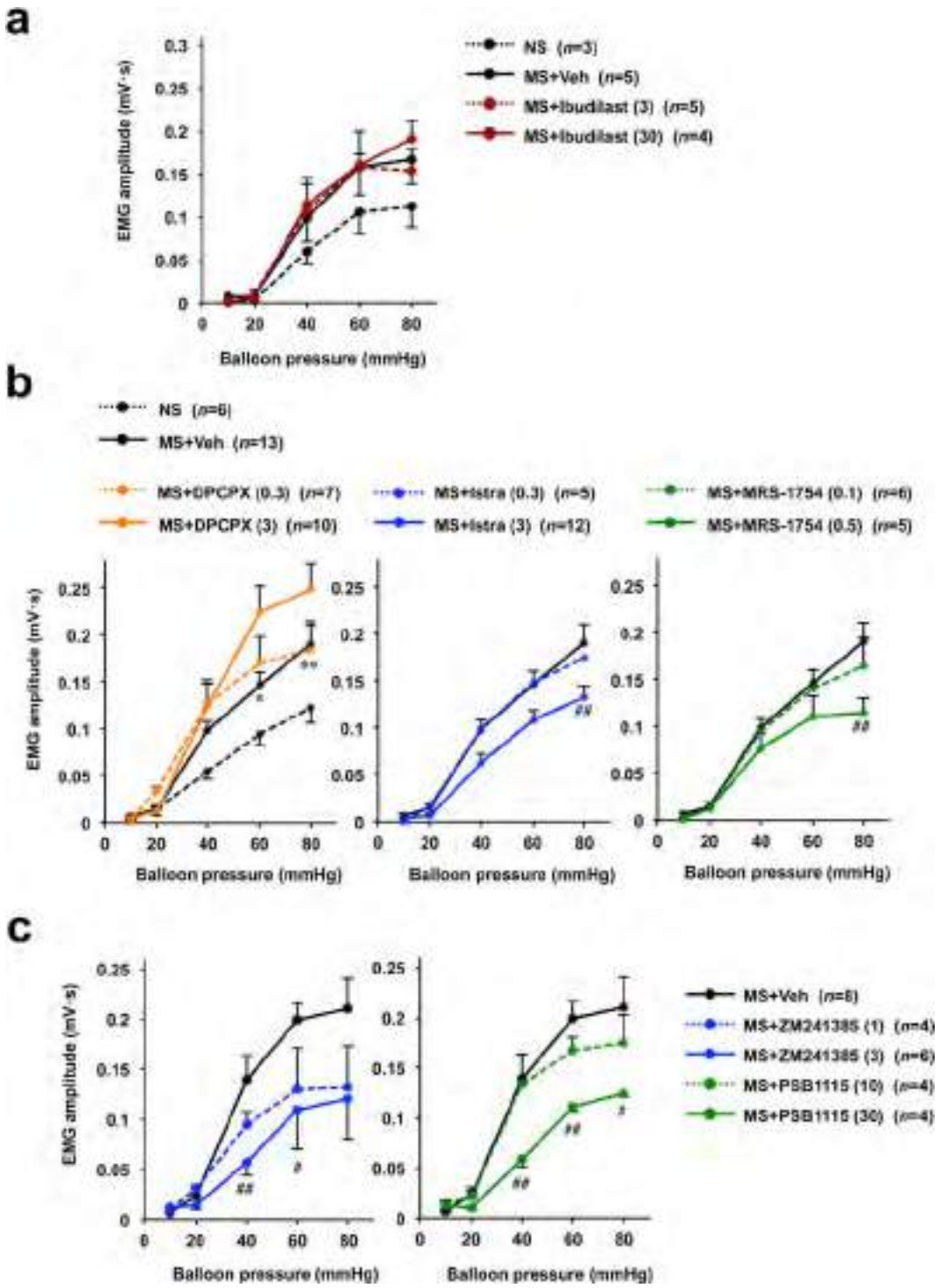

Figure 5. Effects of AR antagonists and PDE inhibitors on maternal separation-induced visceral hypersensitivity to CRD in rats. Rats subjected to maternal separation (MS) (**a**–**c**) or non-separation (NS) (**a**,**b**) were intraperitoneally administered the indicated dose (mg kg^{-1}) of ibudilast (a subtype non-selective PDE inhibitor) (**a**), DCPCX (a selective A_1AR antagonist) (**b**), istradefylline (Istra) (a selective A_{2A}AR antagonist) (**b**), MRS-1754 (a selective A_{2B}AR antagonist) (**b**), ZM241385 (a selective A_{2A}AR antagonist) (**c**), PSB1115 (a selective A_{2B}AR antagonist) (**c**) or vehicle (Veh: 1% methylcellulose) (**a**–**c**). Fifteen minutes later, the VMR to CRD was monitored. The values are the mean ± s.e.m. * or $^{\#}P < 0.05$; ** or $^{\#\#}P < 0.01$ (*, vs Ctrl; $^{\#}$, vs Veh) (Tukey test). The data for the MS + Veh in the three panels in (**b**) and the two panels in (**c**) are the same.

aminophylline on maternal separation-induced visceral hypersensitivity to CRD is mediated by its inhibitory effect on both A_{2A}ARs and A_{2B}ARs. To confirm this hypothesis, we used another subtype-specific antagonist of

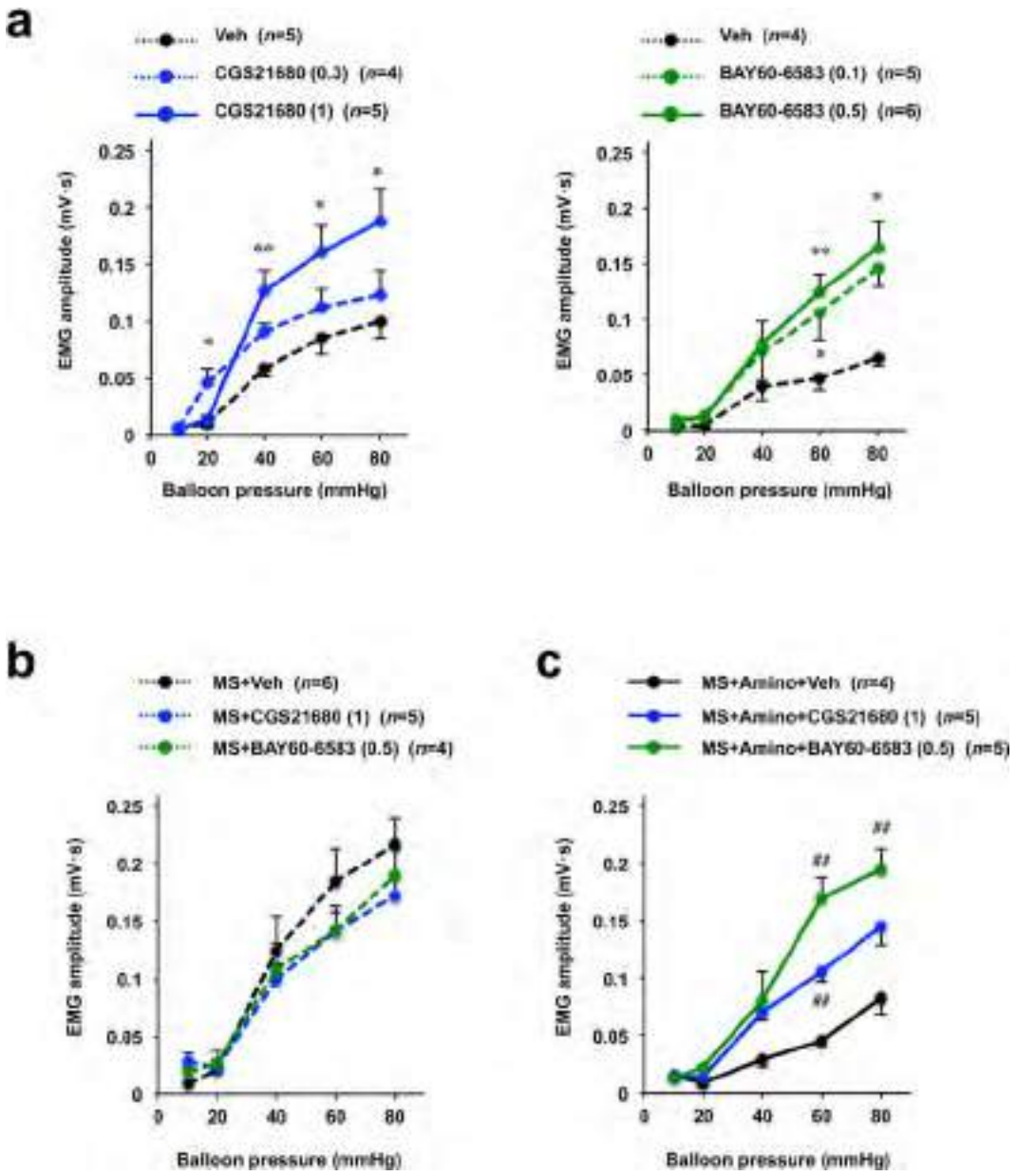

Figure 6. Effects of AR agonists on visceral sensitivity to CRD in control and maternally separated rats. Control rats (**a**) and maternally separated (MS) (**b**,**c**) rats were intraperitoneally administered the indicated dose (mg kg^{-1}) of CGS21680 (a selective A_{2A}AR agonist) (**a**–**c**), BAY60-6583 (a selective A_{2B}AR agonist) (**a**–**c**), or vehicle (Veh: 1% methylcellulose) (**a**–**c**). Fifteen minutes later, the VMR to CRD was monitored. A 60 mg/kg of aminophylline (Amino) was orally administered to rats 2 h before the CRD test (**c**). The values are the mean ± s.e.m. * or $^{\#}P < 0.05$; ** or $^{\#\#}P < 0.01$ (*, vs Veh; $^{\#}$, vs MS + Amino + Veh) (Tukey test).

A_{2A}ARs and A_{2B}ARs. As shown in Fig. 5c, both ZM241385 and PSB1115 (a subtype-specific antagonist of A_{2A}ARs and A_{2B}ARs, respectively) significantly suppressed the VMR to CRD in rats subjected to maternal separation.

To investigate the involvement of A_{2A}AR and A_{2B}AR activation in the development of visceral hypersensitivity to CRD, we examined the effect of CGS21680 (a subtype-specific A_{2A}AR agonist) and BAY60-6583 (a subtype-specific A_{2B}AR agonist) on VMR to CRD in normal rats. We found that both CGS21680 and BAY60-6583 produced a stimulatory effect on VMR to CRD in normal rats (Fig. 6a). We also assessed the effect of CGS21680 and BAY60-6583 on the rats subjected to maternal separation, and found neither agonist affected the VMR to CRD in maternally separated rats (Fig. 6b). Finally, we examined whether an A_{2A}AR or A_{2B}AR agonist could inhibit the ameliorative effect of aminophylline on maternal separation-induced visceral hypersensitivity to CRD. Both CGS21680 and BAY60-6583 significantly stimulated the VMR to CRD in maternally separated rats pretreated with aminophylline (Fig. 6c).

Discussion

Although various types of drugs are prescribed for IBS-D patients and several target proteins for IBS-D drugs have been proposed, an appropriate pharmacological therapy has not yet been established. Furthermore, the adverse effects of the current IBS-D drugs restrict the clinical use of these drugs (see introduction). Thus, novel drugs that target novel proteins and enable long-term treatment without serious adverse effects are required. Here we adopted a phenotypic screening approach and a drug re-positioning strategy to search for suitable drug candidates. Specifically, we screened for compounds that could suppress both the VMR to CRD and stress-induced defecation in rats, and identified aminophylline as a promising candidate. Aminophylline or theophylline has been clinically used as a bronchodilator and both its antagonizing activity on ARs and its inhibitory activity on PDEs have been reported[23]. However, thus far, the potential beneficial effects of these drugs on IBS have not been proven in pre-clinical or clinical studies.

Here, the oral administration of aminophylline prevented not only WRS-induced defecation but also novel stress-induced defecation in rats and RS-induced defecation in mice. However, in rats, aminophylline did not affect defecation under normal conditions and the serum level of corticosterone under stress conditions, suggesting that aminophylline specifically prevented stress-induced defecation independent of the function of the hypothalamic-pituitary-adrenal axis. The lack of an effect on normal defecation would appear to be beneficial for its clinical application in IBS patients. The dose-response profiles of aminophylline in terms of its inhibitory effect on fecal pellet output and its bronchodilatory effect were similar in mice. Theophylline also showed an inhibitory effect on WRS-induced fecal pellet output. These results suggest that the inhibitory effect of aminophylline on stress-induced defecation is mediated by a mechanism similar to that for its bronchodilatory effect. In other words, by antagonizing ARs and/or inhibiting PDEs. We showed that pre-administration of a subtype-specific antagonist of A_{2B}ARs but not of A_1ARs or A_{2A}ARs significantly suppressed WRS-induced fecal pellet output in rats. We also demonstrated that a subtype non-specific inhibitor of PDE and a subtype-specific inhibitor of PDE4 but not PDE3 had a similar effect. These results suggest that the inhibitory effect of aminophylline on WRS-induced fecal pellet output is mediated by its inhibitory effect on both PDE4 and A_{2B}ARs. However, no direct evidence for this effect was presented in this study. Therefore, confirmation that a selective PDE4 activator or a selective A_{2B}AR agonist can inhibit the ameliorating effect of aminophylline is warranted. Furthermore, these results are consistent with those of previous reports showing that A_{2B}AR-knockout mice have decreased stool frequency[32] and that inhibition of PDE4 suppresses stress-induced defecation[35]. Nevertheless, they do not agree with the finding by Antonioli *et al.* that A_{2B}AR antagonists enhance colonic contraction in rats[30]. Thus, our findings are in contrast to those of Antonioli *et al.* We believe that the results of Antonioli *et al.* may not necessarily reflect the overall effect on colonic propulsive activity *in vivo* because their experiments were tested *in vitro* using a longitudinal smooth muscle strip. On the other hand, Chandrasekharan *et al.* reported that A_{2B}AR knockout mice and A_{2B}AR antagonist-treated mice showed delayed colonic emptying, decreased stool retention and decreased stool frequency[32]. The authors also suggested that these phenotypes were mediated by inhibition of colonic circular muscle relaxation through the blockade of A_{2B}ARs, which are involved in NO release from enteric neurons. We postulate that such a mechanism may underlie our results.

Oral administration of aminophylline or theophylline prevented maternal separation- and acetic acid administration-induced visceral hypersensitivity to CRD but did not affect the visceral sensitivity under normal conditions. The inability of these drugs to affect normal visceral sensitivity may be beneficial for their clinical application in IBS patients. Regarding the mechanism governing the inhibitory effect of aminophylline on visceral hypersensitivity to CRD, we showed that a subtype non-specific inhibitor of PDE did not significantly affect the hypersensitivity response. In contrast, pre-administration of subtype-specific antagonists of A_{2A}ARs and A_{2B}ARs but not A_1ARs significantly suppressed the VMR to CRD in rats subjected to maternal separation. These results suggest that the inhibitory effect of aminophylline on maternal separation-induced visceral hypersensitivity to CRD is mediated by its inhibitory effect on both A_{2A}ARs and A_{2B}ARs. We confirmed this hypothesis using additional subtype-specific A_{2A}AR and A_{2B}AR antagonists (ZM241385 and PSB1115, respectively) and subtype-specific A_{2A}AR and A_{2B}AR agonists (CGS21680 and BAY60-6583, respectively) in the presence of aminophylline. Given that it is known that PSB1115 does not cross the blood-brain barrier[38], this result suggests that A_{2B}ARs expressed on peripheral tissues (such as the large intestine) rather than those expressed in the central nervous system mediate the inhibitory effect of aminophylline on visceral hypersensitivity. Furthermore, we found that A_{2A}AR and A_{2B}AR subtype-specific agonists stimulated visceral sensitivity to CRD in normal rats but not in maternally separated rats. We speculate that A_{2A}R and A_{2B}R receptor sensitivity is decreased in maternally separated rats because these receptors are already bound by adenosine. Thus, we also infer that the occurrence (or enhancement) of a tonic adenosine release during stress rather than an increased expression of A_{2A}AR and A_{2B}AR is involved in the development of visceral hypersensitivity to CRD in stressed rats. As described in the introduction, previous studies have shown that A_{2A}AR and A_{2B}AR antagonists produce an analgesic effect in an animal model of somatic pain[31]. However, to the best of our knowledge, our study is the first to demonstrate the inhibitory effect of A_{2A}AR and A_{2B}AR antagonists on visceral pain and hypersensitivity. On the other hand, we found that administration of a higher dose of an A_1AR antagonist stimulated the VMR to CRD, which was consistent with the finding of a previous study showing that the activation of A_1ARs produced an analgesic effect[34].

We propose that aminophylline and theophylline are candidate drugs for IBS-D due to their ameliorating effects on both stress-induced defecation and visceral hypersensitivity. Their ability to suppress maternal separation-induced visceral hypersensitivity to CRD is particularly important, given that most current IBS-D drugs, except for 5-HT_3 receptor antagonists, have not been reported to affect visceral hypersensitivity in this model. Furthermore, since the inhibitory effect of aminophylline on WRS-induced defecation appears to be mediated by a mechanism similar to that which underlies its bronchodilatory effect, aminophylline may show therapeutic efficacy at a dose used clinically and of which the safety has already been confirmed in humans.

Our results have also revealed a novel target protein class for IBS-D drugs: the A_{2B}ARs. Specific antagonists for these receptors may therefore be beneficial for the treatment of IBS-D patients, although it is possible that aminophylline may still prove superior to such specific antagonists. We therefore propose that a pilot clinical study in which the efficacy of aminophylline in IBS-D patients is tested should be performed, given that this is already possible without the need of pre-clinical and phase 1 clinical studies.

Methods

Chemicals and animals. PSB1115 was purchased from Santa Cruz Biotechnology, Inc (Santa Cruz, CA). Methylcellulose, ibudilast and rolipram were obtained from Wako Pure Chemical Industries (Osaka, Japan). Medetomidine chloride (Domitor®) and butorphanol tartrate (Vetorphale®) were obtained from Meiji Seika Pharma Co., Ltd. (Tokyo, Japan) and midazolam was purchased from SANDOZ (Tokyo, Japan). Istradefylline and theophylline were purchased from Sigma (St. Louis, MO). Cilostazol and aminophylline were obtained from LKT laboratories, Inc. (St Paul, MN). MRS-1754 and BAY60-6583 were from Tocris Bioscience (Bristol, UK) and 1,3-dipropyl-8-cyclopentylxanthine (DCPCX), ZM241385 and CGS21680 were from Abcam (Cambridge, UK). ICR mice (5- or 6-week-old males, 28–33 g), primiparous late pregnant Wistar female rats and normal male Wistar rats (4- or 5-week-old, 150–250 g) were obtained from Charles River Laboratories Japan (Yokohama, Japan). The animals were housed under conditions of controlled temperature (22–24 °C) and illumination (12-h light cycle) conditions for 1 or 2 weeks before experiments. The experiments and procedures described here were performed in accordance with the Guide for the Care and Use of Laboratory Animals as adopted and promulgated by the National Institutes of Health, and were approved by the Animal Care Committees of Keio University and St. Marianna University.

Measurement of VMR to CRD. The VMR to CRD was monitored as described[39], with some modifications. Briefly, rats were deeply anesthetized with a mixture of medetomidine chloride (0.5 mg kg^{-1}), midazolam (2.5 mg kg^{-1}), and butorphanol tartrate (2.5 mg kg^{-1}), and electromyography electrodes (Star Medical, Tokyo, Japan) were sutured into the external oblique muscle of the abdomen for electromyogram (EMG) recording. Electrode leads were tunneled subcutaneously and were exteriorized at the nape of the neck for future access. After the surgery, rats were housed individually and allowed to recuperate for 6 days before being used for measurement of the VMR. The rats were restrained in a plastic conical-shape tube (diameter, 6 cm; height, 15 cm), 15 min before the EMG recording. A polyethylene bag (length, 2 cm) was inserted in the distal colon, positioned 1 cm proximal to the rectum and connected to a balloon catheter. The pressure and volume of the balloon were controlled and monitored by a pressure controller-timing device (Distender Series II; G & J Electronics, Toronto, Canada), connected to the balloon. The rats were subjected to repeated CRD (12 times at 80 mm Hg; duration, 30 s; interstimulus interval, 300 s) for drug screening or to phasic CRD (10, 20, 40 60 and 80 mm Hg; duration, 20 s; interstimulus interval, 150 s) for the estimation of drug activity. Aminophylline or theophylline in saline or ramosetron in 1% methylcellulose were administered orally 2 h before CRD. The other drugs (AR antagonists, AR agonists and PDE inhibitors) were dissolved in 1% methylcellulose and were intraperitoneally administered 15 min before CRD. EMG data were collected and analyzed using the 8 STAR software package (version 6.0–19.2 for Windows; Star Medical, Tokyo, Japan). VMR evoked by contraction of the external oblique muscle was quantified by calculating the area under the curve (AUC) of the voltage alteration graph. The data were expressed as the result of the subtraction of the baseline VMR from the VMR during CRD (EMG amplitude). The baseline was consisted of the data collected 20 s before each CRD.

Maternal separation- and acetic acid-induced colonic hypersensitivity to CRD. Neonatal maternal separation was performed as described previously[10] with some modifications. Primiparous late pregnant Wistar female rats were individually housed for about a week prior to giving birth (10–15 pups/rat). The pups were separated from their dams for 3 h every day for 10 days (from postnatal day 2 to 12). Separations were conducted between 9 AM and 12 AM. The pups were placed in plastic cages that contained a heater pad (30 °C–33 °C), and were placed in a room separated from the dams. Non-maternally separated group (control pups) was left undisturbed with their dams. From postnatal day 12, both groups of rats were left undisturbed except for routine cage cleaning every two days. At 5–6 weeks of age, the VMR to CRD was examined in both groups of rats.

Acetic acid-induced colonic hypersensitivity was performed as described previously[40] with some modifications. At 10 days of age, rat pups were subjected to intracolonic injection of 0.2 ml of 0.5% acetic acid in saline in a position 2 cm from the anus; control rats received an equal volume of saline. At 5–6 weeks of age, the VMR to CRD in both groups of rats was measured.

Stress-induced fecal pellet output. WRS-, RS-, and novel stress-induced fecal pellet output was monitored as described previously[36,39], with some modifications.

To monitor the WRS-induced fecal pellet output in rats, the rats received an oral dose of aminophylline or theophylline in saline (2 ml kg^{-1}) or ramosetron in 1% methylcellulose (2 ml kg^{-1}) 2 h before WRS. The other drugs (AR antagonists or PDE inhibitors) were dissolved in 1% methylcellulose and were injected intraperitoneally 15 min before WRS. Rats were subjected to WRS for 1 h and the number or wet weight of fecal pellets excreted during this period was determined. The wet weight of fecal pellets excreted during 24 hours was measured to evaluate the influence of aminophylline on defecation in non-stressed rats. WRS was performed as described previously[36]. Briefly, the rats were lightly anesthetized with isoflurane and their foreshoulders, upper forelimbs and thoracic trunk were wrapped in paper tape to restrict but not prevent movement. The animals recovered from isoflurane within 2–5 min and mobile immediately thereafter. The control rats were anesthetized with isoflurane but were not wrapped.

To monitor RS-induced fecal pellet output in mice, the mice were placed individually into a 50 ml Falcon tube (Becton Dickinson, Franklin Lakes, NJ) for 1 h. These tubes were small enough to restrain each mouse but were large enough to allow breathing. The control mice were left to move freely in their cage. Aminophylline in saline ($10\,ml\,kg^{-1}$) was orally administered 2 h before RS. The number of fecal pellets excreted during the RS period (1 h) was counted.

Control (non-maternally separated) and maternally separated rats (see above) were tested for responsiveness to a novel stress stimulus. This was induced by transferring the rats from their home cage with a white paper towel to a new cage with a wired mesh, as described previously[10]. Aminophylline was orally administered 2 h prior to exposure to a novel stress stimulus. The rats were placed in the new cage for 1 h, and the number of fecal pellets excreted during this period was counted.

Measurement of lung airway resistance. Measurement of lung airway resistance was performed with a computer-controlled small animal ventilator (FlexiVent, SCIREQ, Montreal, Canada) as described previously[37]. The mice were anesthetized with chloral hydrate ($500\,mg\,kg^{-1}$), a tracheotomy was performed, and an 8-mm section of metallic tube was inserted into the trachea. Mice were mechanically ventilated at a rate of 150 breaths per min, using a tidal volume of $8.7\,ml\,kg^{-1}$ and a positive end-expiratory pressure of 2–3 cm H_2O. For measurement of the methacholine-induced increase in airway resistance, mice were exposed to nebulized methacholine ($1\,mg\,ml^{-1}$) five times for 20 s, with a 40 s interval, and airway resistance was measured after each methacholine challenge by the snap shot technique. Aminophylline was orally administered to mice 1 h before the test. All data were analyzed using the FlexiVent software (FlexiVent, SCIREQ, Montreal, Canada).

Measurement of the plasma corticosterone level. After completion of the WRS experiment, the rats were euthanized and blood was collected to measure the plasma corticosterone level, using an ELISA kit (Cayman Chemical, Ann Arbor, MI), according to the manufacturer's instructions.

Statistical analysis. All values are expressed as the mean ± s.e.m. For the defecation experiments, one or two-way ANOVA followed by the Tukey test for unpaired results was used to evaluate differences between more than two groups or between two groups. For the bronchodilation and visceral hypersensitivity to CRD study, two-way ANOVA with repeated measures followed by the Tukey test was used. Differences were considered significant at $P < 0.05$.

References

1. Chang, L., Lembo, A. & Sultan, S. American Gastroenterological Association Institute Technical Review on the pharmacological management of irritable bowel syndrome. *Gastroenterology* **147,** 1149–1172 e1142 (2014).
2. Canavan, C., West, J. & Card, T. Review article: the economic impact of the irritable bowel syndrome. *Aliment Pharmacol Ther* **40,** 1023–1034 (2014).
3. Longstreth, G. F. *et al.* Functional bowel disorders. *Gastroenterology* **130,** 1480–1491 (2006).
4. Matricon, J. *et al.* Review article: Associations between immune activation, intestinal permeability and the irritable bowel syndrome. *Aliment Pharmacol Ther* **36,** 1009–1031 (2012).
5. Simren, M. *et al.* Intestinal microbiota in functional bowel disorders: a Rome foundation report. *Gut* **62,** 159–176 (2013).
6. Spiller, R. & Garsed, K. Postinfectious irritable bowel syndrome. *Gastroenterology* **136,** 1979–1988 (2009).
7. Dinan, T. G. *et al.* Hypothalamic-pituitary-gut axis dysregulation in irritable bowel syndrome: plasma cytokines as a potential biomarker? *Gastroenterology* **130,** 304–311 (2006).
8. Mayer, E. A. & Collins, S. M. Evolving pathophysiologic models of functional gastrointestinal disorders. *Gastroenterology* **122,** 2032–2048 (2002).
9. Videlock, E. J. *et al.* Childhood trauma is associated with hypothalamic-pituitary-adrenal axis responsiveness in irritable bowel syndrome. *Gastroenterology* **137,** 1954–1962 (2009).
10. O'Mahony, S. M. *et al.* Early life stress alters behavior, immunity, and microbiota in rats: implications for irritable bowel syndrome and psychiatric illnesses. *Biol Psychiatry* **65,** 263–267 (2009).
11. Mertz, H. R. Irritable bowel syndrome. *N Engl J Med* **349,** 2136–2146 (2003).
12. Hammerle, C. W. & Surawicz, C. M. Updates on treatment of irritable bowel syndrome. *World J Gastroenterol* **14,** 2639–2649 (2008).
13. Chey, W. D. *et al.* Linaclotide for Irritable Bowel Syndrome With Constipation: A 26-Week, Randomized, Double-blind, Placebo-Controlled Trial to Evaluate Efficacy and Safety. *Am J Gastroenterol* (2012).
14. Menees, S. B., Maneerattannaporn, M., Kim, H. M. & Chey, W. D. The efficacy and safety of rifaximin for the irritable bowel syndrome: a systematic review and meta-analysis. *Am J Gastroenterol* **107,** 28–35 quiz 36 (2012).
15. Traynor, K. Eluxadoline approved for irritable bowel syndrome with diarrhea. *Am J Health Syst Pharm* **72,** 1078 (2015).
16. Camilleri, M. Pharmacology of the new treatments for lower gastrointestinal motility disorders and irritable bowel syndrome. *Clin Pharmacol Ther* **91,** 44–59 (2012).
17. Mayer, E. A. & Bradesi, S. Alosetron and irritable bowel syndrome. *Expert Opin Pharmacother* **4,** 2089–2098 (2003).
18. Shah, E. & Pimentel, M. Evaluating the functional net value of pharmacologic agents in treating irritable bowel syndrome. *Aliment Pharmacol Ther* **39,** 973–983 (2014).
19. Mizushima, T. Drug discovery and development focusing on existing medicines: drug re-profiling strategy. *J Biochem* **149,** 499–505 (2011).
20. Segal, M. S., Levinson, L. *et al.* Evaluation of therapeutic substances employed for the relief of bronchospasm; aminophylline. *J Clin Invest* **28,** 1190–1195 (1949).
21. Hendeles, L. & Weinberger, M. Theophylline. A "state of the art" review. *Pharmacotherapy* **3,** 2–44 (1983).
22. Vassallo, R. & Lipsky, J. J. Theophylline: recent advances in the understanding of its mode of action and uses in clinical practice. *Mayo Clin Proc* **73,** 346–354 (1998).
23. Ukena, D., Schudt, C. & Sybrecht, G. W. Adenosine receptor-blocking xanthines as inhibitors of phosphodiesterase isozymes. *Biochem Pharmacol* **45,** 847–851 (1993).
24. Choi, O. H., Shamim, M. T., Padgett, W. L. & Daly, J. W. Caffeine and theophylline analogues: correlation of behavioral effects with activity as adenosine receptor antagonists and as phosphodiesterase inhibitors. *Life Sci* **43,** 387–398 (1988).
25. Fredholm, B. B., Irenius, E., Kull, B. & Schulte, G. Comparison of the potency of adenosine as an agonist at human adenosine receptors expressed in Chinese hamster ovary cells. *Biochem Pharmacol* **61,** 443–448 (2001).
26. Jacobson, K. A. & Gao, Z. G. Adenosine receptors as therapeutic targets. *Nat Rev Drug Discov* **5,** 247–264 (2006).
27. Christofi, F. L. Purinergic receptors and gastrointestinal secretomotor function. *Purinergic Signal* **4,** 213–236 (2008).

28. Feoktistov, I. & Biaggioni, I. Adenosine A2B receptors. *Pharmacol Rev* **49,** 381–402 (1997).
29. Maurice, D. H. *et al.* Advances in targeting cyclic nucleotide phosphodiesterases. *Nat Rev Drug Discov* **13,** 290–314 (2014).
30. Antonioli, L. *et al.* Role of the A(2B) receptor-adenosine deaminase complex in colonic dysmotility associated with bowel inflammation in rats. *Br J Pharmacol* **171,** 1314–1329 (2014).
31. Abo-Salem, O. M. *et al.* Antinociceptive effects of novel A2B adenosine receptor antagonists. *J Pharmacol Exp Ther* **308,** 358–366 (2004).
32. Chandrasekharan, B. P. *et al.* Adenosine 2B receptors (A(2B)AR) on enteric neurons regulate murine distal colonic motility. *FASEB J* **23,** 2727–2734 (2009).
33. Hussey, M. J., Clarke, G. D., Ledent, C., Hourani, S. M. & Kitchen, I. Reduced response to the formalin test and lowered spinal NMDA glutamate receptor binding in adenosine A2A receptor knockout mice. *Pain* **129,** 287–294 (2007).
34. Zhang, X. J. *et al.* Analgesic effect of paeoniflorin in rats with neonatal maternal separation-induced visceral hyperalgesia is mediated through adenosine A(1) receptor by inhibiting the extracellular signal-regulated protein kinase (ERK) pathway. *Pharmacol Biochem Behav* **94,** 88–97 (2009).
35. Barone, F. C. *et al.* Inhibition of phosphodiesterase type 4 decreases stress-induced defecation in rats and mice. *Pharmacology* **81,** 11–17 (2008).
36. Yamamoto, O. *et al.* Effect of YNS-15P, a new alpha-2 adrenoceptor antagonist, on stress-stimulated colonic propulsion in rats. *J Pharmacol Exp Ther* **287,** 691–696 (1998).
37. Tanaka, K. *et al.* Mepenzolate bromide displays beneficial effects in a mouse model of chronic obstructive pulmonary disease. *Nat Commun* **4,** 2686 (2013).
38. Baumgold, J., Nikodijevic, O. & Jacobson, K. A. Penetration of adenosine antagonists into mouse brain as determined by *ex vivo* binding. *Biochem Pharmacol* **43,** 889–894 (1992).
39. Asano, T. *et al.* Effects of beta-(1,3-1,6)-D-glucan on irritable bowel syndrome-related colonic hypersensitivity. *Biochem Biophys Res Commun* **420,** 444–449 (2012).
40. Qian, A. H. *et al.* Voltage-gated potassium channels in IB4-positive colonic sensory neurons mediate visceral hypersensitivity in the rat. *Am J Gastroenterol* **104,** 2014–2027 (2009).

Acknowledgements

The authors gratefully acknowledge Ayumi Kanada for technical assistance with the animal experiments. This work was supported by Grants-in-Aid for Scientific Research from the Ministry of Health, Labour, and Welfare of Japan, and Grants-in-Aid for Scientific Research from the Ministry of Education, Culture, Sports, Science and Technology, Japan.

Author Contributions

Conception and design: T.A., K.T. and T.M.; analysis and interpretation: T.A., K.T., A.T., R.T., H.S., H.M. and M.T.; drafting of the manuscript for important intellec.tual content: T.A. and T.M.

Additional Information

Competing financial interests: Tohru Mizushima is the chairman and director of LTT Bio-Pharma Co., Ltd, which may develop aminophylline for IBS-D. Teita Asano and Mitsuko Takenaga belong to an endowed research division of LTT Bio-Pharma Co., Ltd.

How to cite this article: Asano, T. *et al.* Aminophylline suppresses stress-induced visceral hypersensitivity and defecation in irritable bowel syndrome. *Sci. Rep.* **7**, 40214; doi: 10.1038/srep40214 (2017).

Publisher's note: Springer Nature remains neutral with regard to jurisdictional claims in published maps and institutional affiliations.

This work is licensed under a Creative Commons Attribution 4.0 International License. The images or other third party material in this article are included in the article's Creative Commons license, unless indicated otherwise in the credit line; if the material is not included under the Creative Commons license, users will need to obtain permission from the license holder to reproduce the material. To view a copy of this license, visit http://creativecommons.org/licenses/by/4.0/

© The Author(s) 2017

Cytotherapy, 2017; ■■: ■■–■■

International Society for Cellular Therapy ISCT®

Intravenous infusion of adipose-derived stem/stromal cells improves functional recovery of rats with spinal cord injury

YUKI OHTA[1], AKEMI HAMAGUCHI[2], MASANORI OOTAKI[1], MINORU WATANABE[3], YUKO TAKEBA[1], TAROH IIRI[1], NAOKI MATSUMOTO[1] & MITSUKO TAKENAGA[2]

[1]*Department of Pharmacology, St. Marianna University School of Medicine, Kawasaki, Kanagawa, Japan,* [2]*Institute of Medical Science, St. Marianna University Graduate School of Medicine, Kawasaki, Kanagawa, Japan, and* [3]*Institute for Animal Experimentation, St. Marianna University Graduate School of Medicine, Kawasaki, Kanagawa, Japan*

Abstract

Background aims. Adipose tissue has therapeutic potential for spinal cord injury (SCI) because it contains multipotent cells known as adipose-derived stem/stromal cells (ASCs). In this study, we attempted intravenous ASC transplantation in rats with SCI to examine the effect on functional recovery. *Methods.* ASCs (2.5×10^6) were intravenously infused into SCI rats, after which hindlimb motor function was evaluated. Distribution of transplanted ASCs was investigated and growth factor/cytokine levels were determined. *Results.* Intravenous transplantation of ASCs promoted the functional recovery in SCI rats and reduced the area of spinal cord cavitation. A distribution study revealed that ASCs gradually accumulated at the site of injury, but long-term survival of these cells was not achieved. Levels of growth factors increased only slightly in the spinal cord after ASC transplantation. Unexpectedly, cytokine-induced neutrophil chemoattractant (CINC)-1 showed a transient but substantial increase in the spinal cord tissue and blood of the ASC group. CINC-1 was secreted by ASCs *in vitro*, and the sponge implantation assay showed that CINC-1 and ASCs induced angiogenesis. CINC-1 promoted functional recovery in SCI rats, which was similar to the ASCs. Expression of glial cell line-derived neurotrophic factor was greater in the ASC group than in the CINC-1 group, although both promoted extracellular signal-regulated kinase (ERK)1/2 phosphorylation; Akt phosphorylation was enhanced in the spinal cord after ASC transplantation. *Conclusions.* Our findings indicated that intravenously transplanted ASCs gradually accumulated in the injured spinal cord, where cytokines such as CINC-1 activated ERK1/2 and Akt, leading to functional recovery.

Key Words: *adipose-derived stem/stromal cells, cytokine-induced neutrophil chemoattractant-1, intravenous infusion, spinal cord injury*

Introduction

Spinal cord injury (SCI) can result in partial or complete paralysis and disability. Currently, there is no effective treatment for SCI. Cell transplantation is being explored as a strategy to promote tissue regeneration, and a variety of cells, including embryonic stem cells, have been tested for their therapeutic potential for SCI [1–4]. However, there are some limitations to their clinical application, which include ethical concerns, problems with immunogenicity and safety issues related to the potential for tumorigenicity [5]. Somatic stem cells, such as bone marrow–derived mesenchymal stromal cells (BM-MSCs), may offset these problems because they are capable of self-renewal and can differentiate into mesodermal lineages as well as neuronal and glial cells [6–8]. MSCs (variously referred to as mesenchymal stromal cells or multipotent stromal cells) have been found in many tissues other than BM [9–11]. Adipose tissues are an attractive source of MSCs because of their ubiquitous distribution, accessibility and the ease with which they can be harvested. Adipose tissue–derived MSCs, called adipose-derived stem/stromal cells (ASCs), are obtained from adherent cultures of the stromal-vascular fraction separated from fatty tissues [9]. ASCs and BM-MSCs have similar characteristics [12] and can undergo multilineage differentiation into fat, bone, cartilage, smooth muscle, and neuronal, endothelial or hepatic cells [9,13–15]. ASCs also secrete a variety of growth factors, such as hepatocyte growth factor (HGF) and vascular endothelial growth factor (VEGF), which might mediate regeneration of the injured spinal cord [16]. Furthermore, adipose tissue contains larger

Correspondence: **Yuki Ohta**, PhD, Department of Pharmacology, St. Marianna University School of Medicine, 2-16-1 Sugao, Miyamae-ku, Kawasaki, Kanagawa 216-8511, Japan. E-mail: yuki-o@marianna-u.ac.jp

(Received 28 December 2016; accepted 7 April 2017)

ISSN 1465-3249 Copyright © 2016 International Society for Cellular Therapy. Published by Elsevier Inc. This is an open access article under the CC BY-NC-ND license (http://creativecommons.org/licenses/by-nc-nd/4.0/).
http://dx.doi.org/10.1016/j.jcyt.2017.04.002

populations of MSCs than does BM [17], thus making ASCs a promising target for regenerative medicine.

One important problem is the delivery of stem cells to the site of injury. In most animal experiments as well as in our previous study [4], cell transplantation was performed by direct injection into the damaged parenchyma, providing effective recovery of motor function and spinal cord preservation after SCI [1–4]. However, direct injection into the lesion is too invasive for human SCI. Intravenous administration has been chosen as the method of transplantation in patients with central nervous system disorders [18,19], with its possible recent report for its effectiveness [20].

In this study, we attempted intravenous ASC transplantation in rats with SCI to examine the effect on functional recovery and to investigate the role of ASCs.

Methods

Animals

Female Sprague-Dawley (SD) (Charles River Laboratories Japan) and green fluorescent protein (GFP) transgenic rats (SD, CAG-EGFP, Japan SLC) were housed in an animal room at a constant temperature (23 ± 1°C) and humidity (50–60%) with a 12-h light/dark cycle and were allowed free access to a standard diet and water. Experimental procedures were performed in accordance with the Guidelines for Animal Experimentation of St. Marianna University Graduate School of Medicine. The experimental protocol was approved by the Animal Research Committee, Institute for Animal Experimentation, St. Marianna University Graduate School of Medicine (approval numbers 1210002 and 1310005).

ASCs

Dorsal fat pads were obtained from 9-week-old rats under anesthesia. The adipose tissue was minced and digested for 1 h in 0.1% collagenase (Thermo Fisher Scientific) at 37°C. The digestion process was stopped by adding Dulbecco's Modified Eagle's Medium (Thermo Fisher Scientific) containing 20% fetal bovine serum (Thermo Fisher Scientific) and 1% antibiotic-antimycotic (Thermo Fisher Scientific). The digested suspension was filtered through a 70-μm nylon mesh cell strainer (BD Biosciences) to remove tissue debris and centrifuged at 1000 rpm for 5 min. The pellet (stromal-vascular fraction) was suspended in medium and cultured in a 10-cm culture dish at 37°C in humidified atmosphere 5% CO_2 and 95% room air. After 24 h, nonadherent cells were gently removed. Adherent cells reached 80% confluence within 5–6 days (passage 0 [P0]). Confluent cells (ASCs) were detached with 0.25% trypsin/1 mmol/L ethylenediamine tetraacetic acid (EDTA; Thermo Fisher Scientific) and plated in 75-cm^2 flasks (P1). The doubling time (DT) was determined by manually counting the number of cells from P1 to P7.

Real-time reverse transcriptase-polymerase chain reaction

Total RNA was extracted from ASCs with TRIzol reagent (Thermo Fisher Scientific). After reverse transcription of 1 μg of total RNA, an aliquot of the cDNA was amplified in a LightCycler system (Roche) with LightCycler FastStart DNA Master SYBR Green I (Roche) according to manufacturer's instructions. Transcript expression of nestin (neural stem cells), βIII tubulin (neurons) and glial fibrillary acidic protein (GFAP; astrocytes) was investigated with hypoxanthine phosphoribosyltransferase as an internal control. Primer sequences were described previously [4].

SCI model, intravenous ASC transplantation and functional evaluation

Spinal cord injury was induced by the weight-drop method [21]. Ten-week-old rats weighing 210–230 g were anesthetized, and dorsal laminectomy was performed at the T10 vertebra. A 10-g weight was then dropped onto the spinal cord from a height of 25 mm. Postoperatively, animals were kept warm on highly absorbent bedding and injected with antibiotics; they received manual bladder expression twice daily until reflex bladder emptying returned.

On day 8 after SCI, the rats were randomly assigned to two groups, and cell transplantation was carried out. ASCs were incubated in growth medium containing 10 ng/mL basic fibroblast growth factor (bFGF; Thermo Fisher Scientific) for 24 h before transplantation. The cells were detached with trypsin/EDTA and resuspended in physiological saline; 2.5×10^6 cells (in 500 μL) were infused via the tail vein at a rate of 25 μL/min using a stereotaxic microinjector (model 310, Muromachi Kikai). SCI control animals received the same volume (500 μL) of physiological saline alone.

Hindlimb motor function was evaluated in SCI rats by using the Basso-Beattie-Bresnahan (BBB) score, a locomotor rating scale developed by Basso et al. [22]. A score from 0 (complete paralysis) to 21 (normal gait) was recorded before and after SCI.

Spinal cord specimens

Under anesthesia, animals were perfused with physiological saline and then with 4% paraformaldehyde in phosphate-buffered saline (PBS) (Wako Pure Chemical Industries) via intracardiac injection.

For hematoxylin and eosin staining, spinal cord specimens were embedded in paraffin, cut into 4-μm

sections and placed on SUPERFROST MAS-coated glass slides (Matsunami Glass). The area of cavitation was measured by using WinROOF software (Mitani Corporation).

For detection of GFP-expressing cells, spinal cord specimens were fixed by immersion for 1 h, followed by cryoprotection in 10%, 20% and 30% sucrose PBS at 4°C, and finally frozen in Tissue-Tek O.T.C. compound (Sakura FineTechnical). Then 10-μm sections were cut and placed on SUPERFROST MAS-coated glass slides. Fluorescence was acquired under a conventional microscope equipped with a CCD camera (IX70, Olympus).

Investigation of ASC distribution

ASCs were labeled with [^{3}H]-thymidine ([methyl, 1′, 2′-^{3}H]thymidine, PerkinElmer Japan). On day 8 after SCI, [^{3}H]-labeled ASCs (1247092 dpm/2.5×10^6 cells) were intravenously infused into rats by the same protocol as mentioned earlier. After 3, 24 and 48 h, a 15-mm spinal cord segment containing the damaged region, blood and target organs were harvested, followed by solubilization with Soluene-350 (PerkinElmer Japan). Aliquots of each solution were then used for the determination of radioactivity with a β counter (LSC-6100, ALOKA).

Measurement of cytokines

Medium with or without bFGF (10 ng/mL) was replaced when ASCs grew to approximately 80% confluence. After culture for 24 h, the supernatant was collected for the measurement of cytokine expression and the number of cells was counted with a hemocytometer.

Serum or plasma (EDTA) was prepared from whole blood collected under anesthesia. Spinal cord (15 mm length) lysate was prepared in buffer containing 20 mmol/L tris(hydroxymethyl)-aminomethane hydrochloride (Tris-HCl; pH 7.5), 2 mol/L NaCl, 0.1% Tween-80, 1 mmol/L phenylmethylsulfonyl fluoride (PMSF; Sigma-Aldrich), and 1 mmol/L EDTA, allowing them to swell on ice before centrifugation at 15000 rpm for 30 min at 4°C.

Levels of HGF (Institute of Immunology), VEGF (Immuno-Biological Laboratories), and cytokine-induced neutrophil chemoattractant (CINC)-1 (Immuno-Biological Laboratories) were measured with enzyme-linked immunosorbent assay kits according to manufacturer's instructions.

Cytokine array analysis

A RayBio rat cytokine antibody array (RayBiotech) was used to assess cytokine expression in the spinal cord lysate and serum according to the manufacturer's instructions. Signals were directly detected with a chemiluminescence imaging system.

Sponge implantation

Sterilized 8-mm sponges (Astellas Pharma) were subcutaneously implanted into the backs of normal rats under anesthesia. The sponges were infused with 100 μL of ASCs (2.5×10^6 cells), CINC-1 (R&D Systems), or saline just before implantation. Four days later, each sponge was harvested for measurement of the hemoglobin content with a hemoglobin determination kit (Wako).

Comparison of ASCs and CINC-1 in SCI rats

On day 8 after SCI, the rats were randomly assigned to three groups, and treatment of ASCs (2.5×10^6 cells in 500 μL saline), CINC-1 (5 μg/kg in 500 μL saline) or saline (500 μL) was carried out. Hindlimb motor function was evaluated by using the BBB score.

Western blot analysis

Spinal cord lysate was prepared in buffer containing 20 mmol/L Tris-HCl (pH 7.5), 150 mmol/L NaCl, 1(v/v)% Triton X-100, 5 mmol/L EDTA, 1 mmol/L PMSF, 5 μg/mL aprotinin, 5 μg/mL leupeptin, Phosphatase Inhibitor Cocktail Set II (Calbiochem, Merck KGaA) or the same buffer as described earlier.

Aliquots of lysate (20–70 μg) were separated by electrophoresis on 5–20% gradient SDS polyacrylamide gels. The protein concentration was determined by using a BCA protein assay kit (Thermo Fisher Scientific). Proteins were transferred to polyvinylidene difluoride membranes (Clearblot P, ATTO Corporation) and incubated with anti-Akt (pan) (C67E7; rabbit, Cell Signaling Technology), phosphor-Akt (Thr308) (C31E5E; rabbit, Cell Signaling), p44/42 mitogen-activated protein kinase (MAPK), extracellular signal-regulated kinase (ERK)1/2; rabbit, Cell Signaling), phosphor-p44/42 MAPK (Thr202/Thr204; rabbit, Cell Signaling), glial cell line–derived neurotrophic factor (GDNF) (D-20; sc-328, rabbit, Santa Cruz Biotechnology), GFAP (clone G-A-5; mouse, Sigma-Aldrich), myelin basic protein (MBP) (D-18; sc-13912, goat; Santa Cruz Biotechnology), or anti-β-actin (clone AC-15; mouse, Sigma-Aldrich). The membranes were then incubated with electrochemiluminescence (ECL) horseradish peroxidase (HRP)-labeled anti-goat immunoglobulin (Ig)G (sc-2020; Santa Cruz Biotechnology), HRP-labeled anti-mouse IgG (GE Healthcare UK), or HRP-labeled anti-rabbit IgG (GE Healthcare UK). Finally, each membrane was incubated with ECL Prime Western blotting detection system (GE Healthcare UK) and exposed to a Polaroid

film. Immunoblot signals were semi-quantified with a densitometer.

Statistical analysis

Results are expressed as the mean ± SE. The BBB scores are expressed as the median and interquartile range (IQR). Data were analyzed by Student's *t*-test (two-group comparisons), Dunnett's test (pairwise comparisons against the control group) or Tukey-Kramer test (multi-group comparisons). Statistical analysis of BBB scores was performed with Mann-Whitney *U*-test (two-group comparisons) or Steel-Dwass test (multi-group comparisons). The statistical analyses were performed with JMP 12 (SAS institute Inc., Cary, NC, USA), and $P < 0.05$ was considered statistically significant.

Results

Characterization of ASCs

ASCs became apparently homogeneous during culture and passage, although freshly isolated cells exhibited heterogeneous features. ASCs could be expanded with a DT of approximately 24 h at the first passage (Figure 1A). Culture and passage were gradually lengthened the DT with morphological change. P2-ASCs (DT: 22.2 ± 0.7 h) had small, spindle-shaped cell bodies (Figure 1B), whereas P7-ASCs (DT: 55.3 ± 1.2 h) had large, flat cell bodies (Figure 1B). ASCs expressed neural lineage mRNAs. Expression of nestin mRNA (neural stem cells) decreased with passaging (P2 versus P7, $P < 0.01$, Figure 1C), whereas expression for both βIII tubulin mRNA (neurons) and GFAP mRNA (astrocytes) was not significantly altered (Figure 1C). Flow cytometry yielded similar results (data not shown). ASCs secreted large amounts of HGF and VEGF *in vitro*. It should be noted that bFGF promoted secretion of HGF ($P < 0.01$, Figure 1D). On the basis of these findings, we used P2-ASCs (ASCs) treated with bFGF as donor cells for SCI rats.

Functional recovery after ASC transplantation through intravenous route

SCI caused complete hindlimb paralysis, after which gradual recovery of locomotion was observed. Before transplantation (day 8 after SCI), there was no difference in BBB score between the saline and ASC groups. Intravenous transplantation of cells into SCI rats was performed without adverse events. As shown

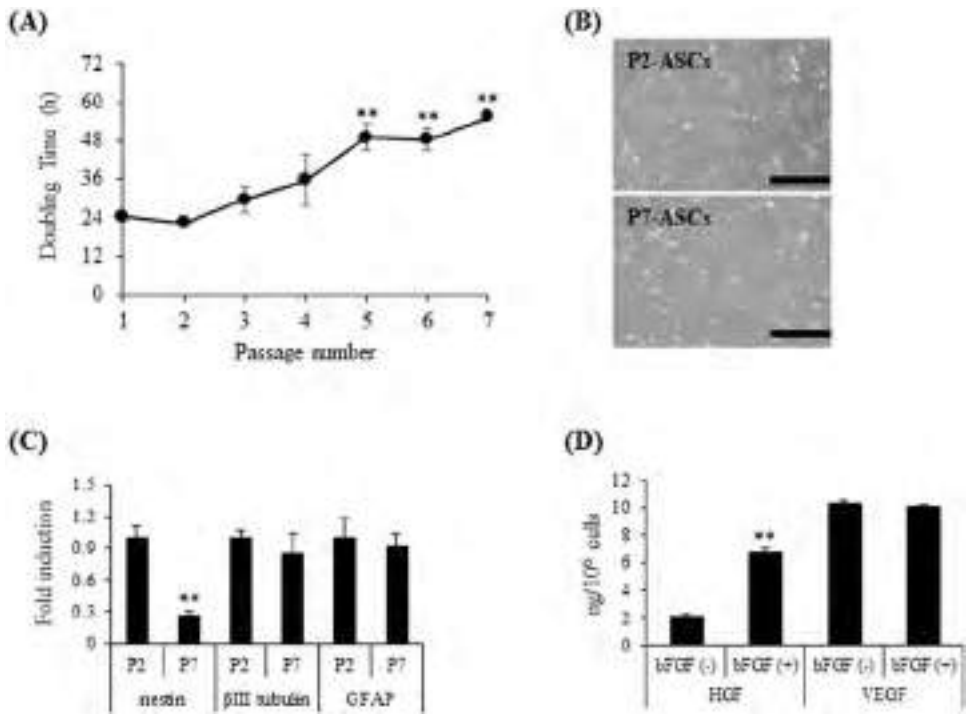

Figure 1. Characterization of cultured ASCs. (A) DT was determined at the indicated number of passages; data represent the mean ± SE (n = 3–4). $^{**}P < 0.01$ versus P1-ASCs. (B) Morphology of P2-ASCs and P7-ASCs. Scale bars = 500 μm. (C) Real-time reverse transcriptase-polymerase chain reaction. Data represent the mean ± SE (n = 5) of the relative ratio when the level of transcripts in P2-ASCs was arbitrarily set as 1. $^{**}P < 0.01$ versus P2-ASCs. (D) Secretion of cytokines. P2-ASCs were cultured for 24 h with or without bFGF. HGF and VEGF in the culture medium and were measured by enzyme-linked immunosorbent assay. Data represent the mean ± SE (n = 4). $^{**}P < 0.01$ versus bFGF (–).

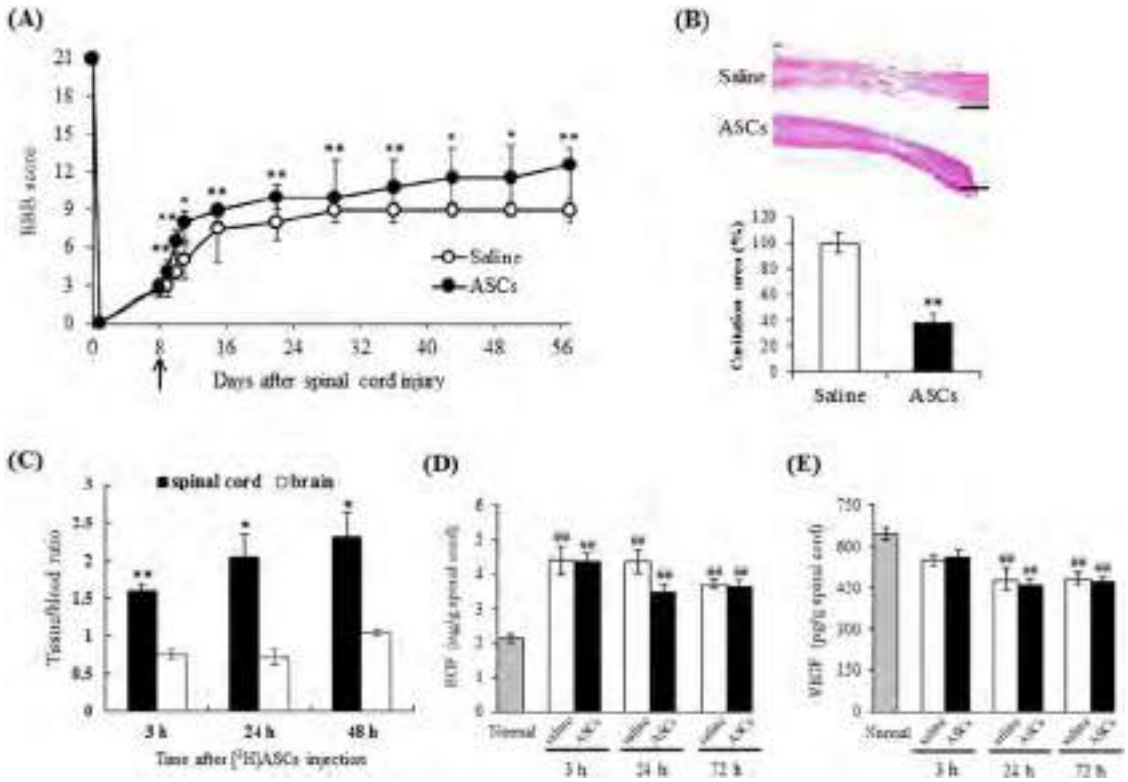

Figure 2. Functional recovery following intravenous ASC transplantation, distribution of ASCs and growth factor expression. (A) On day 8 after injury (arrow), ASCs (2.5×10^6 cells) were infused into SCI rats via the tail vein (n = 20). BBB scores were determined before and after transplantation. The median score is plotted; bars show the IQR. $^*P < 0.05$ and $^{**}P < 0.01$ versus the saline (n = 15). (B) After behavioral observation, hematoxylin-eosin staining of spinal cord specimens was performed for evaluation of cavity area. Scale bars = 1 mm. Data represent the mean ± SE (ASCs; n = 8, saline; n = 5) relative to the area in the saline (defined as 100%). $^{**}P < 0.01$ versus the saline. (C) From the data shown in Table I, the tissue:blood ratio was calculated for the injured spinal cord and brain. Data represent the mean ± SE (n = 3). $^*P < 0.05$ and $^{**}P < 0.01$ versus the ratio for brain. (D) HGF and (E) VEGF in the spinal cord were determined at the indicated times following ASC infusion on day 8 after injury. Data represent the mean ± SE (n = 3–7). $^{\#\#}P < 0.01$ vs. the normal controls.

in Figure 2A, ASC-treated SCI rats showed marked improvement of hindlimb locomotive function after one day (versus saline-treated SCI rats, $P < 0.05$). During the observation period, the ASC group showed significantly better recovery compared with the saline group. In the ASC group, the BBB score was 12.5 (IQR: 4.38), and some animals showed frequent-consistent weight-bearing plantar walking with good forelimb-hindlimb coordination. Although the saline group also recovered, the BBB score was 9 (IQR: 2). Some animals crawled and moved without weight-bearing. After behavioral observation, the cavity at the site of spinal cord injury was smaller in the ASC group than in the saline group ($P < 0.01$, Figure 2B).

In an attempt to identify grafted cells, GFP-expressing ASCs were infused into SCI rats under the same conditions. However, GFP-positive cells were undetectable in the injured spinal cords 8 weeks after transplantation (the median of BBB score: 14, IQR: 5.25, n = 8, data not shown).

In vivo distribution of transplanted ASCs

[^{3}H]-Labeled ASCs were infused into SCI rats under the same conditions to determine the fate of the cells (Table I). The highest radioactivity (~30% of the injected amount) was detected in the lungs 3 h after infusion, while radioactivity in the injured spinal cord was much lower (0.029% of the injected amount at 3 h). The tissue:blood ratio (an index of cell distribution) was calculated at 3, 24 and 48 h after infusion (Figure 2C). Compared with the brain:blood ratio, the spinal cord:blood ratio was significantly higher, indicating that ASCs gradually accumulated in the damaged spinal cord.

Cytokine levels in the spinal cord

In the injured spinal cord, the HGF level was significantly higher than in the normal cords ($P < 0.01$) (Figure 2D), whereas the VEGF level was lower with significance ($P < 0.01$, Figure 2E). However, both HGF

Table I. Distribution of [^{3}H]-labeled ASCs following intravenous infusion into SCI rats.

	Spinal cord (15 mm length)	Blood	Brain	Heart
3 h	0.029 ± 0.003	5.6 ± 0.2	0.42 ± 0.03	0.41 ± 0.08
24 h	0.055 ± 0.005	6.8 ± 0.2	0.49 ± 0.05	0.38 ± 0.07
48 h	0.068 ± 0.013	7.7 ± 0.2	0.80 ± 0.01	0.58 ± 0.02
	Lungs	Liver	Kidneys	Spleen
3 h	30 ± 4	0.47 ± 0.03	0.68 ± 0.06	0.54 ± 0.04
24 h	3.5 ± 1.3	0.30 ± 0.09	0.66 ± 0.09	0.35 ± 0.04
48 h	3.3 ± 0.5	0.45 ± 0.03	1.1 ± 0.6	0.43 ± 0.04

On day 8 after injury, SCI rats received an injection of [^{3}H]-labeled ASCs (1247092 dpm/2.5 × 10^6 cells) via the tail vein. Radioactivity was measured in the blood and each target organ. Data represent the mean ± SE (n = 3) of the percent relative to the radioactivity in injected cells.

and VEGF levels did not differ between the saline and ASC groups.

CINC-1 expression

Cytokine array analysis was performed to search for other possible factors in functional recovery. CINC-1, a member of the CXC chemokine family, was strongly expressed in both the injured spinal cord (Figure 3A) and serum (Figure 3B) 3 h after ASC injection.

CINC-1 was then the focus of additional exploration and was found at 84.5 ± 19.9 pg/g tissue (n = 4) in the normal spinal cord. SCI induced a greater than 150-fold increase (12.9 ± 1.1 ng/g tissue) at 5 h after injury (n = 4, $P < 0.01$). The level in serum was also more than eightfold higher than in normal serum

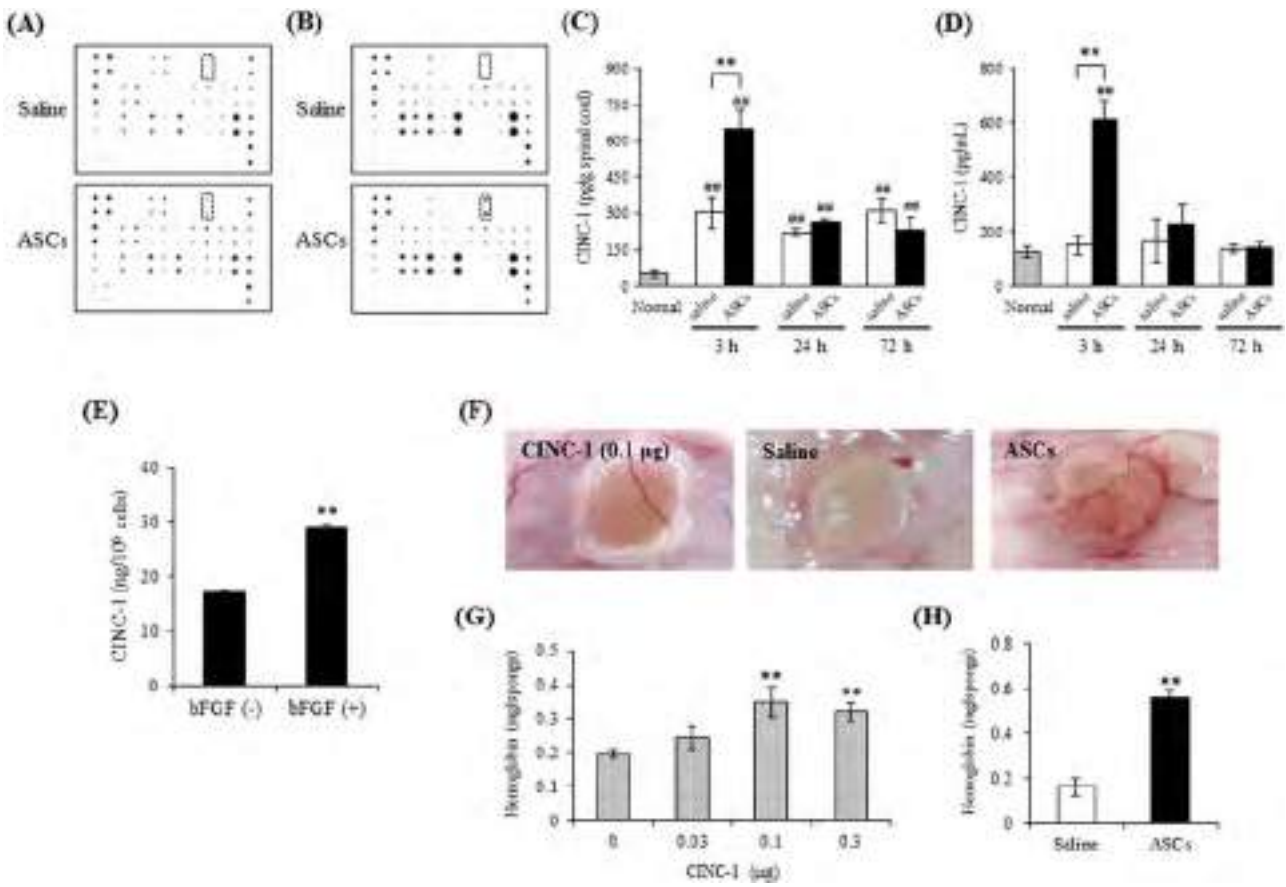

Figure 3. CINC-1 expression *in vivo* and *in vitro*, and angiogenesis. On day 8 after injury, ASCs (2.5 × 10^6 cells) were infused intravenously. (A) Spinal cord and (B) serum cytokine array at 3 h. CINC-1 signals are shown in dotted rectangles. (C) CINC-1 levels in the spinal cord and (D) serum at the indicated times after ASC infusion. Data represent the mean ± SE (n = 3–10). $^{\#\#}P < 0.01$ and $^{**}P < 0.01$ versus the normal and saline controls, respectively. (E) ASCs were cultured for 24 h with or without bFGF, and CINC-1 in the culture medium was measured by enzyme-linked immunosorbent assay. Data represent the mean ± SE (n = 4). $^{**}P < 0.01$ versus bFGF (–). (F–H) Sponges treated with CINC-1, ASCs (2.5 × 10^6 cells), or saline were subcutaneously implanted into the backs of normal rats and harvested on day 4. (F) Representative photographs of CINC-1 (0.1 μg)-, saline-, and ASC-treated sponges. (G, H) Hemoglobin content in the implanted sponges treated with CINC-1 (G) and ASCs (H). Data represent the mean ± SE (each dose of CINC-1, n = 6; ASCs, n = 4). $^{**}P < 0.01$ versus the controls.

(100 ± 22 pg/mL versus 837 ± 27 pg/mL, n = 4, $P < 0.01$). At the time of ASC transplantation (day 8 after injury), CINC-1 levels in the injured spinal cord remained high (Figure 3C). It should be noted that the CINC-1 level in the ASC-treated spinal cords (687 ± 74 pg/g tissue) was transiently but significantly higher than that in the saline-treated spinal cords (305 ± 65 pg/g tissue; $P < 0.01$). Similar results were obtained for the serum ($P < 0.01$, Figure 3D).

Secretion from cultured ASCs *in vitro* was high and further augmented by addition of bFGF ($P < 0.01$, Figure 3E).

To investigate the role of CINC-1 in functional recovery, a sponge implantation assay was performed. Four days after sponge implantation, neocapillaries were detected around the sponges treated with CINC-1 (0.1 μg; Figure 3F), whereas few were observed around the saline sponges. The hemoglobin content of CINC-1-treated sponges increased in a dose-dependent manner, reflecting neovascularization (Figure 3G). ASCs also induced neocapillary formation (Figure 3F) with the increase of hemoglobin content ($P < 0.01$, Figure 3H).

In vivo comparative study of ASCs and CINC-1 in SCI rats

When assessed by the BBB score, a single intravenous injection of CINC-1 also produced significant recovery of hindlimb locomotive function. Compared with CINC-1 (Figure 4A), the BBB scores in the ASC group were better all the time, but there was no significant difference. GFAP and GDNF were more strongly expressed in ASC-transplanted animals than in the saline-injected animals ($P < 0.05$ and 0.01, respectively, Figure 4C–D). In the CINC-1 group, GFAP expression, but not GDNF, was slightly increased (Figure 4C–D). In addition, GDNF expression in the ASC group was superior to that in the CINC-1 group ($P < 0.01$), similar to normal level (Figure 4D).

Phosphorylation of ERK1/2 and Akt was then examined at 3 and 24 h after CINC-1 injection or ASC transplantation. The enhanced potency of ERK1/2 phosphorylation was similar between the two (Figure 4E), although Akt phosphorylation was enhanced in the ASC group (Figure 4F).

Discussion

The present study demonstrated that the intravenous infusion of ASCs into SCI rats could be performed without difficulty and promoted the restoration of motor function. Thus, intravenous infusion could be a promising method for less invasive cell therapy. The fact that smaller cavities were observed at the site of injury led us to hypothesize that grafted ASCs accumulated at the target site and differentiated into neuronal cells, leading to functional improvement.

ASCs express some neural markers, as do BM-MSCs [23]; our results were consistent with this observation. Cell proliferation and nestin expression were reduced with multiple passages; hence, P2-ASCs were used for the transplantation. In addition to rapid growth, ASCs have the potential for differentiation into neuronal or glial lineages *in vitro* [9,13]. We confirmed that ASCs formed neurosphere-like spheroids and then shifted to neurite morphology (data not shown). Therefore, the ASCs were expected to differentiate at the target site into neuronal or glial lineage *in vivo*.

A distribution study revealed that ASCs gradually accumulated at the site of injury, but long-term survival of these cells was not apparent. Radiolabeling showed few ASCs in the injured spinal cord, where around 1300 cells were found 24 h after infusion. Still, compared with the brain in SCI animals, the cell distribution index revealed gradual accumulation in the injured spinal cord. Furthermore, about twice the number of ASCs were detected in the injured spinal cord compared with the normal cord in our preliminary study. These findings prompt us to conclude that some ASCs must have survived for a short time but are unlikely to have differentiated into neuronal or glial cells *in vivo*.

ASCs secrete angiogenic growth factors such as HGF and VEGF [16], which have already been reported to contribute to functional recovery and tissue repair after SCI through angiogenetic and anti-apoptotic activity [24,25]. Our study also showed that ASCs secreted abundant growth factors after pre-incubation with bFGF *in vitro*. Therefore, we hypothesized that growth factors secreted from transplanted ASCs might contribute to functional recovery. However, the intravenous infusion of ASCs into SCI rats produced little increase in these growth factors in the injured spinal cords. Systemic transplantation of ASCs in rats with elastase-induced pulmonary emphysema enhanced the HGF expression in the lung tissue [16]. Indeed, we found that ASCs accumulated in the lungs at a high level, perhaps accounting for the high HGF levels observed in the pulmonary emphysema model, but not in the SCI model.

CINC-1 was clearly a promising candidate for promoting functional recovery after ASC transplantation. CINC-1 belongs to the CXC chemokine family, is a counterpart of human growth–related oncogene (GRO) in the interleukin (IL)-8 family and plays a key role in neutrophil migration [26]. SCI markedly increases the CINC-1 levels in the spinal cord within several hours after injury and is related to the secondary injury process [27]. Indeed, a dramatic increase (>150-fold) was observed 5 h after SCI. On the other

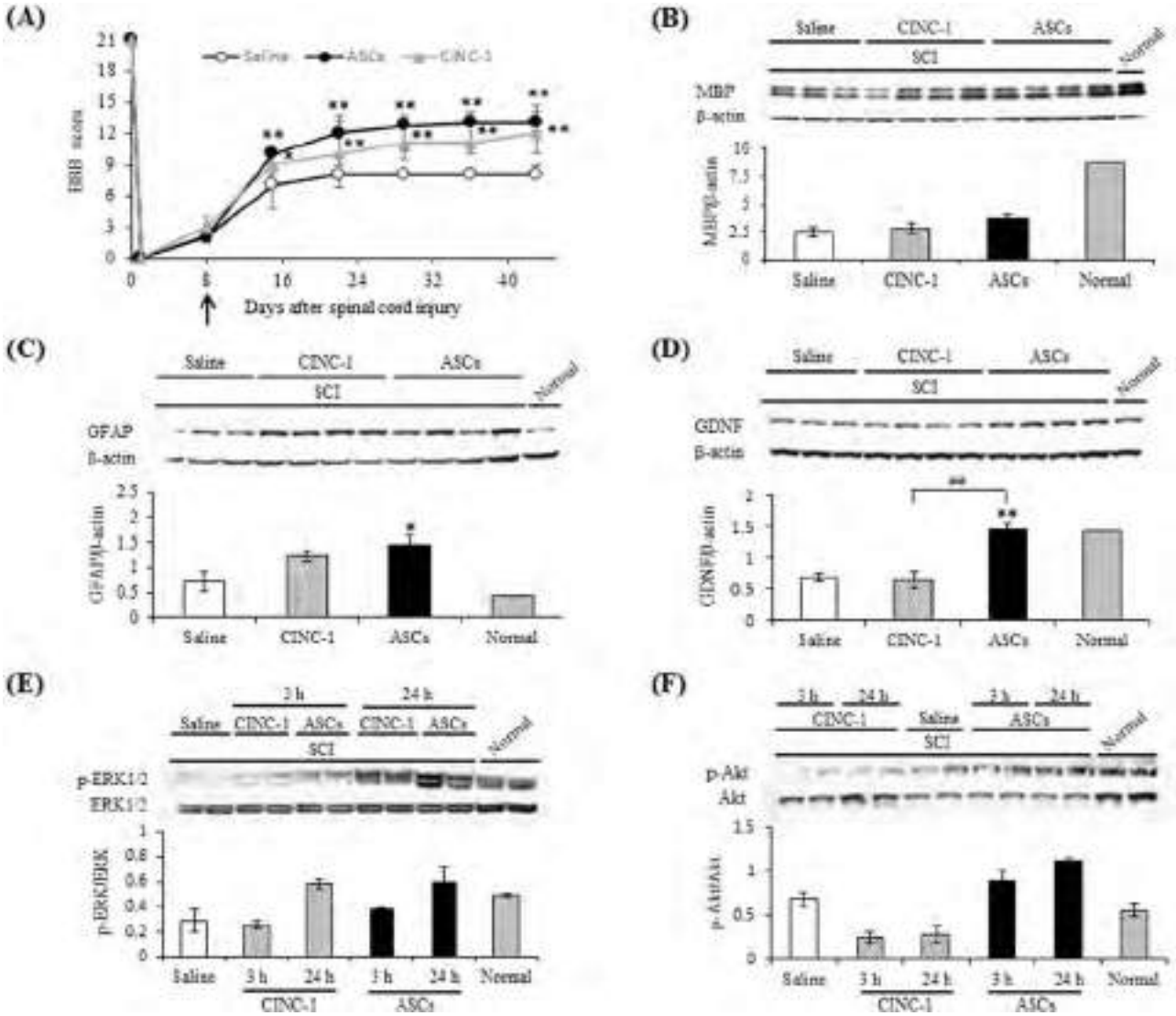

Figure 4. *In vivo* comparative study of ASCs and CINC-1 in SCI rats. (A) On day 8 after injury (arrow), ASCs (2.5×10^6 cells, n = 8) or CINC-1 (5 μg/kg, n = 13) were administered into SCI rats via the tail vein. BBB scores were determined before and after treatments. The median score is shown: bars represent IQR (*$P < 0.05$ and **$P < 0.01$ for both groups versus the saline (n = 9). (B–D) After behavioral observation, spinal cord lysates were isolated for Western blot analysis. Data represent the mean ± SE (n = 3–4) relative to β-actin. Normal is a reference value (n = 1), is excluded from statistical analysis. *$P < 0.05$ and **$P < 0.01$ versus saline. $^{\#\#}p < 0.01$ versus CINC-1. (F) Three hours or 24 h after treatment, spinal cord lysates were prepared for Western blotting. Data represent the mean ± SE (n = 2) relative intensity.

hand, the significant increase of CINC-1 expression at 3 h after ASC infusion was quite unlike the early response after injury. The increase was only moderate (<10 fold). Induction of CINC-1 is considered important for tissue repair because activation and infiltration of neutrophils are essential for eliminating damaged cells, cell debris and extracellular matrix proteins before regeneration can occur [28]. In addition, CINC-1 has been reported to have an angiogenic effect [29]. In fact, CINC-1 induced angiogenesis in the sponge implantation study, but under low-dose condition rather than in high-dose conditions. These findings suggest that the moderate increased CINC-1 may have contributed to tissue repair and to the promotion of functional recovery. GRO/IL-8 regulates stem cell homing [30]. GRO-α has also been shown to act with platelet-derived growth factor to enhance rat spinal cord oligodendrocyte precursor proliferation [31], and CINC-1 protects neurons from apoptosis [32]. These reports support our hypothesis that CINC-1 may have an important role in the repair of the nervous system.

CINC-1 promoted functional recovery of SCI rats, and the potency was similar to ASCs. Although partly statistically not significant, both augmented GFAP expression, perhaps due to the increase in activated astrocytes [33]. It is of note that GDNF

expression in the ASC group was larger than that in the CINC-1 group. Some growth factors that mediate cell survival and tissue repair are produced through signal induction [34–36]. CINC-1 and ASCs enhanced ERK1/2 phosphorylation, although Akt phosphorylation was more greatly enhanced after ASC transplantation. These findings suggest that unidentified factors derived from ASCs may also contribute to activation of upstream kinases triggering cell survival, tissue repair and regeneration. Gradual cell distribution from the blood to the damaged area would have resulted in bringing about sustained secretion and signal induction via some soluble cytokines/chemokines such as CINC-1.

In conclusion, the intravenous infusion of ASCs accelerated motor function recovery and tissue repair in SCI rats. Although undetectable, ASCs gradually migrated to the site of injury and secreted soluble factors such as CINC-1, which activated ERK1/2 and Akt phosphorylation, leading to cell survival, tissue repair and functional recovery. Intravenous route is minimally invasive and thus an attractive approach in clinical settings. Our findings thus contribute to the development of cell therapy.

Acknowledgments

We are grateful to Ms. Yukie Tokura for her helpful discussion and technical assistance. This work was supported by Japan Society for the Promotion of Science KAKENHI grants JP21791758 and P24791925 and St. Marianna University School of Medicine Research Grant.

Disclosure of interest: The authors have no commercial, proprietary, or financial interest in the products or companies described in this article.

References

[1] McDonald JW, Liu XZ, Qu Y, Liu S, Mickey SK, Turetsky D, et al. Transplanted embryonic stem cells survive, differentiate and promote recovery in injured rat spinal cord. Nat Med 1999;5:1410–12.

[2] Hofstetter CP, Schwarz EJ, Hess D, Widenfalk J, El Manira A, Prockop DJ, et al. Marrow stromal cells form guiding strands in the injured spinal cord and promote recovery. Proc Natl Acad Sci USA 2002;99:2199–204.

[3] Ogawa Y, Sawamoto K, Miyata T, Miyao S, Watanabe M, Nakamura M, et al. Transplantation of in vitro-expanded fetal neural progenitor cells results in neurogenesis and functional recovery after spinal cord contusion injury in adult rats. J Neurosci Res 2002;69:925–33.

[4] Ohta Y, Takenaga M, Tokura Y, Hamaguchi A, Matsumoto T, Kano K, et al. Mature adipocyte-derived cells, dedifferentiated fat cells (DFAT), promoted functional recovery from spinal cord injury-induced motor dysfunction in rats. Cell Transplant 2008;17:877–86.

[5] Fujikawa T, Oh SH, Pi L, Hatch HM, Shupe T, Petersen BE. Teratoma formation leads to failure of treatment for type I diabetes using embryonic stem cell-derived insulin-producing cells. Am J Pathol 2005;166:1781–91.

[6] Pittenger MF, Mackay AM, Beck SC, Jaiswal RK, Douglas R, Mosca JD, et al. Multilineage potential of adult human mesenchymal stem cells. Science 1999;284:143–7.

[7] Kopen GC, Prockop DJ, Phinney DG. Marrow stromal cells migrate throughout forebrain and cerebellum, and they differentiate into astrocytes after injection into neonatal mouse brains. Proc Natl Acad Sci USA 1999;96:10711–16.

[8] Sanchez-Ramos J, Song S, Cardozo-Pelaez F, Hazzi C, Stedeford T, Willing A, et al. Adult bone marrow stromal cells differentiate into neural cells in vitro. Exp Neurol 2000;164:247–56.

[9] Zuk PA, Zhu M, Mizuno H, Huang J, Futrell JW, Katz AJ, et al. Multilineage cells from human adipose tissue: implications for cell-based therapies. Tissue Eng 2001;7:211–28.

[10] Bieback K, Kern S, Kluter H, Eichler H. Critical parameters for the isolation of mesenchymal stem cells from umbilical cord blood. Stem Cells 2004;22:625–34.

[11] Shih DT, Lee DC, Chen SC, Tsai RY, Huang CT, Tsai CC, et al. Isolation and characterization of neurogenic mesenchymal stem cells in human scalp tissue. Stem Cells 2005;23:1012–20.

[12] Lee RH, Kim B, Choi I, Kim H, Choi HS, Suh K, et al. Characterization and expression analysis of mesenchymal stem cells from human bone marrow and adipose tissue. Cell Physiol Biochem 2004;14:311–24.

[13] Safford KM, Hicok KC, Safford SD, Halvorsen YD, Wilkison WO, Gimble JM, et al. Neurogenic differentiation of murine and human adipose-derived stromal cells. Biochem Biophys Res Commun 2002;294:371–9.

[14] Planat-Benard V, Silvestre JS, Cousin B, Andre M, Nibbelink M, Tamarat R, et al. Plasticity of human adipose lineage cells toward endothelial cells: physiological and therapeutic perspectives. Circulation 2004;109:656–63.

[15] Seo MJ, Suh SY, Bae YC, Jung JS. Differentiation of human adipose stromal cells into hepatic lineage in vitro and in vivo. Biochem Biophys Res Commun 2005;328:258–64.

[16] Furuya N, Takenaga M, Ohta Y, Tokura Y, Hamaguchi A, Sakamaki A, et al. Cell therapy with adipose tissue-derived stem/stromal cells (ASC) for elastase-induced pulmonary emphysema in rats. Regen Med 2012;7:503–12.

[17] De Ugarte DA, Morizono K, Elbarbary A, Alfonso Z, Zuk PA, Zhu M, et al. Comparison of multi-lineage cells from human adipose tissue and bone marrow. Cells Tissues Organs 2003;174:101–9.

[18] Akiyama Y, Radtke C, Honmou O, Kocsis JD. Remyelination of the spinal cord following intravenous delivery of bone marrow cells. Glia 2002;39:229–36.

[19] Cizkova D, Rosocha J, Vanicky I, Jergova S, Cizek M. Transplants of human mesenchymal stem cells improve functional recovery after spinal cord injury in the rat. Cell Mol Neurobiol 2006;26:1167–80.

[20] Zhang D, He X. A meta-analysis of the motion function through the therapy of spinal cord injury with intravenous transplantation of bone marrow mesenchymal stem cells in rats. PLoS ONE 2014;9:e43987.

[21] Basso DM, Beattie MS, Bresnahan JC. A sensitive and reliable locomotor rating scale for open field testing in rats. J Neurotrauma 1995;12:1–21.

[22] Basso DM, Beattie MS, Bresnahan JC, Anderson DK, Faden AI, Gruner JA, et al. MASCIS evaluation of open field locomotor scores: effects of experience and teamwork on reliability. Multicenter Animal Spinal Cord Injury Study. J Neurotrauma 1996;13:343–59.

[23] Deng J, Petersen BE, Steindler DA, Jorgensen ML, Laywell ED. Mesenchymal stem cells spontaneously express neural proteins in culture and are neurogenic after transplantation. Stem Cells 2006;24:1054–64.
[24] Kitamura K, Iwanami A, Nakamura M, Yamane J, Watanabe K, Suzuki Y, et al. Hepatocyte growth factor promotes endogenous repair and functional recovery after spinal cord injury. J Neurosci Res 2007;85:2332–42.
[25] Widenfalk J, Lipson A, Jubran M, Hofstetter C, Ebendal T, Cao Y, et al. Vascular endothelial growth factor improves functional outcome and decreases secondary degeneration in experimental spinal cord contusion injury. Neuroscience 2003;120:951–60.
[26] Watanabe K, Konishi K, Fujioka M, Kinoshita S, Nakagawa H. The neutrophil chemoattractant produced by the rat kidney epithelioid cell line NRK-52E is a protein related to the KC/gro protein. J Biol Chem 1989;264:19559–63.
[27] Tonai T, Shiba K, Taketani Y, Ohmoto Y, Murata K, Muraguchi M, et al. A neutrophil elastase inhibitor (ONO-5046) reduces neurologic damage after spinal cord injury in rats. J Neurochem 2001;78:1064–72.
[28] Takahashi S, Kobayashi N, Okabe S. Regulation by endogenous interleukin-1 of mRNA expression of healing-related factors in gastric ulcers in rats. J Pharmacol Exp Ther 1999;291:634–41.
[29] Kobayashi T, Hamano K, Li TS, Katoh T, Kobayashi S, Matsuzaki M, et al. Enhancement of angiogenesis by the implantation of self bone marrow cells in a rat ischemic heart model. J Surg Res 2000;89:189–95.
[30] Leu S, Lin YC, Yuen CM, Yen CH, Kao YH, Sun CK, et al. Adipose-derived mesenchymal stem cells markedly attenuate brain infarct size and improve neurological function in rats. J Transl Med 2010;8:63.
[31] Robinson S, Tani M, Strieter RM, Ransohoff RM, Miller RH. The chemokine growth-regulated oncogene-alpha promotes spinal cord oligodendrocyte precursor proliferation. J Neurosci 1998;18:10457–63.
[32] Wang Y, Luo W, Reiser G. Activation of protease-activated receptors in astrocytes evokes a novel neuroprotective pathway through release of chemokines of the growth-regulated oncogene/cytokine-induced neutrophil chemoattractant family. Eur J Neurosci 2007;26:3159–68.
[33] Windelborn JA, Mitchell GS. Glial activation in the spinal ventral horn caudal to cervical injury. Respir Physiol Neurobiol 2012;180:61–8.
[34] Koelsch A, Feng Y, Fink DJ, Mata M. Transgene-mediated GDNF expression enhances synaptic connectivity and GABA transmission to improve functional outcome after spinal cord contusion. J Neurochem 2010;113:143–52.
[35] Rolfe A, Sun D. Stem cell therapy in brain trauma: implications for repair and regeneration of injured brain in experimental TBI models, Chapter 7. In: Kobeissy FH, editor. Brain neurotrauma: molecular, neuropsychological, and rehabilitation aspects. Boca Raton (FL): Taylor & Francis Group, LLC; 2015 [Chapter 7].
[36] Chen MR, Dai P, Wang SF, Song SH, Wang HP, Zhao Y, et al. BDNF overexpression exhibited bilateral effect on neural behavior in SCT mice associated with AKT signal pathway. Neurochem Res 2016;41:2585–97.

British Journal of Pharmacology

British Journal of Pharmacology (2017) **174** 3370–3381 3370

RESEARCH PAPER

Ameliorative effect of chlorpromazine hydrochloride on visceral hypersensitivity in rats: possible involvement of 5-HT_{2A} receptor

Correspondence Teita Asano, Institute of Medical Science, St. Marianna University School of Medicine, 2-16-1 Sugao, Miyamae-ku, Kawasaki 216-8512, Japan. E-mail: asano-ti@marianna-u.ac.jp

Received 7 March 2017; **Revised** 13 July 2017; **Accepted** 17 July 2017

Teita Asano[1], Ken-ichiro Tanaka[2], Arisa Tada[3], Hikaru Shimamura[3], Rikako Tanaka[3], Hiroki Maruoka[3], Tohru Mizushima[4] and Mitsuko Takenaga[1]

[1]Institute of Medical Science, St. Marianna University School of Medicine, Kawasaki, Japan, [2]Department of Pharmaceutical Sciences, Musashino University, Tokyo, Japan, [3]Faculty of Pharmacy, Keio University, Tokyo, Japan, and [4]LTT Bio-Pharma Co., Ltd, Tokyo, Japan

BACKGROUND AND PURPOSE

Visceral hypersensitivity is responsible for pathogenesis of irritable bowel syndrome (IBS). Therefore, its prevention can help avoid abdominal pain and discomfort in IBS. To find candidate drugs for visceral hypersensitivity, we screened existing medicines for their ability to prevent visceral sensitivity induced by colorectal distension (CRD) in rats and identified chlorpromazine, a typical antipsychotic drug, as a candidate compound. In this study, we investigated the effect of chlorpromazine on visceral hypersensitivity.

EXPERIMENTAL APPROACH

Visceral sensitivity (visceromotor response) was monitored by measuring the electrical activity of the abdominal external oblique muscle contraction in response to CRD using a barostat apparatus. Visceral hypersensitivity was induced by a colonic instillation of sodium butyrate or acetic acid in neonates.

KEY RESULTS

Oral administration of chlorpromazine suppressed butyrate-induced visceral hypersensitivity to CRD. Interestingly, atypical antipsychotic drugs, quetiapine and risperidone, ameliorated butyrate-induced visceral hypersensitivity, whereas the typical antipsychotic drugs, haloperidol and sulpiride, did not. Pharmacological analysis using specific inhibitors showed that a selective 5-HT_{2A} receptor antagonist, ketanserin, suppressed butyrate-induced visceral hypersensitivity, whereas a selective dopamine D_2 receptor antagonist, L-741626, did not. Furthermore, the 5-HT_{2A} receptor agonist AL-34662 stimulated visceral sensitivity to CRD in healthy control rats but not in butyrate-treated rats. These findings suggest that increased 5-HT levels in the colon contribute to the induction of visceral hypersensitivity.

CONCLUSIONS AND IMPLICATIONS

Our results indicate that chlorpromazine ameliorates visceral hypersensitivity and that the 5-HT_{2A} receptor is a potential therapeutic target for treating abdominal pain and discomfort in IBS.

Abbreviations

7OH-Cpz, 7-hydroxy chlorpromazine; ASIC, acid-sensing ion channel; CRD, colorectal distension; DRG, dorsal root ganglion; IBS, irritable bowel syndrome; *p*-CPA, *p*-chlorphenylalanine; TRPV1, transient receptor potential vanilloid 1; VMR, visceromotor response

DOI:10.1111/bph.13960

© 2017 The British Pharmacological Society

Introduction

Irritable bowel syndrome (IBS) is a complex functional gastrointestinal disorder characterized by chronic, recurrent abdominal pain and altered bowel habits (diarrhoea, constipation or alternating diarrhoea/constipation). Its prevalence in the general population is remarkably high (~11% of the world's population) (Chang *et al.,* 2014). Although not life-threatening, it imposes a large burden on global healthcare and considerably reduces patient quality of life (Canavan *et al.,* 2014). However, no satisfactory pharmacological therapy has been identified for IBS.

Psychiatric comorbidities are highly common in IBS patients (Ladabaum *et al.,* 2012). Centrally acting agents including antidepressants, anxiolytics, antipsychotics and sedatives are two to four times more likely to be prescribed to presumed IBS patients compared to other patients (Grover and Drossman, 2011). Atypical antipsychotic drugs have been effective in patients with severe IBS and abdominal pain (Grover *et al.,* 2009; Martin-Blanco *et al.,* 2010; Pae *et al.,* 2013). However, the mechanisms underlying the efficacy of these drugs in ameliorating pain are unclear.

Visceral hypersensitivity plays an important role in IBS pathogenesis, and IBS patients have been shown to present visceral hypersensitivity in response to colorectal distension (CRD) (Azpiroz *et al.,* 2007). Therefore, suppression of this pathology could be an effective treatment option for IBS. The mechanisms responsible for visceral hypersensitivity are not completely understood. However, several contributing factors have been suggested, including enhanced visceral perception, altered intestinal microbiota, post-inflammatory changes in gastrointestinal function and enhanced immunological reactivity (Keszthelyi *et al.,* 2012; Matricon *et al.,* 2012; Simren *et al.,* 2013; Brierley and Linden, 2014). In particular, butyrate, a short-chain fatty acid produced by bacterial fermentation in the colon, appears to be important in the development of visceral hypersensitivity. Increased faecal butyrate levels have been observed in IBS patients with diarrhoea, and rectal instillation of butyrate increases visceral sensitivity to colonic distension in rats (Treem *et al.,* 1996; Bourdu *et al.,* 2005). **5-HT** (serotonin) is another key molecule regulating visceral perception (Cremon *et al.,* 2011). In fact, a 5-HT_3 receptor antagonist (alosetron) and 5-HT_4 receptor agonist (tegaserod) have been approved for the clinical treatment of diarrhoea- and constipation-predominant IBS respectively. However, adverse effects, such as ischaemic colitis and cardiac toxicity, limit the use of these drugs (Pasricha, 2007). The role of other 5-HT receptor subtypes, including **5-HT_{2A} receptor**, in visceral sensitivity, has not been fully investigated.

The 5-HT_{2A} receptor is mainly located in the brain, spinal cord, sensory neurons and intestines. Recently, the 5-HT_{2A} receptor antagonist cyproheptadine has been found effective against abdominal pain in children with IBS (Madani *et al.,* 2016). Moreover, the 5-HT_{2A} receptor antagonist **ketanserin** showed an antinociceptive effect on abdominal pain in the acetic acid-induced writhing test (Alhaider, 1991). These findings indicate that the 5-HT_{2A} receptor is involved in visceral pain sensitivity. In addition to visceral pain, the 5-HT_{2A} receptor is associated with the potentiation of pain sensation. Further, activation of the 5-HT_{2A} receptor enhances transient receptor potential vanilloid 1 (TRPV1) function in colon sensory neurons and acid-sensing ion channels (ASICs) in dorsal root ganglion (DRG) neurons *in vitro* (Sugiuar *et al.,* 2004; Qiu *et al.,* 2012). These results suggest that the 5-HT_{2A} receptor participates in peripheral sensitization.

We previously screened a compound library of clinically available drugs for their ability to prevent the visceral pain response to noxious CRD (Asano *et al.,* 2017) and identified aminophylline, a bronchodilator, as a potential candidate. As **chlorpromazine** strongly suppressed visceral sensitivity to noxious CRD in the same phenotypic screen, it was also considered a candidate drug for abdominal pain. Chlorpromazine is traditionally used for treating schizophrenia, nausea and vomiting and severe hiccups (Adams *et al.,* 2005) and has antagonistic activity at various receptors, including the dopamine **D_2 receptor** and 5-HT_{2A} receptors (Horacek *et al.,* 2006). Chlorpromazine's antagonistic activity against the dopamine D_2 and 5-HT_{2A} receptors is involved in its efficacy in regulating positive or negative symptoms and cognitive symptoms in schizophrenia respectively (Horacek *et al.,* 2006).

In this study, we investigated the effect of chlorpromazine on visceral hypersensitivity to CRD. Our results suggest that 5-HT_{2A} receptor activation and increased 5-HT levels in the colon are involved in visceral hypersensitivity.

Methods

Animals

Male Wistar rats (4 to 5 weeks old, 150–200 g) or primiparaous late pregnant Wistar female rats were obtained from Charles River Laboratories Japan (Yokohama, Japan). Animals were housed under conditions of controlled temperature (22–24°C) and light (12 h light: 12 h dark cycle) for 1–2 weeks before experiments. The standard pellet diets (Rodent Diet CE-2, CLEA Japan, Inc.) were fed to the experimental animals ad libitum. The experiments and procedures described here were performed in accordance with the Guide for the Care and Use of Laboratory Animals as adopted and promulgated by the National Institutes of Health (NIH, USA) and were approved by the Animal Care Committees of Keio University and St. Marianna University. Animal studies are reported in compliance with the ARRIVE guidelines (Kilkenny *et al.,* 2010; McGrath and Lilley, 2015).

Assessment of visceromotor response (VMR) to CRD

VMR to CRD was monitored as described previously (Asano *et al.,* 2017). Briefly, rats were deeply anaesthetized with an intraperitoneal injection of mixture of medetomidine chloride (0.5 $mg \cdot kg^{-1}$), midazolam (2.5 $mg \cdot kg^{-1}$) and butorphanol tartrate (2.5 $mg \cdot kg^{-1}$). We ensured adequate depth of anesthesia by testing pedal withdrawal and palpebral reflexes. The skin was incised (1 cm-long incision), and the external oblique muscle of the abdomen was exposed. Electromyography electrodes (Starmedical, Tokyo, Japan) were sutured into the external oblique muscle to record the EMG. Electrode leads were tunnelled s.c. and exteriorized at the nape of the neck for future access. Incised skin was closed with nylon sutures, and the rats were given butorphanol tartrate

(2.5 mg·kg^{-1}) and viccillin (30 mg·kg^{-1}) s.c. After surgery, rats were housed individually and allowed to recuperate for 5 to 7-days before being used in the CRD study. During the recovery period, several rats broke the EMG electrodes and were excluded from VMR assessment. On the day of the CRD test, rats were restrained in a plastic conical tube cage (diameter, 6 cm; height, 15 cm), 15 min before electromyography. Rats were not habituated to the tube prior to experiments. A polyethylene barostat balloon (length, 2 cm; maximum diameter, 1.5 cm; volume, 2–3 mL) was inserted in the colon, positioned 1 cm proximal to the rectum and connected to a balloon catheter, which was anchored with tape to the base of the tail. Pressure and volume of the balloon were controlled and monitored by a barostat device (Distender Series II; G & J Electronics, Toronto, Canada) connected to it. Conscious rats were subjected to graded phasic CRD (10, 20, 40, 60 and 80 mmHg; each distension in triplicate; duration, 20 s; interstimulus interval, 150 s) to estimate drug activity.

EMG data were collected and analysed using the 8 STAR software package (Star Medical, Tokyo, Japan). EMG amplitude (mV·s) resulting from contraction of the external oblique muscle was quantified by calculating the AUC of the voltage alteration graph during CRD. EMG amplitude data were corrected by subtracting the baseline EMG data, which were collected 20 s before each CRD. The AUC (mmHg·mV·s) of EMG amplitude (mV·s) – balloon pressure (mmHg) curve – was also determined.

Colonic compliance (pressure–volume curves) was monitored during phasic CRD in control rats and presented as change in cylinder volume and balloon pressure.

Chlorpromazine, **sulpiride**, **haloperidol**, **risperidone** or **quetiapine** were administered p.o. 2 h before the CRD test. Chlorpromazine was dissolved in saline, whereas other drugs were suspended in 1% methylcellulose. Ketanserin, **L-741,626**, AL-34662 and 7OH-Cpz were also suspended in 1% methylcellulose but were administered i.p. 15 min before the CRD study. In the 5-HT depletion experiment, rats were administered **p-chlorphenylalanine** (*p*-CPA; 300 mg·kg^{-1}, p.o.) with 0.1% Tween-80 or vehicle 30 min before butyrate application, once daily for 3 days.

Sodium butyrate- or acetic acid-induced visceral hypersensitivity to CRD

A butyrate enema was performed using a previously described method with some modifications (Asano *et al.*, 2012). Briefly, rats were instilled with 1 mL sodium butyrate solution (110 mg·mL^{-1}, pH 6.9) or saline into the colon twice daily for 3 days (day 1 to 3). On day 4, rats were subjected to CRD experiments.

Acetic acid-induced colonic hypersensitivity was induced as described previously (Winston *et al.*, 2007). Primiparous late pregnant Wistar female rats were individually housed for about a week prior to giving birth (10–15 pups per rat). The 10-day-old rat pups were subjected to intracolonic injection of 0.2 mL acetic acid (0.5% in saline) 2 cm from the anus; control rats received an equal volume of saline. At 5–6 weeks of age, VMR to CRD was measured in both groups of male rats.

Western blot analysis

Rats were killed by decapitation, and tissue samples from the sigmoid colon and L5-S1 dorsal root ganglia were collected, frozen with liquid nitrogen and stored at −80°C until Western blot analysis. Tissue samples were homogenized in RIPA buffer [50 mM Tris–HCl (pH 7.2), 150 mM NaCl, 1% sodium deoxycholate, 1% SDS, 1% NP-40] containing protease inhibitor cocktail (Sigma, St. Louis, MO, USA) and phosphatase inhibitor cocktail (Santa Cruz Biotechnology, Santa Cruz, CA, USA). Samples were centrifuged at 15 000 × *g* at 4°C, and the supernatants were collected. Total protein concentration of the sample was determined using the Bradford method. Samples were subjected to electrophoresis on 10% polyacrylamide SDS gel (Thermo Fisher Scientific, Rockford, IL, USA), after which the separated proteins were transferred to PVDF membranes. Membranes were blocked for 30 min with Tris phosphate buffer containing 0.1% Tween-80 (T-TBS) and 5% skimmed milk and incubated overnight at 4°C with T-TBS containing the appropriate primary antibodies. Antibodies, including mouse monoclonal anti-5-HT_{2A} receptor (5-HT_{2A} R) antibody (MABN1595, Merck Millipore, Darmstadt, Germany), rabbit polyclonal anti-phosphorylated **ERK1/2** antibody (#9101, Cell Signalling Technology), rabbit polyclonal anti-ERK1/2 antibody (#9102, Cell Signalling Technology) and mouse monoclonal anti-β-actin antibody (Sigma, St. Louis, MO, USA) were used at 1:2000, 1:2000, 1:2000 and 1:1000 dilutions respectively. The membranes were washed three times with T-TBS, incubated for 60 min at room temperature with horseradish peroxidase-conjugated secondary antibodies in T-TBS containing 2% skimmed milk and washed three times with T-TBS. Signal was developed in ECL™ Prime solution (GE Healthcare) and imaged using ImageQuant™ LAS4000 image analyser (GE Healthcare). Intensity of immunoreactive bands was quantified using Image J software (NIH) and normalized to β-actin levels. Data are expressed as the fold change over saline groups.

Measurement of 5-HT levels in colonic tissues

After the 3 day butyrate treatment, the rats were killed and colon tissues were collected to determine tissue 5-HT levels using an enzyme immunoassay kit (Beckman Coulter, Inc., Fullerton, CA, USA), according to the manufacturer's instructions.

Statistical analyses

Data and statistical analysis comply with the recommendations on experimental design and analysis in pharmacology (Curtis *et al.*, 2015). In all animal studies, a co-worker blinded to the experimental protocol randomized animals into groups. The values presented were derived from at least two independent experiments. All data are expressed as mean ± SEM values. Normalization was performed for the quantitative analysis of Western blots. Statistical analyses were performed using SPSS 24.0 software (IBM, Armonk, NY, USA). One or two-way ANOVA followed by Dunnett's test or Student's *t*-test for unpaired results was used to evaluate differences between more than two groups or between two groups respectively. Two-way ANOVA with repeated measures followed by Bonferroni's method was used for the phasic CRD test. Differences were considered significant at $P < 0.05$.

Chemicals

7-Hydroxy chlorpromazine (7OH-Cpz) was purchased from Santa Cruz Biotechnology, Inc. (Santa Cruz, CA, USA).

Methylcellulose, sodium butyrate, haloperidol and quetiapine were obtained from Wako Pure Chemical Industries (Osaka, Japan). Medetomidine chloride (Domitor®) and butorphanol tartrate (Vetorphale®) were purchased from Meiji Seika Pharma Co., Ltd. (Tokyo, Japan). Midazolam was purchased from SANDOZ (Tokyo, Japan). 5-HT, *p*-chlorphenylalanine, sulpiride and chlorpromazine hydrochloride (chlorpromazine) were purchased from Sigma (St. Louis, MO, USA). Risperidone (Ris) was obtained from LKT laboratories, Inc. (St Paul, MN, USA). AL-34662 was obtained from Cayman Chemical Company (Ann Arbor, MI, USA). L-741,626 and ketanserin tartrate (ketanserin) were obtained from Abcam (Cambridge, UK).

Nomenclature of targets and ligands

Key protein targets and ligands in this article are hyperlinked to corresponding entries in http://www.guidetopharmacology.org/, the common portal for data from the IUPHAR/BPS Guide to PHARMACOLOGY (Southan *et al.,* 2016), and are permanently archived in the Concise Guide to PHARMACOLOGY 2015/16 (Alexander *et al.,* 2015a,b).

Results

Effect of chlorpromazine on butyrate-induced visceral hypersensitivity in rats

Effect of oral administration of chlorpromazine on butyrate-induced visceral hypersensitivity, which is a model of IBS, was investigated in rats. Rats subjected to butyrate treatment showed increase in VMR to CRD compared with that in saline-treated control rats (Figure 1A, B). Oral pre-administration of chlorpromazine significantly decreased this response in a dose–response manner (Figure 1A, B). Interestingly, chlorpromazine did not affect visceral sensitivity in healthy control rats except at a high dose of 40 $mg{\cdot}kg^{-1}$ (Figure 1C) nor was colonic compliance affected (Figure 1D). In a preliminary experiment, we observed that 12 $mg{\cdot}kg^{-1}$ chlorpromazine significantly induced a cataleptic response in healthy rats (an adverse effect). However, there was no significant difference between inhibitory actions of 4 and 12 $mg{\cdot}kg^{-1}$ chlorpromazine in Figure 1A, B. Thus, we decided to use 4 $mg{\cdot}kg^{-1}$ chlorpromazine for subsequent experiments. We also assessed the effect of chlorpromazine on visceral hypersensitivity induced by colonic instillation of dilute acetic acid to neonatal rats, another model of IBS. As shown in Figure 1E, chlorpromazine restored visceral sensitivity stimulated by acetic acid to the levels observed in control rats.

The effect of antipsychotics other than chlorpromazine on visceral hypersensitivity to CRD was also evaluated. Typical antipsychotic drugs sulpiride and haloperidol and atypical antipsychotics quetiapine and risperidone were analysed. In addition to inhibiting the dopamine D_2 receptor, quetiapine and risperidone are 5-HT_{2A} receptor antagonists. According to a previous report, sulpiride, haloperidol, quetiapine and risperidone show <500, 20, 0.13 and 0.33 5-HT_{2A}/D_2 K_i ratios respectively (Horacek *et al.,* 2006). We examined whether the inhibition of 5-HT_{2A} receptor by antipsychotic drugs is associated with the suppression of visceral hypersensitivity. As shown in Figure 2A, B, quetiapine and risperidone suppressed butyrate-induced visceral hypersensitivity to CRD, whereas sulpiride and haloperidol did not.

Role of 5-HT_{2A} receptor in visceral hypersensitivity

Next, it was investigated whether 5-HT_{2A} or dopamine D_2 receptor antagonists could inhibit sodium butyrate-induced increase in visceral sensitivity. Results showed that a selective 5-HT_{2A} receptor antagonist, ketanserin, ameliorated butyrate-induced visceral hypersensitivity to CRD, whereas a selective dopamine D_2 receptor antagonist, L-741,626, did not. To confirm these findings, the effect of 7OH-Cpz, which does not bind to 5-HT_{2A} receptors, was also assessed. 7OH-Cpz (4.2 $mg{\cdot}kg^{-1}$) was administered p.o. to rats at a dose equivalent to that of chlorpromazine. 7OH-Cpz did not suppress butyrate-induced visceral hypersensitivity to CRD (Figure 3A, B).

Moreover, we investigated whether a 5-HT_{2A} receptor agonist stimulated visceral sensitivity to CRD in healthy rats to study the involvement of 5-HT_{2A} receptor activation in the stimulation of visceral sensitivity. AL-34662, a selective 5-HT_{2A} receptor agonist, stimulated visceral sensitivity to CRD in control rats (Figure 3C). Additionally, we investigated the effect of AL-34662 on visceral sensitivity in rats treated with butyrate to determine the sensitivity of 5-HT_{2A} receptor in butyrate-treated rats. AL-34662 did not affect the VMR to CRD in butyrate-treated rats (Figure 3D) and significantly restored butyrate-induced visceral hypersensitivity to CRD in the presence of chlorpromazine (Figure 3E).

Mechanisms underlying the inhibitory effect of chlorpromazine on visceral hypersensitivity

Activation of ERK1/2 in DRG neurons plays an important role in butyrate-induced colonic hypersensitivity to CRD (Xu *et al.,* 2013). We examined the effect of chlorpromazine on the expression of phospho-ERK1/2 in DRG neurons after butyrate treatment. As shown in Figure 4A, B, administration of sodium butyrate increased the expression of phospho-ERK1/2, whereas oral pre-administration of chlorpromazine inhibited this effect. To determine whether 5-HT_{2A} receptor antagonism is involved in the attenuation of ERK1/2 activation, we examined the effects of ketanserin and L-741626 on the expression of phospho-ERK1/2 in butyrate-treated rats. Application of ketanserin but not L-741626 to butyrate-treated rats decreased phospho-ERK1/2 expression in DRG neurons (Figure 4C, D).

Moreover, expression of 5-HT_{2A} receptors in DRG neurons and colon was evaluated and shown not to change after butyrate treatment (Figure 5A–C). Next, we determined colonic 5-HT levels. Butyrate treatment significantly increased 5-HT levels in colonic tissues (Figure 5D). Subsequently, we investigated the effect of a 5-HT synthesis inhibitor *p*-CPA on butyrate-induced hypersensitivity (Qin *et al.,* 2010). After oral administration of *p*-CPA for 3 days, colonic 5-HT levels significantly decreased in butyrate-treated rats (Figure 6A), whereas stimulated visceral sensitivity to CRD improved (Figure 6B).

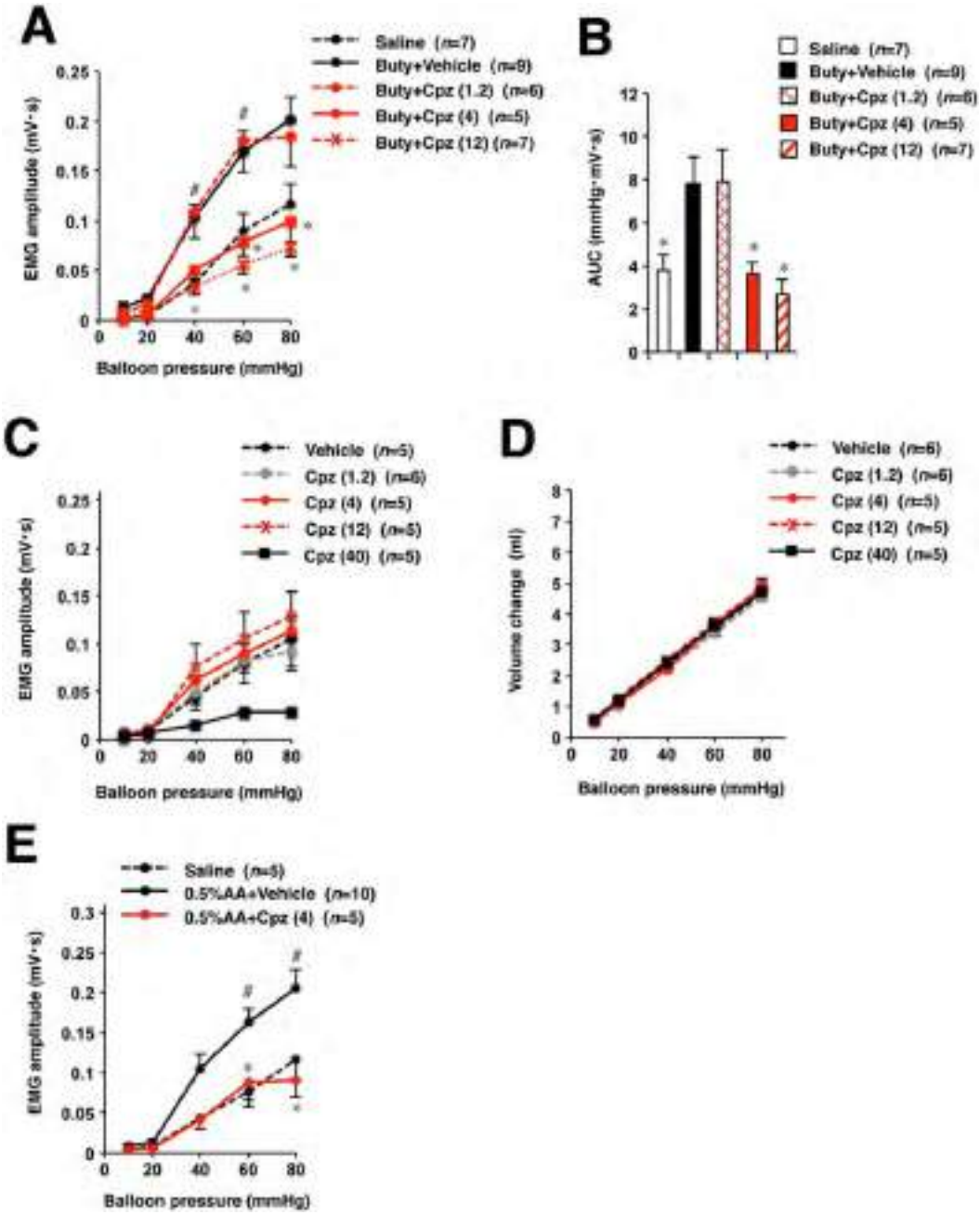

Figure 1

Effects of chlorpromazine on visceral sensitivity to CRD in rats without or with butyrate or acetic acid treatment. Rats were administered saline, sodium butyrate (Buty) or 0.5% acetic acid (0.5% AA) in neonates (A, B, E). Rats were orally administered the indicated doses of chlorpromazine (Cpz) (mg·kg^{-1}) or vehicle (saline), then two hours later, the CRD study was performed (A–E). (A) Visceral sensitivity to CRD (EMG amplitude) was determined. (B) Collective AUC data from (A). (C, D) Visceral sensitivity to CRD and colonic compliance in healthy control rats were examined. Values are mean ± SEM; * or $^{\#}P < 0.05$ (*, vs. vehicle; $^{\#}$, vs. saline).

Discussion

Various types of drugs including psychoactive agents are prescribed to IBS patients, and many target molecules for IBS drugs have been proposed. However, an appropriate pharmacological therapy has not yet been established. Furthermore, although some antipsychotic drugs are prescribed to treat pain symptoms in IBS, their pain amelioration mechanisms are unclear. Previously, in a phenotypic screening, we identified aminophylline as a drug that suppressed visceral sensitivity response to repeated CRD. Aminophylline suppressed stress-induced visceral hypersensitivity by inhibiting adenosine A_2 receptors (Asano *et al.,* 2017). In the same screen, chlorpromazine showed similar effects. Chlorpromazine has been used clinically as an antipsychotic drug for a long time. However, the effects of chlorpromazine on IBS have not been

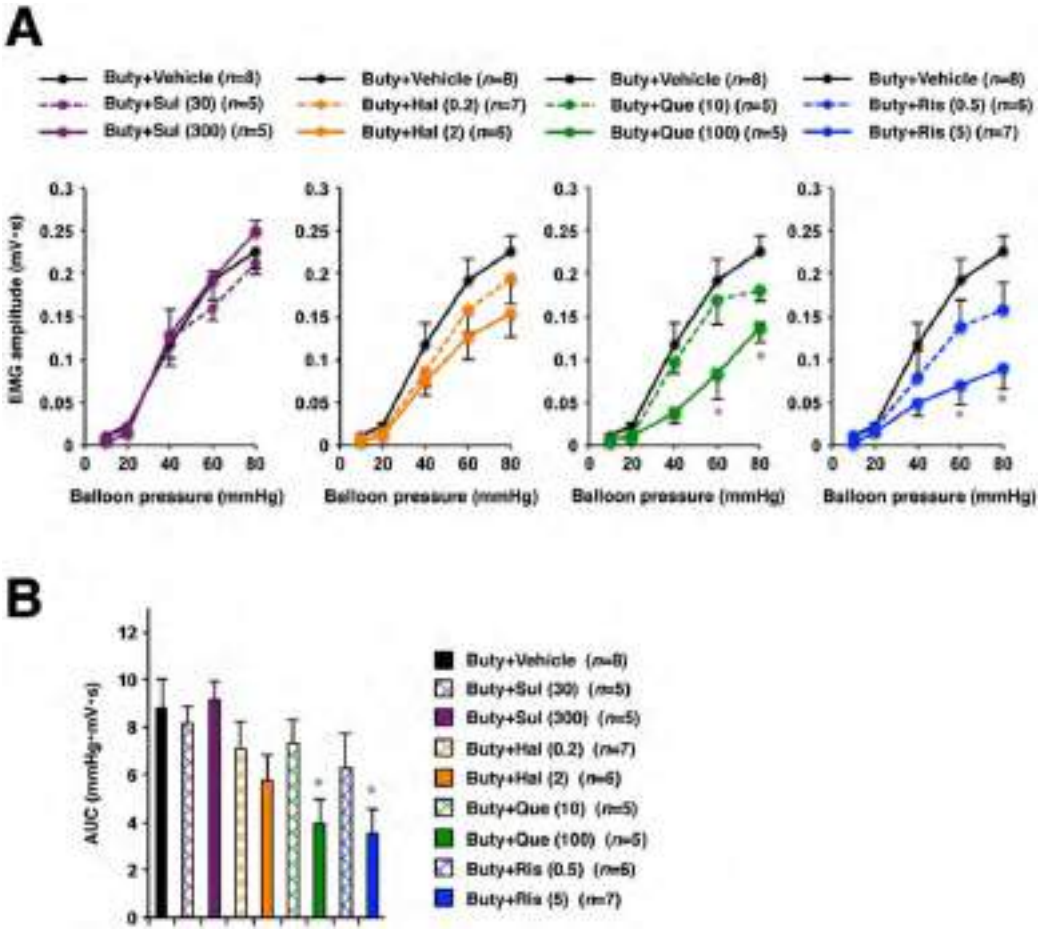

Figure 2

Effects of antipsychotic drugs on butyrate-induced visceral hypersensitivity to CRD in rats. The indicated doses (mg·kg^{-1}) of sulpiride (Sul), haloperidol (Hal), quetiapine (Que), risperidone (Ris) or vehicle (1% methylcellulose) were administered p.o. to butyrate (Buty)-treated rats. Two hours later, the CRD study was performed (A, B). (B) shows the collective AUC data from (A). Values are mean ± SEM; $^{*}P < 0.05$ vs. vehicle. Each graph of Buty + Vehicle group in four panels represents the same data as in (A).

investigated in any non-clinical or clinical study. Herein, we demonstrated that chlorpromazine suppressed visceral hypersensitivity in an IBS animal model, by inhibiting 5-HT$_{2A}$ receptor signalling.

Oral administration of chlorpromazine prevented butyrate- or acetic acid-induced visceral hypersensitivity to CRD without affecting visceral sensitivity under normal conditions or affecting colonic compliance. This activity profile suggests that chlorpromazine could be beneficial for IBS patients. Furthermore, atypical antipsychotic drugs risperidone and quetiapine improved colonic hypersensitivity in rats. Whereas sulpiride and haloperidol, which did not show this effect in our analysis, are preferential dopamine D$_2$ receptor antagonists, quetiapine and risperidone inhibit both 5-HT$_{2A}$ receptor and dopamine D$_2$ receptor. Therefore, 5-HT$_{2A}$ receptor inhibition may be involved in the suppression of visceral hypersensitivity. Although previous studies have suggested the possibility of atypical antipsychotics as a treatment option for IBS (Pae *et al.*, 2013), this is the first report in an animal model.

Pre-administration of a subtype-specific 5-HT$_{2A}$ receptor antagonist significantly suppressed visceral sensitivity to CRD in rats subjected to butyrate treatment. In contrast, preferential dopamine D$_2$ receptor inhibitor did not affect visceral hypersensitivity. This result does not conflict with previous reports suggesting that central activation of dopamine D$_2$ receptor produces antinociceptive action against CRD (Nozu *et al.*, 2016; Okumura *et al.*, 2016). Our results indicate that chlorpromazine-induced amelioration of visceral hypersensitivity could have been mediated by 5-HT$_{2A}$ receptor antagonism. To confirm this, we examined 7OH-Cpz, which does not bind to 5-HT$_{2A}$ receptor (Suzuki *et al.*, 2013), and AL-34662, a subtype-specific 5-HT$_{2A}$ receptor agonist, in the presence of chlorpromazine. As 7OH-Cpz does not inhibit 5-HT$_{2A}$ receptor but does bind to D$_2$ receptor (Suzuki *et al.*, 2013), we anticipated that 7OH-Cpz treatment would have no inhibitory effect on visceral hypersensitivity. As expected, 7OH-Cpz did not suppress butyrate-induced visceral hypersensitivity to CRD, indicating that 5-HT$_{2A}$ receptor antagonism was involved in chlorpromazine-induced inhibition of visceral hypersensitivity. Moreover, AL-34662 induced visceral hypersensitivity in response to CRD in normal rats, but not in butyrate-treated rats, suggesting that the activation of 5-HT$_{2A}$ receptor might be the mechanism

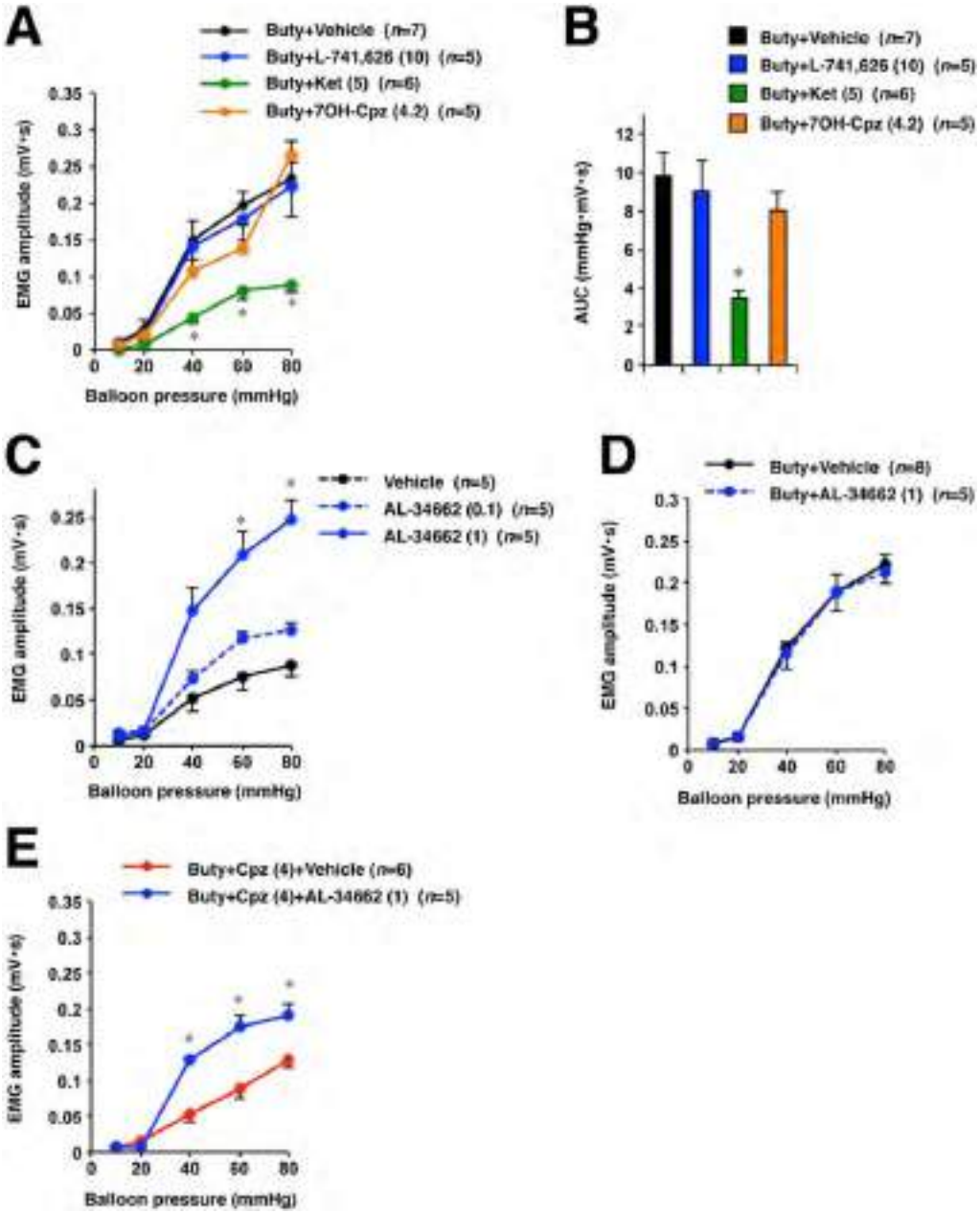

Figure 3

Pharmacological study of role of the 5-HT_{2A} receptor in visceral sensitivity to CRD. Rats treated with sodium butyrate (Buty) for 3 days were administered, i.p., the indicated doses (mg·kg^{-1}) of L-741626 (a selective dopamine D_2 receptor antagonist) (A, B), ketanserin (Ket) (a selective 5-HT_{2A} receptor antagonist) (A, B), AL-34662 (a selective 5-HT_{2A} receptor agonist) (D, E) or vehicle (1% methylcellulose), 15 min before the CRD study. The indicated doses (mg·kg^{-1}) of chlorpromazine (Cpz) (E) or 7OH-Cpz (A, B) were administered, p.o., to butyrate-treated rats, 2 h before the CRD test. (C) The indicated doses of AL-34662 (mg·kg^{-1}) or vehicle (1% methylcellulose) were administered, i.p., to healthy control rats. Fifteen minutes later, the CRD study was performed. (B) Collective AUC data from (A). Values are mean ± SEM; $^{*}P < 0.05$, vs. vehicle.

responsible for sodium butyrate-induced visceral hypersensitivity to CRD. Lack of visceral sensitivity to CRD stimulation by AL-34662 in butyrate-treated rats may imply that the 5-HT_{2A} receptor was already fully occupied by 5-HT produced due to butyrate treatment. Additionally, as AL-34662 is unable to cross the blood–brain barrier (Sharif *et al.*, 2007), 5-HT_{2A} receptors expressed in peripheral tissues (such as the colon) rather than those in the central nervous system appear to be involved in the inhibitory effects of chlorpromazine. However, our data do not exclude the possibility of a central mechanism of chlorpromazine, as 5-HT_{2A} receptors are expressed in the brain and spinal cord and chlorpromazine is a centrally acting agent. Furthermore, inhibition of spinal 5-HT_{2A} receptors was reported to decrease nociceptive responses to noxious stimuli (Rahman *et al.*, 2011), and chlorpromazine was shown to elicit a spinal blockade of

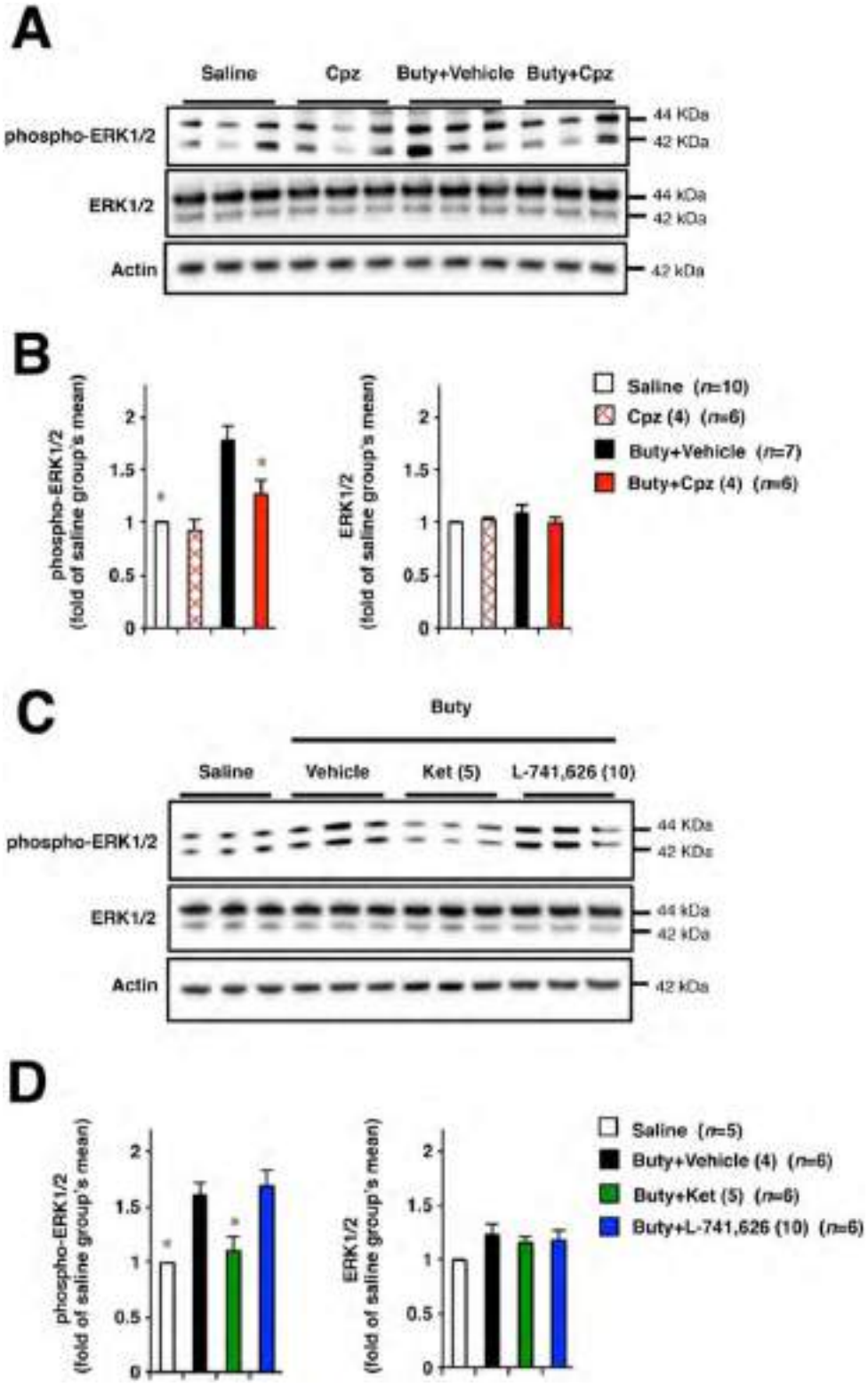

Figure 4

Effect of chlorpromazine, ketanserin or L-741626 on the butyrate-induced activation of ERK1/2 in DRG neurons. Rats were intracolonically administered sodium butyrate or saline twice daily for 3 days (A–D). On the next day after the last administration, chlorpromazine (4 mg·kg^{-1}) or vehicle (saline) was administered p.o. to these rats (A, B). Rats treated with butyrate were given ketanserin (5 mg·kg^{-1}), L-741626 (10 mg·kg^{-1}) or vehicle (1% methylcellulose) (C, D), i.p. Two hours (A, B) or 15 min (C, D) later, the L5-S1 DRG were removed from rats and tissues were subjected to Western blot analysis. (A) and (C) show representative data of immunoblotting. (B) and (D) show the relative data of band intensity at (A) and (C) respectively. Values are mean ± SEM; $^{*}P < 0.05$, vs. vehicle.

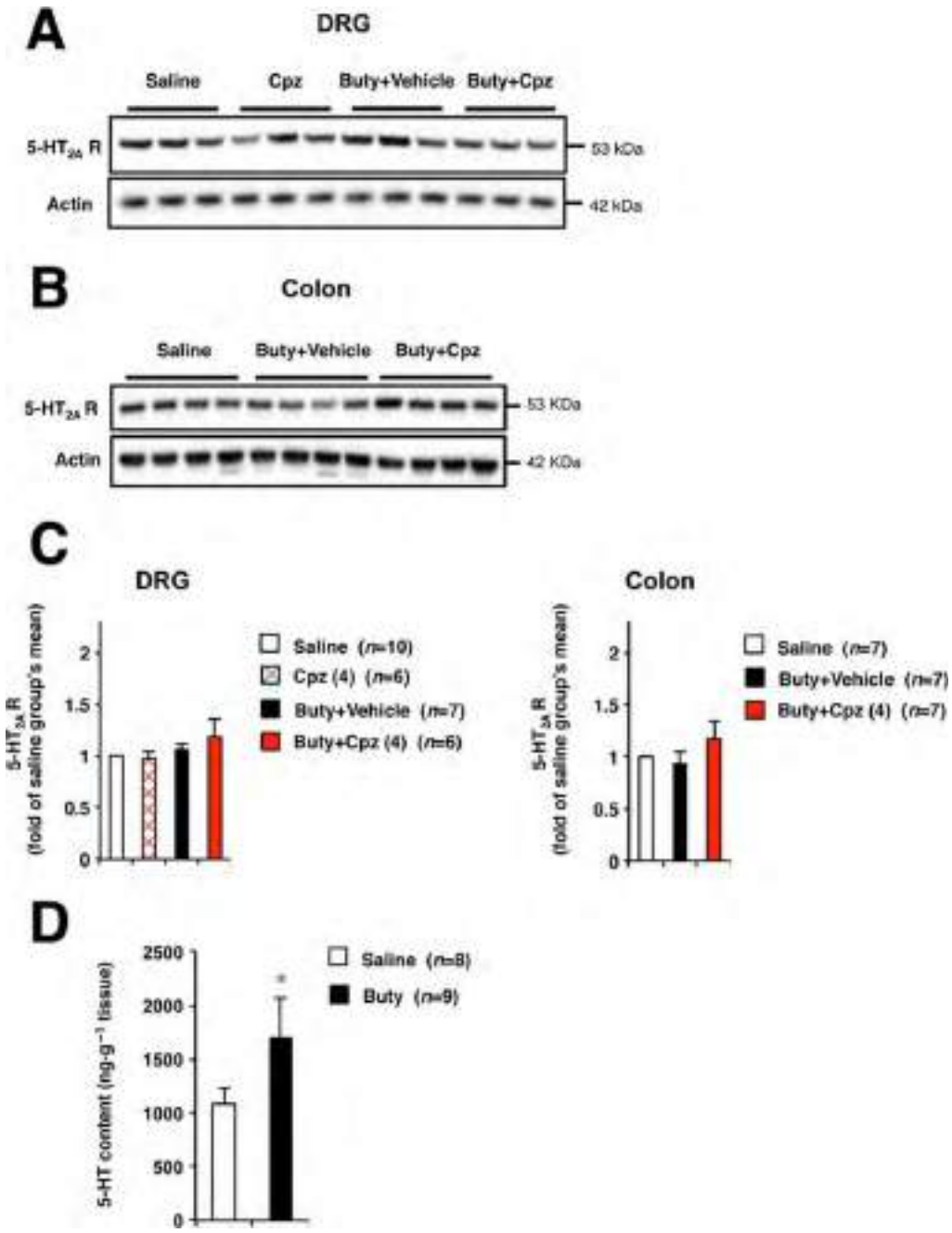

Figure 5

The expression of 5-HT_{2A} receptors in DRG neurons and colon, and colonic 5-HT contents. Rats were administered sodium butyrate or saline *via* colonic instillation twice daily for 3 days (A–D). After the last administration, chlorpromazine (4 mg·kg^{-1}) or vehicle (saline) was administered p.o. Two hours later, the L5-S1 DRG or colon was removed from the rats and tissues were subjected to Western blot analysis (A–C) or 5-HT ELISA assay (D). (A) and (B) show representative data of immunoblotting. (C) The relative data of band intensity at (A) and (B). Values are mean ± SEM; $^{*}P < 0.05$ vs. saline.

nociception in rats (Chen *et al.*, 2012). Thus, further studies are required to determine whether the amelioration of colonic hypersensitivity by chlorpromazine originates from peripheral or central actions of this drug.

As demonstrated earlier, 5-HT_{2A} receptor antagonists have an analgesic effect on inflammatory pain (Nitanda *et al.*, 2005; Cervantes-Duran *et al.*, 2016). In the present study, we demonstrated the inhibitory effect of a 5-HT_{2A} antagonist on the visceral pain response in non-inflammatory models (Bourdu *et al.*, 2005). Inflammatory pain models, such as neuropathic pain and formalin stimulation, were shown to increase the expression of 5-HT_{2A} receptors in DRG neurons (Okamoto *et al.*, 2002; Cervantes-Duran *et al.*, 2016); however, colonic butyrate application did not alter the expression

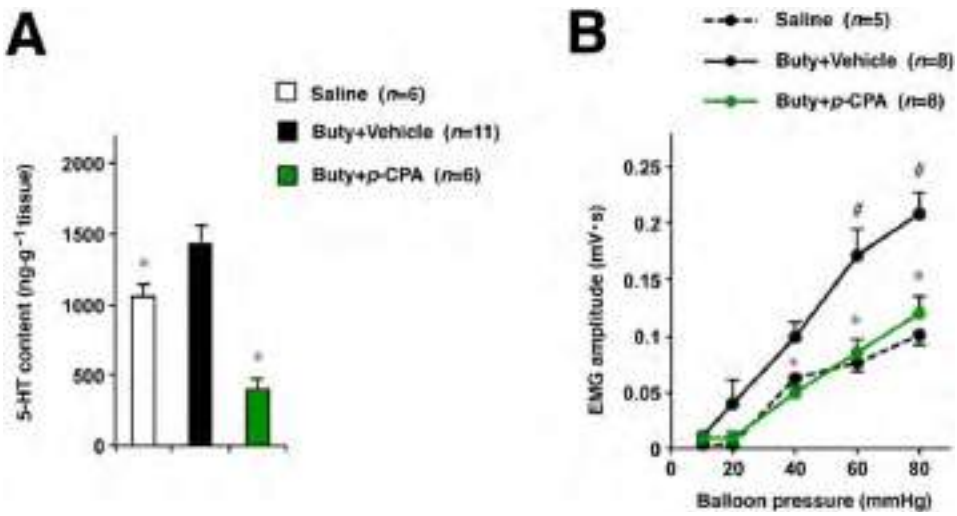

Figure 6

Effects of *p*-CPA on butyrate-induced visceral hypersensitivity to CRD in rats. Rats were administered 300 mg·kg^{-1} *p*-CPA (a 5-HT synthesis inhibitor) or vehicle (0.1% Tween-80), p.o., once daily for 3 days. Thirty minutes after each treatment, sodium butyrate or saline was administered *via* colonic administration. The next day, after the last administration of butyrate, the CRD test was performed (A). Colonic tissues removed from rats were subjected to 5-HT ELISA assay (B). Values are mean ± SEM; * or $^{\#}P < 0.05$ (*, vs. vehicle; $^{\#}$, vs. saline).

of 5-HT$_{2A}$ receptors in this study. This may be because the pathophysiology of pain sensation differs between our models and previous inflammatory pain models.

In rat DRG neurons, butyrate-induced colonic hypersensitivity is mediated by ERK1/2 activation (induction of ERK1/2 phosphorylation) (Xu *et al.*, 2013). Prevention of ERK1/2 phosphorylation in DRG neurons by an MEK inhibitor attenuated the butyrate-induced enhancement of DRG neuronal excitability and colonic hypersensitivity (Xu *et al.*, 2013). However, mechanisms based on an overexpression of acid-sensing ion channels (ASICs), the T-type calcium channel (Ca$_v$3.2) or phosphorylated voltage-gated potassium channel subunit 4.2 (pK$_v$4.2) in colonic sensory neurons have also been proposed (Marger *et al.*, 2011; Xu *et al.*, 2013). These changes would result in the stimulation of neuronal firing, leading to colonic hypersensitivity. In this study, butyrate treatment increased the phosphorylation of ERK1/2, whereas chlorpromazine prevented this activation without altering 5-HT$_{2A}$ receptor expression in DRG neurons. Moreover, ketanserin but not L-741626 suppressed butyrate-induced ERK1/2 activation, suggesting that 5-HT$_{2A}$ receptors may be involved in ERK1/2 activation in DRG neurons. Additionally, chlorpromazine improved visceral hypersensitivity induced by intracolonic injection of dilute acetic acid in neonatal rats. Recent study using the acetic acid model has shown that increased expression of 5-HT and 5-HT$_{2A}$ receptors in colon and DRG neurons is involved in the induction of visceral hypersensitivity (Chen *et al.*, 2016). Present study focused on the role of 5-HT$_{2A}$ receptor and 5-HT in butyrate-induced visceral hypersensitivity, as these mechanisms have not been investigated previously in this model.

Expression of 5-HT$_{2A}$ receptors in DRG neurons and colon did not change after butyrate instillation, in agreement with AL-34662 not stimulating visceral pain response in rats treated with butyrate. Therefore, we focused on colonic 5-HT levels. Butyrate treatment increased 5-HT levels in the colon, in agreement with the findings of a previous study (Grider and Piland, 2007), which showed that butyrate causes 5-HT release in the rat colon. These findings indicate that the change in 5-HT$_{2A}$ receptor expression does not contribute to the inhibitory effect of chlorpromazine on visceral hypersensitivity, whereas increased levels of 5-HT may be responsible for inducing visceral hypersensitivity. To confirm this hypothesis, we examined the effect of *p*-CPA, an inhibitor of 5-HT synthesis, on visceral hypersensitivity. 5-HT depletion *via p*-CPA treatment attenuated butyrate-induced colonic hypersensitivity. As elevated 5-HT levels or 5-HT$_{2A}$ receptor expression in the colon and DRG neurons are associated with acetic acid-induced visceral hypersensitivity (Chen *et al.*, 2016), increased colon 5-HT levels may be a visceral hypersensitivity mechanism shared by butyrate and acetic acid models. Moreover, inhibition of 5-HT$_{2A}$ receptor signalling by chlorpromazine may account for antinociceptive effects in these models. As ASIC3 and TRPV1 are required for visceral sensitivity to CRD, and 5-HT$_{2A}$ receptor signalling enhances TRPV1 and ASICs activity in sensory neurons (Sugiuar *et al.*, 2004; Jones *et al.*, 2005; Qiu *et al.*, 2012), activation of 5-HT$_{2A}$ receptors in our study may also be associated with modulation of these channels. However, we could not exclude the possibility that other effects of chlorpromazine, including histamine H$_1$ receptor antagonism and anti-calmodulin activity, may also be involved in the inhibitory effect observed in this study (Horacek *et al.*, 2006; Olah *et al.*, 2007). Taken together, our results indicate that butyrate-induced increase in colonic 5-HT levels potentiates visceral sensitivity *via* the 5-HT$_{2A}$ receptor, with chlorpromazine potentially preventing the binding of released 5-HT to 5-HT$_{2A}$ receptors.

In conclusion, we propose that the ameliorating effects of chlorpromazine on visceral hypersensitivity may be beneficial for IBS patients with abdominal pain and discomfort. The inhibitory effect of chlorpromazine on visceral hypersensitivity is likely to be mediated by inhibition of 5-HT$_{2A}$

receptor signalling, and we suggest the 5-HT_{2A} receptor as a potential therapeutic target protein for abdominal pain and discomfort in IBS.

Acknowledgements

We gratefully acknowledge Ayumi Kanada for technical assistance with animal experiments. We would like to thank Editage for English language editing. This work was supported by Grants-in-Aid for Scientific Research from the Ministry of Health, Labour, and Welfare of Japan, as well as the Center of Innovation Program from Japan Science and Technology Agency, Scientific Technique Research Promotion Program for Agriculture, Forestry and Food Industry, and Grants-in-Aid for Scientific Research from the Ministry of Education, Culture, Sports, Science and Technology, Japan.

Author contributions

T.A., K.T., M.T. and T.M. conceived and designed the experiments; T.A., A.T., K.T., R.T., H.S. and H.M. carried out the analysis and interpretation; and T.A performed the drafting and critical revising of the manuscript.

Conflict of interest

T.M. is the chairman and director of LTT Bio-Pharma Co., Ltd. T.A. and M.T. belong to an endowed research division of LTT Bio-Pharma Co., Ltd. The other authors declare no conflicts of interest.

Declaration of transparency and scientific rigour

This Declaration acknowledges that this paper adheres to the principles for transparent reporting and scientific rigour of preclinical research recommended by funding agencies, publishers and other organisations engaged with supporting research.

References

Adams CE, Rathbone J, Thornley B, Clarke M, Borrill J, Wahlbeck K *et al*. (2005). Chlorpromazine for schizophrenia: a Cochrane systematic review of 50 years of randomised controlled trials. BMC Med 3: 15.

Alexander SPH, Davenport AP, Kelly E, Marrion N, Peters JA, Benson HE *et al*. (2015a). The Concise Guide to PHARMACOLOGY 2015/16: G protein-coupled receptors. Br J Pharmacol 172: 5744–5869.

Alexander SPH, Fabbro D, Kelly E, Marrion N, Peters JA, Benson HE *et al*. (2015b). The Concise Guide to PHARMACOLOGY 2015/16: Enzymes. Br J Pharmacol 172: 6024–6109.

Alhaider AA (1991). Antinociceptive effect of ketanserin in mice: involvement of supraspinal 5-HT2 receptors in nociceptive transmission. Brain Res 543: 335–340.

Asano T, Tanaka K, Suemasu S, Ishihara T, Tahara K, Suzuki T *et al*. (2012). Effects of beta-(1,3-1,6)-D-glucan on irritable bowel syndrome-related colonic hypersensitivity. Biochem Biophys Res Commun 420: 444–449.

Asano T, Tanaka KI, Tada A, Shimamura H, Tanaka R, Maruoka H *et al*. (2017). Aminophylline suppresses stress-induced visceral hypersensitivity and defecation in irritable bowel syndrome. Sci Rep 7: 40214.

Azpiroz F, Bouin M, Camilleri M, Mayer EA, Poitras P, Serra J *et al*. (2007). Mechanisms of hypersensitivity in IBS and functional disorders. Neurogastroenterol Motil 19: 62–88.

Bourdu S, Dapoigny M, Chapuy E, Artigue F, Vasson MP, Dechelotte P *et al*. (2005). Rectal instillation of butyrate provides a novel clinically relevant model of noninflammatory colonic hypersensitivity in rats. Gastroenterology 128: 1996–2008.

Brierley SM, Linden DR (2014). Neuroplasticity and dysfunction after gastrointestinal inflammation. Nat Rev Gastroenterol Hepatol 11: 611–627.

Canavan C, West J, Card T (2014). Review article: the economic impact of the irritable bowel syndrome. Aliment Pharmacol Ther 40: 1023–1034.

Cervantes-Duran C, Vidal-Cantu GC, Godinez-Chaparro B, Granados-Soto V (2016). Role of spinal 5-HT2 receptors subtypes in formalin-induced long-lasting hypersensitivity. Pharmacol Rep 68: 434–442.

Chang L, Lembo A, Sultan S (2014). American Gastroenterological Association Institute Technical Review on the pharmacological management of irritable bowel syndrome. Gastroenterology 147: 1149–1172.e2.

Chen MX, Chen Y, Fu R, Liu SY, Yang QQ, Shen TB (2016). Activation of 5-HT and NR2B contributes to visceral hypersensitivity in irritable bowel syndrome in rats. Am J Transl Res 8: 5580–5590.

Chen YW, Chu CC, Chen YC, Kan CD, Wang JJ (2012). Promazine and chlorpromazine for prolonged spinal anesthesia in rats. Neurosci Lett 521: 115–118.

Cremon C, Carini G, Wang B, Vasina V, Cogliandro RF, De Giorgio R *et al*. (2011). Intestinal serotonin release, sensory neuron activation, and abdominal pain in irritable bowel syndrome. Am J Gastroenterol 106: 1290–1298.

Curtis MJ, Bond RA, Spina D, Ahluwalia A, Alexander SP, Giembycz MA *et al*. (2015). Experimental design and analysis and their reporting: new guidance for publication in BJP. Br J Pharmacol 172: 3461–3471.

Grider JR, Piland BE (2007). The peristaltic reflex induced by short-chain fatty acids is mediated by sequential release of 5-HT and neuronal CGRP but not BDNF. Am J Physiol Gastrointest Liver Physiol 292: G429–G437.

Grover M, Dorn SD, Weinland SR, Dalton CB, Gaynes BN, Drossman DA (2009). Atypical antipsychotic quetiapine in the management of severe refractory functional gastrointestinal disorders. Dig Dis Sci 54: 1284–1291.

Grover M, Drossman DA (2011). Centrally acting therapies for irritable bowel syndrome. Gastroenterol Clin North Am 40: 183–206.

Horacek J, Bubenikova-Valesova V, Kopecek M, Palenicek T, Dockery C, Mohr P *et al*. (2006). Mechanism of action of atypical antipsychotic drugs and the neurobiology of schizophrenia. CNS Drugs 20: 389–409.

Jones RC 3rd, Xu L, Gebhart GF (2005). The mechanosensitivity of mouse colon afferent fibers and their sensitization by inflammatory

mediators require transient receptor potential vanilloid 1 and acid-sensing ion channel 3. J Neurosci 25: 10981–10989.

Keszthelyi D, Troost FJ, Masclee AA (2012). Irritable bowel syndrome: methods, mechanisms, and pathophysiology. Methods to assess visceral hypersensitivity in irritable bowel syndrome. Am J Physiol Gastrointest Liver Physiol 303: G141–G154.

Kilkenny C, Browne W, Cuthill IC, Emerson M, Altman DG (2010). Animal research: reporting *in vivo* experiments: the ARRIVE guidelines. Br J Pharmacol 160: 1577–1579.

Ladabaum U, Boyd E, Zhao WK, Mannalithara A, Sharabidze A, Singh G *et al*. (2012). Diagnosis, comorbidities, and management of irritable bowel syndrome in patients in a large health maintenance organization. Clin Gastroenterol Hepatol 10: 37–45.

Madani S, Cortes O, Thomas R (2016). Cyproheptadine use in children with functional gastrointestinal disorders. J Pediatr Gastroenterol Nutr 62: 409–413.

Marger F, Gelot A, Alloui A, Matricon J, Ferrer JF, Barrere C *et al*. (2011). T-type calcium channels contribute to colonic hypersensitivity in a rat model of irritable bowel syndrome. Proc Natl Acad Sci U S A 108: 11268–11273.

Martin-Blanco A, Pascual JC, Soler J, Valdeperez A, Perez V (2010). Quetiapine in the treatment of refractory irritable bowel syndrome: a case report. Prog Neuropsychopharmacol Biol Psychiatry 34: 715–716.

Matricon J, Meleine M, Gelot A, Piche T, Dapoigny M, Muller E *et al*. (2012). Review article: Associations between immune activation, intestinal permeability and the irritable bowel syndrome. Aliment Pharmacol Ther 36: 1009–1031.

McGrath JC, Lilley E (2015). Implementing guidelines on reporting research using animals (ARRIVE etc.): new requirements for publication in BJP. Br J Pharmacol 172: 3189–3193.

Nitanda A, Yasunami N, Tokumo K, Fujii H, Hirai T, Nishio H (2005). Contribution of the peripheral 5-HT2A receptor to mechanical hyperalgesia in a rat model of neuropathic pain. Neurochem Int 47: 394–400.

Nozu T, Miyagishi S, Nozu R, Takakusaki K, Okumura T (2016). Water avoidance stress induces visceral hyposensitivity through peripheral corticotropin releasing factor receptor type 2 and central dopamine D2 receptor in rats. Neurogastroenterol Motil 28: 522–531.

Okamoto K, Imbe H, Morikawa Y, Itoh M, Sekimoto M, Nemoto K *et al*. (2002). 5-HT2A receptor subtype in the peripheral branch of sensory fibers is involved in the potentiation of inflammatory pain in rats. Pain 99: 133–143.

Okumura T, Nozu T, Kumei S, Takakusaki K, Miyagishi S, Ohhira M (2016). Levodopa acts centrally to induce an antinociceptive action against colonic distension through activation of D2 dopamine receptors and the orexinergic system in the brain in conscious rats. J Pharmacol Sci 130: 123–127.

Olah Z, Josvay K, Pecze L, Letoha T, Babai N, Budai D *et al*. (2007). Anti-calmodulins and tricyclic adjuvants in pain therapy block the TRPV1 channel. PLoS One 2: e545.

Pae CU, Lee SJ, Han C, Patkar AA, Masand PS (2013). Atypical antipsychotics as a possible treatment option for irritable bowel syndrome. Expert Opin Investig Drugs 22: 565–572.

Pasricha PJ (2007). Desperately seeking serotonin …. A commentary on the withdrawal of tegaserod and the state of drug development for functional and motility disorders. Gastroenterology 132: 2287–2290.

Qin HY, Luo JL, Qi SD, Xu HX, Sung JJ, Bian ZX (2010). Visceral hypersensitivity induced by activation of transient receptor potential vanilloid type 1 is mediated through the serotonin pathway in rat colon. Eur J Pharmacol 647: 75–83.

Qiu F, Qiu CY, Liu YQ, Wu D, Li JD, Hu WP (2012). Potentiation of acid-sensing ion channel activity by the activation of 5-HT(2) receptors in rat dorsal root ganglion neurons. Neuropharmacology 63: 494–500.

Rahman W, Bannister K, Bee LA, Dickenson AH (2011). A pronociceptive role for the 5-HT2 receptor on spinal nociceptive transmission: an in vivo electrophysiological study in the rat. Brain Res 1382: 29–36.

Sharif NA, McLaughlin MA, Kelly CR (2007). AL-34662: a potent, selective, and efficacious ocular hypotensive serotonin-2 receptor agonist. J Ocul Pharmacol Ther 23: 1–13.

Simren M, Barbara G, Flint HJ, Spiegel BM, Spiller RC, Vanner S *et al*. (2013). Intestinal microbiota in functional bowel disorders: a Rome foundation report. Gut 62: 159–176.

Southan C, Sharman JL, Benson HE, Faccenda E, Pawson AJ, Alexander SPH *et al*. (2016). The IUPHAR/BPS guide to PHARMACOLOGY in 2016: towards curated quantitative interactions between 1300 protein targets and 6000 ligands. Nucl Acids Res 44: D1054–D1068.

Sugiuar T, Bielefeldt K, Gebhart GF (2004). TRPV1 function in mouse colon sensory neurons is enhanced by metabotropic 5-hydroxytryptamine receptor activation. J Neurosci 24: 9521–9530.

Suzuki H, Gen K, Inoue Y (2013). Comparison of the anti-dopamine D(2) and anti-serotonin 5-HT(2A) activities of chlorpromazine, bromperidol, haloperidol and second-generation antipsychotics parent compounds and metabolites thereof. J Psychopharmacol 27: 396–400.

Treem WR, Ahsan N, Kastoff G, Hyams JS (1996). Fecal short-chain fatty acids in patients with diarrhea-predominant irritable bowel syndrome: in vitro studies of carbohydrate fermentation. J Pediatr Gastroenterol Nutr 23: 280–286.

Winston J, Shenoy M, Medley D, Naniwadekar A, Pasricha PJ (2007). The vanilloid receptor initiates and maintains colonic hypersensitivity induced by neonatal colon irritation in rats. Gastroenterology 132: 615–627.

Xu D, Wu X, Grabauskas G, Owyang C (2013). Butyrate-induced colonic hypersensitivity is mediated by mitogen-activated protein kinase activation in rat dorsal root ganglia. Gut 62: 1466–1474.

Acta Biomaterialia 64 (2017) 116–125

Contents lists available at ScienceDirect

Acta Biomaterialia

journal homepage: www.elsevier.com/locate/actabiomat

Full length article

In situ depot formation of anti-HIV fusion-inhibitor peptide in recombinant protein polymer hydrogel

Daisuke Asai [a,*], Taisei Kanamoto [a,1], Mitsuko Takenaga [b], Hideki Nakashima [a]

[a] Department of Microbiology, St. Marianna University, School of Medicine, 2-16-1 Sugao, Miyamae, Kawasaki 216-8511, Japan
[b] Institute of Medical Science, St. Marianna University, School of Medicine, 2-16-1 Sugao, Miyamae, Kawasaki 216-8512, Japan

ARTICLE INFO

Article history:
Received 8 July 2017
Received in revised form 11 October 2017
Accepted 13 October 2017
Available online 14 October 2017

Keywords:
Drug depot
Anti-HIV peptide
Polypeptide
Drug delivery

ABSTRACT

Most peptide drugs have short half-lives, necessitating frequent injections that may induce skin sensitivity reactions; therefore, versatile prolonged-release delivery platforms are urgently needed. Here, we focused on an oxidatively and thermally responsive recombinant elastin-like polypeptide with periodic cysteine residues (cELP), which can rapidly and reversibly form a disulfide cross-linked network in which peptide can be physically incorporated. As a model for proof of concept, we used enfuvirtide, an antiretroviral fusion-inhibitor peptide approved for treatment of human immunodeficiency virus (HIV) infection. cELP was mixed with enfuvirtide and a small amount of hydrogen peroxide (to promote cross-linking), and the soluble mixture was injected subcutaneously. The oxidative cross-linking generates a network structure, causing the mixture to form a hydrogel *in situ* that serves as an enfuvirtide depot. We fabricated a series of enfuvirtide-containing hydrogels and examined their stability, enfuvirtide-releasing profile and anti-HIV potency *in vitro*. Among them, hydrophobic cELP hydrogel provided effective concentrations of enfuvirtide in blood of rats for up to 8 h, and the initial concentration peak was suppressed compared with that after injection of enfuvirtide alone. cELP hydrogels should be readily adaptable as platforms to provide effective depot systems for delivery of other anti-HIV peptides besides enfuvirtide.

Statement of Significance

In this paper, we present an anti-HIV peptide delivery system using oxidatively and thermally responsive polypeptides that contain multiple periodic cysteine residues as an injectable biomaterial capable of *in situ* self-gelation, and we demonstrate its utility as an injectable depot capable of sustained release of anti-HIV peptides. The novelty of this work stems from the platform employed to provide the depot encapsulating the peptide drugs (without chemical conjugation), which consists of rationally designed, genetically engineered polypeptides that enable the release rate of the peptide drugs to be precisely controlled.

© 2017 Acta Materialia Inc. Published by Elsevier Ltd. All rights reserved.

1. Introduction

The application of effective antiretroviral therapy (ART) has transformed human immunodeficiency virus (HIV) infection into a long-term and manageable disorder [1]. Enfuvirtide (also known as Fuzeon, T-20 or DP178) is a potent antiretroviral fusion inhibitor composed of a linear sequence of 36 naturally occurring L-amino acid residues with an acetylated N-terminus and a carboxamide C-terminus, and prevents HIV from entering host cells [2–4]. Enfuvirtide interferes with an earlier stage of infection than standard ART regimens, and has been used in combination with other antiretroviral agents for the treatment of HIV-infected individuals and AIDS patients with multidrug-resistant HIV infections that no longer respond to standard ART. Despite its therapeutic efficacy, the clinical use of enfuvirtide is limited, as the peptide is rapidly cleared from the circulation, principally by degradation in the liver and renal clearance, resulting in a short plasma half-life of approximately 2 h [2]. To maintain an effective blood concentration, a twice-daily subcutaneous (*s.c.*) injection schedule has been established clinically, but due to the frequency of administration, skin

* Corresponding author.
E-mail address: asai@marianna-u.ac.jp (D. Asai).
[1] Present address: Laboratory of Microbiology, Showa Pharmaceutical University, Machida, Tokyo 194-8543, Japan.

https://doi.org/10.1016/j.actbio.2017.10.024
1742-7061/© 2017 Acta Materialia Inc. Published by Elsevier Ltd. All rights reserved.

sensitivity reaction side effects often occur at the injection sites [5,6], and this eventually decreases patient compliance.

Significant effort has hence been expended to develop longer-acting analogs of enfuvirtide with the goal of generating a drug that will provide a well-sustained, flat concentration-versus-time profile in the therapeutic range. Such an agent would not only reduce the necessary number of injections, but also prevent "peak-and-valley" fluctuations associated with *s.c.* injections of short-acting analogs that provide a therapeutically effective drug concentration for only short time and may also have undesired side effects, including development of drug-resistant strains of HIV. Several groups have proposed the attachment of enfuvirtide to carrier molecules such as polyethylene glycol (PEG) [7], xten [8], sialyllactose [9], pentasaccharide [10], dihydrosphingosine [11], serum albumin [12], or Fc fragments [13] as a strategy to obtain prolonged circulation. However, these chemical modifications require site-specific covalent bond formation, which generally has a low yield and is often difficult to scale-up. After enfuvirtide, second- and third-generation derivatives with increased antiviral potency were developed [14,15], and many synthetic peptides that interact with HIV *in vitro* [16,17] are candidates for stopping the lifecycle of HIV via different mechanisms from those of standard drugs used in ART. A general methodology for *in vivo* delivery without the need for chemical conjugation of individual peptides is therefore needed. Kapoor et al. approached this issue by *in situ* formation of enfuvirtide-containing implants using poly (D,L-lactide-co-glycolide) with organic solvents [18].

Elastin-like polypeptides (ELPs) are a class of artificial polypeptides composed of the pentameric repeat Val-Pro-Gly-Xaa-Gly (where Xaa is any amino acid except Pro). ELPs are increasingly utilized for many biomedical applications, as they are non-cytotoxic, biodegradable, and show good pharmacokinetics [19]. We are interested in the design of *in situ* depot using ELPs for peptide drugs that need drug delivery system, especially anti-HIV peptides. Herein we describe the design and characterization of injectable hydrogels as a platform for *in situ* formation of subcutaneous drug depots to provide sustained release of anti-HIV peptides. The central hypothesis underlying this design is that hydrogels can entrap a sufficient amount of peptide to form a drug depot, which would be slowly degraded, resulting in prolonged release of active peptide into the circulation. To validate this idea, we selected enfuvirtide as a model anti-HIV peptide. In this system, enfuvirtide is physically mixed with a recombinant elastin-like polypeptide that incorporates periodic cysteine (Cys) residues (cELP), and then with a small amount of hydrogen peroxide that serves as an oxidant to rapidly form a disulfide cross-linked network [20]. The preparation remains in a soluble, injectable state, but undergoes gelation and phase transition (dehydration) between room and body temperature. Therefore, a hydrogel is formed *in situ* after *s.c.* injection. This hydrogel depot is slowly degraded, resulting in prolonged release of enfuvirtide. Our present results confirm the validity of this strategy, and we show that a single *s.c.* injection of enfuvirtide-containing hydrophobic cELP in rats forms a hydrogel depot that provides prolonged anti-HIV activity as compared with injection of the naked peptide. We believe this cELP hydrogel platform should be readily adaptable to provide novel delivery systems for a variety of anti-HIV peptides besides enfuvirtide.

2. Materials and methods

2.1. Materials

Escherichia coli (*E. coli*) EB5alpha and BL21 (DE3) cells were purchased from EdgeBio (Gaithersburg, MD) and EMD Chemicals (San Diego, CA), respectively. All cultures were grown in Terrific Broth (TB) Dry medium from MO Bio Laboratories (Carlsbad, CA). Tris (2-carboxyethyl)phosphine (TCEP) hydrochloride and Slide-A-Lyzer dialysis cassette were purchased from Pierce Biotechnology (Rockford, IL). Polymyxin B sulfate was purchased from EMD Chemicals. Enfuvirtide was purchased from ProSpec-Tany TechnoGene (Ness Ziona, Israel). Hydrogen peroxide (H_2O_2; 30 wt% solution), sodium sulfite (Na_2SO_3), and elastase (from porcine pancreas) were purchased from Wako Pure Chemical Industries (Osaka, Japan). 5,5′-Dithiobis(2-nitrobenzoic acid) (DTNB) was purchased from Dojindo Laboratories (Kumamoto, Japan). Copper chloride, polyethyleneimine (PEI; 50% (w/v) solution), azidothymidine (AZT), 3-(4,5-dimethylthiazol-2-yl)-2,5-diphenyltetrazolium bromide (MTT), and RPMI 1640 medium were purchased from Sigma-Aldrich (St. Louis, MO). Sodium curdlan sulfate (79 kDa) was from Ajinomoto (Tokyo, Japan). Precast SDS-PAGE 5–15% Tris-HCl gradient gel was obtained from D.R.C. (Tokyo, Japan). A human T-cell leukemia virus type I (HTLV-I) positive T-cell line, MT-4 [21] was used for evaluating anti-HIV activity. MOLT-4 cells [22], a lymphoblastoid T-cell line, were used for obtaining HIV-1_{IIIB} (an X4 HIV-1 stain). HIV-1_{IIIB} was prepared from culture supernatant of persistently infected MOLT-4/HIV-1_{IIIB} cells and stored at −80 °C, and the titer of the virus stock was determined as 50% tissue culture infectious doses ($TCID_{50}$) using MT-4 cells [23]. MT-4 cells and MOLT-4 cells were cultured at 37 °C a humidified atmosphere of 5% CO_2 in air, using RPMI 1640 medium with 10% heat-inactivated fetal bovine serum (FBS), 100 units mL^{-1} of penicillin, and 100 μg mL^{-1} of streptomycin (Gibco Life Technologies, Grand Island, NY).

2.2. Nomenclature

ELPs are described with the nomenclature ELP[$A_xV_yC_z$-*n*], where *n* refers to the number of pentapeptide repeats and x, y, and z refer to the relative fractions of alanine, valine, and cysteine in the guest residue position along the length of the polypeptide, respectively. The polypeptides used in this study have the composition ELP [$A_{14}V_1C_1$-160] (cELP1) and ELP[$V_{15}C_1$-160] (cELP2). ELP[V-160] (ELP_{ctrl}), which does not contain Cys residues, was used as a control polypeptide. Cys-containing ELPs are denoted as cELP throughout the paper to distinguish them from general ELPs (for full sequence details, see Fig. S1).

2.3. Construction of ELPs

ELPs were designed and synthesized as described previously [20]. Briefly, BL21(DE3) *E. coli* cells were transformed with recombinant pET-24a(+) vector containing ELP genes. The synthesis of ELPs was based on constitutive expression from the leaky T7 promoter in the host *E. coli* cells. 1 L of TB media supplemented with 50 μg mL^{-1} kanamycin was inoculated with 35 mL of an overnight culture, and incubated overnight at 37 °C on an orbital shaker. The *E. coli* cells were harvested by centrifugation at 2500*g* for 10 min and then re-suspended in phosphate-buffered saline (PBS) and lysed by ultrasonication. To precipitate genomic DNA with insoluble cell debris, the lysate was supplemented with polyethyleneimine (at 1.2 wt%) and centrifuged at 16,000*g* at 4 °C. Each cELP was purified from the soluble fraction of cell lysate by 5 rounds of inverse transition cycling (ITC) [24] with TCEP solution (pH 7.0) and re-suspended in 20 mM TCEP (pH 7.0) supplemented with 1500 units mL^{-1} polymyxin B sulfate. ELP_{ctrl} was also purified by means of 5 rounds of ITC with PBS instead of TCEP. The purified ELPs were dialyzed at 4 °C for 16 h against PBS using 10-kDa molecular weight cut-off Slide-A-Lyzer dialysis cassettes. The purity and molecular weight (MW) of ELPs were examined by SDS-PAGE. The gels were stained with 0.5 M copper chloride, and ELP concentration was determined spectrophotometrically using the

molar extinction coefficient of 5630 M^{-1} cm^{-1} at 280 nm for the sole tryptophan present in each ELP. The content of thiol moieties was quantified by DTNB. The presence of endotoxin was quantified by a gel clot assay using Limulus amoebocyte lysate (LAL) PYROGENT (Lonza, Walkersville, MD). ELP stocks were stored at −80 °C until required.

2.4. Hydrogel formation

cELP hydrogels were formed by mixing a cELP with an appropriate amount of H_2O_2 solution. In brief, cELP solution was mixed with H_2O_2 solution on ice, then the mixture was further incubated on ice for at least 3 min. H_2O_2 accelerates the formation of disulfide bonds in cELP, promoting the formation of a cross-linked network. The final concentrations of cELP and H_2O_2 were 2.2–5.0 wt% and 0.3 wt%, respectively. Hydrogel formation was determined by means of the tube inversion test [25]. Briefly, for 1 mL of hydrogels in vials (12 × 75 mm size), no flow within 1 min upon inverting the vial at 4 °C is regarded as the gel state.

2.5. Hydrogel degradation study

We examined hydrogel degradation via spontaneous fracture and proteolytic degradation. For the former experiments, cELP solutions (2.5 wt%) were mixed with 0.3 wt% H_2O_2 on ice to form hydrogels, and the mixtures were incubated at 20 °C or 37 °C. The resulting hydrogels (50 μL) were inspected daily until complete fracture occurred, for a maximum of 3 weeks. For the latter experiments, 100 μL of PBS was added on top of the hydrogels (50 μL) after their formation, and the mixture was incubated on ice for 1 h to extract excess H_2O_2. After 1 h, the upper solution was replaced with either fresh PBS or PBS containing 0.5 units mL^{-1} elastase (100 μL). Incubation was continued at 20 °C or 37 °C for 2 h or 16 h. The remaining hydrogels were completely fractured by ultrasonication using a Bioruptor UCD-250 (Diagenode; Liege, Belgium) with three runs of 5 min (30-s pulses, 30-s intervals) in ice water, then the samples were subjected to SDS-PAGE. The gels were stained with 0.5 M $CuCl_2$ staining solution. cELPs without H_2O_2 were used as a control for the sol state.

2.6. Enfuvirtide release from cELP hydrogels in vitro

Enfuvirtide (400 μM) was added to aqueous cELP solution (5.0 wt%), and 0.3 wt% H_2O_2 was then added on ice to trigger hydrogel formation, and incubation was continued on ice for 30 min. Then 1.5 mL of RPMI 1640 medium containing 10% heat-inactivated FBS was added to a vial containing the prepared enfuvirtide/cELP hydrogel (1 mL). The vial was incubated at 37 °C and 300 μL aliquots of the supernatant were collected at scheduled time points, *i.e.*, 0, 2, 4, 8, 16, 24, 48, 72, 96, 120, 144, and 168 h. After each removal of supernatant, fresh RPMI 1640 medium containing FBS, 100 units mL^{-1} of penicillin, and 100 μg mL^{-1} of streptomycin was added to keep the total volume of supernatant at 1.5 mL. The activity of released enfuvirtide was evaluated by anti-HIV activity assay. As a control, enfuvirtide was mixed with ELP_{ctrl} solution under the same conditions.

2.7. Anti-HIV activity assay

The recovered supernatants containing enfuvirtide from the *in vitro* experiments were subjected to anti-HIV activity assay after quenching residual H_2O_2 with 35 mM Na_2SO_3. The inhibitory effects of *in vitro* supernatant and/or rat serum samples on HIV-1_{IIIB} replication were estimated in terms of the level of inhibition of virus-induced cytopathic effects (CPE) in MT-4 cells. Aliquots of 3 × 105 MT-4 cells mL^{-1} were infected with HIV-1_{IIIB} at a multiplicity of infection (MOI) of 0.01. HIV- and mock-infected MT-4 cells were cultured for 5 days with different concentrations of enfuvirtide-containing *in vitro* supernatants and/or rat sera and the cell viability was quantified by MTT assay, as described previously [23,26,27]. The 50% cytotoxic concentration (CC_{50}) and the 50% effective concentration (EC_{50}) were determined from the dose–response curves with mock-infected and HIV-infected cells, respectively.

2.8. Animal studies

Four-week-old male Sprague-Dawley (SD) rats with an average body weight of about 100 g were purchased from Charles River Laboratories Japan (Yokohama, Japan). SD rats were housed in an isolated animal room at constant temperature (23 ± 1 °C) and humidity (50–60%) with a 12 h light/dark cycle, and were allowed free access to 30 kGy CL-2 diet (Clea Japan, Tokyo) and sterilized water. All animal experiments were performed in accordance with the Guidelines for Animal Experimentation of St. Marianna University Graduate School of Medicine. The experimental protocol was approved by the Animal Research Committee, Institute for Animal Experimentation, St. Marianna University Graduate School of Medicine (approval number 1604013).

2.9. In vivo pharmacokinetic study of enfuvirtide depots

In vivo studies of enfuvirtide depots were carried out in male SD rats. The animals were randomly divided into 4 groups of 4 animals each to receive different treatment. Group I and II rats were administered pure enfuvirtide solution in PBS (pH 7.4) as a single *s.c.* dose of 9 mg kg^{-1} or 18 mg kg^{-1}, respectively, at the back. Group III and VI rats were given a single *s.c.* injection of cELP2 hydrogel (3.3 wt% in PBS (pH 7.4)) containing enfuvirtide at 9 mg kg^{-1} and 18 mg kg^{-1}, respectively. All rats were anesthetized with sodium pentobarbital (40 mg kg^{-1}) throughout the injection procedures. Blood from all animals was obtained from the inferior ophthalmic vein for serum preparation at pre-determined time points, *i.e.*, 0 (predose), 0.5, 4, 8, 24 h after *s.c.* administration of enfuvirtide. Serum samples were stored at −80 °C until used for anti-HIV activity assay and HPLC analysis. The release of enfuvirtide was quantified by reversed-phase HPLC using a Purospher® STAR RP-18 endcapped column (4.6 × 250 mm, 5 μm; Merck, Darmstadt, Germany) with acetonitrile; fluorescence detection was performed with excitation and emission wavelengths of 280 and 350 nm, respectively. Enfuvirtide concentration was determined from the peak area by reference to a standard curve. The residual amount of enfuvirtide in hydrogels was estimated as follows: the hydrogels excised from rats were immersed in Tris-HCl (pH 8.0) buffer and physically fractured with a spatula, and then the mixture was ultrasonicated in a Bioruptor UCD-250 using three runs of 10 min (30-s pulses, 30-s intervals) in ice water. After centrifugation at 16,000*g* at 4 °C, the supernatants were analyzed by reversed-phase HPLC as described above.

2.10. Histological studies

We evaluated *in vivo* gel formation and the duration of the gel state after injection of cELP2 hydrogel containing enfuvirtide into male SD rats. Formulations comprising 3.3 wt% cELP2, 0.3 wt% H_2O_2, and enfuvirtide (18 mg kg^{-1}) in 0.5 mL of PBS (pH7.4) were injected subcutaneously using a syringe with a 26-gauge needle after anesthetizing the rats with sodium pentobarbital (40 mg kg^{-1}). The rats were sacrificed on day 10 after gel implantation and tissue specimens with residual hydrogels were rinsed with PBS, fixed with 4% formaldehyde in PBS, dehydrated, embedded in paraffin blocks, sectioned (4 μm), and stained with hematoxylin

and eosin (HE) for light-microscopic examination. Histological profiles of individual skin samples were observed under a light microscope.

2.11. Statistical methods

Results are expressed as the mean ± SEM from at least three independent experiments. Data from the *in vitro* and *in vivo* release studies were analyzed with unpaired Student's *t* test.

3. Results and discussion

3.1. Production of ELPs

ELPs were expressed in *E. coli* without isopropyl β-D-1-thiogalactopyranoside (IPTG) and purified by means of the ITC protocol; typically, a yield of 100–200 mg L^{-1} was obtained, with >95% purity (Table 1). Polymyxin B is known to have high affinity for the lipid A moiety of endotoxins [28], and has been used in a commercial affinity chromatography support to remove endotoxin molecules from biological and aqueous solutions. In the ITC protocol, polymyxin B can remove bacterial pyrogen without the need for chromatography. Polymyxin B *per se* was successfully removed by centrifugation at 37 °C, at which ELPs undergo phase transition and are precipitated. The product thus obtained was finally subjected to overnight dialysis. ITC purification in the presence of TCEP together with polymyxin B afforded cELPs with endotoxin levels that are below the FDA-required limit of 5 EU $dose^{-1}$ (1 dose = 1 mg) for biologics. cELPs were purified as thiol-free monomers (over 80%) after overnight dialysis against PBS. cELP2 and ELP_{ctrl} have a T_t below body temperature (37 °C), whereas cELP1 has a T_t well above body temperature.

3.2. Formation of enfuvirtide/cELP hydrogels

We have previously demonstrated in rheological experiments that cELP hydrogels have typical characteristics of covalent cross-linked networks at both 4 °C and 37 °C: (1) the storage moduli are larger than the loss moduli and moduli do not exhibit frequency dependence during a linear frequency sweep; (2) the gelation kinetics are fast: too fast, in many cases, to be characterized in the rheometer (Fig. S2) [20]. To enable effective drug depot formation, the formulation of cELP, H_2O_2 solution, and enfuvirtide should be optimized to ensure rapid gelation *in situ* after *s.c.* injection, so that a sufficient amount of enfuvirtide is entrapped and the initial burst is kept to a minimum. Gelation of cELPs proceeds well even with a very limited amount of H_2O_2: over 0.1 wt% is enough to induce gelation, and the concentration requirement is not strict [29]. The key factors that control the sol-gel phase transition rate are the concentrations of cELP and enfuvirtide. To determine the relationship between hydrogel formation and concentrations of cELP and enfuvirtide, the sol (flow) and gel (no flow) states of mixtures of cELP and enfuvirtide was differentiated by means of the tube inversion test. Enfuvirtide/cELP hydrogels were fabricated simply by mixing the three components: cELP, enfuvirtide, and 0.3 wt% H_2O_2 solution. The sol-gel transition plot of enfuvirtide/cELP hydrogels at various concentrations is shown in Fig. 1. The sol-gel transition patterns of cELP1 and cELP2 were almost the same, with a critical gelation concentration of ~2.2 wt% in the presence or in the absence of enfuvirtide (≤900 μM).

3.3. Assessment of cELP hydrogel depot viability

Technologies that create a change in properties of bulk hydrogel in response to an environmental cue have been developed for biomedical applications [30–33]. Our enfuvirtide/cELP hydrogel is formed by disulfide cross-linking polymerization. Meanwhile, inter- and/or intramolecular reshuffling of disulfide bonds, especially in unfolded proteins, is a well characterized phenomenon [34]. Since we intend to use cELP as an erosion-based drug release depot, it is important to know whether the hydrogel shows self-depolymerization chain-reaction due to cleavage of intermolecular disulfide bonds, leading to fracture of the hydrogel and spontaneous solution formation. Therefore, we investigated the reversibility of the sol-to-gel transition of cELPs using the tube inversion test, as described above. When TCEP solution (100 mM,

Table 1
ELP polymers evaluated in this article.

ELP	n[a]	MW (kDa)	$[A_xV_yC_z]$[b]	Ratio of VPGC̲G	T_t (°C)[c]
cELP1	160	62.5	$A_{14}V\underline{C}$	1/16	42.9
cELP2	160	66.5	$V_{15}\underline{C}$	1/16	23.0
ELP_{ctrl}	160	66.4	V	1/10	24.1

[a,b] $ELP[A_xV_yC_z\text{-}n]$, where the capital letters in bracket are single-letter amino acid codes of a guest residue, the subscripts denote the ratios of the guest residues in the monomer, and n indicates the number of pentapeptides in the ELP.
[c] T_t of ELP monomers in PBS at 2.5 wt%. T_t was defined as the solution temperature that corresponded to the maximum in the first derivative of the absorbance (350 nm) [20]. Cysteine (C) residue available for cross-linking in each ELP is underlined.

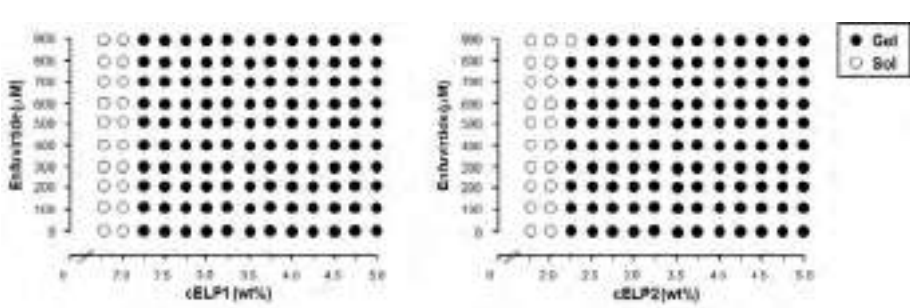

Fig. 1. Sol-gel transition plot of enfuvirtide/cELP hydrogels. The sol (flow) and gel (no flow) states of enfuvirtide/cELP hydrogel were identified by the test tube inversion method. No flow within 1 min upon inverting the vial was regarded as the gel state. The concentration of H_2O_2 was maintained at 0.3 wt%.

pH 7.0) was added on top of the hydrogels in a vial and incubation was carried out at 20 °C (at which temperature none of the three ELPs shows phase transition), partial fracturing was confirmed after 16 h, and the hydrogels of both cELP1 and cELP2 completely reverted to solution form after 3 days. Higher concentrations of TCEP tended to accelerate the transition rate from gel to sol. Next, we examined the time course of spontaneous unraveling of the network structure, leading to fracture of the hydrogel. The transition from gel to sol started to occur between 18 and 21 days upon incubation at 20 °C. The reverted solutions were analyzed by SDS-PAGE and free thiol was quantified using DTNB reagent. Under reducing conditions (β-mercaptoethanol), major bands corresponding to cELP monomers with MW of 60–70 kDa were detected, as observed with fresh stocks of cELPs (Fig. 2A); this result indicates that cELP monomer molecules did not degrade during the incubation. On the other hand, under non-reducing conditions, smeared bands ranging of over approximately 250 kDa appeared, suggesting that the reverted cELP existed as oligomers (tetramer or larger) in the reverted solution. In accordance with this, the content of free thiol in the reverted solution was very low compared with that of fresh cELP solution (Fig. 2B). These results suggest that free thiols in the hydrogel may attack intermolecular disulfide cross-links that sustain the network structure of cELPs and preferentially form intramolecular disulfide bonds, giving rise to a self-unraveling chain-reaction.

As the cELP/enfuvirtide hydrogel depot was designed to reside in subcutaneous space for a prolonged period of time, we were interested in testing its stability to elastase, a degradative enzyme [35] that is released from neutrophils (known as leukocyte elastase). The hydrophilic cELP1 hydrogel was almost completely fractured, whereas the hydrophobic cELP2 hydrogel remained partially intact, after 16 h incubation with elastase at 37 °C. Complete fracture of cELP2 hydrogels required incubation for over 36 h. After the enzymatic digestion, the mixtures were ultrasonicated to fracture the hydrogels completely, and the extent of proteolytic degradation was analyzed by SDS-PAGE. In the gel state, bands corresponding to each cELP monomer were detected after elastase digestion for 2 h, and a weak band of hydrophobic cELP2 monomer was detected even after 16 h, whereas those bands had disappeared in the sol state (Figs. 3A and S3). These results indicate that cELPs in the sol state were completely degraded by elastase. Similarly, hydrophobic ELP_{ctrl} was completely degraded after 2 h, indicating that the resistance of hydrophobic cELP2 to elastase is not due to the intrinsic phase-transition character of ELPs. In the case of digestion with elastase at 20 °C, similar results were observed, though the degradation rate was slower (data not shown). Shah et al. reported that ELP coacervate, a viscous liquid, was formed after the phase transition, and was completely degraded by elastase [36], in accordance with our present findings. We have reported that cELP hydrogels retain thermally triggered phase transition behavior [20]. Indeed, the hydrophobic cELP2 hydrogel at 2.5 wt% displayed a strong phase transition at 37 °C, forming an opaque gel (Fig. 3B). Overall, these results demonstrate that hydrophobic cELP2 hydrogel is proteolytically more stable than hydrophilic cELP1 hydrogel, presumably because the hydrophobic environment in the cross-linked network of cELP2 and low water content impede access of elastase to potential cleavage sites. Seo et al. also reported that tuning the physical properties of hydrogel was an efficient strategy to control drug release rate, although they focused on the relationship between weight decrease behavior and hydrophobicity [37]. Thus, we concluded that the hydrophobic cELP2 hydrogel is a promising candidate as a depot for sustained delivery of enfuvirtide.

3.4. In vitro activity of enfuvirtide released from hydrogels

Next, we examined the anti-HIV activity of enfuvirtide released from hydrogels in human T lymphocyte assay using MT-4 cells. HIV infection reduced the viability of the cells to almost zero during incubation for 5 days in our assay system. Enfuvirtide inhibited the virus-induced CPE in HIV-1_{IIIB}-infected MT-4 cells and the results of anti-HIV activity evaluated in terms of MTT assay are shown in Table 2. The nucleoside analog reverse-transcriptase inhibitor (NRTI) AZT and the virus adsorption inhibitor curdlan sulfate were included as control compounds, and displayed antiviral activity in this assay system. Prolonged incubation of enfuvirtide with 0.3 wt% H_2O_2 at 37 °C slightly reduced the anti-HIV activity. When gelatinous enfuvirtide formed by cELPs was incubated under the same conditions, we did not observe this reduction, probably because the buffering effect of cELPs shielded enfuvirtide from oxidation by H_2O_2. The concentration of H_2O_2 in the assay system was very critical for MT-4 cell viability (CC_{50} was estimated to be 0.00011 wt%), so all recovered sample solutions were quenched with Na_2SO_3 and diluted with RPMI 1640 medium (see Materials and Methods). We evaluated whether the recovered sample solutions retained anti-HIV activity using the parameter RND_{50}, which is the reciprocal number of the dilution affording 50% inhibition of the HIV-induced cytopathic effect [27]. As shown in Fig. 4A,

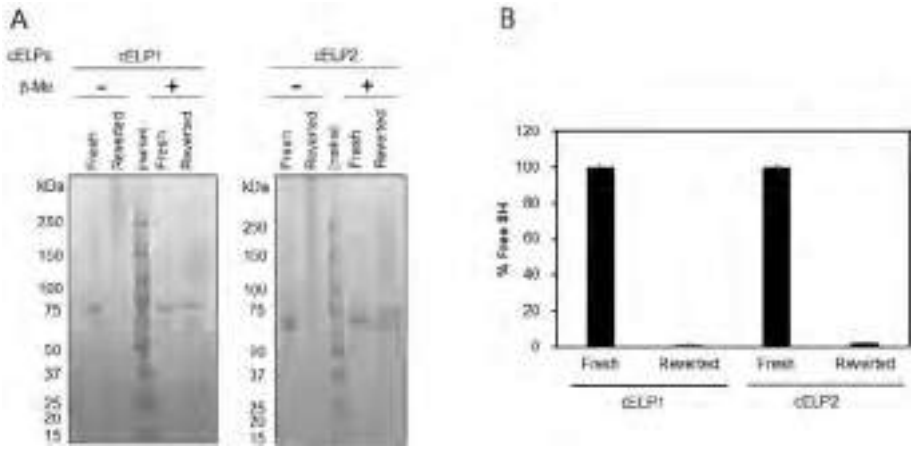

Fig. 2. (A) Representative copper-stained SDS-PAGE gel of cELPs. Each cELP was mixed with 0.3 wt% H_2O_2, and then the mixtures were incubated on ice to form hydrogels, which were incubated at 20 °C until they completely fractured spontaneously. The resulting sample solutions were analyzed by SDS-PAGE. (B) The thiol content of cELP in the resulting solutions formed by reversion from the gel state was also quantified by DTNB with L-cysteine as a standard.

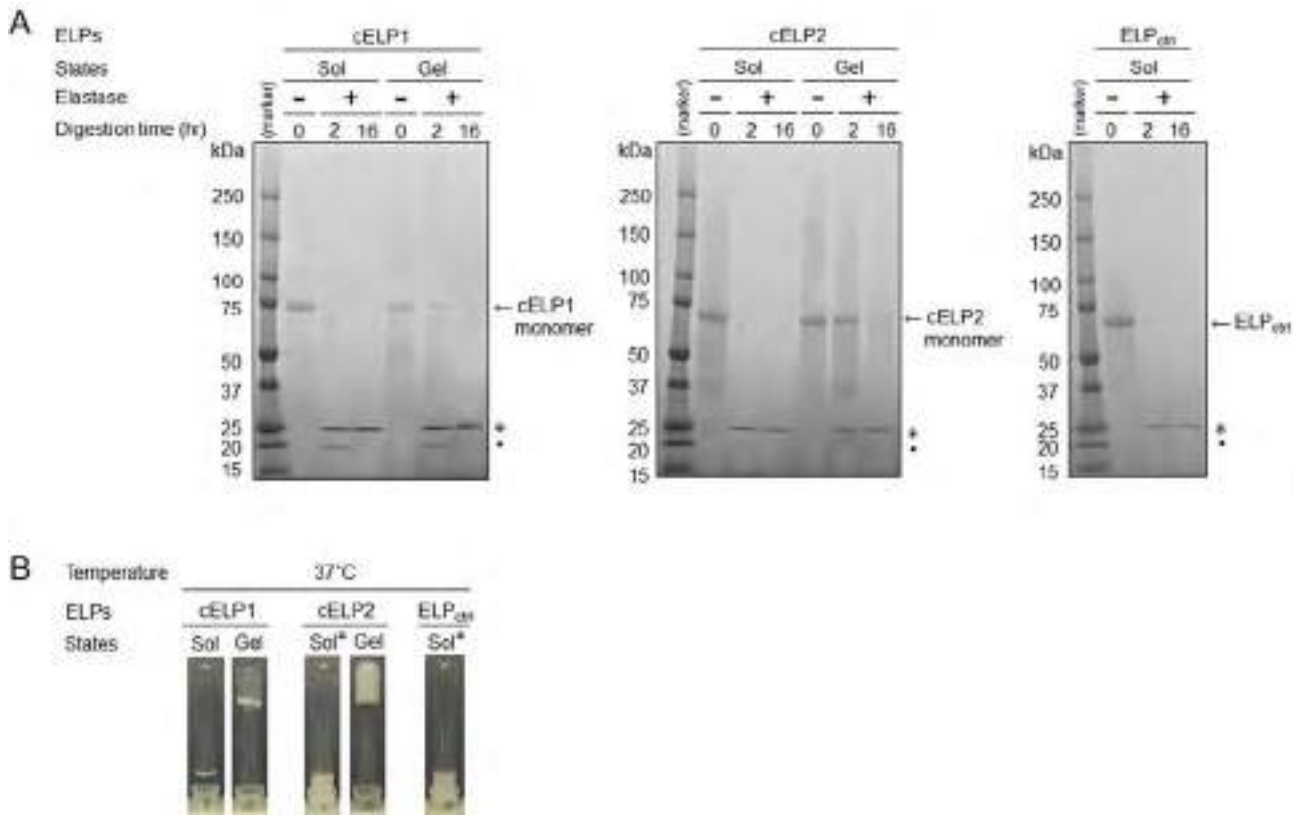

Fig. 3. SDS-PAGE analysis of hydrogel degradation by elastase. (A) Representative SDS-PAGE gels stained with copper chloride. Elastase solution was added on top of hydrogels, and each mixture was incubated at 37 °C for the time indicated in the text. The mixture was treated by ultrasonication and then examined by SDS-PAGE. *Asterisks* show elastase, and *dots* show digested ELPs. (B) Thermally responsive behavior of ELPs in sol and gel states. Mixtures of ELPs and H_2O_2 or water were incubated on ice for 3 min, and the further incubated at 37 °C for 10 min. The vials were inverted to assess the fluidity of the ELPs. *Asterisks* show liquid colloidal suspension of ELP.

Table 2
Anti-HIV activities determined by MTT assay.

Compound	EC_{50} (nM)	CC_{50} (nM)
Enfuvirtide	3.3	5620
Enfuvirtide w/H_2O_2[a]	24.2	3498
AZT	14.7	230,110
Curdlan sulfate[b]	184.9	>1,000,000

MT-4 cells were infected with HIV-1_{IIIB} at an MOI of 0.01. The values are the averages of at least three separate experiments.
[a] Enfuvirtide (100 μM) was incubated with 0.3 wt% H_2O_2 for 168 h, then Na_2SO_3 was added to quench H_2O_2, and the mixture was assayed for anti-HIV activity.
[b] Results are shown as ng mL^{-1}.

sustained release was observed with both cELP1 and cELP2 hydrogels. The supernatant of cELP1 hydrogel showed more potent anti-HIV activity than that of cELP2 hydrogel at the early stage of the assay (~48 h), while the supernatant of cELP2 hydrogel showed far more potent anti-HIV activity after 120 h. ELP_{ctrl}, in which enfuvirtide is not encapsulated in coacervate, showed potent anti-HIV activity at the initial stage, but the activity diminished over time due to the successive samplings and medium replacements (see Materials and Methods). When the hydrogels were physically fractured (after 168 h) and the supernatants were examined, increased anti-HIV activity was confirmed, especially for cELP2 hydrogels (Fig. 4B). The time-dependent release of enfuvirtide analyzed by reversed-phase HPLC paralleled the anti-HIV activity *in vitro* (Fig. S4). These results suggest that enfuvirtide was entrapped in these hydrogels even after 7 days (168 h) and there was a greater amount of residual enfuvirtide in cELP2 hydrogel. These release profiles are similar to the reported pattern for bovine serum albumin (BSA) [20]. cELP1 hydrogel is more hydrophilic than cELP2, and thus water would move more easily in and out of the hydrogel to extract enfuvirtide. In addition, fractures of cELP1 hydrogel were grossly visible by day 2–3, which was earlier than in the case of cELP2 hydrogels; this would be another reason why the supernatant of cELP1 hydrogel contains more enfuvirtide at an earlier stage.

3.5. In vitro anti-HIV activity of rat serum following s.c. administration of the formulation

Next, we examined whether a single injection of enfuvirtide/cELP2 hydrogel depot provides extended anti-HIV activity compared with enfuvirtide alone. Negative control sera collected before the injection showed weak anti-HIV activity at concentrations of more than 5–10% in our assay. Serum mannose-binding protein (MBP) was reported to inhibit infection by HIV [38], and thus we used rat sera at a concentration below 5% and confirmed that the diluted sera showed neither anti-HIV activity nor significant cytotoxicity in MT-4 cells. Enfuvirtide/cELP2 hydrogels afforded dose-dependent blood anti-HIV activity at 4 h: 4.5, 9, 18 mg kg^{-1} gave RND_{50} values of 49, 91, and 167, respectively (Fig. 5A). After a single injection (18 mg kg^{-1}), enfuvirtide/cELP2 hydrogel showed prolonged anti-HIV activity that persisted for 8 h post injection (Fig. 5B). Also, the rapid increase of anti-HIV activity seen at 0.5 and 4 h after injection of enfuvirtide alone was suppressed in the case of enfuvirtide/cELP2 hydrogel. No significant activity was observed after 24 h post injection, though serum samples were monitored for up to 10 days. In contrast, injection of enfuvirtide alone resulted in undetectable blood anti-HIV activity by 8 h post injection. We further examined the residual amount

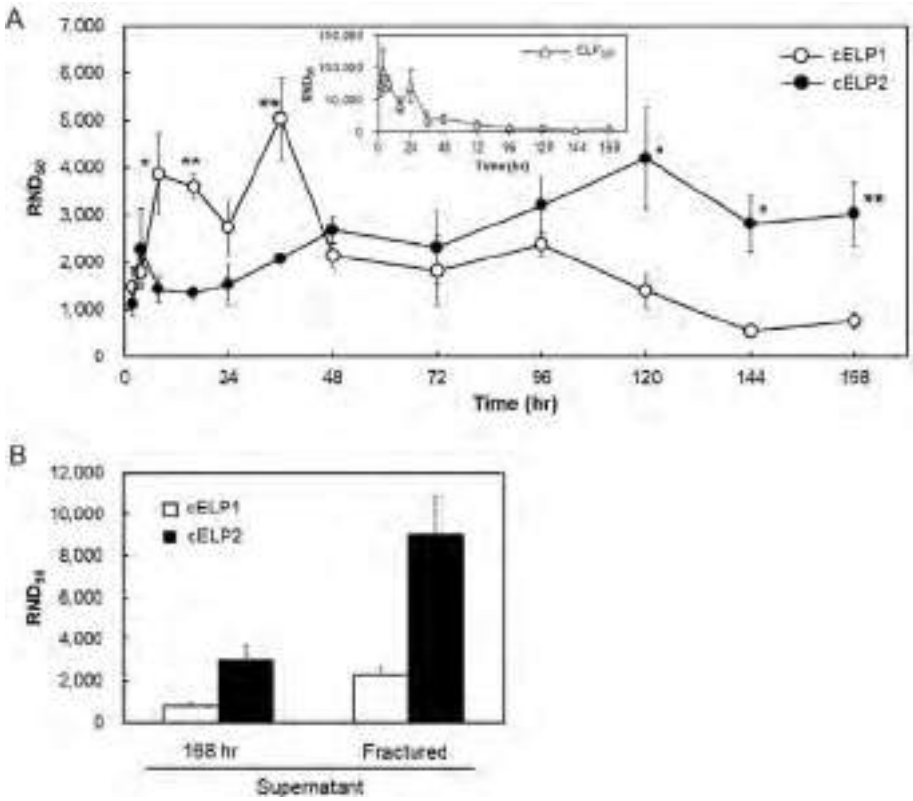

Fig. 4. Anti-HIV activity of enfuvirtide released from cELP hydrogel depots in human T-cell line MT-4 cell assay. The activity was assessed in terms of the parameter RND_{50}, which is the reciprocal number of the dilution affording 50% inhibition of the HIV-induced cytopathic effect. (A) Time-course analyses of anti-HIV activity. ELPs pre-mixed with enfuvirtide were mixed with H_2O_2 solution, then the mixtures were incubated for 3 min. RPMI medium containing 10% FBS was added to the resulting hydrogels, and incubation was continued at 37 °C for the time indicated in the text. The anti-HIV activity of released enfuvirtide was evaluated by MTT assay. ELP_{ctrl}, which does not form a hydrogel, was used as a control. Each data point represents the mean value ± SEM (n = 3–5). *, $P < .06$; **, $P < .03$. (B) Residual enfuvirtide in cELP hydrogel depots after incubation at 37 °C for 1 week (168 h). After 1 week incubation, the hydrogels were fractured physically with a spatula followed by ultrasonication, then the mixtures were centrifuged, and the supernatants were subjected to MTT assay. Data shown are the mean ± SEM and are representative of three independent experiments.

of enfuvirtide in enfuvirtide/cELP hydrogel on days 1 and 10 after *s.c.* injection. When the hydrogels were excised from subcutaneous tissue and analyzed by reversed-phase HPLC, 11% of the injected dose of enfuvirtide was detected in the hydrogel samples at day 1 on average, while no enfuvirtide was detected in the samples at day 10. These results suggest that enfuvirtide was successfully entrapped in the hydrogel, resulting in suppression of the initial burst and slow release over a whole day. It seems likely that time-dependent change of blood anti-HIV activity would continue to occur in parallel with erosion of the hydrogel thereafter, but we could not confirm that this is the case because of the detection limit of the method of analysis.

Hydrogel formation *in vivo*, the lifetime of the gel state, and biocompatibility were investigated after *s.c.* injection of enfuvirtide/cELP2 hydrogels into SD rats. Fig. 5C shows representative photograph of enfuvirtide/cELP2 hydrogel on day 10 after the *s.c.* injection. Transformed enfuvirtide/cELP2 hydrogels were observed at the injection sites, and little inflammation was apparent macroscopically. This was confirmed by HE staining (Fig. 5D). We further evaluated the thermal responsiveness, which is an intrinsic feature of ELP. As shown in Fig. 5E, the enfuvirtide/cELP2 hydrogel excised from the injection site was opaque at 37 °C, but was transparent on ice. This means that the enfuvirtide/cELP2 hydrogels retained the thermally triggered phase-transition behavior of cELP even after indwelling *in vivo* for 10 days.

There could be two major reasons for the apparent disconnect between *in vitro* and *in vivo* release profiles. One is the thermally triggered phase transition of cELP and the other is the *in vivo* setting of the enfuvirtide depot. At body temperature, gelation driven by intermolecular disulfide bond formation and thermally triggered phase transition both occur simultaneously. As shown in Fig. 1, the concentration of cELP should be above 2.2 wt% to form the hydrogel. The phase transition removes cELP from the aqueous phase to form a precipitate that does not contain enfuvirtide, leading to a decreased concentration of cELP, especially at the contact interface with the skin. This would cause an initial burst of enfuvirtide after subcutaneous injection. Another possible reason is that the rats move about freely after recovering from anesthesia, so that enfuvirtide/cELP hydrogels under the skin are subjected to external pressure from that time point. This might cause loss of enfuvirtide from the hydrogels.

H_2O_2 solution is commonly used as an antiseptic for wound clearing at concentrations that are 10-fold those used in the present studies (*i.e.*, 3 wt%). Additionally, H_2O_2 is rapidly metabolized by enzymes to oxygen and water that are non-toxic to cells. Indeed, we carefully checked in detail under skin after implantation, but no significant inflammation was not observed macroscopically. Hence, we believe that subcutaneous administration of a concentration of 0.3 wt% H_2O_2 solution is likely to be non-toxic. More prolonged retention of enfuvirtide under the skin might be achieved by covalent attachment to cELPs. Also, design of ELPs that undergo thermally triggered phase transition more slowly (or that do not undergo the phase transition) at body temperature might be an effective strategy. We are currently exploring these possibilities by changing the number of Cys residues and the chain length of cELP, aiming to design more stable, longer-lasting depots for a range of anti-HIV peptides. Further studies on the generality and limitations of injectable cELP hydrogels are in progress.

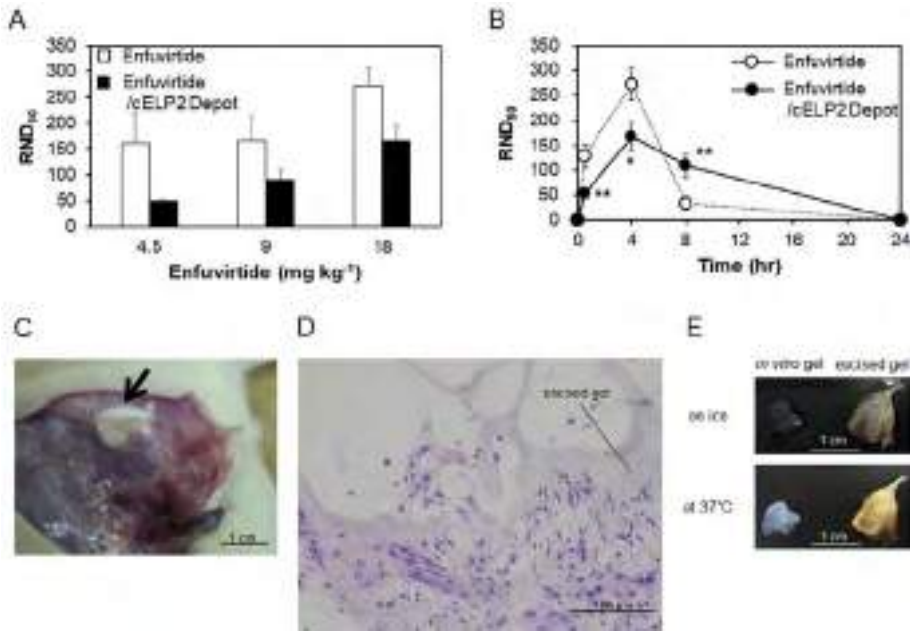

Fig. 5. Anti-HIV activity of sera and characteristics of *in situ*-formed enfuvirtide depots. The activity was assessed in terms of the parameter RND_{50}, which is the reciprocal number of the dilution affording 50% inhibition of the HIV-induced cytopathic effect. (A) Subcutaneous (*s.c.*) injection of cELP2/enfuvirtide/H_2O_2 in rats was carried out to form depots *in situ*. Four hours after injection, blood was collected and centrifuged to obtain serum, and anti-HIV activity was evaluated by MTT assay. Data shown are the mean ± SEM and are representative of four independent experiments. (B) Time-course analyses of anti-HIV activity of rat sera prepared at scheduled time points as indicated in the text after single injection (18 mg kg^{-1}). Anti-HIV activity was evaluated by MTT assay. Each data point represents the mean value ± SEM (n = 4). *, $P < .07$; **, $P < .05$. (C) Photograph of enfuvirtide/cELP2 hydrogel in rat on day 10 after *s.c.* injection. Ten days after injection, the rats were incised to confirm hydrogel formation. The arrows indicate the hydrogel depots. (D) Histological analysis of tissue specimens with residual hydrogel at day 10 after *s.c.* injection into rats. The cells were stained with HE. (E) Photograph of enfuvirtide/cELP2 hydrogel excised from rats on day 10 after *s.c.* injection. Ten days after injection, the hydrogel was excised from the injection site, incubated on ice for 10 min, and then further incubated at 37 °C for 10 min. Enfuvirtide/cELP2 hydrogel incubated at 20 °C for 10 days in a vial was used as a control as *in vitro* gel.

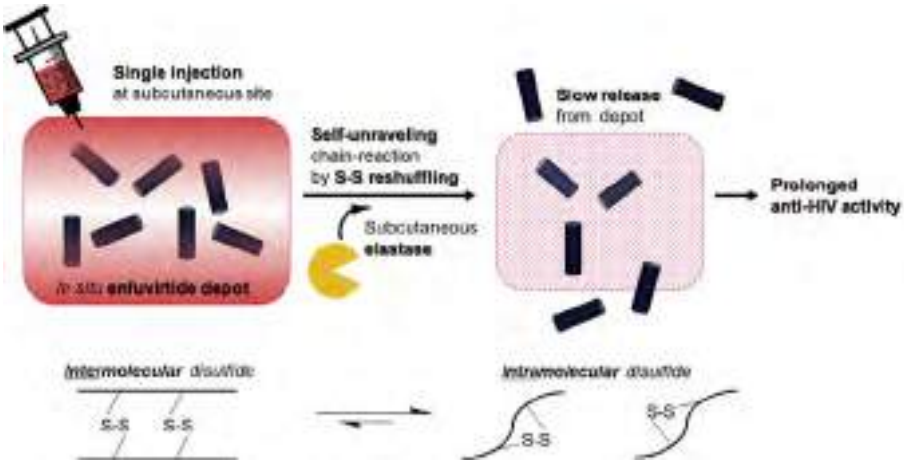

Fig. 6. Schematic illustration of our system for sustained release of enfuvirtide. Hydrogel was formed by disulfide cross-linking in cELP. However, disulfide formation is a reversible process in a state of dynamic equilibrium, and intramolecular disulfide bond formation is favored over intermolecular disulfide bond formation. Consequently, the dynamic equilibrium leads to unraveling of the network structure, fracture of the hydrogel, and spontaneous solution formation. In addition, proteolytic degradation by subcutaneous proteinases, such as elastase, also promotes fracture of the hydrogel. These changes result in sustained release of enfuvirtide from the hydrogel depot.

4. Conclusion

In this study, we have developed a sustained-release enfuvirtide formulation, consisting of an injectable material capable of *in situ* self-gelation followed by spontaneous degradation, employing recombinant polypeptide cELP. The key feature of this system is the erosion-based drug-release behavior of cELP hydrogels in the context of reversible gelation (Fig. 6). Three polypeptides with different characteristics (two cELPs and ELP_{ctrl}) were synthesized. Hydrogels incorporating enfuvirtide were formed by both cELPs under conditions of mild oxidation. The hydrogel systems showed different enfuvirtide release patterns, and hydrophobic character of cELP (as in cELP2) is critical for high resistance to fracture and proteolytic degradation of the hydrogel, so that enfuvirtide can be entrapped for long period of time. The released enfuvirtide retained anti-HIV activity, and no significant inflammation was observed in the tissues surrounding the hydrogel depot. Injectable hydrogels have emerged as promising materials for controlled drug delivery applications because they offer important advantages; for example, they do not require surgical implantation, which is

necessary for prefabricated sustained-release implants, and they are biodegradable, being bioresorbable as well as being cytocompatible. Substantial work has been done on monitoring the controlled-release properties of hydrogels [39–41], including antiretroviral long-acting injectable depot formulations for HIV [42]. In connection with the current standard ART therapy, development of depot-type anti-HIV drugs would offer the following advantages: (1) the development of easy-to-use gel formulations for preventing rectal HIV infection [43,44]; (2) convenient introduction of drugs and formulations to treat drug-resistant HIV variants, which may require drugs with different mechanisms to stop the HIV lifecycle and/or delivery systems optimized for individual drugs. The duration of an effective anti-HIV activity level in blood using the present hydrogel system is only several hours. However, this system has considerable potential for improvement, because rational design of the number of cross-linking points in cELPs by genetic modification enables easy tuning of the mesh size and hydrophobicity of the resulting hydrogel, as well as other parameters that determine the drug release profile from the hydrogel depot. Thus, the cELP hydrogel system may hold the promise of tailor-made long-lasting depot systems for a variety of drugs.

Acknowledgements

We thank Dr. Ashutosh Chilkoti (Duke University) for his contribution to the early stage of this study. We also thank Ms. Sigemi Terakubo, Ms. Niño Okamura, Ms. Yukie Tokura, and Ms. Akemi Hamaguchi (St. Marianna University School of Medicine) for technical assistance. This work was supported by a Grant-in-Aid for Scientific Research (C) (15K01319, 26460050, and 17K08254) of Japan.

Appendix A. Supplementary data

Supplementary data associated with this article can be found, in the online version, at https://doi.org/10.1016/j.actbio.2017.10.024.

References

[1] R. Ellis, D. Langford, E. Masliah, HIV and antiretroviral therapy in the brain: neuronal injury and repair, Nat. Rev. Neurosci. 8 (1) (2007) 33–44.
[2] J.M. Kilby, S. Hopkins, T.M. Venetta, B. DiMassimo, G.A. Cloud, J.Y. Lee, L. Alldredge, E. Hunter, D. Lambert, D. Bolognesi, T. Matthews, M.R. Johnson, M.A. Nowak, G.M. Shaw, M.S. Saag, Potent suppression of HIV-1 replication in humans by T-20, a peptide inhibitor of gp41-mediated virus entry, Nat. Med. 4 (11) (1998) 1302–1307.
[3] T. Matthews, M. Salgo, M. Greenberg, J. Chung, R. DeMasi, D. Bolognesi, Enfuvirtide: the first therapy to inhibit the entry of HIV-1 into host CD4 lymphocytes, Nat. Rev. Drug Discov. 3 (3) (2004) 215–225.
[4] C. Wild, T. Greenwell, T. Matthews, A synthetic peptide from HIV-1 gp41 is a potent inhibitor of virus-mediated cell-cell fusion, AIDS Res. Hum. Retroviruses 9 (11) (1993) 1051–1053.
[5] R.A. Ball, T. Kinchelow, Injection site reactions with the HIV-1 fusion inhibitor enfuvirtide, J. Am. Acad. Dermatol. 49 (5) (2003) 826–831.
[6] P. Maggi, N. Ladisa, E. Cinori, A. Altobella, G. Pastore, R. Filotico, Cutaneous injection site reactions to long-term therapy with enfuvirtide, J. Antimicrob. Chemother. 53 (4) (2004) 678–681.
[7] S. Cheng, Y. Wang, Z. Zhang, X. Lv, G.F. Gao, Y. Shao, L. Ma, X. Li, Enfuvirtide-PEG conjugate: a potent HIV fusion inhibitor with improved pharmacokinetic properties, Eur. J. Med. Chem. 121 (2016) 232–237.
[8] S. Ding, M. Song, B.C. Sim, C. Gu, V.N. Podust, C.W. Wang, B. McLaughlin, T.P. Shah, R. Lax, R. Gast, R. Sharan, A. Vasek, M.A. Hartman, C. Deniston, P. Srinivas, V. Schellenberger, Multivalent antiviral XTEN-peptide conjugates with long in vivo half-life and enhanced solubility, Bioconjug. Chem. 25 (7) (2014) 1351–1359.
[9] S. Cheng, X. Chang, Y. Wang, G.F. Gao, Y. Shao, L. Ma, X. Li, Glycosylated enfuvirtide: a long-lasting glycopeptide with potent anti-HIV activity, J. Med. Chem. 58 (3) (2015) 1372–1379.
[10] T. Huet, O. Kerbarh, D. Schols, P. Clayette, C. Gauchet, G. Dubreucq, L. Vincent, H. Bompais, R. Mazinghien, O. Querolle, A. Salvador, J. Lemoine, B. Lucidi, J. Balzarini, M. Petitou, Long-lasting enfuvirtide carrier pentasaccharide conjugates with potent anti-human immunodeficiency virus type 1 activity, Antimicrob. Agents Chemother. 54 (1) (2010) 134–142.
[11] A. Ashkenazi, M. Viard, L. Unger, R. Blumenthal, Y. Shai, Sphingopeptides: dihydrosphingosine-based fusion inhibitors against wild-type and enfuvirtide-resistant HIV-1, FASEB J. 26 (11) (2012) 4628–4636.
[12] C.A. Stoddart, G. Nault, S.A. Galkina, K. Thibaudeau, P. Bakis, N. Bousquet-Gagnon, M. Robitaille, M. Bellomo, V. Paradis, P. Liscourt, A. Lobach, M.E. Rivard, R.G. Ptak, M.K. Mankowski, D. Bridon, O. Quraishi, Albumin-conjugated C34 peptide HIV-1 fusion inhibitor: equipotent to C34 and T-20 in vitro with sustained activity in SCID-hu Thy/Liv mice, J. Biol. Chem. 283 (49) (2008) 34045–34052.
[13] C.H. Chang, J. Hinkula, M. Loo, T. Falkeborn, R. Li, T.M. Cardillo, E.A. Rossi, D.M. Goldenberg, B. Wahren, A novel class of anti-HIV agents with multiple copies of enfuvirtide enhances inhibition of viral replication and cellular transmission in vitro, PLoS One 7 (7) (2012) e41235.
[14] R.S. Veazey, T.A. Ketas, P.J. Klasse, D.K. Davison, M. Singletary, L.C. Green, M.L. Greenberg, J.P. Moore, Tropism-independent protection of macaques against vaginal transmission of three SHIVs by the HIV-1 fusion inhibitor T-1249, Proc. Natl. Acad. Sci. U.S.A. 105 (30) (2008) 10531–10536.
[15] Y. He, Y. Xiao, H. Song, Q. Liang, D. Ju, X. Chen, H. Lu, W. Jing, S. Jiang, L. Zhang, Design and evaluation of sifuvirtide, a novel HIV-1 fusion inhibitor, J. Biol. Chem. 283 (17) (2008) 11126–11134.
[16] K. Chandra, M. Maes, A. Friedler, Interactions of HIV-1 proteins as targets for developing anti-HIV-1 peptides, Future Med. Chem. 7 (8) (2015) 1055–1077.
[17] A. Qureshi, N. Thakur, M. Kumar, HIPdb: a database of experimentally validated HIV inhibiting peptides, PLoS One 8 (1) (2013) e54908.
[18] D.N. Kapoor, O.P. Katare, S. Dhawan, In situ forming implant for controlled delivery of an anti-HIV fusion inhibitor, Int. J. Pharm. 426 (1–2) (2012) 132–143.
[19] S. Roberts, M. Dzuricky, A. Chilkoti, Elastin-like polypeptides as models of intrinsically disordered proteins, FEBS Lett. 589 (19 Pt A) (2015) 2477–2486.
[20] D. Asai, D. Xu, W. Liu, F. Garcia Quiroz, D.J. Callahan, M.R. Zalutsky, S.L. Craig, A. Chilkoti, Protein polymer hydrogels by in situ, rapid and reversible self-gelation, Biomaterials 33 (21) (2012) 5451–5458.
[21] I. Miyoshi, H. Taguchi, I. Kubonishi, S. Yoshimoto, Y. Ohtsuki, Y. Shiraishi, T. Akagi, Type C virus-producing cell lines derived from adult T-cell leukemia, Gann. Monogr. Cancer Res. 28 (1982) 219–228.
[22] J. Minowada, T. Onuma, G.E. Moore, Rosette-forming human lymphoid cell lines. I. Establishment and evidence for origin of thymus-derived lymphocytes, J. Natl. Cancer Inst. 49 (3) (1972) 891–895.
[23] H. Nakashima, M. Masuda, T. Murakami, Y. Koyanagi, A. Matsumoto, N. Fujii, N. Yamamoto, Anti-human immunodeficiency virus activity of a novel synthetic peptide, T22 ([Tyr-5,12, Lys-7]polyphemusin II): a possible inhibitor of virus-cell fusion, Antimicrob. Agents Chemother. 36 (6) (1992) 1249–1255.
[24] D.E. Meyer, A. Chilkoti, Purification of recombinant proteins by fusion with thermally-responsive polypeptides, Nat. Biotechnol. 17 (11) (1999) 1112–1115.
[25] R. Jin, C. Hiemstra, Z. Zhong, J. Feijen, Enzyme-mediated fast in situ formation of hydrogels from dextran-tyramine conjugates, Biomaterials 28 (18) (2007) 2791–2800.
[26] R. Pauwels, J. Balzarini, M. Baba, R. Snoeck, D. Schols, P. Herdewijn, J. Desmyter, E. De Clercq, Rapid and automated tetrazolium-based colorimetric assay for the detection of anti-HIV compounds, J. Virol. Methods 20 (4) (1988) 309–321.
[27] H. Nakashima, K. Inazawa, K. Ichiyama, M. Ito, N. Ikushima, T. Shoji, K. Katsuraya, T. Uryu, N. Yamamnoto, A.S. Juodawlkis, R.F. Schinazi, Sulfated alkyl oligosaccharides inhibit human immunodefency virus in vitro and provide sustained drug level in mammals, Antivir. Chem. Chemother. 6 (4) (1995) 271–280.
[28] D.C. Morrison, D.M. Jacobs, Binding of polymyxin B to the lipid A portion of bacterial lipopolysaccharides, Immunochemistry 13 (10) (1976) 813–818.
[29] D. Xu, D. Asai, A. Chilkoti, S.L. Craig, Rheological properties of cysteine-containing elastin-like polypeptide solutions and hydrogels, Biomacromolecules 13 (8) (2012) 2315–2321.
[30] Y. Li, J. Rodrigues, H. Tomas, Injectable and biodegradable hydrogels: gelation, biodegradation and biomedical applications, Chem. Soc. Rev. 41 (6) (2012) 2193–2221.
[31] A.H. Van Hove, M.J. Beltejar, D.S. Benoit, Development and in vitro assessment of enzymatically-responsive poly(ethylene glycol) hydrogels for the delivery of therapeutic peptides, Biomaterials 35 (36) (2014) 9719–9730.
[32] A.H. Van Hove, K. Burke, E. Antonienko, E. Brown 3rd, D.S. Benoit, Enzymatically-responsive pro-angiogenic peptide-releasing poly(ethylene glycol) hydrogels promote vascularization in vivo, J. Control. Release 217 (2015) 191–201.
[33] J. Hu, Y. Quan, Y. Lai, Z. Zheng, Z. Hu, X. Wang, T. Dai, Q. Zhang, Y. Cheng, A smart aminoglycoside hydrogel with tunable gel degradation, on-demand drug release, and high antibacterial activity, J. Control. Release 247 (2017) 145–152.
[34] E. Welker, M. Narayan, W.J. Wedemeyer, H.A. Scheraga, Structural determinants of oxidative folding in proteins, Proc. Natl. Acad. Sci. U.S.A. 98 (5) (2001) 2312–2316.
[35] D.L. Nettles, A. Chilkoti, L.A. Setton, Applications of elastin-like polypeptides in tissue engineering, Adv. Drug Deliv. Rev. 62 (15) (2010) 1479–1485.
[36] M. Shah, P.Y. Hsueh, G. Sun, H.Y. Chang, S.M. Janib, J.A. MacKay, Biodegradation of elastin-like polypeptide nanoparticles, Protein Sci. 21 (6) (2012) 743–750.
[37] B.B. Seo, J.T. Koh, S.C. Song, Tuning physical properties and BMP-2 release rates of injectable hydrogel systems for an optimal bone regeneration effect, Biomaterials 122 (2017) 91–104.

[38] R.A. Ezekowitz, M. Kuhlman, J.E. Groopman, R.A. Byrn, A human serum mannose-binding protein inhibits in vitro infection by the human immunodeficiency virus, J. Exp. Med. 169 (1) (1989) 185–196.
[39] K. Manokruang, D.S. Lee, Albumin-conjugated pH/thermo responsive poly (amino urethane) multiblock copolymer as an injectable hydrogel for protein delivery, Macromol. Biosci. 13 (9) (2013) 1195–1203.
[40] K. Li, L. Yu, X. Liu, C. Chen, Q. Chen, J. Ding, A long-acting formulation of a polypeptide drug exenatide in treatment of diabetes using an injectable block copolymer hydrogel, Biomaterials 34 (11) (2013) 2834–2842.
[41] C.V. Duffy, L. David, T. Crouzier, Covalently-crosslinked mucin biopolymer hydrogels for sustained drug delivery, Acta Biomater. 20 (2015) 51–59.
[42] A. Owen, S. Rannard, Strengths, weaknesses, opportunities and challenges for long acting injectable therapies: insights for applications in HIV therapy, Adv. Drug Deliv. Rev. 103 (2016) 144–156.
[43] L. Van Damme, R. Govinden, F.M. Mirembe, F. Guedou, S. Solomon, M.L. Becker, B.S. Pradeep, A.K. Krishnan, M. Alary, B. Pande, G. Ramjee, J. Deese, T. Crucitti, D. Taylor, Lack of effectiveness of cellulose sulfate gel for the prevention of vaginal HIV transmission, N. Engl. J. Med. 359 (5) (2008) 463–472.
[44] C.W. Dobard, A. Taylor, S. Sharma, P.L. Anderson, L.R. Bushman, D. Chuong, C.P. Pau, D. Hanson, L. Wang, J.G. Garcia-Lerma, I. McGowan, L. Rohan, W. Heneine, Protection against rectal chimeric simian/human immunodeficiency virus transmission in macaques by rectal-specific gel formulations of maraviroc and tenofovir, J. Infect. Dis. 212 (12) (2015) 1988–1995.

Journal of
Clinical Medicine

MDPI

Review

Adenosine A_{2B} Receptors: An Optional Target for the Management of Irritable Bowel Syndrome with Diarrhea?

Teita Asano * and Mitsuko Takenaga

Institute of Medical Science, St. Marianna University School of Medicine, 2-16-1, Sugao, Miyamae-ku, Kawasaki 216-8512, Japan; m2take@marianna-u.ac.jp
* Correspondence: asano-ti@marianna-u.ac.jp; Tel./Fax: +81-44-976-3747

Received: 9 October 2017; Accepted: 2 November 2017; Published: 3 November 2017

Abstract: Irritable bowel syndrome (IBS) is a functional gastrointestinal disorder, with the characteristic symptoms of chronic abdominal pain and altered bowel habits (diarrhea, constipation, or both). IBS is a highly prevalent condition, which negatively affects quality of life and is a significant burden on global healthcare costs. Although many pharmacological medicines have been proposed to treat IBS, including those targeting receptors, channels, and chemical mediators related to visceral hypersensitivity, successful pharmacotherapy for the disease has not been established. Visceral hypersensitivity plays an important role in IBS pathogenesis. Immune activation is observed in diarrhea-predominant patients with IBS and contributes to the development of visceral hypersensitivity. Adenosine is a chemical mediator that regulates many physiological processes, including inflammation and nociception. Among its receptors, the adenosine A_{2B} receptor regulates intestinal secretion, motor function, and the immune response. We recently demonstrated that the adenosine A_{2B} receptor is involved in visceral hypersensitivity in animal models of IBS. In this review, we discuss the possibility of the adenosine A_{2B} receptor as a novel therapeutic target for IBS.

Keywords: adenosine A_{2B} receptor; irritable bowel syndrome; visceral hypersensitivity; diarrhea; abdominal pain; immune response

1. Introduction

Irritable bowel syndrome (IBS) is a chronic functional gastrointestinal disorder involving abdominal pain or discomfort, bloating, diarrhea, and/or constipation [1]. IBS is defined by the symptom-based Rome criteria without the detection of organic causes [2,3]. The prevalence of IBS in the general population is remarkably high (affecting approximately 11% of the world's population) [3]. Although IBS is not life-threatening, it accords a large burden on global healthcare and markedly reduces quality of life [4]. Four subtypes of IBS are recognized, depending on the predominant stool pattern: IBS with constipation (IBS-C), IBS with diarrhea (IBS-D), mixed IBS (IBS-M), and un-subtyped IBS (IBS-U) [2,3]. Pharmacological treatments effective against abdominal pain are insufficient in IBS-D therapy, and drugs targeting chemical mediators or receptors involved in visceral sensitivity have recently been developed. Alosetron and ramosetron, both antagonists of the serotonin 3 (5-hydroxytryptamine 3; 5-HT_3) receptors, are approved for use in patients with IBS [5,6]. Rifaximin, an antibacterial drug, and eluxadoline, which has both μ-opioid receptor agonist and δ-opioid receptor antagonist activities, were also recently approved for IBS-D treatment [6,7]. However, although these advances have significantly improved IBS-D treatment, additional pharmacological therapeutic options are required [8].

The mechanism of IBS pathogenesis is not fully understood. However, visceral hypersensitivity plays a vital role in its development [9]. Therefore, drugs targeting visceral hypersensitivity

could represent a novel pharmacological approach to IBS treatment. Enhanced visceral perception, psychological factors, altered intestinal microbiota, and immune activation all contribute to visceral hypersensitivity [10–12]. In particular, immune activation in the gastrointestinal tract has recently attracted much attention as a potential mechanism. This is because inflammatory mediators in the intestinal mucosa, such as adenosine 5′-triphosphate (ATP), bradykinin, and adenosine, activate primary afferent nerve endings. This indirectly triggers the release of nociceptor ligands such as histamine and 5-HT, or causes increased intestinal permeability, which allows exposure to bacteria or their products [12,13]. These harmful events enhance visceral sensitivity. Among inflammatory cells, mast cells appear to be key players. This suggests that anti-inflammatory agents might be a promising therapeutic strategy for visceral hypersensitivity.

Adenosine is a purine nucleoside metabolized from ATP. Among its receptor subtypes, the A_{2B} receptor has low affinity and is activated by high concentrations of adenosine arising from pathological conditions [14]. Until recently, our understanding of this receptor was limited by the lack of pharmacological and molecular tools, including genetically modified mouse models. However, progress in developing these tools has revealed multiple functions, including immunomodulation, relaxation of smooth muscle, and intestinal secretion, in various cell types [14,15]. Recently, we suggested that blockade of the A_{2B} receptor could be therapeutically beneficial for IBS-D, based on the attenuation of visceral hypersensitivity and reduced stress-induced defecation in animal models [16]. The presence of functional A_{2B} receptors has been demonstrated in various tissue types. Furthermore, A_{2B} receptors have been found to be potential therapeutic targets in several diseases. In this review, we focus on the role of the A_{2B} receptor in gut function and the immune response, and its involvement in IBS pathogenesis, particularly in the control of intestinal secretion, motility, and sensation.

2. Etiology of IBS

Regardless of the subtype, visceral hypersensitivity is a common feature of patients with IBS. It is thought that increased visceral sensitivity predominantly contributes to the abdominal pain experienced in IBS. In fact, patients with IBS have a lowered threshold for abdominal pain in response to colorectal distension (CRD) compared with healthy control individuals [9]. Stimulation of visceral sensitivity in the gastrointestinal tract might be linked not only to abdominal pain, but also to other symptoms, including diarrhea, as chemical mediators facilitating visceral sensitivity such as 5-HT and ATP can also directly or indirectly activate secretion and sensorimotor functions. IBS is defined as a functional gastrointestinal disorder without any obvious abnormalities. However, increasing evidence indicates that low-grade inflammation is important for IBS symptoms and visceral hypersensitivity. In particular, low-grade inflammation is consistently observed in patients with IBS-D.

3. Visceral Hypersensitivity

Visceral hypersensitivity is a multifactorial process. Recent studies have revealed the presence of low-grade mucosal inflammation and immune activation, related with impaired epithelial barrier function (increased paracellular permeability) and aberrant neuronal sensitivity in patients with IBS [11,13,17]. Chemical mediators from inflammatory cells sensitize primary afferent nerves, favoring the recruitment of silent nociceptors, which results in secondary spinal sensitization. The release of mediators such as potassium ions, ATP, bradykinin, and prostaglandin E_2 (PGE_2) directly activates nerve endings and indirectly triggers the release of algesic mediators such as histamine, 5-HT, and nerve growth factor from other cells. These mediators in turn stimulate proximal afferent nerve endings and nociceptors, leading to pain sensitization or diarrhea. In particular, consistent observations in human and animal studies support an important role in mast cells and their mediators in exciting visceral sensory neurons [17–19].

4. Immune Activation in IBS

Evidence of immune activation in patients with IBS has been obtained from blood samples and intestinal biopsies [20–24]. Consistent with this, previous digestive infections and long-lasting inflammatory features are often observed in patients with IBS (termed post-infectious IBS and post-inflammatory IBS, respectively) [25,26]. Although a variety of inflammatory cell types are involved in visceral hypersensitivity, a recent meta-analysis has suggested that increased numbers of mast cells and $CD3^+$ T cells in the intestinal mucosa are reliable markers of immune activation in IBS [24]. Mucosal inflammatory cells change the luminal environment to an inflammatory state. Supernatants of colonic biopsies from patients with IBS display increased levels of proteolytic activity, which depends on the activation of nuclear factor (NF)-κB [22]. In addition to local inflammation in the intestinal mucosa, systemic inflammatory changes have been reported in patients with IBS [21,23]. Higher levels of plasma interleukin (IL)-6 and IL-8 have been observed in patients with IBS than in control individuals [21]. In particular, elevated IL-6 levels correlate significantly with IBS symptoms, including abdominal pain and bloating [21,27]. Elevated levels of cytokines and chemokines, including tumor necrosis factor (TNF)-α, IL-1β, and IL-6, were observed in peripheral blood mononuclear cell supernatants from patients with IBS-D, and their levels correlated with the frequency and intensity of abdominal pain [23]. These supernatants caused mechanical hypersensitivity in colonic afferent nerve endings, and this was suppressed by infliximab, a monoclonal antibody against TNF-α. These findings demonstrate that immune activation in patients with IBS is associated with clinical outcomes, and that anti-inflammatory agents can be effective in the treatment of IBS. However, a recent clinical study showed that the anti-inflammatory agent 5-aminosalicylic acid (mesalazine) did not improve abdominal pain or stool consistency in patients with IBS-D compared with placebo groups, nor did it provide satisfactory relief [28].

Increasing evidence suggests that mast cells located at the host-environment interface, in close proximity to sensory nerves, play a significant role in abdominal pain or discomfort. Mast cell mediators such as histamine, tryptase, leukotriene, 5-HT, and platelet-activating factor can activate sensory nerves [17,29]. Sustained sensitization by such mediators could lead to the enhancement of visceral sensitivity. It has been demonstrated that a high density of degranulated mast cells exists in the colonic mucosa of patients with IBS, and the proximity of activated mast cells to mucosal nerve fibers is correlated with the severity of abdominal pain [29]. These observations have suggested that mast cell–nerve interactions are a therapeutic target for visceral pain. Clinical trials have recently been conducted on drugs targeting mast cells. Inhibition of the histamine H_1 receptor by ebastine reduces visceral hypersensitivity, global symptoms, and abdominal pain in patients with IBS [30]. Furthermore, the mast cell stabilizer ketotifen increases the threshold for discomfort during IBS with visceral hypersensitivity and improves IBS symptoms, including abdominal pain [31]. However, no relationship has been observed among mast cell number, visceral perception, and IBS symptoms.

Although further studies are required to confirm that immune activation is associated with alterations in gut function—particularly visceral sensitivity and IBS symptoms—taken together, the available literature provides valuable insights into the potential mechanisms underlying IBS.

5. The Adenosine A_{2B} Receptor

Adenosine is an extracellular purine nucleoside signaling molecule responsible for diverse actions in the nervous, cardiopulmonary, renal, and gastrointestinal systems [32]. It is produced by the dephosphorylation of its precursor, ATP. Under stressful or injurious conditions, ATP is released from cells and is rapidly degraded to adenosine by sequential hydrolysis. Extracellular ATP and adenosine diphosphate (ADP) are mainly hydrolyzed by ecto-apyrase to adenosine monophosphate (AMP), which is further metabolized by ecto-5′-nucleotidase (CD73). The biological actions of adenosine are mediated by binding to G protein-coupled receptors, classified into four subtypes: A_1, A_{2A}, A_{2B}, and A_3. The regulation of biological functions by adenosine is strictly related to its extracellular concentration. A_1, A_{2A}, and A_3 receptors possess high-affinity ligand-binding characteristics and are

activated by physiological adenosine concentrations in the submicromolar range (10–200 nM), whereas A_{2B} receptors are activated by micromolar levels of adenosine (10–100 μM), which are achieved in pathological conditions, including hypoxia, ischemia, and inflammation, or in other stressful environments [32].

Adenosine A_{2B} receptors are expressed in a wide variety of cell types and exert tissue- and cell-specific effects [32,33]. A_{2B} receptor activation triggers the stimulation of adenylate cyclase and phospholipase C by coupling to Gs and Gq proteins, respectively. This stimulation leads to increases in intracellular cyclic AMP (cAMP) and calcium ion levels [32,33]. Transcriptional induction of the A_{2B} receptor is caused by hypoxia, bacterial lipopolysaccharide, or inflammatory mediators, including PGE_2, IL-1β, and TNF-α [32]. The presence of functional A_{2B} receptors has been demonstrated in hematopoietic, mast, myocardial, intestinal epithelial, muscle, retinal pigment epithelial, endothelium, and neurosecretory cells [15,32,33]. The functions of A_{2B} receptors have highlighted their promise as therapeutic targets for asthma, inflammatory bowel diseases, respiratory diseases, and arteriosclerosis [14,32,34]. The recent development of pharmacological and molecular tools, including genetically modified mice, has advanced our understanding of the roles of the adenosine A_{2B} receptor in pathophysiological processes, including intestinal inflammation [32,34,35]. Previous studies have demonstrated significant A_{2B} receptor involvement in the control of intestinal secretion, motility, and sensation [14,33]. In the following section, we focus on the roles of the A_{2B} receptor in gut function and immune responses associated with IBS pathogenesis.

6. Intestinal Fluid Secretion

In the alimentary tract, adenosine A_{2B} receptors are predominantly expressed in the colon, particularly in intestinal epithelial cells and enteric neurons [14]. In the intestinal epithelia, adenosine mediates chloride secretion via the A_{2B} adenosine receptor, which results in the movement of isotonic fluid into the lumen [36]. This physiological process naturally serves to hydrate the mucosal surface and contributes to mucosal defenses against luminal pathogens. However, the extreme secretory flush also produces secretory diarrhea. Studies performed using human intestinal epithelial cells suggest that the stimulation of chloride secretion through apical A_{2B} receptors is a potential target for the treatment of diarrheal diseases [36]. The activation of the A_{2B} receptor by adenosine or agonists produces electrogenic chloride secretion in a polarized human intestinal epithelial cell line [36]. In addition, adenosine A_{2B} receptor-deficient mice display reduced stool water content, suggesting a role of the receptors in chloride secretion [37]. CD73 knockout mice exhibit a defect in converting ATP into adenosine, suggesting that the stimulation of colonic water movement by luminal ATP involves metabolized adenosine and apical A_{2B} receptors [38]. Furthermore, bacterial toxins trigger the chloride secretion response through the A_{2B} receptor. The A_{2B} receptor antagonist MRS-1754 prevents the stimulation of secretion by conditioned medium containing ATP released from cells infected with enteropathogenic *Escherichia coli* [39]. Clostridium difficile toxins upregulate the expression of the A_{2B} receptor in the human colon cell line HCT-8, and the receptor antagonist ATL-692 decreases toxin-induced secretion [40]. These observations indicate that the adenosine A_{2B} receptor regulates intestinal fluid secretion in epithelial cells, and that excess activation could cause diarrhea.

7. Release of 5-HT from Enterochromaffin Cells

Enterochromaffin (EC) cells are neuroendocrine cells in the epithelial lining of the gastrointestinal tract lumen. These cells secrete 5-HT and modulate gut motility, secretion, and pain. EC cells express the adenosine A_{2B} receptor and are thought to function as mechanosensors. A recent study demonstrated that the adenosine receptor agonist 5′-*N*-ethylcarboxamidoadenosine (NECA) stimulates 5-HT release, while the antagonist MRS-1754 inhibits its secretion from EC cells [41]. Moreover, stimulation using a flex-based mechanical stress model induced the release of 5-HT, and this was inhibited by MRS-1754 and amplified by NECA [41]. The release of 5-HT induced by mechanical stretch might be involved in A_{2B} receptor function. This is supported by the finding that A_2 receptor

antagonists suppressed mechanically evoked 5-HT release in the human carcinoid cell line, BON cells, suggesting that endogenous adenosine can activate excitatory A_{2A}/A_{2B} receptor signaling pathways in EC cells to regulate 5-HT release [42,43]. Another study showed that the A_{2B} receptor localizes in human epithelial cells lining both the villi and crypts of the intestine [44]. The A_{2B} receptor has also been found to be overexpressed in EC cells from patients with diseases such as Crohn's disease [41,43]. Thus, the A_{2B} receptor might be expressed in human EC cells and induced by inflammatory stress, which modulates 5-HT release.

8. Colonic Motility

In addition to regulatory roles in intestinal epithelial cells, the A_{2B} adenosine receptor participates in the modulation of colonic motor function. Nonadrenergic noncholinergic (NANC) inhibitory neurotransmission plays a pivotal role in colonic motility. ATP and nitric oxide (NO) are major mediators of NANC transmission. Recent experiments using A_{2B} receptor-knockout/β-gal-knock-in mice and ATL-801, an A_{2B} receptor antagonist, demonstrated that A_{2B} receptors expressed on enteric neurons regulate distal colonic motility [37]. That study revealed a constipation-like phenotype, with delayed colonic transit, impaired colonic motility, and increased stool retention [37]. Mechanistically, the phenotype might be caused by defects in colonic relaxation, through aberrant A_{2B} receptor activation via the NO-cyclic guanosine monophosphate (cGMP) pathway. Subsequently, another group demonstrated that A_{2B} receptors are located in the neuromuscular compartment, and that the A_{2B} receptor antagonist MRS-1754 enhances both electrically and carbachol-induced cholinergic contractions in normal longitudinal muscles [45]. This result suggests that the activation of A_{2B} receptors is associated with the inhibition of excitatory cholinergic pathways. Although this differs from the findings of Chandrasekharan et al., suggesting that the A_{2B} receptor contributes to the facilitation of inhibitory nitrergic nerve control [37], both observations result in similar inhibitory modulation in the colon. Furthermore, we recently found that MRS-1754 suppresses defecation induced by wrap-restraint stress in normal rats and by novel environmental stress in maternally separated rats [16]. These findings indicate that the specific inhibition of A_{2B} receptors could be used as a therapeutic approach for diarrhea or motility disorders, but further investigations are needed to fully understand the function of the receptor.

9. Modulation of the Inflammatory Response

The extracellular accumulation of adenosine contributes to the regulation of inflammation. A_{2B} receptors regulate the immune response in various cell types, including mast cells, epithelial cells, and macrophages. Here, we describe the roles of the A_{2B} receptor in the inflammatory response related to IBS pathogenesis.

Intestinal adenosine A_{2B} receptors modulate inflammation in both acute and chronic models of colitis [46–49]. Genetic ablation or pharmacological blockade of the A_{2B} receptor with ATL-801 attenuated the clinical and histological features of intestinal inflammation in experimental colitis, in parallel with reductions in IL-6 and keratinocyte-derived chemokine secretion [46,47]. In contrast, the A_{2B} antagonist PSB-1115 promoted intestinal inflammation in an acute colitis model, and this was related to the modulation of IL-10 production [49]. The enhancement of the inflammatory response observed with the loss of the A_{2B} receptor might depend on the protective effects of intestinal epithelial cells rather than immune cells. Recently, it was reported that intestinal epithelial-specific A_{2B} receptors confer protective roles against intestinal inflammation [48]. The reason for the disparate results of these studies remains unclear.

Mast cells are increasingly appreciated as a crucial cell type in initiating inflammation and the immune response. As described above, activated mast cells in the intestinal mucosa play an important role in the pathogenesis of IBS. Adenosine is known to potentiate the antigen-induced degranulation of mast cells, based on the observation that inhaled adenosine causes bronchoconstriction in patients with asthma [50]. There is evidence that enprofylline and theophylline, two clinically used anti-asthmatic

agents, block adenosine-induced IL-8 production by the human mast cell line HMC-1 by targeting the A_{2B} receptor, attracting increased interest in this receptor [51]. Moreover, A_{2B} receptors stimulate the release of IL-4, IL-13, vascular endothelial growth factor, and IL-8 from mast cells [52,53]. Conversely, the genetic deletion of the A_{2B} receptor in mice enhances antigen-induced mast cell degranulation [54].

Although we have described the anti-inflammatory actions of the A_{2B} receptor, it is difficult to reconcile the evidence into either pro-inflammatory or anti-inflammatory roles for the receptor, as A_{2B} receptor knockout mice appear to have a pro-inflammatory phenotype compared to wild-type controls, characterized by elevated plasma TNF-α levels and increased vascular permeability for albumin in the colon, kidneys, and lungs [55]. This discrepancy in receptor function may be derived from differences in tissue type (lung or intestine), inflammation type (pro-inflammatory or allergic), or the time scale over which inflammatory response progression was observed (acute or chronic).

10. Anti-Nociceptive Actions

Studies on pain sensitivity in relation to the A_{2B} receptor have been limited due to a lack of selective pharmacological tools. However, several studies have recently demonstrated that pharmacological blockade of the A_{2B} receptor is effective in inflammatory pain models. In a formalin-induced pain model, systemic or local administration of the selective A_{2B} receptor antagonist PSB-1115 attenuated nociception in both the first and second phases of the test [56]. Moreover, this inhibitor produced robust dose-dependent analgesia and enhanced morphine-induced anti-nociception in a hot plate test [57]. In addition to effects on the somatic pain response, our study showed that A_{2B} receptor antagonists affect visceral hypersensitivity in response to CRD. We found that the systemic administration of MRS-1754 and PSB-1115 suppressed this pain response in rats [16]. In addition to acute pain, adenosine and the adenosine A_{2B} receptor play major roles in chronic pain by promoting immune–neuronal interaction. A recent study using adenosine deaminase knockout or complete Freund's adjuvant-injected mice revealed that sustained elevated extracellular adenosine activates adenosine A_{2B} receptors on myeloid cells, which in turn transactivates the nociceptors of sensory neurons, causing neuronal hypersensitivity and chronic pain [58]. These findings imply that the inhibition of the adenosine A_{2B} receptor can suppress pain responses.

11. Conclusions and Remarks

Visceral hypersensitivity plays a crucial role in IBS pathogenesis. Previous studies have demonstrated altered inflammatory responses in IBS, and immune activation is likely to be responsible for the stimulation of visceral sensitivity and clinical outcomes. Consistent observations suggest that mast cells are key players in the development of visceral hypersensitivity. Conversely, the adenosine A_{2B} receptor regulates both intestinal fluid secretion into the lumen and colonic motility. These actions can be beneficial for diarrhea in IBS. Although the A_{2B} receptor is involved in the immune response, it is not clear whether it plays a pro-inflammatory or anti-inflammatory role in the gastrointestinal tract. It is also controversial whether the A_{2B} receptor can stimulate mast cell activity. Importantly, blocking the A_{2B} receptor suppresses both somatic and visceral pain. Taken together, although the inhibition of the A_{2B} receptor might be effective for the treatment of pain and diarrhea associated with IBS, with the exception of our recent work, the role of the A_{2B} adenosine receptor in IBS development has not been investigated. Further research is warranted to evaluate the possibility of targeting the A_{2B} receptor for IBS-D treatment.

Conflicts of Interest: T.A. and M.T. belong to an endowed research division of LTT Bio-Pharma Co., Ltd. (Tokyo, Japan).

References

1. Chang, L.; Lembo, A.; Sultan, S. American Gastroenterological Association Institute Technical Review on the pharmacological management of irritable bowel syndrome. *Gastroenterology* **2014**, *147*, 1149–1172. [CrossRef] [PubMed]
2. Ford, A.C.; Lacy, B.E.; Talley, N.J. Irritable bowel syndrome. *N. Engl. J. Med.* **2017**, *376*, 2566–2578. [CrossRef] [PubMed]
3. Mearin, F.; Lacy, B.E.; Chang, L.; Chey, W.D.; Lembo, A.J.; Simren, M.; Spiller, R. Bowel disorders. *Gastroenterology* **2016**. [CrossRef]
4. Canavan, C.; West, J.; Card, T. Review article: The economic impact of the irritable bowel syndrome. *Aliment. Pharmacol. Ther.* **2014**, *40*, 1023–1034. [CrossRef] [PubMed]
5. Fukudo, S.; Kinoshita, Y.; Okumura, T.; Ida, M.; Akiho, H.; Nakashima, Y.; Nishida, A.; Haruma, K. Ramosetron reduces symptoms of irritable bowel syndrome with diarrhea and improves quality of life in women. *Gastroenterology* **2016**, *150*, 358–366. [CrossRef] [PubMed]
6. Lacy, B.E. Emerging treatments in neurogastroenterology: Eluxadoline—A new therapeutic option for diarrhea-predominant IBS. *Neurogastroenterol. Motil.* **2016**, *28*, 26–35. [CrossRef] [PubMed]
7. Menees, S.B.; Maneerattannaporn, M.; Kim, H.M.; Chey, W.D. The efficacy and safety of rifaximin for the irritable bowel syndrome: A systematic review and meta-analysis. *Am. J. Gastroenterol.* **2012**, *107*, 28–35. [CrossRef] [PubMed]
8. Camilleri, M. Pharmacological agents currently in clinical trials for disorders in neurogastroenterology. *J. Clin. Investig.* **2013**, *123*, 4111–4120. [CrossRef] [PubMed]
9. Drossman, D.A. Functional gastrointestinal disorders: History, pathophysiology, clinical features and Rome IV. *Gastroenterology* **2016**, *150*, 1262–1279. [CrossRef] [PubMed]
10. Keszthelyi, D.; Troost, F.J.; Masclee, A.A. Irritable bowel syndrome: Methods, mechanisms, and pathophysiology. Methods to assess visceral hypersensitivity in irritable bowel syndrome. *Am. J. Physiol. Gastrointest. Liver Physiol.* **2012**, *303*, G141–G154. [CrossRef] [PubMed]
11. Akbar, A.; Walters, J.R.; Ghosh, S. Review article: Visceral hypersensitivity in irritable bowel syndrome: Molecular mechanisms and therapeutic agents. *Aliment. Pharmacol. Ther.* **2009**, *30*, 423–435. [CrossRef] [PubMed]
12. Matricon, J.; Meleine, M.; Gelot, A.; Piche, T.; Dapoigny, M.; Muller, E.; Ardid, D. Review article: Associations between immune activation, intestinal permeability and the irritable bowel syndrome. *Aliment. harmacol. Ther.* **2012**, *36*, 1009–1031. [CrossRef] [PubMed]
13. Bueno, L.; Fioramonti, J. Effects of inflammatory mediators on gut sensitivity. *Can. J. Gastroenterol.* **1999**, *13* (Suppl. A), 42A–46A. [CrossRef] [PubMed]
14. Antonioli, L.; Fornai, M.; Colucci, R.; Ghisu, N.; Tuccori, M.; Del Tacca, M.; Blandizzi, C. Regulation of enteric functions by adenosine: Pathophysiological and pharmacological implications. *Pharmacol. Ther.* **2008**, *120*, 233–253. [CrossRef] [PubMed]
15. Feoktistov, I.; Biaggioni, I. Adenosine A_{2B} receptors. *Pharmacol. Rev.* **1997**, *49*, 381–402. [PubMed]
16. Asano, T.; Tanaka, K.I.; Tada, A.; Shimamura, H.; Tanaka, R.; Maruoka, H.; Takenaga, M.; Mizushima, T. Aminophylline suppresses stress-induced visceral hypersensitivity and defecation in irritable bowel syndrome. *Sci. Rep.* **2017**, *7*. [CrossRef] [PubMed]
17. Wouters, M.M.; Vicario, M.; Santos, J. The role of mast cells in functional GI disorders. *Gut* **2016**, *65*, 155–168. [CrossRef] [PubMed]
18. Demaude, J.; Salvador-Cartier, C.; Fioramonti, J.; Ferrier, L.; Bueno, L. Phenotypic changes in colonocytes following acute stress or activation of mast cells in mice: Implications for delayed epithelial barrier dysfunction. *Gut* **2006**, *55*, 655–661. [CrossRef] [PubMed]
19. Serna, H.; Porras, M.; Vergara, P. Mast cell stabilizer ketotifen (4-(1-methyl-4-piperidylidene)-4h-benzo(4,5)cyclohepta(1,2-b)thiophen-10(9H)-one fumarate) prevents mucosal mast cell hyperplasia and intestinal dysmotility in experimental *Trichinella spiralis* inflammation in the rat. *J. Pharmacol. Exp. Ther.* **2006**, *319*, 1104–1111. [CrossRef] [PubMed]
20. Cremon, C.; Gargano, L.; Morselli-Labate, A.M.; Santini, D.; Cogliandro, R.F.; De Giorgio, R.; Stanghellini, V.; Corinaldesi, R.; Barbara, G. Mucosal immune activation in irritable bowel syndrome: Gender-dependence and association with digestive symptoms. *Am. J. Gastroenterol.* **2009**, *104*, 392–400. [CrossRef] [PubMed]

21. Dinan, T.G.; Clarke, G.; Quigley, E.M.; Scott, L.V.; Shanahan, F.; Cryan, J.; Cooney, J.; Keeling, P.W. Enhanced cholinergic-mediated increase in the pro-inflammatory cytokine IL-6 in irritable bowel syndrome: Role of muscarinic receptors. *Am. J. Gastroenterol.* **2008**, *103*, 2570–2576. [CrossRef] [PubMed]
22. Cenac, N.; Andrews, C.N.; Holzhausen, M.; Chapman, K.; Cottrell, G.; Andrade-Gordon, P.; Steinhoff, M.; Barbara, G.; Beck, P.; Bunnett, N.W.; et al. Role for protease activity in visceral pain in irritable bowel syndrome. *J. Clin. Investig.* **2007**, *117*, 636–647. [CrossRef] [PubMed]
23. Hughes, P.A.; Harrington, A.M.; Castro, J.; Liebregts, T.; Adam, B.; Grasby, D.J.; Isaacs, N.J.; Maldeniya, L.; Martin, C.M.; Persson, J.; et al. Sensory neuro-immune interactions differ between irritable bowel syndrome subtypes. *Gut* **2013**, *62*, 1456–1465. [CrossRef] [PubMed]
24. Bashashati, M.; Moossavi, S.; Cremon, C.; Barbaro, M.R.; Moraveji, S.; Talmon, G.; Rezaei, N.; Hughes, P.A.; Bian, Z.X.; Choi, C.H.; et al. Colonic immune cells in irritable bowel syndrome: A systematic review and meta-analysis. *Neurogastroenterol. Motil.* **2017**. [CrossRef] [PubMed]
25. Thabane, M.; Kottachchi, D.T.; Marshall, J.K. Systematic review and meta-analysis: The incidence and prognosis of post-infectious irritable bowel syndrome. *Aliment. Pharmacol. Ther.* **2007**, *26*, 535–544. [CrossRef] [PubMed]
26. Spiller, R.; Garsed, K. Infection, inflammation, and the irritable bowel syndrome. *Dig. Liver Dis.* **2009**, *41*, 844–849. [CrossRef] [PubMed]
27. Bashashati, M.; Moradi, M.; Sarosiek, I. Interleukin-6 in irritable bowel syndrome: A systematic review and meta-analysis of IL-6 (-g174c) and circulating IL-6 levels. *Cytokine* **2017**, *99*, 132–138. [CrossRef] [PubMed]
28. Lam, C.; Tan, W.; Leighton, M.; Hastings, M.; Lingaya, M.; Falcone, Y.; Zhou, X.; Xu, L.; Whorwell, P.; Walls, A.F.; et al. A mechanistic multicentre, parallel group, randomised placebo-controlled trial of mesalazine for the treatment of IBS with diarrhoea (IBS-D). *Gut* **2016**, *65*, 91–99. [CrossRef] [PubMed]
29. Barbara, G.; Wang, B.; Stanghellini, V.; de Giorgio, R.; Cremon, C.; Di Nardo, G.; Trevisani, M.; Campi, B.; Geppetti, P.; Tonini, M.; et al. Mast cell-dependent excitation of visceral-nociceptive sensory neurons in irritable bowel syndrome. *Gastroenterology* **2007**, *132*, 26–37. [CrossRef] [PubMed]
30. Wouters, M.M.; Balemans, D.; Van Wanrooy, S.; Dooley, J.; Cibert-Goton, V.; Alpizar, Y.A.; Valdez-Morales, E.E.; Nasser, Y.; Van Veldhoven, P.P.; Vanbrabant, W.; et al. Histamine receptor H1-mediated sensitization of TRPV1 mediates visceral hypersensitivity and symptoms in patients with irritable bowel syndrome. *Gastroenterology* **2016**, *150*, 875–887. [CrossRef] [PubMed]
31. Klooker, T.K.; Braak, B.; Koopman, K.E.; Welting, O.; Wouters, M.M.; van der Heide, S.; Schemann, M.; Bischoff, S.C.; van den Wijngaard, R.M.; Boeckxstaens, G.E. The mast cell stabiliser ketotifen decreases visceral hypersensitivity and improves intestinal symptoms in patients with irritable bowel syndrome. *Gut* **2010**, *59*, 1213–1221. [CrossRef] [PubMed]
32. Aherne, C.M.; Kewley, E.M.; Eltzschig, H.K. The resurgence of A_{2B} adenosine receptor signaling. *Biochim. Biophys. Acta* **2011**, *1808*, 1329–1339. [CrossRef] [PubMed]
33. Kolachala, V.L.; Obertone, T.S.; Wang, L.; Merlin, D.; Sitaraman, S.V. Adenosine 2b receptor (A_{2B} R) signals through adenylate cyclase (AC) 6 isoform in the intestinal epithelial cells. *Biochim. Biophys. Acta* **2006**, *1760*, 1102–1108. [CrossRef] [PubMed]
34. Feoktistov, I.; Biaggioni, I. Role of adenosine A(2B) receptors in inflammation. *Adv. Pharmacol.* **2011**, *61*, 115–144. [PubMed]
35. Haskó, G.; Csóka, B.; Németh, Z.H.; Vizi, E.S.; Pacher, P. A_{2B} adenosine receptors in immunity and inflammation. *Trends Immunol.* **2009**, *30*, 263–270. [CrossRef] [PubMed]
36. Strohmeier, G.R.; Reppert, S.M.; Lencer, W.I.; Madara, J.L. The A_{2B} adenosine receptor mediates camp responses to adenosine receptor agonists in human intestinal epithelia. *J. Biol. Chem.* **1995**, *270*, 2387–2394. [CrossRef] [PubMed]
37. Chandrasekharan, B.P.; Kolachala, V.L.; Dalmasso, G.; Merlin, D.; Ravid, K.; Sitaraman, S.V.; Srinivasan, S. Adenosine 2B receptors (A_{2B}AR) on enteric neurons regulate murine distal colonic motility. *FASEB J.* **2009**, *23*, 2727–2734. [CrossRef] [PubMed]
38. Weissmuller, T.; Campbell, E.L.; Rosenberger, P.; Scully, M.; Beck, P.L.; Furuta, G.T.; Colgan, S.P. PMNs facilitate translocation of platelets across human and mouse epithelium and together alter fluid homeostasis via epithelial cell-expressed ecto-NTPDases. *J. Clin. Investig.* **2008**, *118*, 3682–3692. [CrossRef] [PubMed]

39. Crane, J.K.; Olson, R.A.; Jones, H.M.; Duffey, M.E. Release of ATP during host cell killing by enteropathogenic *E. coli* and its role as a secretory mediator. *Am. J. Physiol. Gastrointest. Liver Physiol.* **2002**, *283*, G74–G86. [CrossRef] [PubMed]
40. Warren, C.A.; Li, Y.; Calabrese, G.M.; Freire, R.S.; Zaja-Milatovic, S.; van Opstal, E.; Figler, R.A.; Linden, J.; Guerrant, R.L. Contribution of adenosine A_{2B} receptors in *Clostridium difficile* intoxication and infection. *Infect. Immun.* **2012**, *80*, 4463–4473. [CrossRef] [PubMed]
41. Chin, A.; Svejda, B.; Gustafsson, B.I.; Granlund, A.B.; Sandvik, A.K.; Timberlake, A.; Sumpio, B.; Pfragner, R.; Modlin, I.M.; Kidd, M. The role of mechanical forces and adenosine in the regulation of intestinal enterochromaffin cell serotonin secretion. *Am. J. Physiol. Gastrointest. Liver Physiol.* **2012**, *302*, G397–G405. [CrossRef] [PubMed]
42. Christofi, F.L. Purinergic receptors and gastrointestinal secretomotor function. *Purinergic Signal.* **2008**, *4*, 213–236. [CrossRef] [PubMed]
43. Linan-Rico, A.; Ochoa-Cortes, F.; Beyder, A.; Soghomonyan, S.; Zuleta-Alarcon, A.; Coppola, V.; Christofi, F.L. Mechanosensory signaling in enterochromaffin cells and 5-HT release: Potential implications for gut inflammation. *Front. Neurosci.* **2016**, *10*, 564. [CrossRef] [PubMed]
44. Christofi, F.L.; Zhang, H.; Yu, J.G.; Guzman, J.; Xue, J.; Kim, M.; Wang, Y.Z.; Cooke, H.J. Differential gene expression of adenosine A1, A2a, A2b, and A3 receptors in the human enteric nervous system. *J. Comp. Neurol.* **2001**, *439*, 46–64. [CrossRef] [PubMed]
45. Antonioli, L.; Fornai, M.; Awwad, O.; Giustarini, G.; Pellegrini, C.; Tuccori, M.; Caputi, V.; Qesari, M.; Castagliuolo, I.; Brun, P.; et al. Role of the A_{2B} receptor–adenosine deaminase complex in colonic dysmotility associated with bowel inflammation in rats. *Br. J. Pharmacol.* **2014**, *171*, 1314–1329. [CrossRef] [PubMed]
46. Kolachala, V.L.; Vijay-Kumar, M.; Dalmasso, G.; Yang, D.; Linden, J.; Wang, L.; Gewirtz, A.; Ravid, K.; Merlin, D.; Sitaraman, S.V. A_{2B} adenosine receptor gene deletion attenuates murine colitis. *Gastroenterology* **2008**, *135*, 861–870. [CrossRef] [PubMed]
47. Kolachala, V.; Ruble, B.; Vijay-Kumar, M.; Wang, L.; Mwangi, S.; Figler, H.; Figler, R.; Srinivasan, S.; Gewirtz, A.; Linden, J.; et al. Blockade of adenosine A_{2B} receptors ameliorates murine colitis. *Br. J. Pharmacol.* **2008**, *155*, 127–137. [CrossRef] [PubMed]
48. Aherne, C.M.; Saeedi, B.; Collins, C.B.; Masterson, J.C.; McNamee, E.N.; Perrenoud, L.; Rapp, C.R.; Curtis, V.F.; Bayless, A.; Fletcher, A.; et al. Epithelial-specific A_{2B} adenosine receptor signaling protects the colonic epithelial barrier during acute colitis. *Mucosal Immunol.* **2015**, *8*, 1324–1338. [CrossRef] [PubMed]
49. Frick, J.S.; MacManus, C.F.; Scully, M.; Glover, L.E.; Eltzschig, H.K.; Colgan, S.P. Contribution of adenosine A_{2B} receptors to inflammatory parameters of experimental colitis. *J. Immunol.* **2009**, *182*, 4957–4964. [CrossRef] [PubMed]
50. Cushley, M.J.; Tattersfield, A.E.; Holgate, S.T. Adenosine-induced bronchoconstriction in asthma. Antagonism by inhaled theophylline. *Am. Rev. Respir. Dis.* **1984**, *129*, 380–384. [PubMed]
51. Feoktistov, I.; Biaggioni, I. Adenosine A_{2B} receptors evoke interleukin-8 secretion in human mast cells. An enprofylline-sensitive mechanism with implications for asthma. *J. Clin. Investig.* **1995**, *96*, 1979–1986. [CrossRef] [PubMed]
52. Ryzhov, S.; Zaynagetdinov, R.; Goldstein, A.E.; Novitskiy, S.V.; Dikov, M.M.; Blackburn, M.R.; Biaggioni, I.; Feoktistov, I. Effect of A_{2B} adenosine receptor gene ablation on proinflammatory adenosine signaling in mast cells. *J. Immunol.* **2008**, *180*, 7212–7220. [CrossRef] [PubMed]
53. Ryzhov, S.; Goldstein, A.E.; Matafonov, A.; Zeng, D.; Biaggioni, I.; Feoktistov, I. Adenosine-activated mast cells induce IgE synthesis by B lymphocytes: An A_{2B}-mediated process involving Th2 cytokines IL-4 and IL-13 with implications for asthma. *J. Immunol.* **2004**, *172*, 7726–7733. [CrossRef] [PubMed]
54. Hua, X.; Kovarova, M.; Chason, K.D.; Nguyen, M.; Koller, B.H.; Tilley, S.L. Enhanced mast cell activation in mice deficient in the A_{2B} adenosine receptor. *J. Exp. Med.* **2007**, *204*, 117–128. [CrossRef] [PubMed]
55. Yang, D.; Zhang, Y.; Nguyen, H.G.; Koupenova, M.; Chauhan, A.K.; Makitalo, M.; Jones, M.R.; St Hilaire, C.; Seldin, D.C.; Toselli, P.; et al. The A_{2B} adenosine receptor protects against inflammation and excessive vascular adhesion. *J. Clin. Investig.* **2006**, *116*, 1913–1923. [CrossRef] [PubMed]
56. Bilkei-Gorzo, A.; Abo-Salem, O.M.; Hayallah, A.M.; Michel, K.; Muller, C.E.; Zimmer, A. Adenosine receptor subtype-selective antagonists in inflammation and hyperalgesia. *Naunyn-Schmiedebergs Arch. Pharmacol.* **2008**, *377*, 65–76. [CrossRef] [PubMed]

57. Abo-Salem, O.M.; Hayallah, A.M.; Bilkei-Gorzo, A.; Filipek, B.; Zimmer, A.; Muller, C.E. Antinociceptive effects of novel A_{2B} adenosine receptor antagonists. *J. Pharmacol. Exp. Ther.* **2004**, *308*, 358–366. [CrossRef] [PubMed]
58. Hu, X.; Adebiyi, M.G.; Luo, J.; Sun, K.; Le, T.T.; Zhang, Y.; Wu, H.; Zhao, S.; Karmouty-Quintana, H.; Liu, H.; et al. Sustained elevated adenosine via ADORA2B promotes chronic pain through neuro-immune interaction. *Cell Rep.* **2016**, *16*, 106–119. [CrossRef] [PubMed]

© 2017 by the authors. Licensee MDPI, Basel, Switzerland. This article is an open access article distributed under the terms and conditions of the Creative Commons Attribution (CC BY) license (http://creativecommons.org/licenses/by/4.0/).

TRADITIONAL & KAMPO MEDICINE

ORIGINAL ARTICLE

Protective effect of boiogito extract with glucosamine HCl against adjuvant-induced arthritis in rats

Mitsuko Takenaga,[1*] Jun Niimi,[1] Akemi Hamaguchi,[1] Teita Asano,[1] Reiko Tsuchiya,[1] Yuki Ohta,[2] Kazuo Yudoh[1] & Hajime Inoue[3,4]

1 Institute of Medical Science, St Marianna University School of Medicine, Kawasaki, Japan
2 Department of Pharmacology, St Marianna University School of Medicine, Kawasaki, Japan
3 Department of Plastic and Reconstructive Surgery, St Marianna University School of Medicine, Kawasaki, Japan
4 Department of Stem Cell Therapy, St Marianna University School of Medicine, Kawasaki, Japan

ABSTRACT

Aim: The effect of boiogito extract combined with glucosamine HCl was assessed in adjuvant-induced arthritis (AIA) rats.

Methods: Rats received a daily oral mixture of boiogito extract (125 mg/kg) and glucosamine HCl (80 mg/kg) before and after once-off adjuvant injection. Treatment was continued up to the day when blood and/or tissue were collected (day 12 or day 21). Paw swelling, arthritis score, and inflammatory mediators were assessed.

Results: Combined treatment was more effective for AIA than either agent alone. Both serum nitric oxide (NO) and tissue NO were significantly suppressed in the adjuvant-uninjected hind paw on day 12. Boiogito extract significantly reduced the tissue level of matrix metalloproteinase (MMP)-13. In addition, interleukin (IL)-1β-induced MMP-13 by SW1353 chondrocytes was dose-dependently suppressed by boiogito extract, while glucosamine HCl had little effect. IL-1β-induced phosphorylation of extracellular signal-related kinase (ERK) was inhibited by the combination of boiogito extract and glucosamine HCl, but was most strongly suppressed by glucosamine HCl alone.

Conclusion: Combined treatment with boiogito extract and glucosamine HCl had a protective effect against AIA in rats. This effect was related to strong suppression of MMP-13 production (mainly by boiogito extract) and inhibition of inflammatory mediator production via ERK signaling (mainly by glucosamine HCl).

KEY WORDS: boiogito, glucosamine HCl, matrix metalloproteinase-13, osteoarthritis

INTRODUCTION

Osteoarthritis (OA) is one of the most common chronic diseases and is a major cause of disability in the elderly. Its incidence is increasing rapidly as the world's population ages. OA is characterized by cellular loss in articular cartilage, an important factor in progressive cartilage deterioration, given that apoptosis of chondrocytes leads to degradation of the extracellular matrix (ECM) in the joint cartilage of OA patients [1]. Matrix metalloproteinases (MMP) play a critical role in the initiation and progression of cartilage destruction together with various cytokines [2,3].

Boiogito is a traditional Japanese herbal medicine containing boi (stem or rhizome of *Sinomenium acutum* (Thnb.) Rehder & E.H. Wilson), ogi (root of *Astragalus membranaceus* Bunge), sojutsu (rhizome of *Atractylodes lancea* DC.), taiso (fruit of *Zizyphus jujuba* Miller var. *inermis* Rehder), kanzo (root of *Glycyrrhiza uralensis* Fisch. ex DC.), and shokyo (rhizome of *Zingiber officinale* Roscoe). In Japan, boiogito has been used clinically for the treatment of edema, arthritic pain, and nephrotic syndrome. Kogure *et al.* reported that treatment with boiogito improved both the Harris hip score and clinical criteria in OA patients [4]. In addition, boiogito has been shown to have a cardioprotective effect in the isolated blood-perfused canine heart [5], to inhibit obesity in ovariectomized rats [6], and to increase fatty acid metabolism by cells of the proximal renal tubules [7]. Furthermore, boiogito has been reported to improve hydrarthrosis in a rat model of knee OA [8].

Glucosamine has been shown to be effective for adjuvant arthritis in rats [9–11]. In addition, Nakamura *et al.* showed that glucosamine significantly improved pain and swelling of arthritic joints compared with placebo in patients with rheumatoid arthritis (RA) [12]. Matsuno *et al.*, however,

*Correspondence. Mitsuko Takenaga
Tel: +81-44-977-8111
Fax: +81-44-976-3747
Email: m2take@marianna-u.ac.jp
DOI:10.1002/tkm2.1089
Received 9 June 2017; revised 7 December 2017; accepted 7 December 2017

© 2018 The Authors. *Traditional & Kampo Medicine* published by John Wiley & Sons Australia, Ltd on behalf of Japan Society for Oriental Medicine and Medical and Pharmaceutical Society for WAKAN-YAKU.
This is an open access article under the terms of the Creative Commons Attribution-NonCommercial License, which permits use, distribution and reproduction in any medium, provided the original work is properly cited and is not used for commercial purposes.

Table 1 | Components of boiogito

Original plant	Plant part(s)	Family name	Japanese name
Sinomenium acutum (Thnb.) Rehder & E.H. Wilson	Stem, rhizome	Menispermaceae	Boi
Astragalus membranaceus Bunge	Root	Leguminosae	Ogi
Atractylodes lancea DC.	Rhizome	Compositae	Sojutsu
Zizyphus jujuba Miller var. *inermis* Rehder	Fruit	Rhamnaceae	Taiso
Glycyrrhiza uralensis Fisch. ex DC.	Root	Leguminosae	Kanzo
Zingiber officinale Roscoe	Rhizome	Zingiberaceae	Shokyo

concluded that glucosamine was more effective for OA than RA [13], and Kulkarni *et al.* reported that glucosamine HCl improved pain in 59 patients with knee OA [14]. Recently, a randomized, double-blind, placebo-controlled trial by Sterzi *et al.* showed that glucosamine HCl combined with chondroitin sulfate and bio-curcumin was effective for knee OA [15].

Locofit GL® (Ohta's Isan, Tokyo, Japan) contains both boiogito extract and glucosamine HCl and has been used to treat hyperhidrosis or arthritic joint swelling and pain associated with obesity in Japan. The efficacy of this combination of boiogito extract and glucosamine HCl, however, has not been evaluated. The aim of this study was therefore to assessed the effect of this combined product in rats with adjuvant-induced arthritis (AIA), and compare it with the effects of boiogito extract or glucosamine HCl alone.

METHODS

Reagents

Boiogito extract (boiogito dried extract-O, Lot No. 10 K176) was provided by Alps Pharmaceutical Industries (Gifu, Japan). Boiogito extract was prepared as follows. The following materials were extracted with 20 volumes of distilled water for 50 min at 95–100°C: boi (X3F138), ogi (E3H176), sojutsu (E3D81), taiso (E4C52), kanzo (S15F119), and shokyo (S15G131) (5.0/5.0/3.0/3.0/1.5/1.0; w/w; Table 1). The solution was filtered and concentrated at 60°C *in vacuo*, followed by spray drying (yield: 17.2%). The extract thus obtained contained 0.77% glycyrrhizic acid and 0.39% sinomenine (Figure S1 and S2).

Glucosamine HCl was purchased from Sigma-Aldrich (St Louis, MO, USA).

Cell lines

Chondrosarcoma cell line (SW1353) was purchased from ATCC (Salisbury, UK). Cells were cultured in D-MEM (Sigma-Aldrich) with 10% fetal bovine serum (Invitrogen, Carlsbad, CA, USA) and 1% antibiotic/antimycotic (Thermo Fisher Scientific, Waltham, MD, USA).

Animals

Wistar rats were purchased from Charles River Laboratories Japan (Yokohama, Japan). The rats were housed in an animal room at a constant temperature (22–24°C) and humidity (50–60%) with a 12 h light/dark cycle, and were allowed free access to a standard diet and water. The animal experiments were performed in accordance with the Guidelines for Animal Experimentation of St Marianna University Graduate School of Medicine (approval no. 1501010).

AIA model

Seven-week-old female rats (215.7 ± 11.5 g) were randomly divided into the following groups (n = 5 each): (i) saline-treated AIA control group; (ii) combined therapy (boiogito extract 125 mg/kg and glucosamine HCl 80 mg/kg) AIA group; (iii) boiogito extract (125 mg/kg)-treated AIA group; (iv) glucosamine HCl (80 mg/kg)-treated AIA group; and (v) a normal control group. Complete Freund's adjuvant (0.5 mg/0.05 mL, Chondrex, Redmond, WA, USA) was injected once, intradermally, into the right hind foot pad. Test compounds suspended in saline (1 mL/kg) were given orally at 1 h before the adjuvant injection, followed by daily treatment up to day 12 or day 21. Although the daily dose of Locofit GL® is 3.6 g in humans (approx. 60 mg/kg), a five-fold higher dose was used in this study, corresponding to 125 mg/kg for boiogito extract and 80 mg/kg for glucosamine HCl.

Paw volume was determined every 3 or 4 days with a plethysmometer (TK-101CMP; Unicom, Chiba, Japan). Paw erythema and swelling were then graded as per the following 5-point scale, and arthritis score [16] calculated: 0, no inflammation; 1, swelling and erythema of the digits; 2, moderate swelling and erythema of the paw; 3, severe swelling and erythema of the limb; and 4, severe swelling, erythema, gross deformity, and difficulty using the limb.

Serum measurements and uninjected paw

After *in vivo* observation, a blood sample was collected under anesthesia, and serum was stored. On day 12, the adjuvant-uninjected hind paw was resected at the ankle under deep anesthesia. Paw tissue samples were homogenized in 20 mmol/L Tris–HCl (pH 7.5), 2 mol/L NaCl, 0.1% Tween-80, 1 mmol/L phenylmethylsulfonylfluoride (PMSF),

© 2018 The Authors. *Traditional & Kampo Medicine* published by John Wiley & Sons Australia, Ltd on behalf of Japan Society for Oriental Medicine and Medical and Pharmaceutical Society for WAKAN-YAKU.

and 1 mmol/L ethylenediaminetetra-acetic acid (EDTA), followed by centrifugation.

Hyaluronic acid (HA), nitric oxide (NO), prostaglandin (PG)E_2, and MMP-13 were measured with an HA assay kit (Seikagaku, Tokyo, Japan), nitrate/nitrite assay kit, PGE_2 EIA kit (Cayman Chemical, Ann Arbor, MI, USA) and MMP-13 ELISA kit (R&D Systems, Minneapolis, MN, USA), respectively.

Chondrocyte activity

SW1353 cells (3×10^5) were cultured for 24 h in serum-free medium, incubated for 2 h with boiogito extract and/or glucosamine HCl, and then cultured in fresh medium containing IL-1β (10 ng/mL) for a further 24 h. Culture supernatants were used for measurement of MMP-13 and tissue inhibitor of matrix metalloproteinase (TIMP)-1 (R&D systems). In addition, cells (2×10^6) incubated for 2 h with reagents were exposed to IL-1β for 15 min, after which phosphorylation of extracellular signal-related kinase (ERK) and p38 was assessed.

Boiogito extract and glucosamine HCl were dissolved in phosphate-buffered saline and sterilized by passage through a 0.45 μm membrane filter.

Western blotting

Lysates were prepared with 20 mmol/L Tris–HCl (pH 7.5), 150 mmol/L NaCl, 1(v/v)% Triton X-100, 5 mmol/L EDTA, 1 mmol/L PMSF, 5 μg/mL aprotinin, 5 μg/mL leupeptin, 2 mmol/L imidazole, 1 mmol/L sodium fluoride, 1.15 mmol/L sodium molybdate, 1 mmol/L sodium orthovanadate, and 4 mmol/L sodium tartrate dihydrate.

After centrifugation, the lysates (20 μg) were separated by electrophoresis on 10% sodium dodecylsulfate polyacrylamide gels and proteins were transferred to polyvinylidene difluoride membranes. The membranes were incubated with antibodies targeting p44/42 mitogen-activated protein kinase (MAPK; ERK, rabbit; Cell Signaling Techology, Danvers, MA, USA), phosphor-p44/42 MAP kinase (p-ERK, rabbit; Cell Signaling Technology), phosphor p38 (mouse; Abcam, Cambridge, UK), or p38 (rabbit, Cell Signaling Technology), followed by incubation with electrochemiluminescence (ECL) horseradish peroxidase (HRP)-labeled anti-mouse IgG or HRP-labeled anti-rabbit IgG (GE Healthcare Japan, Tokyo, Japan). Then the membranes were incubated with the ECL Prime Western blotting detection system (GE Healthcare Japan) and signals were quantified on densitometry.

Statistical analysis

Data are given as mean ± SEM. One-way analysis of variance followed by Tukey test or Dunnett's test was used to evaluate differences, which were considered to be significant for $P < 0.05$.

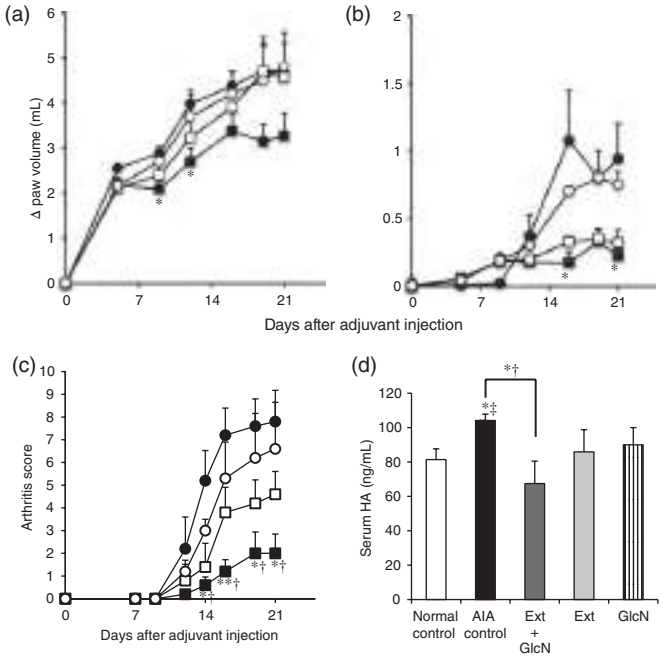

Figure 1 | Effect of (■) boiogito extract with glucosamine HCl (Ext + GlcN), (□) boiogito extract alone (Ext); and (○) glucosamine HCl alone (GlcN) on (a,b) change in paw volume (a, adjuvant-injected paw; b, uninjected paw) and (c) arthritis score up to day 21 in rats with adjuvant-induced arthritis (AIA; ●, AIA control). (d) Serum hyaluronic acid (HA) on day 21. *$P < 0.05$, **$P < 0.01$ †vs AIA control, ‡vs normal control.

RESULTS

Hind paw swelling and arthritis score

In saline-treated AIA control rats, rapid swelling of the right hind paw was noted after adjuvant injection and there was a subsequent steady increase of paw swelling until day 21 (Fig. 1a). In the combined boiogito extract and glucosamine HCl (Ext + GlcN)-treated AIA group, however, significant reduction of hind paw swelling was achieved during the observation period.

In the AIA control group, swelling of the adjuvant-uninjected left hind paw was detected on day 12 and increased until day 21 (Fig. 1b). In the AIA control, the mean increase of paw volume was >1.0 mL. In the Ext + GlcN AIA group, however, the increase in paw volume was significantly suppressed.

In the AIA control, the arthritis score increased to 7.80 ± 1.38 by day 21 (Fig. 1c), while in the Ext + GlcN AIA group, arthritis score was significantly reduced. Boiogito extract alone also reduced the score, but it was not significant; and glucosamine HCl alone had little effect. Thus, combined treatment (Ext + GlcN) was more effective than either agent alone for alleviating the signs and symptoms of AIA.

© 2018 The Authors. *Traditional & Kampo Medicine* published by John Wiley & Sons Australia, Ltd on behalf of Japan Society for Oriental Medicine and Medical and Pharmaceutical Society for WAKAN-YAKU.

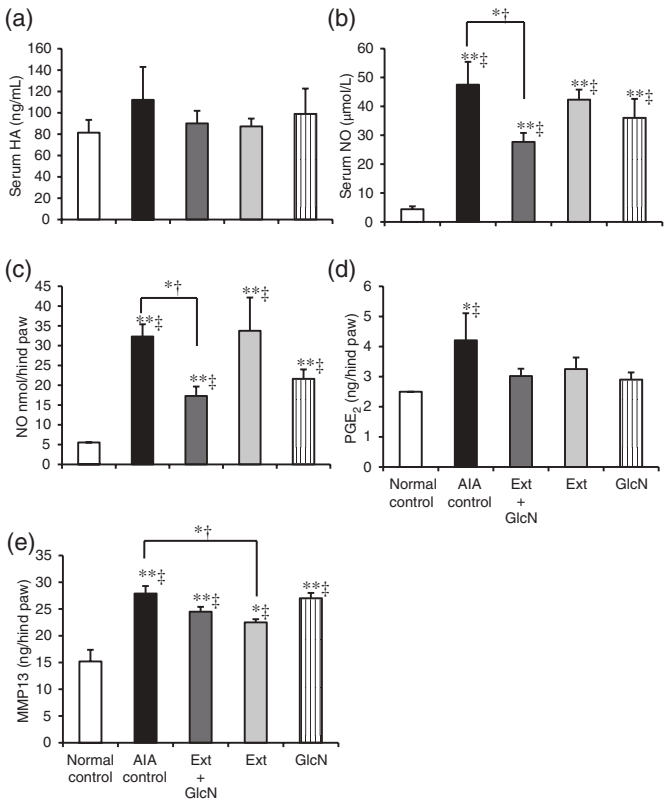

Figure 2 | Effect of boiogito extract (Ext), glucosamine HCl (GlcN) and their combination (Ext + GlcN) in adjuvant-induced arthritis (AIA) rats on day 12. (a,b) Serum (a) hyaluronic acid (HA) and (b) nitric oxide (NO). (c–e) Tissue (c) NO, (d) prostaglandin (PG)E_2, and (e) matrix metalloproteinase (MMP)-13 in the adjuvant-uninjected hind paw. *$P < 0.05$, **$P < 0.01$ †vs AIA control, ‡vs normal control.

Serum HA was significantly elevated in the AIA control compared with the normal control (Fig. 1d), while in the combined treatment group the increase was significantly suppressed.

Serum HA and NO on day 12

Next, we focused on day 12, which was when the volume of the adjuvant-uninjected hind paw began to increase.

Serum HA was slightly elevated in the AIA control. The increase was suppressed in all other treatment groups, but the effect was not significant (Fig. 2a).

In the AIA control, serum NO was dramatically elevated to 48.7 ± 7.5 μmol/L on day 12 (Fig. 2b). In the combined treatment AIA group, serum NO was reduced to 27.7 ± 3.1 μmol/L. Both boiogito extract alone and glucosamine HCl alone suppressed serum NO, but neither agent had a significant effect.

Adjuvant-uninjected hind paw on day 12

Tissue NO was significantly higher in the AIA control compared with the normal control (32.3 ± 3.1 nmol vs 5.4 ± 0.3 nmol per hind paw). Combined treatment lowered the increase (Fig. 2c). Glucosamine HCl suppressed the NO, but the boiogito extract had little effect.

Tissue PGE_2 was significantly higher in the AIA control than in the normal control group (4.21 ± 0.90 ng vs 1.64 ± 0.28 ng per hind paw). PGE_2 was lowered in all treatment groups, but this was not significant (Fig. 2d).

Tissue MMP-13 was significantly increased in the AIA control than in the normal control group (27.9 ± 1.4 ng vs 16.6 ± 2.1 ng per hind paw; Fig. 2e). It was significantly lower in the boiogito extract-treated group.

SW1353 chondrocyte MMP-13 and TIMP-1 production *in vitro*

When chondrocytes were exposed to IL-1β, there was a significant increase in MMP-13, while boiogito extract caused

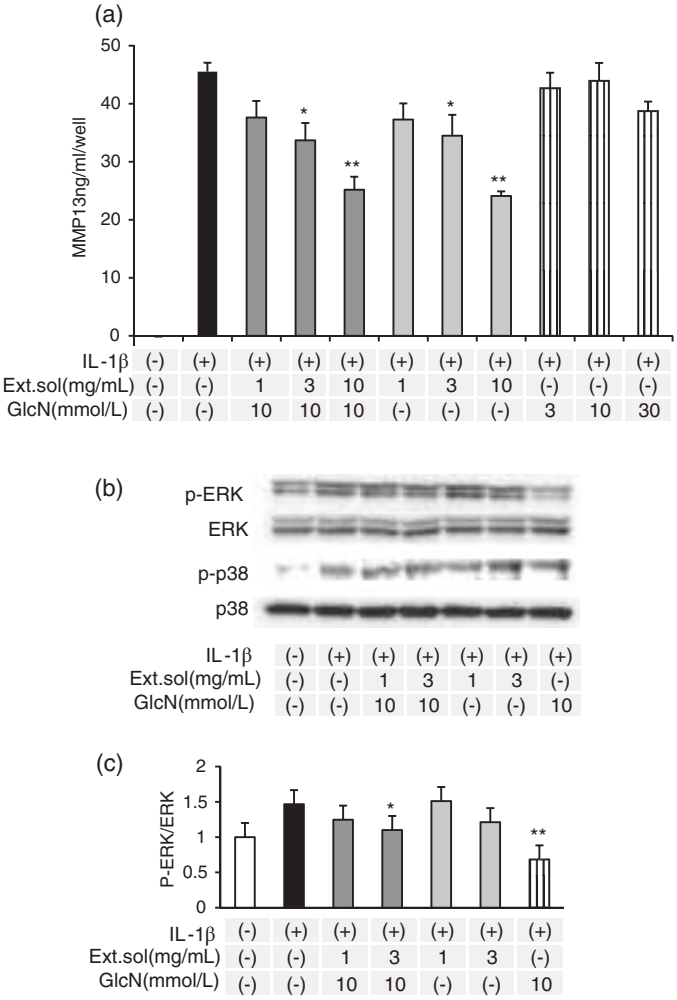

Figure 3 | (a) Effect of boiogito extract (Ext.) and/or glucosamine HCl (GlcN) on interleukin (IL)-1β-stimulated SW1353 cell matrix metalloproteinase (MMP)-13 production *in vitro* and on (b,c) phosphorylation (p-) of extracellular signal-related kinase (ERK) and p38. *$P < 0.05$, **$P < 0.01$ vs control (IL-1β alone).

© 2018 The Authors. *Traditional & Kampo Medicine* published by John Wiley & Sons Australia, Ltd on behalf of Japan Society for Oriental Medicine and Medical and Pharmaceutical Society for WAKAN-YAKU.

Table 2 | Effect of boiogito and/or glucosamine on IL-1β-induced MMP-13 and TIMP-1 SW1353 cell production

Boiogito extract	Glucosamine HCl	IL-1β	MMP-13 (ng/mL) Mean ± SEM	TIMP-1 (ng/mL) Mean ± SEM	MMP-13/TIMP-1 ratio
(–)	(–)	(–)	−0.05 ± 0.02	19.5 ± 0.81	(–)
(–)	(–)	(+)	45.8 ± 1.05	21.4 ± 0.93	2.16 ± 0.09
(+)	(+)	(+)	40.5 ± 0.46*,†	26.8 ± 1.23*,†	1.60 ± 0.07**,†
(+)	(–)	(+)	40.3 ± 0.77*,†	26.8 ± 1.43*,†	1.73 ± 0.14**,†
(–)	(+)	(+)	45.4 ± 1.50	24.1 ± 1.43	1.90 ± 0.08

* $P < 0.05$;
** $P < 0.01$;
† vs control (IL-1β alone).
Final concentration was 3 mg/mL for boiogito extract and 10 mmol/L for glucosamine HCl.
IL, interleukin; MMP, matrix metalloproteinase; TIMP-1, tissue inhibitor of matrix metalloproteinase.

dose-dependent suppression (Fig. 3a). The response to combined treatment was similar to the effect of boiogito extract alone, while glucosamine HCl alone had little influence. Cell viability was similar under all culture conditions.

Boiogito extract increased TIMP-1, and decreased the MMP-13/TIMP-1 ratio, regardless of the presence or absence of glucosamine HCl (Table 2).

Phosphorylation of ERK and p38 by chondrocytes *in vitro*

Exposure of cells to IL-1β increased phosphorylation of ERK by 1.5-fold, while this was dose-dependently decreased by boiogito extract and/or glucosamine HCl. The maximum decrease was noted after addition of glucosamine HCl alone (Fig. 3b,c).

In contrast, a 1.8-fold increase of p38 phosphorylation following exposure to IL-1β was not suppressed by either boiogito extract or glucosamine HCl.

DISCUSSION

In the present study, combined treatment with boiogito extract and glucosamine HCl significantly reduced paw edema and the arthritis score in AIA rats. Boiogito extract alone was less potent, indicating that combined therapy may be more effective for joint inflammation in diseases such as OA.

Hyaluronic acid is an inflammatory mediator [17], and its level was significantly decreased by boiogito extract. Both serum and tissue (adjuvant-uninjected hind paw) NO were also significantly suppressed by boiogito extract. Furthermore, tissue PGE_2 was reduced by boiogito extract, although not significant. This suggests that suppression of inflammatory mediators contributes to the anti-arthritic activity of boiogito extract.

Glucosamine has already been reported to be effective in AIA rats [9–11]. Following oral treatment, glucosamine is absorbed and metabolized, after which it may be incorporated into arthritic joints and support chondrocyte function [18]. Nakamura *et al.* reported that glucosamine reduced joint pain and swelling in RA patients [12], while Matsuno *et al.* concluded that glucosamine was more effective for OA than RA [13]. A recent randomized, double-blind, placebo-controlled study showed that glucosamine HCl combined with chondroitin sulfate and bio-curcumin was effective for knee OA [15]. The equivalent dose of glucosamine HCl alone, however, had little influence on AIA in the present rat model. Therefore, it seems that glucosamine-HCl itself was not effective against AIA in the present study, but acted to promote the pharmacological effects of boiogito extract.

The TIMP regulate tissue breakdown by blocking the activity of MMP, and the balance between these enzymes is assumed to be a critical determinant of ECM turnover, especially during progression of OA. Boiogito extract significantly reduced tissue MMP-13 in the adjuvant-uninjected hind paw. Boiogito extract also suppressed IL-1β-induced MMP-13 production by SW1353 chondrocytes, while increasing TIMP-1, suggesting that not only a decrease of MMP-13 but also reduction of the MMP-13/TIMP-1 ratio may play an important role in suppressing paw edema *in vivo*. Glucosamine HCl had little effect on MMP-13 and TIMP-1 by chondrocytes.

The MAPK participate in inflammation and joint destruction in both RA and OA, and MAPK inhibitors have been reported to decrease synovial inflammation and cartilage damage in an animal model of arthritis [19]. MAPK are also activated by treating cultured chondrocytes with IL-1β [20]. Lu *et al.* found that MMP-13 was suppressed by inhibiting the phosphorylation of MAPK such as ERK and p38 [21]. In the present study, boiogito extract suppressed ERK phosphorylation in association with a decrease of MMP-13, while glucosamine HCl markedly suppressed ERK phosphorylation with little effect on MMP-13. Scotto d'Abusco *et al.* reported that glucosamine HCl suppressed MMP-13 production by inhibiting the phosphorylation of p38, but not ERK [22], which is inconsistent with the present results. Although further investigation of this issue is required, the present results

© 2018 The Authors. *Traditional & Kampo Medicine* published by John Wiley & Sons Australia, Ltd on behalf of Japan Society for Oriental Medicine and Medical and Pharmaceutical Society for WAKAN-YAKU.

suggest that ERK signaling might be involved in MMP-13 production by chondrocytes, but glucosamine HCl seems to have little influence on MMP-13 despite suppressing the ERK pathway. Kim *et al.* and Jang *et al.* reported that suppression of ERK had an anti-inflammatory effect [23,24], and glucosamine has been reported to alleviate oxidative stress by inhibition of MAPK signaling [25]. In the present study, both serum and tissue NO were lower on day 12 in rats treated with glucosamine HCl, although the differences were not significant. Therefore, although glucosamine HCl had little influence on MMP-13, it may have had an anti-inflammatory effect via the ERK pathway that contributed to greater *in vivo* reduction of NO.

In conclusion, the combination of boiogito extract and glucosamine-HCl could be an effective treatment for joint inflammation in diseases such as OA. In addition to strong suppression of MMP-13 production by boiogito extract, the anti-inflammatory effect of glucosamine HCl mediated via ERK signaling suggests the more potent anti-arthritic activity of this combination.

It is also important to determine which component of boiogito extract has the most potent anti-arthritic activity. Sinomenine, a major component of boi, has been reported to ameliorate arthritis by acting on MMP [26,27]. The doses of sinomenine tested in this study were equivalent to 0.48 mg/kg (125 mg/kg *in vivo*) and 32 μmol/L (3 mg/mL *in vitro*), being much lower than in previous reports. Although the data are not shown, 50 μmol/L sinomenine alone had a weak inhibitory effect, but a high dose (250 μmol/L) had similar efficacy to that of boiogito extract (Table 2). Therefore, other components of boiogito extract must have contributed to its activity in addition to sinomenine.

ACKNOWLEDGMENTS

This work was partly supported by a grant from the Ministry of Education, Culture, Sports, Science and Technology of Japan under the Academic Frontier project for Private Universities (S1591006). We thank K. BaBa, T. Yamazaki and T. Yoshie (Ohta's Isan) for their contribution to the analysis of boiogito extract.

CONFLICT OF INTEREST

The authors declare no conflicts of interest.

REFERENCES

1. Johnson EO, Babis GC, Soultanis KC, Soucacos PN. Functional neuroanatomy of proprioception. *J. Surg. Orthop. Adv.* 2008; **17**: 159–164.
2. Klatt AR, Klinger G, Neumuller O *et al*. TAK1 downregulation reduces IL-1beta induced expression of MMP13, MMP1 and TNF-alpha. *Biomed. Pharmacother.* 2006; **60**: 55–61.
3. Pujol JP, Chadjichristos C, Legendre F *et al*. Interleukin-1 and transforming growth factor-beta 1 as crucial factors in osteoarthritic cartilage metabolism. *Connect. Tissue Res.* 2008; **49**: 293–297.
4. Kogure T, Tatsumi T, Shigeta T, Fujinaga H, Sato T, Niizawa A. Effect of kampo medicine on pain and range of motion of osteoarthritis of the hip accompanied by acetabular dysplasia: Case report and literature review. *Integr. Med. Insights* 2011; **6**: 13–17.
5. Yamakawa J, Moriya J, Takeuchi K, Nakatou M, Motoo Y, Kobayashi JA. Kampo medicine, boi-ogi-to, inhibits obesity in ovariectomized rats. *Evid. Based Complement. Alternat. Med.* 2010; **7**: 87–95.
6. Sugiyama A, Takahara A, Satoh Y, Yoneyama M, Saegusa Y, Hashimoto K. Cardiac effects of clinically available kampo medicine assessed with canine isolated, blood-perfused heart preparations. *Jpn. J. Pharmacol.* 2002; **88**: 307–313.
7. Kobayashi K, Matsuyama W, Arai Y *et al*. Boiogito increases the metabolism of fatty acids in proximal tubular cells through peroxisome proliferator-activated receptor (PPAR) alpha agonistic activity. *Biol. Pharm. Bull.* 2016; **39**: 143–147.
8. Fujitsuka N, Tamai M, Tsuchiya K *et al*. Boiogito, a kampo medicine, improves hydrarthrosis in a rat model of knee osteoarthritis. *BMC Complement. Altern. Med.* 2015; **15**: 451.
9. Aghazadeh-Habashi A, Kohan MH, Asghar W, Jamali F. Glucosamine dose/concentration-effect correlation in the rat with adjuvant arthritis. *J. Pharm. Sci.* 2014; **103**: 760–767.
10. Beren J, Hill SL, Diener-West M, Rose NR. Effect of pre-loading oral glucosamine HCl/chondroitin sulfate/manganese ascorbate combination on experimental arthritis in rats. *Exp. Biol. Med.* 2001; **226**: 144–151.
11. Hua J, Suguro S, Hirano S, Sakamoto K, Nagaoka I. Preventive actions of a high dose of glucosamine on adjuvant arthritis in rats. *Inflamm. Res.* 2005; **54**: 127–132.
12. Nakamura H, Masuko K, Yudoh K, Kato T, Kamada T, Kawahara T. Effects of glucosamine administration on patients with rheumatoid arthritis. *Rheumatol. Int.* 2007; **27**: 213–218.
13. Matsuno H, Nakamura H, Katayama K *et al*. Effects of an oral administration of glucosamine-chondroitin-quercetin glucoside on the synovial fluid properties in patients with osteoarthritis and rheumatoid arthritis. *Biosci. Biotechnol. Biochem.* 2009; **73**: 288–292.
14. Kulkarni C, Leena A, Lohit K, Mishra D, Saji MJA. Randomized comparative study of safety and efficacy of immediate release glucosamine HCL and glucosamine HCL sustained release formulation in the treatment of knee osteoarthritis: A proof of concept study. *J. Pharmacol. Pharmacother.* 2012; **3**: 48–54.

© 2018 The Authors. *Traditional & Kampo Medicine* published by John Wiley & Sons Australia, Ltd on behalf of Japan Society for Oriental Medicine and Medical and Pharmaceutical Society for WAKAN-YAKU.

15. Sterzi S, Giordani L, Morrone M *et al*. The efficacy and safety of a combination of glucosamine hydrochloride, chondroitin sulfate and bio-curcumin with exercise in the treatment of knee osteoarthritis: A randomized, double-blind, placebo-controlled study. *Eur. J. Phys. Rehabil. Med.* 2016; **52**: 321–330.
16. Chen H, Shoumura S, Emura S, Isono H. Tibetan medicated-bath therapy may improve adjuvant arthritis in rat. *Evid. Based Complement. Alternat. Med.* 2009; **6**: 211–217.
17. Goldberg RL, Huff JP, Lenz ME, Glickman P, Katz R, Thonar EJ. Elevated plasma levels of hyaluronate in patients with osteoarthritis and rheumatoid arthritis. *Arthritis Rheum.* 1991; **34**: 799–807.
18. Laverty S, Sandy JD, Celeste C, Vachon P, Marier JF, Plaas AH. Synovial fluid levels and serum pharmacokinetics in a large animal model following treatment with oral glucosamine at clinically relevant doses. *Arthritis Rheum.* 2005; **52**: 181–191.
19. Zheng Y, Li X, Qian X *et al*. Secreted and O-GlcNAcylated MIF binds to the human EGF receptor and inhibits its activation. *Nat. Cell Biol.* 2015; **17**: 1348–1355.
20. Geng Y, Valbracht J, Lotz M. Selective activation of the mitogen-activated protein kinase subgroups c-Jun NH2 terminal kinase and p38 by IL-1 and TNF in human articular chondrocytes. *J. Clin. Invest.* 1996; **98**: 2425–2430.
21. Lu S, Xiao X, Cheng M. Matrine inhibits IL-1beta-induced expression of matrix metalloproteinases by suppressing the activation of MAPK and NF-κB in human chondrocytes in vitro. *Int. J. Clin. Exp. Pathol.* 2015; **8**: 4764–4772.
22. Scotto d'Abusco A, Calamia V, Cicione C, Grigolo B, Politi L, Scandurra R. Glucosamine affects intracellular signalling through inhibition of mitogen-activated protein kinase phosphorylation in human chondrocytes. *Arthritis Res. Ther.* 2007; **9**: R104.
23. Kim DH, Jung WS, Kim ME *et al*. Genistein inhibits proinflammatory cytokines in human mast cell activation through the inhibition of the ERK pathway. *Int. J. Mol. Med.* 2014; **34**: 1669–1674.
24. Jang BC, Sung SH, Park JG *et al*. Glucosamine hydrochloride specifically inhibits COX-2 by preventing COX-2 N-glycosylation and by increasing COX-2 protein turnover in a proteasome-dependent manner. *J. Biol. Chem.* 2007; **282**: 27622–27632.
25. YL W, Lin AH, Chen CH *et al*. Glucosamine attenuates cigarette smoke-induced lung inflammation by inhibiting ROS-sensitive inflammatory signaling. *Free Radic. Biol. Med.* 2014; **69**: 208–218.
26. Zhou H, Wong YF, Wang J, Cai X, Liu L. Sinomenine ameliorates arthritis via MMPs, TIMPs, and cytokines in rats. *Biochem. Biophys. Res. Commun.* 2008; **376**: 352–357.
27. Lan Z, Wei M, Chen L, Xie G, Liu X, Zhang X. Role of sinomenine on complete Freund's adjuvant-induced arthritis in rats. *IUBMB Life* 2016; **68**: 429–435.

SUPPORTING INFORMATION

Additional Supporting Information may be found in the online version of this article:

Appendix S1 Supplementary Material.
Figure S1 Glycyrrhizic acid.
Figure S2 sinomenine in boiogito extract.

© 2018 The Authors. *Traditional & Kampo Medicine* published by John Wiley & Sons Australia, Ltd on behalf of Japan Society for Oriental Medicine and Medical and Pharmaceutical Society for WAKAN-YAKU.

frontiers in Pharmacology

ORIGINAL RESEARCH
published: 10 April 2018
doi: 10.3389/fphar.2018.00344

Identification of Mepenzolate Derivatives With Long-Acting Bronchodilatory Activity

Ken-Ichiro Tanaka[1†], Naoki Yamakawa[2†], Yasunobu Yamashita[3], Teita Asano[4], Yuki Kanda[1], Ayaka Takafuji[1], Masahiro Kawahara[1], Mitsuko Takenaga[4], Yoshifumi Fukunishi[3] and Tohru Mizushima[5]*

[1] Research Institute of Pharmaceutical Sciences, Faculty of Pharmacy, Musashino University, Nishi-Tokyo, Japan, [2] School of Pharmacy, Shujitsu University, Okayama, Japan, [3] Molecular Profiling Research Center for Drug Discovery, National Institute of Advanced Industrial Science and Technology, Tokyo, Japan, [4] Institute of Medical Science, School of Medicine, St. Marianna University, Kawasaki, Japan, [5] LTT Bio-Pharma Co., Ltd., Tokyo, Japan

The standard treatment for chronic obstructive pulmonary disease is a combination of anti-inflammatory drugs and bronchodilators. We recently found that mepenzolate bromide (**MP**), an antagonist for human muscarinic M3 receptor (hM_3R), has both anti-inflammatory and short-acting bronchodilatory activities. To obtain **MP** derivatives with longer-lasting bronchodilatory activity, we synthesized hybrid compounds based on **MP** and two other muscarinic antagonists with long-acting bronchodilatory activity glycopyrronium bromide (**GC**) and aclidinium bromide (**AD**). Of these three synthesized hybrid compounds (**MP-GC**, **GC-MP**, **MP-AD**) and **MP**, **MP-AD** showed the highest affinity for hM_3R and had the longest lasting bronchodilatory activity, which was equivalent to that of **GC** and **AD**. Both **MP-GC** and **MP-AD** exhibited an anti-inflammatory effect equivalent to that of MP, whereas, in line with **GC** and **AD**, **GC-MP** did not show this effect. We also confirmed that administration of **MP-AD** suppressed elastase-induced pulmonary emphysema in a mouse model. These findings provide important information about the structure-activity relationship of **MP** for both bronchodilatory and anti-inflammatory activities.

Keywords: chronic obstructive pulmonary disease, anti-inflammatory, long-acting bronchodilatory activity, mepenzolate

OPEN ACCESS

Edited by:
Weien Yuan,
Shanghai Jiao Tong University, China

Reviewed by:
Thiago J. Borges,
Universidade La Salle-Canoas, Brazil
Michela De Bellis,
Università degli Studi di Bari Aldo Moro, Italy
Erzsébet Bartolák-Suki,
Boston University, United States

****Correspondence:***
Tohru Mizushima
t.mizushima@ltt.co.jp

† These authors have contributed equally to this work.

Specialty section:
This article was submitted to Translational Pharmacology, a section of the journal Frontiers in Pharmacology

Received: *28 September 2017*
Accepted: *26 March 2018*
Published: *10 April 2018*

Citation:
Tanaka K-I, Yamakawa N, Yamashita Y, Asano T, Kanda Y, Takafuji A, Kawahara M, Takenaga M, Fukunishi Y and Mizushima T (2018) Identification of Mepenzolate Derivatives With Long-Acting Bronchodilatory Activity. Front. Pharmacol. 9:344. doi: 10.3389/fphar.2018.00344

INTRODUCTION

Chronic obstructive pulmonary disease (COPD) is a serious health problem and the world's fourth leading cause of death (Mannino and Kiriz, 2006). This disease state is defined by a progressive and not fully reversible airflow limitation and an abnormal inflammatory response (Rabe et al., 2007; Vestbo et al., 2013; Vogelmeier et al., 2017). For the clinical treatment of COPD, it is therefore important not only to improve airflow limitations by inducing bronchodilation, but also to hinder disease progression by suppressing inflammatory responses.

The standard treatment for COPD is to use bronchodilators such as β2-agonists and muscarinic receptor antagonists, with this approach being effective in overcoming airflow limitations (Barnes and Stockley, 2005; Vestbo et al., 2013; Vogelmeier et al., 2017). Short-acting β2-agonists (SABAs) and muscarinic antagonists (SAMAs) were previously used for COPD treatment; however, long-acting β2-agonists (LABAs) and muscarinic antagonists [LAMAs, of which tiotropium bromide

(**TP**), glycopyrronium bromide (**GC**), and aclidinium bromide (**AD**) are common examples] have shown superior eÿc acy over the short-acting bronchodilators for the treatment of COPD (Vestbo et al., 2013; Vogelmeier et al., 2017). Thus, LABAs and LAMAs (or combinations of the two) are now used as first-line drugs for COPD treatment.

On the other hand, the inflammatory responses associated with COPD are generally treated with steroids; however, their impact on reducing disease progression and mortality (Barnes and Stockley, 2005; Calverley et al., 2007; Tashkin et al., 2008) is attenuated because COPD-associated inflammation often shows resistance to steroid treatment (Alsaeedi et al., 2002; Calverley et al., 2007). Thus, it is important for new types of anti-inflammatory compounds to be developed for the treatment of COPD.

Based on the aforementioned, we previously screened a library of approved medicines to identify compounds capable of preventing elastase-induced pulmonary emphysema in mice (an animal model of COPD), and selected mepenzolate bromide (**MP**) (Tanaka et al., 2013), which is an orally administered muscarinic receptor antagonist used to treat gastrointestinal disorders (Long and Keasling, 1954; Buckley et al., 1957; Chen, 1959). We showed that **MP** not only exerts an anti-inflammatory effect via a muscarinic receptor-independent mechanism, but also possesses a short-acting bronchodilatory effect via a muscarinic receptor-dependent mechanism [via its binding to human muscarinic M3 receptor (hM_3R)] (Tanaka et al., 2013, 2014; Kurotsu et al., 2014). The anti-inflammatory activity of **MP**, which was more potent than that of steroids (Tanaka et al., 2012, 2013), is mediated via a decreased level of reactive oxygen species (ROS) in the lung due to the inhibition of NADPH oxidase activity and the induction of superoxide dismutase (SOD) and glutathione-*S*-transferase (GST) expression (Tanaka et al., 2013).

In the present study, we examined **MP** derivatives that have both anti-inflammatory and longer-acting bronchodilatory activities, as these could be beneficial for the treatment of COPD. To this end, we synthesized hybrid compounds from **MP** and long-acting muscarinic antagonists (**GC** and **AD**) and identified one compound that showed both a longer duration of bronchodilatory activity (equivalent to **GC** and **AD**) together with anti-inflammatory properties consistent with those of **MP**.

MATERIALS AND METHODS

Chemistry

Muscarinic M3 receptor antagonists were purchased from commercial sources; mepenzolate bromide **(MP)** was from Sigma-Aldrich (St. Louis, MO, United States); tiotropium bromide (**TP**) and glycopyrronium bromide (**GC**) were from Tokyo Chemical Industry, Co., Ltd. (Tokyo, Japan); aclidinium bromide (**AD**) was from Toronto Research Chemicals (Toronto, ON, Canada). All other solvents and reagents for organic syntheses were purchased from Tokyo Chemical Industry, Co., Ltd. (Tokyo, Japan) or Wako Pure Chemical Industries (Tokyo, Japan) and used without further purification. The precursor of hybrid compound (**pre-Hyb**) was synthesized by the condensation of carboxylic acid (**BA** or **CA**) and amino-alcohol (**PR**, **PP,** or **QC**). The each final quaternary salt of hybrid compounds (**MP-GC, GC-MP, MP-AD**) was prepared as described previously (Yamashita et al., 2014), with some modifications (see below). Column chromatography was performed using Silica gel 60N (Kanto Chemical, Co., Tokyo, Japan).

Melting point (mp) data were recorded on Yanaco MP-J3 micro-melting point apparatus. ^{1}H-NMR spectra and ^{13}C-NMR spectra were measured at 400 and 100 MHz, respectively, on a VARIAN 400-MR spectrometer. High resolution mass spectra were detected with an ESI-TOF mass spectrometer (Bruker MicroTOF, Bruker, Bremen, Germany) in the positive mode. HPLC data were recorded on a Waters 2695 Alliance separation module and a Waters 2996 photodiode array detector (Waters, Milford, MA, United States) with a reverse-phase column (TSKgel Super-ODS, 150 mm × 4.6 mm, 2 μm, Tosoh, Co., Tokyo, Japan). CH_3CN/20 mM KH_2PO_4 buffer (3:7) was used as the mobile phase at a flow rate of 0.3 ml/min, with detection performed at an optical density of 210 nm.

General Procedure for the Preparation of pre-Hyb

To a solution of 2-alkyl-2-hydroxy-2-phenylacetic acid (**BA** or **CA**) (1.0 eq.) in DMF, carbonyldiimidazole (1.6 eq.) was added and the mixture was stirred for 15 min at room temperature. A solution of *N*-alkyl amino alcohol (**PR**, **PP**, or **QC**) (1.2 eq.) in DMF was added dropwise into the mixture at 80°C and the mixture was stirred for 18 h at that temperature. The reaction was quenched with H_2O at room temperature and organic materials were extracted with EtOAc. The combined extract was washed with brine, dried over Na_2SO_4 and concentrated *in vacuo*. The residue was then applied to a short silica gel column, eluted with EtOAc and concentrated *in vacuo* to give title compound (**pre-Hyb**), which was used for the next step without further purification.

(±)-3-(2-Hydroxy-2,2-diphenylacetoxy)-1,1-dimethylpyrrolidinium Bromide (MP-GC)

2.0 g (8.7 mmol) of benzilic acid **(BA)** and 1.3 mL (11 mmol) of 1-methylpyrrolidin-3-ol (**PR**) were used to give **pre-Hyb**. To a solution of **pre-Hyb** (2.2 g, 7.0 mmol) in CH_3CN (12 mL), CH_3Br (2.0 M in THF, 18 mL) was added and stirred for 5 h at room temperature. The precipitate was filtered off and the filtrate re-crystallized with CH_3CN and diethyl ether to give the title compound as a white solid (2.0 g, 69% 2 steps). mp: 211–212°C; ^{1}H-NMR (DMSO-*d*6): δ = 7.29–7.38 (m, 10H), 6.81 (s, 1H), 5.51 (brs, 1H), 3.84–3.89 (m, 1H), 3.52–3.70 (m, 3H), 3.6 (s, 3H), 2.93 (s, 3H), 2.62–2.74 (m, 1H), 2.08–2.14 (m, 1H); ^{13}C-NMR (DMSO-*d*6): *d* = 172.3, 142.9, 127.9, 127.7, 127.0, 80.6, 73.3, 69.3, 64.0, 52.7, 51.9, 40.2, 38.9, 29.9; HRMS: calcd. for $C_{20}H_{24}NO_3$ (M^+): 326.1751; found: m/z = 326.1755; HPLC: t_R (min) = 3.12 (98%). This is a known compound, but its spectrum data are not covered by patents or non-patent literature documents.

(±)-3-(2-Cyclopentyl-2-hydroxy-2-phenylacetoxy)-1,1-dimethylpiperidinium Bromide (GC-MP)

1.5 g (6.8 mmol) of 2-cyclopentyl-2-hydroxy-2-phenylacetic acid (**CA**) and 1.0 mL (8.1 mmol) of 1-methylpiperidin-3-ol (**PP**) were used to give **pre-Hyb**. To a solution of **pre-Hyb** (0.41 g, 1.3 mmol) in CH_3CN (5 mL), CH_3Br (2.0 M in THF, 6.4 mL) was added and stirred for 5 h at room temperature. The precipitate was filtered off and the filtrate re-crystallized with CH_3CN and diethyl ether to give the title compound as a white solid (0.38 g, 22% 2 steps). mp: 164–165°C; ^{1}H-NMR (DMSO-*d*6): δ = 7.56–7.59 (d, *J* = 7.5, 2H), 7.25–7.37 (m, 3H), 5.14 (brs, 1H), 3.37–3.62 (m, 4H), 2.89–3.06 (m, 7H), 1.23–1.79 (m, 12H); ^{13}C-NMR (DMSO-*d*6): δ = 173.0, 142.2, 142.7, 128.0, 127.3, 125.7, 79.3, 66.1, 61.5, 60.8, 46.4, 40.1, 38.9, 26.6, 26.0, 25.6, 25.4, 16.4; HRMS calcd. for $C_{20}H_{30}NO_3$ (M^+): 332.2220; found: m/z = 332.2224; HPLC: t_R (min) = 4.94 (98%). This is a known compound, but its spectrum data are not covered by patents or non-patent literature documents.

(±)-3-(2-Hydroxy-2,2-diphenylacetoxy)-1-(3-phenoxypropyl)-1-azoniabicyclo[2.2.2]octane Bromide (MP-AD)

1.6 g (0.60 mmol) of benzilic acid (**BA**) and 1.0 g (7.9 mmol) of quinuclidin-3-ol (**QC**) were used to give **pre-Hyb**. To a solution of **pre-Hyb** (0.10 g, 0.30 mmol) in 1,4-dioxane (5 mL) (3-bromopropoxy)benzene (0.11 g, 11 mmol) was added and stirred for 6 days at room temperature. The precipitate was filtered off and the filtrate re-crystallized with CH_3CN and diethyl ether to give the title compound as a white solid (50 mg, 30% 2 steps). mp: 177–178°C; ^{1}H-NMR (DMSO-*d*6): δ = 7.23–7.42 (m, 12H), 6.86–6.89 (m, 3H), 6.78 (s, 1H), 5.22 (brs, 1H), 3.94–4.04 (m, 2H), 3.85–3.88 (m, 1H), 3.25–3.44 (m, 5H), 3.01–3.07 (m, 1H), 1.45–2.25 (m, 7H); ^{13}C-NMR (DMSO-*d*6): δ = 173.0, 158.6, 143.6, 143.5, 130.1, 128.5, 128.4, 128.2, 127.6, 127.5, 121.5, 115.0, 81.3, 69.1, 65.1, 61.1, 60.0, 54.3, 53.2, 24.0, 22.2, 20.9, 18.1; HRMS calcd. for $C_{30}H_{34}NO_4$ (M^+): 472.2482; found: m/z = 472.2488; HPLC: t_R (min) = 9.26 (99%). This is a known compound whose ^{1}H-NMR spectrum was similar to that previously reported as (*R*)-**MP-GC** (Yamashita et al., 2014).

Chemicals

Porcine pancreatic elastase (PPE) and methacholine chloride (methacholine) were obtained from Sigma-Aldrich (St. Louis, MO, United States). Novo-Heparin for injection was from Mochida Pharmaceutical, Co. (Tokyo, Japan). Chloral hydrate was from Nacalai Tesque (Kyoto, Japan). Diff-Quik was from Sysmex, Co. (Kobe, Japan). Formalin neutral buffer solution was from WAKO Pure Chemicals (Tokyo, Japan). Mayer's hematoxylin, 1% eosin alcohol solution and malinol were from MUTO Pure Chemicals (Tokyo, Japan).

Animals

ICR mice (6–7 weeks old, male) were purchased from Charles River (Yokohama, Japan). The experiments and procedures described here were carried out in accordance with the Guide for the Care and Use of Laboratory Animals as adopted and promulgated by the National Institutes of Health, and were approved by the Animal Care Committee of Musashino University (Approval NOs. 16004 and 17006).

Treatment of Mice With PPE and Each Drug

Mice maintained under anesthesia with isoflurane were administered one intratracheal bolus of PPE (15 or 20 U/kg), **MP** (3.8, 37.5 μg/kg), **TP** (8.4 μg/kg), **GC** (7.1, 35.5 μg/kg), **AD** (10.1, 50.4 μg/kg), **MP-GC** (3.6, 36.2 μg/kg), **GC-MP** (3.7, 36.8 μg/kg), and **MP-AD** (4.9, 49.3 μg/kg) in 0.9% NaCl via micropipette (P200). For control mice, 0.9% NaCl alone was administered by the same procedure.

Figure 3; MP, **GC**, **AD**, **MP-AD**, **MP-GC,** or **GC-MP** were administered intratracheally. After 1, 24, 48, or 72 h, mice were exposed to nebulized methacholine 5 times and airway resistance was determined after each methacholine challenge.

Figure 4 and **Table 2**; **MP**, **TP**, **GC**, **AD**, **MP-AD**, **MP-GC,** and **GC-MP** were administered intratracheally once only. After 1 h, mice were treated with or without (control) PPE (20 U/kg) once only. Six (**Figure 4**) or twenty-four (**Table 2**) hours after the PPE administration, BALF was prepared and the total cell number and the number of neutrophils were determined.

Figure 5; MP-AD was administered intratracheally once daily for 16 days (from day 0 to day 15). 1 h after the first administration, mice were treated with or without (control) PPE (15 U/kg) once only on day 0. 21 days after the PPE administration, lung mechanics was monitored, and sections of pulmonary tissue were prepared.

Preparation of Bronchoalveolar Lavage Fluid (BALF) and Cell Count Method

BALF was collected from mice by cannulating the trachea and lavaging the lung with 1 ml of sterile PBS containing 50 U/ml heparin (2 times). About 1.8 ml of BALF was routinely recovered from each animal. The total cell number in the BALF was counted using a hemocytometer and a manual counter. Cells were stained with Diff-Quik reagents after centrifugation with Cytospin® 4 (Thermo Electron Corporation, Waltham, MA, United States), and differential counts of more than 50 inflammatory cells were done in each of four or more separate sections of smear using fluorescence microscopy (Olympus DP71). The ratio of number of neutrophils to total cell number was determined by counting the number of neutrophils. This cell counting was conducted by an investigator blinded to the study protocol.

Measurement of Lung Mechanics and Airway Resistance

Lung mechanics and airway resistance were monitored with a computer-controlled small-animal ventilator (FlexiVent, SCIREQ, Montreal, QC, Canada), as described previously (Shalaby et al., 2010; Tanaka et al., 2012). Mice were anesthetized

with chloral hydrate (500 mg/kg), a tracheotomy was performed, and an 8 mm section of metallic tube was inserted into the trachea. Mice were mechanically ventilated at a rate of 150 breaths/min, using a tidal volume of 8.7 ml/kg and a positive end-expiratory pressure of 2–3 cmH_2O.

Total respiratory system compliance was measured by the snapshot. All data were analyzed using FlexiVent software (version 5.3; SCIREQ, Montreal, QC, Canada).

Mice were exposed to nebulized methacholine (5 mg/ml) five times for 20 s with a 40 s interval, and airway resistance was measured after each methacholine challenge by the snapshot technique. All data were analyzed using FlexiVent software.

Histopathological Analysis

Twenty one days after PPE treatment, mice were euthanized with an excess of isoflurane. Lung tissue samples were fixed in 10% formalin neutral buffer solution for 24 h at a pressure of 25 cmH_2O, and then embedded in paraÿn before being cut into 4 μm-thick sections. Sections were stained first with Mayer's hematoxylin and then with 1% eosin alcohol solution (H&E staining). Samples were mounted with malinol and scanned using a NanoZoomer-XR digital slide scanner (Hamamatsu Photonics, Shizuoka, Japan). All images were analyzed using NDP.view2 software (Hamamatsu Photonics, Shizuoka, Japan).

To determine the mean linear intercept (MLI) (an indicator of airspace enlargement), 20 lines (800 μm) were drawn randomly on the image of a section and intersection points with alveolar walls were counted to determine the MLI, as described previously (Weibel, 1963). This morphometric analysis was conducted by an investigator blinded to the study protocol.

TABLE 2 | Effect of intratracheal administration of compounds on PPE-induced inflammatory responses.

	Total cells ($\times 10^5$ cells)	Neutrophils ($\times 10^5$ cells)
Control	1.26 ± 0.25	0.12 ± 0.07
PPE	9.66 ± 0.54**	7.46 ± 0.57**
PPE + MP (37.5 μg/kg)	6.30 ± 0.90##	4.11 ± 0.68##
PPE + TP (8.4 μg/kg)	10.00 ± 1.27	6.81 ± 1.03
PPE + TP (42.1 μg/kg)	10.05 ± 0.57	7.31 ± 0.22
PPE + GC (7.1 μg/kg)	10.20 ± 0.93	7.34 ± 0.92
PPE + GC (35.5 μg/kg)	9.09 ± 1.09	6.25 ± 0.83
PPE + AD (10.1 μg/kg)	11.88 ± 2.01	9.06 ± 1.63
PPE + AD (50.4 μg/kg)	9.75 ± 1.12	6.86 ± 0.88

*Mice were treated with or without (control) PPE (20 U/kg) once only on day 0. The indicated doses (μg/kg) of each compound were administered intratracheally once only on day 0. Twenty-four hours after the PPE administration, BALF was prepared and the total cell number and the number of neutrophils were determined as described in Section "Materials and Methods." Values represent mean ± SEM ($n = 4–8$). **$P < 0.01$ (versus control); ##$P < 0.01$ (versus PPE only). Data are representative of two independent experiments.*

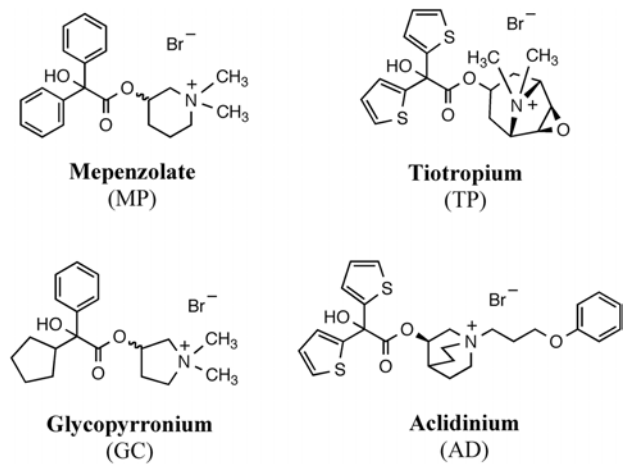

FIGURE 1 | Structure of clinically-used muscarinic antagonists.

TABLE 1 | Binding of compounds to hM2R or hM3R.

Compound	*Ki* (nM)	
	hM_3R	hM_2R
Mepenzolate (MP)	4.6	1.8
Tiotropium (TP)	0.22	0.64
Glycopyrronium (GC)	0.7	1.0
Aclidinium (AD)	0.34	0.39
MP-GC	1.1	0.79
GC-MP	1.2	0.53
MP-AD	0.72	0.64

Membrane fractions prepared from CHO-K1 cells expressing hM2R or hM3R were incubated with 2 nM [^{3}H]NMS (85.5 Ci/mmol) in the presence of each compound. A range of concentrations (10^{-11} to 10^{-6} M) for each compound was tested in triplicate to generate competitive binding curves to determine Ki values. The shown value is an average of at least two independent experiments.

Filter-Binding Assay

The filter-binding assay was performed as described previously (Yamashita et al., 2014), with some modifications. Membrane fractions prepared from Chinese Hamster Ovary (CHO)-K1 cells expressing human muscarinic M2 receptor (hM_2R) or hM_3R (Membrane Target Systems, Perkin-Elmer Life and Analytical Sciences, Boston, MA, United States; protein concentration, 8 μg/well) were incubated with 2 nM [^{3}H]NMS (*N*-methyl-[^{3}H]-scopolamine methylchloride) (85.5 Ci/mmol) at room temperature for 2 h in 200 μL PBS in the presence of each compound. A range of concentrations (10^{-11} to 10^{-6} M) for each compound was tested in triplicate to generate competitive binding curves. Non-specific binding was determined in the presence of atropine (2.5 μM). The samples were passed through a GF/C filter (Filtermat A, PerkinElmer Life and Analytical Sciences, Boston, MA, United States) pre-incubated for 1 h with 1.0% polyethylenimine, and washed four times with ice-cold wash buffer [50 mM Tris/HCl (pH 7.4), 100 mM NaCl, 0.05% Tween-80]. Filters were then dried for 30 min before attachment to a MeltiLex A melt-on scintillation sheet (PerkinElmer Life and Analytical Sciences, Boston, MA, United States). The radioactivity remaining on the filter was monitored with a MicroBeta Trilux microplate scintillation counter (PerkinElmer Life and Analytical Sciences, Boston, MA,

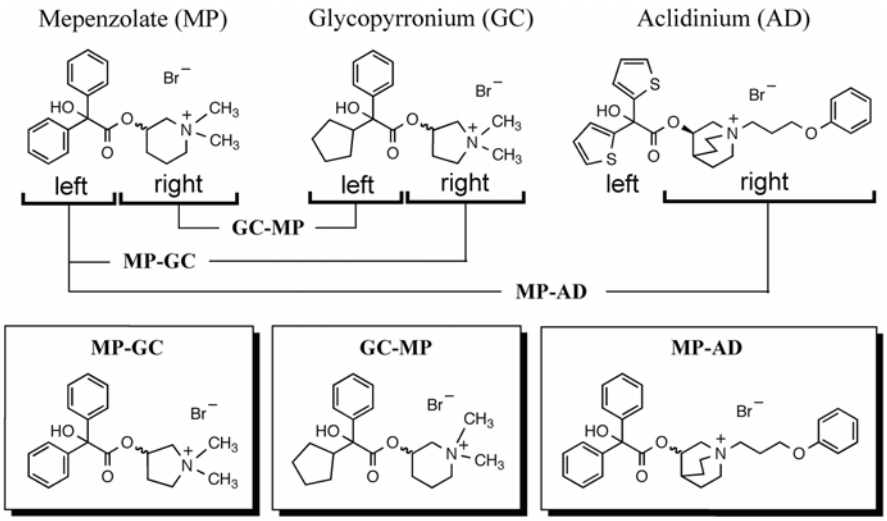

FIGURE 2 | Structure of hybrid compounds. The chemical structure of each compound [mepenzolate (**MP**), glycopyrronium (**GC**), and aclidinium (**AD**)] was separated into parts left and right of the ester bond. These parts were then used to synthesize the shown hybrid structures.

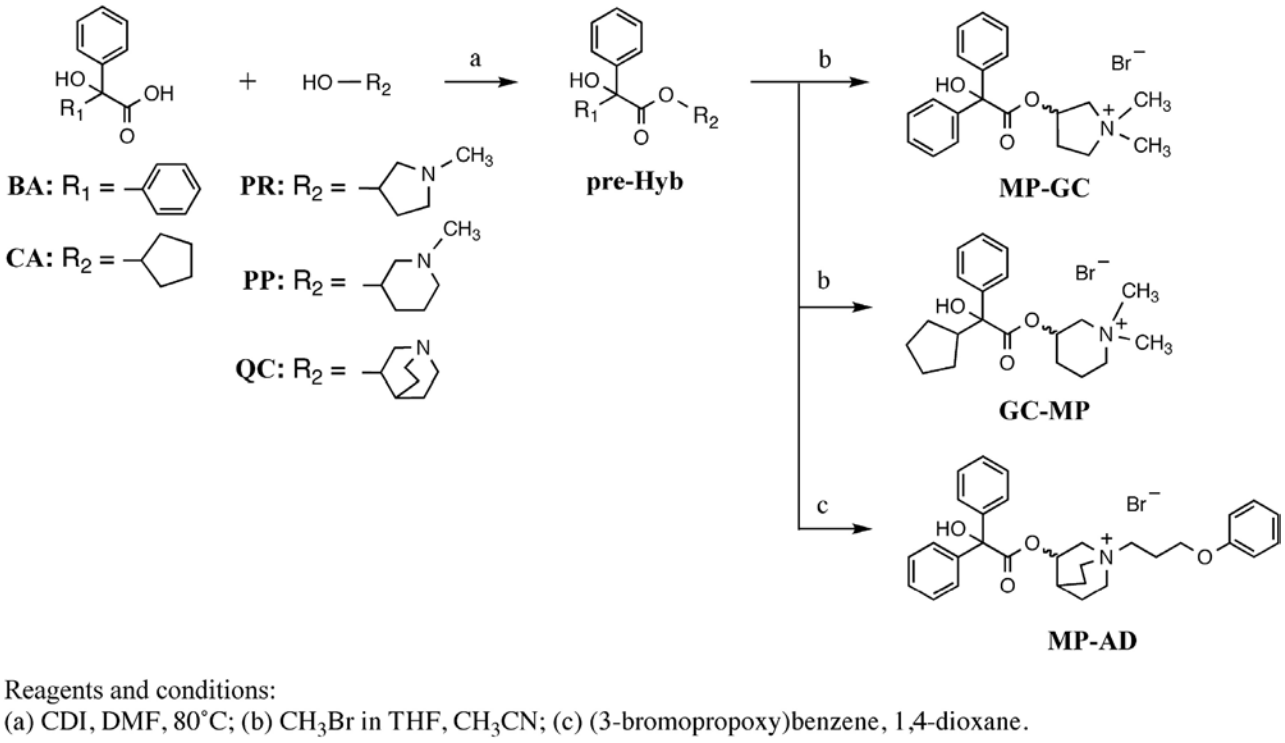

SCHEME 1 | Synthesis of compounds **MP-GC, GC-MP, and MP-AD.**

United States). Aÿnitie s at equilibrium were determined as antagonist dissociation constant (*K*i) values after correcting the experimentally determined IC_{50} values with the experimentally determined *K*d value of NMS for hM_2R or hM_3R and the concentration of NMS, as described previously (Yamashita et al., 2014). Shown values are an average of at least two independent experiments. The *K*i value was obtained from three independent curves. All curve-fitting procedures were performed using Prism (GraphPad Software, Inc., San Diego, CA, United States).

Statistical Analysis

All values are expressed as the mean ± SEM. Homoscedasticity of data were verified by Levene test, then, data were examined

using one-way ANOVA followed by the Tukey test or Games-Howell test for unpaired results was used to evaluate differences between three or more groups. Differences were considered to be statistically significant for values of $P < 0.05$.

RESULTS

Affinity for hM_3R and Anti-inflammatory Activities of MP, TP, GC, and AD

We first compared the binding of **MP**, **TP**, **GC**, **and AD** to hM_3R and hM_2R (**Figure 1**). The binding aÿnity of each compound to each receptor was determined by carrying out [^{3}H]NMS displacement studies on each receptor. A higher *K*i value means a lower aÿnity for hM_3R, because *K*i value is related to the concentration of each compound that causes 50% inhibition of NMS-binding to hM_3R. As shown in **Table 1**, **MP** showed the highest *K*i value (by a factor of at least five compared with **TP**, **GC**, **and AD**), thus indicating it had the lowest aÿnity for hM_3R. Similar results were observed for hM_2R (**Table 1**).

The total number of leucocytes and the individual number of neutrophils in BALF are indicators of pulmonary inflammatory responses; these increased after PPE treatment in a manner that could be partially suppressed by the simultaneous intratracheal administration of **MP** (**Table 2**), as described previously (Tanaka et al., 2013, 2014). Because compared to neutrophils, neither the macrophage nor eosinophil number was so apparently increased in BALF after PPE treatment (Tanaka et al., 2013, 2014), we did not count them here. As none of **TP**, **GC**, **and AD** showed anti-inflammatory activity equivalent to that of **MP** (**Table 2**), we attempted to identify **MP** derivatives that had an aÿnity for hM_3R equivalent to that of **TP**, **GC**, **and AD** and an anti-inflammatory activity equivalent to that of **MP**.

Synthesis of Hybrid Compounds and Their Affinities for hM_3R

We synthesized hybrid compounds based on **MP** and LAMAs used in the clinical setting (**GC** and **AD**). The structures of **MP** and these LAMAs were separated into two parts with a view to synthesizing hybrid compounds by substitution of each of the parts (**Figure 2**). We synthesized mepenzolate-glycopyrronium **(MP-GC)**, glycopyrronium-mepenzolate **(GC-MP)** and mepenzolate-aclidinium **(MP-AD)** (**Figure 2**). The synthetic route for these compounds are outlined in **Scheme 1**. First, the ester compound (**pre-Hyb**) was synthesized by the condensation of an appropriate carboxylic acid (**BA** or **CA**) and aminoalcohol (**PR**, **PP**, or **QC**). The precursor of target compound (**pre-Hyb**) was quaternized with the appropriate methyl bromide or phenoxy alkyl bromide to give target compounds (**MP-GC**, **GC-MP**, **and MP-AD**). These compounds are known and were identified by their melting points, NMR spectra, and mass spectra. On the other hand, we could not synthesize a hybrid compound based on aclidinium-mepenzolate.

As shown in **Table 1**, all of the hybrid compounds had a lower *K*i value for hM_3R than **MP**. Of the target compounds, **MP-AD**

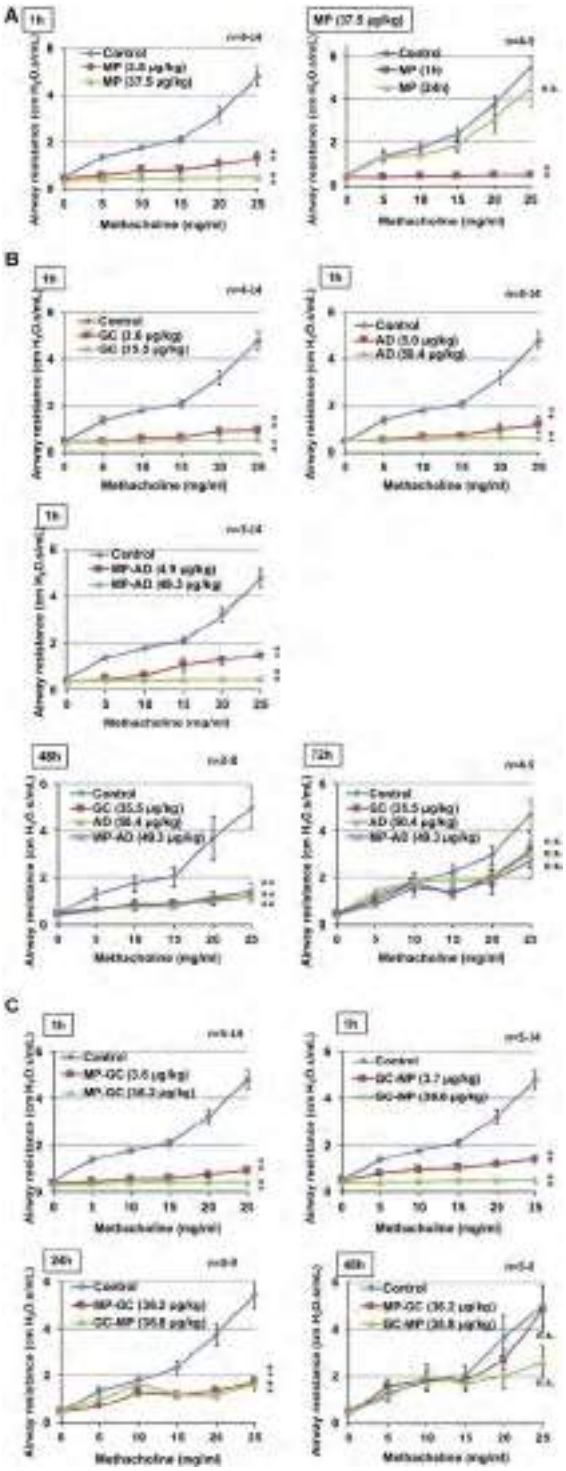

FIGURE 3 | Effect of compounds on methacholine-induced airway constriction. Indicated doses of **MP (A)**, **GC**, **AD,** and **MP-AD (B)** or **MP-GC** or **GC-MP (C)** were administered intratracheally. After the indicated period, mice were exposed to nebulized methacholine 5 times and airway resistance was determined after each methacholine challenge as described in Section "Materials and Methods." Values represent mean ± SEM. $^*P < 0.05$; $^{**}P < 0.01$; n.s., not significant. The control data is the same in all graphs. Data are representative of two independent experiments.

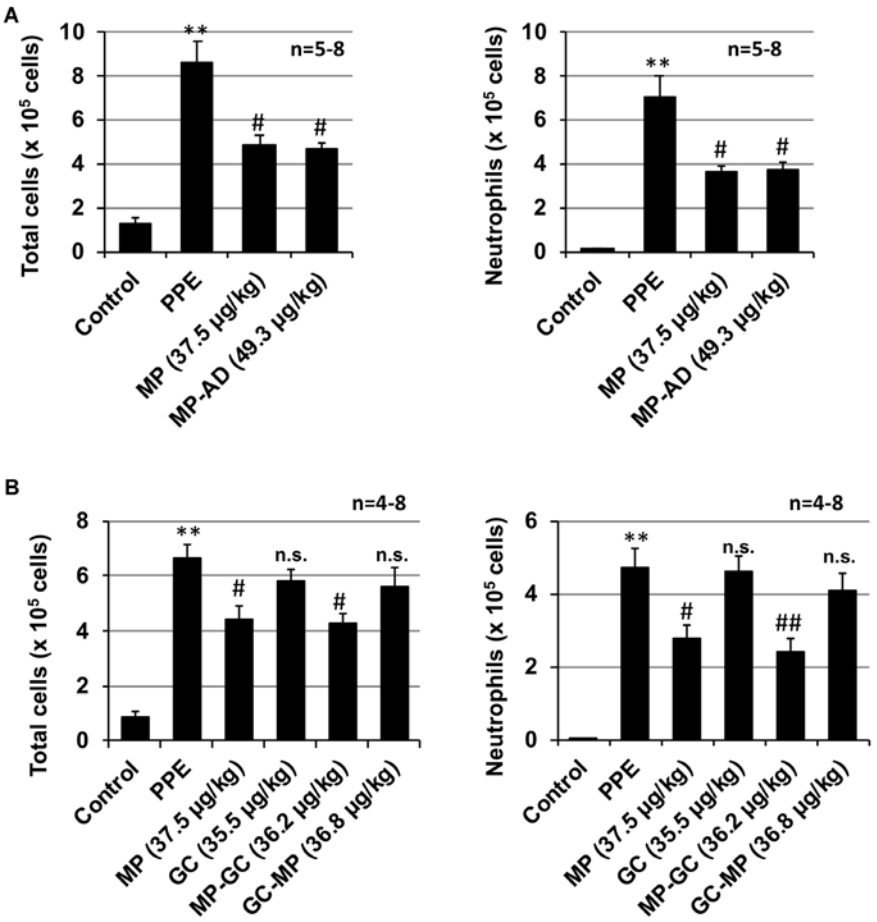

FIGURE 4 | Effect of compounds on PPE-induced inflammatory responses. Mice were treated with or without (control) PPE (20 U/kg) once only on day 0. The indicated doses (μg/kg) of **MP** and **MP-AD (A)** or **MP**, **GC, MP-GC,** or **GC-MP (B)** were administered intratracheally once only. Six hours after the PPE administration, BALF was prepared and the total cell number and the number of neutrophils were determined as described in Section "Materials and Methods." Values represent mean ± SEM. $^{**}P < 0.01$ (versus control); $^{\#}P < 0.05$, $^{\#\#}P < 0.01$ (versus PPE only); n.s., not significant. Data are representative of two independent experiments.

showed the lowest *K*i value for hM_3R (highest aÿnity for hM_3R), while **GC-MP** showed the lowest *K*i value for hM_2R.

Bronchodilation Activities of Hybrid Compounds

As shown in **Figure 3A**, the intratracheal administration of **MP** induced bronchodilation in a dose-dependent manner, which is consistent with our previously reported findings (Tanaka et al., 2013, 2014). We also confirmed that the bronchodilatory activity of **MP** disappeared within 24 h (**Figure 3A**), suggesting that its effects were short-acting.

We then compared these results with the duration of bronchodilatory activity of **GC**, **AD**, and **MP-AD**. As shown in **Figure 3B**, these compounds all exhibited dose-dependent bronchodilatory activity within 1 h of their administration. Compared to baseline, significantly increased bronchodilation (reduced airway resistance) was observed 48 h (but not 72 h) after the administration, suggesting that **MP-AD** has a long-lasting bronchodilatory activity, similar to that of **GC** and **AD**. We also examined the duration of bronchodilation for **MP-GC** and **GC-MP**. Both of these compounds showed bronchodilatory activity at 1 and 24 h, but not at 48 h (**Figure 3C**), suggesting that **MP-GC** and **GC-MP** exhibit bronchodilatory activity intermediate to that of **MP** and **MP-AD**.

Anti-inflammatory and Anti-emphysemic Activities of Hybrid Compounds

As shown in **Figure 4A**, the anti-inflammatory activity of **MP-AD** was similar to that of **MP**. We also found that **MP-GC** exhibited anti-inflammatory activity, but as for **GC**, **GC-MP** did not (**Figure 4B**). These results suggest that the double phenyl rings in **MP** are important for its anti-inflammatory activity.

We next examined the effect of the long-term (up to 15 days) administration of **MP-AD** on PPE-induced lung injury. Histopathological analysis revealed that while PPE administration damaged the alveolar walls and increased MLI, this effect could be partially suppressed by the administration of **MP-AD** (**Figures 5A,B**). We could not find any adverse effects

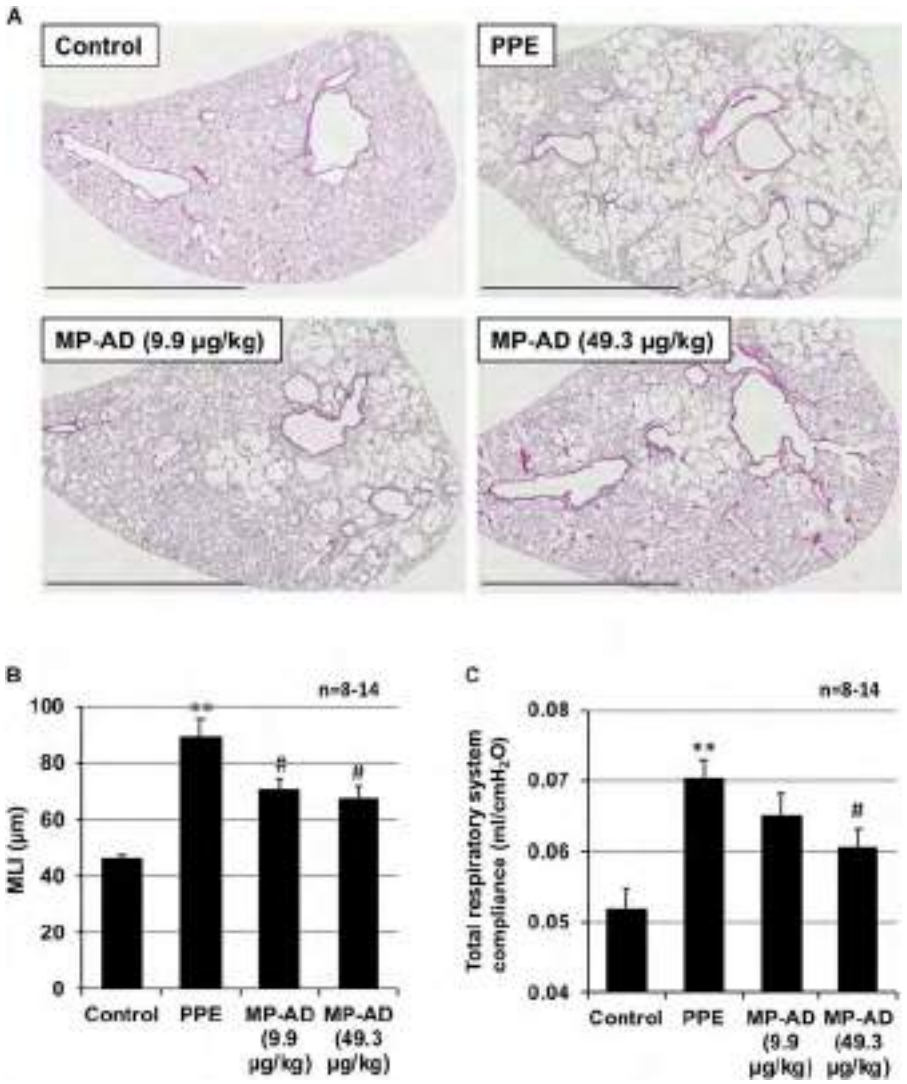

FIGURE 5 | Effect of **MP-AD** on PPE-induced pulmonary damage. Mice were treated with or without (control) PPE (15 U/kg) once only on day 0. The indicated doses of **MP-AD** were administered intratracheally once daily for 16 days (from day 0 to day 15). Sections of pulmonary tissue were prepared on day 21 and subjected to histopathological examination (H&E staining) (scale bar: 2.5 mm). **(A)** Airspace size was estimated by determining the MLI as described in Section "Materials and Methods." **(B)** Total respiratory system compliance was determined on day 21 as described in Section "Materials and Methods." **(C)** Values represent mean ± SEM. $^{**}P < 0.01$ (versus control); $^{\#}P < 0.05$ (versus PPE only). Data are representative of two independent experiments.

(such as decrease in body weight or behavior abnormalities) in mice subjected to the long-term administration of **MP-AD**. Treatment of mice with PPE increased total respiratory system compliance (**Figure 5C**), as described previously (Hamakawa et al., 2011). We here found that treatment of mice with **MP-AD** restored total respiratory system compliance (**Figure 5C**). Based on these results, we suggest that **MP-AD** suppresses PPE-induced emphysema through its anti-inflammatory activity.

DISCUSSION

To obtain **MP** derivatives with longer-acting bronchodilatory activity, we synthesized hybrid compounds based on **MP** and **GC** or **AD**. Among the compounds identified (**MP-GC, GC-MP, and MP-AD**), **MP-AD** showed the highest aÿnity for hM_3R and the longest bronchodilatory activity. It should be noted that the duration of bronchodilation associated with **MP-AD** is equivalent to that of **GC** and **AD**, which are clinically used LAMAs. Based on these results, we speculate that the *N*-substituted 3-quinuclidinyl ester of **AD** is important for its long-acting bronchodilatory properties. On the other hand, both **MP-GC** and **MP-AD** showed anti-inflammatory effects similar to **MP**, whereas **GC-MP**, like **GC** and **AD**, did not exhibit this effect. Based on these results, we speculate that the double phenyl rings in **MP** are important for its anti-inflammatory activity. Our findings thus provide important information concerning the structure-activity relationship for **MP**, which underlies its bronchodilatory and anti-inflammatory

activities. We consider that *in silico* drug design should be done for this target, because such trial for other diseases was successfully done for other studies (Corbo et al., 2007; De Luca et al., 2012). Such structure-activity investigation may also help to identify compounds with better toxicological profile avoiding off target effects (De Bellis et al., 2017).

As for the mechanism underlying these effects, the results from this study support the notion that the bronchodilatory effect is mediated through an antagonistic action toward hM_3R. Concerning the anti-inflammatory effects seen here, we previously showed that **MP** decreases ROS levels in the lung by inhibiting NADPH oxidase activity and by inducing the expression of SOD and GST, both of which are endogenous anti-oxidants (Tanaka et al., 2013). Furthermore, we previously described inhibitory effects of **MP** on nuclear factor-κB and histone deacetylase 2, both of which are involved in the pathogenesis of COPD (Tanaka et al., 2013). Although we did not examine the effect of **MP-AD** on these inflammation-related proteins, a similar mechanism may underlie the anti-inflammatory properties of **MP-AD**. In order to confirm this, immunohistochemical experiments would be useful.

We measured airway resistance in mice exposed to nebulized methacholine, which is the most representative method for monitoring bronchodilatory effects (Ather et al., 2016; Murad et al., 2017). Although this method is convenient, it seems to be an asthmatic-like condition rather than COPD-like condition. Therefore, the effect of each drug on airway resistance should be examined in COPD animal model in future. Furthermore, in emphysema, the most important parameter is a compliance of pulmonary alveolus or total respiratory system. The compliance correlates best with lung structure (structural parameters) (Hamakawa et al., 2011). We here showed that treatment of mice with PPE increased total respiratory system compliance and that treatment of mice with **MP-AD restored** total respiratory system compliance (**Figure 5C**).

In this study, we used intratracheal administration of each drug, because this method is convenient for experiments. However, it is possible that the compound does not distribute evenly through this method (Tanaka et al., 2010; Sato et al., 2015). The patchy appearance of airspace enlargement on the histological section following treatment with **MP-AD** may be explained by this uneven distribution of the drug. Thus, we should examine the distribution of this drug in the lung after intratracheal administration in future.

We also confirmed here that **MP-AD** suppressed elastase-induced pulmonary damage and emphysema in a COPD mouse model. Taken together, we propose that **MP-AD** could serve as a new drug candidate for the treatment of COPD, given its long-lasting bronchodilatory and anti-inflammatory activity.

AUTHOR CONTRIBUTIONS

K-IT, NY, YY, YF, and TM: participated in research design. K-IT, NY, YY, TA, YK, and AT: conducted experiments. MK, MT, and YF: contributed new reagents or analytic tools. K-IT, NY, YY, TA, and TM: performed data analysis. K-IT, NY, YY, TA, YK, AT, MK, MT, YF, and TM: wrote or contributed to the writing of the manuscript.

FUNDING

This work was supported by Grants-in-Aid for Scientific Research from the Ministry of Health, Labour and Welfare of Japan. This research was also supported by the Suzuken Memorial Foundation, the Pharmacological Research Foundation Tokyo, and the Takeda Science Foundation.

REFERENCES

Alsaeedi, A., Sin, D. D., and McAlister, F. A. (2002). The effects of inhaled corticosteroids in chronic obstructive pulmonary disease: a systematic review of randomized placebo-controlled trials. *Am. J. Med.* 113, 59–65. doi: 10.1016/S0002-9343(02)01143-9

Ather, J. L., Chung, M., Hoyt, L. R., Randall, M. J., Georgsdottir, A., Daphtary, N. A., et al. (2016). Weight loss decreases inherent and allergic methacholine hyperresponsiveness in mouse models of diet-induced obese asthma. *Am. J. Respir. Cell Mol. Biol.* 55, 176–187. doi: 10.1165/rcmb.2016-0070OC

Barnes, P. J., and Stockley, R. A. (2005). COPD: current therapeutic interventions and future approaches. *Eur. Respir. J.* 25, 1084–1106. doi: 10.1183/09031936.05.00139104

Buckley, J. P., De, F. J., and Reif, E. C. (1957). The comparative antispasmodic activity of N-methyl-3-piperidyl diphenylglycolate methobromide (JB-340) and atropine sulfate. *J. Am. Pharm. Assoc. Am. Pharm. Assoc.* 46, 592–594. doi: 10.1002/jps.3030461007

Calverley, P. M., Anderson, J. A., Celli, B., Ferguson, G. T., Jenkins, C., Jones, P. W., et al. (2007). Salmeterol and fluticasone propionate and survival in chronic obstructive pulmonary disease. *N. Engl. J. Med.* 356, 775–789. doi: 10.1056/NEJMoa063070

Chen, J. Y. (1959). Antispasmodic activity of JB-340 (N-methyl-3-piperidyl-diphenylglycolate methobromide) with special reference to its relative selective action on the sphincter of Oddi, colon and urinary bladder of the dog. *Arch. Int. Pharmacodyn. Ther.* 121, 78–84.

Corbo, F., Franchini, C., Lentini, G., Muraglia, M., Ghelardini, C., Matucci, R., et al. (2007). Synthesis and biological evaluation of chiral alpha-aminoanilides with central antinociceptive activity. *J. Med. Chem.* 50, 1907–1915. doi: 10.1021/jm061078e

De Bellis, M., Carbonara, R., Roussel, J., Farinato, A., Massari, A., Pierno, S., et al. (2017). Increased sodium channel use-dependent inhibition by a new potent analogue of tocainide greatly enhances in vivo antimyotonic activity. *Neuropharmacology* 113(Pt A), 206–216. doi: 10.1016/j.neuropharm.2016.10.013

De Luca, A., De Bellis, M., Corbo, F., Franchini, C., Muraglia, M., Catalano, A., et al. (2012). Searching for novel anti-myotonic agents: pharmacophore requirement for use-dependent block of skeletal muscle sodium channels by N-benzylated cyclic derivatives of tocainide. *Neuromuscul. Disord.* 22, 56–65. doi: 10.1016/j.nmd.2011.07.001

Hamakawa, H., Bartolak-Suki, E., Parameswaran, H., Majumdar, A., Lutchen, K. R., and Suki, B. (2011). Structure-function relations in an elastase-induced mouse model of emphysema. *Am. J. Respir. Cell Mol. Biol.* 45, 517–524. doi: 10.1165/rcmb.2010-0473OC

Kurotsu, S., Tanaka, K., Niino, T., Asano, T., Sugizaki, T., Azuma, A., et al. (2014). Ameliorative effect of mepenzolate bromide against pulmonary fibrosis. *J. Pharmacol. Exp. Ther.* 350, 79–88. doi: 10.1124/jpet.114.213009

Long, J. P., and Keasling, H. H. (1954). The comparative anticholinergic activity of a series of derivatives of 3-hydroxy piperidine. *J. Am. Pharm. Assoc. Am. Pharm. Assoc.* 43, 616–619. doi: 10.1002/jps.3030431013

Mannino, D. M., and Kiriz, V. A. (2006). Changing the burden of COPD mortality. *Int. J. Chron. Obstruct. Pulmon. Dis.* 1, 219–233.

Murad, H. A., Habib, H. S., Rafeeq, M. M., Sulaiman, M. I., Abdulrahman, A. S., and Khabaz, M. N. (2017). Co-inhalation of roflumilast, rather than formoterol, with fluticasone more effectively improves asthma in asthmatic mice. *Exp. Biol. Med.* 242, 516–526. doi: 10.1177/1535370216685006

Rabe, K. F., Hurd, S., Anzueto, A., Barnes, P. J., Buist, S. A., Calverley, P., et al. (2007). Global strategy for the diagnosis, management, and prevention of chronic obstructive pulmonary disease: GOLD executive summary. *Am. J. Respir. Crit. Care Med.* 176, 532–555. doi: 10.1164/rccm.200703-456SO

Sato, S., Bartolak-Suki, E., Parameswaran, H., Hamakawa, H., and Suki, B. (2015). Scale dependence of structure-function relationship in the emphysematous mouse lung. *Front. Physiol.* 6:146. doi: 10.3389/fphys.2015.00146

Shalaby, K. H., Gold, L. G., Schuessler, T. F., Martin, J. G., and Robichaud, A. (2010). Combined forced oscillation and forced expiration measurements in mice for the assessment of airway hyperresponsiveness. *Respir. Res.* 11:82. doi: 10.1186/1465-9921-11-82

Tanaka, K., Ishihara, T., Azuma, A., Kudoh, S., Ebina, M., Nukiwa, T., et al. (2010). Therapeutic effect of lecithinized superoxide dismutase on bleomycin-induced pulmonary fibrosis. *Am. J. Physiol. Lung Cell. Mol. Physiol.* 298, L348–L360. doi: 10.1152/ajplung.00289.2009

Tanaka, K., Ishihara, T., Sugizaki, T., Kobayashi, D., Yamashita, Y., Tahara, K., et al. (2013). Mepenzolate bromide displays beneficial effects in a mouse model of chronic obstructive pulmonary disease. *Nat. Commun.* 4:2686. doi: 10.1038/ncomms3686

Tanaka, K., Kurotsu, S., Asano, T., Yamakawa, N., Kobayashi, D., Yamashita, Y., et al. (2014). Superiority of pulmonary administration of mepenzolate bromide over other routes as treatment for chronic obstructive pulmonary disease. *Sci. Rep.* 4:4510. doi: 10.1038/srep04510

Tanaka, K., Sato, K., Aoshiba, K., Azuma, A., and Mizushima, T. (2012). Superiority of PC-SOD to other anti-COPD drugs for elastase-induced emphysema and alteration in lung mechanics and respiratory function in mice. *Am. J. Physiol. Lung Cell. Mol. Physiol.* 302, L1250–L1261. doi: 10.1152/ajplung.00019.2012

Tashkin, D. P., Celli, B., Senn, S., Burkhart, D., Kesten, S., Menjoge, S., et al. (2008). A 4-year trial of tiotropium in chronic obstructive pulmonary disease. *N. Engl. J. Med.* 359, 1543–1554. doi: 10.1056/NEJMoa0805800

Vestbo, J., Hurd, S. S., Agusti, A. G., Jones, P. W., Vogelmeier, C., Anzueto, A., et al. (2013). Global strategy for the diagnosis, management, and prevention of chronic obstructive pulmonary disease: GOLD executive summary. *Am. J. Respir. Crit. Care Med.* 187, 347–365. doi: 10.1164/rccm.201204-0596PP

Vogelmeier, C. F., Criner, G. J., Martinez, F. J., Anzueto, A., Barnes, P. J., Bourbeau, J., et al. (2017). Global strategy for the diagnosis, management, and prevention of chronic obstructive lung disease 2017 report. GOLD executive summary. *Am. J. Respir. Crit. Care Med.* 195, 557–582. doi: 10.1164/rccm.201701-0218PP

Weibel, E. R. (1963). Principles and methods for the morphometric study of the lung and other organs. *Lab. Invest.* 12, 131–155.

Yamashita, Y., Tanaka, K., Asano, T., Yamakawa, N., Kobayashi, D., Ishihara, T., et al. (2014). Synthesis and biological comparison of enantiomers of mepenzolate bromide, a muscarinic receptor antagonist with bronchodilatory and anti-inflammatory activities. *Bioorg. Med. Chem.* 22, 3488–3497. doi: 10.1016/j.bmc.2014.04.029

Conflict of Interest Statement: LTT Bio-Pharma Co., Ltd. is developing **MP-AD**-related compounds (such as **MP**) as drugs for the treatment of COPD. TM is Chairman of LTT Bio-Pharma Co., Ltd. TA and MT are employees of an endowed research division of LTT Bio-Pharma Co., Ltd.

The other authors declare that the research was conducted in the absence of any commercial or financial relationships that could be construed as a potential conflict of interest.

Copyright © 2018 Tanaka, Yamakawa, Yamashita, Asano, Kanda, Takafuji, Kawahara, Takenaga, Fukunishi and Mizushima. This is an open-access article distributed under the terms of the Creative Commons Attribution License (CC BY). The use, distribution or reproduction in other forums is permitted, provided the original author(s) and the copyright owner are credited and that the original publication in this journal is cited, in accordance with accepted academic practice. No use, distribution or reproduction is permitted which does not comply with these terms.

International Journal of
Molecular Sciences

MDPI

Article

Isolation of Adipose-Derived Stem/Stromal Cells from Cryopreserved Fat Tissue and Transplantation into Rats with Spinal Cord Injury

Yuki Ohta [1,*], Mitsuko Takenaga [2], Akemi Hamaguchi [2], Masanori Ootaki [1], Yuko Takeba [1], Tsukasa Kobayashi [1], Minoru Watanabe [3], Taroh Iiri [1] and Naoki Matsumoto [1]

1 Department of Pharmacology, St. Marianna University School of Medicine, 2-16-1 Sugao, Miyamae-ku, Kawasaki, Kanagawa 216-8511, Japan; m_ootaki@marianna-u.ac.jp (M.O.); takebay@marianna-u.ac.jp (Y.T.); kobayashit@marianna-u.ac.jp (T.K.); tiiri@marianna-u.ac.jp (T.I.); matsumoto@marianna-u.ac.jp (N.M.)
2 Institute of Medical Science, St. Marianna University School of Medicine, 2-16-1 Sugao, Miyamae-ku, Kawasaki, Kanagawa 216-8512, Japan; m2take@marianna-u.ac.jp (M.T.); hamaguch@marianna-u.ac.jp (A.H.)
3 Institute for Animal Experimentation, St. Marianna University Graduate School of Medicine, 2-16-1 Sugao, Miyamae-ku, Kawasaki, Kanagawa 216-8511, Japan; m4wata@marianna-u.ac.jp
* Correspondence: yuki-o@marianna-u.ac.jp; Tel.: +81-44-977-8111

Received: 30 May 2018; Accepted: 30 June 2018; Published: 5 July 2018

Abstract: Adipose tissue contains multipotent cells known as adipose-derived stem/stromal cells (ASCs), which have therapeutic potential for various diseases. Although the demand for adipose tissue for research use remains high, no adipose tissue bank exists. In this study, we attempted to isolate ASCs from cryopreserved adipose tissue with the aim of developing a banking system. ASCs were isolated from fresh and cryopreserved adipose tissue of rats and compared for proliferation (doubling time), differentiation capability (adipocytes), and cytokine (hepatocyte growth factor and vascular endothelial growth factor) secretion. Finally, ASCs (2.5×10^6) were intravenously infused into rats with spinal cord injury, after which hindlimb motor function was evaluated. Isolation and culture of ASCs from cryopreserved adipose tissue were possible, and their characteristics were not significantly different from those of fresh tissue. Transplantation of ASCs derived from cryopreserved tissue significantly promoted restoration of hindlimb movement function in injured model rats. These results indicate that cryopreservation of adipose tissue may be an option for clinical application.

Keywords: adipose tissue; adipose-derived stem/stromal cells; cryopreservation; spinal cord injury; transplantation; tissue bank

1. Introduction

Regenerative medicine has advanced rapidly in recent years. Embryonic stem (ES) cells, induced pluripotent stem (iPS) cells, and somatic stem cells have all become candidates for transplantation in regenerative therapy. However, ES or iPS cells have some limitations to their clinical application, including ethical concerns, problems with immunogenicity, and safety issues related to the potential for tumorigenicity [1]. Somatic stem cells, such as mesenchymal stem cells (MSCs), may offset these problems, as they are capable of self-renewal and can differentiate into multi-lineages [2–4]. In addition, MSCs are known to have low immunogenicity [5]. Therefore, MSCs are prioritized over ES or iPS cells in clinical trials. MSCs have been found in many tissues, including adipose tissue, which possesses its own advantages for use in regenerative medicine [6–8]. These advantages include its ubiquitous distribution, its accessibility, and the ease with which it can be harvested. Moreover, it contains two kinds of regenerative cells, de-differentiated fat cells (DFAT) and adipose-derived stem/stromal cells (ASCs). Spinal cord injury (SCI) results in partial or complete paralysis and disability. Currently, cell

ubiquitous distribution, its accessibility, and the ease with which it can be harvested. Moreover, it contains two kinds of regenerative cells, de-differentiated fat cells (DFAT) and adipose-derived stem/stromal cells (ASCs). Spinal cord injury (SCI) results in partial or complete paralysis and disability. Currently, cell transplantation is being explored as a strategy to promote tissue regeneration, and a variety of cells have been tested for their therapeutic potential for SCI [9–11]. We have reported that the transplantation of DFAT or ASCs improved hindlimb motor dysfunction in rats with SCI [12,13]. The mechanism of their treatment in this injury may be paracrine effect by humoral factors, not neuronal differentiation [12,13].

For research use, the demand for adipose tissue remains high, but its supply system is lacking. We have operated the human tissue bank since 2001, gathering liver and small intestine tissue that have been removed by surgery and have stopped unnecessary colon supply. Although we began gathering adipose tissue, whether or not cells for transplantation can be obtained from cryopreserved tissue remains unknown. In this study, we attempted to isolate ASCs from cryopreserved adipose tissue, with the aim of evaluating adipose tissue banking as a source of cells for regenerative medicine, including SCI.

2. Results

2.1. Isolation of ASCs from Cryopreserved Adipose Tissue

Adherent cells were observed the day after seeding and isolated from fresh adipose tissue with collagenase. ASCs became apparently homogeneous during culture and passage, although the isolated cells exhibited heterogeneous features. When cryopreserved tissues were treated with collagenase, the cells adhered on the culture dish and grew, similar to the treatment of fresh tissue. ASCs isolated from two- and four-week cryopreserved tissue (Cryo-ASCs) could be amplified with a doubling time (DT) of approximately 24–28 h at the first passage (P1), while ASCs isolated from fresh tissue (Fresh-ASCs) showed a doubling time of approximately 26 h (Figure 1). DT was longer in the 12-week-Cryo-ASCs (approximately 35 h) than in Fresh-ASCs ($n = 4$, $p < 0.05$). Culture and passage progressively lengthened DT in all Fresh- and Cryo-ASCs, with P5 or P6 as the peak (Figure 1). There was no significant difference in the proliferative activity between the two.

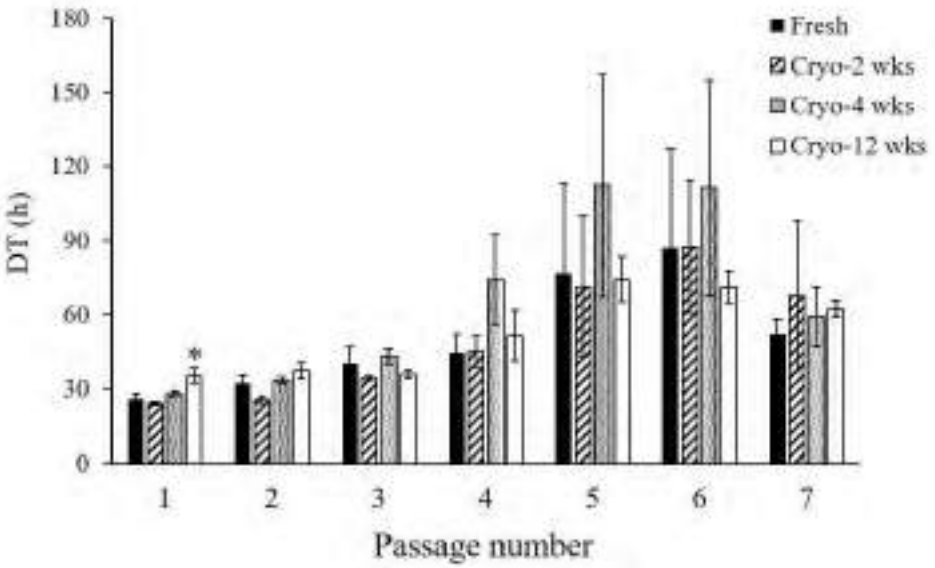

Figure 1. Doubling time of adipose-derived stem/stromal cells (ASCs). ASCs derived from fresh or cryopreserved adipose tissue were cultured for up to seven passages. Doubling time (DT) was determined at the indicated number of passages (as described in the Materials and Methods section). Data are expressed as the mean ± standard error (SE) ($n = 4$). * $p < 0.05$ vs. Fresh.

2.2. Adipogenic and Osteogenic Differentiation

Adipogenic differentiation of Fresh- and Cryo-ASCs was evaluated. When confluent cells were subsequently cultured in adipogenic medium, intracellular lipid droplets formed (Figure 2).

Int. J. Mol. Sci. **2018**, *19*, x 3 of 9

2.2. Adipogenic and Osteogenic Differentiation

2.2. Adipogenic and Osteogenic Differentiation

Adipogenic differentiation of Fresh- and Cryo-ASCs was evaluated. When confluent cells were subsequently cultured in adipogenic medium, intracellular lipid droplets formed (Figure 2). Adipose differentiation was observed in both Fresh- and Cryo-ASCs. However, the efficiency of adipogenic differentiation was lower in 12-week-Cryo-ASCs (Table 1).

Adipogenic differentiation of Fresh- and Cryo-ASCs was evaluated. When confluent cells were subsequently cultured in adipogenic medium, intracellular lipid droplets formed (Figure 2). Adipose differentiation was observed in both Fresh- and Cryo-ASCs. However, the efficiency of adipogenic differentiation was lower in 12-week-Cryo-ASCs (Table 1).

Figure 2. Adipogenic differentiation in ASCs. Fresh or cryopreserved adipose-derived stem/stromal cells (Fresh- or Cryo-ASCs) were differentiated into adipocytes (as described in the Materials and Methods section). Adipogenesis was revealed by Oil red O staining for lipid droplets. (−): confluent state without adipogenic induction; (+): 28 days after adipogenic induction.

Figure 2. Adipogenic differentiation in ASCs. Fresh or cryopreserved adipose-derived stem/stromal cells (Fresh- or Cryo-ASCs) were differentiated into adipocytes (as described in the Materials and Methods section). Adipogenesis was revealed by Oil red O staining for lipid droplets. (−): confluent state without adipogenic induction; (+): 28 days after adipogenic induction.

Table 1. Efficiency of adipogenic differentiation.

	Fresh	Cryo-2 weeks	Cryo-4 weeks	Cryo-12 weeks
Efficiency	4/4 (100%)	4/4 (100%)	4/4 (100%)	2/4 (50%)

Table 1. Efficiency of adipogenic differentiation.

	Fresh	Cryo-2 weeks	Cryo-4 weeks	Cryo-12 weeks
Efficiency	4/4 (100%)	4/4 (100%)	4/4 (100%)	2/4 (50%)

Fresh- or Cryo-ASCs were differentiated into adipocytes (as described in the Materials and Methods section). Adipogenesis was revealed by Oil red O staining, and the ratio was calculated ($n = 4$).

Fresh- or Cryo-ASCs were differentiated into adipocytes (as described in the Materials and Methods section). Adipogenesis was revealed by Oil red O staining, and the ratio was calculated ($n = 4$).

When Fresh- or Cryo-ASCs were cultured in osteogenic medium, the positive cells for alkaline phosphatase (ALP) were observed (Figure 3).

When Fresh- or Cryo-ASCs were cultured in osteogenic medium, the positive cells for alkaline phosphatase (ALP) were observed (Figure 3).

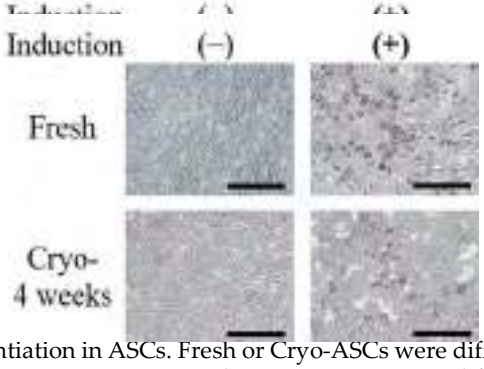

Figure 3. Osteogenic differentiation in ASCs. Fresh or Cryo-ASCs were differentiated into osteoblasts (as described in the Materials and Methods section). Osteogenesis was revealed by alkaline phosphatase staining. (−): confluent state without osteogenic induction; (+): 21 days after osteogenic induction. Scale bars = 500 μm.

Figure 3. Osteogenic differentiation in ASCs. Fresh or Cryo-ASCs were differentiated into osteoblasts (as described in the Materials and Methods section). Osteogenesis was revealed by alkaline phosphatase staining. (−): confluent state without osteogenic induction; (+): 21 days after osteogenic induction. Scale bars = 500 μm.

Int. J. Mol. Sci. 2018, 19, x 4 of 9

2.3. Secretion of Cytokines

To investigate the effect of cryopreservation on cytokine secretion from ASCs, hepatocyte growth factor (HGF) and vascular endothelial growth factor (VEGF) were measured in their culture media. Both Fresh- and Cryo-ASCs secreted large amounts of HGF and VEGF in vitro (Figure 4).

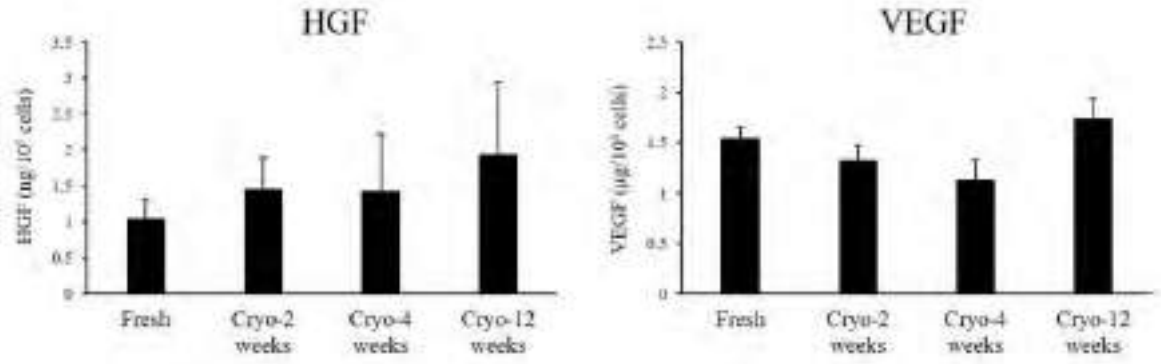

Figure 4. Cytokine secretion from ASCs. P2-ASCs were cultured for four days. Supernatants were harvested for cytokine assay. Hepatocyte growth factor (HGF) and vascular endothelial growth factor (VEGF) in the culture medium were measured by enzyme-linked immunosorbent assay. Data are expressed as the mean ± SE ($n = 4$).

2.4. Transplantation of ASCs into Rats with SCI

Next, we investigated whether Cryo-ASCs were effective for improvement of SCI. SCI caused complete hindlimb paralysis, after which gradual recovery of locomotion was observed. As shown in Figure 5, the Cryo-ASC group showed greater improvement than the saline group in hindlimb locomotive function during the early period after transplantation. The Basso–Beattie–Bresnahan (BBB) score of all SCI animals reached a plateau at four weeks after injury, though ASC-treated animals showed significantly better recovery (median: 13, interquartile range (IQR): 3) than the saline group (median: 8, IQR: 2.75) ($p < 0.05$). In the ASC group, some animals showed frequent-consistent weight-bearing plantar walking with good forelimb–hindlimb coordination. While the saline group also recovered, some animals crawled and moved without weight-bearing.

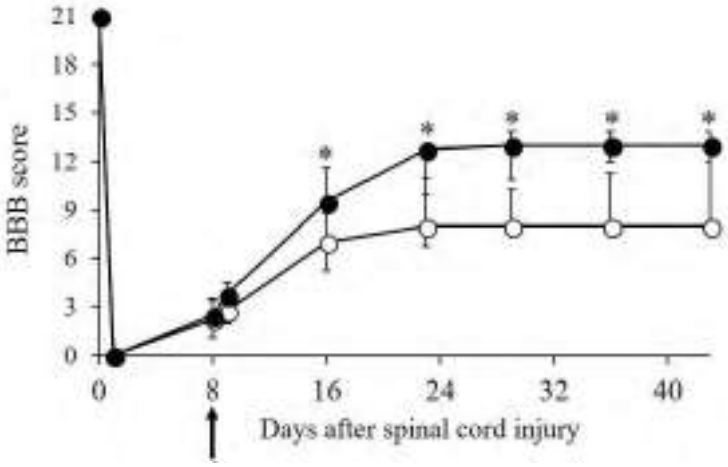

Figure 5. Functional recovery following ASC transplantation. On day eight after injury (arrow), 12-week-Cryo-ASCs (2.5×10^6 cells) were infused into spinal cord injury (SCI) rats via the tail vein ($n = 8$). Basso–Beattie–Bresnahan (BBB) scores were determined before and after transplantation. Black and white circles are ASC and saline group, respectively. The median score is plotted; bars show the inter quartile range (IQR). * $p < 0.05$ vs. saline controls ($n = 10$).

Figure 5. Functional recovery following ASC transplantation. On day eight after injury (arrow), 12-week-Cryo-ASCs (2.5×10^6 cells) were infused into spinal cord injury (SCI) rats via the tail vein ($n = 8$). Basso–Beattie–Bresnahan (BBB) scores were determined before and after transplantation. Black and white circles are ASC and saline group, respectively. The median score is plotted; bars show the inter quartile range (IQR). * $p < 0.05$ vs. saline controls ($n = 10$).

2.5. Long-Term Cryopreservation of Adipose Tissue

Finally, we attempted to isolate ASCs from adipose tissue that had undergone long-term cryopreservation (24 weeks). ASCs with proliferative patterns similar to those of Fresh-ASCs were obtained. Moreover, there was no significant difference in proliferative activity between the two, although DT at P1 was longer (approximately 33 h, Figure 6A) in Cryo-ASCs. Adipogenic differentiation was even lower in Cryo-ASCs (Figure 6B), which showed a 25% (1/4) ratio of adipocyte differentiation.

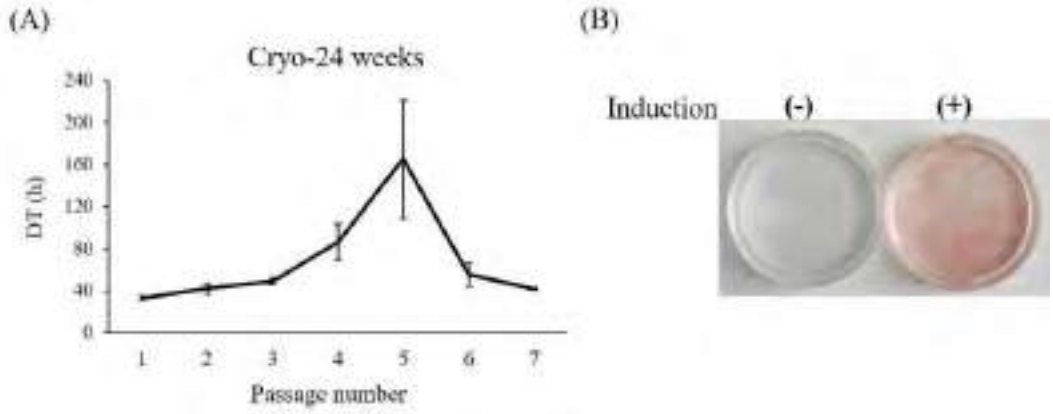

Figure 6. Long-term cryopreserved adipose-derived ASCs were isolated from 24-week cryopreserved tissues and examined for proliferation and adipogenic differentiation. (**A**) DT; (**B**) Oil red O staining. Data are expressed as the SE (*n* = 4).

3. Discussion

The present study demonstrated that the isolation of ASCs from cryopreserved tissue was possible, and a therapeutic effect was observed when they were transplanted into rats with SCI. In fact, intravenous infusion of Cryo-ASCs into SCI rats promoted the restoration of motor function, just as we observed in our previous study using Fresh-ASCs [12]. Therefore, transplantation of Cryo-ASCs improved motor function in SCI rats just as Fresh-ASCs did.

When comparing Fresh- and Cryo-ASCs, the cell proliferative patterns were similar, while DT at P1 tended to be longer with a longer cryopreservation period. In addition, cryopreservation has been reported not to alter expression of cell surface markers [14], characterizing ASCs. ASCs are known to secrete angiogenic growth factors such as HGF and VEGF [15]. The paracrine effect of cytokines secreted from ASCs is considered to play a major role in cell therapy, including SCI [16]. In our study, Fresh- and Cryo-ASCs were equivalent in cytokine secretion, with both Fresh- and Cryo-ASCs secreting abundant growth factors. On the other hand, adipogenic differentiation decreased as cryopreservation time increased. These results indicate that cryopreservation might have affected cell differentiation but did not affect cell proliferation and cytokine secretion. For other mesenchymal lineage differentiation abilities, the positive cells were recorded when stained for alkaline phosphatase activity as an evaluation of osteogenic differentiation. However, in addition to osteogenic differentiation, more detailed studies are needed for chondrogenic differentiation ability.

ASCs were successfully isolated from tissues cryopreserved at −80 °C for six months. However, adipose differentiation was unsatisfactory. Therefore, we will need to reconsider the temperature and agent for cryopreservation of adipose tissue. Indeed, even after this study, optimum conditions for the storage of adipose tissue remain unknown, and previous studies have produced a variety of results. For example, some studies reported that storage at −20 °C was comparable to storage in liquid nitrogen (−196 °C), while others reported that storage in liquid nitrogen was favorable to storage at −20 °C, and still others reported that storage at −80 and −196 °C was equivalent [17–20]. In clinical application, Cryo-ASCs are most likely to be used as allograft rather than autograft. There

will be not concerns about the potential risks of immuno-response even in such circumstances because MSCs containing ASCs are known to have low immunogenicity, and immunologically tolerant [5,21].

In conclusion, ASCs were obtained from cryopreserved adipose tissue, and, with the exception of adipose differentiation, they were functionally equivalent to freshly isolated ASCs. These findings show that banking of adipose tissue is possible, suggesting the use of cryopreserved adipose tissue in future clinical applications.

4. Materials and Methods

4.1. Animals

Female Sprague–Dawley rats (Charles River Laboratories Japan, Yokohama, Japan) were housed in an animal room at a constant temperature (23 ± 1 °C) and humidity (50%–60%) with a 12-h light/dark cycle and were allowed free access to a standard diet and water. Experimental procedures were performed in accordance with the Guidelines for Animal Experimentation of St. Marianna University Graduate School of Medicine (Kawasaki, Japan). The experimental protocol was approved by the Animal Research Committee, Institute for Animal Experimentation, St. Marianna University Graduate School of Medicine (approval number 1310005, 25 October 2013).

4.2. Cryopreservation of Adipose Tissue

Dorsal fat pads were obtained from eight–nine-week-old rats (n = 4) under anesthesia. The weight of adipose tissues was measured, and they were divided into five parts. Adipose tissues were soaked in a cryoprotectant (TC-Protecter, DS Pharma Biomedical, Osaka, Japan), and then stored in a freezer at −80 °C.

4.3. Isolation of ASCs

Frozen tissues were fast-thawed in a water bath at 37 °C and washed with phosphate-buffered saline (PBS). The fresh or thawed adipose tissue was minced and digested for 1 h in 0.1% collagenase (Thermo Fisher Scientific, Waltham, MA, USA) at 37 °C. The digestion process was stopped by adding Dulbecco's Modified Eagle's Medium (DMEM, Thermo Fisher Scientific) containing 20% fetal bovine serum (FBS, Thermo Fisher Scientific) and 1% antibiotic-antimycotic (Thermo Fisher Scientific). The digested suspension was filtered through a 70-µm nylon mesh cell strainer (BD Biosciences, Franklin Lakes, NJ, USA) to remove tissue debris and centrifuged at 1000 rpm for 5 min. The pellet (stromal-vascular fraction) was suspended in medium and cultured in a 10-cm culture dish at 37 °C in a humidified atmosphere of 5% CO_2 and 95% room air. After 24 h, non-adherent cells were gently removed. When adherent cells reached 80% confluence (passage 0: P0), confluent cells (ASCs) were detached with 0.25% trypsin/1 mM ethylenediamine tetraacetic acid (EDTA) (Thermo Fisher Scientific) and plated in flasks at a density of 2.5×10^5 cells/75 cm^2 (P1). DT was determined by manually counting the number of cells from P1 to P7. The numbers of cells and culture times (CT) were used to calculated DTs based on the following formula: $DT = \log 2 \times CT/(\log N - \log N_0)$ where N_0 represents the initial cell number and N represents cell number at the time of harvest.

4.4. Adipogenic and Osteogenic Differentiation

Differentiation into adipocytes was performed using a modification of the previously described methods [2,22]. Confluent cells were incubated in adipogenic induction medium (a 3:1 mixture of DMEM and Ham's F-12 Medium (Thermo Fisher Scientific) containing 10% FBS, 1% antibiotic-antimycotic, 5 µg/mL insulin (Thermo Fisher Scientific), 5 µg/mL transferrin (Thermo Fisher Scientific), 0.25 µM dexamethasone (DEX, MP Biomedicals, Aurora, OH, USA), and 500 µM 3-isobutyl-1-methylxanthine (IBMX, Wako, Osaka, Japan)) for three days, followed by culture in maintenance medium (induction medium without DEX and IBMX) for several days. After this culture procedure was repeated three times, the cells were cultured in maintenance medium for seven days.

Cells were fixed in 10% phosphate-buffered formalin for 1 h and stained with Oil Red O (Sigma-Aldrich, St. Louis, MO, USA) to visualize lipid droplet accumulation.

Differentiation into osteoblasts was performed using Osteoblast-Inducer Reagent (Takara Bio, Shiga, Japan). ASCs were incubated in osteoblastic induction medium (DMEM containing 20% FBS, 5 μg/ml ascorbic acid, 100 nM hydrocortisone, and 10 mM β-glycerophosphate) for 21 days. The medium change was performed each three day. ALP as an osteoblast marker was detected by an ALP stain kit according to the manufacturer's instructions (Takara Bio).

4.5. Measurement of Cytokines

After P2-ASCs were cultured for four days, the supernatant was collected for the measurement of cytokines, and the number of cells was counted with a hemocytometer. After centrifuged at 1000 rpm for 5 min, and aliquots of supernatant were used for assay.

Levels of HGF (Institute of Immunology, Tokyo, Japan) and VEGF (Immuno-Biological Laboratories, Gunma, Japan) were measured by a sandwich method with enzyme-linked immunosorbent assay kits according to manufacturer's instructions. The value was represented as per 10^5 cells.

4.6. SCI Model, Intravenous ASC Transplantation, and Functional Evaluation

Spinal cord injury was induced by the weight-drop method [23]. Ten-week-old rats weighing 210–230 g were anesthetized, and dorsal laminectomy was performed at the T10 vertebra. Then, a 10 g weight was dropped onto the spinal cord from a height of 25 mm. Postoperatively, animals were kept warm on highly absorbent bedding, injected with antibiotics, and given manual bladder expression twice daily until reflex bladder emptying returned.

On day eight after SCI, rats were randomly assigned to two groups, and cell transplantation was carried out using the method reported in our previous study [13]. ASCs were incubated in growth medium containing 10 ng/mL basic fibroblast growth factor (bFGF, Thermo Fisher Scientific) for 24 h before transplantation. The cells were detached with trypsin/EDTA and resuspended in physiological saline; 2.5×10^6 cells (in 500 μL) were infused via the tail vein at a rate of 25 μL/min using a stereotaxic microinjector (model 310, Muromachi Kikai, Tokyo, Japan). SCI control animals received the same volume (500 μL) of physiological saline alone.

Hindlimb motor function was evaluated in SCI rats using the BBB score, a locomotor rating scale developed by Basso et al. [24]. A score from 0 (complete paralysis) to 21 (normal gait) was recorded before and after SCI.

4.7. Statistical Analysis

Results are expressed as the mean ± standard error (SE). BBB scores are expressed as the median and IQR. Data were analyzed by Dunnett's test (pairwise comparisons against the control group). Statistical analysis of BBB scores was performed using the Mann-Whitney U-test. The statistical analyses were performed with JMP 13 (SAS Institute Inc., Cary, NC, USA), and $p < 0.05$ was considered statistically significant.

Author Contributions: Y.O. conceived and designed the experiments. Y.O., M.T., A.H., Y.T., T.K., and M.W. performed the experiments. Y.O. and M.O. analyzed the data. T.I. and N.M. supervised the entire process. Y.O. wrote the manuscript. All authors approved the final version of the manuscript.

Funding: This research received no external funding.

Acknowledgments: We are grateful to Yukie Tokura for her technical assistance. This work was supported by JSPS KAKENHI (Grants-in-Aid for Scientific Research) Grant Number JP24791925 and St. Marianna University School of Medicine Research Grant.

Conflicts of Interest: The authors declare no conflicts of interest.

Abbreviations

ALP	alkaline phosphatase
ASCs	adipose-derived stem/stromal cells
BBB	Basso–Beattie–Bresnahan
bFGF	basic fibroblast growth factor
CT	culture time
Cryo-ASCs	cryopreserved adipose-derived stem/stromal cells
DEX	dexamethasone
DFAT	de-differentiated fat cells
DMEM	Dulbecco's Modified Eagle's Medium
DT	doubling time
EDTA	ethylenediamine tetraacetic acid
ES	embryonic stem
FBS	fetal bovine serum
Fresh-ASCs	fresh adipose-derived stem/stromal cells
HGF	hepatocyte growth factor
IBMX	3-isobutyl-1-methylxanthine
iPS	induced pluripotent stem
IQR	interquartile range
MSCs	mesenchymal stem cells
P	passage
PBS	phosphate buffered saline
SCI	spinal cord injury
SE	standard error
VEGF	vascular endothelial growth factor

References

1. Fujikawa, T.; Oh, S.H.; Pi, L.; Hatch, H.M.; Shupe, T.; Petersen, B.E. Teratoma formation leads to failure of treatment for type I diabetes using embryonic stem cell-derived insulin-producing cells. *Am. J. Pathol.* **2005**, *166*, 1781–1791. [CrossRef]
2. Pittenger, M.F.; Mackay, A.M.; Beck, S.C.; Jaiswal, R.K.; Douglas, R.; Mosca, J.D.; Moorman, M.A.; Simonetti, D.W.; Craig, S.; Marshak, D.R. Multilineage potential of adult human mesenchymal stem cells. *Science* **1999**, *284*, 143–147. [CrossRef] [PubMed]
3. Kopen, G.C.; Prockop, D.J.; Phinney, D.G. Marrow stromal cells migrate throughout forebrain and cerebellum, and they differentiate into astrocytes after injection into neonatal mouse brains. *Proc. Natl. Acad. Sci. USA* **1999**, *96*, 10711–10716. [CrossRef] [PubMed]
4. Sanchez-Ramos, J.; Song, S.; Cardozo-Pelaez, F.; Hazzi, C.; Stedeford, T.; Willing, A.; Freeman, T.B.; Saporta, S.; Janssen, W.; Patel, N.; et al. Adult bone marrow stromal cells differentiate into neural cells in vitro. *Exp. Neurol.* **2000**, *164*, 247–256. [CrossRef] [PubMed]
5. Massimo, D.N.; Carmelo, C.S.; Magni, M.; Milanesi, M.; Longoni, P.D.; Matteucci, P.; Grisanti, S.; Gianni, A.M. Human bone marrow stromal cells suppress T-lymphocyte proliferation induced by cellular or nonspecific mitogenic stimuli. *Blood* **2002**, *15*, 3838–3843. [CrossRef]
6. Zuk, P.A.; Zhu, M.; Mizuno, H.; Huang, J.; Futrell, J.W.; Katz, A.J.; Benhaim, P.; Lorenz, H.P.; Hedrick, M.H. Multilineage cells from human adipose tissue: Implications for cell-based therapies. *Tissue Eng.* **2001**, *7*, 211–228. [CrossRef] [PubMed]
7. Bieback, K.; Kern, S.; Kluter, H.; Eichler, H. Critical parameters for the isolation of mesenchymal stem cells from umbilical cord blood. *Stem Cells* **2004**, *22*, 625–634. [CrossRef] [PubMed]
8. Shih, D.T.; Lee, D.C.; Chen, S.C.; Tsai, R.Y.; Huang, C.T.; Tsai, C.C.; Shen, E.Y.; Chiu, W.T. Isolation and characterization of neurogenic mesenchymal stem cells in human scalp tissue. *Stem Cells* **2005**, *23*, 1012–1020. [CrossRef] [PubMed]

9. McDonald, J.W.; Liu, X.; Qu, Y.; Mickey, S.K.; Turetsky, D.; Gottlieb, D.I.; Choi, D.W. Transplanted embryonic stem cells survive, differentiate and promote recovery in injured rat spinal cord. *Nat. Med.* **1999**, *5*, 1410–1412. [CrossRef] [PubMed]
10. Hofstetter, C.P.; Schwarz, E.J.; Hess, D.; Widenfalk, J.; El Manira, A.; Prockop, D.J.; Olson, L. Marrow stromal cells form guiding strands in the injured spinal cord and promote recovery. *Proc. Natl. Acad. Sci. USA* **2002**, *99*, 2199–2204. [CrossRef] [PubMed]
11. Ogawa, Y.; Sawamoto, K.; Miyata, T.; Miyao, S.; Watanabe, M.; Nakamura, M.; Bregman, B.S.; Koike, M.; Uchiyama, Y.; Toyama, Y.; et al. Transplantation of in vitro-expanded fetal neural progenitor cells results in neurogenesis and functional recovery after spinal cord contusion injury in adult rats. *J. Neurosci. Res.* **2002**, *69*, 925–933. [CrossRef] [PubMed]
12. Ohta, Y.; Takenaga, M.; Tokura, Y.; Hamaguchi, A.; Matsumoto, T.; Kano, K.; Mugishima, H.; Okano, H.; Igarashi, R. Mature adipocyte-derived cells, dedifferentiated fat cells (DFAT), promoted functional recovery from spinal cord injury-induced motor dysfunction in rats. *Cell Transplant.* **2008**, *17*, 877–886. [CrossRef] [PubMed]
13. Ohta, Y.; Hamaguchi, A.; Ootaki, M.; Watanabe, M.; Takeba, Y.; Iiri, T.; Matsumoto, N.; Takenaga, M. Intravenous Infusion of Adipose-derived Stem/Stromal Cells Improves Functional Recovery of Rats with Spinal Cord Injury. *Cytotherapy* **2017**, *19*, 839–848. [CrossRef] [PubMed]
14. Choudhery, M.S.; Badowski, M.; Muise, A.; Pierce, J.; Harris, D.T. Cryopreservation of whole adipose tissue for future use in regenerative medicine. *J. Surg. Res.* **2014**, *187*, 24–35. [CrossRef] [PubMed]
15. Furuya, N.; Takenaga, M.; Ohta, Y.; Tokura, Y.; Hamaguchi, A.; Sakamaki, A.; Kida, H.; Handa, H.; Nishine, H.; Mineshita, M.; et al. Cell therapy with adipose tissue-derived stem/stromal cells (ASC) for elastase-induced pulmonary emphysema in rats. *Regen. Med.* **2012**, *7*, 503–512. [CrossRef] [PubMed]
16. Dasari, V.R.; Veeravalli, K.K.; Dinh, D.H. Mesenchymal stem cells in the treatment of spinal cord injuries: A review. *World J. Stem Cells* **2014**, *6*, 120–133. [CrossRef] [PubMed]
17. Li, B.W.; Liao, W.C.; Wu, S.H.; Ma, H. Cryopreservation of fat tissue and application in autologous fat graft: In vitro and in vivo study. *Aesthet. Plast. Surg.* **2012**, *36*, 714–722. [CrossRef] [PubMed]
18. MacRae, J.W.; Tholpady, S.S.; Ogle, R.C.; Morgan, R.M.; Carraway, J.H.; Vasconez, H.C. Ex Vivo Fat Graft Preservation: Effects and Implications of Cryopreservation. *Ann. Plast. Surg.* **2004**, *52*, 281–282. [CrossRef] [PubMed]
19. Moscatello, D.K.; Dougherty, M.; Narins, R.S.; Lawrence, N. Cryopreservation of human fat for soft tissue augmentation: Viability requires use of cryoprotectant and controlled freezing and storage. *Dermatol. Surg.* **2005**, *31*, 1506–1510. [CrossRef] [PubMed]
20. Roato, I.; Alotto, D.; Belisario, D.C.; Casarin, S.; Fumagalli, M.; Cambieri, I.; Piana, R.; Stella, M.; Ferracini, R.; Castagnoli, C. Adipose Derived-Mesenchymal Stem Cells Viability and Differentiating Features for Orthopaedic Reparative Applications: Banking of Adipose Tissue. *Stem Cells Int.* **2016**, *2016*, 4968724. [CrossRef] [PubMed]
21. Gonzalez-Rey, E.; Gonzalez, M.A.; Varela, N.; O'Valle, F.; Hernandez-Cortes, P.; Rico, L.; Büscher, D.; Delgado, M. Human adipose-derived mesenchymal stem cells reduce inflammatory and T cell responses and induce regulatory T cells in vitro in rheumatoid arthritis. *Ann. Rheum. Dis.* **2010**, *69*, 241–248. [CrossRef] [PubMed]
22. Shimba, S.; Ishii, N.; Ohta, Y.; Ohno, T.; Watabe, Y.; Hayashi, M.; Wada, T.; Aoyagi, T.; Tezuka, M. Brain and muscle Arnt-like protein-1 (BMAL1), a component of the molecular clock, regulates adipogenesis. *Proc. Natl. Acad. Sci. USA* **2005**, *102*, 12071–12076. [CrossRef] [PubMed]
23. Basso, D.M.; Beattie, M.S.; Bresnahan, J.C. A sensitive and reliable locomotor rating scale for open field testing in rats. *J. Neurotrauma* **1995**, *12*, 1–21. [CrossRef] [PubMed]
24. Basso, D.M.; Beattie, M.S.; Bresnahan, J.C.; Anderson, D.K.; Faden, A.I.; Gruner, J.A.; Holford, T.R.; Hsu, C.Y.; Noble, L.J.; Nockels, R.; et al. MASCIS evaluation of open field locomotor scores: Effects of experience and teamwork on reliability. Multicenter Animal Spinal Cord Injury Study. *J. Neurotrauma* **1996**, *13*, 343–359. [CrossRef] [PubMed]

© 2018 by the authors. Licensee MDPI, Basel, Switzerland. This article is an open access article distributed under the terms and conditions of the Creative Commons Attribution (CC BY) license (http://creativecommons.org/licenses/by/4.0/).

European Journal of Pharmacology 844 (2019) 253–258

Contents lists available at ScienceDirect

European Journal of Pharmacology

journal homepage: www.elsevier.com/locate/ejphar

Translational pharmacology

Antinociception by fluoro-loxoprofen, a novel non-steroidal anti-inflammatory drug with less ulcerogenic effects, in rat models of inflammatory pain

Teita Asano[a,*,1], Tomoki Hattori[b,1], Ken-ichiro Tanaka[c], Naoki Yamakawa[d], Shintaro Suemasu[b], Shuji Aida[b], Marika Kataoka[b], Tohru Mizushima[e,*], Mitsuko Takenaga[a]

[a] Institute of Medical Science, St. Marianna University School of Medicine, 2-16-1, Sugao, Miyamae-ku, Kawasaki 216-8512, Japan
[b] Division of Drug Discovery and Development, Faculty of Pharmacy, Keio University, 1-5-30, Shibakoen, Minato-ku, Tokyo 105-8512, Japan
[c] Research Institute of Pharmaceutical Sciences, Faculty of Pharmacy, Musashino University, 1-1-20, Shin-machi, Nishi-Tokyo 202-8585, Japan
[d] School of Pharmacy, Shujitsu University, 1-6-1, Nishi-kawahara, Naka-ku, Okayama 703-8516, Japan
[e] LTT Bio-Pharma Co., Ltd, Shiodome Building 3 F, 1-2-20 Kaigan, Minato-ku, Tokyo 105-0022, Japan

ARTICLE INFO

Keywords:
NSAID
Inflammatory pain
Loxoprofen
Antinociception
Rapid action

ABSTRACT

The use of non-steroidal anti-inflammatory drugs (NSAIDs) for the treatment of inflammatory pain is limited by gastrointestinal complications. The rapid action of NSAIDs is associated with better pain relief. Previously, we demonstrated that fluoro-loxoprofen, a novel NSAID, has less ulcerogenic potential than other NSAIDs, attributable to its gastroprotective properties. The aim of this study was to investigate and compare the effects of fluoro-loxoprofen on inflammatory pain in rats with those of other NSAIDs. Oral administration of fluoro-loxoprofen, loxoprofen, and celecoxib resulted in equivalent analgesic action against yeast-induced inflammatory pain. The antinociceptive effect of fluoro-loxoprofen was maximized within 1 h after administration, which is less time than that observed for loxoprofen (2 h) and celecoxib (3 h). We confirmed that both fluoro-loxoprofen and loxoprofen suppressed the increases in prostaglandin E_2 in inflamed paws. In addition to yeast-induced pain, fluoro-loxoprofen produced a similar effect against adjuvant-induced inflammatory pain, with faster peak analgesic effects than those observed for loxoprofen and celecoxib. Taken together, these results suggest that the analgesic effect of fluoro-loxoprofen is equivalent to that of loxoprofen and celecoxib. Moreover, the analgesic effect of fluoro-loxoprofen against inflammatory pain was more rapid than that of other NSAIDs, and this may be associated with its rapid absorption property.

1. Introduction

Non-steroidal anti-inflammatory drugs (NSAIDs) are among the most commonly used drugs worldwide for the treatment of pain, inflammation, and fever (Biederman, 2005; Wongrakpanich et al., 2018). NSAIDs inhibit the production of prostaglandins by blocking cyclooxygenase (COX), which is essential for prostaglandin synthesis (Rao and Knaus, 2008). Since prostaglandins are key mediators for inducing inflammation and nociception, the suppression of prostaglandin production by NSAIDs is responsible for the analgesic and anti-inflammatory effects of these drugs (Dahl and Kehlet, 1991). Among COX subtypes, COX-1 and COX-2 play pivotal roles in the protection of gastrointestinal mucosa and inflammatory response in peripheral tissues, respectively (McCarberg and Cryer, 2015; Rao and Knaus, 2008).

Although NSAIDs are very effective and useful for pain management, their use is associated with gastrointestinal, cardiovascular, and renal complications (Harirforoosh et al., 2013; Ungprasert et al., 2015). Gastrointestinal toxicity is the major problem in chronic NSAID users. Previous studies have shown that arthritis patients who use NSAIDs have a high incidence of adverse events in upper and lower gastrointestinal mucosa (Graham et al., 2005; Sostres et al., 2013). Recently, selective COX-2 inhibitors (mainly celecoxib) have been reported to be associated with fewer gastrointestinal problems than nonselective NSAIDs (*e.g.,* ibuprofen, aspirin, and diclofenac), because COX-2 inhibitors do not influence COX-1 activity, which is responsible for mucosal protection (Targownik et al., 2008). In contrast, gastroprotective agents, such as proton pump inhibitors, are also effective in preventing NSAID-induced gastrointestinal injuries (Arora et al., 2009; Targownik

* Corresponding authors.
E-mail addresses: asano-ti@marianna-u.ac.jp (T. Asano), t.mizushima@ltt.co.jp (T. Mizushima).
[1] These authors have equally contributed this work.

https://doi.org/10.1016/j.ejphar.2018.12.008
Received 20 August 2018; Received in revised form 1 December 2018; Accepted 5 December 2018
Available online 06 December 2018
0014-2999/ © 2018 Elsevier B.V. All rights reserved.

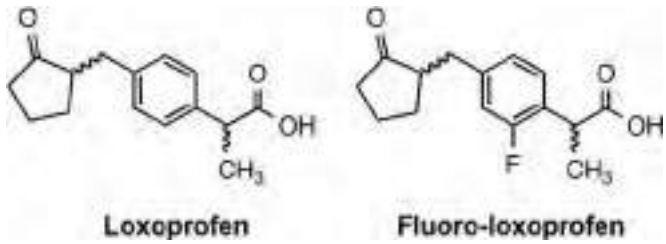

Fig. 1. Structures of loxoprofen and fluoro-loxoprofen.

et al., 2008). Therefore, selective COX-2 inhibitors or nonselective NSAIDs plus gastroprotective agents are presently considered beneficial for preventing adverse events in NSAID users (McCarberg and Cryer, 2015; Targownik et al., 2008).

Loxoprofen, a nonselective NSAID prodrug, is widely used in Japan and several other countries (Arakawa et al., 2009; Greig and Garnock-Jones, 2016) (Fig. 1). It is prescribed for the treatment of inflammation and pain in post-operative or trauma patients, as well as those with osteoarthritis, myalgia, or trauma-induced swelling (Arakawa et al., 2009; Greig and Garnock-Jones, 2016). The pharmacodynamic profile of loxoprofen shows anti-inflammatory and anti-analgesic activities similar to or greater than those of other NSAIDs, including indomethacin, ketoprofen, flurbiprofen, and felbinac, in both human and animal studies (Greig and Garnock-Jones, 2016). Furthermore, loxoprofen has a characteristic rapid absorption profile (Greig and Garnock-Jones, 2016). Although it is reported to be safe (Arakawa et al., 2009; Kawano et al., 1995; Yamakawa et al., 2010a), recent clinical studies have reported that loxoprofen may cause more gastrointestinal complications than celecoxib (Fujimori et al., 2016; Sakamoto et al., 2013).

Recently, we identified fluoro-loxoprofen, a loxoprofen derivative and novel NSAID, that causes less gastrointestinal injuries than loxoprofen (Fig. 1). The anti-inflammatory activity and pharmacokinetics of fluoro-loxoprofen have been determined previously (Suemasu et al., 2012; Yamakawa et al., 2010b, 2012). In the present study, we investigated the effect of fluoro-loxoprofen on acute or chronic pain using rat models of inflammatory pain.

2. Material and methods

2.1. Chemicals

Fluoro-loxoprofen sodium salt (fluoro-loxoprofen-Na) was synthesized as described previously (Yamakawa et al., 2010b, 2012). Loxoprofen sodium salt dihydrate (loxoprofen-Na) was obtained from Tokyo Chemical Industry Co., Ltd. (Tokyo, Japan). Celecoxib was purchased from LKT Laboratories (Saint Paul, USA). Brewer's yeast extract was purchased from Sigma (St. Louis, USA). The prostaglandin E_2 (PGE_2) ELISA kit was obtained from Cayman Chemical Company (Ann Arbor, USA). Complete Freund's adjuvant (CFA) was purchased from Difco Laboratories (Detroit, USA). Methylcellulose was purchased from Wako Pure Chemical Industries (Osaka, Japan).

2.2. Animals

Female Lewis rats were obtained from Charles River Laboratories Japan (Yokohama, Japan). Male Wistar-Imamichi rats were obtained from Sankyo Labo Service Corporation (Tokyo, Japan). All animals were housed under controlled temperatures (22–24 °C) and illumination (12 h light cycle starting at 8:00 A.M.). The experiments and procedures described here were performed in accordance with the Guide for the Care and Use of Laboratory Animals as adopted and promulgated by the National Institutes of Health and were approved by the Animal Care Committee of Keio University and St. Marianna University.

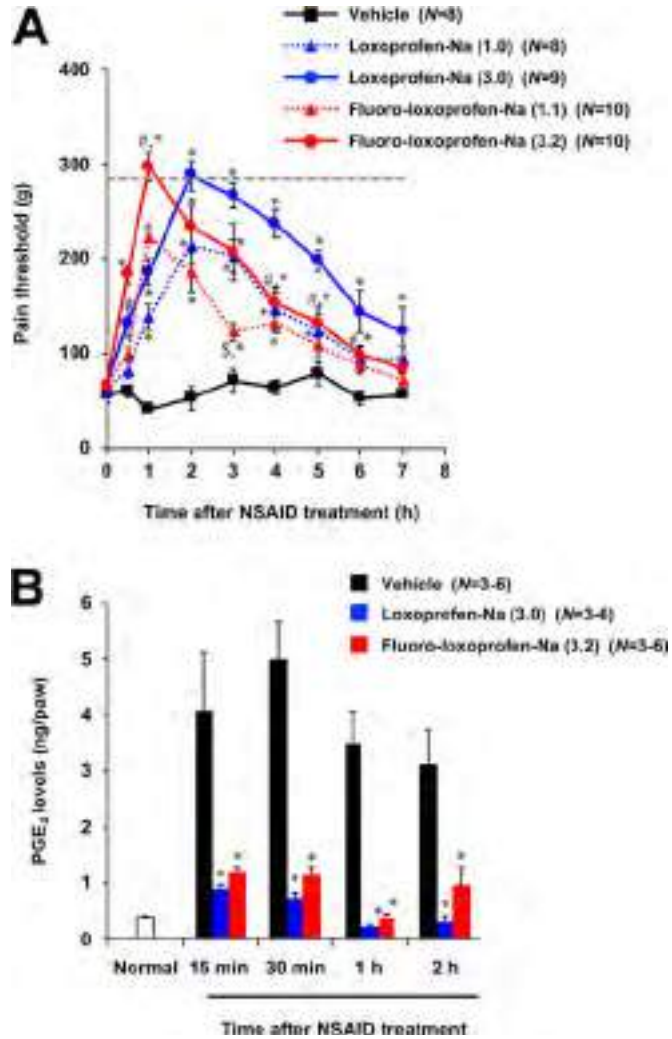

Fig. 2. Effects of fluoro-loxoprofen or loxoprofen against acute pain and paw prostaglandin E_2 (PGE_2) levels after yeast injections. Wistar-Imamichi rats were given a sub-plantar injection of a 20% yeast suspension (**A**, **B**). The rats were orally administered vehicle (1% methylcellulose) or the indicated doses (mg/kg) of fluoro-loxoprofen-Na or loxoprofen-Na after 4.5 h (**A**, **B**). (**A**), Pain thresholds in the paw were measured 0.5–7 h after drug administration. The broken line in gray represents the mean of the rat thresholds before yeast injection (normal levels). (**B**) PGE_2 levels in the inflamed paws were determined at indicated times *via* an enzyme-linked immunoassay (ELISA) kit. Values are means ± S.E.M. One-way analysis of variance (ANOVA) followed by Tukey (**A**) or Dunnett's (**B**) post hoc test was performed. *, $P < 0.05$ *vs.* vehicle. $, $P < 0.05$ *vs.* loxoprofen-Na (1.0). #, $P < 0.05$ *vs.* loxoprofen-Na (3.0).

2.3. Yeast-induced inflammatory pain

Yeast-induced peripheral inflammatory pain was induced as described previously (Ushiyama et al., 2008). Male Wistar-Imamichi rats (4–5 weeks old) were fasted for 16 h before the experiments. Acute inflammation was induced *via* sub-plantar injections of 0.1 ml of a 20% suspension of brewer's yeast in saline into the right hind paw. After injecting yeast (2, 4, or 4.5 h), the rats were subjected to a paw pressure test; rats with a threshold of less than 120 g were selected and evenly divided into five groups. Immediately, test drugs or vehicle (1% methylcellulose) were orally administered at a volume of 5 ml/kg. Pain threshold to pressure of the inflamed paw was measured from 0.5 h to 7 h using the Randall-Selitto method. The threshold in naïve rats was also determined before injecting yeast. Randall-Selitto method is a well-established method for assessment of acute inflammatory pain. Younger Wistar-Imamichi rats are susceptible to acute inflammation and suitable

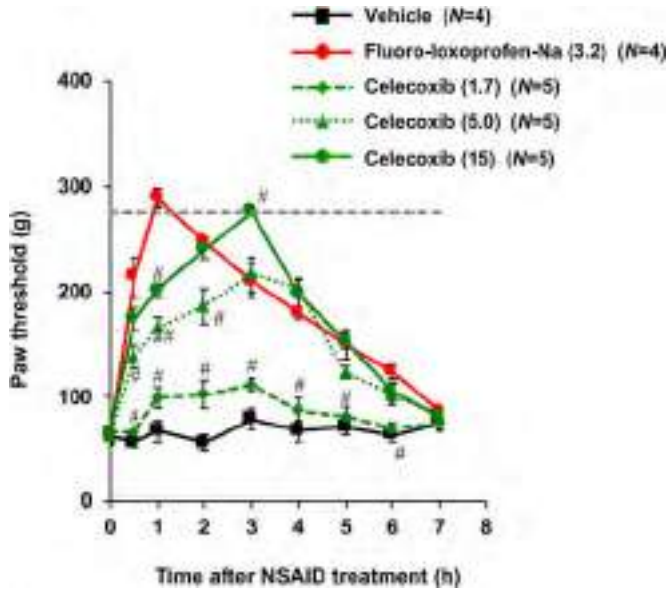

Fig. 3. Analgesic effects of fluoro-loxoprofen against yeast-induced paw hyperalgesia in rats. Wistar-Imamichi rats were given a sub-plantar injection of a 20% yeast suspension. The rats were orally administered vehicle (1% methylcellulose) or the indicated doses (mg/kg) of fluoro-loxoprofen-Na or celecoxib after 4.5 h. Paw thresholds were measured 0.5–7 h after drug administration. The broken line in gray represents the means of the rat thresholds before yeast injection (normal levels). Values are means ± S.E.M. One-way analysis of variance (ANOVA) followed by Tukey post hoc test was performed. #, $P < 0.05$ *vs.* fluoro-loxoprofen-Na (3.2).

for measuring vocalization in response to paw pressure as a marker of pain behavior. Forty-five or 23 rats were used to compare the analgesic action of loxoprofen (Fig. 2A) or celecoxib (Fig. 3) with that of fluoro-loxoprofen, respectively. Fluoro-loxoprofen was prepared at an equivalent molecular weight of loxoprofen. Our previous study showed the anti-inflammatory action by oral fluoro-loxoprofen at a concentration range of 1.1–11 mg/kg in rats (Yamakawa et al., 2010b, 2012). Celecoxib at a dose of 10 mg/kg has indicated anti-inflammatory activity in previous studies (Pinheiro and Calixto, 2002; Suleyman et al., 2004). In addition, loxoprofen or celecoxib is orally applied at around 3 or 5 mg/kg per day in clinical practice, respectively. Therefore, we adopted 1.0–3.0 mg/kg of loxoprofen, 1.1–3.2 mg/kg of fluoro-loxoprofen, or 1.7–15 mg/kg of celecoxib in this experiment, respectively.

2.4. Adjuvant-induced inflammatory pain

Arthritis-induced inflammatory pain was induced as described previously with some modifications (Magari et al., 2003). Female Lewis rats (4–5 weeks old) were subjected to sub-plantar injections of CFA (0.1 ml, 0.5 mg/ml *Mycobacterium butyricum* with paraffin oil) into the left paw. Test drugs or vehicle (1% methylcellulose) were orally administered 18–21 days later. Since our preliminary experiments and previous reports have shown that pain threshold reaches a plateau of reduction until 18 days after CFA injection, we examined the analgesic effects at this period (Magari et al., 2003). The first pressure test was performed on the experiment day before drug treatment (time 0 h). After that, the rats were evenly divided into four groups to have a similar threshold. Pain threshold to pressure of right paw was measured from 0.5 h to 7 h after drug application. Sixteen or 14 rats were used to compare the analgesic action of loxoprofen (Fig. 4A) or celecoxib (Fig. 4B) with that of fluoro-loxoprofen, respectively. Lewis rats are known as a high responder strain to CFA-mediated arthritis. Arthritis is more frequent in females than in males in clinical practice. Therefore, in this study, we used female Lewis rats for the evaluation.

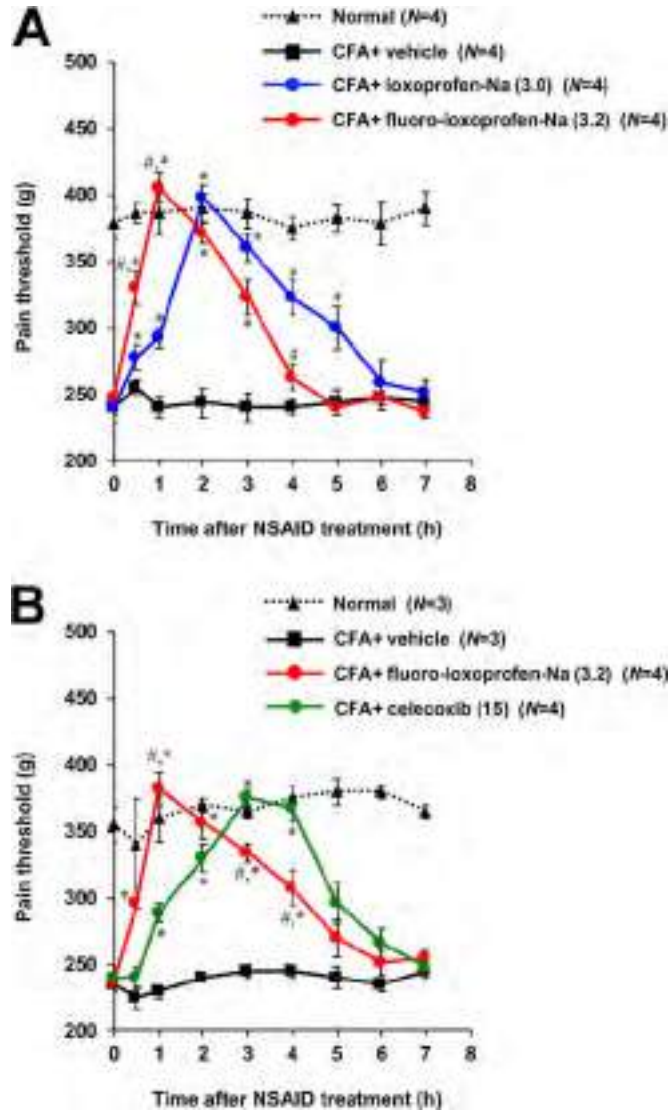

Fig. 4. Analgesic effects of fluoro-loxoprofen, loxoprofen, or celecoxib against adjuvant-induced paw hyperalgesia in rats. Lewis rats were given a sub-plantar injection of complete Freund's adjuvant (CFA) (0.5 mg/ml *Mycobacterium butyricum* with paraffin oil) into the left paw (Day 0) (**A**, **B**). On days 18 to day 21, the rats were orally administered vehicle (1% methylcellulose) or the indicated doses (mg/kg) of fluoro-loxoprofen-Na (**A**, **B**), loxoprofen-Na (**A**), or celecoxib (**B**). The pain thresholds in the right paws were then measured 0.5–7 h after drug administration (**A**, **B**). Values are means ± S.E.M. One-way analysis of variance (ANOVA) followed by Tukey post hoc test was performed. *, $P < 0.05$ *vs.* vehicle. #, $P < 0.05$ *vs.* loxoprofen-Na (3.0) (**A**) or celecoxib (15) (**B**).

2.5. Randall-Selitto paw pressure test

A modified Randall-Selitto paw pressure test was used to measure pain threshold (Randall and Selitto, 1957). Wistar-Imamichi or Lewis rats experienced hyperalgesia attributable to yeast- or adjuvant-induced inflammation and paw edema. Pain threshold was measured by using an Analgesy-Meter (Ugo Basile, Italy). We observed the reaction while gradually increasing the pressure on the inflamed paw. Pain was deemed to be present if the rats exhibited a vocal reaction response to pressure.

2.6. Measurement of tissue PGE_2 levels

The drugs were orally administered approximately 4.5 h after

injecting yeast. The rats were then killed with an overdose of isoflurane from 15 min to 2 h after drug administration, and the tissues were removed from the injected paws. Tissue PGE_2 levels were determined by an enzyme immuno-linked assay (EIA) according to the manufacturer's instructions, as described previously (Yamakawa et al., 2010b). Each group comprising 3 rats (total 9 rats) or 6 rats (total 18 rats) was used in experiments at 15 and 30 min, or 1 and 2 h after NSAID administration, respectively. The PGE_2 levels in 3 naïve rats were determined to serve as normal control.

2.7. Statistical analyses

All data are expressed as mean ± S.E.M. values. Statistical analyses were performed using SPSS 24.0 software (IBM, Armonk, USA). One-way analysis of variance (ANOVA) followed by post hoc Dunnett's or Tukey multiple comparison test was used to evaluate differences between more than two groups. Differences were considered significant at $P < 0.05$.

3. Results

3.1. Effects of loxoprofen and fluoro-loxoprofen on yeast-induced inflammatory pain and PGE_2 levels in rat paws

Loxoprofen is currently used in clinical practice and has a safer profile and equivalent or greater anti-inflammatory and anti-nociception activity than other NSAIDs (Greig and Garnock-Jones, 2016; Kawano et al., 1995). In the present study, we examined the effect of various NSAIDs on acute pain response in rats using a yeast-induced inflammatory pain model. As shown in Fig. 2A, yeast injections decreased the pain threshold in rat paws from 285 ± 25 g to 61.8 ± 4.4 g, and this hyperalgesia persisted 7 h after vehicle treatment. We also confirmed the elevations in PGE_2 levels in rat paws after yeast injection, as an indicator of acute inflammation (Fig. 2B). Oral administration of 3.0 mg/kg of loxoprofen suppressed the reduction of pain threshold from 30 min to 7 h, and restored it to normal (healthy control) levels at 2 h after treatment (*, $P < 0.05$) (Fig. 2A). The NSAID doses that exerted antinociceptive action were similar to those reported previously (Futaki et al., 2009). In contrast, oral fluoro-loxoprofen (3.2 mg/kg) showed significant pain reduction at 30 min to 6 h, with a peak time of 1 h after administration (*, $P < 0.05$). Notably, the time required for fluoro-loxoprofen (3.2 mg/kg) to reach its maximum analgesic effect was shorter than that for loxoprofen (3.0 mg/kg) (1 h and 2 h after NSAID treatment, respectively) (#, $P < 0.05$) (Fig. 2A). Moreover, we observed that analgesic action by fluoro-loxoprofen was eliminated more rapidly than that by loxoprofen from 3 to 6 h after treatment (#, $P < 0.05$ and $, $P < 0.05$). Both loxoprofen (3.0 mg/kg) and fluoro-loxoprofen (3.2 mg/kg) significantly suppressed yeast-dependent increases in PGE_2 in rat-injected paws from 15 min to 2 h after oral administration (*, $P < 0.05$) (Fig. 2B).

3.2. Analgesic effect of fluoro-loxoprofen and celecoxib on yeast-induced inflammatory pain

Next, we compared the analgesic activity of fluoro-loxoprofen to that of celecoxib. Celecoxib is a representative NSAID that is effective for treating inflammatory pain with mild onset (Brune et al., 2010); therefore, we determined whether fluoro-loxoprofen produces antinociceptive action more rapidly than celecoxib in this model. As shown in Fig. 3, celecoxib exerted antinociceptive action against yeast-induced pain in a dose-dependent manner. At 3 h after oral administration, we found the peak time of analgesic action of celecoxib, suggesting mild onset. Both fluoro-loxoprofen (3.2 mg/kg) and celecoxib (15 mg/kg) restored the decreased pain threshold produced by yeast injections to levels observed in rats without yeast treatment (1 h and 3 h after NSAID treatment, respectively). Compared with celecoxib (15 mg/kg), fluoro-loxoprofen (3.2 mg/kg) showed stronger analgesic action at 1 h and weaker action at 3 h (#, $P < 0.05$).

3.3. Antinociceptive effects of loxoprofen, fluoro-loxoprofen, and celecoxib on adjuvant-induced inflammatory pain

Finally, we evaluated the effect of fluoro-loxoprofen on adjuvant-induced inflammatory pain in rats. This model mimics patients with rheumatoid arthritis and is a representative rodent model to investigate the analgesic activity of NSAIDs (Nagakura et al., 2003). The pain threshold was significantly lower in adjuvant-treated rats than in non-treated rats (Fig. 4A). In addition, oral administration of both fluoro-loxoprofen (3.2 mg/kg) and loxoprofen (3.0 mg/kg) significantly suppressed the hyperalgesic response and restored the response to levels observed in rats without adjuvant treatment (*, $P < 0.05$). We observed differences in pain threshold between fluoro-loxoprofen and loxoprofen, indicating that fluoro-loxoprofen has superior action at 30 min and 1 h and inferior action at 4 h to loxoprofen after administration (#, $P < 0.05$). The time of peak antinociceptive action was 1 and 2 h after application of fluoro-loxoprofen and loxoprofen, respectively. We also compared the antinociceptive action of fluoro-loxoprofen (3.2 mg/kg) to that of celecoxib (15 mg/kg) in this model. The results of adjuvant-induced pain model showed that the time required for fluoro-loxoprofen to reach maximum analgesic activity is shorter than that for celecoxib, suggesting that fluoro-loxoprofen is a fast-acting analgesic (Fig. 4B). We found significant differences in analgesic activity between the two NSAIDs at 1, 3, and 4 h after treatment. At 1 h after treatment, fluoro-loxoprofen acted more rapidly than celecoxib (#, $P < 0.05$). In addition, its effect was eliminated more rapidly than celecoxib at 3 and 4 h after treatment (#, $P < 0.05$). Moreover, we calculated the area under the curve (AUC, g*h) (Fig. 4A and B) to compare the analgesic activity between fluoro-loxoprofen, loxoprofen, and celecoxib; no significant differences in AUC were observed (data not shown).

4. Discussion

Although NSAIDs are widely used to treat pain, adverse effects associated with their use, especially gastrointestinal complications, are problematic in clinical practice. Many studies suggest that the side effects associated with celecoxib are tolerable than those associated with other nonselective NSAIDs (Targownik et al., 2008). However, celecoxib is not suitable for the treatment of acute pain, such as dental pain and post-operative pain, because it is slowly absorbed and does not reduce pain rapidly (Brune et al., 2010; Mamidi et al., 2002). Therefore, a fast-acting NSAID with fewer gastrointestinal side effects is required. We recently identified fluoro-loxoprofen as a novel NSAID causing fewer gastrointestinal injuries (Suemasu et al., 2012; Yamakawa et al., 2012). In addition, the pharmacokinetic profile of oral fluoro-loxoprofen showed that it is absorbed more rapidly with higher peak plasma concentration (C_{max}), and it is cleared from the plasma faster than loxoprofen (Yamakawa et al., 2013). In the present study, we investigated the analgesic effect of fluoro-loxoprofen on inflammatory pain in rats.

We used a yeast-induced inflammatory pain model to evaluate the effects on acute pain and compared the analgesic activity of fluoro-loxoprofen to that of loxoprofen. The antinociceptive action of fluoro-loxoprofen was similar to that of loxoprofen, and both NSAIDs restored the pain threshold levels of yeast-treated rats to those observed before injection. However, we found that the peak time of analgesic effect for fluoro-loxoprofen was faster than that for loxoprofen. Moreover, we observed that fluoro-loxoprofen has an equivalent potency and more rapid action against acute inflammatory pain than celecoxib. The peak time of antinociceptive effects for fluoro-loxoprofen, loxoprofen, and celecoxib was 1, 2, and 3 h after oral administration, respectively, suggesting that fluoro-loxoprofen is the most rapid analgesic among the

three NSAIDs. A recent clinical study reported that a single administration of loxoprofen results in a more rapid onset and superior efficacy against pain after spinal surgery than celecoxib (Sekiguchi et al., 2015). In addition, it has been reported that the analgesic activity of celecoxib is inferior to that of ibuprofen (film-coated tablet) during the early pain period (0–8 h) (Malmstrom et al., 2002). Thus, celecoxib might not be an appropriate analgesic to treat pain during the early pain period when compared to fast-acting NSAIDs such as ibuprofen and loxoprofen. The results of our animal studies (Figs. 2 and 3) are in agreement with the findings in humans.

Furthermore, we examined the effect of fluoro-loxoprofen on arthritis-induced pain response in rats. NSAIDs are commonly used to treat patients with rheumatoid arthritis (Crofford, 2013). We used this animal model as it closely mimics the symptoms observed in clinical practice. In some cases, loxoprofen is clinically used for episodes of pain to manage pain. We considered the availability of fluoro-loxoprofen for pain management in arthritis patients. Fluoro-loxoprofen showed antinociceptive action against arthritis-induced pain more rapidly than loxoprofen and celecoxib in this model as well as in yeast model. At the peak point of analgesia, all NSAIDs restored the pain thresholds to those observed in naive rats. These results suggest that fluoro-loxoprofen may provide rapid relief of pain symptoms in patients with rheumatoid arthritis. As described above, arthritis patients chronically using NSAIDs have a high incidence of gastrointestinal toxicity (Graham et al., 2005; Sostres et al., 2013). Since fluoro-loxoprofen provides both rapid analgesia and fewer gastrointestinal injuries than loxoprofen, it could be therapeutic option for treating pain in arthritis patients.

The key factors for achieving better pain relief clinically with fewer adverse effects, include the choice of NSAID, the lowest effective dose, rapid onset, and a short duration (Brune and Patrignani, 2015; Brune et al., 2010; Masso Gonzalez et al., 2010). When treating acute pains, such as dental and post-surgical pain, time to onset and rapid absorption play particularly vital roles for eliciting better analgesic effects. It has been suggested that the time to maximum concentration (T_{max}) (absorption speed) of NSAIDs is related to their effectiveness in humans. Fast-acting formulations of ibuprofen (arginine, lysine, and sodium salt) provide better pain relief than standard ibuprofen, which is associated with shorter T_{max} and higher C_{max} (Moore et al., 2014). Moreover, it has been suggested that diclofenac potassium is better at relieving pain than diclofenac sodium salt, a phenomenon that is dependent on its shorter T_{max} (Derry et al., 2009). Therefore, rapid-acting NSAIDs can contribute to better pain relief. Since the antinociceptive action of fluoro-loxoprofen is faster than that of loxoprofen, it could produce better outcomes in patients. Furthermore, fast elimination (short half-life) from non-target tissues is important in preventing adverse events (Brune et al., 2010). Because long half-life NSAIDs, such as piroxicam and phenylbutazone, cause long-term inhibition of COX, they can increase the risk of toxicities, especially if administered repeatedly. Previously, we demonstrated a faster elimination rate of fluoro-loxoprofen than that of loxoprofen (Yamakawa et al., 2013). In this study, we observed that fluoro-loxoprofen eliminated analgesic activity more rapidly than loxoprofen. We speculate that the characteristic profile of fluoro-loxoprofen, which is rapid absorption with higher C_{max} and faster elimination from plasma than loxoprofen, contributes to its rapid analgesic action and possible lower gastrointestinal toxicities. The absorption and distribution of fluoro-loxoprofen *in vivo* are controlled by its balance of lipophilicity and hydrophilicity, and iconicity. It is well-known that incorporation of fluorine or fluorinated groups increases the lipophilicity of a drug, particularly aromatic benzenes, which contribute to the enhancement of pharmacological action, cell permeability (absorption), and plasma concentration (Iwao, 2009). Such a mechanism may be associated with the properties of fluoro-loxoprofen.

Our study has several limitations. First, we examined both the ulcerogenic and analgesic activities of fluoro-loxoprofen using only a single dose. Although the analgesic properties of fluoro-loxoprofen may be more appropriate for treating acute pain, such as dental pain (that is, short-term), rather than chronic pain, such as arthritis, the effects of repeated doses remain to be determined. Secondly, we did not measure the differences in the degree of antinociception between fluoro-loxoprofen and loxoprofen in this study. Our previous results showed that the C_{max} of fluoro-loxoprofen was approximately 1.4 times higher than that of loxoprofen; therefore, we expected that fluoro-loxoprofen could have a stronger analgesic activity than loxoprofen. However, we did not measure any differences between fluoro-loxoprofen and loxoprofen. This may be because we assessed hyperalgesic pain responses to mechanical pressure but not spontaneous pain in this study. Spontaneous pain is also an important indicator to investigate analgesic activity in both humans and animals. Thus, future experiments to determine spontaneous pain should be performed. Moreover, we did not statistically analyze tissue PGE_2 levels between each time point (15 min, 30 min, 1 h, and 2 h) after NSAID treatment, because these experiments were performed on different days and not on the same day. Under such an experimental condition, it was deemed difficult to obtain appropriate results by statistical analysis of insufficient number of animals ($N = 3$). However, it is likely that there is no difference in PGE_2 reduction between the two NSAIDs within 1 h after administration. Thus, fluoro-loxoprofen might show antinociceptive mechanisms other than COX-2 inhibition. The changes in other inflammatory mediators responsible for acute pain should be examined in future studies.

5. Conclusion

Based on these results, it can be suggested that the analgesic effects of fluoro-loxoprofen may be equivalent to those of loxoprofen and celecoxib. Moreover, fluoro-loxoprofen could produce analgesic effects against inflammatory pain more rapidly than other NSAIDs, which might be associated with its rapid absorption property. Thus, fluoro-loxoprofen could be beneficial for the treatment of acute pain.

CRediT authorship contribution statement

Teita Asano: Conceptualization, Methodology, Investigation, Formal analysis, Writing-original draft, Writing-review & editing. **Tomoki Hattori:** Conceptualization, Methodology, Investigation, Formal analysis, Writing-original draft, Writing-review & editing. **Ken-ichiro Tanaka:** Conceptualization, Methodology, Writing-original draft. **Naoki Yamakawa:** Investigation, Writing-original draft, Writing-review & editing. **Shintaro Suemasu:** Investigation, Formal analysis. **Shuji Aida:** Investigation. **Marika Kataoka:** Investigation. **Tohru Mizushima:** Conceptualization, Methodology, Formal analysis, Writing-original draft. **Mitsuko Takenaga:** Conceptualization, Methodology, Writing-original draft.

Acknowledgements

The authors acknowledge Ayumi Kanada for technical assistance with the animal experiments. We would like to thank Editage for English language editing.

Financial disclosure

TM is the chairman and director of LTT Bio-Pharma Co., Ltd. TA and MT are affiliated to an endowed research division of LTT Bio-Pharma Co., Ltd. TM and NY hold a patent on fluoro-loxoprofen. Other authors have no conflict of interest to declare.

All authors have confirmed the submission of this paper and agree with their contribution to this work.

References

Arakawa, T., Fujiwara, Y., Sollano, J.D., Zhu, Q., Kachintorn, U., Rani, A.A., Hahm, K.B., Takahashi, S., Joh, T., Kinoshita, Y., Matsumoto, T., Naito, Y., Takeuchi, K.,

Yamagami, H., Agustanti, N., Xiong, H., Chen, X., Jang, E.J., Furuta, K., Terano, A., group, Is, 2009. A questionnaire-based survey on the prescription of non-steroidal anti-inflammatory drugs by physicians in East Asian countries in 2007. Digestion 79, 177–185.
Arora, G., Singh, G., Triadafilopoulos, G., 2009. Proton pump inhibitors for gastroduodenal damage related to nonsteroidal anti-inflammatory drugs or aspirin: twelve important questions for clinical practice. Clin. Gastroenterol. Hepatol. 7, 725–735.
Biederman, R.E., 2005. Pharmacology in rehabilitation: nonsteroidal anti-inflammatory agents. J. Orthop. Sports Phys. Ther. 35, 356–367.
Brune, K., Patrignani, P., 2015. New insights into the use of currently available nonsteroidal anti-inflammatory drugs. J. Pain. Res. 8, 105–118.
Brune, K., Renner, B., Hinz, B., 2010. Using pharmacokinetic principles to optimize pain therapy. Nat. Rev. Rheumatol. 6, 589–598.
Crofford, L.J., 2013. Use of NSAIDs in treating patients with arthritis. Arthritis Res. Ther. 15 (Suppl. 3), S2.
Dahl, J.B., Kehlet, H., 1991. Non-steroidal anti-inflammatory drugs: rationale for use in severe postoperative pain. Br. J. Anaesth. 66, 703–712.
Derry, P., Derry, S., Moore, R.A., McQuay, H.J., 2009. Single dose oral diclofenac for acute postoperative pain in adults. Cochrane Database Syst. Rev. CD004768.
Fujimori, S., Hanada, R., Hayashida, M., Sakurai, T., Ikushima, I., Sakamoto, C., 2016. Celecoxib monotherapy maintained small intestinal mucosa better compared with loxoprofen plus lansoprazole treatment: a double-blind, randomized, controlled trial. J. Clin. Gastroenterol. 50, 218–226.
Futaki, N., Harada, M., Sugimoto, M., Hashimoto, Y., Honma, Y., Arai, I., Nakaike, S., Hoshi, K., 2009. The importance of brain PGE2 inhibition versus paw PGE2 inhibition as a mechanism for the separation of analgesic and antipyretic effects of lornoxicam in rats with paw inflammation. J. Pharm. Pharmacol. 61, 607–614.
Graham, D.Y., Opekun, A.R., Willingham, F.F., Qureshi, W.A., 2005. Visible small-intestinal mucosal injury in chronic NSAID users. Clin. Gastroenterol. Hepatol. 3, 55–59.
Greig, S.L., Garnock-Jones, K.P., 2016. Loxoprofen: a review in pain and inflammation. Clin. Drug. Investig. 36, 771–781.
Harirforoosh, S., Asghar, W., Jamali, F., 2013. Adverse effects of nonsteroidal antiinflammatory drugs: an update of gastrointestinal, cardiovascular and renal complications. J. Pharm. Pharm. Sci. 16, 821–847.
Iwao, O., 2009. Fluorine in Medicinal Chemistry and Chemical Biology. Blackwell Publishing Ltd, Chichester.
Kawano, S., Tsuji, S., Hayashi, N., Takei, Y., Nagano, K., Fusamoto, H., Kamada, T., 1995. Effects of loxoprofen sodium, a newly synthesized non-steroidal anti-inflammatory drug, and indomethacin on gastric mucosal haemodynamics in the human. J. Gastroenterol. Hepatol. 10, 81–85.
Magari, K., Miyata, S., Ohkubo, Y., Mutoh, S., Goto, T., 2003. Calcineurin inhibitors exert rapid reduction of inflammatory pain in rat adjuvant-induced arthritis. Br. J. Pharmacol. 139, 927–934.
Malmstrom, K., Fricke, J.R., Kotey, P., Kress, B., Morrison, B., 2002. A comparison of rofecoxib versus celecoxib in treating pain after dental surgery: a single-center, randomized, double-blind, placebo- and active-comparator-controlled, parallel-group, single-dose study using the dental impaction pain model. Clin. Ther. 24, 1549–1560.
Mamidi, R.N., Mullangi, R., Kota, J., Bhamidipati, R., Khan, A.A., Katneni, K., Datla, S., Singh, S.K., Rao, K.Y., Rao, C.S., Srinivas, N.R., Rajagopalan, R., 2002. Pharmacological and pharmacokinetic evaluation of celecoxib prodrugs in rats. Biopharm. Drug. Dispos. 23, 273–282.
Masso Gonzalez, E.L., Patrignani, P., Tacconelli, S., Garcia Rodriguez, L.A., 2010. Variability among nonsteroidal antiinflammatory drugs in risk of upper gastrointestinal bleeding. Arthritis Rheum. 62, 1592–1601.
McCarberg, B.H., Cryer, B., 2015. Evolving therapeutic strategies to improve nonsteroidal anti-inflammatory drug safety. Am. J. Ther. 22, e167–178.
Moore, R.A., Derry, S., Straube, S., Ireson-Paine, J., Wiffen, P.J., 2014. Faster, higher, stronger? Evidence for formulation and efficacy for ibuprofen in acute pain. Pain 155, 14–21.
Nagakura, Y., Okada, M., Kohara, A., Kiso, T., Toya, T., Iwai, A., Wanibuchi, F., Yamaguchi, T., 2003. Allodynia and hyperalgesia in adjuvant-induced arthritic rats: time course of progression and efficacy of analgesics. J. Pharmacol. Exp. Ther. 306, 490–497.
Pinheiro, R.M., Calixto, J.B., 2002. Effect of the selective COX-2 inhibitors, celecoxib and rofecoxib in rat acute models of inflammation. Inflamm. Res. 51, 603–610.
Randall, L.O., Selitto, J.J., 1957. A method for measurement of analgesic activity on inflamed tissue. Arch. Int. Pharmacodyn. Ther. 111, 409–419.
Rao, P., Knaus, E.E., 2008. Evolution of nonsteroidal anti-inflammatory drugs (NSAIDs): cyclooxygenase (COX) inhibition and beyond. J. Pharm. Pharm. Sci. 11, 81s–110s.
Sakamoto, C., Kawai, T., Nakamura, S., Sugioka, T., Tabira, J., 2013. Comparison of gastroduodenal ulcer incidence in healthy Japanese subjects taking celecoxib or loxoprofen evaluated by endoscopy: a placebo-controlled, double-blind 2-week study. Aliment. Pharmacol. Ther. 37, 346–354.
Sekiguchi, H., Inoue, G., Nakazawa, T., Imura, T., Saito, W., Uchida, K., Miyagi, M., Takahira, N., Takaso, M., 2015. Loxoprofen sodium and celecoxib for postoperative pain in patients after spinal surgery: a randomized comparative study. J. Orthop. Sci. 20, 617–623.
Sostres, C., Gargallo, C.J., Lanas, A., 2013. Nonsteroidal anti-inflammatory drugs and upper and lower gastrointestinal mucosal damage. Arthritis Res. Ther. 15 (Suppl 3), S3.
Suemasu, S., Yamakawa, N., Ishihara, T., Asano, T., Tahara, K., Tanaka, K., Matsui, H., Okamoto, Y., Otsuka, M., Takeuchi, K., Suzuki, H., Mizushima, T., 2012. Identification of a unique nsaid, fluoro-loxoprofen with gastroprotective activity. Biochem. Pharmacol. 84, 1470–1481.
Suleyman, H., Demircan, B., Karagoz, Y., Oztasan, N., Suleyman, B., 2004. Anti-inflammatory effects of selective COX-2 inhibitors. Pol. J. Pharmacol. 56, 775–780.
Targownik, L.E., Metge, C.J., Leung, S., Chateau, D.G., 2008. The relative efficacies of gastroprotective strategies in chronic users of nonsteroidal anti-inflammatory drugs. Gastroenterology 134, 937–944.
Ungprasert, P., Cheungpasitporn, W., Crowson, C.S., Matteson, E.L., 2015. Individual non-steroidal anti-inflammatory drugs and risk of acute kidney injury: a systematic review and meta-analysis of observational studies. Eur. J. Intern. Med. 26, 285–291.
Ushiyama, S., Yamada, T., Murakami, Y., Kumakura, S., Inoue, S., Suzuki, K., Nakao, A., Kawara, A., Kimura, T., 2008. Preclinical pharmacology profile of CS-706, a novel cyclooxygenase-2 selective inhibitor, with potent antinociceptive and anti-inflammatory effects. Eur. J. Pharmacol. 578, 76–86.
Wongrakpanich, S., Wongrakpanich, A., Melhado, K., Rangaswami, J., 2018. A comprehensive review of non-steroidal anti-inflammatory drug use in the elderly. Aging Dis. 9, 143–150.
Yamakawa, N., Suemasu, S., Kimoto, A., Arai, Y., Ishihara, T., Yokomizo, K., Okamoto, Y., Otsuka, M., Tanaka, K., Mizushima, T., 2010a. Low direct cytotoxicity of loxoprofen on gastric mucosal cells. Biol. Pharm. Bull. 33, 398–403.
Yamakawa, N., Suemasu, S., Matoyama, M., Kimoto, A., Takeda, M., Tanaka, K., Ishihara, T., Katsu, T., Okamoto, Y., Otsuka, M., Mizushima, T., 2010b. Properties and synthesis of 2-{2-fluoro (or bromo)-4-[(2-oxocyclopentyl)methyl]phenyl}propanoic acid: nonsteroidal anti-inflammatory drugs with low membrane permeabilizing and gastric lesion-producing activities. J. Med. Chem. 53, 7879–7882.
Yamakawa, N., Suemasu, S., Okamoto, Y., Tanaka, K., Ishihara, T., Asano, T., Miyata, K., Otsuka, M., Mizushima, T., 2012. Synthesis and biological evaluation of derivatives of 2-{2-fluoro-4-[(2-oxocyclopentyl)methyl]phenyl}propanoic acid: nonsteroidal anti-inflammatory drugs with low gastric ulcerogenic activity. J. Med. Chem. 55, 5143–5150.
Yamakawa, N., Suemasu, S., Watanabe, H., Tahara, K., Tanaka, K., Okamoto, Y., Ohtsuka, M., Maruyama, T., Mizushima, T., 2013. Comparison of pharmacokinetics between loxoprofen and its derivative with lower ulcerogenic activity, fluoro-loxoprofen. Drug. Metab. Pharmacokinet. 28, 118–124.

Bioorganic & Medicinal Chemistry 27 (2019) 3339–3346

Contents lists available at ScienceDirect

Bioorganic & Medicinal Chemistry

journal homepage: www.elsevier.com/locate/bmc

Chemical modification-mediated optimisation of bronchodilatory activity of mepenzolate, a muscarinic receptor antagonist with anti-inflammatory activity

Yasunobu Yamashita[a,1], Ken-ichiro Tanaka[b,1], Naoki Yamakawa[c,1], Teita Asano[d], Yuki Kanda[b], Ayaka Takafuji[b], Masahiro Kawahara[b], Mitsuko Takenaga[d], Yoshifumi Fukunishi[e], Tohru Mizushima[f,*]

[a] Technology Research Association for Next-Generation Natural Products Chemistry, 2-3-26 Aomi, Koto-ku, Tokyo 135-0064, Japan
[b] Department of Pharmaceutical Sciences, Musashino University, 1-1-20 Shinmachi, Nishi-Tokyo 202-8585, Japan
[c] Shujitsu University School of Pharmacy, 1-6-1, Nishigawara, Naka-ku, Okayama 703-8516, Japan
[d] Institute of Medical Science, St. Marianna University School of Medicine, 2-16-1, Sugao, Miyamae-ku, Kawasaki 216-8512, Japan
[e] Molecular Profiling Research Center for Drug Discovery (molprof), National Institute of Advanced Industrial Science and Technology (AIST), 2-3-26, Aomi, Koto-ku, Tokyo 135-0064, Japan
[f] LTT Bio-Pharma Co., Ltd, Shiodome Building 3F, 1-2-20 Kaigan, Minato-ku, Tokyo 105-0022, Japan

ARTICLE INFO

Keywords:
Chemical modification
Mepenzolate
COPD
Inflammatory
Long-acting muscarinic antagonist

ABSTRACT

The treatment for patients with chronic obstructive pulmonary disease (COPD) usually involves a combination of anti-inflammatory and bronchodilatory drugs. We recently found that mepenzolate bromide (**1**) and its derivative, 3-(2-hydroxy-2, 2-diphenylacetoxy)-1-(3-phenoxypropyl)-1-azoniabicyclo[2.2.2]octane bromide (**5**), have both anti-inflammatory and bronchodilatory activities. We chemically modified **5** with a view to obtain derivatives with both anti-inflammatory and longer-lasting bronchodilatory activities. Among the synthesized compounds, (*R*)-(–)-**12** ((*R*)-3-(2-hydroxy-2,2-diphenylacetoxy)-1-(3-phenylpropyl)-1-azoniabicyclo[2.2.2]octane bromide) showed the highest affinity *in vitro* for the human muscarinic M3 receptor (hM_3R). Compared to **1** and **5**, (*R*)-(–)-**12** exhibited longer-lasting bronchodilatory activity and equivalent anti-inflammatory effect in mice. The long-term intratracheal administration of (*R*)-(–)-**12** suppressed porcine pancreatic elastase-induced pulmonary emphysema in mice, whereas the same procedure with a long-acting muscarinic antagonist used clinically (tiotropium bromide) did not. These results suggest that (*R*)-(–)-**12** might be therapeutically beneficial for use with COPD patients given the improved effects seen against both inflammatory pulmonary emphysema and airflow limitation in this animal model.

1. Introduction

Chronic obstructive pulmonary disease (COPD) is a serious health problem that is defined by a progressive and not fully reversible airflow limitation and an abnormal inflammatory response.[1–3] To treat COPD and to concomitantly elicit improved airflow by bronchodilation, it is important to suppress the inflammatory processes associated with this disease.

Both β2-agonists and muscarinic receptor antagonists are used clinically to achieve bronchodilation in the treatment of COPD.[2–4] Short-acting bronchodilators were previously used; however, in recent times long-acting -agonists (LABAs) and muscarinic receptor

Abbreviations: aclidinium, aclidinium bromide; BALF, bronchoalveolar lavage fluid; CDI, carbonyldiimidazole; COPD, chronic obstructive pulmonary disease; FEV0.1, forced expiratory volume in 0.1 s; FVC, forced vital capacity; glycopyrronium, glycopyrronium bromide; GST, glutathione S-transferase; hM_2R, human muscarinic M2 receptor; hM_3R, human muscarinic M3 receptor; HDAC2, Histone deacetylase 2; IFN, interferon; IL, interleukin; KC, keratinocyte chemoattractant; LABA, long-acting β2-agonist; LAMA, long-acting muscarinic antagonist; mepenzolate, mepenzolate bromide; MLI, mean linear intercept; [^{3}H]NMS, *N*-methyl-[^{3}H]-scopolamine methylchloride; PPE, porcine pancreatic elastase; QNB, 3-quinuclidinyl benzilate; ROS, reactive oxygen species; SOD, superoxide dismutase; tiotropium, tiotropium bromide; TNF, tumor necrosis factor

* Corresponding author.
E-mail address: t.mizushima@ltt.co.jp (T. Mizushima).
[1] These authors contributed equally to this work.

https://doi.org/10.1016/j.bmc.2019.06.016
Received 7 May 2019; Received in revised form 6 June 2019; Accepted 6 June 2019
Available online 08 June 2019
0968-0896/ © 2019 Elsevier Ltd. All rights reserved.

antagonists (LAMAs) have replaced the shorter-acting ones due to their superior efficacy.[2,3] Tiotropium bromide (tiotropium), glycopyrronium bromide (glycopyrronium), and aclidinium bromide (aclidinium) are representative LAMAs used in the clinical setting.

The inflammation associated with COPD is typically treated with steroids; however, COPD disease progression is not fully suppressed by steroid treatment[4–6] because of resistance in part of the inflammatory processes to steroid treatment.[6,7] Histone deacetylase 2 (HDAC2) seems to play an important role in the inflammatory responses associated with COPD.[8–10] Because corticosteroids use HDAC2 to suppress inflammation,[8,11,12] the inhibitory effect of cigarette smoke on HDAC2 may be responsible for the reduced sensitivity of COPD patients to steroid treatment.[8] It is therefore important for new types of anti-inflammatory compounds to be developed to treat COPD.

From a library of medicines approved in Japan, we screened for compounds that suppress porcine pancreatic elastase (PPE)-induced pulmonary emphysema and inflammation in mice, and selected mepenzolate bromide (mepenzolate),[13] an orally administered muscarinic receptor antagonist used for the treatment of gastrointestinal disorders.[14–16] Mepenzolate exhibits not only anti-inflammatory effects via a muscarinic receptor-independent mechanism, but also provides short-acting bronchodilatory effects via a muscarinic receptor-dependent mechanism.[13,17,18] We previously reported that mepenzolate showed anti-inflammatory activity in PPE-induced pulmonary emphysema in mice.[13] We also showed that steroids and other anti-inflammatory drugs did not demonstrate anti-inflammatory activity in the same PPE models,[19] suggesting that the anti-inflammatory activity of mepenzolate is more potent than that of steroids. The anti-inflammatory activity of mepenzolate is mediated via a decreased level of reactive oxygen species (ROS) in the lung due to the NADPH oxidase activity and the induction of superoxide dismutase (SOD) and glutathione S-transferase (GST) expression.[13]

We previously postulated that mepenzolate derivatives possessing both anti-inflammatory and long-acting bronchodilatory activities might be beneficial for the treatment of COPD. To obtain such derivatives, we synthesized hybrid compounds based on mepenzolate and glycopyrronium or aclidinium, and found that one of these hybrid compounds (3-(2-hydroxy-2, 2-diphenylacetoxy)-1-(3-phenoxypropyl)-1-azoniabicyclo[2.2.2]octane bromide **(5)** showed both a longer-acting bronchodilatory activity (equivalent to glycopyrronium and aclidinium) and possessed anti-inflammatory properties (equivalent to mepenzolate).[20] Based on these results, in the present study we chemically modified **5** to obtain derivative compounds with both anti-inflammatory and even longer-acting bronchodilatory activities. As for synthesized hybrid compounds based on mepenzolate bromide (**MP**), glycopyrronium bromide (**GC**), and aclidinium bromide (**AD**), both **MP-GC** and **MP-AD** showed anti-inflammatory effects similar to **MP**, whereas **GC-MP**, like **GC** and **AD** alone, did not.[20] Based on these results, we speculated here that the double phenyl rings in **MP** (Fig. 1) are important for its anti-inflammatory activity and therefore, we avoided modifying this part. Instead, we chemically modified the terminal phenyl ring combined with the nitrogen atom of quinuclidine. Among the derivatives obtained, (*R*)-(–)-**12** showed the highest affinity for hM_3R *in vitro* and the longest bronchodilatory activity *in vivo*, with an anti-inflammatory effect similar to that of **5** and mepenzolate. These results suggest that (*R*)-(–)-**12** might be therapeutically beneficial in a clinical setting for COPD patients.

2. Results

2.1. Chemistry

The route followed to synthesize target compounds **6–14** and **15–27** is outlined in Scheme 1. QNB (3-quinuclidinyl benzilate) (**28**) was the key compound used for synthesizing all target compounds. Subsequent quaternization of **28** with an appropriate alkyl bromide (**29–50**) in 1,4-dioxane provided the desired corresponding target compounds **6–27**. The enantiomers (*R*)-(–)-**12** and (*S*)-(+)-**12** were synthesized in the same manner as that for (*R*)-(–)-**1** and (*S*)-(+)-**1** with enantiomerically pure 3-quinuclidinol instead of racemic 3-quinuclidinol.[21] All of the new target compounds were characterized by NMR and HRMS. Protocols for the synthesis and characterization of final compounds **6–27** and intermediates **29–50** are described in the supporting information.

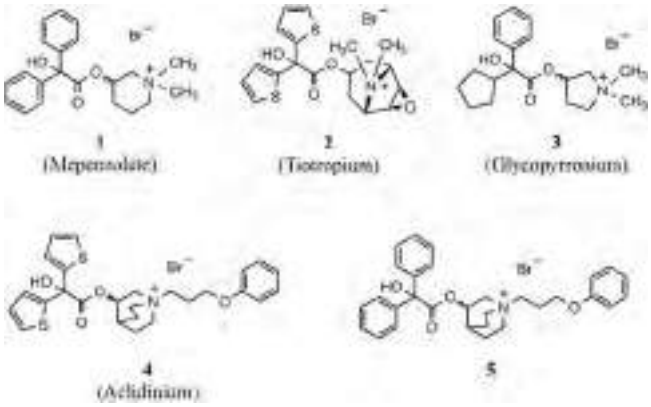

Fig. 1. Structure of clinically-used muscarinic antagonists **1–4** and hybrid compound **5**.

2.2. Chemical modifications to mepenzolate

The binding affinity of each compound to hM_3R was determined by carrying out *N*-methyl-[^{3}H]-scopolamine methylchloride ([^{3}H]NMS) displacement studies on this receptor. The binding affinities of mepenzolate (**1**), tiotropium (**2**), glycopyrronium (**3**), aclidinium (**4**) and compound **5** (Fig. 1) are shown in Table 1 (data for **1–5** are from our previous report[20]). The affinity of **5** for hM_3R was higher than that of **1** but lower than that of **2**.[20]

The total number of leucocytes and the individual number of neutrophils in bronchoalveolar lavage fluid (BALF) are indicators of pulmonary inflammatory responses; we previously showed that increases in these numbers after PPE treatment were partially suppressed by the simultaneous intratracheal administration of **1** and **5**.[13,17,20] On the other hand, none of **2–4** showed anti-inflammatory activity.[20] Based on these findings, we attempted to identify derivatives of **5** that have an affinity for hM_3R similar to that of **2** and an anti-inflammatory activity similar to that of **1** and **5**. Because the high affinities of drugs for hM_2R are associated with adverse effects on cardiac function,[22] compounds that showed a higher affinity for hM_3R than for hM_2R were preferred and thus the focus of the selection process used in this study.

The strategy used for making chemical modifications to **5** is shown in Fig. 2. We modified the linker moiety of **5** (Scheme 1), first shortening (**6** and **7**) or extending (**8** and **9**) the linker length of **5**. We also changed the linker moiety of **5** into a carbon chain without a heteroatom (**10–14**), with **12** found to have the highest affinity for hM_3R (Table 1). As for hM_2R, **12** showed a slightly lower affinity (Table 1).

A variety of substituents were then introduced into the terminal phenyl ring combined with the linker of **12** to obtain derivatives thereof (**15–27**) (Scheme 1). However, the simplest analogue **12**, which had no substituent on the terminal phenyl ring, showed the highest affinity for hM_3R. Based on these results, **12** was selected for further analysis.

2.3. Synthesis and activity of enantiomers of mepenzolate derivatives

As for **1**, **12** has one asymmetric carbon atom, enabling it to exist in two enantiomeric forms (Fig. 2), for which a racemic mixture of these two enantiomers was used in the experiments described above. We recently reported that although anti-inflammatory activity was

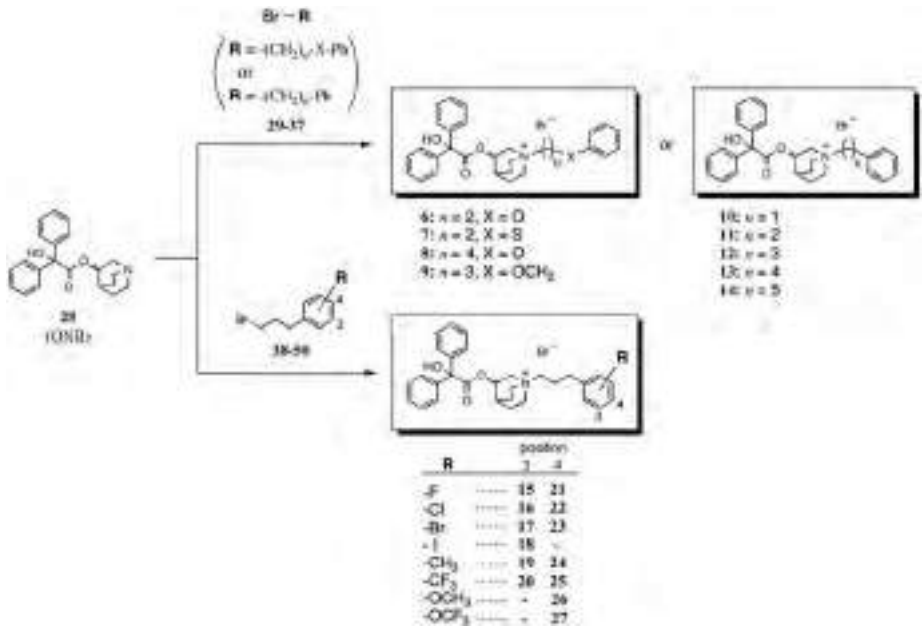

Scheme 1.

indistinguishable between enantiomers (*R*)- (–)-mepenzolate (*R*)-(–)-**1** and (*S*)-mepenzolate (*S*)-(+)-**1**, the binding affinity of (*R*)-(–)-**1** to hM_3R *in vitro* and its bronchodilatory activity *in vivo* were superior to that of (*S*)-(+)-**1**[21].

We have synthesized (*R*)-(–)-**12** and (*S*)-(+)-**12**, and examined their biochemical and pharmacological activities. As shown in Table 1, (*R*)-(–)-**12** exhibited a higher affinity for hM_3R than (*S*)-(+)-**12**. We also compared their bronchodilatory activities. As shown in Fig. 3A, at a dose of 48 μg/kg, **12** and (*R*)-(–)-**12** but not (*S*)-(+)-**12** showed bronchodilatory activity. These *in vivo* results were consistent with the *in vitro* results for hM_3R affinity (Table 1). On the other hand, the measured anti-inflammatory activity was indistinguishable among **12** and its enantiomers ((*R*)-(–)-**12** and (*S*)-(+)-**12**) (Fig. 4A). Taken together, these results suggest that (*R*)-(–)-**12** may be preferable to (*S*)-(+)-**12**, and that the higher affinity for hM_3R of the (*R*)-enantiomer compared with the (*S*)-enantiomer was a general property of mepenzolate derivatives.

2.4. Bronchodilatory and anti-inflammatory activities of R-12

We next compared the bronchodilatory activities of **1**–**5** and (*R*)-(–)-**12**, beginning with their dose–response profiles. A dose of 38 μg/kg for **1** corresponds to 42, 36, 50, 49 and 48 μg/kg for **2**, **3**, **4**, **5**, and (*R*)-(–)-**12**, respectively, based on their molecular weights. As shown in Fig. 3B, 1 h after administration of each drug, complete suppression of the methacholine-induced increase in airway resistance was observed with **2** and (*R*)-(–)-**12** at doses of 4.2 and 4.8 μg/kg, respectively. We recently reported that complete suppression of the methacholine-induced increase in airway resistance was observed with **1**, **3**, **4**, and **5** at doses of 38, 3.6, 5.0 and 4.9, respectively.[20] These results suggest that (*R*)-(–)-**12** has a strong bronchodilatory activity, similar to that of **2** which is currently used in the clinical setting.

We subsequently compared the duration of bronchodilatory activity exhibited by the derivative compounds. We previously found that the bronchodilatory activity of **1** disappeared within 24 h of its administration.[20] We also showed that the bronchodilatory activities of **3** and **4** (clinically used LAMAs) were still present 48 h after their administration, but had disappeared by 72 h.[20] As shown in Fig. 5A, bronchodilatory activity with **3**, **4**, and **5** was not observed up to 96 h after drug administration. On the other hand, (*R*)-(–)-**12** and **2** still showed bronchodilatory activity at 96 or 120 h, respectively, after administration (Fig. 5A, B), suggesting that (*R*)-(–)-**12** exhibits long-acting bronchodilatory activity, similar to that of **2**.

An examination of anti-inflammatory activity revealed that **1** and (*R*)-(–)-**12** significantly suppressed the PPE-induced increase in the total number of leucocytes and the individual number of neutrophils in BALF (Fig. 4B). We recently reported a similar anti-inflammatory effect for **5**, but not for **2**-**4**.[20]

We next examined the mechanism underlying (*R*)-(–)-**12**'s anti-inflammatory activity. As shown in Fig. 4C, PPE-induced an increase in the mRNA expression of tumor necrosis factor (*TNF*)-*α*, interleukin (*IL-6*), interferon (*IFN*)-γ, and keratinocyte chemoattractant (*KC*); this expression was suppressed by the administration of (*R*)-(–)-**12** in all cases. Furthermore, administration of (*R*)-(–)-**12** to healthy mice increased GST activity in the lung, suggesting that this effect is involved in the anti-inflammatory activity of (*R*)-(–)-**12**, as in the case of **1**.[13]

2.5. Effect of 2 and R-12 on PPE-induced lung injury and dysfunction

The effects of the long-term administration of **2** and (*R*)-(–)-**12** on lung injury and dysfunction induced by PPE were compared. Histopathological analysis revealed that PPE induced damage to the alveolar walls and an increase in the mean linear intercept (MLI; an indicator of airspace enlargement). These effects could be partly suppressed by the administration of (*R*)-(–)-**12** but not by **2** (Fig. 6A and B).

PPE-induced lung dysfunction can be monitored by using the $FEV_{0.1}/FVC$[19,23]. While the PPE treatment decreased the $FEV_{0.1}/FVC$ ratio, administration of (*R*)-(–)-**12** but not **2** significantly restored the towards control values (Fig. 6C). The results presented in Fig. 6 suggest that the long-term administration of (*R*)-(–)-**12**, but not of **2**, suppress PPE-induced lung injury and dysfunction.

3. Discussion

We have chemically modified **5** to produce derivatives with both anti-inflammatory and longer-lasting bronchodilatory activities. Although a drug's affinity for hM_3R is not always correlated with its duration of action, we selected this index for the initial screening of drugs given that hM_3R affinity can be rapidly determined for large panels of compounds. Of all the derivatives synthesized, **12** showed the highest affinity for hM_3R. Compound **12** has an asymmetric carbon atom, with (*R*)-(–)-**12** exhibiting a higher affinity for hM_3R *in vitro* and

Table 1
Binding of compounds to hM2R or hM3R. Membrane fractions prepared from CHO-K1 cells expressing hM2R or hM3R were incubated with 2 nM [^{3}H]NMS (85.5 Ci/mmol) in the presence of each compound. A range of concentrations (10^{-11} to 10^{-6} M) for each compound was tested to generate competition curves to determine K_i values. At the initial screening, we examined affinity values from triplicate measurements and determined mean values. For some compounds that showed a relatively high affinity at the initial screening, we re-examined the affinity in independent experiments and confirmed the results. Mean values of triplicate data for each one experiments are shown in the table. Compounds whose affinity values were re-examined in additional experiments are denoted by an asterisk (*). Data for **1–5** are from our previous report [20]. Values represent mean ± S.E.M.

Compound	K_i (nM)	
	hM_3R	hM_2R
1	5.3 ± 2*	2.1 ± 2*
2	0.20 ± 0.02*	0.49 ± 0.2*
3	0.81 ± 0.2*	1.6 ± 0.7*
4	0.56 ± 0.3*	0.43 ± 0.04*
5	0.88 ± 0.1*	0.68 ± 0.1*
6	2.8 ± 0.08	—
7	0.65 ± 0.4*	0.40 ± 0.2*
8	41 ± 21	12 ± 0.2
9	42 ± 12	12 ± 1
10	81 ± 39	21 ± 3*
11	0.86 ± 0.4	2.3 ± 0.2*
12	0.44 ± 0.04*	0.72 ± 0.01
13	4.7 ± 0.6*	12 ± 0.5
14	17 ± 0.4	7.1 ± 2
15	1.1 ± 0.3	0.69 ± 0.04
16	6.5 ± 2	2.1 ± 1*
17	20 ± 16	9.2 ± 2
18	3.8 ± 2	—
19	1.9 ± 0.6	1.4 ± 0.5
20	19 ± 4	—
21	1.7 ± 0.2	0.49 ± 0.2
22	0.51 ± 0.1*	0.11 ± 0.1
23	2.6 ± 0.4	1.6 ± 0.3
24	0.86 ± 0.4*	1.1 ± 0.5
25	2.3 ± 2	0.18 ± 0.1
26	7.8 ± 2	0.91 ± 0.7
27	1.5 ± 0.1	2.6 ± 0.3
(*R*)-(–)-12	0.40 ± 0.06*	1.0 ± 0.2*
(*S*)-(+)-12	184 ± 30*	68 ± 28*

—, not tested.
* , more than two independent experiments were performed.

longer bronchodilatory activity *in vivo* than (*S*)-(+)-**12**. Compound (*R*)-(–)-**12** was thus selected for further study of its pharmacological activities compared to those of clinically used LAMAs.

The results in this study suggest that the length of the linker moiety (between the nitrogen atom of quinuclidine and the terminal phenyl ring) is an important parameter determining a compound's affinity for hM_3R, and that chemical modification of the terminal phenyl ring is not an effective measure to increase affinity for hM_3R. It was reported that the mode of interaction of **2** with the muscarinic receptors is unique,[24] with the results in this study suggesting that (*R*)-(–)-**12** has a similar interaction mode to that of tiotropium. Further study is needed to examine the nature of (*R*)-(–)-**12**′s mode of interaction with hM_3R. In addition, investigation of interaction of (*R*)-(–)-**12** with the other muscarinic receptor subtypes is also important in order to understand the molecular mechanism of its pharmacological action.

Previously, we examined the effect of intratracheal administration of **2** on increased fecal pellet output induced by restraint stress. As a result, compared to the protective effect of **2** against PPE-induced lung injury, more than 100 times higher dose of **2** was required to affect fecal pellet output.[17] We assumed that this is due to the low efficiency of intratracheally administered **2** to transfer to blood, because we showed that the blood concentration of **2**, 1 min after the intratracheal administration (10 mg) was 3 μg/ml, whereas that of intravenous administration (7.5 mg) was 40 μg/ml.[17] Based on these results, we speculate that intratracheally administered (*R*)-(–)-**12** also has less effect on organs (such as colon) other than lung and bronchi, compared to its respiratory effects.

Comparison of the activities of (*R*)-(–)-**12** and of clinically used LAMAs (**2–4**) revealed that the duration of bronchodilation by (*R*)-(–)-**12** was longer than that of **3–5** and similar to that of **2**. The long-term intratracheal administration of (*R*)-(–)-**12**, but not of **2**, also suppressed PPE-induced pulmonary emphysema and respiratory dysfunction. These results suggest that (*R*)-(–)-**12** might be therapeutically beneficial for the treatment of COPD patients given that (*R*)-(–)-**12** appears to have beneficial effects against both inflammation-induced pulmonary emphysema and airflow limitation. While we selected the elastase model for the initial evaluation of candidate drugs given the rapid and acute effects seen therein, further studies with other models, such as the cigarette smoke model,[25] would be important to further characterize the properties of candidate drugs. Patent applications have been submitted for (*R*)-(–)-**12** and related compounds.

4. Materials and methods

More detailed descriptions concerning the methods are provided in the Supplementary Information.

4.1. Synthesis of targeted compounds and purity analyses.

Methods for the synthesis of targeted compounds are described in the Supplementary Information. HPLC analysis was used for determining the purity of targeted compounds, with a purity of greater than 95% purity confirmed for all cases.

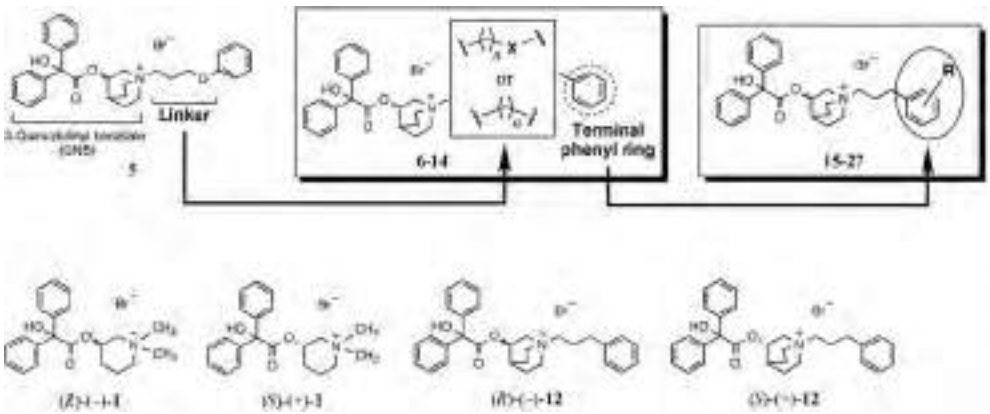

Fig. 2. Strategy used for making chemical modifications to **5** and structures of enantiomers of **1** ((*R*)-(–)-**1** and (*S*)-(+)-**1**) and **12** ((*R*)-(–)-**12** and (*S*)-(+)-**12**)..

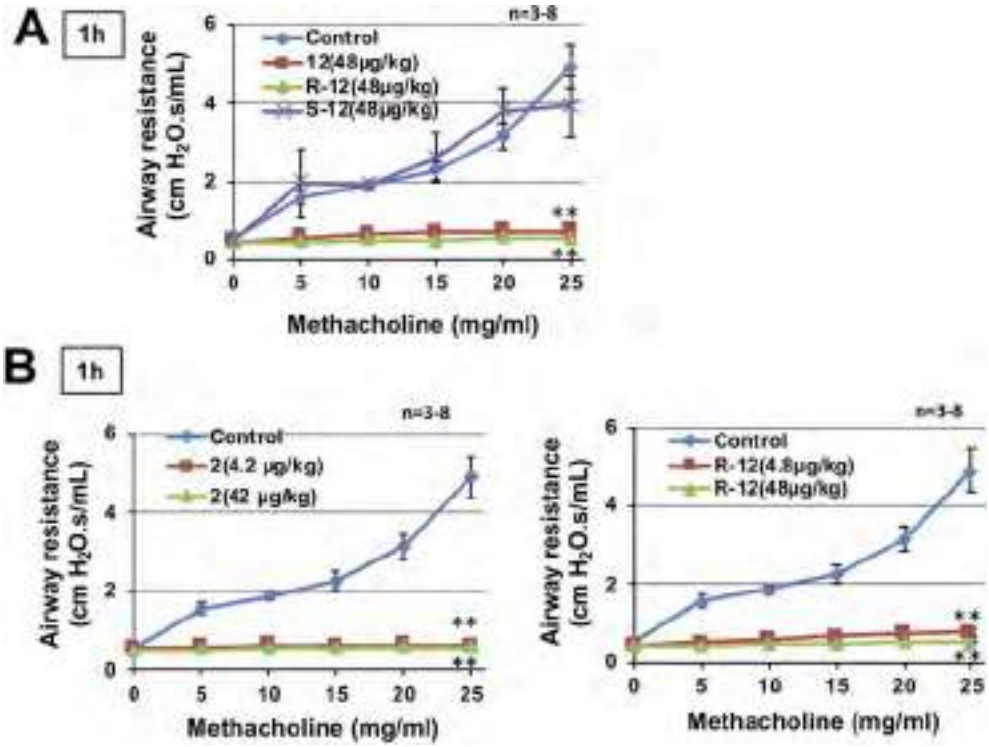

Fig. 3. Dose-response curves for compounds **12**, (*R*)-(–)-**12**, and (*S*)-(+)-**12** (A) or **2** and (*R*)-(–)-**12** (B) for methacholine-induced airway constriction. Indicated doses were administered intratracheally. After 1 h, mice were exposed to nebulized methacholine five times and airway resistance was determined after each methacholine challenge as described in the Materials and Methods. Values represent mean ± S.E.M. $^{*}P < 0.05$. Control data are the same in all graphs. Data are representative of two independent experiments.

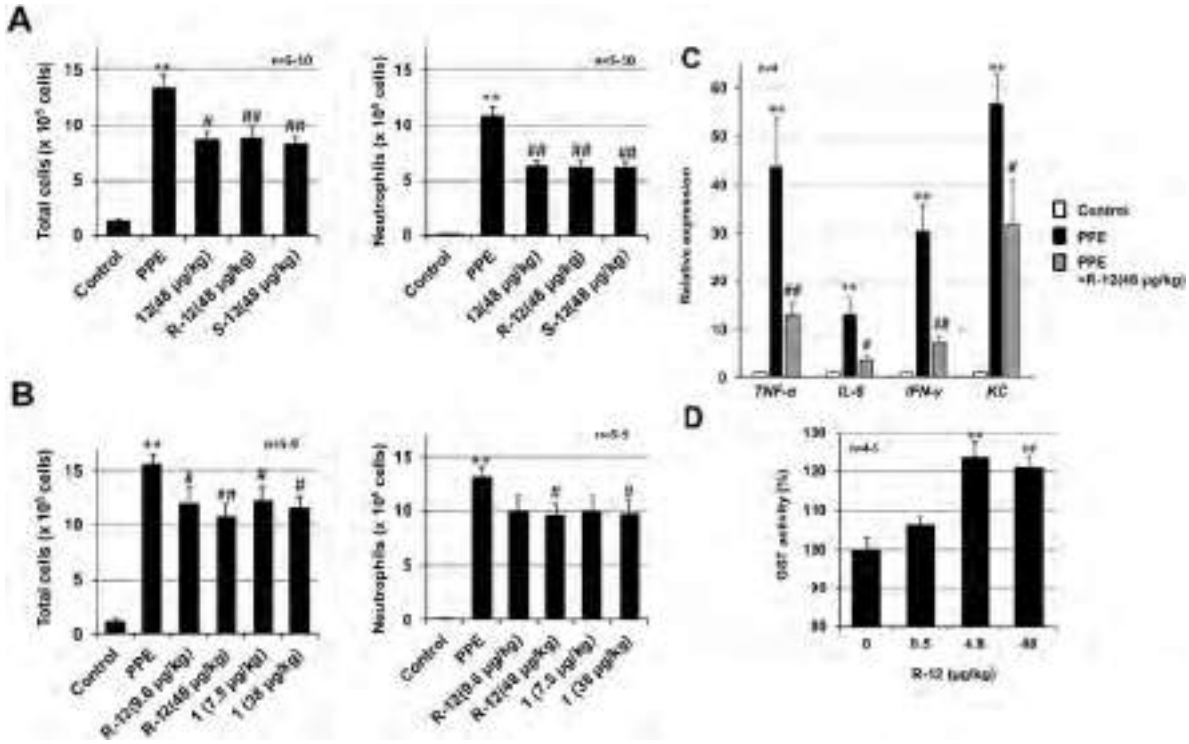

Fig. 4. Effect of compounds on PPE-induced inflammatory responses. Mice were treated with or without (control) PPE (20 U/kg) once only on day 0 (A, B, C). The indicated doses (μg/kg) of compounds were administered intratracheally once only (A, B, C). Twenty-four hours after the PPE administration, BALF was prepared and the total cell number and the number of neutrophils were determined as described in the Materials and Methods (A, B). Twenty-four hours after the PPE administration, total RNA was extracted from lung tissue and subjected to real-time RT-PCR using a specific primer set for each gene. Values were normalized to *Hprt1* and expressed relative to the Control (C). Male ICR mice were administered intratracheally with indicated doses (μg/kg) of (*R*)-(–)-**12** or vehicle (saline) once only. Twenty-four hours after the (*R*)-(–)-**12** administration, lung homogenates were prepared. GST activity was determined as described in the Materials and Methods (D). Values represent mean ± S.E.M. $^{**}P < 0.01$ (versus control); $^{\#}P < 0.05$, $^{\#\#}P < 0.01$ (versus PPE only); n.s., not significant. Data are representative of two independent experiments.

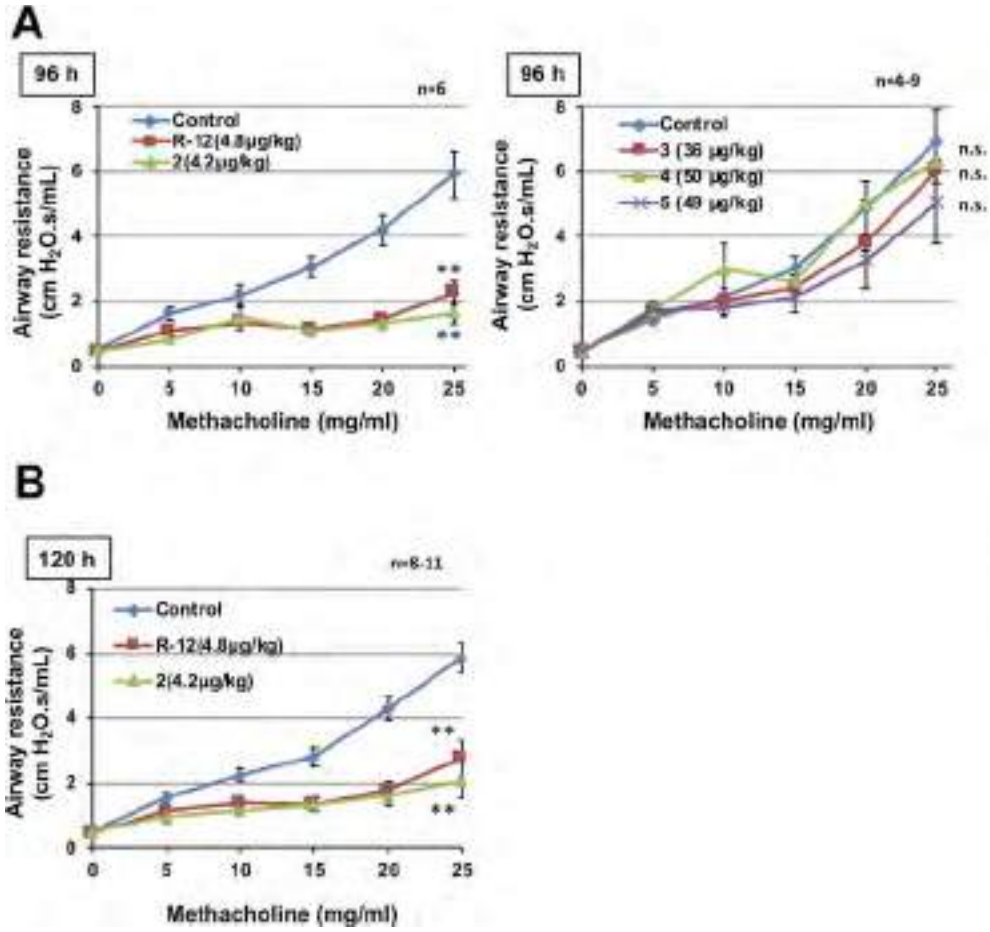

Fig. 5. Time-course of effect of compounds **2**, **3**, **4**, **5** and (*R*)-(–)-**12** (A) or **2** and (*R*)-(–)-**12** (B) on methacholine-induced airway constriction. Indicated doses were administered intratracheally. After 96 h (A) or 120 h (B), mice were exposed to five cycles of nebulized methacholine and airway resistance was determined after each methacholine challenge as described in the Materials and Methods. Values represent mean ± S.E.M. $^{**}P < 0.01$; n.s., not significant. The control data are the same as in Fig. 6A. Data are representative of two independent experiments.

4.2. Treatment of mice with PPE and test drugs

Mice were sedated with 2% isoflurane and then administered intratracheally with PPE (15 or 20 U/kg) followed by the test compound (various doses) contained in a vehicle (0.9% NaCl; 1 ml/kg) via micropipette (P200). For control mice, the 0.9% NaCl vehicle alone was administered by the same procedure.

4.3. Preparation of BALF and cell count method

BALF was collected by cannulating the trachea and lavaging the lung with 1 ml of sterile PBS containing 50 U/ml heparin (2 times). About 1.8 ml of BALF was routinely recovered from each animal. The total cell number was counted using a hemocytometer. Cells were stained with Diff-Quik reagents after centrifugation in a Cytospin® 4 (Thermo Electron Corporation, Waltham, MA), and the ratio of number of neutrophils to total cell number was determined to calculate the number of neutrophils.

4.4. Histopathological analysis

Lung tissue samples were fixed in 10% formalin neutral buffer solution for 24 h at a pressure of 25 cmH_2O, and then embedded in paraffin before being cut into 4 μm-thick sections. Sections were stained first with Mayer's hematoxylin and then with 1% eosin alcohol solution (H & E staining). Samples were mounted with malinol and inspected with the aid of an Olympus BX51 microscope (Tokyo, Japan).

To determine the MLI, 20 lines (800 μm) were drawn randomly on the image of a section and intersection points with alveolar walls were counted to determine the MLI.[26] This morphometric analysis was conducted by an investigator blinded to the study protocol.

4.5. Measurement of airway resistance and $FEV_{0.1}/FVC$

Respiratory function and airway resistance were monitored with a computer-controlled small-animal ventilator (FlexiVent, SCIREQ, Montreal, Canada), as described previously.[19,23] Mice were anesthetized with chloral hydrate (500 mg/kg), a tracheotomy was performed, and an 8 mm section of metallic tube was inserted into the trachea. Mice were mechanically ventilated at a rate of 150 breaths/min, using a tidal volume of 8.7 ml/kg and a positive end-expiratory pressure of 2–3 cmH_2O.

For measurement of methacholine-induced increases in airway resistance, mice were exposed to nebulized methacholine (5 mg/ml) five times for 20 *sec* with a 40 *sec* interval, and airway resistance was measured after each methacholine challenge by the snapshot technique. All data were analysed using FlexiVent software.

Determination of the FEV0.1/FVC (forced expiratory volume in the first 0.1 s to forced vital capacity) ratio was performed with the same computer-controlled small-animal ventilator connected to a negative pressure reservoir (SCIREQ, Montreal, Canada), as described previously.[19,23] Mice were tracheotomised and ventilated as described above. The lung was inflated to 30 cmH_2O over one second and held at this pressure. After 0.2 *sec*, the pinch valve (connected to ventilator) was closed and after a further 0.3 *sec*, the shutter valve (connected to negative pressure reservoir) was opened for exposure of the lung to the negative pressure. The negative pressure was held for 1.5 *sec* to ensure complete expiration. The FEV0.1/FVC ratio was determined using FlexiVent software.

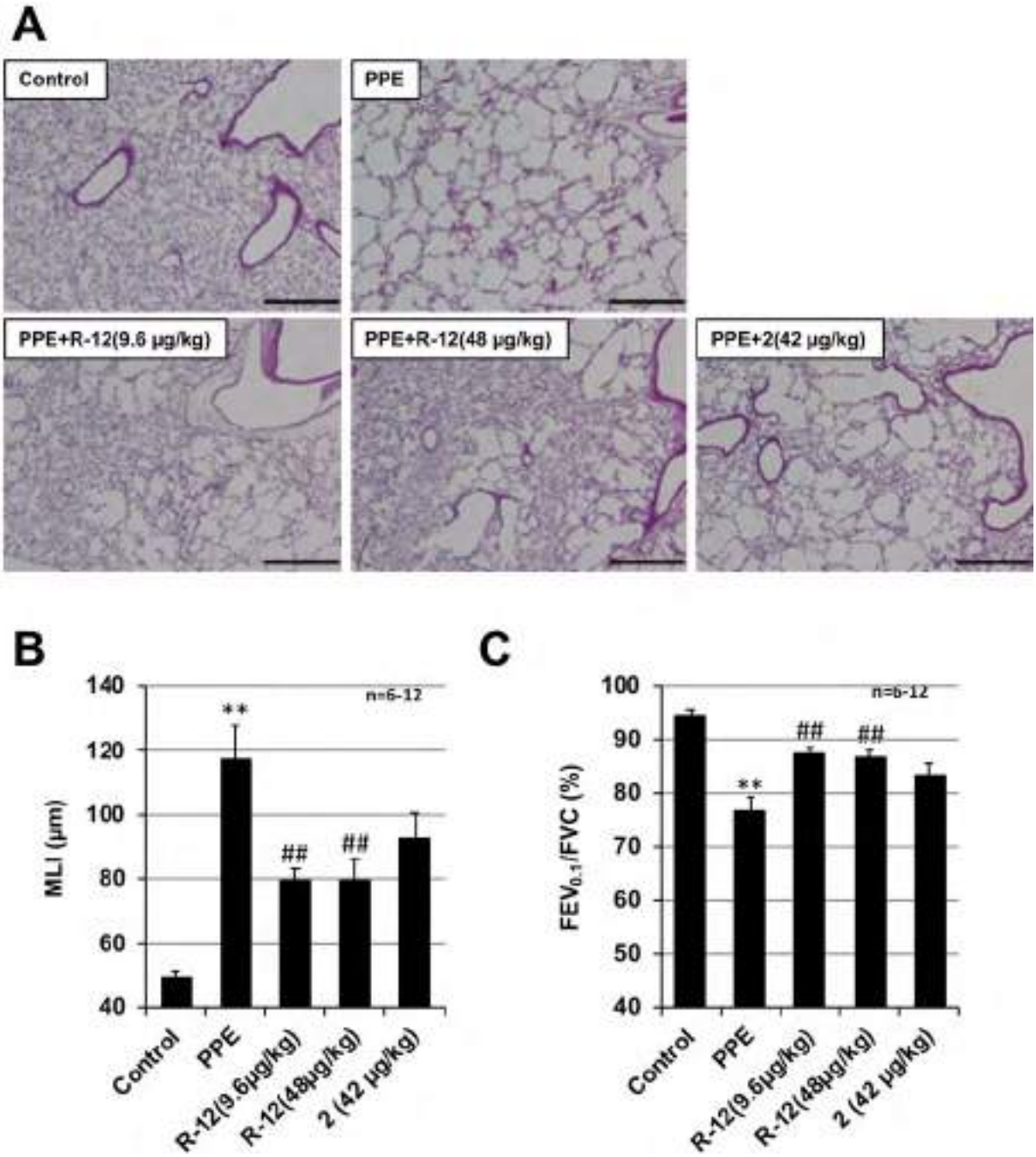

Fig. 6. Effect of **2** and (*R*)-(–)-**12** on PPE-induced pulmonary damage and dysfunction. Mice were treated with or without (control) PPE (15 U/kg) once only on day 0. The indicated doses of **2** or (*R*)-(–)-**12** were administered intratracheally once daily for 14 days (from day 0 to day 13) (A-C). Sections of pulmonary tissue were prepared on day 14 and subjected to histopathological examination (H & E staining) (scale bar, 500 μm) (A). Airspace size was estimated by determining the MLI as described in the Materials and Methods (B). $FEV_{0.1}$/FVC values were determined on day 14 as described in the Materials and Methods (C). Values represent mean ± S.E.M. $^{**}P < 0.01$ (versus control); $^{\#}P < 0.05$ (versus PPE only). Data are representative of two independent experiments.

4.6. Real-time reverse transcription polymerase chain reaction (RT-PCR) analysis.

Total RNA was extracted from lung tissue using an RNeasy kit according to the manufacturer's protocol. Samples were reverse-transcribed using the PrimeScript® kit described above. The synthesized cDNA was used in real-time PCR experiments with SsoAdvanced Universal SYBR Green Supermix and analyzed with a Bio-Rad (Hercules, CA) CFX96™ real-time system and CFX Manager™ software. Specificity was confirmed by electrophoretic analysis of reaction products and by the inclusion of template- or reverse transcriptase-free controls. To normalize the amount of total RNA present in each reaction, hypoxanthine phosphoribosyltransferase 1 (HPRT1) cDNA was used as an internal standard. Primers were designed using Primer-BLAST websites. Primers sequences will be provided upon request.

4.7. Measurement of GST activity

Left lung homogenates were prepared 24 h after (*R*)-(–)-**12** administration, GST activity in the homogenates was measured with the aid of a GST assay kit according to the manufacturer's protocol. GST activity was expressed relative to activity in the control sample.

4.8. Filter-binding assay

The filter-binding assay was performed as described previously[21] with some modifications. Membrane fractions prepared from Chinese Hamster Ovary (CHO)-K1 cells expressing human muscarinic M2 receptor (hM_2R) or human muscarinic M3 receptor (hM_3R) (Membrane Target Systems, Perkin-Elmer Life and Analytical Sciences, Boston, MA; protein concentration, 8 μg/well) were incubated with 2 nM [^{3}H]NMS (*N*-methyl-[^{3}H]-scopolamine methylchloride) (85.5 Ci/mmol) at room temperature for 2 h in 200 μL PBS in the presence of each compound. A range of concentrations (10^{-11} to 10^{-6} M) of each compound was tested in triplicate to generate competition curves. Non-specific binding was determined in the presence of atropine (2.5 μM). The samples were passed through a GF/C filter (Filtermat A, PerkinElmer Life and Analytical Sciences, Boston, MA) that was pre-incubated for 1 h with 1.0% polyethylenimine, and washed four times with ice-cold wash buffer (50 mM Tris/HCl (pH 7.4), 100 mM NaCl, 0.05% Tween-80). Filters were then dried for 30 min before attachment to MeltiLex A (melt-on scintillation sheet; PerkinElmer Life and Analytical Sciences, Boston, MA). The radioactivity remaining on the filter was monitored with a MicroBeta Trilux microplate scintillation counter (PerkinElmer Life and Analytical Sciences, Boston, MA). Affinities at equilibrium were determined as equilibrium dissociation constant (K_i) values after correcting the experimentally determined IC_{50} values with the experimentally determined NMS K_d value for hM_2R or hM_3R and the concentration of NMS, as described previously.[21] All adjustments were performed using Prism (GraphPad Software, Inc., San Diego, CA).

4.9. Statistical analysis

All values are expressed as the mean ± S.E.M. Two-way ANOVA followed by the Tukey test or Dunnett test for unpaired results was used to evaluate differences between three or more groups. Differences were considered to be significant for values of $P < 0.05$.

5. Financial disclosure

This work was supported by Grants-in-Aid for Scientific Research from the Ministry of Health, Labour, and Welfare of Japan, as well as the Japan Science and Technology Agency and Grants-in-Aid for Scientific Research from the Ministry of Education, Culture, Sports, Science and Technology, Japan. This research was also supported by the Pharmacological Research Foundation Tokyo, the Takeda Science Foundation, and the Suzuken Memorial Foundation.

6. Author contributions statement

Participated in research design: YY, KT, NY, YF, TM.
Conducted experiments: YY, KT, NY, TA, YK, AT.
Contributed new reagents or analytic tools: MK, MT, YF.
Performed data analysis: YY, KT, NY, TA, TM.
Wrote or contributed to the writing of the manuscript:
YY, KT, NY, TA, YK, AT, MK, MT, YF, TM.

Declaration of Competing Interest

Tohru Mizushima is Chairman of LTT Bio-Pharma Co., Ltd. Teita Asano and Mitsuko Takenaga are employees of an endowed research division of LTT Bio-Pharma Co., Ltd.

Appendix A. Supplementary data

Supplementary data to this article can be found online at https://doi.org/10.1016/j.bmc.2019.06.016.

References

1. Rabe KF, Hurd S, Anzueto A, et al. Global strategy for the diagnosis, management, and prevention of chronic obstructive pulmonary disease: GOLD executive summary. *Am J Respir Crit Care Med.* 2007;176:532–555.
2. Vogelmeier CF, Criner GJ, Martinez FJ, et al. Global Strategy for the Diagnosis, Management, and Prevention of Chronic Obstructive Lung Disease 2017 Report. GOLD Executive Summary. *Am J Respir Crit Care Med.* 2017;195(2017):557–582.
3. Vestbo J, Hurd SS, Agusti AG, et al. Global strategy for the diagnosis, management, and prevention of chronic obstructive pulmonary disease: GOLD executive summary. *Am J Respir Crit Care Med.* 2013;187:347–365.
4. Barnes PJ, Stockley RA. COPD: current therapeutic interventions and future approaches. *Eur Respir J.* 2005;25:1084–1106.
5. Tashkin DP, Celli B, Senn S, et al. A 4-year trial of tiotropium in chronic obstructive pulmonary disease. *N Engl J Med.* 2008;359:1543–1554.
6. Calverley PM, Anderson JA, Celli B, et al. Salmeterol and fluticasone propionate and survival in chronic obstructive pulmonary disease. *N Engl J Med.* 2007;356:775–789.
7. Alsaeedi A, Sin DD, McAlister FA. The effects of inhaled corticosteroids in chronic obstructive pulmonary disease: a systematic review of randomized placebo-controlled trials. *Am J Med.* 2002;113:59–65.
8. Barnes PJ. Role of HDAC2 in the pathophysiology of COPD. *Annu Rev Physiol.* 2009;71:451–464.
9. Ito K, Ito M, Elliott WM, et al. Decreased histone deacetylase activity in chronic obstructive pulmonary disease. *N Engl J Med.* 2005;352:1967–1976.
10. Di Stefano A, Caramori G, Oates T, et al. Increased expression of nuclear factor-kappaB in bronchial biopsies from smokers and patients with COPD. *Eur Respir J.* 2002;20:556–563.
11. Rajendrasozhan S, Yang SR, Edirisinghe I, Yao H, Adenuga D, Rahman I. Deacetylases and NF-kappaB in redox regulation of cigarette smoke-induced lung inflammation: epigenetics in pathogenesis of COPD. *Antioxid Redox Signal.* 2008;10:799–811.
12. Ito K, Yamamura S, Essilfie-Quaye S, et al. Histone deacetylase 2-mediated deacetylation of the glucocorticoid receptor enables NF-kappaB suppression. *J Exp Med.* 2006;203:7–13.
13. Tanaka K, Ishihara T, Sugizaki T, et al. Mepenzolate bromide displays beneficial effects in a mouse model of chronic obstructive pulmonary disease. *Nat Commun.* 2013;4:2686.
14. Chen JY. Antispasmodic activity of JB-340 (N-methyl-3-piperidyl-diphenylglycolate methobromide) with special reference to its relative selective action on the sphincter of Oddi, colon and urinary bladder of the dog. *Arch Int Pharmacodyn Ther.* 1959;121:78–84.
15. Buckley JP, De FJ, Reif EC. The comparative antispasmodic activity of N-methyl-3-piperidyl diphenylglycolate methobromide (JB-340) and atropine sulfate. *J Am Pharm Assoc Am Pharm Assoc (Baltim).* 1957;46:592–594.
16. Long JP, Keasling HH. The comparative anticholinergic activity of a series of derivatives of 3-hydroxy piperidine. *J Am Pharm Assoc Am Pharm Assoc (Baltim).* 1954;43:616–619.
17. Tanaka K, Kurotsu S, Asano T, et al. Superiority of pulmonary administration of mepenzolate bromide over other routes as treatment for chronic obstructive pulmonary disease. *Sci Rep.* 2014;4:4510.
18. Kurotsu S, Tanaka K, Niino T, et al. Ameliorative effect of mepenzolate bromide against pulmonary fibrosis. *J Pharmac Exp Therapeutics.* 2014;350:79–88.
19. Tanaka K, Sato K, Aoshiba K, Azuma A, Mizushima T. Superiority of PC-SOD to other anti-COPD drugs for elastase-induced emphysema and alteration in lung mechanics and respiratory function in mice. *Am J Physiol Lung Cell Mol Physiol.* 2012;302:L1250–1261.
20. Tanaka KI, Yamakawa N, Yamashita Y, et al. Identification of Mepenzolate Derivatives With Long-Acting Bronchodilatory Activity. *Front Pharmacol.* 2018;9:344.
21. Yamashita Y, Tanaka K, Asano T, et al. Synthesis and biological comparison of enantiomers of mepenzolate bromide, a muscarinic receptor antagonist with bronchodilatory and anti-inflammatory activities. *Bioorg Med Chem.* 2014;22:3488–3497.
22. Olshansky B, Ebinger U, Brum J, Egermark M, Viegas A, Rekeda L. Differential pharmacological effects of antimuscarinic drugs on heart rate: a randomized, placebo-controlled, double-blind, crossover study with tolterodine and darifenacin in healthy participants > or = 50 years. *J Cardiovasc Pharmacol Ther.* 2008;13:241–251.
23. Tanaka K, Tanaka Y, Miyazaki Y, et al. Therapeutic effect of lecithinized superoxide dismutase on pulmonary emphysema. *J Pharmacol Exp Therapeutics.* 2011;338:810–818.
24. Kruse AC, Hu J, Pan AC, et al. Structure and dynamics of the M3 muscarinic acetylcholine receptor. *Nature.* 2012;482:552–556.
25. Ghorani V, Boskabady MH, Khazdair MR, Kianmeher M. Experimental animal models for COPD: a methodological review. *Tob Induc Dis.* 2017;15:25.
26. Weibel ER. Principles and methods for the morphometric study of the lung and other organs. *Lab Invest.* 1963;12:131–155.

SCIENTIFIC REPORTS
natureresearch

OPEN

A_{2B} adenosine receptor inhibition by the dihydropyridine calcium channel blocker nifedipine involves colonic fluid secretion

Teita Asano[1*], Yuto Noda[2], Ken-Ichiro Tanaka[3], Naoki Yamakawa[4], Mitsuhito Wada[5], Tadaaki Mashimo[6,7], Yoshifumi Fukunishi[6], Tohru Mizushima[2*] & Mitsuko Takenaga[1]

The adenosine A_{2B} receptor is a critical protein in intestinal water secretion. In the present study, we screened compound libraries to identify inhibitors of the A_{2B} receptor and evaluated their effect on adenosine-induced intestinal fluid secretion. The screening identified the dihydropyridine calcium antagonists nifedipine and nisoldipine. Their respective affinities for the A_{2B} receptor (K_i value) were 886 and 1,399 nM. Nifedipine and nisoldipine, but not amlodipine or nitrendipine, inhibited both calcium mobilization and adenosine-induced cAMP accumulation in cell lines. Moreover, adenosine injection into the lumen significantly increased fluid volume in the colonic loop of wild-type mice but not A_{2B} receptor-deficient mice. PSB-1115, a selective A_{2B} receptor antagonist, and nifedipine prevented elevated adenosine-stimulated fluid secretion in mice. Our results may provide useful insights into the structure–activity relationship of dihydropyridines for A_{2B} receptor. As colonic fluid secretion by adenosine seems to rely predominantly on the A_{2B} receptor, nifedipine could be a therapeutic candidate for diarrhoea-related diseases.

Adenosine is an important mediator of multiple functions, such as intestinal secretion, contraction, inflammation, and sensation in the gastrointestinal tract[1–3]. Among adenosine receptors, the A_{2B} receptor is highly expressed in the colon and has critical roles in pathological conditions[4]. In general, adenosine levels and A_{2B} receptor expression are low under normal conditions, but increase in response to ischemia, inflammation, and tissue injuries. The activated A_{2B} receptor stimulates intestinal water secretion and sensation or modulates inflammatory response and colonic motility[5,6]. As a result, it is associated with the development of gastrointestinal diseases, such as irritable bowel syndrome (IBS), secretary diarrhoea, and inflammatory bowel disease[7,8]. Therefore, this receptor has attracted substantial attention as a therapeutic target. Although pharmacological and molecular tools, including genetically modified mouse models, have revealed multiple functions of the A_{2B} receptor, such as immunomodulation, relaxation of smooth muscle, and intestinal secretion[5,9], our understanding of its biology remains unclear.

Diarrhoea is caused by bacterial and viral infections, inflammatory processes, drugs, genetic disorders, and abnormal intestinal secretion or electrolyte absorption[10,11]. However, the pathophysiology of diarrhoea is not fully understood. Chloride secretion into the lumen following activation of the cystic fibrosis transmembrane conductance regulator (CFTR) channel in intestinal epithelial cells plays a crucial role in secretory diarrhoea[1,12]. Several studies suggest that A_{2B} receptor activation causes fluid secretion into the lumen. *In vitro* studies using colonic epithelial cells have demonstrated that adenosine increases luminal water volume through apical or basolateral

[1]Institute of Medical Science, St. Marianna University School of Medicine, 2-16-1, Sugao, Miyamae-ku, Kawasaki, 216-8512, Japan. [2]LTT Bio-Pharma Co., Ltd, Shiodome Building 3F, 1-2-20 Kaigan, Minato-ku, Tokyo, 105-0022, Japan. [3]Research Institute of Pharmaceutical Sciences, Faculty of Pharmacy, Musashino University, 1-1-20, Shinmachi, Nishi-Tokyo, 202-8585, Japan. [4]School of Pharmacy, Shujitsu University, 1-6-1, Nishi-kawahara, Naka-ku, Okayama, 703-8516, Japan. [5]Technology Research Association for Next Generation Natural Products Chemistry, 2-3-26, Aomi, Koto-ku, Tokyo, 135-0064, Japan. [6]Molecular Profiling Research Center for Drug Discovery (molprof), National Institute of Advanced Industrial Science and Technology (AIST), 2-3-26, Aomi, Koto-ku, Tokyo, 135-0064, Japan. [7]IMSBIO Co., Ltd., Owl Tower, 4-21-1, Higashi-Ikebukuro, Toshima-ku, Tokyo, 170-0013, Japan. *email: asano-ti@marianna-u.ac.jp; t.mizushima@ltt.co.jp

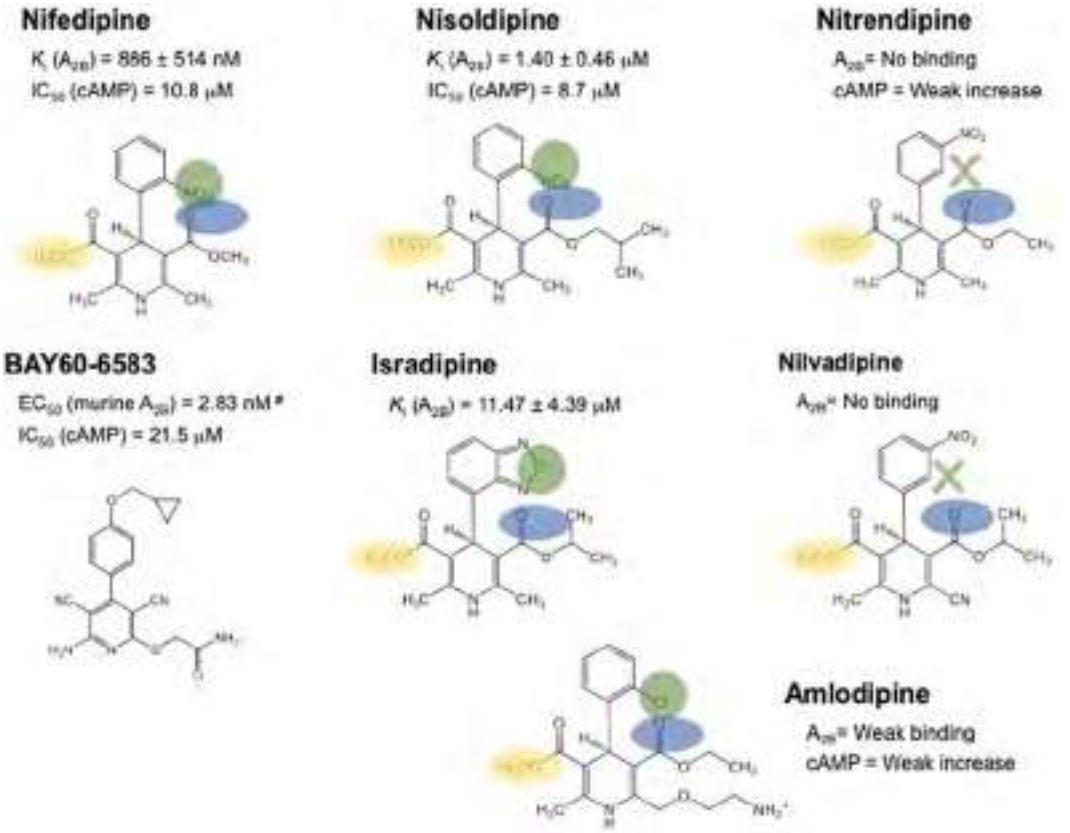

Figure 1. Summary of the compounds. 'K_i (A_{2B})' values are the [^{3}H]-DPCPX binding assay results and 'cAMP' values are the adenosine-induced cAMP assay results. Pharmacophore analysis of the compounds was performed. Green, blue, and orange circles represent the hydrogen donor site binding His280$^{7.43}$, a hydrogen donor with side-chain binding to Tyr10$^{1.35}$, and the common $-OCH_3$ group close to Ser279$^{7.42}$, respectively. Green cross 'X' represents the mismatch between the ligand NO_2 group and the pharmacophore. $^{\#}$, the values of BAY60-6583 were adopted from van der Hoeven *et al.*[44].

A_{2B} receptors[13,14]. Although both cAMP activation via Gs proteins and the intracellular calcium pathway contribute to chloride or water secretion in epithelial cells, chloride release is most likely due to cAMP elevation following A_{2B} receptor activation[1,15]. A recent report has shown that A_{2B} receptor-mediated direct activation of the CFTR channel is associated with water secretion in epithelial cells[12]. Nevertheless, evidence that the A_{2B} receptor modulates fluid secretion has remained limited, in part because of a lack of appropriate pharmacological agents or genetically modified mice.

Recently, we reported that blockade of the A_{2B} receptor could be beneficial for diarrhoea-predominant IBS[8]. Inhibition of the receptor by pharmacological agents ameliorated colonic hypersensitivity and stress-induced defecation in rodent models of IBS. In the present study, we screened a library of approved medicinal compounds for candidate drugs that could suppress adenosine A_{2B} receptor activation. We also determined the role of various adenosine receptor subtypes involved in colonic fluid secretion induced by luminal adenosine and examined the effect of the candidate drug on fluid secretion in mice.

Results

Identification of nifedipine through screening for adenosine A2B receptor binding compounds.

Screening of a compound library identified 12 candidate drugs with binding affinity for the A_{2B} receptor (Supplementary Table 1). Of these, three were already known, four had a xanthine-like structure, and two were dihydropyridine calcium channel blockers. We focused on the latter, nifedipine and nisoldipine, because dihydropyridine is similar to the structure of BAY60-6583, a known adenosine A_{2B} receptor agonist (Fig. 1). Nifedipine inhibited [^{3}H]-DPCPX binding to the A_{2B} receptor membrane in a dose-dependent manner and its K_i value was 886 ± 514 nM (Fig. 2a). We also examined the binding activity of other dihydropyridine calcium channel blockers and Fig. 1 summarizes the results. Nisoldipine but not nitrendipine and nilvadipine significantly suppressed [^{3}H]-DPCPX binding, whereas isradipine and amlodipine exhibited only weak binding to the A_{2B} receptor (Fig. 2a). The K_i values of nisoldipine and isradipine were 1.40 ± 0.46 µM and 11.47 ± 4.39 µM, respectively. We confirmed the effect of nifedipine on adenosine-induced calcium mobilization in CHO cells stably expressing the A_{2B} receptor. Dose-dependent calcium mobilization by adenosine was observed, with fluorescence being nearly maximal with 10 µM of adenosine (data not shown). As shown in Fig. 2b,c, adenosine caused immediate calcium mobilization while nifedipine dose-dependently blocked it but did not stimulate it. Nisoldipine had a

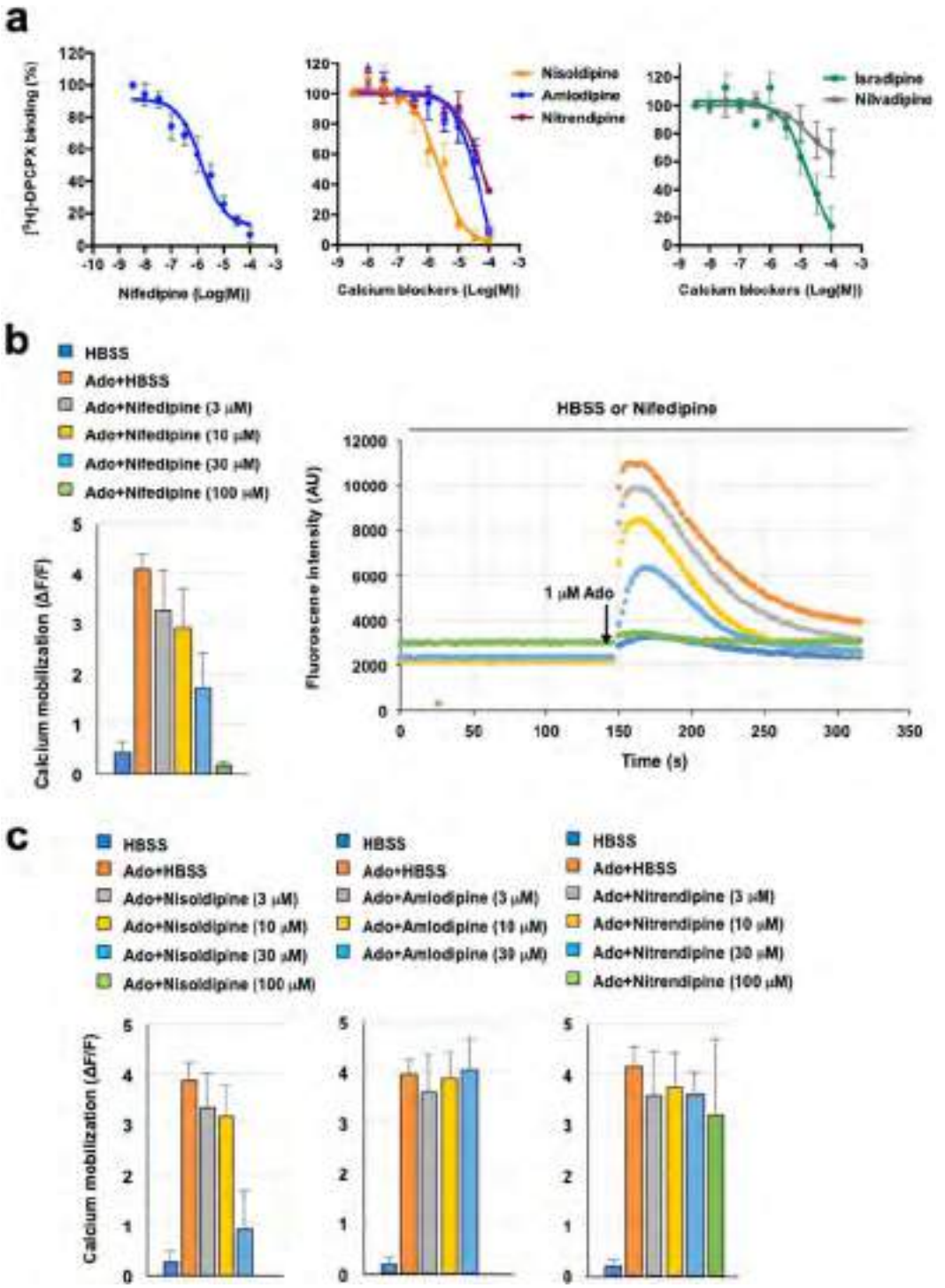

Figure 2. Binding affinity of dihydropyridine calcium blockers for the A_{2B} receptor and effect on calcium mobilization. (**a**) Curves generated from competition displacement experiments in HEK293 cells expressing human adenosine A_{2B} receptor in the presence of [^{3}H]-DPCPX and various calcium antagonists (nifedipine, nisoldipine, amlodipine, isradipine, nitrendipine, and nilvadipine). Data represent the average of three independent experiments. (**b**) Calcium mobilization assay in CHO cells stably expressing both human adenosine A_{2B} receptor and Gα15 protein and incubated with various concentrations of nifedipine. Cells were stimulated by injection with 1 μM adenosine (Ado) solution or HBSS. Calcium mobilization (ΔF/F) was calculated based on fluorescence intensity readings. (**c**) Calcium mobilization assay in the presence of various concentrations of nisoldipine, amlodipine, and nitrendipine. All data are expressed as mean ± SEM. [^{3}H]-DPCPX, 8-cyclopentyl-1,3-dipropylxanthine, [dipropyl-2,3-^{3}H(N)].

similar effect, whereas amlodipine and nitrendipine did not. The IC_{50} values of nifedipine and nisoldipine were 42.4 μM and 34.0 μM, respectively.

Effect of dihydropyridine calcium blockers on adenosine-induced cAMP production in intestinal epithelial cells. Next, we examined the effect of nifedipine on intracellular cAMP levels in colonic epithelial T84 cells. Fluid secretion and dominant A_{2B} receptor expression have already been reported in this cell line[13]. First, we characterized the cells' cAMP response to adenosine agonists. Adenosine or BAY60-6583 (a specific A_{2B} receptor agonist) induced cAMP accumulation in a significant dose-dependent manner, whereas a selective A_{2B} antagonist, PSB-1115, suppressed adenosine-produced cAMP elevation (IC_{50} = 84.0 nM) (Fig. 3a,b). Pharmacological analysis using specific agonists showed that CPA (A_1 receptor) increased cAMP levels in T84 cells and both BAY60-6583 (A_{2B} receptor) and IB-MECA (A_3 receptor) induced modest stimulation, whereas CGS21680 (A_{2A} receptor) had only a minor effect (Fig. 3b). cAMP elevation by CPA, CGS21680, and IB-MECA was completely blocked by PSB-1115 (Fig. 3c), suggesting that the observed effect was mediated by their non-specific binding to the A_{2B} receptor. Thus, cAMP accumulation induced by adenosine in T84 cells likely involves the A_{2B} receptor.

We then examined the effect of dihydropyridine calcium blockers on cAMP response in T84 cells. In the absence of adenosine, both nifedipine and nisoldipine slightly decreased intracellular cAMP levels, nitrendipine caused an increase, and amlodipine had no significant effect (Fig. 4a). In addition, nifedipine dose-dependently inhibited cAMP accumulation (Fig. 4b) induced by either adenosine (IC_{50} = 10.8 μM) or BAY60-6583 (IC_{50} = 21.5 μM). Nisoldipine, but not amlodipine or nitrendipine, exhibited similar dose-dependent inhibition of adenosine-induced cAMP levels (IC_{50} = 8.7 μM) (Fig. 4c). The results are summarized in Fig. 1. To determine whether nifedipine decreases intracellular cAMP levels independent of its A_{2B} receptor blockade, we examined the effect of nifedipine on an adenylate cyclase activator, forskolin, which induced increases in cAMP levels. We observed no influence by nifedipine on elevated cAMP by the compounds, suggesting that adenosine-stimulated cAMP elevation is dependent on the A_{2B} receptor (data not shown).

Effect of nifedipine on adenosine-induced colonic fluid secretion in mice. Finally, we investigated whether the A_{2B} receptor stimulated intestinal fluid secretion and whether nifedipine suppressed it *in vivo*. First, we characterized fluid secretion induced by luminal adenosine in C57BL/6 mice. As shown in Fig. 5a, adenosine injection into the colonic lumen increased fluid content in a dose-dependent manner. Analysis of subtype-specific agonists revealed that only the adenosine A_{2B} receptor agonist BAY60-6583 significantly increased luminal fluid content (Fig. 5b). Confirming this point, increased fluid production by luminal adenosine was absent from A_{2B} receptor-knockout mice (Fig. 5c). These results suggest that stimulation of fluid secretion by luminal adenosine is dependent on the A_{2B} receptor, and it was suppressed by nifedipine and PSB-1115 (Fig. 5d).

Discussion

Increased intestinal fluid secretion plays an important role in diarrhoea-related diseases such as IBS, and infection- or drug-induced diarrhoea[10,11]. Several studies have reported an association between adenosine A_{2B} receptor and intestinal fluid secretion. Inhibition of the A_{2B} receptor has been shown to be effective against IBS with diarrhoea in rodents[8]. To identify candidate A_{2B} receptor inhibitors, we screened a library of medicines in clinical use. As their pharmacokinetics, pharmacodynamics, metabolism, tolerability, and toxicity are already known in humans, they can be relatively easily included in a pilot study[16]. Using a competitive binding assay, we identified four drugs with xanthine-like structures and three known A_{2B} receptor binding compounds, including aminophylline, confirming the specificity of the screening (Supplementary Table 1). Considering that A_{2B} receptor antagonists without a xanthine backbone had not been reported previously, we focused on two dihydropyridine calcium antagonists, nifedipine and nisoldipine, whose structure is similar to BAY60-6583, a selective A_{2B} receptor agonist (Fig. 1). The inhibitory action of nifedipine and nisoldipine could reveal important structure–activity information.

Unlike other calcium antagonists (e.g., nitrendipine, amlodipine, nilvadipine, and isradipine), nifedipine and nisoldipine exhibited significant binding affinity for the A_{2B} receptor. This property may be explained by the presence of an ortho-nitric oxide substitute on the benzene ring of nifedipine and nisoldipine that is absent from other compounds (Fig. 1). This nitric oxide group might be critical in preventing the binding of adenosine to the A_{2B} receptor. To confirm the competition assay results, we performed a calcium mobilization test in CHO cells stably expressing the A_{2B} receptor. Both nifedipine and nisoldipine inhibited but did not stimulate this calcium response, with the former exhibiting a stronger inhibitory action, in line with the competitive binding assay results. This result also suggested that both calcium blockers have antagonistic activity for A_{2B} receptor.

As a mechanism of colonic fluid secretion by A_{2B} receptor activation, intracellular cAMP elevation by Gs protein and mobilisation of intracellular calcium by Gq protein have been suggested[1]. Nichols *et al.* recently reported that cAMP elevation but not calcium mobilisation mediated by Gq-protein in T84 colonic epithelial cells predominantly contributes to secretary activity into the lumen through CFTR channel activation[17]. Therefore, we confirmed the antagonistic activities of nifedipine and nisoldipine on adenosine- or BAY60-6583-dependent activation in T84 cells using a cAMP accumulation assay. Again, amlodipine and nitrendipine showed no effect, consistent with the calcium assay results. We also determined a weak inhibition of intracellular cAMP levels by nifedipine and nisoldipine in the absence of adenosine stimulation. Amlodipine and nitrendipine did not inhibit adenosine-induced cAMP levels and showed a weak increase in cAMP without adenosine stimulation.

While the expression profiles of adenosine receptors and intestinal fluid secretion have been extensively characterized in T84 cells[18], responsiveness to specific agonists for each adenosine receptor has not been examined. Here, we investigated the cAMP response to activation of each adenosine receptor. We speculated that cAMP production by adenosine receptor agonists originated predominantly from A_{2B} receptor activation in the cells. In

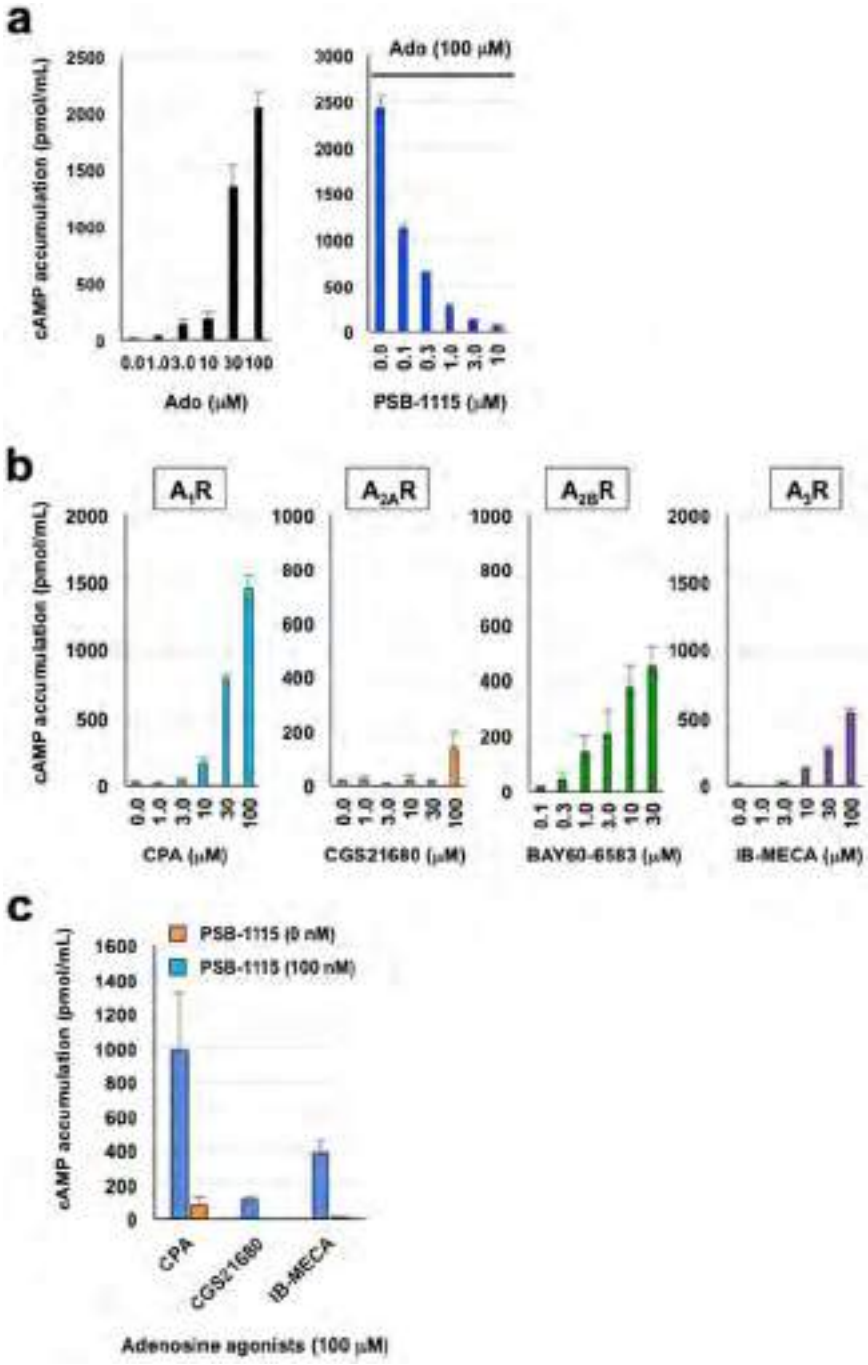

Figure 3. Responsiveness of cAMP production to adenosine receptor agonists in T84 cells. (**a**) Intracellular cAMP levels in confluent epithelial T84 cells incubated with various concentrations of either adenosine (Ado) or the selective A_{2B} receptor antagonist PSB-1115 for 15 min. (**b**) Intracellular cAMP levels in confluent T84 cells incubated with various concentrations of the selective receptor agonists CPA (A_1R), CGS21680 (A_{2A}R), BAY60-6583 (A_{2B}R), or IB-MECA (A_3R). (**c**) Intracellular cAMP levels in confluent T84 cells incubated with various concentrations of selective receptor agonists (100 μM) and the A_{2B} receptor antagonist PSB-1115 (100 nM). All data are expressed as mean ± SEM.

Fig. 3b, CPA, CGS21680, and IB-MECA caused cAMP elevation at a concentration of nearly 100 μM. However, we consider that these results are derived from non-specific A_{2B} receptor binding of these agonists, because the K_i values of CPA, CGS21680, and IB-MECA for A_{2B} receptors are 18,600 nM, >10,000 nM, and 11,000 nM, respectively[19]. In addition, elevated intracellular cAMP levels by these agonists were blocked by a selective A_{2B} antagonist, PSB-1115 (Fig. 3c). Furthermore, a previous study showed low or undetectable expression of A_1 and A_3 receptors in T84 cells[18]. Thus, adenosine- or BAY60-6583-induced cAMP accumulation may be predominantly mediated by A_{2B} receptor. Although we do not evaluate this in normal intestinal epithelial cells and cannot fully

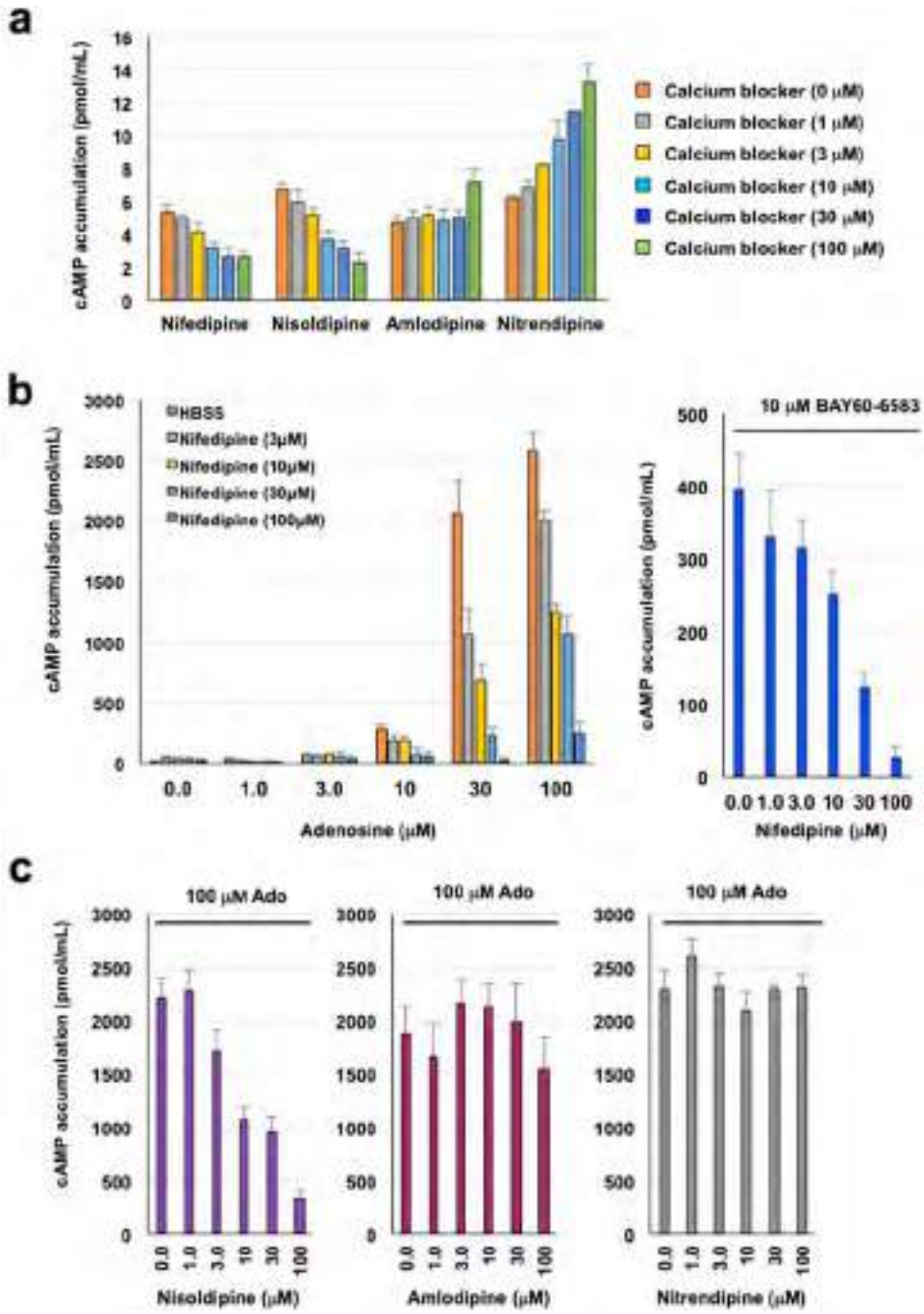

Figure 4. Effect of calcium blockers on adenosine-induced cAMP accumulation in T84 cells. (**a**) Intracellular cAMP levels in confluent T84 cells incubated with various concentrations of nifedipine, nisoldipine, amlodipine, or nitrendipine. (**b**) Intracellular cAMP levels in the presence of varying concentrations of adenosine (0–100 μM) or 10 μM BAY60-6583 for 15 min. (**c**) Intracellular cAMP levels in the presence of 100 μM adenosine (Ado) and various concentrations of nisoldipine, amlodipine, or nitrendipine. All data are expressed as mean ± SEM.

exclude the association with A_{2A} receptor, activation of A_{2B} receptor by binding of extracellular adenosine might cause an increase in intracellular cAMP levels through Gs protein, followed by CFTR channel activation in intestinal epithelial cells, leading to fluid secretion.

Moreover, we observed that both adenosine- and BAY60-6583-stimulated cAMP increases were blocked by nifedipine. The latter may bind to an active site shared by both agonists. Site-directed mutagenesis suggests that Phe173$^{2.52}$ and Trp247$^{6.48}$ on the A_{2B} receptor are important for BAY60-6583 and adenosine binding[20,21]. The present docking study supported the above mutagenesis analysis. Namely, our docking model shows that these amino acid residues can form ionic interactions with nifedipine (Fig. 6). Therefore, Phe173$^{2.52}$ and Trp247$^{6.48}$ may

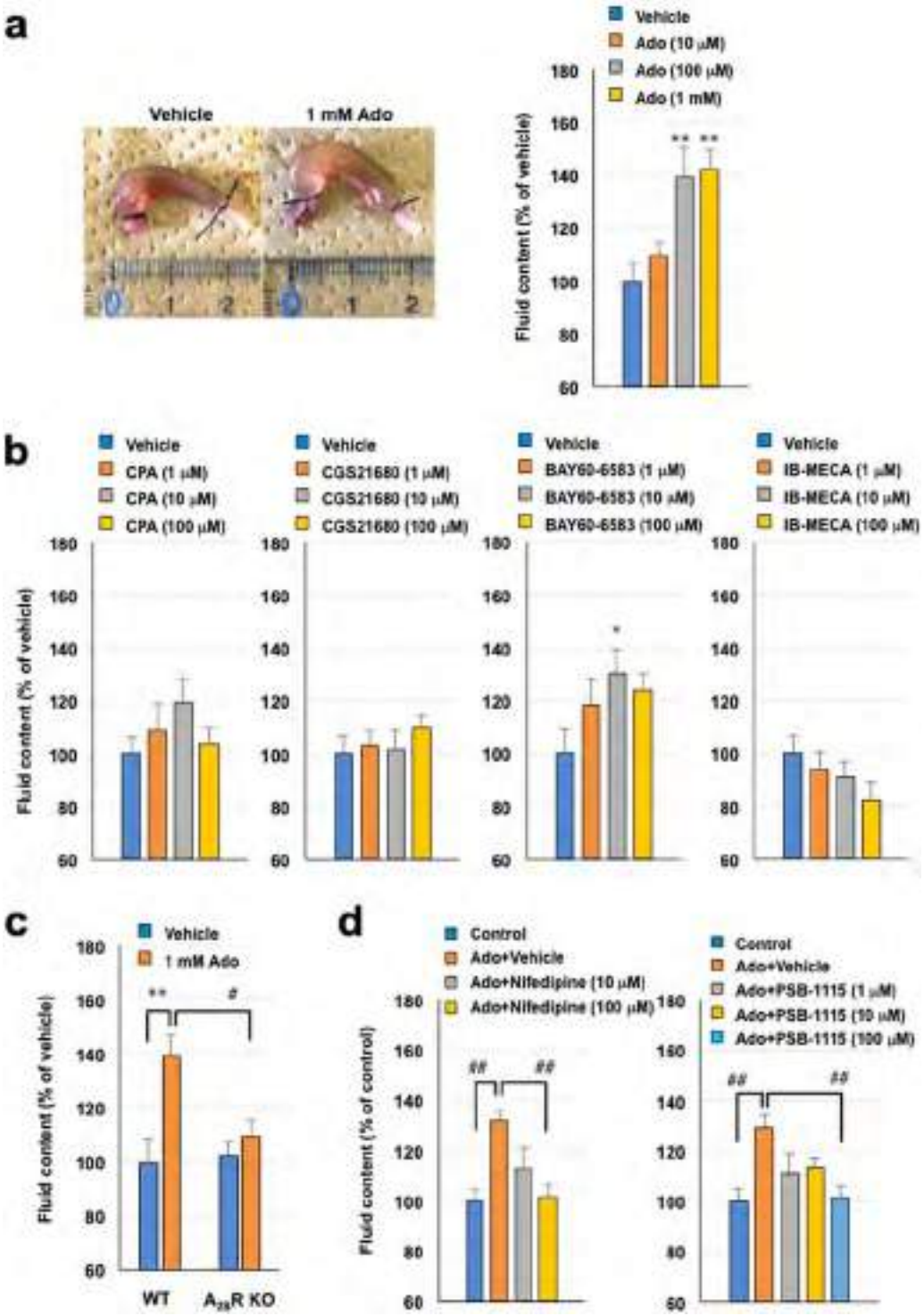

Figure 5. Involvement of adenosine A_{2B} receptor and effectiveness of nifedipine in colonic fluid secretion in mice. (**a**) Representative image of colonic loop treated with vehicle (saline containing 2.5% DMSO) or 1 mM adenosine (Ado), and colonic fluid volume following injection of various doses of adenosine. (**b**) Effect of the selective adenosine receptor agonists CPA (A_1R), CGS21680 ($A_{2A}R$), BAY60-6583 ($A_{2B}R$), and IB-MECA (A_3R) on colonic fluid volume in C57/BL6 mice. (**c**) Adenosine-induced colonic fluid secretion in C57/BL6 and A_{2B} receptor-deficient mice. (**d**) Effect of nifedipine or PSB-1115 on adenosine (1 mM)-induced colonic fluid secretion in mice. All data are expressed as mean ± SEM. $^{*}P < 0.05$ or $^{**}P < 0.01$ (*vs*. vehicle). $^{\#}P < 0.05$ or $^{\#\#}P < 0.01$ (*vs* Ado in wild-type).

be required for the interaction between nifedipine and the A_{2B} receptor. The present docking study also suggested the pharmacophore model. Figure 1 shows the pharmacophore analysis of the calcium antagonists based on the present assay results. The NO group should be essential in the A_{2B} binding and bind the NH of His280[7.43]. The

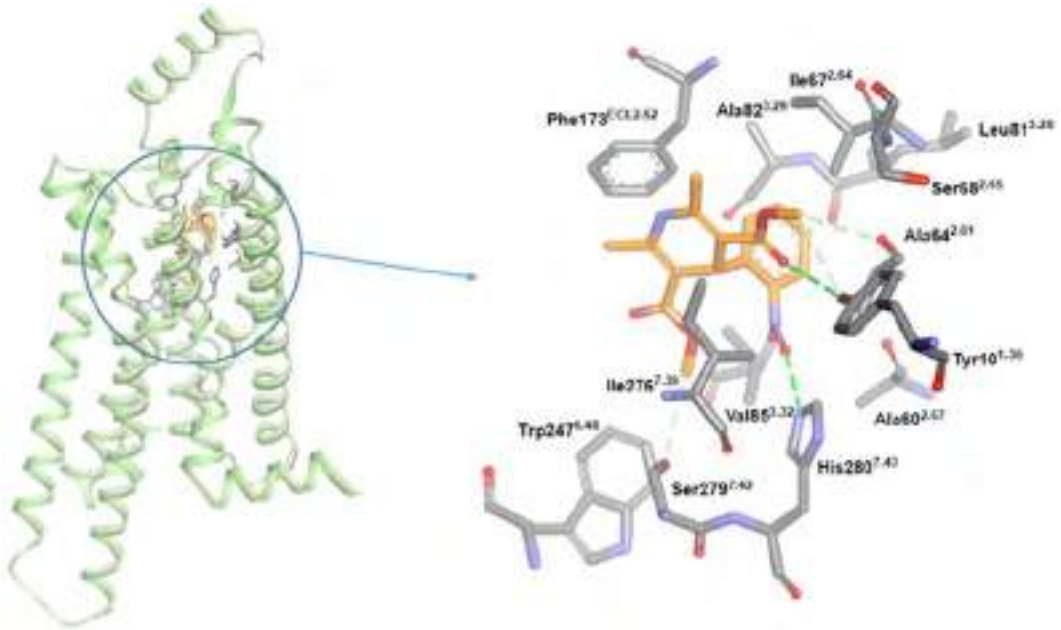

Figure 6. Docking model of the interaction between human adenosine A_{2B} receptor and nifedipine. Nifedipine is shown as a stick model, with carbon coloured in yellow, nitrogen in blue, hydrogen in white, and oxygen in red. Broken lines connecting Tyr10$^{1.35}$, Ala64$^{2.61}$, His280$^{7.42}$, and Ser279$^{7.42}$ represent possible hydrogen bonds (or CH…O interactions) with nifedipine. The distances of nifedipine from Tyr10$^{1.35}$, Ala64$^{2.61}$, Phe173$^{ECL2.52}$, His280$^{7.42}$, and Ser279$^{7.42}$ were calculated to be 3.38 Å, 3.42 Å, 3.35 Å, 2.86 Å, and 3.54 Å, respectively, without taking account of hydrogens. The dihydropyridine of nifedipine can form a π–π stacking interaction with Phe173$^{ECL2.52}$.

ester parts indicated by the blue circles are common structures binding the OH group of Tyr10$^{1.35}$and the variation of the side chains suggests that these parts should locate toward the outside of the A_{2B} receptor. The $-OCH_3$ groups are common structures among these compounds, and are located towards the inside of the receptor, with no additional space. The pharmacophore analysis of the assay results and the docking results are consistent with each other.

Finally, we sought to confirm the *in vitro* results by examining the effect of nifedipine on luminal adenosine-induced intestinal fluid secretion in mice. Specifically, we investigated the effect of adenosine receptor agonists on fluid secretion in the colon. Only BAY60-6583, an A_{2B} receptor agonist, significantly increased intestinal fluid content (Fig. 5b). This finding was confirmed using A_{2B} receptor-deficient mice. These results agreed with those for cAMP accumulation in T84 cells. To our knowledge, this is the first evidence that the colonic A_{2B} receptor is predominantly involved in water secretion into the lumen. We confirmed that adenosine-induced increases in fluid contents were blocked by the selective A_{2B} antagonist PSB-1115 as well as nifedipine, suggesting that the latter's inhibitory action relied on blocking the A_{2B} receptor. However, A_{2B} receptor in the colon is also expressed in various cell types, such as enteric neurons, vascular cells, and mast cells[18], which can indirectly contribute to water secretion *in vivo*. Thus, we need to examine this possibility using epithelial cell-specific A_{2B} receptor-deficient mice in our next study. The dose required to inhibit fluid secretion by adenosine was higher for nifedipine than PSB-1115. This is supported by the fact that the affinity of nifedipine for the receptor was lower than that of PSB-1115. However, nifedipine possesses antagonistic calcium activity at a nanomolar level[22], which may also contribute to the suppression of fluid secretion, a possibility we could not exclude.

Nifedipine is commonly used in medication. In general, anti-diarrhoea drugs can cause constipation in humans. Nifedipine treatment also seems to be associated with constipation[23]. According to adverse events from prescribing information, constipation in nifedipine users has been reported approximately 1% of patients (versus 0% in placebo). Previous reports have showed that nifedipine slows small intestinal transit or suppresses colonic motility in humans[24,25]. Although these results suggest the potential of nifedipine as an anti-diarrhoea agent, its A_{2B} receptor antagonistic activity for intestinal epithelial cells as well as its calcium inhibitory activity in intestinal smooth muscle cells can contribute to the effects.

Our study has also some limitations. First, we did not assess the binding affinity of other adenosine receptor subtypes. We have recently conducted preliminary experiments to determine whether nifedipine binds to A_1 and A_{2A} receptors. We have found a weak affinity of nifedipine for both receptors (the K_i values of A_1 and A_{2A} receptors were 4.3 μM and 4.1 μM, respectively). Thus, we could not fully exclude the involvement of other receptor subtypes in the present study. Although our pharmacological studies using selective agonists indicate the specific involvement of the A_{2B} receptor, experiments using genetically modified cells (e.g., A_{2B} receptor-knockout T84 cells) or mice (e.g., epithelial cell-specific A_{2B} receptor-deficient mice) could be beneficial in future studies. Second, future studies should investigate normal intestinal cell lines, as their receptor expression profiles and responsiveness to adenosine may be different from those of cancer cells. In addition, other types of fluid secretion

assays such as the Ussing chamber assay and 2D or 3D secretion assays are necessary to validate our idea. Third, in the present study we did not determine the influence of nifedipine or PSB-1115 on luminal fluid contents in the absence of adenosine treatment. Because A_{2B} receptor can be mainly activated by extracellular adenosine in pathophysiological conditions, we focused on these conditions in this study. However, it is important to investigate whether nifedipine or PSB-1115 affect fluid secretory activity in normal conditions or modulate absorption processes in luminal fluid dynamics, as fluid absorption from epithelial cells occurs before secretion. Here, we observed colonic fluid contents 2 h after adenosine injection. Thus, we could not exclude the possibility that adenosine A_{2B} receptor suppresses absorption.

In summary, the identification of nifedipine, an already approved drug, as an inhibitor of the A_{2B} receptor could facilitate its application in clinical trials as a therapeutic candidate for diarrhoea-related diseases. Moreover, modelling of its interaction with the receptor's active site could drive the design of specific modifications that ameliorate its function.

Methods

Chemicals. Nifedipine, nisoldipine, nitrendipine, nilvadipine, and isradipine were obtained from Tokyo Chemical Industry (Tokyo, Japan) and Wako Pure Chemical Industries (Osaka, Japan). PSB-1115 was purchased from Santa Cruz Biotechnology. Amlodipine besylate (amlodipine), adenosine deaminase (ADA), *N*6-cyclopentyladenosine (CPA), forskolin, and adenosine were purchased from Sigma (St. Louis, MO). CGS21680, IB-MECA, and EHNA hydrochloride (EHNA) were obtained from Abcam (Cambridge, UK). BAY60-6583 was purchased from Tocris Bioscience (Bristol, UK). The compound library consisting of 1,241 existing medicines was a kind gift from LTT Bio-Pharma Co., Ltd (Tokyo, Japan).

Animals. Male C57/BL6N mice (9–12 weeks old, 22–28 g) and male adenosine A_{2B} receptor (A_{2B}AR)-deficient mice were purchased from Charles River Laboratories Japan and Deltagen Inc[26], respectively. Animals were housed in controlled temperature (22–24 °C) and light (12-h light/12-h dark cycle) conditions for more than 4 days before experiments. The heterozygous mice were backcrossed to C57BL/6 N strain mice for four generations to generate congenic C57BL/6 N strain *ADORA2B* gene mutant mice. Crossbreeding of C57BL/6 N strain *ADORA2B* mutant heterozygous mice generated the same background strain as wild-type (WT) or *ADORA2B* gene knockout homozygous mice. We have confirmed that both WT and C57BL/6 N mice showed similar colonic fluid secretion in normal conditions. The phenotypic properties of the genetically modified mice have also been characterized in previous studies[27–29]. All animal studies were performed in accordance with the ARRIVE[30,31] and National Institutes of Health guidelines, and were approved by the Animal Care Committees of St. Marianna University (approval numbers: TG180529-5 and 1804015).

Competitive receptor binding assay. The ligand binding assay was performed using 8-cyclopentyl-1,3-dipropylxanthine,[dipropyl-2,3-^{3}H(N)] ([^{3}H]-DPCPX). Membrane fractions (20 µg) prepared from human embryonic kidney (HEK) 293 cells expressing human adenosine A_{2B} receptor (Perkin-Elmer) were incubated with 30.5 nM [^{3}H]-DPCPX, test drugs, and assay buffer (50 mM HEPES pH 7.4, 5 mM $MgCl_2$, 1 mM EDTA) in a 96-well microplate at room temperature for 1 h. A range of concentrations (3 nM to 100 µM) for each compound was tested in triplicate to generate competition curves. The samples were passed through a GF/C filter (Perkin-Elmer) pre-soaked for 1 h with 0.5% BSA and washed four times with wash buffer (5 mM HEPES pH 7.4, 5 mM $MgCl_2$, 1 mM EDTA, 0.25% BSA). Filters were then dried for 30 min before attachment to a MeltiLex A (Perkin-Elmer). The radioactivity remaining on the filter was monitored with a MicroBeta Trilux microplate scintillation counter (Perkin-Elmer). Inhibitory binding constant (K_i) values were determined from IC_{50} and K_D values according to the Cheng & Prusoff equation[32]. K_i and IC_{50} values were calculated by non-linear regression analysis using the equation for a sigmoid concentration-response curve (Graph-PAD Prism). The K_D value for [^{3}H]-DPCPX binding to A_{2B}R was determined by saturation assay ($K_D = 10.9$ nM). Non-specific binding was examined in the presence of PSB-1115 (10 µM). All experiments were performed in triplicate. Data were normalized to the results of each compound at 3 nM. The data represent the average of the values from at least three independent experiments.

Test drugs or control drugs (aminophylline, CGS21680, BAY60-6583, PSB-1115, NECA) (approximately 10 µM) were screened using 96-well microplates, each of which included a non-specific binding control (without [^{3}H]-DPCPX), buffer control (without drug), and aminophylline and PSB-1115 as positive controls. Before drug screening, we confirmed that the K_i values of the positive control drugs were similar to those in previous reports and that a selective A_{2A} agonist, CGS21680, had no affinity for the A_{2B} receptor membrane. Each plate was normalized to the buffer control. From the screening, we selected drugs with higher affinity than aminophylline. Then, these candidates were tested at three different concentrations (0.1–10 µM) in triplicate. Finally, we identified 12 candidates that had equivalent binding affinity to aminophylline.

Calcium mobilization assay. Calcium mobilization was assayed using the FRIPR® calcium-6 assay kit (Molecular Devices) according to the manufacturer's instructions. Chinese hamster ovary (CHO) cells stably expressing both human adenosine A_{2B} receptor and Gα15 protein (GeneScript) were seeded in a 96-well microplate (poly-D-lysine-coated black plate) at a density of 3×10^4 cells/well with 100 µL Ham's F12 containing heat-inactivated 10% FBS, 1% penicillin/streptomycin (Gibco), 400 µg/mL G418, and 100 µg/mL hygromycin. Cells were incubated for 24 h at 37 °C in 5% CO_2. After that, 100 µL loading buffer containing 2.5 mM probenecid was added to each well, and incubation proceeded for another 2 h. A 20-µL test drug solution was added to the appropriate wells and the plates were kept at room temperature for 10 min. Cells were stimulated by the addition of 20 µL 1 µM adenosine solution or Hank's balanced salt solution (HBSS) with an injector. Fluorescence intensity (F) was measured by a TECAN plate reader (excitation 485 nm; emission 525 nm; 80 cycles; single detection).

Serial concentrations of test drugs dissolved in DMSO were prepared with HBSS (3 to 100 μM). Calcium mobilization (ΔF/F) was calculated as follows: ΔF/F = [(maximum F value after adenosine treatment) – (maximum F value before adenosine treatment)] / (maximum F value before adenosine treatment). As these cells overexpress not only the A_{2B} receptor but also the Gα15 protein, this cell line was suitable for the evaluation of A_{2B} receptor binding activity.

cAMP accumulation assay. Colonic epithelial T84 cells (CCL-248; ATCC) were plated into a 24-well microplate at a density of 2×10^5 cells/well with 500 μL DMEM/Ham's F12 (1:1 mixture) supplemented with 5% FBS and 1% penicillin/streptomycin. Cells were incubated for approximately 7 days at 37 °C in 5% CO_2 until confluent. During preculture, the medium was changed twice a week. Confluent cells were washed with 300 μL HBSS containing 1 unit/mL adenosine deaminase (ADA) before further incubation for 2 h with HBSS without ADA. After that, cells were preincubated with 100 μL 50 μM rolipram for 15 min, and then with 100 μL adenosine receptor agonist and calcium blockers for another 15 min. During adenosine stimulation, ADA inhibitor EHNA (50 μM) was added with rolipram to avoid adenosine degradation. T84 cells were washed with HBSS and lysed with 250 μL 0.1 N HCl at room temperature for 20 min. Intracellular cAMP levels were determined by an enzymatic cAMP assay kit from Cayman Chemical Company (Ann Arbor, MI) according to the instruction manual.

Assessment of colonic fluid secretion and absorption. To determine the intestinal luminal fluid volume, a mouse intestinal loop model was used as described previously with some modifications[2]. Mice fasted for 18 h were anesthetized with 2% isoflurane. The intestinal tract was exposed using a 1-cm middle incision. The colon was ligated with silk approximately 1 cm distal to the caecal–colon junction. Then 100 μL drug solution or vehicle (saline containing 2.5% DMSO) was injected from the ligated point into the colonic lumen. Immediately, one loop of approximately 2 cm was prepared by ligating the colon around 3 cm distal to the caecal–colon junction. The tract was returned to the peritoneal cavity, and the abdominal incision was closed with sutures. Mice were allowed to recover from the anaesthesia. After 2 h, the colonic loop was removed, and its length and weight (including intraluminal contents) were measured. Then, the loop was opened and wiped to remove residual contents. The volume of residual intraluminal fluid was calculated as follows: Residual fluid volume (μL/cm) = [(isolated loop weight with intraluminal contents) – (isolated loop weight without intraluminal contents)] / loop length. Finally, data were normalized to 100% vehicle. Control mice were treated with saline containing 2.5% DMSO (vehicle) alone. For assessment of the inhibitory activity of nifedipine or PSB-1115 on adenosine-produced colonic water secretion, a 1 mM adenosine solution was used.

Homology modelling. As no experimental structures of A_{2B} were available at the time, homology-based models were built for A_{2B}. These were based on a crystal structure of the closely related A_{2A}, which has 55% sequence identity to A_{2B} in the transmembrane region. The crystal structure of A_{2A} (PDB entry 5N2R[33]); complexed with an antagonist (PSB36) served as a structural template. The sequence of human A_{2B} (UniProt entry P29275) was aligned to that of the A_{2A} crystal structure using MATRAS[34] Subsequently, the alignment in the second extracellular loop (ECL2) was manually edited (Supplementary Fig. 1). The C-terminus was excluded from the model because the coordinates were missing in the template. The cytochrome b_{562}RIL fused between TM5 and TM6 was replaced with the corresponding wild-type amino acid sequence (QLRTELMD) of A_{2B}. According to a mutagenesis study of the four cysteine residues in the ECL2, the $C171^{45.50}$S mutant lost its capacity for high-affinity binding to the A_{2B} antagonist, whereas cysteine-to-serine mutants in the other three positions behaved like the wild-type receptor[35]. Therefore, we considered only the $C78^{3.25}$–$C171^{45.50}$ disulphide bond, which is highly conserved in class A G protein-coupled receptors. The antagonist PSB36 was incorporated and placed in the same position as in the A_{2A} crystal structure. All modelling procedures were performed using Modeller v9.13[36].

Docking simulation. The crystal structures of nifedipine found in the Crystallography Open Database[37] were computationally docked into the A_{2B} model using the sievgene/myPresto docking engine[38] implemented in MolDesk ver. 1.1[39]. The partial charge was derived by quantum chemical calculations using Gaussian03[40] at the HF/6-31 G* level followed by RESP fitting[41]. The AMBER99 force field parameters[42] were applied to A_{2B}. All acidic residues (Asp and Glu) and all basic residues (Lys and Arg) were set to be negatively and positively charged, respectively. The $His280^{7.43}$ residue was assumed to be positively charged whereas all other His residues were set to be neutrally charged and protonated at the δ-nitrogen atom. The binding pocket of A_{2B} was specified as a collection of probe points, which were located as the heavy atoms of PSB36 modelled with A_{2B}. Flexible docking was performed by twisting the rotatable bonds of nifedipine, while the coordinates of the A_{2B} model remained fixed. The plausibility of docking was evaluated by the scores of the docking program. The best pose giving the highest score is shown in Fig. 6.

Statistical analysis. Data and statistical analysis were compiled using recommendations on experimental design and analysis in pharmacology[43]. Values obtained from animal experiments were derived from at least two independent experiments. All data are expressed as mean ± standard error of the mean (SEM). For the assessment of colonic fluid secretion, normalization was performed after collection of all data. Statistical analyses were performed using SPSS 24.0 software (IBM). One- or two-way ANOVA followed by Dunnett's test or Tukey's test were used to evaluate differences between more than two groups. Differences were considered significant at $P < 0.05$.

Received: 18 April 2019; Accepted: 28 January 2020;
Published online: 26 February 2020

References

1. Bucheimer, R. E. & Linden, J. Purinergic regulation of epithelial transport. *J. Physiol.* **555**, 311–321 (2004).
2. Weissmuller, T. *et al*. PMNs facilitate translocation of platelets across human and mouse epithelium and together alter fluid homeostasis via epithelial cell-expressed ecto-NTPDases. *J. Clin. Invest.* **118**, 3682–3692 (2008).
3. Sohn, C. I., Park, H. J. & Gebhart, G. F. Adenosine receptor agonists modulate visceral hyperalgesia in the rat. *Gut Liver* **2**, 39–46 (2008).
4. Feoktistov, I. & Biaggioni, I. Adenosine A2B receptors. *Pharmacol. Rev.* **49**, 381–402 (1997).
5. Chandrasekharan, B. P. *et al*. Adenosine 2B receptors (A(2B)AR) on enteric neurons regulate murine distal colonic motility. *FASEB J.* **23**, 2727–2734 (2009).
6. Antonioli, L. *et al*. Role of the A(2B) receptor-adenosine deaminase complex in colonic dysmotility associated with bowel inflammation in rats. *Br. J. Pharmacol.* **171**, 1314–1329 (2014).
7. Asano, T. & Takenaga, M. Adenosine A2B Receptors: An Optional Target for the Management of Irritable Bowel Syndrome with Diarrhea? *J. Clin. Med.* **6**, (2017).
8. Asano, T. *et al*. Aminophylline suppresses stress-induced visceral hypersensitivity and defecation in irritable bowel syndrome. *Sci. Rep.* **7**, 40214 (2017).
9. Warren, C. A. *et al*. Contribution of adenosine A(2B) receptors in Clostridium difficile intoxication and infection. *Infect. Immun.* **80**, 4463–4473 (2012).
10. Camilleri, M. Intestinal secretory mechanisms in irritable bowel syndrome-diarrhea. *Clin Gastroenterol Hepatol* **13**, 1051–1057; quiz e1061–1052, (2015).
11. Thiagarajah, J. R., Donowitz, M. & Verkman, A. S. Secretory diarrhoea: mechanisms and emerging therapies. *Nat. Rev. Gastroenterol. Hepatol.* **12**, 446–457 (2015).
12. Watson, M. J. *et al*. The Cystic Fibrosis Transmembrane Conductance Regulator (CFTR) Uses its C-Terminus to Regulate the A2B Adenosine Receptor. *Sci. Rep.* **6**, 27390 (2016).
13. Strohmeier, G. R., Reppert, S. M., Lencer, W. I. & Madara, J. L. The A2b adenosine receptor mediates cAMP responses to adenosine receptor agonists in human intestinal epithelia. *J. Biol. Chem.* **270**, 2387–2394 (1995).
14. Barrett, K. E., Huott, P. A., Shah, S. S., Dharmsathaphorn, K. & Wasserman, S. I. Differing effects of apical and basolateral adenosine on colonic epithelial cell line T84. *Am. J. Physiol.* **256**, C197–203 (1989).
15. Kolachala, V. L., Obertone, T. S., Wang, L., Merlin, D. & Sitaraman, S. V. Adenosine 2b receptor (A2bR) signals through adenylate cyclase (AC) 6 isoform in the intestinal epithelial cells. *Biochim. Biophys. Acta* **1760**, 1102–1108 (2006).
16. Mizushima, T. Identification of a molecular mechanism for actions of existing medicines and its application for drug development]. *Yakugaku Zasshi* **132**, 713–720 (2012).
17. Nichols, J. M., Maiellaro, I., Abi-Jaoude, J., Curci, S. & Hofer, A. M. "Store-operated" cAMP signaling contributes to Ca^{2+}-activated Cl^{-}secretion in T84 colonic cells. *Am. J. Physiol. Gastrointest. Liver Physiol* **309**, G670–G679 (2015).
18. Christofi, F. L. *et al*. Differential gene expression of adenosine A1, A2a, A2b, and A3 receptors in the human entericnervous system. *J. Comp. Neurol.* **439**, 46–64 (2001).
19. Müller, C. E. & Jacobson, K. A. Recent developments in adenosine receptor ligands and their potential as novel drugs. *Biochim. Biophys. Acta* **1808**, 1290–1308 (2011).
20. Thimm, D. *et al*. Ligand-specific binding and activation of the human adenosine A(2B) receptor. *Biochem.* **52**, 726–740 (2013).
21. Peeters, M. C. *et al*. Domains for activation and inactivation in G protein-coupled receptors–a mutational analysis of constitutive activity of the adenosine A2B receptor. *Biochem. Pharmacol.* **92**, 348–357 (2014).
22. Morel, N. *et al*. The action of calcium channel blockers on recombinant L-type calcium channel alpha1-subunits. *Br. J. Pharmacol.* **125**, 1005–1012 (1998).
23. Bharucha, A. E., Pemberton, J. H. & Locke, G. R. 3rd American Gastroenterological Association Technical Review on Constipation. *Gastroenterology* **144**, 218–238 (2013).
24. Chiarioni, G., Scattolini, C., Bonfante, F., Brentegani, M. T. & Vantini, I. Effect of nifedipine on mouth-to-cecum transit of liquid meal in normal subjects. *Dig. Dis. Sci.* **38**, 1022–1025 (1993).
25. Zar, M. & Gooptu, D. Effect of nifedipine on the contractile responses of human colonic muscle. *Br. J. Clin. Pharmacol.* **16**, 339–340 (1983).
26. Eckle, T. *et al*. Cardioprotection by ecto-5′-nucleotidase (CD73) and A2B adenosine receptors. *Circulation* **115**, 1581–1590 (2007).
27. Eckle, T., Grenz, A., Laucher, S. & Eltzschig, H. K. A2B adenosine receptor signaling attenuates acute lung injury by enhancing alveolar fluid clearance in mice. *J. Clin. Invest.* **118**, 3301–3315 (2008).
28. Yang, D. *et al*. The A2B adenosine receptor protects against inflammation and excessive vascular adhesion. *J. Clin. Invest.* **116**, 1913–1923 (2006).
29. Grenz, A. *et al*. The Reno-Vascular A2B Adenosine Receptor Protects the Kidney from Ischemia. *PLoS Med.* **5**, e137 (2008).
30. Kilkenny, C. *et al*. Animal research: reporting *in vivo* experiments: the ARRIVE guidelines. *Br. J. Pharmacol.* **160**, 1577–1579 (2010).
31. McGrath, J. C. & Lilley, E. Implementing guidelines on reporting research using animals (ARRIVE etc.): new requirements for publication in BJP. *Br. J. Pharmacol.* **172**, 3189–3193 (2015).
32. Cheng, Y. & Prusoff, W. H. Relationship between the inhibition constant (K1) and the concentration of inhibitor which causes 50 per cent inhibition (I50) of an enzymatic reaction. *Biochem. Pharmacol.* **22**, 3099–3108 (1973).
33. Cheng, R. K. Y. *et al*. Structures of Human A1 and A2A Adenosine Receptors with Xanthines Reveal Determinants of Selectivity. *Structure* **25**, 1275–1285 e1274 (2017).
34. Kawabata, T. MATRAS: A program for protein 3D structure comparison. *Nucleic Acids Res.* **31**, 3367–3369 (2003).
35. Schiedel, A. C. *et al*. The four cysteine residues in the second extracellular loop of the human adenosine A2B receptor: role in ligand binding and receptor function. *Biochem. Pharmacol.* **82**, 389–399 (2011).
36. Sali, A. & Blundell, T. L. Comparative protein modelling by satisfaction of spatial restraints. *J. Mol. Biol.* **234**, 779–815 (1993).
37. Merkys, A. *et al*. COD::CIF::Parser: an error-correcting CIF parser for the Perl language. *J. Appl. Crystallogr.* **49**, 292–301 (2016).
38. Fukunishi, Y., Mikami, Y. & Nakamura, H. Similarities among receptor pockets and among compounds: analysis and application to in silico ligand screening. *J. Mol. Graph. Model.* **24**, 34–45 (2005).
39. MolDesk ver.1.1, IMSBIO Co., Ltd., Tokyo, https://www.moldesk.com/ (2018).
40. Gaussian 03, Revision E.01. *Frisch, M. J. et al*. Gaussian, Inc., Wallingford CT, http://gaussian.com/ (2004).
41. Bayly, C. I., Cieplak, P., Cornell, W. & Kollman, P. A. A well-behaved electrostatic potential based method using charge restraints for deriving atomic charges: the RESP model. *J. Phys. Chem.* **97**, 10269–10280 (1993).
42. Wang, J., Cieplak, P. & Kollman, P. A. How well does a restrained electrostatic potential (RESP) model perform in calculating conformational energies of organic and biological molecules? *J. Comput. Chem.* **21** 1049–1074. 10.1002/1096-987X(200009)21:12%3C1049::AID-JCC3%3E3.0.CO;2-F (2000).
43. Curtis, M. J. *et al*. Experimental design and analysis and their reporting: new guidance for publication in BJP. *Br. J. Pharmacol.* **172**, 3461–3471 (2015).
44. van der Hoeven, D. *et al*. A role for the low-affinity A_{2B} adenosine receptor in regulating superoxide generation by murine neutrophils. *J. Pharmacol. Exp. Ther.* **338**, 1004–1012 (2011).

Acknowledgements
The authors acknowledge Ayumi Kanada for technical assistance with the *in vitro* experiments. We also thank the Isotope Research Institute at St. Marianna University for help with the receptor binding assay. This work was supported by Grants-in-Aid for Young Scientists from the Japan Society for the Promotion of Science (JSPS KAKENHI grant number JP18K15033). Finally, we thank Edanz Group for editing a draft of this manuscript.

Author contributions
Conception and design: T.A., K.T., T. Mizushima, and M.T. Conducted experiments: T.A., M.W., T. Mashimo, and Y.N. Analysis and interpretation: T.A., K.T., N.Y., Y.F., T. Mizushima, and M.T. Drafting and critically revising the manuscript: Y.F., T. Mizushima, M.T., and T.A.

Competing interests
T.M. and Y.N. are employees of LTT Bio-Pharma Co., Ltd., and T.M. is the chairman and director of the company. T.A. and M.T. are affiliated to an endowed research division of LTT Bio-Pharma Co., Ltd. All other authors have no conflict of interest to declare.

Additional information
Supplementary information is available for this paper at https://doi.org/10.1038/s41598-020-60147-7.

Correspondence and requests for materials should be addressed to T.A. or T.M.

Reprints and permissions information is available at www.nature.com/reprints.

Publisher's note Springer Nature remains neutral with regard to jurisdictional claims in published maps and institutional affiliations.

Open Access This article is licensed under a Creative Commons Attribution 4.0 International License, which permits use, sharing, adaptation, distribution and reproduction in any medium or format, as long as you give appropriate credit to the original author(s) and the source, provide a link to the Creative Commons license, and indicate if changes were made. The images or other third party material in this article are included in the article's Creative Commons license, unless indicated otherwise in a credit line to the material. If material is not included in the article's Creative Commons license and your intended use is not permitted by statutory regulation or exceeds the permitted use, you will need to obtain permission directly from the copyright holder. To view a copy of this license, visit http://creativecommons.org/licenses/by/4.0/.

© The Author(s) 2020

5 リピッドマイクロスフェア（リポ）製剤

Lipid Microsphere Formulation

聖マリアンナ医科大学 難病治療研究センター[1]，慶應義塾大学 薬学部[2]
武永美津子[1]，五十嵐理慧[1]，星 恵子[1]，水島 徹[2]
MITSUKO TAKENAGA[1], RIE IGARASHI[1], KEIKO HOSHI[1], TOHRU MIZUSHIMA[2]
Institute of Medical Science, St. Marianna University School of Medicine [1]
Faculty of Pharmacy, Keio University [2]

はじめに

世界に先駆け日本で実用化を果たしたリピッドマイクロスフェア製剤（通称：リポ製剤）（図1）は，イントラリポス®，イントラファット®，イントラリピッド®等の栄養補給剤がリピッドマイクロスフェア（脂肪微粒子）形状をとり，血管傷害部位や炎症組織に集積しやすいことに着眼して，水島裕らによって臨床適用された薬物封入注射用DDS製剤である。リピッドマイクロスフェアは優れた脂溶性薬物キャリアとして薬物動態を変化させ，結果として薬用量の低下および副作用の軽減に寄与している。

これまで実用化されたリポ製剤は，承認順に，リメタゾン®（1988年6月），パルクス®（1988年10月）／リプル®（同年11月），ロピオン®（1992年6月）である。パルクス®／リプル®に代表されるプロスタグランジンE_1（PGE_1）を封入したリポPGE_1製剤は，その後アリプロスト®，プリンク®，アルプロスタジル®が後発品として承認され医療に貢献している（表1）。

薬物キャリアとしてリピッドマイクロスフェア（o/wエマルション：200～300nm）に注目したのは，1960年代から研究されてきたリポソーム（w/o/wエマルション）と，構成成分および体内動態でいくつかの類似点があったことが大きい。さらに，欧米，日本等で上記脂肪微粒子製剤が栄養補給を目的として臨床の場で使用されていたことから，安全性や安定性が確立しており，大量生産も可能で開発しやすい，と判断したためである。また構成するレシチンは生体膜成分でもあり，体内動態を左右する因子としての魅力も備えていた。これは，その後のレシチン化DDS製剤[1]の研究につながっていく。本稿では，実用化されたリポ製剤のそれぞれの特徴，また関連ある基礎研究および臨床研究報告に触れたい。

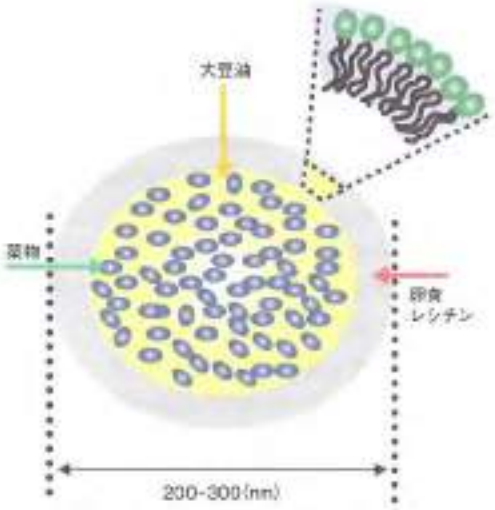

図1 リピッドマイクロスフェア

1 リポデキサメタゾンパルミチン酸エステル（リポステロイド）

リポデキサメタゾンパルミチン酸エステル（リメタゾン®）は，関節リウマチ疾患に適用されている（デキサメタゾン

表1 臨床適用されたリピッドマイクロスフェア製剤（リポ製剤）と諸外国での販売状況

封入薬物	商品名	日本での承認（年）	適応症	中国	韓国	インド
パルミチン酸デキサメタゾン	リメタゾン	1988	関節リウマチ	利美达松*1)（LI MEI DA SONG）	*2)	Lipotalon*1)
プロスタグランジンE1	パルクス／リプル	1988	①慢性動脈閉塞症（バージャー病、閉塞性動脈硬化症）における間歇跛行ならびに安静時疼痛の改善	凱時*1)（KAI SHI）	Eglandin*1)	
	アリプロスト	2002	②進行性全身性硬化症、全身性エリテマトーデスにおける皮膚潰瘍の改善 ③糖尿病性皮膚潰瘍の改善			
	プリンク	2004	④振動病における末梢血行障害に伴う自覚症状の改善ならびに末梢循環・神経・運動機能障害の回復 ⑤動脈管依存性先天性心疾患における動脈管の開存			
	アルプロスタジル	2009	⑥経上腸管腸骨静脈性門脈造影後の改善			
フルルビプロフェンアキセチル	ロピオン	1992	術後・各種疼痛	財鈴*1)（KAI FEN）		

*1) 商品名
*2) 2014年現在、販売していない

として2.5 mg を2週に1回静注）。1990年にはドイツで痛みを伴う変形性関節症に適用承認され、中国でも実用化されている（表1）。

活性本体であるデキサメタゾンは、半減期が長く、受容体に高い親和性をもち、ヒドロコルチゾンの25倍の力価をもつステロイドである。少量で抗炎症作用や鎮痛作用を示す一方、ステロイド特有の副作用も多い。とりわけ関節リウマチのような長期にわたる使用が想定される慢性疾患では、副作用を軽減させることはとりわけ重要である。

デキサメタゾンがリピッドマイクロスフェアに封入する薬物の候補となったのは、少量で高い活性を示すのに加え、水にほとんど溶けず脂溶性が高いことにある。パルミチン酸をエステル結合させたプロドラッグ（図2）とすることで、リピッドマイクロスフェアの大豆油への溶解性をさらに上げ、製剤としての安定性を増すことにつながった。投与後炎症巣局所へ集積するとともに、体内エステラーゼによって活性体（デキサメタゾン）へと変換する。

Mizushima et al[2] は、デキサメタゾンパルミチン酸エステルを封入したリポ製剤が、膵臓に代表される細網内皮系、およびカラゲニン足浮腫部位に顕著に集積した一方で、対照のデキサメタゾンリン酸塩の取り込みはわずかであることを明らかにした。さらに、リウマチ患者や慢性閉塞性動脈硬化症患者に^{99m}Tc標識リピッドマイクロスフェアを投与すると、関節炎部位など病巣部位にきわめて集積することも明らかになっている[3]。

健常男子6名にリメタゾン®5 mg（デキサメタゾンとして）を静脈内投与すると、デキサメタゾンパルミチン酸エステル（封入薬物）の血中半減期は1.13時間であった。一方デキサメタゾンの血漿中濃度は、1.68時間後に最高値（6.62 μg/ml）に達し、また半減期は5.2時間であった。これは体内でエステラーゼによってデキサメタゾンに変換することを示している[1]。

138名のリウマチ患者に対する多施設二重盲検比較試験[4]で、リポステロイド（デキサメタゾンとして2.5mg）を2週間に一度静注あるいは筋注した群は、対照としたデカドロン®3.3mg投与群に比べ改善効果が有意に高く、しかも副作用が少ないとの結果を得た。自己免疫疾患である関節リウマチは、細胞工学・遺伝子工学の進歩を背景に標的分子が次々明らかとなるなか、疾患特異的なサイトカイン分子あるいはその受容体をターゲットとした生物学的製剤が続々登場し、奏効している。一方で多発関節炎および関節痛などの症状に合わせて、関節疼痛や腫脹の軽減を目的に消炎鎮痛薬などを適宜用いることが求められ、ステロイドは現在も症状の改善に処方される選択肢の1つとなっている。

近年、リメタゾン®を用いた臨床研究がいくつか報告

デキサメタゾンパルミチン酸エステル

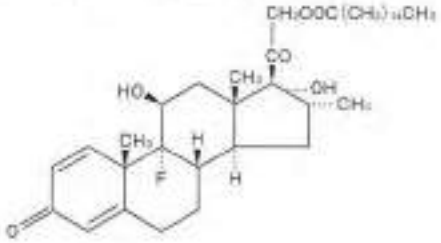

フルルビプロフェンアキセチル

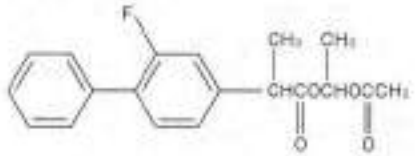

プロスタグランジンE₁（PGE₁）

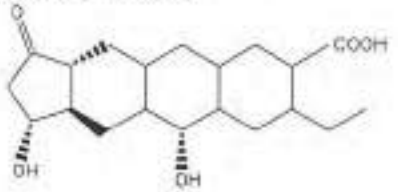

図2　臨床適用されたリポ製剤に封入されている薬物

されている。同種造血幹細胞移植後に血球貪食症を発症した3名にリメタゾン®5 mg/dayを3日間投与したところ，高い血清フェリチン値，およびAST/ALT/LDH値は低下し，一方で，白血球，リンパ球，血小板の数は正常値に近づいたことをNishiwaki et al[6]が報告している。白血球減少症や懸念される感染症などはみられず，症状の改善が速やかに認められた。これまで高用量のステロイドを投与しても症状の悪化は食い止められなかったという。彼らはヒト単球由来の活性化したマクロファージにデキサメタゾンパルミチン酸エステルを添加して細胞生存率をみたところ，デキサメタゾンリン酸塩に比べ有意に低下させた*in vitro*の成績も示している。

また毛細管からの出血を繰り返す難病疾患の1つ，小児特発性ヘモジデローシス症に対するリメタゾン®投与が有効であったことをDoi et al[7]が報告している。特発性ヘモジデローシス症患者9名（発症年齢：平均2.3歳，1.2－8.6歳）に，出血がみられたその日から3日間リメタゾン®（0.8mg/kg/day）を投与する治療を続けた結果，平均11年間（2.4～16.9年）の観察期間中に死亡例はなく，5名はリポ療法から離脱でき，1名は離脱中，離脱できないのは残る3名（活動期のため）であったという。離脱できない3名を含む4名には骨密度の低下がみられたものの，身長や肥満には大きな影響はなく，呼吸困難もなく学校生活を過ごしていることが報告されている。リポステロイド療法は生存率を上げるとともに，ステロイドのもつ副作用の低減に効果があると結論づけている。

② リポフルルビプロフェンアキセチル（リポNSAID）

リポフルルビプロフェンアキセチル（ロピオン®）は，呼吸循環に影響が少ない非ステロイド系抗炎症薬（NSAID）フルルビプロフェンのプロドラッグを封入したリポ製剤である。わが国唯一のNSAID静注薬で術後疼痛や各種癌に適用され，リポフルルビプロフェンアキセチルとして50mg/5mlをできるだけ緩徐に静注する。

活性本体であるフルルビプロフェンは，関節リウマチ，変形性関節症，抜歯後疼痛に，また消炎を目的に処方されるプロピオン酸系NSAIDである。プロスタグランジン生合成阻害（シクロオキシゲナーゼ阻害）作用が強く，血中半減期は比較的短く，ヒトではほとんど尿中排泄され腸肝循環が少ない。注射剤とすることで，①速効性，②十分な効力の発現，③投与量依存的血中濃度の確保，④胃腸肝障害の軽減，⑤経口摂取不能な患者への使用が可能，といった点が期待できる。

フルルビプロフェンがリピッドマイクロスフェアに封入するNSAID候補となったのは，薬効に加え，脂溶性の高さによるところが大きい。水にはほとんど溶けない。さらにエステル体（プロドラッグ）（図2）とすることで脂溶性が一段と上がり，大豆油に安定に存在するリポ製剤となった。投与後体内で速やかにエステラーゼによって活性体となる。

健常男子6名にロピオン®を静脈内投与（フルルビプロフェンアキセチルとして50mg）すると，フルルビプロフェンの血漿中濃度は，6.7分後に最高値（8.9μg/ml）に達し，半減期は5.8時間であった[8]。一方フルルビプロフェン（40mg）の経口投与では，1.4時間後に最高値（5.6μg/ml）に達し，半減期は2.7時間である[9]。リポNSAIDとすることで，生物学的利用率の高さとともに，速やかな効きめと効果の持続が期待できる。

医療で痛みの除去・抑制は欠かせない。腹腔鏡下大腸

切除術後にロピオン®の静脈内投与（4mg/kg/24h）を行い，中枢性鎮痛薬トラマドール塩酸塩（2mg/kg/24h）を併用することで，除痛効果がより長時間持続したことがMihara et al[10]によって報告されている。

またロピオン®の執刀前投与が，手術中に投与する麻薬性鎮痛薬フェンタニル®の減量につながる可能性をKodaka et al[11]は報告している。手術前にロピオン®投与（1mg/kg）すると，体動を抑制するために必要なフェンタニル®を約50%減量でき，かつ催眠効果や血流には影響を及ぼさないという。フェンタニル®を減量できれば，麻薬本来のもつ呼吸や循環抑制のほか，吐き気などの副作用を回避できる可能性が高い。

さらに，全身麻酔の導入・維持に使用されるプロポフォール注射による痛みを，ロピオン®が抑制する可能性について，Zhang et al[12]が過去の文献からメタ解析を行っている。プラセボ群に比べて，ロピオン®50mg群では痛みを感じない（RR3.51，95%CI 2.22-5.55，P＝0.000）との解析結果が得られたことから，プロポフォール注射を起因とする痛みをロピオン®50mgは抑制すると結論づけている。

本剤は，中国でも凱扮®（2004年～）として術後，各種癌の鎮痛を目的に臨床適用されている（表1）。

3 リポプロスタグランジンE_1（リポPGE_1）

リポPGE_1製剤は，適応疾患（表1）に応じて5－10μgをそのまま，あるいは輸液などに混和して静注する。造影能の改善には，カテーテルを用いて上腸間膜動脈内投与を行う。

PGE_1（図2）は，EP受容体を介してcAMP増加による血小板凝集抑制作用，および平滑筋弛緩作用から強力な血管拡張能を示すプロスタノイドの1つで，血流改善効果が期待できる。PGE_1は，肺に豊富に存在する脱水素酵素によって15位水酸基がケト基に代謝されると生物活性を失うため，肺を一過すると活性が極端に低下する。リピッドマイクロスフェアに封入されることで，肺での不活化が抑えられ，作用時間も長くなる。また，PGE_1は局所刺激性が強い。これはラット背部皮膚へ皮内投与後，エバンスブルー色素斑の大きさからも明らかである[13]。リポPGE_1投与では色素斑の大きさは抑えられており，リピッドマイクロスフェアから遊離するPGE_1量の低下を反映している。これは血管痛や静脈炎などの副作用の低下につながる。

リポPGE_1は，障害血管部位，炎症部位などの病変部位に効率よく送り込まれる。^{3}[H]－リポPGE_1は，ウサギで作製した腹部大動脈硬化部位へ正常血管部位に比べて2～5倍[14]，SHR胸部大動脈部位へは，1.5倍[15]集積した。リポPGE_1投与後のSHR腹部大動脈血管壁には，PGE_1の集積が組織免疫染色によって証明されている[16]。またコットンペレットを埋め込んだ周囲にみられるラット新生血管部位に，PGE_1が効率よく集積することが共焦点レーザー蛍光顕微鏡で捉えられている。ラット新生仔動脈管内皮細胞への集積も確認されている[17]。以上は，血管病変部では血管内皮細胞間隙が広がっており，貪食能や透過性が亢進するEPR（enhanced permeability and retention）効果によるものと考えられている。

リポPGE_1は，末梢動脈疾患（peripheral arterial disease：PAD）に有効性・有用性を発揮する。わが国におけるPADは，1970年代まではバージャー病（閉塞性血栓血管炎）が慢性閉塞性動脈疾患の中心を占めてきたが，食生活の変化や高齢化によって，糖尿病や高脂血症，肥満，高血圧など生活習慣病の罹病率が高まり，心筋梗塞や狭心症などの虚血性心疾患や脳梗塞などの動脈硬化性血管疾患が増加してきた。血流障害の進展に応じて，四肢の冷感，しびれ，間歇性跛行，安静時疼痛，皮膚潰瘍，壊死が出現し，下肢切断に至る例もあり，日常生活，社会生活に支障をきたす疾患となっている。

PAD患者79名にリポPGE_1（10μg）を短期投与（10～14日間）した林田ら[18]の成績では，間歇性跛行症状を示す患者の最大歩行距離が飛躍的に有意に延び，有用率は83%と高かった。重症例での有用率は低かったが，これは高血圧症，高脂血症，糖尿病などの多リスク因子をもつ症例が多かったことも関連している可能性がある。一方，足関節／上腕血圧比（ABI：ankle-brachial pressure index）からみると，Fontaine分類Ⅱ度のABI（0.57±0.22）は，Ⅲ度（0.31±0.31）およびⅣ度（0.36±0.24）に比べ明らかに高かったものの，全症例でみたリポPGE_1有効群（0.42±0.27）と無効群（0.44±0.29）との間に統計学的有意差はなかった。

一方ABI0.9未満のPAD患者169名にリポPGE_1（5～10μg）を8週間投与したMatsuo et al[19]の成績では，日本脈管学会基準のWalking Impairment Questionnaire（WIQ）スコアで評価したところ，重症PAD患者＜0.5（n＝16）では歩行距離および階段上りに有意な差がみられなかっ

たものの，他の評価項目はすべて投与前に比べ有意な改善を示した。また軽症：0.8－＜0.9（n＝54），中程度：0.5－＜0.8（n＝97），および重症：＜0.5（n＝16）と症状別に冷感，しびれ，安静時疼痛を評価した場合も，すべての項目で有意な改善がみられている。

Muruta et al[20]は，皮膚潰瘍を伴う膠原病患者にリポPGE_1（10μg）を2週間投与した結果，潰瘍面積の著明な縮小（100％治癒も含め平均30％）とともに，CRP（1.48mg/dL→0.38mg/dL）など炎症マーカー値が低下したと報告した。病態局所へターゲットされたPGE_1がこれらの産生制御にかかわったためと考えている。また皮膚潰瘍を伴う全身性進行性硬化症およびSLE患者192名に3カ月間にわたってリポPGE_1（5～10μg）投与を実施した成績[21]では，潰瘍面積が有意に縮小し，SF-36スコア（QOL）も有意に改善した。さらにMiyata et al[22]は，388名の糖尿病性壊疽皮膚潰瘍患者にリポPGE_1（5～10μg）を4週間投与するprospective studyを行っている。その結果，虚血性皮膚潰瘍患者71名の42.5％，神経障害性潰瘍患者70名の61.8％，また神経障害性虚血性皮膚潰瘍患者125名の33％に，潰瘍サイズの縮小がみられ，潰瘍の状態も改善したことが明らかとなった。病態別では，神経障害性潰瘍の83.6％が，他疾患に比べ，優れた改善効果を示した。一方，副作用発生頻度は4.1％（16名）で，安全性に問題ないと結論づけている。

肺動脈と大動脈とをつなぐ動脈管は，胎児ではプロスタグランジン生成によって開存が維持されているが，出生により閉鎖する。動脈管閉鎖によって循環状態が維持できなくなる動脈管先天性心疾患では，肺動脈狭窄を伴う肺血流型，大動脈縮窄や左心室低形成を伴う体血流型，混合型，いずれも手術までの間，動脈管の開存維持のために投与するリポPGE_1を含むPGE_1製剤が新生児の命を支えている[23]。

4 日本から世界へ

リポ製剤は，永島裕日本DDS学会元名誉理事長（当時聖マリアンナ医科大学内科学教授）のアイデアから，大正製薬株式会社，ミドリ十字株式会社（現田辺三菱製薬株式会社），科研製薬株式会社などとの共同開発で実用化となった日本発のDDS化医薬品である。

リポPGE_1製剤は，パルクス®（大正製薬株式会社）／リプル®（田辺三菱製薬株式会社）に加え，後発品としてアリプロスト®（富士製薬工業株式会社 2002年～），プリンク®（科研製薬株式会社，テバ製薬株式会社 2004年～），アルプロスタジル®（沢井製薬株式会社 2009年～）も臨床適用に至っている。韓国および中国でも，それぞれエグランディンEglandin®（Mitsubishi Tanabe Pharma Korea株式会社），凱時（KAI SHI）®（北京泰德製薬有限公司；適応疾患，①慢性動脈閉塞症（バージャー病，閉塞性動脈硬化症）における四肢潰瘍ならびに安静時疼痛の改善，②臓器移植後の抗血栓治療，③動脈管依存性先天性心疾患における動脈管の開存，④慢性肝炎の補助的な治療）として末梢動脈疾患をはじめ，種々症状の改善に多大な貢献をしている[24]。

さらにリポステロイドはドイツや中国で，リポNSAIDは中国でも臨床適用されている。日本発の医薬品がこのような形で世界の病める方々に届き，また医療に貢献していることは誇らしいことである。さらに発展していくことを期待したい。

■引用文献

1) 永島 裕：レシチン化スーパーオキシドジスムターゼ（PC-SOD）の特発性間質性肺炎治療薬としての開発．YAKUGAKU ZASSHI 134 (1)：69-76, 2014
2) Mizushima Y, Hamano T, Yokoyama K：Tissue distribution and anti-inflammatory activity of corticosteroids incorporated in lipid emulsion. Ann Rheum Dis 41：263-267, 1982
3) 清田重人，五十嵐理恵，岩田克志 他：^{99m}Tc標識lipid microsphere（LM）を用いたLMのtargeting効果の検討と画像診断への応用．癌 7：551-557, 1987
4) リメタゾン医薬品インタビューフォーム
5) Hoshi K, Mizushima Y, Shiokawa Y, et al：Double-blind study with liposteroid in rheumatoid arthritis. Drugs Exp Clin Res 11：621-626, 1985
6) Nishiwaki S, Nakayama T, Murata M, et al：Dexamethasone palmitate successfully attenuates hemophagocytic syndrome after allogeneic stem cell transplantation：macrophage-targeted steroid therapy. Int J Hematol 95：428-433, 2012
7) Doi T, Ohga S, Ishimura M, et al：Long-term liposteroid therapy for idiopathic pulmonary hemosiderosis. Eur J Pediatr 172：1475-1481, 2013
8) 東野正男，小西与志雄，小島博 他：LFP83単回及び連続静脈内投与時のヒト血中濃度推移及び代謝．基礎と臨床26 (9)：3907-3921, 1992
9) フルルビプロフェン医薬品インタビューフォーム
10) Mihara R, Soen M, Kusaka H, et al：Effect of continuous intravenous infusion of flurbiprofen axetil and tramadol hydrochloride for postoperative pain management of laparoscopic colectomy. Masui 60：1364-1369, 2011
11) Kodaka M, Tsukakoshi M, Miyao H, et al：The fentanyl concentration required for immobility under propofol

anesthesia is reduced by pre-treatment with flurbiprofen axetil. Can J Anaesth 60 : 1204-1211, 2013
12) Zhang L, Zhu J, Xu L, et al : Efficacy and safety of flurbiprofen axetil in the prevention of pain on propofol injection : a systematic review and meta-analysis. Med Sci Monit 20 : 995-1002, 2014
13) 武永美津子、太田有紀、都倉京恵 他：静注用リポプロスタグランディン(PG)E₁製剤の比較YAKUGAKU ZASSHI 127(8)：1237-1243, 2007
14) 清川重人、塚本俊一、王手純子 他：PG含有リピッドマイクロスフェアの動脈硬化部位へのターゲティングDrug Delivery System 2 (1) : 35-40, 1987
15) Mizushima Y, Hamano T, Haranoto S, et al : Distribution of lipid microspheres incorporating prostaglandin E₁ to vascular lesions. Prostaglandins Leukot Essent Fatty Acids 41 (4) : 269-272, 1990
16) Igarashi R, Takenaga M, Takeuchi J, et al : Marked hypotensive and blood flow-increasing effects of a new lipo-PGE₁ (lipo-AS013) due to vascular wall targeting. J Controlled Release 71 : 157-164, 2001
17) Chino Y, Minagawa T, Kohno Y, et al : Vasodilating effect and tissue accumulation of prostaglandin E₁ incorporated in lipid microspheres on the rat ductus arteriosus. Jpn J Pharmacol 81 : 107-114, 1999
18) 林田直樹、中島伸之、堀田征久 他：PADに対するLipo PGE₁の臨床効果の検討—短期静注療法における諸因子の解析—脈管学 48 : 213-220, 2008
19) Matsuo H, Shigematsu H : Patient-based outcomes using the Walking Impairment Questionnaire for patients with peripheral arterial occlusive disease treated with Lipo-PGE₁. Circ J 74 : 365-370, 2010
20) Murata H, Kotobuki Y : New aspect of anti-inflammatory action of lipo-prostaglandin E₁ in the management of collagen diseases-related skin ulcer. Rheumatol Int 28 : 1127-1135, 2008
21) Hoshi K, Fukuhara S : Effect of Lipo-PGE₁ on health-related quality of life in patients with systemic sclerosis and systemic lupus erythematosus in Japan. J Inter Med Res 36 : 187-197, 2008
22) Miyata T, Yamada N, Miyachi Y : Efficacy by ulcer type and safety of lipo-PGE₁ for Japanese patients with diabetic foot ulcers. J Atheroscler Thromb 17 : 805-816, 2010
23) 長和俊：動脈管依存性先天性心疾患治療の現状とLipo PGE₁製剤の意義 診療と新薬 51 (7) : 644-648, 2014
24) 五十嵐理慧、星恵子、松田隆秀 他：リポPGE₁製剤開発から20年—日本発のDDS製剤を韓国、中国、そして欧米へ—Drug Delivery System 18 (5) : 426-430, 2003

Aberrant Glycosylation of Lumican in Aortic Valve Stenosis Revealed by Proteomic Analysis

Hirotoshi SUZUKI,[1,2] MD, Masahide CHIKADA,[1] MD, Michiyo K. YOKOYAMA,[2] BSc, Manae S. KUROKAWA,[3] MD, Takashi ANDO,[1] MD, Hiroshi FURUKAWA,[1] MD, Mitsumi ARITO,[2] PhD, Takeshi MIYAIRI,[1] MD, *and* Tomohiro KATO,[2] MD

SUMMARY

To identify proteins related to the pathophysiology of aortic valve stenosis (AS), we investigated the protein profiles of AS aortic valves. Specifically, proteins were extracted from a thickened and calcified area (AS-C) and an apparently non-thickened and non-calcified area (AS-N) in an identical aortic valve leaflet in each of 6 AS patients. The proteins were then separated by 2-dimensional gel electrophoresis (2DE). Protein spots detected by 2DE were compared between the AS-C and AS-N samples. Protein spots of interest were subjected to protein identification by mass spectrometry.

In total, 670 protein spots were detected by 2DE, 28 of which showed more than 1.5-fold different intensity ($P < 0.05$) between the AS-C and AS-N samples. Proteins were identified in 17 out of the 28 spots. Fibrinogen and lumican were identified in 9 and 3 spots, respectively. Intensity of these 12 spots was lower in the AS-C samples than in the AS-N samples. In the 1D-Western blot analysis, 4 lumican bands (80 kDa, 75 kDa, 65 kDa, and 53 kDa) were detected, of which 2 bands with 80 kDa and 75 kDa showed lower intensity in the AS-C samples than in the AS-N samples. When de-glycosylated protein samples were used in the 1D-Western blot, only a single lumican band with ~40 kDa was detected, indicating that lumican was variously glycosylated and that highly glycosylated lumican molecules were decreased in AS-C.

Collectively, insufficient glycosylation of lumican in the thickened and calcified areas of AS aortic valves may be involved in the pathophysiology of AS. (Int Heart J 2016; 57: 104-111)

Key words: Calcification, 2-dimensional gel electrophoresis, Mass spectrometry, Peptide:N-glycosidase F, Proteoglycan

Aortic valve stenosis (AS) is one of the most common cardiovascular diseases. Several decades ago, the main cause of AS used to be rheumatic fever, however, it was recently replaced by degenerative changes with calcification.[1] Risk factors for AS, which include aging, gender, dyslipidemia, hypertension, and smoking, largely overlap those for atherosclerosis.[1-3] Macroscopically, AS is characterized by thickening and calcification in irregular areas of aortic valves. AS is thought to develop via the three processes of lipid accumulation, inflammation, and calcification.[4] Infiltration of lipoproteins into aortic valve tissue and oxidation of the lipoproteins were reported.[5,6] Infiltration of macrophages and T cells into aortic valve tissue, which indicates chronic inflammation, has been reported.[7] These processes lead to osteoblastic transformation of valvular interstitial cells, resulting in the calcification of valve tissue.[8,9] However, the precise mechanisms for the processes are still not fully understood.

Recent years have seen great advances in proteomics to analyze proteins comprehensively using 2-dimensional gel electrophoresis (2DE) and mass spectrometry (MS). The 2DE-MS methods have been recently applied to the analyses of cardiovascular diseases. For example, up-regulation of complement C4 and fibrinogen fragments in aortic walls were demonstrated in abdominal aortic aneurysm (AAA).[10] Furthermore, modification of carbonic anhydrase I and autoimmunity against the enzyme were reported in AAA.[11] In terms of techniques, Gil-Dones, *et al* reported an effective protein extraction protocol for the proteome analysis of AS valves[12] and their group reported up-regulation of 35 proteins and down-regulation of 8 proteins in AS valves.[13]

To find novel molecules involved in the pathophysiology of AS, we here applied 2DE-MS to the elucidation of protein profile differences between a thickened and calcified area (AS-C) and an apparently non-thickened and non-calcified area (AS-N) of an identical AS valve leaflet, since AS-C areas were expected to contain protein alteration related to the pathophysiology of AS. By this approach, we found that lumican with a high molecular weight (MW), ie, glycan-rich lumican, was specifically decreased in the AS-C areas of AS-affected valves. This insufficient glycosylation of lumican may be involved in the pathophysiology of AS.

From the Departments of [1] Cardiovascular Surgery, [2] Clinical Proteomics & Molecular Medicine, and [3] Disease Biomarker Analysis & Molecular Regulation, St. Marianna University Graduate School of Medicine, Kanagawa, Japan.

Address for correspondence: Tomohiro Kato, MD, Department of Clinical Proteomics & Molecular Medicine, St. Marianna University Graduate School of Medicine, 2-16-1, Sugao, Miyamae, Kawasaki, Kanagawa, 216-8511, Japan. E-mail: tkato@marianna-u.ac.jp

Received for publication June 22, 2015. Revised and accepted August 28, 2015.

Released in advance online on J-STAGE January 8, 2016.

All rights reserved by the International Heart Journal Association.

METHODS

Patients and clinical samples: Seven patients with AS were enrolled in this study. Aortic valve samples were obtained during therapeutic aortic valve replacement for AS. All the samples were obtained with written informed consent. This study was approved by the institutional ethics committee of St. Marianna University School of Medicine. One of the 7 AS valve leaflets was used for photographic presentation in Figure 1 and the remaining 6 leaflets were subjected to proteomic analyses. Clinical information of the 6 AS patients is summarized in Table I.

Protein preparation: In each of the 6 AS aortic valve leaflets, AS-C and AS-N areas were separately recovered and were respectively subjected to protein extraction (Figure 1). Specifically, the valve tissue samples were washed in phosphate-buffered saline to eliminate blood contaminants and then were minced and homogenized in a cell lysis buffer (7 M urea, 2 M thiourea, 4% 3-[(3-cholamidopropyl) dimethylammonio]-1-propanesulfonate) using HG30 homogenizer (Hitachi Koki Co., Ltd., Tokyo). The samples were then frozen and thawed 5 times and centrifuged at 4°C for 30 minutes. The supernatants containing extracted proteins were then collected and stored at -80°C until use.

A part of the extracted proteins were de-glycosylated by the treatment with Peptide:N-glycosidase F (PNGase F, Sigma, MO, USA) at the ratio of 50 units PNGase F per mg protein at 37°C for 3 hours and then were used in Western blot.

2DE: The extracted proteins were separated by 2DE as described previously.[10] Briefly, the protein samples were subjected to isoelectric focusing (IEF) using gels with the range of pH 3.0-11.0. The IEF-separated proteins were then further separated by 12.5% sodium dodecyl sulfate-polyacrylamide gel electrophoresis (SDS-PAGE). Protein spots on the 2DE gels were stained with a fluorescent dye (SYPRO Ruby, Invitrogen Co., CA, USA). The intensity of the separated protein spots was quantified by the Progenesis program (PerkinElmer, MA, USA).

Protein identification: Protein spots of interest were recovered and subjected to in-gel digestion with trypsin. Next, the mass-to-charge ratios (m/z) of the generated peptides were measured by a matrix assisted laser desorption ionization-time of flight/time of flight (MALDI-TOF/TOF) mass spectrometer (Ultraflex; Bruker Daltonics, Ettlingen, Germany). In each sample, MS/MS data were also obtained for some of the peptides. The obtained MS and MS/MS data were compiled to allow searches of the National Center for Biotechnology Information (NCBI) protein database using the Mascot software program (Matrix Science, London, UK).

Western blot: Western blot analysis was performed as described previously.[10] Briefly, protein samples were separated by SDS-PAGE under reducing conditions. The separated proteins on the SDS-PAGE gels were stained with SYPRO Ruby to precisely assess the amounts of the loaded proteins, after which the separated proteins were transferred onto polyvinylidene difluoride membranes. The membranes were reacted with antibodies to human lumican (Abnova, Taipei, Taiwan) for 1 hour. The membranes were then washed and reacted with horseradish peroxidase (HRP)-labeled antibodies to mouse IgG (Invitrogen) for 1 hour. After washing, bound antibodies were detected by 3, 3'-diaminobenzidine, tetrahydrochloride (Dojin, Kumamoto, Japan). For the relative quantification of lumican, the intensity of a whole area of each lane in the SYPRO Ruby-stained SDS-PAGE gels was measured and used as the "total protein intensity" of each sample. After membrane transfer and Western blotting, the intensity of lumican bands detected by the anti-lumican antibodies was corrected by the "total protein intensity" in each sample. Finally, the corrected lumican band intensity was compared between the samples.

Statistical Analysis: Statistical significance was calculated using Student's *t*-test. A value of $P < 0.05$ was considered to be statistically significant.

RESULTS

First, we prepared AS-C and AS-N samples from an identical valve leaflet in each of the 7 patients with AS. Representa-

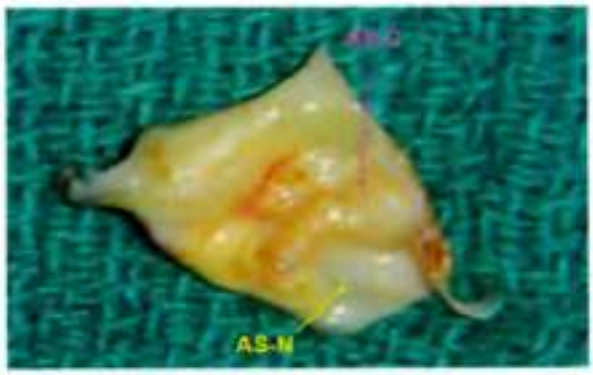

Figure 1. Preparation of valve tissue samples. Tissue samples were obtained from an AS-C area and an AS-N area of each aortic valve leaflet in 6 patients with AS. Proteins extracted from the 6 AS-C and 6 AS-N samples were subjected to 2DE analysis.

Table I. Summary of Patients Whose Valve Protein Samples Were Analyzed by 2DE

Patient	Age	M/F	Pre-existing conditions				Medication		
			HT	DL	DM	Smoking	Anti-HT	Statins	Anticoagulants
AS1	73	F	+	+	-	+	+	+	-
AS2	75	F	+	-	-	-	+	-	-
AS3	78	F	+	+	+	-	+	+	-
AS4	43	F	-	-	-	-	-	-	-
AS5	80	F	+	+	+	-	+	+	+
AS6	63	M	+	-	+	+	+	-	+

M/F indicates male or female; HT, hypertension; DL, dyslipidemia; and DM, diabetes mellitus.

tive sampling areas are shown using one of the 7 valves (Figure 1). We then separated proteins extracted from the remaining 6 samples by 2DE (Figure 2). We detected 670 protein spots in total, and 57 of the 670 protein spots showed significantly different intensity between the AS-C and AS-N samples ($P < 0.05$, Table II). Among the 57 spots, 28 showed more than 1.5-fold intensity differences and 13 of these 28 spots showed more than 2.0-fold intensity differences (Table II). Our data indicate that the protein profiles of the AS-C areas are different from those of the AS-N areas.

Next, we attempted to identify the proteins of the 28 protein spots by mass spectrometry, and successfully identified the proteins of 17 protein spots (Table III). The locations of the identified spots are shown in Figure 3. Among the 17 protein spots identified, 2 showed higher intensity in the AS-C samples than in the AS-N samples. The remaining 15 spots showed lower intensity in the AS-C samples than in the AS-N samples. Interestingly, 10 of the 15 spots were identified as fibrinogen peptides (6 alpha, 3 beta, and 2 gamma chains, Table III). Similarly, 3 of the remaining 5 spots were identified as lumican (ID503, ID504, and ID637, Table III).

Next, we investigated the decrease of lumican in the AS-C areas, since lumican, a proteoglycan with keratin sulfate (KS)-glycosaminoglycans (GAGs), is known to play critical roles in the maintenance of tissue structure.[15-17] In the 1D-Western blot of lumican, 4 lumican bands (80 kDa, 75 kDa, 65 kDa, and 53 kDa) were detected both in the AS-C and AS-N samples (Figure 4A). This indicates that there are at least 4 subtypes of lumican in the AS aortic valves. On the 2DE gels, the lumican spots of ID503 and ID504 were 80 kDa and the

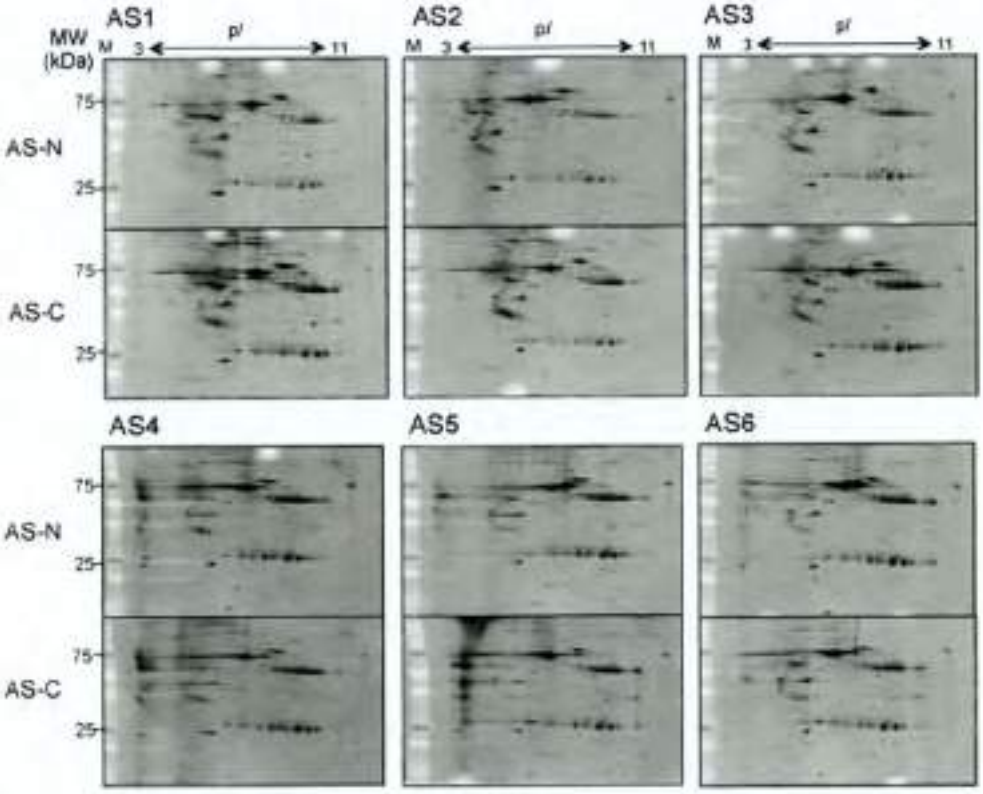

Figure 2. 2DE analysis of valve tissue proteins. The 6 AS-C and 6 AS-N protein samples were separated by 2DE (IEF with the range of pI 3-11 and 12.5% SDS-PAGE). The separated proteins were stained with SYPRO Ruby. pI indicates isoelectric point; and MW, molecular weight.

Table II. Number of Protein Spots That Showed Different Intensity Between the AS-C and AS-N Samples on 2DE

Total number of detected protein spots	Number of spots with different intensity ($P < 0.05$)	Fold difference (x, AS-C/AS-N)	Number of spots
		$3.0 < x$	1
		$2.0 < x \leq 3.0$	2
		$1.5 < x \leq 2.0$	4
670	57	$-1.5 < x \leq 1.5$	29
		$-2.0 < x \leq -1.5$	11
		$-3.0 < x \leq -2.0$	10
		$x < -3.0$	0

In the fold difference, -1.5, -2.0, and -3.0 indicate 1/1.5, 1/2, and 1/3, respectively.

Table III. Summary of the Identified Proteins

Spot ID	MW observed	pI	Difference (C/N)	Protein	Accession no.	MW theoretical	pI	NPM	Mascot score	Coverage (%)	Confirmed sequences (Mascot ion score)
557	74	7.2	-2.97	Fibrinogen alpha chain (FIBA_HUMAN)	gi|1706799	94.9	5.7	10	181	14	^{72}GLIDEVNQDFTNR^{84} (68) ^{218}MKPVPDLVPGNFK^{230} (40) ^{511}HRHPDEAAFFDTASTGK^{527} (22)
2010	74	7.9	-2.58	Fibrinogen alpha chain (FIBA_HUMAN)	gi|1706799	94.9	5.7	10	129	13	^{72}GLIDEVNQDFTNR^{84} (59) ^{218}MKPVPDLVPGNFK^{230} (27)
560	74	7.5	-2.52	Fibrinogen alpha chain (FIBA_HUMAN)	gi|1706799	94.9	5.7	14	174	20	^{72}GLIDEVNQDFTNR^{84} (73) ^{511}HRHPDEAAFFDTASTGK^{527} (19)
561	74	7.7	-2.08	Fibrinogen alpha chain (FIBA_HUMAN)	gi|1706799	94.9	5.7	8	84	11	^{72}GLIDEVNQDFTNR^{84} (66) ^{511}HRHPDEAAFFDTASTGK^{527} (2)
591	72	7.8	-2.43	Fibrinogen alpha chain (FIBA_HUMAN)	gi|1706799	94.9	5.7	8	94	11	^{72}GLIDEVNQDFTNR^{84} (57) ^{511}HRHPDEAAFFDTASTGK^{527} (12)
586	72	7.6	-1.97	Fibrinogen alpha chain (FIBA_HUMAN)	gi|1706799	94.9	5.7	9	76	13	^{72}GLIDEVNQDFTNR^{84} (59) ^{511}HRHPDEAAFFDTASTGK^{527} (2)
763	51	5.5	-2.25	Fibrinogen gamma chain (FIBG_HUMAN)	gi|20178780	51.4	5.3	7	116	29	^{250}IHLISTQSAIPYALR^{270} (80)
765	51	5.7	-1.74	Fibrinogen gamma chain (FIBG_HUMAN)	gi|20178780	51.4	5.3	12	84	47	^{250}IHLISTQSAIPYALR^{270} (1)
671	60	6.9	-1.74	Fibrinogen beta chain (FIBG_HUMAN)	gi|399492	55.8	8.5	11	199	28	^{53}REEAPSLRPAPPPSGGGYR^{72} (4) ^{56}FNALQYLR^{72} (37) ^{170}HQLYIDETVNSNIPTNLR^{190} (63) ^{207}KGGETSEMYLIQPDSSVKPYR^{202} (87)
674	60	7.1	-1.68	Fibrinogen beta chain (FIBG_HUMAN)	gi|399492	55.8	8.5	9	168	30	^{56}FNALQYLR^{72} (37) ^{170}HQLYIDETVNSNIPTNLR^{190} (1) ^{207}KGGETSEMYLIQPDSSVKPYR^{202} (91)
503	80	5.2	-2.45	Lumican (LUM_HUMAN)	gi|20141464	38.4	6.1	9	208	31	^{195}SLEYLDLSFNQIAR^{198} (96) ^{229}FNALQYLR^{239} (47)
504	80	5.3	-2.56	Lumican (LUM_HUMAN)	gi|20141464	38.4	6.1	11	198	34	^{195}SLEYLDLSFNQIAR^{198} (74) ^{229}FNALQYLR^{239} (53)
637	65	5.4	-1.68	Lumican (LUM_HUMAN)	gi|20141464	38.4	6.1	6	81	25	^{195}SLEYLDLSFNQIAR^{198} (19) ^{229}FNALQYLR^{239} (30)
727	53	9.2	-1.64	Ig gamma-1 chain C region (IGHG1_HUMAN)	gi|121039	36.0	8.4	6	272	25	^{156}TPEVTCVVVDVSHEDPEVK^{177} (50) ^{178}FNWYVDGVEVHNAK^{191} (106) ^{220}EPQVYTLPPSR^{230} (32) ^{220}EPQVYTLPPSRDELTK^{244} (34)
2064	48	6.4	-1.52	Procollagen C-endopeptidase enhancer 1 (PCOC1_HUMAN)	gi|6919941	47.9	7.4	6	87	17	^{83}VFDLELHPACR^{93} (26) ^{95}YDALEVFAGSGTSGQR^{110} (15)
1260	28	6.0	1.68	Extracellular superoxide dismutase [Cu-Zn] (SODE_HUMAN)	gi|108885292	25.8	6.1	6	76	37	^{62}VTEIWQEVMQR^{72} (4) ^{79}VTGVVLFR^{87} (14)
2004	38	5.9	4.52	Fibrinogen beta chain (FIBG_HUMAN)	gi|399492	55.8	8.5	8	134	18	^{170}HQLYIDETVNSNIPTNLR^{190} (59) ^{466}IRPFFPQQ^{481} (26)

pI indicates isoelectric point; MW, molecular weight; and NPM, number of peptides matched.

other lumican spot of ID637 was 65 kDa. Therefore, the former 2 spots and the latter one spot were concluded to correspond to the 80 kDa and 65 kDa bands in the 1D-Western blot, respectively.

We then compared the intensity of the 4 lumican bands between the AS-C and AS-N samples in each of the 6 patients. The 80 kDa- and 75 kDa-lumican bands showed significantly lower intensity in the AS-C samples than in the AS-N samples ($P = 0.01$, Figure 4B). The 65 kDa-lumican band also showed lower intensity in the AS-C samples than in the AS-N samples, although the difference did not meet statistical significance ($P = 0.07$, Figure 4B). On the other hand, the intensity of the 53 kDa-lumican band was not significantly different between the AS-C and AS-N samples ($P = 0.42$, Figure 4B). From these data, we concluded that the production of lumican with high MWs was decreased in the AS-C areas compared to the AS-N areas.

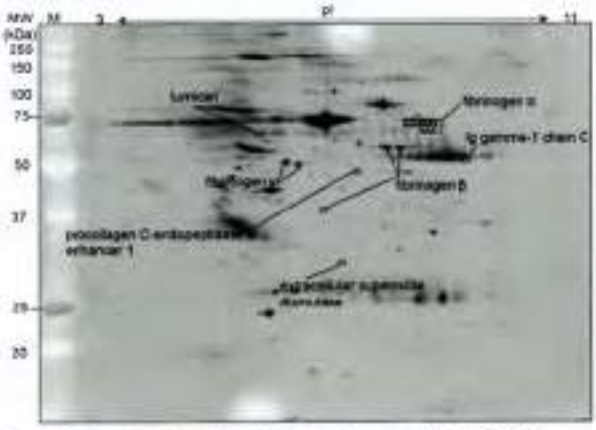

Figure 3. Location of the identified protein spots on the 2DE gel. 28 protein spots with more than 1.5-fold differences ($P < 0.05$) were subjected to protein identification by mass spectrometry. Proteins in 17 of the 28 spots were identified (Table III). The identified spots are circled with their protein names. MW indicates molecular weight; and M, MW markers.

We then investigated what modifications produced the 4 different lumican subtypes in aortic valves. Since lumican has been reported to possess glycosylation,[18-22] we examined whether these 4 lumican subtypes represented different glycosylations, using de-glycosylation with PNGase F. None of the 4 lumican bands (80 kDa, 75 kDa, 65 kDa, and 53 kDa) was detected after de-glycosylation, instead, a single band with approximately 40 kDa was newly detected in the 1D-Western blot (Figure 5A). Since the observed MW of the new band was very close to the theoretical MW of the lumican core protein (38.4 kDa, Table III), the 4 lumican subtypes (80 kDa, 75 kDa, 65 kDa, and 53 kDa) were concluded to possess different levels of glycosylation.

Interestingly, the intensity of the 40 kDa lumican band generated by de-glycosylation was not significantly different ($P = 0.62$) between the AS-C and AS-N samples (Figure 5B and 5C). This indicates that the production of the lumican core protein itself is not significantly different between the AS-C and AS-N areas. Taking these data together, we concluded that glycosylation of lumican was insufficient in the AS-C areas of AS aortic valves.

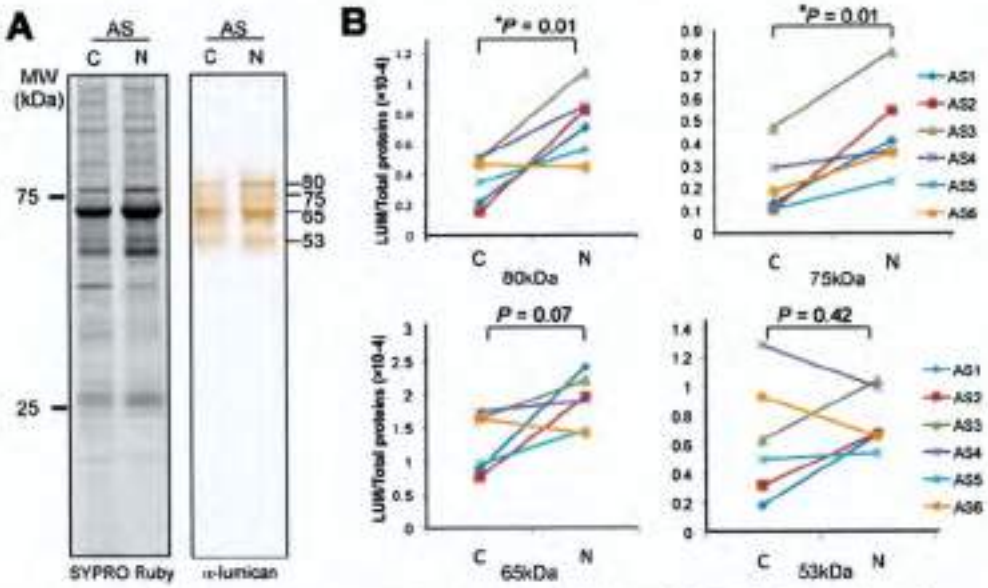

Figure 4. Comparison of lumican molecules between the AS-C and AS-N areas. **A:** The AS valve protein samples were separated by 15% SDS-PAGE and then stained with SYPRO Ruby to detect total protein. Next, the separated proteins were transferred onto membranes and lumican molecules were detected by Western blot. Results from a representative case of AS3 are shown. **B:** Four lumican bands (80 kDa, 75 kDa, 65 kDa, and 53 kDa) were detected in the Western blot. Intensity of these 4 lumican bands, corrected by the intensity of total protein detected by SYPRO Ruby (LUM/Total proteins), was compared between the AS-C and AS-N samples ($n = 6$). MW indicates molecular weight; C, AS-C; and N, AS-N.

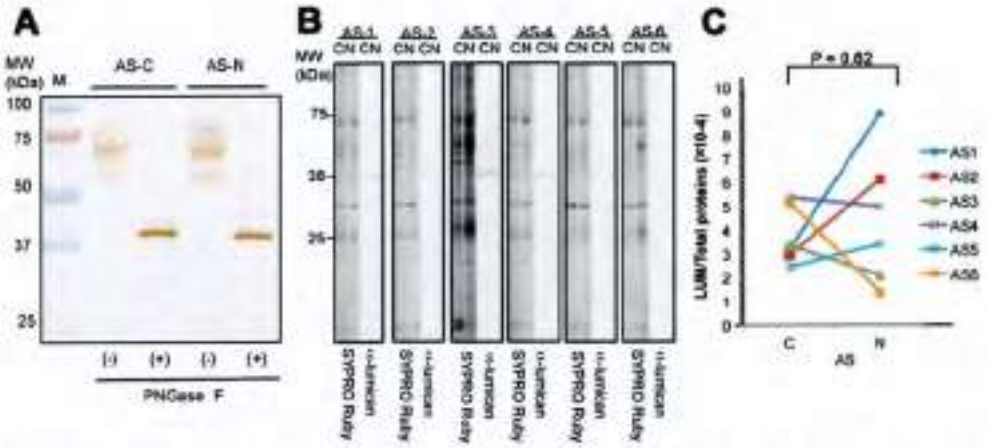

Figure 5. Comparison of de-glycosylated lumican molecules between the AS-C and AS-N areas. **A:** The AS-C and AS-N samples de-glycosylated by PNGase F and non-treated as a negative control were separated by 15% SDS-PAGE. The separated proteins were then transferred onto membranes and lumican molecules were detected by Western blot. Results from a representative case of AS3 are shown. **B:** De-glycosylated lumican was detected and compared between the AS-C and AS-N samples by same Western blot as A. **C:** Intensity of the de-glycosylated lumican bands, corrected by the intensity of total protein detected by SYPRO Ruby (LUM/Total proteins), was compared between the AS-C and AS-N samples ($n = 6$). MW indicates molecular weight; M, MW markers; C, AS-C; and N, AS-N.

Discussion

In this study, we compared protein profiles between the AS-C and AS-N samples of AS valves. Our findings are as follows: 1) 57 (8.5%) out of the detected 670 protein spots showed significantly different expression between the 2 areas. 2) Fibrinogen chains (10 spots) and lumican (3 spots) showed lower expression in the AS-C samples than in the AS-N samples. 3) The amounts of high MW lumican (glycan-rich lumican) were lower in the AS-C samples than in the AS-N samples, even though the amounts of the lumican core protein were not significantly different between the 2 samples.

Lumican, a member of small leucine-rich proteoglycans with KS-GAGs, shows wide distribution such as in cornea, heart valves, and brain.[18-21] Qin, *et al* reported 4 types of lumican with different MWs of 68 kDa, 62 kDa, 50 kDa, and 37 kDa in rat aortic smooth muscle cells, where 68 kDa-lumican and 62 kDa-lumican corresponded to proteoglycan forms, 50 kDa-lumican corresponded to a glycoprotein form without GAGs, and 37 kDa-lumican corresponded to the core protein alone.[22] Taking our data and theirs together, the 80 kDa-, 75 kDa-, and 65 kDa-lumican molecules detected here were thought to be proteoglycan forms and the 53 kDa-lumican was speculated to be a glycoprotein form without GAGs. The 40 kDa-lumican produced by de-glycosylation was thought to be the core protein form of lumican. Therefore, our data indicate that the amounts of KS-GAG-rich lumican with 80 kDa and 75 kDa are decreased in the AS-C samples compared to the AS-N samples in AS aortic valves.

Structurally, lumican plays a critical role in the formation and maintenance of collagen fibril architecture, interacting with fibrillar collagens.[15-17] Quite recently, mineral crystals have been suggested to nucleate and grow in the interior of the collagen fibers in the absence of surface events in calcified aortic valves.[23] This suggests the existence of impaired collagen architecture in AS valves. The decrease of KS-GAG-rich lumican detected here may be one of the causes of the impairment of collagen architecture.

The roles of inflammation in the pathogenesis of AS have been demonstrated.[24] Infiltration of macrophages as well as T cells and mast cells into AS valves has been reported.[7,25] Infiltrating macrophages have been reported to be involved in the calcification of aortic walls.[26] Interestingly, lumican has been reported to be involved in the recruitment of macrophages to inflammation sites.[27] Furthermore, lumican is also reported to be involved in the recruitment of neutrophils to inflammation sites,[28] possibly via binding to CXCL1.[29] These reports indicate critical roles for lumican in the recruitment of inflammatory cells. On this point, Funderburgh, *et al* reported the interesting finding that macrophages did not adhere to intact corneal KS proteoglycans, but attached to lumican core protein and spread rapidly on it after the removal of KS chains.[27] Thereby, the decrease of KS-GAG of the lumican molecule in the AS-C area detected here would promote adhesion of macrophages to aortic valve tissue. This may lead to the calcification of AS valves as a result of chronic inflammation. The roles of KS-GAG in the functions of lumican would be important and thus should be investigated in more detail in the future.

A previous study suggested that MMP-9 was involved in calcification of the aortic walls.[30] Furthermore, lumican-transfected pancreatic cancer cells were reported to secret 70 kDa lumican (KS-GAG-rich lumican) and to decrease the production of MMP-9.[31] Thus, the decrease of KS-GAG-rich lumican in the AS-C samples detected here may increase the production of MMP-9. This may in turn promote calcification of the aortic valves. Further studies are needed to clarify this point.

Lumican is one of 35 protein species that were reported to be more highly expressed in AS valves than in necropsy-derived normal control valves in a previous proteomic study.[1] Since we compared protein profiles within the same AS valves, our study did not provide information on the comparison of lumican expression between AS and normal valves. This point

would be a limitation of our study. On the other hand, considering that glycosylation is thought to play critical roles in the functions of lumican as described above, simple quantitative comparison would not be sufficient. Analyses of post-translational modifications including glycosylation as performed here would be of great importance.

With respect to fibrinogen, large amounts of fibrin were previously demonstrated within valve leaflets of patients with advanced AS.[32] An increase of fibrinogen gamma chains in AS aortic valves was also reported.[33] Impaired fibrinolysis in AS was suggested recently.[34] Here, among the identified 11 fibrinogen spots, 10 spots (6 alpha, 2 beta, and 2 gamma chains) showed lower intensity in the AS-C samples than in the AS-N samples. Considering the observed MWs of these fibrinogen spots, ie, 74-72 kDa for the alpha chain, 60 kDa for the gamma chain, and 51 kDa for the beta chain, these spots appeared to be mostly intact fibrin chains. Thereby, our data indicates that the thickened and calcified areas are rather resistant to fibrin deposition. The relationship between calcification and the deposition of fibrin should be investigated in detail in the future.

In conclusion, we here found that the amounts of KS-GAG-rich lumican were decreased in the thickened and calcified areas of AS aortic valves, compared to the non-thickened and non-calcified areas. The insufficient glycosylation of lumican may contribute to the development of AS, possibly via the impairment of collagen fibrils and promotion of inflammation.

Disclosure

Conflict of interest: None

References

1. Rose AG. Etiology of valvular heart disease. Curr Opin Cardiol 1996; 11: 98-113. (Review)
2. Mohler ER 3rd, Gannon F, Reynolds C, Zimmerman R, Keane MG, Kaplan FS. Bone formation and inflammation in cardiac valves. Circulation 2001; 103: 1522-8.
3. Newby DE, Cowell SJ, Boon NA. Emerging medical treatments for aortic stenosis: statins, angiotensin converting enzyme inhibitors, or both? Heart 2006; 92: 729-34. (Review)
4. Olszowska M. Pathogenesis and pathophysiology of aortic valve stenosis in adults. Pol Arch Med Wewn 2011; 121: 409-13. (Review. English, Polish)
5. Rabuş MB, Kayalar N, Sarıyüpoğlu B, Erkin A, Karali K, Yakut C. Hypercholesterolemia association with aortic stenosis of various etiologies. J Card Surg 2009; 24: 146-50.
6. O'Brien KD, Reichenbach DD, Marcovina SM, Kuusisto J, Alpers CE, Otto CM. Apolipoproteins B, (a), and E accumulate in the morphologically early lesion of 'degenerative' valvular aortic stenosis. Arterioscler Thromb Vasc Biol 1996; 16: 523-32.
7. Otto CM, Kuusisto J, Reichenbach DD, Gown AM, O'Brien KD. Characterization of the early lesion of 'degenerative' valvular aortic stenosis. Histological and immunohistochemical studies. Circulation 1994; 90: 844-53.
8. Miller JD, Weiss RM, Heistad DD. Calcific aortic valve stenosis: methods, models, and mechanisms. Circ Res 2011; 108: 1392-412. (Review)
9. Winchester R, Wiesendanger M, O'Brien W, *et al.* Circulating activated and effector memory T cells are associated with calcification and clonal expansions in bicuspid and tricuspid valves of calcific aortic stenosis. J Immunol 2011; 187: 1006-14.
10. Ando T, Nagai K, Chikada M, *et al.* Proteomic analyses of aortic wall in patients with abdominal aortic aneurysm. J Cardiovasc Surg (Torino) 2011; 52: 545-55.
11. Ando T, Iizuka N, Sato T, *et al.* Autoantigenicity of carbonic anhydrase 1 in patients with abdominal aortic aneurysm, revealed by proteomic surveillance. Hum Immunol 2013; 74: 852-7.
12. Gil-Dones F, Martin-Rojas T, López-Almodovar LF, *et al.* Development of an optimal protocol for the proteomic analysis of stenotic and healthy aortic valves. Rev Esp Cardiol 2010; 63: 46-53. (English, Spanish)
13. Martin-Rojas T, Gil-Dones F, Lopez-Almodovar LF, Padial LR, Vivanco F, Barderas MG. Proteomic profile of human aortic stenosis: insights into the degenerative process. J Proteome Res 2012; 11: 1537-50.
14. Matsuo K, Xiang Y, Nakamura H, *et al.* Identification of novel citrullinated autoantigens of synovium in rheumatoid arthritis using a proteomic approach. Arthritis Res Ther 2006; 8: R175.
15. Blochberger TC, Vergnes JP, Hempel J, Hassell JR. cDNA to chick lumican (corneal keratan sulfate proteoglycan) reveals homology to the small interstitial proteoglycan gene family and expression in muscle and intestine. J Biol Chem 1992; 267: 347-52.
16. Svensson L, Narlid I, Oldberg A. Fibromodulin and lumican bind to the same region on collagen type I fibrils. FEBS Lett 2000; 470: 178-82.
17. Chakravarti S, Petroll WM, Hassell JR, *et al.* Corneal opacity in lumican-null mice: defects in collagen fibril structure and packing in the posterior stroma. Invest Ophthalmol Vis Sci 2000; 41: 3365-73.
18. Embery G, Hall R, Waddington R, Septier D, Goldberg M. Proteoglycans in dentinogenesis. Crit Rev Oral Biol Med 2001; 12: 331-49. (Review)
19. Funderburgh JL, Caterson B, Conrad GW. Keratan sulfate proteoglycan during embryonic development of the chicken cornea. Dev Biol 1986; 116: 267-77.
20. Funderburgh JL, Funderburgh ML, Mann MM, Conrad GW. Arterial lumican. Properties of a corneal-type keratan sulfate proteoglycan from bovine aorta. J Biol Chem 1991; 266: 24773-7.
21. Cheng H, Caterson B, Neame PJ, Lester GE, Yamauchi M. Differential distribution of lumican and fibromodulin in tooth cementum. Connect Tissue Res 1996; 34: 87-96.
22. Qin H, Ishiwata T, Asano G. Effects of the extracellular matrix on lumican expression in rat aortic smooth muscle cells in vitro. J Pathol 2001; 195: 604-8.
23. Perrotta I, Davoli M. Collagen mineralization in human aortic valve stenosis: a field emission scanning electron microscopy and energy dispersive spectroscopy analysis. Ultrastruct Pathol 2014; 38: 281-4.
24. Dweck MR, Boon NA, Newby DE. Calcific aortic stenosis: a disease of the valve and the myocardium. J Am Coll Cardiol 2012; 60: 1854-63. (Review)
25. Wypasek E, Natorska J, Grudzień G, Filip G, Sadowski J, Undas A. Mast cells in human stenotic aortic valves are associated with the severity of stenosis. Inflammation 2013; 36: 449-56.
26. Otsuka F, Sakakura K, Yahagi K, Joner M, Virmani R. Has our understanding of calcification in human coronary atherosclerosis progressed? Arterioscler Thromb Vasc Biol 2014; 34: 724-36. (Review)
27. Funderburgh JL, Mitschler RR, Funderburgh ML, Roth MR, Chapes SK, Conrad GW. Macrophage receptors for lumican. A corneal keratan sulfate proteoglycan. Invest Ophthalmol Vis Sci 1997; 38: 1159-67.
28. Hayashi Y, Call MK, Chikama T, *et al.* Lumican is required for neutrophil extravasation following corneal injury and wound healing. J Cell Sci 2010; 123: 2987-95.
29. Carlson EC, Sun Y, Auletta J, *et al.* Regulation of corneal inflammation by neutrophil-dependent cleavage of keratan sulfate proteoglycans as a model for breakdown of the chemokine gradient. J Leukoc Biol 2010; 88: 517-22.
30. Chen NX, O'Neill KD, Chen X, Kiattisunthorn K, Gattone VH, Moe SM. Activation of arterial matrix metalloproteinases leads to vascular calcification in chronic kidney disease. Am J Nephrol

2011; 34: 211-9.
31. Yamamoto T, Matsuda Y, Kawahara K, Ishiwata T, Naito Z. Secreted 70kDa lumican stimulates growth and inhibits invasion of human pancreatic cancer. Cancer Lett 2012; 320: 31-9.
32. Natorska J, Marek G, Hlawaty M, Sadowski J, Tracz W, Undas A. Fibrin presence within aortic valves in patients with aortic stenosis: association with in vivo thrombin generation and fibrin clot properties. Thromb Haemost 2011; 105: 254-60.
33. Martin-Rojas T, Gil-Dones F, Lopez-Almodovar LF, Padial LR, Vivanco F, Barderas MG. Proteomic profile of human aortic stenosis: insights into the degenerative process. J Proteome Res 2012; 11: 1537-50.
34. Natorska J, Wypasek E, Grudzień G, Sadowski J, Undas A. Impaired fibrinolysis is associated with the severity of aortic stenosis in humans. J Thromb Haemost 2013; 11: 733-40.

Altered acetylation of proteins in patients with rheumatoid arthritis revealed by acetyl-proteomics

M. Arito[1], K. Nagai[2], S. Ooka[3], T. Sato[1], Y. Takakuwa[3], M.S. Kurokawa[4], T. Sase[5], K. Okamoto[1], N. Suematsu[1], T. Kato[1]

[1]Clinical Proteomics and Molecular Medicine, St. Marianna University Graduate School of Medicine, Kanagawa, Japan; [2]Department of Genetic Engineering, Kinki University, Wakayama, Japan; [3]Division of Rheumatology, Department of Internal Medicine, [4]Disease Biomarker Analysis and Molecular Regulation, and [5]Department of Neurosurgery, St. Marianna University Graduate School of Medicine, Kanagawa, Japan.

Abstract

Objective

Post-translational modifications (PTMs) are often critical for the function of proteins as well as antigenicity of proteins. We here tried to elucidate alteration of PTMs in Rheumatoid arthritis (RA), focusing on acetylation. We applied acetyl-proteomics to peripheral blood mononuclear cells (PBMCs) to elucidate PTM difference between patients with RA and healthy donors.

Methods

Proteins, extracted from peripheral blood mononuclear cells (PBMCs) of 7 RA patients and 7 healthy donors, were separated by 2-dimensional electrophoresis. Acetylation ratios of each protein spot were estimated by the combination of Sypro Ruby staining and anti-acetylated lysine antibodies. Proteins highly acetylated in the RA group were identified by mass spectrometry. Focusing on α-enolase (ENO1), one of the identified proteins, involvement of histone deacetylases (HDACs) in the high acetylation was investigated. Furthermore, the effects of acetylation on the activity of ENO1 were investigated.

Results

In PBMCs from the patients with RA, 29 acetylated protein spots were detected. One of highly acetylated proteins in the RA patients was identified as ENO1. The acetylation of ENO1 was found to be regulated in part by HDAC1. The enzymatic activity of ENO1 was up-regulated by acetylation.

Conclusion

Highly acetylated ENO1 may play roles in the pathophysiology of RA through the maintenance of activated lymphocytes by increasing glycolysis-derived energy supply.

Key words

rheumatoid arthritis, acetylation, proteomics

Mitsumi Arito, PhD
Kouhei Nagai, PhD
Sosuke Ooka, MD, PhD
Yoshiyuki Sato, PhD
Yukiko Takakuwa, MD, PhD
Manae S. Kurokawa, MD, PhD
Taigen Suzu, MD
Kazuki Okamoto, PhD
Naoya Suematsu, PhD
Tomohiro Kato, MD, PhD

Please address correspondence to: Tomohiro Kato, MD, PhD, Clinical Proteomics and Molecular Medicine, St. Marianna University Graduate School of Medicine, 2-16-1, Sugao, Miyamae, Kawasaki, Kanagawa 216-8512, Japan. E-mail: t3kato@marianna-u.ac.jp

Received on August 27, 2014; accepted in revised form on July 7, 2015.

© Copyright CLINICAL AND EXPERIMENTAL RHEUMATOLOGY 2015.

Funding: this work was supported by MEXT KAKENHI (Grant-in-Aid for Young Scientists (B)), grant no. 24790563
Competing interests: none declared.

Introduction

Rheumatoid arthritis (RA) is chronic polyarthritis of unknown cause, characterised by proliferation of synoviocytes and infiltration of inflammatory cells into expanded synovial tissue in affected joints (1-3). Although recent therapies with biologics, like anti TNF-α antibodies and soluble TNF α receptors, have been found successful (4-8), more specific therapies based on the pathogenesis of RA should be established in the future. Thus, better understanding of the pathogenesis of RA is needed.

In the pathogenesis of RA, the involvement of altered post-translational modifications (PTMs) has been reported. Specifically, abnormal citrullination is detected on synovial proteins and autoantibodies to the citrullinated proteins are generated. In fact, the detection of anti-citrullinated peptides antibodies has been widely used for the diagnosis of RA (9-11).

Another example of the altered PTM would be IgG molecules. IgG in patients with RA is reported to exhibit decreased galactosylation of its conservative N glycans (Asn-297) in the domains of its heavy chains (12). Similarly as the case of citrullination, autoantibodies to the agalactosyl IgG are frequently detected in RA, which are also used for the diagnosis of RA clinically (13).

Generally speaking, PTMs are often critical for the function of proteins as well as antigenicity of proteins. Thereby it is interesting whether such an aberrant PTM is limited to the citrullination and glycosylation in RA. We hypothesised that proteins in patients with RA possess various kinds of aberrant PTMs that might affect the pathophysiology of RA. Thereby, we here tried to elucidate alteration of PTM, focusing on acetylation.

The expression and activity of histone deacetylase (HDAC) 1 and HDAC2 in synovial tissue were reported to be lower in patients with RA than in patients with osteoarthritis and in healthy donors (14). Increased acetylation of histone proteins has been reported to be associated with the activation of NF-κB and activator protein 1, 2 major transcription factors involved in the pathogenesis of RA (14). Although the HDAC family catalyses the deacetylation of histone proteins (15), it also catalyses the deacetylation of non-histone proteins like p53 (16). This indicates the possibility that acetylation of other various proteins is also promoted in patients with RA. Thus, we here tried to detect proteins predominantly acetylated in peripheral blood mononuclear cells (PBMCs) from patients with RA, compared to PBMCs from healthy donors by proteomic analysis.

We first confirmed that the expression of HDAC1 and HDAC2 were decreased not only in synovial tissues but also in PBMCs of patients with RA compared to healthy donors. We then detected and identified several protein spots which were predominantly acetylated in the RA patients by 2-dimensional electrophoresis (2-DE), one of which was identified as α-Enolase (ENO1). Further, we found that the acetylation of ENO1 was regulated at least in part by HDAC1. Interestingly, the enzymatic activity of ENO1 was found up-regulated by acetylation. The enhanced acetylation of ENO1 may play roles in the pathophysiology of RA through the up-regulation of the ENO activity.

Materials and methods

PBMCs and serum samples

PBMCs were isolated by density-gradient centrifugation using Ficoll-Paque Plus (Pharmacia Biotech, Uppsala, Sweden) from blood samples of 7 patients with RA (7 female; mean age 56.7 years old [range 49–80]) and 7 healthy donors (7 female; mean age 56.5 years [range 42–74]). T cells and monocytes were isolated from PBMCs of 3 patients with RA (3 female; mean age 73.6 [range 68–74]) and 3 healthy donors (3 female; mean age 69.3 [range 63–80]). B cells were also isolated from PBMCs of 3 patients with RA (3 female; mean age 66.7 [range 41–89]) and the 3 healthy donors (3 female, mean age 69.3 [range 63–80]). Serum samples were obtained from 14 patients with RA (1 male; age 74 years, 12 female; mean age 53.4 years [range 38–77]). The patients were diagnosed according to the criteria of the disease (17). All the samples were obtained with written informed consent

and this study was approved by the institutional ethics committee of Ethics Committee of St. Marianna University Graduate School of Medicine. Proteins were extracted into a lysis buffer (7M urea, 2M thiourea, 4% CHAPS) from each of the PBMC samples. 2-DE was performed as described previously (18, 19). 100 μg of the extracted protein samples were loaded onto 13 cm drystrips (Immobiline, pH range of 3-11, GE Healthcare, Buckinghamshire, UK) and the drystrips were kept at 20 degrees centigrade for 12 hours. Then isoelectric focusing was performed using Ettan IPGphor (GE Healthcare). The proteins separated by the isoelectric focusing were further separated by 12.5% sodium dodecyl sulfate polyacrylamide gel electrophoresis (SDS-PAGE). The separated proteins, stained with SYPRO Ruby Protein Gel Stain (GE Healthcare) to detect total proteins, were transferred onto a polyvinylidene difluoride (PVDF) membrane (Millipore, Massachusetts, USA). The membrane was subjected to western blot with anti-acetylated lysine polyclonal antibodies (Abcam, Cambridge, UK) to detect acetylated proteins. Intensity of the protein spots were measured by an image analyser (Typhoon 9400, GE Healthcare). Intensity of acetylation of the protein spots was measured by LAS-3000 Luminolimager (FUJIFILM, Tokyo, Japan).

Isolation of T cells, B cells, and monocytes from PBMCs

T cells, B cells, and monocytes were isolated from PBMCs using EasySep™ NEGATIVE SELECTION Human T Cell Enrichment Kit, Human B Cell Enrichment Kit, and Human Monocyte Enrichment Kit (STEMCELL Technologies Inc., Vancouver, Canada), according to the manufacturer's instructions.

Mass spectrometric analysis

Interest spots excised from the SYPRO Ruby-stained 2-DE gels were digested by trypsin as described previously (20). The obtained peptides were analysed using a MALDI-TOF/TOF mass spectrometer (Ultraflex, Bruker Daltonics, Ettlingen, Germany). For the MALDI-TOF/TOF analysis, a 1 μl aliquot was spotted onto a MALDI target plate using a μ-C18 Zip-Tip (Millipore, Billerica, MA) for desalting and concentration. MS spectra (m/z 500-4,400) were acquired in the positive ion mode. The peptides were fragmented by the laser induced dissociation (LID) for MS/MS analysis. Peak lists were generated by Flex Analysis (v. 2.2). Database searching was performed with Mascot (v. 1.0) against the human Swiss Prot protein database (v. 56.7) using the following search parameters: trypsin was selected with 1 missed cleavage, mass tolerance of 100 ppm for MS and 1.0 Da for MS/MS, N-terminal acetylation, lysine acetylation, cysteine carbamidomethylation, and methionine oxidation were set as variable modifications. The acquired MS/MS data were used for peptide identification using a searching program of Mascot MS/MS Ion search (Matrix Science, London, UK) against the human Swiss Prot protein database. Peptide identifications were accepted when the Mascot search results delivered the significant MOWSE scores ($p<0.05$). Peptides with PTM were identified using the Mascot error tolerant search (21).

Cell culture

PBMCs were isolated from the blood samples as described above. The isolated PBMCs were cultured in RPMI1640 (Invitrogen/GIBCO, Carlsbad, CA). These media containing 100 units/ml penicillin and 100 μg/ml streptomycin (Sigma Aldrich), were supplemented with 10% fetal bovine serum (Wako Pure Chemical Industries, Osaka, Japan). The cells were cultured at 37 degrees centigrade in 5% CO_2.

Expression vectors and transfection

The pcDNA3.1-HA-HDAC1 and pcDNA3.1-HA-HDAC2 expression vectors were constructed in our laboratory. These vectors as well as pcDNA3.1 as a negative control vector were used for transfection of PBMCs using Lipofectamine LTX (Invitrogen), according to the manufacturer's instructions.

Western blot

Anti-acetyl lysine and anti-ENO1 polyclonal antibodies (Abcam and LifeSpan Biosciences, Seattle, WA, USA, respectively) were used as the 1st antibodies and HRP-conjugated rabbit anti-mouse IgG antibodies (Invitrogen/Zymed) were used as the 2nd antibody. The bound antibodies were visualised using an enhanced chemiluminescence detection system (GE healthcare).

Analysis of acetylated sites

Peptides were extracted from the ENO1 spot after in-gel digestion by trypsin. Then the extracted peptide solution was diluted at 1:5 with ice-cold 0.1% trifluoroacetic acid (TFA) solution. Then the peptides were analysed using a nano-HPLC system (1200 Series; Agilent Technologies Inc., PaloAlto, CA, USA), connected to the HCT Ultra ion trap mass spectrometer (Bruker Daltonics). The ZORBAX 300SB-C18 trap column (length: 5mm, inside diameter: 300μm, particle diameter: 5μm, pore diameter: 300 ångström, Agilent Technologies) was used to concentrate and desalt the injected samples. Chromatographic separation of the peptides was carried out using the ZORBAX™ 300SB-C18 analytical column (length: 150mm, inside diameter: 100μm, particle diameter: 3.5μm, pore diameter: 300 ångström, Agilent Technologies). Sample elution through the analytical column was obtained at a flow rate of 300 nl/min by starting the following gradient: 0–60% solvent B for 75 min; a step with 80% solvent B for 5 min; and a step with 95% solvent A for 15 min. Solvent A was water containing 0.1% formic acid and solvent B was acetonitrile containing 0.1% formic acid. The mass spectrometer was operated in the positive ion mode with a maximum accumulation time of 200ms in an m/z range of 350–3000. From a single MS spectrum, the three most intense peaks were selected for MS/MS analysis with an absolute threshold of 10000 and an active ion precursor exclusion after two MS/MS spectra for 0.5 min. The peptides were fragmented in the CID mode. Fragmentation parameters were as follows: width 4.0 m/z and time of fragmentation 200 ms.

The MS/MS data of the peptides, acquired by the ESI-ion trap mass spectrometer, were used for acetylated peptide identification using a search-

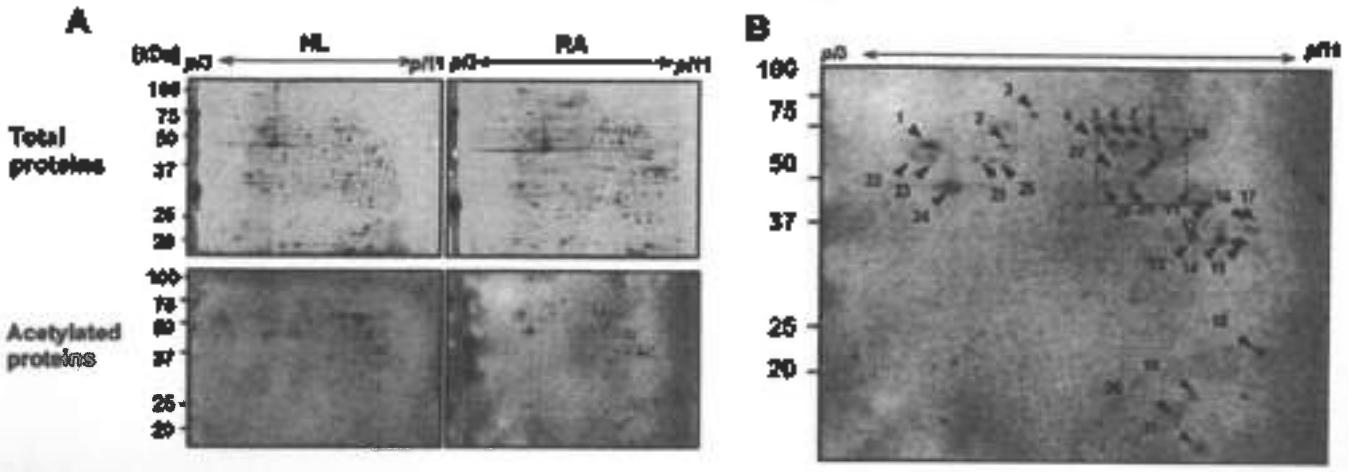

Fig. 1. Detection of total or acetylated proteins in PBMCs from patients with RA and healthy donors.
A. Proteins extracted from PBMCs were separated by 2-DE. The separated proteins, stained with SYPRO Ruby®, were transferred onto PVDF membranes (upper panels) and then were reacted to anti-acetylated lysine polyclonal antibodies (lower panels). Representative results from HL4 and RA6 are shown. B. In total, 29 acetylated protein spots were detected in the RA group. The 29 acetylated protein spots were indicated by arrow heads in the enlarged image of the right lower panel of Fig. 1A (RA6). HL: healthy

ing program of the Mascot MS/MS ion search against the Swiss Prot human protein sequence database. Peptide tolerance for precursor ions was set at 0.5Da. MS/MS tolerance for fragment ions was set at 1.0Da. Variable modifications such as acetylation of lysine and carbamidomethylation and oxidation of methionine were taken into consideration. Peptide identification was accepted when the Mascot search results delivered significant MOWSE scores ($p<0.05$).

In vitro acetylation

In vitro acetylation was performed as described previously (22). GST-ENO1 (Abnova) were incubated with acetyl co enzyme A (Sigma) and 0.2 μg of p300 in 50 μl of an acetylation buffer containing 50 mM Tris (pH 8.0), 5% glycerol, 0.1 mM EDTA, 50 mM KCl, 1 mM DTT, and 1 mM PMSF. The acetylation reaction was performed at 30°C for 1 hour.

Measurement of the ENO1 enzymatic activity

The enzymatic activity of ENO1 was measured using the conversion of sodium 2-phospho-glycerate to phosphoenolpyruvate, as described previously (23, 24).

Statistical analysis

All the statistical significance was calculated by Student's *t*-test. All the tests were two-tailed.

Results

Identification of proteins highly acetylated in RA

First, we compared acetylated protein profiles of PBMCs between RA and healthy groups. Specifically, proteins extracted from PBMCs of 7 RA patients and 7 healthy donors were separated by 2-DE. The separated proteins, labelled with SYPRO Ruby®, were transferred onto PVDF membranes. Representative results are shown in the upper panels of Fig. 1A. Then acetylated proteins were detected by anti-acetylated lysine antibodies, as representative results are shown in the lower panels of Fig. 1A. In the both RA and healthy cases, only a small part of the separated proteins were found acetylated. In the RA and healthy groups, we detected 29 acetylated protein spots in total (Fig. 1B).

Next, acetylation levels of the 29 protein spots were compared between the RA and healthy groups. Specifically, we compared the frequency of positive acetylation for each of the 29 acetylated protein spots in the RA and healthy groups (Table I). Interestingly, spot no.28 and no.29 were acetylated only in the RA group and the difference of the frequency was statistically significant. Further, we compared acetylation levels corrected by the spot intensity on the SYPRO Ruby®-stained gel image in each spot between the RA and healthy groups. This comparison revealed that spots no. 9 and no. 27 were acetylated more strongly in the RA group than in the healthy group with statistical significance (Table I). On the other hand, there was no spot that showed higher acetylation in the healthy group than in the RA group. There was also no spot that was acetylated only in the healthy group (Table I). We thus selected these 4 spots of nos. 9, 27, 28, and 29 for identification. The location and the corrected acetylation intensity of the 4 spots are shown in Fig. 2A and 2B, respectively.

We successfully identified all the 4 protein spots by mass spectrometry and protein database searching. Both of the spots no. 9 and no. 27 were identified as ENO1 and both of the spots no. 28 and no. 29 were identified as isocitrate dehydrogenase 1 (IDH1) (Table II).

Expression of ENO1 in PBMCs from the patients with RA

From the above experiments, ENO1, one of the glycolytic enzymes, was found to be highly acetylated in RA. We then asked whether the total amount of ENO1 was increased or not in the RA patients. Western blot with anti-ENO1 antibodies revealed that the total amount of ENO1 was found similar to each other between the RA and healthy groups (Fig. 3A, left). This indicates the increased ratio of the acetylated ENO1 to the total ENO1 in PBMCs from the patient with RA.

Table I. Comparison of the frequency of detection and the relative acetylation levels of acetylated protein spots between the RA and healthy groups.

Spot no	The frequency of detection (%)		The normalised intensity
	HL	RA	
1	100 (7/7)	100 (7/7)	1.05
2	71 (5/7)	71 (5/7)	1.14
3	86 (6/7)	100 (7/7)	1.06
4	86 (6/7)	100 (7/7)	1.00
5	86 (6/7)	100 (7/7)	1.41
6	86 (6/7)	100 (7/7)	1.40
7	71 (5/7)	71 (5/7)	1.22
8	57 (4/7)	43 (3/7)	0.83
9	100 (7/7)	100 (7/7)	3.19**
10	71 (5/7)	57 (4/7)	1.11
11	29 (2/7)	43 (3/7)	1.15
12	100 (7/7)	100 (7/7)	1.06
13	100 (7/7)	100 (7/7)	1.01
14	100 (7/7)	100 (7/7)	1.21
15	100 (7/7)	100 (7/7)	1.15
16	100 (7/7)	86 (6/7)	1.30
17	14 (1/7)	14 (1/7)	1.10
18	29 (2/7)	14 (1/7)	0.95
19	43 (3/7)	29 (2/7)	1.11
20	29 (2/7)	43 (3/7)	1.05
21	43 (3/7)	29 (2/7)	1.31
22	86 (6/7)	100 (7/7)	1.11
23	86 (6/7)	100 (7/7)	1.22
24	100 (7/7)	100 (7/7)	1.03
25	71 (5/7)	86 (6/7)	1.22
26	71 (5/7)	86 (6/7)	1.21
27	14 (1/7)	71 (5/7)	4.51*
28	0 (0/7)	86 (6/7)	-
29	0 (0/7)	86 (6/7)	

HL: healthy, RA: rheumatoid arthritis, * $p<0.05$ ** $p<0.01$.

The regulation of deacetylation of ENO1 by HDAC1 in human PBMCs

Recently, Huber *et al.* reported that the expression and activity of both HDAC1 and HDAC2 in synovial tissue was lower in patients with RA than in patients with osteoarthritis and healthy donors (14). The HDAC family was reported to catalyse the deacetylation of histone proteins (15). However, HDACs were reported to deacetylate several non-histone proteins like p53 (16). This indicates the possibility that HDACs are also involved in the increased acetylation of ENO1 in PBMCs from the patient with RA. Thereby, we first investigated the expression of HDAC1 and HDAC2 in PBMCs from the patients with RA and healthy donors. As a result, the protein levels of HDAC1 and HDAC2 were lower in PBMCs from the patients with RA than in those from the healthy donors, like the previous reports on synovial tissue (Fig. 3A, middle and right). Next, to examine the involvement of HDACs in the acetylation of ENO1, we treated the cells from the healthy donors with trichostatin A (TSA) of an HDAC family inhibitor (25) and then measured the degree of

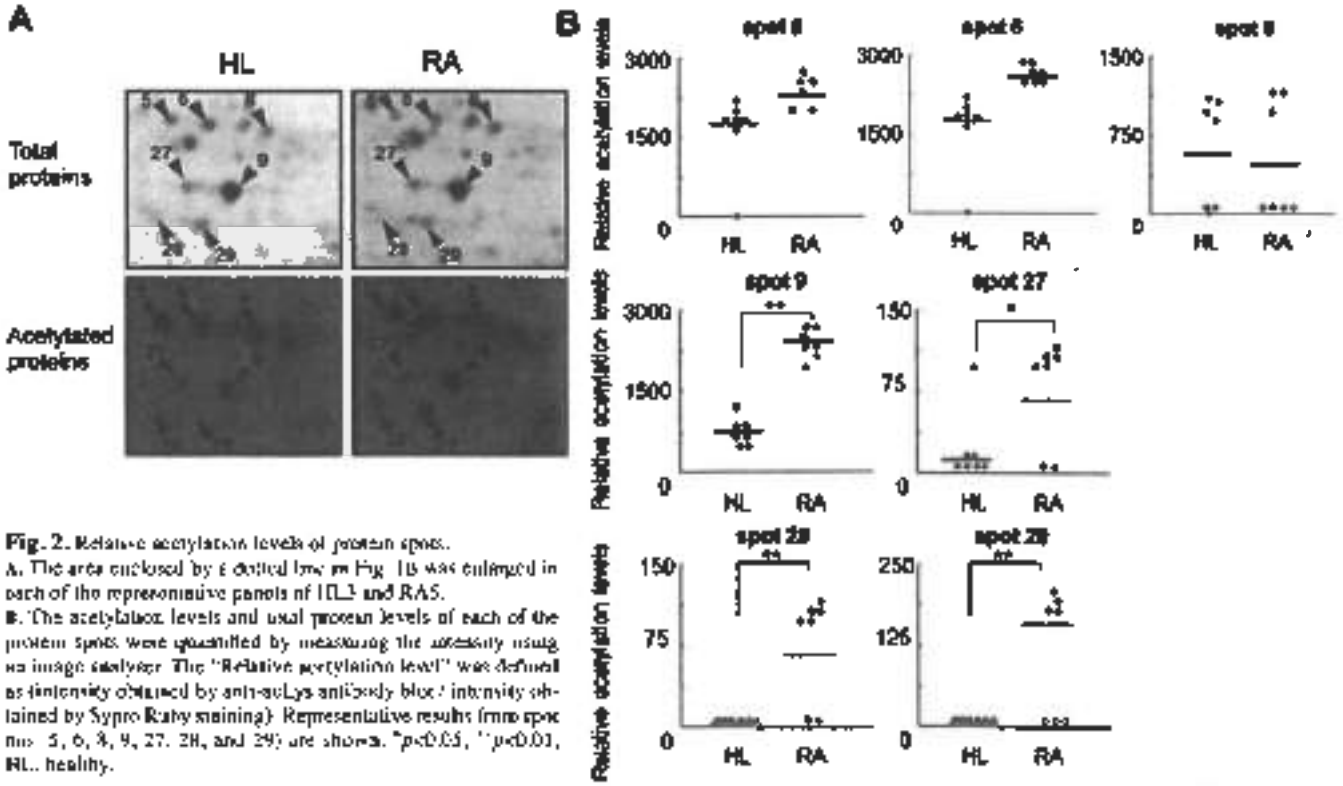

Fig. 2. Relative acetylation levels of protein spots.
A. The area enclosed by a dotted line in Fig. 1B was enlarged in each of the representative panels of HL3 and RA5.
B. The acetylation levels and total protein levels of each of the protein spots were quantified by measuring the intensity using an image analyzer. The "Relative acetylation level" was defined as (intensity obtained by anti-acLys antibody blot / intensity obtained by Sypro Ruby staining). Representative results from spot no. 5, 6, 8, 9, 27, 28, and 29 are shown. *$p<0.05$, **$p<0.01$, HL: healthy.

Table II. Identified highly acetylated proteins in RA.

Spot no	Observed M.W./pI	Protein name	Accession ID (Accession NO.)	Calculated M.W. (kDa/pI)	Matched / Searched	Seq. Cov (%)	Score	Sequence confirmed by LID (Mascot ion score)
9	47/8.2	α-enolase	ENOA_HUMAN (gi|6507965)	47.1/7.0	26/61	52	392	[12]AAVPSGASTGIYEALELR[29] (99) [30]VVIGMDVAASEFFR[43] (56) [201]YISPDQLADLYK[211] (54)
27	47/8.0	α-enolase	ENOA_HUMAN (gi|6507965)	47.1/7.0	20/68	46	135	[19]GNPTVEVDLFTSK[31] (52) [12]AAVPSGASTGIYEALELR[29] (75) [30]VVIGMDVAASEFFR[43] (64) [201]YISPDQLADLYK[211] (68)
28	50/7.9	isocitrate dehydrogenase	IDHC_HUMAN (gi|28178824)	46.6/6.5	27/61	68	280	[227]FKDIIQEIYDK[237] (35)
29	50/8.1	isocitrate dehydrogenase	IDHC_HUMAN (gi|28178824)	46.6/6.5	26/69	68	147	[91]NIIGGTVFR[99] (43) [195]SDYLNTFEFMDK[206] (15)

Acetylation levels of protein spots were compared between the RA and healthy groups. By matching the western blot image and the Sypro Ruby image, we identified the location of the highly acetylated protein spots on the 2D gel. Then the proteins, digested with trypsin in the gel, were identified by MALDI-TOF/TOF mass spectrometry. M.W.: molecular weight, Seq. Cov.: sequence coverage, LID, laser-induced dissociation, M: Oxidised methionine, C: carbamidomethylated cysteine.

acetylation of ENO1 by western blot. As a result, the acetylation of ENO1 was found significantly increased by the treatment with TSA (Fig. 3B). This indicates that the acetylation of ENO1 is regulated by HDACs. Again, the expression of HDAC1 and HDAC2 in PBMCs was lower in the patients with RA than in the healthy donors. Thus, to further clarify which of HDAC1 and HDAC2 was involved in the deacetylation of ENO1, HDAC1 with a tag of HA (HA-HDAC1) and HDAC2 with a tag of HA (HA-HDAC2) were respectively over expressed in PBMCs from the patients with RA and then the acetylation degree of ENO1 was measured by western blot. As a result, the acetylation of ENO1 was significantly down-regulated by the over-expression of HDAC1, but not by that of HDAC2 (Fig. 3C). In an additional experiment using PBMCs from a healthy donor, TSA treatment up-regulated the ENO1 acetylation, but did not up-regulate it when HDAC1 was knocked down (data not shown). Collectively, among the HDAC family, HDAC1 is thought to be mainly involved in the regulation of ENO1 acetylation.

Identification of the acetylation sites of ENO1

Since no study has been reported on the acetylation sites of ENO1, it was structurally interesting to identify which lysine residues in ENO1 were acetylated. We thus tried to identify the acetylation sites of the spot no.9 of ENO1, by nanoLC-CID-MS/MS, although ENO1 contained as many as 38 lysine residues. As a result, we found that 3 lysine residues (K120, K126, and K256) of ENO1 were acetylated in the healthy samples (Fig. 3D). In the RA samples, peptides containing the 3 lysine residues were detected but the 3 lysine residues were not acetylated (data not shown). Including these 3 lysine residues, mass spectrometric analysis failed to identify acetylated lysine residues in the RA samples. Again ENO1 possesses 38 lysine residues in total. However, no information has been obtained on more than half of the 38 lysine residues of ENO1 in spite of the extensive analysis (data not shown).

Acetylation levels of ENO1 in T cells, B cells, and monocytes

We then investigated which subsets of PBMCs, T cells, B cells, and monocytes, showed the high ENO1 acetylation. Using pooled lysates of T cells, B cells, and monocytes isolated from PBMCs of 3 patients with RA and 3 healthy donors, we investigated acetylation levels similarly as above. As a result, in the T cells, the acetylated level of ENO1 was higher in the RA sample than in the healthy sample (1.76-fold, Fig. 3E). In contrast, in the B cells and monocytes, the acetylated levels of ENO1 were found similar to each other between the RA and healthy samples (0.91- and 0.84-fold, respectively, Fig. 3E). This data indicates that acetylation of ENO1 was specifically up-regulated in T cells.

The effect of acetylation on the enzymatic activity of ENO1

Next, we examined the effect of acetylation on the function of ENO1. ENO1 catalyses the generation of phosphoenolpyruvic acid from 2-phosphoglyceric acid. Thus, we measured this activity of non-acetylated ENO1 and acetylated ENO1. The acetylated ENO1 was prepared by *in vitro* acetylation of bacterially expressed ENO1, after which the acetylation of ENO1 was confirmed by western blot using anti-acetylated lysine antibodies (Fig. 4A). As a result, the enzymatic activity of the acetylated ENO1 was found significantly higher than the non-acetylated ENO1 (Fig. 4B). This indicates that acetylation up-regulates the enzymatic activity of ENO1.

The effect of acetylation on the antigenicity of ENO1

Finally, we examined whether acetylation affect the antigenicity of ENO1 in patients with RA, since another PTM of citrullination was evidenced to contribute to the acquirement of antigenicity in RA. Specifically, we first checked whether RA serum samples reacted to the acetylated ENO1 or not. We found that 5 out of the tested 14 RA

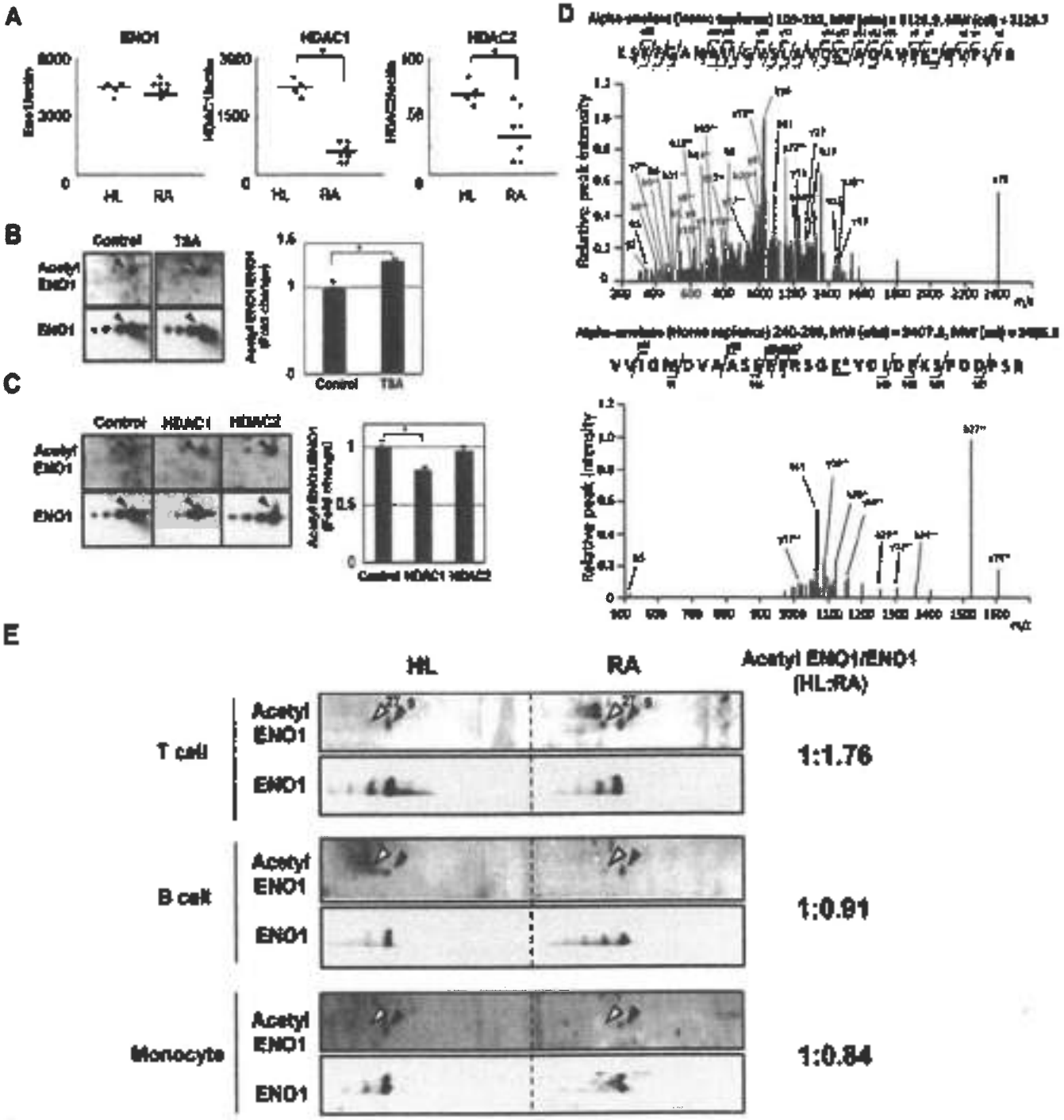

Fig. 3. Effect of HDACs on the acetylation of ENO1.

A. Proteins extracted from PBMCs of 7 patients with RA and 4 healthy donors were separated by 1-DE. The separated proteins were transferred onto PVDF membranes and each membrane was subjected to western blot with anti-ENO1 polyclonal antibodies, anti-HDAC1 polyclonal antibodies, anti-HDAC2 polyclonal antibodies, or anti-α-actin monoclonal antibodies. The relative intensity of ENO1, HDAC1 and HDAC2, corrected by that of α-actin, are shown (ENO1/actin, HDAC1/actin, and HDAC2/actin).

B and C. PBMCs of 3 healthy donors were incubated with 300nM TSA for 24 hours (B) and PBMCs of 3 patients with RA, transfected with expression plasmids for HA-HDAC1 and HA-HDAC2 or HA alone, were incubated for 24 hours (C). Each of the whole cell extracts was subjected to 2-DE and western blot with the anti-acetylated lysine polyclonal antibodies and with anti-ENO1 polyclonal antibodies. Representative images of the western blot are shown in the left. Acetylation levels and total protein levels of ENO1 were quantified as described in Fig. 2B. Then the acetylation levels of ENO1 were corrected by the total protein levels of ENO1 (Acetyl ENO1/ENO1 (Fold change)). The relative intensity averages of "control" were defined as 1. *$p<0.05$, **$p<0.01$

D. ENO1 peptides from spot no. 9 were subjected to nano LC-ESI-MS/MS analysis. The MS/MS spectrum of acetylated peptides are shown. K*: acetylated lysine, M*: oxidized methionine, HL: healthy (E) T cells, B cells, and monocytes were isolated from PBMCs of 3 patients with RA and 3 healthy donors. The pooled lysates of T cell, B cell and monocyte were subjected to 2-DE and western blot with the anti-acetylated lysine polyclonal antibodies and with anti-ENO1 polyclonal antibodies. Acetylation levels and total protein levels of ENO1 were quantified as described in Fig. 2B. The acetylation levels of ENO1, corrected by the total protein levels of ENO1, are shown (Acetyl ENO1/ENO1)

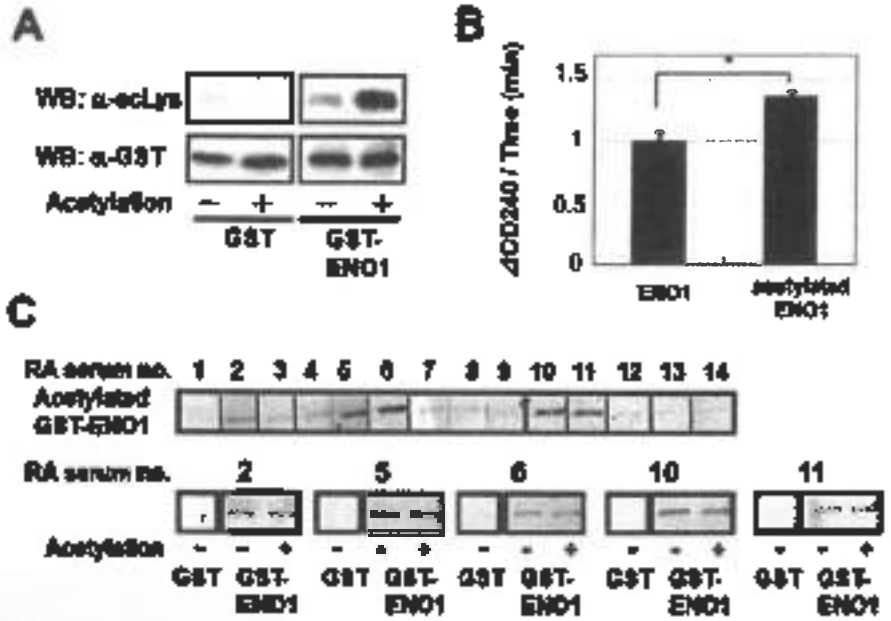

Fig. 4. The effect of the acetylation on the enzymatic activity of ENO1

A. GST and GST-ENO1 were acetylated *in vitro* by p300 of histone acetyltransferase. Acetylated GST-ENO1 and GST and non-acetylated ones were subjected to western blot with the anti-acetyl lysine polyclonal antibodies (WB: α-acLys) and anti-GST polyclonal antibodies (WB: α-GST).

B. The enzymatic activity of non-acetylated ENO1 and acetylated ENO1 were evaluated by the absorbance of phosphoenolpyruvic acid (wave length=230nm). *p<0.05

C. Recombinant acetylated GST-ENO1 was subjected to western blot with 14 RA serum samples (nos. 1~14) (upper panel). Non-acetylated GST, non-acetylated GST-ENO1, and acetylated GST-ENO1 were subjected to western blot with 5 RA serum samples (nos. 2, 5, 6, 10, 11) that positively reacted to the acetylated GST-ENO1 (lower panel). WB; Western blot.

serum samples reacted to the acetylated ENO1 (Fig. 4C upper panel). We then compared the reactivity of the 5 serum sample to the non-acetylated ENO1 and the acetylated ENO1. As a result, the reactivity was not different between the acetylated ENO1 and the non-acetylated ENO1. Thus, we concluded that the acetylation did not contribute to the antigenicity of ENO1 in RA, although autoantibodies to ENO1 were generated in a part of patients with RA.

Discussion

We here tried to elucidate altered PTMs focusing on proteins acetylation in PBMCs of patients with RA by proteomic analysis. We selected PBMCs as a subject, since PBMCs would reflect the immune condition of RA, one of the autoimmune diseases (26). Further, PBMCs are suitable materials when the acetylation detected here is used as a medical examination in the near future.

Our findings are as follows; 1) multiple proteins in PBMCs were highly acetylated in the RA groups compared to the healthy groups. 2) ENO1 and IDH1 were identified as protein spots highly acetylated in RA. 3) Acetylation of ENO1 was regulated in part by HDAC1. 4) The expression of HDAC1 and HDAC2 was decreased in PBMCs in RA. 5) Three lysine residues (K120, K126, and K256) of ENO1 were acetylated in the healthy samples. 6) Acetylation up-regulated the enzymatic activity of ENO1. 7) The acetylation level of ENO1 was high specifically in T cells in RA. In addition, 8) Acetylation did not affect the antigenicity of ENO1.

On the first and second points, altered acetylation was found in PBMCs of the RA patients. Previously, over-citrullination of proteins and galactose deficiency of IgG were reported as characteristics of RA (8-12). Combining these facts with our data, RA would possess a wide range of PTM dysregulation. The amount of ENO1 in PBMCs of the RA group was similar to that of the healthy group (Fig. 3A). The amount of ENO1 was not changed by the incubation with TSA of a HDAC inhibitor (Fig. 3B and C). These data indicate that acetylation would not affect the stability of ENO1, even though acetylation is known to often alter the stability of proteins (27).

On the third point, the overexpression of HDAC1 decreased the acetylation of ENO1, however, ENO1 was still acetylated at a lower level (Fig. 3C). This indicates that other deacetylases participate in the deacetylation of ENO1. Alternatively, it is possible that activities of acetyltransferases remained in the cells, by which a certain level of acetylation was observed. Such deacetylases and acetyltransferases should be investigated in the future.

On the fourth point, recently, the expression and activity of the HDAC family was reported to be involved in the pathogenesis of RA recently (14, 28-29). However, the results were controversial. It has been reported that TSA, which inhibits the HDAC family, suppressed IL-6 production in fibroblast-like synoviocytes and macrophages by accelerating decay of IL-6 mRNA in RA (28). Furthermore it has been reported that an HDAC3-selective inhibitor reduced IL-6 production in PBMCs of RA patients (29). Thus, acetylation increased by the inhibition of HDACs, in particular, HDAC3, appeared to have anti-inflammatory roles. On the other hand, the expression and activity of HDAC1 and HDAC2 in synovial tissue were reported to be lower in RA than in osteoarthritis and in the healthy condition (14). We here showed that the expression of HDAC1 and HDAC2 in PBMCs was also lower in RA than in the healthy condition. Thus, the ENO1 acetylation increased by the decreased HDAC1 expression may participate in the inflammation of RA. Alternatively, the expression of HDAC1 and HDAC2 may result in compensatory decrease to suppress the inflammation of RA. This point should be investigated in the future.

On the fifth point, to identify acetylated lysine residues, we performed mass spectrometric analysis extensively using MALDI-TOF/TOF and nanoLC-CID-MS/MS, by which we identified in total 3 acetylated lysine residues from the healthy samples. In the RA samples, peptides containing these 3 lysine residues were detected, but the 3 lysine residues were not acetylated. ENO1 possesses 38 lysine residues

in total. However, no information has been obtained on more than half of the 38 lysine residues in spite of the extensive analysis. This would be technical limitation of mass spectrometric analysis at present. Some of the remaining undetected lysine residues would possess acetylation in the RA samples. In the future, it would be needed to establish more effective methods to identify acetylated lysine residues.

On the sixth and seventh point, ENO1, one of the glycolytic enzymes, converts 2-phosphoglycerric acid to phosphoenolpyruvic acid. Our data indicates that acetylation up-regulates the enzymatic activity of ENO1 and that ENO1 is highly acetylated in the patients with RA. Thus, the enzymatic activity of ENO1 would be higher in RA than in the healthy condition in PBMCs, in particular, in T cells. Activated T cells are known to induce production of various inflammatory cytokines in RA (30) and abatacept of a T cell co-stimulation blocker has been shown to be very effective in the treatment of RA (30), indicating critical roles of T cells in the pathology of RA. The supposed high activity of ENO1 would support the activation of T cells in RA, providing much energy through glycolysis. It was reported that acetylation played roles in the intracellular transfer of proteins (31). Thereby, we investigated the effect of acetylation on ENO1 from this viewpoint. ENO1 was localised in not only cytosol but also nuclei. We thus compared the ratios of acetylated ENO1 to the total ENO1 between nuclei and cytosol, however, the ratios were similar to each other in PBMCs (data not shown). Therefore, we concluded that acetylation did not affect the localisation of ENO1.

A recent study reported other new functions of ENO1. In inflamed lung, ENO1 binds with plasminogen at the cell surface and promotes the production of local plasmin, one of the inflammatory agents, and invasion of inflammatory cells are mediated by increased cell-surface expression of ENO1 (32). Further, ENO1 that was expressed on the surfaces of monocytes and macrophages induces synovial inflammation in RA (33). The relation between the high acetylation of ENO1 and the inflammatory process in RA should be investigated in the future.

On the eighth point, it is well known that citrullinated proteins are highly antigenic in RA. In the case of acetylation, the anti-ENO1 positive RA serum samples reacted to acetylated ENO1 and non-acetylated one at similar levels. Thus, acetylation would not contribute to the antigenicity of ENO1. Recently the affinity interaction between DEK and anti-DEK autoantibodies has been reported to be enhanced by acetylation of DEK in juvenile idiopathic arthritis (34). Thus, alteration of antigenicity by acetylation appears to depend on property of each protein.

Besides ENO1 (spot nos. 9 and 27), we identified IDH1 from the other 2 protein spots (spot nos. 28 and 29) that were highly acetylated in RA. IDH1 converts isocitrate to α-ketoglutarate in the citric acid cycle (35). IDH possesses 3 isotypes of IDH1, 2, and 3. IDH2, which shows about 70% homology with IDH1, was reported to be deacetylated by class III HDAC (36, 37). This indicates that IDH1 might be acetylated similarly as IDH2. In our data, IDH1 (spot nos. 28 and 29) was highly acetylated in the RA samples, but was little acetylated in the healthy condition. Therefore, the acetylated IDH1 may be a new candidate biomarker for RA.

In conclusion, highly acetylated ENO1 may play roles in the pathophysiology of RA through the maintenance of activated lymphocytes by increasing energy supply by glycolysis.

Acknowledgements

The authors thank Ms M. Konke, Ms K.M. Yokoyama, and Ms J. Asano for their excellent technical assistance.

References

1. ARNETT FC, EDWORTHY SM, BLOCH DA *et al.*: The American Rheumatism Association 1987 revised criteria for the classification of rheumatoid arthritis. *Arthritis Rheum* 1988; 31: 315-24.
2. BUCHELER C: Fibroblast biology. Effector signals released by the synovial fibroblast in arthritis. *Arthritis Res* 2000; 2: 356-60.
3. MUELLER-LADNER U, KRIEGSMANN J, FRANKLIN BN *et al.*: Synovial fibroblasts of patients with rheumatoid arthritis attach to and invade normal human cartilage when engrafted into SCID mice. *Am J Pathol* 1996; 149: 1607-15.
4. BRENNAN FM, MAINI RN, FELDMANN M: TNF alpha—a pivotal role in rheumatoid arthritis? *Br J Rheumatol* 1992; 31: 293-8.
5. MAINI RN, FELDMANN M: How does infliximab work in rheumatoid arthritis? *Arthritis Res* 2002; 4: S22-8.
6. BOUSSIAC EA, DEVOGELAER JP, VAN DAMME J, DE DEUXCHAISNES CN, VAS SNECK J: Interleukin-6 in synovial fluid and serum of patients with rheumatoid arthritis and other inflammatory arthritides. *Arthritis Rheum* 1988; 31: 784-8.
7. MIHARA M, NISHIMOTO N, OHSUGI Y: The therapy of autoimmune diseases by anti-interleukin-6 receptor antibody. *Expert Opin Biol Ther* 2005; 5: 683-90.
8. INGEGNOLI F, FANTINI F, FAVALLI EG *et al.*: Inflammatory and prothrombotic biomarkers in patients with rheumatoid arthritis: effects of tumor necrosis factor-alpha blockade. *J Autoimmun* 2008; 31: 175-9.
9. VAN VENROOIJ WJ, VAN BEERS JJ, PRUIJN GJ: Anti CCP Antibody, a Marker for the Early Detection of Rheumatoid Arthritis. *Ann N Y Acad Sci* 2008; 1143: 268-85.
10. VAN VENROOIJ WJ: The diagnostic accuracy of anti-citrulline antibody assessment in the diagnosis of patients suspected of rheumatoid arthritis by a general practitioner. *Ned Tijdschr Geneeskd* 2008; 152: 1243-4, author reply 1244-5.
11. VAN VENROOIJ WJ, ZENDMAN AJ: Anti-CCP2 antibodies: an overview and perspective of the diagnostic abilities of this serological marker for early rheumatoid arthritis. *Clin Rev Allergy Immunol* 2008; 34: 26-34.
12. ARNOLD JN, WORMALD MR, SIM RB, RUDD PM, DWEK RA: The impact of glycosylation on the biological function and structure of human immunoglobulins. *Annu Rev Immunol* 2007; 25: 21-50.
13. PAREKH RB, DWEK RA, SUTTON BJ *et al.*: Association of rheumatoid arthritis and primary osteoarthritis with changes in the glycosylation pattern of total serum IgG. *Nature* 1985; 316: 452-7.
14. HUBER LC, BROCK M, HEMMATAZAD H *et al.*: Histone deacetylase/acetylase activity in total synovial tissue derived from rheumatoid arthritis and osteoarthritis patients. *Arthritis Rheum* 2007; 56: 1087-93.
15. TAUNTON J, HASSIG CA, SCHREIBER SL: A mammalian histone deacetylase related to the yeast transcriptional regulator Rpd3p. *Science* 1996; 272: 408-11.
16. TUAN LL, SHIA WJ, CHEN MH *et al.*: Histone deacetylases specifically down-regulate p53-dependent gene activation. *J Biol Chem* 2000; 275: 20594-43.
17. ALTMAN R, ASCH E, BLOCH D *et al.*: Development of criteria for the classification and reporting of osteoarthritis. Classification of osteoarthritis of the knee. Diagnostic and Therapeutic Criteria Committee of the American Rheumatism Association. *Arthritis Rheum* 1986; 29: 1039-49.
18. UCHIYAMA T, ISHIJIMA Y, MATSUSHITA H, YOSHIDA M, KIMURA S: Detection of thrombopoietin-responsive proteins in nude mouse spleen cells by two-dimensional polyacrylamide gel

electrophoresis and image processing. *Electrophoresis* 1994; 15: 98–7.

19. SANCHEZ JC, ROUGE V, BISTEUR M *et al.*: Improved and simplified in-gel sample application using rehydrating of dry immobilized pH gradients. *Electrophoresis* 1997; 18: 324-7.
20. FUJISAWA-OKIANI KANEKO R, NATSUME *et al.*: Involvement of post-translational modification of neuronal cytoskeleton-related proteins in hyperalgesia revealed by a proteomic analysis. *Proteomics* 2008; 8: 1706–19.
21. CREASY DM, COTTRELL JS. Error tolerant searching of uninterpreted tandem mass spectrometry data. *Proteomics* 2002; 2: 1426-34.
22. CHAKRAVARTI D, OGRYZKO V, KAO HY *et al.*: A viral mechanism for inhibition of p300 and PCAF acetyltransferase activity. *Cell* 96: 393-403.
23. KHAIER A, SCARNA H, MERMET A, PUIGO JF: Biochemical and immunological properties of the mouse brain enolases purified by a simple method. *J Neurochem* 1981; 36: 1389-97.
24. JIN X, WANG LS, XIA L *et al.*: Hyper-phosphorylation of alpha-enolase in hypertrophied left ventricle of spontaneously hypertensive rat. *Biochem Biophys Res Commun* 2006; 371: 804-9.
25. YOSHIDA M, KUDMA M, AKITA M, BEPPU T: Potent and specific inhibition of mammalian histone deacetylase both in vivo and in vitro by trichostatin A. *J Biol Chem* 1990; 265: 17174-9.
26. DAVIDSON A, DIAMOND B: Autoimmune diseases. *N Engl J Med* 2001; 345: 340-50.
27. GIANNOPENICO V, SIMONSSON M, GRONROOS E, ERICSSON J: Coactivator-dependent acetylation stabilizes members of the SREBP family of transcription factors. *Mol Cell Biol* 2003; 23: 2587-99.
28. GILABIEC AM, KORCZYNSKI O, TAK PP, RIPOLL VT KA: Histone deacetylase inhibitors suppress rheumatoid arthritis fibroblast-like synoviocyte and macrophage IL-6 production by accelerating mRNA decay. *Ann Rheum Dis* 2012; 71: 424-31.
29. GILLESPIE J, SAVIC S, WONG C *et al.*: Histone deacetylases are dysregulated in rheumatoid arthritis and a novel histone deacetylase 3-selective inhibitor reduces interleukin-6 production by peripheral blood mononuclear cells from rheumatoid arthritis patients. *Arthritis Rheum* 2012; 64: 418-22.
30. KADIR JL: Abatacept for the treatment of rheumatoid arthritis: A review. *Curr Ther Res Clin Exp* 2007; 68: 379-99.
31. BECK KM, PEMBERTON LF: Histone chaperones link histone nuclear import and chromatin assembly. *Biochim Biophys Acta* 2012; 1819: 277-89.
32. WYGRECKA M, MARSH LM, MORTY RE *et al.*: Enolase-1 promotes plasminogen-mediated recruitment of monocytes to the stretch injured lung. *Blood* 2009; 113: 3588-98.
33. BAE S, KIM H, LEE N *et al.*: α-Enolase expressed on the surface of monocytes and macrophages induces robust synovial inflammation in rheumatoid arthritis. *J Immunol* 2012; 189: 365-72.
34. MOR-VAKNIN N, KAPHES F, DICK AE *et al.*: DEK in the synovium of JIA patients: Characterization of DEK antibodies and post-translational modification of the DEK autoantigen. *Arthritis Rheum* 2011; 63: 536-67.
35. FRIEDEN C: Protein-Protein Interaction and Enzymatic Activity. *Annual Review of Biochemistry* 1971; 40: 653-96.
36. SOMDYA S, YU W, HATTLOWS WC *et al.*: Sirt3 mediates reduction of oxidative damage and prevention of age-related hearing loss under caloric restriction. *Cell* 2010; 143: 802-12.
37. SCHLICKER C, GRUBE M, PAPATHEODOROU P, KACHOLZ B, BECKER CW, STEGBUHN C: Substrates and regulatory mechanisms for the human mitochondrial sirtuins Sirt3 and Sirt5. *J Mol Biol* 2008; 382: 790-801.

Biochemical and Biophysical Research Communications 467 (2015) 63–69

Contents lists available at ScienceDirect

Biochemical and Biophysical Research Communications

journal homepage: www.elsevier.com/locate/ybbrc

Roles of layilin in TNF-α-induced epithelial-mesenchymal transformation of renal tubular epithelial cells

Takayuki Adachi [a, b], Mitsumi Arito [a], Naoya Suematsu [a], Atsuko Kamijo-Ikemori [c], Kazuki Omoteyama [a], Toshiyuki Sato [a], Manae S. Kurokawa [d], Kazuki Okamoto [a], Kenjiro Kimura [e], Yugo Shibagaki [b], Tomohiro Kato [a, *]

[a] Clinical Proteomics and Molecular Medicine, St. Marianna University Graduate School of Medicine, Kanagawa, Japan
[b] Division of Nephrology and Hypertension, Department of Internal Medicine, St. Marianna University School of Medicine, Kanagawa, Japan
[c] Department of Anatomy, St. Marianna University School of Medicine, Kanagawa, Japan
[d] Disease Biomarker Analysis and Molecular Regulation, St. Marianna University Graduate School of Medicine, Kanagawa, Japan
[e] Japan Community Health Care Organization Tokyo Takanawa Hospital, Tokyo, Japan

ARTICLE INFO

Article history:
Received 15 September 2015
Accepted 22 September 2015
Available online 26 September 2015

Keywords:
Epithelial-mesenchymal transformation
Renal tubular epithelium
Glomerulonephritis
Layilin
TNF-α

ABSTRACT

Background: Tumor necrosis factor (TNF)-α is suggested to induce epithelial-mesenchymal transformation (EMT) of renal tubular epithelial cells that possibly exacerbates renal interstitial fibrosis in glomerulonephritis (GN). We here investigated whether layilin (LAYN), a c-type lectin-homologous protein, was involved in the EMT process.
Methods: Expression of LAYN was investigated in kidneys of mice administered with TNF-α and in a clear cell renal carcinoma cell line of KMRC-1 stimulated with TNF-α by quantitative polymerase chain reaction (qPCR) and/or western blotting. Expression of LAYN was assessed immunohistochemically in renal biopsy samples of patients with various types of GN. Changes of EMT markers and cell morphology by TNF-α and transforming growth factor (TGF)-β in LAYN-knocked down KMRC-1 cells were investigated by qPCR and immunocytochemistry.
Results: Administration of TNF-α increased expression of LAYN in renal tubular epithelia in mice. TNF-α but not TGF-β increased expression of LAYN in KMRC-1 cells. Renal biopsy samples from the patients with GN showed high expression of LAYN in tubular epithelial cells. TNF-α induced up-regulation of vimentin, down-regulation of E-cadherin, and fibroblast-like morphological change in KMRC-1 cells, indicating occurrence of EMT. These changes were not observed in the LAYN-knocked down cells. In contrast, similarly occurred TGF-β-induced EMT was not affected by the LAYN knockdown.
Conclusion: Our data indicate that LAYN is involved in the TNF-α-induced EMT of renal tubular epithelial cells. LAYN may play roles in the generation of renal interstitial fibrosis in GN via TNF-α-induced EMT.
© 2015 Elsevier Inc. All rights reserved.

1. Introduction

Glomerulonephritis (GN) is one of the major causes of chronic renal failure. Although pathological mechanisms for the onset and progression of GN have not been fully understood, roles of cytokines such as tumor necrosis factor (TNF)-α have been suggested. For example, high expression of TNF-α in patients with IgAN was reported [1]. TNF-α derived from mesangial cells has been reported to stimulate renal tubular epithelia (RTE) cells to secrete TNF-α in IgA nephropathy (IgAN) [2]. TNF-α derived from mesangial cells has been reported to damage podcytes [3]. Increased renal production of TNF-α has been reported in lupus nephritis (LN) and anti-neutrophil cytosol antibody (ANCA)-associated GN (AAGN) [4,5].

In GN, inflammation of glomeruli is the central phenomenon, however, it has been suggested that decrease of glomerular filtration rates is promoted by RTE damages rather than glomerular damages themselves [6]. Although mechanisms for the generation of RTE damages have been poorly understood, epithelial-mesenchymal transformation (EMT) is recently thought to be involved in the RTE damages [7,8]. On the one hand, that lack of RTE cells by EMT would

* Corresponding author. Clinical Proteomics and Molecular Medicine, St. Marianna University Graduate School of Medicine, 2–16–1 Sugao, Miyamae, Kawasaki, Kanagawa, 216–8511, Japan.
E-mail address: t3kato@marianna-u.ac.jp (T. Kato).

http://dx.doi.org/10.1016/j.bbrc.2015.09.121
0006-291X/© 2015 Elsevier Inc. All rights reserved.

cause damages of the renal tubular basement membrane [9,10]. On the other hand, proliferation of fibroblastic cells by progression of EMT would cause renal interstitial fibrosis that hampers glomerular functions [9,10]. In general, transforming growth factor (TGF)-β is a well-known inducer of EMT in various cell types [11]. However, several studies indicate that TNF-α is an EMT inducer in GN [12–15].

Layilin (LAYN) is a transmembrane protein with homology with c-type lectin [16]. Studies on mice showed that LAYN was expressed in various organs such as liver, heart, kidney, and spleen [16], however, distribution of LAYN in human has not been fully investigated. LAYN has been reported as a receptor for hyaluronic acid [17], but also reported to bind to cytoskeletal proteins such as talin and merlin to regulate cell adhesion [18,19]. In fact, some studies showed that LAYN was involved in the infiltration and metastasis of cancer cells [20]. Largely, functions of LAYN remain to be fully elucidated.

Recently, we reported that TNF-α increased expression of LAYN in human chondrocytes [21]. Thereby we here hypothesize that LAYN plays roles in the TNF-α-mediated EMT induction of RTE cells. To test this hypothesis, we investigated whether TNF-α increased renal expression of LAYN in mice and in a human clear cell renal carcinoma cell line, whether renal expression of LAYN was increased in patients with GN, and whether LAYN was involved in TNF-α-induced EMT of the cell line.

2. Materials and methods

2.1. Clinical samples

Renal needle biopsy samples were obtained from 4 patients with IgAN of H-grade I (2 males and 2 females; mean age 26.8 years old [range 22–39]), 4 patients with IgAN of H-grade II (4 males; mean age 36.5 years old [range 16–59]), 4 patients with IgAN of H-grade III (2 males and 2 females; mean age 48.8 years old [range 35–67]), 4 patients with LN (1 male and 3 females; mean age 38.8 years old [range 27–51]), 4 patients with AAGN (2 males and 2 females; mean age 67.8 years old [range 44–80]), and 4 donors of renal transplantation (0 h protocol biopsies) (4 males; mean age 39.3 years old [range 30–51]). The diagnoses of IgAN, LN, and AAGN were made by their respective criteria [22–24]. Histological lesions of the biopsy samples in the IgAN patients were classified into H-grade I–IV, according to the reported guideline [22].

Written informed consent was obtained from each of the patients and donors. This study protocol was approved by the ethics committee of St. Marianna University School of Medicine. The study was performed in compliance with the World Medical Association Declaration of Helsinki.

2.2. Animal experiments

Six Slc:ICR mice were intraperitoneally injected with 20 μg of human TNF-α (PROSPEC, Ness Ziona, Israel). Three Slc:ICR mice were intraperitoneally injected with phosphate buffered saline (PBS) as a negative control (non-treated, NT). After 48 h, 3 out of the 6 TNF-α-injected mice and the control mice were sacrificed (TNF-α (×1) and NT, respectively). The remaining 3 mice were again intraperitoneally injected with 20 μg of human TNF-α (TNF-α (×2)). After 48 h, the TNF-α (×2) mice was sacrificed. Kidneys of the mice were subjected to western blotting and immunohistochemical staining. The animal experiments were carried out in KAC, Co., Inc. (Kyoto, Japan) in accordance with protocols reviewed and approved by the animal care and use committee of KAC.

2.3. Immunohistochemistry

Formalin-fixed paraffin-embedded mouse and human kidney samples, sectioned to be 2 μm-thick, were deparaffinized with xylene. Then the mouse and human kidney sections, incubated at 121 °C for 15 min and 93 °C for 20 min respectively, were reacted with goat anti-LAYN polyclonal antibodies (R&D, MN, USA) and mouse anti-LAYN monoclonal (IgG1) antibodies (Santa Cruz Biotechnology, TX, USA), respectively. As a negative control, normal goat IgG and normal mouse IgG1 (DAKO cytomation, Glostrup, Denmark) were used in place of the anti-LAYN antibodies, respectively. Horseradish peroxidase (HRP)-conjugated anti-goat and anti-mouse immunoglobulin antibodies (ImmPRESS Reagent, VECTOR LABORATORIES, INC., Burlingame, CA, USA) were used as the 2nd antibodies, respectively. Bound 2nd antibodies were detected by DAB + Substrate Chromogen System (Dako). Nuclei of the mouse kidney sections were stained by Mayer's hematoxylin solution (Wako Pure Chemical Industries, Osaka, Japan).

2.4. Cell culture

A human clear cell renal carcinoma cell line of KMRC-1 was obtained from Japanese Collection of Research Bioresources Cell Bank (Osaka, Japan). KMRC-1 cells were cultured in Dulbecco's modified Eagle's medium (DMEM, GIBCO, Carsbad, CA) supplemented with 10% fetal calf serum (FBS, Wako), 100 units/ml penicillin, and 100 μg/ml streptomycin (Sigma-Aldrich, St. Louis, MO, USA). The cells were cultured at 37 °C in 5% CO_2.

2.5. Treatment of KMRC-1 cells with small interfering RNA (siRNA)

KMRC-1 cells were transfected with 200 pmol/ϕ100 mm dish or 100 pmol/ϕ35 mm dish of siRNA for human LAYN (nucleotides 462–486 (GGGAGGGACACAGAGGCCTTGTTAT) in NM_001258390.1, Invitrogen, Carlsbad, CA, USA) using Lipofectamine RNAiMAX (Invitrogen). As a negative control, the cells were transfected with the same doses of control siRNA (Stealth™ RNAi Negative Control Medium GC Duplex, Invitrogen). After 24 h, the KMRC-1 cells were cultured in the starvation condition of DMEM supplemented with 1% FBS, 100 units/ml penicillin, and 100 μg/ml streptomycin for 24 h. The cells were treated with 10 ng/ml human TNF-α (PROSPEC) or 10 ng/ml human TGF-β (PEPROTECH, Rocky Hill, NJ, USA) for 24 h and subjected to the following experiments.

2.6. Western blotting

Western blotting was performed as described previously [25]. The mouse kidneys, washed in PBS, were minced and homogenized in a lysis buffer (20 mM Tris-HCl, 250 mM NaCl, 1% NP-40, 1 mM dithiothreitol) including protease inhibitor cocktail (Roche, Basel, Switzerland). KMRC-1 cells, washed in PBS, were sonicated in the same lysis buffer. After centrifugation, collected supernatants were used as protein samples. The protein samples were separated by 15% SDS-PAGE and transferred into nylon membranes. The membranes were reacted to the same antibodies as above. Bound antibodies were visualized using an enhanced chemiluminescence detection system (GE healthcare, Buckinghamshire, UK).

2.7. RNA extraction, reverse transcription, and quantitative polymerase chain reaction (qPCR)

Total RNA, purified from the KMRC-1 cells using RNeasy® (Qiagen, Venlo, the Netherlands), was converted to cDNA by High Capacity cDNA Reverse Transcription Kits® (Life Technologies, Rockville, MD, USA), according to the manufacturer's instructions.

qPCR was performed by ABI Prism 7000 Sequence Detection System (Applied Biosystems, Foster city, CA, USA). To measure mRNA for LAYN and GAPDH, the mixture of 2 μg of cDNA, 300 nM each of forward and reverse primers, and Power SYBR® Master Mix (Applied Biosystems) was subjected to qPCR. Nucleotide sequences of the primers are as follows: LAYN: 5′-CACAGCCTGCCAGGACCTTTA and 5′-TGCACCGGTCATCATTCCA, and GAPDH: 5′-TGGTATGGTG-GAAGGACTCA and 5′-ATGCCAGTGAGCTTCCCGTT. To measure mRNA for vimentin and E-cadherin, the mixture of 2 μg of cDNA, 2 solutions of TaqMan® Gene Expression Assays (Hs00185584_m1 and Hs01023894_m1, respectively, Applied Biosystems), and TaqMan® Gene Expression Master Mix (Applied Biosystems) was subjected to qPCR. The thermal cycle condition was as follows: 95 °C for 10 min, followed by 40 cycles of 95 °C for 15 s and 60 °C for 60 s.

2.8. Immunocytochemistry

KMRC-1 cells cultured in 35 mm dishes (ASAHI GLASS, Tokyo, Japan) were fixed in PBS containing 4% paraformaldehyde. The fixed cells were reacted to Alexa 488-labeled phalloidin (Cytoskelton Inc., Denver, CO, USA) to detect F-actin and Alexa 488-labeled anti-zona occludens (ZO)-1 antibodies (Abcam, Cambridge, UK) to detect ZO-1. Nuclei were stained with DAPI (Wako). The bound Alexa 488 and DAPI were detected using a fluorescence microscope (BIOREVO (BZ-9000), KEYENCE, Jena, Germany). The width and length of the cells were measured using BZ-II Analyzer Ver. 1.42 (KEYENCE).

2.9. Statistical analysis

Statistical significance was calculated by Student's t-test. A value of $p < 0.05$ was considered to be statistically significant.

3. Results

3.1. Renal expression of LAYN is up-regulated by TNF-α in vivo

First, to investigate effects of TNF-α on renal expression of LAYN *in vivo*, we intraperitoneally administered TNF-α to mice once or twice (TNF-α (×1) and TNF-α (×2), n = 3 for each) as well as PBS once as a negative control (NT, n = 3). Then renal expression of LAYN was analyzed by western blotting and immunohistochemistry. As a result, we found that renal expression of LAYN was significantly increased in the TNF-α (×2) mice ($p = 3.0 \times 10^{-4}$, Fig. 1A), although the increase was not obvious in the TNF-α (×1) mice (Fig. 1A). In the immunohistochemistry, high expression of LAYN in kidneys was also demonstrated in the TNF-α (×2) mice (Fig. 1B), where LAYN was highly expressed in renal tubules and, to lesser extent, in mesangial areas of glomeruli (Fig. 1B). These data indicate that TNF-α up-regulates expression of LAYN mainly in renal tubules.

3.2. High expression of LAYN in kidneys of patients with GN

Next, we immunohistochemically investigated expression of LAYN in kidney sections of patients with various types of GN. Specifically, we prepared renal biopsy sections from patients with IgAN of H grade (HG) I–III (n = 4 for each grade), LN (n = 4), and AAGN (n = 4), and from kidney donors of renal transplantation as a healthy control (HL, n = 4). As a result, 18 out of the 20 GN patients showed high expression of LAYN, compared to HL, although 2 out of the 4 LN patients (LN-2 and -3) did not show high LAYN expression (Fig. 2). LAYN was mainly expressed in renal tubules, cellular crescents, and infiltrating inflammatory cells (Fig. 2) and, to lesser extent, in mesangial areas of glomeruli. These data was largely in consistent with the results from the mouse experiment as above described. Taking these data together, TNF-α is likely involved in the high expression of LAYN in patients with GN.

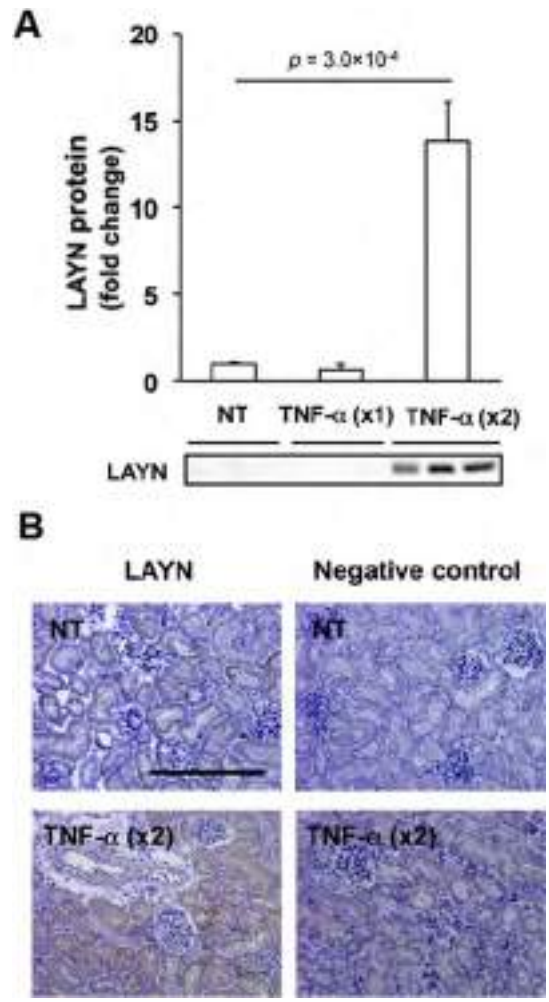

Fig. 1. Effects of TNF-α on LAYN expression in mouse kidneys. A: Kidney samples were obtained from mice intraperitoneally injected with 20 μg TNF-α once (n = 3, TNF-α (×1)) or twice (n = 3, TNF-α (×2)) and also from mice intraperitoneally injected with PBS as a negative control (n = 3, non-treated (NT)). Then proteins extracted from the kidney samples were subjected to western blotting to detect LAYN (lower panel). Intensity of LAYN bands was measured with a densitometer. The average of the LAYN intensity in the NT group was defined as 1.0. Mean values with SD are shown (upper panel). B: LAYN was immunohistochemically detected in mouse renal sections. Representative results from the TNF-α (×2) and NT groups are shown. As a negative control, goat non-specific IgG was used in place of goat anti-LAYN antibodies. A black bar indicates 100 μm.

3.3. Suppression of LAYN inhibited TNF-α-induced change of EMT markers

We hypothesize that TNF-α causes EMT of RTE cells via LAYN. To test this hypothesis, we first investigated whether TNF-α increased expression of LAYN using a clear cell renal carcinoma cell line of KMRC-1 by western blotting. As a result, expression of LAYN was significantly increased by the treatment with TNF-α ($p = 0.011$, Fig. 3A). In contrast, expression of LAYN was significantly decreased by treatment with TGF-β ($p = 2.3 \times 10^{-6}$, Fig. 3A). Next, we assessed EMT markers in LAYN-knocked down KMRC-1 cells with or without TNF-α treatment. By a preliminary experiment on the efficiency of siRNA for LAYN, we confirmed that LAYN mRNA was hardly

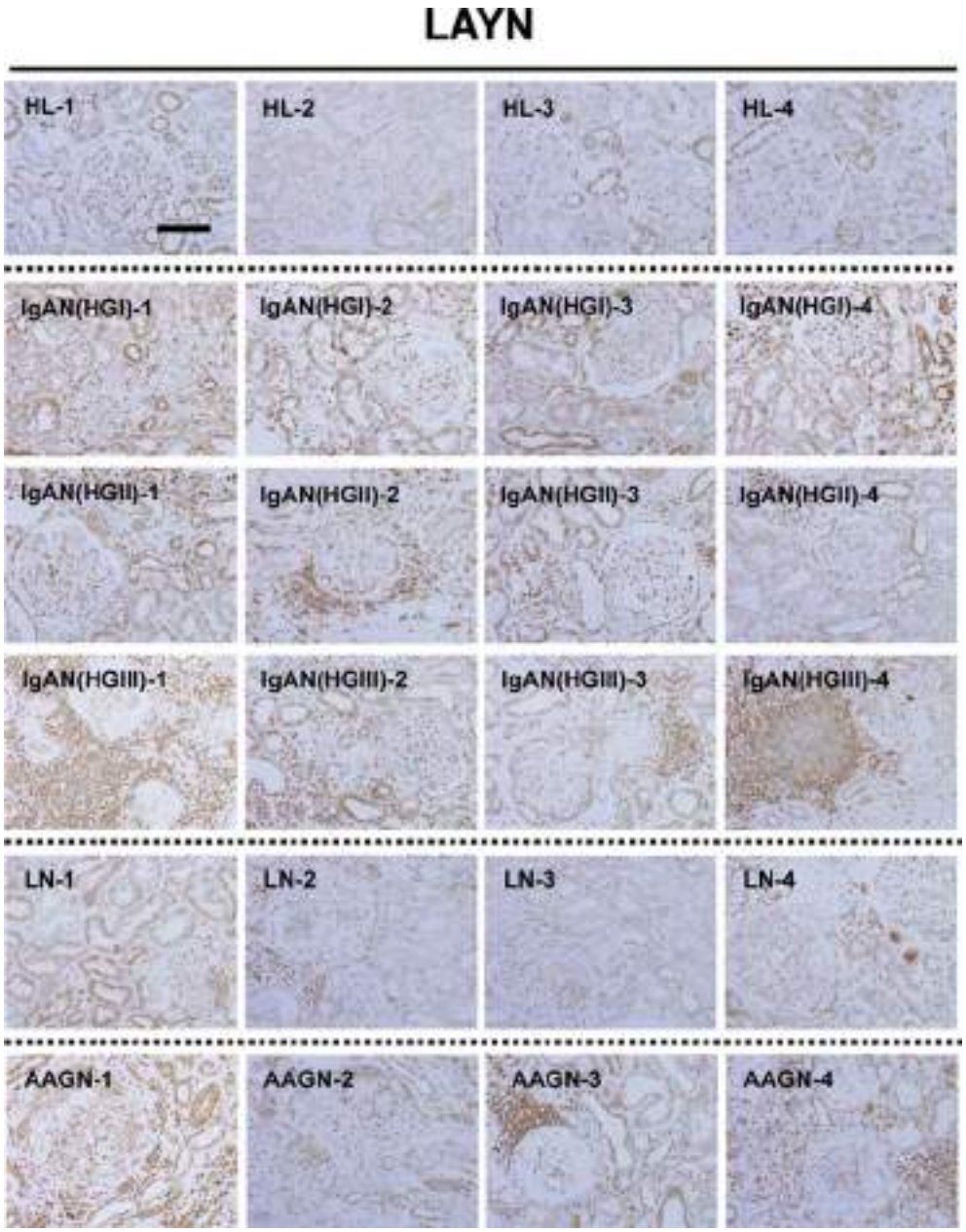

Fig. 2. Renal expression of LAYN in patients with GN. LAYN was detected in renal sections from patients with IgAN (H-grade (HG) I–III, n = 4 for each grade), LN (n = 4), and AAGN (n = 4) and from donors of renal transplantation (0 h protocol biopsies, Healthy, HL) using anti-LAYN antibodies. A black bar indicates 100 μm.

detected even in the TNF-α-treated condition (Fig. 3B). We then evaluated effects of LAYN knockdown on the induction of EMT by assessing mRNA for EMT markers of vimentin and E-cadherin. As a result, mRNA levels of vimentin were significantly increased by the TNF-α treatment in the control cells ($p = 0.028$), however, the TNF-α mediated increase of vimentin mRNA was totally suppressed in the LAYN-knocked down cells (Fig. 3C, left panel). On the other hand, mRNA levels of vimentin were significantly increased by the treatment with TGF-β, regardless of whether LAYN was knocked down or not ($p = 0.001$ and $p = 0.001$, respectively, Fig. 3C, right panel). In the case of E-cadherin, the mRNA levels were significantly decreased by the TNF-α treatment in the control cells ($p = 0.014$), however, such decrease was not observed in the LAYN-knocked down cells (Fig. 3D, left panel). On the other hand, mRNA levels of E-cadherin were not actually affected by the TGF-β treatment, regardless of whether LAYN was knocked down or not (Fig. 3D, right panel). These data indicate that LAYN is an essential factor for TNF-α-induced EMT but not for TGF-β-induced EMT.

In addition, in KMRC-1 cells transfected with control siRNA, mRNA levels of LAYN were significantly increased by the treatment with TNF-α ($p = 0.0064$), whereas the levels tended to be decreased by the treatment with TGF-β (Fig. 3B). This result was largely in accordance with the changes of the LAYN protein levels as shown in Fig. 3A.

3.4. Suppression of LAYN inhibited TNF-α-induced morphological changes

Finally, we evaluated effects of the LAYN knockdown on morphological changes of KMRC-1 cells by the treatment with TNF-

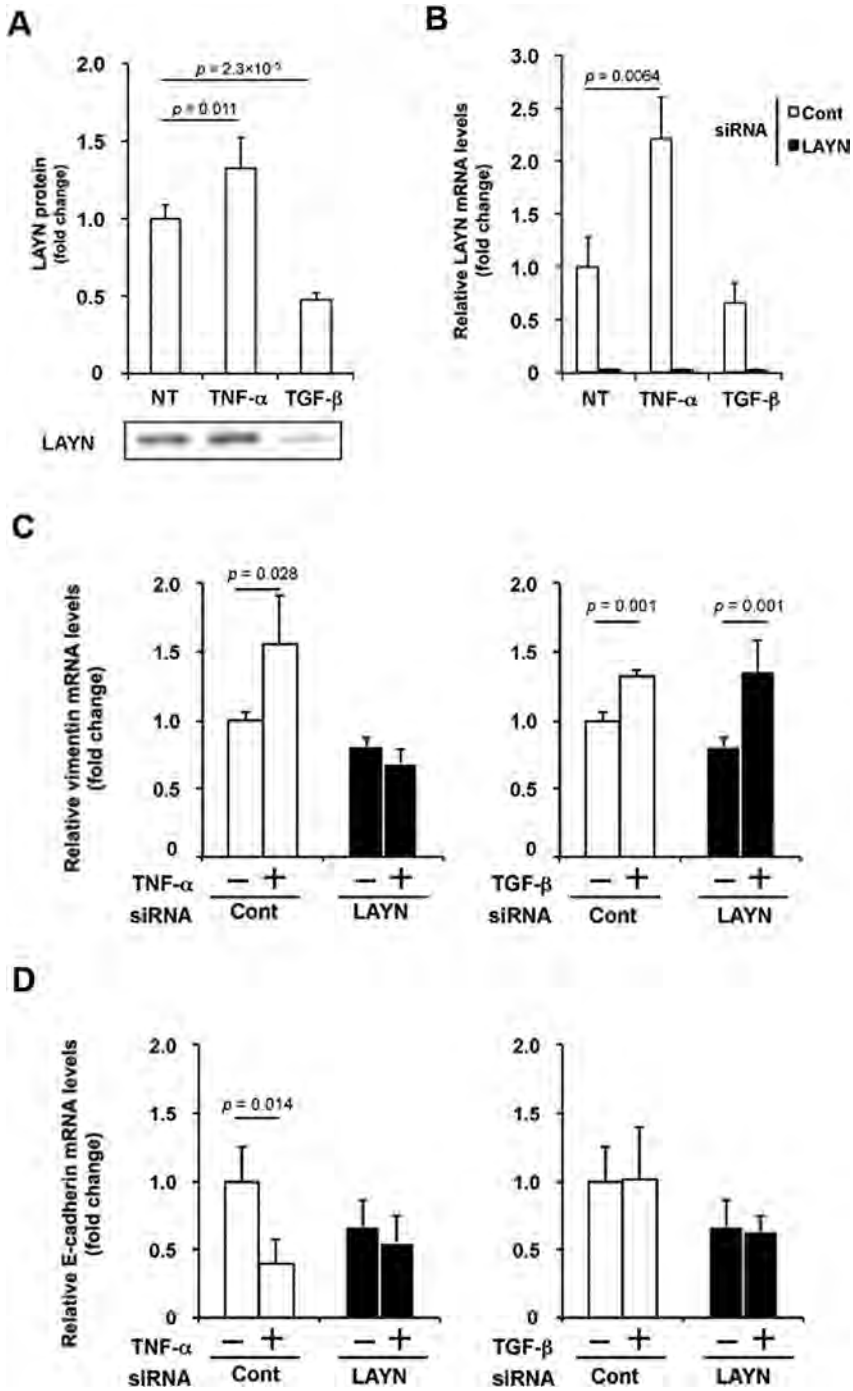

Fig. 3. Effects of LAYN siRNA on the expression of EMT markers in KMRC-1 cells. A: KMRC-1 cells were cultured with or without 10 ng/ml TNF-α and TGF-β for 24 h (n = 3). Then LAYN was detected by western blotting (lower panel). Intensity of LAYN bands was measured by a densitometer. The average of the LAYN intensity in the NT samples was defined as 1.0. B–D: KMRC-1 cells were transfected with control or LAYN siRNA. Then the cells were cultured with or without 10 ng/ml TNF-α and TGF-β for 24 h (n = 3). Then, RNA extracted from the cells was used for reverse-transcription and the subsequent quantitative real time-PCR to estimate amounts of mRNA for LAYN, vimentin, E-cadherin, and GAPDH. mRNA levels of LAYN (B), vimentin (C), and E-cadherin (D) were corrected using those of GAPDH. In each panel, the average of the corrected mRNA levels in the NT samples transfected with control siRNA was defined as 1.0. Mean values with SD are shown.

α. As a result, in the F-actin staining, the control cells, which were originally round in shape, changed to be fibroblast-like in shape by the TNF-α treatment, however, the LAYN-knocked down cells remained rather round in shape against the TNF-α treatment (Fig. 4A). On the other hand, the control cells appeared to become partially dendritic in shape by the TGF-β treatment and this change was suppressed by the knockdown of LAYN (Fig. 4A). We tried to quantify the morphological changes of KMRC-1 cells by measuring the length/width ratios of the cells. As a result, the change of length/width ratios on average was significantly increased by the TNF-α treatment as well as by the TGF-β treatment (Fig. 4B, lower left panel). Importantly, in the control cells, the average length/width ratio increased to 2.1-folds (from 1.7 to 3.6) by the TNF-α treatment, however, in the LAYN-knocked down cells, the ratio

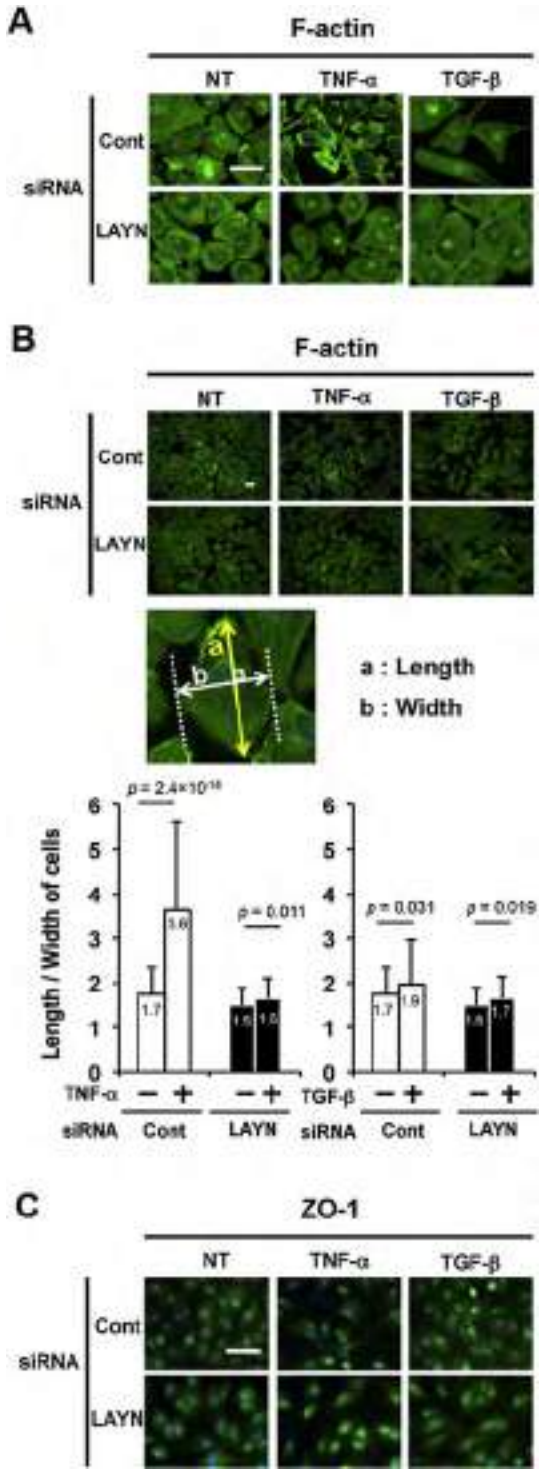

Fig. 4. Effects of LAYN siRNA on morphology of KMRC-1 cells and ZO-1 localization. A: KMRC-1 cells were transfected with control or LAYN siRNA. Then the cells were cultured with or without 10 ng/ml TNF-α and TGF-β for 24 h (n = 3). After fixation, F-actin was detected using Alexa 488-labeled phalloidin (green). Nuclei were stained with DAPI (blue). A white bar indicates 100 μm. B: [Upper panels] KMRC-1 cells in the Fig. 4A were observed in low-power fields. A white bar indicates 100 μm. Length and width of all the cells in each of these 6 panels were measured using BZ-II Analyzer Ver. 1.42. [Middle and lower panels] The length/width ratios of the cells defined as 'length (a)/width (b)' were calculated. Mean values with SD are shown. C: Localization of ZO-1 in fixed KMRC-1 cells was investigated using Alexa 488-labeled anti-ZO-1 antibodies (green). Nuclei were stained with DAPI (blue). A white bar indicates 100 μm.

change was only 1.1-folds (from 1.5 to 1.6), as shown in Fig. 4B-lower left panel. This data quantitatively demonstrate that LAYN is an essential molecule for the TNF-α-induced EMT from the morphological viewpoint. On the other hand, the changes of the length/width ratios by the TGF-β treatment were very similar between the control and LAYN-knocked down cells (1.2-folds vs. 1.1-folds, Fig. 4B, lower right panel). This indicates that TGF-β-induced EMT does little needs LAYN.

Furthermore, we examined localization of ZO-1, a tight junction protein, which was known to move from periphery to cytosol in cells by EMT [26]. As a result, in the control cells, ZO-1 was found to move from periphery to cytosol of cells by the TNF-α treatment, however, in the LAYN-knocked down cells, ZO-1 remained in periphery against the TNF-α treatment (Fig. 4C). On the other hand, ZO-1 did not change its localization by the TGF-β treatment, regardless of whether LAYN was knocked down or not (Fig. 4C).

These morphological data largely support that LAYN is an essential molecule for the TNF-α-induced EMT but not for the TGF-β-induced EMT.

4. Discussion

Our findings are summarized as follows: 1) TNF-α up-regulated expression of LAYN in mouse kidneys and in KMRC-1 cells, 2) Renal expression of LAYN in patients with GN were higher than that in healthy donors, and 3) LAYN was essential for TNF-α-induced EMT, but not for TGF-β-induced EMT in KMRC-1 cells.

On the first and second points, the main renal cells that increased expression of LAYN by the TNF-α treatment of mice were RTE cells (Fig. 1B). KMRC-1 we used *in vitro* is a human clear cell renal carcinoma cell line. In general, clear cell renal carcinomas are known to be derived from renal proximal tubules, displaying epithelial cell-like morphology [27,28]. Thereby, TNF-α is highly speculated to up-regulate LAYN expression in RTE cells in human. Together with the facts that LAYN was highly expressed mainly in RTE cells in patients with GN (Fig. 2) and many studies demonstrated high renal levels of TNF-α in patients with GN [1,29], TNF-α would be a responsible molecule for the high LAYN expression in RTE cells of GN patients.

On the third point, several studies have suggested that TNF-α causes EMT of RTE cells by experiments using clear cell renal carcinoma cells [12–14]. We here also used a clear cell renal carcinoma cell line of KMRC-1 to investigate roles of LAYN in EMT. Since TGF-β is a well-known EMT inducer in various epithelial cells [9,11], TGF-β would be involved in EMT in GN. We thus investigated roles of LAYN in the TNF-α-induced EMT as well as in TGF-β-induced EMT. Importantly, TNF-α up-regulated expression of LAYN but TGF-β down-regulated the expression (Fig. 3A). TNF-α-induced changes of EMT marker expression and cell shape were almost completely suppressed by the knockdown of LAYN, whereas the changes by TGF-β were not affected by the knockdown of LAYN (Figs. 3 and 4). From these data, LAYN is an essential molecule for TNF-α-induced EMT of KMRC-1 cells, but would not be involved in the TGF-β-induced EMT. TNF-α-induced EMT and TGF-β-induced EMT would have different pathological roles in GN, even if the both EMT-inducing pathways are involed in the pathophysiology of GN. Considering together that expression of LAYN was up-regulated by TNF-α but down-regulated by TGF-β (Fig. 3A) and that RTE cells strongly expressed LAYN in GN patients, TNF-α may be a dominant EMT inducer of RTE cells in GN.

In conclusion, our data indicate that LAYN is involved in the TNF-α-induced EMT of RTE cells. LAYN may play critical roles in the pathophysiology of GN from the viewpoint of EMT.

Conflict of interest statement

None.

Acknowledgments

We thank Ms. Michiyo Katano, Ms. Atsuko Nozawa, Ms. Seiko Hoshino, and Mr. Kazuho Inoue for their technical assistance.

Transparency document

Transparency document related to this article can be found online at http://dx.doi.org/10.1016/j.bbrc.2015.09.121.

References

[1] K. Yoshioka, T. Takemura, K. Murakami, et al., In situ expression of cytokines in IgA nephritis, Kidney Int. 44 (1993) 825–833.
[2] L.Y. Chan, J.C. Leung, A.W. Tsang, et al., Activation of tubular epithelial cells by mesangial-derived TNF-α: glomerulotubular communication in IgA nephropathy, Kidney Int. 67 (2005) 602–612.
[3] K.N. Lai, J.C. Leung, L.Y. Chan, et al., Podocyte injury induced by mesangial-derived cytokines in IgA nephropathy, Nephrol. Dial. Transpl. 24 (2009) 62–72.
[4] S. Yung, K.F. Cheung, Q. Zhang, et al., Mediators of inflammation and their effect on resident renal cells: implications in lupus nephritis, Clin. Dev. Immunol. (2013) 317682.
[5] I.L. Noronha, C. Kruger, K. Andrassy, et al., In situ production of TNF-α, IL-1 β and IL-2R in ANCA-positive glomerulonephritis, Kidney Int. 43 (1993) 682–692.
[6] E.I. Christensen, P.J. Verroust, Interstitial fibrosis: tubular hypothesis versus glomerular hypothesis, Kidney Int. 74 (2008) 1233–1236.
[7] F.M. Strutz, EMT and proteinuria as progression factors, Kidney Int. 75 (2009) 475–481.
[8] S.E. Quaggin, A. Kapus, Scar wars: mapping the fate of epithelial-mesenchymal-myofibroblast transition, Kidney Int. 80 (2011) 41–50.
[9] M. Iwano, D. Plieth, T.M. Danoff, et al., Evidence that fibroblasts derive from epithelium during tissue fibrosis, J. Clin. Invest. 110 (2002) 341–350.
[10] M. Zeisberg, R. Kalluri, The role of epithelial-to-mesenchymal transition in renal fibrosis, J. Mol. Med. 82 (2004) 175–181.
[11] J. Xu, S. Lamouille, R. Derynck, TGF-β-induced epithelial to mesenchymal transition, Cell Res. 19 (2009) 156–172.
[12] M.J. Chuang, K.H. Sun, S.J. Tang, et al., Tumor-derived tumor necrosis factor-alpha promotes progression and epithelial-mesenchymal transition in renal cell carcinoma cells, Cancer Sci. 99 (2008) 905–913.
[13] S.T. Wu, G.H. Sun, C.Y. Hsu, et al., Tumor necrosis factor-α induces epithelial-mesenchymal transition of renal cell carcinoma cells via a nuclear factor kappa B-independent mechanism, Exp. Biol. Med. 236 (2011) 1022–1029.
[14] M.Y. Ho, S.J. Tang, M.J. Chuang, et al., TNF-α induces epithelial-mesenchymal transition of renal cell carcinoma cells via a GSK3β-dependent mechanism, Mol. Cancer Res. 10 (2012) 1109–1119.
[15] J. Wan, X. Zhou, J. Cui, et al., Role of complement 3 in TNF-α-induced mesenchymal transition of renal tubular epithelial cells in vitro, Mol. Biotechnol. 54 (2013) 92–100.
[16] M.L. Borowsky, R.O. Hynes, Layilin, a novel talin-binding transmembrane protein homologous with C-type lectins, is localized in membrane ruffles, J. Cell Biol. 143 (1998) 429–442.
[17] P. Bono, K. Rubin, J.M. Higgins, et al., Layilin, a novel integral membrane protein, is a hyaluronan receptor, Mol. Biol. Cell 12 (2001) 891–900.
[18] P. Bono, E. Cordero, K. Johnson, et al., Layilin, a cell surface hyaluronan receptor, interacts with merlin and radixin, Exp. Cell Res. 308 (2005) 177–187.
[19] K.L. Wegener, J. Basran, C.R. Bagshaw, et al., Structural basis for the interaction between the cytoplasmic domain of the hyaluronate receptor layilin and the talin F3 subdomain, J. Mol. Biol. 382 (2008) 112–126.
[20] Z. Chen, W. Zhuo, Y. Wang, et al., Down-regulation of layilin, a novel hyaluronan receptor, via RNA interference, inhibits invasion and lymphatic metastasis of human lung A549 cells, Biotechnol. Appl. Biochem. 50 (2008) 89–96.
[21] K. Asano, M. Arito, M.S. Kurokawa, et al., Secretion of inflammatory factors from chondrocytes by layilin signaling, Biochem. Biophys. Res. Commun. 452 (2014) 85–90.
[22] T. Kawamura, K. Joh, H. Okonogi, et al., A histologic classification of IgA nephropathy for predicting long-term prognosis: emphasis on end-stage renal disease, J. Nephrol. 26 (2013) 350–357.
[23] B.H. Hahn, M.A. McMahon, A. Wilkinson, et al., American College of Rheumatology guidelines for screening, treatment, and management of lupus nephritis, Arthritis Care Res. 64 (2012) 797–808.
[24] J.C. Jennette, R.J. Falk, P.A. Bacon, et al., 2012 revised International Chapel Hill Consensus Conference Nomenclature of Vasculitides, Arthritis Rheum. 65 (2013) 1–11.
[25] K. Matsuo, M. Arito, K. Noyori, et al., Arthritogenicity of annexin VII revealed by phosphoproteomics of rheumatoid synoviocytes, Ann. Rheum. Dis. 70 (2011) 1489–1495.
[26] M. Zeisberg, E.G. Neilson, Biomarkers for epithelial-mesenchymal transitions, J. Clin. Invest. 119 (2009) 1429–1437.
[27] J.C. Presti Jr., P.H. Rao, Q. Chen, et al., Histopathological, cytogenetic, and molecular characterization of renal cortical tumors, Cancer Res. 51 (1991) 1544–1552.
[28] V.F. Muglia, A. Prando, Renal cell carcinoma: histological classification and correlation with imaging findings, Radiol. Bras. 48 (2015) 166–174.
[29] T. Ernandez, T.N. Mayadas, Immunoregulatory role of TNFα in inflammatory kidney diseases, Kidney Int. 76 (2009) 262–276.

RESEARCH ARTICLE

Effects of methotrexate and salazosulfapyridine on protein profiles of exosomes derived from a human synovial sarcoma cell line of SW982

Hirotaka Tsuno[1,2], Naoya Suematsu[1], Toshiyuki Sato[1], Mitsumi Arito[1], Toshihiro Matsui[2], Nobuko Iizuka[1], Kazuki Omoteyama[1], Kazuki Okamoto[1], Shigeto Tohma[3], Manae S. Kurokawa[1] and Tomohiro Kato[1]

[1] Clinical Proteomics and Molecular Medicine, St. Marianna University Graduate School of Medicine, Sugao, Miyamae, Kawasaki, Kanagawa, Japan
[2] Department of Rheumatology, Sagamihara National Hospital, National Hospital Organization, Sakuradai, Minami, Sagamihara, Kanagawa, Japan
[3] Department of Rheumatology, Clinical Research Center for Allergy and Rheumatology, Sagamihara National Hospital, National Hospital Organization, Sakuradai, Minami, Sagamihara, Kanagawa, Japan

Purpose: To elucidate effects of salazosulfapyridine (SASP) and methotrexate (MTX), major anti-rheumatic drugs, on exosomes derived from SW982 of a human synovial sarcoma cell line.
Experimental design: SW982 was treated with SASP and/or MTX under interleukin-1β (IL-1β)-treated or nontreated conditions. Exosomes were isolated from the culture media, and exosomal proteome was analyzed by 2D-DIGE. Protein spots whose intensity was significantly altered by the above treatments were identified by MS.
Results: Two hundred ninety-four protein spots were detected in the exosome preparations by 2D-DIGE. Compared to the nontreated cells, SASP-, MTX-, and (SASP + MTX)-treated cells displayed 8, 10, and 21 exosomal protein spots with more than ±2.0-fold intensity differences ($p < 0.05$), respectively. Similarly, the IL-1β-treated cells displayed 58 exosomal protein spots with more than ±1.5-fold intensity differences ($p < 0.05$). In about half of the 58 spots, the IL-1β-induced intensity changes were suppressed by simultaneous addition of SASP and/or MTX. Most of the identified proteins were immunity- or anti-oxidation-related proteins.
Conclusions and clinical relevance: The SASP and/or MTX treatments altered the protein profiles of exosomes and suppressed the effects of IL-1β on the exosomal proteome. Exosomes may play roles in the actions of these anti-rheumatic drugs.

Received: September 26, 2014
Revised: June 12, 2015
Accepted: July 7, 2015

Keywords:
2D-DIGE / Exosome / Methotrexate / Rheumatoid arthritis / Salazosulfapyridine

Additional supporting information may be found in the online version of this article at the publisher's web-site

Correspondence: Dr. Tomohiro Kato, Clinical Proteomics and Molecular Medicine, St. Marianna University Graduate School of Medicine, 2-16-1, Sugao, Miyamae, Kawasaki, Kanagawa 216–8511, Japan
E-mail: t3kato@marianna-u.ac.jp
Fax: +81-44-976-7553

Abbreviations: DMARD, disease-modifying antirheumatic drug; **ESCRT**, endosomal sorting complex required for transport; **IL-1β**, interleukin-1β; **MMP**, metalloproteinase; **MTX**, methotrexate; **MVE**, multivesicular endosome; **RA**, rheumatoid arthritis; **SASP**, salazosulfapyridine; **SP**, sulfapyridine; **TLR**, Toll-like receptor

1 Introduction

Exosomes are membranous extracellular vesicles with diameters of 30–100 nm [1]. They are initially formed as intracellular vesicles of multivesicular endosomes (MVEs) and then are secreted from cells by fusion of MVEs with plasma membrane [2]. Functionally, exosomes have been reported to play roles in various immune reactions [1, 3, 4], intercellular communication [5], and transfer of RNAs and proteins [6].

Rheumatoid arthritis (RA) is a systemic autoimmune disorder characterized by synovial inflammation and hyperplasia. Chronic inflammation in multiple joints sometimes

© 2015 WILEY-VCH Verlag GmbH & Co. KGaA, Weinheim

Clinical Relevance

Exosomes are membranous extracellular vesicles with diameters of 30–100 nm, which have recently attracted much attention for their various immunomodulatory functions. Since rheumatoid arthritis (RA), characterized by systemic synovial inflammation, is associated with various immunological disorders, exosomes are presumed to be related to the pathophysiology and treatment of RA. However, roles of exosomes in the pathophysiology and treatment of RA have been poorly understood. This study showed that salazosulfapyridine (SASP) and methotrexate (MTX) of representative anti-rheumatic drugs greatly affected protein profiles of exosomes derived from SW982 of a synovial sarcoma cell line. Our findings would help understanding of roles of exosomes in the pathogenesis and treatment of RA.

leads to severe joint destruction. Methotrexate (MTX) and salazosulfapyridine (SASP) are oral disease-modifying antirheumatic drugs (DMARDs) used widely in the world. MTX, a folate antagonist, is one of the most effective DMARDs. MTX prevents de novo pyrimidine and purine syntheses, and consequently inhibits proliferation of lymphocytes [7]. Further, MTX suppresses synthesis of synovial metalloproteinases (MMPs) [8]. SASP, consisting of sulfapyridine (SP) and 5-aminosalicylic acid, is also commonly used in the treatment of RA. Action mechanisms of SASP include inhibition of dendritic cell maturation [9], suppression of IL-2 production by T cells [10], and inhibition of synovial cell proliferation [11]. Clinically, MTX and SASP are often used in combination, since the combination therapy was found more effective than a mono-therapy with MTX or SASP [12].

Since RA is associated with various immunological disorders and exosomes are involved in various immunoreactions, exosomes are presumed to play roles in the pathophysiology and treatment of RA. For example, exosomes derived from synovial fibroblasts were reported to contain a membrane form of tumor necrosis factor-α [13]. It was also reported that exosomes from interleukin-1β (IL-1β)-stimulated synovial fibroblasts upregulated MMP-13 expression in chondrocytes [14]. As for effects of DMARDs on exosomes, no report has been available to our knowledge, although many studies have focused on effects of DMARDs on synovial cells themselves.

Based on these backgrounds, we here tried to analyze effects of MTX and SASP on the protein profiles of exosomes derived from a synovial sarcoma cell line of SW982 under IL-1β-stimulated or nonstimulated conditions by 2D-DIGE and subsequent MS analysis. SW982 has been frequently used as a substitute of synovial cells in studies on arthritis, although synovial sarcoma including SW982 is classified as a miscellaneous tumor of uncertain histological origin [15–17]. We found that the treatments with SASP and/or MTX altered the protein profiles of exosomes and that the treatments with SASP, MTX, and in particular, the combination of SASP and MTX suppressed a part of the protein profile changes induced by IL-1β. Our data would promote understanding of roles of exosomes in the pathogenesis and treatments of RA.

2 Materials and methods

2.1 Reagent preparation, cell culture, and stimulation with drugs

A synovial sarcoma cell line of SW982 was obtained from American Type Culture Collection (Manassas, Va., USA, Cell number HTB-93). SW982 cells were cultured and stimulated as described in the Supporting Information. Preparation of SASP, MTX, and IL-1β is also described in the Supporting Information. The cells were treated with SASP, MTX, SASP + MTX, IL-1β, IL-1β + SASP, IL-1β + MTX, and IL-1β + SASP + MTX in triplicate for 48 h. Nontreated cells were used as a negative control. Then supernatants of the culture were collected for preparation of exosomes. On the other hand, the cells were washed in PBS and proteins were extracted into a cell lysis buffer (30 mM Tris-HCl pH 8.0, 7 M Urea, 2 M Thiourea, 4% CHAPS). The resulting cell lysates were used for cellular protein analyses.

2.2 Preparation of cellular and exosomal proteins, transmission electron microscopic analysis, and Western blotting for exosome markers

For preparation of exosomal proteins, exosomes were isolated from the collected supernatants using ExoQuick-TC® (System Bioscience, Mountain View, CA). Briefly, the supernatants were centrifuged at 3000 × *g* for 15 min at 4°C to remove cell debris. Then, the resulting supernatants were subjected to 0.22-μm vacuum filters to remove impurities such as apoptotic bodies, and then an appropriate volume of ExoQuick-TC was added, according to the manufacturer's instructions. The Exoquick-TC/supernatant mixtures were refrigerated at 4°C overnight, and then were centrifuged at 1500 × *g* for 30 min at 4°C. The pellets consisting of exosomes were collected and dissolved in the cell lysis buffer. The protein concentrations of the resulting exosome lysates were determined by the Bradford method. In some cases, a part of the exosome pellets was resuspended in PBS for transmission electron microscopic analysis. Preparation of the cellular proteins, transmission electron microscopic

© 2015 WILEY-VCH Verlag GmbH & Co. KGaA, Weinheim

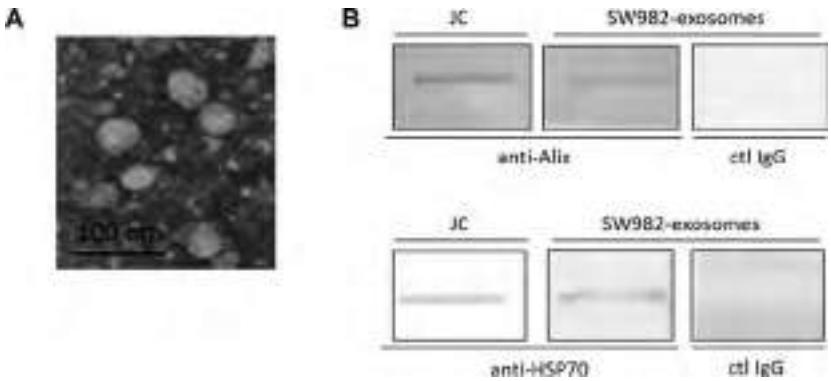

Figure 1. A transmission electron micrograph of the isolated exosomes and detection of exosome markers by Western blotting in the isolated exosomes. (A) A part of the exosomes isolated using Exoquick-TC was subjected to transmission electron microscopic analysis. A representative result is shown. (B) Lysates from the isolated SW982 exosomes were separated by SDS-PAGE and transferred onto nylon membranes. Then Alix and HSP70, representative exosome markers, were detected by their specific antibodies. Whole cell lysates from Jurkat cells were used as a positive control. JC: Jurkat cells, ctl IgG: control IgG.

analysis, and Western blotting for exosome markers are described in the Supporting Information.

2.3 2D-DIGE analysis and protein identification

The exosome lysates and the parent cell lysates were separated by 2D-DIGE, respectively, as described previously [18]. The procedures were briefly described in the Supporting Information. Protein identification is also described in the Supporting Information.

2.4 Statistical analysis

Statistical significance was calculated by Student's *t*-test. A *p* value of less than 0.05 was considered to be statistically significant.

3 Results

3.1 Isolation of exosomes from culture supernatants of SW982 cells

We stimulated SW982 cells with above drugs and then isolated exosomes from the culture supernatants. As a result, almost all the isolated extracellular vesicles showed diameters of 30–100 nm in transmission electron microscopic analysis, as shown in Fig. 1A. The observed sizes were compatible with the definition of the exosome [1]. Furthermore, representative exosomal markers of Alix and HSP70 were detected in lysates of the isolated exosomes by Western blotting, as shown in Fig. 1B. These results indicated the successful isolation of exosomes. In addition, we confirmed the cell viability in these culture conditions was nearly 100% in our preliminary experiments (data not shown).

3.2 Effects of SASP, MTX, and SASP + MTX on the exosomal protein profile

We then extracted proteins from the isolated exosome samples for 2D-DIGE to compare protein profiles among the four groups of SASP-treated, MTX-treated, (SASP + MTX)-treated, and nontreated as a negative control. As a result, the extracted exosomal proteins were separated to make 294 protein spots in total on the gels, as shown in Fig. 2A. Then intensity of the separated protein spots, adjusted by that of the internal control, was compared among the groups. The number of protein spots whose intensity was significantly altered by these drugs is summarized in Table 1. In the SASP-, MTX-, and (SASP + MTX)-treated group, 58, 44, and 42 out of the 294 protein spots showed significantly altered intensity compared to the nontreated group, respectively ($p < 0.05$) (Table 1). These data demonstrated that the SASP and/or MTX treatments altered the protein profiles of exosomes considerably. Representative spots whose intensity was

Table 1. Number of exosomal protein spots intensity of which was significantly altered with SASP and/or MTX treatments

Drug	Number of protein spots with altered intensity ($p < 0.05$)	Difference (x-fold)	Number of spots
SASP	58	$2.0<x$	2
		$1.5<x$	8
		$1.0<x$	16
		$x<1.0$	42
		$x<1/1.5$	24
		$x<1/2.0$	6
MTX	44	$2.0<x$	8
		$1.5<x$	25
		$1.0<x$	31
		$x<1.0$	13
		$x<1/1.5$	11
		$x<1/2.0$	2
SASP + MTX	42	$2.0<x$	20
		$1.5<x$	28
		$1.0<x$	33
		$x<1.0$	9
		$x<1/1.5$	8
		$x<1/2.0$	1

In total, 294 protein spots were detected in the exosome preparation. Numbers of the protein spots intensity of which was significantly altered by the drugs are shown ($p < 0.05$).

© 2015 WILEY-VCH Verlag GmbH & Co. KGaA, Weinheim

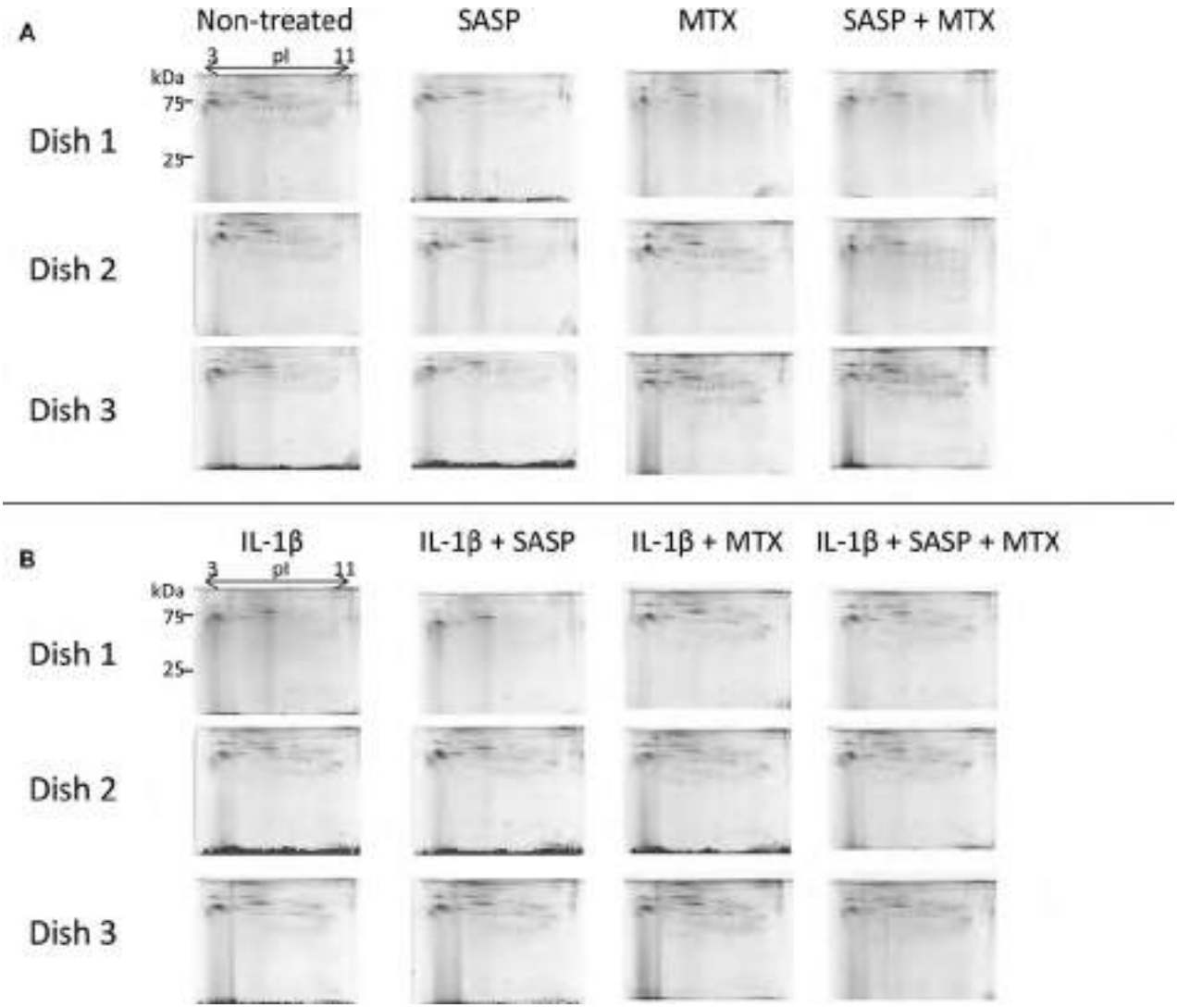

Figure 2. 2D-DIGE images showing protein profiles of exosomes derived from SW982 cells. (A) SW982 cells were treated with 100 μg/mL SASP alone, 1 μg/mL MTX alone, 100 μg/mL SASP + 1 μg/mL MTX, and with media alone as a negative control. Then exosomes were isolated from the cell culture supernatants. Extracted exosomal proteins were separated by 2D-DIGE. (B) SW982 cells were treated with 100 μg/mL SASP, 1 μg/mL MTX, and 100 μg/mL SASP + 1 μg/mL MTX with the simultaneous addition of 2 ng/mL IL-1β. Then exosomal proteins were analyzed similarly as (A).

significantly altered by the drug stimulation are shown in Supporting Information Fig. 1.

Of note, the 58 protein spots affected by SASP and the 44 spots affected by MTX shared only ten spots (Fig. 3A), indicating different pharmacological mechanisms of the two drugs. Again, focusing on the 21 protein spots that changed their intensity more than 2.0-fold or less than 1/2.0-fold ($p < 0.05$), 17 spots (81.0%) showed significant intensity changes only by the SASP + MTX treatment, not by the SASP treatment alone or by the MTX treatment alone (Fig. 3B). The result indicates additive or synergistic effects of SASP and MTX to form the exosomal protein profile change.

3.3 Effects of SASP, MTX, and SASP + MTX on the IL-1β-induced changes of the exosomal protein profiles

Next, we investigated whether IL-1β affected the protein profiles of exosomes and if affected, whether SASP and MTX suppressed the effects of IL-1β. For this aim, we treated SW982 cells with SASP, MTX, or SASP + MTX under the IL-1β-stimulated condition and then compared exosomal protein profiles among these groups by 2D-DIGE similarly as above (Fig. 2B). As a result, out of the 294 detected protein spots, 62 spots (21.1%) changed their intensity by the IL-1β treatment

© 2015 WILEY-VCH Verlag GmbH & Co. KGaA, Weinheim

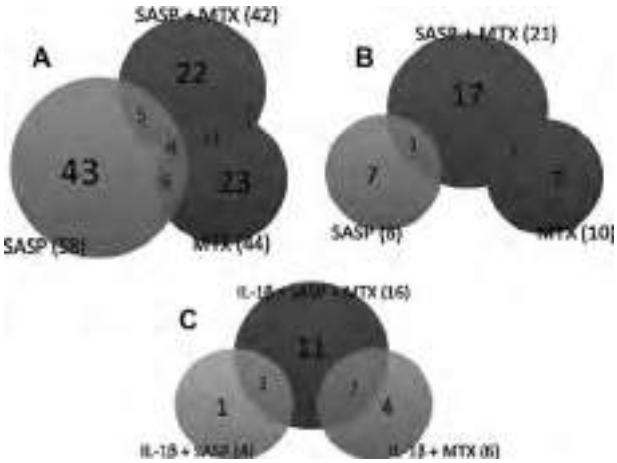

Figure 3. Venn diagrams showing shared protein spots intensity of which was significantly altered by SASP, MTX, and/or IL-1β. (A) Classification of all the exosomal protein spots whose intensity was significantly altered by the SASP and/or MTX treatments. (B) Classification of exosomal protein spots whose intensity was significantly altered more than 2.0-fold or less than 1/2.0-fold by the SASP and/or MTX treatments. (C) The spots whose IL-1β-induced alterations were significantly suppressed by simultaneous addition of SASP and/or MTX.

($p < 0.05$). Fifty-eight out of the 62 spots showed more than 1.5-fold or less than 1/1.5-fold changes (Table 2).

Focusing on the 58 protein spots, we then examined whether the SASP and/or MTX treatments suppressed the effects of IL-1β. As a result, the addition of SASP, MTX, SASP + MTX suppressed the IL-1β-induced changes ($p < 0.05$) in 4 (6.9%), 6 (10.3%), and 16 (27.6%) out of the 58 spots, respectively (Table 2, Fig. 3C, Supporting Information Fig. 2). A representative image of spot ID 464 is shown in Supporting Information Fig. 1.

Of note, the addition of SASP, MTX, and SASP + MTX enhanced the IL-1β-induced changes with significance only in 1 (1.7%), 1 (1.7%), and none (0%) out of the 58 spots, respectively (Table 2). Thus, we concluded that IL-1β affected the exosomal protein profiles greatly and that SASP, MTX, and SASP + MTX, in particular, SASP + MTX suppressed a considerable part of the effects of IL-1β.

3.4 Comparison of protein profile change between exosomes and their parent cells

It would be of interest whether the changes of exosomal protein profiles are simple reflections of those of the parent cells treated by the drugs. To investigate this point, we treated SW982 cells with SASP + MTX, which greatly affected the exosomal protein profiles. Then we detected cellular protein spots with significant intensity changes using 2D-DIGE, similarly as the analysis of exosomal proteins. As a result, we detected 994 protein spots in total (Supporting Information Fig. 3), out of which ten spots changed their intensity more than 1.5-fold or less than 1/1.5-fold ($p < 0.05$) (Supporting Information Table 1A). Importantly, seven out of the ten spots were not detected in the 2D panels of the exosomal proteins. The intensity of the remaining three spots, which showed 1.77-, 1.86-, and 2.08-fold increases by the SASP + MTX treatment in the whole cell extract, did not show any increase in the exosomal extracts (0.82-, 0.99-, and 0.92-fold change by the SASP + MTX treatment, respectively). On the other hand, in the 2D panels of the exosomal proteins, we detected 36 protein spots whose intensity was changed by SASP + MTX more than 1.5-fold or less than 1/1.5-fold ($p < 0.05$) (Table 1, Supporting Information Table 1B). Intensity of 32 out of the 36 exosomal spots did not show actual changes (0.92~1.20-fold) in the 2D panels of SW982 cellular proteins (Supporting Information Table 1B). Three (ID 673, 134, 40) out of the remaining four spots were not detected in the panel from the cell bodies, and remaining one (ID131) spot showed increased intensity in the panels of the cellular proteins in contrast with the decreased intensity in the panels of the exosomal proteins. Taking these data together, we concluded that the protein profile changes of exosomes by the SASP + MTX treatment were distinct from those of their parent cells.

3.5 Identification of exosomal proteins affected by SASP, MTX, and SASP + MTX under the conditions with/without IL-1β-treatment

We tried to identify the 35 exosomal protein spots which showed more than 2.0-fold or less than 1/2.0-fold intensity

Table 2. Number of protein spots intensity of which was significantly altered by the stimulation with IL-1β and the additional treatment with SASP and/or MTX

IL-1β-/nontreated			(IL-1β + SASP and/or MTX)- /IL-1β-treated			
Number of spots ($p < 0.05$, Difference >1.5 or 1/1.5)			Difference	SASP	MTX	SASP + MTX
58	Upregulated	16	Upregulated ($p < 0.05$)	1	1	0
			Not significant ($p \geqq 0.05$)	15	15	16
			Downregulated ($p < 0.05$)	0	0	0
	Downregulated	42	Upregulated ($p < 0.05$)	4	6	16
			Not significant ($p \geqq 0.05$)	38	36	26
			Downregulated ($p < 0.05$)	0	0	0

© 2015 WILEY-VCH Verlag GmbH & Co. KGaA, Weinheim

changes ($p < 0.05$) by the treatment with SASP and/or MTX as shown in Fig. 3B and Supporting Information Fig. 4. By MS analysis, we identified 17 out of the 35 protein spots as listed in Supporting Information Table 2. They were classified into three groups from the standpoint of biological function: immune system-related proteins of Ras-related protein Rab-7b and GTP-binding nuclear protein Ran; oxidative stress-related proteins of cytoglobin, NAD(P)H dehydrogenase 1, and glyceraldehyde-3-phosphate dehydrogenase; and others. The two immune system-related proteins were upregulated by the MTX treatment and more greatly by the SASP + MTX treatment. The three oxidative stress-related proteins were upregulated by the MTX treatment and more greatly by the SASP + MTX treatment.

Similarly, we tried to identify 21 exosomal protein spots, which showed more than 1.5-fold or less than 1/1.5-fold intensity changes ($p < 0.05$) by the treatment with IL-1β and the changes were suppressed by the simultaneous addition of SASP and/or MTX as shown in Fig. 3C and Supporting Information Figs. 2 and 4. By MS analysis, we identified 14 out of the 21 protein spots as listed in Supporting Information Table 3. They were also classified into three groups: immune system-related proteins of GTP-binding nuclear protein Ran and SH2 domain containing protein 1B; oxidative stress-related proteins of Clusterin, Thioredoxin-interacting protein, NAD(P)H dehydrogenase 1, and glyceraldehyde-3-phosphate dehydrogenase; and others. The two immune system-related proteins were downregulated by IL-1β treatment and the IL-1β-induced decreases were canceled by MTX or SASP + MTX treatment. The four oxidative stress-related proteins were downregulated by IL-1β treatment and the IL-1β-induced decreases were canceled by SASP or SASP + MTX treatment.

4 Discussion

In this study, we analyzed effects of SASP, MTX, and/or IL-1β on protein profiles of exosomes derived from a human synovial sarcoma cell line of SW982. Our findings are summarized as follows: (1) The SASP and/or MTX treatments altered the protein profiles of exosomes considerably. (2) IL-1β affected the exosome protein profiles greatly and SASP and/or MTX, in particular, SASP + MTX suppressed a considerable part of the effects of IL-1β. (3) In exosomes, the number of detected protein spots by 2D-DIGE was only about one-thirds of that in the cell bodies and protein spots greatly affected by the SASP + MTX treatment were different between the cell bodies and exosomes. (4) The proteins affected by SASP and/or MTX under the conditions with/without IL-1β were mostly those related to the immune system and oxidative stress.

On the first point, this study demonstrated for the first time that anti-rheumatic drugs affected the protein profiles of exosomes, to our knowledge (Table 1). The main body of the affected proteins was different between the SASP- and MTX-treated groups, which would reflect different pharmacological functions of the two drugs. Interestingly, a considerable number of protein spots were affected only by the combination of SASP and MTX. This indicates the additive and/or synergistic effects between SASP and MTX. This is in accordance with the actual clinical use of the two drugs in combination and the fact that the combination therapy is more effective than mono-therapy with only one of the two [12].

On the second point, IL-1β is known to stimulate synovium to produce inflammatory cytokines such as IL-6 and enzymes like cyclooxygenase-2 and MMPs in RA [19]. Exosomes from IL-1β-stimulated synovial fibroblasts were reported to upregulate MMP-13 expression in chondrocytes [14]. Thereby, IL-1β was expected to affect exosomal proteins. Here, we demonstrated that IL-1β greatly altered the protein profile of exosomes. Furthermore, a considerable part of the IL-1β-induced changes of the exosomal protein profiles was suppressed by the simultaneous treatments with SASP, MTX, and in particular, SASP + MTX (Table 2). Previous reports have revealed that SASP and MTX inhibit the IL-1β-induced inflammation [8, 11]. The suppression of the IL-1β-induced changes of exosomal proteins by SASP and/or MTX would be resulted from the blockage of the IL-1β signal pathway in the cell bodies.

On the third point, the changes of exosomal proteins by the SASP + MTX treatment were distinct from those of the cell bodies, in other words, the exosomal protein profiles were not a reflection of whole cell protein profiles. It has been reported that endosomal sorting complex required for transport (ESCRT) machinery are essential for both the formation of MVEs and the sorting of proteins into MVEs [20]. A part of the protein-sorting process by ESCRT machinery occurs in an ATP-dependent manner [20, 21]. MTX, which increases extracellular adenosine levels by inhibition of AMP deaminase and adenosine deaminase [7, 8], could influence ATP metabolism and affect the sorting process by ESCRT machinery. This point needs to be investigated in the future.

On the last point, we identified several functionally notable exosomal proteins altered by the treatment of SW982 cells with SASP, MTX, and/or IL-1β. Generally, exosomes released to the extracellular environment from parent cells have been reported to affect target cells by several mechanisms such as cellular binding via receptor-ligand interactions, fusing with target cell membrane or internalization by target cells by endocytosis [2]. Since exosomes have an ability to transfer specific proteins to target cells to deliver signals [22], functions of exosomes in target cells would be affected by change of exosomal protein profiles.

The identified proteins in this study were classified into three functional groups: immune system-related, oxidative stress-related, and others (Supporting Information Tables 2 and 3). The three immune system-related proteins suppress immune reaction by monocytes, T cells or NK cells [23–26], and the five oxidative stress-related proteins have protective functions from oxidative stress [27–30] or inhibit anti-oxidative molecule [31].

© 2015 WILEY-VCH Verlag GmbH & Co. KGaA, Weinheim

One example of the immune system-related proteins, Ras-related protein Rab-7b is one of Rab proteins that are small guanosine triphosphatases. Rab-7b is localized to late endosomes, lysosomes, and Trans Golgi Network, directing the transport between these compartments [32]. It has been reported that Rab-7b promotes degradation of Toll-like receptor (TLR) 4 and TLR9 and downregulates TLR4- and TLR9-mediated inflammatory responses in macrophages [23, 24]. It has been also reported that exosomes are taken up more effectively into macrophages than into nonphagocytic cells [33]. Together with our result that exosomal Rab-7b was increased by the SASP + MTX treatment, intake of the increased exosomal Rab-7b may provide anti-inflammatory effects in macrophages.

One example of the oxidative stress-related proteins, Cytoglobin, whose expression is elevated in response to oxidant exposure, exerts a protective influence against oxidative stress [27]. Several reports have shown that both SASP and MTX induce ROS, which inhibit cell proliferation and induce apoptosis [7, 34]. In our study, Cytoglobin in exosomes were increased by the treatment with SASP and MTX. Thereby, exosomes secreted from the SASP + MTX-treated cells may have protective functions from oxidative stress.

Lastly, differences between synovial sarcoma and synovial cells should be noted. The name of "synovial sarcoma" was originally given because it occurs primarily in the vicinity of large joints and resembles developing synovium [35, 36]. However, later, significant differences between synovial sarcoma and synovial cells have been evidenced [17, 36, 37]. Furthermore, synovial sarcoma has been found to arise in organs without synovial structure [36]. Thereby, synovial sarcoma is now classified as a miscellaneous tumor of uncertain histological origin, and is thought to arise from undifferentiated mesenchymal cells [15, 16]. On the other hand, SW982 has been frequently used as a substitute of synovial cells in studies on arthritis like RA, probably because it is extremely difficult to establish cell lines from primary synovial cells. Since SW982 and primary synovial cells have been reported to share similar physiological and immunological properties such as cytokine expression and signaling profiles [38, 39], SW982 would still be a useful cell line in studies on arthritis. Considering these circumstances, it should be investigated whether our findings from the experiments using SW982 can be applied to primary synovial cells in the future.

In conclusion, we have demonstrated that SASP and MTX changed exosomal protein profiles and that the drugs suppressed the IL-1β induced change of exosomal protein profiles. Our data implies possible roles of exosomes in the actions of SASP and MTX.

We would like to thank Professor M. Takagi and Mr. Y. Natsuki for their help in transmission electron microscopic analysis, Dr. S. Tatsunami for his help in statistical analysis and Ms. M. Katano for her excellent technical assistance.

The authors have declared no conflict of interest.

5 References

[1] Théry, C., Zitvogel, L., Amigorena, S., Exosomes: composition, biogenesis and function. *Nat. Rev. Immun.* 2002, *2*, 569–579.

[2] Simpson, R. J., Jensen, S. S., Lim, J. W., Proteomic profiling of exosomes: current perspectives. *Proteomics* 2008, *8*, 4083–4099.

[3] Clayton, A., Mitchell, J. P., Court, J., Mason, M. D., Human tumor-derived exosomes selectively impair lymphocyte responses to interleukin-2. *Cancer Res.* 2007, *67*, 7458–7466.

[4] Raposo, G., Nijman, H. W., Stoorvogel, W., Liejendekker, R. et al., B lymphocytes secrete antigen-presenting vesicles. *J. Exp. Med.* 1996, *183*, 1161–1172.

[5] Denzer, K., van Eijk, M., Kleijmeer, M. J., Jakobson, E. et al., Follicular dendritic cells carry MHC class II-expressing microvesicles at their surface. *J. Immunol.* 2000, *165*, 1259–1265.

[6] Valadi, H., Ekström, K., Bossios, A., Sjöstrand, M. et al., Exosome-mediated transfer of mRNAs and microRNAs is a novel mechanism of genetic exchange between cells. *Nat. Cell Biol.* 2007, *9*, 654–659.

[7] Wessels, J. A., Huizinga, T. W., Guchelaar, H. J., Recent insights in the pharmacological actions of methotrexate in the treatment of rheumatoid arthritis. *Rheumatology* 2008, *47*, 249–255.

[8] Cutolo, M., Sulli, A., Pizzorni, C., Seriolo, B. et al., Anti-inflammatory mechanisms of methotrexate in rhematoid arthritis. *Ann. Rheum. Dis.* 2001, *60*, 729–735.

[9] Matasic, R., Dietz, A. B., Vuk-Pavlovic, S., Maturation of human dendritic cells as sulfasalazine target. *Croat. Med. J.* 2001, *42*, 440–445.

[10] Fujiwara, M., Mitsui, K., Yamamoto, I., Inhibition of proliferative responses and interleukin-2 productions by salazosulfapyridine and its metabolites. *Jpn. J. Pharmacol.* 1990, *54*, 121–131.

[11] Aono, H., Hasunuma, T., Fujisawa, K., Nakajima, T. et al., Direct suppression of human synovial cell proliferation in vitro by salazosulfapyridine and bucillamine. *J. Rheumatol.* 1996, *23*, 65–70.

[12] Haagsma, C. J., van Riel, P. L., de Rooij, D. J., Vree, T. B. et al., Combination of methotrexate and sulphasalazine vs methotrexate alone: a randomized openclinical trial in rheumatoid arthritis patients resistant to sulphasalazine therapy. *Br. J. Rheumatol.* 1994, *33*, 1049–1055.

[13] Zhang, H. G., Liu, C., Su, K., Yu, S. et al., A membrane form of TNF-alpha presented by exosomes delays T cell activation-induced cell death. *J. Immunol.* 2006, *176*, 7385–7393.

[14] Kato, T., Miyaki, S., Ishitobi, H., Nakamura, Y. et al., Exosomes from IL-1β stimulated synovial fibroblasts induce osteoarthritic changes in articular chondrocytes. *Arthritis Res. Ther.* 2014, *16*, R163.

[15] Flecher, C. D. M., Unni, K. K., Mertens, F. (eds.), *World Health Organization Classification of Tumours. Pathology and Genetics of Tumours of Soft Tissue and Bone*, IARC Press, Lyon 2002, pp. 200–204.

© 2015 WILEY-VCH Verlag GmbH & Co. KGaA, Weinheim

[16] Liu, A., Feng, B., Gu, W., Cheng, X. et al., The CD133+ subpopulation of the SW982 human synovial sarcoma cell line exhibits cancer stem-like characteristics. *Int. J. Oncol.* 2013, *42*, 1399–1407.

[17] Miettinen, M., Virtanen, I., Synovial sarcoma—a misnomer. *Am. J. Pathol.* 1984, *117*, 18–25.

[18] Shimada, S., Nakamura, M., Tanaka, Y., Tsutsumi, K. et al., Crosslinking of the CD69 molecule enhances S100A9 production in activated neutrophils. *Microbiol. Immunol.* 2007, *51*, 87–98.

[19] Choy, E. H., Panayi, G. S., Cytokine pathways and joint inflammation in rheumatoid arthritis. *N. Engl. J. Med.* 2001, *344*, 907–916.

[20] Hurley, J. H., ESCRT complexes and the biogenesis of multivesicular bodies. *Curr. Opin. Cell Biol.* 2008, *20*, 4–11.

[21] Record, M., Subra, C., Silvente-Poirot, S., Poirot, M., Exosomes as intercellular signalosomes and pharmacological effectors. *Biochem. Pharmacol.* 2011, *81*, 1171–1182.

[22] Taylor, D. D., Gercel-Taylor, C., Exosomes/microvesicles: mediators of cancer-associated immunosuppressive microenvironments. *Semin. Immunopathol.* 2011, *33*, 441–454.

[23] Wang, Y., Chen, T., Han, C., He, D. et al., Lysosome-associated small rab GTPase Rab7b negatively regulates TLR4 signaling in macrophages by promoting lysosomal degradation of TLR4. *Blood* 2007, *110*, 962–971.

[24] Yao, M., Liu, X., Li, D., Chen, T. et al., Late endosome/lysosome-localized Rab7b suppresses TLR9-initiated proinflammatory cytokine and type I IFN production in macrophages. *J. Immunol.* 2009, *183*, 1751–1758.

[25] Qiao, X., Pham, D. N., Luo, H., Wu, J., Ran overexpression leads to diminished T cell responses and selectively modulates nuclear levels of c-Jun and c-Fos. *J. Biol. Chem.* 2010, *285*, 5488–5496.

[26] Roncagalli, R., Taylor, J. E., Zhang, S., Shi, X. et al., Negative regulation of natural killer cell function by EAT-2, a SAP-related adaptor. *Nat. Immunol.* 2005, *6*, 1002–1010.

[27] Oleksiewicz, U., Liloglou, T., Field, J. K., Xinarianos, G., Cytoglobin: biochemical, functional and clinical perspective of the newest member of the globin family. *Cell Mol. Life Sci.* 2011, *68*, 3869–3883.

[28] Ralser, M., Wamelink, M. M., Kowald, A., Gerisch, B. et al., Dynamic rerouting of the carbohydrate flux is key to counteracting oxidative stress. *J. Biol.* 2007, *6*, 10.

[29] Dinkova-Kostova, A. T., Talalay, P., NAD(P)H: quinone acceptor oxidoreductase 1 (NQO1), a multifunctional antioxidant enzyme and exceptionally versatile cytoprotector. *Arch. Biochem. Biophys.* 2010, *501*, 116–123.

[30] Poon, S., Easterbrook-Smith, S. B., Rybchyn, M. S., Carver, J. A. et al., Clusterin is an ATP-independent chaperone with very broad substrate specificity that stabilizes stressed proteins in a folding-competent state. *Biochemistry* 2000, *39*, 15953–15960.

[31] Nishiyama, A., Matsui, M., Iwata, S., Hirota, K. et al., Identification of thioredoxin-binding protein-2/vitamin D(3) up-regulated protein 1 as a negative regulator of thioredoxin function and expression. *J. Biol. Chem.* 1999, *274*, 21645–21650.

[32] Bucci, C., Bakke, O., Progida, C., Rab7b and receptors trafficking. *Commun. Integr. Biol.* 2010, *3*, 401–404.

[33] Feng, D., Zhao, W. L., Ye, Y. Y., Bai, X. C., Liu, R. Q. et al., Cellular internalization of exosomes occurs through phagocytosis. *Traffic* 2010, *11*, 675–687.

[34] Linares, V., Alonso, V., Domingo, J. L., Oxidative stress as a mechanism underlying sulfasalazine-induced toxicity. *Expert. Opin. Drug Saf.* 2011, *10*, 253–263.

[35] Smith, L. W., Synoviomata. *Am. J. Pathol.* 1927, *3*, 355–364.

[36] Nagayama, S., Katagiri, T., Tsunoda, T., Hosaka, T. et al., Genome-wide analysis of gene expression in synovial sarcomas using a cDNA microarray. *Cancer Res.* 2002, *62*, 5859–5866.

[37] Smith, M. E., Fisher, C., Wilkinson, L. S., Edwards, J. C., Synovial sarcoma lacks synovial differentiation. *Histopathology* 1995, *26*, 279–281.

[38] Yamazaki, T., Yokoyama, T., Akatsu, H., Tukiyama, T. et al., Phenotypic characterization of a human synovial sarcoma cell line, SW982, and its response to dexamethasone. *In Vitro Cell Dev. Biol. Anim.* 2003, *39*, 337–339.

[39] Chang, J. H., Lee, K. J., Kim, S. K., Yoo, D. H. et al., Validity of SW982 synovial cell line for studying the drugs against rheumatoid arthritis in fluvastatin-induced apoptosis signaling model. *Indian J. Med. Res.* 2014, *139*, 117–124.

© 2015 WILEY-VCH Verlag GmbH & Co. KGaA, Weinheim

RESEARCH ARTICLE

International Journal of Geriatric Psychiatry

Serum peptides as candidate biomarkers for dementia with Lewy bodies

Itsuku Suzuki[1], Miwa Noguchi[1], Mitsumi Arito[2], Toshiyuki Sato[2], Kazuki Omoteyama[2], Mioto Maedomari[1], Hiroshi Hasegawa[1], Naoya Suematsu[2], Kazuki Okamoto[2], Tomohiro Kato[2], Noboru Yamaguchi[1] and Manae S. Kurokawa[3]

[1]Department of Neuropsychiatry, St. Marianna University School of Medicine, Kawasaki, Japan
[2]Clinical Proteomics and Molecular Medicine, St. Marianna University Graduate School of Medicine, Kawasaki, Japan
[3]Disease Biomarker Analysis and Molecular Regulation, St. Marianna University Graduate School of Medicine, Kawasaki, Japan
Correspondence to: M. S. Kurokawa, MD, PhD, E-mail: manae@marianna-u.ac.jp

Objective: For diagnosis of dementia with Lewy bodies (DLB), we tried to find blood biomarkers for the disease.

Methods: Serum peptides were comprehensively detected by mass spectrometry. Peptides of interest were identified by tandem mass spectrometry.

Results: One hundred forty-six peptides were detected in a training set consisting of 30 DLB patients, 30 patients with Alzheimer's disease (AD), and 28 healthy control (HC) subjects. Multivariate analysis for discriminating the DLB group from the non-DLB (AD and HC) group using ion intensity of four peptides (2898, 4052, 4090, and 5002 m/z) showed sensitivity of 93.3% and specificity of 87.9% (DLB/nonDLB-4P model). In a testing set consisting of 20 DLB patients, 30 AD patients, and 14 HC subjects, this model showed sensitivity of 90.0% and specificity of 88.6%. DLB/nonDLB-4P model detected 86.7% and 90.0% of the AD patients as non-DLB in the training and testing sets, respectively, and discriminated all the 15 patients with amnestic mild cognitive impairment as non-DLB. Notably, a combination of two peptides (1737 and 5002 m/z) showed sensitivity of 95.0% and specificity of 93.3% for discriminating the DLB group from the AD group (DLB/nonDLB-2P model) in the testing set. The peptides used in these models included fragments from complement 4b, Wnt-2b, and lipopolysaccharide-binding protein, which were reported to be involved in the pathology of DLB or Parkinson's disease and hippocampal neurogenesis.

Conclusions: Serum peptide profiles would provide useful DLB biomarker candidates, which may be implicated in the pathophysiology of the disease. Copyright © 2015 John Wiley & Sons, Ltd.

Key words: dementia with Lewy bodies; biomarkers; serum peptides; mass spectrometry
History: Received 25 October 2014; Accepted 29 January 2015; Published online 6 March 2015 in Wiley Online Library (wileyonlinelibrary.com)
DOI: 10.1002/gps.4274

Introduction

Dementia with Lewy bodies (DLB) is a neurodegenerative disorder associated with cognitive decline, visual hallucinations, and parkinsonism. DLB is the second most common subtype of senile dementia after Alzheimer's disease (AD), accounting for 10–15% of the dementia (McKeith *et al.*, 2004). At present, diagnosis of DLB is made by the revised criteria in 2005 (McKeith *et al.*, 2005), in which the diagnosis is based on clinical symptoms and brain imaging. However, evaluation of the symptoms and imaging could be different among experts. Furthermore, differential diagnosis of DLB from AD is difficult because of the overlap in clinical presentation. Simple and non-invasive biomarkers that can differentiate DLB from AD are essential for the diagnosis of DLB.

Several biological fluid markers have been explored for the diagnosis of DLB such as α-synuclein, amyloid beta 40/42, tau/phosphorylated-tau, neurofilaments,

Copyright © 2015 John Wiley & Sons, Ltd.

DJ-1, heart-type fatty acid-binding protein (H-FABP), and biogenic amines and their metabolites (Mollenhauer *et al.*, 2008; Ohrfelt *et al.*, 2009; Bibl *et al.*, 2006; Parnetti *et al.*, 2008; Clark *et al.*, 2003; Mollenhauer *et al.*, 2005; de Jong *et al.*, 2007; Waragai *et al.*, 2007; Mollenhauer *et al.*, 2007; Wada-Isoe *et al.*, 2008; Steinacker *et al.*, 2004; Herbert *et al.*, 2014). Comprehensive studies have also found several proteins as potential biomarkers for DLB (Wada-Isoe *et al.*, 2007; Abdi *et al.*, 2006). Among them, α-synuclein, the main constituent of Lewy bodies, has been the most intensively studied biomarker; however, the results are still controversial (Mollenhauer *et al.*, 2008; Ohrfelt *et al.*, 2009). Although most of these markers have been examined in cerebrospinal fluid, blood would be a more convenient material for biomarkers.

In this study, we tried to find novel blood biomarkers for DLB, which could efficiently differentiate DLB from AD. For this aim, we comprehensively detected serum peptides from DLB patients, AD patients, and healthy control (HC) subjects. Our analysis would provide useful blood biomarker candidates for the diagnosis of DLB.

Materials and methods

Patients

The diagnoses of DLB, AD, and mild cognitive impairment (MCI) were made according to the respective criteria (McKeith *et al.*, 2005; American Psychiatric Association, 1994; McKhann *et al.*, 1984; Petersen *et al.*, 1999). Japanese patients with those diseases and HC subjects, who were 55 years old or more, were enrolled in this study (Table 1). Patients with Parkinson's disease (PD), dementia other than DLB and AD, and psychiatric diseases other than dementia were excluded. Either brain computed tomography or magnetic resonance imaging was performed in the enrolled patients. All the MCI patients were with amnestic MCI.

Peripheral blood was obtained from the subjects with written informed consents. The study protocol conformed to the ethical guidelines of the Declaration of Helsinki revised in 2008 and was approved by the ethics committee of St. Marianna University School of Medicine.

Analysis of serum peptide profiles

Serum peptides were purified by weak cation exchange (MB-WCX, Bruker Daltonics, Ettlingen, Germany). Ion intensity of peptides was measured by matrix-assisted laser desorption/ionization time-of-flight mass spectrometer (Ultraflex, Bruker Daltonics). The ion intensity was compared among the DLB, AD, MCI, and HC groups by ClinPro Tools (Bruker Daltonics). Peptides were designated as p + peptide mass/charge ratio (i.e., p2989 indicates a peptide with 2989 m/z). Amino acid sequences of peptides were identified by tandem mass spectrometry using nano-HPLC system (1200 Series; Agilent Technologies, Palo Alto, CA, USA) connected to an ion trap mass spectrometer (HCT Ultra, Bruker Daltonics) as described previously (Noguchi *et al.*, 2014).

Statistical analysis

Significance of peptide ion intensity difference was calculated by Student's *t*-test. Discriminant models were generated using orthogonal partial least square-discriminant analysis (OPLS-DA; SIMCA-P+, Umetrics, Umea, Sweden). Receiver operating characteristic (ROC) analysis was conducted by JMP software (SAS Institute, Cary, NC, USA). Significance of prediction values of the discriminant models was calculated by Wilcoxon signed-rank test.

Results

Comparison of serum peptide ion intensity among the DLB, AD, and HC groups

To find serum peptides useful for the discrimination of DLB from AD and HC, we comprehensively compared ion intensity of serum peptides between DLB patients and AD patients, and between DLB patients and HC subjects in the training set (Table 1). A total of 146 peptide ion peaks were detected (data not shown). Nineteen peptides showed at least 1.2-fold higher ion intensity in the DLB group than in the AD group ($p < 0.05$) (Table 2). Conversely, 10 peptides showed at least 1.2-fold lower ion intensity in the DLB group than in the AD group. Similarly, 32 and 11 peptides showed at least 1.2-fold higher and lower ion intensity in the DLB group than in the HC group, respectively. Serum peptide profiles of DLB were different from those of AD and HC.

Discriminant models between the DLB and AD groups

To discriminate DLB from AD, we performed supervised multivariate analysis of serum peptide profiles. Ion

Copyright © 2015 John Wiley & Sons, Ltd.

Table 1 Clinical information of the subjects

	DLB ($n = 50$)		AD ($n = 60$)		MCI ($n = 15$)	HC ($n = 42$)	
	Training set ($n = 30$)	Testing set ($n = 20$)	Training set ($n = 30$)	Testing set ($n = 30$)		Training set ($n = 28$)	Testing set ($n = 14$)
Male : female	15:15	12:8	16:14	16:14	7:8	15:13	9:5
Age[#] (years old)	78.5 ± 5.8	8.4 ± 5.0	9.4 ± 6.0	79.4 ± 5.0	77.7 ± 4.8	70.8 ± 7.1*	70.6 ± 6.9*
MMSE[#]	15.7 ± 9.7	20.4 ± 7.1	18.3 ± 3.4	22.5 ± 5.6	26.9 ± 1.3	29.1 ± 1.4	29.2 ± 1.2
Disease duration[#]	3y2m ± 1y10m		1y9m ± 1y4m		2y3m ± 1y9m	NA	
Physical disease[$]	37		44		12	NA	
	HT, 12; MT, 10; DM, 8; IHD, 6; HL 3; HU, 3; Others, 11		HT, 28; HL, 13; MT, 12; IHD, 7; DM, 6; COPD, 3; CI, 3; Others, 6		HT, 8; MT, 4; HL, 3; HU, 3; DM, 2; IHD, 2; Others, 5		
Inflammatory disease[$]	1 (SSc)		1 (RA)		1 (SjS)	NA	
Liver/renal dysfunction[$]	4/3		2/1		0/1	NA	
Medication[$]	37		44		1	NA	
	23 DON, 6 GAL, 5 MEM, 3 DON+MEM		(44 DON)		(1 GAL)		

[#]Means ± standard deviations are shown. Statistical significance of age difference was calculated by Wilcoxon Signed-rank test. The HC groups showed significant differences of age against all the disease groups.

*$p < 0.05$.

[$]Number of patients are shown. A part of the patients were with multiple physical diseases. One MCI patient was prophylactically treated.

DLB, dementia with Lewy bodies; AD, Alzheimer's disease; HC, healthy control; MCI, mild cognitive impairment; MMSE, Mini-Mental State Examination; y, years; m, months; HT, hypertension, MT, malignant tumors; DM, diabetes mellitus; IHD, ischemic heart diseases; HL, hyperlipidemia; HU, hyperuricemia; COPD, chronic obstructive pulmonary disease; CI, cerebral infarction; SSc, systemic sclerosis; RA, rheumatoid arthritis; SjS, Sjogren's syndrome; DON, donepezil; GAL, galantamine; MEM, memantine; NA, not applicable.

Copyright © 2015 John Wiley & Sons, Ltd.

Table 2 Comparison of peptide ion intensity

Peptides ion intensity	Differences (x-folds)	Numbers of peptides	
		DLB/AD	DLB/HC
	$2.0 \leq x$	0	1
Increased	$1.5 \leq x$	5	10
	$1.2 \leq x$	19	32
	$-1.2 < x < 1.2$	2	6
	$-1.2 \geq x$	10	11
Decreased	$-1.5 \geq x$	1	4
	$-2.0 \geq x$	0	2

Numbers of peptides, ion intensity of which was significantly different in the DLB group from that in the AD group or the HC group, are shown ($p < 0.05$).
DLB, dementia with Lewy bodies; AD, Alzheimer's disease; HC, healthy control.

intensity of all the 146 peptides was analyzed to generate discriminant models between the DLB and AD groups in the training set. As a result, a discriminant model generated with all the 146 peptides (DLB/AD-146P model) accurately distinguished the 30 DLB patients from the 30 AD patients (Figure 1(A)). Explanatory variable (R^2) of this model was 0.858, which indicated its high potential for the discrimination. Predictor variable (Q^2) of this model was 0.563, indicating its high potential for the prediction, because Q^2 is desired to exceed 0.4 in biological studies (Hatsugai *et al.*, 2010).

We next tried to completely discriminate between the DLB and AD groups using a minimal number of peptides. For this aim, we selected peptides from the 146 peptides in the DLB/AD-146P model, using their variable importance of the projection (VIP) and S-plot parameters. VIP indicates contribution of each peptide to generate the model. S-plot shows reliability (p(corr)) and magnitude (w) of each peptide, indicating the usefulness as a biomarker candidate and the difference of its ion intensity between the two groups, respectively (Figure 1 (B)). We found that a combination of 13 peptides completely discriminated between the two groups (DLB/AD-13P model) (Figure 1(C)). DLB/AD-13P model provided a high R^2 of 0.803 and Q^2 of 0.625. VIP of the 13 peptides was varied from 0.231 to 2.100, indicating different contributions of the individual peptides to generate this model (Figure 1(D)). These peptides would be useful for discriminating DLB from AD.

Discriminant models between the DLB and HC groups

We next tried to discriminate between the DLB and HC groups in the training set. The model generated with 146 peptides (DLB/HC-146P model) accurately distinguished the two groups with a relatively high R^2 of 0.750 and a high Q^2 of 0.546 (Figure 1(E)). We selected important peptides according to the VIP and S-plot parameters and found that only six peptides were necessary for complete discrimination (DLB/HC-6P model, Figure 1(F)–(H)). This model showed a fairly high R^2 of 0.707 and a high Q^2 of 0.606. VIP of the six peptides was from 0.768 to 1.351, indicating a relatively similar contribution of the peptides to generate this model (Figure 1(H). These peptides were thought to have a pivotal role in the discrimination of DLB from HC.

Discriminant models between the DLB and non-DLB groups

To find a specific biomarker for DLB, we tried to discriminate the DLB group from the AD and HC (non-DLB) group in the training set. The model generated with all the 146 peptides (DLB/nonDLB-146P model) completely discriminated between the DLB and non-DLB groups with a high R^2 of 0.898, but with a relatively low Q^2 of 0.339 (Figure 1(I), Table 3). When a part of the peptides was selected according to the VIP and S-plot parameters, no DLB/nonDLB-discriminant model that completely discriminated the two groups was obtained (data not shown). Therefore, we used the ion intensity of the 13 peptides of DLB/AD-13P model and the six peptides of DLB/HC-6P model to create a new model that discriminated the DLB group from the non-DLB group. Because two peptides overlapped between the 13 and six peptides, 17 peptides in total were used for the discrimination (DLB/nonDLB-17P model). This model nearly completely discriminated between the two groups, in which only one DLB patient was diagnosed as non-DLB (Figure 1(J)–(L), Table 3). We subsequently started to select important peptides from the 17 peptides to find a minimal number of peptides that efficiently discriminated the DLB group from the non-DLB group.

We first examined the ability of each of the 17 peptides' ion intensity to discriminate between the DLB and non-DLB groups, using area under the ROC curve (AUROC) (Figure 2(A)). The AUROC of the 17 peptides' ion intensity ranged from 0.541 to 0.836. Next, we removed the peptide with the lowest AUROC and then generated a DLB/nonDLB-discriminant model with the remaining peptides. By repeating this process, we generated 17 models. The AUROC of these models was gradually decreased from

Copyright © 2015 John Wiley & Sons, Ltd.

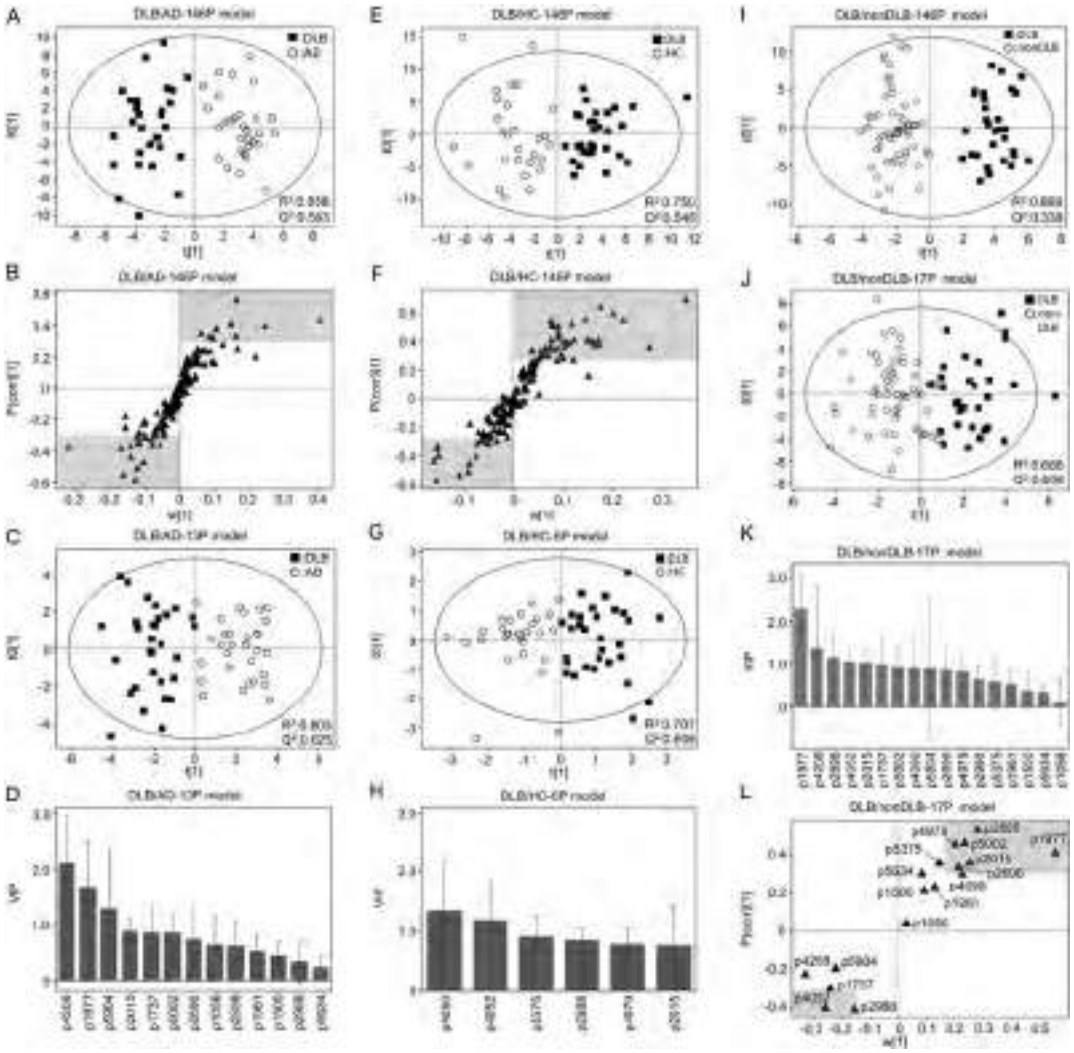

Figure 1 Generation of dementia with Lewy bodies (DLB)-discriminant models. (A). Ion intensity of the 146 peptides detected in 30 DLB patients and 30 Alzheimer's disease (AD) patients in the training set was subjected to orthogonal partial least square-discriminant analysis (OPLS-DA) (DLB/AD-146P model). X axis indicates the first principal component for the discrimination. (B). S-plot of the peptides in DLB/AD-146P model. Magnitude (w and x axis) and reliability (p(corr) and y axis) of the peptides are visualized. Shaded areas of p(corr) > | ± 0.2956 | included 27 peptides. (C). The second discriminant model between the DLB and AD groups using a minimum number of peptides. To generate this model, the 27 peptides with p(corr) > | ± 0.2956 | in DLB/AD-146 model were selected (Figure 1(B)). A discriminant model generated with the 27 peptides completely differentiated DLB and AD (data not shown). Each of the 27 peptides was examined to be necessary for the complete discrimination, by which a combination of 13 peptides was found to discriminate completely between the DLB and AD groups (DLB/AD-13P model). (D). variable importance of the projection (VIP) of the 13 peptides. (E). Ion intensity of the 146 peptides detected in 30 DLB patients and 28 healthy control (HC) subjects in the training set was subjected to OPLS-DA (DLB/HC-146P model). (F). S-plot of the peptides in DLB/HC-146P model. Shaded areas of p(corr) ≥ 0.28 and p(corr) ≤ -0.27 included 36 peptides. (G). The second discriminant model between the DLB and HC groups using a minimum number of peptides. To generate this model, the 36 peptides with p(corr) ≥ 0.28 or p(corr) ≤ -0.27 (Figure 1(F)), which completely differentiated the DLB group from the HC group (data not shown), were selected and examined one by one to be necessary for the complete discrimination. A combination of six peptides was found to discriminate completely between the DLB and HC groups (DLB/HC-6 model). (H). VIP of the peptides in DLB/HC-6P model. (I). Ion intensity of the 146 peptides detected in 30 DLB patients and 58 non-DLB patients and subjects in the training set was subjected to OPLS-DA (DLB/nonDLB-146P model). (J). The second discriminant model between the DLB and non-DLB groups using 17 peptides (DLB/nonDLB-17P model) is shown. (K). VIP values of the 17 peptides. (L). S-plot of the 17 peptides. Shaded areas show those with p(corr) ≥ | ± 0.3 | and w ≥ | ± 0.15 |.

0.997 to 0.836 according to the decrease of the number of peptides (Figure 2(B)). The model generated with six peptides (DLB/nonDLB-6P model) showed sensitivity and specificity of more than 80.0% (Figure 2 (C) and (D), Table 3). Interestingly, a model generated with two peptides (DLB/nonDLB-2P model) showed higher AUROC than the model generated with three peptides (Figure 2(B)), displaying

Copyright © 2015 John Wiley & Sons, Ltd.

Table 3 Evaluation and validation of DLB/nonDLB-discriminant models

Models (Peptides)		Training set (DLB 30, nonDLB 58)					Testing set (DLB 20, nonDLB 44)				
		DLB	nonDLB	Sens (%)	Spec (%)	AUROC	DLB	nonDLB	Sens (%)	Spec (%)	AUROC
146P				100.0	100.0	1.000			45.0	97.7	0.920
	DLB	30	0				9	1			
	nonDLB	0	58				11	43			
17P				96.7	100.0	0.998			65.0	95.5	0.966
	DLB	29	0				13	2			
	nonDLB	1	58				7	42			
6P				90.0	81.0	0.923			90.0	90.9	0.943
(p1737,p2898, p2988	DLB	27	11				18	4			
p4052,p4979, p5002)	nonDLB	3	47				2	40			
2P				80.0	87.9	0.882			95.0	86.4	0.928
(p1737, p5002)	DLB	24	7				19	6			
	nonDLB	6	51				1	38			
3P				96.7	81.0	0.925			95.0	84.1	0.936
(p4052, p4090,	DLB	29	11				19	7			
p4979)	nonDLB	1	47				1	37			
4P				93.3	87.9	0.956			90.0	88.6	0.935
(p2898, p4052,	DLB	28	7				18	5			
p4090, p5002)	nonDLB	2	51				2	39			

Sens, sensitivity; Spec, specificity ; DLB, dementia with Lewy bodies; AUROC, area under the receiver operating characteristic.

sensitivity and specificity of 80.0% or more (Figure 2 (C) and (E), Table 3).

Furthermore, we used S-plot parameters of the DLB/nonDLB-17P model to select valuable peptides from the 17 peptides. Specifically, nine peptides with $p(corr) > |\pm 0.3|$ and $w > |\pm 0.15|$ were selected (Figure 1(L)), and all the 84 combinations of three out of the nine peptides were subjected to generation of DLB/nonDLB-discriminant models. As a result, 7 out of the 84 models showed sensitivity and specificity of 80.0% or more (data not shown). To find more useful models, we added one out of the nine peptides to these seven models with three peptides to generate models with four peptides. Similarly, we deleted one peptide from the seven models with three peptides to generate models with two peptides. As a result, 19 models with four peptides and one model with two peptides showed sensitivity and specificity of 80.0% or more (data not shown). These 26 DLB/nonDLB-discriminant models consisting of two to four peptides were subjected to validation together with the aforementioned models.

Validation of the DLB/nonDLB-discriminant models

To find useful models for discrimination of DLB, the models generated using the training set were validated using a testing set (Table 1). As a result, specificity of DLB/nonDLB-146P model and DLB/nonDLB-17P model was also high in the testing set (97.7% and 95.5%, respectively), whereas sensitivity of these models was low (45.0% and 65.0%, respectively) (Table 3). Notably, the DLB/nonDLB-6P model showed high sensitivity of 90.0% and high specificity of 90.9% in the testing set. The DLB/nonDLB-2P model also showed high sensitivity of 95.0% and high specificity of 86.4%. Among the 26 models generated using S-plot parameters, two models generated with three peptides and eight models generated with four peptides showed sensitivity and specificity of 80.0% or more in the testing set (data not shown). Among these 10 models, a model generated with three peptides of p4052, p4090, and p4979 showed sensitivity of 95.0% and specificity of 84.1% (DLB/nonDLB-3P model) (Figure 2(F), Table 3). Similarly, another model generated with four peptides of p2898, p4052, p4090, and p5002 showed sensitivity of 90.0% and specificity of 88.6% (DLB/nonDLB-4P model) (Figure 2(G), Table 3). These DLB/nonDLB-6P, DLB/nonDLB-2P, DLB/nonDLB-3P, and DLB/nonDLB-4P models would be useful biomarker candidates for discriminating DLB from non-DLB.

Discriminant ability for the AD, MCI, and HC groups by DLB/nonDLB-discriminant models

We examined the ability of the DLB/nonDLB-6P, DLB/nonDLB-2P, DLB/nonDLB-3P, and DLB/nonDLB-

Copyright © 2015 John Wiley & Sons, Ltd.

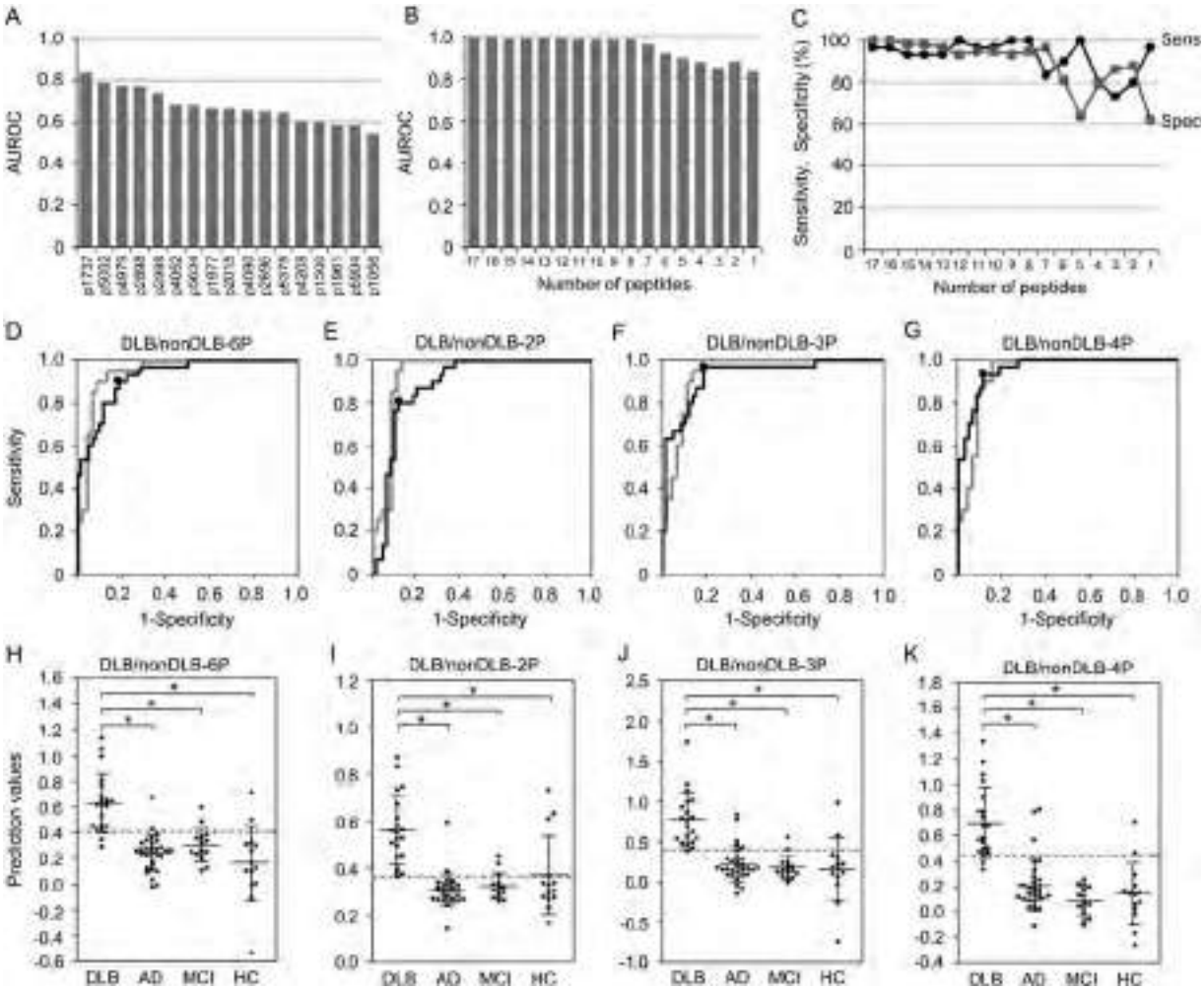

Figure 2 Generation of dementia with Lewy bodies (DLB)/nonDLB-discriminant models with a small number of peptides. (A). Ion intensity of each of the 17 peptides was used to generate an orthogonal partial least square-discriminant analysis (OPLS-DA) model to discriminate between the DLB and non-DLB groups in the training set. Prediction values of individual patients and subjects were calculated in each model as an ideal DLB patient as 1.0 and as an ideal non-DLB patient or subject as 0.0. Area under the receiver operating characteristic (AUROC) of each peptide model, calculated using the prediction values, are shown. (B). To detect useful DLB/nonDLB-discriminant models with a small number of peptides, the peptide with the lowest AUROC was deleted, and the models were generated with the remaining peptides. Seventeen models were obtained by repetition of this process. AUROC of each DLB/nonDLB-discriminant model are shown by the number of peptides used in the models. (C). Sensitivity and specificity of the 17 DLB/nonDLB-discriminant models (Figure 2(B)) are shown. (D)–(K). ROC curves in the training and testing sets and prediction values in the testing set are shown ((D) and (H), DLB/nonDLB-6P model; (E), and (I), DLB/nonDLB-2P model; (F) and (J), DLB/nonDLB-3P model; (G) and (K), DLB/nonDLB-4P model). Black lines, training set; gray lines, testing sets (D–G). Dots (D–G) and dotted lines (H–K) shows the cutoff points that shows the maximal values of "sensitivity + specificity" in the training set. Significance of the differences between the DLB group and the other groups is shown (*$p < 0.05$, H–K).

4P models to discriminate the AD patients, MCI patients, and HC subjects as non-DLB, using the testing set and 15 MCI patients. All four models showed good discriminant ability for the AD group, detecting 83.3–93.3% of the AD patients as non-DLB (Figure 2(H)–(K)). The DLB/nonDLB-6P and DLB/nonDLB-2P models showed the best discriminant ability, detecting 93.3% of the AD patients as non-DLB (Figure 2(H) and (I)). The DLB/nonDLB-4P model also showed good ability, detecting 90.0% of the AD patients as non-DLB (Figure 2(K)). This model detected 86.7% of the AD patients as non-DLB in the training set (data not shown). The discriminant ability for the MCI patients by the four models was 86.7–100.0% in the testing set (Figure 2(H)–(K)). The DLB/nonDLB-4P model showed the best result, detecting all the MCI patients as non-DLB (Figure 2(K)). The discriminant ability for the HC group was 85.7% in all the models except the DLB/nonDLB-2P model (71.4%) (Figure 2(H)–(K)). These four models overall showed good discriminant ability for the AD, MCI, and

Copyright © 2015 John Wiley & Sons, Ltd.

HC groups, except the DLB/nonDLB-2P model for the HC group.

Identification of the peptides

Finally, we tried to identify the peptides involved in the discrimination of DLB. Peptides, the ion intensity of which showed at least 1.5-fold difference between the DLB and AD groups (six peptides, Table 2) or between the DLB and HC groups (14 peptides) and which were used in DLB/AD-13P model (13 peptides) or DLB/HC-6P model (six peptides), were subjected to the identification. As eight peptides were overlapped among the four peptide-groups, a total of 27 peptides were subjected to the identification. As a result, 11 peptides and their parent proteins were identified (Table 4). The p1462, p1613, p2860, and p2988 were identified as fragments derived from fibrinogen alpha chain (FIBA). Among the peptides used in DLB/nonDLB-6P, DLB/nonDLB-2P, DLB/nonDLB-3P, and DLB/nonDLB-4P models, p1737, p2898, and p4052 were identified as fragments of complement C4b, Wnt-2b, and lipopolysaccharide-binding protein (LBP), respectively. Different expressions and/or fragmentations of these proteins between the DLB group and the AD or HC group may be due to the specific disease mechanism of DLB.

Discussion

We comprehensively analyzed serum peptides to find a blood biomarker for DLB. Serum peptide profiles would reflect characteristic dynamics of proteins such as production and fragmentation of proteins and peptides. In the case of neurodegenerative diseases, aberrant production and fragmentation of proteins and peptides in neural tissue can be reflected by serum peptide profiles. Indeed, DLB showed different serum peptide profiles from those in AD and HC (Table 2). The number of peptides that showed different ion intensities between the DLB and HC groups was larger than that between the DLB and AD groups, indicating that DLB and AD possess relatively similar serum peptide profiles.

Because our subjects displayed broad ranges of age and dementia degrees, we examined whether these factors influenced serum peptide profiles. As for dementia degrees, serum protein profiles hardly discriminated severe/moderate dementia patients (Mini-Mental State Examination (MMSE) < 20, $n = 45$) from mild dementia patients ($20 \leq$ MMSE $<$ 24, $n = 32$) (data not shown). The dementia degrees would not influence serum protein profiles. On the other hand, serum peptide profiles were found to roughly discriminate the elder half (age ≥ 72 years, $n = 21$) and the younger half (age < 72 years, $n = 21$) of the HC subjects (data not shown). Age would influence serum peptide profiles. However, DLB/non-DLB discrimination by age itself showed only 107.3% of "sensitivity + specificity" in the testing set at the maximum (cutoff age, 74 years) (data not shown). In contrast, our DLB/nonDLB-2P, DLB/nonDLB-3P, DLB/nonDLB-4P, and DLB/nonDLB-6P models showed much higher "sensitivity + specificity" of 178.6–181.4% in the testing set (Table 3). Thus, our peptide models are thought to contain critical discriminant factors independent from age.

When we validated DLB/nonDLB-discriminant models using the testing set, the models with a small number of peptides showed better results than the DLB/nonDLB-146P and DLB/nonDLB-17P models (Table 3). Selection of peptides that greatly contributed to the discrimination was effective for generation of good models. The DLB/nonDLB-6P model showed high sensitivity of 90.0% and high specificity of 90.9% in the testing set, therefore, this model would be useful for screening of DLB (Figure 2(H), Table 3). Similarly, because the DLB/nonDLB-2P model showed the best discriminant ability between the DLB and AD groups in the testing set (sensitivity of 95.0% and specificity of 93.3%, Figure 2(I), Table 3), the model would be a useful biomarker for the differential diagnosis of DLB and AD. Collectively, the DLB/nonDLB-4P model showed the best result among the models, detecting 90.0% of the DLB group as DLB, 88.6% of the non-DLB group as non-DLB, 90.0% of the AD group as non-DLB, and 85.7% of the HC group as non-DLB in the testing set (Table 3, Figure 2(K)). Interestingly, this model also detected 100% of the amnestic MCI patients as non-DLB. This result was compatible with the report that amnestic MCI is at risk of developing AD rather than DLB (Ferman *et al.*, 2013). The establishment of a simultaneous measurement system of the peptides in these models by enzyme-linked immunosorbent assay or quantitative mass spectrometry would facilitate the use of these biomarker candidates.

We examined correlations between prediction values of DLB/nonDLB-2P, DLB/nonDLB-3P, DLB/nonDLB-4P, and DLB/nonDLB-6P models and disease duration in groups of the 50 DLB patients, the 60 AD patients, and the 15 MCI patients, however, no correlation was found (data not shown). Thus, these models would be useful in patients with various disease durations. The

Copyright © 2015 John Wiley & Sons, Ltd.

Table 4 Identification of characteristic serum peptides in DLB

Peptides*	Selections#		Proteins	Accession ID	MW (Da)*		Ion	Errors	Confirmed sequences	Modification$
	folds	Models			Theoretical	Observed	scores	(Da)		
p1462	1.560 (/HC)	–	Fibrinogen alpha chain	FIBA_HUMAN (gil1706799)	1464.6	1464.8	103	0.2013	^{21}DSGEGDFLAEGGGVR^{35}	–
p1613	1.572 (/HC)	–	Fibrinogen alpha chain	FIBA_HUMAN (gil1706799)	1615.7	1615.9	115	0.2819	^{20}ADSGEGDFLAEGGGVR^{35}	Phospho(ST)
p1737	−2.609 (/HC)	D/A13P D/N6P	Complement C4A	CO4A_HUMAN (gil476007827)	1738.9	1738.9	71	0.0115	^{1337}NGFKSHALQLNNRQI^{1351}	–
	−1.668 (/AD)	D/N2P –	Complement C4B	CO4B_HUMAN (gil476007828)						
p2860	2.822 (/HC)		Fibrinogen alpha chain	FIBA_HUMAN (gil1706799)	2860.3	2860.7	89	0.3881	^{603}MADEAGSEADHEGTHST KRGHAKSRPV^{629}	–
p2898	1.786 (/HC)	D/A13P D/N6P D/N4P	Protein Wnt-2b	WNT2B_HUMAN (gil14424481)	2893.6	2895.1	65	1.5403	^{12}QLPLRRASAPVPVPSPAAP DGSRASARLG^{40}	–
p2988	−1.242 (/AD)	D/A13P D/H6P	Fibrinogen alpha chain	FIBA_HUMAN (gil1706799)	2988.4	2989.8	56	1.3409	^{602}KMADEAGSEADHEGTHS TKRGHAKSRPV^{629}	–
	−1.587 (/HC)	D/N6P								
p3239	1.563 (/HC)	–	Collagen alpha-1(IV) chain	CO4A1_HUMAN (gil125987809)	3241.5	3240.1	60	−1.4931	^{402}SLPGPSGRDGLPGPPGSPG PPGQPGYTNGIVECQ^{435}	–
p4052	−1.368 (/AD)	D/H6P D/N4P	Lipopolysaccharide-binding protein	LBP_HUMAN (gil116242615)	4049.3	4049.1	60	−0.1413	^{390}TLTFNTSKITGFLKPGKVK VELKESKVGLFNAELLEA^{426}	–
	−1.554 (/HC)	D/N3P								
p4208	−1.372 (/AD)	D/A13P	Diacylglycerol kinase iota	DGKI_HUMAN (gil12643642)	4207.8	4209.2	72	1.3695	^{58}SAGEEKGATGGSSSSGSGA GSCCLGAEGGADPRGAGSA AAAGAAALDEPA^{107}	–
p5017	1.600 (/AD)	–	One cut domain family member 3	ONEC3_HUMAN (gil122064635)	5018.2	5017.2	57	−1.0005	^{49}GMASLLDGGGGGGGGGA GGAGGAGSAGGGADFRGE LAGPLHPAMGMACEAPGLG GTYTT^{107}	–
p5904	−1.281 (/AD)	D/A13P	Gamma-aminobutyric acid type B receptor subunit 1	GABR1_HUMAN (gil12643873)	5901.8	5900.9	67	−0.9075	^{178}MSGGWPGGQACQPAVEM ALEDVNSRRDILPDYELKLI HHDSKCDPGQATKYLY^{230}	–

*Mass/charge ratios used for the designation of peptides were obtained by MALDI-TOF/MS, whereas those for "observed MW" were obtained by LC–MS.
#Peptides, which showed at least 1.5-fold different ion intensity between the DLB and AD groups (/AD) or between the DLB and HC groups (/HC) in the training sets ($p < 0.05$), or which were used in either of DLB/AD-13P model (D/A13P), DLB/HC-6P model (D/H6P), DLB/nonDLB-6P model (D/N6P), DLB/nonDLB-4P model (D/N4P), DLB/nonDLB-3P model (D/N3P), or DLB/nonDLB-2P model (D/N2P), were selected for the identification.
$Possible modifications deduced from the results of LC–MS analysis are shown. Letters in the parentheses show the targeted amino acids.
AD, Alzheimer's disease; HC, health control; MW, molecular weights; MALDI-TOF/MS, matrix-assisted laser desorption/ionization time-of-flight mass spectrometry; LC–MS, liquid chromatography–mass spectrometry; DLB, dementia with Lewy bodies.

Copyright © 2015 John Wiley & Sons, Ltd.

models can be applied to the screening of early phase DLB as well as diagnosis of DLB. Furthermore, because most DLB patients are known to have AD pathology in addition to Lewy pathology, our DLB patients would include both "DLB with AD" type and "pure DLB" type. Because our DLB/nonDLB-2P, DLB/nonDLB-3P, DLB/nonDLB-4P and DLB/nonDLB-6P models efficiently discriminated DLB from AD (Figure 2(H)–(K)), these models would detect changes of serum peptide profiles derived from Lewy pathology.

As blood biomarker candidates for DLB, DJ-1 and H-FABP have been reported (Waragai *et al.*, 2007; Mollenhauer *et al.*, 2007; Wada-Isoe *et al.*, 2008). Plasma DJ-1 levels were higher in DLB than in HC and in early stage of PD (Waragai *et al.*, 2007). The ability of DJ-1 to discriminate DLB from AD would be interesting. Serum H-FABP levels were higher in DLB and PD than in AD, and the ratio of serum H-FABP to cerebrospinal fluid tau showed sensitivity of 91% and specificity of 66% to discriminate DLB from AD (Mollenhauer *et al.*, 2007). However, the ability of H-FABP to discriminate DLB from AD was inferior to that of the delayed heart to mediastinum ratio measured by ^{123}I-metaiodobenzylguanidine cardiac scintigraphy (Wada-Isoe *et al.*, 2008). Our DLB/nonDLB-2P, DLB/nonDLB-3P, DLB/nonDLB-4P, and DLB/nonDLB-6P models requiring only serum samples showed better discriminant ability between the DLB and AD groups in the validation (Figure 2(H)–(K), Table 3). The discriminant ability of our models between DLB and PD should be investigated in future. A serum proteomic study found a combination of three serum proteins with 3883, 4964, or 10,534 m/z showed good discriminant ability of DLB from non-DLB, indicating sensitivity of 83.3% and specificity of 95.8% in the training set (Wada-Isoe *et al.*, 2007). The high specificity needs to be validated.

Several interesting peptides were found in our identification results (Table 4). The FIBA-derived peptides of p1462, p1613, p2860, and p2988 were also identified as peptides that contributed to the discrimination of AD from HC in our previous study (Noguchi *et al.*, 2014). The increase of p1462, p1613, and p2860, and the decrease of p2988 in DLB compared with HC in this study were compatible with the previous results comparing AD to HC. Thus, aberrant degradation of FIBA may similarly occur in DLB, which causes abnormal coagulation and fibrinolysis, leading to vascular damage as suggested in AD (Noguchi *et al.*, 2014; Cortes-Canteli *et al.*, 2010).

In the DLB/nonDLB-2P, DLB/nonDLB-3P, DLB/nonDLB-4P, and DLB/nonDLB-6P models, p1737, p2898, and p4052 were identified (Table 4). The p1737, decreased in the DLB group compared with both AD and HC groups, was identified as a fragment of C4b. Interestingly, C4d, an inactive fragment from a different part of C4b from p1737, was detected in the Lewy bodies in DLB (Iseki *et al.*, 2000; Togo *et al.*, 2001). Because C4d is known to be precipitated according to the activation of classical component pathway, activation of the classical component pathway may occur in degenerated Lewy body-bearing neurons (Iseki *et al.*, 2000). The decrease of p1737 in sera of the DLB patients may indicate its precipitation into Lewy bodies similarly as the case of C4d precipitation. The p2898, identified as a fragment of Wnt-2b, was increased in the DLB group compared with the HC group (1.786-fold, $p < 0.01$, Table 3) and also to the AD group (1.323-fold, $p < 0.05$). Wnt-2b, a stem cell factor for neural cells during embryogenesis, was reported to be highly expressed in fetal hippocampus (Katoh, 2005; Zhang *et al.*, 2002). The increased Wnt-2b fragment may indicate an increased expression of Wnt-2b protein. The relatively highly expressed Wnt-2b in DLB compared with AD may be involved in the regeneration of neurons in hippocampus to rescue memory function in DLB. The p4052, identified as a fragment of LBP, was decreased in the DLB group compared with both AD and HC groups (Table 4). LBP transfers bacterial endotoxin of lipopolysaccharide to CD14 to enhance the innate immune response *via* toll-like receptor 4 (Jerala, 2007). The plasma concentration of LBP was lower in PD than in its control group, suggesting increased inflammatory signaling in PD (Forsyth *et al.*, 2011). The decrease of the LBP-derived peptide in our study suggested the low concentration of blood LBP in DLB similarly to PD. Collectively, parent proteins of all the identified peptides in the DLB/nonDLB-2P, DLB/nonDLB-3P, DLB/nonDLB-4P, and DLB/nonDLB-6P models have been previously reported as important proteins in the pathology of DLB, AD, or PD, and in the hippocampal neurogenesis. Because a single peptide was not enough for the efficient discrimination of DLB (Figure 2(B), one peptide model), the combination of multiple peptides would be essential for generating useful biomarkers. Further identification of the serum peptides used in the four DLB/nonDLB-discriminant models may provide a new insight both in biomarker analysis and in elucidation of the disease-mechanism.

In conclusion, we found the usefulness of serum peptides as biomarker candidates for DLB. The discriminant models generated with a small number of peptides showed sensitivity and specificity of

Copyright © 2015 John Wiley & Sons, Ltd.

approximately 90% in the validation. Several limitations of this study such as a relatively small sample size, limited demographic and clinical information, and no biological diagnostic data (^{123}I-metaiodobenzylguanidine cardiac scintigraphy or dopamine transporter imaging in basal ganglia) should be overcome before clinical application of these models. Confirmation of usefulness of the models with more number of subjects and identification of all the used peptides would promote DLB treatment.

Acknowledgements

We are indebted to Ms A. Nozawa and Mr Y Iizuka for their technical assistance. This study was partly supported by the Promotion and Mutual Aid Corporation for Private Schools of Japan.

Conflict of Interest

None declared.

Key points

- Serum peptide profiles of patients with dementia with Lewy bodies (DLB) were different from those of patients with Alzheimer's disease (AD) and healthy control (HC) subjects.
- Serum peptide profiles would provide useful DLB biomarker candidates. Multivariate analysis for discriminating a DLB group from the a non-DLB (AD and HC) group using ion intensity of four peptides of 2898, 4052, 4090, and 5002 m/z (DLB/nonDLB-4P model) showed sensitivity of 93.3% and specificity of 87.9% in a training set, and sensitivity of 90.0% and specificity of 88.6% in a testing set. This model detected 86.7% and 90.0% of the AD patients as non-DLB in the training and testing sets, respectively, and discriminated all the patients with amnestic mild cognitive impairment as non-DLB.

  Furthermore, DLB/nonDLB-2P model using ion intensity of two peptides (1737 and 5002 m/z) showed sensitivity of 95.0% and specificity of 93.3% for discriminating the DLB group from the AD group in the testing set.
- The peptides used in the aforementioned models included fragments from complement 4b, Wnt-2b, and LPS-binding protein, which would be involved in the pathophysiology of DLB.

References

Abdi F, Quinn JF, Jankovic J, *et al.* 2006. Detection of biomarkers with a multiplex quantitative proteomic platform in cerebrospinal fluid of patients with neurodegenerative disorders. *J Alzheimers Dis* **9**: 293–348.

American Psychiatric Association. 1994. Diagnostic and Statistical Manual of Mental Disorders. 4th edn.Washington: American Psychiatric Association.

Bibl M, Mollenhauer B, Esselmann H, *et al.* 2006. CSF amyloid-beta-peptides in Alzheimer's disease, dementia with Lewy bodies and Parkinson's disease dementia. *Brain* **129**: 1177–1187.

Clark CM, Xie S, Chittams J, *et al.* 2003. Cerebrospinal fluid tau and beta-amyloid: how well do these biomarkers reflect autopsy-confirmed dementia diagnoses? *Arch Neurol* **60**: 1696–1702.

Cortes-Canteli M, Paul J, Norris EH, *et al.* 2010. Fibrinogen and beta-amyloid association alters thrombosis and fibrinolysis: a possible contributing factor to Alzheimer's disease. *Neuron* **66**: 695–709. DOI:10.1016/j.neuron.2010.05.014.

de Jong D, Jansen RW, Pijnenburg YA, *et al.* 2007. CSF neurofilament proteins in the differential diagnosis of dementia. *J Neurol Neurosurg Psychiatry* **78**: 936–938.

Ferman TJ, Smith GE, Kantarci K, *et al.* 2013. Nonamnestic mild cognitive impairment progresses to dementia with Lewy bodies. *Neurology* **81**: 2032–2038. DOI:10.1212/01.wnl.0000436942.55281.47.

Forsyth CB, Shannon KM, Kordower JH, *et al.* 2011. Increased intestinal permeability correlates with sigmoid mucosa alpha-synuclein staining and endotoxin exposure markers in early Parkinson's disease. *PLoS One* **6**: e28032. DOI:10.1371/journal.pone.0028032.

Hatsugai M, Kurokawa MS, Kouro T, *et al.* 2010. Protein profiles of peripheral blood mononuclear cells are useful for differential diagnosis of ulcerative colitis and Crohn's disease. *J Gastroenterol* **45**: 488–500. DOI:10.1007/s00535-009-0183-y.

Herbert MK, Aerts MB, Kuiperij HB, *et al.* 2014. Addition of MHPG to Alzheimer's disease biomarkers improves differentiation of dementia with Lewy bodies from Alzheimer's disease but not other dementias. *Alzheimers Dement* **10**: 448–455. DOI:10.1016/j.jalz.2013.05.1775.

Iseki E, Marui W, Akiyama H, Uéda K, Kosaka K. 2000. Degeneration process of Lewy bodies in the brains of patients with dementia with Lewy bodies using alpha-synuclein-immunohistochemistry. *Neurosci Lett* **286**: 69–73.

Jerala R. 2007. Structural biology of the LPS recognition. *Int J Med Microbiol* **297**: 353–363.

Katoh M. 2005. WNT2B: comparative integromics and clinical applications (Review). *Int J Mol Med* **16**: 1103–1108.

McKeith IG, Dickson DW, Lowe J, et al. Consortium on DLB. 2005. Diagnosis and management of dementia with Lewy bodies: third report of the DLB Consortium. *Neurology* **65**: 1863–1872.

McKeith I, Mintzer J, Aarsland D, *et al.*, International Psychogeriatric Association Expert Meeting on DLB. 2004. Dementia with Lewy bodies. *Lancet Neurol* **3**: 19–28.

McKhann G, Drachman D, Folstein M, *et al.* 1984. Clinical diagnosis of Alzheimer's disease: report of the NINCDS-ADRDA Work Group under the auspices of Department of Health and Human Services Task Force on Alzheimer's Disease. *Neurology* **34**: 939–944.

Mollenhauer B, Cepek L, Bibl M, *et al.* 2005. Tau protein, Abeta42 and S-100B protein in cerebrospinal fluid of patients with dementia with Lewy bodies. *Dement Geriatr Cogn Disord* **19**: 164–170.

Mollenhauer B, Cullen V, Kahn I, *et al.* 2008. Direct quantification of CSF alpha-synuclein by ELISA and first cross-sectional study in patients with neurodegeneration. *Exp Neurol* **213**: 315–325. DOI:10.1016/j.expneurol.2008.06.004.

Mollenhauer B, Steinacker P, Bahn E, *et al.* 2007. Serum heart-type fatty acid-binding protein and cerebrospinal fluid tau: marker candidates for dementia with Lewy bodies. *Neurodegener Dis* **4**: 366–375.

Noguchi M, Sato T, Nagai K, *et al.* 2014. Roles of serum fibrinogen α chain-derived peptides in Alzheimer's disease. *Int J Geriatr Psychiatry* **29**: 808–818. DOI:10.1002/gps.4047.

Ohrfelt A, Grognet P, Andreasen N, *et al.* 2009. Cerebrospinal fluid alpha-synuclein in neurodegenerative disorders-a marker of synapse loss? *Neurosci Lett* **450**: 332–335. DOI:10.1016/j.neulet.2008.11.015.

Parnetti L, Tiraboschi P, Lanari A, *et al.* 2008. Cerebrospinal fluid biomarkers in Parkinson's disease with dementia and dementia with Lewy bodies. *Biol Psychiatry* **64**: 850–855. DOI:10.1016/j.biopsych.2008.02.016.

Petersen RC, Smith GE, Waring SC, et al. 1999. Mild cognitive impairment: clinical characterization and outcome. *Arch Neurol* **56**: 303–308.

Steinacker P, Mollenhauer B, Bibl M, *et al.* 2004. Heart fatty acid binding protein as a potential diagnostic marker for neurodegenerative diseases. *Neurosci Lett* **370**: 36–39.

Togo T, Iseki E, Marui W, *et al.* 2001. Glial involvement in the degeneration process of Lewy body-bearing neurons and the degradation process of Lewy bodies in brains of dementia with Lewy bodies. *J Neurol Sci* **184**: 71–75.

Copyright © 2015 John Wiley & Sons, Ltd.

Wada-Isoe K, Imamura K, Kitamaya M, Kowa H, Nakashima K. 2008. Serum heart-fatty acid binding protein levels in patients with Lewy body disease. *J Neurol Sci* **266**: 20–24.

Wada-Isoe K, Michio K, Imamura K, *et al.* 2007. Serum proteomic profiling of dementia with Lewy bodies: diagnostic potential of SELDI-TOF MS analysis. *J Neural Transm* **114**: 1579–1583.

Waragai M, Nakai M, Wei J, *et al.* 2007. Plasma levels of DJ-1 as a possible marker for progression of sporadic Parkinson's disease. *Neurosci Lett* **425**: 18–22.

Zhang Y, Mei P, Lou R, *et al.* 2002. Gene expression profiling in developing human hippocampus. *J Neurosci Res* **70**: 200–208.

Supporting information

Additional supporting information may be found in the online version of this article at the publisher's web-site.

Copyright © 2015 John Wiley & Sons, Ltd.

Japan College of Rheumatology
MODERN RHEUMATOLOGY

http://informahealthcare.com/mor
ISSN 1439-7595 (print), 1439-7609 (online)

Mod Rheumatol, 2015; 25(4): 522–527
© 2015 Japan College of Rheumatology
DOI: 10.3109/14397595.2014.995874

Taylor & Francis
Taylor & Francis Group

ORIGINAL ARTICLE

Effects of tofacitinib on nucleic acid metabolism in human articular chondrocytes

Hideki Koizumi[1], Mitsumi Arito[1], Wataru Endo[1], Manae S. Kurokawa[2], Kazuki Okamoto[1], Kazuki Omoteyama[1], Naoya Suematsu[1], Moroe Beppu[3], and Tomohiro Kato[1]

[1]*Clinical Proteomics & Molecular Medicine, St. Marianna University Graduate School of Medicine, Sugao, Miyamae, Kawasaki, Kanagawa, Japan,* [2]*Disease Biomarker Analysis & Molecular Regulation, St. Marianna University Graduate School of Medicine, Sugao, Miyamae, Kawasaki, Kanagawa, Japan, and* [3]*Department of Orthopedic Surgery, St. Marianna University School of Medicine, Sugao, Miyamae, Kawasaki, Kanagawa, Japan*

Mod Rheumatol Downloaded from informahealthcare.com by St Marianna University on 06/29/15
For personal use only.

Abstract

Objective. In our previous screening of chondrocyte protein profiles, the amount of adenosine monophosphate deaminase (AMPD) 2 was found to be decreased by tofacitinib. Extending the study, here we confirmed the decrease of AMPD2 by tofacitinib and further investigated effects of tofacitinib on purine nucleotide metabolism.
Methods. Human articular chondrocytes and a chondrosarcoma cell line: OUMS-27 were stimulated with tofacitinib. Then the levels of AMPD2 and its related enzymes were investigated by Western blot. The levels of AMP and adenosine were assessed by mass spectrometry.
Results. We confirmed the significant decrease of AMPD2 by tofacitinib in chondrocytes ($p = 0.025$). The levels of adenosine kinase and 5′-nucleotidase were decreased in chondrocytes, although they did not meet statistical significance ($p = 0.067$ and $p = 0.074$, respectively). The results from OUMS-27 were similar to those from the chondrocytes. The cellular adenosine levels were significantly decreased by tofacitinib in OUMS-27 ($p = 0.014$). The cellular AMP levels were increased, although they did not meet statistical significance in OUMS-27 ($p = 0.066$).
Conclusion. Our data indicate that tofacitinib increases the cellular levels of adenosine, which is known to have anti-inflammatory activity, through the downregulation of AMPD2. This would be a novel functional aspect of tofacitinib.

Keywords

Adenosine, AMP deaminase, Chondrocytes, Tofacitinib

History

Received 20 August 2014
Accepted 1 December 2014
Published online 9 January 2015

Introduction

Tofacitinib is a recently approved oral anti-rheumatic drug. Tofacitinib, inhibiting the actions of Janus kinase (JAK) 1–3, blocks the JAK-signal transducers and activator of transcription pathway [1–3]. Consequently, tofacitinib displays its anti-inflammatory effects by suppressing transcription of various pro-inflammatory cytokine genes such as interleukin 2 (IL-2) in lymphocytes and by decreasing nuclear localization of nuclear factor kappa B (NF-κB) subunits in tumor necrosis factor (TNF)-stimulated macrophages and in rheumatoid arthritis (RA) synovial macrophages [4,5]. Strong anti-inflammatory actions of tofacitinib have been evidenced both in humans and in animal arthritis models [6–10]. Tofacitinib is expected to show high therapeutic efficacy similar to that of biological drugs like anti-TNF agents in the treatment of RA [2].

As mentioned above, the functions of tofacitinib in lymphocytes have been extensively investigated; however, effects of tofacitinib on other cell types have not been fully investigated. Thereby, we recently conducted screening of effects of tofacitinib on human articular chondrocytes using 2-dimensional difference gel electrophoresis (2D-DIGE), where we found that tofacitinib suppressed a part of protein profile changes brought by IL-1β stimulation [11]. One of the protein spots whose expression was increased by IL-1β stimulation and also suppressed by the simultaneous addition of tofacitinib was adenosine monophosphate deaminase (AMPD) 2 [11].

AMPD2 (EC 3.5.4.6) converts AMP to inosine monophosphate (IMP) in purine nucleotide catabolism. In human, 3 subtypes of AMPD have been reported until now (AMPD1, 2, and 3) [12–18]. In chondrocytes, it remains to be solved which subtypes are expressed. In our screening by 2D-DIGE in both IL-1β present and absent conditions, the expression of AMPD2 spot was decreased by tofacitinib alone, thereby the suppressive effect of tofacitinib on AMPD2 was thought to be independent of the IL-1β pathway.

Extending the study, here we investigated effects of tofacitinib on purine nucleotide metabolism, focusing on AMPD2 and its related molecules. As a result, we confirmed the decrease of AMPD2 by tofacitinib and further found that tofacitinib increased the amounts of cellular adenosine. Our data would elucidate novel functional aspects of tofacitinib in articular chondrocytes.

Materials and methods

Clinical samples and preparation of chondrocytes

Human articular chondrocytes were obtained from rather less-degraded parts of cartilage of 9 patients with osteoarthritis (OA) (4 males and 5 females, mean age: 74.4 years [range: 70–80 years]) who underwent knee joint arthroplasty. The diagnosis of OA was made according to the criteria by Kellgren and Lawrence [19].

Correspondence to: Mitsumi Arito, Clinical Proteomics and Molecular Medicine, St. Marianna University Graduate School of Medicine, 2-16-1, Sugao, Miyamae, Kawasaki, Kanagawa, 216-8511, Japan. Tel: + 81-44-977-8111. Fax: + 81-44-976-7553. E-mail: m-ari@marianna-u.ac.jp

RIGHTSLINK

Mod Rheumatol Downloaded from informahealthcare.com by St Marianna University on 06/29/15
For personal use only.

Written informed consent was obtained from each of the patients and this study protocol was approved by the ethics committee of St. Marianna University School of Medicine. The study was performed in compliance with the World Medical Association's Declaration of Helsinki.

After careful removal of synovial tissue, cartilage was minced, washed, and treated with collagenase (Wako Pure Chemical Industries, Osaka, Japan). Isolated chondrocytes (Passage 0, P0) were then washed and grown in vitro in monolayer culture in Dulbecco's modified Eagle's medium (DMEM, GIBCO, Carsbad, CA) supplemented with 10% fetal calf serum (Wako), 100 units/ml of penicillin, and 100 μg/ml of streptomycin (Sigma-Aldrich, St. Louis, MO, USA) on type-I collagen-coated culture dishes. The production of type-II collagen in the isolated chondrocytes was confirmed (data not shown)

In addition to chondrocytes, a human chondrosarcoma cell line of OUMS-27 cells, purchased from Health Science Research Resource Bank (Osaka, Japan), was used. Similarly, OUMS-27 cells were cultured in DMEM prepared as mentioned above. The cells were cultured at 37 degrees centigrade in 5% CO_2.

Treatment of chondrocytes and OUMS-27 cells with reagents

The prepared articular chondrocytes (P1-P3, 1.0×10^7 cells/ϕ100mm dish) and OUMS-27 cells were treated with or without 10–100 μM of tofacitinib for 48 h, which was the same stimulating period as used in our previous study [11]. Tofacitinib, dissolved in dimethyl sulfoxide (DMSO) (Wako) at a concentration of 10–100 mM, was added to the culture to make the final concentration of 10–100 μM. Since the culture contained 0.1% DMSO, control cultures were adjusted to contain 0.1% DMSO to avoid DMSO-derived biases in the comparison. In our preliminary experiments, we confirmed that these concentrations of DMSO and tofacitinib did not affect survival of the chondrocytes and OUMS-27 (data not shown).

Western blotting

Proteins were extracted from the chondrocytes into a lysis buffer (7M urea, 2M thiourea, 4% CHAPS) for Western blotting. Monoclonal antibodies to human AMPD2 (Abnova, Taipei, Taiwan), adenosine kinase (ADK, LifeSpan Biosciences, Seattle, WA, USA), 5′-nucleotidase (5′-NT, Abnova), and adenosine deaminase (ADA, abcam, Cambridge, England) were used as the primary antibodies. Horseradish peroxidase-conjugated rabbit anti-mouse immunoglobulin G antibodies (Invitrogen/Zymed) were used as the secondary antibody. The bound antibodies were visualized using an enhanced chemiluminescence detection system (GE healthcare).

Reverse transcription-polymerase chain reaction (RT-PCR)

Extraction and purification of RNA from the cells and reverse transcription of the RNA samples were performed using RNeasy® (Qiagen, Venlo, The Netherlands). Primer sets were designed to amplify parts of protein-coding regions of AMPD1, AMPD2, and AMPD3. PCR for AMPD1 was performed for 33 cycles (98 °C for 1 min, 58 °C for 45 s, and 72 °C for 30 s). PCR for AMPD2 and AMPD3 were similarly performed for 33 cycles (98 °C for 1 min, 63 °C for 45 s, and extension at 72 °C for 30 s). Nucleotide sequences of the 3 primers are as follows. For AMPD1: 5′ -GCTTGCATGAACCAGAAACA and 5′ -ATGCTGGTACTTGGCCTCC, for AMPD2: 5′-TACAAGGAACAGGGTGAGGG and 5′ -ACAGTGCTCATACGGGTGCT, and for AMPD3: 5′ -TGACAGGACTGTGGCAGAGA and 5′ -CCGTGGCTCTGAGTACTGGT.

Quantitative real-time PCR

Real-time PCR was performed using ABI Prism 7000 Sequence Detection System (Applied Biosystems, Foster city, CA, USA), according manufacturer's instructions. To measure AMPD2 and β-actin mRNA, 2 μg of total RNA-derived cDNA was mixed with TaqMan® Gene Expression Assays (Hs01092053_g1 and Hs01060665_g1, respectively, Applied Biosystems) and TaqMan® Gene Expression Master Mix (Applied Biosystems). To measure AMPD3 mRNA, 2 μg of total RNA-derived cDNA was mixed with 300 nM each of the forward and reverse primers and Power SYBR® Master Mix (Applied Biosystems). Nucleotide sequences of the primers for the amplification of an AMPD3 DNA fragment is as follows: 5′ -TGACAGGACTGTGGCAGAGA and 5′ -CCGTGGCTCTGAGTACTGGT. Then the mixture was subjected to real-time PCR. The thermal cycle conditions were as follows: 95°C for 10 min, followed by 40 cycles of 95°C for 15 s and 60°C for 60 s.

Assessment of intracellular adenosine and AMP

The assessment of intracellular adenosine and AMP was carried out in accordance with protocols reviewed and approved by Kazusa DNA Research Institute (Chiba, Japan). Briefly, from OUMS-27 cells, a lysate fraction containing AMP and adenosine were extracted into 100% methanol, removing insoluble protein aggregates by centrifugation and lipids by C18 spin column treatment. The extracts were dried up and then were dissolved in 0.1% formic acid solution. Adenosine and AMP in the samples were analyzed using a high-performance liquid chromatography system (1200 Series; Agilent Technologies Inc., PaloAlto, CA, USA), connected to the orbitrap and ion trap mass spectrometer (LTQ ORBITRAP XL, Thermo Fisher Scientific Inc., Waltham, MA, USA). Detected peak areas of adenosine and AMP were calculated by Xcalibur (Thermo Fisher Scientific Inc.). Then, relative amounts of adenosine and AMP per weight of the cells were assessed by the peak areas.

Statistical analysis

Statistical significance was calculated by Student's *t*-test.

Results

Our recent 2D-DIGE analysis revealed that tofacitinib affected protein profiles of human articular chondrocytes [11]. One of the affected proteins is AMPD2. The protein spot assigned to AMPD2 increased its intensity by IL-1β stimulation and the increase was suppressed by the simultaneous addition of tofacitinib. Since tofacitinib treatment alone also decreased the AMPD2 spot intensity, the effect was thought to be independent of the IL-1β pathway.

AMPD2 is an enzyme that converts AMP to IMP. Decrease of AMPD2 may suppress the conversion from AMP to IMP and increase AMP levels, which in turn leads to increase of adenosine, since adenosine is synthesized from AMP. Based on this hypothesis, here we investigated whether tofacitinib decreased AMP or not. Further, we investigated effects of tofacitinib on several nucleotide metabolism-related enzymes.

Human AMPD consists of at least 3 subtypes, AMPD1–3 [12–18]. AMPD1 is mainly produced in skeletal muscle, AMPD2 is produced abundantly in liver and spleen, and AMPD3 is produced in hematopoietic cells [12–18]. However, it remains unclear which AMPD subtypes are produced in chondrocytes. Thereby we first tested the expression of AMPD1–3 in chondrocytes from patients with OA by RT-PCR. As a result, we found that the chondrocytes produced AMPD2 and 3, but not AMPD1 (Figure 1A).

Next, we confirmed that the amount of AMPD2 was decreased by the treatment with tofacitinib and tested whether the amount of

RIGHTSLINK

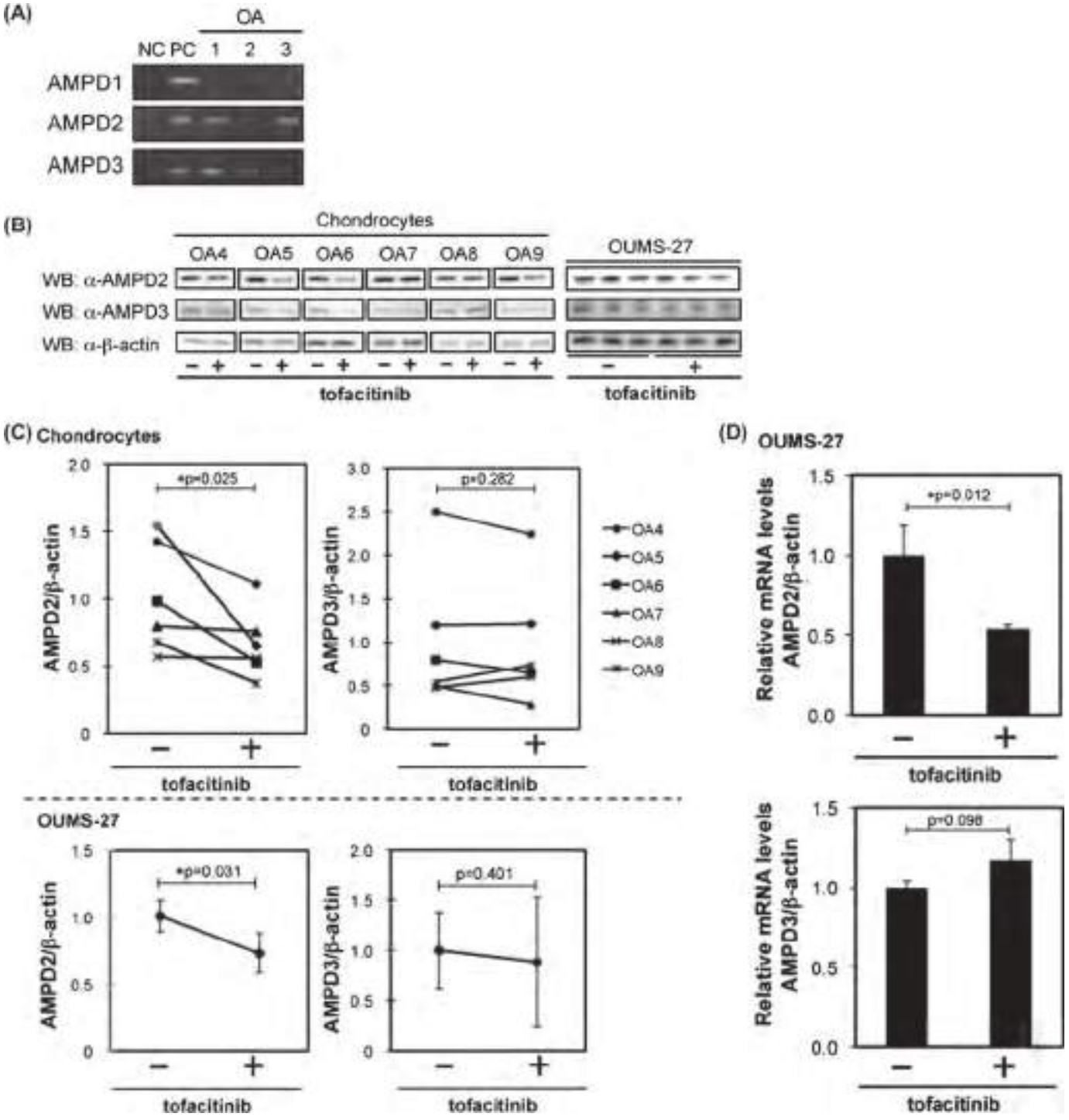

Figure 1. Expression of the AMPD family and effects of tofacitinib on it in human articular chondrocytes. (A) Total RNA, extracted from human articular chondrocytes ($n = 3$) or HepG2 as a positive control, was subjected to reverse transcription and then were used for PCR of AMPD1-3 DNA fragments. HepG2 was used as a positive control in the amplification of AMPD2 and 3, and cDNA for AMPD1 was used as a positive control in the amplification of AMPD1, since no cell type that expressed AMPD1 was available. NC: negative control, PC: positive control. (B) Human articular chondrocytes ($n = 6$) and a chondrosarcoma cell line, OUMS-27 ($n = 3$) were incubated with or without 10μM of tofacitinib for 48 h. Then proteins were extracted and subjected to Western blotting with antibodies to AMPD2, AMPD3, and β-actin. (C) Intensity of the band for AMPD2, AMPD3, and β-actin was measured by densitometry. In each patient and in the OUMS-27 samples, the intensity of the band for AMPD2 and AMPD3, corrected using that of β-actin, was compared between the non-treated and tofacitinib-treated conditions. An average of the corrected intensity in the non-treated group was defined as 1.0. $^*p < 0.05$.

AMPD3 was altered by the treatment with tofacitinib. Specifically, human articular chondrocytes were treated with 10 μM tofacitinib for 48 h, and then whole cell lysate, extracted from the cells and from non-treated chondrocytes as a control, were subjected to Western blotting with anti-AMPD2 and anti-AMPD3 antibodies, respectively. As a result, the amount of AMPD2 was decreased by the tofacitinib treatment in accordance with our result in the 2D-DIGE screening ($p = 0.025$, Figure 1B and C). However, the amount of AMPD3 was not affected by the tofacitinib treatment (Figure 1B and C). Further, we confirmed these effects of tofacitinib in a chondrosarcoma cell line of OUMS-27. As shown in Figure 1B and C, the amount of AMPD2 was significantly

Mod Rheumatol Downloaded from informahealthcare.com by St Marianna University on 06/29/15
For personal use only.

RIGHTSLINK

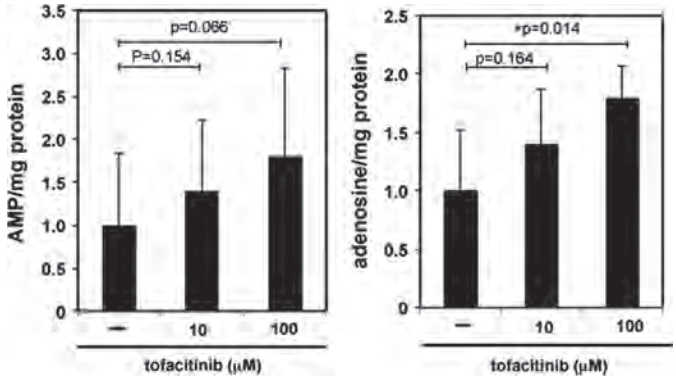

Figure 2. Effects of tofacitinib on the intracellular levels of AMP and adenosine. OUMS-27 was incubated with 0, 10, and 100 μM of tofacitinib for 48 h ($n = 3$). After washing, the cell lysate was used for the measurement of AMP and adenosine by LC-MS. Average peak areas of AMP and adenosine in LC–MS of the lysate from the non-treated (0 μM of tofacitinib) cells are defined as 1.0, respectively. $^*p < 0.05$.

decreased by the tofacitinib treatment ($p = 0.031$), while the amount of AMPD3 was not affected by the tofacitinib treatment ($p = 0.401$).

Since OUMS-27 and OA chondrocytes showed nearly the same behavior from the viewpoint of tofacitinib's effects on AMPDs, we next investigated whether the decreased expression of AMPD2 was a result of decreased transcription of mRNA for AMPD2 by quantitative real-time PCR using OUMS-27. As a result, the level of mRNA for AMPD2 was found to be decreased significantly by the tofacitinib treatment (Figure 1D). Additionally, the same experiment using an OA chondrocyte sample also showed very similar results (data not shown). From these data, we concluded that tofacitinib downregulated the amount of AMPD2 through the decrease in level of its mRNA.

Next, we investigated whether tofacitinib increased adenosine levels or not, since decrease of AMPD2 possibly increases adenosine by supplying abundant AMP. Specifically, we treated OUMS-27 with 10 μM and 100 μM of tofacitinib for 48 h; then we measured relative amounts of AMP and adenosine by liquid chromatography–mass spectrometry (LC–MS). As a result, the relative AMP amount tended to be increased by tofacitinib in a dose-dependent manner even though the difference did not meet statistical significance (Figure 2). The relative adenosine levels were also increased by the tofacitinib treatment in a dose-dependent manner and the increase was statistically significant ($p = 0.014$, 100 μM of tofacitinib, Figure 2). From these data, it was concluded that tofacitinib increases AMP and adenosine levels probably due to the decrease of AMPD2. Since the increase in the adenosine level was more distinct than the increase of AMP, enzymes that use AMP or adenosine as a substrate may be affected by tofacitinib. We thus investigated whether tofacitinib affected the levels of ADK (EC; 2.7.1.20) that converts adenosine to AMP, 5'-NT (EC; 3.1.3.5) that converts AMP to adenosine, and ADA (EC; 3.5.4.4) that converts adenosine to inosine in human articular chondrocytes and OUMS-27. As a result of Western blotting with antibodies to ADK, 5'-NT, and ADA, the levels of ADK and 5'-NT tended to be decreased although the decreases did not meet statistical significance in human articular chondrocytes ($p = 0.067$ and $p = 0.074$, respectively, Figure 3A and B). Similar experiments were also performed in OUMS-27. As a result, the amount of ADK was decreased significantly and the amount of 5'-NT tended to be decreased by the tofacitinib treatment in OUMS-27 ($p = 0.038$ and $p = 0.108$, respectively, Figure 3A and B). The results from OUMS-27 were very similar to those from OA chondrocytes. The distinct increase of adenosine compared with the increase of AMP may be due to the subtle balance of ADK and 5'-NT, both of which tended to be decreased by tofacitinib. On the other hand, the amount of ADA was not affected by tofacitinib in both human articular chondrocytes and OUMS-27 ($p = 0.222$ and $p = 0.403$, respectively, Figure 3A and B). This indicates that ADA is not involved in the increase of adenosine levels by tofacitinib.

Discussion

Previously, we comprehensively analyzed the changes of protein profiles by tofacitinib in human articular chondrocytes, where the amount of AMPD2 appeared to be decreased by tofacitinib. Extending the study, (1) here we confirmed the decrease of AMPD2 by tofacitinib quantitatively and (2) we further found that the amounts of cellular AMP and adenosine were increased by tofacitinib. In addition, (3) we found that ADK and 5'-NT, which affect AMP and adenosine, tended to be decreased by tofacitinib and the amount of ADA did not show obvious change by tofacitinib.

The decrease of AMPD2 by tofacitinib would decrease the conversion of AMP to IMP, which would lead to the increase of AMP concentration detected here. The increase of AMP, a material for the synthesis of adenosine, would lead to the increase of adenosine concentration detected here (Figure 4).

Other enzymes that affect the amounts of AMP and adenosine directly are ADK and 5'-NT. ADK catalyzes the conversion of adenosine to AMP and 5'-NT catalyzes the conversion of AMP to adenosine. Since both the enzymes tended to be decreased by tofacitinib, the conversion of AMP to adenosine and adenosine to AMP may be suppressed by tofacitinib; however, it would not affect the balance of AMP and adenosine. This point should be clarified in the future.

The most impressive finding here is that tofacitinib increased the cellular adenosine level. Adenosine is known to possess anti-inflammatory and analgesic activities [20]. Intracellular adenosine is released through the adenosine transporter [20,21]. Released adenosine binds to adenosine receptors (ARs) on the surface of cells in autocrine and paracrine fashions [20,21]. Until now, 4 types of ARs have been reported: A_1R, $A_{2A}R$, $A_{2B}R$, A_3R [20,21]. In chondrocytes, it was reported that $A_{2A}R$ is the major functional AR [21]. $A_{2A}R$ has been reported to be expressed on T-cells, neutrophils, and platelets as well as chondrocytes [20–22]. It was reported that adenosine suppressed type-II collagen-induced arthritis, where binding of adenosine to $A_{2A}R$ suppressed the synthesis of TNF-α and enhanced the synthesis of IL-10 [23]. Further, it was reported that adenosine inactivated NF–κB and also suppressed production of NO and prostaglandin E2 [24]. In RA, an increased level of ADA promotes degradation of adenosine, leading to the exacerbation of arthritis [25]. In this study, the amount of ADA was not affected by tofacitinib, thereby the conversion of adenosine to inosine would not be affected by tofacitinib.

Methotrexate and sulfasalazine of anti-rheumatic drugs have been reported to inhibit aminoimidazole 4-carboxamide ribonucleotide (AICAR) transformylase and thus increase intracellular AICAR levels, in addition to their main pharmacological functions [26–30]. AICAR was reported to increase the adenosine level, inhibiting AMPD and ADA [26–30]. Similarly, tofacitinib would increase the adenosine level and thus show anti-inflammatory activities, in addition to its main pharmacological function of JAK inhibition.

The expression of AMPD2 was downregulated by the tofacitinib treatment, while the expression of AMPD3 was not affected by the treatment. AMPD2 and AMPD3 are encoded by different genes. AMPD2 is predominantly produced in liver and spleen,

Mod Rheumatol Downloaded from informahealthcare.com by St Marianna University on 06/29/15
For personal use only.

RIGHTSLINK

Mod Rheumatol Downloaded from informahealthcare.com by St Marianna University on 06/29/15
For personal use only.

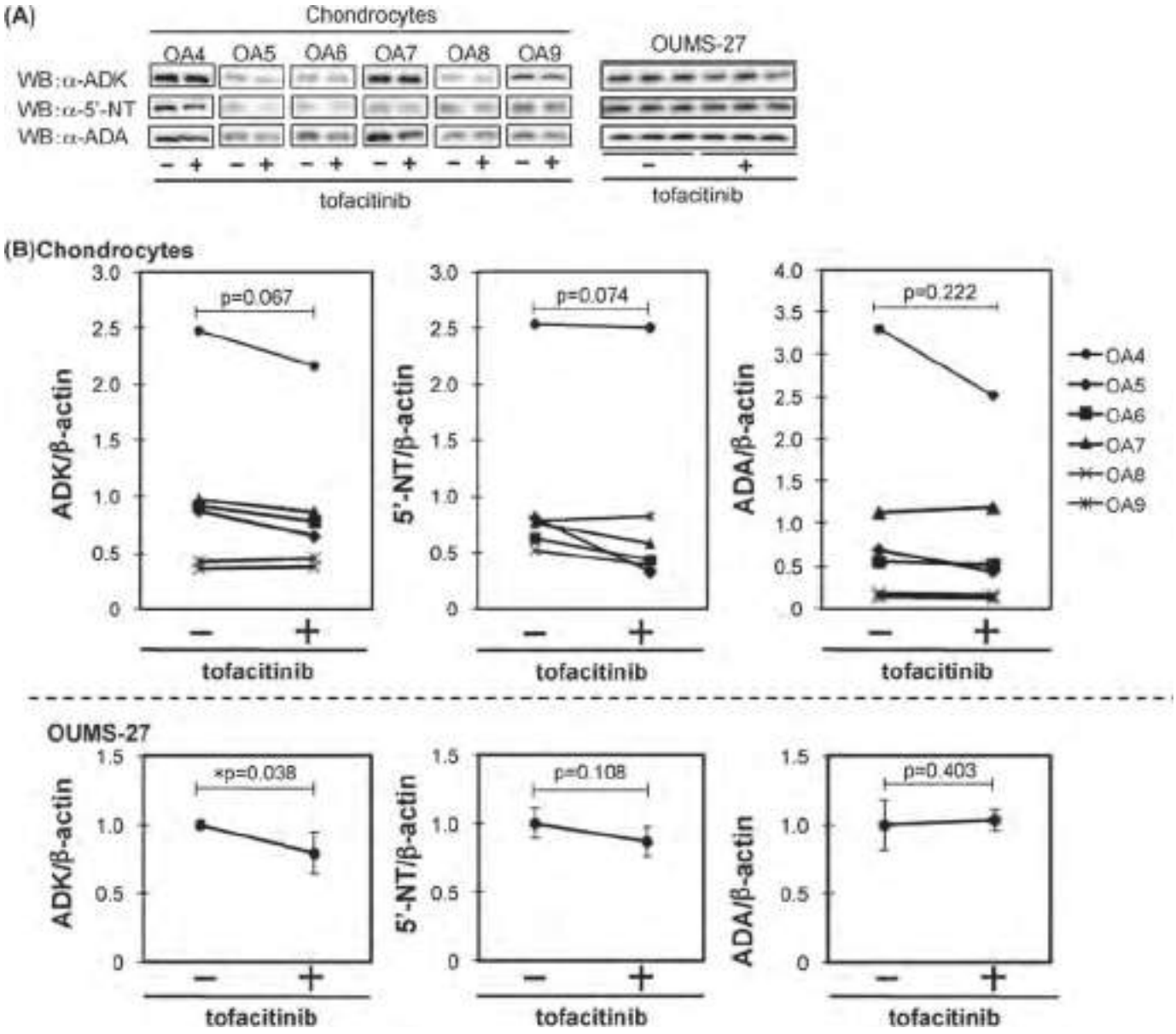

Figure 3. Effects of tofacitinib on the levels of ADK, 5'-NT, and ADA. (A) Human articular chondrocytes ($n = 6$) and OUMS-27 ($n = 3$) were incubated with or without 10 μM of tofacitinib for 48 h. Then proteins were extracted and subjected to Western blotting with antibodies to ADK, 5'-NT, ADA, and β-actin. (B) Intensity of the band for ADK, 5'-NT, ADA, and β-actin was measured by densitometry. In each patient and in the OUMS-27 samples, the intensity of the band for ADK, 5'-NT, and ADA, corrected using that of β-actin, was compared between the non-treated and tofacitinib-treated conditions. An average of the corrected intensity in the non-treated group is defined as 1.0. $^*p < 0.05$.

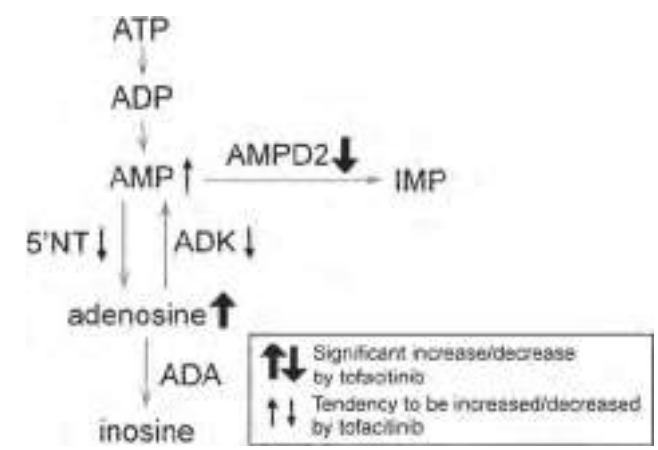

Figure 4. Schema of nucleic metabolism related to AMP and adenosine. Our findings are described in the rectangle. AMPD2: AMP deaminase 2, ADK: adenosine kinase, 5'-NT: 5'-nucleotidase, and ADA: adenosine deaminase.

while AMPD3 is predominantly produced in hematopoietic cells [12–18]. Thus, the mechanisms regulating the expression of AMPD2 and AMPD3 are speculated to be different from each other. Tofacitinib would suppress the AMPD2-specific expression-regulating mechanism.

Here we stimulated chondrocytes with tofacitinib for 48 h, since the tofacitinib treatment for 48 h decreased AMPD2 spot intensity in 2D-DIGE screening of our previous study [11]. Considering daily oral administration of tofacitinib in the clinical use, longer stimulation periods should be investigated in the future.

The expression levels of AMPD2 appeared to be different among the patients (Figure 1). Additional real-time PCR using 3 samples revealed that AMPD2 mRNA levels did not show more than 3 times difference among the samples (data not shown). Thereby it should be investigated whether the effects of tofacitinib detected here were affected by the expression levels of AMPD2 in the future.

Our data would promote understanding of roles of tofacitinib in the treatment of RA.

RIGHTSLINK

Acknowledgements

We thank Ms. Sawada Y, Ms. Yokoyama MK, Ms. Asano J, Ms. Tamaki M, Ms. Mogi T, and Ms. Suzuki M for their technical assistance.

Conflict of interest

None.

References

1. O'Shea JJ, Kontzias A, Yamaoka K, Tanaka Y, Laurence A. Janus kinase inhibitors in autoimmune diseases. Ann Rheum Dis. 2013;72(Suppl 2):111–15.
2. Tanaka Y, Yamaoka K. JAK inhibitor tofacitinib for treating rheumatoid arthritis: from basic to clinical. Mod Rheumatol. 2013;23(3):415–24.
3. Kontzias A, Kotlyar A, Laurence A, Changelian P, O'Shea JJ. Jakinibs: a new class of kinase inhibitors in cancer and autoimmune disease. Curr Opin Pharmacol. 2012;12(4):464–70.
4. O'Shea JJ, Gadina M, Schreiber RD. Cytokine signaling in 2002: new surprises in the Jak/Stat pathway. Cell. 2002;109 Suppl:S121–31.
5. Yarilina A, Xu K, Chan C, Ivashkiv LB. Regulation of inflammatory responses in tumor necrosis factor-activated and rheumatoid arthritis synovial macrophages by JAK inhibitors. Arthritis Rheum. 2012;64(12):3856–66.
6. Milici AJ, Kudlacz EM, Audoly L, Zwillich S, Changelian P. Cartilage preservation by inhibition of Janus kinase 3 in two rodent models of rheumatoid arthritis. Arthritis Res Ther. 2008;10(1):R14.
7. Flanagan ME, Blumenkopf TA, Brissette WH, Brown MF, Casavant JM, Shang-Poa C, et al. Discovery of CP-690,550: a potent and selective Janus kinase (JAK) inhibitor for the treatment of autoimmune diseases and organ transplant rejection. J Med Chem. 2010;53(24):8468–84.
8. Tanaka Y, Suzuki M, Nakamura H, Toyoizumi S, Zwillich SH, Tofacitinib Study Investigators. Phase II study of tofacitinib (CP-690,550) combined with methotrexate in patients with rheumatoid arthritis and an inadequate response to methotrexate. Arthritis Care Res (Hoboken). 2011;63(8):1150–8.
9. Fleischmann R, Kremer J, Cush J, Schulze-Koops H, Connell CA, Bradley JD, et al. Placebo-Controlled Trial of Tofacitinib Monotherapy in Rheumatoid Arthritis. N Engl J Med. 2012;367(6):495–507.
10. van Vollenhoven RF, Fleischmann R, Cohen S, Lee EB, García Meijide JA, Wagner S, et al. Tofacitinib or adalimumab versus placebo in rheumatoid arthritis. N Engl J Med. 2012;367(6):508–19.
11. Endo W, Arito M, Sato T, Kurokawa MS, Omoteyama K, Iizuka N, et al. Effects of sulfasalazine and tofacitinib on the protein profile of articular chondrocytes. Mod Rheumatol. 2013. doi:10.3109/14397595.2013.864225.
12. Ogasawara N, Goto H, Watanabe T. Isozymes of rat AMP deaminase. Biochim Biophys Acta. 1975;403(2):530–7.
13. Ogasawara N, Goto H, Yamada Y, Watanabe T. Distribution of AMP-deaminase isozymes in rat tissues. Eur J Biochem. 1978;87(2):297–304.
14. Ogasawara N, Goto H, Yamada Y, Watanabe T, Asano T. AMP deaminase isozymes in human tissues. Biochim Biophys Acta. 1982;714(2):298–306.
15. Ogasawara N, Goto H, Yamada Y, Watanabe T. Distribution of AMP deaminase isozymes in various human blood cells. Int J Biochem. 1984;16(3):269–73.
16. Sabina RL, Morisaki T, Clarke P, Eddy R, Shows TB, Morton CC, Holmes EW. Characterization of the human and rat myoadenylate deaminase genes. J Biol Chem. 1990;265(16):9423–33.
17. Bausch-Jurken MT, Mahnke-Zizelman DK, Morisaki T, Sabina RL. Molecular cloning of AMP deaminase isoform L. Sequence and bacterial expression of human AMPD2 cDNA. J Biol Chem. 1992;267(31):22407–13.
18. Mahnke-Zizelman DK, Sabina RL. Cloning of human AMP deaminase isoform E cDNAs. Evidence for a third AMPD gene exhibiting alternatively spliced 5'-exons. J Biol Chem. 1992;267(29):20866–77.
19. Kellgren JH, Lawrence JS. Radiological assessment of osteo-arthrosis. Ann Rheum Dis. 1957;16(4):494–502.
20. Fredholm BB, IJzerman AP, Jacobson KA, Linden J, Müller CE. International Union of Basic and Clinical Pharmacology. LXXXI. Nomenclature and Classification of Adenosine Receptors—An Update. Pharmacol Rev. 2011;63(1):1–34.
21. Mediero A, Cronstein BN. Adenosine and Bone Metabolism. Trends Endocrinol Metab. 2013;24(6):290–300.
22. Cronstein BN, Levin RI, Philips M, Hirschhorn R, Abramson SB, Weissmann G. Neutrophil adherence to endothelium is enhanced via adenosine A1 receptors and inhibited via adenosine A2 receptors. J Immunol. 1992;148(7):2201–6.
23. Bitto A, Polito F, Irrera N, D'Ascola A, Avenoso A, Nastasi G, et al. Polydeoxyribonucleotide reduces cytokine production and the severity of collagen-induced arthritis by stimulation of adenosine A(2A) receptor. Arthritis Rheum. 2011;63(11):3364–71.
24. Petrov R, MacDonald MH, Tesch AM, Benton HP. Inhibition of adenosine kinase attenuates interleukin-1- and lipopolysaccharide-induced alterations in articular cartilage metabolism. Osteoarthritis Cartilage. 2005;13(3):250–7.
25. Mazzon E, Esposito E, Impellizzeri D, DI Paola R, Melani A, Bramanti P, et al. CGS 21680, an agonist of the adenosine (A2A) receptor, reduces progression of murine type II collagen-induced arthritis. J Rheumatol. 2011;38(10):2119–29.
26. Baggott JE, Morgan SL, Ha T, Vaughn WH, Hine RJ. Inhibition of folate-dependent enzymes by non-steroidal anti-inflammatory drugs. Biochem J. 1992;282(Pt 1):197–202.
27. Baggott JE, Morgan SL, Ha TS, Alarcon GS, Koopman WJ, Krumdieck CL. Antifolates in rheumatoid arthritis: a hypothetical mechanism of action. Clin Exp Rheumatol. 1993;11 (Suppl 8):S101–5.
28. Cronstein BN, Eberle MA, Gruber HE, Levin RI. Methotrexate inhibits neutrophil function by stimulating adenosine release from connective tissue cells. Proc Natl Acad Sci U S A. 1991;88(6):2441–5.
29. Cronstein BN, Naime D, Ostad E. The antiinflammatory mechanism of methotrexate. Increased adenosine release at inflamed sites diminishes leukocyte accumulation in an in vivo model of inflammation. J Clin Invest. 1993;92(6):2675–82.
30. Gadangi P, Longaker M, Naime D, Levin RI, Recht PA, Montesinos MC, et al. The anti-inflammatory mechanism of sulfasalazine is related to adenosine release at inflamed sites. J Immunol. 1996;156(5):1937–41.

Mod Rheumatol Downloaded from informahealthcare.com by St Marianna University on 06/29/15
For personal use only.

RIGHTSLINK

Biochemical and Biophysical Research Communications 482 (2017) 50–56

Contents lists available at ScienceDirect

Biochemical and Biophysical Research Communications

journal homepage: www.elsevier.com/locate/ybbrc

Hypoxia-induced production of peptidylarginine deiminases and citrullinated proteins in malignant glioma cells

Taigen Sase [a, b], Mitsumi Arito [a, *], Hidetaka Onodera [b], Kazuki Omoteyama [a], Manae S. Kurokawa [c], Yayoi Kagami [d], Akihito Ishigami [d], Yuichiro Tanaka [b], Tomohiro Kato [a]

[a] Clinical Proteomics and Molecular Medicine, St. Marianna University Graduate School of Medicine, 2-16-1 Sugao, Miyamae, Kawasaki, Kanagawa 216-8511, Japan
[b] Department of Neurosurgery, St. Marianna University Graduate School of Medicine, 2-16-1 Sugao, Miyamae, Kawasaki, Kanagawa 216-8511, Japan
[c] Disease Biomarker Analysis and Molecular Regulation, St. Marianna University Graduate School of Medicine, 2-16-1 Sugao, Miyamae, Kawasaki, Kanagawa 216-8511, Japan
[d] Tokyo Metropolitan Institute of Gerontology, 35-2 Sakae-cho, Itabashi-ku, Tokyo 173-0015, Japan

ARTICLE INFO

Article history:
Received 22 October 2016
Accepted 25 October 2016
Available online 3 November 2016

Keywords:
Citrullinated proteins
Hypoxia
Malignant gliomas
Peptidylarginine deiminase

ABSTRACT

Background: Recently, it has been reported that hypoxia highly enhances expression of peptidylarginine deiminase (PAD) 4 and production of citrullinated proteins in some tumor cells. However, little is known about malignant gliomas on this issue. Therefore, we here investigated whether expression of PADs was induced by hypoxia and whether PADs citrullinated intracellular proteins if induced using U-251 MG cells of a human malignant glioma cell line.
Methods: Expression of PADs in U-251 MG cells, cultured under hypoxia or normoxia for 24 h, was investigated by quantitative polymerase chain reaction (qPCR). Citrullination of proteins in the cells and the cell lysates incubated for 48 h with or without Ca^{2+} was detected by western blotting. Citrullinated proteins were identified by mass spectrometry.
Results: The mRNA levels of PAD1, 2, 3, and 4 were up-regulated by hypoxia in a hypoxia-inducible factor-1-dependent manner in U-251 MG cells. In spite of the increased expression, intracellular proteins were not citrullinated. However, the induced PADs citrullinated U-251 MG cell-derived proteins when the cells were lysed. Multiple proteins citrullinated by hypoxia-induced PADs were identified. In addition, the extracellular domain of vascular endothelial growth factor receptor 2 was citrullinated by human PAD2 *in vitro*.
Conclusion: Our data may contribute to understanding of pathophysiology of malignant gliomas from the aspects of protein citrullination.

© 2016 Elsevier Inc. All rights reserved.

1. Introduction

Malignant gliomas are characterized by high invasiveness, neovascularization, and necrosis [1]. These features have been reported to be triggered by hypoxia, which is a rather common condition caused by insufficient blood supply [2–5]. Generally speaking, cellular responses to hypoxia are mainly regulated by a transcriptional factor of hypoxia-inducible factor (HIF)-1 [6]. HIF-1 is a heterodimer composed of HIF-1α and HIF-1β, formation of which is triggered by hypoxia. The HIF-1 heterodimer binds to hypoxia responsive elements (HRE) of various target genes like glycolysis-related enzymes and angiogenic factor [6].

Peptidylarginine deiminases (PADs; EC 3.5.3.15) are calcium (Ca^{2+})-dependent post-translational citrullination enzymes that convert an arginine residue into a citrulline residue [7]. In human, 5 isoforms of PAD have been reported (PAD1, 2, 3, 4, and 6) [7]. In *in vitro* studies, it was reported that hypoxia induced production of PAD2 and citrullinated glial fibrillary acidic protein (GFAP) in human astrocytes [8] and that hypoxia highly enhanced production of

* Corresponding author.
E-mail addresses: sasetaigen@marianna-u.ac.jp (T. Sase), m-ari@marianna-u.ac.jp (M. Arito), dera@marianna-u.ac.jp (H. Onodera), omoteyama@marianna-u.ac.jp (K. Omoteyama), manae@marianna-u.ac.jp (M.S. Kurokawa), yakagami@tmig.or.jp (Y. Kagami), ishigami@tmig.or.jp (A. Ishigami), tanaka@marianna-u.ac.jp (Y. Tanaka), t3kato@marianna-u.ac.jp (T. Kato).

http://dx.doi.org/10.1016/j.bbrc.2016.10.154
0006-291X/© 2016 Elsevier Inc. All rights reserved.

PAD4 in various kinds of tumor cells [9–11]. In an *in vivo* study, hypoxia was found to induce production of PADs, and the produced PADs citrullinated proteins of brains in rats [12,13]. Citrullination is often critical for functions and antigenicity of proteins. Aberrant citrullination was suggested to relate to pathogenesis and pathology of some diseases [14–17]. For example, in patients with alzheimer's disease, citrullinated proteins were reported to be abnormally detected in hippocampi [14]. In sera and synovial fluid of patients with rheumatoid arthritis (RA), autoantibodies to aberrantly citrullinated proteins were reported [15–20].

In malignant gliomas, it has been poorly investigated whether hypoxia induces expression of PADs and whether PADs citrullinate intracellular proteins, if induced. In addition, it is unclear whether HIF-1 is involved in induction of PADs by hypoxia in malignant gliomas. Therefore, we here investigated whether hypoxia induced production of PADs in U-251 MG cells of a human malignant glioma cell line. We also investigated whether the induced PADs citrullinated intracellular proteins. We identified target proteins of PADs in the cell line by proteomic analysis.

2. Materials and methods

2.1. Cell culture

U-251 MG cells of a human malignant glioma cell line (DS Pharma Biomedical Co., Ltd, Osaka, Japan) were cultured in EMEM (NISSUI PHARMACEUTICAL Co., Ltd, Tokyo, Japan) containing 7% Sodium Bicarbonate (Otsuka Pharmaceutical Co., Ltd., Tokyo, Japan) and L-Glutamine (NISSUI PHARMACEUTICAL Co., Ltd), and supplemented with 10% fetal bovine serum (MP Biomedical LLC, Santa Ana, CA, USA). The U-251 MG cells were cultured at 37 °C in humidified air with 5% CO_2. For the exposure of cells to hypoxia, U-251 MG cells were cultured in a hypoxic chamber (Hypoxia incubator chamber, STEMCELL TECHNOLOGIES, Vancouver, BC, Canada) containing 1% O_2, 5% CO_2, and 94% N_2 for 24 h as described previously [21].

2.2. Activation of HIF-1

U-251 MG cells were cultured with 0, 20, and 40 μM dimethyloxaloylglycine (DMOG, Enzo life Sciences, Inc., NY, USA) of a HIF-1 activator for 24 h.

2.3. RNA extraction and reverse transcription-PCR (RT-PCR)

RNA extraction and RT-PCR were performed as described previously [22,23]. Briefly, extraction and purification of RNA from U-251 MG cells and reverse transcription of the RNA samples were performed using RNeasy (Qiagen, Venlo, The Netherlands) and High Capacity cDNA Reverese Transcription Kits (Life Technologies, Rockville, MD, USA), respectively. Then, 2 μg of total RNA-derived cDNA, mixed with 1 μM each of the forward and reverse primers and Premix Taq™ (Ex Taq™ Version 2.0, Takara, Shiga, Japan), was subjected to PCR. Nucleotide sequences of the primers for the amplification of a vascular endothelial growth factor (VEGF) fragment and a β-actin (ACTB) fragment are as follows: for VEGF; 5′ -GCCTCCGAAACCATGAACTTTCTGCTG and 5′ -TGGTGATGTTGGACTCCTCA, and for ACTB; 5′ -AGGCACCAGGGCGTGAT and 5′ -TGCTCCCAGTTGGTGACGAT. The thermal cycle conditions were as follows: for VEGF; 95 °C for 5 min, 25 cycles (95 °C for 15 s, 60 °C for 30 s, 72 °C for 20 s), and 72 °C for 5 min, and for ACTB; 98 °C for 5 min, 25 cycles (98 °C for 15 s, 58 °C for 30 s, 72 °C for 20 s), and 72 °C for 5 min.

2.4. Quantitative PCR (qPCR)

qPCR was performed as described previously [23]. Briefly, qPCR was performed using ABI Prism 7000 Sequence Detection System (Applied Biosystems™, Foster city, CA, USA), according the manufacturer's instructions. 1 μg of total RNA-derived cDNA, mixed with TaqMan® Gene Expression Assays (PAD1: Hs00203458_m1, PAD2: Hs00247108_m1, PAD3: Hs00212088_m1, PAD4: Hs00202612_m1, PAD6: Mm00462201_m1, VEGF: Hs0090055_m1, and ACTB: Mm00607939_s1, Applied Biosystems™) and TaqMan® Gene Expression Master Mix (Applied Biosystems™), was subjected to qPCR. The thermal cycle conditions were as follows: 95 °C for 10 min, followed by 40 cycles of 95 °C for 15 s and 60 °C for 60 s.

2.5. In vitro citrullination by endogenious PADs

The U-251 MG cells, suspended in a sonication buffer (50 mM Tris-HCl (pH 7.5), 1 mM 1, 4-dithiothreitol (DTT)), were sonicated by Bioruptor UCD-250 (SONIC BIO Corporation, Kanagawa, Japan). The cell lysates were incubated at 37 °C for 48 h, with or without 1 mM $CaCl_2$.

2.6. In vitro citrullination by human PAD2

Recombinant human VEGF receptor (VEGFR) 2 protein (aa1-764, abcam, Cambridge, UK) was subjected to *in vitro* citrullination in a solution (50 mM Tris-HCl (pH7.4), 1 mM $CaCl_2$, and 20 U/mg human PAD2 (abcam)) for 2 h.

2.7. Western blotting (WB)

The procedure for WB was described previously [24]. Briefly, an equal amount of protein (1μg/lane) was separated by 15% sodium dodecyl sulfate-polyacrylamide gel electrophoresis (SDS-PAGE). The separated proteins were transferred onto a membranepolyvinylidence difluoride (PVDF membrane; Merck Millipore, Billerica, MA, USA). For detection of citrullinated proteins, citrulline residues of proteins on the PVDF membrane were chemically modified by overnight incubation at 37 °C in 0.0125% $FeCl_3$, 2.3 M H_2SO_4, 1.7 M H_3PO_4, 0.25% 2, 3-butanedion monoxime, 0.125% antipyrine, and 0.25 M acetic acid (a modification medium) [13,25]. Then, the modified citrulline residues were detected by rabbit anti-modified citrulline polyclonal antibodies diluted at 1:2000 [13,24,25] and horseradish peroxidase (HRP)-conjugated goat anti-rabbit IgG antibodies (Merck Millipore) diluted at 1:2000. The bound antibodies were visualized using 3,3′-diaminobenxide, tetrahydrochloride (DAB; DOJINDO, Kumamoto, Japan).

2.8. 2-Dimensional electrophoresis (2-DE) analysis

Proteins were extracted into a lysis buffer (7 M urea, 2 M thiourea, 4% CHAPS) from each of U-251 MG samples. 2-DE was perfomed as described previously [26]. Briefly, 200 μg of the extracted protein samples were loaded onto 13 cm drystrips (Imobiline, pH range of 3–11, GE Healthcare, Buckinghamshire, UK) and the drystrips were kept at 20 °C for 12 h. Then isoelectric focusing (IEF) was performed using Ettan IPGphor (GE Healthcare). The proteins separated by IEF were further separated by 12.5% SDS-PAGE. The separated proteins, stained with SYPRO Ruby Protein Gel Stain (GE Healthcare), were transferred onto a PVDF membrane. The membrane was subjected to WB with rabbit anti-modified citrulline polyclonal antibodies to detect citrullinated proteins. Intensity of protein spots were measured by an image analyzer (Typhoon 9400, GE Healthcare).

2.9. Protein identification

Protein identification was performed as described previously [27–29]. For identification of citrullinated proteins, gel fragments that corresponded to protein spots of interest were recovered. Peptides, generated by in-gel digestion with trypsin, were extracted from the gel fragments and were subjected to MALDI-TOF/TOF mass spectrometry (MS, Ultraflex, Bruker Daltonics, Bremen, Germany). The determined peptide masses were compiled to allow searches of protein database of National Center for Biotechnology Information (NCBI) using the Mascot software program (Matrix Svience, London, UK).

2.10. Statistical analysis

Statistical significance was calculated by Student's t-test.

3. Result

3.1. Induction of PAD expression by hypoxia in U-251 MG cells

To investigate whether hypoxia induced expression of PADs in malignant glioma cells, we cultured U-251 MG cells under hypoxia or normoxia for 24 h. First, we checked exposure of U-251 MG cells to hypoxia by the assessment of mRNA levels of VEGF. As a result, the mRNA levels of VEGF were significantly increased in the hypoxia samples compared to the normoxia samples (8.7-folds, Fig. 1A). This indicated that the U-251 MG cells were surely exposed to hypoxia in our experiments.

Next, we measured mRNA levels of PAD1, 2, 3, 4, and 6 in the normoxia and hypoxia samples by qPCR. As a result, mRNA levels of PAD1, 2, 3, and 4 were significantly increased in the hypoxia samples compared to the normoxia samples (5.2, 31.6, 5.6, and 6.4-folds, respectively, Fig. 1A). On the other hand, mRNA of PAD6 was not detected under the hypoxic and the normoxic conditions.

We next investigated whether mRNA levels of PAD1, 2, 3 and 4 were up-regulated by HIF-1 in hypoxic U-251 MG cells specifically. We cultured U-251 MG cells for 24 h after the treatment with DMOG, a HIF-1α activator (0, 20, and 40 μM) and then evaluated mRNA for PADs. As a result, the mRNA levels of PAD1, 2, and 4 were significantly increased both in the 20 and 40 μM DMOG-treated samples compared to the non-treated samples, as was the case of VEGF (Fig. 1B). The levels of PAD3 were significantly increased in the 40 μM DMOG-treated samples compared to the non-treated samples (Fig. 1B). Therefore, we concluded that up-regulation of mRNA levels of PAD1, 2, 3, and 4 in hypoxic U-251 MG cells was HIF-1-dependent.

3.2. Citrullination of proteins by PADs in hypoxic U-251 MG cells

Based on the above finding, we then investigated whether the induced PADs citrullinated intracellular proteins in the hypoxic U-251 MG cells by WB. As a result, in spite of the increased expression of PADs, citrullination of intracellular proteins were not detected (data not shown). Thereby, we next investigated whether the induced PADs citrullinated proteins in lysates of the cells. Specifically, cell lysates of the normoxic or hypoxic U-251 MG cells were

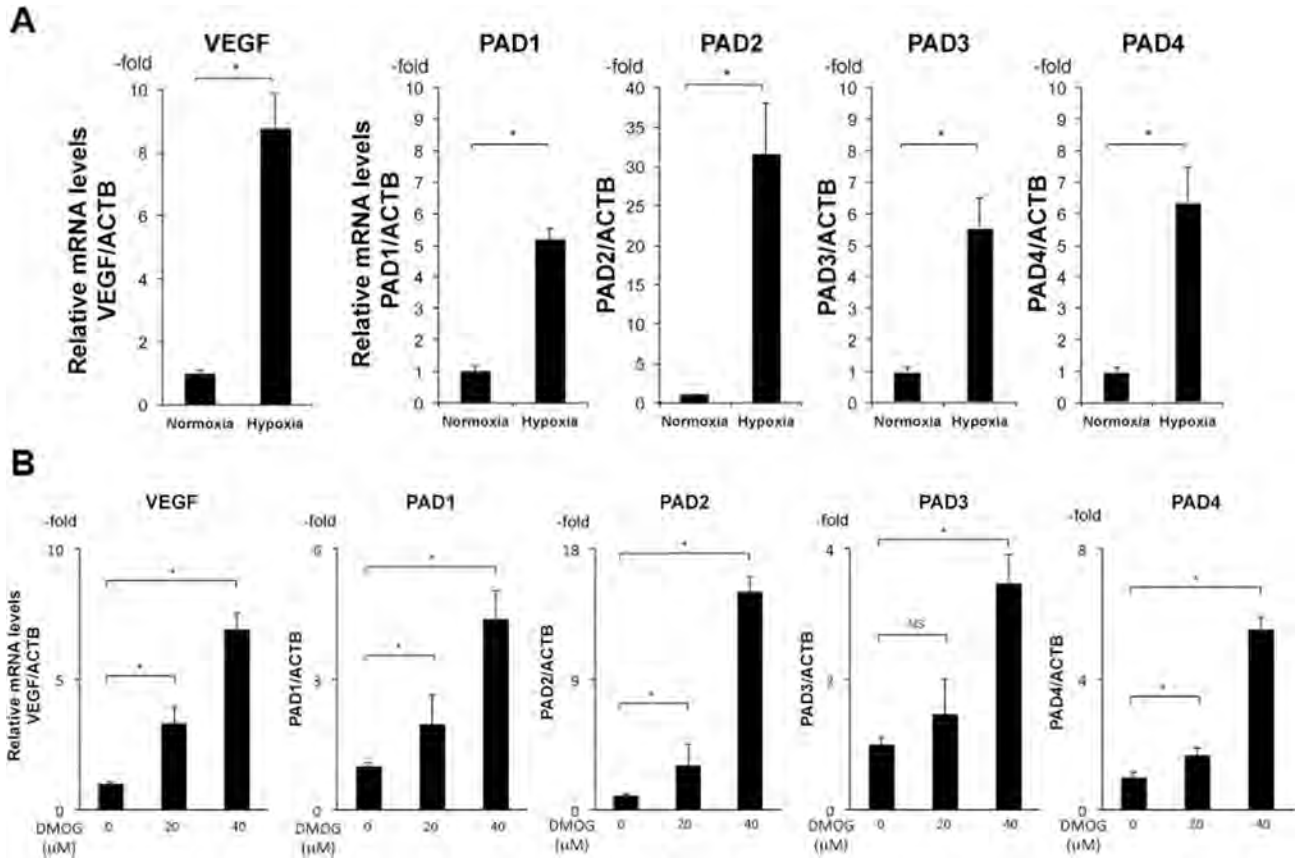

Fig. 1. Measurement of mRNA levels of VEGF and PADs in U-251 MG cells. U-251 MG cells were cultured under hypoxia or normoxia for 24 h (**A**) mRNA for VEGF, PAD1-4 and ACTB were assayed by qPCR. The mRNA levels of VEGF and PAD1-4 were normalized by the mRNA level of ACTB as an internal control. The average value in the normoxia group was defined as 1.0. Mean values with SD are shown. *p < 0.01. (B) U-251 MG cells were cultured under normoxia with DMOG (0, 20 or 40 μM) for 24 h. Then mRNA for VEGF, PAD1-4 and ACTB were assayed by qPCR. The mRNA level of VEGF and PAD1-4 were normalized by the mRNA level of ACTB as an internal control. The average value in the normoxia group was defined as 1.0. Mean values with SD are shown. *p < 0.01. NS: not significant.

incubated at 37 °C for 48 h with or without 1 mM $CaCl_2$. Then the lysates were subjected to WB to detect citrullinated proteins. As a result, in the condition without $CaCl_2$, citrullinated proteins were not detected in the lysates both from hypoxic and normoxic cells. On the other hand, in the $CaCl_2$-treated samples, citrullinated proteins were clearly detected in the lysates both from hypoxic and normoxic cells. The citrullination levels were much higher in the hypoxia samples than in the normoxia samples (2.0-fold, Fig. 2A). These data indicates that endogeneous PADs do not citrullinate detectable amount of intracellular proteins when U-251 MG cells are alive, but citrullinate considerable amounts of them when the cells are lysed and intracellular proteins are exposed to Ca^{2+}. Furthermore, the data indicates that increased PADs by hypoxia enhance the citrullination.

3.3. Indentification of PADs target proteins in hypoxic U-251 MG cells

As above demonstrated, citrullinated proteins were increased in the cell lysates of hypoxic U-251 MG cells. To identify the citrullinated proteins, the proteins were separated by 2-DE. The separated proteins labeled with SYPRO Ruby® are shown in the upper panels of Fig. 2B. Then citrullinated proteins were detected by WB, as shown in the lower panels of Fig. 2B. By the comparision of citrullination levels between the normoxia and hypoxia samples, we selected 18 protein spots citrullination of which increased by hypoxia (Fig. 2B–D). We identified proteins corresponding to all the 18 citrullinated protein spots using MALDI-TOF/TOF MS. Protein spot nos. 1–4 and 10–13 were identified as vimentin (VIME). Nos. 5 and 6 were identified as glial fibrillary acidic protein (GFAP). No. 7 was identified as filamin-A (FLNA). Nos. 8 and 9 were identified as 78 kDa glucose-regulated protein (GRP78). Nos. 14 and 15 were identified as actin cytoplasmic 1 or 2 (ACTB or ACTG). No. 16 was identified as glyceraldehyde-3-phosphate dehydrogenase (G3P), and nos. 17 and 18 were identified as alpha-crystallin B chain (CRYAB) (Table 1). The identified proteins were roughly mainly classified into the three categories of cytoskeletal proteins, stress-related proteins, and glycolytic proteins (Table 1).

3.4. Citrullination of VEGFR2 by human PAD2

Recently, autoantibodies to VEGFR2 have been reported in patients with high-grade malignant glioma [30]. It is well-known that autoantibodies are generated against aberrantly citrullinated

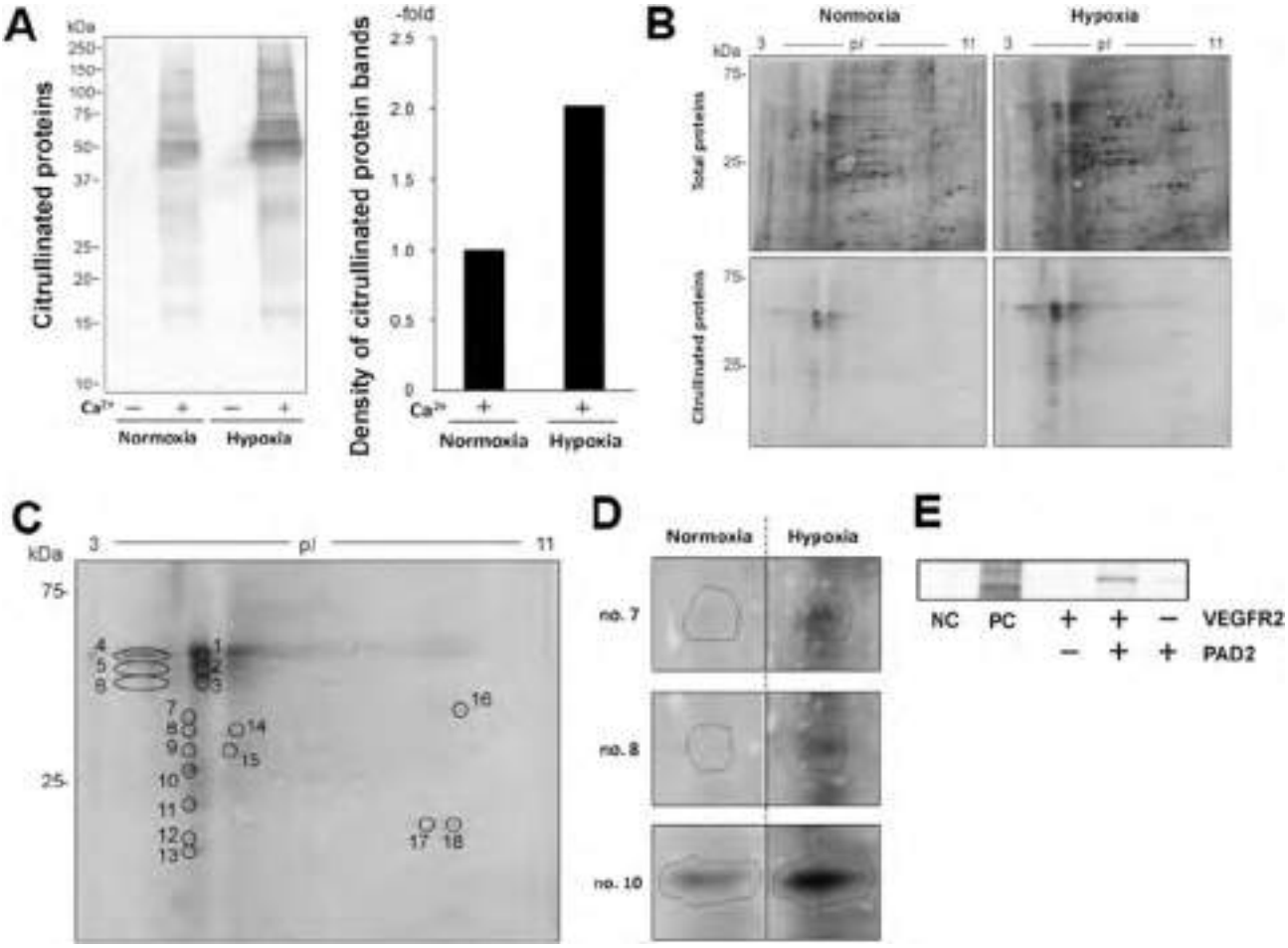

Fig. 2. Citrullinated proteins in hypoxic U-251 MG cells. (A) Left panel: U-251 MG cells were cultured under hypoxia or normoxia for 24 h. U-251 MG cells suspended in a sonication buffer (50 mM Tris-HCl (pH 7.5), and 1 mM DTT) were sonicated. The cell lysates were incubated at 37 °C for 48 h, with or without 1 mM $CaCl_2$ (Ca^{2+}). The incubated lysates were subjected to WB using rabbit anti-modified citrulline polyclonal antibodies. Right panel: density of the citrullinated protein bands in the normoxia- and hypoxia-treated samples incubated with Ca^{2+} were measured by using Progeneosis software (Nonliner Dynamics, Newcastle, UK). **(B)** The normoxic and hypoxic U-251 MG cells-derived lysates (with 1 mM Ca^{2+}) described in (A) were subjected to 2-DE. Separated protein spots were stained by SYPRO Ruby (Upper panels). Then, the proteins were transferred onto a PVDF membrane and reacted with a rabbit anti-modified citrulline polyclonal antibody (Lower panels). (C) The locations of 18 protein spots, intensity of which were increased in the hypoxia samples compared to the normoxia samples, are shown by circles with spot numbers. (D) Out of the 18 citrulinated protein spots, representative cases (nos. 7, 8, and 10) are shown (5.5, 3.0, and 1.6-folds, respectively). (E) The recombinant extracellular domain of human VEGFR2 (aa1-764) was treated with or without human PAD2 for 2 h in a solution (50 mM Tris-HCl pH7.4 and 1 mM $CaCl_2$) for 2 h. The samples were subjected to WB using rabbit anti-modified citrulline polyclonal antibodies.

proteins in RA [18–20]. Therefore, citrullination of VEGFR2 may trigger the generation of the anti-VEGFR2 autoantibodies, if it occurs. We investigated whether VEGFR2 could be citrullinated by PAD2 *in vitro*. As a result, we found that the extracellular domain of human VEGFR2 was citrullinated by PAD2 *in vitro* (Fig. 2E).

4. Discussion

The findings in this study are summarized as follows: 1) The mRNA levels of PAD1, 3, and 4 as well as PAD2 were up-regulated by hypoxia in a HIF-1-dependent manner in U-251 MG cells of a malignant glioma cell line; 2) The induced PADs citrullinated proteins of the cells when tested using cell lysates; 3) Multiple proteins citrullinated by hypoxia-induced PADs were identified; 4) The extracellular domain of human VEGFR2 was citrullinated by human PAD2 *in vitro*.

On the first point, the mRNA levels of PAD1, 2, 3, and 4 were drastically up-regulated by hypoxia in a HIF-1-dependent manner in malignant glioma cells. An inner part of malignant gliomas easily becomes hypoxic due to insufficient blood supply [1,4,5]. These

Table 1
Identification of citrullinated protein spots whose intensity was significantly increased by hypoxia condition.

Category	Spot no.	Fold changes of citrullination (Hypoxia/ Normoxia)	MW/p*I* (observed)	Protein	Accession no. (GI)	MW/p*I* (calculated)	Matched peptides	Coverage (%)	Sequence confirmed by LID (Mascot ion score)
Cytoskeltal protein	1	1.3	42/5.2	Vimentin VIME_HUMAN	62414289	53.6/5.06	295	39	^{197}EEAENTLQSFR^{207}(60) ^{295}FADLSEAANRNNDALR^{310} (57) + Deiminated (R) ^{411}ISLPLPNFSSLNLR^{424}(81)
	2	1.3	38/5.2	Vimentin VIME_HUMAN	62414289	53.6/5.06	303	37	^{197}EEAENTLQSFR^{207}(71) ^{346}EMEENFAVEAANYQDTIGR^{364}(28) + Oxidation (M) ^{411}ISLPLPNFSSLNLR^{424}(111)
	3	1.6	36/5.2	Vimentin VIME_HUMAN	62414289	53.6/5.06	203	32	^{197}EEAENTLQSFR^{207}(71) ^{295}FADLSEAANRNNDALR^{310}(50) + Deiminated (R) ^{411}ISLPLPNFSSLNLR^{424}(17)
	4	2.9	42/4.5	Vimentin VIME_HUMAN	62414289	53.6/5.06	152	25	^{197}EEAENTLQSFR^{207}(20) ^{411}ISLPLPNFSSLNLR^{424}(71)
	10	1.6	25/5.1	Vimentin VIME_HUMAN	62414289	53.6/5.06	173	18	^{346}EMEENFAVEAANYQDTIGR^{364}(126) + Oxidation (M) ^{411}ISLPLPNFSSLNLR^{424}(15)
	11	1.6	22/5.1	Vimentin VIME_HUMAN	62414289	53.6/5.06	124	12	^{197}EEAENTLQSFR^{207}(2) ^{346}EMEENFAVEAANYQDTIGR^{364}(96) + Oxidation (M)
	12	2.9	19/5.1	Vimentin VIME_HUMAN	62414289	53.6/5.06	287	28	^{295}FADLSEAANRNNDALR^{310} (58) + Deiminated (R) ^{346}EMEENFAVEAANYQDTIGR^{364}(129) + Oxidation (M) ^{391}MALDIEIATYR^{401}(46) + Oxidation (M)
	13	1.5	18/5.1	Vimentin VIME_HUMAN	62414289	53.6/5.06	227	20	^{346}EMEENFAVEAANYQDTIGR^{364}(152)+ Oxidation (M) ^{391}MALDIEIATYR^{401}(46) + Oxidation (M)
	5	3.7	38/4.5	Glial fibrillary acidic protein GFAP_HUMAN	4503979	49.9/5.42	185	43	^{96}ALAAELNQLR^{105}(34) ^{377}ITIPVQTFSNLQIR^{390}(80)
	6	2.3	36/4.5	Glial fibrillary acidic protein GFAP_HUMAN	4503979	49.9/5.42	71	15	^{96}ALAAELNQLR^{105}(10) ^{377}ITIPVQTFSNLQIR^{390}(42)
	7	5.5	29/5.1	Filamin-A FLNA_HUMAN	116063573	280.6/5.7	87	3	^{1516}EGPYSISVLYGDEEVPR^{1532}(35) ^{1622}YGGDEIPFSPYR^{1633}(55)
	14	1.8	27/5.3	Actin, cytoplasmic 1 ACTB_HUMAN	4501885	41.8/5.29	117	19	^{239}SYELPDGQVITIGNER^{254}(86)
				Actin, cytoplasmic 2 ACTG_HUMAN	4501887	41.8/5.31	117	19	^{239}SYELPDGQVITIGNER^{254}(86)
	15	1.6	26/5.3	Actin, cytoplasmic 1 ACTB_HUMAN	4501885	41.8/5.29	163	26	^{239}SYELPDGQVITIGNER^{254}(118)
				Actin, cytoplasmic 2 ACTG_HUMAN	4501887	41.8/5.31	163	26	^{239}SYELPDGQVITIGNER^{254}(118)
Stress-related protein	8	3.0	27/5.1	78 kDa glucose-regulated protein GRP78_HUMAN	16507237	72.3/5.07	83	3	^{475}DNHLLGTFDLTGIPPAPR^{492}(77)
	9	3.1	26/5.1	78 kDa glucose-regulated protein GRP78_HUMAN	16507237	72.3/5.07	119	10	^{475}DNHLLGTFDLTGIPPAPR^{492}(109)
	17	2.4	20/7.5	Alpha-crystallin B chain CRYAB_HUMAN	4503057	20.1/6.76	71	38	^{12}RPFFPFHSPSR^{22}(41)
	18	1.2	20/7.9	Alpha-crystallin B chain CRYAB_HUMAN	4503057	20.1/6.76	71	45	^{57}APSWFDTGLSEMR^{69}(41)+ Oxidation (M)
Glycolytic protein	16	1.6	29/8.0	Glyceraldehyde-3-phosphate dehydrogenase G3P_HUMAN	7669492	36.3/8.57	189	17	^{67}LVINGNPITIFQER^{80}(76) + Deiminated (R) ^{310}LISWYDNEFGYSNR^{323}(93)

MW; molecular weight (kDa), p*I*; isoelectric point, LID; laser-induced dissociation.

indicate that PAD1-4 would be highly expressed in a part of malignant gliomas.

Each of the 5 PADs is expressed in a tissue-specific manner to some degree [7]. PAD1 and PAD3 are mainly expressed in epidermis, uterus, and hair follicles [7,31,32]. PAD2 is expressed in various tissue, including the central nervous system [7]. Although PAD4 is poorly expressed in normal tissue, PAD4 is highly expressed in various malignant tumor tissue [10]. PAD6 is expressed only in germ cells [33]. Levels of plasma PAD4 were reported to be higher in patients with malignant tumors than in that of healthy donors, which was consistent with increased production of PAD4 in malignant tumor tissue [11]. Thus, PAD4 is proposed as a diagnostic marker and a therapeutic target of malignant tumors [11]. Taking our data together with the reports, PAD1, 2, 3 as well as PAD4 would be released from glioma cells into blood. Diagnostic and therapeutic roles of PADs 1–3 should be investigated in the future.

On the second point, endogenious PADs were drastically increased by hypoxia, but nevertheless intracellular citrullination of proteins were not detected when malignant glioma cells were alive. In contrast, citrullination of intracellular proteins were massively detected when the cells were lysed and exposed to Ca^{2+}. Further, more the citrullination were much greater in the hypoxic samples than in the normoxic samples, reflecting the increase of PADs expression. Thereby, when malignant glioma cells undergo necrosis by hypoxia, the induced PADs would be easily activated by exposure to Ca^{2+} in the body fluid and then possibly citrullinate glioma cell- and other cell-derived proteins.

Even in the PAD-increased condition by hypoxia, citrullinated proteins were not detected when the cells were alive. Because the enzymatic activity of PADs depends on the intracellular Ca^{2+} concentration around PADs, we speculate that the intracellular Ca^{2+} concentration in live cells is too low to activate PADs. Even though hypoxia was reported to induce Ca^{2+} influx temporarily, it would be still low to activate PADs [34]. Alternatively, localization of PADs might limit the access of Ca^{2+}. Those points should be investigated in the near future.

On the third point, we identified 7 kinds of proteins that were citrullinated by the hypoxia-induced PADs when malignant glioma cells were lysed. Cytoskeletal proteins such as VIME and GFAP, stress-related proteins such as GRP78 and glycolytic proteins such as G3P were identified (Table 1). The concentration of citrullinated antithrombin in plasma was reported to be higher in patients with malignant tumors than in healthy donors [11]. The plasma levels of citrullinated antithrombin were reported to be correlated with levels of tumor markers such as CA19-9 in blood of patients with breast carcinoma, bladder cancer, renal cell carcinoma, and pancreastic cancer [10]. Further, higher levels of citrullinated antithrombin are considered to cause hypercoagulation in patients with malignant tumors [11,35]. From our data, the induced PADs derived from glioma cells possibly citrullinate glioma cell- and other cell-derived proteins. The citrullinated proteins including the proteins identified here may circulate in blood of patients with malignant gliomas. Detection of them should be tried in the future. In RA, aberrant citrullination of synovial proteins and generation of autoantibodies to the citrullinated proteins have been reported [17–20]. Therefore, the citrullinated proteins, derived from malignant gliomas, may get autoantigenicity in patients with malignant glioma. These points should be investigated in the near future.

On the fourth point, again, autoantibodies to the citrullinated proteins are generated in RA [17–20]. Recently, autoantibodies to VEGFR2 have been reported in patients with high-grade malignant glioma [30]. VEGFR2 is known to be expressed on the surface of brain microvascular endothelial cells near to glia cells. We here demonstrated that the extracellular domain of VEGFR2 was citrullinated by PAD2 *in vitro*. Therefore, we speculate that PADs derived from hypoxic glioma cells citrullinates the extracellular domain of VEGFR2 on the surface of brain microvascular endothelial cells and that the citrullination of VEGFR2 contributes to the acquirement of antiginecity. It is needed to investigate whether VEGFR2 in patients with high-grade malignant glioma is citrullinated or not.

In conclusion, we here found induction of PADs expression by hypoxia in malignant glioma cells and identified multiple proteins that were citrullinated by the hypoxia-induced PADs when malignant glioma cells were lysed. Our data may contribute to understanding of pathophysiology of malignant gliomas from the aspects of protein citrullination.

Conflict of interest statement

All authors have nothing to disclose.

Acknowledgments

We thank Ms. Y. Sawada and Ms. M.K. Yokoyama for their technical assistance.

Transparency document

Transparency document related to this article can be found online at http://dx.doi.org/10.1016/j.bbrc.2016.10.154.

References

[1] S. Fujiwara, K. Nakagawa, H. Harada, et al., Silencing hypoxia-inducible factor-1alpha inhibits cell migration and invasion under hypoxic environment in malignant gliomas, Int. J. Oncol. 30 (2007) 793–802.
[2] M. Hockel, P. Vaupel, Tumor hypoxia: definitions and current clinical, biologic, and molecular aspects, J. Natl. Cancer. Inst. 93 (2001) 266–276.
[3] P. Vaupel, A. Mayer, Hypoxia in cancer: significance and impact on clinical outcome, Cancer. Metastasis. Rev. 26 (2007) 225–239.
[4] D. Zagzag, H. Zhong, J.M. Scalzitti, et al., Expression of hypoxia-inducible factor 1alpha in brain tumors: association with angiogenesis, invasion, and progression, Cancer 88 (2000) 2606–2618.
[5] K.L. Søndergaard, D.A. Hilton, M. Penneym, et al., Expression of hypoxia-inducible factor 1alpha in tumours of patients with glioblastoma, Neuropathol. Appl. Neurobiol. 28 (2000) 210–217.
[6] G.L. Semenza, Targeting HIF-1 for cancer therapy, Nat. Rev. Cancer 3 (2003) 721–732.
[7] E.R. Vossenaar, A.J. Zendman, W.J. van Venrooij, et al., PAD, a groeing family of citrullinating enzymes: genes, features and involvement in disease, Bioessays 25 (2003) 1106–1118.
[8] T. Sambandam, M. Belousova, M.A. Accaviti-Loper, et al., Increased peptidylarginine deiminase type II in hypoxic astrocytes, Biochem. Biophys. Res. Commun. 325 (2007) 1324–1329.
[9] X. Chang, J. Han, Expression of peptidylarginine deiminase type 4 (PAD4) in various tumors, Mol. Carcinoge 45 (2006) 183–196.
[10] X. Chang, J. Han, L. Pang, et al., Increased PADI4 expression in blood and tissue of patients with malignant tumors, B.M.C. Cancer 40 (2009).
[11] X. Chang, K. fang, PADI4 and tumourigenesis, Cancer. Cell. Int. 10 (2010), http://dx.doi.org/10.1186/1475-2867-10-7.
[12] S. Lange, E. Rocha-Ferreira, L. Thei, et al., Peptidylarginine deiminases: novel drug targets for prevention of neuronal damage following hypoxic ischemic insult (HI) in neonates, J. Neurochem. 130 (2014) 555–562.
[13] H. Asaga, A. Ishigami, Protein deamination in the rat brain: generation of citrulline-containing proteins in cerebrum perfused with oxygen-deprived media, Biomed. Res. 21 (2000) 197–205.
[14] A. Ishigami, T. Ohsawa, M. Hiratsuka, et al., Abnormal accumulation of citrullinated proteins catalyzed by peptidylarginine deiminase in hippocampal extracts from patients with Alzheimer's disease, J. Neurosci. Res. 80 (2005) 120–128.
[15] X. Chang, R. Yamada, A. Suzuki, et al., Citrullination of fibronectin in rheumatoid arthritis synovial tissue, Rheumatol. Oxf. 44 (2005) 1374–1382.
[16] X. Chang, R. Yamada, T. Sawada, et al., The inhibition of antithrombin by peptidylarginine deiminase 4 may contribute to pathogenesis of rheumatoid arthritis, Rheumatol. Oxf. 44 (2005) 293–298.
[17] A. Kinloch, K. Lundberg, R. Wait, et al., Venables, Synovial fluid is a site of citrullination of autoantigens in inflammatory arthritis, Arthritis. Rheum. 58 (2008) 2287–2295.
[18] W.J. van Venrooij, J.J. van Beers, G.J. Pruijn, Anti-ccp antibody, a marker for the early detection of rheumatoid arthritis, Ann. N. Y. Acad. Sci. 1143 (2008)

268–285.
[19] W.J. van Venrooij, The diagnostic accuracy of anti-citrulline antibody assessment in the diagnosis of patients suspected of rheumatoid arthritis by a general practitioner, Ned. Tijdschr. Geneeskd. 152 (2008) 1243–1244 author reply 1244–1245.
[20] W.J. van Venrooij, A.J. Zendman, Anti-CCP2 antibodies: an overview and perspective of the diagnostic abilities of this serological marker for early rheumatoid arthritis, Clin. Rev. Allergy. Immunol. 34 (2008) 36–39.
[21] T. Sase, M. Arito, H. Onodera, et al., Effects of edaravone on hypoxic human astrocytes revealed by a proteomic approach, Biomed. Res. 27 (2016) 1064–1070.
[22] K. Asano, M. Arito, M.S. Kurokawa, et al., Secretion of inflammatory factors from chondrocytes by layilin signaling, Biochem. Biophys. Res. Commun. 452 (2014) 85–90.
[23] H. Koizumi, M. Arito, W. Endo, et al., Effects of tofacitinib on nucleic acid metabolism in human articular chondrocytes, Mod. Rheumatol. 25 (2015) 522–527.
[24] K. Matsuo, Y. Xiang, H. Nakamura, et al., Identification of novel citrullinated autoantigens of synovium in rheumatoid arthritis using a proteomic approach, Arthritis. Res. Ther. 8 (2006) R175.
[25] T. Senshu, T. Sato, T. Akiyama, et al., Detection of citrulline residues in deiminated proteins on polyvinylidene difluoride membrane, Anal. Biochem. 203 (1992) 94–100.
[26] M. Arito, K. Nagai, S. Ooka, et al., Altered acetylation of proteins in patients with rheumatoid arthritis revealed by acetyl-proteomics, Clin. Exp. Rheumatol. 33 (2015) 877–886.
[27] M. Fukasawa, K. Okamoto, M. Nakamura, et al., Proteomic analysis of the rat cerebellar flocculus during vestibular compensation, J. Vestib. Res. 19 (2009) 83–94.
[28] H. Onodera, M. Arito, T. Sato, et al., Novel effect of edaravone on human brain microvascular endothelial cells revealed by a proteomic approach, Brain. Res. 1534 (2013) 87–94.
[29] W. Endo, M. Arito, T. Sato, et al., Effects of sulfasalazine and tofacitinib on the protein profile of articular chondrocytes, Mod. Rheumatol. 24 (2013) 844–850.
[30] A. Iizuka, M. Komiyama, C. Oshita, et al., Anti-vascular endothelial growth factor receptor (VEGFR) 2 autoantibody identification in glioblastoma patient using single B cell-based antibody gene cloning, Immunol. Lett. 159 (2014) 15–22.
[31] R. Nachat, M.C. Mechin, M. Charveron, et al., Peptidylarginine deiminase isoforms are differentially expressed in the anagen hair follicles and other human skin appendages, J. Investig. Dermatol. 125 (2005) 34–41.
[32] R. Nachat, M.C. Mechin, H. Takahara, et al., Peptidylarginine deiminase isoforms 1-3 are expressed in the epidermis and involved in the deamination of K1 and filaggrin, J. Investig. Dermatol. 124 (2005) 384–393.
[33] P.W. Wright, L.C. Bolling, M.E. Calvert, et al., ePAD, an oocyte and early embryo-abundant peptidylarginine deiminase-like protein that localizes to egg cytoplasmic sheets, Dev. Biol. 256 (2003) 73–88.
[34] S. Duffy, B.A. MacVicar, *In vitro* ischemia promotes calcium influx and intracellular calcium release in hippocampal astrocytes, J. Neurosci. 16 (1996) 71–81.
[35] A. Ordóñez, J. Yélamos, S. Pedersen, et al., Increased levels of citrullinated antithrombin in plasma of patients with rheumatoid arthritis and colorectal adenocarcinoma determined by a newly developed ELISA using a specific monoclonal antibody, Thromb. Haemost. 104 (2010) 1143–1149.

前 田 賞

聖マリアンナ医科大学雑誌
Vol. 44, pp. 13–16, 2016

新規抗炎症薬の発明
—ステロイド薬と同程度に強力で副作用の少ないペプチド抗炎症薬—

岡本 一起　佐藤 政秋　表山 和樹　佐藤 利行
有戸 光美　黒川（鈴木） 真奈絵　末松 直也　加藤 智啓

（受付：平成 28 年 3 月 30 日）

緒　言

アレルギー，感染，熱傷，外傷などに起因する様々な炎症反応は種々のサイトカインにより生体組織に伝播する。これらサイトカインシグナルは細胞質中に存在する IκB/NF-κB 複合体の IκB（inhibitor of NF-κB）をリン酸化し，リン酸化した IκB は NF-κB を解離する。IκB から離れた NF-κB はただちに核内に移行する。核内に移行した NF-κB は炎症反応に呼応して，シクロオキシゲナーゼ（COX2）を含む多くの炎症関連遺伝子の転写を促進することにより炎症やストレス反応を増幅し，生体の炎症反応を賦活化する[1]。一方，ステロイド薬は，ホルモンリガンドとしてステロイド受容体（グルココルチコイド受容体：GR）と結合し，非活性型 GR を活性化する。この活性型 GR はただちに核内に移行し，核内で NF-κB に直接結合することにより NF-κB の転写活性を阻害する。このようにステロイド薬は炎症反応の中核的役割を担っている転写因子 NF-κB を直接抑えることにより，幅広くかつ強力に炎症を抑える（**Figure 1A**）。しかし，ステロイド薬と結合した活性型 GR は同時に炎症部位以外のところで，強力なグルココルチコイドホルモン作用を発揮する（**Figure 1B**）。これがステロイド薬の副作用である。GR の NF-κB 阻害活性は残して（すなわち，抗炎症作用は残して），GR のホルモン作用がない（副作用が少ない）ステロイド薬の合成はステロイド薬が使われ始めてから 60 年間試みられてきたが，未だに成功していない[1]。

聖マリアンナ医科大学　疾患プロテオーム・分子病態治療学

著者らが見いだした新しいタイプの核内受容体コアクティベーター（MTI-II）[2] は NF-κB に直接結合して，NF-κB の転写共役阻害因子（コリプレッサー）として働き，その転写活性を抑制した。すなわち，MTI-II は，GR と同様の作用機序で強力な抗炎症作用を示すと考えられる（**Figure 1C**）[3)4)]。また，MTI-II 自体には DNA 結合能もホルモン作用もないので（**Figure 1D**），ステロイド薬のような副作用が少ないと考えられる。MTI-II を抗炎症薬として利用できれば，ステロイド薬と同様に全ての炎症性疾患及び，アレルギー疾患，難病を含む自己免疫疾患等に使用することができる。また，ステロイド薬より安全で非ステロイド系抗炎症薬より有効性の高い治療薬となるので，これまでステロイド薬の適応外であった軽微な炎症治療への適応や長期投与，家庭での投薬が可能となり，アトピー，花粉症，関節リウマチ等の患者さんの QOL を劇的に向上させることができる。

結　果

MTI-II は 101 アミノ酸残基から成る分子量 11.5 κDa の小さなタンパク質（**Figure 2A, 2B**）で，中央部の B 領域（40 アミノ酸残基）はグルタミン酸（24 アミノ酸残基）とアスパラギン酸（7 アミノ酸残基）の連打から構成される。この中央部酸性アミノ酸領域が NF-κB 転写活性の阻害に必要であることが分っている。タンパク質やペプチドは，そのままでは細胞膜を通過出来ない。そこで，MTI-II にアルギニン 11 連打から成る細胞導入ペプチド[5]を付加した MTI 抗炎症剤（MTI Anti-Inflammatory Drugs: MAIDs）と

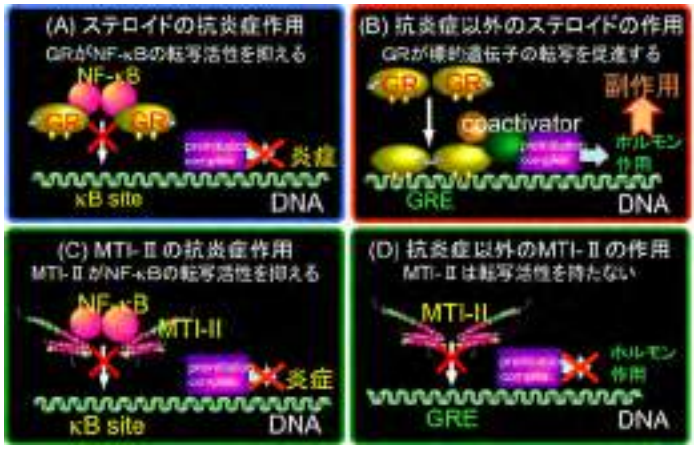

Figure 1. Anti-inflammatory action of glucocorticoid-receptor (GR) and MTI-II.

(**A**) GR directly binds to NF-κB and inhibits binding of NF-κB to specific DNA (κB site) in inflamed area, (**B**) GR specifically binds to specific DNA (GRE) and exerts glucocorticoid hormone action in whole body, (**C**) MTI-II also directly binds to NF-κB and inhibits the binding of NF-κB to κB site, (**D**) MTI-II has neither DNA binding ability nor hormone action.

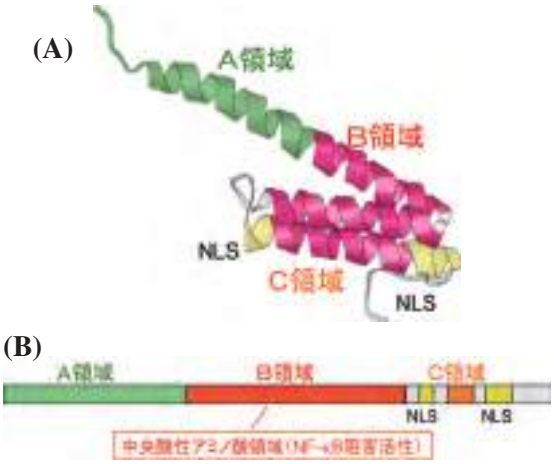

Figure 2. Predicted 3D structure (**A**) and schematic representation (**B**) of MTI-II.

Abbreviation NLS indicates nuclear localization signal.

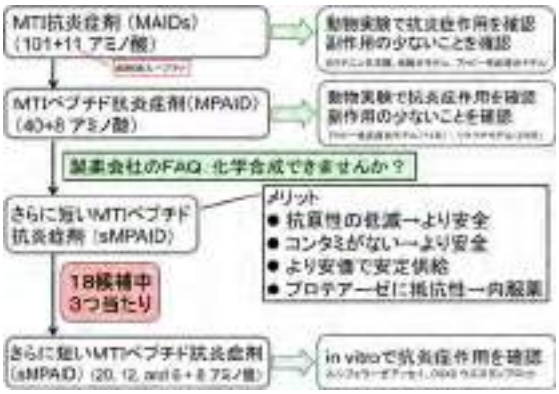

Figure 3. Brief summary of this study.

中央部酸性アミノ酸領域 (40 アミノ酸残基) に細胞導入ペプチド (アルギニン 8 連打) を付加した MTI ペプチド抗炎症剤 (MTI Peptide Anti-Inflammatory Drug: MPAID) を作製し，その抗炎症作用と副作用を検討した (**Figure 3**)。その結果，MAIDs と MPAID は炎症モデル動物 (カラゲニン足浮腫，結膜炎，アトピー性皮膚炎，リウマチ) で強力な抗炎症作用を示したが，著明な副作用 (血液生化学検査，反復投与毒性) は認められなかった[3)4)]。

次に，新たな創薬候補の開発を目的に抗炎症作用を持つアミノ酸領域の絞り込みを行い，さらに短い MTI ペプチド抗炎症剤 (short MTI Peptide Anti-Inflammatory Drug: sMPAID) の作製を試みた (**Figure 3**)。MPAID をさらに短くすることにより，(1) 抗原性が低減され，より安全なバイオ医薬品となる，(2)

化学合成がより簡便になり，合成に伴うコンタミが激減する，(3) 製造コストが低下し，安定供給が可能になる等のメリットが望める。

中央部酸性アミノ酸領域 (B 領域) から sMPAID 候補として 30 アミノ酸残基のペプチドを 3 種類，20 アミノ酸残基のペプチドを 5 種類，12 アミノ酸残基のペプチドを 5 種類の計 13 種類のペプチドを選んだ (**Figure 4**)。これらペプチドの C 末端に細胞導入ペプチド (アルギニン 8 連打) を付加したペプチドを発現するベクターを構築し，レポーター遺伝子 (NF-κB により転写が促進されるルシフェラーゼ) と共に HeLa 細胞にトランスフェクトした。選択した候補ペプチドには核移行シグナル (**Figure 2B**) が欠失しているが，細胞導入ペプチドが核移行シグナルとして働いている[5]。TNFα 刺激後のルシフェラーゼの発現を解析した結果，30 アミノ酸残基のペプチド 3 種類は NF-κB の転写活性を阻害しなかった。20 アミノ酸残基のペプチド 5 種類中のペプチド 20A-5 と 12 アミノ酸残基のペプチド 5 種類中のペプチド 12A-3 が NF-κB の転写活性を阻害した。さらにペプチド 12A-3 の配列から 6 アミノ酸残基の配列 5 種類をさらに短い sMPAID 候補ペプチドとして選んだ。これらペプチドを発現させて TNFa 刺激後のルシフェラーゼの発現を解析した結果，6 アミノ酸残基のペプチド 5 種類中のペプチド 6A-3 だけが NF-κB の転写活性を阻害した。結果，18 候補ペプチドから 3 つの抗炎症ペプチド (sMPAID) を見つけることができた[6]。次にペプチド 12A-3 とペプチド 6A-3 を化学合成し，HeLa 細胞の培養液中に添加し，それらの NF-κB の転写活性に及ぼす効果を検討した。その結果，両方のペプチドは添加した濃度依存的に TNFα 刺激後のルシフェラーゼの発現を抑えることがわかった。さらに，外因性のレポーター遺伝子だけでなく，内在する COX2 遺伝子の発現を抑えることもわかった[6]。すなわち，ペプチド 12A-3 とペプチド 6A-3 は抗炎症剤として働きうることが示唆された。

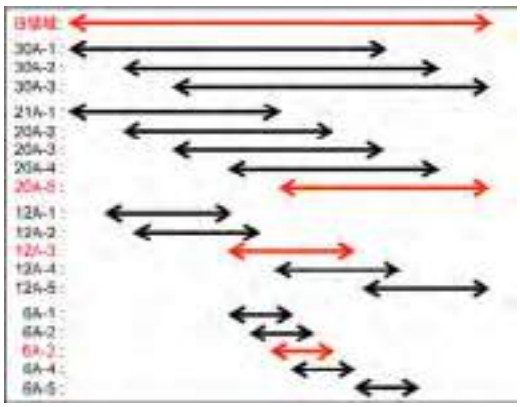

Figure 4. Locations of sMPAID candidates.

Out of 18 candidates, the 3 peptides (shown in red) inhibit the transcriptional activity of NF-κB.

考　察

MTI-II の作用機序は核内で NF-κB に直接結合して，その転写活性を阻害することがわかっている[3)4)]。今回見いだした sMPAID (20A-5，12A-3 と 6A-3) も細胞導入ペプチド部分が核移行シグナルとして働くので，その作用場所は核内で，MTI-II と同様に核移行した NF-κB に結合すると考えられる。しかし，その仔細な作用機構や sMPAID が結合する NF-κB の部位は判っていない。また，現在判明している NF-κB 阻害活性を持つ最小単位であるペプチド 6A-3 の配列を含むペプチド 30A-1～30A-3，20A-3，20A-4 に NF-κB 阻害活性がない理由も不明である。現在 sMPAID の作用機構を仔細に解明する目的で，sMPAID と NF-κB の共結晶の X 線構造解析を行い，sMPAID と NF-κB の結合部位の分析を行っている (他大学との共同プロジェクト)。この sMPAID が結合する NF-κB の部位の解明は，ペプチドミメティックを用いた新しい低分子創薬 (NF-κB 阻害薬) に繋がる研究である。

MPAID と sMPAID はバイオ医薬品 (タンパク質医薬品，ペプチド医薬品) であるが，他のバイオ医薬品にはない大きな利点がある。一般的にバイオ医薬品は，1) 遺伝子組み換え技術を用いた微生物や動物細胞内での産生とその後の精製が複雑でコストが掛かる，2) 細胞膜を透過できないので細胞内の標的分子に作用できない，3) タンパク質の変性により生体内での安定性が悪い，4) 抗体ができるなどの問題を持っている。しかし，MPAID と sMPAID は，1) 化学合成できるので製造が簡便安価である (鎖長を短くすることで合成コストをさらに下げることができた)，2) 細胞膜を透過して，核内の標的分子 NF-κB に作用している，3) タンパク質の高次構造 (ジスルフィド結合や疎水性相互作用など) を持たないので変性しない (実際にアトピー性皮膚炎に軟膏に混合して塗布することで抗炎症効果を確認している)，

4) 酸性アミノ酸が連打される領域には抗体が出来にくい (短くすることで抗原性をさらに下げることができる)，などの利点を持っている。このようにMPAID と sMPAID は非常に使い易いバイオ医薬品となりえる。現在，sMPAID を内服薬として応用する目的で，sMPAID の生体内での安定性を高める研究を進めている。

謝　辞

前田賞受賞の対象となりました本発明は，発明委員会の先生方，教学部石井様，MPO 天野様をはじめ多くの方々のご支援，ご声援の賜物です。この場をお借りして厚く御礼申し上げます。

引用文献

1) 岡本一起，三井寛之，加藤智啓．抗炎症療法における unmet needs．NF-κB 阻害薬．炎症と免疫 2013; 21: 229–233.
2) Oкamoto κ, Isohashi F. Macromolecular-translocation inhibitor-II (Zn^{2+}-binding protein, parathymosin) interacts with the glucocorticoid receptor and enhances transcription in vivo. J Biol Chem 2005; 280: 36986–36993.
3) 職務発明　発明の名称：NFκB 作用抑制剤及び抗炎症剤並びにステロイド作用増強剤，特許番号：4,874,798，出願人：聖マリアンナ医科大学，発明者：岡本一起，礒橋文秀.
4) 職務発明　United State Patent：NFκB ACTION INHIBITOR AND ANTIINFLAMMATORY AGENT, AND STEROID ACTION FORTIFIER, Patent No.: 7,932,226, Assignee: St.Marianna University School of Medicine, Inventors: κazuкi Oкamoto, and Fumihide Isohashi
5) Futaкi S, Suzuкi T, Ohashi W, Yagami T, Tanaкa S, Ueda κ, Sugiura Y. Arginine-rich peptides. An abundant source of membrane-permeable peptides having potential as carriers for intracellular protein delivery. J Biol Chem 2001; 276: 5836–5840.
6) 職務発明　発明の名称：ペプチド，ポリヌクレオチド，ベクター，形質転換体，NFκB 阻害剤，及び NFκB 亢進性疾患の治療剤，出願番号：特願 2014–257827，出願人：聖マリアンナ医科大学，発明者：岡本一起.

International Journal of
Rheumatic Diseases

International Journal of Rheumatic Diseases 2017; **20:** 708–721

ORIGINAL ARTICLE

Phosphoproteome analysis of synoviocytes from patients with rheumatoid arthritis

Masayoshi KATANO,[1,2] Manae S. KUROKAWA,[3] Kosuke MATSUO,[4] Kayo MASUKO,[5] Naoya SUEMATSU,[2] Kazuki OKAMOTO,[2] Toshikazu KAMADA,[6] Hiroshi NAKAMURA[7] and Tomohiro KATO[2]

[1]*Research and Development, Clinical Department, LSI Medience Corporation, Tokyo,* [2]*Clinical Proteomics and Molecular Medicine, St. Marianna University Graduate School of Medicine,* [3]*Disease Biomarker Analysis and Molecular Regulation, St. Marianna University Graduate School of Medicine, Kawasaki,* [4]*Department of Orthopaedic Surgery, Yokohama City University School of Medicine, Yokohama,* [5]*Preventive Medical Center, Sanno Hospital Medical Center,* [6]*Department of Rheumatology, Nippon Medical School, and* [7]*Department of Orthopedic Surgery, International University of Health and Welfare, Tokyo, Japan*

Abstract

Aim: To explore disease-associated molecules in rheumatoid arthritis (RA), we comprehensively analyzed phosphoproteins purified from RA synoviocytes.

Method: Synoviocytes were obtained from three patients with RA and three patients with osteoarthritis (OA). Profiles of phosphoproteins purified from the synoviocytes were compared by two-dimensional differential gel electrophoresis (2D-DIGE) between the RA and OA groups. Protein spots with significantly different phosphorylation levels were identified by mass spectrometry. Recombinant protein of annexin A4 (ANXA4), one of the identified phosphoproteins, was transfected into synoviocytes from an OA patient to mimic RA synoviocytes and humoral factor secretion was compared between rANXA4-transfected and non-transfected synoviocytes under a tumor necrosis factor-α (TNFα)-stimulated condition.

Results: In 2D-DIGE, 318 phosphoprotein spots were detected, of which 94 spots showed significantly different intensities between the two groups ($P < 0.05$). Among the 94 spots, 22 spots showed two-fold or higher intensity and one spot showed less than 1/2-fold intensity in the RA group compared to the OA group. From the 22 spots, 11 phosphoproteins were identified, which included kinases, carrier and chaperone proteins, cytoskeletal proteins, proteases and calcium-binding proteins. One of the identified calcium-binding proteins was ANXA4, an exocytosis-regulating protein. The transfected rANXA4 was found to be phosphorylated intracellularly, and secretion of chemokine (C-X-C motif) ligand 1 and interleukin-8 induced by TNFα stimulation was significantly suppressed by the transfection ($P < 0.01$).

Conclusion: The phosphoprotein profile of RA synoviocytes was different from that of OA synoviocytes. This difference would reflect the different pathophysiologies of the diseases. ANXA4 may be one of therapeutic targets in RA.

Key words: annexin A4, phosphoprotein, rheumatoid arthritis, synoviocytes.

Correspondence: Professor Manae S. Kurokawa, Disease Biomarker Analysis and Molecular Regulation, St. Marianna University Graduate School of Medicine, 2–16–1, Sugao, Miyamae-ku, Kawasaki, 216–8511 Japan. Fax: 81-44-975-7553.
Email: manae@marianna-u.ac.jp

INTRODUCTION

Rheumatoid arthritis (RA) is a systemic inflammatory disease characterized by progressive destruction of synovial joints.[1] Although the pathogenesis of RA remains

© 2017 Asia Pacific League of Associations for Rheumatology and John Wiley & Sons Australia, Ltd

unclear, it has been elucidated that activated synoviocytes in affected joints play an important role.[2,3] Infiltration of inflammatory cells into synovium and proliferation of synoviocytes lead to severe cartilage and bone erosion via formation of pannus.[4,5] Production of proinflammatory cytokines and chemokines by synoviocytes and the infiltrating cells promote the process of joint destruction.[4,5]

Phosphorylation, one of the important post-translational modifications of proteins, plays a key role in cellular signal transduction in inflammation.[6,7] Thus, phosphoprotein profiles should be investigated in RA as well as in other diseases. Recent studies have focused on protein profiles of RA synoviocytes or synovial tissue;[8–13] however, only a few studies are available on the phosphoproteome of RA.[14]

In this paper, we found that phosphoprotein profiles of synoviocytes were different between RA and osteoarthritis (OA). Annexin A4 (ANXA4), one of the highly phospholyrated proteins in RA was found to regulate inflammatory chemokine secretion from synoviocytes. Our analysis of synovial phosphoproteins would help understanding of the pathophysiology of RA.

MATERIALS AND METHODS

Patients

Diagnosis of RA and OA were made according to the criteria of American College of Rheumatology.[15,16] Three RA patients (RA1–3) and four OA patients (OA1–4) were enrolled in this clinical study that was approved by the Ethics Committee in St. Marianna University School of Medicine, Kawasaki, Japan. The protocol of this study conformed to the provisions of the World Medical Association's Declaration of Helsinki.

Synovial membrane samples were obtained from RA1, RA2 and OA3 when they underwent total knee arthroplasty, and from RA3, OA1, OA2 and OA4 when they underwent total hip arthroplasty with their written informed consents. Clinical information of the patients are as follows: sex, all female; age (mean ± standard deviation, SD), RA1–3, 68 ± 9 years old, OA1–3 68 ± 8 years old, OA4 50 years old; disease duration (mean ± SD), RA1–3 18 ± 6 years, OA1–3 22 ± 18 years, OA4 7 years; C-reactive protein (CRP) (mean ± SD), RA1–3 0.80 ± 0.47 mg/dL, OA1–3 0.20 ± 0.26 mg/dL, OA4 0.17 mg/dL; X-ray grades (RA, Larsen grade; OA, Kellgren-Lawrence grade), RA1 V, RA2 IV, RA3 IV, OA1 IV, OA2 III, OA3 IV, OA4 IV; drugs, RA1 bucillamine 100 mg/day, loxoprofen 120 mg/day, RA2 prednisolone 9 mg/day, penicillamine 200 mg/day, mizoribine 150 mg/day, RA3 prednisolone 9 mg/day, loxoprofen 180 mg/day, salazosulfapyridine 3000 mg/day, OA1 none, OA2 loxoprofen 120 mg/day, OA3 none, OA4 none.

Preparation of synoviocyte-derived proteins and phosphoproteins

The synovial membrane samples were digested with collagenases (Sigma, St. Louis, MO, USA). Obtained synoviocytes were cultured in Ham's F-12 (Gibco, Carlsbad, CA, USA) containing 20% fetal bovine serum (FBS). After the first passage, the cells were cultured in Ham's F-12 containing 10% FBS. Proteins were extracted into cell lysis buffer (4% 3-[(3-cholamidopropryl)dimethylamino]-1-propanesulfonate (CHAPS)/7 mol/L urea/2 mol/L thiourea/30 mmol/L tris pH8.0). Phosphoproteins were purified from the extracted proteins using Pro-Q Diamond Phosphoprotein Enrichment Kit (Invitrogen, Carlsbad, CA, USA). After the treatment with 2-D clean-up kit (GE Healthcare, Piscataway, NJ, USA), the purified phosphoproteins were dissolved into the cell lysis buffer.

Two-dimensional differential gel electrophoresis (2D-DIGE)

The purified phosphoproteins were separated by 2D-DIGE according to the manufacture's protocol (CyDye DIGE fluor labeling kits for scarce samples, GE Healthcare).[17] Briefly, phosphoprotein amounts were quantified by Bradford assay and an equal amount of the phosphoproteins obtained from each of six synoviocyte samples (RA1–3 and OA 1–3) were mixed and labeled with Cy3 saturation dye (Cy Dye DIGE Saturation dye; GE Healthcare) for preparation of an internal control, 'standard sample'. Then each of the six samples (RA1–3 and OA 1–3) was labeled with Cy5 saturation dye; 2.5 μg of the individual Cy5-labeled sample was mixed with 2.5 μg of the Cy3-labeled standard sample. Then phosphoproteins in the mixture were separated by isoelectric focusing (Immobiline Drystrip pH 4–7, 24 cm, linear; GE Healthcare) and subsequently by sodium dodecyl sulfate-polyacrylamide gel electrophoresis (SDS-PAGE). The separated phosphoprotein spots were scanned using an image analyzer (Typhoon 9400 Imager, GE Healthcare). The Cy5-fluorescent intensity of each protein spot was normalized by the Cy3-fluorescent intensity of an identical spot by using a quantitative analysis program of Progenesis (Nonlinear Dynamics, Newcastle, UK). The normalized Cy5-intensity was compared between the RA and OA synoviocytes using Progenesis.

Identification of phosphoproteins

Phosphoproteins were identified by mass spectrometry (MS).[17] In brief, 50 μg of the phosphoproteins were separated by two-dimensional electrophoresis (2DE). Gel specimens corresponding to the phosphoprotein spots of interest were recovered. Then the phosphoproteins in the gel fragments were digested with trypsin.

Peptides produced by the digestion were analyzed using a matrix-assisted laser desorption/ionization time of flight (MALDI-TOF) mass spectrometer (Ultraflex; Bruker Daltonics, Ettlingen, Germany). Ten microliters of the peptide solution were applied to C18 Zip-Tip (Millipore, Billerica, MA, USA) for desalting, and then bound peptides were eluted using 2 μL 50% acetonitrile/0.1% trifluoroacetic acid. One microliter of the eluent was mixed with 1 μL of a matrix solution (0.3 mg/mL alpha-cyano-4-hydroxycinnamic acid in ethanol/acetone 2 : 1) and the mixture was spotted onto a MALDI target plate (AnchorChip; Bruker Daltonics). Then mass spectra of the peptide peaks were obtained in the automatic positive reflector mode with the mass range of 500–4400 m/z. The data were subjected to external calibration with nine standard peptides (Peptide calibration standard II; Bruker Daltonics). Based on the mass spectra, some peptides were selected for tandem mass spectrometry (MS/MS) analysis. The MS/MS spectra were measured in LIFT™-TOF/TOF mode using fragment ions produced by post-source decay. Ion peaks were detected using flexAnalysis (Bruker Daltonics). The signal-to-noise threshold for the peak detection was set at 5.0.

The obtained MS and MS/MS spectra were used to identify the phosphoproteins by database searching (Mascot, http://www.matrixscience.com) against the Swiss Prot human protein sequence database 54.3–8. The charge of the precursor ion was set as 1. Mass and peptide tolerances for precursor ions were set at 150 ppm and 1 Da, respectively. Variable modification of phosphorylation of serine, threonine and tyrosine were taken into consideration. Protein identification was accepted when Mascot search results delivered significant molecular weight search (MOWSE) scores ($P < 0.05$).

Western blotting

Expression of ANXA4 was examined by Western blotting. In brief, 10 μg of whole cell lysates of RA and OA synoviocytes were electrophoresed on 12.5% SDS-PAGE. Alternatively, phosphoproteins derived from 70 μg of whole cell lysates of OA synoviocytes were similarly electrophoresed. The separated proteins on the SDS-PAGE gels were transferred to polyvinylidene fluoride membranes. After blocking for 1 h in phosphate-buffered saline containing 1% bovine serum albumin and 0.1% Tween-20, the membranes were reacted with anti-ANXA4 antibody for 1 h (R&D Systems, Minneapolis, MN, USA), followed by incubation with horseradish peroxidase-conjugated rabbit anti-goat immunoglobulin G (Zymed, San Francisco, CA, USA). Immunoreactive bands were detected by Enhanced Chemi Luminescence (ECL)-Plus (GE Healthcare). The results were scanned using Typhoon 9400 Imager. Intensity of the resultant bands was measured by Science Lab 2001 Image Gauge (Fujifilm, Tokyo, Japan).

Transfection of recombinant ANXA4 to synoviocytes

Recombinant ANXA4 (rANXA4) fused with His-tag (GenWay, San Diego, CA, USA) was transfected to OA synoviocytes using Chariot (Active Motif, Carlsbad, CA, USA). After 16 h, a part of the cells were stimulated with 10 ng/mL recombinant tumor necrosis factor α (TNFα) (R&D Systems) for 6–48 h. Then proteins were extracted from the cells into the cell lysis buffer.

Analysis of humoral factor secretion

The culture medium of the OA4 synoviocytes was applied to a cytokine array (Proteome Profiler kit, R&D Systems) to examine levels of humoral factors. The analyzed humoral factors were as follows: complement 5a (C5a), CD40 ligand (CD40L), granulocyte-colony stimulating factor (G-CSF), granulocyte macrophage-colony stimulating factor (GM-CSF), chemokine (C-X-C motif) ligand 1 (CXCL1), small inducible cytokine A1 precursor (I-309), soluble intercellular adhesion molecule-1 (sICAM-1), interferon-γ (IFN-γ), interleukin-1α (IL-1α), IL-1β, IL-1 receptor antagonist (IL-1ra), IL-2, IL-4, IL-5, IL-6, IL-8, IL-10, IL-12 p70, IL-13, IL-16, IL-17, IL-17E, IL-23, IL-27, IL-32α, IFN-γ inducible protein 10 (IP-10), IFN-inducible T cell-α chemoattractant (ITAC), monocyte chemotactic protein-1 (MCP-1), macrophage migration inhibitory factor (MIF), macrophage inflammatory protein-1α (MIP-1α), MIP-1β, Serpin E1, regulated on activation, normal T cell expressed and secreted (RANTES), stromal cell-derived factor-1 (SDF-1), TNF-α, and soluble triggering receptor expressed on myeloid cells-1 (sTREM-1). Humoral factors detected as specific spots were visualized by ECL Plus, and the spots were scanned using Typhoon 9400

Imager. Intensity of each spot, measured by Science Lab 2001 Image Gauge, was normalized using that of the positive control. CXCL1 and IL-8 were measured by the respective enzyme-linked immunosorbent assay (ELISA) kits (R&D Systems).

Statistical analysis

Statistical significance was calculated by Student's *t*-test.

RESULTS

Comparison of phosphoprotein spot intensity between the RA and OA synoviocytes

To detect phosphoproteins differently expressed in RA, we analyzed phosphoprotein profiles of synoviocytes from three RA patients and three OA patients by 2D-DIGE. In total, 318 phosphoprotein spots were obtained (Fig. 1a). Ninety-four out of the 318 phosphoprotein spots showed significantly different intensities between the RA and OA groups ($P < 0.05$, Table 1). Among the 94 spots, 22 phosphoprotein spots were at least two-fold higher in intensity in the RA group than in the OA group (Table 1, Fig. 1b). Another phosphoprotein spot showed less than 1/2-fold intensity in the RA group than in the OA group (Table 1, Fig. 1b). As a representative result, spots of ID 8, 18 and 39 showed higher intensity in the RA group than in the OA group (Fig. 1c–e). The different intensities of phosphoprotein spots indicated different phosphoprotein levels of proteins between RA and OA synoviocytes.

Identification of the phosphoprotein spots differently expressed between the RA and OA synoviocytes

We tried to identify proteins for the above described 22 and one spots (Table 1, Fig. 1b). As a result, proteins were identified in 11 out of the former 22 spots and the latter one spot (Table 2, Fig. 2). Spots of ID 8 and ID 10, both of which showed higher intensity in RA, were identified as the same protein of ferritin light chain (FTL). The identified 10 phosphoproteins, which showed increased intensity in RA, were categorized into five groups: (i) proteins involved in phosphorylation (mitogen-activated protein kinase 4 [MAPK4] and COP9 signalosome complex subunit 8 [COPS8]); (ii) carrier or chaperone proteins (FTL, sodium/bile acid cotransporter 4 [SLC10A4], and heat shock protein beta-6 [HSPB6]); (iii) a cytoskeletal protein (4.1 protein/ezrin/radixin/moesin domain-containing protein 8 [FRMD8]); (iv) proteases (calpain small subunit 2 [CAPNS2] and sentrin-specific protease 8 [SENP8]); and (v) calcium-binding proteins (sorcin [SRI] and ANXA4). A cytoskeletal protein of myosin regulatory light chain 12A (ML12A) was identified from the spot, intensity of which was lower in RA (Table 2).

Comparison of ANXA4 expression between RA and OA synoviocytes

Among the identified phosphoproteins, we extended our study focusing on ANXA4, intensity of which was 2.3-fold higher in the RA group than in the OA group (spot ID 39, Fig. 1b,e, Table 2). ANXA4 belongs to the annexin family of calcium-dependent phospholipid binding proteins.[18] ANXA4 has been involved in diverse cellular processes, including exocytosis.[18,19] Interestingly, ANXA4 mediates aggregation of phospholipid-containing vesicles prior to fusion; however, it loses this activity when phosphorylated by protein kinase C (PKC).[20] Thus, we hypothesized that phosphorylation of ANXA4 regulates secretion of inflammatory cytokines and/or chemokines from RA synoviocytes.

First, to elucidate whether the increase of phosphorylated ANXA4 is due to the increase of protein expression or its phosphorylation, we compared the total amount of ANXA4 in the RA and OA synoviocytes. As a result, the total amount of ANXA4 was significantly higher in the RA synoviocytes compared to the OA synoviocytes (approximately 1.5-fold, $P < 0.01$, Fig. 3a,b). Thus, the up-regulated intensity of the phosphorylated ANXA4 spot in the RA synoviocytes (2.3-fold, Table 2) was at least in part due to the up-regulated expression of ANXA4.

Effects of rANXA4 protein transfection on secretion of inflammatory cytokines and chemokines from OA synoviocytes

Next, we tried to examine whether the phosphorylated ANXA4 regulates the secretion of inflammatory cytokines and chemokines from synoviocytes, since the phosphorylation of ANXA4 has been reported to inhibit vesicle aggregation.[20] To achieve this, we transfected rANXA4 into OA synoviocytes, mimicking RA synoviocytes. We compared inflammatory cytokine and chemokine secretion between the rANXA4-transfected OA synoviocytes and non-transfected OA synoviocytes after TNFα stimulation.

First, we examined effects of TNFα on endogenous ANXA4 (eANXA4) expression. In the Western blotting result, eANXA4 bands showed similar intensity between the TNFα-treated and non-treated conditions ($P > 0.05$, Fig. 3c,d). This indicates that TNFα does not affect the

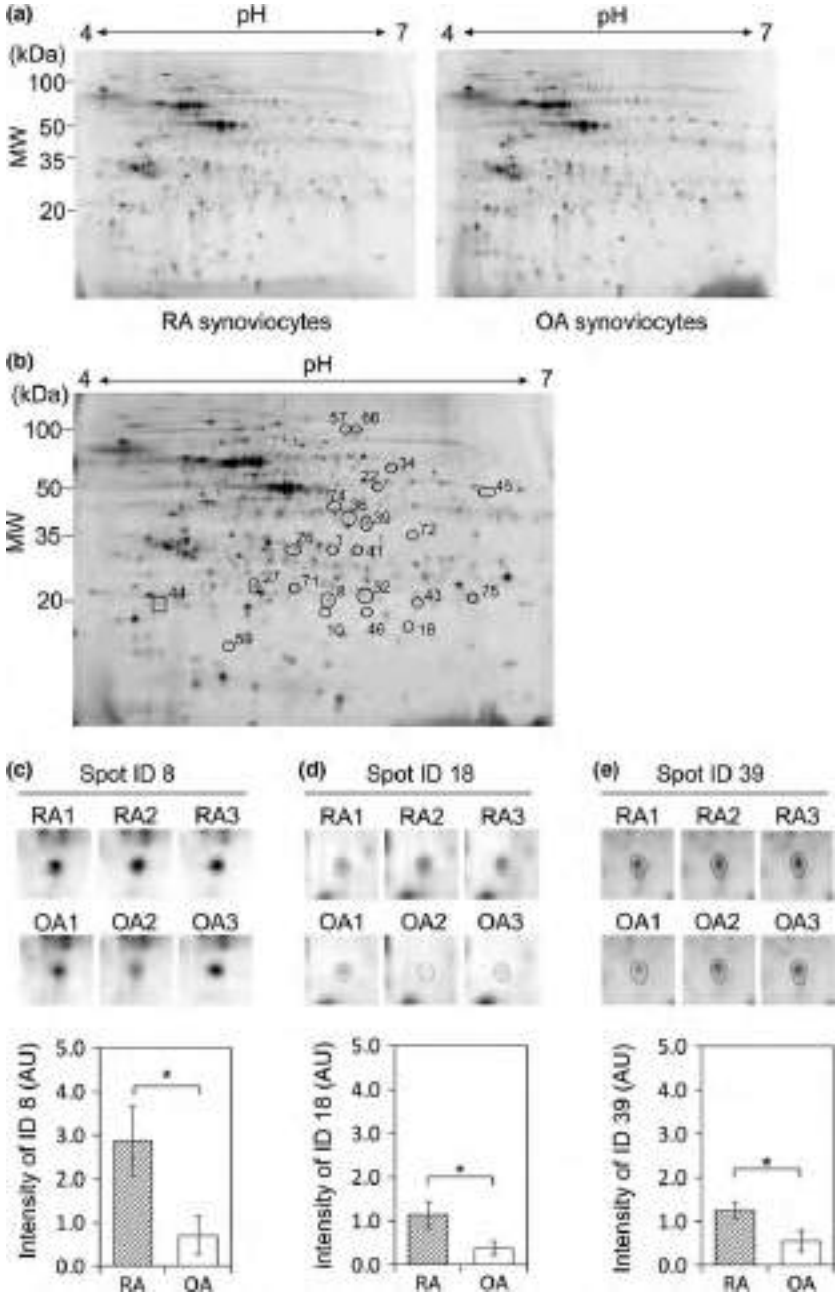

Figure 1 Two-dimensional differential gel electrophoresis (2D-DIGE) analysis of phosphoproteins extracted from rheumatoid arthritis (RA) and osteoarthritis (OA) synoviocytes. (a) Representative results from RA1 and OA1 synoviocytes are shown. (b) A representative result of the internal control sample that was a mixture of an equal amount of phosphoprotein samples from the three RA and three OA synoviocytes, is shown. Circles indicate 22 phosphoprotein spots that showed two-fold or more intensity in the RA synoviocytes compared to the OA synoviocytes ($P < 0.05$). The square indicates a phosphoprotein spot that showed less than 1/2-fold intensity in the RA synoviocytes compared to the OA synoviocytes ($P < 0.05$). ID numbers of those 23 spots are shown. (c–e) Results of three phosphoprotein spots (spot IDs 8, 18 and 39) that showed two-fold or more intensity in the RA synoviocytes compared to the OA synoviocytes. Error bars, SD. *$P < 0.05$. MW, molecular weights.

Table 1 Number of phosphoprotein spots detected from RA and OA synoviocytes

Change of spot intensity (x-fold)	Number of spots	Number of spots
(RA/OA)	($P < 0.05$)	($P \geq 0.05$)
$3.0 \leq x$	4	0
$2.0 \leq x < 3.0$	18	2
$1.5 \leq x < 2.0$	54	17
$1/1.5 < x < 1.5$	14	188
$1/2 < x \leq 1/1.5$	3	15
$1/3 < x \leq 1/2$	1	2
$x \leq 1/3$	0	0
Subtotal	94	224
Total	318	

expression of eANXA4 in the OA synoviocytes. Second, we transfected rANXA4 into OA synoviocytes. As a result, rANXA4 was detected as a band with slightly heavier molecular weight compared to eANXA4 because of addition of 6xHis-tag, which indicated successful transfection (Fig. 3e). Finally, we compared the total amount of phosphorylated ANXA4 between TNFα-treated and non-treated conditions. For this aim, after the TNFα treatment, phosphoproteins were purified from the samples and then ANXA4 was detected by anti-ANXA4 antibodies. As a result, in the non-transfected synoviocytes, phosphorylated eANXA4 were detected at similar levels between the TNFα-treated and non-treated conditions (Fig. 3f,g). In the rANXA4-transfected synoviocytes, relatively large amounts of phosphorylated rANXA4 were detected in addition to the phosphorylated eANXA4. The total amounts of phosphorylated ANXA4 were not affected by the TNFα treatment. Transfection of rANXA4 increased phosphorylated ANXA4 in the synovial cells ($P < 0.01$, Fig. 3f,g). The TNFα treatment did not affect the phosphorylation of eANXA4 or rANXA4.

To examine functions of phosphorylated ANXA4 in synoviocytes, we compared secretion of humoral factors, including inflammatory cytokines and chemokines between rANXA4-transfected and non-transfected synoviocytes. Since TNFα treatment was considered to facilitate the comparison, we first tried to find humoral factors up-regulated by TNFα in the non-transfected condition. Among the examined 36 humoral factors, secretion of CXCL1 and IL-8 was up-regulated to more than four-fold levels by the TNFα treatment (CXCL1, 4.04-fold; IL-8, 7.38-fold; Fig. 4a–c). Interestingly, the up-regulated secretion of CXCL1 and IL-8 by the TNFα treatment tended to be decreased after the transfection of rANXA4, which increased intracellular phosphorylated ANXA4 by approximately 10-fold (Figs 3g,4a–c). The CXCL1 secretion in the non-treated condition also tended to be decreased after the rANXA4 transfection (Fig. 4a,b).

To confirm the immunosuppressive effect of the transfected rANXA4, we quantitatively measured the secretion of CXCL1 and IL-8 by ELISA between rANXA4-transfected and non-transfected conditions in the presence or absence of TNFα. As a result, secretion of CXCL1 and IL-8 was markedly increased by TNFα treatment also in the ELISA results (Fig. 4d,e). In the TNFα-treated condition, the significantly up-regulated secretion of CXCL1and IL-8 was found to be suppressed by the transfection of rANXA4 (Fig. 4d,e, 24 and 48 h). Even in the non-treated synovial cells, the basic secretion levels of CXCL1 were suppressed by the transfection of rANXA4 (Fig. 4d, 24 and 48 h). In the case of IL-8, its basic secretion levels were too low to be estimated. These results suggested that the transfected rANXA4 that was phosphorylated intracellularly suppressed the secretion of these two inflammatory chemokines from synoviocytes.

DISCUSSION

To explore pathophysiology-related molecules from the aspect of phosphorylation in RA, we compared phosphoprotein profiles of synoviocytes between RA and OA synoviocytes. Among the detected 318 phosphoprotein spots in the 2D-DIGE results, 94 phosphoprotein spots (30%) showed different intensities between the two diseases. These differences would reflect the different mechanisms of the diseases. In particular, 23 spots showed two-fold or more different intensities between the RA and OA synoviocytes (Table 1, Fig. 1b,c). Previously, we compared the phosphoprotein profiles between RA and OA synovial tissue by staining phosphoproteins on 2-DE gels, where 408 phosphoprotein spots were obtained, and 121 spots out of them showed more than two-fold different intensities between the two diseases.[14] The relatively low number of spots with different intensities in this study would be the difference of the materials and methods, that is, cultured synoviocytes versus synovial tissue, and purification of phosphoproteins versus staining of phosphoproteins.

It is interesting that 76 of the 94 (81%) differently expressed phosphoprotein spots showed higher intensity in RA than in OA. Limiting to the 23 spots that showed more than two-fold differences, 22 (96%) showed higher intensity in RA than in OA (Table 1). This indicates that phosphorylation of proteins in

Table 2 Identification of the phosphoproteins

Spot numbers	Proteins	pI/MW (kDa) (observed)	pI/MW (kDa) (theoretical)†	Accession nos.	Matched peptides	Mascot score	Coverage (%)	Confirmed sequences (Mascot ion score)	Ratios (RA/OA)	Kinases
1	Mitogen-activated protein kinase 4 (MAPK4)	5.6/28.0	6.1/62.3	P31152	7	106	8	^{72}LDHDNIVKVYEVLGPK^{87} (86)	10.8	MAPK-activated protein kinase 5, group I p21-activated kinases
8	Ferritin light chain (FTL)	5.6/20.0	5.5/20.0	P02792	1	75	8	^{155}LGGPEAGLGEYLFER^{169} (53)	4.1	n. r.
10	Ferritin light chain (FTL)	5.6/19.0	5.5/20.0	P02792	1	88	8	^{155}LGGPEAGLGEYLFER^{169} (66)	3.7	n. r.
22	4.1 protein/ezrin/radixin/moesin (FERM) domain- containing protein 8 (FRMD8)	5.9/50.0	5.8/51.2	Q9BZ67	1	106	2	^{135}RELQIHDEEVLR^{146} (89)	2.9	n. r.
26	Calpain small subunit 2 (CAPNS2)	5.3/28.0	5.5/27.6	Q96L46	1	110	6	^{14}GLGEALGGLFGGGGQRR^{30} (90)	2.6	n. r.
27	Sorcin (SRI)	5.1/22.0	5.3/21.7	P30626	1	77	5	^{107}QHFISFDTDR^{116} (56)	2.6	cAMP-dependent protein kinase, polo-like kinase 1
32	Sentrin-specific protease 8 (SENP8)	5.8/22.0	5.6/24.1	Q96LD8	1	82	5	^{113}NSFFHYDSHSR^{123} (62)	2.5	n. r.
39	Annexin A4 (ANXA4)	5.8/40.0	5.8/36.0	P09525	1	94	3	^{203}NHLLHVFDEYKR^{214} (74)	2.3	protein kinase C (PKC), cAMP-dependent protein kinase
43	Heat shock protein, alpha-crystallin- related, B6 (HSPB6)	6.1/20.0	6.0/17.1	O14558	1	56	8	^{1}MEIPVPVQPSWLRR^{14} (34)	2.3	cAMP-dependent protein kinase
71	Constitutive photomorphogenesis 9 signalosome complex subunit 8 (COPS8)	5.4/22.0	5.3/23.0	Q99627	1	60	6	^{166}KPVAGALDVSFNK^{178} (39)	2.0	n. r.
74	Sodium/bile acid cotransporter 4 (SLC10A4)	5.6/42.0	5.1/46.5	Q96EP9	1	70	2	^{384}MYGSEMLHK^{392} (55)	2.0	n. r.
44	Myosin regulatory light chain 2 (ML12A)	4.5/20.0	4.7/19.8	P19105	6	70	12	^{151}GNFNYIEFTR^{160} (33) ^{133}FTDEEVDELYR^{143} (17)	0.4	myosin light chin kinase, Rho-kinase

n. r., not reported.
†Data calculated in Swiss-Prot data base.

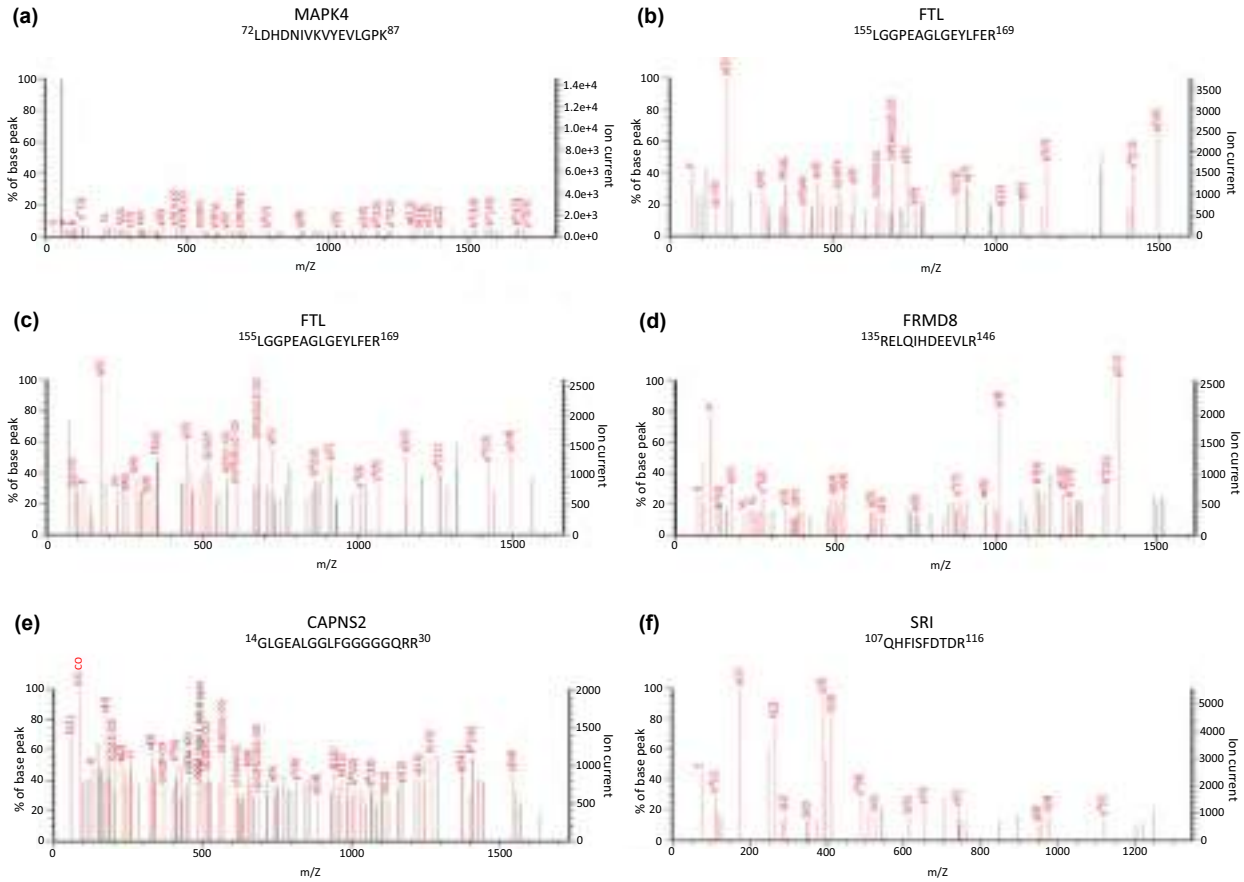

Figure 2 Tandem mass (MS/MS) spectra of the identified phosphoproteins. MS/MS spectra of the 13 peptides derived from the identified phosphoproteins (Table 2) are shown. (a) mitogen-activated protein kinase 4 (MAPK4) (spot ID 1); (b) ferritin light chain (FTL) (spot ID 8); (c) FTL (spot ID 10); (d) 4.1 protein/ezrin/radixin/moesin domain-containing protein 8 (FRMD8) (spot ID 22); (e) calpain small subunit 2 (CAPNS2) (spot ID 26); (f) sorcin (SR1) (spot ID 27); (g) sentrin-specific protease 8 (SENP8) (spot ID 32), (h) annexin A4 (ANXA4) (spot ID 39); (i) heat shock protein beta-6 (HSPB6) (spot ID 43); (j) COP9 signalosome complex subunit 8 (COPS8) (spot ID 71); (k) sodium/bile acid cotransporter 4 (SLC10A4) (spot ID 74); (l, m) myosin regulatory light chain 12A (ML12A) (spot ID 44).

synoviocytes would be up-regulated in RA compared to OA. Since protein phosphorylation plays critical roles in a broad spectrum of physiological mechanisms, including transcription and signal transduction, the mechanisms may be dysregulated in RA synoviocytes. From functions of the identified protein spots (Table 2), protein phosphorylation and degradation, cellular transportation, cytoskeletal formation and calcium-signaling would be differently regulated in RA synoviocytes compared to OA synoviocytes.

We are specifically interested in ANXA4, a calcium-dependent phospholipid binding protein, since the protein was highly phosphorylated in the RA synoviocytes compared to the OA synoviocytes (Fig. 1e, Table 2). Not only phosphorylation but also expression of ANXA4 was increased in RA synoviocytes (Fig. 2a,b). The predominant expression of ANXA4 in RA synovium compared to OA and non-inflamed synovium has been previously reported.[21] ANXA4 is also expressed predominantly in epithelial cells, especially at the apical site.[22] The expression level of ANXA4 is up-regulated in cancer cells according to the increase of tumor stages, suggesting its ability to promote cell migration.[23,24] These reports indicate that ANXA4 may be associated with dissemination of cancer cells. RA shows massive proliferation of synoviocytes and migration of synovial cells similar to cancer cells. Thus, the up-regulated expression of ANXA4 may be involved in the proliferation and invasion of synoviocytes.

Roles of ANXA4 have been also implicated in a variety of cellular process such as membrane aggregation, exocytosis, ion-transport and modulation of nuclear

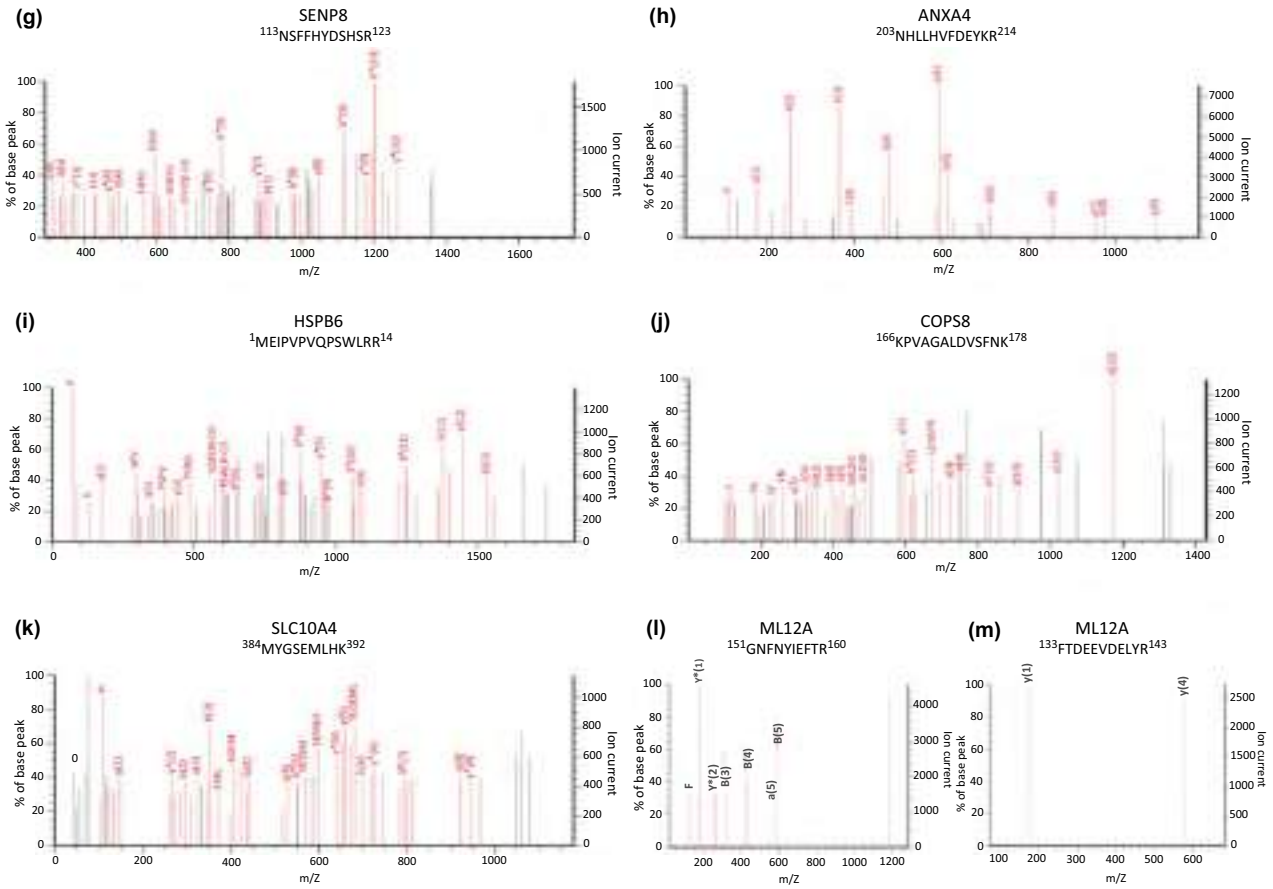

Figure 2 continued

factor-κB.[18–20,25–27] We here investigated roles of ANXA4 in RA synoviocytes, focusing on exocytosis. Since the exocytotic activity of ANXA4 is inhibited by phosphorylation by PKC,[20] we hypothesized that the relatively highly phosphorylated ANXA4 in RA synoviocytes regulates the secretion of inflammatory cytokines and/or chemokines. To mimic the inflammatory condition of RA, we used TNFα, a major inflammatory cytokine secreted in the RA joints. If we use other inflammatory cytokines such as IL-1β, IL-6 and lymphotoxin-αβ (LTαβ), we might detect other increased humoral factors than CXCL1 and IL-8.[28] We stimulated OA synoviocytes with TNFα, not RA synoviocytes. This is because OA synoviocytes would be in a relatively naïve state, but RA synoviocytes are already activated by the so-called cytokine storm and still in an activated condition even if cultured for a while.[29,30] Use of healthy synoviocytes might be more suitable, which is worthwhile to be tested.

We found increased amounts of phosphorylated ANXA4 after the transfection of rANXA4 (Fig. 3f,g). The phosphorylated ANXA4 would reduce the secretion of CXCL1 and IL-8 from TNFα-stimulated synoviocytes (Fig. 4). CXCL1 and IL-8 are expressed in RA synoviocytes and their expression is up-regulated by the stimulation with TNFα and/or IL-1β and also in the inflamed joints.[31–33] CXCL1 and IL-8, which belong to a group of CXC chemokines with an ELR motif, are potent chemoattractants and activators for neutrophils and potent promoters of angiogenesis.[34–36] These chemokines would promote the inflammation of RA by recruiting neutrophils into the joints and promoting angiogenesis in the synovium.[37,38] Furthermore, it was reported that CXCL1 and IL-8 down-regulated collagen expression in rheumatoid synovial fibroblasts.[39] Phosphorylation of ANXA4 may suppress these events by down-regulating CXCL1 and IL-8 in RA and thus may contribute to the amelioration of the disease.

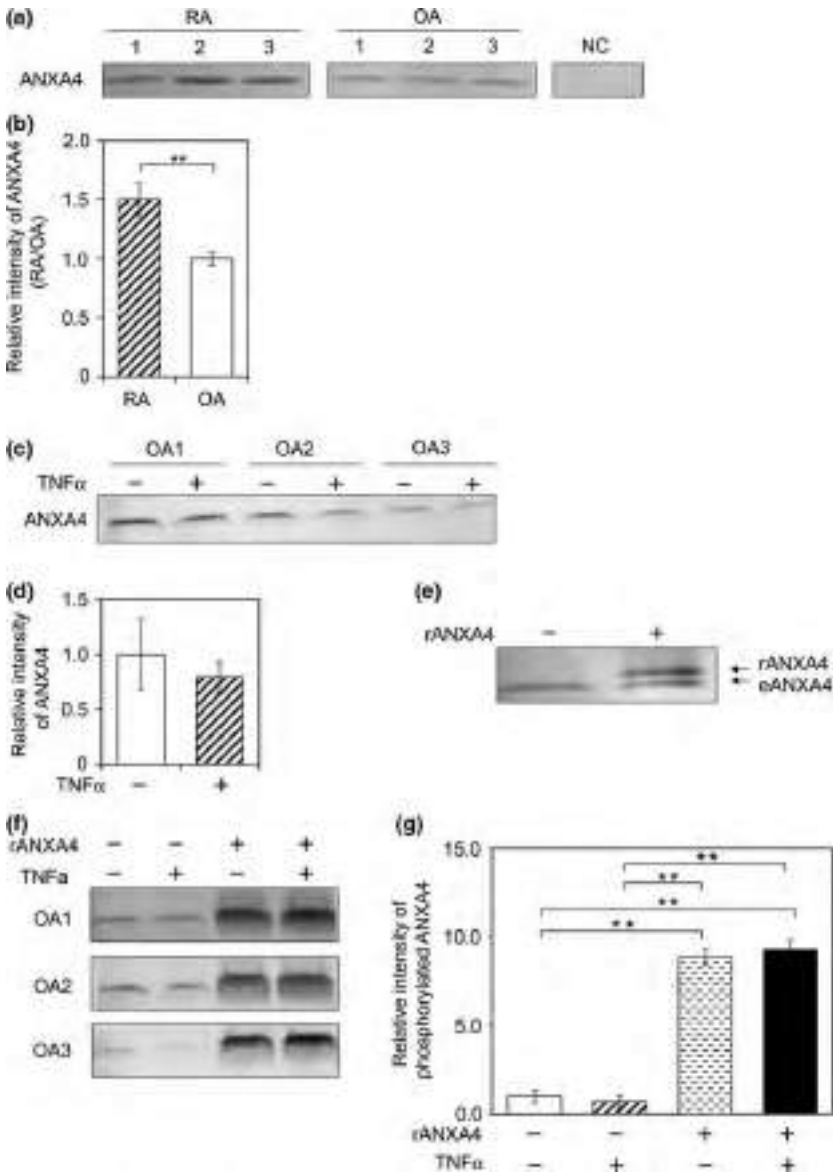

Figure 3 Annexin A4 (ANXA4) expression in rheumatoid arthritis (RA) and osteoarthritis (OA) synoviocytes. (a) Total ANXA4 expression in RA1–3 and OA1–3 synoviocytes was examined by Western blotting using antibodies to human ANXA4. In the negative control (NC), the blocking solution was used in place of the anti-ANXA4 antibody solution. (b) Intensity of the ANXA4 band in (a) was measured. The relative intensity of the RA group to the OA group is shown. Error bars, SD. $^{**}P < 0.01$. (c) OA synoviocytes were cultured in a medium alone or that containing tumor necrosis factor alpha (TNFα) for 24 h. Whole cell lysates were electrophoresed, and expression of total ANXA4 protein was examined by Western blotting. (d) Intensity of the ANXA4 band in c was compared between the non-treated and TNFα-treated synoviocytes. Error bars, SD. (e) Recombinant ANXA4 (rANXA4) was transfected into osteoarthritis (OA) synoviocytes. Since the rANXA4 was fused with 6xHis-tag, the molecular weight of rANXA4 is slightly higher than that of endogenous ANXA4 (eANXA4). Expression of eANXA4 and the transfected rANXA4 were examined by Western blotting. A representative result from OA4 synoviocytes is shown. (f) OA1–3 synoviocytes were cultured in a medium alone or that containing TNFα for 24 h. The synoviocytes transfected with rANXA4 were similarly cultured. Phosphoproteins were extracted from those synoviocytes, and phosphorylation of eANXA4 and rANXA4 was examined by Western blotting. (g) Total intensity of the phosphorylated eANXA4 bands and the phosphorylated rANXA4 bands in f were compared among the four types of treatments. Error bars, SD. $^{**}P < 0.01$.

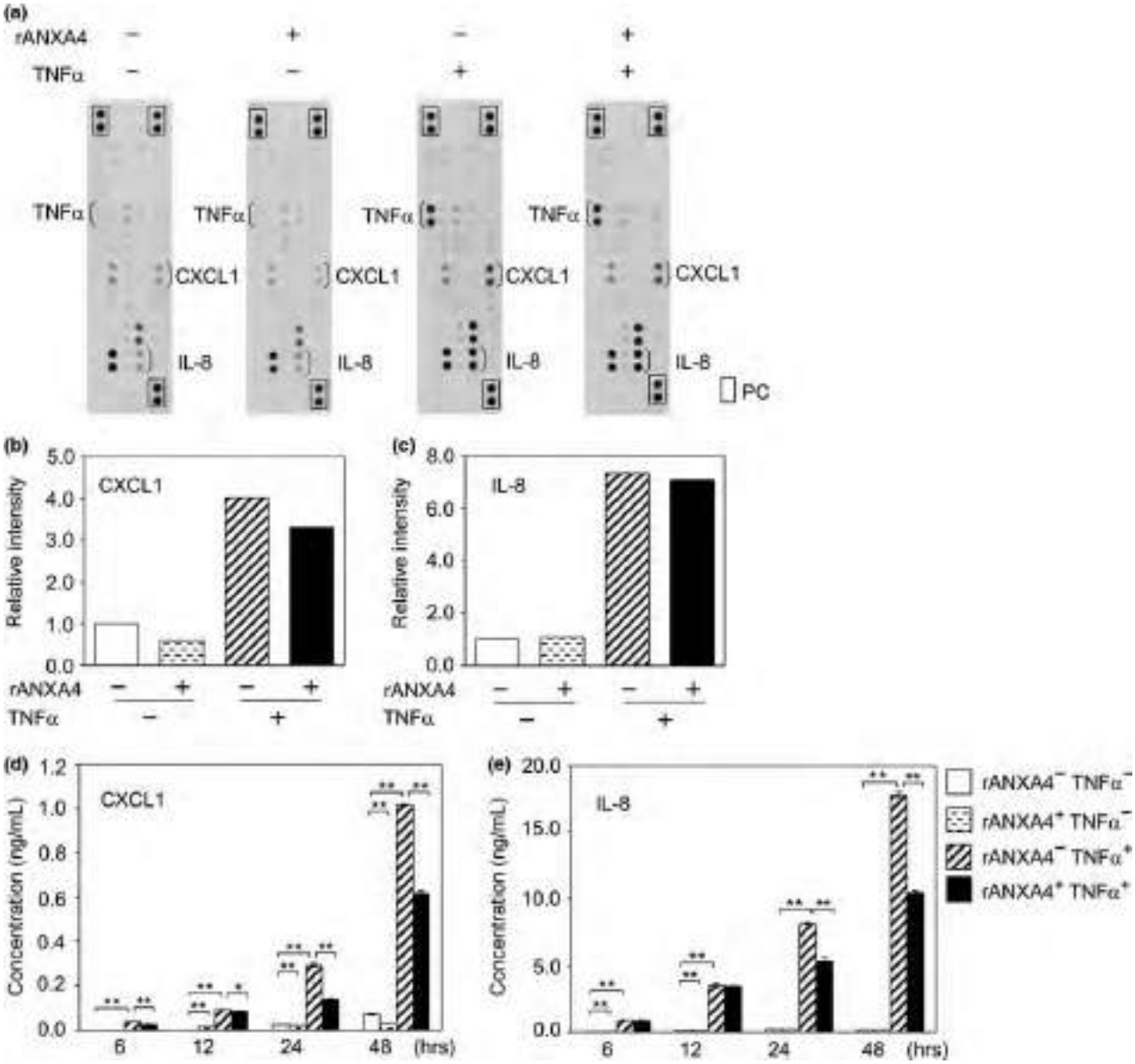

Figure 4 Down-regulation of the secretion of chemokine (C-X-C motif) ligand 1 (CXCL1) and interleukin 8 (IL-8) by transfection of recombinant annexin A4 (rANXA4). (a) OA4 synoviocytes were cultured in a medium alone or that containing tumor necrosis factor alpha (TNFα) for 24 h. The synoviocytes transfected with rANXA4 were similarly cultured. Levels of humoral factor secretion in the four types of treatments were analyzed by a humoral factor array, in which 36 different anti-humoral factor antibodies were blotted. PC, positive control. (b, c) Results of CXCL1 (b) and IL-8 (c) spots in a, which showed more than four-fold intensity increase by TNFα treatment in the non-transfected condition, are shown. (d, e) OA4 synoviocytes were cultured in a medium alone or that containing TNFα for 6, 12, 24 and 48 h. The synoviocytes transfected with rANXA4 were similarly cultured. Concentration of CXCL1 (d) and IL-8 (e) in the culture supernatants were measured by enzyme-linked immunosorbent assay. Significance between the presence and absence of TNFα in the non-transfected condition, between the presence and absence of rANXA4 in the non-treated condition, and between the presence and absence of rANXA4 in the TNFα-treated condition, is specifically shown. $^{*}P < 0.05$, $^{**}P < 0.01$.

Annexins consist of 12 members of $Ca^{2\pm}$ and phospholipid-binding proteins, involved in endocytosis and exocytosis, membrane traffic and organization, calcium signaling, cell growth and apoptosis.[18,40] Molecular mechanisms of the annexin-mediated exocytosis have been mainly investigated on ANXA2.[41–43] Cytosolic

ANXA2 translocates to plasma membrane, following a rise in cytosolic Ca^{2+} and binds to S100A10 proteins to form a tetramer, in which two ANXA2 were connected through a homodimer of S100A10 (ANXA2t). ANXA2t promotes formation of lipid rafts necessary for exocytosis, which contain clusters of soluble N-ethylmaleimide-sensitive factor attachment protein receptor (SNARE), phosphatidylinositol 4,5-bisphosphate (PIP_2), and monosialotetrahexosyl-ganglioside (GM1).[41–43] Furthermore, AnxA2t bundles actin filaments to stabilize the lipid rafts and the bundled actin filaments may connect granules to the plasma membrane to exert a mechanical force for compressing granules and favoring release of their contents.[41,43] Phosphorylation is an important post-translational modification to control the functions of ANXA2 during exocytosis.[41,42] Several phosphorylation sites of ANXA2 have been reported such as Ser 11, Ser 25 and Tyr 23.[41,42,44–47] However, it has been controversial whether the sites are phosphorylated or dephosphorylated to exert the exocytotic functions.[44,45] As in the case of Ser 11, ANXA2 may be first phosphorylated to be activated and then dephosphorylated to stabilize an ANXA2t complex in the release of humoral factors.[46] ANXA4 is considered to be involved in exocytosis in a similar manner to the case of ANXA2. The precise mechanisms need to be elucidated.

Several members of annexins such as ANXA1 and ANXA7 have been reported to be involved in the pathophysiology of rheumatic diseases.[14,48] We previously found up-regulated phosphorylation of synovial ANXA7 in RA compared to OA and that the ANXA7 was associated with increased secretion of IL-8 from RA synoviocytes.[14] Involvement of phosphorylated annexins, ANXA4 and ANXA7, in exocytosis of RA synoviocytes was found by our studies (this study and Matsuo *et al.*[14]) for the first time. The reason why ANXA7 was not detected in this study would be difference of the materials and methods between the two studies (see the first paragraph of Discussion). As an advantage of this study, we found intracellular phosphorylation of the transfected ANXA4 protein (Fig. 3f,g) and that the transfection of ANXA4 reduced CXCL1 and IL-8 secretion from the TNFα-treated synoviocytes (Fig. 4). This result is in accordance with the reports that phosphorylation of annexins make them lose the exocytotic functions.[20,45,47] Analysis of phosphorylation sites of ANXA4 and ANXA7 and phosphorylation/dephosphorylation status of the sites during exocytosis is the next challenge.

One of the limitations of this study is that the number of analyzed samples was rather small to provide good statistical power. Another is that important supporting data for the upregulated phosphorylation of ANXA4 in RA synoviocytes such as increased intracellular Ca^{2+} levels, activation of kinases, and the phosphorylation sites of ANXA4 were not provided. We would like to conduct these experiments using more numbers of RA and OA synoviocyte samples in the near future.

Taken together, the potential mechanism indicated by this study is as follows: inflammatory cytokines such as TNFα and LTαβ stimulate RA synoviocytes to increase the secretion of CXCL1 and IL-8 (Fig. 4).[28] ANXA4 would be involved in the exocytosis of CXCL1 and IL-8 in a similar manner to the case of ANXA2.[41–43] Secreted CXCL1 and IL-8 recruit neutrophils to the joints and exaggerate the arthritis.[31–38] Because PKC phosphorylates a broad spectrum of proteins, ANXA4 can be a specific therapeutic target for down-regulation of the inflammatory chemokine secretion in RA. Further investigation of other differently phosphorylated proteins between RA and OA detected in this study would help understanding of the disease mechanisms in RA.

ACKNOWLEDGEMENTS

The authors are indebted to Ms Michiyo Katano, Ms Mie Kanke and Ms Atsuko Nozawa for their technical assistance. This work was supported by a grant from St. Marianna University School of Medicine.

CONFLICTS OF INTEREST

The authors have no financial conflicts of interest.

AUTHOR CONTRIBUTIONS

Masayoshi Katano: data acquisition and analysis, interpretation of data, preparation of manuscript. Manae S. Kurokawa: study design, data analysis, interpretation of data, preparation and revision of manuscript. Kosuke Matsuo: data analysis, interpretation of data. Kayo Masuko, Naoya Suematsu, Kazuki Okamoto, Toshikazu Kamada: data acquisition and analysis. Hiroshi Nakamura: data analysis, interpretation of data. Tomohiro Kato: study design, interpretation of data, revision of manuscript

REFERENCES

1 McInnes IB, Schett G (2011) The pathogenesis of rheumatoid arthritis. *N Engl J Med* **365**, 2205–19.

2 Meinecke I, Rutkauskaite E, Gay S, Pap T (2005) The role of synovial fibroblasts in mediating joint destruction in rheumatoid arthritis. *Curr Pharm Des* **11**, 563–8.

3 Huber LC, Distler O, Tarner I, Gay RE, Gay S, Pap T (2006) Synovial fibroblasts: key players in rheumatoid arthritis. *Rheumatology* **45**, 669–75.

4 Ritchlin C (2000) Fibroblast biology. Effector signals released by the synovial fibroblast in arthritis. *Arthritis Res* **2**, 356–60.

5 Knedla A, Neumann E, Müller-Ladner U (2007) Developments in the synovial biology field 2006. *Arthritis Res Ther* **9**, 209.

6 Cole PA, Courtney AD, Shen K *et al.* (2003) Chemical approaches to reversible protein phosphorylation. *Acc Chem Res* **36**, 444–52.

7 Ehrentraut SF, Colgan SP (2012) Implications of protein post-translational modifications in IBD. *Inflamm Bowel Dis* **18**, 1378–88.

8 Dasuri K, Antonovici M, Chen K *et al.* (2004) The synovial proteome: analysis of fibroblast-like synoviocytes. *Arthritis Res Ther* **6**, R161–8.

9 Tilleman K, Van Beneden K, Dhondt A *et al.* (2005) Chronically inflamed synovium from spondyloarthropathy and rheumatoid arthritis investigated by protein expression profiling followed by tandem mass spectrometry. *Proteomics* **5**, 2247–57.

10 Zhang H, Fan LY, Zong M, Sun LS, Lu L (2012) Proteins related to the functions of fibroblast-like synoviocytes identified by proteomic analysis. *Clin Exp Rheumatol* **30**, 213–21.

11 Li XJ, Xu M, Zhao XQ, *et al.* (2013) Proteomic analysis of synovial fibroblast-like synoviocytes from rheumatoid arthritis. *Clin Exp Rheumatol* **31**, 552–8.

12 Bo GP, Zhou LN, He WF *et al.* (2009) Analyses of differential proteome of human synovial fibroblasts obtained from arthritis. *Clin Rheumatol* **28**, 191–9.

13 Kriegsmann M, Seeley EH, Schwarting A *et al.* (2012) MALDI MS imaging as a powerful tool for investigating synovial tissue. *Scand J Rheumatol* **41**, 305–9.

14 Matsuo K, Arito M, Noyori K *et al.* (2011) Arthritogenicity of annexin VII revealed by phosphoproteomics of rheumatoid synoviocytes. *Ann Rheum Dis* **70**, 1489–95.

15 Altman R, Asch E, Bloch D *et al.* (1986) Development of criteria for the classification and reporting of osteoarthritis. Classification of osteoarthritis of the knee. Diagnostic and Therapeutic Criteria Committee of the American Rheumatism Association. *Arthritis Rheum* **29**, 1039–49.

16 Arnett FC, Edworthy SM, Bloch DA *et al.* (1988) The American Rheumatism Association 1987 revised criteria for the classification of rheumatoid arthritis. *Arthritis Rheum* **31**, 315–24.

17 Hatsugai M, Kurokawa MS, Kouro T *et al.* (2010) Protein profiles of peripheral blood mononuclear cells are useful for differential diagnosis of ulcerative colitis and Crohn's disease. *J Gastroenterol* **45**, 488–500.

18 Gerke V, Moss SE (2002) Annexins: from structure to function. *Physiol Rev* **82**, 331–71.

19 Willshaw A, Grant K, Yan J *et al.* (2004) Identification of a novel protein complex containing annexin A4, rabphilin and synaptotagmin. *FEBS Lett* **559**, 13–21.

20 Kaetzel MA, Mo YD, Mealy TR *et al.* (2001) Phosphorylation mutants elucidate the mechanism of annexin IV-mediated membrane aggregation. *Biochemistry* **40**, 4192–9.

21 Goulding NJ, Dixey J, Morand EF *et al.* (1995) Differential distribution of annexins-I, -II, -IV, and -VI in synovium. *Ann Rheum Dis* **54**, 841–5.

22 Kaetzel MA, Chan HC, Dubinsky WP, Dedman JR, Nelson DJ (1994) A role for annexin IV in epithelial cell function. Inhibition of calcium-activated chloride conductance. *J Biol Chem* **269**, 5297–302.

23 Zimmermann U, Balabanov S, Giebel J *et al.* (2004) Increased expression and altered location of annexin IV in renal clear cell carcinoma: a possible role in tumour dissemination. *Cancer Lett* **209**, 111–8.

24 Duncan R, Carpenter B, Main LC, Telfer C, Murray GI (2008) Characterisation and protein expression profiling of annexins in colorectal cancer. *Br J Cancer* **98**, 426–33.

25 Crosby KC, Postma M, Hink MA, Zeelenberg CH, Adjobo-Hermans MJ, Gadella TW (2013) Quantitative analysis of self-association and mobility of annexin A4 at the plasma membrane. *Biophys J* **104**, 1875–85.

26 Chan HC, Kaetzel MA, Gotter AL, Dedman JR, Nelson DJ (1994) Annexin IV inhibits calmodulin-dependent protein kinase II-activated chloride conductance. A novel mechanism for ion channel regulation. *J Biol Chem* **269**, 32464–8.

27 Jeon YJ, Kim DH, Jung H *et al.* (2010) Annexin A4 interacts with the NF-kappaB p50 subunit and modulates NF-kappaB transcriptional activity in a Ca2 + -dependent manner. *Cell Mol Life Sci* **67**, 2271–81.

28 Young J, Yu X, Wolslegel K *et al.* (2010) Lymphotoxin-alphabeta heterotrimers are cleaved by metalloproteinases and contribute to synovitis in rheumatoid arthritis. *Cytokine* **51**, 78–86.

29 Zhou JJ, Ma JD, Mo YQ *et al.* (2014) Down-regulating peroxisome proliferator-activated receptor-gamma coactivator-1 beta alleviates the proinflammatory effect of rheumatoid arthritis fibroblast-like synoviocytes through inhibiting extracellular signal-regulated kinase, p38 and nuclear factor-kappaB activation. *Arthritis Res Ther* **16**, 472.

30 Bartok B, Firestein GS (2010) Fibroblast-like synoviocytes: key effector cells in rheumatoid arthritis. *Immunol Rev* **233**, 233–55.

31 Heller RA, Schena M, Chai A *et al.* (1997) Discovery and analysis of inflammatory disease-related genes using cDNA microarrays. *Proc Natl Acad Sci USA* **94**, 2150–5.

32 Kraan MC, Patel DD, Haringman JJ *et al.* (2001) The development of clinical signs of rheumatoid synovial inflammation is associated with increased synthesis of the chemokine CXCL8 (interleukin-8). *Arthritis Res* **3**, 65–71.

33 Koch AE, Kunkel SL, Burrows JC *et al.* (1991) Synovial tissue macrophage as a source of the chemotactic cytokine IL-8. *J Immunol* **147**, 2187–95.
34 Zlotnik A, Yoshie O (2000) Chemokines: a new classification system and their role in immunity. *Immunity* **12**, 121–7.
35 Clark-Lewis I, Dewald B, Geiser T, Moser B, Baggiolini M (1993) Platelet factor 4 binds to interleukin 8 receptors and activates neutrophils when its N terminus is modified with Glu-Leu-Arg. *Proc Natl Acad Sci USA* **90**, 3574–7.
36 Strieter RM, Polverini PJ, Kunkel SL *et al.* (1995) The functional role of the ELR motif in CXC chemokine-mediated angiogenesis. *J Biol Chem* **270**, 27348–57.
37 Koch AE, Kunkel SL, Shah MR *et al.* (1995) Growth-related gene product alpha. A chemotactic cytokine for neutrophils in rheumatoid arthritis. *J Immunol* **155**, 3660–6.
38 Kaneko S, Satoh T, Chiba J, Ju C, Inoue K, Kagawa J (2000) Interleukin-6 and interleukin-8 levels in serum and synovial fluid of patients with osteoarthritis. *Cytokines Cell Mol Ther* **6**, 71–9.
39 Unemori EN, Amento EP, Bauer EA, Horuk R (1993) Melanoma growth-stimulatory activity/GRO decreases collagen expression by human fibroblasts. Regulation by C-X-C but not C-C cytokines. *J Biol Chem* **268**, 1338–42.
40 Fatimathas L, Moss SE (2010) Annexins as disease modifiers. *Histol Histopathol* **25**, 527–32.
41 Gabel M, Chasserot-Golaz S (2016) Annexin A2, an essential partner of the exocytotic process in chromaffin cells. *J Neurochem* **137**, 890–6.
42 Bharadwaj A, Bydoun M, Holloway R, Waisman D (2013) Annexin A2 heterotetramer: structure and function. *Int J Mol Sci* **14**, 6259–305.
43 Hitchcock JK, Katz AA, Schäfer G (2014) Dynamic reciprocity: the role of annexin A2 in tissue integrity. *J Cell Commun Signal* **8**, 125–33.
44 Sarafian T, Pradel LA, Henry JP, Aunis D, Bader MF (1991) The participation of annexin II (calpactin I) in calcium-evoked exocytosis requires protein kinase C. *J Cell Biol* **114**, 1135–47.
45 Regnouf F, Sagot I, Delouche B *et al.* (1995) "In vitro" phosphorylation of annexin 2 heterotetramer by protein kinase C. Comparative properties of the unphosphorylated and phosphorylated annexin 2 on the aggregation and fusion of chromaffin granule membranes. *J Biol Chem* **270**, 27143–50.
46 Brandherm I, Disse J, Zeuschner D, Gerke V (2013) cAMP-induced secretion of endothelial von Willebrand factor is regulated by a phosphorylation/dephosphorylation switch in annexin A2. *Blood* **122**, 1042–51.
47 Rescher U, Ludwig C, Konietzko V, Kharitonenkov A, Gerke V (2008) Tyrosine phosphorylation of annexin A2 regulates Rho-mediated actin rearrangement and cell adhesion. *J Cell Sci* **121**, 2177–85.
48 Yang YH, Morand E, Leech M (2013) Annexin A1: potential for glucocorticoid sparing in RA. *Nat Rev Rheumatol* **9**, 595–603.

Biomedical Research 2016; 27 (4): 1064-1070 *ISSN 0970-938X*
www.biomedres.info

Effects of edaravone on hypoxic human astrocytes revealed by a proteomic approach.

Taigen Sase[1,2], Mitsumi Arito[1*], Hidetaka Onodera[2], Manae S. Kurokawa[1], Yuichiro Tanaka[2], Tomohiro Kato[1]

[1]Clinical Proteomics and Molecular Medicine, St. Marianna University Graduate School of Medicine, 2-16-1 Sugao, Miyamae, Kawasaki, Kanagawa 216-8511, Japan

[2]Department of Neurosurgery, St. Marianna University Graduate School of Medicine, 2-16-1 Sugao, Miyamae, Kawasaki, Kanagawa 216-8511, Japan

Abstract

Introduction: Edaravone (3-methyl-1-phenyl-2-pyrazolin-5-one) of a free radical scavenger has been widely used in treatment of acute ischemic stroke. However, effects of edaravone on hypoxic astrocytes have not been fully understood. Therefore, we investigated the effects by proteomic analysis.
Methods: We cultured human astrocytes under hypoxia and normoxia with or without edaravone. Then, we compared protein profiles of the astrocytes using 2-dimensional differential gel electrophoresis (2D-DIGE). Further, we identified proteins affected by hypoxia and/or edaravone by mass spectrometry.
Results: We detected 507 protein spots by 2D-DIGE. Among them, intensity of 22 spots showed more than 1.5-fold increase or less than 1/1.5-fold decrease with statistical significance ($p<0.05$) by hypoxia. We were able to identify 6 out of the 22 protein spots (increased: alpha-enolase (ENO1, from 2 spots) and ephrin-B2, decreased: adenosine triphosphate synthase subunit alpha (ATPA), mitochondrial heat shock 70 kDa protein 1A/1B, and ferritin light chain). In addition, in 61 out of the 507 spots, the spot intensity showed more than 1.3-fold increase or less than 1/1.3-fold decrease with statistical significance ($p<0.05$) by hypoxia. In 9 out of the 61 spots, the hypoxia-induced intensity alteration was suppressed by the simultaneous addition of edaravone. Three out of the 9 protein spots were identified (ENO1, ATPA, and rab-interacting lysosomal protein-like protein 1).
Conclusion: Edaravone suppressed a part of molecular responses of human astrocytes to hypoxia. Our data would support use of edaravone in acute ischemic stroke.

Keywords: Astrocyte, Edaravone, Hypoxia, Proteomics

Accepted on March 25, 2016

Introduction

The neurovascular unit (NVU) is a functionally integrated structure that is mainly composed of neuronal cells, astrocytes, and microvascular endothelial cells [1,2]. NVU is thought to regulate the interaction between brain circulation and neuronal functions [1,2]. Thereby, sparing of the NVU functions would be important in treatment of acute ischemic stroke [3]. In brain parenchyma, endothelial cells of blood vessels are connected to astrocytes via the foot processes of astrocytes [4]. Similarly, neurons are also connected to astrocytes via other foot processes of astrocytes [1]. Thus, astrocytes play a central role in NVU as a regulator of the interactions between blood vessels and neurons. Furthermore, astrocytes also play a role in maintenance of homeostasis and regulation of responses of the central nervous system to injury [5,6]. From these backgrounds, sparing of astrocyte functions would be of critical importance for sparing of NVU functions in the treatment of acute ischemic stroke.

Edaravone (3-methyl-1-phenyl-2-pyrazolin-5-one) of a free radical scavenger has been widely used in the treatment of acute ischemic stroke [7,8]. Use of edaravone reduces infarction areas and ameliorates neurological deficits in patients with acute ischemic stroke [9]. Similarly, use of edaravone was suggested to improve outcomes of the patients with acute ischemic stroke who were treated with tissue plasminogen activator [10]. Edaravone is thought to work mainly as an antioxidant to inhibit lipid peroxidation [11-13]. However other effects of edaravone have been reported. For example, we reported that edaravone promoted formation of the tight junction between microvascular endothelial cells partly via the down-regulation of monocyte chemoattractant protein-1 secretion [14]. Furthermore, in hypoxic astrocytes, edaravone has been reported to down-regulate hypoxia-inducible factor (HIF)-1 and inhibit the production of vascular endothelial growth factor (VEGF) that promotes brain edema [15,16]. However, effects of edaravone on hypoxic astrocytes

have not been fully understood. Based on these backgrounds, we here attempted to investigate effects of edaravone on human brain astrocytes in the hypoxic condition by 2-dimensional fluorescence difference gel electrophoresis (2D-DIGE) of a comprehensive protein profile analysis.

Materials and Methods

Cell culture

Human astrocytes (Lonza Group Ltd., Basel, Switzerland) were cultured in Astrocyte Basal Medium (ABMTM, Lonza Walkersville, Inc., USA) containing 0.1% recombinant human epidermal growth factor, 0.25% insulin, 3% fetal bovine serum, 0.1% ascorbic acid, 1% L-Glutamine, and 0.1% GA-1000 (AGMTM BulletKitTM, AGMTM plus SingleQuotsTM of Growth Supplements, Lonza Walkersville, Inc., USA). The astrocytes were cultured at 37 degrees centigrade in humidified air with 5% CO_2.

Treatment of astrocytes with edaravone

Astrocytes were cultured under hypoxia and normoxia condition with or without 10 μM edaravone (Mitsubishi Tanabe Pharma Corporation, Osaka, Japan). The hypoxia condition (1% O_2, 5% CO_2, and 94% N_2) was achieved using a hypoxic chamber (Hypoxia Chamber, Stemcell Technologies).

RNA extraction and reverse transcription-PCR (RT-PCR)

RNA extraction and RT-PCR were performed as described previously [17,18]. Extraction and purification of RNA from the astrocytes and reverse transcription of the RNA samples were performed using RNeasy (Qiagen, Venlo, The Netherlands) and High Capacity cDNA Reverse Transcription Kits (Life Technologies, Rockville, MD, USA), respectively. Then, 2 μg of total RNA-derived cDNA was mixed with 1 μM each of the forward and reverse primers and Premix TaqTM (Ex TaqTM Version 2.0, Takara, Shiga, Japan) and subjected to PCR. Nucleotide sequences of the primers for the amplification of a VEGF fragment and β-actin (ACTB) fragment are as follows: for VEGF; 5'-GCCTCCGAAACCATGAACTTTCTGCTG and 5'-TGGTGATGTTGGACTCCTCA, and for ACTB; 5'-AGGCACCAGGGCGTGAT and 5'-TGCTCCCAGTTGGTGACGAT. The thermal cycle conditions were as follows: for VEGF; 95 for 5 min, 25 cycles (95°C for 15 s, 60°C for 30 s, and 72°C for 20 s), and 72°C for 5 min, and for ACTB; 98°C for 5 min, 25 cycles (98°C for 15 s, 58°C for 30 s, and 72°C for 20 s), and 72°C for 5 min.

Quantitative PCR (qPCR)

qPCR was performed as described previously [18]. qPCR was performed using ABI Prism 7000 Sequence Detection System (Applied BiosystemsTM, Foster city, CA, USA), according manufacturer's instructions. 1 μg of total RNA-derived cDNA was mixed with TaqMan® Gene Expression Assays (VEGF: Hs00900055_m1, and ACTB: Mm00607939_s1, Applied Biosystems™) and TaqMan® Gene Expression Master Mix (Applied Biosystems™) and then was subjected to qPCR. The thermal cycle conditions were as follows: 95°C for 10 min, followed by 40 cycles of 95°C for 15 s and 60°C for 60 s.

2-dimensional fluorescence difference gel electrophoresis analysis (2D-DIGE)

Proteins extracted from the astrocytes were separated by 2D-DIGE. 2D-DIGE was performed as described previously [14,19,20]. An internal control sample was prepared by mixing an equal amount of samples from the 4 conditions of normoxia without edaravone, normoxia with edaravone, hypoxia without edaravone, and hypoxia with edaravone. The internal control sample was labeled with Cy3 (Cy Dye DIGE Saturation dye; GE Healthcare, Buckinghamshire, UK). Similarly, each of the treated protein samples was labeled with Cy5. Then, 2.5 μg of the Cy3-labeled internal control sample and 2.5 μg of the Cy5-labeled samples were mixed and applied onto an isoelectric focusing (IEF) gel (pH3-11, GE Healthcare). After IEF, the proteins were further separated by 12.5% SDS-PAGE, separated protein spots were detected using an image analyzer (Typhoon 9400 Imager, GE Healthcare). To compare protein spot intensity among the 4 groups, Cy5-fluorescent intensity of protein spots in each gel was normalized by Cy3-fluorescent intensity of the identical spots by using the Progeneosis software (Nonlinear Dynamics, Newcastle, UK), and the normalized Cy5-intensity was used for the comparison.

Protein identification

Protein identification was performed as described previously [14,19,20]. For identification of proteins, gel fragments that corresponded to protein spots of interest were recovered. Peptides, generated by in-gel digestion with trypsin, were extracted from the gel fragments and were subjected to MALDI-TOF/TOF mass spectrometry (Ultraflex, Bruker Daltonics, Bremen, Germany). The determined peptide masses were compiled to allow searches of the NCBI (National Center for Biotechnology Information) protein database using the Mascot software program (Matrix Svience, London, UK).

Statistical analysis

Statistical significance was calculated by Student's t-test.

Results

Changes of astrocyte protein profiles by hypoxia

To understand effects of edaravone on hypoxic human astrocytes, we here investigated protein profile changes of human astrocytes by hypoxia and effects of edaravone on the changes using 2D-DIGE.

Specifically, we cultured human astrocytes under hypoxia and normoxia for 24 hours with or without 10 μM edaravone (n=3 for each of the 4 conditions; normoxia without edaravone,

hypoxia without edaravone, normoxia with edaravone, and hypoxia with edaravone). Before the 2D-DIGE analysis, we confirmed that the astrocytes were exposed to hypoxia by the assessment of mRNA levels of VEGF between the normoxia and hypoxia samples without edaravone. As a result, the levels of VEGF were significantly high in the hypoxia samples compared to the normoxia samples (3.2-folds, Figure 1). This indicated that the astrocytes were exposed to hypoxia condition in our experiment.

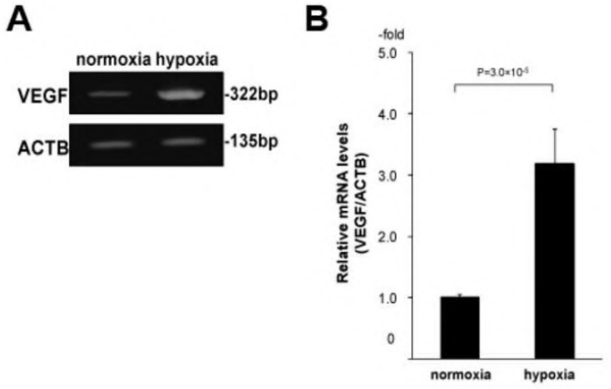

Figure 1. *Hypoxic responses of human astrocytes. Human astrocytes were cultured under hypoxia and normoxia for 24 hours (n=3). Then mRNA for VEGF and ACTB were assayed by RT-PCR. A: A DNA fragment for VEGF (322bp) as a hypoxic marker and a DNA fragment for ACTB (135bp) as an internal control were amplified. A representative case is shown. B: The mRNA level of VEGF was normalized by the mRNA level of ACTB. The average value in the normoxia group was defined as 1.0. Mean values with SD are shown.*

Next, we separated proteins of each sample by 2D-DIGE as shown in figure 2, by which we detected 507 protein spots in total (Table 1). In the comparison of astrocyte protein profiles between normoxia and hypoxia conditions, we found that intensity of 116 out of the 507 protein spots were different with statistical significance as shown in Table 1. Out of the 116 protein spots, 39 protein spots showed more than 1.3-fold higher intensity in the hypoxia condition than in the normoxia condition. 15 out of the 39 protein spots showed more than 1.5-fold higher intensity. Similarly, 22 protein spots showed less than 1/1.3-fold lower intensity in the hypoxia condition than in normoxia condition.

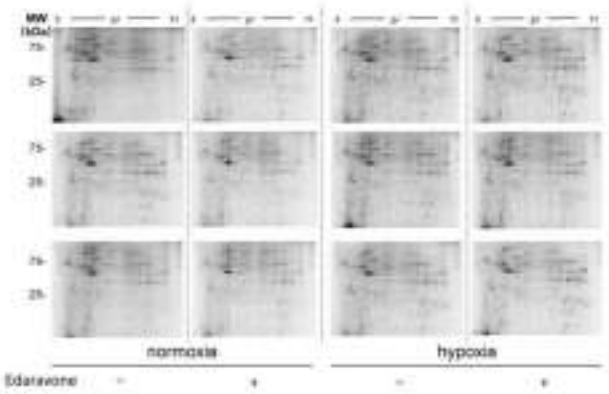

Figure 2. *2D-DIGE detection of proteins affected by edaravone in hypoxic human astrocytes. Human astrocytes were cultured under hypoxia and normoxia with or without 10 μM edaravone for 24 hours (n=3, each). Proteins extracted from each of the astrocyte samples mixed with the internal standard sample were separated by 2D-DIGE. MW; molecular weight, pI: isoelectric point.*

Table 1. *Numbers of protein spots whose intensity was altered more than 1.3-fold by hypoxia and the alternation was suppressed by edaravone.*

Detected spots on 2-DE gels	hypoxia/normoxia (p<0.05)			Effects of edaravone (under hypoxia) (p<0.05)	
	Total	Difference	Spot count	Difference	Spot count
507	116	↑ (1.5 ≤)	15	↓	2
				→	13
				↑	0
		↑ (1.3 ≤)	39	↓	5
				→	34
				↑	0
		↓ (≤ -1.3)	22	↓	0
				→	18
				↑	4
		↓ (≤ -1.5)	7	↓	0
				→	4
				↑	3

7 out of the 22 protein spots showed less than 1/1.5-fold lower intensity. Focusing on the 22 protein spots that showed more than 1.5- or less than 1/1.5- fold changes, we tried to identify protein names using MALDI-TOF/TOF mass spectrometry. As a result, protein names were identified in 6 protein spots (nos. 633, 685, 686, 1114, 1133, and 1196), as summarized in figure 3 and table 2. Three out of the 6 identified spots (no.685 of alpha-enolase (ENO1), no.686 of ENO1, and no.1113 of ephrin-B2 (EFNB2), showed higher intensity in the hypoxia condition than in the normoxia condition. The remaining 3 spots (no. 633 of adenosine triphosphate synthase subunit alpha (ATPA), no. 1196 of mitochondrial heat shock 70 kDa protein 1A/1B (HSPA1A), and no.1114 of ferritin light chain (FTL)) showed lower intensity in the hypoxia condition than in the normoxia condition.

Table 2. *Identification of protein spots whose intensity was altered more than 1.5-fold by hypoxia with statistical significance.*

Spot no.	Fold changes (hypoxia/ normoxia)	MW/pI (observed)	Protein	Accession no.	MW/pI (calculated)	Matched peptides	Coverage (%)	Sequence confirmed by LID (Mascot ion score)
685	1.6	48.9/7.4	Alpha-enolase (ENO1_HUMAN)	GI:4503571	47.1/7.01	238	14	33AAVPSGASTGIYEALELR50 (106) 163LAMQEFMILPVGAANFR179 + 2 Oxidation (M) (41)
686	1.6	48.7/7.8	Alpha-enolase (ENO1_HUMAN)	GI:4503571	47.1/7.01	184	22	33AAVPSGASTGIYEALELR50 (78) 240VVIGMDVAASEFFR253 + Oxidation (M) (58)
1133	1.6	16.7/7.9	Ephrin-B2 (EFNB2_HUMAN)	GI:4758250	36.9/9.04	59	15	182RPELEAGTNGR192 (8) 295TADSVFCPHYEK306 (17)
633	-1.7	53.1/8.7	ATP synthase subunit alpha, mitochondrial (ATPA_HUMAN)	GI:4757810	59.7/9.16	106	15	335EAYPGDVFYLHSR347 (31) 403GIRPAINVGLSVSR416 (17)
1196	-2.1	66.7/5.6	Heat shock 70 kDa protein1A/1B (HSPA1A_HUMAN)	GI: 194248072	70.0/5.48	158	19	160DAGVIAGLNVLR171(21) 172IINEPTAAAIAYGLDR187(33) 329AQIHDLVLVGGSTR342(46)
1114	-3.3	18.0/5.7	Ferritin light chain (FTL_HUMAN)	GI:20149498	20.0/5.52	62	23	155LGGPEAGLGEYLFER169(19)

MW: molecular weight (kDa), pI: isoelectric point, LID: laser-induced dissociation

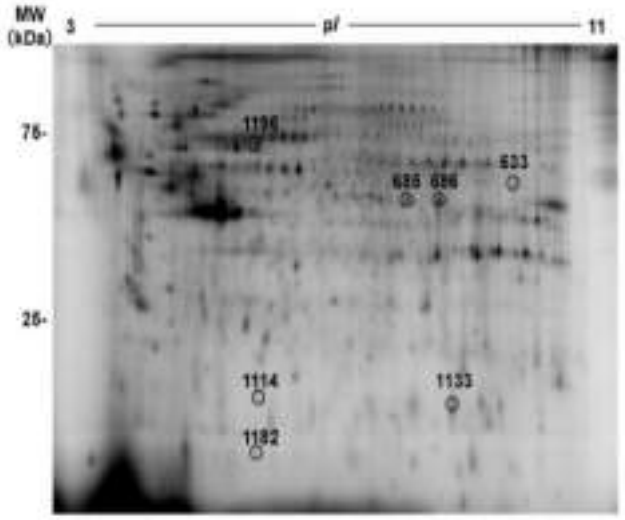

Figure 3. *Location of identified protein spots. Identified protein spots on the 2D gel are shown by circles with spot numbers. MW; molecular weight, pI: isoelectric point.*

Effects of edaravone on the hypoxia-induced protein profile changes in astrocytes

We then investigated effects of edaravone on the hypoxia-induced protein profile changes in astrocytes. Specifically, we compared the protein profiles between the edaravone-treated and non-treated samples (under hypoxia) using the 2D-DIGE results. Among the 39 protein spots that showed more than 1.3-fold higher intensity by the hypoxia induction, 5 spots showed significant suppression of the intensity increase by the treatment with edaravone ($p<0.05$, Table 1). Similarly, 22 protein spots that showed less than 1/1.3-fold lower intensity by the hypoxia induction, 4 protein spots showed significant suppression of the intensity decrease by the treatment with edaravone ($p<0.05$, Table 1). In addition, edaravone did not enhance significantly the hypoxia-induced intensity changes in any of the 116 protein spots.

Then, we tried to identify the 9 protein spots in which hypoxia-induced intensity changes were suppressed by the treatment with edaravone, using MALDI-TOF-TOF/MS. As a result, we identified 3 protein spots (no. 686 of ENO1, no. 1182 of rab-interacting lysosomal protein-like protein 1 (RILPL1), and no. 633 of ATPA, Fig. 3 and Table 3). Of note, the intensity of

these 3 protein spots was not significantly changed by the treatment with edaravone under normoxia (Figure 4). These data showed that edaravone suppressed the hypoxia-induced change of these protein spots.

Table 3.*Identification of proteins whose intensity changes by hypoxia were suppressed by edaravone with statistical significance.*

Spot no.	Effects of hypoxia	Effects of edaravone under hypoxia	MW/pI (observed)	Protein	Accession no.	MW/pI (calculated)	Matched peptides	Coverage (%)	Sequence confirmed by LID (Mascot ion score)
a	↑	↓	48.7/7.8	Alpha-enolase (ENO1_HUMAN)	GI:4503571	47.1/7.01	184	22	33AAVPSGASTGIYEALELR50 (78) 240VVIGMDVAASEFFR253 + Oxidation (M) (58)
1182	↑	↓	13.4/5.6	RILP-like protein 1 (RILPL1_HUMAN)	GI: 195947382	47.1/5.13	72	16	201LMKINHDLR209 + Oxidation (M) (24)
633	↓	↑	53.1/8.7	ATP synthase subunit alpha, mitochondrial (ATPA_HUMAN)	GI:4757810	59.7/9.16	106	15	335EAYPGDVFYLHSR347 (31) 403GIRPAINVGLSVSR416 (17)

MW; molecular weight (kDa), pI; isoelectric point, LID; laser-induced dissociation

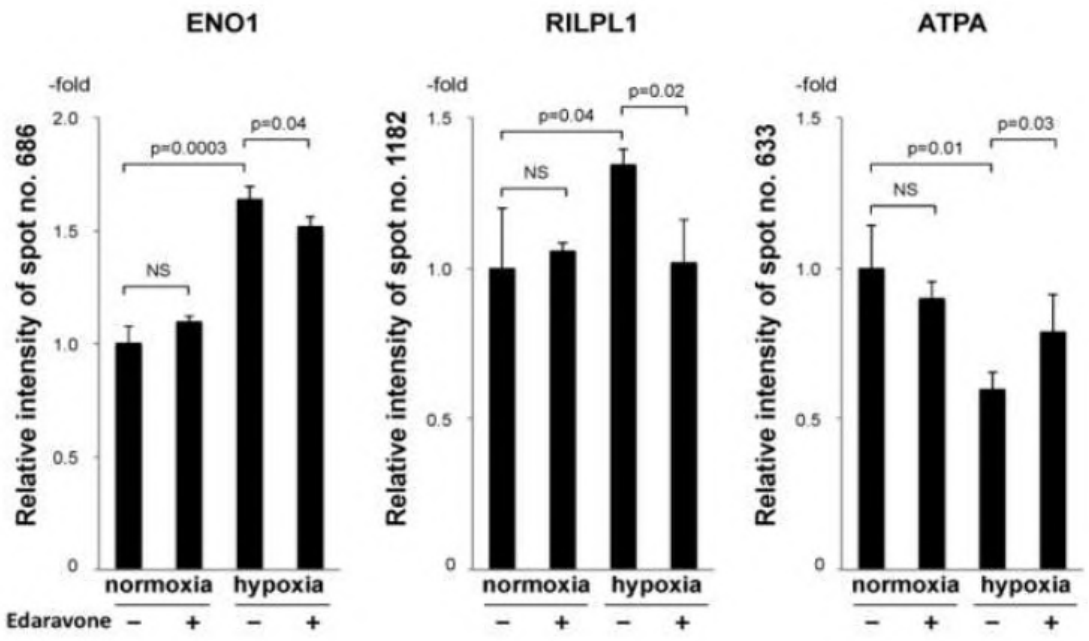

Figure 4. *Relative intensity of the 3 identified protein spots. The normalized intensity of the 3 identified protein spots (nos. 686, 1182 and 633) was compared between normoxia and hypoxia conditions and between edaravone-treated and non-treated conditions. The average of the normalized protein spot intensity in "normoxia without edaravone" group are defined as 1.0. Mean values with SD are shown.*

Discussion

We here found that edaravone suppressed a part of hypoxia-induced protein profile changes of astrocytes and that edaravone did not enhance the hypoxia-induced alteration of the profile. Our data indicate that use of edaravone in the treatment of acute ischemic stroke would be beneficial to protect astrocytes from hypoxia-induced damages. First, intensity of the protein spots of nos. 685, 1133, and 1182, which were assigned to ENO1, EFNB2, and RILPL1 respectively, was increased by hypoxia. The increase of these 3 proteins was in accordance with previous reports. Specifically, expression of ENO1 and EFNB2 was reported to be increased in hypoxic human astrocytes [21] and in hypoxic human trophoblast-derived cell lines [22], respectively. Since EFNB2 is an essential factor for differentiation of vascular endothelial cells into arterial endothelial cells [23], it is reasonable that the expression of EFNB2 was increased by hypoxia to maintain arterial endothelial structures.

Protein spots of nos. 633, 1114, and 1196 whose intensity was decreased by hypoxia were identified as ATPA, FTL, and HSPA1A respectively. ATPA was reported to be decreased by hypoxia in human macrophages [24]. It was reported that the

protein level of FTL was increased in lens epithelial cells of mixed breeding dog [25]. The change of FTL expression by hypoxia is likely to be different among tissue type. Then, we thus need to investigate this point in the future. Next, we focused on the effects of edaravone on hypoxic human astrocytes. The intensity of protein spot no. 686, identified as ENO1, was increased by hypoxia and the change was suppressed by the simultaneous treatment with edaravone. ENO1, one of the glycolytic enzymes, converts 2-phosphoglyceric acid to phosphoenolpyruvic acid. The expression of ENO1 was reported to be increased by hypoxia via enhancement of anaerobic metabolism [26,27]. ENO1 was reported to be produced by hypoxia in a HIF-1-dependent manner [21]. Furthermore, it was reported that edaravone inhibited HIF-1 activity [15]. Taking these reports together with ours, edaravone would suppress the expression of ENO1 by the inhibition of HIF-1 activity.

Intensity of protein spot no. 633, identified as ATPA, was decreased by hypoxia and the change was suppressed by the simultaneous treatment with edaravone. ATPA is one of the 5 subunits of ATP synthesize. The ATP synthase contains subunits and among which decrease of ATP synthase subunit (ATPB) in hypoxic rats, decrease of ATPB and ATP synthase subunit in hypoxic mice, and decrease of ATPA and ATPB in hypoxic human macrophages were reported previously [28,29]. We found that edaravone suppressed the decrease of ATPA in hypoxic human astrocytes. It was recently reported that ATPA was decreased by hypoxia at least in part in a HIF-1-independent manner [24]. HIF-1 activity was suppressed by edaravone as above mentioned [15]. Taking these data together with ours, edaravone would suppress expression of ATPA in the hypoxia condition via both HIF-1-dependent and -independent pathways.

It was reported that hypoxia and/or oxidative stress suppressed the synthesis level of ATP in mitochondria, promoting the production of reactive oxygen species (ROS) [30-35]. Therefore, edaravone may suppress ROS production by maintaining the expression of ATPA in the hypoxic condition. The intensity of protein spot no. 1182, identified as RILPL1, was increased by hypoxia and the increase was fully suppressed by the treatment with edaravone. Thereby, RILPL1 would be deeply involved in the functions of edaravone in hypoxia, however, functions of RILPL1 have been little understood. The relationship among hypoxia, RILPL1, and edaravone should be investigated in the future. In conclusion, edaravone suppressed a part of molecular responses of human astrocytes to hypoxia, but did not enhance any of the responses. Although molecular functions of edaravone should be investigated in more detailed, our data here would support the current clinical use of edaravone for the treatment of acute ischemic stroke.

Acknowledgments

We thank Ms. Y. Sawada, Ms. M. Yokoyama and Ms. A. Nozawa for their technical assistance.

References

1. del Zoppo GJ. The neurovascular unit in the setting of stroke. J Intern Med 2010; 267: 156-171.
2. Lo EH, Dalkara T, Moskowitz MA. Mechanisms, challenges and opportunities in stroke. Nat Rev Neurosci 2003; 4: 399-415.
3. Lo EH, Rosenberg GA. The neurovascular unit in health and disease: introduction. Stroke 2009; 40: S2-3.
4. Mathiisen TM, Lehre KP, Danbolt NC, Ottersen OP. The perivascular astroglial sheath provides a complete covering of the brain microvessels: an electron microscopic 3D reconstruction. Glia 2010; 58: 1094-1103.
5. Liberto CM, Albrecht PJ, Herx LM, Yong VW, Levison SW. Pro-regenerative properties of cytokine-activated astrocytes. J Neurochem 2004; 89: 1092-1100.
6. Tsacopoulos M, Magistretti PJ. Metabolic coupling between glia and neurons. J Neurosci 1996; 16: 877-885.
7. Abe K, Yuki S, Kogure K. Strong attention of ischemic and postischemic brain edema in rats by a novel free radical scavenger. Stroke 1988; 19: 480-485.
8. Albers GW, Goldstein LB, Hess DC, Wechsler LR, Furie KL, Gorelick PB, Hurn P, Liebeskind DS, Nogueira RG, Saver JV, and for the STAIR VII Consortium. Stroke Treatment Academic Industry Roundtable (STAIR) recommendations for maximizing the use of intravenous thrombolytics and expanding treatment options with intra-arterial and neuroprotective therapies. Stroke 2011; 42: 2645-2650.
9. Nakase T, Yoshida S, Suzuki, A. Free radical scavenger, edaravone, reduces the lesion size of lacunar infarction in human brain ischemic stroke. BMC Neurol 2011; 11: 39.
10. Wada T, Yasunaga H, Inokuchi R, Horiguchi H, Fushimi K, Matsubara T, Nakajima S, Yahagi N. Effects of edaravone on early outcomes in acute ischemic stroke patients treated with recombinant tissue plasminogen activator. J Neurol Sci 2014; 345: 106-111.
11. Lukic-Panin V, Deguchi K, Yamashita T, Shang J, Zhang X, Tian F, Liu N, Kawai H, Matsuura T, Abe K. Free radical scavenger edaravone administration protects against tissue plasminogen activator induced oxidative stress and blood brain barrier damage. Curr Neurovasc Res 2010; 7: 319-29.
12. Mizuno A, Umemura K, Nakashima M. Inhibitory effect of MCI-186, a free radical scavenger, on cerebral ischemia following rat middle cerebral artery occlusion. Gen Pharmacol 1998; 30: 575-578.
13. Watanabe T, Yuki S, Egawa M, Nishi H. Protective effects of MCI-186 on cerebral ischemia: possible involvement of free radical scavenging and antioxidant actions. J Pharmacol Exp Ther 1994; 268: 1597-1604.
14. Onodera H, Arito M, Sato T, Ito H, Hashimoto T, Tanaka Y, Kurokawa MS, Okamoto K, Suematsu N, Kato T. Novel effects of edaravone on human brain microvascular endothelial cells revealed by a proteomic approach. Brain Res 2013; 1534: 87-94.

15. Ishikawa A, Yoshida H, Metoki N, Toki T, Imaizumi T, Matsumiya T, Yamashita K, Taima K, Satoh K. Edaravone inhibits the expression of vascular endothelial growth factor in human astrocytes exposed to hypoxia. Neurosci Res 2007; 59: 406-412.
16. Jośko J, Knefel K. The role of vascular endothelial growth factor in cerebral oedema formation. Folia Neuropathol 2003; 41: 161-166.
17. Asano K, Arito M, Kurokawa MS, Omoteyama K, Okamoto K, Suematsu N, Yudoh K, Nakamura H, Beppu M, Kato T. Secretion of inflammatory factors from chondrocytes by layilin signaling. Biochem Biophys Res Commun 2014; 452: 85-90.
18. Koizumi H, Arito M, Endo W, Kurokawa MS, Okamoto K, Omoteyama K, Suematsu N, Beppu M, Kato T. Effects of tofacitinib on nucleic acid metabolism in human articular chondrocytes. Mod Rheumatol 2015; 25: 522-7.
19. Fukasawa M, Okamoto K, Nakamura M, Mikami K, Shimada S, Tanaka Y, Nagai K, Arito M, Kurokawa MS, Masuko K, Suematsu N, Koizuka I, Kato T. Proteomic analysis of the rat cerebellar flocculus during vestibular compensation. J Vestib Res 2009; 19: 83-94.
20. Endo W, Arito M, Sato T, Kurokawa MS, Omoteyama K, Iizuka N, Okamoto K, Suematsu N, Nakamura H, Beppu M, Kato T. Effects of sulfasalazine and tofacitinib on the protein profile of articular chondrocytes. Mod Rheumatol 2014; 24: 844-50.
21. Mense SM, Sengupta A, Zhou M, Lan C, Bentsman G, Volsky DJ, Zhang L. Gene expression profiling reveals the profound upregulation of hypoxia-responsive genes in primary human astrocytes. Physiol Genomics 2006; 25: 435-49.
22. Chennakesava CS, Di Sabto S, Ziemiecki A, Schneiber H, Andres AC. Differential expression of the receptor tyrosine kinase ephB4 and its ligand ephrin-B2 during human placental development. Placenta 2006; 27: 959-967.
23. Adams RH, Wilkinson GA, Weiss C, Diella F, Gale NW, Deutsch U, Risau W, Klein R. Roles of ephrinB ligands and EphB receptors in cardiovascular development: demarcation of arterial/venous domains, vascular morphogenesis, and sprouting angiogenesis. Genes Dev 1999; 13: 295-306.
24. Fuhrmann DC, Wittig I, Heide H, Dehne N, Brüne B. Chronic hypoxia alters mitochondrial composition in human macrophages. Biochim Biophys Acta 2013; 1834: 2750-2760.
25. Goralska M, Fleisher LN, McGahan MC. Hypoxia induced changes in expression of proteins involved in iron uptake and storage in cultured lens epithelial cells. Exp Eye Res 2014; 125: 135-141.
26. Sedoris KC, Thomas SD, Miller DM. Hypoxia induces differential translation of enolase/MBP-1. BMC Cancer 2010; 10: 157.
27. Pancholi V. Multifunctional alpha-enolase: its role in diseases. Cell Mol Life Sci 2001; 58: 902-20.
28. Li J, Qi Y, Liu H, Cui Y, Zhang L, Gong H, Li Y, Li L, Zhang Y. Acute high-altitude hypoxic brain injury: Identification of ten differential proteins. Neural Regen Res 2013; 8: 2932-2941.
29. Dukhande VV, Sharma GC, Lai JCK, Farahani R. Chronic hypoxia-induced alterations of key enzymes of glucose oxidative metabolism in developing mouse liver are mTOR dependent. Mol Cell Biochem 2011; 357: 189-197.
30. Hoffman DL, Salter JD, Brookes PS. Response of mitochondrial reactive oxygen species generation to steady-state oxygen tension: implications for hypoxic cell signaling. Am J Physiol Heart Circ Physiol 2007; 292: H101-108.
31. Murphy MP. How mitochondria produce reactive oxygen species. Biochem J 2009; 417: 1-13.
32. Yang J, Chi Y, Burkhardt BR, Guan Y, Wolf BA. Leucine metabolism in regulation of insulin secretion from pancreatic beta cells. Nutr Rev 2010; 68: 270-279.
33. Diaz F, Enríquez JA, Moraes CT. Cells lacking Rieske iron-sulfur protein have a reactive oxygen species-associated decrease in respiratory complexes I and IV. Mol Cell Biol 2012; 32: 415-429.
34. Sena LA, Chandel NS. Physiological roles of mitochondrial reactive oxygen species. Mol Cell 2012; 48: 158-167.
35. Huang WY, Jou MJ, Peng TI. mtDNA T8993G mutation-induced F1F0-ATP synthase defect augments mitochondrial dysfunction associated with hypoxia/reoxygenation: the protective role of melatonin. PLoS One 2013; 8: e81546.

***Correspondence to:**

Mitsumi Arito, PhD

Clinical Proteomics and Molecular Medicine

St. Marianna University Graduate School of Medicine

Japan

A Small Nuclear Acidic Protein (MTI-II, Zn^{2+} Binding Protein, Parathymosin) That Inhibits Transcriptional Activity of NF-κB and Its Potential Application to Antiinflammatory Drugs

Kazuki Okamoto, Shizu Hirata-Tsuchiya, Chiaki Kitamura, Kazuki Omoteyama, Toshiyuki Sato, Mitsumi Arito, Manae S. Kurokawa, Naoya Suematsu, and Tomohiro Kato

Departments of Clinical Proteomics and Molecular Medicine (K.Ok., K.Om., T.S., M.A., N.S., T.K.) and Disease Biomarker Analysis and Molecular Regulation (M.S.K.), St Marianna University Graduate School of Medicine, Kawasaki, Kanagawa 216-8511, Japan; Department of Biological Endodontics (S.H.-T.), Institute of Biomedical and Health Science, Hiroshima University, Hiroshima 734-8553, Japan; and Division of Endodontics and Restorative Dentistry (C.K.), Kyushu Dental University, Kitakyushu, Fukuoka 803-8580, Japan

Nuclear factor-κB (NF-κB) is the most potent proinflammatory transactivator, and an inhibitor of NF-κB is a good antiinflammatory drug. Glucocorticoids (GCs) are the strongest and the most frequently used antiinflammatory drugs. GC-bound glucocorticoid receptor (GR) inhibits the transcriptional activity of NF-κB and thereby suppresses a broad range of inflammatory processes. Concurrently, in whole body outside the inflammation area, the GR exerts a lot of hormone action, which results in severe side effects. There is a long-awaited need for a new NF-κB inhibitor. Previously we found a small nuclear acidic protein (named MTI-II, also known as Zn^{2+}-binding protein or parathymosin), which worked as a coactivator of GR. Here we showed that overexpression of MTI-II inhibited a transcriptional activity of NF-κB independently of GCs and the GR. Vise versa, RNA interference suppression of inherent MTI-II enhanced the transcriptional activity of NF-κB. An immunoprecipitation analysis showed that MTI-II precipitated NF-κB after the stimulation of TNFα. Deletion mutants of MTI-II showed that central acidic region is essential for the inhibition of the transcriptional activity of NF-κB. These results suggest that MTI-II would be an inherent inhibitor that interacts with NF-κB. Next, we constructed MTI-II-based antiinflammatory drugs (three fusion proteins of MTI-II with a protein transduction domain and a fusion peptide of the central acidic region with protein transduction domain). These drugs had significant antiinflammatory effects on acute inflammation models and on animal models of human chronic inflammation diseases without an increase of the blood glucose level and repeated-dose toxicity. The MTI-II-based antiinflammatory drug will be a good alternative of GCs. (***Endocrinology* 157: 4973–4986, 2016)**

An inhibitor of proinflammatory transactivator, nuclear factor-κB (NF-κB), is the most potent antiinflammatory drug. Glucocorticoids (GCs) are the strongest and the most frequently used inhibitors of NF-κB. As for mechanism of the antiinflammatory action of GCs, it has been suggested that the GC-bound glucocorticoid receptor (GR) interacts with NF-κB (1–3) and then inhibits the transcriptional activity of NF-κB. Furthermore, recent reports suggest that GR induces

ISSN Print 0013-7227 ISSN Online 1945-7170
Printed in USA
Copyright © 2016 by the Endocrine Society
Received October 7, 2016. Accepted October 10, 2016.
First Published Online October 14, 2016

Abbreviations: AR, acidic region; BM, betamethasone valerate; CIA, collagen-induced arthritis; COX2, cyclooxygenase 2; DC-FBS, dextran-charcoal-treated FBS; Dex, dexamethasone; FBS, fetal bovine serum; GAPDH, glyceraldehyde-3-phosphate dehydrogenase; GC, glucocorticoid; GFP, green fluorescent protein; GR, glucocorticoid receptor; GRE, GC response element; IκB, inhibitory-κB; IDM, indomethacin; MAID, MTI-II-based antiinflammatory drug; MPAID, MTI-II peptide antiinflammatory drug; NC, negative control; NF-κB, nuclear factor-κB; NLS, nuclear localization signal; PTD, protein transduction domain; R, arginine; RFP, red fluorescent protein; RNAi, RNA interference; siRNA, small interfering RNA.

genes that contribute to the inhibition of NF-κB (4–9). Thus GCs suppress a broad range of inflammatory processes by inhibiting NF-κB in active inflammation areas. At the same time, outside the inflammation areas, the GR binds to specific DNA and induces both gene transactivation (eg, genes for enzymes involved in gluconeogenesis) and gene transrepression, which result in severe side effects such as diabetes, atrophy of skin, apoptosis of immune cells, and suppression of the hypothalamic-pituitary-adrenal axis (10). There is a long-awaited need for a new NF-κB inhibitor.

Previously we found a small nuclear acidic protein (named MTI-II [11], also known as Zn^{2+} binding protein [12] or parathymosin [13]). MTI-II is ubiquitously expressed in whole mammalian tissues with the highest concentrations in liver followed by kidney and the lowest concentrations in thymus, spleen, and muscle (13–16). And its amino acid sequence (17) is highly conserved among rat, cow, and human (18). In the last paper (19), we found that the overexpression of MTI-II enhanced a transcriptional activity of GR as strong as steroid receptor coactivator-1, whereas MTI-II had little effect on the transcriptional activity of estrogen receptor-α. RNA interference (RNAi) suppression of inherent MTI-II reduced the transcriptional activity of the GR (19). An immunoprecipitation assay revealed that MTI-II directly bound both to the GR and to CBP/p300 (19). MTI-II is very small (101 amino acid residues, 11.5 kDa) and very acidic (pI = 4.0, 47 of 101 amino acid residues are acidic) (17). MTI-II has neither protein-protein interaction domains (eg, LXXLL domain) nor enzymatic activities (eg, histone acetyltransferase activity) as well no DNA binding motif. Thus, an expected molecular mechanism of MTI-II is that MTI-II may slide into GR/coactivators complex and plays as electrostatic glue that binds the GR and CBP/p300. Thereby MTI-II enhances the transcriptional activity of GR. MTI-II is an important component of the GR/coactivator complex (19).

In this report, we examined the effect of MTI-II on a transcriptional activity of NF-κB and found that the overexpression of MTI-II inhibited the transcriptional activity of NF-κB independently of GCs and the GR. The inhibition was caused by a formation of a complex of MTI-II with NF-κB. Furthermore, we constructed four kinds of MTI-II-based antiinflammatory drugs and found that they had significant in vivo antiinflammatory effects on acute inflammation models (carrageenan induced paw edema and croton oil induced conjunctival inflammation) and also on animal models of human chronic inflammation diseases (mite-antigens induced atopic dermatitis and collagen induced arthritis) without an increase of the blood glucose level and repeated-dose toxicity. The MTI-II-based antiinflammatory drugs will fulfill the unmet need as an alternative to GCs.

Materials and Methods

Cell culture, transient transfection, and luciferase assay

HeLa cells (DS Pharma Biomedical; 03-117) were grown in DMEM with 10% fetal bovine serum (FBS) in the presence of penicillin-streptomycin. The cells were plated at a density of 0.12×10^5 cells/well in 48-well plates. At 24 hours after the cell plating, the medium was changed to DMEM plus 10% dextran-charcoal-treated FBS (DC-FBS; HyClone). At 24 hours after the medium change, the cells were transfected with 60 ng of κB-Luc2P (pGL4.32; Promega) or glucocorticoid response element (GRE)-Luc2P and 20 ng of TK-hRLuc (pGL4.74; Promega) together with 120 ng of pTriEx-MTI (MTI-II cDNA inserted into *Nco*I-*Hin*dIII site of pTriEx-4 [Novagen] vector) or pTriEx-NC (expressing only his-tag) to a total 200 ng of DNA per well by using a cationic lipid reagent (FuGENE HD; Promega). The GRE-Luc2P was constructed from a GRE promoter of pGRE-Luc vector (PT3339-5; CLONTECH) and basic Luc2P vector (pGL4.11; Promega). At 48 hours after the transfection, the cells were treated with 1 ng/mL of TNFα and/or 120 nM dexamethasone (Dex). The cells were harvested at 4.5 hours after the treatment, and the luciferase activities were detected by a dual-luciferase assay system (Promega).

As for the luciferase assay in COS7 cells (Health Science Research Resources Bank; JCRB9127), the procedures were essentially the same as above, except that the cells were plated at a density of 1.2×10^5 cells/well in 12-well plates and transfected with 100 ng of κB-Luc2P, 20 ng of TK-hRLuc, and 880 ng of pTriEx-MTI plus pTriEx-NC to a total 1000 ng/well.

Antibodies and Western blot detection

The following antibodies are used: anticyclooxygenase 2 (COX2; Abcam; ab52237), antiglyceraldehyde-3-phosphate dehydrogenase (GAPDH; Abcam; ab9485), anti-GR (20), antiinhibitory-κB (IκB; Abcam; ab7217), anti-MTI-II (19), and anti-NF-κB p65 (Abcam; ab7970) rabbit polyclonal antibodies anti-IκB phosphorylated at serine 32 rabbit monoclonal antibody (Abcam; ab92700) and anti-his-tag mouse monoclonal antibody (Merck Millipore; 70796). For the second antibody, horseradish peroxidase-labeled antirabbit IgG (Merck Millipore; 12-348), horseradish peroxidase-labeled antimouse IgG (Abcam; ab1801), and fluorescein isothiocyanate-labeled antimouse IgG (Sigma; F0257) polyclonal antibodies were used. Proteins were separated with 12.5% SDS-PAGE and transferred to polyvinyl difluoride membrane (Amersham Hybond 0.2 μm; GE Healthcare). As for the immunodetection of MTI-II, proteins separated with 12.5% SDS-PAGE were transferred to nitrocellulose membrane (Immobilon NY+; Merck Millipore) and fixed with 0.5% glutaraldehyde as described previously (19). Detection was performed with ECL Select (GE Healthcare). Band intensities were measured by Image Studio software (LI-COR BIOSCIENCES).

RNA interference

For RNAi suppression of MTI-II, we used a 27-nt hairpin small interfering RNA (siRNA) expression vector (psiLentGene; Promega) containing MTI-II cDNA corresponding to nucleotides 72–98 (19). Transfection of the siRNA vector together with

the reporter genes and the luciferase assay were performed as described above.

Immunoprecipitation

HeLa cells were plated at a density of 8.5×10^5 cells per 100-mm diameter plate. At 24 hours after the cell plating, the medium was changed to DMEM plus 10% DC-FBS. At 24 hours after the medium change, the cells were transfected with 10 μg of pTriEx-MTI(+H) (MTI-II cDNA inserted into *Pst*I-*Hin*dIII sites of pTriEx-4 vector expressing his-tag and 63 amino acid linker followed by MTI-II) (19). At 48 hours after transfection, the cells were treated with 1 ng/mL of TNFα and/or 120 nM Dex. The cells were harvested at 2 hours after the treatment. The procedures of cell-lysate preparation and the immunoprecipitation were essentially same as mentioned in a previous paper (19) except that the supernatants of the cell lysates were incubated with anti-his-tag antibody-conjugated Protein G-agarose beads for 3 hours at 4°C in a rotator.

Fluorescence microscopy

For the plasmids expressing green fluorescent protein (GFP)-fused MTI-II and red fluorescent protein (RFP)-fused p65, we subcloned the MTI-II cDNA and the p65 cDNA into the *Eco*RV-*Not*I sites of pQBI25-fC1 (Qbiogene) (19) and the *Sac*I-*Kpn*I sites of pDsRed2-C1 (CLONTECH), respectively. We also subcloned the IκBα cDNA into the *Sma*I site of pTriEx-4 vector.

The HeLa cells were plated at a density of 2.0×10^5 cells per 35-mm coverslip-bottom dishes (Becton Dickinson). After 24 hours, the medium was changed to DMEM plus 10% DC-FBS. At 24 hours after the medium change, the cells were transfected with 200 ng of the GFP-MTI-II, 200 ng of the RFP-NF-κB and 200 ng of the IκBα expression vectors. At 24 hours after the transfection, the cells were treated with 1 ng/mL of TNFα for 6 hours. The cells were viewed on a Carl Zeiss LSM 510 META laser-scanning confocal microscope.

Purification of MTI-II-based antiinflammatory drugs

H11RM was expressed in yeast Pichia (Life Technologies). Proteins were extracted with an extraction reagent (YeastBuster; Merck Millipore) and the extract was centrifuged at 113 000 $\times$ *g* for 60 minutes at 4°C. The resultant supernatant was loaded onto Ni-NTA column (Merck Millipore). The column was washed with buffer A (20 mM Tris-HCl, pH 7.5; 500 mM NaCl) containing 20 mM imidazole and then developed with a linear gradient of 20–500 mM imidazole in the buffer A. Fractions containing H11RM were pooled and diluted by addition of the same volume of the ice-cold buffer A. The diluted sample was loaded onto HisTrap column (GE Healthcare). The column was washed with the buffer A containing 20 mM imidazole and then developed with a linear gradient of 20–500 mM imidazole in the buffer A (Supplemental Figure 1A). The fractions containing H11RM were pooled, concentrated using a centrifugal concentrator (Amicon Ultra-15; Merck Millipore) and dialyzed against 20 mM Tris-HCl (pH 7.5) and 250 mM NaCl at 4°C overnight. The dialyzed sample was then loaded onto a MonoQ column (GE Healthcare). The column was developed with a liner gradient of 250–500 mM NaCl in 20 mM Tris-HCl (pH 7.5) at 4°C (Supplemental Figure 1B). The eluent was concentrated to approximately 50 mg/mL using the centrifugal concentrator. The protein concentration of the purified MTI-II-based antiinflammatory drugs (MAIDs; H11RM, HM11R, and M11R) was estimated by absorbance at 214 nm using BSA (Pierce; 23209) as a standard because the MAIDs have no absorbance at 280 nm. The concentrated sample was dialyzed against PBS at 4°C overnight and then stored at −80°C in aliquots. H11RM was confirmed by the immunoblot analysis using both anti-his-tag and anti-MTI antibodies.

For purification of HM11R (Supplemental Figure 2), the procedure was essentially the same as above, except that H11RM was expressed in *Escherichia coli* Rosetta2 (DE3; Merck Millipore) and that the proteins were extracted with the extraction reagent BugBuster (Merck Millipore). HM11R was also confirmed by the immunoblot analysis using both anti-his-tag and anti-MTI antibodies.

For the purification of M11R, M11R was expressed in *E coli* CL1, which is a hyperexpression mutant derived from JM109 (CHOTOSE Laboratory). Proteins were extracted with BugBuster (Merck Millipore) and the extract was centrifuged as above. To the resultant supernatant, 70% ammonium sulfate was added on ice. After centrifugation at 28 000 $\times$ *g* for 20 minutes at 4°C, the resultant supernatant solution was loaded onto a HiTrap Phenyl HP column (GE Healthcare). The column was developed with a liner gradient of 70%–0% ammonium sulfate in 20 mM Tris-HCl (pH 7.5) and 50 mM NaCl. The fractions containing M11R were pooled and dialyzed against 20 mM Tris-HCl (pH 7.5) and 200 mM NaCl at 4°C overnight. The dialyzed sample was then loaded onto a MonoS column (GE Healthcare). The column was developed with a liner gradient of 200–1200 mM NaCl in 20 mM Tris-HCl (pH 7.5) at 4°C (Supplemental Figure 3). The eluent was dialyzed against PBS at 4°C overnight and then concentrated to approximately 25 mg/mL using a centrifugal concentrator (Amicon Ultra-3K). The concentrated sample was stored at −80°C in aliquots. M11R was confirmed by the nanoliquid chromatography-electrospray ionization-quadrupole-time-of-flight-tandem mass spectrometry analysis after asparaginyl endopeptidase digestion (Hokkaido System Science Co, Ltd).

Preparation of MTI-II peptide antiinflammatory drug (MPAID)

MPAID was chemically synthesized (Biomatik Corp) and dissolved in PBS. The pH of the solution was adjusted to pH 7.4 by the addition of NaOH.

Immunohistochemical staining of HM11R

HeLa cells were plated at a density of 0.3×10^5 cells/well in an eight-well culture slide. At 24 hours after the cell plating, the medium was changed to DMEM plus 10% DC-FBS. At 24 hours after the medium change, the medium was changed to that containing 3.0 mg/mL of HM11R. After the incubation time (30, 60, 120 min), the cells were washed twice with ice-cold PBS and fixed by 4% paraformaldehyde in 0.1 M phosphate buffer (pH 7.3). After membrane permeabilization with 1.5% Triton X-100 in PBS, HM11R was detected by the anti-his-tag monoclonal antibody and fluorescein isothiocyanate labeled antimouse IgG polyclonal antibody.

In vitro antiinflammatory action of MPAID

HeLa cells were plated at a density of 0.12×10^5 cells/well in 48-well plates. At 24 hours after the cell plating, the medium was changed to DMEM plus 10% DC-FBS. At 24 hours after the

medium change, the cells were transfected with 60 ng of κB-Luc2P, 20 ng of TK-hRLuc, and 120 ng of pTriEx-NC as described above. At 24 hours after the transfection, the medium was changed to the medium containing MPAID (0.2, 0.5 mg/mL) or α-polyglutamate peptide (10 glutamate residues, 0.2, 0.5 mg/mL). At 24 hours after the medium exchange, the cells were treated with 1 ng/mL of TNFα. The luciferase activities were detected as above.

Statement of compliance for animal experiments

Experimental procedures involving animals were reviewed and approved by the Institutional Animal Committee of St Marianna University School of Medicine and the president of St Marianna University School of Medicine (approval number 1502011). The experiments were carried out under the approved protocols by the Internal Regulations for the Animal Care and Use at Animal Experiment Committee of KAC Co, Ltd and by the Animal Experiment Committee of Nihon Bioresearch Inc in compliance with the Fundamental Guidelines for Proper Conduct of Animal Experiment and Related Activities in Academic Research Institutions under the jurisdiction of the Ministry of Education, Culture, Sports, Science, and Technology (Japan; Notice, number 71, 2006).

Animals (male and female Slc:Wister rats, female NC/Nga slc mice, and female DA/Slc rats) were purchased from Japan SLC 1 week before the experiment and acclimatized. They were housed one per cage and were maintained on a 12-hour light, 12-hour dark cycle (lights on from 7:00 AM to 7:00 PM) with access to food (certified diet CRF-1; Oriental Yeast Co, Ltd) and water ad libitum. To assess animal health, body condition, and well-being, we observed the appearance, posture, awareness, and behavior of the animals essentially twice a day and additionally during the experiment time. When at least one of the auricular reflex, auditory reflex, and pain reflection is lost, we immediately put the animal painlessly to death by anesthesia. During the following experiments, fortunately, we had observed no adverse outcomes and animal death before they could be euthanized.

Carrageenan-induced foot edema model

This test was performed at KAC Co, Ltd, essentially according to the method reported elsewhere(21) except that male Slc:Wister rats (6 wk old, 143.3 ± 1.24 g) were fasted for 16 hours before the injection of λ-carrageenan. Edema was induced in right hind foot of the rats by the plantar injection of 0.1 mL of 1% λ-carrageenan. Test samples (PBS [negative control [NC]], indomethacin [IDM; 0.4 mg], Dex [0.14 mg], H11RM [3, 6, 12 mg], and HM11R [6 mg]) were injected ip at 1 hour before and at the same time of the carrageenan injection. Each subject group consists of six rats. Significance of differences was evaluated with a Student's *t* test. The blood samples of the three randomly chosen rats from each group were collected from the abdominal aorta under the isoflurane anesthesia at 6 hours after the carrageenan injection.

Croton oil-induced conjunctival inflammation model

This test was performed at Nihon Bioresearch Inc. According to the method (22), female Slc:Wister rats (5 wk old, 89.5 ± 1.0 g) were received by repeated binocular instillation of 2-(2-ethoxyethoxy)ethanol and croton oil, according to the schedule that 2.5 μL of 100% 2-(2-ethoxyethoxy)ethanol was instilled at 0 and 40 minutes, and 5.0 μL of 10% croton oil was at 80, 140, and 200 minutes. This condition enhances the conjunctival inflammation and reduces vision for the animals, but neither induces opacification of the lens nor makes the animal blind (Nihon Bioresearch Inc, personal communication). Test samples (PBS [NC], 0.1% Dex, H11RM [50, 150, 250 μg], and HM11R [200 μg]) were binocularly instilled according to the schedule that the 5.0 μL of the sample was instilled at 120 and 60 minutes before and at 30, 70, 130, and 190 minutes after the first 2-(2-ethoxyethoxy)ethanol instillation. Each subject group consists of three rats, and each rat underwent an experimental intervention in both eyes. The instillation of 2-(2-ethoxyethoxy)ethanol and croton oil into a single eye has no influence on the opposite eye and conjunctiva for at least 320 minutes after the first instillation (Nihon Bioresearch Inc, personal communication), indicating that the croton oil-induced conjunctival inflammation is caused independently for each eye. Therefore, the experimental intervention in both eyes of a single animal reduces the number of animals. At 320 minutes after the first 2-(2-ethoxyethoxy)ethanol instillation, the eyelid was removed and the upper conjunctiva was weighted. Significance of differences was evaluated with a Student's *t* test.

Mite antigens induced atopic dermatitis model

This test was performed at KAC Co, Ltd. According to the method (23), 5 μL of mite antigen (1 mg/mL) was given intradermally to the right auricular region of female NC/Nga slc mice (8 wk old, 20.7 ± 1.4 g) at days 0 (the first administration), 3, 7, 10, and 14. Total clinical severity score for atopic dermatitis-like skin lesions and thickness of the right auricular region were measured at days 0, 1, 4, 8, 11, and 15 by animal pathologists at KAC Co, Ltd. The clinical severity score was defined as described previously (24). Briefly, the total score is the sum of individual scores graded as 0 (none), 1 (mild), 2 (moderate), or 3 (severe) for each of the four signs and symptoms: erythema/hemorrhage, edema, erosion, and dryness. The test samples are hydrophilic ointment base (negative control; Maruishi Pharmaceutical), 0.12% betamethasone valerate (BM; Shionogi & Co, Ltd), M11R (0.04, 0.2 mg per 5 μL), and MPAID (0.2, 1.0 mg per 5 μL). MPAID and M11R were mixed with the ointment base and applied. The samples (5 μL) were applied to the skin of the right auricular region every day from day 1 to day 15. Each subject group consists of eight mice. The blood samples were collected from the abdominal aorta under the isoflurane anesthesia at day 15. The significance of differences was evaluated with a Student's *t* test.

Collagen-induced arthritis model

This test was performed at KAC Co, Ltd. According to the method (25), the emulsion of bovine type II collagen and incomplete Freund's adjuvant was injected intracutaneously at three sites on the back of female DA/Slc rats (9 wk old, 133.2 ± 5.5 g) at day 0. PBS (NC) and MPAID (0.7, 3.5 mg) were injected ip every day from day 0. The clinical severity score of arthritis and a volume of right and left feet were measured at days 0, 3, 7, 10, 14, 17, 21, 24, and 28 by animal pathologists at KAC Co, Ltd. The score was defined as described previously (26). Briefly, the total score is the sum of individual scores graded as 0 (normal), 1 (swelling in one joint), 2 (swelling in more than one joint), 3 (swelling in the entire paw), or 4 (deformity and/or ankylosis) for all four paws of each rat. Each subject group consists of eight rats.

Blood samples were collected from the abdominal aorta under isoflurane anesthesia at day 28. The significance of differences was evaluated with Student's *t* test.

Results

Effects of overexpression of MTI-II on transcriptional activity of NF-κB

For further elucidation of a function of MTI-II that works as a coactivator of GR, we examined the effect of MTI-II on the proinflammatory transactivator, NF-κB. We overexpressed MTI-II in HeLa cells and measured the NF-κB-induced luciferase activity after TNFα stimulation. To avoid an effect of serum GC, we used DC-FBS (GC free serum) as the culture medium of the HeLa cells. As shown in Figure 1A, addition of TNFα enhanced the NF-κB-induced luciferase activity in the HeLa cells transfected with mock vector (NC cells). Further addition of Dex to the NC cells reduced the luciferase activity to approximately 57% of that without Dex. The overexpression of MTI-II also inhibited the NF-κB-induced luciferase activity. Magnitude of the inhibition by MTI-II was comparable with that of the addition of Dex to the NC cells. Further addition of Dex to the MTI-II-overexpressed cells inhibited NF-κB-induced luciferase activity to approximately 58% of that in the MTI-II-overexpressed cells without Dex. Next, to avoid the possible contribution of GR, we measured the NF-κB-induced luciferase activity in COS-7 cells, which lack detectable endogenous GR (27, 28). Figure 1B shows that the overexpression of MTI-II in the COS-7 cells inhibited the luciferase activity in a dose-dependent manner. Thus, the inhibition by MTI-II is independent of GC and GR. In Figure 1, C and D, we examined whether the overexpression of MTI-II inhibited NF-κB-induced endogenous gene expression in addition to the exogenous reporter gene. Temporal changes in COX2 expression were measured by immunoblot detection. As shown, the overexpression of MTI-II also inhibited the NF-κB-induced COX2 expression.

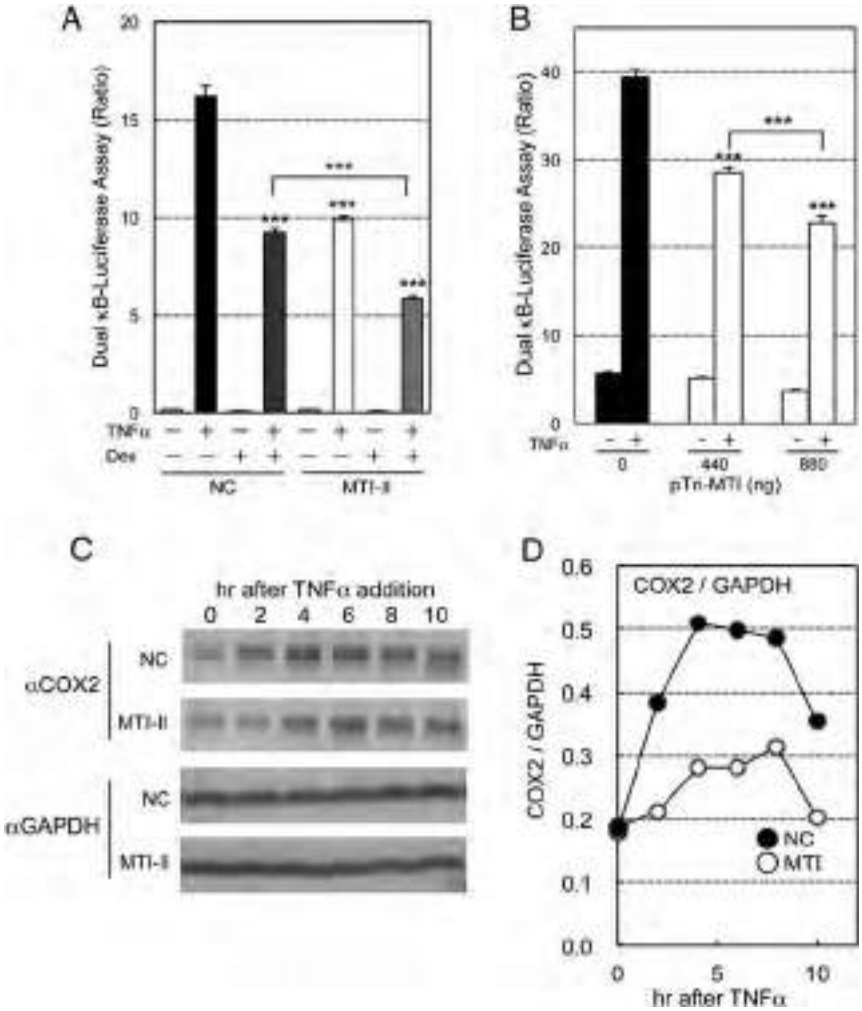

Figure 1. Effect of overexpression of MTI-II on the transcriptional activity of NF-κB. A, NF-κB-induced luciferase activities were measured in HeLa cells transfected with an MTI-II expression vector. The cells were cultured in DMEM plus 10% DC-FBS and transfected with MTI-II expression vector (MTI-II) or mock vector (NC) together with luciferase reporter genes (κB-Luc2P and TK-hRLuc). Luciferase activities were measured 4.5 hours after stimulation of TNFα and/or Dex. Values are expressed as a ratio of κB to Luc2P activity divided by TK-hRLuc activity (internal control) and are represented as mean ± SEM (n = 12). Significance of differences was evaluated with a Student's *t* test, and *P* values are indicated on graphs as follows. ***, $P < .001$ vs NC. B, NF-κB-induced luciferase activities were measured in COS-7 cells transfected with MTI-II expression vector as in panel A. C, Temporal changes of COX2 and GAPDH after the stimulation of TNFα in the HeLa cells transfected with MTI-II expression vector (MTI-II) or mock vector (NC) were detected by the immunoblot. D, The band intensity of the COX2 was measured and normalized by that of GAPDH.

Mechanism of the inhibition of the transcriptional activity of NF-κB by MTI-II

To elucidate the mechanism of the inhibition by MTI-II, we first examined whether the overexpression of MTI-II changes protein levels of GR and the p65 subunit of NF-κB. As shown in Figure 2A, there were no marked change in these protein levels. Thus, the inhibition by the overexpression of MTI-II is not caused by an increase of GR or by a decrease of

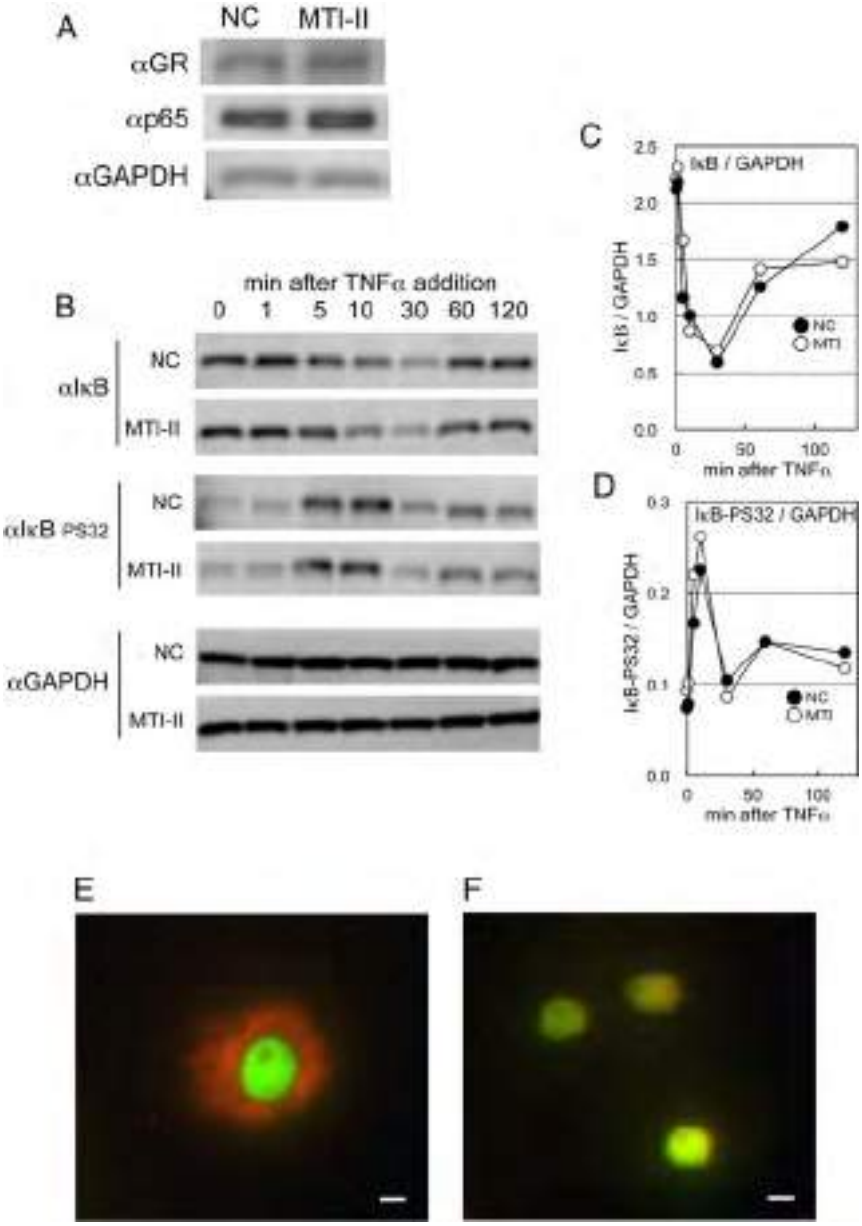

Figure 2. Mechanism of the inhibition of the transcriptional activity of NF-κB by MTI-II. A, Protein levels of GR, p65, and GAPDH in the HeLa cells transfected with MTI-II expression vector (MTI-II) or mock vector (NC) were detected by the immunoblot. B, Temporal changes in IκB, IκB phosphorylated at serine 32 (PS32), and GAPDH after the stimulations of TNFα in the HeLa cells transfected with MTI-II expression vector (MTI-II) or mock vector (NC) were detected by the immunoblot. C and D, The band intensities of IκB (C) and IκB PS32 (D) were measured and normalized by that of GAPDH. E and F, Fluorescence microscopy analysis of GFP-MTI-II and RFP-p65 was performed in HeLa cells in the absence (E) or presence (F) of TNFα. Bar, 5 μm.

NF-κB. Next, we examined the effect of MTI-II on TNFα signaling of upstream of NF-κB. In Figure 2B, we measured the emporal changes in IκB and S32-phosphorylated IκB proteins after the TNFα stimulation. Band intensities were measured and are shown in Figure 2, C and D. As shown, the overexpression of MTI-II had no remarkable effect on the temporal changes in these proteins. Furthermore, we examined whether the overexpression of MTI-II inhibits the nuclear localization of NF-κB. We transiently transfected HeLa cells with an expression vector of GFP-fused MTI-II and RFP-fused p65. Confocal microscopy analysis of the living cells in the absence of TNFα showed that RFP-fused p65 was localized in the cytosol, whereas GFP-fused MTI-II was localized in the nuclei (Figure 2E). When we added TNFα to the culture medium, RFP-fused p65 translocated into the nuclei and GFP-fused MTI-II remained in the nuclei (Figure 2F). This observation indicates that MTI-II does not inhibit the nuclear localization of p65. Taken together, these results suggest that the target of MTI-II would be the IκB released and nuclear localized NF-κB.

Effects of siRNA-mediated reduction of inherent MTI-II on the transcriptional activity of NF-κB

We examined effect of reduction of inherent MTI-II on the NF-κB-induced luciferase activity. To reduce the inherent MTI-II, we used a 27-nt hairpin siRNA expression vector containing a sequence (72–98 nt) from the MTI-II mRNA (19). HeLa cells were transiently transfected with the hairpin siRNA expression vector (siRNA) or with mock vector (NC) together with the κB-luciferase reporter vector. Figure 3A shows an immunoblot detection of the inherent MTI-II after siRNA-mediated reduction. As reported previously (19), the inherent MTI-II (11.5 kDa) gave a higher apparent molecular mass (~20 kDa). In Figure 3B, band intensities showed that the siRNA reduced the inherent MTI-II to approximately 40% of that in NC. We examined whether the reduction of MTI-II changes protein levels of GR and p65 in the presence or absence of TNFα. As shown in Figure 3C, there were no marked changes in the protein levels after the reduction of MTI-II. Under this condition, we measured the NF-κB-induced luciferase activity (Figure 3D). In the siRNA cells, the NF-κB-induced luciferase activity was increased to approximately 140% of that in the NC cells. This result suggests that MTI-II would be

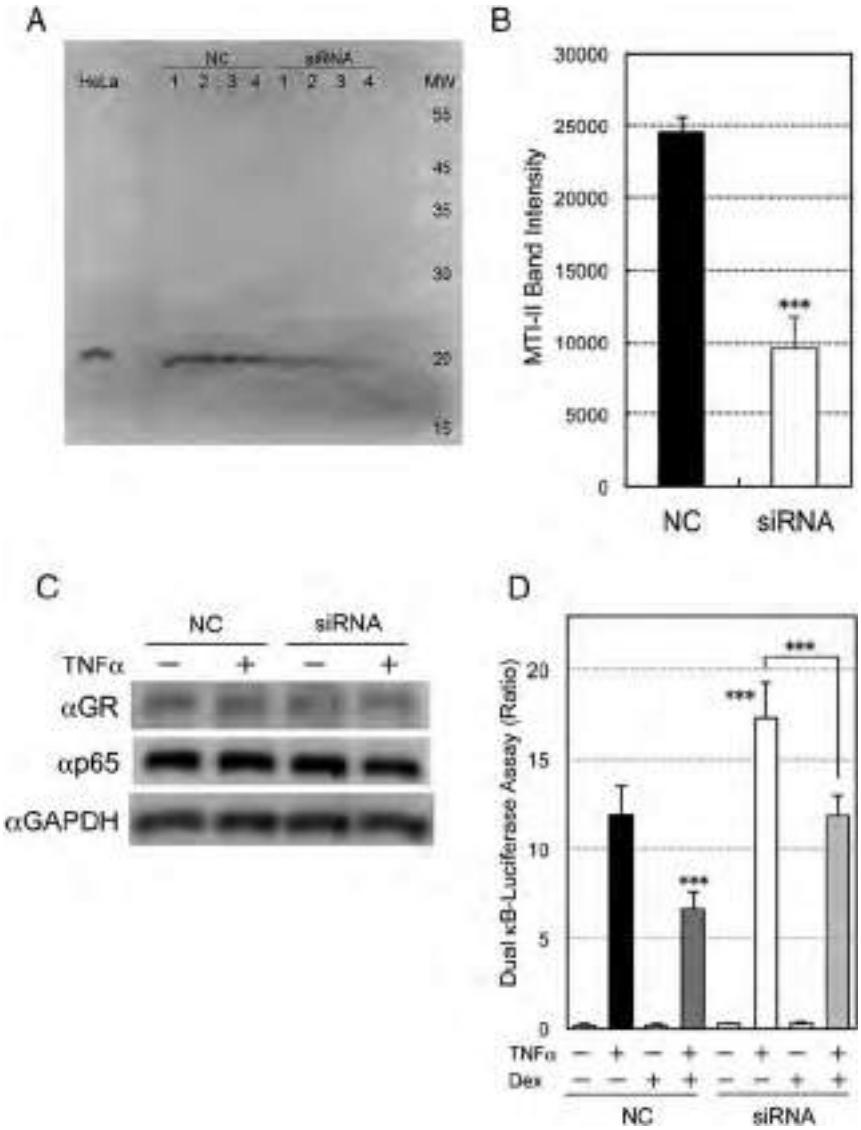

Figure 3. Effects of RNAi-mediated reduction of inherent MTI-II on the transcriptional activity of NF-κB. A, HeLa cells were transfected with the expression vector of the 27-nt hairpin siRNA of MTI-II (siRNA) or mock vector (NC) together with the luciferase reporter genes. Inherent MTI-II in HeLa cells was detected by immunoblot 48 hours after the transfection. The lane (HeLa) represented the sample from nontransfected HeLa cells. The lanes numbered 1–4 represented the samples from four independent culture wells. B, The band intensity of the inherent MTI-II was measured. Values are represented as mean ± SEM (n = 4). Significance of differences was evaluated with a Student's *t* test, and *P* values are indicated on graphs as follows: ***, $P < .001$ vs NC. C, Protein levels of GR, p65, and GAPDH in the HeLa cells transfected with siRNA expression vector or NC vector were detected by the immunoblot in the presence or absence of TNFα. D, NF-κB-induced luciferase assay was performed in HeLa cells transfected with siRNA expression vector or NC vector. The dual-luciferase activities were measured 4.5 hours after the stimulations of TNFα and/or Dex. Values are expressed as in Figure 1A and are represented as mean ± SEM (n = 12). Significance of differences was evaluated with a Student's *t* test, and *P* values are indicated on graphs as follows: ***, $P < .001$ vs NC.

an inherent inhibitor of NF-κB. In the NC cells, addition of Dex inhibited the NF-κB-induced luciferase activity to approximately 56% of that without Dex. Interestingly, in the siRNA cells, the addition of Dex also inhibited the NF-κB-induced luciferase activity to approximately 68% of that without Dex. The magnitude of the inhibition by Dex in the siRNA cells is almost of the same level as that in the NC cells. Thus, MTI-II may not be involved in the GR-induced inhibition of NF-κB transactivation.

Immunoprecipitation of NF-κB with MTI-II

We examined whether MTI-II interacts with NF-κB in the presence of TNFα and/or Dex by an immunoprecipitation assay. Because the anti-MTI-II antibody was not available for immunoprecipitation (19), we transfected the his-tagged MTI-II (his-tag plus 64 amino acid linker in the N terminal of MTI-II) expression vector into HeLa cells and performed the immunoprecipitation assay using an anti-his-tag antibody. As shown in Figure 4, the p65 subunit of NF-κB was coprecipitated with the his-tagged MTI-II in the presence of TNFα but not in the absence of TNFα. The p65 precipitation was independent of Dex. This result indicates that at least MTI-II forms a complex with the p65 subunit of NF-κB after the TNFα stimulation.

Inhibitory active region within MTI-II

We examined which region of MTI-II was required for the inhibition. MTI-II is approximately divided into three portions (Figure 5A): the N-terminal thymosin homolog region (amino acids 1–34), the central acidic region (amino acids 35–74), and the C-terminal nuclear localization signal (NLS) region (amino acids 76–101) (19). The amino acid sequence of MTI-II is shown in Figure 5B. The C-terminal NLS region contains two NLSs (amino acids 78–80 and 91–95) separated by a short acidic domain (amino acids 83–87). Thus, we constructed three expression vectors of deletion mutants (Figure 5A). The first contained thymosin homolog region plus one NLS motif (amino acids 1–27 + 88–101), the second contained the central acidic region (AR) plus the NLS region (amino acids 28–101), and the

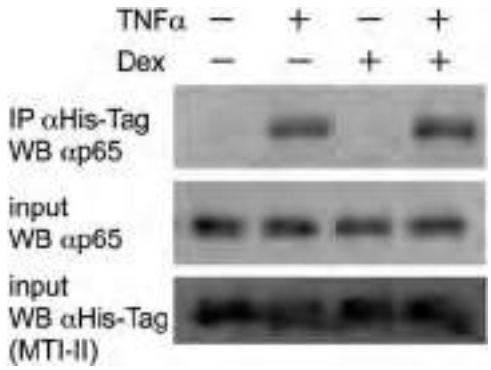

Figure 4. Immunoprecipitation of p65 subunit of NF-κB with MTI-II. HeLa cells were transfected with the expression vector of MTI-II fused with his-tag. The cells were stimulated with TNFα and/or Dex for 2 hours and were harvested for the immunoprecipitation by the anti-his-tag antibody. Immunoblot detection was performed with anti-p65 antibody and anti-his-tag antibody. IP, immunoprecipitation; WB, Western blot.

third contained only the NLS region (amino acids 76–101). Effects of these mutants on the NF-κB-induced luciferase activity were measured. Figure 5C shows that only the second mutant (AR) inhibited the NF-κB-induced luciferase activity as the full-length MTI-II. Both the thymosin homolog and the NLS mutants had no detectable effect. This result indicates that at least the central acidic region is essential for the inhibition.

Design of MAIDs and MPAIDs

To apply MTI-II to antiinflammatory drugs, we made fusion proteins of MTI-II with the protein transduction domain (PTD) (29). Of several kinds of PTDs, we selected monotonous runs of 8 or 11 arginine (R) residues. First, we constructed three types of fusion proteins of MTI-II with 11R (MAIDs; H11RM, HM11R, and M11R) as schematically shown in Figure 6A. As for H11RM, we were afraid that the basic 11R affects the antiinflammatory action of the acidic region in MTI-II. Thus, we added a 65-amino acid linker to separate them. When only the linker was expressed in the HeLa cell, it had little inhibitory effect on the NF-κB-induced luciferase activity (data not shown). In HM11R and M11R, the 11R was placed beside the NLS that consisted of basic amino acids. Next, we constructed a short peptide drug (MPAID) that consisted of the AR (40 amino acid residues) and 8R. The MPAID lacks the NLSs; however, the PTD (8R) works in place of the NLS. The MPAID is a chemically synthesizable length. A short peptide drug reduces the risk of production of antibodies. Moreover, a chemically synthesized peptide drug has great advantage of low cost and little contamination compared with biosynthesized protein drugs.

We examined whether these fusion proteins inhibited the transcriptional activity of NF-κB by the luciferase reporter assay. As shown in Figure 6B, overexpression of

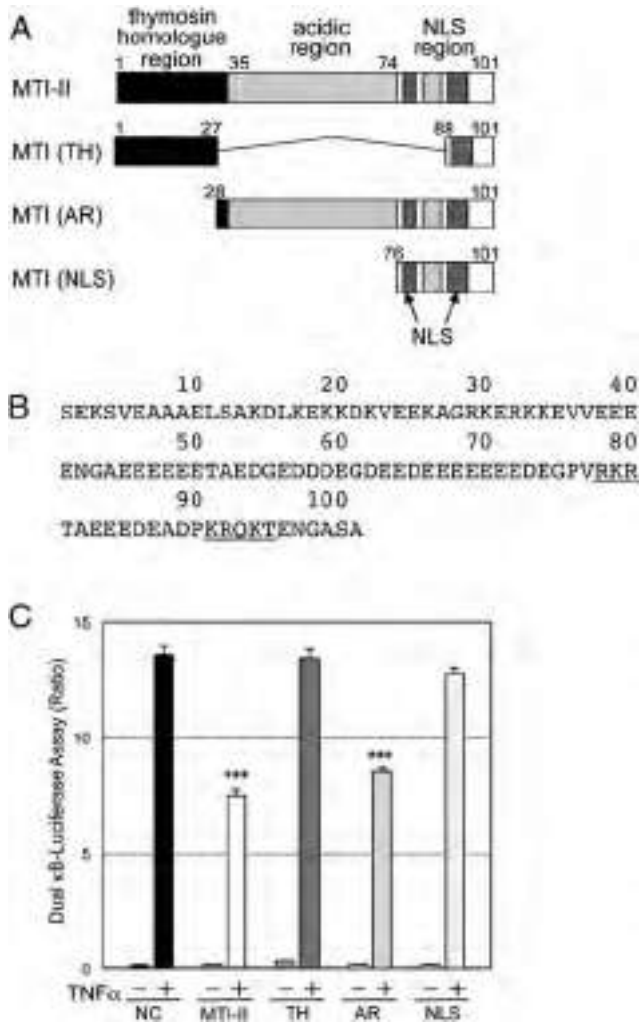

Figure 5. Effects of overexpression of deletion mutants of MTI-II on the transcriptional activity of NF-κB. A, Full-length MTI-II and the deletion mutants were schematically represented. TH, thymosin homologue. B, Amino acid sequence of MTI-II. NLSs are underlined. C, NF-κB-luciferase assay was performed in HeLa cells transfected with the mock vector (NC), the full-length MTI-II expression vector (MTI-II), or the deletion mutant expression vectors with luciferase reporter genes. The dual-luciferase activities were measured and values are expressed as in Figure 1A. Values are represented as mean ± SEM (n = 12). Significance of differences was evaluated with a Student's *t* test, and *P* values are indicated on graphs as follows: ***, $P < .001$ vs NC.

these fusion proteins inhibited the NF-κB-induced luciferase activity as well as MTI-II in the HeLa cells. As mentioned in the last paper (19), MTI-II and the AR+NLS region worked as a coactivator of GR. Therefore, it would be interesting to examine whether these proteins enhanced the transcriptional activity of GR. MAIDs as well as MTI-II enhanced it (data not shown). However, interestingly, the MPAID did not enhance the GR-induced luciferase activity (Figure 6C). This indicates that the replacement of the NLS region with 8R results in the loss of the coactivator activity, that is, both the AR and the in-

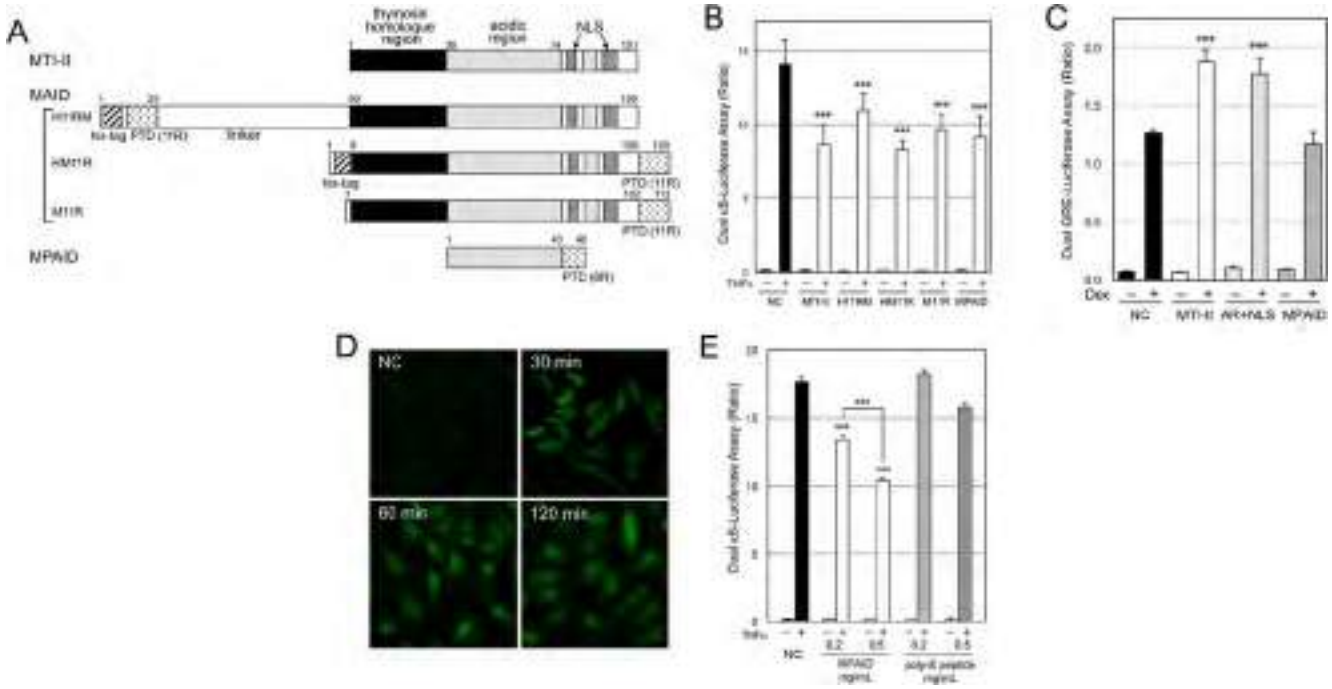

Figure 6. Preparation of three MTI-II-based antiinflammatory drugs and a MTI peptide antiinflammatory drug. A, The full-length MTI-II, three MAIDs, and a MPAID were schematically represented. 11R, 11 arginine residues; 8R, 8 arginine residues. B, NF-κB-luciferase assay was performed in HeLa cells transfected with the mock vector (NC), the full-length MTI-II expression vector (MTI-II), the MAID expression vectors, or MPAID expression vector with luciferase reporter genes. The dual-luciferase activities were measured and values are expressed as in Figure 1A. Values are represented as mean $\pm$ SEM (n = 12). Significance of differences was evaluated with a Student's *t* test, and *P* values are indicated on graphs as follows: ***, $P < .001$ vs NC. C, GRE-luciferase assay was performed in HeLa cells transfected with the mock vector (NC), the full-length MTI-II (MTI-II), the deletion mutant (AR+NLS), or MPAID expression vectors with GRE-luciferase reporter genes. The GRE-luciferase activity was measured 4.5 hours after the addition of Dex. The dual-luciferase activities were measured and values are expressed as in Figure 1A. Values are represented as mean $\pm$ SEM (n = 12). D, Purified HM11R protein (3.0 mg/mL) was added to the culture medium of HeLa cells and detected by anti-his-tag antibody after the incubation time as indicated. As for negative control (NC), PBS was added and the cells were incubated for 120 minutes. E, NF-κB-induced luciferase activities were measured in HeLa cells. MPAID (0.2, 0.5 mg/mL) or α-polyglutamate peptide (10 glutamate residues, 0.2, 0.5 mg/mL) was added to the culture medium of HeLa cells, to which the luciferase reporter genes were transfected at 24 hours before the additions of the peptides. At 24 hours after the addition of MPAID, the cells were treated with TNFα. The dual-luciferase activities were measured and values are expressed as in Figure 1A. Values are represented as mean $\pm$ SEM (n = 12).

herent NLS region are required for the enhancement of the transcriptional activity of GR, whereas the AR with alternate NLS (8R) is sufficient for the inhibition of NF-κB.

Next, to confirm that the PTD could transport the fusion protein into cells, we added the purified HM11R protein to the culture medium of HeLa cells and detected the HM11R by immunohistochemical staining using an anti-his-tag antibody. Figure 6D shows that HM11R was detected mainly in cytoplasm at 30 minutes after the addition and then in both cytoplasm and nuclei at 60 and 120 minutes. As for MPAID, it has neither his-tag nor the antigenic region for the anti-MTI antibody. Therefore, using the luciferase reporter assay, we examined whether MPAID enters HeLa cells and inhibits the NF-κB-induced luciferase activity. We added MPAID to the culture medium of HeLa cells, which were already transfected with the luciferase reporter genes. As shown in Figure 6E, MPAID inhibited the NF-κB-induced luciferase activity in a dose-dependent manner. As a negative control, α-polyglutamate peptide (10 residues) that mimics the acidic amino acid residues in the MPAID was added, whereas it had little effect on the NF-κB-induced luciferase activity.

In vivo antiinflammatory actions of MAIDs in acute inflammation models

Using two kinds of acute inflammation model animals, we examined the in vivo antiinflammatory action of MAIDs (H11RM and HM11R). First, H11RM and HM11R were injected into the peritoneal cavity of rats with carrageenan-induced foot edema 1 hour before and at the same time of the λ-carrageenan injection. Figure 7A shows the temporal change in foot volume after the carrageenan injection. MAIDs significantly inhibited the increase of foot volume at 2–5 hours after the λ-carrageenan injection. The antiinflammatory action of H11RM (12 mg/rat $\times$ 2 injections) achieved statistical significance compared with PBS-injected rats (NC rats), but it was weaker than Dex (0.14 mg/rat $\times$ 2 injections) and a nonsteroidal antiinflammatory drug (IDM; 0.4 mg/rat $\times$ 2 injections). In contrast, HM11R (6 mg/rat $\times$ 2 injections) showed a strong antiinflammatory action comparable with IDM.

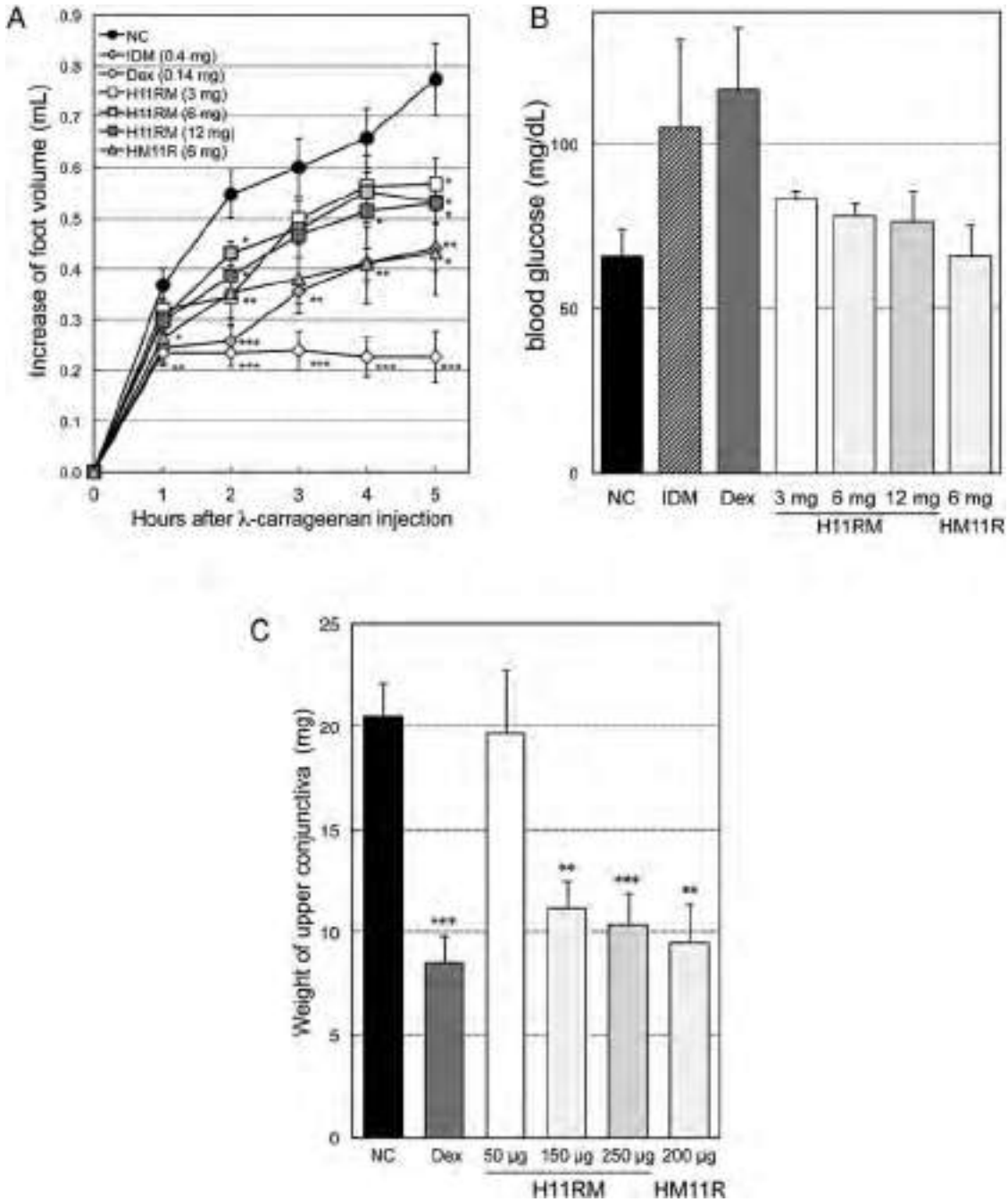

Figure 7. In vivo antiinflammatory actions of MAIDs (H11RM and HM11R) in acute inflammation models. A, Foot volume of rat with carrageenan-induced foot edema was measured. PBS (NC), IDM (0.4 mg/rat per injection), Dex (0.14 mg/rat per injection), H11RM (3, 6, 12 mg/rat per injection), and HM11R (6 mg/rat per injection) were injected ip 1 hour before and at the same time of the λ-carrageenan injection. The foot volume was measured at the time indicated in the figure. Values are represented as mean ± SEM (n = 6). Significance of differences was evaluated with a Student's *t* test, and *P* values are indicated on graphs as follows: *, $P < .05$, **, $P < .01$, ***, $P < .001$ vs NC. B, Blood glucose level of the carrageenan-induced foot edema rats was measured 6 hours after the λ-carrageenan injection. Values are represented as mean ± SEM (n = 3). C, The weight of the upper conjunctiva of rat with conjunctival inflammation was measured. PBS (NC) (5 μL/rat per instillation), 0.1% Dex (5 μL/rat per instillation), H11RM (50, 150, 250 μg/5 μL per rat per instillation), or HM11R (200 μg per 5 μL/rat per instillation) was binocular instilled according to the schedule described in *Materials and Methods*. At 320 minutes after the first instillation of the phlogistic substances, the eyelid was removed and the upper conjunctiva was weighed. Values are represented as mean ± SEM (n = 6). Significance of differences was evaluated with a Student's *t* test, and *P* values are indicated on graphs as follows: **, $P < .01$, ***, $P < .001$ vs NC.

As mentioned above, MAIDs enhanced the transcriptional activity of GR in vitro. Therefore, we were afraid that the ip injections of MAIDs enhanced intrinsic GC hormone actions that resulted in severe side effects. To elucidate this possibility, we measured the blood glucose level of the rats. In this carrageenan-induced paw

edema experiment, the rats were fasted for 16 hours before the λ-carrageenan injection. Under this starvation condition, release of intrinsic GC would be enhanced and release of insulin would be reduced. Thereby the metabolism of the whole body should be sifted to gluconeogenesis. The average blood glucose level of nonfasted (healthy) rats was known to be 119 ± 9.9 mg/dL (KAC Co, Ltd, personal communication). As shown in Figure 7B, the blood glucose level of the fasted and PBS-injected rats (NC rats) decreased to 55% of that of the healthy rats. The ip injections of Dex and IDM increased the blood glucose level to nearly equal to that of the healthy rats, whereas the blood glucose level of the MAID-injected rats are nearly equal to that of the NC rats. Thus, the ip injection of MAIDs had a significant antiinflammatory effect but had little effect on the blood glucose levels.

Next, the MAIDs were instilled into the eyes of the rats with croton oil-induced conjunctival inflammation. As shown in Figure 7C, ocular instillation of 50 μg of H11RM did not show a significant antiinflammatory effect. However, the ocular instillations of H11RM (150 μg and 250 μg) and HM11R (200 μg) showed a strong antiinflammatory effect comparable with Dex (0.1%). An average weight of the upper conjunctiva of a healthy rat was approximately 10 mg (Nihon Bioresearch Inc, personal communication). Therefore, the ocular instillations of the MAIDs (150–250 μg) as well as Dex (0.1%) almost completely suppressed the swelling of the eyelid.

In vivo antiinflammatory actions of MPAID and M11R in animal models of human chronic inflammation disease

Using two kinds of animal models of human chronic inflammation diseases, we examined the in vivo antiinflammatory action of MPAID and M11R. First, MPAID and M11R were transdermally applied to mite antigensinduced atopic dermatitis mice daily for 15 days. We measured their antiinflammatory effect on clinical skin severity scoring (Figure 8A) and on the measurement of thickness in the inflamed auricular region (Figure 8B). As shown, MPAID showed a marked antiinflammatory effect both on the scoring and on the thickness. M11R also showed a significant antiinflammatory effect on the scoring. However, the decrease of the thickness was statistically insignificant. As for the advantage in drug development, it should be emphasized here that MPAID and M11R have antiinflammatory effect, even after mixing with the ointment base. As a GC control, we applied 0.12% betamethasone valerate (BM). The BM showed a remarkable antiinflammatory effect on the scoring and the thickness. However, the BM-applied mice also showed severe atrophy of skin (data not shown), which is one of the serious side effects of GC. Therefore, we cannot determine whether the low score and the low thickness in the BM-applied mice (Figure 8, A and B) are the results from the severe atrophy or from the strong antiinflammatory action of BM.

Next, we examined the effects of repeated ip injections of MPAID on collagen-induced arthritis (CIA) rats. The rats were ip injected with MPAID daily for 28 days. In the clinical severity scoring of the arthritis (Figure 8C), MPAID showed significant antiinflammatory actions at day 21 and day 24. In the measurement of foot volumes (Figure 8D), MPAID slightly suppressed swelling, although their difference from PBS-injected (NC) rats was insignificant. It should be mentioned here that the autopsy of the peritoneal cavity of the rats that received daily ip injections of MPAID for 28 days showed neither apparent dilatation nor atrophy of the mesentery, the peritoneum, the portal vain, the liver, the spleen, the stomach, the small intestine, and the large intestine (data not shown, KAC Co, Ltd, personal communication). Furthermore, the injections of MPAID showed no gastrointestinal tract ulcer and bleedings. These observations indicate that MPAID has little repeated-dose toxicity.

Discussion

Previously we showed that MTI-II was a member of the GR/coactivator complex and enhanced the transcriptional activity of GR (19). Here we showed that the overexpression of MTI-II inhibited the transcriptional activity of NF-κB in a dose-dependent manner. It should be emphasized here that the inhibition by MTI-II is independent of the presence of GCs and GR. The overexpression of MTI-II did not have an affect on the TNFα signaling of the upstream NF-κB and on the nuclear translocation of NF-κB. The p65 subunit of NF-κB was coimmunoprecipitated with MTI-II only after TNFα stimulation. Because MTI-II is a nuclear-localized protein (19) and NF-κB also localizes in the nucleus after the release of IκB, the interaction of MTI-II with NF-κB will arise in the nucleus. Taking these data together, MTI-II would interact with NF-κB in the nucleus or at least form a complex with NF-κB and other coactivators; thereby MTI-II inhibits the transcriptional activity of NF-κB. The data from the siRNA-mediated reduction of MTI-II suggest that MTI-II would be an inherent inhibitor of NF-κB. MTI-II is ubiquitously expressed in whole mammalian tissues at different concentrations for each tissue (13–16). Therefore, it is possible that the amount of the inherent MTI-II may regulate the intensity of inflammation in each tissue.

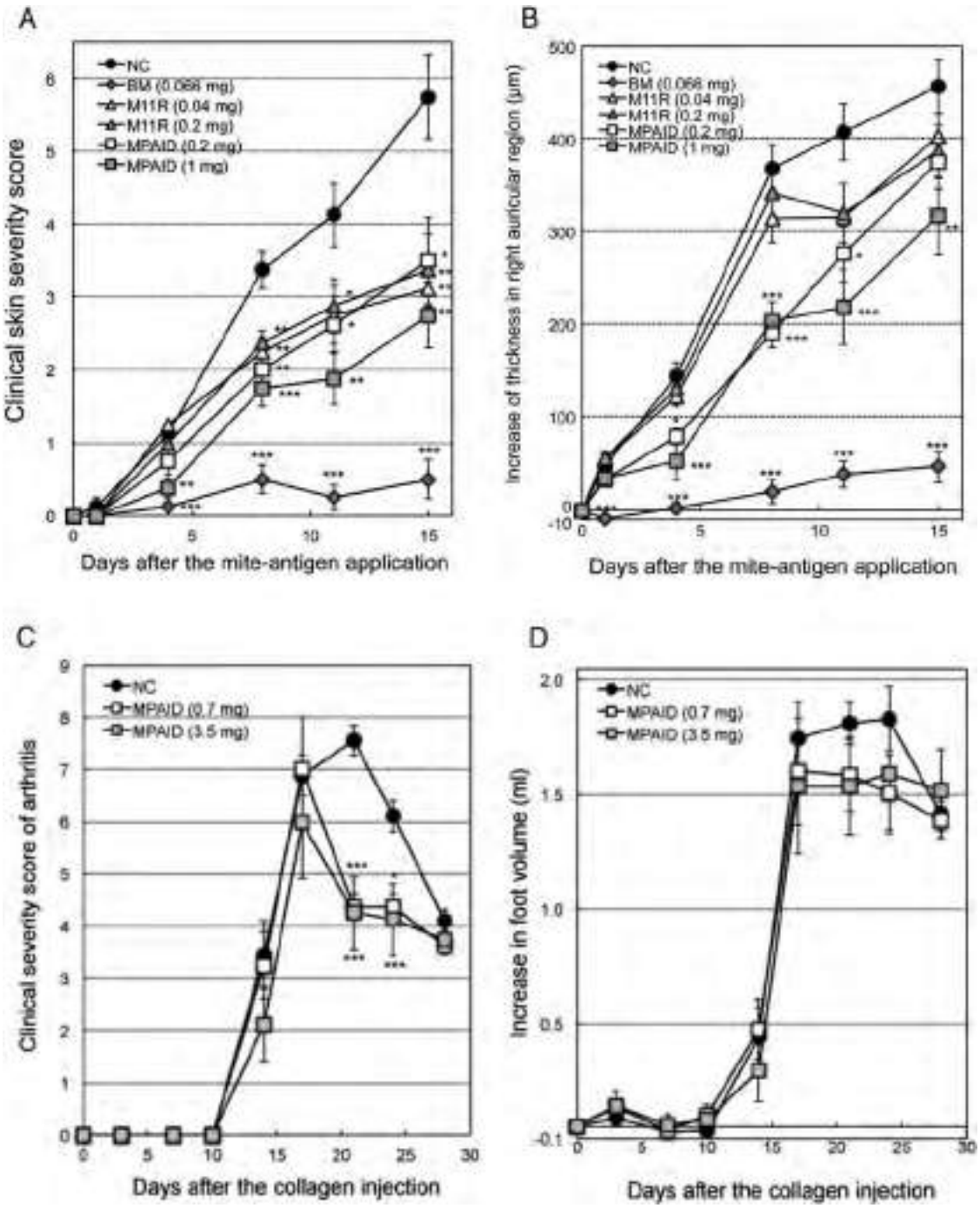

Figure 8. In vivo antiinflammatory actions of MPAID and M11R in animal models of human chronic inflammation disease. Clinical skin severity score (A) and the thickness of the right auricular region of mite antigen-induced atopic dermatitis mice (B) were measured. Mite antigen was intradermally administrated to the right auricular region of female mice at days 0, 3, 7, 10, and 14. Ointment base (NC), BM (0.066 mg/mouse per application), M11R (0.04, 0.2 mg/mouse per application per day), and MPAID (0.2, 1.0 mg/mouse per application per day) were applied to the skin of the right auricular region every day from day 1 to day 15. Values are represented as mean ± SEM (n = 8). Significance of differences was evaluated with a Student's *t* test. *, $P < .05$, **, $P < .01$, ***, $P < .001$ vs NC. Clinical severity score of arthritis (C) and volume of right and left feet in the CIA rats (D) were measured. Arthritis was induced by intracutaneous injection of type II collagen at day 0. PBS (NC) and MPAID (0.7, 3.5 mg/rat per injection per day) were ip injected every day from day 0 to day 28. Values are represented as mean ± SEM (n = 8).

The central acidic region (40 amino acid residues) of MTI-II was found to be essential for the inhibition of the transcriptional activity of NF-κB. Therefore, MTI-II would interact with NF-κB through the central acidic region. However, the precise mechanisms of the inhibition by MTI-II, especially the region of NF-κB with which MTI-II interacts and how the interaction inhibits the transcriptional activity of NF-κB, remained unclear. Because

the central acidic region consists of simple monotonous runs of either glutamic or aspartic acidic residues, one possible model is that the acidic region may mimic κB-response element DNA, in this case, the acidic region may inhibit the DNA binding of NF-κB. Alternatively, MTI-II may interact with another part of NF-κB. This issue will be revealed by a cocrystallization analysis of MTI-II and NF-κB. Wherever MTI-II binds, the binding point should be the weak point of NF-κB, which reduces the transcriptional activity of NF-κB. Pharmaceuticals, which mimic the three-dimensional structure of the acidic region and thereby bind to the weak point of NF-κB, will be an ideal NF-κB inhibitor and an antiinflammatory drug. The cocrystallization analysis is now in progress.

Previously we showed that MTI-II enhanced the transcriptional activity of GR, probably by strengthening the interaction of GR with other coactivators (19). Thus, we presupposed that MTI-II might enhance the GR-induced antiinflammatory effect, probably by strengthening the interaction of GR with NF-κB. However, the inhibitory effect of MTI-II and Dex on the NF-κB-induced luciferase activity appeared to be additive. Moreover, the siRNA-mediated reduction of MTI-II did not reduce the GR-induced inhibition, although the siRNA-mediated reduction of MTI-II reduced the transcriptional activity of GR (19). Therefore, the contribution of MTI-II on the GR-mediated inhibition might be small in the in vitro luciferase assay. Recently, in addition to the interaction of GR with NF-κB, several lines of evidence indicate that GR induces antiinflammatory genes, such as IκB (30, 31), GC-induced leucine zipper (*GILZ*) (4), dual GC-induced specificity phosphatase 1 (*DUSP1*) (32), GR-interacting protein 1 (*GRIP1*) (33), and *A20* (also known as TNF-α induced protein 3) (7, 34–36). As mentioned, MTI-II/MAIDs work as a coactivator of GR. Therefore, it is possible that MTI-II/MAIDs would enhance the GR-induced transcriptions of these antiinflammatory genes in vivo. Further elucidation will be required.

The in vivo experiments of the MTI-II-based antiinflammatory drugs (MAIDs and MPAID) showed that they had a significant antiinflammatory effect both on acute inflammation models and on animal models of human chronic inflammation diseases. The antiinflammatory effect of MAPID injected into the ip cavity of CIA rats was statistically significant but weak. However, taking into consideration the fact that MPAID is nonspecifically and rapidly imported into cells (29), it is somewhat surprising that the ip injection of the peptide had the effects on inflammation of the legs. In contrast, ocular instillations of H11RM and HM11R showed a strong antiinflammatory effect comparable with Dex. Thus, localized administration of MAIDs and MPAID into the inflamed knee joint (for example, transdermal absorption) will show a stronger antiinflammatory effect than the ip administration.

In applying MAIDs as a drug, it should be very important to elucidate that they do not have toxicity and severe side effects. As of now, we have only two in vivo data: 1) when MAIDs were ip injected into the fasted rat, MAIDs did not increase the blood glucose level, unlike Dex or IDM; and 2) prolonged and repeated ip injections of MPAID for 28 days caused little damage to the whole internal organs. These results indicate that MAIDs did not show the most prominent example of GC side effects in vivo, although the overexpression of MAIDs increased GR-induced luciferase assay in vitro. And these results also indicate that at least MPAID is not toxic. A lot of further experiments including observations of systemic symptoms and conditions will be required. However, the MTI-II-based antiinflammatory drugs would become good candidates for novel NF-κB inhibitors and antiinflammatory drugs. Especially, instead of long-term GC therapy, they will be conveniently applied to atopic dermatitis, pollinosis, asthma, rheumatoid arthritis, and so on. Furthermore, they will be also effective for GC-resistant inflammatory diseases.

Acknowledgments

Address all correspondence and requests for reprints to: Kazuki Okamoto, PhD, Department of Clinical Proteomics and Molecular Medicine, St Marianna University Graduate School of Medicine, Sugao 2-16-1, Miyamae-ku, Kawasaki, Kanagawa 216-8511, Japan. E-mail: k2oka@marianna-u.ac.jp.

This work was supported in part by Grants-in-Aid for Scientific Research from the Ministry of Education, Science, Sports, and Culture of Japan, Commercialization Promotion Program for Biotechnology-Related Studies 2008 from Kanagawa Prefecture, Adaptable and Seamless Technology Transfer Program through target-drive Research and Development Feasibility Study stage: Seeds Validation 2010 and Exploratory Research 2012 from the Japan Science and Technology Agency, and by a grant from the Vitamin Society of Japan.

Disclosure Summary: The authors have nothing to disclose.

References

1. **Almawi WY, Melemedjian OK.** Negative regulation of nuclear factor-κB activation and function by glucocorticoids. *J Mol Endocrinol*. 2002;28:69–78.
2. **Baschant U, Tuckermann J.** The role of the glucocorticoid receptor in inflammation and immunity. *J Steroid Biochem Mol Biol*. 2010; 120:69–75.
3. **De Bosscher K, Haegeman G.** Minireview: latest perspectives on

antiinflammatory actions of glucocorticoids. *Mol Endocrinol*. 2009;23:281–291.
4. **Ayroldi E, Macchiarulo A, Riccardi C.** Targeting glucocorticoid side effects: selective glucocorticoid receptor modulator or glucocorticoid induced leucine zipper? A perspective. *FASEB J*. 2014;28: 5055–5070.
5. **Cruz-Topete D, Cidlowski JA.** One hormone, two actions: anti- and pro-inflammatory effects of glucocorticoids. *Neuroimmunomodulation*. 2015;22:20–32.
6. **Vandevyver S, Dejager L, Tuckermann J, Libert C.** New insights into the anti-inflammatory mechanisms of glucocorticoids: an emerging role for glucocorticoid receptor-mediated transactivation. *Endocrinology*. 2013;154:993–1007.
7. **Kadiyala V, Sasse SK, Altonsy MO, et al.** Cistrome-based cooperation between airway epithelial glucocorticoid receptor and NF-κB orchestrates anti-inflammatory effects. *J Biol Chem*. 2016;291: 12673–12687.
8. **King EM, Chivers JE, Rider CF, Minnich A, Giembycz MA, Newton R.** Glucocorticoid repression of inflammatory gene expression shows differential responsiveness by transactivation- and transrepression-dependent mechanisms. *Plos One*. 2013;8(1):e53936.
9. **Uhlenhaut NH, Barish GD, Yu RT, et al.** Insights into negative regulation by the glucocorticoid receptor from genome-wide profiling of inflammatory cistromes. *Mol Cell*. 2013;49:158–171.
10. **Schäcke H, Döcke W-D, Asadullah K.** Mechanisms involved in the side effects of glucocorticoids. *Pharmacol Ther*. 2002;96:23–43.
11. **Okamoto K, Isohashi F, Horiuchi M, Sakamoto Y.** Three forms of macromolecular translocation inhibitor of the nuclear binding of "activated" receptor-glucocorticoid complex and their interaction with ATP. *Biochem Biophys Res Commun*. 1982;108:1655–1660.
12. **Brand IA, Söling H-D.** Zn^{2+}-dependent reversible inactivation of rat liver phosphofructokinase-1. Purification of the inactivating protein and characterization of the inactivation reaction. *J Biol Chem*. 1986; 261:5892–5900.
13. **Haritos AA, Salvin SB, Blacher R, Stein S, Horecker BL.** Parathymosin α: a peptide from rat tissues with structural homology to prothymosin α. *Proc Natl Acad Sci USA*. 1985;82:1050–1053.
14. **Brand IA, Heinickel A, Söling H-D.** Localization of a 11.5 kDa Zn(2+)-binding protein (parathymosin) in different rat tissues. Cell type-specific distribution between cytosolic and nuclear compartment. *Eur J Cell Biol*. 1991;54:157–165.
15. **Clinton M, Frangou-Lazaridis M, Panneerselvam C, Horecker BL.** Prothymosin α and parathymosin: mRNA and polypeptide levels in rodent tissues. *Arch Biochem Biophys*. 1989;269:256–263.
16. **Panneerselvam C, Caldarella J, Horecker BL.** A radioimmunoassay for parathymosin. *J Immunol Methods*. 1987;104:131–136.
17. **Okamoto K, Isohashi F.** Purification and primary structure of a macromolecular-translocation inhibitor II of glucocorticoid-receptor binding to nuclei from rat liver. Inhibitor II is the 11.5-kDa Zn^{2+}-binding protein (parathymosin). *Eur J Biochem*. 2000;267: 155–162.
18. **Clinton M, Frangou-Lazaridis M, Panneerselvam C, Horecker BL.** The sequence of human parathymosin deduced from a cloned human kidney cDNA. *Biochem Biophys Res Commun*. 1989;158: 855–862.
19. **Okamoto K, Isohashi F.** Macromolecular translocation inhibitor II (Zn^{2+}-binding protein, parathymosin) interacts with the glucocorticoid receptor and enhances transcription in vivo. *J Biol Chem*. 2005;280:36986–36993.
20. **Okamoto K, Liu G, Yu W-G, Ochiai T, Isohashi F.** Effect of macromolecular-translocation inhibitor-III on binding of activated glucocorticoid-receptor complex to specific DNA. *J Biochem*. 1996; 119:920–925.
21. **Swingle KF, Grant TJ, Jaques LW, Kvam DC.** Interactions of anti-inflammatory drugs in carrageenan-induced foot edema of the rat. *J Pharmacol Exp Ther*. 1970;172:423–425.
22. **Maistrello I, Rigamonti G, Frova C, De Ruggieri P.** Quantitative effect of topically applied anti-inflammatory agents on external ocular inflammation in rats. *J Pharm Sci*. 1973;62:1455–1460.
23. **Sasakawa T, Higashi Y, Sakuma S, et al.** Atopic dermatitis-like skin lesions induced by topical application of mite antigens in NC/Nga mice. *Int Arch Allergy Immunol*. 2001;126:239–247.
24. **Matsumoto J, Ishikawa S, Doi M, Kishida T, Ebihara K.** Protease-resistant fraction of smoked, dried bonito alleviates atopic dermatitis-like skin lesions in NC/Nga mice. *J Nutr Sci Vitaminol*. 2007; 53:451–456.
25. **Trentham DE, Townes AS, Kang AH.** Autoimmunity to type II collagen: an experimental model of arthritis. *J Exp Med*. 1977;146: 857–868.
26. **Hu Y, Liu R, Li J, Yue Y, Cheng W, Zhang P.** Attenuation of collagen-induced arthritis in rat by nicotinic α7 receptor partial agonist GTS-21. *Biomed Res Int*. 2014;2014:325875.
27. **Picard D, Yamamoto KR.** Two signals mediate hormone-dependent nuclear localization of the glucocorticoid receptor. *EMBO J*. 1987; 6:3333–3340.
28. **Zhang Z, Jones S, Hagood JS, Fuentes NL, Fuller GM.** STAT3 acts as a co-activator of glucocorticoid receptor signaling. *J Biol Chem*. 1997;272:30607–30610.
29. **Futaki S, Suzuki T, Ohashi W, et al.** Arginine-rich peptides, an abundant source of membrane-permeable peptides having potential as carriers for intracellular protein delivery. *J Biol Chem*. 2001;276: 5836–5840.
30. **Scheinman RI, Cogswell PC, Lofquist AK, Baldwin AS Jr.** Role of transcriptional activation of IκB α in mediation of immunosuppression by glucocorticoids. *Science*. 1995;270:283–286.
31. **Auphan, N, DiDonato, JA, Rosette, C, Helmberg, A, Karin, M.** Immunosuppression by glucocorticoids: inhibition of NF-κB activity through induction of IκB synthesis. *Science*. 1995;270:286–290.
32. **Tchen CR, Martins JRS, Paktiawal N, Perelli R, Saklatvala J, Clark AR.** Glucocorticoid regulation of mouse and human dual specificity phosphatase 1 (DUSP1) genes. Unusual cis-acting elements and unexpected evolutionary divergence. *J Biol Chem*. 2010;285:2642–2652.
33. **Chinenov Y, Gupte R, Dobrovolna J, et al.** Role of transcriptional coregulator GRIP1 in the anti-inflammatory actions of glucocorticoids. *Proc Natl Acad Sci USA*. 2012;109:11776–11781.
34. **Ma A, Malynn BA.** A20: linking a complex regulator of ubiquitylation to immunity and human disease. *Nat Rev Immunol*. 2012; 12:774–785.
35. **Kelly C, Shields MD, Elborn JS, Schock BC.** A20 regulation of nuclear factor-κB, Perspectives for inflammatory lung disease. *Am J Resp Cell Mol*. 2011;44:743–748.
36. **Altonsy MO, Sasse SK, Phang TL, Gerber AN.** Context-dependent cooperation between nuclear factor κB (NF-κB) and the glucocorticoid receptor at a TNFAIP3 intronic enhancer: a mechanism to maintain negative feedback control of inflammation. *J Biol Chem*. 2014;289:8231–8239.

Integrative Molecular Medicine

Research Article ISSN: 2056-6360

Effects of soy peptides on IL-1β-induced matrix-degrading enzymes in human articular chondrocytes

Mitsumi Arito[1], Hiroyuki Mitsui[2], Manae S Kurokawa[3], Kazuo Yudoh[4], Toshikazu Kamada[5], Hisateru Niki[2] and Tomohiro Kato[1]

[1]Clinical Proteomics and Molecular Medicine, St. Marianna University Graduate School of Medicine, 2-16-1, Sugao, Miyamae, Kawasaki, Kanagawa, 216-8511, Japan

[2]Department of Orthopaedic Surgery, St. Marianna University School of Medicine, 2-16-1, Sugao, Miyamae, Kawasaki, Kanagawa 216-8511, Japan

[3]Disease Biomarker Analysis and Molecular Regulation, St. Marianna University Graduate School of Medicine, 2-16-1, Sugao, Miyamae, Kawasaki, Kanagawa, 216-8511, Japan

[4]Institute of Medical Science, St. Marianna University Graduate School of Medicine, 2-16-1, Sugao, Miyamae, Kawasaki, Kanagawa, 216-8512, Japan

[5]Department of Orthopedic Surgery and Rheumatology, Hara Orthopedic Hospital, 3-36-23, Nishi-ikebukuro, Toshima-ku, Tokyo, 171-0021 Japan

Abstract

Background: In osteoarthritis (OA) of the most common joint disease, inflammation is deeply involved in the cartilage degradation. Specifically, inflammatory cytokines like IL-1β are known to enhance production of matrix-degrading enzymes like matrix metalloproteinase (MMP) and a disintegrin and metalloproteinase with thrombospondin motifs (ADAMTS). Recently, soy peptides, generated by hydrolytic enzymatic digestion of soy proteins, have been found to show anti-inflammatory activity. Thereby we investigated whether soy peptides affected IL-1β-induced expression of matrix-degrading enzymes in human articular chondrocytes. Methods: Articular chondrocytes derived from 4 patients with bone fracture and 11 patients with OA were cultured with 0, 10, or 100 μM soy peptides for 4 hours. Then, the cells were stimulated with IL-1β for 24 hours. Non-stimulated cells were used as a control. RNA extracted from the cells was subjected to quantitative real time-PCR to assess amounts of mRNA for MMP-3 and ADAMTS-4. Results: Treatment with 100 μM soy peptides significantly suppressed mRNA levels of MMP-3 and ADAMTS-4 enhanced by the IL-1β stimulation (p=0.036 and p=0.005, respectively), although the treatment with 10 μM soy peptides did not show significant suppression (p=0.91 and p=0.20, respectively). In the 100 μM soy peptides treatment, the suppression of MMP-3 mRNA levels was correlated with that of ADAMTS-4 mRNA levels (R^2=0.534). Conclusion: Soy peptides suppressed the IL-1β-induced expression of matrix-degrading enzymes in human articular chondrocytes. Soy peptides may have potential to ameliorate cartilage degradation in OA.

Introduction

Osteoarthritis (OA), the most common joint disease, is histologically characterized by degeneration of cartilage and formation of osteophytes, which lead to destruction of joints [1]. Many patients with OA suffer from pain and disability [1]. Thus, to suppress the symptoms of OA and prevent the progress of OA, novel agents should be developed.

Articular chondrocytes maintain the cartilage matrix by producing and degrading matrix proteins such as type II collagen and proteoglycans [2]. In OA, imbalance between production and degradation of the matrix protein leads to cartilage degradation [1]. Inflammation is deeply involved in the cartilage degradation in OA [1]. Inflammatory cytokines like IL-1β are known to be increased in synovial fluid of patients with OA [3]. In particular, IL-1β was reported to enhance secretion of matrix metalloproteinase (MMP)-1, -3, and -13 from chondrocytes that digest multiple types of collagens [4]. Furthermore, IL-1β was reported to enhance secretion of a disintegrin and metalloproteinase with thrombospondin motifs (ADAMTS)-4 and -5 from chondrocytes that digest aggrecan of a representative proteoglycan [5].

Soybeans contain a large amount of nutrients such as proteins, fats, and carbohydrates. Recently, novel biological roles of soybeans have been highlighted in addition to the roles as nutrients. Specifically, so-called soy peptides, generated by hydrolytic enzymatic digestion of soy proteins, have been reported to show various functions beneficial to health such as cholesterol-lowering properties, cognitive impairment-prevention, antiviral effects, and anti-inflammatory effects [6-12]. As to the anti-inflammatory effects, soy peptides were reported to suppress lipopolysaccharide (LPS)-induced production of cyclooxygenase-2 and prostaglandin E2 in a murine macrophage cell line [10]. Furthermore, soy peptides were reported to suppress LPS-induced production of pro-inflammatory cytokines such as IL-6 and IL-8 in human umbilical vein endothelial cells [11]. *In vivo*, soy-derived di- and tri-rich peptides were reported to alleviate colon and ileum inflammation in pigs with dextran sodium sulfate-induced colitis [12]. Therefore, soy peptides are expected to show anti-inflammatory effects also in human articular chondrocytes, which may lead to suppression of cartilage degradation in OA. However, effects of soy peptides on human articular chondrocytes have not been investigated to our knowledge. We here investigated whether soy peptides suppressed IL-1β-induced expression of matrix-degrading enzymes in human articular chondrocytes.

Correspondence to: Mitsumi Arito, Clinical Proteomics and Molecular Medicine, St. Marianna University Graduate School of Medicine, 2-16-1, Sugao, Miyamae, Kawasaki, Kanagawa, 216-8511, Japan, Tel: +81-44-977-8111 (ext. 3523); Fax: +81-44-976-7553; **E-mail:** m-ari@marianna-u.ac.jp

Key words: *A disintegrin and metalloproteinase with thrombospondin motifs-4 (ADAMTS-4), Chondrocytes, IL-1β, Matrix metalloproteinase-3 (MMP-3), Osteoarthritis; Soy peptides*

Received: May 08, 2016; **Accepted:** May 23, 2016; **Published:** May 26, 2016

Materials and methods

Clinical samples and preparation of chondrocytes

Human articular cartilage samples were obtained from 4 patients with bone fracture (Normal, N1-4, 1 male; age 58 years, 3 female; mean age 78.0 years [range58-88]) at therapeutic surgery of total hip arthroplasty. Cartilage samples were also obtained from 11 patients with OA (OA1-11, 1 male; age 82 years, 10 female; mean age 78.7 years [range 66-86 years]) at therapeutic surgery of total knee arthroplasty.

The diagnosis of OA was made according to the Kellgren and Lawrence criteria [13]. Written informed consent was obtained from each of the patients and this study protocol was approved by the ethics committee of St. Marianna University School of Medicine. The study was performed in compliance with the World Medical Association Declaration of Helsinki.

For chondrocyte preparation, after careful removal of synovial tissue from cartilage samples, the cartilage was minced, washed, and treated with collagenase (Wako Pure Chemical Industries, Osaka, Japan). Isolated chondrocytes (Passage 0, P0) were washed and grown in monolayer culture in Dulbecco's modified Eagle's medium (DMEM, GIBCO, Carlsbad, CA) supplemented with 10% fetal calf serum (Wako), 100 units/ml penicillin, and 100 μg/ml streptomycin (Sigma-Aldrich, St. Louis, MO, USA) on type I collagen-coated culture dishes.

Treatment of chondrocytes with IL-1β and soy peptides

Soy peptides (Hinute-AM, FUJI OIL Co. Ltd., Osaka, Japan), which were mainly composed of di- and tri-peptides, were used [14].

The prepared chondrocytes (P1-P3, 1.0×10^7 cells/φ100mm dish) were cultured with 0, 10, and 100 μM soy peptides for 4 hours. Then, the cells were treated with 1 μg/ml IL-1β alone (R&D, Minneapolis, MN, USA), 1 μg/ml IL-1β and 10 μM soy peptides, and 1 μg/ml IL-1β and 100 μM soy peptides for 24 hours. Non-treated cells were used as a control.

Evaluation of cell viability

Cell viability was evaluated by trypan blue staining. Chondrocytes, cultured with 0, 10, or 100 μM soy peptides for 24 hours, were harvested by treatment with 0.1% trypsin-EDTA (Sigma-Aldrich). The cell pellet, collected by centrifugation for 10 min at 1000×g, was stained with 0.5% trypan blue (Sigma-Aldrich). The number of the blue -stained (dead) cells and the total number of cells were counted using a haemocytometer under a microscopy.

Extraction and reverse transcription (RT) of RNA

Extraction of RNA from the chondrocyte samples and reverse-transcription of the RNA samples were performed using RNeasy® (Qiagen, Venlo, the Netherlands) and High Capacity cDNA Reverse Transcription Kits® (Life Technologies, Rockville, MD, USA), respectively.

Quantitative real time PCR

Real time PCR was performed using ABI Prism 7000 Sequence Detection System (Applied Biosystems, Foster city, CA, USA), according to the manufacturer's instructions. To measure mRNA levels for MMP-3 and ADAMTS-4, 1 μg of total RNA-derived cDNA was mixed with TaqMan® Gene Expression Assays (Hs00968305_m1 and Hs00192708_m1, respectively, Applied Biosystems) and TaqMan® Gene Expression Master Mix (Applied Biosystems). Then the mixture was subjected to real time PCR. The thermal cycle condition was as follows: 95°C for 10 min, followed by 40 cycles of 95°C for 15 s and 60°C for 60 s. To measure mRNA levels for GAPDH, 1 μg of total RNA-derived cDNA was mixed with 300 nM each of the forward and reverse primers and Power SYBR® Master Mix (Applied Biosystems). Nucleotide sequences of the primers for amplification of a GAPDH DNA fragment are as follows: for GAPDH: 5'-TGGTATGGTGGAAGGACTCA and 5'-ATGCCAGTGAGCTTCCCGTT. Real time PCR was performed under the same condition as above.

Statistical analysis

Statistical analysis was performed by IBM SPSS Statistics (Ver.22.0). Effects of soy peptides on IL-1β-induced matrix-degrading enzymes were analyzed by Wilcoxon signed-rank test ($p<0.05$).

Results

Effects of soy peptides on IL-1β-induced matrix-degrading enzymes in human articular chondrocytes

Firstly, we tested whether the concentrations of soy peptides used here showed cytotoxicity against human articular chondrocytes. As a result, we confirmed that up to 100 μM soy peptides did not affect viability of the chondrocytes (Figure 1A). We then investigated effects of the soy peptides on IL-1β-induced expression of MMP-3 and ADAMTS-4 in the chondrocytes. We cultured chondrocytes with or without the soy peptides for 4 hours and then stimulated with IL-1β. We then assessed mRNA levels of MMP-3 and ADAMTS-4.

In the assessment of mRNA levels of MMP-3, we first confirmed that mRNA levels of MMP-3 were significantly increased by the IL-1β stimulation ($p<0.01$, Table 1 and Figure 1B, left panel). Of note, in each of the stimulated chondrocyte sample, the mRNA levels of MMP-3 were increased by the IL-1β stimulation. We then evaluated effects of the soy peptides on the IL-1β-induced expression of MMP-3 in chondrocytes. As a result, the treatment with 100 μM soy peptides significantly

Table 1. Effects of soy peptides on IL-1β-induced MMP-3 mRNA levels in human chondrocytes.

Sample no.	Control	IL-1β	IL-1β +10μM HN-AM	IL-1β +100μM HN-AM
N1	0.063	13.2	16.2	15.9
N2	1.49	60.0	73.3	54.4
N3	2.13	13.5	13.0	11.9
N4	1.45	10.3	10.1	9.27
OA1	1.09	4.62	4.49	2.58
OA2	2.93	7.98	6.98	6.62
OA3	0.77	3.17	2.85	2.48
OA4	0.91	6.50	4.60	5.52
OA5	0.81	42.5	19.2	5.72
OA6	0.33	15.9	20.7	25.0
OA7	0.02	15.9	16.3	10.3
OA8	1.58	12.1	7.93	4.04
OA9	0.20	10.9	10.9	9.13
OA10	1.02	13.0	14.2	8.11
OA11	0.22	3.55	3.91	3.50
Average	1.00	15.5	15.0	11.6
STDEV	0.82	15.4	17.1	13.2
p value	-	<0.01 (vs Control)	0.91 (vs IL-1β)	0.036 (vs IL-1β)

SP: soy peptides

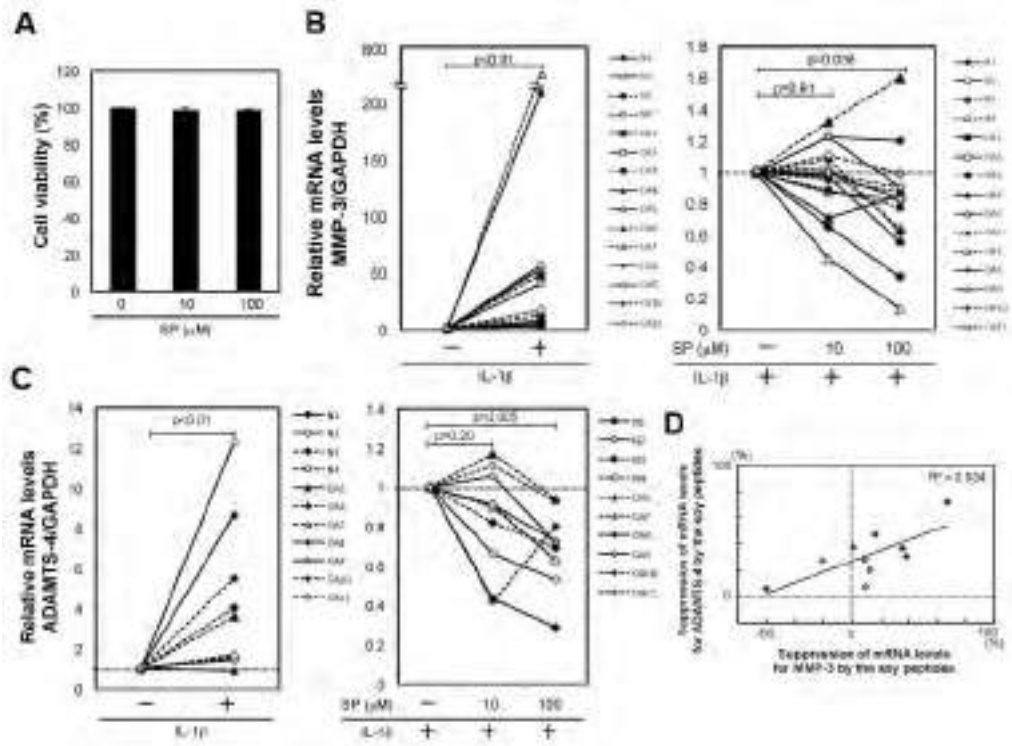

Figure 1. Effects of soy peptides on IL-1β-induced expression of MMP-3 and ADAMTS-4 in human articular chondrocytes**. (A)** Articular chondrocytes from 3 patients with OA (OA1-3) were cultured with 0, 10, and 100 μM soy peptides for 24 hours. The cells were subjected to trypan blue staining. The cell viability (%) was calculated using the following formula; (the number of unstained cells/the total number of cells)×100. SP, soy peptides. **(B)** Articular chondrocytes from 4 patients with bone fracture (N1-4) and 11 patients with OA (OA1-11) were cultured with 0, 10, and 100 μM soy peptides for 4 hours. Then, the cells were stimulated with IL-1β for 24 hours. Non-stimulated cells were used as a control. The mRNA levels for MMP-3 and GAPDH were assessed by RT-qPCR. The mRNA levels of MMP-3 were corrected using those of GAPDH. Left: The corrected mRNA level of MMP-3 was as 1.0 in each of the non-treated samples. Right: The corrected mRNA level of MMP-3 was as 1.0 in each of the IL-1β-treated samples. p-values were calculated by Wilcoxon signed-rank test using the values listed in Table 1. **(C)** Articular chondrocytes from 4 patients with bone fracture (N1-4) and 7 patients with OA (OA5-11) were treated similarly as described in (A). The mRNA levels of ADAMTS-4 were corrected using those of GAPDH. Left: The corrected mRNA level of ADAMTS-4 was as 1.0 in each of the non-treated samples. Right: The corrected mRNA level of ADAMTS-4 was as 1.0 in each of the IL-1β-treated samples. p-values were calculated by Wilcoxon signed-rank test using the values listed in Table 2. SP, soy peptides. **(D)** Suppression rates (%) of mRNA levels for MMP-3 and ADAMTS-4 in each of the chondrocyte samples (4 patients with bone fracture (N1-4) and 6 patients with OA (OA6-11)) were calculated by using the values listed in Table 1 and 2, respectively. A correlation diagram between the suppression of mRNA levels for MMP-3 and ADAMTS-4 in the treatment with 100 ^{2}) was calculated by regression analysis.

suppressed mRNA levels of MMP-3 enhanced by the IL-1β stimulation (p=0.036, Table 1 and Figure 1B, right panel), although the treatment with 10 μM soy peptides did not show significant suppression (p=0.91, Table 1 and Figure 1B, right panel).

In the assessment of ADAMTS-4, we first confirmed that mRNA levels of ADAMTS-4 were significantly increased by IL-1β stimulation (p<0.01, Table 2 and Figure 1C, left panel). Ten out of the 11 chondrocyte samples up-regulated the mRNA levels of ADAMTS-4 by the IL-1β stimulation. We thus evaluated effects of the soy peptides on the IL-1β-induced expression of ADAMTS-4 using the 10 chondrocyte samples that positively responded to IL-1β. As a result, the treatment with 100 μM soy peptides significantly suppressed mRNA levels of ADAMTS-4 enhanced by the IL-1β stimulation (p=0.005, Table 2 and Figure 1C, right panel), although the treatment with 10 μM soy peptides did not show significant suppression (p=0.20, Table 2 and Figure 1C, right panel).

Finally, we investigated correlation of the suppressing effect of the soy peptides on the MMP-3 expression to that of ADAMTS-4 expression. As a result, in the treatment with 100 μM soy peptides, the suppression of MMP-3 mRNA levels was correlated with that of ADAMTS-4 mRNA levels (R^2=0.534, Figure 1D). In addition, the suppressive effect of the soy peptides on the expression of MMP-3 and ADAMTS-4 tended to be higher in patients with OA than in those with bone fracture (Figure 1D).

Discussion

We here found that soy peptides suppressed IL-1β-induced production of MMP-3 and ADAMTS-4 in human articular chondrocytes.

The possible mechanisms for the actions of soy peptides are as follows: 1) soy peptides inhibit the input of IL-1β signal transduction by binding to IL-1β or IL-1β receptors, 2) soy peptides, taken up into chondrocytes, inhibit the intracellular IL-1β signal transduction, and 3) soy peptides bind to their unknown receptors and then block the IL-1β signal transduction.

On the first possible mechanism, IL-1β activates the signal transduction system by specific binding to IL-1β receptors. In the majority of the tested chondrocytes samples, the mRNA levels of MMP-3 of the IL-1β-stimulated chondrocytes group were suppressed by the treatment with 100 μM soy peptides (Figure 1B). However, in a small part of the tested chondrocytes samples, the mRNA levels of MMP-3 were increased by the soy peptides treatment (Figure 1B). If soy peptides bound to IL-1β or IL-1β receptors, the mRNA levels of MMP-

Table 2. Effects of soy peptides on IL-1β-induced ADAMTS-4 mRNA levels in human chondrocytes.

Sample no.	Control	IL-1β	IL-1β +10μM HN-AM	IL-1β +100μM HN-AM
N1	0.16	1.37	1.25	1.00
N2	0.23	2.78	2.94	2.00
N3	0.13	0.74	0.31	0.59
N4	0.92	1.49	1.65	1.38
OA5	2.03	1.77	-	-
OA6	1.30	4.71	5.53	4.43
OA7	1.70	2.96	2.66	1.88
OA8	1.02	1.51	0.66	0.43
OA9	1.47	2.20	1.46	1.16
OA10	0.91	3.64	2.98	2.52
OA11	1.11	1.83	1.66	1.14
Average	1.00	2.27	2.11	1.65
STDEV	0.63	1.16	1.50	1.17
p value	-	<0.01 (*vs.* Control)	0.20 (*vs.* IL-1β)	0.005 (*vs.* IL-1β)

SP: soy peptides

3 would have been suppressed in all the tested chondrocytes samples. Thus, it would be unlikely that soy peptides inhibit the binding between IL-1β and IL-1β receptors.

On the second possible mechanism, we showed that suppression of mRNA levels for MMP-3 were well correlated with that of mRNA levels for ADAMTS-4 in the soy peptides-treated chondrocyte samples (R^2=0.5343, Figure 1D). Thus, we thought that soy peptides suppressed the IL-1β-induced production of MMP-3 and ADAMTS-4 by inhibiting their common pathway. IL-1β activates the signal transduction systems through the activation of multiple protein kinases such as p38 mitogen-activated protein kinase (MAPK), c-Jun N-terminal kinase (JNK), and Akt [15-18]. The activated MAPK, JNK, and Akt enhance production of various inflammatory cytokines and matrix degrading proteins, activating transcription factors such as AP-1 and NF-κB [19]. Akt, phosphorylated by activated phosphoinositol 3-kinase (PI3K), leads to activation of NF-κB [20]. NF-κB activates transcription of pro-inflammatory cytokines and matrix-degrading enzymes including MMP-3 and ADAMTS-4 [4,5]. Peptides derived from β-conglycinin of a representative soy protein have been reported to inactivate NF-κB by suppressing phosphorylation of Akt in liver and aorta of LPS-induced inflammatory model mice [11]. Thus, we speculate that soy peptides suppress the IL-1β-induced production of MMP-3 and ADAMTS-4, probably by inhibiting their PI3K-Akt-NF-κB signaling by suppressing the phosphorylation of Akt.

On the third possible mechanism, although receptors for soy peptides have not yet been identified, such receptors may exist and deliver signals. For example, M. Chimen *et al.* reported that PEPITEM, a peptide proteolytically derived from 14.3.3 zeta delta protein, used cadherin-15 as a receptor and lead to release of sphingosine-1-phosphate from endothelial cells [21]. Like the case of PEPITEM, receptors for soy peptides may exist, which should be investigated. Including these 3 possible mechanisms, the mechanisms for the action of soy peptides should be investigated in the near future.

We here found that soy peptides significantly suppressed the IL-1β-induced production of MMP-3 and ADAMTS-4 in human articular chondrocytes. In the majority of the tested chondrocytes samples, both the mRNA levels of MMP-3 and those of ADAMTS-4 were suppressed by the treatment with 100 μM soy peptides (Figure 1C). However, in a small part of the tested chondrocytes samples, neither the mRNA levels of MMP-3 nor those of ADAMTS-4 were suppressed by the soy peptides treatment (Figure 1C). Thus, the effect of soy peptides would be influenced by the individual genetic backgrounds. There might be subpopulations that show different sensitivity to soy peptides.

It is interesting that the suppressive effect of the soy peptides on the expression of MMP-3 and ADAMTS-4 tended to be higher in the patients with OA than in those with bone fracture (Figure 1D). OA chondrocytes might show higher sensitivity to soy peptides than normal chondrocytes.

Soy peptides used in this study are mainly composed of di- and tri-peptides [14]. However, specific peptides that suppressed the IL-1β-induced production of MMP-3 and ADAMTS-4 have not been identified yet. Recently, a tri-peptide of Val-Pro-Tyr, derived from glycinin of a major soy protein, has been reported to down-regulate the expression of pro-inflammatory cytokines in intestinal epithelial cells and macrophages [22]. The soy peptides used in this study are expected to contain glycinin and thus would contain Val-Pro-Tyr. A tri-peptide of Val-Pro-Tyr might be one of the soy peptides that suppressed the effects of IL-1β in this study. On this point, further investigation is required.

Our data showed that soy peptides suppressed the IL-1β-induced production of MMP-3 and ADAMTS-4 in human articular chondrocytes *in vitro*. Our data indicate that soy peptides may be useful to prevent or suppress cartilage degradation in OA.

Acknowledgements

We thank Ms. Sawada Y, Ms. Tamaki M, Ms. Mogi T, and Ms. Suzuki M for their technical assistance. This work was supported by FUJI OIL CO., LTD.

Conflict of interest statement

Arito M, Mitsui H, Kurokawa MS, Niki H, Yudoh K, and Kato T report grants and non-financial support from FUJI OIL Co. Ltd., during the conduct of the study. Kato T reports grants and non-financial support from Chugai Pharmaceutical Co. Ltd., outside the submitted work. Yudoh K reports non-financial support from Vitamin C60 BioResearch Corporation, outside the submitted work. Kamada T has nothing to disclose.

References

1. Loeser RF, Goldring SR, Scanzello CR, Goldring MB (2012) Osteoarthritis: a disease of the joint as an organ. *Arthritis Rheum* 64: 1697-1707. [Crossref]

2. Goldring MB, Marcu KB (2009) Cartilage homeostasis in health and rheumatic diseases. *Arthritis Res Ther* 11: 224. [Crossref]

3. Kaneyama K, Segami N, Nishimura M, Suzuki T, Sato J (2002) Importance of cytokines in synovial from 121 joints with temporomandibular disorders. *Br J Oral Maxillofac Surg* 40: 418-423. [Crossref]

4. Richardson DW, Dodge GR (2000) Effects of interleukin-1beta and tumor necrosis factor-alpha on expression of matrix-related genes by cultured equine articular chondrocytes. *Am J Vet Res* 61: 624-630. [Crossref]

5. Bau B, Gebhard PM, Haag J, Knorr T, Bartnik E, et al. (2002) Relative messenger RNA expression of collagenases and aggrecanases in human articular chondrocytes *in vivo* and *in vitro*. *Arthritis Rheum* 46: 2648-2657. [Crossref]

6. Inoue N, Nagao K, Sakata K, Yamano N, Gunawardena PE, et al. (2011) Screening of soy protein-derived hypotriglyceridemic di-peptides in vitro and in vivo. *Lipids Health Dis* 10: 85. [Crossref]

7. Maebuchi M, Kishi Y, Koikeda T, Fruya S (2013) Soy Peptide Dietary Supplementation Increases Serum Dopamine Level and Improves Cognitive Dysfunction in Subjects with Mild Cognitive Impairment. *Jpn Pharmacol Ther* 41: 67-73.

8. Katayama S, Imai R, Sugiyama H, Nakamura S (2014) Oral administration of soy peptides suppresses cognitive decline by induction of neurotrophic factors in SAMP8 mice. *J Agric Food Chem* 62: 3563-3569. [Crossref]

9. Matemu AO, Nakamura K, Kayahara H, Murasawa H, Katayama S, et al. (2011) Enhanced antiviral activity of soybean ß-conglycinin-derived peptides by acylation with saturated fatty acids. *J Food Sci* 76: M299-M304.[Crossref]

10. Martinez-Villaluenga C, Dia VP, Berhow M, Bringe NA, Gonzalez de Mejia E (2009) Protein hydrolysates from beta-conglycinin enriched soybean genotypes inhibit lipid accumulation and *in vitro. Mol Nutr Food Res* 53: 1007-1018. [Crossref]

11. Burris RL, Ng HP, Nagarajan S (2014) Soy protein inhibits VCAM-1 and cytokine induction by inhibiting the NF-κB and AKT signaling pathway in apolipoprotein mice. *Eur J Nutr* 53: 135-148. [Crossref]

12. Young D, Ibuki M, Nakamori T, Fan M, Mine Y (2012) Soy-derived di- and tripeptides alleviate colon and ileum in pigs with dextran sodium sulfate-induced colitis. *J Nutr* 142: 363-368. [Crossref]

13. Kellgren JH, Lawrence JS (1957) Radiological assessment of osteo-arthrosis. *Ann Rheum Dis* 16: 494-502. [Crossref]

14. Nakamori T (2010) Soy peptides as functional food materials. In: Bioactive proteins and peptides as functional foods and nutraceuticals. (Mine Y, Li-Chan ECY, Jiang B, eds.) Wiley-Blackwell Publishing, Hoboken, pp. 265-271

15. Guy GR, Philp R, Tan YH (1995) Activation of protein kinases and the inactivation of protein phosphatase 2A in tumour necrosis factor and interleukin-1 signal-transduction pathways. *Eur J Biochem* 229: 503-511. [Crossref]

16. Bankers-Fulbright JL, Kalli KR, McKean DJ (1996) Interleukin-1 signal transduction. *Life Sci* 59: 61-83. [Crossref]

17. Li X, Tupper JC, Bannerman DD, Winn RK, Rhodes CJ, et al. (2003) Phosphoinositide 3 kinase mediates Toll-like receptor 4-induced activation of NF-kappa B in endothelial cells. *Infect Immun* 71: 4414-4420. [Crossref]

18. Tsuzaki M, Guyton G, Garrett W, Archambault JM, Herzog W, et al. (2003) IL-1 beta induces COX2, MMP-, -3 and -13, ADAMTS-4, IL-1 beta and IL-6 in human tendon cells. *J Orthop Res* 21: 256-264. [Crossref]

19. Williams DH, Jeffery LJ, Murray EJ (1992) Aurothioglucose inhibits induced NF-kB and AP-1 activity by acting as an IL-1 functional antagonist. *Biochim Biophys Acta* 1180: 9-14. [Crossref]

20. Yap TA, Garrett MD, Walton MI, Raynaud F, de Bono JS, et al. (2008) Targeting the PI3K-AKT-mTOR pathway: progress, pitfalls, and promises. *Curr Opin Pharmacol* 8: 393-412. [Crossref]

21. Chimen M, McGettrick HM, Apta B, Kuravi SJ, Yates CM, et al. (2015) Homeostatic regulation of T cell by a B cell-derived peptide is impaired in autoimmune *Nat Med* 21: 467-475. [Crossref]

22. Kovacs-Nolan J, Zhang H, Ibuki M, Nakamori T, Yoshiura K, et al. (2012) The PepT1-transportable soy tripeptide VPY reduces intestinal *Biochim Biophys Acta* 1820: 1753-1763. [Crossref]

Copyright: ©2016 Arito M. This is an open-access article distributed under the terms of the Creative Commons Attribution License, which permits unrestricted use, distribution, and reproduction in any medium, provided the original author and source are credited.

Integrative Molecular Medicine

Research Article ISSN: 2056-6360

Comprehensive analysis of surface proteins of peripheral blood mononuclear cells in patients with systemic lupus erythematosus

Nozawa Y[1], Arito M[1], Omoteyama K[1], Sato M[1], Takakuwa Y[2], Ooka S[2], Kurokawa MS[3] and Kato T[1]

[1]Clinical Proteomics and Molecular Medicine, St. Marianna University Graduate School of Medicine, Japan
[2]Division of Rheumatology, Department of Internal Medicine, St. Marianna University School of Medicine, Japan
[3]Disease Biomarker Analysis and Molecular Regulation, St. Marianna University Graduate School of Medicine, Japan

Abstract

Background: To understand pathophysiology of systemic lupus erythematosus (SLE), we here tried to identify profiles of cell surface (CS) molecules of peripheral blood mononuclear cells (PBMCs) using targeted proteomics.

Methods: PBMCs prepared from 5 patients with SLE and 5 healthy donors (HLs), were subjected to live cell-biotinylation. Then the biotinylated CS proteins were analyzed by 2-dimensional fluorescence difference gel electrophoresis (2D-DIGE). Protein spots that showed different intensity between the SLE and HL groups were identified by mass spectrometry.

Results: In total, 468 protein spots were detected by 2D-DIGE, out of which 151 spots (32.3%) showed significantly different intensity between the two groups. Among the 151 spots, 137 spots (29.3%) showed > ±1.5-fold different intensity and 44 spots (9.4%) showed > ±2.5-fold different intensity between the two groups. Proteins in 17 out of the 44 spots were identified.

Conclusion: Our study comprehensively investigated CS protein profiles of PBMCs in SLE for the first time, to our knowledge. We found that CS protein profiles of PBMCs from patients with SLE were greatly different from those from HLs. Our study would provide a new strategy to investigate the pathophysiology of SLE.

Introduction

Systemic lupus erythematosus (SLE) is a prototype of systemic autoimmune diseases, characterized by generation of various autoantibodies. Patients with SLE display clinical features in multiple organs such as kidney, skin, and central nerve systems and also display various abnormalities in laboratory examinations like anti-nuclear antibodies (ANAs) and low levels of serum complements. Since the clinical features and abnormalities are considerably different among patients with SLE, the diagnosis of SLE is made by referring the revised classification criteria for SLE 1997 [1] or more recently by the systemic lupus international collaborating clinics classification criteria for SLE 2012 [2,3]. Only a limited part of autoantibodies such as SS-A antibodies has been evidenced to cause damages of an organ [4,5]. However, direct roles of the remaining large part of the autoantibodies in the clinical features have not been elucidated.

Although mechanisms for the autoantibody production in SLE have not been fully understood, both B cells and T cells are thought to be involved in the autoantibody production [6,7]. For example, expansion of memory B cells has been demonstrated and thus SLE is suggested to be characterized by frequent cycles of B cell activation and differentiation [8]. T cells are thought to abnormally assist the activation and differentiation of autoreactive B cells. Expansion of the Th17 population and perturbation of T cell receptor (TCR) physiology and downstream signaling of TCRs have been reported [9]. However, molecular mechanisms for the alterations in T and B cells have been not fully understood.

In general, any type of cells possesses various molecules on their surface. Cell surface (CS) molecules that receive extracellular information mediate intracellular signal transduction. Thus, abnormal expression or post-translational modification of CS molecules can be directly linked to the pathophysiology of SLE. As a tool to analyze CS proteins, fluorescence-activated cell sorting (FACS) analysis has been established. In fact, FACS has provided various findings on abnormalities of CS proteins of PBMCs in SLE [10-13]. However, FACS can analyze only a limited kinds of CS proteins and thereby cannot comprehensively analyze CS proteins. Based on these backgrounds, we here tried to comprehensively analyze CS protein profiles using targeted proteomics, the combination of live cell-biotinylation and 2-dimensional fluorescence difference gel electrophoresis (2D-DIGE), to understand pathophysiology of SLE.

Correspondence to: Mitsumi Arito, PhD, Clinical Proteomics and Molecular Medicine, St. Marianna University Graduate School of Medicine, 2-16-1 Sugao, Miyamae, Kawasaki, Kanagawa, 216-8511, Japan, E-mail: m-ari@marianna-u.ac.jp

Key words: *surface proteins, systemic lupus erythematosus, proteomics*

Received: November 20, 2016; **Accepted:** December 06, 2016; **Published:** December 12, 2016

Materials and methods

Clinical specimens

PBMCs were isolated by density-gradient centrifugation using Ficoll-Paque Plus (Pharmacia Biotech, Uppsala, Sweden) from blood samples of 5 patients with SLE and 5 healthy donors (HLs). All the samples were obtained with written informed consent and this study was approved by the institutional ethics committee of St. Marianna University School of Medicine.

Isolation of CS proteins by biotin labeling

CS proteins were isolated by a commercially available CS protein isolation kit (Thermo Fisher Scientific Inc., Waltham, MA, USA), according to the manufacturer's instructions. Briefly, CS proteins of live PBMCs were biotinylated with sulfo-NHS-S-S-biotin, which was a cell-impermeable and cleavable biotinylation reagent. After the biotinylation, PBMCs were lysed and the biotinylated CS proteins were recovered by avidin beads (Thermo Scientific NeutrAvidin Agarose Resin). Then CS proteins were released from the avidin-bound biotin by cleavage of the S-S bonds using a reducing reagent.

2-dimensional fluorescence difference gel electrophoresis (2D-DIGE)

The isolated CS proteins were separated by 2D-DIGE. 2D-DIGE was performed as described previously [14]. Each of the CS protein samples was labeled with Cyanine dye 5 (Cy5, Cy Dye DIGE Saturation dye; GE Healthcare, Buckinghamshire, UK). An internal control "standard sample" was prepared by mixing an equal amount of each of the samples. The standard sample was then labeled with Cyanine dye 3 (Cy3, GE Healthcare). Then, each of the Cy5-labeled protein samples (2.5 μg) were mixed with the Cy3-labeled standard sample (2.5 μg). The mixture was applied onto an isoelectric focusing (IEF) gel (pH 3-11, GE Healthcare). Subsequently, proteins separated by IEF were further separated by 12.5% sodium dodecyl sulfate-polyacrylamide gel electrophoresis (SDS-PAGE). The separated proteins were scanned using an image analyzer (Typhoon 9400 Imager, GE Healthcare). Intensity of the separated protein spots was quantified by Progenesis program (PerkinElmer, MA, US). To compare protein spot intensity between the SLE patient group and the HL group, Cy5-fluorescent intensity of each protein spot was normalized by Cy3-fluorescent intensity of the identical spot. The normalized Cy5-intensity was used for the comparison.

Protein identification

Protein spots of interest, excised from the 2D gels, were digested by trypsin as described previously [15]. Produced peptides were subjected to matrix-assisted laser desorption ionization-time of flight/time of flight mass spectrometry (MALDI-TOF/TOF-MS) (Ultraflex, Bruker Daltonics, Bremen, Germany). Determined peptide masses were compiled to allow searches of the National Center for Biotechnology Information (NCBI) protein database using Mascot software program (Matrix Science, London, UK).

Results

Analysis of CS proteins of PBMCs from patients with SLE and HL by 2D-DIGE

To identify SLE-specific CS protein profiles of PBMCs, we comprehensively compared CS proteins of PBMCs between 5 patients with SLE and 5 HLs using 2D-DIGE of isolated CS proteins by cell surface biotinylation. Clinical features of the 5 patients with SLE are described in Table 1.

As a result, in total 468 definite protein spots were detected (Figure 1A). We then compared intensity of the 468 protein spots between the SLE patient group and the HL group. We found that 151 (32.3%) out of the 468 protein spots showed significantly different intensity between the two groups (Table 2). Among them, 137 spots (29.3%) showed >±1.5-fold intensity differences between the two groups. Furthermore, 44 spots (9.4%) showed >±2.5-fold intensity differences (Table 2). This study revealed that CS protein profiles of PBMCs in SLE patients were greatly skewed compared to those in HLs.

Table 1. Clinical information of enrolled patients with SLE.

Patients	**SLE1**	**SLE2**	**SLE3**	**SLE4**	**SLE5**
Sex/Age (y.o.)	F/23	F/45	F/46	F/36	F/54
Disease duration (y)	9y	17y	1y	11y	33y
Clinical manifestations at the onset and during the course	Malar rash, Pericarditis, Nephritis, Anti-Sm(+), ANA(+), Plateletpenia, Psychosis	Non-erosive arthritis, Malar rash, Nephritis, Fever, Skin ulcer, Hyper-CK-emia, Hypocomplementemia	Non-erosive arthritis, ANA(+), Malar rash, Anti-DNA(+), Nephritis Hypocomplementemia,	Fever, anti-DNA(+), ANA(+), Pancytopenia, Nephritis, CNS lesion	Malar rash, Fever, Pleuritis, Nephritis, ANA(+), Anti-DNA(+)
Clinical symptoms at the day of sampling	Malar rash, Discoid rash, Photosensitivity, Psychosis, Nephritis	Malar rash, Photosensitivity, Non-erosive arthritis	Malar rash, Non-erosive arthritis	Malar rash	Non-erosive arthritis
Laboratory examinations*					
WBC (/μL) Lymphocytes (/μL) Hemoglobin (g/dL) Platelets (x10^3/μL)	7,000 210 11.9 200	7,900 893 13.7 196	11,100 2142 12.2 204	8,100 599 12.3 317	6,300 762 13.3 209
CH50 (U/mL)	14.9	53.7	<10	40.9	43.9
Anti-dsDNA-IgG (IU/mL) (negative≤10)	29.7	≤10	323	23.5	≤10
ANA	1:320	1:2560	1:1280	1:160	1:320
SLEDAI*	18	10	12	8	4
Treatment*	PSL (8mg)	PSL (40mg)	PSL (20mg)	PSL (10mg)	PSL (12mg), Tacrolimus (3mg)

*Findings and drugs at the day of sampling are shown.

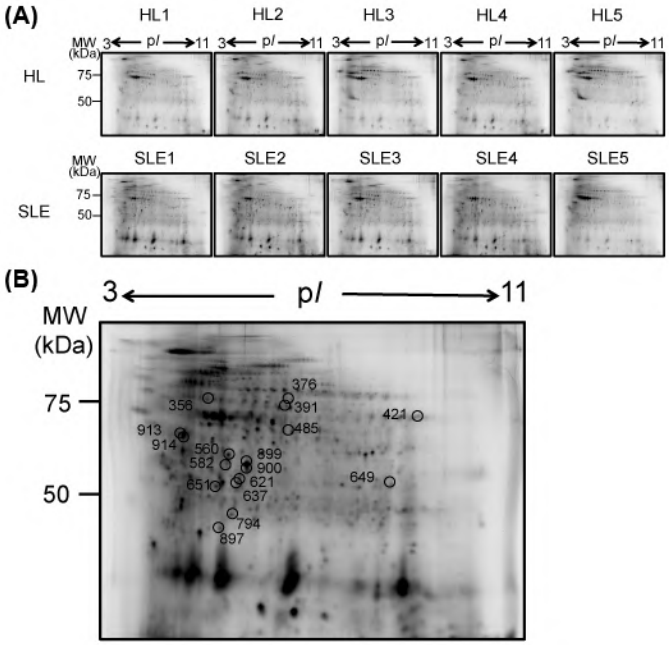

Figure 1. 2D-DIGE analysis of CS proteins of PBMCs from patients with SLE and HLs. A) CS proteins were extracted from PBMCs obtained from 5 patients with SLE and 5 HLs and then were subjected to 2D-DIGE. Each protein sample labeled with Cy5 and an internal control "standard sample" labeled with Cy3 were mixed and applied onto an IEF gel. The protein samples were separated on 24 cm pH 3-11 non-linear IEF strips and further separated by 12.5% SDS-PAGE. Results from the patients with SLE (Cy5, SLE1-5) and HLs (Cy5, HL1-5) are shown. MW, molecular weight. B) 44 protein spots that showed different intensity between the SLE patient group and the HL group were subjected to the MS/MS analysis to identify proteins. Proteins in 17 out of the 44 protein spots were as summarized in Table 3. Positions of the 17 spots on the 2D gel are shown by circles with spot numbers.

Table 2: Numbers of protein spots that showed different intensity between the SLE patient group and the HL group.

Total number of detected protein spots	Number of spots with different intensity (p <0.05)	Fold difference (X, SLE / HL)	Number of spots
468	151	X ≥ 3.5	6
		3.5 > X ≥ 2.5	23
		2.5 > X ≥ 1.5	41
		1.5 > X > -1.5	14
		-1.5 ≥ X > -2.5	52
		-2.5 ≥ X > -3.5	13
		-3.5 ≥ X	2

Identification of proteins with significant intensity differences between the SLE patient group and the HL group: The 44 protein spots that showed > ±2.5-fold intensity differences were subjected to MS/MS analysis to identify protein names (Figure 1B). As a result, proteins in 17 out of the 44 spots were identified as summarized in (Table 3).

Thirteen out of the 17 identified spots showed higher intensity in the SLE patient group than in the HL group (no. 649 of myeloblastin, no. 899 of cyclin-L1, no. 485 of leukocyte elastase inhibitor, no. 897 of DNA-directed RNA polymerase II subunit RPB11-b2, no. 900 of POTE ankyrin domain family member F, and nos. 651, 582, 734, 913, 560, 914, 637, and 621 of actins) (Figure 2, upper and middle). The remaining 4 spots showed lower intensity in the SLE group than in the HL patient group (no. 421 of meiosis 1 arrest protein, no. 376 of heterogeneous nuclear ribonucleoprotein H, no. 391 of pyruvate kinase PKM and no. 356 of tubulin alpha-4A chain) (Figure 2, lower).

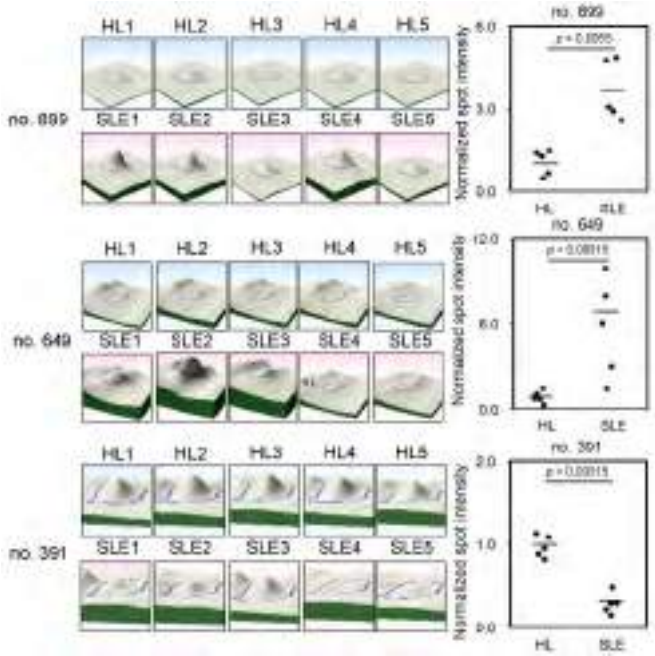

Figure 2. Representative protein spots that showed different intensity between the SLE patient group and the HL group.

Representative results from nos. 899, 649, and 391 are shown. 3D image of the protein spot (nos. 649, 899, and 391) was constructed by Progenesis program (Left panel). Normalized intensity of the spot was compared between the SLE patient group and the HL group (Right panel). An average of the normalized protein spot intensity in the HL group was as 1.0. A bar shows an average of the normalized protein spot intensity in each group.

Discussion

Our study revealed that CS protein profiles of PBMCs in patients with SLE were greatly different from those in HLs. Of the differently expressed CS proteins, 10 proteins from 17 proteins spots were identified.

CS proteins have been generally analyzed by FACS. In FACS, targeted CS proteins of live cells are labelled with fluorescence-conjugated target-specific antibodies, after which intensity of bound fluorescence are measured. It is well recognized that FACS is a very effective tool to analyze CS proteins. In fact, FACS has been often used in the analysis of the pathophysiology of SLE [10-13]. However, FACS can analyze only limited kinds (usually 1-4 kinds, at most 8 kinds) of CS proteins. FACS cannot comprehensively analyze CS proteins. In comparison, biotin labeling of CS proteins combined with 2D-DIGE as used here can comprehensively detect and quantitate CS proteins. This is a great advantage of our method. Another point different from FACS is that proteins that bind to biotinylated CS proteins are also isolated together with CS proteins themselves, even if they themselves do not exist on the outside of cell membranes. In this regard, the method used here would be also adequate to analyze translocation of proteins from cytosol or nucleus to the plasma membrane and vice versa. Our strategy and FACS should be differently used depending on aims of studies.

Our study revealed that approximately one-thirds (32.3%) of the detected protein spots showed significantly different expression between the SLE patient group and the HL group. This indicates that CS protein profiles of PBMCs of SLE patients skews very widely. Out of the 44 protein spots with highly different intensity (> ±2.5 folds), proteins of 17 spots were identified, which were composed of 10 kinds of proteins.

Table 3: Protein from the protein spots with different intensity between the SLE patient group and the HL group.

Spot no.	MW pI Observed	Difference (SLE/HL)	Protein	Accession no.	MW pI Theoretical	Matched peptides	Mascot score	Coverage (%)	(Mascot ion score)
649	27.3 7.84	5.85	Myeloblastin (PRTN3_HUMAN)	gi: 6174926	27.8 8.72	3	73	11	^{80}LVNNVLGAHNVR^{91} (9) ^{228}LFPDFFTR^{235} (16) ^{236}VALYVDWIR^{244} (26)
899	31.8 6.27	3.72	Cyclin-L1 (CCNL_HUMAN)	gi: 74753368	59.6 10.7	6	72	13	^{99}LPQVAMATGQVLFHR^{113} (17)
651	27.2 5.07	3.24	Actin, cytoplasmic 1 (ACTB_HUMAN) Actin, cytoplasmic 2 (ACTG_HUMAN)	gi: 46397333 gi: 54036678	41.7 5.29 41.8 5.31	5	161	21	^{29}AVFPSOVGRPR^{39} (10) ^{40}HQGVMVGMGQK^{50} (2) ^{85}IWHHTFYNELR^{95} (73) ^{96}VAPEEHPVLLTEAPLNPK^{113} (49)
485	40.6 62.7	2.90	Leukocyte elastase inhibitor (ILEU_HUMAN)	gi: 266344	42.7 5.90	3	108	7	^{57}TFHFNTVEEVHSR^{69} (57)
									^{276}FKLEESYTLNSDLAR^{290} (28)
582	32 5.26	2.82	Actin, cytoplasmic 1(ACTB_HUMAN) Actin, cytoplasmic 2 (ACTG_HUMAN)	gi: 46397333 gi: 4501887	41.7 5.29 41.8 5.31	6	119	19	^{239}SYELPDGQVITIGNER^{254} (74) ^{285}CDVDIR^{290} (5)
734	23.4 5.32	2.81	Actin, cytoplasmic 1(ACTB_HUMAN) Actin, cytoplasmic 2 (ACTG_HUMAN) Beta-actin-like protein 2 (ACTBL_HUMAN)	gi: 46397333 gi: 4501887 gi: 172046825	41.7 5.29 41.8 5.31 42.0 5.39	3	74	6	^{239}SYELPDGQVITIGNER^{254} (59) ^{285}CDVDIR^{290} (2) ^{240}SYELPDGQVITIGNER^{250} (59) ^{286}CDVDIR^{291} (2)
913	40.2 4.56	2.81	Actin, cytoplasmic 1(ACTB_HUMAN) Actin, cytoplasmic 2 (ACTG_HUMAN)	gi: 46397333 gi: 4501887	41.7 5.29 41.8 5.31	4	265	14	^{29}AVFPSIVGRPR^{39} (37) ^{85}IWHHTFYNELR^{95}(74) ^{239}SYELPDGQVITIGNER^{254} (127)
560	34 5.27	2.76	Actin, cytoplasmic 1(ACTB_HUMAN) Actin, cytoplasmic 2 (ACTG_HUMAN)	gi: 46397333 gi: 4501887	4.17 5.29 41.8 5.31	4	96	14	^{239}SYELPDGQVITIGNER^{254} (83) ^{285}CDVDIR^{290} (6)
914	40 4.62	2.70	Actin, cytoplasmic 1 (ACTB_HUMAN) Actin, cytoplasmic 2 (ACTG_HUMAN) Actin, gamma-enteric smooth muscle (ACTH_HUMAN) Actin, aortic smooth muscle (ACTA_HUMAN) Actin, alpha cardiac muscle 1 (ACTC_HUMAN) Actin, alpha skeletal muscle (ACTS_HUMAN)	gi: 46397333 gi: 4501887 gi: 54036679 gi: 51316972 gi: 54036697 gi: 61218043	41.7 5.29 41.8 5.31 41.9 5.31 42.0 5.23 42.0 5.23 42.0 5.23	2	110	7	^{29}AVFPSIVGRPR^{39} (9) ^{239}SYELPDGQVITIGNER^{254} (87) ^{30}AVFPSIVGRPR^{40} (9) ^{240}SYELPDGQVITIGNER^{255} (87) ^{31}AVFPSIVGRPR^{41} (9) ^{241}SYELPDGQVITIGNER^{256} (87)
897	22.1 5.14	2.66	DNA-directed RNA polymeraseII subunit RPB11-b2 (RPB1C_HUMAN)	gi: 74725032	13.1 5.88	4	56	27	^{104}FRTCLLPLR^{112} (9)
900	30 5.57	2.66	POTE ankyrin domain family member F	gi: 153791352	121 5.83	3	67	4	^{939}SYELPDGQVITIGNER^{954} (59)
637	27.9 5.43	2.55	Actin, cytoplasmic 1(ACTB_HUMAN) Actin, cytoplasmic 2 (ACTG_HUMAN) Beta-actin-like protein 2 (ACTBL_HUMAN)	gi: 46397333 gi: 4501887 gi: 172046825	41.7 5.29 41.8 5.31 42.0 5.39	3	101	6	^{239}SYELPDGQVITIGNER^{254} (88)
621	28.7 5.45	2.53	Putative beta-actin-like protein3 (ACTBM_HUMAN) Actin, cytoplasmic 1 (ACTB_HUMAN) Actin, cytoplasmic 2 (ACTG_HUMAN) Bate-actin-like protein 2 (ACTBL_HUMAN) Actin, gamma-enteric smooth muscle (ACTH_HUMAN) Actin, aortic smooth muscle (ACTA_HUMAN) Actin, alpha cardiac muscle 1 (ACTC_HUMAN) Actin, alpha skeletal muscle (ACTS_HUMAN)	gi: 74739412 gi; 46397333 gi: 4501887 gi: 172046825 gi: 54036679 gi: 51316972 gi: 54036697 gi: 61218043	42.0 5.91 41.7 5.29 41.8 5.31 42.0 5.39 41.9 5.31 42.0 5.23 42.0 5.23 42.0 5.23	2	62	4	^{239}YELPDGQVITIGNER^{254} (54) ^{240}YELPDGQVITIGNER^{255} (54) ^{241}YELPDGQVITIGNER^{256} (54)
421	47.7 8.28	-2.75	Meiosis 1 arrest protein (M1AR_HUMAN)	gi: 74730556	59.3 6.40	7	72	17	^{379}IPASTFYVIMPSHSLTLLVK^{398} (22)
376	55.8 6.29	-3.09	Heterogeneous nuclear ribonucleoprotein H (HNRH1_HUMAN)	gi: 1710632	49.2 5.89	7	77	24	^{300}ATENDIYNFFSPLNPVR^{316} (26)
391	52.9 6.19	-3.21	Pyruvate kinase PKM (KPYM_HUMAN)	gi: 20178296	57.9 7.96	10	92	21	^{384}EAEAAIYHLQLFEELR^{399} (13)
356	59 4.92	-3.40	Tubulin alpha-4A chain (TBA4A_HUMAN)	gi: 55977476	49.9 4.95	11	104	30	^{65}AVFVDLEPTVIDEIR^{79} (27)

Peptides recovered from the 17 protein spots after in-gel digestion with trypsin were subjected to MALDI-TOF/TOF-MS analysis. MW; molecular weight, p*I;* Isoelectric points, LID; laser-induced dissociation

First, spot no. 649, which showed 5.85-fold higher intensity in the SLE patient group than in the HL group, was identified as myeloblastin. It is also known as proteinase 3 (PR3). PR3 is a serine protease that is mainly located in granules of neutrophils and eosinophils [16]. PR3 is also known as a target of anti-neutrophil cytoplasm antibodies (ANCA) [17]. It was reported that mRNA for PR3 in monocytes was increased in patients with SLE compared to HL [18]. Furthermore, it was reported that amounts of cell surface PR3 were increased by TNF-α stimulation in neutrophils of patients with SLE and monocytes of patients with ANCA-associated vasculitis [19,20]. In addition, serum TNF-α levels were reported to be increased in patients with SLE [21]. Taking our data together with these reports, both PR3 expression and its translocation to the plasma membrane fraction would be increased in PBMCs of patients with SLE. Roles of the increase in the pathogenesis of SLE should be investigated in the future.

Second, spot no. 899, which showed 3.72-fold higher intensity in the SLE patient group than in the HL group, was identified as cyclin L1. Cyclin L1 is usually located in cytoplasm. It was reported that cyclin L1 was involved in the splicing of mRNA [22,23]. In T cells of patients with SLE, abnormal splicing of TCR zeta chain was reported [24,25]. Our data and their reports indicate possible involvement of translocation of cyclin L1 in the abnormal splicing in T cells of patients with SLE. This point should be also investigated in detail in the future.

Third, spot nos. 560, 582, 621, 637, 651, 734, 913, and 914, intensity

of which was 2,53~3,24-fold higher in the SLE patient group than in the HL group, were assigned to members of the actin family. The existence of multiple spots would indicate different isoforms of actin and/or different post-translational modification of actin. Since actin is an important component of cytoskeleton, PBMCs in patients with SLE would alter the structure of cytoskeleton, reflecting functional abnormalities of lymphocytes. Further studies are needed to clarify the relation between the actin alteration and functional abnormalities of lymphocytes.

Conclusion

In conclusion, our study comprehensively investigated CS protein profiles of PBMCs from patients with SLE for the first time, to our knowledge. We found that CS protein profiles from PBMCs from patients with SLE are greatly different from those of HLs. Our study would provide a new strategy to investigate the pathophysiology of SLE.

Acknowledgement

We thank Ms. Yokoyama MK for her technical assistance.

Conflicts of interest

The authors has no conflicts of interest.

References

1. Tan EM, Cohen AS, Fries JF, Masi AT, McShane DJ, et al. (1982) The 1982 revised criteria for the of systemic lupus erythematosus. *Arthritis Rheum* 25: 1271-1277. [Crossref]
2. Yu C, Gershwin ME, Chang C (2014) Diagnostic criteria for systemic lupus erythematosus: a critical review. *J Autoimmun* 48-49: 10-3. [Crossref]
3. Petri M, Orbai AM, Alarcon GS, Gordon C, Merrill JT, et al. (2012) Derivation and validation of the systemic lupus international collaborating clinics criteria for systemic lupus erythematosus. *Arthritis Rheum* 64: 2677–2686. [Crossref]
4. Miranda-Carús ME, Askanase AD, Clancy RM, Di Donato F, Chou TM, et al. (2000) Anti-SSA/Ro and anti-SSB/La autoantibodies bind the surface of apoptotic fetal cardiocytes and promote secretion of TNF-alpha by macrophages. *J Immunol*. 165: 5345-5351.
5. Cozzani E, Agnoletti AF, Pappalardo F, Schiavetti I, Torino A, et al. (2016) The high incidence of anti-Ro/SSA and anti-p200 antibodies in female patients with connective tissue diseases the importance of screening for congenital heart block-associated autoantibodies during pregnancy. *Arch Dermatol Res*. 308: 139-143.
6. Mak A, Kow NY (2014) The pathology of T cells in systemic lupus erythematosus. *J Immunol Res* 2014: 419029. [Crossref]
7. Shlomchik MJ, Craft JE, Mamula MJ (2001) From T to B and back again: positive feedback in systemic autoimmune disease. *Nat Rev Immunol* 1: 147-153. [Crossref]
8. Anolik JH (2013) B cell biology: implications for treatment of systemic lupus erythematosus. *Lupus* 22: 342-349. [Crossref]
9. Kow NY, Mak A. (2013) Costimulatory pathways: physiology and potential therapeutic manipulation in systemic lupus erythematosus. *Clin Dev Immunol* 16: 245928.
10. Hase K, Tani K, Shimizu T, Ohmoto Y, Matsushima K, et al. (2001) Increased CCR4 expression in active systemic lupus erythematosus. *J Leukoc Biol* 70: 749-755. [Crossref]
11. Bohgaki T, Amasaki Y, Nishimura N, Bohgaki M, Yamashita Y, et al. (2005) Up regulated expression of tumour necrosis factor α converting enzyme in peripheral monocytes of patients with early systemic sclerosis. *Ann Rheum Dis* 64: 1165-1173.
12. Nakano S, Morimoto S, Suzuki J, Nozawa K, Amano H, et al. (2008) Role of pathogenic auto-antibody production by Toll-like receptor 9 of B cells in active systemic lupus erythematosus. *Rheumatology* (Oxford) 47: 145-149.
13. Herrada AA, Llanos C, Mackern-Oberti JP, Carreño LJ, Henriquez C, et al. (2012) Haem oxygenase 1 expression is altered in monocytes from patients with systemic lupus erythematosus. *Immunology* 136: 414-424.
14. Onodera H, Arito M, Sato T, Ito H, Hashimoto T, et al. (2013) Novel effects of edaravone on human brain microvascular endothelial cells revealed by a proteomic approach. *Brain Res* 1534: 87-94. [Crossref]
15. Fujisawa H, Ohtani-Kaneko R, Naiki M, Okada T, Masuko K, et al. (2008) Involvement of post-translational of neuronal plasticity-related proteins in hyperalgesia revealed by a proteomic analysis. *Proteomics* 8: 1706-1719.
16. Kettritz R (2016) Neutral serine proteases of neutrophils. *Immunol Rev* 273: 232-248. [Crossref]
17. van der Geld YM, Limburg PC, Kallenberg CG (2001) Proteinase 3, Wegener's autoantigen: from gene to antigen. *J Leukoc Biol* 69: 177-190. [Crossref]
18. Ohlsson S, Hellmark T, Pieters K, Sturfelt G, Wieslander J, et al. (2005) Increased monocyte transcription of the proteinase 3 gene in small vessel vasculitis. *Clin Exp Immunol* 141: 174-182. [Crossref]
19. van Rossum AP, Huitema MG, Stegeman CA, Bijl M, de Leeuw K, et al. (2007) Standardised assessment of membrane proteinase 3 expression. Analysis in ANCA-associated vasculitis and controls. *Ann Rheum Dis* 66: 1350-1355.
20. Hattar K, Bickenbach A, Csernok E, Rosseau S, Grandel U, et al. (2002) Wegener's granulomatosis: antiproteinase 3 antibodies induce monocyte cytokine and prostanoid release-role of autocrine cell activation. *J Leukoc Biol* 71: 996-1004. [Crossref]
21. Weckerle CE, Mangale D, Franek BS, Kelly JA, Kumabe M, et al. (2012) Large-scale analysis of tumor necrosis factor α levels in systemic lupus erythematosus. *Arthritis Rheum* 64: 2947-2952.
22. Chen HH, Wang YC, Fann MJ (2006) and characterization of the CDK12/cyclin L1 complex involved in alternative splicing regulation. *Mol Cell Biol* 26: 2736-2745.
23. Loyer P, Trembley JH, Grenet JA, Busson A, Corlu A, et al. (2008) Characterization of cyclin L1 and L2 interactions with CDK11 and splicing factors: of cyclin L isoforms on splice site selection. *J Biol Chem*. 283: 7721-7732.
24. Tsuzaka K, Onoda N, Yoshimoto K, Setoyama Y, Suzuki K, et al. (2002) T-cell receptor ζ mRNA with an alternatively spliced 3' untranslated region is generated predominantly in the peripheral blood T cells of systemic lupus erythematosus patients. *Mod Rheumatol* 12: 167-173.
25. Tsuzaka K, Nozaki K, Kumazawa C, Shiraishi K, Setoyama Y, et al. (2006) TCR 3mRNA splice variant forms observed in the peripheral blood T cells from systemic lupus erythematosus patients. *Springer Semin Immun* 28: 185-193.

Copyright: ©2016 Nozawa Y. This is an open-access article distributed under the terms of the Creative Commons Attribution License, which permits unrestricted use, distribution, and reproduction in any medium, provided the original author and source are credited.

Journal of Dermatological Science 87 (2017) 36–49

Contents lists available at ScienceDirect

Journal of Dermatological Science

journal homepage: www.jdsjournal.com

Serum peptides as putative modulators of inflammation in psoriasis

Tetsuhiko Matsuura[a], Masaaki Sato[b], Kouhei Nagai[c], Toshiyuki Sato[b], Mitsumi Arito[b], Kazuki Omoteyama[b], Naoya Suematsu[b], Kazuki Okamoto[b], Tomohiro Kato[b], Yoshinao Soma[a], Manae S. Kurokawa[d,*]

[a] Department of Dermatology, St. Marianna University School of Medicine, Japan
[b] Clinical Proteomics and Molecular Medicine, St. Marianna University Graduate School of Medicine, Japan
[c] Department of Genetic Engineering, Faculty of Biology-Oriented Science and Technology, Kindai University, Japan
[d] Disease Biomarker Analysis and Molecular Regulation, St. Marianna University Graduate School of Medicine, Japan

ARTICLE INFO

Article history:
Received 28 November 2016
Accepted 21 March 2017

Keywords:
Psoriasis vulgaris
Psoriatic arthritis
Serum peptides
Mass spectrometry
Fibrinogen α chain
Filaggrin

ABSTRACT

Background: Psoriasis is a refractory inflammatory disease, however, its pathophysiology is still not fully understood.
Objective: We tried to identify novel serum peptides associated with the pathophysiology of psoriasis.
Methods: Serum peptides from 24 patients with psoriasis vulgaris (PV), 10 patients with psoriatic arthritis (PsA), 14 patients with atopic dermatitis (AD), and 23 healthy control (HC) subjects were analyzed by mass spectrometry. The effects of some peptides on the secretion of humoral factors from dermal cells were investigated by cytokine arrays and ELISAs.
Results: A total of 93 peptides were detected. 24, 20, 23, and 2 peptides showed at least 1.2-fold difference in ion intensity between the psoriasis (PV + PsA) and HC groups, between the PV + PsA and AD groups, between the PV and PsA groups, and between patients with severe-to-moderate PV ($n = 6$) and those with mild PV ($n = 18$), respectively ($p < 0.05$). 13 out of 27 peptides that showed at least 1.5-fold ion intensity difference in the abovementioned 4 comparisons were identified. The parent proteins of the identified peptides included a coagulation factor, proteins involved in the maintenance of skin, and a protein relating to cytoskeleton. We focused on 2 peptides that were increased in the PV + PsA group: a fibrinogen α chain-derived peptide (1462 m/z), the unmodified form of which was fibrinopeptide A-des-alanine (FPAdA), and a filaggrin (FLG)-derived peptide (1977 m/z), a modified form of $FLG_{2099-2118}$ (Q_{2099}pE, Q_{2115}E; FLG-pEE). FPAdA stimulation increased the secretion of GROα from dermal microvascular endothelial cells (dMVECs) and decreased the secretion of lipocalin-2 from keratinocytes in comparison to FPAdA-resequenced peptide stimulation (GROα, 280.9 ± 7.3 pg/mL vs. 229.6 ± 5.0 pg/mL, $p < 0.001$; lipocalin-2, 273 ± 13 pg/mL vs. 350 ± 10 pg/mL, $p < 0.01$). Interestingly, FLG-pEE stimulation decreased the secretion of GROα, IL-8, and MCP-1 from dMVECs in comparison to FLG-derived control peptide stimulation (GROα, 844.3 ± 47.5 pg/mL vs. 1038.5 ± 96.9 pg/mL, $p < 0.05$; IL-8, 2240.1 ± 172.6 pg/mL vs. 3221.8 ± 523.7 pg/mL, $p < 0.05$; MCP-1, 4057.8 ± 157.2 pg/mL vs. 4619.1 ± 213.4 pg/mL, $p < 0.05$).

Abbreviations: AD, atopic dermatitis; α2HS-GP, alpha-2-HS-glycoprotein; CCL20, C–C motif ligand 20; CCR2, C–C chemokine receptor type 2; CRP, C-reactive protein; CYA, ciclosporin; DC, dendritic cells; Dkk-1, dickkopf-related protein 1; dMVECs, dermal microvascular endothelial cells; E, glutamate; ELISA, enzyme-linked immunosorbent assay; ELR, glutamate-leucine-arginine; FIBA, fibrinogen alpha chain; FIBA-αCDC, C-terminal portion of the αC-domain of FIBA; FLG, filaggrin; FPA, fibrinopeptide A; FPAdA, fibrinopeptide A-des-alanine; GROα, growth-regulated oncogene alpha; HC, healthy control; HLA, human leukocyte antigen; HPLC, high-performance liquid chromatography; IL-1ra, interleukin 1 receptor antagonist; IMQ, imiquimod; M, methionine; MALDI-TOF/MS, matrix-assisted laser desorption/ionization time-of-flight mass spectrometry; MCP-1, monocyte chemoattractant protein 1; MIF, macrophage migration inhibitory factor; MMP, matrix metalloproteinase; mPV, mild psoriasis vulgaris; MS, mass spectrometry; MTX, methotrexate; NSAIDs, non-steroidal anti-inflammatory drugs; PASI, Psoriatic Area and Severity Index; pE, pyroglutamate; PsA, psoriatic arthritis; PSL, prednisolone; PV, psoriasis vulgaris; Q, glutamine; SD, standard deviation; SHBG, sex hormone binding globulin; sPV, severe-to-moderate psoriasis vulgaris; TGFα, transforming growth factor alpha; TNF, tumor necrosis factor; VEGF, vascular endothelial growth factor.

* Corresponding author at: Disease Biomarker Analysis and Molecular Regulation, St. Marianna University Graduate School of Medicine, 2-16-1, Sugao, Miyamae-ku, Kawasaki, Japan.
E-mail address: manae@marianna-u.ac.jp (M.S. Kurokawa).

http://dx.doi.org/10.1016/j.jdermsci.2017.03.014
0923-1811/ © 2017 Japanese Society for Investigative Dermatology. Published by Elsevier Ireland Ltd. All rights reserved.

Conclusions: The results suggested that some serum peptides are involved in the pathophysiology of psoriasis, regulating the secretion of inflammatory chemokines and an antimicrobial protein. The modulation of serum peptides may be a potential therapeutic strategy for psoriasis.

© 2017 Japanese Society for Investigative Dermatology. Published by Elsevier Ireland Ltd. All rights reserved.

1. Introduction

Psoriasis is a chronic inflammatory multi-organ disease that mainly manifests in the skin [1,2]. The estimated prevalence of psoriasis is approximately 2% worldwide and 0.34% in Japan [1,3]. The most common type of psoriasis is psoriasis vulgaris (PV), which accounts for approximately 90% of cases [1,4]. The typical lesions are monomorphic and well-demarcated erythematous plaques covered by silvery scales [1,5]. Patients with PV suffer from pain, itching, and bleeding of the skin lesions. Furthermore, patients with psoriasis are at risk of developing other chronic inflammatory diseases such as arthritis (psoriatic arthritis, PsA), metabolic syndrome, cardiovascular disorders, depression, and cancer [1,4,5]. Since the pathophysiology of psoriasis remains unclear, it is imperative to elucidate the pathophysiology in order to establish effective treatments for the disease.

It is widely accepted that aberrant immune responses shifting toward the IL-23/Th17 and Th1 axes play major roles in the pathophysiology of psoriasis [1,5]. IL-17, which is produced by Th17 cells, γδT cells, neutrophils, and mast cells, activates keratinocytes to produce ELR^+ chemokines such as GROα and IL-8 and CCL20 bringing neutrophils, dendritic cells (DCs), and T cells into the psoriatic lesion [6–10]. IL-22, which is produced by Th17 cells, Th1 cells, and Th22 cells, promotes the proliferation of keratinocytes and hyperkeratosis [6]. The activation of keratinocytes by TGFα, which is overexpressed in psoriatic epidermis, increases the secretion of VEGFα from the cells [11]. VEGFα binds to its receptors, kdr and flt-1, which are expressed by papillary dermal microvascular endothelial cells (dMVECs) to induce hyperpermeability. VEGF, hypoxia-inducible factors, angiopoietins, and proangiogenic cytokines such as TNF, IL-8, and IL-17, are up-regulated in psoriatic lesions, which increases dermal vascularity [11,12]. On the other hand, keratinocytes overexpress antimicrobial peptides such as LL37 and β-defensin 2, which trigger the self-nucleic acid-mediating activation of plasmacytoid DCs through toll-like receptor 9 [13,14]. Furthermore, genetic risk factors such as HLA-Cw6 are associated with the onset [1,15]. Nonetheless, the precise pathophysiology of psoriasis is not fully understood. The identification of novel disease-related molecules will thus be necessary to elucidate of the pathophysiology.

In the present study, we comprehensively analyzed the serum peptides in PV and PsA patients. We found that the serum peptide profiles of psoriasis differed from those of healthy individuals and atopic dermatitis (AD) patients. Some of the peptides that were increased in psoriasis were found to modulate the secretion of inflammatory chemokines from dermal cells. Our data suggested a novel disease mechanism of psoriasis, which involves the degradation of proteins in the skin and blood.

2. Materials and methods

2.1. Patients and serum samples

The diagnosis of PV was clinically made. The diagnoses of PsA and AD were made according to the respective criteria [16,17]. Serum samples were obtained from 24 patients with PV, 10 patients with PsA, 14 patients with AD, and 23 healthy control (HC) subjects after they provided written informed consents (Table 1). The study protocol conformed to the ethical guidelines of the 1964 Declaration of Helsinki and its later amendments and was approved by the ethics committee of St. Marianna University School of Medicine.

Table 1
The clinical information of the subjects.

	PV (n = 24)	PsA (n = 10)	AD (n = 14)	HC (n = 23)
Male:female	15:9	5:5	8:6	15:8
Age (years)[a]	56.8 ± 18.2	53.1 ± 17.6	38.8 ± 12.1	57.6 ± 18.5
Disease duration (years)[a]	12.1 ± 7.8	6.0 ± 4.7	24.7 ± 10.1	–
PASI[a]	7.0 ± 4.9	3.9 ± 3.5	–	–
BSA (%)[a]	15.8 ± 17.0	6.2 ± 7.4	–	–
CRP (mg/dL)[a,b]	0.20 ± 0.30 (n = 18)	0.33 ± 0.33	–	–
Comorbid diseases[c]	2 HT, 2 HT/DM, 1 HT/DM/CI, 1 HT/DL/FL/ML, 1 DL/HU, 1 HU, 1 BD, 1 CB, 1 PP, 1 PC	2 DM, 1 FL, 1 HT/DM/HU, 1 HT/HU/FL/R, 1 CB	None	None
Treatment[d]	24 ext CS/VD3; 3 CYA, 1 ADA, 1 IFX, 1 UST; 1 VA	3 ext CS/VD3, 1 ext CS/VD3/IND; 1 LOX, 3 MTX, 1 CYA/LOX, 1 PSL/CEL, 1 PSL/CYA/LOX	13 ext CS; 2 CYA, 1 FX	–

PV, psoriasis vulgaris; PsA, psoriatic arthritis; AD, atopic dermatitis; HC, healthy control; PASI, Psoriasis Area and Severity Index; BSA, body surface area; HT, hypertension; DM, diabetes mellitus; CI, cerebral infarction; DL, dyslipidemia; FL, fatty liver; ML, malignant lymphoma; HU, hyperuricemia; BD, Basedow's disease; CB, chronic bronchitis; PP, palmoplantar pustulosis; PC, prostatic carcinoma; R, rhinitis; CYA, ciclosporin; ADA, adalimumab; IFX, infliximab; UST, ustekinumab; VA, vitamin A derivative; LOX, loxoprofen; MTX, methotrexate; CEL, celecoxib; FX, fexofenadine.

[a] Mean ± standard deviations.

[b] C-reactive protein (CRP) was measured in 18 out of 24 PV patients and in all the 10 PsA patients.

[c] Comorbid diseases such as metabolic diseases, cardiovascular diseases, and other inflammatory diseases are shown.

[d] The external use of corticosteroids (CS), vitamin D3 (VD3), and indomethacin (IND) were counted independently from other treatments.

The disease severity of PV was estimated according to the Psoriatic Area and Severity Index (PASI) [18,19]. The 24 PV patients were divided into 2 groups according to their PASI values [20]; the severe-to-moderate PV (sPV, PASI > 10) group ($n = 6$; male, $n = 3$; female, $n = 3$; mean ± standard deviation [SD] age, 42.7 ± 15.7 years; disease duration, 19.5 ± 8.6 years; PASI, 14.3 ± 2.8) and the mild PV (mPV; PASI ≤ 10) group ($n = 18$; male, $n = 12$; female, $n = 6$; age, 61.6 ± 16.4 years; disease duration, 9.6 ± 5.7 years; PASI, 4.6 ± 2.4).

To analyze the correlation between peptide ion intensity and treatment, we designed a treatment score in which the treatments for psoriasis in this study were classified into five groups as follows: Score 0 ($n = 0$), no treatment; Score 1 ($n = 19$), external medication and/or internal vitamin A derivative; Score 2 ($n = 3$), non-steroidal anti-inflammatory drugs (NSAIDs), with or without drugs in score 1; Score 3 ($n = 9$), prednisolone (PSL) ≤ 5 mg/day, methotrexate (MTX) ≤ 8 mg/week, ciclosporin (CYA) ≤ 3 mg/kg/day, or maintenance dosages of biological drugs, with or without drugs in scores 1 and 2; Score 4 ($n = 3$), (i) PSL > 5 mg/day, MTX > 8 mg/week, CYA > 3 mg/kg/day, or increased dosages of biological drugs, (ii) at least two of PSL, immunosuppressants (MTX or CYA), and biological drugs, both (i) and (ii) are with or without drugs in scores 1 and 2.

2.2. The comparison of peptide profiles and the identification of peptide sequences

Serum peptides were purified using weak cation exchange chromatography (Bruker Daltonics, Ettlingen, Germany). The concentration of each peptide was measured according to the ion intensity on matrix-assisted laser desorption/ionization time-of-flight mass spectrometry (MALDI-TOF/MS, Ultraflex, Bruker Daltonics). The ion intensity of the peptides was obtained as the peak heights using ClinPro Tools software program (Bruker Daltonics). The peptides were designated according to the mass to charge ratios (i.e., p1056 indicates a peptide with 1056 m/z).

The amino acid sequences of the peptides were identified by tandem mass spectrometry using a nano-HPLC system (Ecksigent nano-LC400 system, AB sciex, Framingham, MA, USA) connected to a Triple TOF5600 system (AB sciex). The MS and MS/MS spectra that were obtained were used to identify the parent proteins of the peptides by searching the Uniprot protein database using a software (Protein Pilot version 4.0, AB sciex).

2.3. The synthesis of peptides and cell culturing

A peptide corresponding to fibrinopeptide A-des-alanine (FPAdA, N-DSGEGDFLAEGGGVR-C) and a control peptide for FPAdA (FPAdA-Cont) in which the 15 amino acids were randomly re-sequenced (N-GDRGEGASGELDVFG-C) were synthesized (Eurofins Genomics, Tokyo, Japan). Peptides derived from filaggrin (FLG), $FLG_{2099-2118}$ (N-QSESTHGQSAPSTGGRQGSH-C, FLG-Q_2), a modified form of $FLG_{2099-2118}$ ($FLG_{2099-2118}$,Q_{2099}pE,Q_{2115}E, N-pESESTHGQ-SAPSTGGREGSH-C, FLG-pEE), and a control peptide, FLG_{52-71} (N-DMVDVFMDHLDIDHNKKIDF-C, FLG-Cont) were similarly synthesized (Eurofins Genomics).

Human dMVECs and human keratinocytes were purchased (Lonza, Walkersville, MD, USA). To prepare the culture supernatants for cytokine assays, 1×10^5 cells were cultured with FPAdA, FPAdA-Cont or medium-alone for 24 h. Similarly, 1×10^5 cells were

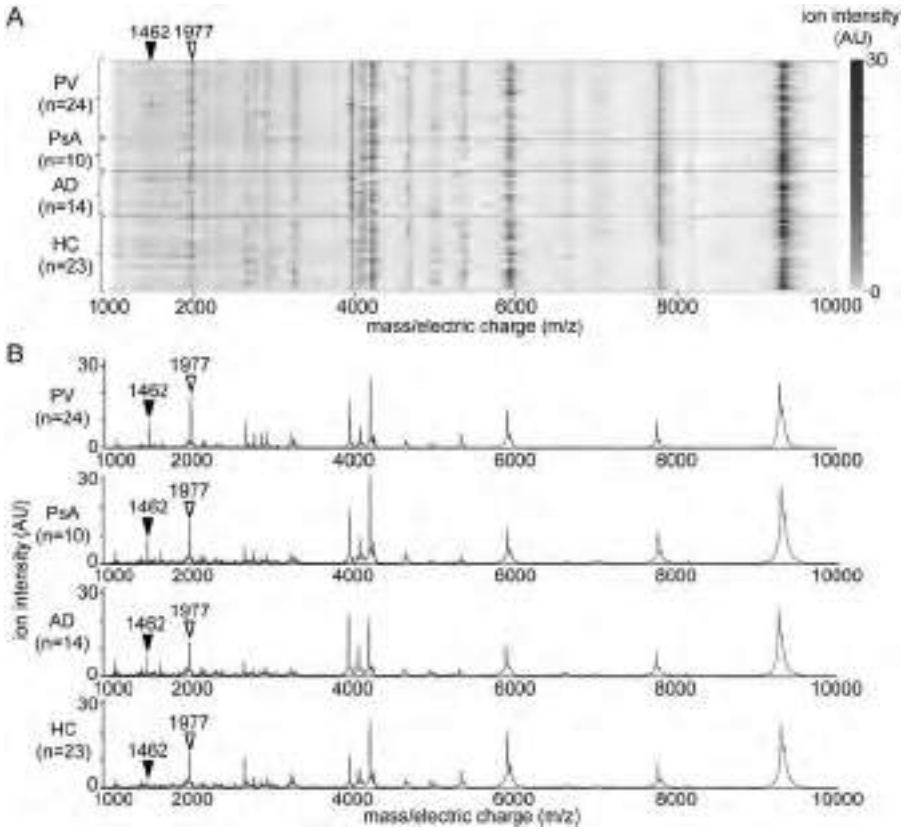

Fig. 1. The serum peptide profiles of the psoriasis patients. (A) A gel image of the ion intensity of the detected peptides. The results of each serum sample are vertically aligned. The numbers of the patients in the PV, PsA, AD, and HC groups are shown in the parentheses. The intensity is shown as black-white gradation, as indicated on the right side of the panel. (B) The average ion intensity of the serum peptides in the PV, PsA, AD, and HC groups. Black arrowheads show p1462, the ion intensity of which was increased 2.99-fold in the PV + PsA group in comparison to the HC group. The white arrowheads show p1977, the ion intensity of which was increased 1.44-fold and 1.45-fold in the PV + PsA group in comparison to the HC and AD groups, respectively.

cultured with FLG-pEE, FLG-Q_2, FLG-Cont, or medium-alone for 24 h. The culture supernatants were recovered and stocked at −80 °C until the analysis.

2.4. The analysis of the secretion of humoral factors from dermal cells stimulated with the peptides

Humoral factors including proinflammatory cytokines and chemokines in culture supernatants were measured in duplicate by cytokine arrays (for dMVECs, Human Cytokine Array, R&D Systems, Minneapolis, MN, USA; for keratinocytes, Human XL Cytokine Array kit, R&D Systems). Humoral factors that were detected as specific spots were visualized using ECL Plus (GE Healthcare, Piscataway, NJ, USA) and a LAS-3000 Imager (Fujifilm, Tokyo, Japan). The intensity of each spot, which was measured using the Science Lab 2001 Image Gauge software program (Fujifilm), was normalized based on the intensity of a positive control sample. The humoral factors that were selected by cytokine arrays were measured in triplicate with their respective ELISA kits (R&D Systems).

2.5. Statistical analysis

The significance of the differences in peptide ion intensity among the PV, PsA, AD and HC groups was calculated using Student's *t*-test. The correlations between the peptide ion intensity and clinical parameters were calculated using Spearman's rank correlation coefficient. The significance of the differences in peptide ion intensity according to the difference in treatment was calculated using Wilcoxon's signed-rank test.

3. Results

3.1. A comparison of the serum peptide profiles among the PV, PsA, AD, and HC groups

To find the serum peptides associated with the pathophysiology of psoriasis (PV + PsA), we comprehensively measured the ion intensity of serum peptides in the PV, PsA, AD, and HC groups. A total of 93 peptide ion peaks were detected (Fig. 1A and B). Among these, we compared the ion intensity between the PV + PsA and HC groups, and between the PV + PsA and AD groups (Table 2). In the PV + PsA group, 18 peptides showed an ion intensity that was at least 1.2-fold higher and 6 peptides showed an ion intensity that was at least 1.3-fold lower in comparison to the HC group ($p < 0.05$). Similarly, in the PV + PsA group, 11 peptides showed an ion intensity that was at least 1.3-fold higher and 9 peptides showed an ion intensity that was at least 1.3-fold lower in comparison to the AD group ($p < 0.05$).

Furthermore, we compared the serum peptide profiles between the subgroups of psoriasis patients. In the PsA group, 7 peptides showed an ion intensity that was at least 1.2-fold higher and 16 peptides showed an ion intensity that was at least 1.3-fold lower in comparison to the PV group ($p < 0.05$) (Table 2). In the sPV group, 2 peptides showed an ion intensity that was at least 1.5-fold lower in comparison to the mPV group ($p < 0.05$).

Collectively, the serum peptide profiles of psoriasis (PV + PsA) patients were found to differ from AD patients and HC subjects. Among the psoriasis patients, there were differences in the peptide profiles of PV and PsA patients, and in the peptide profiles of sPV and mPV patients.

3.2. The identification of the disease-specific peptides in psoriasis

We tried to identify the peptides with an ion intensity that showed a ≥1.5-fold difference in the 4 comparisons (Table 2). Although Table 2 shows 35 of these peptides, the actual number was 27 because some of the peptides overlapped.

We identified 13 out of the 27 peptides and found 4 parent proteins (Table 3). It is noteworthy that 9 of the 13 identified peptides were derived from the fibrinogen alpha chain (FIBA); in the PV + PsA group, the ion intensity of most of these peptides was higher in comparison to the HC and/or AD groups. Two out of the 9 FIBA peptides were derived from FPA; the other 7 were derived from the αC-domain (Fig. 2). In the PV + PsA group, the ion intensity of p1462 derived from FPA was 2.99-fold higher than that in the HC group. p1462 was identified as FPA_{1-15},$S_{3phospho}$ or N-terminal alanine-defective FPA, FPA_{2-16} (FPAdA) (Table 3).

Interestingly, in the PV + PsA group, the ion intensity of p1977 was 1.44-fold and 1.45-fold higher than that in the HC and AD groups, respectively. p1977 was identified as being derived from FLG, which is involved in the terminal differentiation of mammalian epidermis (Table 3) [21,22]. This peptide included two types of post-translational modifications; the N-terminal (2099th) glutamine (Q) was changed to pyroglutamate (pE) and the 17th (2115th) Q was deamidated (changed to glutamate, E) ($FLG_{2099-2118}$,Q_{2099}pE,Q_{2115}E; FLG-pEE). Two peptides, p4964 and p4979, were derived from the thymosin β4 protein, which is associated with actin filament organization [23]. In the PsA group, the ion intensities of p4964 and p4979 were 1.95- and 1.67-fold

Table 2
The comparison of peptide ion intensity.

Peptide ion intensity	Differences (*x*-folds)	Numbers of peptides			
		(PV + PsA)/HC ($n = 34/n = 23$)	(PV + PsA)/AD ($n = 34/n = 14$)	PsA/PV ($n = 10/n = 24$)	sPV/mPV ($n = 6/n = 18$)
Increased	$2.0 \leq x$	1	1	0	0
	$1.5 \leq x < 2.0$	2	7	1	0
	$1.3 \leq x < 1.5$	10	3	5	0
	$1.2 \leq x < 1.3$	5	0	1	0
	$-1.2 < x < 1.2$	0	0	0	0
Decreased	$-1.2 \geq x > -1.3$	0	0	0	0
	$-1.3 \geq x > -1.5$	3	3	4	0
	$-1.5 \geq x > -2.0$	2	6	11	2
	$-2.0 \geq x$	1	0	1	0

The numbers of peptides, for which the ion intensity was significantly different between the 2 indicated groups, are shown ($p < 0.05$). The numbers in the parentheses indicate the numbers of subjects.
PV, psoriasis vulgaris; PsA, psoriatic arthritis; HC, healthy control; AD, atopic dermatitis; sPV, severe-to-moderate psoriasis vulgaris; mPV, mild psoriasis vulgaris.

Table 3
The identification of the serum peptides in psoriasis.

m/z	Selections	Proteins	Accession ID[a]	Theoretical	Observed	Confidence	dMass	Confirmed sequences[a]	Modification
1056	−1.76 (PV + PsA)/AD	cDNA FLJ55606, highly similar to alpha-2-HS-glycoprotein	B7Z8Q2_HUMAN	1055.6	1056.2	99	−1.15E−04	^{407}TVVQPSVGAAAG^{418}	–
1462	2.99 (PV + PsA)/HC	Fibrinogen alpha chain	FIBA_HUMAN	1459.6	1459.6	99	−1.02E−03	^{1}ADSGEGDFLAEGGGV^{15}	Phospho (S)
		Fibrinogen alpha chain	FIBA_HUMAN	1464.6	1465.5	99	−5.59E−05	^{2}DSGEGDFLAEGGGVR^{16}	–
1613	1.90 (PV + PsA)/HC	Fibrinogen alpha chain	FIBA_HUMAN	1615.7	1616.5	99	−8.21E−05	^{1}ADSGEGDFLAEGGGVR^{16}	Phospho (S)
1977	1.44 (PV + PsA)/HC 1.45 (PV + PsA)/AD	Filaggrin	FILA_HUMAN	1978.8	1980.0	98.14	−1.2E−02	^{2099}QSESTHGQSAPSTGGRQGSH^{2118}	pyro-Glu (N-term) Deamidated (^{2115}Q)
2658	−1.61 PsA/PV	Fibrinogen alpha chain	FIBA_HUMAN	2658.2	2659.8	99	9.69E−04	^{586}DEAGSEADHEGTHSTKRGH AKSRPV^{610}	–
2681	1.45 (PV + PsA)/AD −1.54 PsA/PV	Fibrinogen alpha chain	FIBA_HUMAN	2680.2	2681.8	99	5.17E−04	^{557}SSSYSKQFTSSTSYNRGDSTF ESK^{580}	–
2767	1.96 (PV + PsA)/AD	Fibrinogen alpha chain	FIBA_HUMAN	2767.2	2768.8	99	−5.05E−04	^{557}SSSYSKQFTSSTSYNRGDSTF ESKS^{581}	–
2930	1.36 (PV + PsA)/HC 1.43 (PV + PsA)/AD −1.75 PsA/PV	Fibrinogen alpha chain	FIBA_HUMAN	2930.3	2932.0	99	−1.33E−03	^{557}SSSYSKQFTSSTSYNRGDSTF ESKSY^{582}	–
3239	1.55 (PV + PsA)/AD −1.57 PsA/PV −1.61 sPV/mPV	Fibrinogen alpha chain	FIBA_HUMAN	3238.5	3240.5	99	3.10E−04	^{581}SYKMADEAGSEADHEGTHS TKRGHAKSRPV^{610}	–
4053	−2.04 (PV + PsA)/HC	Fibrinogen alpha chain	FIBA_HUMAN	4049.9	4052.3	99	1.29E−02	^{518}LGEFVSETESRGSESGIFTN TKESSSHHPGIAEFPSRG^{555}	–
4964	−1.95 PsA/PV	TMSB4X protein	Q0P5N8_HUMAN	4960.5	4963.5	99	3.72E−04	^{27}SDKPDMAEIEKFDKSKLKKTETQ EKNPLPSKETIEQEKQAGES^{69}	Protein terminal acetyl (N-term)
4979	−1.67 PsA/PV	TMSB4X protein	Q0P5N8_HUMAN	4976.5	4979.5	96.74	−2.06E−03	^{27}SDKPDMAEIEKFDKSKLKKTETQ EKNPLPSKETIEQEKQAGES^{69}	Protein terminal acetyl (N-term), Oxidation (M)
5337	1.89 (PV + PsA)/AD −1.73 PsA/PV	Fibrinogen alpha chain	FIBA_HUMAN	5333.3	5336.5	99	2.74E−03	^{557}SSSYSKQFTSSTSYNRGDSTFESKSYKMADEAGSEADHEGTHSTKRGHA^{605}	–

The mass to charge ratios used for the designation of peptides were obtained by MALDI-TOF/MS, whereas those for "observed" were obtained by LC–MS.
The peptides that showed a ≥1.5-fold difference in ion intensity between the PV + PsA and HC groups, between the PV + PsA and AD groups, between the PsA and PV groups, and between the sPV and mPV groups were selected for identification.
[a] The positions of amino acids of the FIBA-derived peptides are specifically shown as the first amino acid of its mature peptide as 1. The positions of amino acids of the other identified peptides are shown according to the indications in the accession ID data files. TMSB4X, thymosin β4.

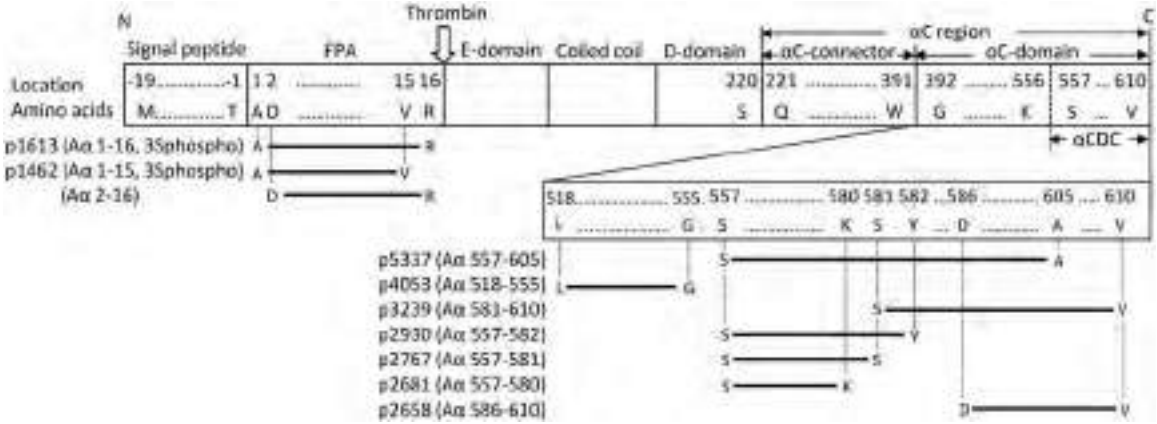

Fig. 2. The intra-molecular locations of the identified FIBA-derived peptides. A schematic illustration of the structure of the FIBA precursor and the locations of the 9 identified FIBA-derived peptides. The mature FIBA protein without its signal peptide consists of FPA, the E-domain, the coiled coil region, the D-domain, and the αC region. The αC region (Aα221–610) consists of the αC-connector (Aα221–391) and the αC-domain (Aα392–610) [59]. The C-terminal region of the αC-domain (Aα557–610) was designated as αCDC [29].

lower than their respective ion intensities in the PV group (Table 3). p1056 was derived from a protein that was highly similar to alpha-2-HS-glycoprotein (α2HS-GP), which may be involved in the development and maintenance of skin [24].

3.3. The effect of FPAdA on the secretion of humoral factors

Among the peptides that were identified, we focused on p1462 and p1977 (FLG-pEE), which showed a higher ion intensity in the PV + PsA group than in the HC and/or AD groups (Table 3). We hypothesized that these peptides may function as modulators of the inflammation in psoriasis. We therefore examined whether these peptides stimulated the dermal cells to alter the secretion of inflammatory humoral factors.

We first synthesized FPAdA, the unmodified form of p1462 (Table 3). dMVECs and keratinocytes were stimulated with FPAdA or its re-sequenced control peptide (FPAdA-Cont). The concentration of FPAdA and FPAdA-Cont in the cell culture (1.6 mg/mL) was calculated from the plasma concentration of fibrinogen. At this concentration, the cell viability of both the dMVEC and keratinocyte cultures was ≥97% (data not shown).

In a cytokine array of dMVEC culture supernatants, spots of GROα, IL-8, MCP-1, MIF, and serpin E1 were detected. FPAdA stimulation caused a ≥1.2-fold change in the spot intensity of those humoral factors in comparison to non-stimulated dMVECs (Fig. 3A). Among these, GROα, IL-8, and MCP-1 that showed a ≥1.3-fold change in the spot intensity were subsequently measured by ELISAs.

As a result, the secretion of GROα following FPAdA stimulation (280.9 ± 7.3 pg/mL) was increased 1.20-fold and 1.22-fold in comparison to non-stimulated (233.5 ± 5.3 pg/mL, $p < 0.001$) and FPAdA-Cont stimulated (229.6 ± 5.0 pg/mL, $p < 0.001$) dMVECs, respectively (Fig. 3B). In contrast, the measured secretion of IL-8 was found to decrease following FPAdA stimulation (679.6 ± 89.3 pg/mL) in comparison to non-stimulated dMVECs (919.2 ± 36.2 pg/mL, $p < 0.05$); this result conflicted with the results of the cytokine array. The secretion of MCP-1 in response to FPAdA stimulation (1404 ± 108 pg/mL) was increased 1.19-fold in comparison to FPAdA-Cont-stimulated dMVECs (1181 ± 47 pg/mL, $p < 0.05$); however, there was no difference in comparison to non-stimulated dMVECs (1368 ± 41 pg/mL, $p = 0.63$) (Fig. 3B).

Next, we analyzed the secretion of humoral factors from keratinocytes in response to FPAdA stimulation. The cytokine array showed that FPAdA stimulation caused a 1.5-fold change in the spot intensities of VEGF, pentraxin-3, MIF, lipocalin-2, osteopontin, and Dkk-1 in comparison to non-stimulated keratinocytes (Fig. 4A). Among these, MIF, lipocalin-2, osteopontin, and Dkk-1 that showed a ≥1.7-fold change in the spot intensity were subsequently measured by ELISAs.

As a result, the secretion of lipocalin-2 following FPAdA stimulation (273 ± 13 pg/mL) was decreased −1.17-fold and −1.28-fold in comparison to non-stimulated (321 ± 10 pg/mL, $p < 0.01$) and FPAdA-Cont-stimulated (350 ± 10 pg/mL, $p < 0.01$) keratinocytes, respectively (Fig. 4B). The secretion of MIF following FPAdA stimulation (12.0 ± 0.7 pg/mL) was decreased −1.28-fold in comparison to non-stimulated keratinocytes (15.3 ± 1.3 pg/mL, $p < 0.05$); however, no difference was found in the FPAdA-Cont-stimulated keratinocytes (12.5 ± 1.4 pg/mL, $p = 0.59$) (Fig. 4B). The secretion of osteopontin following FPAdA stimulation (172.0 ± 2.7 pg/mL) was increased 1.15-fold in comparison to that in FPAdA-Cont-stimulated keratinocytes (150.2 ± 2.7 pg/mL, $p < 0.001$); however, no difference was found in comparison to non-stimulated keratinocytes (175.2 ± 4.7 pg/mL, $p = 0.37$) (Fig. 4B). After FPAdA stimulation, there were no significant changes in the secretion of Dkk-1 in comparison to FPAdA-Cont-stimulated and non-stimulated keratinocytes.

3.4. The effect of FLG-pEE on humoral factor secretion

We similarly examined the effects of FLG-pEE on the secretion of humoral factors from dMVECs and keratinocytes. The concentrations of FLG-pEE and its control peptides, FLG-Q_2 and FLG-Cont, were determined by examining the cell viability. As a result, 1.4 mg/mL for dMVECs and 1.5 mg/mL for keratinocytes were found to be the highest concentrations to provide ≥95% cell viability (data not shown).

First, the secretion of humoral factors from dMVECs was analyzed. A cytokine array detected the spots of 5 humoral factors, GROα, IL-8, MCP-1, MIF, and Serpin E1. The spot intensities of GROα, IL-8, and MCP-1 were changed ≤−1.3-fold by FLG-pEE stimulation in comparison to non-stimulated dMVECs (Fig. 5A). These 3 humoral factors were subsequently measured by ELISAs.

As a result, the secretion of GROα following FLG-pEE stimulation (844.3 ± 47.5 pg/mL) was found to decrease −1.46-fold and −1.23-fold in comparison to non-stimulated dMVECs (1230.9 ± 32.3 pg/mL, $p < 0.001$) and FLG-Cont stimulated dMVECs (1038.5 ± 96.9 pg/mL, $p < 0.05$), respectively (Fig. 5B). However, no difference was found between the secretion of GROα following FLG-pEE stimulation or FLG-Q_2 stimulation (768.2 ± 49.9 pg/mL, $p = 0.13$). The secretion of IL-8 following FLG-pEE stimulation

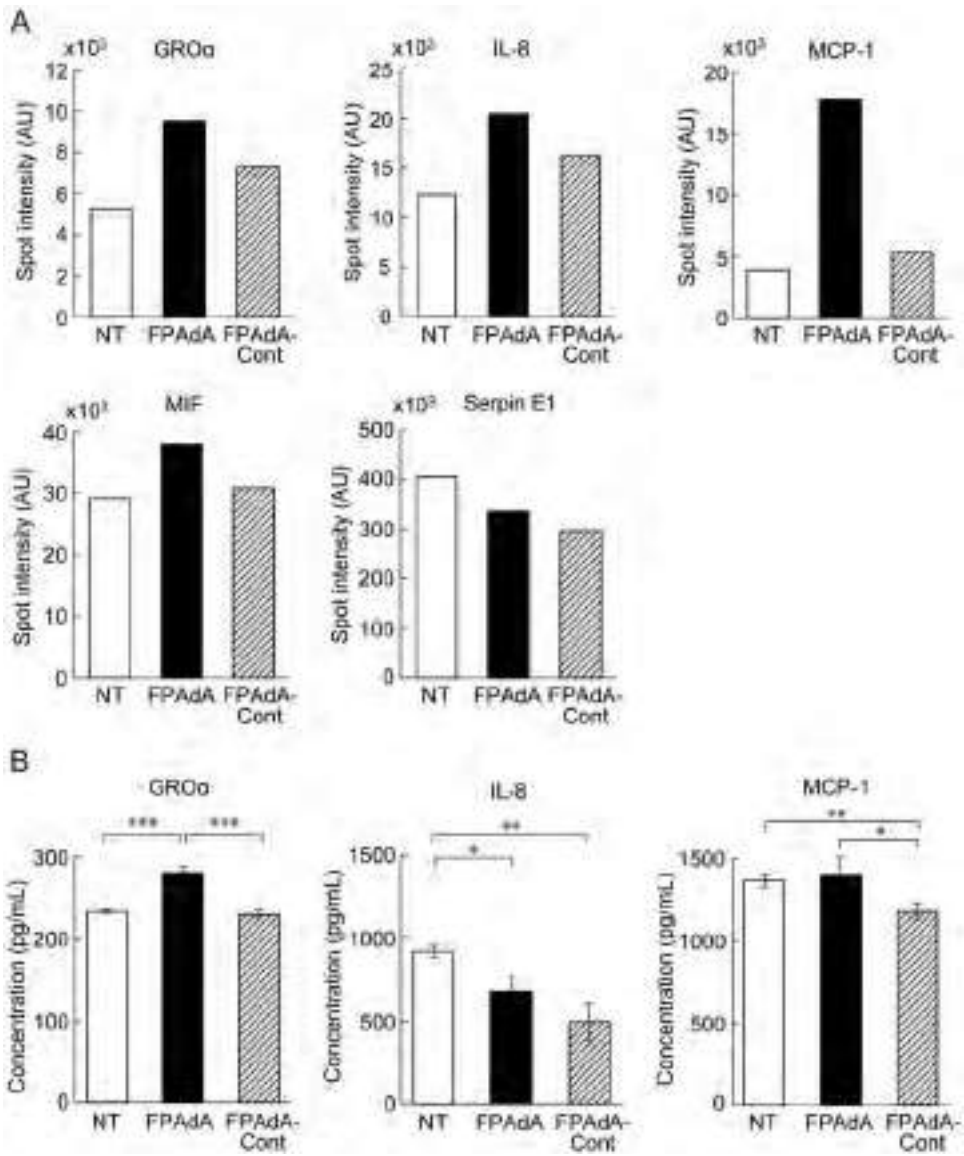

Fig. 3. The secretion of humoral factors from FPAdA-stimulated dMVECs. (A) The secretion of humoral factors from dMVECs cultured with medium-alone (no treatment, NT), with FPAdA, and with FPAdA-Cont was assayed using a cytokine array. The spot intensities of GROα, IL-8, MCP-1, MIF, and serpin E1, spots of which were detected in the cytokine array, are shown. (B) The secretion of GROα, IL-8, and MCP-1 from dMVECs, which was found to be increased more than 1.3-fold following FPAdA stimulation in comparison to non-stimulated dMVECs in the cytokine array, was measured by ELISAs. $^{*}p < 0.05$, $^{**}p < 0.01$, $^{***}p < 0.001$.

(2240.1 ± 172.6 pg/mL) decreased −1.35-fold and −1.44-fold in comparison to non-stimulated dMVECs (3032.3 ± 28.9 pg/mL, $p < 0.01$) and FLG-Cont-stimulated dMVECs (3221.8 ± 523.7 pg/mL, $p < 0.05$), respectively. However, no difference was found between the secretion of IL-8 following FLG-pEE stimulation or FLG-Q_2 stimulation (1967.8 ± 17.9 pg/mL, $p = 0.05$). Interestingly, the secretion of MCP-1 following FLG-pEE stimulation (4057.8 ± 157.2 pg/mL) decreased −1.23-fold and −1.14-fold in comparison to non-stimulated dMVECs (4986.1 ± 238.7 pg/mL, $p < 0.01$) and FLG-Q_2-stimulated dMVECs (4619.1 ± 213.4 pg/mL, $p < 0.05$), respectively. However, no difference was found between the secretion of MCP-1 following FLG-pEE stimulation or FLG-Cont stimulation (4524.0 ± 323.3 pg/mL, $p = 0.09$) (Fig. 5B).

Next, the secretion of humoral factors from keratinocytes was analyzed after FLG-pEE stimulation. The cytokine array detected the spots of all of the humoral factors except IL-5. IL-1ra, lipocalin-2, MMP-9, and SHBG showed a ≥1.2-fold change in intensity following FLG-pEE stimulation in comparison to non-stimulated keratinocytes. These 4 humoral factors were subsequently measured by ELISAs (Fig. 6A).

Among the 4 humoral factors, the secretion of lipocalin-2 following FLG-pEE stimulation (648.2 ± 88.3 pg/mL) was increased 1.35-fold in comparison to non-stimulated keratinocytes (480.8 ± 25.5 pg/mL, $p < 0.05$); however, no changes were observed in comparison to FLG-Cont stimulation (643.0 ± 15.0 pg/mL, $p = 0.93$) and FLG-Q_2 stimulation (568.8 ± 3.0 pg/mL, $p = 0.19$) (Fig. 6B). The secretion of IL-1ra and MMP-9 after FLG-pEE stimulation was not significantly different from that in non-stimulated keratinocytes (Fig. 6B). All of the SHBG results were below the detection limits (data not shown).

3.5. Correlation of peptide ion intensity and clinical parameters

To detect the peptides that would be associated with the pathophysiology of psoriasis in another way, we analyzed correlations between intensity of the identified peptides and

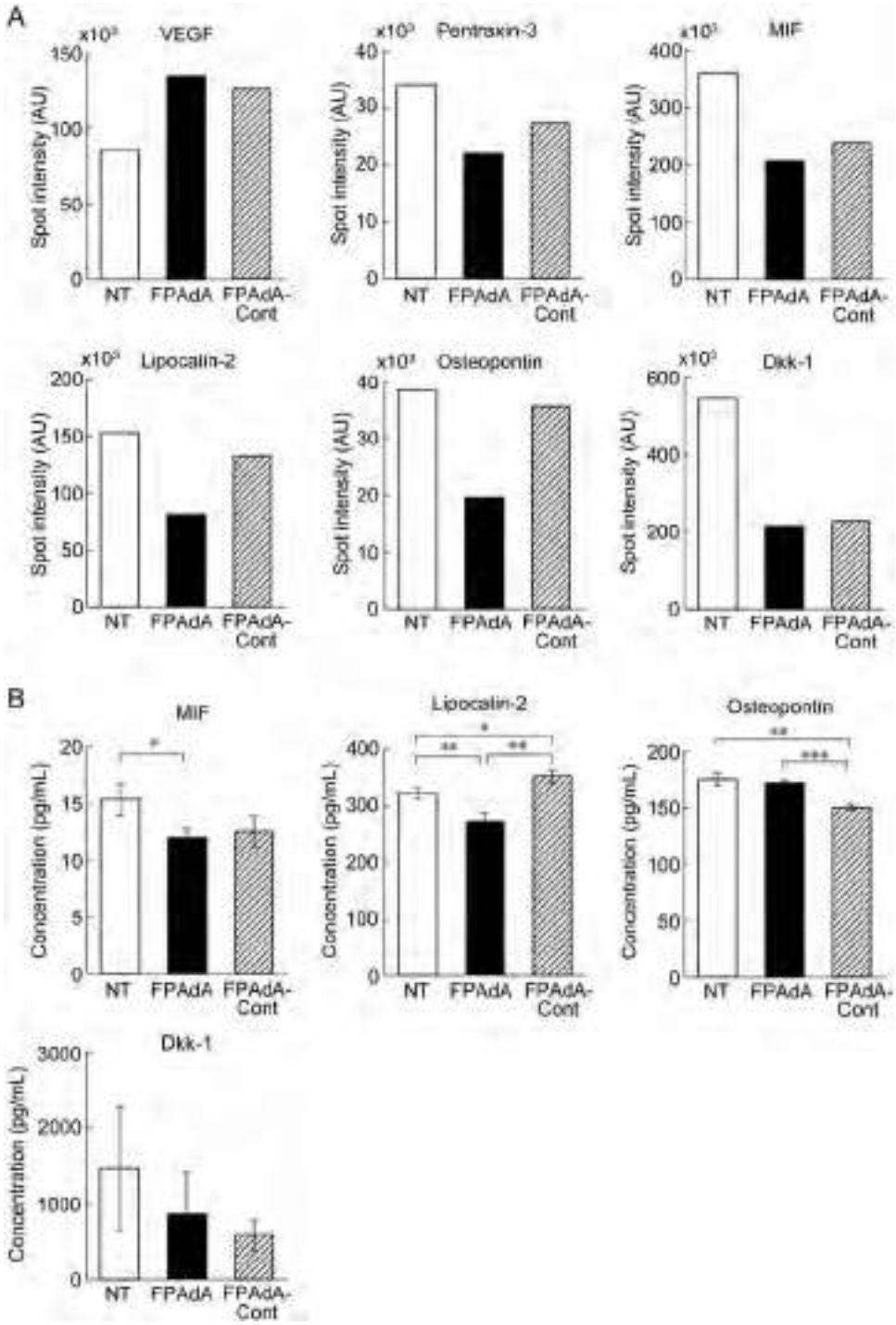

Fig. 4. The secretion of humoral factors from FPAdA-stimulated keratinocytes. (A) The secretion of humoral factors from keratinocytes cultured with medium-alone (NT), with FPAdA, and with FPAdA-Cont was assayed using a cytokine array. The spot intensities of VEGF, pentraxin-3, MIF, lipocalin-2, osteopontin, and Dkk-1, which showed more than 30,000 AU and increased ≥1.5-fold following FPAdA-stimulation in comparison to non-stimulated keratinocytes, are shown. (B) The secretion of MIF, lipocalin-2, osteopontin, and Dkk-1 from dMVECs, which was found to be decreased less than −1.7-fold following FPAdA-stimulation in comparison to non-stimulated keratinocytes in the cytokine array, was measured by ELISAs. $^{*}p < 0.05$, $^{**}p < 0.01$, $^{***}p < 0.001$.

clinical parameters. PASI, C-reactive protein (CRP), and treatment were selected as the clinical parameters because they reflected the disease severity, activity, and demands for the disease control, respectively. To analyze the correlation between peptide ion intensity and treatment, we specifically designed a treatment score in which the treatments for psoriasis in this study were classified into five groups as described in Section 2.

As a result, we found that p1056, derived from a protein highly similar to α2HS-GP, was negatively correlated with PASI ($\rho = -0.481$, $p < 0.01$; Fig. 7A). p2681, an N-terminal peptide of FIBA-αCDC (C-terminal portion of the αC-domain of FIBA, Fig. 2), was negatively correlated with CRP ($\rho = -0.394$, $p < 0.05$; Fig. 7B). p2930, p3239, and p5337, the relatively long FIBA-αCDC-derived peptides, were negatively correlated with the treatment score

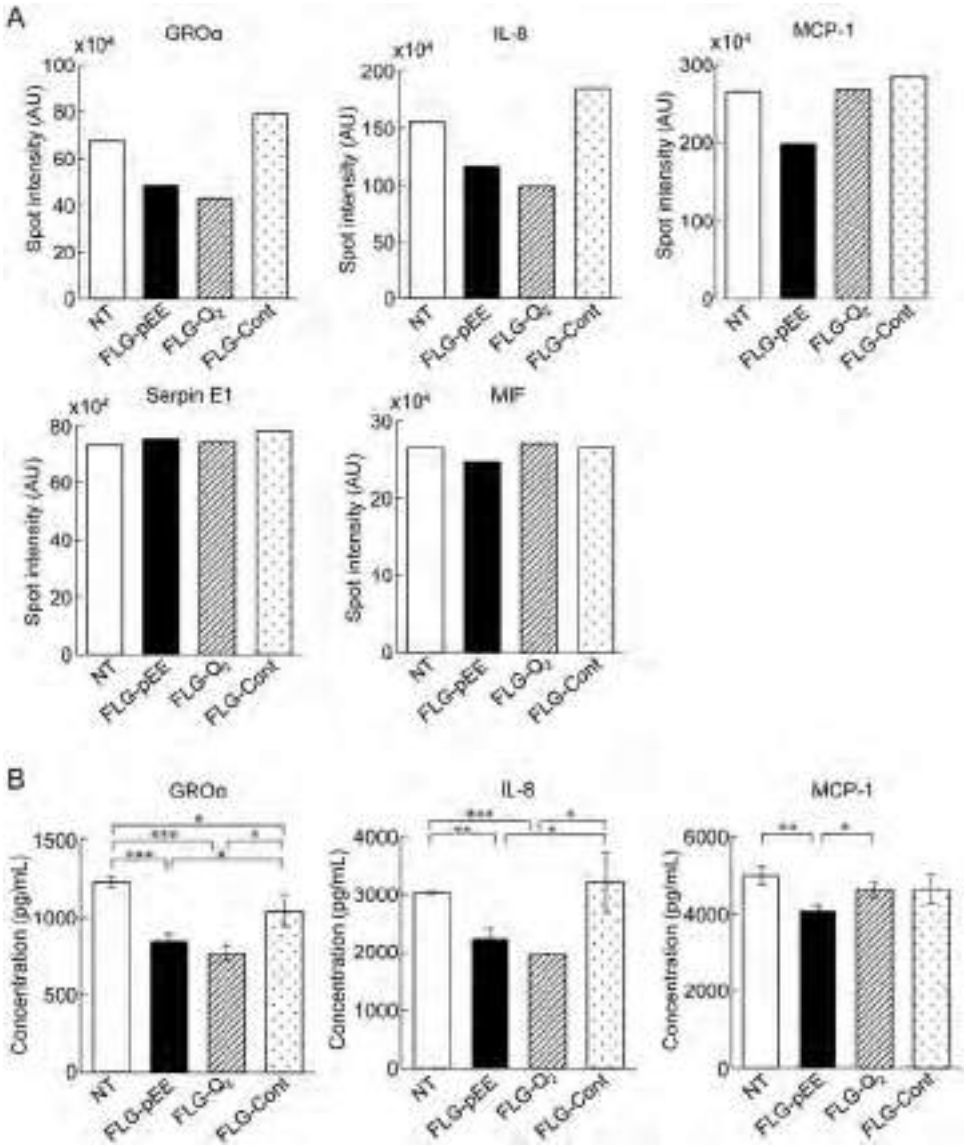

Fig. 5. The secretion of humoral factors from dMVECs stimulated with FLG-pEE. (A) The secretion of humoral factors from dMVECs cultured with medium-alone (NT), with FLG-pEE, with FLG-Q_2, and with FLG-Cont was assayed using a cytokine array. The spot intensities of GROα, MCP-1, IL-8, MIF, and serpin E1, spots of which were detected, are shown. (B) The secretion of GROα, MCP-1, and IL-8 from dMVECs, which was decreased less than −1.3-fold following FLG-pEE stimulation in comparison to non-stimulated dMVECs in the cytokine array, was measured by ELISAs. $^{*}p < 0.05$, $^{**}p < 0.01$, $^{***}p < 0.001$.

(p2930, $\rho = -0.531$, $p < 0.01$, Fig. 7C; p3239, $\rho = -0.440$, $p < 0.01$, Fig. 7D; p5337, $\rho = -0.451$, $p < 0.01$, Fig. 7E).

As shown in Fig. 7C–E, psoriasis patients treated with NSAIDs (treatment score 2) showed relatively low ion intensity of the FIBA-derived peptides. We therefore specifically compared ion intensity of all the identified peptides between the psoriasis patients treated with NSAIDs ($n = 6$) and those treated without NSAIDs ($n = 28$), between the psoriasis patients treated with immunosuppressants (MTX and CYA) ($n = 8$) and those treated without immunosuppressants ($n = 26$), and between the psoriasis patients treated with biological drugs ($n = 3$) and those treated without biological drugs ($n = 31$). Interestingly, the ion intensity of p2658, p2681, p2930, and p3239, which are all derived from FIBA-αCDC, was significantly decreased in the NSAID-treated group compared to the NSAID-non-treated group (Fig. 7F–I). The ion intensity of p4979, which is derived from thymosin β4, was also significantly decreased in the NSAID-treated group compared to the NSAID-non-treated group (Fig. 7J). Furthermore, the ion intensity of p2930 was significantly decreased in the immunosuppressant-treated group compared to the immunosuppressant-non-treated group (Fig. 7K). No peptide showed ion intensity difference between the psoriasis patients treated with biological drugs and those treated without biological drugs (data not shown). The production of those peptides and/or their parent proteins may be suppressed by NSAIDs and/or immunosuppressants.

4. Discussion

We analyzed serum peptide profiles to find peptides that are involved in the pathophysiology of psoriasis. The major psoriasis-affected site is the skin, however, the inflammation also affects the joints and other organs such as the eyes, lungs, and heart. To explore novel molecules that are associated with the inflammation in psoriasis, we selected serum peptidome that contained processed proteins as a source of unknown molecules with pathophysiologic effects.

We comprehensively analyzed the serum peptides of PV, PsA, and AD patients and HC subjects, and found 93 serum peptides that

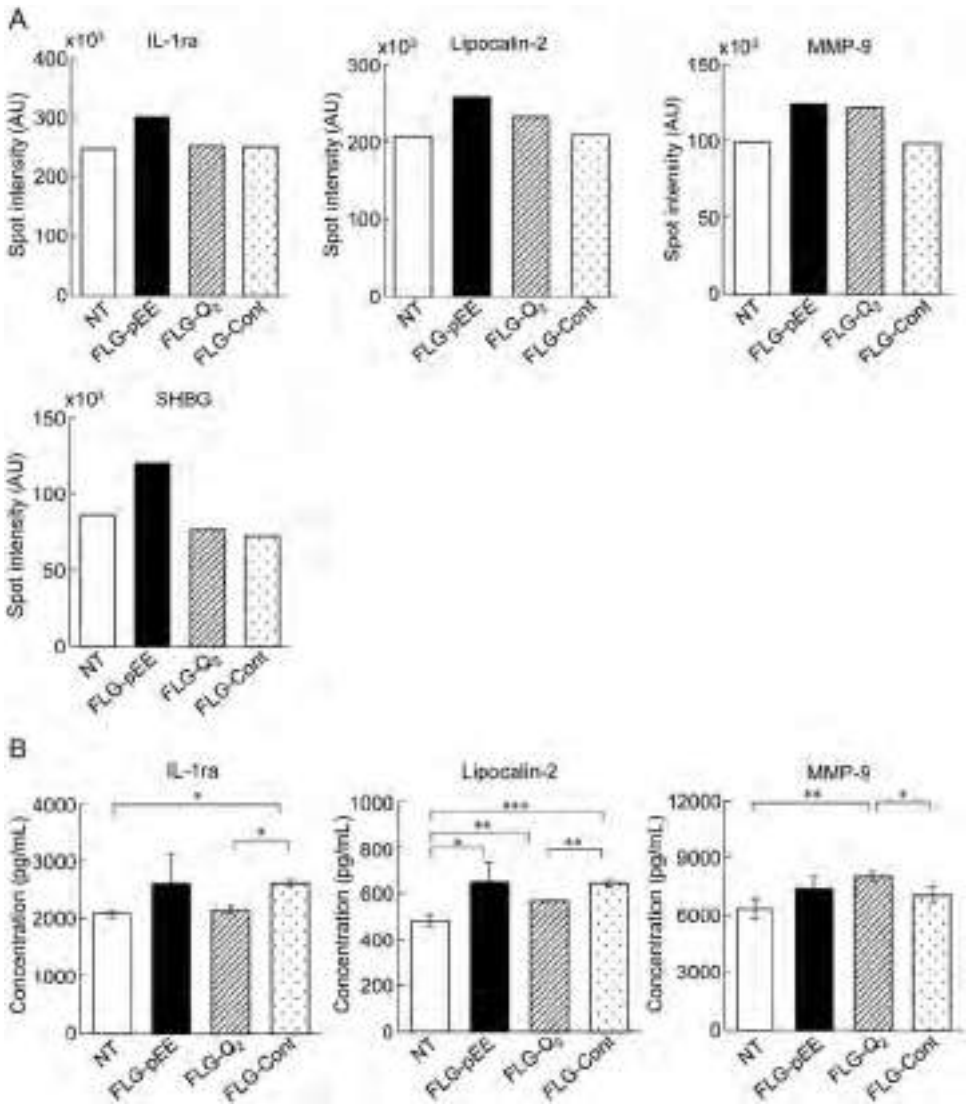

Fig. 6. The secretion of humoral factors from keratinocytes stimulated with FLG-pEE. (A) The secretion of humoral factors from keratinocytes cultured with medium-alone (NT), with FLG-pEE, with FLG-Q_2, and with FLG-Cont was assayed using a cytokine array. The spot intensities of IL-1ra, lipocalin-2, MMP-9, and SHBG, which increased ≥1.2-fold following FLG-pEE stimulation in comparison to non-stimulated keratinocytes, are shown. (B) The results of ELISAs measuring IL-1ra, lipocalin-2, and MMP-9. $^{*}p < 0.05$, $^{**}p < 0.01$, $^{***}p < 0.001$.

possibly contained the disease-related peptides (Fig. 1A and B). There were significant differences in the ion intensities of 24 of these peptides between the PV + PsA and HC groups, and 20 of the peptides between the PV + PsA and AD groups ($p < 0.05$) (Table 2). These peptides were considered to be candidates that are involved in the pathophysiology of psoriasis. Interestingly, in the PsA group, the number of peptides for which the ion intensity-decreased was greater than the numbers of peptides for which the ion intensity-increased in comparison to the PV group; a similar finding was observed in the sPV group in comparison to the mPV group (Table 2). The decrease of serum peptides may be associated with the onset of arthritis and the severity of psoriasis.

Nine of the 13 identified peptides were FIBA-derived, and were fragments of FPA and the αC-domain (Table 3 and Fig. 2). Physiologically, cleavage of FIBA by thrombin releases FPA and initiates the conversion of fibrinogens to fibrins that polymerize themselves to form fibrin clots [25]. The ion intensity of the FPA-derived peptides, p1462 and p1613, was higher in the PV + PsA group than in the HC group ($p < 0.05$) (Table 3). Fibrinogen and FPA have been reported to be increased in psoriasis patients in comparison to healthy individuals [26,27]. The increase in FPA-derived peptides may reflect the increased expression of the parent protein, suggesting the activation of coagulation due to the microvascular abnormalities of the psoriatic lesion.

On the other hand, 7 FIBA-derived peptides were from the αC-domain, 6 of which were from αCDC, the C-terminal portion of the αC-domain (Fig. 2) [28,29]. The αC-domain is the site at which fibrins interact intermolecularly for the polymerization [30]. The overall results of the ion intensity of αC-domain-derived peptides were as follows: (1) the PV + PsA group > the AD group; (2) the PsA group < the PV group; and (3) the sPV group < the mPV group ($p < 0.05$) (Table 3). Since fibrinogen was reported to be increased in psoriasis patients in comparison to healthy individuals [26], the fragmentation of the αC-domain can be expected to be decreased in psoriasis, especially in PsA and sPV. The decrease of αC-domain-derived peptides may be associated with the onset of arthritis and the severity of psoriasis, which suggests a protective effect of αC-domain fragmentation and/or the αC-domain-derived peptides in

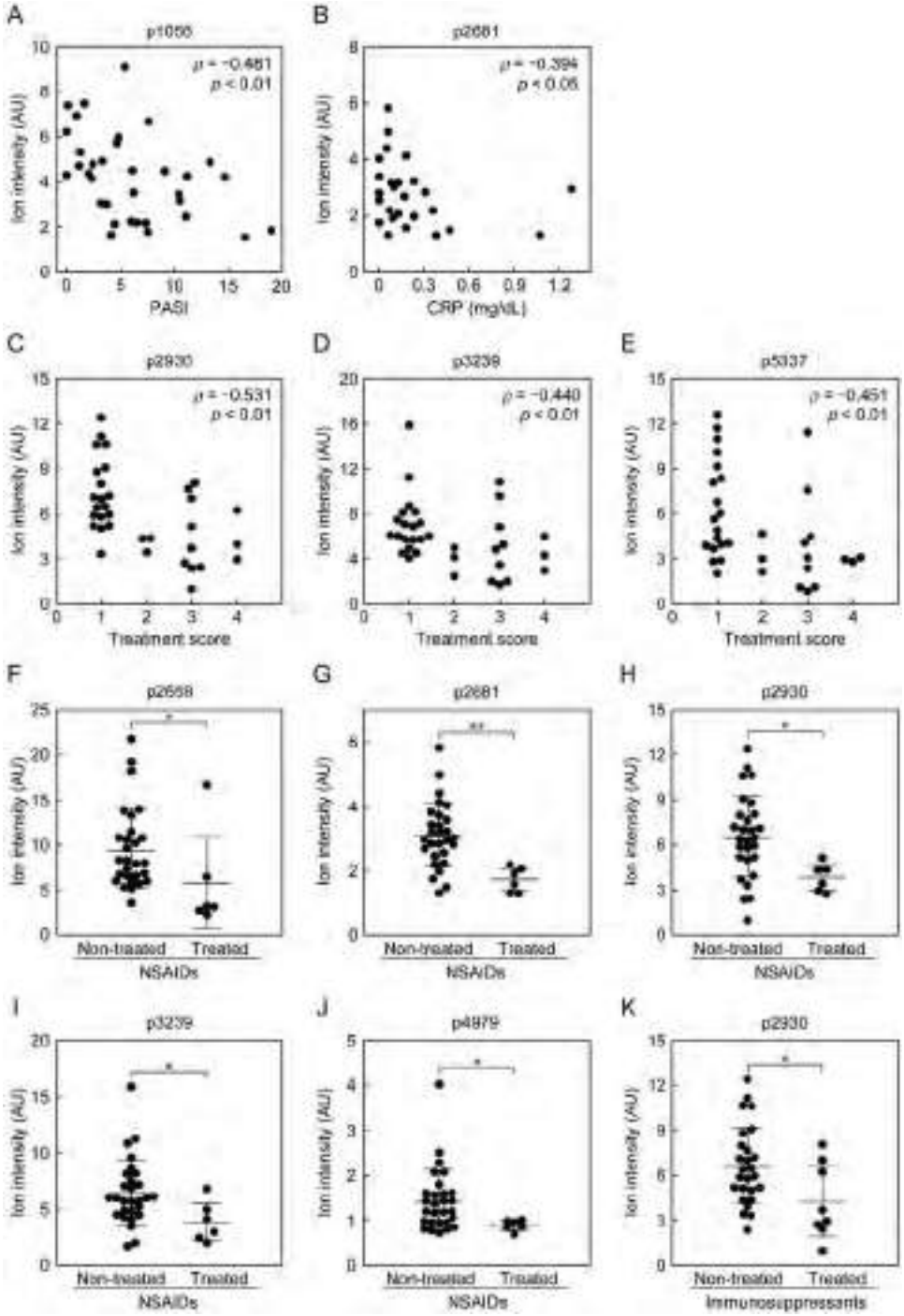

Fig. 7. The correlations between the peptide ion intensity and clinical parameters in the psoriasis patients. The correlations between the ion intensity of the 13 identified peptides and clinical parameters of PASI ($n = 34$), CRP ($n = 26$), and the treatment score ($n = 34$) were examined in the psoriasis (PV + PsA) patients (Table 1). In the correlation analysis of CRP, a PV patient with malignant lymphoma (ML) and a PsA patient with rhinitis (R) were excluded. CRP values of <0.03 were regarded as 0. The results of the 5 peptides that showed correlations are shown (A–E). The results of the 5 peptides that showed differences in ion intensity between the NSAID-treated group ($n = 6$) and the NSAID-non-treated group ($n = 28$) and between the immunosuppressant-treated group ($n = 8$) and the immunosuppressant-non-treated group ($n = 26$) are also shown (F–K). $^{*}p < 0.05$, $^{**}p < 0.01$.

psoriasis. p2681 was negatively correlated with CRP values ($\rho = -0.394$, $p < 0.05$), however, most of the psoriasis patients showed CRP values within normal limits (Table 1 and Fig. 7B). Therefore, this correlation should be confirmed using a large cohort of psoriatic patients that includes a sufficient number of CRP-positive patients. p2930, p3239, and p5337, relatively longer αCDC-derived peptides, were negatively correlated with the treatment score ($\rho = -0.531$, $\rho = -0.440$, and $\rho = -0.451$; $p < 0.01$) (Fig. 7C–E). These FIBA-derived peptides are expected to be decreased according to the intensity of the treatment. In addition, the ion intensity of p2658, p2681, p2930, and p3239, which are all derived from FIBA-αCDC, was decreased in the NSAID-treated group compared to the NSAID-non-treated group, and the ion intensity of p2930 was also decreased in the immunosuppressant-treated group compared to the immunosuppressant-non-treated group ($p < 0.05$) (Fig. 7F–I and K). Thus, NSAIDs and

immunosuppressants, especially NSAIDs, may effectively suppress the inflammatory process of psoriasis, which results in a decrease in the production of fibrinogen.

It is noteworthy that the ion intensity of p1977, FLG-pEE, was higher in the PV + PsA group than in the HC and AD groups ($p < 0.05$) (Table 3). FLG is processed from its large precursor protein, profilaggrin. FLG aggregates the keratin filaments to form tight bundles that promote the flattering of corneocytes [22]. FLG monomers are degraded into free amino acids and further metabolized to constitute natural moisturizing factors. Mutations of FLG cause ichthyosis vulgaris and FLG deficiency is known to contribute to the pathogenesis of AD [22,31]. FLG monomers, FLG1-FLG23, are located in tandem in profilaggrin and FLG-pEE was derived from an interventing sequence located between FLG12 and FLG13 [32]. The expression of FLG has been reported to be decreased in the skin of PV patients in comparison to the skin of healthy individuals and AD patients [33]. Although the mechanism by which FLG-interventing peptides are catabolized is unclear, FLG-pEE may escape from further degradation because of its post-translational modification. p1056, which is decreased in the PV + PsA group in comparison to the AD group, was derived from a protein that is highly similar to α2HS-GP ($p < 0.05$) (Table 3). α2HS-GP is associated with skin development and wound healing [24]. p1056 was also negatively correlated with PASI in psoriasis patients ($\rho = -0.481$, $p < 0.01$) (Fig. 7A). These results suggest that the expression of the parent protein decreased in psoriasis, according to their disease severity, which would also function as a skin-protective protein in a manner similar to α2HS-GP. p1056 may be a candidate biomarker for the severity of psoriasis.

p4964 and p4979, which are derived from thymosin β4 protein, were decreased in the PsA group in comparison to the PV group ($p < 0.05$) (Table 3). Thymosin β4 is one of the regulators of actin polymerization [34]. Thymosin β4 is thought to participate in anti-inflammation and wound healing, through its relationship to the secretion of MMPs and inflammatory cytokines and the upregulation of anti-oxidative enzymes [35–37]. Thus, thymosin β4 may suppress the onset of arthritis in psoriasis. The decrease of thymosin β4-derived peptides suggests the decreased expression of thymosin β4 in PsA. Interestingly, the ion intensity of p4979, the oxidated thymosin β4-derived peptide, was decreased in the NSAID-treated group compared to the NSAID-non-treated group ($p < 0.05$) (Fig. 7J). This suggested that the oxidation at the 32nd methionine (M) was decreased by the treatment with NSAIDs which may be involved in the inflammation of psoriasis (Table 3).

It was noteworthy that FLG-pEE stimulation resulted in the decreased secretion of GROα and IL-8 from dMVECs in comparison to FLG-Cont-stimulated and non-stimulated dMVECs ($p < 0.05$) (Fig. 5B). IL-17, a key inflammatory cytokine in psoriasis is abundantly produced by the Th17 cells, γδT cells, neutrophils and mast cells in psoriatic skin [7–10,38]. IL-17A acts on the keratinocytes to increase the expression of ELR^+ chemokines such as GROα and IL-8, recruiting neutrophils and T cells to the lesion sites [39,40]. IL-17 receptors are expressed on vascular endothelial cells [41–43], and human dermal endothelial cells migrated following IL-17A stimulation [44]. Thus, dMVECs as well as keratinocytes could be stimulated by IL-17A. Our data showed that FLG-pEE downregulated the secretion of GROα and IL-8 from dMVECs, which would lead to a reduction of the neutrophil- and T cell-mediated inflammation in psoriasis. FLG-pEE stimulation also led to a decrease in the secretion of MCP-1 from dMVECs in comparison to non-stimulated and FLG-Q_2-stimulated dMVECs ($p < 0.05$) (Fig. 5B). In psoriasis, the keratinocytes are known to produce MCP-1 and to recruit CCR2- and CD163-positive macrophages/monocytes to the skin lesions [45–47]. The injection of MCP-1 together with TNFα induced psoriasiform skin inflammation in a CD18-hypomorphic psoriasis mouse model, thus, MCP-1 is considered to be the disease-causing inflammatory chemokine in psoriasis [48]. Our data showed that FLG-pEE stimulation downregulated the secretion of MCP-1 from dMVECs, which may lead to a reduction in the macrophage-mediated inflammation of psoriasis. Interestingly, this downregulation of MCP-1 was not found after the stimulation with FLG-Q_2 (Fig. 5B). Since N-terminal glutamine (Q_{2099}) is spontaneously changed to pyroglutamate (pE) when a peptide is solved, the other post-translational modification, Q_{2115}E, may be specifically involved in the downregulation of MCP-1 by FLG-pEE.

In contrast, FPAdA-stimulation increased the secretion of GROα from dMVECs in comparison to FPAdA-Cont-stimulated and non-stimulated dMVECs ($p < 0.001$) (Fig. 3B). This result suggested that FPAdA upregulates neutrophil chemotaxis to aggravate the inflammation. On the other hand, FPAdA decreased the secretion of lipocalin-2 from keratinocytes in comparison to FPAdA-Cont-stimulated and non-stimulated keratinocytes ($p < 0.01$) (Fig. 4B). Lipocalin-2 is an antimicrobial protein that is highly expressed in the psoriatic skin [49]. Since the intraperitoneal injection of lipocalin-2 exacerbated erythema and scaling and the neutralization of lipocalin-2 alleviated the epidermal inflammation in a murin model of IMQ-treated psoriatic skin, lipocalin-2 has been recognized to contribute to the pathogenesis of psoriasis [49,50]. Because FPAdA downregulated the secretion of lipocalin-2 from keratinocytes, this peptide may reduce inflammation. The elucidation of the overall contribution of FPAdA to inflammation in psoriasis will require further studies.

As a limitation of this study, we analyzed serum but not skin peptide profiles of psoriasis. Analyzing the peptide profiles in skin and comparing them to the profiles in sera would be extremely useful. Peptidomics analyze the native fragmentation of proteins, and clinical peptidomics are generally conducted using body fluids such as plasma/serum and urine, which are uniform and have low protease-activity [51–53]. Tissue samples contain a large amount of proteases, which are probably activated during the peptide extraction, resulting in artificial digestion of the parent proteins. Therefore, to reduce protease activity in tissue samples, a number of methods for a variety of tissue have been proposed for sample preparation, such as heat inactivation and the addition of acetone, trichloroacetic acid, and protease inhibitors [54–56]. To the best of our knowledge, however, no method involving a protease activity-reducing treatment has been established in human skin peptidomics. In the near future, we will attempt to establish a novel method for analyzing natively digested peptides to compare the peptide profiles between skin and serum in psoriasis. In addition, most of the psoriasis patients in this study possessed comorbid diseases such as metabolic diseases and cardiovascular diseases, and all of the patients were treated with external and/or internal medication (Table 1). Therefore, production of some peptides has been probably affected by such comorbid diseases as well as treatments as shown in Fig. 7C–K.

It was reported that anti-microbial peptides such as β-defensin 2, LL37, and psoriasin are increased in sera from psoriasis patients compared to those from healthy individuals [57]. However, we did not detect MS peaks for those anti-microbial peptides in our serum peptidomic results (data not shown). This may be due to the differences in the sensitivity between ELISA and peptidomics. The sensitivity of proteomics/peptidomics with standard sample preparation remains in the μg/mL orders [58], which is lower than the sensitivity of ELISA that detects proteins/peptides in the ng/mL to pg/mL orders. Proteomics/peptidomics are useful methods for detecting novel proteins/peptides related to the pathophysiology of targeted diseases, however, already-identified proteins/peptides at low concentrations should be detected and quantified by specific and sensitive methods such as ELISA. If the concentration of the overexpressed anti-microbial peptides in skin

is much higher than in that in sera, they may be detectable via the novel peptidomic strategy that we will try to establish as described above.

In conclusion, serum peptides are thus considered to be involved in the pathophysiology of psoriasis, as well as in the onset of arthritis and the severity of psoriasis. p1056, derived from a protein highly similar to α2HS-GP, may be a candidate biomarker for the severity of psoriasis, if the correlation can be confirmed with a large cohort of psoriasis patients. FLG-pEE may reduce inflammation in psoriasis by downregulating the chemotaxis of neutrophils, T cells, and macrophages. FPAdA may aggravate inflammation by inducing neutrophils; however, it may alleviate inflammation by downregulating the anti-microbial activity. Modulating the fragmentation of serum proteins is a potential therapeutic strategy for the treatment of psoriasis.

Funding

This work was partly supported by the Supported Program for the Strategic Research Foundation at Private Universities of Ministry of Education, Culture, Sports, Science and Technology. The other part of this work was supported by St. Marianna University School of Medicine.

Conflict of interest

The authors have no conflict of interest to declare.

Acknowledgements

The authors are indebted to Ms Atsuko Nozawa and Ms Fumiko Oikawa for their technical assistance.

References

[1] W.H. Boehncke, M.P. Schön, Psoriasis, Lancet 386 (2015) 983–994.
[2] S.K. Raychaudhuri, E. Maverakis, S.P. Raychaudhuri, Diagnosis and classification of psoriasis, Autoimmun. Rev. 13 (2014) 490–495.
[3] K. Kubota, Y. Kamijima, T. Sato, N. Ooba, D. Koide, H. Iizuka, H. Nakagawa, Epidemiology of psoriasis and palmoplantar pustulosis: a nationwide study using the Japanese national claims database, BMJ Open 5 (2015) e006450.
[4] C.E.M. Griffiths, J.N.W.N. Barker, Pathogenesis and clinical features of psoriasis, Lancet 370 (2007) 263–271.
[5] F.O. Nestle, D.H. Kaplan, J. Barker, Psoriasis, N. Engl. J. Med. 361 (2009) 496–509.
[6] K.E. Nograles, L.C. Zaba, E. Guttman-Yassky, J. Fuentes-Duculan, M. Suárez-Fariñas, I. Cardinale, A. Khatcherian, et al., Th17 cytokines interleukin (IL)-17 and IL-22 modulate distinct inflammatory and keratinocyte-response pathways, Br. J. Dermatol. 159 (2008) 1092–1102.
[7] M.A. Lowes, T. Kikuchi, J. Fuentes-Duculan, I. Cardinale, L.C. Zaba, A.S. Haider, E. P. Bowman, et al., Psoriasis vulgaris lesions contain discrete populations of Th1 and Th17 T cells, J. Invest. Dermatol. 128 (2008) 1207–1211.
[8] Y. Cai, X. Shen, C. Ding, C. Qi, K. Li, X. Li, V.R. Jala, et al., Pivotal role of dermal IL-17-producing γδ T cells in skin inflammation, Immunity 35 (2011) 596–610.
[9] R.R.M.C. Keijsers, A.G.M. Hendriks, P.E.J. van Erp, B. van Cranenbroek, P.C.M. van de Kerkhof, H.J.P.M. Koenen, I. Joosten, In vivo induction of cutaneous inflammation results in the accumulation of extracellular trap-forming neutrophils expressing RORγt and IL-17, J. Invest. Dermatol. 134 (2014) 1276–1284.
[10] A.M. Lin, C.J. Rubin, R. Khandpur, J.Y. Wang, M. Riblett, S. Yalavarthi, E.C. Villanueva, et al., Mast cells and neutrophils release IL-17 through extracellular trap formation in psoriasis, J. Immunol. 187 (2011) 490–500.
[11] M. Detmar, L.F. Brown, K.P. Claffey, K.T. Yeo, O. Kocher, R.W. Jackman, B. Berse, et al., Overexpression of vascular permeability factor/vascular endothelial growth factor and its receptors in psoriasis, J. Exp. Med. 180 (1994) 1141–1146.
[12] R. Heidenreich, M. Röcken, K. Ghoreschi, Angiogenesis drives psoriasis pathogenesis, Int. J. Exp. Pathol. 90 (2009) 232–248.
[13] R. Lande, J. Gregorio, V. Facchinetti, B. Chatterjee, Y.H. Wang, B. Homey, W. Cao, et al., Plasmacytoid dendritic cells sense self-DNA coupled with antimicrobial peptide, Nature 449 (2007) 564–569.
[14] R. Lande, G. Chamilos, D. Ganguly, O. Demaria, L. Frasca, S. Durr, C. Conrad, et al., Cationic antimicrobial peptides in psoriatic skin cooperate to break innate tolerance to self-DNA, Eur. J. Immunol. 45 (2015) 203–213.
[15] L. Puig, A. Julià, S. Marsal, The pathogenesis and genetics of psoriasis, Actas Dermosifiliogr. 105 (2014) 535–545.
[16] CASPAR Study Group, W. Taylor, D. Gladman, P. Helliwell, A. Marchesoni, P. Mease, H. Mielants, Classification criteria for psoriatic arthritis: development of new criteria from a large international study, Arthritis Rheum. 54 (2006) 2665–2673.
[17] J.M. Hanifin, G. Rajka, Diagnostic features of atopic dermatitis, Acta. Dermatovener. (Stockholm) Suppl. 92 (1980) 44–47.
[18] T. Fredriksson, U. Pettersson, Severe psoriasis – oral therapy with a new retinoid, Dermatologica 157 (1978) 238–244.
[19] U. Mrowietz, K. Kragballe, K. Reich, P. Spuls, C.E. Griffiths, A. Nast, J. Franke, et al., Definition of treatment goals for moderate to severe psoriasis: a European consensus, Arch. Dermatol. Res. 303 (2011) 1–10.
[20] A.Y. Finlay, Current severe psoriasis and the rule of tens, Br. J. Dermatol. 152 (2005) 861–867.
[21] J.P. Thyssen, S. Kezic, Causes of epidermal filaggrin reduction and their role in the pathogenesis of atopic dermatitis, J. Allergy Clin. Immunol. 134 (2014) 792–799.
[22] B. Cabanillas, N. Novak, Atopic dermatitis and filaggrin, Curr. Opin. Immunol. 42 (2016) 1–8.
[23] D. Rengaraj, Y.S. Hwang, X.H. Liang, W.B. Deng, Z.M. Yang, J.Y. Han, Comparative expression and regulation of TMSB4X in male reproductive tissues of rats and chickens, J. Exp. Zool. A: Ecol. Genet. Physiol. 319 (2013) 584–595.
[24] G. Nistor, A.J. Poole, Z. Draelos, M. Lupo, T. Tzikas, J.H. Liu, H.S. Keirstead, Human stem cell-derived skin progenitors produce alpha 2-HS glycoprotein (fetuin): a revolutionary cosmetic ingredient, J. Drugs Dermatol. 15 (2016) 583–598.
[25] M.W. Mosesson, Fibrinogen and fibrin structure and functions, J. Thromb. Haemost. 3 (2005) 1894–1904.
[26] P. Rocha-Pereira, A. Santos-Silva, I. Rebelo, A. Figueiredo, A. Quintanilha, F. Teixeira, The inflammatory response in mild and in severe psoriasis, Br. J. Dermatol. 150 (2004) 917–928.
[27] F. Marongiu, G.G. Sorano, C. Bibbò, M.P. Pistis, M. Conti, P. Mulas, A. Balestrieri, et al., Abnormalities of blood coagulation and fibrinolysis in psoriasis, Dermatology 189 (1994) 32–37.
[28] S. Yakovlev, I. Mikhailenko, G. Tsurupa, A.M. Belkin, L. Medved, Polymerisation of fibrin αC-domains promotes endothelial cell migration and proliferation, Thromb. Haemost. 112 (2014) 1244–1251.
[29] M. Noguchi, T. Sato, K. Nagai, I. Utagawa, I. Suzuki, M. Arito, N. Iizuka, et al., Roles of serum fibrinogen α chain-derived peptides in Alzheimer's disease, Int. J. Geriatr. Psychiatry 29 (2014) 808–818.
[30] J.W. Weisel, L. Medved, The structure and function of the alpha C domains of fibrinogen, Ann. N. Y. Acad. Sci. 936 (2001) 312–327.
[31] F.J. Smith, A.D. Irvine, A. Terron-Kwiatkowski, A. Sandilands, L.E. Campbell, Y. Zhao, H. Liao, et al., Loss-of-function mutations in the gene encoding filaggrin cause ichthyosis vulgaris, Nat. Genet. 38 (2006) 337–342.
[32] Universal Protein Resource. UniProtKB – P20930 (FILA_HUMAN) http://www.uniprot.org/uniprot/P20930 (accessed 15.11.16).
[33] T. Makino, M. Mizawa, T. Yamakoshi, M. Takaishi, T. Shimizu, Expression of filaggrin-2 protein in the epidermis of human skin diseases: a comparative analysis with filaggrin, Biochem. Biophys. Res. Commun. 449 (2014) 100–106.
[34] M.C. Sanders, A.L. Goldstein, Y.L. Wang, Thymosin beta 4 (Fx peptide) is a potent regulator of actin polymerization in living cells, Proc. Natl. Acad. Sci. U. S. A. 89 (1992) 4678–4682.
[35] H.M. Choi, Y.A. Lee, H.I. Yang, M.C. Yoo, K.S. Kim, Increased levels of thymosin β4 in synovial fluid of patients with rheumatoid arthritis: association of thymosin β4 with other factors that are involved in inflammation and bone erosion in joints, Int. J. Rheum. Dis. 14 (2011) 320–324.
[36] D. Philp, B. Scheremeta, K. Sibliss, M. Zhou, E.L. Fine, M. Nguyen, L. Wahl, et al., Thymosin beta4 promotes matrix metalloproteinase expression during wound repair, J. Cell. Physiol. 208 (2006) 195–200.
[37] J.H. Ho, K.C. Tseng, W.H. Ma, K.H. Chen, O.K. Lee, Y. Su, Thymosin beta-4 upregulates anti-oxidative enzymes and protects human cornea epithelial cells against oxidative damage, Br. J. Ophthalmol. 92 (2008) 992–997.
[38] S. Pantelyushin, S. Haak, B. Ingold, P. Kulig, F.L. Heppner, A.A. Navarini, B. Becher, Rorγt+ innate lymphocytes and γδ T cells initiate psoriasiform plaque formation in mice, J. Clin. Invest. 122 (2012) 2252–2256.
[39] G. Girolomoni, U. Mrowietz, C. Paul, Psoriasis: rationale for targeting interleukin-17, Br. J. Dermatol. 167 (2012) 717–724.
[40] K. Reich, K.A. Papp, R.T. Matheson, J.H. Tu, R. Bissonnette, M. Bourcier, D. Gratton, et al., Evidence that a neutrophil-keratinocyte crosstalk is an early target of IL-17A inhibition in psoriasis, Exp. Dermatol. 24 (2015) 529–535.
[41] M.C. Honorati, R. Meliconi, L. Pulsatelli, S. Canè, L. Frizziero, A. Facchini, High in vivo expression of interleukin-17 receptor in synovial endothelial cells and chondrocytes from arthritis patients, Rheumatology (Oxf.) 40 (2001) 522–527.
[42] J.Z. Yang, Y. Li, L.X. Sun, J. Fang, L.J. Kong, J.Q. Zhang, Interleukin-17 receptor expression on vascular endothelial cells of masses of skeletal extramedullary disease in myeloma patients, Pathol. Res. Pract. 210 (2014) 586–590.
[43] H. Fujie, K. Niu, M. Ohba, Y. Tomioka, H. Kitazawa, K. Nagashima, T. Ohrui, et al., A distinct regulatory role of Th17 cytokines IL-17A and IL-17F in chemokine secretion from lung microvascular endothelial cells, Inflammation 35 (2012) 1119–1131.
[44] E.M. Moran, M. Connolly, W. Gao, J. McCormick, U. Fearon, D.J. Veale, Interleukin-17A induction of angiogenesis, cell migration, and cytoskeletal rearrangement, Arthritis Rheum. 63 (2011) 3263–3273.
[45] R. Gillitzer, K. Wolff, D. Tong, C. Müller, T. Yoshimura, A.A. Hartmann, G. Stingl, et al., MCP-1 mRNA expression in basal keratinocytes of psoriatic lesions, J. Invest. Dermatol. 101 (1993) 127–131.

[46] G. Martin, S. Guérard, M.M. Fortin, D. Rusu, J. Soucy, P.E. Poubelle, R. Pouliot, Pathological crosstalk in vitro between T lymphocytes and lesional keratinocytes in psoriasis: necessity of direct cell-to-cell contact, Lab. Invest. 92 (2012) 1058–1070.
[47] C. Vestergaard, H. Just, J. Baumgartner Nielsen, K. Thestrup-Pedersen, M. Deleuran, Expression of CCR2 on monocytes and macrophages in chronically inflamed skin in atopic dermatitis and psoriasis, Acta Derm. Venereol. 84 (2004) 353–358.
[48] H. Wang, T. Peters, D. Kess, A. Sindrilaru, T. Oreshkova, N. Van Rooijen, A. Stratis, et al., Activated macrophages are essential in a murine model for T cell-mediated chronic psoriasiform skin inflammation, J. Clin. Invest. 116 (2006) 2105–2114.
[49] S. Shao, T. Cao, L. Jin, B. Li, H. Fang, J. Zhang, Y. Zhang, et al., Increased lipocalin-2 contributes to the pathogenesis of psoriasis by modulating neutrophil chemotaxis and cytokine secretion, J. Invest. Dermatol. 136 (2016) 1418–1428.
[50] C.S. Hau, N. Kanda, Y. Tada, S. Shibata, H. Uozaki, T. Fukusato, S. Sato, et al., Lipocalin-2 exacerbates psoriasiform skin inflammation by augmenting T-helper 17 response, J. Dermatol. 43 (2016) 785–794.
[51] S. Mahboob, A. Mohamedali, S.B. Ahn, P. Schulz-Knappe, E. Nice, M.S. Baker, Is isolation of comprehensive human plasma peptidomes an achievable quest? J. Proteomics 127 (Pt B) (2015) 300–309.
[52] P. Zhu, P. Bowden, D. Zhang, J.G. Marshall, Mass spectrometry of peptides and proteins from human blood, Mass Spectrom. Rev. 30 (2011) 685–732.
[53] A. Albalat, H. Mischak, W. Mullen, Clinical application of urinary proteomics/peptidomics, Expert Rev. Proteomics 8 (2011) 615–629.
[54] D.C. Dallas, A. Guerrero, E.A. Parker, R.C. Robinson, J. Gan, J.B. German, D. Barile, et al., Current peptidomics: applications, purification, identification, quantification, and functional analysis, Proteomics 15 (2015) 1026–1038.
[55] A. Secher, C.D. Kelstrup, K.W. Conde-Frieboes, C. Pyke, K. Raun, B.S. Wulff, J.V. Olsen, Analytic framework for peptidomics applied to large-scale neuropeptide identification, Nat. Commun. 7 (2016) 11436.
[56] A.D. Tinoco, D.M. Tagore, A. Saghatelian, Expanding the dipeptidyl peptidase 4-regulated peptidome via an optimized peptidomics platform, J. Am. Chem. Soc. 132 (2010) 3819–3830.
[57] T. Gambichler, F.G. Bechara, N. Scola, S. Rotterdam, P. Altmeyer, M. Skrygan, Serum levels of antimicrobial peptides and proteins do not correlate with psoriasis severity and are increased after treatment with fumaric acid esters, Arch. Dermatol. Res. 304 (2012) 471–474.
[58] L. Anderson, C.L. Hunter, Quantitative mass spectrometric multiple reaction monitoring assays for major plasma proteins, Mol. Cell. Proteomics 5 (2006) 573–588.
[59] R.I. Litvinov, S. Yakovlev, G. Tsurupa, O.V. Gorkun, L. Medved, J.W. Weisel, Direct evidence for specific interactions of the fibrinogen alphaC-domains with the central E region and with each other, Biochemistry 46 (2007) 9133–9142.

J Gastroenterol (2017) 52:1051–1063
DOI 10.1007/s00535-017-1316-3

ORIGINAL ARTICLE—LIVER, PANCREAS, AND BILIARY TRACT

Effects of vaccine-acquired polyclonal anti-HBs antibodies on the prevention of HBV infection of non-vaccine genotypes

Masaki Kato[1,2] · Susumu Hamada-Tsutsumi[3] · Chiaki Okuse[4] · Aiko Sakai[5] · Nobuyuki Matsumoto[2] · Masaaki Sato[6] · Toshiyuki Sato[6] · Mitsumi Arito[6] · Kazuki Omoteyama[6] · Naoya Suematsu[6] · Kazuki Okamoto[6] · Takanobu Kato[7] · Fumio Itoh[2] · Ryo Sumazaki[5] · Yasuhito Tanaka[3] · Hiroshi Yotsuyanagi[8] · Tomohiro Kato[6] · Manae Suzuki Kurokawa[1]

Received: 8 November 2016 / Accepted: 31 January 2017 / Published online: 14 February 2017
© Japanese Society of Gastroenterology 2017

Abstract

Background In universal hepatitis B (HB) vaccination, single vaccine-derived polyclonal anti-HBs antibodies (anti-HBs) need to inhibit infection of HB viruses (HBV) of non-vaccine genotypes. We experimentally addressed this issue.

Methods Anti-HBs-positive sera were obtained by vaccination with genotype A- or C-derived HBs antigen (HBsAg, gtA-sera or gtC-sera). Their reactivity to genotype A- and C-derived HBsAg (gtA-Ag and gtC-Ag) was measured by ELISA. The capacity of sera to neutralize HBV was evaluated using an in vitro infection model.

Results Of 135 anti-gtA-Ag-reactive gtA-sera, 134 (99.3%) were anti-gtC-Ag-reactive. All (100%) 120 anti-gtC-Ag-reactive gtC-sera were anti-gtA-Ag-reactive. The reactivity to gtA-Ag was strongly correlated with that to gtC-Ag (gtA-sera, $\rho = 0.989$; gtC-sera, $\rho = 0.953$; $p < 0.01$). In gtA-sera ($n = 10$), anti-HBs to gtA-Ag were less completely absorbed with gtC-Ag (96.4%) than with gtA-Ag (100%, $p < 0.05$). Similarly, in gtC-sera ($n = 10$), anti-HBs to gtC-Ag were less completely absorbed with gtA-Ag (96.0%) than with gtC-Ag (100%, $p < 0.01$). Thus, 3.6 and 4.0% of anti-HBs in gtA-sera and gtC-sera were vaccine genotype HBsAg-specific, respectively. In the neutralization test, gtA-sera ($n = 4$) and gtC-sera ($n = 3$) with anti-HBs titers adjusted to 100 mIU/mL equally inhibited genotype C HBV infection (92.8 vs. 95.4%, $p = 0.44$). However, at 30 mIU/mL, the gtA-sera less effectively inhibited infection than the gtC-sera (60.2 vs. 90.2%, $p < 0.05$).

Conclusions Vaccination with genotype A- or C-derived HBsAg provided polyclonal anti-HBs that sufficiently bound to non-vaccine genotype HBsAg. However, a small portion of anti-HBs were specific to the vaccine genotype HBsAg. High anti-HBs titers would be required to prevent HBV infection of non-vaccine genotypes. *UMIN/CTR* UMIN000014363.

Keywords Hepatitis B virus · Genotypes · Universal vaccination · Polyclonal anti-HBs antibodies

Abbreviations

Anti-HBs	Anti-hepatitis B surface antibodies
DNA	Deoxyribonucleic acid
ELISA	Enzyme-linked immunosorbent assay

Electronic supplementary material The online version of this article (doi:10.1007/s00535-017-1316-3) contains supplementary material, which is available to authorized users.

✉ Manae Suzuki Kurokawa
manae@marianna-u.ac.jp

1 Disease Biomarker Analysis and Molecular Regulation, St. Marianna University Graduate School of Medicine, 2-16-1, Sugao, Miyamae-Ku, Kawasaki 216-8511, Japan

2 Division of Gastroenterology and Hepatology, Department of Internal Medicine, St. Marianna University School of Medicine, Kawasaki, Japan

3 Department of Virology and Liver Unit, Nagoya City University Graduate School of Medical Sciences, Nagoya, Japan

4 Division of Gastroenterology and Hepatology, Kawasaki Municipal Tama Hospital, Kawasaki, Japan

5 Department of Child Health, Faculty of Medicine, University of Tsukuba, Tsukuba, Japan

6 Clinical Proteomics and Molecular Medicine, St. Marianna University Graduate School of Medicine, Kawasaki, Japan

7 Department of Virology II, National Institute of Infectious Diseases, Tokyo, Japan

8 Department of Infectious Diseases, Graduate School of Medicine, The University of Tokyo, Tokyo, Japan

F	Female
HB	Hepatitis B
HBIG	Immunoglobulins containing high-titer antibodies against HBsAg
HBsAg	Hepatitis B surface antigen
HBV	Hepatitis B virus
HCC	Hepatocellular carcinoma
gtA-Ag	Genotype A-derived hepatitis B surface antigen
gtC-Ag	Genotype C-derived hepatitis B surface antigen
gtA-sera	Anti-HBs-antibody-positive sera from Heptavax-II-immunized individuals
gtC-sera	Anti-HBs-antibody-positive sera from Bimmugen-immunized individuals
M	Male
NC	Negative control
NI-sera	Anti-HBs-negative sera from HB vaccine-non-immunized individuals
OD	Optical density
PCR	Polymerase chain reaction
SD	Standard deviation

Introduction

Hepatitis B virus (HBV) infection is an important public health problem worldwide, leading to chronic hepatitis, liver cirrhosis, and hepatocellular carcinoma (HCC) [1, 2]. Approximately 248 million individuals were estimated to be HBs antigen (HBsAg)-positive globally in 2010 [3], and more than 600,000 individuals die annually due to liver cirrhosis and cancer [4]. The prevention of HBV infection by vaccination is crucial for eradicating HBV-associated life-threatening diseases, as well as for treating infection with anti-viral drugs.

Safe and effective universal vaccination against HBV infection has been available since 1981 [1, 5]. By 2014, 184 countries had introduced childhood vaccination against HBV including birth dose vaccination [6]. Ten HBV genotypes (A-J) have been identified at present and are an important factor for developing strategies to prevent HBV infection [7, 8]. Infection of various genotypes of HBV has been found in most countries [9]. HB vaccines, most of which are derived from genotype A HBV, have an excellent record of effectiveness, reducing the rate of chronic infection in children from 8–15% to less than 1% [6]. This result indicates that HB vaccines made from a single genotype-derived HBsAg are capable of neutralizing HBV of non-vaccine genotypes [9]. For example, although almost all HBV infection in Taiwan were caused by genotypes B and C [10], systematic vaccination using a genotype A-derived vaccine decreased the HBsAg seropositivity in children from 9.8 to 1.3% by 10 years after the start of vaccination [11]. Furthermore, the HBsAg seropositivity and HCC incidence in Thailand, where genotype B and C were dominant, were markedly reduced in cohorts immunized with a genotype A-derived vaccine [12, 13]. These observations also indicate that single genotype-derived HB vaccines are largely effective in neutralizing HBV of non-vaccine genotypes.

However, whether single genotype-derived HB vaccines prevent infection of non-vaccine genotype HBV as effectively as they do vaccine genotype HBV remains unclear. Interestingly, surveillance of blood donors in the United States detected nine HBV-seronegative but HBV-DNA-positive donors, six of whom had received a genotype A2-vaccine and showed low or undetectable levels of anti-HBs antibody (anti-HBs) titers [14]. The infecting genotypes were significantly different between the vaccinated and unvaccinated donors: five out of the six vaccinated donors were exclusively or predominantly infected with non-A2 strains, while the remaining one vaccinated and the three unvaccinated donors were infected with A2 strain. We also reported that an anti-HBs monoclonal antibody derived from a recipient of a genotype C-derived vaccine efficiently neutralized genotype C HBV, however, it failed to neutralize genotype A HBV at a low anti-HBs titer [15]. These studies indicate an insufficient capacity of single genotype-derived HB vaccines to prevent infection of non-vaccine genotype HBV. However, no experimental study has examined the capacity of vaccine-acquired polyclonal anti-HBs to bind to and neutralize non-vaccine genotype HBV.

In Japan, universal vaccination against HBV launched in October 2016. Japan had already introduced HB vaccination for infants born to HBV-infected mothers in combination with hepatitis B immunoglobulin approximately 30 years before this launch [16]. This strategy was found to be very effective, reducing the rate of HBsAg-positivity in children from 0.75 to 0.04%. However, recently, HBV infection in children via their fathers and unknown origins has been shown to be a relatively common cause of chronic hepatitis B [17, 18]. In Japan, 82% and 14% of HBV-infected individuals are infected with genotypes C and B, respectively [19, 20]. Recently, the rate of infection with genotype A HBV has been increasing, especially among young individuals [21, 22]. Indeed, in 52% of patients with acute hepatitis B, the hepatitis was caused by genotype A HBV [22]. Therefore, universal HB vaccination in Japan needs to mainly prevent infection of genotype C HBV in children as well as infection of genotype A HBV in adults. In this regard, it is important to evaluate whether single genotype-derived HB vaccines sufficiently prevent infection of non-vaccine genotype HBVs. At present, two kinds of HB vaccines of recombinant small S antigens are available in Japan: genotype A2 HBV-derived Heptavax-II,

which is commonly used worldwide, and genotype C-derived Bimmugen, which is generated in Japan.

In this study, we examined whether polyclonal anti-HBs generated by genotype A-derived HBsAg vaccination bound to genotype C-derived HBsAg and vice versa. Both Heptavax-II and Bimmugen vaccinations provided polyclonal anti-HBs that bound to HBsAgs of the other genotypes. However, a small portion of the polyclonal anti-HBs repertoire did not bind to HBsAgs of the other genotypes. Heptavax-II vaccination-derived anti-HBs as well as Bimmugen vaccination-derived anti-HBs neutralized genotype C HBV at a high anti-HBs titer, whereas the former neutralized genotype C HBV less effectively than the latter at a low titer. Our data suggested that high titers of anti-HBs should be maintained for the prevention of non-vaccine genotype HBV infection.

Materials and methods

Subjects and serum samples

The subjects were medical students and health care providers ≥18 years of age who needed to be immunized with HB vaccines for their future work. Subjects with a fever or acute diseases were excluded from the vaccination. In total, 474 subjects were enrolled in this study at St. Marianna University School of Medicine (including its branch, Kawasaki Municipal Tama Hospital) and University of Tsukuba. Of these, 196 subjects were vaccinated with Heptavax-II (MSD, Kenilworth, NJ, USA) (genotype A-derived vaccine). The anti-HBs titers were evaluated by Stacia (LSI Medience, Tokyo, Japan) or Architect (Abbott, Abbott Park, IL, USA). Anti-HBs-positive sera (≥10 mIU/mL) were selected as genotype A-derived vaccine-immunized sera (gtA-sera). A total of 150 gtA-sera with low-to-high anti-HBs titers, obtained 3–52 months after the last vaccination, were subjected to our analyses. Another gtA-serum, the anti-HBs titer of which was 842.7 mIU/mL measured by Stacia, was used as an internal control serum sample. Similarly, 148 subjects were vaccinated with Bimmugen (Kaketsuken, Kumamoto, Japan). Their anti-HBs titers were evaluated by Stacia or Architect. Anti-HBs-positive sera (≥10 mIU/mL) were selected as genotype C-derived vaccine-immunized sera (gtC-sera). A total of 124 gtC-sera with low-to-high anti-HBs titers, obtained 1–2 months after the last vaccination, were subjected to our analyses. The anti-HBs titers were evaluated by Stacia in 130 university freshmen, 101 of whom were anti-HBs-negative and had no experience of HB vaccination. Sera from these 101 students were subjected to our analyses as HB vaccine-non-immunized sera (NI-sera). The age and sex of the subjects were as follows: 150 gtA-sera providers, mean ± standard deviation (SD) of age 22.7 ± 2.9 years, male (M)/female (F) ratio 67/83; 124 gtC-sera providers, age 20.0 ± 2.7 years, M/F 31/93; 101 NI-sera providers, age 20.3 ± 3.3 years, M/F 60/41. The protocol of this clinical study, which conformed to the provisions of the 1964 Declaration of Helsinki and its later amendments, was approved by the ethics committees of St. Marianna University School of Medicine and University of Tsukuba (UMIN000014363). All of the subjects gave their informed consent prior to their inclusion in this study.

Sandwich ELISA for genotype A- and C-derived HBsAg

Genotype A2-derived HBs small Ag (gtA-Ag) was purchased (adw2; Abcam, Cambridge, UK), and genotype C-derived HBs small Ag (gtC-Ag) was kindly provided by Kaketsuken (Bimmugen, adrq+). A total of 5 μg/mL of each antigen was immobilized onto 8-well strips (Immobilizer amino F8 module; Thermo Fisher Scientific, Waltham, MA, USA) for 2 h at room temperature. The sera and peroxidase-conjugated HBsAg (ad + ay, Enzygnost Anti-HBs II; Siemens, München, Germany) were added and incubated for 1 h at 37 °C. The reactivity was developed in accordance with the protocol of Enzygnost Anti-HBs II. When the sera showed optical density (OD) values exceeding 1.5, they were diluted until their OD values fell into the range of 0.25–1.5; the obtained OD values were then multiplied by the serum dilutions. The multiplied values were compensated by the OD value of the internal control serum sample in each experiment, and the compensated values were shown as reactivity specific to gtA- and gtC-Ag.

Alternatively, the reactivity of some gtA- and gtC-sera were absorbed with serially diluted soluble gtA- and gtC-Ags, and the resultant reactivity to the HBsAgs of the vaccine genotypes was measured. The absorption ratios with HBsAgs of non-vaccine genotypes were calculated using the following formula: (OD values without absorption—OD values absorbed with the non-vaccine genotype-derived HBsAg)/(OD values without absorption—OD values absorbed with the vaccine genotype-derived HBsAg).

HBV-neutralization

Genotype C HBVs (7×10^5 copies) were suspended in 90 μL of dHCGM medium [15]. gtA- and gtC-sera were serially diluted with the negative control (NC) serum (Enzygnost Anti-HBs II) to adjust their anti-HBs titers to 100, 200, 300, 500, 1,000, and 10,000 mIU/mL. The anti-HBs titers of the diluted sera were confirmed by measurement using Enzygnost Anti-HBs II. Three NI sera (no dilution) and immunoglobulins containing high-titer

antibodies against HBsAg (HBIG) (Hebsbulin, Japan Blood Products Organization, Tokyo, Japan), anti-HBs titers of which were adjusted to 10, 100, 1,000 and 10,000 mIU/mL, were also prepared. Each serum sample or HBIG (10 μL) was added to 90 μL of the virus-suspended medium, and incubated at 37 °C for 2 h. After the incubation, primary human hepatocytes (PhoenixBio, Higashi-hiroshima, Japan), seeded at 7.0×10^4 cells/well, were cultured in 100 μL of the medium containing the HBV and the serum sample above (Day 0). On Days 2 and 3, the culture supernatants of mock wells (10 μL of dHCGM was added in place of sera) were recovered, and the supernatants of the other wells were discarded. The cells were washed in 100 μL of DMEM 3 times and again cultured in 100 μL of fresh dHCGM. On Day 7, the culture supernatants of each well were replaced with 100 μL of fresh dHCGM. On Days 12, 17, and 22, the culture supernatants were recovered. On Days 12 and 17, 100 μL of fresh dHCGM was added to each well. HBV genomic DNA was extracted using Smitest (Medical Biology, Nagoya, Japan) from the supernatants on Day 17.

The extracted HBV-DNA was quantified by real-time polymerase chain reaction (PCR) using Eagle Taq Universal Master Mix (Roche Diagnostics, Basel, Switzerland). The sequences of the primers and probes were as follows: forward, 5′-CACATCAGGATTCCTAGGACC-3′; reverse, 5′-AGGTTGGTGAGTGATTGGAG-3′; probe, 5′-CAGAGTCTAGACTCGTGGTGGACTTC-3′. Serially diluted pHBV/Aa-1.24, in which the whole genome of HBV was sub-cloned, was used as the template for the standard samples. The amplification program was performed as follows using a StepOne Plus PCR system (Thermo Fisher Scientific): 50 °C for 2 min, 95 °C for 10 min, and (95 °C for 15 s and 60 °C for 1 min) for 45 cycles.

Statistical analyses

The significance of differences in the reactivity between gtA- and gtC-sera was calculated using Wilcoxon's signed-rank test (Fig. 1a, b) and Student's *t* test (Fig. 2c). The correlations between the reactivity to gtA-Ag and that to gtC-Ag were calculated using Spearman's rank correlation coefficient (Fig. 2a, b). The significance of differences in the absorption ratios between sera absorbed with vaccine genotype HBsAg and those absorbed with the non-vaccine genotype HBsAg was calculated by Wilcoxon's signed-rank test (Fig. 3a, b). The significance of differences in the absorption ratios between a serum sample absorbed with the vaccine genotype HBsAg and that absorbed with the non-vaccine genotype HBsAg was calculated using Student's *t* test (Fig. 3c–e). The significance of differences in the HBV neutralization levels between gtA- and gtC-sera was also calculated using Student's *t* test (Fig. 4b, d).

Results

gtA-sera were cross-reactive to gtC-Ag and gtC-sera were cross-reactive to gtA-Ag

First, we examined whether gtA-sera (anti-HBs-positive sera from Heptavax-II-immunized individuals) were reactive to gtC-Ag and whether gtC-sera (anti-HBs-positive sera from Bimmugen-immunized individuals) were reactive to gtA-Ag. The reactivity of 147 gtA-sera, 120 gtC-sera, and 101 NI-sera (anti-HBs-negative sera from HB vaccine-non-immunized individuals) to gtA- and gtC-Ag was measured by sandwich ELISA (Fig. 1a, b). The mean + 2SD of the OD values of the NI-sera were set as the cut-off values to determine whether the examined gtA- and gtC-sera were anti-HBs-positive or -negative (0.067 AU in gtA-Ag ELISA, and 0.078 AU in gtC-Ag ELISA) (Fig. 1a, b, broken lines).

We found that 135 out of the 147 gtA-sera (91.8%) were positive for anti-gtA-Ag (2.94 ± 4.04 AU), and 134 out of the 135 anti-gtA-Ag-positive sera (99.3%) were also positive for anti-gtC-Ag (4.54 ± 6.21 AU) (Fig. 1a–c). The titer of the remaining 1 gtA-serum sample, A56, was 0.085 AU to gtA-Ag and 0.075 AU to gtC-Ag, which were close to the cutoff values (Table 1). All of the examined 120 gtC-sera (100%) were positive for anti-gtC-Ag (38.4 ± 49.4 AU) as well as anti-gtA-Ag (19.5 ± 28.9 AU) (Fig. 1a–c). Thus, almost all of the anti-HBs-positive sera obtained by vaccination with Heptavax-II and Bimmugen were found to be cross-reactive to gtC-Ag and gtA-Ag, respectively.

We found 13 gtA-sera that were not reactive to gtA- or gtC-Ag (Fig. 1a–c; Table 1). Eleven of these 13 gtA-sera were both anti-gtA-Ag- and anti-gtC-Ag-negative. Regarding the remaining two sera, the results of one A56 were described above; the other sample (A142) was anti-gtA-Ag-negative but anti-gtC-Ag-positive (Table 1).

In addition, the 120 gtC-sera showed significantly higher reactivity to both gtA-Ag and gtC-Ag than the 147 gtA-sera (gtA-sera vs. gtC-sera: 2.70 ± 3.95 vs. 19.5 ± 28.9 AU to gtA-Ag, $p < 0.001$; 4.15 ± 6.06 vs. 38.4 ± 49.4 AU to gtC-Ag, $p < 0.001$) (Fig. 1a, b).

gtC-sera bound more strongly to gtC-Ag than to gtA-Ag compared to gtA-sera, and vice versa for gtA-sera

We compared the reactivity to gtA-Ag with that to gtC-Ag in the 135 anti-gtA-Ag-positive gtA-sera and the 120 anti-

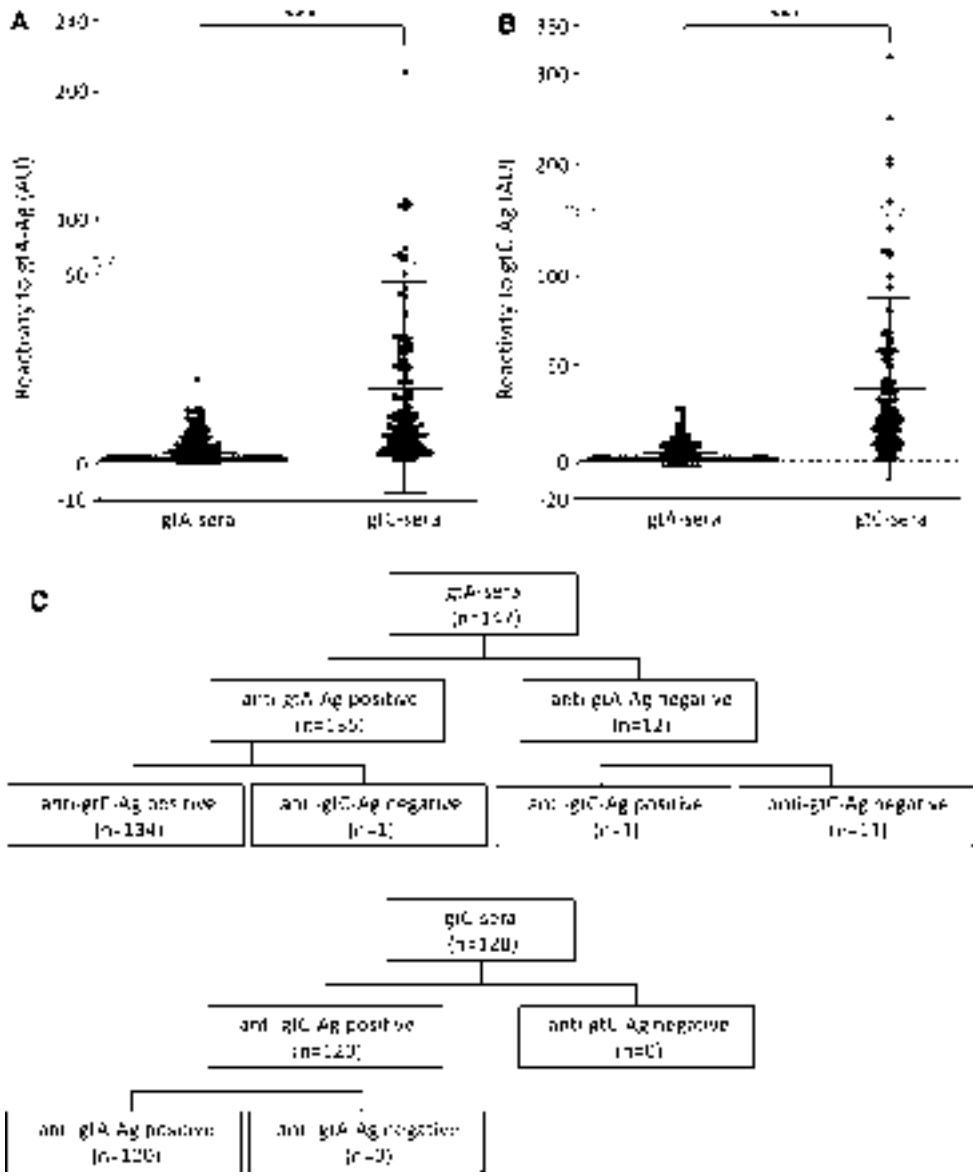

Fig. 1 Reactivity of gtA-sera to gtC-Ag and that of gtC-sera to gtA-Ag. A total of 147 gtA-sera and 120 gtC-sera, determined as anti-HBs-positive by clinical examinations, were measured for their reactivity to gtA-Ag and gtC-Ag by respective sandwich ELISAs. The resultant OD values were compensated using the OD values of an internal control serum in every ELISA experiment, and the compensated values are shown as the reactivity. The cut-off values were determined as the mean + 2SD of 101 NI-sera (*broken lines*). The results of gtA-Ag (**a**) and gtC-Ag (**b**) are shown. A summary of the results is shown (**c**). ***$p < 0.001$

gtC-Ag-positive gtC-sera. We examined the correlation between the gtA-serum reactivity to gtA-Ag and that to gtC-Ag, and the correlation between the gtC-serum reactivity to gtA-Ag and that to gtC-Ag. In the 135 gtA-sera, the reactivity to gtA-Ag and that to gtC-Ag showed a strong positive correlation ($\rho = 0.989$, $p < 0.01$) (Fig. 2a). In the 120 gtC-sera, the reactivity to gtA-Ag and that to gtC-Ag also showed a strong positive correlation ($\rho = 0.953$, $p < 0.01$) (Fig. 2b).

We next examined the difference between the serum reactivity to vaccine genotype HBsAg and that to non-vaccine genotype HBsAg. To analyze the difference, we calculated the ratio of "the reactivity to gtC-Ag/the reactivity to gtA-Ag" (y/x in Fig. 2a, b). Interestingly, the ratio was higher in gtC-sera than in gtA-sera (2.40 ± 0.80 vs. 1.54 ± 0.42, $p < 0.001$) (Fig. 2a, b). To demonstrate the different reactivity between gtA- and gtC-sera more clearly, we calculated the normalized ratio of "the reactivity to gtC-Ag/the reactivity to gtA-Ag" by setting the average ratio of the total samples as 1.0. gtC-sera showed an average normalized ratio of more than 1.0, while gtA-sera showed an average normalized ratio of less than 1.0 (1.23 [−7.41 to 3.03] vs. −1.25 [−2.64 to 2.00], $p < 0.001$) (Fig. 2c). These results suggested that the gtC-sera were more strongly reactive to gtC-Ag than to gtA-Ag and that the gtA-sera were more strongly reactive to gtA-Ag than to gtC-Ag.

A small fraction of polyclonal anti-HBs was vaccine genotype HBsAg-specific

Next, we investigated whether vaccine genotype-specific anti-HBs fractions were present in gtA- and gtC-sera by

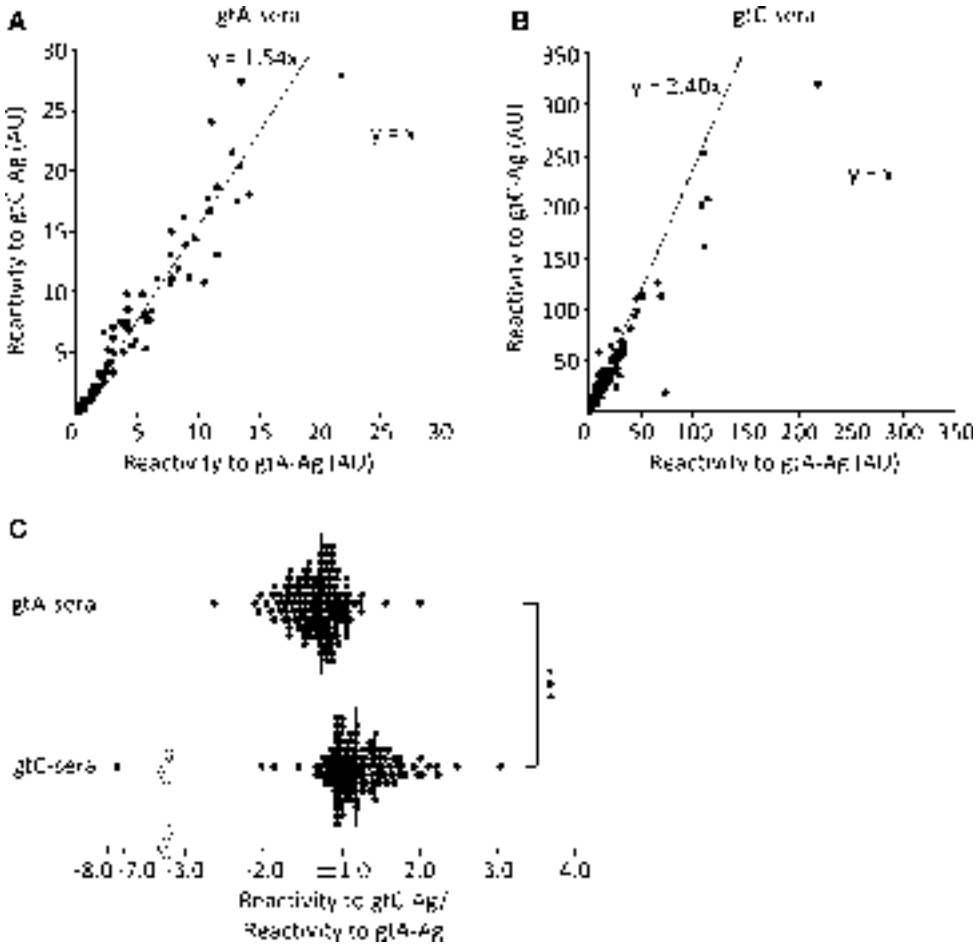

Fig. 2 The correlations of gtA- and gtC-serum reactivity to gtA-Ag and gtC-Ag. **a**, **b** The correlations of gtA- and gtC-serum reactivity to gtA-Ag and gtC-Ag were examined. The results of 135 gtA-sera (**a**, $\rho = 0.989$, $p < 0.01$) and 120 gtC-sera (**b**, $\rho = 0.953$, $p < 0.01$) are shown. **c** The difference in the reactivity between gtA- and gtC-sera was examined by calculating the ratio of "the reactivity to gtC-Ag/the reactivity to gtA-Ag." The ratios were normalized as the average of all examined sera as 1.0. "-x" indicates "1/x". ***$p < 0.001$

an antibody-absorption test using gtA- and gtC-Ag. Ten samples each of gtA- and gtC-sera adjusted to show anti-HBs values of approximately 1.0 OD were absorbed with serial concentrations of soluble gtA- and gtC-Ag, respectively (Table 2). The reactivity of the absorbed gtA-sera to gtA-Ag, and that of the absorbed gtC-sera to gtC-Ag was measured by ELISA. In all 10 examined gtA-sera, the reactivity to gtA-Ag was completely (100%) absorbed with 5 μg/mL gtA-Ag (data not shown). Similarly, in all 10 examined gtC-sera, the reactivity to gtC-Ag was completely (100%) absorbed with 5 μg/mL gtC-Ag (data not shown). Given these results, we determined the concentration of soluble antigens for the absorption as 5 μg/mL.

We then measured the absorption ratios of the OD-adjusted gtA-sera and gtC-sera absorbed with 5 μg/mL gtC-Ag and gtA-Ag, respectively. On average, 96.4 ± 6.5% of the reactivity of gtA-sera to gtA-Ag was absorbed with gtC-Ag ($p < 0.01$) (Table 2; Fig. 3a). Similarly, 96.0 ± 2.6% of the reactivity of gtC-sera to gtC-Ag was absorbed with gtA-Ag ($p < 0.001$) (Table 2; Fig. 3b). Thus, 3.6 and 4.0% anti-HBs in gtA- and gtC-sera were not absorbed with gtC- and gtA-Ag, respectively. Sixteen of the 20 sera showed 91.1–99.8% absorption ratios (Table 2, a representative case of C24 is shown in Fig. 3c). Three gtA-sera (A74, A75, and A93) showed 100% absorption with gtC-Ag (Table 2; Fig. 3d). Interestingly, in 1 gtA-serum sample, A72, only 79.2% of the reactivity to gtA-Ag was absorbed with gtC-Ag (Table 2; Fig. 3e). Collectively, almost all of the examined gtA- and gtC-sera showed identical or slightly less reactivity to non-vaccine genotype HBsAg than to the vaccine genotype HBsAg. In each anti-HBs-positive serum, most polyclonal anti-HBs were cross-reactive to non-vaccine genotype HBsAg, however, a small fraction of the anti-HBs was vaccine genotype HBsAg-specific.

gtA- and gtC-sera with a high anti-HBs titer effectively neutralized genotype C HBV

Finally, we examined whether or not the genotype C HBV-neutralization levels were different between gtA-sera ($n = 4$) and gtC-sera ($n = 3$) (Table 3). The sera were serially diluted to show anti-HBs titers of 100–10,000 mIU/mL. The resultant titers of the diluted sera were confirmed to be within ±20% of each titer (data

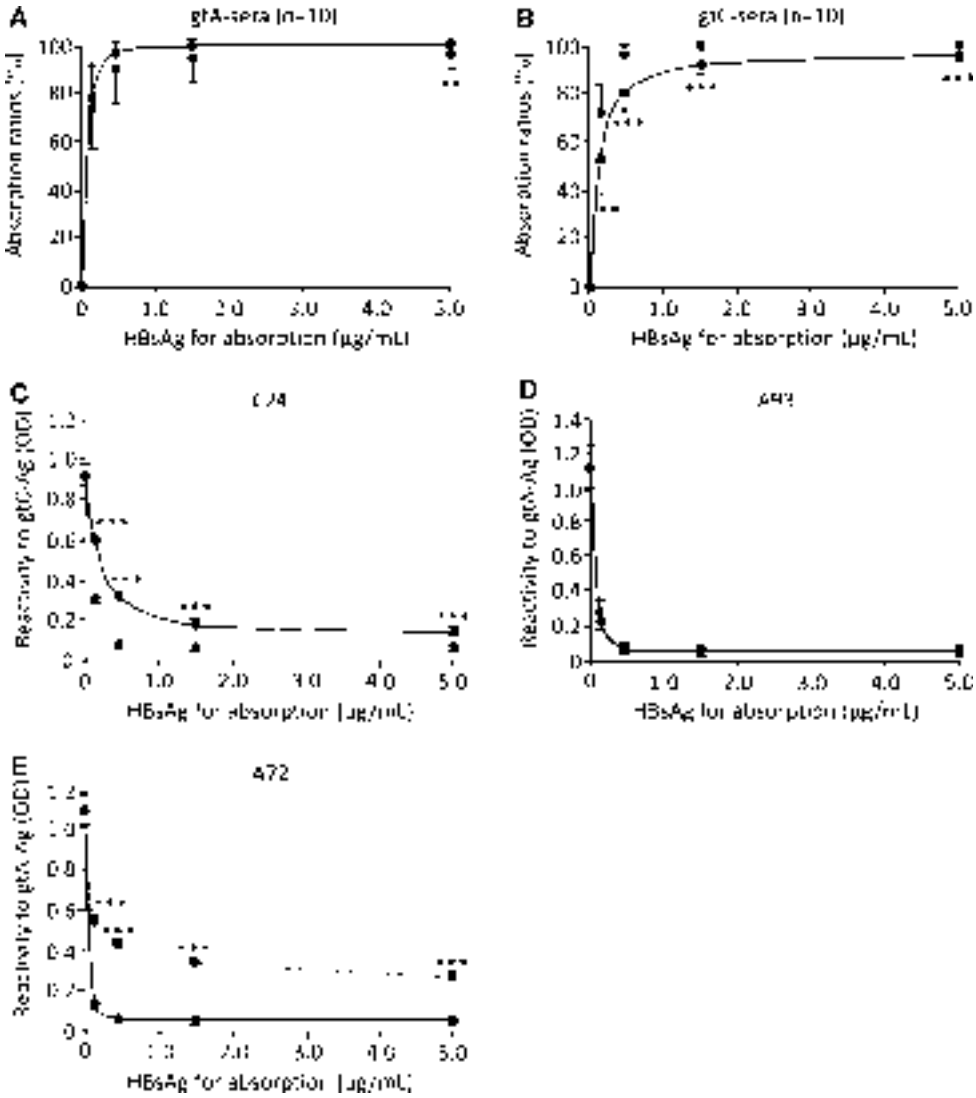

Fig. 3 gtA-serum reactivity absorbed with gtC-Ag and gtC-serum reactivity absorbed with gtA-Ag. A total of 10 gtA-sera and 10 gtC-sera (Table 2) were absorbed with serially diluted gtA-Ag and gtC-Ag. The resultant reactivity of the gtA-sera was measured by gtA-ELISA, and that of the gtC-sera was measured by gtC-ELISA. When the gtA-sera absorbed with gtA-Ag and the gtC-sera absorbed with gtC-Ag showed the same or lower reactivity than the reactivity of anti-HBs-negative control serum (NC serum in Enzygnost anti-HBs II), we determined that those sera had been completely absorbed. The averages of the absorption ratios of gtA-sera (**a**) and gtC-sera (**b**), and the representative results of 3 sera (the absorption ratios with the non-vaccine genotype HBsAg were 91.1%, **c**; 100%, **d**; and 79.2%, **e**) are shown. *Solid lines*, absorption with gtA-Ag; *dotted lines*, absorption with gtC-Ag. $^{**}p < 0.01$, $^{***}p < 0.001$

not shown). We then mixed the diluted sera with HBV-suspended culture media to obtain final anti-HBs titers at 1/10 of the adjusted titers (10–1,000 mIU/mL) (Fig. 4a).

First, we tried to determine the anti-HBs titers of HBIG and gtC-sera that sufficiently neutralized HBV in this experiment. We found that 100 and 1,000 mIU/mL HBIG sufficiently neutralized the genotype C HBV (the extracellular HBV-DNA, 7.1 and 4.3 copies, respectively) (Fig. 4a). Similarly, 100 and 1,000 mIU/mL gtC-sera sufficiently neutralized the genotype C HBV (6.5 ± 7.4 and 4.6 ± 5.9 copies, respectively). In contrast, 10 mIU/mL HBIG was insufficient for the neutralization (405.5 copies) (Fig. 4a), showing a level similar to that of anti-HBs-negative sera (NI 1–3 and NC, 309.3 ± 115.1 copies).

In this condition, the gtA-sera sufficiently neutralized genotype C HBV at an anti-HBs titer of 100 mIU/mL (10.7 ± 5.5 copies) (Fig. 4a). The gtA-sera showed inhibition ratios similar to those of the gtC-sera at 100 mIU/mL (92.8 ± 3.7 vs. 95.4 ± 4.8%, $p = 0.44$) (Fig. 4b). The A72 serum sample that showed low absorption with gtC-Ag (79.2%, Fig. 3e) provided an inhibition ratio similar to those of the other three gtA-sera at 100 mIU/mL anti-HBs (92.0 vs. 93.0 ± 4.5%) (Fig. 4a, b).

Interestingly, the inhibition ratios at a relatively low anti-HBs titer of 30 mIU/mL were significantly lower in the gtA-sera than the gtC-sera (60.2 ± 17.0 vs. 90.2 ± 8.2%, $p < 0.05$) (Fig. 4b). To compare the genotype C HBV-neutralizing capacity between the gtA- and gtC-sera, we compared the anti-HBs titers of those sera that showed an inhibition ratio of 87.0% (Fig. 4c, broken line). This ratio, which was equal to that of 92.2 mIU/mL HBIG, was selected because all 7 sera were able to be evaluated. As a result, the anti-HBs titers of the gtA-sera that showed an inhibition ratio of 87.0% were significantly higher than those of the gtC-sera (72.8 ± 23.7 vs. 25.6 ± 14.2 mIU/mL, $p < 0.05$) (Fig. 4d). This indicates that the genotype C

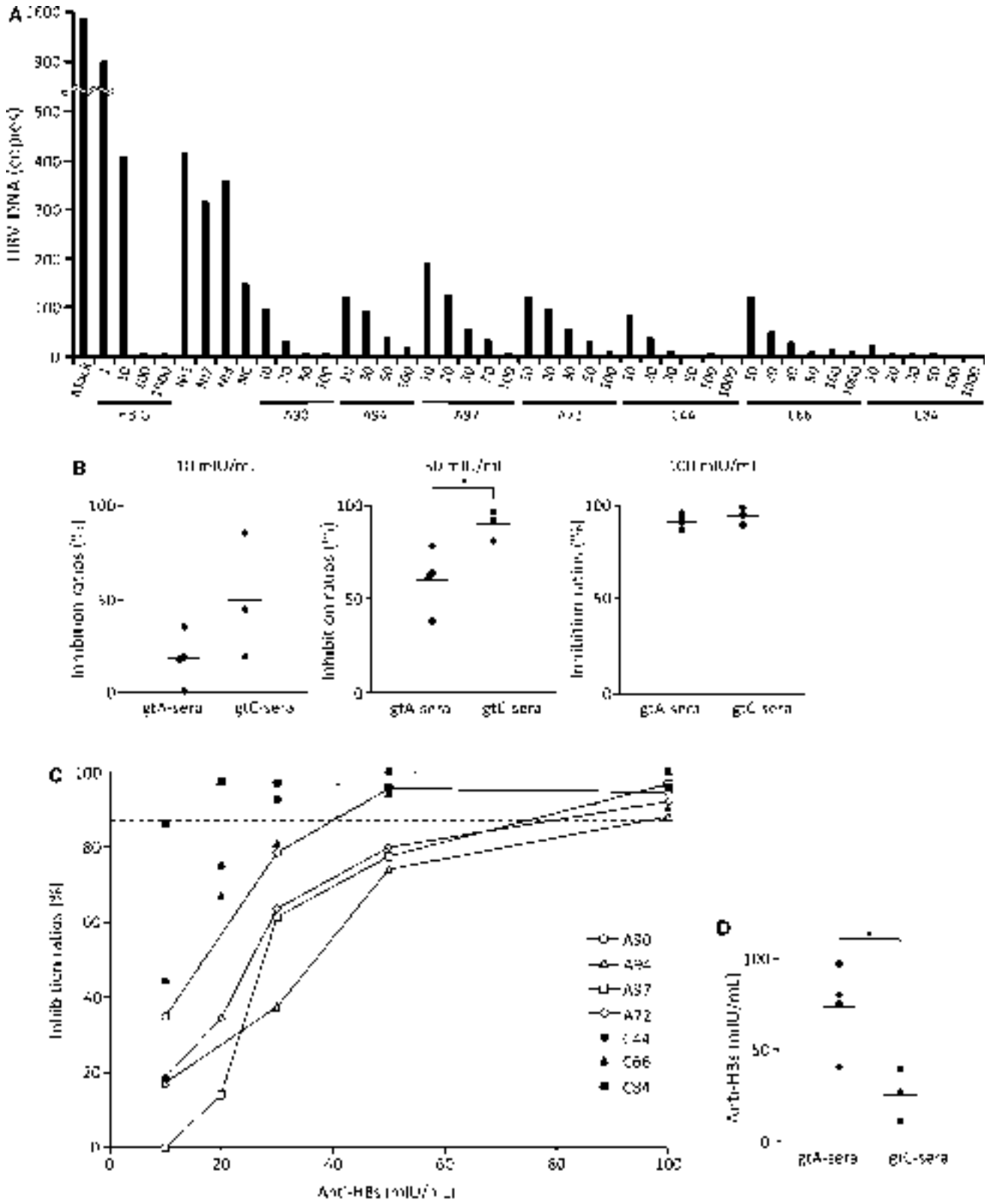
A
B
gtA-sera
gtC-sera
C
D
gtA-sera
gtC-sera

◀**Fig. 4** Genotype C HBV-neutralization by gtA-sera and gtC-sera. **a** Four gtA-sera and three gtC-sera (Table 3) were diluted until their anti-HBs titers were 100, 200, 300, 500, 1,000, and 10,000 (gtC-sera only) mIU/mL and subsequently mixed with genotype C HBV. The final anti-HBs titers were at 1/10 of the adjusted titers (10–1,000 mIU/mL). The mixture was incubated at 37 °C for 2 h, and infected into primary human hepatocytes. The HBV-DNA copy numbers in the culture supernatants on Day 17 were quantified. HBV-DNA copy numbers of medium-alone wells, in which HBV was not infected, were subtracted from the resultant HBV-DNA copy numbers of all experiments. **b** Since all of the gtA- and gtC-sera were diluted with NC serum, we calculated the inhibition ratios of the genotype C-HBV infection as 0% inhibition for NC serum (147.45 copies) and as 100% for 0 copies (C44, 50 mIU/mL; C84, 100 and 1,000 mIU/mL). The inhibition ratios of genotype C HBV infection by gtA- and gtC-sera, diluted to anti-HBs titers of 10, 30, and 100 mIU/mL, are shown. **c**, **d** The anti-HBs titers of the 4 gtA-sera and the 3 gtC-sera that showed an inhibition ratio of 87.0% (*broken line*, **c**) were compared. Mock: HBV was infected, and either HBIG or serum was not added. $*p < 0.05$

HBV-neutralizing capacity of the gtA-sera was lower than that of the gtC-sera. In addition, the A72 serum sample showed an anti-HBs titer of 79.5 mIU/mL with over 87.0% inhibition, which was similar to the anti-HBs titers of the other 3 gtA-sera (70.5 ± 28.5 mIU/mL) (Fig. 4c, d).

Discussion

To examine whether or not vaccine-acquired polyclonal anti-HBs effectively bound to the HBsAg of non-vaccine genotypes, we established gtA-Ag ELISA and gtC-Ag ELISA. Of 101 NI sera that were anti-HBs-negative in a clinical examination, 99 (98%) and 94 (93%) samples showed compensated OD values less than the cut-off values of the gtA-Ag ELISA and gtC-Ag ELISA, respectively (data not shown). In contrast, of 147 gtA-sera and 120 gtC-sera that were ant-HBs-positive in clinical examinations, 135 gtA-sera (92%) and all 120 gtC-sera (100%) showed OD values exceeding the cut-off values in the gtA-Ag ELISA and gtC-Ag ELISA, respectively (Fig. 1a–c; Table 1). Collectively, at most 8% of the examined gtA-sera were judged to be anti-HBs-negative in the gtA-Ag ELISA. It was reported that approximately 7% of serum samples showed conflicting results between the 2 established anti-HBs measurement methods [23]. Thus, our ELISAs were considered to be accurate enough to measure the reactivity to single genotype-derived HBsAgs.

Notably, 134 of the 135 gtA-sera (99.3%) and all 120 gtC-sera (100%) were both anti-gtA-Ag-positive and anti-gtC-Ag-positive (Fig. 1a–c). Indeed, gtA- and gtC-sera showed very high correlations between the reactivity to gtA-Ag and that to gtC-Ag (gtA-sera, $\rho = 0.989, p < 0.01$; gtC-sera, $\rho = 0.953$, $p < 0.01$) (Fig. 2a, b). Heptavax-II and Bimmugen were therefore concluded to provide polyclonal anti-HBs that bound not only to HBsAgs of the vaccine genotypes but also to those of non-vaccine genotypes. This finding concurs with that from a previous study in Uzbekistan in which both adr- and adw2-type vaccines were reported to provide equally high anti-HBs acquisition ratios [24]. We therefore believe that vaccine recipients who become anti-HBs-positive can still prevent infection

Table 1 gtA-sera not reactive to either or both gtA-Ag or gtC-Ag

Sera	Age (years)	Sex	Anti-HBs* (mIU/mL)	Anti-HBs (AU)**		Duration*** (months)
				gtA-Ag	gtC-Ag	
A56	24	F	*21.0*	*0.085*	0.075	33
A126	22	M	125.6	0.041	0.047	4
A128	20	M	52.0	0.040	0.044	33
A130	22	M	21.5	0.032	0.043	16
A131	20	F	191.8	0.042	0.046	16
A132	20	M	70.6	0.043	0.056	16
A136	22	M	108.2	0.063	0.058	16
A137	21	M	681.5	0.065	0.053	4
A139	22	M	27.9	0.047	0.063	16
A142	22	M	340.2	0.050	*0.114*	4
A143	22	M	24.4	0.040	0.055	33
A144	23	M	15.3	0.039	0.060	16
A147	20	F	21.5	0.042	0.051	33

* The anti-HBs titers of the sera were measured by Architect (A56, italic) or Stacia (others)

** The reactivity to single genotype-derived HBsAg was measured. The cut-off values were 0.067 and 0.078 AU for reactivity to gtA-Ag and gtC-Ag, respectively. A56 was anti-gtA-Ag-positive, whereas A142 was anti-gtC-Ag-positive (italic). The other sera were anti-gtA-Ag-negative and anti-gtC-Ag-negative

*** Duration from the last vaccination to blood sampling

Table 2 gtA-sera and gtC-sera examined by the absorption test

Sera	Age/sex	Anti-HBs* (mIU/mL)	Anti-HBs (AU) to		Absorption (%) with		Duration (months)
			gtA-Ag	gtC-Ag	gtA-Ag	gtC-Ag	
A9	24/F	361.0	13.474	20.340	100	99.2	52
A40	23/F	436.5	11.561	13.062	100	99.8	4
A53	22/M	>1000	11.562	18.632	100	98.4	4
A57	24/F	>1000	9.752	14.369	100	98.9	16
A72	19/F	840.3	4.863	5.996	100	79.2	4
A74	20/F	>1000	10.787	17.663	100	100	16
A75	20/F	>1000	–	–	100	100	4
A80	20/F	847.5	7.730	10.665	100	92.4	4
A93	34/M	>1000	12.785	21.514	100	100	4
A105	21/F	>1000	8.805	16.118	100	96.3	4
C10	19/F	2111.3	72.841	19.197	95.1	100	1
C11	19/F	1415.9	13.473	25.743	99.4	100	1
C13	21/F	1334.2	33.233	63.650	96.2	100	1
C24	20/F	1519.5	29.919	54.688	91.1	100	1
C49	19/F	2990.8	112.926	208.351	96.6	100	2
C56	19/M	1681.1	25.290	50.826	98.1	100	2
C77	19/F	3792.2	45.235	111.681	96.1	100	2
C81	21/F	1379.7	21.172	33.248	95.4	100	2
C91	21/F	17173.6	217.508	320.561	98.8	100	2
C121	19/F	1913.6	–	–	93.0	100	2

* The anti-HBs titers of gtA-sera and gtC-sera were measured by Stacia and Architect, respectively

Table 3 gtA-sera and gtC-sera examined by the neutralization test

Sera	Age (years)	Sex	Anti-HBs* (mIU/mL)	Anti-HBs (AU)		Durations (months)
				gtA-Ag	gtC-Ag	
A72	19	F	840.3	4.863	5.996	4
A90	19	F	>1000	–	–	4
A94	20	F	>1000	21.855	27.878	4
A97	19	M	>1000	–	–	4
C44	19	F	15675.8	–	–	1
C66	19	M	11862.7	–	–	2
C84	21	M	34646.0	–	–	2

* The anti-HBs titers of gtA-sera and gtC-sera were measured by Stacia and Architect, respectively

with a non-vaccine genotype HBV. Our results provide evidence to support efforts to promote universal HB vaccination using single genotype-derived HB vaccines from the viewpoint of anti-HBs values to HBsAg of non-vaccine genotypes. In addition, the gtC-sera showed higher reactivity to both gtA- and gtC-Ag than did gtA-sera (Fig. 1a, b). This would be mainly because the durations from the last vaccination to blood sampling were shorter in the gtC-sera providers (1–2 months) than in the gtA-sera providers (3–52 months) (Supplementary Figures).

We hypothesized that the reactivity of anti-HBs-positive sera to vaccine genotype HBsAg was stronger than that to non-vaccine genotype HBsAg. Since gtC-Ag-ELISA and gtA-Ag-ELISA were two independent assays, the OD values of those ELISAs could not be directly compared. To analyze the difference in the serum reactivity, we calculated the ratio of "the reactivity to gtC-Ag/the reactivity to gtA-Ag". The ratio was higher in gtC-sera than in gtA-sera (2.40 ± 0.80 vs. 1.54 ± 0.42, $p < 0.001$) (Fig. 2a, b), which suggested stronger reactivity of anti-HBs-positive sera to vaccine-genotype HBsAg than to non-vaccine genotype HBsAg. However, it was difficult to comprehend, as both sera showed average "the reactivity to gtC-Ag/the reactivity to gtA-Ag" values exceeding 1.0 (gtA-sera,

1.54 ± 0.42; gtC-sera, 2.40 ± 0.80) (Fig. 2a, b). In other words, anti-HBs values to gtC-Ag were apparently higher than those to gtA-Ag in both gtA- and gtC-sera. Although the possibility that the reactivity to gtC-Ag was really higher than that to gtA-Ag in both sera could not be completely excluded, it was unlikely that most anti-sera (gtA-sera in this case) would show higher reactivity to another antigen than to the immunized antigen. We therefore considered the apparently higher anti-HBs to gtC-Ag than to gtA-Ag to be because of higher sensitivity of gtC-Ag-ELISA than gtA-Ag-ELISA. Indeed, the OD values of anti-HBs showed higher values in gtC-Ag-ELISA than in gtA-Ag-ELISA (gtA-sera, 4.15 ± 6.06 AU to gtC-Ag, 2.70 ± 3.95 AU to gtA-Ag; gtC-sera, 38.4 ± 49.4 AU to gtC-Ag, 19.5 ± 28.9 AU to gtA-Ag) (Fig. 1a, b). To exclude the assay difference from the analysis, we calculated the normalized ratio of "the reactivity to gtC-Ag/the reactivity to gtA-Ag." This normalization suggested that vaccine-acquired polyclonal anti-HBs preferentially recognize vaccine genotype HBsAg compared to non-vaccine genotype HBsAg (gtA-sera, −1.25 [−2.64 to 2.00] vs. gtC-sera, 1.23 [−7.41 to 3.03]; $p < 0.001$) (Fig. 2c).

Consistent with the above result, in the absorption test, almost all of the polyclonal anti-HBs repertoire was absorbed by non-vaccine genotype HBsAg; however, the absorption was not complete (gtA-sera, 96.4%; gtC-sera 96.0%) (Table 2; Fig. 3a, b). The different ratios between the absorption with vaccine genotype HBsAg and that with non-vaccine genotype HBsAg is due to the differences in the HBsAg epitopes covered by polyclonal anti-HBs. Whole HBsAg epitopes of gtA- and gtC-Ag consist of gtA-Ag-specific epitopes, gtC-Ag-specific epitopes, and epitopes common to both. The ratios of absorption with non-vaccine genotype HBsAg indicate the ratios of the common epitope-covering anti-HBs repertoire to the whole anti-HBs repertoire. The common epitopes of gtA-Ag and gtC-Ag include "a"-determinant (aa124-149) and "d" epitope (aa122) but not "w" or "r" epitopes (aa160) [25–27]. Interestingly, among 222 B-cell lines secreting anti-HBs antibodies, established from 34 good responders to HB vaccine, 216 (97.3%) and 5 (2.3%) lines recognized the "a" and "d" epitopes, respectively, whereas only one (0.4%) line recognized "w" epitope [28]. The ratio of 99.6% recognition of "a" and "d" epitopes by the B cell lines was within the range of our non-vaccine genotype HBsAg-absorption ratios of 19 out of the 20 examined sera, 91.1–100% (Table 2). Collectively, more than 90% of the whole anti-HBs repertoire would recognize the common major epitopes in almost all vaccine recipients. This part of the anti-HBs repertoire may contribute to the neutralization of non-vaccine genotype HBV.

We directly assessed the neutralizing capacity and found that the gtA-sera as well as the gtC-sera showed sufficient levels of genotype C HBV-neutralization at a high anti-HBs titer of 100 mIU/mL (92.8 ± 3.7 vs. 95.4 ± 4.8%, $p = 0.44$) (Fig. 4b). Thus, vaccine-acquired polyclonal anti-HBs with high titers would be capable of preventing infection of both vaccine and non-vaccine genotype HBV equally. This result is in accordance with previous epidemiological studies that reported that single genotype-derived HBsAg vaccination effectively decreased multiple genotype HBV infection [9, 11–13]. Our result is also in accordance with our previous in vitro study, where we found that monoclonal anti-HBs prevented HBV infection of non-vaccine genotype at high titers [15]. These findings indicate that the neutralizing capacity through the common major epitopes such as "a"-determinant and C(K/R)TC motif (aa121-124) is critical for preventing HBV infection of multiple genotypes [25, 29].

However, we also found that the gtA-sera showed lower inhibition levels than the gt-C sera at a low anti-HBs titer of 30 mIU/mL (60.2 ± 17.0 vs. 90.2 ± 8.2%, $p < 0.05$) (Fig. 4b). Furthermore, the gtA-sera required higher anti-HBs titers than the gtC-sera to provide a particular inhibition ratio (72.8 ± 23.7 vs. 25.6 ± 14.2 mIU/mL, $p < 0.05$) (Fig. 4c, d). Thus, vaccination with a single genotype HBsAg may be less effective in preventing the infection of non-vaccine genotype HBV than that of vaccine genotype HBV. The neutralizing capacity through genotype-specific epitopes was also important for preventing HBV infection of individual genotypes, as suggested in our previous observation [30]. Taken together, these present and previous findings indicate that high titers of anti-HBs are required to prevent infection with non-vaccine genotype HBV. In addition, we tried to compare the capacity of the gtA- and gtC-sera to neutralize genotype A HBV. However, genotype A HBV available at that time did not sufficiently infect the primary hepatocytes (data not shown). In the near future, we will prepare a new genotype A HBV and attempt to perform the neutralizing study again.

Of the 20 sera examined by the absorption test, 17 showed incomplete absorption with non-vaccine genotype HBsAg (Table 2; Fig. 3c, e). Among these 17 sera, 1 gtA-serum sample (A72) showed a relatively low ratio of absorption with gtC-Ag (79.2%) (Fig. 3e). However, the inhibition ratios of genotype C HBV infection were similar between the A72 serum sample and the other gtA-sera (Fig. 4c). In the polyclonal anti-HBs repertoire of each of the 17 sera, a portion was against the epitopes common to gtA-Ag and gtC-Ag, while another portion was against gtA-Ag- or gtC-Ag-specific epitopes. It is well known that the titers of vaccine-acquired polyclonal anti-HBs decrease over time: indeed, a notable proportion of complete vaccine recipients lost their immune memories 15–18 years

after vaccination [31, 32]. In the above 17 sera, the anti-HBs repertoire that can neutralize non-vaccine genotype HBV is smaller than the anti-HBs repertoire that can neutralize vaccine genotype HBV; as such, the former would be lost earlier than the latter. This speculation is supported by the different neutralization capacities between gtA- and gtC-sera at 30 mIU/mL anti-HBs titer (Fig. 4b). When the anti-HBs titers against the common epitopes drop below the threshold of the minimum necessary titer for HBV neutralization, infection with non-vaccine genotype HBV would preferentially occur compared to infection with vaccine genotype HBV. Stramer et al. reported that a majority of individuals with low anti-HBs titers (5 out of 6 cases), who were found to be HBV-DNA-positive 7–16 years after the vaccination, were exclusively or predominantly infected with non-vaccine genotype HBV [14]. These cases may be examples of vaccine recipients who were infected with non-vaccine genotype HBV due to the time-dependent decrease in the polyclonal anti-HBs. To maintain anti-HBs titers, booster vaccination has been proposed, especially for cohorts with a high risk of HBV infection such as immunocompromised patients and health care providers [33–36]. Taken together, these findings suggested that booster vaccination would be useful for preventing infection of non-vaccine genotype HBV in individuals with low anti-HBs titers.

In conclusion, single genotype HBsAg vaccination with Heptavax-II and Bimmugen provided polyclonal anti-HBs that possessed sufficient capacity to bind to non-vaccine HBsAg. The vaccine-acquired polyclonal anti-HBs sufficiently neutralized non-vaccine genotype HBV at a high anti-HBs titer; however, the neutralization was insufficient at a low anti-HBs titer. It is recommended to maintain high anti-HBs titers to prevent infection of non-vaccine genotype HBV as well as vaccine genotype HBV.

Acknowledgements The authors are indebted to Ms Atsuko Nozawa and Ms Fumiko Oikawa for their technical assistance. The authors are also grateful to Kaketsuken, Abbott, Siemens, Abcam, and Thermo Fisher Scientific for their support for this study. This work was partly supported by a Grant from Ministry of Health, Labour and Welfare.

Compliance with ethical standards

Conflict of interest Chiaki Okuse received a research grant from Takeda Pharma. Yasuhito Tanaka received lecture fees from Chugai Pharma, Bristol-Myers Squibb, and GlaxoSmithKline. Hiroshi Yotsuyanagi received lecture fees from MSD K.K. and Bristol-Myers Squibb. Tomohiro Kato received a research grant from FUJI OIL.

References

1. Trépo C, Chan HL, Lok A. Hepatitis B virus infection. Lancet. 2014;384:2053–63.
2. Lin CL, Kao JH. Novel therapies for hepatitis B virus cure-advances and perspectives. Aliment Pharmacol Ther. 2016;44:213–22.
3. Schweitzer A, Horn J, Mikolajczyk RT, et al. Estimations of worldwide prevalence of chronic hepatitis B virus infection: a systematic review of data published between 1965 and 2013. Lancet. 2015;386:1546–55.
4. GBD 2013 Mortality and Causes of Death Collaborators. Global, regional, and national age-sex specific all-cause and cause-specific mortality for 240 causes of death, 1990–2013: a systematic analysis for the Global Burden of Disease Study 2013. Lancet. 2015;385:117–71.
5. Zanetti AR, Van Damme P, Shouval D. The global impact of vaccination against hepatitis B: a historical overview. Vaccine. 2008;26:6266–73.
6. World Health Organization. Hepatitis B. 2016. http://www.who.int/mediacentre/factsheets/fs204/en/. Accessed 31 Oct 2016.
7. Norder H, Hammas B, Löfdahl S, et al. Comparison of the amino acid sequences of nine different serotypes of hepatitis B surface antigen and genomic classification of the corresponding hepatitis B virus strains. J Gen Virol. 1992;73:1201–8.
8. Tian Q, Jia J. Hepatitis B virus genotypes: epidemiological and clinical relevance in Asia. Hepatol Int. 2016;10:854–60 **(in press)**.
9. Cassidy A, Mossman S, Olivieri A, et al. Hepatitis B vaccine effectiveness in the face of global HBV genotype diversity. Expert Rev Vaccines. 2011;10:1709–15.
10. Kao JH, Chen PJ, Lai MY, et al. Clinical and virological aspects of blood donors infected with hepatitis B virus genotypes B and C. J Clin Microbiol. 2002;40:22–5.
11. Chen HL, Chang MH, Ni YH, et al. Seroepidemiology of hepatitis B virus infection in children: ten years of mass vaccination in Taiwan. JAMA. 1996;276:906–8.
12. Chongsrisawat V, Yoocharoen P, Theamboonlers A, et al. Hepatitis B seroprevalence in Thailand: 12 years after hepatitis B vaccine integration into the national expanded programme on immunization. Trop Med Int Health. 2006;11:1496–502.
13. Wichajarn K, Kosalaraksa P, Wiangnon S. Incidence of hepatocellular carcinoma in children in Khon Kaen before and after national hepatitis B vaccine program. Asian Pac J Cancer Prev. 2008;9:507–9.
14. Stramer SL, Wend U, Candotti D, et al. Nucleic acid testing to detect HBV infection in blood donors. N Engl J Med. 2011;364:236–47.
15. Hamada-Tsutsumi S, Iio E, Watanabe T, et al. Validation of cross-genotype neutralization by hepatitis B virus-specific monoclonal antibodies by in vitro and in vivo infection. PLoS One. 2015;10:e0118062.
16. Koyama T, Matsuda I, Sato S, et al. Prevention of perinatal hepatitis B virus transmission by combined passive–active immunoprophylaxis in Iwate, Japan (1981–1992) and epidemiological evidence for its efficacy. Hepatol Res. 2003;26:287–92.
17. Komatsu H, Inui A, Fujisawa T, et al. Transmission route and genotype of chronic hepatitis B virus infection in children in Japan between 1976 and 2010: A retrospective, multicenter study. Hepatol Res. 2015;45:629–37.
18. Tajiri H, Tanaka Y, Kagimoto S, et al. Molecular evidence of father-to-child transmission of hepatitis B virus. J Med Virol. 2007;79:922–6.
19. Matsuura K, Tanaka Y, Hige S, et al. Distribution of hepatitis B virus genotypes among patients with chronic infection in Japan shifting toward an increase of genotype A. J Clin Microbiol. 2009;47:1476–83.
20. Ito K, Yotsuyanagi H, Sugiyama M, Japanese AHB CHB Study Group, et al. Geographic distribution and characteristics of genotype A hepatitis B virus infection in acute and chronic

hepatitis B patients in Japan. J Gastroenterol Hepatol. 2016;31:180–9.
21. Suzuki Y, Kobayashi M, Ikeda K, et al. Persistence of acute infection with hepatitis B virus genotype A and treatment in Japan. J Med Virol. 2005;76:33–9.
22. Yano K, Tamada Y, Yatsuhashi H, Japan National Hospital Acute Hepatitis Study Group, et al. Dynamic epidemiology of acute viral hepatitis in Japan. Intervirology. 2010;53:70–5.
23. Oone K, Kani S, Oohashi M, et al. Comparative Study for Anti-Hepatitis B Surface Antigen Titers Based on Two Measurement Methods: Using Monoclonal Antibodies Isolated from Hepatitis B Vaccinated Recipients. Rinsho Byori. 2015;63:907–12.
24. Avazova D, Kurbanov F, Tanaka Y, et al. Hepatitis B virus transmission pattern and vaccination efficiency in Uzbekistan. J Med Virol. 2008;80:217–24.
25. Romanò L, Paladini S, Galli C, et al. Hepatitis B vaccination. Hum Vaccin Immunother. 2015;11:53–7.
26. Okamoto H, Imai M, Tsuda F, et al. Point mutation in the S gene of hepatitis B virus for a d/y or w/r subtypic change in two blood donors carrying a surface antigen of compound subtype adyr or adwr. J Virol. 1987;61:3030–4.
27. Kay A, Zoulim F. Hepatitis B virus genetic variability and evolution. Virus Res. 2007;127:164–76.
28. Shokrgozar MA, Shokri F. Subtype specificity of anti-HBs antibodies produced by human B-cell lines isolated from normal individuals vaccinated with recombinant hepatitis B vaccine. Vaccine. 2002;20:2215–20.
29. Qiu X, Schroeder P, Bridon D. Identification and characterization of a C (K/R) TC motif as a common epitope present in all subtypes of hepatitis B surface antigen. J Immunol. 1996;156:3350–6.
30. Aono J, Yotsuyanagi H, Miyoshi H, et al. Amino acid substitutions in the S region of hepatitis B virus in sera from patients with acute hepatitis. Hepatol Res. 2007;37:731–9.
31. Lu CY, Ni YH, Chiang BL, et al. Humoral and cellular immune responses to a hepatitis B vaccine booster 15–18 years after neonatal immunization. J Infect Dis. 2008;197:1419–26.
32. Wu TW, Lin HH, Wang LY. Chronic hepatitis B infection in adolescents who received primary infantile vaccination. Hepatology. 2013;57:38–45.
33. European Consensus Group on Hepatitis B Immunity. Are booster immunisations needed for lifelong hepatitis B immunity? Lancet. 2000;355:561–5.
34. Chaves SS, Fischer G, Groeger J, et al. Persistence of long-term immunity to hepatitis B among adolescents immunized at birth. Vaccine. 2012;30:1644–9.
35. Tajiri K, Shimizu Y. Unsolved problems and future perspectives of hepatitis B virus vaccination. World J Gastroenterol. 2015;21:7074–83.
36. Hahné S, van Houdt R, Koedijk F, et al. Selective hepatitis B virus vaccination has reduced hepatitis B virus transmission in the Netherlands. PLoS One. 2013;8:e67866.

International Journal of
Rheumatic Diseases

International Journal of Rheumatic Diseases 2017; **20:** 708–721

ORIGINAL ARTICLE

Phosphoproteome analysis of synoviocytes from patients with rheumatoid arthritis

Masayoshi KATANO,[1,2] Manae S. KUROKAWA,[3] Kosuke MATSUO,[4] Kayo MASUKO,[5] Naoya SUEMATSU,[2] Kazuki OKAMOTO,[2] Toshikazu KAMADA,[6] Hiroshi NAKAMURA[7] and Tomohiro KATO[2]

[1]*Research and Development, Clinical Department, LSI Medience Corporation, Tokyo,* [2]*Clinical Proteomics and Molecular Medicine, St. Marianna University Graduate School of Medicine,* [3]*Disease Biomarker Analysis and Molecular Regulation, St. Marianna University Graduate School of Medicine, Kawasaki,* [4]*Department of Orthopaedic Surgery, Yokohama City University School of Medicine, Yokohama,* [5]*Preventive Medical Center, Sanno Hospital Medical Center,* [6]*Department of Rheumatology, Nippon Medical School, and* [7]*Department of Orthopedic Surgery, International University of Health and Welfare, Tokyo, Japan*

Abstract

Aim: To explore disease-associated molecules in rheumatoid arthritis (RA), we comprehensively analyzed phosphoproteins purified from RA synoviocytes.

Method: Synoviocytes were obtained from three patients with RA and three patients with osteoarthritis (OA). Profiles of phosphoproteins purified from the synoviocytes were compared by two-dimensional differential gel electrophoresis (2D-DIGE) between the RA and OA groups. Protein spots with significantly different phosphorylation levels were identified by mass spectrometry. Recombinant protein of annexin A4 (ANXA4), one of the identified phosphoproteins, was transfected into synoviocytes from an OA patient to mimic RA synoviocytes and humoral factor secretion was compared between rANXA4-transfected and non-transfected synoviocytes under a tumor necrosis factor-α (TNFα)-stimulated condition.

Results: In 2D-DIGE, 318 phosphoprotein spots were detected, of which 94 spots showed significantly different intensities between the two groups ($P < 0.05$). Among the 94 spots, 22 spots showed two-fold or higher intensity and one spot showed less than 1/2-fold intensity in the RA group compared to the OA group. From the 22 spots, 11 phosphoproteins were identified, which included kinases, carrier and chaperone proteins, cytoskeletal proteins, proteases and calcium-binding proteins. One of the identified calcium-binding proteins was ANXA4, an exocytosis-regulating protein. The transfected rANXA4 was found to be phosphorylated intracellularly, and secretion of chemokine (C-X-C motif) ligand 1 and interleukin-8 induced by TNFα stimulation was significantly suppressed by the transfection ($P < 0.01$).

Conclusion: The phosphoprotein profile of RA synoviocytes was different from that of OA synoviocytes. This difference would reflect the different pathophysiologies of the diseases. ANXA4 may be one of therapeutic targets in RA.

Key words: annexin A4, phosphoprotein, rheumatoid arthritis, synoviocytes.

Correspondence: Professor Manae S. Kurokawa, Disease Biomarker Analysis and Molecular Regulation, St. Marianna University Graduate School of Medicine, 2–16–1, Sugao, Miyamae-ku, Kawasaki, 216–8511 Japan. Fax: 81-44-975-7553.
Email: manae@marianna-u.ac.jp

INTRODUCTION

Rheumatoid arthritis (RA) is a systemic inflammatory disease characterized by progressive destruction of synovial joints.[1] Although the pathogenesis of RA remains

© 2017 Asia Pacific League of Associations for Rheumatology and John Wiley & Sons Australia, Ltd

unclear, it has been elucidated that activated synoviocytes in affected joints play an important role.[2,3] Infiltration of inflammatory cells into synovium and proliferation of synoviocytes lead to severe cartilage and bone erosion via formation of pannus.[4,5] Production of proinflammatory cytokines and chemokines by synoviocytes and the infiltrating cells promote the process of joint destruction.[4,5]

Phosphorylation, one of the important post-translational modifications of proteins, plays a key role in cellular signal transduction in inflammation.[6,7] Thus, phosphoprotein profiles should be investigated in RA as well as in other diseases. Recent studies have focused on protein profiles of RA synoviocytes or synovial tissue;[8–13] however, only a few studies are available on the phosphoproteome of RA.[14]

In this paper, we found that phosphoprotein profiles of synoviocytes were different between RA and osteoarthritis (OA). Annexin A4 (ANXA4), one of the highly phospholyrated proteins in RA was found to regulate inflammatory chemokine secretion from synoviocytes. Our analysis of synovial phosphoproteins would help understanding of the pathophysiology of RA.

MATERIALS AND METHODS

Patients

Diagnosis of RA and OA were made according to the criteria of American College of Rheumatology.[15,16] Three RA patients (RA1–3) and four OA patients (OA1–4) were enrolled in this clinical study that was approved by the Ethics Committee in St. Marianna University School of Medicine, Kawasaki, Japan. The protocol of this study conformed to the provisions of the World Medical Association's Declaration of Helsinki.

Synovial membrane samples were obtained from RA1, RA2 and OA3 when they underwent total knee arthroplasty, and from RA3, OA1, OA2 and OA4 when they underwent total hip arthroplasty with their written informed consents. Clinical information of the patients are as follows: sex, all female; age (mean ± standard deviation, SD), RA1–3, 68 ± 9 years old, OA1–3 68 ± 8 years old, OA4 50 years old; disease duration (mean ± SD), RA1–3 18 ± 6 years, OA1–3 22 ± 18 years, OA4 7 years; C-reactive protein (CRP) (mean ± SD), RA1–3 0.80 ± 0.47 mg/dL, OA1–3 0.20 ± 0.26 mg/dL, OA4 0.17 mg/dL; X-ray grades (RA, Larsen grade; OA, Kellgren-Lawrence grade), RA1 V, RA2 IV, RA3 IV, OA1 IV, OA2 III, OA3 IV, OA4 IV; drugs, RA1 bucillamine 100 mg/day, loxoprofen 120 mg/day, RA2 prednisolone 9 mg/day, penicillamine 200 mg/day, mizoribine 150 mg/day, RA3 prednisolone 9 mg/day, loxoprofen 180 mg/day, salazosulfapyridine 3000 mg/day, OA1 none, OA2 loxoprofen 120 mg/day, OA3 none, OA4 none.

Preparation of synoviocyte-derived proteins and phosphoproteins

The synovial membrane samples were digested with collagenases (Sigma, St. Louis, MO, USA). Obtained synoviocytes were cultured in Ham's F-12 (Gibco, Carlsbad, CA, USA) containing 20% fetal bovine serum (FBS). After the first passage, the cells were cultured in Ham's F-12 containing 10% FBS. Proteins were extracted into cell lysis buffer (4% 3-[(3-cholamidopropryl)dimethylamino]-1-propanesulfonate (CHAPS)/7 mol/L urea/2 mol/L thiourea/30 mmol/L tris pH8.0). Phosphoproteins were purified from the extracted proteins using Pro-Q Diamond Phosphoprotein Enrichment Kit (Invitrogen, Carlsbad, CA, USA). After the treatment with 2-D clean-up kit (GE Healthcare, Piscataway, NJ, USA), the purified phosphoproteins were dissolved into the cell lysis buffer.

Two-dimensional differential gel electrophoresis (2D-DIGE)

The purified phosphoproteins were separated by 2D-DIGE according to the manufacture's protocol (CyDye DIGE fluor labeling kits for scarce samples, GE Healthcare).[17] Briefly, phosphoprotein amounts were quantified by Bradford assay and an equal amount of the phosphoproteins obtained from each of six synoviocyte samples (RA1–3 and OA 1–3) were mixed and labeled with Cy3 saturation dye (Cy Dye DIGE Saturation dye; GE Healthcare) for preparation of an internal control, 'standard sample'. Then each of the six samples (RA1–3 and OA 1–3) was labeled with Cy5 saturation dye; 2.5 μg of the individual Cy5-labeled sample was mixed with 2.5 μg of the Cy3-labeled standard sample. Then phosphoproteins in the mixture were separated by isoelectric focusing (Immobiline Drystrip pH 4–7, 24 cm, linear; GE Healthcare) and subsequently by sodium dodecyl sulfate-polyacrylamide gel electrophoresis (SDS-PAGE). The separated phosphoprotein spots were scanned using an image analyzer (Typhoon 9400 Imager, GE Healthcare). The Cy5-fluorescent intensity of each protein spot was normalized by the Cy3-fluorescent intensity of an identical spot by using a quantitative analysis program of Progenesis (Nonlinear Dynamics, Newcastle, UK). The normalized Cy5-intensity was compared between the RA and OA synoviocytes using Progenesis.

Identification of phosphoproteins

Phosphoproteins were identified by mass spectrometry (MS).[17] In brief, 50 μg of the phosphoproteins were separated by two-dimensional electrophoresis (2DE). Gel specimens corresponding to the phosphoprotein spots of interest were recovered. Then the phosphoproteins in the gel fragments were digested with trypsin.

Peptides produced by the digestion were analyzed using a matrix-assisted laser desorption/ionization time of flight (MALDI-TOF) mass spectrometer (Ultraflex; Bruker Daltonics, Ettlingen, Germany). Ten microliters of the peptide solution were applied to C18 Zip-Tip (Millipore, Billerica, MA, USA) for desalting, and then bound peptides were eluted using 2 μL 50% acetonitrile/0.1% trifluoroacetic acid. One microliter of the eluent was mixed with 1 μL of a matrix solution (0.3 mg/mL alpha-cyano-4-hydroxycinnamic acid in ethanol/acetone 2 : 1) and the mixture was spotted onto a MALDI target plate (AnchorChip; Bruker Daltonics). Then mass spectra of the peptide peaks were obtained in the automatic positive reflector mode with the mass range of 500–4400 m/z. The data were subjected to external calibration with nine standard peptides (Peptide calibration standard II; Bruker Daltonics). Based on the mass spectra, some peptides were selected for tandem mass spectrometry (MS/MS) analysis. The MS/MS spectra were measured in LIFT™-TOF/TOF mode using fragment ions produced by post-source decay. Ion peaks were detected using flexAnalysis (Bruker Daltonics). The signal-to-noise threshold for the peak detection was set at 5.0.

The obtained MS and MS/MS spectra were used to identify the phosphoproteins by database searching (Mascot, http://www.matrixscience.com) against the Swiss Prot human protein sequence database 54.3–8. The charge of the precursor ion was set as 1. Mass and peptide tolerances for precursor ions were set at 150 ppm and 1 Da, respectively. Variable modification of phosphorylation of serine, threonine and tyrosine were taken into consideration. Protein identification was accepted when Mascot search results delivered significant molecular weight search (MOWSE) scores ($P < 0.05$).

Western blotting

Expression of ANXA4 was examined by Western blotting. In brief, 10 μg of whole cell lysates of RA and OA synoviocytes were electrophoresed on 12.5% SDS-PAGE. Alternatively, phosphoproteins derived from 70 μg of whole cell lysates of OA synoviocytes were similarly electrophoresed. The separated proteins on the SDS-PAGE gels were transferred to polyvinylidene fluoride membranes. After blocking for 1 h in phosphate-buffered saline containing 1% bovine serum albumin and 0.1% Tween-20, the membranes were reacted with anti-ANXA4 antibody for 1 h (R&D Systems, Minneapolis, MN, USA), followed by incubation with horseradish peroxidase-conjugated rabbit anti-goat immunoglobulin G (Zymed, San Francisco, CA, USA). Immunoreactive bands were detected by Enhanced Chemi Luminescence (ECL)-Plus (GE Healthcare). The results were scanned using Typhoon 9400 Imager. Intensity of the resultant bands was measured by Science Lab 2001 Image Gauge (Fujifilm, Tokyo, Japan).

Transfection of recombinant ANXA4 to synoviocytes

Recombinant ANXA4 (rANXA4) fused with His-tag (GenWay, San Diego, CA, USA) was transfected to OA synoviocytes using Chariot (Active Motif, Carlsbad, CA, USA). After 16 h, a part of the cells were stimulated with 10 ng/mL recombinant tumor necrosis factor α (TNFα) (R&D Systems) for 6–48 h. Then proteins were extracted from the cells into the cell lysis buffer.

Analysis of humoral factor secretion

The culture medium of the OA4 synoviocytes was applied to a cytokine array (Proteome Profiler kit, R&D Systems) to examine levels of humoral factors. The analyzed humoral factors were as follows: complement 5a (C5a), CD40 ligand (CD40L), granulocyte-colony stimulating factor (G-CSF), granulocyte macrophage-colony stimulating factor (GM-CSF), chemokine (C-X-C motif) ligand 1 (CXCL1), small inducible cytokine A1 precursor (I-309), soluble intercellular adhesion molecule-1 (sICAM-1), interferon-γ (IFN-γ), interleukin-1α (IL-1α), IL-1β, IL-1 receptor antagonist (IL-1ra), IL-2, IL-4, IL-5, IL-6, IL-8, IL-10, IL-12 p70, IL-13, IL-16, IL-17, IL-17E, IL-23, IL-27, IL-32α, IFN-γ inducible protein 10 (IP-10), IFN-inducible T cell-α chemoattractant (ITAC), monocyte chemotactic protein-1 (MCP-1), macrophage migration inhibitory factor (MIF), macrophage inflammatory protein-1α (MIP-1α), MIP-1β, Serpin E1, regulated on activation, normal T cell expressed and secreted (RANTES), stromal cell-derived factor-1 (SDF-1), TNF-α, and soluble triggering receptor expressed on myeloid cells-1 (sTREM-1). Humoral factors detected as specific spots were visualized by ECL Plus, and the spots were scanned using Typhoon 9400

Imager. Intensity of each spot, measured by Science Lab 2001 Image Gauge, was normalized using that of the positive control. CXCL1 and IL-8 were measured by the respective enzyme-linked immunosorbent assay (ELISA) kits (R&D Systems).

Statistical analysis

Statistical significance was calculated by Student's *t*-test.

RESULTS

Comparison of phosphoprotein spot intensity between the RA and OA synoviocytes

To detect phosphoproteins differently expressed in RA, we analyzed phosphoprotein profiles of synoviocytes from three RA patients and three OA patients by 2D-DIGE. In total, 318 phosphoprotein spots were obtained (Fig. 1a). Ninety-four out of the 318 phosphoprotein spots showed significantly different intensities between the RA and OA groups ($P < 0.05$, Table 1). Among the 94 spots, 22 phosphoprotein spots were at least two-fold higher in intensity in the RA group than in the OA group (Table 1, Fig. 1b). Another phosphoprotein spot showed less than 1/2-fold intensity in the RA group than in the OA group (Table 1, Fig. 1b). As a representative result, spots of ID 8, 18 and 39 showed higher intensity in the RA group than in the OA group (Fig. 1c–e). The different intensities of phosphoprotein spots indicated different phosphoprotein levels of proteins between RA and OA synoviocytes.

Identification of the phosphoprotein spots differently expressed between the RA and OA synoviocytes

We tried to identify proteins for the above described 22 and one spots (Table 1, Fig. 1b). As a result, proteins were identified in 11 out of the former 22 spots and the latter one spot (Table 2, Fig. 2). Spots of ID 8 and ID 10, both of which showed higher intensity in RA, were identified as the same protein of ferritin light chain (FTL). The identified 10 phosphoproteins, which showed increased intensity in RA, were categorized into five groups: (i) proteins involved in phosphorylation (mitogen-activated protein kinase 4 [MAPK4] and COP9 signalosome complex subunit 8 [COPS8]); (ii) carrier or chaperone proteins (FTL, sodium/bile acid cotransporter 4 [SLC10A4], and heat shock protein beta-6 [HSPB6]); (iii) a cytoskeletal protein (4.1 protein/ezrin/radixin/moesin domain-containing protein 8 [FRMD8]); (iv) proteases (calpain small subunit 2 [CAPNS2] and sentrin-specific protease 8 [SENP8]); and (v) calcium-binding proteins (sorcin [SRI] and ANXA4). A cytoskeletal protein of myosin regulatory light chain 12A (ML12A) was identified from the spot, intensity of which was lower in RA (Table 2).

Comparison of ANXA4 expression between RA and OA synoviocytes

Among the identified phosphoproteins, we extended our study focusing on ANXA4, intensity of which was 2.3-fold higher in the RA group than in the OA group (spot ID 39, Fig. 1b,e, Table 2). ANXA4 belongs to the annexin family of calcium-dependent phospholipid binding proteins.[18] ANXA4 has been involved in diverse cellular processes, including exocytosis.[18,19] Interestingly, ANXA4 mediates aggregation of phospholipid-containing vesicles prior to fusion; however, it loses this activity when phosphorylated by protein kinase C (PKC).[20] Thus, we hypothesized that phosphorylation of ANXA4 regulates secretion of inflammatory cytokines and/or chemokines from RA synoviocytes.

First, to elucidate whether the increase of phosphorylated ANXA4 is due to the increase of protein expression or its phosphorylation, we compared the total amount of ANXA4 in the RA and OA synoviocytes. As a result, the total amount of ANXA4 was significantly higher in the RA synoviocytes compared to the OA synoviocytes (approximately 1.5-fold, $P < 0.01$, Fig. 3a,b). Thus, the up-regulated intensity of the phosphorylated ANXA4 spot in the RA synoviocytes (2.3-fold, Table 2) was at least in part due to the up-regulated expression of ANXA4.

Effects of rANXA4 protein transfection on secretion of inflammatory cytokines and chemokines from OA synoviocytes

Next, we tried to examine whether the phosphorylated ANXA4 regulates the secretion of inflammatory cytokines and chemokines from synoviocytes, since the phosphorylation of ANXA4 has been reported to inhibit vesicle aggregation.[20] To achieve this, we transfected rANXA4 into OA synoviocytes, mimicking RA synoviocytes. We compared inflammatory cytokine and chemokine secretion between the rANXA4-transfected OA synoviocytes and non-transfected OA synoviocytes after TNFα stimulation.

First, we examined effects of TNFα on endogenous ANXA4 (eANXA4) expression. In the Western blotting result, eANXA4 bands showed similar intensity between the TNFα-treated and non-treated conditions ($P > 0.05$, Fig. 3c,d). This indicates that TNFα does not affect the

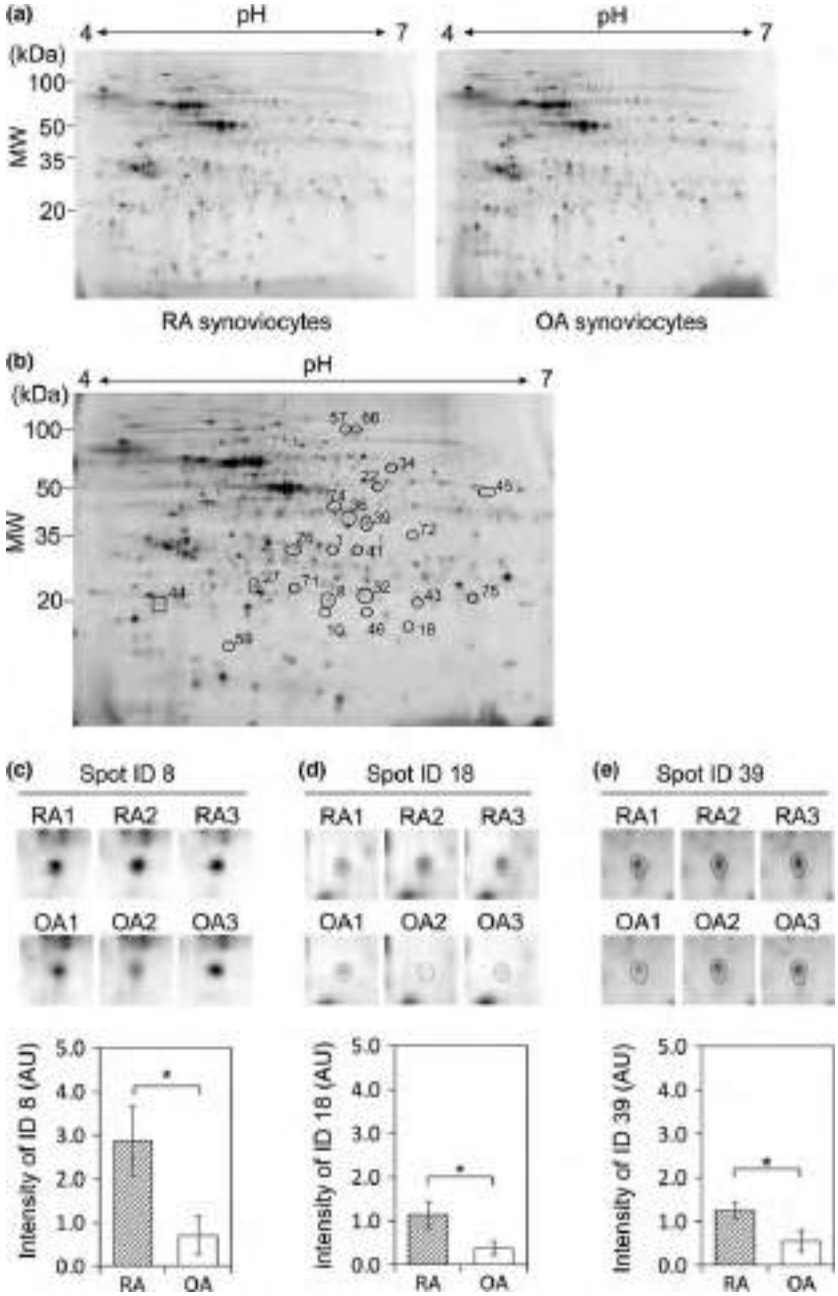

Figure 1 Two-dimensional differential gel electrophoresis (2D-DIGE) analysis of phosphoproteins extracted from rheumatoid arthritis (RA) and osteoarthritis (OA) synoviocytes. (a) Representative results from RA1 and OA1 synoviocytes are shown. (b) A representative result of the internal control sample that was a mixture of an equal amount of phosphoprotein samples from the three RA and three OA synoviocytes, is shown. Circles indicate 22 phosphoprotein spots that showed two-fold or more intensity in the RA synoviocytes compared to the OA synoviocytes ($P < 0.05$). The square indicates a phosphoprotein spot that showed less than 1/2-fold intensity in the RA synoviocytes compared to the OA synoviocytes ($P < 0.05$). ID numbers of those 23 spots are shown. (c–e) Results of three phosphoprotein spots (spot IDs 8, 18 and 39) that showed two-fold or more intensity in the RA synoviocytes compared to the OA synoviocytes. Error bars, SD. *$P < 0.05$. MW, molecular weights.

Table 1 Number of phosphoprotein spots detected from RA and OA synoviocytes

Change of spot intensity (x-fold)	Number of spots	Number of spots
(RA/OA)	($P < 0.05$)	($P \geq 0.05$)
$3.0 \leq x$	4	0
$2.0 \leq x < 3.0$	18	2
$1.5 \leq x < 2.0$	54	17
$1/1.5 < x < 1.5$	14	188
$1/2 < x \leq 1/1.5$	3	15
$1/3 < x \leq 1/2$	1	2
$x \leq 1/3$	0	0
Subtotal	94	224
Total	318	

expression of eANXA4 in the OA synoviocytes. Second, we transfected rANXA4 into OA synoviocytes. As a result, rANXA4 was detected as a band with slightly heavier molecular weight compared to eANXA4 because of addition of 6xHis-tag, which indicated successful transfection (Fig. 3e). Finally, we compared the total amount of phosphorylated ANXA4 between TNFα-treated and non-treated conditions. For this aim, after the TNFα treatment, phosphoproteins were purified from the samples and then ANXA4 was detected by anti-ANXA4 antibodies. As a result, in the non-transfected synoviocytes, phosphorylated eANXA4 were detected at similar levels between the TNFα-treated and non-treated conditions (Fig. 3f,g). In the rANXA4-transfected synoviocytes, relatively large amounts of phosphorylated rANXA4 were detected in addition to the phosphorylated eANXA4. The total amounts of phosphorylated ANXA4 were not affected by the TNFα treatment. Transfection of rANXA4 increased phosphorylated ANXA4 in the synovial cells ($P < 0.01$, Fig. 3f,g). The TNFα treatment did not affect the phosphorylation of eANXA4 or rANXA4.

To examine functions of phosphorylated ANXA4 in synoviocytes, we compared secretion of humoral factors, including inflammatory cytokines and chemokines between rANXA4-transfected and non-transfected synoviocytes. Since TNFα treatment was considered to facilitate the comparison, we first tried to find humoral factors up-regulated by TNFα in the non-transfected condition. Among the examined 36 humoral factors, secretion of CXCL1 and IL-8 was up-regulated to more than four-fold levels by the TNFα treatment (CXCL1, 4.04-fold; IL-8, 7.38-fold; Fig. 4a–c). Interestingly, the up-regulated secretion of CXCL1 and IL-8 by the TNFα treatment tended to be decreased after the transfection of rANXA4, which increased intracellular phosphorylated ANXA4 by approximately 10-fold (Figs 3g,4a–c). The CXCL1 secretion in the non-treated condition also tended to be decreased after the rANXA4 transfection (Fig. 4a,b).

To confirm the immunosuppressive effect of the transfected rANXA4, we quantitatively measured the secretion of CXCL1 and IL-8 by ELISA between rANXA4-transfected and non-transfected conditions in the presence or absence of TNFα. As a result, secretion of CXCL1 and IL-8 was markedly increased by TNFα treatment also in the ELISA results (Fig. 4d,e). In the TNFα-treated condition, the significantly up-regulated secretion of CXCL1and IL-8 was found to be suppressed by the transfection of rANXA4 (Fig. 4d,e, 24 and 48 h). Even in the non-treated synovial cells, the basic secretion levels of CXCL1 were suppressed by the transfection of rANXA4 (Fig. 4d, 24 and 48 h). In the case of IL-8, its basic secretion levels were too low to be estimated. These results suggested that the transfected rANXA4 that was phosphorylated intracellularly suppressed the secretion of these two inflammatory chemokines from synoviocytes.

DISCUSSION

To explore pathophysiology-related molecules from the aspect of phosphorylation in RA, we compared phosphoprotein profiles of synoviocytes between RA and OA synoviocytes. Among the detected 318 phosphoprotein spots in the 2D-DIGE results, 94 phosphoprotein spots (30%) showed different intensities between the two diseases. These differences would reflect the different mechanisms of the diseases. In particular, 23 spots showed two-fold or more different intensities between the RA and OA synoviocytes (Table 1, Fig. 1b,c). Previously, we compared the phosphoprotein profiles between RA and OA synovial tissue by staining phosphoproteins on 2-DE gels, where 408 phosphoprotein spots were obtained, and 121 spots out of them showed more than two-fold different intensities between the two diseases.[14] The relatively low number of spots with different intensities in this study would be the difference of the materials and methods, that is, cultured synoviocytes versus synovial tissue, and purification of phosphoproteins versus staining of phosphoproteins.

It is interesting that 76 of the 94 (81%) differently expressed phosphoprotein spots showed higher intensity in RA than in OA. Limiting to the 23 spots that showed more than two-fold differences, 22 (96%) showed higher intensity in RA than in OA (Table 1). This indicates that phosphorylation of proteins in

Table 2 Identification of the phosphoproteins

Spot numbers	Proteins	pI/MW (kDa) (observed)	pI/MW (kDa) (theoretical)†	Accession nos.	Matched peptides	Mascot score	Coverage (%)	Confirmed sequences (Mascot ion score)	Ratios (RA/OA)	Kinases
1	Mitogen-activated protein kinase 4 (MAPK4)	5.6/28.0	6.1/62.3	P31152	7	106	8	^{72}LDHDNIVKVYEVLGPK^{87} (86)	10.8	MAPK-activated protein kinase 5, group I p21-activated kinases
8	Ferritin light chain (FTL)	5.6/20.0	5.5/20.0	P02792	1	75	8	^{155}LGGPEAGLGEYLFER^{169} (53)	4.1	n. r.
10	Ferritin light chain (FTL)	5.6/19.0	5.5/20.0	P02792	1	88	8	^{155}LGGPEAGLGEYLFER^{169} (66)	3.7	n. r.
22	4.1 protein/ezrin/radixin/moesin (FERM) domain- containing protein 8 (FRMD8)	5.9/50.0	5.8/51.2	Q9BZ67	1	106	2	^{135}RELQIHDEEVLR^{146} (89)	2.9	n. r.
26	Calpain small subunit 2 (CAPNS2)	5.3/28.0	5.5/27.6	Q96L46	1	110	6	^{14}GLGEALGGLFGGGGQRR^{30} (90)	2.6	n. r.
27	Sorcin (SRI)	5.1/22.0	5.3/21.7	P30626	1	77	5	^{107}QHFISFDTDR^{116} (56)	2.6	cAMP-dependent protein kinase, polo-like kinase 1
32	Sentrin-specific protease 8 (SENP8)	5.8/22.0	5.6/24.1	Q96LD8	1	82	5	^{113}NSFFHYDSHSR^{123} (62)	2.5	n. r.
39	Annexin A4 (ANXA4)	5.8/40.0	5.8/36.0	P09525	1	94	3	^{203}NHLLHVFDEYKR^{214} (74)	2.3	protein kinase C (PKC), cAMP-dependent protein kinase
43	Heat shock protein, alpha-crystallin- related, B6 (HSPB6)	6.1/20.0	6.0/17.1	O14558	1	56	8	^{1}MEIPVPVQPSWLRR^{14} (34)	2.3	cAMP-dependent protein kinase
71	Constitutive photomorphogenesis 9 signalosome complex subunit 8 (COPS8)	5.4/22.0	5.3/23.0	Q99627	1	60	6	^{166}KPVAGALDVSFNK^{178} (39)	2.0	n. r.
74	Sodium/bile acid cotransporter 4 (SLC10A4)	5.6/42.0	5.1/46.5	Q96EP9	1	70	2	^{384}MYGSEMLHK^{392} (55)	2.0	n. r.
44	Myosin regulatory light chain 2 (ML12A)	4.5/20.0	4.7/19.8	P19105	6	70	12	^{151}GNFNYIEFTR^{160} (33) ^{133}FTDEEVDELYR^{143} (17)	0.4	myosin light chin kinase, Rho-kinase

n. r., not reported.
†Data calculated in Swiss-Prot data base.

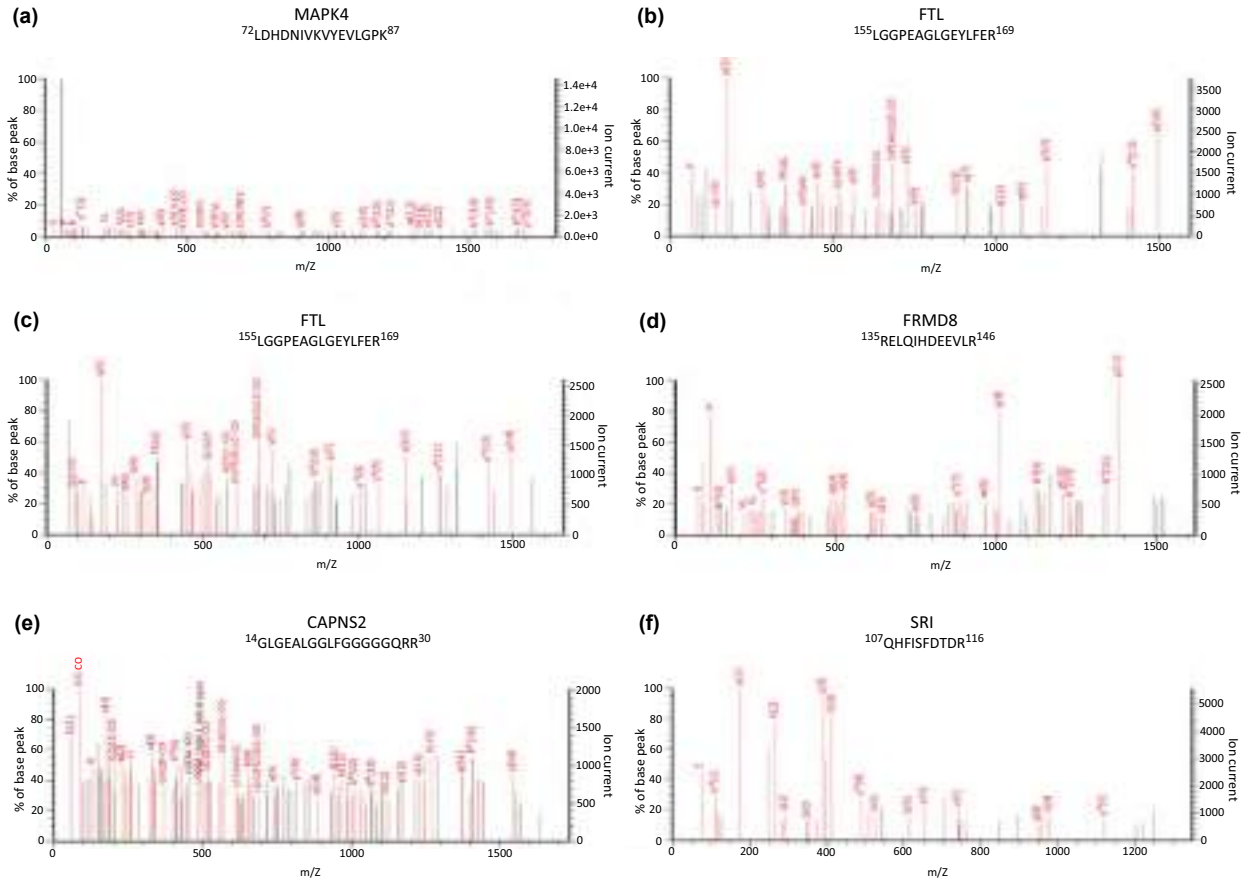

Figure 2 Tandem mass (MS/MS) spectra of the identified phosphoproteins. MS/MS spectra of the 13 peptides derived from the identified phosphoproteins (Table 2) are shown. (a) mitogen-activated protein kinase 4 (MAPK4) (spot ID 1); (b) ferritin light chain (FTL) (spot ID 8); (c) FTL (spot ID 10); (d) 4.1 protein/ezrin/radixin/moesin domain-containing protein 8 (FRMD8) (spot ID 22); (e) calpain small subunit 2 (CAPNS2) (spot ID 26); (f) sorcin (SR1) (spot ID 27); (g) sentrin-specific protease 8 (SENP8) (spot ID 32), (h) annexin A4 (ANXA4) (spot ID 39); (i) heat shock protein beta-6 (HSPB6) (spot ID 43); (j) COP9 signalosome complex subunit 8 (COPS8) (spot ID 71); (k) sodium/bile acid cotransporter 4 (SLC10A4) (spot ID 74); (l, m) myosin regulatory light chain 12A (ML12A) (spot ID 44).

synoviocytes would be up-regulated in RA compared to OA. Since protein phosphorylation plays critical roles in a broad spectrum of physiological mechanisms, including transcription and signal transduction, the mechanisms may be dysregulated in RA synoviocytes. From functions of the identified protein spots (Table 2), protein phosphorylation and degradation, cellular transportation, cytoskeletal formation and calcium-signaling would be differently regulated in RA synoviocytes compared to OA synoviocytes.

We are specifically interested in ANXA4, a calcium-dependent phospholipid binding protein, since the protein was highly phosphorylated in the RA synoviocytes compared to the OA synoviocytes (Fig. 1e, Table 2). Not only phosphorylation but also expression of ANXA4 was increased in RA synoviocytes (Fig. 2a,b). The predominant expression of ANXA4 in RA synovium compared to OA and non-inflamed synovium has been previously reported.[21] ANXA4 is also expressed predominantly in epithelial cells, especially at the apical site.[22] The expression level of ANXA4 is up-regulated in cancer cells according to the increase of tumor stages, suggesting its ability to promote cell migration.[23,24] These reports indicate that ANXA4 may be associated with dissemination of cancer cells. RA shows massive proliferation of synoviocytes and migration of synovial cells similar to cancer cells. Thus, the up-regulated expression of ANXA4 may be involved in the proliferation and invasion of synoviocytes.

Roles of ANXA4 have been also implicated in a variety of cellular process such as membrane aggregation, exocytosis, ion-transport and modulation of nuclear

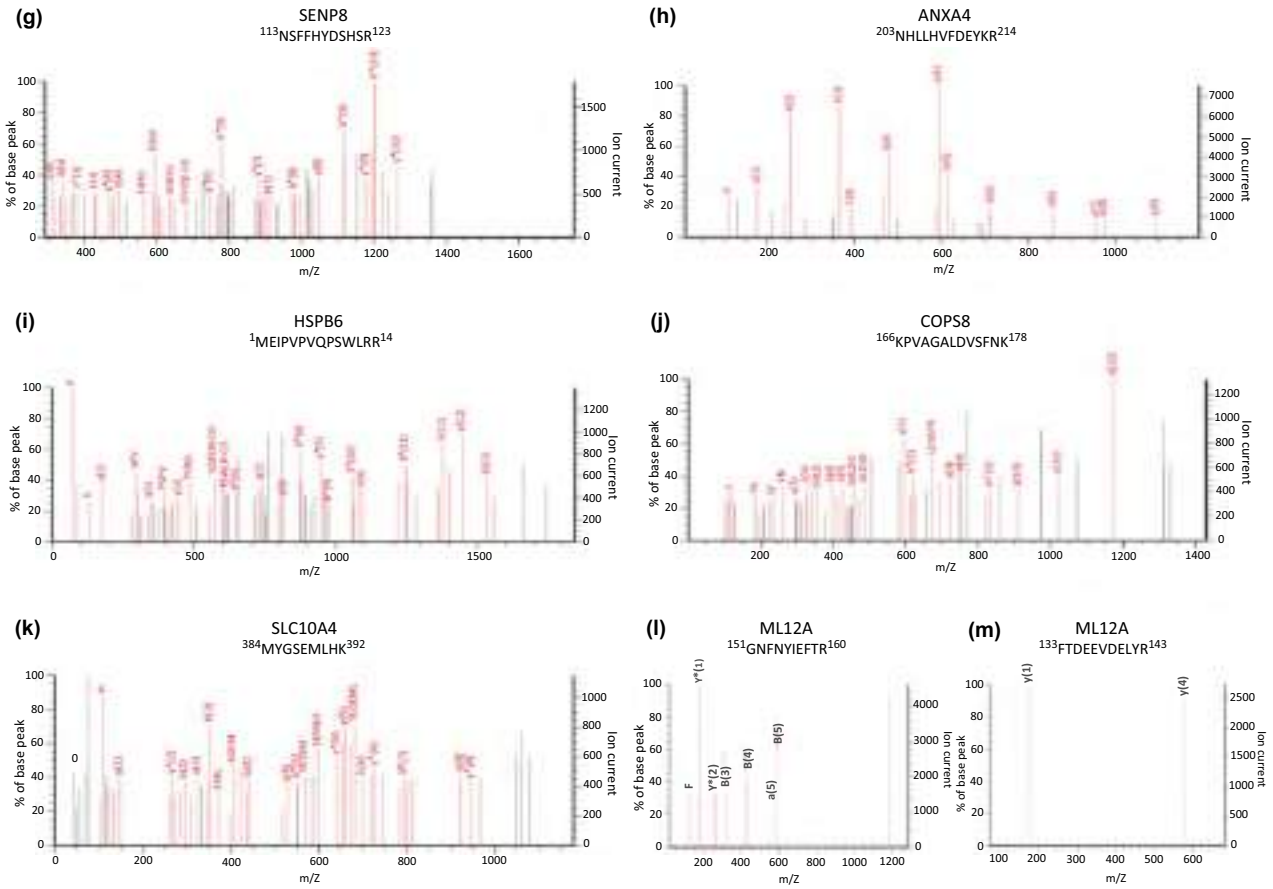

Figure 2 continued

factor-κB.[18–20,25–27] We here investigated roles of ANXA4 in RA synoviocytes, focusing on exocytosis. Since the exocytotic activity of ANXA4 is inhibited by phosphorylation by PKC,[20] we hypothesized that the relatively highly phosphorylated ANXA4 in RA synoviocytes regulates the secretion of inflammatory cytokines and/or chemokines. To mimic the inflammatory condition of RA, we used TNFα, a major inflammatory cytokine secreted in the RA joints. If we use other inflammatory cytokines such as IL-1β, IL-6 and lymphotoxin-αβ (LTαβ), we might detect other increased humoral factors than CXCL1 and IL-8.[28] We stimulated OA synoviocytes with TNFα, not RA synoviocytes. This is because OA synoviocytes would be in a relatively naïve state, but RA synoviocytes are already activated by the so-called cytokine storm and still in an activated condition even if cultured for a while.[29,30] Use of healthy synoviocytes might be more suitable, which is worthwhile to be tested.

We found increased amounts of phosphorylated ANXA4 after the transfection of rANXA4 (Fig. 3f,g). The phosphorylated ANXA4 would reduce the secretion of CXCL1 and IL-8 from TNFα-stimulated synoviocytes (Fig. 4). CXCL1 and IL-8 are expressed in RA synoviocytes and their expression is up-regulated by the stimulation with TNFα and/or IL-1β and also in the inflamed joints.[31–33] CXCL1 and IL-8, which belong to a group of CXC chemokines with an ELR motif, are potent chemoattractants and activators for neutrophils and potent promoters of angiogenesis.[34–36] These chemokines would promote the inflammation of RA by recruiting neutrophils into the joints and promoting angiogenesis in the synovium.[37,38] Furthermore, it was reported that CXCL1 and IL-8 down-regulated collagen expression in rheumatoid synovial fibroblasts.[39] Phosphorylation of ANXA4 may suppress these events by down-regulating CXCL1 and IL-8 in RA and thus may contribute to the amelioration of the disease.

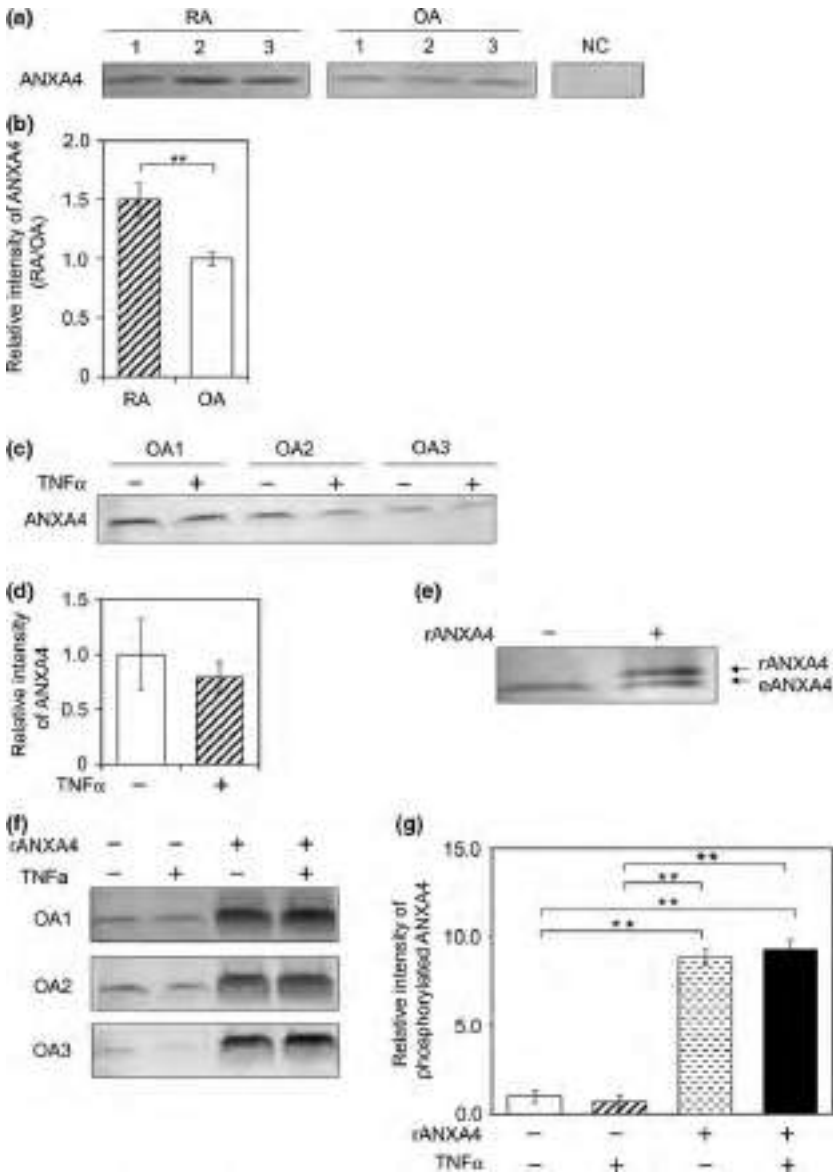

Figure 3 Annexin A4 (ANXA4) expression in rheumatoid arthritis (RA) and osteoarthritis (OA) synoviocytes. (a) Total ANXA4 expression in RA1–3 and OA1–3 synoviocytes was examined by Western blotting using antibodies to human ANXA4. In the negative control (NC), the blocking solution was used in place of the anti-ANXA4 antibody solution. (b) Intensity of the ANXA4 band in (a) was measured. The relative intensity of the RA group to the OA group is shown. Error bars, SD. $^{**}P < 0.01$. (c) OA synoviocytes were cultured in a medium alone or that containing tumor necrosis factor alpha (TNFα) for 24 h. Whole cell lysates were electrophoresed, and expression of total ANXA4 protein was examined by Western blotting. (d) Intensity of the ANXA4 band in c was compared between the non-treated and TNFα-treated synoviocytes. Error bars, SD. (e) Recombinant ANXA4 (rANXA4) was transfected into osteoarthritis (OA) synoviocytes. Since the rANXA4 was fused with 6xHis-tag, the molecular weight of rANXA4 is slightly higher than that of endogenous ANXA4 (eANXA4). Expression of eANXA4 and the transfected rANXA4 were examined by Western blotting. A representative result from OA4 synoviocytes is shown. (f) OA1–3 synoviocytes were cultured in a medium alone or that containing TNFα for 24 h. The synoviocytes transfected with rANXA4 were similarly cultured. Phosphoproteins were extracted from those synoviocytes, and phosphorylation of eANXA4 and rANXA4 was examined by Western blotting. (g) Total intensity of the phosphorylated eANXA4 bands and the phosphorylated rANXA4 bands in f were compared among the four types of treatments. Error bars, SD. $^{**}P < 0.01$.

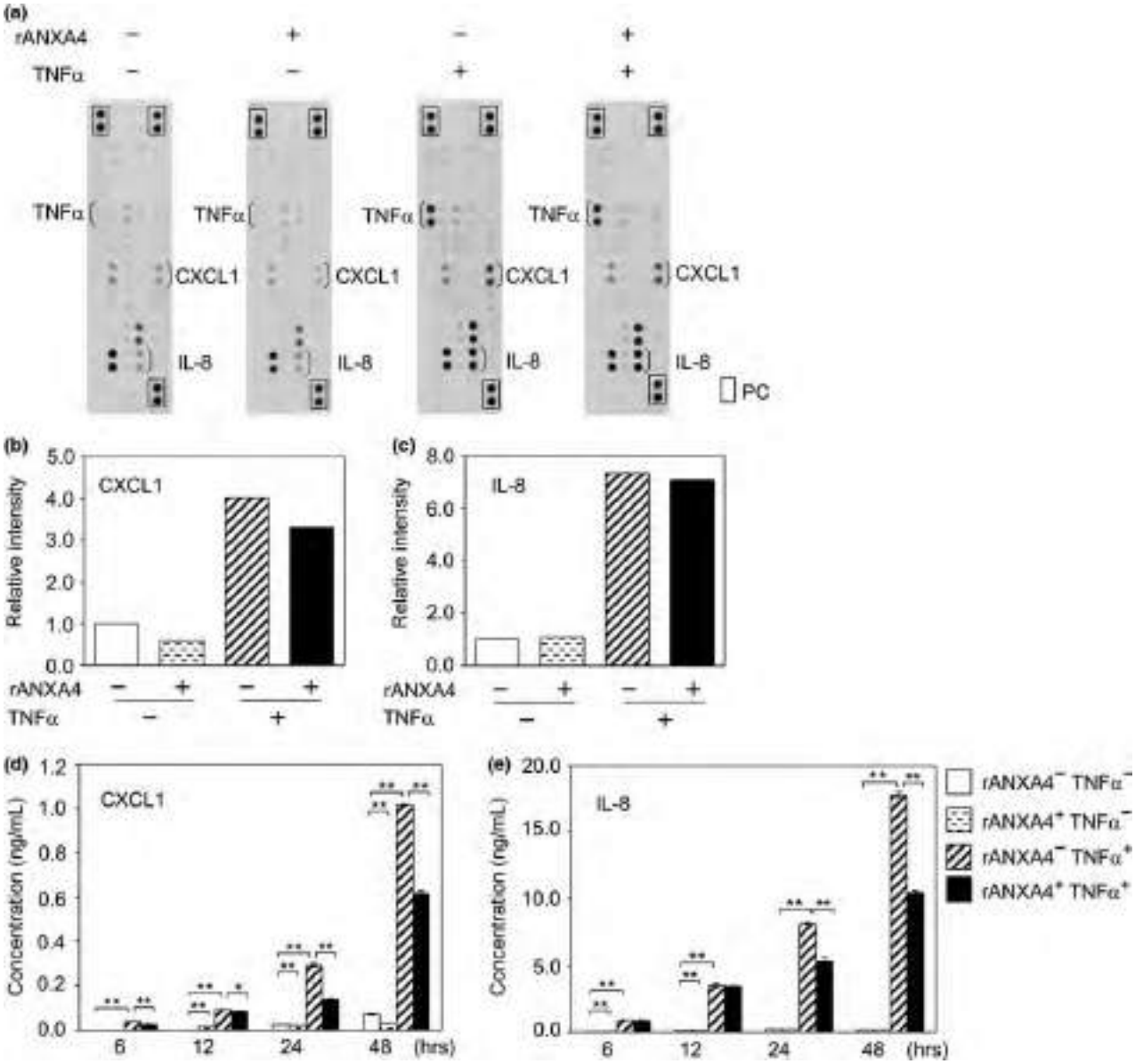

Figure 4 Down-regulation of the secretion of chemokine (C-X-C motif) ligand 1 (CXCL1) and interleukin 8 (IL-8) by transfection of recombinant annexin A4 (rANXA4). (a) OA4 synoviocytes were cultured in a medium alone or that containing tumor necrosis factor alpha (TNFα) for 24 h. The synoviocytes transfected with rANXA4 were similarly cultured. Levels of humoral factor secretion in the four types of treatments were analyzed by a humoral factor array, in which 36 different anti-humoral factor antibodies were blotted. PC, positive control. (b, c) Results of CXCL1 (b) and IL-8 (c) spots in a, which showed more than four-fold intensity increase by TNFα treatment in the non-transfected condition, are shown. (d, e) OA4 synoviocytes were cultured in a medium alone or that containing TNFα for 6, 12, 24 and 48 h. The synoviocytes transfected with rANXA4 were similarly cultured. Concentration of CXCL1 (d) and IL-8 (e) in the culture supernatants were measured by enzyme-linked immunosorbent assay. Significance between the presence and absence of TNFα in the non-transfected condition, between the presence and absence of rANXA4 in the non-treated condition, and between the presence and absence of rANXA4 in the TNFα-treated condition, is specifically shown. $^{*}P < 0.05$, $^{**}P < 0.01$.

Annexins consist of 12 members of $Ca^{2\pm}$ and phospholipid-binding proteins, involved in endocytosis and exocytosis, membrane traffic and organization, calcium signaling, cell growth and apoptosis.[18,40] Molecular mechanisms of the annexin-mediated exocytosis have been mainly investigated on ANXA2.[41–43] Cytosolic

ANXA2 translocates to plasma membrane, following a rise in cytosolic Ca^{2+} and binds to S100A10 proteins to form a tetramer, in which two ANXA2 were connected through a homodimer of S100A10 (ANXA2t). ANXA2t promotes formation of lipid rafts necessary for exocytosis, which contain clusters of soluble N-ethylmaleimide-sensitive factor attachment protein receptor (SNARE), phosphatidylinositol 4,5-bisphosphate (PIP_2), and monosialotetrahexosyl-ganglioside (GM1).[41–43] Furthermore, AnxA2t bundles actin filaments to stabilize the lipid rafts and the bundled actin filaments may connect granules to the plasma membrane to exert a mechanical force for compressing granules and favoring release of their contents.[41,43] Phosphorylation is an important post-translational modification to control the functions of ANXA2 during exocytosis.[41,42] Several phosphorylation sites of ANXA2 have been reported such as Ser 11, Ser 25 and Tyr 23.[41,42,44–47] However, it has been controversial whether the sites are phosphorylated or dephosphorylated to exert the exocytotic functions.[44,45] As in the case of Ser 11, ANXA2 may be first phosphorylated to be activated and then dephosphorylated to stabilize an ANXA2t complex in the release of humoral factors.[46] ANXA4 is considered to be involved in exocytosis in a similar manner to the case of ANXA2. The precise mechanisms need to be elucidated.

Several members of annexins such as ANXA1 and ANXA7 have been reported to be involved in the pathophysiology of rheumatic diseases.[14,48] We previously found up-regulated phosphorylation of synovial ANXA7 in RA compared to OA and that the ANXA7 was associated with increased secretion of IL-8 from RA synoviocytes.[14] Involvement of phosphorylated annexins, ANXA4 and ANXA7, in exocytosis of RA synoviocytes was found by our studies (this study and Matsuo *et al.*[14]) for the first time. The reason why ANXA7 was not detected in this study would be difference of the materials and methods between the two studies (see the first paragraph of Discussion). As an advantage of this study, we found intracellular phosphorylation of the transfected ANXA4 protein (Fig. 3f,g) and that the transfection of ANXA4 reduced CXCL1 and IL-8 secretion from the TNFα-treated synoviocytes (Fig. 4). This result is in accordance with the reports that phosphorylation of annexins make them lose the exocytotic functions.[20,45,47] Analysis of phosphorylation sites of ANXA4 and ANXA7 and phosphorylation/dephosphorylation status of the sites during exocytosis is the next challenge.

One of the limitations of this study is that the number of analyzed samples was rather small to provide good statistical power. Another is that important supporting data for the upregulated phosphorylation of ANXA4 in RA synoviocytes such as increased intracellular Ca^{2+} levels, activation of kinases, and the phosphorylation sites of ANXA4 were not provided. We would like to conduct these experiments using more numbers of RA and OA synoviocyte samples in the near future.

Taken together, the potential mechanism indicated by this study is as follows: inflammatory cytokines such as TNFα and LTαβ stimulate RA synoviocytes to increase the secretion of CXCL1 and IL-8 (Fig. 4).[28] ANXA4 would be involved in the exocytosis of CXCL1 and IL-8 in a similar manner to the case of ANXA2.[41–43] Secreted CXCL1 and IL-8 recruit neutrophils to the joints and exaggerate the arthritis.[31–38] Because PKC phosphorylates a broad spectrum of proteins, ANXA4 can be a specific therapeutic target for down-regulation of the inflammatory chemokine secretion in RA. Further investigation of other differently phosphorylated proteins between RA and OA detected in this study would help understanding of the disease mechanisms in RA.

ACKNOWLEDGEMENTS

The authors are indebted to Ms Michiyo Katano, Ms Mie Kanke and Ms Atsuko Nozawa for their technical assistance. This work was supported by a grant from St. Marianna University School of Medicine.

CONFLICTS OF INTEREST

The authors have no financial conflicts of interest.

AUTHOR CONTRIBUTIONS

Masayoshi Katano: data acquisition and analysis, interpretation of data, preparation of manuscript. Manae S. Kurokawa: study design, data analysis, interpretation of data, preparation and revision of manuscript. Kosuke Matsuo: data analysis, interpretation of data. Kayo Masuko, Naoya Suematsu, Kazuki Okamoto, Toshikazu Kamada: data acquisition and analysis. Hiroshi Nakamura: data analysis, interpretation of data. Tomohiro Kato: study design, interpretation of data, revision of manuscript

REFERENCES

1 McInnes IB, Schett G (2011) The pathogenesis of rheumatoid arthritis. *N Engl J Med* **365**, 2205–19.

2 Meinecke I, Rutkauskaite E, Gay S, Pap T (2005) The role of synovial fibroblasts in mediating joint destruction in rheumatoid arthritis. *Curr Pharm Des* **11**, 563–8.

3 Huber LC, Distler O, Tarner I, Gay RE, Gay S, Pap T (2006) Synovial fibroblasts: key players in rheumatoid arthritis. *Rheumatology* **45**, 669–75.

4 Ritchlin C (2000) Fibroblast biology. Effector signals released by the synovial fibroblast in arthritis. *Arthritis Res* **2**, 356–60.

5 Knedla A, Neumann E, Müller-Ladner U (2007) Developments in the synovial biology field 2006. *Arthritis Res Ther* **9**, 209.

6 Cole PA, Courtney AD, Shen K *et al.* (2003) Chemical approaches to reversible protein phosphorylation. *Acc Chem Res* **36**, 444–52.

7 Ehrentraut SF, Colgan SP (2012) Implications of protein post-translational modifications in IBD. *Inflamm Bowel Dis* **18**, 1378–88.

8 Dasuri K, Antonovici M, Chen K *et al.* (2004) The synovial proteome: analysis of fibroblast-like synoviocytes. *Arthritis Res Ther* **6**, R161–8.

9 Tilleman K, Van Beneden K, Dhondt A *et al.* (2005) Chronically inflamed synovium from spondyloarthropathy and rheumatoid arthritis investigated by protein expression profiling followed by tandem mass spectrometry. *Proteomics* **5**, 2247–57.

10 Zhang H, Fan LY, Zong M, Sun LS, Lu L (2012) Proteins related to the functions of fibroblast-like synoviocytes identified by proteomic analysis. *Clin Exp Rheumatol* **30**, 213–21.

11 Li XJ, Xu M, Zhao XQ, *et al.* (2013) Proteomic analysis of synovial fibroblast-like synoviocytes from rheumatoid arthritis. *Clin Exp Rheumatol* **31**, 552–8.

12 Bo GP, Zhou LN, He WF *et al.* (2009) Analyses of differential proteome of human synovial fibroblasts obtained from arthritis. *Clin Rheumatol* **28**, 191–9.

13 Kriegsmann M, Seeley EH, Schwarting A *et al.* (2012) MALDI MS imaging as a powerful tool for investigating synovial tissue. *Scand J Rheumatol* **41**, 305–9.

14 Matsuo K, Arito M, Noyori K *et al.* (2011) Arthritogenicity of annexin VII revealed by phosphoproteomics of rheumatoid synoviocytes. *Ann Rheum Dis* **70**, 1489–95.

15 Altman R, Asch E, Bloch D *et al.* (1986) Development of criteria for the classification and reporting of osteoarthritis. Classification of osteoarthritis of the knee. Diagnostic and Therapeutic Criteria Committee of the American Rheumatism Association. *Arthritis Rheum* **29**, 1039–49.

16 Arnett FC, Edworthy SM, Bloch DA *et al.* (1988) The American Rheumatism Association 1987 revised criteria for the classification of rheumatoid arthritis. *Arthritis Rheum* **31**, 315–24.

17 Hatsugai M, Kurokawa MS, Kouro T *et al.* (2010) Protein profiles of peripheral blood mononuclear cells are useful for differential diagnosis of ulcerative colitis and Crohn's disease. *J Gastroenterol* **45**, 488–500.

18 Gerke V, Moss SE (2002) Annexins: from structure to function. *Physiol Rev* **82**, 331–71.

19 Willshaw A, Grant K, Yan J *et al.* (2004) Identification of a novel protein complex containing annexin A4, rabphilin and synaptotagmin. *FEBS Lett* **559**, 13–21.

20 Kaetzel MA, Mo YD, Mealy TR *et al.* (2001) Phosphorylation mutants elucidate the mechanism of annexin IV-mediated membrane aggregation. *Biochemistry* **40**, 4192–9.

21 Goulding NJ, Dixey J, Morand EF *et al.* (1995) Differential distribution of annexins-I, -II, -IV, and -VI in synovium. *Ann Rheum Dis* **54**, 841–5.

22 Kaetzel MA, Chan HC, Dubinsky WP, Dedman JR, Nelson DJ (1994) A role for annexin IV in epithelial cell function. Inhibition of calcium-activated chloride conductance. *J Biol Chem* **269**, 5297–302.

23 Zimmermann U, Balabanov S, Giebel J *et al.* (2004) Increased expression and altered location of annexin IV in renal clear cell carcinoma: a possible role in tumour dissemination. *Cancer Lett* **209**, 111–8.

24 Duncan R, Carpenter B, Main LC, Telfer C, Murray GI (2008) Characterisation and protein expression profiling of annexins in colorectal cancer. *Br J Cancer* **98**, 426–33.

25 Crosby KC, Postma M, Hink MA, Zeelenberg CH, Adjobo-Hermans MJ, Gadella TW (2013) Quantitative analysis of self-association and mobility of annexin A4 at the plasma membrane. *Biophys J* **104**, 1875–85.

26 Chan HC, Kaetzel MA, Gotter AL, Dedman JR, Nelson DJ (1994) Annexin IV inhibits calmodulin-dependent protein kinase II-activated chloride conductance. A novel mechanism for ion channel regulation. *J Biol Chem* **269**, 32464–8.

27 Jeon YJ, Kim DH, Jung H *et al.* (2010) Annexin A4 interacts with the NF-kappaB p50 subunit and modulates NF-kappaB transcriptional activity in a Ca2 + -dependent manner. *Cell Mol Life Sci* **67**, 2271–81.

28 Young J, Yu X, Wolslegel K *et al.* (2010) Lymphotoxin-alphabeta heterotrimers are cleaved by metalloproteinases and contribute to synovitis in rheumatoid arthritis. *Cytokine* **51**, 78–86.

29 Zhou JJ, Ma JD, Mo YQ *et al.* (2014) Down-regulating peroxisome proliferator-activated receptor-gamma coactivator-1 beta alleviates the proinflammatory effect of rheumatoid arthritis fibroblast-like synoviocytes through inhibiting extracellular signal-regulated kinase, p38 and nuclear factor-kappaB activation. *Arthritis Res Ther* **16**, 472.

30 Bartok B, Firestein GS (2010) Fibroblast-like synoviocytes: key effector cells in rheumatoid arthritis. *Immunol Rev* **233**, 233–55.

31 Heller RA, Schena M, Chai A *et al.* (1997) Discovery and analysis of inflammatory disease-related genes using cDNA microarrays. *Proc Natl Acad Sci USA* **94**, 2150–5.

32 Kraan MC, Patel DD, Haringman JJ *et al.* (2001) The development of clinical signs of rheumatoid synovial inflammation is associated with increased synthesis of the chemokine CXCL8 (interleukin-8). *Arthritis Res* **3**, 65–71.

33 Koch AE, Kunkel SL, Burrows JC *et al.* (1991) Synovial tissue macrophage as a source of the chemotactic cytokine IL-8. *J Immunol* **147**, 2187–95.
34 Zlotnik A, Yoshie O (2000) Chemokines: a new classification system and their role in immunity. *Immunity* **12**, 121–7.
35 Clark-Lewis I, Dewald B, Geiser T, Moser B, Baggiolini M (1993) Platelet factor 4 binds to interleukin 8 receptors and activates neutrophils when its N terminus is modified with Glu-Leu-Arg. *Proc Natl Acad Sci USA* **90**, 3574–7.
36 Strieter RM, Polverini PJ, Kunkel SL *et al.* (1995) The functional role of the ELR motif in CXC chemokine-mediated angiogenesis. *J Biol Chem* **270**, 27348–57.
37 Koch AE, Kunkel SL, Shah MR *et al.* (1995) Growth-related gene product alpha. A chemotactic cytokine for neutrophils in rheumatoid arthritis. *J Immunol* **155**, 3660–6.
38 Kaneko S, Satoh T, Chiba J, Ju C, Inoue K, Kagawa J (2000) Interleukin-6 and interleukin-8 levels in serum and synovial fluid of patients with osteoarthritis. *Cytokines Cell Mol Ther* **6**, 71–9.
39 Unemori EN, Amento EP, Bauer EA, Horuk R (1993) Melanoma growth-stimulatory activity/GRO decreases collagen expression by human fibroblasts. Regulation by C-X-C but not C-C cytokines. *J Biol Chem* **268**, 1338–42.
40 Fatimathas L, Moss SE (2010) Annexins as disease modifiers. *Histol Histopathol* **25**, 527–32.
41 Gabel M, Chasserot-Golaz S (2016) Annexin A2, an essential partner of the exocytotic process in chromaffin cells. *J Neurochem* **137**, 890–6.
42 Bharadwaj A, Bydoun M, Holloway R, Waisman D (2013) Annexin A2 heterotetramer: structure and function. *Int J Mol Sci* **14**, 6259–305.
43 Hitchcock JK, Katz AA, Schäfer G (2014) Dynamic reciprocity: the role of annexin A2 in tissue integrity. *J Cell Commun Signal* **8**, 125–33.
44 Sarafian T, Pradel LA, Henry JP, Aunis D, Bader MF (1991) The participation of annexin II (calpactin I) in calcium-evoked exocytosis requires protein kinase C. *J Cell Biol* **114**, 1135–47.
45 Regnouf F, Sagot I, Delouche B *et al.* (1995) "In vitro" phosphorylation of annexin 2 heterotetramer by protein kinase C. Comparative properties of the unphosphorylated and phosphorylated annexin 2 on the aggregation and fusion of chromaffin granule membranes. *J Biol Chem* **270**, 27143–50.
46 Brandherm I, Disse J, Zeuschner D, Gerke V (2013) cAMP-induced secretion of endothelial von Willebrand factor is regulated by a phosphorylation/dephosphorylation switch in annexin A2. *Blood* **122**, 1042–51.
47 Rescher U, Ludwig C, Konietzko V, Kharitonenkov A, Gerke V (2008) Tyrosine phosphorylation of annexin A2 regulates Rho-mediated actin rearrangement and cell adhesion. *J Cell Sci* **121**, 2177–85.
48 Yang YH, Morand E, Leech M (2013) Annexin A1: potential for glucocorticoid sparing in RA. *Nat Rev Rheumatol* **9**, 595–603.

Integrative Molecular Medicine

Review Article ISSN: 2056-6360

Effects of iguratimod on protein profiles of chondrosarcoma cells

Seido Ooka[1*], Manae S Kurokawa[2], Michiyo Yokoyama[3], Mitsumi Arito[3], Toshiyuki Sato[3], Masaaki Sato[3], Yukiko Takakuwa[1], Kazuki Omoteyama[3], Naoya Suematsu[3], Kimito Kawahata[1] and Tomohiro Kato[3]

[1]Division of Rheumatology and Allergy, Department of Internal Medicine, St. Marianna University School of Medicine, Kawasaki, Japan

[2]Disease Biomarker Analysis and Molecular Medicine, St. Marianna University Graduate School of Medicine, Kawasaki, Japan

[3]Clinical Proteomics and Molecular Medicine, St. Marianna University Graduate School of Medicine, Kawasaki, Japan

Abstract

Objective: To explore novel mechanisms for the effect of iguratimod (IGU) on rheumatoid arthritis (RA), we analyzed protein profile changes caused by IGU using chondrosarcoma cells. Methods: OUMS-27 cells were cultured in the presence or absence of 100 μM IGU. Proteins were extracted and separated by 2 dimensional-differential image gel electrophoresis (2D-DIGE). Protein spots of interest were identified by mass spectrometry. Results: 776 and 803 protein spots were detected in the 2D-DIGE results of 24 hour- and 6 day-treatment with IGU, respectively. In the 6 day-treatment, 22 protein spots showed 1.3-fold or higher intensity by IGU-treatment than no-treatment, whereas 15 spots showed -1.3 (1/1.3) -fold or lower intensity ($p<0.05$). We identified 15 out of the 37 spots, which included proteins involved in packaging and splicing of pre-mRNA, regulation of signaling pathways/protein folding, innate immunity and inflammation, transcription, ATP synthesis, cytoprotection, and cytoskeleton organization. Interestingly, intensity of multiple spots of heterogenous nuclear ribonucleoprotein (hnRNP) A2/B1 and A1 was decreased by the IGU treatment, which are highly expressed in synovia of RA and/or its animal model. Specifically, hnRNP A2/B1 are known as autoantigens in RA and also as proinflammatory activators for NF-κB, the target of IGU. Conclusion: IGU affected protein profiles of chondrosarcoma cells. The decreased expression of hnRNPs suggests novel mechanisms for anti-rheumatic effects of IGU.

Introduction

Rheumatoid arthritis (RA) is a systemic inflammatory disease that causes progressive joint destruction and functional loss [1]. Although its etiology remains unknown, early diagnosis and a treat-to-target approach are recommended as standard care to achieve the remission [2]. Developments of biologics and small-molecule immunosuppressive disease-modifying anti-rheumatic drugs (DMARDs) such as methotrexate and janus kinase inhibitors have enabled this strategy [1, 2]. Nonetheless, it is difficult to use the immunosuppressive drugs in a considerable portion of RA patients with comorbidities such as malignant tumors and chronic infection. Furthermore, for RA patients that achieved the remission, application of treatments with immunomodulatory drugs should be considered.

From these points of view, the role of conventional disease-modifying anti-rheumatic drugs (cDMARDs) is important in RA treatment. The immunomodulatory cDMARDs include salazosulfapyridine and bucillamine which are recommended as alternatives for methotrexate-intolerant patients by RA treatment guidelines [3, 4]. The immunomodulatory cDMARDs can be used in the patients with malignancy and infection. Iguratimod (IGU), a novel immunomodulatory cDMARD developed in Japan, inhibits the production of immunoglobulins and proinflammatory cytokines such as TNFα, IL-1β, and IL-6 [5-8]. IGU has been considered to exhibit its anti-rheumatic effects through suppression of NF-κB, by the inhibition of phosphorylation and nuclear translocation of RelA/p65 without interfering with IκB [6, 7, 9]. IGU also suppresses ERK and NF-κB pathways in RANKL-induced osteoclast differentiation [9-11]. Recently, IGU was found to block IL-17 signaling in a murine arthritis model, targeting an IL-17 receptor adaptor protein, Act-1 [12]. However, mechanisms of the effects of IGU, especially those on chondrocytes, are still obscured.

In this study, we comprehensively analyzed changes of protein expression of chondrosarcoma cells caused by IGU. We found that IGU affected the protein profile of chondrosarcoma cells. Interestingly, IGU suppressed expression of heterogenous nuclear protein (hnRNP) A2/B1 and A1. Specifically, hnRNP A2/B1 play roles as autoantigens and proinflammatory regulators in RA and also as coactivators for NF-κB, the target of IGU. Our findings suggested novel mechanisms of the effect of IGU on RA treatment.

Methods

Cell culture

A chondrosarcoma cell line, OUMS-27 (C-2012-1583, Human Science Research Resources Bank, Sennan, Osaka, Japan) [13], was cultured in DMEM (Sigma-Aldrich, St. Louis, MO, USA) and 10% FBS

Correspondence to: Seido Ooka, MD, PhD, Division of Rheumatology and Allergy, Department of Internal Medicine, St. Marianna University School of Medicine, 2-16-1, Sugao, Miyamae-ku, Kawasaki, 216-8511, Japan, Tel: 81-44-977-8111; Fax: 81-44-976-7553; E-mail: ooka@marianna-u.ac.jp

Key words: *chondrosarcoma cells, iguratimod, mass spectrometry, proteomics, rheumatoid arthritis*

Received: November 20, 2017; **Accepted:** December 11, 2017; **Published:** December 14, 2017

(Hyclone, South Logan, Utah, USA) in type I collagen-coated dishes (AGC techno glass, Haibara-gun, Shizuoka, Japan). To analyze effects of IGU (Tokyo chemical industry, Chuo-ku, Tokyo, Japan) on the cell viability and growth, $1.5x10^5$ of OUMS-27 cells were seeded and cultured for 24 hours in the presence or absence of 10-300 μM of IGU. Similarly, to analyze a longer term (6 days) effect, $1.5x10^5$ of the cells were seeded and 100 μM IGU was added three times every 48 hours. The cells were harvested after 48 hours from the last treatment. All the experiments were performed in triplicates.

Two dimensional-differential image gel electrophoresis (2D-DIGE)

Proteins, extracted from the OUMS-27 cells, were analyzed by 2D-DIGE as previously described [14]. Briefly, an equal weight of proteins taken from six lysates from the 24 hour-cultured cell samples (three of 100 μM IGU-treated and three non-treated) were mixed and labeled with Cyanine dye 3 (Cy3, Cy Dye DIGE Saturation dye, GE Healthcare, Piscataway, NJ, USA) for preparation of an internal control "standard sample". Each of the six samples was labeled with Cyanine dye 5 (Cy5, GE Healthcare). 2.5 μg of the individual Cy5-labeled samples were mixed with 2.5 μg of the Cy3-labeled standard sample. Then each of the mixed protein sample was applied to an isoelectric focusing (IEF) gel strip (Immobiline Drystrip pH 3-11, 24 cm, non-linear, GE Healthcare). After the proteins were separated by IEF, they were further separated by sodium dodecyl sulfate-polyacrylamide gel electrophoresis. The resultant protein spots were scanned using an image analyzer (Typhoon 9400 Imager, GE Healthcare). The Cy5-fluorescent intensity of each protein spot was normalized by the Cy3-fluorescent intensity of an identical spot by using a quantitative analysis program (Progenesis, Nonlinear Dynamics, Newcastle, UK). The normalized Cy5-intensity was compared between the IGU-treated and non-treated protein samples using Progenesis. Similarly, protein profiles of the 6 day-cultured cells were compared between the IGU-treated and non-treated OUMS-27 cells.

Identification of proteins

Proteins were identified by mass spectrometry (MS) [14]. In brief, 50 μg of proteins was separated by 2-dimensional electrophoresis. Gel specimens corresponding to protein spots of interest were recovered. Then proteins in the gel fragments were digested with trypsin. Peptides produced by the digestion were analyzed using a matrix-assisted laser desorption/ionization time of flight mass spectrometer (MALDI-TOF/MS) (Ultraflex, Bruker Daltonics, Ettlingen, Germany). Based on the mass spectra, some peptides were selected for MS/MS analysis. The obtained MS and MS/MS spectra were used to identify the proteins by database searching (Mascot, http://www.matrixscience.com) against the Swiss Prot human protein sequence database. Protein identification was accepted when MASCOT search results delivered significant MOWSE scores ($p<0.05$).

Analysis of protein interaction

Interactions among the identified proteins were searched by Ingenuity Pathway Analysis (IPA) (Qiagen, Venlo, NLD). Core analysis was performed using names and the fold differences (IGU/Control) of all the identified proteins and information of all the cells in all the species in IPA database.

Statistical analysis

Significance of differences of cell viability, cell growth, and protein spot intensity in 2D-DIGE was calculated by Student's t-test.

Results

Effects of 24 hour-treatment by IGU on OUMS-27 cells

We first treated OUMS-27 cells for 24 hours with 0-300 μM IGU to examine its effect on viability and growth of the cells. OUMS-27 cells showed viability of more than 94% in the presence of 10-300 μM IGU as well as in the absence of IGU (100%). The cell growth in all the conditions was also at similar levels (0.95- to 1.05-fold) except that in the presence of 300 μM iguratimod (0.84-fold), which showed slightly lower level ($p<0.05$). Thus, we determined the concentration of IGU as 100 μM and analyzed protein profile of OUMS-27 cells at this condition.

We compared protein profiles of OUMS-27 cells between the 100 μM IGU-treatment and no-treatment by 2D-DIGE. We found 776 protein spots in total (Figure 1A, B). In the 776 protein spots, 41 protein spots showed different intensity between the two conditions ($p<0.05$) (Table 1). Among the 41 protein spots, 11 protein spots showed 1.3-fold or higher intensity in the IGU-treated cells compared to the non-treated cells. In contrast, 5 spots showed -1.3 (1/1.3)-fold or lower intensity in the IGU-treated cells compared to the non-treated cells. It was shown that IGU affected the protein profile of OUMS-27 cells.

Effects of 6 day-treatment by IGU on OUMS-27 cells

Next, we treated OUMS-27 cells for a longer term of 6 days with 100 μM IGU. The levels of cell viability and growth were high enough and at similar levels at 6 days between the IGU-treated and non-treated cells (100 μM; cell viability, 100.1 %, $p=0.92$; cell growth, 1.05-fold, $p=0.64$). Thus, we performed 2D-DIGE using those cell lysates.

In total, 803 protein spots were detected in the 2D-DIGE results (Figure 1C, D). In the 803 protein spots, 150 protein spots showed different intensity between the IGU-treated and non-treated cells ($p<0.05$, Table 1). Among the 150 protein spots, 22 protein spots showed 1.3-fold or higher intensity in the IGU-treated cells compared to the non-treated cells. On the other hand, 15 spots showed -1.3-fold or lower intensity in the IGU-treated cells compared to the non-treated cells. Protein spots that changed to ±1.3-fold or more in the 6-day treatment (150 spots) showed 3.7-fold in number compared to those in the 24-hour treatment (41 spots) (Table 1).

To follow a time course of the protein expression, we observed intensity change of the protein spots that showed ±1.3-fold or more change by the 24 hour-treatment with IGU. In the case of 9 intensity-increased spots, intensity of almost all the spots were decreased in the 6 day-treatment (Figure 2A). Similarly, in the case of 4 intensity-

Table 1.

Culture periods	Total number of detected protein spots	Number of protein spots with ($p<0.05$)	IGU/Control	Number of the protein spots
24 hours	776	41	$x \geq 1.5$ $1.5 > x \geq 1.3$ $1.3 > x \geq -1.3$ $-1.3 > x \geq -1.5$ $-1.5 \geq x$	2 9 25 3 2
6 days	803	150	$x \geq 1.5$ $1.5 > x \geq 1.3$ $1.3 > x \geq -1.3$ $-1.3 > x \geq -1.5$ $-1.5 \geq x$	7 15 113 11 4

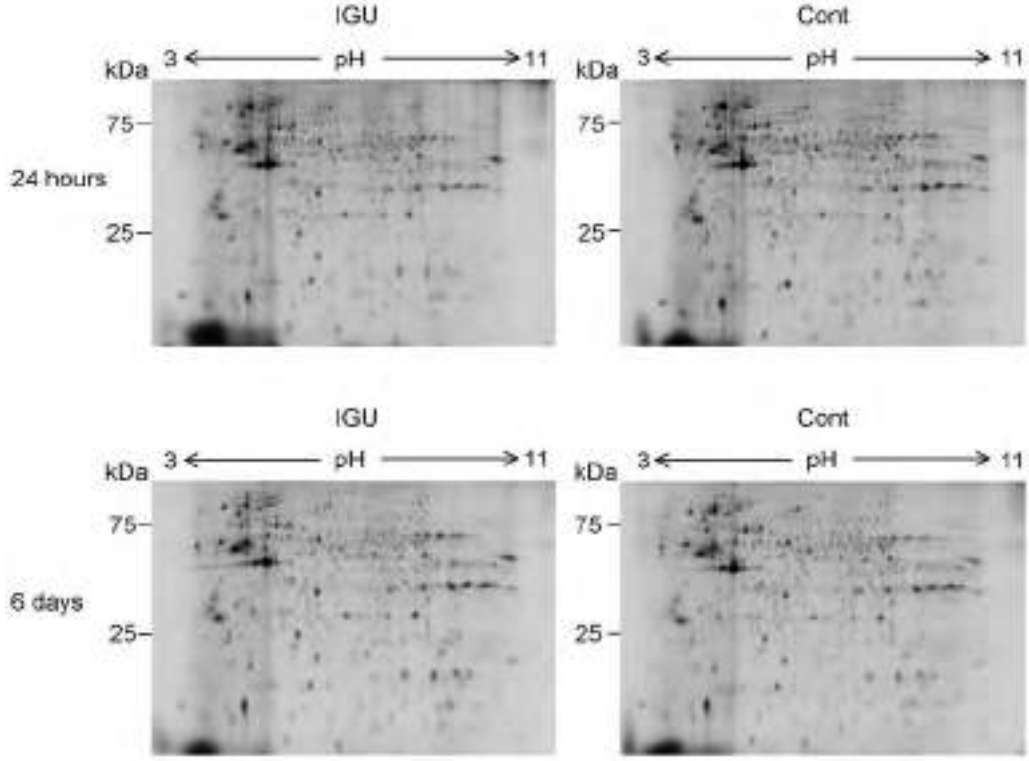

Figure 1. Protein of OUMS-27 cells treated with IGU. Representative results of 2D-DIGE of proteins from OUMS-27 cells cultured in the presence (left upper) or absence (right upper) of 100 μM IGU for 24 hours are shown. Similarly, those cultured in the presence (left lower) or absence (right lower) of 100 μM IGU for 6 days are shown.

decreased spots, intensity of 3 spots were increased in the 6 day-treatment (Figure 2B). The effect of the 24 hour-treatment on OUMS-27 cells was tentative. In contrast, when we observed intensity of the protein spots that showed ±1.3-fold or more change in the 6 day-treatment, almost all the spots of the 22 intensity-increased spots and the 15 intensity-decreased spots similarly increased and decreased in the 24 hour-treatment, respectively (Figure 2C, D). The 6 day-treatment was considered to reflect a long term effect of IGU on OUMS-27 cells.

Identification of the proteins expression of which was changed by IGU

We tried to identify the proteins in the spots intensity of which was changed by the 6 day-treatment with IGU. 37 protein spots that showed ±1.3-fold or more intensity change by the treatment were subjected to the identification. As a result, 14 proteins were identified from 15 out of the 37 spots (Figure 3, 4 and Table 2).

Seven proteins were identified from the 7 spots intensity of which was increased by the treatment with IGU. They were 1) proteins involved in splicing of pre-mRNA (cyclin L1 [CCLN1]; and tuftelin-interacting protein 11 [TFIP11]), 2) proteins that regulate signaling pathways and protein folding (14-3-3 protein epsilon, tyrosine 3-monooxygenase/tryptophan 5-monooxygenase activation protein epsilon [YWHAE]; and cyclophilin A, peptidyl-prolyl cis-trans isomerase A [PPIA]), 3) a protein involved in innate immunity and inflammation (NACHT, LRR and PYD domains-containing protein 3 [NLRP3]), 4) a transcription factor (human immunodeficiency virus type 1 enhancer-binding protein 2 [HIVEP2]), and 5) a protein with unknown function (transmembrane protein 95 [TMM95]).

The other 7 proteins were included in the 8 spots intensity of which was decreased by the treatment with IGU. They were 1) proteins involved

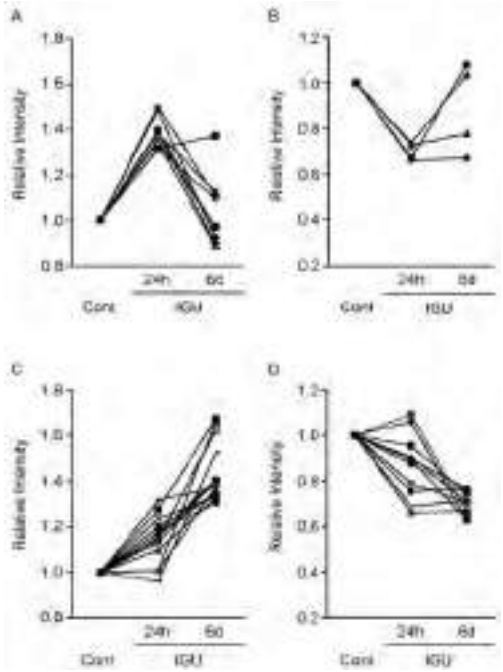

Figure 2. Time course of each protein expression of OUMS-27 cells in the presence of IGU. A, B. Nine out of the 11 protein spots and 4 out of the 5 protein spots, intensity of which were increased to 1.3-fold or more (A) and decreased to -1.3-fold or less (B) in the 24 hour-treatment, respectively (Table 1), were detected both in the 24 hour- and 6 day-treatments and applied for time course analysis. C, D. 14 out of the 22 protein spots and 11 out of the 15 protein spots, intensity of which were increased to 1.3-fold or more (C) and decreased to -1.3-fold or less (D) in the 6 day-treatment, respectively (Table 1), were detected both in the 24 hour- and 6 day-treatments and applied for time course analysis. Control samples (Cont) were proteins from OUMS-27 cells cultured without IGU for 24 hours (A, B) and 6 days (C, D).

Table 2.

Spot		Proteins	Accession ID	MW (kDa)		pI		Mascot	Coverage	
ID	(folds)			Theoret	Observed	Theoret	Observed	scores	(%)	(Mascot ion scores)
1072	1.67	NACHT, LRR and PYD domains-containing protein 3 (NLRP3)	NLRP3_HUMAN	118.1	23	6.22	6.1	71	13	^{661}MDHMVSSFCIENCHR^{675} (11)
487	1.53	Cyclin-L1 (CCNL1)	CCNL1_HUMAN	59.6	60	10.7	6.2	75	18	^{99}LPQVAM*ATGQVLFHR^{113} (21)
1033	1.50	Transmembrane protein 95 (TMM95)	TMM95_HUMAN	19.6	24	8.98	7.8	57	37	^{31}LARLCSQMEAR^{41} (2) ^{79}EAVSSLPSYWSWLRK^{93} (3)
763	1.40	Transcription factor HIVEP2 (HIVEP2)	ZEP2_HUMAN	228.9	41	6.5	5.8	65	8	^{436}NALSVTTTSQERAAM*GR^{452} (11)
445	1.37	Tuftelin-interacting protein 11 (TFIP11)	TFP11_HUMAN	96.8	64	5.45	5.8	61	12	^{262}ELSQVKVIDMTGR^{274} (25) ^{387}M*QPDCSNPLTLDECAR^{402} (7)
924	1.34	14-3-3 protein epsilon (YWHAE)	1433E_HUMAN	29.2	29	4.63	4.5	189	18	^{131}YLAEFATGNDR^{141} (54) ^{131}YLAEFATGNDRK^{142} (16) ^{154}AASDIAMTELPPTHPIR^{170} (77) ^{216}DSTLIMQLLR^{225} (18)
1107	1.34	Cyclophilin A (PPIA)	PPIA_HUMAN	18.0	21	7.68	8.0	74	10	^{2}VNPTVFFDIAVDGEPLGR^{19} (66)
87	−1.35	Hypoxia up-regulated protein 1 (HYOU1)	HYOU1_HUMAN	111.3	98	5.16	5.3	66	12	^{439}DAVVYPILVEFTR^{451} (24)
599	−1.34	ATP synthase subunit alpha, mitochondrial (ATP5A1)	ATPA_HUMAN	59.7	53	9.16	8.0	185	11	^{134}TGAIVDVPVGEELLGR^{139} (72) ^{335}EAYPGDVFYLHSR^{347} (72) ^{403}GIRPAINVGLSVSR^{416} (15)
376	−1.49	Keratin, type II cytoskeletal 1, (KRT1) Keratin, type II cytoskeletal 6B (K2C6B)	K2C1_HUMAN K2C6B_HUMAN	66.0 66.0	69	8.15 8.09	6.9	106 82	9 1	^{377}YEELQITAGR^{386} (78) ^{360}YEELQITAGR^{369} (78)
784	−1.31	Heterogenous nuclear ribonucleoproteins A2/B1 (hnRNP A2/B1)	ROA2_HUMAN	37.4	39	8.97	9.5	99	8	^{23}LFIGGLSFETTEESLR^{38} (38) ^{214}GGGGNFGPGPGSNFR^{228} (46)
797	−1.35	Heterogenous nuclear ribonucleoproteins A2/B1 (hnRNP A2/B1)	ROA2_HUMAN	37.4	38	8.97	8.8	256	23	^{23}LFIGGLSFETTEESLR^{38} (52) ^{154}GFGFVTFDDHDPVDK^{168} (83) ^{214}GGGGNFGPGPGSNFR^{228} (64)
794	−1.42	Heterogenous nuclear ribonucleoproteins A2/B1 (hnRNP A2/B1)	ROA2_HUMAN	37.4	38	8.97	8.7	129	13	^{23}LFIGGLSFETTEESLR^{38} (47) ^{214}GGGGNFGPGPGSNFR^{228} (60)
773	−1.52	Heterogenous nuclear ribonucleoproteins A1 (hnRNP A1) Heterogenous nuclear ribonucleoproteins A1-like 2 (hnRNP A1L2)	ROA1_HUMAN RA1L2_HUMAN	38.7 34.2	40	9.17 9.08	9.2	77 61	24 23	^{16}LFIGGLSFETTDESLR^{31} (9) ^{337}SSGPYGGGGQYFAKPR^{352} (5) ^{16}LFIGGLSFETTDESLR^{31} (9)
775	−1.60	Heterogenous nuclear ribonucleoproteins A1 (hnRNP A1)	ROA1_HUMAN	38.7	39	9.17	8.8	62	8	^{15}KLFIGGLSFETTDESLR^{31}(15) ^{16}LFIGGLSFETTDESLR^{31} (25)

37 protein spots, intensity of which changed to ±1.3-fold or more by the 6 day-treatment with IGU, were selected for the protein Proteins of 15 out of the 37 spots were

*Oxidation of methionine.

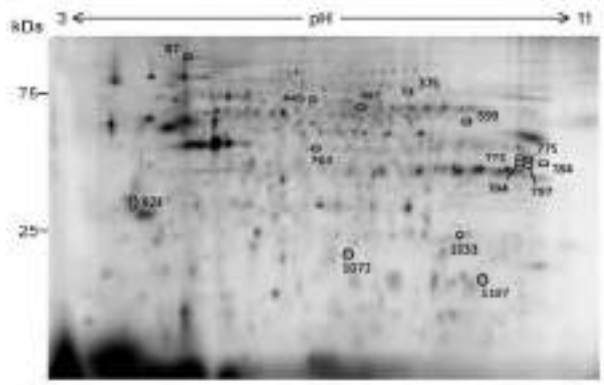

Figure 3. Locations of the protein spots on a 2D-DIGE gel. Proteins included in 15 spots out of the 37 spots that showed ±1.3-fold or more change in intensity by the 6 day-treatment with IGU were A representative result of the standard sample is shown.

in packaging of pre-mRNA (heterogenous nuclear ribonucleoproteins A2/B1 [hnRNP A2/B1]; heterogenous nuclear ribonucleoproteins A1 [hnRNP A1]; and heterogenous nuclear ribonucleoproteins A1-like 2 [hnRNP A1L2]), 2) a cytoprotective protein from hypoxia (hypoxia up-regulated protein 1 [HYOU1]), 3) an ATP synthase (ATP synthase subunit alpha, mitochondrial [ATP5A1]), and 4) Cytoskeletal proteins (keratin, type II cytoskeletal 1 [KRT1]; and keratin, type II cytoskeletal 6B [K2C6B]).

Interestingly, hnRNP A2/B1 was identified in 3 protein spots (spot ID 784, 794, and 797) (Table 2). Similarly, hnRNP A1 was identified in 2 protein spots (spot ID 773 and 775). In spot ID 773, only hnRNP A1 or both hnRNP A1 and hnRNP A1L2 were considered to be included. Spot ID 376 included KRT1 and/or K2C6B. The observed molecular weights of TFIP11 in the spot ID 445, HIVEP2 in the spot ID 763, and NLRP3 in the spot ID 1072 were smaller than their theoretical weights, indicating that the detected proteins were fragments of those

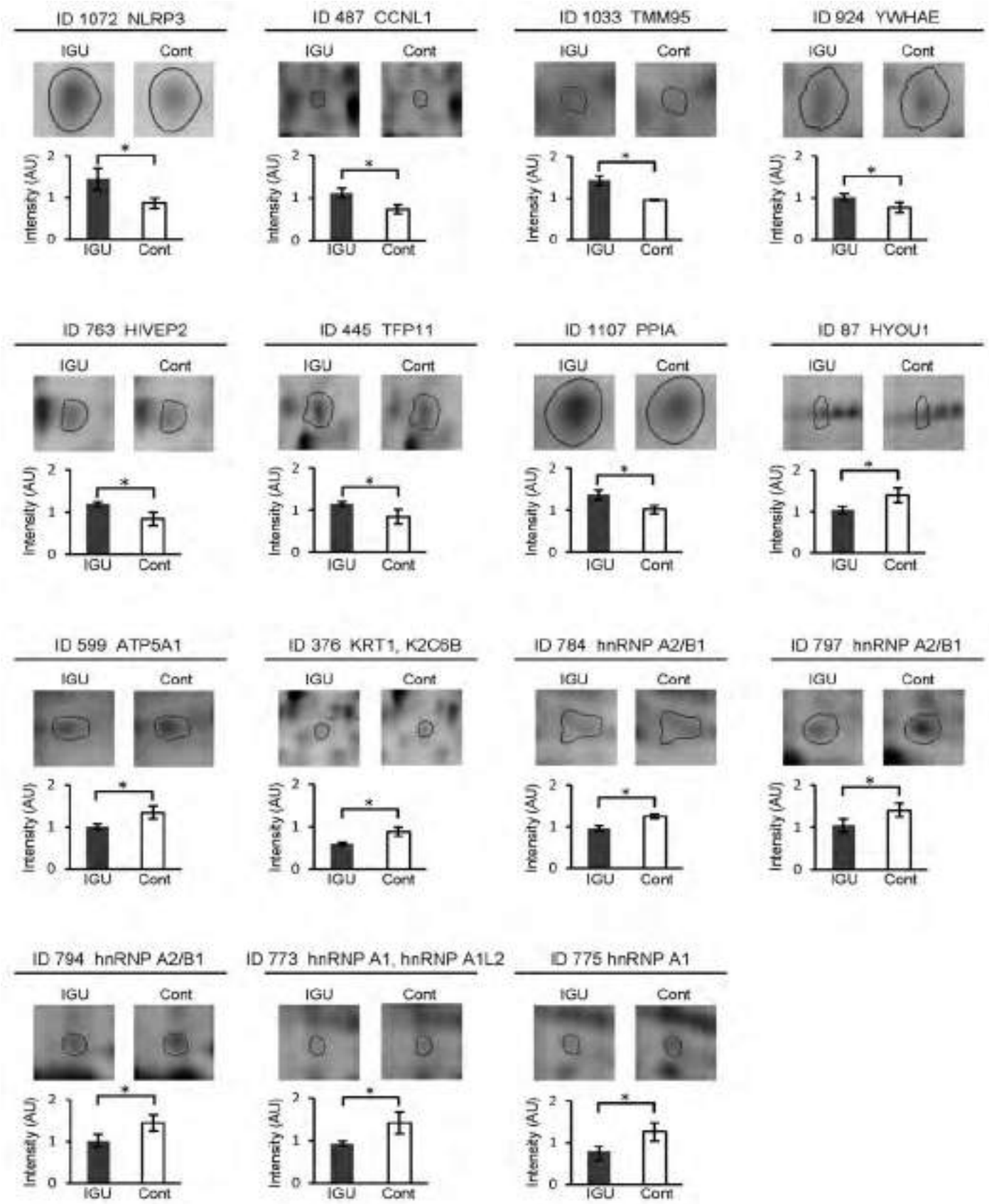

Figure 4. Comparisons of spot intensity of the 15 protein spots and intensity proteins between IGU-treated and non-treated conditions. Representative results of the Error bars, standard deviations, *p<0.05.

proteins. The pathway analysis showed deduced interactions of 11 out of the 14 identified proteins (Figure 5). hnRNP A2/B1, hnRNP A1 and their complex located at the center of the network. Of note, NF-κB, Akt, and p53 (encoded by TP53 gene) appeared as relay points of the network. These proteins would directly and/or indirectly interact with the identified proteins.

Discussion

We compared protein profiles of a chondrosarcoma cell line OUMS-27 cells between the presence and absence of IGU. Although the maximal plasma concentration after repetitive administration of 50 mg/day IGU for 14 days was 5 μM, the concentration is ununiform in vivo and would reach much higher levels in tissue such as RA-affected joints [15]. Treatment with 100 μM IGU caused significant changes in protein profiles of OUMS-27 cells, that is, intensity of 41 and 150 protein spots was changed by the 24 hour- and 6 day-treatment, respectively ($p<0.05$) (Table 1). When we examined time courses, intensity of most of the examined spots was much increased or decreased at 6 days compared to that at 24 hours (Figure 2C, D). Continuous treatment with IGU would augment its effect on protein expression.

The 6-day treatment changed intensity of 37 protein spots by 1.3-fold or more (Table 1). Such change levels of protein expression were considered to affect the function of proteins. Among the 14 identified proteins, we focused on three proteins, hnRNP A2/B1, hnRNP A1, and PPIA (Table 2, Figure 4, 5). Of note, intensity of multiple spots of hnRNP A2/B1 and hnRNP A1 was decreased by IGU (Table 2). This indicated that total expression of these proteins would be decreased by IGU regardless of differences of isoforms and/or post-translational modifications.

The main function of hnRNP A/B proteins, components of hnRNP particles, is to package pre-mRNA into hnRNP particles [16]. hnRNP A/B also play roles in telomere maintenance, transcription, pre-mRNA splicing, mRNA nucleo-cytoplasmic export, mRNA stability, and translation. Interestingly, high expression of hnRNP A2/B1 and A1 has been found in inflamed joints of RA patients and/or arthritis models [17-19]. Autoantibodies and autoreactive T cells against hnRNP A2/B1 have been detected in approximately 30% and 60% of RA patients, respectively [17, 20, 21]. Since depletion of hnRNP A2/B1 almost completely blocked development of arthritis both in collagen-induced arthritis (CIA) and K/BxN serum-transfer arthritis, hnRNP A2/B1 was considered to play a crucial role in the pathogenesis of inflammatory arthritis [22]. Besides their role as autoantigens in arthritis, hnRNP A2/B1 act as proinflammatory regulators. hnRNP A2 activates the Raf-MEK-ERK signaling pathway, located at the upstream of NF-κB, by elevating full length A-Raf transcription and reducing production of short dominant-negative isoform of A-Raf [23]. Furthermore, hnRNP A2, phosphorylated and activated by the serine/threonine kinase Akt1, also functions as a transcriptional coactivator for NF-κB c-Rel [24, 25].

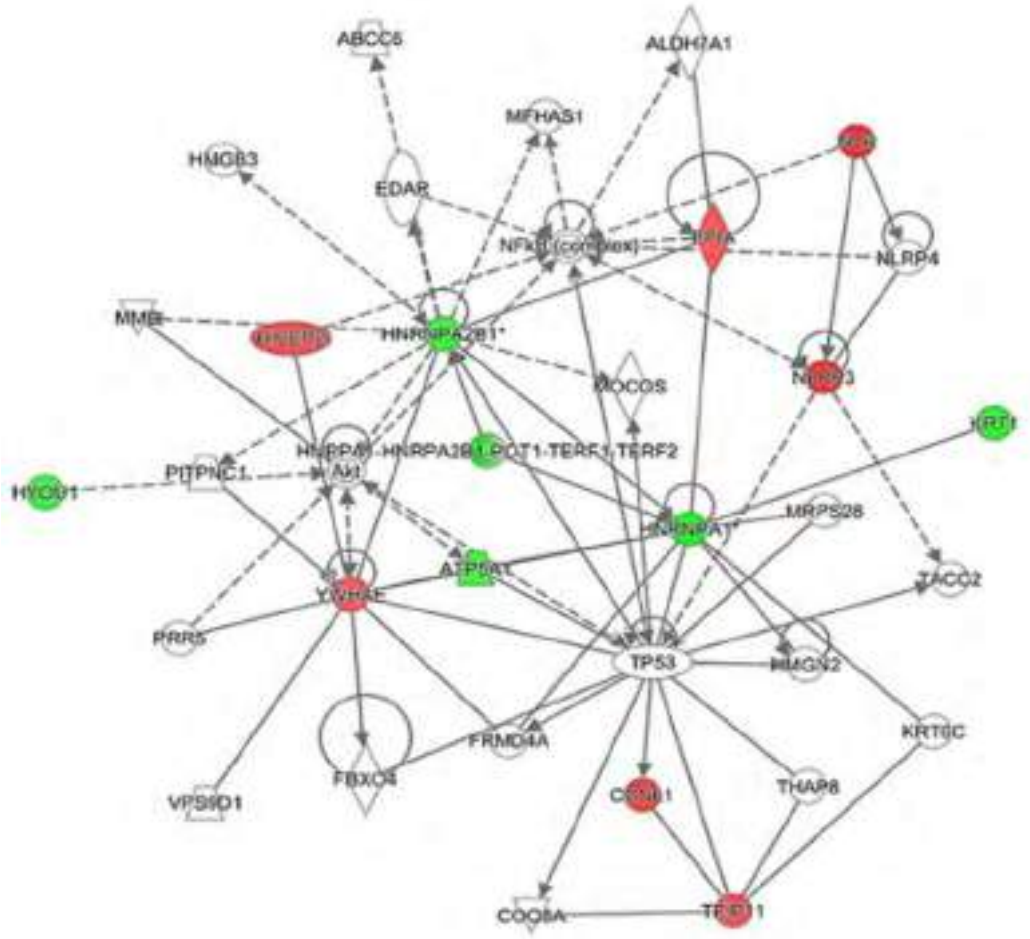

Figure 5. Interaction of the ident proteins. Result of a pathway analysis. Symbols in red and green show the proteins intensity of which were increased and decreased by the IGU-treatment, respectively. Solid lines and dotted lines show direct and indirect interactions, respectively. Arrows indicate activation.

NF-κB p65 and p50 are known to be targets of IGU [6, 7, 9, 11]. Thus, NF-κB c-Rel activated by hnRNP A2 would be also a target of IGU. Moreover, depletion of hnRNP A2/B1 almost completely inhibited bone erosion in RA models [22]. Since IGU suppresses bone erosion via RANKL- and ERK-mediating pathways [9, 11, 26, 27], its effect to suppress bone erosion may be also associated with the decrease of hnRNP A2/B1.

Our IPA result indicated that both hnRNP A2/B1 and hnRNP A1 could interact with p53 (Figure 5). However, p53 of OUMS-27 cells as well as that of most cancer cells is a mutant-type and thus does not function as a tumor suppressor [13]. Interestingly, suppression of hnRNP A1/A2 induces apoptosis in a variety of human cancer cells irrespective of p53 expression [28]. This was considered because hnRNP A1/A2 have a capping function of telomeres as G-tail binding proteins in cancer cells [28]. Suppression of hnRNPs may inhibit the tumorigenic growth of RA synovial cells.

The other protein of interest, PPIA, was increased by IGU, which has dual function as a chaperone and a signal transducer (Table 2, Figure 4, 5) [29]. Interestingly, PPIA was highly expressed in RA and CIA synovia [30]. PPIA aggravated the arthritis by polarizing macrophages toward proinflammatory M1 phenotypes that produced IL-1β, IL-6, MMP-2, and MMP-9 [30, 31]. The polarization was dependent on the activation of ERK-NF-κB p65 pathway and also on the PPIase activity [30, 32]. On the other hand, in concert with NF-κB p65, PPIA mediates BMP-2-induced Sox9 production and regulation of chondrogenesis signaling [33]. These processes may contribute to repairment of destructed cartilage in RA. Since IGU targets NF-κB, PPIA may be increased to recover the reduced functions of NF-κB.

In conclusion, we found that IGU affected protein profiles of OUMS-27 cells. IGU specifically decreased expression of hnRNP A2/B1 and A1, which are highly expressed in synovia of RA and its arthritis model. Since hnRNP A2/B1 are autoantigens in RA and activators for NF-κB, the decrease of hnRNPs would downregulate the autoimmune responses and also be involved in the NF-κB-targeting mechanism of IGU. The reduction of hnRNP A2/B1 may be further associated with the inhibition of bone erosion by IGU. The present data should be validated using RA chondrocytes and synovial cells in near future. Our results suggest novel mechanisms of the effect of IGU.

Acknowledgement

The authors indebted Ms Kumi Aso for her technical assistance.

Conflict of interest

Kimito Kawahata received research grants from Astellas, Eli lilly, Chugai Pharma, and Pfizer, and a personal fee from Ono Pharma.

References

1. McInnes IB, Schett G (2017) Pathogenetic insights from the treatment of rheumatoid arthritis. *Lancet* 389: 2328-2337. [Crossref]
2. Burmester GR, Pope JE (2017) Novel treatment strategies in rheumatoid arthritis. *Lancet* 389: 2338-2348. [Crossref]
3. Lau CS, Chia F, Harrison A, Hsieh TY, Jain R, et al. (2015) APLAR rheumatoid arthritis treatment recommendations. *Int J Rheum Dis* 18: 685-713. [Crossref]
4. Gaujoux-Viala C, Gossec L, Cantagrel A, Dougados M, Fautrel B, et al. (2014) Recommendations of the French Society for Rheumatology for managing rheumatoid arthritis. *Joint Bone Spine* 81: 287-297. [Crossref]
5. Tanaka K, Aikawa Y, Kawasaki H, Asaoka K, Inaba T, et al. (1992) Pharmacological studies on 3-formylamino-7-methylsulfonylamino-6-phenoxy-4H-1-benzopyran-4-one (T-614), a novel agent. 4th communication: inhibitory on the production of interleukin-1 and interleukin-6. *J Pharmacobiodyn* 15: 649-655. [Crossref]
6. Kohno M, Aikawa Y, Tsubouchi Y, Hashiramoto A, Yamada R, et al. (2001) Inhibitory of T-614 on tumor necrosis factor-alpha induced cytokine production and nuclear factor-kappaB activation in cultured human synovial cells. *J Rheumatol* 28: 2591-2596. [Crossref]
7. Aikawa Y, Yamamoto M, Yamamoto T, Morimoto K, Tanaka K (2002) An anti-rheumatic agent T-614 inhibits NF-kappaB activation in LPS- and TNF-alpha-stimulated THP-1 cells without interfering with IkappaBalpha degradation. *Inflamm Res* 51: 188-194. [Crossref]
8. Tanaka K, Yamamoto T, Aikawa Y, Kizawa K, Muramoto K, et al. (2003) Inhibitory of an anti-rheumatic agent T-614 on immunoglobulin production by cultured B cells and rheumatoid synovial tissues engrafted into SCID mice. *Rheumatology* 42: 1365-1371. [Crossref]
9. Gan K, Yang L, Xu L, Feng X, Zhang Q, et al. (2016) Iguratimod (T-614) suppresses RANKL-induced osteoclast and migration in RAW264.7 cells via NF-κB and MAPK pathways. *Int Immunopharmacol* 35: 294-300. [Crossref]
10. Sun Y, Ye DW, Zhang P, Wu YX, Wang BY, et al. (2016) Anti-rheumatic drug iguratimod (T-614) alleviates cancer-induced bone destruction via down-regulating interleukin-6 production in a nuclear factor-κB-dependent manner. *J Huazhong Univ Sci Technolog Med Sci* 36: 691-699. [Crossref]
11. Wei Y, Sun X, Hua M, Tan W, Wang F, et al. (2015) Inhibitory of a Novel Antirheumatic Drug T-614 on the IL-6-Induced RANKL/OPG, IL-17, and MMP-3 Expression in Synovial Fibroblasts from Rheumatoid Arthritis Patients. *Biomed Res Int* 2015: 214683. [Crossref]
12. Luo Q, Sun Y, Liu W, Qian C, Jin B, et al. (2013) A novel disease-modifying antirheumatic drug, iguratimod, ameliorates murine arthritis by blocking IL-17 signaling, distinct from methotrexate and *J Immunol* 191: 4969-4978. [Crossref]
13. Katano M, Kurokawa MS, Matsuo K, Masuko K, et al. (2017) Phosphoproteome analysis of synoviocytes from patients with rheumatoid arthritis. *Int J Rheum Dis* 20: 708-721. [Crossref]
14. Fiehn C (2010) Methotrexate transport mechanisms: the basis for targeted drug delivery *Clin Exp Rheumatol* 28: S40-45. [Crossref]
15. He Y, Smith R (2009) Nuclear functions of heterogeneous nuclear ribonucleoproteins A/B. *Cell Mol Life Sci* 66: 1239-1256. [Crossref]
16. Fritsch R, Eselböck D, Skriner K, Jahn-Schmid B, Scheinecker C, et al. (2002) Characterization of autoreactive T cells to the autoantigens heterogeneous nuclear ribonucleoprotein A2 (RA33) and in patients with rheumatoid arthritis. *J Immunol* 169: 1068-1076. [Crossref]
17. Hayer S, Tohidast-Akrad M, Haralambous S, Jahn-Schmid B, Skriner K, et al. (2005) Aberrant expression of the autoantigen heterogeneous nuclear ribonucleoprotein-A2 (RA33) and spontaneous formation of rheumatoid arthritis-associated anti-RA33 autoantibodies in TNF-alpha transgenic mice. *J Immunol* 175: 8327-8336. [Crossref]
18. MH, Tuncel J, Skriner K, Tohidast-Akrad M, Türk B, et al. (2007) The rheumatoid arthritis-associated autoantigen hnRNP-A2 (RA33) is a major stimulator of autoimmunity in rats with pristane-induced arthritis. *J Immunol* 179: 7568-7576. [Crossref]
19. Nell VP, Machold KP, Stamm TA, Eberl G, Heinzl H, et al. (2005) Autoantibody as early diagnostic and prognostic tool for rheumatoid arthritis. *Ann Rheum Dis* 64: 1731-1736. [Crossref]
20. Steiner G (2007) Auto-antibodies and autoreactive T-cells in rheumatoid arthritis: pathogenetic players and diagnostic tools. *Clin Rev Allergy Immunol* 32: 23-36. [Crossref]
21. Herman S, Fischer A, Presumey J, M, Koenders MI, et al. (2015) Inhibition of ation and bone erosion by RNA interference-mediated silencing of heterogeneous nuclear RNP A2/B1 in two experimental models of rheumatoid arthritis. *Arthritis Rheumatol* 67: 2536-2546. [Crossref]
22. Shilo A, Ben Hur V, Denichenko P, Stein I, Pikarsky E, et al. (2014) Splicing factor hnRNP A2 activates the Ras-MAPK-ERK pathway by controlling A-Raf splicing in hepatocellular carcinoma development. *RNA* 20: 505-515. [Crossref]
23. Guha M, Tang W, Sondheimer N, Avadhani NG (2010) Role of calcineurin, hnRNPA2 and Akt in mitochondrial respiratory stress-mediated transcription activation of nuclear gene targets. *Biochim Biophys Acta* 1797: 1055-1065. [Crossref]
24. Guha M, Fang JK, Monks R, Birnbaum MJ, Avadhani NG (2010) Activation of Akt is essential for the propagation of mitochondrial respiratory stress signaling and activation of the transcriptional coactivator heterogeneous ribonucleoprotein A2. *Mol Biol Cell* 21: 3578-3589. [Crossref]
25. Sun Y, Wu YX, Zhang P, Peng G, Yu SY (2017) Anti-rheumatic drug iguratimod protects against cancer-induced bone pain and bone destruction in a rat model. *Oncol Lett* 13: 4849-4856. [Crossref]

26. Wu YX, Sun Y, Ye YP, Zhang P, Guo JC, et al. (2017) Iguratimod prevents ovariectomy-induced bone loss and suppresses osteoclastogenesis via inhibition of peroxisome proliferator-activated receptor-γ. *Mol Med Rep* 16: 8200-8208. [Crossref]

27. Kunisada T, Miyazaki M, Mihara K, Gao C, Kawai A, et al. (1998) A new human chondrosarcoma cell line (OUMS-27) that maintains chondrocytic *Int J Cancer* 77: 854-859. [Crossref]

28. Patry C, Bouchard L, Labrecque P, Gendron D, Lemieux B, et al. (2003) Small interfering RNA-mediated reduction in heterogeneous nuclear ribonucleoparticule A1/A2 proteins induces apoptosis in human cancer cells but not in normal mortal cell lines. *Cancer Res* 63: 7679-7688. [Crossref]

29. Fischer G, Aumüller T (2003) Regulation of peptide bond cis/trans isomerization by enzyme catalysis and its implication in physiological processes. *Rev Physiol Biochem Pharmacol* 148: 105-150. [Crossref]

30. Dongsheng Z, Zhiguang F, Junfeng J, Zifan L, Li W (2010) Cyclophilin A Aggravates Collagen-Induced Arthritis via Promoting Classically Activated Macrophages. *Inflammation* 40: 1761-1772. [Crossref]

31. Wang L, Wang CH, Jia JF, Ma XK, Li Y, et al. (2010) Contribution of cyclophilin A to the regulation of processes in rheumatoid arthritis. *J Clin Immunol* 30: 24-33. [Crossref]

32. Wang L, Jia J, Wang C, Ma X, Liao C, et al. (2013) Inhibition of synovitis and joint destruction by a new single domain antibody for cyclophilin A in two mouse models of rheumatoid arthritis. *Arthritis Res Ther* 15: R208. [Crossref]

33. Guo M, Shen J, Kwak JH, Choi B, Lee M, et al. (2015) Novel role for cyclophilin A in regulation of chondrogenic commitment and endochondral *Mol Cell Biol* 35:2119-2130. [Crossref]

Copyright: ©2017 Ooka S. This is an open-access article distributed under the terms of the Creative Commons Attribution License, which permits unrestricted use, distribution, and reproduction in any medium, provided the original author and source are credited.

Integrative Molecular Medicine

Research Article ISSN: 2056-6360

Roles of layilin in human synovial fibroblasts revealed by proteomic analysis

Kosuke Shimazaki[1,2], Mitsumi Arito[1*], Toshiyuki Sato[1], Kazuki Omoteyama[1], Masaaki Sato[1], Manae S Kurokawa[3], Naoya Suematsu[1], Hisateru Niki[2] and Tomohiro Kato[1]

[1]Clinical Proteomics and Molecular Medicine, St. Marianna University Graduate School of Medicine, 2-16-1, Sugao, Miyamae, Kawasaki, Kanagawa, 216-8511, Japan

[2]Department of Orthopedic Surgery, St. Marianna University School of Medicine, 2-16-1, Sugao, Miyamae, Kawasaki, Kanagawa, 216-8511, Japan

[3]Disease Biomarker Analysis and Molecular Regulation, St. Marianna University Graduate School of Medicine, 2-16-1, Sugao, Miyamae, Kawasaki, Kanagawa, 216-8511, Japan

Abstract

Aim: To understand physiological and pathological roles of layilin in synovial fibroblasts, we comprehensively investigated protein profile changes caused by layilin-silencing. Methods: Immortalized human synovial membrane fibroblasts (HSFs) were transfected with siRNA for layilin (siL) in TNF-α-treated and -non-treated conditions. Proteins affected by siL were comprehensively detected by 2-dimensional fluorescence difference gel electrophoresis (2D-DIGE). Proteins of interest were identified by mass spectrometry. Results: In the 2D-DIGE analysis, intensity of approximately one-fifth of the detected protein spots was significantly changed by siL both in the TNF-α-treated and –non-treated conditions (239/1092 spots and 201/1092 spots, respectively). Proteins were identified in 25 out of 87 protein spots with ± 1.3-fold or greater intensity changes by siL. 15 (62.5%) of the 24 protein spots were assigned to epithelial-mesenchymal transition (EMT)-related proteins. Conclusion: Our data suggest that layilin is deeply involved in the regulation of EMT-related proteins. Functions of layilin in synovial fibroblasts should be investigated in the context of EMT, although synovial fibroblasts are not epithelial cells. Furthermore, the EMT-related proteins affected by layilin may be involved in the pathogenesis of rheumatoid arthritis, which was characterized by proliferation and invasion of synovial fibroblasts.

Introduction

Layilin is a type 1 transmembrane protein with a C-type lectin-like motif [1]. Layilin has been reported to be a receptor for hyaluronic acid [1] and also reported to bind to cytoskeletal proteins such as talin and merlin to regulate cell adhesion [2-4]. In fact, several studies showed that down-regulation of layilin inhibited infiltration and metastasis of cancer cells [5, 6]. Recently, it has been reported that layilin is highly expressed in an exhausted subset of $CD8^+$ T cells in liver cancer [7]. We have reported that renal tubular epithelial cells in patients with glomerulonephritis more strongly express layilin than those in healthy people [8]. Taking these reports together, layilin is expected to play pathophysiological roles in various diseases. However, physiological and pathological roles of layilin have been poorly understood.

Accordingly, roles of layilin in rheumatoid arthritis (RA) remain also unclear. RA, a chronic polyarthritis, is histologically characterized by proliferation and invasion of synovial fibroblasts and infiltration of inflammatory cells into the expanded synovia in affected joints. In RA, inflammatory cytokines like tumor necrosis factor-α (TNF-α) are known to play pathological roles [9]. In fact, blockage of the inflammatory cytokines is used as effective therapies in RA [10]. Recently, Snail, a transcriptional factor, has been reported to regulate TNF-α-mediated activation of synovial fibroblasts in rheumatoid joints. We have reported that TNF-α up-regulates expression of layilin in human chondrocytes and also in a human clear cell renal carcinoma cell line of KMRC-1 [8, 11]. We have demonstrated that layilin is involved in TNF-α-mediated epithelial-mesenchymal transformation (EMT) of KMRC-1 [8]. We thus speculate that layilin is involved in the TNF-α-mediated inflammatory processes in RA. However, physiological roles of layilin as well as pathological roles in synovial fibroblasts have been poorly understood. To promote understanding of roles of layilin in synovial fibroblasts, we here comprehensively investigated effects of layilin-silencing on human synovial membrane fibroblasts (HSFs) in the TNF-α-treated and -non-treated conditions using proteomics.

Materials and Methods

Cell culture

Immortalized human synovial membrane fibroblasts (HSFs) were purchased from Applied Biological Materials Inc. (abm, Richmond, Canada). HSFs were cultured in a Prigrow III medium (abm) supplemented with 10% fetal calf serum (FBS, Wako, Japan), 100 units/ml penicillin, and 100 μg/ml streptomycin (Sigma-Aldrich, St. Louis, MO, USA). The cells were cultured at 37°C in 5% CO_2.

Treatment of HSFs with siRNA and TNF-α

HSFs were transfected with 200 pmol/φ100 mm dish of siRNA for human LAYN (nucleotides 462-486

Correspondence to: Mitsumi Arito, PhD, Clinical Proteomics and Molecular Medicine, St. Marianna University Graduate School of Medicine, 2-16-1 Sugao, Miyamae, Kawasaki, Kanagawa, 216-8511, Japan, Tel: +81-44-977-8111 (ext. 3522); FAX: +81-44-976-7553; E-mail: m-ari@marianna-u.ac.jp

Key words: *Layilin, synovial membrane fibroblasts, TNF-α*

Received: November 28, 2017; **Accepted:** December 19, 2017; **Published:** December 22, 2017

(GGGAGGGACACAGAGGCCTTGTTAT) in NM_001258390.1, Invitrogen, Carlsbad, CA, USA)) using Lipofectamine RNAiMAX (Invitrogen). As a negative control, the cells were transfected with the same doses of control siRNA (Stealth™ RNAi Negative Control Medium GC Duplex, Invitrogen). After 24 hours, the HSFs were further cultured in the starvation condition of a Prigrow III medium supplemented with 1% FBS, 100 units/ml penicillin, and 100 μg/ml streptomycin for 24 hours. Then the cells were incubated with or without 10 ng/ml human TNF-α (PROSPEC, Ness Ziona, Israel) for 24 hours. Proteins were extracted from the cells into a lysis buffer (7M urea, 2M thiourea, 4% CHAPS). The protein samples were stored at -80 °C until use.

RNA extraction, reverse transcription, and quantitative polymerase chain reaction (qPCR)

Total RNA, purified from HSFs using RNeasy® (Qiagen, Venlo, the Netherlands), was converted to cDNA by High Capacity cDNA Reverse Transcription Kits® (Life Technologies, Rockville, MD, USA), according to the manufacturer's instructions.

qPCR was performed by ABI Prism 7000 Sequence Detection System (Applied Biosystems, Foster city, CA, USA). To measure mRNA for layilin and glyceraldehyde 3-phosphate dehydrogenase (GAPDH), a mixture of 2 μg cDNA, 300 nM each of forward and reverse primers, and Power SYBR® Master Mix (Applied Biosystems) was subjected to qPCR. Nucleotide sequences of the primers are as follows: layilin: 5' -CACAGCCTGCCAGGACCTTTA and 5' -TGCACCGGTCATCATTCCA, and GAPDH: 5'-TGGTATGGTGGAAGGACTCA and 5'-ATGCCAGTGAGCTTCCCGTT. The thermal cycle condition was as follows: 95°C for 10 min, followed by 40 cycles of 95°C for 15 sec and 60°C for 60 sec.

2-dimensional fluorescence difference gel electrophoresis (2D-DIGE)

The extracted proteins were separated by 2D-DIGE as described previously [12, 13]. Briefly, each of the protein samples was labeled with Cyanine dye 5 (Cy5, Cy Dye DIGE Saturation dye; GE Healthcare, Buckinghamshire, UK). An internal standard sample was prepared by mixing an equal amount of each of the samples. The standard sample was then labeled with Cyanine dye3 (Cy3, GE Healthcare). Then, each of the Cy5-labeled protein samples (2.5 μg) were mixed with the Cy3-labeled standard sample (2.5 μg). The mixture was applied onto a non-liner isoelectric focusing (IEF) gel (24 cm in width, pH 3-11, GE Healthcare). Subsequently, proteins separated by IEF were further separated by 12.5 % sodium dodecyl sulfate-polyacrylamide gel electrophoresis (SDS-PAGE). Then, the separated protein spots were scanned using an image analyzer (Typhoon 9400 Imager, GE Healthcare). On each protein spot, Cy5- and Cy3-fluorescence intensity was separately quantified by the Progenesis program (PerkinElmer, MA, US) and the Cy5-fluorescence intensity was normalized by Cy3-fluorescence intensity. The normalized Cy5-intensity was used for the quantitative comparison among the samples.

Protein identification

Protein spots of interest, excised from the 2D gels, were digested by trypsin as described previously [14]. Produced peptides were subjected to matrix-assisted laser desorption ionization-time of flight/time of flight mass spectrometry (MALDI-TOF/TOF-MS) (Ultraflex, BrukerDaltonics, Bremen, Germany). Obtained peptide masses were compiled to allow searches of the National Center for Biotechnology Information (NCBI) protein database using the Mascot software program (Matrix Science, London, UK).

Statistical analysis

Statistical significance was calculated using Student's t-test.

Results

Detection of proteins affected by layilin-silencing

We here comprehensively investigated changes of protein profiles of HSFs caused by siRNA for layilin in TNF-α-treated and non-treated conditions, using 2D-DIGE and mass spectrometry. First, HSFs were transfected with siRNA for human layilin (siL) or control siRNA (siC). In part, the cells were further treated with TNF-α for 24 hours. Then the cultured cell samples were subjected to 2D-DIGE. Prior to the experiments, the efficacy of layilin-silencing by siL was checked by qPCR. As a result, expression of layilin was suppressed down to approximately 7% (Figure 1), indicating that layilin-silencing was enough for the analysis.

Comprehensive analysis of proteins affected by layilin-silencing in the TNF-α- treated or non-treated condition by 2D-DIGE

By the 2D-DIGE analysis, in total, 1092 protein spots were detected on the 2D-gels (Figure 2A). In the condition without TNF-α, 239 (21.9%) out of the 1092 spots showed significantly different intensity between the siL and siC conditions (Table 1). Among the 239 spots, 29 spots showed 1.3-fold or higher intensity in the siL condition than in the siC condition and 24 spots showed 1/1.3-fold or lower intensity in the siL condition than in the siC condition (Table 1). Focusing on the 29 and 24 protein spots, we then compared intensity between the siL and siC conditions under the TNF-α-treated condition (Table 1). As a result, 17 out of the 29 spots showed significantly higher intensity in the siL condition than in the siC condition even under the TNF-α-treated condition (Category 1). The other 12 spots did not show significant difference between the siL and siC conditions under the TNF-α-treated condition (Category 2). No spots showed significantly lower intensity in the siL condition than in the siC condition (Category 3). Similarly, 2 out of the 24 spots showed significantly lower intensity in the siL

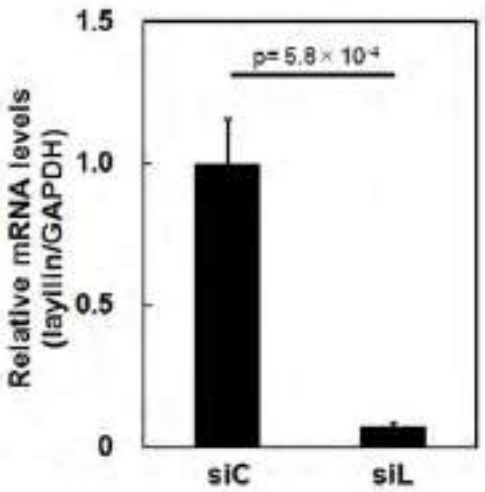

Figure 1. Silencing of layilin by siRNA in HSFs

HSFs cells were transfected with layilin or control siRNA (siL or siC, respectively). Then, RNA extracted from the cells was used for quantitative real time-PCR to estimate amounts of mRNA for layilin and GAPDH as a control. The measured mRNA levels of layilin were corrected using those of GAPDH. The average of the corrected mRNA levels in the cells

Table 1.

Total number of protein spots	TNF-α (-)			TNF-α (+)		Category in this study
1092	239	siL/siC≥1.3	29	↑	17	1
				→	12	2
				↓	0	3
		siL/siC≤-1.3	24	↑	0	4
				→	22	5
				↓	2	6

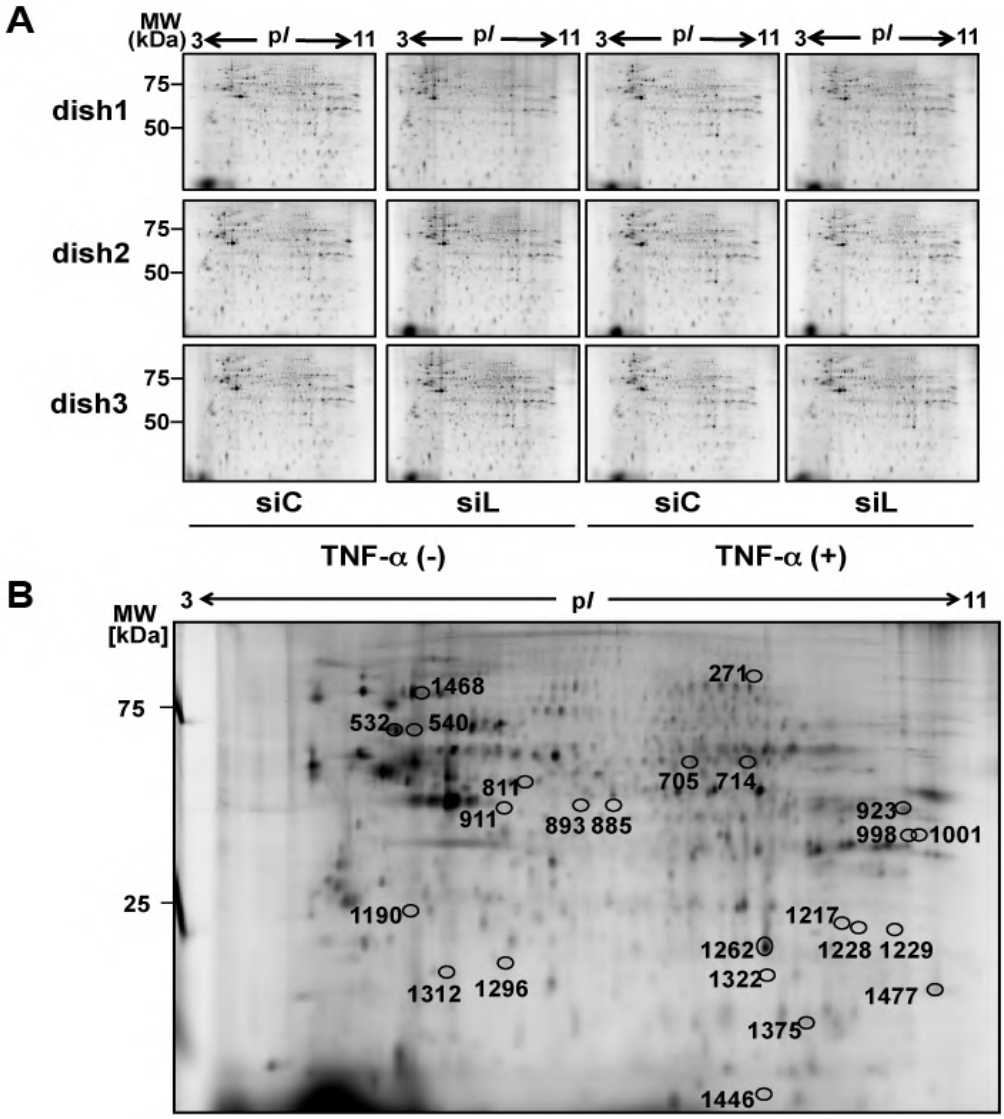

Figur ?on HSFs

(A) HSFs were transfected with siRNA for layilin (siL) or control siRNA (siC). Then the cells were cultured for 24 hours and then subjected to 24 hours starvation. Next, a part of the cultured cells were further treated with 10 ng/ml TNF-α for 24 hours. Proteins, extracted from the HSFs were subjected to 2D-DIGE (n=3). MW, molecular weight.

(B) Protein spots intensity of which was altered by siL were subjected to protein by MALDI-TOF-TOF/MS. Locations of the spots on the 2D gel are shown by circles with spot numbers.

condition than in the siC condition even under the TNF-α-treated condition (Category 6). The other 22 spots did not show significant difference between the siL and siC conditions (Category 5). No spots showed significantly higher intensity in the siL condition than in the siC condition (Category 4). Proteins of the spots in Categories 1 and 6 are thought to be affected by layilin, regardless of presence or absence of TNF-α. Proteins of the spots in Categories 2 and 5 are thought to be affected by layilin only in the TNF-α-non-treated condition.

On the other hand, in the TNF-α-treated condition, 201 (18.4%) out of the 1092 spots showed significantly different intensity between the siL and siC conditions (Table 2). Among the 201 spots, 14 spots showed

1.3-fold or higher intensity in the siL condition than in the siC condition and 20 spots showed 1/1.3-fold or lower intensity in the siL condition than in the siC condition (Table 2). Focusing on the 14 and 20 protein spots, we then compared intensity between the siL and siC conditions under the TNF-α-non-treated condition (Table 2). As a result, 5 out of the 14 spots showed significantly higher intensity in the siL condition than in the siC condition even under the TNF-α-non-treated condition (Category 7). The other 9 spots did not show significant difference between the siL and siC conditions under the TNF-α-non-treated condition (Category 8). No spots showed significantly lower intensity in the siL condition than in the siC condition (Category 9). Similarly, 4 out of the 20 spots showed significantly lower intensity in the siL condition than in the siC condition even under the TNF-α-non-treated condition (Category 12). The other 16 spots did not show significant difference between the siL and siC conditions under the TNF-α-non-treated condition (Category 11). No spots showed significantly higher intensity in the siL condition than in the siC condition (Category 10). Proteins of the spots in Categories 7 and 12 are thought to be affected by layilin, regardless of presence or absence of TNF-α. Proteins of the spots in Categories 8 and 11 are thought to be affected by layilin only in the TNF-α-non-treated condition.

Identification of proteins that are affected by layilin-silencing

Next, we tried to identify proteins of the 53 protein spots affected by layilin-silencing in the TNF-α-non-treated condition (29 up-regulated and 24 down-regulated, Table1), using MALDI-TOF-TOF mass spectrometry. As a result, 15 out of the 53 protein spots were identified (Figure 2B, Table 3).

Proteins of the spots in Category 1, which were thought to be down-regulated by layilin regardless of presence or absence of TNF-α, were identified as follows: ID1217: superoxide dismutase [Mn] mitochondrial (SODM), ID893: calcium-binding mitochondrial carrier protein SCaMC-1 (SCMC1), ID923: serpin H1 (SERPH), ID532: 78kDa glucose-regulated protein (GRP78), ID1001: heterogeneous nuclear ribonucleoproteins A2/B1 (ROA2), and ID1477: peptidyl-prolyl cis-trans isomerase B. Proteins of the spots in Category 2, which were thought to be down-regulated by layilin only under the TNF-α-non-treated condition, were identified as follows: ID1262: SODM, ID998: ROA2, ID714: nicotinamide phosphoribosyltransferase (NAMPT), ID911: keratin, type II cytoskeletal 1 (K2C1), and ID885: SCMC1. Proteins of the spots in Category 5, which were thought to be up-regulated by layilin only under the TNF-α-non-treated condition, were identified as follows: ID540: GRP78, ID271: growth /differentiation factor 10 (GDF10), ID811: glutathione synthetase (GSHB), and ID1190: melanoma-associated antigen B3 (MAGB3).

Similarly, we tried to identify proteins of the 34 protein spots affected by layilin-silencing under the TNF-α-treated condition (14 up-regulated and 20 down-regulated, Table 4). As a result, 10 out of the 34 proteins spots were identified (Figure 2B, Table 4).

Proteins of the spots in Category 7, which were thought to be down-regulated by layilin regardless of presence or absence of TNF-α, were identified as follows: ID1217: SODM and ID1312: peroxyiredoxin-2. Proteins of the spots in Category 8, which were thought to be down-regulated by layilin only under the TNF-α-treated condition, were identified as follows: IDs1228 and 1229: protein NipSnap homolog 3A (NPS3A). Proteins of the spots in Category 11, which were thought to be up-regulated by layilin only under the TNF-α-treated condition, were identified as follows: ID1468: vimentin, ID705: cdc42-interacting protein 4 (CIP4), ID1322: peroxisomal bifunctional enzyme (ECHP), ID1375: zinc finger protein 350 (ZN350), ID1446: cystatin-B (CYTB 2), and ID1296: peroxyiredoxin-2 (PRDX2).

Discussion

We here comprehensively investigated effects of layilin-silencing on HSFs under TNF-α-treated and -non-treated conditions using proteomics. We found that layilin-silencing significantly changed the expression of approximately one-fifth of the detected protein spots both in the two conditions. The 53 spots that showed ±1.3-fold or greater intensity changes in the TNF-α-non-treated condition were further classified into Categories 1-6, according to the changes by layilin-silencing under the TNF-α-treated condition. Similarly, the 34 protein spots that showed ±1.3-fold or greater intensity changes in the TNF-α-treated condition were further classified into Categories 7-12, according to the changes by layilin-silencing under the TNF-α-non-treated condition.

The protein spots of Categories 1 and 7 and Categories 6 and 12 are thought to contain proteins that regulated by layilin independently from TNF-α signaling. Here, 7 proteins were identified in Categories 1 and 7. Interestingly, 5 out of the 7 proteins were reported to be related with EMT (ID1217: SODM ID923: SERPH ID532: GRP78 ID1001: ROA2 ID1312: Peroxiredoxin-2.). Specifically, SODM, an enzyme that catalyzes the superoxide radical, has been reported to be up-regulated during EMT induced by TNF-α and to enhance expression of CD44, which are strongly expressed on highly malignant cancer cells [15]. SERPH, one of heat shock proteins, has been reported to be increased during cyclosporine-induced EMT of renal epithelial cells in mice [16]. GRP78, one of heat shock proteins, has been reported to increase fibronectin and integrin β1 to enhance adhesiveness of colon cancer cells [17]. Moreover, expression of GRP78 has been reported to be increased at EMT of human colon adenocarcinoma [17]. ROA2, a nuclear ribonucleoprotein, has been reported to be highly expressed in lung cancer cells [18]. Silencing of ROA2 have been reported toup-regulate E-cadherin and down-regulate transcriptional repressors of E-cadherin [18], thereby, ROA2 is thought to promote EMT. Collectively, these 4 proteins are thought to be involved in induction and/or promotion of EMT. The up-regulation of these 4 proteins by layilin-silencing observed here indicates that layilin constitutively suppresses these 4 proteins. On the other hand, PRDX2 has been reported to inhibit TNF-α-induced EMT in colon cancer cells [19]. The up-regulation of PRDX2 by layilin-silencing observed here indicates that layilin constitutively suppresses PRDX2.

The protein spots of Categories 2 and 5 are thought to contain proteins that appear to be affected by layilin only under the TNF-α-non-treated condition. These proteins may be regulated oppositely by TNF-α and layilin-silencing. Alternatively, if TNF-α down-regulates layilin, layilin-silencing would not actually affect the proteins under the TNF-α-treated condition. In Categories 2 and 5, 9 proteins were identified. Five out of the 9 proteins, i.e., ID1262: SODM ID998: ROA2 ID714: NAMPT ID271: GDF10 ID811: GSHB, were reported to be related to EMT. Specifically, SODM identified from ID1262 and ROA2 identified from ID998 were also identified from the spots of ID1217 and ID1001 in Category 1, respectively. This indicates existence of different post-translational modifications on SODM and ROA2. As above described, both SODM and ROA2 have been reported to induce or promote EMT. NAMPT, a rate-limiting enzyme of NAD^+ synthesis, has been recently reported to promote EMT, independently from its enzyme activity [20]. GDF10, a member of the TGF-β super family, has been reported to suppress EMT in oral squamous cell carcinoma [21]. On GSHB of a glutathione synthase, decrease of GSHB has been

Table 2.

Total number of protein spots	TNF-α (+)			TNF-α (-)		Category in this study
1092	201	siL/siC≥1.3	14	↑	5	7
				→	9	8
				↓	0	9
		siL/siC≤-1.3	20	↑	0	10
				→	16	11
				↓	4	12

Table 3.

Category	Spot ID	Observed MW	Observed p*I*	siL/siC	Protein	Accession no.	Theoretical MW	Theoretical p*I*	Mascot score	Coverage (%)	
1	1217	26	8.5	1.7	Superoxide dismutase [Mn], mitochondrial	P04179	24.7	8.35	59	24	^{203}AIWNVINWENVTER^{216}(31)
					SODM_HUMAN						
	893	41	5.8	1.6	Calcium-binding mitochondrial carrier protein SCaMC-1	Q6NUK1	53.3	6.00	61	16	^{24}YETLFQALDR^{33}(11)
					SCMC1_HUMAN						^{34}NGDGVVDIGELQEGLR^{49}(17)
	923	44	9.5	1.4	Serpin H1	P50454	46.4	8.75	288	23	^{134}LYGPSSVSFADDFVR^{148}(92)
					SERPH_HUMAN						^{264}LSSLIILMPHHVEPLER^{280}(85)
											^{264}LSSLIILMPHHVEPLER^{280} + Oxidation (M)(50)
											^{381}LFYADHPFIFLVR^{393}(89)
	532	68	5.2	1.3	78 kDa glucose-regulated protein	P11021	72.3	5.07	622	33	^{61}ITPSYVAFTPEGER^{74}(99)
					GRP78_HUMAN						^{165}VTHAVVTVPAYFNDAQR^{181}(141)
											^{325}AKFEELNMDLFR^{336}(96)
											^{475}DNHLLGTFDLTGIPPAPR^{492}(155)
	1001	38	9.8	1.3	Heterogeneous nuclear ribonucleoproteins A2/B1	P22626	37.4	8.97	272	30	^{22}KLFIGGLSFETTEESLR^{28}(28)
					ROA2_HUMAN						^{23}LFIGGLSFETTEESLR^{38}(84)
											^{138}IDTIEIITDR^{147}(10)
											^{214}GGGGNFGPGPGSNFR^{228}(72)
	1477	20	10.0	1.3	Peptidyl-prolyl cis-trans isomerase B	P23284	23.7	9.42	131	16	^{96}VIKDFMIQGGDFTR^{109}(33)
					PPIB_HUMAN						^{96}VIKDFMIQGGDFTR^{109} + Oxidation (M)(26)
											^{99}DFMIQGGDFTR^{109}(79)
											^{99}DFMIQGGDFTR^{109} + Oxidation (M) (44)
2	1262	23	7.5	1.4	Superoxide dismutase [Mn], mitochondrial	P04179	24.7	8.35	247	33	^{54}HHAAYVNNLNVTEEK^{68}(18)
					SODM_HUMAN						^{76}GDVTAQIALQPALK^{89}(57)
											^{115}GELLEAIKR^{123}(28)
											^{203}AIWNVINWENVTER^{216}(96)
	998	38	9.5	1.4	Heterogeneous nuclear ribonucleoproteins A2/B1	P22626	37.4	8.97	108	13	^{22}KLFIGGLSFETTEESLR^{28}(15)
					ROA2_HUMAN						^{23}LFIGGLSFETTEESLR^{38}(37)
											^{214}GGGGNFGPGPGSNFR^{228}(34)
	714	54	7.2	1.4	Nicotinamide phosphoribosyltransferase	P43490	55.5	6.69	92	13	^{197}GVSSQETAGIGASAHLVNFK^{216}□5□
					NAMPT_HUMAN						^{479}NAQLNIELEAAHH^{491}□48□
	911	44	5.5	1.4	Keratin, type II cytoskeletal 1		66	8.15	78	4	^{212}WELLQQVDTSTR^{223}(23)
					K2C1_HUMAN						^{224}THNLEPYFESFINNLR^{239}(51)
	885	41	6.0	1.4	Calcium-binding mitochondrial carrier protein SCaMC-1	Q6NUK1	53.3	6.00	71	18	^{24}YETLFQALDR^{33}(7)
					SCMC1_HUMAN						^{34}NGDGVVDIGELQEGLR^{49}(24)
5	540	67	5.2	-1.6	78 kDa glucose-regulated protein	P11021	72.3	5.07	88	17	^{165}VTHAVVTVPAYFNDAQR^{181}(33)
					GRP78_HUMAN						^{198}IINEPTAAAIAYGLDKR^{214}(19)
	271	90	7.2	-1.4		P55107	53.1	9.58	95	31	^{89}QGARPGGGNTVR^{100}(36)
					GDF10_HUMAN						
	811	51	5.5	-1.4	Glutathione synthetase	P48637	52.4	5.67	80	5	^{113}EGIAQTVFLGLNR^{125}(44)
					GSHB_HUMAN						^{254}LFVDGQEIAVVYFR^{267}(25)
	1190	28	5.2	-1.4	Melanoma-associated antigen B3	O15480	39.2	10.1	59	29	^{156}ASFNMEVVFGVDLKK^{170}(19)
					MAGB3_HUMAN						

MW; molecular weight, pI; isoelectric point

Table 4.

Category	Spot ID	Observed			Protein	Accession no.	Theoretical		Mascot	Coverage	
		MW	p*I*	siL/siC			MW	p*I*	score	(%)	
7	1217	26	8.5	2.2	Superoxide dismutase [Mn], mitochondrial	P04179	24.7	8.35	59	24	^{203}AIWNVINWENVTER^{216}(31)
					SODM_HUMAN						
	1312	20	5.2	1.4	Peroxiredoxin-2	P32119	21.9	5.66	222	17	^{92}KEGGLGPLNIPLLADVTR^{109}(95)
					PRDX2_HUMAN						^{93}EGGLGPLNIPLLADVTR^{109}(64)
											^{140}QITVNDLPVGR^{150}(33)
8	1228	25	8.9	1.5	Protein NipSnap homolog 3A	Q9UFN0	28.4	9.21	61	13	^{31}QYDGIFYEFR^{40}(23)
					NPS3A_HUMAN						^{180}LVGVFHTEYGALNR^{193}(6)
	1229	24	9.2	1.5	Protein NipSnap homolog 3A	Q9UFN0	28.4	9.21	57	20	^{180}LVGVFHTEYGALNR^{193}(15)
					NPS3A_HUMAN						
11	1468	85	5.2	-1.5	Vimentin	P08670	53.6	5.06	215	21	^{37}TYSLGSALRPSTSR^{50}(19)
					VIME_HUMAN						^{197}EEAENTLQSFR^{207}(69)
											^{411}ISLPLPNFSSLNLR^{424}(72)
	705	54	6.7	-1.4	Cdc42-interacting protein 4	Q15642	68.3	5.55	58	13	^{464}YEAWLAEAESRVLSNR^{479}□3□
					CIP4_HUMAN		52.7	6.39			
	1322	20	7.7	-1.4	Peroxisomal bifunctional enzyme	Q08426	79.4	9.24	58	15	^{223}QHPGCLAQEACVR^{235}(10)
					ECHP_HUMAN						^{468}KIGVVVGNCFGFVGNR^{483}(6)
	1375	17	8.0	-1.3		Q9GZX5	60	8.92	65	24	^{101}KPCHEHDAFENIVHCSK^{117}(4)
					ZN350_HUMAN						^{118}SQFLLGQNHDIFDLRGK^{134}(2)
											^{311}IHTGEKPYICNECGKGFIQK^{330}(2)
	1446	13	7.5	-1.3	Cystatin-B	P04080	11.1	6.96	68	35	^{57}VHVGDEDFVHLR^{68}(27)
					CYTB_HUMAN						
	1296	21	5.4	-1.3	Peroxiredoxin-2	P32119	21.9	5.66	167	14	^{92}KEGGLGPLNIPLLADVTR^{109}(65)
					PRDX2_HUMAN						^{93}EGGLGPLNIPLLADVTR^{109}(48)
											^{140}QITVNDLPVGR^{150}(31)

MW; molecular weight, pI; isoelectric point

reported to promote EMT, resulting in fibrosis [22]. Thus, all the 5 EMT-related proteins, SODM, ROA2, NAMPT, GDF10, and GSHB are thought to induce or promote EMT.

The protein spots of Categories 8 and 11 are thought to contain proteins that are regulated by layilin in the TNF-α signaling pathway. Out of the 8 identified proteins in Categories 8 and 11, 4 proteins (50%), CIP4, CYTB, PRDX2, and VIME, were reported to be related to EMT. Since all the 4 proteins were down-regulated by layilin-silencing, these 4 proteins were thought to be up-regulated by TNF-α via layilin. CYTB and PRDX2 have been reported to be suppressed during EMT or to suppress EMT [19, 23]. On the other hand, CIP4 and VIME have been reported to be increased during EMT or to promote EMT [24, 25].

Collectively, 15 (62.5%) out of the 24 identified proteins spots were found to be EMT-related ones. Among the 15 proteins, 10 proteins are related to induction or promotion of EMT as above discussed. Here, layilin-silencing up-regulated 7 out of the 10 proteins, and at the same time, down-regulated the remaining 3 proteins. Similarly, the remaining 5 out of the 16 proteins are related to suppression of EMT as above discussed. Here, layilin-silencing down-regulated 4 out of the 5 proteins, and at the same time, up-regulated the remaining 1 protein. Thereby, overall effects of layilin on EMT cannot be easily determined at present, although layilin is thought to be involved in EMT. Further studies should be needed to elucidate precise roles of layilin in EMT and EMT-like changes.

Again, 15 (62.5%) out of the 24 identified protein were found to be EMT-related ones. This result suggests EMT-related roles of layilin in the pathogenesis of RA. Synovial fibroblasts in patients with RA are known to possess high growth potential and high invasiveness into cartilage and bone [26]. Recently, it has been reported that these character changes of synovial fibroblasts in RA are associated with up-regulation of various EMT markers [27, 28]. Thereby, mechanisms that cause EMT are probably involved in the character changes of synovial fibroblasts, although synovial fibroblasts are not epithelial cells.

In conclusion, this study suggests that layilin is deeply involved in the regulation of EMT-related proteins in synovial fibroblasts. Functions of layilin in synovial fibroblasts in RA as well as in healthy conditions should be investigated from the viewpoint of EMT.

Acknowledgements

We thank Ms. Yokoyama MK and Ms. Sawada Y for their technical assistance.

Conflict of interest statement

None.

References

1. Bono P, Rubin K, Higgins JM, Hynes RO (2001) Layilin, a novel integral membrane protein, is a hyaluronan receptor. *Mol Biol Cell* 12(4): 891-900. [Crossref]

2. Borowsky ML, Hynes RO (1998) Layilin, a novel talin-binding transmembrane protein homologous with C-type lectins, is localized in membrane *J Cell Biol* 143(2): 429-442. [Crossref]

3. Wegener KL, Basran J, Bagshaw CR, Campbell ID, Roberts GC, et al. (2008) Structural basis for the interaction between the cytoplasmic domain of the hyaluronate receptor layilin and the talin F3 subdomain. *J Mol Biol* 382(1): 112-126. [Crossref]

4. Scoles DR. (2008) The merlin interacting proteins reveal multiple targets for NF2 therapy. *Biochim Biophys Acta* 1785(1): 32-54. [Crossref]

5. Zhuo W, Wang Y, Chen Z (2006) Inhibitory of shRNA targeting layilin on adhesion and invasion behavior of human lung adenocarcinoma A549 cells induced by hyaluronan in vitro. *Zhongguo Fei Ai Za Zhi* 9(3): 236-240. [Crossref]

6. Chen Z, Zhuo W, Wang Y, Ao X, An J (2008) Down-regulation of layilin, a novel hyaluronan receptor, via RNA interference, inhibits invasion and lymphatic metastasis of human lung A549 cells. *Biotechnol Appl Biochem* 50(Pt 2): 89-96. [Crossref]

7. Zheng C, Zheng L, Yoo JK, Guo H, Zhang Y, et al. (2017) Landscape of T Cells in Liver Cancer Revealed by Single-Cell Sequencing. *Cell* 169: 1342-1356. [Crossref]

8. Adachi T, Arito M, Suematsu N, Kamijo-Ikemori A, Omoteyama K, et al. (2015) Roles of layilin in TNF-a-induced epithelial-mesenchymal transformation of renal tubular epithelial cells. *Biochem Biophys Res Commun* 467(1): 63-69. [Crossref]

9. Brennan FM, Maini RN, Feldmann M (1992) TNF alpha--a pivotal role in rheumatoid arthritis? *Br J Rheumatol* 31: 293-298. [Crossref]

10. Maini RN, Feldmann M (2002) How does work in rheumatoid arthritis? *Arthritis Res* 4 Suppl 2: S22-28. [Crossref]

11. Asano K, Arito M, Kurokawa MS, Omoteyama K, Okamoto K, et al. (2014) Secretion of factors from chondrocytes by layilin signaling. *Biochem Biophys Res Commun* 452: 85-90. [Crossref]

12. Toda T, Ishijima Y, Matsushita H, Yoshida M, Kimura N (1994) Detection of thymopoietin-responsive proteins in nude mouse spleen cells by two-dimensional polyacrylamide gel electrophoresis and image processing. *Electrophoresis* 15: 984-987. [Crossref]

13. Onodera H, Arito M, Sato T, Ito H, Hashimoto T, et al. (2013) Novel of edaravone on human brain microvascular endothelial cells revealed by a proteomic approach. *Brain Res* 1534: 87-94. [Crossref]

14. Fujisawa H, Ohtani-Kaneko R, Naiki M, Okada T, Masuko K, et al. (2008) Involvement of post-translational of neuronal plasticity-related proteins in hyperalgesia revealed by a proteomic analysis. *Proteomics* 8: 1706-1719. [Crossref]

15. Kinugasa H, Whelan KA, Tanaka K, Natsuizaka M, Long A, et al. (2015) Mitochondrial SOD2 regulates epithelial-mesenchymal transition and cell populations by *Oncogene* 34(41): 5229-5239. [Crossref]

16. Galichon P, Vittoz N, Xu-Dubois YC, Cornaire E, Vandermeersch S, et al. (2011) Epithelial phenotypic changes detect cyclosporine in vivo nephrotoxicity at a reversible stage. *Transplantation* 92(9): 993-998. [Crossref]

17. Zhang L, Li Z, Fan Y, Li H, Li Z, et al. (2015) Overexpressed GRP78 EMT and cell-matrix adhesion via autocrine TGF-Î²/Smad2/3 signaling. *Int J Biochem Cell Biol* 64: 202-211. [Crossref]

18. Tauler J, Zudaire E, Liu H, Shih J, Mulshine JL (2010) hnRNP A2/B1 modulates epithelial-mesenchymal transition in lung cancer cell lines. *Cancer Res* 70: 7137-7147. [Crossref]

19. Feng J, Fu Z, Guo J, Lu W, Wen K, et al. (2014) Overexpression of peroxiredoxin 2 inhibits TGF-β1-induced epithelial-mesenchymal transition and cell migration in colorectal cancer. *Mol Med Rep* 10: 867-873. [Crossref]

20. Soncini D, I, Zoppoli G, Cea M, Cagnetta A, et al. (2014) Nicotinamide phosphoribosyltransferase promotes epithelial-to-mesenchymal transition as a soluble factor independent of its enzymatic activity. *J Biol* Chem 289(49): 34189-34204. [Crossref]

21. Cheng CW, Hsiao JR, Fan CC, Lo YK, Tzen CY, et al. (2016) Loss of GDF10/BMP3b as a prognostic marker collaborates with TGFBR3 to enhance chemotherapy resistance and epithelial-mesenchymal transition in oral squamous cell carcinoma. *Mol Carcinog* 55(5): 499-513. [Crossref]

22. Liu RM, Gaston Pravia KA (2010) Oxidative stress and glutathione in TGF-beta- *Free Radic Biol Med* 48: 1-15. [Crossref]

23. Xiong Y, Ji W, Fei Y, Zhao Y, Wang L, et al. (2017) Cathepsin L is involved in X-ray-induced invasion and migration of human glioma U251 cells. *Cell Signal* 2017 29:181-191. [Crossref]

24. Bai S, Zeng R, Zhou Q, Liao W, Zhang Y, et al. (2012) Cdc42-interacting protein-4 promotes TGF-β1-induced epithelial-mesenchymal transition and extracellular matrix deposition in renal proximal tubular epithelial cells. *Int J Biol Sci* 8(6):859-69. [Crossref]

25. Kokkinos MI, Wafai R, Wong MK, Newgreen DF, Thompson EW, et al. (2007) Vimentin and epithelial-mesenchymal transition in human breast cancer--observations in vitro and in vivo. *Cells Tissues Organs* 185(1-3): 191-203. [Crossref]

26. Firestein GS (1996) Invasive synoviocytes in rheumatoid arthritis: passive responders or transformed aggressors? *Arthritis Rheum* 39: 1781–1790. [Crossref]

27. Steenvoorden MM, Tolboom TC, van der Pluijm G, Löwik C, Visser CP, et al. (2006) Transition of healthy to diseased synovial tissue in rheumatoid arthritis is associated with gain of characteristics. *Arthritis Res Ther* 8(6):R165. [Crossref]

28. NJ (2006) Relevance of the stroma and epithelial-mesenchymal transition (EMT) for the rheumatic diseases. *Arthritis Res Ther* 8: 210. [Crossref]

Copyright: ©2017 Shimazaki K. This is an open-access article distributed under the terms of the Creative Commons Attribution License, which permits unrestricted use, distribution, and reproduction in any medium, provided the original author and source are credited.

Integrative Molecular Medicine

Research Article ISSN: 2056-6360

Effects of memantine on the growth and protein profiles of neuroblastoma cells

Kiyoshi Sekiguchi[1], Masaaki Sato[2], Michiyo K Yokoyama[2], Toshiyuki Sato[2], Atsuhiro Tsutiya[2], Kazuki Omoteyama[2], Mitsumi Arito[2], Naoya Suematsu[2], Tomohiro Kato[2] and Manae S Kurokawa[3*]

[1]Advanced Medical Research, St. Marianna University Graduate School of Medicine, Japan

[2]Clinical Proteomics and Molecular Medicine, St. Marianna University Graduate School of Medicine, Japan

[3]Disease Biomarker Analysis and Molecular Regulation, St. Marianna University Graduate School of Medicine, Japan

Abstract

Objective: Memantine, a low-affinity N-methyl-D-aspartate receptor antagonist, is one of the primary pharmacological therapies for Alzheimer's disease. To explore novel actions of memantine, we analyzed effects of memantine on cell viability, cell growth, and protein profile of neuroblastoma cells. Methods: A human neuroblastoma cell line of GIMEN was used. GIMEN cells were cultured in the presence or absence of 1-100 μM memantine for 48 hours. Effects of memantine on the cell viability and growth were evaluated by counting cell numbers. Proteins, extracted from GIMEN cells treated or non-treated with 10 μM memantine, were separated by 2 dimensional-differential image gel electrophoresis (2D-DIGE). Protein spots of interest were subjected to protein identification by mass spectrometry. Results: The viability of GIMEN cells was 99.0% or more in the range of 1-10 μM memantine compared to that in the absence of memantine. The viability was slightly decreased in the presence of 100 μM memantine (97.5%, $p<0.01$). In contrast, the cell growth was suppressed by memantine in a dose-dependent manner (2-100 μM, 85.5-63.0%; 2-10 μM, $p<0.05$; 20-100 μM, $p<0.01$). For the protein profile analysis, we used GIMEN cells treated with 10 μM memantine which showed the viability of 99.4% and the growth of 76.1%. As a result, 892 protein spots were detected in the 2D-DIGE results of 10 μM memantine-treated and non-treated GIMEN cells. 13 protein spots showed 1.2-fold or higher intensity and 19 protein spots showed -1.2 (1/1.2)-fold or lower intensity in the memantine-treated cells than in the non-treated cells ($p<0.05$). We identified proteins in 7 out of the 32 spots: coronin-1C (1.44-fold increased), β-actin (-1.21-fold decreased), γ-enolase (-1.21-fold decreased), glutathione synthetase (-1.28-fold decreased), spermatogenesis-associated protein 24 (-1.46-fold decreased), and V-set transmembrane domain-containing protein 2B (-1.46-fold decreased). Interestingly, β-actin, γ-enolase, and glutathione synthetase are known to be involved in cell proliferation. Conclusion: Memantine suppressed the growth of GIMEN cells and affected their protein profiles. Our data suggested a novel action of memantine to suppress the neuroblastoma cell growth, which may be associated with the decreased expression of β-actin, γ-enolase, and glutathione synthetase.

Introduction

Alzheimer's disease (AD), a neurodegenerative disorder, is the main cause of dementia [1, 2]. Although the etiology of AD remains obscure, it is believed to be associated with the formation of senile plaques and neurofibrillary tangles in the brain due to the extracellular deposition of amyloid β (Aβ) peptides and hyperphosphorylation of intracellular tau protein [2]. Vaccines or antibodies targeting these aberrant peptides/protein and inhibitors for β-secretase or γ-secretase, which interfere with the production of amyloid β peptides, are under investigation for treatment of AD [3]. However, none of these drugs has brought a fundamental breakthrough [4]. Choline esterase inhibitors and N-methyl D-aspartate (NMDA) receptor antagonist are currently the main treatment for AD, the latter of which has a unique neuroprotective effect [4, 5].

NMDA receptors, one of ion channel-type glutamate receptors, are crucial for neuronal communication [6]. To date, 7 different subunits of NMDA receptors have been identified: NR1, NR2A-D, and NR3A and B [6, 7]. NMDA receptors are heterotetramers that consist of two NR1 subunits and two NR2 subunits or two NR1 subunits and a mixture of NR2 and NR3 subunits [6]. Glycine and glutamate bind to NR1 and NR2, respectively, and the glycine sites must be occupied before the glutamate-binding for the activation of the receptors [7]. NMDA receptors that are non-selective cation channels have a potential for high Ca^{2+} permeability [6]. At rest, Mg^{2+} binds to NMDA receptors to block the activation. On sufficient depolarization of the synaptic membrane, Mg^{2+} dissociates from NMDA receptors in a voltage-dependent manner [6, 7]. Simultaneously, glutamate must bind to the receptors for their activation. The activation of NMDA receptors opens their ion channels for Ca^{2+} influx to mediate long-term potentiation (LTP) [6, 8]. LTP has been implicated to play a crucial role in the processes of learning and memory formation [8].

In the brains of AD patients, Aβ peptides mediate an increase in extracellular glutamate by increasing glutamate release from presynaptic neurons, induction of glutamate release from astrocytes and microglia, and inhibition of glutamate uptake by astrocytes and microglia [9, 10]. Prolonged activation of synaptic NMDA receptors and another ion channel-type glutamate receptor, α-amino-3-hydroxy-5-methylisoxazole-4-propionic acid (AMPA) receptors, leads to their

Correspondence to: Manae S Kurokawa, MD, PhD, Disease Biomarker Analysis and Molecular Regulation, St. Marianna University Graduate School of Medicine, 2-16-1, Sugao, Miyamae-ku, Kawasaki, 216-8511, Japan, Tel: 81-44-977-8111, ext. 3521; Fax +81-44-976-7553; E-mail: manae@marianna-u.ac.jp

Key words: *Alzheimer's disease, cell growth, mass spectrometry, memantine, neuroblastoma cells, protein profiles*

Received: December 23, 2017; **Accepted:** January 12, 2018; **Published:** January 15, 2018

desensitization and internalization, resulting in synaptic depression. Finally, excess glutamate activates extra-synaptic NMDA receptors, which results in multiple deleterious downstream events, including cell death and impairment of LTP [6, 9]. Hyperphosphorylated tau targets the receptor protein kinase Fyn that phosphorylates NR2B to stabilize their association with postsynaptic density 95 (PSD95), which enhances the above glutamatergic excitotoxicity induced by Aβ peptides.

Memantine is a low affinity, voltage-dependent, non-competitive NMDA receptor antagonist which is currently used in the treatment of moderate to severe AD [6, 11, 12]. Compared to other NMDA receptor channel blockers, memantine has a higher affinity than that of Mg^{2+}, but a lower affinity than those of ketamine, phencyclidine, and MK-801 [13]. Memantine enters NMDA receptor channel preferentially when the channel is excessively open [14]. Thereby, memantine inhibits the Ca^{2+} influx by blocking the channel activity that is induced by relatively low, tonic levels of glutamate [11-13]. This may contribute to symptomatic improvement of AD and protect neuronal cells from the glutamatergic excitotoxicity [12, 13]. Most importantly, the off-rate of memantine from NMDA receptors is relatively fast, which allows for the preservation of the physiological function of the receptors including expression of LTP [11, 14]. NMDA receptors blocked by memantine can be activated by higher concentrations of glutamate released after depolarization of the presynaptic neurons [11, 13].

Besides the above-mentioned action as an NMDA receptor antagonist, memantine has been found to influence protein expression of neuronal cells. Memantine reduces levels of total Aβ precursor protein (APP), APPα isoform, and $A\beta_{1-40}$ secreted from neuroblastoma cells, and lowers the amyloidogenic $A\beta_{1-42}$ secretion in primary rat cortical neuronal culture [15, 16]. Memantine also inhibits and reverses protein phosphatase 2A inhibition-induced abnormal hyperphosphorylation and accumulation of tau in organotypic culture of rat hippocampal slices [17]. Furthermore, memantine affects physiologically expressed genes/proteins in rat and mouse brains [18, 19]. However, no comprehensive study of physiologically expressed proteins in human neuronal cells under the effect of memantine has been conducted to date as far as we searched. It is important to collect information concerning the molecular pharmacology of memantine to understand its actions and anticipate potential adverse effects.

In this study, we analyzed effects of memantine on the viability, growth, and protein profile of neuroblastoma cells. We found that memantine almost did not affect the cell viability but decreased the cell growth in a dose-dependent manner. Protein profile of neuroblastoma cells was changed by memantine, showing altered expression levels of at least 6 proteins. Our findings suggest novel actions of memantine, which may underlie the success of AD treatment.

Materials and methods

Cell culture

A human neuroblastoma cell line of GIMEN (CLS Cell Lines Service GmbH, Eppelheim, Germany) was used in this study. GIMEN cells were cultured in DMEM supplemented with 10% FBS. To investigate effects of memantine on the cell viability and proliferation, GIMEN cells were cultured in the presence or absence of 1-100 μM memantine for 48 hours. Specifically, the cells were plated onto a 96-well plate at 7.0×10^4 cells/cm^2. Then, the culture medium was replaced with FBS-free DMEM that contained or did not contain 1-100 μM memantine. After culturing for 48 hours, the cell viability was calculated as ratios of the viable cell numbers to the total cell numbers. The cell growth was calculated as ratios of the viable cell numbers (at 48 hours) to the seeded cell numbers (2.2×10^4 cells, at 0 hour). To perform 2-dimensional differential image gel electrophoresis (2D-DIGE), cytokine array, and ELISA, the cells were cultured for 48 hours in the presence or absence of 10 μM memantine. All the experiments were performed in triplicates.

Reverse-transcription polymerase chain reaction (RT-PCR)

RNA extraction and RT-PCR were performed using TaqMan Gene Expression Cells-to-CT Kit (Thermo Fisher Scientific, Waltham, MA, USA) and ExTaq (Takara Bio Inc., Shiga, Japan). Sequences of primers for NMDA receptor subunits and 18S ribosomal RNA were previously reported [20]. PCR products were separated by 3% agarose gel electrophoresis.

2D-DIGE

Proteins extracted from GIMEN cells were separated by 2D-DIGE as described previously [21]. Briefly, an equal weight of proteins taken from six lysates (three of 10 μM memantine-treated and three non-treated) were mixed and labeled with Cyanine dye 3 (Cy3, Cy Dye DIGE Saturation dye, GE Healthcare, Buckinghamshire, UK) for preparation of an internal control "standard sample". Each of the six samples was labeled with Cyanine dye 5 (Cy5, GE Healthcare). 2.5 μg of the individual Cy5-labeled samples were mixed with 2.5 μg of the Cy3-labeled standard sample. Then each of the mixed protein sample was applied to an isoelectric focusing (IEF) gel strip (Immobiline Drystrip pH 3-11, 24 cm, non-linear, GE Healthcare). After the proteins were separated by IEF, they were further separated by sodium dodecyl sulfate-polyacrylamide gel electrophoresis. The resultant protein spots were scanned using an image analyzer (Typhoon 9400 Imager, GE Healthcare). The Cy5-fluorescent intensity of each protein spot was normalized by the Cy3-fluorescent intensity of an identical spot by using a quantitative analysis program (Progenesis, Nonlinear Dynamics, Newcastle, UK). The normalized Cy5-fluorescent intensity was compared between the memantine-treated and non-treated samples using Progenesis.

Protein identification

Proteins were identified by mass spectrometry (MS) [21]. In brief, 50 μg of proteins was separated by 2-dimensional electrophoresis. Gel specimens corresponding to protein spots of interest were recovered. Then proteins in the gel fragments were digested with trypsin. Peptides produced by the digestion were analyzed using a matrix-assisted laser desorption/ionization time of flight mass spectrometer (MALDI-TOF/MS) (Ultraflex, Bruker Daltonics, Ettlingen, Germany). Based on the mass spectra, some peptides were selected for MS/MS analysis. The obtained MS and MS/MS spectra were used to identify the proteins by database searching (Mascot, http://www.matrixscience.com) against the Swiss Prot human protein sequence database. Protein identification was accepted when MASCOT search results delivered significant MOWSE scores ($p<0.05$).

Analysis of the secretion of humoral factors from GIMEN cells treated with memantine

Humoral factors in culture supernatants were measured in duplicate by a cytokine array (Human Neuro Discovery Array C1, RayBiotech, Norcross, GA, USA). The analyzed humoral factors were as follows: BDNF, βNGF, GCSF, GDNF, HB-EGF, IFNγ, IGF-1, IL-10, IL-1α, IL-1β, IL-6, IL-8, MCP-1, MIP-1α, MMP-2, MMP-3, S100B, TGFβ, TNFα, and VEGF-A. Humoral factors detected as specific spots were visualized using an image analyzer (LAS-3000, Fujifilm, Tokyo,

Japan). The intensity of each spot, which was measured by Science Lab 2003 Image Gauge software program (Fujifilm), was normalized based on the intensity of positive control spots. MCP-1, a chemokine selected by the cytokine array, was measured in triplicate using an ELISA kit (R&D Systems, Minneapolis, MN, USA).

Statistical analysis

Significance of differences in cell viability, cell growth, intensity of protein spots in 2D-DIGE, and humoral factor secretion was calculated using Student's *t*-test.

Results

Expression of all the NMDA receptor subunits in GIMEN cells

We first examined which subunits of NMDA receptors GIMEN cells expressed. As a result, all the subunits of NR1, NR2A-D, and NR3A, B were expressed on GIMEN cells (Figure 1A). Thus, memantine was considered to affect GIMEN cells by binding NMDA receptors.

Effects of memantine on the viability and growth of GIMEN cells

To investigate effects of memantine on the viability and growth of GIMEN cells, the cells were treated with 1-100 μM memantine under FBS-free condition. The viability of GIMEN cells was 99.0% or more in the range of 1-10 μM memantine compared that in the absence of memantine (100%) (Figure 1B). The viability was slightly increased by 1 μM memantine (101.0%, $p<0.05$) and slightly decreased by 100 μM memantine (97.5%, $p<0.01$). On the other hand, the viable cell numbers in the range of 0-100 μM memantine were 4.22 to 2.66 x 10^4 cells after the 48 hour treatment, all of which was increased from the seeded cell numbers (2.2 x 10^4 cells). Interestingly, the growth of GIMEN cells was decreased in a dose-dependent manner (2-100 μM, 85.5-63.0%; 2-10 μM, $p<0.05$; 20-100 μM, $p<0.01$) (Figure 1C). From these results, we determined to treat GIMEN cells with 10 μM memantine in the subsequent protein profile analysis. This was because the cell viability was high enough (99.4%, $p\geq0.05$), while the cell growth was decreased to less than 80% (76.1%, $p<0.05$) by that concentration (Figure 1B, C).

Change of the protein profile of GIMEN cells by treatment with memantine

We compared protein profiles between 10 μM memantine-treated and non-treated GIMEN cells by 2D-DIGE to find proteins involved in the suppression of cell growth. As a result, 892 protein spots were detected (Figure 2A, B). 45 out of the 892 protein spots showed different intensity between the memantine-treated and non-treated cells ($p<0.05$) (Table 1). Among the 45 protein spots, 13 protein spots showed 1.2-fold or higher intensity in the memantine-treated cells compared to the non-treated cells. In contrast, 19 protein spots showed -1.2 (1/1.2)-fold or lower intensity in the memantine-treated cells compared to the non-treated cells. Protein profile of GIMEN cells was changed by the treatment with memantine.

Identification of the proteins expression of which was changed by memantine

We tried to identify the proteins in the spots, intensity of which was changed by the treatment with memantine. 32 protein spots that showed ±1.2-fold or more intensity change by memantine were subjected to the identification. As a result, 6 proteins were identified from 7 out of the 32 spots (Figure 2C, Table 2). Coronin-1C was identified from the 1 spot, intensity of which was increased 1.44-fold by the treatment with memantine (Figure 2C, Figure 3A, Table 2). In contrast, 5 proteins were identified from the 6 spots, intensity of which was decreased by the treatment with memantine (Figure 2C, Figure 3B-G). They were β-actin (-1.21-fold decreased), γ-enolase (-1.21-fold decreased), glutathione synthetase (-1.28-fold decreased), spermatogenesis-associated protein 24 (-1.46-fold decreased), and V-set transmembrane domain-containing protein 2B (-1.46-fold decreased). β-actin was identified from 2 spots (ID 798 and ID 804).

Effects of memantine on humoral factor secretion from GIMEN cells

Finally, we compared levels of humoral factor secretion between the memantine-treated and non-treated GIMEN cells. A cytokine array analysis using the culture supernatants showed clear spots of 2 humoral factors, MCP-1 and BDNF (Figure 4A). After the normalization using the positive control spot intensity, intensity of MCP-1 spots tended to be higher in the memantine-treated cells than in the non-treated cells (Figure 4B). We quantified the secreted MCP-1 by ELISA, however, no difference in MCP-1 secretion was found between the memantine-treated and non-treated cells (Figure 4C). Memantine did not affect secretion of the examined 20 humoral factors from GIMEN cells.

Discussion

In this study, we explored novel actions of memantine by comparing the memantine-treated GIMEN cells to the non-treated cells. GIMEN cells expressed all the 7 NMDA receptor subunits, including NR2B that is related to the glutamatergic excitotoxicity (Figure 1A) [6, 9]. Memantine was considered to affect GIMEN cells through NMDA receptors as well as it affects neuronal cells in the AD brain. The subunit composition of NMDA receptors is known to be plastic [6], therefore, all the 7 subunits may be used to form heterotetrameric complexes of the receptors in various combinations. Protein expression of the NMDA receptor subunits in GIMEN cells should be further confirmed.

The viability of GIMEN cells was not decreased by memantine except the 100 μM treatment (97.3%, $p<0.01$) Figure 1B. This result was different from the previous study using another neuroblastoma cell line, SK-N-SH [16]. The viability of SK-N-SH cells was relatively increased by 10 μM and 100 μM memantine [16]. Since SK-N-SH cells do not express functional NMDA receptors [22], memantine may decrease the viability of GIMEN cells through NMDA receptors.

In contrast, the growth of GIMEN cells was apparently decreased in a dose-dependent manner in the range of 2-100 μM memantine (2-10 μM, 85.5-76.1%, $p<0.05$; 20-100 μM, 70.0-63.0%, $p<0.01$) Figure 1C. Thus, memantine was considered to suppress the growth of GIMEN neuroblastoma cells by its pharmacological effect. In several neuroblastoma cell lines, mRNA expression of NR1 subunit of NMDA receptors was shown, however, the expression of NR2A-D was not shown or was controversial among the studies [22-24]. In contrast, protein expression of NMDA receptors and/or their involvement in cell proliferation have been reported in other types of tumor cells such as glioma, prostatic cancer, breast cancer, colon cancer, and small cell lung cancer [25-27]. In such tumor cells, 20-900 μM memantine reduced the cell growth probably by limiting signals from NMDA receptors. In our results, relatively low doses of 2-50 μM memantine showed suppression of the cell growth without affecting the cell viability Figure 1BC. Interestingly, 1 μM memantine that is within therapeutic serum concentrations for AD [28] also tended to suppress the cell growth (89.1%, $p\geq0.05$) (Figure 1C). Memantine may have an effect

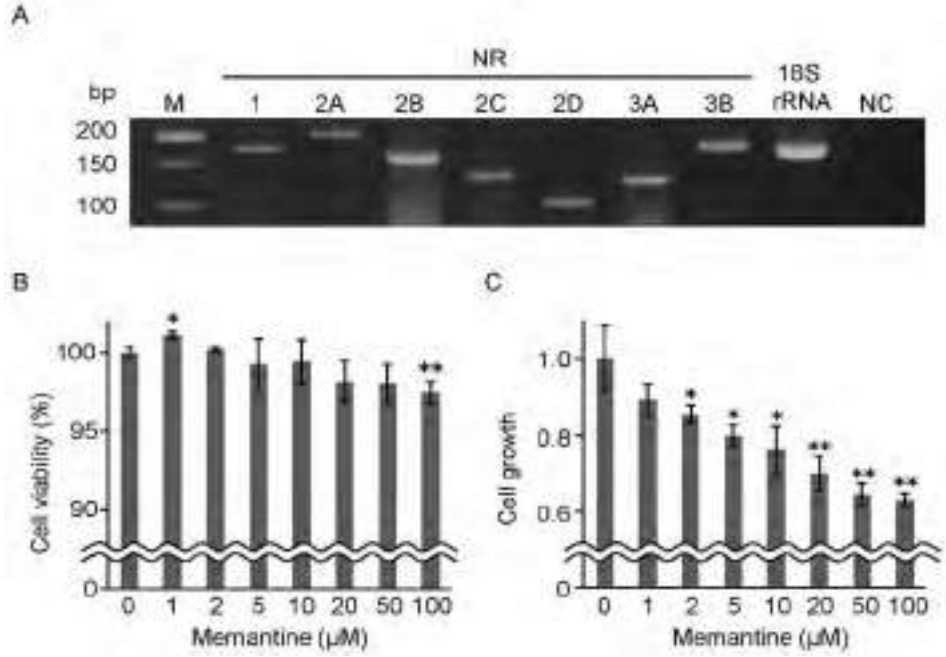

Figure 1. Effects of memantine on the viability and growth of GIMEN cells. A. Expression of NMDA receptor subunits in GIMEN cells was examined by RT-PCR. 18S ribosomal RNA was used as a template as positive control. Distilled water was similarly used as negative control (NC). M, DNA size marker. B. The viability of GIMEN cells cultured for 48 hours in the presence or absence of 1-100 μM memantine. Relative values of the viability to that in the absence of memantine are shown. C. The growth of GIMEN cells cultured for 48 hours in the presence or absence of 1-100 μM memantine. Relative values of the growth to that in the absence of memantine are shown. All the experiments were performed in triplicates. Error bars, standard deviations. $^{*}p<0.05$, $^{**}p<0.01$.

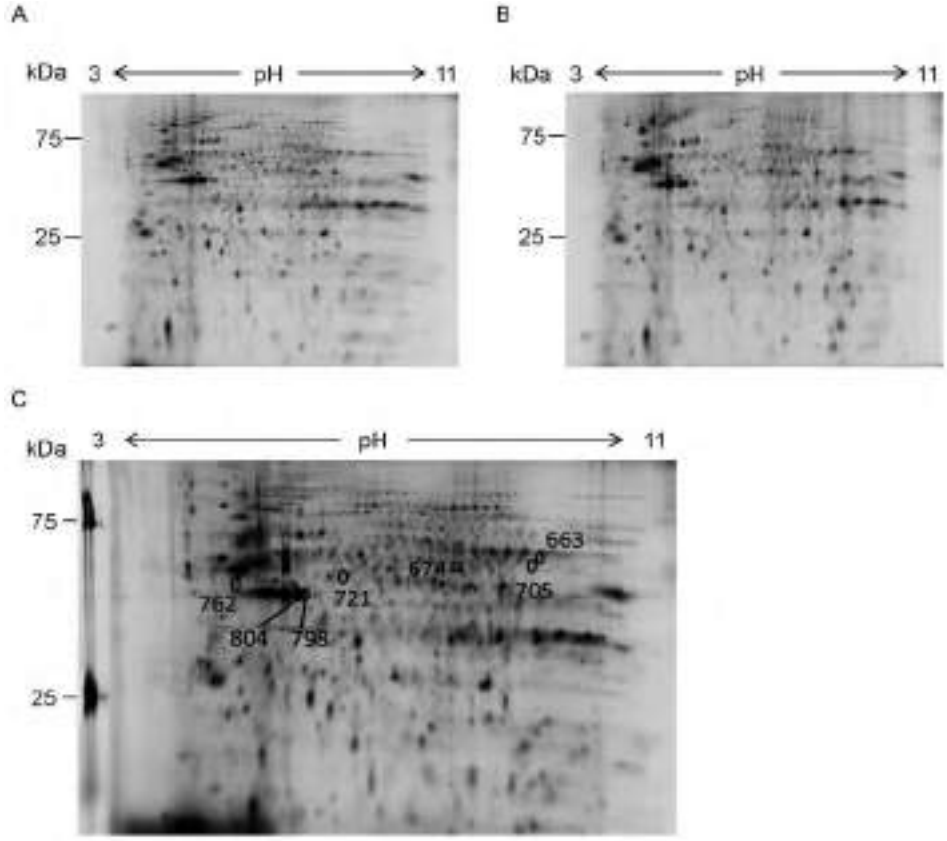

Figure 2. Protein of GIMEN cells treated with memantine. A, B. Proteins extracted from 10 μM memantine-treated GIMEN cells (A) and non-treated GIMEN cells (B) were separated by 2D-DIGE. Each analysis was performed in triplicates. Representative 2D-DIGE results are shown. C. Proteins in 7 out of the 32 protein spots, intensity of which were changed able 2). A square and circles show 1 and 6 spots, intensity of which was increased and decreased by the treatment with memantine, respectively.

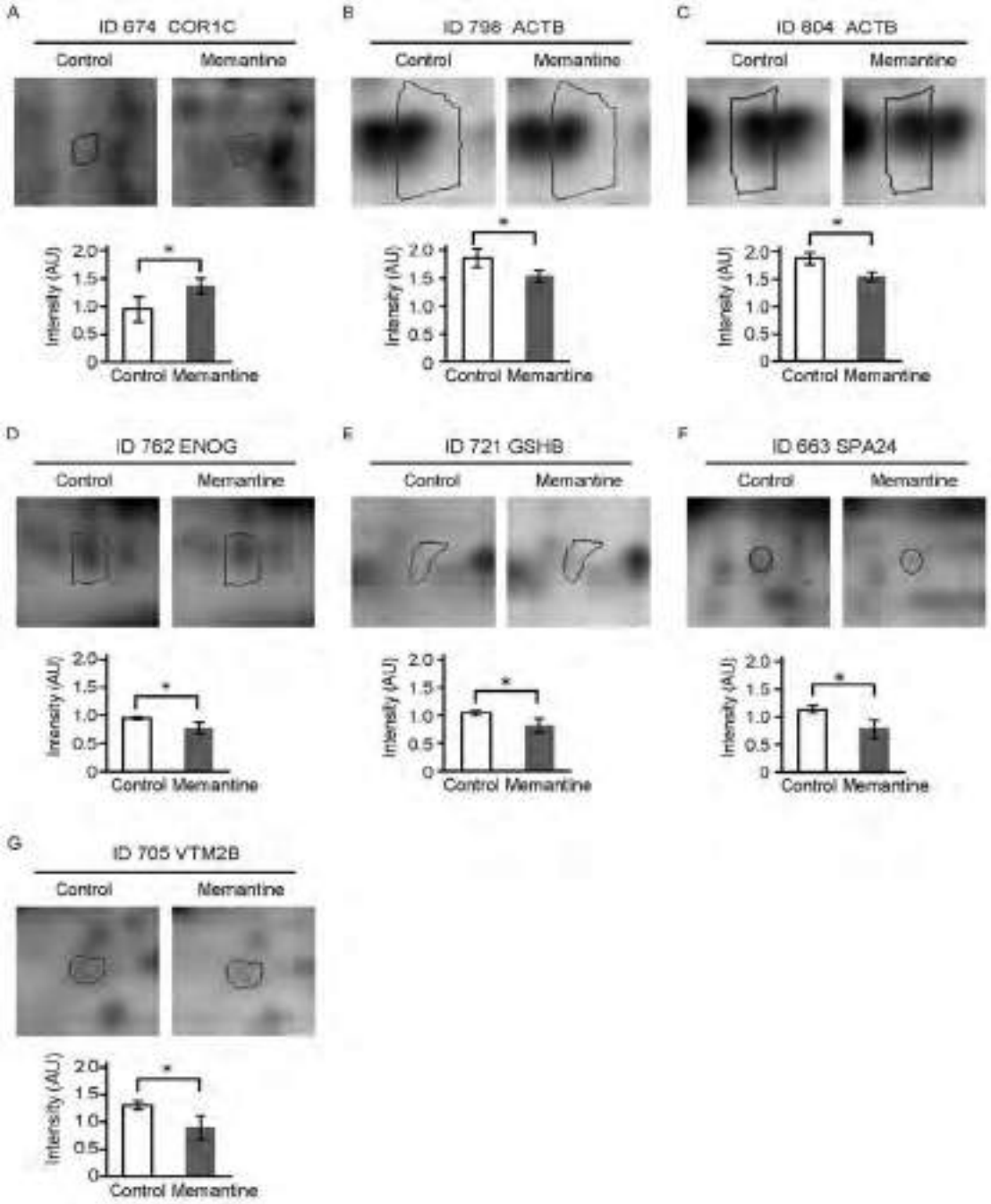

Figure 3. Comparisons of spot intensity of the proteins between the memantine-treated and non-treated conditions. Representative results of the 7 protein spots and intensity difference of those spots between the memantine-treated and non-treated (control) GIMEN cells are shown.

Error bars, standard deviations. *p<0.05.

Table 1.

Total number of detected protein spots	Number of protein spots with different intensity (p<0.05)	Fold difference, Memantine/Control	Number of the protein spots
		x ≥ 1.5	5
892	45	1.5 > x ≥ 1.3 1.3 > x ≥ 1.2 1.2 > x > −1.2 −1.2 ≥ x > -1.3 −1.3 ≥ x > -1.5	6 2 13 11 8
		−1.5 ≥ x	0

on the inhibition of neuroblastoma cell growth. On the other hand, the therapeutic concentration of memantine, 1μM, may suppress growth of normal neural cells in adult brains, i.e., the growth of adult neural stem/progenitor cells. The suppressive effect on GIMEN cell growth should be validated using other neuroblastoma cell lines expressing NMDA receptors and also using normal neural cells.

Under therapeutic condition, serum concentrations of memantine in man with daily maintenance doses of 20 mg range from 0.5-1.0 μM, while the concentrations in cerebrospinal fluid (man) and brain

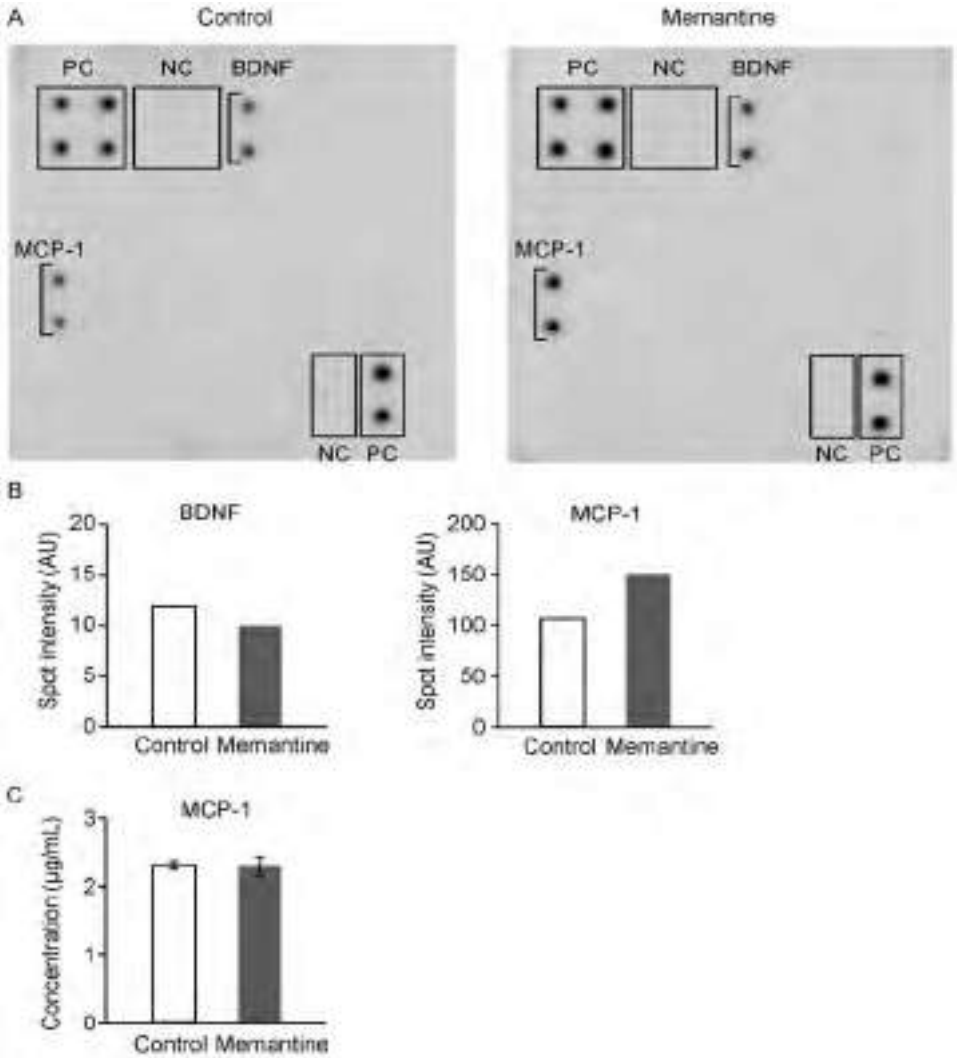

Figure 4. Effects of memantine on humoral factor secretion from GIMEN cells. A. The secretion of humoral factors from GIMEN cells which cultured with medium-alone (left) or 10 μM memantine (right) was assayed using a humoral factor array, in which 20 different anti-humoral factor antibodies were blotted. PC, positive control; NC, negative control. B. The spot intensity of BDNF and MCP-1, which were detected in the humoral factor array results, are shown. C. Concentration of MCP-1 was measured by ELISA. Error bars, standard deviations.

Table 2.

Spot	Fold	Proteins	Accession ID	MW (kDa)		*pI*		Mascot	Coverage	
ID	difference			Theoret	Observed	Theoret	Observed	scores	%	(Mascot ion scores)
674	1.44	Coronin-1C	COR1C_HUMAN	53.2	53	6.65	6.7	74	21	^{224}AIFLADGNVFTTGFSR^{239} (25)
798	-1.21	Actin, cytoplasmic 1	ACTB_HUMAN	41.7	42	5.29	5.4	195	25	^{29}AVFPSIVGRPR^{39} (23) ^{239}SYELPDGQVITIGNER^{254} (111) ^{360}QEYDESGPSIVHR^{372} (14)
804	-1.21	Actin, cytoplasmic 1	ACTB_HUMAN	41.7	42	5.29	5.35	182	31	^{29}AVFPSIVGRPR^{39} (6) ^{239}SYELPDGQVITIGNER^{254} (97) ^{360}QEYDESGPSIVHR^{372} (28)
762	-1.21	Gamma-enolase	ENOG_HUMAN	47.2	48	4.91	5.1	69	16	^{33}AAVPSGASTGIYEALELR^{50} (8) ^{240}IVIGM*DVAASEFYR^{253} (4) ^{270}YITGDQLGALYQDFVR^{285} (19)
721	-1.28	Glutathione synthetase	GSHB_HUMAN	52.4	50	5.67	5.5	67	15	^{113}EGIAQTVFLGLNR^{125} (7) ^{142}QIEINTISASFGGLASR^{158} (8) ^{254}LFVDGQEIAVVYFR^{267}(24)
663	-1.46	Spermatogenesis-associated protein 24	SPA24_HUMAN	23.6	55	7.77	8.0	59	30	^{24}DVIESQEELIHQLR^{37} (16)
705	-1.46	V-set and transmembrane domain-containing protein 2B	VTM2B_HUMAN	30.3	50	7.88	7.9	69	35	^{41}EGDDIEMPCAFR^{52} (26)

*Oxidation of methionine.
MW: molecular weights.

microdialysates (rat) are 20-50% lower due to albumin binding in serum [28]. However, the brain homogenates in both man and rodents contain much higher concentrations of memantine (10-30 fold) probably due to lysosomal accumulation [28]. Recently, it was found that macroautophagy occurs in neurons of an AD mouse model to increase Aβ incorporation into secondary lysosomes [29]. A part of such neurons undergo atypical cell death to release undegraded Aβ to extracellular space [29]. In such condition, neurons can be exposed to higher concentrations of memantine similarly released from lysosomes of the dead cells. Taken together the above-mentioned reasons with the results of cell viability and growth, we determined the concentration of memantine to be 10 μM for the analysis of protein expression. Among 892 protein spots detected in the 2D-DIGE results, intensity of 32 spots was changed ±1.2-fold or more between the memantine-treated and non-treated GIMEN cells ($p<0.05$) (Table 1). The number of the protein spots, intensity of which was changed, was comparable with those in the other proteomic studies that similarly examined actions of drugs or cytokines [30, 31].

We identified proteins in 7 out of the 32 spots and found the decreased expression of β-actin, γ-enolase, and glutathione synthetase by the treatment with memantine (Table 2, Figure 3B-E). β-actin, a cytoskeletal protein, involves in cytokinesis as well as in cell migration and cell morphogenesis [32]. The decreased expression of β-actin is considered to be associated with the suppression of GIMEN cell growth. In contrast, expression of coronin-1C that contains multiple actin-binding sites [33] was increased by the treatment with memantine (Table 2, Figure 3A). Since coronin-1C has been suggested to act as an integrator of actin filaments [34], coronin-1C may be increased to recover the down-regulated functions of β-actin. γ-enolase, predominantly expressed in neurons and cells of the neuroendocrine system, is an enzyme of the glycolytic pathway which catalyzes the dehydration of 2-phospho-D-glycerate to phosphoenol-pyruvate [35]. γ-enolase promotes survival of neuronal cells by regulating neuronal growth factor receptor-dependent signaling pathway, which results in extensive actin cytoskeleton remodeling [35]. Interestingly, $p19^{ras}$ was suggested to suppress proliferation of cancer cells through the interaction with γ-enolase [36]. The decrease of γ-enolase may be also involved in the suppression of GIMEN cell growth, relating to the decrease of β-actin.

Glutathione is a tripeptide formed by glutamate, cysteine, and glycine, which plays an important role in a multitude of cellular processes, including cell proliferation and apoptosis [37]. Glutathione synthetase is involved in the subpathway of glutathione biosynthesis, in which glutathione is synthesized from γ-glutamylcysteine and glycine. Glutathione is required for cell proliferation and is essential for the cells to enter the S phase [38, 39]. The level of glutathione is up-regulated by glutathione synthetase and is correlated with cell growth rate [39]. The decrease of glutathione synthetase by the treatment with memantine would reduce the glutathione level in GIMEN cells, which may further lead to the suppression of cell growth.

Effects of memantine on molecular profiles of neuronal cells were previously studied by analyses of mRNA expression of rat cortex using cDNA microarray [18] and protein expression and modification of mouse hippocampus and cortex using reverse phase protein arrays [19]. However, none of molecules found in these studies was detected in our study. This may be due to the difference of materials (human neuroblastoma vs mouse or rat brain tissue) and methods (2D-DIGE and mass spectrometry vs cDNA or protein arrays). The effects of memantine on protein profiles found in this study should be validated using other neuroblastoma cells and normal neural cells in near future.

In conclusion, we found that memantine suppressed the growth of GIMEN cells and affected the protein profile. Memantine may have an effect to inhibit growth of neuroblastoma cells, whereas it may suppress growth of normal neural cells even at the therapeutic concentrations. The suppression of cell growth may be caused by the decreased expression of β-actin, γ-enolase, and glutathione synthase due to the loss of their functions associated with cell proliferation. Further investigations are needed to validate the above results and to elucidate mechanisms of the newly found actions of memantine in this study.

Acknowledgement

The authors are indebted to Ms. Kumi Aso for her technical assistance. The authors are also grateful to Daiichi Sankyo for the support for this study.

Conflict of interest

None.

References

1. Scheltens P, Blennow K, Breteler MM, de Strooper B, Frisoni GB, et al. (2016) Alzheimer's disease. *Lancet* 388: 505-517. [Crossref]
2. Magi S, Castaldo P, Macrì ML, Maiolino M, Matteucci A, et al. (2016) Intracellular Calcium Dysregulation: Implications for Alzheimer's Disease. *Biomed Res Int* 2016: 6701324. [Crossref]
3. Hung SY, Fu WM (2017) Drug candidates in clinical trials for Alzheimer's disease. *J Biomed Sci* 24: 47. [Crossref]
4. Wang T (2017) New Drug Research and Development for Alzheimer's Pathology: Present and Prospect. *Shanghai Arch Psychiatry* 29: 237-239. [Crossref]
5. Rosini M, Simoni E, Minarini A, Melchiorre C (2014) Multi-target design strategies in the context of Alzheimer's disease: acetylcholinesterase inhibition and NMDA receptor antagonism as the driving forces. *Neurochem Res* 39: 1914-1923. [Crossref]
6. Paoletti P, Bellone C, Zhou Q (2013) NMDA receptor subunit diversity: impact on receptor properties, synaptic plasticity and disease. *Nat Rev Neurosci* 14: 383-400. [Crossref]
7. Albensi BC (2007) The NMDA receptor/ion channel complex: a drug target for modulating synaptic plasticity and excitotoxicity. *Curr Pharm Des* 13: 3185-3194. [Crossref]
8. Rezvani AH (2006) Involvement of the NMDA System in Learning and Memory. In: Levin ED, Buccafusco JJ, editors. Animal Models of Cognitive Impairment. Boca Raton (FL): CRC Press/Taylor & Francis. Chapter 4.
9. Rudy CC, Hunsberger HC, Weitzner DS, Reed MN (2015) The role of the tripartite glutamatergic synapse in the pathophysiology of Alzheimer's disease. *Aging Dis* 6: 131-148. [Crossref]
10. Lewerenz J, Maher P (2015) Chronic Glutamate Toxicity in Neurodegenerative Diseases-What is the Evidence? *Front Neurosci* 9: 469. [Crossref]
11. Bello O, Blair K, Chapleau C, Larimore JL (2013) Is memantine a potential therapeutic for Rett syndrome? *Front Neurosci* 7: 245. [Crossref]
12. Zdanys K, Tampi RR (2008) A systematic review of off-label uses of memantine for psychiatric disorders. *Prog Neuropsychopharmacol Biol Psychiatry* 32: 1362-1374. [Crossref]
13. Rogawski MA, Wenk GL (2003) The neuropharmacological basis for the use of memantine in the treatment of Alzheimer's disease. *CNS Drug Rev* 9: 275-308. [Crossref]
14. Lipton SA (2004) Paradigm shift in NMDA receptor antagonist drug development: molecular mechanism of uncompetitive inhibition by memantine in the treatment of Alzheimer's disease and other neurologic disorders. *J Alzheimers Dis* 6: S61-74. [Crossref]
15. Ray B, Banerjee PK, Greig NH, Lahiri DK (2010) Memantine treatment decreases levels of secreted Alzheimer's amyloid precursor protein (APP) and amyloid beta (A beta) peptide in the human neuroblastoma cells. *Neurosci Lett* 470: 1-5. [Crossref]

16. Alley GM, Bailey JA, Chen D, Ray B, Puli LK, et al. (2010) Memantine lowers amyloid-ß peptide levels in neuronal cultures and in APP/PS1 transgenic mice. *J Neurosci Res* 88: 143-154. [Crossref]

17. Li L, Sengupta A, Haque N, Grundke-Iqbal I, Iqbal K (2004) Memantine inhibits and reverses the Alzheimer type abnormal hyperphosphorylation of tau and associated neurodegeneration. *FEBS Lett* 566: 261-269. [Crossref]

18. Marvanová M, Lakso M, Wong G (2004) of genes regulated by memantine and MK-801 in adult rat brain by cDNA microarray analysis. *Neuropsychopharmacology* 29: 1070-1079. [Crossref]

19. Ahmed MM, Dhanasekaran AR, Block A, Tong S, Costa ACS, et al. (2014) Protein associated with context fear conditioning and their modulation by memantine. *Mol Cell Proteomics* 13: 919-937. [Crossref]

20. Anaparti V, Ilarraza R, Orihara K, Stelmack GL, Ojo OO, et al. (2015) NMDA receptors mediate contractile responses in human airway smooth muscle cells. *Am J Physiol Lung Cell Mol Physiol* 308: L1253-L1264.

21. Katano M, Kurokawa MS, Matsuo K, Masuko K, Suematsu N, et al. (2017) Phosphoproteome analysis of synoviocytes from patients with rheumatoid arthritis. *Int J Rheum Dis* 20:708-721.[Crossref]

22. Pizzi M, Boroni F, Bianchetti A, Moraitis C, Sarnico I, et al. (2002) Expression of functional NR1/NR2B-type NMDA receptors in neuronally differentiated SK-N-SH human cell line. *Eur J Neurosci* 16: 2342-2350. [Crossref]

23. Yoshioka A, Ikegaki N, Williams M, Pleasure D (1996) Expression of N-methyl-D-aspartate (NMDA) and non-NMDA glutamate receptor genes in neuroblastoma, medulloblastoma, and other cell lines. *J Neurosci Res* 46: 164-178. [Crossref]

24. North WG, Fay MJ, Du J, Cleary M, Gallagher JD, et al. (1997) Presence of functional NMDA receptors in a human neuroblastoma cell line. *Mol Chem Neuropathol* 30: 77-94. [Crossref]

25. Takano T, Lin JH, Arcuino G, Gao Q, Yang J, et al. (2001) Glutamate release promotes growth of malignant gliomas. *Nat Med* 7:1010-1015. [Crossref]

26. Abdul M, Hoosein N (2005) N-methyl-D-aspartate receptor in human prostate cancer. *J Membr Biol* 205: 125-128. [Crossref]

27. North WG, Gao G, Jensen A, Memoli VA, Du J (2010) NMDA receptors are expressed by small-cell lung cancer and are potential targets for effective treatment. *Clin Pharmacol* 2: 31-40. [Crossref]

28. Parsons CG, Danysz W, Quack G (1999) Memantine is a clinically well tolerated N-methyl-D-aspartate (NMDA) receptor antagonist--a review of preclinical data. *Neuropharmacology* 38: 735-767. [Crossref]

29. Chen X, Kondo K, Motoki K, Homma H, Okazawa H (2015) Fasting activates macroautophagy in neurons of Alzheimer's disease mouse model but is to degrade amyloid-beta. *Sci Rep* 5: 12115.

30. Endo W, Arito M, Sato T, Kurokawa MS, Omoteyama K, et al. (2014) Effects of sulfasalazine and tofacitinib on the protein of articular chondrocytes. *Mod Rheumatol* 24: 844-850. [Crossref]

31. Tsuno H, Suematsu N, Sato T, Arito M, Matsui T, et al. (2016) Effects of methotrexate and salazosulfapyridine on protein of exosomes derived from a human synovial sarcoma cell line of SW982. *Proteomics Clin Appl* 10: 164-171. [Crossref]

32. Pollard TD, Cooper JA (2009) Actin, a central player in cell shape and movement. *Science* 326: 1208-1212. [Crossref]

33. Tilley FC, Williamson RC, Race PR, Rendall TC, Bass MD (2015) Integration of the Rac1- and actin-binding properties of Coronin-1C. *Small GTPases* 6: 36-42. [Crossref]

34. Behrens J, Solga R, Ziemann A, Rastetter RH, Berwanger C, et al. (2016) Coronin 1C-free primary mouse exhibit robust rearrangements in the orientation of actin microtubules, and intermediate *Eur J Cell Biol* 95: 239-251. [Crossref]

35. Vizin T, Kos J (2015) Gamma-enolase: a well-known tumor marker, with a less-known role in cancer. *Radiol Oncol* 49: 217-226. [Crossref]

36. Jang S, Kim J, Kim C, Kim D, Rhee S, et al. (2010) p19ras represses proliferation of non-small cell lung cancer possibly through interaction with enolase (NSE). *Cancer Lett* 289: 91-98. [Crossref]

37. Traverso N, Ricciarelli R, Nitti M, Marengo B, Furfaro AL, et al. (2013) Role of glutathione in cancer progression and chemoresistance. *Oxid Med Cell Longev* 2013: 972913. [Crossref]

38. Messina JP, Lawrence DA (1989) Cell cycle progression of glutathione-depleted human peripheral blood mononuclear cells is inhibited at S phase. *J Immunol* 143: 1974-1981. [Crossref]

39. Huang Z, Chen C, Zeng Z, Yang H, Oh J, et al. (2001) Mechanism and of increased glutathione level in human hepatocellular carcinoma and liver regeneration. *FASEB J* 15: 19-21. [Crossref]

Copyright: ©2018 Kurokawa MS. This is an open-access article distributed under the terms of the Creative Commons Attribution License, which permits unrestricted use, distribution, and reproduction in any medium, provided the original author and source are credited.

BBA - Proteins and Proteomics 1867 (2019) 47–56

Contents lists available at ScienceDirect

BBA - Proteins and Proteomics

journal homepage: www.elsevier.com/locate/bbapap

Effects of salazosulfapyridine on the profile of cell surface proteins, revealed by biotinylation of cell surface proteins and 2-dimentional electrophoresis☆

Kazuki Omoteyama[a,*], Toshiyuki Sato[a], Mitsumi Arito[a], Masaaki Sato[a], Naoya Suematsu[a], Manae S. Kurokawa[b], Tomohiro Kato[a]

[a] Clinical Proteomics and Molecular Medicine, St. Marianna University Graduate School of Medicine
[b] Disease Biomarker Analysis and Molecular Regulation, St. Marianna University Graduate School of Medicine

ARTICLE INFO

Keywords:
Salazosulfapyridine
Rheumatoid arthritis
Cell surface protein
Biotinylation
Two-dimensional electrophoresis

ABSTRACT

Objective: We investigated effects of salazosulfapyridine (SASP) on the protein profile of cell surface (CS)-proteins of SW982, a human synovial sarcoma cell line, using biotinylation of CS-proteins and 2-dimensional fluorescence difference gel electrophoresis (2D-DIGE).

Methods: SW982 cells were treated with SASP and its metabolites, sulfapyridine (SP) and 5-aminosalicylic acid (5ASA). Then the cells were treated with a membrane-impermeable biotinylating reagent. Biotinylated CS-proteins were isolated using NeutrAvidin-bound beads. CS-proteins affected by the drugs were detected by 2D-DIGE and subjected to mass spectrometry.

Results: By the 2D-DIGE analysis, in total 576 spots were detected, 29 out of which showed more than ± 1.5-fold different intensity in the SASP-, SP-, and 5ASA-treated cells, compared to non-treated cells ($p < 0.05$). Interestingly, 7 out of the 29 spots changed their intensity only by SASP and 17 spots changed their intensity only by SP. We identified 9 protein from 15 out of the 29 spots, most of which were evidenced to exist on the cell surface by flow cytometry.

Conclusion: We found novel effects of SASP and its metabolites on SW982 cells by the combination of biotinylation of cell surface proteins and 2D-DIGE analysis. These data would help understanding of anti-rheumatic actions of SASP. Furthermore, the combination would be a useful method for the analysis of CS-proteins in various conditions.

1. Introduction

Salazosulfapyridine (SASP) has been used as an anti-rheumatic drug for > 30 years. In the human body, a part of oral administrated SASP is catabolized to generate sulfapyridine (SP) and 5-aminosalicylic acid (5ASA), as the chemical structures of SASP, SP, and 5ASA are depicted in Fig. 1A. In fact, all the three forms were detected in plasma samples of volunteers with oral administration of SASP [1]. SASP, SP, and 5ASA have been reported to possess their unique pharmacological effects. For example, SASP inhibits production of matrix metalloproteases (MMP) in chondrocytes, differentiation from peripheral blood mononuclear cells to osteoclasts, and activation of peripheral dendritic cells [2–4]. 5ASA inhibits proliferation of T cells by suppression of IL-2 production [5]. SP inhibits production of IL-8, chemokine (C-X-C motif) ligand 1 (CXCL1), and monocyte chemotactic protein-1 (MCP-1) in synovial cells from patients with rheumatoid arthritis (RA) [6]. Thereby orally administrated SASP is thought to show anti-rheumatic functions through the forms of SASP, SP, and 5ASA.

In RA, it has been reported that synoviocytes invade into cartilage and bone with aggressive proliferative potential [7,8] and exhibit epithelial-mesenchymal transition (EMT) phenotypes [9]. Thereby, expression of CS-proteins on synoviocytes is expected to be changed during the pathophysiology of RA and SASP may cancel the changes of CS-proteins on synoviocytes. However, effects of SASP on non-immune cells including synoviocytes remain unclear, even though synoviocytes play key roles in the pathology of RA. If anti-rheumatic actions of SASP through the analysis of CS-proteins of synoviocytes, it would contribute to develop a new treatment against activated synoviocytes. Therefore, it would be effective to investigate changes of CS-proteins for the elucidation of molecular mechanisms of SASP. However, this strategy has been hampered by the lack of comprehensive analysis methods of CS-proteins. In 1967, Anderson GW et al. synthesized N-hydroxysuccinimide ester, which was used to label proteins [10]. By the coupling of biotin with this molecule, biotin started to be used to label

☆ This article is part of a Special Issue entitled: Electrophoresis in Proteomics, edited by Dr. Tadashi Kondo.

* Corresponding author at: Clinical Proteomics and Molecular Medicine, St. Marianna University Graduate School of Medicine, Sugao 2-16-1, Kawasaki, Kanagawa 216-5811, Japan.
E-mail address: omoteyama@marianna-u.ac.jp (K. Omoteyama).

https://doi.org/10.1016/j.bbapap.2018.05.007
Received 16 February 2018; Received in revised form 18 April 2018; Accepted 8 May 2018
Available online 09 May 2018
1570-9639/ © 2018 Elsevier B.V. All rights reserved.

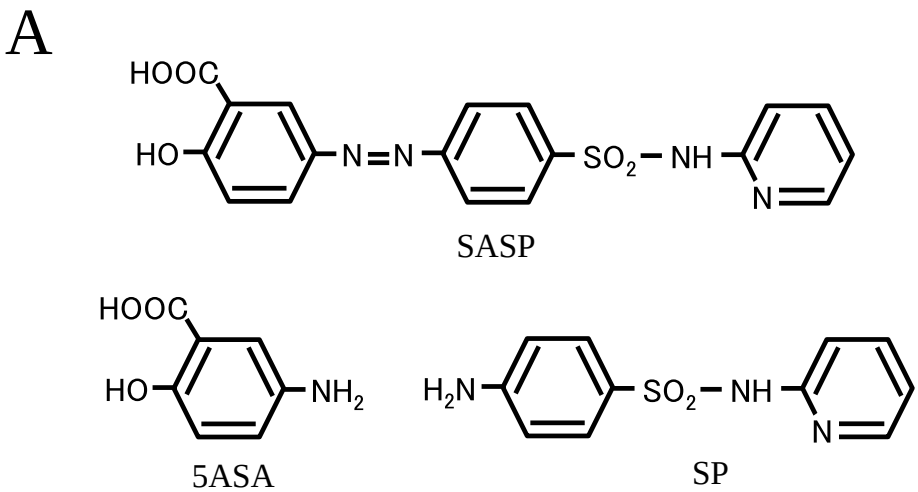

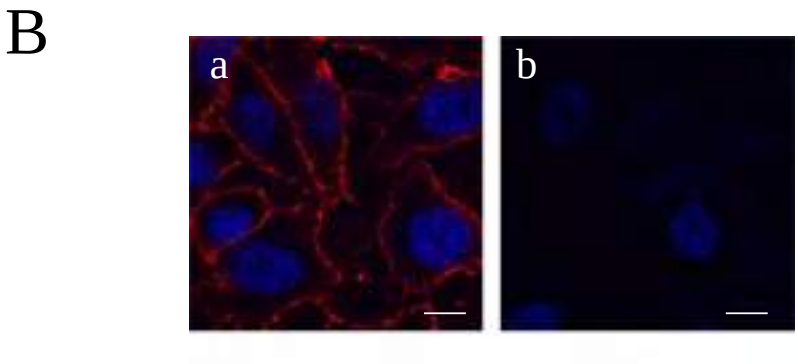

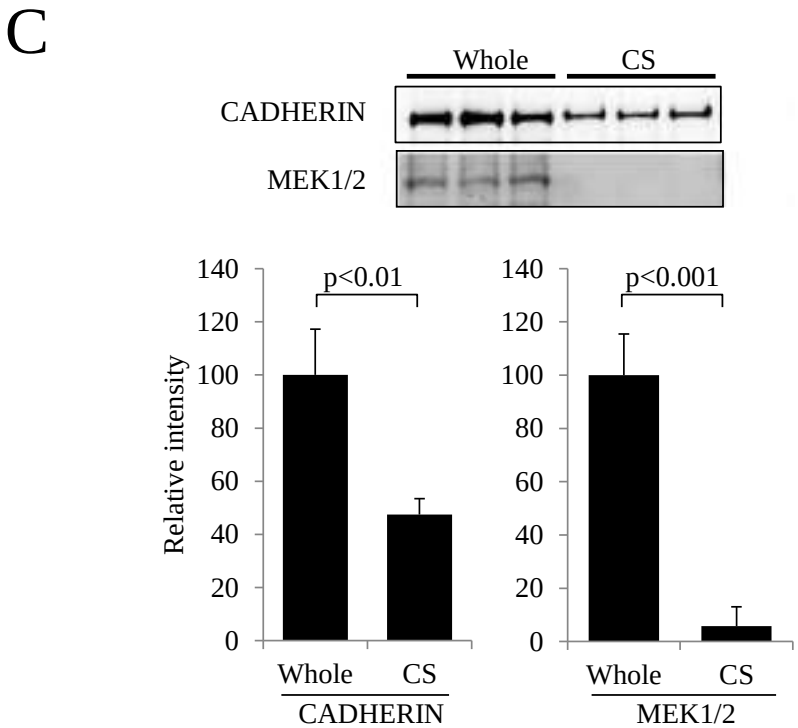

Fig. 1. Isolation of CS-proteins.
(A) The chemical structures of SASP and its metabolites.
(B) Confirmation of biotinylation of CS-proteins. Living SW982 cells, incubated (a) with or (b) without a biotinylation reagent, were further incubated with streptavidin-Alexa Fluor 647 conjugate. The cells, stained with DAPI (blue) and Alexa Fluor 647 (red), were fixed with 4% PHA and subjected to confocal laser-scanning microscopy. Scale bar; 10 μm.
(C) Confirmation of isolation of CS-proteins. A CS-protein sample and a whole cell lysate sample were respectively prepared from biotinylated SW982 cells and were subjected to western blot with an antibody against CADHERIN (a cell surface marker) and that against MEK1/2 (a cytosolic maker). Intensity of the detected bands was quantified. Whole; whole cell lysate, CS; isolated CS-protein fraction.

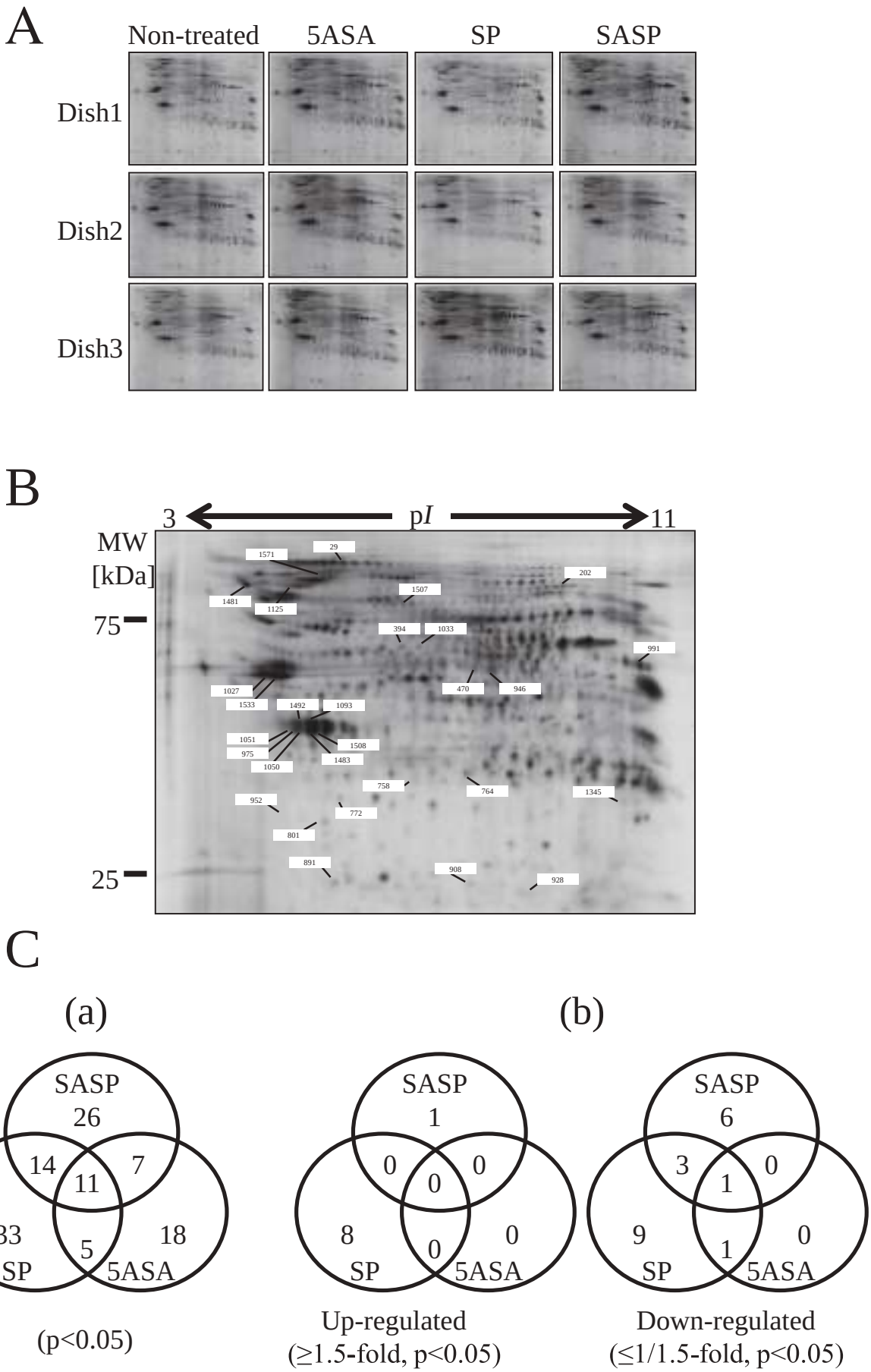

(caption on next page)

Fig. 2. 2D-DIGE analyses of CS-proteins.
(A) Detection of CS-proteins by 2D-DIGE. CS-proteins isolated from SW982 cells treated with SASP, SP, and 5ASA and non-treated cells (n = 3 for each of the 4 groups) were separated and quantified by 2D-DIGE. Proteins were visualized by the detection of Cy5 in all the 12 samples.
(B) Location of 29 CS-protein spots that showed more than ± 1.5-fold intensity changes with statistical significances in the SASP-, SP- and 5ASA-treated cells compared to the non-treated cells on the 2D gels are shown.
(C) Overlap of the effects of SASP, SP, and 5ASA on the 29 CS-protein spots is shown by Venn diagram.

proteins [11]. Furthermore, use of N-hydroxysulfosuccinimide ester made it possible to specifically label cell surface proteins [12]. Recently, the combination of labelling of CS-proteins on living cells with a membrane-impermeable biotinylating reagent and subsequent insolation of the biotinylated proteins by streptavidin was found to be an effective way to isolate CS-proteins. We here applied this method to isolate CS-proteins of cells treated with SASP, SP, and 5ASA. Furthermore, we comprehensively and quantitatively investigated profile changes of these isolated CS-proteins caused by SASP, SP, and 5ASA, using 2-dimensional fluorescence difference gel electrophoresis (2D-DIGE) [13]. Finally, we identified multiple proteins affected by SASP, SP, and 5ASA using mass spectrometric analysis. Our data would help understanding of molecular mechanisms of SASP.

2. Materials and methods

2.1. Cell culture

A human synovial sarcoma cell line of SW982 was cultured in Dulbecco's Modified Eagle's Medium (DMEM) (GIBCO, Carlsbad, CA) supplemented with 10% fetal bovine serum (FBS) (Wako Pure Chemical Industries, Ltd., Osaka, Japan), 100 U/ml penicillin and 100 μg/ml streptomycin (Sigma-Aldrich, St. Louis, MO) in a humidified atmosphere with 5% CO_2 at 37 °C. The medium was replaced twice a week. The SW982 cells were cultured in the medium containing 250 μM SASP (Sigma-Aldrich), 250 μM SP (Sigma-Aldrich), and 250 μM 5ASA (Sigma-Aldrich) for 24 h.

2.2. Isolation of CS-proteins

CS-proteins were isolated using a cell surface protein isolation kit (Pierce, Rockford, IL), according to the manufacturer's instructions. Briefly, living SW982 cells were incubated with a biotinylation reagent at 4 °C, harvested, and then were lysed by sonication in a lysis buffer. After centrifugation, the supernatants were incubated with NeutrAvidin-bound beads. Captured proteins were eluted from the beads into the 1× Laemmli sample buffer. For 2D-DIGE analysis, CS-proteins were precipitated using trichloroacetic acid/ethanol and then were dissolved in 50 μl of a urea lysis buffer (8 M Urea, 4% CHAPS, 40 mM Tris).

2.3. Western blot analysis

Proteins were separated by sodium dodecyl sulfate-polyacrylamide gel electrophoresis (SDS-PAGE) and transferred to polyvinylidene difluoride (PVDF) membranes. The membranes were incubated in a solution containing a mouse anti-pan-cadherin antibody (C1821, Sigma-Aldrich) and a mouse anti-MEK1/2 antibody (4694, Cell Signaling Technology, Danvers, MA). After washing, the bound antibodies were reacted with a horseradish peroxidase (HRP)-conjugated rabbit anti-mouse IgG antibody (61–6520, Invitrogen, Camarillo, CA). Immunoreactive bands were detected using an enhanced chemiluminescence system (ECL Select Western Blotting Detection Reagent, RPN2235, GE Healthcare, Buckinghamshire, UK).

2.4. Confocal laser-scanning microscopy

Living SW982 cells cultured in an 8-chamber slide (AGC techno glass, Tokyo, Japan) were incubated with or without the biotinylation reagent at 4 °C. After washing, the cells were incubated with a streptavidin-Alexa Fluor 647 conjugate (Life Technologies, Carlsbad, CA) at 4 °C. After washing, the cells were fixed with 4% paraformaldehyde (PHA) and were mounted with SlowFade Gold Antifade Mountant with 4′, 6-diamidino-2-phenylindole (DAPI) (Life Technologies). Finally, the samples were subjected to confocal laser-scanning microscopy (LSM 510 META, Zeiss, Oberkochen, Germany).

2.5. 2D-DIGE analysis

CS-protein samples from SASP-, SP-, and 5ASA-treated cells and from non-treated cells (n = 3, respectively) were labelled with Cyanine saturation dye 5 (Cy5) (GE Healthcare), according to the manufacturer's instructions. An internal control sample was prepared by mixing an equal amount of each of the 12 CS-protein samples. The internal control sample was labelled with Cy3. Each of the Cy5-labelled samples 2.5 μg was mixed with 2.5 μg of the Cy3-labelled control sample. The mixture was subjected to isoelectric focusing (IEF) (24 cm-long, pH 3–11 non-liner gradient gels, GE Healthcare) and then to separation by 10% SDS-PAGE. The separated proteins were detected using an image analyzer (Typhoon 9400 Imager, GE Healthcare).

Intensity of detected protein spots was quantified by the Progenesis Same Spots software (Nonlinear Dynamics, Newcastle, UK). Briefly, the Cy5-fluorescent intensity of the protein spots was normalized by the Cy3-fluorescent intensity of the identical spots. Then the normalized Cy5-intensity was used for the comparison. Protein spots that showed more than ± 1.5-fold intensity changes with significant differences ($p < 0.05$) were rated as valid.

2.6. Protein identification

200 μg of CS-protein samples labelled with Cy3 was subjected to IEF (24 cm-long, pH 3–11 non-liner gradient gels) and then were separation by 10% SDS-PAGE. Gel fragments that corresponded to protein spots of interest were subjected to in-gel digestion with trypsin (37 °C, 16 h). Then generated peptides, extracted from the gel fragments into a solution containing 5% TFA and 50% acetonitrile, were desalted using a Zip Tip c18 (Millipore corporation, Billerica, MA), which were then subjected to matrix-assisted laser desorption ionization-time of flight/time of flight mass spectrometry (MALDI-TOF/TOF MS) (Ultraflex, BrukerDaltonics, Bremen, Germany). Peptide masses obtained by the MS and MS/MS analysis were compiled to allow searches of the Swiss-Prot database using the Mascot software program (Matrix Science, London, UK).

2.7. Flow cytometric analysis

Cells, harvested by scraping in a trypsin-free condition, were suspended in PBS containing EDTA. The cells were reacted with first antibodies. The first antibodies used are as follows: a rabbit antibody against human peroxiredoxin 6 (PRDX6) (sc-134,478, Santa Cruz Biotechnology, Dallas, TX), a rabbit antibody against human procollagen-lysine, 2-oxoglutarate 5-dioxygenase 3 (PLOD3) (sc-98,453, Santa Cruz Biotechnology), a rabbit antibody against human non-POU domain-containing octamer-binding protein (NONO) (sc-67,016, Santa Cruz Biotechnology), a rabbit antibody against human heat shock protein 90 kDa, beta member 1 (HSP90B1) (2104, Cell signaling

Table 1
Identification of cell surface proteins.

Spot no.	MW	p*I*	Difference			Protein name	GI accession no.	MW	p*I*	NPM	Mascot score	Coverage (%)	Sequence confirmed (Mascot ion score)
	Observed		5ASA	SP	SASP			Theoretical					
801	30	5.3	−1.04	−1.09	−1.51*	Prohibitin (PHB_HUMAN)	gi|464,371	29.7	5.5	13	91	33	^{94}ILFRPVASQLPR^{105} (24)
908	25	6.3	−1.62*	−1.76**	−1.46*	Peroxiredoxin-6 (PRDX6_HUMAN)	gi|1,718,024	25.0	6.0	10	180	60	^{2}PGGLLLGDVAPNFEANTTVGR^{22} (46) ^{98}LPFPIIDDR^{106} (20)
991	66	10.1	−1.37	−1.72*	−1.59	Non-POU domain-containing octamer-binding protein (NONO_HUMAN)	gi|67,469,924	54.1	9.0	16	329	37	^{76}LFVGNLPPDITEEEMR^{91} (82) ^{257}FAQPGSFEYEYAMR^{270} (62) ^{435}GQAATMEGIGAIGGTPPAFNR^{456} (90)
975	42	5.15	1.25*	1.51*	1.49*	Actin, cytoplasmic1 (ACTB_HUMAN)	gi|46,397,333	41.7	5.2	8	316	43	^{29}AVFPSIVGRPR^{39} (38) ^{96}VAPEEHPVLLTEAPLNPK^{113} (111) ^{239}SYELPDGQVITIGNER^{254} (104)
1027	60	4.9	−1.05	−1.15	−1.66***	Vimentin (VIM_HUMAN)	gi|55,977,767	53.6	5.0	14	264	37	^{346}EMEENFAVEAANYQDTIGR^{364} (91) ^{346}E**M**EENFAVEAANYQDTIGR^{364} (23) ^{411}ISLPLPNFSSLNLR^{424} (79)
1050	42	5.2	−1.42*	−1.77**	−1.61*	Actin, cytoplasmic1 (ACTB_HUMAN)	gi|46,397,333	41.7	5.2	6	184	22	^{96}VAPEEHPVLLTEAPLNPK^{113} (63) ^{239}SYELPDGQVITIGNER^{254} (82)
1051	42	5.1	−1.34	−1.84*	−1.56	Actin, cytoplasmic1 (ACTB_HUMAN) Actin, cytoplasmic2 (ACTG_HUMAN)	gi|46,397,333 gi|54,036,678	41.7 41.8	5.2 5.3	7	293	30	^{85}IWHHTFYNELR^{95} (79) ^{96}VAPEEHPVLLTEAPLNPK^{113} (46) ^{239}SYELPDGQVITIGNER^{254} (113) ^{285}CDVDIR^{290} (8)
1093	44	5.2	−1.36*	−1.56**	−1.28	Actin, cytoplasmic1 (ACTB_HUMAN)	gi|46,397,333	41.7	5.2	11	228	37	^{85}IWHHTFYNELR^{95} (54) ^{239}SYELPDGQVITIGNER^{254} (92) ^{285}CDVDIR^{290} (12)
1481	96	4.6	1.12	1.52*	1.30*	HSP90B1 (HSP90B1_HUMAN)	gi|119,360	92.4	4.7	21	280	29	^{76}FAFQAEVNR^{84} (43) ^{385}SILFVPTSAPR^{395} (54) ^{512}FQSSHHPTDITSLDQYVER^{530} (72)
1483	42	5.25	−1.50**	−1.72**	−1.69*	Actin, cytoplasmic1 (ACTB_HUMAN)	gi|46,397,333	41.7	5.2	10	408	44	^{29}AVFPSIVGRPR^{39} (43) ^{85}IWHHTFYNELR^{95} (74) ^{96}VAPEEHPVLLTEAPLNPK^{113} (80) ^{239}SYELPDGQVITIGNER^{254} (119) ^{285}CDVDIR^{290} (19)
1492	44	5.0	−1.35	−1.74*	−1.39	Actin, cytoplasmic1 (ACTB_HUMAN)	gi|46,397,333	41.7	5.2	9	264	37	^{29}AVFPSIVGRPR^{39} (16) ^{85}IWHHTFYNELR^{95} (56) ^{239}SYELPDGQVITIGNER^{254} (116)
1507	85	5.8	1.33	1.53*	1.07	lysyl hydroxylase-3 (PLOD3_HUMAN)	gi|6,093,731	84.7	5.6	8	77	14	–
1508	42	5.3	−1.50*	−1.63*	−1.56*	Actin, cytoplasmic1 (ACTB_HUMAN)	gi|46,397,333	41.7	5.2	9	284	37	^{29}AVFPSIVGRPR^{39} (49) ^{85}IWHHTFYNELR^{95} (73) ^{239}SYELPDGQVITIGNER^{254} (93)
1533	60	5.0	−1.06	−1.12	−1.62*	Vimentin (VIM_HUMAN)	gi|55,977,767	53.6	5.0	23	707	51	^{130}ILLAELEQLK^{139} (77) ^{223}KVESLQEEIAFLK^{235} (94) ^{346}EMEENFAVEAANYQDTIGR^{364} (92) ^{365}LQDEIQNMKEEMAR^{378} (87) ^{391}MALDIEIATYR^{401} (74) ^{411}ISLPLPNFSSLNLR^{424} (109)
1571	100	5.25	−1.08	2.16**	1.24	α-actinin-4 (ACTN4_HUMAN)	gi|13,123,943	104.7	5.2	14	129	20	–

MW = molecular weight; p*I* = isoelectric point; NPM = number of peptides matched. **M**, oxidated methionine. Statistical significance was calculated using Student' s *t*-test. Results of statistical analyses are presented on a scale of significance levels: $p < 0.05$ being significant (*), $p < 0.01$ being highly significant (**), and $p < 0.001$ being extremely significant (***).

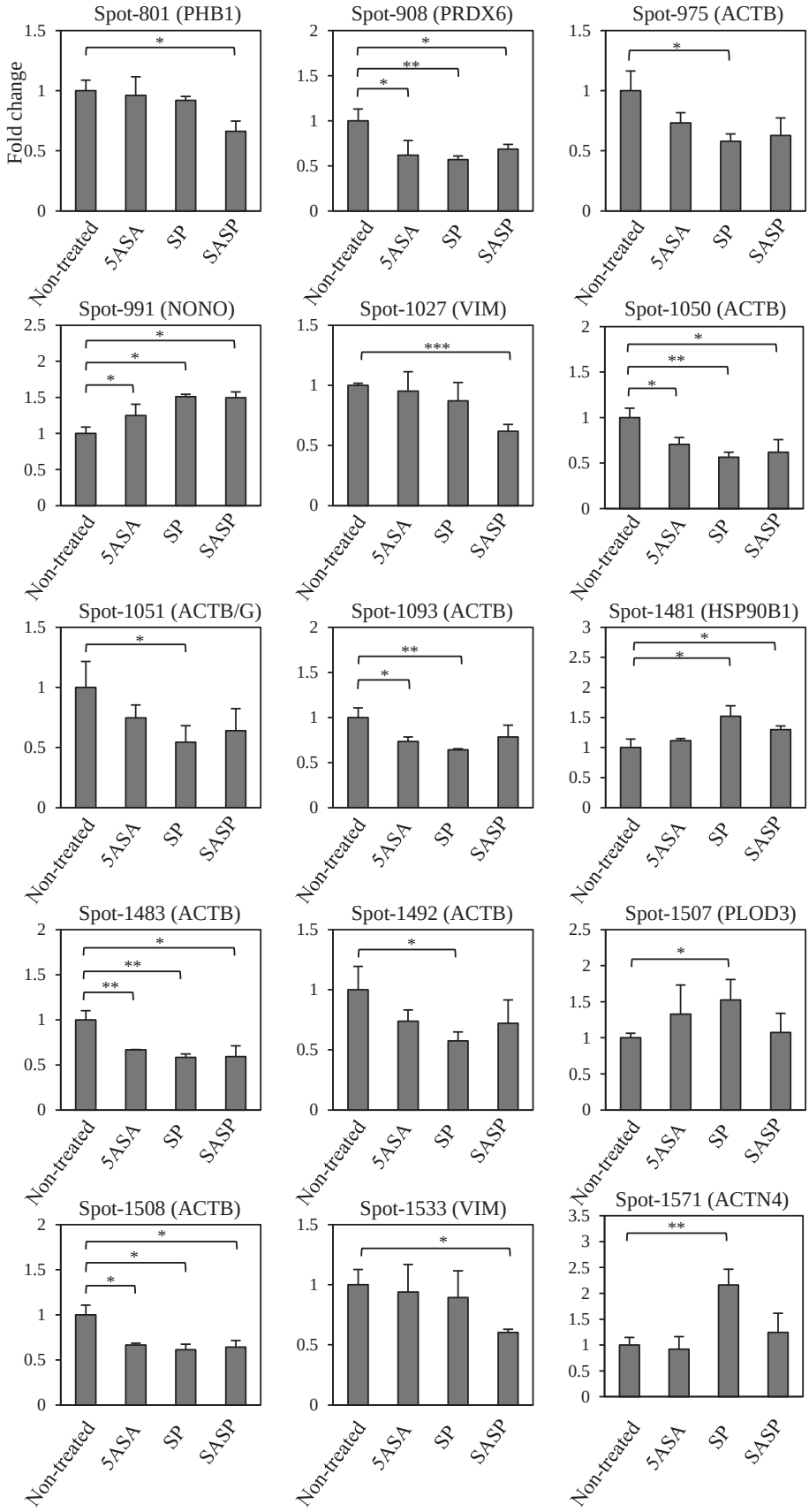

Fig. 3. Effects of SASP, SP, and 5ASA on the expression of CS-proteins.
(A) Intensity changes of the 15 proteins spots in which proteins were identified by mass spectrometry is shown. The average intensity of the non-treated cell samples was defined as 1.0. *$p < 0.05$, **$p < 0.01$, ***$p < 0.001$.

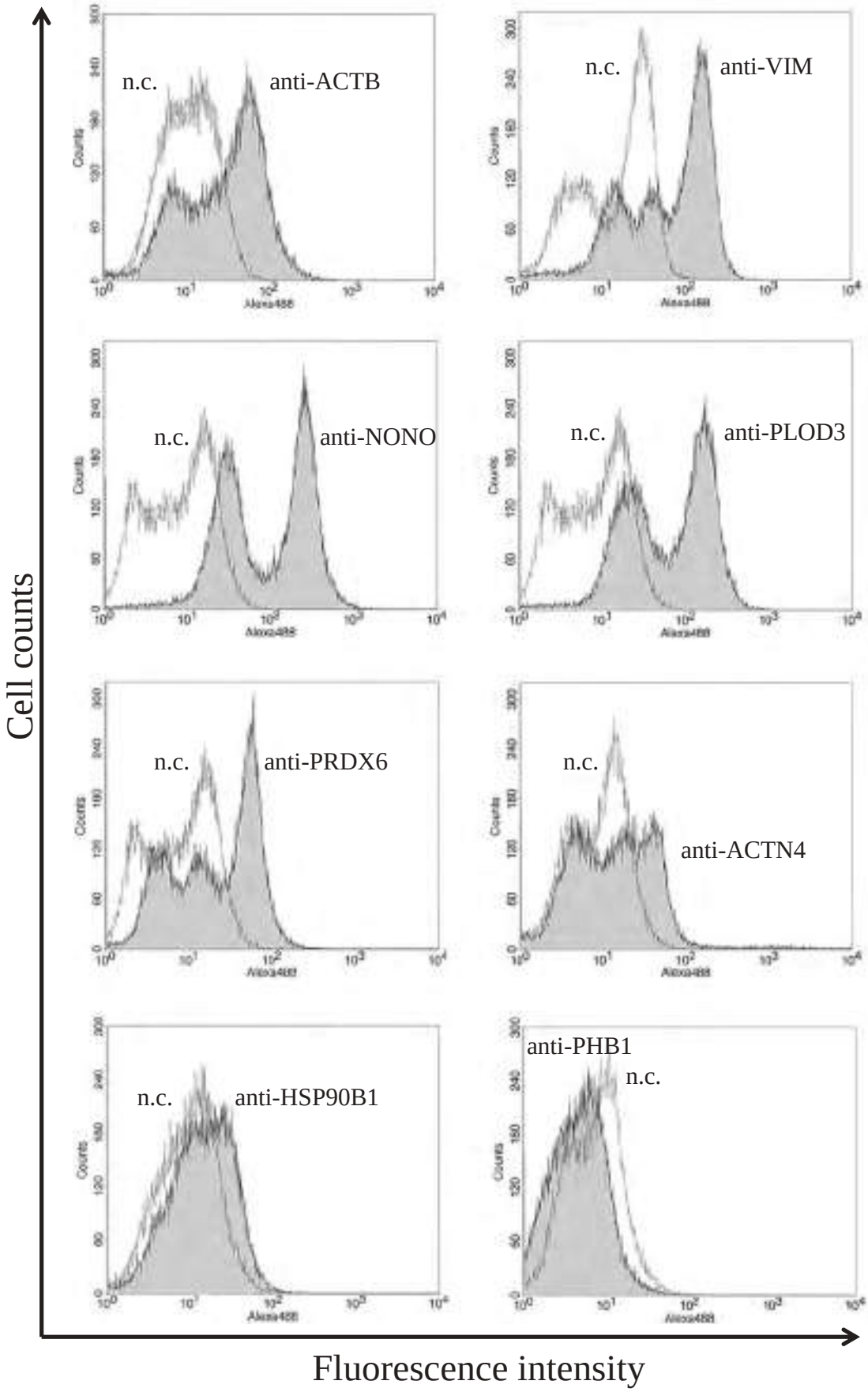

Fig. 4. Expression of the identified CS-proteins evaluated by flow cytometry. Living SW982 cells were reacted with antibodies against each of the identified proteins and Alexa Fluor 488-conjugated secondary antibodies. Then Alexa Fluor 488-positive cells were detected by flow cytometry. N·C; negative control using isotype-control antibodies.

Technology), a rabbit antibody against human prohibitin 1 (PHB1) (2426, Cell signaling Technology) and a mouse IgG_1 antibody against human β-actin (ACTB) (sc-47,778, Santa Cruz Biotechnology), a mouse IgG_{2a} antibody against human actinin4 (ACTN4) (ab117445, abcam, Cambridge, UK), and a goat antibody against VIMENTIN (VIM) (AB1620, CHEMICON International, Temecula, CA). Negative control antibodies used are as follows: a rabbit immunoglobulin fraction (×0936, Dako, Denmark), mouse IgG_1 (×0931, Dako), mouse IgG_{2a} (×0943, Dako), and normal goat serum (sc-2043, Santa Cruz Biotechnology). After washing, the bound antibodies were reacted with the second antibodies of an Alexa Fluor 488-conjugated goat anti-rabbit IgG antibody (ab150077, abcam), an Alexa Fluor 488-conjugated goat anti-mouse IgG antibody (ab150113, abcam), and an Alexa Fluor 488-conjugated rabbit anti-goat IgG antibody (A11078, Molecular probes, Waltham, MA). After washing, the cells were subjected to flow cytometry (BD FACS Calibur, Becton, Dickinson and Company, Franklin Lakes, NJ).

2.8. Statistical analysis

Results were presented as the mean ± standard deviation of triplicate samples, and difference was assessed by Student's *t*-test. P-values of < 0.05 were considered to be statistically significant.

3. Results

3.1. Isolation of CS-proteins using sulfo-NHS-SS-biotin and NeutrAvidin

We first labelled CS-proteins of living SW982 cells by sulfo-NHS-SS-biotin and confirmed biotinylation of CS-proteins by fluorescence-conjugated streptavidin using confocal laser-scanning microscopy. As a result, only the plasma membrane part of the SW982 cells were positive for the fluorescence, indicating that CS-proteins were specifically labelled with sulfo-NHS-SS-biotin (Fig. 1B). Next, we similarly labelled CS-proteins of living SW982 cells by sulfo-NHS-SS-biotin, after which we isolated the biotinylated proteins by NeutrAvidin-bound beads. We then compared the amounts of MEK1/2 (a cytosolic protein) and CADHERIN (a membrane protein) between whole cell lysate of the biotin-labelled cells and the isolated biotinylated proteins using western blotting. As a result, only < 5% of MEK1/2 in the whole cell lysate was detected in the isolated biotinylated protein fraction (Fig. 1C). On the other hand, an approximately half of the CADHERIN in the whole cell lysate was detected in the isolated biotinylated protein fraction (Fig. 1C). These data indicated that enough amounts of CS-proteins were isolated from SW982 cells with high purity.

3.2. 2D-DIGE analysis of CS-proteins of SW982 cells treated with SASP, SP, and 5ASA

We treated SW982 cells with 250 μM SASP, SP, and 5ASA for 24 h (n = 3 for each treatment). Non-treated cells were prepared as a control (n = 3). We then isolated CS-proteins from the cells by the biotinylation and NeutrAvidin capture method as above mentioned. We thus obtained 12 samples, which were dissolved in 50 μl of a urea lysis buffer. The protein concentration of the samples were 1.19–1.83 g/l. Next, we separated the isolated CS-proteins by 2D-DIGE as shown in Fig. 2A. As a result, in total, 576 protein spots were detected on the gels. Among them, 114 spots (19.8%) changed their intensity by SASP, SP and/or 5ASA ($p < 0.05$) as shown in Fig. 2C-(a). This indicates that SASP and its metabolites considerably affect the profile of CS-proteins. The 114 spots consisted of 58 (50.9%) SASP-affected spots, 63 (55.3%) SP-affected spots, and 41 (36.0%) 5ASA-affected spots, including overlap. This indicates that SASP and SP more widely affected the profile of CS-proteins than 5ASA. Restricted to the spots that showed more than ± 1.5-fold intensity changes, specific effects of SASP and SP were also demonstrated. Specifically, 29 out of the 114 spots showed more than ± 1.5-fold intensity changes as shown in Fig. 2C-(b). Location of the 29 spots on the 2D-gel is shown in Fig. 2B. In the SASP-treated group, 11 spots showed more than ± 1.5-fold intensity difference compared to the non-treated group [1 up and 10 down, $p < 0.05$, Fig. 2C-(b)]. Interestingly, intensity of 7 (63.6%) out of the 11 spots were affected only by SASP, not by SP and 5ASA as shown in Fig. 2C-(b). In the SP-treated group, 22 spots showed more than ± 1.5-fold intensity difference compared to the non-treated group (8 up and 14 down, $p < 0.05$). Interestingly, intensity of 17 (77.3%) out of the 22 spots were affected only by SP, not by SASP and 5ASA as shown in Fig. 2C-(b). In contrast, in the 5ASA-treated group, only 2 spots showed more than ± 1.5-fold intensity difference compared to the non-treated group (0 up and 2 down, $p < 0.05$). The intensity of the 2 spots was also down-regulated by SASP as shown in Fig. 2C-(b). In addition, only 5 out of the 29 spots changed their intensity by two or more drugs (1 by all the 3 drugs, 3 by SASP and SP, and 1 by SP and 5ASA). These results suggests that SASP and SP possess their unique effects on the CS-protein profiles. On the other hand, 5ASA was thought to possess less effects on the CS-protein profiles.

3.3. Identification of proteins by mass spectrometry

We tried to identify proteins of these 29 spots by mass spectrometric analysis. As a result, we were able to identify proteins in 15 spots, which consisted of 9 proteins as shown in Table 1. ACTB was identified in 7 spots with slightly different molecular weights and/or p*I*s. Intensity of all the ACTB spots were significantly decreased or tend to be decreased by each of the SASP, SP, and 5ASA treatments, among which the suppressing effect by SP was most distinct (Fig. 3). In the case of Spot-1051, both ACTB and ACTG were identified. VIM was identified from 2 spots with slightly different p*I*s. Intensity of the both VIM spots significantly decreased only by SASP. 5ASA and SP did not appear to affect expression of VIM (Fig. 3). PRDX6 identified from Spot-908 was significantly decreased by all of the 3 drugs (Fig. 3). PHB1 was significantly decreased only by SASP (Fig. 3). NONO was significantly increased by each of the 3 drugs (Fig. 3). HSP90B1 was significantly increased by SASP and SP (Fig. 3). PLOD3 and ACTN4 were significantly increased by SP (Fig. 3). Interestingly, these identified 9 proteins were not transmembrane proteins.

3.4. Confirmation of expression of the identified proteins on the cell surface

We then validated the results of the biotinylation/2D-DIGE analysis of CS-proteins by another method of flow cytometry. As a result, ACTB, VIM, NONO, PLOD3, PRDX6, ACTN4, and HSP90B1 were evidenced to exist on the cell surface of SW982 cells, but PHB1 was not (Fig. 4). Together with the results of the biotinylation/2D-DIGE analysis, these 7 identified proteins were confirmed to exist on the cell surface, even though they were not transmembrane proteins.

4. Discussion

We here comprehensively investigated profile changes of CS-proteins by SASP and its metabolites, SP and 5ASA, using biotinylation-based isolation and 2D-DIGE. Our findings are as follows. 1) The combination of the biotinylation-based isolation and 2D-DIGE is useful for the investigation of CS-protein profiles affected by drugs. 2) A considerable part (114 spots, 19.8%) of the detected protein spots were affected by SASP, SP, and/or 5ASA, in which 29 spots showed more than ± 1.5-fold intensity differences. 3) SASP and SP appeared to more widely affect the profile compared to 5ASA. 4) Proteins were identified in 15 out of the affected 29 spots by SASP and its metabolites. They consisted of 9 proteins, all of which were not transmembrane proteins. 5) Existence of most of the 9 proteins, ACTB, VIM, NONO, PLOD3, PRDX6, ACTN4, and HSP90B1, on the cell surface was confirmed by flow cytometry.

On the first point, we recently reported the different profiles of CS-proteins of peripheral blood mononuclear cells between patients with systemic lupus erythematosus and healthy donors [14]. In that study, we detected 468 protein spots using the same biotinylation/2D-DIGE method. Here, we detected 567 protein spots on the 2D gels in the analysis of SW982 cells. Thereby, the biotinylation/2D-DIGE method is thought to be able to detect approximately 500 kinds of CS-proteins including differences of post-translational modifications. At present, it is unclear how many percent of the total CS-proteins were detected by this method. Use of longer IEF gels and larger SDS-PAGE gels may enable us to detect more numbers of protein spots in the 2D separation. The points should be investigated in the future. Furthermore, biotinylated proteins were captured by avidin beads and then disulfide bonds in the spacer region of the biotinylation reagent were cut to elute the proteins. The eluted sample may be contaminated with originally non-biotinylated proteins, thus, it would be needed to confirm that detected CS-proteins really exist on the cell surface by another method. Thereby we here confirmed the existence of the identified proteins on the cell surface by flow cytometry.

On the second and third points, although unique actions of SASP, SP, and 5ASA have been reported as described in the introduction, the effect of 5ASA on the expression of CS-proteins appeared to be weak compared to SASP and SP, as far as counting the affected protein spots in 2D-DIGE. In the 9 identified proteins, PRDX6, NONO, and ACTB were affected by 5ASA, all of which were similarly affected by SASP, SP, or both. In contrast, PHB1 and VIM were affected only by SASP and also PLOD3 and ACTN4 were affected only by SP. Moreover, HSP90B1 was affected by SASP and SP, but not by 5ASA. Thereby, viewing the list of identified proteins, the effect of 5ASA on the expression of CS-proteins also appeared to be week compared to SASP and SP.

On the fourth point, a puzzling point is that no transmembrane proteins were identified. It may simply indicate that the effects of SASP and its metabolites on the expression of transmembrane proteins is rather weak so that the effects were not detected with significance here. Alternatively, extraction of hydrophobic transmembrane proteins into a cell lysis buffer is generally more difficult than that of cytosolic or secretary proteins. More effective extraction of hydrophobic transmembrane proteins may contribute to identification of affected hydrophobic transmembrane proteins. This point should be investigated in the future.

On the fifth point, localization of all the identified proteins but NONO on the cell surface has been reported, even though they are not transmembrane proteins.

Specifically, actin on the cell surface (CS-actin) has been reported to be a receptor for plasminogen and tissue plasminogen activator and to be involved in activation of plasminogen [15]. It has been also reported that CS-actin promotes endocytosis of plasminogen and plasmin and the endocytosed plasminogen and plasmin are targeted to lysosomes for degradation [16]. Plasmin activates matrix metalloprotease (MMPs) that promote degradation of cartilage and bone [17]. On the other hand, it has been reported that SASP blocks release of MMPs and activation of a disintegrin-like and metalloprotease domain with thrombospondin (ADAMTS) [18]. Here, intensity of all the identified ACTB spots were significantly decreased or tend to be decreased by each of the SASP, SP, and 5ASA treatments. Taking these reports together with ours, SASP and its metabolites may enhance endocytosis of CS-ACTB, resulting the decrease of RA activity through the decrease of plasminogen, MMP, and ADAMTS.

We here found that cell surface ACTN4 (CS-ACTN4) was increased by SP. VIM, identified from 2 spots, was decreased by SASP. CS-ACTN4 has been reported to suppress proliferation of cancer cells [19]. Cell surface VIM (CS-VIM) has been highlighted from the aspects of viral infection and EMT. On the former aspect, it has been reported that CS-VIM plays a critical role as a receptor for some viruses [20,21]. A virus infection is one of the risk factors for an autoimmune disease such as RA. On the latter aspect, it has been reported that existence of CS-VIM without CD133 is a marker of hepatocellular carcinoma cells with EMT phenotypes and CS-VIM-positive/CD133-negative cells are aggressively metastatic [22]. Furthermore, it has been reported that recruitment of VIM to the cell surface on lymphocytes is induced by cell activation [23]. In RA, synoviocytes are known to invade into cartilage and bone with aggressive proliferative potential [7,8] and to exhibit EMT phenotypes [9]. As mentioned above, RA is characterized by proliferation of synoviocytes, which may be suppressed by SP through the increase of CS-ACTN4. The suppression of CS-VIM by SASP may reflect the suppression of such rheumatic changes of synoviocytes by SASP. Further studies are needed to clarify these points.

We here found that cell surface HSP90B1 (CS-HSP90B1) was increased by SASP and SP. CS-HSP90B1 has been reported to be essential to activation of a disintegrin-like and metalloprotease domain with thrombospondin type 1 motifs 9 (ADAMTS9) [24]. ADAMTS9 has been reported to inhibit angiogenesis [25]. Since angiogenesis plays a key role in the pathology of RA [26], SASP and SP may inhibit angiogenesis in RA by enhancing the activation of ADAMTS9.

PRDX6 was significantly decreased by all of the 3 drugs. PRDX6 has been reported to be produced in synoviocytes of patients with arthritis [27]. It has been reported that PRDX6 is translocated from cytosol to plasma membranes by hydrogen peroxide that mediates lipid peroxide in plasma membranes in A549 cells [28]. It has been reported that TNF-α mediates production of IL-8, monocyte chemotactic protein-1 (MCP-1), and collagenases through the induction of reactive oxygen species (ROS) in synoviocytes [29]. On the other hand, SASP, 5ASA, and SP are known to scavenge ROS [30–32]. Thereby, decrease of ROS by SASP and its metabolites may decrease production of ROS, resulting in the decrease of CS-PRDX6.

Taken together, SASP and its metabolites may contribute to the decrease of RA activity through changes of CS-proteins by them and their scavenging functions.

In conclusion, we found novel effects of SASP and its metabolites on SW982 cells by the combination of biotinylation of CS-proteins and 2D-DIGE analysis. These data would help understanding of anti-rheumatic actions of SASP. In addition, the method would be useful for the analysis of CS-proteins.

Transparency document

The http://dx.doi.org/10.1016/j.bbapap.2018.05.007 associated with this article can be found, on online version.

Acknowledgement

This work was supported by a grant from the St. Marianna University School of Medicine Research Grant (2014). We thank Ms. Michiyo Yokoyama for her technical assistance.

References

[1] G.Z. Gu, H.M. Xia, Z.Q. Pang, Z.Y. Liu, X.G. Jiang, J. Chen, Determination of sulphasalazine and its main metabolite sulphapyridine and 5-aminosalicylic acid in human plasma by liquid chromatography/tandem mass spectrometry and its application to a pharmacokinetic study, J. Chromatogr. B Analyt. Technol. Biomed. Life Sci. 879 (2011) 449–456.

[2] M. Nose, M. Sasano, Y. Kawashima, Salazosulfapyridine suppresses chondrocyte mediated degradation induced by interleukin 1beta, J. Rheumatol. 24 (1997) 550–554.

[3] C.K. Lee, E.Y. Lee, S.M. Chung, S.H. Mun, B. Yoo, H.B. Moon, Effects of disease-modifying antirheumatic drugs and antiinflammatory cytokines on human osteoclastogenesis through interaction with receptor activator of nuclear factor kappaB, osteoprotegerin, and receptor activator of nuclear factor kappaB ligand, Arthritis Rheum. 50 (2004) 3831–3843.

[4] R. Matasic, A.B. Dietz, S. Vuk-Pavlovic, Maturation of human dendritic cells as sulfasalazine target, Croat. Med. J. 42 (2001) 440–445.

[5] C. Stevens, M. Lipman, S. Fabry, M. Moscovitch-Lopatin, W. Almawi, S. Keresztes, M.A. Peppercorn, T.B. Strom, 5-Aminosalicylic acid abrogates T-cell proliferation by blocking interleukin-2 production in peripheral blood mononuclear cells, J. Pharmacol. Exp. Ther. 272 (1995) 399–406.

[6] M.V. Volin, P.L. Campbell, M.A. Connors, D.C. Woodruff, A.E. Koch, The effect of sulfasalazine on rheumatoid arthritic synovial tissue chemokine production, Exp. Mol. Pathol. 73 (2002) 84–92.
[7] Z. Qu, C.H. Garcia, L.M. O'Rourke, S.R. Planck, M. Kohli, J.T. Rosenbaum, Local proliferation of fibroblast-like synoviocytes contributes to synovial hyperplasia. Results of proliferating cell nuclear antigen/cyclin, c-myc, and nucleolar organizer region staining, Arthritis Rheum. 37 (1994) 212–220.
[8] A. Lauzier, M. Charbonneau, K. Harper, M. Jilaveanu-Pelmus, C.M. Dubois, Formation of invadopodia-like structures by synovial cells promotes cartilage breakdown in collagen-induced arthritis: involvement of the protein tyrosine kinase Src, Arthritis Rheum. 63 (2011) 1591–1602.
[9] G.Q. Li, Y. Zhang, D. Liu, Y.Y. Qian, H. Zhang, S.Y. Guo, M. Sunagawa, T. Hisamitsu, Y.Q. Liu, PI3 kinase/Akt/HIF-1alpha pathway is associated with hypoxia-induced epithelial-mesenchymal transition in fibroblast-like synoviocytes of rheumatoid arthritis, Mol. Cell. Biochem. 372 (2013) 221–231.
[10] G.W. Anderson, F.M. Callahan, J.E. Zimmerman, Synthesis of N-hydroxysuccinimide esters of acyl peptides by the mixed anhydride method, J. Am. Chem. Soc. 89 (1967) 178.
[11] H. Heitzmann, F.M. Richards, Use of the avidin-biotin complex for specific staining of biological membranes in electron microscopy, Proc. Natl. Acad. Sci. U. S. A. 71 (1974) 3537–3541.
[12] J.V. Staros, N-hydroxysulfosuccinimide active esters: bis(N-hydroxysulfosuccinimide) esters of two dicarboxylic acids are hydrophilic, membrane-impermeant, protein cross-linkers, Biochemistry 21 (1982) 3950–3955.
[13] M. Unlü, M.E. Morgan, J.S. Minden, Difference gel electrophoresis: a single gel method for detecting changes in protein extracts, Electrophoresis 18 (1997) 2071–2077.
[14] Y. Nozawa, M. Arito, K. Omoteyama, M. Sato, Y. Takakuwa, S. Ooka, M.S. Kurokawa, T. Kato, Comprehensive analysis of surface proteins of peripheral mononuclearblood cells in patients with systemic lupus erythematosus, Integr. Mol. Med. 3 (2016) 1–5.
[15] A.K. Dudani, P.R. Ganz, Endothelial cell surface actin serves as a binding site for plasminogen, tissue plasminogen activator and lipoprotein(a), Br. J. Haematol. 95 (1996) 168–178.
[16] A. Briens, I. Bardou, H. Lebas, L.A. Miles, R.J. Parmer, D. Vivien, F. Docagne, Astrocytes regulate the balance between plasminogen activation and plasmin clearance via cell-surface actin, Cell Discov. 3 (2017) 17001.
[17] J. Li, A. Ny, G. Leonardsson, K.S. Nandakumar, R. Holmdahl, T. Ny, The plasminogen activator/plasmin system is essential for development of the joint inflammatory phase of collagen type II-induced arthritis, Am. J. Pathol. 166 (2005) 783–792.
[18] R.L. Lakey, T.E. Cawston, Sulfasalazine blocks the release of proteoglycan and collagen from cytokine stimulated cartilage and down-regulates metalloproteinases, Rheumatology (Oxford) 48 (2009) 1208–1212.
[19] J. Menez, B. Le Maux Chansac, G. Dorothee, I. Vergnon, A. Jalil, M.F. Carlier, S. Chouaib, F. Mami-Chouaib, Mutant alpha-actinin-4 promotes tumorigenicity and regulates cell motility of a human lung carcinoma, Oncogene 23 (2004) 2630–2639.
[20] Y.T. Yu, S.C. Chien, I.Y. Chen, C.T. Lai, Y.G. Tsay, S.C. Chang, M.F. Chang, Surface vimentin is critical for the cell entry of SARS-CoV, J. Biomed. Sci. 23 (2016) 14.
[21] N. Du, H. Cong, H. Tian, H. Zhang, W. Zhang, L. Song, P. Tien, Cell surface vimentin is an attachment receptor for enterovirus 71, J. Virol. 88 (2014) 5816–5833.
[22] A. Mitra, A. Satelli, X. Xia, J. Cutrera, L. Mishra, S. Li, Cell-surface vimentin: a mislocalized protein for isolating csVimentin(+) CD133(−) novel stem-like hepatocellular carcinoma cells expressing EMT markers, Int. J. Cancer 137 (2015) 491–496.
[23] S. Bilalic, A. Michlmayr, V. Gruber, E. Buchberger, C. Burghuber, G.A. Bohmig, R. Oehler, Lymphocyte activation induces cell surface expression of an immunogenic vimentin isoform, Transpl. Immunol. 27 (2012) 101–106.
[24] B.H. Koo, S.S. Apte, Cell-surface processing of the metalloprotease pro-ADAMTS9 is influenced by the chaperone GRP94/gp96, J. Biol. Chem. 285 (2010) 197–205.
[25] M.E. Clark, G.S. Kelner, L.A. Turbeville, A. Boyer, K.C. Arden, R.A. Maki, ADAMTS9, a novel member of the ADAM-TS/metallospondin gene family, Genomics 67 (2000) 343–350.
[26] F.P. Cantatore, N. Maruotti, A. Corrado, D. Ribatti, Anti-angiogenic effects of biotechnological therapies in rheumatic diseases, Biologics 11 (2017) 123–128.
[27] D.H. Kim, D.H. Lee, M.R. Jo, D.J. Son, M.H. Park, C.J. Hwang, J.H. Park, D.Y. Yuk, D.Y. Yoon, Y.S. Jung, Y. Kim, J.H. Jeong, S.B. Han, J.T. Hong, Exacerbation of collagen antibody-induced arthritis in transgenic mice overexpressing peroxiredoxin 6, Arthritis Rheumatol. 67 (2015) 3058–3069.
[28] Y. Manevich, T. Shuvaeva, C. Dodia, A. Kazi, S.I. Feinstein, A.B. Fisher, Binding of peroxiredoxin 6 to substrate determines differential phospholipid hydroperoxide peroxidase and phospholipase A(2) activities, Arch. Biochem. Biophys. 485 (2009) 139–149.
[29] M. Sato, T. Miyazaki, T. Nagaya, Y. Murata, N. Ida, K. Maeda, H. Seo, Antioxidants inhibit tumor necrosis factor-alpha mediated stimulation of interleukin-8, monocyte chemoattractant protein-1, and collagenase expression in cultured human synovial cells, J. Rheumatol. 23 (1996) 432–438.
[30] D. Couto, D. Ribeiro, M. Freitas, A. Gomes, J.L. Lima, E. Fernandes, Scavenging of reactive oxygen and nitrogen species by the prodrug sulfasalazine and its metabolites 5-aminosalicylic acid and sulfapyridine, Redox Rep. 15 (2010) 259–267.
[31] R. Joshi, S. Kumar, M. Unnikrishnan, T. Mukherjee, Free radical scavenging reactions of sulfasalazine, 5-aminosalicylic acid and sulfapyridine: mechanistic aspects and antioxidant activity, Free Radic. Res. 39 (2005) 1163–1172.
[32] I. Kimura, T. Kumamoto, A. Matsuda, M. Kataoka, Y. Kokuba, Effects of BX661A, a new therapeutic agent for ulcerative colitis, on reactive oxygen species in comparison with salazosulfapyridine and its metabolite sulfapyridine, Arzneimittelforschung 48 (1998) 1007–1011.

Tsuno et al. BMC Rheumatology (2018) 2:35
https://doi.org/10.1186/s41927-018-0041-8

BMC Rheumatology

RESEARCH ARTICLE Open Access

A proteomic analysis of serum-derived exosomes in rheumatoid arthritis

Hirotaka Tsuno[1,2*], Mitsumi Arito[1], Naoya Suematsu[1], Toshiyuki Sato[1], Atsushi Hashimoto[2], Toshihiro Matsui[2], Kazuki Omoteyama[1], Masaaki Sato[1], Kazuki Okamoto[5], Shigeto Tohma[3], Manae S. Kurokawa[4] and Tomohiro Kato[1]

Abstract

Background: To understand the roles of serum exosomes in rheumatoid arthritis (RA), we comprehensively investigated the protein profiles of serum exosomes in patients with RA.

Methods: Exosomes were isolated from serum samples obtained from 33 patients (12 with active RA [aRA], 11 with inactive RA [iRA], 10 with osteoarthritis [OA]) and 10 healthy donors (HLs). Proteins extracted from the exosomes were separated by two-dimensional differential gel electrophoresis (2D-DIGE) and identified by mass spectrometry.

Results: In total, 204 protein spots were detected by 2D-DIGE. In the aRA, iRA, and OA groups, 24, 5, and 7 spots showed approximately ≥ ±1.3-fold intensity differences compared with the HL group, respectively. We were able to identify proteins in six protein spots. Among them, the protein spot identified as Toll-like receptor 3 (TLR3) showed approximately 6-fold higher intensity in the aRA group than in the other groups.

Conclusions: Patients with active RA possessed considerably different protein profiles of serum exosomes from patients with iRA, patients with OA, and healthy donors. The unique protein profile of serum exosomes, such as the possession of abundant TLR3 fragments, may reflect the pathophysiology of active RA.

Keywords: Exosome, Proteomics, Rheumatoid arthritis, Osteoarthritis, Toll like receptor 3

Background

Exosomes are nanometer-sized (50–100 nm) membranous extracellular vesicles secreted from various types of cells [1]. Exosomes are initially generated by inward budding of late endosomes, called "multivesicular bodies (MVBs)", in cells and then released from the cells by the fusion of MVBs with plasma membranes [1]. Exosomes are involved in intercellular communications via the delivery of proteins, lipids, and RNAs (mRNA and microRNA) through exosome-cell fusion and via signal delivery through exosome-cell interactions [2, 3].

Immunologically, exosomes play roles in the presentation of antigens to T cells [4]. Exosomes derived from antigen-presenting cells (APCs) were reported to possess major histocompatibility complex (MHC) class I and II molecules, co-stimulatory molecules of CD80 and CD86, and adhesion molecule of intercellular adhesion molecule (ICAM)-1, which are essential to antigen presentation [5, 6]. In fact, exosomes derived from dendritic cells (DCs) have been shown to induce CD8+ T cells to produce interferon (IFN)-γ and tumor necrosis factor (TNF)-α in an exosomal MHC class I-dependent manner [7]. Furthermore, mature DC-derived exosomes have been reported to induce the proliferation of CD4+ T cells in an antigen-specific manner [8].

In the field of cancer, the immunosuppressive and immunostimulatory properties of exosomes have been demonstrated [4]. For example, tumor-derived exosomes were reported to induce T cell apoptosis via Fas ligand [9] and to inhibit interleukin (IL)-2-induced proliferation of T cells [10]. Quite recently, exosomal programmed death-ligand 1 (PD-L1) was shown to inhibit the function of CD8+ T cells and facilitate the progression of melanoma [11].

* Correspondence: h-tsuno@sagamihara-hosp.gr.jp
[1]Clinical Proteomics and Molecular Medicine, St. Marianna University Graduate School of Medicine, 2-16-1, Sugao, Miyamae, Kawasaki, Kanagawa 216-8511, Japan
[2]Department of Rheumatology, National Hospital Organization Sagamihara National Hospital, 18-1, Sakuradai, Minami, Sagamihara, Kanagawa 252-0392, Japan
Full list of author information is available at the end of the article

© The Author(s). 2018 **Open Access** This article is distributed under the terms of the Creative Commons Attribution 4.0 International License (http://creativecommons.org/licenses/by/4.0/), which permits unrestricted use, distribution, and reproduction in any medium, provided you give appropriate credit to the original author(s) and the source, provide a link to the Creative Commons license, and indicate if changes were made. The Creative Commons Public Domain Dedication waiver (http://creativecommons.org/publicdomain/zero/1.0/) applies to the data made available in this article, unless otherwise stated.

Collectively, exosomes are thought to play immunopathological roles in various diseases. Rheumatoid arthritis (RA) is a systemic autoimmune disorder characterized by inflammation and proliferation of synovial tissue, destruction of cartilage and bone, and production of autoantibodies, such as anti-citrullinated peptide antibodies [12]. Although the pathogenesis of RA remains unclear, the pathophysiology is thought to be as follows: First, innate immunity activates DCs [13]. Subsequently, DCs migrate into central lymphoid organs and present autoantigens, such as type II collagen and citrullinated proteins, to T cells [13]. The activated T cells then induce B cells to produce autoantibodies [14]. These lymphocytes migrate into synovial tissue and enhance adaptive immune responses, leading to synovial angiogenesis and hyperplasia of synovial tissue [14]. Inflammatory cytokines such as IL-1, IL-6, IL-17, and TNF-α produced in this process amplify osteoclast differentiation and activation, which results in the destruction of cartilage and bone [12].

As mentioned above, exosomes have various immunological functions and are thus expected to play roles in the pathophysiology of RA. For instance, fibroblast-like synoviocyte (FLS)-derived exosomes were reported to contain citrullinated proteins [15] and a membrane form of TNF-α [16]. IL-1β-stimulated FLS-derived exosomes were reported to up-regulate the matrix metalloproteinase (MMP)-13 expression in chondrocytes [17]. We showed that IL-1β and anti-rheumatic drugs of salazosulfapyridine (SASP) and methotrexate (MTX) considerably altered the protein profiles of exosomes derived from SW982 of synovial sarcoma cell line [18]. Recently, it was reported that some serum exosomal proteins in patients with RA might be useful parameters of disease activity [19]. In terms of bone formation and resorption, osteoclast-derived exosomes containing microRNA (miR-214) were reported to play an inhibitory role in osteoblast activity [20, 21]. However, at present, the roles of exosomes in RA are largely unclear.

These previous findings suggest that characterizing the exosomes generated in patients with RA would be quite useful. We therefore characterized the protein profile of serum exosomes in patients with RA by two-dimensional differential gel electrophoresis (2D-DIGE) and a subsequent mass spectrometry (MS) analysis. We found that the serum exosomes in patients with active RA (aRA) possessed considerably different protein profiles from those in patients with inactive RA (iRA), patients with osteoarthritis (OA), and healthy donors (HLs). In particular, the serum exosomes in patients with aRA contained abundant Toll-like receptor (TLR) 3 fragments. Our data will help promote the understanding of the roles of exosomes in the pathophysiology of RA.

Materials and methods

Preparation of blood samples

Blood samples were obtained from 33 patients (12 patients with aRA, 11 with iRA, 10 with OA) and 10 HLs. Clinical information on the patients with RA is shown in Table 1. The diagnoses of RA and OA were made according to the respective criteria by American College of Rheumatology [22, 23]. We defined aRA as "Disease Activity Score 28 using C-reactive protein (DAS28-CRP) > 2.7" and iRA as "DAS28-CRP < 2.3" [24]. Blood samples were drawn into vacuum tubes (Venoject II, VPAS109K50; Terumo Corporation, Tokyo, Japan) and centrifuged at 1500 *g* for 10 min to separate the sera at room temperature. The separated serum samples were then stored at − 80 °C until use.

This study was approved by the ethics committee of Sagamihara National Hospital and that of St. Marianna University School of Medicine. All of the blood samples were obtained with written informed consent.

Preparation of serum exosomal proteins

Exosomes were isolated from the serum samples using ExoQuick® (System Bioscience, Mountain View, CA, USA) according to the manufacturer's instructions. The collected exosomes were dissolved in a cell lysis buffer (30 mM Tris-HCl pH 8.0, 7 M Urea, 2 M Thiourea, 4% 3-(3-cholamidepropyl) dimethylammonio-1-propanesulfonate [CHAPS]). The protein concentrations of the resulting exosome lysates were then determined by the Bradford assay. A portion of the collected exosomes was suspended in phosphate-buffered saline (PBS) for a transmission electron microscopic analysis.

Transmission electron microscopic analyses

A 5-μl aliquot of PBS-suspended exosomes was placed onto a support grid (Cu, 200 mesh). After 60 s, the grid was washed twice in double distilled water and incubated in 5% aqueous solution of phosphotungstic acid for 10 s. The size and morphology of the collected exosomes were examined using a transmission electron microscope (JEOL Ltd., Tokyo, Japan).

The 2D-DIGE analysis and protein identification

The exosome lysates were separated by 2D-DIGE, as described previously [25]. In brief, each protein sample was labeled with Cy5 saturation dye. Similarly, 2.5 μg of an internal standard sample (a mixture of equal amounts of all 43 samples) was labeled with Cy3 saturation dye. Then, 2.5 μg of the Cy3-labeled internal standard sample and 2.5 μg of the individual Cy5-labeled protein samples were mixed and subjected to 2D-DIGE. Separated proteins were detected using an image analyzer (Typhoon 9400 Imager; GE Healthcare UK, Buckinghamshire, UK).

Table 1 Clinical information of patients with aRA, iRA, and OA and of HL

	Active RA ($n = 12$)	Inactive RA ($n = 11$)	p Value (aRA vs. iRA)	OA ($n = 10$)	HL ($n = 10$)
Age (years), mean (range)	62.2 (31 to 79)	63.4 (41 to 80)	0.85	62.5 (41 to 74)	60.5 (41 to 82)
Sex, male/female	2/10	3/8	0.93	1/9	2/8
Disease duration (years), mean (range)	5.6 (0.25 to 20)	10.9 (0.25 to 38)	0.22	(–)	(–)
ESR (mm/h), mean (range)	56.3 (16 to 100)	21.0 (2 to 41)	< 0.01	(–)	(–)
CRP (mg/L), mean (range)	3.19 (0.07 to 7.16)	0.14 (0.02 to 0.33)	< 0.01	(–)	(–)
MMP-3 (ng/mL), mean (range)	252.0 (18.8 to 602.4)	52.7 (10 to 121.5)	< 0.01	(–)	(–)
SJC, mean (range)	3.7 (1 to 8)	0	< 0.01	(–)	(–)
TJC, mean (range)	6.3 (0 to 17)	0.8 (0 to 3)	< 0.01	(–)	(–)
RF positive (%)	83.3	72.7	0.56	(–)	(–)
ACPA positive (%)	90.0	77.8	0.49	(–)	(–)
DAS28-ESR, mean (range)	4.80 (4.21 to 5.72)	2.33 (0.51 to 3.02)	< 0.01	(–)	(–)
DAS28-CRP, mean (range)	3.84 (3.10 to 4.64)	1.49 (0.98 to 2.2)	< 0.01	(–)	(–)
Medication					
DMARDs (%)	75.0	90.9	0.34	(–)	(–)
Methotrexate (%)	50.0	81.8	0.11	(–)	(–)
Biologics (%)	8.0	18.1	0.51	(–)	(–)
Prednisolone (%)	41.7	0	0.01	(–)	(–)

ESR erythrocyte sedimentation rate, *CRP* C-reactive protein, *MMP-3* matrix metalloproteinase-3, *SJC* swollen joint count, *TJC* tender joint count, *RF* rheumatoid factor, *ACPA* anti-cyclic citrullinated peptide antibody, *DAS28-ESR* disease activity score 28 joints using erythrocyte sedimentation rate, *DAS28-CRP* disease activity score 28 joints using C-reactive protein, *DMARDs* disease-modifying anti-rheumatic drugs

Acquired gel images were analyzed using the Progenesis software program (PerkinElmer, Waltham, MA, USA), in which the intensity of the protein spots in the gel image of each sample was corrected using that of the internal standard sample.

Proteins were identified by a mass spectrometric analysis as described previously [25]. In brief, the gel fragments that corresponded to protein spots of interest were recovered from 2D gels. Peptides generated by in-gel digestion with trypsin were extracted from the gel fragments. The extracted peptides were then subjected to matrix-assisted laser desorption/ionization time-of-flight/time-of-flight mass spectrometry (Ultraflex; Bruker Daltonics, Bremen, Germany). The determined peptide masses were compiled to allow a search of the National Center for Biotechnology Information protein database using the Mascot software program (Matrix Science, London, UK).

Detection of TLR3 by Western blotting (WB)

Proteins were extracted from the purified exosomes into lysis buffer (7 M urea, 2 M thiourea, and 4% CHAPS) for WB. The extracted proteins were separated by sodium dodecyl sulfate-polyacrylamide gel electrophoresis (SDS-PAGE) or by 2D electrophoresis (2DE). In 2DE, the protein samples were first subjected to isoelectric focusing (IEF) using gels with the range of p*I*3.0–11.0. The IEF-separated proteins were then further separated by 12.5% SDS-PAGE. The proteins separated by SDS-PAGE or 2DE were transferred onto polyvinylidene difluoride membranes. In WB, the membranes were incubated with rabbit anti-human TLR3 polyclonal antibodies (Abcam, Cambridge, UK) followed by horseradish peroxidase (HRP)-conjugated goat anti-rabbit immunoglobulin G antibodies (Dako, Glostrup, Denmark). The bound antibodies were visualized using ImmunoStar LD (Wako Pure Chemical Industries, Ltd., Tokyo, Japan). In each membrane, the intensity of a blank area in each membrane was defined as 1.0.

Statistical analyses

The statistical significance of differences in parameters clinical features between the aRA and iRA groups and that of differences in protein spot intensity in 2D-DIGE among the 4 groups was calculated by Student's *t*-test and a one-way analysis of variance, respectively. The expression of TLR3 fragments (17–18 kDa) in the 4 groups was statistically evaluated by Fisher's exact test. *P*-values of less than 0.05 were considered to indicate statistical significance.

Results

Clinical information of the participants

Clinical information of the 43 participants is shown in Table 1. No significant differences were found between the aRA and iRA groups with regard to age, sex, disease

duration, and test items other than markers for inflammatory condition (Table 1). Regarding the medication, the percentage of patients receiving oral corticosteroids in the aRA group (41.7%) was significantly higher than that in the iRA group (0%) (Table 1).

Isolation of exosomes from serum samples

We isolated exosomes from serum samples and checked for successful isolation of exosomes using a transmission electron microscopic analysis. Almost all of the isolated extracellular vesicles were found to have a diameter of 50–100 nm, as shown in Fig. 1. The observed sizes were compatible with the definition of exosomes [1, 2].

The comparison of the protein profiles of serum-derived exosomes among patients with RA and OA and HLs

We investigated the protein profiles of exosomes in each of the 43 serum samples by 2D-DIGE. As a result, a total of 204 protein spots were detected on the gels, as shown in Fig. 2. The spot intensities in each group are shown in Additional file 1: Table S1. We first compared the intensity of the separated protein spots between the whole RA (wRA; aRA + iRA) and HL groups and between the OA and HL groups. In the comparison between the wRA and HL groups, 28 of the 204 protein spots showed significantly different intensities ($p < 0.05$) (Table 2A). Of these 28 spots, 7 showed a difference in intensity exceeding ±1.3-fold (Table 2A). In the comparison between the OA and HL groups, 21 protein spots showed different intensities ($p < 0.05$) (Table 2D). Of these 21 spots, 7 showed a difference in intensity exceeding ±1.3-fold (Table 2D). As shown in Fig. 3a-(i), only 4 spots overlapped between the 28 spots that differed in the wRA group and the 21 spots that differed in the OA group (14% and 19%, respectively). Furthermore, no spots overlapped between these 2 groups when we focused on the spots with a difference in intensity exceeding ±1.3-fold (Fig. 3a-[ii]). These results indicate that the protein profiles of exosomes are quite different between the wRA and OA groups.

We next compared the protein profiles between the aRA and HL groups and between the iRA and HL groups. On comparing the aRA and HL groups, 31 spots showed different intensities ($p < 0.05$) (Table 2B). Of these 31 spots, 24 showed a difference in intensity exceeding ±1.3-fold (Table 2B). On comparing the iRA and HL groups, 14 protein spots showed different intensities ($p < 0.05$) (Table 2C). Of these 14 spots, 5 showed a difference in intensity exceeding ±1.3-fold (Table 2C). Of note, as shown in Fig. 3b-(i), only 2 spots overlapped between the 31 spots that differed in the aRA group and the 14 spots that differed in the iRA group (6.5% and 14%, respectively). Furthermore, no spots overlapped between the 2 groups when we focused on the spots with a difference in intensity exceeding ±1.3-fold (Fig. 3b-[ii]). These results indicate that the protein profiles of exosomes differ markedly between the aRA and iRA groups. In addition, only 4 spots overlapped between the 31 spots that differed in the aRA group and the 21 spots that differed in the OA group (13% and 19%, respectively) (Fig. 3b-[i]). No spots overlapped between the 2 groups when we focused on the spots with a difference in intensity exceeding ±1.3-fold (Fig. 3b-[ii]). These results indicate that the protein profiles of exosomes differ markedly between the aRA and OA groups. In contrast, 6 spots overlapped between the 14 spots that differed in the iRA group and the 21 spots that differed in the OA group (43% and 29%, respectively) (Fig. 3b-[i]). The location of spots that showed an intensity with more than ±1.3-fold difference ($p < 0.05$) compared to that in the HL group were marked on the 2D-DIGE images of the aRA, iRA, and OA groups (Additional file 1: Figure S1).

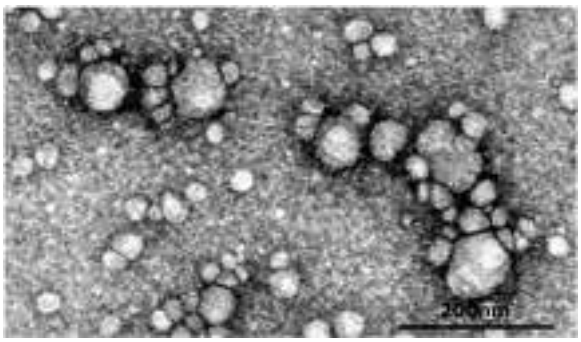

Fig. 1 A transmission electron micrograph of exosomes isolated from serum samples. Serum exosomes isolated using Exoquick® were analyzed by transmission electron microscopy. A representative result from the serum exosome samples is shown

Identification of proteins in the spots with different intensity

We then compared the spot intensity of the 14 spots shown in Fig. 3a-(ii) between the wRA and OA groups. As a result, 7 spots (ID208, ID564, ID407, ID416, ID420, ID236, and ID325, rectangle in Fig. 3a-[ii]) showed different intensities ($p < 0.05$) between the wRA and OA groups. Similarly, we compared the spot intensity of the 34 spots (including 2 overlapping spots) shown in Fig. 3b-(ii) between the aRA and OA groups and between the aRA and iRA groups. As a result, 5 spots (ID370, ID407, ID494, ID564, and ID704, rectangle in Fig. 3b[ii]) showed different intensity ($p < 0.05$) between the aRA and OA groups and between the aRA and iRA groups.

We tried to identify the protein names of the former 7 spots and the latter 5 spots (actually 10 spots because of

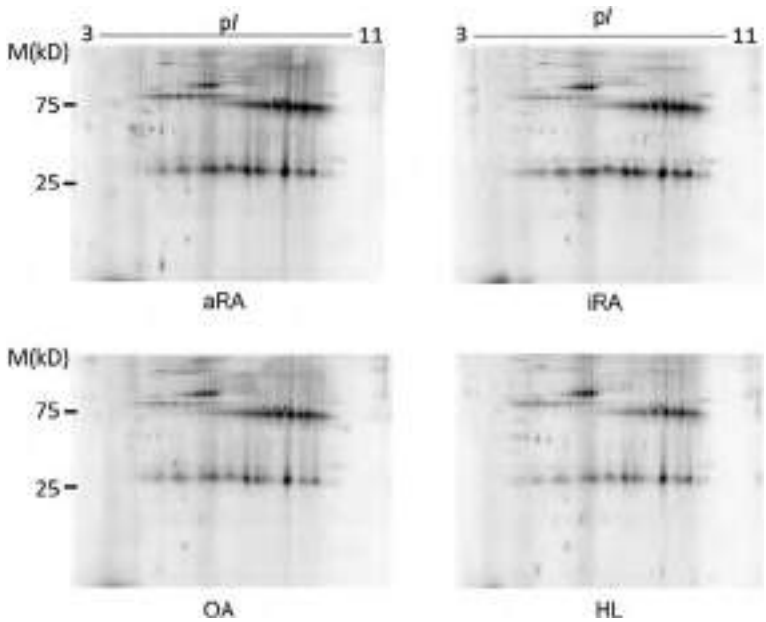

Fig. 2 Representative 2D-DIGE images showing protein profiles of exosomes isolated from the serum samples of the aRA, iRA, OA, and HL groups. A representative image from each group is shown

2 overlapped spots [ID407 and ID564]) by a mass spectrometric analysis (Fig. 4). As a result, we were able to name 6 out of the 10 protein spots, as listed in Table 3. ID208 (increased only in the wRA group) was found to be a membrane-bound isoform of Pro-neuregulin-3. ID564 (increased in the wRA and aRA groups) was found to be TLR3. ID370 (increased only in the aRA group) was found to be alpha-1-antitrypsin. ID494 (decreased only in the aRA group) was found to be keratin of type II cytoskeletal 1. ID236 (increased only in the

Table 2 Differences in the exosomal protein profiles among the disease categories detected by 2D-DIGE

A. wRA vs. HL			
Total number of detected protein spots	Number of spots with different intensities ($p < 0.05$)	fold difference (wRA/HL)	number of spots
204	28	X ≥ 1.3	5
		1.3 > X > −1.3	21
		−1.3 ≥ X	2
B. aRA vs. HL			
Total number of detected protein spots	Number of spots with different intensities ($p < 0.05$)	fold difference (aRA/HL)	number of spots
204	31	X ≥ 1.3	13
		1.3 > X > −1.3	7
		− 1.3 ≥ X	11
C. iRA vs. HL			
Total number of detected protein spots	Number of spots with different intensities ($p < 0.05$)	fold difference (iRA/HL)	number of spots
204	14	X ≥ 1.3	1
		1.3 > X > −1.3	9
		−1.3 ≥ X	4
D. OA vs. HL			
Total number of detected protein spots	Number of spots with different intensities ($p < 0.05$)	fold difference (OA/HL)	number of spots
204	21	X ≥ 1.3	1
		1.3 > X > −1.3	14
		−1.3 ≥ X	6

wRA whole RA, *aRA* active RA, *iRA* inactive RA, *OA* osteoarthritis, *HL* healthy donor

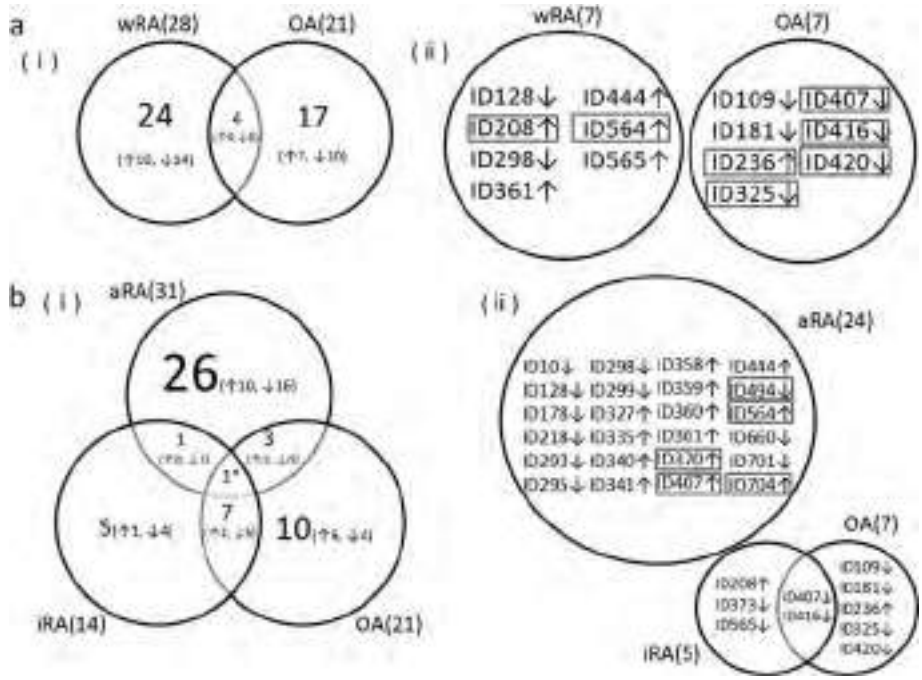

Fig. 3 Venn diagrams showing the numbers of protein spots with significantly different intensities between the HL group and each disease group. (**a**) (i) Numbers of protein spots with significantly different intensities between the wRA and HL groups and between the OA and HL groups ($p < 0.05$). Up and down arrows indicate the spots whose intensity was higher and lower, respectively, in the disease groups than that in HL group. (ii) IDs of protein spots with an intensity ≥ ±1.3-fold different in the diagram (i). IDs of protein spots with a significantly different intensity between the wRA and OA groups are boxed. Up and down arrows indicate the spots whose intensity was higher and lower, respectively, compared to the intensity of the identical spots in the HL group. (**b**) (i) Numbers of protein spots with significantly different intensities between the aRA and HL groups, between the iRA and HL groups, and between the OA and HL groups ($p < 0.05$). Up and down arrows indicate the spots whose intensity was higher and lower, respectively, in the disease groups than that in HL group. The spots with "*" showed a higher intensity in the aRA group and a lower intensity in the iRA and OA groups than in the HL group. (ii) IDs of protein spots with an intensity ≥ ±1.3-fold different in the diagram (i). IDs of protein spots with a significantly different intensity between the aRA and OA groups and between the aRA and iRA groups are boxed. Up and down arrows indicate the spots whose intensity was higher and lower, respectively, compared to the intensity of the identical spots in the HL group

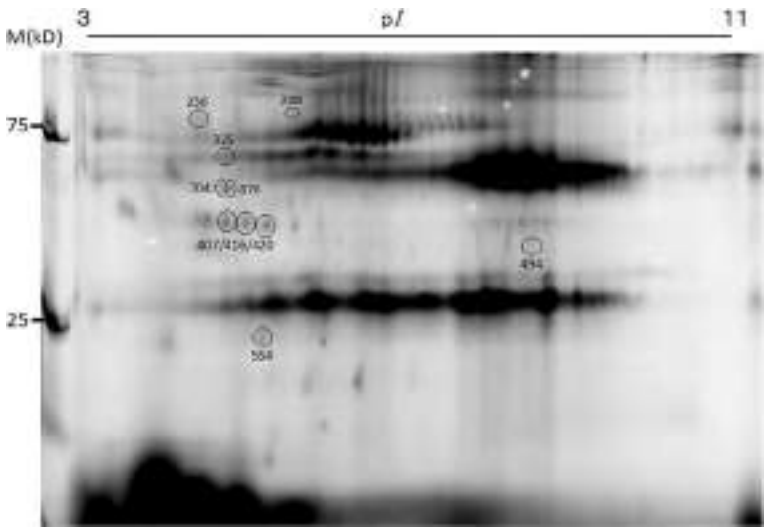

Fig. 4 Location and IDs of exosomal protein spots subjected to identification

Table 3 Proteins identified by mass spectrometry

Spot ID	Observed		Fold difference				Protein	Theoretical		Masscot Score	Coverage (%)	Confirmed Sequences (Masscot ion score)	Search log
	MW	p*I*	wRA		OA	HL		MW	p*I*				
			aRA	iRA									
208	90	5.3	1.4*		1.0	1.0	Pro-neuregulin-3, membrane-bound isoform NRG3_HUMAN	78	7.8	61	12	^{388}QAKQIQEQLK^{397}(19)	38,220
236	87	5.1	1.1		1.3*	1.0	Cathepsin F CATF_HUMAN	53	8.5	26	3	^{103}TLLCSFQVLDELGRHVLLR^{121}(26)	38,210 peptide summary
325	65	5.1	0.9		0.7*	1.0	Ig alpha-2 chain C region IGHA2_HUMAN	37	5.7	132	10	^{251}WLQGSQELPR^{260}(53) ^{270}QEPSQGTTTFAVTSILR^{286}(70)	38,207
370	53	5.1	1.3*	0.9	0.9	1.0	Alpha-1-antitrypsin A1AT_HUMAN	47	5.4	170	33	^{50}ITPNLAEFAFSLYR^{63}(79) ^{216}GKWERPFEVK^{225}(10)	38,190
494	40	7.0	0.7*	0.9	0.9	1.0	Keratin, type II cytoskeletal 1 K2C1_HUMAN	66	8.2	62	9	^{212}WELLQQVDTSTR^{223}(14) ^{224}THNLEPYFESFINNLR^{239}(41)	38,206
564	24	5.2	6.3*	1.2	1.1	1.0	Toll-like receptor 3 TLR3_HUMAN	104	6.7	68	19	^{532}LEILDLQHNNLAR^{544}(7)	38,215

MW molecular weight, *wRA* whole RA, *aRA* active RA, *iRA* inactive RA, *OA* osteoarthritis, *HL* healthy donor
Fold differences are shown with the intensity of the protein spots in HLs defined as 1.0. Asterisks indicate that the spot intensity is significantly different ($p < 0.05$) from that in HLs

OA group) was found to be cathepsin F. ID 325 (decreased only in the OA group) was found to be Ig alpha-2 chain C region. We confirmed that these 6 identified proteins were registered in Vesiclepedia, a database of extracellular vesicle components [26].

Among these six protein spots, the difference in ID564 (assigned as TLR3) was most drastic, as shown in Fig. 5. Since the observed molecular weight (MW) (24 kD) of ID564 was rather small compared to the theoretical MW (104 kD) of full-length TLR3, ID564 was thought to be a part of TLR3. Mass spectrometry detected a peptide corresponding to the 532–544 amino acid residues of TLR3 (Table 3), indicating that the spot ID564 was a middle part of TLR3.

Detection of the TLR3 fragment by 1DE- and 2DE-WB

We tried to detect the TLR3 fragment (24 kDa) corresponding to the ID564 spot using 2DE-WB and a mixture of 4 aRA exosomal protein samples with a relatively high intensity of ID564 using antibodies raised against the human TLR3 fragment of amino acid 464–647. However, the ID564 spot was not detected by the antibody; instead, 3 protein spots of 17–18 kDa were detected (Fig. 6a). We therefore focused on the TLR3 fragments (17–18 kDa) and compared the expression of these fragments among the HL ($n = 10$), aRA ($n = 12$), iRA ($n = 11$), and OA ($n = 10$) groups by 1DE-WB. The 17- to 18-kDa TLR3 spots were ultimately detected as doublet bands on 1DE-WB (Fig. 6b [i]). In 6 of the 12 aRA samples, 5 of the 11 iRA samples and 1 of the 10 OA samples, the band intensity of the TLR3 fragments was higher than the mean of that in the HL group + 2.5 standard deviations (Fig. 6b [ii] and [iii]). In the aRA and iRA groups, the ratios of samples with a high band intensity of TLR3 fragments (17–18 kDa) were significantly higher than in the HL group (Fig. 6b [ii] and [iii]). These results suggest that patients with RA more frequently have large amounts of TLR3 fragments (17–18 kDa) in serum-derived exosomes than HLs.

Discussion

To our knowledge, this is the first report to compare the protein profiles of serum exosomes among patients with RA, those with OA, and HLs.

In the aRA group, ID564, identified as TLR3, showed about 6-fold higher intensity than the other groups. Given the observed small MW (24 kDa) of ID564 and the mass spectrometric data, ID564 was thought to represent a middle part fragment of TLR3. Furthermore, patients with RA more frequently had large amounts of the TLR3 fragments (17–18 kDa) in serum-derived exosomes than HLs.

TLR3 is a member of the TLR family of pattern recognition receptors of the innate immune system [27]. TLR3 is an endosomal TLR that recognizes double-stranded RNA (dsRNA), a molecular pattern associated with viral infection [27, 28]. TLR3 signal activates transcription factors of NF-κB and interferon regulatory factor (IRF) 3, which leads to the secretion of type I interferons and proinflammatory cytokines, such as IL-6

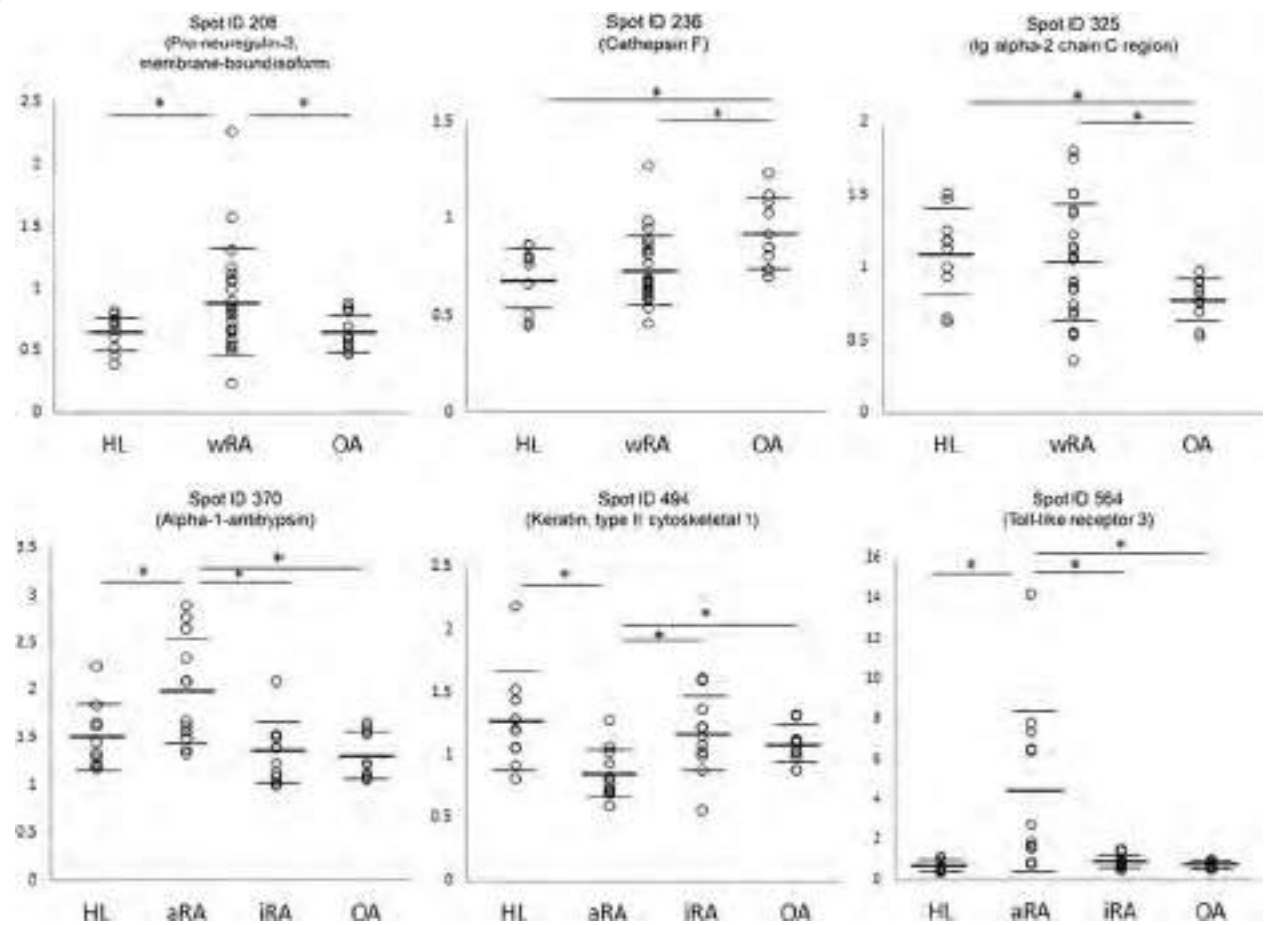

Fig. 5 Differences in the relative spot intensities of the identified proteins. Open circles show the relative intensity of individual samples. Bars show the mean ± SD. *, $p < 0.05$

and IL-8 [27, 28]. In the intracellular trafficking and maturation of TLR3, a precursor form of TLR3 is transported to endosomes through the endoplasmic reticulum (ER) and Golgi apparatus [29]. In the endosomes, the precursor form of TLR3 is cleaved to produce a C-terminal 70-kDa fragment of TLR3 that can deliver signals [29]. The amino acid sequences of ID564 identified by the mass spectrometric analysis were located in the range of the C-terminal 70-kDa fragment (Table 3). We therefore considered that the 24-kDa fragments of TLR3 had been generated by additional proteolytic cleavage of the C-terminal 70-kDa fragment in endosomes and then taken up into exosomes after the cleavage.

Several reports have suggested that the expression of TLR3 and the activation of its pathways are associated with the pathogenesis of RA. For example, TLR3 was found to be more highly expressed in RA synovial tissue than in OA synovial tissue [30]. The stimulation of cultured fibroblast-like synoviocytes (FLSs) with poly (I-C), a synthetic TLR3 ligand, up-regulated the TLR3 expression in FLSs [30]. RNA released from necrotic synovial fluid cells of RA patients activated the TLR3 pathway in FLSs and up-regulated the expression of IFN-β mRNA and the production of IL-6 [30]. It was recently reported that poly (I:C) of a TLR3 ligand associated with extracellular vesicles (EVs) was able to selectively activate antiviral and proinflammatory responses in synovial fibroblasts [31]. In addition, it has been reported that the expression of TLR3 is increased in the spleen of rats with collagen-induced arthritis as well as in those with pritane-induced arthritis, and that the increased expression of TLR3 was decreased by treatment with MTX [32]. Thus, TLR3, which is highly expressed in synoviocytes and possibly in the spleen of patients with active RA as well, is thought to play a role in the production of proinflammatory cytokines. The markedly high levels of the TLR3 fragment in serum exosomes may be caused by the high expression of TLR3 in FLSs in patients with active RA. From this viewpoint, the 24- and the

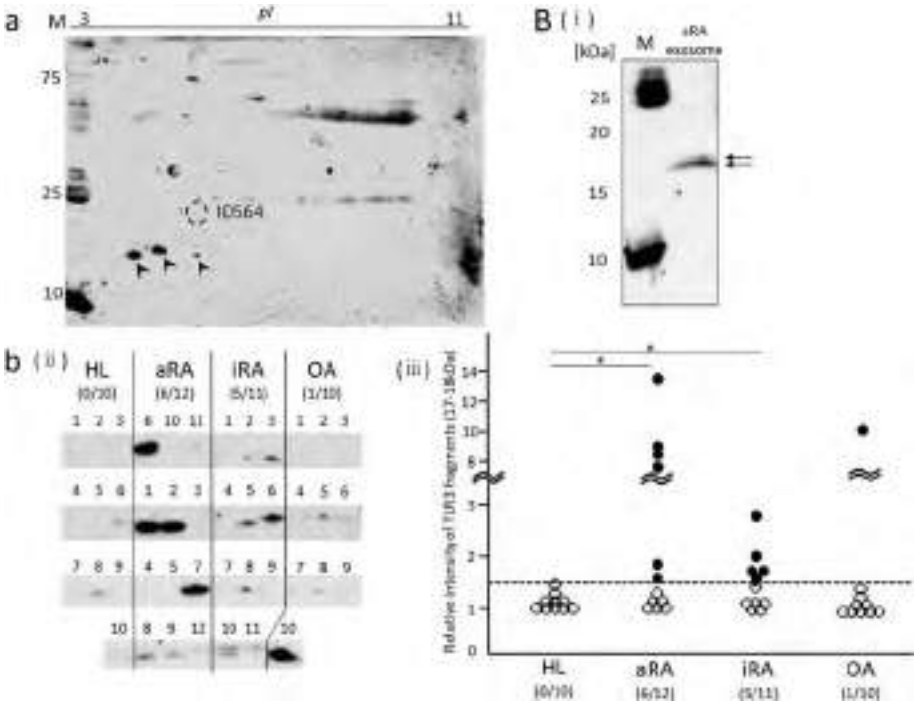

Fig. 6 Detection of TLR3 in the serum-derived exosome protein. (**a**) TLR3 was detected by 2DE-WB from the exosomal protein sample mixture from 4 aRA patients (aRA 1, 6, 10, and 11) with a relatively high ID564 intensity. Arrowheads, TLR3 fragments (17–18 kDa). (**b**) (i) The TLR3 fragments (17–18 kDa) in the exosomal protein samples described in (**a**) were detected by 1DE-WB. (ii) The TLR3 fragments (17–18 kDa) in the exosomal protein samples from the HLs ($n = 10$) and patients with aRA ($n = 12$), iRA ($n = 11$), and OA ($n = 10$) were detected by 1DE-WB. (iii) The intensity of the bands was measured using a densitometer. The intensity of the blank area in each membrane was defined as 1.0. The obtained relative expression of the TLR3 fragments (17–18 kDa) was compared among the 4 groups. The dotted line indicates the mean + 2.5SD of the band intensity in the HL group. The intensity of the TLR3 fragments (17–18 kDa) was higher in 6 of the 12 aRA samples, 5 of the 11 iRA samples, and 1 of the 10 OA samples than the mean of that in HL groups + 2.5SD (filled circles). The ratios of samples with a high intensity of TLR3 fragments (17–18 kDa) were significantly higher in the aRA and iRA groups than in the HL group. * $p < 0.05$

17–18 kDa TLR3 fragments in serum exosomes may be useful markers of the activation of FLSs in patients with RA.

While the TLR3 fragments (17–18 kDa and 24 kDa) are likely non-functional, they may still have some pathological significance. We previously reported that a degradation product of Apo-AI has a biological function of promoting IL-8 secretion from cells [33]. The TLR3 fragments detected in the present study might therefore perform some biological functions that differ from those of full-length TLR3. Further studies will be needed to investigate this possibility.

A membrane-bound isoform of pro-neuregulin-3 showed 1.4-fold higher expression in the wRA group than in the OA and HL groups (Table 3, Fig. 5). Pro-neuregulin-3 is a precursor of neureglin-3, which is a ligand for ErbB4, a member of the epidermal growth factor receptor (EGFR) family [34]. It has been reported that the binding of neureglin-3 to ErbB4 promotes the proliferation, migration, and differentiation of neuroblasts [34, 35]. Although little is known about the involvement of neuregulin in the pathogenesis of rheumatic diseases, it has been reported that EGFR is expressed in fibroblasts and vascular endothelial cells and that EGFR signaling induces FLS proliferation and cytokine production in patients with RA [36]. Given the high expression of pro-neuregulin-3 in serum-derived exosomes of patients with RA detected in our study, the neuregulin-3-ErbB4 pathway may be activated to promote proliferation in FLSs. Furthermore, pro-neuregulin-3 in serum exosomes may be converted to neuregulin-3 and act as a ligand for ErbB4 in FLSs. Further studies are needed to elucidate these points.

The intensity of the spot ID236, identified as cathepsin F, was higher in the OA group than in the other three groups. Cathepsin F is a member of the papain family cysteine proteinases [37]. Given that another member of cathepsin K was reported to be involved in the pathogenesis of OA [38, 39], cathepsin F might also be involved in the pathogenesis of OA. This point needs to be investigated in the future.

The observed MWs of the proteins identified in this study were slightly different from their theoretical MWs (Table 3). Post-translational modifications, such as glycosylation, have

been reported for the spots ID208 (pro-neuregulin-3, membrane-bound isoform), ID236 (cathepsin F), and ID325 (Ig alpha-2 chain C region), which may have contributed to this discrepancy in MW findings [40–42]. For spot ID494 (Keratin, type II cytoskeletal), the observed MW was smaller than the theoretical MW, suggesting that ID494 might be a keratin degradate, similar to the case of TLR3.

Exosomal lymphatic vessel endothelial hyaluronic acid receptor-1 (LYVE-1) was very recently reported to be a candidate marker of RA activity by a 2D-LC-MS/MS (two-dimensional liquid chromatography-tandem mass spectrometry) analysis of serum exosomal proteins from RA patients with complete remission and those with non-complete remission [19]. However, in that study, none of the six proteins we identified in our own were found to be candidate markers of RA activity [19]. Similarly, LYVE-1 was not identified as a differently expressed protein in our study [19]. This difference may be due to differences in the serum donors (we analyzed exosomal samples from OA patients and HLs in addition to patients with RA) and different methods used in these two studies (2D-LC-MS/MS vs. 2D-DIGE followed by MS/MS).

In addition, we isolated serum exosomes using Exoquick®, which was useful to isolate exosomes from a large number of blood samples. However, similarly as other methods, contamination of serum proteins cannot be completely avoided. It would be needed to investigate characters and functions of the individual identified proteins as exosomal proteins.

Conclusions

In the present study, we demonstrated that the serum exosomes of patients with aRA have different protein profiles from those of patients with iRA, patients with OA, and HLs. The 24- and the 17- to 18-kDa TLR3 fragments, which were found to be markedly increased in patients with aRA, may reflect the inflammatory condition of FLSs. Our findings may aid in the clarification of the roles of exosomes in the pathophysiology of RA.

Additional file

Additional file 1: Figure S1. Location of differently enriched protein spots. **Table S1.** Averages of spot intensities of each group. (DOCX 101 kb)

Abbreviations

2D-DIGE: Two-dimensional differential image gel electrophoresis; 2D-LC-MS/MS: Two-dimensional liquid chromatography-tandem mass spectrometry; ACPA: Anti-cyclic citrullinated peptide antibody; APC: Antigen-presenting cell; aRA: Active RA; CHAPS: 3-(3-cholamidepropyl) dimethylammonio-1-propanesulfonate; CRP: C-reactive protein; DAS28-CRP: Disease activity score 28 joints using C-reactive protein; DAS28-ESR: Disease activity score 28 joints using erythrocyte sedimentation rate; DC: Dendritic cell; DMARDs: Disease-modifying anti-rheumatic drugs; dsRNA: Double-stranded RNA; EGFR: Epidermal growth factor receptor; ER: Endoplasmic reticulum; ESR: Erythrocyte sedimentation rate; FLS: Fibroblast-like synoviocyte; HL: Healthy control; ICAM: Intercellular adhesion molecule; IFN: Interferon; IL: Interleukin; iRA: Inactive RA; IRF: Interferon regulatory factor; LYVE-1: Lymphatic vessel endothelial hyaluronic acid receptor-1; MHC: Major histocompatibility complex; MMP: Matrix metalloproteinase; MS: Mass spectrometry; MTX: Methotrexate; MVBs: Multivesicular bodies; MW: Molecular weight; NF-κB: Nuclear factor-kappa B; OA: Osteoarthritis; PBS: Phosphate-buffered saline; PD-L1: Programmed death-ligand 1; RA: Rheumatoid arthritis; RF: Rheumatoid factor; SASP: Salazosulfapyridine; SJC: Swollen joint count; TJC: Tender joint count; TLR: Toll-like receptor; TNF: Tumor necrosis factor; wRA: Whole RA

Acknowledgements

We would like to thank Professor M. Takagi and Mr. Y. Natsuki for their help in the transmission electron microscopic analysis, Professor N. Fukui for the collection of the sera of the patients with OA, and Ms. M. Katano for her excellent technical assistance.

Funding

No funding was obtained for this study.

Availability of data and materials

The datasets used and/or analyzed during the current study are available from the corresponding author on reasonable request.

Authors' contributions

HT participated in the study design, performed the experiments and drafted the manuscript. MA participated in its design, contributed to the interpretation of the results, and helped draft the manuscript. NS, TS, and MS participated in the acquisition and analysis of the data and contributed to editing the manuscript. KO (Kazuki Omoteyama) participated in the acquisition and analysis of the data and contributed to editing the manuscript. KO (Kazuki Okamoto) participated in the acquisition and analysis of the data and contributed to editing the manuscript. AH, TM, and ST participated in the acquisition and analysis of the data and helped edit the manuscript. MSK participated in the study design and contributed to the interpretation of the results and editing the manuscript. TK conceived the study, participated in its design and coordination, and revised the manuscript. All authors read and approved the final manuscript.

Ethics approval and consent to participate

This study was approved by the ethics committee of Sagamihara National Hospital and that of St. Marianna University School of Medicine. All of the blood samples were obtained with written informed consent.

Consent for publication

Not applicable.

Competing interests

AH has received research funding from Chugai Pharmaceutical Co., Ltd. TM was a member of the Department of Lifetime Clinical Immunology (LCI) at Tokyo Medical and Dental University (TMDU). TMDU received unrestricted research grants for the Department of LCI from AbbVie GK, Ayumi Pharmaceutical Corporation, Chugai Pharmaceutical Co., Ltd., CSL Behring K.K., Japan Blood Products Organization, Mitsubishi Tanabe Pharma Corporation, Nippon Kayaku Co., Ltd., Ono Pharmaceutical Co., Ltd., Towa Pharmaceutical Co., Ltd., and UCB Japan Co. Ltd., with which TMDU paid the salary of TM. ST was supported by research grants from nine pharmaceutical companies: Abbott Japan Co., Ltd., Astellas Pharma Inc., Chugai Pharmaceutical Co., Ltd., Eisai Co., Ltd., Mitsubishi Tanabe Pharma Corporation, Pfizer Japan Inc., Takeda Pharmaceutical Company Limited, and Teijin Pharma Limited. ST received honoraria from Asahi Kasei Pharma Corporation, Astellas Pharma Inc., AbbVie GK., Chugai Pharmaceutical Co., Ltd., Ono Pharmaceutical Co., Ltd., Mitsubishi Tanabe Pharma Corporation, and Pfizer Japan, Inc. The other authors have no financial or commercial conflicts of interest to declare.

Publisher's Note

Springer Nature remains neutral with regard to jurisdictional claims in published maps and institutional affiliations.

Author details
[1]Clinical Proteomics and Molecular Medicine, St. Marianna University Graduate School of Medicine, 2-16-1, Sugao, Miyamae, Kawasaki, Kanagawa 216-8511, Japan. [2]Department of Rheumatology, National Hospital Organization Sagamihara National Hospital, 18-1, Sakuradai, Minami, Sagamihara, Kanagawa 252-0392, Japan. [3]National Hospital Organization Tokyo National Hospital, 3-1-1, Takeoka, Kiyose, Tokyo 204-8585, Japan. [4]Disease Biomarker Analysis and Molecular Regulation, St. Marianna University Graduate School of Medicine, 2-16-1, Sugao, Miyamae, Kawasaki, Kanagawa 216-8511, Japan. [5]The Institute of Scientific and Industrial Research, Osaka University, 8-1, Mihogaoka, Osaka, Ibaraki 567-0047, Japan.

Received: 10 May 2018 Accepted: 18 October 2018
Published online: 27 November 2018

References

1. Théry C, Ostrowski M, Segura E. Membrane vesicles as conveyors of immune responses. Nat Rev Immunol. 2009;9:581–93.
2. Record M, Subra C, Silvente-Poirot S, Poirot M. Exosomes as intercellular signalosomes and pharmacological effectors. Biochem Pharmacol. 2011;81:1171–82.
3. Valadi H, Ekström K, Bossios A, Sjöstrand M, Lee JJ, Lötvall JO. Exosome-mediated transfer of mRNAs and microRNAs is a novel mechanism of genetic exchange between cells. Nat Cell Biol. 2007;9:654–9.
4. Chaput N, Théry C. Exosomes: immune properties and potential clinical implementations. Semin Immunopathol. 2011;33:419–40.
5. Clayton A, Court J, Navabi H, Adams M, Mason MD, Hobot JA, et al. Analysis of antigen presenting cell derived exosomes, based on immuno-magnetic isolation and flow cytometry. J Immunol Methods. 2001;247:163–74.
6. Raposo G, Nijman HW, Stoorvogel W, Liejendekker R, Harding CV, Melief CJ, et al. B lymphocytes secrete antigen-presenting vesicles. J Exp Med. 1996;183:1161–72.
7. Admyre C, Johansson SM, Paulie S, Gabrielsson S. Direct exosome stimulation of peripheral human T cells detected by ELISPOT. Eur J Immunol. 2006;36:1772–81.
8. Segura E, Nicco C, Lombard B, Véron P, Raposo G, Batteux F, et al. ICAM-1 on exosomes from mature dendritic cells is critical for efficient naive T-cell priming. Blood. 2005;106:216–23.
9. Andreola G, Rivoltini L, Castelli C, Huber V, Perego P, Deho P, et al. Induction of lymphocyte apoptosis by tumor cell secretion of FasL-bearing microvesicles. J Exp Med. 2002;195:1303–16.
10. Clayton A, Mitchell JP, Court J, Mason MD, Tabi Z. Human tumor-derived exosomes selectively impair lymphocyte responses to interleukin-2. Cancer Res. 2007;67:7458–66.
11. Chen G, Huang AC, Zhang W, Zhang G, Wu M, Xu W, et al. Exosomal PD-L1 contributes to immunosuppression and is associated with anti-PD-1 response. Nature. 2018;560:382–6.
12. McInnes IB, Schett G. The pathogenesis of rheumatoid arthritis. N Engl J Med. 2011;365:2205–19.
13. Gary SF. Etiology and pathogenesis of rheumatoid arthritis. In: Gary SE, Ralph CB, Ted H, Ian BM, Shaun R, John SS, editors. Kelley's textbook of rheumatology. 8th ed. Philadelphia: Saunders; 2009. p. 1035–87.
14. Gary SF. Pathogenesis of rheumatoid arthritis. In: Paul LR, editor. UpToDate. Waltham, MA: UpToDate; 2016.
15. Skriner K, Adolph K, Jungblut PR, Burmester GR. Association of citrullinated proteins with synovial exosomes. Arthritis Rheum. 2006;54:3809–14.
16. Zhang HG, Liu C, Su K, Yu S, Zhang L, Zhang S, et al. A membrane form of TNF-alpha presented by exosomes delays T cell activation-induced cell death. J Immunol. 2006;176:7385–93.
17. Kato T, Miyaki S, Ishitobi H, Nakamura Y, Nakasa T, Lotz MK, et al. Exosomes from IL-1β stimulated synovial fibroblasts induce osteoarthritic changes in articular chondrocytes. Arthritis Res Ther. 2014;16:R163.
18. Tsuno H, Suematsu N, Sato T, Arito M, Matsui T, Iizuka N, et al. Effects of methotrexate and salazosulfapyridine on protein profiles of exosomes derived from a human synovial sarcoma cell line of SW982. Proteomics Clin Appl. 2016;10:164–71.
19. Yoo J, Lee SK, Lim M, Sheen D, Choi EH, Kim SA. Exosomal amyloid a and lymphatic vessel endothelial hyaluronic acid receptor-1 proteins are associated with disease activity in rheumatoid arthritis. Arthritis Res Ther. 2017;19:119.
20. Sun W, Zhao C, Li Y, Wang L, Nie G, Peng J, et al. Osteoclast-derived microRNA-containing exosomes selectively inhibit osteoblast activity. Cell discov. 2016;2:16015.
21. Li D, Liu J, Guo B, Liang C, Dang L, Lu C, et al. Osteoclast-derived exosomal miR-214-3p inhibits osteoblastic bone formation. Nat Commun. 2016;7:10872.
22. Arnett FC, Edworthy SM, Bloch DA, McShane DJ, Fries JF, Cooper NS, et al. The American rheumatism association 1987 revised criteria for the classification of rheumatoid arthritis. Arthritis Rheum. 1988;31:315–24.
23. Altman R, Asch E, Bloch D, Bole G, Borenstein D, Brandt K, et al. The American College of Rheumatology criteria for the classification and reporting of osteoarthritis of the knee. Arthritis Rheum. 1986;29:1039–49.
24. Inoue E, Yamanaka H, Hara M, Tomatsu T, Kamatani N. Comparison of disease activity score (DAS)28- erythrocyte sedimentation rate and DAS28-C-reactive protein threshold values. Ann Rheum Dis. 2007;66:407–9.
25. Shimada S, Nakamura M, Tanaka Y, Tsutsumi K, Katano M, Masuko K, et al. Crosslinking of the CD69 molecule enhances S100A9 production in activated neutrophils. Microbiol Immunol. 2007;51:87–98.
26. Kalra H, Simpson RJ, Ji H, Aikawa E, Altevogt P, Askenase P, et al. Vesiclepedia: a compendium for extracellular vesicles with continuous community annotation. PLoS Biol. 2012;10:e1001450.
27. Alexopoulou L, Holt AC, Medzhitov R, Flavell RA. Recognition of double-stranded RNA and activation of NF-kappaB by toll-like receptor 3. Nature. 2001;413:732–8.
28. Botos I, Liu L, Wang Y, Segal DM, Davies DR. The toll-like receptor 3: dsRNA signaling complex. Biochim Biophys Acta. 2009;1789:667–74.
29. Garcia-Cattaneo A, Gobert FX, Müller M, Toscano F, Flores M, Lescure A, et al. Cleavage of toll-like receptor 3 by cathepsins B and H is essential for signaling. Proc Natl Acad Sci U S A. 2012;109:9053–8.
30. Brentano F, Schorr O, Gay RE, Gay S, Kyburz D. RNA released from necrotic synovial fluid cells activates rheumatoid arthritis synovial fibroblasts via toll-like receptor 3. Arthritis Rheum. 2005;52:2656–65.
31. Frank-Bertoncelj M, Pisetsky DS, Kolling C, Michel BA, Gay RE, Jüngel A, et al. TLR3 ligand poly (I:C) exerts distinct actions in synovial fibroblasts when delivered by extracellular vesicles. Front Immunol. 2018;9:28.
32. Zhu W, Meng L, Jiang C, Xu J, Wang B, Han Y, et al. Overexpression of toll-like receptor 3 in spleen is associated with experimental arthritis in rats. Scand J Immunol. 2012;76:263–70.
33. Takakuwa Y, Kurokawa MS, Ooka S, Sato T, Nagai K, Arito M, et al. AC13, a C-terminal fragment of apolipoprotein A-I, is a candidate biomarker for microscopic polyangiitis. Arthritis Rheum. 2011;63:3613–24.
34. Zhang D, Sliwkowski MX, Mark M, Frantz G, Akita R, Sun Y, et al. Neuregulin-3 (NRG3): a novel neural tissue-enriched protein that binds and activates ErbB4. Proc Natl Acad Sci U S A. 1997;94:9562–7.
35. Kao WT, Wang Y, Kleinman JE, Lipska BK, Hyde TM, Weinberger DR, et al. Common genetic variation in Neuregulin 3 (NRG3) influences risk for schizophrenia and impacts NRG3 expression in human brain. Proc Natl Acad Sci U S A. 2010;107:15619–24.
36. Yuan FL, Li X, Lu WG, Sun JM, Jiang DL, Xu RS. Epidermal growth factor receptor (EGFR) as a therapeutic target in rheumatoid arthritis. Clin Rheumatol. 2013;32:289–92.
37. Wang B, Shi GP, Yao PM, Li Z, Chapman HA, Bromme D. Human cathepsin F Molecular cloning, functional expression, tissue localization, and enzymatic characterization. J Biol Chem. 1998;273:32000–8.
38. Kozawa E, Nishida Y, Cheng XW, Urakawa H, Arai E, Futamura N, Shi GP, Kuzuya M, Hu L, Sasaki T, Ishiguro N. Osteoarthritic change is delayed in a Ctsk-knockout mouse model of osteoarthritis. Arthritis Rheum. 2012;64:454–64.
39. Kozawa E, Cheng XW, Urakawa H, Arai E, Yamada Y, Kitamura S, Sato K, Kuzuya M, Ishiguro N, Nishida Y. Increased expression and activation of cathepsin K in human osteoarthritic cartilage and synovial tissues. J Orthop Res. 2016;34:127–34.
40. Carteron C, Ferrer-Montiel A, Cabedo H. Characterization of a neural-specific splicing form of the human neuregulin 3 gene involved in oligodendrocyte survival. J Cell Sci. 2006;119:898–909.
41. Somoza JR, Palmer JT, Ho JD. The crystal structure of human cathepsin F and its implications for the development of novel immunomodulators. J Mol Biol. 2002;322:559–68.
42. Picariello G, Ferranti P, Mamone G, Roepstorff P, Addeo F. Identification of N-linked glycoproteins in human milk by hydrophilic interaction liquid chromatography and mass spectrometry. Proteomics. 2008;8:3833–47.

Brain Research 1719 (2019) 140–147

Contents lists available at ScienceDirect

Brain Research

journal homepage: www.elsevier.com/locate/brainres

Research report

Layilin enhances the invasive ability of malignant glioma cells via SNAI1 signaling

Tomohiro Kaji[a,b], Mitsumi Arito[a,*], Atsuhiro Tsutiya[a], Taigen Sase[b], Hidetaka Onodera[b], Toshiyuki Sato[a], Kazuki Omoteyama[a], Masaaki Sato[a], Naoya Suematsu[a], Manae S. Kurokawa[c], Yuichiro Tanaka[b], Tomohiro Kato[a]

[a] *Clinical Proteomics and Molecular Medicine, St. Marianna University Graduate School of Medicine, 2-16-1 Sugao, Miyamae, Kawasaki, Kanagawa 216-8511, Japan*
[b] *Department of Neurosurgery, St. Marianna University Graduate School of Medicine, 2-16-1 Sugao, Miyamae, Kawasaki, Kanagawa 216-8511, Japan*
[c] *Disease Biomarker Analysis and Molecular Regulation, St. Marianna University Graduate School of Medicine, 2-16-1 Sugao, Miyamae, Kawasaki, Kanagawa 216-8511, Japan*

HIGHLIGHTS

- Malignant glioma cells highly expressed layilin, compared to astrocytes.
- Layilin was mainly localized in the cytoplasm of A172 and T98G cells.
- Layilin up-regulated SNAI1 to increase expression of MMP2, MMP9 and COL1A1.
- Transcription of SNAI1 was up-regulated via down-regulation of MTA3 by layilin.
- Layilin enhanced the invasive ability of malignant glioma cells.

ARTICLE INFO

Keywords:
Glial-mesenchymal transition
Layilin
Malignant gliomas
MTA3
SNAI1

ABSTRACT

Background: Malignant gliomas are characterized by high invasive ability. In this study, we investigated roles of layilin, a C-type lectin-homologous protein, in the invasive ability of malignant glioma cells.
Methods: Expression of layilin was investigated by western blotting in the malignant glioma cell lines of U251-MG, A172, and T98G and in astrocytes. The effects of layilin-knockdown on the expression and protein levels of snail family transcriptional repressor 1 (SNAI1), a transcriptional factor involved in the acquisition and enhancement of invasive ability in malignant gliomas, and on the expression of its target genes, matrix metalloproteinase 2 (*MMP2*), *MMP9*, and collagen type I alpha 1 chain (*COL1A1*), were investigated by qPCR and/or western blotting. Furthermore, the effects of layilin-knockdown on the expression and protein levels of metastasis associated 1 family member 3 (MTA3), a transcriptional repressor of *SNAI1*, were also investigated by qPCR and western blotting. Finally, the effects of layilin-knockdown on the invasive ability of the cells were investigated by a wound healing assay.
Results: All the tested malignant glioma cells highly expressed layilin, compared to astrocytes, one of representative glial cell types. Layilin-knockdown reduced SNAI1 both at the mRNA and protein levels in A172 cells, and consequently mRNA levels of MMP2, MMP9, and COL1A1 were also reduced. Furthermore, layilin-knockdown increased nuclear protein levels of MTA3 in A172 cells. Notably, layilin-knockdown suppressed the invasive ability of the cells.
Conclusion: Layilin up-regulates the expression of *SNAI1* via down-regulation of MTA3. This process enhances the invasive ability of malignant glioma cells.

* Corresponding author.
E-mail addresses: t2kaji@marianna-u.ac.jp (T. Kaji), m-ari@marianna-u.ac.jp (M. Arito), atsuchi@marianna-u.ac.jp (A. Tsutiya), sasetaigen@marianna-u.ac.jp (T. Sase), dera@marianna-u.ac.jp (H. Onodera), stoshi@marianna-u.ac.jp (T. Sato), omoteyama@marianna-u.ac.jp (K. Omoteyama), msato@marianna-u.ac.jp (M. Sato), n2sue@marianna-u.ac.jp (N. Suematsu), manae@marianna-u.ac.jp (M.S. Kurokawa), tanaka@marianna-u.ac.jp (Y. Tanaka), t3kato@marianna-u.ac.jp (T. Kato).

https://doi.org/10.1016/j.brainres.2019.05.034
Received 8 January 2019; Received in revised form 15 May 2019; Accepted 26 May 2019
Available online 27 May 2019
0006-8993/ © 2019 Published by Elsevier B.V.

1. Introduction

Gliomas account for 25–30% of brain tumors (Goodenberger and Jenkins, 2012) and arise from glial cells, which support brain neuronal cells in the central nervous system (Goodenberger and Jenkins, 2012). Malignant gliomas (World Health Organization grades III and IV) are particularly lethal tumors and characterized by their diffuse invasion into surrounding brain parenchyma and unclear their boundaries (Cuddapah et al., 2014; Louis et al., 2007; Louis et al., 2016).

Recently, a transcriptional factor, snail family transcriptional repressor 1 (SNAI1) has been reported to play roles in the acquisition and enhancement of invasiveness in malignant gliomas (Han et al., 2011). Generally, cell motility is activated by the reconstruction of actin filaments and the degradation of extracellular matrix by matrix metalloproteinases (MMPs), which mechanisms have been reported to contribute to the invasiveness of tumor cells (Kahlert et al., 2013; Iwadate, 2016). In malignant glioma cells, it has been reported that SNAI1 up-regulates the gene expression of MMP2 and/or MMP9, which degrade type IV collagen in peripheral basement membranes to promote cell invasion (Han et al., 2011; Yokoyama et al., 2003; Wu et al., 2017; Myung et al., 2014). From the viewpoint of expression patterns of epithelial mesenchymal transition (EMT)-related genes, the process of the acquisition and enhancement of invasive ability in malignant gliomas has similarities to EMT (Kalluri and Weinberg, 2009). During EMT, epithelial cells lose polarity and cell-cell adhesion and acquire migratory and invasive properties. Accordingly, the levels of epithelial cell markers such as E-cadherin decrease and the levels of mesenchymal cell markers such as vimentin, “actin alpha 2, smooth muscle” (ACTA2), and MMP2/MMP9 increase. These changes are also observed in malignant gliomas. Thereby, mesenchymal transition of glioma cells is sometimes called the “glial-mesenchymal transition” (GMT) (Mahabir et al., 2014; Kühnöl et al., 2017).

Layilin is a type 1 transmembrane protein with a C-type lectin-like motif (Bono et al., 2001). Layilin has been reported to be a receptor for hyaluronic acid and to bind to cytoskeletal proteins such as talin and merlin to regulate cell adhesion (Bono et al., 2001; Bono et al., 2005; Borowsky and Hynes, 1998; Wegener et al., 2008; Scoles, 2008). On the relation with EMT, we demonstrated that layilin is involved in the TNF-α-mediated EMT of epithelial like-clear cell renal carcinoma cells (Adachi et al., 2015).

Based on the abovementioned facts, we here hypothesized that layilin could induce GMT to enhance invasive ability in malignant glioma cells. To test this hypothesis, we investigated whether layilin was expressed in human malignant glioma cell lines and if so, whether layilin was involved in GMT to enhance invasive ability of the cells in the present study.

2. Results

2.1. Malignant glioma cells showed highly expressed layilin

We first investigated expression levels of layilin in U251-MG, A172, and T98G cells of malignant glioma cell lines and in astrocytes by western blotting. As a result, all the three cell lines expressed high levels of layilin, compared to astrocytes (Fig. 1A). We next investigated the localization of layilin in A172 and T98G cells immunocytochemically. As a result, layilin was mainly localized not on the cell surface but to the cytoplasm in both cell types (Fig. 1B). Based on these data, we then examined whether layilin was localized to the endoplasmic reticulum (ER) and/or to Golgi bodies. As a result, layilin did not co-localize with calnexin, an ER marker (Fig. 1C, upper), but some did co-localized with golgin 97, a Golgi marker (Fig. 1C, lower). These data suggest that some layilin is localized to Golgi bodies and that the remainder of the cytoplasmic layilin is not localized to the ER; thus, layilin may have a function other than that of a hyaluronan receptor.

2.2. Layilin-knockdown decreased the expression of SNAI1 and its target genes

SNAI1 has been recently reported to play critical roles in the acquisition and enhancement of invasive ability in malignant gliomas (Han et al., 2011). We therefore investigated whether layilin-knockdown by treatment with siRNA (siL-1 and siL-2) affected molecules that were involved in invasiveness of A172 cells. We first confirmed that the expression of layilin mRNA was nearly completely suppressed both by the treatment with siL-1 and by that with siL-2 (Fig. 2A, left). We then evaluated the effects of layilin-knockdown on the expression of *SNAI1* and *SNAI2* genes. As a result, SNAI1 mRNA levels were significantly decreased by the treatment with siL-1 and siL-2 (Fig. 2A, center), whereas SNAI2 mRNA levels were not changed (Fig. 2A, right). We next assessed protein levels of SNAI1 in whole cell and nuclear extracts of layilin-knockdown A172 cells. After we confirmed that both extracts were successfully prepared (Fig. 2B, upper left), we checked the protein levels of SNAI1. As a result, protein levels of SNAI1 were significantly decreased by the treatment with siL-1 and siL-2 in both the whole cell and nuclear extracts (Fig. 2B, upper right and lower). Accordingly, mRNA levels of vitronectin and occludin, both well-known target genes of SNAI1, were significantly decreased by the treatment with siL-1 and siL-2 (Fig. 2C, upper). Similarly, mRNA levels of MMP2, MMP9, and COL1A1, which are other target genes of SNAI1 involved in cellular invasive ability, were also significantly decreased by the treatment with siL-1 and siL-2 (Fig. 2C, lower). These data indicate that layilin up-regulates the expression of *SNAI1* to promote the expression of *MMP2*, *MMP9*, and *COL1A1*, as well as other SNAI1 target genes.

2.3. Layilin-knockdown increased nuclear metastasis associated 1 family member 3 (MTA3) level

Cellular protein levels of SNAI1 are known to be regulated by transcription and post-translational modification (Aomatsu et al., 2011; Liang et al., 2017; Fujita et al., 2003; Toh and Nicolson, 2008; Chen et al., 2013; Zhou et al., 2004; Yamaguchi et al., 2012).

The transcription of the *SNAI1* gene is up-regulated by phosphorylated smad 2/3 and down-regulated by nuclear MTA3 (Aomatsu et al., 2011; Liang, et al., 2017; Fujita et al., 2003; Toh and Nicolson, 2008; Chen et al., 2013). We therefore investigated whether layilin-knockdown decreased phosphorylated smad 2/3 levels in A172 cells. As a result, phosphorylated smad 2/3 levels could not be detected in either whole cell or nuclear extracts (data not shown). We next investigated whether layilin-knockdown increased MTA3 at mRNA and protein levels. As a result, mRNA levels of MTA3 were not changed by treatment with siL-1 and siL-2 (Fig. 3A, upper left), whereas the amounts of whole and nuclear MTA3 protein were significantly increased (Fig. 3A, upper middle, upper right, and lower). These data indicate that layilin down-regulates nuclear MTA3. The transcriptional up-regulation of *SNAI1* by layilin is thought to be mainly due to down-regulation of nuclear MTA3.

2.4. Layilin-knockdown up-regulated phosphorylation of ERK, Akt, and GSK3β

Again, cellular protein levels of SNAI1 are regulated by post-translational modification as well as by transcription (Zhou et al., 2004; Yamaguchi et al., 2012). Specifically, SNAI1 phosphorylated by kinases such as GSK3β is degraded by the ubiquitin-proteasome degradation system (Zhou et al., 2004; Yamaguchi et al., 2012). Since GSK3β acts down-stream of ERK and Akt (Zhou et al., 2004; Yamaguchi et al., 2012), we investigated whether layilin-knockdown affected the levels of ERK, Akt, and GSK3β proteins and their phosphorylation (p-ERK, p-Akt, and p-GSK3β) in A172 cells. As a result, total ERK (t-ERK) and total Akt (t-Akt), as well as p-ERK and p-Akt were significantly increased by the treatment with siL-1 and siL-2 (Fig. 3B). The ratio of p-ERK to t-ERK and that of p-Akt to t-Akt were significantly increased by the treatment

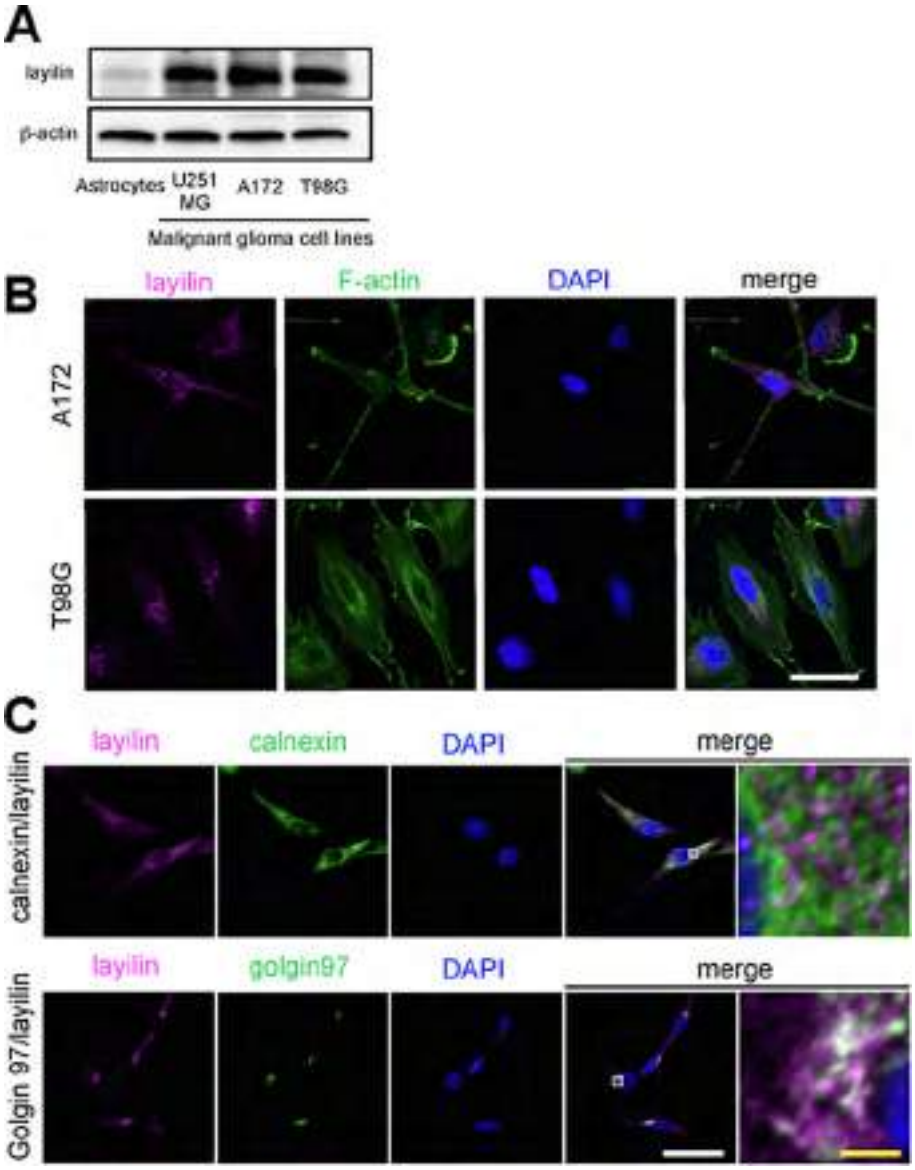

Fig. 1. Protein levels and localization of layilin. (A) Proteins extracted from astrocytes and malignant glioma cell lines (U251MG, A172, and T98G cells) were subjected to western blotting with anti-layilin and anti-actin antibodies. (B) Layilin was immunocytochemically detected in A172 and T98G cells. After fixation of cultured A172 and T98G cells, layilin was detected using mouse monoclonal anti-layilin antibodies and Alexa 647-labeled anti-mouse IgG (magenta). F-actin was detected using Alexa 488-labeled phalloidin (green). Nuclei were stained with DAPI (blue). A white bar indicates 50 μm. (C) Layilin, calnexin, and golgin 97 were immunocytochemically detected in A172 cells. For double staining of layilin and calnexin, layilin was detected with the mouse anti-layilin antibodies and Alexa 647-labeled anti-mouse IgG antibodies (magenta in upper panels). Calnexin was detected using rabbit anti-calnexin antibodies and Alexa 488-labeled anti-rabbit IgG (green in upper panels). For double staining of layilin and golgin 97, layilin was detected with the goat anti-layilin antibodies and Alexa 647-labeled anti-goat IgG antibodies (magenta in lower panels). Golgin 97 was detected using mouse anti-golgin 97 antibodies and Alexa 488-labeled anti-mouse IgG (green in lower panels). The areas enclosed by open squares in the left panels of the merged panels are enlarged in the right panels. White and yellow bars indicate 50 and 2 μm, respectively.

with siL-1 and siL-2 (Fig. 3B). These data indicate that active ERK (p-ERK) and active Akt (p-Akt) were significantly increased by the treatment with siL-1 and siL-2. Accordingly, p-GSK3β, an inactive form of GSK3β, were also significantly increased by the treatment with siL-1 and siL-2 (Fig. 3B). In addition, total GSK3β (t-GSK3β) were significantly increased by the treatment with siL-1 and siL-2 (Fig. 3B). Since the ratio of p-GSK3β to t-GSK3β were also significantly increased, it could not be determined whether active GSK3β (the non-phosphorylated form) were increased or not.

2.5. Layilin-knockdown suppressed invasive ability of cells

Finally, we investigated the effects of layilin-knockdown on the invasive ability of the cells by a wound healing assay. As a result, both the areas and numbers of migrating cells were significantly decreased by treatment with siL-1 and siL-2 (Fig. 4A). These data indicate that layilin is involved in the invasive ability of malignant glioma cells.

3. Discussion

Our findings can be summarized as follows: 1) Malignant glioma cells expressed high levels of layilin; 2) Layilin was mainly localized to the cytoplasm not the cell surface; 3) Layilin up-regulated the gene expression of SNAI1, which increased the expression of *MMP2*, *MMP9*, and *COL1A1*; 4) Up-regulation of *SNAI1* expression by layilin was mainly due to down-regulation of nuclear MTA3; 5) Layilin suppressed the phosphorylation of ERK, Akt, and GSK3β, and 6) Layilin enhanced the invasive ability of malignant glioma cells (Fig. 4B).

On the first point, all the tested malignant glioma cells expressed high levels of layilin, compared to astrocytes. We previously reported that TNF-α up-regulated expression of layilin in chondrocytes and renal carcinoma cells (Adachi et al., 2015; Asano et al., 2014). However, malignant glioma cells seem to spontaneously express layilin strongly without any stimulation. Unknown mechanisms other than TNF-α-induced signaling may therefore promote the expression of layilin in malignant glioma cells. This point needs to be addressed in future studies.

On the second point, layilin has been reported to function as a hyaluronan receptor at the cell surface (Bono et al., 2001; Bono et al., 2005). However, in this study, we found that layilin was mainly localized not on the cell surface but to the cytoplasm of malignant glioma cells. Moreover, we also found that layilin-knockdown was enough to down-regulate expression of several genes contributing to cellular invasive ability in the absence of hyaluronan treatment. Therefore, we

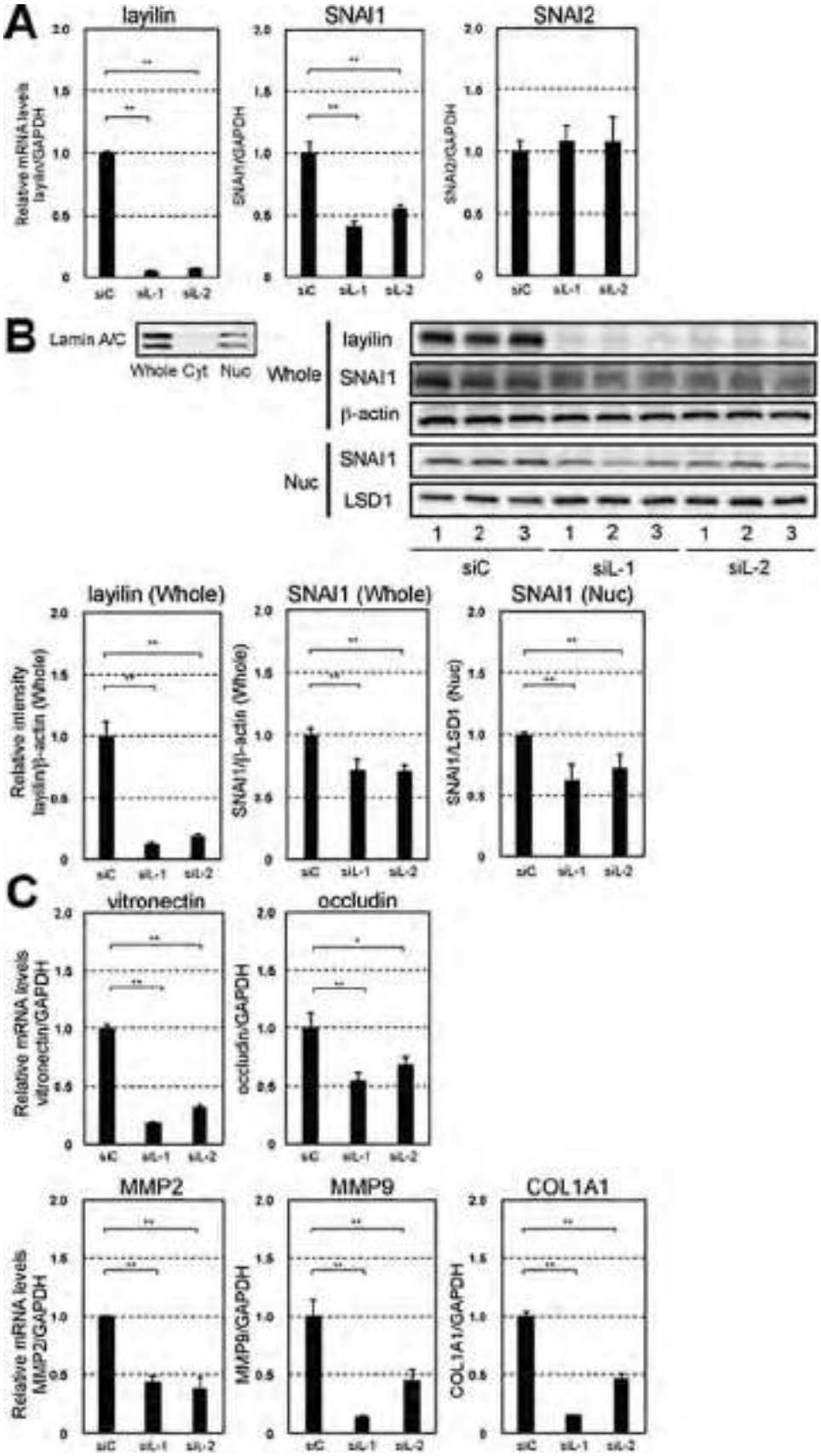

Fig. 2. Effects of layilin knockdown on the expression of *SNAI1* and its target genes in A172 cells. A172 cells were transfected with control siRNA (siC) and 2 kinds of layilin siRNA (siL-1 or siL-2/n = 3 for each condition). (A) RNA extracted from the cells was used for reverse-transcription and the subsequent quantitative PCR to estimate amounts of mRNA for layilin, SNAI1, SNAI2, and GAPDH. Measured mRNA levels of layilin, SNAI1, and SNAI2 were corrected using those of GAPDH. In each panel, the average of the corrected mRNA levels in the samples transfected with siC was defined as 1.0. (B) Proteins were extracted from whole cells (Whole). Cytosol and nuclei (Cyt and Nuc, respectively) were fractionated. The protein samples were subjected to western blotting. Lamin A/C was used as a nuclear marker. The intensity of the detected bands was measured by a densitometer. Measured intensities of layilin and SNAI1 (Whole) and SNAI1 (Nuc) were normalized using that of β-actin and lysine-specific histone demethylase 1 (LSD1), respectively. The averages of the normalized layilin (Whole) and SNAI1 (Whole and Nuc) intensities in the "siC" samples were defined as 1.0. (C) RNA extracted from cells was used for reverse transcription and the subsequent quantitative PCR to estimate the amounts of mRNA for vitronectin, occludin, MMP2, MMP9, COL1A1, and GAPDH. Measured mRNA levels for vitronectin, occludin, MMP2, MMP9, and COL1A1 were corrected using those of GAPDH. In each panel, the average of the corrected mRNA levels in samples transfected with siC was defined as 1.0. Mean values with SD are shown. * < 0.05, ** < 0.01.

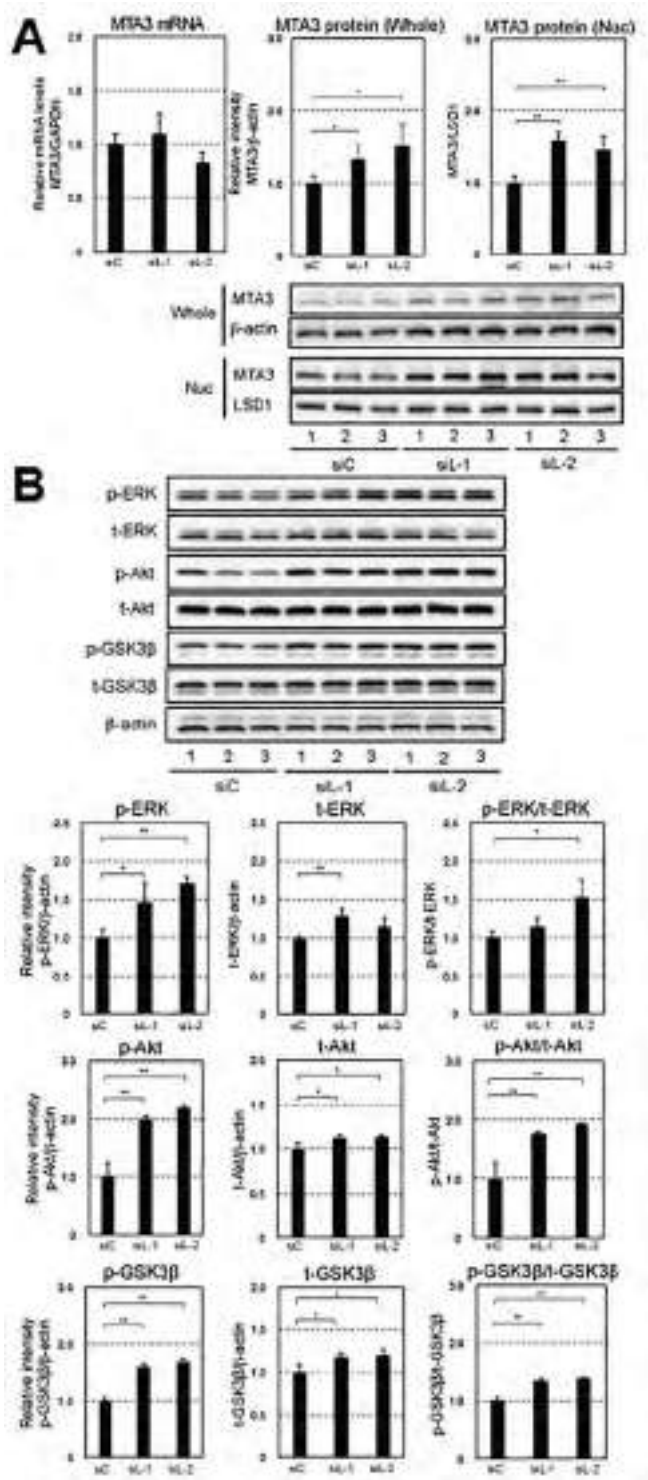

Fig. 3. Effects of layilin knockdown on regulators of SNAI1. A172 cells were transfected with siC, siL-1 and siL-2 (n = 3 for each condition). (A) RNA extracted from the cells was used for reverse transcription and the subsequent quantitative PCR to estimate amounts of mRNA for MTA3 and GAPDH. Measured mRNA levels of MTA3 were corrected using those of GAPDH. In each panel, the average of the corrected mRNA levels in samples transfected with siC was defined as 1.0 (Upper left panel). Proteins were extracted from whole cells (Whole) and isolated nuclei (Nuc). The measured intensities of MTA3 (Whole) and MTA3 (Nuc) were normalized using those of β-actin and LSD1, respectively. The averages of the normalized MTA3 (Whole and Nuc) intensities in the "siC" samples were defined as 1.0 (Upper middle and right panels). The images of the western blotting are shown in the lower panels. (B) Proteins were extracted from whole cells and the samples were subjected to western blotting. β-actin was used as an internal control. Intensities of the detected bands were measured by a densitometer. The averages of the normalized p/t-ERK, p/t-Akt and p/t-GSK3β intensities and the calculated p-ERK/t-ERK, p-Akt/t-Akt, and p-GSK3β/t-GSK3β values in the "siC" samples were defined as 1.0. Mean values with SD are shown. * < 0.05, ** < 0.01.

speculate that layilin enhances the invasive ability of malignant glioma cells, independently of its function as a hyaluronan receptor. In addition, our data suggest that some layilin is localized to Golgi bodies. Layilin in Golgi bodies may play a role in Golgi function or may simply be in the process of post-translational modification like glycosylation. The precise localization of the remaining pool of layilin has not been determined, although it may be present in cytoplasmic vesicles. We plan to clarify the localization and functions of layilin in the cytoplasm and in Golgi bodies in more detail in the future.

On the third and sixth points, layilin up-regulated expression of *MMP2*, *MMP9*, and *COL1A1* via SNAI1 and enhanced the invasive ability of A172 cells, and these three molecules have been reported to enhance the invasive ability in malignant glioma cells (Han et al., 2011; Yokoyama et al., 2003; Wu et al., 2017; Myung et al., 2014; Sun et al., 2018). Furthermore, layilin enhanced the motility of A172 cells in a wound healing assay. Since cell motility generally contributes to the invasiveness of tumor cells, layilin is thought to contribute to invasive ability of malignant glioma cells. In addition, SNAI1 has various target genes other than *MMP2*, *MMP9*, and *COL1A1*. For example, SNAI1 has been reported to increase the expression of cyclin-dependent kinase 1 (*CDK1*) and decrease the expression of cyclin dependent kinase inhibitor 1A (*P21*) to promote cell proliferation (Yang et al., 2017). In addition, SNAI1 has been reported to increase the expression of caspases and tumor protein p53 (*TP53*) to inhibit apoptosis (Barrallo-Gimeno and Nieto, 2005). Therefore, layilin would contribute to both cell proliferation and death resistance in malignant glioma cells via the regulation of SNAI1 targets. This point needs further investigation in future studies.

On the fourth point, layilin-knockdown did not affect the expression of *MTA3* (Fig. 3A, upper left). On the other hand, it increased the amounts of whole cellular MTA3 protein and that present in the nuclei (Fig. 3A, upper middle and right). We therefore speculate that layilin increases the stability of MTA3 proteins. This point should be also investigated in the near future.

On the fifth point, layilin-knockdown increased the amounts of t-GSK3β and p-GSK3β (Fig. 3B). It is unlikely that layilin promotes phosphorylation of SNAI1 by GSK3β, although it cannot be denied that the amounts of non-phosphorylated GSK3β is increased by layilin-knockdown. In contrast, SNAI1 has been reported to activate PI3K and ERK, which phosphorylate GSK3β (Barrallo-Gimeno and Nieto, 2005). In this study, layilin-knockdown decreased expression of *SNAI1*, whereas it increased phosphorylation of ERK and GSK3β. Our data are inconsistent with theirs. This discrepancy should be clarified in future studies using various types of malignant glioma cells.

4. Conclusion

Layilin up-regulates the expression of *SNAI1* via MTA3, which enhances the invasive ability of malignant glioma cells.

5. Materials and methods

5.1. Cell culture

Human astrocytes (Lonza Group Ltd., Basel, Switzerland) were cultured in Astrocyte Basal Medium (ABMTM, Lonza Walkersville, Inc., USA) containing 0.1% recombinant human epidermal growth factor,

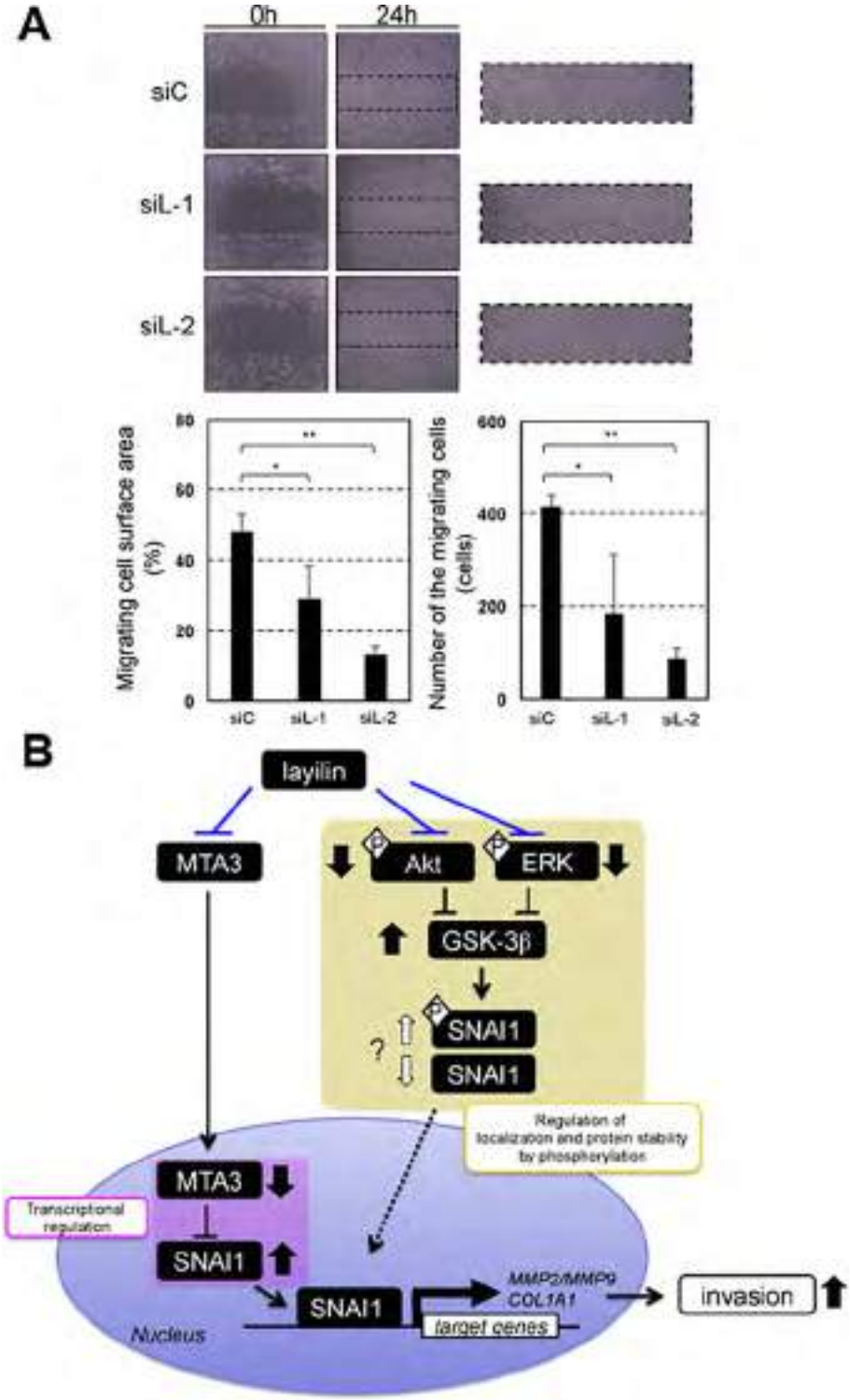

Fig. 4. Effects of layilin-knockdown on the invasive ability and summary of this study. (A) A172 cells transfected with siC, siL-1 and siL-2 were cultured in 24 well plates for a wound healing assay (n = 3 for each condition). Representative images of the wound fields at 0 and 24 h after removal of the wound-creating inserts (upper left 6 panels). Areas and numbers of cells migrating into the wound areas enclosed by the dotted lines in the 24-h panels (upper right 3 panels) were measured. The invasive ability was evaluated by < equation: migrating cell-occupying area/the wound fields enclosed by dotted lines × 100 (%) > (lower left panel). The invasive ability was also evaluated by counting the cells that had migrated into the wound fields enclosed by the dotted lines (lower right panel). Mean values with SD are shown. * < 0.05, ** < 0.01 (B) Summary of the results of this study.

0.25% insulin, 3% fetal bovine serum (FBS, Sigma-Aldrich, St. Louis, MO, USA), 0.1% ascorbic acid, 1% L-glutamine, and 0.1% GA-1000 (AGM™ BulletKit™, AGM™ plus SingleQuots™ of Growth Supplements). A-172 and T98G of human malignant glioma cell lines (DS Pharma Biomedical Co., LTD, Osaka, Japan) were cultured in RPMI1640 (Sigma-Aldrich) supplemented with 10% FBS, 100 U/ml penicillin, and 100 μg/ml streptomycin (Sigma-Aldrich). U-251 MG cells of a human malignant glioma cell line (DS Pharma Biomedical Co. Ltd) were cultured in EMEM (NISSUI PHARMACEUTICAL Co., Ltd, Tokyo, Japan) containing 7% sodium bicarbonate (Otsuka Pharmaceutical Co., Ltd., Tokyo, Japan) and 1% L-glutamine (NISSUI PHARMACEUTICAL Co., Ltd) and supplemented with 10% FBS (MP Biomedical LLC, Santa Ana, CA, USA), 100 U/ml penicillin, and 100 μg/ml streptomycin. The cells were cultured at 37 °C in an atmosphere containing 5% CO_2.

5.2. Protein extraction from cultured cells

Cultured cells, washed in phosphate buffered saline (PBS) and collected, were sonicated in a lysis buffer (20 mM Tris-HCl (pH7.4), 250 mM NaCl, 1% NP-40, 1 mM dithiothreitol) including protease

inhibitor cocktail (Roche, Basel, Switzerland). After centrifugation, collected supernatants were used as protein samples. Nuclear and cytosolic fractions were prepared using Nuclear/Cytosolic Fractionation Kit (CELL BIOLABS INC, San Diego, CA, USA) by following the manufacturer's instruction.

5.3. Western blotting

Western blotting was performed as described previously (Asano et al., 2014). Briefly, the protein samples, separated by 15% SDS-PAGE, were transferred onto polyvinylidene difluoride membranes. Goat polyclonal antibodies to human layilin (R&D Systems Inc., Minneapolis, MN, USA), rabbit polyclonal antibodies to human MTA3 (abcam, Cambridge, UK), LSD1 (Cell Signaling Technology Inc. (CST), Danvers, MA, USA), p-ERK (CST), p-Akt (CST), Akt (CST), p-GSK-3β (CST), and GSK-3β (CST), and mouse monoclonal antibodies to human SNAI1 (CST), β-actin (Sigma), and ERK (CST) were used as primary antibodies. Horseradish peroxidase (HRP)-conjugated rabbit anti-goat IgG antibodies (Agilent/DAKO, Santa Clara, CA, USA), anti-mouse IgG antibodies (CST), and goat anti-rabbit IgG antibodies (Agilent/DAKO) were used as secondary antibodies. The bound antibodies were visualized using ImmunoStar® LD (FUJI FILM, Osaka, Japan).

5.4. Immunocytochemistry

A172 and T98G cells were fixed in PBS containing 4% paraformaldehyde. The fixed cells were treated with Alexa Fluor 488-labeled phalloidin (Cytoskeleton Inc., Denver, CO, USA) to stain F-actin and then with mouse monoclonal anti-layilin antibodies (Santa Cruz, Dallas, TX, USA). In the latter, the bound antibodies were further reacted with goat anti-mouse IgG antibodies conjugated with Alexa Fluor 647 (Invitrogen, Carlsbad, CA, USA). For double staining of layilin and calnexin, the fixed cells were treated with the mouse monoclonal anti-layilin antibodies (Santa Cruz)/rabbit monoclonal anti-calnexin antibodies (CST). The bound antibodies were further reacted with anti-mouse IgG antibodies conjugated with Alexa Fluor 647 (Invitrogen)/anti-rabbit IgG antibodies conjugated with Alexa Fluor 488 (Invitrogen). For double staining of layilin and golgin 97, the fixed cells were treated with the goat anti-layilin antibodies (R&D Systems Inc)/mouse monoclonal anti-golgin 97 antibodies (Santa Cruz). The bound antibodies were further reacted with anti-goat IgG antibodies conjugated with Alexa Fluor 647 (Invitrogen)/anti-mouse IgG antibodies conjugated with Alexa Fluor 488 (Invitrogen). Nuclei were stained with DAPI (Wako Pure Chemical Industries, Osaka, Japan). Nuclei and the bound antibodies were visualized by confocal fluorescence microscopy (LSM510 META, Carl Zeiss, Jena, Germany).

5.5. Treatment of A172 cells with siRNA

A172 cells were transfected with 200 pmol/100 mm dish of 2 kinds of siRNA for human layilin mRNA (siL-1; nucleotides 844–868 (CAGT GGAATGATGACCGGTGCAACA) and siL-2; nucleotides 1019–1043 (AAGCTGCCTTGAATCTGGCCTACAT) in NM_001258390.1, Invitrogen) using Lipofectamine RNAiMAX (Invitrogen) according to manufacturer's instructions. As a negative control, A172 cells were transfected with the same doses of control siRNA (siC, Stealth™ RNAi Negative Control Medium GC Duplex, Invitrogen). Cells were used for subsequent experiments after 24 h.

5.6. RNA extraction and reverse transcription

RNA extraction and RT-PCR were performed as described previously (Asano et al., 2014). Briefly, extraction and purification of RNA from A172 cells and reverse transcription of the RNA samples were performed using RNeasy (Qiagen, Venlo, The Netherlands) and High Capacity cDNA Reverse Transcription Kits (Life Technologies, Rockville, MD, USA), respectively, according to the manufacturer's instructions.

5.7. Quantitative PCR

Quantitative PCR (qPCR) was performed by ABI Prism 7000 Sequence Detection System (Applied Biosystems, Foster city, CA, USA). To measure mRNA for layilin and glyceraldehyde 3-phosphate dehydrogenase (GAPDH), mixtures of 2 μg of total RNA-derived cDNA, 300 nM each of forward and reverse primers, and Power SYBR® Master Mix (Applied Biosystems) were subjected to qPCR. Nucleotide sequences of the primers are as follows: layilin, 5′-CACAGCCTGCCAGG ACCTTTA and 5′ -TGCACCGGTCATCATTCCA, and GAPDH, 5′-TGGTA TGGTGGAAGGACTCA and 5′-ATGCCAGTGAGCTTCCCGTT. To measure mRNA for SNAI1, SNAI2, vitronectin, occludin, MMP2, MMP9, COL1A1, and MTA3, mixtures of 2 μg of total RNA-derived cDNA, 8 solutions of TaqMan® Gene Expression Assays (Hs00195591_m1, Hs00161904_m1, Hs00940758_g1, Hs00928613_m1, Hs01548727_m1, Hs00957562-m1, Hs00164004_m1, and Hs00383033_m1, respectively, Applied Biosystems), and TaqMan® Gene Expression Master Mix (Applied Biosystems) were subjected to qPCR. The thermal cycle conditions were as follows: 95 °C for 10 min, followed by 40 cycles of 95 °C for 15 sec and 60 °C for 60 sec.

5.8. Wound healing assay

Effects of layilin-knockdown on invasive ability were investigated by CytoSelect™ Wound Healing Assay Kit (Cell Biolabs, Inc., San Diego, USA). A172 cells transfected with siL-1, siL-2 or siC (7.5×10^5/750 μl) in RPMI containing 10% FBS were seeded onto 24-wells culture plates containing plastic inserts for creation of "wound fields". After the cells reached confluence by incubation for 24 h, the inserts were removed and the wells were washed with PBS. The cells were then further cultured in RPMI containing 10% FBS for 24 h. Microscopic images of "wound closure" were analyzed using the software of "Fiji" (Schindelin et al., 2012). Invasive ability was assessed by areas and numbers of cells migrating into the original wound field.

5.9. Statistical analysis

Statistical significance was calculated by Student *t*-test. Values of $p < 0.05$ were considered statistically significant.

Declaration of Competing Interest

T. Kaji, M. Arito, A. Tsutiya, T. Sase, H. Onodera, T. Sato, K. Omoteyama, M. Sato, N. Suematsu, and M.S. Kurokawa have nothing to disclose. Y. Tanaka reports grants from Daiichi Sankyo Company, Limited, grants from Eisai Co., Ltd., grants from NGK Spark Plug Co., Ltd., grants from Novartis Pharma K.K., and grants from TEIJIN PHARMA LIMITED outside the submitted work. T. Kato reports grants from Astellas Pharma Inc., grants from CHUGAI PHARMACEUTICAL CO., LTD., grants from Daiichi Sankyo Company, Limited, grants from Pfizer Inc., and grants from Sanofi K.K. outside the submitted work.

Acknowledgment

We thank Ms. Sawada Y. and Ms. Yokoyama M. for their technical assistance.

References

Adachi, T., Arito, M., Suematsu, N., Kamijo-Ikemori, A., Omoteyama, K., Sato, T., Kurokawa, M.S., Okamoto, K., Kimura, K., Shibagaki, Y., Kato, T., 2015. Roles of layilin in TNF-α-induced epithelial-mesenchymal transformation of renal tubular epithelial cells. Biochem. Biophys. Res. Commun. 467, 63–69.

Aomatsu, K., Arao, T., Sugioka, K., Matsumoto, K., Tamura, D., Kudo, K., Kaneda, H., Tanaka, K., Fujita, Y., Shimomura, Y., Nishio, K., 2011. TGF-β induces sustained

upregulation of SNAI1 and SNAI2 through Smad and non-Smad pathways in a human corneal epithelial cell line. Invest. Ophthalmol. Vis. Sci. 52, 2437–2443.
Asano, K., Arito, M., Kurokawa, M.S., Omoteyama, K., Okamoto, K., Suematsu, N., Yudoh, K., Nakamura, H., Beppu, M., Kato, T., 2014. Secretion of inflammatory factors from chondrocytes by layilin signaling. Biochem. Biophys. Res. Commun. 452, 85–90.
Barrallo-Gimeno, A., Nieto, M.A., 2005. The snail genes as inducers of cell movement and survival: implications in development and cancer. Development 132, 3151–3161.
Bono, P., Cordero, E., Johnson, K., Borowsky, M., Ramesh, V., Jacks, T., Hynes, R.O., 2005. Layilin, a cell surface hyaluronan receptor, interacts with merlin and radixin. Exp. Cell Res. 308, 177–187.
Bono, P., Rubin, K., Higgins, J.M., Hynes, R.O., 2001. Layilin, a novel integral membrane protein, is a hyaluronan receptor. Mol. Biol. Cell. 12, 891–900.
Borowsky, M.L., Hynes, R.O., 1998. Layilin, a novel talin-binding transmembrane protein homologous with C-type lectins, is localized in membrane ruffles. J. Cell Biol. 143, 429–442.
Chen, Y., Miyazaki, J., Nishizawa, H., Kurahashi, H., Leach, R., Wang, K., 2013. MTA3 regulates CGB5 and Snail genes in trophoblast. Biochem. Biophys. Res. Commun. 433, 379–384.
Cuddapah, V.A., Robel, S., Watkins, S., Sontheimer, H., 2014. A neurocentric perspective on glioma invasion. Nat. Rev. Neurosci. 15, 455–465.
Fujita, N., Jaye, D.L., Kajita, M., Geigerman, C., Moreno, C.S., Wade, P.A., 2003. MTA3, a Mi-2/NuRD complex subunit, regulates an invasive growth pathway in breast cancer. Cell 113, 207–219.
Goodenberger, M.L., Jenkins, R.B., 2012. Genetics of adult glioma. Cancer Genet. 205, 613–621.
Han, S.P., Kim, J.H., Han, M.E., Sim, H.E., Kim, K.S., Yoon, S., Baek, S.Y., Kim, B.S., Oh, S.O., 2011. SNAI1 is involved in the proliferation and migration of glioblastoma cells. Cell Mol. Neurobiol. 31, 489–496.
Iwadate, Y., 2016. Epithelial-mesenchymal transition in glioblastoma progression. Oncol. Lett. 11, 1615–1620.
Kahlert, U.D., Nikkhah, G., Maciaczyk, J., 2013. Epithelial-to-mesenchymal(-like) transition as a relevant molecular event in malignant gliomas. Cancer Lett. 331, 131–138.
Kalluri, R., Weinberg, R.A., 2009. The basics of epithelial-mesenchymal transition. J. Clin. Invest. 119, 1420–1428.
Kühnöl, C.D., Würfel, C., Staege, M.S., Kramm, C., 2017. Snail homolog 1 is involved in epithelial-mesenchymal transition-like processes in human glioblastoma cells. Oncol. Lett. 13, 3882–3888.
Liang, D., An, G., Zhu, Z., Wang, Y., Yang, G., Li, X., Niu, P., Chen, L., Tian, L., 2017. The protective effects of bone morphogenetic protein-7 against epithelial injury and matrix metalloproteases upregulation induced by silica in vitro. Hum. Exp. Toxicol. 36, 892–900.
Louis, D.N., Ohgaki, H., Wiestler, O.D., Cavenee, W.K., Burger, P.C., Jouvet, A., Scheithauer, B.W., Kleihues, P., 2007. The 2007 WHO classification of tumours of the central nervous system. Acta Neuropathol. 114, 97–109.
Louis, D.N., Perry, A., Reifenberger, G., von Deimling, A., Figarella-Branger, D., Cavenee, W.K., Ohgaki, H., Wiestler, O.D., Kleihues, P., Ellison, D.W., 2016. The 2016 world health organization classification of tumors of the central nervous system: a summary. Acta Neuropathol. 131, 803–820.
Mahabir, R., Tanino, M., Elmansuri, A., Wang, L., Kimura, T., Itoh, T., Ohba, Y., Nishihara, H., Shirato, H., Tsuda, M., Tanaka, S., 2014. Sustained elevation of Snail promotes glial-mesenchymal transition after irradiation in malignant glioma. Neuro Oncol. 16, 671–685.
Myung, J.K., Choi, S.A., Kim, S.K., Wang, K.C., Park, S.H., 2014. Snail plays an oncogenic role in glioblastoma by promoting epithelial mesenchymal transition. Int. J. Clin. Exp. Pathol. 7, 1977–1987.
Schindelin, J., Arganda-Carreras, I., Frise, E., Kaynig, V., Longair, M., Pietzsch, T., Preibisch, S., Rueden, C., Saalfeld, S., Schmid, B., Tinevez, J.Y., White, D.J., Hartenstein, V., Eliceiri, K., Tomancak, P., Cardona, A., 2012. Fiji: an open-source platform for biological-image analysis. Nat. Methods 9, 676–682.
Scoles, D.R., 2008. The merlin interacting proteins reveal multiple targets for NF2 therapy. Biochim. Biophys. Acta 1785, 32–54.
Sun, S., Wang, Y., Wu, Y., Gao, Y., Li, Q., Abdulrahman, A.A., Liu, X.F., Ji, G.Q., Gao, J., Li, L., Wan, F.P., Li, Y.Q., Gao, D.S., 2018. Identification of COL1A1 as an invasion-related gene in malignant astrocytoma. Int. J. Oncol. 53, 2542–2554.
Toh, Y., Nicolson, G.L., 2008. The role of the MTA family and their encoded proteins in human cancers: molecular functions and clinical implications. Clin. Exp. Metastasis 26, 215–227.
Wegener, K.L., Basran, J., Bagshaw, C.R., Campbell, I.D., Roberts, G.C., Critchley, D.R., Barsukov, I.L., 2008. Structural basis for the interaction between the cytoplasmic domain of the hyaluronate receptor layilin and the talin F3 subdomain. J. Mol. Biol. 382, 112–126.
Wu, W.S., You, R.I., Cheng, C.C., Lee, M.C., Lin, T.Y., Hu, C.T., 2017. Snail collaborates with EGR-1 and SP-1 to directly activate transcription of MMP 9 and ZEB1. Sci. Rep. 7, 17753.
Yamaguchi, H., Hsu, J.L., Hung, M.C., 2012. Regulation of ubiquitination-mediated protein degradation by survival kinases in cancer. Front. Oncol. 2, 1–15.
Yang, X., Han, M., Han, H., Wang, B., Li, S., Zhang, Z., Zhao, W., 2017. Silencing Snail suppresses tumor cell proliferation and invasion by reversing epithelial-to-mesenchymal transition and arresting G2/M phase in non-small cell lung cancer. Int. J. Oncol. 50, 1251–1260.
Yokoyama, K., Kamata, N., Fujimoto, R., Tsutsumi, S., Tomonari, M., Taki, M., Hosokawa, H., Nagayama, M., 2003. Increased invasion and matrix metalloproteinase-2 expression by Snail-induced mesenchymal transition in squamous cell carcinomas. Int. J. Oncol. 22, 891–898.
Zhou, B.P., Deng, J., Xia, W., Xu, J., Li, Y.M., Gunduz, M., Hung, M.C., 2004. Dual regulation of Snail by GSK-3beta-mediated phosphorylation in control of epithelial-mesenchymal transition. Nat. Cell Biol. 6, 931–940.

Journal of Assisted Reproduction and Genetics (2018) 35:627–636
https://doi.org/10.1007/s10815-018-1166-9

TECHNOLOGICAL INNOVATIONS

Preliminary human application of optical coherence tomography for quantification and localization of primordial follicles aimed at effective ovarian tissue transplantation

Seido Takae[1] · Kosuke Tsukada[2] · Ichiro Maeda[3] · Naoki Okamoto[1] · Yorino Sato[1] · Haruhiro Kondo[1] · Kiemi Shinya[1] · Yuki Motani[2] · Nao Suzuki[1]

Received: 20 September 2017 / Accepted: 15 March 2018 / Published online: 2 April 2018
© The Author(s) 2018

Abstract

Purpose The purpose of this study was to evaluate the possible clinical application of optical coherence tomography for assessing ovarian reserve in individual specimens of human ovarian tissue for fertility preservation.

Methods Ovarian tissue examination by optical coherence tomography was performed before ovarian tissue cryopreservation. Three of the four subjects had hematological disease or cancer, and they faced a threat to their fertility due to impending chemotherapy. One patient underwent ovarian tissue extraction for in vitro activation of dormant follicles as fertility treatment.

Results The current full-field optical coherence tomography technique can detect primordial follicles in non-fixed and non-embedded human ovarian tissue. These images are well correlated with histological evaluation and the ovarian reserve test, including follicle counts.

Conclusion It was demonstrated that optical coherence tomography could assess localization of primordial follicles and ovarian reserve in specimens of non-fixed human ovarian cortex, although optimization for examination of human ovarian tissue is needed for clinical application. Additionally, this technique holds the possibility of assessing the ovarian reserve of patients with unevaluable ovarian reserve.

Trial registration number UMIN000023141

Keywords Optical coherence tomography · Ovarian tissue transplantation · Ovarian tissue cryopreservation · Ovarian reserve · Fertility preservation

✉ Nao Suzuki
nao@marianna–u.ac.jp

Seido Takae
s2takae@marianna-u.ac.jp

Kosuke Tsukada
ktsukada@appi.keio.ac.jp

Ichiro Maeda
ichirou@marianna-u.ac.jp

Naoki Okamoto
na-okamoto@marianna-u.ac.jp

Yorino Sato
yorinos@marianna-u.ac.jp

Haruhiro Kondo
haru@marianna-u.ac.jp

Kiemi Shinya
k2shinya@marianna-u.ac.jp

Yuki Motani
yukimotani@keio.jp

[1] Department of Obstetrics and Gynecology, St. Marianna University School of Medicine, 2-16-1 Sugao, Miyamae-ku, Kawasaki City, Kanagawa 216-8511, Japan

[2] Graduate School of Fundamental Science and Technology, Keio University, 3-14-1 Hiyoshi, Kouhoku-ku, Yokohama, Kanagawa 223-8522, Japan

[3] Department of Pathology, St. Marianna University School of Medicine, 2-16-1 Sugao, Miyamae-ku, Kawasaki City, Kanagawa 216-8511, Japan

Introduction

Ovarian tissue cryopreservation has become the standard procedure for fertility preservation in young cancer patients who are facing loss of fertility due to impending chemotherapy and radiation therapy. According to the guidelines of the American Society of Clinical Oncology (ASCO) [1], although ovarian tissue cryopreservation is still an experimental and viable option for fertility preservation, more than 130 live births have already been reported [2–4]. Furthermore, in Germany, around 400 ovarian tissue cryopreservation procedures are carried out each year [5]. To date, more than 1500 ovarian tissue cryopreservation procedures have been performed in the Nordic countries [6]. In addition, two live births were reported applying the new clinical procedure of ovarian tissue transplantation (IVA: in vitro activation) as a fertility treatment for patients with primary ovarian insufficiency (POI) [7, 8]. Globally, the live birth rate from transplanted frozen-thawed ovarian tissue is approximately 30% [3, 5, 9, 10]. Although ovarian function is well recovered among most transplanted cases [3, 11], only 67–75% of patients had at least 1 year of ovarian tissue activity [10]. The duration of ovarian tissue activity normally depends on the number of remaining primordial follicles contained in the transplanted ovarian tissue. The main reasons for follicle loss are "burst" or "activation" of primordial follicle recruitment and ischemic apoptosis [3]. However, selection of ovarian tissue that includes a maximum number of primordial follicles is important for improving the outcome of ovarian tissue transplantation. Therefore, a procedure needs to be established for the assessment of ovarian reserve in ovarian tissue.

Optical coherence tomography (OCT) is a non-invasive imaging technique that provides high-resolution images for a range of clinical applications [12, 13]. By measuring backscattered light from microstructural features in tissues, OCT images include micron-scale detail to a penetration depth of 1–3 mm [12, 14]. OCT has recently been used for the imaging of tissues for clinical examination of areas that can be accessed directly or by using an endoscope or catheter. OCT is used in such fields as ophthalmology [15, 16] and dentistry [17, 18], and to evaluate such areas of the body as the gastrointestinal tract [19, 20], coronary blood vessels [21, 22], colon [23], breast [24, 25], and more [12, 14]. Some researchers have been investigating the application of OCT in evaluating the anatomical features of normal ovarian tissue [13, 14, 26–29]. In particular, a study has been reported on the clinical application of OCT for the detection of malignant cells and to search for primordial follicles in formalin-fixed and embedded ovarian tissue for fertility preservation [30]. In addition, researchers have recently reported a study using mice ovaries to investigate the possibility of using OCT to assess ovarian reserve [31].

The present study investigated the possibility of using OCT to assess the localization of primordial follicles and ovarian reserve in ovarian tissue, using non-fixed human ovarian tissue that had been cryopreserved for fertility preservation due to POI and impending treatment of hematological disease and cancer.

Material and methods

Preparation of human ovarian tissue

Human ovaries were obtained from 4 patients who underwent ovariectomy for ovarian tissue cryopreservation between November 2013 and February 2017 for fertility preservation or fertility treatment at our university hospital. Ovarian tissue from Patients 1 and 2 was cryopreserved-thawed by vitrification methods using a commercial ovarian cryopreservation kit (Ova Cryo Kit Type M; KITAZATO Biopharma Co., Ltd., Shizuoka, Japan), as previously reported [7, 8]. The ovarian tissue from Patients 3 and 4 was fresh. A small (4–8 mm × 2 mm) 1-mm-thick section of ovarian cortex was cut out from part of each ovary. This process was performed in a petri dish (Bacteriological Petri Dish 60 × 15 mm, FALCON 351007; Becton, Dickinson and Company, Franklin Lakes, NJ, USA) containing modified HTF (mHTF) culture medium (with HEPES; KITAZATO Biopharma Co., Ltd.). For the present study, in accordance with the principles of the Declaration of Helsinki, all patients provided written, informed consent, and the study was approved by the institutional review board of our university (institutional approval No. 3311, UMIN000023141).

Optical coherence tomography examination

The OCT system (Light-CT scanner; LL Tech, Paris, France) was used in the present study. The light source of this equipment is a halogen lamp. The mechanical characteristics of the Light-CT scanner included images with 1-μm resolution in all three dimensions that can be manipulated using a standard DICOM viewer. The wavelength of the OCT examination was 700–800 nm (near-infrared), the width of the wave was 125 nm, and the area of examination was 0.64 mm^2. Images were obtained to a depth of 100 μm, which was the maximum depth at which high-resolution images could be taken. The mean exposure time during the OCT examination was approximately 2–3 min for each 0.64-mm^2 section. The recorded images were modified using a Gaussian filter to reduce the speckle noise, and then contrast and brightness were adjusted to clarify the follicle boundaries. These modified images were reconstructed as representative images in accordance with histological images.

Histological study of human ovarian tissue

The specimens of ovaries examined with OCT were fixed by 10% buffered formalin. The specimens were embedded in paraffin and sectioned into 4-μm-thick slices, placed on silane-coated glass slides, and stained with hematoxylin and eosin (H&E). OCT images were compared with H&E-stained histological images.

Follicle counting

To verify the accuracy of OCT examination, the number of counted follicles was compared between OCT and histological imaging to a depth of 65 μm. In performing histological follicle counts on human ovaries, primordial follicles were defined as those containing flat follicular cells, and primary follicles were defined as those with one cuboidal follicular cell on histological study [32]. Follicles were counted only when the dark-staining nucleolus was seen within the nucleus of the oocytes to prevent recounting of the same follicle [33]. Meanwhile, when performing OCT follicle counts on human ovaries, a black dot of around 20–30 μm was regarded as a primordial and/or primary follicle. To avoid duplicate counting of follicles on OCT imaging, the black dots were counted carefully every 20 μm. With this OCT equipment, it is difficult to make an accurate distinction between primordial and primary follicles. Accordingly, the sum of primordial and primary follicles was compared between OCT and histological imaging. In this regard, it was difficult to count follicles in whole ovarian tissue due to the penetration of OCT (no more than 100 μm). Therefore, the follicles were counted on histological images after calculating the degree of shrinkage after fixation and paraffin embedding. Also, to reduce the bias of this process, follicle count was performed by three collaborators.

Statistical analysis

JMP Pro version 12 (SAS Institute Inc., Cary, NC, USA) was used for statistical analysis. The numbers of follicles are expressed as means ± standard error (SE). The Wilcoxon signed-rank test was performed, and a P value < 0.05 was considered significant.

Results

Medical history and characteristics of the subjects

The characteristics of the patients are shown in Table 1. Patient 1 was 32 years of age with anal cancer. Her ovarian reserve was normal (a "normal ovarian reserve case"); her basal follicle-stimulating hormone (FSH) level was 4.34 mIU/ml, and her anti-Müllerian hormone (AMH) level was 5.01 ng/ml. Her ovarian tissue was cryopreserved for fertility preservation, but after her treatment for anal cancer, she became pregnant naturally.

Patient 2 (a "menopausal case") was 45 years of age and had severely diminished ovarian reserve (DOR). She underwent ovariectomy for IVA. Her basal FSH level was 20.1 mIU/ml, and her AMH level was 0.51 ng/ml at 1.5 years prior to ovariectomy. This patient had primary amenorrhea and was diagnosed with Mayer-Rokitansky-Küster-Hauser syndrome (MRKH syndrome) because she had a hypoplastic uterus. Although she received ovarian tissue transplantation for IVA, she could not become pregnant. The cryopreserved-thawed ovarian tissues of patients 1 and 2 were investigated by OCT.

Patients 3 and 4 were investigated as "unknown ovarian reserve cases." These patients had not yet experienced menarche. Patient 3 was 15 years of age with aplastic anemia, and she underwent ovarian tissue cryopreservation before bone marrow transplantation. Her basal FSH level was 6.0 mIU/ml, and her AMH level was 1.99 ng/ml. Patient 4 was 11 years of age with acute lymphatic leukemia; she underwent ovarian tissue cryopreservation before bone marrow transplantation. In addition, she received chemotherapy (3250 mg of cyclophosphamide) before consultation for fertility preservation. Her basal FSH level was 3.0 mIU/ml, and her AMH level was 0.07 ng/ml. In these teenaged patients, basal FSH and AMH levels are not reliable markers for assessing real ovarian reserve.

Comparison between OCT images and histological images of human ovarian tissue

Patient 1 (normal ovarian reserve case)

Figure 1a–d shows a set of OCT images and H&E-stained histological images from patient 1. The OCT images show several follicles including primary-primordial and antral follicles, in accordance with the H&E-stained histological images.

Patient 2 (menopausal case)

Figure 2a, b shows a set of OCT images and H&E-stained histological images from patient 2. No follicles were detected by OCT, in accordance with the H&E-stained histological images. These images represent very low ovarian reserve, corresponding with basal FSH and AMH levels.

Patients 3 and 4 (unknown ovarian reserve cases)

Figures 3a–d) and 4a, b show a set of OCT images and H&E-stained histological images from patients 3 and 4. Although their AMH levels were low (patient 3, 1.99 ng/ml; patient 4, 0.07 ng/ml), many primordial follicles were detected in the ovarian cortex of both patients.

On pathological examination, malignant cells were not detected in the ovarian tissues of patients 1 through 4.

Table 1 Characteristics of patients received ovarian tissue cryopreservation

Patient	1	2	3	4
Case	Normal OR	Menopausal OR	Unknown OR	Unknown OR
Disease/condition	Anal cancer	Severe DOR	Aplastic anemia	ALL
Age at OTC	32	45	15	11
Menstruation	Regular (30 days)	Primary amenorrhea	Before menarche	Before menarche
Basal FSH (mIU/ml)	4.34	20.1	6.0	3.0
AMH (ng/ml)	5.01	0.51 (before 1.5 year of ovariectomy)	1.99	0.07
Chemotherapy before OTC	—	—	—	CPA 3250 mg
Past history	Crohn disease	MRKH syndrome Unilateral ovarian cystectomy	—	—

OTC ovarian tissue cryopreservation, *FSH* follicle-stimulating hormone, *AMH* anti-Müllerian Hormone, *OR* ovarian reserve, *DOR* diminished ovarian reserve, *ALL* acute lymphocytic leukemia, *CPA* cyclophosphamide, *MRKH syndrome* Mayer-Rokitansky-Kuster-Hauser syndrome

Meanwhile, there were no differences among fresh (patients 1, 2) and vitrified-thawed (patients 3, 4) ovarian tissue in terms of image quality and appearance of primordial-primary follicles.

Accuracy of follicle counts using OCT

On the follicle counting of four serial ovarian sections obtained from girls with hematological disease and before menarche, the means of the sum of primordial and primary follicles of ovarian tissue were 84.5 ± 43.0 (OCT) and 83.7 ± 52.9 (histology); there was no significant difference between OCT and histological evaluation ($P = 0.78$). Also, Fig. 5 shows the follicle counts for OCT and histological imaging (sample number 1–3: patient 3, sample number 4: patient 4).

Discussion

Advantage of OCT for assessment of the numbers of primordial follicle intend for effective ovarian tissue transplantation

Comparison of OCT imaging and H&E-stained histological images demonstrated that OCT could detect primordial follicles clearly. Detection of primordial follicles on formalin-

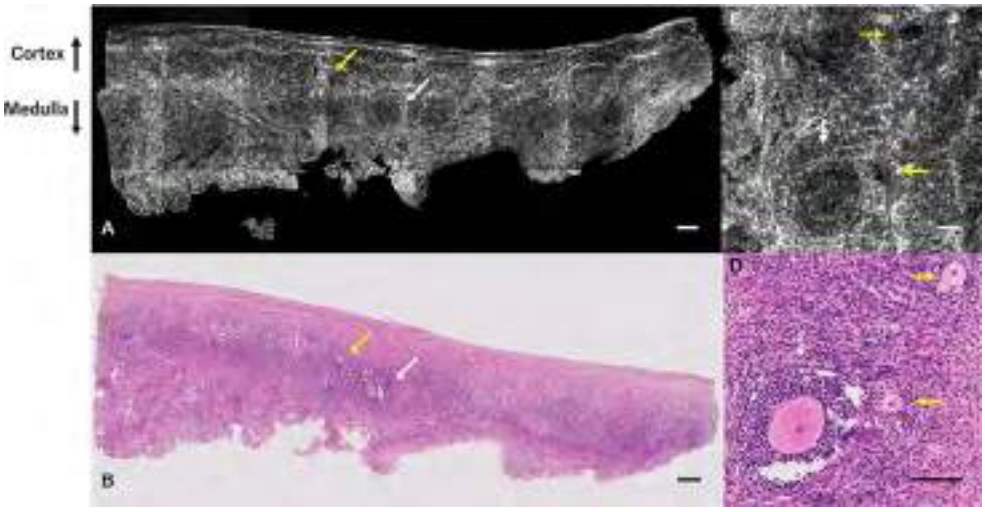

Fig. 1 OCT images and H&E-stained histological images of ovarian tissue from patient 1 (normal ovarian reserve case). Results of OCT examination of ovarian tissue from patient 1, who was 32 years of age with anal cancer. Several developing follicles (primordial-primary: yellow arrows, and antral follicles: white arrows) are detected by OCT (**a**), in accordance with histological examination (**b**). This OCT image reflects the normal result of the ovarian reserve test (FSH 4.34 mIU/ml, AMH 5.01 ng/ml). Magnified OCT image (**c**) demonstrates the details of developing follicles (primordial-primary: yellow arrows, and antral follicles: white arrows) in accordance with magnified histological examination (**d**). Scale bar = 200 μm (**a**, **b**), 100 μm (**c**, **d**). *OCT* optical coherence tomography, *H&E* hematoxylin and eosin, *FSH* follicle-stimulating hormone, *AMH* anti-Müllerian hormone

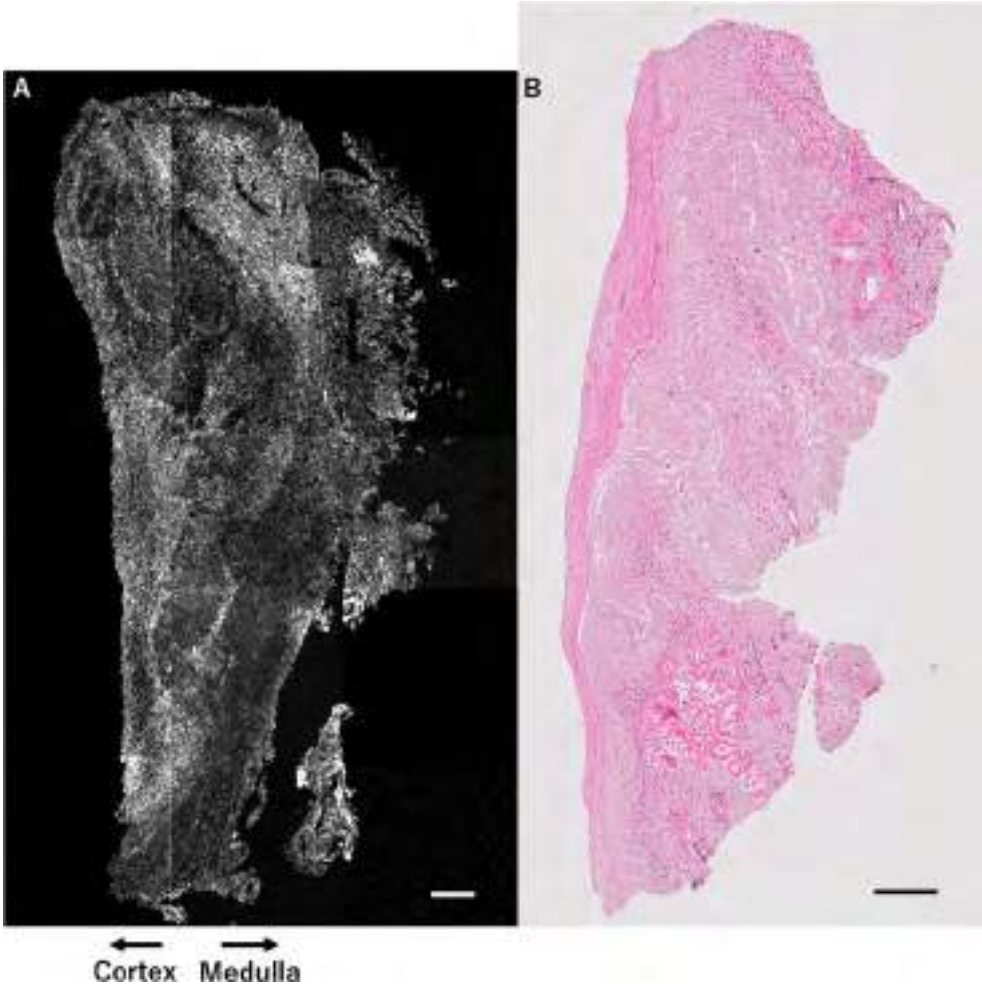

Fig. 2 OCT image and H&E-stained histological image of ovarian tissue from patient 2 (menopausal case). Results of OCT examination of ovarian tissue from patient 2, who was 45 years of age with severely diminished ovarian reserve. No follicles are detected by OCT (**a**), in accordance with histological examination (**b**). This OCT image reflects the poor result of the ovarian reserve test (FSH 20.1 mIU/ml, AMH 0.51 ng/ml at 1.5 years prior to ovariectomy). Scale bar = 200 μm (**a**, **b**). *OCT* optical coherence tomography, *H&E* hematoxylin and eosin, *FSH* follicle-stimulating hormone, *AMH* anti-Müllerian hormone

fixed and embedded human ovarian tissue was reported in 2016 [30]; this was the first report of detection of primordial follicles in fresh human ovarian tissue with clear OCT images. In 2017, researchers reported the detection of primordial follicles in fresh murine ovaries [31]. Through non-invasive detection of primordial follicles in fresh human ovarian tissue, localization of primordial follicles can be assessed. Primordial follicles have been shown to be very unevenly distributed in the cortex of ovaries [34]; these findings indicate that OCT can assist in selecting the most productive ovarian tissue for ovarian tissue transplantation. The present study is the first case series of OCT examination using clinical samples intended for assessment of the quantity and localization of primordial follicles as the first step for clinical application.

OCT images were compared between patient 1 (normal ovarian reserve case) and patient 2 (menopausal case), and the outcomes were correlated with H&E-stained histological images and the ovarian reserve test (basal FSH and AMH levels). Although present study is the first report that showed certain accuracy of OCT, and indicated correlation with basal FSH and AMH levels, at present, the accuracy of OCT compared with histological examination remains debatable [31]. Although OCT examination does not have any advantage in terms of image quality compared with histological studies, the biggest advantage of OCT examination is that there is no need for any fixation and paraffin embedding, unlike conventional histological studies. This means we can transplant ovarian tissue whose follicle count has already been evaluated. We believe that the ovarian tissue selection may improve the efficacy of ovarian tissue transplantation, because primordial follicles were very unevenly distributed throughout the ovarian cortex [34]. As a matter of course, more investigation is needed to confirm the correlation between the numbers of counted follicles using OCT and ovarian function after ovarian auto-transplantation, although such confirmation is very difficult with human fresh ovaries because the testable depth of high-resolution OCT still extends only to 100 μm [31]. Nevertheless, to apply OCT in clinical medicine, establishment of a follicle count system in conjunction with OCT, such as an automatic cell counter and a statistical computing method, is needed. A rapid screening and rapid counting system would be vital for the effective practice of clinical medicine.

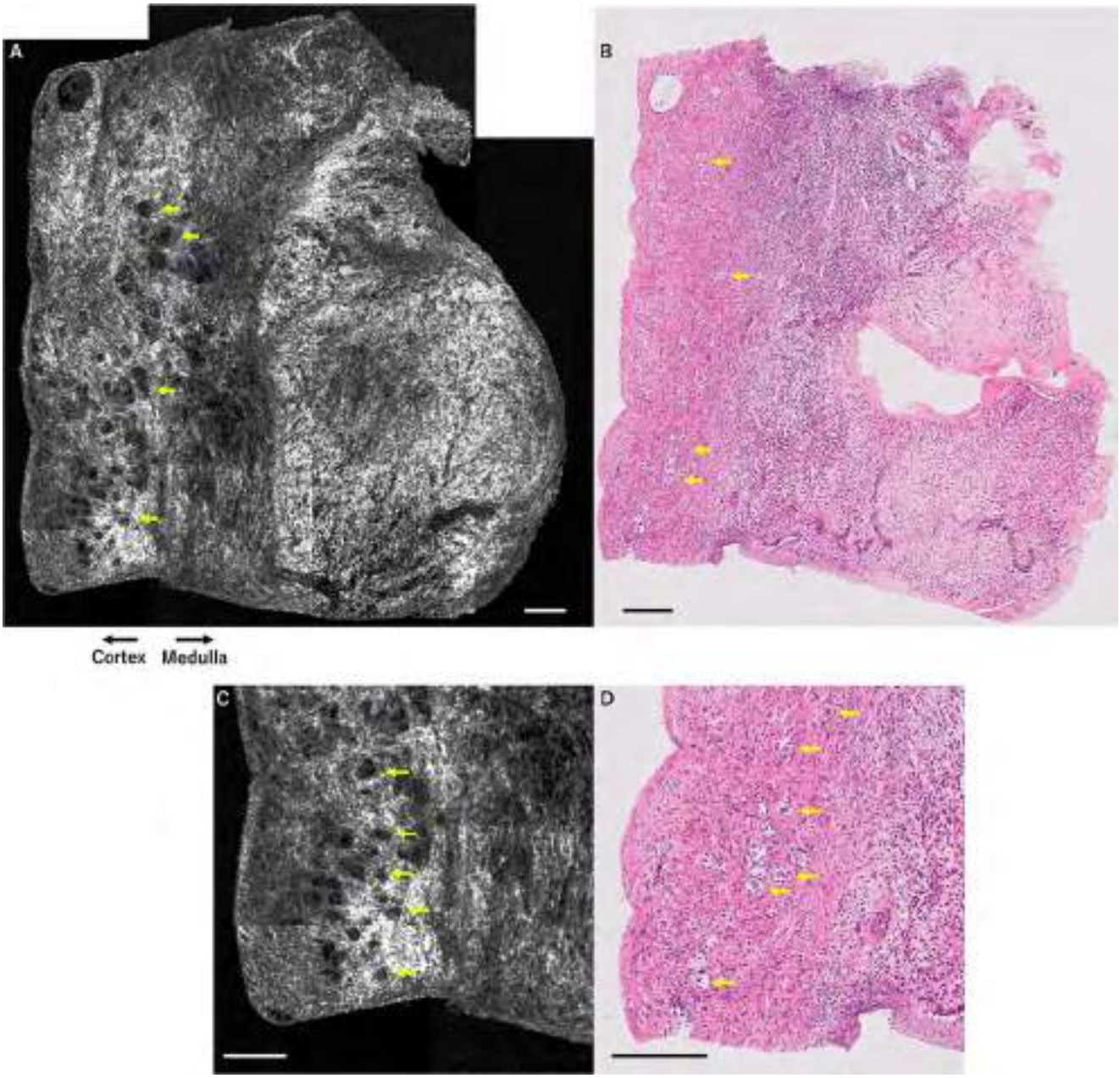

Fig. 3 OCT images and H&E-stained histological images of ovarian tissue from patient 3 (unknown ovarian reserve case). Results of OCT examination of ovarian tissue from patient 3, who was 15 years of age with aplastic anemia. Her AMH and basal FSH levels were unevaluable for ovarian reserve assessment because she was premenarcheal. Several primordial-primary follicles (yellow arrows) are detected by OCT (**a**), in accordance with histological examination (**b**). Magnified OCT images (**c**) demonstrate the details of primordial-primary follicles (yellow arrows) in accordance with magnified histological examination (**d**). Scale bar = 200 μm (**a**–**d**). *OCT* optical coherence tomography, *H&E* hematoxylin and eosin, *FSH* follicle-stimulating hormone, *AMH* anti-Müllerian hormone

Development and modification of OCT for primordial follicle detection

Exciting developments have occurred in OCT. The first generation of OCT was time-domain OCT (TD-OCT), which can be used to compose an image that is acquired by point-by-point scanning of both the interferometer reference arm length and the laser beam. Subsequently, frequency-domain (Fourier-domain) OCT was developed, which replaced the reference arm length scan with parallel spectroscopic measurements (spectral-domain OCT) or sequential measurements made by scanning the wavelength of a tunable laser (swept-source OCT). Full-field OCT differs from TD-OCT and frequency-domain OCT in that it does not use a scanning light beam to produce tomographic images in the *en face* orientation (orthogonal to the optical axis). Unlike with conventional OCT,

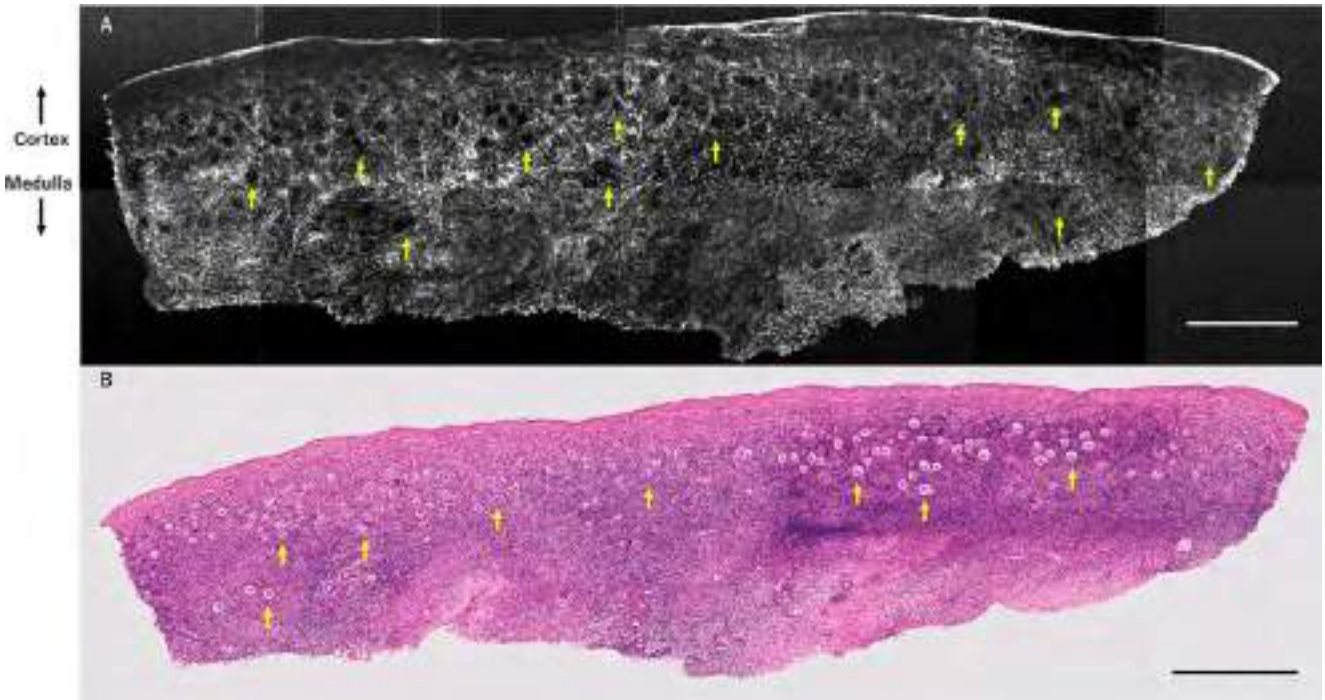

Fig. 4 OCT image and H&E-stained histological image of ovarian tissue from patient 4 (unknown ovarian reserve case). Results of OCT examination of ovarian tissue from patient 4, who was 11 years of age with acute lymphatic leukemia. Although her AMH and basal FSH levels were unevaluable for ovarian reserve assessment because she was premenarcheal and in the midst of a chemotherapy treatment cycle, several primordial-primary follicles (yellow arrows) are detected by OCT (**a**), in accordance with histological examination (**b**). Scale bar = 500 μm (**a**, **b**). *OCT* optical coherence tomography, *H&E* hematoxylin and eosin, *FSH* follicle-stimulating hormone, *AMH* anti-Müllerian hormone

low spatial coherence light illuminates the entire field of the image [35]. The present study used a full-field OCT system to pursue rapid image creation and high-resolution imaging. Some improvements of the OCT technique (e.g., a wavelength or scanning system) are needed to investigate human ovarian tissue for assessment of actual follicle localization and ovarian reserve. Indeed, OCT technology has evolved rapidly, and attempts have been made to achieve ultra-high-speed imaging with a modified luminous source and a high scanning rate system [36, 37]. Methods of speckle noise reduction (e.g., Gaussian filtering) for improvement of image quality have been investigated [38, 39]. These investigations may allow OCT to move closer to practical use. Although the present study was preliminary, it indicated the possibility of clinical application. Certainly, histological study is superior in terms of accuracy for ovarian reserve assessment, though OCT has advantages in terms of swiftness and non-invasiveness, although it is still under development. Further, OCT is a unique method for assessing follicle localization and ovarian reserve without fixation, dyeing, or contact.

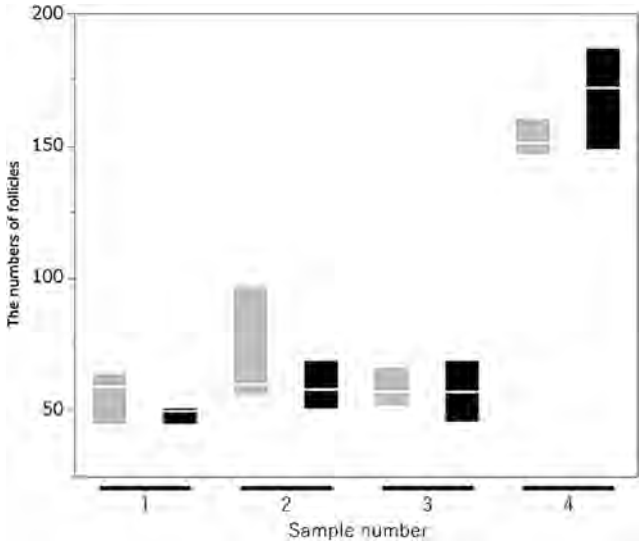

Fig. 5 A comparison of follicle counts between OCT and histological examination. There is no significant difference in follicle counts between OCT and histological examination ($P = 0.78$, Wilcoxon signed-rank test). Sample number 1–3: patient 3, 4: patient 4. Gray boxplot: OCT examination, Black boxplot: histological study

Utility of OCT to assess the ovarian reserve for patients with unevaluable ovarian reserve

In the present study, OCT was applied effectively for patients who had unknown ovarian reserve (patients 3 and 4). These patients were prepubertal and premenarcheal, so the serum FSH level was not reliable for assessing the ovarian reserve of these patients. Additionally, AMH levels are low during

prepubertal development, rise during early puberty, and reach a plateau at 20–25 years of age [40, 41]. Serum AMH levels decline immediately after initiation of chemotherapy and increase after several months of chemotherapy, but no markers attain the pretreatment values [42]. In particular, patient 4 received chemotherapy (3250 mg of cyclophosphamide) before consultation for fertility preservation; therefore, the AMH level was not reliable for assessing her ovarian reserve. Although supplementary data of the ASCO guidelines has set a high-risk POI dosage for cyclophosphamide treatment [1], the innate amount of ovarian reserve varies between individuals. Consequently, the total dosage of cyclophosphamide is not a conclusive factor in determining the ovarian reserve of a patient. However, assessment of the ovarian reserve of such patients is greatly needed to evaluate the efficacy of ovarian tissue cryopreservation and transplantation. Unfortunately, at present, there is no procedure to accurately assess ovarian reserve and distribution, as with histological examination. With optimization of inspection of the ovary, OCT examination could assess the ovarian reserve of child patients and chemotherapy patients who have low AMH levels, which indicate a seemingly low ovarian reserve.

Further investigation of OCT for fertility preservation

To accurately assess fresh ovarian reserve by OCT, several issues need to be resolved regarding OCT equipment. One issue is testable depth; as mentioned above, the current testable depth of high-resolution OCT reaches only 100 μm. The existing model of OCT equipment does not readily support testable depth and resolution simultaneously. Second, modification of the method for examining human ovarian tissue is needed. In the present study, ex vivo OCT examination was performed on dissected ovarian cortex. To assess ovarian reserve before ovarian tissue cryopreservation, in vivo OCT examination is needed, for example, integrated with endoscopy or laparoscopy or a catheter [21, 22, 26]. Implementation of in vivo laparoscopic or catheter examination for ovarian reserve assessment and a faster acquisition rate and downsizing are also needed while maintaining high resolution [26]. Third, the scanning area is too shallow to obtain OCT imaging of the ovary. The scanning area of the OCT equipment used in the present study was 0.64 mm^2. Expansion of the scanning area would be important for clinical application. In the area of ophthalmological research, megahertz OCT for ultrawide-field retinal imaging with a 1050-nm Fourier-domain mode-locked laser has been reported [43], having seven times the width of the current scanning area and 200 times the scanning speed of the conventional system.

Ideally, we hope to investigate the use of OCT for assessing ovarian reserve from the surface of the body as with ultrasonography by high-speed, real-time image processing. This would be a truly non-invasive and effective method for assessment of ovarian reserve and primordial follicle localization. Additionally, further safety assessments are needed for clinical application of OCT; only one paper mentioned the reproductive safety of OCT technique using mice, and there are no reports to date that mentioned human reproductive safety [30]. In addition, more investigation is needed to confirm the "non-invasiveness for reproductive cells" of OCT examination through evaluation of follicle viability after NIR irradiation, although a report indicated its non-invasiveness using a glucose uptake assay and neutral red staining with bovine ovarian tissue [30]. Further verification of the non-invasiveness for reproductive cells under various study conditions (wavelength, illuminance, irradiation time, and energy) will bring OCT closer to clinical application in reproductive medicine.

Conclusion

In the present study, the possibility of the clinical application of OCT for assessment of the localization of primordial follicles and ovarian reserve was demonstrated. OCT could also assess ovarian reserve in patients with unevaluable ovarian reserve. Although clinical applications of OCT are not feasible with the current technology, the optimization and improvement of OCT equipment will make it possible to select the most suitable ovarian tissue containing abundant follicles for the purpose of successful ovarian tissue transplantation. As a next step, it will be necessary to compare the effectiveness of OCT imaging and conventional methods for ovarian tissue selection.

Acknowledgements We are appreciative of Professor Kohei M Itoh for coordinating our research team. The authors are grateful to Shigeko Onuma for creating the histologic sections.

Authors' contributions S.T., K.T., and N.S. designed the research and wrote the critical discussion. S.T., N.O., Y.S., and K.S. performed the experiments and analyzed the data. H.K. and S.T. performed the laparoscopic surgery. I.M. conducted pathological and histological examination. Y.M. performed expert image modification. S.T. and K.T. drafted the manuscript.

Compliance with ethical standards

Financial support This research did not receive any specific grant from funding agencies in the public, commercial, or not-for-profit sectors.

Conflicts of interest The authors declare that they have no conflicts of interest.

Open Access This article is distributed under the terms of the Creative Commons Attribution 4.0 International License (http://creativecommons.org/licenses/by/4.0/), which permits unrestricted use, distribution, and reproduction in any medium, provided you give appropriate credit to the original author(s) and the source, provide a link to the Creative Commons license, and indicate if changes were made.

References

1. Loren AW, Mangu PB, Beck LN, Brennan L, Magdalinski AJ, Partridge AH, et al. Fertility preservation for patients with cancer: American Society of Clinical Oncology clinical practice guideline update. J Clin Oncol. 2013;31:2500–10.
2. Donnez J, Dolmans MM. Ovarian cortex transplantation: 60 reported live births brings the success and worldwide expansion of the technique towards routine clinical practice. J Assist Reprod Genet. 2015;32:1167–70.
3. Silber S. Ovarian tissue cryopreservation and transplantation: scientific implications. J Assist Reprod Genet. 2016;33:1595–603.
4. Donnez J, Dolmans MM. Fertility preservation in women. N Engl J Med. 2017;377:1657–65.
5. Van der Ven H, Liebenthron J, Beckmann M, Toth B, Korell M, Krussel J, et al. Ninety-five orthotopic transplantations in 74 women of ovarian tissue after cytotoxic treatment in a fertility preservation network: tissue activity, pregnancy and delivery rates. Hum Reprod. 2016;31:2031–41.
6. Rodriguez-Wallberg KA, Tanbo T, Tinkanen H, Thurin-Kjellberg A, Nedstrand E, Kitlinski ML, et al. Ovarian tissue cryopreservation and transplantation among alternatives for fertility preservation in the Nordic countries—compilation of 20 years of multicenter experience. Acta Obstet Gynecol Scand. 2016;95:1015–26.
7. Kawamura K, Cheng Y, Suzuki N, Deguchi M, Sato Y, Takae S, et al. Hippo signaling disruption and Akt stimulation of ovarian follicles for infertility treatment. Proc Natl Acad Sci U S A. 2013;110:17474–9.
8. Suzuki N, Yoshioka N, Takae S, Sugishita Y, Tamura M, Hashimoto S, et al. Successful fertility preservation following ovarian tissue vitrification in patients with primary ovarian insufficiency. Hum Reprod. 2015;30:608–15.
9. Jensen AK, Kristensen SG, Macklon KT, Jeppesen JV, Fedder J, Ernst E, et al. Outcomes of transplantations of cryopreserved ovarian tissue to 41 women in Denmark. Hum Reprod. 2015;30:2838–45.
10. von Wolff M, Stute P, Fluck C. Autologous transplantation of cryopreserved ovarian tissue to induce puberty-the endocrinologists' view. Eur J Pediatr. 2016;
11. Meirow D, Ra'anani H, Shapira M, Brenghausen M, Derech Chaim S, Aviel-Ronen S, et al. Transplantations of frozen-thawed ovarian tissue demonstrate high reproductive performance and the need to revise restrictive criteria. Fertil Steril. 2016;106:467–74.
12. Wang T, Brewer M, Zhu Q. An overview of optical coherence tomography for ovarian tissue imaging and characterization. Wiley interdisciplinary reviews. Nanomed NanoBiotechnol. 2015;7:1–16.
13. Yang Y, Wang T, Brewer M, Zhu Q. Quantitative analysis of angle-resolved scattering properties of ovarian tissue using optical coherence tomography. J Biomed Opt. 2012;17:90503–1.
14. Yang Y, Li X, Wang T, Kumavor PD, Aguirre A, Shung KK, et al. Integrated optical coherence tomography, ultrasound and photoacoustic imaging for ovarian tissue characterization. Biomedical optics express. 2011;2:2551–61.
15. Li P, An L, Lan G, Johnstone M, Malchow D, Wang RK. Extended imaging depth to 12 mm for 1050-nm spectral domain optical coherence tomography for imaging the whole anterior segment of the human eye at 120-kHz A-scan rate. J Biomed Opt. 2013;18:16012.
16. Yu L, Chen Z. Doppler variance imaging for three-dimensional retina and choroid angiography. J Biomed Opt. 2010;15:016029.
17. Holtzman JS, Osann K, Pharar J, Lee K, Ahn YC, Tucker T, et al. Ability of optical coherence tomography to detect caries beneath commonly used dental sealants. Lasers Surg Med. 2010;42:752–9.
18. Otis LL, Everett MJ, Sathyam US, Colston BW Jr. Optical coherence tomography: a new imaging technology for dentistry. J Am Dent Assoc. 2000;131:511–4.
19. Cobb MJ, Hwang JH, Upton MP, Chen Y, Oelschlager BK, Wood DE, et al. Imaging of subsquamous Barrett's epithelium with ultrahigh-resolution optical coherence tomography: a histologic correlation study. Gastrointest Endosc. 2010;71:223–30.
20. Testoni PA, Mangiavillano B. Optical coherence tomography in detection of dysplasia and cancer of the gastrointestinal tract and bilio-pancreatic ductal system. World J Gastroenterol. 2008;14:6444–52.
21. Barlis P, Serruys PW, Gonzalo N, van der Giessen WJ, de Jaegere PJ, Regar E. Assessment of culprit and remote coronary narrowings using optical coherence tomography with long-term outcomes. Am J Cardiol. 2008;102:391–5.
22. Tearney GJ, Yabushita H, Houser SL, Aretz HT, Jang IK, Schlendorf KH, et al. Quantification of macrophage content in atherosclerotic plaques by optical coherence tomography. Circulation. 2003;107:113–9.
23. Shen B, Zuccaro G Jr, Gramlich TL, Gladkova N, Trolli P, Kareta M, et al. In vivo colonoscopic optical coherence tomography for transmural inflammation in inflammatory bowel disease. Clin Gastroenterol Hepatol. 2004;2:1080–7.
24. Boppart SA, Luo W, Marks DL, Singletary KW. Optical coherence tomography: feasibility for basic research and image-guided surgery of breast cancer. Breast Cancer Res Treat. 2004;84:85–97.
25. Curatolo A, McLaughlin RA, Quirk BC, Kirk RW, Bourke AG, Wood BA, et al. Ultrasound-guided optical coherence tomography needle probe for the assessment of breast cancer tumor margins. AJR Am J Roentgenol. 2012;199:W520–2.
26. Boppart SA, Goodman A, Libus J, Pitris C, Jesser CA, Brezinski ME, et al. High resolution imaging of endometriosis and ovarian carcinoma with optical coherence tomography: feasibility for laparoscopic-based imaging. Br J Obstet Gynaecol. 1999;106:1071–7.
27. Nandy S, Sanders M, Zhu Q. Classification and analysis of human ovarian tissue using full field optical coherence tomography. Biomed Optics Express. 2016;7:5182–7.
28. Pitris C, Goodman A, Boppart SA, Libus JJ, Fujimoto JG, Brezinski ME. High-resolution imaging of gynecologic neoplasms using optical coherence tomography. Obstet Gynecol. 1999;93:135–9.
29. Yang Y, Wang T, Biswal NC, Wang X, Sanders M, Brewer M, et al. Optical scattering coefficient estimated by optical coherence tomography correlates with collagen content in ovarian tissue. J Biomed Opt. 2011;16:090504.
30. Peters IT, Stegehuis PL, Peek R, Boer FL, van Zwet EW, Eggermont J, et al. Non-invasive detection of metastases and follicle density in ovarian tissue using full-field optical coherence tomography. Clin Cancer Res. 2016;22:5506–13.
31. Takae S, Tsukada K, Sato Y, Okamoto N, Kawahara T, Suzuki N. Accuracy and safety verification of ovarian reserve assessment technique for ovarian tissue transplantation using optical coherence tomography in mice ovary. Sci Rep. 2017;7:43550.
32. Adashi EY, Leung PCK. The ovary. 2nd ed. Amsterdam: Elsevier Academic Press; 2004.
33. Hreinsson JG, Scott JE, Rasmussen C, Swahn ML, Hsueh AJ, Hovatta O. Growth differentiation factor-9 promotes the growth, development, and survival of human ovarian follicles in organ culture. J Clin Endocrinol Metab. 2002;87:316–21.
34. Schmidt KL, Byskov AG, Nyboe Andersen A, Muller J, Yding Andersen C. Density and distribution of primordial follicles in single pieces of cortex from 21 patients and in individual pieces of cortex from three entire human ovaries. Hum Reprod. 2003;18:1158–64.
35. Greenbaum E, Drexler W, Fujimoto JG, SpringerLink (Online service). Optical coherence tomography technology and applications. In: Biological and medical physics, biomedical engineering,. Berlin, Heidelberg: Springer Berlin Heidelberg,, 2008.

36. Choi W, Moult EM, Waheed NK, Adhi M, Lee B, Lu CD, et al. Ultrahigh-speed, swept-source optical coherence tomography angiography in nonexudative age-related macular degeneration with geographic atrophy. Ophthalmology. 2015;122:2532–44.
37. Park HC, Mavadia-Shukla J, Yuan W, Alemohammad M, Li X. Broadband rotary joint for high-speed ultrahigh-resolution endoscopic OCT imaging at 800 nm. Opt Lett. 2017;42:4978–81.
38. Gong G, Zhang H, Yao M. Speckle noise reduction algorithm with total variation regularization in optical coherence tomography. Opt Express. 2015;23:24699–712.
39. Cheng J, Tao D, Quan Y, Wong DW, Cheung GC, Akiba M, et al. Speckle reduction in 3D optical coherence tomography of retina by A-scan reconstruction. IEEE Trans Med Imaging. 2016;35:2270–9.
40. Broer SL, Broekmans FJ, Laven JS, Fauser BC. Anti-Mullerian hormone: ovarian reserve testing and its potential clinical implications. Hum Reprod Update. 2014;20:688–701.
41. Kelsey TW, Wright P, Nelson SM, Anderson RA, Wallace WH. A validated model of serum anti-mullerian hormone from conception to menopause. PLoS One. 2011;6:e22024.
42. Rosendahl M, Andersen CY, la Cour Freiesleben N, Juul A, Lossl K, Andersen AN. Dynamics and mechanisms of chemotherapy-induced ovarian follicular depletion in women of fertile age. Fertil Steril. 2010;94:156–66.
43. Klein T, Wieser W, Eigenwillig CM, Biedermann BR, Huber R. Megahertz OCT for ultrawide-field retinal imaging with a 1050 nm Fourier domain mode-locked laser. Opt Express. 2011;19:3044–62.

Human Reproduction, Vol.33, No.2 pp. 303–310, 2018
Advanced Access publication on December 28, 2017 doi:10.1093/humrep/dex368

human reproduction

ORIGINAL ARTICLE *Reproductive endocrinology*

Aromatase inhibitor use during ovarian stimulation suppresses growth of uterine endometrial cancer in xenograft mouse model

Tai Kawahara[1], Naoki Okamoto[1], Seido Takae[1], Megumi Kashiwagi[1], Mariko Nakajima[1], Atsushi Uekawa[1], Junya Ito[2], Naomi Kashiwazaki[2], Yodo Sugishita[1], and Nao Suzuki[1,*]

[1]Department of Obstetrics and Gynecology, St. Marianna University School of Medicine, Sugao, Miyamae, Kawasaki, Kanagawa 216-8511, Japan [2]Laboratory of Animal Reproduction, School of Veterinary Medicine, Azabu University, Sagamihara 229-8501, Japan

*Correspondence address. Department of Obstetrics and Gynecology, St. Marianna University School of Medicine, Kawasaki, Kanagawa 216-8511, Japan. E-mail: nao@marianna-u.ac.jp

Submitted on June 13, 2017; resubmitted on November 14, 2017; accepted on December 4, 2017

STUDY QUESTION: Could aromatase inhibitors (AI) be used to reduce risks of uterine endometrial cancer growth or recurrence during ovarian stimulation?

SUMMARY ANSWER: In a xenograft mouse model of endometrial cancer, concomitant AI administration suppressed the growth of endometrial cancer during ovarian stimulation.

WHAT IS KNOWN ALREADY: Recurrence and mortality rates of estrogen receptor-positive early breast cancer are reduced by long-term AI administration. Concomitant AI use for ovarian stimulation in patients with breast cancer is recommended for reducing estrogen-related potential risks. However, the efficacy of concomitant AI use for estrogen receptor-positive endometrial cancer have not been demonstrated conclusively by clinical or experimental animal studies.

STUDY DESIGN, SIZE, DURATION: Forty nude mice xenografted with uterine endometrial cancer cells were allocated to four groups. Group 1: no ovarian stimulation (control). Group 2: ovarian stimulation. Group 3: AI administration + ovarian stimulation. Group 4: ovariectomy and ovarian stimulation. Tumor growth was evaluated during the 6-week treatment period.

PARTICIPANTS/MATERIALS, SETTING, METHODS: Ishikawa 3-H-12 uterine endometrial cancer cells (estrogen and progesterone receptors-positive) were transplanted into 6-week-old BALB/cSlc-nu/nu nude mice, followed by interventions 2 weeks later.

MAIN RESULTS AND THE ROLE OF CHANCE: Compared to ovarian stimulation alone (Group 2), significant suppressions of tumor growth were observed in other three groups (Groups 1, 3 and 4, all at $P < 0.05$) and correlated with estrogen levels. AI administration had no apparent impact on embryo development.

LIMITATIONS, REASONS FOR CAUTION: In this study, we examined the growth of endometrial cancer tumors using one endometrial cancer cell line. Clinical endometrial cancer or hyperplasia cells can have diverse origins and AI may not be effective against other cancer cell types.

WIDER IMPLICATIONS OF THE FINDINGS: Concomitant AI use may provide a chance for safer childbirth by for patients with endometrial cancer or hyperplasia.

STUDY FUNDING/CONPETING INTEREST(S): This study was supported by the Graduate Student Aid from the St. Marianna University School of Medicine. The authors declare no competing interests.

Key words: fertility preservation / endometrial cancer / ovarian stimulation / estrogen / aromatase inhibitor

© The Author(s) 2017. Published by Oxford University Press on behalf of the European Society of Human Reproduction and Embryology. All rights reserved.
For Permissions, please e-mail: journals.permissions@oup.com

Downloaded from https://academic.oup.com/humrep/article-abstract/33/2/303/4781342 by St.Marianna University School of Medicine Library user on 29 November 2019

Introduction

Uterine endometrial cancer is one of the very common types of cancer in women. In the USA, for example, there were 54 870 cases in 2015, including 10 170 deaths, and these numbers have been increasing in recent years (Siegel et al., 2015). The standard treatment for uterine endometrial cancer is the combination of surgery, chemotherapy and radiotherapy (Rutledge, 1974; Signorelli et al., 2009), but young patients with early stage cancer (equivalent to the International Federation of Gynecology and Obstetrics stage IA) or endometrial hyperplasia sometimes request consideration of fertility preservation. In countries where surrogate pregnancy is recognized, women can have children by surrogate pregnancy after total hysterectomy, including bilateral adnexectomy so long as the collection of oocytes is performed before surgery (Azim and Oktay, 2007). However, for patients who do not have the option of surrogate pregnancy, fertility preservation implies conception by patient's own uterus and is associated with higher risks. For those patients, endometrial curettage is initially performed to physically remove cancer or hyperplasia cells, followed by hormone therapy.

Uterine endometrial cancer is classified as the estrogen-dependent type I and estrogen-independent type II. The former represents more than 80% of cases, and its carcinogenesis is associated with estrogen (Setiawan et al., 2013). Progesterone therapy has been demonstrated as an effective treatment for type I uterine endometrial cancers (Kelley and Baker, 1961). When medroxyprogesterone acetate (MPA) was used for the treatment of endometrial cancer and atypical endometrial hyperplasia, the overall complete response (CR) rate was 67%, hence, treatment with MPA has become the standard approach for patients who choose not to undergo hysterectomy to preserve fertility potential (Ushijima et al., 2007).

In premenopausal women, estrogen is synthesized primarily in the ovaries. In postmenopausal women, the estrogen level decreases as ovarian function declines and estrogen production relies on synthesis from androgens in the adrenal glands by the enzymatic reaction of aromatase. Estrogen is also produced from androgens in the aromatase pathway through the interaction of tumors and interstitial cells (Takahashi-Shiga et al., 2009). Aromatase inhibitors (AI) inhibit the enzymatic activity of aromatase and thus suppresses estrogen biosynthesis.

Recurrence and mortality rates of estrogen receptor (ER)-positive early breast cancer are reduced by long-term AI administration, which is more effective than the selective ER modulator tamoxifen (Early Breast Cancer Trialists' Collaborative Group, 2015). Therefore, AI have been used as long-term hormone therapy for breast cancer.

Ovarian stimulation elevates blood estrogen to non-physiological levels for limited periods by promoting the development of oocytes. Although, the short-term rise of blood estrogen caused by ovarian stimulation has been reported not to increase the risk of developing breast cancer in general population (Venn et al., 1999; Silva Idos et al., 2009), co-administration of AI for ovarian stimulation in patients with breast cancer is recommended due to the potential risk of cancer recurrence (Reddy and Oktay, 2012; Oktay et al., 2015; Rodgers et al., 2017).

Concomitant AI use has been previously investigated for ovarian stimulation in patients with endometrial cancer for similar reasons (Azim and Oktay, 2007), however, reported cases are limited and surrogate pregnancy is recommended.

Given the lack of evidence, in this experimental animal study we aimed to investigate the efficacy and safety of concomitant AI use by evaluation of tumor growth and blood estrogen concentrations as well as ovulation, insemination and embryo maturation under the internal use of AI.

Materials and Methods

Ethical approval

This study was performed upon the approval by the Animal Experiment Review Committee of St. Marianna University School of Medicine.

Animals

Mice were kept at 23 ± 2°C with a humidity of, 55 ± 5% humidity, 12-h light and 12-h dark cycle, and constant ad libitum access to feed food and water.

AI administration for estrogen measurements

C57BL/6 J, 4-week-old, female mice (Japan SLC, Inc., Shizuoka, Japan) (N = 16) were divided into four groups. Using a gastric tube, the third-generation AI letrozole (Femara®; Novartis Pharmaceuticals, AG, East Hanover, NJ) was administered at 0, 2, 10 or 25 μg/kg for 3 consecutive days. On the second day of letrozole administration, 7 IU of pregnant mare serum gonadotropin (PMSG; ASKA Animal Health Co., Ltd., Tokyo, Japan) was intraperitoneally administered to induce follicular development.

Measurement of the serum estrogen concentration

Mice were euthanized using carbon dioxide (CO_2) 2 days after the administration of PMSG. The blood was collected from their hearts, and centrifuged for 5 min at 684 g at 4 °C in a 1.5-ml microtube. Supernatant serum was transferred to a 1.5-ml microtube and stored in a freezer. Serum 17β-estradiol (E2) concentrations were measured using an Estradiol EIA Kit (Cayman Chemical Co., Ltd, Ann Arbor, MI) in accordance with the manufacturer's protocol.

AI administration and ovarian stimulation

For four groups of C57BL/6 J, 4-week-old, female mice (N = 36), letrozole was orally administered at 0, 2, 10 or 25 μg/kg/day for 4 days. On Day 2 of the letrozole administration, 7 IU of PMSG was intraperitoneally administered to induce follicular development, and on Day 4, of the letrozole administration, 7 IU of hCG (ASKA Pharmaceutical Co., Ltd, Tokyo, Japan) was intraperitoneally administered to induce hyperovulation.

Harvesting cumulus oocyte complexes

Mice were euthanized 16 h after hCG administration, and cumulus oocyte complexes (COCs) were collected through an incision made in the ampulla of the Fallopian tube. Collected COCs were transferred to 100-μl TYH (LSI Medience Corp., Tokyo, Japan) culture drops covered with mineral oil (Irvine Scientific, Santa Ana, CA), and then cultured at 37°C under 5% CO_2 in air until insemination. Fertilized oocytes and embryos were cultured in the KSOM-AA medium (Merck Millipore Corp., Billerica, MA).

Downloaded from https://academic.oup.com/humrep/article-abstract/33/2/303/4781342 by St.Marianna University School of Medicine Library user on 29 November 2019

Sperm collection and pre-culture

Caudal parts of the epididymis were collected from 8-week-old to 12-week-old, male C57BL/6J mice, and washed with the M16 culture medium (Global Stem, Rockville, MD). Blood and fat were removed on filter paper, and the sperm mass was collected from the tip of the caudal parts of the epididymis using a 23-G syringe needle. Then the collected sperm mass was submerged in 500 μl of the TYH medium in a 1.5-ml microtube and pre-cultured at 37°C and 5% CO_2 in air.

IVF and embryo culture

A 10-μl pre-cultured sperm was collected from the upper layer, and transferred to a TYH culture drop containing COCs and kept at 37°C under 5% CO_2 for 5–6 h to facilitate fertilization. After fertilization, ova were recovered from the TYH culture drops, transferred to drops of the KSOM medium, and cultured at 37°C, under 5% CO_2 in air. After culture for 16 h, two-cell embryos were transferred to fresh KSOM medium drops, and cultured at 37°C under 5% CO_2 to observing development up to the blastocyst stage.

Preparation and hematoxylin–eosin staining of mouse ovary tissue sections

Collected mouse ovaries were submerged in Bouin's solution (Wako Pure Chemical Industries, Ltd., Osaka, Japan) for 24 h at 4°C and saturated with paraffin by sequentially submerging them in the following: 70% *v/v* ethanol at room temperature for 1 h, 90% *v/v* ethanol at room temperature for 1 h, 100% ethanol at room temperature for 30 min, xylene at room temperature for 30 min, a mixture of paraffin and xylene at 65°C for 24 h, and paraffin at 65°C. Sequential 6-μm thick sections were prepared. Next, the paraffin sections were melted at 65°C, followed by deparaffinization with xylene, 100% ethanol, 90% *v/v* ethanol and 70% *v/v* ethanol. Tissue sections were stained with hematoxylin–eosin (HE), mounted, dried and evaluated.

Histological evaluation of ovaries

Histological evaluation of ovarian tissues was performed after HE staining. In ovaries collected during ovum collection and IVF, numbers of luteinized unruptured follicles (LUFs) were counted to evaluate any effects on the numbers of oocytes ovulated. Only nucleated ova were counted to avoid double counting.

Xenografting

The Ishikawa 3-H-12 cell line (National Research and Development Foundation JCRB Cell Bank, Osaka, Japan) (Nishida *et al.*, 1996), a cell strain expressing ER and progesterone receptor (PR), was used. Cells were cultured in minimum essential medium (Gibco Earle's salts$^+$ and L-glutamine; Thermo Fisher Scientific, Inc., Waltham, MA), with 15% w/v fetal bovine serum (Bovogen Biologicals Pty., Ltd, East Keilor, Australia) and 1% *w/v* Gibco Antibiotic–Antimycotic (Thermo Fisher Scientific, Inc., Waltham, MA). BALB/cSlc-nu/nu nude, 6-week-old, female mice (Japan SLC, Inc., Shizuoka, Japan) ($N = 40$) were used. We subcutaneously transplanted 1.0×10^7 Ishikawa 3-H-12 cells in the center of the mice's back using a 1-ml syringe with a 21-G syringe needle. Transplantation sites were monitored for 2 weeks to confirm grafting of the tumor. Four groups of 10 mice each were assigned to the following treatments.

Schedule for ovarian stimulation and AI administration

Group 1: Control group (no ovarian stimulation)
No drug administration after transplantation (oral and intraperitoneal injections of the physiological saline).

Group 2: Ovarian stimulation group
Starting 2 weeks after transplantation, intraperitoneal administrations of PMSG and hCG, once per week for 6 weeks.

Group 3: Ovarian stimulation + letrozole group
Oral daily administration of letrozole.
Starting 2 weeks after transplantation, intraperitoneal administrations of PMSG and hCG once per week for 6 weeks.

Group 4: Ovariectomy + ovarian stimulation group
Bilateral ovariectomy was performed 2 weeks after transplantation.
Starting 2 weeks after transplantation, intraperitoneal administrations of PMSG and hCG, once per week for 6 weeks.

For ovarian stimulation, follicular development was induced by intraperitoneal injection of 7-IU PMSG (ASKA Animal Health Co., Ltd). Hyperovulation was induced 2 days later by an intraperitoneal injection of 7-IU hCG (ASKA Animal Health Co.). Femara® (2.5-mg tablet; Novartis Pharmaceuticals, AG) was pulverized using a mortar and pestle and dissolved in sterilized water. A 25 μg/kg was administered orally using a gastric tube.

Sizes of subcutaneous tumors were measured weekly using a caliper with a vernier dial, and measurements in mm^3 (length × width × height) were recorded. On Day 4 of the sixth week after starting ovarian stimulation, mice were euthanized 2 days after PMSG administration using CO_2, tumors were excised, and bloods samples were collected.

Tumor evaluation and measurement of blood E2 concentration

(i) After euthanasia of mice using CO_2, blood was collected from their hearts, and the blood 17β-estradiol level was measured using the Estradiol EIA Kit (Cayman Chemical Co.).
(ii) Tumors on body surfaces were photographed.
(iii) Tumors were excised, photographed and weighed.
(iv) Each excised tumor was cut into at least four pieces. Two pieces were placed in a 1.5-ml microtube and then stored at −80°C. *ERα* and *ERβ* expression levels of each tumor tissue were measured by reverse transcription real-time polymerase chain reaction (RT-rPCR).
(v) Half of the remaining pieces were fixed using the Bouin solution, followed by HE staining.
(vi) Remaining pieces were fixed using a neutral formalin solution, followed by Ki67 staining.

Statistical analysis

Results are expressed as the mean ± standard error of the mean. The effects of treatment were compared among the groups using one-way analysis of variance with the post-hoc Tukey honestly significant difference test. Differences were considered significant if P was < 0.05. All analyses were computed using SAS JMP Pro 12.2.0 (SAS Institute Inc., Cary, NC).

Results

Reduction of blood E2 level by letrozole

The effect of AI on the blood estrogen concentration was examined using letrozole. Increasing concentrations of letrozole were administered orally for 3 days in C57BL/6J, female, 4-week-old mice ($N = 16$). The blood E2 concentration decreased from 29.0 ± 6.0 pg/ml to 25 ± 2.7, 11.4 ± 4.4 and 0.71 ± 0.4 pg/ml dose dependently with increasing concentrations of 2, 10 and 25 μg/kg of letrozole, respectively (Fig. 1). Significant decreases were obtained by 10 and 25 μg/kg of letrozole ($P < 0.05$).

Downloaded from https://academic.oup.com/humrep/article-abstract/33/2/303/4781342 by St.Marianna University School of Medicine Library user on 29 November 2019

Ovarian stimulation and letrozole administration

The effect of reduced E2 levels due to letrozole administration on superovulation for IVF was investigated. C57BL/6 J, female, 4-week-old mice ($N = 36$) were divided into four groups that received 0, 2, 10 or 25 μg/kg of letrozole orally.

The numbers of retrieved oocytes in the 0, 2, 10 and 25-μg/kg letrozole groups were 48 ± 2.8, 50 ± 1.8, 39 ± 2.7 and 36 ± 4.1, respectively. Therefore, retrieved oocytes were significantly fewer in the 25-μg/kg group than in the control group ($P < 0.05$; Fig. 2A). Fertilization rates were 79.9 ± 3.6%, 80.6 ± 4.1%, 74.7 ± 8.9% and 69.4 ± 5.3%, respectively, in the 0, 2, 10 and 25 μg/kg groups with no significant differences ($P > 0.05$; Fig. 2B). Blastocyst achievement rates were 94.7 ± 1.3%, 97.0 ± 1.3%, 90.6 ± 3.9% and 89.5 ± 3.6%, respectively, in the 0, 2, 10 and 25-μg/kg groups, demonstrating no significant differences ($P > 0.05$; Fig. 2C). Numbers of LUFs in ovarian tissue sections at the time of IVF were 5 ± 1.5, 3 ± 0.9, 2 ± 0.3 and 4 ± 0.9, respectively, in the 0, 2, 10 and 25-μg/kg letrozole groups. No correlation was observed between LUFs numbers and AI dose ($P > 0.05$; Fig. 2D).

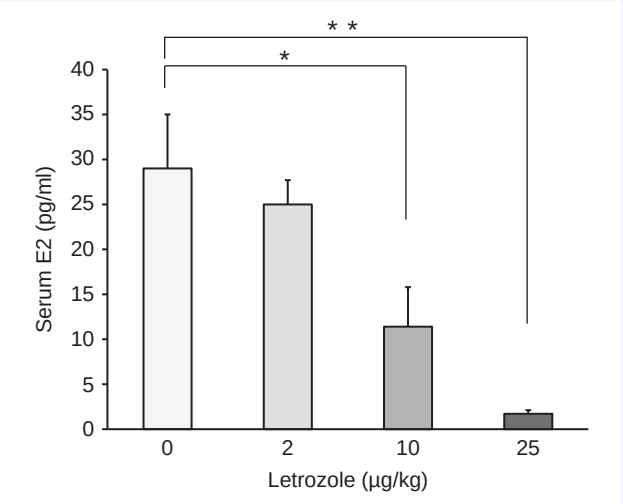

Figure 1 Effect of letrozole (aromatase inhibitor) on serum estrogen (E2) concentrations. Mice were divided into four groups according to the doses of letrozole (0, 2, 10 and 25 μg/kg). Letrozole was given orally for 3 days. A 7 IU of pregnant mare serum gonadotropin (PMSG) was given i.p., 2 days after the letrozole administration. All mice were sacrificed 2 days after PMSG administration, and E2 concentrations in sera were measured. *$P < 0.05$ versus the control.

Suppression of uterine endometrial cancer growth by letrozole

Ishikawa 3-H-12 cells (1×10^7) were transplanted subcutaneously in the back of BALB/cSlc-nu/nu mice. After 2 weeks, 40 mice were divided into four groups and treated as described in Fig. 3. Tumor size increased significantly in the ovarian stimulation group compared to the control group and was reduced by letrozole administration (Fig. 4). The blood E2 concentration, similar to the result with female C57BL/6 J mice (Fig. 1), was significantly lower in the letrozole and ovariectomy groups than in the ovarian stimulation group in BALB/cSlc-nu/nu mice ($P < 0.05$; Fig. 5A). As measured by RT-rPCR, the *ERα* messenger RNA expression level in tumor tissue was significantly higher in the ovarian stimulation group than in the other three groups ($P < 0.05$, Fig. 5B). No significant differences in the *ERβ* expression level were found between any of the four groups ($P > 0.05$, Fig. 5B).

Tumor tissues in all groups, after HE staining, showed characteristics of endometrial adenocarcinoma, including the formation of ductal structures, nuclear stratification with mild atypia, and cribriform pattern in the periductal region (Fig. 6A). In addition, Ki67 staining-positive cells were found in all groups (Fig. 6B).

Discussion

The present study demonstrated that the growth of endometrial cancer cells was promoted during ovarian stimulation and suppressed by letrozole in correlation with blood estrogen levels.

In general, long-term exposure to unopposed estrogen increases the incidence of endometrial cancer (Weiderpass *et al.*, 1999). On the other hand, no increase in the incidence of hormone-sensitive tumors due to ovarian stimulation has been reported in the general population (Venn *et al.*, 1999; Silva Idos *et al.*, 2009). This is because

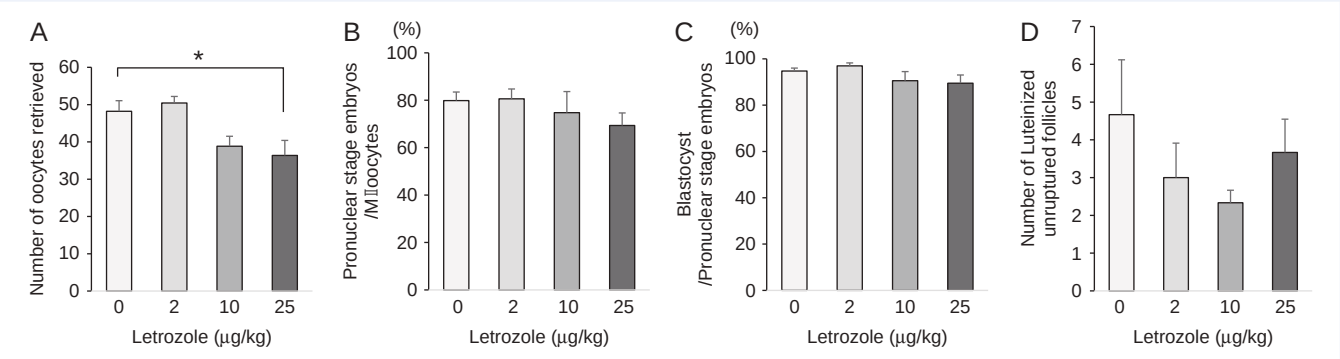

Figure 2 Efficacy of letrozole on fertility and embryogenesis. The aromatase inhibitor (AI) was administered orally at 0, 2, 10 and 25 μg/kg for 4 days. Pregnant mare serum gonadotropin and human chorionic gonadotropin were administered at seven IU/mouse intraperitoneally on Days 2 and 4, respectively, after AI administration. IVF was performed on Day 5 after AI administration. *$P < 0.05$ versus the control.

Downloaded from https://academic.oup.com/humrep/article-abstract/33/2/303/4781342 by St.Marianna University School of Medicine Library user on 29 November 2019

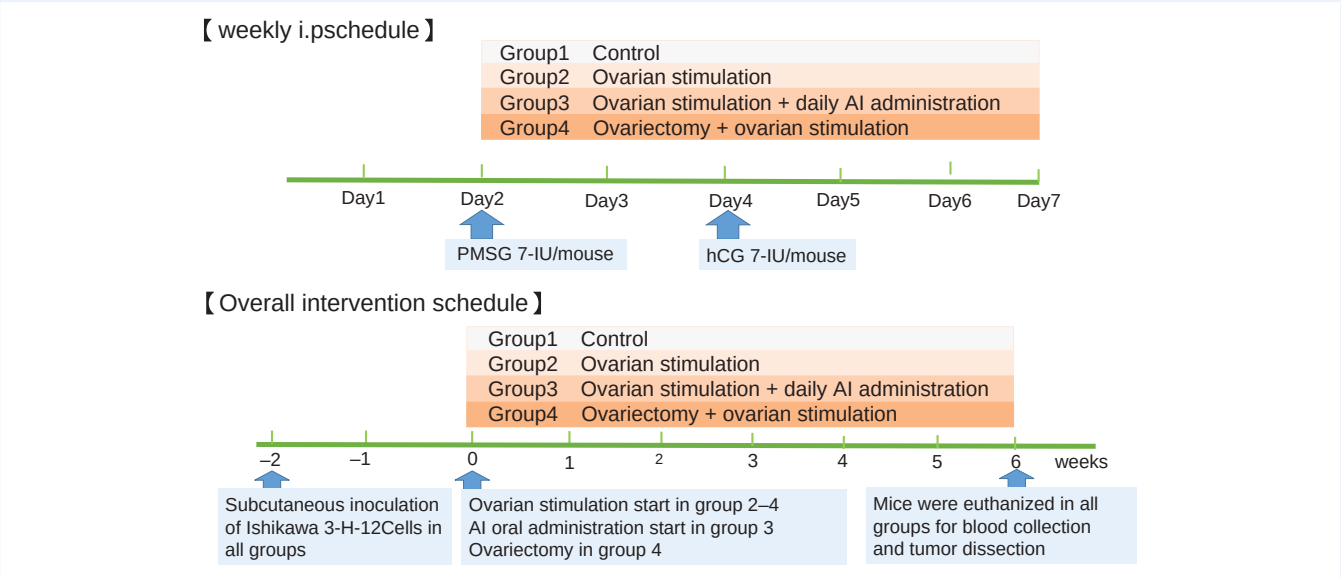

Figure 3 Experimental schedules of treatments started 2 weeks after tumor xenografting in all four groups. Group 1: no treatment; group 2: weekly intraperitoneal injections of 7 IU/mouse of pregnant mare serum gonadotropin, followed by intraperitoneal injections of 7 IU/mouse hCG 2 days later; Group 3: ovarian stimulation with daily oral administration of 25 μg/kg of the aromatase inhibitor; and Group 4: ovariectomy and ovarian stimulation 2 weeks after xenograft placement.

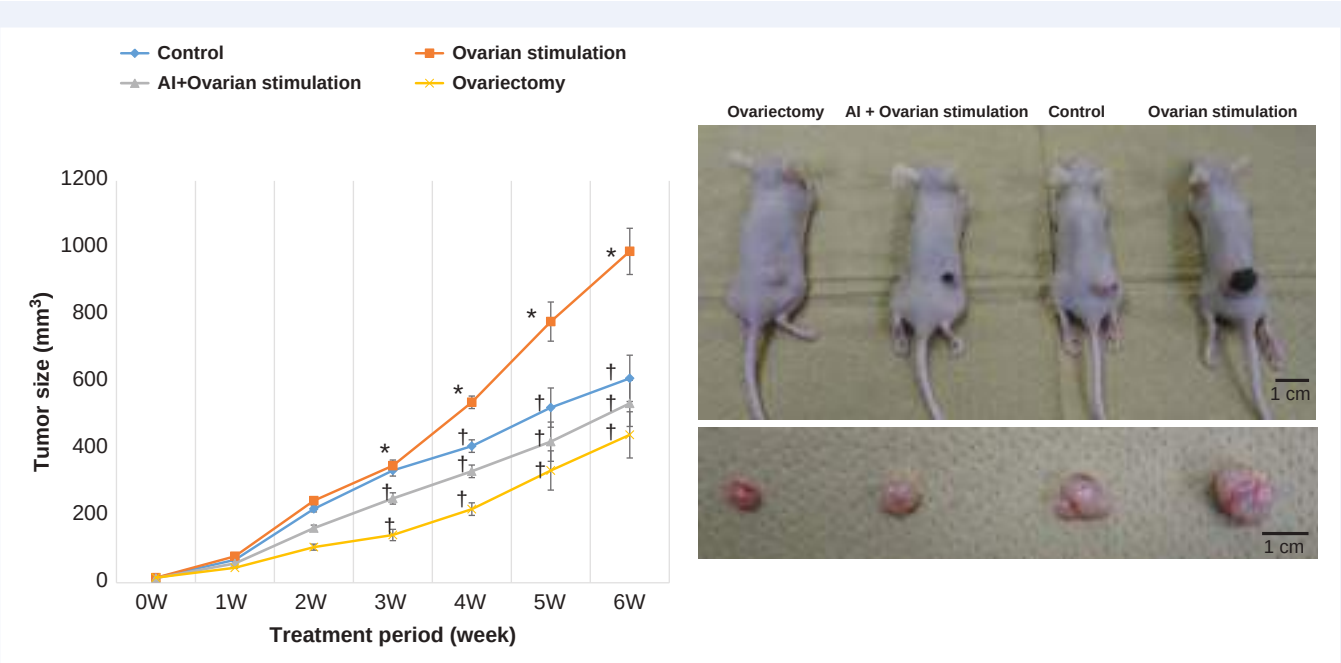

Figure 4 Tumor growth after xenografting. Endometrial cancer cells (Ishikawa 3-H-12) were xenografted subcutaneously in the back of nude mice, as described in Fig. 3. Tumor sizes were measured weekly. *A significant difference between the ovarian stimulation group and each of three other groups (marked by †) for the same weeks ($P < 0.05$).

the development of cancer is a long-term process in which mutations accumulate in genes such as tumor suppressor genes and mismatch repair genes while endometrial cells repeat cell divisions under stimulation by estrogen (Banno *et al.*, 2014). On the other hand, the increase in blood estrogen levels due to ovarian stimulation and accompanying follicular development is usually a temporary environmental change.

This study was undertaken to examine whether a short-term increase in blood estrogen concentrations contributes to the proliferation of a small number of established endometrial cancer cells, as predicted from

Downloaded from https://academic.oup.com/humrep/article-abstract/33/2/303/4781342 by St.Marianna University School of Medicine Library user on 29 November 2019

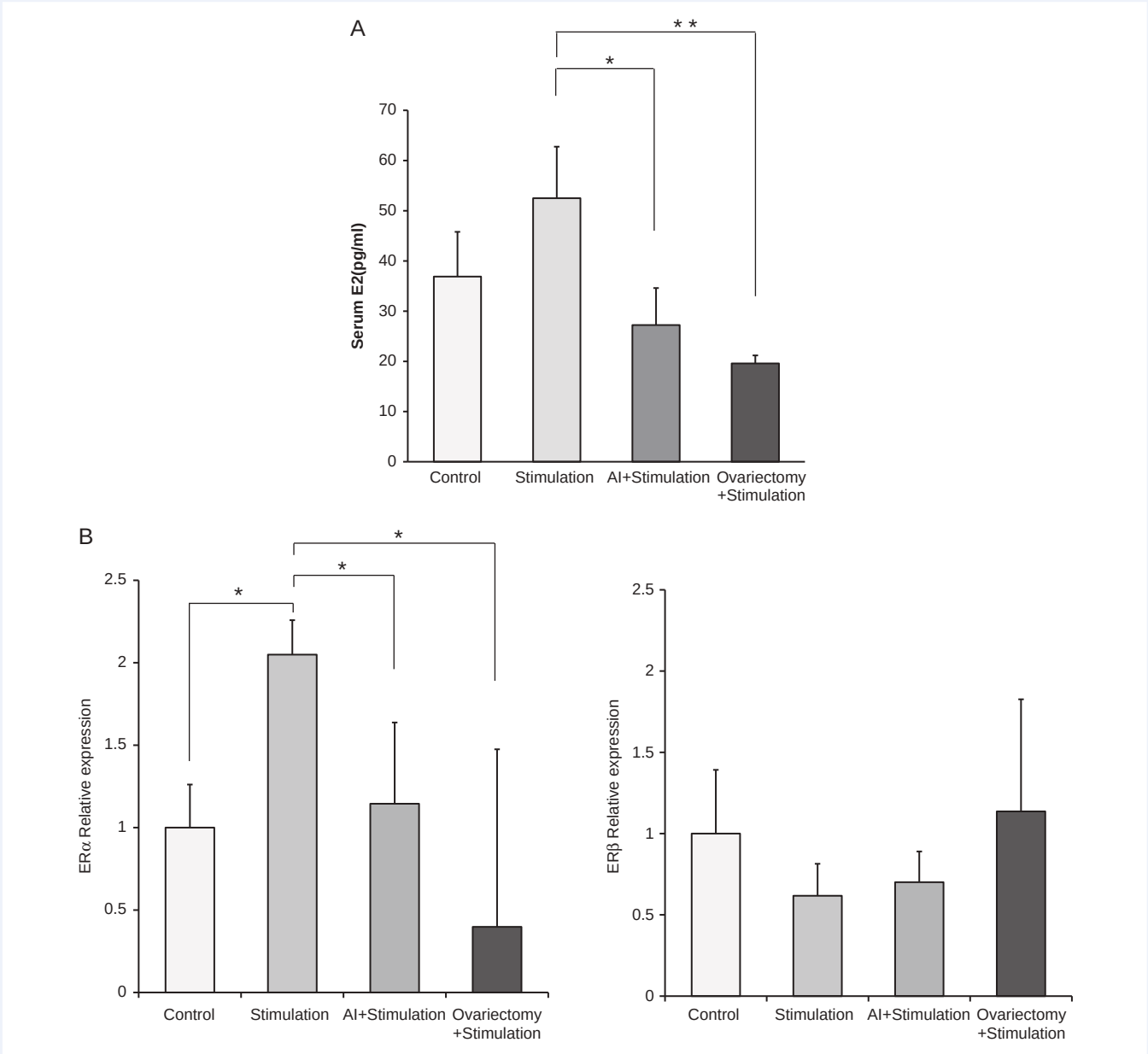

Figure 5 (**A**) Estrogen (E2) concentrations after 6-week intervention. Blood E2 concentrations in the plasma were measured by enzyme-linked immunosorbent assay. *$P < 0.05$ versus the stimulation group. (**B**) Expression levels of estrogen receptor (ER) α and β. mRNAs were measured by reverse transcription real-time polymerase chain reaction. *$P < 0.05$ versus the stimulation group.

past xenograft experiments (Clarke and Satyaswaroop, 1985). As it is difficult to reproduce residual endometrial cancer cells remaining in the uterus after endometrial curettage and MPA therapy in animal experiments, risks of clinical recurrence were approximately evaluated by implanting a small number of tumor cells subcutaneously in nude mouse and observing proliferation of these tumor cells. In the present study, we demonstrated that ovarian stimulation as a risk factor for endometrial cancer growth or recurrence and that the AI use is beneficial during ovarian stimulation against hormone-sensitive endometrial cancer growth.

Letrozole reduced the blood E2 concentration dose dependently (Fig. 1), without apparent effects on embryo development (Fig. 2C). However, the oocyte yield decreased at the highest dose of letrozole in the 25 μg/kg group as compared to the control group (Fig. 2A). Since no correlation was observed between LUF number and AI doses (Fig. 2D), the decrease in the number of oocytes retrieved did not appear to be due to dysfunction in ovulation; instead it appeared to be caused by effects on the maturation process of oocytes. In clinical practice, trigger timing by hCG or gonadotropin-releasing hormone agonist is determined by measuring the diameter of leading follicles. Since it was difficult to measure follicle sizes in mouse experiments, our experimental protocol, in which the same dose of hCG was administered 48 h after PMSG administration in all groups, may have affected the number of oocytes yielded. Since no significant decreases in oocyte yields nor risks on embryogenesis have been reported with

Downloaded from https://academic.oup.com/humrep/article-abstract/33/2/303/4781342 by St.Marianna University School of Medicine Library user on 29 November 2019

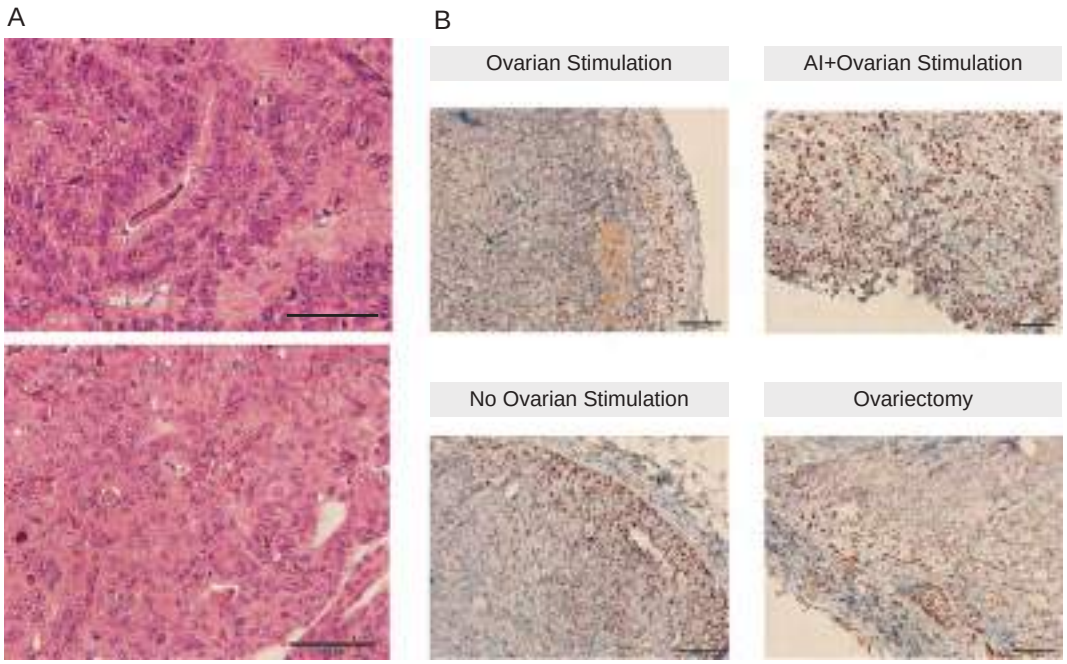

Figure 6 Histological analyses of Ishikawa 3-H-12 tumors. (**A**) Typical hematoxylin–eosin staining of uterine endometrial cancer seen in all groups. Scale bars, 100 μm. (**B**) Ki67 positive cells in all groups.

AI administration in clinical studies (Oktay *et al.*, 2005; Tulandi *et al.*, 2006; Lee and Oktay, 2012; Rodgers *et al.*,2017), this could be due to the use of prolific animals such as mice. Although further studies are required for the impact of high dose AI uses on folliculogenesis, AI appears not to have serious effects on the fertilization or embryo development.

Based on the present study, *ER α* expression, was highest in the ovarian stimulation group than in the other three groups (Fig. 5B), which is consistent with a previous report that E2 acts on ER α, inducing *c-Fos* expression and thus cell proliferation (Vivacqua *et al.*, 2006). The proliferative and prognostic indicator Ki67 staining did not change significantly in the present study (Fig. 6B), although it was previously shown to correlate with the suppression of endometrial cancer growth by neoadjuvant anastrozole treatment (Thangavelu *et al.*, 2013). Loci that showed strong Ki67-staining were uneven in all tumors, indicating complexities of tumors where proliferation and necrosis occurred even in the same tumor mass and which could have caused Ki67 staining irrespective of proliferation rates.

Previous reports on the therapeutic effect of AI against endometrial cancer are unclear. A phase II clinical study, in which 23 patients with recurrent uterine endometrial cancers were treated by the administration of anastrozole (a third-generation AI) showed minimal therapeutic effect (Rose *et al.*,2000). In another study of 28 postmenopausal women with advanced or recurrent uterine endometrial cancer treated with letrozole, the overall response rate was 9.4% and the authors concluded that letrozole was well tolerated but had little overall activity (Ma *et al.*, 2014). Recently, researchers reported that AI was effective against low-grade endometrial cancer after failure with progesterone treatment in three cases (Straubhar *et al.*, 2017). These reports indicate that AI may have therapeutic effect only for a limited number of ER-positive endometrial cancer cases, suggesting the diverse developmental mechanisms of endometrial cancer.

As our results are based on one type of endometrial cancer cell line, we cannot conclude that the concomitant AI use is effective for fertility preservation treatment of all endometrial cancer or hyperplasia patients, since it is currently not possible to fully identify the nature of the tumor in each case.

Since fertility preservation treatments for endometrial cancer or hyperplasia with atypia involve potential major risks which cannot be ignored, concomitant AI use during ovarian stimulation is worth considering to minimize those risks. In fact, there were cases in our institution in which endometrial cancer recurred after the ovarian stimulation during MPA therapy, resulting in patient death, although the causal relationship is unknown. Our research is motivated by these difficult experiences.

We focused on the ovarian stimulation in this study, but the influence of estrogen rise during pregnancy period on endometrial cancer or hyperplasia is also controversial. Regarding this point, the rise of progesterone and so-called healthy mother effect should be also taken into consideration (Valachis *et al.*, 2010).

Conclusion

Ovarian stimulation is a potential option for fertility preservation in reproductive age women with low-grade endometrial cancer or endometrial hyperplasia. It is however associated with risks of their recurrence or growth which can be mitigated by the concomitant AI use by decreasing serum estrogen concentrations.

Downloaded from https://academic.oup.com/humrep/article-abstract/33/2/303/4781342 by St.Marianna University School of Medicine Library user on 29 November 2019

Acknowledgements

We thank Dr Koko Murakami of New York Medical College for critically reading the article.

Authors' roles

N.S., S.T., Y.S., J.I. and N.K. designed the study. T.K., N.O., M.K., M.N. and A.U. conducted the experiments. T.K. wrote the article. T.K. and A.U. performed the statistical analysis. S.T., Y.S. and N.S. participated in the critical discussion and article editing.

Funding

This work was supported by the Graduate Student Aid from the St. Marianna University School of Medicine.

Conflict of interest

The authors declare no conflict of interest.

References

Azim A, Oktay K. Letrozole for ovulation induction and fertility preservation by embryo cryopreservation in young women with endometrial carcinoma. *Fertil Steril* 2007;**88**:657–664.

Banno K, Yanokura M, Iida M, Masuda K, Aoki D. Carcinogenic mechanisms of endometrial cancer: involvement of genetics and epigenetics. *J Obstet Gynaecol Res* 2014;**40**:1957–1967.

Clarke C, Satyaswaroop P. Photoaffinity labeling of the progesterone receptor from human endometrial carcinoma. *Cancer Res* 1985;**45**: 5417–5420.

Early Breast Cancer Trialists' Collaborative Group. Aromatase inhibitors versus tamoxifen in early breast cancer: patient-level meta-analysis of the randomised trials. *Lancet* 2015;**386**:1341–1352.

Kelley RM, Baker WH. Progestational agents in the treatment of carcinoma of the endometrium. *N Engl J Med* 1961;**264**:216–222.

Lee S, Oktay K. Does higher starting dose of FSH stimulation with letrozole improve fertility preservation outcomes in women with breast cancer? *Fertil Steril* 2012;**98**:961–964.

Ma BB, Oza A, Eisenhauer E, Stanimir G, Carey M, Chapman W, Latta E, Sidhu K, Powers J, Walsh W *et al*. The activity of letrozole in patients with advanced or recurrent endometrial cancer and correlation with biological markers—a study of the National Cancer Institute of Canada Clinical Trials Group. *Int J Gynecol Cancer* 2014;**4**:650–658.

Nishida M, Kasahara K, Oki A, Satoh T, Arai Y, Kubo T. Establishment of eighteen clones of Ishikawa cells. *Hum Cell* 1996;**9**:109–116.

Oktay K, Buyuk E, Libertella N, Akar M, Rosenwaks Z. Fertility preservation in breast cancer patients: a prospective controlled comparison of ovarian stimulation with tamoxifen and letrozole for embryo cryopreservation. *J Clin Oncol* 2005;**23**:4347–4353.

Oktay K, Turan V, Bedoschi G, Pacheco FS, Moy F. Fertility preservation success subsequent to concurrent aromatase inhibitor treatment and ovarian stimulation in women with breast cancer. *J Clin Oncol* 2015;**33**: 2424–2429.

Reddy J, Oktay K. Ovarian stimulation and fertility preservation with the use of aromatase inhibitors in women with breast cancer. *Fertil Steril* 2012;**98**:1363–1369.

Rodgers R, Reid G, Koch J, Deans R, Ledger W, Friedlander M, Abbott J. The safety and efficacy of controlled ovarian hyperstimulation for fertility preservation in women with early breast cancer: a systematic review. *Hum Reprod* 2017;**32**:1033–1045.

Rose PG, Brunetto VL, VanLe L, Bell J, Walker JL, Lee RB. A phase II trial of anastrozole in advanced recurrent or persistent endometrial carcinoma: a Gynecologic Oncology Group study. *Gynecol Oncol* 2000;**78**:212–216.

Rutledge F. The role of radical hysterectomy in adenocarcinoma of the endometrium. *Gynecol Oncol* 1974;**2**:331–347.

Setiawan V, Yang H, Pike M, McCann S, Yu H, Xiang Y, Wolk A, Wentzensen N, Weiss N, Webb P *et al*. Type I and II endometrial cancers: have they different risk factors? *J Clin Oncol* 2013;**31**:2607–2618.

Siegel RL, Miller KD, Jemal A. Cancer statistics. *CA Cancer J Clin 2015* 2015; **65**:5–29.

Signorelli M, Lissoni AA, Cormio G, Katsaros D, Pellegrino A, Selvaggi L, Ghezzi F, Scambia G, Zola P, Grassi R *et al*. Modified radical hysterectomy versus extrafascial hysterectomy in the treatment of stage I endometrial cancer: results from the ILIADE randomized study. *Ann Surg Oncol* 2009;**16**:3431–3441.

Silva Idos S, Wark I, McCormack A, Mayer A, Overton D, Little C, MacLean A. Ovulation-stimulation drugs and cancer risks: a long-term follow-up of a British cohort. *Br J Cancer* 2009;**100**:1824–1831.

Straubhar A, Soisson A, Dodson M, Simons E. Successful treatment of low-grade endometrial cancer in premenopausal women with an aromatase inhibitor after failure with oral or intrauterine progesterone. *Gynecol Oncol Rep* 2017;**21**:10–12.

Takahashi-Shiga N, Utsunomiya H, Miki Y, Nagase S, Kobayashi R, Matsumoto M, Niikura H, Ito K, Yaegashi N. Local biosynthesis of estrogen in human endometrial carcinoma through tumor-stromal cell interactions. *Clin Cancer Res* 2009;**15**:6028–6034.

Thangavelu A, Hewitt M, Quinton N, Duffy S. Neoadjuvant treatment of endometrial cancer using anastrozole: a randomised pilot study. *Gynecol Oncol* 2013;**131**:613–618.

Tulandi T, Martin J, Al-Fadhli R, Kabli N, Forman R, Hitkari J, Casper RF. Congenital malformations among 911 newborns conceived after infertility treatment with letrozole or clomiphene citrate. *Fertil Steril* 2006;**85**: 1761–1765.

Ushijima K, Yahata H, Yoshikawa H, Konishi I, Yasugi T, Saito T, Nakanishi T, Sasaki H, Saji F, Iwasaka T *et al*. Multicenter phase II study of fertility-sparing treatment with medroxyprogesterone acetate for endometrial carcinoma and atypical hyperplasia in young women. *J Clin Oncol* 2007; **25**:2798–2803.

Valachis A, Tsali L, Pesce LL, Polyzos NP, Dimitriadis C, Tsalis K, Mauri D. Safety of pregnancy after primary breast carcinoma in young women: a meta-analysis to overcome bias of healthy mother effect studies. *Obstet Gynecol Surv* 2010;**65**:786–793.

Venn A, Watson L, Bruinsma F, Giles G, Healy D. Risk of cancer after use of fertility drugs with in-vitro fertilisation. *Lancet* 1999;**354**:1586–1590.

Vivacqua A, Bonofiglio D, Recchia AG, Musti AM, Picard D, Andò S, Maggiolini M. The G protein-coupled receptor GPR30 mediates the proliferative effects induced by 17β-estradiol and hydroxytamoxifen in endometrial cancer cells. *Mol Endocrinol* 2006;**20**:631–646.

Weiderpass E, Adami H, Baron J, Magnusson C, Bergström R, Lindgren A, Persson I. Risk of endometrial cancer following estrogen replacement with and without progestins. *J Natl Cancer Inst* 1999;**91**:1131–1137.

Downloaded from https://academic.oup.com/humrep/article-abstract/33/2/303/4781342 by St.Marianna University School of Medicine Library user on 29 November 2019

Journal of Assisted Reproduction and Genetics (2019) 36:2251–2257
https://doi.org/10.1007/s10815-019-01599-3

FERTILITY PRESERVATION

Radiofrequency identification tag system improves the efficiency of closed vitrification for cryopreservation and thawing of bovine ovarian tissues

T. Sato[1] · Yodo Sugishita[1,4] · Y. Suzuki[1] · M. Kashiwagi[1] · S. Furuyama[1] · S. Nishimura[1] · A. Uekawa[1] · T. Koizumi[1] · M. Awaji[3] · T. Sawa[2] · A. Tozawa[1] · V. Komatsu[2] · Nao Suzuki[1]

Received: 18 April 2019 / Accepted: 26 September 2019 / Published online: 5 November 2019
© Springer Science+Business Media, LLC, part of Springer Nature 2019

Abstract

Purpose A radiofrequency identification (RFID) tag system was designed to streamline cryopreservation and thawing procedures. This study evaluated the usefulness of the RFID tag system for improving the efficiency of cryopreserving/thawing bovine ovarian tissue by the closed vitrification protocol.

Methods Six participants carried out closed vitrification and thawing of bovine ovarian tissues procedures using either the conventional or the new RFID tag method, and the time required to perform each step of the respective methods was measured. After normality of data was confirmed by the Shapiro-Wilk test, the significance of differences was assessed by the unpaired *t* test.

Results When closed vitrification was performed, the time required for each step showed a significant difference between the two methods ($t(4) = 2.938$, $p = 0.042$, $d = 2.40$), and the total cryopreservation time was 11 min shorter using the RFID tag system. When thawing was performed, the time required for each step also showed a significant difference between the two methods ($t(4) = 2.797$, $p = 0.049$, $d = 2.28$), and the total thawing time was 2 min shorter using the RFID tag system.

Conclusion The RFID tag system tested in this study seems to be suitable for managing biological samples stored in liquid nitrogen. Adoption of an RFID tag system by fertility centers may not only improve the efficiency of cryopreserving/thawing reproductive tissues but could also reduce human error.

Keywords Infertility treatment · Cryopreservation · Thawing · Ovarian tissue closed vitrification · Frozen samples · RFID tag · Storage system

Introduction

Advances in medical treatment have led to an increase of patients surviving cancer, resulting in more healthcare providers recognizing the importance of fertility preservation for cancer patients. It is important to offer cancer patients the option to preserve their reproductive tissues (oocytes, sperm, embryos, or ovaries) before initiation of treatment since many anticancer therapies reduce fertility [1–9]. Cryopreservation of reproductive tissues can be performed by fertility centers until a cancer survivor is ready to start a family, but storage time of the reproductive tissues may be as long as decades in the case of children with cancer [10]. Accordingly, meticulous management of the stored reproductive tissues from many patients over a prolonged period is required and this is a challenge for every fertility centers.

Conventional methods for managing cryopreserved tissues have several flaws. Since most steps in the cryopreservation process are carried out manually, human error can be a significant problem, as emphasized by several reported cases (Kagawa, Japan, in 2008, Singapore in 2010, and Rome, Italy, in 2013). In recent years, two-dimensional barcode

✉ Nao Suzuki
nao@marianna-u.ac.jp

1 Department of Obstetrics and Gynecology, St. Marianna University School of Medicine, 2-16-1 Sugao, Miyamae-ku, Kawasaki City, Kanagawa 216-8511, Japan

2 KRD Corporation, City, Yamato, Kanagawa 242-0007, Japan

3 Its Corporation, Kawasaki City, Kanagawa 211-0041, Japan

4 Department of Frontier Medicine Institute of Medical Science, St. Marianna University, School of Medicine, Kawasaki City, Kanagawa 216-8511, Japan

systems marketed by Merk or Oligio have improved the efficiency of managing cryopreserved tissues by minimizing manual data entry, but practical use of such systems is challenging for samples stored in liquid nitrogen (LN2) because frost forms on cryogenic vials and interferes with readability. Therefore, it is necessary to wipe the label dry before reading it with a reader, which leads to a risk of damaging the sample if its temperature rises to about − 135 °C. In addition, the current design of storage systems contributes to low efficiency in tracking and retrieving patient samples. The need for an efficient storage system that allows easy tracking/retrieval of cryopreserved tissues and reduces manual data entry has never been stronger in the fertility preservation field. We have designed a new storage system and a new device for preserving ovarian tissues that combines the use of two-dimensional barcode labels with radiofrequency identification (RFID) tags. The major advantages of using RFID tags are to eliminate manual data entry and allow readability when samples are stored in LN2. Patient information is transferred to the RFID tag from a computer, and by using an RFID reader, the same information can then be retrieved from the tag attached to sample devices that are stored in LN2. The new storage system has many sub-compartments for samples to maximize storage space in the LN2 tank. In the present study, we evaluated the influence of this RFID tag system on the efficiency of closed vitrification and thawing of bovine ovarian tissue.

Materials and methods

In total, 6 participants were asked to carry out the procedures of closed vitrification and thawing of bovine ovaries by either the conventional or the RFID tag method. Three participants were randomly selected by computer to perform the conventional method while the other 3 participants perform the RFID tagged method. Each participant processed 1 bovine ovary. The conventional method involved manual processing, while the RFID tag method employed a combination of two-dimensional barcode labels and RFID tag technology.

The following eight components were used in the RFID tag method:

1. Two-dimensional barcode label (Fig. 1A)

Both vertical and horizontal matrices are used in the barcode label, making it possible to read more information than provided by the original Universal Product Code. The code also has an error correction function that restores data if part of the code is missing.

2. RFID tags (Fig. 1B and C)

RFID uses electromagnetic radiation to wirelessly read and capture information stored in tags attached to objects. While a laser bar code scanner can only scan bar codes within direct view, an RFID reader can read multiple tags up to several feet away and does not need direct line-of-sight access to the tags. Another advantage of RFID is that it can identify tags in soiled or non-translucent bags. Each RFID tag stores data in the embedded IC chip and transmits data at a frequency of 13.56 MHz. We designed a round RFID tag (16 mm in diameter and 1 mm in thickness) for ovarian tissue cryopreservation devices by taking the size of the device and the data storage limit into consideration (Fig. 1B). Each device holds one ovarian tissue sample and the round RFID tag attached to the device can function after being stored in LN2 (− 196 °C). To prevent the slowing of the electrical circuit at low temperatures, which sometimes causes RFID tags to become unresponsive, we redesigned the circuit and improved the sensitivity of the tag. The RFID tag thus obtained was more sensitive and functioned better after storage in LN2 (Fig. 1C).

3. RFID reader (Fig. 1D)

The RFID reader uses radiofrequency waves to read information stored in the RFID tags. In our new RFID system, the antenna of the reader was modified to increase sensitivity for reading data from tags that had been stored in LN2. The modifications included lengthening the antenna, using copper wire, and increasing the magnetic field density by narrowing the antenna edge.

4. Device box (Fig. 1E)

The device box was made from SUS304 stainless steel containing chromium and nickel, with the metal inert gas welding method being used to seal any gaps so that the samples remained in LN2 after being taken out of the storage tank. Each cuboidal device box was designed to store up to 20 ovarian tissue cryopreservation devices from one patient, since an average of approximately 17 ovarian tissue samples are harvested per patient.

5. Storage box (Fig. 1F)

The storage box was also made from SUS304 stainless steel by spot welding and was large enough to contain 6 device boxes (120 cryopreservation devices with ovarian tissue samples from 6 patients).

6. Canister (Fig. 1G)

The cylindrical canister was used for the conventional method. Each canister could store samples from 4 patients. In the RFID tag system, each cuboidal canister had an

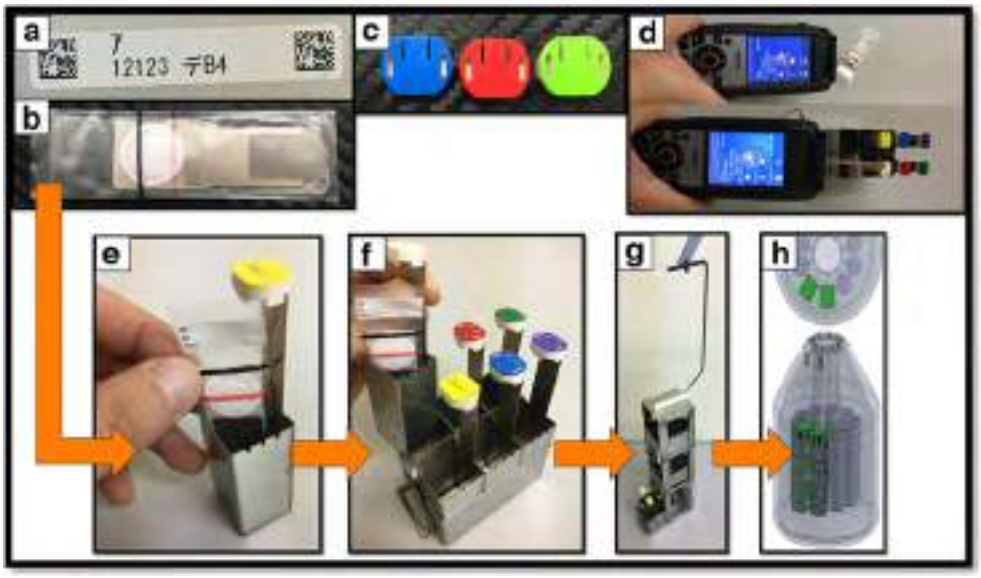

Fig. 1 The RFID tag system. (A) A two-dimensional barcode label. (B) An ovarian tissue cryopreservation device with a round RFID tag. (C) RFID tag for the device box. Tags of different colors are available for easy identification. (D) RFID reader (top). The reader shows patient information in the monitor (bottom). (E) Device box. Each device box holds 20 cryopreservation devices. (F) Storage box. Each storage box holds 6 device boxes. (G) Cuboidal canister. Each canister holds 3 storage boxes. (H) LN2 tank. Each tank holds 10 canisters

RFID tag attached to the handle and held 3 storage boxes, which could store up to 360 cryopreservation devices with ovarian tissues from 18 patients.

7. LN2 tank (Fig. 1H)

The tanks used in this study were the HC35 (Taylor Wharton) and KD32-10 LN2 (Kitazato). Each LN2 tank held 10 canisters storing samples from 40 patients (conventional method) or 180 patients (RFID tag method).

8. Computer

A computer was used to manage storage efficiently, with the computer screen showing the location of each RFID tag and indicating empty space in the tank.

9. Pretest

The Uchida-Kraepelin (U-K) test is a questionnaire that requires intense concentration by the participants and is used to assess mental agility, long-term attention, and recovery from fatigue. Each participant was asked to perform the U-K test prior to carry out the closed vitrification and thawing procedures. All participants achieved similar U-K test scores, indicating a similar ability to follow instructions irrespective of their professional background.

10. Steps in closed vitrification procedure

Conventional method (cryopreservation of bovine ovarian tissue; Fig. 2):

Step 1.The patient's hospital card was swiped through a card reader to obtain patient information. Then the patient information sheet (name, date of birth, hospital ID number, diagnosis, date of operation) was filled in manually.

Step 2.The resected ovary was placed in a cup filled with PBS and the cup was labeled (patient's name, hospital ID number, and date of birth).

Step 3.The same patient information was written on a Petri dish.

Step 4.The ovary was transferred from the cup to the Petri dish and cut into small pieces.

Step 5.Each ovarian tissue piece was assigned a number and photographed with the number.

Step 6.Patient information was written on 3 dishes containing graduated concentrations of cryoprotectant and the ovarian tissue samples were processed through the dishes.

Step 7.Each ovarian tissue sample was placed in a cryopreservation device (one per device). Then each device was placed in a plastic pouch and patient information (name, hospital ID number, date of birth, and ovarian tissue sample number) was written on the pouch.

Step 8.The labeled device was placed in a metal holder and successively into a canister and LN2 tank.

RFID tag method (cryopreservation of bovine ovarian tissue; Fig. 2):

Step 1.The patient's hospital card was swiped through a card reader to print out two-dimensional barcode labels with patient information (name, hospital ID number, and date of birth).

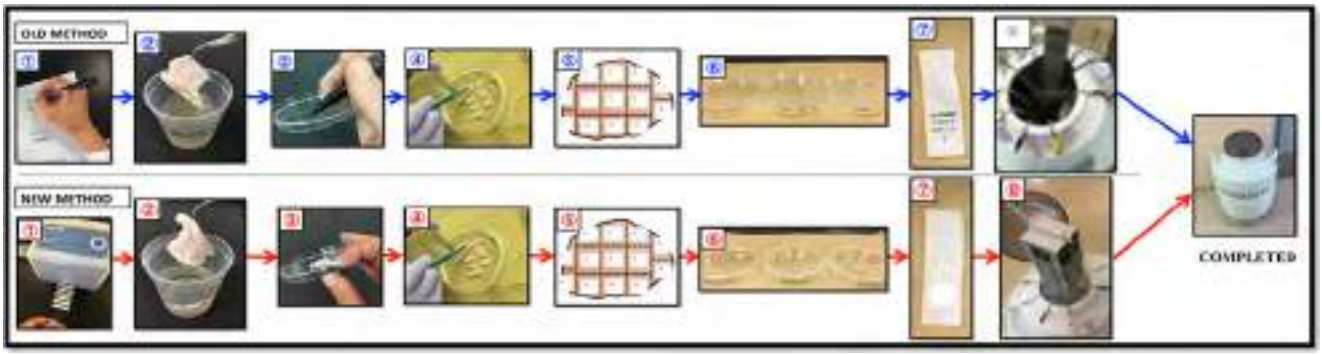

Fig. 2 Conventional and RFID tag methods for cryopreservation of ovarian tissue samples

Step 2.The resected ovary was placed in a cup filled with PBS and a barcode label was attached to the cup.

Step 3.A barcode label was attached to a Petri dish.

Step 4.The ovary was transferred from the cup to the Petri dish and cut it into small pieces.

Step 5.Each ovarian tissue piece was assigned a number and a single photograph was taken of that included all of the numbered tissue pieces. The camera was linked to a computer, allowing automatic recognition of the numbered tissues.

Step 6.Labels were attached to 3 dishes containing graduated concentrations of cryoprotectant and the ovarian tissue samples were processed through the dishes.

Step 7.Each ovarian tissue sample was placed in a cryopreservation device with an RFID tag, which stored patient information (name, hospital ID number, date of birth, and ovarian tissue sample number).

Step 8.The cryopreservation device was placed in a device box with an RFID tag and then successively in a storage box, canister, and LN2 tank.

11. Steps in thawing procedure

Conventional method (thawing bovine ovarian tissue; Fig. 3):

Step 1.The patient's information sheet was identified in a ledger.

Step 2.The ovarian tissue sample number and location in the LN2 tank were obtained from the patient information sheet.

Step 3.The cryopreservation device containing the ovarian tissue sample of interest was retrieved from the LN2 tank and compared with the handwritten information in the ledger.

Step 4.Patient information was written on a Petri dish.

RFID tag method (thawing bovine ovarian tissue; Fig. 3):

Step 1.Patient information was retrieved on a computer by swiping the patient's hospital card through a card reader and two-dimensional barcode labels were printed.

Step 2.The ovarian tissue sample number and location in the LN2 tank were obtained from the computer.

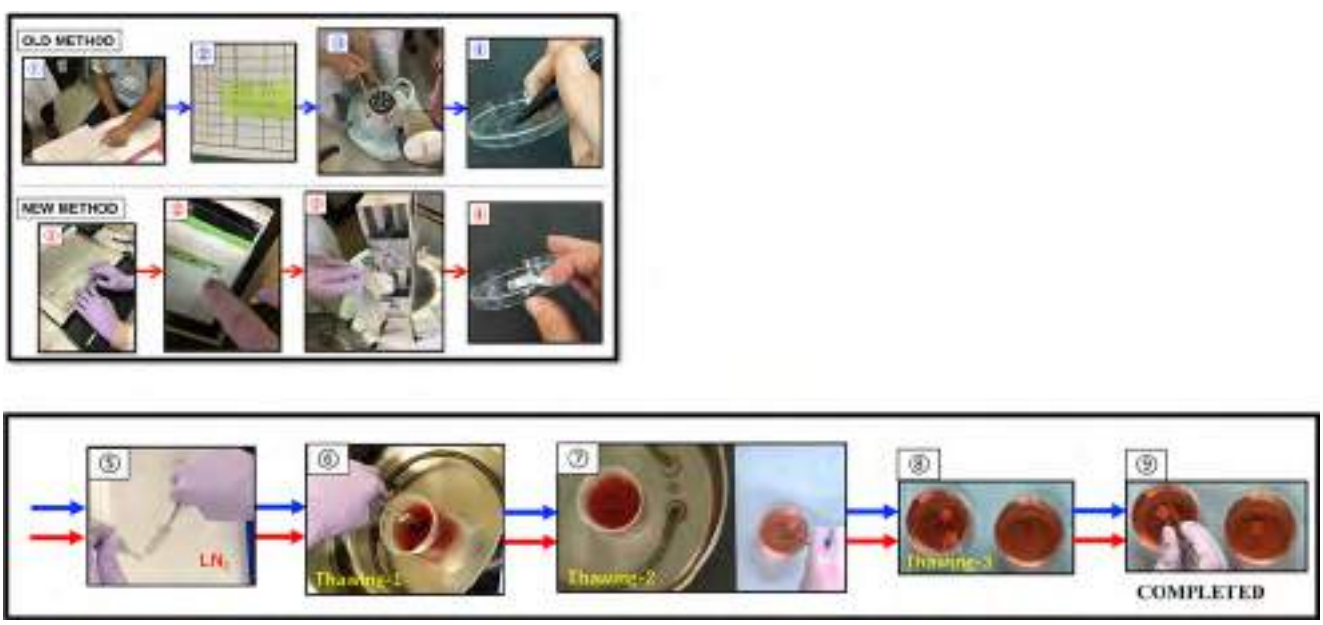

Fig. 3 Conventional and RFID tag methods for thawing ovarian tissue samples

Step 3.The cryopreservation device containing the ovarian tissue sample of interest was retrieved from the LN2 tank and its RFID tag was scanned with an RFID reader to confirm the patient information stored in the tag.

Step 4.A barcode label was attached to a Petri dish.

The remaining steps were the same for both methods and were not timed in this study.

Step 5 – The cryopreservation device with the sample of interest was removed from the plastic pouch in LN2.

Step 6.The cryopreservation device was placed in thawing solution 1.

Step 7.The cryopreservation device was transferred to thawing solution 2.

Step 8.The cryopreservation device was transferred to thawing solution 3.

Step 9.The ovarian tissue sample was removed from the cryopreservation device.

Statistical analysis

The time required to perform each step of the two methods was measured in seconds. Normality of data was determined by using the Shapiro-Wilk test. After normality was confirmed, the time for each step was treated as the dependent variable and the unpaired *t* test was performed without logarithmic transformation.

Results

All 6 participants underwent the Uchida-Kraepelin (U-K) test before performing the closed vitrification and thawing procedures by either the conventional or RFID tag method. The U-K test scores indicated that all participants had a similar ability to follow instructions and none was particularly slow or fast, irrespective of their professional background.

Performance with the two methods

When the RFID tag method was used for closed vitrification [11], the total time required for ovarian tissue cryopreservation was significantly shorter than that for the conventional method ($t(4) = 2.938$, $p = 0.042$, $d = 2.40$). The mean time required for cryopreservation was 1412.33 (± 130.5) seconds by the RFID tag method versus 2073.0 (± 367.0) seconds by the conventional method, and the use of the RFID tag method reduced the cryopreservation time by a mean of 11 min. A similar result was obtained with the thawing procedure, and the total time required for thawing samples was significantly shorter with the RFID tag method than the conventional method ($t(4) = 2.797$, $p = 0.049$, $d = 2.28$). The mean time required thawing ovarian tissue samples was 260.67 (± 38.7) seconds by the RFID tag method versus 405.0 (± 80.6) seconds by the conventional method, and using the RFID tag method reduced the thawing time by a mean of 2 min. The time differences between the two methods were calculated for each step. During closed vitrification procedure, the largest time difference was observed in step 3, where additional time was taken to correct patient information after incorrect information was written on the cup when performing the conventional method. During the thawing procedure, the largest time difference was noted when locating and retrieving the device with the target ovarian tissue sample. In the conventional method, retrieving the cryopreservation device took longer due to time required to confirm the handwritten information on the device pouch matched the patient information in the ledger. Also, when participants were searching for the target cryopreserved device, some incorrect devices were removed from the LN2 storage. In contrast, locating and retrieving the RFID-tagged cryopreserved device was performed efficiently, since the computer system showed the exact location of the device and the RFID reader was used to confirm patient information stored in the tag before removing the device from the LN2 tank.

Discussion

In Japan, the need for cryopreservation of ovarian tissue is increasing. The Japanese Ministry of Health, Labour and Welfare has conducted research in this field and launched a program to promote fertility preservation for adolescents and young adults with cancer in 2016 [12]. To date, 201 patients have undergone ovarian tissue cryopreservation [12]. The Obstetrics and Gynecology Department of St. Marianna Medical University is the one of the major fertility preservation centers in Japan and co-operates with The Ministry of Health, Labour and Welfare to support adolescents and young adults with cancer who require fertility preservation. In this study, we evaluated the usefulness of the RFID tag method for improving the efficiency of the closed vitrification protocol because our group has achieved 3 live births using vitrified/thawed ovarian tissues. Two of these live births have been reported already, although the third case has not been reported (unpublished observations) [13, 14]. Slow freezing is currently the standard method of ovarian tissue cryopreservation, but there is ongoing debate as to which, slow freezing or vitrification, is superior [15, 16]. Automatic vitrification systems have been developed for oocytes and embryos. However, an automatic system has not yet been developed for vitrification or slow freezing of ovarian tissue samples [17, 18].

Against this background, we aimed to develop a system that could streamline the cryopreservation and thawing procedures, and we performed this study to evaluate the usefulness of our RFID tag method in closed vitrification and thawing of bovine ovarian tissue samples. We found that application of

the RFID tag system improved the efficiency of both procedures, with the total time required for cryopreservation being reduced by 11 min when using the RFID tag system and the thawing time being reduced by 2 min.

Efficiency and control of human error are closely associated. The key advantages of utilizing an RFID tag system at fertility centers are improved efficiency and reduced the risk of human error. When the RFID tag system is integrated into a hospital network, swiping the hospital ID card transfers patient information to the IC chip on an RFID tag without manual entry, thus minimizing the risk of typing or writing errors associated with manual procedures. For tracking patient samples, the computer shows the exact location of each cryopreserved tissue sample in the LN2 tank and the RFID reader identifies the cryopreservation device with the target sample while it remains under LN2. The new round RFID tag that we developed has been tested to confirm readability while under LN2. If the IC chip in the RFID tag is damaged, the identification number etched on the surface of the device can still be used to retrieve patient information. In the future, we hope to focus on total elimination of human error and devising a backup system, such as cloud technology, to support this RFID tag method.

The RFID tag method can be applied to other forms of fertility preservation. The devices that are used for cryopreservation depend on the type of tissue being cryopreserved and the method of cryopreservation adopted. For example, the cryotop and the cryovial with a screw cap are usually employed for cryopreservation of oocytes, embryos, and sperm by vitrification, while the cryovial with metal pins attached to the screw cap is used for cryopreservation of ovarian tissue by open vitrification and a flat metal device (Fig. 1B) is used for cryopreservation by closed vitrification. The RFID tag manufacturer (KRD in Japan) can modify the tag size and sensitivity to fit the needs of each device.

Conclusion

Combining two-dimensional barcode labels with an RFID tag system improved the efficiency of cryopreservation and thawing by closed vitrification and reduced human error.

Acknowledgments Dr. David Robert McQuire (Yamada Translation Bureau, Tokyo, Japan) assisted with manuscript editing.

Authors' roles Y.S., T.S., N.S., T.S., and H.K. participated in study conception and design; Y.S., T.S., and H.K. developed the device; T.S, Y.S., Y.S., M.K., S.F., and U.A. performed the study; T.K. performed the statistical analysis; M.A., T.S., and H.K. built the computer system; N.S. edited the English manuscript; N.S, A.T., and N.S. gave suggestions for this research.

Funding information Grant-in-Aid for Scientific Research (B) from the Japan Society for the Promotion of Science to Nao Suzuki.

Compliance with ethical standards

Conflict of interest The authors declare that they have no conflicts of interest.

References

1. Green DM, Liu W, Kutteh WH, Ke RW, Shelton KC, Sklar CA, et al. Cumulative alkylating agent exposure and semen parameters in adult survivors of childhood cancer: a report from the St Jude Lifetime Cohort Study. The Lancet Oncology. 2014;15(11):1215–23.
2. Thomson AB, Campbell AJ, Irvine DC, Anderson RA, Kelnar CJ, Wallace WH. Semen quality and spermatozoal DNA integrity in survivors of childhood cancer: a case-control study. Lancet. 2002;360(9330):361–7.
3. Aubier F, Flamant F, Brauner R, Caillaud JM, Chaussain JM, Lemerle J. Male gonadal function after chemotherapy for solid tumors in childhood. J Clin Oncol. 1989;7(3):304–9.
4. Williams D, Crofton PM, Levitt G. Pediatr Blood Cancer. 2008;50(2):347–51.
5. Lampe H, Horwich A, Norman A, Nicholls J, Dearnaley DP. Fertility after chemotherapy for testicular germ cell cancers. J Clin Oncol. 1997;15(1):239–45.
6. Green DM, Kawashima T, Stovall M, Leisenring W, Sklar CA, Mertens AC, et al. Fertility of male survivors of childhood cancer: a report from the Childhood Cancer Survivor Study. J Clin Oncol. 2010;28(2):322–9.
7. Howell SJ, Shalet SM. Testicular function following chemotherapy. Hum Reprod Update. 2001;7(4):363–9.
8. Shalet SM, Tsatsoulis A, Whitehead E, Read G. Vulnerability of the human Leydig cell to radiation damage is dependent upon age. J Endocrinol. 1989;120(1):161–5.
9. Fisch B, Abir R. Female fertility preservation: past, present and future. Reproduction. 2018;156(1):F11–27.
10. Kristensen SG, Andersen CY. Cryopreservation of ovarian tissue: opportunities beyond fertility preservation and a positive view into the future. Front Endocrinol (Lausanne). 2018;9:347.
11. Sugishita Y, Okamoto N, Uekawa A, Yamochi T, Nakajima M, Namba C, et al. Oocyte retrieval after heterotopic transplantation of ovarian tissue cryopreserved by closed vitrification protocol. J Assist Reprod Genet. 2018;35(11):2037–48.
12. Suzuki N. Research on the effectiveness of cancer and reproductive health care for young cancer patients (fertility preservation), Degree the Ministry of Health, Labor and Welfare of children, Child care support promotion research project. 2018 (in Japanese)
13. Kawamura K, Cheng Y, Suzuki N, Deguchi M, Sato Y, Takae S, et al. Hippo signaling disruption and Akt stimulation of ovarian follicles for infertility treatment. Proc Natl Acad Sci U S A. 2013;110(43):17474–9.
14. Suzuki N, Yoshioka N, Takae S, Sugishita Y, Tamura M, Hashimoto S, et al. Successful fertility preservation following ovarian tissue vitrification in patients with primary ovarian insufficiency. Hum Reprod. 2015;30(3):608–15.
15. Amorim CA, Curaba M, Van Langendonckt A, Dolmans MM, Donnes J. Vitrification as an alternative means of cryopreserving ovarian tissue. Reprod BioMed Online. 2011;23(2):160–86.

16. Abir R, Fisch B, Fisher N, Samara N, Lerer-Serfaty G, Magen R, et al. Attempts to improve human ovarian transplantation outcomes of needle immersed vitrification and slow-freezing by host and graft treatments. J Assist Reprod Genet. 2017;34(5):633–44.
17. Arav A, Natan Y, Kalo D, Komsky-Elbaz A, Roth Z, Levi-Setti PE, et al. A new, simple, automatic vitrification device; preliminary results with murine and bovine oocytes and embryos. J Assist Reprod Genet. 2018;35(7):1161–8.
18. Roy TK, Brandi S, Tappe NM, Bradley CK, Vom E, Henderson C, et al. Embryo vitrification using a novel semi-automated closed system yields in vitro outcomes equivalent to the manual Cryotop method. Hum Reprod. 2014;29(11):2431–8.

Publisher's note Springer Nature remains neutral with regard to jurisdictional claims in published maps and institutional affiliations.

SCIENTIFIC REPORTS

OPEN

High co-expression of IL-34 and M-CSF correlates with tumor progression and poor survival in lung cancers

Received: 12 July 2017
Accepted: 18 December 2017
Published online: 11 January 2018

Muhammad Baghdadi[1], Hiraku Endo[1,2], Atsushi Takano[3,4], Kozo Ishikawa[1], Yosuke Kameda[1], Haruka Wada[1], Yohei Miyagi[5], Tomoyuki Yokose[6], Hiroyuki Ito[7], Haruhiko Nakayama[7], Yataro Daigo[3,4], Nao Suzuki[2] & Ken-ichiro Seino[1]

Despite recent advances in diagnosis and treatment of lung cancers, the 5-year survival rate remains unsatisfactory, which necessitates the identification of novel factors that associates with disease progression and malignant degree for improving diagnostic and therapeutic strategies. Recent progress in cancer immunology research has unveiled critical roles for colony stimulating factor 1 receptor (CSF1R) in multiple aspects of the tumor microenvironment. CSF1R is expressed on tumor-associated macrophages (TAMs), and mediates important pro-tumorigenic functions. CSF1R also provides critical autocrine signals that promote cancer cell survival and proliferation. Activation of CSF1R can be achieved by two independent ligands; macrophage colony-stimulating factor (M-CSF) and interleukin 34 (IL-34). Accordingly, the expression of these ligands in cancer is expected to result in poor prognosis. In this study, we show that IL-34 and M-CSF expression correlates with poor survival in a cohort of lung cancer patients. Importantly, high co-expression of IL-34 and M-CSF associates with the poorest survival compared to cancers that show weak or absent expression of the two ligands. Furthermore, high expression of IL-34 and M-CSF associates with advanced stages of lung cancers. Together, these results indicate a correlation between IL-34/M-CSF expression with poor survival and disease progression in lung cancer patients.

Lung cancer is the leading cause of cancer death and one of the most common cancers among both men and women worldwide[1]. In contrast to the steady increase in survival for most cancers, lung cancer still shows the poorest survival with less than 18% of 5-year relative survival, which results largely from poor detection and insufficient prediction of prognosis at early stages[1]. Obviously, an accurate assessment of prognosis is critical for an effective clinical decision and survival improvement.

With an aim to identify the molecular mechanisms that control the biological process of disease progression in cancer, several studies have focused on the genetic backgrounds of cancer cells and its relative impact on prognosis and clinical outcome of cancer therapy, such as RRM1, EGFR and KRAS mutations[2–6]. However, recent advances in cancer immunology research have unveiled a critical role for the interaction between cancer cells and immune cells at the tumor microenvironment (TME) in tumor progression and therapeutic resistance[7–9]. Thus, tumors that express critical immune-modulators are expected to be associated with high malignancy and thus related to poor prognosis. Indeed, patients with advanced stage cancers showed enhanced expression levels of several immune modulators including MIF, TNFα, IL-6, IL-8, IL-10, IL-18 and TGFβ[10]. Accordingly, accurate

[1]Division of Immunobiology, Institute for Genetic Medicine, Hokkaido University, Kita-15 Nishi-7, Sapporo, 060-0815, Japan. [2]Department of Obstetrics and Gynecology, St. Marianna University School of Medicine, 2-16-1 Sugao, Miyamae-ku, Kawasaki City, Kanagawa, 216–8512, Japan. [3]Department of Medical Oncology and Cancer Center, Shiga University of Medical Science, Otsu, 520-2192, Japan. [4]Center for Antibody and Vaccine, Research Hospital, Institute of Medical Science, University of Tokyo, Tokyo, 108-8639, Japan. [5]Molecular Pathology and Genetics Division, Kanagawa Cancer Center, Yokohama, 241-0815, Japan. [6]Department of Pathology, Kanagawa Cancer Center, Yokohama, 241-8515, Japan. [7]Department of Thoracic Surgery, Kanagawa Cancer Center, Yokohama, 241-8515, Japan. Muhammad Baghdadi, Hiraku Endo and Atsushi Takano contributed equally to this work. Correspondence and requests for materials should be addressed to K.-i.S. (email: seino@igm.hokudai.ac.jp)

prediction of prognosis in cancer patients may require the assessment of such factors in addition to the genetic backgrounds of cancer cells.

Among several immune cells, tumor-associated macrophages (TAMs) consist the most abundant cell population in many tumors, which play crucial roles in multiple aspects of the TME, including tumor progression, invasion, metastasis and angiogenesis[11–13]. Importantly, TAMs infiltration has been considered as an independent poor prognostic factor in several cancers[7–9]. TAMs depend largely on CSF1R signaling for survival, proliferation and function, which can be achieved by two independent ligands; M-CSF and IL-34[14,15]. M-CSF and IL-34 share no sequence homology, but show comparable biological activities in myeloid cells[16,17]. Both cytokines correlate with tumor progression, metastasis, angiogenesis and therapeutic resistance[9]. It has been suggested that expression of IL-34 or M-CSF is accompanied with increased infiltration of M2-polarized TAMs that show enhanced pro-tumorigenic functions[18,19]. Based on these backgrounds, the expression of IL-34 and/or M-CSF at the TME may characterize tumors with enhanced aggression and has an impact on the patient's survival. In this regard, previous reports have related M-CSF expression with poor survival in cancer patients[20,21]. However, IL-34 expression has not been evaluated in these studies, since it was discovered for the first time in 2008[22]. In this study, we analyze the expression of IL-34 and M-CSF in primary lung cancer tissues and its correlation with survival and tumor progression in a cohort of lung cancer patients, providing for the first time an evidence that show the association between IL-34 and M-CSF expression with disease progression and poor survival in lung cancer patients.

Results

IL-34 or M-CSF expression correlates with poor survival in lung cancer patients. We have previously described a correlation between high expression of IL-34 and poor survival in a cohort of lung cancer patients (Fig. 1a)[19]. The clinicopathological characteristics of this cohort were described in detail in our previous report[19]. In this cohort, 45% of patients were Japanese women over 60 years without smoking history, and 77.4% of cases were diagnosed as non-small lung cancers (stage I) with 5 years of follow-up period[19]. Immunohistochemical staining of IL-34, M-CSF, CSF1R and CD163 was performed on lung cancer tissues obtained from patients by surgical resection. Antibodies specificity was confirmed before staining (Supplementary Fig. 1). Similar with IL-34, M-CSF expression was detected in lung adenocarcinomas (ADCs), squamous cell carcinomas (SCCs) and small cell lung cancers (SCLCs) with a variety among patients (Fig. 1b). In contrast, M-CSF was undetectable at protein level in normal lung tissues (Fig. 1b). Kaplan-Meier analysis of overall survival in lung cancer patients showed that high expression of M-CSF correlates with poor survival of lung cancer patients (Fig. 1c), in accordance with previous reports[20,21].

High co-expression of IL-34 and M-CSF correlates with the poorest survival in lung cancer patients. Next, we evaluated the association between IL-34 and M-CSF expression in lung cancers and the related impact on patients' survival. Interestingly, 91% of cancer tissues that showed strong staining of IL-34 were accompanied with high (48%) or weak (43%) expression of M-CSF (Supplementary Table 1). Similarly, 77% of cancer tissues that showed strong staining of M-CSF were accompanied with high (56%) or weak (21%) expression of IL-34 (Supplementary Table 1). On the other hand, the absence of IL-34 staining in cancer tissues was frequently associated with the absence of M-CSF staining, and vice versa, (Supplementary Table 1) which may suggest a reciprocal relationship between the expression of IL-34 and M-CSF in lung cancers. Furthermore, we categorized patients in this cohort depending on the expression levels of M-CSF and IL-34 into 4 groups: 1) weak or absent expression of both M-CSF and IL-34, 2) High expression of IL-34 with weak or absent expression of M-CSF, 3) High expression of M-CSF with weak or absent expression of IL-34, 4) high expression of both M-CSF and IL-34. Kaplan-Meier analysis of overall survival in lung cancer patients based on this classification showed that high expression of M-CSF or IL-34 correlates with poor survival compared to groups that showed weak or absent expression of the two ligands (Fig. 2a,b). Importantly, patients with high expression of both M-CSF and IL-34 have the poorest survival compared to other groups (Fig. 2c). Together, these results suggest that high co-expression of both IL-34 and M-CSF correlates with poorer survival in lung cancer patients.

CSF1R expression correlates with poor survival in lung cancers. CSF1R is tyrosine-protein kinase that acts as a cell-surface receptor for M-CSF and IL-34[14–16]. CSF1R is expressed mainly in cells of the myeloid lineage and is a key regulator of macrophage differentiation[23]. However, several reports have showed that CSF1R expression can be also detected in other cells such as endothelial cells and importantly in cancer cell lines and primary cancer tissues[24,25]. Thus, we next evaluated the expression of CSF1R in lung cancer tissues. Similar with IL-34 and M-CSF, immunohistochemical staining showed that CSF1R is expressed in lung cancer tissues with a variety among patients (Fig. 3a). Again, high expression of CSF1R correlates with poor survival in lung cancer patients, similar with IL-34 and M-CSF expression (Fig. 3b).

CD163 expression correlates with poor survival in lung cancers. Accumulating evidence from clinical and experimental studies indicates that TAMs play critical roles in the promotion of tumor development, progression, metastasis and therapeutic resistance[26]. CD163 is a member of the scavenger family receptor, with high specificity for monocyte/macrophage lineage[27], and has been considered as a specific marker to enumerate TAMs[28]. Thus, CD163 staining is expected to reflect the status of macrophage infiltration into tumors and predict poor prognosis in cancer patients[29]. Immunohistochemical staining showed that CD163 expression could be detected in lung cancer tissues with a variety among patients (Fig. 4a,b). Furthermore, Kaplan-Meier analysis of overall survival in this cohort of lung cancer patients showed that CD163 expression correlates with poor survival, in consistent with previous reports[29] (Fig. 4c).

IL-34 and M-CSF expression correlates with CD163 expression and poor survival in lung cancers. Next, we examined the relation between M-CSF or IL-34 with CD163 expression and its impact on

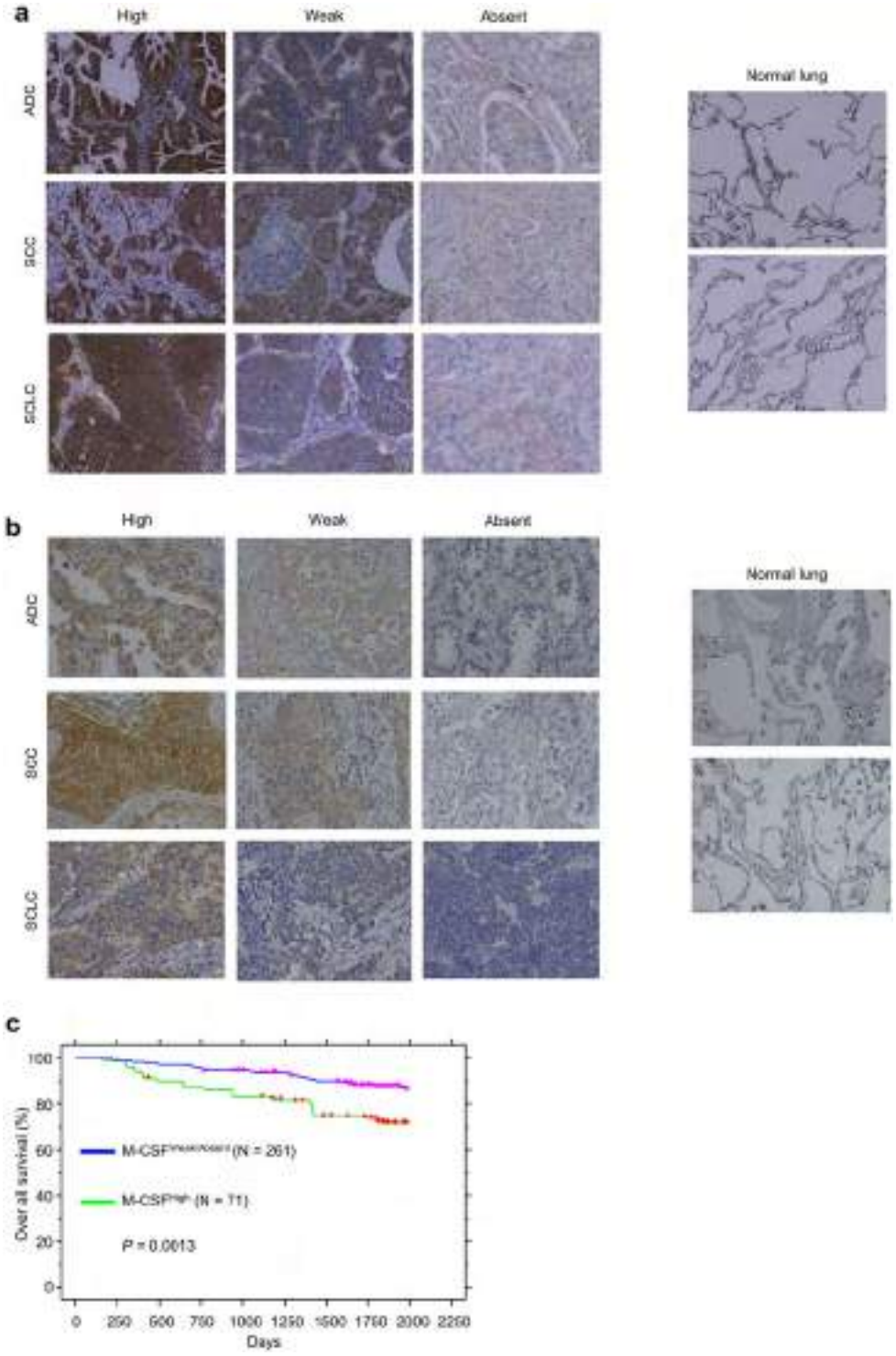

Figure 1. Correlation between IL-34 and M-CSF expression with poor survival in lung cancer patients. (**A**) and (**b**), Immunohistochemistry staining of IL-34 (**a**) or M-CSF (**b**) in primary lung cancer tissues from patients diagnosed with adenocarcinoma (ADC), squamous cell carcinoma (SCC) or small cell lung cancers (SCLC) compared to normal lung tissues. (**c**) Kaplan-Meier analysis showing overall survival in lung cancer patients according to M-CSF expression.

survival in this cohort of lung cancer patients. High expression of M-CSF was frequently accompanied with high expression of CD163 (Fig. 5a; Supplementary Table 1), and the absence of CD163 staining was frequently associated with absent or weak staining of M-CSF (Fig. 5a; Supplementary Table 1). Kaplan-Meier analysis of overall survival in lung cancer patients based on M-CSF and CD163 expression showed that high expression of both M-CSF and CD163 in cancer tissues correlates with poor survival compared to other groups (Fig. 5b),

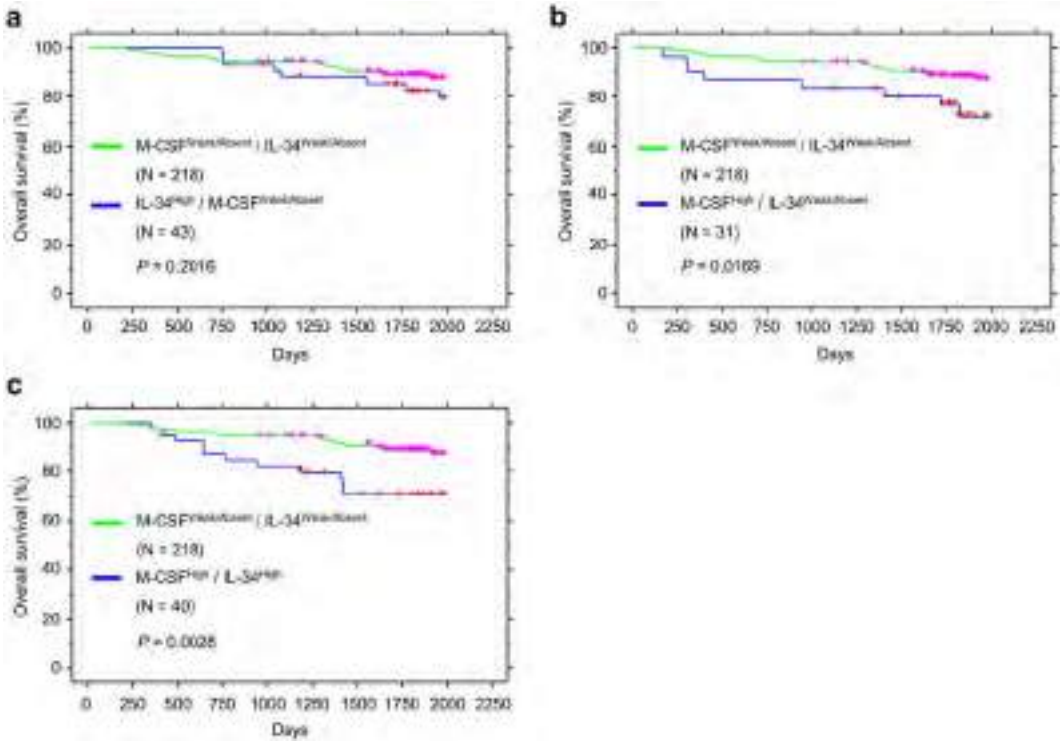

Figure 2. Correlation between M-CSF/IL-34 expression with poor survival in lung cancer patients. (**a**) Kaplan-Meier analysis showing overall survival in lung cancer patients that show M-CSF$^{Weak/Absent}$/IL-34$^{Weak/absent}$ expression compared to M-CSF$^{Weak/Absent}$/IL-34^{High} group. (**b**) Kaplan-Meier analysis of overall survival in lung cancer patients that show M-CSF$^{Weak/Absent}$/IL-34$^{Weak/absent}$ expression compared to M-CSF^{High}/IL-34^{High} group. (**c**) Kaplan-Meier analysis of overall survival in lung cancer patients that show M-CSF$^{Weak/Absent}$/IL-34$^{Weak/absent}$ expression compared to M-CSF^{High}/IL-34^{High} group.

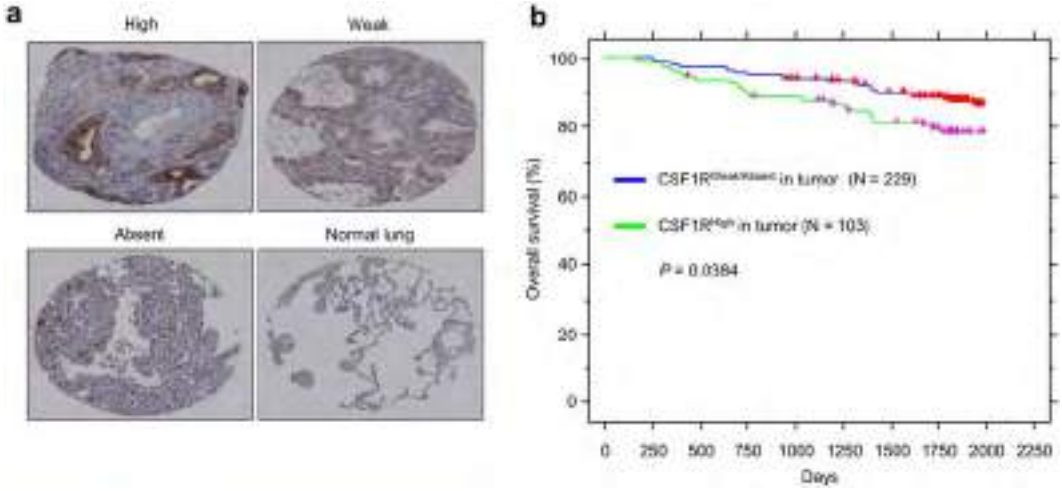

Figure 3. Correlation between CSF1R expression with poor survival in lung cancer patients. (**a**) Representative data of immunohistochemistry staining of CSF1R in primary lung cancer tissues compared to normal lung tissues. (**b**) Kaplan-Meier analysis showing overall survival in lung cancer patients according to CSF1R expression.

consistent with previous reports[28]. Similarly, we evaluated the relation between IL-34 and CD163. As expected, 60% of cancer tissues that showed high expression of IL-34 were accompanied with high expression of CD163 (Fig. 5c; Supplementary Table 1), and the absence of CD163 staining was frequently associated with negative staining of IL-34 (Fig. 5c; Supplementary Table 1), which indeed suggests a correlation between IL-34 and CD163 expression in lung cancers. Kaplan-Meier analysis of overall survival in lung cancer patients based on IL-34 and

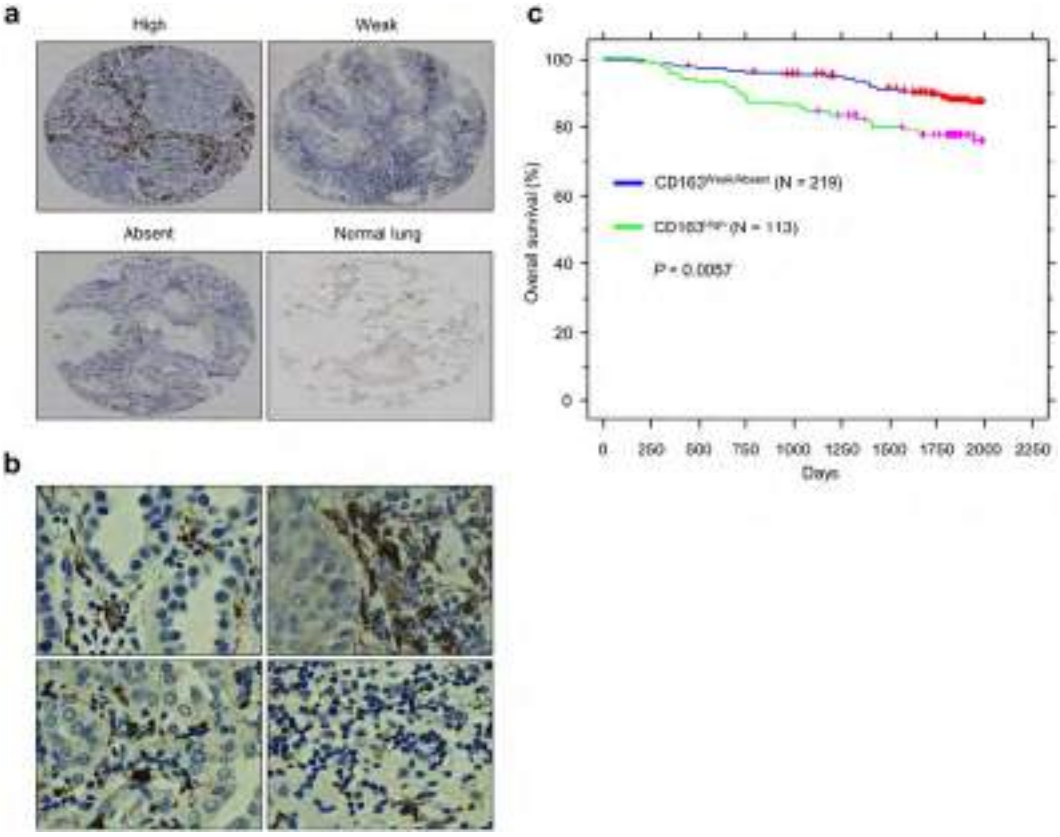

Figure 4. Correlation between CD163 expression with poor survival in lung cancer patients. (**a**) Representative data of immunohistochemistry staining of CD163 in primary lung cancer tissues compared to normal lung tissues. (**b**) High magnification images of CD163 staining in lung cancer tissues. (**c**) Kaplan-Meier analysis showing overall survival in lung cancer patients based on CD163 expression.

CD163 expression showed that patients with high expression of both IL-34 and CD163 have the poorest survival compared to other groups (Fig. 5d). Collectively, these results indicate a correlation between high expression of IL-34, M-CSF, CSF1R and CD163 with poor survival, which was further confirmed in univariate analysis using Cox's proportional hazards model (Table 1), although multivariate analysis in this model did not reach a statistical significance except for T and N factors (Table 1).

IL-34 and M-CSF expression is enhanced in advanced stages of lung cancers. Finally, we evaluated the expression level of IL-34 and M-CSF according to each stage in lung cancer patients (Supplementary Tables 2 and 3). By calculating positivity rates in each group, patients with high expression of IL-34 or M-CSF showed increased frequencies from stage IA (17.2%, 15.3%), stage IB (25%, 22%), stage IIA (40%, 20%), stage IIB (37.5%, 50%) to stage IIIA (44.8%, 37.9%) (Fig. 6a,b). Similarly, frequencies of patients with high co-expression of IL-34 and M-CSF associated with stages, starting from 8.3% at stage IA, 11% at stage IB, 16.7% at stage IIA, 25% at stage IIB, to 24.13% at stage IIIA (Fig. 6c). Statistically, the expression of IL-34 (Supplementary Table 4, $P = 0.0004$) or M-CSF (Supplementary Table 4, $P = 0.0062$) showed a tendency to be enhanced in stage II and III compared to stage I. Similarly, high co-expression of IL-34 and M-CSF was observed more frequently in stage II and IIIA compared to stage I (Supplementary Table 4, $P = 0.0081$). In a combined analysis, patients' groups that showed high expression of IL-34 (Table 2, $P = 0.0095$), M-CSF (Table 2, $P = 0.00829$) or high co-expression of both IL-34 and M-CSF (Table 2, $P = 0.0011$) were associated with stage II and IIIA rather than stage I compared to other groups with weak or absent expression. Together, these findings indicate an association between IL-34 and M-CSF expression with stages in lung cancers, and thus may serve as progression parameters.

Discussion

In this paper, we describe for the first time the clinicopathological relevance of M-CSF and IL-34 expression with disease stages and poor survival in a cohort of lung cancer patients. Our data showed that single expression of M-CSF or IL-34 can be observed in primary lung cancer tissues and correlated with poor survival. High expression of both cytokines correlates with CD163 expression, which collectively correlates with poor survival. Additionally, high co-expression of M-CSF or IL-34 correlates with disease stages and the poorest survival compared to groups that showed weak or absent expression of the two ligands. Thus, evaluating the expression of both M-CSF and IL-34 may help to estimate disease progression and malignant degree in lung cancer patients.

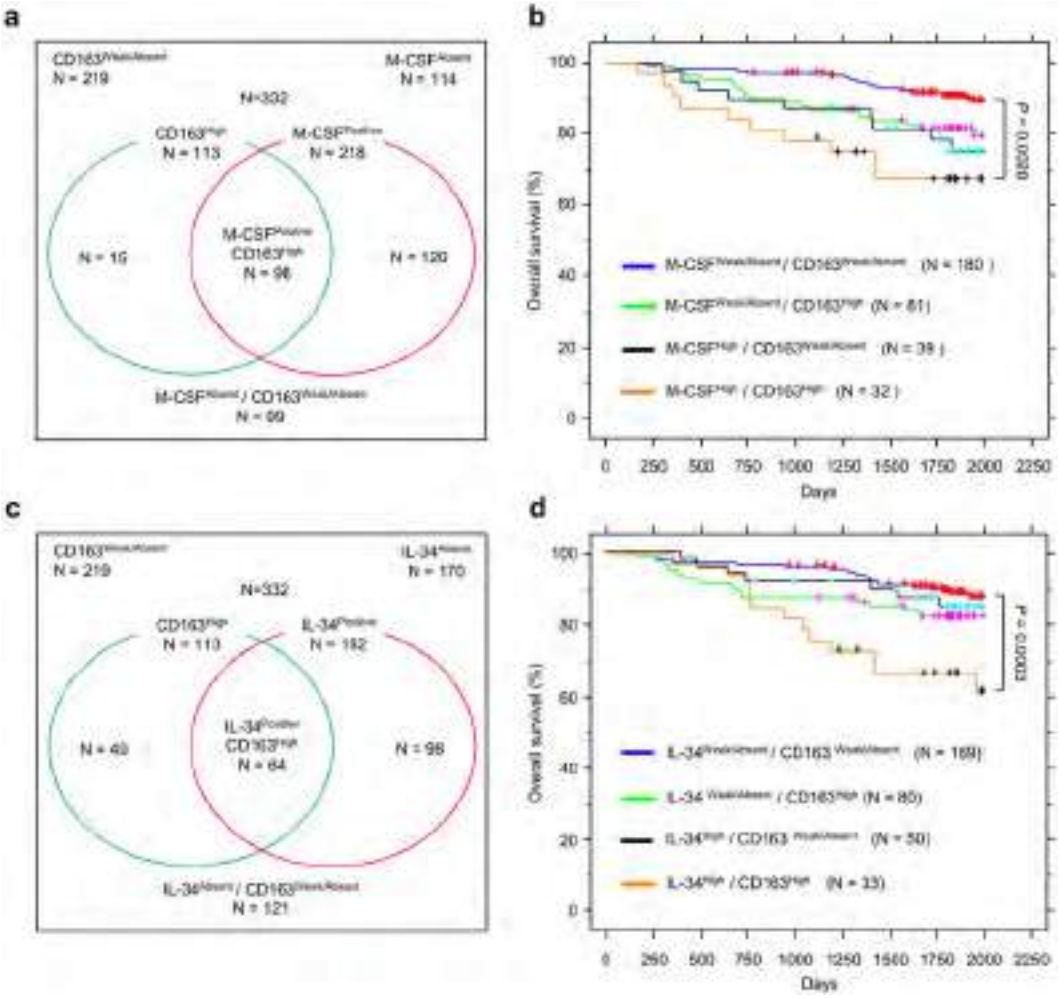

Figure 5. Correlation between M-CSF or IL-34 with CD163 expression in lung cancers. (**a**) Classification of lung cancer patients based on M-CSF and CD163 expression. M-CSF positive refers to samples that show high or weak expression of M-CSF. (**b**) Kaplan-Meier analysis showing overall survival in lung cancer patients based on M-CSF and CD163 expression. (**c**) Classification of lung cancer patients based on IL-34 and CD163 expression. IL-34 positive refers to samples that show high or weak expression of IL-34. (**d**) Kaplan-Meier analysis showing overall survival in lung cancer patients based on IL-34 and CD163 expression.

In the cohort of lung cancer patients described in this study, IL-34 and M-CSF were naturally expressed in cancer tissues prior to any therapeutic procedures. Oncogenic mutations in cancer cells are frequently accompanied by activation of certain signaling pathways that induce the expression of a wide range of cytokines and chemokines, which in turn contribute to tumor progression and ultimately resistance to cancer therapy such as chemotherapy or tyrosine kinase inhibitors[30,31]. In this context, it is of great interest to identify oncogenic mutations that lead to IL-34 and M-CSF production by cancer cells and its impact on the tumor microenvironment, therapeutic resistance.

One remaining important issue is to unveil how can two ligands of the same receptor co-exist and exert their functions at the same microenvironment. The co-expression of both IL-34 and M-CSF has been previously observed in cancers such as giant cell tumors and malignant pleural mesothelioma[32–34]. In this study, we also observed a co-expression of M-CSF and IL-34 in a sub-population of lung cancer patients, which correlates with poorer prognosis. Under physiological conditions, M-CSF and IL-34 show tissue-restricted expression patterns with specific functions[14,15]. In *vitro*, both cytokines exhibit comparable biological functions in myeloid cells[14,15]. While expected to act as competitors, IL-34 and M-CSF can induce dual additive biological effects under certain conditions[17]. Additionally, IL-34 has the potential to interact with M-CSF to form a novel heterodimer that induce a specific activation pattern on CSF1R[17]. Accordingly, in tumors that naturally express both M-CSF and IL-34, or acquired the ability to produce both cytokines under certain therapeutic conditions, IL-34 has the possibility to act through interaction with M-CSF resulting in unique functions of CSF1R in both myeloid and cancer cells, which should be elucidated experimentally in further basic studies. Based on these backgrounds, co-expression of both IL-34 and M-CSF - naturally or induced under therapeutic conditions - may characterize malignancies with enhanced aggression and has an impact on the clinical outcome of cancer therapy. Indeed, our data shown in this study indicates an association between high expression of IL-34 and M-CSF in cancer tissues with disease stages

Variables	Hazards ratio	95% CI	Unfavorable/Favorable	*P*-value
Univariate analysis				
High IL-34 expression	1.862	1.058–3.275	High/Weak and absent	0.031*
High M-CSF expression	2.445	1.390–4.303	High/Weak and absent	0.0019*
High CSF1R expression	1.774	1.023–3.077	High/Weak and absent	0.0411*
CD163 expression in TAM#	2.115	1.228–3.644	High/Weak and absent	0.0069*
Age (years)	1.624	0.910–2.899	≧65/< 65	0.101
Gender	1.539	0.875–2.706	Male/Female	0.1346
Histology	3.014	1.671–5.436	Non-ADC/ADC	0.0002*
T-factor	2.834	1.572–5.109	T2-3/T1	0.0005*
N-factor	3.67	2.097–6.422	N1-2/N0	<0.0001*
Smoking status	1.321	0.751–2.323	Ex or Current/Never	0.3342
Multivariate analysis				
High IL-34 expression	1.016	0.547–1.886	High/Weak and absent	0.9604
High M-CSF expression	1.492	0.799–2.785	High/Weak and absent	0.2089
High CSF1R expression	1.469	0.842–2.564	High/Weak and absent	0.1757
CD163 expression in TAM#	1.557	0.888–2.730	High/Weak and absent	0.1225
Histology	1.999	1.063–3.759	Non-ADC/ADC	0.0316*
T-factor	1.884	1.016–3.493	T2-3/T1	0.0445*
N-factor	2.911	1.617–5.241	N1-2/N0	0.0004*

Table 1. Cox's proportional hazards model analysis of prognostic factors in lung cancer patients. *$P < 0.05$ #TAM: Tumor associated macrophage ADC: Adenocarcinoma, Non-ADC includes Squamous cell carcinoma, Large cell carcinoma and others.

and poor survival in lung cancer patients. In conclusion, IL-34 and M-CSF may help to predict poor survival and tumor progression in lung cancer patients, which should be further evaluated in other cohorts of lung cancer patients and various cancers in future studies.

Materials and Methods

Clinical Samples. Primary NSCLC tissues were collected from patients who had undergone surgical lobectomy or pneumonectomy at Kanagawa Cancer Center (Yokohama, Japan) after the acquirement of informed consent. A total of 332 resected tumor specimens were preserved at Kanagawa Cancer Center Biospecimen Center (KCC-BSC) and utilized for immunohistochemical analysis. All tumors were staged based on the pTNM pathologic classification of the UICC (International Union Against Cancer). All formalin-fixed samples of primary NSCLCs (Gender: 151 female and 181 male patients; Age: median age of 68 with a range of 35–90 years; Smoking history: 138 with no history of smoking, 192 ex- or current smokers and 2 unknown; Tissue type: 277 adenocarcinomas (ADC), 32 squamous cell carcinomas (SCC), 5 large cell carcinoma (LCC), and 18 other types of histological cancer; Stage: 157 pstage IA, 100 pstage IB, 30 pstage IIA, 16 pstage IIB, and 29 pstage IIIA cases) had been obtained earlier along with clinicopathologic data from KCC-BSC. A median follow-up period was 118.0 months for living patients (range, 8.0–138.9 months). The primary endpoint was overall survival as measured from the date of surgery to the time of death. Written informed consent was obtained from all patients, and the use of related clinical materials was approved by institutional ethics committees of Hokkaido University Hospital, Institute for Genetic Medicine and Kanagawa Cancer Center, and all experiments were performed in accordance with all guidelines and regulations indicated by these committees.

TMA Construction. Tumor tissue microarrays were constructed with 332 formalin-fixed primary lung cancers, each of which had been obtained with an identical protocol to collect, fix, and preserve the tissues after resection. The tissue area for sampling was selected based on visual alignment with the corresponding hematoxylin and eosin (H&E)-stained section on a slide. Three to five tissue cores (diameter, 0.6 mm; depth, 3–4 mm) taken from a donor tumor block were placed into a recipient paraffin block with a tissue microarray (Beecher Instruments). A core of normal tissue was punched from each case, and 5-μm sections of the resulting microarray block were used for immunohistochemical analysis.

Immunohistochemical analysis. To investigate the expression levels of IL-34, M-CSF, CSF1R and CD163 protein in clinical samples from lung cancer patients, tissue sections were stained the in the following manner. TMA slides were immersed in antigen retrieval solution (pH 9.0) (Nichirei, Tokyo, Japan) and boiled for 15 min in an autoclave. Endogenous peroxidase activity was blocked by incubation in 0.3% H_2O_2 in methanol for 15 min. After protein blocking (Catalog No. X0909, Abcam), TMA slides were incubated with a mouse anti-IL-34 antibody (Catalog No. ab101443), a rabbit anti-M-CSF antibody (Catalog No. ab52864, Abcam) in 1:100 dilution, a rabbit anti-CSF1R antibody (Catalog No. HPA012323, SIGMA) in 1:100 dilution or a mouse anti-CD163 antibody in 1:100 dilution (Catalog No. MCA1853, Bio-Rad) in Antibody Diluent (Catalog No. S0809, DakoCytomation) for 30 min at room temperature in a moist chamber. The sections were incubated with HRP-labeled polymer

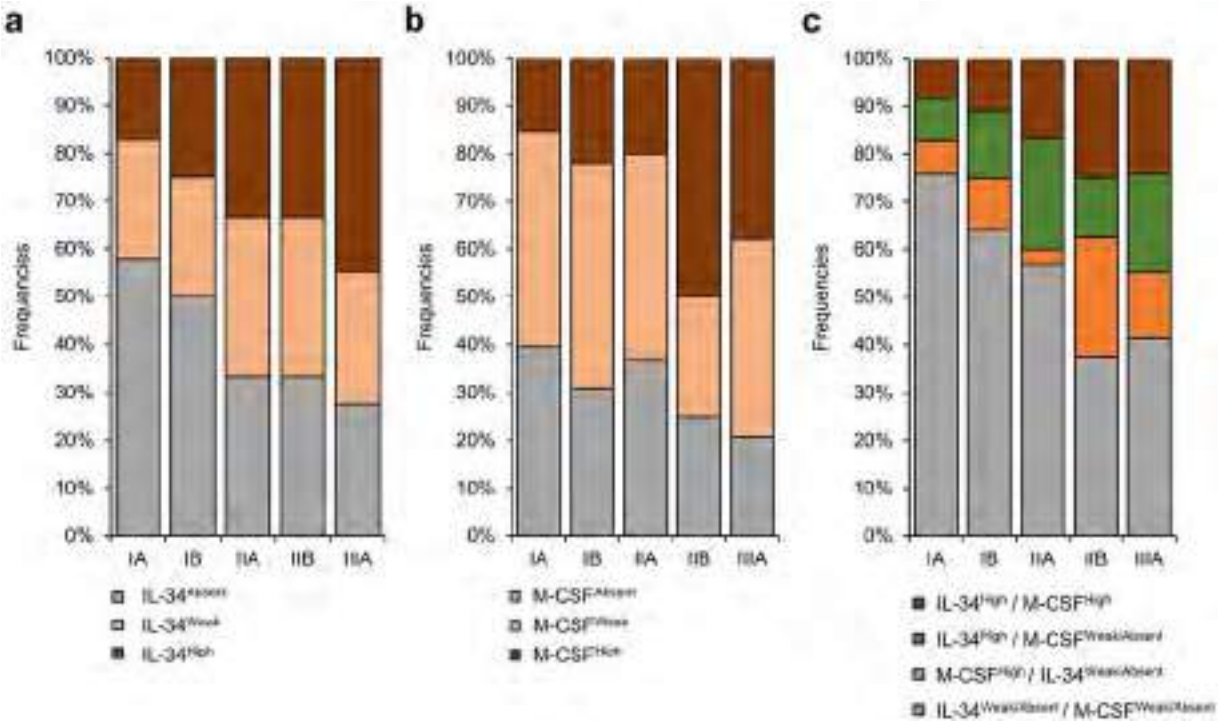

Figure 6. Association between IL-34/M-CSF expression with advanced stages in lung cancers. Bar graph analysis resembles the association between M-CSF or IL-34 expression with disease stages in lung cancer patients. Positivity rates of IL-34 (**a**), M-CSF (**b**) or both IL-34 and M-CSF (**c**) were calculated in each group according to disease stage.

Correlation between high IL-34 expression and disease stages				
	Total	**IL-34$^{W/A}$/M-CSF$^{W/A}$**	**IL-34^{High}/M-CSF$^{W/A}$**	
	n = 261	**n = 218**	**n = 43**	***P*-value**
Stage				
IA	133	119	14	0.0095*,#
IB	78	64	14	
IIA	24	17	7	
IIB	8	6	2	
IIIA	18	12	6	
Correlation between high M-CSF expression and disease stages				
	Total	**IL-34$^{W/A}$/M-CSF$^{W/A}$**	**IL-34$^{W/A}$/M-CSF^{High}**	***P*-value**
	n = 249	**n = 218**	**n = 31**	
Stage				
IA	130	119	11	0.00829*,#
IB	75	64	11	
IIA	18	17	1	
IIB	10	6	4	
IIIA	16	12	4	
Correlation between high IL-34 and M-CSF co-expression and disease stages				
	Total	**IL-34$^{W/A}$/M-CSF$^{W/A}$**	**IL-34^{High}/M-CSF^{High}**	***P*-value**
	n = 258	**n = 218**	**n = 40**	
Stage				
IA	132	119	13	0.0011*,#
IB	75	64	11	
IIA	22	17	5	
IIB	10	6	4	
IIIA	19	12	7	

Table 2. Correlation between IL-34/M-CSF expression and disease stages in lung cancer patients. *$P < 0.05$ (Fisher's exact test) #stage I vs stage II-IIIA W/A: Weak or Absent.

anti-mouse (Catalog No. K4007, DakoCytomation) or anti-rabbit IgG (Catalog No. K4002, DakoCytomation) as the secondary antibody for 30 min at room temperature in a moist chamber. Substrate-chromogen was added, and the specimens were counterstained with hematoxylin.

Evaluation of Immunohistochemical Staining and Statistical analysis. Two independent investigators semiquantitatively assessed IL-34, M-CSF, CSF1R and CD163 positivity without prior knowledge of clinicopathologic data. Since the staining intensities of IL-34 and M-CSF were mostly homogenous in cytoplasm of cancer cells, they were semiquantitatively scored as high, weak or absent. As CSF1R staining was detected in cytoplasm and membrane, they were semiquantitatively scored as high, weak or absent. CD163 staining was mainly detected in cytoplasm of stromal macrophage. $CD163^+$ macrophage infiltration in stroma was semiquantitatively scored as high, weak or absent, (high: many infiltrating $CD163^+$ macrophages, weak: some infiltrating $CD163^+$ macrophages and absent: no or few infiltrating $CD163^+$ macrophages)[35]. If there is a discrepancy among them, a consensus was reached using simultaneous examination by two investigators.

Statistics. Statistical analysis was done using the StatView software. Tumor-specific survival curves were calculated from the date of surgery to the time of death related to NSCLC or to the last follow-up observation. Kaplan–Meier curves were calculated for each relevant variable and for IL-34, M-CSF, CSF1R or CD163 expression; differences in survival times among patient subgroups were analyzed using the log-rank test.

References

1. Miller, K. D. *et al*. Cancer treatment and survivorship statistics, 2016. *CA Cancer J. Clin.* **66**, 271–89 (2016).
2. Bepler, G. *et al*. RRM1 modulated *in vitro* and *in vivo* efficacy of gemcitabine and platinum in non-small-cell lung cancer. *J. Clin. Oncol.* **24**, 4731–7 (2006).
3. Lee, J. J. *et al*. The immunohistochemical overexpression of ribonucleotide reductase regulatory subunit M1 (RRM1) protein is a predictor of shorter survival to gemcitabine-based chemotherapy in advanced non-small cell lung cancer (NSCLC). *Lung Cancer* **70**, 205–10 (2010).
4. Paez, J. G. *et al*. EGFR mutations in lung cancer: correlation with clinical response to gefitinib therapy. *Science* **304**, 1497–500 (2004).
5. Pao, W. *et al*. Acquired resistance of lung adenocarcinomas to gefitinib or erlotinib is associated with a second mutation in the EGFR kinase domain. *PLOS Med.* **2**, e73 (2005).
6. Eberhard, D. A. *et al*. Mutations in the epidermal growth factor receptor and in KRAS are predictive and prognostic indicators in patients with non-small-cell lung cancer treated with chemotherapy alone and in combination with erlotinib. *J. Clin. Oncol.* **23**, 5900–9 (2005).
7. Noy, R. & Pollard, J. W. Tumor-associated macrophages: from mechanisms to therapy. *Immunity* **41**, 49–61 (2014).
8. De Palma, M. & Lewis, C. E. Macrophage regulation of tumor responses to anticancer therapies. *Cancer Cell* **223**, 277–86 (2013).
9. Ruffell, B. & Coussens, L. M. Macrophages and therapeutic resistance in cancer. *Cancer Cell* **27**, 462–72 (2015).
10. Lippitz, B. E. Cytokine patterns in patients with cancer: a systematic review. *Lancet Oncol.* **14**, e218–28 (2013).
11. Allavena, P., Sica, A., Solinas, G., Porta, C. & Mantovani, A. The inflammatory micro-environment in tumor progression: the role of tumor-associated macrophages. *Crit. Rev. Oncol. Hematol.* **66**, 1–9 (2008).
12. Mantovani, A., Schioppa, T., Porta, C., Allavena, P. & Sica, A. Role of tumor-associated macrophages in tumor progression and invasion. *Cancer Metastasis Rev.* **25**, 315–22 (2006).
13. Condeelis, J. & Pollard, J. W. Macrophages: obligate partners for tumor cell migration, invasion, and metastasis. *Cell* **124**, 263–6 (2006).
14. Droin, N. & Solary, E. Editorial: CSF1R, CSF-1, and IL-34, a "menage a trois" conserved across vertebrates. *J. Leukoc. Biol.* **87**, 745–7 (2010).
15. Nakamichi, Y., Udagawa, H. & Takahashi, N. IL-34 and CSF-1: similarities and differences. *J. Bone Miner. Metab.* **31**, 486–95 (2013).
16. Chihara, T. *et al*. IL-34 and M-CSF share the receptor Fms but are not identical in biological activity and signal activation. *Cell Death Differ.* **17**, 1917–27 (2010).
17. Ségaliny, A. I. *et al*. IL-34 and M-CSF form a novel heteromeric cytokine and regulate the M-CSF receptor activation and localization. *Cytokine* **76**, 170–81 (2015).
18. Chockalingam, S. & Ghosh, S. S. Macrophage colony-stimulating factor and cancer: a review. *Tumour Biol.* **35**, 10635–44 (2014).
19. Baghdadi, M. *et al*. Chemotherapy-Induced IL34 Enhances Immunosuppression by Tumor-Associated Macrophages and Mediates Survival of Chemoresistant Lung Cancer Cells. *Cancer Res.* **76**, 6030–6042 (2016).
20. McDermott, R. S. *et al*. Circulating macrophage colony stimulating factor as a marker of tumour progression. *Eur. Cytokine Netw.* **13**, 121–7 (2002).
21. Scholl, S. M. *et al*. Circulating levels of the macrophage colony stimulating factor CSF-1 in primary and metastatic breast cancer patients. A pilot study. *Breast Cancer Res. Treat.* **39**, 275–83 (1996).
22. Lin, H. *et al*. Discovery of a cytokine and its receptor by functional screening of the extracellular proteome. *Science* **320**, 807–11 (2008).
23. Stanley, E. R. & Chitu, V. CSF-1 receptor signaling in myeloid cells. *Cold Spring Harb. Perspect. Biol.* **6**, a021857 (2014).
24. Hung, J. Y. *et al*. Colony-stimulating factor 1 potentiates lung cancer bone metastasis. *Lab. Invest.* **94**, 371–81 (2014).
25. Patsialou, A. *et al*. Autocrine CSF1R signaling mediates switching between invasion and proliferation downstream of TGFbeta in claudin-low breast tumor cells. *Oncogene* **34**, 2721–31 (2015).
26. Achkova, D. & Maher, J. Role of the colony-stimulating factor (CSF)/CSF-1 receptor axis in cancer. *Biochem. Soc. Trans.* **44**, 333–41 (2016).
27. Fabriek, B. O. & Dijkstra, C. D. & Van den Berg, T. K. The macrophage scavenger receptor CD163. *Immunobiology* **210**, 153–60 (2005).
28. Heusinkveld, M. & der Burg, V. S.H. Identification and manipulation of tumor associated macrophages in human cancers. *J. Transl. Med.* **9**, 216 (2011).
29. Medrek, C., Pontén, F., Jirström, K. & Leandersson, K. The presence of tumor associated macrophages in tumor stroma as a prognostic marker for breast cancer patients. *BMC Cancer* **12**, 306 (2012).
30. Castells, M. *et al*. Implication of tumor microenvironment in chemoresistance: tumor-associated stromal cells protect tumor cells from cell death. *Int. J. Mol. Sci.* **13**, 9545–71 (2012).
31. Naugler, W. E. & Karin, M. NF-kappaB and cancer-identifying targets and mechanisms. *Curr. Opin. Genet. Dev.* **18**, 19–26 (2008).
32. Baud'huin, M. *et al*. Interleukin-34 is expressed by giant cell tumours of bone and plays a key role in RANKL-induced osteoclastogenesis. *J. Pathol.* **221**, 77–86 (2010).
33. Cioce, M. *et al*. Autocrine CSF-1R signaling drives mesothelioma chemoresistance via AKT activation. *Cell Death Dis.* **5**, e1167 (2014).

34. Baghdadi, M., Endo, H., Tanaka, Y., Wada, H. & Seino, K. Interleukin 34, from pathogenesis to clinical applications. *Cytokine* **99**, 139–147 (2017).
35. Maniecki, M. B. *et al*. Tumor-promoting macrophages induce the expression of the macrophage-specific receptor CD163 in malignant cells. *Int. J. Cancer* **131**, 2320–31 (2012).

Acknowledgements

This work was supported in part by Japan Agency for Medical Research and Development AMED (KI Seino) and Grant-in-Aid for Scientific Research on Innovative Areas from The Japan Society for the Promotion of Science (JSPS KAKENHI Grant Number JP: 16H06277; Group for Supporting Research using Biospecimen, Platform of Supporting Cohort Study and Biospecimen Analysis).

Author Contributions

H.E., M.B., A.T., K.I., Y.K., H.W., Y.M., T.Y., H.I. and H.N. performed research; Y.M., H.I., Y.D. and K.S. contributed new reagents/analytic tools; H.E., M.B., A.T., K.I., Y.K., H.W., Y.M., T.Y., H.I., H.N., Y.D., N.S. and K.S. analyzed data; and H.E., M.B., and K.S. wrote and revised the manuscript.

Additional Information

Supplementary information accompanies this paper at https://doi.org/10.1038/s41598-017-18796-8.

Competing Interests: The authors declare that they have no competing interests.

Publisher's note: Springer Nature remains neutral with regard to jurisdictional claims in published maps and institutional affiliations.

Open Access This article is licensed under a Creative Commons Attribution 4.0 International License, which permits use, sharing, adaptation, distribution and reproduction in any medium or format, as long as you give appropriate credit to the original author(s) and the source, provide a link to the Creative Commons license, and indicate if changes were made. The images or other third party material in this article are included in the article's Creative Commons license, unless indicated otherwise in a credit line to the material. If material is not included in the article's Creative Commons license and your intended use is not permitted by statutory regulation or exceeds the permitted use, you will need to obtain permission directly from the copyright holder. To view a copy of this license, visit http://creativecommons.org/licenses/by/4.0/.

© The Author(s) 2017

THE JOURNAL OF
Obstetrics and Gynaecology Research

doi:10.1111/jog.13359 J. Obstet. Gynaecol. Res. Vol. 43, No. 8: 1326–1334, August 2017

Glycan profiling using formalin-fixed, paraffin-embedded tissues: Hippeastrum hybrid lectin is a sensitive biomarker for squamous cell carcinoma of the uterine cervix

Akiko Tozawa-Ono[1], Manabu Kubota[2], Chika Honma[1], Yuko Nakagawa[1], Noriyuki Yokomichi[1], Norihito Yoshioka[1], Chiharu Tsuda[1], Tatsuru Ohara[1], Hirotaka Koizumi[2] and Nao Suzuki[1]

[1]*Department of Obstetrics and Gynecology, St. Marianna University School of Medicine and* [2]*Department of Pathology, St. Marianna University School of Medicine, Miyamae, Kawasaki, Japan*

Abstract

Aim: Glycosylation of proteins is altered in cancer cells and distinctive glycan structures are associated with specific cancers, but little is known about the complete glycan profile of particular tumors. In this study, glycomic analysis of squamous cell carcinoma (SCC) of the uterine cervix was performed to search for useful markers.

Methods: A lectin microarray containing 45 lectins with different binding preferences that covered N- and O-linked glycans was coupled with evanescent field-activated fluorescent detection for glycomic analysis of SCC and normal squamous epithelium (NSE) of the cervix. Formalin-fixed, paraffin-embedded tissue specimens were obtained from 16 patients with uterine cervical cancer. Sections that included both tumor and non-tumor tissues were examined to detect alterations of glycans based on the lectin-binding pattern.

Results: Hippeastrum hybrid lectin was found to be a sensitive marker for distinguishing SCC of the cervix from NSE. It was the best lectin for discriminating SCC from other tissues according to receiver–operator curve analysis, as it showed a high sensitivity (81.8%), a high specificity (70.1%), and a large area under the curve (0.8182). Histochemistry confirmed specific cytoplasmic staining of SCC cells by Hippeastrum hybrid lectin, while there was little staining of cervical intraepithelial neoplasia and no staining of NSE.

Conclusion: The present lectin microarray technique could be applied for tissue-based glycomic analysis of various tumors and for discovery of glycan-related biomarkers.

Key words: glycan, lectin, squamous cell carcinoma, uterine cervical cancer.

Introduction

The human glycome is of particular interest in cancer research because aberrant glycans, such as β1–6 branched N-glycans and the truncated O-glycan known as Tn antigen, are found in a wide variety of cancers.[1–6] Since glycans are synthesized by the cooperative action of multiple genes, each glycan molecule reflects a variety of genetic anomalies. While progress in exploiting the human glycome as a source of disease markers has generally been slow due to the complexity of the glycans themselves and lack of suitable methods for investigating their structures, technical developments have allowed the analysis of glycans in cancer cells[4] and tissues.[7]

Glycosylation of proteins plays an important role in various cellular events, including differentiation, adhesion, proliferation, and maintenance of immunity.[8] Cell differentiation and proliferation are associated with changes of glycosylation, and there seems to be significant variation of the glycosylation machinery among different types of cells.[9,10]

Received: October 31 2016.
Accepted: March 20 2017.
Correspondence: Assistant Professor Akiko Tozawa-Ono, Department of Obstetrics and Gynecology, St. Marianna University School of Medicine, 2-16-1 Sugao, Miyamae, Kawasaki 216-8511, Japan. Email: a2ono@marianna-u.ac.jp

 © 2017 Japan Society of Obstetrics and Gynecology

In order to profile glycans, complex mixtures of these molecules must be resolved accurately enough to determine quantitative differences, so a highly sensitive method of detection is required. A useful test would assess the quantity of a target glycan and would not depend on detecting certain glycan structures. Capillary electrophoresis, liquid chromatography, and mass spectrometry are commonly used for glycome profiling.[11] However, these techniques are not well suited to screening a large number of samples for differences because they are time-consuming, low-throughput methods that are sensitive to sample contamination, require expensive equipment, and generate complex data. In 2005, several research groups independently reported the development of lectin arrays for rapid multiplex analysis of protein glycosylation. Since then, lectin arrays have been used to analyze the glycomes of bacteria,[12] viruses,[13] and mammals.[14] An evanescent field is a field that cannot propagate, so its amplitude decreases as a function of distance. Evanescent field fluorescence-assisted lectin microarray technology[15] has been adopted for glycome profiling using formalin-fixed, paraffin-embedded tissue specimens.[16] In the present study, a microarray containing 45 lectins with defined binding preferences covering N- and O-linked glycans was coupled with evanescent field activated fluorescent detection to perform glycomic analysis of specimens of primary cervical cancer and normal cervical epithelium in order to identify specific lectin-binding patterns associated with squamous cell carcinoma (SCC) of the cervix.

Methods

Specimens

We investigated formalin-fixed, paraffin-embedded uterine cervical tissue specimens obtained by radical hysterectomy between 2007 and 2011 that were stored in the surgical pathology archives of the Department of Pathology at St. Marianna University School of Medicine, Kawasaki, Japan. Specimens of SCC and normal squamous epithelium were obtained from 16 patients with a mean age of 49.7 ± 3.6 years, and tissue sections 1.5 mm in diameter and 10 μm thick were cut for microarray analysis.

We also retrieved formalin-fixed, paraffin-embedded cervical tissue specimens obtained by punch biopsy, cone biopsy, or hysterectomy between 2002 and 2010 from the surgical pathology archives of the Department of Pathology at St. Marianna University School of Medicine, for histochemical analysis. Specimens of cervical intraepithelial neoplasia (CIN; mild to severe dysplasia/carcinoma *in situ*) were obtained from 63 patients, including 26 patients with CIN1 (mean age: 35.2 ± 8.8 years), 17 patients with CIN2 (mean age: 33.9 ± 5.5 years), and 20 patients with CIN3 (mean age: 35.6 ± 8.3 years). These samples had been fixed in 10% buffered formalin for 24–48 h and then embedded in paraffin.

This study was approved by the Human Ethics Review Committee of St. Marianna University School of Medicine.

Extraction of proteins from tissue sections

Each section was deparaffinized and removed from the glass slide by using a 21-G needle under a microscope, after which the tissue fragments were collected into a 1.5-mL microtube containing 200 μL of 10 mM citrate buffer (pH 6.0) and incubated for 5 min at 95°C for antigen retrieval. After washing with phosphate-buffered saline (PBS; Seikagaku Kogyo Co.) by centrifugation, the pellet was solubilized with 20 μL of PBS containing 0.5% Nonidet P40 and gently sonicated. The resulting tissue suspension was incubated on ice for 60 min and then was centrifuged at 20 000 *g* for 5 min at 4°C to obtain the supernatant (detergent-solubilized glycoprotein extract).

Lectin microarray analysis

Aliquots (20 μL) of the glycoprotein extract were incubated with 100 μg of Cy3 Mono-Reactive dye (GE Healthcare) for 60 min at room temperature in the dark and the reaction products were loaded onto a Zeba Spin Desalting Column (Thermo Scientific) to remove the excess fluorescent reagent. After centrifugation, the solution was adjusted to 300 μL with probe buffer (Tris-buffered saline, pH 7.5, containing 1.0% Triton X-100 and 500 mM glycine). After washing three times with probinding solution, 80 μL of Cy3-labeled glycoprotein solution was added to a LecChip (GP BioScience) in each well of the glass slide, and incubation was done overnight at 20°C in a humidified chamber. Then a fluorescent image of the array was acquired by using a GlycoStation Reader 1200 evanescent field fluorescence scanner (GP Bioscience). Data were analyzed with GlycoStation Tools Pro Suite 1.5 software (GP Bioscience), and values were normalized by the average signal for all lectins.

Lectin staining of cervical tissues

Lectin staining of the tissue sections was performed by using Histofine Simple Stain MAX-PO (Nichirei Co.).

© 2017 Japan Society of Obstetrics and Gynecology

After deparaffinization, tissue arrays on glass slides were placed in 10-mM citrate buffer (pH 6.0) and autoclaved for 10 min at 121°C to enhance lectin reactivity. After cooling to room temperature, the arrays were incubated for 10 min in methanol containing 0.3% hydrogen peroxide to deplete endogenous peroxidases. Then washing was done three times with PBS and the arrays were incubated with PBS containing 1% bovine serum albumin for 10 min at room temperature in a humidified chamber. This was followed by incubation with 5 μg/mL of biotinylated lectin dissolved in PBS for 1 h at room temperature. After washing three times with PBS, streptavidin–peroxidase reagent was applied for 5 min at room temperature. Finally, reaction products were visualized by incubation with 3,3-diaminobenzidine tetrahydrochloride and the sections were counterstained with hematoxylin.

The percentage of Hippeastrum hybrid lectin (HHL)-stained cells was calculated from the stained area relative to the total area of epithelial cells and a staining score was assigned as follows: 0 (0%), 1 (1–5%), 2 (6–50%), and 3 (51–100%). All parts of the section were evaluated at 200× magnification under a light microscope and all of the entire epithelial cell areas were assessed for staining.

Statistical analysis

Lectin microarray data are presented as the mean ± standard error (SEM). A two-sided χ^2-test was used for comparison of clinicopathological variables between groups.

Receiver–operator curve (ROC) analysis was performed to evaluate differences between SCC and normal squamous epithelium by calculating the sensitivity and specificity at various cut-off values. The area under the ROC (AUC) was calculated, with an AUC of 1.0 indicating perfect discrimination, whereas an AUC of 0.5 indicated that the test was no better than random chance at discriminating epithelium from SCC.

For comparison of the lectin staining scores between normal epithelium, CIN, and SCC, Steel's multiple comparison method of Dwass was employed (Statcel4, version 4.0). A P-value < 0.05 was considered significant in all analyses.

Results

Lectin microarray analysis

To identify the lectin that was most specific for SCC, we performed differential glycan profiling using paraffin-embedded, formalin-fixed tissue sections. This analysis revealed significant differences for four of the 45 lectins tested, with the signal intensities of four α2–3Sia-binding lectins (*Agrocybe Cylindracea* galectin [ACG], *Maackia amurensis* lectin [MAL], HHL that binds to1,6-branched mannose, and *Maclura pomifera* agglutinin [MPA]) being either significantly higher or lower (all $P < 0.05$) in SCC tissues than in normal squamous epithelium. Among the four lectins, HHL staining showed the largest difference of intensity between SCC and normal squamous epithelium from the same patient ($P < 0.05$; Fig. 1). HHL and ACG were both useful for discriminating SCC from other tissues according to ROC analysis, as HHL and ACG showed a high sensitivity (81.8% and 74.9%, respectively), a high specificity (70.1% and 84.9%), and a large AUC (0.8182 and 0.849; Fig. 2). However, there was a difference in the SCC /normal epithelium signal intensity ratio (tumor tissue/normal tissue ratio [T/N ratio]) between these two lectins, with it being 0.8 for ACG and 2.1 for HHL (Table 1). These results suggested that strong binding of HHL to SCC tissues was related to changes of glycosylation that were specific for this malignancy.

Histochemical analysis of HHL-reactive glycans

To confirm the above results, we employed histochemistry with biotinylated HHL to visualize the expression of HHL-reactive glycans in specimens of SCC, CIN, and normal squamous epithelium. CIN tissues and normal squamous epithelium showed little or no staining by HHL (Fig. 3a-d). In contrast, SCC tissues were stained by HHL, especially at the sites of tumor infiltration. HHL was strongly expressed in the interstitial regions of SCC, suggesting a correlation of this lectin with infiltration (Fig. 3e-f). The results of histochemical analysis are summarized in Table 2. SCC showed a very high rate of staining by HHL (14/16 tumors: 87.5%), while there was little staining of CIN (7/26 (26.9%) for CIN1, 5/19 (26.3%) for CIN2, and 2/20 (10.0%) for CIN3 and no staining of normal squamous epithelium (0/16; 0%). These results also suggested that HHL-reactive glycans were specifically expressed by SCC.

The HHL staining score was significantly higher for SCC than for either normal squamous epithelium or CIN ($P < 0.05$, Fig. 4), while there was no significant difference of HHL expression between normal epithelium and CIN (Fig. 4).

© 2017 Japan Society of Obstetrics and Gynecology

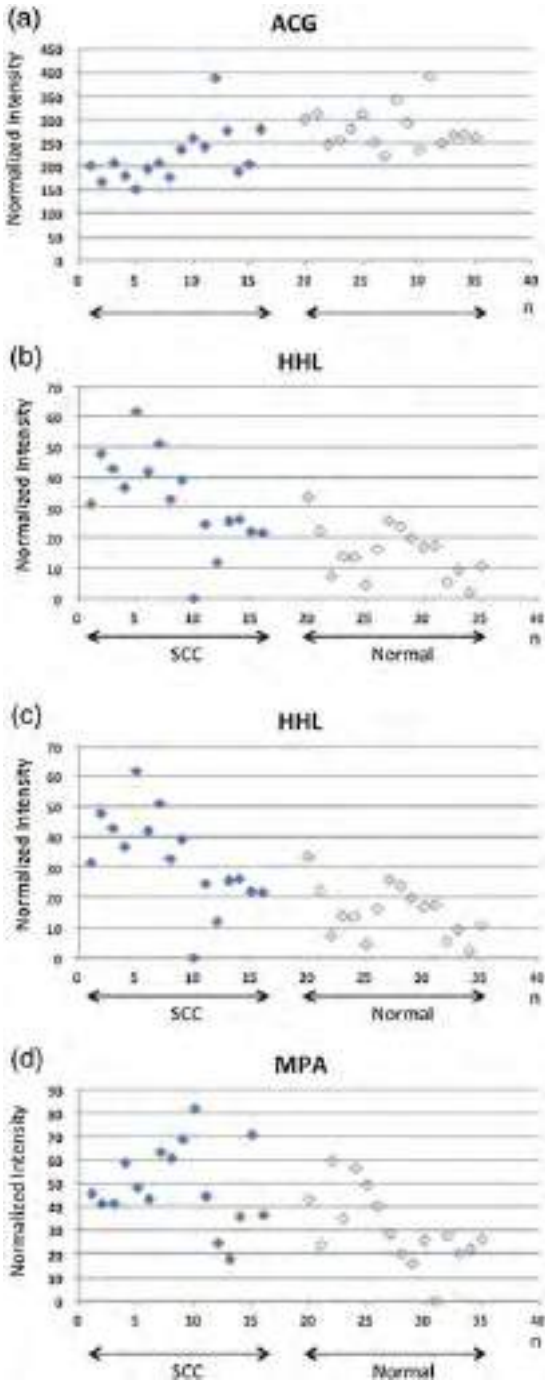

Figure 1 Glycan analysis of normal squamous epithelium (NSE) and squamous cell carcinoma (SCC). Graphs display normalized intensity data for the four lectins that showed significant differences between NSE and SCC (by the two-sided χ^2-test using normalized lectin data). (a) *Agrocybe Cylindracea* galectin (ACG). (b) *Maackia amurensis* lectin (MAL). (c) Hippeastrum hybrid lectin (HHL). (d) *Maclura pomifera* agglutinin (MPA). Cases 1–16: SCC. Cases 20–36: NSE.

Discussion

Treating cervical cancer at an early stage does not reduce the incidence of invasive cancer, and tumors that relapse are often refractory with a high mortality rate.[17] Therefore, an accurate biomarker is needed for this cancer, as cytological diagnosis of cervical cancer is a subjective process. In the present study, we investigated potential glycoprotein biomarkers by performing glycoproteomic analysis of cervical tissue sections containing both normal squamous epithelium and SCC.[18,19] We found that ACG,[20] MAL, HHL,[21] and MPA[22] showed marked differences of binding to SCC tissues compared with normal epithelium.

Lectin microarray analysis is a highly sensitive technique for multiplex analysis of small tissue sections (approximately 500 cells), using 45 lectins to investigate the N- and O-glycans attached to glycoproteins. This method has already been employed to identify lectin-binding patterns associated with a poor prognosis of colon cancer by Matsuda *et al.*, who performed glycan analysis of adenocarcinoma tissues and normal colon epithelium to reveal that staining with *Wisteria floribunda* agglutinin clearly differentiated cancer from normal epithelium.[16] Their findings agreed well with those of a subsequent histochemical study using biotinylated *Wisteria floribunda* agglutinin.[16] Thus, it seems reasonable to employ lectin microarray analysis for investigation of glycan-related tumor biomarkers.

In the present study, lectin microarray analysis demonstrated several differences of the lectin-binding pattern between SCC and normal squamous epithelium, with stronger binding of HHL and MPA to SCC tissues along with weaker binding of MAL and ACG. ROC analysis revealed that HHL was the best of these four lectins for discriminating between normal squamous epithelium and SCC ($P < 0.05$). In addition, the T/N ratio of HHL showed the largest difference between normal squamous epithelium and SCC (Table 1). These findings suggested that HHL was the best lectin marker for SCC among those investigated in the present study.

The evanescent field fluorescence-assisted method of lectin microarray analysis used in this study allows high-throughput, rapid, and sensitive glycome profiling of clinical samples. The greatest advantage of a lectin microarray over alternative methods of glycan profiling is that simultaneous quantitative analysis of N- and O-linked glycans can be performed in intact biological structures after minimal preparation of samples without the need for extraction of glycans. The 45 lectins in the microarray we used cover the majority of known human

© 2017 Japan Society of Obstetrics and Gynecology

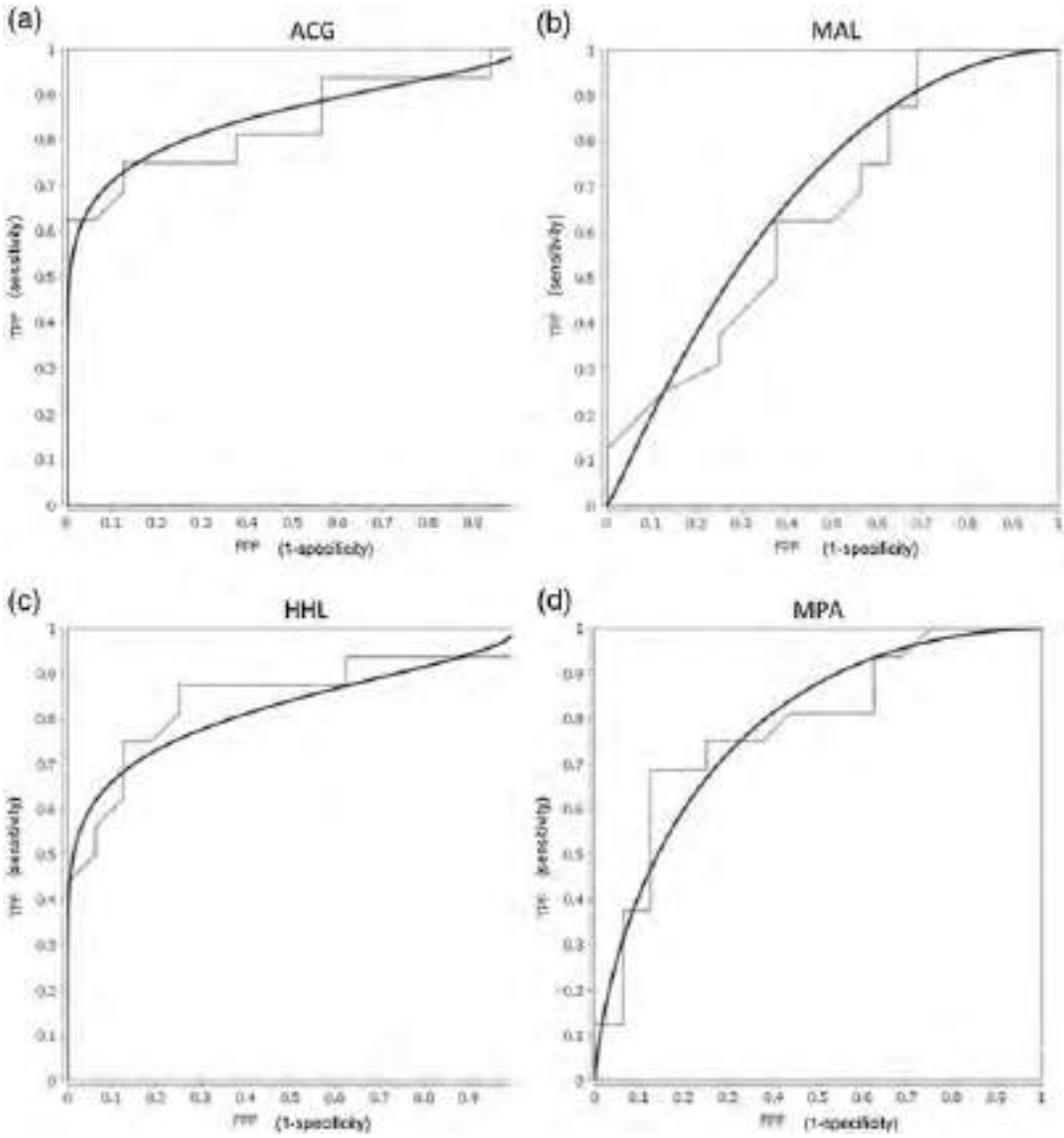

Figure 2 Results of receiver–operator curve (ROC) analysis for (a) *Agrocybe Cylindracea* galectin (ACG), (b) *Maackia amurensis* lectin (MAL), (c) Hippeastrum hybrid lectin (HHL), and (d) *Maclura pomifera* agglutinin (MPA). (•) Best-fit ROC obtained with the Metz system and (•) actual data were compared for differentiating normal squamous epithelium (NSE) from squamous cell carcinoma (SCC). The area under the ROC (AUC) was larger for ACG and HHL than for MAL and MPA. ACG and HHL showed a higher sensitivity (74.6% and 70.1%) and higher AUC values (0.85 and 0.82) than MAL or MPA. Data were normalized by the average value for all lectins tested. (a) ACG: AUC = 0.849; false-positive fraction (FPF) = 0.415 at true-positive fraction (TPF) = 0.85; TPF = 0.746 at FPF = 0.15; sensitivity = 74.6%; specificity = 84.9%. (b) MAL: AUC = 0.6785; FPF = 0.596 at TPF = 0.85; TPF = 0.294 at FPF = 0.15; sensitivity = 29.4%; specificity = 67.8%. (c) HHL: AUC = 0.8182; FPF = 0.534 at TPF = 0.85; TPF = 0.701 at FPF = 0.15; sensitivity = 70.1%; specificity = 81.8%. (d) MPA: AUC = 0.7857; FPF = 0.451 at TPF = 0.85; TPF = 0.517 at FPF = 0.15; sensitivity = 51.7%; specificity = 78.5%.

oligosaccharides, allowing the detection of subtle differences.[18,19] Although the patient population investigated in this study was too small to confidently define the lectin-binding pattern of cervical cancer, we still identified differences of glycosylation between neoplastic and non-neoplastic cervical tissues. The lectins that showed differences between SCC and normal epithelium in this study may be good candidates for

© 2017 Japan Society of Obstetrics and Gynecology

Table 1 Results of microarray analysis of 45 lectins in normal squamous epithelium and SCC of the cervix

Lectin	Normal epithelium (SEM)		Tumor tissue (SEM)		T/N ratio	Staining†
LTL	46.2	(8.9)	44.7	(3.1)	1.0	+/−
PSA	94.5	(8.3)	83.5	(4.7)	0.9	+/−
LCA	117.9	(7.0)	100.2	(4.8)	0.9	+/−
UEA_I	27.1	(5.2)	31.2	(5.1)	1.2	+
AOL	196.5	(21.6)	182.1	(18.3)	0.9	+/−
AAL	172.8	(18.7)	154.9	(15.7)	0.9	+/−
MAL_I	40.4	(4.4)	31.0	(3.2)	0.8	−
SNA	177.9	(11.2)	180.6	(11.3)	1.0	+/−
SSA	174.1	(13.0)	185.6	(13.6)	1.1	+/−
TJA-I	285.1	(17.0)	278.2	(16.5)	1.0	+/−
PHA(L)	14.4	(3.0)	21.4	(2.7)	1.5	++
ECA	27.1	(4.7)	27.1	(4.3)	1.0	+/−
RCA120	67.8	(5.7)	85.4	(6.6)	1.3	+
PHA(E)	93.2	(4.4)	76.3	(5.7)	0.8	−
DSA	331.8	(15.2)	278.6	(11.1)	0.8	−
GSL-II	11.5	(2.6)	8.5	(1.6)	0.7	−
NPA	121.3	(12.8)	148.6	(14.7)	1.2	+
ConA	155.4	(8.1)	195.4	(12.9)	1.3	+
GNA	64.7	(7.4)	97.9	(8.7)	1.5	++
HHL	15.0	(2.1)	32.2	(3.8)	2.1	+++
ACG	279.5	(10.8)	221.7	(14.4)	0.8	−
TxLC_I	18.6	(2.9)	20.7	(3.5)	1.1	+/−
BPL	21.3	(4.1)	34.2	(5.3)	1.6	++
TJA-II	72.6	(13.4)	64.3	(5.5)	0.9	+/−
EEL	15.8	(6.1)	12.2	(2.4)	0.8	−
ABA	115.8	(11.1)	108.8	(5.0)	0.9	+/−
LEL	372.8	(11.6)	348.7	(18.8)	0.9	+/−
STL	340.2	(16.7)	325.0	(23.2)	1.0	+/−
UDA	300.2	(12.2)	344.6	(22.7)	1.1	+/−
PWM	19.4	(3.2)	32.7	(4.5)	1.7	++
Jacalin	124.4	(6.8)	134.7	(7.1)	1.1	+/−
PNA	7.6	(3.5)	9.5	(3.0)	1.3	+
WFA	30.2	(4.9)	36.5	(4.4)	1.2	+
ACA	88.5	(9.4)	91.4	(7.3)	1.0	+/−
MPA	30.9	(3.9)	48.8	(4.3)	1.6	++
HPA	97.8	(24.6)	53.8	(12.7)	0.5	−
VVA	9.3	(2.2)	16.0	(3.7)	1.7	++
DBA	25.8	(7.8)	24.9	(4.7)	1.0	+/−
SBA	9.9	(3.1)	16.1	(3.5)	1.6	++
Calsepa	65.5	(4.5)	90.5	(8.5)	1.4	+
PTL_I	7.3	(3.3)	7.6	(3.1)	1.0	+/−
MAH	33.4	(5.4)	33.5	(4.2)	1.0	+/−
WGA	162.8	(8.8)	157.2	(7.9)	1.0	+/−
GSL_I_A4	11.4	(2.9)	14.8	(3.1)	1.3	+
GSL_I_B4	4.3	(1.5)	8.4	(3.2)	1.9	++

†+++ = T/N > 1.9; ++ = T/N 1.5–1.9; + = T/N 1.2–1.5; +/− = T/N 0.9–1.1, − = T/N < 0.9. SEM, standard error of the mean; T/N ratio, tumor tissue/normal tissue ratio.

isolating glycoprotein subsets before performing proteomic and glycomic analyses to identify novel biomarkers.

While lectin microarray technology can demonstrate the lectin-binding patterns associated with cervical cancer, identifying specific disease-associated glycans is impossible by this method because the structures of the glycan molecules can only be inferred from lectin-binding data.

To confirm our findings, we performed histochemistry with biotin-labeled HHL, which revealed cytoplasmic staining of cancer cells in nearly all SCC specimens (Fig. 3e,f). On the other hand, there was little HHL staining of cells in CIN1 and CIN2 tissues (Fig. 3b–d),

© 2017 Japan Society of Obstetrics and Gynecology

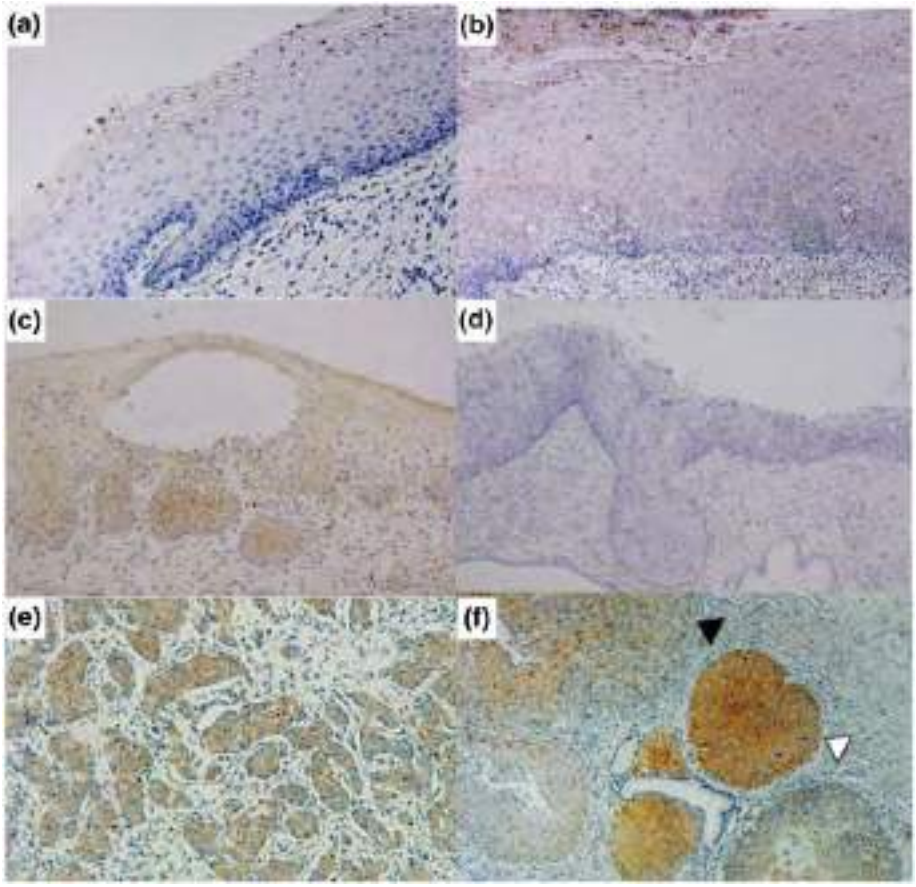

Figure 3 Staining of cervical tissues for Hippeastrum hybrid lectin (HHL). (a) Normal squamous epithelium (score = 0). (b) Cervical intraepithelial neoplasia (CIN)1 (score = 1). (c) CIN2 (score = 1). (d) CIN3 (score = 0). (e,f) Squamous cell carcinoma (SCC) (score = 3). (f) (▶) Basement membrane. (▷) Site of infiltration.

Table 2 Summary of histochemistry with HHL

Tissue specimens	HHL staining score			
	0	1	2	3
NSE (n = 16)	16	0	0	0
CIN1 (n = 26)	19	7	0	0
CIN2 (n = 19)	14	5	0	0
CIN3 (n = 20)	18	2	0	0
SCC (n = 16)	4	6	3	3

HHL staining score: 0 (0%), 1 (1%–5%), 2 (6%–50%), or 3 (51%–100%). CIN, cervical intraepithelial neoplasia; HHL, Hippeastrum hybrid lectin; NSE, normal squamous epithelium; SCC, squamous cell carcinoma.

and no staining of normal squamous epithelium (Fig. 3a). The reason why HHL preferentially stains cancer cells is unclear, but may possibly be related to the mechanism of tumor infiltration. A recent lectin microarray analysis of non-small cell lung cancer examined whether lectins can be used to estimate the lung cancer tissue type based on examination of lung cancer specimens and cultured cells. It was an effective study of a disease such as lung cancer for which tissue diagnosis is difficult before treatment.[23] In addition, lectins have been studied as predictors of recurrence and the prognosis.[24] However, the actual roles of lectins and their binding glycoproteins have not been clarified in any research. In this study, our results suggested that HHL might be associated with infiltration of SCC, which means it could become a marker of the prognosis or relapse in the future. To clarify the significance of the staining pattern of HHL, we will also analyze the binding glycoprotein and related genes in the future. After identification and structural analysis of its target glycoprotein has been performed by glycoprofiling, HHL might become a useful biomarker for identification of SCC of the uterine cervix.

The present lectin microarray method was effective for analyzing glycans in glycoproteins without the need to

© 2017 Japan Society of Obstetrics and Gynecology

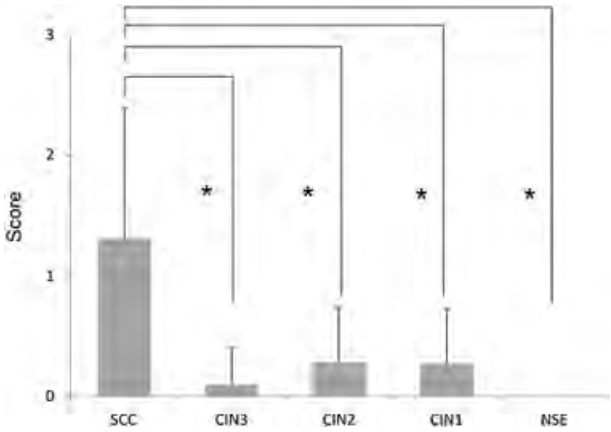

Figure 4 Histochemical expression of Hippeastrum hybrid lectin in cervical tissues. Staining scores for normal squamous epithelium (NSE, n = 16), cervical intraepithelial neoplasia (CIN)1 (n = 26), CIN2 (n = 17), CIN3 (n = 20), and squamous cell carcinoma (SCC; n = 16) are presented as the mean and standard error. The staining score for SCC was significantly higher than that for NSE and each grade of CIN (*$P < 0.05$, Steel's multiple comparison method).

release the glycan moieties or perform purification, unlike other available methods. Differential profiling with tissue microarrays could become a valuable tool if glycan-related biomarkers can be identified.

Cytoplasmic HHL staining of SCC cells (Fig. 3e,f) could distinguish cancer cells from normal epithelial cells or dysplastic cells, but HHL positivity was not associated with the histological tumor grade and the strength of staining varied among different SCC specimens. Despite this, HHL staining achieved a high sensitivity (87.5%) and high specificity (100%) for detection of SCC. As the HHL-positive tumor cells were often at sites of infiltration, this method may be useful for assessing the risk of infiltration by SCC. Currently, follow-up of CIN is required after diagnosis, but there is a possibility that HHL expression can be used to more easily detect tumor infiltration.

In conclusion, HHL is a potential new marker for distinguishing uterine cervical cancer from normal squamous epithelium by glycan profiling of formalin-fixed, paraffin-embedded tissues. Both cytology and histology are associated with overdiagnosis in elderly women with atrophic changes, and HHL staining might be to facilitate the diagnosis of SCC in these women compared to the combination of conventional cytology and histology. Moreover, as HHL positivity was uncommon in CIN, this lectin may be useful when diagnosis is difficult or for detecting recurrence of SCC.

Disclosure

The authors declare that they have no conflicts of interest.

References

1. Feizi T. Demonstration by monoclonal antibodies that carbohydrate structures of glycoproteins and glycolipids are onco-developmental antigens. *Nature* 1985; **314**: 53–57.
2. Dennis JW, Laferte S, Waghorne C *et al.* Beta 1–6 branching of Asn-linked oligosaccharides is directly associated with metastasis. *Science* 1987; **236**: 582–585.
3. Hakomori S. Tumor malignancy defined by aberrant glycosylation and sphingo(glyco)lipid metabolism. *Cancer Res* 1996; **56**: 5309–5318.
4. Goetz JA, Mechref Y, Kang P *et al.* Glycomic profiling of invasive and non-invasive breast cancer cells. *Glycoconj J* 2009; **26**: 117–131.
5. Satomaa T, Heiskanen A, Leonardsson I *et al.* Analysis of the human cancer glycome identifies a novel group of tumor-associated N-acetylglucosamine glycan antigens. *Cancer Res* 2009; **69**: 5811–5819.
6. Pinho SS, Figueiredo J, Cabral J *et al.* E-cadherin and adherens junctions stability in gastric carcinoma: Functional implications of glycosyltransferases involving N-glycan branching biosynthesis, N-acetylglucosaminyltransferases III and V. *Biochim Biophys Acta* 2012; **1830**: 2690–2700.
7. Mitra I, Zhuang Z, Zhang Y *et al.* N-glycan profiling by microchip electrophoresis to differentiate disease states related to esophageal adenocarcinoma. *Anal Chem* 2012; **84**: 3621–3627.
8. Varki A. Biological roles of oligosaccharides: All of the theories are correct. *Glycobiology* 1993; **3**: 97–130.
9. Hakomori S. Glycosylation defining cancer malignancy: New wine in an old bottle. *Proc Natl Acad Sci U S A* 2002; **99**: 10231–10233.
10. Fukuda M. Possible roles of tumor-associated carbohydrate antigens. *Cancer Res* 1996; **56**: 2237–2244.
11. Vanderschaeghe D, Festjens N, Delanghe J *et al.* Glycome profiling using modern glycomics technology: Technical aspects and applications. *Biol Chem* 2010; **391**: 149–161.
12. Hsu KL, Pilobello KT, Mahal LK. Analyzing the dynamic bacterial glycome with a lectin microarray approach. *Nat Chem Biol* 2006; **2**: 153–157.
13. Krishnamoorthy L, Bess JW Jr, Preston AB *et al.* HIV-1 and microvesicles from T cells share a common glycome, arguing for a common origin. *Nat Chem Biol* 2009; **5**: 244–250.
14. Pilobello KT, Slawek DE, Mahal LK. A ratiometric lectin microarray approach to analysis of the dynamic mammalian glycome. *Proc Natl Acad Sci U S A* 2007; **104**: 11534–11539.
15. Kuno A, Uchiyama N, Koseki-Kuno S *et al.* Evanescent-field fluorescence-assisted lectin microarray: A new strategy for glycan profiling. *Nat Methods* 2005; **2**: 851–856.
16. Matsuda A, Kuno A, Ishida H *et al.* Development of an all-in-one technology for glycan profiling targeting formalin-embedded tissue sections. *Biochem Biophys Res Commun* 2008; **370**: 259–263.

© 2017 Japan Society of Obstetrics and Gynecology

17. Wells M, Ostor AG, Crum CP *et al. World Health Organization Classification of Tumours – Pathology and genetics: Tumours of the breast and female genital organs*. Lyon: IARC Press, 2003.
18. Monsonego J. Cervical cancer prevention: Current perspectives. *Endocr Dev* 2012; **22**: 222–229.
19. Ito H, Kuno A, Sawaki H *et al.* Strategy for glycoproteomics: Identification of glyco-alteration using multiple glycan profiling tools. *J Proteome Res* 2009; **8**: 1358–1367.
20. Narimatsu H, Sawaki H, Kuno A *et al.* A strategy for discovery of cancer glyco-biomarkers in serum using newly developed technologies for glycoproteomics. *FEBS J* 2010; **277**: 95–105.
21. Ban M, Yoon HJ, Demirkan E *et al.* Structural basis of a fungal galectin from Agrocybe cylindracea for recognizing sialoconjugate. *J Molec Biol* 2005; **351**: 695–706.
22. Veau B, Guillot J, Damez M *et al.* Purification and characterization of an anti-(A + B) specific lectin from the mushroom Hygrophorus hypothejus. *Biochim Biophys Acta* 1999; **1428**: 39–44.
23. Hirao Y, Matsuzaki H, Iwaki J *et al.* Glycoproteomics approach for identifying Glycobiomarker candidate molecules for tissue type classification of non-small cell lung carcinoma. *J Proteome Res* 2014; **13**: 4705–4716.
24. Yazawa S, Takahashi R, Yokobori T *et al.* Fucosylated glycans in α1-acid glycoprotein for monitoring treatment outcomes and prognosis of cancer patients. *PLoS ONE* 2016; **11**: e0156277.

© 2017 Japan Society of Obstetrics and Gynecology

Journal of Assisted Reproduction and Genetics (2018) 35:2037–2048
https://doi.org/10.1007/s10815-018-1298-y

FERTILITY PRESERVATION

Oocyte retrieval after heterotopic transplantation of ovarian tissue cryopreserved by closed vitrification protocol

Yodo Sugishita[1] · Naoki Okamoto[1] · Atsushi Uekawa[1] · Takayuki Yamochi[2] · Mariko Nakajima[1] · Chie Namba[1] · Suguru Igarashi[1] · Takumi Sato[1] · Sei Ohta[3] · Makoto Takenoshita[3] · Shu Hashimoto[2] · Akiko Tozawa[4] · Yoshiharu Morimoto[5] · Nao Suzuki[1]

Received: 27 May 2018 / Accepted: 22 August 2018 / Published online: 1 September 2018
© Springer Science+Business Media, LLC, part of Springer Nature 2018

Abstract

Purpose A device for closed vitrification was designed to reduce the risk of contamination and investigated on its efficacy for ovarian function recovery after cryopreservation and heterotopic transplantation.

Methods Ovarian tissues from green fluorescence protein transgenic mice (10 GFP mice) were vitrified using the device, and warmed ovarian tissues were transplanted into the ovarian bursa region in wild-type female mice (6 mice). Fresh ovarian tissues were similarly transplanted as a control. After recovery of the estrous cycle, mice were mated with male mice. Ovarian tissues from six cynomolgus monkeys were vitrified and warmed with the device for autologous, heterotopic transplantation. Fresh tissue transplantation was not performed for the control. Ovarian function was examined by recovery of the hormonal cycle. Histological examination was conducted.

Results The number of live pups per recipient mouse was not significantly different after transplantation of fresh or vitrified-warmed ovarian tissue, although the pregnancy rate was reduced with vitrified tissues. The hormonal cycle was restored in 5/6 monkeys after heterotopic transplantation of vitrified-warmed ovarian tissue. Follicles were harvested at eight sites in the omentum and 13 sites in the mesosalpinx. In vitro maturation (IVM)/IVF produced embryo but did not develop.

Conclusions Resumption of the hormonal cycles, follicle development, and oocyte retrieval from vitrified-warmed ovarian tissue transplants may indicate that the use of vitrification for ovarian tissue in a closed system has a potential of clinical application without the risk of contaminations. More detailed analyses of the effects of vitrification on ovarian tissue, such as gene expression patterns in oocytes and granulosa cells, may be needed for establishing a standard procedure for cryopreservation of ovarian tissues in human.

Keywords Ovarian tissue cryopreservation · Vitrification · Closed device · Cynomolgus monkey · Fertility preservation · Autologous transplantation

✉ Nao Suzuki
nao@marianna-u.ac.jp

[1] Department of Obstetrics and Gynecology, St. Marianna University School of Medicine, 2-16-1 Sugao, Miyamae-ku, Kawasaki, Kanagawa 216-8511, Japan

[2] Namba IVF Clinic, Osaka 550-0015, Japan

[3] Eve Bioscience, Co, Ltd., Wakayama 648-0003, Japan

[4] Institute of Medical Science, St. Marianna University Graduate School of Medicine, 2-16-1 Sugao, Miyamae-ku, Kawasaki, Kanagawa 216-8511, Japan

[5] HORAC IVF Grand Front, Osaka 530-0011, Japan

Introduction

Medical and technical advances have given women better chances to preserve fertility and to have children at a later time, including the cryopreservation of embryos, oocytes, and ovarian tissue. Ovarian tissue cryopreservation benefits women more broadly, since ovarian tissue contains steroidogenesis and gametogenesis activities and a large number of primordial follicles and can be harvested irrespective of the stage of the menstrual cycle or be applied to pre-pubertal girls. Since the first successful transplantation of frozen–thawed ovarian tissues was reported by Oktay and Karlikaya in 2000 [1], about 130 live births have been reported after

transplantation of cryopreserved ovarian tissue around the world [2], and the FertiPROTEKT network registry has listed more than 1000 ovarian tissue cryopreservation procedures [3]. Nonetheless, no validated standard protocol has been established for cryopreservation of ovarian tissue [4].

Some studies comparing slow freezing and vitrification by rapid freezing have shown that vitrification is superior for cryopreservation of ovarian tissue with respect to follicle density, cell proliferation, stromal cell preservation, and cell viability [5–8]. Recently, several protocols for vitrification have been reported [5, 6, 9–11], and at least one vitrification system is currently available for clinical use. Cryopreservation by vitrification is achieved by elevating the cooling rate and concentration of cryoprotectants and forming a glassy, vitrified state by extreme elevation of viscosity during cooling [12]. There are two main challenges to improving vitrification techniques: (i) high concentrations of cryoprotectant, which may be toxic to oocytes, embryos, and ovaries, are required and (ii) intracellular ice may develop if the cooling or warming rates are incorrect [13, 14]. Several methods have been developed to overcome these problems. The logical way to make cooling more rapid is to use the smallest possible volume of cryoprotectant around the sample and to directly expose it to liquid nitrogen without any insulation. It is a process known as open vitrification [13]. Successful open vitrification of ovarian tissues has been achieved in mice [5, 15, 16], cattle [9], monkeys [10, 11], and humans [6]. Two healthy babies have been born from vitrified ovarian tissues preserved by open vitrification [17, 18]. However, there is concern about the sterility of liquid nitrogen and the risk of cross-contamination during long-term storage [19, 20]. Because ovaries are larger than oocytes or embryos, the risk of cross-contamination is increased with ovarian cryopreservation by direct contact between solution containing ovarian tissue and liquid nitrogen. To avoid the risk of contamination, a closed vitrification method was developed and used in vitro for development of preantral follicles from the macaque ovarian cortex [21]. However, in vivo tissue transplantation studies are needed to confirm long-term function and fertility of vitrified-warmed ovarian tissues.

In the present study, we developed a new closed vitrification protocol. The efficacy of the protocol was assessed using ovarian tissues of mice and cynomolgus monkeys for long-term functions of vitrified-warmed ovarian tissues after transplantation.

Materials and methods

This investigation of closed vitrification process was based on previous research into open vitrification by Suzuki et al. [11]. The study protocol was approved by the ethics committee of St. Marianna University School of Medicine (Kanagawa, Japan) and IVF Namba Clinic (Osaka, Japan). This study was performed in accordance with the guidelines for use of animals at the experimental facilities of St. Marianna University School of Medicine (Kanagawa, Japan), Kinki University (Wakayama, Japan), and Eve Bioscience Ltd. (Wakayama, Japan).

Studies in mice

Animal care and management

Female and male C57BL/6J mice and green fluorescence protein (GFP)-transgenic [C57BL/6J-Tg (CAG-EGFP)] mice were purchased from SLC Japan Inc. (Tokyo, Japan). Mice were housed under a 12-h light/12-h dark cycle at 22 °C with 55% humidity and received food and water ad libitum.

Collection, cryopreservation, and thawing of donor mouse ovaries

Donor ovaries were collected from 4-week-old C57BL/6J-Tg (CAG-EGFP) mice and placed into disposable Petri dishes containing Dulbecco's modified Eagle's medium/Ham's F-12 [1:1 (*v*/*v*)]. Then, each ovary was cut in half for cryopreservation using the new closed device. After 1–2 months, the cryopreserved ovarian tissues were warmed and stored in H199 supplemented with 20% (*V*/*V*) SSS medium until transplantation.

Transplantation of mouse ovaries

Orthotopic transplantation of vitrified-warmed half ovaries was performed in 6-week-old female C57BL/6J mice, while fresh ovaries harvested from 4-week-old CAG-EGFP female mice were cut in half and used as control grafts. Orthotopic transplantation was done as described previously [15] with some modifications. In brief, anesthesia was induced by intraperitoneal injection of pentobarbital sodium salt (7.5 g/kg body weight). A midline longitudinal skin incision was made in the lower back, followed by small bilateral incisions in the fascia and muscles immediately above each ovary through which the recipient's reproductive tract was lifted out. Then, a small slit was made in each ovarian bursa, and the recipient's ovary was removed under an operating microscope and was replaced with a fresh or thawed half ovary. Subsequently, the bursal membrane was sutured, the reproductive tract was replaced inside the body, and the skin incision was sutured.

Mating of mice

One recipient mouse was paired for 1 day with one male C57BL/6J mice 10 days after transplantation to allow recruitment of primordial follicles before mating. When mating was confirmed by the presence of a vaginal plug, pregnant females were moved to separate cages. The number of pups (both dead and alive) was recorded.

Monkey experiments

Animal care and management

Six cynomolgus monkeys (4 years old and weighing 3.0–3.5 kg) imported from Vietnam by Eve Bioscience (Wakayama, Japan) were used in this study. After importation, the monkeys were quarantined for 1 month and were examined for pathogenic bacteria and changes of appearance and/or behavior. Monkeys were housed individually in special cages (550 mm × 72 mm × 780 mm) in an animal room with a temperature of 25–38 °C, ventilation 5 times/h, and a 12-h light/12-h dark cycle (07:00–19:00). Food (AS; Oriental Yeast Co., Ltd., Tokyo, Japan) was supplied every morning, and drinking water (municipal tap water of Hashimoto City, Wakayama, Japan) was provided ad libitum. The estrous cycle was confirmed in each female by monitoring vaginal bleeding.

Anesthesia and surgery

Laparotomy was performed after induction of anesthesia by intramuscular injection of a 2:1 mixture of ketamine (20 mg/kg Ketalar 50; Sankyo Yell Pharmaceutical, Tokyo, Japan) and xylazine (1 mg/kg Celactal Bayer Yakuhin, Osaka, Japan). During surgery, additional doses of these anesthetics were administered as appropriate to maintain the depth of anesthesia. After resection of the bilateral ovaries, adherent tissues were removed, and the organs washed twice in modified Human Tubal Fluid (m-HTF, Kitazato BioPharma Co., Ltd., Shizuoka, Japan). Then, the cortical tissue was removed from each pair of ovaries and placed in m-HTF. Monkeys were recovered from anesthesia following suture. Relaparotomy for transplantation was performed generally after about 5 h, including 1 h for tissue preparation, 3 h of soaking in liquid nitrogen, and 1 h for warming.

Ovarian tissue cryopreservation and transplantation

The monkey ovarian tissue was cut into strips (10 mm × 10 mm × 1 mm) for vitrification, and cryopreservation was performed using the closed device by the same procedure as that for mice (Fig. 1d, e). Tissue strips were maintained in liquid nitrogen for at least 3 h. Laparotomy was performed for transplantation of vitrified-thawed ovarian tissue, with a minced graft (cut into 20~25 pieces measuring 1 mm × 1 mm × 1 mm) on the right side and an intact strip (10 mm × 10 mm × 1 mm) on the left side of the omentum or the mesosalpinx. Altogether, four tissue grafts, two preparations each for strips and minces, were transplanted in each monkey, one graft each on each side of two sites, the omentum, and the mesosalpinx. For omental transplantation, the graft was wrapped in the omentum that was sutured to form a bag. For transplantation into the mesosalpinx, an incision was made in the right side of the mesosalpinx to create a pocket, into which graft was placed and incision was sutured. To prevent adhesions, Seprafilm® (Kaken Pharmaceutical Co., Ltd. Tokyo, Japan) was used during closure of the abdomen.

Stimulation of ovarian tissue

Ovarian stimulation was conducted after down-regulation with a gonadotropin-releasing hormone (GnRH) agonist (1.88 mg of Leuplin injection 3.75; Takeda Pharmaceutical, Osaka, Japan). Six female monkeys were administered various doses of recombinant human follicle-stimulating hormone (rhFSH; Follistim®; MSD, Osaka, Japan) after down-regulation in three trials, as described below. On the evening of the final day of rhFSH injection, 400 IU/kg of human chorionic gonadotrophin (hCG; Puberogen; Nippon Yakkyoku, Tokyo, Japan) was administered, and ova were collected 40 h later. In the first trial, 25 IU/kg of rhFSH was administered once daily in the morning on days 1 to 9 (initiation of FSH injection = day 0). The second and third trials were initiated 6 months and 1 year after transplantation. In the second trial, 50 IU/kg of rhFSH was administered once daily in the morning on days 1 to 9, after which 100 IU/kg of rhFSH was administered twice daily in the morning and evening on days 10 and 11. In third trial, 50 IU/kg of rhFSH was administered once daily in the morning on days 1 to 4, 75 IU/kg of rhFSH was administered twice daily in the morning and evening on days 5 to 11, and 100 IU/kg of rhFSH was administered twice daily in the morning and evening on day 12. Ovarian stimulation was initiated 2 weeks after estradiol elevation in the trial 1 and between estradiol elevations 6 months and 1 year after transplantation in the trials 2 and 3, respectively. All three trials were performed on all monkeys, except the monkey 6 which was subjected to only the trials 2 and 3.

Oocyte collection and transportation

Laparotomy was performed under general anesthesia as described above. After confirming mature follicle development, oocytes were aspirated, and a small piece of ovarian tissue containing the follicle growth area was excised and placed in the culture medium. Oocytes were collected by puncturing the follicle in a culture dish to avoid loss of oocytes. Aspiration of mature follicles was performed by using a 2.5-ml syringe with a 21-G needle that contained a small amount of HEPES-Tyrode's albumin with lactate and pyruvate (HEPES-TALP, pH 7.4) and 0.3% bovine serum albumin, after pre-washing the needle and syringe with heparin sodium (Ajinomoto Pharmaceutical, Tokyo, Japan). The retrieved ova were transferred to HEPES-TALP in a dish on a warming plate maintained at 38 °C and maturation was examined by stereomicroscopy (×80). Then, the collected ova were placed into HEPES-TALP in a sealed round-bottom tube (2058, Becton Dickinson Labware, NJ, USA) kept in warm water (38 °C). The ovarian tissue was placed in 15-ml tubes (Polypropylene Conical Centrifuge Tube, BD Falcon, Bedford,

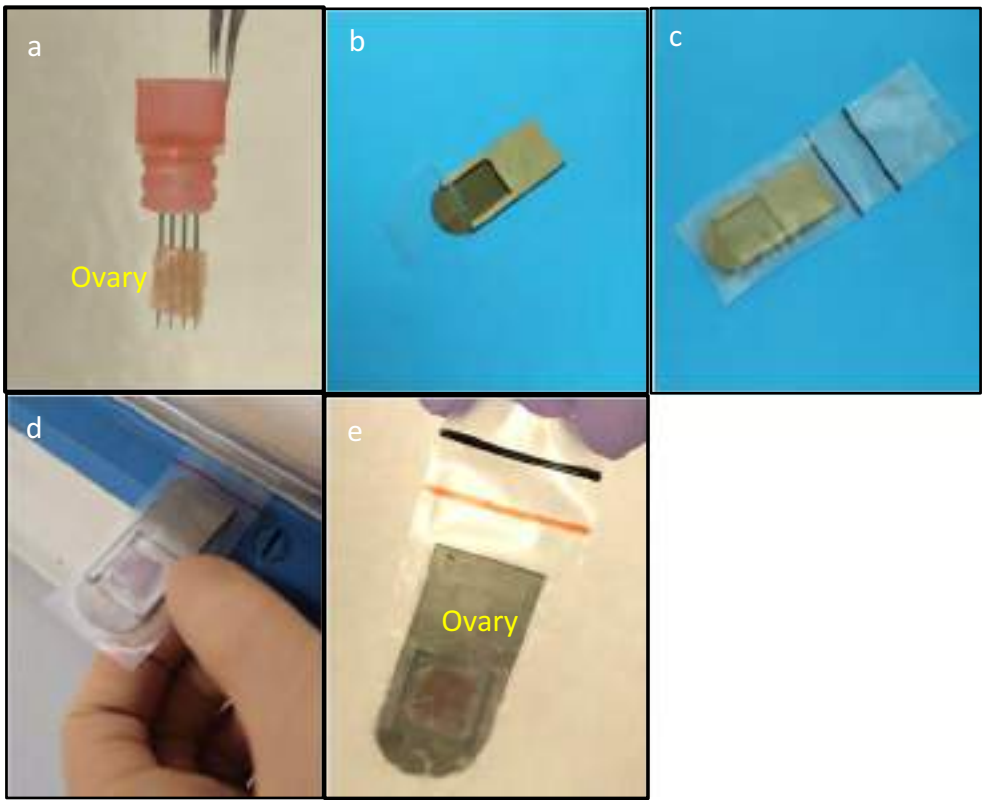

Fig. 1 Devices for vitrification. **a** Ova Cryo Device Type M (open device [11]). **b** Closed device. **c** Closed device in the pouch. **d** The sealed pouch. **e** Vitrified ovarian tissue

MA, USA) containing the same culture medium. The specimens were transferred from Eve Bioscience to Namba IVF Clinic (Namba, Osaka, Japan) within 2 h.

In vitro maturation of immature monkey oocytes

In the first and second trials, we examined whether oocytes obtained at the germinal vesicle (GV) stage or metaphase I (MI) stage could reach metaphase II (MII). The oocytes were incubated at 37 °C for 24–72 h under an atmosphere of 5% O_2, 5% CO_2, and 90% N_2 in TALP medium containing L-glutamine, lactic acid, pyruvic acid, and 20% (*v*/*v*) fetal bovine serum. In the third trial, 20 ng/ml of epidermal growth factor (EGF; Sigma-Aldrich Chemical Co., St. Louis, MO, USA) was added to the abovementioned TALP medium, and the oocytes were cultured for 24–72 h.

Intracytoplasmic sperm injection: fertilization of monkey oocytes

Semen was obtained from a male monkey under anesthesia with ketamine HCl (10 mg /kg) by electrical induction of ejaculation. The methods used for freezing and thawing sperm were described previously [21]. Intracytoplasmic injection (ICSI) of cryopreserved sperm was performed as reported previously [11] with minor modifications. Briefly, cumulus cell-oocyte complexes were treated with 0.01% (*w*/*v*) hyaluronidase (H3757; Sigma-Aldrich) dissolved in HEPES-TALP, and then oocytes were denuded by pipetting at room temperature. After maturation of the denuded oocytes was evaluated, culture was performed at 37 °C under an atmosphere of 5% O_2, 5% CO_2, and 90% N_2 in TALP until the time of ICSI. The sperm suspension and oocytes were placed in HEPES-TALP and covered with mineral oil (M8410; Sigma-Aldrich). A single sperm with normal morphology was captured by an injection pipette (MIC-SI-30-NTP; Humagen Fertility Diagnostics, Charlottesville, VA, USA) and then was washed and immobilized in an injection pipette containing 10% polyvinylpyrrolidone (PVP360; Sigma-Aldrich) dissolved in HEPES-TALP. The immobilized sperm was injected into a mature oocyte in HEPES-TALP. After injection, culture was done for 24 h at 37 °C under an atmosphere of 5% O_2, 5% CO_2, and 90% N_2 in TALP. Fertilization was evaluated on basis of detecting two pronuclei and two polar bodies at 18 h after sperm injection, and cleavage was confirmed at 24 h after sperm injection. Then, the embryos were cultured for 144 h in CMRL-1066 medium (11530-037; Life Technologies, Carlsbad, CA, USA) containing L-glutamine, lactic acid, pyruvate, and 20% (*v*/*v*) fetal bovine serum under the same atmosphere.

Morphological investigation of monkey ovarian tissue

Monkey ovarian tissues were fixed overnight at 4 °C in Bouin's fixative (Polysciences, Warrington, PA, USA), embedded in paraffin, and cut into 1–5-μm-thick

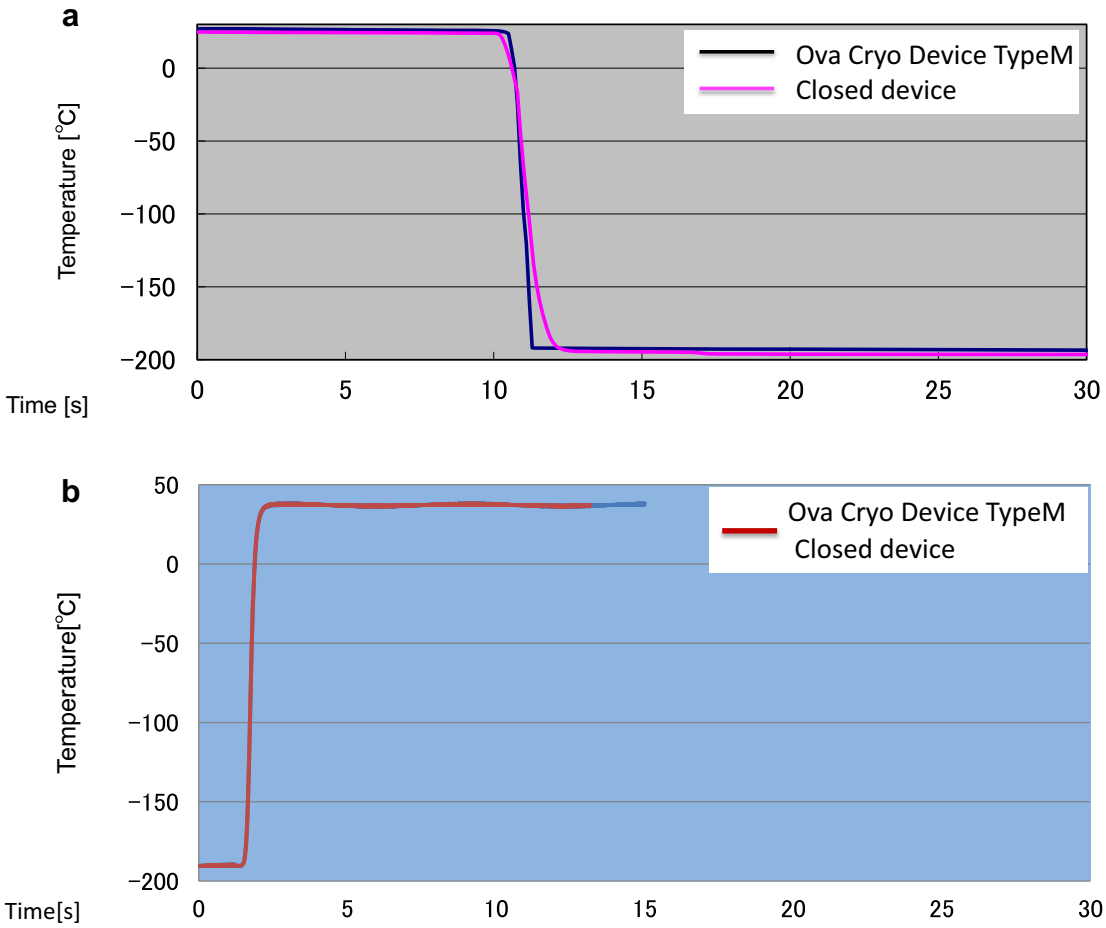

Fig. 2 Cooling and warming rates of vitrification devices. **a** Cooling rate of the open (black) and closed (pink) devices. The cooling rates of the open devise and the closed devise were − 19,500 and − 12,000 °C/min, respectively. **b** Warming rates of the open and closed devices were identical and shown in red. The warming rate was 42,000 °C/min

sections. Sections were stained with toluidine blue (Certistain® Toluidine blue O (C.I.52040), Millipore, MA, USA) and hematoxylin-eosin (Sakura Finetek Japan, Tokyo, Japan), followed by observation under a microscope. Follicular development stages were defined as follows: primordial follicles were in a single layer of flattened pre-granulosa cells, primary follicles were follicles with only one granulosa cell layer, early secondary follicles had two to four granulosa cell layers without an antrum, late secondary follicles had more than four granulosa cell layers without an antrum, and antral follicles had multiple layers of cuboidal granulosa cells with an antrum [22].

Hormone assays

Estradiol (E_2) and progesterone (P_4) were measured by SRL Inc. (SRL, Tokyo, Japan) to confirm the hormone cycle of the monkeys before ovarian tissue cryopreservation and approximately every 2 weeks after transplantation of vitrified-thawed ovarian tissue. This procedure was performed in the same manner as reported previously [11].

Open vs. closed vitrification

Loading with cryoprotectant

Cryopreservation of ovarian tissues using an open device was performed as described previously with some modifications [10, 11]. Strips of ovarian tissue were first equilibrated in HEPES-buffered 199 (H199, Invitrogen, Carlsbad, CA, USA) supplemented with 20% (*V*/*V*) SSS (Irvine Scientific, Santa Ana, CA, USA) and 1.61 mol/l ethylene glycol for 5 min, followed by equilibration in H199 supplemented with 20% (*V*/*V*) SSS and 3.22 mol/l ethylene glycol for 5 min. Subsequently, the ovarian strips were transferred into H199 supplemented with 20% (*V*/*V*) SSS, 5.64 mol/l ethylene glycol, 5% (*w*/*v*) polyvinylpyrrolidone (Sigma-Aldrich, St. Louis, Mo, USA), and 0.5 mol/l sucrose EMPROVE®bio

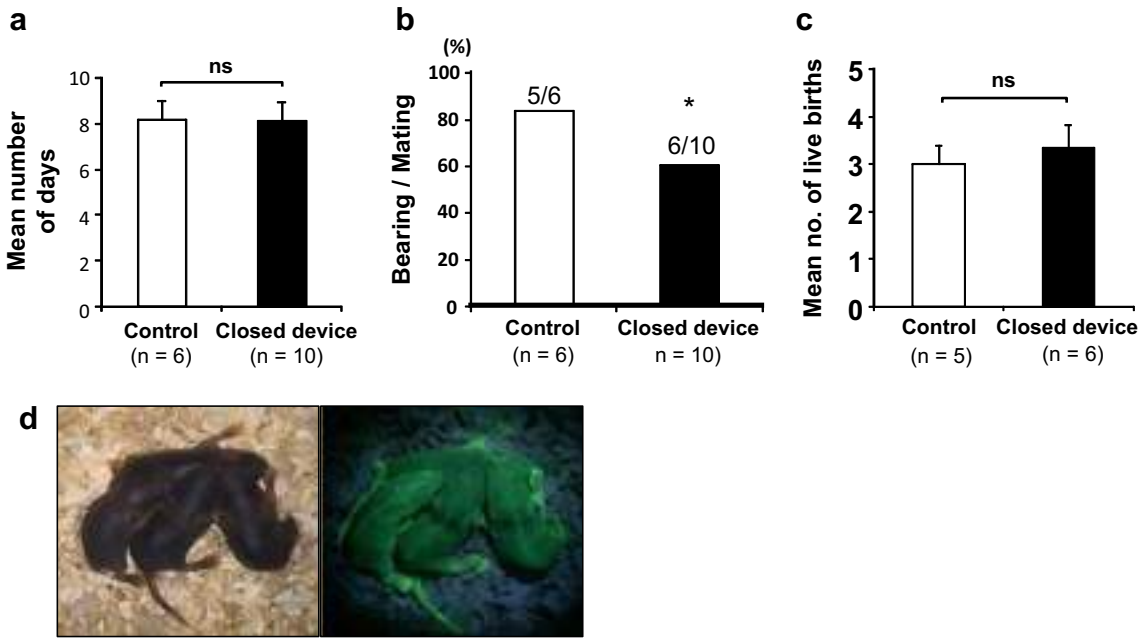

Fig. 3 Orthotopic ovarian tissue transplantation in mice. Fresh and vitrified/warmed ovarian tissues were transplanted for functional evaluation. Graph shows the mean with the standard deviation for 6 mice (fresh tissue) and 10 mice (vitrified/warmed tissue). *$p < 0.05$. **a** Days required before the initial increase of estradiol. **b** Rates of pregnancy. **c** Number of live pups per pregnancy. **d** Pups from transplants of fresh (**a**) or cryopreserved GFP mouse ovaries (**b**)

(EMD Millipore, Billerica, MA, USA). All steps were performed at 26 °C.

Vitrification procedure

Open device Within 25 min, the strips were loaded into an ovarian storage device (Ova Cryo Device TypeM®; Kitazato BioPharma Co., Shizuoka, Japan; Fig. 1a) and the device was immersed vertically into liquid nitrogen. Then the frozen strips were individually placed into cryogenic vials and were stored in liquid nitrogen until further use.

Closed device The device was made from titanium (500 and 800 μm in thickness) for excellent thermal conductivity (CDT × 10, titanium, Kitazato BioPharma Co., Ltd., Shizuoka, Japan). Two sizes of thickness (500 and 800 μm) were tested in consideration of conductance and structural stability. However, the similar stability and conductance were obtained with both thicknesses. The 500-μm thickness was used in mice. The 800-μm one was used only for one monkey as comparison after testing both thicknesses. For vitrification, a piece of ovarian tissue equilibrated with vitrification solution was placed on the titanium plate and covered with polypropylene film (Kitazato BioPharma Co., Ltd., Shizuoka, Japan). To prevent viral contamination, the device was placed in a bag made from the same polypropylene material as the film cover, which was heat-sealed and immersed in liquid nitrogen. This extra step for inserting vitrified tissue in a bag took only 10~30 s; thus, we did not feel there was any difference between open and closed device in the effect of cryoprotectants. The polypropylene material used for the film cover and bag was demonstrated to be safe by a cytotoxicity test before this study (Fig. 1b–e).

Warming procedure

For thawing, pouch is cut open and the device is directly placed into the thawing solution. The vitrified samples were thawed in 20 ml of H199 containing 20% (*V*/*V*) SSS and 0.8 mol/l sucrose, which had been warmed at 37 °C for 1 min in a water bath, followed by dilution in H199 containing 20% (*V*/*V*) SSS and 0.4 mol/l sucrose for 3 min at room temperature, and then dilution twice in H199 containing 20% (*V*/*V*) SSS for 5 min at room temperature. After removal of the cryoprotectant, the ovarian sections were placed in H199 containing 20% (*V*/*V*) SSS. No devitrification was observed in any tissue preparation.

Heat conduction rate

Cooling was assessed by measuring the heat conduction rate using a K-type thermocouple and a data logger GL900-4 (Graphtec Inc., Kanagawa, Japan), with the mean of 10 temperature measurements being plotted to generate a graph (Kitazato

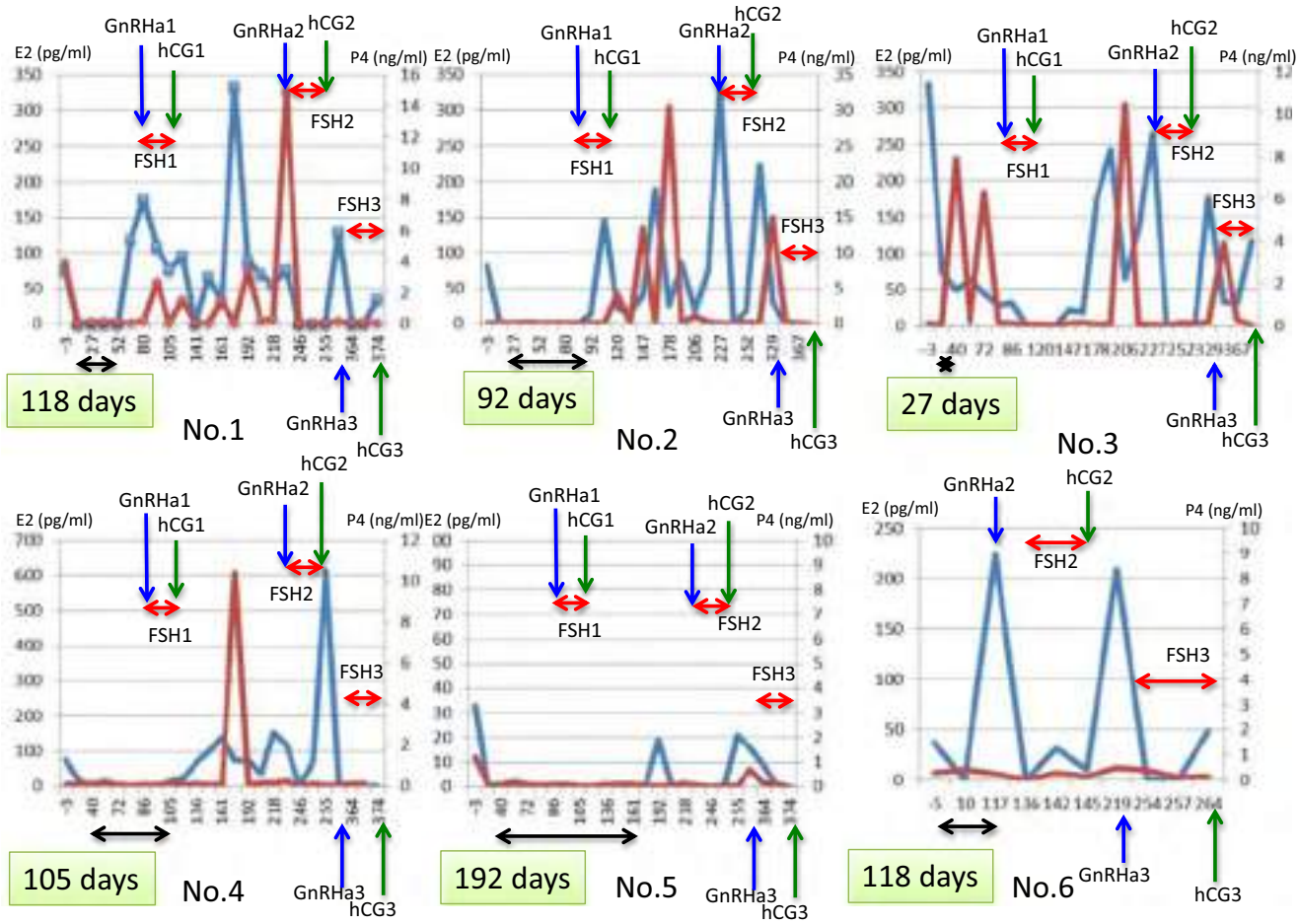

Fig. 4 Hormonal cycles in monkeys. Estradiol (blue line) and progesterone (red line) in blood after ovarian transplantation. Number in green square: days required before hormone detection in blood. IVF cycles are indicated by arrows: GnRH (blue), FSH (red), and hCG (green)

BioPharma Co., Ltd., Shizuoka, Japan). The heat conduction rate was compared between the open device (Ova Cryo Device TypeM®) and the closed device (CDT × 10; Fig. 2a, b).

Statistical analysis

All statistical analyses were performed by using EZR (Saitama Medical Center, Jichi Medical University, Saitama, Japan), which is a graphical user interface for R (The R Foundation for Statistical Computing, Vienna, Austria).

Results

Thermal conductivity

The cooling rates of the open and closed vitrification devices were − 19,500 and − 12,000 °C/min, respectively (Fig. 2a), while the warming rate of both devices was 42,000 °C/min (Fig. 2b). There were no differences of thermal conductivity, especially the cooling speed, between devices with a thickness of 500 or 800 μm.

Fertility of mice after transplantation of vitrified-warmed ovarian tissues

Six mice received transplantation of fresh ovarian tissue as controls. Vitrified-warmed ovarian tissue was transplanted into 10 mice. The estrous cycle was recovered in all recipients. Estradiol increased at 5–11 days after transplantation of fresh ovarian grafts and after 7–14 days in mice receiving vitrified-warmed grafts. There were no significant differences in the time required until recovery of the estrous cycle between mice receiving fresh grafts (8.2 ± 0.9 days) and vitrified-warmed grafts (8.1 ± 0.9 days) (Fig. 3a). Recipient mice were kept for 3 weeks after transplantation to allow recruitment of primordial follicles before mating. The delivery rate was significantly lower for mice with vitrified-warmed ovarian grafts

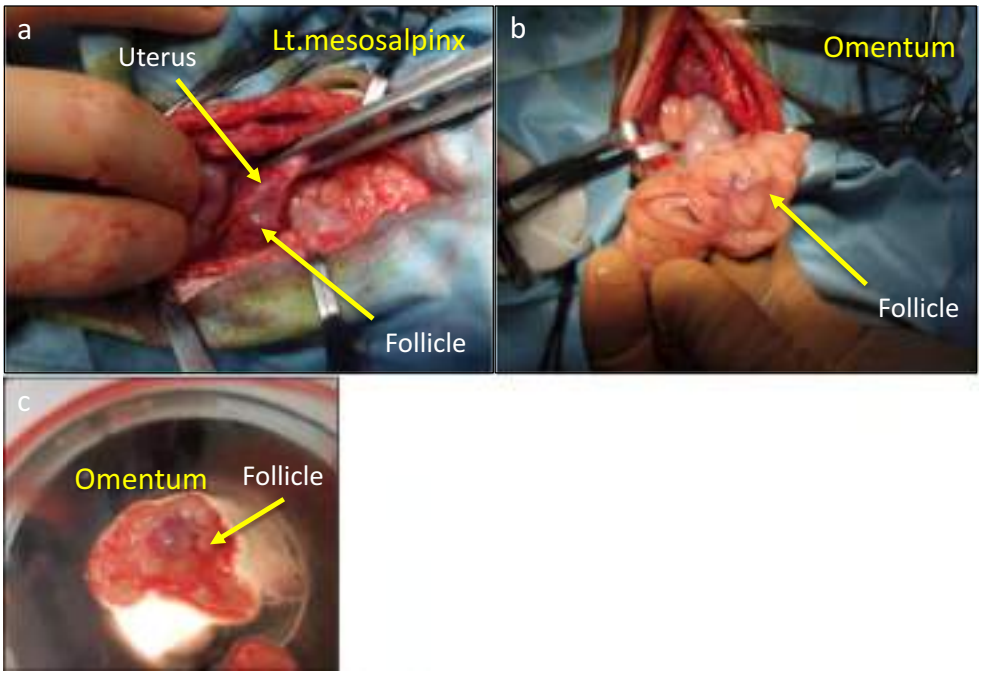

Fig. 5 Laparotomy for oocyte retrieval in monkey no. 4. Follicles are evident in the left mesosalpinx (**a**) and omentum (**b**) on the post-transplantation day 252. A pre-ovulatory follicle dissected from the omentum, shown in **b**, is shown in an enlarged scale (**c**)

(60%) than for mice with fresh grafts (83%) (Fig. 3b). However, the number of live pups delivered per recipient was not significantly different between the two groups (Fig. 3c, d).

Hormonal cycle in monkeys

Transplantation of vitrified-warmed ovarian tissues was performed in six cynomolgus monkeys. No monkey received fresh ovarian tissue as control due to the cost of each monkey. Five monkeys received ovarian tissue that had been vitrified using 500-μm closed device, and one monkey (no. 3) received tissue vitrified using 800-μm closed device. Follicle development was assessed by estradiol measurements every 2 weeks. Harvesting of ova was successful in five monkeys, while it failed in monkey no. 4. Resumption of the hormonal cycle was confirmed at 111 days (27–192 days) after transplantation (Fig. 4). The five monkeys used for egg collection exhibited periodic hormonal cycles by 367 days after transplantation. Oocyte collection was performed via laparotomy, with a small piece of tissue around the site of follicle formation being excised carefully while avoiding rupture of the follicle (Fig. 5). It was found that transplanted ovarian tissue had been incorporated into the omentum and the mesosalpinx, and minimal resection was required for oocyte harvesting. Three monkeys (no. 1, no. 3, and no. 6) were still alive at the time of writing, and their hormonal cycles had continued for > 1240 days.

Follicle development

Follicle development was found at eight graft sites in the omentum and 13 sites in the mesosalpinx. In addition, it was detected at 10 sites after transplantation of minced grafts (1-mm cubes) and at 11 sites after transplantation of strip grafts (10 mm × 10 mm × 1 mm), while the number of oocytes recovered was eight and nine, respectively. There were no significant differences of follicle development between transplantation into the omentum or the mesosalpinx, between transplantation of strips or minced grafts, and between cryopreservation with the 500- or 800-μm devices.

IVM and IVF

Seventeen oocytes were retrieved from five monkeys. To perform in vitro maturation (IVM), EGF was not used in the first and second trials in case immature oocytes were collected. A total of seven GV-stage oocytes, one MI oocyte, and two MII oocytes were obtained by the initial two egg collections. When the eight GV-stage oocytes were cultured for up to 72 h, only three reached MI stage but did not progress further. ICSI was performed with the two MII oocytes, and fertilization was confirmed by detection of two pronuclei, but development did not proceed beyond the one-cell stage. A total of six oocytes were obtained at the third egg collection, including four GV-stage oocytes, one MII oocyte, and one degenerated embryo. IVM was performed with four GV-stage oocytes by adding EGF at 20 ng/ml. One of these oocytes reached MII stage but failed to fertilize by ICSI (Table 1).

Table 1 IVM and IVF of oocytes retrieved from transplanted ovarian tissue in monkeys

Ovarian stimulation	No of Monkey	Thickness of device	Days between hormonal measurement and oocyte harvest	Serum estradiol (E2) level (pg/ml) / Serum progesterone (P4) level (ng/ml)	Days between hormone measurement and oocyte harvest	Site	Side	Follicle number	Gained oocyte number	Stage	IVM	Reached to MII	ICSI	Fertilized
Trial 1	1	500	110	E2: 76 / P4: 0.06	5	Mesosalpinx	Lt	1	1	GV	yes	No		
	2	500		E2: 146 / P4: 0.1	5	Omentum	Rt	1	1	GV	yes	No		
Trial 2	2	500	258	E2: 223 / P4: 0.08	3	Mesosalpinx	Lt	4	4	GV	yes	No		
						Omentum	Lt	1	0					
	4	800		E2: 61 / P4: 0.04	3	Mesosalpinx	Lt	2	2	MII	No		Yes	2PN
						Omentum	Lt	1	1	MI	yes	No		
						Mesosalpinx	Rt	1	1	GV	yes	No		
						Omentum	Rt	1	1	GV	yes	No		
Trial 3	1	500	377	E2: 34 / P4: 0.03	3	Omentum	Rt	1	1	MII	No		Yes	No
	3	800		E2: 116 / P4: 0.04	3	Omentum	Lt	1	1	Degeneration				
						Omentum	Rt	1	0					
	6	500		E2: 49 / P4: 0.16	3	Mesosalpinx	Rt	4	4	GV	Yes	Yes	Yes	No
						Mesosalpinx	Lt	1	0					
						Omentum	Rt	1	0					

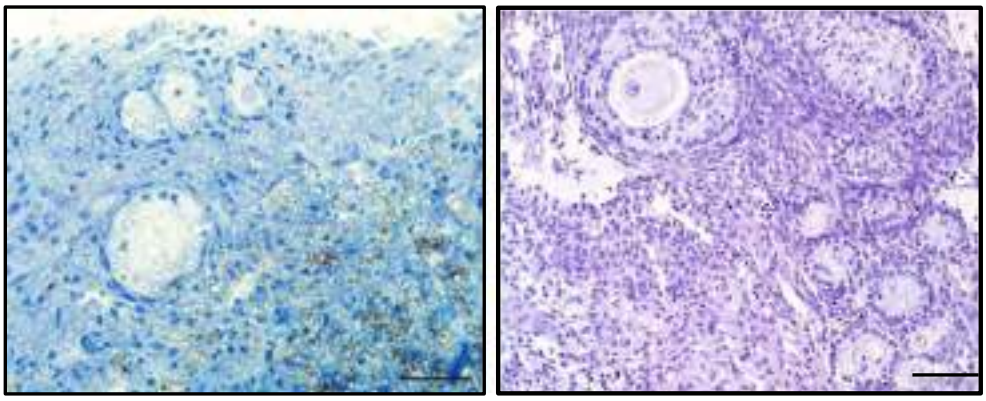

Fig. 6 Post-transplantation histological analyses. **a** Ovarian tissue adjacent to pre-ovulatory follicles excised for oocyte harvest from the omentum on the post-transplantation day 258 that yielded a MI oocyte (monkey no. 4). **b** The omentum which yielded GV oocytes (monkey no. 2). A Toluidine blue staining. **b** H&E staining. Scale bar = 50 μm

Histological findings

After collection of oocytes, the residual tissues were fixed for histological examination. At a site of ovarian tissue transplantation into the omentum, two primary follicles and one early secondary follicle were detected. Also, at another omental transplantation site, there were primordial follicles, primary follicles, and late secondary follicles, having the potential to develop for oocyte collection (Fig. 6a, b).

Discussion

A closed vitrification devise was developed using a titanium plate for housing ovarian tissue which is sealed inside a polypropylene pouch to avoid viral contamination during exposure to liquid nitrogen. Due to the excellent thermal conductivity of titanium, similar cooling and warming rates, which are important for maintaining the structural integrity of tissue, were observed by closed vitrification method to those by the standard open one.

The in vivo function was examined by transplanting ovarian tissues after cryopreservation by the closed vitrification devise on mice and cynomolgus monkeys. The number of live pups per litter was similar with both tissues in mice (Fig. 4a). However, the birth rate by cryopreserved tissue with the closed vitrification method was lower than that from fresh ovarian tissue in mice (Fig. 4b). Using similar vitrification conditions to the one used in the present study, follicle counts were similar to fresh tissue transplants, and pregnancy rates were higher than those of transplants from slow freezing or conventional vitrification and similar to the fresh tissue transplants [5, 16]. These studies may indicate that vitrification conditions influence the integrity and potentials of follicles. The lower birth rates observed in the current study could indicate interferences on follicle maturation by vitrification method utilized here, for which further studies may be needed for improvement of vitrification protocol.

In monkeys, vitrified-warmed ovarian tissues were transplanted into the mesosalpinx and the omentum which were shown to be suitable sites for engraftment in our previous study [11]. Heterotopic transplantation was conducted with minced or strip grafts, but the type of graft did not affect oocyte collection. Grafts were wrapped with the omentum tissue, while they were put into a pouch by incision made in the mesosalpinx. These procedures made harvesting easier. Six follicles formed in grafts transplanted to the mesosalpinx and eight follicles were obtained after transplantation to the omentum (with no difference in follicle formation between the two sites). The ovarian cycle was restored after transplantation in most animals, while there were developments of pre-ovulatory follicles and mature oocytes which could fertilize after ICSI. Our study thus demonstrated the mesosalpinx and the omentum as viable options for transplantation of cryopreserved ovarian tissues which would be clinically available for those patients with bilateral ovariectomy or pelvic irradiation.

Multiple follicles were observed in both transplantation sites of the mesosalpinx and the omentum. Some are more mature or immature than others among these follicles. Therefore, the mechanism for selection of a dominant follicle could have been lost by the vitrification process. On the other hand, since the present study was performed by the IVF cycle, it is not apparent if the dominant follicle selection mechanism is preserved. Even in clinics, oocytes can be obtained from smaller follicles rather than the dominant follicle. As many follicles develop at one transplantation site due to ovarian stimulation by FSH, we tried to harvest as many oocytes as can be identified, thus resulting in the harvest of more immature oocytes. Thus, the number of follicles which could yield competent oocytes could have been very limited, even in the presence of cyclic steroid hormone production.

When oocytes were retrieved from transplanted vitrified-warmed ovarian tissues of monkeys after the return of the hormonal cycle, embryos did not develop after fertilization in vitro. Could the failure of embryogenesis be caused by injuries/damages during cryopreservation process? When murine ovarian tissues were processed for cryopreservation by different vitrification methods, transmission electron microscopy demonstrated varying degrees of damages in subcellular structures even in the presence of apparently normal delivery of pups [16]. Using

both murine and human tissues, changes in follicle morphology, particularly in granulosa and stromal cells, were seen after cryopreservation [5]. In ovarian tissue cryopreservation, stromal cells were demonstrated to be more vulnerable to cryoinjuries than primordial follicles [23, 24]. The ovary includes heterogenous cellular and structural components with different properties, and their interactions are needed for follicle maturation and embryogenesis [25]. Apparent structural integrity of ovarian tissue after cryopreservation does not appear to guaranty the quality and function of follicles. It might be informative to analyze effects of cryopreservation on gene expression pattern of oocytes, stromal cells, etc. during maturation for establishing a standard procedure of ovarian tissue cryopreservation.

One of the six monkeys monitored for more than 1 year after transplantation showed a weak response to ovarian stimulation, but its estradiol level was still restored. It is possible that engraftment of ovarian tissue might have been poor in this animal. Among the monkeys monitored for less than 1 year after transplantation, one did not show stable recovery of the hormonal cycle by 8 months after transplantation, although it is possible that the hormonal cycle would have resumed if the follow-up period had been extended. Recovery of the hormonal cycle was confirmed in five of six monkeys, with menstruation returning between 50 and 90 days after transplantation. The time required for recovery of menstruation was shorter than that expected for growth of primordial follicles, indicating the presence of primary and secondary follicles in vitrified ovarian tissues as well as primordial follicles. In three of these monkeys, the hormonal cycle has persisted for over 1200 days since resumption after transplantation.

In conclusion, a closed vitrification procedure was developed to improve the efficacy for ovarian cryopreservation and to avoid the risk of cross-contamination during storage in liquid nitrogen. Live birth was achieved in mice, but our results were unsatisfactory in terms of fertilization and embryo development in primates. This outcome may have occurred because follicle development was only monitored by blood tests and might not have been fully matured. On the other hand, vitrification procedure may have caused damages to cellular structures and genetic activities interfering developmental processes in primates. As we confirmed persistence of the hormonal cycle for longer than 1 year, we are confident that heterotopic engraftment of ovarian tissue was successful. We hope that our closed device will help advance the vitrification technology for clinical application.

Acknowledgments We thank Dr. Ikko Kawashima for support with IVM/IVF; Ms. Ami Amou for cryopreserving and thawing of ovarian tissues; Ms. Asami Onimal for the support in conducting the histological examinations; Tomohiro Noguchi, M.S. (Kitazato Co., Ltd., Shizuoka, Japan) for supplying the devices and solutions and for allowing us to conduct thermal conductivity measurements; Kaken Pharmaceutical Co., Ltd., Tokyo, Japan for supplying Seprafilm; and Dr. David Robert McQuire (Yamada Translation Bureau, Tokyo, Japan) for assistance with manuscript editing.

Author's contribution Y.S., Y.M., A.T., and N.S. participated in the study conception and design; Y.S., A.U., M.N., S.H., and N.S. developed the device; N.O. and M.N. performed mouse studies; Y.S. and M.N. completed freeze–thawing of ovarian tissue in the monkey study; Y.S., N.S., C.N., and S.I. performed surgery on the monkeys; S.O. and M.T. performed ovarian stimulation and management in the monkeys; T.Y. performed collection of monkey oocytes and IVM/IVF; and Y.S. and T.S. conducted histological examination.

Funding This study was funded by grant no. AS2522901P, Adaptable and Seamless Technology transfer Program through target driven R&D (A-STEP), and no. 16gk0110014h0001, Japan Agency for Medical Research and Development (AMED).

Compliance with ethical standards

Conflict of interest The authors declare that they have no conflicts of interest.

References

1. Oktay K, Karlikaya G. Ovarian function after transplantation of frozen, banked autologous ovarian tissue. N Engl J Med. 2000;342(25):1919.
2. Donnez J, Dolmans MM. Fertility preservation in women. NEJM. 2017;377:1658–65.
3. von Wolff M, Dittrich R, Liebenthron J, Nawroth F, Schüring AN, Bruckner T, et al. Fertility-preservation counselling and treatment for medical reasons: data from a multinational network of over 5000 women. Reprod BioMed Online. 2015;31:605–12.
4. Amorim CA, Curaba M, Van Langendonckt A, Dolmans MM, Donnez J. Vitrification as an alternative means of cryopreserving ovarian tissue. Reprod BioMed Online. 2011;23:160–86.
5. Wang Y, Xiao Z, Li L, Fan W, Li SW. Novel needle immersed vitrification: a practical and convenient method with potential advantages in mouse and human ovarian tissue cryopreservation. Hum Reprod. 2008;23:2256–65.
6. Keros V, Xella S, Hultenby K, Pettersson K, Sheikhi M, Volpe A, et al. Vitrification versus controlled-rate freezing in cryopreservation of human ovarian tissue. Hum Reprod. 2009;24:1670–83.
7. Amorim CA, Dolmans MM, David A, Jaeger J, Vanacker J, Camboni A, et al. Vitrification and xenografting of human ovarian tissue. Fertil Steril. 2012;98:1291–8.e1–2.
8. Herraiz S, Novella-Maestre E, Rodríguez B, Díaz C, Sánchez-Serrano M, Mirabet V, et al. Improving ovarian tissue cryopreservation for oncologic patients: slow freezing versus vitrification, effect of different procedures and devices. Fertil Steril. 2014;101:775–84.
9. Kagawa N, Silber S, Kuwayama M. Successful vitrification of bovine and human ovarian tissue. Reprod BioMed Online. 2009;18:568–77.
10. Hashimoto S, Suzuki N, Yamanaka M, Hosoi Y, Ishizuka B, Morimoto Y. Effects of vitrification solutions and equilibration times on the morphology of cynomolgus ovarian tissues. Reprod BioMed Online. 2010;21:501–9.
11. Suzuki N, Hashimoto S, Igarashi S, Takae S, Yamanaka M, Yamochi T, et al. Assessment of long-term function of heterotopic transplants of vitrified ovarian tissue in cynomolgus monkeys. Hum Reprod. 2012;27:2420–9.
12. Fahy GM, MacFarhlane DR, Angell CA, Meyman HT. Vitrification as an approach to cryopreservation. Cryobiology. 1984;21:407–26.

13. Mazur P, Cole KW, Hall WH, Schreuders PD, Mahowald AP. Cryobiological preservation of Drosophila embryos. Science. 1992;258:1932–5.
14. Vajta G, Nagy ZP. Are programmable freezers still needed in the embryo laboratory? Review on vitrification. Reprod BioMed Online. 2006;12:779–96.
15. Migishima F, Suzuki-Migishima R, Song SY, Kuramochi T, Azuma S, Nishijima M, et al. Successful cryopreservation of mouse ovaries by vitrification. Biol Reprod. 2003;68:881–7.
16. Chen SU, Chien CL, Wu MY, Chen TH, Lai SM, Lin CW, et al. Novel direct cover vitrification for cryopreservation of ovarian tissues increases follicle viability and pregnancy capability in mice. Hum Reprod. 2006;21:2794–800.
17. Kawamura K, Cheng Y, Suzuki N, Deguchi M, Sato Y, Takae S, et al. Hippo signaling disruption and Akt stimulation of ovarian follicles for infertility treatment. Proc Natl Acad Sci U S A. 2013;110:17474–9.
18. Suzuki N, Yoshioka N, Takae S, Sugishita Y, Tamura M, Hashimoto S, et al. Successful fertility preservation following ovarian tissue vitrification in patients with primary ovarian insufficiency. Hum Reprod. 2015;30(3):608–15.
19. Bielanski A. The potential for animal and human germplasm contamination through assisted reproductive technologies. Trends Reprod Biol. 2006;2:13–36.
20. Bielanski A, Vajta G. Risk of contamination of germplasm during cryopreservation and cryobanking in IVF units. Hum Reprod. 2009;24:2457–67.
21. Sankai T, Terao K, Yanagimachi R, Cho F, Yoshikawa Y. Cryopreservation of spermatozoa from cynomolgus monkeys (Macaca fascicularis). J Reprod Fertil. 1994;101:273–8.
22. Wulff C, Wilson H, Wiegand SJ, Rudge JS, Fraser HM. Prevention of thecal angiogenesis, antral follicular growth, and ovulation in the primate by treatment with vascular endothelial growth factor trap R1R2. Endocrinology. 2002;7:2797–807.
23. Kim SS, Yang HW, Kang HG, Lee HH, Lee HC, Ko DS, et al. Quantitative assessment of ischemic tissue damage in ovarian cortical tissue with or without antioxidant (ascorbic acid) treatment. Fertil Steril. 2004;82:670–85.
24. Hreinsson J, Zhang P, Swahn ML, Hultenby K, Hovatta O. Cryopreservation of follicles in human ovarian cortical tissue. Comparison of serom and human serum albumin in the cryoprotectant solutions. Hum Reprod. 2003;11:2420–8.
25. Da Broi MG, Giorgi VSI, Wang F, Keefe DL, Albertini D, Navarro PA. Influence of follicular fluid and cumulus cells on oocyte quality: clinical implications. J Assist Reprod Genet. 2018;35(5):735–51.

Human Reproduction, Vol.33, No.2 pp. 303–310, 2018
Advanced Access publication on December 28, 2017 doi:10.1093/humrep/dex368

human reproduction

ORIGINAL ARTICLE *Reproductive endocrinology*

Aromatase inhibitor use during ovarian stimulation suppresses growth of uterine endometrial cancer in xenograft mouse model

Tai Kawahara[1], Naoki Okamoto[1], Seido Takae[1], Megumi Kashiwagi[1], Mariko Nakajima[1], Atsushi Uekawa[1], Junya Ito[2], Naomi Kashiwazaki[2], Yodo Sugishita[1], and Nao Suzuki[1,*]

[1]Department of Obstetrics and Gynecology, St. Marianna University School of Medicine, Sugao, Miyamae, Kawasaki, Kanagawa 216-8511, Japan [2]Laboratory of Animal Reproduction, School of Veterinary Medicine, Azabu University, Sagamihara 229-8501, Japan

*Correspondence address. Department of Obstetrics and Gynecology, St. Marianna University School of Medicine, Kawasaki, Kanagawa 216-8511, Japan. E-mail: nao@marianna-u.ac.jp

Submitted on June 13, 2017; resubmitted on November 14, 2017; accepted on December 4, 2017

STUDY QUESTION: Could aromatase inhibitors (AI) be used to reduce risks of uterine endometrial cancer growth or recurrence during ovarian stimulation?

SUMMARY ANSWER: In a xenograft mouse model of endometrial cancer, concomitant AI administration suppressed the growth of endometrial cancer during ovarian stimulation.

WHAT IS KNOWN ALREADY: Recurrence and mortality rates of estrogen receptor-positive early breast cancer are reduced by long-term AI administration. Concomitant AI use for ovarian stimulation in patients with breast cancer is recommended for reducing estrogen-related potential risks. However, the efficacy of concomitant AI use for estrogen receptor-positive endometrial cancer have not been demonstrated conclusively by clinical or experimental animal studies.

STUDY DESIGN, SIZE, DURATION: Forty nude mice xenografted with uterine endometrial cancer cells were allocated to four groups. Group 1: no ovarian stimulation (control). Group 2: ovarian stimulation. Group 3: AI administration + ovarian stimulation. Group 4: ovariectomy and ovarian stimulation. Tumor growth was evaluated during the 6-week treatment period.

PARTICIPANTS/MATERIALS, SETTING, METHODS: Ishikawa 3-H-12 uterine endometrial cancer cells (estrogen and progesterone receptors-positive) were transplanted into 6-week-old BALB/cSlc-nu/nu nude mice, followed by interventions 2 weeks later.

MAIN RESULTS AND THE ROLE OF CHANCE: Compared to ovarian stimulation alone (Group 2), significant suppressions of tumor growth were observed in other three groups (Groups 1, 3 and 4, all at $P < 0.05$) and correlated with estrogen levels. AI administration had no apparent impact on embryo development.

LIMITATIONS, REASONS FOR CAUTION: In this study, we examined the growth of endometrial cancer tumors using one endometrial cancer cell line. Clinical endometrial cancer or hyperplasia cells can have diverse origins and AI may not be effective against other cancer cell types.

WIDER IMPLICATIONS OF THE FINDINGS: Concomitant AI use may provide a chance for safer childbirth by for patients with endometrial cancer or hyperplasia.

STUDY FUNDING/CONPETING INTEREST(S): This study was supported by the Graduate Student Aid from the St. Marianna University School of Medicine. The authors declare no competing interests.

Key words: fertility preservation / endometrial cancer / ovarian stimulation / estrogen / aromatase inhibitor

© The Author(s) 2017. Published by Oxford University Press on behalf of the European Society of Human Reproduction and Embryology. All rights reserved.
For Permissions, please e-mail: journals.permissions@oup.com

Downloaded from https://academic.oup.com/humrep/article-abstract/33/2/303/4781342 by St.Marianna University School of Medicine Library user on 29 November 2019

Introduction

Uterine endometrial cancer is one of the very common types of cancer in women. In the USA, for example, there were 54 870 cases in 2015, including 10 170 deaths, and these numbers have been increasing in recent years (Siegel et al., 2015). The standard treatment for uterine endometrial cancer is the combination of surgery, chemotherapy and radiotherapy (Rutledge, 1974; Signorelli et al., 2009), but young patients with early stage cancer (equivalent to the International Federation of Gynecology and Obstetrics stage IA) or endometrial hyperplasia sometimes request consideration of fertility preservation. In countries where surrogate pregnancy is recognized, women can have children by surrogate pregnancy after total hysterectomy, including bilateral adnexectomy so long as the collection of oocytes is performed before surgery (Azim and Oktay, 2007). However, for patients who do not have the option of surrogate pregnancy, fertility preservation implies conception by patient's own uterus and is associated with higher risks. For those patients, endometrial curettage is initially performed to physically remove cancer or hyperplasia cells, followed by hormone therapy.

Uterine endometrial cancer is classified as the estrogen-dependent type I and estrogen-independent type II. The former represents more than 80% of cases, and its carcinogenesis is associated with estrogen (Setiawan et al., 2013). Progesterone therapy has been demonstrated as an effective treatment for type I uterine endometrial cancers (Kelley and Baker, 1961). When medroxyprogesterone acetate (MPA) was used for the treatment of endometrial cancer and atypical endometrial hyperplasia, the overall complete response (CR) rate was 67%, hence, treatment with MPA has become the standard approach for patients who choose not to undergo hysterectomy to preserve fertility potential (Ushijima et al., 2007).

In premenopausal women, estrogen is synthesized primarily in the ovaries. In postmenopausal women, the estrogen level decreases as ovarian function declines and estrogen production relies on synthesis from androgens in the adrenal glands by the enzymatic reaction of aromatase. Estrogen is also produced from androgens in the aromatase pathway through the interaction of tumors and interstitial cells (Takahashi-Shiga et al., 2009). Aromatase inhibitors (AI) inhibit the enzymatic activity of aromatase and thus suppresses estrogen biosynthesis.

Recurrence and mortality rates of estrogen receptor (ER)-positive early breast cancer are reduced by long-term AI administration, which is more effective than the selective ER modulator tamoxifen (Early Breast Cancer Trialists' Collaborative Group, 2015). Therefore, AI have been used as long-term hormone therapy for breast cancer.

Ovarian stimulation elevates blood estrogen to non-physiological levels for limited periods by promoting the development of oocytes. Although, the short-term rise of blood estrogen caused by ovarian stimulation has been reported not to increase the risk of developing breast cancer in general population (Venn et al., 1999; Silva Idos et al., 2009), co-administration of AI for ovarian stimulation in patients with breast cancer is recommended due to the potential risk of cancer recurrence (Reddy and Oktay, 2012; Oktay et al., 2015; Rodgers et al., 2017).

Concomitant AI use has been previously investigated for ovarian stimulation in patients with endometrial cancer for similar reasons (Azim and Oktay, 2007), however, reported cases are limited and surrogate pregnancy is recommended.

Given the lack of evidence, in this experimental animal study we aimed to investigate the efficacy and safety of concomitant AI use by evaluation of tumor growth and blood estrogen concentrations as well as ovulation, insemination and embryo maturation under the internal use of AI.

Materials and Methods

Ethical approval

This study was performed upon the approval by the Animal Experiment Review Committee of St. Marianna University School of Medicine.

Animals

Mice were kept at 23 ± 2°C with a humidity of, 55 ± 5% humidity, 12-h light and 12-h dark cycle, and constant ad libitum access to feed food and water.

AI administration for estrogen measurements

C57BL/6 J, 4-week-old, female mice (Japan SLC, Inc., Shizuoka, Japan) (N = 16) were divided into four groups. Using a gastric tube, the third-generation AI letrozole (Femara®; Novartis Pharmaceuticals, AG, East Hanover, NJ) was administered at 0, 2, 10 or 25 μg/kg for 3 consecutive days. On the second day of letrozole administration, 7 IU of pregnant mare serum gonadotropin (PMSG; ASKA Animal Health Co., Ltd., Tokyo, Japan) was intraperitoneally administered to induce follicular development.

Measurement of the serum estrogen concentration

Mice were euthanized using carbon dioxide (CO_2) 2 days after the administration of PMSG. The blood was collected from their hearts, and centrifuged for 5 min at 684 g at 4 °C in a 1.5-ml microtube. Supernatant serum was transferred to a 1.5-ml microtube and stored in a freezer. Serum 17β-estradiol (E2) concentrations were measured using an Estradiol EIA Kit (Cayman Chemical Co., Ltd, Ann Arbor, MI) in accordance with the manufacturer's protocol.

AI administration and ovarian stimulation

For four groups of C57BL/6 J, 4-week-old, female mice (N = 36), letrozole was orally administered at 0, 2, 10 or 25 μg/kg/day for 4 days. On Day 2 of the letrozole administration, 7 IU of PMSG was intraperitoneally administered to induce follicular development, and on Day 4, of the letrozole administration, 7 IU of hCG (ASKA Pharmaceutical Co., Ltd, Tokyo, Japan) was intraperitoneally administered to induce hyperovulation.

Harvesting cumulus oocyte complexes

Mice were euthanized 16 h after hCG administration, and cumulus oocyte complexes (COCs) were collected through an incision made in the ampulla of the Fallopian tube. Collected COCs were transferred to 100-μl TYH (LSI Medience Corp., Tokyo, Japan) culture drops covered with mineral oil (Irvine Scientific, Santa Ana, CA), and then cultured at 37°C under 5% CO_2 in air until insemination. Fertilized oocytes and embryos were cultured in the KSOM-AA medium (Merck Millipore Corp., Billerica, MA).

Downloaded from https://academic.oup.com/humrep/article-abstract/33/2/303/4781342 by St.Marianna University School of Medicine Library user on 29 November 2019

Sperm collection and pre-culture

Caudal parts of the epididymis were collected from 8-week-old to 12-week-old, male C57BL/6J mice, and washed with the M16 culture medium (Global Stem, Rockville, MD). Blood and fat were removed on filter paper, and the sperm mass was collected from the tip of the caudal parts of the epididymis using a 23-G syringe needle. Then the collected sperm mass was submerged in 500 μl of the TYH medium in a 1.5-ml microtube and pre-cultured at 37°C and 5% CO_2 in air.

IVF and embryo culture

A 10-μl pre-cultured sperm was collected from the upper layer, and transferred to a TYH culture drop containing COCs and kept at 37°C under 5% CO_2 for 5–6 h to facilitate fertilization. After fertilization, ova were recovered from the TYH culture drops, transferred to drops of the KSOM medium, and cultured at 37°C, under 5% CO_2 in air. After culture for 16 h, two-cell embryos were transferred to fresh KSOM medium drops, and cultured at 37°C under 5% CO_2 to observing development up to the blastocyst stage.

Preparation and hematoxylin–eosin staining of mouse ovary tissue sections

Collected mouse ovaries were submerged in Bouin's solution (Wako Pure Chemical Industries, Ltd., Osaka, Japan) for 24 h at 4°C and saturated with paraffin by sequentially submerging them in the following: 70% *v/v* ethanol at room temperature for 1 h, 90% *v/v* ethanol at room temperature for 1 h, 100% ethanol at room temperature for 30 min, xylene at room temperature for 30 min, a mixture of paraffin and xylene at 65°C for 24 h, and paraffin at 65°C. Sequential 6-μm thick sections were prepared. Next, the paraffin sections were melted at 65°C, followed by deparaffinization with xylene, 100% ethanol, 90% *v/v* ethanol and 70% *v/v* ethanol. Tissue sections were stained with hematoxylin–eosin (HE), mounted, dried and evaluated.

Histological evaluation of ovaries

Histological evaluation of ovarian tissues was performed after HE staining. In ovaries collected during ovum collection and IVF, numbers of luteinized unruptured follicles (LUFs) were counted to evaluate any effects on the numbers of oocytes ovulated. Only nucleated ova were counted to avoid double counting.

Xenografting

The Ishikawa 3-H-12 cell line (National Research and Development Foundation JCRB Cell Bank, Osaka, Japan) (Nishida *et al.*, 1996), a cell strain expressing ER and progesterone receptor (PR), was used. Cells were cultured in minimum essential medium (Gibco Earle's salts$^+$ and L-glutamine; Thermo Fisher Scientific, Inc., Waltham, MA), with 15% w/v fetal bovine serum (Bovogen Biologicals Pty., Ltd, East Keilor, Australia) and 1% *w/v* Gibco Antibiotic–Antimycotic (Thermo Fisher Scientific, Inc., Waltham, MA). BALB/cSlc-nu/nu nude, 6-week-old, female mice (Japan SLC, Inc., Shizuoka, Japan) ($N = 40$) were used. We subcutaneously transplanted 1.0×10^7 Ishikawa 3-H-12 cells in the center of the mice's back using a 1-ml syringe with a 21-G syringe needle. Transplantation sites were monitored for 2 weeks to confirm grafting of the tumor. Four groups of 10 mice each were assigned to the following treatments.

Schedule for ovarian stimulation and AI administration

Group 1: Control group (no ovarian stimulation)
No drug administration after transplantation (oral and intraperitoneal injections of the physiological saline).

Group 2: Ovarian stimulation group
Starting 2 weeks after transplantation, intraperitoneal administrations of PMSG and hCG, once per week for 6 weeks.

Group 3: Ovarian stimulation + letrozole group
Oral daily administration of letrozole.
Starting 2 weeks after transplantation, intraperitoneal administrations of PMSG and hCG once per week for 6 weeks.

Group 4: Ovariectomy + ovarian stimulation group
Bilateral ovariectomy was performed 2 weeks after transplantation.
Starting 2 weeks after transplantation, intraperitoneal administrations of PMSG and hCG, once per week for 6 weeks.

For ovarian stimulation, follicular development was induced by intraperitoneal injection of 7-IU PMSG (ASKA Animal Health Co., Ltd). Hyperovulation was induced 2 days later by an intraperitoneal injection of 7-IU hCG (ASKA Animal Health Co.). Femara® (2.5-mg tablet; Novartis Pharmaceuticals, AG) was pulverized using a mortar and pestle and dissolved in sterilized water. A 25 μg/kg was administered orally using a gastric tube.

Sizes of subcutaneous tumors were measured weekly using a caliper with a vernier dial, and measurements in mm^3 (length × width × height) were recorded. On Day 4 of the sixth week after starting ovarian stimulation, mice were euthanized 2 days after PMSG administration using CO_2, tumors were excised, and bloods samples were collected.

Tumor evaluation and measurement of blood E2 concentration

(i) After euthanasia of mice using CO_2, blood was collected from their hearts, and the blood 17β-estradiol level was measured using the Estradiol EIA Kit (Cayman Chemical Co.).
(ii) Tumors on body surfaces were photographed.
(iii) Tumors were excised, photographed and weighed.
(iv) Each excised tumor was cut into at least four pieces. Two pieces were placed in a 1.5-ml microtube and then stored at −80°C. *ERα* and *ERβ* expression levels of each tumor tissue were measured by reverse transcription real-time polymerase chain reaction (RT-rPCR).
(v) Half of the remaining pieces were fixed using the Bouin solution, followed by HE staining.
(vi) Remaining pieces were fixed using a neutral formalin solution, followed by Ki67 staining.

Statistical analysis

Results are expressed as the mean ± standard error of the mean. The effects of treatment were compared among the groups using one-way analysis of variance with the post-hoc Tukey honestly significant difference test. Differences were considered significant if P was < 0.05. All analyses were computed using SAS JMP Pro 12.2.0 (SAS Institute Inc., Cary, NC).

Results

Reduction of blood E2 level by letrozole

The effect of AI on the blood estrogen concentration was examined using letrozole. Increasing concentrations of letrozole were administered orally for 3 days in C57BL/6J, female, 4-week-old mice ($N = 16$). The blood E2 concentration decreased from 29.0 ± 6.0 pg/ml to 25 ± 2.7, 11.4 ± 4.4 and 0.71 ± 0.4 pg/ml dose dependently with increasing concentrations of 2, 10 and 25 μg/kg of letrozole, respectively (Fig. 1). Significant decreases were obtained by 10 and 25 μg/kg of letrozole ($P < 0.05$).

Downloaded from https://academic.oup.com/humrep/article-abstract/33/2/303/4781342 by St.Marianna University School of Medicine Library user on 29 November 2019

Ovarian stimulation and letrozole administration

The effect of reduced E2 levels due to letrozole administration on superovulation for IVF was investigated. C57BL/6 J, female, 4-week-old mice ($N = 36$) were divided into four groups that received 0, 2, 10 or 25 μg/kg of letrozole orally.

The numbers of retrieved oocytes in the 0, 2, 10 and 25-μg/kg letrozole groups were 48 ± 2.8, 50 ± 1.8, 39 ± 2.7 and 36 ± 4.1, respectively. Therefore, retrieved oocytes were significantly fewer in the 25-μg/kg group than in the control group ($P < 0.05$; Fig. 2A). Fertilization rates were 79.9 ± 3.6%, 80.6 ± 4.1%, 74.7 ± 8.9% and 69.4 ± 5.3%, respectively, in the 0, 2, 10 and 25 μg/kg groups with no significant differences ($P > 0.05$; Fig. 2B). Blastocyst achievement rates were 94.7 ± 1.3%, 97.0 ± 1.3%, 90.6 ± 3.9% and 89.5 ± 3.6%, respectively, in the 0, 2, 10 and 25-μg/kg groups, demonstrating no significant differences ($P > 0.05$; Fig. 2C). Numbers of LUFs in ovarian tissue sections at the time of IVF were 5 ± 1.5, 3 ± 0.9, 2 ± 0.3 and 4 ± 0.9, respectively, in the 0, 2, 10 and 25-μg/kg letrozole groups. No correlation was observed between LUFs numbers and AI dose ($P > 0.05$; Fig. 2D).

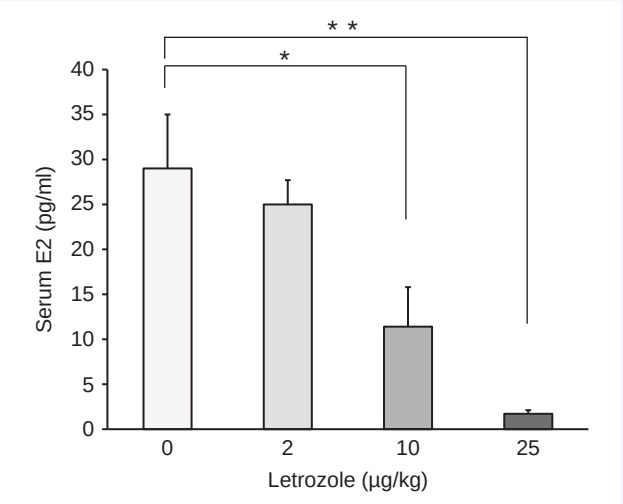

Figure 1 Effect of letrozole (aromatase inhibitor) on serum estrogen (E2) concentrations. Mice were divided into four groups according to the doses of letrozole (0, 2, 10 and 25 μg/kg). Letrozole was given orally for 3 days. A 7 IU of pregnant mare serum gonadotropin (PMSG) was given i.p., 2 days after the letrozole administration. All mice were sacrificed 2 days after PMSG administration, and E2 concentrations in sera were measured. *$P < 0.05$ versus the control.

Suppression of uterine endometrial cancer growth by letrozole

Ishikawa 3-H-12 cells (1×10^7) were transplanted subcutaneously in the back of BALB/cSlc-nu/nu mice. After 2 weeks, 40 mice were divided into four groups and treated as described in Fig. 3. Tumor size increased significantly in the ovarian stimulation group compared to the control group and was reduced by letrozole administration (Fig. 4). The blood E2 concentration, similar to the result with female C57BL/6 J mice (Fig. 1), was significantly lower in the letrozole and ovariectomy groups than in the ovarian stimulation group in BALB/cSlc-nu/nu mice ($P < 0.05$; Fig. 5A). As measured by RT-rPCR, the *ERα* messenger RNA expression level in tumor tissue was significantly higher in the ovarian stimulation group than in the other three groups ($P < 0.05$, Fig. 5B). No significant differences in the *ERβ* expression level were found between any of the four groups ($P > 0.05$, Fig. 5B).

Tumor tissues in all groups, after HE staining, showed characteristics of endometrial adenocarcinoma, including the formation of ductal structures, nuclear stratification with mild atypia, and cribriform pattern in the periductal region (Fig. 6A). In addition, Ki67 staining-positive cells were found in all groups (Fig. 6B).

Discussion

The present study demonstrated that the growth of endometrial cancer cells was promoted during ovarian stimulation and suppressed by letrozole in correlation with blood estrogen levels.

In general, long-term exposure to unopposed estrogen increases the incidence of endometrial cancer (Weiderpass *et al.*, 1999). On the other hand, no increase in the incidence of hormone-sensitive tumors due to ovarian stimulation has been reported in the general population (Venn *et al.*, 1999; Silva Idos *et al.*, 2009). This is because

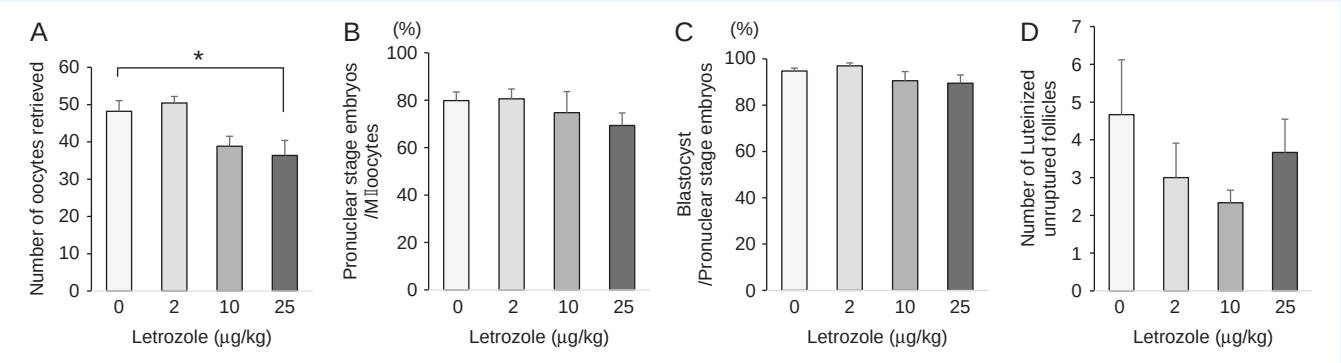

Figure 2 Efficacy of letrozole on fertility and embryogenesis. The aromatase inhibitor (AI) was administered orally at 0, 2, 10 and 25 μg/kg for 4 days. Pregnant mare serum gonadotropin and human chorionic gonadotropin were administered at seven IU/mouse intraperitoneally on Days 2 and 4, respectively, after AI administration. IVF was performed on Day 5 after AI administration. *$P < 0.05$ versus the control.

Downloaded from https://academic.oup.com/humrep/article-abstract/33/2/303/4781342 by St.Marianna University School of Medicine Library user on 29 November 2019

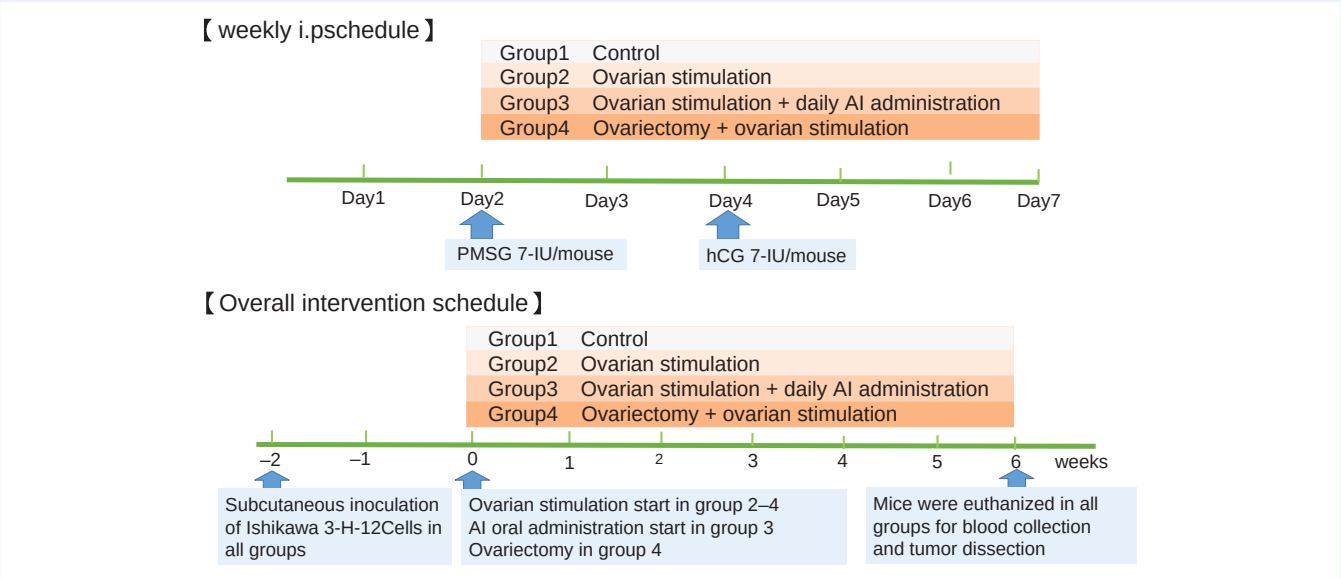

Figure 3 Experimental schedules of treatments started 2 weeks after tumor xenografting in all four groups. Group 1: no treatment; group 2: weekly intraperitoneal injections of 7 IU/mouse of pregnant mare serum gonadotropin, followed by intraperitoneal injections of 7 IU/mouse hCG 2 days later; Group 3: ovarian stimulation with daily oral administration of 25 μg/kg of the aromatase inhibitor; and Group 4: ovariectomy and ovarian stimulation 2 weeks after xenograft placement.

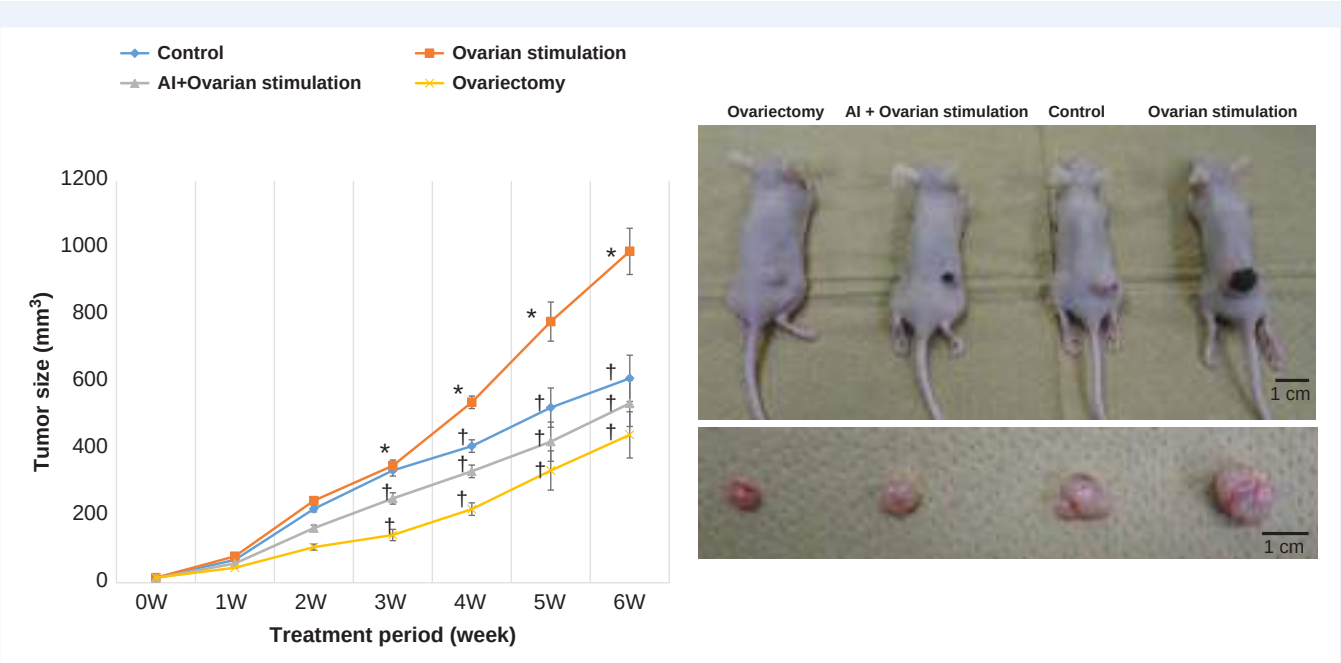

Figure 4 Tumor growth after xenografting. Endometrial cancer cells (Ishikawa 3-H-12) were xenografted subcutaneously in the back of nude mice, as described in Fig. 3. Tumor sizes were measured weekly. *A significant difference between the ovarian stimulation group and each of three other groups (marked by †) for the same weeks ($P < 0.05$).

the development of cancer is a long-term process in which mutations accumulate in genes such as tumor suppressor genes and mismatch repair genes while endometrial cells repeat cell divisions under stimulation by estrogen (Banno *et al.*, 2014). On the other hand, the increase in blood estrogen levels due to ovarian stimulation and accompanying follicular development is usually a temporary environmental change.

This study was undertaken to examine whether a short-term increase in blood estrogen concentrations contributes to the proliferation of a small number of established endometrial cancer cells, as predicted from

Downloaded from https://academic.oup.com/humrep/article-abstract/33/2/303/4781342 by St.Marianna University School of Medicine Library user on 29 November 2019

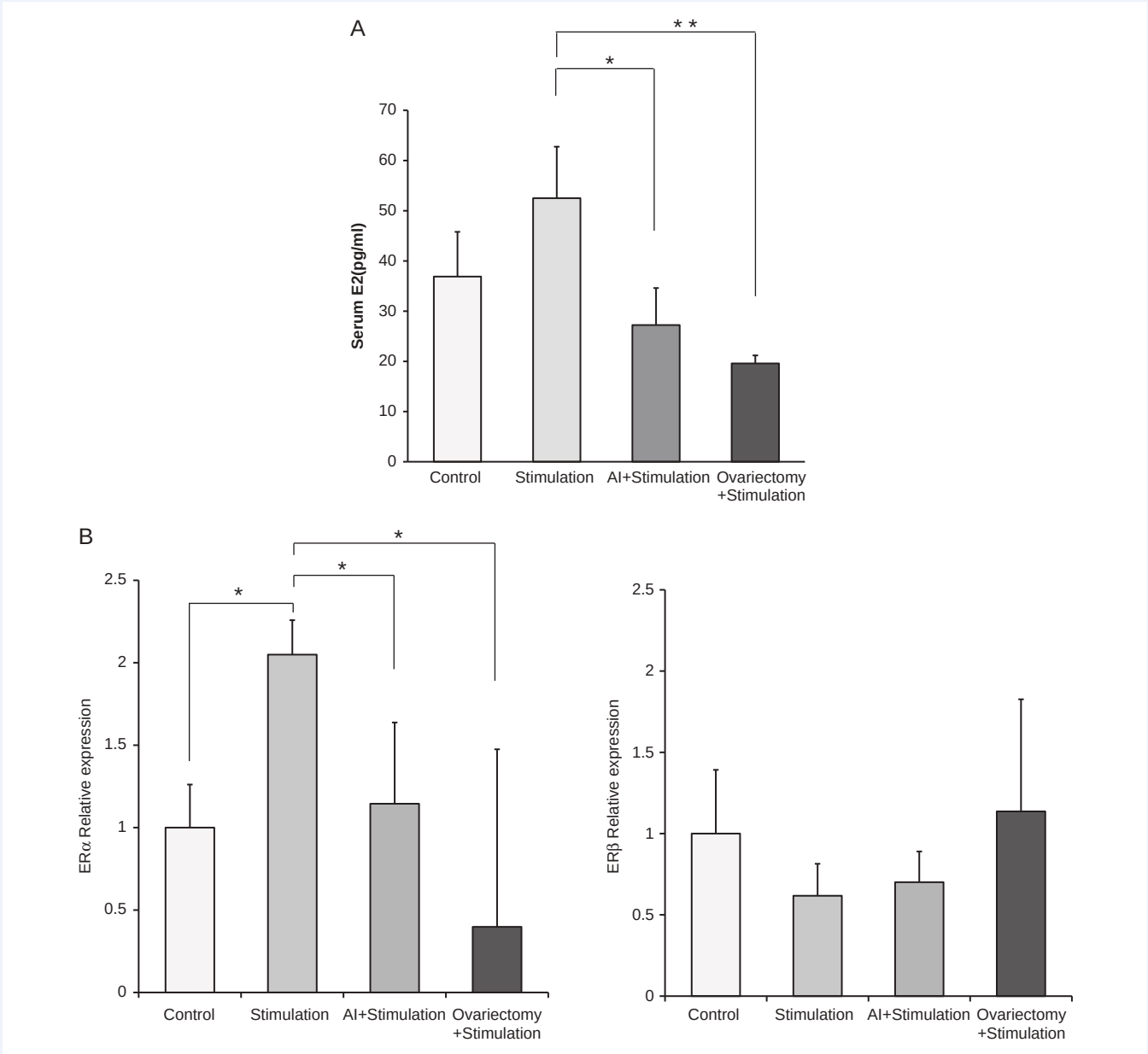

Figure 5 (**A**) Estrogen (E2) concentrations after 6-week intervention. Blood E2 concentrations in the plasma were measured by enzyme-linked immunosorbent assay. *$P < 0.05$ versus the stimulation group. (**B**) Expression levels of estrogen receptor (ER) α and β. mRNAs were measured by reverse transcription real-time polymerase chain reaction. *$P < 0.05$ versus the stimulation group.

past xenograft experiments (Clarke and Satyaswaroop, 1985). As it is difficult to reproduce residual endometrial cancer cells remaining in the uterus after endometrial curettage and MPA therapy in animal experiments, risks of clinical recurrence were approximately evaluated by implanting a small number of tumor cells subcutaneously in nude mouse and observing proliferation of these tumor cells. In the present study, we demonstrated that ovarian stimulation as a risk factor for endometrial cancer growth or recurrence and that the AI use is beneficial during ovarian stimulation against hormone-sensitive endometrial cancer growth.

Letrozole reduced the blood E2 concentration dose dependently (Fig. 1), without apparent effects on embryo development (Fig. 2C). However, the oocyte yield decreased at the highest dose of letrozole in the 25 μg/kg group as compared to the control group (Fig. 2A). Since no correlation was observed between LUF number and AI doses (Fig. 2D), the decrease in the number of oocytes retrieved did not appear to be due to dysfunction in ovulation; instead it appeared to be caused by effects on the maturation process of oocytes. In clinical practice, trigger timing by hCG or gonadotropin-releasing hormone agonist is determined by measuring the diameter of leading follicles. Since it was difficult to measure follicle sizes in mouse experiments, our experimental protocol, in which the same dose of hCG was administered 48 h after PMSG administration in all groups, may have affected the number of oocytes yielded. Since no significant decreases in oocyte yields nor risks on embryogenesis have been reported with

Downloaded from https://academic.oup.com/humrep/article-abstract/33/2/303/4781342 by St.Marianna University School of Medicine Library user on 29 November 2019

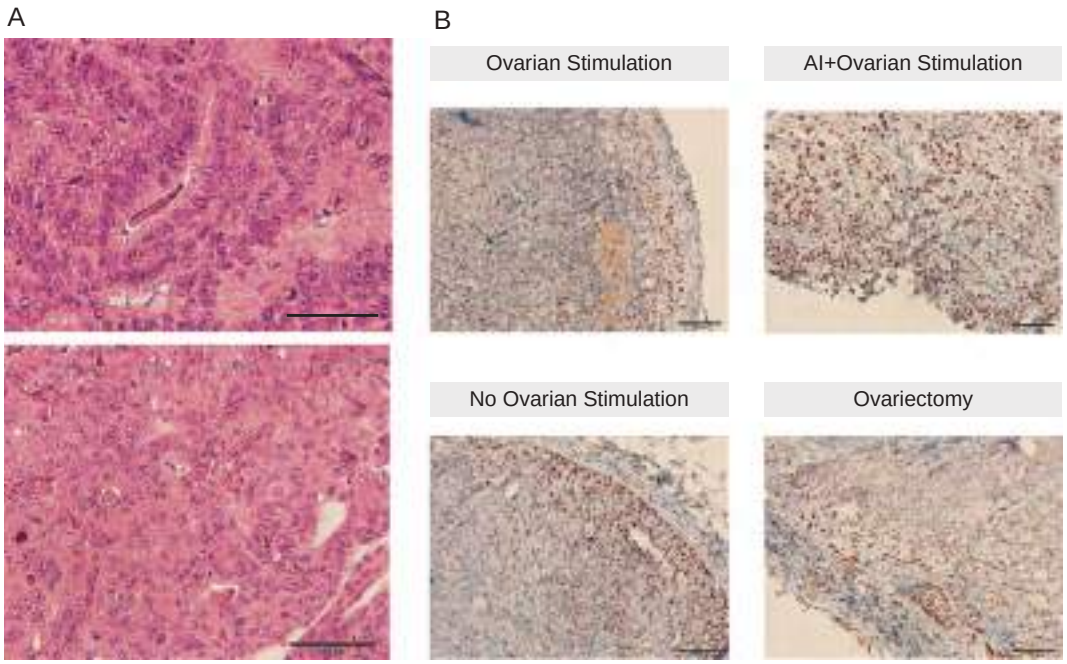

Figure 6 Histological analyses of Ishikawa 3-H-12 tumors. (**A**) Typical hematoxylin–eosin staining of uterine endometrial cancer seen in all groups. Scale bars, 100 μm. (**B**) Ki67 positive cells in all groups.

AI administration in clinical studies (Oktay *et al.*, 2005; Tulandi *et al.*, 2006; Lee and Oktay, 2012; Rodgers *et al.*,2017), this could be due to the use of prolific animals such as mice. Although further studies are required for the impact of high dose AI uses on folliculogenesis, AI appears not to have serious effects on the fertilization or embryo development.

Based on the present study, *ER α* expression, was highest in the ovarian stimulation group than in the other three groups (Fig. 5B), which is consistent with a previous report that E2 acts on ER α, inducing *c-Fos* expression and thus cell proliferation (Vivacqua *et al.*, 2006). The proliferative and prognostic indicator Ki67 staining did not change significantly in the present study (Fig. 6B), although it was previously shown to correlate with the suppression of endometrial cancer growth by neoadjuvant anastrozole treatment (Thangavelu *et al.*, 2013). Loci that showed strong Ki67-staining were uneven in all tumors, indicating complexities of tumors where proliferation and necrosis occurred even in the same tumor mass and which could have caused Ki67 staining irrespective of proliferation rates.

Previous reports on the therapeutic effect of AI against endometrial cancer are unclear. A phase II clinical study, in which 23 patients with recurrent uterine endometrial cancers were treated by the administration of anastrozole (a third-generation AI) showed minimal therapeutic effect (Rose *et al.*,2000). In another study of 28 postmenopausal women with advanced or recurrent uterine endometrial cancer treated with letrozole, the overall response rate was 9.4% and the authors concluded that letrozole was well tolerated but had little overall activity (Ma *et al.*, 2014). Recently, researchers reported that AI was effective against low-grade endometrial cancer after failure with progesterone treatment in three cases (Straubhar *et al.*, 2017). These reports indicate that AI may have therapeutic effect only for a limited number of ER-positive endometrial cancer cases, suggesting the diverse developmental mechanisms of endometrial cancer.

As our results are based on one type of endometrial cancer cell line, we cannot conclude that the concomitant AI use is effective for fertility preservation treatment of all endometrial cancer or hyperplasia patients, since it is currently not possible to fully identify the nature of the tumor in each case.

Since fertility preservation treatments for endometrial cancer or hyperplasia with atypia involve potential major risks which cannot be ignored, concomitant AI use during ovarian stimulation is worth considering to minimize those risks. In fact, there were cases in our institution in which endometrial cancer recurred after the ovarian stimulation during MPA therapy, resulting in patient death, although the causal relationship is unknown. Our research is motivated by these difficult experiences.

We focused on the ovarian stimulation in this study, but the influence of estrogen rise during pregnancy period on endometrial cancer or hyperplasia is also controversial. Regarding this point, the rise of progesterone and so-called healthy mother effect should be also taken into consideration (Valachis *et al.*, 2010).

Conclusion

Ovarian stimulation is a potential option for fertility preservation in reproductive age women with low-grade endometrial cancer or endometrial hyperplasia. It is however associated with risks of their recurrence or growth which can be mitigated by the concomitant AI use by decreasing serum estrogen concentrations.

Downloaded from https://academic.oup.com/humrep/article-abstract/33/2/303/4781342 by St.Marianna University School of Medicine Library user on 29 November 2019

Acknowledgements

We thank Dr Koko Murakami of New York Medical College for critically reading the article.

Authors' roles

N.S., S.T., Y.S., J.I. and N.K. designed the study. T.K., N.O., M.K., M.N. and A.U. conducted the experiments. T.K. wrote the article. T.K. and A.U. performed the statistical analysis. S.T., Y.S. and N.S. participated in the critical discussion and article editing.

Funding

This work was supported by the Graduate Student Aid from the St. Marianna University School of Medicine.

Conflict of interest

The authors declare no conflict of interest.

References

Azim A, Oktay K. Letrozole for ovulation induction and fertility preservation by embryo cryopreservation in young women with endometrial carcinoma. *Fertil Steril* 2007;**88**:657–664.

Banno K, Yanokura M, Iida M, Masuda K, Aoki D. Carcinogenic mechanisms of endometrial cancer: involvement of genetics and epigenetics. *J Obstet Gynaecol Res* 2014;**40**:1957–1967.

Clarke C, Satyaswaroop P. Photoaffinity labeling of the progesterone receptor from human endometrial carcinoma. *Cancer Res* 1985;**45**: 5417–5420.

Early Breast Cancer Trialists' Collaborative Group. Aromatase inhibitors versus tamoxifen in early breast cancer: patient-level meta-analysis of the randomised trials. *Lancet* 2015;**386**:1341–1352.

Kelley RM, Baker WH. Progestational agents in the treatment of carcinoma of the endometrium. *N Engl J Med* 1961;**264**:216–222.

Lee S, Oktay K. Does higher starting dose of FSH stimulation with letrozole improve fertility preservation outcomes in women with breast cancer? *Fertil Steril* 2012;**98**:961–964.

Ma BB, Oza A, Eisenhauer E, Stanimir G, Carey M, Chapman W, Latta E, Sidhu K, Powers J, Walsh W *et al*. The activity of letrozole in patients with advanced or recurrent endometrial cancer and correlation with biological markers—a study of the National Cancer Institute of Canada Clinical Trials Group. *Int J Gynecol Cancer* 2014;**4**:650–658.

Nishida M, Kasahara K, Oki A, Satoh T, Arai Y, Kubo T. Establishment of eighteen clones of Ishikawa cells. *Hum Cell* 1996;**9**:109–116.

Oktay K, Buyuk E, Libertella N, Akar M, Rosenwaks Z. Fertility preservation in breast cancer patients: a prospective controlled comparison of ovarian stimulation with tamoxifen and letrozole for embryo cryopreservation. *J Clin Oncol* 2005;**23**:4347–4353.

Oktay K, Turan V, Bedoschi G, Pacheco FS, Moy F. Fertility preservation success subsequent to concurrent aromatase inhibitor treatment and ovarian stimulation in women with breast cancer. *J Clin Oncol* 2015;**33**: 2424–2429.

Reddy J, Oktay K. Ovarian stimulation and fertility preservation with the use of aromatase inhibitors in women with breast cancer. *Fertil Steril* 2012;**98**:1363–1369.

Rodgers R, Reid G, Koch J, Deans R, Ledger W, Friedlander M, Abbott J. The safety and efficacy of controlled ovarian hyperstimulation for fertility preservation in women with early breast cancer: a systematic review. *Hum Reprod* 2017;**32**:1033–1045.

Rose PG, Brunetto VL, VanLe L, Bell J, Walker JL, Lee RB. A phase II trial of anastrozole in advanced recurrent or persistent endometrial carcinoma: a Gynecologic Oncology Group study. *Gynecol Oncol* 2000;**78**:212–216.

Rutledge F. The role of radical hysterectomy in adenocarcinoma of the endometrium. *Gynecol Oncol* 1974;**2**:331–347.

Setiawan V, Yang H, Pike M, McCann S, Yu H, Xiang Y, Wolk A, Wentzensen N, Weiss N, Webb P *et al*. Type I and II endometrial cancers: have they different risk factors? *J Clin Oncol* 2013;**31**:2607–2618.

Siegel RL, Miller KD, Jemal A. Cancer statistics. *CA Cancer J Clin 2015* 2015; **65**:5–29.

Signorelli M, Lissoni AA, Cormio G, Katsaros D, Pellegrino A, Selvaggi L, Ghezzi F, Scambia G, Zola P, Grassi R *et al*. Modified radical hysterectomy versus extrafascial hysterectomy in the treatment of stage I endometrial cancer: results from the ILIADE randomized study. *Ann Surg Oncol* 2009;**16**:3431–3441.

Silva Idos S, Wark I, McCormack A, Mayer A, Overton D, Little C, MacLean A. Ovulation-stimulation drugs and cancer risks: a long-term follow-up of a British cohort. *Br J Cancer* 2009;**100**:1824–1831.

Straubhar A, Soisson A, Dodson M, Simons E. Successful treatment of low-grade endometrial cancer in premenopausal women with an aromatase inhibitor after failure with oral or intrauterine progesterone. *Gynecol Oncol Rep* 2017;**21**:10–12.

Takahashi-Shiga N, Utsunomiya H, Miki Y, Nagase S, Kobayashi R, Matsumoto M, Niikura H, Ito K, Yaegashi N. Local biosynthesis of estrogen in human endometrial carcinoma through tumor-stromal cell interactions. *Clin Cancer Res* 2009;**15**:6028–6034.

Thangavelu A, Hewitt M, Quinton N, Duffy S. Neoadjuvant treatment of endometrial cancer using anastrozole: a randomised pilot study. *Gynecol Oncol* 2013;**131**:613–618.

Tulandi T, Martin J, Al-Fadhli R, Kabli N, Forman R, Hitkari J, Casper RF. Congenital malformations among 911 newborns conceived after infertility treatment with letrozole or clomiphene citrate. *Fertil Steril* 2006;**85**: 1761–1765.

Ushijima K, Yahata H, Yoshikawa H, Konishi I, Yasugi T, Saito T, Nakanishi T, Sasaki H, Saji F, Iwasaka T *et al*. Multicenter phase II study of fertility-sparing treatment with medroxyprogesterone acetate for endometrial carcinoma and atypical hyperplasia in young women. *J Clin Oncol* 2007; **25**:2798–2803.

Valachis A, Tsali L, Pesce LL, Polyzos NP, Dimitriadis C, Tsalis K, Mauri D. Safety of pregnancy after primary breast carcinoma in young women: a meta-analysis to overcome bias of healthy mother effect studies. *Obstet Gynecol Surv* 2010;**65**:786–793.

Venn A, Watson L, Bruinsma F, Giles G, Healy D. Risk of cancer after use of fertility drugs with in-vitro fertilisation. *Lancet* 1999;**354**:1586–1590.

Vivacqua A, Bonofiglio D, Recchia AG, Musti AM, Picard D, Andò S, Maggiolini M. The G protein-coupled receptor GPR30 mediates the proliferative effects induced by 17β-estradiol and hydroxytamoxifen in endometrial cancer cells. *Mol Endocrinol* 2006;**20**:631–646.

Weiderpass E, Adami H, Baron J, Magnusson C, Bergström R, Lindgren A, Persson I. Risk of endometrial cancer following estrogen replacement with and without progestins. *J Natl Cancer Inst* 1999;**91**:1131–1137.

Downloaded from https://academic.oup.com/humrep/article-abstract/33/2/303/4781342 by St.Marianna University School of Medicine Library user on 29 November 2019

Journal of Assisted Reproduction and Genetics (2019) 36:2251–2257
https://doi.org/10.1007/s10815-019-01599-3

FERTILITY PRESERVATION

Radiofrequency identification tag system improves the efficiency of closed vitrification for cryopreservation and thawing of bovine ovarian tissues

T. Sato[1] · Yodo Sugishita[1,4] · Y. Suzuki[1] · M. Kashiwagi[1] · S. Furuyama[1] · S. Nishimura[1] · A. Uekawa[1] · T. Koizumi[1] · M. Awaji[3] · T. Sawa[2] · A. Tozawa[1] · V. Komatsu[2] · Nao Suzuki[1]

Received: 18 April 2019 / Accepted: 26 September 2019 / Published online: 5 November 2019
© Springer Science+Business Media, LLC, part of Springer Nature 2019

Abstract

Purpose A radiofrequency identification (RFID) tag system was designed to streamline cryopreservation and thawing procedures. This study evaluated the usefulness of the RFID tag system for improving the efficiency of cryopreserving/thawing bovine ovarian tissue by the closed vitrification protocol.

Methods Six participants carried out closed vitrification and thawing of bovine ovarian tissues procedures using either the conventional or the new RFID tag method, and the time required to perform each step of the respective methods was measured. After normality of data was confirmed by the Shapiro-Wilk test, the significance of differences was assessed by the unpaired *t* test.

Results When closed vitrification was performed, the time required for each step showed a significant difference between the two methods ($t(4) = 2.938$, $p = 0.042$, $d = 2.40$), and the total cryopreservation time was 11 min shorter using the RFID tag system. When thawing was performed, the time required for each step also showed a significant difference between the two methods ($t(4) = 2.797$, $p = 0.049$, $d = 2.28$), and the total thawing time was 2 min shorter using the RFID tag system.

Conclusion The RFID tag system tested in this study seems to be suitable for managing biological samples stored in liquid nitrogen. Adoption of an RFID tag system by fertility centers may not only improve the efficiency of cryopreserving/thawing reproductive tissues but could also reduce human error.

Keywords Infertility treatment · Cryopreservation · Thawing · Ovarian tissue closed vitrification · Frozen samples · RFID tag · Storage system

Introduction

Advances in medical treatment have led to an increase of patients surviving cancer, resulting in more healthcare providers recognizing the importance of fertility preservation for cancer patients. It is important to offer cancer patients the option to preserve their reproductive tissues (oocytes, sperm, embryos, or ovaries) before initiation of treatment since many anticancer therapies reduce fertility [1–9]. Cryopreservation of reproductive tissues can be performed by fertility centers until a cancer survivor is ready to start a family, but storage time of the reproductive tissues may be as long as decades in the case of children with cancer [10]. Accordingly, meticulous management of the stored reproductive tissues from many patients over a prolonged period is required and this is a challenge for every fertility centers.

Conventional methods for managing cryopreserved tissues have several flaws. Since most steps in the cryopreservation process are carried out manually, human error can be a significant problem, as emphasized by several reported cases (Kagawa, Japan, in 2008, Singapore in 2010, and Rome, Italy, in 2013). In recent years, two-dimensional barcode

✉ Nao Suzuki
nao@marianna-u.ac.jp

1 Department of Obstetrics and Gynecology, St. Marianna University School of Medicine, 2-16-1 Sugao, Miyamae-ku, Kawasaki City, Kanagawa 216-8511, Japan

2 KRD Corporation, City, Yamato, Kanagawa 242-0007, Japan

3 Its Corporation, Kawasaki City, Kanagawa 211-0041, Japan

4 Department of Frontier Medicine Institute of Medical Science, St. Marianna University, School of Medicine, Kawasaki City, Kanagawa 216-8511, Japan

systems marketed by Merk or Oligio have improved the efficiency of managing cryopreserved tissues by minimizing manual data entry, but practical use of such systems is challenging for samples stored in liquid nitrogen (LN2) because frost forms on cryogenic vials and interferes with readability. Therefore, it is necessary to wipe the label dry before reading it with a reader, which leads to a risk of damaging the sample if its temperature rises to about − 135 °C. In addition, the current design of storage systems contributes to low efficiency in tracking and retrieving patient samples. The need for an efficient storage system that allows easy tracking/retrieval of cryopreserved tissues and reduces manual data entry has never been stronger in the fertility preservation field. We have designed a new storage system and a new device for preserving ovarian tissues that combines the use of two-dimensional barcode labels with radiofrequency identification (RFID) tags. The major advantages of using RFID tags are to eliminate manual data entry and allow readability when samples are stored in LN2. Patient information is transferred to the RFID tag from a computer, and by using an RFID reader, the same information can then be retrieved from the tag attached to sample devices that are stored in LN2. The new storage system has many sub-compartments for samples to maximize storage space in the LN2 tank. In the present study, we evaluated the influence of this RFID tag system on the efficiency of closed vitrification and thawing of bovine ovarian tissue.

Materials and methods

In total, 6 participants were asked to carry out the procedures of closed vitrification and thawing of bovine ovaries by either the conventional or the RFID tag method. Three participants were randomly selected by computer to perform the conventional method while the other 3 participants perform the RFID tagged method. Each participant processed 1 bovine ovary. The conventional method involved manual processing, while the RFID tag method employed a combination of two-dimensional barcode labels and RFID tag technology.

The following eight components were used in the RFID tag method:

1. Two-dimensional barcode label (Fig. 1A)

Both vertical and horizontal matrices are used in the barcode label, making it possible to read more information than provided by the original Universal Product Code. The code also has an error correction function that restores data if part of the code is missing.

2. RFID tags (Fig. 1B and C)

RFID uses electromagnetic radiation to wirelessly read and capture information stored in tags attached to objects. While a laser bar code scanner can only scan bar codes within direct view, an RFID reader can read multiple tags up to several feet away and does not need direct line-of-sight access to the tags. Another advantage of RFID is that it can identify tags in soiled or non-translucent bags. Each RFID tag stores data in the embedded IC chip and transmits data at a frequency of 13.56 MHz. We designed a round RFID tag (16 mm in diameter and 1 mm in thickness) for ovarian tissue cryopreservation devices by taking the size of the device and the data storage limit into consideration (Fig. 1B). Each device holds one ovarian tissue sample and the round RFID tag attached to the device can function after being stored in LN2 (− 196 °C). To prevent the slowing of the electrical circuit at low temperatures, which sometimes causes RFID tags to become unresponsive, we redesigned the circuit and improved the sensitivity of the tag. The RFID tag thus obtained was more sensitive and functioned better after storage in LN2 (Fig. 1C).

3. RFID reader (Fig. 1D)

The RFID reader uses radiofrequency waves to read information stored in the RFID tags. In our new RFID system, the antenna of the reader was modified to increase sensitivity for reading data from tags that had been stored in LN2. The modifications included lengthening the antenna, using copper wire, and increasing the magnetic field density by narrowing the antenna edge.

4. Device box (Fig. 1E)

The device box was made from SUS304 stainless steel containing chromium and nickel, with the metal inert gas welding method being used to seal any gaps so that the samples remained in LN2 after being taken out of the storage tank. Each cuboidal device box was designed to store up to 20 ovarian tissue cryopreservation devices from one patient, since an average of approximately 17 ovarian tissue samples are harvested per patient.

5. Storage box (Fig. 1F)

The storage box was also made from SUS304 stainless steel by spot welding and was large enough to contain 6 device boxes (120 cryopreservation devices with ovarian tissue samples from 6 patients).

6. Canister (Fig. 1G)

The cylindrical canister was used for the conventional method. Each canister could store samples from 4 patients. In the RFID tag system, each cuboidal canister had an

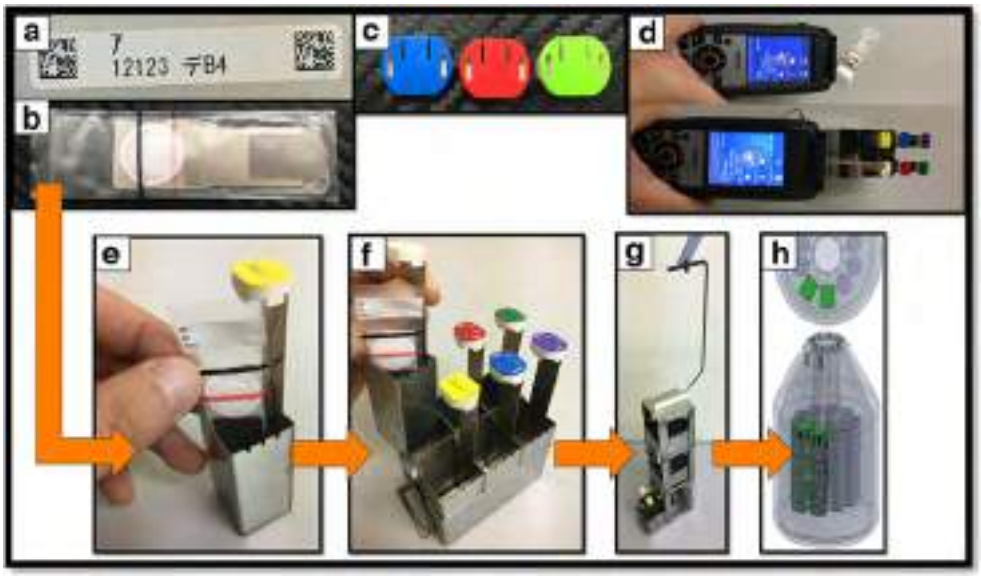

Fig. 1 The RFID tag system. (A) A two-dimensional barcode label. (B) An ovarian tissue cryopreservation device with a round RFID tag. (C) RFID tag for the device box. Tags of different colors are available for easy identification. (D) RFID reader (top). The reader shows patient information in the monitor (bottom). (E) Device box. Each device box holds 20 cryopreservation devices. (F) Storage box. Each storage box holds 6 device boxes. (G) Cuboidal canister. Each canister holds 3 storage boxes. (H) LN2 tank. Each tank holds 10 canisters

RFID tag attached to the handle and held 3 storage boxes, which could store up to 360 cryopreservation devices with ovarian tissues from 18 patients.

7. LN2 tank (Fig. 1H)

The tanks used in this study were the HC35 (Taylor Wharton) and KD32-10 LN2 (Kitazato). Each LN2 tank held 10 canisters storing samples from 40 patients (conventional method) or 180 patients (RFID tag method).

8. Computer

A computer was used to manage storage efficiently, with the computer screen showing the location of each RFID tag and indicating empty space in the tank.

9. Pretest

The Uchida-Kraepelin (U-K) test is a questionnaire that requires intense concentration by the participants and is used to assess mental agility, long-term attention, and recovery from fatigue. Each participant was asked to perform the U-K test prior to carry out the closed vitrification and thawing procedures. All participants achieved similar U-K test scores, indicating a similar ability to follow instructions irrespective of their professional background.

10. Steps in closed vitrification procedure

Conventional method (cryopreservation of bovine ovarian tissue; Fig. 2):

Step 1.The patient's hospital card was swiped through a card reader to obtain patient information. Then the patient information sheet (name, date of birth, hospital ID number, diagnosis, date of operation) was filled in manually.

Step 2.The resected ovary was placed in a cup filled with PBS and the cup was labeled (patient's name, hospital ID number, and date of birth).

Step 3.The same patient information was written on a Petri dish.

Step 4.The ovary was transferred from the cup to the Petri dish and cut into small pieces.

Step 5.Each ovarian tissue piece was assigned a number and photographed with the number.

Step 6.Patient information was written on 3 dishes containing graduated concentrations of cryoprotectant and the ovarian tissue samples were processed through the dishes.

Step 7.Each ovarian tissue sample was placed in a cryopreservation device (one per device). Then each device was placed in a plastic pouch and patient information (name, hospital ID number, date of birth, and ovarian tissue sample number) was written on the pouch.

Step 8.The labeled device was placed in a metal holder and successively into a canister and LN2 tank.

RFID tag method (cryopreservation of bovine ovarian tissue; Fig. 2):

Step 1.The patient's hospital card was swiped through a card reader to print out two-dimensional barcode labels with patient information (name, hospital ID number, and date of birth).

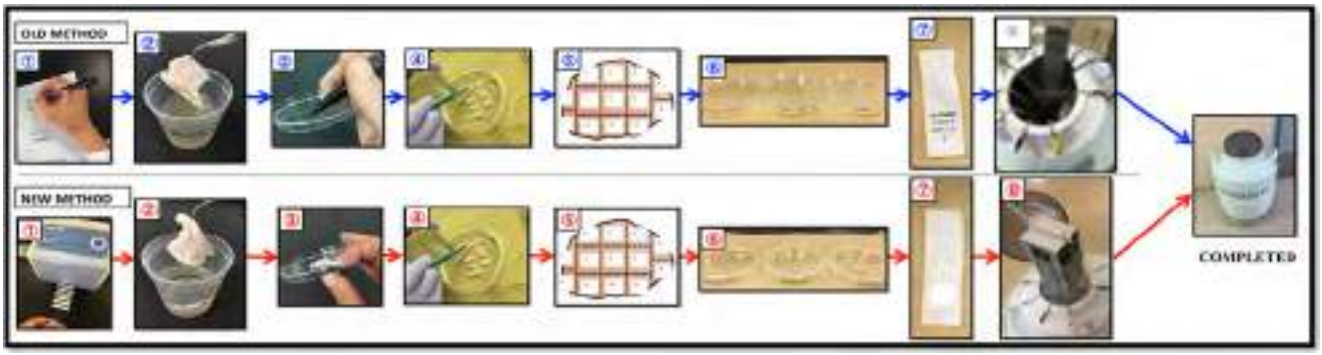

Fig. 2 Conventional and RFID tag methods for cryopreservation of ovarian tissue samples

Step 2.The resected ovary was placed in a cup filled with PBS and a barcode label was attached to the cup.

Step 3.A barcode label was attached to a Petri dish.

Step 4.The ovary was transferred from the cup to the Petri dish and cut it into small pieces.

Step 5.Each ovarian tissue piece was assigned a number and a single photograph was taken of that included all of the numbered tissue pieces. The camera was linked to a computer, allowing automatic recognition of the numbered tissues.

Step 6.Labels were attached to 3 dishes containing graduated concentrations of cryoprotectant and the ovarian tissue samples were processed through the dishes.

Step 7.Each ovarian tissue sample was placed in a cryopreservation device with an RFID tag, which stored patient information (name, hospital ID number, date of birth, and ovarian tissue sample number).

Step 8.The cryopreservation device was placed in a device box with an RFID tag and then successively in a storage box, canister, and LN2 tank.

11. Steps in thawing procedure

Conventional method (thawing bovine ovarian tissue; Fig. 3):

Step 1.The patient's information sheet was identified in a ledger.

Step 2.The ovarian tissue sample number and location in the LN2 tank were obtained from the patient information sheet.

Step 3.The cryopreservation device containing the ovarian tissue sample of interest was retrieved from the LN2 tank and compared with the handwritten information in the ledger.

Step 4.Patient information was written on a Petri dish.

RFID tag method (thawing bovine ovarian tissue; Fig. 3):

Step 1.Patient information was retrieved on a computer by swiping the patient's hospital card through a card reader and two-dimensional barcode labels were printed.

Step 2.The ovarian tissue sample number and location in the LN2 tank were obtained from the computer.

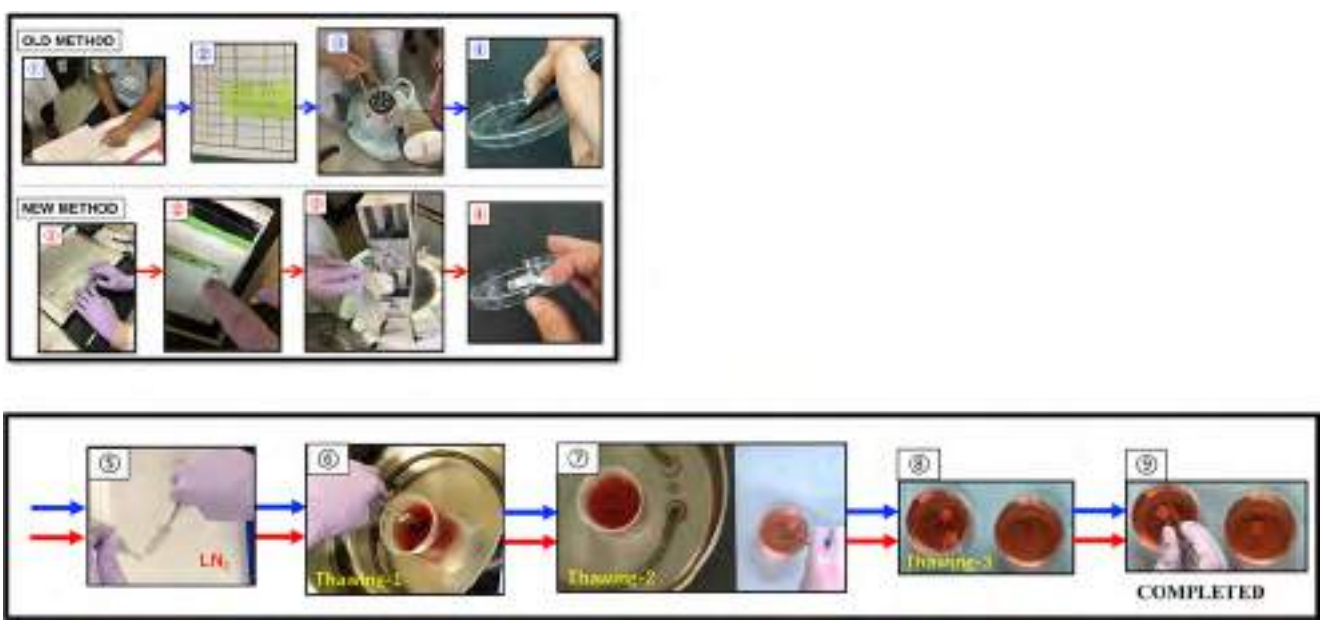

Fig. 3 Conventional and RFID tag methods for thawing ovarian tissue samples

Step 3.The cryopreservation device containing the ovarian tissue sample of interest was retrieved from the LN2 tank and its RFID tag was scanned with an RFID reader to confirm the patient information stored in the tag.

Step 4.A barcode label was attached to a Petri dish.

The remaining steps were the same for both methods and were not timed in this study.

Step 5 – The cryopreservation device with the sample of interest was removed from the plastic pouch in LN2.

Step 6.The cryopreservation device was placed in thawing solution 1.

Step 7.The cryopreservation device was transferred to thawing solution 2.

Step 8.The cryopreservation device was transferred to thawing solution 3.

Step 9.The ovarian tissue sample was removed from the cryopreservation device.

Statistical analysis

The time required to perform each step of the two methods was measured in seconds. Normality of data was determined by using the Shapiro-Wilk test. After normality was confirmed, the time for each step was treated as the dependent variable and the unpaired *t* test was performed without logarithmic transformation.

Results

All 6 participants underwent the Uchida-Kraepelin (U-K) test before performing the closed vitrification and thawing procedures by either the conventional or RFID tag method. The U-K test scores indicated that all participants had a similar ability to follow instructions and none was particularly slow or fast, irrespective of their professional background.

Performance with the two methods

When the RFID tag method was used for closed vitrification [11], the total time required for ovarian tissue cryopreservation was significantly shorter than that for the conventional method ($t(4) = 2.938$, $p = 0.042$, $d = 2.40$). The mean time required for cryopreservation was 1412.33 (± 130.5) seconds by the RFID tag method versus 2073.0 (± 367.0) seconds by the conventional method, and the use of the RFID tag method reduced the cryopreservation time by a mean of 11 min. A similar result was obtained with the thawing procedure, and the total time required for thawing samples was significantly shorter with the RFID tag method than the conventional method ($t(4) = 2.797$, $p = 0.049$, $d = 2.28$). The mean time required thawing ovarian tissue samples was 260.67 (± 38.7) seconds by the RFID tag method versus 405.0 (± 80.6) seconds by the conventional method, and using the RFID tag method reduced the thawing time by a mean of 2 min. The time differences between the two methods were calculated for each step. During closed vitrification procedure, the largest time difference was observed in step 3, where additional time was taken to correct patient information after incorrect information was written on the cup when performing the conventional method. During the thawing procedure, the largest time difference was noted when locating and retrieving the device with the target ovarian tissue sample. In the conventional method, retrieving the cryopreservation device took longer due to time required to confirm the handwritten information on the device pouch matched the patient information in the ledger. Also, when participants were searching for the target cryopreserved device, some incorrect devices were removed from the LN2 storage. In contrast, locating and retrieving the RFID-tagged cryopreserved device was performed efficiently, since the computer system showed the exact location of the device and the RFID reader was used to confirm patient information stored in the tag before removing the device from the LN2 tank.

Discussion

In Japan, the need for cryopreservation of ovarian tissue is increasing. The Japanese Ministry of Health, Labour and Welfare has conducted research in this field and launched a program to promote fertility preservation for adolescents and young adults with cancer in 2016 [12]. To date, 201 patients have undergone ovarian tissue cryopreservation [12]. The Obstetrics and Gynecology Department of St. Marianna Medical University is the one of the major fertility preservation centers in Japan and co-operates with The Ministry of Health, Labour and Welfare to support adolescents and young adults with cancer who require fertility preservation. In this study, we evaluated the usefulness of the RFID tag method for improving the efficiency of the closed vitrification protocol because our group has achieved 3 live births using vitrified/thawed ovarian tissues. Two of these live births have been reported already, although the third case has not been reported (unpublished observations) [13, 14]. Slow freezing is currently the standard method of ovarian tissue cryopreservation, but there is ongoing debate as to which, slow freezing or vitrification, is superior [15, 16]. Automatic vitrification systems have been developed for oocytes and embryos. However, an automatic system has not yet been developed for vitrification or slow freezing of ovarian tissue samples [17, 18].

Against this background, we aimed to develop a system that could streamline the cryopreservation and thawing procedures, and we performed this study to evaluate the usefulness of our RFID tag method in closed vitrification and thawing of bovine ovarian tissue samples. We found that application of

the RFID tag system improved the efficiency of both procedures, with the total time required for cryopreservation being reduced by 11 min when using the RFID tag system and the thawing time being reduced by 2 min.

Efficiency and control of human error are closely associated. The key advantages of utilizing an RFID tag system at fertility centers are improved efficiency and reduced the risk of human error. When the RFID tag system is integrated into a hospital network, swiping the hospital ID card transfers patient information to the IC chip on an RFID tag without manual entry, thus minimizing the risk of typing or writing errors associated with manual procedures. For tracking patient samples, the computer shows the exact location of each cryopreserved tissue sample in the LN2 tank and the RFID reader identifies the cryopreservation device with the target sample while it remains under LN2. The new round RFID tag that we developed has been tested to confirm readability while under LN2. If the IC chip in the RFID tag is damaged, the identification number etched on the surface of the device can still be used to retrieve patient information. In the future, we hope to focus on total elimination of human error and devising a backup system, such as cloud technology, to support this RFID tag method.

The RFID tag method can be applied to other forms of fertility preservation. The devices that are used for cryopreservation depend on the type of tissue being cryopreserved and the method of cryopreservation adopted. For example, the cryotop and the cryovial with a screw cap are usually employed for cryopreservation of oocytes, embryos, and sperm by vitrification, while the cryovial with metal pins attached to the screw cap is used for cryopreservation of ovarian tissue by open vitrification and a flat metal device (Fig. 1B) is used for cryopreservation by closed vitrification. The RFID tag manufacturer (KRD in Japan) can modify the tag size and sensitivity to fit the needs of each device.

Conclusion

Combining two-dimensional barcode labels with an RFID tag system improved the efficiency of cryopreservation and thawing by closed vitrification and reduced human error.

Acknowledgments Dr. David Robert McQuire (Yamada Translation Bureau, Tokyo, Japan) assisted with manuscript editing.

Authors' roles Y.S., T.S., N.S., T.S., and H.K. participated in study conception and design; Y.S., T.S., and H.K. developed the device; T.S, Y.S., Y.S., M.K., S.F., and U.A. performed the study; T.K. performed the statistical analysis; M.A., T.S., and H.K. built the computer system; N.S. edited the English manuscript; N.S, A.T., and N.S. gave suggestions for this research.

Funding information Grant-in-Aid for Scientific Research (B) from the Japan Society for the Promotion of Science to Nao Suzuki.

Compliance with ethical standards

Conflict of interest The authors declare that they have no conflicts of interest.

References

1. Green DM, Liu W, Kutteh WH, Ke RW, Shelton KC, Sklar CA, et al. Cumulative alkylating agent exposure and semen parameters in adult survivors of childhood cancer: a report from the St Jude Lifetime Cohort Study. The Lancet Oncology. 2014;15(11):1215–23.
2. Thomson AB, Campbell AJ, Irvine DC, Anderson RA, Kelnar CJ, Wallace WH. Semen quality and spermatozoal DNA integrity in survivors of childhood cancer: a case-control study. Lancet. 2002;360(9330):361–7.
3. Aubier F, Flamant F, Brauner R, Caillaud JM, Chaussain JM, Lemerle J. Male gonadal function after chemotherapy for solid tumors in childhood. J Clin Oncol. 1989;7(3):304–9.
4. Williams D, Crofton PM, Levitt G. Pediatr Blood Cancer. 2008;50(2):347–51.
5. Lampe H, Horwich A, Norman A, Nicholls J, Dearnaley DP. Fertility after chemotherapy for testicular germ cell cancers. J Clin Oncol. 1997;15(1):239–45.
6. Green DM, Kawashima T, Stovall M, Leisenring W, Sklar CA, Mertens AC, et al. Fertility of male survivors of childhood cancer: a report from the Childhood Cancer Survivor Study. J Clin Oncol. 2010;28(2):322–9.
7. Howell SJ, Shalet SM. Testicular function following chemotherapy. Hum Reprod Update. 2001;7(4):363–9.
8. Shalet SM, Tsatsoulis A, Whitehead E, Read G. Vulnerability of the human Leydig cell to radiation damage is dependent upon age. J Endocrinol. 1989;120(1):161–5.
9. Fisch B, Abir R. Female fertility preservation: past, present and future. Reproduction. 2018;156(1):F11–27.
10. Kristensen SG, Andersen CY. Cryopreservation of ovarian tissue: opportunities beyond fertility preservation and a positive view into the future. Front Endocrinol (Lausanne). 2018;9:347.
11. Sugishita Y, Okamoto N, Uekawa A, Yamochi T, Nakajima M, Namba C, et al. Oocyte retrieval after heterotopic transplantation of ovarian tissue cryopreserved by closed vitrification protocol. J Assist Reprod Genet. 2018;35(11):2037–48.
12. Suzuki N. Research on the effectiveness of cancer and reproductive health care for young cancer patients (fertility preservation), Degree the Ministry of Health, Labor and Welfare of children, Child care support promotion research project. 2018 (in Japanese)
13. Kawamura K, Cheng Y, Suzuki N, Deguchi M, Sato Y, Takae S, et al. Hippo signaling disruption and Akt stimulation of ovarian follicles for infertility treatment. Proc Natl Acad Sci U S A. 2013;110(43):17474–9.
14. Suzuki N, Yoshioka N, Takae S, Sugishita Y, Tamura M, Hashimoto S, et al. Successful fertility preservation following ovarian tissue vitrification in patients with primary ovarian insufficiency. Hum Reprod. 2015;30(3):608–15.
15. Amorim CA, Curaba M, Van Langendonckt A, Dolmans MM, Donnes J. Vitrification as an alternative means of cryopreserving ovarian tissue. Reprod BioMed Online. 2011;23(2):160–86.

16. Abir R, Fisch B, Fisher N, Samara N, Lerer-Serfaty G, Magen R, et al. Attempts to improve human ovarian transplantation outcomes of needle immersed vitrification and slow-freezing by host and graft treatments. J Assist Reprod Genet. 2017;34(5):633–44.
17. Arav A, Natan Y, Kalo D, Komsky-Elbaz A, Roth Z, Levi-Setti PE, et al. A new, simple, automatic vitrification device; preliminary results with murine and bovine oocytes and embryos. J Assist Reprod Genet. 2018;35(7):1161–8.
18. Roy TK, Brandi S, Tappe NM, Bradley CK, Vom E, Henderson C, et al. Embryo vitrification using a novel semi-automated closed system yields in vitro outcomes equivalent to the manual Cryotop method. Hum Reprod. 2014;29(11):2431–8.

Publisher's note Springer Nature remains neutral with regard to jurisdictional claims in published maps and institutional affiliations.

SCIENTIFIC REPORTS

OPEN

High co-expression of IL-34 and M-CSF correlates with tumor progression and poor survival in lung cancers

Received: 12 July 2017
Accepted: 18 December 2017
Published online: 11 January 2018

Muhammad Baghdadi[1], Hiraku Endo[1,2], Atsushi Takano[3,4], Kozo Ishikawa[1], Yosuke Kameda[1], Haruka Wada[1], Yohei Miyagi[5], Tomoyuki Yokose[6], Hiroyuki Ito[7], Haruhiko Nakayama[7], Yataro Daigo[3,4], Nao Suzuki[2] & Ken-ichiro Seino[1]

Despite recent advances in diagnosis and treatment of lung cancers, the 5-year survival rate remains unsatisfactory, which necessitates the identification of novel factors that associates with disease progression and malignant degree for improving diagnostic and therapeutic strategies. Recent progress in cancer immunology research has unveiled critical roles for colony stimulating factor 1 receptor (CSF1R) in multiple aspects of the tumor microenvironment. CSF1R is expressed on tumor-associated macrophages (TAMs), and mediates important pro-tumorigenic functions. CSF1R also provides critical autocrine signals that promote cancer cell survival and proliferation. Activation of CSF1R can be achieved by two independent ligands; macrophage colony-stimulating factor (M-CSF) and interleukin 34 (IL-34). Accordingly, the expression of these ligands in cancer is expected to result in poor prognosis. In this study, we show that IL-34 and M-CSF expression correlates with poor survival in a cohort of lung cancer patients. Importantly, high co-expression of IL-34 and M-CSF associates with the poorest survival compared to cancers that show weak or absent expression of the two ligands. Furthermore, high expression of IL-34 and M-CSF associates with advanced stages of lung cancers. Together, these results indicate a correlation between IL-34/M-CSF expression with poor survival and disease progression in lung cancer patients.

Lung cancer is the leading cause of cancer death and one of the most common cancers among both men and women worldwide[1]. In contrast to the steady increase in survival for most cancers, lung cancer still shows the poorest survival with less than 18% of 5-year relative survival, which results largely from poor detection and insufficient prediction of prognosis at early stages[1]. Obviously, an accurate assessment of prognosis is critical for an effective clinical decision and survival improvement.

With an aim to identify the molecular mechanisms that control the biological process of disease progression in cancer, several studies have focused on the genetic backgrounds of cancer cells and its relative impact on prognosis and clinical outcome of cancer therapy, such as RRM1, EGFR and KRAS mutations[2–6]. However, recent advances in cancer immunology research have unveiled a critical role for the interaction between cancer cells and immune cells at the tumor microenvironment (TME) in tumor progression and therapeutic resistance[7–9]. Thus, tumors that express critical immune-modulators are expected to be associated with high malignancy and thus related to poor prognosis. Indeed, patients with advanced stage cancers showed enhanced expression levels of several immune modulators including MIF, TNFα, IL-6, IL-8, IL-10, IL-18 and TGFβ[10]. Accordingly, accurate

[1]Division of Immunobiology, Institute for Genetic Medicine, Hokkaido University, Kita-15 Nishi-7, Sapporo, 060-0815, Japan. [2]Department of Obstetrics and Gynecology, St. Marianna University School of Medicine, 2-16-1 Sugao, Miyamae-ku, Kawasaki City, Kanagawa, 216–8512, Japan. [3]Department of Medical Oncology and Cancer Center, Shiga University of Medical Science, Otsu, 520-2192, Japan. [4]Center for Antibody and Vaccine, Research Hospital, Institute of Medical Science, University of Tokyo, Tokyo, 108-8639, Japan. [5]Molecular Pathology and Genetics Division, Kanagawa Cancer Center, Yokohama, 241-0815, Japan. [6]Department of Pathology, Kanagawa Cancer Center, Yokohama, 241-8515, Japan. [7]Department of Thoracic Surgery, Kanagawa Cancer Center, Yokohama, 241-8515, Japan. Muhammad Baghdadi, Hiraku Endo and Atsushi Takano contributed equally to this work. Correspondence and requests for materials should be addressed to K.-i.S. (email: seino@igm.hokudai.ac.jp)

prediction of prognosis in cancer patients may require the assessment of such factors in addition to the genetic backgrounds of cancer cells.

Among several immune cells, tumor-associated macrophages (TAMs) consist the most abundant cell population in many tumors, which play crucial roles in multiple aspects of the TME, including tumor progression, invasion, metastasis and angiogenesis[11–13]. Importantly, TAMs infiltration has been considered as an independent poor prognostic factor in several cancers[7–9]. TAMs depend largely on CSF1R signaling for survival, proliferation and function, which can be achieved by two independent ligands; M-CSF and IL-34[14,15]. M-CSF and IL-34 share no sequence homology, but show comparable biological activities in myeloid cells[16,17]. Both cytokines correlate with tumor progression, metastasis, angiogenesis and therapeutic resistance[9]. It has been suggested that expression of IL-34 or M-CSF is accompanied with increased infiltration of M2-polarized TAMs that show enhanced pro-tumorigenic functions[18,19]. Based on these backgrounds, the expression of IL-34 and/or M-CSF at the TME may characterize tumors with enhanced aggression and has an impact on the patient's survival. In this regard, previous reports have related M-CSF expression with poor survival in cancer patients[20,21]. However, IL-34 expression has not been evaluated in these studies, since it was discovered for the first time in 2008[22]. In this study, we analyze the expression of IL-34 and M-CSF in primary lung cancer tissues and its correlation with survival and tumor progression in a cohort of lung cancer patients, providing for the first time an evidence that show the association between IL-34 and M-CSF expression with disease progression and poor survival in lung cancer patients.

Results

IL-34 or M-CSF expression correlates with poor survival in lung cancer patients. We have previously described a correlation between high expression of IL-34 and poor survival in a cohort of lung cancer patients (Fig. 1a)[19]. The clinicopathological characteristics of this cohort were described in detail in our previous report[19]. In this cohort, 45% of patients were Japanese women over 60 years without smoking history, and 77.4% of cases were diagnosed as non-small lung cancers (stage I) with 5 years of follow-up period[19]. Immunohistochemical staining of IL-34, M-CSF, CSF1R and CD163 was performed on lung cancer tissues obtained from patients by surgical resection. Antibodies specificity was confirmed before staining (Supplementary Fig. 1). Similar with IL-34, M-CSF expression was detected in lung adenocarcinomas (ADCs), squamous cell carcinomas (SCCs) and small cell lung cancers (SCLCs) with a variety among patients (Fig. 1b). In contrast, M-CSF was undetectable at protein level in normal lung tissues (Fig. 1b). Kaplan-Meier analysis of overall survival in lung cancer patients showed that high expression of M-CSF correlates with poor survival of lung cancer patients (Fig. 1c), in accordance with previous reports[20,21].

High co-expression of IL-34 and M-CSF correlates with the poorest survival in lung cancer patients. Next, we evaluated the association between IL-34 and M-CSF expression in lung cancers and the related impact on patients' survival. Interestingly, 91% of cancer tissues that showed strong staining of IL-34 were accompanied with high (48%) or weak (43%) expression of M-CSF (Supplementary Table 1). Similarly, 77% of cancer tissues that showed strong staining of M-CSF were accompanied with high (56%) or weak (21%) expression of IL-34 (Supplementary Table 1). On the other hand, the absence of IL-34 staining in cancer tissues was frequently associated with the absence of M-CSF staining, and vice versa, (Supplementary Table 1) which may suggest a reciprocal relationship between the expression of IL-34 and M-CSF in lung cancers. Furthermore, we categorized patients in this cohort depending on the expression levels of M-CSF and IL-34 into 4 groups: 1) weak or absent expression of both M-CSF and IL-34, 2) High expression of IL-34 with weak or absent expression of M-CSF, 3) High expression of M-CSF with weak or absent expression of IL-34, 4) high expression of both M-CSF and IL-34. Kaplan-Meier analysis of overall survival in lung cancer patients based on this classification showed that high expression of M-CSF or IL-34 correlates with poor survival compared to groups that showed weak or absent expression of the two ligands (Fig. 2a,b). Importantly, patients with high expression of both M-CSF and IL-34 have the poorest survival compared to other groups (Fig. 2c). Together, these results suggest that high co-expression of both IL-34 and M-CSF correlates with poorer survival in lung cancer patients.

CSF1R expression correlates with poor survival in lung cancers. CSF1R is tyrosine-protein kinase that acts as a cell-surface receptor for M-CSF and IL-34[14–16]. CSF1R is expressed mainly in cells of the myeloid lineage and is a key regulator of macrophage differentiation[23]. However, several reports have showed that CSF1R expression can be also detected in other cells such as endothelial cells and importantly in cancer cell lines and primary cancer tissues[24,25]. Thus, we next evaluated the expression of CSF1R in lung cancer tissues. Similar with IL-34 and M-CSF, immunohistochemical staining showed that CSF1R is expressed in lung cancer tissues with a variety among patients (Fig. 3a). Again, high expression of CSF1R correlates with poor survival in lung cancer patients, similar with IL-34 and M-CSF expression (Fig. 3b).

CD163 expression correlates with poor survival in lung cancers. Accumulating evidence from clinical and experimental studies indicates that TAMs play critical roles in the promotion of tumor development, progression, metastasis and therapeutic resistance[26]. CD163 is a member of the scavenger family receptor, with high specificity for monocyte/macrophage lineage[27], and has been considered as a specific marker to enumerate TAMs[28]. Thus, CD163 staining is expected to reflect the status of macrophage infiltration into tumors and predict poor prognosis in cancer patients[29]. Immunohistochemical staining showed that CD163 expression could be detected in lung cancer tissues with a variety among patients (Fig. 4a,b). Furthermore, Kaplan-Meier analysis of overall survival in this cohort of lung cancer patients showed that CD163 expression correlates with poor survival, in consistent with previous reports[29] (Fig. 4c).

IL-34 and M-CSF expression correlates with CD163 expression and poor survival in lung cancers. Next, we examined the relation between M-CSF or IL-34 with CD163 expression and its impact on

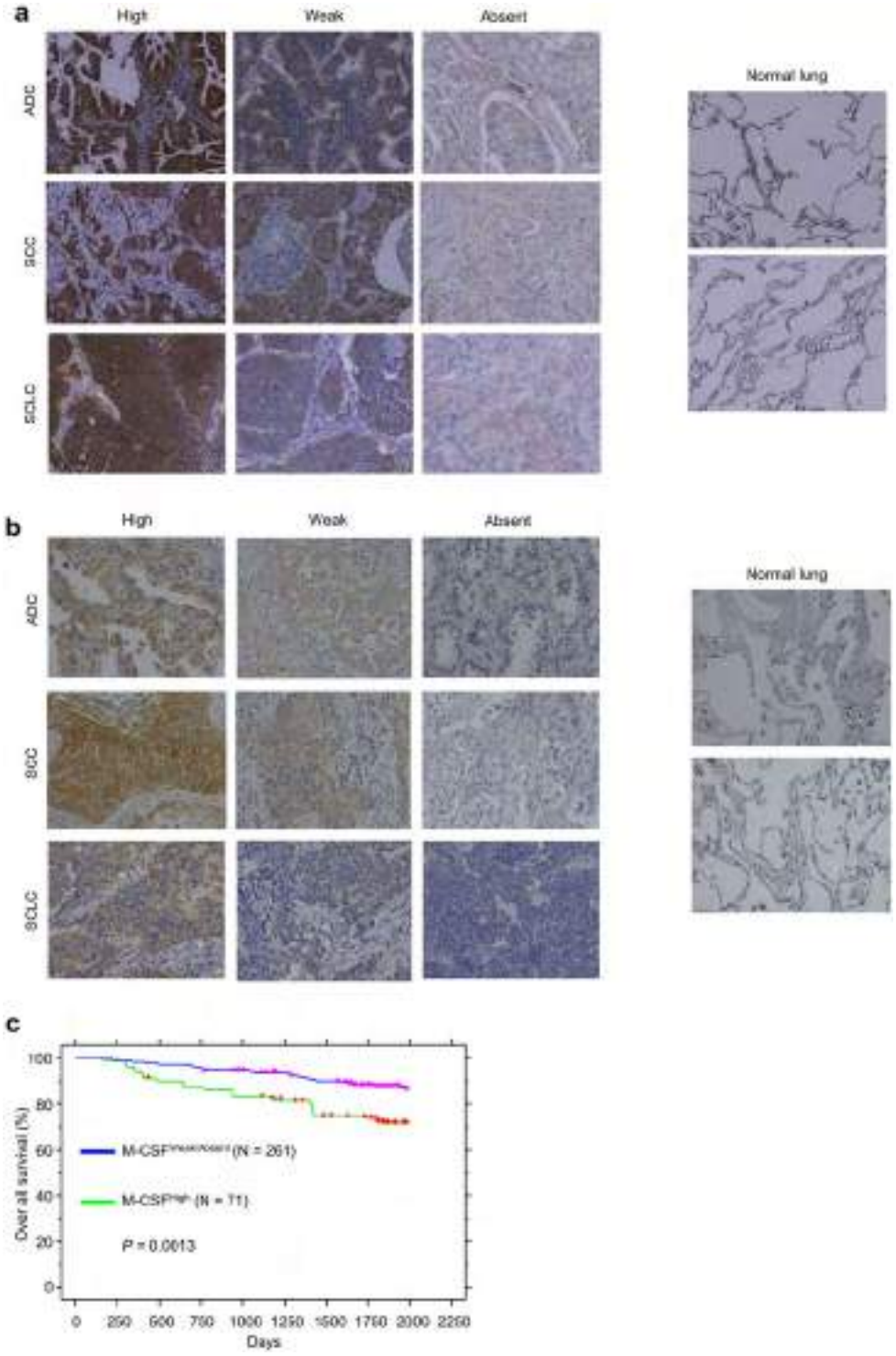

Figure 1. Correlation between IL-34 and M-CSF expression with poor survival in lung cancer patients. (**A**) and (**b**), Immunohistochemistry staining of IL-34 (**a**) or M-CSF (**b**) in primary lung cancer tissues from patients diagnosed with adenocarcinoma (ADC), squamous cell carcinoma (SCC) or small cell lung cancers (SCLC) compared to normal lung tissues. (**c**) Kaplan-Meier analysis showing overall survival in lung cancer patients according to M-CSF expression.

survival in this cohort of lung cancer patients. High expression of M-CSF was frequently accompanied with high expression of CD163 (Fig. 5a; Supplementary Table 1), and the absence of CD163 staining was frequently associated with absent or weak staining of M-CSF (Fig. 5a; Supplementary Table 1). Kaplan-Meier analysis of overall survival in lung cancer patients based on M-CSF and CD163 expression showed that high expression of both M-CSF and CD163 in cancer tissues correlates with poor survival compared to other groups (Fig. 5b),

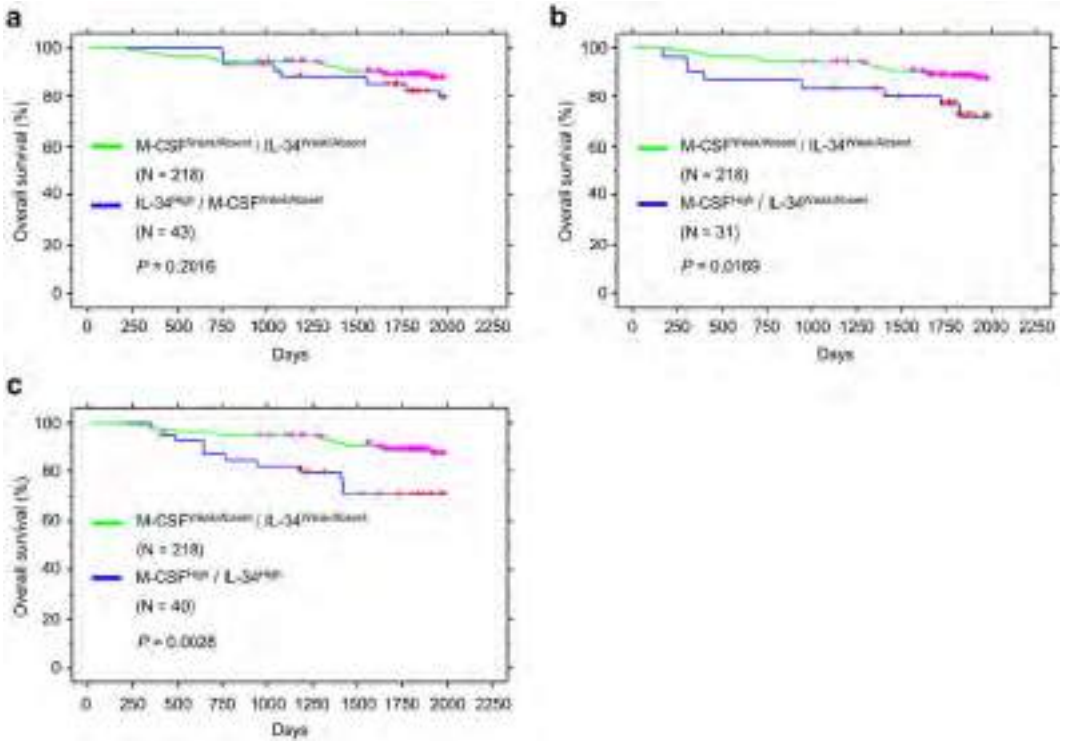

Figure 2. Correlation between M-CSF/IL-34 expression with poor survival in lung cancer patients. (**a**) Kaplan-Meier analysis showing overall survival in lung cancer patients that show M-CSF$^{Weak/Absent}$/IL-34$^{Weak/absent}$ expression compared to M-CSF$^{Weak/Absent}$/IL-34^{High} group. (**b**) Kaplan-Meier analysis of overall survival in lung cancer patients that show M-CSF$^{Weak/Absent}$/IL-34$^{Weak/absent}$ expression compared to M-CSF^{High}/IL-34^{High} group. (**c**) Kaplan-Meier analysis of overall survival in lung cancer patients that show M-CSF$^{Weak/Absent}$/IL-34$^{Weak/absent}$ expression compared to M-CSF^{High}/IL-34^{High} group.

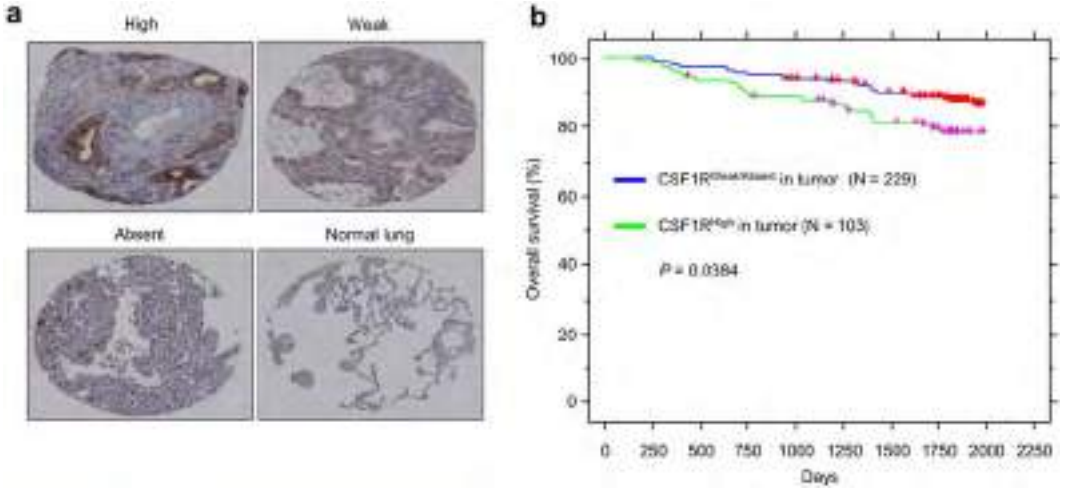

Figure 3. Correlation between CSF1R expression with poor survival in lung cancer patients. (**a**) Representative data of immunohistochemistry staining of CSF1R in primary lung cancer tissues compared to normal lung tissues. (**b**) Kaplan-Meier analysis showing overall survival in lung cancer patients according to CSF1R expression.

consistent with previous reports[28]. Similarly, we evaluated the relation between IL-34 and CD163. As expected, 60% of cancer tissues that showed high expression of IL-34 were accompanied with high expression of CD163 (Fig. 5c; Supplementary Table 1), and the absence of CD163 staining was frequently associated with negative staining of IL-34 (Fig. 5c; Supplementary Table 1), which indeed suggests a correlation between IL-34 and CD163 expression in lung cancers. Kaplan-Meier analysis of overall survival in lung cancer patients based on IL-34 and

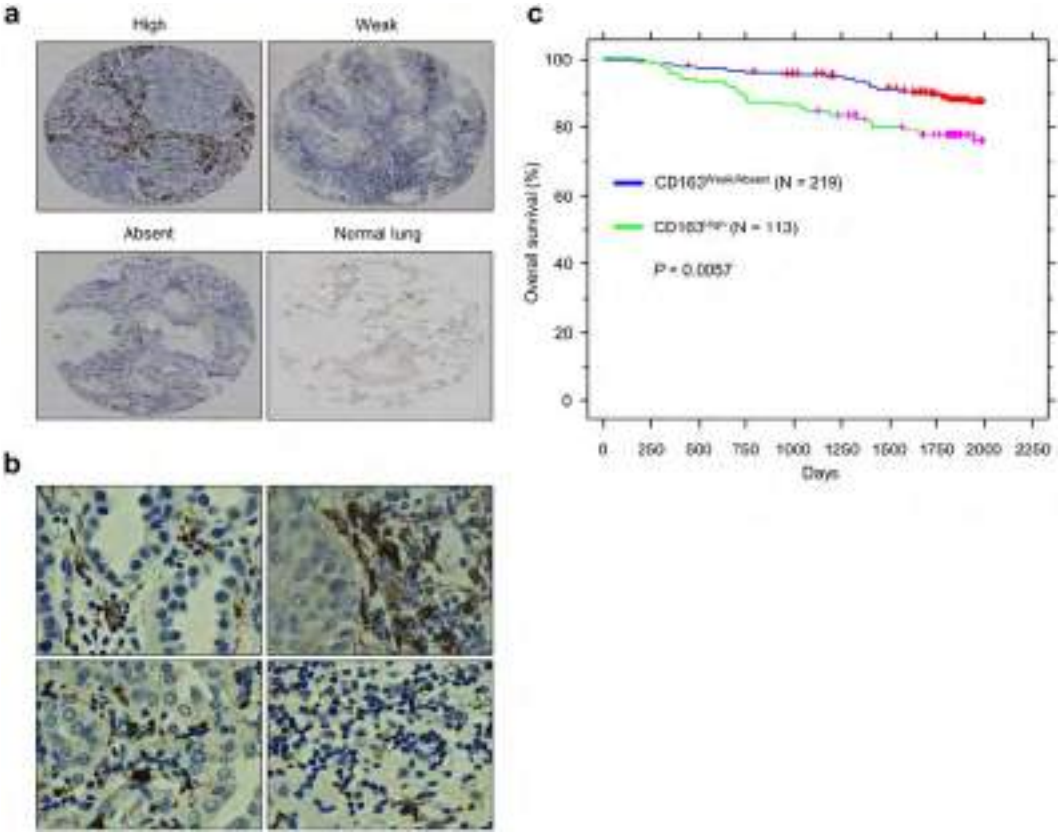

Figure 4. Correlation between CD163 expression with poor survival in lung cancer patients. (**a**) Representative data of immunohistochemistry staining of CD163 in primary lung cancer tissues compared to normal lung tissues. (**b**) High magnification images of CD163 staining in lung cancer tissues. (**c**) Kaplan-Meier analysis showing overall survival in lung cancer patients based on CD163 expression.

CD163 expression showed that patients with high expression of both IL-34 and CD163 have the poorest survival compared to other groups (Fig. 5d). Collectively, these results indicate a correlation between high expression of IL-34, M-CSF, CSF1R and CD163 with poor survival, which was further confirmed in univariate analysis using Cox's proportional hazards model (Table 1), although multivariate analysis in this model did not reach a statistical significance except for T and N factors (Table 1).

IL-34 and M-CSF expression is enhanced in advanced stages of lung cancers. Finally, we evaluated the expression level of IL-34 and M-CSF according to each stage in lung cancer patients (Supplementary Tables 2 and 3). By calculating positivity rates in each group, patients with high expression of IL-34 or M-CSF showed increased frequencies from stage IA (17.2%, 15.3%), stage IB (25%, 22%), stage IIA (40%, 20%), stage IIB (37.5%, 50%) to stage IIIA (44.8%, 37.9%) (Fig. 6a,b). Similarly, frequencies of patients with high co-expression of IL-34 and M-CSF associated with stages, starting from 8.3% at stage IA, 11% at stage IB, 16.7% at stage IIA, 25% at stage IIB, to 24.13% at stage IIIA (Fig. 6c). Statistically, the expression of IL-34 (Supplementary Table 4, $P = 0.0004$) or M-CSF (Supplementary Table 4, $P = 0.0062$) showed a tendency to be enhanced in stage II and III compared to stage I. Similarly, high co-expression of IL-34 and M-CSF was observed more frequently in stage II and IIIA compared to stage I (Supplementary Table 4, $P = 0.0081$). In a combined analysis, patients' groups that showed high expression of IL-34 (Table 2, $P = 0.0095$), M-CSF (Table 2, $P = 0.00829$) or high co-expression of both IL-34 and M-CSF (Table 2, $P = 0.0011$) were associated with stage II and IIIA rather than stage I compared to other groups with weak or absent expression. Together, these findings indicate an association between IL-34 and M-CSF expression with stages in lung cancers, and thus may serve as progression parameters.

Discussion

In this paper, we describe for the first time the clinicopathological relevance of M-CSF and IL-34 expression with disease stages and poor survival in a cohort of lung cancer patients. Our data showed that single expression of M-CSF or IL-34 can be observed in primary lung cancer tissues and correlated with poor survival. High expression of both cytokines correlates with CD163 expression, which collectively correlates with poor survival. Additionally, high co-expression of M-CSF or IL-34 correlates with disease stages and the poorest survival compared to groups that showed weak or absent expression of the two ligands. Thus, evaluating the expression of both M-CSF and IL-34 may help to estimate disease progression and malignant degree in lung cancer patients.

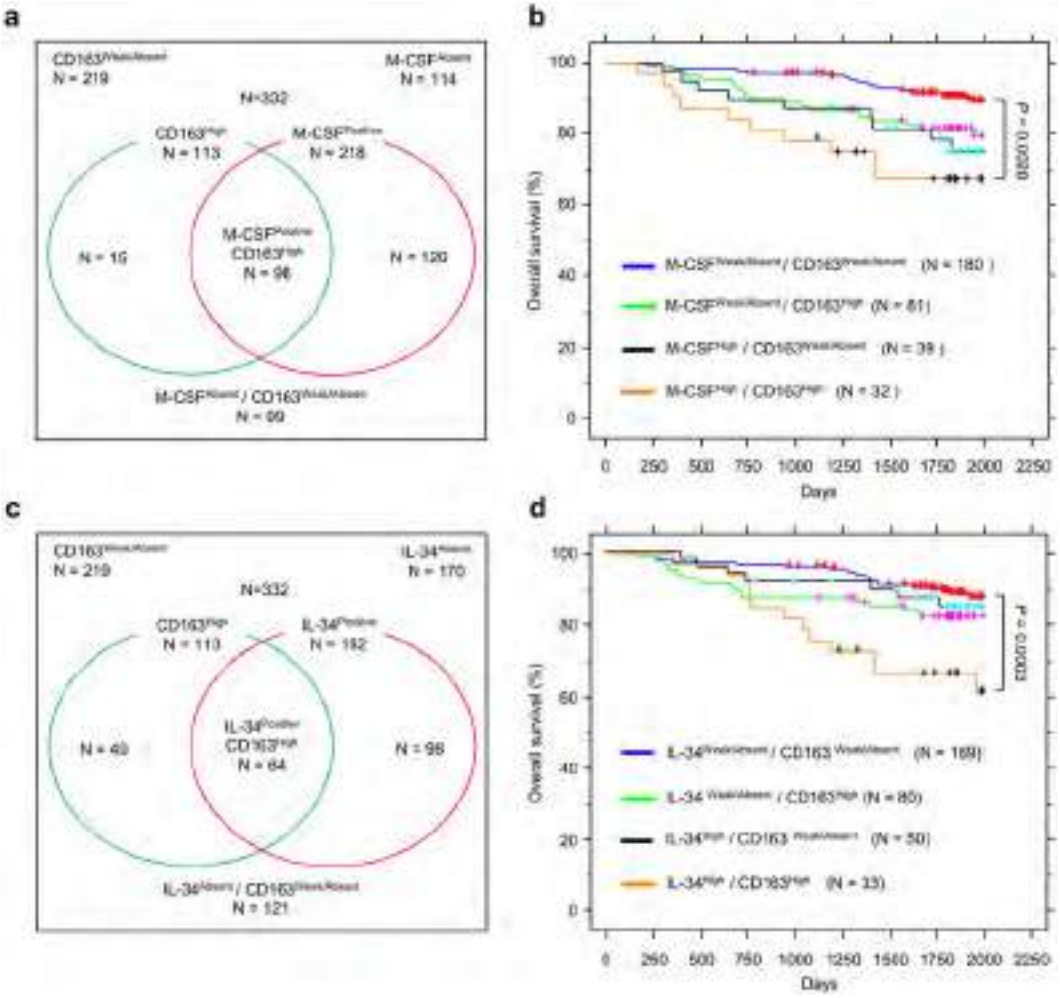

Figure 5. Correlation between M-CSF or IL-34 with CD163 expression in lung cancers. (**a**) Classification of lung cancer patients based on M-CSF and CD163 expression. M-CSF positive refers to samples that show high or weak expression of M-CSF. (**b**) Kaplan-Meier analysis showing overall survival in lung cancer patients based on M-CSF and CD163 expression. (**c**) Classification of lung cancer patients based on IL-34 and CD163 expression. IL-34 positive refers to samples that show high or weak expression of IL-34. (**d**) Kaplan-Meier analysis showing overall survival in lung cancer patients based on IL-34 and CD163 expression.

In the cohort of lung cancer patients described in this study, IL-34 and M-CSF were naturally expressed in cancer tissues prior to any therapeutic procedures. Oncogenic mutations in cancer cells are frequently accompanied by activation of certain signaling pathways that induce the expression of a wide range of cytokines and chemokines, which in turn contribute to tumor progression and ultimately resistance to cancer therapy such as chemotherapy or tyrosine kinase inhibitors[30,31]. In this context, it is of great interest to identify oncogenic mutations that lead to IL-34 and M-CSF production by cancer cells and its impact on the tumor microenvironment, therapeutic resistance.

One remaining important issue is to unveil how can two ligands of the same receptor co-exist and exert their functions at the same microenvironment. The co-expression of both IL-34 and M-CSF has been previously observed in cancers such as giant cell tumors and malignant pleural mesothelioma[32–34]. In this study, we also observed a co-expression of M-CSF and IL-34 in a sub-population of lung cancer patients, which correlates with poorer prognosis. Under physiological conditions, M-CSF and IL-34 show tissue-restricted expression patterns with specific functions[14,15]. In *vitro*, both cytokines exhibit comparable biological functions in myeloid cells[14,15]. While expected to act as competitors, IL-34 and M-CSF can induce dual additive biological effects under certain conditions[17]. Additionally, IL-34 has the potential to interact with M-CSF to form a novel heterodimer that induce a specific activation pattern on CSF1R[17]. Accordingly, in tumors that naturally express both M-CSF and IL-34, or acquired the ability to produce both cytokines under certain therapeutic conditions, IL-34 has the possibility to act through interaction with M-CSF resulting in unique functions of CSF1R in both myeloid and cancer cells, which should be elucidated experimentally in further basic studies. Based on these backgrounds, co-expression of both IL-34 and M-CSF - naturally or induced under therapeutic conditions - may characterize malignancies with enhanced aggression and has an impact on the clinical outcome of cancer therapy. Indeed, our data shown in this study indicates an association between high expression of IL-34 and M-CSF in cancer tissues with disease stages

Variables	Hazards ratio	95% CI	Unfavorable/Favorable	*P*-value
Univariate analysis				
High IL-34 expression	1.862	1.058–3.275	High/Weak and absent	0.031*
High M-CSF expression	2.445	1.390–4.303	High/Weak and absent	0.0019*
High CSF1R expression	1.774	1.023–3.077	High/Weak and absent	0.0411*
CD163 expression in TAM#	2.115	1.228–3.644	High/Weak and absent	0.0069*
Age (years)	1.624	0.910–2.899	≧65/< 65	0.101
Gender	1.539	0.875–2.706	Male/Female	0.1346
Histology	3.014	1.671–5.436	Non-ADC/ADC	0.0002*
T-factor	2.834	1.572–5.109	T2-3/T1	0.0005*
N-factor	3.67	2.097–6.422	N1-2/N0	<0.0001*
Smoking status	1.321	0.751–2.323	Ex or Current/Never	0.3342
Multivariate analysis				
High IL-34 expression	1.016	0.547–1.886	High/Weak and absent	0.9604
High M-CSF expression	1.492	0.799–2.785	High/Weak and absent	0.2089
High CSF1R expression	1.469	0.842–2.564	High/Weak and absent	0.1757
CD163 expression in TAM#	1.557	0.888–2.730	High/Weak and absent	0.1225
Histology	1.999	1.063–3.759	Non-ADC/ADC	0.0316*
T-factor	1.884	1.016–3.493	T2-3/T1	0.0445*
N-factor	2.911	1.617–5.241	N1-2/N0	0.0004*

Table 1. Cox's proportional hazards model analysis of prognostic factors in lung cancer patients. *$P < 0.05$ #TAM: Tumor associated macrophage ADC: Adenocarcinoma, Non-ADC includes Squamous cell carcinoma, Large cell carcinoma and others.

and poor survival in lung cancer patients. In conclusion, IL-34 and M-CSF may help to predict poor survival and tumor progression in lung cancer patients, which should be further evaluated in other cohorts of lung cancer patients and various cancers in future studies.

Materials and Methods

Clinical Samples. Primary NSCLC tissues were collected from patients who had undergone surgical lobectomy or pneumonectomy at Kanagawa Cancer Center (Yokohama, Japan) after the acquirement of informed consent. A total of 332 resected tumor specimens were preserved at Kanagawa Cancer Center Biospecimen Center (KCC-BSC) and utilized for immunohistochemical analysis. All tumors were staged based on the pTNM pathologic classification of the UICC (International Union Against Cancer). All formalin-fixed samples of primary NSCLCs (Gender: 151 female and 181 male patients; Age: median age of 68 with a range of 35–90 years; Smoking history: 138 with no history of smoking, 192 ex- or current smokers and 2 unknown; Tissue type: 277 adenocarcinomas (ADC), 32 squamous cell carcinomas (SCC), 5 large cell carcinoma (LCC), and 18 other types of histological cancer; Stage: 157 pstage IA, 100 pstage IB, 30 pstage IIA, 16 pstage IIB, and 29 pstage IIIA cases) had been obtained earlier along with clinicopathologic data from KCC-BSC. A median follow-up period was 118.0 months for living patients (range, 8.0–138.9 months). The primary endpoint was overall survival as measured from the date of surgery to the time of death. Written informed consent was obtained from all patients, and the use of related clinical materials was approved by institutional ethics committees of Hokkaido University Hospital, Institute for Genetic Medicine and Kanagawa Cancer Center, and all experiments were performed in accordance with all guidelines and regulations indicated by these committees.

TMA Construction. Tumor tissue microarrays were constructed with 332 formalin-fixed primary lung cancers, each of which had been obtained with an identical protocol to collect, fix, and preserve the tissues after resection. The tissue area for sampling was selected based on visual alignment with the corresponding hematoxylin and eosin (H&E)-stained section on a slide. Three to five tissue cores (diameter, 0.6 mm; depth, 3–4 mm) taken from a donor tumor block were placed into a recipient paraffin block with a tissue microarray (Beecher Instruments). A core of normal tissue was punched from each case, and 5-μm sections of the resulting microarray block were used for immunohistochemical analysis.

Immunohistochemical analysis. To investigate the expression levels of IL-34, M-CSF, CSF1R and CD163 protein in clinical samples from lung cancer patients, tissue sections were stained the in the following manner. TMA slides were immersed in antigen retrieval solution (pH 9.0) (Nichirei, Tokyo, Japan) and boiled for 15 min in an autoclave. Endogenous peroxidase activity was blocked by incubation in 0.3% H_2O_2 in methanol for 15 min. After protein blocking (Catalog No. X0909, Abcam), TMA slides were incubated with a mouse anti-IL-34 antibody (Catalog No. ab101443), a rabbit anti-M-CSF antibody (Catalog No. ab52864, Abcam) in 1:100 dilution, a rabbit anti-CSF1R antibody (Catalog No. HPA012323, SIGMA) in 1:100 dilution or a mouse anti-CD163 antibody in 1:100 dilution (Catalog No. MCA1853, Bio-Rad) in Antibody Diluent (Catalog No. S0809, DakoCytomation) for 30 min at room temperature in a moist chamber. The sections were incubated with HRP-labeled polymer

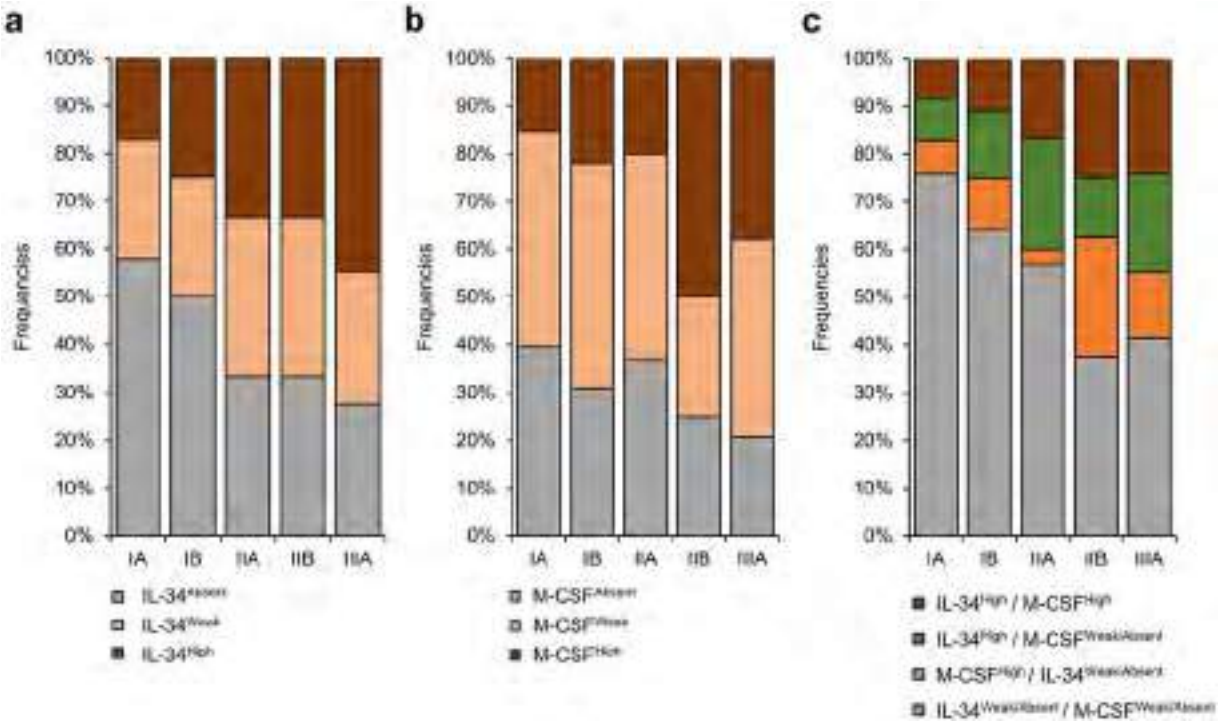

Figure 6. Association between IL-34/M-CSF expression with advanced stages in lung cancers. Bar graph analysis resembles the association between M-CSF or IL-34 expression with disease stages in lung cancer patients. Positivity rates of IL-34 (**a**), M-CSF (**b**) or both IL-34 and M-CSF (**c**) were calculated in each group according to disease stage.

Correlation between high IL-34 expression and disease stages				
	Total	**IL-34$^{W/A}$/M-CSF$^{W/A}$**	**IL-34^{High}/M-CSF$^{W/A}$**	
	n = 261	**n = 218**	**n = 43**	***P*-value**
Stage				
IA	133	119	14	0.0095*,#
IB	78	64	14	
IIA	24	17	7	
IIB	8	6	2	
IIIA	18	12	6	
Correlation between high M-CSF expression and disease stages				
	Total	**IL-34$^{W/A}$/M-CSF$^{W/A}$**	**IL-34$^{W/A}$/M-CSF^{High}**	***P*-value**
	n = 249	**n = 218**	**n = 31**	
Stage				
IA	130	119	11	0.00829*,#
IB	75	64	11	
IIA	18	17	1	
IIB	10	6	4	
IIIA	16	12	4	
Correlation between high IL-34 and M-CSF co-expression and disease stages				
	Total	**IL-34$^{W/A}$/M-CSF$^{W/A}$**	**IL-34^{High}/M-CSF^{High}**	***P*-value**
	n = 258	**n = 218**	**n = 40**	
Stage				
IA	132	119	13	0.0011*,#
IB	75	64	11	
IIA	22	17	5	
IIB	10	6	4	
IIIA	19	12	7	

Table 2. Correlation between IL-34/M-CSF expression and disease stages in lung cancer patients. *$P < 0.05$ (Fisher's exact test) #stage I vs stage II-IIIA W/A: Weak or Absent.

anti-mouse (Catalog No. K4007, DakoCytomation) or anti-rabbit IgG (Catalog No. K4002, DakoCytomation) as the secondary antibody for 30 min at room temperature in a moist chamber. Substrate-chromogen was added, and the specimens were counterstained with hematoxylin.

Evaluation of Immunohistochemical Staining and Statistical analysis. Two independent investigators semiquantitatively assessed IL-34, M-CSF, CSF1R and CD163 positivity without prior knowledge of clinicopathologic data. Since the staining intensities of IL-34 and M-CSF were mostly homogenous in cytoplasm of cancer cells, they were semiquantitatively scored as high, weak or absent. As CSF1R staining was detected in cytoplasm and membrane, they were semiquantitatively scored as high, weak or absent. CD163 staining was mainly detected in cytoplasm of stromal macrophage. $CD163^+$ macrophage infiltration in stroma was semiquantitatively scored as high, weak or absent, (high: many infiltrating $CD163^+$ macrophages, weak: some infiltrating $CD163^+$ macrophages and absent: no or few infiltrating $CD163^+$ macrophages)[35]. If there is a discrepancy among them, a consensus was reached using simultaneous examination by two investigators.

Statistics. Statistical analysis was done using the StatView software. Tumor-specific survival curves were calculated from the date of surgery to the time of death related to NSCLC or to the last follow-up observation. Kaplan–Meier curves were calculated for each relevant variable and for IL-34, M-CSF, CSF1R or CD163 expression; differences in survival times among patient subgroups were analyzed using the log-rank test.

References

1. Miller, K. D. *et al*. Cancer treatment and survivorship statistics, 2016. *CA Cancer J. Clin.* **66**, 271–89 (2016).
2. Bepler, G. *et al*. RRM1 modulated *in vitro* and *in vivo* efficacy of gemcitabine and platinum in non-small-cell lung cancer. *J. Clin. Oncol.* **24**, 4731–7 (2006).
3. Lee, J. J. *et al*. The immunohistochemical overexpression of ribonucleotide reductase regulatory subunit M1 (RRM1) protein is a predictor of shorter survival to gemcitabine-based chemotherapy in advanced non-small cell lung cancer (NSCLC). *Lung Cancer* **70**, 205–10 (2010).
4. Paez, J. G. *et al*. EGFR mutations in lung cancer: correlation with clinical response to gefitinib therapy. *Science* **304**, 1497–500 (2004).
5. Pao, W. *et al*. Acquired resistance of lung adenocarcinomas to gefitinib or erlotinib is associated with a second mutation in the EGFR kinase domain. *PLOS Med.* **2**, e73 (2005).
6. Eberhard, D. A. *et al*. Mutations in the epidermal growth factor receptor and in KRAS are predictive and prognostic indicators in patients with non-small-cell lung cancer treated with chemotherapy alone and in combination with erlotinib. *J. Clin. Oncol.* **23**, 5900–9 (2005).
7. Noy, R. & Pollard, J. W. Tumor-associated macrophages: from mechanisms to therapy. *Immunity* **41**, 49–61 (2014).
8. De Palma, M. & Lewis, C. E. Macrophage regulation of tumor responses to anticancer therapies. *Cancer Cell* **223**, 277–86 (2013).
9. Ruffell, B. & Coussens, L. M. Macrophages and therapeutic resistance in cancer. *Cancer Cell* **27**, 462–72 (2015).
10. Lippitz, B. E. Cytokine patterns in patients with cancer: a systematic review. *Lancet Oncol.* **14**, e218–28 (2013).
11. Allavena, P., Sica, A., Solinas, G., Porta, C. & Mantovani, A. The inflammatory micro-environment in tumor progression: the role of tumor-associated macrophages. *Crit. Rev. Oncol. Hematol.* **66**, 1–9 (2008).
12. Mantovani, A., Schioppa, T., Porta, C., Allavena, P. & Sica, A. Role of tumor-associated macrophages in tumor progression and invasion. *Cancer Metastasis Rev.* **25**, 315–22 (2006).
13. Condeelis, J. & Pollard, J. W. Macrophages: obligate partners for tumor cell migration, invasion, and metastasis. *Cell* **124**, 263–6 (2006).
14. Droin, N. & Solary, E. Editorial: CSF1R, CSF-1, and IL-34, a "menage a trois" conserved across vertebrates. *J. Leukoc. Biol.* **87**, 745–7 (2010).
15. Nakamichi, Y., Udagawa, H. & Takahashi, N. IL-34 and CSF-1: similarities and differences. *J. Bone Miner. Metab.* **31**, 486–95 (2013).
16. Chihara, T. *et al*. IL-34 and M-CSF share the receptor Fms but are not identical in biological activity and signal activation. *Cell Death Differ.* **17**, 1917–27 (2010).
17. Ségaliny, A. I. *et al*. IL-34 and M-CSF form a novel heteromeric cytokine and regulate the M-CSF receptor activation and localization. *Cytokine* **76**, 170–81 (2015).
18. Chockalingam, S. & Ghosh, S. S. Macrophage colony-stimulating factor and cancer: a review. *Tumour Biol.* **35**, 10635–44 (2014).
19. Baghdadi, M. *et al*. Chemotherapy-Induced IL34 Enhances Immunosuppression by Tumor-Associated Macrophages and Mediates Survival of Chemoresistant Lung Cancer Cells. *Cancer Res.* **76**, 6030–6042 (2016).
20. McDermott, R. S. *et al*. Circulating macrophage colony stimulating factor as a marker of tumour progression. *Eur. Cytokine Netw.* **13**, 121–7 (2002).
21. Scholl, S. M. *et al*. Circulating levels of the macrophage colony stimulating factor CSF-1 in primary and metastatic breast cancer patients. A pilot study. *Breast Cancer Res. Treat.* **39**, 275–83 (1996).
22. Lin, H. *et al*. Discovery of a cytokine and its receptor by functional screening of the extracellular proteome. *Science* **320**, 807–11 (2008).
23. Stanley, E. R. & Chitu, V. CSF-1 receptor signaling in myeloid cells. *Cold Spring Harb. Perspect. Biol.* **6**, a021857 (2014).
24. Hung, J. Y. *et al*. Colony-stimulating factor 1 potentiates lung cancer bone metastasis. *Lab. Invest.* **94**, 371–81 (2014).
25. Patsialou, A. *et al*. Autocrine CSF1R signaling mediates switching between invasion and proliferation downstream of TGFbeta in claudin-low breast tumor cells. *Oncogene* **34**, 2721–31 (2015).
26. Achkova, D. & Maher, J. Role of the colony-stimulating factor (CSF)/CSF-1 receptor axis in cancer. *Biochem. Soc. Trans.* **44**, 333–41 (2016).
27. Fabriek, B. O. & Dijkstra, C. D. & Van den Berg, T. K. The macrophage scavenger receptor CD163. *Immunobiology* **210**, 153–60 (2005).
28. Heusinkveld, M. & der Burg, V. S.H. Identification and manipulation of tumor associated macrophages in human cancers. *J. Transl. Med.* **9**, 216 (2011).
29. Medrek, C., Pontén, F., Jirström, K. & Leandersson, K. The presence of tumor associated macrophages in tumor stroma as a prognostic marker for breast cancer patients. *BMC Cancer* **12**, 306 (2012).
30. Castells, M. *et al*. Implication of tumor microenvironment in chemoresistance: tumor-associated stromal cells protect tumor cells from cell death. *Int. J. Mol. Sci.* **13**, 9545–71 (2012).
31. Naugler, W. E. & Karin, M. NF-kappaB and cancer-identifying targets and mechanisms. *Curr. Opin. Genet. Dev.* **18**, 19–26 (2008).
32. Baud'huin, M. *et al*. Interleukin-34 is expressed by giant cell tumours of bone and plays a key role in RANKL-induced osteoclastogenesis. *J. Pathol.* **221**, 77–86 (2010).
33. Cioce, M. *et al*. Autocrine CSF-1R signaling drives mesothelioma chemoresistance via AKT activation. *Cell Death Dis.* **5**, e1167 (2014).

34. Baghdadi, M., Endo, H., Tanaka, Y., Wada, H. & Seino, K. Interleukin 34, from pathogenesis to clinical applications. *Cytokine* **99**, 139–147 (2017).
35. Maniecki, M. B. *et al*. Tumor-promoting macrophages induce the expression of the macrophage-specific receptor CD163 in malignant cells. *Int. J. Cancer* **131**, 2320–31 (2012).

Acknowledgements

This work was supported in part by Japan Agency for Medical Research and Development AMED (KI Seino) and Grant-in-Aid for Scientific Research on Innovative Areas from The Japan Society for the Promotion of Science (JSPS KAKENHI Grant Number JP: 16H06277; Group for Supporting Research using Biospecimen, Platform of Supporting Cohort Study and Biospecimen Analysis).

Author Contributions

H.E., M.B., A.T., K.I., Y.K., H.W., Y.M., T.Y., H.I. and H.N. performed research; Y.M., H.I., Y.D. and K.S. contributed new reagents/analytic tools; H.E., M.B., A.T., K.I., Y.K., H.W., Y.M., T.Y., H.I., H.N., Y.D., N.S. and K.S. analyzed data; and H.E., M.B., and K.S. wrote and revised the manuscript.

Additional Information

Supplementary information accompanies this paper at https://doi.org/10.1038/s41598-017-18796-8.

Competing Interests: The authors declare that they have no competing interests.

Publisher's note: Springer Nature remains neutral with regard to jurisdictional claims in published maps and institutional affiliations.

Open Access This article is licensed under a Creative Commons Attribution 4.0 International License, which permits use, sharing, adaptation, distribution and reproduction in any medium or format, as long as you give appropriate credit to the original author(s) and the source, provide a link to the Creative Commons license, and indicate if changes were made. The images or other third party material in this article are included in the article's Creative Commons license, unless indicated otherwise in a credit line to the material. If material is not included in the article's Creative Commons license and your intended use is not permitted by statutory regulation or exceeds the permitted use, you will need to obtain permission directly from the copyright holder. To view a copy of this license, visit http://creativecommons.org/licenses/by/4.0/.

© The Author(s) 2017

THE JOURNAL OF
Obstetrics and Gynaecology Research

doi:10.1111/jog.13359 J. Obstet. Gynaecol. Res. Vol. 43, No. 8: 1326–1334, August 2017

Glycan profiling using formalin-fixed, paraffin-embedded tissues: Hippeastrum hybrid lectin is a sensitive biomarker for squamous cell carcinoma of the uterine cervix

Akiko Tozawa-Ono[1], Manabu Kubota[2], Chika Honma[1], Yuko Nakagawa[1], Noriyuki Yokomichi[1], Norihito Yoshioka[1], Chiharu Tsuda[1], Tatsuru Ohara[1], Hirotaka Koizumi[2] and Nao Suzuki[1]

[1]*Department of Obstetrics and Gynecology, St. Marianna University School of Medicine and* [2]*Department of Pathology, St. Marianna University School of Medicine, Miyamae, Kawasaki, Japan*

Abstract

Aim: Glycosylation of proteins is altered in cancer cells and distinctive glycan structures are associated with specific cancers, but little is known about the complete glycan profile of particular tumors. In this study, glycomic analysis of squamous cell carcinoma (SCC) of the uterine cervix was performed to search for useful markers.

Methods: A lectin microarray containing 45 lectins with different binding preferences that covered N- and O-linked glycans was coupled with evanescent field-activated fluorescent detection for glycomic analysis of SCC and normal squamous epithelium (NSE) of the cervix. Formalin-fixed, paraffin-embedded tissue specimens were obtained from 16 patients with uterine cervical cancer. Sections that included both tumor and non-tumor tissues were examined to detect alterations of glycans based on the lectin-binding pattern.

Results: Hippeastrum hybrid lectin was found to be a sensitive marker for distinguishing SCC of the cervix from NSE. It was the best lectin for discriminating SCC from other tissues according to receiver–operator curve analysis, as it showed a high sensitivity (81.8%), a high specificity (70.1%), and a large area under the curve (0.8182). Histochemistry confirmed specific cytoplasmic staining of SCC cells by Hippeastrum hybrid lectin, while there was little staining of cervical intraepithelial neoplasia and no staining of NSE.

Conclusion: The present lectin microarray technique could be applied for tissue-based glycomic analysis of various tumors and for discovery of glycan-related biomarkers.

Key words: glycan, lectin, squamous cell carcinoma, uterine cervical cancer.

Introduction

The human glycome is of particular interest in cancer research because aberrant glycans, such as β1–6 branched N-glycans and the truncated O-glycan known as Tn antigen, are found in a wide variety of cancers.[1–6] Since glycans are synthesized by the cooperative action of multiple genes, each glycan molecule reflects a variety of genetic anomalies. While progress in exploiting the human glycome as a source of disease markers has generally been slow due to the complexity of the glycans themselves and lack of suitable methods for investigating their structures, technical developments have allowed the analysis of glycans in cancer cells[4] and tissues.[7]

Glycosylation of proteins plays an important role in various cellular events, including differentiation, adhesion, proliferation, and maintenance of immunity.[8] Cell differentiation and proliferation are associated with changes of glycosylation, and there seems to be significant variation of the glycosylation machinery among different types of cells.[9,10]

Received: October 31 2016.
Accepted: March 20 2017.
Correspondence: Assistant Professor Akiko Tozawa-Ono, Department of Obstetrics and Gynecology, St. Marianna University School of Medicine, 2-16-1 Sugao, Miyamae, Kawasaki 216-8511, Japan. Email: a2ono@marianna-u.ac.jp

 © 2017 Japan Society of Obstetrics and Gynecology

In order to profile glycans, complex mixtures of these molecules must be resolved accurately enough to determine quantitative differences, so a highly sensitive method of detection is required. A useful test would assess the quantity of a target glycan and would not depend on detecting certain glycan structures. Capillary electrophoresis, liquid chromatography, and mass spectrometry are commonly used for glycome profiling.[11] However, these techniques are not well suited to screening a large number of samples for differences because they are time-consuming, low-throughput methods that are sensitive to sample contamination, require expensive equipment, and generate complex data. In 2005, several research groups independently reported the development of lectin arrays for rapid multiplex analysis of protein glycosylation. Since then, lectin arrays have been used to analyze the glycomes of bacteria,[12] viruses,[13] and mammals.[14] An evanescent field is a field that cannot propagate, so its amplitude decreases as a function of distance. Evanescent field fluorescence-assisted lectin microarray technology[15] has been adopted for glycome profiling using formalin-fixed, paraffin-embedded tissue specimens.[16] In the present study, a microarray containing 45 lectins with defined binding preferences covering N- and O-linked glycans was coupled with evanescent field activated fluorescent detection to perform glycomic analysis of specimens of primary cervical cancer and normal cervical epithelium in order to identify specific lectin-binding patterns associated with squamous cell carcinoma (SCC) of the cervix.

Methods

Specimens

We investigated formalin-fixed, paraffin-embedded uterine cervical tissue specimens obtained by radical hysterectomy between 2007 and 2011 that were stored in the surgical pathology archives of the Department of Pathology at St. Marianna University School of Medicine, Kawasaki, Japan. Specimens of SCC and normal squamous epithelium were obtained from 16 patients with a mean age of 49.7 ± 3.6 years, and tissue sections 1.5 mm in diameter and 10 μm thick were cut for microarray analysis.

We also retrieved formalin-fixed, paraffin-embedded cervical tissue specimens obtained by punch biopsy, cone biopsy, or hysterectomy between 2002 and 2010 from the surgical pathology archives of the Department of Pathology at St. Marianna University School of Medicine, for histochemical analysis. Specimens of cervical intraepithelial neoplasia (CIN; mild to severe dysplasia/carcinoma *in situ*) were obtained from 63 patients, including 26 patients with CIN1 (mean age: 35.2 ± 8.8 years), 17 patients with CIN2 (mean age: 33.9 ± 5.5 years), and 20 patients with CIN3 (mean age: 35.6 ± 8.3 years). These samples had been fixed in 10% buffered formalin for 24–48 h and then embedded in paraffin.

This study was approved by the Human Ethics Review Committee of St. Marianna University School of Medicine.

Extraction of proteins from tissue sections

Each section was deparaffinized and removed from the glass slide by using a 21-G needle under a microscope, after which the tissue fragments were collected into a 1.5-mL microtube containing 200 μL of 10 mM citrate buffer (pH 6.0) and incubated for 5 min at 95°C for antigen retrieval. After washing with phosphate-buffered saline (PBS; Seikagaku Kogyo Co.) by centrifugation, the pellet was solubilized with 20 μL of PBS containing 0.5% Nonidet P40 and gently sonicated. The resulting tissue suspension was incubated on ice for 60 min and then was centrifuged at 20 000 *g* for 5 min at 4°C to obtain the supernatant (detergent-solubilized glycoprotein extract).

Lectin microarray analysis

Aliquots (20 μL) of the glycoprotein extract were incubated with 100 μg of Cy3 Mono-Reactive dye (GE Healthcare) for 60 min at room temperature in the dark and the reaction products were loaded onto a Zeba Spin Desalting Column (Thermo Scientific) to remove the excess fluorescent reagent. After centrifugation, the solution was adjusted to 300 μL with probe buffer (Tris-buffered saline, pH 7.5, containing 1.0% Triton X-100 and 500 mM glycine). After washing three times with probinding solution, 80 μL of Cy3-labeled glycoprotein solution was added to a LecChip (GP BioScience) in each well of the glass slide, and incubation was done overnight at 20°C in a humidified chamber. Then a fluorescent image of the array was acquired by using a GlycoStation Reader 1200 evanescent field fluorescence scanner (GP Bioscience). Data were analyzed with GlycoStation Tools Pro Suite 1.5 software (GP Bioscience), and values were normalized by the average signal for all lectins.

Lectin staining of cervical tissues

Lectin staining of the tissue sections was performed by using Histofine Simple Stain MAX-PO (Nichirei Co.).

© 2017 Japan Society of Obstetrics and Gynecology

After deparaffinization, tissue arrays on glass slides were placed in 10-mM citrate buffer (pH 6.0) and autoclaved for 10 min at 121°C to enhance lectin reactivity. After cooling to room temperature, the arrays were incubated for 10 min in methanol containing 0.3% hydrogen peroxide to deplete endogenous peroxidases. Then washing was done three times with PBS and the arrays were incubated with PBS containing 1% bovine serum albumin for 10 min at room temperature in a humidified chamber. This was followed by incubation with 5 μg/mL of biotinylated lectin dissolved in PBS for 1 h at room temperature. After washing three times with PBS, streptavidin–peroxidase reagent was applied for 5 min at room temperature. Finally, reaction products were visualized by incubation with 3,3-diaminobenzidine tetrahydrochloride and the sections were counterstained with hematoxylin.

The percentage of Hippeastrum hybrid lectin (HHL)-stained cells was calculated from the stained area relative to the total area of epithelial cells and a staining score was assigned as follows: 0 (0%), 1 (1–5%), 2 (6–50%), and 3 (51–100%). All parts of the section were evaluated at 200× magnification under a light microscope and all of the entire epithelial cell areas were assessed for staining.

Statistical analysis

Lectin microarray data are presented as the mean ± standard error (SEM). A two-sided χ^2-test was used for comparison of clinicopathological variables between groups.

Receiver–operator curve (ROC) analysis was performed to evaluate differences between SCC and normal squamous epithelium by calculating the sensitivity and specificity at various cut-off values. The area under the ROC (AUC) was calculated, with an AUC of 1.0 indicating perfect discrimination, whereas an AUC of 0.5 indicated that the test was no better than random chance at discriminating epithelium from SCC.

For comparison of the lectin staining scores between normal epithelium, CIN, and SCC, Steel's multiple comparison method of Dwass was employed (Statcel4, version 4.0). A P-value < 0.05 was considered significant in all analyses.

Results

Lectin microarray analysis

To identify the lectin that was most specific for SCC, we performed differential glycan profiling using paraffin-embedded, formalin-fixed tissue sections. This analysis revealed significant differences for four of the 45 lectins tested, with the signal intensities of four α2–3Sia-binding lectins (*Agrocybe Cylindracea* galectin [ACG], *Maackia amurensis* lectin [MAL], HHL that binds to1,6-branched mannose, and *Maclura pomifera* agglutinin [MPA]) being either significantly higher or lower (all $P < 0.05$) in SCC tissues than in normal squamous epithelium. Among the four lectins, HHL staining showed the largest difference of intensity between SCC and normal squamous epithelium from the same patient ($P < 0.05$; Fig. 1). HHL and ACG were both useful for discriminating SCC from other tissues according to ROC analysis, as HHL and ACG showed a high sensitivity (81.8% and 74.9%, respectively), a high specificity (70.1% and 84.9%), and a large AUC (0.8182 and 0.849; Fig. 2). However, there was a difference in the SCC /normal epithelium signal intensity ratio (tumor tissue/normal tissue ratio [T/N ratio]) between these two lectins, with it being 0.8 for ACG and 2.1 for HHL (Table 1). These results suggested that strong binding of HHL to SCC tissues was related to changes of glycosylation that were specific for this malignancy.

Histochemical analysis of HHL-reactive glycans

To confirm the above results, we employed histochemistry with biotinylated HHL to visualize the expression of HHL-reactive glycans in specimens of SCC, CIN, and normal squamous epithelium. CIN tissues and normal squamous epithelium showed little or no staining by HHL (Fig. 3a-d). In contrast, SCC tissues were stained by HHL, especially at the sites of tumor infiltration. HHL was strongly expressed in the interstitial regions of SCC, suggesting a correlation of this lectin with infiltration (Fig. 3e-f). The results of histochemical analysis are summarized in Table 2. SCC showed a very high rate of staining by HHL (14/16 tumors: 87.5%), while there was little staining of CIN (7/26 (26.9%) for CIN1, 5/19 (26.3%) for CIN2, and 2/20 (10.0%) for CIN3 and no staining of normal squamous epithelium (0/16; 0%). These results also suggested that HHL-reactive glycans were specifically expressed by SCC.

The HHL staining score was significantly higher for SCC than for either normal squamous epithelium or CIN ($P < 0.05$, Fig. 4), while there was no significant difference of HHL expression between normal epithelium and CIN (Fig. 4).

© 2017 Japan Society of Obstetrics and Gynecology

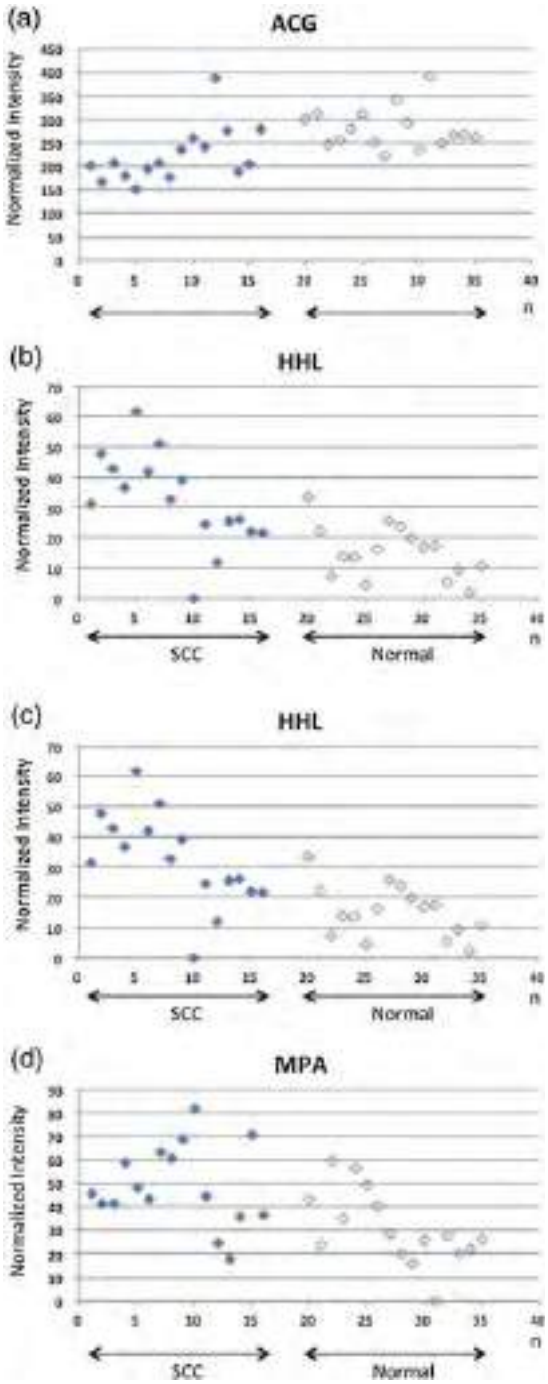

Figure 1 Glycan analysis of normal squamous epithelium (NSE) and squamous cell carcinoma (SCC). Graphs display normalized intensity data for the four lectins that showed significant differences between NSE and SCC (by the two-sided χ^2-test using normalized lectin data). (a) *Agrocybe Cylindracea* galectin (ACG). (b) *Maackia amurensis* lectin (MAL). (c) Hippeastrum hybrid lectin (HHL). (d) *Maclura pomifera* agglutinin (MPA). Cases 1–16: SCC. Cases 20–36: NSE.

Discussion

Treating cervical cancer at an early stage does not reduce the incidence of invasive cancer, and tumors that relapse are often refractory with a high mortality rate.[17] Therefore, an accurate biomarker is needed for this cancer, as cytological diagnosis of cervical cancer is a subjective process. In the present study, we investigated potential glycoprotein biomarkers by performing glycoproteomic analysis of cervical tissue sections containing both normal squamous epithelium and SCC.[18,19] We found that ACG,[20] MAL, HHL,[21] and MPA[22] showed marked differences of binding to SCC tissues compared with normal epithelium.

Lectin microarray analysis is a highly sensitive technique for multiplex analysis of small tissue sections (approximately 500 cells), using 45 lectins to investigate the N- and O-glycans attached to glycoproteins. This method has already been employed to identify lectin-binding patterns associated with a poor prognosis of colon cancer by Matsuda *et al.*, who performed glycan analysis of adenocarcinoma tissues and normal colon epithelium to reveal that staining with *Wisteria floribunda* agglutinin clearly differentiated cancer from normal epithelium.[16] Their findings agreed well with those of a subsequent histochemical study using biotinylated *Wisteria floribunda* agglutinin.[16] Thus, it seems reasonable to employ lectin microarray analysis for investigation of glycan-related tumor biomarkers.

In the present study, lectin microarray analysis demonstrated several differences of the lectin-binding pattern between SCC and normal squamous epithelium, with stronger binding of HHL and MPA to SCC tissues along with weaker binding of MAL and ACG. ROC analysis revealed that HHL was the best of these four lectins for discriminating between normal squamous epithelium and SCC ($P < 0.05$). In addition, the T/N ratio of HHL showed the largest difference between normal squamous epithelium and SCC (Table 1). These findings suggested that HHL was the best lectin marker for SCC among those investigated in the present study.

The evanescent field fluorescence-assisted method of lectin microarray analysis used in this study allows high-throughput, rapid, and sensitive glycome profiling of clinical samples. The greatest advantage of a lectin microarray over alternative methods of glycan profiling is that simultaneous quantitative analysis of N- and O-linked glycans can be performed in intact biological structures after minimal preparation of samples without the need for extraction of glycans. The 45 lectins in the microarray we used cover the majority of known human

© 2017 Japan Society of Obstetrics and Gynecology

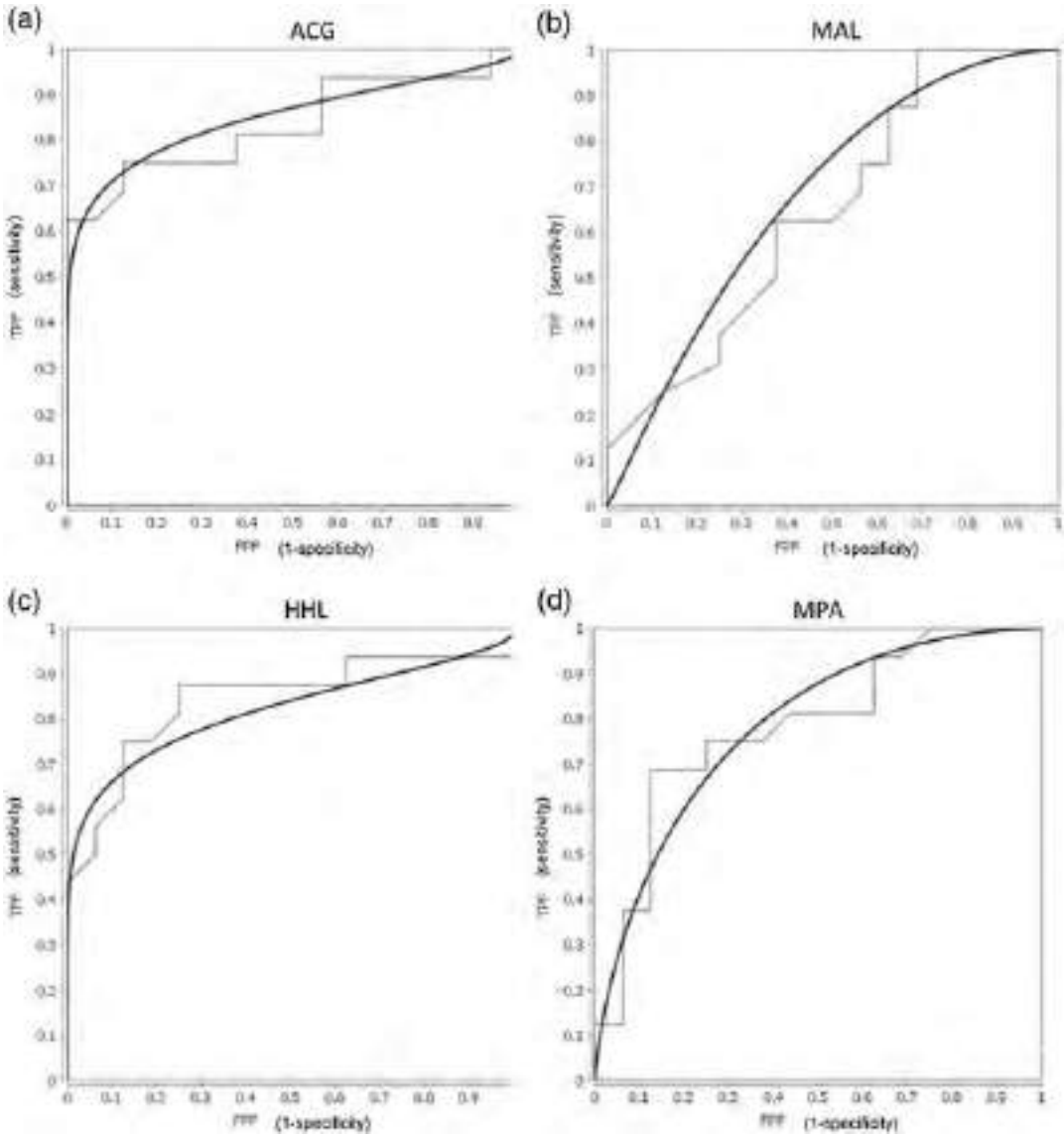

Figure 2 Results of receiver–operator curve (ROC) analysis for (a) *Agrocybe Cylindracea* galectin (ACG), (b) *Maackia amurensis* lectin (MAL), (c) Hippeastrum hybrid lectin (HHL), and (d) *Maclura pomifera* agglutinin (MPA). (•) Best-fit ROC obtained with the Metz system and (•) actual data were compared for differentiating normal squamous epithelium (NSE) from squamous cell carcinoma (SCC). The area under the ROC (AUC) was larger for ACG and HHL than for MAL and MPA. ACG and HHL showed a higher sensitivity (74.6% and 70.1%) and higher AUC values (0.85 and 0.82) than MAL or MPA. Data were normalized by the average value for all lectins tested. (a) ACG: AUC = 0.849; false-positive fraction (FPF) = 0.415 at true-positive fraction (TPF) = 0.85; TPF = 0.746 at FPF = 0.15; sensitivity = 74.6%; specificity = 84.9%. (b) MAL: AUC = 0.6785; FPF = 0.596 at TPF = 0.85; TPF = 0.294 at FPF = 0.15; sensitivity = 29.4%; specificity = 67.8%. (c) HHL: AUC = 0.8182; FPF = 0.534 at TPF = 0.85; TPF = 0.701 at FPF = 0.15; sensitivity = 70.1%; specificity = 81.8%. (d) MPA: AUC = 0.7857; FPF = 0.451 at TPF = 0.85; TPF = 0.517 at FPF = 0.15; sensitivity = 51.7%; specificity = 78.5%.

oligosaccharides, allowing the detection of subtle differences.[18,19] Although the patient population investigated in this study was too small to confidently define the lectin-binding pattern of cervical cancer, we still identified differences of glycosylation between neoplastic and non-neoplastic cervical tissues. The lectins that showed differences between SCC and normal epithelium in this study may be good candidates for

© 2017 Japan Society of Obstetrics and Gynecology

Table 1 Results of microarray analysis of 45 lectins in normal squamous epithelium and SCC of the cervix

Lectin	Normal epithelium (SEM)		Tumor tissue (SEM)		T/N ratio	Staining†
LTL	46.2	(8.9)	44.7	(3.1)	1.0	+/−
PSA	94.5	(8.3)	83.5	(4.7)	0.9	+/−
LCA	117.9	(7.0)	100.2	(4.8)	0.9	+/−
UEA_I	27.1	(5.2)	31.2	(5.1)	1.2	+
AOL	196.5	(21.6)	182.1	(18.3)	0.9	+/−
AAL	172.8	(18.7)	154.9	(15.7)	0.9	+/−
MAL_I	40.4	(4.4)	31.0	(3.2)	0.8	−
SNA	177.9	(11.2)	180.6	(11.3)	1.0	+/−
SSA	174.1	(13.0)	185.6	(13.6)	1.1	+/−
TJA-I	285.1	(17.0)	278.2	(16.5)	1.0	+/−
PHA(L)	14.4	(3.0)	21.4	(2.7)	1.5	++
ECA	27.1	(4.7)	27.1	(4.3)	1.0	+/−
RCA120	67.8	(5.7)	85.4	(6.6)	1.3	+
PHA(E)	93.2	(4.4)	76.3	(5.7)	0.8	−
DSA	331.8	(15.2)	278.6	(11.1)	0.8	−
GSL-II	11.5	(2.6)	8.5	(1.6)	0.7	−
NPA	121.3	(12.8)	148.6	(14.7)	1.2	+
ConA	155.4	(8.1)	195.4	(12.9)	1.3	+
GNA	64.7	(7.4)	97.9	(8.7)	1.5	++
HHL	15.0	(2.1)	32.2	(3.8)	2.1	+++
ACG	279.5	(10.8)	221.7	(14.4)	0.8	−
TxLC_I	18.6	(2.9)	20.7	(3.5)	1.1	+/−
BPL	21.3	(4.1)	34.2	(5.3)	1.6	++
TJA-II	72.6	(13.4)	64.3	(5.5)	0.9	+/−
EEL	15.8	(6.1)	12.2	(2.4)	0.8	−
ABA	115.8	(11.1)	108.8	(5.0)	0.9	+/−
LEL	372.8	(11.6)	348.7	(18.8)	0.9	+/−
STL	340.2	(16.7)	325.0	(23.2)	1.0	+/−
UDA	300.2	(12.2)	344.6	(22.7)	1.1	+/−
PWM	19.4	(3.2)	32.7	(4.5)	1.7	++
Jacalin	124.4	(6.8)	134.7	(7.1)	1.1	+/−
PNA	7.6	(3.5)	9.5	(3.0)	1.3	+
WFA	30.2	(4.9)	36.5	(4.4)	1.2	+
ACA	88.5	(9.4)	91.4	(7.3)	1.0	+/−
MPA	30.9	(3.9)	48.8	(4.3)	1.6	++
HPA	97.8	(24.6)	53.8	(12.7)	0.5	−
VVA	9.3	(2.2)	16.0	(3.7)	1.7	++
DBA	25.8	(7.8)	24.9	(4.7)	1.0	+/−
SBA	9.9	(3.1)	16.1	(3.5)	1.6	++
Calsepa	65.5	(4.5)	90.5	(8.5)	1.4	+
PTL_I	7.3	(3.3)	7.6	(3.1)	1.0	+/−
MAH	33.4	(5.4)	33.5	(4.2)	1.0	+/−
WGA	162.8	(8.8)	157.2	(7.9)	1.0	+/−
GSL_I_A4	11.4	(2.9)	14.8	(3.1)	1.3	+
GSL_I_B4	4.3	(1.5)	8.4	(3.2)	1.9	++

†+++ = T/N > 1.9; ++ = T/N 1.5–1.9; + = T/N 1.2–1.5; +/− = T/N 0.9–1.1, − = T/N < 0.9. SEM, standard error of the mean; T/N ratio, tumor tissue/normal tissue ratio.

isolating glycoprotein subsets before performing proteomic and glycomic analyses to identify novel biomarkers.

While lectin microarray technology can demonstrate the lectin-binding patterns associated with cervical cancer, identifying specific disease-associated glycans is impossible by this method because the structures of the glycan molecules can only be inferred from lectin-binding data.

To confirm our findings, we performed histochemistry with biotin-labeled HHL, which revealed cytoplasmic staining of cancer cells in nearly all SCC specimens (Fig. 3e,f). On the other hand, there was little HHL staining of cells in CIN1 and CIN2 tissues (Fig. 3b–d),

© 2017 Japan Society of Obstetrics and Gynecology

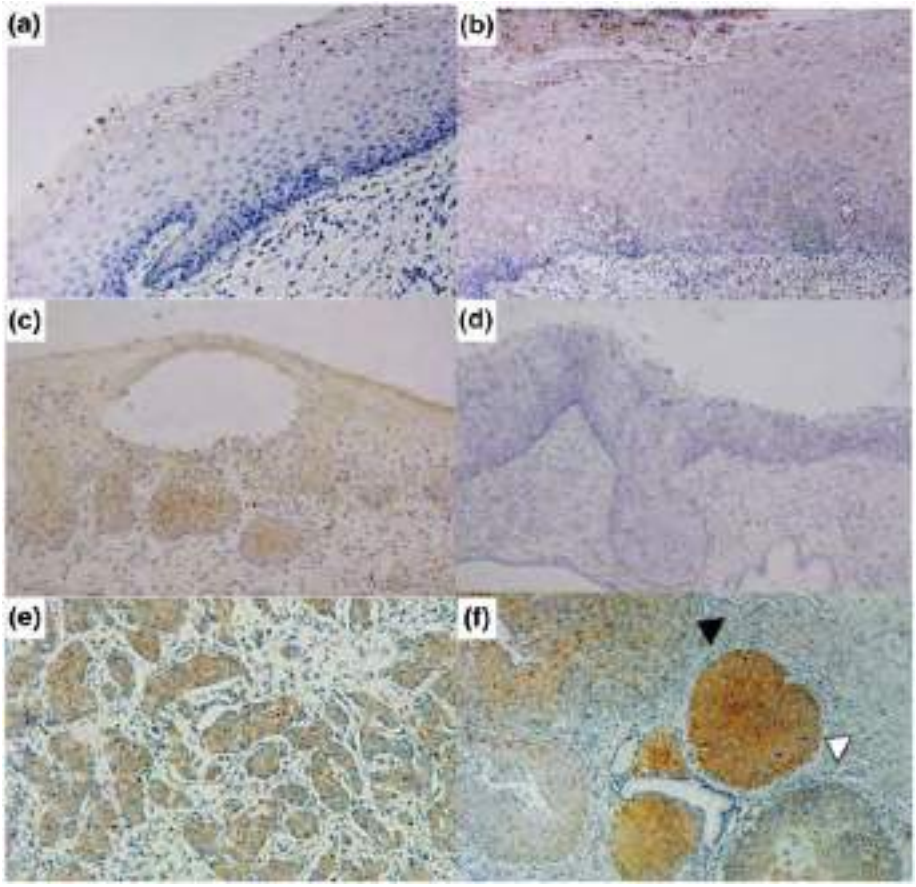

Figure 3 Staining of cervical tissues for Hippeastrum hybrid lectin (HHL). (a) Normal squamous epithelium (score = 0). (b) Cervical intraepithelial neoplasia (CIN)1 (score = 1). (c) CIN2 (score = 1). (d) CIN3 (score = 0). (e,f) Squamous cell carcinoma (SCC) (score = 3). (f) (▶) Basement membrane. (▷) Site of infiltration.

Table 2 Summary of histochemistry with HHL

Tissue specimens	HHL staining score			
	0	1	2	3
NSE (n = 16)	16	0	0	0
CIN1 (n = 26)	19	7	0	0
CIN2 (n = 19)	14	5	0	0
CIN3 (n = 20)	18	2	0	0
SCC (n = 16)	4	6	3	3

HHL staining score: 0 (0%), 1 (1%–5%), 2 (6%–50%), or 3 (51%–100%). CIN, cervical intraepithelial neoplasia; HHL, Hippeastrum hybrid lectin; NSE, normal squamous epithelium; SCC, squamous cell carcinoma.

and no staining of normal squamous epithelium (Fig. 3a). The reason why HHL preferentially stains cancer cells is unclear, but may possibly be related to the mechanism of tumor infiltration. A recent lectin microarray analysis of non-small cell lung cancer examined whether lectins can be used to estimate the lung cancer tissue type based on examination of lung cancer specimens and cultured cells. It was an effective study of a disease such as lung cancer for which tissue diagnosis is difficult before treatment.[23] In addition, lectins have been studied as predictors of recurrence and the prognosis.[24] However, the actual roles of lectins and their binding glycoproteins have not been clarified in any research. In this study, our results suggested that HHL might be associated with infiltration of SCC, which means it could become a marker of the prognosis or relapse in the future. To clarify the significance of the staining pattern of HHL, we will also analyze the binding glycoprotein and related genes in the future. After identification and structural analysis of its target glycoprotein has been performed by glycoprofiling, HHL might become a useful biomarker for identification of SCC of the uterine cervix.

The present lectin microarray method was effective for analyzing glycans in glycoproteins without the need to

© 2017 Japan Society of Obstetrics and Gynecology

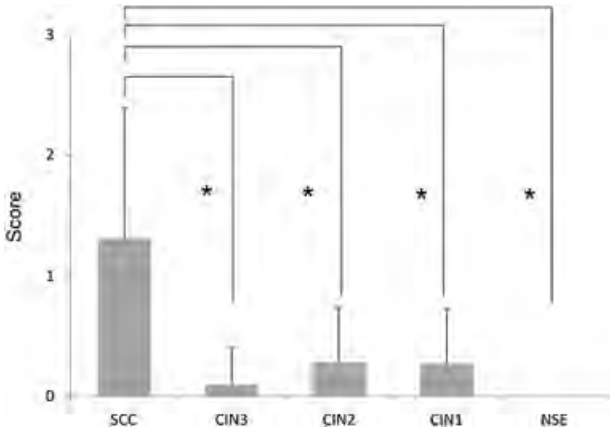

Figure 4 Histochemical expression of Hippeastrum hybrid lectin in cervical tissues. Staining scores for normal squamous epithelium (NSE, n = 16), cervical intraepithelial neoplasia (CIN)1 (n = 26), CIN2 (n = 17), CIN3 (n = 20), and squamous cell carcinoma (SCC; n = 16) are presented as the mean and standard error. The staining score for SCC was significantly higher than that for NSE and each grade of CIN (*$P < 0.05$, Steel's multiple comparison method).

release the glycan moieties or perform purification, unlike other available methods. Differential profiling with tissue microarrays could become a valuable tool if glycan-related biomarkers can be identified.

Cytoplasmic HHL staining of SCC cells (Fig. 3e,f) could distinguish cancer cells from normal epithelial cells or dysplastic cells, but HHL positivity was not associated with the histological tumor grade and the strength of staining varied among different SCC specimens. Despite this, HHL staining achieved a high sensitivity (87.5%) and high specificity (100%) for detection of SCC. As the HHL-positive tumor cells were often at sites of infiltration, this method may be useful for assessing the risk of infiltration by SCC. Currently, follow-up of CIN is required after diagnosis, but there is a possibility that HHL expression can be used to more easily detect tumor infiltration.

In conclusion, HHL is a potential new marker for distinguishing uterine cervical cancer from normal squamous epithelium by glycan profiling of formalin-fixed, paraffin-embedded tissues. Both cytology and histology are associated with overdiagnosis in elderly women with atrophic changes, and HHL staining might be to facilitate the diagnosis of SCC in these women compared to the combination of conventional cytology and histology. Moreover, as HHL positivity was uncommon in CIN, this lectin may be useful when diagnosis is difficult or for detecting recurrence of SCC.

Disclosure

The authors declare that they have no conflicts of interest.

References

1. Feizi T. Demonstration by monoclonal antibodies that carbohydrate structures of glycoproteins and glycolipids are onco-developmental antigens. *Nature* 1985; **314**: 53–57.
2. Dennis JW, Laferte S, Waghorne C *et al.* Beta 1–6 branching of Asn-linked oligosaccharides is directly associated with metastasis. *Science* 1987; **236**: 582–585.
3. Hakomori S. Tumor malignancy defined by aberrant glycosylation and sphingo(glyco)lipid metabolism. *Cancer Res* 1996; **56**: 5309–5318.
4. Goetz JA, Mechref Y, Kang P *et al.* Glycomic profiling of invasive and non-invasive breast cancer cells. *Glycoconj J* 2009; **26**: 117–131.
5. Satomaa T, Heiskanen A, Leonardsson I *et al.* Analysis of the human cancer glycome identifies a novel group of tumor-associated N-acetylglucosamine glycan antigens. *Cancer Res* 2009; **69**: 5811–5819.
6. Pinho SS, Figueiredo J, Cabral J *et al.* E-cadherin and adherens junctions stability in gastric carcinoma: Functional implications of glycosyltransferases involving N-glycan branching biosynthesis, N-acetylglucosaminyltransferases III and V. *Biochim Biophys Acta* 2012; **1830**: 2690–2700.
7. Mitra I, Zhuang Z, Zhang Y *et al.* N-glycan profiling by microchip electrophoresis to differentiate disease states related to esophageal adenocarcinoma. *Anal Chem* 2012; **84**: 3621–3627.
8. Varki A. Biological roles of oligosaccharides: All of the theories are correct. *Glycobiology* 1993; **3**: 97–130.
9. Hakomori S. Glycosylation defining cancer malignancy: New wine in an old bottle. *Proc Natl Acad Sci U S A* 2002; **99**: 10231–10233.
10. Fukuda M. Possible roles of tumor-associated carbohydrate antigens. *Cancer Res* 1996; **56**: 2237–2244.
11. Vanderschaeghe D, Festjens N, Delanghe J *et al.* Glycome profiling using modern glycomics technology: Technical aspects and applications. *Biol Chem* 2010; **391**: 149–161.
12. Hsu KL, Pilobello KT, Mahal LK. Analyzing the dynamic bacterial glycome with a lectin microarray approach. *Nat Chem Biol* 2006; **2**: 153–157.
13. Krishnamoorthy L, Bess JW Jr, Preston AB *et al.* HIV-1 and microvesicles from T cells share a common glycome, arguing for a common origin. *Nat Chem Biol* 2009; **5**: 244–250.
14. Pilobello KT, Slawek DE, Mahal LK. A ratiometric lectin microarray approach to analysis of the dynamic mammalian glycome. *Proc Natl Acad Sci U S A* 2007; **104**: 11534–11539.
15. Kuno A, Uchiyama N, Koseki-Kuno S *et al.* Evanescent-field fluorescence-assisted lectin microarray: A new strategy for glycan profiling. *Nat Methods* 2005; **2**: 851–856.
16. Matsuda A, Kuno A, Ishida H *et al.* Development of an all-in-one technology for glycan profiling targeting formalin-embedded tissue sections. *Biochem Biophys Res Commun* 2008; **370**: 259–263.

© 2017 Japan Society of Obstetrics and Gynecology

17. Wells M, Ostor AG, Crum CP *et al. World Health Organization Classification of Tumours – Pathology and genetics: Tumours of the breast and female genital organs*. Lyon: IARC Press, 2003.
18. Monsonego J. Cervical cancer prevention: Current perspectives. *Endocr Dev* 2012; **22**: 222–229.
19. Ito H, Kuno A, Sawaki H *et al.* Strategy for glycoproteomics: Identification of glyco-alteration using multiple glycan profiling tools. *J Proteome Res* 2009; **8**: 1358–1367.
20. Narimatsu H, Sawaki H, Kuno A *et al.* A strategy for discovery of cancer glyco-biomarkers in serum using newly developed technologies for glycoproteomics. *FEBS J* 2010; **277**: 95–105.
21. Ban M, Yoon HJ, Demirkan E *et al.* Structural basis of a fungal galectin from Agrocybe cylindracea for recognizing sialoconjugate. *J Molec Biol* 2005; **351**: 695–706.
22. Veau B, Guillot J, Damez M *et al.* Purification and characterization of an anti-(A + B) specific lectin from the mushroom Hygrophorus hypothejus. *Biochim Biophys Acta* 1999; **1428**: 39–44.
23. Hirao Y, Matsuzaki H, Iwaki J *et al.* Glycoproteomics approach for identifying Glycobiomarker candidate molecules for tissue type classification of non-small cell lung carcinoma. *J Proteome Res* 2014; **13**: 4705–4716.
24. Yazawa S, Takahashi R, Yokobori T *et al.* Fucosylated glycans in α1-acid glycoprotein for monitoring treatment outcomes and prognosis of cancer patients. *PLoS ONE* 2016; **11**: e0156277.

© 2017 Japan Society of Obstetrics and Gynecology

Journal of Assisted Reproduction and Genetics (2018) 35:2037–2048
https://doi.org/10.1007/s10815-018-1298-y

FERTILITY PRESERVATION

Oocyte retrieval after heterotopic transplantation of ovarian tissue cryopreserved by closed vitrification protocol

Yodo Sugishita[1] · Naoki Okamoto[1] · Atsushi Uekawa[1] · Takayuki Yamochi[2] · Mariko Nakajima[1] · Chie Namba[1] · Suguru Igarashi[1] · Takumi Sato[1] · Sei Ohta[3] · Makoto Takenoshita[3] · Shu Hashimoto[2] · Akiko Tozawa[4] · Yoshiharu Morimoto[5] · Nao Suzuki[1]

Received: 27 May 2018 / Accepted: 22 August 2018 / Published online: 1 September 2018
© Springer Science+Business Media, LLC, part of Springer Nature 2018

Abstract

Purpose A device for closed vitrification was designed to reduce the risk of contamination and investigated on its efficacy for ovarian function recovery after cryopreservation and heterotopic transplantation.

Methods Ovarian tissues from green fluorescence protein transgenic mice (10 GFP mice) were vitrified using the device, and warmed ovarian tissues were transplanted into the ovarian bursa region in wild-type female mice (6 mice). Fresh ovarian tissues were similarly transplanted as a control. After recovery of the estrous cycle, mice were mated with male mice. Ovarian tissues from six cynomolgus monkeys were vitrified and warmed with the device for autologous, heterotopic transplantation. Fresh tissue transplantation was not performed for the control. Ovarian function was examined by recovery of the hormonal cycle. Histological examination was conducted.

Results The number of live pups per recipient mouse was not significantly different after transplantation of fresh or vitrified-warmed ovarian tissue, although the pregnancy rate was reduced with vitrified tissues. The hormonal cycle was restored in 5/6 monkeys after heterotopic transplantation of vitrified-warmed ovarian tissue. Follicles were harvested at eight sites in the omentum and 13 sites in the mesosalpinx. In vitro maturation (IVM)/IVF produced embryo but did not develop.

Conclusions Resumption of the hormonal cycles, follicle development, and oocyte retrieval from vitrified-warmed ovarian tissue transplants may indicate that the use of vitrification for ovarian tissue in a closed system has a potential of clinical application without the risk of contaminations. More detailed analyses of the effects of vitrification on ovarian tissue, such as gene expression patterns in oocytes and granulosa cells, may be needed for establishing a standard procedure for cryopreservation of ovarian tissues in human.

Keywords Ovarian tissue cryopreservation · Vitrification · Closed device · Cynomolgus monkey · Fertility preservation · Autologous transplantation

✉ Nao Suzuki
nao@marianna-u.ac.jp

[1] Department of Obstetrics and Gynecology, St. Marianna University School of Medicine, 2-16-1 Sugao, Miyamae-ku, Kawasaki, Kanagawa 216-8511, Japan

[2] Namba IVF Clinic, Osaka 550-0015, Japan

[3] Eve Bioscience, Co, Ltd., Wakayama 648-0003, Japan

[4] Institute of Medical Science, St. Marianna University Graduate School of Medicine, 2-16-1 Sugao, Miyamae-ku, Kawasaki, Kanagawa 216-8511, Japan

[5] HORAC IVF Grand Front, Osaka 530-0011, Japan

Introduction

Medical and technical advances have given women better chances to preserve fertility and to have children at a later time, including the cryopreservation of embryos, oocytes, and ovarian tissue. Ovarian tissue cryopreservation benefits women more broadly, since ovarian tissue contains steroidogenesis and gametogenesis activities and a large number of primordial follicles and can be harvested irrespective of the stage of the menstrual cycle or be applied to pre-pubertal girls. Since the first successful transplantation of frozen–thawed ovarian tissues was reported by Oktay and Karlikaya in 2000 [1], about 130 live births have been reported after

transplantation of cryopreserved ovarian tissue around the world [2], and the FertiPROTEKT network registry has listed more than 1000 ovarian tissue cryopreservation procedures [3]. Nonetheless, no validated standard protocol has been established for cryopreservation of ovarian tissue [4].

Some studies comparing slow freezing and vitrification by rapid freezing have shown that vitrification is superior for cryopreservation of ovarian tissue with respect to follicle density, cell proliferation, stromal cell preservation, and cell viability [5–8]. Recently, several protocols for vitrification have been reported [5, 6, 9–11], and at least one vitrification system is currently available for clinical use. Cryopreservation by vitrification is achieved by elevating the cooling rate and concentration of cryoprotectants and forming a glassy, vitrified state by extreme elevation of viscosity during cooling [12]. There are two main challenges to improving vitrification techniques: (i) high concentrations of cryoprotectant, which may be toxic to oocytes, embryos, and ovaries, are required and (ii) intracellular ice may develop if the cooling or warming rates are incorrect [13, 14]. Several methods have been developed to overcome these problems. The logical way to make cooling more rapid is to use the smallest possible volume of cryoprotectant around the sample and to directly expose it to liquid nitrogen without any insulation. It is a process known as open vitrification [13]. Successful open vitrification of ovarian tissues has been achieved in mice [5, 15, 16], cattle [9], monkeys [10, 11], and humans [6]. Two healthy babies have been born from vitrified ovarian tissues preserved by open vitrification [17, 18]. However, there is concern about the sterility of liquid nitrogen and the risk of cross-contamination during long-term storage [19, 20]. Because ovaries are larger than oocytes or embryos, the risk of cross-contamination is increased with ovarian cryopreservation by direct contact between solution containing ovarian tissue and liquid nitrogen. To avoid the risk of contamination, a closed vitrification method was developed and used in vitro for development of preantral follicles from the macaque ovarian cortex [21]. However, in vivo tissue transplantation studies are needed to confirm long-term function and fertility of vitrified-warmed ovarian tissues.

In the present study, we developed a new closed vitrification protocol. The efficacy of the protocol was assessed using ovarian tissues of mice and cynomolgus monkeys for long-term functions of vitrified-warmed ovarian tissues after transplantation.

Materials and methods

This investigation of closed vitrification process was based on previous research into open vitrification by Suzuki et al. [11]. The study protocol was approved by the ethics committee of St. Marianna University School of Medicine (Kanagawa, Japan) and IVF Namba Clinic (Osaka, Japan). This study was performed in accordance with the guidelines for use of animals at the experimental facilities of St. Marianna University School of Medicine (Kanagawa, Japan), Kinki University (Wakayama, Japan), and Eve Bioscience Ltd. (Wakayama, Japan).

Studies in mice

Animal care and management

Female and male C57BL/6J mice and green fluorescence protein (GFP)-transgenic [C57BL/6J-Tg (CAG-EGFP)] mice were purchased from SLC Japan Inc. (Tokyo, Japan). Mice were housed under a 12-h light/12-h dark cycle at 22 °C with 55% humidity and received food and water ad libitum.

Collection, cryopreservation, and thawing of donor mouse ovaries

Donor ovaries were collected from 4-week-old C57BL/6J-Tg (CAG-EGFP) mice and placed into disposable Petri dishes containing Dulbecco's modified Eagle's medium/Ham's F-12 [1:1 (*v*/*v*)]. Then, each ovary was cut in half for cryopreservation using the new closed device. After 1–2 months, the cryopreserved ovarian tissues were warmed and stored in H199 supplemented with 20% (*V*/*V*) SSS medium until transplantation.

Transplantation of mouse ovaries

Orthotopic transplantation of vitrified-warmed half ovaries was performed in 6-week-old female C57BL/6J mice, while fresh ovaries harvested from 4-week-old CAG-EGFP female mice were cut in half and used as control grafts. Orthotopic transplantation was done as described previously [15] with some modifications. In brief, anesthesia was induced by intraperitoneal injection of pentobarbital sodium salt (7.5 g/kg body weight). A midline longitudinal skin incision was made in the lower back, followed by small bilateral incisions in the fascia and muscles immediately above each ovary through which the recipient's reproductive tract was lifted out. Then, a small slit was made in each ovarian bursa, and the recipient's ovary was removed under an operating microscope and was replaced with a fresh or thawed half ovary. Subsequently, the bursal membrane was sutured, the reproductive tract was replaced inside the body, and the skin incision was sutured.

Mating of mice

One recipient mouse was paired for 1 day with one male C57BL/6J mice 10 days after transplantation to allow recruitment of primordial follicles before mating. When mating was confirmed by the presence of a vaginal plug, pregnant females were moved to separate cages. The number of pups (both dead and alive) was recorded.

Monkey experiments

Animal care and management

Six cynomolgus monkeys (4 years old and weighing 3.0–3.5 kg) imported from Vietnam by Eve Bioscience (Wakayama, Japan) were used in this study. After importation, the monkeys were quarantined for 1 month and were examined for pathogenic bacteria and changes of appearance and/or behavior. Monkeys were housed individually in special cages (550 mm × 72 mm × 780 mm) in an animal room with a temperature of 25–38 °C, ventilation 5 times/h, and a 12-h light/12-h dark cycle (07:00–19:00). Food (AS; Oriental Yeast Co., Ltd., Tokyo, Japan) was supplied every morning, and drinking water (municipal tap water of Hashimoto City, Wakayama, Japan) was provided ad libitum. The estrous cycle was confirmed in each female by monitoring vaginal bleeding.

Anesthesia and surgery

Laparotomy was performed after induction of anesthesia by intramuscular injection of a 2:1 mixture of ketamine (20 mg/kg Ketalar 50; Sankyo Yell Pharmaceutical, Tokyo, Japan) and xylazine (1 mg/kg Celactal Bayer Yakuhin, Osaka, Japan). During surgery, additional doses of these anesthetics were administered as appropriate to maintain the depth of anesthesia. After resection of the bilateral ovaries, adherent tissues were removed, and the organs washed twice in modified Human Tubal Fluid (m-HTF, Kitazato BioPharma Co., Ltd., Shizuoka, Japan). Then, the cortical tissue was removed from each pair of ovaries and placed in m-HTF. Monkeys were recovered from anesthesia following suture. Relaparotomy for transplantation was performed generally after about 5 h, including 1 h for tissue preparation, 3 h of soaking in liquid nitrogen, and 1 h for warming.

Ovarian tissue cryopreservation and transplantation

The monkey ovarian tissue was cut into strips (10 mm × 10 mm × 1 mm) for vitrification, and cryopreservation was performed using the closed device by the same procedure as that for mice (Fig. 1d, e). Tissue strips were maintained in liquid nitrogen for at least 3 h. Laparotomy was performed for transplantation of vitrified-thawed ovarian tissue, with a minced graft (cut into 20~25 pieces measuring 1 mm × 1 mm × 1 mm) on the right side and an intact strip (10 mm × 10 mm × 1 mm) on the left side of the omentum or the mesosalpinx. Altogether, four tissue grafts, two preparations each for strips and minces, were transplanted in each monkey, one graft each on each side of two sites, the omentum, and the mesosalpinx. For omental transplantation, the graft was wrapped in the omentum that was sutured to form a bag. For transplantation into the mesosalpinx, an incision was made in the right side of the mesosalpinx to create a pocket, into which graft was placed and incision was sutured. To prevent adhesions, Seprafilm® (Kaken Pharmaceutical Co., Ltd. Tokyo, Japan) was used during closure of the abdomen.

Stimulation of ovarian tissue

Ovarian stimulation was conducted after down-regulation with a gonadotropin-releasing hormone (GnRH) agonist (1.88 mg of Leuplin injection 3.75; Takeda Pharmaceutical, Osaka, Japan). Six female monkeys were administered various doses of recombinant human follicle-stimulating hormone (rhFSH; Follistim®; MSD, Osaka, Japan) after down-regulation in three trials, as described below. On the evening of the final day of rhFSH injection, 400 IU/kg of human chorionic gonadotrophin (hCG; Puberogen; Nippon Yakkyoku, Tokyo, Japan) was administered, and ova were collected 40 h later. In the first trial, 25 IU/kg of rhFSH was administered once daily in the morning on days 1 to 9 (initiation of FSH injection = day 0). The second and third trials were initiated 6 months and 1 year after transplantation. In the second trial, 50 IU/kg of rhFSH was administered once daily in the morning on days 1 to 9, after which 100 IU/kg of rhFSH was administered twice daily in the morning and evening on days 10 and 11. In third trial, 50 IU/kg of rhFSH was administered once daily in the morning on days 1 to 4, 75 IU/kg of rhFSH was administered twice daily in the morning and evening on days 5 to 11, and 100 IU/kg of rhFSH was administered twice daily in the morning and evening on day 12. Ovarian stimulation was initiated 2 weeks after estradiol elevation in the trial 1 and between estradiol elevations 6 months and 1 year after transplantation in the trials 2 and 3, respectively. All three trials were performed on all monkeys, except the monkey 6 which was subjected to only the trials 2 and 3.

Oocyte collection and transportation

Laparotomy was performed under general anesthesia as described above. After confirming mature follicle development, oocytes were aspirated, and a small piece of ovarian tissue containing the follicle growth area was excised and placed in the culture medium. Oocytes were collected by puncturing the follicle in a culture dish to avoid loss of oocytes. Aspiration of mature follicles was performed by using a 2.5-ml syringe with a 21-G needle that contained a small amount of HEPES-Tyrode's albumin with lactate and pyruvate (HEPES-TALP, pH 7.4) and 0.3% bovine serum albumin, after pre-washing the needle and syringe with heparin sodium (Ajinomoto Pharmaceutical, Tokyo, Japan). The retrieved ova were transferred to HEPES-TALP in a dish on a warming plate maintained at 38 °C and maturation was examined by stereomicroscopy (×80). Then, the collected ova were placed into HEPES-TALP in a sealed round-bottom tube (2058, Becton Dickinson Labware, NJ, USA) kept in warm water (38 °C). The ovarian tissue was placed in 15-ml tubes (Polypropylene Conical Centrifuge Tube, BD Falcon, Bedford,

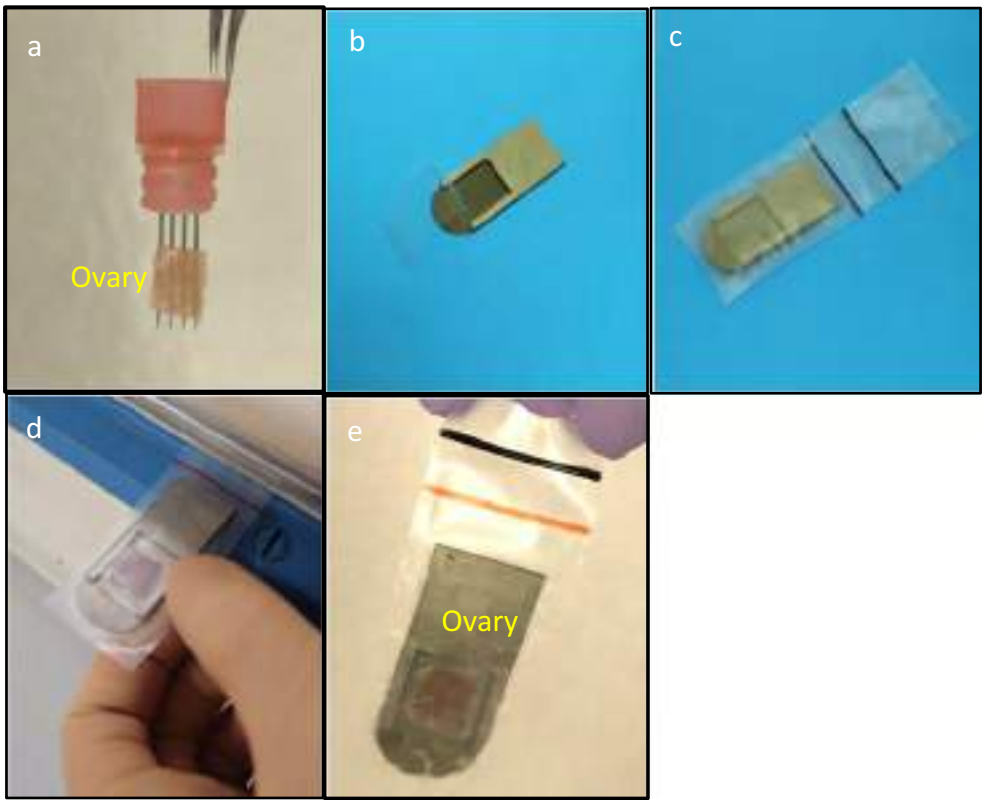

Fig. 1 Devices for vitrification. **a** Ova Cryo Device Type M (open device [11]). **b** Closed device. **c** Closed device in the pouch. **d** The sealed pouch. **e** Vitrified ovarian tissue

MA, USA) containing the same culture medium. The specimens were transferred from Eve Bioscience to Namba IVF Clinic (Namba, Osaka, Japan) within 2 h.

In vitro maturation of immature monkey oocytes

In the first and second trials, we examined whether oocytes obtained at the germinal vesicle (GV) stage or metaphase I (MI) stage could reach metaphase II (MII). The oocytes were incubated at 37 °C for 24–72 h under an atmosphere of 5% O_2, 5% CO_2, and 90% N_2 in TALP medium containing L-glutamine, lactic acid, pyruvic acid, and 20% (*v*/*v*) fetal bovine serum. In the third trial, 20 ng/ml of epidermal growth factor (EGF; Sigma-Aldrich Chemical Co., St. Louis, MO, USA) was added to the abovementioned TALP medium, and the oocytes were cultured for 24–72 h.

Intracytoplasmic sperm injection: fertilization of monkey oocytes

Semen was obtained from a male monkey under anesthesia with ketamine HCl (10 mg /kg) by electrical induction of ejaculation. The methods used for freezing and thawing sperm were described previously [21]. Intracytoplasmic injection (ICSI) of cryopreserved sperm was performed as reported previously [11] with minor modifications. Briefly, cumulus cell-oocyte complexes were treated with 0.01% (*w*/*v*) hyaluronidase (H3757; Sigma-Aldrich) dissolved in HEPES-TALP, and then oocytes were denuded by pipetting at room temperature. After maturation of the denuded oocytes was evaluated, culture was performed at 37 °C under an atmosphere of 5% O_2, 5% CO_2, and 90% N_2 in TALP until the time of ICSI. The sperm suspension and oocytes were placed in HEPES-TALP and covered with mineral oil (M8410; Sigma-Aldrich). A single sperm with normal morphology was captured by an injection pipette (MIC-SI-30-NTP; Humagen Fertility Diagnostics, Charlottesville, VA, USA) and then was washed and immobilized in an injection pipette containing 10% polyvinylpyrrolidone (PVP360; Sigma-Aldrich) dissolved in HEPES-TALP. The immobilized sperm was injected into a mature oocyte in HEPES-TALP. After injection, culture was done for 24 h at 37 °C under an atmosphere of 5% O_2, 5% CO_2, and 90% N_2 in TALP. Fertilization was evaluated on basis of detecting two pronuclei and two polar bodies at 18 h after sperm injection, and cleavage was confirmed at 24 h after sperm injection. Then, the embryos were cultured for 144 h in CMRL-1066 medium (11530-037; Life Technologies, Carlsbad, CA, USA) containing L-glutamine, lactic acid, pyruvate, and 20% (*v*/*v*) fetal bovine serum under the same atmosphere.

Morphological investigation of monkey ovarian tissue

Monkey ovarian tissues were fixed overnight at 4 °C in Bouin's fixative (Polysciences, Warrington, PA, USA), embedded in paraffin, and cut into 1–5-μm-thick

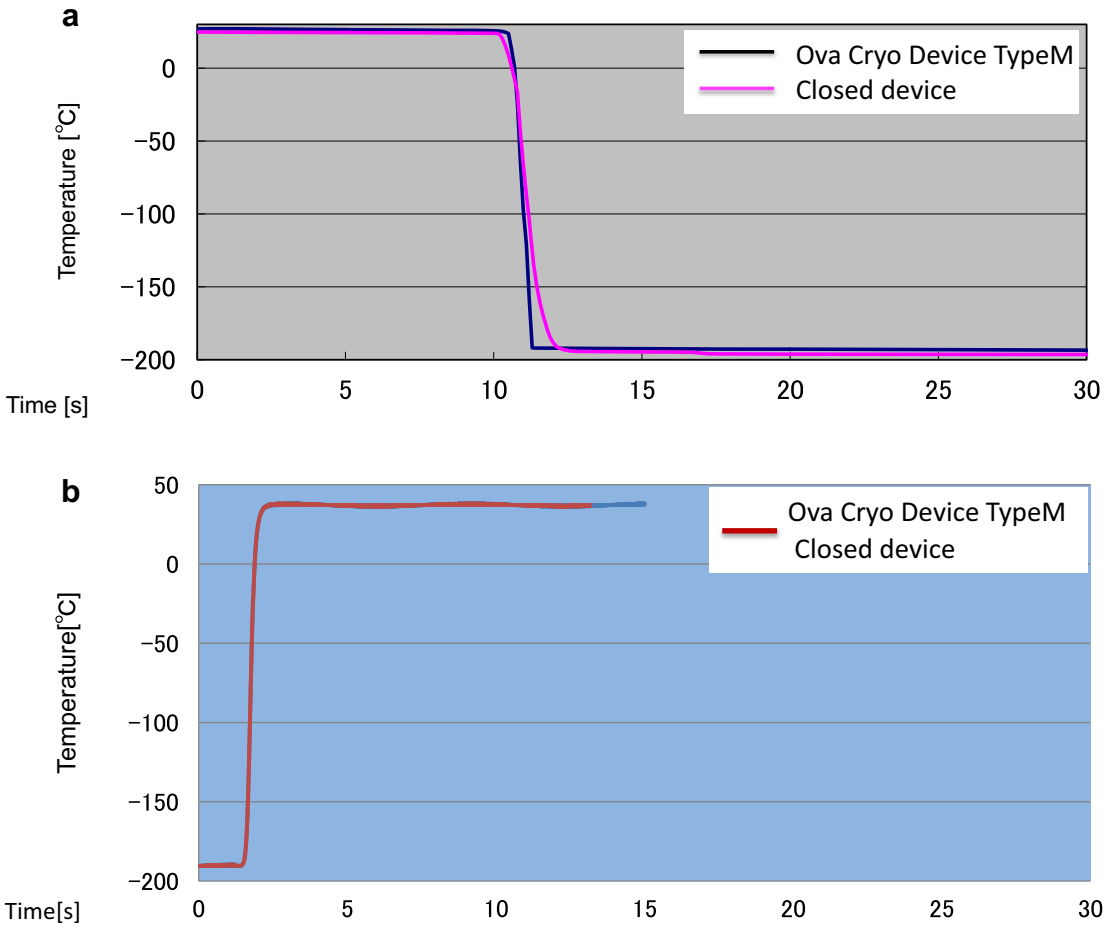

Fig. 2 Cooling and warming rates of vitrification devices. **a** Cooling rate of the open (black) and closed (pink) devices. The cooling rates of the open devise and the closed devise were − 19,500 and − 12,000 °C/min, respectively. **b** Warming rates of the open and closed devices were identical and shown in red. The warming rate was 42,000 °C/min

sections. Sections were stained with toluidine blue (Certistain® Toluidine blue O (C.I.52040), Millipore, MA, USA) and hematoxylin-eosin (Sakura Finetek Japan, Tokyo, Japan), followed by observation under a microscope. Follicular development stages were defined as follows: primordial follicles were in a single layer of flattened pre-granulosa cells, primary follicles were follicles with only one granulosa cell layer, early secondary follicles had two to four granulosa cell layers without an antrum, late secondary follicles had more than four granulosa cell layers without an antrum, and antral follicles had multiple layers of cuboidal granulosa cells with an antrum [22].

Hormone assays

Estradiol (E_2) and progesterone (P_4) were measured by SRL Inc. (SRL, Tokyo, Japan) to confirm the hormone cycle of the monkeys before ovarian tissue cryopreservation and approximately every 2 weeks after transplantation of vitrified-thawed ovarian tissue. This procedure was performed in the same manner as reported previously [11].

Open vs. closed vitrification

Loading with cryoprotectant

Cryopreservation of ovarian tissues using an open device was performed as described previously with some modifications [10, 11]. Strips of ovarian tissue were first equilibrated in HEPES-buffered 199 (H199, Invitrogen, Carlsbad, CA, USA) supplemented with 20% (*V*/*V*) SSS (Irvine Scientific, Santa Ana, CA, USA) and 1.61 mol/l ethylene glycol for 5 min, followed by equilibration in H199 supplemented with 20% (*V*/*V*) SSS and 3.22 mol/l ethylene glycol for 5 min. Subsequently, the ovarian strips were transferred into H199 supplemented with 20% (*V*/*V*) SSS, 5.64 mol/l ethylene glycol, 5% (*w*/*v*) polyvinylpyrrolidone (Sigma-Aldrich, St. Louis, Mo, USA), and 0.5 mol/l sucrose EMPROVE®bio

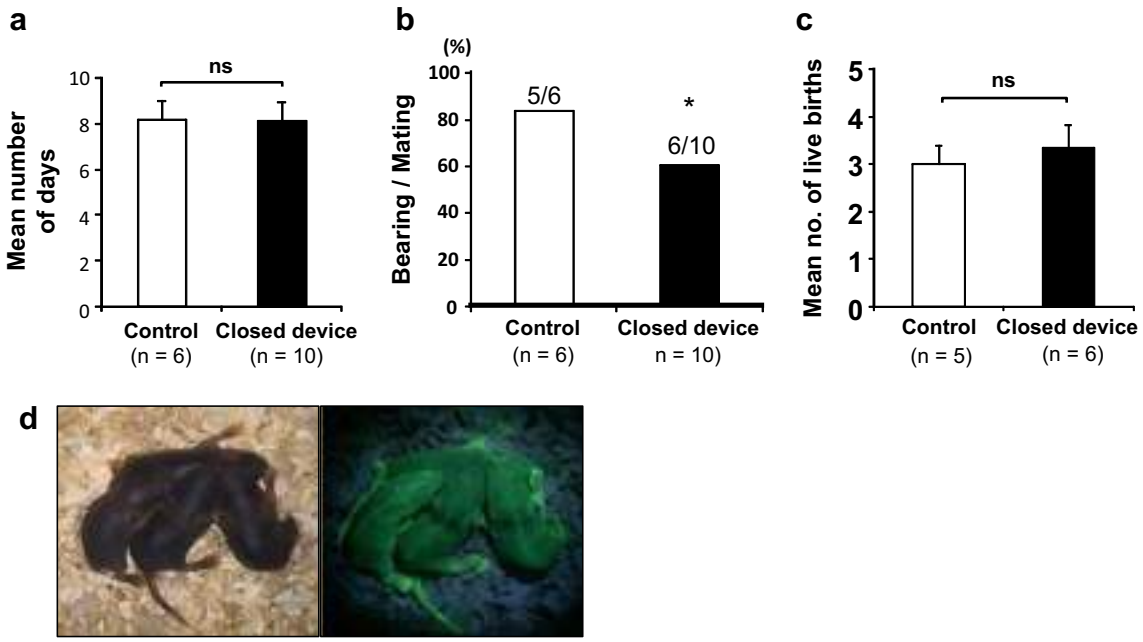

Fig. 3 Orthotopic ovarian tissue transplantation in mice. Fresh and vitrified/warmed ovarian tissues were transplanted for functional evaluation. Graph shows the mean with the standard deviation for 6 mice (fresh tissue) and 10 mice (vitrified/warmed tissue). *$p < 0.05$. **a** Days required before the initial increase of estradiol. **b** Rates of pregnancy. **c** Number of live pups per pregnancy. **d** Pups from transplants of fresh (**a**) or cryopreserved GFP mouse ovaries (**b**)

(EMD Millipore, Billerica, MA, USA). All steps were performed at 26 °C.

Vitrification procedure

Open device Within 25 min, the strips were loaded into an ovarian storage device (Ova Cryo Device TypeM®; Kitazato BioPharma Co., Shizuoka, Japan; Fig. 1a) and the device was immersed vertically into liquid nitrogen. Then the frozen strips were individually placed into cryogenic vials and were stored in liquid nitrogen until further use.

Closed device The device was made from titanium (500 and 800 μm in thickness) for excellent thermal conductivity (CDT × 10, titanium, Kitazato BioPharma Co., Ltd., Shizuoka, Japan). Two sizes of thickness (500 and 800 μm) were tested in consideration of conductance and structural stability. However, the similar stability and conductance were obtained with both thicknesses. The 500-μm thickness was used in mice. The 800-μm one was used only for one monkey as comparison after testing both thicknesses. For vitrification, a piece of ovarian tissue equilibrated with vitrification solution was placed on the titanium plate and covered with polypropylene film (Kitazato BioPharma Co., Ltd., Shizuoka, Japan). To prevent viral contamination, the device was placed in a bag made from the same polypropylene material as the film cover, which was heat-sealed and immersed in liquid nitrogen. This extra step for inserting vitrified tissue in a bag took only 10~30 s; thus, we did not feel there was any difference between open and closed device in the effect of cryoprotectants. The polypropylene material used for the film cover and bag was demonstrated to be safe by a cytotoxicity test before this study (Fig. 1b–e).

Warming procedure

For thawing, pouch is cut open and the device is directly placed into the thawing solution. The vitrified samples were thawed in 20 ml of H199 containing 20% (*V*/*V*) SSS and 0.8 mol/l sucrose, which had been warmed at 37 °C for 1 min in a water bath, followed by dilution in H199 containing 20% (*V*/*V*) SSS and 0.4 mol/l sucrose for 3 min at room temperature, and then dilution twice in H199 containing 20% (*V*/*V*) SSS for 5 min at room temperature. After removal of the cryoprotectant, the ovarian sections were placed in H199 containing 20% (*V*/*V*) SSS. No devitrification was observed in any tissue preparation.

Heat conduction rate

Cooling was assessed by measuring the heat conduction rate using a K-type thermocouple and a data logger GL900-4 (Graphtec Inc., Kanagawa, Japan), with the mean of 10 temperature measurements being plotted to generate a graph (Kitazato

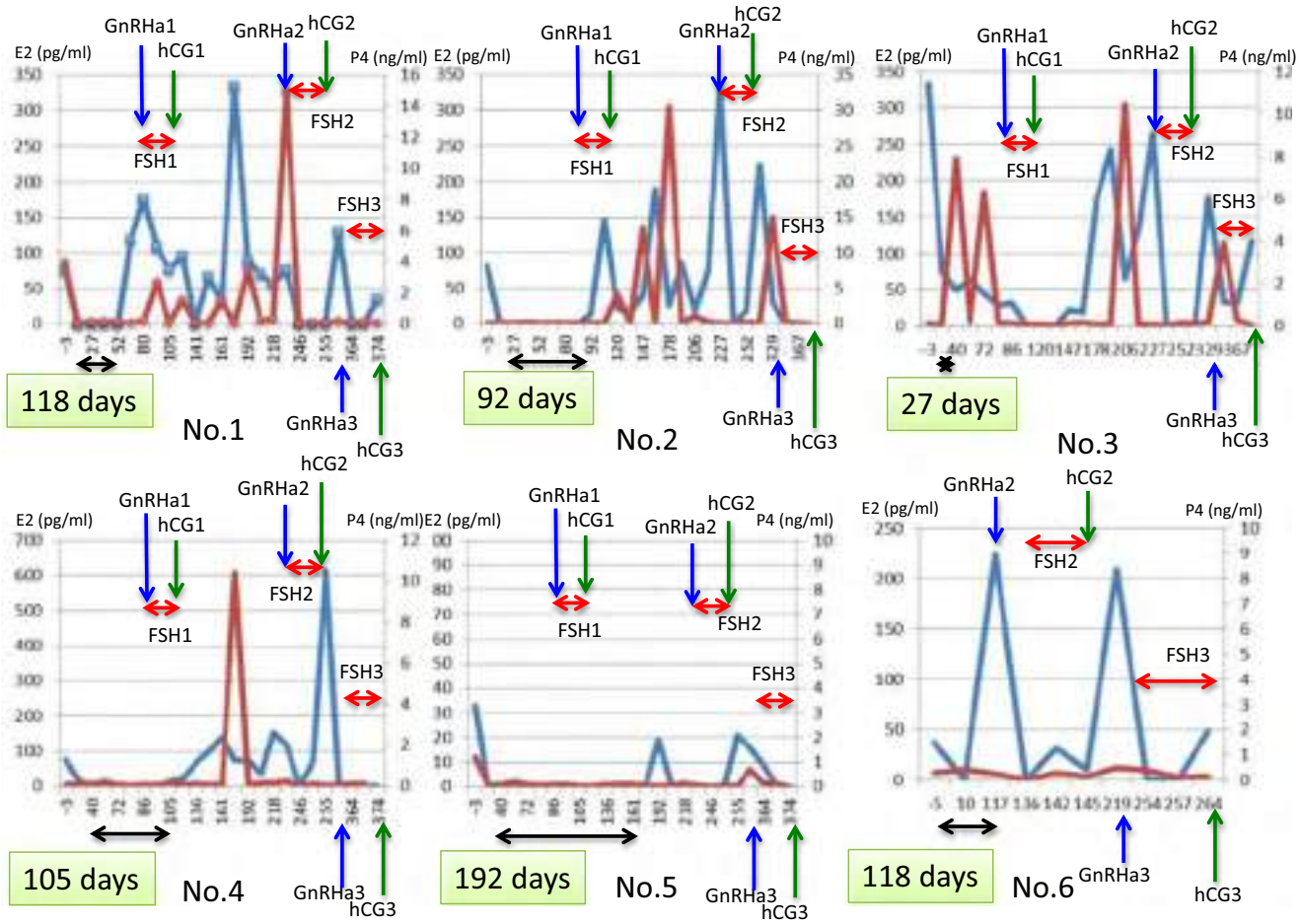

Fig. 4 Hormonal cycles in monkeys. Estradiol (blue line) and progesterone (red line) in blood after ovarian transplantation. Number in green square: days required before hormone detection in blood. IVF cycles are indicated by arrows: GnRH (blue), FSH (red), and hCG (green)

BioPharma Co., Ltd., Shizuoka, Japan). The heat conduction rate was compared between the open device (Ova Cryo Device TypeM®) and the closed device (CDT × 10; Fig. 2a, b).

Statistical analysis

All statistical analyses were performed by using EZR (Saitama Medical Center, Jichi Medical University, Saitama, Japan), which is a graphical user interface for R (The R Foundation for Statistical Computing, Vienna, Austria).

Results

Thermal conductivity

The cooling rates of the open and closed vitrification devices were − 19,500 and − 12,000 °C/min, respectively (Fig. 2a), while the warming rate of both devices was 42,000 °C/min (Fig. 2b). There were no differences of thermal conductivity, especially the cooling speed, between devices with a thickness of 500 or 800 μm.

Fertility of mice after transplantation of vitrified-warmed ovarian tissues

Six mice received transplantation of fresh ovarian tissue as controls. Vitrified-warmed ovarian tissue was transplanted into 10 mice. The estrous cycle was recovered in all recipients. Estradiol increased at 5–11 days after transplantation of fresh ovarian grafts and after 7–14 days in mice receiving vitrified-warmed grafts. There were no significant differences in the time required until recovery of the estrous cycle between mice receiving fresh grafts (8.2 ± 0.9 days) and vitrified-warmed grafts (8.1 ± 0.9 days) (Fig. 3a). Recipient mice were kept for 3 weeks after transplantation to allow recruitment of primordial follicles before mating. The delivery rate was significantly lower for mice with vitrified-warmed ovarian grafts

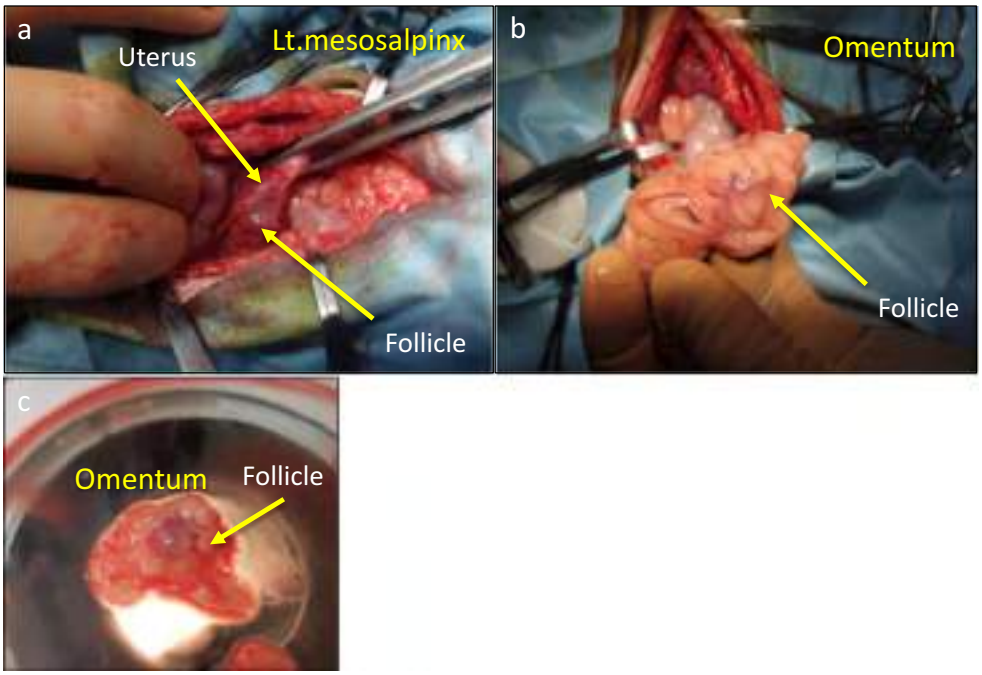

Fig. 5 Laparotomy for oocyte retrieval in monkey no. 4. Follicles are evident in the left mesosalpinx (**a**) and omentum (**b**) on the post-transplantation day 252. A pre-ovulatory follicle dissected from the omentum, shown in **b**, is shown in an enlarged scale (**c**)

(60%) than for mice with fresh grafts (83%) (Fig. 3b). However, the number of live pups delivered per recipient was not significantly different between the two groups (Fig. 3c, d).

Hormonal cycle in monkeys

Transplantation of vitrified-warmed ovarian tissues was performed in six cynomolgus monkeys. No monkey received fresh ovarian tissue as control due to the cost of each monkey. Five monkeys received ovarian tissue that had been vitrified using 500-μm closed device, and one monkey (no. 3) received tissue vitrified using 800-μm closed device. Follicle development was assessed by estradiol measurements every 2 weeks. Harvesting of ova was successful in five monkeys, while it failed in monkey no. 4. Resumption of the hormonal cycle was confirmed at 111 days (27–192 days) after transplantation (Fig. 4). The five monkeys used for egg collection exhibited periodic hormonal cycles by 367 days after transplantation. Oocyte collection was performed via laparotomy, with a small piece of tissue around the site of follicle formation being excised carefully while avoiding rupture of the follicle (Fig. 5). It was found that transplanted ovarian tissue had been incorporated into the omentum and the mesosalpinx, and minimal resection was required for oocyte harvesting. Three monkeys (no. 1, no. 3, and no. 6) were still alive at the time of writing, and their hormonal cycles had continued for > 1240 days.

Follicle development

Follicle development was found at eight graft sites in the omentum and 13 sites in the mesosalpinx. In addition, it was detected at 10 sites after transplantation of minced grafts (1-mm cubes) and at 11 sites after transplantation of strip grafts (10 mm × 10 mm × 1 mm), while the number of oocytes recovered was eight and nine, respectively. There were no significant differences of follicle development between transplantation into the omentum or the mesosalpinx, between transplantation of strips or minced grafts, and between cryopreservation with the 500- or 800-μm devices.

IVM and IVF

Seventeen oocytes were retrieved from five monkeys. To perform in vitro maturation (IVM), EGF was not used in the first and second trials in case immature oocytes were collected. A total of seven GV-stage oocytes, one MI oocyte, and two MII oocytes were obtained by the initial two egg collections. When the eight GV-stage oocytes were cultured for up to 72 h, only three reached MI stage but did not progress further. ICSI was performed with the two MII oocytes, and fertilization was confirmed by detection of two pronuclei, but development did not proceed beyond the one-cell stage. A total of six oocytes were obtained at the third egg collection, including four GV-stage oocytes, one MII oocyte, and one degenerated embryo. IVM was performed with four GV-stage oocytes by adding EGF at 20 ng/ml. One of these oocytes reached MII stage but failed to fertilize by ICSI (Table 1).

Table 1 IVM and IVF of oocytes retrieved from transplanted ovarian tissue in monkeys

Ovarian stimulation	No of Monkey	Thickness of device	Days between hormonal measurement and oocyte harvest	Serum estradiol (E2) level (pg/ml) / Serum progesterone (P4) level (ng/ml)	Days between hormone measurement and oocyte harvest	Site	Side	Follicle number	Gained oocyte number	Stage	IVM	Reached to MII	ICSI	Fertilized
Trial 1	1	500	110	E2: 76 / P4: 0.06	5	Mesosalpinx	Lt	1	1	GV	yes	No		
	2	500		E2: 146 / P4: 0.1	5	Omentum	Rt	1	1	GV	yes	No		
Trial 2	2	500	258	E2: 223 / P4: 0.08	3	Mesosalpinx	Lt	4	4	GV	yes	No		
						Omentum	Lt	1	0					
	4	800		E2: 61 / P4: 0.04	3	Mesosalpinx	Lt	2	2	MII	No		Yes	2PN
						Omentum	Lt	1	1	MI	yes	No		
						Mesosalpinx	Rt	1	1	GV	yes	No		
						Omentum	Rt	1	1	GV	yes	No		
Trial 3	1	500	377	E2: 34 / P4: 0.03	3	Omentum	Rt	1	1	MII	No		Yes	No
	3	800		E2: 116 / P4: 0.04	3	Omentum	Lt	1	1	Degeneration				
						Omentum	Rt	1	0					
	6	500		E2: 49 / P4: 0.16	3	Mesosalpinx	Rt	4	4	GV	Yes	Yes	Yes	No
						Mesosalpinx	Lt	1	0					
						Omentum	Rt	1	0					

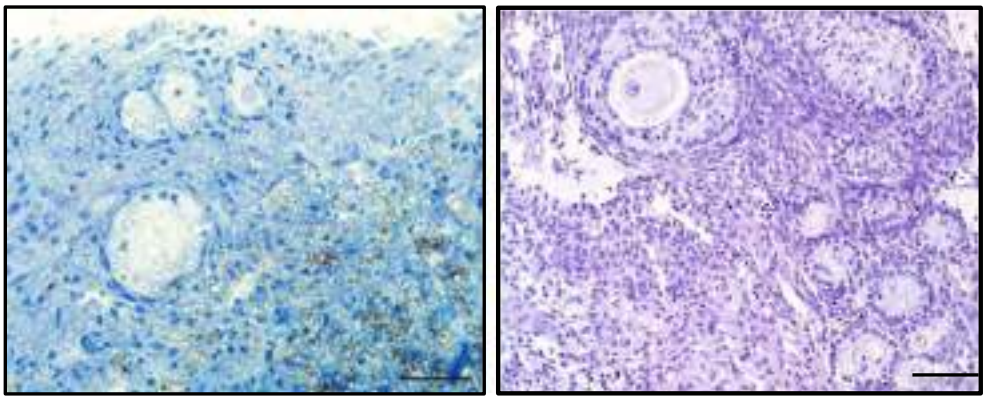

Fig. 6 Post-transplantation histological analyses. **a** Ovarian tissue adjacent to pre-ovulatory follicles excised for oocyte harvest from the omentum on the post-transplantation day 258 that yielded a MI oocyte (monkey no. 4). **b** The omentum which yielded GV oocytes (monkey no. 2). A Toluidine blue staining. **b** H&E staining. Scale bar = 50 μm

Histological findings

After collection of oocytes, the residual tissues were fixed for histological examination. At a site of ovarian tissue transplantation into the omentum, two primary follicles and one early secondary follicle were detected. Also, at another omental transplantation site, there were primordial follicles, primary follicles, and late secondary follicles, having the potential to develop for oocyte collection (Fig. 6a, b).

Discussion

A closed vitrification devise was developed using a titanium plate for housing ovarian tissue which is sealed inside a polypropylene pouch to avoid viral contamination during exposure to liquid nitrogen. Due to the excellent thermal conductivity of titanium, similar cooling and warming rates, which are important for maintaining the structural integrity of tissue, were observed by closed vitrification method to those by the standard open one.

The in vivo function was examined by transplanting ovarian tissues after cryopreservation by the closed vitrification devise on mice and cynomolgus monkeys. The number of live pups per litter was similar with both tissues in mice (Fig. 4a). However, the birth rate by cryopreserved tissue with the closed vitrification method was lower than that from fresh ovarian tissue in mice (Fig. 4b). Using similar vitrification conditions to the one used in the present study, follicle counts were similar to fresh tissue transplants, and pregnancy rates were higher than those of transplants from slow freezing or conventional vitrification and similar to the fresh tissue transplants [5, 16]. These studies may indicate that vitrification conditions influence the integrity and potentials of follicles. The lower birth rates observed in the current study could indicate interferences on follicle maturation by vitrification method utilized here, for which further studies may be needed for improvement of vitrification protocol.

In monkeys, vitrified-warmed ovarian tissues were transplanted into the mesosalpinx and the omentum which were shown to be suitable sites for engraftment in our previous study [11]. Heterotopic transplantation was conducted with minced or strip grafts, but the type of graft did not affect oocyte collection. Grafts were wrapped with the omentum tissue, while they were put into a pouch by incision made in the mesosalpinx. These procedures made harvesting easier. Six follicles formed in grafts transplanted to the mesosalpinx and eight follicles were obtained after transplantation to the omentum (with no difference in follicle formation between the two sites). The ovarian cycle was restored after transplantation in most animals, while there were developments of pre-ovulatory follicles and mature oocytes which could fertilize after ICSI. Our study thus demonstrated the mesosalpinx and the omentum as viable options for transplantation of cryopreserved ovarian tissues which would be clinically available for those patients with bilateral ovariectomy or pelvic irradiation.

Multiple follicles were observed in both transplantation sites of the mesosalpinx and the omentum. Some are more mature or immature than others among these follicles. Therefore, the mechanism for selection of a dominant follicle could have been lost by the vitrification process. On the other hand, since the present study was performed by the IVF cycle, it is not apparent if the dominant follicle selection mechanism is preserved. Even in clinics, oocytes can be obtained from smaller follicles rather than the dominant follicle. As many follicles develop at one transplantation site due to ovarian stimulation by FSH, we tried to harvest as many oocytes as can be identified, thus resulting in the harvest of more immature oocytes. Thus, the number of follicles which could yield competent oocytes could have been very limited, even in the presence of cyclic steroid hormone production.

When oocytes were retrieved from transplanted vitrified-warmed ovarian tissues of monkeys after the return of the hormonal cycle, embryos did not develop after fertilization in vitro. Could the failure of embryogenesis be caused by injuries/damages during cryopreservation process? When murine ovarian tissues were processed for cryopreservation by different vitrification methods, transmission electron microscopy demonstrated varying degrees of damages in subcellular structures even in the presence of apparently normal delivery of pups [16]. Using

both murine and human tissues, changes in follicle morphology, particularly in granulosa and stromal cells, were seen after cryopreservation [5]. In ovarian tissue cryopreservation, stromal cells were demonstrated to be more vulnerable to cryoinjuries than primordial follicles [23, 24]. The ovary includes heterogenous cellular and structural components with different properties, and their interactions are needed for follicle maturation and embryogenesis [25]. Apparent structural integrity of ovarian tissue after cryopreservation does not appear to guaranty the quality and function of follicles. It might be informative to analyze effects of cryopreservation on gene expression pattern of oocytes, stromal cells, etc. during maturation for establishing a standard procedure of ovarian tissue cryopreservation.

One of the six monkeys monitored for more than 1 year after transplantation showed a weak response to ovarian stimulation, but its estradiol level was still restored. It is possible that engraftment of ovarian tissue might have been poor in this animal. Among the monkeys monitored for less than 1 year after transplantation, one did not show stable recovery of the hormonal cycle by 8 months after transplantation, although it is possible that the hormonal cycle would have resumed if the follow-up period had been extended. Recovery of the hormonal cycle was confirmed in five of six monkeys, with menstruation returning between 50 and 90 days after transplantation. The time required for recovery of menstruation was shorter than that expected for growth of primordial follicles, indicating the presence of primary and secondary follicles in vitrified ovarian tissues as well as primordial follicles. In three of these monkeys, the hormonal cycle has persisted for over 1200 days since resumption after transplantation.

In conclusion, a closed vitrification procedure was developed to improve the efficacy for ovarian cryopreservation and to avoid the risk of cross-contamination during storage in liquid nitrogen. Live birth was achieved in mice, but our results were unsatisfactory in terms of fertilization and embryo development in primates. This outcome may have occurred because follicle development was only monitored by blood tests and might not have been fully matured. On the other hand, vitrification procedure may have caused damages to cellular structures and genetic activities interfering developmental processes in primates. As we confirmed persistence of the hormonal cycle for longer than 1 year, we are confident that heterotopic engraftment of ovarian tissue was successful. We hope that our closed device will help advance the vitrification technology for clinical application.

Acknowledgments We thank Dr. Ikko Kawashima for support with IVM/IVF; Ms. Ami Amou for cryopreserving and thawing of ovarian tissues; Ms. Asami Onimal for the support in conducting the histological examinations; Tomohiro Noguchi, M.S. (Kitazato Co., Ltd., Shizuoka, Japan) for supplying the devices and solutions and for allowing us to conduct thermal conductivity measurements; Kaken Pharmaceutical Co., Ltd., Tokyo, Japan for supplying Seprafilm; and Dr. David Robert McQuire (Yamada Translation Bureau, Tokyo, Japan) for assistance with manuscript editing.

Author's contribution Y.S., Y.M., A.T., and N.S. participated in the study conception and design; Y.S., A.U., M.N., S.H., and N.S. developed the device; N.O. and M.N. performed mouse studies; Y.S. and M.N. completed freeze–thawing of ovarian tissue in the monkey study; Y.S., N.S., C.N., and S.I. performed surgery on the monkeys; S.O. and M.T. performed ovarian stimulation and management in the monkeys; T.Y. performed collection of monkey oocytes and IVM/IVF; and Y.S. and T.S. conducted histological examination.

Funding This study was funded by grant no. AS2522901P, Adaptable and Seamless Technology transfer Program through target driven R&D (A-STEP), and no. 16gk0110014h0001, Japan Agency for Medical Research and Development (AMED).

Compliance with ethical standards

Conflict of interest The authors declare that they have no conflicts of interest.

References

1. Oktay K, Karlikaya G. Ovarian function after transplantation of frozen, banked autologous ovarian tissue. N Engl J Med. 2000;342(25):1919.
2. Donnez J, Dolmans MM. Fertility preservation in women. NEJM. 2017;377:1658–65.
3. von Wolff M, Dittrich R, Liebenthron J, Nawroth F, Schüring AN, Bruckner T, et al. Fertility-preservation counselling and treatment for medical reasons: data from a multinational network of over 5000 women. Reprod BioMed Online. 2015;31:605–12.
4. Amorim CA, Curaba M, Van Langendonckt A, Dolmans MM, Donnez J. Vitrification as an alternative means of cryopreserving ovarian tissue. Reprod BioMed Online. 2011;23:160–86.
5. Wang Y, Xiao Z, Li L, Fan W, Li SW. Novel needle immersed vitrification: a practical and convenient method with potential advantages in mouse and human ovarian tissue cryopreservation. Hum Reprod. 2008;23:2256–65.
6. Keros V, Xella S, Hultenby K, Pettersson K, Sheikhi M, Volpe A, et al. Vitrification versus controlled-rate freezing in cryopreservation of human ovarian tissue. Hum Reprod. 2009;24:1670–83.
7. Amorim CA, Dolmans MM, David A, Jaeger J, Vanacker J, Camboni A, et al. Vitrification and xenografting of human ovarian tissue. Fertil Steril. 2012;98:1291–8.e1–2.
8. Herraiz S, Novella-Maestre E, Rodríguez B, Díaz C, Sánchez-Serrano M, Mirabet V, et al. Improving ovarian tissue cryopreservation for oncologic patients: slow freezing versus vitrification, effect of different procedures and devices. Fertil Steril. 2014;101:775–84.
9. Kagawa N, Silber S, Kuwayama M. Successful vitrification of bovine and human ovarian tissue. Reprod BioMed Online. 2009;18:568–77.
10. Hashimoto S, Suzuki N, Yamanaka M, Hosoi Y, Ishizuka B, Morimoto Y. Effects of vitrification solutions and equilibration times on the morphology of cynomolgus ovarian tissues. Reprod BioMed Online. 2010;21:501–9.
11. Suzuki N, Hashimoto S, Igarashi S, Takae S, Yamanaka M, Yamochi T, et al. Assessment of long-term function of heterotopic transplants of vitrified ovarian tissue in cynomolgus monkeys. Hum Reprod. 2012;27:2420–9.
12. Fahy GM, MacFarhlane DR, Angell CA, Meyman HT. Vitrification as an approach to cryopreservation. Cryobiology. 1984;21:407–26.

13. Mazur P, Cole KW, Hall WH, Schreuders PD, Mahowald AP. Cryobiological preservation of Drosophila embryos. Science. 1992;258:1932–5.
14. Vajta G, Nagy ZP. Are programmable freezers still needed in the embryo laboratory? Review on vitrification. Reprod BioMed Online. 2006;12:779–96.
15. Migishima F, Suzuki-Migishima R, Song SY, Kuramochi T, Azuma S, Nishijima M, et al. Successful cryopreservation of mouse ovaries by vitrification. Biol Reprod. 2003;68:881–7.
16. Chen SU, Chien CL, Wu MY, Chen TH, Lai SM, Lin CW, et al. Novel direct cover vitrification for cryopreservation of ovarian tissues increases follicle viability and pregnancy capability in mice. Hum Reprod. 2006;21:2794–800.
17. Kawamura K, Cheng Y, Suzuki N, Deguchi M, Sato Y, Takae S, et al. Hippo signaling disruption and Akt stimulation of ovarian follicles for infertility treatment. Proc Natl Acad Sci U S A. 2013;110:17474–9.
18. Suzuki N, Yoshioka N, Takae S, Sugishita Y, Tamura M, Hashimoto S, et al. Successful fertility preservation following ovarian tissue vitrification in patients with primary ovarian insufficiency. Hum Reprod. 2015;30(3):608–15.
19. Bielanski A. The potential for animal and human germplasm contamination through assisted reproductive technologies. Trends Reprod Biol. 2006;2:13–36.
20. Bielanski A, Vajta G. Risk of contamination of germplasm during cryopreservation and cryobanking in IVF units. Hum Reprod. 2009;24:2457–67.
21. Sankai T, Terao K, Yanagimachi R, Cho F, Yoshikawa Y. Cryopreservation of spermatozoa from cynomolgus monkeys (Macaca fascicularis). J Reprod Fertil. 1994;101:273–8.
22. Wulff C, Wilson H, Wiegand SJ, Rudge JS, Fraser HM. Prevention of thecal angiogenesis, antral follicular growth, and ovulation in the primate by treatment with vascular endothelial growth factor trap R1R2. Endocrinology. 2002;7:2797–807.
23. Kim SS, Yang HW, Kang HG, Lee HH, Lee HC, Ko DS, et al. Quantitative assessment of ischemic tissue damage in ovarian cortical tissue with or without antioxidant (ascorbic acid) treatment. Fertil Steril. 2004;82:670–85.
24. Hreinsson J, Zhang P, Swahn ML, Hultenby K, Hovatta O. Cryopreservation of follicles in human ovarian cortical tissue. Comparison of serom and human serum albumin in the cryoprotectant solutions. Hum Reprod. 2003;11:2420–8.
25. Da Broi MG, Giorgi VSI, Wang F, Keefe DL, Albertini D, Navarro PA. Influence of follicular fluid and cumulus cells on oocyte quality: clinical implications. J Assist Reprod Genet. 2018;35(5):735–51.

Lung (2017) 195:179–184
DOI 10.1007/s00408-017-9985-5

COPD

Decrease in Small Pulmonary Vessels on Chest Computed Tomography in Light Smokers Without COPD: An Early Change, but Correlated with Smoking Index

Shinji Saruya[1] · Tsuneo Yamashiro[1,2] · Shin Matsuoka[1] · Shoichiro Matsushita[1] · Kunihiro Yagihashi[1] · Yasuo Nakajima[1]

Received: 20 August 2016 / Accepted: 7 February 2017 / Published online: 21 February 2017
© Springer Science+Business Media New York 2017

Abstract

Purpose The aim of this study was to evaluate the relationship between the amount of smoking and the cross-sectional area (CSA) of small pulmonary vessels in light smokers without a diagnosis of chronic obstructive pulmonary disease (COPD).

Methods This retrospective study was approved by our institutional review board, which waived the need for informed consent from patients. The study included 34 current smokers without COPD, who were defined as light smokers based on their smoking history (≤25 pack years). The CSA of small pulmonary vessels (<5 mm^2 [$CSA_{<5}$]) was measured on computed tomography (CT) scans, and the percentage of total CSA of the lung ($\%CSA_{<5}$) was calculated. The extent of emphysema was also assessed as the percentage of low attenuation area (%LAA, <−950 Hounsfield units). The correlations of $\%CSA_{<5}$ and %LAA with pack years were determined using the Spearman rank correlation.

Results There was a significant negative correlation between $\%CSA_{<5}$ and pack years, whereas no significant correlation was found between %LAA and pack years. The correlations between pack years and percent predicted forced expiratory volume in 1 s (FEV_1) and FEV_1/forced vital capacity were not significant.

Conclusions The percentage of total CSA of the lung made up of small pulmonary vessels in light smokers without COPD significantly decreases with increasing amount of smoking, in contrast to emphysema measurements. This suggests that small pulmonary vessels might have been injured or might have degenerated because of smoking, and might represent an initial stage in the development of COPD.

Keywords COPD · Current smokers · Smoking habits · Pack years · Pulmonary vessels · Cross-sectional area

Introduction

Cigarette smoking is a major risk factor for various diseases, including hypertension, atherosclerosis, and chronic obstructive pulmonary disease (COPD) [1, 2]. Since endothelial dysfunction is an early event in these vascular diseases and in pulmonary emphysema, the effect of smoking on endothelial function has been the focus of several studies, which have shown that both active and passive smoking lead to impaired endothelial function, even in healthy individuals without COPD [3–6]. Because the endothelium plays an important role in the regulation of vascular tone and control of cell growth, pulmonary arteries with endothelial dysfunction have a diminished ability to dilate [7]. Consequently, reduced blood flow in the small precapillary blood vessels may lead to loss of alveolar septa, finally leading to emphysema. Considering the previous reports that vascular changes may precede emphysema, vascular changes might be detectable before pulmonary emphysema on a clinical imaging modality such as computed tomography (CT).

✉ Shinji Saruya
bubi_11_22@yahoo.co.jp

[1] Department of Radiology, St. Marianna University School of Medicine, 2-16-1 Sugao, Miyamae-ku, Kawasaki, Kanagawa 216-8511, Japan

[2] Department of Radiology, Graduate School of Medical Sciences, University of the Ryukyus, 207 Uehara, Nishihara, Okinawa 903-0215, Japan

Several recent studies have shown that the cross-sectional area (CSA) of small pulmonary vessels, which can be quantitatively measured on chest CT, is reliable for the in vivo evaluation of vascular changes in small pulmonary vessels [8–12]. A previous study [8] finding of a significant negative correlation between the extent of emphysema and %CSA of small pulmonary vessels can be supported by the findings of early angiographic studies of patients with emphysema, which showed narrowing and diminution of small pulmonary arteries [13–15]. While it is already known that the diameter of the brachial artery measured on ultrasound images decreases with an increasing amount of smoking [3], to the best of our knowledge, it is unknown how small pulmonary vessels change in relation to the amount of smoking. Based on previous observations, we hypothesized that changes in small pulmonary vessels, which can be expressed by reduction in the CSA of pulmonary vessels on chest CT, would be correlated with the amount of smoking in smokers, thereby representing an initial stage in the development of COPD before the appearance of pulmonary emphysema on CT. Thus, the aim of this study was to evaluate the relationship between the amount of smoking and the CSA of small pulmonary vessels on chest CT in light smokers without a diagnosis of COPD.

Materials and Methods

This retrospective study was approved by our institutional review board, which waived the need for informed consent from patients.

Participants

We initially identified 85 eligible participants who were all current light smokers (≤25 pack years) and had undergone pulmonary function testing (PFT) within 1 month of chest CT at our institution from August 2004 to December 2013. The definition of "light smoker" was reported in a previous study [16]. Every participant underwent preoperative pulmonary evaluation by identical multi-detector (MD) CT scanners. Every participant had received a diagnosis of an operable neoplasm outside the thorax and filled out questionnaires on smoking habits at the time of CT scanning. None of the patients were found to have COPD or had received cardiovascular agents, antihypertensive drugs, or treatment for COPD (including pharmacotherapy, oxygen inhalation therapy, and respiratory rehabilitation). A single radiologist retrospectively reviewed the participants' medical records and chest CT scans. Thirty-one participants were excluded from the study because of inadequate CT images due to motion or metallic artifacts ($n=4$) or use of contrast medium ($n=27$). Furthermore, 20 patients were also excluded because of the following coexisting pulmonary conditions or other systemic diseases that affected quantitative CT measurements: post-infectious changes in the lung ($n=7$), heart failure and valvular disease ($n=4$), interstitial pneumonia ($n=5$), large volume of atelectasis ($n=1$), current pneumonia ($n=1$), pneumothorax ($n=1$), and history of pneumonectomy ($n=1$).

A total of 34 patients were eventually included in this study (23 men and 11 women; mean age, 53 years; age range, 28–77 years). Data on smoking habits were obtained from the questionnaires and included number of packs smoked per day and duration of smoking, data which were converted to pack years. The mean number of pack years was 15.7 (range 1.8–25.0). Participants' characteristics are shown in Table 1.

Pulmonary Function Testing

PFT was performed within 1 month of chest CT. Forced vital capacity (FVC) and forced expiratory volume in 1 s (FEV_1) were measured using standard techniques, and were expressed as percentages of predicted values.

CT Scanning

All patients were scanned using identical 64-detector MDCT scanners (Aquilion 64; Toshiba Medical Systems, Otawara, Tochigi, Japan). All patients were examined at full inspiration in the supine position, without contrast material. The rotation time was 0.5 s, tube voltage was 120 kV_p, and tube current was varied by automatic exposure control (upper limit, 300 mA). Helical scanning was performed in the cranio-caudal direction, with a beam pitch of 0.828 (helical pitch of 53 divided by 64 detector

Table 1 Characteristics of participants, including smoking habits and pulmonary function testing ($N=34$)

	Mean (SD)	Range
Patient characteristics		
Age (years)	53 (12)	28–77
BMI	22.2 (3.9)	17.4–40.1
Smoking habits		
Pack years	15.7 (7.2)	1.8–25.0
Number of cigarettes smoked per day (packs)	0.57 (0.24)	0.1–1.0
Smoking period (years)	28.6 (10.7)	8–50
Pulmonary function testing		
FEV_1 % predicted (%)	95.1 (11.4)	67.1–120.8
FEV_1/FVC	0.80 (0.06)	0.71–0.95

SD standard deviation, *BMI* body mass index, *FEV_1* forced expiratory volume in 1 s, *FVC* forced vital capacity

rows). Images were contiguously reconstructed with 7-mm-thick slices without image interval. The matrix size was 512×512 pixels (pixel size, 0.625 mm).

Quantitative Assessment of Small Pulmonary Vessels and Lung Attenuation

All quantitative analyses for pulmonary vascular CSA and low attenuation area (LAA) measurements were performed as described elsewhere [8–12]. To measure these values, 3 CT images were selected from the entire CT series. The upper cranial slice was taken approximately 1 cm above the upper margin of the aortic arch, the middle slice was taken approximately 1 cm below the carina, and the lower caudal slice was taken approximately 1 cm below the right inferior pulmonary vein. These CT images were analyzed using a semiautomatic image-processing program (ImageJ Version 1.46, a public domain Java image-processing program available on the Internet at: http://rsb.info.nih.gov/ij/).

In brief, pulmonary vessel CSA and LAA were measured as follows (Fig. 1): first, the lung field was segmented from other tissues and structures using a threshold technique with an upper threshold value of −500 Hounsfield units (HU) on each CT image. To measure pulmonary vessel CSA, segmented CT images were converted into binary images using a window setting level of −720 HU. The vessel size was set to range from 0 to 5 mm^2, and the range of circularity was set from 0.9 to 1.0 ($CSA_{<5}$). To measure LAA, defined as the lung area < −950 HU [7], segmented CT images were converted into binary images with an upper threshold value of −950 HU. The pulmonary vessel CSA and LAA were each expressed as a percentage of the total area of each CT slice ($\%CSA_{<5}$ and %LAA). Finally, we calculated the mean $\%CSA_{<5}$ and %LAA of the 3 CT images, and these mean values were used in the final analysis.

Statistical Analysis

Spearman rank correlation analysis was used to evaluate the relationship between the pack years and CT parameters ($\%CSA_{<5}$ and %LAA). All statistical analyses were performed using JMP10.0 software (SAS Institute, Cary, NC). Data are expressed as the mean ± standard deviation for all continuous variables. For all statistical analyses, a P value < 0.05 was considered significant.

Results

CT parameters and their correlations with pack years are shown in Table 2. There was a significant negative correlation between $\%CSA_{<5}$ and pack years ($\rho = -0.629$,

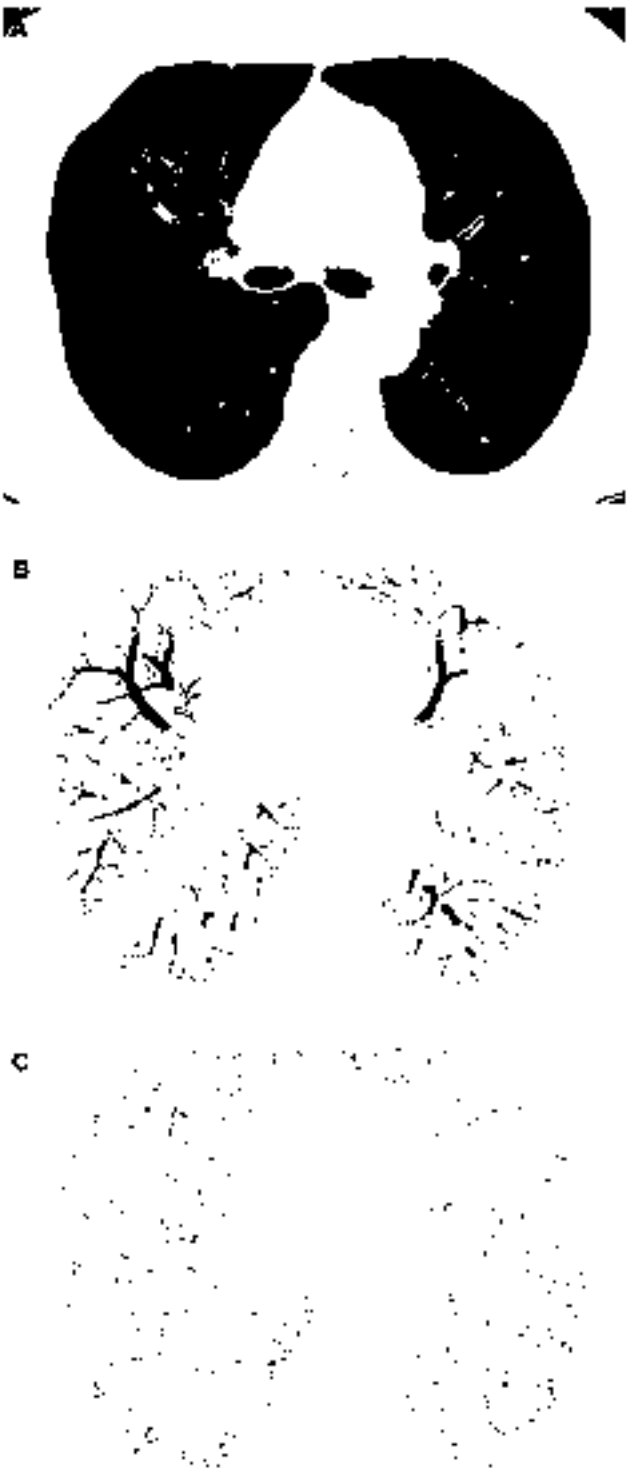

Fig. 1 Method for measuring the cross sectional area (CSA) of small pulmonary vessels using Image J software. **a** Computed tomography image taken approximately 1 cm below the carina (the *middle* of the 3 slices used in the analysis). **b** Binary image converted from the original image **a** with a window level of −720 HU. Pulmonary vessels are displayed in black. **c** Masked image for particle analysis after setting vessel size parameters within 0 to 5 mm^2 and the range of circularity within 0.9 to 1.0

Table 2 Computed tomography (CT) parameters and correlation with pack years

CT Parameter	Mean (SD)	Correlation with pack years	
		Correlation coefficient (ρ)	*P* value
$\%CSA_{<5}$ (%)	0.37 (0.14)	−0.629	<0.0001
%LAA (%)	3.0 (4.3)	0.125	0.480

CSA = the cross-sectional area of pulmonary vessels; $\%CSA_{<5}$ = the percentage of CSA < 5 mm^2 of the lung area; LAA = low attenuation area; % LAA = the percentage of LAA of the lung area

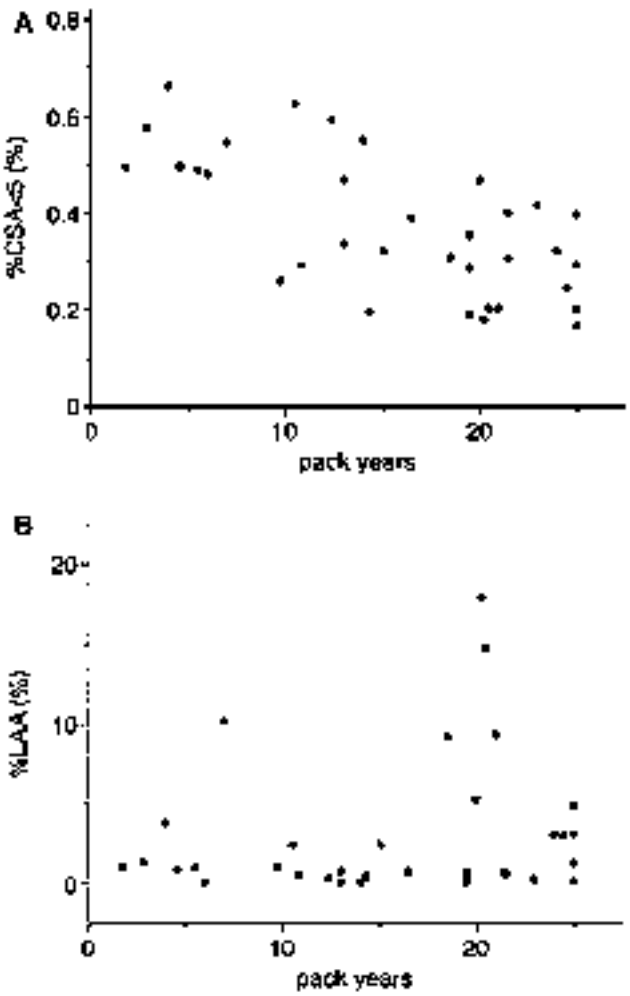

Fig. 2 Plots of the relationships between number of pack years and $\%CSA_{<5}$ a or %LAA b. There was a significant negative correlation between pack years and $\%CSA_{<5}$ (a, ρ = −0.629, *P* < 0.0001), whereas the correlation between pack years and %LAA was not significant (b, ρ=0.125; *P*=0.480)

P < 0.0001), whereas no significant correlation was found between %LAA and pack years (ρ=0.125, *P* = 0.480) (Fig. 2). The correlations between pack years and FEV_1% predicted and FEV_1/FVC were not significant (ρ = −0.208, *P* = 0.237; ρ=0.138, *P*=0.438, respectively).

Discussion

In this study, we found that $\%CSA_{<5}$ was negatively correlated with pack years in light smokers without COPD. The extent of emphysema was not significantly correlated with pack years in these participants. To our knowledge, this is the first in vivo study to describe the relationship between pulmonary vessel morphology and the amount of smoking.

Endothelial dysfunction caused by oxidants in cigarette smoking leads to the production of vasoconstrictor and vasoproliferative agents and interferes with the effects of vasodilators [18]. Vascular remodeling is the eventual result. Furthermore, Kasahara et al. [19] demonstrated that inhibition of vascular endothelial growth factor receptors led to the pruning of the pulmonary arterial tree on angiograms of rat lungs. The reduced blood flow in small precapillary blood vessels due to vascular remodeling might induce the disappearance of alveolar septa, eventually leading to emphysema [19–24]. Although early reports suggested that destruction of the pulmonary vascular bed by emphysema led to pulmonary hypertension, correlations between pulmonary hypertension and emphysema or vascular changes have not yet been proven. However, vascular remodeling has consistently indicated changes in the pulmonary vascular intima of patients with moderate to severe COPD [25, 26] and is believed to be the most important factor involved in the development of pulmonary hypertension in severe emphysema. Thus, dynamic morphological changes in the pulmonary vascular bed are very important findings when considering vascular disease caused by cigarette smoking. Although previous studies have shown that the extent of emphysema increases with the amount of smoking [27, 28], our study found that in light smokers without COPD, the extent of emphysema did not significantly increase with an increasing amount of smoking. These observations support the view that vascular changes resulting from the reduction in the pulmonary vascular bed may precede detectable emphysema [19, 29–32], even in smokers who have neither airflow limitation nor signs of progression to COPD. In other words, the CSA of pulmonary vessels depicted on chest CT scans may be an interesting parameter for identifying very early vascular changes caused by smoking. In contrast, parameters of quantitative emphysema do not provide information on the effects of smoking by light smokers without COPD.

A dose response relationship between the number of smoked cigarettes and the inflammatory response has been reported [33]. Celermajer et al. [3] also demonstrated a stronger association between the impairment of

endothelium-dependent dilation and number of pack years (reflecting chronic exposure) than with cotinine levels (reflecting acute exposure), suggesting that that the effect of smoking on endothelial function was unlikely to be an acute phenomenon. In light of these previous observations, we speculate that the correlation observed in this study between the CSA of small pulmonary vessels and the amount of smoking may reflect a dose-related impairment of endothelial function, which could lead to morphological and histological changes in the pulmonary vessels of light smokers without COPD.

Our study has several limitations. First, the information on smoking habits was not objective, because the data were collected from a questionnaire that the participants were asked to complete at the time of CT scanning; we do not know the accuracy of self-reported smoking status. Second, the amounts of tar and nicotine in cigarettes vary; therefore, similar amounts of smoking may have different effects on small pulmonary vessels. There have been conflicting reports on which has a larger effect on endothelial function, the number of cigarettes smoked in a day or the amount of tar and nicotine contained in a cigarette [5, 6, 34–39]. Third, the sample size was relatively small. Fourth, the CSA measurement might have been affected by the automatic exposure control provided by the scanner. Fifth, we did not measure the CSA of pulmonary vessels on histological sections; therefore, there may be some differences between the vascular CSA measured on CT scans and the actual CSA of small pulmonary vessels in histological specimens. Sixth, we did not have data from body plethysmography. Thus, the effect of air trapping or hyperinflation, which can be expressed as an increase in residual volume, as determined by plethysmography, on the CSA of pulmonary vessels is still ambiguous. Seventh, every participant in our study had received a diagnosis of a neoplasm outside the thorax. Although there have been no published data on vasodilation or vasoconstriction associated with neoplasms outside the thorax, we cannot rule out any effects by neoplasms on the sizes of pulmonary vessels. Eighth, the method we employed for vascular measurement was a two-dimensional analysis of axial CT slices, which has recently been reported to be less accurate than analysis of three-dimensional CT data [40]. Finally, we do not have data on arterial blood gas parameters obtained just before or immediately after chest CT. Hence, we cannot evaluate if hypoxia-induced vasoconstriction and vascular remodeling might have affected the CSA of small pulmonary vessels. Dupuy et al. [41] reported that exposure to cigarette smoke induced a rapid, consistent, and reversible drop in pulmonary artery pressure, which suggests that exposure to cigarette smoke results in the selective reversal of acute hypoxic vasoconstriction. Ueijima et al. [42] demonstrated that $\%CSA_{<5}$ is significantly positively correlated with FEV_1/FVC, even in healthy nonsmokers without airway obstruction, and suggested that subtle airflow impairment may be connected with morphological changes such as vasoconstriction in small pulmonary vessels. Further studies are needed to determine the effect of hypoxia on the decreased CSA of small pulmonary vessels that is observed on chest CT.

In conclusion, we found that $\%CSA_{<5}$ of small pulmonary vessels in light smokers without COPD significantly decreases with increasing amount of smoking, while the extent of emphysema does not significantly increase. These findings suggest that there is a dose–response relationship between the amount of smoking and vascular changes/vasoconstriction, and also support the assumption that vascular changes may precede detectable pulmonary emphysema.

Compliance with Ethical Standards

Conflict of interest None of the authors have any conflicts of interest to disclose.

References

1. Erhardt L. (2009) Cigarette smoking: an underrated risk factor for cardiovascular disease. Atherosclerosis 205:23–32
2. Nussbaumer-Ochsner Y, Rabe KF (2011) Systemic manifestations of COPD. Chest 139:165–172
3. Celermajer DS, Sorensen KE, Georgakopoulos D, Bull C, Thomas O, Robinson J et al (1993) Cigarette smoking is associated with dose-related and potentially reversible impairment of endothelium-dependent dilation in healthy young adults. Circulation 88:2149–2155
4. Celermajer DS, Adams MR, Clarkson P, Robinson J, McCredie R, Donald A et al (1996) Passive smoking and impaired endothelium-dependent arterial dilation in healthy young adults. N Engl J Med 334:150–154
5. Lekakis J, Papamichael C, Vemmos C, Nanas J, Kontoyannis D, Stamatelopoulos S et al (1997) Effect of acute cigarette smoking on endothelium-dependent brachial artery dilation in healthy individuals. Am J Cardiol 79:529–531
6. Lekakis J, Papamichael C, Vemmos C, Stamatelopoulos K, Voutsas A, Stamatelopoulos S (1998) Effects of acute cigarette smoking on endothelium dependent arterial dilation in normal subjects. Am J Cardiol 81:1223–1228
7. Dinh-Xuan AT, Higenbottam TW, Clelland CA, Pepke-Zaba J, Cremona G, Butt AY et al (1991) Impairment of endothelium-dependent pulmonary-artery relaxation in chronic obstructive lung disease. N Engl J Med 324:1539–1547
8. Matsuoka S, Washko GR, Dransfield MT, Yamashiro T, San Jose Estepar R, Diaz A et al (2010) Quantitative CT measurement of cross-sectional area of small pulmonary vessel in COPD: correlations with emphysema and airflow limitation. Acad Radiol 17:93–99
9. Matsuoka S, Washko GR, Yamashiro T, Estepar RS, Diaz A, Silverman EK et al (2010) Pulmonary hypertension and computed tomography measurement of small pulmonary vessels in severe emphysema. Am J Respir Crit Care Med 181:218–225
10. Matsuoka S, Yamashiro T, Diaz A, Estépar RS, Ross JC, Silverman EK et al (2011) The relationship between small pulmonary vascular alterations and aortic atherosclerosis in chronic

obstructive pulmonary disease: quantitative CT analysis. Acad Radiol 18:40–46
11. Matsuoka S, Yamashiro T, Matsushita S, Fujikawa A, Yagihashi K, Kurihara Y et al (2014) Relationship between quantitative CT of pulmonary small vessels and pulmonary perfusion. AJR Am J Roentgenol 202:719–724
12. Matsuoka S, Yamashiro T, Matsushita S, Kotoku A, Fujikawa A, Yagihashi K et al (2014) Usefulness of coronal reconstruction CT images for quantitative evaluation of the cross-sectional area of small pulmonary vessels. Acad Radiol 21:1411–1415
13. Scarrow GD (1965) The pulmonary angiogram in chronic bronchitis and emphysema. Proc R Soc Med 58:684–687
14. Cordasco EM, Becerra FR, Vance JW, Wende RW, Toffolo RR (1968) Newer aspects of the pulmonary vasculature in chronic lung disease. A comparative study. Angiology 19:399–407
15. Jacobson G, Turner AF, Balchum OJ, Jung R (1967) Vascular changes in pulmonary emphysema. The radiologic evaluation by selective and peripheral pulmonary wedge angiography. Am J Roentgenol Radium Ther Nucl Med 100:374–396
16. Price JF, Mowbray PI, Lee AJ, Rumley A, Lowe GD, Fowkes FG (1999) Relationship between smoking and cardiovascular risk factors in the development of peripheral arterial disease and coronary artery disease: Edinburgh Artery Study. Eur Heart J 20:344–353
17. Coxson HO, Dirksen A, Edwards LD, Yates JC, Agusti A, Bakke P et al (2013) The presence and progression of emphysema in COPD as determined by CT scanning and biomarker expression: a prospective analysis from the ECLIPSE study. Lancet Respir Med 1:129–136
18. Wright JL, Levy RD, Churg A (2005) Pulmonary hypertension in chronic obstructive pulmonary disease: current theories of pathogenesis and their implications for treatment. Thorax 60:605–609
19. Kasahara Y, Tuder RM, Taraseviciene-Stewart L, Le Cras TD, Abman S, Hirth PK et al (2000) Inhibition of VEGF receptors causes lung cell apoptosis and emphysema. J Clin Invest 106:1311–1319
20. Santos S, Peinado VI, Ramirez J, Morales-Blanhir J, Bastos R, Roca J et al (2002) Enhanced expression of vascular endothelial growth factor in pulmonary arteries of smokers and patients with moderate chronic obstructive pulmonary disease. Am J Respir Crit Care Med 167:1250–1256
21. Barr RG, Mesia-Vela S, Austin JH, Basner RC, Keller BM, Reeves AP et al (2007) Impaired flow-mediated dilation is associated with low pulmonary function and emphysema in ex-smokers: the emphysema and cancer action project (EMCAP) Study. Am J Respir Crit Care Med 176:1200–1207
22. Kasahara Y, Tuder RM, Cool CD, Lynch DA, Flores SC, Voelkel NF (2001) Endothelial cell death and decreased expression of vascular endothelial growth factor and vascular endothelial growth factor receptor 2 in emphysema. Am J Respir Crit Care Med 163:737–744
23. Kanazawa H, Asai K, Hirata K, Yoshikawa J (2003) Possible effects of vascular endothelial growth factor in the pathogenesis of chronic obstructive pulmonary disease. Am J Med 114:354–358
24. Tuder RM, Zhen L, Cho CY, Taraseviciene-Stewart L, Kasahara Y, Salvemini D et al (2003) Oxidative stress and apoptosis interact and cause emphysema due to vascular endothelial growth factor receptor blockade. Am J Respir Cell Mol Biol 29:88–97
25. Wright JL, Petty T, Thurlbeck WM (1992) Analysis of the structure of the muscular pulmonary arteries in patients with pulmonary hypertension and COPD: national Institutes of Health nocturnal oxygen therapy trial. Lung 170:109–124
26. Barbera JA, Peinado VI, Santos S (2005) Pulmonary hypertension in chronic obstructive pulmonary disease. Eur Respir J 21:892–905
27. Grydeland TB, Dirksen A, Coxson HO, Pillai SG, Sharma S, Eide GE et al (2009) Quantitative computed tomography emphysema and airway wall thickness by sex, age and smoking. Eur Respir J 34:858–865
28. Mohamed Hoesein FA, Zanen P, de Jong PA, van Ginneken B, Boezen HM, Groen HJ et al (2013) Rate of progression of CT-quantified emphysema in male current and ex-smokers: a follow-up study. Respir Res 14:55
29. Liebow AA (1959) Pulmonary emphysema with special reference to vascular changes. Am Rev Respir Dis 80:67–93
30. Eriksson S (1965) Studies in alpha 1-antitrypsin deficiency. Acta Med Scand Suppl 432:1–85
31. Cudkowicz L, Armstrong JB (1953) The bronchial arteries in pulmonary emphysema. Thorax 8:46–58
32. Isenschmid K (1871) Pathologisch-anatomische Veränderungen der Lungengefässe beim Emphysem. Virchows Arch A Pathol Pathol Anat 53:466–469
33. Kuschner WG, D'Alessandro A, Wong H, Blanc PD (1996) Dose-dependent cigarette smoking-related inflammatory responses in healthy adults. Eur Respir J 9:1989–1994
34. Barua RS, Ambrose JA, Eales-Reynolds LJ, DeVoe MC, Zervas JG, Saha DC (2002) Heavy and light cigarette smokers have similar dysfunction of endothelial vasoregulatory activity: an in vivo and in vitro correlation. J Am Coll Cardiol 39:1758–1765
35. Ciftçi O, Gunday M, Calişkan M, Gullu H, Guven A, Müderrisoğlu H (2013) Light cigarette smoking and vascular function. Acta Cardiol 68:255–261
36. Amato M, Frigerio B, Castelnuovo S, Ruvani A, Sansaro D, Tremoli E et al (2013) Effects of smoking regular or light cigarettes on brachial artery flow-mediated dilation. Atherosclerosis 228:153–160
37. Papamichael CM, Aznaouridis KA, Stamatelopoulos KS, Karatzis EN, Protogerou AD, Papaioannou TG et al (2004) Endothelial dysfunction and type of cigarette smoked: the impact of 'light' versus regular cigarette smoking. Vasc Med 9:103–105
38. Neunteufl T, Heher S, Kostner K, Mitrovic G, Lehr S, Khoschsorur G et al (2002) Contribution of nicotine to acute endothelial dysfunction in long-term smokers. J Am Coll Cardiol 39:351–356
39. Higashi T, Mai Y, Noya Y, Horinouchi T, Terada K, Hoshi A et al (2014) A simple and rapid method for standard preparation of gas phase extract of cigarette smoke. PLOS ONE 9:e107856
40. San Jose Estepar R, Kinney GL, Black-Shinn JL, Bowler RP, Kindlmann GL, Ross JC et al (2013) Computed tomographic measures of pulmonary vascular morphology in smokers and their clinical implications. Am J Respir Crit Care Med 188:231–239
41. Dupuy PM, Lançon JP, Françoise M, Frostel CG (1995) Inhaled cigarette smoke selectively reverses hypoxic vasoconstriction. Intensive Care Med 21:941–944
42. Uetani T, Matsuoka S, Yamashiro T, Yagihashi K, Kurihara Y, Nakajima Y (2011) Quantitative computed tomographic measurement of a cross-sectional area of a small pulmonary vessel in nonsmokers without airflow limitation. Jpn J Radiol 29:251–255

This copy is for personal use only. To order printed copies, contact reprints@rsna.org

Idiopathic Pulmonary Fibrosis:

Data-driven Textural Analysis of Extent of Fibrosis at Baseline and 15-Month Follow-up[1]

Stephen M. Humphries, PhD
Kunihiro Yagihashi, MD
Jason Huckleberry, MD
Byung-Hak Rho, MD
Joyce D. Schroeder, MD
Matthew Strand, PhD
Marvin I. Schwarz, MD
Kevin R. Flaherty, MD
Elie A. Kazerooni, MD
Edwin J. R. van Beek, MD
David A. Lynch, MB

Purpose: To evaluate associations between pulmonary function and both quantitative analysis and visual assessment of thin-section computed tomography (CT) images at baseline and at 15-month follow-up in subjects with idiopathic pulmonary fibrosis (IPF).

Materials and Methods: This retrospective analysis of preexisting anonymized data, collected prospectively between 2007 and 2013 in a HIPAA-compliant study, was exempt from additional institutional review board approval. The extent of lung fibrosis at baseline inspiratory chest CT in 280 subjects enrolled in the IPF Network was evaluated. Visual analysis was performed by using a semiquantitative scoring system. Computer-based quantitative analysis included CT histogram-based measurements and a data-driven textural analysis (DTA). Follow-up CT images in 72 of these subjects were also analyzed. Univariate comparisons were performed by using Spearman rank correlation. Multivariate and longitudinal analyses were performed by using a linear mixed model approach, in which models were compared by using asymptotic χ^2 tests.

Results: At baseline, all CT-derived measures showed moderate significant correlation ($P < .001$) with pulmonary function. At follow-up CT, changes in DTA scores showed significant correlation with changes in both forced vital capacity percentage predicted ($\rho = -0.41$, $P < .001$) and diffusing capacity for carbon monoxide percentage predicted ($\rho = -0.40$, $P < .001$). Asymptotic χ^2 tests showed that inclusion of DTA score significantly improved fit of both baseline and longitudinal linear mixed models in the prediction of pulmonary function ($P < .001$ for both).

Conclusion: When compared with semiquantitative visual assessment and CT histogram-based measurements, DTA score provides additional information that can be used to predict diminished function. Automatic quantification of lung fibrosis at CT yields an index of severity that correlates with visual assessment and functional change in subjects with IPF.

©RSNA, 2017

[1]From the Department of Radiology (S.M.H., D.A.L.) and Division of Biostatistics and Bioinformatics (M.S.), National Jewish Health, 1440 Jackson St, Denver, CO 80206-2761; Department of Radiology, St. Marianna University School of Medicine, Kawasaki, Japan (K.Y.); Department of Radiology, Kaiser Permanente, Denver, Colo (J.H.); Department of Radiology, Kyunghee University School of Medicine, Seoul, Republic of Korea (B.H.R.); Department of Radiology and Imaging Sciences, University of Utah, Salt Lake City, Utah (J.D.S.); Division of Pulmonary Sciences & Critical Care Medicine, University of Colorado, Aurora, Colo (M.S.); Departments of Pulmonology (K.R.F.) and Radiology (E.A.K.), University of Michigan, Ann Arbor, Mich; and Clinical Research Imaging Centre, University of Edinburgh, Edinburgh, Scotland (E.J.R.v.B.). Received June 6, 2016; revision requested August 5; revision received January 2, 2017; accepted February 6; final version accepted February 23. Address correspondence to S.M.H. (e-mail: humphriesS@nsh.org).

Supported by the National Institutes of Health and the National Heart, Lung, and Blood Institute (R01 HL091747).

©RSNA, 2017

Idiopathic pulmonary fibrosis (IPF) is characterized by progressive scarring of the lungs and declining lung function, and it has a variable clinical course. Some patients experience periods of relative stability, while others have acute progression and rapid decline. Accurate diagnosis and prediction of disease course are difficult, prompting interest in standardized quantitative measures of severity to assist in clinical decision making and assessment of treatment efficacy in clinical trials (1,2). In clinical practice, disease severity is assessed with physiology, most commonly by using pulmonary function tests (PFTs), including measurement of forced vital capacity (FVC) and lung diffusing capacity for carbon monoxide (DLco), which are also the most common primary outcome variables used to assess progression in clinical trials. Known limitations of FVC and DLco in this context include lack of sensitivity to change and difficulty interpreting marginal changes of 5%–10% (2), emphasizing the need for more precise anatomically based measures of severity.

Extent of lung fibrosis on computed tomographic (CT) images is a recognized marker of disease severity (3); correlates with prognosis, including mortality (4), and can replace DLco in a clinical model to determine risk of death (1). The ability to evaluate the extent of fibrosis noninvasively, capturing the spatial and temporal heterogeneity typical of usual interstitial pneumonia (UIP), makes CT particularly useful. However, visual identification of a UIP pattern is impaired by interobserver variation, and results are generally communicated in nonspecific qualitative terms (5). Computer-based quantitative methods capitalize on detailed information available on images and have the potential to increase precision and reproducibility in evaluation of IPF on CT images.

The relatively recent approval of drug therapies for IPF has generated excitement that better treatments are within reach (6). As new treatments are evaluated, there is a need for an objective anatomy-based measure of IPF that could be provided by quantitative CT. Such a technique would be valuable in clinical practice to assess prognosis, identify progression, and standardize assessment across a diverse group of radiologists. In clinical trials, quantitative CT could be useful in the stratification of baseline severity of disease and in the assessment of progression or improvement in response to treatment.

Our group has developed a computer algorithm, dubbed data-driven textural analysis (DTA), which is capable of quantifying the extent of lung fibrosis on CT images. On the basis of initial technical validation (7), we hypothesized that serial DTA measurements are predictive of progression in patients with IPF. The purpose of this work was to evaluate associations between pulmonary function and both quantitative analysis and visual assessment of thin-section CT images at baseline and 15 month follow-up in patients with IPF.

Advances in Knowledge

- Extent of lung fibrosis determined with data-driven textural analysis (DTA) is associated with forced vital capacity (FVC) percentage predicted ($\rho = -0.60$, $P < .001$) and lung diffusing capacity for carbon monoxide (DLco) percentage predicted ($\rho = -0.68$, $P < .001$) at baseline.
- Change in DTA score is correlated with change in FVC percentage predicted ($\rho = -0.41$, $P < .001$) and DLco percentage predicted ($\rho = -0.40$, $P < .001$) at 15-month follow-up.
- Subjects with disease progression ($n = 34$) at visual assessment had greater mean DTA score at baseline (32.90 vs 23.43, $P = .003$), poorer function (mean FVC percentage predicted: 69.82 vs 78.34, $P = .019$; mean DLco percentage predicted: 41.91 vs 51.1, $P < .001$), and greater rates of change in these indexes over the follow-up period (change in DTA score: 6.6 vs 0.7, $P < .001$; change in FVC percentage predicted: −5.15 vs −1.27, $P = .003$; change in DLco percentage predicted: −5.59 vs −1.85, $P = .004$) when compared with patients who did not have disease progression.

Implication for Patient Care

- Automatic quantification of lung fibrosis on CT images yields an index of severity that correlates with visual assessment and functional change in subjects with idiopathic pulmonary fibrosis.

Materials and Methods

The original prospective study (8–10) was compliant with the Health Insurance Portability and Accountability Act and was approved by the institutional review board at all participating institutions; informed consent was obtained from all patients. As an analysis of preexisting anonymized data, this retrospective study of prospectively collected data was exempt from additional institutional review board approval.

https://doi.org/10.1148/radiol.2017161177
Content code: CH
Radiology 2017; 285:270–278

Abbreviations:
DLco = lung diffusing capacity for carbon monoxide
DTA = data-driven textural analysis
FVC = forced vital capacity
IPF = idiopathic pulmonary fibrosis
PFT = pulmonary function test
ROI = region of interest
SVM = support vector machine
UIP = usual interstitial pneumonia

Author contributions:
Guarantor of integrity of entire study, S.M.H., M.I.S., D.A.L.; study concepts/study design or data acquisition or data analysis/interpretation, all authors; manuscript drafting or manuscript revision for important intellectual content, all authors; approval of final version of submitted manuscript, all authors; agreeing to ensure any questions related to the work are appropriately resolved, all authors; literature research, S.M.H., D.J.R., K.R.F., E.A.K., E.J.R.v.B., D.A.L.; clinical studies, K.Y., J.H., B.H.R., M.I.S., E.A.K., E.J.R.v.B., D.A.L.; statistical analysis, S.M.H., M.S.; and manuscript editing, S.M.H., K.Y., J.H., M.S., M.I.S., K.R.F., E.A.K., E.J.R.v.B., D.A.L.

Conflicts of interest are listed at the end of this article.

Subjects

For inclusion in the original studies, patients were required to have received a diagnosis of IPF according to standardized criteria similar to the subsequently published American Thoracic Society–European Respiratory Society criteria (11). Baseline CT examinations were performed within 3 months of enrollment. The minimal CT acquisition requirements for study entry were 0.3–1.25-mm thick sections obtained at 1-cm intervals and at full inspiration. When feasible, subjects underwent multidetector thin-section CT according to a prespecified protocol, which was customized according to CT scanner manufacturer and model. PFTs to measure FVC and DLco were performed according to standardized protocols (8–10). Data were acquired between 2007 and 2013.

CT studies that met minimal acquisition requirements were available in 539 subjects enrolled in the STEP, PANTHER, and ACE IPFnet trials (8–10). For this work, we selected subjects (n = 335) based on availability of thin-section volumetric CT (image reconstructions ≤ 1.25 mm) and PFT data. From this group, we selected a subset from the ACE cohort for algorithm training data (n = 55; mean age, 65.8 years; age range, 50–78 years [38 men; mean age, 65.3 years; age range, 50–78 years; 17 women; mean age, 67.1 years; age range, 54–75 years]). These subjects were selected for training because they had been examined with equipment from the most commonly used manufacturers (GE Healthcare, Waukesha, Wis; Siemens Healthineers, Erlangen, Germany) and because they had appropriate examples of the fibrotic UIP pattern. Twenty-two of these studies were acquired with Siemens equipment, and 33 were obtained with GE units. The remaining subjects with thin-section volumetric CT studies comprise the study subjects for this project (n = 280; mean age, 67.5 years; age range, 43–86 years [216 men; mean age, 67.9 years; age range, 48–85 years; 64 women; mean age, 66.3 years; age range, 43–84 years]). A total of 139 study subjects were examined with GE equipment, 89 were examined with Siemens equipment, and 52 were examined with Philips equipment.

Data in all subjects have been reported previously (8–10); however, prior articles dealt with experimental drug therapies, whereas we report a new method to quantify lung fibrosis on CT images.

Quantitative CT Analysis

DTA is based on an unsupervised feature-learning paradigm. Briefly, this method uses an initial clustering analysis to "learn" feature representations directly from a large collection of unlabeled images (7). Unsupervised clustering produces a set of basis elements, called a dictionary, which can be used to encode other image regions. Dictionary elements tend to be simple features, like directed edges or blobs, and they can be considered a collection of the elemental low-level pixel patterns that occur at lung CT. Weighting coefficients on dictionary elements needed to reconstruct novel image regions provide quantitative features useful for subsequent classification with machine learning. Unsupervised feature learning differs from feature engineering, which is a more traditional approach in which features are designed manually, often by using combinations of standard statistical or image processing calculations.

In our implementation, feature representations were produced by clustering thousands of small (3 × 3-mm) patches randomly sampled from lung regions on CT images in patients with IPF and in those without IPF. Images of the 55 subjects from the IPFnet ACE study, none of whom were included in this study cohort, served as examples of IPF. Images in nonsmoking control subjects from the Genetic Epidemiology of COPD (COPDGene) cohort (n = 35) (12) were used as examples of non-IPF lungs. A modified k-means clustering process (13) on the pixel intensities in those small patches yielded a 512-element dictionary of low-level CT patterns found in the lungs.

Separately, an experienced radiologist (K.Y., 10 years of experience) delineated regions of interest (ROIs) showing the characteristic patterns of UIP (honeycombing, reticular abnormality, and traction bronchiectasis) on CT images in 55 subjects from the IPFnet ACE cohort that were used in dictionary construction. A senior thoracic radiologist (D.L., more than 20 years of experience) verified each ROI. Quantitative features were computed for 14 × 14 mm ROIs by using the previously constructed dictionary. The features for a given 14 × 14 mm ROI can be thought of as the frequency with which 3 × 3 mm subregions matching learned dictionary elements occur in that ROI. These labeled exemplars were used to train a support vector machine (SVM) classifier. The SVM was trained in a binary fashion so that novel image regions described in terms of the established dictionary are classified as either a normal lung or a fibrotic lung (7). Hard negative mining, an iterative approach to training that emphasizes difficult-to-classify normal samples to reduce false-positive results, was used (14). Images of the 280 study subjects were not used to construct the dictionary or train the SVM classifier.

Analysis of study population CT studies began with semiautomatic lung segmentation with commercially available software (Apollo; Vida Diagnostics, Coralville, Iowa). Pixel histogram statistics (mean, standard deviation, skewness, and kurtosis) were computed over whole-lung volumes by using custom software developed in-house. Square 14 × 14 mm ROIs were sampled from within lung segmentation volumes and were classified with DTA as fibrotic or not fibrotic. DTA fibrosis score was computed as the number of ROIs classified as fibrotic divided by the total number of ROIs sampled from the lung segmentation volume.

Baseline CT Analysis

Volumetric CT of 280 subjects enrolled in ACE, PANTHER, and STEP IPFnet studies were used for testing (8–10). Two radiologists (J.H., K.Y.; 5 and 10 years of experience, respectively) scored extent of fibrosis, expressing the visual extent of fibrotic abnormality to the nearest 10% on a scale from 0 (no fibrosis) to 10 (100% fibrosis) (15). Baseline PFT data (FVC, FVC percentage predicted, DLco, and DLco percentage predicted) were available in all subjects.

Serial CT Evaluation

A subset of 72 subjects (51 men; mean age, 65.9 years; age range, 49–82 years; 21 women; mean age, 65.8 years; age range, 43–84 years) enrolled in the PANTHER study underwent both baseline and follow-up volumetric CT. The resultant images were evaluated independently by three senior thoracic radiologists (D.L., E.K., E.A.R.; all with more than 15 years of experience). Semiquantitative scores (scale, 0–10) for extent of fibrosis were assigned for each study. Visual assessment of change in fibrosis at follow-up was performed by comparing both studies and was scored on a five-point ordinal scale (0, much better; 1, slightly better; 2, same; 3, slightly worse; 4, much worse). Baseline and follow-up PFT results were available for all 72 subjects. FVC and FVC percentage predicted were measured at baseline and at 15, 30, 45, and 60 weeks thereafter. DL_{CO} and DL_{CO} percentage predicted were measured at baseline and at 30 and 60 weeks thereafter.

Statistical Analyses

Statistical analyses were performed by using two software packages (R, version 3.0.0, R Foundation for Statistical Computing, Vienna, Austria; SAS, version 9.4, SAS Institute, Cary, NC). Level of significance was set to $P < .05$ for all experiments, and correction for multiple comparisons was not applied. Spearman correlation coefficients were used to quantify univariate relationships between DTA scores, CT histogram-based measures (mean lung attenuation, standard deviation of lung pixel intensities, skewness, and kurtosis), semiquantitative visual scores, and physiologic measures (FVC, FVC percentage predicted, DL_{CO}, and DL_{CO} percentage predicted). Follow-up data were analyzed descriptively with Spearman correlation coefficients by considering change scores (last follow-up measurement minus baseline measurement) and rate of change (slope determined by linear regression of all follow-up measurements). For visual assessments, the mean of readers' scores was used in all analyses. Interrater agreement was evaluated with weighted κ scores. The κ agreement scores were interpreted by using the following criteria: κ of 0.0–0.2 indicated slight agreement; κ of 0.21–0.40, fair agreement; κ of 0.41–0.60, moderate agreement; κ of 0.61–0.80, substantial agreement; and κ of 0.81–1.0, almost perfect agreement (16). Subjects whose follow-up CT images were scored as slightly worse or much worse by at least two readers were considered to have progressed. Welch two sample t tests were performed to compare baseline scores and rates of change between subjects whose disease had progressed and those whose disease had not.

Linear mixed models were used to evaluate multiple CT-derived approaches in predicting FVC or DL_{CO} for both baseline and longitudinal data. In particular, histogram, DTA, and visual based variables were included as predictors in FVC or DL_{CO} models separately or together to determine their predictive utility or added benefit. Asymptotic χ^2 tests using the difference in two log likelihoods between nested models were used to determine whether DTA fibrosis score significantly improved prediction of clinical outcomes (17). Base models used visual score, CT histogram-based measures (mean, standard deviation, skewness, and kurtosis of lung voxel values), or both. Models for baseline data included one term per predictor (1 for visual score, 4 for CT histogram-based measures, 1 for DTA fibrosis score), while longitudinal models included two terms for each predictor (variable itself plus time by variable interaction). Thus, asymptotic tests for added benefit of DTA score used one degree of freedom in models for baseline data and two degrees of freedom in longitudinal models. Linear mixed models included a random intercept term for CT reconstruction kernel plus random terms for subject (in longitudinal models) and reader (in models for visual extent).

Table 1

Study Subject Characteristics

Characteristic	Baseline IPFNet (ACE, PANTHER, and STEP) (n = 292)	PANTHER (n = 72)		
		Baseline	Change at Follow-up	P Value[1]
Age (y)	67.5 ± 8.8	66.0 ± 9.2	...	<.001
Visual extent of fibrosis score[2]	4.74 ± 1.5	1.7 ± 0.7	0.2 ± 0.5	<.001
Visual assessment of change score[2]	...	..	2.6 ± 0.8	<.001
DTA fibrosis score	36.6 ± 16.1	27.9 ± 13.4	4.0 ± 5.7	<.001
Mean lung attenuation (HU)	−714.0 ± 85.5	−728.9 ± 53.7	9.5 ± 32.8	.020
Standard deviation of lung attenuation (HU)	223.1 ± 34.2	238.8 ± 27.7	1.7 ± 15.8	.570
Skewness	1.7 ± 0.5	1.9 ± 0.5	−0.1 ± 0.2	<.001
Kurtosis	3.1 ± 2.8	3.9 ± 2.3	−0.4 ± 1.1	.002
CT total lung capacity (L)	3.7 ± 1.1	3.9 ± 1.3	−0.1 ± 0.4	.230
FVC (L)	2.7 ± 0.9	2.9 ± 0.7	−0.1 ± 0.2	<.001
FVC percentage predicted	66.2 ± 17.5	74.3 ± 15.4	−3.4 ± 6.5	<.001
DL_{CO} (mL of CO/min/mm Hg)	11.3 ± 4.4	13.8 ± 4.2	−1.2 ± 2.2	<.001
DL_{CO} percentage predicted	38.0 ± 13.4	46.8 ± 13.1	4.3 ± 7.1	<.001

[1] P values were calculated with two-sample t test.

[2] Semiquantitative extent of fibrosis was scored on a scale from 0 to 10. For subjects in the PANTHER study, scores at baseline were assigned by two readers (K.K., J.H.). For patients in the PANTHER study, scores at baseline and follow-up were assigned by three readers (D.A.L., E.J.R.B., E.A.K.), and change at follow-up was calculated as follow-up score minus baseline score.

[3] Average of three readers (D.A.L., E.J.R.B., E.A.K.); a follow-up score of 0 indicated fibrosis was much better; a score of 1, fibrosis was slightly better; a score of 2, fibrosis was the same; a score of 3, fibrosis was worse; and a score of 4, fibrosis was much worse.

Results

Table 1 summarizes subject demographics. A subset of 72 subjects from

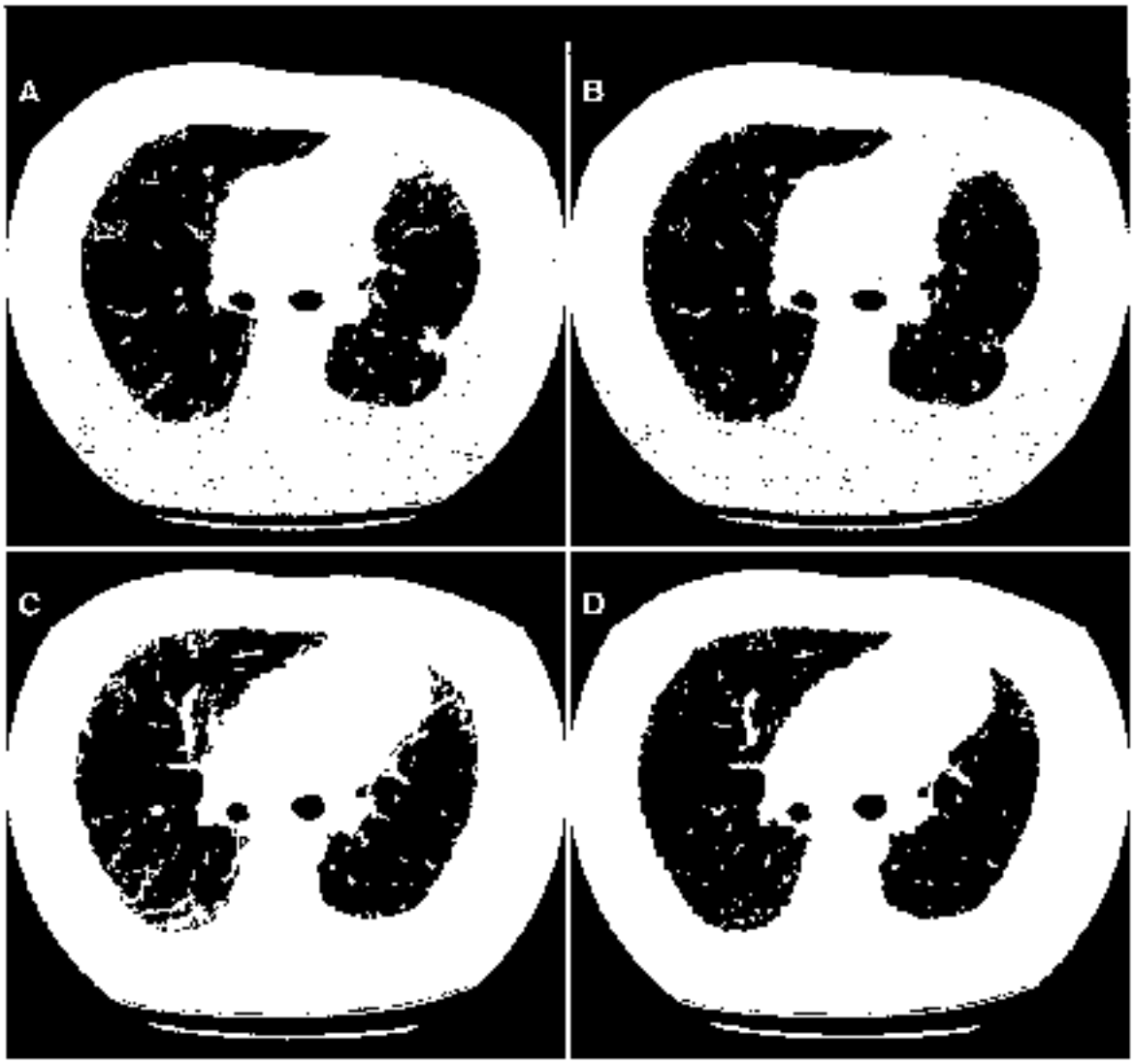

A, Axial baseline unenhanced CT image in a 60-year-old man. *B*, Areas of fibrosis identified with DTA are indicated (red). Baseline DTA fibrosis score was 22.3%, average visual extent of fibrosis as assessed by three readers (D.L., E.vB., E.K.) was 1.67, baseline FVC percentage predicted was 53.15, and Dlco percentage predicted was 36.1. *C*, Similar axial unenhanced CT image in the same subject at 18.2-month follow-up. *D*, DTA fibrosis score was 40.6% at follow-up, average visual extent of fibrosis (D.L., E.vB., and E.K.) was 3.37, with all three readers scoring the follow-up image as slightly worse. Follow-up FVC percentage predicted was 44.4 and Dlco percentage predicted was 30.5.

the PANTHER study underwent volumetric CT and PFT both at baseline and at follow-up. The follow-up interval ranged from 13.1 to 18.2 months (mean, 14.9 months ± 0.93 [standard deviation]; median, 14.7 months). The Figure shows visualization of DTA analysis results for baseline and follow-up images.

Table 2 shows associations between baseline values and rates of change of CT-derived measures, visual assessment, and PFTs. Radiologist agreement for semiquantitative fibrosis scores at baseline (assigned by two radiologists) was poor by weighted κ (κ = 0.3, $P < .001$, n = 280). However, DTA score showed moderate correlation with average visual score (Spearman ρ = 0.50, $P < .001$).

In the 72 subjects who underwent follow-up CT, the evaluation of agreement between three reviewers' visual assessment of change showed poor agreement (mean of pairwise weighted κ = 0.3, $P < .05$, n = 72). Agreement for extent of fibrosis scores at baseline and at follow-up (assigned by the same three readers) was moderate (mean pairwise κ = 0.33, $P < .001$). Subjects identified at visual assessment as having disease progression had higher DTA score and poorer PFT at baseline and had greater rates of change in these measurements over the follow-up period (Table 3).

Table 2

Associations between Baseline Values and Rates of Change for Visual Scores, Quantitative CT Measures, and Pulmonary Function

Characteristic	Visual Extent of Fibrosis Score[a]	Based on IPFnet (ACT, PANTHER, and STEP) (n = 280)						PANTHER (n = 72)					
		FVC	FVC Percentage Predicted	DLco	DLco Percentage Predicted	Visual Follow-up Score	Change in FVC	Change in FVC Percentage Predicted	Change in DLco	Change in DLco Percentage Predicted
Visual extent of fibrosis score[a]	...	−0.22	−0.28	−0.46	−0.49	...	...	...	.	. .
Visual assessment of change score[a]	...	. .	. .	.	.	. .	−0.26 (P = .030)	−0.41	−0.41	−0.36
DTA fibrosis score	0.5	−0.54	−0.60	−0.64	−0.68	0.63	−0.42	−0.41	−0.47	−0.40
Mean (HU)	0.31	−0.62	−0.68	0.54	0.55	0.55	0.38	0.37	0.32 (P = .007)	0.26 (P = .029)
Standard deviation (HU)	0.45	−0.46	−0.55	−0.42	−0.45	0.30 (P = .010)	−0.52	−0.40	−0.07 (P = .564)	−0.03 (P = .816)
Skewness	0.48	0.62	0.70	0.64	0.67	−0.48	0.47	0.44	0.21 (P = .040)	0.27 (P = .030)
Kurtosis	−0.49	0.62	0.68	0.62	0.65	−0.38	0.46	0.45	0.16 (P = .140)	0.16 (P = .196)
CT TLC (L)	−0.06 (P = .360)	0.83	0.57	0.45	0.31	−0.32	0.28	0.40	0.08 (P = .500)	0.08 (P = .529)

Note — P < .001, except where indicated. Change at follow-up was computed as follow-up value minus baseline value.

[a] Number of lung lobes (0, 1, 2, 3, 4, 5) where extent of fibrosis was scored ≥ 3–10.

[b] Average of three readers (D.M.C., E.J.R.H.S., E.A.K.), with a visual follow-up score of 0 (stable or fibrosis was much better) or 1 (fibrosis was much worse). Results was the average score of 3 fibrosis visual scores and a score of 4, fibrosis with high value.

CT-derived measurements were predictive of PFT outcomes for both baseline and longitudinal data based on linear mixed models. The main outcome variables analyzed (FVC, DLco) are approximately normally distributed based on examination of histograms. Table 4 shows the added benefit, based on asymptotic χ^2 tests, of including DTA score in models predicting FVC or DLco by using visual score, histogram measurement metrics, or both. The most significant improvements occurred when we included DTA score in models with visual score only (P < .001) and for all longitudinal models of DLco, including those with visual score, histogram measurements, or both (P < .001).

Discussion

We have developed a computer algorithm capable of quantifying extent of lung fibrosis on CT images. In 280 subjects with IPF, DTA fibrosis score showed correlation with semiquantitative visual scores and PFTs at baseline. In a subset of 72 subjects with baseline and follow-up CT images, DTA score showed moderate significant correlation with the degree of change in PFTs. This indicates that extent of lung fibrosis captured on CT images and quantified with DTA is associated with change in lung function. The purpose of comparing quantitative CT images with lung function is not to suggest that CT can or should replace PFTs. Our intent is to perform a clinical validation of CT analysis methods to show that measurement of morphology is associated with measures of disease severity; however, textural analysis may yield a more sensitive index of longitudinal change that may be in part independent of physiologic change. We focused on FVC and DLco because these measures are recommended for evaluation of disease course by the American Thoracic Society, European Respiratory Society, Japanese Respiratory Society, and Latin American Thoracic Association official guidelines on IPF (11). Multivariate analysis for prediction of lung function showed

DTA score adds information beyond histogram-based measurements and semiquantitative visual scores.

It is known that lung pixel histogram statistics, including skewness and kurtosis, correlate with baseline physiologic parameters, including FVC and DLco (4,17). Although these measures are attractive in that they are easy to calculate and are fairly intuitive, they are coarse global metrics that are not sufficiently precise for longitudinal analysis (4,18).

Automatic localization of interstitial lung disease on CT images is a challenging task. Fibrotic patterns are complex and are not defined adequately by using simple quantitative descriptors. Kliment et al (19) studied a large population and showed that attenuation value alone, separated by applying a threshold, is not sufficient to identify regions of interstitial lung abnormality. Local pixel histograms can yield more information. Iwasawa et al (20) described a method in which histograms of pixel intensities and gradients within ROIs were compared by using normalized correlation. They determined that the extent of a histogram pattern associated with honeycombing based on comparison with radiologist-identified exemplars was associated with mortality in a group of 40 patients with IPF. Bartholmai et al (21) and Maldonado et al (22) also used local histograms but classified small volumes of interest on thin-section CT images by using an approach based on clustering of expert-labeled volumes of interest by affinity propagation. By using this method to determine extents of UIP patterns on CT images, they reported correlations between automatic scores and other clinical measures in 119 subjects with interstitial lung disease.

Histograms count frequency of individual pixel intensities but do not explicitly capture local visually distinct patterns like edges or curves. The characteristic appearance of UIP on CT images is formed by patterns in both pixel intensity and spatial arrangement, a quality called image texture. Researchers have applied image texture methods to the problem of automatic analysis of interstitial lung disease on CT images and have shown impressive results (18,23,24). Kim et al (25) developed a method in which texture features computed by using local first- and second-order pixel statistics are classified with an SVM

Table 3

Comparison of Baseline Values and Change in Subjects Who Had Progressed and Those Who Had Not Based on 5% Decline in FVC Percentage Predicted and Visual Assessment

At 5% Decline in FVC Percentage Predicted

Characteristic	Nonprogressors (n = 47)	Progressors (n = 32)	P Value*
Baseline			
DTA score	25.86 ± 13.21	28.41 ± 11.42	.273
DLco percentage predicted	47.72 ± 11.46	45.42 ± 12.97	.439
Visual score†	1.70 ± 0.63	1.80 ± 0.74	.561
Rate of change (per year)			
DTA score	1.71 ± 5.0	6.92 ± 7.63	.007
DLco percentage predicted	−2.07 ± 6.56	−6.32 ± 6.04	.029
Visual assessment of change†	0.35 ± 0.61	0.822 ± 0.56	<.001

By Visual Assessment

Characteristic	Nonprogressors (n = 38)	Progressors (n = 34)	P Value*
Baseline			
DTA score	23.43 ± 11.02	32.93 ± 14.16	.003
FVC percentage predicted	75.34 ± 13.53	69.82 ± 16.23	.020
DLco percentage predicted	53.10 ± 12.80	41.91 ± 9.49	<.001
Rate of change (per year)			
DTA score	0.20 ± 3.61	6.8 ± 5.66	<.001
FVC percentage predicted	1.27 ± 4.54	−5.15 ± 5.56	.003
DLco percentage predicted	−1.65 ± 9.67	−5.58 ± 5.55	.004

Note.—Unless otherwise indicated, data are mean ± standard deviation.

* Welch two-sample t test.

† Average of two readers.

Table 4

P Values for Improvement in Goodness of Fit after Adding Algorithm Score as a Predictor in Clinical Outcome Models

	Baseline Data		Longitudinal Data	
Adding DTA score to Model with the Following Base Predictors	FVC Percentage Predicted	DLco Percentage Predicted	FVC Percentage Predicted	DLco Percentage Predicted
Visual score	<.001 (81.6) [1]	<.001 (93.9) [1]	<.001 (47.2) [2]	<.001 (53.5) [2]
Histogram measures	.007 (7.2) [1]	.006 (7.9) [1]	.061 (5.6) [2]	<.001 (25.2) [2]
Histogram measures and visual score	.008 (7) [1]	.032 (4.6) [1]	.301 (2.4) [2]	<.001 (14.6) [2]

Note.—Data are P values. Double parentheses are the χ^2 statistic, and data in brackets are degrees of freedom. Asymptotic χ^2 tests for difference in −2 log likelihood values were used to detect statistical significance of improvement of including algorithm score as a predictor in linear mixed models; see text for more detail.

trained in a supervised fashion using radiologist-delineated regions of lung fibrosis. In a study of 57 subjects with IPF and sequential CT examinations selected from a database of standardized scans, fibrosis scores computed with their method were associated with baseline FVC and DLco and change in these measurements after 7 months (18). Yoon et al (26) used a similar texture-based system to quantify disease patterns of fibrotic interstitial pneumonia at sequential CT in 89 subjects with clinically proven and/or biopsy proven UIP or nonspecific interstitial pneumonia. They showed there was an association between quantitative and visual scores, FVC and DLco at baseline, and change in FVC and DLco at 1 year follow-up. Correlations between DTA score and PFTs in the present study were similar to those reported by these investigators. Several recently developed classification systems have sought to subcategorize disease patterns into specific categories, including ground-glass abnormality, reticulation, and honeycombing (15,27). However, we chose to focus this analysis on the extent of fibrosis because in patients with IPF, the extent of fibrosis or reticular abnormality is invariably the most important in correlating with pulmonary function and outcome (28,29).

Most established image texture methods are based on engineered features, meaning calculation strategies designed to capture particular characteristics anticipated to be useful in distinguishing patterns of interest. These approaches can be limited in that they are based on assumptions regarding which characteristics are important, and they generally rely on multiple parameters that must be tuned, often by trial and error. The typical approach computes a battery of features then applies feature selection to identify those that are useful in the classification task. Unsupervised feature learning distills descriptive feature representations directly from a large collection of relevant data. Mounting evidence suggests this type of approach yields image features that are more powerful than engineered features (30), thereby providing more discriminative information for classifier training. This is the strategy used in DTA. A supervised classifier was trained by using radiologist-labeled regions, from which features were extracted by using a framework developed in an unsupervised process rather than by using designed features. There was no overlap in images used to develop the DTA algorithm, including construction of the feature dictionary and training the classifier, and the images analyzed in this study. Classification systems based on learned features are thought to be more flexible and easier to generalize to similar tasks (eg, classification of other CT patterns) than those based on engineered features (31).

Limitations of this study include variation in CT technical parameters, the relatively small number of subjects who underwent a follow-up examination, and the absence of mortality data. CT technical parameters, such as reconstruction kernel, affect image sharpness and noise level, which likely affect quantitative CT measures. The use of a random intercept term for reconstruction kernel in the linear mixed model accounts for this in multivariate analysis, but variation in CT technical parameters may contribute to the relatively low correlations at univariate analysis. The use of FVC and DLco as the reference standard for disease severity is inherently flawed because of known variation in these measures and because of the inevitable incongruity of physiologic and anatomic measurements. This may explain the relatively modest correlations between the CT-based and physiologic measurements. The lack of correction for multiple comparisons can also be considered a limitation; however, we chose to present individual P values for the planned comparisons. The observer variation for visual assessment is a known limitation that has been demonstrated in this study and in prior studies, but it emphasizes the difficulty of visual quantification and the need for an automated method. We also did not perform a direct comparison of DTA with other published fibrosis quantification methods. Nevertheless, a key conclusion from this and related work is that CT captures useful prognostic information that can be quantified by using computational techniques.

We conclude that DTA fibrosis score applied to CT from a multicenter study of IPF correlates with visual assessment and PFTs at baseline and when assessing change. Multivariate analysis indicates that DTA score improves the ability to predict change in function over time. Our findings that DTA fibrosis score is associated with baseline measurements of disease severity and with change over time suggest that CT captures anatomic information that can be quantified by using automatic computational methods to provide useful indexes of disease severity and progression in patients with IPF.

Disclosures of Conflicts of Interest: S.M.H. Activities related to the present article: disclosed no relevant relationships. Activities not related to the present article: has a patent pending for a system and method for automatic detection and quantification of pathology using dynamic texture classification (62/335,816). Other relationships: disclosed no relevant relationships. **K.Y.** disclosed no relevant relationships. **J.H.** disclosed no relevant relationships. **D.H.R.** disclosed no relevant relationships. **J.D.S.** disclosed no relevant relationships. **M.S.** disclosed no relevant relationships. **M.L.S.** disclosed no relevant relationships. **K.H.F.** disclosed no relevant relationships. **E.A.K.** disclosed no relevant relationships. **R.J.Kaul** Activities related to the present article: disclosed no relevant relationships. Activities not related to the present article: is the founder and owner of Quantitative Clinical Imaging Tools. Other relationships: disclosed no relevant relationships. **D.A.L.** Activities related to the present article: disclosed no relevant relationships. Activities not related to the present article: received personal fees from Pfizer, Genentech, and Boehringer Ingelheim; received a grant from Veracyte; has a patent pending for a system and method for automatic detection and quantification of pathology using dynamic texture classification (62/335,816). Other relationships: disclosed no relevant relationships.

References

1. Ley B, Ryerson CJ, Vittinghoff E, et al. Idiopathic pulmonary fibrosis: CT and risk of death. Radiology 2014;273(2):570–579.

2. Hansell DM, Goldin JG, King TE Jr, Lynch DA, Richeldi L, Wells AU. CT staging and monitoring of fibrotic interstitial lung diseases in clinical practice and treatment trials: a position paper from the Fleischner Society. Lancet Respir Med 2015;3(6):483–496.

3. Wells AU, Desai SR, Rubens MB, et al. Idiopathic pulmonary fibrosis: a composite physiologic index derived from disease extent observed by computed tomography. Am J Respir Crit Care Med 2003;167(7):962–969.

4. Best AC, Meng J, Lynch AM, et al. Idiopathic pulmonary fibrosis: physiologic tests, quantitative CT indexes, and CT visual scores as predictors of mortality. Radiology 2008;246(3):935–940.

5. Wyndham T, Sokai F, Johkoh T, et al. Interobserver variability in the CT assessment of honeycombing in the lungs. Radiology 2010;266(3):936–944.

6. Hurwitz GM. A new hope for idiopathic pulmonary fibrosis. N Engl J Med 2014;370(22):2142–2143.

7. Humphries S, Yagihashi K, Sood H, Rho BH, Schroeder J, Lynch DA. Quantification of IPF on chest CT using unsupervised feature learning. ATS Journals Web site. https://www.atsjournals.org/doi/abs/10.1164/ajrccm-conference.2015.191.1. Meeting Abstracts.A4973. Accessed September 29, 2015.

8. Idiopathic Pulmonary Fibrosis Clinical Research Network, Zisman DA, Schwarz M, et al. A controlled trial of sildenafil in advanced idiopathic pulmonary fibrosis. N Engl J Med 2010;363(7):620–628.

9. Idiopathic Pulmonary Fibrosis Clinical Research Network, Raghu G, Anstrom KJ, King TE Jr, Lasky JA, Martinez FJ. Prednisone, azathioprine, and N-acetylcysteine for pulmonary fibrosis. N Engl J Med 2012;366(21):1968–1977.

10. Noble PW, Albera C, Bradford WZ, et al. A placebo-controlled randomized trial of pirfenidone in idiopathic pulmonary fibrosis. Am J Respir Crit Care Med 2011;183(1):88–95.

11. Raghu G, Collard HR, Egan JJ, et al. An official ATS/ERS/JRS/ALAT statement: idiopathic pulmonary fibrosis—evidence-based guidelines for diagnosis and management. Am J Respir Crit Care Med 2011;183(6):788–824.

12. Zach JA, Newell JD Jr, Schroeder J, et al. Quantitative computed tomography of the lungs and airways in healthy nonsmoking adults. Invest Radiol 2012;47(10):596–602.

13. Cootes A, Ng AY. Learning feature representations with K-means. In: Montavon G, Orr GB, Müller KR, eds. Neural networks: tricks of the trade. Berlin, Germany: Springer; 2012: 561–580.

14. Dalal N, Triggs B. Histograms of oriented gradients for human detection. In: IEEE Computer Society Conference on Computer Vision and Pattern Recognition, 2005. CVPR 2005. Piscataway, NJ: IEEE, 2005: 886–893.

15. Salisbury ML, Lynch DA, van Beek EJ, et al. Idiopathic pulmonary fibrosis: adaptive multiple features method fibrosis association with outcomes. Am J Respir Crit Care Med 2016 Oct 21. [Epub ahead of print]

16. Landis JR, Koch GG. The measurement of observer agreement for categorical data. Biometrics. 1977;33(1):159–174.

17. Best AC, Lynch AM, Bozic CM, Miller D, Grunwald GK, Lynch DA. Quantitative CT indexes in idiopathic pulmonary fibrosis: relationship with physiologic impairment. Radiology 2003;228(2):407–414.

18. Kim EJ, Brown MS, Chong D, et al. Comparison of the quantitative CT imaging biomarkers of idiopathic pulmonary fibrosis at baseline and early change with an interval of 7 months. Acad Radiol 2015;22(1):70–80.

19. Kliment CR, Araki T, Doyle TJ, et al. A comparison of visual and quantitative methods to identify interstitial lung abnormalities. BMC Pulm Med 2015;15(1):134.

20. Iwasawa T, Asakura A, Sakai F, et al. Assessment of prognosis of patients with idiopathic pulmonary fibrosis by computer-aided analysis of CT images. J Thorac Imaging 2009;24(3):218–222.

21. Bartholmai BJ, Raghunath S, Karwoski RA, et al. Quantitative computed tomography imaging of interstitial lung diseases. J Thorac Imaging 2013;28(5):298–307.

22. Mendonça E, Moss T, Rajagopalan S, et al. Automated quantification of radiological patterns predicts survival in idiopathic pulmonary fibrosis. Eur Respir J 2014;43(1):204–212.

23. Uppaluri R, Hoffman EA, Sonka M, Hunninghake GW, McLennan G. Interstitial lung disease: a quantitative study using the adaptive multiple feature method. Am J Respir Crit Care Med 1999;159(2):519–525.

24. Kum HJ, Li G, Qiersce D, et al. Classification of parenchymal abnormality in scleroderma lung using a novel approach to denoise images collected via a multicenter study. Acad Radiol 2008;15(8):1004–1016.

25. Kim HG, Tashkin DP, Clements PJ, et al. A computer-aided diagnosis system for quantitative scoring of extent of lung fibrosis in scleroderma patients. Clin Exp Rheumatol 2010;28(5,Suppl 62):S26–S35.

26. Yoon JG, Seo JB, Kim N, et al. Quantitative assessment of change in regional disease patterns on serial HRCT of fibrotic interstitial pneumonia with texture-based automated quantification system. Eur Radiol 2013;23(3):692–701.

27. Jacob J, Bartholmai BJ, Rajagopalan S, et al. Automated quantitative computed tomography versus visual computed tomography scoring in idiopathic pulmonary fibrosis: validation against pulmonary function. J Thorac Imaging 2016;31(5):304–311.

28. Lynch DA, Godwin JD, Safrin S, et al. High-resolution computed tomography in idiopathic pulmonary fibrosis: diagnosis and prognosis. Am J Respir Crit Care Med 2005;172(4):488–493.

29. Park HJ, Lee SM, Song JW, et al. Texture-based automated quantitative assessment of regional patterns on initial CT in patients with idiopathic pulmonary fibrosis: relationship to decline in forced vital capacity. AJR Am J Roentgenol 2016;207(3):976–983.

30. Halevy A, Norvig P, Pereira F. The unreasonable effectiveness of data. IEEE Intell Syst 2009;24(2):8–12.

31. Cyntas A, Ng AY, Lee H. An analysis of single-layer networks in unsupervised feature learning. In: International Conference on Artificial Intelligence and Statistics, 2011: 215–25.

■ 特集　小児にかかわる診療ガイドライン

血管腫・血管奇形・リンパ管奇形診療ガイドライン 2017

三村秀文*

はじめに

血管腫・脈管奇形（血管奇形・リンパ管奇形）の診断，治療法は確立しておらず，とくに血管腫・血管奇形は慣用的表現である「血管腫」と一括して呼称されることが多かったため，治療方針について混乱を招き，誤った治療が行われることも少なくなかった。血管腫・脈管奇形の診療の指針が求められていた。

I．疾患群の臨床的特徴

血管腫・脈管奇形（血管奇形・リンパ管奇形）の大半は原因不明で，根本的な治療法が確立しておらず，多くの患者は専門医を求めて多数の医療機関を受診し，とくに重症度の高い患者は治療難民といえる状態にある。血管腫・血管奇形は慣用的に「血管腫」と呼称されることが多いが，血管腫・脈管奇形診療の国際学会が提唱しているISSVA分類（ISSVA：The International Society for the Study of Vascular Anomalies）では両者は別の疾患であり，この分類は国際的に標準化されつつある。一般に「血管腫」と診断されるものでもっとも頻度の高いのは乳児血管腫であり，多くは小児期に自然消退する。一方，血管奇形は自然消退することはなく，疼痛，腫脹，患肢の成長異常，機能障害，整容上の問題などをきたす。脈管奇形は動脈，静脈，毛細血管，リンパ管といった構成要素により細分され，その混合型も存在する。脈管奇形には，病変がかなり切除治療が可能なものから，多発性あるいは巨大で解剖組織に浸潤し治療に抵抗性を示す難治性のものまで幅広く含まれる。

II．ガイドライン作成の目的

血管腫・脈管奇形に関してevidence based medicine（EBM）の手法に基づいて，効果的・効率的診療を整理し，安全性を検証し，体系化し，現時点で最適の治療を行うための指針を作成することを目的とした。疼痛，腫脹，整容障害，機能障害など，アウトカムの改善を目標とした。

III．ガイドライン作成の意図と作成・改訂にいたる経過

2009年度厚生労働科学研究費補助金（難治性疾患克服研究事業）「難治性血管腫・血管奇形についての調査研究班」（研究代表者 2009〜2011年度佐々木 了，2012〜2013年度三村秀文）が発足し，「難治性血管腫・血管奇形」についての研究を行ったが，難治性病変の診療についての研究を行う前提として「血管腫・血管奇形」の疾患概念，診断，治療を整理し，解説する必要があると考えられ，診療ガイドラインを作成することとなった。日本形成外科学会，日本IVR学会からも委員を選出し，研究班と協力して「血管腫・血管奇形診療ガイドライン 2013」[1]が作成され，2013年3月に完成した。

「血管腫・血管奇形・リンパ管奇形診療ガイドライン 2017」[2]は，その改訂版として作成された。作成主体は厚生労働科学研究費補助金［難治性疾患等政策研究事業（難治性疾患政策研究事業）］「難治性血管腫・血管奇形・リンパ管腫・リンパ管腫症および関連疾患についての調査研究」班（研究代表者 2014〜2016年度三村秀文）であり，リンパ

Hidefumi Mimura
* 慶応義塾大学医学部小児外科学講座
（〒216-851）川崎市宮前区菅生 2-16-1）

Presented by Medical*Online

管疾患は「小児期からの難治性血管疾患の移行期を包含するガイドラインの確立に関する研究」班（研究代表者 田口智章），「小児呼吸器形成異常・低形成疾患に関する実態調査ならびに診療ガイドライン作成に関する研究」班（研究代表者 白井規弘）のリンパ管奇形疾患研究グループとの共同作成となった。主に頭部・体表リンパ管疾患は三村班，縦隔胸部疾患は白井班，腹部疾患は田口班で作成され，最終的に本ガイドラインに統一された。

IV. 組織編成

ガイドライン策定委員会委員は形成外科，皮膚科，放射線科，小児外科，基礎分野のそれぞれの代表者が選定された。クリニカルクエスチョン（CQ）および推奨作成のためのガイドライン作成グループ・システマティックレビューチームは，動静脈奇形・静脈奇形・混合型・症候群担当，毛細血管奇形・乳児血管腫担当，リンパ管系担当，基礎分野担当の4つのグループからなる構成とした。動静脈奇形・静脈奇形・混合型・症候群グループは主に形成外科医，放射線科医が担当，毛細血管奇形・乳児血管腫グループは主に形成外科医，皮膚科医が担当，リンパ管系グループは主に小児外科医，形成外科医，小児科医が担当した。ガイドライン総説も各グループから選ばれた担当者が作成した。総説基礎分野は病理医，分子生物学研究者が担当した。

V. 重要臨床課題

①切除術の有効性，②塞栓/閉塞術の有効性，③薬物療法，レーザー治療，放射線治療，そのほか保存的治療の有効性，④病変の部位による適切な治療の違い，⑤症状による適切な治療の違い，⑥適切な治療・経過の期間，⑦診断の決め手となる病理診断を重要臨床課題とした。

VI. ガイドラインがカバーする範囲

血管腫，脈管奇形が対象である。ISSVの分類にしたがい，血管腫と脈管奇形を分けて記載した。血管腫では乳児血管腫を対象とした。そのほかの血管性腫瘍については適宜記載した。脈管奇形では静脈奇形，動静脈奇形，リンパ管奇形（リンパ管腫），毛細血管奇形，混合型脈管奇形，脈管奇形症候群，リンパ管腫症・ゴーハム病などを対象とした。これらの疾患の診断・治療について総説，CQ推奨を作成した。

VII. ガイドライン改訂の工程

本ガイドラインは2014年に発表された「Minds診療ガイドライン作成の手引き 2014」[3]および「Minds診療ガイドライン作成マニュアル Ver. 1.0〜2.0」[2]にしたがって改訂された。ガイドライン作成組織は新たなガイドラインの作成方法は手慣れであったため，2014年度は新規に10個のCQを設定し，Mindsの手法にならって文献検索，システマティックレビューを行い，推奨案・解説案の試作を行った。2015〜2016年度にかけて本格的な改訂作業にとりかかり，三村班では13個のCQを改訂し，1個のCQを新たに加え，CQは計24個となった。ガイドラインは田口班，白井班との共同作成であったため，田口班CQ 4個，白井班CQ 5個を加え，計33個のCQとなった（表）。

システマティックレビューに関しては，おのおののCQごとに文献検索のためのキーワードを設定し，文献をPubMed，Cochrane Library，医学中央雑誌を用いて検索した。既存の診療ガイドラインについては，Guideline International Networkの International Guideline Library，日本医療機能評価機構EBM普及推進事業（Minds）を用いた。文献検索期間は1980〜2014年9月末とした。文献検索は特定非営利活動法人日本医学図書館協会に依頼した。文献検索後「Minds診療ガイドライン作成の手引き 2014」[3]に基づき，エビデンス総体の評価と統合を行った。

推奨作成方法は「Minds診療ガイドライン作成の手引き 2014」に準じたが，エビデンスが乏しい，あるいはエビデンスが弱いCQ推奨の決定には作成グループの議論およびその合意を反映させた。各グループに分かれて作業が行われたため，作成された推奨文の様式にばらつきが生じたが，複数の研究班で作成された経緯があり，スコープにしたがっていれば各グループの意向を尊重した。

本ガイドラインでは疾患の解説が必要と考えら

Presented by Medical*Online

表　クリニカルクエスチョン（CQ）リスト

CQ 1. 動静脈奇形において硬化療法開始の目安は何か？	CQ 20. 青色ゴムまり様母斑症候群（Blue rubber bleb nevus 母斑症）を疑った患児には，どのような画像検査が有用か？　また，いつから検査を開始したらよいのか？
CQ 2. 動静脈奇形の切除に際して水腫による術中出血は皮膚による母斑よりも再発（再増大）が多いか？	CQ 21. 血管奇形や症候群でみられる臓器の過成長に対する対応としてどのようなものがあるか？
CQ 3. 動静脈奇形の流入血管に対する原位（中枢側）での閉塞術・コイル塞栓術は有効か？	CQ 22. 頭部・体表リンパ管奇形（リンパ管腫）に対する切除術は可能か？
CQ 4. 動静脈奇形に対する切除術前画像検査法の実施時期として，適当なのはいつか？	CQ 23. 頭部・体表リンパ管奇形（リンパ管腫）に対する適切な手術時期はいつか？
CQ 5. 頭部の動静脈奇形の適切な治療は何か？	CQ 24. 縦隔ミクロシスティックリンパ管奇形（リンパ管腫）に対する硬化療法は有効か？
CQ 6. 手指の動静脈奇形の適切な治療は何か？	CQ 25. 腹部リンパ管奇形（リンパ管腫）に硬化療法は有効か？
CQ 7. 痛みを伴える治療奇形にはどのような治療が有効か？	CQ 26. 臨床症状のない腹部リンパ管奇形（リンパ管腫）は治療すべきか？
CQ 8. 静脈奇形に対するレーザー色素照射法は有効か？	CQ 27. 新生児性乳び胸水に対して有効な治療は何か？
CQ 9. 静脈奇形に対する硬化療法は有効か？	CQ 28. 腹部リンパ管奇形（リンパ管腫）手術における合併症はどのようなものか？
CQ 10. 静脈奇形による血液凝固異常に対して抗凝固療法の適応はあるか？	CQ 29. 胸郭内で気道圧迫を生じているリンパ管奇形（リンパ管腫）に対して効果的な治療法は何か？
CQ 11. 毛細血管奇形に対する色素レーザー照射は部位によって効果に差があるか？	CQ 30. 頸部の気道閉塞に分布するリンパ管奇形（リンパ管腫）に対して，乳児期から硬化療法をすべきか？
CQ 12. 毛細血管奇形に対するQ-スイッチレーザー照射において特異があるか？	CQ 31. 舌のリンパ管奇形（リンパ管腫）に対して外科的切除は有効か？
CQ 13. 毛細血管奇形に対する色素レーザー照射は治療開始年齢が若いほど有効性が高いか？	CQ 32. 新生児期の乳び胸水に対して積極的な外科的介入は有効か？
CQ 14. 乳児血管腫に対してプロプラノロール内服療法は安全で有効か？	CQ 33. 難治性の乳び胸水や心嚢液貯留，呼吸障害を呈するリンパ管腫症やゴーハム病に対して有効な治療法は何か？
CQ 15. 乳児血管腫における治癒形成に対する有効な治療法は何か？	
CQ 16. 乳児血管腫に対するステロイドの局所注射は全身投与に比べて有効か？	
CQ 17. 乳児血管腫に対する表面外用療法は有効か？	
CQ 18. 乳児血管腫に対して圧迫療法は有効か？	
CQ 19. 乳児血管腫の診断にGLUT-1免疫染色は有効であるか？	

れ，総説として総論，各論を掲載した。総説は各専門家が執筆したが，とくに各論は複数の診療科の専門家が協力して担当した。こうして多領域の専門医が作成し，多領域の専門医のコンセンサスを得たガイドライン草案が作成された。

ガイドライン草案は2016年12月に完成し，2016年12月～2017年1月にかけて日本形成外科学会，日本皮膚科学会，日本医学放射線学会，日本IVR学会，日本小児外科学会，日本病理学会に査読を依頼し，査読結果から修正を行った。また2016年12月～2017年1月にかけて「難治性血管腫・血管奇形・リンパ管腫・リンパ管腫症および関連疾患についての調査研究」班ホームページにガイドライン案が公開され，パブリックコメントを募った。関係する2つの患者会「血管腫・血管奇形の患者会」，「混合型脈管奇形の会」にガイドライン案を提示し，コメントを受けた。これらを基にガイドライン案が検討・ブラッシュアップされ，2017年3月に最終化され完成した。

なお，総説形式の「乳幼児巨大肝血管腫診療ガイドライン」（作成担当：黒田達夫）も併せて作成された。肝血管腫のなかで稀ではあるが，ときに致死的な経過をとる一群の症例があり，その診療に関するガイドラインである。

VII. 目玉となる点

前ガイドラインとの違いは，形成外科医，放射

Presented by Medical*Online

線科医（IVR 医），基礎研究者以外に，皮膚科医，小児科医，放射線科医（画像診断医）からそれぞれ多数の委員を募り，関係学会の意見を集約することを目標とした。また刷新された「Minds 診療ガイドライン作成の手引き 2014」[1]および「Minds 診療ガイドライン作成マニュアル」[4]にしたがって作成したため，全面改定となった。本ガイドラインは 2017 年 3 月発刊となり，2017 年 5 月までに日本形成外科学会，日本皮膚科学会，日本医学放射線学会，日本 IVR 学会，日本小児外科学会，日本病理学会から承認を受けた。

ガイドライン改訂と同時期に，乳児血管腫に対するプロプラノロールの有用性が広く認められ，その臨床での適切な使用のための指針が必要と考えられた。「CQ 14. 乳児血管腫に対してプロプラノロール内服療法は安全で有効か？」は「推奨文：慎重な観察の下に施行されるのであれば，プロプラノロール内服療法は乳児血管腫に対し第 1 選択となる可能性のある薬剤である。推奨の強さ 1（行うことを強く推奨する），エビデンス A」と提示された。

IX. 苦労した点

本ガイドライン関連疾患の診療を担当する診療科，関与する学会は多岐にわたる。ガイドラインは多診療科の協力の下作成されたが，各診療科の意見は必ずしも一致せず，議論のあるところが多かった。各診療科には疾患の診療についてそれぞれの考え方，歴史があるが，文献によるエビデンスを基にガイドラインを作成することにより，なんとか折り合いをつけることができたのではないかと思われる。

X. 効　果

ガイドライン[2]は研究班ホームページ（http://www.marianna-u.ac.jp/va/guideline.html）から無料でダウンロードが可能である。多学会の承認が得られたため，本ガイドラインが関連各科に広く使用され，状況の認識の下に診療が行われることが期待される。

XI. 今後の予定

2017 年度より「難治性血管腫・血管奇形・リンパ管腫・リンパ嚢胞症および関連疾患についての調査研究」班は秋田定伯が研究代表者となり，次回改訂のためのガイドライン統括委員会が新たに組織される予定である。

文　献

1) 日本脈管・血管奇形診療ガイドライン 2013（http://www.marianna-u.ac.jp/va/files/vascular%20anomalies%20practice%20guideline%202013.pdf）
2) 血管腫・血管奇形・リンパ管奇形診療ガイドライン 2017（http://www.marianna-u.ac.jp/va/files/vascular%20anomalies%20practice%20guideline%202017.pdf?view=FitV）
3) 福井次矢，山口直人（監修），森實敏夫，他（編）：Minds 診療ガイドライン作成の手引き 2014．医学書院，東京，2014
4) 小島原典子，中山健夫，森實敏夫，他（編）：Minds 診療ガイドライン作成マニュアル．公益財団法人 日本医療機能評価機構，東京，2014

＊　＊　＊

Presented by Medical Online

画像診断の実際

はじめに

血管腫・血管奇形，リンパ管奇形において，画像は病変の鑑別診断や病変分布の評価のために用いられる．図1に血管腫・脈管奇形診断のフローチャートを提示する[1]．以下，フローチャートを参照しながら読み進めていただきたい．鑑別診断のために必要な情報として，病変が嚢胞性病変であるかどうか，内部血流の有無，血流の性状などの情報が必要であることがわかる．

病変が嚢胞性病変であるかの質的評価のためには超音波，MRI が有用で，まずはこのいずれかで評価を行う．次に，内部の血流の有無を評価するためには，カラードプラ像を用いた超音波検査や，造影 MRI，造影 CT 検査などが有用である．さらに，内部血流の流速を評価するために，超音波ドプラ法での内部血流の観察や，ダイナミック造影による早期相から静脈相までの造影増強効果の観察がなされる．

モダリティの選択については，表在病変であれば超音波による評価で十分であるが，深部を含む病変分布を評価するには組織コントラストのよい MRI が有用である．一方で，generalized lymphatic anomaly (GLA) や Gorham-Stout disease (GSD) のような骨間質への浸潤性病変や骨浸潤の病巣の変形を評価するには，CT や単純 X 線写真が有用である．血管撮影は血流のダイナミックな評価が可能であるが侵襲を伴う検査であり，診断目的のみでは通常，選択されない．

診断対象に応じた検査法を選択する必要があり，ここからは各モダリティごとの評価方法と至適撮像方法について述べる．なお，画像診断の対象となるのが小児または若年成人であることが多い背景を考慮すると，可能な限り X 線被曝の少ない方法で評価することが望ましい．

超音波検査

表在病変の評価に有用である．B モード像でサイズの大きな嚢胞性病変は，無エコーで後方エコー増強を伴う病変として確認される．拡張した異常血管も嚢胞様に描出されるため，純粋な嚢胞との鑑別にカラードプラ画像による内部血流の評価を行う．カラードプラ画像で fast flow 病変は容易に血流が検出できるが，slow flow 病変は内部血流が不明瞭であることがままある．嚢胞様に見える病変がリンパ管奇形なのか，血流を拾いがたい静脈奇形なのかの判断に，病変の圧迫による虚脱がみられるかどうかを確認する方法があり（図2）[2]，圧迫が容易な表在病変に対しては，有用である．また，静脈奇形では静脈石を伴うことがあり，内部にアコースティックシャドーを伴う結石像が確認されれば，静脈奇形の特徴的所見となる（図3）．

内部血流が確認されたら，その血流が動脈性かどうかを判断する必要があり，血流が検出された部位のパルスドプラでの計測を行う．Slow flow 病変では通常単相性の血流が確認され，fast flow 病変では拍動性の波形が検出できる（図4）．

最後に，嚢胞性病変の評価としてリンパ管奇形の所見について解説する．大嚢胞性リンパ管奇形は隔壁で境界された無エコー病変が典型的であるが，出血や感染により内部に高輝度のデブリス様構造や液面形成を含むことがある（図5）．カラードプラでは小さな動静脈構造が嚢胞壁や隔壁内，周囲間質にみられるが，嚢胞内に血流は確認されない．一方，小嚢胞性リンパ管奇形は嚢胞性病変であるにもかかわらず，小嚢胞の無数の壁が interface になり高輝度に描出されることがあり，充実性成分との鑑別がむずかしいことがある．

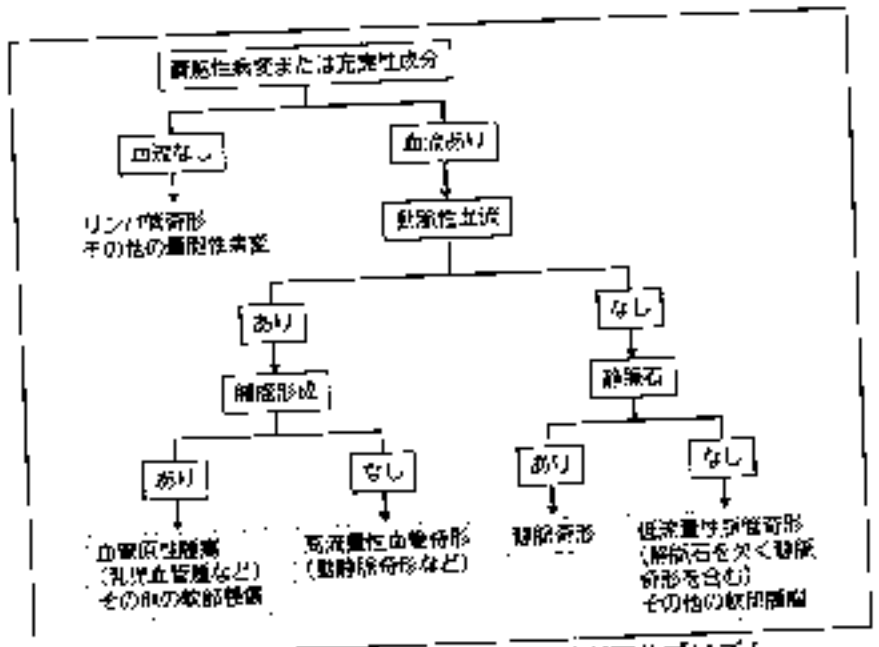

図1　血管腫・血管奇形・リンパ管奇形画像診断アルゴリズム

[日本形成外科学会・日本皮膚科学会・日本放射線腫瘍学会・日本小児外科学会・日本小児皮膚科学会・日本小児放射線学会・日本血管腫・血管奇形・リンパ管奇形診療ガイドライン2017 関連疾患についての調査研究班（編）：血管腫・血管奇形・リンパ管奇形診療ガイドライン2017．<http://www.eurekin-s.org/va/guideline.html>（2017年7月アクセス）をもとに筆者作成]

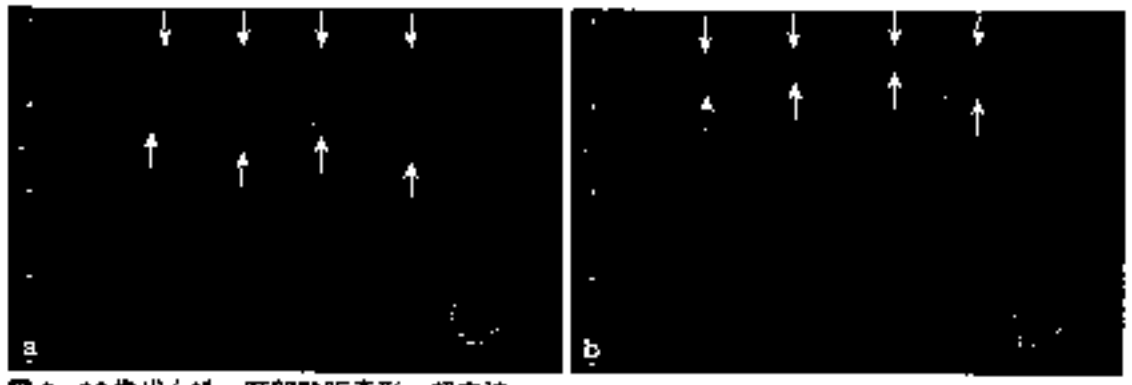

図2　30歳代女性，頭部静脈奇形，超音波

a) 圧迫前Bモード像．
b) 圧迫後Bモード像．
皮下に低輝度の軟部組織を認めている．病変内部の血流は乏しく，検出が困難であったがプローブによる圧迫で病変は虚脱し静脈奇形の所見に合致している

MRI

MRI はその優れた組織分解能により脈管奇形の分布と性状を評価する最良のモダリティである．皮下組織から，筋内や筋間，時に骨内といった，複数の組織に分布する脈管奇形の分布をも正確に描出することができる（図6）．経静脈的な造影剤投与を行うことにより，病変内部の充実成分の含有の有無や血流評価が可能となる．撮像の際には適切なサイズのコイルと FOV を選択し，軸位断像に冠状断像あるいは矢状断像を加えた2方向以上からの評価が望ましい[3]．基本となるシークエンスは fast SE（FSE）法の脂肪抑制 T2 強調画像または short TI inversion recovery (STIR) spin echo (SE) と，FSE 法の T1 強調画像である[3]．Slow flow の脈管奇形はおおむね水信号に近く，脂肪抑制画像となる STIR や脂肪抑制 T2 強調画像では，背景の軟部組織に比して強い高信号となるため，分布を判断しやすい．T1 強調画像で造影剤投与前後の造影効果を対比することによって，病変が血管性なのか，嚢胞性なのかの判断に役立つ．Slow flow 病変では病変内への造影剤分布に時間がかかることがあるため，造影後画像の撮像は造影剤投与後5～10分経過した時点で行うことが望ましい[3]．fast flow 病変では，流速の早い血管成分が signal void となり低信号から無信号に描出される．低信号病変は静脈奇形で特徴的な静脈石の無信号が鑑別に挙がるが，静脈石が結節状構造であるのに対し，signal void の脈

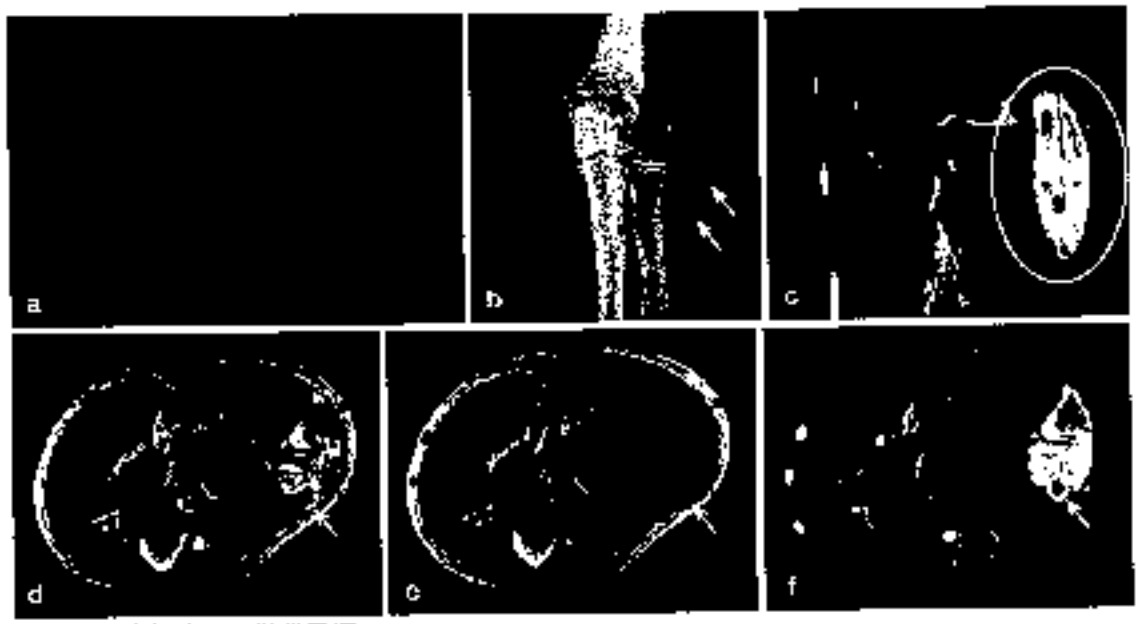

図3　静脈奇形，10歳代男児

a) 超音波(Bモード)像：静脈石は音響陰影 (acoustic shadow)を伴う結節構造として検出される．
b) 肘関節部単純写真：肘関節外側の軟部組織が腫脹し，内部に静脈石と考える石灰化を認める(矢印)．
c) MRI, STIR 冠状断像：同部位に一致して高信号を示す軟部腫瘤があり(丸囲み)，内部に静脈石の低信号の結節構造として複数みられる．単純写真でみられるより多くの結節構造があるが，石灰化する前の静脈石もMRI では描出されるためと考えられる．
d) MR, T2 強調画像
e) MR, T1 強調画像
f) MRI, STIR 像：静脈奇形は大部分が T2WI，STIR で高信号，T1WI で中間信号の病変として描出されている．静脈奇形内部には血栓成分を反映できる T2WI 低信号，T1WI 高信号領域を認める(矢頭)．静脈石はいずれのシーケンスでも低信号の類円形構造として描出される(矢印)．
[厚生労働省難治性血管疾患克服研究事業「難治性血管腫・血管奇形・リンパ管腫，リンパ管奇形および血管炎症についての調査研究」班(編)：血管腫・血管奇形・リンパ管奇形診療ガイドライン 2017 < http://www.mariannu-u.ac.jp/va/guidelines/ > (2017年7月アクセス)より]

皆病変に帯状の連続性を有する点や，造影動脈相における造影効果で鑑別が可能である．Fast flow 病変の血流を捉えるためには，3D T1fast GRE 法を用いた造影ダイナミック MRA を用いて，少なくとも1相の動脈相，2相の静脈相での撮像を行い，評価する必要がある[3]．近年，より高い空間分解能を有した高速造影 3D time resolved MRA 法を用いることができるようになり，短い間隔で多相撮像をすることが可能となっている．これにより病変の血流が動脈性なのか，静脈性なのかの判断のみならず，feeding vessel の指出，シャントの有無，血流の方向など，詳細な血行動態までも評価を行うことができるようになった[4]．以上，病変評価のための MRI 評価の方法を述べたが，経過観察時に病変サイズの変化のみが必要な場合には，造影検査を行う必要はない．

CT

CT の有用性は，きわめて短時間に広範囲の画像を撮像することができる点にある．MRI と比較して組織コントラストが不良となるため，病変分布が必ずしも完全に評価できるわけではないが，周囲組織との位置関係も含めて，おおむね把握することができる．造影剤を使用するとコントラストが改善し，より病変の評価がしやすくなる．造影ダイナミック撮像により動脈，静脈との位置関係，血流評価も可能である．術前のマッピングなど，正確な空間的位置関係の情報が必要な際には有用な検査法である(図7)．しかしながら，CT における多相撮影は被曝が多く，ALARA (as low as reasonably achievable)の原則に準じて適応や撮像方法を考慮する必要がある．

リンパ管奇形の中でも GLA や GSD といった，

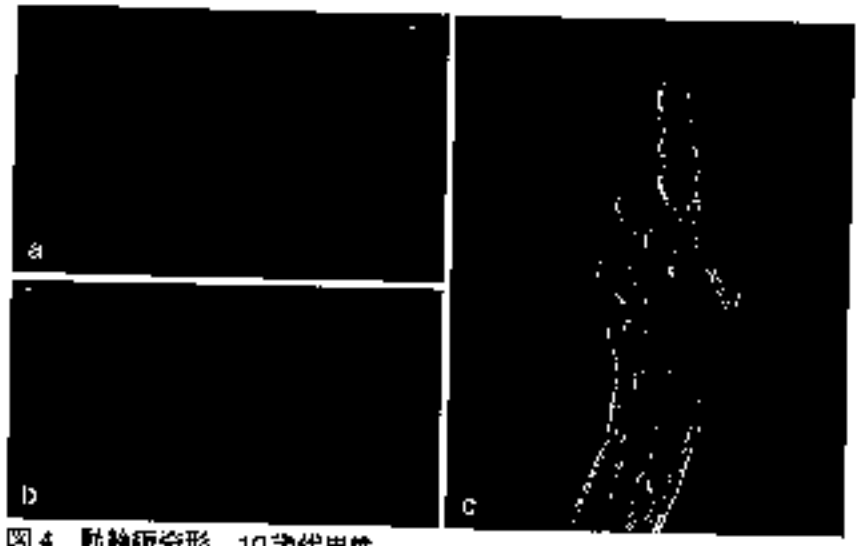

図4　動静脈奇形，10歳代男性

a) 超音波パルスドプラ像．
b) カラードプラ像．
c) 造影 CT，MIP 画像
造影 CT MIP 像で第3相に拡張した血管構造が集簇しており，ナイダスを含む動静脈奇形を見ているものである．近位側には血流量増加に伴い，拡張した動脈血管が蛇行し分布している．ナイダス部分はカラードプラ像でモザイク状となり，末梢部の血流が乱流を呈している状況である．同部分をパルスドプラ像で確認すると拍動性の波形が確認される．

図5　大嚢胞性リンパ管奇形と小嚢胞性リンパ管奇形

a) 2歳男児小嚢胞性リンパ管奇形．
b) 20歳代男性腹部大嚢胞性リンパ管奇形．
いずれも3モード像．a)小嚢胞性リンパ管奇形で皮下に嚢胞壁の低エコー部分が認められるが，その周囲に高輝度の軟部組織が分布している．これらはいずれもリンパ管奇形で，明かな嚢胞の部分は高輝度に描出されている．b)は大嚢胞性リンパ管奇形で厚い隔壁構造を有する嚢胞群が集簇してみられている．

間質への分布が広範なものについては，CT 肺野条件での評価が有用である(図8)[5]．

単純写真

単純写真は，脈管奇形そのものの評価には用いられないが，静脈奇形における静脈石の確認，GLA や GSD などの骨浸潤によって起こる溶骨性変化や，Klippel-Trenaunay 症候群や Parkes Weber 症候群などで知られる過成長状態の全貌を評価するために利用されている．

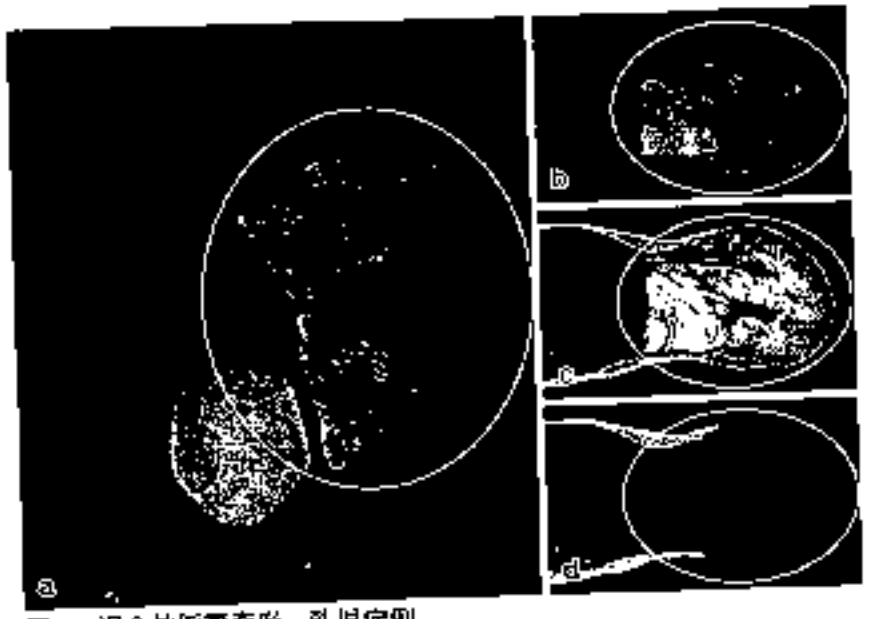

図8　混合性脈管奇形，乳児症例

a) STIR 冠状断，
b) STIR 水平断，
c) T2強調画像水平断，
d) T1強調画像水平断
病変部は○囲いの部分で，STIR や T2強調像で高信号，T1強調像では低信号に描出されている．STIR では脂肪成分の信号が抑制されており，分布範囲がより明瞭に把握できる．

おわりに

血管腫，血管・リンパ管奇形における画像診断について，概容を述べた．症例ごとに分布や背景，合併疾患など，さまざまであるため，診断アルゴリズムに準じつつ，状況に応じて適切な画像モダリティを選択することが肝要である．

1) Nozaki T, et al : Radiographics 33 : 175-195, 2013
2) Trop I, et al : Radiology 212 : 841-845, 1999
3) Flors L, et al : AJR Am J Roentgenol 201 : W554-562, 2013
4) Kramer U, et al : AJR Am J Roentgenol 196 : 702-711, 2011
5) Wunderbaldinger P, et al : AJR Am J Roentgenol 174 : 827-832, 2000

図7　20歳代女性，ダイナミック造影 CT による手指 AVM の描出

a) リブトラクション画像による血管描出．動脈相からナイダスを介して早期還流する血流が確認できる．
b) ボリュームレンダリング再構成画像．骨格や軟部組織と異常血管の位置関係が明瞭に描出されている．

図8　GIA における広義間質への病変浸潤，10歳代女児

a) 肺野条件水平断，
b) 造影 CT 縦隔条件水平断．
肺野条件では広義間質肥厚が広範に認められており，病変浸潤やリンパ路の閉塞異常による変化が示唆される．縦隔条件では縦隔や肺門部の気管支血管周囲に分布する低吸収の軟部組織が認められる(矢印)．病変浸潤を見ているものである．
[厚生労働省難治性疾患克服研究事業「難治性血管腫・血管奇形・リンパ管腫・リンパ管腫症および関連疾患について の調査研究」(班)：血管腫・血管奇形・リンパ管の形態学ガイドライン 2012 < http://www.marunouchi-u.ac.jp/ja/guidline.html >(2012年7月アクセスより)]

急性呼吸窮迫症候群（ARDS）

Acute respiratory distress syndrome

松本純一[1]　細野[illegible][2]　大塚[illegible][3]

診断のポイント

- （肺内・肺外の）感染症などの主病態の経過を追うなかで，両肺に影が広がってきた際には，透過性亢進型肺水腫の最重症型であるARDSを考える。
- ARDSは，併存病態によっても，解剖学的要因でも，水漏れの程度や持続期間によっても，さまざまな陰影パターンを呈しうる。

症例 1 肺炎からのARDS（60歳代，男性）

細菌性肺炎の診断で近医から転院搬送され，加療中。画像所見の経時変化を示す。

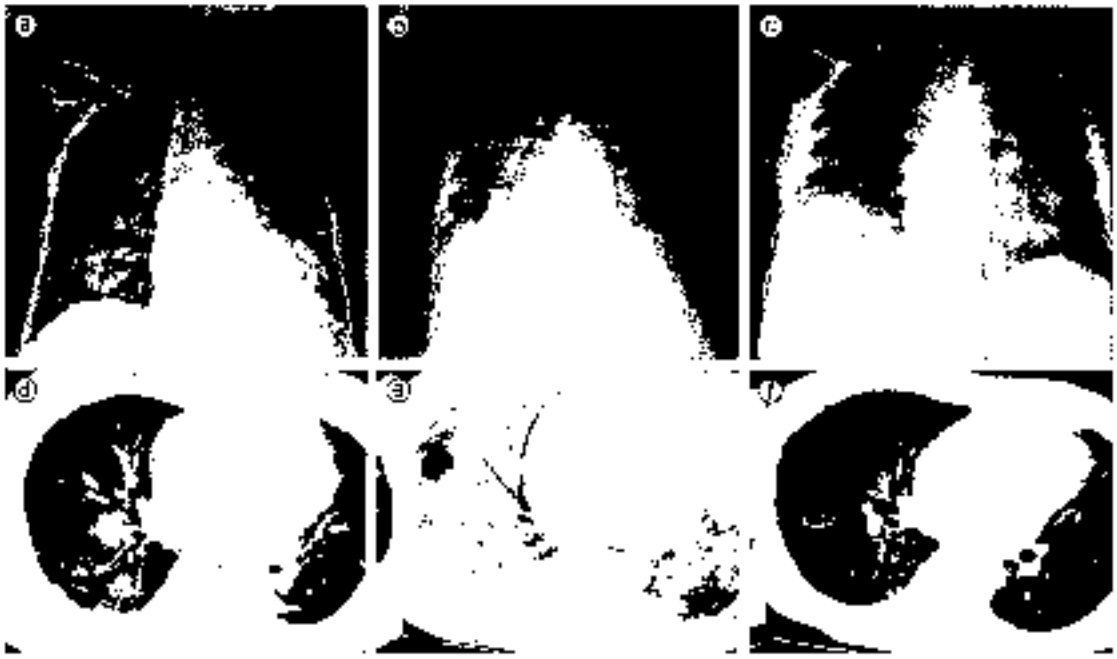

a：ポータブル胸部単純X線写真（臥位）第1病日　b：同第3病日　c：同第16病日
d：非造影CT横断像肺野条件第1病日　e：同第5病日　f：同第16病日

臥位ポータブル胸部単純X線写真では，右肺優位の不均一な濃度の浸潤影が認められ（a），肺炎と診断されたが，第5病日では，陰影は密度の高い浸潤影として両側に広範に広がっている（b）。臨常上はARDSを疑わせる所見である。主病態と考えた肺炎の治療後，第16病日には，陰影は改善傾向を示した（c）。CTでは，上記陰影の性状が，右肺の実質のすりガラス状陰影～浸潤影（第1病日）から，両肺に広がるすりガラス状陰影～浸潤影（air space consolidation）へと進展し（第5病日），CT上もARDSの経過に矛盾しない。主病態の治療が進むにつれ，両側肺の病変は不均一な濃度のすりガラス状陰影となって消退していく様子が確認できる。ARDSの病態モデルとも一致していることがわかる。本病態は改善していったものの，陰影はしばらく消えなかった（非掲載）。

1. Matsumoto J：聖マリアンナ医科大学病院 放射線科
2. Hosoi K：聖マリアンナ医科大学 放射線医学
3. Otsuka M：横浜市西部病院 放射線科

Presented by Medical*Online

症例 2 尿路感染症からのARDS(30歳代，男性)
尿路感染症の診断で近医から転院搬送された。画像所見の経時変化を示す。

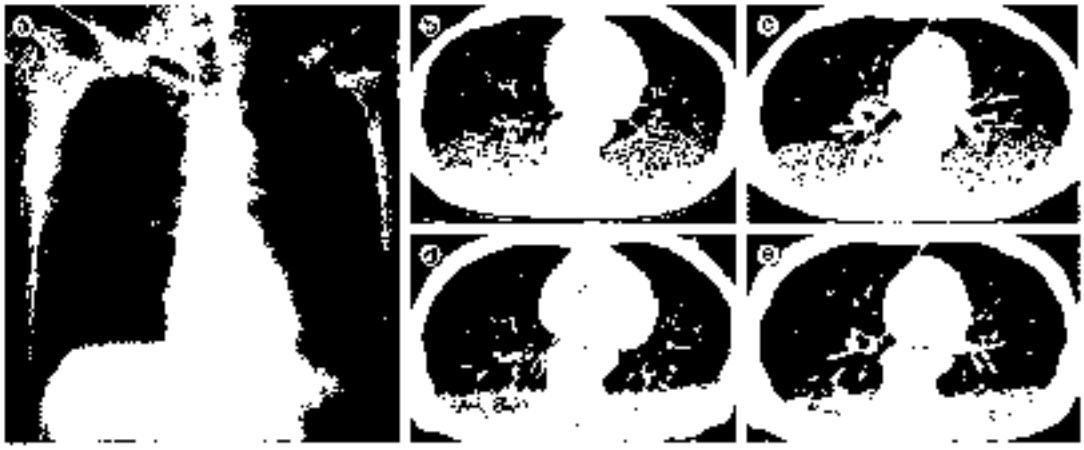

a：ポータブル胸部単純X線写真(臥位) 第1病日　b，c：同日の胸部非造影CT　d，e：4日後の胸部非造影CT
転院搬送時の胸部単純X線写真では，両肺で淡い不均一なすりガラス状陰影を認める(a)。一部網状にみえるところもあり，非定型の発生も疑った。同日後行された胸部非造影CTでは，腹側から背側に行くにしたがって濃度の濃くなるすりガラス状陰影から密度の低い浸潤影を認める(b，c)。これより頭側のスライスでは小葉中心性肺気腫像も認められた(非掲載)。尿路感染症からの敗血症に対し治療を行ったところ，4日後には陰影は中等領同で，その分布は，まゆで液面形成(air-fluid level)を形成しているようである。

一般的知識

■ 症例1

急性呼吸窮迫症候群(acute respiratory distress syndrome：ARDS)とは，大まかには，「感染症などのさまざまな侵襲に生体がさらされた際に，反応として起こる透過性亢進が，肺を結合に異常となり，ただならぬ水漏れが生じた状態」ととらえることができる。ARDSと聞くと，大変なことが肺で起きている，ということは感じることができるが，それがどんなイベントなのか大まかにでも整理できていないと，肺が白っぽい画像を目の前にして「うーん……ARDSですねぇ……」と発するときの言葉の重みが随分と変わってくる。ARDSとは結局，細胞レベルでみて，毛細血管という河の堤防が破壊した結果生じる大洪水であり，流れ出る水の中には破壊された家屋やなぎ倒された樹木や車などが含まれており，水が引いた後もかなり荒廃した状態と復興とが混じり合った風景となるのに似て，簡単に元通りの状態にはならないのである。このとき，毛細血管の内皮細胞から肺胞上皮(すなわち，河の縁から堤防，そして住宅街の外周循環？)までが広く全層性に障害されるため，病理像は「びまん性」肺胞傷害(diffuse alveolar damage)とよばれる(肺のあちこちが全体的に侵される，という意味ではないことに注意)。このようなことを考えながら画像所見とその推移をみてみると，ARDSというものがなんとなくわかった気がするのではないかと思う。

(松本，細井)

■ 症例2

ARDSは，基本的には，毛細血管から肺胞壁で構成される血液空気関門が破壊されて，高度の水漏れが生じる病態である。漏れ出る水の勢いによっては，換気運動や血管・リンパの流れなどによって水がきばきされず，どんどんと陰影が濃くなってしまう。その際，水をなんとかきばかせようと，正常部である小葉辺縁部分の血管やリンパ路がフル活用されるため，小葉間隔壁の肥厚はみられうる。しかし，左心不全の際(水力学的肺水腫)と異なり，心臓方向へのうっ滞は生病態ではないため，小葉間隔壁の肥

Presented by Medical*Online

原に主たる病態ではない。あくまでも大部に漏れ出た水の回収路の破綻化としてみられる，ということである。本例では，敗血症に伴う透過性亢進から水漏れが生じたが，水の漏れ出し合が軽度であったため，敗血症の治療により比較的速やかに水が引いていく様子が観察されている。結局は肺の陰影を形作っているのは漏れた水が主体であり，臥位を続けている患者では，CTでみると腹側から背側にかけて重力荷重側に水が溜まったようになる（グラデーションまたは液面形成）。水を多く含んだ肺は当然重さを増すので，背側の肺は腹自体の重さによって潰されている。このため背側の濃度は高くなる。漏れ出る勢いが強い場合には，全体がすりガラス状陰影や浸潤影を示すようになるが，その違いは漏れ出る勢い（主病態の病勢などと）と回収する能力（心機能や胸郭運動などを含む）の差によると思われる。

（松本，紺井，大野）

文献

1）松本純一：ARDSと画像診断：病態と画像所見についての考察，救急医学，39：6：655-660，2015.

2）Ware LB, et al.: The Acute respiratory distress syndrome. N Engl J Med. 342：1334-1349, 2000.

Presented by Medical*Online

硬化療法・塞栓術の実際

はじめに

硬化療法・塞栓術は，切除術と並んで軟部腫瘍奇形の積極的な治療法である．静脈奇形（海綿状血管腫），リンパ管奇形（リンパ管腫）に対しては直接穿刺の硬化療法，動静脈奇形（arteriovenous malformation：AVM）に対しては経動脈的，直接穿刺あるいは経静脈的な塞栓術が行われる．切除術と比較して根治性は劣るものの，機能・形態の温存が可能で，より低侵襲で反復しやすい治療である．施設による治療方法の違いがあり，また疾患の部位が多岐にわたり，まとまった症例数の蓄積が少なく，治療の標準化についてはまだ今後の課題である．

静脈奇形（海綿状血管腫）の硬化療法

1 適応

硬化療法の適応は症状があるか，あるいは病変の拡大であり，症状の緩和あるいは病変の縮小を目的とする．症状としては，疼痛，腫脹，機能障害，整容的問題などが挙げられる．とくに疼痛緩和は硬化療法の重要な役割である．症状がない病変は必ずしも治療を必要としない．

2 術前評価

症状のうち，疼痛はその部位，誘因，頻度を問診し，疼痛スコア（visual analog scale：VAS あるいは numerical rating scale：NRS）で評価する．整容面の評価は写真で行う．画像診断としては MRI，超音波検査が有用である．MRI では STIR あるいは脂肪抑制 T2 強調像が病変の進展範囲の描出にとくに有用である．

3 硬化剤の比較

静脈奇形に対する硬化療法は，2017年の時点で保険認可されていない．本邦で使用可能な硬化剤としてはポリドカノール，無水エタノール，エタノールアミンオレイトなどがあり，硬化作用の強さ，注入時の疼痛，推奨最大使用量は表1のとおりである．ポリドカノールやエタノールアミンオレイトは洗浄性硬化剤である．

4 手技

病変部の腫脹によるコンパートメント症候群や，頭頸部病変で気道狭窄の危険性が高い場合は，術前からステロイドを投与する．気道狭窄の危険性がある場合は術前の気管切開も検討する．エタノールを使用する場合は全身麻酔，他の硬化剤では局所麻酔を選択する．われわれは，小学校中学年までは基本的に全身麻酔下に施行している．

a) フォーム硬化療法

フォームは硬化剤とガスを混和したもので，作成方法は Tessari 法を用いる．本邦においては入手可能なポリドカノール，エタノールアミンオレイトと，CO_2 あるいは空気を混和する．具体的に，当院では1～3%ポリドカノールと CO_2 を1:4の割合で，二つのシリンジと三方活栓を用いて20往復パンピングして混和したものを使用している．フォーム硬化療法の利点としては，硬化剤容積の増加，硬化剤と血管壁の接着性の向上，血管壁縮小による血管容積の減少により，液体硬化剤より効果が高く，より大きい血管腔に対しても有効と考えられる．

超音波ガイドトに病変を22ゲージ針で直接穿刺し，血流の逆流を確認する．Digital subtraction angiography（DSA）下あるいは透視下に生理食塩水で希釈した造影剤を注入し，造影剤の血管外漏出の有無，硬化剤の病変内への停滞の程度などを評価する．造影剤の停滞が得られない場合，駆血や流出静脈の圧迫による血流コントロールが必要となり，治療の成否にかかわる．ただし，駆血解除時に硬化剤や血栓が体循環に流入する可能性があり，長時間の駆血は望ましくない．

フォーム注入は DSA 下に行い，フォームは陰性造影剤として観察される．われわれは炭酸ガスを用いたフォームを使用しており，成人ではフォームの1回注入量は原則として5 mL以下で，5分間隔で注入している．また，成人での1セッションでの最大使用量は，1%ポリドカノールと CO_2 によるフォームを用いた場合，成人では30 mL程度までとしている．ヨーロッパにおける下肢静脈瘤に対するフォーム硬化療法のコンセンサスミーティングでは，空気を用いたフォームを使用する場合，10 mLまでが望ましい，としている．

b) エタノール硬化療法

エタノール濃度としては無水エタノールを使用する報告が多いが，透視や DSA で観察するために造影剤と混和して70～80%で使用することも可能である．ただし，造影剤によってはエタノールとの混和により混濁する製品もある．無水エタノールの推奨総注入量は，文献的には1 mL/kg以下との記載が多いが，筆者の意見では日本人の場合0.5 mL/kg程度までが望ましく，また1回注入量0.1 mL/kg以下，注入間隔は5～10分間以上が望ましい．エタノール硬化療法の重篤な合併症である心肺虚脱を防ぐうえでも，1回注入量，注入間隔，総注入量の管理は重要と思われる．十分な輸液を行い，利尿を保つ．

5 術後管理

われわれは，前腕・顔面病変以外に対しては術後3日間，弾性包帯を装着としている．1～3か月後に合併症，治療効果の評価を行う．術前と同様に疼痛は疼痛スコア・頻度で，病変の大きさは MRI・写真で評価する．効果が十分でなければ，硬化療法を繰り返す．

病変が大きい場合，病変の縮小などによる合併症が問題となる場合に，数回に分けて段階的な硬化療法を施行する（図1）．術前に長期的な治療方針を患者と相談しておくことは重要である．

6 成績

Yakes らは四肢静脈奇形36患者に対してエタノール硬化療法を施行し，90%で症状の消失が得られたと報告している[6]．Goyal らは小児の静脈奇形59例にエタノール硬化療法を施行し，病変の大きさ，患者の症状を評価したところ，59%で著効あるいは有効であったとしている[7]．MRI による彼らの分類では，5 cm以下の境界明瞭な病変では効果が良好で，5 cm以上の浸潤性の病変では効果が不良であった，と報告している．Cabrera らは静脈奇形50例に対してポリドカノールフォーム硬化療法を施行し，外観と疼痛について，それぞれ50例，39例を評価した．病変の消失は36%，縮小は56%，不変は8%であり，疼痛の消失は54%，改善は36%であった[8]．これらの成績の評価基準はさまざまで，比較は困難である．

7 合併症

手技そのものによる合併症と，硬化剤に特徴的な合併症とがある．手技による合併症としては皮膚壊死，水疱，蜂窩織炎，神経障害，筋拘縮，コンパートメント症候群，血栓性静脈炎，深部静脈血栓症／肺塞栓症などが挙げられる．

皮膚壊死，神経障害は硬化剤の血管外漏出が主たる原因である．神経障害は術後の腫脹により起こる場合もある．深部静脈血栓症・肺塞栓症は硬化剤の深部静脈への流出が主たる原因である．コンパートメント症候群・気道閉塞は前腕や顔面病変で生じる危険性がある．筋肉内の静脈奇形では，病変の縮小に伴って筋拘縮をきたす可能性がある．

硬化剤に特徴的な合併症は以下のとおりである．エタノールアミンオレイトは溶血を起こしやすく，血尿をきたす．高度の溶血は急性腎不全の原因となる．溶血の予防にはハプトグロビンの投与が有効で，具体的には，成人では治療直前～治療中にハプトグロビン4,000単位を点滴静注する．また，補液，尿のアルカリ化が有用といわれている．ポリドカノールは多量に使用した場合，麻酔作用として痙攣，血圧低下をきたす．一時的な心停止の報告もある．エタノールは血管を透過して浸透する性質があり，皮膚壊死，神経障害の危険性が高いといわれている．エタノール硬化療法・塞栓術の重篤な合併症として心肺虚脱が報告されているが，原因は明らかではない．心肺虚脱は肺動脈塞栓が関連しているとの推論があり，Swan-Ganz カテーテルによる肺動脈圧測定が有用かもしれない．また，とくに日本人では急性アルコール毒にも注意が必要である．

リンパ管奇形（リンパ管腫）の硬化療法

静脈奇形硬化療法と類似の治療法であり，前項に記載する．

表1　硬化剤の比較

硬化剤	硬化剤の効力	注入時の疼痛	推奨最大使用量（成人）
無水エタノール	強	高度	0.5～1 mL/kg
5%エタノールアミンオレイト	中	軽度	0.4 mL/kg
3%ポリドカノール	弱	ほぼなし（フォームでは軽度）	2 mg/kg

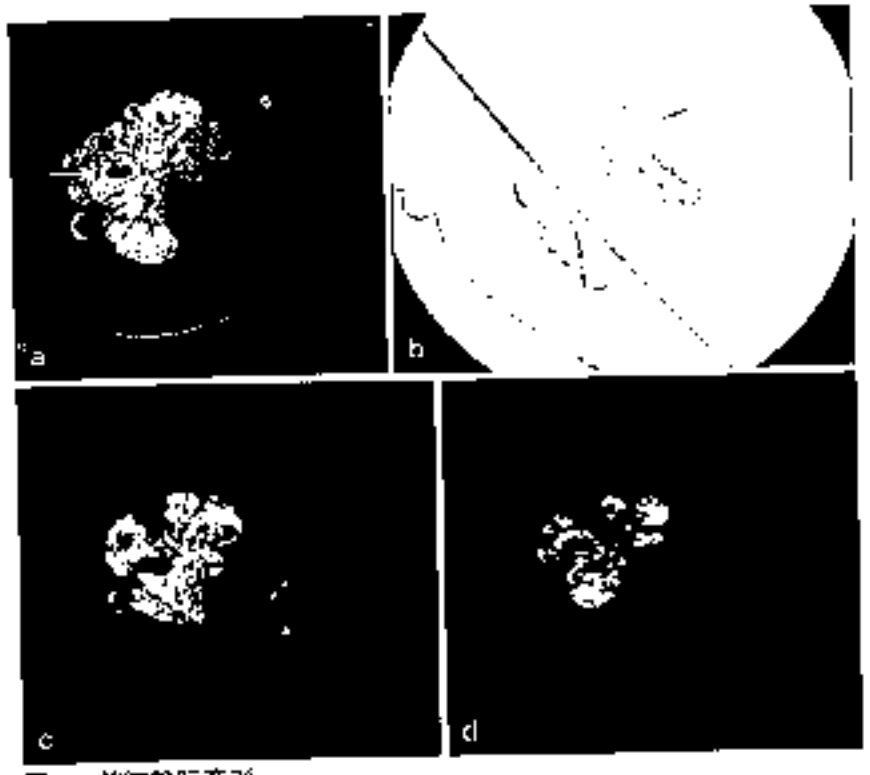

図1　前腕静脈奇形

主訴は疼痛．コンパートメント症候群の予防のため，ステロイド症併用し，少量の硬化剤を用いて段階的な硬化療法を施行した
a) 硬化療法前 MRI STIR 横断像：病変は著明な高信号を呈する．病変内を上腕動脈が貫通している(→)．
b) フォーム注入：フォームは陽性造影剤として認められる．
c, d) 1回目硬化療法後3ヵ月，5回目硬化療法後3ヵ月 MRI STIR 横断像：病変は徐々に縮小し，疼痛は改善した
[三村秀文ほか：臨放 59：321-332, 2014 より許可を得て転載]

E. 適応

リンパ管奇形では，疼痛，腫脹，機能障害，増大傾向などが積極的治療の適応となる．リンパ管奇形の治療法として，硬化療法は外科的切除術と並ぶ積極的治療であり，機能・形態の温存が可能な治療として，まず考慮されるべき治療である．

F. 硬化剤

硬化剤としてはOK-432（ピシバニール®），無水エタノール，マキシサイクリン，ブレオマイシンなどが用いられ，本邦ではOK-432のみ保険適用となっている．以下，本邦で一般的なOK-432を用いた硬化療法について述べる．

G. 手技

硬化剤は1KEのOK-432を10 mLの生理食塩水に溶解したものを使用する．OK-432の1回治療での最大使用量は2 KEとされている．超音波ガイド下あるいは直視下に病変を直接穿刺し，リンパ液を吸引し，吸引したリンパ液と同量の硬化剤を注入する．必要に応じて造影剤を混和し，透視下あるいはDSA下に注入する．静脈奇形との違いは，リンパ管奇形では内容液吸引により虚脱し，注入した硬化剤が溜まりにくいと考えられる．OK-432硬化療法が効果を発揮するのは治療後約1ヵ月以降なので，治療間隔はそれ以上とする(図2，3)．

H. 成績

硬化療法はマクロシスティックタイプには有効性が高いが，ミクロシスティックタイプでは効果が得られにくいとされている．OK-432を使用した硬化療法の治療成績のレビューでは[4]，マクロシスティックタイプの治療成績は，111例中98例(88%)がexcellent（90%以上の縮小），9例(8%)がgood（50～90%の縮小），4例(4%)がpoor（50%以下の縮小）であった．ミクロシスティックタイプの治療成績は，49例中13例(27%)がexcellent，16例(33%)がgood，19例(40%)がpoorであった．

図2　リンパ管奇形の乳児

[赤坂医療センター 大原圏夫先生ご提供]

図3　OK-432で治療後，1年4カ月

[赤坂医療センター 大原圏夫先生ご提供]

I. 合併症

副作用としては発熱と局所の腫脹・発赤・疼痛があり，発熱はほぼ全例に認められ，38～39℃台の発熱が2～4日間みられる．合併症として，眼窩内のリンパ管奇形に視神経の圧迫，眼球突出をきたす可能性があり，頭部のリンパ管奇形は気道狭窄や上大静脈症候群と同様の症状をきたす可能性があるため，これらの部位の治療に際してはとくに慎重な対応が必要である．また，OK-432はペニシリンGを含むため，ペニシリンアレルギーの患者には禁忌である．

動静脈奇形（AVM）の塞栓術

J. 適応

疼痛，腫脹，潰瘍，出血，機能障害などの症状あるいは増大傾向があれば，積極的治療（塞栓術あるいは切除術）の適応となる．出血は生死にかかわるため，治療方針にとくに影響を与えやすい．症状がなく整容目的の場合の積極的治療については，リスクとベネフィットを十分検討する必要がある．

AVMは悪化するため，発見すれば早めに積極的な治療をするべき，との意見がある．しかし，小児期のAVMはほぼ例外なく増大するが，成人になってからは増大しない病変も多い．小児期に根治的な治療ができれば望ましいが，残存すれば思春期にかけて悪化する可能性があり，長期的なコントロールを目標とする．

K. 術前評価

術前評価は静脈奇形と同様である．疼痛にはVAS スコア・疼痛の頻度などで，病変の外観は写真で評価する．画像診断は，ドプラ超音波，MR angiography（MRA）を含めたMRIに加えて，空間分解能に優れる造影CTも有用であるが，経過観察で頻回にCTを使用すると被曝の問題がある．

L. 塞栓物質

塞栓物質の主役は液体塞栓物質であり，n-butyl-2-cianoacrylate（NBCA）・エタノールが使用される．しかしながら，本邦において前者は胃静脈瘤の内視鏡的血管塞栓材料としてのみ薬事承認され，また後者の血管内投与は承認されていない．粒状塞栓物質，コイルも使用されるが，対象は限られる．

M. 手技

術中の疼痛対策としてエタノールを使用する場合は全身麻酔下に施行するが，NBCA，粒状塞栓物質，コイルを使用する場合は局所麻酔でも施行可能である．

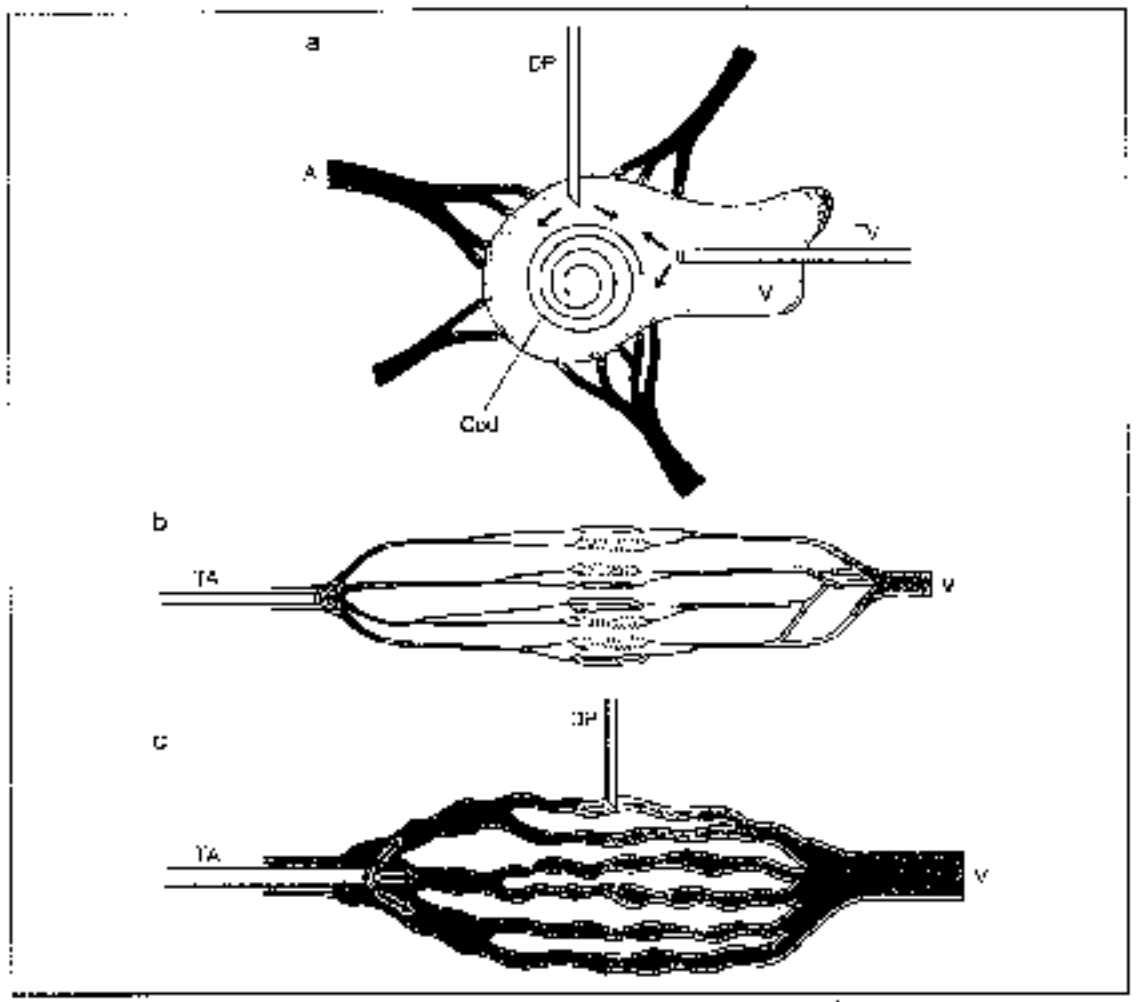

図4　血管造影によるAVMの分類と対応するエタノール塞栓術のアプローチ方法

TA(transarterial)：経動脈的，DP(direct puncture)：直接穿刺，Tv(transvenous)：経静脈的
a) Type Ⅰ：さほど多い流入動脈が1本の静脈にシャントしている．直接穿刺あるいは経静脈的に静脈側を塞栓する．彼らの方法ではコイルを留置し，エタノールを追加する．
b) Type Ⅱa：流入動脈が多数，流出静脈多数で，シャント部の拡張はない．経動脈的にアプローチする．
c) Type Ⅱb：流入動脈が多数，流出静脈が多数で，シャント部が拡張している．経動脈的にあるいは直接穿刺でアプローチする．

[Cho SK, et al.：J Endovasc Ther 13：527-535, 2006 より作成]

a) NBCAを用いた塞栓術

NBCAは接着剤であり，油性造影剤のリピオドール®と混和した溶液を使用する．NBCAとリピオドール®の混合比は1:4～1:2(20～33%)を主に用いる．リピオドール®の量を増やすと重合時間が延長するが，粘調となって流れにくくなる可能性があり，リピオドール®を温めて粘調度を低下させるなどの工夫が有用かもしれない．

b) エタノールを用いた塞栓術

エタノールを用いた直接穿刺の治療は，文献的に凝固術とも硬化療法とも呼ばれている．エタノールは，細く流速の遅い血管には有効だが，太く流速の速い血管には効果が乏しい．AVMの塞栓術でエタノールを使用する場合は基本的にフロー・コントロールが必要である．また，太く流速の速い血管には後述のコイルの併用が有効である．

c) コイルを用いた塞栓術

動脈と静脈が一対一で交通しているAVFに対して，コイル塞栓はよい適応である．コイルによる動脈の近位塞栓は側副血行路の発達を促し，病変が悪化する可能性があり，術前塞栓の場合などの限られた症例で施行するべきである．また，コイルは後述のtype Ⅱ AVMの静脈側の塞栓に寄与し，重要な役割を担う．

d) 粒状塞栓物質を用いた塞栓術

粒状塞栓物質単独の塞栓術で対象となるAVMは，後述のSamsungの分類でtype Ⅲaと思われる．粒状塞栓物質にシャントを通過する可能性があり，肺塞栓症や右左シャントによる奇異性脳梗塞をきたす可能性があるが，大きめの粒子を用いると近位塞栓になり，効果が乏しいかもしれず，粒子の選択はむずかしい．マイクロスフィアを用いる場合は複数のサイズの製品をそろえ，シャントの径よりも大きめの粒子を使い，すり抜けるようであればより大きい粒子を使う．ゼラチンスポンジは一時的塞栓物質で，閉塞した血管は2～4週間程度で再開通するが，炎症を惹起し，血栓を伴い，ある程度は血管を閉塞させる．

Ⅲ AVMのタイプ別の治療戦略

動脈造影により，治療が必要な血管の同定，造影上のAVM形態による経皮塞栓術のアプローチ方法の選択を行う．Choらは，66例の百肢・体幹AVMの塞栓術を検討し，Samsungの分類のtype Ⅱで全例に有効，type Ⅲbでは83%に有効であり，type Ⅲaあるいは混合型での有効率は50%以下であったと述べている(図4)[9]．彼らの分類を元に症例を提示して実際の治療を述べる．

Type Ⅰでは直接穿刺あるいは経静脈的なアプ

図5　3歳女性，顔面動静脈奇形(type Ⅲa)

主訴は口腔内出血
a) 治療前：右口唇からの出血，舌内の腫瘍がみられる
b) 右外頸動脈造影：主として右顔動脈枝を流入動脈とするtype ⅢaのAVMがみられる．
c) 右下行口蓋動脈造影：出血源の流入動脈と考えられ，粒状塞栓物質エンボスフィア®300～500 μmで塞栓した
d) 塞栓術2週間後　口唇からの出血，舌内の腫瘍はあらかたなくなった．

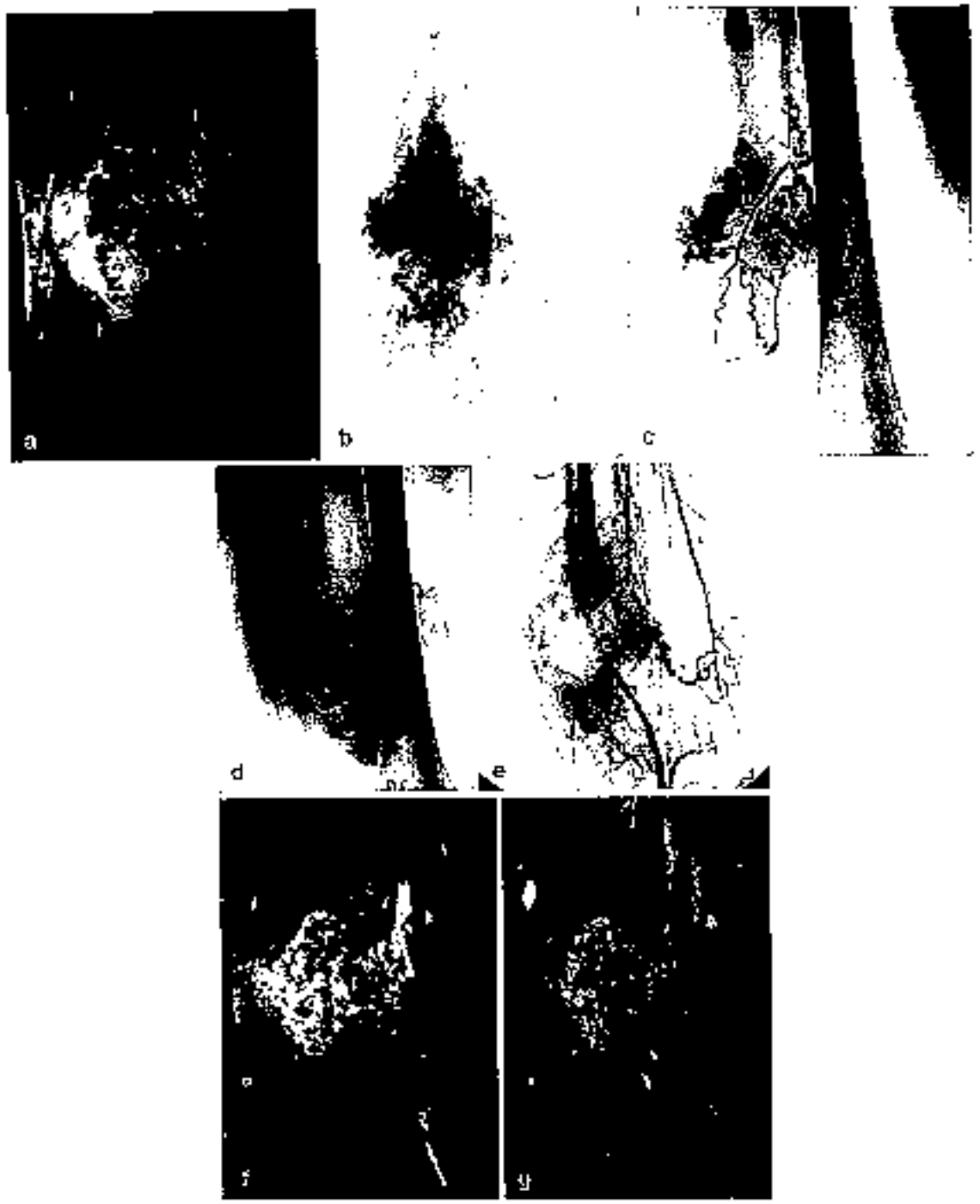

図6　16歳女性，左大腿動静脈奇形（type Ⅲb）

主訴は疼痛．
a) MRI 脂肪抑制造影 T1 強調像：左大腿部に flow void を呈する屈曲蛇行する血管がみられ，周囲に造影効果がみられる．
b) 左総大腿動脈造影：左浅大腿動脈，深大腿動脈の両者から多数の流入動脈をもつ type Ⅲb の AVM がみられる．
c) 経動脈的塞栓術後：経カテーテル的にリピオドール®と混和した NBCA を注入した．
d) 直接穿刺塞栓術後：直接穿刺で NBCA を追加注入した．
e) 直接穿刺塞栓術後の総大腿動脈造影：5割程度のシャントは閉塞されたと考えられた．
f, g) 塞栓術の 1 年後と 13 年後の MRI 脂肪抑制造影 T1 強調像：術後疼痛は消失し，疼痛の再発や病変の増大はみられない．

コ・チが主となる．直接穿刺は超音波ガイド下に行う．シャントの静脈側を塞栓することにより，シャントを閉鎖することが可能である．静脈側が細ければエタノールやNBCA 単独で塞栓可能だが，太く血流が速ければ困難であり，コイルを使用し必要があればエタノールやNBCA を追加する．

Type Ⅲa では経動脈的なアプローチが主となり，一般に治療はむずかしい．NBCA は選択的に注入してもシャントを貫通させることがむずかしい．出血や疼痛などの症状の緩和を目指すのであれば，効果は限局的であるかもしれないが，マイクロスフィアなどの粒状塞栓物質が有効かもしれない（図5）．

Type Ⅲb では経動脈的あるいは直接穿刺の手技が主となる（図6）．塞栓物質はエタノール，NBCA が使用される．動脈を NBCA で塞栓した後，シャント部を直接穿刺しエタノールアミンオレイトで硬化療法を施行し，よい成績であった報告もみられる．

Type Ⅲa，Ⅲb ではシャントが多く，一度の手技で大部分を塞栓することは難しくむずかしい．部分的であってもシャント部を閉鎖すれば術後側副血行路がただちに発達することは少なく，数回に分けて治療することは一般に可能であり，合併症の予防のためにも段階的な塞栓術が施行されるべきと思われる．

術後管理

1〜3ヵ月後に合併症，治療効果の評価を行う．術前と同様に疼痛は疼痛スコア・疼痛の頻度などで，病変の外観，大きさは写真・MRI で評価する．

合併症

手技による合併症として，水腫，びらん，壊死，潰瘍，二次感染，神経障害，横紋筋融解，筋拘縮，腔コンパートメント，血栓性静脈炎，深部静脈血栓症／肺塞栓症，播種性血管内凝固症候群（DIC）が挙げられる．

塞栓物質と関連した合併症としては，NBCA による血管壁へのカテーテル固着，NBCA のカテーテルへの付着や断片の飛散，シャントを通過した肺動脈への流入，NBCA そのものによる硬い腫瘤の形成，皮膚・粘膜からの NBCA の排出が挙げられる．

エタノールの合併症に関しては酵素奇形のエタノール硬化療法の項を参照されたい．

おわりに

静脈奇形，リンパ管奇形硬化療法，動静脈奇形塞栓術の実際について述べた．同じ疾患でも患者の症状，個々の病変の性状により，治療方針は異なる．合併症を予防し，良好な治療効果を得るためには，リスクとベネフィットの十分な理解が必要である．

1) Yakes WF : Semin intervent Radiol 11 : 332-339, 1994
2) Goyal M, et al : Radiology 223 : 639-644, 2002
3) Cabrera J, et al : Arch Dermatol 139 : 1400-1416, 2003
4) Poldervaart MT, et al : J Craniofac Surg 20 : 1159-1162, 2009
5) Cho SK, et al : J Endovasc Ther 13 : 527-538, 2006

閉塞性肺疾患と急性病態の合併

Coexistence of chronic obstructive pulmonary disease and acute lesion

松本純一[1]，[illegible]，[illegible]

診断のポイント

- 急性呼吸不全の画像診断では，必ず水力学的肺水腫の可能性を念頭に間質肺炎がないか確認する。CTでは，肺尖部と肺底部で輪郭模様がないかを確認する。
- 肺気腫や既存病変があると，新たに加わった病変の画像所見は修飾される。目の前の所見一つ一つを解きながら，そして解釈を統合しながら診断していく。

症例 1 肺気腫に合併した肺水腫(60歳代，男性)

肺気腫にて経過観察中の患者。数日前から続く呼吸苦が増悪し，来院。

a：胸部単純X線写真(臥位)　b，c：胸部非造影CT肺野条件(前回通常時)　d，e：胸部非造影CT肺野条件(今回，前回と同じスライス)

画像所見

胸部単純X線写真では，明らかな浸潤影やKerley線のような目立った正質の肥厚は指摘できないが，全体としては気管支血管影が顕在化してみえ，しかしその輪郭は不明瞭である。肺底部傍脊椎領域の透過性は低く，かなり白い。胸水の存在を疑わせる所見である。肺尖部の含気低下をみているだけの可能性もある。中上肺野はバラーで肺気腫に矛盾しないが，(本来は陰影所見をもっと観察すべきであるが)単純X線写真のみでは，病態をとらえきれない。前回のCTの肺底部近くのスライス(b，c)では，不均一に透過性の低下した肺野と気管支壁の肥厚

1. Matsumoto J.：聖マリアンナ医科大学救急医学 救急救命科部門
2. Kon Y，Okuno M：横浜市西部病院 放射線科
3. Hosui K：聖マリアンナ医科大学 放射線医学

Presented by Medical*Online

を認める。慢性気管支炎＋肺気腫の所見である。今回のほぼ同じスライスの画像(d, e)では，気管支壁の肥厚が強調されており(d)，また，肺底域では小葉間隔壁の肥厚と小葉中心腺造の顕在化が，亀の甲羅の模様のようにみえる(特に右肺底部)。両肺に胸水も指摘できる。間質の肥厚像は肺気腫浮腫を反映した像であり，今回の呼吸苦の原因は水力学的肺水腫，おそらく心原性肺水腫と考えられる。

一般的知識

肺気腫が存在すると画像所見が修飾され，また，臨床像も修飾され，診断が難しいことがある。肺気腫の存在が単純写真でわかる程度であれば，それだけ呼吸機能に余力はないと考えられるので，画像で明らかな増悪が出てくる以前に呼吸苦の症状が前面に出てくることは十分ありうる。また，それだけ呼吸機能に余裕がないような状態では，肺自体が肺気腫だけでなく，炎症後の変化や胸膜肥厚，線維化巣などを伴って，どこまでが元の状態かを判断することも難しいことはよくある。そんなときでもまずは，治療反応性のよい病態として水力学的肺水腫の存在を診断，否定するようにする。その際の鍵となる所見は小葉間隔壁の肥厚や気管支壁の肥厚だが，肺尖部と肺底部で観察しやすいので，この両方をまずみるようにする。しばしばどちらかだけでしか確認できないことはあり，さらに水力学的肺水腫であっても(おそらく病期というかタイミングによって)間質の肥厚像が目立たないことも経験する。過去画像との比較は基本であり，単純X線写真も含め，必ず行うようにする。そうすることで病態を短時間で経済的に高く解釈できる可能性が高くなる。特に背景病態があるときはなおさらである。前回だけでなく，さらに古い画像もあれば比較するとよい。

(松本，氏，大熊)

参考症例 症例1図e拡大図
(亀甲状の肺底部間質肥厚)

画像化した小葉間隔壁が網目に亀甲様を呈している。

症例 2 肺気腫に合併した肺炎(70歳代，男性)

50年来の喫煙歴がある。3日前から呼吸困難および湿性痰を自覚。当日から右背部痛があり，外来を受診した。

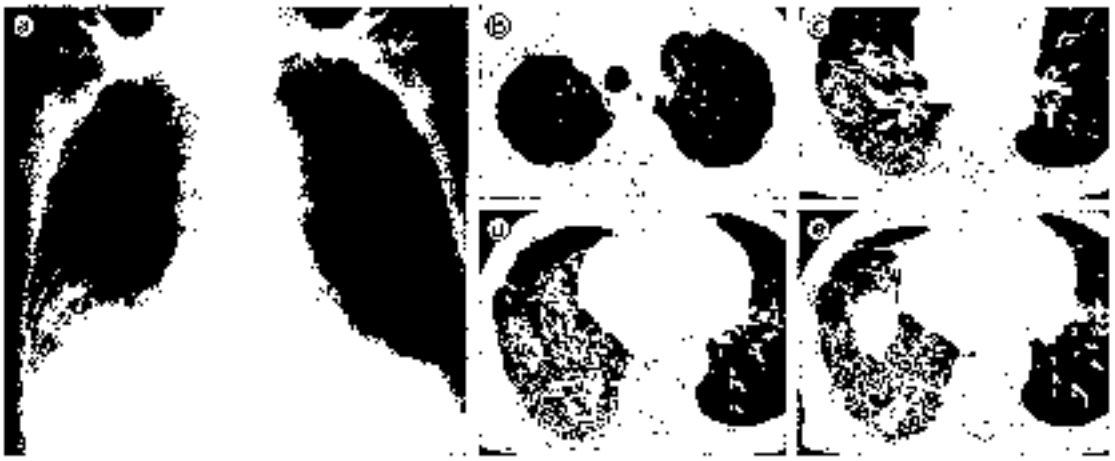

a：胸部単純X線写真(臥位)　b～e：胸部非造影CT肺野条件

Presented by Medical Online

画像所見

胸部単純X線写真(a)では，右下肺野に浸潤影を認める。左下肺野にも浸潤影を指摘できる。肺野の濃度は不均一で肺気腫に矛盾しない。縦隔では上縦隔がアンバランスに大きく，動脈硬化性の蛇行かつ拡張傾向を呈う。胸部もあり，CTが施行されている。肺尖部(b)では，相変わらず心性の肺気腫が目立つ。肺門より下位レベルの肺では，一見すると不均一なすりガラス状陰影から浸潤影が斑状影の様相を呈してもみえる。もう少し詳しくみると，肺門付近(c)では気管支壁の肥厚があり，ほかのスライスに降りていくと，これらの気管支血管束に沿うような浸潤影(d，e)の存在も推測することができる。主病態は気管支肺炎であり，一見斑状ガラス＋斑状の陰影は，肺気腫を背景としてこの気管支肺炎に重畳して出現してきた炎症性浸潤であると考えられる。自覚症状は3日前からと記載されているが，陰影の様子からは実際にはもう少し前から症状をひき起こすような病態が存在していたという印象をもつ。肺気腫を背景としていれば，症状発現はなおさら早かったのではないかと疑う。画像所見と臨床情報が乖離する場合には，安易に流さず，臨床情報を確認しなおすなど，疑問点や問題点を解決する姿勢が非常に大切である(なお，本例でのこれ以上の詳細な情報は不明である)。

一般的知識

肺気腫や慢性炎症性病変，炎症後瘢痕や器質化巣など，既存の陳旧変があると，画像所見が修飾されて，さまざまな鑑別が想起されるような所見となることがある。肺気腫を背景とした場合，肺炎や肺水腫が斑状影となってみえ，蜂巣肺のようにみえる。肺気腫に限ったことではないが，既存の病変により，肺自体の運動や免疫や血流が制限されたり変化した場合にも，病変の広がりや波及のしかたが修飾され，さまざまな陰影パターンを経過をたどりうると思われる。また，自分が画像をみることになったタイミングは，教科書的には典型的な像を呈するタイミングでなかったりすることもあるので，時期的な制限や変化といった要因でのバリエーションもありうる。教科書に記載されたパターンでの認識だけでなく，目の前にある画像所見をマクロ病理あるいは病態生理，あるいは起こりうる現象を想像しながら，矛盾のない範囲で物語を作っていく(詰めていく)作業が，肺の病変を評価する際には時に多く求められるように思う。そのためには代表的な病態生理と典型的な画像所見は知っておかなければならないが，パターン認識に縛られて，「読影」という思考作業が行われていないレジデントに遭遇する機会は多い。

(松本，昆，大熊，細井)

文献

1) 松本純一，ほか：安本和正編．呼吸器学における不思議53．2．原発性肺水腫と非心原性肺水腫は画像上どうすれば見分けられるのか？ アトムス p28-33, 2011.

Presented by Medical Online

頭頸部

血管奇形

5. vascular anomalies（脈管異常）

[illegible]

ISSVA 分類（2018 年改訂）

本分類の定義・意義

vascular anomalies（脈管異常）は，脈管奇形（血管奇形・リンパ管奇形）と脈管性腫瘍を指す．全身のあらゆる部位に発症し，診療を担当する科は多岐にわたり，疾患概念と治療法に混乱がみられる．

vascular anomaliesの国際学会であるThe International Society for Study of Vascular Anomalies（ISSVA）は，1996年の学術会議でISSVA分類（表1）[1]を採択した．分類の利点は，わかりやすい世界共通の病名を用いて脈管奇形と脈管性腫瘍を区別することにより（表2[2]，3[3]），適切な臨床診断と治療方針を導くことにある[2-4]（▶NOTE 1）．

表1　オリジナルISSVA分類（1996年）

tumors	malformations			
hemangioma other	simple			complicated
	capillary (C)	lymphatic (L)	venous (V)	AVF，AVM，CVM，CLVM，LVM，CAVM，CLAVM

（文献1）を元に作成）

表2　ISSVA分類（2018年改訂）

vascular anomalies				
vascular tumors	vascular malformations			
	simple	combined	of major named vessels	associated with other anomalies
benign infantile hemangioma congenital hemangioma other locally aggressive or borderline kaposiform hemangioendothelioma others malignant angiosarcoma others	CM LM VM AVM AVF	CVM CLM LVM CVLM CAVM CLAVM others	affect lymphatics, veins, arteries anomalies of origin, course, number length, diameter, valves, communication, persistence	Klippel-Trenaunay syndrome Parkes Weber syndrome Servelle-Martorell syndrome Sturge-Weber syndrome Limb CM＋congenital nonprogressive limb overgrowth Maffucci syndrome others

AVF：arteriovenous fistula，AVM：arteriovenous malformations，CM：capillary malformations，LM：lymphatic malformations，VM：venous malformations．
CAVM：CM＋AVM，CLAVM：CM＋LM＋AVM，CLM：CM＋LM，CLVM：CM＋LM＋VM，CVM：CM＋VM，LVM：LM＋VM（文献2）を元に作成）

表3　ISSVA分類と従来の分類との対比

ISSVA分類	従来の分類
[illegible]	
乳児血管腫　infantile hemangioma	いちご状血管腫　strawberry hemangioma
[illegible]	
毛細血管奇形 capillary malformation	単純性血管腫　hemangioma simplex 毛細血管拡張症　telangiectasia ポートワイン斑　portwine stain
リンパ管奇形 lymphatic malformation	リンパ管腫　lymphangioma, cystic hygroma
静脈奇形　venous malformation	海綿状血管腫　cavernous hemangioma 静脈性血管腫　venous hemangioma 筋肉内血管腫　intramuscular hemangioma 滑膜血管腫　synovial hemangioma
動静脈奇形 arteriovenous malformation	動静脈性血管腫　arteriovenous hemangioma

典型的な組み合わせの例を示しているが，明瞭な対応ではなく，表現とは異なる場合もある．
（文献3）より転載）

NOTE

[illegible]

分類の解説

脈管性腫瘍は，細胞（主に内皮）の腫瘍性増殖を来すことで発育する．その一方，脈管奇形では内皮細胞のturnoverは正常であり，形態形成の局所的な異常と考えられ，血管形成・脈管形成を制御する経路の機能障害により引き起こされたと考えられる．

A. 脈管奇形（vascular malformation）（図1）

脈管奇形は，発生学的には胎生4～10週の末梢脈管系形成期の異常によって生じ，その構成成分によって，静脈奇形（図1-B）[5,6]，動静脈奇形（図1-C）[5,6]，リンパ管奇形（図1-D）[5,6]，および毛細血管奇形などに分類され，その混合型も存在する．発生頻度に性差はなく，成長期などにゆっくりと増大し，退縮はしない．

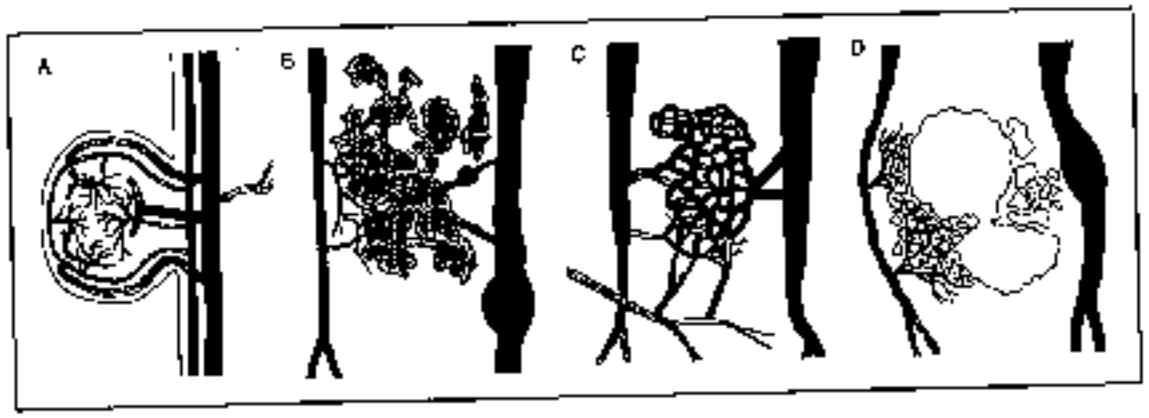

図1　vascular anomaliesのシェーマ
A：乳児血管腫．多血性病変の形態を呈する．
B：静脈奇形．形成異常を来した拡張した静脈腔からなる．
C：動静脈奇形．毛細血管を介さない動静脈の短絡がみられる．
D：リンパ管奇形．形成異常を示した拡張したリンパ腔からなる．
（文献5，6）を元に作成）

症例1

10歳台，女性，下肢痛を認める．

A　STIR像

B　超音波像
（プローブによる圧迫前）

C　超音波像
（プローブによる圧迫後）

A：筋肉内に蜂巣状の病変がみられ，（－），内容は高信号を呈する．
B，C：低エコーの立体腔は圧迫にて虚脱する
図2　静脈奇形

1）静脈奇形（venous malformation：VM）

静脈奇形は，筋層外皮の低形成を来した拡張した静脈腔で構成される（症例1）．周囲組織の圧迫，血栓形成による疼痛や機能障害を生じ，頭頸部病変などでは整容的な問題が生じる．消費性凝固障害（consumption coagulopathy, localized intravascular coagulopathy：LIC）を来すことがある．

2）動静脈奇形（arteriovenous malformation：AVM）

動静脈奇形は，動脈と静脈が正常の毛細血管床を介さずに，異常な交通を生じた病変である（症例2）．疼痛，腫脹，潰瘍，出血を来し，大きな病変では心不全を呈することがある．皮膚に温かく，拍動，血管雑音がある．

症例2

40歳台，女性，上肢痛を認める．

A　血管造影（動脈早期相）

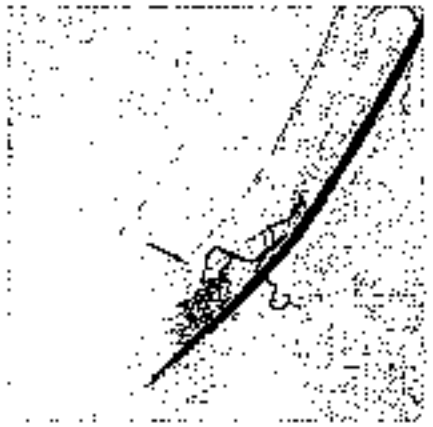

B　血管造影（動脈後期相）

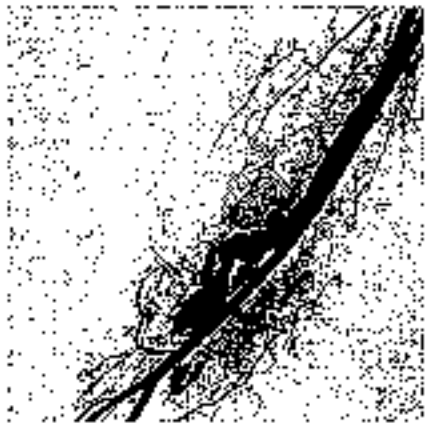

A，B：流入動脈（A：→），動静脈短絡（B：→），拡張した流出静脈（B：→）がみられる．
図3　動静脈奇形

症例3

40歳台，男性，鼠径部腫瘤を認める．

A　STIR冠状断像

B　T1強調像

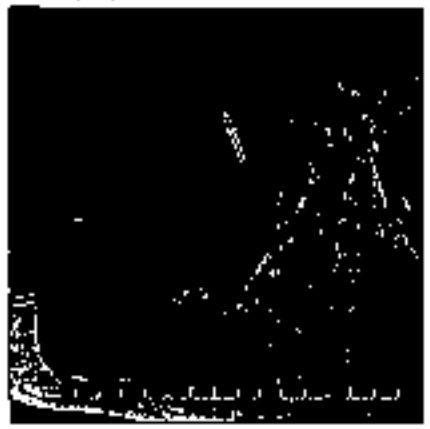

A：右鼠径部皮下の嚢胞性病変は，分葉状の形態で内部は高信号を呈する（→）
B：内容液は，漿液と同程度の低信号を呈する（→）．
図4　リンパ管奇形（macrocystic type）

3）リンパ管奇形（lymphatic malformation：LM）

リンパ管奇形はリンパ管の形成不全であり，胎生期の未熟リンパ組織がリンパ管に接合できずに孤立して嚢胞状に拡張した病変と考えられている（症例3）．皮下病変は，多房性あるいは単房性嚢胞性腫瘤として認められ，microcystic, macrocystic typeに分類される．しばしば炎症を伴い，一時的に増大し，腫脹・発赤・熱感・疼痛を来す．

4）毛細血管奇形（capillary malformation：CM）

毛細血管奇形は，皮膚の毛細血管拡張による赤色から暗赤色の色素斑である

5）脈管奇形関連症候群

脈管奇形関連症候群は患肢の肥大を伴う代表的な病変として，slow-flowのKlippel-Trenaunay症候群（CM＋VM＋/－LM，症例4），fast-flowのParkes Weber症候群（CM＋arteriovenous fistula：AVF）が挙げられる（表2参照）．Klippel-Trenaunay-Weber症候群は，この両者を併せた疾患名であり，便宜的に用いられている．

症例 4　20歳代，男性．下肢肥大を認める．

A　下肢正面写真　　B　STIR冠状断像

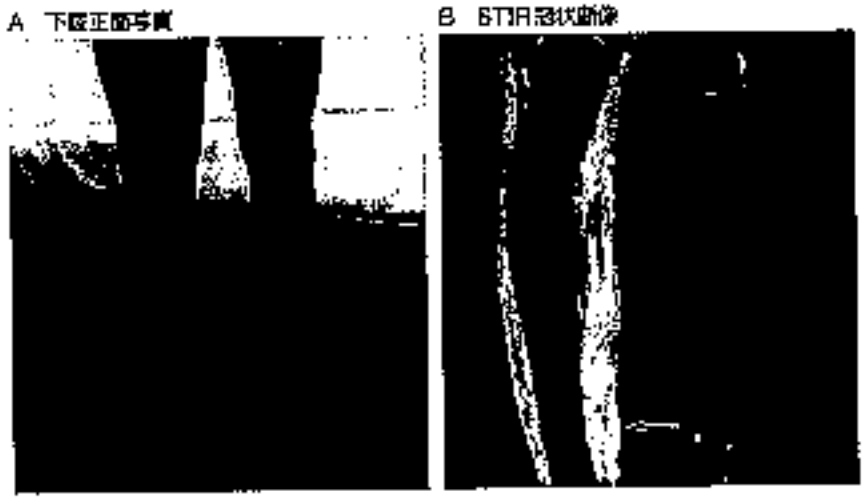

A：患肢の肥大．毛細血管奇形がみられる
B：患肢の肥大．皮下・筋肉内の静脈奇形（→）がみられる．

診断 Klippel-Trenaunay症候群

症例 5　3か月，女児．腫瘤触診を認める．

A　T1強調冠状断像（生後3か月）　　B　T1強調冠状断像（7歳時）

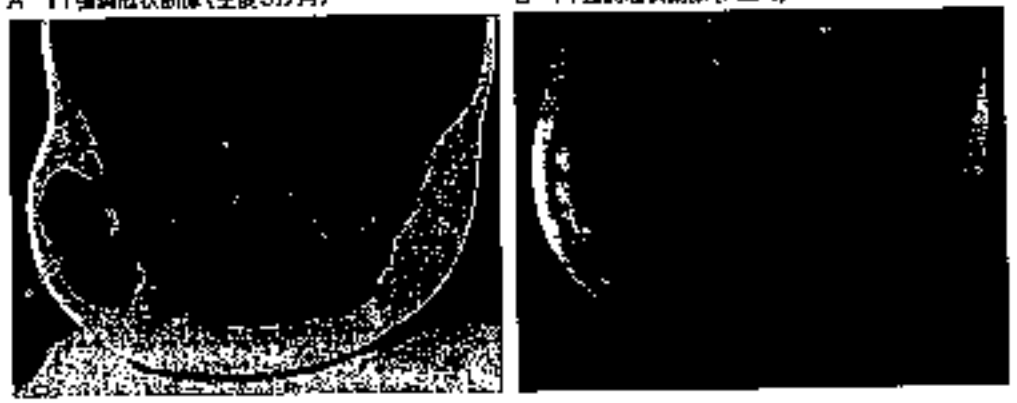

A：右頬部皮下脂肪織内に低信号を呈する腫瘤がみられる（→）．
B：腫瘤は消退し，線状瘢痕組織に置換されている
（文献5）より転載）

診断 乳児血管腫（深在型）

B. 脈管性腫瘍

代表的な乳児血管腫（infantile hemangioma）について記載する．

乳児血管腫は女児期に最も多い腫瘍で，血管内皮細胞の増殖性増殖とアポトーシスによる消退を示す（図1-A[5][6]，症例5[5]）．3～9：1の頻度で女性に多い．生下時は存在しないか，あるいは前駆病変が存在するが，生後2週程度で顕在化し，1.5歳頃まで増大する（増殖期）．その後，90%以上の血管腫は，5～7歳までに数年かけて徐々に自然消退する（消退期）．

表在型（superficial type），深在型（deep type），混合型（mixed type）などがあり，深在型は血管奇形と混同されやすい．

鑑別診断のポイント

①静脈奇形

超音波検査では病変内に血エコーの管腔構造がみられ，圧迫にて虚脱する．網状にみえる線状な血流，石灰，静脈石がみられる．MRI T1強調像では血液による低～中間の信号を呈し，T2強調像で高信号を呈する．病変の造影範囲の観察にSTIR像あるいは脂肪抑制T2強調像が有用である．造影により，均一ないしは不均一な増強効果を受ける．直接穿刺で静脈血が吸引され，造影で分葉状・静脈瘤状の拡張した静脈の描出が描出される．

②動静脈奇形

超音波検査では，拡張蛇行した流入動脈，流出静脈および動静脈の異常接合が無エコーとして描出され，ドプラでは，静脈側まで動静脈短絡を示唆する拍動流が描出される．MRIでは，血流による信号欠損（flow void）がみられる．MRAやCTAで，異常血管を描出した画像が得られる．動脈造影では拡張した流入動脈，短絡，拡張した流出静脈の早期描出がみられる．

③リンパ管奇形

超音波検査では，macrocystic typeは無エコーの単房性あるいは多房性嚢胞である．macrocystic typeは多数の小さな房をもち（明確な定義はないが，長径5cmあるいは1cm以下），隔壁が高エコーとなり，充実性にみえることがある．MRIでは，リンパ管奇形内部はリンパ液の信号を反映し，T1強調像で低信号，T2強調像で高信号を呈する．内部に出血があればfluid-fluid levelを形成する．内壁は造影されないが，隔壁は造影され，充実性にみえることもある．

④乳児血管腫

超音波検査では，腫瘍の大部分がechogenicである．増殖期には，ドプラ超音波検査で腫瘍内の動脈に拍動流がみられる．MRI T1強調像で中間の信号，T2強調像では高信号を呈する．多血性腫瘍の像であり，早期より均一な造影効果を受ける．消退期，消失期には線維脂肪変性がみられ，造影効果は減弱する．なお，病理検査で特筆すべき所見として，乳児血管腫はerythrocyte-type glucose transporter-1（GLUT1）免疫染色が陽性であるのに対し，脈管奇形では陰性である．

参考文献

1) Enjolras O: Classification and management of the various superficial vascular anomalies: hemangiomas and vascular malformations. J Dermatol 24: 701-710, 1997.
2) ISSVA classification for vascular anomalies© (Approved at the 20th ISSVA Workshop, Melbourne, April 2014. Last revision May 2018) (http://www.issva.org/UserFiles/file/ISSVA-Classification-2018.pdf)
3) 「奇形性血管腫・血管奇形・リンパ管腫・リンパ管奇形症および関連疾患についての調査研究」班：血管腫・血管奇形・リンパ管奇形診療ガイドライン2017，第2版．p.46-50, 2017 (https://www.mariann-u.ac.jp/va/guideline.html)
4) Wassef M, Blei F, Adams D, et al: ISSVA Board and Scientific Committee. Vascular anomalies classification: recommendations from the International Society for the Study of Vascular Anomalies. Pediatrics 136: e203-e214, 2015.
5) Burrows PE, Fellows KE: Techniques for management of pediatric vascular anomalies. In Cope C (ed): Current techniques in interventional radiology, 2nd ed. Current Science, Philadelphia, p.11-27, 1995.
6) 三村秀文，安井裕利，藤原俊輝・他：ISSVAの分類とその臨床的意義．西日本皮膚 32: 974-985, 2012.

下し，代償性に赤血球増加症が生じる．右室造影で太い大動脈と細い肺動脈が同時に造影される．術後は，心臓 MRI による右室機能計価が有用である．

全例が外科手術の適応となる．右室流出路形成と心室中隔欠損閉鎖により，チアノーゼを改善する．手術時期は施設によるが，概ね体重 6 ~ 8 kg を目安に実施される．新生児・乳児期にチアノーゼが強い例，無酸素発作例，肺動脈が細い例では，まず体肺短絡手術が必要となる．術前・術後（遠隔期・成人期を含む）の内科的管理は重要である．乳幼児の無酸素発作の治療は膝胸位，酸素投与，鎮静薬，アシドーシス補正，β 遮断薬，昇圧薬（α_1 刺激薬）である．術後の心不全，不整脈に留意し，症例毎に運動制限および薬物療法（血管拡張薬，利尿薬，抗不整脈薬等）を考慮する．肺動脈狭窄，肺動脈弁閉鎖不全にはカテーテル治療や肺動脈弁置換術などの再手術を検討する．

術前に肺動脈狭窄の程度，術後は合併症・残遺症により決まる．

外科治療なしでは，1 年生存率 75 %，3 年生存率 60 %，10 年生存率 30 % である．手術予後は良好で，術後 30 年の生存率は 98 % である．

（山岸敬幸）

4 クリッペル・トレノネー・ウェーバー症候群 ［指定難病 291］

四肢のうち一肢またはそれ以上のほぼ全体にわたる混合型脈管奇形に片側肥大症を伴った疾患である．古典的には四肢の片側肥大，皮膚毛細血管奇形，二次性静脈瘤を三徴とするが，近年は低流速型脈管奇形（静脈奇形）を主とするものをクリッペル・トレノネー症候群，高流速病変（動静脈奇形）を主とするものをパークスウェーバー症候群と分けられている．しかし，両者を厳密に区分することは特に小児例では困難であり，本対象疾病としてはクリッペル・トレノネー・ウェーバー症候群（Klippel-Trenaunay-Weber syndrome）とする．

脈管奇形は先天性であり，胎生期における脈管形成異常により生じた病変と考えられている．原因は明らかでないが，その一部として遺伝子変異が同定され，遺伝子治療や分子標的薬の可能性が模索されている．

混合型脈管奇形と片側肥大が生下時ないしは幼児期に気づかれ，加齢と成長に伴って増悪する．側臥位が高度になると疼痛や代償性等性腎障症をきたす．疼痛，腫脹，潰瘍，発熱，感染，出血，変色など，各脈管奇形の症状を呈する．低流速型では多くの場合で血液凝固能低下をきたし，高流速型では血行動態にも影響を及ぼして心不全などによる致死的な病態に至りやすい．

病的過成長に対する根治的治療法はなく，骨軟部組織の過剰発育に対しては，下肢補高装具や外科的矯正手術（骨端線成長抑制術，骨延長術）が行われる．軟部組織の肥大については病変切除などの減量手術などが行われるが，病変はびまん性であり，完全切除は不可能である．弾性ストッキングによる圧迫，切除手術，硬化療法・塞栓術，レーザー凝固などが用いられるが，これらの治療に抵抗性であることが多い．

modified Rankin Scale（mRS），出血，感染に関するそれぞれの評価スケールを用いて，いずれかが 3 度以上の場合を重症と判定する．

一般に成長とともに病変は増大する傾向にあり，時間経過に伴い成人後も進行する．塞栓術・硬化療法，切除術により症状が改善することもあるが，治癒することは稀である．皮膚潰瘍は難治性であり，感染を繰り返す場合や動脈性出血を認める場合は致死的となる．

（三村秀文，佐々木　淳）

5 半心室症 ［指定難病 216］

房室弁がすべてまたはほとんどが主

Evaluation of pain incidence due to venous malformation based on data from 85 institutions in Japan

Naoaki Rikihisa, MD, PhD,[a] Sadanori Akita, MD, PhD,[b] Keigo Osuga, MD, PhD,[c] Hidefumi Mimura, MD, PhD,[d] Shunsuke Yuzuriha, MD, PhD,[e] *and* Satoru Sasaki, MD, PhD,[f] *Ichihara, Fukuoka, Suita, Kawasaki, Matsumoto, and Sapporo, Japan*

ABSTRACT

Background: Depending on the size and site of the venous malformation (VM), patients with VM often experience pain and swelling. VMs in the head and neck typically have lower pain rates due to complications than VMs in the limbs and trunk. We evaluated the heuristics on VM pain by statistically analyzing data of patients with VM from a multicenter database in Japan.

Methods: We collected data on age, sex, pain, lesion site, lesion depth, and lesion size for 2199 clinical cases with common VMs. We created categories for lesion depth and size and excluded multiple lesion cases that overlapped in these categories. Next, we constructed cross-tabulation tables to analyze the factors that contributed to pain. Finally, we evaluated the risk of pain in patients with VM by performing binomial logistic regression analysis based on age, sex, lesion site, lesion depth, and lesion size.

Results: For patients with limb and trunk VMs, the most frequent site of pain was the muscle, tendon, and bone, with an incidence of 79%, followed by the skin and subcutis, with an incidence of 43%. For patients with head and neck VMs, the most frequent site of pain was the muscle, tendon, and bone, with an incidence of 28%, followed by the skin and subcutis, with an incidence of 11% ($P < .01$). For pain incidence by lesion size, pain most frequently occurred in lesions >10 cm (67%), followed by lesions between 5 cm and 10 cm (56%) and lesions <5 cm (29%).

Conclusions: Our study indicated a clear order of factors that contributed to pain: lesion site > lesion depth > lesion size. Age was also an important factor. Infants and children had low pain complication frequencies with limb and trunk VMs. As the patients aged, the pain frequency became higher, reaching 50% at almost 7 years of age. (J Vasc Surg: Venous and Lym Dis 2020;8:244-50.)

Keywords: Pain; Venous malformation; Epidemiologic survey; Site; Depth

Venous malformations (VMs) are the most common vascular anomalies seen in clinical practice. VMs can be superficial, affecting the dermis and subcutis, or deeper, involving the muscle or bone. They can occur throughout the body, including visceral locations.[1]

Common VMs that bring pain, stiffness, swelling, infection, and bleeding are deeply troubling for patients. Depending on the lesion size and site, patients often experience pain and swelling. Stiffness and pain on walking are common in patients with VMs in the extremities.[2]

VMs in the head and neck are likely to have lower pain complication rates than those in the limbs and trunk. Among the various complications of VM, we chose to focus on pain in this study and evaluated VM pain heuristics by statistically analyzing data of patients with VM from a multicenter database in Japan.

METHODS

Epidemiologic study of vascular malformations in Japan. A large epidemiologic survey on vascular malformation was conducted in Japan between July 2013 and February 2014. Eighty-five institutions that were certified facilities of the Japan Society of Plastic and Reconstructive Surgery and the Japanese Society of Interventional Radiology restarted a web system for the survey. Clinical data were collected from 3695 cases that included venous, lymphatic, arteriovenous, or mixed malformations treated at these 85 institutions between January 2009 and December 2011.

From the Department of Plastic Surgery, Chiba Rosai Hospital, Ichihara[a]; the Department of Plastic Surgery, Wound Repair and Regeneration, Fukuoka University, School of Medicine, Fukuoka[b]; the Department of Diagnostic and Interventional Radiology, Osaka University, Graduate School of Medicine, Suita[c]; the Department of Radiology, St. Marianna University, School of Medicine, Kawasaki[d]; the Department of Plastic and Reconstructive Surgery, Shinshu University, School of Medicine, Matsumoto[e]; and the Center for Vascular Anomalies, KKR Sapporo Medical Center Tonan Hospital, Sapporo.[f]

This study was supported by a Survey on Intractable hemangioma, vascular malformation, lymphangioma, lymphangiomatosis and related diseases (H29-Nanchi-Ippan-014), Health and Labor Sciences Research Grants intractable diseases such as policy research projects (intractable disease policy research project).

Author conflict of interest: none.

Correspondence: Naoaki Rikihisa, MD, PhD, Department of Plastic Surgery, Chiba Rosai Hospital, 2-16 Tatsumidai-Higashi, Ichihara, Chiba 290-0003, Japan (e-mail: rikihisa@faculty.chiba-u.jp).

The editors and reviewers of this article have no relevant financial relationships to disclose per the Journal policy that requires reviewers to decline review of any manuscript for which they may have a conflict of interest.

2213-333X

Copyright © 2019 by the Society for Vascular Surgery. Published by Elsevier Inc.

https://doi.org/10.1016/j.jvsv.2019.03.008

Table I. Summary of patients with common venous malformations (VMs) in the head and neck and the limbs and trunk

	Head and neck	Limbs and trunk
No. of cases	878	1265
Male/female	334/544	481/784
Age at first visit, years		
Average	31	24
Median	27	20
Pain incidence at first visit	20%	63%

Before grouping, we excluded multiple lesion cases that belonged to both groups from 2199 cases.

This study was performed after ethical approval was received from the university ethical review committees of Kawasaki Medical School, Nagasaki University, Chiba University, and Osaka University. This ethical approval included discussions about the acquisition of informed consent and personal information management.

Common VM data. Common VM data were extracted from the database. Data included lesion size, lesion depth, lesion site, sex, birth year and month, year and month of the first visit, and major complaints at the first visit.

We calculated the sex ratio, average age at first visit, median age at first visit, and pain incidence from the common VM data. Patients with VM were divided into two groups by affected site: head and neck or limbs and trunk. To simplify the epidemiologic survey, we did not include the pain site as a survey item. For example, in a case with VMs in the neck and upper arm with pain, it is not clear which part is causing the pain. Thus, we excluded patients with multiple VM lesions that belonged to both groups. We also calculated the sex ratio, average age at first visit, median age at first visit, and pain incidence for both groups.

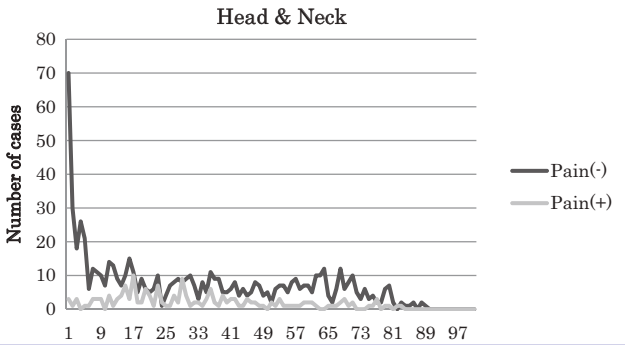

Fig 1. Cross-sectional analysis of patients' age and pain at first visit for patients with head and neck venous malformations (VMs).

ARTICLE HIGHLIGHTS

- **Type of Research:** Multicenter, retrospective, cross-sectional study
- **Key Findings:** For limb and trunk venous malformations (VMs), the pain incidence was 79% in muscle, tendon, and bone and 43% in the skin and subcutis. For head and neck VMs, the pain incidence was 28% in muscle, tendon, and bone and 11% in the skin and subcutis. The pain incidence in accordance with lesion size was 67% for >10 cm, 56% for 5 to 10 cm, and 29% for <5 cm.
- **Take Home Message:** The order of factors contributing to the occurrence of pain due to VM was lesion site > depth > size. Age was also an important factor, with younger patients experiencing less pain than older patients.

Analysis of factors that contributed to pain. We summarized the ages of patients with or without pain at their first visit by a cross-sectional approach in the head and neck group and the limbs and trunk group. We evaluated differences in pain incidence by the patient's sex and age at first visit using the same approach.

The two groups were further categorized by lesion depth (ie, in the skin and subcutis vs in the muscle, tendon, or bone). We excluded multiple lesion cases that belonged to both subgroups and compared the pain incidence between the four subgroups.

We also calculated the pain incidence during treatment (excluding pain at the first visit) by lesion size (lesion diameter <5 cm, lesion diameter ≥5 cm and ≤10 cm, or lesion diameter ≥10 cm). We excluded multiple lesion cases that overlapped in these categories and summarized patient age and lesion size during treatment using a cross-sectional approach.

Finally, we constructed a cross-tabulation table for lesion size, lesion depth, and pain for the head and neck group and the limbs and trunk group.

Statistical analysis. The χ^2 tests were performed for the cross-tabulation table analysis of the site, depth, and size of the lesion.

We evaluated the risk of pain in patients with VM by binomial logistic regression analysis (forward selection method, likelihood ratio) based on age at first visit to the physician, sex, lesion site, lesion depth, and lesion size. The significance level in the analysis was set at <5%, and Excel Tokei 2012 (Social Survey Research Information Co, Ltd, Tokyo, Japan) was used for the statistical analysis. Pain was scored as 0 (no pain) or 1 (pain) and was set as the objective variable. We coded the explanatory variables as follows: sex, 0 (male) or 1 (female); lesion site, 0 (head and neck) or 1 (limbs and

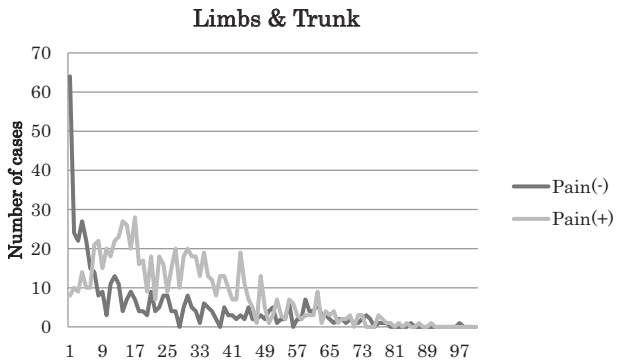

Fig 2. Cross-sectional analysis of patients' age and pain at first visit for patients with limb and trunk venous malformations (VMs).

trunk); lesion depth, 0 (skin and subcutis) or 1 (muscle, tendon, and bone); and lesion size, 0 (<5 cm in diameter), 1 (≥5 cm but ≤10 cm in diameter), or 2 (>10 cm in diameter).

RESULTS

We obtained 3681 cases that included venous, lymphatic, arteriovenous, and mixed malformations from patient data collected from 85 hospitals in an epidemiologic survey conducted in Japan. Of these patients, there were 2199 with common VMs. The sex distribution (male/female) was 839/1360. The average age at first visit was 27 years, and the median age at first visit was 22 years.

Of these cases, 878 were head and neck VMs; 1265 were limb and trunk VMs (Table I). In the head and neck group, the male to female ratio was 334/544. Fig 1 shows the age distribution at first visit in the head and neck group; the average age at first visit was 31 years, and the median age at first visit was 27 years (Table I). In the limbs and trunk group, the male to female ratio was 481/784. Fig 2 shows the age distribution at first visit in the limbs and trunk group; the average age at first visit was 24 years, and the median age at first visit was 20 years (Table I). The χ^2 test showed no significant differences in sex distribution between the head and neck group and the limbs and trunk group; however, both the lesion depth and age distribution at first visit significantly differed between the head and neck group and the limbs and trunk group ($P < .01$).

In the skin and subcutis subgroup of the head and neck group, 11% of patients reported pain at their first visit. In the muscle, tendon, and bone subgroup of the head and neck group, 28% of patients reported pain at their first visit. In the skin and subcutis subgroup of the limbs and trunk group, 43% of patients reported pain at their first visit. In the muscle, tendon, and bone subgroup of the limbs and trunk group, 79% of patients reported pain at their first visit. The χ^2 test showed that the pain incidence significantly differed between the four subgroups for lesion site and depth ($P < .01$; Table II).

In the head and neck group, 20% of patients reported pain at their first visit. In the limbs and trunk group, 63% of patients reported pain at their first visit (Table I). Figs 1 and 2 show the ages of patients who reported pain at their first visit. Interestingly, the numbers of patients with or without pain reversed at around 7 years of age in the limbs and trunk group (Fig 2). The presence of pain and the age at first visit did not significantly differ between men and women (Table III).

Pain at the first visit was reported by 29% of patients with lesions <5 cm in diameter, 56% of patients with lesions ≥5 cm but ≤10 cm in diameter, and 67% of patients with lesions >10 cm in diameter. Pain incidence significantly differed between the three lesion sizes ($P < .01$; Table IV). Fig 3 shows a cross-sectional analysis of the maximum lesion size during treatment in the limbs and trunk group.

Finally, we analyzed the pain incidence for VMs in the head and neck and in the limbs and trunk. For each group, we listed the lesion size, lesion depth, pain, and pain incidence and constructed cross-tabulation tables (Tables V and VI).

Binomial logistic regression analysis regarding pain associated with VM was performed using the forward selection method and likelihood ratio. The regression equation and its variables are shown in Table VII. The sample size was large enough to appropriately perform

Table II. Pain incidence and lesion site and depth at first visit

Site	Depth	Cases without pain	Cases with pain	Pain incidence, %	Significant difference[a]
Head and neck	Skin, subcutis	388	50	11	
	Muscle, tendon, bone	298	116	28	
Limbs and trunk	Skin, subcutis	308	230	43	
	Muscle, tendon, bone	144	541	79	

Before subgrouping, we excluded multiple lesion cases that belonged to both the head and neck and the limbs and trunk groups.
[a]The χ^2 test, $P < .01$.

Table III. Comparison of pain incidence at first visit between men and women

	Cases without pain	Cases with pain	Pain incidence, %
VMs in skin and subcutis			
Men	283	51	15
Women	421	123	23
VMs in muscle, bone, and tendon			
Men	188	294	61
Women	282	503	64
Summation of data			
Men	471	345	42
Women	703	626	47

VMs, Venous malformations.

binomial logistic regression analysis with five variables. Assessment of the linearity of the objective variable and the logit of the explanatory variable showed that there were no linearly coupled variables. A significant regression equation was found (the model had a likelihood ratio of 676.1006, five degrees of freedom, and $P < .0000$ with an R^2 of 0.2354 and Nagelkerke's R^2 of 0.03703). The percentage of correct classifications was 74.93%.

DISCUSSION

We showed that patients with limb and trunk VMs experienced higher rates of pain than patients with head and neck VMs. For patients with limb and trunk VMs, the most frequent site of pain was the muscle, tendon, and bone, with an incidence of 79%, followed by the skin and subcutis, with an incidence of 43%. For patients with head and neck VMs, the most frequent site of pain was the muscle, tendon, and bone, with an incidence of 28%, followed by the skin and subcutis, with an incidence of 11%.

VMs are traditionally thought to be most prevalent in the head and neck.[3,4] However, this was not reflected in our sample population. Although VM in the head and neck is treated by plastic surgeons and otolaryngologists in Japan, the epidemiologic survey was completed only by plastic surgeons and interventional radiology physicians. Thus, the data from patients who were undergoing otolaryngology treatment are missing. Even considering this departmental bias, the number of cases of VM in the head and neck is smaller than expected.

Another contradiction is that although there is traditionally thought to be no sex predilection for VM,[5] there seems to be a higher prevalence of VM in women than in men in this sample population. Although there was no sex difference in the entire data set of the epidemiologic survey that included VMs, arteriovenous malformations, and lymphatic malformations, the sex difference appeared when patients with VM were extracted from the original data. Compared with arteriovenous and lymphatic malformations, VMs are more likely to cause aesthetic problems that decrease quality of life, which may cause a relatively greater psychological burden on women compared with men. Moreover, plastic surgeons who treat aesthetic problems provided a large amount of clinical data to the survey. These factors may explain the unexpectedly higher proportion of women in the sample population.

VMs that affect the skeletal muscle are more common in the head and neck, followed by the lower and upper extremities and the thorax.[3,4] However, in this survey, VMs affecting the skeletal muscle were more common in the limbs and trunk; this lesion type had the highest pain incidence (80%) among all subgroups. Based on clinical data from 115 subjects, Vogel et al[6] reported that the incidence of pain in those with VMs limited to the skin or subcutis (60%) was significantly less than in those with VMs restricted to the intramuscular compartment (79%).

Of the patients with limb and trunk VMs, infants and children had a low pain complication frequency. As the patients aged, the frequency increased until it reached 50% at almost 7 years of age. After the age of 7 years, the pain frequency reached 60% to 80%. Similarly, of the patients with head and neck VMs, infants and children had a low pain complication frequency. As the patients aged, the pain incidence increased until around

Table IV. Pain incidence and lesion size during treatment

Maximum size (diameter)	Cases without pain	Cases with pain	Pain incidence, %	Significant difference[a]
<5 cm	716	290	29	
>5 cm and <10 cm	237	274	56	
>10 cm	185	373	67	

Before subgrouping by lesion size, we excluded multiple lesion cases that overlapped in these categories.
[a]The χ^2 test, $P < .01$.

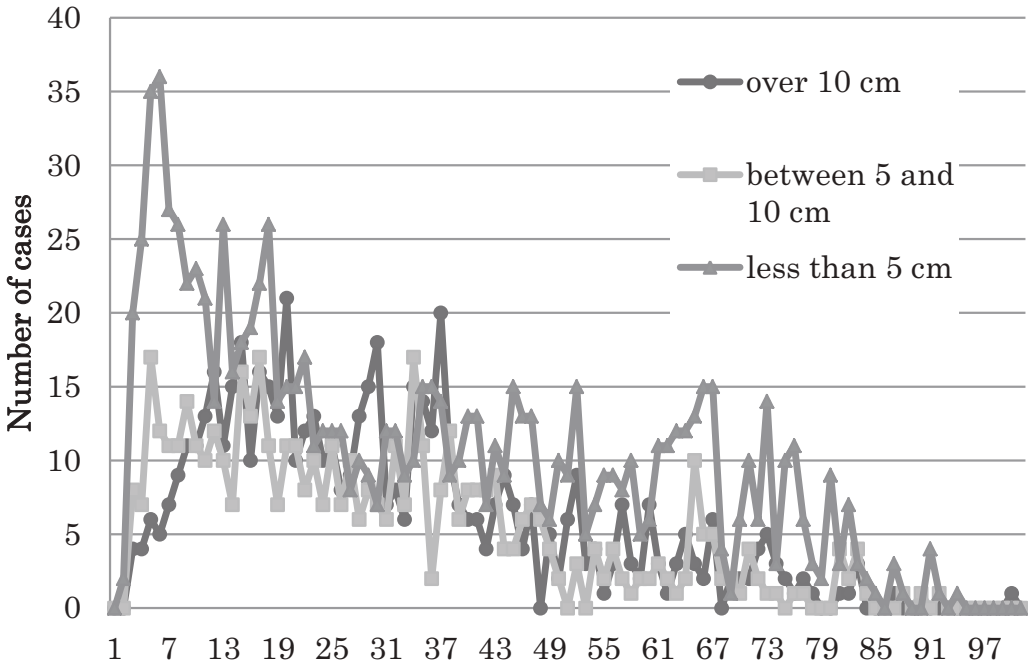

Fig 3. Cross-sectional analysis of maximum lesion size (diameter) during treatment in patients with limb and trunk venous malformations (VMs).

13 years of age. However, the upper limit of this pain incidence was approximately 50%. We examined the differences in pain complications between male and female patients and in age at first visit for patients with limb and trunk VMs and found no differences between the sexes.

Both the VM pain incidence and the lesion size increased as the patients' ages increased. Thus, we analyzed the relationship between lesion size, pain incidence, and age in patients with limb and trunk VMs. The lesion size in infants was small, usually <5 cm, and increased with age. At approximately 12 years of age, the lesion size ratio was 1:1:1 (<5 cm:5-10 cm:>10 cm). As the lesion size increased, the pain incidence increased.

Patients with VM experience severe pain that often leads to walking dysfunction and may cause them to temporarily miss school. Although the mechanism of VM pain is unclear, compression of the affected limbs with elastic stockings often relieves pain in the clinical setting. Elastic stockings prevent dilation of the affected veins and congestion of blood flow. The main state of VM probably involves stagnation of blood that may induce intralesional thrombosis or localized intravascular coagulation.[7] Avoidance of blood stasis is expected to

Table V. Summary of pain incidence with head and neck venous malformations (VMs) by lesion site and depth during treatment

	Skin and subcutis			Muscle, tendon, and bone			
Maximum size (diameter)	Cases without pain	Cases with pain	Pain incidence, %	Cases without pain	Cases with pain	Pain incidence, %	Total, %
<5 cm	338	30	8	134	29	18	11
>5 cm and <10 cm	38	13	25	101	48	32	30
>10 cm	12	7	37	63	39	38	38
Total	388	50	11	298	116	28	19

Before subgrouping by lesion size and site, we excluded multiple lesion cases that overlapped in these categories.

Table VI. Summary of pain incidence with limb and trunk venous malformations (VMs) by site and depth during treatment

Maximum size (diameter)	Skin and subcutis			Muscle, tendon, and bone			Total, %
	Cases without pain	Cases with pain	Pain incidence, %	Cases without pain	Cases with pain	Pain incidence, %	
<5 cm	198	125	39	46	106	70	49
>5 cm and <10 cm	69	61	46	29	152	84	68
>10 cm	41	44	51	69	283	80	75
Total	308	230	43	144	541	79	63

Before subgrouping by lesion size and site, we excluded multiple lesion cases that overlapped in these categories.

indirectly or directly reduce pain. These positive effects have already been established in treatment of varicose veins.[8] Although many patients younger than 5 years dislike wearing the elastic stockings because of their tight fit, most patients older than 5 years understand the effects of the stockings and will wear them.[9] These stockings can be custom-made to fit babies' and children's affected limbs, thus reaping the benefits of industry advancement. However, there are some controversies about compression therapy. Although compression therapy is commonly used to treat low-flow vascular malformations, the available literature provides no high-quality evidence to validate its use.[10] The appropriate time to begin using elastic stockings, the appropriate limb compression pressure, the time of day, and the effectiveness of elastic stockings in preventing or postponing the first severe pain attack in the limbs of patients with VM are also unclear.

CONCLUSIONS

The results of our binomial logistic regression analysis based on age, sex, lesion site, lesion depth, and lesion size and our cross-tabulation table analysis of lesion site, depth, and size indicated a clear order of factors that contribute to pain: site > depth > size. Age was also an important factor, whereas sex was not. These results may be fundamental for further surveys on preventing and treating VM pain. For example, elastic stockings are expected to be more effective on the basis of lesion site and depth rather than lesion size and patient age. As pain often impairs the patient's quality of life, the findings of our epidemiologic survey may be used for individual clinical practice and basic medical research studies based on the principle "think globally, act locally." It is important for physicians and patients to share short-term expectations when setting up treatment strategies. Furthermore, these findings

Table VII. Result of binomial logistic regression analysis

Explanatory variable	Partial regression coefficient	Standard error	Standard partial regression coefficient	Wald test for the partial regression coefficient	Degrees of freedom for the partial regression coefficient	*P* value for the partial regression coefficient	95% Confidence intervals of the partial regression coefficient	Odds ratio	95% Confidence intervals of the odds ratio
Age	0.0124	0.0025	0.2732	25.1463	1	.0000[a]	0.0075-0.0172	1.0124	1.0076-1.0173
Sex	0.2027	0.1077	0.0985	3.5444	1	.0597	−0.0083 to 0.4138	1.2247	0.9117-1.5125
Lesion site	2.0553	0.1179	1.0108	303.7818	1	.0000[a]	1.8242-2.2864	7.8092	6.1977-9.8397
Lesion depth	1.2303	0.1151	0.6140	114.2484	1	.0000[a]	1.0047-1.4559	3.4224	2.7312-4.2885
Lesion size	0.4014	0.0677	0.3374	35.1336	1	.0000[a]	0.2687-0.5341	1.4939	1.3082-1.7059
Constant term	−2.9424	0.1664		312.4961	1	.0000[a]	−3.2686 to −2.6162	0.0527	0.0381-0.0731

[a] $P < .001$.

reconfirmed the need to investigate the cause of VM pain and to explore its solutions, including oral treatment, sclerotherapy, surgery, and compression therapy with elastic stockings.

We thank Kelly Zammit, BVSc, and Traci Raley, MS, ELS, from Edanz Group (www.edanzediting.com/ac) for editing a draft of this manuscript.

AUTHOR CONTRIBUTIONS

Conception and design: NR, SA, KO, HM, SY, SS
Analysis and interpretation: NR, SA, KO, HM, SY, SS
Data collection: NR, SA, KO, HM, SY, SS
Writing the article: NR, SA, KO, HM, SY, SS
Critical revision of the article: NR, SA, KO, HM, SY, SS
Final approval of the article: NR, SA, KO, HM, SY, SS
Statistical analysis: NR
Obtained funding: NR, SA, KO, HM, SY, SS
Overall responsibility: NR

REFERENCES

1. Dasgupta R, Patel M. Venous malformations. Semin Pediatr Surg 2014;23:198-202.
2. Enjolras O, Wassef M, Chapot R. Color atlas of vascular tumors and vascular malformations. New York: Cambridge University Press; 2007. p. 168.
3. Behravesh S, Yakes W, Gupta N, Naidu S, Chong BW, Khademhosseini A, et al. Venous malformations: clinical diagnosis and treatment. Cardiovasc Diagn Ther 2016;6:557-69.
4. Hein KD, Mulliken JB, Kozakewich HP, Upton J, Burrows PE. Venous malformations of the skeletal muscle. Plast Reconstr Surg 2002;110:1625-35.
5. Wassef M, Blei F, Adams D, Alomari A, Baselga E, Berenstein A, et al. Vascular anomalies classification: recommendations from the International Society for the Study of Vascular Anomalies. Pediatrics 2015;136:e203-14.
6. Vogel SA, Hess CP, Dowd CF, Hoffman WY, Kane AJ, Rajaii R, et al. Early versus later presentations of venous malformations: where and why? Pediatr Dermatol 2013;30:534-40.
7. Hermans C, Dessomme B, Lambert C, Deneys V. Venous malformations and coagulopathy. Ann Chir Plast Esthet 2006;51:388-93.
8. Kakkos SK, Timpilis M, Patrinos P, Nikolakopoulos KM, Papageorgopoulou CP, Kouri AK, et al. Acute effects of graduated elastic compression stockings in patients with symptomatic varicose veins: a randomised double blind placebo controlled trial. Eur J Vasc Endovasc Surg 2018;55:118-25.
9. Chute C, Stein B, Sylvia MB, Spera E. Perioperative care of the vascular anomaly patient. Semin Pediatr Surg 2014;23:233-7.
10. Langbroek GB, Horbach SE, van der Vleuten CJ, Ubbink DT, van der Horst CM. Compression therapy for congenital low-flow vascular malformations of the extremities: a systematic review. Phlebology 2018;33:5-13.

Submitted Sep 27, 2018; accepted Mar 12, 2019.

Japanese Dermatological Association
The Journal of Dermatology
doi: 10.1111/1346-8138.15189
Journal of Dermatology 2020; ●●: 1–46

GUIDELINE

Japanese Clinical Practice Guidelines for Vascular Anomalies 2017

Hidefumi MIMURA,[1] Sadanori AKITA,[2] Akihiro FUJINO,[3] Masatoshi JINNIN,[4] Mine OZAKI,[5] Keigo OSUGA,[6] Hiroki NAKAOKA,[7] Eiichi MORII,[8] Akira KURAMOCHI,[9] Yoko AOKI,[10] Yasunori ARAI,[1] Noriko ARAMAKI,[11] Masanori INOUE,[12] Yuki IWASHINA,[5] Tadashi IWANAKA,[13] Shigeru UENO,[14] Akihiro UMEZAWA,[15] Michio OZEKI,[16] Junko OCHI,[17] Yoshiaki KINOSHITA,[18] Masakazu KURITA,[19] Shien SEIKE,[20] Nobuyuki TAKAKURA,[21] Masataka TAKAHASHI,[15] Takao TACHIBANA,[22] Kumiko CHUMAN,[23] Shuji NAGATA,[24] Mitsunaga NARUSHIMA,[25] Yasunari NIIMI,[26] Shunsuke NOSAKA,[27] Taiki NOZAKI,[28] Kazuki HASHIMOTO,[1] Ayato HAYASHI,[29] Satoshi HIRAKAWA,[30] Atsuko FUJIKAWA,[1] Yumiko HORI,[8] Kentaro MATSUOKA,[31] Hideki MORI,[7] Yuki YAMAMOTO,[4] Shunsuke YUZURIHA,[32] Naoaki RIKIHISA,[33] Shoji WATANABE,[34] Shinichi WATANABE,[35] Tatsuo KURODA,[36] Shunsuke SUGAWARA,[37] Kosuke ISHIKAWA,[38] Satoru SASAKI[39]

[1]Department of Radiology, St. Marianna University School of Medicine, Kawasaki, [2]Department of Plastic Surgery, Wound Repair and Regeneration, Fukuoka University, School of Medicine, Fukuoka, [3]Division of Surgery, National Center for Child Health and Development, Tokyo, [4]Department of Dermatology, Wakayama Medical University, Wakayama, [5]Department of Plastic, Reconstructive and Aesthetic Surgery, Kyorin University School of Medicine, Mitaka, [6]Department of Diagnostic and Interventional Radiology, Osaka University Graduate School of Medicine, Suita, [7]Department of Plastic Surgery, Ehime University Hospital, Toon, [8]Department of Pathology, Osaka University Graduate School of Medicine, Suita, [9]Department of Dermatology, Saitama Medical University, Iruma-gun, [10]Department of Medical Genetics, Tohoku University School of Medicine, Sendai, [11]Department of Plastic and Reconstructive Surgery, [12]Department of Radiology, Keio University School of Medicine, [13]Department of Pediatric Surgery, The University of Tokyo Hospital, Tokyo, [14]Department of Pediatric Surgery, Tokai University School of Medicine, Isehara, [15]Department of Reproductive Biology, Center for Regenerative Medicine, National Center for Child Health and Development, Tokyo, [16]Department of Pediatrics, Gifu University Graduate School of Medicine, Gifu, [17]Department of Diagnostic Radiology, Tohoku University Graduate School of Medicine, Sendai, [18]Department of Pediatric Surgery, Niigata University Graduate School of Medical and Dental Sciences, Niigata, [19]Department of Plastic and Reconstructive Surgery, The University of Tokyo Hospital, Tokyo, [20]Department of Plastic Surgery, Osaka University Graduate School of Medicine, [21]Department of Signal Transduction, Research Institute for Microbial Diseases, Osaka University, Suita, [22]Department of Dermatology, Osaka Red Cross Hospital, Osaka, [23]Department of Dermatology, Kanto Central Hospital, Tokyo, [24]Department of Radiology, Kurume University School of Medicine, Kurume, [25]Department of Plastic and Reconstructive Surgery, Graduate School of Medicine, Mie University, Tsu, [26]Department of Neuroendovascular Therapy, St. Luke's International Hospital, [27]Division of Radiology, National Center for Child Health and Development, [28]Department of Radiology, St. Luke's International Hospital, Tokyo, [29]Department of Plastic and Reconstructive Surgery, Juntendo University Urayasu Hospital, Urayasu, [30]Department of Dermatology, Hamamatsu University School of Medicine, Hamamatsu, [31]Department of Pathology, Dokkyo Medical University Saitama Medical Center, Koshigaya, [32]Department of Plastic and Reconstructive Surgery, Shinshu University School of Medicine, Matsumoto, [33]Department of Plastic and Reconstructive Surgery, Oyumino Central Hospital, Chiba, [34]Department of Plastic and Reconstructive Surgery, Saitama Children's Medical Center, Saitama, [35]Department of Dermatology, Teikyo University School of Medicine, [36]Department of Pediatric Surgery, Keio University School of Medicine, [37]Department of Diagnostic Radiology, National Cancer Center Hospital, Tokyo, [38]Department of Plastic and Reconstructive Surgery, Faculty of Medicine and Graduate School of Medicine, Hokkaido University, [39]Department of Plastic and Reconstructive Surgery, Center for Vascular Anomalies, Tonan Hospital, Sapporo, Japan

Correspondence: Hidefumi Mimura, M.D., Department of Radiology, St Marianna University School of Medicine, 2-16-1 Sugao, Miyamae, Kawasaki, Kanagawa 216-8511, Japan. Email: mimura@marianna-u.ac.jp

The Japanese Clinical Practice Guidelines for Vascular Anomalies 2017 were published in Japanese in 2017. We provide these guidelines in English to inform health-care professionals and the general public worldwide to improve medical practice and patient outcomes. This article has been co-published in *The Journal of Dermatology*, *Japanese Journal of Radiology* and *Pediatrics International* based on the agreement of the Editors-in-Chief of the three journals.

Received 19 November 2019; accepted 20 November 2019.

This article has been co-published with the permission of *The Journal of Dermatology*, *Pediatrics International* and *Japanese Journal of Radiology*. All rights reserved. © 2020 The Authors. The articles are identical except for minor stylistic and spelling differences in keeping with each journal's style. Either citation can be used when citing this article. This is an open access article under the terms of the Creative Commons Attribution License, which permits use, distribution and reproduction in any medium, provided the original work is properly cited.

ABSTRACT

The objective was to prepare guidelines to perform the current optimum treatment by organizing effective and efficient treatments of hemangiomas and vascular malformations, confirming the safety and systematizing treatment, employing evidence-based medicine techniques and aimed at improvement of the outcomes. Clinical questions (CQ) were decided based on the important clinical issues. For document retrieval, key words for published work searches were set for each CQ, and work published from 1980 to the end of September 2014 was searched in PubMed, Cochrane Library and Japana Centra Revuo Medicina databases. The strengths of evidence and recommendations acquired by systematic reviews were determined following the Medical Information Network Distribution System technique. A total of 33 CQ were used to compile recommendations and the subjects included efficacy of resection, sclerotherapy/embolization, drug therapy, laser therapy, radiotherapy and other conservative treatment, differences in appropriate treatment due to the location of lesions and among symptoms, appropriate timing of treatment and tests, and pathological diagnosis deciding the diagnosis. Thus, the Japanese Clinical Practice Guidelines for Vascular Anomalies 2017 have been prepared as the evidence-based guidelines for the management of vascular anomalies.

Key words: clinical practice, guidelines, hemangioma, vascular anomalies, vascular malformation.

INTRODUCTION

The etiology of vascular anomalies on the body surface and in soft tissue are mostly unclear and no fundamental treatment methods have been established. Many patients visit many medical institutions seeking an expert, being a disadvantage in treatment. Hemangiomas and vascular malformations are frequently termed "hemangioma", but these are different diseases in the classification proposed by the International Society for Study of Vascular Anomalies (ISSVA),[1,2] and this classification has been internationally standardized.

The *Clinical Practice Guidelines for Vascular Anomalies 2013* (1st edition)[3] target general practitioners and the general public, and were prepared aiming at organizing effective and efficient treatments for hemangiomas/vascular malformations, confirming the safety and systematizing treatment using evidence-based medicine (EBM) techniques. The organization responsible for preparation was the Health, Labor and Welfare Sciences Research Grants (Research on Measures for Intractable Diseases), Research Committee for "Intractable Vascular Anomalies", and the main committee members were selected from academic societies of plastic surgery and radiology mainly treating hemangiomas and vascular malformations: the Japanese Society of Plastic and Reconstructive Surgery and Japanese Society of Interventional Radiology, and the guidelines were prepared by them.

The *Clinical Practice Guidelines for Vascular Anomalies 2017* were prepared as a revised edition of the *Clinical Practice Guidelines for Vascular Anomalies 2013*. The organization responsible for preparation was the Health, Labor and Welfare Sciences Research Grants (Research on Policy Planning and Evaluation for Rare and Intractable Diseases), Research Committee for Intractable Vascular Anomalies, and the differences from the previous guidelines are setting the objective of summarizing opinions from related academic societies by inviting many committee members from dermatologists, pediatric surgeons, pediatricians, radiologists (diagnostic radiology), and basic researchers including the pathology, molecular biology and epidemiology fields, in addition to plastic surgeons and radiologists (interventional radiology). Because the guidelines were prepared following the reformed *Minds Handbook for Clinical Practice Guideline Development 2014*[4] and *Minds Manual for Clinical Practice Guideline Development Ver. 1.0–2.0*,[5,6] it was fully revised.

The original text of the guidelines (Japanese version) is comprised of reviews and clinical questions (CQ), but only CQ are presented in this report.

PURPOSE OF THE GUIDELINES

The objective was to prepare guidelines to perform the current optimum treatment by organizing effective and efficient treatments of hemangiomas and vascular malformations, confirming the safety and systematizing treatment, employing the EBM techniques and aimed at improvement of the following outcomes: pain, swelling, esthetic impairment and functional disorder.

METHODS

Organization

For the Guidelines Executive Committee members, representatives of the plastic surgery, dermatology, radiology, pediatric surgery and basic science fields were selected. The guidelines preparation group and systematic review (SR) team for preparation of CQ and recommendations were comprised of four groups: (i) groups in charge of arteriovenous malformation (AVM), venous malformation (VM), combined type and syndrome; (ii) in charge of capillary malformation (CM) and infantile hemangioma; (iii) in charge of the lymphatic malformation (lymphangioma) (LM); and (iv) in charge of the basic field. To the group in charge of AVM, VM, combined type and syndrome, plastic surgeons and radiologists were mainly assigned. To the group in charge of CM and infantile

This article has been co-published with the permission of *The Journal of Dermatology, Pediatrics International* and *Japanese Journal of Radiology*. All rights reserved. © 2020 The Authors. The articles are identical except for minor stylistic and spelling differences in keeping with each journal's style. Either citation can be used when citing this article.

hemangioma, plastic surgeons and dermatologists were mainly assigned. To the group in charge of the lymphatic system, pediatric surgeons, plastic surgeons and pediatricians were mainly assigned. The reviews of the guidelines were also prepared by those selected from each group. Pathologists and molecular biologists were in charge of the reviews of the basic fields.

Preparation process

The guidelines were revised following the *Minds Handbook for Clinical Practice Guideline Development 2014* and *Minds Manual for Clinical Practice Guideline Development Ver. 1.0–2.0*.

Clinical questions were decided based on the following important clinical issues: (i) efficacy of resection; (ii) efficacy of sclerotherapy/embolization; (iii) efficacy of drug therapy, laser therapy, radiotherapy and other conservative treatment; (iv) differences in appropriate treatment due to the location of lesions; (v) differences in appropriate treatment among symptoms; (vi) appropriate timing of treatment and tests; and (vii) pathological diagnosis deciding the diagnosis.

For document retrieval, key words for published work searches were set for each CQ and work published from 1980 to the end of September 2014 was searched in PubMed, Cochrane Library and Japana Centra Revuo Medicina (JCRM) databases. A published work search was requested from the Japan Medical Library Association. For decisions on CQ and recommendations lacking evidence or having weak evidence, discussion and agreement in the preparation group were reflected.

The strengths of evidence and recommendations acquired by SR were determined following the Minds technique as described below and this follows the GRADE guidelines preparation method.[7,8]

Determination of the strength of evidence of the body of evidence (Table 1)

The strength of evidence of the body of evidence was determined according to the *Minds Handbook for Clinical Practice Guideline Development 2014*.

> In the case of RCTs [randomized controlled trials], the score "A (strong)" is given at the start of evaluation, and the final score might be downgraded to B, C, or D, according to the results of evaluation of five items, including risk of bias, inconsistency in results, indirectness of evidence, data imprecision and high possibility of publication bias. In the case of observational studies, the score "C (weak)" is given at the start of evaluation, and five items lowering the strength are evaluated similarly as for RCTs. In addition, three items, including large effect with no confounding factors, dose–response gradient, and possible confounding factors, are weaker than actual effects increasing the strength are evaluated as well. . .

Table 1. Recommendation grade and definition of the strength of body of evidence in evaluation of systematic review

Recommendation grade
1: strongly recommended
2: weakly recommended (suggested)
Definition of the Strength of Body of Evidence in Evaluation of Systematic Review
A (strong): strongly confident of the estimate of effect
B (moderate): moderately confident of the estimate of effect
C (weak): limited confidence of the estimate of effect
D (very weak): very little confident of the estimate of effect

Presentation of the strength of recommendations

The strength of recommendation was also determined according to the *Minds Handbook for Clinical Practice Guideline Development 2014* (Table 1).

> The strength of recommendations is usually presented in two ways: "1": strongly recommended, and "2": weakly recommended (suggested). If the strength of recommendations cannot be determined by any means, it is occasionally presented as "no definite recommendation can be made." Recommendations will be entered as follows by indicating the strength of evidence (A, B, C, D) with the strength of recommendations "1": strong or "2": weak.

Finalization

Preparation of the draft guidelines was completed in December 2016 and review was requested from the Japanese Society of Plastic and Reconstructive Surgery, Japanese Dermatological Association, Japan Radiology Society, Japanese Society of Interventional Radiology, Japanese Society of Pediatric Surgeons and Japanese Society of Pathology between December 2016 and January 2017, and corrections were made based on the results of the reviews. In addition, from December 2016 to January 2017, the guidelines were disclosed on the home page of the Research Committee for "Intractable Vascular Anomalies" and public comments were collected. The draft guidelines were presented to two related patient organizations, the Patients Association of Vascular Anomalies and the Patients Association of Combined Vascular Malformations, and comments were received. Based on these, the draft guidelines were revised and CQ, recommendations and explanations were completed. It was finalized in March 2017.

RESULTS

CQ and recommendations

CQ1: What are the guidelines for the time to begin treatment for AVM?

Recommendation: It is necessary to judge the time to begin endovascular or surgical treatment for AVM individually by evaluating the stage of symptoms and lesion extent and in consideration of the risk of complications.

Strength of recommendation: 2 (weak).

This article has been co-published with the permission of *The Journal of Dermatology, Pediatrics International* and *Japanese Journal of Radiology*. All rights reserved. © 2020 The Authors. The articles are identical except for minor stylistic and spelling differences in keeping with each journal's style. Either citation can be used when citing this article.

Evidence: D (very weak).

Comments: As a result of primary screening, 92, three and 27 papers were extracted from PubMed, JCRM and Cochrane Library, respectively, and, as a result of secondary screening, 37 and three papers were extracted from PubMed and JCRM, respectively. However, as all of these references were observational or case series studies, the strength of evidence is rated as D (very weak).

There has been no report in which time to begin treatment for AVM in itself was the end-point, and only some reports described the view on the time to begin treatment in the discussion. Therefore, as it is difficult to objectively evaluate the validity of the time to begin treatment, we determined whether guidelines can be derived from the patient age, lesion site, symptoms, clinical stage, effectiveness of treatment and frequency of complications in each report.

In the two reports on the treatment for AVM,[9,10] symptomatic AVM is primarily addressed, and treatment can be suspended (follow up) while the lesion remains asymptomatic. However, as AVM often progresses when left untreated, it is considered important to begin the treatment at an appropriate time depending on the stage of symptoms. In addition, as there is the tendency that the response rate decreases, and the complication rate increases, with progression of symptoms, some reports from particular pediatric institutions where patients are concentrated recommend early therapeutic intervention in relatively "early" or "mild" stages without waiting for progression of the disease.

Localized lesions may be radically treated by early intervention.[11] Among endovascular procedures, the response (cure) rate tends to be high by ethanol embolization, but the complication rate is also high.[12,13] By surgery, localized lesions are unlikely to recur if they are completely resected, although adverse events, such as postoperative cicatrization/deformation or functional impairment, have been seldom discussed.[10] On the other hand, in diffuse lesions, limitations of effectiveness, such as recurrence and persistence and the risk of treatment, are higher by both endovascular treatment and surgery, with the risks outweighing the benefits.[13] It should also be considered that children, in particular, are not mentally ready to accept such invasive treatments.[14]

As discussed above, it is difficult to give guidelines for the time to begin treatment for AVM at present, and individual judgment is necessary depending on the symptom stage and lesion extent in consideration of the complication risk.

CQ2: Is recurrence (regrowth) after resection of AVM more frequent by wound closure with a skin graft than by reconstruction using a flap?

Recommendation: Whether recurrence (regrowth) is more frequent by wound closure with a skin graft compared with reconstruction using a flap is unclear.

Strength of recommendation: 2 (weak).

Evidence: D (very weak).

Comments: The number of references retrieved by searches using key words was 40 from JCRM, 75 from PubMed and zero from Cochrane, and 39 were extracted by secondary screening. For AVM of a certain size, reconstruction is necessary after resection, and wound closure by skin grafting or reconstruction using a flap is performed according to common reconstruction methods for tissue defects. The reports discussing reconstruction after resection of AVM that we could retrieve were all descriptive studies (case reports or case series studies). Therefore, the evidence level of all of these references is D (very weak).

The concept of a regulating flap,[15,16] that reconstruction using a free flap controls the recurrence or regrowth after resection of AVM, has been proposed. However, no report has evaluated whether free flaps[16–37] and other flap types[17,19,25,28,38–49] clearly prevent the recurrence or regrowth compared with skin grafts.[21,23,50–52]

According to the present knowledge on the recurrence or regrowth after resection of AVM,[15,16,39,53] whether AVM can be completely resected is important, and, concerning cases in which complete resection is difficult, it has been reported that the hemodynamics in the residual lesions contribute to the recurrence and regrowth, and that they can be controlled by a flap with rich blood flow.

CQ3: Is proximal ligation/coil embolization of the feeding artery of AVM effective?

Recommendation: The therapeutic effect of ligation/coil embolization of the feeding artery on the proximal side may be poor, and the possibility of recurrence may be high. In addition, in the event of recurrence, treatment may become difficult due to the development of collateral vessels. Therefore, these procedures are recommended to be avoided, in principle.

Strength of recommendation: 2 (weak).

Evidence: D (very weak).

Comments: As a result of secondary screening, one and 14 papers were extracted from PubMed and JCRM, respectively, and were reviewed. As a result, all of these papers were case reports. In addition, six papers retrieved by manual searches were also reviewed, but they were all case series studies at the maximum. Therefore, the strength of evidence as a collection of published work concerning this CQ is D (very weak).

To summarize the evaluation of this collection of papers, AVM was treated by proximal ligation/coil embolization of the feeding artery, but as there have been reports of recurrence following the development of collateral channels (reports of cases of the occurrence of unfavorable situations), the treatment is recommended to be avoided, but the evidence level of this recommendation is low as mentioned above.

The objective of embolization for AVM is obliteration of the nidus, and embolization at or near the nidus is necessary as much as possible. If ligation/coil embolization of the feeding artery is performed on the proximal/central side, the nidus is not obliterated, and the development of several collateral channels is promoted. In many cases, the collateral channels are thin, complicated and markedly tortuous, and transcatheter treatment is often difficult.

Wu *et al.*[14] performed proximal ligation in nine of 29 patients treated for AVM of the auricle but the condition was

This article has been co-published with the permission of *The Journal of Dermatology, Pediatrics International* and *Japanese Journal of Radiology*. All rights reserved. © 2020 The Authors. The articles are identical except for minor stylistic and spelling differences in keeping with each journal's style. Either citation can be used when citing this article.

exacerbated in all patients with eight requiring auricular resection and one requiring additional treatment. They excluded proximal ligation from treatment options for AVM, because it makes subsequent transcatheter treatments difficult.

Slaba *et al.*[54] evaluated 25 patients with AVM of the tongue and reported that three of the 12 symptomatic patients who underwent ipsilateral external carotid artery ligation at another facility showed marked development of collateral channels.

Other reports include those of a case in which a large number of collateral channels developed as a result of ligation of the feeding artery for AVM of the shoulder with serious complications including high-output heart failure;[55] three cases in which proximal ligation/embolization was performed for AVM of the limbs and pelvis, collateral vessels developed, but the condition was controlled by multidisciplinary treatment consisting of transcatheter treatment and direct puncture sclerotherapy;[56] and several cases in which external carotid artery ligation was performed for AVM of the head and neck, but the subsequent treatment was difficult.

Suyama *et al.*[35] reported a case in which AVM of the auricle, treated by proximal embolization using coils and gelatin sponge, recurred and was treated again by ligation at a proximal part of the artery, but the lesion recurred again. Also, Aikawa *et al.*[57] reported a case of intrapelvic AVM that underwent coil embolization of the left ovarian artery and left internal iliac artery but showed little change in the area of the nidus or the state of arterial or venous dilatation. In addition, Yamamoto *et al.*[58] reported a case in which transarterial embolization (TAE) was performed for AVM of the mandible through the maxillary artery, facial artery, lingual artery and ocular artery, but was not effective due to the development of collateral channels from the internal carotid artery and vertebral artery.

As observed above, it is recommended not to select proximal/central ligation/coil embolization as a treatment for AVM. However, AV fistulas with direct connection of a large artery and a vessel may be treated by coil embolization if the shunt area is directly accessible with a catheter. Proximal coil embolization may also be accepted as preoperative embolization, but careful evaluation of its indications is necessary, and embolization at a site near the shunt is necessary to leave room for catheter insertion in the event of future recurrence.

CQ4: What is the appropriate timing for embolization before resection of AVM?

Recommendation: It is recommended to perform resection within 3 days (72 h) after embolization. If the interval is prolonged, the risk of massive intraoperative hemorrhage may increase due to recanalization of the embolized vessel and development of collateral channels. In addition, surgery has been reported to be made difficult by enlargement of the lesion after embolization.

Strength of recommendation: 2 (weak).

Evidence: D (very weak).

Comments: While it is difficult to generalize the therapeutic approach as it varies with the affected area and extent of the lesion, there were a few reports that preoperative embolization was useful for the treatment of AVM of the head and neck region.

As a result of secondary screening, 10 and three papers from PubMed and JCRM, respectively, were reviewed. All of the papers selected by this screening procedure were case reports or case series, and the strength of evidence is D (very weak). Mentions about the timing of preoperative embolization and volume of hemorrhage also varied among the papers. Although it is difficult to draw a conclusion, among the papers that mentioned specific timing of preoperative embolization and volume of hemorrhage, Deng *et al.*[59] performed embolization within 48–72 h before surgery in 16 patients with maxillofacial AVM and reported that the volume of hemorrhage was 200 mL or less in all patients and that there were no complications. Erdmann *et al.*[60] performed embolization within 24 h before surgery in four patients with head and neck AVM, and the lesion was resected with hemorrhage of 100 mL or less in three. It is recommended to perform resection within 72 h to prevent increases in difficulty of resection due to inflammation after embolization.

There have also been reports that embolization was performed intraoperatively or within a few days before surgery, resulting in decreases in the volume of hemorrhage or favorable long-term outcomes. Most papers reported no or only mild complications, but as for relatively severe complications, Goldberg *et al.*[61] reported temporary visual impairment in two of the three patients with orbital AVM.

Factors that affect the appropriate timing of preoperative embolization include recanalization of the target vessel, development of collateral channels, and swelling and reactive changes after embolization, which make surgery difficult. To avoid the effects of these phenomena, many papers supported relatively early resection, namely within 72 h after embolization. Clinically, also, there is no benefit in taking a long interval, and it is considered valid to recommend resection within 72 h of embolization.

In conclusion, adequate control of hemorrhage may be achieved with fewer complications by performing vascular embolization within a few days before surgery, but no sufficient evidence that supports this view has been provided.

CQ5: What treatments are appropriate for maxillomandibular AVM?

Recommendation: Although surgery alone is not recommended, a combination of surgery with endovascular embolization (including sclerotherapy) can be recommended depending on the case.

Radiotherapy is not recommended.

Endovascular embolization (including sclerotherapy) alone or as a preoperative treatment can be recommended.

Strength of recommendation: 2 (weak).

Evidence: D (very weak).

Comments: AVM of the maxilla and mandible is a rare disorder. Most of the published works are reports of a small number of cases except a few case series reported from some special institutions. Only five reports[62–66] of a series of 10 or more cases were retrieved by the search of PubMed. Because there is no cohort study or randomized trial comparing various treatments, strong evidence regarding the best treatment is lacking.

This article has been co-published with the permission of *The Journal of Dermatology, Pediatrics International* and *Japanese Journal of Radiology*. All rights reserved. © 2020 The Authors. The articles are identical except for minor stylistic and spelling differences in keeping with each journal's style. Either citation can be used when citing this article.

Maxillomandibular AVM may involve the maxilla, mandible or both, and it often presents with massive oral hemorrhage around the age of 10 years when milk teeth are lost, but may also be detected due to swelling of the soft tissue.

According to Persky *et al.*,[62] embolization alone resulted in cure in 42%, improvement in 16% and stabilization of symptoms in 23% of the 26 patients with a maxillomandibular AVM. Liu *et al.*[63] treated 25 patients by transarterial or transvenous embolization alone or in combination with curettage and reported anatomical cure in 14 and clinical cure in 21. Chen *et al.*[65] treated 15 patients by bone wax packing (BWP) alone in four, TAE + BWP in three, TAE + resection in four and TAE + radiotherapy + resection in four, and reported clinical cure in 14.

The following are considered as treatment options for AVM of the maxilla and mandible:

1. A: Surgical treatment
   a. A-1: Resection and reconstruction
   b. A-2: Curettage
   c. A-3: BWP
2. B: Endovascular embolization (including sclerotherapy)
   a. B-1: TAE
   b. B-2: Transvenous embolization
   c. B-3: Embolization by direct puncture
3. C: Combination of A and B
4. D: Radiotherapy

The published work is mostly about B, namely endovascular embolization (including sclerotherapy) alone, or surgical treatment after B. There was no report of case series of surgical treatment alone, but there was only one report[65] of case series of surgery + radiotherapy. Surgery alone and radiotherapy are generally not recommended. Endovascular embolization is performed by various approaches including transarterial and transvenous routes and direct puncture, sometimes in combination. Concerning embolic agents, polyvinyl alcohol and Gelfoam® (Pfizer, New York, NY, USA) are used for embolization as an adjuvant therapy immediately before surgery as they allow recanalization. Cyanoacrylate liquid embolic agents are considered effective for embolization performed preoperatively or alone in expectation of a long-term occlusive effect.[64,67,68] Coils are often used for transvenous embolization. Recently, there have been reports[69,70] that favorable outcomes were obtained by TAE using Onyx® (Medtronic, Irvine, CA, USA), a non-adhesive liquid embolic agent. Concerning sclerotherapy, there is a case series study of ethanol sclerotherapy alone, reporting relatively favorable outcomes.[71] Infection and bone necrosis are frequent complications of embolization, and they may occur when an embolic agent, a foreign body, is injected into lesions that were in contact with the external environment due to direct puncture or hemorrhage. Surgical treatments as listed above are performed primarily after endovascular embolization. Invasive radical resection and reconstruction should be avoided at least as the initial treatment, because many lesions can now be controlled by endovascular embolization alone with the advancement of endovascular technique.

As mentioned above, endovascular embolization is performed using various approaches and embolic agents selected depending on the facility and patient. There are also a wide variety of surgical treatment options. Because the treatment may be performed by combining these options, AVM of the maxilla and mandible should be treated at the institutions where multidisciplinary treatment can be performed by experienced physicians.

CQ6: What treatments are appropriate for AVM of the fingers?

Recommendation: Although embolization or sclerotherapy are effective because they alleviate symptoms, such as pain, sufficient evaluation is necessary because of the risk of finger necrosis and nerve damage. In surgical resection, total resection is recommended, because partial resection is likely to result in enlargement of the lesion. Occasionally, the disorder results in finger amputation.

Strength of recommendation: 2 (weak).

Evidence: D (very weak).

Comments: As a result of primary screening, 38, 16 and 35 papers were retrieved from PubMed, Cochrane Library and JCRM, respectively. However, during secondary screening, many reports concerned AV shunts in dialysis patients and AVM at sites other than the fingers. Eventually, only 10 papers comprising three case series and seven case reports remained as references, and the evidence level is extremely low (D: very weak).

Arteriovenous malformation of the fingers is often difficult to treat, and treatments are likely to be ineffective, particularly when the lesion extends from the fingers to the palm. In addition, when AVM is localized in the fingers, complications are likely to occur after treatment.[72] It is recommended to conduct treatment by a team from several departments including plastic surgery, vascular surgery and radiology.[73] 3-D computed tomography (CT) angiography is useful for preoperative examination.[74] Because complete cure is difficult to obtain by embolization therapy, it is recommended to be performed for alleviation of symptoms such as pain only in symptomatic areas.[75] In addition, as there is the possibility of re-enlargement after embolization, it is recommended to periodically follow up the condition and repeatedly perform embolization each time symptoms appear.[73] Surgical resection is necessary for permanent cure, and total resection is recommended as there is the possibility of re-enlargement after partial resection.[76–78] Reconstruction is occasionally necessary, but treatment may end in finger amputation. In this event, preoperative embolization or sclerotherapy is effective.[79] The present review has fallen short of clarifying situations in which preoperative embolization is useful in fingers to which a tourniquet can be applied.

CQ7: What treatments are effective for painful VM?

Recommendation: Sclerotherapy and surgical resection, as well as conservative treatments, such as compression, oral

This article has been co-published with the permission of *The Journal of Dermatology, Pediatrics International* and *Japanese Journal of Radiology*. All rights reserved. © 2020 The Authors. The articles are identical except for minor stylistic and spelling differences in keeping with each journal's style. Either citation can be used when citing this article.

aspirin and low-molecular-weight heparin, are reported to be effective depending on the site and size of the lesion and symptoms. Endovascular laser treatment, percutaneous cryotherapy and photodynamic therapy have also been suggested to be effective.

Strength of recommendation: 2 (weak).

Evidence: D (very weak).

Comments: As a result of the published work search, 54 reports in English and four in Japanese were retrieved by primary screening. Of these reports, 39 in English and four in Japanese were extracted by secondary screening. Many options were reported as treatments for pain associated with VM, but all of these documents were case series or case reports without comparison of treatments. Therefore, the evidence level was rated as very weak and the recommendation level as weak.

Pain is one of the major symptoms of VM. It may respond to conservative treatments that are relatively easy to manage, such as compression and oral aspirin, depending on the site and size of the lesion and symptoms. Particularly when pain is localized, surgery should also be considered. Relatively novel treatments, such as endovascular laser therapy, percutaneous cryotherapy and photodynamic therapy, have been reported to be effective for controlling local VM, and they have also been reported to be effective for the control of pain. Limb lesions accompanied by localized intravascular coagulopathy may be indications for low-molecular-weight heparin. Reports on various treatments are mentioned below.

1. Compression

Although there has been no report of comparative evaluation, compression is reportedly effective according to reviews by specialized medical facilities.[80–82]

2. Oral aspirin

The published work is also limited, but the treatment has been mentioned in reviews.[80–82] Nguyen *et al.*[83] reported that pain was alleviated in 17 (77%) of 22 patients in whom oral aspirin therapy was initiated for pain.

3. Sclerotherapy

Sclerotherapy has often been performed using ethanol or polidocanol. The published work concerning other sclerosing agents is scarce, and their effectiveness remains largely unclear.

Each sclerosing agent is commented on below.

(i) Ethanol

Shireman *et al.*[84] reported remission in six of 12 patients, and Rimon *et al.*[85] reported alleviation or remission in 14 patients with painful VM (including eight with lower limb lesions) except in four of those with lower limb lesions. Marrocco-Trischitta *et al.*[86] reported that pain was resolved in both (100%) of two women with external genital lesions.

Concerning the use of ethanol, Suh *et al.*[87] reported alleviation to 50% or less of the pretreatment state according to a VAS in 12 (71%) of 17 patients who underwent sclerotherapy using its mixture with lipiodol, and Dompmartin *et al.*[88] reported 37 patients who underwent sclerotherapy using its mixture with ethylcellulose. According to Schumacher *et al.*,[89] also, 77 patients underwent sclerotherapy using ethylcellulose ethanol in a multicenter study, and significant improvement compared with the pretreatment state was observed in all patients.

(ii) Polidocanol (including foam sclerotherapy)

Mimura *et al.*[90] reported remission in six, alleviation in four and no change in one of 11 patients with painful VM, and remission in 12 (41%), alleviation in 14 (48%), no change in two (7%) and exacerbation in one (3%) of 29 patients in another study.[91] Cabrera *et al.*[92] treated 50 patients (including 15 with Klippel–Trenaunay syndrome) using a foamed sclerosing agent and reported remission in 25 (50%) and alleviation in 14 (28%). Marrocco-Trischitta *et al.*[86] reported resolution of pain in all three women with external genital lesions.

(iii) Ethanolamine oleate

Ozaki *et al.*[93] reported remission in two (20%) and alleviation in eight (80%) of 10 patients.

(iv) Sodium tetradecyl sulfate (STS)

Krokidis *et al.*[94] reported alleviation of pain in four of five women with external genital lesions.

4. Surgical resection

Enjolras *et al.*[95] performed surgical resection in seven of 13 patients with VM involving a wide area including the knee joint and reported alleviation of pain in five (71%). Steiner *et al.*[96] reported alleviation to 50% or less of the pretreatment state by a VAS in 24 (89%) of 27 patients with background pain and 12 (92%) of 13 patients with acute episodic pain. In addition, Noel *et al.*[97] performed surgical resection and compression therapy for VM of the lower extremities in 20 patients with Klippel–Trenaunay syndrome and reported disappearance of pain in 18 (90%) (mean follow-up period, 63 months).

5. Endovascular laser therapy

Sidhu *et al.*[98] and Lu *et al.*[99] reported alleviation of pain in all eight and 51 lesions in six and 33 patients, respectively. Liu *et al.*[100] also reported marked responses in 46 (35%), responses in 84 (63%) and no change in three (2%) of 133 patients.

6. Low-molecular-weight heparin

According to Mazoyer *et al.*,[101] only low-molecular-weight heparin was effective when VM were complicated by localized intravascular coagulation, resulting in disappearance of pain.

7. Percutaneous cryotherapy

Cornelis *et al.*[102,103] reported remission of pain in a report of one case (observation period, 2 months) and a report of four cases (observation period, 6 months).

8. Photodynamic therapy

Betz *et al.*[104] reported remission in two and alleviation in one of three patients.

This article has been co-published with the permission of *The Journal of Dermatology, Pediatrics International* and *Japanese Journal of Radiology*. All rights reserved. © 2020 The Authors. The articles are identical except for minor stylistic and spelling differences in keeping with each journal's style. Either citation can be used when citing this article.

CQ8: Is laser therapy effective for VM?

Recommendation: With appropriate selection of the type of laser according to the site, size and symptoms of the lesion, laser therapy can be effective for the treatment of VM. It is recommended to evaluate whether the net benefit by laser therapy is worth the cost and resources by comparison with other treatments such as sclerotherapy and surgical resection.

Strength of recommendation: 2 (weak).

Evidence: C (weak).

Comments: VM is a lesion that has been called cavernous hemangioma, and it causes pain, functional impairment and cosmetic defect depending on the affected site. In addition to conventional resection of the lesion, sclerotherapy has been widely performed in recent years. While reports of laser therapy for VM have increased, there have not been prospective studies (PS) comparing the results of laser therapy with those of surgery or sclerotherapy, among types of laser equipment different in wavelength, or using the same equipment type but changing the irradiation method or parameter setting. We analyzed 134 papers extracted by primary screening and 98 papers extracted by secondary screening. Concerning more than 30 cases, the answer to the CQ was based primarily on seven reports summarizing the methods and sites of treatment and benefits and harms derived from treatment (decrease in size of the lesion, alleviation of symptoms, complications).

In the facial skin, pigmentation and scar formation after irradiation can be serious treatment-related complications compared with unexposed areas. In the airway and digestive tract, the mass effect of the lesion and chronic bleeding from the lesion can be causes of serious symptoms. Thus, as the goal to achieve varies with the anatomical site of the lesion, we reviewed the published work by the anatomical site (the neurosurgery field was excluded). For this reason, we also extracted benefits and harms of treatment from the text of the reports of less than 30 cases. The relevant departments surveyed included ear, nose and throat, dental and oral surgery, gastrointestinal surgery, ophthalmology, plastic surgery and dermatology, and secondary screening overviewed laser therapy for VM and vasodilatory lesions.

When a new laser instrument is developed and put into use, reports of therapeutic results using the equipment are presented. The types of laser used for treatment varied widely. The types of laser that have been reported are summarized chronologically in a graph (Fig. 1). While the type of laser with more reports is not necessarily more effective, the graph is

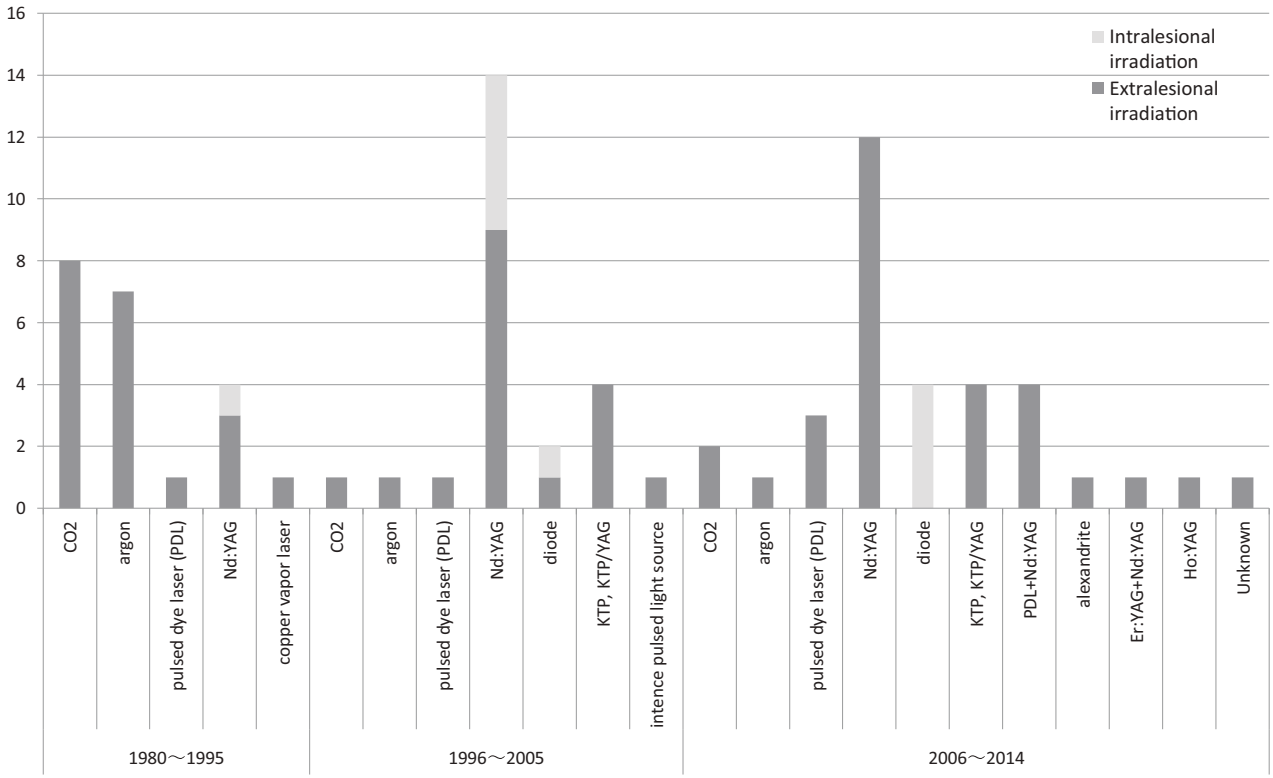

Figure 1. Reports of laser therapy for hemangiomas/vascular malformations (primarily venous) in various periods and types of laser used in the reports (CQ8). CO_2: 10 of 11 reports recommend the use for surgical resection. Argon: there are four reports of mixed treatments for CM and VM. Neodymium:yttrium–aluminum–garnet (Nd:YAG): there are 12 reports of its use in combination therapy with surgery, sclerotherapy or other lasers. Alexandrite: there is only one report summarizing cases treated with alexandrite in combination therapy with other lasers. CQ, clinical question; Er:YAG, erbium:yttrium–aluminum–garnet; Ho:YAG, holmium:yttrium–aluminum–garnet; KTP, potassium titanyl phosphate laser; YAG, yttrium–aluminum–garnet.

This article has been co-published with the permission of *The Journal of Dermatology, Pediatrics International* and *Japanese Journal of Radiology*. All rights reserved. © 2020 The Authors. The articles are identical except for minor stylistic and spelling differences in keeping with each journal's style. Either citation can be used when citing this article.

considered to reflect tendencies of laser types that are established and gain favorable appraisal or no longer in use.

Because dye laser used for the treatment of port-wine stain (wavelength, 595 nm) uses hemoglobin as the observer/heater, photothermal conversion occurs efficiently in the blood vessel, and the thermal energy reaches endothelial cells.[105] However, its optical penetration depth is shallow, being approximately 1 mm in both the skin and mucosa.[105] However, in an erbium: yttrium–aluminum–garnet (Er:YAG) laser with a longer wavelength (1064 nm), the optical penetration depth is approximately 3 mm in the skin and approximately 6 mm in the mucosa.[105] Although an neodymium:yttrium–aluminum–garnet (Nd:YAG) laser is advantageous compared with dye laser for the treatment of deep lesions, heat is generated also in perivascular tissues, because light is converted to heat as it is absorbed by water contained in the skin and mucosa.

The target of laser treatment for VM is the endothelium of morbidly dilated blood vessels. There is no light that is specifically absorbed by endothelial cells and emits heat. Satisfactory therapeutic results cannot be expected unless treatment is performed by selecting the laser type and modifying the irradiation method based on the understanding of such principles and limitations of phototherapy.

Concerning small VM of the mucosa, tongue, lips and glans penis, in which scar formation after treatment poses no serious problem, there are a number of reports[106–108] that lesions were resolved by treatment using Nd:YAG laser. There have also been cases in which favorable results were obtained by treatment of anemia due to gastrointestinal bleeding[109] and of symptoms, such as airway obstruction, due to the mass effect of the lesion.[110] While transient purpura and swelling after treatment are unavoidable, they often resolve rapidly.[99] Modifications of the irradiation setting and method are necessary to obtain satisfactory results and avoid serious complications, such as peroneal neuropathy[100] and pigmentation and scar formation of the facial skin,[106,108] and we must learn from the experience of experts.

Neodymium:yttrium–aluminum–garnet laser irradiation by insertion into the lesion under ultrasound guidance has begun to be performed as a treatment to avoid damaging important organs and nerves,[98–100] therapeutic experience using this technique has been accumulated, and detailed records and reports have been presented. At present, the results have been satisfactory in terms of safety and efficacy, and standardization of the procedure is anticipated.

CQ9: Is sclerotherapy effective for VM?

Recommendation: Sclerotherapy for VM is effective for alleviating symptoms and reducing the size of the lesion and is recommended.

Strength of recommendation: 2 (weak).

Evidence: D (very weak).

Comments: VM is a lesion that used to be called cavernous hemangioma or intramuscular hemangioma and differs from infantile hemangioma. VM poses problems, such as pain, swelling and functional impairment, and has been treated conventionally by surgical resection. In Western countries, percutaneous sclerotherapy has a long history. In 1989, Yakes *et al.*[111] reported ethanol sclerotherapy for VM, and the treatment has since been performed worldwide. Recently, sclerotherapy, which is mildly invasive, permits functional and morphological preservation, and can be performed repeatedly, has become widely used. However, as of 2016, sclerotherapy is not covered by medical insurance in Japan. In addition, there has been no RCT on the usefulness of sclerotherapy for VM compared with surgery or placebo.

As a result of secondary screening, 76, three and three papers were extracted from PubMed, Cochrane and JCRM, respectively. They include three semi-RCT, but randomization and blinding were insufficient, and their quality as an RCT was low. Also, the theme evaluated by all these RCT was "comparison of sclerosing agents in sclerotherapy", and none compared sclerotherapy with other treatments. Therefore, control groups related to this CQ were not established, and their contribution as a whole is weak. The other published work was all case reports or case series, and the evidence level is D (very weak). As mentioned above, while the evidence level is low, most of the studies reported alleviation of symptoms and regression of lesions in a high percentage (70–90%) of the patients, suggesting the usefulness of sclerotherapy.

The sclerosing agents used included absolute ethanol, polidocanol, ethanolamine oleate, STS and bleomycin. Polidocanol is approved as a sclerosing agent for lower limb varices and esophageal varices, and ethanolamine oleate as a sclerosing agent for esophageal varices. STS is not marketed in Japan. Each sclerosing agent has characteristic complications. Recently, injection of polidocanol, STS, as a foam by mixing with CO_2 or air has been increasingly performed. Sclerotherapy using ethanol is often performed under general anesthesia, but sclerotherapy using polidocanol or ethanolamine oleate can be performed under local anesthesia.

Three RCT have been reported as studies that evaluated differences in therapeutic effect according to the sclerosing agent. However, randomization and blinding are insufficient, and their quality as an RCT is low. In addition, the theme evaluated in these RCT was "comparison of sclerosing agents in sclerotherapy" rather than comparison with other treatments.

Although the evidence level is low, there have been a few case series that reported the usefulness of sclerotherapy, and a wide variety of sclerosing agents including ethanol, polidocanol, ethanolamine oleate, STS and bleomycin were used. Among studies with a relatively large number of patients, there is a report[112] that sclerotherapy using ethanol in 87 patients with craniofacial VM resulted in a 75% or more decrease in size in 23 (32%) and a 25–75% decrease in size in 37 (52%). The results of sclerotherapy using polidocanol in 50 patients with VM were excellent in 19, good in 16, moderate improvement in 13 and unchanged or worse in two.[92] The results of sclerotherapy using ethanolamine oleate performed in 83 patients, who were mostly children, were complete remission of symptoms in 79 lesions and significant alleviation in six lesions.[113] Sclerotherapy using STS resulted in subjective improvements in 174 (85.3%) of 204 patients.[114] The results of sclerotherapy using bleomycin were complete cure in 185 of 260 patients, marked improvement in 44 and some

This article has been co-published with the permission of *The Journal of Dermatology, Pediatrics International* and *Japanese Journal of Radiology*. All rights reserved. © 2020 The Authors. The articles are identical except for minor stylistic and spelling differences in keeping with each journal's style. Either citation can be used when citing this article.

improvement or no change in 31.[115] In addition, regarding the size of the lesion, a very satisfactory decrease was achieved in 104, and a satisfactory decrease was achieved in 10 of 120 patients.[116]

Papers that evaluated the types of VM that are likely to respond to sclerotherapy include those by Goyal *et al.*,[117] Yun *et al.*,[118] Mimura *et al.*,[91] Rautio *et al.*,[119] Lee *et al.*,[112] Yamaki *et al.*[120] and Nagao *et al.*[121] Types of lesions that were likely to be sclerosed were reported to be well-defined small (≤5 cm) lesions by Goyal *et al.*;[117] those in females, lesions showing no or delayed delineation of the draining vein and lesions well-defined on magnetic resonance imaging (MRI) by Yun *et al.*;[118] small lesions, well-defined lesions and lesions that show prolonged drug retention by Mimura *et al.*;[91] localized lesions by Lee *et al.*[112] and Yamaki *et al.*;[120] and slow flow type lesions by Nagao *et al.*[121] Nomura *et al.*[122] evaluated the therapeutic effect according to the degrees of functional and gross improvements and reported that the therapeutic effect was greater in head and neck and trunk lesions than in the upper or lower limb lesions. Moreover, Rautio *et al.*[119] reported that the treatment-related improvement in the quality of life was higher when the lesion did not involve the muscle or was 5 cm or less in size.

Various complications ranging from mild complications, such as transient neuropathy and local inflammation, to serious ones, such as myopathy, skin necrosis and deep venous thrombosis/pulmonary embolism, have been reported. In sclerotherapy using ethanol or polidocanol, particularly serious life-threatening complications have been reported. Qiu *et al.*[123] reviewed the published work concerning sclerotherapy for VM and reported that shock and pulmonary embolism occurred in 0.19% each of 522 patients who underwent sclerotherapy using ethanol and that ethanol was used at 1 mL/kg in those who developed shock. They also reported that a decrease in blood pressure/bradycardia was noted in 0.61% of 163 patients who underwent sclerotherapy using polidocanol but that its differentiation from vagus nerve reflex was clinically difficult. Wong *et al.*[124] reported a case of shock after sclerotherapy using 0.86 g/kg ethanol but could be saved. Tachibana *et al.*[125] reported that two patients (1.1%) developed pulmonary embolism and that the amounts of ethanol used were 0.71 and 0.16 mL/kg. Concerning sclerotherapy using polidocanol, also, cardiac arrest in children has been reported by authors including Marrocco-Trischitta *et al.*[126] and Shimo *et al.*,[127] who used 4 mL of 1% polidocanol (bodyweight, 20 kg) and 10 mL of 3% polidocanol (15.6 kg), respectively.

In conclusion, sclerotherapy is generally considered effective for VM, but its problems are that the evidence level is low and that the procedure has not been standardized. In addition, serious complications that are rare but life-threatening have been reported, and caution is needed in deciding the dose of the sclerosing agent.

CQ10: Are clotting abnormalities due to VM an indication for radiotherapy?

Recommendation: Radiotherapy should not be performed without careful evaluation because malignant neoplasm, growth disorders and functional impairment have been reported as late complications.

Many reports included both VM and vascular tumors in the subjects, which make it difficult to assess the therapeutic effects of radiotherapy.

Strength of recommendation: 2 (weak).

Evidence: D (very weak).

Comments: As a result of primary screening, six and two documents were retrieved from PubMed and JCRM. However, as a result of secondary screening, liver hemangioma was excluded, and 10 papers including the references from the previous guideline were reviewed. The reviewed papers were case series or case reports, and the evidence level of the published work as a whole is D (very weak).

While there have been reports that radiotherapy was performed for the treatment of vascular tumors and vascular malformations, it is difficult to judge whether the treatment was performed by determining the disorders.

According to many reports,[128–132] radiotherapy has been performed to treat Kasabach–Merritt phenomenon. However, while there is no mention of Kasabach–Merritt phenomenon, there is a report[133] of five cases in which giant hemangiomas accompanied by clotting disorders, thrombocytopenia, heart failure and bleeding were controlled by multidisciplinary treatment including radiotherapy.

Vascular tumors that cause Kasabach–Merritt phenomenon are considered to be kaposiform hemangioendothelioma or tufted angioma rather than infantile hemangioma.[134] Because VM and infantile hemangiomas are included in other vascular tumors in the lesions described in these reports, they are not considered to be indications of radiotherapy for VM or infantile hemangiomas.

Schild *et al.*[128] reported 13 cases of symptomatic hemangioma (11 of which were pathologically diagnosed as cavernous hemangioma, but as the report is old, vascular tumors and vascular malformations were not distinguished and were probably included). Radiotherapy at 6.25–40 Gy was carried out in these 13 cases. The lesions were located in the limbs in five, face in two, vertebral bodies in three, pituitary fossa in one, sacrum in one and bladder in one. Note that organs that should be excluded in this CQ were included.

Of these patients, two (one each with a limb and facial lesion) exhibited Kasabach–Merritt phenomenon and showed normalization of clotting disorder (evaluated according to the platelet count and fibrinogen level) after treatment. However, they were aged 3 years and 5 months, and the lesions might not have been VM.

When the subjects were limited to patients with limb or facial lesions, complete response (CR) was observed in two, partial response (PR) in four and no response in one in terms of decrease in the lesion size, and CR was observed in four, PR in one and no response in two in terms of the control of symptoms.

A serious treatment-related complication, which was unilateral visual impairment, was noted in one (14 Gy/8 fr).[128] These problems have been recognized as late complications of radiotherapy for vascular tumors or vascular malformations;

This article has been co-published with the permission of *The Journal of Dermatology, Pediatrics International* and *Japanese Journal of Radiology*. All rights reserved. © 2020 The Authors. The articles are identical except for minor stylistic and spelling differences in keeping with each journal's style. Either citation can be used when citing this article.

malignant neoplasms, such as breast cancer,[135] thyroid cancer[136] and vascular sarcoma,[137] visual impairment mentioned above,[128] and shortening of the lower limb and restriction of the joint motion range.[131]

According to Coldwell *et al.*,[137] late complications of radiotherapy for hemangiomas in infancy include bruise and Stewart–Treves syndrome after the patients reach adulthood. Angiosarcoma is also observed. They reported that the median survival period was 24 months, and the 5-year survival rate was approximately 10%, in those who developed angiosarcoma.

As observed above, the diagnosis was not confirmed in the reports that have suggested the effectiveness of radiotherapy, and its indications have not been specified. In addition, there have been a considerable number of reports of late complications due to radiotherapy. Thus radiotherapy should not be performed without careful evaluation.

CQ11: Is there difference in the effectiveness of dye laser treatment for CM according to the site of the body?

Recommendation: Dye laser treatment for CM is likely more effective in the face and neck region compared with other sites, and it is more likely to cause complications such as pigmentation in the limbs.

Strength of recommendation: 2 (weak).

Evidence: C (weak).

Comments: As a result of published work searches, 176 papers consisting of 139 from PubMed and 37 from JCRM were extracted. They included a few reports that were allegedly RCT but were not actual RCT. Therefore, a total of 26 papers consisting of 15 from PubMed and 11 from JCRM including case series with a large number (≥100) of relevant cases were selected by secondary screening. In addition, a total of 17 papers were adopted as references for the comments in the guidelines by adding three papers in English extracted by manual search to six from PubMed and eight from JCRM considered to be relevant or closely related to the CQ among those selected by secondary screening. Because there was no RCT, the evidence as a whole was rated as C (weak).

Concerning the effect of dye laser treatment for CM, most of the reports were about the effects for hemangioma simplex or port-wine hemangioma in Japan and port-wine stain abroad.

There have been a few papers[138–152] that evaluated the therapeutic results of dye laser treatment according to the site in a small to relatively large number of patients. The laser equipment used varies from early dye laser to pulsed-dye laser with adjustable pulse duration with a cooling system, and reports limited to variable-pulse pulsed-dye laser with a cooling system, which is widely used today, are extremely few.

According to many reports,[138–149] the response rate is higher in the face and neck region than in the trunk and limbs. In the face, it has been reported that the response rate is higher in the palpebral, forehead and temporal, and lateral buccal regions but is significantly lower in the territory of the second division of the trigeminal nerve (dermatome V2), and that the number of irradiations tends to increase in the midline region, frequently resulting in persistence of redness.[150] There is a report[151] that the response rate did not differ significantly among regions in the lower limb. While the number of patients was small, it has been reported that treatment of the foot involves stronger pain but was less effective than in the face but that the degree of patient satisfaction was relatively high.[152]

The incidence of complications of dye laser (bleb formation, depigmentation, pigmentation, scar formation) is reported to be low, being 1.7% in adults, 0.6% in children and approximately 1.4% in all patients even when all sites of the body are included, and no significant difference has been reported in the age at the beginning of treatment, Fitzpatrick skin type,[153] site, number of treatments or irradiation energy between those who developed complications and those who did not, but complications may occur more frequently in the lower limbs.[154] Moreover, there is a report[152] that complications, such as pigmentation, depigmentation and atrophic scar, were observed more frequently in the lower limbs.

CQ12: Do CM recur after dye laser treatment?

Recommendation: Although the effectiveness of dye laser treatment for CM is established, the recurrence rate may increase with time after treatment.

Strength of recommendation: 2 (weak).

Evidence: C (weak).

Comments: As a result of published work searches, a total of 211 papers consisting of 149 from PubMed, 53 from Cochrane and nine from JCRM were retrieved. They did not include RCT, and a total of 30 papers consisting of 23 from PubMed and seven from Cochrane, which were mostly case reports and case series studies, were extracted by secondary screening. In addition, a total of 10 papers that were relevant and closely related to the CQ (including eight case series) consisting of seven from PubMed, two from Cochrane and one in English retrieved by manual search were adopted as references for the guidelines. Because there was no RCT, the strength of evidence of the group of published work concerning this CQ is C (weak).

Concerning papers that referred to "whether CM recur after dye laser treatment", there are four retrospective studies[155–158] after treatment by pulsed-dye laser (wavelength, 585 nm) with a cooling system, and the recurrence rate was 15.9–35%. Also, there is a report[155] that the recurrence rate increased with time after treatment and was 3.1% after 1 year, 20.8% after 2 years, 40% after 3 years and 50% after 4 years. Therefore, it is necessary to treat CM with the recurrence after dye laser treatment in mind.

It is difficult to strictly distinguish whether the recurrence is generation of new dilated vessels after laser therapy or regeneration of blood vessels damaged due to treatment or re-proliferation of remaining vessels. However, there have been reports that, in an experiment using mice, angiogenesis occurred in the process of wound healing at the site of

This article has been co-published with the permission of *The Journal of Dermatology, Pediatrics International* and *Japanese Journal of Radiology*. All rights reserved. © 2020 The Authors. The articles are identical except for minor stylistic and spelling differences in keeping with each journal's style. Either citation can be used when citing this article.

irradiation in early recurrence[159] and that, in an experiment using hamsters, complete treatment was difficult, and morbid vessels persisted, because coagulation was difficult to induce by dye laser irradiation in vessels ranging 2 μm or less to16 μm in diameter.[160] While there is a report[161] that genes affected by dye laser therapy early after treatment were identified, further evaluation is necessary to clarify their relationships with the recurrence.

Concerning the prevention of recurrence, there is a report[162] that the recurrence-free period was long in the patients treated with a variable-pulse pulsed-dye laser with a cooling system (wavelength, 595 nm), which is widely used today, and they were treated within 6 months after birth. In addition, there have been reports of animal experiments using rapamycin, which inhibits angiogenesis after laser irradiation,[159,163] and of prospective RCT using imiquimod,[164,165] and these treatments were considered effective for the prevention of recurrence. However, careful evaluation by large-scale investigations, including the assessment of the safety concerning drugs, is considered necessary.

CQ13: Is dye laser irradiation for CM more effective as it is initiated at a younger age?

Recommendation: Laser therapy before the age of 1 year may be effective, and the earliest possible initiation of treatment is recommended as an option.

Strength of recommendation: 2 (weak).

Evidence: D (very weak).

Comments: Concerning the timing of treatment for CM, there is the opinion that early initiation of treatment is recommended because in young children the skin is thinner, so the depth of penetration is larger, the vascular wall is also immature, cure after laser irradiation is better, pigmentation is less and the irradiation area is small, so the treatment efficiency is higher. However, there is still controversy. As a result of secondary screening of past reports, six and one were extracted from PubMed and JCRM, respectively. While the papers selected by these screening procedures include two papers on PS as described below, their conclusions differed, and the evidence level is considered to decline when these references are reviewed together.

Oguri *et al.*[138] performed a non-RCT by dividing children into those aged 0–12 months, 13–24 months and 25–36 months, and observed significant differences in the response rate combining "markedly effective" and "effective" among the groups. They also compared the response rate according to the age in months at the beginning of treatment in the 0-year-old group and reported that the response rate was higher as the treatment was initiated earlier. Furthermore, Nguyen *et al.*[166] divided their patients into those aged less than 1 year, those aged 1–6 years and those aged 6 or more years, and investigated the correlation between treatment response and age. They reported that those aged less than 1 year and lesions with a size of less than 20 cm^2 located in the center of the face showed the best treatment response.

Among reports suggesting no difference in the therapeutic effect according to the age at the beginning of treatment, van der Horst *et al.*[167] studied 100 patients with untreated CM of the head and neck region prospectively and concluded from the results of colorimetry and clinical evaluation that there was no significant difference in the therapeutic effect of pulsed-dye laser among the four groups in which the treatment was started at the age of 0–5, 6–11, 12–17 and 18–31 years. In the retrospective study of Katugampola *et al.*,[140] also, comparison of four groups in which treatment was started at the age of 0–5, 6–12, 13–50 and 50 years or more showed no significant difference in the therapeutic effect.

Among the above reports, those that did not affirm the usefulness of early laser treatment were relatively old. Also, reports of Oguri *et al.*[138] and Nguyen *et al.*[166] indicated that laser therapy may be more effective in those aged less than 1 year. In addition, the effectiveness of laser clearly declines when the lesion is elevated or thickens with time. In consideration of "benefits" of early laser treatment and "harms", which include the occasional necessity of general anesthesia for laser treatment around the eye in small children, the recommendation level was rated as 2D based on the consensus of this guidelines drafting committee.

CQ14: Is propranolol safe and effective for infantile hemangiomas?

Recommendation: If administrated under careful monitoring, oral propranolol therapy may be the first choice for the treatment of infantile hemangioma.

Strength of recommendation: 1 (strong).

Evidence: A (strong).

Comments:

1. Effectiveness

There was the serendipity that regression of hemangioma was induced in a child under steroid therapy with a giant infantile hemangioma by propranolol administrated for obstructive hypertrophic cardiomyopathy in 2008.[168] Based on this report, oral propranolol therapy began to be used for the treatment of infantile hemangioma, and its high efficacy against alarming hemangioma/life-threatening hemangioma in the proliferating phase and in patients with cosmetic problems, such as giant lesions in the face, those with ulcerated and hemorrhagic lesions and those who may develop functional impairment, has been demonstrated, resulting in its use (Hemangiol®, Pierre Fabre Dermatologie, Boulogne, France) as the first choice in Western countries. In addition, its effectiveness for the treatment of hemangiomas after the proliferating phase was also described. Moreover, a group of physicians used propranolol earlier due to cosmetic significance and at the request of the family even in cases of small or localized lesions, and it is also effective in such cases.

A total of 131 papers consisting of 25 from JCRM, 106 from PubMed and zero from Cochrane were extracted as related to the CQ, "Is propranolol safe and effective for infantile hemangioma?", and they were subjected to primary and secondary screenings with reduction of hemangioma (effectiveness of propranolol) and treatment-related complications (adverse effects) as outcomes. Twenty-six papers,[169–194] most of which were RCT or observational studies, were adopted.

This article has been co-published with the permission of *The Journal of Dermatology, Pediatrics International* and *Japanese Journal of Radiology*. All rights reserved. © 2020 The Authors. The articles are identical except for minor stylistic and spelling differences in keeping with each journal's style. Either citation can be used when citing this article.

For example, Hogeling *et al.*[180] administrated placebo or propranolol at 2 mg/kg per day for 6 months with randomization to 40 patients aged 9 weeks to 5 years with infantile hemangiomas in the face or sites with the potential for disfigurement. They reported significant improvements in size, redness and elevation in the propranolol group. Elevated lesions disappeared in four of the 19 patients in the propranolol group but none of the 18 patients in the placebo group. As for adverse events, the trial was interrupted in one patient due to upper respiratory tract infection (URTI), and conditions including bronchiolitis, gastroenteritis, streptococcal infection, cool extremities, dental caries and sleep disturbance were observed.

Zaher *et al.*[181] observed 45 patients by randomly dividing them into 15 each treated by p.o. administration, topical application and intralesional injection of propranolol. Responses were observed in 60% in the oral group, 20% in the topical ointment group and 13.3% in the injection group. No major adverse events were noted, and the trial was discontinued in one in the oral group and three in the injection group due to inconvenience or pain of the treatment.

Malik *et al.*[182] randomly allotted 30 patients aged 1 week to 8 months to propranolol alone, prednisolone alone or both propranolol and prednisolone. They found that the mean initial response times were lower in the propranolol group than in the prednisolone group but that there was no clear difference between the propranolol + prednisolone group and propranolol alone group. All 10 patients in the propranolol group and nine patients in the corticosteroid group responded to the 3-month treatment. However, adverse events were observed in two of the 10 patients in the propranolol group (asymptomatic hypoglycemia, insomnia) and nine of the 10 patients in the steroid group (cushingoid appearance, gastrointestinal upset), and were more frequent in the latter group.

Bauman *et al.*[183] performed a phase 2, investigator-blinded, multicenter RCT in 44 patients aged 2 weeks to 6 months. Propranolol or prednisolone (2 mg/kg per day) was administrated p.o. until halted due to toxic effects or clinical response. During 4 months of treatment, no significant difference was observed between the two groups, for example, with regression of five of the six tumors in the corticosteroid group and nine of the 10 tumors in the propranolol group. For long-term analyses, the effect of prednisolone appeared earlier. While the incidence of adverse events as a whole did not differ between the two groups, severe adverse events were observed in one of the 11 patients in the propranolol group but five of the seven patients in the prednisolone group, being significantly more frequently in the latter group.

Léauté-Labrèze *et al.*[184] carried out an RCT in patients aged less than 4 months by comparing seven administrated and seven not administrated propranolol. Because color changes and softening were observed within 24 h, and the thickness and size of the lesions decreased within 4 weeks in the propranolol group, the treatment was considered useful for the prevention of scarring. No serious adverse effect was observed except asymptomatic mild decreases in heart rate and diastolic blood pressure.

There have also been comparisons between atenolol and propranolol and between laser and laser + topical propranolol.[185,186] In 2015, the largest RCT was published in the *New England Journal of Medicine*, also reporting that propranolol was significantly effective for hemangioma compared with placebo.[187] Hemangioma showed complete or nearly complete resolution after 6 months of treatment in two (4%) of 55 patients in the placebo group and 61 (60%) of 101 patients in the 3 mg/kg per day propranolol group.

Furthermore, there have also been a few SR and meta-analyses primarily of observational studies. Menezes *et al.*[188] reviewed 49 English-language papers published between June 2008 and September 2010, and summarized six studies with 10 or more patients administrated propranolol (154 patients in total). Propranolol was administrated to infants with a mean age of 4.5 months at a dose of 2 mg/kg per day in 65% and 3 mg/kg per day in 25.3%. Two-thirds of the patients were treated with propranolol alone. Recurrence was observed in 21% after treatment for a mean of 4.3 months, and adverse events including hypotension, somnolence, wheezing, insomnia, agitation, nightmare, cool hands, night sweat, gastroesophageal reflux disease and psoriasiform rash appeared in 18.1%.

Marqueling *et al.*[189] reviewed the therapeutic results in 1264 patients (including 806 girls) in 41 reports published from 2008 to 2012 retrieved from Medline and Cochrane. The treatment was initiated at a mean age of 6.6 months at 2.1 mg/kg per day and continued for a mean of 6.4 months. The overall response rate was 98%, and the treatment was also effective in clinically problematic areas such as the face (100%), airway (100%), periorbital (98%), head and neck region (97%), and parotid gland (82%). However, recurrence was observed in 17% after treatment. Adverse effects were noted in 371 of 1189 patients. Changes in sleep (136 patients) and acrocyanosis ($n = 61$) were the most frequent among them, and hypotension was observed in 44, bradycardia in nine and hypoglycemia in four as serious complications. In conclusion, the grade of recommendation was 1, quality of evidence is A and propranolol was recommended as the first-line drug for complicated infantile hemangiomas. Regarding adverse effects, the grade of recommendation was 1, and the quality of evidence was A or B. While serious adverse effects may be observed, their frequency is low, and they can be usually avoided by proper monitoring at initiation of treatment.

Xu *et al.*,[190] on the other hand, evaluated volume changes, improvement in overall appearance, visual function and adverse effects using 15 online databases. The data of 419 cases were analyzed, but meta-analysis was not performed because of the wide differences among studies. Some studies showed superiority of propranolol compared with corticosteroid in reducing volume and improving the overall appearance. No marked difference was noted in adverse effects or visual function.

In addition, in a meta-analysis of 16 studies (2629 cases) and 25 studies (795 cases) published in 1965–2012, 69% of the patients responded to 12-month corticosteroid therapy, but the response rate to propranolol was 97% with a significant difference.[191]

In periorbital hemangiomas, the response rate to propranolol was found to be significantly higher than that to corticosteroid by meta-analysis of papers published before 2013,[192] and propranolol showed the strongest effect against airway

This article has been co-published with the permission of *The Journal of Dermatology, Pediatrics International* and *Japanese Journal of Radiology*. All rights reserved. © 2020 The Authors. The articles are identical except for minor stylistic and spelling differences in keeping with each journal's style. Either citation can be used when citing this article.

hemangiomas compared with steroid, CO_2 laser and vincristine on meta-analysis.[193,194]

From these observations, we concluded that propranolol was significantly more effective than placebo and to be similarly effective compared with corticosteroid. Concerning the safety, propranolol is considered to have significantly fewer adverse effects than corticosteroid. Because there have been several RCT and SR or meta-analyses directly related to this CQ, the evidence level is considered to be extremely high.

2. Meta-analysis

Regarding the effectiveness and adverse effects of propranolol, a large number of SR and meta-analyses based on observational studies are already present in the above 26 papers. We, therefore, used only four reports[180,182,183,187] on interventional studies for meta-analysis.

As a result of meta-analysis, regarding "tumor reduction", it was found that propranolol had significantly stronger reducing effects than placebo and that it had a stronger reducing effect, which, however, was not significant, compared with corticosteroid. Concerning "complications", propranolol was compared with steroid and was shown by two RCT to have significantly fewer adverse events than corticosteroid. Because this meta-analysis found significantly stronger reducing effect of propranolol compared with placebo and in fewer complications compared with steroid, and because our results were similar to those of SR of many existing observational studies considered to have high-quality evidence, we considered that there was a major tendency in this CQ and judged the evidence level as A.

3. Estimated action mechanism

Beta-blockers have a wide range of actions on the blood vessels and vascular endothelium, and have diverse actions on cell proliferation and vascular remodeling. Thus, the mechanism of action of propranolol on infantile hemangiomas is still unclear. In vascular endothelial cells, propranolol is considered to induce vascular contraction by suppressing NO production, inhibit renin production, control angiogenesis by regulating the expression of vascular endothelial growth factor·basic fibroblast growth factor·matrix metallopeptidase (MMP)2/MMP9, and induce apoptosis, but it may also affect pericytes and hemangioma stem cells.[195–197]

4. Adverse events associated with propranolol in children

In conducting propranolol therapy, it is necessary to have knowledge of possible adverse effects, their symptoms and their management. In addition, as there are also preventive measures for, and points of attention about, adverse effects and the timing for discontinuation of propranolol, sufficient explanation to the patients and their families is essential.

Adverse events that have been reported include sleep disorders, peripheral cyanosis, hypotension (symptomatic, asymptomatic), bradycardia (symptomatic, asymptomatic), hypoglycemia, respiratory disorders, gastrointestinal disorders and mental disorders. Severe cases that require interruption of treatment are few, but particular caution is needed regarding the following points.[189,196–200]

1. Because there is the risk of hypoglycemia, the patient should be fed before and after propranolol administration. If the patient cannot be fed, or is vomiting, for some reason, the administration should be suspended.
2. Because propranolol has cardiovascular adverse effects, such as hypotension and bradycardia, interviewing for the past history and familial history, examination and electrocardiography are recommended before treatment. Even if no abnormality is noted on these examinations, hypotension and bradycardia may occur during treatment. In such cases, interruption of the administration is necessary.
3. Propranolol is contraindicated for bronchial asthma as it causes bronchial contraction due to its β2-blocking action. Caution is also necessary in patients who have been suspected to have bronchial asthma.

CQ15: What treatments are effective for ulcer formation in infantile hemangioma?

1. Propranolol

Recommendation: The administration of propranolol is recommended for ulcer formation.
Strength of recommendation: 2 (weak).
Evidence: C (weak).

2. Topical administration of antibiotics

Recommendation: Topical and systemic administration of antibiotics is recommended for ulcer formation.
Strength of recommendation: 2 (weak).
Evidence: D (very weak).

3. Dressings

Recommendation: The use of dressings is recommended for ulcer formation.
Strength of recommendation: 2 (weak).
Evidence: D (very weak).

4. Laser therapy

Recommendation: Although laser therapy may be effective in some patients with ulcer formation, the evidence is not considered sufficient at present.
Strength of recommendation: 2 (weak).
Evidence: D (very weak).

5. Systemic administration of steroid

Recommendation: Systemic administration of steroid is recommended not to be performed for ulcer formation.
Strength of recommendation: 2 (weak).
Evidence: D (very weak).

6. Platelet-derived growth factor preparations

Recommendation: The accumulation of cases is insufficient for the judgment of the recommendability of the use of platelet-derived growth factor preparations for ulcer formation.
Strength of recommendation: No recommendation.

This article has been co-published with the permission of *The Journal of Dermatology, Pediatrics International* and *Japanese Journal of Radiology*. All rights reserved. © 2020 The Authors. The articles are identical except for minor stylistic and spelling differences in keeping with each journal's style. Either citation can be used when citing this article.

Evidence: D (very weak).

Comments: Concerning this CQ, 42 papers in Japanese and 156 in English were retrieved. As a result of their primary screening, 47 papers were submitted to secondary screening for this CQ. None of them were about studies with a high level of evidence, such as RCT, and they were all retrospective studies, case series or case reports.

As a result, 15 papers in English were adopted, and the evidence level was C for propranolol alone, because of the presence of a prospective controlled trial, but D for other treatments, because the related papers were case reports or case series.

According to cross-sectional analysis in a multicenter prospective cohort study in 1096 cases of infantile hemangioma by Chamlin *et al.*,[201] it was complicated by ulcer, which was or was not bleeding, in 173 (15.8%), the median age of the patients was 4.0 months (standard deviation, 8.5; mean, 6.6 months), and the age at the first examination was significantly lower in patients with ulcerated hemangioma (median, 3.5 months; mean, 3.98 months) than in those with non-ulcerated hemangioma.

By the site, ulcer formation was observed in 21 (30%) of 71 patients in the lower lip, 25 (25%) of 100 patients in the neck and 46 (50%) of 93 patients in the perianal/perigenital area, and the frequency was statistically lowest in the upper eyelid ($P = 0.0140$).

Ulcer formation was observed more frequently in mixed or segmental hemangiomas. Bleeding was noted in 78 lesions (41%) and was mild in 56 (29%), moderate in 11 (6%) and severe in four (2%). Severe bleeding occurred in three lesions in the limbs and one lesion in the face, and bleeding occurred in two cases at home. Two cases required blood transfusion by hospitalization, because they showed symptoms due to serious bleeding. Of the ulcerated hemangiomas, 67 (35%) were in the proliferating phase.

Ulcerated hemangiomas required treatment (odds ratio [OR], 6.86; 95% CI, 3.70–12.71; $P < 0.0001$), and non-ulcerated hemangiomas were observed (OR, 19.01; 95% CI, 11.23–28.88; $P < 0.0001$). Ulcerated hemangiomas tended to be treated by conventional wound care and pulsed-dye laser (OR, 2.03; 95% CI, 1.19–3.46; $P < 0.0091$), and non-ulcerated hemangiomas were treated by topical glucocorticoid administration (OR, 2.57; 95% CI, 1.49–4.43; $P < 0.0007$) and surgical resection (OR, 2.04; 95% CI, 1.08–3.86; $P < 0.0286$).

However, propranolol has recently been suggested to be effective regardless of the presence or absence of ulcer formation, and as it has few adverse effects, it is expected to become the first choice treatment in the future.

Treatments

1. Oral propranolol

Hermans *et al.*[172] treated 20 previously treated patients with ulcerated infantile hemangioma using propranolol and compared them with 36 patients treated without propranolol. The administration was initiated by hospitalization, and the dose was increased from 0.7–1.0 to 2.0–2.5 mg/kg per day in three divided doses at an interval of at least 3 days. The blood pressure, heart rate and blood sugar level were monitored during the initial administration period, and the administration was continued on an outpatient basis until the age of 1 year. The mean age at the beginning of propranolol administration was 3.5 months, and the mean duration of administration was 9.1 months. Not only the color and elevation of the lesion but also pain was reduced from early after the beginning of administration. The administration was concluded before the age of 1 year in 19 patients, and no recurrence of ulcer was noted in any of these patients except that some reactivation (enlargement) of hemangioma was observed after the discontinuation in four of these patients.

The mean time until complete cure of ulcer was 8.7 weeks, and those in whom the administration was initiated later (>3.5 months) tended to require a longer time until cure than those in whom the administration was initiated earlier ($P = 0.025$). Also, analysis using Student's *t*-test showed a significant difference in the time until disappearance of the tumor, which was 8.7 and 22.4 weeks ($t = 2.6$, d.f. = 38, $P = 0.012$; 95% CI, 3.2–24.2) in the treated and control groups, respectively. Temporary sleepiness/malaise was observed in six patients, irritability before falling asleep in two patients, coldness of the limbs in six patients, anorexia in two patients and gastrointestinal disorders (diarrhea, vomiting) in one patient, but no adverse event was noted in nine patients.

Vercellino *et al.*,[202] who started the administration at 1 mg/kg per day and increased to 2 mg/kg per day, and Sadykov *et al.*,[203] who started the administration at 2 mg/kg per day, also reported that propranolol was effective.

2. Topical and/or systemic administration of antibiotics

Kim *et al.*[204] topically administrated antibiotics in 40 patients with ulcerated hemangioma and reported that the results were better in 37 patients (92.5%), worse in none and no change in three patients (7.5%). They also systemically administrated antibiotics in 26 patients and reported that the results were better in 24 patients (92.3%), worse in two patients (7.7%) and no change in zero patients.

Wananukul *et al.*[205] topically and/or systemically administrated antibiotics in 41 patients with ulcerated hemangioma and reported improvement in 19 patients (46%).

Pandey *et al.*[206] treated 608 patients showing ulcer formation with an ointment containing an antibiotic (mupirocin, sodium fusidate, sisomicin or metronidazole) combined with systemic administration of an antibiotic (amoxiclav at 20–40 mg/kg per day) in those with ulcers with an area of more than 10 cm^2 and examined the effectiveness of treatment according to the time until cure. The time until cure was 32.63 ± 13.06 days in superficial lesions, 42.89 ± 19.89 days in mixed lesions and 57.03 ± 16.12 days in extensive lesions, with a mean of 40.09 ± 19.41 days in all lesions combined, showing significant differences among the three groups ($P < 0.05$). They also reported that the time until cure was significantly longer in larger (>10 cm^2) than smaller ulcers ($P < 0.05$).

This article has been co-published with the permission of *The Journal of Dermatology, Pediatrics International* and *Japanese Journal of Radiology*. All rights reserved. © 2020 The Authors. The articles are identical except for minor stylistic and spelling differences in keeping with each journal's style. Either citation can be used when citing this article.

3. Dressings

Kim *et al.*[204] treated 25 patients using dressings and reported that the results were better in 23 patients (92%) and no change in two patients (8%). Oranje *et al.*[207] applied polyurethane film and reported rapid relief of pain and cure of ulcer in 1–2 months. In addition, Bauland *et al.*[208] treated 41 patients using a non-adhering dressing containing an antibiotic and reported that the results were good in 26 patients (63.4%), moderate in five patients (12.2%) and little change in 10 patients (24.4%).

4. Laser therapy

In the 1980s–1990s, there were reports[209,210] of argon, Nd: YAG and potassium titanyl phosphate laser, but recent reports[211,212] are primarily about treatment using dye laser. Morelli *et al.*[209] treated 37 patients with ulcerated hemangioma by dye laser irradiation (SPTL1b® [Candela Corporation, Wyland, MA, USA]; wavelength, 585 nm; spot size, 5–7 mm; irradiation power, 5–6.8 J/cm^2; pulse width, 0.45 ms) and reported that the number of irradiations until cure was one in 26 patients (68%) and two in eight patients (21%), and that the mean period from the first treatment until cure of ulcer was 2.84 $\pm$ 0.22 weeks. Lacour *et al.*[210] irradiated eight patients with ulcerated hemangioma that resisted conventional treatments using the same equipment and reported acceleration of cure. David *et al.*[211] performed dye laser irradiation (PhotoGenica V® [Cynosure, Westford, MA, USA]; wavelength, 585 nm; spot size, 5–7 mm; irradiation power, 5–6.8 J/cm^2; pulse width, 0.3–0.5 ms) in 78 patients and reported the effectiveness of laser therapy alone in 72 (92.3%). Also, Michel[212] performed one or two irradiations using Dermobeam 2000® (Deka MELA, Calenzano, Italy) with a cooling system 595 nm (two pulsed irradiations with a 10% overlap; spot size, 7 mm; irradiation power, 4–8 J/cm^2) and reported resolution of pain in 10 of the 12 patients. Moreover, Di Maio *et al.*[213] performed laser treatment in 65 patients with hemangioma with ulcer and reported that the effect was excellent and that no clear adverse events were observed, because scarring, which was noted in a few patients, did not differ markedly compared with scarring that occurs after conventional treatments.

However, Kim *et al.*[204] treated 22 patients with pulsed-dye laser and reported that the results were better in 11 patients (50%), worse in one patient (4.5%) and no change in four patients (18.2%), but warned that five patients in the proliferating phase showed ulcer formation after irradiation.

As observed above, although there have been several reports of the effectiveness of laser therapy against ulcer as factors of "benefit", many reports are relatively old and lack controls, and the evidence is not considered sufficient. Further accumulation of cases is necessary. Laser may be effective in limited patients, but as there is the risk of ulcer formation as an adverse effect of laser irradiation of infantile non-ulcerated hemangioma, greater caution is needed in treating already ulcerated lesions.

5. Steroids

There have been few reports on steroid therapy focusing on ulcer. Kim *et al.*[204] treated seven patients by local steroid injections and reported that the results were better in four patients (57.1%), worse in one patient (14.3%) and no change in one patient (14.3%). They also systemically administrated steroid to 22 patients and reported that the results were better in 16 patients (72.7%), worse in one patient (4.5%) and no change in five patients (22.7%). Based on these results, they considered that the treatment was effective for reducing the lesion size, and there are few other reports suggesting the effectiveness of steroid. Considering that the patients are infants and that there are other treatment options, steroid cannot be recommended at present.

6. Topical preparations of recombinant human platelet-derived growth factor

Becaplermin 0.01% (Regranex®, Ortho-McNeil Pharmaceutical, Raritan, NJ, USA) is a preparation for diabetic foot ulcer approved by the US Food and Drug Administration in 1997. Sugarman *et al.*[214] and Metz *et al.*[215] reported its effectiveness for the treatment of ulcerated hemangioma in one and eight patients, respectively, but its effectiveness cannot be appraised at present because of the small number of cases.

CQ16: Is intralesional corticosteroid injection more effective than systemic administration for infantile hemangioma?

Recommendation: Treatment using corticosteroid is effective for inducing early regression of hemangioma. While no significant difference is observed in the effectiveness between intralesional injection and systemic administration, attention to complications including those at the administration site, such as the periocular region, on local injection and those, such as hypertension and growth retardation, on systemic administration is necessary.

Strength of recommendation: 2 (weak).

Evidence: B (moderate).

Comments: As a result of primary screening, 99, nine and 35 papers were extracted from PubMed, Cochrane and JCRM, respectively, and four papers in English were subjected to secondary screening for this CQ. There was one report of an RCT, but the other reports were about case series while they evaluated a large number of cases. In addition, two papers on complications considered important in relation to intralesional corticosteroid injection for periocular lesions were added by manual search. Because there is a report of an RCT, and because other case series studies with a large number of subjects presented the results that there was no significant difference in the effectiveness of corticosteroid depending on the administration method, the strength of evidence was rated as B.

There was one report[216] of an RCT focusing on "Is intralesional corticosteroid injection more effective than systemic administration for infantile hemangioma?". In this trial, the subjects were divided into control, p.o. administration (prednisolone at 2 mg/kg per day every other day for 6 weeks) and intralesional injection (triamcinolone at 1–5 mg/kg with a maximum of 30 mg once a month for 6 months) groups, and the lesion size was significantly reduced in the treated groups

This article has been co-published with the permission of *The Journal of Dermatology, Pediatrics International* and *Japanese Journal of Radiology*. All rights reserved. © 2020 The Authors. The articles are identical except for minor stylistic and spelling differences in keeping with each journal's style. Either citation can be used when citing this article.

compared with the control group. While no significant difference was noted between the p.o. administration and the intralesional injection groups, the reduction rate tended to be larger in the local injection group, and local injection was concluded to be slightly superior.[216]

There were reports[217,218] of case series with more than 1000 subjects, but the findings were not statistically analyzed. Although both intralesional injection and p.o. administration were effective, there was also a mixed group of intralesional injection and p.o. administration, the condition of patients varied among the three groups (intralesional injection, p.o. administration, mixed), and the effectiveness according to the administration method was not shown. Regarding complications, systemic symptoms, such as hypertension, retarded bodyweight gains and cushingoid appearance, were reported to be more frequent on p.o. administration than intralesional injection.[217,218] Moreover, concerning complications, in one report,[219] periocular lesions were excluded from the targets of intralesional injection to avoid its effect on visual function. Indeed, there have also been case reports[220,221] that visual impairment was caused by occlusion of the retinal artery after intralesional corticosteroid injection for periocular hemangiomas. Currently, in Japan, intralesional corticosteroid injection is a treatment unapproved by the national health insurance system.

CQ17: Is topical therapy effective for infantile hemangioma?

Recommendation: Although it must be noted that there are no reports of comparison with placebo and that the degree of improvement is smaller compared with systemically administrated drugs, topical medication can be an option for the treatment of infantile hemangioma with no risk of complications if drugs with milder adverse effects are selected.

Strength of recommendation: 2 (weak).

Evidence: C (weak).

Comments: As a result of published work searches, a total of 111 papers consisting of 70, seven and 34 papers from PubMed, Cochrane and JCRM, respectively, were extracted. They included one RCT study. Including this RCT, 48 papers were extracted by secondary screening. In addition to the papers selected by secondary screening as closely related to the CQ, a total of 47 papers obtained by manual search were adopted as reference for the preparation of guidelines. There was one RCT, and comparative studies of therapeutic results by topical therapy and case series studies with a relatively large number of subjects were adopted as papers of relatively high quality, the strength of evidence was rated as C (weak).

In the reports related to the CQ:

1. Drug type: The drugs were classified as imiquimod, timolol, propranolol, corticosteroid and others.[215,222–225]
2. Drug concentration and dosage form: Imiquimod was used as a 5% cream,[222,226–233] timolol as 0.5% ophthalmic solution or gel,[222,223,232,234–243] propranolol as 1% ointment,[181,234,241,244,245] and corticosteroid were often used as ointments of agents ranked as relatively strong such as clobetasol propionate, halobetasol propionate and betamethasone dipropionate.[246,247]
3. Methods for topical application: Frequent administration methods were once a day every other day for imiquimod, two times a day every day at 1–2 drops each time for timolol, two times a day every day for propranolol and two times a day every day for corticosteroid.
4. Methods for efficacy evaluation: Comparison of gross findings and photographs were adopted in all papers. The area was compared using photographs in one report.[227] There was also a report[228] of half-side test for a control.
5. Adverse effects: No systemic adverse effect was reported, and most adverse effects were local. Imiquimod caused pain, flare and erosion relatively frequently.[231,233] Few local adverse effects were reported for timolol and propranolol.[232,234,241,242,245] No local adverse effects were reported also by corticosteroid.[246,247]
6. Relative advantages of drugs: Imiquimod has been reported to have usefulness comparable with that of topical beta-blockers, but it is not considered superior in terms of adverse effects.[226,228,230,232]

Corticosteroid was not shown to be superior in efficacy compared with beta-blockers.

There was also one RCT study[181] concerning the CQ, which is related to topical propranolol concerning drugs. In this RCT, 15 each of a total of 45 subjects were allotted to oral (propranolol at 2 mg/kg per day, two times a day), topical (1% propranolol water soluble ointment, applied two times a day) and local injection (1 mg/1 mL, 0.2 mL/1 cm in diameter, 1 mL/injection at the maximum, one time a week) groups. Ten patients (66.7%) in the topical group responded, but they were fewer than 13 (86.7%) in the oral group. The time until the appearance of the effect and time until complete cure were also longer in the topical group than in the oral group. Concerning complications, none were observed in the topical group, but one patient in the oral group showed unexplained syncope as an adverse effect and was excluded. While decreases in the heart rate and blood pressure were observed in three in the oral group, they did not necessitate interruption of the study. In the local injection group, eight (53.3%) responded, but three were lost due to pain. From these results, the study concluded that topical therapy is an option to be evaluated for patients with a risk of adverse reactions to oral medication. While there were no reports of comparison under the same conditions, comparative studies of therapeutic results by topical therapy and case series studies with a relatively large number were adopted as relatively high-quality papers. In all these reports, topical therapy of beta-blockers (propranolol, timolol) was effective to an extent with no serious complications.

Thus, topical therapy, particularly of beta-blockers is considered generally useful, but there has not been a report of its comparison with placebo, and further accumulation of cases is necessary.

Research by comparison between dye laser treatment and topical beta-blocker therapy is considered to be necessary.

This article has been co-published with the permission of *The Journal of Dermatology, Pediatrics International* and *Japanese Journal of Radiology*. All rights reserved. © 2020 The Authors. The articles are identical except for minor stylistic and spelling differences in keeping with each journal's style. Either citation can be used when citing this article.

CQ18: Is compression therapy effective for infantile hemangioma?

Recommendation: Although an appropriate compression method must be performed for individual patients, compression therapy may be regarded as an option on condition that the therapy is carried out by a skilled physician. Sufficient attention to skin abnormalities and local/neighboring growth disturbance due to the compression are needed.

Strength of recommendation: 2 (weak).

Evidence: D (very weak).

Comments: While 23, one and 14 papers were extracted from PubMed, Cochrane and JCRM, respectively, only three case reports remained to be reviewed as a result of primary and secondary screening. Thus, the evidence level is very low at D (very weak).

According to a case report of ulcerated infantile hemangiomas of the limbs by Kaplan *et al.*,[248] the ulcers of most patients showed rapid improvements and cure within 2 weeks by compression therapy using the self-adherent wrap Coban® (3M, St. Paul, MN, USA) combined with topical treatment with an antibiotic ointment (or early systemic antibiotic administration when secondary infection was apparent). They concluded that, compared with antibiotic ointment alone, its combination with compression therapy was more effective, and is a safe and easy treatment that promotes regression of hemangiomas.

Ochi *et al.*[249] reported 12 cases of infantile hemangioma (nine girls and three boys with a mean age of 8.4 months; sites of the lesion were limbs in six, head and neck in five and trunk in one). By treatment using elastic bandages (five patients), Presnet® (ALCARE, Tokyo, Japan) (four), supporter (one), or Elatex® (ALCARE, Tokyo, Japan) and cryotherapy (two), the hemangiomas disappeared or decreased in size in 11 of the 12 patients, with only one (head and neck) showing no improvement. The time until the disappearance of the lesion in the 11 responders was 2 months to 3 years (mean, 19.5 months), no complications associated with compression therapy were noted, and the authors recommended early initiation of compression therapy if the site of the lesion can be compressed.

Totsuka *et al.*[250] treated three girls with parotid gland hemangiomas (mean age, 4.3 months) by splinting using a resin plate and compression using a handmade cap. The mean duration of treatment was 13 months (8–16 months), and the patients were followed up until a mean age of 4.6 years (2–7 years), resulting in clinical and echographic disappearance of hemangioma in all three. Because infantile hemangiomas often regress spontaneously, it is impossible to conclude that they regressed due to compression therapy, but they reported the therapy to be safe and effective.

Thus, concerning factors related to "benefits" of compression therapy, there are reports that suggest the effectiveness of compression methods appropriate for sites (elastic bandages, Presnet, splinting with a resin plate). However, it must be noted that they are all old reports. Concerning factors related to "harm", while compression is a relatively safe and simple method without reports of serious complications, the occurrence of dermatitis and growth disturbance at the site of compression or surrounding areas is considered possible. The recommendation level was set at 2D with consensus of the present guidelines preparation committee on condition that the treatment is performed carefully by a skilled physician in consideration of these points. The present guidelines do not exclude compression therapy, but it is necessary to consider oral propranolol, p.o. administration or local injection of steroid, and laser therapy first for infantile hemangiomas that need treatment.

CQ19: Is glucose transporter 1 (GLUT-1) immunostaining useful for the diagnosis of infantile hemangioma?

Recommendation: Immunostaining for GLUT-1 is positive in the proliferating, involuting and involuted phases, shows high sensitivity and specificity, and is useful for the diagnosis of infantile hemangiomas if the clinical diagnosis is difficult.

Strength of recommendation: 2 (weak).

Evidence: C (weak).

Comments: To evaluate whether GLUT-1 immunostaining is useful for the diagnosis of infantile hemangiomas, the published work was searched first for the following key words: infantile OR juvenile AND hemangioma AND marker AND immunohistochemistry.

The search of JCRM resulted in 26 hits, but none of them performed analysis of GLUT-1 or evaluated its usefulness by comparing infantile hemangioma with other hemangiomas/vascular malformations even if GLUT-1 was analyzed. The search of PubMed resulted in 182 hits. From these papers, those that deserved detailed analysis were selected according to the following criteria:

1. Those in which GLUT-1 immunostaining was performed for infantile hemangioma or other hemangiomas/vascular malformations.
2. Those that were retrospective epidemiological studies rather than reports of one case.

Fifteen research papers selected by these criteria were analyzed in detail.

In seven of these reports,[251–257] infantile hemangiomas were stained using GLUT-1 simultaneously with other hemangiomas/vascular malformations, and differences in positive/negative results were evaluated. Of all cases reported in the seven papers, GLUT-1 was positive in 268 of the 273 cases of infantile hemangioma and negative in 244 of the 247 cases of lesions other than infantile hemangioma. There were also four papers[258–261] in which GLUT-1 staining was performed for clinically typical infantile hemangiomas and hemangiomas that need to be differentiated from infantile hemangioma although they were not simultaneously stained in the same paper. When the four papers were combined, GLUT-1 was positive in all eight cases of infantile hemangioma and negative in all 49 cases of non-infantile hemangioma. When the above cases are totaled, GLUT-1 was positive in 276 of the 281 cases of infantile hemangioma and negative in 293 of the 296 cases of non-infantile hemangioma, and the sensitivity and specificity of GLUT-1 positivity for infantile hemangioma were 98.2% and 99.0%, respectively.

The usefulness of GLUT-1 staining has also been confirmed by re-evaluation of cases that were initially examined

This article has been co-published with the permission of *The Journal of Dermatology, Pediatrics International* and *Japanese Journal of Radiology*. All rights reserved. © 2020 The Authors. The articles are identical except for minor stylistic and spelling differences in keeping with each journal's style. Either citation can be used when citing this article.

by hematoxylin–eosin (HE) staining alone.[262–265] There have been four papers in which cases were re-evaluated using GLUT-1 staining, and one paper reported that the diagnosis was impossible by HE staining alone in 18% of the cases.[262]

CQ20: What gastrointestinal examinations are useful for children suspected to have blue rubber bleb nevus syndrome? When should the examinations be started?

Recommendation: It is recommended to start screening by examinations including blood tests and fecal occult blood test as early as possible. In children suspected to have gastrointestinal bleeding, the usefulness of endoscopic examination, red blood cell scintigraphy (technetium-99*m* [^{99m}Tc]-labeled red blood cells), and single photon emission CT–CT (SPECT-CT) has been reported for the identification of the source of bleeding. If no abnormality is detected by screening, and search for gastrointestinal lesions needs to be performed to diagnose this disease or evaluate the future risk of bleeding, there is no standard for its timing. Among the examinations that led to the detection of gastrointestinal lesions in past reports, CT and MRI can be performed with relatively mild invasion and from an early stage.

Strength of recommendation: 2 (weak).

Evidence: D (very weak).

Comments: Gastrointestinal lesions of blue rubber bleb nevus syndrome (bean syndrome) are observed in the entire digestive tract, but they frequently appear, particularly in the small intestine. Because it is an extremely rare disease, the published work is primarily case reports and reviews, and there have been no reports of clinical studies of many cases that are relevant for the CQ. Therefore, we investigated examinations that were useful for the detection of gastrointestinal lesions in reports, primarily of child cases. Lesions in the small intestine are difficult to observe by conventional endoscopy, but techniques such as double-balloon endoscopy, capsule endoscopy, CT enterography, CT and MRI as well as upper and lower gastrointestinal endoscopy have been reported to be useful.[266–276]

As a result of database searching, 11 papers in English were adopted through primary and secondary screening. All papers selected by these screening processes were case reports or case series, and the strength of evidence is D (very weak).

There is no clear standard as to when the examinations should be initiated. However, neonates who developed gastrointestinal bleeding shortly after birth have been reported,[270] and the earliest possible examinations are necessary if this disease is suspected. Invasive examinations are difficult to perform in small children, but blood tests (presence or absence of anemia or consumption coagulopathy) and fecal occult blood tests can be performed. If gastrointestinal bleeding is suspected, procedures such as endoscopy, particularly double-balloon endoscopy and capsule endoscopy, ^{99m}Tc-labeled red blood cell scintigraphy and ^{99m}Tc-labeled red blood cell SPECT-CT have been reported to be useful for the determination of the source of bleeding.[266,268,271,275]

If no abnormality has been detected by screening tests, and if a search for gastrointestinal lesions needs to be performed non-emergently to diagnose this disease or evaluate the future risk of bleeding, there is no standard for the timing, which may vary among facilities. Among the above examinations, CT and MRI can be performed earlier and with relatively milder invasion, and are worth attempting if this disease is suspected. The necessity of the other examinations for the gastrointestinal lesions mentioned above should be considered when the patient reaches the age that tolerates the examinations.

CQ21: How are limb overgrowths to be managed in vascular malformations and syndromes?

Recommendation: If leg-length inequality is insignificant, shoe lift is recommended. As significant inequality causes gait disturbance complicated with scoliosis, surgical treatment aimed to arrest epiphyseal growth is performed in the growth period. Shortening of the femur or tibia may be performed as an additional treatment. Bone elongation of the intact side is considered effective for the correction of leg-length inequality.

Strength of recommendation: 2 (weak).

Evidence: D (very weak).

Comments: As a result of published work searches, 40 papers in English and four papers in Japanese were retrieved by primary screening. Of these papers, 17 in English and four in Japanese were extracted by secondary screening. As for the control of overgrowth of limbs, measures against leg-length inequality and soft tissue hypertrophy are separately discussed and regarded as effective, but these papers were all classified either as case reports or as general discussions. Therefore, the evidence level is rated as “very weak”, and the recommendation level as “weak”.

In vascular malformations, typical disorders with hypertrophy of the affected limbs are Klippel–Trenaunay syndrome and Parkes Weber syndrome, and most of the papers refer to the management of limb overgrowth due to vascular malformations were written about these disorders. The published work regarding lesions at different sites is commented on below.

Lower limbs: In most reports, treatment for the overgrowth of the lower limbs were aimed to prevent physical disorders caused by leg-length inequality. Some reports particularly mentioned treatment for foot lesions.

1. Correction of leg-length inequality

If the leg-length inequality is less than 2 cm, the management of leg length difference and accompanying scoliosis is considered possible by the use of shoe lift.[277–281] If the leg-length inequality is 2 cm or more, significant gait disturbance, postural abnormalities and compensatory changes in the contralateral limb are likely to develop, and before consequent unphysiological gait leads to irreversible impairment, surgical treatment to correct the leg-length inequality should be considered.[277–281] Long-leg radiography is useful for determining the best time for surgery,[282] and the measurement of the leg length by long-leg radiography or CT is reported to be effective.[278] Surgical treatment reported in the papers are as follows:

This article has been co-published with the permission of *The Journal of Dermatology, Pediatrics International* and *Japanese Journal of Radiology*. All rights reserved. © 2020 The Authors. The articles are identical except for minor stylistic and spelling differences in keeping with each journal’s style. Either citation can be used when citing this article.

Treatment for overgrown limbs affected by vascular malformations: Jacob *et al.*[277] performed epiphysiodesis in 41 patients with a leg-length inequality of 2 cm or more among 252 patients with Klippel–Trenaunay syndrome and reported improvement in more than 90% of the patients. The effectiveness of this surgery is also confirmed by other review articles.[277–281] The effectiveness of shortening of the femur and tibia was reported in the review by Capraro *et al.*[278] The fixation period is considered to be shortened as a whole by simultaneously performing femoral or tibial shortening in addition to epiphysiodesis. Redondo *et al.*[280] recommended endoscopic growth control of the epiphyseal plate in the distal end of the femur for patients with a leg-length inequality of 2 cm or more. Capraro *et al.*[278] did not recommend growth control with the epiphyseal stapling because of the unpredictability of the results and high frequency of complications. The appropriate time for surgical intervention on affected limbs is reported to be around the age of 11 years.[280]

Elongation of the intact leg: Tanaka *et al.*[283] performed bone elongation of the intact limbs using an external fixator in adult patients with mild structural scoliosis and reported that the procedure was effective for correcting the leg-length inequality and scoliosis. Jacob *et al.*[277] also recommended bone elongation of the intact limb using Ilizarov external fixation apparatus in their review.

Popliteal vein ligation: Servelle[284] hypothesized that elongation of the affected limbs was due to a high venous pressure and performed ligation of the popliteal vein of the intact limb in 48 children, and they reported significant improvement in leg-length inequality. However, there are also negative views, saying its effectiveness is uncertain.[278]

2. Foot lesions

Redondo *et al.*[280] recommended resection of the toes (ray resection) and debulking for wearing shoes and cosmetic improvement. Gates *et al.*[285] notably reported that compared with ray resection, wound healing of the stumps was poor after major resection.

Upper limbs: Asymmetry due to hypertrophy of the upper limb less frequently causes impairment of activities of daily living than that of the lower limb. In one article, resection in patients with functional impairment due to marked finger deformities is reported,[282] but articles reporting treatment for upper limb overgrowth are very few. While debulking has been reported to be advantageous from the cosmetic viewpoint,[279] it has also been reported to induce or exacerbate edema of the affected limb,[284] causing complications including cicatricial contracture, recurrence of the lesion and refractory ulcer,[278] and sufficient caution is necessary.

CQ22: Is surgical resection effective for soft tissue/superficial LM?

Recommendation: Although surgical resection is an effective treatment, it should be performed after comprehensive evaluation of cosmetic aspects, prognosis, functional prognosis, resectability and possibility of recurrence/complications.

Strength of recommendation: 2 (weak).

Evidence: D (very weak).

Comments:

Process of preparation of recommendation

Surgical resection is one of the major treatment options performed for LM. Although LM can be cured by total resection, the objective of treatment is not necessarily total resection, because the disease is not malignant, and surgical resection is often carried out for cosmetic, functional and symptomatic improvements. Cosmetic problems are considered to be particularly serious if the lesion is located in superficial areas such as the body surface and soft tissue. However, surgical resection has been known to cause complications including hemorrhage, infection, deformation and nerve paralysis.

In evaluating whether resection is effective, the balance between its positive aspects and negative aspects, such as complications, is important. For soft tissue/superficial LM, in which cosmetic improvement is important, problems including in what situations resection can be performed, whether there are criteria for the selection of resection and, as there are differences in the incidence of complications, cure rate and recurrence rate depending on the circumstances, whether its indications should be evaluated under different conditions are unclear. Therefore, the CQ, "Is surgical resection effective for soft tissue/superficial LM effective?", was formulated, and the current knowledge was summarized.

Published work search and screening

As a result of the published work search, 105 papers in Japanese and 348 papers in English were subjected to primary screening. Of these papers, five in Japanese and 42 in English were subjected to secondary screening concerning this CQ. They did not include papers with a high level of evidence, such as an SR and RCT, and all of them were case series or case reports. As a result, in the evaluation of this CQ, the results and discussion in each case series were integrated.

Review of observational studies (case series)

The effectiveness of resection of LM was evaluated from the following five viewpoints: (i) effectiveness regarding the prognosis (mortality); (ii) resection rate of the lesions (resectability); (iii) functional outcome after resection (function); (iv) recurrence rate (recurrence); and (v) complications.

Results of review: Generally, the rate of successful surgical resection is high, and 90% or more resection is reported to be possible in 60% or more of the patients.[286–288] This also applies to the head and neck region, which is the frequent site of the lesion.[286] However, the percentage of resectable lesions decreases from the cystic to mixed and to cavernous type.[286] Because many LM are distributed diffusely in the skin and subcutaneous adipose tissue and around structures including muscles, blood vessels and nerves, resection of the lesion involves resection of normal tissues in varying degrees. In lesions that show complicated distribution in the head and neck region, complications after surgical resection are observed relatively frequently. Serious complications including nerve paralysis, hematoma, local necrosis, sepsis, deformation, salivary fistula, hoarseness, airway obstruction and malocclusion have been reported,[286,287,289–297] and facial nerve

This article has been co-published with the permission of *The Journal of Dermatology, Pediatrics International* and *Japanese Journal of Radiology*. All rights reserved. © 2020 The Authors. The articles are identical except for minor stylistic and spelling differences in keeping with each journal's style. Either citation can be used when citing this article.

paralysis is likely to result from resection, particularly of LM infiltrating the parotid region.[289] By the site, the incidence of complications increases as the area of involvement widens from unilateral to bilateral, from below to above the lingual bone, both sides, and both above and below the lingual bone.[293,296] Postoperative death may occur in patients with a severe neck lesion, but the extent of the effect of surgical resection is unclear.[287,288,298] Postoperative recurrence is closely related to the resectability of the lesion depending on its distribution, and lesions that are difficult to resect due to a wide area of involvement and a strong tendency of infiltration have been reported to be associated with recurrence.[296]

Limitations: Indications for surgical resection vary among papers, and differences in the patient background must be considered in the evaluation of the effectiveness of resection. While there were many reports that surgical resection was performed in combination with sclerotherapy, and resection is considered to have been performed when more favorable results were expected from resection rather than sclerotherapy, criteria for their selection are unclear. Therefore, there is certainly the large bias of individual variation in the circumstances, and it was clearly impossible to conclude that resection is uniformly effective.

SUMMARY

While the effectiveness of surgical resection for soft tissue/superficial LM was evaluated, there was no published work with a high level of evidence. One of the major reasons is the diversity of the lesion type (cystic or cavernous), area of involvement and history of other treatments. Because of this diversity, the condition of patients is considered to show an extremely wide variation, and their generalization is impossible. However, if conditions, such as the type of the lesion (cystic or cavernous), site of origin and relationship with other treatments are restricted, tendencies were observed in functional prognosis, recurrence rate, and contents and incidence of complications.

While the resection rate of lesions by surgical treatment was suggested to be generally high, selection criteria for resection were unclear. Therefore, it is speculated that resection was performed for patients clinically judged to be treated more effectively by surgery. However, because there were some serious complications of surgical resection that persist as sequelae, their possibility should be evaluated carefully in performing surgical resection. The risk of resection has been suggested to vary with conditions of the lesion. The functional outcome is poor, and the recurrence rate and incidence of complications after resection are high, in those that occupy a wide area and those that are accompanied by symptoms such as airway obstruction.

From these observations, we propose at present, "While surgical resection is often effective, it must be selected in consideration of cosmetic aspects, prognosis, functional prognosis, resectability, and possibility of recurrence and complications", despite limited scientific grounds. If complete resection of the lesion is possible, surgical resection may be performed as the first-line treatment, but the possibility of other treatments including sclerotherapy in particular, should be evaluated according to the diverse conditions of individual patients, and surgical resection should be performed when other treatments are ineffective or when surgical resection is considered clearly superior.

CQ23: What is the optimal timing of surgery for soft tissue/superficial LM?

Recommendation: It is impossible to recommend optimal timing of surgery, and judgments according to the condition of each case are necessary.

Strength of recommendation: 2 (weak).

Evidence: D (very weak).

Comments:

Process of preparation of recommendation

Soft tissue/superficial LM are not malignant lesions. Emergent treatment may be necessitated by life-threatening symptoms, such as airway obstruction, but the initiation of treatment immediately after the diagnosis is generally considered unnecessary. The natural course of the disease differs considerably among individuals, particularly in infancy, and the lesions may show a tendency of spontaneous regression but may also cause various functional problems due to rapid enlargement. Moreover, there are cosmetic problems characteristic of this disease in addition to functional problems, and early therapeutic effects are necessary to make social life comfortable. For these reasons, the selection of optimal timing of treatment, surgery in particular, is a major issue.

For the selection of the timing of surgical resection, conditions to obtain the best results as well as indications for resection must be evaluated, and sufficient consideration of the balance between merits and demerits depending on the timing of resection is necessary. Therefore, in this CQ, we attempted to summarize the presently available knowledge about "What is the optimal timing of surgery for soft tissue/superficial lesions?".

Published work search and screening

As a result of a published work search, 67 papers in Japanese and 231 papers in English were subjected to primary screening. Of these papers, five in Japanese and 42 in English were subjected to secondary screening for this CQ. They included none with a high level of evidence, such as an SR and RCT, and all papers were case series or case reports. Therefore, the results and discussion in each case series were integrated in the evaluation of this CQ.

Review of observational studies (case series)

Defining "the optimal timing of surgery" mentioned in the CQ as "the timing of surgery at which good results can be obtained", we aimed to evaluate the timing of surgery at which resection is effective, problems, such as complications are few, and namely "the best results" can be obtained as a whole. Conditions must be evaluated on the basis of the timing in addition to the effectiveness of surgery, but objective judgments were considered difficult in this evaluation. However, as it was considered possible to obtain information about the age and time of surgery from the published work reviewed in the

This article has been co-published with the permission of *The Journal of Dermatology, Pediatrics International* and *Japanese Journal of Radiology*. All rights reserved. © 2020 The Authors. The articles are identical except for minor stylistic and spelling differences in keeping with each journal's style. Either citation can be used when citing this article.

previous CQ concerning the effectiveness, papers that evaluated the age at surgery were searched.

Results of review: Despite a careful review of the published work by secondary screening, there was no paper that analyzed cases from the viewpoint of optimal timing of surgery. There was information concerning the age at surgery, but its appropriateness was not evaluated. Papers that mentioned the timing of surgery are shown below.

Concerning the timing (age) of surgery, unless the size of the lesion is small or there are symptoms that require urgent treatment, such as respiratory disturbance, it is recommended to delay surgery until the age of 3 years by expecting spontaneous regression or for the ease of identification of surrounding structures during surgery, ease of control of bleeding and less problems with postoperative management.[294] There was also a paper[295] that suggested the necessity of the determination of the time of surgery in consideration of problems that change with age including the priority of securing the airway and appropriate nutritional management in neonates with head and neck and giant lesions, control of hemorrhage and infection and measures to prevent dysarthria and dental problems in infants, and skeletal and cosmetic problems in school-age children, although it did not mention the optimal timing of surgery.

However, there was no paper that positively recommended resection without considering the time after the diagnosis or grounds for such a recommendation.

SUMMARY

As a result of the published work search for evaluating the CQ, "What is the optimal timing of surgery for soft tissue/superficial LM?", there were papers that mentioned the timing of surgery, but none of them objectively evaluated its appropriateness. Therefore, no suggestion about the appropriate timing of surgery was obtained from the published work available at present, but there were a few papers suggesting that the decision to perform surgery should be made carefully.

Similar to the previous CQ, soft tissue/superficial LM of which the background vary in individual cases, and it is difficult to uniformly evaluate the effectiveness of resection. In clinical practice, in addition to medical reasons, social reasons including school attendance are considered to largely influence the decision of the time of resection. The results of RCT are necessary to obtain objective data, but it is practically very difficult to arrange an RCT fulfilling the above conditions.

While this CQ is a very important issue for patients and families as well as clinicians, there has not been objective evaluation of the optimal timing of surgery in the past. Presently, as quick decisions to perform surgery should be avoided, this guideline proposes, "The optimal timing of surgery cannot be decided in general, and judgments according to the condition of each case are necessary".

CQ24: Is sclerotherapy effective for facial microcystic LM?

Recommendation: A wide range of drugs are used for sclerotherapy. Although comparison among drugs has not been made, and consensus regarding the methods or frequency of their administration has not been reached, improvements are observed after sclerotherapy in various symptomatic, functional and cosmetic (esthetic) aspects. However, complications including functional impairment have also been reported.

Strength of recommendation: 2 (weak).

Evidence: D (very weak).

Comments:

Process of preparation of recommendation

Published work search and screening

Concerning this CQ, 35 papers in Japanese and 92 papers in English (60 from PubMed, 32 from Cochrane) were retrieved. After their primary screening, six in Japanese and 18 in English were subjected to secondary screening concerning this CQ. Although they included three RCT, many of the other papers were case series or case reports. Therefore, in the evaluation of the draft recommendation concerning this CQ, the results and discussion in each RCT and case series were integrated. While the evidence is scarce, the papers judged to be useful for the preparation of the draft recommendation are presented as review data.

Review of case series

As a result of published work screening, it was found that the effectiveness of sclerotherapy for facial microcystic LM has been evaluated from the following viewpoints:

1. Treatment responses
   a. Size
   b. Symptoms
   c. Functions
   d. Cosmetics
2. Complications

The contents of the accounts concerning the effectiveness of sclerotherapy are summarized according to these viewpoints.

However, there were few reports that exclusively analyzed facial (and microcystic) LM, and lesions of the neck and other regions as well as the face were evaluated or different types of LM, such as cystic and mixed types, were reported together. In addition, the definition of the cavernous type and standard procedure of sclerotherapy (method and number of administrations) varied among reports, and these differences in background should be considered in the evaluation of the effectiveness of sclerotherapy.

The sclerosing agents used for the published work search ranged widely from OK-432, bleomycin, ethanol, doxycycline to STS. However, as none of the papers reviewed for the preparation of these guidelines evaluated differences in the effectiveness for facial microcystic lesions among drugs or the method or number of administrations of each drug, these evaluation items were excluded in discussing this CQ.

1. Responses

A. Size: Many of the papers that referred to the regression rate of the lesion classified the responses into (i) excellent or complete (regression rate ≥90%); (ii) good or substantial (regression rate

This article has been co-published with the permission of *The Journal of Dermatology, Pediatrics International* and *Japanese Journal of Radiology*. All rights reserved. © 2020 The Authors. The articles are identical except for minor stylistic and spelling differences in keeping with each journal's style. Either citation can be used when citing this article.

≥50% and <90%); (iii) fair or intermediate (regression rate ≥20% and <50%); and (iv) poor or none (regression rate <20%).

Although there was no paper that collected cases of facial lesions alone, Yang *et al.*[299] reported that the regression rate after sclerotherapy was 90% or more in 19 (63%) of the 30 patients with head and neck lesions and 50% or more in 10 (33%). In addition, the regression rate was reported to be 50% or more in 18 (85.7%) of the 21 patients with head and neck lesions by Alomari *et al.*,[300] and in 30 of the 31 patients to be 50% or more, who included those with mixed type lesions, by Chaudry *et al.*[301]

Smith *et al.*[302] reported that none showed a response (complete or substantial) in 17 patients who underwent sclerotherapy, some of whom had mediastinal lesions. Giguere *et al.*[303] also reported that all five patients with head and neck lesions showed no response (poor) to the therapy. While these studies were RCT evaluating the time of sclerotherapy, the results suggest that sclerotherapy is not effective for microcystic lesions regardless of the time of treatment.

There was no paper that compared sclerotherapy and resection for facial microcystic LM.

B. Symptoms: There is no published work that evaluated this item based on objective data, and few reports referred to symptoms themselves. The information was limited to the report by Chaudry *et al.*[301] that symptoms disappeared after sclerotherapy using bleomycin in 75% of the patients who complained of pain and a few case reports[304,305] that symptoms, such as hemorrhage and respiratory impairment, were relieved after sclerotherapy.

C. Functions: Ravindranathan *et al.*[306] performed sclerotherapy in three patients with diffuse microcystic lesions extending from the face to the tongue and pharynx and reported that respiratory impairment and swallowing disorder due to airway obstruction observed before treatment were mitigated. Poonyathalang *et al.*[307] administrated STS to a patient with orbital lesions primarily complaining of visual defect and reduced visual acuity due to retrobulbar hemorrhage and reported alleviation of the symptoms, but relevant published work similar to that concerning symptoms was scarce.

D. Cosmetic aspects: Cosmetic improvements are difficult to evaluate objectively. Poonyathalang *et al.*[307] administrated STS to three patients with orbital lesions with exophthalmos as the primary symptom and reported improvement by measuring the degree of protrusion before and after the treatment. There have also been reports of objective assessment based on the degree of satisfaction in the patients' families. According to Chaudry *et al.*,[301] all patients with head and neck lesions (nine with microcystic lesions, 22 with mixed lesions) and their families reported improvements in the size and appearance of the lesions. In addition, Alomari *et al.*[300] treated 32 patients with mostly microcystic but including some cystic LM of the head and neck region by sclerotherapy and reported improvements compared with the condition before treatment by the families of 26 patients (81.3%).

2. Complications

As complications in the facial region, there are a large number of reports[299,301,307–312] of transient complications associated with sclerotherapy, such as fever, local swelling and pain, intracystic hemorrhage and infection, although the lesions were poorly characterized in some reports. In addition, complications considered to have been caused by the effect of treatment, such as ulcer of the oral mucosa and tongue, facial nerve paralysis, leakage of saliva and respiratory insufficiency due to airway obstruction, have been occasionally reported.[303,306,307] There have also been reports[307,313,314] of an elevation of the intraorbital pressure, exophthalmos, intraorbital hemorrhage, corneal damage and external ocular muscle paralysis due to enlargement of the mass after sclerotherapy for ocular LM. There was also no published work showing the incidence of complications in facial microcystic LM.

As complications caused by sclerosing agents, skin ulcer and necrosis and nerve damage due to ethanol leakage, hypotension during anhydrous ethanol injection and epidermal detachment due to doxycycline have been reported.[300,315] However, there was no report of serious complications due to OK-432. Pulmonary fibrosis is widely known to be a complication of bleomycin, but, according to Chaudry *et al.*[301] and Yang *et al.*,[299] impairment of respiratory function does not occur at a dose routinely employed for sclerotherapy.

SUMMARY

In evaluating the CQ, "Is sclerotherapy effective for facial microcystic LM?", analysis was performed from the viewpoints of responses to the treatment in terms of symptoms, functions and cosmetic (esthetic) aspects and complications, but few papers with a high level of evidence were found. While the degree of regression of the lesions by sclerotherapy varied widely, the size-reducing effect of the therapy was consistently small unlike that in cystic lesions. Some papers referred to symptoms, functional outcome and cosmetic improvement, but they were insufficient for general discussion of sclerotherapy for facial microcystic LM. As complications characteristic of sclerotherapy, serious impairment may be caused by leakage of the sclerosing agent (ethanol in particular), and this point needs attention. Based on the above observations, it is difficult at present to evaluate indications for sclerotherapy against microcystic LM by formulating criteria. Therefore, for the future, it is considered necessary to evaluate the usefulness of sclerotherapy addressed by this CQ by designs such as RCT.

CQ25: Is sclerotherapy effective for intra-abdominal LM?

Recommendation: Although there are many reports that sclerotherapy is useful, there is the risk of complications, and careful judgments about matters including the resectability of the lesion and selection of the sclerosing agent are necessary.

Strength of recommendation: 2 (weak).

Evidence: D (very weak).

Comments:

Process of preparation of recommendation

Lymphangioma is the most frequent lymphatic vessel disorder of the abdomen. Intra-abdominal lesions are estimated to

This article has been co-published with the permission of *The Journal of Dermatology, Pediatrics International* and *Japanese Journal of Radiology*. All rights reserved. © 2020 The Authors. The articles are identical except for minor stylistic and spelling differences in keeping with each journal's style. Either citation can be used when citing this article.

account for 10–20% of all LM, and the selection of treatment is difficult depending on the site of the lesion. While surgical resection is expected to be effective, less invasive treatments are considered necessary in view of stress to the patient and the possibility of severe complications such as lymphatic fluid leakage and bowel obstruction. Sclerotherapy, which is a major treatment for LM, is considered to be less invasive than surgery. Although positive therapeutic effects are expected, sclerotherapy is known to induce marked inflammation. Whether it can be performed safely without negative effects including complications and its long-term effects are major clinical concerns. In addition, what therapeutic effects are expected or what complications should be anticipated after sclerotherapy for the intra-abdominal lesion is also unclear. Therefore, the CQ, "Is sclerotherapy effective for intra-abdominal LM?", was formulated, and knowledge available at present was compiled.

Published work search and screening

As a result of the published work search, 19 papers in Japanese and 38 papers in English (32 from PubMed, six from Cochrane) were subjected to primary screening. Of these papers, two in Japanese and nine in English were subjected to secondary screening concerning this CQ. They included no papers with a high level of evidence, such as SR and RCT, and all were case series or case reports. Consequently, the results and discussion in each case series were integrated in the evaluation of this CQ.

Review of observational studies (case series)

The published work concerning the effectiveness of sclerotherapy for intra-abdominal LM was reviewed from the viewpoints of: (i) therapeutic effects (decrease in lesion size, symptoms); and (ii) complications.

The drugs used for sclerotherapy ranged widely from OK-432 to bleomycin, ethanol, doxycycline, STS, acetic acid, steroid/tetracycline and 50% glucose solution. According to our review, there was no paper that evaluated the differences in effectiveness of sclerotherapy in the abdomen according to the drug type or administration method or number of administrations of each drug.

Results of review:

1. Therapeutic effects

A. Regression rate of the lesion: Regression of lesions of intra-abdominal LM by sclerotherapy was mentioned in five papers.[288,316–319] According to the report by Chaudry *et al.*,[316] the reduction rate was 90% or more in seven and 20% or more in one of the 10 patients with LM of the mesentery and retroperitoneum treated with doxycycline, and evaluation using imaging examination was not performed in two cases. The patient who showed a low regression rate had a mixed type of cystic and cavernous lymphangiomas, and the other patients had cystic lesions. Oliveira *et al.*[317] reported that the lesion regressed by 70% in one of the two patients with cystic lymphangiomas treated with OK-432. Won *et al.*[318] reported one patient who showed complete disappearance of cystic retroperitoneal lesions after sclerotherapy using acetic acid. Shiels *et al.*[319] reported that cystic lesions responded to sclerotherapy using STS and ethanol in two patients, but there was no mention of the reduction rate. However, according to Alqahtani *et al.*,[288] no effect was observed in 10 patients who underwent sclerotherapy using steroid/tetracycline or 50% glucose solution.

B. Symptoms: There were three papers that referred to symptoms of patients treated by sclerotherapy for intra-abdominal LM.[316,317]

According to Chaudry *et al.*,[316] of the 10 patients who underwent sclerotherapy, three had chronic abdominal pain, three had acute abdominal pain, one had fever/chill, one had anemia and two had palpable masses, but the symptoms were alleviated by treatment in all patients, and no recurrence was noted.

Oliveira *et al.*[317] reported that sclerotherapy was performed in a patient with a palpable mass and in one with a palpable mass, abdominal compartment syndrome and a poor general condition. While the condition was alleviated in the patient who only showed a palpable mass after two courses of OK-432 sclerotherapy, the treatment was changed to surgery in the patient who had abdominal compartment syndrome because of enlargement of the mass due to intracystic hemorrhage.

2. Complications

Three papers specifically mentioned complications of sclerotherapy for intra-abdominal LM. There was no report of deaths due to treatment-related complications. Oliveira *et al.*[317] treated three patients by sclerotherapy using OK-432 and reported that one of them developed sub-bowel obstruction after the treatment and another required emergency surgery due to exacerbation of abdominal compartment syndrome induced by intracystic hemorrhage. Chaudry *et al.*[316] reported that doxycycline used for sclerotherapy leaked into the retroperitoneal space in one of the 10 patients but that the lesion regressed without any particular problem. Won *et al.*[318] performed sclerotherapy using acetic acid in one patient with retroperitoneal cystic lymphangioma. Although pain and hematuria were observed, they concluded that the relationship of hematuria with the therapy was unclear, because it was observed during menstruation.

Limitations: Sclerotherapy was often performed before, after or during surgical resection, and papers that reported the results of sclerotherapy alone were few. There was no paper that directly compared observation without treatment, sclerotherapy and surgical resection. Few papers analyzed intra-abdominal lesions alone, and many papers included lesions in other areas or evaluated lesions in different intra-abdominal regions including the mesentery, retroperitoneum and viscera collectively.

Moreover, differences in properties of LM, such as cystic, cavernous and mixed types, their definitions, criteria for the selection of sclerotherapy (combination with surgery, types of sclerosing agents and methods of their use, number of administrations) varied among papers, and few papers evaluated these matters separately.

This article has been co-published with the permission of *The Journal of Dermatology, Pediatrics International* and *Japanese Journal of Radiology*. All rights reserved. © 2020 The Authors. The articles are identical except for minor stylistic and spelling differences in keeping with each journal's style. Either citation can be used when citing this article.

Such differences in the patient background and contents of treatment must be considered in evaluating the effectiveness of sclerotherapy. In evaluating this CQ, particularly differences in morphology of LM and sclerosing agents were excluded.

SUMMARY

The CQ, "Is sclerotherapy effective for intra-abdominal LM?" was evaluated from the viewpoints of therapeutic effect, symptoms/functions and complications, but no paper with a high level of evidence was found. While sufficient regression of the lesion and alleviation of symptoms were achieved by sclerotherapy in some patients, the response rate varied among reports, and information was insufficient for general discussion of sclerotherapy. Concerning treatment-related complications, there have been reports of bowel obstruction associated with sclerotherapy, and attention to this condition as well as intracystic hemorrhage is considered necessary. However, there was no report of chylorrhea, which was reportedly caused by surgery.

Based on the above observations, it is presently difficult to determine indications for sclerotherapy in intra-abdominal LM by setting up criteria, but as there was no published work that strongly ruled out intra-abdominal LM as indications of sclerotherapy, these guidelines propose, "Although there are many reports that sclerotherapy is useful, there is the risk of complications, and careful judgments about matters including the resectability of the lesion and selection of the sclerosing agent are necessary". For the future evaluation of this CQ, validation by a design with a high level of evidence, such as RCT, is considered necessary.

CQ26: Are patients with scarcely symptomatic intra-abdominal LM candidates for treatment?

Recommendation: Because there is risk of treatment-related complications, it is proposed to consider therapeutic intervention when the lesion tends to enlarge or has become symptomatic.

Strength of recommendation: 2 (weak).

Evidence: D (very weak).

Comments:

Process of preparation of recommendation

Intra-abdominal LM occasionally presents with severe symptoms, such as abdominal pain, giant mass and bowel obstruction, but may also be asymptomatic and detected incidentally. Lesions may gradually enlarge and cause serious symptoms due to infection and intraluminal hemorrhage.

Under such circumstances, whether patients with nearly asymptomatic intra-abdominal LM should be aggressively treated, or when intervention should be optimally performed during their long follow-up period, are major problems that pose a clinical dilemma. Therefore, the CQ, "Are patients with scarcely symptomatic intra-abdominal LM candidates for treatment?", was formulated, and knowledge available at present was summarized.

Published work search and screening

As a result of the published work search, 206 papers in Japanese and 237 papers in English (230 from PubMed, seven from Cochrane) were subjected to primary screening. Of these papers, six in Japanese and nine in English were subjected to secondary screening concerning CQ26. They included no papers with a high level of evidence, such as an SR or RCT, and many of them were case series or case reports. Because seven papers among them described asymptomatic LM, their results and discussions were integrated to answer the CQ.

Review of observational studies (case series)

Seven papers[316,317,320–324] among reviewed published work described asymptomatic LM. Fifteen cases reported in these papers were considered to have actually presented few symptoms (including asymptomatic patients who were incidentally detected by imaging studies to have intra-abdominal masses at the sites as greater omentum, mesentery and retroperitoneum).

The published work was screened, and papers addressing issues concerning therapeutic intervention for scarcely symptomatic intra-abdominal LM including, "What symptoms they may present with if they are left untreated?", "By what studies and how often should they be examined?" and "What other treatments are available and how serious are complications or risk of each treatment?" were reviewed.

Results of review: From the published work reviewed, symptoms of intra-abdominal LM (abdominal pain, bowel obstruction, torsion, infection, hemorrhage, vomiting/sucking difficulty, frequent urination and abdominal mass)[320–326] are considered to be dependent on factors such as site, size and age. It is necessary to determine risk factors by stratification of these factors in the future.[320,322,325]

Reported complications in treated cases include recurrence that required re-treatment,[321] bowel obstruction,[317,323,324] chylous ascites,[324,326] embolism,[317] hemorrhage[317] and wound infection. Embolism of the inferior vena cava after surgery[317] and abdominal compartment syndrome after adhesion therapy[317] were reported as severe complications. It deserves special attention that, if surgical resection is performed for mesenteric LM, the intestine may have to be resected with the lesion.[326]

While there have been reports[320,322] that intra-abdominal LM with few clinical symptoms regressed during follow up, they may become symptomatic later (as observed in many case reports). For that reason, the opinion that intervention should not been chosen during the follow up until the lesion enlarges or new symptoms appear was frequently described.

Limitations: It should be noted that many asymptomatic cases may be left unreported and some asymptomatic lesions that had been detected were treated. There is no study with a high level of evidence indicating explicit criteria concerning the age, site or situation about whether intervention should be made for asymptomatic intra-abdominal LM.

SUMMARY

The necessity of treatment of a patient with intra-abdominal LM with few symptoms should be determined after evaluating the balance between the risk of treatment and non-treatment

This article has been co-published with the permission of *The Journal of Dermatology, Pediatrics International* and *Japanese Journal of Radiology*. All rights reserved. © 2020 The Authors. The articles are identical except for minor stylistic and spelling differences in keeping with each journal's style. Either citation can be used when citing this article.

considering its site and size as well as patient age. However, because research on indications for treatments has been insufficient so far and serious complications after treatment have been reported, deliberate evaluation for each patient is mandatory. When observation is selected, periodic imaging studies are recommended to optimize therapeutic intervention by detecting enlargement of the lesion. Also, if any symptom has developed during follow up, intervention should be considered. For these reasons, the recommendation, "Because there is risk of treatment-related complications, it is proposed to consider therapeutic intervention when the lesion tends to enlarge or has become symptomatic" was adopted.

CQ27: What treatments are effective for refractory chylous ascites?

Recommendation: Conservative treatments, such as fasting, high-calorie infusion and medium chain triglyceride (MCT), should be performed first, but, if they are ineffective, drug treatment, sclerotherapy and surgery may also be considered.

Strength of recommendation: 2 (weak).

Evidence: D (very weak).

Comments:

Process of preparation of recommendation

Refractory chylous ascites causes loss of large amounts of protein and lymphocytes, decreases in the blood lipid levels, and abdominal pain, unpleasantness and dyspnea due to abdominal distention and markedly reduces quality of life. The cause of ascites often remains unknown. Treatment of chylous ascites may require drainage to avoid abdominal distention. It is a very important point for clinicians to make proper judgments by understanding treatments and their effects and demerits. Therefore, it is considered beneficial to collect information about chylous ascites over a long period and compile guidelines. For this purpose, the presently available knowledge was collected by formulating the CQ, "What treatments are effective for refractory chylous ascites?".

Published work search and screening

As a result of the search, 161 papers in Japanese and 728 papers in English (564 from PubMed, 164 from Cochrane) were subjected to primary screening. Of these papers, 15 in Japanese and 12 in English were subjected to secondary screening for CQ27. They included none with a high level of evidence, such as SR and RCT, and consisted of one multicenter and two single-center case series and case reports. Consequently, we used the results and discussion of 27 papers judged for the preparation of the draft recommendation were integrated, although evidence was insufficient for the evaluation of this CQ.

Review of observational studies (case series)

As for causes of chylous ascites, congenital chylous ascites,[327–342] idiopathic chylous ascites,[328] chylous ascites after laparotomy,[343–346] protein-losing enteropathy,[345] LM,[347,348] lymphangiectasis,[349,350] lymphangiomatosis[351,352] and lymphatic dysplasia[353] were reported. None of the papers evaluated treatments according to the cause.

When treatments are categorized, conservative treatments (fasting, high-calorie infusion, MCT), drug treatments, sclerotherapy and surgical treatment were performed.

Results of review: The results of review are presented below according to the treatment.

1. Conservative treatments

Whether the amount of ascites changes by fasting should be checked first.

High-calorie infusion is often used with fasting, and because there was no report that ascites increased under the effect of high-calorie infusion according to our review, it is recommended for nutritional support during fasting. In the multicenter case series reported by Bellini *et al.*,[327] high-calorie infusion/total parenteral nutrition was performed in 15 patients without adverse effects.

Medium chain triglyceride was used before, after and during treatment.[327,328,330–335,337,339–341,343,345,346,348–352] In the multicenter case series by Bellini *et al.*,[327] MCT was reportedly performed in 14 patients without adverse effects.

2. Drug treatments

In drug therapy for chylous ascites, primarily octreotide (a long-acting somatostatin analog) was used, and no report that discussed the effectiveness of other drug therapies was found by the present published work search.

In the multicenter case series by Bellini *et al.*,[327] octreotide was administrated to six of the 16 patients with chylous ascites for 8–38 days, and a decrease in chylous ascites was reported in all of them. In the single-center case series by Huang *et al.*,[344] two of the four patients with chylous ascites treated by high-calorie infusion and octreotide administration were reported to have shown a decrease in ascites within 10 days. However, there has been a report[330] that no effect was observed despite the administration of octreotide for 3 weeks. Concerning the dose of octreotide, it was administrated at 1 μg/kg per h,[327] at 3 μg/kg per h,[332] began to be administrated at 0.5 μg/kg per h and increased to 10 μg/kg per h by 1 μg/kg per h,[329] administrated by continuous i.v. infusion at 0.5–2.0 μg/kg per h,[333] and began to be administrated by s.c. injection at 2.5 μg/kg two times a day and increased every 2 days to 8 μg/kg two times a day.[330] Regarding the time of the beginning of administration, the administration was started as no improvement was observed in chylous ascites after conservative treatments for 2 weeks,[330,334] and as chylous ascites was alleviated by conservative treatments but was exacerbated again.[333] No adverse effects of octreotide administration were noted in the present review of the published work. Thus, no control study that evaluated the effect of octreotide on chylous ascites was found by the present published work search, and the level of evidence concerning the efficacy is low, but as there are case series and many case reports that chylous ascites was reduced by octreotide administration, it appears reasonable to consider drug treatment using octreotide for chylous ascites that does not respond to conservative treatments.

3. Sclerotherapy

Sclerotherapy was performed in six patients in five case reports.[339,347,349,351,352] The sclerosing agent was OK-432 in

This article has been co-published with the permission of *The Journal of Dermatology, Pediatrics International* and *Japanese Journal of Radiology*. All rights reserved. © 2020 The Authors. The articles are identical except for minor stylistic and spelling differences in keeping with each journal's style. Either citation can be used when citing this article.

five of the six patients and was Beta-isodona® (Mundipharma GmbH, Cambridge, UK) solution in one.[349] OK-432 was locally injected into the lesion in four,[347,351,352] administrated i.p. in one[352] and administrated through the drain in two.[347,352] Concerning sclerotherapy, the number of reported cases that were reviewed was limited, and further accumulation of cases is considered necessary to establish its usefulness.

4. Abdominal drainage, abdominal puncture and surgical treatment

Abdominal drainage and abdominal puncture are performed when organ compression symptoms (compartment syndrome and respiratory insufficiency) due to abdominal distention are present or possible, or when the drain is inserted postoperatively. However, drainage itself cannot improve chylous ascites, and treatments, such as infusion, blood preparations and blood transfusion, are necessary to supplement the ascites lost due to drainage.[327,330–333,337–340,343,345–347,349,351,352]

Surgical treatment is reported to be frequently performed after conservative or drug treatments. According to the single-center case series by Zeidan *et al.*,[343] surgical treatment was performed in patients who responded poorly to conservative treatments for over a mean of 25.3 days. In other reports, surgical treatment was performed after conservative treatments for 1–3 months[328,329] and in patients with congenital chylous ascites 1–4 months after birth.[330,334,350] Because it is often impossible to identify the leakage site of chylous ascites,[330] there have been attempts to identify the leakage site by p.o. administration of a lipophilic dye (Sudan black, Sudan III) before operation.[328,329,336,343] When the leakage site can be identified, ligation, suturing, clipping and cauterization have been performed.[328,334,336,343,350] In addition to reports of the usefulness of techniques to stop leakage, such as applying or sprinkling fibrin glue at the leakage site of chylous ascites or over the surrounding retroperitoneum,[329,331,343,350] and applying a patch of oxidized cellulose/resorbable local hemostatic agent,[331,343] there have also been reports of peritoneovenous shunting[349,353] and peritoneoamniotic shunting for fetal cases.[338]

There was no large clinical study in the past published work. Therefore, although the level of evidence is low, we consider that surgical treatment is recommendable for chylous ascites that does not respond to conservative or drug treatments, because it has been performed in case series and case reports for chylous ascites that did not respond to conservative or drug treatments for over approximately 1 month. Although techniques to enhance the response rate of surgical treatment, such as identifying the leakage site by using a lipophilic dye and applying fibrin glue or a patch of oxidized cellulose/resorbable local hemostatic agent, have been attempted, there are only case series and case reports, and none of the papers retrieved by the present published work search evaluated their usefulness.

Limitations: There was no published work that defined refractory chylous ascites based on the duration of illness or treatment responses. Therefore, we extracted and summarized factors that were considered to contribute to clinical refractoriness, such as the duration of illness and treatment responses, in each paper related to the treatment for chylous ascites. Also, as the cause of chylous ascites varies widely, the therapeutic effect is expected to differ depending on the cause, but no paper that was reviewed evaluated treatments according to the cause. Therefore, in the present evaluation, the statements are limited to treatments and their effects regardless of the cause.

SUMMARY

It was difficult to comprehensively discuss treatments, because its cause varied widely, and treatments for various causes were performed. Therefore, treatments were classified into conservative treatments (fasting, high-calorie infusion, MCT), drug treatments (octreotide), sclerotherapy, abdominal drainage, abdominal puncture and surgical treatment, and the effects of each treatment were evaluated.

Treatments effective for refractory chylous ascites can be summarized as follows with the understanding that they may depend on the cause and that the level of evidence of the available reports concerning treatments and their effects is low. Conservative treatments, such as fasting, high-calorie infusion and MCT, should be performed first because of the rareness of adverse effects. In patients who respond insufficiently to conservative treatments, drug treatments using octreotide can be considered as there have been case series and many case reports. Concerning sclerotherapy, the number of reported cases is small, and further large clinical studies will be needed to confirm its usefulness. Abdominal paracentesis and surgical treatments may be considered for chylous ascites that does not response to conservative or drug treatments for approximately 1 month.

Thus, the draft recommendation is “Conservative treatments, such as fasting, high-calorie infusion and MCT, should be performed first, and, if they are ineffective, drug treatments, sclerotherapy and surgical treatments may be considered”. However, evaluation of this CQ by a design with a higher level of evidence, such as RCT, is considered necessary for the future.

CQ28: What kinds of complications are associated with treatments for intra-abdominal LM?

Recommendation: Complications associated with sclerotherapy for intra-abdominal LM include bowel obstruction, hemorrhage, pain, hematuria and chylous ascites. Surgical treatment of the disease can be associated with serious complications such as occlusion of the inferior vena cava and massive resection of the intestine as well as more common, wound infection, bowel obstruction, hemorrhage and chylous ascites.

Strength of recommendation: No recommendation.

Evidence: D (very weak).

Comments:

Process of preparation of recommendation

Patients with intra-abdominal LM are treated with various modalities from non-surgical therapy to surgical procedures.

This article has been co-published with the permission of *The Journal of Dermatology, Pediatrics International* and *Japanese Journal of Radiology*. All rights reserved. © 2020 The Authors. The articles are identical except for minor stylistic and spelling differences in keeping with each journal’s style. Either citation can be used when citing this article.

Treatment modality is selected depending on the patient's state. Therefore, it is necessary for the clinician, patient and family to share information concerning complications that may be associated with treatments for implementing them smoothly. However, there are no resources that give a clear answer to this problem, and both clinicians and patients may become disconcerted. Therefore, the CQ "What kinds of complications are associated with treatments for intra-abdominal LM?" was formulated, and information available at present was accumulated and integrated for the answer.

Published work search and screening

As a result of the published work search, 203 papers in Japanese and 602 papers in English (593 from PubMed, nine from Cochrane) were subjected to primary screening. Of these papers, 23 in Japanese and 27 in English were subjected to secondary screening concerning this CQ. They included no papers with a high level of evidence, such as SR or RCT, and all of them were case series or case reports. To answer CQ28, the results and discussion in each case series were integrated.

Review of observational studies (case series)

Complications in the CQ were evaluated by defining them as those encountered when patients with intra-abdominal LM were treated, and reports on sclerotherapy and surgery were reviewed.

Results of review:

1. Complications associated with sclerotherapy

Sclerotherapy using OK-432 was reported to be associated with bowel obstruction and hemorrhage for mesenteric LM,[317] and chylous ascites for retroperitoneal LM.[326] Sclerotherapy using acetic acid was reported to be associated with pain and hematuria in patients with retroperitoneal LM.[318]

2. Complications associated with surgical procedures

Complete resection of both mesenteric and retroperitoneal LM by laparotomy was reported to be associated with wound infection[324,354] and bowel obstruction[323,354,355] as common complications. There were reports of serious complications such as occlusion of the inferior vena cava[317] and massive resection of the intestine was necessary due to diffuse infiltration of the LM tissue to the intestinal wall.[356]

In a report about complications associated with complete laparoscopic resection of intra-abdominal LM by Tran *et al.*,[357] resection was attempted in 47 patients, and conversion to laparotomy was necessary in three (6.4%) due to tight adhesion in two and intraoperative hemorrhage in one.

Partial resection by laparotomy was reported to be associated with persistent ascites over a long period that was refractory to the treatment.[355]

Limitations: Patients with intra-abdominal LM are treated with various modalities including sclerotherapy and surgical procedures. Modalities were combined in many cases, and complications are often reported as those of entire treatment without more detailed information about those associated with individual treatment.

SUMMARY

For answering the CQ, "What kinds of complications are associated with treatments for intra-abdominal LM?", no published work with a high level of evidence was found, but foreseeable complications were listed from many case reports. Bowel obstruction, hemorrhage, pain, hematuria and chylous ascites were reported as complications of sclerotherapy. Serious conditions, such as occlusion of the inferior vena cava and massive resection of the intestine, as well as common complications, such as wound infection, bowel obstruction, hemorrhage and chylous ascites were reported as complications after surgical procedures.

Although the incidences and differences in complications in respect of the site and histological type are not shown in the published work, each patient with intra-abdominal LM should be treated with sufficient evaluation of the site, size and symptoms. In addition, treatment must be implemented with sufficient understanding of the possible complications.

Thus, we propose "Complications associated with sclerotherapy for intra-abdominal LM include bowel obstruction, hemorrhage, pain, hematuria and chylous ascites. Surgical treatment of the disease can be associated with serious complications such as occlusion of the inferior vena cava and massive resection of the intestine as well as more common, wound infection, bowel obstruction, hemorrhage and chylous ascites" as a recommendation draft.

CQ29: What treatments are effective for LM causing airway obstruction in the mediastinum?

Recommendation: Sclerotherapy is effective for macrocystic lesions, and surgical resection is effective for microcystic lesions. However, as the complication rate is relatively high, treatments should be selected according to the condition of each case.

Strength of recommendation: 2 (weak).

Evidence: D (very weak).

Comments:

Process of preparation of recommendation

Among LM, those that may cause airway obstruction due to their sites are life-threatening. Lesions in the mediastinum cause respiratory disorders if they physically compress the trachea or bronchi and obstruct the airway or markedly protrude into the thoracic cavity and narrow it.

In such situations, aggressive and effective treatment is necessary, but the therapeutic approach must be selected carefully in consideration of the relationship of the lesion with the important organs around it such as the large cardiac vessels, mediastinal nerve and thoracic duct. However, the judgment is often difficult in clinical settings.

Therefore, the CQ, "What treatments are effective for LM causing airway obstruction in the mediastinum?" was formulated, and the presently available knowledge concerning matters including the risk of complications and prognosis of treatments, such as surgical resection and sclerotherapy, was summarized.

This article has been co-published with the permission of *The Journal of Dermatology, Pediatrics International* and *Japanese Journal of Radiology*. All rights reserved. © 2020 The Authors. The articles are identical except for minor stylistic and spelling differences in keeping with each journal's style. Either citation can be used when citing this article.

Published work search and screening

As a result of the published work search, 134 papers in Japanese and 227 in English (226 from PubMed, one from Cochrane) were subjected to primary screening. Of these papers, five in Japanese and 16 in English were subjected to secondary screening concerning this CQ. Because they included none with a high level of evidence, such as an SR or RCT, and all were case series or case reports, the results and discussion in each case series were integrated.

Review of observational studies (case series)

By screening of the published work, the following approaches were found for the treatment of LM in the mediastinum.

Therapeutic options are surgical resection, puncture and drainage, sclerotherapy (OK-432, bleomycin, Ethiblock [Ethicon, Hamburg, Germany], anhydrous ethanol), drug treatments (Chinese herbal medicines such as *eppikajutsuto* and *ogikenchuto*) and no treatment. Of these approaches, surgical resection and sclerotherapy using OK-432 have been evaluated in a relatively large number of cases, and reports of other therapy had an extremely limited number of cases, for example, reports of only one case.

Results of review: Boardman *et al.*[358] reported that, of the 97 patients with LM of the head and neck region, surgical treatments were necessary in six of the 12 patients with mediastinal lesions, that complications of surgery occurred in four of the six patients, and that long-term nerve damage was observed in three of them. In addition, they reported that management by tracheotomy was necessary in 15% of all patients. Complete or nearly complete remission was observed in 92% of the patients, but they suggested that surgical treatments should be indicated only when there is airway obstruction or there is the risk of it, because surgical treatment of mediastinal lesions frequently causes complications.

Park *et al.*[359] reported that they surgically resected mediastinal LM in 12 patients. Seven of them had dyspnea and three were asymptomatic, but they were all judged to have indications for surgery due to symptoms or the tendency of the lesions to enlarge. A total of five recurrences were observed in four patients (33%) during a mean period of 3.6 years after the initial surgery, and all underwent by re-resection. No perioperative death was observed, and, in a total of 25 cases including past cases, the overall survival was not different compared with that in healthy individuals over a follow-up period of 11.5 years.

Smith *et al.*[302] performed local injection of OK-432 in 16 patients with mediastinal LM and reported 60% or more regression of the lesion in 13 (81%). They also mentioned treatment responses according to the histological types and, by reporting responses (complete or nearly complete remission) in 94% of those with macrocystic lesions, 63% of those with mixed lesions, but 0% in those with microcystic lesions, suggested a macrocystic lesion to be a good indication for sclerotherapy using OK-432. Although not from the viewpoint of airway obstruction, they reported that treatment using OK-432 was more effective than surgical resection and less frequently caused serious complications.

Limitations: There have been no papers that directly analyzed treatments effective for mediastinal lesions expected to cause airway obstruction, and many papers reported cases of mediastinal lesions that responded to treatments. Therefore, we simply extracted matters relevant to this CQ from these reports.

SUMMARY

There was no published work with a high level of evidence concerning effective treatments for LM in the mediastinum causing airway obstruction. A few case reports that referred to the effects of surgery and sclerotherapy were observed, but it was difficult to present objective and specific figures concerning their effectiveness or safety. However, according to the available information, it should be noted that favorable responses have been obtained by OK-432 local injection in macrocystic lesions and that complications due to surgical resection are likely to occur relatively frequently.

From these observations, we consider the following to be a therapeutic approach that can be proposed: "Sclerotherapy, such as that by local injection of OK-432, should be considered for macrocystic lesions, and, for lesions that are technically difficult to treat by sclerotherapy or microcystic lesions, surgical resection should be considered with attention to complications. In addition, it is necessary to pay attention to the appearance of respiratory disturbances before and after these treatments and to constantly evaluate indications for securing the airway by intratracheal intubation or tracheostomy." Therefore, at present, we recommend, "Sclerotherapy is effective for macrocystic lesions, and surgical resection is effective for microcystic lesions. However, as the complication rate is relatively high, treatments should be selected according to the condition of each case."

CQ30: Should sclerotherapy be performed in infancy for a patient with head and neck LM affecting the airway?

Recommendation: In a patient with LM around the airway, there is risk of respiratory distress in infancy, while airway obstruction is likely to be exacerbated by sclerotherapy. Particularly when risk of airway obstruction is judged to be high or when the patient has already presented symptoms, it is proposed to perform sclerotherapy with sufficient preparations including airway management.

Strength of recommendation: 2 (weak).

Evidence: D (very weak).

Comments:

Process of preparing recommendation

Lymphangiomas of the neck, which are located in an exposed part of the body, may cause cosmetic problems that are important, but airway obstruction can be a particularly serious problem in some cases.

Sclerotherapy, which is one of the major treatment modalities, is most effective in patients with cystic LM, but swelling of the treated portion after the therapy may cause or exacerbate

This article has been co-published with the permission of *The Journal of Dermatology, Pediatrics International* and *Japanese Journal of Radiology*. All rights reserved. © 2020 The Authors. The articles are identical except for minor stylistic and spelling differences in keeping with each journal's style. Either citation can be used when citing this article.

airway obstruction symptoms, especially in neonates. The upper airway will become less vulnerable to obstruction because it becomes less frail and wider as patients grow and respiratory distress tends to be unlikely. Therefore, it is occasionally difficult to determine how a patient who does not present any obstructive symptoms should be treated in infancy.

Thus, we evaluated this problem by formulating the CQ, "Should sclerotherapy be performed in infancy for a patient with the neck LM affecting airway?".

Published work search and screening

As a result of search, 86 papers in Japanese and 135 papers in English (130 from PubMed, five from Cochrane) were subjected to primary screening. Of these papers, six in Japanese and 20 in English were subjected to secondary screening concerning this CQ. They included one SR, one RCT, two PS and one retrospective cohort study, but all the others were case series or case reports. Therefore, the results and discussion, primarily, in these SR, RCT, PS and retrospective cohort study, but also in other case series were integrated.

Review of observational studies

The published work concerning the effectiveness of sclerotherapy for head and neck LM in infancy was reviewed from the viewpoints of responses (prognosis [survival rate or mortality], size, symptoms and cosmetic improvement) and complications.

Sclerosing agents used as key words for the present published work search varied widely and included OK-432, bleomycin, ethanol, doxycycline, STS and fibrin glue. No paper evaluated differences in effectiveness of various agents due to their methods of administration for lesions around the neck affecting the airway. Therefore, differences among agents were excluded from the evaluation of this CQ.

Results of Review:

1. Responses

A. Prognosis (survival rate or mortality): According to the SR by Adams *et al.*,[360] the mortality was 4.7% in 277 cases with head and neck LM. Because lesions around the airway were not the only target, and because sclerotherapy was not the only treatment modality, the paper has not quite rightly answered the CQ. However, because patients who died were all younger than 1 year of age and their causes of death are considered to have been mostly airway problems, such as airway obstruction and aspiration due to vocal cord paralysis in eight, and as at least one patient is judged to have died due to complications of invasive treatment, the paper is considered to indicate the risk of this disorder during infancy.

B. Size: Many of the papers that referred to the size regression evaluated it by four categories: (i) excellent or complete (≥90% regression); (ii) good or substantial (≥50% and <90% regression); (iii) fair or intermediate (≥20% and <50% regression); and (iv) poor or none (≤20% regression).

Ravindranathan *et al.*[306] treated five patients (aged 4–19 months) with cervicofacial LM by sclerotherapy using OK-432 (in addition to Fibrovein® [STD Pharmaceutical Products Ltd, Hereford, UK] in two) and reported that the responses were good in one (20%) (cystic), partial in one (20%) (cavernous) and poor in three (60%) (two with cavernous lesions that required tracheotomy and one with cystic lesions in whom the condition improved to good after surgical resection). However, they did not mention the evaluation criteria for good, partial and poor.

According to the report of eight cases with head and neck LM by Leung *et al.*,[361] all patients underwent sclerotherapy and 50% or more regression was observed in all patients, with complete regression in two. However, the patient age varied from 2 months to 11 years, and the types of LM were not mentioned.

Ogawa *et al.*[362] reported nine patients (including five preschoolers and toddlers, two school children and two adults) who underwent OK-432 sclerotherapy for the neck LM and evaluated it to be markedly effective in eight, in whom the lesions mostly disappeared, and effective in one, who showed a 50% or more regression. Eight patients in whom the treatment was markedly effective consisted of one with mixed and seven with cystic lesions, and the one in whom the treatment was effective had a mixed type.

Cahill *et al.*[315] reported doxycycline sclerotherapy in 17 patients with head and neck LM (cystic in 10, mixed in seven [three required tracheotomy]), and its size regression was reported to be more than 90% in seven (41.2%) (cystic in six, mixed in one), 75–89% in four (23.5%) (cystic in two, mixed in two), 51–74% in four (23.5%) (cystic in one, mixed in three) and 25–50% in two (11.8%) (mixed in two).

Nehra *et al.*[311] reported doxycycline sclerotherapy in 11 patients with head and neck LM (cystic in seven, mixed in four; aged 2 days to 21 months) (later combined with surgical resection in three). The treatment results were excellent in five (45.5% of all patients) and satisfactory in two (18.2% of all patients) among seven patients with cystic lesions but poor in all four patients with mixed type lesions (36.4% of all patients). Particularly, three of the four patients with mixed type lesions required tracheal intubation shortly after birth and underwent sclerotherapy while intubated, but the effects were poor in all of them. Surgical resection was added in one and was under consideration in another.

C. Symptoms: According to Ravindranathan *et al.*,[306] who reported five patients with cervicofacial LM (aged 4–19 months) treated with sclerotherapy using OK-432 (in addition to Fibrovein in two), four exhibited symptoms of airway obstruction before treatment. Symptoms included dysphagia in two and dyspnea (including croup-like symptoms) in four (some both). Symptoms were alleviated by sclerotherapy in two out of four (cystic one, cavernous one), but tracheotomy was necessary in the remaining two (cavernous in both) without improvement.

In the report of eight patients with head and neck LM and five patients with VM (aged 2 months to 11 years) by Leung *et al.*,[361] their symptoms noted before treatment were mass or swelling (10 patients [77%]), pain after hemorrhage (two patients [15%]), skin discoloration (blue) (one patient [8%]), obstructive airway symptoms (six patients [46%]) and swallowing difficulty (one

This article has been co-published with the permission of *The Journal of Dermatology, Pediatrics International* and *Japanese Journal of Radiology*. All rights reserved. © 2020 The Authors. The articles are identical except for minor stylistic and spelling differences in keeping with each journal's style. Either citation can be used when citing this article.

patient [8%]). All symptoms were alleviated by sclerotherapy (doxycycline for LM, STS foam for VM).

Arimoto *et al.*[363] reported a patient with cystic LM in the neck presenting 3 months after birth. The patient presented with respiratory distress at the age of 10 months due to enlargement of the LM following upper respiratory infection. While left vocal cord fixation due to the mass was confirmed by ultrasonography before treatment, aspiration of the cyst and steroid administration resulted in opening of the glottic area and regression of the mass with relief of wheezing and distress. Because they underwent sclerotherapy 2 months after the disappearance of symptoms, aspiration of internal fluid and steroid administration rather than sclerotherapy were directly effective for the alleviation of symptoms.

Kitagawa *et al.*[364] reported a patient with giant LM of the neck which had been prenatally diagnosed and was treated under *ex utero* intrapartum treatment by tracheal intubation after aspiration of the cyst. The lesion was reported to be refractive to subsequent sclerotherapy and tracheotomy was eventually needed.

Nehra *et al.*[311] reported that, among 11 patients with head and neck LM (cystic type in seven and mixed type of cystic + cavernous in four; aged 2 days to 21 months), three out of four with mixed LM presented respiratory distress soon after birth and were managed by intubation, but that all were extubated after sclerotherapy using doxycycline (1–3 times; median, 1.6 times).

D. Cosmetic improvements: No paper has reported cosmetic results in detail. Only sporadically they mentioned surgery for redundant skin after regression of cystic lesions by sclerotherapy.

2. Complications

Complications associated with treatment for LM around the airway have been reported in many papers. They include temporary conditions caused by sclerotherapy such as fever,[292,303,312,362,365–371] local swelling,[303,312,365,367,368,370,371] pain,[288,312,362,367,370–372] hemorrhage into the cyst[288,303,312,368] and infection.[288,292,303,310,312,360,365,372] The effects of treatment for head and neck lesions, such as respiratory distress due to airway obstruction[292,303,306,312,362,365,366] as well as nerve palsy,[288,292,312,360,365] have also been reported.

According to an SR about head and neck LM by Adams *et al.*,[360] both nerve damage due to sclerotherapy and post-therapeutic infection were reported in one (0.8%) out of 123 patients. Because nerve damage and infection after surgery were observed in 12 (10.2%) and seven (5.9%) out of 118 patients, respectively, the complication rate would be lower by sclerotherapy than by surgery.

Ogawa *et al.*[362] reported a patient aged 1 year and 5 months who developed airway edema after OK-432 sclerotherapy for a cystic neck LM necessitating tracheal intubation for 3 days, and cautioned against sclerotherapy for LM around the airway in young children (particularly those <2 years old).

Kudo *et al.*[369] also reported two patients aged 11 months and 1 year and 11 months who were treated with OK-432 sclerotherapy intubated in advance for fear of airway obstruction due to post-therapeutic swelling. Tomemori *et al.*[373] also cautioned against sclerotherapy for LM in children aged less than 2 years as in the report by Ogawa *et al.*[362]

On the other hand, Kudo *et al.*[369] reported two cases whose neck LM having been enlarged rapidly after suffering from measles or URTI. Arimoto *et al.*[363] also reported a patient with cystic LM of the neck 3 months after birth, who developed dyspnea due to enlargement of the lesion after URTI at 10 months and was about to be intubated.

Regarding complications due to sclerosing agents, Cahill *et al.*[315] reported those by doxycycline, STS and absolute ethanol. They reported delayed complications, such as Horner's syndrome, transient left lip weakness, right facial nerve palsy and transient left hemidiaphragm paralysis, in addition to periprocedural complications such as hemolytic anemia after doxycycline injection in two patients, hypoglycemic and metabolic acidosis in three neonates, transient hypotension during absolute alcohol instillation and self-limiting skin excoriation secondary to pericatheter leakage of doxycycline. Other reported complications include permanent vocal cord paralysis after local ethanol injection,[374] serious complications after OK-432 injection such as death due to pulmonary embolism,[375] deaths due to pulmonary complications after treatment using bleomycin[376,377] and leukocytopenia due to bleomycin.[368]

Limitations: There are few papers that solely analyzed LM around the cervical airway. Most papers included lesions involving not only the neck but also the craniofacial and other parts of the body and reported LM with different properties such as cystic and mixed types. In addition, definition of cavernous lesions and methods of sclerotherapy (injection techniques, number of injections) were not similar among papers, and differences in these backgrounds must be taken into consideration to evaluate the effectiveness of sclerotherapy.

SUMMARY

The CQ, "Should sclerotherapy be performed in infancy for a patient with head and neck LM affecting the airway?", was evaluated from the viewpoints of responses (prognosis [survival rate or mortality], decrease in size, symptoms, cosmetic improvements) and complications. Because there have been some reports on the risk of respiratory distress due to LM around the airway in infants, and therapeutic intervention is necessary even in infants when the risk is high or they have already developed symptoms. Such intervention is made by sclerotherapy or surgery, and as surgical resection is associated with the risk of more serious complications than sclerotherapy, intervention by less invasive sclerotherapy is recommended. Sclerotherapy is considered to be very effective because of the high regression rate of the lesion and symptom/function-improving effect. However, its effect varies depending on the disease type, being somewhat less effective in the cavernous and mixed types than in the cystic type. Furthermore, when it is performed for the lesions around the airway, it may be associated with the risk of exacerbation of airway obstruction symptoms due to reactive enlargement of the lesion. Thus, we formulated the recommendation, "In LM around the airway, there is the risk of respiratory disturbances from infancy, but airway obstruction is likely to be

This article has been co-published with the permission of *The Journal of Dermatology, Pediatrics International* and *Japanese Journal of Radiology*. All rights reserved. © 2020 The Authors. The articles are identical except for minor stylistic and spelling differences in keeping with each journal's style. Either citation can be used when citing this article.

exacerbated by sclerotherapy. Particularly when the risk of airway obstruction is judged to be high or when symptoms have appeared, it is proposed to perform sclerotherapy with sufficient preparations including securing the airway."

CQ31: Is surgical resection effective for LM of the tongue?

Recommendation: Surgical resection is effective for reducing the size of the lesion and alleviating symptoms and functional impairment. However, total resection is often difficult, and careful decision-making is required in consideration of the possibility of complications and recurrence.

Strength of recommendation: 2 (weak).

Evidence: D (very weak).

Comments:

Process of preparation of recommendation

While the tongue is one of the frequent sites of LM, the lesion is often distributed widely over the neck rather than localized in the tongue. LM of the tongue not only cause cosmetic problems, such as protrusion from the mouth and bleeding, but also readily occupy the oropharyngeal cavity and cause functional problems such as disorder of mouth closing, difficulty in speaking, respiratory disturbances and impairment of oral food intake. These conditions are treated at departments including plastic surgery, oral surgery, otorhinolaryngology and pediatric surgery. LM of the tongue are treated by surgical resection or sclerotherapy, but comprehensive evaluation of the condition of individual cases including the distribution of the lesion in the tongue, involvement of other areas and cyst components, and vascular distribution in addition to general information, such as the risk of complications and recurrence in each treatment, is necessary.

Therefore, the CQ, "Is surgical resection effective for LM of the tongue?" was formulated, and the present knowledge about the effectiveness of surgical resection of the lesion, particularly by partial glossectomy was summarized.

Published work search and screening

As a result of the published work search, 29 papers in Japanese and 76 papers in English (75 from PubMed, one from Cochrane) were subjected to primary screening. Of these papers, two in Japanese and 10 in English were subjected to secondary screening concerning this CQ. They included one retrospective cohort study, but most other papers were case series or case reports. Consequently, in the evaluation of this CQ, the results and discussion of the cohort study and each case series were integrated.

Review of observational studies (case series)

The effectiveness of surgical resection of LM of the tongue was evaluated from the viewpoints of resectability of the lesion, symptoms, function and cosmetic improvements as elements of responses as well as complications and recurrence.

Results of Review:

1. Responses

A. Resectability of the lesion: Twenty-four cases of tongue lesions treated by surgical resection alone were reported in four papers. Catalfamo *et al.*[378] performed surgical resection of localized masses including normal structures with a margin of 1 cm in the horizontal direction and reported that the size of tongue lesions was reduced in eight (88.9%) of the nine patients.

Concerning large lesions impossible to resect totally, Boardman *et al.*[358] reported 13 cases of partial surgical resection, but several operations were often necessary to reduce lesion size. A total of two case have been reported,[379,380] and the lesion size was reduced in both. Although differences were observed in re-enlargement after surgery, they are discussed in detail in "(2) Complications".

In one case report, sclerotherapy was performed 15 times, but the lesion size could not be reduced, and surgical resection was performed, eventually resulting in a favorable outcome without recurrence.[381]

According to a report of 89 cases of head and neck LM by Lei *et al.*,[291] the outcome was excellent in 73 (82%) and good in 16 (18%) although it was not a report of cases of tongue lesions alone. They included 43 cases of tongue lesions.

In addition, a few papers[382–385] that suggested the effectiveness of combinations of surgical resection with sclerotherapy and laser therapy were observed. Wiegand *et al.*[383] classified the disease into four stages according to the area of involvement and reported that the stage can be a prognostic factor. Surgery was effective, and complications were rare, when the lesion was localized in the superficial layer and part of the muscle layer. Surgical resection can also be effective, but complete resection is difficult, when the lesion extends over the entire muscle layer or to the tongue base and neck. Therefore, partial resection is often repeated and combined with laser therapy and sclerotherapy, but the recurrence is observed very frequently, and the results did not contradict the reports mentioned below in the section of the recurrence rate.[291,358]

B. Symptoms: A wide variety of symptoms have been reported depending on the site of the mass, and they include tongue discomfort, bleeding, pain and difficulty in oral feeding.[386] Roy *et al.*[387] reported that bleeding from the tongue surface, pain and eating difficulty were alleviated by cauterization.

C. Functions: In most patients who exhibited functional impairment, the lesions were so extended that they were no longer indications for one-time surgical resection. Large masses located at sites such as the tongue base cause respiratory disturbances, swallowing disorders and difficulty in speech. According to the report by Azizkhan *et al.*,[385] oral intake of normally cooked food became possible in 14, and normal vocalization became possible in eight, of the 21 patients with tongue base lesions. In addition, five of the 17 patients who needed tracheotomy were weaned.

D. Cosmetic improvements: Objective evaluation of cosmetic effects is also difficult.

Azizkhan *et al.*[385] reported that, of the 20 patients, excluding one with severe deformity who died, deformity of structures around the tongue, such as the mandible and maxilla, was mild in six, moderate in five and severe in nine. There have been a few reports that cosmetic improvements were also observed in

This article has been co-published with the permission of *The Journal of Dermatology, Pediatrics International* and *Japanese Journal of Radiology*. All rights reserved. © 2020 The Authors. The articles are identical except for minor stylistic and spelling differences in keeping with each journal's style. Either citation can be used when citing this article.

patients who showed a reduction of the tongue size by surgical resection, but objective evaluation is insufficient.

2. Complications

Although the properties of the lesions are unclear in some papers, facial nerve paralysis, vagus nerve paralysis, infection, hematoma, seroma, salivary leakage, ruptured suture and skin flap necrosis have been reported as complications of the facial region. There have also been reports of temporary complications such as pain and hemorrhage.

3. Recurrence

There have been a few postoperative evaluations reporting that no reactivation that clinically required treatment was observed. Lei *et al.*[291] reported greater details: recurrence was observed in 21 (23.6%) of 89 patients and was more frequent in those aged less than 1 year, those with lesions in the oral cavity/face, those with lesions at three or more sites and those with microcystic lesions. According to Boardman *et al.*,[358] LM of the tongue recurred in 12 (48%) of 28 patients, more often than other head and neck lesions. As factors related to this more frequent recurrence of lingual LM, more frequent involvement of other regions, such as the floor of the mouth, and a high percentage of microcystic lesions (70%) have been suggested. Of the two patients treated by surgical resection alone, one who underwent resection of the middle part of the tongue showed no re-enlargement for 1 year or longer after surgery,[379] but surgery was repeated three times in the one who underwent marginal resection.[380] This patient who underwent repeated resections also showed no re-enlargement, although the time of the last resection is unclear.

Limitations: In some papers, surgical resection was combined with other treatments,[381–385,387] lesions in other areas such as the neck were included[291] and the lesion types were unknown. The lack of standardization of subjects and uniformity of the definition or time of recurrence must be considered in the evaluation of the effectiveness of surgical resection.

SUMMARY

Many papers suggest that surgical resection is effective for reducing the size of lingual LM. However, in patients with large lesions, lesions extending to structures other than the tongue, and microcystic lesions, several resections or combination of resection with other treatments such as sclerotherapy and laser therapy were necessary, and the recurrence rate tended to be higher. While a few papers referred to symptoms, functional outcome and cosmetic improvements, none showed a high level of evidence, and the evidence was insufficient for general discussion of the effectiveness of surgical resection.

Therefore, concerning the effectiveness of surgical resection for LM of the tongue, "Surgical resection is effective for reducing the size of the lesion and alleviating symptoms and functional impairment. However, total resection is often difficult depending on the distribution of the lesion, and careful decision-making is required in consideration of the possibility of complications and recurrence", was proposed as a draft recommendation.

CQ32: Is aggressive surgical intervention effective for chylous pleural effusion in the neonatal period?

Recommendation: For chylous pleural effusion refractory to conservative treatments, surgical procedures, such as pleurodesis, ligation of the thoracic duct and pleuroperitoneal shunting, may be effective.

Strength of recommendation: 2 (weak).

Evidence: D (very weak).

Comments:

Process of determining recommendation

Primary chylous pleural effusion during the neonatal period is often refractory and can be fatal. Thoracic drainage is performed for respiratory insufficiency due to accumulation of pleural effusion, followed by conservative treatments, such as nutritional therapy, steroid and octreotide therapy, conducted primarily by a neonatologist until resolution of chylous pleural effusion.

In refractory cases that do not respond to these conservative therapies, surgical intervention, such as ligation of the thoracic duct and pleurodesis, may be performed. However, no sufficient consensus has been obtained concerning their effects. To evaluate problems, such as at what point surgical intervention should be made and whether aggressive surgical intervention is effective for such a condition, the CQ, "Is aggressive surgical intervention effective for chylous pleural effusion in the neonatal period?", was formulated, and the knowledge available at present was summarized.

Published work search and screening

As a result of the published work search, 98 papers in Japanese and 264 papers in English (262 from PubMed, two from Cochrane) were subjected to primary screening. Of these papers, eight in Japanese and nine in English were subjected to secondary screening concerning this CQ. They included none with a high level of evidence, such as an SR or RCT that evaluated surgical treatment, and all papers were case series or case reports. Consequently, the results and discussion in each of the case series judged to be useful for the preparation of the draft recommendation were integrated although they were weak as the evidence for the evaluation of this CQ.

Review of observational studies (case series)

The published work concerning the effectiveness of surgical treatment for chylous pleural effusion in the neonatal period was reviewed from the viewpoints of responses and complications.

Results of Review:

1. Responses

Surgical treatment for neonatal chylothorax is performed in patients who respond insufficiently even to thoracic drainage in addition to nutritional therapy using MCT milk or total parenteral nutrition or drug treatment such as octreotide administration.

This article has been co-published with the permission of *The Journal of Dermatology, Pediatrics International* and *Japanese Journal of Radiology*. All rights reserved. © 2020 The Authors. The articles are identical except for minor stylistic and spelling differences in keeping with each journal's style. Either citation can be used when citing this article.

The methods for surgical intervention found by the present published work review included ligation of the thoracic duct and pleuroperitoneal shunting as well as pleurodesis with OK-432 administration, intrathoracic infusion of fibrin and povidone-iodine administration, and some patients diagnosed *in utero* underwent pleuro-amniotic shunting. Cases in which mildly invasive treatments, such as thoracoscopic ligation of the thoracic duct and intrathoracic fibrin application, have been reported in addition to those who underwent thoracic duct ligation by thoracotomy.

Treatments that were performed before surgery and their periods were not uniform. In addition, because there are cases that developed chylous pleural effusion after surgery and those of congenital chylothorax, the diversity of the patient background must be taken into consideration in the efficacy evaluation.

Among the surgically treated cases, those in whom chylous plural effusion disappeared, respiratory symptoms were alleviated and weaning from the respirator became possible have been reported.[388,389] In addition, the absence of recurrence or reactivation is considered to be a point.[388–391] There were reports that chylous pleural effusion after thoracic surgery was resolved by drainage alone. Cleveland *et al.*[392] considered conservative treatments, such as total parenteral nutrition, octreotide and diuretic administration, to be the best and, observing that, of the poor responders, the mortality was 80% in five who continued to be managed by conservative treatments but 0% in four who underwent additional surgery, reporting that surgical treatment contributed to the reduction of the mortality. According to the guidelines for the treatment of chylous thoracic effusion by Buttiker *et al.*,[393] conservative treatment should be continuing for approximately 3 weeks but should be abandoned thereafter because of the risk of nutritional disturbance, and increased susceptibility to infection and liver disorders. However, Kaji *et al.*[394] reported that it is difficult to set a clear period of conservative therapy, because the effectiveness and success rate of surgical treatment are unclear.

2. Complications

As complications due to sclerosing agents, fever and increased inflammatory reaction due to the administration of OK-432 as well as pulmonary abscess and temporary flaccidity and protrusion of the upper abdominal region considered to have been due to intercostal nerve damage have been reported. While chyle leakage in the abdominal cavity was noted in a patient who underwent pleuroperitoneal shunting, there were no reports of fatal complications.

Limitations: Surgical treatment was performed in most reported cases when responses to conservative therapy were not obtained. Therefore, it must be assumed that the results of evaluation of this CQ are based on data concerning the effectiveness of surgery performed with conservative therapy.

SUMMARY

The published work was reviewed concerning the effectiveness of aggressive surgical intervention for neonatal chylous thoracic effusion from the viewpoints of responses and complications, but no objective study with a high level of evidence was found. In most reported cases, surgical treatment was performed when responses to conservative treatments were poor. Therefore, it is difficult to compare surgery with other therapies, and the evaluation of the period of conservative treatment before surgery remains insufficient. However, there was a paper that proposed surgical intervention after attempting conservative treatments for 3 weeks as a standard.

Thus, surgical intervention for neonatal chylous pleural effusion is characterized at present as an approach that may be effective but should be evaluated when the condition is not improved by other treatments, and "Surgical procedures, such as pleurodesis, ligation of the thoracic duct, and pleuroperitoneal shunting, may be effective for chylous pleural effusion refractory to conservative treatments" is proposed as a draft recommendation.

CQ33: What treatments are effective for refractory chylous pleural, and pericardial effusion and respiratory disturbances of the patients with generalized lymphatic anomaly (GLA) and Gorham–Stout disease (GSD)?

Recommendation: While treatments including surgery, sclerotherapy, radiotherapy, nutritional therapy and drug therapy are conducted, there is presently no effective treatment with a high level of evidence. Treatments should be selected in consideration of complications and adverse effects according to individual symptoms.

Strength of recommendation: 2 (weak).

Evidence: D (very weak).

Comments:

Process of preparation of recommendation

Generalized lymphatic anomaly and GSD are refractory diseases that cause a wide variety of symptoms in the entire body and are difficult to diagnose and treat. The investigation by the Health and Labour Sciences Research group (Ozeki group) carried out by 2013 showed that the mortality is particularly high when the patients had thoracic lesions.

Among the thoracic symptoms, chylous pleural effusion/pericardial effusion are often refractory and occasionally fatal. While information about the disease is extremely limited because of its rareness, case reports are being globally accumulated as chronic cases are managed on an outpatient basis, and as severe cases are treated intensively.

Presently, no radical treatment for these refractory diseases is known, but the CQ, "What treatments are effective for refractory chylous pleural, and pericardial effusion and respiratory disturbances of the patients with GLA and GSD?" was formulated to compile the knowledge about what treatments are effective as it is a problem of clinical importance.

Published work search and screening

As a result of the published work search, 208 papers in Japanese and 617 papers in English (598 from PubMed, 19 from Cochrane) were subjected to primary screening. Of these papers, two in Japanese and 25 in English were subjected to

This article has been co-published with the permission of *The Journal of Dermatology, Pediatrics International* and *Japanese Journal of Radiology*. All rights reserved. © 2020 The Authors. The articles are identical except for minor stylistic and spelling differences in keeping with each journal's style. Either citation can be used when citing this article.

secondary screening concerning CQ37. They included no studies with a high level of evidence, such as an SR and RCT, and all were reports of 1–2 cases. Therefore, the evaluation of this CQ was performed by integrating the results and discussion in case series judged to be useful for the preparation of the draft recommendation despite the lack of evidence.

Review of observational studies (case series)

The effectiveness of various treatments for refractory GLA and GSD was evaluated according to the prognosis and the presence or absence of improvement in imaging findings, improvement in symptoms, improvement in airway obstruction, enlargement of the lesion, regression, treatment-related complications, recurrence and reactivation.

Conditions of patients: The cause of chylous pleural and pericardial effusion is lymphorrhea from lymphatic vessel tissue lesions that have primarily invaded the mediastinum and pleura, and lymphorrhea from osteolytic lesions of the ribs and vertebrae was also observed. Respiratory disturbances were caused by pleural effusion, chylous pleural effusion, pericardial effusion, and direct invasion of the mediastinum and lungs.

Results of review: As surgical treatments for chylous pleural effusion, procedures, such as thoracentesis, thoracic drainage, ligation of the thoracic duct and pleural decortication, have been performed, and local lesions were surgically resected. In most cases, thoracentesis and thoracic drainage were performed, but chyle leakage was not resolved. As for complications, there were patients who developed hypovolemic shock and required blood transfusion and catecholamine administration or supplementation of albumin, immunoglobulin and clotting factors.[395–397] While chylous pleural effusion was controlled in some patients who underwent ligation of the thoracic duct,[397–408] the treatment was performed in combination with other surgical procedure or radiotherapy in all cases.[400,402,408] There was one case that showed improvement in respiratory disturbance.[406] As complications of ligation of the thoracic duct, splenomegaly and lymphorrhea[405] and left-sided pleural effusion[397,405] have been reported. In the patients who showed marked improvements in chylous pleural effusion[395,405,408] after pleural decortication,[395,396,401,403–405,408,409] the procedure was performed in combination with other surgical treatments or sclerotherapy, and there was no mention of complications. There were cases that showed marked improvements in chylous pleural effusion[396,400,405,408] among those who underwent surgical resection of local lesions including splenectomy,[396,397,400,405,408,410–412] but the procedure was performed in combination with other surgical treatments in most of them. Hemorrhage was reported as a complication.[410] Among other treatments, pleuroperitoneal shunting[403] and lung transplantation[413] were performed, and alleviation of respiratory disturbance was noted in the patient who underwent lung transplantation.

As a surgical treatment for pericardial effusion, pericardiocentesis was performed,[396,414–416] and pericardial fenestration was performed when pericardial effusion could not be controlled by pericardiocentesis.[396,416] There was no mention of complications.

As sclerotherapy, pleurodesis was performed using OK-432, talc and minocycline.[395,397–399,404,408,411,416–418] There were patients who responded markedly to sclerotherapy alone and sclerotherapy combined with surgical procedures such as pleural decortication or local radiotherapy. There was no mention of complications of sclerotherapy.

There have also been reports[399,400,402–404,410–412,415,416,418–420] on local (e.g. lesion area, thoracic duct region) and thoracic radiotherapy for chylous pleural effusion and local lesions, and marked responses of chylous pleural effusion and responses of respiratory symptoms were noted, but other treatments were performed concomitantly in some patients. Radiation pneumonitis has been reported as a complication.[416]

Concerning nutritional therapy, fasting, high-calorie infusion and MCT diet have been performed alone or in combinations, but few cases that showed alleviation of chylous pleural effusion were observed.[395,396,398–400,403,405,408,421]

For drug therapy against chylous pleural effusion, drugs including interferon (IFN)-α, propranolol, anticancer agents (e.g. vincristine), bisphosphonate, octreotide, steroid, sirolimus and low-molecular-weight heparin were used. IFN-α was used most frequently,[395–398,400,401,403,415,421] and marked improvement in chylothorax was reported in five cases. Of these cases, IFN-α was used with propranolol in one[395] and with low-molecular-weight heparin and local radiotherapy (15 Gy) in one.[400] As for complications of drug therapy using IFN-α, there were reports of fever, nausea and headache,[421] and thrombocytopenia and hepatic toxicity.[397] There was no report of improvement in chylous pleural effusion by the use of steroid[395,399,403,415] or octreotide[395,397,398,400,403,405] alone. Concerning other drug therapies, only a few cases have been reported with no improvement in chylous pleural effusion. One case that showed regression of mediastinal invasion of GLA and alleviation of respiratory disturbance by sirolimus treatment has been reported,[414] and hypertension was noted as a complication. In drug therapy for pericardial effusion, diuretics were used for conservative therapy.[400]

Limitations: Although cases that responded to various therapies have been reported, treatments are often performed in combinations, and the evaluation of the effectiveness of each treatment alone is difficult at this point.

SUMMARY

Treatments effective for GLA and GSD presenting with refractory chylous pleural effusion, pericardial effusion and respiratory disturbances were evaluated by a review of the published work, which was primarily case reports. Various treatments, such as surgery, sclerotherapy, radiotherapy, nutritional therapy and drug therapy, have been performed, but there was no study with a sufficient number of cases and a high level of evidence because of the rareness of the disease and diversity of symptoms. Although cases that responded to various treatments have been reported, treatments are frequently performed in combinations, and the evaluation of the effectiveness of individual therapies is difficult at present. Sirolimus (a mammalian target of rapamycin inhibitor) is considered

This article has been co-published with the permission of *The Journal of Dermatology, Pediatrics International* and *Japanese Journal of Radiology*. All rights reserved. © 2020 The Authors. The articles are identical except for minor stylistic and spelling differences in keeping with each journal's style. Either citation can be used when citing this article.

promising as a drug for this disease, and some clinical trials are currently underway in Japan and abroad.

In clinical situations, these diseases are not recognized as indications of various drug therapies by the Japanese health insurance system, and the therapeutic effects of other treatments are also uncertain. Therefore, the above treatments cannot be recommended, but we propose that treatments "should be selected in consideration of complications and adverse effects according to individual symptoms". It is necessary to evaluate the invasiveness, complications and adverse effects, and select the treatments judged to be appropriate for each case.

CONCLUSION

These practice guidelines for vascular anomalies have been prepared as the EBM guidelines for the management of vascular anomalies.

ACKNOWLEDGMENTS: We thank all members of the systematic review team as follows. Tomoko Izaki, Ryohei Ishiura, Yohei Iwata, Tatsuo Ueda, Naoki Okura, Sachiyo Osawa, Jun Otaka, Kuniaki Ohara, Shinya Ogishima, Takuro Kazama, Motoi Kato, Takahide Kaneko, Motohiro Kano, Tamihiro Kawakami, Tatsuki Kono, Eisuke Shibata, Yohsuke Suyama, Kazuhiro Takahashi, Yuichi Takama, Takaya Takeguchi, Kensuke Tashiro, Masashi Tamura, Atsushi Tamura, Masato Tsuchiya, Kyoichi Deie, Toshihide Tokuda, Asami Tozawa, Fumio Nagai, Michiko Nagahama, Yasuhiro Nakamura, Akifumi Nozawa, Naoki Hashizume, Takuya Hara, Koji Higuchi, Masahito Hibi, Takaya Fukumoto, Shinji Fujizuka, Megumi Furuya, Seiji Houbara, Kyoko Hoshino, Tomohiro Hori, Takanobu Maekawa, Junko Miyata, Kenji Murakami, Kiichiro Yaguchi, Daisuke Yasui, Kentaro Yamada, Yohei Yamada, Yuki Yamamoto, and Azusa Watanabe. The funding for preparation of the Japanese Clinical Practice Guidelines for Vascular Anomalies 2017 was from Health, Labor and Welfare Sciences Research Grants (Research on Policy Planning and Evaluation for Rare and Intractable Diseases) provided to "Japanese Research Committees for Intractable Vascular Anomalies" (main funding source), "Japanese Study Group for Intractable Diseases of Pediatric Gastrointestinal Tract" and "Japanese Research Committees for Survey and Establishment of Guidelines for Pediatric Respiratory Dysplastic/hypoplastic Disease". No financial support was received from any other organization or corporation.

CONFLICT OF INTEREST: Conflict of interest of the guidelines preparation organization was managed by the Guidelines Executive Committee. The following corporations were disclosed by self-declaration of the Guidelines Committee members in the 3-year period before 1 April 2017: Japan Pharmaceuticals and Medical Devices Agency (PMDA), Mitsubishi Foundation, Rohto Pharmaceutical, Mitsubishi Tanabe Pharma and Shionogi.

REFERENCES

1 ISSVA Classification of Vascular Anomalies ©2014 International Society for the Study of Vascular Anomalies. [Cited April 2014.] Available from URL: issva.org/classification.
2 Wassef M, Blei F, Adams D *et al.* Vascular anomalies classification: recommendations from the International Society for the Study of Vascular Anomalies. *Pediatrics* 2015; **136**: e203–e214.
3 [Clinical practice guidelines for vascular anomalies 2013]. The Research Committee of Intractable Vascular Anomalies, Research on Measures for Intractable Diseases, Health, Labour and Welfare Sciences Research Grants, the Ministry of Health, Labour and Welfare, Japan. [Cited 29 March 2013.] Available from URL: http://www.marianna-u.ac.jp/va/files/vascular%20anomalies%20practice%20guideline%202013.pdf. Japanese.
4 Fukui T, Yamaguchi N (editorial supervisors), Morizane T, Yoshida M, Kojimahara N (eds). *Minds Handbook for Clinical Practice Guideline Development 2014*. Ver 1.0, Tokyo: Minds Guideline Center, Japan Council for Quality Health Care, [Cited 1 February 2015.] Available from URL: http://minds4.jcqhc.or.jp/minds/guideline/pdf/MindsHB2014.pdf.
5 Morizane T, Yoshida M (eds). *[Minds Manual for Guideline Development Ver. 1.0]*. Tokyo: Japan Council for Quality Health Care, [Cited 31 March 2014.]. Japanese.
6 Kojimahara N, Nakayama T, Morizane T, Yamaguchi N, Yoshida M. (eds). *[Minds Manual for Guideline Development Ver. 2.0]*. Tokyo: Japan Council for Quality Health Care, [Cited 15 March 2016.] Available from URL: http://minds4.jcqhc.or.jp/minds/guideline/pdf/manual_all_2.0.pdf. Japanese.
7 Balshem H, Helfand M, Schunemann HJ *et al.* GRADE guidelines: 3. rating the quality of evidence. *J Clin Epidemiol* 2011; **64**: 401–406.
8 Andrews J, Guyatt G, Oxman AD *et al.* GRADE guidelines: 14. Going from evidence to recommendations: the significance and presentation of recommendations. *J Clin Epidemiol* 2013; **66**: 719–725.
9 Liu AS, Mulliken JB, Zurakowski D, Fishman SJ, Greene AK. Extracranial arteriovenous malformations: natural progression and recurrence after treatment. *Plast Reconstr Surg* 2010; **125**: 1185–1194.
10 Kohout MP, Hansen M, Pribaz JJ, Mulliken JB. Arteriovenous malformations of the head and neck: natural history and management. *Plast Reconstr Surg* 1998; **102**: 643–654.
11 Richter GT, Suen J, North PE, James CA, Waner M, Buckmiller LM. Arteriovenous malformations of the tongue: a spectrum of disease. *Laryngoscope* 2007; **117**: 328–335.
12 Hyun D, Do YS, Park KB *et al.* Ethanol embolotherapy of foot arteriovenous malformations. *J Vasc Surg* 2013; **58**: 1619–1626.
13 Park KB, Do YS, Kim DI *et al.* Predictive factors for response of peripheral arteriovenous malformations to embolization therapy: analysis of clinical data and imaging findings. *J Vasc Interv Radiol* 2012; **23**: 1478–1486.
14 Wu JK, Bisdorff A, Gelbert F, Enjolras O, Burrows PE, Mulliken JB. Auricular arteriovenous malformation: evaluation, management, and outcome. *Plast Reconstr Surg* 2005; **115**: 985–995.
15 DesPrez JD, Kiehn CL, Vlastou C, Bonstelle C. Congenital arteriovenous malformation of the head and neck. *Am J Surg* 1978; **136**: 424–429.
16 Dompmartin A, Labbé D, Barrellier MT, Théron J. Use of a regulating flap in the treatment of a large arteriovenous malformation of the scalp. *Br J Plast Surg* 1998; **51**: 561–563.
17 Yamamoto Y, Ohura T, Minakawa H *et al.* Experience with arteriovenous malformations treated with flap coverage. *Plast Reconstr Surg* 1994; **94**: 476–482.
18 Hartzell LD, Stack BC Jr, Yuen J, Vural E, Suen JY. Free tissue reconstruction following excision of head and neck arteriovenous malformations. *Arch Facial Plast Surg* 2009; **11**: 171–177.
19 Visser A, FitzJohn T, Tan ST. Surgical management of arteriovenous malformation. *J Plast Reconstr Aesthet Surg* 2011; **64**: 283–291.
20 Hong JP, Choi JW, Chang H, Lee TJ. Reconstruction of the face after resection of arteriovenous malformations using anterolateral thigh perforator flap. *J Craniofac Surg* 2005; **16**: 851–855.
21 Koshima I, Takahashi Y, Namba Y *et al.* Treatment for arteriovenous malformation. *Keisei Geka* 2001; **44**: 665–673. Japanese.
22 Toh S, Tsubo K, Arai H, Harata S. Vascularized free flaps for reconstruction after resection of congenital arteriovenous malformations of the hand. *J Reconstr Microsurg* 2000; **16**: 511–517.
23 Yokoo K, Nishihori K, Kono A, Ishiguchi T, Ohta T. [Surgical treatment of arteriovenous malformations in the head and neck combined with antecedent embolization]. *Keisei Geka* 2009; **52**: 1201–1208. Japanese.

This article has been co-published with the permission of *The Journal of Dermatology, Pediatrics International* and *Japanese Journal of Radiology*. All rights reserved. © 2020 The Authors. The articles are identical except for minor stylistic and spelling differences in keeping with each journal's style. Either citation can be used when citing this article.

24 Koshima I, Nanba Y, Tsutsui T, Takahashi Y, Watanabe A, Ishii R. Free perforator flap for the treatment of defects after resection of huge arteriovenous malformations in the head and neck regions. *Ann Plast Surg* 2003; **51**: 194–199.
25 Kajitani N, Ikuta Y, Ishida O, Mochizuki Y, Kimori K. [Surgical treatment of arteriovenous fistula of the hand]. *Nihon Te No Geka Gakkai Zasshi* 1999; **15**: 758–761. Japanese.
26 Minami A, Kato H, Hirachi K. Complete removal plus dorsalis pedis flap for arteriovenous malformation in the hypothenar region. *J Reconstr Microsurg* 1998; **14**: 439–443.
27 Koshima I, Soeda S, Murashita T. Extended wrap-around flap for reconstruction of the finger with recurrent arteriovenous malformation. *Plast Reconstr Surg* 1993; **91**: 1140–1144.
28 Wojcicki P, Wojcicka K. The treatment of extensive arteriovenous malformations in the head. *Pol Przegl Chir* 2013; **85**: 83–89.
29 Ermer MA, Gutwald R, Schumacher M, Schmelzeisen R, Taschner C. Use of the radial forearm artery for secondary embolization of an extensive life-threatening arteriovenous malformation of the mid-face and anterior skull base – a case report. *J Craniomaxillofac Surg* 2013; **41**: 258–264.
30 Ueda K, Oba S, Nakai K, Okada M, Kurokawa N, Nuri T. Functional reconstruction of the upper and lower lips and commissure with a forearm flap combined with a free gracilis muscle transfer. *J Plast Reconstr Aesthet Surg* 2009; **62**: e337–e340.
31 Ninkovic M, Sucur D, Starovic B, Markovic S. Arteriovenous fistulae after free flap surgery in a replanted hand. *J Hand Surg Br* 1992; **17**: 657–659.
32 Bit N, Vidyasagaran T, Amalorpavanathan J, Balakrishnan TM, Sritharan N. Management of a challenging arteriovenous malformation of the scalp and orbit in a patient with polycystic kidney disease. *Ann Vasc Surg* 2012; **26**: 1129.e9–1129.e11.
33 Righi PD, Bade MA, Coleman JJ 3rd, Allen M. Arteriovenous malformation of the base of tongue: case report and literature review. *Microsurgery* 1996; **17**: 706–709.
34 Minagawa T, Itaya Y, Furukawa H. Resection of an arteriovenous malformation of the scalp using a modified tumescent technique. *Nihon Keisei Geka Gakkai Kaishi* 2010; **30**: 87–89.
35 Suyama Y, Nakayama B, Fukuoka K *et al.* Auricular reconstruction with a free radial forearm flap for necrotized ear after sclerotherapy for arteriovenous malformation: a case report. *Nihon Maikuro Sajari Gakkai Kaishi* 2010; **23**: 311–315. Japanese.
36 Urayama H, Harada T, Kawase H, Watanabe Y. Surgical management of soft tissue arteriovenous malformations and hemangiomas. *Shoni Geka* 1993; **25**: 415–419. Japanese.
37 Yamamoto Y, Sugihara T, Minakawa H, Ohkubo Y, Hayashi T. [Surgical treatment of massive arteriovenous malformation with application of hypothermia and cardiopulmonary bypass]. *Nihon Keisei Geka Gakkai Kaishi* 1996; **16**: 863–871. Japanese.
38 Hormozi AK, Shafii MR. Supraclavicular flap: reconstructive strategy for massive facial arteriovenous malformations. *J Craniofac Surg* 2011; **22**: 931–936.
39 Hurwitz DJ, Kerber CW. Hemodynamic considerations in the treatment of arteriovenous malformations of the face and scalp. *Plast Reconstr Surg* 1981; **67**: 421–434.
40 Kiyokawa K, Takagi M, Fukushima J, Kizuka Y, Inoue Y, Tai Y. Surgical treatment following huge arteriovenous malformation extending from the lower lip to the chin: combination of embolization, total resection, and a double cross lip flap. *J Craniofac Surg* 2005; **16**: 443–448.
41 Thomas WO. Facial arteriovenous malformation managed with ablative surgery and dual rotational flap reconstruction. *South Med J* 1994; **87**: 1178–1182.
42 Warwick DJ, Milling MA. Growth of a vascular malformation into a cross-finger flap. *Br J Clin Pract* 1993; **47**: 48.
43 Agir H, Sen C, Onyedi M. Extended lateral supramalleolar flap for very distal foot coverage: a case with arteriovenous malformation. *J Foot Ankle Surg* 2007; **46**: 310–313.
44 Sakurai H, Nozaki M, Sasaki K *et al.* Successful management of a giant arteriovenous fistula with a combination of selective embolization and excision: report of a case. *Surg Today* 2002; **32**: 189–193.
45 Watanabe T, Asato H, Umekawa K, Nomura H, Suzuki Y. [Resurfacing the index finger after resection of an arteriovenous malformation using a reverse forearm flap combined with additional venous anastomosis: a case report]. *Nihon Keisei Geka Gakkai Kaishi* 2012; **32**: 335–339. Japanese.
46 Ishisaka T, Naitoh H, Akiyama K, Shigeyoshi N. [A case of lower lip arteriovenous malformation with verrucous carcinoma]. *Nihon Keisei Geka Gakkai Kaishi* 2009; **29**: 7–11. Japanese.
47 Kitagawa S, Kizaki K, Yajima H, Mii Y, Tamai S. [Treatment of hemangiomas associated with arteriovenous fistulae in a family]. *Chubu Nihon Seikei Geka Saigai Geka Gakkai Zasshi* 1997; **40**: 331–332. Japanese.
48 Gunji H, Suda K, Ono I, Ariga T, Kaneko F. [Arteriovenous fistula of auricle treated with a temporoparietal fascial flap: a case report]. *Nihon Keisei Geka Gakkai Kaishi* 1993; **13**: 221–227. Japanese.
49 Fujita A, Asada M, Saitoh M *et al.* A case of congenital arteriovenous malformation of the scalp treated with rotation flap. *No Shinkei Geka Janaru* 2000; **9**: 86–91. Japanese.
50 Nakamura E, Suzuki S, Imagawa K, Akamatsu T, Miyasaka M. Experience of two patients with auricular arteriovenous malformation. *Skin Surgery* 2014; **23**: 73–78. Japanese.
51 Yoshimura Y, Mizuno M, Kobayashi T *et al.* [Case reports: extracranial arteriovenous malformation]. *Hifuka No Rinsho* 2014; **56**: 1180–1183. Japanese.
52 Matsuzaki K, Nakamura T, Tahara T, Kashiwa H, Oshima H, Souzumi T. [Congenital arteriovenous malformation of the auricle]. *Jibi Inkoka Tokeibu Geka* 1995; **67**: 337–341. Japanese.
53 Schultz RC, Hermosillo CX. Congenital arteriovenous malformation of the face and scalp. *Plast Reconstr Surg* 1980; **65**: 496–501.
54 Slaba S, Herbreteau D, Jhaveri HS *et al.* Therapeutic approach to arteriovenous malformations of the tongue. *Eur Radiol* 1998; **8**: 280–285.
55 Toker ME, Eren E, Akbayrak H *et al.* Combined approach to a peripheral congenital arteriovenous malformation: surgery and embolization. *Heart Vessels* 2006; **21**: 127–130.
56 Doppman JL, Pevsner P. Embolization of arteriovenous malformations by direct percutaneous puncture. *AJR Am J Roentgenol* 1983; **140**: 773–778.
57 Aikawa H, Okino Y, Yamada Y *et al.* [A review of embolization for arteriovenous malformations (fistulae)]. *Oita Kenritsu Byoin Igaku Zasshi* 1997; **26**: 77–82. Japanese.
58 Yamamoto T, Kanamura N, Tsukitani K *et al.* Direct embolization for a life-threatening mandibular arteriovenous malformation by means of hypothermic cardio-pulmonary arrest. *Kyoto Furitsu Ika Daigaku Zasshi* 1999; **108**: 981–994.
59 Deng W, Huang D, Chen S *et al.* Management of high-flow arteriovenous malformation in the maxillofacial region. *J Craniofac Surg* 2010; **21**: 916–919.
60 Erdmann MW, Jackson JE, Davies DM, Allison DJ. Multidisciplinary approach to the management of head and neck arteriovenous malformations. *Ann R Coll Surg Engl* 1995; **77**: 53–59.
61 Goldberg RA, Garcia GH, Duckwiler GR. Combined embolization and surgical treatment of arteriovenous malformation of the orbit. *Am J Ophthalmol* 1993; **116**: 17–25.
62 Persky MS, Yoo HJ, Berenstein A. Management of vascular malformations of the mandible and maxilla. *Laryngoscope* 2003; **113**: 1885–1892.
63 Liu DG, Ma XC, Zhao FY, Zhang JG. A preliminary study of angiographic classification and its correlation to treatment of central arteriovenous malformation in the jaw. *Oral Surg Oral Med Oral Pathol Oral Radiol Endod* 2005; **100**: 473–480.
64 Rodesch G, Soupre V, Vazquez MP, Alvarez H, Lasjaunias P. Arteriovenous malformations of the dental arcades. The place of endovascular therapy: results in 12 cases are presented. *J Craniomaxillofac Surg* 1998; **26**: 306–313.

This article has been co-published with the permission of *The Journal of Dermatology, Pediatrics International* and *Japanese Journal of Radiology*. All rights reserved. © 2020 The Authors. The articles are identical except for minor stylistic and spelling differences in keeping with each journal's style. Either citation can be used when citing this article.

65 Chen W, Wang J, Li J, Xu L. Comprehensive treatment of arteriovenous malformations in the oral and maxillofacial region. *J Oral Maxillofac Surg* 2005; **63**: 1484–1488.
66 Chen WL, Ye JT, Xu LF, Huang ZQ, Zhang DM. A multidisciplinary approach to treating maxillofacial arteriovenous malformations in children. *Oral Surg Oral Med Oral Pathol Oral Radiol Endod* 2009; **108**: 41–47.
67 Churojana A, Khumtong R, Songsaeng D, Chongkolwatana C, Suthipongchai S. Life-threatening arteriovenous malformation of the maxillomandibular region and treatment outcomes. *Interv Neuroradiol* 2012; **18**: 49–59.
68 Liu D, Ma XC. Clinical study of embolization of arteriovenous malformation in the oral and maxillofacial region. *Chin J Dent Res* 2000; **3**: 63–70.
69 Chandra RV, Leslie-Mazwi TM, Orbach DB, Kaban LB, Rabinov JD. Transarterial embolization of mandibular arteriovenous malformations using ONYX. *J Oral Maxillofac Surg* 2014; **72**: 1504–1510.
70 Fifi J, Niimi Y, Berenstein A. Onyx embolization of an extensive mandibular arteriovenous malformation via a dual lumen balloon catheter: a technical case report. *J Neurointerv Surg* 2013; **5**: e5.
71 Fan XD, Su LX, Zheng JW, Zheng LZ, Zhang ZY. Ethanol embolization of arteriovenous malformations of the mandible. *AJNR Am J Neuroradiol* 2009; **30**: 1178–1183.
72 Park HS, Do YS, Park KB *et al.* Ethanol embolotherapy of hand arteriovenous malformations. *J Vasc Surg* 2011; **53**: 725–731.
73 Park UJ, Do YS, Park KB *et al.* Treatment of arteriovenous malformations involving the hand. *Ann Vasc Surg* 2012; **26**: 643–648.
74 Hibino N, Hamada Y, Goda Y *et al.* [Arterial graft for reconstruction after complete removal of the arteriovenous malformation]. *Nihon Maikuro Sajari Gakkai Kaishi* 2005; **18**: 78–82. Japanese.
75 Widlus DM, Murray RR, White RI Jr *et al.* Congenital arteriovenous malformations: tailored embolotherapy. *Radiology* 1988; **169**: 511–516.
76 Hattori Y, Doi K, Kawakami F, Watanabe M. Extended wrap-around flap for thumb reconstruction following radical excision of a congenital arteriovenous fistula. *J Hand Surg Br* 1998; **23**: 72–75.
77 Sugioka T, Sunagawa T, Suzuki O, Kijima Y, Ochi M. [Surgical treatment for arteriovenous malformation involving the hand and forearm]. *Nihon Te No Geka Gakkai Zasshi* 2008; **24**: 940–943. Japanese.
78 Furuya T, Nakazawa T. Congenital arteriovenous malformation of the index finger: a case report. *Myakkangaku* 2009; **49**: 430–433. Japanese.
79 Moore JR, Weiland AJ. Embolotherapy in the treatment of congenital arteriovenous malformations of the hand: a case report. *J Hand Surg Am* 1985; **10**: 135–139.
80 Arneja JS, Gosain AK. Vascular malformations. *Plast Reconstr Surg* 2008; **121**: 195e–206e.
81 Hein KD, Mulliken JB, Kozakewich HP, Upton J, Burrows PE. Venous malformations of skeletal muscle. *Plast Reconstr Surg* 2002; **110**: 1625–1635.
82 Marler JJ, Mulliken JB. Current management of hemangiomas and vascular malformations. *Clin Plast Surg* 2005; **32**: 99–116, ix.
83 Nguyen JT, Koerper MA, Hess CP *et al.* Aspirin therapy in venous malformation: a retrospective cohort study of benefits, side effects, and patient experiences. *Pediatr Dermatol* 2014; **31**: 556–560.
84 Shireman PK, McCarthy WJ, Yao JS, Vogelzang RL. Treatment of venous malformations by direct injection with ethanol. *J Vasc Surg* 1997; **26**: 838–844.
85 Rimon U, Garniek A, Galili Y, Golan G, Bensaid P, Morag B. Ethanol sclerotherapy of peripheral venous malformations. *Eur J Radiol* 2004; **52**: 283–287.
86 Marrocco-Trischitta MM, Nicodemi EM, Nater C, Stillo F. Management of congenital venous malformations of the vulva. *Obstet Gynecol* 2001; **98**: 789–793.
87 Suh JS, Shin KH, Na JB, Won JY, Hahn SB. Venous malformations: sclerotherapy with a mixture of ethanol and lipiodol. *Cardiovasc Intervent Radiol* 1997; **20**: 268–273.
88 Dompmartin A, Blaizot X, Théron J *et al.* Radio-opaque ethylcellulose-ethanol is a safe and efficient sclerosing agent for venous malformations. *Eur Radiol* 2011; **21**: 2647–2656.
89 Schumacher M, Dupuy P, Bartoli JM *et al.* Treatment of venous malformations: first experience with a new sclerosing agent–a multicenter study. *Eur J Radiol* 2011; **80**: e366–e372.
90 Mimura H, Kanazawa S, Yasui K *et al.* Percutaneous sclerotherapy for venous malformations using polidocanol under fluoroscopy. *Acta Med Okayama* 2003; **57**: 227–234.
91 Mimura H, Fujiwara H, Hiraki T *et al.* Polidocanol sclerotherapy for painful venous malformations: evaluation of safety and efficacy in pain relief. *Eur Radiol* 2009; **19**: 2474–2480.
92 Cabrera J, Cabrera J Jr, Garcia-Olmedo MA, Redondo P. Treatment of venous malformations with sclerosant in microfoam form. *Arch Dermatol* 2003; **139**: 1409–1416.
93 Ozaki M, Kurita M, Kaji N *et al.* Efficacy and evaluation of safety of sclerosants for intramuscular venous malformations: clinical and experimental studies. *Scand J Plast Reconstr Surg Hand Surg* 2010; **44**: 75–87.
94 Krokidis M, Venetucci P, Hatzidakis A, Iaccarino V. Sodium tetradecyl sulphate direct intralesional sclerotherapy of venous malformations of the vulva and vagina: report of five cases. *Cardiovasc Intervent Radiol* 2011; **34**(Suppl 2): S228–S231.
95 Enjolras O, Ciabrini D, Mazoyer E, Laurian C, Herbreteau D. Extensive pure venous malformations in the upper or lower limb: a review of 27 cases. *J Am Acad Dermatol* 1997; **36**: 219–225.
96 Steiner F, FitzJohn T, Tan ST. Surgical treatment for venous malformation. *J Plast Reconstr Aesthet Surg* 2013; **66**: 1741–1749.
97 Noel AA, Gloviczki P, Cherry KJ Jr, Rooke TW, Stanson AW, Driscoll DJ. Surgical treatment of venous malformations in Klippel-Trenaunay syndrome. *J Vasc Surg* 2000; **32**: 840–847.
98 Sidhu MK, Perkins JA, Shaw DW, Bittles MA, Andrews RT. Ultrasound-guided endovenous diode laser in the treatment of congenital venous malformations: preliminary experience. *J Vasc Interv Radiol* 2005; **16**: 879–884.
99 Lu X, Ye K, Shi H *et al.* Percutaneous endovenous treatment of congenital extratruncular venous malformations with an ultrasound-guided and 810-nm diode laser. *J Vasc Surg* 2011; **54**: 139–145.
100 Liu G, Liu X, Li W *et al.* Ultrasound-guided intralesional diode laser treatment of congenital extratruncular venous malformations: mid-term results. *Eur J Vasc Endovasc Surg* 2014; **47**: 558–564.
101 Mazoyer E, Enjolras O, Laurian C, Houdart E, Drouet L. Coagulation abnormalities associated with extensive venous malformations of the limbs: differentiation from Kasabach-Merritt syndrome. *Clin Lab Haematol* 2002; **24**: 243–251.
102 Cornelis F, Neuville A, Labreze C *et al.* Percutaneous cryotherapy of vascular malformation: initial experience. *Cardiovasc Intervent Radiol* 2013; **36**: 853–856.
103 Cornelis F, Havez M, Labreze C *et al.* Percutaneous cryoablation of symptomatic localized venous malformations: preliminary short-term results. *J Vasc Interv Radiol* 2013; **24**: 823–827.
104 Betz CS, Jager HR, Brookes JA, Richards R, Leunig A, Hopper C. Interstitial photodynamic therapy for a symptom-targeted treatment of complex vascular malformations in the head and neck region. *Lasers Surg Med* 2007; **39**: 571–582.
105 Bashkatov AN, Genina EA, Kochubey VI, Tuchin VV. Optical properties of human skin, subcutaneous and mucous tissues in the wavelength range from 400 to 2000 nm. *J Phys D Appl Phys* 2005; **38**: 2543–2555.
106 Sarig O, Kimel S, Orenstein A. Laser treatment of venous malformations. *Ann Plast Surg* 2006; **57**: 20–24.
107 Vesnaver A, Dovsak DA. Treatment of vascular lesions in the head and neck using Nd:YAG laser. *J Craniomaxillofac Surg* 2006; **34**: 17–24.
108 Asai T, Suzuki H, Enomoto Y *et al.* Clinical evaluation of 74 vascular malformations of the oral region treated by photocoagulation with an Nd:YAG laser. *Nihon Reza Shigakkaishi* 2013; **24**: 3–9. Japanese.

This article has been co-published with the permission of *The Journal of Dermatology, Pediatrics International* and *Japanese Journal of Radiology*. All rights reserved. © 2020 The Authors. The articles are identical except for minor stylistic and spelling differences in keeping with each journal's style. Either citation can be used when citing this article.

109 Ng EK, Cheung FK, Chiu PW. Blue rubber bleb nevus syndrome: treatment of multiple gastrointestinal hemangiomas with argon plasma coagulator. *Dig Endosc* 2009; **21**: 40–42.
110 Cholewa D, Waldschmidt J. Laser treatment of hemangiomas of the larynx and trachea. *Lasers Surg Med* 1998; **23**: 221–232.
111 Yakes WF, Haas DK, Parker SH *et al.* Symptomatic vascular malformations: ethanol embolotherapy. *Radiology* 1989; **170**: 1059–1066.
112 Lee IH, Kim KH, Jeon P *et al.* Ethanol sclerotherapy for the management of craniofacial venous malformations: the interim results. *Korean J Radiol* 2009; **10**: 269–276.
113 Hoque S, Das BK. Treatment of venous malformations with ethanolamine oleate: a descriptive study of 83 cases. *Pediatr Surg Int* 2011; **27**: 527–531.
114 Stuart S, Barnacle AM, Smith G, Pitt M, Roebuck DJ. Neuropathy after sodium tetradecyl sulfate sclerotherapy of venous malformations in children. *Radiology* 2015; **274**: 897–905.
115 Zhao JH, Zhang WF, Zhao YF. Sclerotherapy of oral and facial venous malformations with use of pingyangmycin and/or sodium morrhuate. *Int J Oral Maxillofac Surg* 2004; **33**: 463–466.
116 Bai N, Chen YZ, Fu YJ, Wu P, Zhang WN. A clinical study of pingyangmycin sclerotherapy for venous malformation: an evaluation of 281 consecutive patients. *J Clin Pharm Ther* 2014; **39**: 521–526.
117 Goyal M, Causer PA, Armstrong D. Venous vascular malformations in pediatric patients: comparison of results of alcohol sclerotherapy with proposed MR imaging classification. *Radiology* 2002; **223**: 639–644.
118 Yun WS, Kim YW, Lee KB *et al.* Predictors of response to percutaneous ethanol sclerotherapy (PES) in patients with venous malformations: analysis of patient self-assessment and imaging. *J Vasc Surg* 2009; **50**: 581–589, 589 e581.
119 Rautio R, Saarinen J, Laranne J, Salenius JP, Keski-Nisula L. Endovascular treatment of venous malformations in extremities: results of sclerotherapy and the quality of life after treatment. *Acta Radiol* 2004; **45**: 397–403.
120 Yamaki T, Nozaki M, Sakurai H, Takeuchi M, Soejima K, Kono T. Prospective randomized efficacy of ultrasound-guided foam sclerotherapy compared with ultrasound-guided liquid sclerotherapy in the treatment of symptomatic venous malformations. *J Vasc Surg* 2008; **47**: 578–584.
121 Nagao M, Sasaki S, Furukawa H, Saito N, Yamamoto Y. [A clinical study of sclerotherapy for venous malformation of an upper extremity]. *Nihon Keisei Geka Gakkai Kaishi* 2012; **32**: 463–468. Japanese.
122 Nomura T, Sakurai A, Nagata I, Terashi H, Tahara S. Our strategy for the treatment of venous malformations. *Jomyakugaku* 2008; **19**: 161–168. Japanese.
123 Qiu Y, Chen H, Lin X, Hu X, Jin Y, Ma G. Outcomes and complications of sclerotherapy for venous malformations. *Vasc Endovascular Surg* 2013; **47**: 454–461.
124 Wong GA, Armstrong DC, Robertson JM. Cardiovascular collapse during ethanol sclerotherapy in a pediatric patient. *Paediatr Anaesth* 2006; **16**: 343–346.
125 Tachibana K, Kobayashi S, Kojima T, Kaseno S, Kemmotsu O. Pulmonary emboli in sclerotherapy for peripheral vascular malformations under general anesthesia; a report of two cases. *Masui* 2004; **53**: 645–649. Japanese.
126 Marrocco-Trischitta MM, Guerrini P, Abeni D, Stillo F. Reversible cardiac arrest after polidocanol sclerotherapy of peripheral venous malformation. *Dermatol Surg* 2002; **28**: 153–155.
127 Shimo T, Hidaka K, Yanagawa S, Kadota W, Kawakami S, Tsuchida H. Two episodes of cardiac arrest in a boy receiving sclerotherapy with polydocanol–a case report. *Masui* 2005; **54**: 57–59. Japanese.
128 Schild SE, Buskirk SJ, Frick LM, Cupps RE. Radiotherapy for large symptomatic hemangiomas. *Int J Radiat Oncol Biol Phys* 1991; **21**: 729–735.
129 Mitsuhashi N, Furuta M, Sakurai H *et al.* Outcome of radiation therapy for patients with Kasabach-Merritt syndrome. *Int J Radiat Oncol Biol Phys* 1997; **39**: 467–473.
130 Ogino I, Torikai K, Kobayasi S, Aida N, Hata M, Kigasawa H. Radiation therapy for life- or function-threatening infant hemangioma. *Radiology* 2001; **218**: 834–839.
131 Miller JG, Orton CI. Long term follow-up of a case of Kasabach-Merritt syndrome successfully treated with radiotherapy and corticosteroids. *Br J Plast Surg* 1992; **45**: 559–561.
132 Frevel T, Rabe H, Uckert F, Harms E. Giant cavernous haemangioma with Kasabach-Merritt syndrome: a case report and review. *Eur J Pediatr* 2002; **161**: 243–246.
133 Stringel G, Mercer S. Giant hemangioma in the newborn and infant. Complications and management. *Clin Pediatr (Phila)* 1984; **23**: 498–502.
134 Enjolras O, Wassef M, Mazoyer E *et al.* Infants with Kasabach-Merritt syndrome do not have "true" hemangiomas. *J Pediatr* 1997; **130**: 631–640.
135 Lundell M, Mattsson A, Hakulinen T, Holm LE. Breast cancer after radiotherapy for skin hemangioma in infancy. *Radiat Res* 1996; **145**: 225–230.
136 Haddy N, Andriamboavonjy T, Paoletti C *et al.* Thyroid adenomas and carcinomas following radiotherapy for a hemangioma during infancy. *Radiother Oncol* 2009; **93**: 377–382.
137 Caldwell JB, Ryan MT, Benson PM, James WD. Cutaneous angiosarcoma arising in the radiation site of a congenital hemangioma. *J Am Acad Dermatol* 1995; **33**: 865–870.
138 Oguri A, Oda M, Yokoo K. [The relation between age and the effectiveness of laser treatment for capillary malformation]. *Nihon Keisei Geka Gakkai Kaishi* 2009; **29**: 407–411. Japanese.
139 Reynolds N, Exley J, Hills S, Falder S, Duff C, Kenealy J. The role of the Lumina intense pulsed light system in the treatment of port wine stains–a case controlled study. *Br J Plast Surg* 2005; **58**: 968–980.
140 Katugampola GA, Lanigan SW. Five years' experience of treating port wine stains with the flashlamp-pumped pulsed dye laser. *Br J Dermatol* 1997; **137**: 750–754.
141 Minato S. Comparison between results of treatment with dye laser and argon laser in cases of hemangioma simplex. *Iwate Igaku Zasshi* 1997; **49**: 299–302.
142 Ryuzaki K, Tamura A, Amano H, Takeuchi Y, Ishikawa O, Miyachi Y. [An overview of dye laser treatment for superficial hemangiomas at the Department of Dermatology, Gunma University]. *Hifuka Kiyo* 1996; **91**: 41–46. Japanese.
143 Matsumoto T. [Comparative study in laser treatment of portwine stains with dye and argon lasers. Part 2: statistical study of clinical effects]. *Nihon Keisei Geka Gakkai Kaishi* 1996; **16**: 246–259. Japanese.
144 Fitzpatrick RE, Lowe NJ, Goldman MP, Borden H, Behr KL, Ruiz-Esparza J. Flashlamp-pumped pulsed dye laser treatment of portwine stains. *J Dermatol Surg Oncol* 1994; **20**: 743–748.
145 Morikawa K, Yamauchi K, Saheki M, Tezuka T. Treatment of portwine stain using pulsed dye laser: comparison of effectiveness with location of lesion, age and wavelength. *Hifu* 1994; **36**: 514–521. Japanese.
146 Matsushita Y, Suzuki S, Koyama H, Akamatsu J, Kawata Y, Kawai K. Treatment of portwine stains with dye lasers. *Hifuka Kiyo* 1994; **89**: 205–210. Japanese.
147 Namba Y, Mae O, Nagase Y, Ao M, Hamaya K, Nose S. [Dye laser treatment of cutaneous simple hemangioma]. *Okayama Saiseikai Sogo Byoin Zasshi* 1991; **22**: 1–10. Japanese.
148 Bandoh Y, Yanai A, Tsuzuki K. Dye laser treatment of port-wine stains. *Aesthetic Plast Surg* 1990; **14**: 287–291.
149 Bandoh Y. [Pulsed dye laser treatment for port-wine stains]. *Rinsho Hifuka* 1989; **43**: 1337–1340. Japanese.
150 Renfro L, Geronemus RG. Anatomical differences of port-wine stains in response to treatment with the pulsed dye laser. *Arch Dermatol* 1993; **129**: 182–188.
151 Lanigan SW. Port wine stains on the lower limb: response to pulsed dye laser therapy. *Clin Exp Dermatol* 1996; **21**: 88–92.
152 Sommer S, Seukeran DC, Sheehan-Dare RA. Efficacy of pulsed dye laser treatment of port wine stain malformations of the lower limb. *Br J Dermatol* 2003; **149**: 770–775.

This article has been co-published with the permission of *The Journal of Dermatology, Pediatrics International* and *Japanese Journal of Radiology*. All rights reserved. © 2020 The Authors. The articles are identical except for minor stylistic and spelling differences in keeping with each journal's style. Either citation can be used when citing this article.

153 Fitzpatrick TB. The validity and practicality of sun-reactive skin types I through VI. *Arch Dermatol* 1988; **124**: 869–871.
154 Wareham WJ, Cole RP, Royston SL, Wright PA. Adverse effects reported in pulsed dye laser treatment for port wine stains. *Lasers Med Sci* 2009; **24**: 241–246.
155 Orten SS, Waner M, Flock S, Roberson PK, Kincannon J. Port-wine stains. An assessment of 5 years of treatment. *Arch Otolaryngol Head Neck Surg* 1996; **122**: 1174–1179.
156 Michel S, Landthaler M, Hohenleutner U. Recurrence of port-wine stains after treatment with the flashlamp-pumped pulsed dye laser. *Br J Dermatol* 2000; **143**: 1230–1234.
157 Soueid A, Waters R. Re-emergence of port wine stains following treatment with flashlamp-pumped dye laser 585 nm. *Ann Plast Surg* 2006; **57**: 260–263.
158 Huikeshoven M, Koster PH, de Borgie CA, Beek JF, van Gemert MJ, van der Horst CM. Redarkening of port-wine stains 10 years after pulsed-dye-laser treatment. *N Engl J Med* 2007; **356**: 1235–1240.
159 Phung TL, Oble DA, Jia W, Benjamin LE, Mihm MC Jr, Nelson JS. Can the wound healing response of human skin be modulated after laser treatment and the effects of exposure extended? Implications on the combined use of the pulsed dye laser and a topical angiogenesis inhibitor for treatment of port wine stain birthmarks. *Lasers Surg Med* 2008; **40**: 1–5.
160 Babilas P, Shafirstein G, Bäumler W *et al.* Selective photothermolysis of blood vessels following flashlamp-pumped pulsed dye laser irradiation: in vivo results and mathematical modelling are in agreement. *J Invest Dermatol* 2005; **125**: 343–352.
161 Laquer VT, Hevezi PA, Albrecht H, Chen TS, Zlotnik A, Kelly KM. Microarray analysis of port wine stains before and after pulsed dye laser treatment. *Lasers Surg Med* 2013; **45**: 67–75.
162 Chapas AM, Eickhorst K, Geronemus RG. Efficacy of early treatment of facial port wine stains in newborns: a review of 49 cases. *Lasers Surg Med* 2007; **39**: 563–568.
163 Jia W, Sun V, Tran N *et al.* Long-term blood vessel removal with combined laser and topical rapamycin antiangiogenic therapy: implications for effective port wine stain treatment. *Lasers Surg Med* 2010; **42**: 105–112.
164 Chang CJ, Hsiao YC, Mihm MC Jr, Nelson JS. Pilot study examining the combined use of pulsed dye laser and topical Imiquimod versus laser alone for treatment of port wine stain birthmarks. *Lasers Surg Med* 2008; **40**: 605–610.
165 Tremaine AM, Armstrong J, Huang YC *et al.* Enhanced port-wine stain lightening achieved with combined treatment of selective photothermolysis and imiquimod. *J Am Acad Dermatol* 2012; **66**: 634–641.
166 Nguyen CM, Yohn JJ, Huff C, Weston WL, Morelli JG. Facial port wine stains in childhood: prediction of the rate of improvement as a function of the age of the patient, size and location of the port wine stain and the number of treatments with the pulsed dye (585 nm) laser. *Br J Dermatol* 1998; **138**: 821–825.
167 van der Horst CM, Koster PH, de Borgie CA, Bossuyt PM, van Gemert MJ. Effect of the timing of treatment of port-wine stains with the flash-lamp-pumped pulsed-dye laser. *N Engl J Med* 1998; **338**: 1028–1033.
168 Léauté-Labrèze C, Dumas de la Roque E, Hubiche T, Boralevi F, Thambo JB, Taïeb A. Propranolol for severe hemangiomas of infancy. *N Engl J Med* 2008; **358**: 2649–2651.
169 Broeks IJ, Hermans DJ, Dassel AC, van der Vleuten CJ, van Beynum IM. Propranolol treatment in life-threatening airway hemangiomas: a case series and review of literature. *Int J Pediatr Otorhinolaryngol* 2013; **77**: 1791–1800.
170 Sharma VK, Fraulin FO, Dumestre DO, Walker L, Harrop AR. Beta-blockers for the treatment of problematic hemangiomas. *Can J Plast Surg* 2013; **21**: 23–28.
171 Zvulunov A, McCuaig C, Frieden IJ *et al.* Oral propranolol therapy for infantile hemangiomas beyond the proliferation phase: a multicenter retrospective study. *Pediatr Dermatol* 2011; **28**: 94–98.
172 Hermans DJ, van Beynum IM, Schultze Kool LJ, van de Kerkhof PC, Wijnen MH, van der Vleuten CJ. Propranolol, a very promising treatment for ulceration in infantile hemangiomas: a study of 20 cases with matched historical controls. *J Am Acad Dermatol* 2011; **64**: 833–838.
173 Saint-Jean M, Léauté-Labrèze C, Mazereeuw-Hautier J *et al.* Propranolol for treatment of ulcerated infantile hemangiomas. *J Am Acad Dermatol* 2011; **64**: 827–832.
174 Caussé S, Aubert H, Saint-Jean M *et al.* Propranolol-resistant infantile haemangiomas. *Br J Dermatol* 2013; **169**: 125–129.
175 Vassallo P, Forte R, Di Mezza A, Magli A. Treatment of infantile capillary hemangioma of the eyelid with systemic propranolol. *Am J Ophthalmol* 2013; **155**: 165–170 e162.
176 Lynch M, Lenane P, O'Donnell BF. Propranolol for the treatment of infantile haemangiomas: our experience with 44 patients. *Clin Exp Dermatol* 2014; **39**: 142–145.
177 Price CJ, Lattouf C, Baum B *et al.* Propranolol vs corticosteroids for infantile hemangiomas: a multicenter retrospective analysis. *Arch Dermatol* 2011; **147**: 1371–1376.
178 Hermans DJ, Bauland CG, Zweegers J, van Beynum IM, van der Vleuten CJ. Propranolol in a case series of 174 patients with complicated infantile haemangioma: indications, safety and future directions. *Br J Dermatol* 2013; **168**: 837–843.
179 de Graaf M, Breur J, Raphael MF, Vos M, Breugem CC, Pasmans S. Adverse effects of propranolol when used in the treatment of hemangiomas: a case series of 28 infants. *J Am Acad Dermatol* 2011; **65**: 320–327.
180 Hogeling M, Adams S, Wargon O. A randomized controlled trial of propranolol for infantile hemangiomas. *Pediatrics* 2011; **128**: e259–e266.
181 Zaher H, Rasheed H, Esmat S *et al.* Propranolol and infantile hemangiomas: different routes of administration, a randomized clinical trial. *Eur J Dermatol* 2013; **23**: 646–652.
182 Malik MA, Menon P, Rao KL, Samujh R. Effect of propranolol vs prednisolone vs propranolol with prednisolone in the management of infantile hemangioma: a randomized controlled study. *J Pediatr Surg* 2013; **48**: 2453–2459.
183 Bauman NM, McCarter RJ, Guzzetta PC *et al.* Propranolol vs prednisolone for symptomatic proliferating infantile hemangiomas: a randomized clinical trial. *JAMA Otolaryngol Head Neck Surg* 2014; **140**: 323–330.
184 Léauté-Labrèze C, Dumas de la Roque E, Nacka F *et al.* Double-blind randomized pilot trial evaluating the efficacy of oral propranolol on infantile haemangiomas in infants < 4 months of age. *Br J Dermatol* 2013; **169**: 181–183.
185 Abarzúa-Araya A, Navarrete-Dechent CP, Heusser F, Retamal J, Zegpi-Trueba MS. Atenolol versus propranolol for the treatment of infantile hemangiomas: a randomized controlled study. *J Am Acad Dermatol* 2014; **70**: 1045–1049.
186 Ehsani AH, Noormohammadpoor P, Abdolreza M, Balighi K, Arianian Z, Daklan S. Combination therapy of infantile hemangioma with pulsed dye laser with topical propranolol: a randomized clinical trial. *Arch Iran Med* 2014; **17**: 657–660.
187 Léauté-Labrèze C, Hoeger P, Mazereeuw-Hautier J *et al.* A randomized, controlled trial of oral propranolol in infantile hemangioma. *N Engl J Med* 2015; **372**: 735–746.
188 Menezes MD, McCarter R, Greene EA, Bauman NM. Status of propranolol for treatment of infantile hemangioma and description of a randomized clinical trial. *Ann Otol Rhinol Laryngol* 2011; **120**: 686–695.
189 Marqueling AL, Oza V, Frieden IJ, Puttgen KB. Propranolol and infantile hemangiomas four years later: a systematic review. *Pediatr Dermatol* 2013; **30**: 182–191.
190 Xu SQ, Jia RB, Zhang W, Zhu H, Ge SF, Fan XQ. Beta-blockers versus corticosteroids in the treatment of infantile hemangioma: an evidence-based systematic review. *World J Pediatr* 2013; **9**: 221–229.
191 Izadpanah A, Izadpanah A, Kanevsky J, Belzile E, Schwarz K. Propranolol versus corticosteroids in the treatment of infantile

This article has been co-published with the permission of *The Journal of Dermatology, Pediatrics International* and *Japanese Journal of Radiology*. All rights reserved. © 2020 The Authors. The articles are identical except for minor stylistic and spelling differences in keeping with each journal's style. Either citation can be used when citing this article.

hemangioma: a systematic review and meta-analysis. *Plast Reconstr Surg* 2013; **131**: 601–613.
192 Xu S, Jia R, Ge S, Lin M, Fan X. Treatment of periorbital infantile haemangiomas: a systematic literature review on propranolol or steroids. *J Paediatr Child Health* 2014; **50**: 271–279.
193 Peridis S, Pilgrim G, Athanasopoulos I, Parpounas K. A meta-analysis on the effectiveness of propranolol for the treatment of infantile airway haemangiomas. *Int J Pediatr Otorhinolaryngol* 2011; **75**: 455–460.
194 Vlastarakos PV, Papacharalampous GX, Chrysostomou M *et al.* Propranolol is an effective treatment for airway haemangiomas: a critical analysis and meta-analysis of published interventional studies. *Acta Otorhinolaryngol Ital* 2012; **32**: 213–221.
195 Storch CH, Hoeger PH. Propranolol for infantile haemangiomas: insights into the molecular mechanisms of action. *Br J Dermatol* 2010; **163**: 269–274.
196 Drolet BA, Frommelt PC, Chamlin SL *et al.* Initiation and use of propranolol for infantile hemangioma: report of a consensus conference. *Pediatrics* 2013; **131**: 128–140.
197 Kum JJ, Khan ZA. Mechanisms of propranolol action in infantile hemangioma. *Dermatoendocrinol* 2014; **6**: e979699.
198 Horev A, Haim A, Zvulunov A. Propranolol induced hypoglycemia. *Pediatr Endocrinol Rev* 2015; **12**: 308–310.
199 Blei F, McElhinney DB, Guarini A, Presti S. Cardiac screening in infants with infantile hemangiomas before propranolol treatment. *Pediatr Dermatol* 2014; **31**: 465–470.
200 Raphael MF, Breugem CC, Vlasveld FA *et al.* Is cardiovascular evaluation necessary prior to and during beta-blocker therapy for infantile hemangiomas?: a cohort study. *J Am Acad Dermatol* 2015; **72**: 465–472.
201 Chamlin SL, Haggstrom AN, Drolet BA *et al.* Multicenter prospective study of ulcerated hemangiomas. *J Pediatr* 2007; **151**: 684–689, 689 e681.
202 Vercellino N, Romanini MV, Pelegrini M, Rimini A, Occella C, Dalmonte P. The use of propranolol for complicated infantile hemangiomas. *Int J Dermatol* 2013; **52**: 1140–1146.
203 Sadykov RR, Podmelle F, Sadykov RA, Kasimova KR, Metellmann HR. Use of propranolol for the treatment infantile hemangiomas in the maxillofacial region. *Int J Oral Maxillofac Surg* 2013; **42**: 863–867.
204 Kim HJ, Colombo M, Frieden IJ. Ulcerated hemangiomas: clinical characteristics and response to therapy. *J Am Acad Dermatol* 2001; **44**: 962–972.
205 Wananukul S, Chatproedprai S. Ulcerated hemangiomas: clinical features and management. *J Med Assoc Thai* 2002; **85**: 1220–1225.
206 Pandey A, Gangopadhyay AN, Sharma SP, Kumar V, Gopal SC, Gupta DK. Conservative management of ulcerated haemangioma–twenty years experience. *Int Wound J* 2009; **6**: 59–62.
207 Oranje AP, de Waard-van der Spek FB, Devillers AC, de Laat PC, Madern GC. Treatment and pain relief of ulcerative hemangiomas with a polyurethane film. *Dermatology* 2000; **200**: 31–34.
208 Bauland CG, Smit JM, Ketelaars R, Rieu PN, Spauwen PH. Management of haemangiomas of infancy: a retrospective analysis and a treatment protocol. *Scand J Plast Reconstr Surg Hand Surg* 2008; **42**: 86–91.
209 Morelli JG, Tan OT, Yohn JJ, Weston WL. Treatment of ulcerated hemangiomas infancy. *Arch Pediatr Adolesc Med* 1994; **148**: 1104–1105.
210 Lacour M, Syed S, Linward J, Harper JI. Role of the pulsed dye laser in the management of ulcerated capillary haemangiomas. *Arch Dis Child* 1996; **74**: 161–163.
211 David LR, Malek MM, Argenta LC. Efficacy of pulse dye laser therapy for the treatment of ulcerated haemangiomas: a review of 78 patients. *Br J Plast Surg* 2003; **56**: 317–327.
212 Michel JL. Treatment of hemangiomas with 595 nm pulsed dye laser dermobeam. *Eur J Dermatol* 2003; **13**: 136–141.
213 Di Maio L, Baldi A, Dimaio V, Barzi A. Use of flashlamp-pumped pulsed dye laser in the treatment of superficial vascular malformations and ulcerated hemangiomas. *In Vivo* 2011; **25**: 117–123.
214 Sugarman JL, Mauro TM, Frieden IJ. Treatment of an ulcerated hemangioma with recombinant platelet-derived growth factor. *Arch Dermatol* 2002; **138**: 314–316.
215 Metz BJ, Rubenstein MC, Levy ML, Metry DW. Response of ulcerated perineal hemangiomas of infancy to becaplermin gel, a recombinant human platelet-derived growth factor. *Arch Dermatol* 2004; **140**: 867–870.
216 Jalil S, Akhtar J, Ahmed S. Corticosteroids therapy in the management of infantile cutaneous hemangiomas. *J Coll Physicians Surg Pak* 2006; **16**: 662–665.
217 Gangopadhyay AN, Sinha CK, Gopal SC, Gupta DK, Sahoo SP, Ahmad M. Role of steroid in childhood haemangioma: a 10 years review. *Int Surg* 1997; **82**: 49–51.
218 Pandey A, Gangopadhyay AN, Gopal SC *et al.* Twenty years' experience of steroids in infantile hemangioma–a developing country's perspective. *J Pediatr Surg* 2009; **44**: 688–694.
219 Tan BH, Leadbitter PH, Aburn NH, Tan ST. Steroid therapy for problematic proliferating haemangioma. *N Z Med J* 2011; **124**: 57–65.
220 Ruttum MS, Abrams GW, Harris GJ, Ellis MK. Bilateral retinal embolization associated with intralesional corticosteroid injection for capillary hemangioma of infancy. *J Pediatr Ophthalmol Strabismus* 1993; **30**: 4–7.
221 Egbert JE, Schwartz GS, Walsh AW. Diagnosis and treatment of an ophthalmic artery occlusion during an intralesional injection of corticosteroid into an eyelid capillary hemangioma. *Am J Ophthalmol* 1996; **121**: 638–642.
222 Craiglow BG, Antaya RJ. Management of infantile hemangiomas: current and potential pharmacotherapeutic approaches. *Paediatr Drugs* 2013; **15**: 133–138.
223 Ni N, Langer P, Wagner R, Guo S. Topical timolol for periocular hemangioma: report of further study. *Arch Ophthalmol* 2011; **129**: 377–379.
224 Elsas FJ, Lewis AR. Topical treatment of periocular capillary hemangioma. *J Pediatr Ophthalmol Strabismus* 1994; **31**: 153–156.
225 Lapidoth M, Ben-Amitai D, Bhandarkar S, Fried L, Arbiser JL. Efficacy of topical application of eosin for ulcerated hemangiomas. *J Am Acad Dermatol* 2009; **60**: 350–351.
226 Barry RB, Hughes BR, Cook LJ. Involution of infantile haemangiomas after imiquimod 5% cream. *Clin Exp Dermatol* 2008; **33**: 446–449.
227 Ho NT, Lansang P, Pope E. Topical imiquimod in the treatment of infantile hemangiomas: a retrospective study. *J Am Acad Dermatol* 2007; **56**: 63–68.
228 Jiang C, Hu X, Ma G *et al.* A prospective self-controlled phase II study of imiquimod 5% cream in the treatment of infantile hemangioma. *Pediatr Dermatol* 2011; **28**: 259–266.
229 Mao XH, Wang JY, Yan JL. Topical imiquimod treatment of cutaneous vascular disorders in pediatric patients: clinical evaluation on the efficacy and safety. *J Zhejiang Univ Sci B* 2012; **13**: 745–750.
230 McCuaig CC, Dubois J, Powell J *et al.* A phase II, open-label study of the efficacy and safety of imiquimod in the treatment of superficial and mixed infantile hemangioma. *Pediatr Dermatol* 2009; **26**: 203–212.
231 Qiu Y, Ma G, Lin X, Jin Y, Chen H, Hu X. Treating protruding infantile hemangiomas with topical imiquimod 5% cream caused severe local reactions and disfiguring scars. *Pediatr Dermatol* 2013; **30**: 342–347.
232 Qiu Y, Ma G, Yang J *et al.* Imiquimod 5% cream versus timolol 0.5% ophthalmic solution for treating superficial proliferating infantile haemangiomas: a retrospective study. *Clin Exp Dermatol* 2013; **38**: 845–850.
233 Welsh O, Olazaran Z, Gomez M, Salas J, Berman B. Treatment of infantile hemangiomas with short-term application of imiquimod 5% cream. *J Am Acad Dermatol* 2004; **51**: 639–642.
234 Blatt J, Morrell DS, Buck S *et al.* β-blockers for infantile hemangiomas: a single-institution experience. *Clin Pediatr (Phila)* 2011; **50**: 757–763.
235 Cante V, Pham-Ledard A, Imbert E, Ezzedine K, Léauté-Labrèze C. First report of topical timolol treatment in primarily ulcerated

This article has been co-published with the permission of *The Journal of Dermatology, Pediatrics International* and *Japanese Journal of Radiology*. All rights reserved. © 2020 The Authors. The articles are identical except for minor stylistic and spelling differences in keeping with each journal's style. Either citation can be used when citing this article.

perineal haemangioma. *Arch Dis Child Fetal Neonatal Ed* 2012; **97**: F155–F156.
236 Chakkittakandiyil A, Phillips R, Frieden IJ *et al.* Timolol maleate 0.5% or 0.1% gel-forming solution for infantile hemangiomas: a retrospective, multicenter, cohort study. *Pediatr Dermatol* 2012; **29**: 28–31.
237 Chambers CB, Katowitz WR, Katowitz JA, Binenbaum G. A controlled study of topical 0.25% timolol maleate gel for the treatment of cutaneous infantile capillary hemangiomas. *Ophthalmic Plast Reconstr Surg* 2012; **28**: 103–106.
238 Khunger N, Pahwa M. Dramatic response to topical timolol lotion of a large hemifacial infantile haemangioma associated with PHACE syndrome. *Br J Dermatol* 2011; **164**: 886–888.
239 Ma G, Wu P, Lin X *et al.* Fractional carbon dioxide laser-assisted drug delivery of topical timolol solution for the treatment of deep infantile hemangioma: a pilot study. *Pediatr Dermatol* 2014; **31**: 286–291.
240 Moehrle M, Léauté-Labrèze C, Schmidt V, Röcken M, Poets CF, Goelz R. Topical timolol for small hemangiomas of infancy. *Pediatr Dermatol* 2013; **30**: 245–249.
241 Ni N, Guo S, Langer P. Current concepts in the management of periocular infantile (capillary) hemangioma. *Curr Opin Ophthalmol* 2011; **22**: 419–425.
242 Oranje AP, Janmohamed SR, Madern GC, de Laat PC. Treatment of small superficial haemangioma with timolol 0.5% ophthalmic solution: a series of 20 cases. *Dermatology* 2011; **223**: 330–334.
243 Pope E, Chakkittakandiyil A. Topical timolol gel for infantile hemangiomas: a pilot study. *Arch Dermatol* 2010; **146**: 564–565.
244 Kunzi-Rapp K. Topical propranolol therapy for infantile hemangiomas. *Pediatr Dermatol* 2012; **29**: 154–159.
245 Xu G, Lv R, Zhao Z, Huo R. Topical propranolol for treatment of superficial infantile hemangiomas. *J Am Acad Dermatol* 2012; **67**: 1210–1213.
246 Garzon MC, Lucky AW, Hawrot A, Frieden IJ. Ultrapotent topical corticosteroid treatment of hemangiomas of infancy. *J Am Acad Dermatol* 2005; **52**: 281–286.
247 Pandey A, Gangopadhyay AN, Sharma SP, Kumar V, Gupta DK, Gopal SC. Evaluation of topical steroids in the treatment of superficial hemangioma. *Skinmed* 2010; **8**: 9–11.
248 Kaplan M, Paller AS. Clinical pearl: use of self-adhesive, compressive wraps in the treatment of limb hemangiomas. *J Am Acad Dermatol* 1995; **32**: 117–118.
249 Ochi G, Ohkawa H, Kaneko M *et al.* [Compression therapy and cryosurgery for hemangiomas in childhood]. *Shoni Geka* 1992; **24**: 539–547. Japanese.
250 Totsuka Y, Fukuda H, Tomita K. Compression therapy for parotid haemangioma in infants. A report of three cases. *J Craniomaxillofac Surg* 1988; **16**: 366–370.
251 Osaki TH, Jakobiec FA, Mendoza PR, Lee Y, Fay AM. Immunohistochemical investigations of orbital infantile hemangiomas and adult encapsulated cavernous venous lesions (malformation versus hemangioma). *Ophthalmic Plast Reconstr Surg* 2013; **29**: 183–195.
252 Laing EL, Brasch HD, Steel R *et al.* Verrucous hemangioma expresses primitive markers. *J Cutan Pathol* 2013; **40**: 391–396.
253 North PE, Waner M, James CA, Mizeracki A, Frieden IJ, Mihm MC Jr. Congenital nonprogressive hemangioma: a distinct clinicopathologic entity unlike infantile hemangioma. *Arch Dermatol* 2001; **137**: 1607–1620.
254 North PE, Waner M, Mizeracki A, Mihm MC Jr. GLUT1: a newly discovered immunohistochemical marker for juvenile hemangiomas. *Hum Pathol* 2000; **31**: 11–22.
255 North PE, Waner M, Mizeracki A *et al.* A unique microvascular phenotype shared by juvenile hemangiomas and human placenta. *Arch Dermatol* 2001; **137**: 559–570.
256 Leon-Villapalos J, Wolfe K, Kangesu L. GLUT-1: an extra diagnostic tool to differentiate between haemangiomas and vascular malformations. *Br J Plast Surg* 2005; **58**: 348–352.
257 Ahrens WA, Ridenour RV 3rd, Caron BL, Miller DV, Folpe AL. GLUT-1 expression in mesenchymal tumors: an immunohistochemical study of 247 soft tissue and bone neoplasms. *Hum Pathol* 2008; **39**: 1519–1526.
258 Trindade F, Kutzner H, Requena L, Tellechea O, Colmenero I. Microvenular hemangioma-an immunohistochemical study of 9 cases. *Am J Dermatopathol* 2012; **34**: 810–812.
259 Sadeghpour M, Antaya RJ, Lazova R, Ko CJ. Dilated lymphatic vessels in tufted angioma: a potential source of diagnostic confusion. *Am J Dermatopathol* 2012; **34**: 400–403.
260 Drut RM, Drut R. Extracutaneous infantile haemangioma is also Glut1 positive. *J Clin Pathol* 2004; **57**: 1197–1200.
261 Lyons LL, North PE, Mac-Moune Lai F, Stoler MH, Folpe AL, Weiss SW. Kaposiform hemangioendothelioma: a study of 33 cases emphasizing its pathologic, immunophenotypic, and biologic uniqueness from juvenile hemangioma. *Am J Surg Pathol* 2004; **28**: 559–568.
262 Al-Adnani M, Williams S, Rampling D, Ashworth M, Malone M, Sebire NJ. Histopathological reporting of paediatric cutaneous vascular anomalies in relation to proposed multidisciplinary classification system. *J Clin Pathol* 2006; **59**: 1278–1282.
263 Badi AN, Kerschner JE, North PE, Drolet BA, Messner A, Perkins JA. Histopathologic and immunophenotypic profile of subglottic hemangioma: multicenter study. *Int J Pediatr Otorhinolaryngol* 2009; **73**: 1187–1191.
264 Hernandez F, Navarro M, Encinas JL *et al.* The role of GLUT1 immunostaining in the diagnosis and classification of liver vascular tumors in children. *J Pediatr Surg* 2005; **40**: 801–804.
265 Mo JQ, Dimashkieh HH, Bove KE. GLUT1 endothelial reactivity distinguishes hepatic infantile hemangioma from congenital hepatic vascular malformation with associated capillary proliferation. *Hum Pathol* 2004; **35**: 200–209.
266 Das KJ, Sharma P, Naswa N *et al.* Hybrid SPECT-CT with 99mTc-labeled red blood cell in a case of blue rubber bleb nevus syndrome: added value over planar scintigraphy. *Diagn Interv Radiol* 2013; **19**: 41–43.
267 Senturk S, Bilici A, Miroglu TC, Bilek SU. Blue rubber bleb nevus syndrome: imaging of small bowel lesions with peroral CT enterography. *Abdom Imaging* 2011; **36**: 520–523.
268 Thomson M, Venkatesh K, Elmalik K, van der Veer W, Jaacobs M. Double balloon enteroscopy in children: diagnosis, treatment, and safety. *World J Gastroenterol* 2010; **16**: 56–62.
269 Agnese M, Cipolletta L, Bianco MA, Quitadamo P, Miele E, Staiano A. Blue rubber bleb nevus syndrome. *Acta Paediatr* 2010; **99**: 632–635.
270 Hansen LF, Wewer V, Pedersen SA, Matzen P, Paerregaard A. Severe blue rubber bleb nevus syndrome in a neonate. *Eur J Pediatr Surg* 2009; **19**: 47–49.
271 Yarlagadda R, Menda Y, Graham MM. Tc-99m red blood cell imaging in a patient with blue rubber bleb nevus syndrome. *Clin Nucl Med* 2008; **33**: 374–376.
272 Mechri M, Soyer P, Boudiaf M, Duchat F, Hamzi L, Rymer R. Small bowel involvement in blue rubber bleb nevus syndrome: MR imaging features. *Abdom Imaging* 2009; **34**: 448–451.
273 Certo M, Lopes L, Ramada J. Blue rubber bleb nevus syndrome: manifestations at computed tomography. *Acta Radiol* 2007; **48**: 962–966.
274 Kopacova M, Tacheci I, Koudelka J, Kralova M, Rejchrt S, Bures J. A new approach to blue rubber bleb nevus syndrome: the role of capsule endoscopy and intra-operative enteroscopy. *Pediatr Surg Int* 2007; **23**: 693–697.
275 De Bona M, Bellumat A, De Boni M. Capsule endoscopy for the diagnosis and follow-up of blue rubber bleb nevus syndrome. *Dig Liver Dis* 2005; **37**: 451–453.
276 Place RJ. Blue rubber bleb nevus syndrome: a case report with long-term follow-up. *Mil Med* 2001; **166**: 728–730.
277 Jacob AG, Driscoll DJ, Shaughnessy WJ, Stanson AW, Clay RP, Gloviczki P. Klippel-Trenaunay syndrome: spectrum and management. *Mayo Clin Proc* 1998; **73**: 28–36.
278 Capraro PA, Fisher J, Hammond DC, Grossman JA. Klippel-Trenaunay syndrome. *Plast Reconstr Surg* 2002; **109**: 2052–2060; quiz 2061–2052.

This article has been co-published with the permission of *The Journal of Dermatology, Pediatrics International* and *Japanese Journal of Radiology*. All rights reserved. © 2020 The Authors. The articles are identical except for minor stylistic and spelling differences in keeping with each journal's style. Either citation can be used when citing this article.

279 Meine JG, Schwartz RA, Janniger CK. Klippel-Trenaunay-Weber syndrome. *Cutis* 1997; **60**: 127–132.
280 Redondo P, Aguado L, Martinez-Cuesta A. Diagnosis and management of extensive vascular malformations of the lower limb: part II. Systemic repercussions [corrected], diagnosis, and treatment. *J Am Acad Dermatol* 2011; **65**: 909–923; quiz 924.
281 Gloviczki P, Hollier LH, Telander RL, Kaufman B, Bianco AJ, Stickler GB. Surgical implications of Klippel-Trenaunay syndrome. *Ann Surg* 1983; **197**: 353–362.
282 McGrory BJ, Amadio PC. Klippel-Trenaunay syndrome: orthopaedic considerations. *Orthop Rev* 1993; **22**: 41–50.
283 Takata M, Watanabe K, Matsubara H, Takato K, Nomura I, Tsuchiya H. Lengthening of the normal tibia in a patient with hemihypertrophy caused by Klippel-Trenaunay-Weber syndrome: a case report. *J Orthop Surg (Hong Kong)* 2011; **19**: 359–363.
284 Servelle M. Klippel and Trenaunay's syndrome. 768 operated cases. *Ann Surg* 1985; **201**: 365–373.
285 Gates PE, Drvaric DM, Kruger L. Wound healing in orthopaedic procedures for Klippel-Trenaunay syndrome. *J Pediatr Orthop* 1996; **16**: 723–726.
286 Bajaj Y, Hewitt R, Ifeacho S, Hartley BE. Surgical excision as primary treatment modality for extensive cervicofacial lymphatic malformations in children. *Int J Pediatr Otorhinolaryngol* 2011; **75**: 673–677.
287 Orvidas LJ, Kasperbauer JL. Pediatric lymphangiomas of the head and neck. *Ann Otol Rhinol Laryngol* 2000; **109**: 411–421.
288 Alqahtani A, Nguyen LT, Flageole H, Shaw K, Laberge JM. 25 years' experience with lymphangiomas in children. *J Pediatr Surg* 1999; **34**: 1164–1168.
289 Wiegand S, Zimmermann AP, Eivazi B, Sesterhenn AM, Werner JA. Lymphatic malformations involving the parotid gland. *Eur J Pediatr Surg* 2011; **21**: 242–245.
290 Chen WL, Zhang B, Wang JG, Ye HS, Zhang DM, Huang ZQ. Surgical excision of cervicofacial giant macrocystic lymphatic malformations in infants and children. *Int J Pediatr Otorhinolaryngol* 2009; **73**: 833–837.
291 Lei ZM, Huang XX, Sun ZJ, Zhang WF, Zhao YF. Surgery of lymphatic malformations in oral and cervicofacial regions in children. *Oral Surg Oral Med Oral Pathol Oral Radiol Endod* 2007; **104**: 338–344.
292 Okazaki T, Iwatani S, Yanai T *et al.* Treatment of lymphangioma in children: our experience of 128 cases. *J Pediatr Surg* 2007; **42**: 386–389.
293 Hamoir M, Plouin-Gaudon I, Rombaux P *et al.* Lymphatic malformations of the head and neck: a retrospective review and a support for staging. *Head Neck* 2001; **23**: 326–337.
294 Fageeh N, Manoukian J, Tewfik T, Schloss M, Williams HB, Gaskin D. Management of head and neck lymphatic malformations in children. *J Otolaryngol* 1997; **26**: 253–258.
295 Padwa BL, Hayward PG, Ferraro NF, Mulliken JB. Cervicofacial lymphatic malformation: clinical course, surgical intervention, and pathogenesis of skeletal hypertrophy. *Plast Reconstr Surg* 1995; **95**: 951–960.
296 de Serres LM, Sie KC, Richardson MA. Lymphatic malformations of the head and neck. A proposal for staging. *Arch Otolaryngol Head Neck Surg* 1995; **121**: 577–582.
297 Riechelmann H, Muehlfay G, Keck T, Mattfeldt T, Rettinger G. Total, subtotal, and partial surgical removal of cervicofacial lymphangiomas. *Arch Otolaryngol Head Neck Surg* 1999; **125**: 643–648.
298 Greinwald J Jr, Cohen AP, Hemanackah S, Azizkhan RG. Massive lymphatic malformations of the head, neck, and chest. *J Otolaryngol Head Neck Surg* 2008; **37**: 169–173.
299 Yang Y, Sun M, Ma Q *et al.* Bleomycin A5 sclerotherapy for cervicofacial lymphatic malformations. *J Vasc Surg* 2011; **53**: 150–155.
300 Alomari AI, Karian VE, Lord DJ, Padua HM, Burrows PE. Percutaneous sclerotherapy for lymphatic malformations: a retrospective analysis of patient-evaluated improvement. *J Vasc Interv Radiol* 2006; **17**: 1639–1648.
301 Chaudry G, Guevara CJ, Rialon KL *et al.* Safety and efficacy of bleomycin sclerotherapy for microcystic lymphatic malformation. *Cardiovasc Intervent Radiol* 2014; **37**: 1476–1481.
302 Smith MC, Zimmerman MB, Burke DK *et al.* Efficacy and safety of OK-432 immunotherapy of lymphatic malformations. *Laryngoscope* 2009; **119**: 107–115.
303 Giguère CM, Bauman NM, Sato Y *et al.* Treatment of lymphangiomas with OK-432 (Picibanil) sclerotherapy: a prospective multi-institutional trial. *Arch Otolaryngol Head Neck Surg* 2002; **128**: 1137–1144.
304 Udagawa A, Yoshimoto S, Matumoto F *et al.* A case of facial cavernous lymphangioma: observation from infancy to adulthood. *Nihon Togai Gaku Ganmen Geka Gakkaishi* 2005; **21**: 302–309.
305 Nagao M, Sasaki S, Furukawa H, Uchiyama E, Yamamoto Y. [Treatments for huge lymphatic malformations of cheek, oral cavity and neck]. *Nihon Keisei Geka Gakkai Kaishi* 2007; **27**: 779–782. Japanese.
306 Ravindranathan H, Gillis J, Lord DJ. Intensive care experience with sclerotherapy for cervicofacial lymphatic malformations. *Pediatr Crit Care Med* 2008; **9**: 304–309.
307 Poonyathalang A, Preechawat P, Jiarakongmun P, Pongpech S. Sclerosing therapy for orbital lymphangioma using sodium tetradecyl sulfate. *Jpn J Ophthalmol* 2008; **52**: 298–304.
308 Emran MA, Dubois J, Laberge L, Al-Jazaeri A, Butter A, Yazbeck S. Alcoholic solution of zein (Ethibloc) sclerotherapy for treatment of lymphangiomas in children. *J Pediatr Surg* 2006; **41**: 975–979.
309 Bai Y, Jia J, Huang XX, Alsharif MJ, Zhao JH, Zhao YF. Sclerotherapy of microcystic lymphatic malformations in oral and facial regions. *J Oral Maxillofac Surg* 2009; **67**: 251–256.
310 Shiels WE 2nd, Kang DR, Murakami JW, Hogan MJ, Wiet GJ. Percutaneous treatment of lymphatic malformations. *Otolaryngol Head Neck Surg* 2009; **141**: 219–224.
311 Nehra D, Jacobson L, Barnes P, Mallory B, Albanese CT, Sylvester KG. Doxycycline sclerotherapy as primary treatment of head and neck lymphatic malformations in children. *J Pediatr Surg* 2008; **43**: 451–460.
312 Asonuma K, Inomata Y. [Current strategy and outcome of treatment of lymphangioma in children: the analysis of a survey in the Kyushu and Okinawa area]. *Nihon Shoni Geka Gakkai Zasshi* 2006; **42**: 215–221. Japanese.
313 Schwarcz RM, Ben Simon GJ, Cook T, Goldberg RA. Sclerosing therapy as first line treatment for low flow vascular lesions of the orbit. *Am J Ophthalmol* 2006; **141**: 333–339.
314 Oyama T, Eguchi K, Cho H, Abe H. A variety of orbital lymphangioma treatments: one case treated with orbital decompression therapy and the other case with intralesional injection of OK-432 therapy. *Nihon Ganka Gakkai Zasshi* 2009; **113**: 732–740. Japanese.
315 Cahill AM, Nijs E, Ballah D *et al.* Percutaneous sclerotherapy in neonatal and infant head and neck lymphatic malformations: a single center experience. *J Pediatr Surg* 2011; **46**: 2083–2095.
316 Chaudry G, Burrows PE, Padua HM, Dillon BJ, Fishman SJ, Alomari AI. Sclerotherapy of abdominal lymphatic malformations with doxycycline. *J Vasc Interv Radiol* 2011; **22**: 1431–1435.
317 Oliveira C, Sacher P, Meuli M. Management of prenatally diagnosed abdominal lymphatic malformations. *Eur J Pediatr Surg* 2010; **20**: 302–306.
318 Won JH, Kim BM, Kim CH, Park SW, Kim MD. Percutaneous sclerotherapy of lymphangiomas with acetic acid. *J Vasc Interv Radiol* 2004; **15**: 595–600.
319 Shiels WE 2nd, Kenney BD, Caniano DA, Besner GE. Definitive percutaneous treatment of lymphatic malformations of the trunk and extremities. *J Pediatr Surg* 2008; **43**: 136–139; discussion 140.
320 Chiappinelli A, Forgues D, Galifer RB. Congenital abdominal cystic lymphangiomas: what is the correct management? *J Matern Fetal Neonatal Med* 2012; **25**: 915–919.
321 Muraoka A, Suzuki N, Niwa Y, Komatsu Y, Tagami K. [A case report of an asymptomatic giant retroperitoneal lymphangioma

This article has been co-published with the permission of *The Journal of Dermatology, Pediatrics International* and *Japanese Journal of Radiology*. All rights reserved. © 2020 The Authors. The articles are identical except for minor stylistic and spelling differences in keeping with each journal's style. Either citation can be used when citing this article.

pointed out at a physical examination]. *Nihon Rinsho Geka Gakkai Zasshi* 2009; **70**: 899–905. Japanese.
322 Oyachi N, Iwashita K, Kubo M. [Diagnosis and management of mesenteric lymphangioma: comparison of prenatal and school-age diagnosed cases]. *Nihon Shoni Geka Gakkai Zasshi* 2008; **44**: 33–37. Japanese.
323 Mendez-Gallart R, Bautista A, Estevez E, Rodriguez-Barca P. Abdominal cystic lymphangiomas in pediatrics: surgical approach and outcomes. *Acta Chir Belg* 2011; **111**: 374–377.
324 Ikeda T, Asai Y, Nango Y *et al.* [Childhood abdominal cystic lymphangioma]. *Nihon Shoni Geka Gakkai Zasshi* 2008; **44**: 959–964. Japanese.
325 Losanoff JE, Kjossev KT. Mesenteric cystic lymphangioma: unusual cause of intra-abdominal catastrophe in an adult. *Int J Clin Pract* 2005; **59**: 986–987.
326 Uchiyama M, Murata H, Ohtaki M. [Acute abdomen by inflammatory infiltration of retroperitoneal lymphangioma to the duodenum: report of a case and review of cases in childhood]. *Nihon Shoni Geka Gakkai Zasshi* 2007; **43**: 938–944. Japanese.
327 Bellini C, Ergaz Z, Radicioni M *et al.* Congenital fetal and neonatal visceral chylous effusions: neonatal chylothorax and chylous ascites revisited. A multicenter retrospective study. *Lymphology* 2012; **45**: 91–102.
328 Matsuo Y, Okada A. The role and use of Sudan Black in the surgical treatment of chylothorax and chylous ascites. *Shoni Geka* 2001; **33**: 186–190. Japanese.
329 Spagnol L, Conforti A, Valfre L, Morini F, Bagolan P. Preoperative administration of Sudan III and successful treatment of persistent chylous ascites in a neonate. *J Pediatr Surg* 2011; **46**: 994–997.
330 Joe K, Kemmotsu H, Mori T, Goto C, Ohkawa H. [Treatment of idiopathic chylous ascites in infants]. *Shoni Geka* 2001; **33**: 134–140. Japanese.
331 Moreira Dde A, Santos MM, Tannuri AC, Tannuri U. Congenital chylous ascites: a report of a case treated with hemostatic cellulose and fibrin glue. *J Pediatr Surg* 2013; **48**: e17–e19.
332 Olivieri C, Nanni L, Masini L, Pintus C. Successful management of congenital chylous ascites with early octreotide and total parenteral nutrition in a newborn. *BMJ Case Rep* 2012; **2012**: bcr2012006196.
333 Huang Y, Zhuang S, Li Y, Liu M, Chen H, Du M. Successful management of congenital chylous ascites in a premature infant using somatostatin analogue. *Indian J Pediatr* 2011; **78**: 345–347.
334 Melo-Filho AA, Souza IJ, Leite CA, Leite RD, Colares JH, Correia JM. Refractory congenital chylous ascites. *Indian J Pediatr* 2010; **77**: 1335–1337.
335 Karagol BS, Zenciroglu A, Gokce S, Kundak AA, Ipek MS. Therapeutic management of neonatal chylous ascites: report of a case and review of the literature. *Acta Paediatr* 2010; **99**: 1307–1310.
336 Kuroiwa M, Toki F, Suzuki M, Suzuki N. Successful laparoscopic ligation of the lymphatic trunk for refractory chylous ascites. *J Pediatr Surg* 2007; **42**: E15–E18.
337 Antao B, Croaker D, Squire R. Successful management of congenital chyloperitoneum with fibrin glue. *J Pediatr Surg* 2003; **38**: E7–E8.
338 Nakagawa J, Nakabayashi M, Kikuchi M *et al.* [A case of congenital chyloperitoneum improved by prenatal treatment]. *Nihon Sanka Fujinka Gakkai Tokyo Chiho Bukai Kaishi* 2002; **51**: 399–403. Japanese.
339 Wakisaka M, Kitagawa H, Satoh Y, Nakada K. Congenital chyloascites treated by laparotomy and OK-432 injection. *Shoni Geka* 2001; **33**: 196–200. Japanese.
340 Sato H, Okamatsu T, Yatsuzuka M *et al.* Chylous ascites resolved by exploratory laparotomy. *Shoni Geka* 2001; **33**: 191–195. Japanese.
341 Takahashi A, Suzuki N, Kuwano H. Neonatal chylous ascites. *Shoni Geka* 2001; **33**: 144–147. Japanese.
342 Komuro H. [Endoscopic surgery for chylothorax and chylous ascites]. *Shoni Geka* 2010; **42**: 805–808. Japanese.
343 Zeidan S, Delarue A, Rome A, Roquelaure B. Fibrin glue application in the management of refractory chylous ascites in children. *J Pediatr Gastroenterol Nutr* 2008; **46**: 478–481.
344 Huang Q, Jiang ZW, Jiang J, Li N, Li JS. Chylous ascites: treated with total parenteral nutrition and somatostatin. *World J Gastroenterol* 2004; **10**: 2588–2591.
345 Nemoto T, Tsuchiya H, Nagashima K. Clinical and experimental analysis for chylothorax and chylous ascites. *Shoni Geka* 2001; **33**: 119–122. Japanese.
346 Ohtsu K, Ueda Y, Kurihara S, Kawashima M. Intractable chylous ascites. *Shoni Geka* 2011; **43**: 747–750. Japanese.
347 Ono S, Iwai N, Chiba F, Furukawa T, Fumino S. OK-432 therapy for chylous pleural effusion or ascites associated with lymphatic malformations. *J Pediatr Surg* 2010; **45**: e7–e10.
348 Tanaka M, Yokomori K, Kamii Y. Chylous ascites caused by a retroperitoneal lymphangioma: a case report. *Shoni Geka* 2001; **33**: 163–167. Japanese.
349 Siebert S, Helbling C, Wolff M *et al.* Peritoneovenous shunting as palliative treatment in an infant with chylous ascites due to generalised congenital lymphangiectasia. *Klin Padiatr* 2010; **222**: 317–318.
350 Densupsoontorn N, Jirapinyo P, Aanpreung P, Laohapensang M, Parichatikanond P. Congenital chylous ascites: the roles of fibrin glue and CD31. *Acta Paediatr* 2009; **98**: 1847–1849.
351 Guvenc BH, Ekingen G, Tuzlaci A, Senel U. Diffuse neonatal abdominal lymphangiomatosis: management by limited surgical excision and sclerotherapy. *Pediatr Surg Int* 2005; **21**: 595–598.
352 Kotera A, Kamagata S, Hirobe S *et al.* A case of diffuse lymphangiomatosis with chylothorax and chylous ascites. *Shoni Geka* 2001; **33**: 128–133. Japanese.
353 Horisawa M, Nishimoto K, Ogura Y, Tainaka T, Matsunaga K, Niinomi N. Generalized lymphatic dysplasia with intermittent chylous discharge from the scrotum: a case report. *Shoni Geka* 2001; **33**: 180–185. Japanese.
354 Katz MS, Finck CM, Schwartz MZ *et al.* Vacuum-assisted closure in the treatment of extensive lymphangiomas in children. *J Pediatr Surg* 2012; **47**: 367–370.
355 Sugito K, Ikeda T, Hagiwara N *et al.* [A case of large mesenteric cyst with inflammatry reaction]. *Shoni Geka* 2001; **33**: 1017–1020. Japanese.
356 Chang TS, Ricketts R, Abramowsky CR *et al.* Mesenteric cystic masses: a series of 21 pediatric cases and review of the literature. *Fetal Pediatr Pathol* 2011; **30**: 40–44.
357 Tran NS, Nguyen TL. Laparoscopic management of abdominal lymphatic cyst in children. *J Laparoendosc Adv Surg Tech A* 2012; **22**: 505–507.
358 Boardman SJ, Cochrane LA, Roebuck D, Elliott MJ, Hartley BE. Multimodality treatment of pediatric lymphatic malformations of the head and neck using surgery and sclerotherapy. *Arch Otolaryngol Head Neck Surg* 2010; **136**: 270–276.
359 Park JG, Aubry MC, Godfrey JA, Midthun DE. Mediastinal lymphangioma: Mayo Clinic experience of 25 cases. *Mayo Clin Proc* 2006; **81**: 1197–1203.
360 Adams MT, Saltzman B, Perkins JA. Head and neck lymphatic malformation treatment: a systematic review. *Otolaryngol Head Neck Surg* 2012; **147**: 627–639.
361 Leung M, Leung L, Fung D *et al.* Management of the low-flow head and neck vascular malformations in children: the sclerotherapy protocol. *Eur J Pediatr Surg* 2014; **24**: 97–101.
362 Ogawa T, Shibayama M, Shimizu T. Clinical analysis of lymphangioma in the neck: the effects of local OK-432 injection therapy. *Jibi Inkoka Rinsho* 2010; **103**: 249–255. Japanese.
363 Arimoto Y, Kudo F, Suzuki H. Usefulness of ultrasonography in the differential diagnosis of respiratory distress disorders including infantile paresis of the vocal cords. *Shoni Jibi Inkoka* 2005; **26**: 37–42. Japanese.
364 Kitagawa H, Kawase H, Wakisaka M *et al.* Six cases of children with a benign cervical tumor who required tracheostomy. *Pediatr Surg Int* 2004; **20**: 51–54.
365 Hiki S, Yamataka A, Kobayashi H, Okada Y, Miyano T. [Treatment of lymphangioma in children. A report of 105 cases]. *Juntendo Igaku* 2003; **48**: 476–483. Japanese.

This article has been co-published with the permission of *The Journal of Dermatology, Pediatrics International* and *Japanese Journal of Radiology*. All rights reserved. © 2020 The Authors. The articles are identical except for minor stylistic and spelling differences in keeping with each journal's style. Either citation can be used when citing this article.

366 Desir A, Ghaye B, Duysinx B, Dondelinger RF. Percutaneous sclerotherapy of a giant mediastinal lymphangioma. *Eur Respir J* 2008; **32**: 804–806.
367 Kim DW. OK-432 sclerotherapy of lymphatic malformation in the head and neck: factors related to outcome. *Pediatr Radiol* 2014; **44**: 857–862.
368 Niramis R, Watanatittan S, Rattanasuwan T. Treatment of cystic hygroma by intralesional bleomycin injection: experience in 70 patients. *Eur J Pediatr Surg* 2010; **20**: 178–182.
369 Kudo F, Arimoto Y, Nakano A. [Sclerosing therapy for cystic hygroma in infants: intracystic injection of OK-432]. *Tokeibu Geka* 2008; **18**: 71–75. Japanese.
370 Kim MG, Kim SG, Lee JH, Eun YG, Yeo SG. The therapeutic effect of OK-432 (picibanil) sclerotherapy for benign neck cysts. *Laryngoscope* 2008; **118**: 2177–2181.
371 Baskota DK, Singh BB, Sinha BK. OK-432: an effective sclerosing agent for the treatment of lymphangiomas of head and neck. *Kathmandu Univ Med J (KUMJ)* 2007; **5**: 312–317.
372 Jamal N, Ahmed S, Miller T *et al.* Doxycycline sclerotherapy for pediatric head and neck macrocystic lymphatic malformations: a case series and review of the literature. *Int J Pediatr Otorhinolaryngol* 2012; **76**: 1127–1131.
373 Tomemori T, Kudo F, Sasamura Y, Numata T. [Cystic hygroma in infants]. *Tokeibu Shuyo* 2003; **29**: 58–63. Japanese.
374 Dasgupta R, Adams D, Elluru R, Wentzel MS, Azizkhan RG. Noninterventional treatment of selected head and neck lymphatic malformations. *J Pediatr Surg* 2008; **43**: 869–873.
375 Hogeling M, Adams S, Law J, Wargon O. Lymphatic malformations: clinical course and management in 64 cases. *Australas J Dermatol* 2011; **52**: 186–190.
376 Acevedo JL, Shah RK, Brietzke SE. Nonsurgical therapies for lymphangiomas: a systematic review. *Otolaryngol Head Neck Surg* 2008; **138**: 418–424.
377 Kim KH, Sung MW, Roh JL, Han MH. Sclerotherapy for congenital lesions in the head and neck. *Otolaryngol Head Neck Surg* 2004; **131**: 307–316.
378 Catalfamo L, Nava C, Lombardo G, Iudicello V, Siniscalchi EN, Saverio DPF. Tongue lymphangioma in adult. *J Craniofac Surg* 2012; **23**: 1920–1922.
379 Magoshi S, Okada M, Shigematsu H, Suzuki S, Kusama K, Sakashita H. [A case of hemangio-lymphangioma of the tongue]. *Nihon Koku Shindan Gakkai Zasshi* 2003; **16**: 250–252. Japanese.
380 Ogiuchi H, Yamazaki T, Yamamura T, Kuwazawa T, Ogiuchi H. A long-term follow-up, case of lymphangioma of tongue and floor of the mouth. *Shoni Koku Geka* 2003; **13**: 17–20. Japanese.
381 Rowley H, Perez-Atayde AR, Burrows PE, Rahbar R. Management of a giant lymphatic malformation of the tongue. *Arch Otolaryngol Head Neck Surg* 2002; **128**: 190–194.
382 Chakravarti A, Bhargava R. Lymphangioma circumscriptum of the tongue in children: successful treatment using intralesional bleomycin. *Int J Pediatr Otorhinolaryngol* 2013; **77**: 1367–1369.
383 Wiegand S, Eivazi B, Zimmermann AP *et al.* Microcystic lymphatic malformations of the tongue: diagnosis, classification, and treatment. *Arch Otolaryngol Head Neck Surg* 2009; **135**: 976–983.
384 Hong JP, Lee MY, Kim EK, Seo DH. Giant lymphangioma of the tongue. *J Craniofac Surg* 2009; **20**: 252–254.
385 Azizkhan RG, Rutter MJ, Cotton RT, Lim LH, Cohen AP, Mason JL. Lymphatic malformations of the tongue base. *J Pediatr Surg* 2006; **41**: 1279–1284.
386 Ogawa-Ochiai K, Sekiya N, Kasahara Y *et al.* A case of mediastinal lymphangioma successfully treated with Kampo medicine. *J Altern Complement Med* 2011; **17**: 563–565.
387 Roy S, Reyes S, Smith LP. Bipolar radiofrequency plasma ablation (Coblation) of lymphatic malformations of the tongue. *Int J Pediatr Otorhinolaryngol* 2009; **73**: 289–293.
388 Kemmotsu T, Takeda Y, Nakamura K, Tateishi I. [A case of congenital chylothorax requiring early OK-432 pleurodesis]. *Nihon Shusanki Shinseiji Igakkai Zasshi* 2012; **48**: 945–950. Japanese.
389 Tani G, Okuyama H, Kubota A, Kawahara H. [Thoracoscopic thoracic duct ligation in a premature infant with congenital chylothorax]. *Nihon Shoni Geka Gakkai Zasshi* 2011; **47**: 844–847. Japanese.
390 Miura K, Yoshizawa K, Tamaki M, Okumura K, Okada M. [Congenital chylothorax treated with video-assisted thoracic surgery]. *Kyobu Geka* 2008; **61**: 1149–1151. Japanese.
391 Amagai T, Nakamura H, Kaneko M, Sugiura M, Hamada H. Use and problems of pleuro-peritoneal shunting tube for neonatal chylothorax. *Shoni Geka* 2001; **33**: 201–207. Japanese.
392 Cleveland K, Zook D, Harvey K, Woods RK. Massive chylothorax in small babies. *J Pediatr Surg* 2009; **44**: 546–550.
393 Buttiker V, Fanconi S, Burger R. Chylothorax in children: guidelines for diagnosis and management. *Chest* 1999; **116**: 682–687.
394 Kaji M, Sakauchi M, Yoshii K *et al.* [A case of chylothorax treated effectively with surgery]. *Tokyo Joshi Ika Daigaku Zasshi* 2013; **83**: E366–E370. Japanese.
395 Haga T, Toida C, Muguruma T, Fujino A. [Two cases of mediastinal lymphangiomatosis that required intensive care management]. *Nihon Shonika Gakkai Zasshi* 2013; **117**: 1483–1488. Japanese.
396 Chen YL, Lee CC, Yeh ML, Lee JS, Sung TC. Generalized lymphangiomatosis presenting as cardiomegaly. *J Formos Med Assoc* 2007; **106**: S10–S14.
397 Pfleger A, Schwinger W, Maier A, Tauss J, Popper HH, Zach MS. Gorham-Stout syndrome in a male adolescent-case report and review of the literature. *J Pediatr Hematol Oncol* 2006; **28**: 231–233.
398 Noda M, Endo C, Hoshikawa Y *et al.* Successful management of intractable chylothorax in Gorham-Stout disease by awake thoracoscopic surgery. *Gen Thorac Cardiovasc Surg* 2013; **61**: 356–358.
399 Fukahori S, Tsuru T, Asagiri K *et al.* Thoracic lymphangiomatosis with massive chylothorax after a tumor biopsy and with disseminated intravenous coagulation–lymphoscintigraphy, an alternative minimally invasive imaging technique: report of a case. *Surg Today* 2011; **41**: 978–982.
400 Brodszki N, Lansberg JK, Dictor M *et al.* A novel treatment approach for paediatric Gorham-Stout syndrome with chylothorax. *Acta Paediatr* 2011; **100**: 1448–1453.
401 Deveci M, Inan N, Corapcioglu F, Ekingen G. Gorham-Stout syndrome with chylothorax in a six-year-old boy. *Indian J Pediatr* 2011; **78**: 737–739.
402 Seok YK, Cho S, Lee E. Early surgical management of chylothorax complicated by Gorham's disease. *Thorac Cardiovasc Surg* 2010; **58**: 492–493.
403 Kose M, Pekcan S, Dogru D *et al.* Gorham-Stout Syndrome with chylothorax: successful remission by interferon alpha-2b. *Pediatr Pulmonol* 2009; **44**: 613–615.
404 Boyle MJ, Alison P, Taylor G, Lightbourne BA. A case of Gorham's disease complicated by bilateral chylothorax. *Heart Lung Circ* 2008; **17**: 64–66.
405 Burgess S, Harris M, Dakin C, Borzi P, Ryan C, Cooper D. Successful management of lymphangiomatosis and chylothorax in a 7-month-old infant. *J Paediatr Child Health* 2006; **42**: 560–562.
406 Underwood J, Buckley J, Manning B. Gorham disease: an intraoperative case study. *AANA J* 2006; **74**: 45–48.
407 Fujiu K, Kanno R, Suzuki H, Nakamura N, Gotoh M. Chylothorax associated with massive osteolysis (Gorham's syndrome). *Ann Thorac Surg* 2002; **73**: 1956–1957.
408 Chavanis N, Chaffanjon P, Frey G, Vottero G, Brichon PY. Chylothorax complicating Gorham's disease. *Ann Thorac Surg* 2001; **72**: 937–939.
409 Konez O, Vyas PK, Goyal M. Disseminated lymphangiomatosis presenting with massive chylothorax. *Pediatr Radiol* 2000; **30**: 35–37.
410 Morita K, Fukumoto K, Mitsunaga M *et al.* [A case of thoracic lymphangiomatosis causing difficulty in treatment due to dyspnea and hemorrhage]. *Nihon Shoni Ketsueki Gan Gakkai Zasshi* 2013; **50**: 644–649. Japanese.
411 Kitami A, Suzuki T, Suzuki S, Usuda R, Kamio Y, Kadokura M. Gorham's disease complicated by chyloma of the chest wall. *Jpn J Thorac Cardiovasc Surg* 2006; **54**: 311–313.

This article has been co-published with the permission of *The Journal of Dermatology, Pediatrics International* and *Japanese Journal of Radiology*. All rights reserved. © 2020 The Authors. The articles are identical except for minor stylistic and spelling differences in keeping with each journal's style. Either citation can be used when citing this article.

412 Lee S, Finn L, Sze RW, Perkins JA, Sie KC. Gorham Stout syndrome (disappearing bone disease): two additional case reports and a review of the literature. *Arch Otolaryngol Head Neck Surg* 2003; **129**: 1340–1343.
413 Reinglas J, Ramphal R, Bromwich M. The successful management of diffuse lymphangiomatosis using sirolimus: a case report. *Laryngoscope* 2011; **121**: 1851–1854.
414 Tamay Z, Saribeyoglu E, Ones U *et al.* Diffuse thoracic lymphangiomatosis with disseminated intravascular coagulation in a child. *J Pediatr Hematol Oncol* 2005; **27**: 685–687.
415 Duffy BM, Manon R, Patel RR, Welsh JS. A case of Gorham's disease with chylothorax treated curatively with radiation therapy. *Clin Med Res* 2005; **3**: 83–86.
416 Kinnier CV, Eu JP, Davis RD, Howell DN, Sheets J, Palmer SM. Successful bilateral lung transplantation for lymphangiomatosis. *Am J Transplant* 2008; **8**: 1946–1950.
417 Huang SY, Lee YM, Tzeng ST *et al.* Gorham syndrome with postoperative respiratory failure and requiring prolonged mechanical ventilation. *Respir Care* 2013; **58**: e144–148.
418 Lee WS, Kim SH, Kim I *et al.* Chylothorax in Gorham's disease. *J Korean Med Sci* 2002; **17**: 826–829.
419 Fontanesi J. Radiation therapy in the treatment of Gorham disease. *J Pediatr Hematol Oncol* 2003; **25**: 816–817.
420 Yoo SY, Goo JM, Im JG. Mediastinal lymphangioma and chylothorax: thoracic involvement of Gorham's disease. *Korean J Radiol* 2002; **3**: 130–132.
421 Timke C, Krause MF, Oppermann HC, Leuschner I, Claviez A. Interferon alpha 2b treatment in an eleven-year-old boy with disseminated lymphangiomatosis. *Pediatr Blood Cancer* 2007; **48**: 108–111.

This article has been co-published with the permission of *The Journal of Dermatology, Pediatrics International* and *Japanese Journal of Radiology*. All rights reserved. © 2020 The Authors. The articles are identical except for minor stylistic and spelling differences in keeping with each journal's style. Either citation can be used when citing this article.

PEDIATRICS INTERNATIONAL Official Journal of the Japan Pediatric Society

Pediatrics International (2020) **0**, 1–48 doi: 10.1111/ped.14077

Guidelines

Japanese clinical practice guidelines for vascular anomalies 2017

Hidefumi Mimura,[1] Sadanori Akita,[2] Akihiro Fujino,[3] Masatoshi Jinnin,[4] Mine Ozaki,[5] Keigo Osuga,[6] Hiroki Nakaoka,[7] Eiichi Morii,[8] Akira Kuramochi,[9] Yoko Aoki,[10] Yasunori Arai,[1] Noriko Aramaki,[11] Masanori Inoue,[12] Yuki Iwashina,[5] Tadashi Iwanaka,[13] Shigeru Ueno,[14] Akihiro Umezawa,[15] Michio Ozeki,[16] Junko Ochi,[17] Yoshiaki Kinoshita,[18] Masakazu Kurita,[19] Shien Seike,[20] Nobuyuki Takakura,[21] Masataka Takahashi,[15] Takao Tachibana,[22] Kumiko Chuman,[23] Shuji Nagata,[24] Mitsunaga Narushima,[25] Yasunari Niimi,[26] Shunsuke Nosaka,[27] Taiki Nozaki,[28] Kazuki Hashimoto,[1] Ayato Hayashi,[29] Satoshi Hirakawa,[30] Atsuko Fujikawa,[1] Yumiko Hori,[8] Kentaro Matsuoka,[31] Hideki Mori,[7] Yuki Yamamoto,[4] Shunsuke Yuzuriha,[32] Naoaki Rikihisa,[33] Shoji Watanabe,[34] Shinichi Watanabe,[35] Tatsuo Kuroda,[36] Shunsuke Sugawara,[37] Kosuke Ishikawa[38] and Satoru Sasaki[39]

[1]*Department of Radiology, St. Marianna University School of Medicine, Kawasaki,* [2]*Department of Plastic Surgery, Wound Repair and Regeneration, School of Medicine, Fukuoka University, Fukuoka,* [3]*Division of Surgery,* [15]*Department of Reproductive Biology, Center for Regenerative Medicine,* [27]*Division of Radiology, National Center for Child Health and Development,* [11]*Departments of Plastic and Reconstructive Surgery,* [12]*Radiology,* [36]*Pediatric Surgery, Keio University School of Medicine,* [37]*Department of Diagnostic Radiology, National Cancer Center Hospital,* [13]*Departments of Pediatric Surgery,* [19]*Plastic and Reconstructive Surgery, The University of Tokyo Hospital,* [23]*Department of Dermatology, Kanto Central Hospital,* [26]*Departments of Neuroendovascular Therapy,* [28]*Radiology, St. Luke's International Hospital,* [35]*Department of Dermatology, Teikyo University School of Medicine, Tokyo,* [4]*Department of Dermatology, Wakayama Medical University, Wakayama,* [5]*Department of Plastic and Reconstructive, Aesthetic Surgery, Kyorin University School of Medicine, Mitaka,* [6]*Departments of Diagnostic and Interventional Radiology,* [8]*Pathology,* [20]*Plastic Surgery, Osaka University Graduate School of Medicine,* [21]*Department of Signal Transduction, Research Institute for Microbial Diseases, Osaka University, Suita,* [7]*Department of Plastic Surgery, Ehime University Hospital, Toon,* [9]*Department of Dermatology, Saitama Medical University, Irumagun,* [10]*Departments of Medical Genetics,* [17]*Diagnostic Radiology, Tohoku University Graduate School of Medicine, Sendai,* [14]*Department of Pediatric Surgery, Tokai University School of Medicine, Isehara,* [16]*Department of Pediatrics, Gifu University Graduate School of Medicine, Gifu,* [18]*Department of Pediatric Surgery, Niigata University Graduate School of Medical and Dental Sciences, Niigata,* [22]*Department of Dermatology, Osaka Red Cross Hospital, Osaka,* [24]*Department of Radiology, Kurume University School of Medicine, Kurume,* [25]*Department of Plastic and Reconstructive Surgery, Graduate School of Medicine, Mie University, Tsu,* [29]*Department of Plastic and Reconstructive Surgery, Juntendo University Urayasu Hospital, Urayasu,* [30]*Department of Dermatology, Hamamatsu University School of Medicine, Hamamatsu,* [31]*Department of Pathology, Dokkyo Medical University Saitama Medical Center, Koshigaya,* [32]*Department of Plastic and Reconstructive Surgery, Shinshu University School of Medicine, Matsumoto,* [33]*Department of Plastic and Reconstructive Surgery, Oyumino Central Hospital, Chiba,* [34]*Department of Plastic and Reconstructive Surgery, Saitama Children's Medical Center, Saitama,* [38]*Department of Plastic and Reconstructive Surgery, Faculty of Medicine and Graduate School of Medicine, Hokkaido University and* [39]*Department of Plastic and Reconstructive Surgery, Center for Vascular Anomalies, Tonan Hospital, Sapporo, Japan*

Correspondence: Hidefumi Mimura, M.D., Department of Radiology, St. Marianna University School of Medicine, 2-16-1, Sugao, Miyamae, Kawasaki, Kanagawa, 216-8511, Japan. Email: mimura@marianna-u.ac.jp

Japanese Clinical Practice Guidelines for Vascular Anomalies 2017 were published in Japanese in 2017. We provide these guidelines in English to inform healthcare professionals and the general public in the world to improve medical practice and patient outcome. This article has been co-published in The Journal of Dermatology, Japanese Journal of Radiology, and Pediatrics International based on the agreement of Editor-In-Chief of the three journals.

Received 19 November 2019; accepted 20 November 2019.

This article has been co-published with the permission of *The Journal of Dermatology, Pediatrics International and Japanese Journal of Radiology*. All rights reserved. © 2020 The Authors. The articles are identical except for minor stylistic and spelling differences in keeping with each journal's style. Either citation can be used when citing this article.

Abstract The objective was to prepare guidelines to perform the current optimum treatment by organizing effective and efficient treatments of hemangiomas and vascular malformations, confirming the safety, and systematizing treatment, employing evidence-based medicine (EBM) techniques and aimed at improvement of the outcomes. Clinical questions (CQs) were decided based on the important clinical issues. For document retrieval, key words for literature searches were set for each CQ and literature published from 1980 to the end of September 2014 was searched in Pubmed, Cochrane Library, and Japana Centra Revuo Medicina (JCRM). The strengths of evidence and recommendations acquired by systematic reviews were determined following the Medical Information Network Distribution System (MINDS) technique. A total of 33 CQs were used to compile recommendations and the subjects included efficacy of resection, sclerotherapy/embolization, drug therapy, laser therapy, radiotherapy, and other conservative treatment, differences in appropriate treatment due to the location of lesions and among symptoms, appropriate timing of treatment and tests, and pathological diagnosis deciding the diagnosis. Thus, the Japanese Clinical Practice Guidelines for Vascular Anomalies 2017 have been prepared as the evidence-based guidelines for the management of vascular anomalies.

Key words clinical practice, guidelines, hemangioma, vascular anomalies, vascular malformation.

The etiology of vascular anomalies on the body surface and in soft tissue are mostly unclear and no fundamental treatment methods have been established. Many patients visit many medical institutions seeking an expert, being a disadvantage in treatment. Hemangiomas and vascular malformations are frequently termed 'hemangioma', but these are different diseases in the ISSVA classification proposed by the International Society for Study of Vascular Anomalies (ISSVA),[1,2] and this classification has been internationally standardized.

"Clinical Practice Guidelines for Vascular Anomalies 2013" (1st edition)[3] target general practitioners and the general public, and were prepared aiming at organizing effective and efficient treatments for hemangiomas/vascular malformations, confirming the safety, and systematizing treatment using evidence-based medicine (EBM) techniques. The organization responsible for preparation was the Health, Labour and Welfare Sciences Research Grants (Research on Measures for Intractable Diseases), Research Committee for "Intractable Vascular Anomalies," and the main committee members were selected from academic societies of plastic surgery and radiology mainly treating hemangiomas and vascular malformations: the Japanese Society of Plastic and Reconstructive Surgery and Japanese Society of Interventional Radiology, and the guidelines were prepared by them.

''Clinical Practice Guidelines for Vascular Anomalies 2017" were prepared as a revised edition of the "Clinical Practice Guidelines for Vascular Anomalies 2013." The organization responsible for preparation was the Health, Labour and Welfare Sciences Research Grants (Research on Policy Planning and Evaluation for Rare and Intractable Diseases), Research Committee for Intractable Vascular Anomalies, and the differences from the previous guidelines are setting the objective at summarizing opinions from related academic societies by inviting many committee members from dermatologists, pediatric surgeons, pediatricians, radiologists (diagnostic radiology), and basic researchers including the pathology, molecular biology, and epidemiology fields, in addition to plastic surgeons and radiologists (interventional radiology). Since the guidelines were prepared following the reformed "Minds Handbook for Clinical Practice Guideline Development 2014"[4] and "Minds Manual for Clinical Practice Guideline Development Ver.1.0-2.0,"[5,6] it was fully revised.

The original text of the guidelines (Japanese version) is comprised of Reviews and Clinical Questions (CQs), but only CQs are presented in this report.

Purpose of the guidelines

The objective was to prepare guidelines to perform the current optimum treatment by organizing effective and efficient treatments of hemangiomas and vascular malformations, confirming the safety, and systematizing treatment, employing the EBM techniques and aimed at improvement of the following outcomes: Pain, swelling, esthetic impairment, and functional disorder.

Materials and methods

Organization

For the Guidelines Executive Committee members, representatives of the plastic surgery, dermatology, radiology, pediatric surgery, and basic science fields were selected. The guidelines preparation group and systematic review team for preparation of CQs and recommendations were comprised of 4 groups: groups in charge of arteriovenous malformation (AVM), venous malformation (VM), combined type, and syndrome, in charge of capillary malformation (CM) and infantile hemangioma, in charge of the lymphatic malformation (lymphangioma) (LM), and in charge of the basic field. To the group in charge of AVM, VM, combined type, and syndrome, plastic surgeons and radiologists were mainly assigned. To the group in charge of CM and infantile hemangioma, plastic surgeons

This article has been co-published with the permission of *The Journal of Dermatology, Pediatrics International and Japanese Journal of Radiology*. All rights reserved. © 2020 The Authors. The articles are identical except for minor stylistic and spelling differences in keeping with each journal's style. Either citation can be used when citing this article.

and dermatologists were mainly assigned. To the group in charge of the lymphatic system, pediatric surgeons, plastic surgeons, and pediatricians were mainly assigned. The Reviews of the guidelines were also prepared by those selected from each group. Pathologists and molecular biologists were in charge of the Reviews of the basic fields.

Preparation process

The guidelines were revised following the "Minds Handbook for Clinical Practice Guideline Development 2014" and "Minds Manual for Clinical Practice Guideline Development Ver.1.0-2.0."

CQs were decided based on the following important clinical issues: (i) Efficacy of resection, (ii) efficacy of sclerotherapy/embolization, (iii) efficacy of drug therapy, laser therapy, radiotherapy, and other conservative treatment, (iv) differences in appropriate treatment due to the location of lesions, (v) differences in appropriate treatment among symptoms, (vi) appropriate timing of treatment and tests, and (vii) pathological diagnosis deciding the diagnosis.

For document retrieval, key words for literature searches were set for each CQ and literature published from 1980 to the end of September 2014 was searched in Pubmed, Cochrane Library, and Japana Centra Revuo Medicina (JCRM). Literature search was requested to the Japan Medical Library Association. For decisions on CQs and recommendations lacking evidence or having weak evidence, discussion and agreement in the preparation group were reflected.

The strengths of evidence and recommendations acquired by systematic reviews were determined following the Minds technique as described below and this follows the GRADE guidelines preparation method.[7,8]

Determination of the strength of evidence of the body of evidence

The Strength of Evidence of the Body of Evidence was determined according to 'Minds Handbook for Clinical Practice Guideline Development 2014' (Table 1).

> In the case of RCTs, the score "A (strong)" is given at the start of evaluation, and the final score might be downgraded to B, C, or D, according to the results of evaluation of five items, including risk of bias, inconsistency in results, indirectness of evidence, data imprecision, and high possibility of publication bias. In the case of observational studies, the score "C (weak)" is given at the start of evaluation, and five items lowering the strength are evaluated similarly as for RCTs. In addition, three items, including large effect with no confounding factors, dose–response gradient, and possible confounding factors, are weaker than actual effects increasing the strength are evaluated as well.

Table 1 Recommendation Grade and Definition of the Strength of Body of Evidence in Evaluation of Systematic Review

Recommendation grade
1 strongly recommended
2 weakly recommended (suggested)
Definition of the Strength of Body of Evidence in Evaluation of Systematic Review
A (strong): strongly confident of the estimate of effect
B (moderate): moderately confident of the estimate of effect
C (weak): limited confidence of the estimate of effect
D (very weak): very little confident of the estimate of effect

Presentation of the strength of recommendations

The strength of recommendation was also determined according to "Minds Handbook for Clinical Practice Guideline Development 2014" (Table 1).

> The strength of recommendations is usually presented in two ways: "1": strongly recommended, and "2": weakly recommended (suggested). If the strength of recommendations cannot be determined by any means, it is occasionally presented as "no definite recommendation can be made." Recommendations will be entered as follows by indicating the strength of evidence (A, B, C, D) with the strength of recommendations "1": strong or "2": weak.

Finalization

Preparation of the draft guidelines was completed in December 2016 and review was requested to the Japanese Society of Plastic and Reconstructive Surgery, Japanese Dermatological Association, Japan Radiology Society, Japanese Society of Interventional Radiology, Japanese Society of Pediatric Surgeons, and Japanese Society of Pathology between December 2016 and January 2017, and corrections were made based on the results of the reviews. In addition, from December 2016 to January 2017, the guidelines were disclosed on the home page of the Research Committee for 'Intractable Vascular Anomalies' and public comments were collected. The draft guidelines were presented to two related patient organizations, 'the Patients Association of Vascular Anomalies' and 'the Patients Association of Combined Vascular Malformations' and comments were received. Based on these, the draft guidelines were revised and CQs, recommendations, and explanations were completed. It was finalized in March 2017.

Results

CQs and recommendations

CQ1: What are the guidelines for the time to begin treatment for AVM?

Recommendation: It is necessary to judge the time to begin endovascular or surgical treatment for AVM individually by

This article has been co-published with the permission of *The Journal of Dermatology, Pediatrics International and Japanese Journal of Radiology*. All rights reserved. © 2020 The Authors. The articles are identical except for minor stylistic and spelling differences in keeping with each journal's style. Either citation can be used when citing this article.

evaluating the stage of symptoms and lesion extent and in consideration of the risk of complications.

Strength of recommendation: 2 (weak)

Evidence: D (very weak)

Comments: As a result of primary screening, 92, 3, and 27 papers were extracted from PubMed, JCRM, and Cochrane Library, respectively, and, as a result of secondary screening, 37 and 3 papers were extracted from PubMed and JCRM, respectively. However, as all these references were observational or case series studies, the strength of evidence is rated as "D (very weak)."

There has been no report in which the time to begin treatment for AVM in itself was the endpoint, and only some reports described the view on the time to begin treatment in the discussion. Therefore, as it is difficult to objectively evaluate the validity of the time to begin treatment, we determined whether guidelines can be derived from the patient age, lesion site, symptoms, clinical stage, effectiveness of treatment, frequency of complications in each report.

In the reports[9,10] on the treatment for AVM, symptomatic AVM is primarily addressed, and treatment can be suspended (follow-up) while the lesion remains asymptomatic. However, as AVM often progresses when left untreated, it is considered important to begin the treatment at an appropriate time depending on the stage of symptoms. In addition, as there is the tendency that the response rate decreases, and the complication rate increases, with progression of symptoms, some reports from particular pediatric institutions where patients are concentrated recommend early therapeutic intervention in relatively "early" or "mild" stages without waiting for progression of the disease.

Localized lesions may be radically treated by early intervention.[11] Among endovascular procedures, the response (cure) rate tends to be high by ethanol embolization, but as the complication rate is also high.[12,13] By surgery, localized lesions are unlikely to recur if they are completely resected, although adverse events, such as postoperative cicatrization/deformation or functional impairment, have been seldom discussed.[10] On the other hand, in diffuse lesions, limitations of effectiveness, such as recurrence and persistence and the risk of treatment, are higher by both endovascular treatment and surgery, with the risks outweighing benefits.[13] It should also be considered that children, in particular, are not mentally ready to accept such invasive treatments.[14]

As discussed above, it is difficult to give guidelines for the time to begin treatment for AVM at present, and individual judgment is necessary depending on the symptom stage and lesion extent in consideration of the complication risk.

CQ2: Is recurrence (regrowth) after resection of AVM more frequent by wound closure with a skin graft than by reconstruction using a flap?

Recommendation: Whether recurrence (regrowth) is more frequent by wound closure with a skin graft compared with reconstruction using a flap is unclear.

Strength of recommendation: 2 (weak)

Evidence: D (very weak)

Comments: The number of references retrieved by searches using keywords was 40 from JCRM, 75 from PubMed, and 0 from Cochrane, and 39 were extracted by secondary screening. For AVM of a certain size, reconstruction is necessary after resection, and wound closure by skin grafting or reconstruction using a flap is performed according to common reconstruction methods for tissue defects. The reports discussing reconstruction after resection of AVM that we could retrieve were all descriptive studies (case reports or case series studies). Therefore, the evidence level of all these references is D (very weak).

The concept of regulating flap,[15,16] that reconstruction using a free flap controls the recurrence or regrowth after resection of AVM, has been proposed. However, no report has evaluated whether free flaps[16–37] and other flap types[17,19,25,28,38–49] clearly prevent the recurrence or regrowth compared with skin grafts.[21,23,50–52]

According to the present knowledge about the recurrence or regrowth after resection of AVM,[15,16,39,53] whether AVM can be completely resected is important, and, concerning cases in which complete resection is difficult, it has been reported that the hemodynamics in the residual lesions contributes to the recurrence and regrowth, and that it can be controlled by a flap with rich blood flow.

CQ3: Is proximal ligation/coil embolization of the feeding artery of AVM effective?

Recommendation: The therapeutic effect of ligation/coil embolization of the feeding artery on the proximal side may be poor, and the possibility of recurrence may be high. In addition, in the event of recurrence, treatment may become difficult due to the development of collateral vessels. Therefore, these procedures are recommended to be avoided, in principle.

Strength of recommendation: 2 (weak)

Evidence: D (very weak)

Comments: As a result of secondary screening, 1 and 14 papers were extracted from PubMed and JCRM, respectively, and were reviewed. As a result, all these papers were case reports. In addition, 6 papers retrieved by manual searches were also reviewed, but they were all case series studies at the maximum. Therefore, the strength of evidence as a collection of literature concerning this CQ is D (very weak).

To summarize the evaluation of this collection of papers, AVM was treated by proximal ligation/coil embolization of the feeding artery, but as there have been reports of recurrence following the development of collateral channels (reports of cases of the occurrence of unfavorable situations), the treatment is recommended to be avoided, but the evidence level of this recommendation is low as mentioned above.

The objective of embolization for AVM is obliteration of the nidus, and embolization at or near the nidus is necessary as much as possible. If ligation/coil embolization of the feeding artery is performed on the proximal/central side, the nidus is not obliterated, and the development of several collateral channels is promoted. In many cases, the collateral channels

This article has been co-published with the permission of *The Journal of Dermatology, Pediatrics International and Japanese Journal of Radiology*. All rights reserved. © 2020 The Authors. The articles are identical except for minor stylistic and spelling differences in keeping with each journal's style. Either citation can be used when citing this article.

are thin, complicated, and markedly tortuous, and trans-catheter treatment is often difficult.

Wu *et al.*[14] performed proximal ligation in 9 of 29 patients treated for AVM of the auricle but that the condition was exacerbated in all patients with 8 requiring auricular resection and 1 requiring additional treatment. They excluded proximal ligation from treatment options for AVM, because it makes subsequent trans-catheter treatments difficult.

Slaba *et al.*[54] evaluated 25 patients with AVM of the tongue and reported that 3 of the 12 symptomatic patients who underwent ipsilateral external carotid artery ligation at another facility showed marked development of collateral channels.

Other reports include those of a case in which a large number of collateral channels developed as a result of ligation of the feeding artery for AVM of the shoulder with serious complications including high-output heart failure,[55] 3 cases in which proximal ligation/embolization was performed for AVM of the limbs and pelvis, collateral vessels developed, but the condition was controlled by multidisciplinary treatment consisting of trans-catheter treatment and direct puncture sclerotherapy,[56] and several cases in which external carotid artery ligation was performed for AVM of the head and neck, but the subsequent treatment was difficult.

Suyama *et al.*[35] reported a case in which AVM of the auricle, treated by proximal embolization using coils and gelatin sponge, recurred and was treated again by ligation at a proximal part of the artery, but the lesion recurred again. Also, Aikawa *et al.*[57] reported a case of intrapelvic AVM that underwent coil embolization of the left ovarian artery and left internal iliac artery but showed little change in the area of the nidus or the state of arterial or venous dilatation. In addition, Yamamoto *et al.*[58] reported a case in which TAE was performed for AVM of the mandible via the maxillary artery, facial artery, lingual artery, and ocular artery but was not effective due to the development of collateral channels from the internal carotid artery and vertebral artery.

As observed above, it is recommended not to select proximal/central ligation/coil embolization as a treatment for AVM. However, AV fistulas with direct connection of a large artery and a vessel may be treated by coil embolization if the shunt area is directly accessible with a catheter. Proximal coil embolization may also be accepted as preoperative embolization, but careful evaluation of its indications is necessary, and embolization at a site near the shunt is necessary to leave the room for catheter insertion in the event of future recurrence.

CQ4: What is the appropriate timing for embolization before resection of AVM?

Recommendation: It is recommended to perform resection within 3 days (72 h) after embolization. If the interval prolongs, the risk of massive intraoperative hemorrhage may increase due to recanalization of the embolized vessel and development of collateral channels. In addition, surgery has been reported to be made difficult by enlargement of the lesion after embolization.

Strength of recommendation: 2 (weak)

Evidence: D (very weak)

Comments: While it is difficult to generalize the therapeutic approach as it varies with the affected area and extent of the lesion, there were a few reports that preoperative embolization was useful for the treatment of AVM of the head and neck region.

As a result of secondary screening, 10 and 3 papers from PubMed and JCRM, respectively, were reviewed. All the papers selected by this screening procedure were case reports or case series, and the strength of evidence is "D (very weak)." Mentions about the timing of preoperative embolization and volume of hemorrhage also varied among the papers. Although it is difficult to draw a conclusion, among the papers that mentioned specific timing of preoperative embolization and volume of hemorrhage, Deng *et al.*[59] performed embolization within 48–72 h before surgery in 16 patients with maxillofacial AVM and reported that the volume of hemorrhage was ≤200 mL in all patients and that there were no complications. Erdmann *et al.*[60] performed embolization within 24 h before surgery in 4 patients with head and neck AVM, and the lesion was resected with hemorrhage of ≤100 mL in 3. It is recommended to perform resection within 72 h to prevent increases in difficulty of resection due to inflammation after embolization.

There have also been reports that embolization was performed intraoperatively or within a few days before surgery, resulting in decreases in the volume of hemorrhage or favorable long-term outcomes. Most papers reported no or only mild complications, but as for relatively severe complications, Goldberg *et al.*[61] reported temporary visual impairment in 2 of the 3 patients with orbital AVM.

Factors that affect the appropriate timing of preoperative embolization include recanalization of the target vessel, development of collateral channels, and swelling and reactive changes after embolization, which make surgery difficult. To avoid the effects of these phenomena, many papers supported relatively early resection, i.e., within 72 h after embolization. Clinically, also, there is no benefit in taking a long interval, and it is considered valid to recommend resection within 72 h after embolization.

In conclusion, adequate control of hemorrhage may be achieved with fewer complications by performing vascular embolization within a few days before surgery, but no sufficient evidence that support this view has been provided.

CQ5: What treatments are appropriate for the maxillo-mandibular AVM?

Recommendation: Although surgery alone is not recommended, a combination of surgery with endovascular embolization (including sclerotherapy) can be recommended depending on the case.

Radiotherapy is not recommended.

Endovascular embolization (including sclerotherapy) alone or as a preoperative treatment can be recommended.

Strength of recommendation: 2 (weak)

Evidence: D (very weak)

This article has been co-published with the permission of *The Journal of Dermatology, Pediatrics International and Japanese Journal of Radiology*. All rights reserved. © 2020 The Authors. The articles are identical except for minor stylistic and spelling differences in keeping with each journal's style. Either citation can be used when citing this article.

Comments: AVM of the maxilla and mandible is a rare disorder. Most of the literature is reports of a small number of cases except a few case series reported from some special institutions. Only 5 reports[62–66] of a series of 10 or more cases were retrieved by the search of PubMed. Because there is no cohort study or randomized trial comparing various treatments, strong evidence regarding the best treatment is lacking.

Maxillo-mandibular AVM may involve the maxilla, mandible, or both, and it often presents with massive oral hemorrhage around the age of 10 years when milk teeth are lost, but may also be detected due to swelling of the soft tissue.

According to Persky *et al*.,[62] embolization alone resulted in cure in 42%, improvement in 16%, and stabilization of symptoms in 23% of the 26 patients with a maxillo-mandibular AVM. Liu *et al*.[63] treated 25 patients by transarterial or transvenous embolization alone or in combination with curettage and reported anatomical cure in 14 and clinical cure in 21. Chen *et al*.[65] treated 15 patients by bone wax packing (BWP) alone in 4, transarterial embolization (TAE) + BWP in 3, TAE + resection in 4, and TAE + radiotherapy + resection in 4 and reported clinical cure in 14.

The following are considered as treatment options for AVM of the maxilla and mandible.

A: Surgical treatment

- A-1: Resection and reconstruction
- A-2: Curettage
- A-3: Bone wax packing

B: Endovascular embolization (including sclerotherapy)

- B-1: Transarterial embolization
- B-2: Transvenous embolization
- B-3: Embolization by direct puncture

C: Combination of A and B

D: Radiotherapy

The literature is mostly about B, i.e., endovascular embolization (including sclerotherapy) alone, or surgical treatment after B. There was no report of case series of surgical treatment alone, but there was only 1 report[65] of case series of surgery + radiotherapy. Surgery alone and radiotherapy are generally not recommended. Endovascular embolization is performed by various approaches including transarterial and transvenous routes and direct puncture, sometimes, in combination. Concerning embolic agents, PVA and Gelfoam® (Pfizer, New York, NY, USA) are used for embolization as an adjuvant therapy immediately before surgery as they allow recanalization. Cyanoacrylate liquid embolic agents are considered effective for embolization performed preoperatively or alone in expectation of a long-term occlusive effect.[64,67,68] Coils are often used for transvenous embolization. Recently, there have been reports[69,70] that favorable outcomes were obtained by TAE using Onyx® (Medtronic, Irvine, CA, USA) a non-adhesive liquid embolic agent. Concerning sclerotherapy, there is a case series study of ethanol sclerotherapy alone, reporting relatively favorable outcomes.[71] Infection and bone necrosis are frequent complications of embolization, and they may occur, when an embolic agent, a foreign body, is injected into lesions that were in contact with the external environment due to direct puncture or hemorrhage. Surgical treatments as listed above are performed primarily after endovascular embolization. Invasive radical resection and reconstruction should be avoided at least as the initial treatment, because many lesions can now be controlled by endovascular embolization alone with the advancement of endovascular technique.

As mentioned above, endovascular embolization is performed using various approaches and embolic agents selected depending on the facility and patient. There are also a wide variety of surgical treatment options. Since the treatment may be performed by combining these options, AVM of the maxilla and mandible should be treated at the institutions where multidisciplinary treatment can be performed by experienced physicians.

CQ6: What treatments are appropriate for AVM of the fingers?

Recommendation: Although embolization or sclerotherapy is effective as it alleviates symptoms, such as pain, sufficient evaluation is necessary because of the risk of finger necrosis and nerve damage. In surgical resection, total resection is recommended, because partial resection is likely to result in enlargement of the lesion. Occasionally, the disorder results in finger amputation.

Strength of recommendation: 2 (weak)

Evidence: D (very weak)

Comments: As a result of primary screening, 38, 16, and 35 papers were retrieved from PubMed, Cochrane Library, and JCRM, respectively. However, during secondary screening, many reports concerned AV shunts in dialysis patients and AVM at sites other than the fingers. Eventually, only 10 papers consisting of 3 case series and 7 case reports remained as references, and the evidence level is extremely low (D: very weak).

AVM of the fingers is often difficult to treat, and treatments are likely to be ineffective, particularly, when the lesion extends from the fingers to the palm. In addition, when AVM is localized in the fingers, complications are likely to occur after treatment.[72] It is recommended to conduct treatment by a team from several departments including the plastic surgery, vascular surgery, and radiology departments.[73] 3D-CTA is useful for preoperative examination.[74] Since complete cure is difficult to obtain by embolization therapy, it is recommended to be performed for alleviation of symptoms such as pain only in symptomatic areas.[75] In addition, as there is the possibility of re-enlargement after embolization, it is recommended to periodically follow-up the condition and repeatedly perform embolization each time symptoms appear.[73] Surgical resection is necessary for permanent cure, and total resection is recommended as there is the possibility of re-enlargement after partial resection.[76–78] Reconstruction is occasionally necessary, but treatment may end in finger amputation. In this event, preoperative embolization or sclerotherapy is effective.[79] The present review has fallen short of clarifying situations in which

This article has been co-published with the permission of *The Journal of Dermatology, Pediatrics International and Japanese Journal of Radiology*. All rights reserved. © 2020 The Authors. The articles are identical except for minor stylistic and spelling differences in keeping with each journal's style. Either citation can be used when citing this article.

preoperative embolization is useful in fingers to which a tourniquet can be applied.

CQ7: What treatments are effective for painful VM?

Recommendation: Sclerotherapy and surgical resection, as well as conservative treatments, such as compression, oral aspirin, and low-molecular-weight heparin, are reported to be effective depending on the site and size of the lesion and symptoms. Endovascular laser treatment, percutaneous cryotherapy, and photodynamic therapy have also been suggested to be effective.

Strength of recommendation: 2 (weak)

Evidence: D (very weak)

Comments: As a result of literature search, 54 reports in English and 4 in Japanese were retrieved by primary screening. Of these reports, 39 in English and 4 in Japanese were extracted by secondary screening. Many options were reported as treatments for pain associated with VM, but all these documents were case series or case reports without comparison of treatments. Therefore, the evidence level was rated as "very weak," and the recommendation level as "weak."

Pain is one of the major symptoms of VM. It may respond to conservative treatments that are relatively easy to manage, such as compression and oral aspirin, depending on the site and size of the lesion and symptoms. Particularly, when pain is localized, surgery should also be considered. Relatively novel treatments, such as endovascular laser therapy, percutaneous cryotherapy, and photodynamic therapy, have been reported to be effective for controlling local VM, and they have also been reported to be effective for the control of pain. Limb lesions accompanied by localized intravascular coagulopathy may be indications for low-molecular-weight heparin. Reports on various treatments are mentioned below.

1. Compression

Although there has been no report of comparative evaluation, compression is reportedly effective according to reviews by specialized medical facilities.[80–82]

2. Oral aspirin

The literature is also limited, but the treatment has been mentioned in reviews.[80–82] Nguyen *et al*.[83] reported that pain was alleviated in 17 (77%) of 22 patients in whom oral aspirin therapy was initiated for pain.

3. Sclerotherapy

Sclerotherapy has often been performed using ethanol or polidocanol. The literature concerning other sclerosing agents is scarce, and their effectiveness remains largely unclear.

Each sclerosing agent is commented below.

(i) Ethanol

Shireman *et al*.[84] reported remission in 6 of 12 patients, and Rimon *et al*.[85] reported alleviation or remission in 14 patients with painful VM (including 8 with lower limb lesions) except in 4 of those with lower limb lesions. Marrocco-Trischitta *et al*.[86] reported that pain was resolved in both (100%) of 2 women with external genital lesions.

Concerning the use of ethanol, Suh *et al*.[87] reported alleviation to 50% or less of the pre-treatment state according to a VAS in 12 (71%) of 17 patients who underwent sclerotherapy using its mixture with lipiodol, and Dompmartin *et al*.[88] reported 37 patients who underwent sclerotherapy using its mixture with ethylcellulose. According to Schumacher *et al*.,[89] also, 77 patients underwent sclerotherapy using ethylcellulose-ethanol in a multicenter study, and significant improvement compared with the pre-treatment state was observed in all patients.

(ii) Polidocanol (including foam sclerotherapy)

Mimura *et al*.[90] reported remission in 6, alleviation in 4, and no change in 1 of 11 patients with painful VM, and remission in 12 (41%), alleviation in 14 (48%), no change in 2 (7%), and exacerbation in 1 (3%) of 29 patients in another study.[91] Cabrera *et al*.[92] treated 50 patients (including 15 with Klippel-Trenaunay syndrome) using a foamed sclerosing agent and reported remission in 25 (50%) and alleviation in 14 (28%). Marrocco-Trischitta *et al*.[86] reported resolution of pain in all 3 women with external genital lesions.

(iii) Ethanolamine oleate

Ozaki *et al*.[93] reported remission in 2 (20%) and alleviation in 8 (80%) of 10 patients.

(iv) Sodium tetradecyl sulfate

Krokidis *et al*.[94] reported alleviation of pain in 4 of 5 women with external genital lesions.

4. Surgical resection

Enjolras *et al*.[95] performed surgical resection in 7 of 13 patients with VM involving a wide area including the knee joint and reported alleviation of pain in 5 (71%). Steiner *et al*.[96] reported alleviation to 50% or less of the pre-treatment state by a VAS in 24 (89%) of 27 patients with background pain and 12 (92%) of 13 patients with acute episodic pain. In addition, Noel *et al*.[97] performed surgical resection and compression therapy for VM of the lower extremities in 20 patients with Klippel-Trenaunay syndrome and reported disappearance of pain in 18 (90%) (mean follow-up period: 63 months).

5. Endovascular laser therapy

Sidhu *et al*.[98] and Lu *et al*.[99] reported alleviation of pain in all 8 and 51 lesions in 6 and 33 patients, respectively. Liu *et al*.[100] also reported marked responses in 46 (35%), responses in 84 (63%), and no change in 3 (2%) of 133 patients.

6. Low-molecular-weight heparin

According to Mazoyer *et al*.,[101] only low-molecular-weight heparin was effective when VM are complicated by localized intravascular coagulation, resulting in disappearance of pain.

This article has been co-published with the permission of *The Journal of Dermatology, Pediatrics International and Japanese Journal of Radiology*. All rights reserved. © 2020 The Authors. The articles are identical except for minor stylistic and spelling differences in keeping with each journal's style. Either citation can be used when citing this article.

7. Percutaneous cryotherapy

Cornelis *et al.*[102,103] reported remission of pain in a report of 1 case (observation period: 2 months) and a report of 4 cases (observation period: 6 months).

8. Photodynamic therapy

Betz *et al.*[104] reported remission in 2 and alleviation in 1 of 3 patients.

CQ8: Is laser therapy effective for VM?

Recommendation: With appropriate selection of the type of laser according to the site, size, and symptoms of the lesion, laser therapy can be effective for the treatment of VM. It is recommended to evaluate whether the net benefit by laser therapy is worth the cost and resources by comparison with other treatments such as sclerotherapy and surgical resection.

Strength of recommendation: 2 (weak)

Evidence: C (weak)

Comments: VM is a lesion that has been called cavernous hemangioma, and it causes pain, functional impairment, and cosmetic defect depending on the affected site. In addition to conventional resection of the lesion, sclerotherapy has been widely performed in recent years. While reports of laser therapy for VM have increased, there have not been prospective studies comparing the results of laser therapy with those of surgery or sclerotherapy, among types of laser equipment different in wavelength, or using the same equipment type but changing the irradiation method or parameter setting. We analyzed 134 papers extracted by primary screening and 98 papers extracted by secondary screening. Concerning more than 30 cases, the answer to the CQ was based primarily on 7 reports summarizing the methods and sites of treatment and benefits and harms derived from treatment (decrease in size of the lesion, alleviation of symptoms, complications).

In the facial skin, pigmentation and scar formation after irradiation can be serious treatment-related complications compared with unexposed areas. In the airway and digestive tract, the mass effect of the lesion and chronic bleeding from the lesion can be causes of serious symptoms. Thus, as the goal to achieve varies with the anatomical site of the lesion, we reviewed the literature by the anatomical site (the neurosurgery field was excluded). For this reason, we also extracted benefits and harms of treatment from the text of the reports of less than 30 cases. The relevant departments surveyed included ENT, dental and oral surgery, gastrointestinal surgery, ophthalmology, plastic surgery, and dermatology, and secondary screening overviewed laser therapy for VM and vasodilatory lesions.

When a new laser instrument is developed and put into use, reports of therapeutic results using the equipment are presented. The types of laser used for treatment varied widely. The types of laser that have been reported are summarized chronologically in a graph (Fig. 1). While the type of laser with more reports is not necessarily more effective, the graph is considered to reflect tendencies of laser types that are established and gain favorable appraisal or no longer in use.

Since dye laser used for the treatment of port wine stain (wavelength: 595 nm) uses hemoglobin as the observer/heater, photothermal conversion occurs efficiently in the blood vessel, and the thermal energy reaches endothelial cells.[105] However, its optical penetration depth is shallow, being about 1 mm in both the skin and mucosa.[105] However, in Nd:YAG laser with a longer wavelength (1,064 nm), the optical penetration depth is about 3 mm in the skin and about 6 mm in the mucosa.[105] Although Nd:YAG laser is advantageous compared with dye laser for the treatment of deep lesions, heat is generated also in perivascular tissues, because light is converted to heat as it is absorbed by water contained in the skin and mucosa.

The target of laser treatment for VM is the endothelium of morbidly dilated blood vessels. There is no light that is specifically absorbed by endothelial cells and emits heat. Satisfactory therapeutic results cannot be expected unless treatment is performed by selecting the laser type and modifying the irradiation method based on the understanding of such principles and limitations of phototherapy.

Concerning small VM of the mucosa, tongue, lips, and glans penis, in which scar formation after treatment poses no serious problem, there are a number of reports[106–108] that lesions were resolved by treatment using Nd:YAG laser. There have also been cases in which favorable results were obtained by treatment of anemia due to gastrointestinal bleeding[109] and of symptoms, such as airway obstruction, due to the mass effect of the lesion.[110] While transient purpura and swelling after treatment are unavoidable, they often resolve rapidly.[99] Modifications of the irradiation setting and method are necessary to obtain satisfactory results and avoid serious complications, such as peroneal neuropathy[100] and pigmentation and scar formation of the facial skin,[106,108] and we must learn from the experience of experts.

Nd:YAG laser irradiation by insertion into the lesion under ultrasound guidance has begun to be performed as a treatment to avoid damage of important organs and nerves,[98–100] therapeutic experience using this technique has been accumulated, and detailed records and reports have been presented. At present, the results have been satisfactory in terms of safety and efficacy, and standardization of the procedure is anticipated.

CQ9: Is sclerotherapy effective for VM?

Recommendation: Sclerotherapy for VM is effective for alleviating symptoms and reducing the size of the lesion and is recommended.

Strength of recommendation: 2 (weak)

Evidence: D (very weak)

Comments: VM is lesion that used to be called cavernous hemangioma or intramuscular hemangioma and differ from infantile hemangioma. VM poses problems, such as pain, swelling, and functional impairment, and has been treated conventionally by surgical resection. In Western countries,

This article has been co-published with the permission of *The Journal of Dermatology, Pediatrics International and Japanese Journal of Radiology*. All rights reserved. © 2020 The Authors. The articles are identical except for minor stylistic and spelling differences in keeping with each journal's style. Either citation can be used when citing this article.

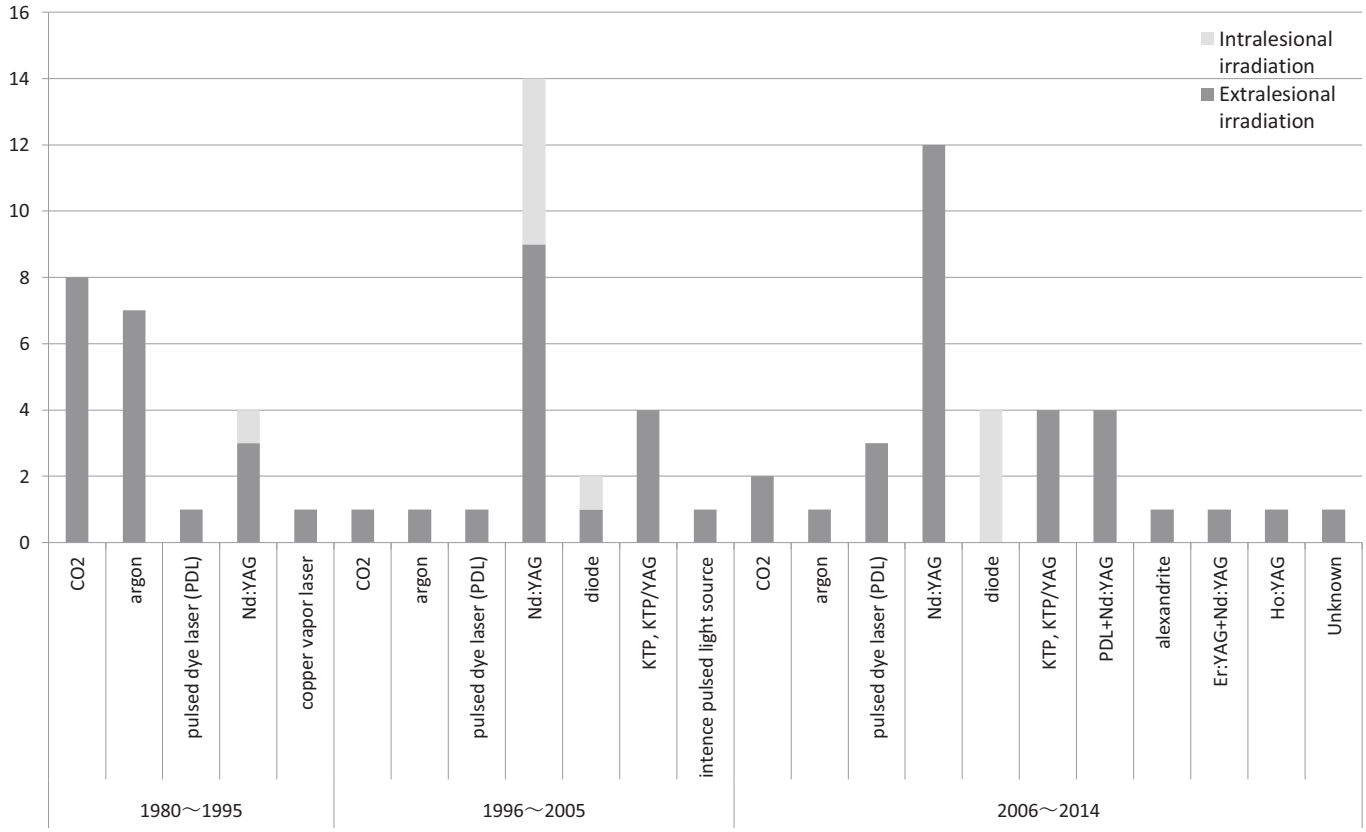

Fig. 1 Reports of laser therapy for hemangiomas/vascular malformations (primarily venous) in various periods and types of laser used in the reports (CQ8). *Notes*: CO2; 10 of 11 reports recommend the use for surgical resection. Argon; There are 4 reports of mixed treatments for CM and VM. Nd:YAG; There are 12 reports of its use in combination therapy with surgery, sclerotherapy, or other lasers. Alexandrite; There is only 1 report summarizing cases treated with alexandrite in combination therapy with other lasers.

percutaneous sclerotherapy has a long history. In 1989, Yakes *et al.*[111] reported ethanol sclerotherapy for VM, and the treatment has since been performed worldwide. Recently, sclerotherapy, which is mildly invasive, permits functional and morphological preservation, and can be performed repeatedly, is widely used. However, as of 2016, sclerotherapy is not covered by medical insurance in Japan. In addition, there has been no randomized controlled trial (RCT) on the usefulness of sclerotherapy for VM compared with surgery or placebo.

As a result of secondary screening, 76, 3, and 3 papers were extracted from PubMed, Cochrane, and JCRM, respectively. They include 3 semi-RCTs, but randomization and blinding were insufficient, and their quality as an RCT was low. Also, the theme evaluated by all these RCTs was "comparison of sclerosing agents in sclerotherapy," and none compared sclerotherapy with other treatments. Therefore, control groups related to this CQ were not established, and their contribution as a whole is weak. The other literature was all case reports or case series, and the evidence level is D (very weak). As mentioned above, while the evidence level is low, most of the studies reported alleviation of symptoms and regression of lesions in a high percentage (70–90%) of the patients, suggesting the usefulness of sclerotherapy.

The sclerosing agents used included absolute ethanol, polidocanol, ethanolamine oleate, sodium tetradecyl sulfate (STS), and bleomycin. Polidocanol is approved as a sclerosing agent for lower limb varices and esophageal varices, and ethanolamine oleate as a sclerosing agent for esophageal varices. STS is not marketed in Japan. Each sclerosing agent has characteristic complications. Recently, injection of polidocanol, STS, as a foam by mixing with CO_2 or air has been increasingly performed. Sclerotherapy using ethanol is often performed under general anesthesia, but sclerotherapy using polidocanol or ethanolamine oleate can be performed under local anesthesia.

Three RCTs have been reported as studies that evaluated differences in therapeutic effect according to the sclerosing agent. However, randomization and blinding are insufficient, and their quality as an RCT is low. In addition, the theme evaluated in these RCTs was "comparison of sclerosing agents in sclerotherapy" rather than comparison with other treatments.

Although the evidence level is low, there have been a few case series that reported the usefulness of sclerotherapy, and a wide variety of sclerosing agents including ethanol, polidocanol, ethanolamine oleate, STS, and bleomycin were used. Among studies with a relatively large number of patients, there is a report[112] that sclerotherapy using ethanol in 87

This article has been co-published with the permission of *The Journal of Dermatology, Pediatrics International and Japanese Journal of Radiology*. All rights reserved. © 2020 The Authors. The articles are identical except for minor stylistic and spelling differences in keeping with each journal's style. Either citation can be used when citing this article.

patients with craniofacial VM resulted in a ≥75% decrease in size in 23 (32%) and a 25–75% decrease in size in 37 (52%). The results of sclerotherapy using polidocanol in 50 patients with VM were excellent in 19, good in 16, moderate improvement in 13, and unchanged or worse in 2.[92] The results of sclerotherapy using ethanolamine oleate performed in 83 patients, who were mostly children, were complete remission of symptoms in 79 lesions and significant alleviation in 6 lesions.[113] Sclerotherapy using STS resulted in subjective improvements in 174 (85.3%) of 204 patients.[114] The results of sclerotherapy using bleomycin were complete cure in 185 of 260 patients, marked improvement in 44, and some improvement or no change in 31.[115] In addition, regarding the size of the lesion, a very satisfactory decrease was achieved in 104, and a satisfactory decrease was achieved in 10, of 120 patients.[116]

Papers that evaluated the types of VM that are likely to respond to sclerotherapy include those by Goyal *et al.*,[117] Yun *et al.*,[118] Mimura *et al.*,[91] Rautio *et al.*,[119] Lee *et al.*,[112] Yamaki *et al.*,[120] and Nagao *et al.*[121] Types of lesions that were likely to be sclerosed were reported to be well-defined small (≤5 cm) lesions by Goyal *et al.*,[117] females, lesions showing no or delayed delineation of the draining vein, and lesions well-defined on MRI by Yun *et al.*,[118] small lesions, well-defined lesions, and lesions that show prolonged drug retention by Mimura *et al.*,[91] localized lesions by Lee *et al.*[112] and Yamaki *et al.*,[120] and slow flow type lesions by Nagao *et al.*[121] Nomura *et al.*[122] evaluated the therapeutic effect according to the degrees of functional and gross improvements and reported that the therapeutic effect was greater in head and neck and trunk lesions than in the upper or lower limb lesions. Moreover, Rautio *et al.*[119] reported that the treatment-related improvement in the quality of life was higher when the lesion did not involve the muscle or was ≤5 cm in size.

Various complications ranging from mild complications, such as transient neuropathy and local inflammation, to serious ones, such as myopathy, skin necrosis, and deep venous thrombosis/pulmonary embolism, have been reported. In sclerotherapy using ethanol or polidocanol, particularly serious life-threatening complications have been reported. Qiu *et al.*[123] reviewed the literature concerning sclerotherapy for VM and reported that shock and pulmonary embolism occurred in 0.19% each of 522 patients who underwent sclerotherapy using ethanol and that ethanol was used at 1 mL/kg in those who developed shock. They also reported that a decrease in blood pressure/bradycardia was noted in 0.61% of 163 patients who underwent sclerotherapy using polidocanol but that its differentiation from vagus nerve reflex was clinically difficult. Wong *et al.*[124] reported a case of shock after sclerotherapy using 0.86 g/kg ethanol but could be saved. Tachibana *et al.*[125] reported that 2 patients (1.1%) developed pulmonary embolism and that the amounts of ethanol used were 0.71 and 0.16 mL/kg. Concerning sclerotherapy using polidocanol, also, cardiac arrest in children has been reported by authors including Marrocco-Trischitta *et al.*[126] and Shimo *et al.*,[127] who used 4 mL of 1% polidocanol (body weight: 20 kg) and 10 mL of 3% polidocanol (15.6 kg), respectively.

In conclusion, sclerotherapy is generally considered effective for VM, but its problems are that the evidence level is low and that the procedure has not been standardized. In addition, serious complications that are rare but life-threatening have been reported, and caution is needed in deciding the dose of the sclerosing agent.

CQ10: Are clotting abnormalities due to VM an indication for radiotherapy?

Recommendation: Radiotherapy should not be performed without careful evaluation because malignant neoplasm, growth disorders, and functional impairment have been reported as late complications.

Many reports included both VM and vascular tumors in the subjects, which make it difficult to assess the therapeutic effects of radiotherapy.

Strength of recommendation: 2 (weak)

Evidence: D (very weak)

Comments: As a result of primary screening, 6 and 2 documents were retrieved from PubMed and JCRM. However, as a result of secondary screening, liver hemangioma was excluded, and 10 papers including the references from the previous guideline were reviewed. The reviewed papers were case series or case reports, and the evidence level of the literature as a whole is D "very weak."

While there have been reports that radiotherapy was performed for the treatment of vascular tumors and vascular malformations, it is difficult to judge whether the treatment was performed by determining the disorders.

According to many reports,[128–132] radiotherapy has been performed to treat Kasabach-Merritt phenomenon. However, while there is no mention about Kasabach-Merritt phenomenon, there is a report[133] of 5 cases in which giant hemangiomas accompanied by clotting disorders, thrombocytopenia, heart failure, and bleeding were controlled by multidisciplinary treatment including radiotherapy.

Vascular tumors that cause Kasabach-Merritt phenomenon are considered to be kaposiform hemangioendothelioma or tufted angioma rather than infantile hemangioma.[134] Because VM and infantile hemangiomas are included in other vascular tumors in the lesions described in these reports, they are not considered to be indications of radiotherapy for VM or infantile hemangiomas.

Schild *et al.*[128] reported 13 cases of symptomatic hemangioma (11 of which were pathologically diagnosed as cavernous hemangioma, but as the report is old, vascular tumors and vascular malformations were not distinguished and were probably included). Radiotherapy at 6.25–40 Gy was carried out in these 13 cases. The lesions were located in the limbs in 5, face in 2, vertebral bodies in 3, pituitary fossa in 1, sacrum in 1, and bladder in 1. Note that organs that should be excluded in this CQ were included.

This article has been co-published with the permission of *The Journal of Dermatology, Pediatrics International and Japanese Journal of Radiology*. All rights reserved. © 2020 The Authors. The articles are identical except for minor stylistic and spelling differences in keeping with each journal's style. Either citation can be used when citing this article.

Of these patients, 2 (1 each with a limb and facial lesion) exhibited Kasabach-Merritt phenomenon and showed normalization of clotting disorder (evaluated according to the platelet count and fibrinogen level) after treatment. However, they were aged 3 years and 5 months, and the lesions may not have been VM.

When the subjects were limited to patients with limb or facial lesions, CR was observed in 2, PR in 4, and no response in 1 in terms of decrease in the lesion size, and CR was observed in 4, PR in 1, and no response in 2 in terms of the control of symptoms.

A serious treatment-related complication, which was unilateral visual impairment, was noted in 1 (14 Gy/8 fr).[128] These problems have been recognized as late complications of radiotherapy for vascular tumors or vascular malformations; malignant neoplasms, such as breast cancer,[135] thyroid cancer,[136] and vascular sarcoma,[137] visual impairment mentioned above,[128] shortening of the lower limb, and restriction of the joint motion range.[131]

According to Coldwell *et al.*,[137] late complications of radiotherapy for hemangiomas in infancy include bruise and Stewart-Treves syndrome after the patients reach adulthood. Angiosarcoma is also observed. They reported that the median survival period was 24 months, and the 5-year survival rate was about 10%, in those who developed angiosarcoma.

As observed above, the diagnosis was not confirmed in the reports that have suggested the effectiveness of radiotherapy, and its indications have not been specified. In addition, there have been a considerable number of reports of late complications due to radiotherapy. Thus radiotherapy should not be performed without careful evaluation.

CQ11: Is there difference in the effectiveness of dye laser treatment for CM according to the site of the body?

Recommendation: Dye laser treatment for CM is likely more effective in the face and neck region compared with other sites, and it is more likely to cause complications such as pigmentation in the limbs.

Strength of recommendation: 2 (weak)

Evidence: C (weak)

Comments: As a result of literature searches, 176 papers consisting of 139 from PubMed and 37 from JCRM were extracted. They included a few reports that were allegedly RCTs but were not actual RCTs. Therefore, a total of 26 papers consisting of 15 from PubMed and 11 from JCRM including case series with a large number (≥100) of relevant cases were selected by secondary screening. In addition, a total of 17 papers were adopted as references for the comments in the guidelines by adding 3 papers in English extracted by manual search to 6 from PubMed and 8 from JCRM considered to be relevant or closely related to the CQ among those selected by secondary screening. Since there was no RCT, the evidence as a whole was rated as C (weak).

Concerning the effect of dye laser treatment for CM, most of the reports were about the effects for hemangioma simplex or port-wine hemangioma in Japan and port-wine stain abroad.

There have been a few papers[138–152] that evaluated the therapeutic results of dye laser treatment according to the site in a small to relatively large number of patients. The laser equipment used varies from early dye laser to pulsed dye laser with adjustable pulse duration with a cooling system, and reports limited to variable-pulse pulsed-dye laser with a cooling system, which is widely used today, are extremely few.

According to many reports,[138–149] the response rate is higher in the face and neck region than in the trunk and limbs. In the face, it has been reported that the response rate is higher in the palpebral, forehead and temporal, and lateral buccal regions but is significantly lower in the territory of the 2nd division of the trigeminal nerve (dermatome V2), and that the number of irradiations tends to increase in the midline region, frequently resulting in persistence of redness.[150] There is a report[151] that the response rate did not differ significantly among regions in the lower limb. While the number of patients was small, it has been reported that treatment of the foot involves stronger pain but was less effective than in the face but that the degree of patient satisfaction was relatively high.[152]

The incidence of complications of dye laser (bleb formation, depigmentation, pigmentation, scar formation) is reported to be low, being 1.7% in adults, 0.6% in children, and about 1.4% in all patients even when all sites of the body are included, and no significant difference has been reported in the age at the beginning of treatment, Fitzpatrick skin type,[153] site, number of treatments, or irradiation energy between those who developed complications and those who did not, but complications may occur more frequently in the lower limbs.[154] Moreover, there is a report[152] that complications, such as pigmentation, depigmentation, and atrophic scar, were observed more frequently in the lower limbs.

CQ12: Do CM recur after dye laser treatment?

Recommendation: Although the effectiveness of dye laser treatment for CM is established, the recurrence rate may increase with time after treatment.

Strength of recommendation: 2 (weak)

Evidence: C (weak)

Comments: As a result of literature searches, a total of 211 papers consisting of 149 from PubMed, 53 from Cochrane, and 9 from JCRM were retrieved. They did not include RCTs, and a total of 30 papers consisting of 23 from PubMed and 7 from Cochrane, which were mostly case reports and case series studies, were extracted by secondary screening. In addition, a total of 10 papers that were relevant and closely related to the CQ (including 8 case series) consisting of 7 from PubMed, 2 from Cochrane, and 1 in English retrieved by manual search were adopted as references for the guidelines. Since there was no RCT, the strength of evidence of the group of literature concerning this CQ is C "weak".

Concerning papers that referred to "whether CM recur after dye laser treatment," there are 4 retrospective studies[155–158] after treatment by pulsed dye laser (wavelength: 585 nm) with a

This article has been co-published with the permission of *The Journal of Dermatology, Pediatrics International and Japanese Journal of Radiology*. All rights reserved. © 2020 The Authors. The articles are identical except for minor stylistic and spelling differences in keeping with each journal's style. Either citation can be used when citing this article.

cooling system, and the recurrence rate was 15.9–35%. Also, there is a report[155] that the recurrence rate increased with time after treatment and was 3.1% after 1 year, 20.8% after 2 years, 40% after 3 years, and 50% after 4 years. Therefore, it is necessary to treat CM with the recurrence after dye laser treatment in mind.

It is difficult to strictly distinguish whether the recurrence is generation of new dilated vessels after laser therapy or it is regeneration of blood vessels damaged due to treatment or reproliferation of remaining vessels. However, there have been reports that, in an experiment using mice, angiogenesis occurred in the process of wound healing at the site of irradiation in early recurrence[159] and that, in an experiment using hamsters, complete treatment was difficult, and morbid vessels persisted, because coagulation was difficult to induce by dye laser irradiation in vessels ≤2–16 μm in diameter.[160] While there is a report[161] that genes affected by dye laser therapy early after treatment were identified, further evaluation is necessary to clarify their relationships with the recurrence.

Concerning the prevention of recurrence, there is a report[162] that the recurrence-free period was long in the patients treated with a variable-pulse pulsed-dye laser with a cooling system (wavelength: 595 nm), which is widely used today, and they were treated within 6 months after birth. In addition, there have been reports of animal experiments using Rapamycin, which inhibits angiogenesis after laser irradiation,[159,163] and of prospective RCT using imiquimod,[164,165] and these treatments were considered effective for the prevention of recurrence. However, careful evaluation by large-scale investigations, including the assessment of the safety concerning drugs, is considered necessary.

CQ13: Is dye laser irradiation for CM more effective as it is initiated at a younger age?

Recommendation: Laser therapy before the age of 1 year may be effective, and the earliest possible initiation of treatment is recommended as an option.

Strength of recommendation: 2 (weak)

Evidence: D (very weak)

Comments: Concerning the timing of treatment for CM, there is the opinion that early initiation of treatment is recommended, because, in young children, the skin is thinner, so the depth of penetration is larger, the vascular wall is also immature, cure after laser irradiation is better, pigmentation is less, and the irradiation area is small, so the treatment efficiency is higher. However, there is still controversy. As a result of secondary screening of past reports, 6 and 1 were extracted from PubMed and JCRM, respectively. While the papers selected by these screening procedures include 2 papers on prospective studies as described below, their conclusions differed, and the evidence level is considered to decline when these references are reviewed together.

Oguri *et al.*[138] performed a non-randomized controlled trial by dividing children into those aged 0–12, 13–24, and 25–36 months and observed significant differences in the response rate combining "markedly effective" and "effective" among the groups. They also compared the response rate according to the age in months at the beginning of treatment in the 0-year-old group and reported that the response rate was higher as the treatment was initiated earlier. Furthermore, Nguyen *et al.*[166] divided their patients into those aged less than 1 year, those aged 1–6 years, and those aged 6 or more years and investigated the correlation between treatment response and age. They reported that those aged less than 1 year and lesions with a size of <20 cm^2 located in the center of the face showed the best treatment response.

Among reports suggesting no difference in the therapeutic effect according to the age at the beginning of treatment, van der Horst *et al.*[167] studied 100 patients with untreated CM of the head and neck region prospectively and concluded from the results of colorimetry and clinical evaluation that there was no significant difference in the therapeutic effect of pulsed dye laser among the 4 groups in which the treatment was started at the age of 0–5, 6–11, 12–17, and 18–31 years. In the retrospective study of Katugampola *et al.*,[140] also, comparison of 4 groups in which treatment was started at the age of 0–5, 6–12, 13–50, and 50+ years showed no significant difference in the therapeutic effect.

Among the above reports, those did not affirm the usefulness of early laser treatment were relatively old. Also, reports of Oguri *et al.*[138] and Nguyen *et al.*[166] indicated laser therapy may be more effective in those aged <1 year. In addition, the effectiveness of laser clearly declines when the lesion is elevated or thickens with time. In consideration of "benefits" of early laser treatment and "harms," which include the occasional necessity of general anesthesia for laser treatment around the eye in small children, the recommendation level was rated as 2D based on the consensus of this guidelines drafting committee.

CQ14: Is propranolol safe and effective for infantile hemangiomas?

Recommendation: If administered under careful monitoring, oral propranolol therapy may be the first choice for the treatment of infantile hemangioma.

Strength of recommendation: 1 (strong)

Evidence: A (strong)

Comments:

(1) Effectiveness: There was the serendipity that regression of hemangioma was induced in a child under steroid therapy with a giant infantile hemangioma by propranolol administered for obstructive hypertrophic cardiomyopathy in 2008.[168] Based on this report, oral propranolol therapy began to be used for the treatment of infantile hemangioma, and its high efficacy against alarming hemangioma/life-threatening hemangioma in the proliferating phase and in patients with cosmetic problems, such as giant lesions in the face, those with ulcerated and hemorrhagic lesions, and those who may develop functional impairment, has been demonstrated, resulting in its use (Hemangiol®, Pierre Fabre Dermatologie, Boulogne, France)

This article has been co-published with the permission of *The Journal of Dermatology, Pediatrics International and Japanese Journal of Radiology*. All rights reserved. © 2020 The Authors. The articles are identical except for minor stylistic and spelling differences in keeping with each journal's style. Either citation can be used when citing this article.

as the first choice in Western countries. In addition, its effectiveness for the treatment of hemangiomas after the proliferating phase was also described. Moreover, a group of physicians used propranolol earlier due to cosmetic significance and at the request of the family even in cases of small or localized lesions, and it is also effective in such cases.

A total of 131 papers consisting of 25 from JCRM, 106 from PubMed, and 0 from Cochrane Library were extracted as related to the CQ, "Is propranolol safe and effective for infantile hemangioma?," and they were subjected to primary and secondary screenings with reduction of hemangioma (effectiveness of propranolol) and treatment-related complications (adverse effects) as outcomes. Twenty-six papers,[169–194] most of which were RCTs or observational studies, were adopted.

For example, Hogeling *et al.*[180] administered placebo or propranolol at 2 mg/kg/day for 6 months with randomization to 40 patients aged 9 weeks to 5 years with infantile hemangiomas in the face or sites with the potential for disfigurement. They reported significant improvements in size, redness, and elevation in the propranolol group. Elevated lesions disappeared in 4 of the 19 patients in the propranolol group but none of the 18 patients in the placebo group. As for adverse events, the trial was interrupted in 1 patient due to upper respiratory tract infection, and conditions including bronchiolitis, gastroenteritis, streptococcal infection, cool extremities, dental caries, and sleep disturbance were observed.

Zaher *et al.*[181] observed 45 patients by randomly dividing them into 15 each treated by oral administration, topical application, and intralesional injection of propranolol. Responses were observed in 60% in the oral group, 20% in the topical ointment group, and 13.3% in the injection group. No major adverse events were noted, and the trial was discontinued in 1 in the oral group and 3 in the injection group due to inconvenience or pain of the treatment.

Malik *et al.*[182] randomly allotted 30 patients aged 1 week to 8 months to propranolol alone, prednisolone alone, or both propranolol and prednisolone. They found that the mean initial response times were lower in the propranolol group than in the prednisolone group but that there was no clear difference between the propranolol + prednisolone group and propranolol alone group. All 10 patients in the propranolol group and 9 patients in the corticosteroid group responded to the 3-month treatment. However, adverse events were observed in 2 of the 10 patients in the propranolol group (asymptomatic hypoglycemia, insomnia) and 9 of the 10 patients in the steroid group (cushingoid appearance, gastrointestinal upset), and were more frequently in the latter group.

Bauman *et al.*[183] performed a phase 2, investigator-blinded, multi-center RCT in 44 patients aged 2 weeks to 6 months. Propranolol or prednisolone (2 mg/kg/day) was administered orally until halted due to toxic effects or clinical response. During 4-months treatment, no significant difference was observed between the two groups, for example, with regression of 5 of the 6 tumors in the corticosteroid group and 9 of the 10 tumors in the propranolol group. For long-term analyses, the effect of prednisolone appeared earlier. While the incidence of adverse events as a whole did not differ between the two groups, severe adverse events were observed in 1 of the 11 patients in the propranolol group but 5 of the 7 patients in the prednisolone group, being significantly more frequently in the latter group.

Léauté-Labrèze *et al.*[184] carried out an RCT in patients aged less than 4 months by comparing 7 administered and 7 not administered propranolol. Since color changes and softening were observed within 24 h, and the thickness and size of the lesions decreased within 4 weeks in the propranolol group, the treatment was considered useful for the prevention of scarring. No serious adverse effect was observed except asymptomatic mild decreases in heart rate and diastolic blood pressure.

There have also been comparisons between atenolol and propranolol and between laser and laser plus topical propranolol.[185,186] In 2015, the largest RCT was published in the New England Journal of Medicine, also reporting that propranolol was significantly effective for hemangioma compared with placebo.[187] Hemangioma showed complete or nearly complete resolution after 6-month treatment in 2 (4%) of 55 patients in the placebo group and 61 (60%) of 101 patients in the 3 mg/kg/day propranolol group.

Furthermore, there have also been a few systematic reviews and meta-analyses primarily of observational studies. Menezes *et al.*[188] reviewed 49 English papers published between June 2008 and September 2010, and summarized 6 studies with 10 or more patients administered propranolol (totally 154 patients). Propranolol was administered to infants with a mean age of 4.5 months at a dose of 2 mg/kg/day in 65% and 3 mg/kg/day in 25.3%. Two-thirds of the patients were treated with propranolol alone. Recurrence was observed in 21% after treatment for a mean of 4.3 months, and adverse events including hypotension, somnolence, wheezing, insomnia, agitation, nightmare, cool hands, night sweat, gastroesophageal reflux disease, and psoriasiform rash appeared in 18.1%.

Marqueling *et al.*[189] reviewed the therapeutic results in 1,264 patients (including 806 girls) in 41 reports published from 2008 to 2012 retrieved from Medline and Cochrane database. The treatment was initiated at a mean age of 6.6 months at 2.1 mg/kg/day and continued for a mean of 6.4 months. The overall response rate was 98%, and the treatment was also effective in clinically problematic areas such as the face (100%), airway (100%), periorbital (98%), head and neck region (97%), and parotid gland (82%). However, recurrence was observed in 17% after treatment. Adverse effects were noted in 371 of 1,189 patients. Changes in sleep (136 patients) and acrocyanosis (61) were the most frequent among them, and hypotension was observed in 44, bradycardia in 9, and hypoglycemia in 4 as serious complications. In conclusion, the grade of recommendation was 1, quality of evidence is A, and propranolol was recommended as the first-line drug for complicated infantile hemangiomas. Regarding adverse effects, the grade of recommendation was 1, quality of evidence was A or B. while serious adverse effects may be observed, their

This article has been co-published with the permission of *The Journal of Dermatology, Pediatrics International and Japanese Journal of Radiology*. All rights reserved. © 2020 The Authors. The articles are identical except for minor stylistic and spelling differences in keeping with each journal's style. Either citation can be used when citing this article.

frequency is low, and they can be usually avoided by proper monitoring at initiation of treatment.

Xu *et al.*,[190] on the other hand, evaluated volume changes, improvement in overall appearance, visual function, and adverse effects using 15 online databases. The data of 419 cases were analyzed, but meta-analysis was not performed because of the wide differences among studies. Some studies showed superiority of propranolol compared with corticosteroid in reducing volume and improving the overall appearance. No marked difference was noted in adverse effects or visual function.

In addition, in meta-analysis of 16 studies (2,629 cases) and 25 studies (795) published in 1965–2012, 69% of the patients responded to 12-month corticosteroid therapy, but the response rate to propranolol was 97% with a significant difference.[191]

In periorbital hemangiomas, the response rate to propranolol was found to be significantly higher than that to corticosteroid by meta-analysis of papers published before 2013,[192] and propranolol showed the strongest effect against airway hemangiomas compared with steroid, CO_2 laser, and vincristine on meta-analysis.[193,194]

From these observations, we concluded that propranolol was significantly more effective than placebo and to be similarly effective compared with corticosteroid. Concerning the safety, propranolol is considered to have significantly fewer adverse effects than corticosteroid. Since there have been several RCTs and systematic reviews or meta-analyses directly related to this CQ, the evidence level is considered to be extremely high.

(2) Meta-analysis: Regarding the effectiveness and adverse effects of propranolol, a large number of systematic reviews and meta-analyses based on observational studies are already present in the above 26 papers. We, therefore, used only 4 reports[180,182,183,187] on interventional studies for meta-analysis.

As a result of meta-analysis, regarding "tumor reduction," it was found that propranolol had significantly stronger reducing effects than placebo and that it had a stronger reducing effect, which, however, was not significant, compared with corticosteroid. Concerning "complications," propranolol was compared with steroid and was shown by 2 RCTs to have significantly fewer adverse events than corticosteroid. Since this meta-analysis found significantly stronger reducing effect of propranolol compared with placebo and in fewer complications compared with steroid, and since our results were similar to those of systematic reviews of many existing observational studies considered to have high-quality evidence, we considered that there was a major tendency in this CQ and judged the evidence level as A.

(3) Estimated action mechanism: Beta-blockers have a wide range of actions on the blood vessels and vascular endothelium, and have diverse actions on cell proliferation and vascular remodeling. Thus, the action mechanism of propranolol on infantile hemangiomas is still unclear. In vascular endothelial cells, propranolol is considered to induce vascular contraction by suppressing NO production, inhibit renin production, control angiogenesis by regulating the expression of VEGF•bFGF•MMP2/MMP9, and induce apoptosis, but it may also affect pericytes and hemangioma stem cells.[195–197]

(4) Adverse events associated with propranolol in children

In conducting propranolol therapy, it is necessary to have knowledge about possible adverse effects, their symptoms, and their management. In addition, as there are also preventive measures for, and points of attention about, adverse effects and the timing for discontinuation of propranolol, sufficient explanation to the patients and their families is essential.

Adverse events that have been reported include sleep disorders, peripheral cyanosis, hypotension (symptomatic, asymptomatic), bradycardia (symptomatic, asymptomatic), hypoglycemia, respiratory disorders, gastrointestinal disorders, and mental disorders. Severe cases that require interruption of treatment are few, but particular caution is needed regarding the following points.[189,196–200]

(a) Since there is the risk of hypoglycemia, the patient should be fed before and after propranolol administration. If the patient cannot be fed, or is vomiting, for some reason, the administration should be suspended.

(b) Since propranolol has cardiovascular adverse effects, such as hypotension and bradycardia, interviewing for the past history and familial history, examination, and electrocardiography are recommended before treatment. Even if no abnormality is noted on these examinations, hypotension, and bradycardia may occur during treatment. In such cases, interruption of the administration is necessary.

(c) Propranolol is contraindicated for bronchial asthma as it causes bronchial contraction due to its β2-blocking action. Caution is also necessary in patients who have been suspected to have bronchial asthma.

CQ15: What treatments are effective for ulcer formation in infantile hemangioma?

1. Propranolol

Recommendation: The administration of propranolol is recommended for ulcer formation.
Strength of recommendation: 2 (weak)
Evidence: C (weak)

2. Topical administration of antibiotics

Recommendation: Topical and systemic administration of antibiotics is recommended for ulcer formation.
Strength of recommendation: 2 (weak)
Evidence: D (very weak)

3. Dressings

Recommendation: The use of dressings is recommended for ulcer formation.

This article has been co-published with the permission of *The Journal of Dermatology, Pediatrics International and Japanese Journal of Radiology*. All rights reserved. © 2020 The Authors. The articles are identical except for minor stylistic and spelling differences in keeping with each journal's style. Either citation can be used when citing this article.

Strength of recommendation: 2 (weak)
Evidence: D (very weak)

4. Laser therapy

Recommendation: Although laser therapy may be effective in some patients with ulcer formation, the evidence is not considered sufficient at present.
Strength of recommendation: 2 (weak)
Evidence: D (very weak)

5. Systemic administration of steroid

Recommendation: Systemic administration of steroid is recommended not to be performed for ulcer formation.
Strength of recommendation: 2 (weak)
Evidence: D (very weak)

6. Platelet-derived growth factor preparations

Recommendation: The accumulation of cases is insufficient for the judgment of the recommendability of the use of platelet-derived growth factor preparations for ulcer formation.
Strength of recommendation: No recommendation
Evidence: D (very weak)

Comments: Concerning this CQ, 42 papers in Japanese and 156 in English were retrieved. As a result of their primary screening, 47 papers were submitted to secondary screening for this CQ. None of them were about studies with a high level of evidence, such as RCT, and they were all retrospective studies, case series, or case reports.

As a result, 15 papers in English were adopted, and the evidence level was C for propranolol alone, because of the presence of a prospective controlled trial, but D for other treatments, because the related papers were case reports or case series.

According to cross-sectional analysis in a multicenter prospective cohort study in 1,096 cases of infantile hemangioma by Chamlin *et al.*,[201] it was complicated by ulcer, which was or was not bleeding, in 173 (15.8%), the median age of the patients was 4.0 months (SD = 8.5, mean = 6.6 months), and the age at the first examination was significantly lower in patients with ulcerated hemangioma (median = 3.5 months, mean = 3.98 months) than in those with non-ulcerated hemangioma.

By the site, ulcer formation was observed in 21 (30%) of 71 patients in the lower lip, 25 (25%) of 100 patients in the neck, and 46 (50%) of 93 patients in the perianal/perigenital area, and the frequency was statistically lowest in the upper eyelid ($P = 0.0140$).

Ulcer formation was observed more frequently in mixed or segmental hemangiomas. Bleeding was noted in 78 lesions (41%) and was mild in 56 (29%), moderate in 11 (6%), and severe in 4 (2%). Severe bleeding occurred in 3 lesions in the limbs and 1 lesion in the face, and bleeding occurred in 2 cases at home. Two cases required blood transfusion by hospitalization, because they showed symptoms due to serious bleeding. Of the ulcerated hemangiomas, 67 (35%) were in the proliferating phase.

Ulcerated hemangiomas required treatment (odds ratio [OR] = 6.86, 95% CI = 3.70–12.71, $P < 0.0001$), and non-ulcerated hemangiomas were observed (OR = 19.01, 95% CI = 11.23–28.88, $P < 0.0001$). Ulcerated hemangiomas tended to be treated by conventional wound care and pulsed dye lase (OR = 2.03, 95% CI = 1.19–3.46, $P < 0.0091$), and non-ulcerated hemangiomas were treated by topical glucocorticoid administration (OR = 2.57, 95% CI = 1.49–4.43, $P < 0.0007$) and surgical resection (OR = 2.04, 95% CI = 1.08–3.86, $P < 0.0286$).

However, propranolol has recently been suggested to be effective regardless of the presence or absence of ulcer formation, and as it has few adverse effects, it is expected to become the first choice treatment in the future.

[Treatments]

1. Oral propranolol

Hermans *et al.*[172] treated 20 previously treated patients with ulcerated infantile hemangioma using propranolol and compared them with 36 patients treated without propranolol. The administration was initiated by hospitalization, and the dose was increased from 0.7–1.0 to 2.0–2.5 mg/kg/day in 3 divided doses at an interval of at least 3 days. The blood pressure, heart rate, and blood sugar level were monitored during the initial administration period, and the administration was continued on an outpatient basis until the age of 1 year. The mean age at the beginning of propranolol administration was 3.5 months, and the mean duration of administration was 9.1 months. Not only the color and elevation of the lesion but also pain was reduced from early after the beginning of administration. The administration was concluded before the age of 1 year in 19 patients, and no recurrence of ulcer was noted in any of these patients except that some reactivation (enlargement) of hemangioma was observed after the discontinuation in 4 of these patients.

The mean time until complete cure of ulcer was 8.7 weeks, and those in whom the administration was initiated later (>3.5 months) tended to require a longer time until cure than those in whom the administration was initiated earlier ($P = 0.025$). Also, analysis using the *t*-test showed a significant difference in the time until disappearance of the tumor, which was 8.7 and 22.4 weeks ($t = 2.6$, d.f. = 38, $P = 0.012$, 95% CI = 3.2–24.2) in the treated and control groups, respectively. Temporary sleepiness/malaise was observed in 6 patients, irritable before falling asleep in 2 patients, coldness of the limbs in 6 patients, anorexia in 2 patients, and gastrointestinal disorders (diarrhea, vomiting) in 1 patient, but no adverse event was noted in 9 patients.

Vercellino *et al.*,[202] who started the administration at 1 mg/kg/day and increased to 2 mg/kg/day, and Sadykov *et al.*,[203] who started the administration at 2 mg/kg/day, also reported that propranolol was effective.

This article has been co-published with the permission of *The Journal of Dermatology, Pediatrics International and Japanese Journal of Radiology*. All rights reserved. © 2020 The Authors. The articles are identical except for minor stylistic and spelling differences in keeping with each journal's style. Either citation can be used when citing this article.

2. Topical and/or systemic administration of antibiotics

Kim *et al.*[204] topically administered antibiotics in 40 patients with ulcerated hemangioma and reported that the results were better in 37 patients (92.5%), worse in none, and no change in 3 patients (7.5%). They also systemically administered antibiotics in 26 patients and reported that the results were better in 24 patients (92.3%), worse in 2 patients (7.7%), and no change in 0 patient.

Wananukul *et al.*[205] topically and/or systemically administered antibiotics in 41 patients with ulcerated hemangioma and reported improvement in 19 patients (46%).

Pandey *et al.*[206] treated 608 patients showing ulcer formation with an ointment containing an antibiotic (mupirocin, sodium fusidate, sisomicin, or metronidazole) combined with systemic administration of an antibiotic (amoxiclav at 20–40 mg/kg/day) in those with ulcers with an area of >10 cm^2 and examined the effectiveness of treatment according to the time until cure. The time until cure was 32.63 ± 13.06 days in superficial lesions, 42.89 ± 19.89 days in mixed lesions, and 57.03 ± 16.12 days in extensive lesions, with a mean of 40.09 ± 19.41 days in all lesions combined, showing significant differences among the 3 groups ($P < 0.05$). They also reported that the time until cure was significantly longer in larger (>10 cm^2) than smaller ulcers ($P < 0.05$).

3. Dressings

Kim *et al.*[204] treated 25 patients using dressings and reported that the results were better in 23 patients (92%), and no change in 2 patients (8%). Oranje *et al.*[207] applied polyurethane film and reported rapid relief of pain and cure of ulcer in 1–2 months. In addition, Bauland *et al.*[208] treated 41 patients using a non-adhering dressing containing an antibiotic and reported that the results were good in 26 patients (63.4%), moderate in 5 patients (12.2%), and little change in 10 patients (24.4%).

4. Laser therapy

In the 1980s–1990s, there were reports[209,210] of argon, NdYAG, and KTP, but recent reports[211,212] are primarily about treatment using dye laser. Morelli *et al.*[209] treated 37 patients with ulcerated hemangioma by dye laser irradiation (SPTL1b® (Candela Corporation, Wyland, MA, USA), wavelength: 585 nm, spot size: 5–7 mm, irradiation power: 5–6.8 J/cm^2, pulse width: 0.45 ms) and reported that the number of irradiations until cure was 1 in 26 patients (68%) and 2 in 8 patients (21%) and that the mean period from the first treatment until cure of ulcer was 2.84 ± 0.22 weeks. Lacour *et al.*[210] irradiated 8 patients with ulcerated hemangioma that resisted conventional treatments using the same equipment and reported acceleration of cure. David *et al.*[211] performed dye laser irradiation (PhotoGenica V® (Cynosure, Westford, MA, USA), wavelength: 585 nm, spot size: 5–7 mm, irradiation power: 5–6.8 J/cm^2, pulse width: 0.3–0.5 ms) in 78 patients and reported the effectiveness of laser therapy alone in 72 (92.3%). Also, Michel[212] performed 1 or 2 irradiations using Dermobeam 2000®(Deka MELA, Calenzano, Italy) with a cooling system 595 nm (2 pulsed irradiations with a 10% overlap, spot size: 7 mm, irradiation power: 4–8 J/cm^2) and reported resolution of pain in 10 of the 12 patients. Moreover, Di Maio *et al.*[213] performed laser treatment in 65 patients with hemangioma with ulcer and reported that the effect was excellent and that no clear adverse events were observed, because scarring, which was noted in a few patients, did not differ markedly compared with scarring that occurs after conventional treatments.

However, Kim *et al.*[204] treated 22 patients with pulsed dye laser and reported that the results were better in 11 patients (50%), worse in 1 patient (4.5%), and no change in 4 patients (18.2%), but warned that 5 patients in the proliferating phase showed ulcer formation after irradiation.

As observed above, although there have been several reports of the effectiveness of laser therapy against ulcer as factors of "benefit," many reports are relatively old and lack controls, and the evidence is not considered sufficient. Further accumulation of cases is necessary. Laser may be effective in limited patients, but as there is the risk of ulcer formation as an adverse effect of laser irradiation of infantile non-ulcerated hemangioma, greater caution is needed in treating already ulcerated lesions.

5. Steroids

There have been few reports on steroid therapy focusing on ulcer. Kim *et al.*[204] treated 7 patients by local steroid injections and reported that the results were better in 4 patients (57.1%), worse in 1 patient (14.3%), and no change in 1 patient (14.3%). They also systemically administered steroid to 22 patients and reported that the results were better in 16 patients (72.7%), worse in 1 patient (4.5%), and no change in 5 patients (22.7%). Based on these results, they considered that the treatment was effective for reducing the lesion size, and there are few other reports suggesting the effectiveness of steroid. Considering that the patients are infants and that there are other treatment options, steroid cannot be recommended at present.

6. Topical preparations of recombinant human platelet-derived growth factor

0.01% becaplermin Regranex® (Ortho-McNeil Pharmaceutical, Raritan, NJ, USA) is a preparation for diabetic foot ulcer approved by the FDA in 1997. Sugarman *et al.*[214] and Metz *et al.*[215] reported its effectiveness for the treatment of ulcerated hemangioma in 1 and 8 patients, respectively, but its effectiveness cannot be appraised at present because of the small number of cases.

CQ16: Is intralesional corticosteroid injection more effective than systemic administration for infantile hemangioma?

Recommendation: Treatment using corticosteroid is effective for inducing early regression of hemangioma. While no significant difference is observed in the effectiveness between

This article has been co-published with the permission of *The Journal of Dermatology, Pediatrics International and Japanese Journal of Radiology*. All rights reserved. © 2020 The Authors. The articles are identical except for minor stylistic and spelling differences in keeping with each journal's style. Either citation can be used when citing this article.

intralesional injection and systemic administration, attention to complications including those at the administration site, such as the periocular region, on local injection and those, such as hypertension and growth retardation, on systemic administration is necessary.

Strength of recommendation: 2 (wean)

Evidence: B (moderate)

Comments: As a result of primary screening, 99, 9, and 35 papers were extracted from PubMed, Cochrane, and JCRM, respectively, and 4 papers in English were subjected to secondary screening for this CQ. There was 1 report of an RCT, but the other reports were about case series while they evaluated a large number of cases. In addition, 2 papers on complications considered important in relation to intralesional corticosteroid injection for periocular lesions were added by manual search. Since there is a report of an RCT, and since other case series studies with a large number of subjects presented the results that there was no significant difference in the effectiveness of corticosteroid depending on the administration method, the strength of evidence was rated as "B."

There was 1 report[216] of an RCT focusing on "Is intralesional corticosteroid injection more effective than systemic administration for infantile hemangioma?." In this trial, the subjects were divided into control, oral administration (prednisolone at 2 mg/kg/day every other day for 6 weeks), and intralesional injection (triamcinolone at 1–5 mg/kg with a maximum of 30 mg once a month for 6 months) groups, and the lesion size was significantly reduced in the treated groups compared with the control group. While no significant difference was noted between the oral administration and the intralesional injection groups, the reduction rate tended to be larger in the local injection group, and local injection was concluded to be slightly superior.[216]

There were reports[217,218] of case series with more than 1,000 subjects, but the findings were not statistically analyzed. Although both intralesional injection and oral administration were effective, there was also a mixed group of intralesional injection and oral administration, the condition of patients varied among the 3 groups (intralesional injection, oral administration, mixed), and the effectiveness according to the administration method was not shown. Regarding complications, systemic symptoms, such as hypertension, retarded body weight gains, and cushingoid appearance, were reported to be more frequent on oral administration than intralesional injection.[217,218] Moreover, concerning complications, in one report,[219] periocular lesions were excluded from the targets of intralesional injection to avoid its effect on visual function. Indeed, there have also been case reports[220,221] that visual impairment was caused by occlusion of the retinal artery after intralesional corticosteroid injection for periocular hemangiomas. Currently, in Japan, intralesional corticosteroid injection is a treatment unapproved by the national health insurance system.

CQ17: Is topical therapy effective for infantile hemangioma?

Recommendation: Although it must be noted that there are no reports of comparison with placebo and that the degree of improvement is smaller compared with systemically administered drugs, topical medication can be an option for the treatment of infantile hemangioma with no risk of complications if drugs with milder adverse effects are selected.

Strength of recommendation: 2 (weak)

Evidence: C (weak)

Comments: As a result of literature searches, a total of 111 papers consisting of 70, 7, and 34 papers from PubMed, Cochrane, and JCRM, respectively, were extracted. They included 1 RCT study. Including this RCT, 48 papers were extracted by secondary screening. In addition to the papers selected by secondary screening as closely related to the CQ, a total of 47 papers obtained by manual search were adopted as reference for the preparation of guidelines. There was 1 RCT, and comparative studies of therapeutic results by topical therapy and case series studies with a relatively large number of subjects were adopted as papers of relatively high quality, the strength of evidence was rated as C "weak."

In the reports related to the CQ:

1. Drug type: The drugs were classified into imiquimod, timolol, propranolol, corticosteroid, and others.[215,222–225]
2. Drug concentration and dosage form: Imiquimod was used as a 5% cream,[222,226–233] timolol as 0.5% ophthalmic solution or gel,[222,223,232,234–243] propranolol as 1% ointment,[181,234,241,244,245] and corticosteroid were often used as ointments of agents ranked as relatively strong such as clobetasol propionate, halobetasol propionate, and betamethasone dipropionate.[246,247]
3. Methods for topical application: Frequent administration methods were once a day every other day for imiquimod, 2 times a day every day at 1–2 drops each time for timolol, 2 times a day every day for propranolol, and 2 times a day every day for corticosteroid.
4. Methods for efficacy evaluation: Comparison of gross findings and photographs were adopted in all papers. The area was compared using photographs in one report.[227] There was also a report[228] of half-side test for a control.
5. Adverse effects: No systemic adverse effect was reported, and most adverse effects were local. Imiquimod caused pain, flare, and erosion relatively frequently.[231,233] Few local adverse effects were reported for timolol and propranolol.[232,234,241,242,245] No local adverse effects were reported also by corticosteroid.[246,247]
6. Relative advantages of drugs Imiquimod has been reported to have usefulness comparable to that of topical beta blockers, but it is not considered superior in terms of adverse effects.[226,228,230,232]

Corticosteroid was not shown to be superior in efficacy compared with beta blockers.

There was also one RCT study[181] concerning the CQ, which is related to topical propranolol concerning drugs. In this RCT, 15 each of a total of 45 subjects were allotted to oral (propranolol at 2 mg/kg/day, 2 times a day), topical (1% propranolol water soluble ointment, applied 2 times a day),

This article has been co-published with the permission of *The Journal of Dermatology, Pediatrics International and Japanese Journal of Radiology*. All rights reserved. © 2020 The Authors. The articles are identical except for minor stylistic and spelling differences in keeping with each journal's style. Either citation can be used when citing this article.

and local injection (1 mg/1 mL, 0.2 mL/1 cm in diameter, 1 mL/injection at the maximum, 1 time/week) groups. Ten patients (66.7%) in the topical group responded, but they were fewer than 13 (86.7%) in the oral group. The time until the appearance of the effect and time until complete cure were also longer in the topical group than in the oral group. Concerning complications, none was observed in the topical group, but 1 patient in the oral group showed unexplained syncope as an adverse effect and was excluded. While decreases in the heart rate and blood pressure were observed in 3 in the oral group, they did not necessitate interruption of the study. In the local injection group, 8 (53.3%) responded, but 3 were lost due to pain. From these results, the study concluded that topical therapy is an option to be evaluated for patients with a risk of adverse reactions to oral medication. While there were no reports of comparison under the same conditions, comparative studies of therapeutic results by topical therapy and case series studies with a relatively large number were adopted as relatively high-quality papers. In all these reports, topical therapy of beta blockers (propranolol, timolol) was effective to an extent with no serious complications.

Thus, topical therapy, particularly, of beta blockers is considered generally useful, but there has not been a report of its comparison with placebo, and further accumulation of cases is necessary.

Research by comparison between dye laser treatment and topical beta blocker therapy is considered to be necessary.

CQ18: Is compression therapy effective for infantile hemangioma?

Recommendation: Although appropriate compression method must be performed for individual patients, compression therapy may be regarded as an option on condition that the therapy is carried out by a skilled physician. Sufficient attention to skin abnormalities and local/neighboring growth disturbance due to the compression are needed.

Strength of recommendation: 2 (weak)

Evidence: D (very weak)

Comments: While 23, 1, and 14 papers were extracted from PubMed, Cochrane, and JCRM, respectively, only 3 case reports remained to be reviewed as a result of primary and secondary screening. Thus, the evidence level is very low at D (very weak).

According to a case report of ulcerated infantile hemangiomas of the limbs by Kaplan *et al.*,[248] the ulcers of most patients showed rapid improvements and cured within 2 weeks by compression therapy using the self-adherent wrap Coban® (3M, St. Paul, MN, USA) combined with topical treatment with an antibiotic ointment (or early systemic antibiotic administration when secondary infection was apparent). They concluded that, compared with antibiotic ointment alone, its combination with compression therapy was more effective, and is a safe and easy treatment that promotes regression of hemangiomas.

Ochi *et al.*[249] reported 12 cases of infantile hemangioma (9 girls and 3 boys with a mean age of 8.4 months; sites of the lesion: limbs in 6, head and neck in 5, and trunk in 1). By treatment using elastic bandages (5 patients), Presnet® (ALCARE, Tokyo, Japan) (4), supporter (1), or Elatex® (ALCARE, Tokyo, Japan) and cryotherapy (2), the hemangiomas disappeared or decreased in size in 11 of the 12 patients, with only 1 (head and neck) showing no improvement. The time until the disappearance of the lesion in the 11 responders was 2 months to 3 years (mean: 19.5 months), no complications associated with compression therapy were noted, and the authors recommended early initiation of compression therapy if the site of the lesion can be compressed.

Totsuka *et al.*[250] treated 3 girls with parotid gland hemangiomas (mean age: 4.3 months) by splinting using a resin plate and compression using a handmade cap. The mean duration of treatment was 13 months (8–16 months), and the patients were followed up until a mean age of 4.6 years (2–7 years), resulting in clinical and echographic disappearance of hemangioma in all 3. Since infantile hemangiomas often regress spontaneously, it is impossible to conclude that they regressed due to compression therapy, but they reported the therapy to be safe and effective.

Thus, concerning factors related to "benefits" of compression therapy, there are reports that suggest the effectiveness of compression methods appropriate for sites (elastic bandages, Presnet, splinting with a resin plate). However, it must be noted that they are all old reports. Concerning factors related to "harm," while compression is a relatively safe and simple method without reports of serious complications, the occurrence of dermatitis and growth disturbance at the site of compression or surrounding areas is considered possible. The recommendation level was set at 2D with consensus of the present guidelines preparation committee on condition that the treatment is performed carefully by a skilled physician in consideration of these points. The present guidelines do not exclude compression therapy, but it is necessary to consider oral propranolol, oral administration or local injection of steroid, and laser therapy first for infantile hemangiomas that need treatment.

CQ19: Is glucose transporter 1 (GLUT-1) immunostaining useful for the diagnosis of infantile hemangioma?

Recommendation: Immunostaining for GLUT-1 is positive in the proliferating, involuting, and involuted phases, shows high sensitivity and specificity, and is useful for the diagnosis of infantile hemangiomas if the clinical diagnosis is difficult.

Strength of recommendation: 2 (weak)

Evidence: C (weak)

Comments: To evaluate whether GLUT-1 immunostaining is useful for the diagnosis of infantile hemangiomas, the literature was searched first for the following key words.

Infantile OR juvenile AND hemangioma AND marker AND immunohistochemistry

The search of JCRM resulted in 26 hits, but none of them performed analysis of GLUT-1 or evaluated its usefulness by

This article has been co-published with the permission of *The Journal of Dermatology, Pediatrics International and Japanese Journal of Radiology*. All rights reserved. © 2020 The Authors. The articles are identical except for minor stylistic and spelling differences in keeping with each journal's style. Either citation can be used when citing this article.

comparing infantile hemangioma with other hemangiomas/vascular malformations even if GLUT-1 was analyzed. The search of PubMed resulted in 182 hits. From these papers, those that deserved detailed analysis were selected according to the following criteria.

1. Those in which GLUT-1 immunostaining was performed for infantile hemangioma or other hemangiomas/vascular malformations.
2. Those that were retrospective epidemiological studies rather than reports of one case.

Fifteen research papers selected by these criteria were analyzed in detail.

In 7 of these reports,[251–257] infantile hemangiomas were stained using GLUT-1 simultaneously with other hemangiomas/vascular malformations, and differences in positive/negative results were evaluated. Of all cases reported in the 7 papers, GLUT-1 was positive in 268 of the 273 cases of infantile hemangioma and negative in 244 of the 247 cases of lesions other than infantile hemangioma. There were also 4 papers[258–261] in which GLUT-1 staining was performed for clinically typical infantile hemangiomas and hemangiomas that need to be differentiated from infantile hemangioma although they were not simultaneously stained in the same paper. When the 4 papers were combined, GLUT-1 was positive in all 8 cases of infantile hemangioma and negative in all 49 cases of non-infantile hemangioma. When the above cases are totaled, GLUT-1 was positive in 276 of the 281 cases of infantile hemangioma and negative in 293 of the 296 cases of non-infantile hemangioma, and the sensitivity and specificity of GLUT-1 positivity for infantile hemangioma were 98.2% and 99.0%, respectively.

The usefulness of GLUT-1 staining has also been confirmed by re-evaluation of cases that were initially examined by hematoxylin-eosin staining alone.[262–265] There have been 4 papers in which cases were re-evaluated using GLUT-1 staining, and 1 paper reported that the diagnosis was impossible by HE staining alone in 18% of the cases.[262]

CQ20: What gastrointestinal examinations are useful for children suspected to have blue rubber bleb nevus syndrome? When should the examinations be started?

Recommendation: It is recommended to start screening by examinations including blood tests and fecal occult blood test as early as possible. In children suspected to have gastrointestinal bleeding, the usefulness of endoscopic examination, red blood cell scintigraphy (^{99m}Tc-labeled red blood cells), and single photon emission computed tomography-CT (SPECT-CT) has been reported for the identification of the source of bleeding. If no abnormality is detected by screening, and search for gastrointestinal lesions needs to be performed to diagnose this disease or evaluate the future risk of bleeding, there is no standard for its timing. Among the examinations that led to the detection of gastrointestinal lesions in past reports, CT and MRI can be performed with relatively mild invasion and from an early stage.

Strength of recommendation: 2 (weak)

Evidence: D (very weak)

Comments: Gastrointestinal lesions of blue rubber bleb nevus syndrome (bean syndrome) are observed in the entire digestive tract, but they frequently appear, particularly, in the small intestine. Since it is an extremely rare disease, the literature is primarily case reports and reviews, and there have been no reports of clinical studies of many cases that are relevant for the CQ. Therefore, we investigated examinations that were useful for the detection of gastrointestinal lesions in reports, primarily, of child cases. Lesions in the small intestine are difficult to observe by conventional endoscopy, but techniques such as double-balloon endoscopy, capsule endoscopy, CT enterography, CT, and MRI as well as upper and lower gastrointestinal endoscopy have been reported to be useful.[266–276]

As a result of database searching, 11 papers in English were adopted through primary and secondary screening. All papers selected by these screening processes were case reports or case series, and the strength of evidence is "D (very weak)."

There is no clear standard as to when the examinations should be initiated. However, neonates who developed gastrointestinal bleeding shortly after birth have been reported,[270] and the earliest possible examinations are necessary if this disease is suspected. Invasive examinations are difficult to perform in small children, but blood tests (presence or absence of anemia or consumption coagulopathy) and fecal occult blood tests can be performed. If gastrointestinal bleeding is suspected, procedures such as endoscopy, particularly, double-balloon endoscopy and capsule endoscopy, ^{99m}Tc-labeled red blood cell scintigraphy, and ^{99m}Tc-labeled red blood cell SPECT-CT have been reported to be useful for the determination of the source of bleeding.[266,268,271,275]

If no abnormality has been detected by screening tests, and if search for gastrointestinal lesions needs to be performed nonemergently to diagnose this disease or evaluate the future risk of bleeding, there is no standard for the timing, which may vary among facilities. Among the above examinations, CT and MRI can be performed earlier and with relatively milder invasion, and are worth attempting if this disease is suspected. The necessity of the other examinations for the gastrointestinal lesions mentioned above should be considered when the patient reaches the age that tolerates the examinations.

CQ21: How are limb overgrowths to be managed in vascular malformations and syndromes?

Recommendation: If leg-length inequality is insignificant, shoe lift is recommended. As significant inequality causes gait disturbance complicated with scoliosis, surgical treatment aimed to arrest epiphyseal growth is performed in the growth period. Shortening of the femur or tibia may be performed as an additional treatment. Bone elongation of the intact side is considered effective for the correction of leg-length inequality.

This article has been co-published with the permission of *The Journal of Dermatology, Pediatrics International and Japanese Journal of Radiology*. All rights reserved. © 2020 The Authors. The articles are identical except for minor stylistic and spelling differences in keeping with each journal's style. Either citation can be used when citing this article.

Strength of recommendation: 2 (weak)

Evidence: D (very weak)

Comments: As a result of literature searches, 40 papers in English and 4 papers in Japanese were retrieved by primary screening. Of these papers, 17 in English and 4 in Japanese were extracted by secondary screening. As for the control of overgrowth of limbs, measures against leg-length inequality and soft tissue hypertrophy are separately discussed and regarded as effective, but these papers were all classified either as case reports or as general discussions. Therefore, the evidence level is rated as "very weak," and the recommendation level as "weak."

In vascular malformations, typical disorders with hypertrophy of the affected limbs are Klippel-Trenaunay syndrome and Parkes Weber syndrome and most of the papers refer to the management of limb overgrowth due to vascular malformations were written about these disorders. The literature regarding lesions at different sites is commented on below.

Lower limbs: In most reports, treatment for the overgrowth of the lower limbs were aimed to prevent physical disorders caused by leg-length inequality. Some reports particularly mentioned treatment for foot lesions.

1. Correction of leg-length inequality

If the leg-length inequality is ≤2 cm, the management of leg length difference and accompanying scoliosis is considered possible by the use of shoe lift.[277–281] If the leg-length inequality is ≥2 cm, significant gait disturbance, postural abnormalities, and compensatory changes in the contralateral limb are likely to develop, and before consequent unphysiological gait leads to irreversible impairment, surgical treatment to correct the leg-length inequality should be considered.[277–281] Long-leg radiography is useful for determining the best time for surgery,[282] and the measurement of the leg length by long-leg radiography or CT is reported to be effective.[278] Surgical treatment reported in the papers are as follows.

Treatment for overgrown limbs affected by vascular malformations: Jacob *et al*.[277] performed epiphysiodesis in 41 patients with a leg-length inequality of ≥2 cm among 252 patients with Klippel-Trenaunay syndrome and reported improvement in more than 90% of the patients. The effectiveness of this surgery is also confirmed by other review articles.[277–281] The effectiveness of shortening of the femur and tibia was reported in the review by Capraro *et al*.[278] The fixation period is considered to be shortened as a whole by simultaneously performing femoral or tibial shortening in addition to epiphysiodesis. Redondo *et al*.[280] recommended endoscopic growth control of the epiphyseal plate in the distal end of the femur for patients with a leg-length inequality of ≥2 cm. Capraro *et al*.[278] did not recommend growth control with the epiphyseal stapling because of the unpredictability of the results and high frequency of complications. The appropriate time for surgical intervention on affected limbs is reported to be around the age of 11 years.[280]

Elongation of the intact leg: Tanaka *et al*.[283] performed bone elongation of the intact limbs using an external fixator in adult patients with mild structural scoliosis and reported that the procedure was effective for correcting the leg-length inequality and scoliosis. Jacob *et al*.[277] also recommended bone elongation of the intact limb using Ilizarov external fixation apparatus in their review.

Popliteal vein ligation: Servelle[284] hypothesized that elongation of the affected limbs was due to a high venous pressure and performed ligation of the popliteal vein of the intact limb in 48 children, and they reported significant improvement in leg-length inequality. However, there are also negative views, saying its effectiveness is uncertain.[278]

2. Foot lesions

Redondo *et al*.[280] recommended resection of the toes (ray resection) and debulking for wearing shoes and cosmetic improvement. Gates *et al*.[285] notably reported that compared with ray resection, wound healing of the stumps was poor after major resection.

Upper limbs: Asymmetry due to hypertrophy of the upper limb less frequently causes impairment of ADL than that of the lower limb. In one article, resection in patients with functional impairment due to marked finger deformities is reported,[282] but articles reporting treatment for upper limb overgrowth are very few. While debulking has been reported to be advantageous from the cosmetic viewpoint,[279] it has also been reported to induce exacerbate of edema of the affected limb,[284] causing complications including cicatricial contracture, recurrence of the lesion, and refractory ulcer,[278] and sufficient caution is necessary.

CQ22: Is surgical resection effective for soft tissue/superficial LM?

Recommendation: Although surgical resection is an effective treatment, it should be performed after comprehensive evaluation of cosmetic aspects, prognosis, functional prognosis, resectability, and possibility of recurrence/complications.

Strength of recommendation: 2 (weak)

Evidence: D (very weak)

Comments

[Process of preparation of recommendation]

Surgical resection is one of the major treatment options performed for LM. Although LM can be cured by total resection, the objective of treatment is not necessarily total resection, because the disease is not malignant, and surgical resection is often carried out for cosmetic, functional, and symptomatic improvements. Cosmetic problems are considered to be particularly serious if the lesion is located in superficial areas such as the body surface and soft tissue. However, surgical resection has been known to cause complications including hemorrhage, infection, deformation, and nerve paralysis.

In evaluating whether resection is effective, the balance between its positive aspects and negative aspects, such as

This article has been co-published with the permission of *The Journal of Dermatology, Pediatrics International and Japanese Journal of Radiology*. All rights reserved. © 2020 The Authors. The articles are identical except for minor stylistic and spelling differences in keeping with each journal's style. Either citation can be used when citing this article.

complications, is important. For soft tissue/superficial LM, in which cosmetic improvement is important, problems including in what situations resection can be performed, whether there are criteria for the selection of resection, and, as there are differences in the incidence of complications, cure rate, and recurrence rate depending on the circumstances, whether its indications should be evaluated under different conditions are unclear. Therefore, the CQ, "Is surgical resection effective for soft tissue/superficial LM effective?," was formulated, and the current knowledge was summarized.

<Literature search and screening>

As a result of literature search, 105 papers in Japanese and 348 papers in English were subjected to primary screening. Of these papers, 5 in Japanese and 42 in English were subjected to secondary screening concerning this CQ. They did not include papers with a high level of evidence, such as a systematic review and RCT, and all of them were case series or case reports. As a result, in the evaluation of this CQ, the results and discussion in each case series were integrated.

<Review of observational studies (case series)>

The effectiveness of resection of LM was evaluated from the following 5 viewpoints: (1) Effectiveness regarding the prognosis (mortality), (2) resection rate of the lesions (resectability), (3) functional outcome after resection (function), (4) recurrence rate (recurrence), and (5) complications.

Results of review

Generally, the rate of successful surgical resection is high, and ≥90% resection is reported to be possible in 60% or more of the patients.[286–288] This also applies to the head and neck region, which is the frequent site of the lesion.[286] However, the percentage of resectable lesions decreases from the cystic to mixed and to cavernous type.[286] Since many LM are distributed diffusely in the skin and subcutaneous adipose tissue and around structures including muscles, blood vessels, and nerves, resection of the lesion involves resection of normal tissues in varying degrees. In lesions that show complicated distribution in the head and neck region, complications after surgical resection are observed relatively frequently. Serious complications including nerve paralysis, hematoma, local necrosis, sepsis, deformation, salivary fistula, hoarseness, airway obstruction, and malocclusion have been reported,[286,287,289–297] and facial nerve paralysis is likely to result from resection, particularly, of LM infiltrating the parotid region.[289] By the site, the incidence of complications increases as the area of involvement widens from unilateral to bilateral, from below to above the lingual bone, both sides, and both above and below the lingual bone.[293,296] Postoperative death may occur in patients with a severe neck lesion, but the extent of the effect of surgical resection is unclear.[287,288,298] Postoperative recurrence is closely related to the resectability of the lesion depending on its distribution, and lesions that are difficult to resect due to a wide area of involvement and a strong tendency of infiltration have been reported to be associated with recurrence.[296]

Limitations

Indications for surgical resection vary among papers, and differences in the patient background must be considered in the evaluation of the effectiveness of resection. While there were many reports that surgical resection was performed in combination with sclerotherapy, and resection is considered to have been performed when more favorable results were expected from resection rather than sclerotherapy, criteria for their selection are unclear. Therefore, there is certainly the large bias of individual variation in the circumstances, and it was clearly impossible to conclude that resection is uniformly effective.

<Summary>

While the effectiveness of surgical resection for soft tissue/superficial LM was evaluated, there was no literature with a high level of evidence. One of the major reasons is the diversity of the lesion type (cystic or cavernous), area of involvement, and history of other treatments. Because of this diversity, the condition of patients is considered to show an extremely wide variation, and their generalization is impossible. However, if conditions, such as the type of the lesion (cystic or cavernous), site of origin, and relationship with other treatments are restricted, tendencies were observed in functional prognosis, recurrence rate, and contents and incidence of complications.

While the resection rate of lesions by surgical treatment was suggested to be generally high, selection criteria for resection were unclear. Therefore, it is speculated that resection was performed for patients clinically judged to be treated more effectively by surgery. However, since there were some serious complications of surgical resection that persist as sequelae, their possibility should be evaluated carefully in performing surgical resection. The risk of resection has been suggested to vary with conditions of the lesion. The functional outcome is poor, and the recurrence rate and incidence of complications after resection are high, in those that occupy a wide area and those that are accompanied by symptoms such as airway obstruction.

From these observations, we propose at present, "While surgical resection is often effective, it must be selected in consideration of cosmetic aspects, prognosis, functional prognosis, resectability, and possibility of recurrence and complications," despite limited scientific grounds. If complete resection of the lesion is possible, surgical resection may be performed as the first line treatment, but the possibility of other treatments including sclerotherapy, in particular, should be evaluated according to the diverse conditions of individual patients, and surgical resection should be performed when other treatments are ineffective or when surgical resection is considered clearly superior.

CQ23: What is the optimal timing of surgery for soft tissue/superficial LM?

Recommendation: It is impossible to recommend optimal timing of surgery, and judgments according to the condition of each case are necessary.

This article has been co-published with the permission of *The Journal of Dermatology, Pediatrics International and Japanese Journal of Radiology*. All rights reserved. © 2020 The Authors. The articles are identical except for minor stylistic and spelling differences in keeping with each journal's style. Either citation can be used when citing this article.

Strength of recommendation: 2 (weak)

Evidence: D (very weak)

Comments

[Process of preparation of recommendation]

Soft tissue/superficial LM are not malignant lesions. Emergent treatment may be necessitated by life-threatening symptoms, such as airway obstruction, but the initiation of treatment immediately after the diagnosis is generally considered unnecessary. The natural course of the disease differs considerably among individuals, particularly, in infancy, and the lesions may show a tendency of spontaneous regression but may also cause various functional problems due to rapid enlargement. Moreover, there are cosmetic problems characteristic of this disease in addition to functional problems, and early therapeutic effects are necessary to make social life comfortable. For these reasons, the selection of optimal timing of treatment, surgery in particular, is a major issue.

For the selection of the timing of surgical resection, conditions to obtain the best results as well as indications for resection must be evaluated, and sufficient consideration of the balance between merits and demerits depending on the timing of resection is necessary. Therefore, in this CQ, we attempted to summarize the presently available knowledge about "What is the optimal timing of surgery for soft tissue/superficial lesions?".

<Literature search and screening>

As a result of literature search, 67 papers in Japanese and 231 papers in English were subjected to primary screening. Of these papers 5 in Japanese and 42 in English were subjected to secondary screening for this CQ. They included none with a high level of evidence, such as a systematic review and RCT, and all papers were case series or case reports. Therefore, the results and discussion in each case series were integrated in the evaluation of this CQ.

<Review of observational studies (case series)>

Defining "the optimal timing of surgery" mentioned in the CQ as "the timing of surgery at which good results can be obtained," we aimed to evaluate the timing of surgery at which resection is effective, problems, such as complications are few, and, i.e., "the best results" can be obtained as a whole. Conditions must be evaluated on the basis of the timing in addition to the effectiveness of surgery, but objective judgments were considered difficult in this evaluation. However, as it was considered possible to obtain information about the age and time of surgery from the literature reviewed in the previous CQs concerning the effectiveness, papers that evaluated the age at surgery were searched.

Results of review

Despite a careful review of the literature by secondary screening, there was no paper that analyzed cases from the viewpoint of optimal timing of surgery. There was information concerning the age at surgery, but its appropriateness was not evaluated. Papers that mentioned the timing of surgery are shown below.

Concerning the timing (age) of surgery, unless the size of the lesion is small or there are symptoms that require urgent treatment, such as respiratory disturbance, it is recommended to delay surgery until the age of 3 years by expecting spontaneous regression or for the ease of identification of surrounding structures during surgery, ease of control of bleeding, and less problems with postoperative management.[294] There was also a paper[295] that suggested the necessity of the determination of the time of surgery in consideration of problems that change with age including the priority of securing the airway and appropriate nutritional management in neonates with head and neck and giant lesions, control of hemorrhage and infection and measures to prevent dysarthria and dental problems in infants, and skeletal and cosmetic problems in school-age children, although it did not mention the optimal timing of surgery.

However, there was no paper that positively recommended resection without considering the time after the diagnosis or grounds for such a recommendation.

<Summary>

As a result of literature search for evaluating the CQ, "What is the optimal timing of surgery for soft tissue/superficial LM," there were papers that mentioned the timing of surgery, but none of them objectively evaluated its appropriateness. Therefore, no suggestion about the appropriate timing of surgery was obtained from the literature available at present, but there were a few papers suggesting that the decision to perform surgery should be made carefully.

Similar to the previous CQ, soft tissue/superficial LM of which the background vary in individual cases, and it is difficult to uniformly evaluate the effectiveness of resection. In clinical practice, in addition to medical reasons, social reasons including school attendance are considered to largely influence the decision of the time of resection. The results of RCTs are necessary to obtain objective data, but it is practically very difficult to arrange an RCT fulfilling the above conditions.

While this CQ is a very important issue for patients and families as well as clinicians, there has not been objective evaluation of the optimal timing of surgery in the past. Presently, as quick decisions to perform surgery should be avoided, this guideline proposes, "The optimal timing of surgery cannot be decided in general, and judgments according to the condition of each case are necessary."

CQ24: Is sclerotherapy effective for facial microcystic LM?

Recommendation: A wide range of drugs are used for sclerotherapy. Although comparison among drugs has not been made, and consensus regarding the methods or frequency of their administration has not been reached, improvements are observed after sclerotherapy in various symptomatic, functional, and cosmetic (esthetic) aspects. However, complications including functional impairment have also been reported.

Strength of recommendation: 2 (weak)

Evidence: D (very weak)

This article has been co-published with the permission of *The Journal of Dermatology, Pediatrics International and Japanese Journal of Radiology*. All rights reserved. © 2020 The Authors. The articles are identical except for minor stylistic and spelling differences in keeping with each journal's style. Either citation can be used when citing this article.

Comments

[Process of preparation of recommendation]

[Literature search and screening]

Concerning this CQ, 35 papers in Japanese and 92 papers in English (60 from PubMed, 32 from Cochrane) were retrieved. After their primary screening, 6 in Japanese and 18 in English were subjected to secondary screening concerning this CQ. Although they included 3 RCTs, many of the other papers were case series or case reports. Therefore, in the evaluation of the draft recommendation concerning this CQ, the results and discussion in each RCT and case series were integrated. While the evidence is scarce, the papers judged to be useful for the preparation of the draft recommendation are presented as review data.

[Review of case series]

As a result of literature screening, it was found that the effectiveness of sclerotherapy for facial microcystic LM has been evaluated from the following viewpoints.

1. Treatment responses

   A. Size
   B. Symptoms
   C. Functions
   D. Cosmetics

2. Complications

The contents of the accounts concerning the effectiveness of sclerotherapy are summarized according to these viewpoints.

However, there were few reports that exclusively analyzed facial (and microcystic) LM, and lesions of the neck and other regions as well as the face were evaluated or different types of LM, such as cystic and mixed types, were reported together. In addition, the definition of the cavernous type and standard procedure of sclerotherapy (method and number of administrations) varied among reports, and these differences in the background should be considered in the evaluation of the effectiveness of sclerotherapy.

The sclerosing agents used for the literature search ranged widely from OK-432, bleomycin, ethanol, doxycycline, and sodium tetradecyl sulfate (STS). However, as none of the papers reviewed for the preparation of these guidelines evaluated differences in the effectiveness for facial microcystic lesions among drugs or the method or number of administrations of each drug, these evaluation items were excluded in discussing this CQ.

1. Responses

A. Size

Many of the papers that referred to the regression rate of the lesion classified the responses into (1) excellent or complete (regression rate ≥90%), (2) good or substantial (regression rate ≥50% and <90%), (3) fair or intermediate (regression rate ≥20% and <50%), and (4) poor or none (regression rate <20%).

Although there was no paper that collected cases of facial lesions alone, Yang *et al.*[299] reported that the regression rate after sclerotherapy was ≥90% in 19 (63%) of the 30 patients with head and neck lesions and ≥50% in 10 (33%). In addition, the regression rate was reported to be ≥50% in 18 (85.7%) of the 21 patients with head and neck lesions by Alomari *et al.*[300] and in 30 of the 31 patients to be ≥50%, who included those with mixed type lesions, by Chaudry *et al.*[301]

Smith *et al.*[302] reported that none showed a response (complete or substantial) in 17 patients who underwent sclerotherapy, some of whom had mediastinal lesions. Giguere *et al.*[303] also reported that all 5 patients with head and neck lesions showed no response (poor) to the therapy. While these studies were RCTs evaluating the time of sclerotherapy, the results suggest that sclerotherapy is not effective for microcystic lesions regardless of the time of treatment.

There was no paper that compared sclerotherapy and resection for facial microcystic LM.

B. Symptoms

There is no literature that evaluated this item based on objective data, and few reports referred to symptoms themselves. The information was limited to the report by Chaudry *et al.*[301] that symptoms disappeared after sclerotherapy using bleomycin in 75% of the patients who complained of pain and a few case reports[304,305] that symptoms, such as hemorrhage and respiratory impairment, were relieved after sclerotherapy.

C. Functions

Ravindranathan *et al.*[306] performed sclerotherapy in 3 patients with diffuse microcystic lesions extending from the face to the tongue and pharynx and reported that respiratory impairment and swallowing disorder due to airway obstruction observed before treatment were mitigated. Poonyathalang *et al.*[307] administered STS to a patient with orbital lesions primarily complaining of visual defect and reduced visual acuity due to retrobulbar hemorrhage and reported alleviation of the symptoms, but relevant literature was scarce similar to that concerning symptoms.

D. Cosmetic aspects

Cosmetic improvements are difficult to evaluate objectively. Poonyathalang *et al.*[307] administered STS to 3 patients with orbital lesions with exophthalmos as the primary symptom and reported improvement by measuring the degree of protrusion before and after the treatment. There have also been reports of objective assessment based on the degree of satisfaction in the patients' families. According to Chaudry *et al.*,[301] all patients with head and neck lesions (9 with microcystic lesions, 22 with mixed lesions) and their families reported improvements in the size and appearance of the lesions. In addition, Alomari *et al.*[300] treated 32 patients with mostly microcystic but including some cystic LM of the head and neck region by sclerotherapy and reported improvements compared with the condition before treatment by the families of 26 patients (81.3%).

This article has been co-published with the permission of *The Journal of Dermatology, Pediatrics International and Japanese Journal of Radiology*. All rights reserved. © 2020 The Authors. The articles are identical except for minor stylistic and spelling differences in keeping with each journal's style. Either citation can be used when citing this article.

2. Complications

As complications in the facial region, there are a large number of reports[299,301,307–312] of transient complications associated with sclerotherapy, such as fever, local swelling and pain, intracystic hemorrhage, and infection, although the lesions were poorly characterized in some reports. In addition, complications considered to have been caused by the effect of treatment, such as ulcer of the oral mucosa and tongue, facial nerve paralysis, leakage of saliva, and respiratory insufficiency due to airway obstruction, have been occasionally reported.[303,306,307] There have also been reports[307,313,314] of an elevation of the intraorbital pressure, exophthalmos, intraorbital hemorrhage, corneal damage, and external ocular muscle paralysis due to enlargement of the mass after sclerotherapy for ocular LM. There was also no literature showing the incidence of complications in facial microcystic LM.

As complications caused by sclerosing agents, skin ulcer and necrosis and nerve damage due to ethanol leakage, hypotension during anhydrous ethanol injection, and epidermal detachment due to doxycycline have been reported.[300,315] However, there was no report of serious complications due to OK-432. Pulmonary fibrosis is widely known to be a complication of bleomycin, but, according to Chaudry *et al.*[301] and Yang *et al.*,[299] impairment of respiratory function does not occur at a dose routinely employed for sclerotherapy.

[Summary]

In evaluating the CQ, "Is sclerotherapy effective for facial microcystic LM?," analysis was performed from the viewpoints of responses to the treatment in terms of symptoms, functions, and cosmetic (esthetic) aspects and complications, but few papers with a high level of evidence were found. While the degree of regression of the lesions by sclerotherapy varied widely, the size-reducing effect of the therapy was consistently small unlike that in cystic lesions. Some papers referred to symptoms, functional outcome, and cosmetic improvement, but they were insufficient for general discussion of sclerotherapy for facial microcystic LM. As complications characteristic of sclerotherapy, serious impairment may be caused by leakage of the sclerosing agent (ethanol, in particular), and this point needs attention. Based on the above observations, it is difficult at present to evaluate indications for sclerotherapy against microcystic LM by formulating criteria. Therefore, for the future, it is considered necessary to evaluate the usefulness of sclerotherapy addressed by this CQ by designs such as RCT.

CQ25: Is sclerotherapy effective for intra-abdominal LM?

Recommendation: Although there are many reports that sclerotherapy is useful, there is the risk of complications, and careful judgments about matters including the resectability of the lesion and selection of the sclerosing agent are necessary.

Strength of recommendation: 2 (weak)

Evidence: D (very weak)

Comments

[Process of preparation of recommendation]

LM is the most frequent lymphatic vessel disorder of the abdomen. Intra-abdominal lesions are estimated to account for 10–20% of all LM, and the selection of treatment is difficult depending on the site of the lesion. While surgical resection is expected to be effective, less invasive treatments are considered necessary in view of stress to the patient and the possibility of severe complications such as lymphatic fluid leakage and bowel obstruction. Sclerotherapy, which is a major treatment for LM, is considered to be less invasive than surgery. Although positive therapeutic effects are expected, sclerotherapy is known to induce marked inflammation. Whether it can be performed safely without negative effects including complications and its long-term effects are major clinical concerns. In addition, what therapeutic effects are expected or what complications should be anticipated after sclerotherapy for the intra-abdominal lesion is also unclear. Therefore, the CQ, "Is sclerotherapy effective for intra-abdominal LM?", was formulated, and knowledge available at present was compiled.

<Literature search and screening>

As a result of literature search, 19 papers in Japanese and 38 papers in English (32 from PubMed, 6 from Cochrane) were subjected to primary screening. Of these papers, 2 in Japanese and 9 in English were subjected to secondary screening concerning this CQ. They included no papers with a high level of evidence, such as systematic reviews and RCTs, and all were case series or case reports. Consequently, the results and discussion in each case series were integrated in the evaluation of this CQ.

<Review of observational studies (case series)>

The literature concerning the effectiveness of sclerotherapy for intra-abdominal LM was reviewed from the viewpoints of (1) therapeutic effects (decrease in lesion size, symptoms) and (2) complications.

The drugs used for sclerotherapy ranged widely from OK-432 to bleomycin, ethanol, doxycycline, STS, acetic acid, steroid/tetracycline, and 50% glucose solution. According to our review, there was no paper that evaluated the differences in effectiveness of sclerotherapy in the abdomen according to the drug type or administration method or number of administrations of each drug.

Results of review

1. Therapeutic effects

A. Regression rate of the lesion

Regression of lesions of intra-abdominal LM by sclerotherapy was mentioned in 5 papers.[288,316–319] According to the report by Chaudry *et al.*,[316] the reduction rate was ≥90% in 7 and ≥20% in 1 of the 10 patients with LM of the mesentery and retroperitoneum treated with doxycycline, and evaluation using imaging examination was not performed in 2 cases. The patient who showed a low regression rate had a mixed type of cystic and cavernous lymphangiomas, and the other patients

This article has been co-published with the permission of *The Journal of Dermatology, Pediatrics International and Japanese Journal of Radiology*. All rights reserved. © 2020 The Authors. The articles are identical except for minor stylistic and spelling differences in keeping with each journal's style. Either citation can be used when citing this article.

had cystic lesions. Oliveira *et al*.[317] reported that the lesion regressed by 70% in 1 of the 2 patients with cystic lymphangiomas treated with OK-432. Won *et al*.[318] reported 1 patient who showed complete disappearance of cystic retroperitoneal lesions after sclerotherapy using acetic acid. Shiels *et al*.[319] reported that cystic lesions responded to sclerotherapy using STS and ethanol in 2 patients, but there was no mention about the reduction rate. However, according to Alqahtani *et al*.,[288] no effect was observed in 10 patients who underwent sclerotherapy using steroid/tetracycline or 50% glucose solution.

B. Symptoms

There were 3 papers that referred to symptoms of patients treated by sclerotherapy for intra-abdominal LM.[316,317]

According to Chaudry *et al*.,[316] of the 10 patients who underwent sclerotherapy, 3 had chronic abdominal pain, 3 had acute abdominal pain, 1 had fever/chill, 1 had anemia, and 2 had palpable masses, but the symptoms were alleviated by treatment in all patients, and no recurrence was noted.

Oliveira *et al*.[317] reported that sclerotherapy was performed in a patient with a palpable mass and in 1 with a palpable mass, abdominal compartment syndrome, and a poor general condition. While the condition was alleviated in the patient who only showed a palpable mass after 2 courses of OK-432 sclerotherapy, but the treatment was changed to surgery in the patient who had abdominal compartment syndrome because of enlargement of the mass due to intracystic hemorrhage.

2. Complications

Three papers specifically mentioned complications of sclerotherapy for intra-abdominal LM. There was no report of deaths due to treatment-related complications. Oliveira *et al*.[317] treated 3 patients by sclerotherapy using OK-432 and reported that one of them developed subbowel obstruction after the treatment and another required emergency surgery due to exacerbation of abdominal compartment syndrome induced by intracystic hemorrhage. Chaudry *et al*.[316] reported that doxycycline used for sclerotherapy leaked into the retroperitoneal space in 1 of the 10 patients but that the lesion regressed without any particular problem. Won *et al*.[318] performed sclerotherapy using acetic acid in 1 patient with retroperitoneal cystic lymphangioma. Although pain and hematuria were observed, they concluded that the relationship of hematuria with the therapy was unclear, because it was observed during menstruation.

Limitations

Sclerotherapy was often performed before, after, or during surgical resection, and papers that reported the results of sclerotherapy alone were few. There was no paper that directly compared observation without treatment, sclerotherapy, and surgical resection. Few papers analyzed intra-abdominal lesions alone, and many papers included lesions in other areas or evaluated lesions in different intra-abdominal regions including the mesentery, retroperitoneum, and viscera collectively.

Moreover, differences in properties of LM, such as cystic, cavernous, and mixed types, their definitions, criteria for the selection of sclerotherapy (combination with surgery, types of sclerosing agents and methods of their use, number of administrations) varied among papers, and few papers evaluated these matters separately.

Such differences in the patient background and contents of treatment must be considered in evaluating the effectiveness of sclerotherapy. In evaluating this CQ, particularly, differences in morphology of LM and sclerosing agents were excluded.

<Summary>

The CQ, "Is sclerotherapy effective for intra-abdominal LM?" was evaluated from the viewpoints of therapeutic effect, symptoms/functions, and complications, but no paper with a high level of evidence was found. While sufficient regression of the lesion and alleviation of symptoms were achieved by sclerotherapy in some patients, the response rate varied among reports, and information was insufficient for general discussion of sclerotherapy. Concerning treatment-related complications, there have been reports of bowel obstruction associated with sclerotherapy, and attention to this condition as well as intracystic hemorrhage is considered necessary. However, there was no report of chylorrhea, which was reportedly caused by surgery.

Based on the above observations, it is presently difficult to determine indications for sclerotherapy in intra-abdominal LM by setting up criteria, but as there was no literature that strongly ruled out intra-abdominal LM as indications of sclerotherapy, these guidelines propose, "Although there are many reports that sclerotherapy is useful, there is the risk of complications, and careful judgments about matters including the resectability of the lesion and selection of the sclerosing agent are necessary." For the future evaluation of this CQ, validation by a design with a high level of evidence, such as RCT, is considered necessary.

CQ26: Are patients with scarcely symptomatic intra-abdominal LM candidates for treatment?

Recommendation: Since there is risk of treatment-related complications, it is proposed to consider therapeutic intervention when the lesion tends to enlarge or has become symptomatic.

Strength of recommendation: 2 (weak)

Evidence: D (very weak)

Comments

[Process of preparation of recommendation]

Intra-abdominal LM occasionally presents with severe symptoms, such as abdominal pain, giant mass, and bowel obstruction, but may also be asymptomatic and detected incidentally. Lesions may gradually enlarge and cause serious symptoms due to infection and intraluminal hemorrhage.

Under such circumstances, whether patients with nearly asymptomatic intra-abdominal LM should be aggressively treated, or when intervention should be optimally performed during their long follow-up period are major problems that

This article has been co-published with the permission of *The Journal of Dermatology, Pediatrics International and Japanese Journal of Radiology*. All rights reserved. © 2020 The Authors. The articles are identical except for minor stylistic and spelling differences in keeping with each journal's style. Either citation can be used when citing this article.

pose clinical dilemma. Therefore, the CQ, "Are patients with scarcely symptomatic intra-abdominal LM candidates for treatment?," was formulated, and knowledge available at present was summarized.

<Literature search and screening>

As a result of literature search, 206 papers in Japanese and 237 papers in English (230 from PubMed, 7 from Cochrane) were subjected to primary screening. Of these papers, 6 in Japanese and 9 in English were subjected to secondary screening concerning CQ 26. They included no papers with a high level of evidence, such as a systematic review or RCT, and many of them were case series or case reports. Since 7 papers among them described asymptomatic LM, their results and discussions were integrated to answer the CQ.

<Review of observational studies (case series)>

Seven papers[316,317,320–324] among reviewed literature described asymptomatic LM. Fifteen cases reported in these papers were considered to have actually presented few symptom (including asymptomatic patients who were incidentally detected by imaging studies to have intra-abdominal masses at the sites as greater omentum, mesentery and retroperitoneum).

The literature was screened, and papers addressing issues concerning therapeutic intervention for scarcely symptomatic intra-abdominal LM including "What symptoms they may present with if they are left untreated?," "By what studies and how often should they be examined?," and "What other treatments are available and how serious are complications or risk of each treatment?" were reviewed.

Results of review

From the literature reviewed, symptoms of intra-abdominal LM (abdominal pain, bowel obstruction, torsion, infection, hemorrhage, vomiting/sucking difficulty, frequent urination and abdominal mass[320–326]) are considered to be dependent on factors such as site, size and age. It is necessary to determine risk factors by stratification of these factors in the future.[320,322,325]

Reported complications in treated cases include recurrence that required re-treatment,[321] bowel obstruction,[317,323,324] chylous ascites,[324,326] embolism,[317] hemorrhage[317] and wound infection. Embolism of the inferior vena cava after surgery[317] and abdominal compartment syndrome after adhesion therapy[317] were reported as severe complications. It deserves special attention that, if surgical resection is performed for mesenteric LM, the intestine may have to be resected with the lesion.[326]

While there have been reports[320,322] that intra-abdominal LM with few clinical symptoms regressed during follow-up, they may become symptomatic later (as observed in many case reports). For that reason, the opinion that intervention should not been chosen during the follow-up until the lesion enlarges or new symptoms appear was frequently described.

Limitations

It should be noted that many asymptomatic cases may be left unreported and some asymptomatic lesions that had been detected were treated. There is no study with a high level of evidence indicating explicit criteria concerning the age, site or situation about whether intervention should be made for asymptomatic intra-abdominal LM.

<Summary>

The necessity of treatment of a patient with intra-abdominal LM with few symptoms should be determined after evaluating the balance between the risk of treatment and non-treatment considering its site and size as well as patient age. However, since research on indications for treatments has been insufficient so far and serious complications after treatment have been reported, deliberate evaluation for each patient is mandatory. When observation is selected, periodic imaging studies are recommended to optimize therapeutic intervention by detecting enlargement of the lesion. Also if any symptom has developed during follow-up, intervention should be considered. For these reasons, the recommendation, "Since there is risk of treatment-related complications, it is proposed to consider therapeutic intervention when the lesion tends to enlarge or has become symptomatic." was adopted.

CQ27: What treatments are effective for refractory chylous ascites?

Recommendation: Conservative treatments, such as fasting, high-calorie infusion, and medium chain triglyceride (MCT), should be performed first, but, if they are ineffective, drug treatment, sclerotherapy, and surgery may also be considered.

Strength of recommendation: 2 (weak)

Evidence: D (very weak)

Comments

[Process of preparation of recommendation]

Refractory chylous ascites causes loss of large amounts of protein and lymphocytes, decreases in the blood lipid levels, and abdominal pain, unpleasantness, and dyspnea due to abdominal distention and markedly reduces the quality of life. The cause of ascites often remains unknown. Treatment of chylous ascites may require drainage to avoid abdominal distention. It is a very important point for clinicians to make proper judgments by understanding treatments and their effects and demerits. Therefore, it is considered beneficial to collect information about chylous ascites over a long period and compile guidelines. For this purpose, the presently available knowledge was collected by formulating the CQ, "What treatments are effective for refractory chylous ascites?"

<Literature search and screening>

As a result of search, 161 papers in Japanese and 728 papers in English (564 from PubMed, 164 from Cochrane) were subjected to primary screening. Of these papers, 15 in Japanese and 12 in English were subjected to secondary screening for CQ 27. They included none with a high level of evidence, such as systematic reviews and RCTs, and consisted of 1 multicenter and 2 single-center case series and case reports. Consequently, we used the results and discussion of 27 papers judged for the preparation of the draft recommendation were integrated although evidence was insufficient for the evaluation of this CQ.

This article has been co-published with the permission of *The Journal of Dermatology, Pediatrics International and Japanese Journal of Radiology*. All rights reserved. © 2020 The Authors. The articles are identical except for minor stylistic and spelling differences in keeping with each journal's style. Either citation can be used when citing this article.

<Review of observational studies (case series)>

As for causes of chylous ascites, congenital chylous ascites,[327–342] idiopathic chylous ascites,[328] chylous ascites after laparotomy,[343–346] protein-losing enteropathy,[345] LM,[347,348] lymphangiectasis,[349,350] lymphangiomatosis,[351,352] and lymphatic dysplasia[353] were reported. None of the papers evaluated treatments according to the cause.

When treatments are categorized, conservative treatments (fasting, high-calorie infusion, MCT), drug treatments, sclerotherapy, and surgical treatment were performed.

Results of review

The results of review are presented below according to the treatment.

1. Conservative treatments

Whether the amount of ascites changes by fasting should be checked first.

High-calorie infusion is often used with fasting, and since there was no report that ascites increased under the effect of high-calorie infusion according to our review, it is recommended for nutritional support during fasting. In the multicenter case series reported by Bellini *et al.*,[327] high-calorie infusion/total parenteral nutrition was performed in 15 patients without adverse effects.

MCT was used before, after, and during treatment.[327,328,330–335,337,339–341,343,345,346,348–352] In the multicenter case series by Bellini *et al.*,[327] MCT was reportedly performed in 14 patients without adverse effects.

2. Drug treatments

In drug therapy for chylous ascites, primarily octreotide (a long-acting somatostatin analogue) was used, and no report that discussed the effectiveness of other drug therapies was found by the present literature search.

In the multicenter case series by Bellini *et al.*,[327] octreotide was administered to 6 of the 16 patients with chylous ascites for 8–38 days, and a decrease in chylous ascites was reported in all of them. In the single-center case series by Huang *et al.*,[344] 2 of the 4 patients with chylous ascites treated by high-calorie infusion and octreotide administration were reported to have shown a decrease in ascites within 10 days. However, there has been a report[330] that no effect was observed despite the administration of octreotide for 3 weeks. Concerning the dose of octreotide, it was administered at 1 μg/kg/h,[327] at 3 μg/kg/h,[332] began to be administered at 0.5 μg/kg/h and increased to 10 μg/kg/h by 1 μg/kg/h,[329] administered by continuous intravenous infusion at 0.5–2.0 μg/kg/h,[333] and began to be administered by subcutaneous injection at 2.5 μg/kg 2 times/day and increased every 2 days to 8 μg/kg 2 times/day.[330] Regarding the time of the beginning of administration, the administration was started as no improvement was observed in chylous ascites after conservative treatments for 2 weeks,[330,334] and as chylous ascites was alleviated by conservative treatments but was exacerbated again.[333] No adverse effects of octreotide administration were noted in the present review of the literature. Thus, no control study that evaluated the effect of octreotide on chylous ascites was found by the present literature search, and the level of evidence concerning the efficacy is low, but as there are case series and many case reports that chylous ascites was reduced by octreotide administration, it appears reasonable to consider drug treatment using octreotide for chylous ascites that does not respond to conservative treatments.

3. Sclerotherapy

Sclerotherapy was performed in 6 patients in 5 case reports.[339,347,349,351,352] The sclerosing agent was OK-432 in 5 of the 6 patients and was Beta-isodona® (MUNDIPHARMA GmbH, Cambridge, UK) solution in 1.[349] OK-432 was locally injected into the lesion in 4,[347,351,352] administered intraperitoneally in 1,[352] and administered via the drain in 2.[347,352] Concerning sclerotherapy, the number of reported cases that were reviewed was limited, and further accumulation of cases is considered necessary to establish its usefulness.

4. Abdominal drainage, abdominal puncture, and surgical treatment

Abdominal drainage and abdominal puncture are performed when organ compression symptoms (compartment syndrome and respiratory insufficiency) due to abdominal distention are present or possible or when the drain is inserted postoperatively. However, drainage itself cannot improve chylous ascites, and treatments, such as infusion, blood preparations, and blood transfusion, are necessary to supplement the ascites lost due to drainage.[327,330–333,337–340,343,345–347,349,351,352]

Surgical treatment is reported to be frequently performed after conservative or drug treatments. According to the single-center case series by Zeidan *et al.*,[343] surgical treatment was performed in patients who responded poorly to conservative treatments for over a mean of 25.3 days. In other reports, surgical treatment was performed after conservative treatments for 1–3 months[328,329] and in patients with congenital chylous ascites 1–4 months after birth.[330,334,350] Since it is often impossible to identify the leakage site of chylous ascites,[330] attempts to identify the leakage site by orally administering a lipophilic dye (Sudan black, Sudan III) before operation.[328,329,336,343] When the leakage site can be identified, ligation, suturing, clipping, and cauterization have been performed.[328,334,336,343,350] In addition to reports of the usefulness of techniques to stop leakage, such as applying or sprinkling fibrin glue at the leakage site of chylous ascites or over the surrounding retroperitoneum[329,331,343,350] and applying a patch of oxidized cellulose/resorbable local hemostatic agent,[331,343] there have also been reports of peritoneovenous shunting[349,353] and peritoneoamniotic shunting for fetal cases.[338]

There was no large clinical study in the past literature. Therefore, although the level of evidence is low, we consider

This article has been co-published with the permission of *The Journal of Dermatology, Pediatrics International and Japanese Journal of Radiology*. All rights reserved. © 2020 The Authors. The articles are identical except for minor stylistic and spelling differences in keeping with each journal's style. Either citation can be used when citing this article.

that surgical treatment is recommendable for chylous ascites that does not respond to conservative or drug treatments, because it has been performed in case series and case reports for chylous ascites that did not respond to conservative or drug treatments for over about 1 month. Although techniques to enhance the response rate of surgical treatment, such as identifying the leakage site by using a lipophilic dye and applying fibrin glue or a patch of oxidized cellulose/resorbable local hemostatic agent, have been attempted, there are only case series and case reports, and none of the papers retrieved by the present literature search evaluated their usefulness.

Limitations

There was no literature that defined refractory chylous ascites based on the duration of illness or treatment responses. Therefore, we extracted and summarized factors that were considered to contribute to clinical refractoriness, such as the duration of illness and treatment responses, in each paper related to the treatment for chylous ascites. Also, as the cause of chylous ascites varies widely, the therapeutic effect is expected to differ depending on the cause, but no paper that was reviewed evaluated treatments according to the cause. Therefore, in the present evaluation, the statements are limited to treatments and their effects regardless of the cause.

<Summary>

It was difficult to comprehensively discuss treatments, because its cause varied widely, and treatments for various causes were performed. Therefore, treatments were classified into conservative treatments (fasting, high-calorie infusion, MCT), drug treatments (octreotide), sclerotherapy, abdominal drainage, abdominal puncture, and surgical treatment, and the effects of each treatment were evaluated.

Treatments effective for refractory chylous ascites can be summarized as follows with the understanding that they may depend on the cause and that the level of evidence of the available reports concerning treatments and their effects is low. Conservative treatments, such as fasting, high-calorie infusion, and MCT, should be performed first because of the rareness of adverse effects. In patients who respond insufficiently to conservative treatments, drug treatments using octreotide can be considered as there have been case series and many case reports. Concerning sclerotherapy, the number of reported cases is small, and further large clinical studies will be needed to confirm its usefulness. Abdominal paracentesis and surgical treatments may be considered for chylous ascites that does not response to conservative or drug treatments for about 1 month.

Thus, the draft recommendation is "Conservative treatments, such as fasting, high-calorie infusion, and MCT, should be performed first, and, if they are ineffective, drug treatments, sclerotherapy, and surgical treatments may be considered." However, evaluation of this CQ by a design with a higher level of evidence, such as RCT, is considered necessary for the future.

CQ28: What kinds of complications are associated with treatments for intra-abdominal LM?

Recommendation: Complications associated with sclerotherapy for intra-abdominal LM include bowel obstruction, hemorrhage, pain, hematuria and chylous ascites. Surgical treatment of the disease can be associated with serious complications such as occlusion of the inferior vena cava and massive resection of the intestine as well as more common, wound infection, bowel obstruction, hemorrhage and chylous ascites.

Strength of recommendation: No recommendation

Evidence: D (very weak)

Comments

[Process of preparation of recommendation]

Patients with intra-abdominal LM are treated with various modalities from non-surgical therapy to surgical procedures. Treatment modality is selected depending on the patient's state. Therefore, it is necessary for the clinician, patient, and family to share information concerning complications that may be associated with treatments for implementing them smoothly. However, there are no resources that give a clear answer to this problem, and both clinicians and patients may become disconcerted. Therefore, the CQ "What kinds of complications are associated with treatments for intra-abdominal LM?" was formulated, and information available at present was accumulated and integrated for the answer.

<Literature search and screening>

As a result of literature search, 203 papers in Japanese and 602 papers in English (593 from PubMed, 9 from Cochrane) were subjected to primary screening. Of these papers, 23 in Japanese and 27 in English were subjected to secondary screening concerning this CQ. They included no papers with a high level of evidence, such as systematic reviews or RCTs, and all of them were case series or case reports. To answer CQ 28, the results and discussion in each case series were integrated.

<Review of observational studies (case series)>

Complications in the CQ were evaluated by defining them as those encountered when patients with intra-abdominal LM were treated, and reports on sclerotherapy and surgery were reviewed.

Results of review

1. Complications associated with sclerotherapy

Sclerotherapy using OK-432 was reported to be associated with bowel obstruction and hemorrhage for mesenteric LM,[317] and chylous ascites for retroperitoneal LM.[326] Sclerotherapy using acetic acid was reported to be associated with pain and hematuria in patients with retroperitoneal LM.[318]

2. Complications associated with surgical procedures

Complete resection of both mesenteric and retroperitoneal LM by laparotomy was reported to be associated with wound infection[324,354] and bowel obstruction[323,354,355] as common

This article has been co-published with the permission of *The Journal of Dermatology, Pediatrics International and Japanese Journal of Radiology*. All rights reserved. © 2020 The Authors. The articles are identical except for minor stylistic and spelling differences in keeping with each journal's style. Either citation can be used when citing this article.

complications. There were reports of serious complications such as occlusion of the inferior vena cava[317] and massive resection of the intestine was necessary due to diffuse infiltration of the LM tissue to the intestinal wall.[356]

In a report[357] about complications associated with complete laparoscopic resection of intra-abdominal LM by Tran *et al*., resection was attempted in 47 patients, and conversion to laparotomy was necessary in 3 (6.4%) due to tight adhesion in 2 and intraoperative hemorrhage in 1.

Partial resection by laparotomy was reported to be associated with persistent ascites over a long period that was refractory to the treatment.[355]

Limitations: Patients with intra-abdominal LM are treated with various modalities including sclerotherapy and surgical procedures. Modalities were combined in many cases, and complications are often reported as those of entire treatment without more detail information about those associated with individual treatment.

<Summary>

For answering the CQ, "What kinds of complications are associated with treatments for intra-abdominal LM?," no literature with a high level of evidence was found, but foreseeable complications were listed from many case reports. Bowel obstruction, hemorrhage, pain, hematuria, and chylous ascites were reported as complications of sclerotherapy. Serious conditions, such as occlusion of the inferior vena cava and massive resection of the intestine, as well as common complications, such as wound infection, bowel obstruction, hemorrhage and chylous ascites were reported as complications after surgical procedures.

Although the incidences and differences in complications in respect of the site and histological type are not shown in the literature, each patient with intra-abdominal LM should be treated with sufficient evaluation of the site, size and symptoms. In addition, treatment must be implemented with sufficient understanding of the possible complications.

Thus, we propose "Complications associated with sclerotherapy for intra-abdominal LM include bowel obstruction, hemorrhage, pain, hematuria, and chylous ascites. Surgical treatment of the disease can be associated with serious complications such as occlusion of the inferior vena cava and massive resection of the intestine as well as more common, wound infection, bowel obstruction, hemorrhage and chylous ascites." as a recommendation draft.

CQ29: What treatments are effective for LM causing airway obstruction in the mediastinum?

Recommendation: Sclerotherapy is effective for macrocystic lesions, and surgical resection is effective for microcystic lesions. However, as the complication rate is relatively high, treatments should be selected according to the condition of each case.

Strength of recommendation: 2 (weak)

Evidence: D (very weak)

Comments

[Process of preparation of recommendation]

Among LM, those that may cause airway obstruction due to their sites are life-threatening. Lesions in the mediastinum cause respiratory disorders if they physically compress the trachea or bronchi and obstruction the airway or markedly protrude into the thoracic cavity and narrow it.

In such situations, aggressive and effective treatment is necessary, but the therapeutic approach must be selected carefully in consideration of the relationship of the lesion with the important organs around it such as the large cardiac vessels, mediastinal nerve, and thoracic duct. However, the judgment is often difficult in clinical settings.

Therefore, the CQ, "What treatments are effective for LM causing airway obstruction in the mediastinum?" was formulated, and the presently available knowledge concerning matters including the risk of complications and prognosis of treatments, such as surgical resection and sclerotherapy, was summarized.

<Literature search and screening>

As a result of literature search, 134 papers in Japanese and 227 in English (226 from PubMed, 1 from Cochrane) were subjected to primary screening. Of these papers, 5 in Japanese and 16 in English were subjected to secondary screening concerning this CQ. Since they included none with a high level of evidence, such as a systematic review or RCT, and all were case series or case reports, the results and discussion in each case series were integrated.

<Review of observational studies (case series)>

By screening of the literature, the following approaches were found for the treatment of LM in the mediastinum.

Therapeutic options are surgical resection, puncture and drainage, sclerotherapy (OK-432, bleomycin, ethiblock, anhydrous ethanol), drug treatments (Chinese herbal medicines such as *eppikajutsuto* and *ogikenchuto*), and no treatment. Of these approaches, surgical resection and sclerotherapy using OK-432 have been evaluated in a relatively large number of cases, and reports of other therapy had extremely limited number of cases, e.g., reports of only 1 case.

Results of review

Boardman *et al*.[358] reported that, of the 97 patients with LM of the head and neck region, surgical treatments were necessary in 6 of the 12 patients with mediastinal lesions, that complications of surgery occurred in 4 of the 6 patients, and that long-term nerve damage was observed in 3 of them. In addition, they reported that management by tracheotomy was necessary in 15% of all patients. Complete or nearly complete remission was observed in 92% of the patients, but they suggested that surgical treatments should be indicated only when there is airway obstruction or there is the risk of it, because surgical treatment of mediastinal lesions frequently causes complications.

Park *et al*.[359] reported that they surgically resected mediastinal LM in 12 patients. Seven of them had dyspnea, and 3 were asymptomatic, but they were all judged to have

This article has been co-published with the permission of *The Journal of Dermatology, Pediatrics International and Japanese Journal of Radiology*. All rights reserved. © 2020 The Authors. The articles are identical except for minor stylistic and spelling differences in keeping with each journal's style. Either citation can be used when citing this article.

indications for surgery due to symptoms or the tendency of the lesions to enlarge. A total of 5 recurrences were observed in 4 patients (33%) during a mean period of 3.6 years after the initial surgery, and all underwent by re-resection. No perioperative death was observed, and, in a total of 25 cases including past cases, the overall survival was not different compared with that in healthy individuals over a follow-up period of 11.5 years.

Smith *et al.*[302] performed local injection of OK-432 in 16 patients with mediastinal LM and reported ≥60% regression of the lesion in 13 (81%). They also mentioned treatment responses according to the histological types and, by reporting responses (complete or nearly complete remission) in 94% of those with macrocystic lesions, 63% of those with mixed lesions, but 0% in those with microcystic lesions, suggested a macrocystic lesion to be a good indication for sclerotherapy using OK-432. Although not from the viewpoint of airway obstruction, they reported that treatment using OK-432 was more effective than surgical resection and less frequently caused serious complications.

Limitations

There have been no papers that directly analyzed treatments effective for mediastinal lesions expected to cause airway obstruction, and many papers reported cases of mediastinal lesions that responded to treatments. Therefore, we simply extracted matters relevant to this CQ from these reports.

<Summary>

There was no literature with a high level of evidence concerning effective treatments for LM in the mediastinum causing airway obstruction. A few case reports that referred to the effects of surgery and sclerotherapy were observed, but it was difficult to present objective and specific figures concerning their effectiveness or safety. However, according to the available information, it should be noted that favorable responses have been obtained by OK-432 local injection in macrocystic lesions and that complications due to surgical resection are likely to occur relatively frequently.

From these observations, we consider the following to be a therapeutic approach that can be proposed: "Sclerotherapy, such as that by local injection of OK-432, should be considered for macrocystic lesions, and, for lesions that are technically difficult to treat by sclerotherapy or microcystic lesions, surgical resection should be considered with attention to complications. In addition, it is necessary to pay attention to the appearance of respiratory disturbances before and after these treatments and to constantly evaluate indications for securing the airway by intratracheal intubation or tracheostomy." Therefore, at present, we recommend, "Sclerotherapy is effective for macrocystic lesions, and surgical resection is effective for microcystic lesions. However, as the complication rate is relatively high, treatments should be selected according to the condition of each case."

CQ30: Should sclerotherapy be performed in infancy for a patient with head and neck LM affecting the airway?

Recommendation: In a patient with LM around the airway, there is risk of respiratory distress in infancy, while airway obstruction is likely to be exacerbated by sclerotherapy. Particularly, when risk of airway obstruction is judged to be high or when the patient has already presented symptoms, it is proposed to perform sclerotherapy with sufficient preparations including airway management.

Strength of recommendation: 2 (weak)

Evidence: D (very weak)

Comments

[Process of preparing recommendation]

LM of the neck, which are located in an exposed part of the body, may cause cosmetic problems that are important, but airway obstruction can particularly be a serious problem in some cases.

Sclerotherapy, which is one of the major treatment modalities, is most effective in patients with cystic LM, but swelling of the treated portion after the therapy may cause or exacerbate airway obstruction symptoms especially in neonates. The upper airway will become less vulnerable to obstruction because it becomes less frail and wider as patients grow and respiratory distress tends to be unlikely. Therefore, it is occasionally difficult to determine how a patient who does not present any obstructive symptom should be treated in infancy.

Thus, we evaluated this problem by formulating the CQ, "Should sclerotherapy be performed in infancy for a patient with the neck LM affecting airway?"

<Literature search and screening>

As a result of search, 86 papers in Japanese and 135 papers in English (130 from PubMed, 5 from Cochrane) were subjected to primary screening. Of these papers, 6 in Japanese and 20 in English were subjected to secondary screening concerning this CQ. They included 1 systematic review (SR), 1 RCT, 2 prospective studies (PS) and 1 retrospective cohort study, but all the others were case series or case reports. Therefore, the results and discussion, primarily, in these SR, RCT, PS, and retrospective cohort study, but also in other case series were integrated.

<Review of observational studies>

The literature concerning the effectiveness of sclerotherapy for head and neck LM in infancy was reviewed from the viewpoints of responses (prognosis (survival rate or mortality), size, symptoms, and cosmetic improvement) and complications.

Sclerosing agents used as keywords for the present literature search varied widely and included OK-432, bleomycin, ethanol, doxycycline, STS and fibrin glue. No paper evaluated differences in effectiveness of various agents due to their methods of administrations for lesions around the neck affecting airway. Therefore, differences among agents were excluded from the evaluation of this CQ.

This article has been co-published with the permission of *The Journal of Dermatology, Pediatrics International and Japanese Journal of Radiology*. All rights reserved. © 2020 The Authors. The articles are identical except for minor stylistic and spelling differences in keeping with each journal's style. Either citation can be used when citing this article.

Results of review

1. Responses

A. Prognosis (survival rate or mortality)

According to the SR by Adams *et al.*,[360] the mortality was 4.7% in 277 cases with head and neck LM. Since lesions around the airway were not the only target, and since sclerotherapy was not the only treatment modality, the paper has not quite rightly answered to the CQ. However, since patients who died were all before one year of age and their causes of death are considered to have been mostly airway problems, such as airway obstruction and aspiration due to vocal cord paralysis in 8, and as at least 1 patient is judged to have died due to complications of invasive treatment, the paper is considered to indicate the risk of this disorder during infancy.

B. Size

Many of the papers that referred to the size regression evaluated it by four categories; (1) excellent or complete (≥90% regression), (2) good or substantial (≥50% and <90% regression), (3) fair or intermediate (≥20% and <50% regression), (4) and poor or none (≤20% regression).

Ravindranathan *et al.*[306] treated 5 patients (aged 4–19 months) with cervicofacial LM by sclerotherapy using OK-432 (in addition to Fibrovein® (STD Pharmaceutical Products Ltd, Hereford, UK) in 2) and reported that the responses were good in 1 (20%) (cystic), partial in 1 (20%) (cavernous), and poor in 3 (60%) (2 with cavernous lesions that required tracheotomy and 1 with cystic lesions in whom the condition improved to good after surgical resection). However, they did not mention the evaluation criteria for good, partial, and poor.

According to the report of 8 cases with head and neck LM by Leung *et al.*,[361] all patients underwent sclerotherapy, ≥50% regression was observed in all patients with complete regression in 2. However, the patient age varied from 2 months to 11 years, and the types of LM were not mentioned.

Ogawa *et al.*[362] reported 9 patients (including 5 preschoolers and toddlers, 2 school children, and 2 adults) who underwent OK-432 sclerotherapy for the neck LM and evaluated it to be markedly effective in 8, in whom the lesions mostly disappeared, and effective in 1, who showed a ≥50% regression. Eight patients in whom the treatment was markedly effective consisted of 1 with mixed and 7 with cystic lesions, and the one in whom the treatment was effective had a mixed type.

Cahill *et al.*[315] reported doxycycline sclerotherapy in 17 patients with head and neck LM (cystic in 10, mixed in 7 (3 required tracheotomy)), and its size regression was reported to be >90% in 7 (41.2%) (cystic in 6, mixed in 1), 75–89% in 4 (23.5%) (cystic in 2, mixed in 2), 51–74% in 4 (23.5%) (cystic in 1, mixed in 3), and 25–50% in 2 (11.8%) (mixed in 2).

Nehra *et al.*[311] reported doxycycline sclerotherapy in 11 patients with head and neck LM (cystic in 7, mixed in 4; aged 2 days-21 months) (later combined with surgical resection in 3). The treatment results were excellent in 5 (45.5% of all patients) and satisfactory in 2 (18.2% of all patients) among 7 patients with cystic lesions but poor in all 4 patients with mixed type lesions (36.4% of all patients). Particularly, 3 of the 4 patients with mixed type lesions required tracheal intubation shortly after birth and underwent sclerotherapy while intubated, but the effects were poor in all of them. Surgical resection was added in 1 and was under consideration in another.

C. Symptoms

According to Ravindranathan *et al.*[306] who reported 5 patients with cervicofacial LM (aged 4–19 months) treated with sclerotherapy using OK-432 (in addition to fibrovein in 2), 4 exhibited symptoms of airway obstruction before treatment. Symptoms included dysphagia in 2 and dyspnea (including croup-like symptoms) in 4 (some both). Symptoms were alleviated by sclerotherapy in 2 out of 4 (cystic 1, cavernous 1), but tracheotomy was necessary in the remaining 2 (cavernous in both) without improvement.

In the report of 8 patients with head and neck LM and 5 patients with VM (aged 2 months-11 years) by Leung *et al.*,[361] their symptoms noted before treatment were mass or swelling (10 patients (77%)), pain after hemorrhage (2 patients (15%)), skin discoloration (blue) (1 patient (8%)), obstructive airway symptoms (6 patients (46%)), and swallowing difficulty (1 patient, (8%)). All symptoms were alleviated by sclerotherapy (doxycycline for LM, STS foam for VM).

Arimoto *et al.*[363] reported a patient with cystic LM in the neck presented 3 months after birth. The patient presented with respiratory distress at the age of 10 months due to enlargement of the LM following upper respiratory infection. While left vocal cord fixation due to the mass was confirmed by ultrasonography before treatment, aspiration of the cyst and steroid administration resulted in opening of the glottic area and regression of the mass with relief of wheezing and distress. Since they underwent sclerotherapy 2 months after the disappearance of symptoms, aspiration of internal fluid and steroid administration rather than sclerotherapy were directly effective for the alleviation of symptoms.

Kitagawa *et al.*[364] reported a patient with giant LM of the neck which had been prenatally diagnosed and was treated under ex utero intrapartum treatment (EXIT) by tracheal intubation after aspiration of the cyst. The lesion was reported to be refractive to subsequent sclerotherapy and tracheotomy was eventually needed.

Nehra *et al.*[311] reported that, among 11 patients with head and neck LM (cystic type in 7 and mixed type of cystic + cavernous in 4; aged 2 days-21 months), 3 out of 4 with mixed LM presented respiratory distress soon after birth and were managed by intubation, but that all were extubated after sclerotherapy using doxycycline (1–3 times, median: 1.6 times).

D. Cosmetic improvements

No paper has reported cosmetic results in detail. Only sporadically they mentioned about surgery for redundant skin after regression of cystic lesions by sclerotherapy.

2. Complications

Complications associated with treatment for LM around the airway have been reported in many papers. They include

This article has been co-published with the permission of *The Journal of Dermatology, Pediatrics International and Japanese Journal of Radiology*. All rights reserved. © 2020 The Authors. The articles are identical except for minor stylistic and spelling differences in keeping with each journal's style. Either citation can be used when citing this article.

temporary conditions caused by sclerotherapy such as fever,[292,303,312,362,365–371] local swelling[303,312,365,367,368,370,371] pain,[288,312,362,367,370–372] hemorrhage into the cyst,[288,303,312,368] and infection.[288,292,303,310,312,360,365,372] There also reported complications as the effects of treatment for head and neck lesions such as respiratory distress due to airway obstruction,[292,303,306,312,362,365,366] as well as nerve palsy.[288,292,312,360,365]

According to a systematic review about head and neck LM by Adams *et al.*,[360] both nerve damage due to sclerotherapy and post-therapeutic infection were reported in 1 (0.8%) out of 123 patients. Since nerve damage and infection after surgery were observed in 12 (10.2%) and 7 (5.9%) out of 118 patients, respectively, the complication rate would be lower by sclerotherapy than by surgery.

Ogawa *et al.*[362] reported a 1-year-and-5-month-old patient who developed airway edema after OK-432 sclerotherapy for the cystic neck LM and necessitated tracheal intubation for 3 days and cautioned against sclerotherapy for LM around the airway in young children (particularly, those less than 2 years old).

Kudo *et al.*[369] also reported 2 patients aged 11 months and 1 year and 11 months who were treated with OK-432 sclerotherapy intubated in advance for fear of airway obstruction due to post-therapeutic swelling. Tomemori *et al.*[373] also cautioned against sclerotherapy for LM in children aged less than 2 years as in the report by Ogawa *et al.*[362]

On the other hand, Kudo *et al.*[369] reported 2 cases whose neck LM having been enlarged rapidly after suffering from measles or upper respiratory tract infection (URTI). Arimoto *et al.*[363] also reported a patient with cystic LM of the neck 3 months after birth, who developed dyspnea due to enlargement of the lesion after URTI at 10 months and was about to be intubated.

Regarding complications due to sclerosing agents, Cahill *et al.*[315] reported those by doxycycline, STS and absolute ethanol. They reported delayed complications, such as Horner's syndrome, transient left lip weakness, right facial nerve palsy, and transient left hemidiaphragm paralysis, in addition to peri-procedural complications such as hemolytic anemia after doxycycline injection in 2 patients, hypoglycemic and metabolic acidosis in 3 neonates, transient hypotension during absolute alcohol instillation and self-limiting skin excoriation secondary to peri-catheter leakage of doxycycline. Other reported complications include permanent vocal cord paralysis after local ethanol injection,[374] serious complications after OK-432 injection such as death due to pulmonary embolism,[375] deaths due to pulmonary complications after treatment using bleomycin[376,377] and leukocytopenia due to bleomycin.[368]

Limitations

There are few papers that solely analyzed LM around the cervical airway. Most papers included lesions involving not only the neck but also the craniofacial and other parts of the body and reported LM with different properties such as cystic and mixed types. In addition, definition of cavernous lesions and methods of sclerotherapy (injection techniques, number of injections) were not similar among papers, and differences in these backgrounds must be taken into consideration to evaluate the effectiveness of sclerotherapy.

<Summary>

The CQ, "Should sclerotherapy be performed in infancy for a patient with head and neck LM affecting the airway?", was evaluated from the viewpoints of responses (prognosis (survival rate or mortality), decrease in size, symptoms, cosmetic improvements) and complications. Since there have been some reports on the risk of respiratory distress due to LM around the airway in infants, and therapeutic intervention is necessary even in infants when the risk is high or they have already developed symptoms. Such intervention is made by sclerotherapy or surgery, and as surgical resection is associated with the risk of more serious complications than sclerotherapy, intervention by less invasive sclerotherapy is recommended. Sclerotherapy is considered to be very effective because of high regression rate of the lesion and symptom/function-improving effect. However, its effect varies depending on the disease type, somewhat less effective in the cavernous and mixed types than in the cystic type. Furthermore, when it was performed for the lesions around the airway, it may be associated with the risk of exacerbation of airway obstruction symptoms due to reactive enlargement of the lesion. Thus, we formulated the recommendation, "In LM around the airway, there is the risk of respiratory disturbances from infancy, but airway obstruction is likely to be exacerbated by sclerotherapy. Particularly, when the risk of airway obstruction is judged to be high or when symptoms have appeared, it is proposed to perform sclerotherapy with sufficient preparations including securing the airway."

CQ31: Is surgical resection effective for LM of the tongue?

Recommendation: Surgical resection is effective for reducing the size of the lesion and alleviating symptoms and functional impairment. However, total resection is often difficult, and careful decision is required in consideration of the possibility of complications and recurrence.

Strength of recommendation: 2 (weak)

Evidence: D (very weak)

Comments

[Process of preparation of recommendation]

While the tongue is one of the frequent sites of LM, the lesion is often distributed widely over the neck rather than is localized in the tongue. LM of the tongue not only cause cosmetic problems, such as protrusion from the mouth and bleeding, but also readily occupy the oropharyngeal cavity and cause functional problems such as disorder of mouth closing, difficulty in speaking, respiratory disturbances, and impairment of oral food intake. These conditions are treated at departments including plastic surgery, oral surgery,

This article has been co-published with the permission of *The Journal of Dermatology, Pediatrics International and Japanese Journal of Radiology*. All rights reserved. © 2020 The Authors. The articles are identical except for minor stylistic and spelling differences in keeping with each journal's style. Either citation can be used when citing this article.

otorhinolaryngology, and pediatric surgery. LM of the tongue are treated by surgical resection or sclerotherapy, but comprehensive evaluation of the condition of individual cases including the distribution of the lesion in the tongue, involvement of other areas and cyst components, and vascular distribution in addition to general information, such as the risk of complications and recurrence in each treatment, is necessary.

Therefore, the CQ, "Is surgical resection effective for LM of the tongue?" was formulated, and the present knowledge about the effectiveness of surgical resection of the lesion, particularly, by partial glossectomy was summarized.

<Literature search and screening>

As a result of search, 29 papers in Japanese and 76 papers in English (75 from PubMed, 1 from Cochrane) were subjected to primary screening. Of these papers, 2 in Japanese and 10 in English were subjected to secondary screening concerning this CQ. They included 1 retrospective cohort study, but most other papers were case series or case reports. Consequently, in the evaluation of this CQ, the results and discussion of the cohort study and each case series were integrated.

<Review of observational studies (case series)>

The effectiveness of surgical resection of LM of the tongue was evaluated from the viewpoints of resectability of the lesion, symptoms, function, and cosmetic improvements as elements of responses as well as complications and recurrence.

Results of review

1. Responses

A. Resectability of the lesion

Twenty-four cases of tongue lesions treated by surgical resection alone were reported in 4 papers. Catalfamo *et al.*[378] performed surgical resection of localized masses including normal structures with a margin of 1 cm in the horizontal direction and reported that the size of tongue lesions was reduced in 8 (88.9%) of the 9 patients.

Concerning large lesions impossible to resect totally, Boardman *et al.*[358] reported 13 cases of partial surgical resection, but several operations were often necessary to reduce lesion size. A total of 2 case have been reported,[379,380] and the lesion size was reduced in both. Although differences were observed in re-enlargement after surgery, they are discussed in detail in "(2) Complications".

In 1 case report, sclerotherapy was performed 15 times, but the lesion size could not be reduced, and surgical resection was performed, eventually resulting in a favorable outcome without recurrence.[381]

According to a report of 89 cases of head and neck LM by Lei *et al.*,[291] the outcome was excellent in 73 (82%) and good in 16 (18%) although it was not a report of cases of tongue lesions alone. They included 43 cases of tongue lesions.

In addition, a few papers[382–385] that suggested the effectiveness of combinations of surgical resection with sclerotherapy and laser therapy were observed. Wiegand *et al.*[383] classified the disease into 4 stages according to the area of involvement and reported that the stage can be a prognostic factor. Surgery was effective, and complications were rare, when the lesion was localized in the superficial layer and part of the muscle layer. Surgical resection can also be effective, but complete resection is difficult, when the lesion extends over the entire muscle layer or to the tongue base and neck. Therefore, partial resection is often repeated and combined with laser therapy and sclerotherapy, but the recurrence is observed very frequently, and the results did not contradict the reports mentioned below in the section of the recurrence rate.[291,358]

B. Symptoms

A wide variety of symptoms have been reported depending on the site of the mass, and they include tongue discomfort, bleeding, pain, and difficulty in oral feeding.[386] Roy *et al.*[387] reported that bleeding from the tongue surface, pain, and eating difficulty were alleviated by cauterization.

C. Functions

In most patients who exhibited functional impairment, the lesions were so extended that they were no longer indications for one-time surgical resection. Large masses located at sites such as the tongue base cause respiratory disturbances, swallowing disorders, and difficulty in speech. According to the report by Azizkhan *et al.*,[385] oral intake of normally cooked food became possible in 14, and normal vocalization became possible in 8, of the 21 patients with tongue base lesions. In addition, 5 of the 17 patients who needed tracheotomy were weaned.

D. Cosmetic improvements

Objective evaluation of cosmetic effects is also difficult.

Azizkhan *et al.*[385] reported that, of the 20 patients, excluding 1 with severe deformity who died, deformity of structures around the tongue, such as the mandible and maxilla, was mild in 6, moderate in 5, and severe in 9. There have been a few reports that cosmetic improvements were also observed in patients who showed a reduction of the tongue size by surgical resection, but objective evaluation is insufficient.

2. Complications

Although the properties of the lesions are unclear in some papers, facial nerve paralysis, vagus nerve paralysis, infection, hematoma, seroma, salivary leakage, ruptured suture, and skin flap necrosis have been reported as complications of the facial region. There have also been reports of temporary complications such as pain and hemorrhage.

3. Recurrence

There have been a few postoperative evaluations reporting that no reactivation that clinically required treatment was observed. Lei *et al.*[291] reported greater details: Recurrence was observed in 21 (23.6%) of 89 patients and was more frequent in those aged less than 1 year, those with lesions in the oral cavity/face, those with lesions at 3 or more sites, and those with microcystic lesions. According to Boardman

This article has been co-published with the permission of *The Journal of Dermatology, Pediatrics International and Japanese Journal of Radiology*. All rights reserved. © 2020 The Authors. The articles are identical except for minor stylistic and spelling differences in keeping with each journal's style. Either citation can be used when citing this article.

et al.,[358] LM of the tongue recurred in 12 (48%) of 28 patients, more often than other head and neck lesions. As factors related to this more frequent recurrence of lingual LM, more frequent involvement of other regions, such as the floor of mouth, and a high percentage of microcystic lesions (70%) have been suggested. Of the 2 patients treated by surgical resection alone, 1 who underwent resection of the middle part of the tongue showed no re-enlargement for 1 year or longer after surgery,[379] but surgery was repeated 3 times in the 1 who underwent marginal resection.[380] This patient who underwent repeated resections also showed no re-enlargement although the time of the last resection is unclear.

Limitations

In some papers, surgical resection was combined with other treatments,[381–385,387] lesions in other areas such as the neck were included,[291] and the lesion types were unknown. The lack of standardization of subjects and uniformity of the definition or time of recurrence must be considered in the evaluation of the effectiveness of surgical resection.

<Summary>

Many papers suggest that surgical resection is effective for reducing the size of lingual LM. However, in patients with large lesions, lesions extending to structures other than the tongue, and microcystic lesions, several resections or combination of resection with other treatments such as sclerotherapy and laser therapy were necessary, and the recurrence rate tended to be higher. While a few papers referred to symptoms, functional outcome, and cosmetic improvements, none showed a high level of evidence, and the evidence was insufficient for general discussion of the effectiveness of surgical resection.

Therefore, concerning the effectiveness of surgical resection for LM of the tongue, "Surgical resection is effective for reducing the size of the lesion and alleviating symptoms and functional impairment. However, total resection is often difficult depending on the distribution of the lesion, and careful decision is required in consideration of the possibility of complications and recurrence." was proposed as a draft recommendation.

CQ32: Is aggressive surgical intervention effective for chylous pleural effusion in the neonatal period?

Recommendation: For chylous pleural effusion refractory to conservative treatments, surgical procedures, such as pleurodesis, ligation of the thoracic duct, and pleuroperitoneal shunting, may be effective.

Strength of recommendation: 2 (weak)

Evidence: D (very weak)

Comments

[Process of determining recommendation]

Primary chylous pleural effusion during the neonatal period is often refractory and can be fatal. Thoracic drainage is performed for respiratory insufficiency due to accumulation of pleural effusion, followed by conservative treatments, such as nutritional therapy, steroid, and octreotide therapy, conducted primarily by neonatologist until resolution of chylous pleural effusion.

In refractory cases that do not respond to these conservative therapies, surgical intervention, such as ligation of the thoracic duct and pleurodesis, may be performed. However, no sufficient consensus has been obtained concerning their effects. To evaluate problems, such as at what point surgical intervention should be made and whether aggressive surgical intervention is effective for such a condition, the CQ, "Is aggressive surgical intervention effective for chylous pleural effusion in the neonatal period?", was formulated, and the knowledge available at present was summarized.

<Literature search and screening>

As a result of search, 98 papers in Japanese and 264 papers in English (262 from PubMed, 2 from Cochrane) were subjected to primary screening. Of these papers, 8 in Japanese and 9 in English were subjected to secondary screening concerning this CQ. They included none with a high level of evidence, such as a systematic review or RCT that evaluated surgical treatment, and all papers were case series or case reports. Consequently, the results and discussion in each of the case series judged to be useful for the preparation of the draft recommendation were integrated although they were weak as the evidence for the evaluation of this CQ.

<Review of observational studies (case series)>

The literature concerning the effectiveness of surgical treatment for chylous pleural effusion in the neonatal period was reviewed from the viewpoints of responses and complications.

Results of review

1. Responses

Surgical treatment for neonatal chylothorax is performed in patients who respond insufficiently even to thoracic drainage in addition to nutritional therapy using MCT milk or total parenteral nutrition or drug treatment such as octreotide administration.

The methods for surgical intervention found by the present literature review included ligation of the thoracic duct and pleuroperitoneal shunting as well as pleurodesis with OK-432 administration, intrathoracic infusion of fibrin, and povidone-iodine administration, and some patients diagnosed in utero underwent pleuro-amniotic shunting. Cases in which mildly invasive treatments, such as thoracoscopic ligation of the thoracic duct and intrathoracic fibrin application, have been reported in addition to those who underwent thoracic duct ligation by thoracotomy.

Treatments that were performed before surgery and their periods were not uniform. In addition, since there are cases that developed chylous pleural effusion after surgery and those of congenital chylothorax, the diversity of the patient background must be taken into consideration in the efficacy evaluation.

Among the surgically treated cases, those in whom chylous plural effusion disappeared, respiratory symptoms were

This article has been co-published with the permission of *The Journal of Dermatology, Pediatrics International and Japanese Journal of Radiology*. All rights reserved. © 2020 The Authors. The articles are identical except for minor stylistic and spelling differences in keeping with each journal's style. Either citation can be used when citing this article.

alleviated, and weaning from the respirator became possible have been reported.[388,389] In addition, the absence of recurrence or reactivation is considered to be a point.[388–391] There were reports that chylous pleural effusion after thoracic surgery was resolved by drainage alone. Cleveland *et al*.[392] considered conservative treatments, such as total parenteral nutrition, octreotide, and diuretic administration, to be the best and, observing that, of the poor responders, the mortality was 80% in 5 who continued to be managed by conservative treatments but 0% in 4 who underwent additional surgery, reported that surgical treatment contributed to the reduction of the mortality. According to the guidelines for the treatment of chylous thoracic effusion by Buttiker *et al*.,[393] conservative treatment should be continuing for about 3 weeks but should be abandoned thereafter because of the risk of nutritional disturbance, increased susceptibility to infection, and liver disorders. However, Kaji *et al*.[394] reported that it is difficult to set a clear period of conservative therapy, because the effectiveness and success rate of surgical treatment are unclear.

2. Complications

As complications due to sclerosing agents, fever and increased inflammatory reaction due to the administration of OK-432 as well as pulmonary abscess and temporary flaccidity and protrusion of the upper abdominal region considered to have been due to intercostal nerve damage have been reported. While chyle leakage in the abdominal cavity was noted in a patient who underwent pleuroperitoneal shunting, there were no reports of fatal complications.

Limitations

Surgical treatment was performed in most reported cases when responses to conservative therapy were not obtained. Therefore, it must be assumed that the results of evaluation of this CQ are based on data concerning the effectiveness of surgery performed with conservative therapy.

<Summary>

The literature was reviewed concerning the effectiveness of aggressive surgical intervention for neonatal chylous thoracic effusion from the viewpoints of responses and complications, but no objective study with a high level of evidence was found. In most reported cases, surgical treatment was performed when responses to conservative treatments were poor. Therefore, it is difficult to compare surgery with other therapies, and the evaluation of the period of conservative treatment before surgery remains insufficient. However, there was a paper that proposed surgical intervention after attempting conservative treatments for 3 weeks as a standard.

Thus, surgical intervention for neonatal chylous pleural effusion is characterized at present as an approach that may be effective but should be evaluated when the condition is not improved by other treatments, and "Surgical procedures, such as pleurodesis, ligation of the thoracic duct, and pleuroperitoneal shunting, may be effective for chylous pleural effusion refractory to conservative treatments." is proposed as a draft recommendation.

CQ33: What treatments are effective for refractory chylous pleural, and pericardial effusion and respiratory disturbances of the patients with generalized lymphatic anomaly (GLA) and Gorham-Stout disease (GSD)?

Recommendation: While treatments including surgery, sclerotherapy, radiotherapy, nutritional therapy, and drug therapy are conducted, there is presently no effective treatment with a high level of evidence. Treatments should be selected in consideration of complications and adverse effects according to individual symptoms.

Strength of recommendation: 2 (weak)

Evidence: D (very weak)

Comments

[Process of preparation of recommendation]

GLA and GSD are refractory diseases that cause a wide variety of symptoms in the entire body and are difficult to diagnose and treat. The investigation by the Health and Labour Sciences Research group (Ozeki group) carried out by 2013 showed that the mortality is particularly high when the patients had thoracic lesions.

Among the thoracic symptoms, chylous pleural effusion/pericardial effusion are often refractory and occasionally fatal. While information about the disease is extremely limited because of its rareness, case reports are being globally accumulated as chronic cases are managed on an outpatient basis, and as severe cases are treated intensively.

Presently, no radical treatment for these refractory diseases is known, but the CQ, "What treatments are effective for refractory chylous pleural, and pericardial effusion and respiratory disturbances of the patients with GLA and GSD?" was formulated to compile the knowledge about what treatments are effective as it is a problem of clinical importance.

<Literature search and screening>

As a result of search, 208 papers in Japanese and 617 papers in English (598 from PubMed, 19 from Cochrane) were subjected to primary screening. Of these papers, 2 in Japanese and 25 in English were subjected to secondary screening concerning CQ 37. They included no studies with a high level of evidence, such as a systematic review and RCT, and all were reports of 1–2 cases. Therefore, the evaluation of this CQ was performed by integrating the results and discussion in case series judged to be useful for the preparation of the draft recommendation despite the lack of evidence.

<Review of observational studies (case series)>

The effectiveness of various treatments for refractory GLA and GSD was evaluated according to the prognosis and the presence or absence of improvement in imaging findings, improvement in symptoms, improvement in airway obstruction, enlargement of the lesion, regression, treatment-related complications, recurrence, and reactivation.

Conditions of patients

This article has been co-published with the permission of *The Journal of Dermatology, Pediatrics International and Japanese Journal of Radiology*. All rights reserved. © 2020 The Authors. The articles are identical except for minor stylistic and spelling differences in keeping with each journal's style. Either citation can be used when citing this article.

The cause of chylous pleural and pericardial effusion is lymphorrhea from lymphatic vessel tissue lesions that have primarily invaded the mediastinum and pleura, and lymphorrhea from osteolytic lesions of the ribs and vertebrae was also observed. Respiratory disturbances were caused by pleural effusion, chylous pleural effusion, pericardial effusion, and direct invasion of the mediastinum and lungs.

Results of review

As surgical treatments for chylous pleural effusion, procedures, such as thoracentesis, thoracic drainage, ligation of the thoracic duct, and pleural decortication, have been performed, and local lesions were surgically resected. In most cases, thoracentesis and thoracic drainage were performed, but chyle leakage was not resolved. As for complications, there were patients who developed hypovolemic shock and required blood transfusion and catecholamine administration or supplementation of albumin, immunoglobulin, and clotting factors.[395–397] While chylous pleural effusion was controlled in some patients who underwent ligation of the thoracic duct,[397–408] the treatment was performed in combination with other surgical procedure or radiotherapy in all cases.[400,402,408] There was 1 case that showed improvement in respiratory disturbance.[406] As complications of ligation of the thoracic duct, splenomegaly and lymphorrhea[405] and left-sided pleural effusion[397,405] have been reported. In the patients who showed marked improvements in chylous pleural effusion[395,405,408] after pleural decortication,[395,396,401,403–405,408,409] the procedure was performed in combination with other surgical treatments or sclerotherapy, and there was no mention about complications. There were cases that showed marked improvements in chylous pleural effusion[396,400,405,408] among those who underwent surgical resection of local lesions including splenectomy,[396,397,400,405,408,410–412] but the procedure was performed in combination with other surgical treatments in most of them. Hemorrhage was reported as a complication.[410] Among other treatments, pleuroperitoneal shunting[403] and lung transplantation[413] were performed, and alleviation of respiratory disturbance was noted in the patient who underwent lung transplantation.

As a surgical treatment for pericardial effusion, pericardiocentesis was performed,[396,414–416] and pericardial fenestration was performed when pericardial effusion could not be controlled by pericardiocentesis.[396,416] There was no mention about complications.

As sclerotherapy, pleurodesis was performed using OK-432, talc, and minocycline.[395,397–399,404,408,411,416–418] There were patients who responded markedly to sclerotherapy alone and sclerotherapy combined with surgical procedures such as pleural decortication or local radiotherapy. There was no mention about complications of sclerotherapy.

There have also been reports[399,400,402–404,410–412,415,416,418–420] on local (e.g., lesion area, thoracic duct region) and thoracic radiotherapy for chylous pleural effusion and local lesions, and marked responses of chylous pleural effusion and responses of respiratory symptoms were noted, but other treatments were performed concomitantly in some patients. Radiation pneumonitis has been reported as a complication.[416]

Concerning nutritional therapy, fasting, high-calorie infusion, and MCT diet have been performed alone or in combinations, but few cases that showed alleviation of chylous pleural effusion were observed.[395,396,398–400,403,405,408,421]

For drug therapy against chylous pleural effusion, drugs including interferon α, propranolol, anticancer agents (e.g., vincristine), bisphosphonate, octreotide, steroid, sirolimus, and low-molecular-weight heparin were used. Interferon α was used most frequently,[395–398,400,401,403,415,421] and marked improvement in chylothorax was reported in 5 cases. Of these cases, interferon α was used with propranolol in 1[395] and with low-molecular-weight heparin and local radiotherapy (15 Gy) in 1.[400] As for complications of drug therapy using interferon α, there were reports of fever, nausea, and headache[421] and thrombocytopenia and hepatic toxicity.[397] There was no report of improvement in chylous pleural effusion by the use of steroid[395,399,403,415] or octreotide[395,397,398,400,403,405] alone. Concerning other drug therapies, only a few cases have been reported with no improvement in chylous pleural effusion. One case that showed regression of mediastinal invasion of GLA and alleviation of respiratory disturbance by sirolimus treatment has been reported,[414] and hypertension was noted as a complication. In drug therapy for pericardial effusion, diuretics were used for conservative therapy.[400]

Limitations

Although cases that responded to various therapies have been reported, treatments are often performed in combinations, and the evaluation of the effectiveness of each treatment alone is difficult at this point.

<Summary>

Treatments effective for GLA and GSD presenting with refractory chylous pleural effusion, pericardial effusion, and respiratory disturbances were evaluated by a review of the literature, which was primarily case reports. Various treatments, such as surgery, sclerotherapy, radiotherapy, nutritional therapy, and drug therapy, have been performed, but, there was no study with a sufficient number of cases and a high level of evidence because of the rareness of the disease and diversity of symptoms. Although cases that responded to various treatments have been reported, treatments are frequently performed in combinations, and the evaluation of the effectiveness of individual therapies is difficult at present. Sirolimus (a mTOR inhibitor) is considered promising as a drug for this disease, and some clinical trials are currently under way in Japan and abroad.

In clinical situations, these diseases are not recognized as indications of various drug therapies by the Japanese health insurance system, and the therapeutic effects of other treatments are also uncertain. Therefore, the above treatments cannot be recommended, but we propose that treatments "should be selected in consideration of complications and adverse effects according to individual symptoms." It is necessary to evaluate the invasiveness, complications, and adverse effects, and select the treatments judged to be appropriate for each case.

This article has been co-published with the permission of *The Journal of Dermatology, Pediatrics International and Japanese Journal of Radiology*. All rights reserved. © 2020 The Authors. The articles are identical except for minor stylistic and spelling differences in keeping with each journal's style. Either citation can be used when citing this article.

Conclusion

The practice guidelines for vascular anomalies have been prepared as the evidence-based guidelines for the management of vascular anomalies.

Acknowledgement

We thank all members of the systematic review team as follows. Tomoko Izaki, Ryohei Ishiura, Yohei Iwata, Tatsuo Ueda, Naoki Okura, Sachiyo Osawa, Jun Otaka, Kuniaki Ohara, Shinya Ogishima, Takuro Kazama, Motoi Kato, Takahide Kaneko, Motohiro Kano, Tamihiro Kawakami, Tatsuki Kono, Eisuke Shibata, Yohsuke Suyama, Kazuhiro Takahashi, Yuichi Takama, Takaya Takeguchi, Kensuke Tashiro, Masashi Tamura, Atsushi Tamura, Masato Tsuchiya, Kyoichi Deie, Toshihide Tokuda, Asami Tozawa, Fumio Nagai, Michiko Nagahama, Yasuhiro Nakamura, Akifumi Nozawa, Naoki Hashizume, Takuya Hara, Koji Higuchi, Masahito Hibi, Takaya Fukumoto, Shinji Fujizuka, Megumi Furuya, Seiji Houbara, Kyoko Hoshino, Tomohiro Hori, Takanobu Maekawa, Junko Miyata, Kenji Murakami, Kiichiro Yaguchi, Daisuke Yasui, Kentaro Yamada, Yohei Yamada, Yuki Yamamoto, and Azusa Watanabe.

Conflict of interest

Conflict of interest of the guidelines preparation organization was managed by the Guidelines Executive Committee. The following corporations were disclosed by self-declaration of the Guidelines Committee members in the 3 year-period before 1 April 2017. Japan Pharmaceuticals and Medical Devices Agency (PMDA), Mitsubishi Foundation, Rohto Pharmaceutical Co., Ltd., Mitsubishi Tanabe Pharma Corporation, and Shionogi & Co., Ltd.

Funding

The funding for preparation of the Japanese Clinical Practice Guidelines for Vascular Anomalies 2017 was from Health, Labour and Welfare Sciences Research Grants (Research on Policy Planning and Evaluation for Rare and Intractable Diseases) provided to 'Japanese Research Committees for Intractable Vascular Anomalies' (main funding source), 'Japanese Study Group for Intractable Diseases of Pediatric Gastrointestinal Tract', and 'Japanese Research Committees for Survey and Establishment of Guidelines for Pediatric Respiratory Dysplastic/hypoplastic Disease'. No financial support was received from any other organization or corporation.

References

1 *ISSVA Classification of Vascular Anomalies ©2014 International Society for the Study of Vascular Anomalies*. [Cited 2014 April.] Available from URL: issva.org/classification

2 Wassef M, Blei F, Adams D *et al*. Vascular anomalies classification: recommendations from the International Society for the Study of Vascular Anomalies. *Pediatrics* 2015; **136**: e203–14.

3 [Clinical practice guidelines for vascular anomalies 2013]. *The Research Committee of Intractable Vascular Anomalies, Research on Measures for Intractable Diseases, Health, Labour and Welfare Sciences Research Grants, the Ministry of Health, Labour and Welfare, Japan*. [Cited 2013 March 29.] Available from URL: http://www.marianna-u.ac.jp/va/files/vascular%20anomalies%20practice%20guideline%202013.pdf. Japanese.

4 Fukui T, Yamaguchi N (editorial supervisors), Morizane T, Yoshida M, Kojimahara N (eds). *Minds Handbook for Clinical Practice Guideline Development 2014*. Ver 1.0. Tokyo: Minds Guideline Center, Japan Council for Quality Health Care. [Cited 2015 February 1.] Available from URL: http://minds4.jcqhc.or.jp/minds/guideline/pdf/MindsHB2014.pdf

5 Morizane T, Yoshida M (eds). *[Minds Manual for Guideline Development Ver. 1.0]*. Tokyo: Japan Council for Quality Health Care, [Cited 2014 March 31]. Japanese.

6 Kojimahara N, Nakayama T, Morizane T, Yamaguchi N, Yoshida M (eds). *[Minds Manual for Guideline Development Ver. 2.0]*. Tokyo: Japan Council for Quality Health Care, [Cited 2016 March 15]. Available from URL: http://minds4.jcqhc.or.jp/minds/guideline/pdf/manual_all_2.0.pdf. Japanese.

7 Balshem H, Helfand M, Schunemann HJ *et al*. GRADE guidelines: 3. Rating the quality of evidence. *J. Clin. Epidemiol.* 2011; **64**: 401–6.

8 Andrews J, Guyatt G, Oxman AD *et al*. GRADE guidelines: 14. Going from evidence to recommendations: the significance and presentation of recommendations. *J. Clin. Epidemiol.* 2013; **66**: 719–25.

9 Liu AS, Mulliken JB, Zurakowski D, Fishman SJ, Greene AK. Extracranial arteriovenous malformations: natural progression and recurrence after treatment. *Plast. Reconstr. Surg.* 2010; **125**: 1185–94.

10 Kohout MP, Hansen M, Pribaz JJ, Mulliken JB. Arteriovenous malformations of the head and neck: natural history and management. *Plast. Reconstr. Surg.* 1998; **102**: 643–54.

11 Richter GT, Suen J, North PE, James CA, Waner M, Buckmiller LM. Arteriovenous malformations of the tongue: a spectrum of disease. *Laryngoscope* 2007; **117**: 328–35.

12 Hyun D, Do YS, Park KB *et al*. Ethanol embolotherapy of foot arteriovenous malformations. *J. Vasc. Surg.* 2013; **58**: 1619–26.

13 Park KB, Do YS, Kim DI *et al*. Predictive factors for response of peripheral arteriovenous malformations to embolization therapy: analysis of clinical data and imaging findings. *J. Vasc. Interv. Radiol.* 2012; **23**: 1478–86.

14 Wu JK, Bisdorff A, Gelbert F, Enjolras O, Burrows PE, Mulliken JB. Auricular arteriovenous malformation: evaluation, management, and outcome. *Plast. Reconstr. Surg.* 2005; **115**: 985–95.

15 DesPrez JD, Kiehn CL, Vlastou C, Bonstelle C. Congenital arteriovenous malformation of the head and neck. *Am. J. Surg.* 1978; **136**: 424–9.

16 Dompmartin A, Labbé D, Barrellier MT, Théron J. Use of a regulating flap in the treatment of a large arteriovenous malformation of the scalp. *Br. J. Plast. Surg.* 1998; **51**: 561–3.

17 Yamamoto Y, Ohura T, Minakawa H *et al*. Experience with arteriovenous malformations treated with flap coverage. *Plast. Reconstr. Surg.* 1994; **94**: 476–82.

This article has been co-published with the permission of *The Journal of Dermatology, Pediatrics International and Japanese Journal of Radiology*. All rights reserved. © 2020 The Authors. The articles are identical except for minor stylistic and spelling differences in keeping with each journal's style. Either citation can be used when citing this article.

18 Hartzell LD, Stack BC Jr, Yuen J, Vural E, Suen JY. Free tissue reconstruction following excision of head and neck arteriovenous malformations. *Arch. Facial Plast. Surg.* 2009; **11**: 171–7.
19 Visser A, FitzJohn T, Tan ST. Surgical management of arteriovenous malformation. *J. Plast. Reconstr. Aesthet. Surg.* 2011; **64**: 283–91.
20 Hong JP, Choi JW, Chang H, Lee TJ. Reconstruction of the face after resection of arteriovenous malformations using anterolateral thigh perforator flap. *J. Craniofac. Surg.* 2005; **16**: 851–5.
21 Koshima I, Takahashi Y, Namba Y *et al*. Treatment for arteriovenous malformation. *Keisei Geka* 2001; **44**: 665–73. Japanese.
22 Toh S, Tsubo K, Arai H, Harata S. Vascularized free flaps for reconstruction after resection of congenital arteriovenous malformations of the hand. *J. Reconstr. Microsurg.* 2000; **16**: 511–7.
23 Yokoo K, Nishihori K, Kono A, Ishiguchi T, Ohta T. [Surgical treatment of arteriovenous malformations in the head and neck combined with antecedent embolization]. *Keisei Geka* 2009; **52**: 1201–8. Japanese.
24 Koshima I, Nanba Y, Tsutsui T, Takahashi Y, Watanabe A, Ishii R. Free perforator flap for the treatment of defects after resection of huge arteriovenous malformations in the head and neck regions. *Ann. Plast. Surg.* 2003; **51**: 194–9.
25 Kajitani N, Ikuta Y, Ishida O, Mochizuki Y, Kimori K. [Surgical treatment of arteriovenous fistula of the hand]. *Nihon Te No Geka Gakkai Zasshi* 1999; **15**: 758–61. Japanese.
26 Minami A, Kato H, Hirachi K. Complete removal plus dorsalis pedis flap for arteriovenous malformation in the hypothenar region. *J. Reconstr. Microsurg.* 1998; **14**: 439–43.
27 Koshima I, Soeda S, Murashita T. Extended wrap-around flap for reconstruction of the finger with recurrent arteriovenous malformation. *Plast. Reconstr. Surg.* 1993; **91**: 1140–4.
28 Wojcicki P, Wojcicka K. The treatment of extensive arteriovenous malformations in the head. *Pol. Przegl. Chir.* 2013; **85**: 83–9.
29 Ermer MA, Gutwald R, Schumacher M, Schmelzeisen R, Taschner C. Use of the radial forearm artery for secondary embolization of an extensive life-threatening arteriovenous malformation of the mid-face and anterior skull base – a case report. *J. Craniomaxillofac. Surg.* 2013; **41**: 258–64.
30 Ueda K, Oba S, Nakai K, Okada M, Kurokawa N, Nuri T. Functional reconstruction of the upper and lower lips and commissure with a forearm flap combined with a free gracilis muscle transfer. *J. Plast. Reconstr. Aesthet. Surg.* 2009; **62**: e337–40.
31 Ninkovic M, Sucur D, Starovic B, Markovic S. Arteriovenous fistulae after free flap surgery in a replanted hand. *J. Hand. Surg. Br.* 1992; **17**: 657–9.
32 Bit N, Vidyasagaran T, Amalorpavanathan J, Balakrishnan TM, Sritharan N. Management of a challenging arteriovenous malformation of the scalp and orbit in a patient with polycystic kidney disease. *Ann. Vasc. Surg.* 2012; **26**: 1129.e9–29.e11.
33 Righi PD, Bade MA, Coleman JJ 3rd, Allen M. Arteriovenous malformation of the base of tongue: case report and literature review. *Microsurgery* 1996; **17**: 706–9.
34 Minagawa T, Itaya Y, Furukawa H. Resection of an arteriovenous malformation of the scalp using a modified tumescent technique. *Nihon Keisei Geka Gakkai Kaishi* 2010; **30**: 87–9.
35 Suyama Y, Nakayama B, Fukuoka K *et al*. Auricular reconstruction with a free radial forearm flap for necrotized ear after sclerotherapy for arteriovenous malformation: a case report. *Nihon Maikuro Sajari Gakkai Kaishi* 2010; **23**: 311–5. Japanese.
36 Urayama H, Harada T, Kawase H, Watanabe Y. Surgical management of soft tissue arteriovenous malformations and hemangiomas. *Shoni Geka* 1993; **25**: 415–9. Japanese.
37 Yamamoto Y, Sugihara T, Minakawa H, Ohkubo Y, Hayashi T. [Surgical treatment of massive arteriovenous malformation with application of hypothermia and cardiopulmonary bypass]. *Nihon Keisei Geka Gakkai Kaishi* 1996; **16**: 863–71. Japanese.
38 Hormozi AK, Shafii MR. Supraclavicular flap: reconstructive strategy for massive facial arteriovenous malformations. *J. Craniofac. Surg.* 2011; **22**: 931–6.
39 Hurwitz DJ, Kerber CW. Hemodynamic considerations in the treatment of arteriovenous malformations of the face and scalp. *Plast. Reconstr. Surg.* 1981; **67**: 421–34.
40 Kiyokawa K, Takagi M, Fukushima J, Kizuka Y, Inoue Y, Tai Y. Surgical treatment following huge arteriovenous malformation extending from the lower lip to the chin: combination of embolization, total resection, and a double cross lip flap. *J. Craniofac. Surg.* 2005; **16**: 443–8.
41 Thomas WO. Facial arteriovenous malformation managed with ablative surgery and dual rotational flap reconstruction. *South Med. J.* 1994; **87**: 1178–82.
42 Warwick DJ, Milling MA. Growth of a vascular malformation into a cross-finger flap. *Br. J. Clin. Pract.* 1993; **47**: 48.
43 Agir H, Sen C, Onyedi M. Extended lateral supramalleolar flap for very distal foot coverage: a case with arteriovenous malformation. *J. Foot Ankle Surg.* 2007; **46**: 310–3.
44 Sakurai H, Nozaki M, Sasaki K *et al*. Successful management of a giant arteriovenous fistula with a combination of selective embolization and excision: report of a case. *Surg. Today* 2002; **32**: 189–93.
45 Watanabe T, Asato H, Umekawa K, Nomura H, Suzuki Y. [Resurfacing the index finger after resection of an arteriovenous malformation using a reverse forearm flap combined with additional venous anastomosis: a case report]. *Nihon Keisei Geka Gakkai Kaishi* 2012; **32**: 335–9. Japanese.
46 Ishisaka T, Naitoh H, Akiyama K, Shigeyoshi N. [A case of lower lip arteriovenous malformation with verrucous carcinoma]. *Nihon Keisei Geka Gakkai Kaishi* 2009; **29**: 7–11. Japanese.
47 Kitagawa S, Kizaki K, Yajima H, Mii Y, Tamai S. [Treatment of hemangiomas associated with arteriovenous fistulae in a family]. *Chubu Nihon Seikei Geka Saigai Geka Gakkai Zasshi* 1997; **40**: 331–2. Japanese.
48 Gunji H, Suda K, Ono I, Ariga T, Kaneko F. [Arteriovenous fistula of auricle treated with a temporoparietal fascial flap: a case report]. *Nihon Keisei Geka Gakkai Kaishi* 1993; **13**: 221–7. Japanese.
49 Fujita A, Asada M, Saitoh M *et al*. A case of congenital arteriovenous malformation of the scalp treated with rotation flap. *No Shinkei Geka Janaru* 2000; **9**: 86–91. Japanese.
50 Nakamura E, Suzuki S, Imagawa K, Akamatsu T, Miyasaka M. Experience of two patients with auricular arteriovenous malformation. *Skin Surg.* 2014; **23**: 73–8. Japanese.
51 Yoshimura Y, Mizuno M, Kobayashi T *et al*. [Case reports: extracranial arteriovenous malformation]. *Hifuka No Rinsho* 2014; **56**: 1180–3. Japanese.
52 Matsuzaki K, Nakamura T, Tahara T, Kashiwa H, Oshima H, Souzumi T. [Congenital arteriovenous malformation of the auricle]. *Jibi Inkoka Tokeibu Geka* 1995; **67**: 337–41. Japanese.

This article has been co-published with the permission of *The Journal of Dermatology, Pediatrics International and Japanese Journal of Radiology*. All rights reserved. © 2020 The Authors. The articles are identical except for minor stylistic and spelling differences in keeping with each journal's style. Either citation can be used when citing this article.

53 Schultz RC, Hermosillo CX. Congenital arteriovenous malformation of the face and scalp. *Plast. Reconstr. Surg.* 1980; **65**: 496–501.
54 Slaba S, Herbreteau D, Jhaveri HS *et al*. Therapeutic approach to arteriovenous malformations of the tongue. *Eur. Radiol.* 1998; **8**: 280–5.
55 Toker ME, Eren E, Akbayrak H *et al*. Combined approach to a peripheral congenital arteriovenous malformation: surgery and embolization. *Heart Vessel.* 2006; **21**: 127–30.
56 Doppman JL, Pevsner P. Embolization of arteriovenous malformations by direct percutaneous puncture. *AJR Am. J. Roentgenol.* 1983; **140**: 773–8.
57 Aikawa H, Okino Y, Yamada Y *et al*. [A review of embolization for arteriovenous malformations (fistulae)]. *Oita Kenritsu Byoin Igaku Zasshi* 1997; **26**: 77–82. Japanese.
58 Yamamoto T, Kanamura N, Tsukitani K *et al*. Direct embolization for a life-threatening mandibular arteriovenous malformation by means of hypothermic cardio-pulmonary arrest. *Kyoto Furitsu Ika Daigaku Zasshi* 1999; **108**: 981–94.
59 Deng W, Huang D, Chen S *et al*. Management of high-flow arteriovenous malformation in the maxillofacial region. *J. Craniofac. Surg.* 2010; **21**: 916–9.
60 Erdmann MW, Jackson JE, Davies DM, Allison DJ. Multidisciplinary approach to the management of head and neck arteriovenous malformations. *Ann. R. Coll. Surg. Engl.* 1995; **77**: 53–9.
61 Goldberg RA, Garcia GH, Duckwiler GR. Combined embolization and surgical treatment of arteriovenous malformation of the orbit. *Am. J. Ophthalmol.* 1993; **116**: 17–25.
62 Persky MS, Yoo HJ, Berenstein A. Management of vascular malformations of the mandible and maxilla. *Laryngoscope* 2003; **113**: 1885–92.
63 Liu DG, Ma XC, Zhao FY, Zhang JG. A preliminary study of angiographic classification and its correlation to treatment of central arteriovenous malformation in the jaw. *Oral Surg. Oral Med. Oral Pathol. Oral Radiol. Endod.* 2005; **100**: 473–80.
64 Rodesch G, Soupre V, Vazquez MP, Alvarez H, Lasjaunias P. Arteriovenous malformations of the dental arcades. The place of endovascular therapy: results in 12 cases are presented. *J. Craniomaxillofac. Surg.* 1998; **26**: 306–13.
65 Chen W, Wang J, Li J, Xu L. Comprehensive treatment of arteriovenous malformations in the oral and maxillofacial region. *J. Oral Maxillofac. Surg.* 2005; **63**: 1484–88.
66 Chen WL, Ye JT, Xu LF, Huang ZQ, Zhang DM. A multidisciplinary approach to treating maxillofacial arteriovenous malformations in children. *Oral Surg. Oral Med. Oral Pathol. Oral Radiol. Endod.* 2009; **108**: 41–7.
67 Churojana A, Khumtong R, Songsaeng D, Chongkolwatana C, Suthipongchai S. Life-threatening arteriovenous malformation of the maxillomandibular region and treatment outcomes. *Interv. Neuroradiol.* 2012; **18**: 49–59.
68 Liu D, Ma XC. Clinical study of embolization of arteriovenous malformation in the oral and maxillofacial region. *Chin. J. Dent. Res.* 2000; **3**: 63–70.
69 Chandra RV, Leslie-Mazwi TM, Orbach DB, Kaban LB, Rabinov JD. Transarterial embolization of mandibular arteriovenous malformations using ONYX. *J. Oral. Maxillofac. Surg.* 2014; **72**: 1504–10.
70 Fifi J, Niimi Y, Berenstein A. Onyx embolization of an extensive mandibular arteriovenous malformation via a dual lumen balloon catheter: a technical case report. *J. Neurointerv. Surg.* 2013; **5**: e5.
71 Fan XD, Su LX, Zheng JW, Zheng LZ, Zhang ZY. Ethanol embolization of arteriovenous malformations of the mandible. *AJNR Am. J. Neuroradiol.* 2009; **30**: 1178–83.
72 Park HS, Do YS, Park KB *et al*. Ethanol embolotherapy of hand arteriovenous malformations. *J. Vasc. Surg.* 2011; **53**: 725–31.
73 Park UJ, Do YS, Park KB *et al*. Treatment of arteriovenous malformations involving the hand. *Ann. Vasc. Surg.* 2012; **26**: 643–8.
74 Hibino N, Hamada Y, Goda Y *et al*. [Arterial graft for reconstruction after complete removal of the arteriovenous malformation]. *Nihon Maikuro Sajari Gakkai Kaishi* 2005; **18**: 78–82. Japanese.
75 Widlus DM, Murray RR, White RI Jr *et al*. Congenital arteriovenous malformations: tailored embolotherapy. *Radiology* 1988; **169**: 511–6.
76 Hattori Y, Doi K, Kawakami F, Watanabe M. Extended wrap-around flap for thumb reconstruction following radical excision of a congenital arteriovenous fistula. *J. Hand Surg. Br.* 1998; **23**: 72–5.
77 Sugioka T, Sunagawa T, Suzuki O, Kijima Y, Ochi M. [Surgical treatment for arteriovenous malformation involving the hand and forearm]. *Nihon Te No Geka Gakkai Zasshi* 2008; **24**: 940–3. Japanese.
78 Furuya T, Nakazawa T. Congenital arteriovenous malformation of the index finger: a case report. *Myakkangaku* 2009; **49**: 430–3. Japanese.
79 Moore JR, Weiland AJ. Embolotherapy in the treatment of congenital arteriovenous malformations of the hand: a case report. *J Hand Surg Am* 1985; **10**: 135–9.
80 Arneja JS, Gosain AK. Vascular malformations. *Plast. Reconstr. Surg.* 2008; **121**: 195e–206e.
81 Hein KD, Mulliken JB, Kozakewich HP, Upton J, Burrows PE. Venous malformations of skeletal muscle. *Plast. Reconstr. Surg.* 2002; **110**: 1625–35.
82 Marler JJ, Mulliken JB. Current management of hemangiomas and vascular malformations. *Clin. Plast. Surg.* 2005; **32**: 99–116**,** ix.
83 Nguyen JT, Koerper MA, Hess CP *et al*. Aspirin therapy in venous malformation: a retrospective cohort study of benefits, side effects, and patient experiences. *Pediatr. Dermatol.* 2014; **31**: 556–60.
84 Shireman PK, McCarthy WJ, Yao JS, Vogelzang RL. Treatment of venous malformations by direct injection with ethanol. *J. Vasc. Surg.* 1997; **26**: 838–44.
85 Rimon U, Garniek A, Galili Y, Golan G, Bensaid P, Morag B. Ethanol sclerotherapy of peripheral venous malformations. *Eur. J. Radiol.* 2004; **52**: 283–7.
86 Marrocco-Trischitta MM, Nicodemi EM, Nater C, Stillo F. Management of congenital venous malformations of the vulva. *Obstet. Gynecol.* 2001; **98**: 789–93.
87 Suh JS, Shin KH, Na JB, Won JY, Hahn SB. Venous malformations: sclerotherapy with a mixture of ethanol and lipiodol. *Cardiovasc. Intervent. Radiol.* 1997; **20**: 268–73.
88 Dompmartin A, Blaizot X, Théron J *et al*. Radio-opaque ethylcellulose-ethanol is a safe and efficient sclerosing agent for venous malformations. *Eur. Radiol.* 2011; **21**: 2647–56.
89 Schumacher M, Dupuy P, Bartoli JM *et al*. Treatment of venous malformations: first experience with a new sclerosing agent–a multicenter study. *Eur. J. Radiol.* 2011; **80**: e366–72.
90 Mimura H, Kanazawa S, Yasui K *et al*. Percutaneous sclerotherapy for venous malformations using polidocanol under fluoroscopy. *Acta Med. Okayama* 2003; **57**: 227–34.
91 Mimura H, Fujiwara H, Hiraki T *et al*. Polidocanol sclerotherapy for painful venous malformations: evaluation of safety and efficacy in pain relief. *Eur. Radiol.* 2009; **19**: 2474–80.
92 Cabrera J, Cabrera J Jr, Garcia-Olmedo MA, Redondo P. Treatment of venous malformations with sclerosant in microfoam form. *Arch. Dermatol.* 2003; **139**: 1409–16.

This article has been co-published with the permission of *The Journal of Dermatology, Pediatrics International and Japanese Journal of Radiology*. All rights reserved. © 2020 The Authors. The articles are identical except for minor stylistic and spelling differences in keeping with each journal's style. Either citation can be used when citing this article.

93 Ozaki M, Kurita M, Kaji N *et al*. Efficacy and evaluation of safety of sclerosants for intramuscular venous malformations: clinical and experimental studies. *Scand. J. Plast. Reconstr. Surg. Hand Surg.* 2010; **44**: 75–87.
94 Krokidis M, Venetucci P, Hatzidakis A, Iaccarino V. Sodium tetradecyl sulphate direct intralesional sclerotherapy of venous malformations of the vulva and vagina: report of five cases. *Cardiovasc. Intervent. Radiol.* 2011; **34** (Suppl 2): S228–31.
95 Enjolras O, Ciabrini D, Mazoyer E, Laurian C, Herbreteau D. Extensive pure venous malformations in the upper or lower limb: a review of 27 cases. *J. Am. Acad. Dermatol.* 1997; **36**: 219–25.
96 Steiner F, FitzJohn T, Tan ST. Surgical treatment for venous malformation. *J. Plast. Reconstr. Aesthet. Surg.* 2013; **66**: 1741–49.
97 Noel AA, Gloviczki P, Cherry KJ Jr, Rooke TW, Stanson AW, Driscoll DJ. Surgical treatment of venous malformations in Klippel-Trenaunay syndrome. *J. Vasc. Surg.* 2000; **32**: 840–7.
98 Sidhu MK, Perkins JA, Shaw DW, Bittles MA, Andrews RT. Ultrasound-guided endovenous diode laser in the treatment of congenital venous malformations: preliminary experience. *J. Vasc. Interv. Radiol.* 2005; **16**: 879–84.
99 Lu X, Ye K, Shi H *et al*. Percutaneous endovenous treatment of congenital extratruncular venous malformations with an ultrasound-guided and 810-nm diode laser. *J. Vasc. Surg.* 2011; **54**: 139–45.
100 Liu G, Liu X, Li W *et al*. Ultrasound-guided intralesional diode laser treatment of congenital extratruncular venous malformations: mid-term results. *Eur. J. Vasc. Endovasc. Surg.* 2014; **47**: 558–64.
101 Mazoyer E, Enjolras O, Laurian C, Houdart E, Drouet L. Coagulation abnormalities associated with extensive venous malformations of the limbs: differentiation from Kasabach-Merritt syndrome. *Clin. Lab. Haematol.* 2002; **24**: 243–51.
102 Cornelis F, Neuville A, Labreze C *et al*. Percutaneous cryotherapy of vascular malformation: initial experience. *Cardiovasc. Intervent. Radiol.* 2013; **36**: 853–6.
103 Cornelis F, Havez M, Labreze C *et al*. Percutaneous cryoablation of symptomatic localized venous malformations: preliminary short-term results. *J. Vasc. Interv. Radiol.* 2013; **24**: 823–7.
104 Betz CS, Jager HR, Brookes JA, Richards R, Leunig A, Hopper C. Interstitial photodynamic therapy for a symptom-targeted treatment of complex vascular malformations in the head and neck region. *Lasers Surg. Med.* 2007; **39**: 571–82.
105 Bashkatov AN, Genina EA, Kochubey VI, Tuchin VV. Optical properties of human skin, subcutaneous and mucous tissues in the wavelength range from 400 to 2000 nm. *J. Phys. D Appl. Phys.* 2005; **38**: 2543–55.
106 Sarig O, Kimel S, Orenstein A. Laser treatment of venous malformations. *Ann. Plast. Surg.* 2006; **57**: 20–24.
107 Vesnaver A, Dovsak DA. Treatment of vascular lesions in the head and neck using Nd:YAG laser. *J. Craniomaxillofac. Surg.* 2006; **34**: 17–24.
108 Asai T, Suzuki H, Enomoto Y *et al*. Clinical evaluation of 74 vascular malformations of the oral region treated by photocoagulation with an Nd:YAG laser. *Nihon Reza Shigakkaishi* 2013; **24**: 3–9. Japanese.
109 Ng EK, Cheung FK, Chiu PW. Blue rubber bleb nevus syndrome: treatment of multiple gastrointestinal hemangiomas with argon plasma coagulator. *Dig. Endosc.* 2009; **21**: 40–2.
110 Cholewa D, Waldschmidt J. Laser treatment of hemangiomas of the larynx and trachea. *Lasers Surg. Med.* 1998; **23**: 221–32.
111 Yakes WF, Haas DK, Parker SH *et al*. Symptomatic vascular malformations: ethanol embolotherapy. *Radiology* 1989; **170**: 1059–66.
112 Lee IH, Kim KH, Jeon P *et al*. Ethanol sclerotherapy for the management of craniofacial venous malformations: the interim results. *Korean J. Radiol.* 2009; **10**: 269–76.
113 Hoque S, Das BK. Treatment of venous malformations with ethanolamine oleate: a descriptive study of 83 cases. *Pediatr. Surg. Int.* 2011; **27**: 527–31.
114 Stuart S, Barnacle AM, Smith G, Pitt M, Roebuck DJ. Neuropathy after sodium tetradecyl sulfate sclerotherapy of venous malformations in children. *Radiology* 2015; **274**: 897–905.
115 Zhao JH, Zhang WF, Zhao YF. Sclerotherapy of oral and facial venous malformations with use of pingyangmycin and/or sodium morrhuate. *Int. J. Oral. Maxillofac. Surg.* 2004; **33**: 463–6.
116 Bai N, Chen YZ, Fu YJ, Wu P, Zhang WN. A clinical study of pingyangmycin sclerotherapy for venous malformation: an evaluation of 281 consecutive patients. *J. Clin. Pharm. Ther.* 2014; **39**: 521–6.
117 Goyal M, Causer PA, Armstrong D. Venous vascular malformations in pediatric patients: comparison of results of alcohol sclerotherapy with proposed MR imaging classification. *Radiology* 2002; **223**: 639–644.
118 Yun WS, Kim YW, Lee KB *et al*. Predictors of response to percutaneous ethanol sclerotherapy (PES) in patients with venous malformations: analysis of patient self-assessment and imaging. *J. Vasc. Surg.* 2009; **50**: 581–9**,** 589 e581.
119 Rautio R, Saarinen J, Laranne J, Salenius JP, Keski-Nisula L. Endovascular treatment of venous malformations in extremities: results of sclerotherapy and the quality of life after treatment. *Acta Radiol.* 2004; **45**: 397–403.
120 Yamaki T, Nozaki M, Sakurai H, Takeuchi M, Soejima K, Kono T. Prospective randomized efficacy of ultrasound-guided foam sclerotherapy compared with ultrasound-guided liquid sclerotherapy in the treatment of symptomatic venous malformations. *J. Vasc. Surg.* 2008; **47**: 578–84.
121 Nagao M, Sasaki S, Furukawa H, Saito N, Yamamoto Y. [A clinical study of sclerotherapy for venous malformation of an upper extremity]. *Nihon Keisei Geka Gakkai Kaishi* 2012; **32**: 463–8. Japanese.
122 Nomura T, Sakurai A, Nagata I, Terashi H, Tahara S. Our strategy for the treatment of venous malformations. *Jomyakugaku* 2008; **19**: 161–8. Japanese.
123 Qiu Y, Chen H, Lin X, Hu X, Jin Y, Ma G. Outcomes and complications of sclerotherapy for venous malformations. *Vasc. Endovascular. Surg.* 2013; **47**: 454–61.
124 Wong GA, Armstrong DC, Robertson JM. Cardiovascular collapse during ethanol sclerotherapy in a pediatric patient. *Paediatr. Anaesth.* 2006; **16**: 343–6.
125 Tachibana K, Kobayashi S, Kojima T, Kaseno S, Kemmotsu O. Pulmonary emboli in sclerotherapy for peripheral vascular malformations under general anesthesia; a report of two cases. *Masui* 2004; **53**: 645–9. Japanese.
126 Marrocco-Trischitta MM, Guerrini P, Abeni D, Stillo F. Reversible cardiac arrest after polidocanol sclerotherapy of peripheral venous malformation. *Dermatol. Surg.* 2002; **28**: 153–5.
127 Shimo T, Hidaka K, Yanagawa S, Kadota W, Kawakami S, Tsuchida H. Two episodes of cardiac arrest in a boy receiving sclerotherapy with polydocanol–a case report. *Masui* 2005; **54**: 57–9. Japanese.
128 Schild SE, Buskirk SJ, Frick LM, Cupps RE. Radiotherapy for large symptomatic hemangiomas. *Int. J. Radiat. Oncol. Biol. Phys.* 1991; **21**: 729–35.

This article has been co-published with the permission of *The Journal of Dermatology, Pediatrics International and Japanese Journal of Radiology*. All rights reserved. © 2020 The Authors. The articles are identical except for minor stylistic and spelling differences in keeping with each journal's style. Either citation can be used when citing this article.

129 Mitsuhashi N, Furuta M, Sakurai H *et al*. Outcome of radiation therapy for patients with Kasabach-Merritt syndrome. *Int. J. Radiat. Oncol. Biol. Phys.* 1997; **39**: 467–73.
130 Ogino I, Torikai K, Kobayasi S, Aida N, Hata M, Kigasawa H. Radiation therapy for life- or function-threatening infant hemangioma. *Radiology* 2001; **218**: 834–9.
131 Miller JG, Orton CI. Long term follow-up of a case of Kasabach-Merritt syndrome successfully treated with radiotherapy and corticosteroids. *Br. J. Plast. Surg.* 1992; **45**: 559–61.
132 Frevel T, Rabe H, Uckert F, Harms E. Giant cavernous haemangioma with Kasabach-Merritt syndrome: a case report and review. *Eur. J. Pediatr.* 2002; **161**: 243–6.
133 Stringel G, Mercer S. Giant hemangioma in the newborn and infant. Complications and management. *Clin. Pediatr. (Phila)* 1984; **23**: 498–502.
134 Enjolras O, Wassef M, Mazoyer E *et al*. Infants with Kasabach-Merritt syndrome do not have "true" hemangiomas. *J. Pediatr.* 1997; **130**: 631–40.
135 Lundell M, Mattsson A, Hakulinen T, Holm LE. Breast cancer after radiotherapy for skin hemangioma in infancy. *Radiat. Res.* 1996; **145**: 225–30.
136 Haddy N, Andriamboavonjy T, Paoletti C *et al*. Thyroid adenomas and carcinomas following radiotherapy for a hemangioma during infancy. *Radiother. Oncol.* 2009; **93**: 377–82.
137 Caldwell JB, Ryan MT, Benson PM, James WD. Cutaneous angiosarcoma arising in the radiation site of a congenital hemangioma. *J. Am. Acad. Dermatol.* 1995; **33**: 865–70.
138 Oguri A, Oda M, Yokoo K. [The relation between age and the effectiveness of laser treatment for capillary malformation]. *Nihon Keisei Geka Gakkai Kaishi* 2009; **29**: 407–11. Japanese.
139 Reynolds N, Exley J, Hills S, Falder S, Duff C, Kenealy J. The role of the Lumina intense pulsed light system in the treatment of port wine stains–a case controlled study. *Br. J. Plast. Surg.* 2005; **58**: 968–80.
140 Katugampola GA, Lanigan SW. Five years' experience of treating port wine stains with the flashlamp-pumped pulsed dye laser. *Br. J. Dermatol.* 1997; **137**: 750–4.
141 Minato S. Comparison between results of treatment with dye laser and argon laser in cases of hemangioma simplex. *Iwate Igaku Zasshi* 1997; **49**: 299–302.
142 Ryuzaki K, Tamura A, Amano H, Takeuchi Y, Ishikawa O, Miyachi Y. [An overview of dye laser treatment for superficial hemangiomas at the Department of Dermatology, Gunma University]. *Hifuka Kiyo* 1996; **91**: 41–6. Japanese.
143 Matsumoto T. [Comparative study in laser treatment of portwine stains with dye and argon lasers. Part 2: statistical study of clinical effects]. *Nihon Keisei Geka Gakkai Kaishi* 1996; **16**: 246–59. Japanese.
144 Fitzpatrick RE, Lowe NJ, Goldman MP, Borden H, Behr KL, Ruiz-Esparza J. Flashlamp-pumped pulsed dye laser treatment of port-wine stains. *J. Dermatol. Surg. Oncol.* 1994; **20**: 743–8.
145 Morikawa K, Yamauchi K, Saheki M, Tezuka T. Treatment of portwine stain using pulsed dye laser: comparison of effectiveness with location of lesion, age and wavelength. *Hifu* 1994; **36**: 514–21. Japanese.
146 Matsushita Y, Suzuki S, Koyama H, Akamatsu J, Kawata Y, Kawai K. Treatment of portwine stains with dye lasers. *Hifuka Kiyo* 1994; **89**: 205–10. Japanese.
147 Namba Y, Mae O, Nagase Y, Ao M, Hamaya K, Nose S. [Dye laser treatment of cutaneous simple hemangioma]. *Okayama Saiseikai Sogo Byoin Zasshi* 1991; **22**: 1–10. Japanese.
148 Bandoh Y, Yanai A, Tsuzuki K. Dye laser treatment of port-wine stains. *Aesthet. Plast. Surg.* 1990; **14**: 287–91.
149 Bandoh Y. [Pulsed dye laser treatment for port-wine stains]. *Rinsho Hifuka* 1989; **43**: 1337–40. Japanese.
150 Renfro L, Geronemus RG. Anatomical differences of port-wine stains in response to treatment with the pulsed dye laser. *Arch. Dermatol.* 1993; **129**: 182–8.
151 Lanigan SW. Port wine stains on the lower limb: response to pulsed dye laser therapy. *Clin. Exp. Dermatol.* 1996; **21**: 88–92.
152 Sommer S, Seukeran DC, Sheehan-Dare RA. Efficacy of pulsed dye laser treatment of port wine stain malformations of the lower limb. *Br. J. Dermatol.* 2003; **149**: 770–5.
153 Fitzpatrick TB. The validity and practicality of sun-reactive skin types I through VI. *Arch. Dermatol.* 1988; **124**: 869–71.
154 Wareham WJ, Cole RP, Royston SL, Wright PA. Adverse effects reported in pulsed dye laser treatment for port wine stains. *Lasers Med. Sci.* 2009; **24**: 241–6.
155 Orten SS, Waner M, Flock S, Roberson PK, Kincannon J. Port-wine stains. An assessment of 5 years of treatment. *Arch. Otolaryngol. Head Neck Surg.* 1996; **122**: 1174–9.
156 Michel S, Landthaler M, Hohenleutner U. Recurrence of port-wine stains after treatment with the flashlamp-pumped pulsed dye laser. *Br. J. Dermatol.* 2000; **143**: 1230–4.
157 Soueid A, Waters R. Re-emergence of port wine stains following treatment with flashlamp-pumped dye laser 585 nm. *Ann. Plast. Surg.* 2006; **57**: 260–3.
158 Huikeshoven M, Koster PH, de Borgie CA, Beek JF, van Gemert MJ, van der Horst CM. Redarkening of port-wine stains 10 years after pulsed-dye-laser treatment. *N. Engl. J. Med.* 2007; **356**: 1235–40.
159 Phung TL, Oble DA, Jia W, Benjamin LE, Mihm MC Jr, Nelson JS. Can the wound healing response of human skin be modulated after laser treatment and the effects of exposure extended? Implications on the combined use of the pulsed dye laser and a topical angiogenesis inhibitor for treatment of port wine stain birthmarks. *Lasers Surg. Med.* 2008; **40**: 1–5.
160 Babilas P, Shafirstein G, Bäumler W *et al*. Selective photothermolysis of blood vessels following flashlamp-pumped pulsed dye laser irradiation: in vivo results and mathematical modelling are in agreement. *J. Invest. Dermatol.* 2005; **125**: 343–52.
161 Laquer VT, Hevezi PA, Albrecht H, Chen TS, Zlotnik A, Kelly KM. Microarray analysis of port wine stains before and after pulsed dye laser treatment. *Lasers Surg. Med.* 2013; **45**: 67–75.
162 Chapas AM, Eickhorst K, Geronemus RG. Efficacy of early treatment of facial port wine stains in newborns: a review of 49 cases. *Lasers Surg. Med.* 2007; **39**: 563–8.
163 Jia W, Sun V, Tran N *et al*. Long-term blood vessel removal with combined laser and topical rapamycin antiangiogenic therapy: implications for effective port wine stain treatment. *Lasers Surg. Med.* 2010; **42**: 105–12.
164 Chang CJ, Hsiao YC, Mihm MC Jr, Nelson JS. Pilot study examining the combined use of pulsed dye laser and topical Imiquimod versus laser alone for treatment of port wine stain birthmarks. *Lasers Surg. Med.* 2008; **40**: 605–10.
165 Tremaine AM, Armstrong J, Huang YC *et al*. Enhanced port-wine stain lightening achieved with combined treatment of selective photothermolysis and imiquimod. *J. Am. Acad. Dermatol.* 2012; **66**: 634–41.
166 Nguyen CM, Yohn JJ, Huff C, Weston WL, Morelli JG. Facial port wine stains in childhood: prediction of the rate of improvement as a function of the age of the patient, size and location of the port wine stain and the number of treatments with the pulsed dye (585 nm) laser. *Br. J. Dermatol.* 1998; **138**: 821–5.

This article has been co-published with the permission of *The Journal of Dermatology, Pediatrics International and Japanese Journal of Radiology*. All rights reserved. © 2020 The Authors. The articles are identical except for minor stylistic and spelling differences in keeping with each journal's style. Either citation can be used when citing this article.

167 van der Horst CM, Koster PH, de Borgie CA, Bossuyt PM, van Gemert MJ. Effect of the timing of treatment of port-wine stains with the flash-lamp-pumped pulsed-dye laser. *N. Engl. J. Med.* 1998; **338**: 1028–1033.
168 Léauté-Labrèze C, de la Roque ED, Hubiche T, Boralevi F, Thambo J-B, Taïeb A. Propranolol for severe hemangiomas of infancy. *N. Engl. J. Med.* 2008; **358**: 2649–51.
169 Broeks IJ, Hermans DJ, Dassel AC, van der Vleuten CJ, van Beynum IM. Propranolol treatment in life-threatening airway hemangiomas: a case series and review of literature. *Int. J. Pediatr. Otorhinolaryngol.* 2013; **77**: 1791–1800.
170 Sharma VK, Fraulin FO, Dumestre DO, Walker L, Harrop AR. Beta-blockers for the treatment of problematic hemangiomas. *Can. J. Plast. Surg.* 2013; **21**: 23–8.
171 Zvulunov A, McCuaig C, Frieden IJ *et al*. Oral propranolol therapy for infantile hemangiomas beyond the proliferation phase: a multicenter retrospective study. *Pediatr. Dermatol.* 2011; **28**: 94–8.
172 Hermans DJ, van Beynum IM, Schultze Kool LJ, van de Kerkhof PC, Wijnen MH, van der Vleuten CJ. Propranolol, a very promising treatment for ulceration in infantile hemangiomas: a study of 20 cases with matched historical controls. *J. Am. Acad. Dermatol.* 2011; **64**: 833–838.
173 Saint-Jean M, Léauté-Labrèze C, Mazereeuw-Hautier J *et al*. Propranolol for treatment of ulcerated infantile hemangiomas. *J. Am. Acad. Dermatol.* 2011; **64**: 827–32.
174 Caussé S, Aubert H, Saint-Jean M *et al*. Propranolol-resistant infantile haemangiomas. *Br. J. Dermatol.* 2013; **169**: 125–9.
175 Vassallo P, Forte R, Di Mezza A, Magli A. Treatment of infantile capillary hemangioma of the eyelid with systemic propranolol. *Am. J. Ophthalmol.* 2013; **155**: 165–70 e162.
176 Lynch M, Lenane P, O'Donnell BF. Propranolol for the treatment of infantile haemangiomas: our experience with 44 patients. *Clin. Exp. Dermatol.* 2014; **39**: 142–5.
177 Price CJ, Lattouf C, Baum B *et al*. Propranolol vs corticosteroids for infantile hemangiomas: a multicenter retrospective analysis. *Arch. Dermatol.* 2011; **147**: 1371–6.
178 Hermans DJ, Bauland CG, Zweegers J, van Beynum IM, van der Vleuten CJ. Propranolol in a case series of 174 patients with complicated infantile haemangioma: indications, safety and future directions. *Br. J. Dermatol.* 2013; **168**: 837–43.
179 de Graaf M, Breur J, Raphael MF, Vos M, Breugem CC, Pasmans S. Adverse effects of propranolol when used in the treatment of hemangiomas: a case series of 28 infants. *J. Am. Acad. Dermatol.* 2011; **65**: 320–7.
180 Hogeling M, Adams S, Wargon O. A randomized controlled trial of propranolol for infantile hemangiomas. *Pediatrics* 2011; **128**: e259–66.
181 Zaher H, Rasheed H, Esmat S *et al*. Propranolol and infantile hemangiomas: different routes of administration, a randomized clinical trial. *Eur. J. Dermatol.* 2013; **23**: 646–52.
182 Malik MA, Menon P, Rao KL, Samujh R. Effect of propranolol vs prednisolone vs propranolol with prednisolone in the management of infantile hemangioma: a randomized controlled study. *J. Pediatr. Surg.* 2013; **48**: 2453–9.
183 Bauman NM, McCarter RJ, Guzzetta PC *et al*. Propranolol vs prednisolone for symptomatic proliferating infantile hemangiomas: a randomized clinical trial. *JAMA Otolaryngol. Head Neck Surg.* 2014; **140**: 323–30.
184 Léauté-Labrèze C, Dumas de la Roque E, Nacka F *et al*. Double-blind randomized pilot trial evaluating the efficacy of oral propranolol on infantile haemangiomas in infants < 4 months of age. *Br. J. Dermatol.* 2013; **169**: 181–3.
185 Abarzúa-Araya A, Navarrete-Dechent CP, Heusser F, Retamal J, Zegpi-Trueba MS. Atenolol versus propranolol for the treatment of infantile hemangiomas: a randomized controlled study. *J. Am. Acad. Dermatol.* 2014; **70**: 1045–9.
186 Ehsani AH, Noormohammadpoor P, Abdolreza M, Balighi K, Arianian Z, Daklan S. Combination therapy of infantile hemangioma with pulsed dye laser with topical propranolol: a randomized clinical trial. *Arch. Iran Med.* 2014; **17**: 657–60.
187 Léauté-Labrèze C, Hoeger P, Mazereeuw-Hautier J *et al*. A randomized, controlled trial of oral propranolol in infantile hemangioma. *N. Engl. J. Med.* 2015; **372**: 735–46.
188 Menezes MD, McCarter R, Greene EA, Bauman NM. Status of propranolol for treatment of infantile hemangioma and description of a randomized clinical trial. *Ann. Otol. Rhinol. Laryngol.* 2011; **120**: 686–95.
189 Marqueling AL, Oza V, Frieden IJ, Puttgen KB. Propranolol and infantile hemangiomas four years later: a systematic review. *Pediatr. Dermatol.* 2013; **30**: 182–91.
190 Xu SQ, Jia RB, Zhang W, Zhu H, Ge SF, Fan XQ. Beta-blockers versus corticosteroids in the treatment of infantile hemangioma: an evidence-based systematic review. *World J. Pediatr.* 2013; **9**: 221–9.
191 Izadpanah A, Izadpanah A, Kanevsky J, Belzile E, Schwarz K. Propranolol versus corticosteroids in the treatment of infantile hemangioma: a systematic review and meta-analysis. *Plast. Reconstr. Surg.* 2013; **131**: 601–13.
192 Xu S, Jia R, Ge S, Lin M, Fan X. Treatment of periorbital infantile haemangiomas: a systematic literature review on propranolol or steroids. *J. Paediatr. Child Health* 2014; **50**: 271–9.
193 Peridis S, Pilgrim G, Athanasopoulos I, Parpounas K. A meta-analysis on the effectiveness of propranolol for the treatment of infantile airway haemangiomas. *Int. J. Pediatr. Otorhinolaryngol.* 2011; **75**: 455–60.
194 Vlastarakos PV, Papacharalampous GX, Chrysostomou M *et al*. Propranolol is an effective treatment for airway haemangiomas: a critical analysis and meta-analysis of published interventional studies. *Acta Otorhinolaryngol. Ital.* 2012; **32**: 213–21.
195 Storch CH, Hoeger PH. Propranolol for infantile haemangiomas: insights into the molecular mechanisms of action. *Br. J. Dermatol.* 2010; **163**: 269–74.
196 Drolet BA, Frommelt PC, Chamlin SL *et al*. Initiation and use of propranolol for infantile hemangioma: report of a consensus conference. *Pediatrics* 2013; **131**: 128–40.
197 Kum JJ, Khan ZA. Mechanisms of propranolol action in infantile hemangioma. *Dermatoendocrinol* 2014; **6**: e979699.
198 Horev A, Haim A, Zvulunov A. Propranolol induced hypoglycemia. *Pediatr. Endocrinol. Rev.* 2015; **12**: 308–10.
199 Blei F, McElhinney DB, Guarini A, Presti S. Cardiac screening in infants with infantile hemangiomas before propranolol treatment. *Pediatr. Dermatol.* 2014; **31**: 465–70.
200 Raphael MF, Breugem CC, Vlasveld FA *et al*. Is cardiovascular evaluation necessary prior to and during beta-blocker therapy for infantile hemangiomas?: A cohort study. *J. Am. Acad. Dermatol.* 2015; **72**: 465–72.
201 Chamlin SL, Haggstrom AN, Drolet BA *et al*. Multicenter prospective study of ulcerated hemangiomas. *J. Pediatr.* 2007; **151**: 684–9, 689 e681.
202 Vercellino N, Romanini MV, Pelegrini M, Rimini A, Occella C, Dalmonte P. The use of propranolol for complicated infantile hemangiomas. *Int. J. Dermatol.* 2013; **52**: 1140–6.
203 Sadykov RR, Podmelle F, Sadykov RA, Kasimova KR, Metellmann HR. Use of propranolol for the treatment infantile hemangiomas in the maxillofacial region. *Int. J. Oral Maxillofac. Surg.* 2013; **42**: 863–7.
204 Kim HJ, Colombo M, Frieden IJ. Ulcerated hemangiomas: clinical characteristics and response to therapy. *J. Am. Acad. Dermatol.* 2001; **44**: 962–72.

This article has been co-published with the permission of *The Journal of Dermatology, Pediatrics International and Japanese Journal of Radiology*. All rights reserved. © 2020 The Authors. The articles are identical except for minor stylistic and spelling differences in keeping with each journal's style. Either citation can be used when citing this article.

205 Wananukul S, Chatproedprai S. Ulcerated hemangiomas: clinical features and management. *J. Med. Assoc. Thai.* 2002; **85**: 1220–5.
206 Pandey A, Gangopadhyay AN, Sharma SP, Kumar V, Gopal SC, Gupta DK. Conservative management of ulcerated haemangioma–twenty years experience. *Int. Wound J.* 2009; **6**: 59–62.
207 Oranje AP, de Waard-van der Spek FB, Devillers ACA, de Laat P, Madern GC. Treatment and pain relief of ulcerative hemangiomas with a polyurethane film. *Dermatology* 2000; **200**: 31–4.
208 Bauland CG, Smit JM, Ketelaars R, Rieu PN, Spauwen PH. Management of haemangiomas of infancy: a retrospective analysis and a treatment protocol. *Scand. J. Plast. Reconstr. Surg. Hand Surg.* 2008; **42**: 86–91.
209 Morelli JG, Tan OT, Yohn JJ, Weston WL. Treatment of ulcerated hemangiomas infancy. *Arch. Pediatr. Adolesc. Med.* 1994; **148**: 1104–5.
210 Lacour M, Syed S, Linward J, Harper JI. Role of the pulsed dye laser in the management of ulcerated capillary haemangiomas. *Arch. Dis. Child.* 1996; **74**: 161–3.
211 David LR, Malek MM, Argenta LC. Efficacy of pulse dye laser therapy for the treatment of ulcerated haemangiomas: a review of 78 patients. *Br. J. Plast. Surg.* 2003; **56**: 317–27.
212 Michel JL. Treatment of hemangiomas with 595 nm pulsed dye laser dermobeam. *Eur. J. Dermatol.* 2003; **13**: 136–41.
213 Di Maio L, Baldi A, Dimaio V, Barzi A. Use of flashlamp-pumped pulsed dye laser in the treatment of superficial vascular malformations and ulcerated hemangiomas. *In Vivo* 2011; **25**: 117–23.
214 Sugarman JL, Mauro TM, Frieden IJ. Treatment of an ulcerated hemangioma with recombinant platelet-derived growth factor. *Arch. Dermatol.* 2002; **138**: 314–6.
215 Metz BJ, Rubenstein MC, Levy ML, Metry DW. Response of ulcerated perineal hemangiomas of infancy to becaplermin gel, a recombinant human platelet-derived growth factor. *Arch. Dermatol.* 2004; **140**: 867–70.
216 Jalil S, Akhtar J, Ahmed S. Corticosteroids therapy in the management of infantile cutaneous hemangiomas. *J. Coll. Physicians Surg. Pak.* 2006; **16**: 662–5.
217 Gangopadhyay AN, Sinha CK, Gopal SC, Gupta DK, Sahoo SP, Ahmad M. Role of steroid in childhood haemangioma: a 10 years review. *Int. Surg.* 1997; **82**: 49–51.
218 Pandey A, Gangopadhyay AN, Gopal SC *et al*. Twenty years' experience of steroids in infantile hemangioma–a developing country's perspective. *J. Pediatr. Surg.* 2009; **44**: 688–94.
219 Tan BH, Leadbitter PH, Aburn NH, Tan ST. Steroid therapy for problematic proliferating haemangioma. *N. Z. Med. J.* 2011; **124**: 57–65.
220 Ruttum MS, Abrams GW, Harris GJ, Ellis MK. Bilateral retinal embolization associated with intralesional corticosteroid injection for capillary hemangioma of infancy. *J. Pediatr. Ophthalmol. Strabismus* 1993; **30**: 4–7.
221 Egbert JE, Schwartz GS, Walsh AW. Diagnosis and treatment of an ophthalmic artery occlusion during an intralesional injection of corticosteroid into an eyelid capillary hemangioma. *Am. J. Ophthalmol.* 1996; **121**: 638–42.
222 Craiglow BG, Antaya RJ. Management of infantile hemangiomas: current and potential pharmacotherapeutic approaches. *Paediatr. Drugs* 2013; **15**: 133–8.
223 Ni N, Langer P, Wagner R, Guo S. Topical timolol for periocular hemangioma: report of further study. *Arch. Ophthalmol.* 2011; **129**: 377–9.
224 Elsas FJ, Lewis AR. Topical treatment of periocular capillary hemangioma. *J. Pediatr. Ophthalmol. Strabismus* 1994; **31**: 153–6.
225 Lapidoth M, Ben-Amitai D, Bhandarkar S, Fried L, Arbiser JL. Efficacy of topical application of eosin for ulcerated hemangiomas. *J. Am. Acad. Dermatol.* 2009; **60**: 350–1.
226 Barry RB, Hughes BR, Cook LJ. Involution of infantile haemangiomas after imiquimod 5% cream. *Clin. Exp. Dermatol.* 2008; **33**: 446–9.
227 Ho NT, Lansang P, Pope E. Topical imiquimod in the treatment of infantile hemangiomas: a retrospective study. *J. Am. Acad. Dermatol.* 2007; **56**: 63–8.
228 Jiang C, Hu X, Ma G *et al*. A prospective self-controlled phase II study of imiquimod 5% cream in the treatment of infantile hemangioma. *Pediatr. Dermatol.* 2011; **28**: 259–66.
229 Mao XH, Wang JY, Yan JL. Topical imiquimod treatment of cutaneous vascular disorders in pediatric patients: clinical evaluation on the efficacy and safety. *J. Zhejiang Univ. Sci. B* 2012; **13**: 745–50.
230 McCuaig CC, Dubois J, Powell J *et al*. A phase II, open-label study of the efficacy and safety of imiquimod in the treatment of superficial and mixed infantile hemangioma. *Pediatr. Dermatol.* 2009; **26**: 203–12.
231 Qiu Y, Ma G, Lin X, Jin Y, Chen H, Hu X. Treating protruding infantile hemangiomas with topical imiquimod 5% cream caused severe local reactions and disfiguring scars. *Pediatr. Dermatol.* 2013; **30**: 342–7.
232 Qiu Y, Ma G, Yang J *et al*. Imiquimod 5% cream versus timolol 0.5% ophthalmic solution for treating superficial proliferating infantile haemangiomas: a retrospective study. *Clin. Exp. Dermatol.* 2013; **38**: 845–50.
233 Welsh O, Olazaran Z, Gomez M, Salas J, Berman B. Treatment of infantile hemangiomas with short-term application of imiquimod 5% cream. *J. Am. Acad. Dermatol.* 2004; **51**: 639–42.
234 Blatt J, Morrell DS, Buck S *et al*. β-blockers for infantile hemangiomas: a single-institution experience. *Clin. Pediatr. (Phila)* 2011; **50**: 757–63.
235 Cante V, Pham-Ledard A, Imbert E, Ezzedine K, Léauté-Labrèze C. First report of topical timolol treatment in primarily ulcerated perineal haemangioma. *Arch. Dis. Child Fetal Neonatal Ed.* 2012; **97**: F155–6.
236 Chakkittakandiyil A, Phillips R, Frieden IJ *et al*. Timolol maleate 0.5% or 0.1% gel-forming solution for infantile hemangiomas: a retrospective, multicenter, cohort study. *Pediatr. Dermatol.* 2012; **29**: 28–31.
237 Chambers CB, Katowitz WR, Katowitz JA, Binenbaum G. A controlled study of topical 0.25% timolol maleate gel for the treatment of cutaneous infantile capillary hemangiomas. *Ophthalmic. Plast. Reconstr. Surg.* 2012; **28**: 103–6.
238 Khunger N, Pahwa M. Dramatic response to topical timolol lotion of a large hemifacial infantile haemangioma associated with PHACE syndrome. *Br. J. Dermatol.* 2011; **164**: 886–8.
239 Ma G, Wu P, Lin X *et al*. Fractional carbon dioxide laser-assisted drug delivery of topical timolol solution for the treatment of deep infantile hemangioma: a pilot study. *Pediatr. Dermatol.* 2014; **31**: 286–91.
240 Moehrle M, Léauté-Labrèze C, Schmidt V, Röcken M, Poets CF, Goelz R. Topical timolol for small hemangiomas of infancy. *Pediatr. Dermatol.* 2013; **30**: 245–9.
241 Ni N, Guo S, Langer P. Current concepts in the management of periocular infantile (capillary) hemangioma. *Curr. Opin. Ophthalmol.* 2011; **22**: 419–25.
242 Oranje AP, Janmohamed SR. Madern GC, de Laat PC. Treatment of small superficial haemangioma with timolol 0.5% ophthalmic solution: a series of 20 cases. *Dermatology* 2011; **223**: 330–4.
243 Pope E, Chakkittakandiyil A. Topical timolol gel for infantile hemangiomas: a pilot study. *Arch. Dermatol.* 2010; **146**: 564–5.

This article has been co-published with the permission of *The Journal of Dermatology, Pediatrics International and Japanese Journal of Radiology*. All rights reserved. © 2020 The Authors. The articles are identical except for minor stylistic and spelling differences in keeping with each journal's style. Either citation can be used when citing this article.

244 Kunzi-Rapp K. Topical propranolol therapy for infantile hemangiomas. *Pediatr. Dermatol.* 2012; **29**: 154–9.
245 Xu G, Lv R, Zhao Z, Huo R. Topical propranolol for treatment of superficial infantile hemangiomas. *J. Am. Acad. Dermatol.* 2012; **67**: 1210–13.
246 Garzon MC, Lucky AW, Hawrot A, Frieden IJ. Ultrapotent topical corticosteroid treatment of hemangiomas of infancy. *J. Am. Acad. Dermatol.* 2005; **52**: 281–286.
247 Pandey A, Gangopadhyay AN, Sharma SP, Kumar V, Gupta DK, Gopal SC. Evaluation of topical steroids in the treatment of superficial hemangioma. *Skinmed* 2010; **8**: 9–11.
248 Kaplan M, Paller AS. Clinical pearl: use of self-adhesive, compressive wraps in the treatment of limb hemangiomas. *J. Am. Acad. Dermatol.* 1995; **32**: 117–8.
249 Ochi G, Ohkawa H, Kaneko M *et al*. [Compression therapy and cryosurgery for hemangiomas in childhood]. *Shoni Geka* 1992; **24**: 539–47. Japanese.
250 Totsuka Y, Fukuda H, Tomita K. Compression therapy for parotid haemangioma in infants. A report of three cases. *J. Craniomaxillofac. Surg.* 1988; **16**: 366–70.
251 Osaki TH, Jakobiec FA, Mendoza PR, Lee Y, Fay AM. Immunohistochemical investigations of orbital infantile hemangiomas and adult encapsulated cavernous venous lesions (malformation versus hemangioma). *Ophthalmic. Plast. Reconstr. Surg.* 2013; **29**: 183–95.
252 Laing EL, Brasch HD, Steel R *et al*. Verrucous hemangioma expresses primitive markers. *J. Cutan. Pathol.* 2013; **40**: 391–6.
253 North PE, Waner M, James CA, Mizeracki A, Frieden IJ, Mihm MC Jr. Congenital nonprogressive hemangioma: a distinct clinicopathologic entity unlike infantile hemangioma. *Arch. Dermatol.* 2001; **137**: 1607–20.
254 North PE, Waner M, Mizeracki A, Mihm MC Jr. GLUT1: a newly discovered immunohistochemical marker for juvenile hemangiomas. *Hum. Pathol.* 2000; **31**: 11–22.
255 North PE, Waner M, Mizeracki A *et al*. A unique microvascular phenotype shared by juvenile hemangiomas and human placenta. *Arch. Dermatol.* 2001; **137**: 559–70.
256 Leon-Villapalos J, Wolfe K, Kangesu L. GLUT-1: an extra diagnostic tool to differentiate between haemangiomas and vascular malformations. *Br. J. Plast. Surg.* 2005; **58**: 348–52.
257 Ahrens WA, Ridenour RV 3rd, Caron BL, Miller DV, Folpe AL. GLUT-1 expression in mesenchymal tumors: an immunohistochemical study of 247 soft tissue and bone neoplasms. *Hum. Pathol.* 2008; **39**: 1519–26.
258 Trindade F, Kutzner H, Requena L, Tellechea O, Colmenero I. Microvenular hemangioma-an immunohistochemical study of 9 cases. *Am. J. Dermatopathol.* 2012; **34**: 810–12.
259 Sadeghpour M, Antaya RJ, Lazova R, Ko CJ. Dilated lymphatic vessels in tufted angioma: a potential source of diagnostic confusion. *Am. J. Dermatopathol.* 2012; **34**: 400–3.
260 Drut RM, Drut R. Extracutaneous infantile haemangioma is also Glut1 positive. *J. Clin. Pathol.* 2004; **57**: 1197–200.
261 Lyons LL, North PE, Mac-Moune Lai F, Stoler MH, Folpe AL, Weiss SW. Kaposiform hemangioendothelioma: a study of 33 cases emphasizing its pathologic, immunophenotypic, and biologic uniqueness from juvenile hemangioma. *Am. J. Surg. Pathol.* 2004; **28**: 559–68.
262 Al-Adnani M, Williams S, Rampling D, Ashworth M, Malone M, Sebire NJ. Histopathological reporting of paediatric cutaneous vascular anomalies in relation to proposed multidisciplinary classification system. *J. Clin. Pathol.* 2006; **59**: 1278–82.
263 Badi AN, Kerschner JE, North PE, Drolet BA, Messner A, Perkins JA. Histopathologic and immunophenotypic profile of subglottic hemangioma: multicenter study. *Int. J. Pediatr. Otorhinolaryngol.* 2009; **73**: 1187–91.
264 Hernandez F, Navarro M, Encinas JL *et al*. The role of GLUT1 immunostaining in the diagnosis and classification of liver vascular tumors in children. *J. Pediatr. Surg.* 2005; **40**: 801–4.
265 Mo JQ, Dimashkieh HH, Bove KE. GLUT1 endothelial reactivity distinguishes hepatic infantile hemangioma from congenital hepatic vascular malformation with associated capillary proliferation. *Hum. Pathol.* 2004; **35**: 200–9.
266 Das KJ, Sharma P, Naswa N *et al*. Hybrid SPECT-CT with 99mTc-labeled red blood cell in a case of blue rubber bleb nevus syndrome: added value over planar scintigraphy. *Diagn. Interv. Radiol.* 2013; **19**: 41–3.
267 Senturk S, Bilici A, Miroglu TC, Bilek SU. Blue rubber bleb nevus syndrome: imaging of small bowel lesions with peroral CT enterography. *Abdom. Imaging* 2011; **36**: 520–3.
268 Thomson M, Venkatesh K, Elmalik K, van der Veer W, Jaacobs M. Double balloon enteroscopy in children: diagnosis, treatment, and safety. *World J. Gastroenterol.* 2010; **16**: 56–62.
269 Agnese M, Cipolletta L, Bianco MA, Quitadamo P, Miele E, Staiano A. Blue rubber bleb nevus syndrome. *Acta Paediatr.* 2010; **99**: 632–5.
270 Hansen LF, Wewer V, Pedersen SA, Matzen P, Paerregaard A. Severe blue rubber bleb nevus syndrome in a neonate. *Eur. J. Pediatr. Surg.* 2009; **19**: 47–9.
271 Yarlagadda R, Menda Y, Graham MM. Tc-99m red blood cell imaging in a patient with blue rubber bleb nevus syndrome. *Clin. Nucl. Med.* 2008; **33**: 374–376.
272 Mechri M, Soyer P, Boudiaf M, Duchat F, Hamzi L, Rymer R. Small bowel involvement in blue rubber bleb nevus syndrome: MR imaging features. *Abdom. Imaging* 2009; **34**: 448–51.
273 Certo M, Lopes L, Ramada J. Blue rubber bleb nevus syndrome: manifestations at computed tomography. *Acta. Radiol.* 2007; **48**: 962–6.
274 Kopacova M, Tacheci I, Koudelka J, Kralova M, Rejchrt S, Bures J. A new approach to blue rubber bleb nevus syndrome: the role of capsule endoscopy and intra-operative enteroscopy. *Pediatr. Surg. Int.* 2007; **23**: 693–7.
275 De Bona M, Bellumat A, De Boni M. Capsule endoscopy for the diagnosis and follow-up of blue rubber bleb nevus syndrome. *Dig. Liver Dis.* 2005; **37**: 451–3.
276 Place RJ. Blue rubber bleb nevus syndrome: a case report with long-term follow-up. *Mil. Med.* 2001; **166**: 728–30.
277 Jacob AG, Driscoll DJ, Shaughnessy WJ, Stanson AW, Clay RP, Gloviczki P. Klippel-Trenaunay syndrome: spectrum and management. *Mayo Clin. Proc.* 1998; **73**: 28–36.
278 Capraro PA, Fisher J, Hammond DC, Grossman JA. Klippel-Trenaunay syndrome. *Plast. Reconstr. Surg.* 2002; **109**: 2052–60; quiz 2061–2052.
279 Meine JG, Schwartz RA, Janniger CK. Klippel-Trenaunay-Weber syndrome. *Cutis* 1997; **60**: 127–32.
280 Redondo P, Aguado L, Martinez-Cuesta A. Diagnosis and management of extensive vascular malformations of the lower limb: part II. Systemic repercussions [corrected], diagnosis, and treatment. *J. Am. Acad. Dermatol.* 2011; **65**: 909–23; quiz 924.
281 Gloviczki P, Hollier LH, Telander RL, Kaufman B, Bianco AJ, Stickler GB. Surgical implications of Klippel-Trenaunay syndrome. *Ann. Surg.* 1983; **197**: 353–62.
282 McGrory BJ, Amadio PC. Klippel-Trenaunay syndrome: orthopaedic considerations. *Orthop. Rev.* 1993; **22**: 41–50.
283 Takata M, Watanabe K, Matsubara H, Takato K, Nomura I, Tsuchiya H. Lengthening of the normal tibia in a patient with hemihypertrophy caused by Klippel-Trenaunay-Weber syndrome: a case report. *J. Orthop. Surg. (Hong Kong)* 2011; **19**: 359–63.

This article has been co-published with the permission of *The Journal of Dermatology, Pediatrics International and Japanese Journal of Radiology*. All rights reserved. © 2020 The Authors. The articles are identical except for minor stylistic and spelling differences in keeping with each journal's style. Either citation can be used when citing this article.

284 Servelle M. Klippel and Trenaunay's syndrome. 768 operated cases. *Ann. Surg.* 1985; **201**: 365–73.
285 Gates PE, Drvaric DM, Kruger L. Wound healing in orthopaedic procedures for Klippel-Trenaunay syndrome. *J. Pediatr. Orthop.* 1996; **16**: 723–6.
286 Bajaj Y, Hewitt R, Ifeacho S, Hartley BE. Surgical excision as primary treatment modality for extensive cervicofacial lymphatic malformations in children. *Int. J. Pediatr. Otorhinolaryngol.* 2011; **75**: 673–7.
287 Orvidas LJ, Kasperbauer JL. Pediatric lymphangiomas of the head and neck. *Ann. Otol. Rhinol. Laryngol.* 2000; **109**: 411–21.
288 Alqahtani A, Nguyen LT, Flageole H, Shaw K, Laberge JM. 25 years' experience with lymphangiomas in children. *J. Pediatr. Surg.* 1999; **34**: 1164–68.
289 Wiegand S, Zimmermann AP, Eivazi B, Sesterhenn AM, Werner JA. Lymphatic malformations involving the parotid gland. *Eur. J. Pediatr. Surg.* 2011; **21**: 242–5.
290 Chen WL, Zhang B, Wang JG, Ye HS, Zhang DM, Huang ZQ. Surgical excision of cervicofacial giant macrocystic lymphatic malformations in infants and children. *Int. J. Pediatr. Otorhinolaryngol.* 2009; **73**: 833–7.
291 Lei ZM, Huang XX, Sun ZJ, Zhang WF, Zhao YF. Surgery of lymphatic malformations in oral and cervicofacial regions in children. *Oral Surg. Oral Med. Oral Pathol. Oral Radiol. Endod.* 2007; **104**: 338–44.
292 Okazaki T, Iwatani S, Yanai T *et al*. Treatment of lymphangioma in children: our experience of 128 cases. *J. Pediatr. Surg.* 2007; **42**: 386–9.
293 Hamoir M, Plouin-Gaudon I, Rombaux P *et al*. Lymphatic malformations of the head and neck: a retrospective review and a support for staging. *Head Neck* 2001; **23**: 326–37.
294 Fageeh N, Manoukian J, Tewfik T, Schloss M, Williams HB, Gaskin D. Management of head and neck lymphatic malformations in children. *J. Otolaryngol.* 1997; **26**: 253–8.
295 Padwa BL, Hayward PG, Ferraro NF, Mulliken JB. Cervicofacial lymphatic malformation: clinical course, surgical intervention, and pathogenesis of skeletal hypertrophy. *Plast. Reconstr. Surg.* 1995; **95**: 951–60.
296 de Serres LM, Sie KC, Richardson MA. Lymphatic malformations of the head and neck. A proposal for staging. *Arch. Otolaryngol. Head Neck Surg.* 1995; **121**: 577–82.
297 Riechelmann H, Muehlfay G, Keck T, Mattfeldt T, Rettinger G. Total, subtotal, and partial surgical removal of cervicofacial lymphangiomas. *Arch. Otolaryngol. Head Neck Surg.* 1999; **125**: 643–8.
298 Greinwald J Jr, Cohen AP, Hemanackah S, Azizkhan RG. Massive lymphatic malformations of the head, neck, and chest. *J. Otolaryngol. Head Neck Surg.* 2008; **37**: 169–73.
299 Yang Y, Sun M, Ma Q *et al*. Bleomycin A5 sclerotherapy for cervicofacial lymphatic malformations. *J. Vasc. Surg.* 2011; **53**: 150–5.
300 Alomari AI, Karian VE, Lord DJ, Padua HM, Burrows PE. Percutaneous sclerotherapy for lymphatic malformations: a retrospective analysis of patient-evaluated improvement. *J. Vasc. Interv. Radiol.* 2006; **17**: 1639–48.
301 Chaudry G, Guevara CJ, Rialon KL *et al*. Safety and efficacy of bleomycin sclerotherapy for microcystic lymphatic malformation. *Cardiovasc. Intervent. Radiol.* 2014; **37**: 1476–81.
302 Smith MC, Zimmerman MB, Burke DK *et al*. Efficacy and safety of OK-432 immunotherapy of lymphatic malformations. *Laryngoscope* 2009; **119**: 107–15.
303 Giguère CM, Bauman NM, Sato Y *et al*. Treatment of lymphangiomas with OK-432 (Picibanil) sclerotherapy: a prospective multi-institutional trial. *Arch. Otolaryngol. Head Neck Surg.* 2002; **128**: 1137–44.
304 Udagawa A, Yoshimoto S, Matumoto F *et al*. A case of facial cavernous lymphangioma: observation from infancy to adulthood. *Nihon Togai Gaku Ganmen Geka Gakkaishi* 2005; **21**: 302–9.
305 Nagao M, Sasaki S, Furukawa H, Uchiyama E, Yamamoto Y. [Treatments for huge lymphatic malformations of cheek, oral cavity and neck]. *Nihon Keisei Geka Gakkai Kaishi* 2007; **27**: 779–82. Japanese.
306 Ravindranathan H, Gillis J, Lord DJ. Intensive care experience with sclerotherapy for cervicofacial lymphatic malformations. *Pediatr. Crit. Care Med.* 2008; **9**: 304–9.
307 Poonyathalang A, Preechawat P, Jiarakongmun P, Pongpech S. Sclerosing therapy for orbital lymphangioma using sodium tetradecyl sulfate. *Jpn. J. Ophthalmol.* 2008; **52**: 298–304.
308 Emran MA, Dubois J, Laberge L, Al-Jazaeri A, Butter A, Yazbeck S. Alcoholic solution of zein (Ethibloc) sclerotherapy for treatment of lymphangiomas in children. *J. Pediatr. Surg.* 2006; **41**: 975–9.
309 Bai Y, Jia J, Huang XX, Alsharif MJ, Zhao JH, Zhao YF. Sclerotherapy of microcystic lymphatic malformations in oral and facial regions. *J. Oral. Maxillofac. Surg.* 2009; **67**: 251–6.
310 Shiels WE 2nd, Kang DR, Murakami JW, Hogan MJ, Wiet GJ. Percutaneous treatment of lymphatic malformations. *Otolaryngol. Head Neck Surg.* 2009; **141**: 219–24.
311 Nehra D, Jacobson L, Barnes P, Mallory B, Albanese CT, Sylvester KG. Doxycycline sclerotherapy as primary treatment of head and neck lymphatic malformations in children. *J. Pediatr. Surg.* 2008; **43**: 451–60.
312 Asonuma K, Inomata Y. [Current strategy and outcome of treatment of lymphangioma in children: the analysis of a survey in the Kyushu and Okinawa area]. *Nihon Shoni Geka Gakkai Zasshi* 2006; **42**: 215–21. Japanese.
313 Schwarcz RM, Ben Simon GJ, Cook T, Goldberg RA. Sclerosing therapy as first line treatment for low flow vascular lesions of the orbit. *Am. J. Ophthalmol.* 2006; **141**: 333–9.
314 Oyama T, Eguchi K, Cho H, Abe H. A variety of orbital lymphangioma treatments: one case treated with orbital decompression therapy and the other case with intralesional injection of OK-432 therapy. *Nihon Ganka Gakkai Zasshi* 2009; **113**: 732–40. Japanese.
315 Cahill AM, Nijs E, Ballah D *et al*. Percutaneous sclerotherapy in neonatal and infant head and neck lymphatic malformations: a single center experience. *J. Pediatr. Surg.* 2011; **46**: 2083–95.
316 Chaudry G, Burrows PE, Padua HM, Dillon BJ, Fishman SJ, Alomari AI. Sclerotherapy of abdominal lymphatic malformations with doxycycline. *J. Vasc. Interv. Radiol.* 2011; **22**: 1431–5.
317 Oliveira C, Sacher P, Meuli M. Management of prenatally diagnosed abdominal lymphatic malformations. *Eur. J. Pediatr. Surg.* 2010; **20**: 302–6.
318 Won JH, Kim BM, Kim CH, Park SW, Kim MD. Percutaneous sclerotherapy of lymphangiomas with acetic acid. *J. Vasc. Interv. Radiol.* 2004; **15**: 595–600.
319 Shiels WE 2nd, Kenney BD, Caniano DA, Besner GE. Definitive percutaneous treatment of lymphatic malformations of the trunk and extremities. *J. Pediatr. Surg.* 2008; **43**: 136–9: discussion 140.
320 Chiappinelli A, Forgues D, Galifer RB. Congenital abdominal cystic lymphangiomas: what is the correct management? *J. Matern. Fetal Neonatal Med.* 2012; **25**: 915–9.
321 Muraoka A, Suzuki N, Niwa Y, Komatsu Y, Tagami K. [A case report of an asymptomatic giant retroperitoneal lymphangioma pointed out at a physical examination]. *Nihon Rinsho Geka Gakkai Zasshi* 2009; **70**: 899–905. Japanese.

This article has been co-published with the permission of *The Journal of Dermatology, Pediatrics International and Japanese Journal of Radiology*. All rights reserved. © 2020 The Authors. The articles are identical except for minor stylistic and spelling differences in keeping with each journal's style. Either citation can be used when citing this article.

322 Oyachi N, Iwashita K, Kubo M. [Diagnosis and management of mesenteric lymphangioma: comparison of prenatal and school-age diagnosed cases]. *Nihon Shoni Geka Gakkai Zasshi* 2008; **44**: 33–7. Japanese.
323 Mendez-Gallart R, Bautista A, Estevez E, Rodriguez-Barca P. Abdominal cystic lymphangiomas in pediatrics: surgical approach and outcomes. *Acta Chir. Belg.* 2011; **111**: 374–7.
324 Ikeda T, Asai Y, Nango Y *et al*. [Childhood abdominal cystic lymphangioma]. *Nihon Shoni Geka Gakkai Zasshi* 2008; **44**: 959–64. Japanese.
325 Losanoff JE, Kjossev KT. Mesenteric cystic lymphangioma: unusual cause of intra-abdominal catastrophe in an adult. *Int. J. Clin. Pract.* 2005; **59**: 986–7.
326 Uchiyama M, Murata H, Ohtaki M. [Acute abdomen by inflammatory infiltration of retroperitoneal lymphangioma to the duodenum: report of a case and review of cases in childhood]. *Nihon Shoni Geka Gakkai Zasshi* 2007; **43**: 938–44. Japanese.
327 Bellini C, Ergaz Z, Radicioni M *et al*. Congenital fetal and neonatal visceral chylous effusions: neonatal chylothorax and chylous ascites revisited. A multicenter retrospective study. *Lymphology* 2012; **45**: 91–102.
328 Matsuo Y, Okada A. The role and use of Sudan Black in the surgical treatment of chylothorax and chylous ascites. *Shoni Geka* 2001; **33**: 186–90. Japanese.
329 Spagnol L, Conforti A, Valfre L, Morini F, Bagolan P. Preoperative administration of Sudan III and successful treatment of persistent chylous ascites in a neonate. *J. Pediatr. Surg.* 2011; **46**: 994–7.
330 Joe K, Kemmotsu H, Mori T, Goto C, Ohkawa H. [Treatment of idiopathic chylous ascites in infants]. *Shoni Geka* 2001; **33**: 134–40. Japanese.
331 Moreira Dde A, Santos MM, Tannuri AC, Tannuri U. Congenital chylous ascites: a report of a case treated with hemostatic cellulose and fibrin glue. *J. Pediatr. Surg.* 2013; **48**: e17–9.
332 Olivieri C, Nanni L, Masini L, Pintus C. Successful management of congenital chylous ascites with early octreotide and total parenteral nutrition in a newborn. *BMJ Case Rep.* 2012; **2012**. https://doi.org/10.1136/bcr-2012-006196
333 Huang Y, Zhuang S, Li Y, Liu M, Chen H, Du M. Successful management of congenital chylous ascites in a premature infant using somatostatin analogue. *Indian J. Pediatr.* 2011; **78**: 345–7.
334 Melo-Filho AA, Souza IJ, Leite CA, Leite RD, Colares JH, Correia JM. Refractory congenital chylous ascites. *Indian J. Pediatr.* 2010; **77**: 1335–7.
335 Karagol BS, Zenciroglu A, Gokce S, Kundak AA, Ipek MS. Therapeutic management of neonatal chylous ascites: report of a case and review of the literature. *Acta Paediatr.* 2010; **99**: 1307–10.
336 Kuroiwa M, Toki F, Suzuki M, Suzuki N. Successful laparoscopic ligation of the lymphatic trunk for refractory chylous ascites. *J. Pediatr. Surg.* 2007; **42**: E15–8.
337 Antao B, Croaker D, Squire R. Successful management of congenital chyloperitoneum with fibrin glue. *J. Pediatr. Surg.* 2003; **38**: E7–8.
338 Nakagawa J, Nakabayashi M, Kikuchi M *et al*. [A case of congenital chyloperitoneum improved by prenatal treatment]. *Nihon Sanka Fujinka Gakkai Tokyo Chiho Bukai Kaishi* 2002; **51**: 399–403. Japanese.
339 Wakisaka M, Kitagawa H, Satoh Y, Nakada K. Congenital chylo-ascites treated by laparotomy and OK-432 injection. *Shoni Geka* 2001; **33**: 196–200. Japanese.
340 Sato H, Okamatsu T, Yatsuzuka M *et al*. Chylous ascites resolved by exploratory laparotomy. *Shoni Geka* 2001; **33**: 191–5. Japanese.
341 Takahashi A, Suzuki N, Kuwano H. Neonatal chylous ascites. *Shoni Geka* 2001; **33**: 144–7. Japanese.
342 Komuro H. [Endoscopic surgery for chylothorax and chylous ascites]. *Shoni Geka* 2010; **42**: 805–8. Japanese.
343 Zeidan S, Delarue A, Rome A, Roquelaure B. Fibrin glue application in the management of refractory chylous ascites in children. *J. Pediatr. Gastroenterol. Nutr.* 2008; **46**: 478–81.
344 Huang Q, Jiang ZW, Jiang J, Li N, Li JS. Chylous ascites: treated with total parenteral nutrition and somatostatin. *World J. Gastroenterol.* 2004; **10**: 2588–91.
345 Nemoto T, Tsuchiya H, Nagashima K. Clinical and experimental analysis for chylothorax and chylous ascites. *Shoni Geka* 2001; **33**: 119–22. Japanese.
346 Ohtsu K, Ueda Y, Kurihara S, Kawashima M. Intractable chylous ascites. *Shoni Geka* 2011; **43**: 747–50. Japanese.
347 Ono S, Iwai N, Chiba F, Furukawa T, Fumino S. OK-432 therapy for chylous pleural effusion or ascites associated with lymphatic malformations. *J. Pediatr. Surg.* 2010; **45**: e7–10.
348 Tanaka M, Yokomori K, Kamii Y. Chylous ascites caused by a retroperitoneal lymphangioma: a case report. *Shoni Geka* 2001; **33**: 163–7. Japanese.
349 Siebert S, Helbling C, Wolff M *et al*. Peritoneovenous shunting as palliative treatment in an infant with chylous ascites due to generalised congenital lymphangiectasia. *Klin. Padiatr.* 2010; **222**: 317–8.
350 Densupsoontorn N, Jirapinyo P, Aanpreung P, Laohapensang M, Parichatikanond P. Congenital chylous ascites: the roles of fibrin glue and CD31. *Acta Paediatr.* 2009; **98**: 1847–9.
351 Guvenc BH, Ekingen G, Tuzlaci A, Senel U. Diffuse neonatal abdominal lymphangiomatosis: management by limited surgical excision and sclerotherapy. *Pediatr. Surg. Int.* 2005; **21**: 595–8.
352 Kotera A, Kamagata S, Hirobe S *et al*. A case of diffuse lymphangiomatosis with chylothorax and chylous ascites. *Shoni Geka* 2001; **33**: 128–33. Japanese.
353 Horisawa M, Nishimoto K, Ogura Y, Tainaka T, Matsunaga K, Niinomi N. Generalized lymphatic dysplasia with intermittent chylous discharge from the scrotum: a case report. *Shoni Geka* 2001; **33**: 180–5. Japanese.
354 Katz MS, Finck CM, Schwartz MZ *et al*. Vacuum-assisted closure in the treatment of extensive lymphangiomas in children. *J. Pediatr. Surg.* 2012; **47**: 367–70.
355 Sugito K, Ikeda T, Hagiwara N *et al*. [A case of large mesenteric cyst with inflammatory reaction]. *Shoni Geka* 2001; **33**: 1017–20. Japanese.
356 Chang TS, Ricketts R, Abramowsky CR *et al*. Mesenteric cystic masses: a series of 21 pediatric cases and review of the literature. *Fetal Pediatr. Pathol.* 2011; **30**: 40–4.
357 Tran NS, Nguyen TL. Laparoscopic management of abdominal lymphatic cyst in children. *J. Laparoendosc. Adv. Surg. Tech. A* 2012; **22**: 505–7.
358 Boardman SJ, Cochrane LA, Roebuck D, Elliott MJ, Hartley BE. Multimodality treatment of pediatric lymphatic malformations of the head and neck using surgery and sclerotherapy. *Arch. Otolaryngol. Head Neck Surg.* 2010; **136**: 270–6.
359 Park JG, Aubry MC, Godfrey JA, Midthun DE. Mediastinal lymphangioma: Mayo Clinic experience of 25 cases. *Mayo Clin. Proc.* 2006; **81**: 1197–203.
360 Adams MT, Saltzman B, Perkins JA. Head and neck lymphatic malformation treatment: a systematic review. *Otolaryngol. Head Neck Surg.* 2012; **147**: 627–39.
361 Leung M, Leung L, Fung D *et al*. Management of the low-flow head and neck vascular malformations in children: the sclerotherapy protocol. *Eur. J. Pediatr. Surg.* 2014; **24**: 97–101.

This article has been co-published with the permission of *The Journal of Dermatology, Pediatrics International and Japanese Journal of Radiology*. All rights reserved. © 2020 The Authors. The articles are identical except for minor stylistic and spelling differences in keeping with each journal's style. Either citation can be used when citing this article.

362 Ogawa T, Shibayama M, Shimizu T. Clinical analysis of lymphangioma in the neck: the effects of local OK-432 injection therapy. *Jibi Inkoka Rinsho* 2010; **103**: 249–55. Japanese.
363 Arimoto Y, Kudo F, Suzuki H. Usefulness of ultrasonography in the differential diagnosis of respiratory distress disorders including infantile paresis of the vocal cords. *Shoni Jibi Inkoka* 2005; **26**: 37–42. Japanese.
364 Kitagawa H, Kawase H, Wakisaka M *et al*. Six cases of children with a benign cervical tumor who required tracheostomy. *Pediatr. Surg. Int.* 2004; **20**: 51–4.
365 Hiki S, Yamataka A, Kobayashi H, Okada Y, Miyano T. [Treatment of lymphangioma in children. A report of 105 cases]. *Juntendo Igaku* 2003; **48**: 476–83. Japanese.
366 Desir A, Ghaye B, Duysinx B, Dondelinger RF. Percutaneous sclerotherapy of a giant mediastinal lymphangioma. *Eur. Respir. J.* 2008; **32**: 804–6.
367 Kim DW. OK-432 sclerotherapy of lymphatic malformation in the head and neck: factors related to outcome. *Pediatr. Radiol.* 2014; **44**: 857–62.
368 Niramis R, Watanatittan S, Rattanasuwan T. Treatment of cystic hygroma by intralesional bleomycin injection: experience in 70 patients. *Eur. J. Pediatr. Surg.* 2010; **20**: 178–82.
369 Kudo F, Arimoto Y, Nakano A. [Sclerosing therapy for cystic hygroma in infants: intracystic injection of OK-432]. *Tokeibu Geka* 2008; **18**: 71–5. Japanese.
370 Kim MG, Kim SG, Lee JH, Eun YG, Yeo SG. The therapeutic effect of OK-432 (picibanil) sclerotherapy for benign neck cysts. *Laryngoscope* 2008; **118**: 2177–81.
371 Baskota DK, Singh BB, Sinha BK. OK-432: an effective sclerosing agent for the treatment of lymphangiomas of head and neck. *Kathmandu Univ. Med. J. (KUMJ)* 2007; **5**: 312–7.
372 Jamal N, Ahmed S, Miller T *et al*. Doxycycline sclerotherapy for pediatric head and neck macrocystic lymphatic malformations: a case series and review of the literature. *Int. J. Pediatr. Otorhinolaryngol.* 2012; **76**: 1127–31.
373 Tomemori T, Kudo F, Sasamura Y, Numata T. [Cystic hygroma in infants]. *Tokeibu Shuyo* 2003; **29**: 58–63. Japanese.
374 Dasgupta R, Adams D, Elluru R, Wentzel MS, Azizkhan RG. Noninterventional treatment of selected head and neck lymphatic malformations. *J. Pediatr. Surg.* 2008; **43**: 869–73.
375 Hogeling M, Adams S, Law J, Wargon O. Lymphatic malformations: clinical course and management in 64 cases. *Australas. J. Dermatol.* 2011; **52**: 186–90.
376 Acevedo JL, Shah RK, Brietzke SE. Nonsurgical therapies for lymphangiomas: a systematic review. *Otolaryngol. Head Neck Surg.* 2008; **138**: 418–24.
377 Kim KH, Sung MW, Roh JL, Han MH. Sclerotherapy for congenital lesions in the head and neck. *Otolaryngol. Head Neck Surg.* 2004; **131**: 307–16.
378 Catalfamo L, Nava C, Lombardo G, Iudicello V, Siniscalchi EN, Saverio PF. Tongue lymphangioma in adult. *J. Craniofac. Surg.* 2012; **23**: 1920–2.
379 Magoshi S, Okada M, Shigematsu H, Suzuki S, Kusama K, Sakashita H. [A case of hemangio-lymphangioma of the tongue]. *Nihon Koku Shindan Gakkai Zasshi* 2003; **16**: 250–2. Japanese.
380 Ogiuchi H, Yamazaki T, Yamamura T, Kuwazawa T, Ogiuchi H. A long-term follow-up, case of lymphangioma of tongue and floor of the mouth. *Shoni Koku Geka* 2003; **13**: 17–20. Japanese.
381 Rowley H, Perez-Atayde AR, Burrows PE, Rahbar R. Management of a giant lymphatic malformation of the tongue. *Arch. Otolaryngol. Head Neck Surg.* 2002; **128**: 190–94.
382 Chakravarti A, Bhargava R. Lymphangioma circumscriptum of the tongue in children: successful treatment using intralesional bleomycin. *Int. J. Pediatr. Otorhinolaryngol.* 2013; **77**: 1367–9.
383 Wiegand S, Eivazi B, Zimmermann AP *et al*. Microcystic lymphatic malformations of the tongue: diagnosis, classification, and treatment. *Arch. Otolaryngol. Head Neck Surg.* 2009; **135**: 976–83.
384 Hong JP, Lee MY, Kim EK, Seo DH. Giant lymphangioma of the tongue. *J. Craniofac. Surg.* 2009; **20**: 252–4.
385 Azizkhan RG, Rutter MJ, Cotton RT, Lim LH, Cohen AP, Mason JL. Lymphatic malformations of the tongue base. *J. Pediatr. Surg.* 2006; **41**: 1279–84.
386 Ogawa-Ochiai K, Sekiya N, Kasahara Y *et al*. A case of mediastinal lymphangioma successfully treated with Kampo medicine. *J. Altern. Complement. Med.* 2011; **17**: 563–5.
387 Roy S, Reyes S, Smith LP. Bipolar radiofrequency plasma ablation (Coblation) of lymphatic malformations of the tongue. *Int. J. Pediatr. Otorhinolaryngol.* 2009; **73**: 289–93.
388 Kemmotsu T, Takeda Y, Nakamura K, Tateishi I. [A case of congenital chylothorax requiring early OK-432 pleurodesis]. *Nihon Shusanki Shinseiji Igakkai Zasshi* 2012; **48**: 945–50. Japanese.
389 Tani G, Okuyama H, Kubota A, Kawahara H. [Thoracoscopic thoracic duct ligation in a premature infant with congenital chylothorax]. *Nihon Shoni Geka Gakkai Zasshi* 2011; **47**: 844–7. Japanese.
390 Miura K, Yoshizawa K, Tamaki M, Okumura K, Okada M. [Congenital chylothorax treated with video-assisted thoracic surgery]. *Kyobu Geka* 2008; **61**: 1149–51. Japanese.
391 Amagai T, Nakamura H, Kaneko M, Sugiura M, Hamada H. Use and problems of pleuro-peritoneal shunting tube for neonatal chylothorax. *Shoni Geka* 2001; **33**: 201–7. Japanese.
392 Cleveland K, Zook D, Harvey K, Woods RK. Massive chylothorax in small babies. *J. Pediatr. Surg.* 2009; **44**: 546–50.
393 Buttiker V, Fanconi S, Burger R. Chylothorax in children: guidelines for diagnosis and management. *Chest* 1999; **116**: 682–7.
394 Kaji M, Sakauchi M, Yoshii K *et al*. [A case of chylothorax treated effectively with surgery]. *Tokyo Joshi Ika Daigaku Zasshi* 2013; **83**: E366–70. Japanese.
395 Haga T, Toida C, Muguruma T, Fujino A. [Two cases of mediastinal lymphangiomatosis that required intensive care management]. *Nihon Shonika Gakkai Zasshi* 2013; **117**: 1483–8. Japanese.
396 Chen YL, Lee CC, Yeh ML, Lee JS, Sung TC. Generalized lymphangiomatosis presenting as cardiomegaly. *J. Formos. Med. Assoc.* 2007; **106**: S10–4.
397 Pfleger A, Schwinger W, Maier A, Tauss J, Popper HH, Zach MS. Gorham-Stout syndrome in a male adolescent-case report and review of the literature. *J. Pediatr. Hematol. Oncol.* 2006; **28**: 231–3.
398 Noda M, Endo C, Hoshikawa Y *et al*. Successful management of intractable chylothorax in Gorham-Stout disease by awake thoracoscopic surgery. *Gen. Thorac. Cardiovasc. Surg.* 2013; **61**: 356–8.
399 Fukahori S, Tsuru T, Asagiri K *et al*. Thoracic lymphangiomatosis with massive chylothorax after a tumor biopsy and with disseminated intravenous coagulation–lymphoscintigraphy, an alternative minimally invasive imaging technique: report of a case. *Surg. Today* 2011; **41**: 978–82.

This article has been co-published with the permission of *The Journal of Dermatology, Pediatrics International and Japanese Journal of Radiology*. All rights reserved. © 2020 The Authors. The articles are identical except for minor stylistic and spelling differences in keeping with each journal's style. Either citation can be used when citing this article.

400 Brodszki N, Lansberg JK, Dictor M *et al*. A novel treatment approach for paediatric Gorham-Stout syndrome with chylothorax. *Acta Paediatr.* 2011; **100**: 1448–53.
401 Deveci M, Inan N, Corapcioglu F, Ekingen G. Gorham-Stout syndrome with chylothorax in a six-year-old boy. *Indian J. Pediatr.* 2011; **78**: 737–9.
402 Seok YK, Cho S, Lee E. Early surgical management of chylothorax complicated by Gorham's disease. *Thorac. Cardiovasc. Surg.* 2010; **58**: 492–3.
403 Kose M, Pekcan S, Dogru D *et al*. Gorham-Stout Syndrome with chylothorax: successful remission by interferon alpha-2b. *Pediatr. Pulmonol.* 2009; **44**: 613–5.
404 Boyle MJ, Alison P, Taylor G, Lightbourne BA. A case of Gorham's disease complicated by bilateral chylothorax. *Heart Lung Circ.* 2008; **17**: 64–6.
405 Burgess S, Harris M, Dakin C, Borzi P, Ryan C, Cooper D. Successful management of lymphangiomatosis and chylothorax in a 7-month-old infant. *J. Paediatr. Child Health* 2006; **42**: 560–2.
406 Underwood J, Buckley J, Manning B. Gorham disease: an intraoperative case study. *AANA J.* 2006; **74**: 45–8.
407 Fujiu K, Kanno R, Suzuki H, Nakamura N, Gotoh M. Chylothorax associated with massive osteolysis (Gorham's syndrome). *Ann. Thorac. Surg.* 2002; **73**: 1956–7.
408 Chavanis N, Chaffanjon P, Frey G, Vottero G, Brichon PY. Chylothorax complicating Gorham's disease. *Ann. Thorac. Surg.* 2001; **72**: 937–9.
409 Konez O, Vyas PK, Goyal M. Disseminated lymphangiomatosis presenting with massive chylothorax. *Pediatr. Radiol.* 2000; **30**: 35–7.
410 Morita K, Fukumoto K, Mitsunaga M *et al*. [A case of thoracic lymphangiomatosis causing difficulty in treatment due to dyspnea and hemorrhage]. *Nihon Shoni Ketsueki Gan Gakkai Zasshi* 2013; **50**: 644–9. Japanese.
411 Kitami A, Suzuki T, Suzuki S, Usuda R, Kamio Y, Kadokura M. Gorham's disease complicated by chyloma of the chest wall. *Jpn. J. Thorac. Cardiovasc. Surg.* 2006; **54**: 311–3.
412 Lee S, Finn L, Sze RW, Perkins JA, Sie KC. Gorham Stout syndrome (disappearing bone disease): two additional case reports and a review of the literature. *Arch. Otolaryngol. Head Neck Surg.* 2003; **129**: 1340–3.
413 Reinglas J, Ramphal R, Bromwich M. The successful management of diffuse lymphangiomatosis using sirolimus: a case report. *Laryngoscope* 2011; **121**: 1851–4.
414 Tamay Z, Saribeyoglu E, Ones U *et al*. Diffuse thoracic lymphangiomatosis with disseminated intravascular coagulation in a child. *J. Pediatr. Hematol. Oncol.* 2005; **27**: 685–7.
415 Duffy BM, Manon R, Patel RR, Welsh JS. A case of Gorham's disease with chylothorax treated curatively with radiation therapy. *Clin. Med. Res.* 2005; **3**: 83–6.
416 Kinnier CV, Eu JP, Davis RD, Howell DN, Sheets J, Palmer SM. Successful bilateral lung transplantation for lymphangiomatosis. *Am. J. Transplant.* 2008; **8**: 1946–50.
417 Huang SY, Lee YM, Tzeng ST *et al*. Gorham syndrome with postoperative respiratory failure and requiring prolonged mechanical ventilation. *Respir. Care* 2013; **58**: e144–8.
418 Lee WS, Kim SH, Kim I *et al*. Chylothorax in Gorham's disease. *J. Korean Med. Sci.* 2002; **17**: 826–9.
419 Fontanesi J. Radiation therapy in the treatment of Gorham disease. *J. Pediatr. Hematol. Oncol.* 2003; **25**: 816–7.
420 Yoo SY, Goo JM, Im JG. Mediastinal lymphangioma and chylothorax: thoracic involvement of Gorham's disease. *Korean J. Radiol.* 2002; **3**: 130–2.
421 Timke C, Krause MF, Oppermann HC, Leuschner I, Claviez A. Interferon alpha 2b treatment in an eleven-year-old boy with disseminated lymphangiomatosis. *Pediatr. Blood Cancer* 2007; **48**: 108–11.

This article has been co-published with the permission of *The Journal of Dermatology, Pediatrics International and Japanese Journal of Radiology*. All rights reserved. © 2020 The Authors. The articles are identical except for minor stylistic and spelling differences in keeping with each journal's style. Either citation can be used when citing this article.

Japanese Journal of Radiology
https://doi.org/10.1007/s11604-019-00885-5

SPECIAL REPORT

Japanese clinical practice guidelines for vascular anomalies 2017

Hidefumi Mimura[1] · Sadanori Akita[2] · Akihiro Fujino[3] · Masatoshi Jinnin[4] · Mine Ozaki[5] · Keigo Osuga[6] · Hiroki Nakaoka[7] · Eiichi Morii[8] · Akira Kuramochi[9] · Yoko Aoki[10] · Yasunori Arai[1] · Noriko Aramaki[11] · Masanori Inoue[12] · Yuki Iwashina[5] · Tadashi Iwanaka[13] · Shigeru Ueno[14] · Akihiro Umezawa[15] · Michio Ozeki[16] · Junko Ochi[17] · Yoshiaki Kinoshita[18] · Masakazu Kurita[19] · Shien Seike[20] · Nobuyuki Takakura[21] · Masataka Takahashi[15] · Takao Tachibana[22] · Kumiko Chuman[23] · Shuji Nagata[24] · Mitsunaga Narushima[25] · Yasunari Niimi[26] · Shunsuke Nosaka[27] · Taiki Nozaki[28] · Kazuki Hashimoto[1] · Ayato Hayashi[29] · Satoshi Hirakawa[30] · Atsuko Fujikawa[1] · Yumiko Hori[8] · Kentaro Matsuoka[31] · Hideki Mori[7] · Yuki Yamamoto[4] · Shunsuke Yuzuriha[32] · Naoaki Rikihisa[33] · Shoji Watanabe[34] · Shinichi Watanabe[35] · Tatsuo Kuroda[36] · Shunsuke Sugawara[37] · Kosuke Ishikawa[38] · Satoru Sasaki[39]

© The Author(s) 2020

Abstract

The objective was to prepare guidelines to perform the current optimum treatment by organizing effective and efficient treatments of hemangiomas and vascular malformations, confirming the safety, and systematizing treatment, employing evidence-based medicine (EBM) techniques and aimed at improvement of the outcomes. Clinical questions (CQs) were decided based on the important clinical issues. For document retrieval, key words for literature searches were set for each CQ and literature published from 1980 to the end of September 2014 was searched in Pubmed, Cochrane Library, and Japana Centra Revuo Medicina (JCRM). The strengths of evidence and recommendations acquired by systematic reviews were determined following the Medical Information Network Distribution System (MINDS) technique. A total of 33 CQs were used to compile recommendations and the subjects included efficacy of resection, sclerotherapy/embolization, drug therapy, laser therapy, radiotherapy, and other conservative treatment, differences in appropriate treatment due to the location of lesions and among symptoms, appropriate timing of treatment and tests, and pathological diagnosis deciding the diagnosis. Thus, the Japanese Clinical Practice Guidelines for Vascular Anomalies 2017 have been prepared as the evidence-based guidelines for the management of vascular anomalies.

Keywords Clinical practice · Guidelines · Hemangioma · Vascular anomalies · Vascular malformation

Introduction

The etiology of vascular anomalies on the body surface and in soft tissue are mostly unclear and no fundamental treatment methods have been established. Many patients visit many medical institutions seeking an expert, being a disadvantage in treatment. Hemangiomas and vascular malformations are frequently termed 'hemangioma', but these are different diseases in the ISSVA classification proposed by the International Society for Study of Vascular Anomalies (ISSVA) [1, 2], and this classification has been internationally standardized.

'Clinical Practice Guidelines for Vascular Anomalies 2013' (1st edition) [3] target general practitioners and the general public, and were prepared aiming at organizing effective and

Japanese Clinical Practice Guidelines for Vascular Anomalies 2017 were published in Japanese in 2017. We provide these guidelines in English to inform healthcare professionals and the general public in the world to improve medical practice and patient outcome. This article has been co-published in The Journal of Dermatology, Japanese Journal of Radiology, and Pediatrics International based on the agreement of Editor-In-Chief of the three journals.

✉ Hidefumi Mimura
mimura@marianna-u.ac.jp

Extended author information available on the last page of the article

Published online: 23 March 2020

efficient treatments for hemangiomas/vascular malformations, confirming the safety, and systematizing treatment using evidence-based medicine (EBM) techniques. The organization responsible for preparation was the Health, Labour and Welfare Sciences Research Grants (Research on Measures for Intractable Diseases), Research Committee for 'Intractable Vascular Anomalies', and the main committee members were selected from academic societies of plastic surgery and radiology mainly treating hemangiomas and vascular malformations: the Japanese Society of Plastic and Reconstructive Surgery and Japanese Society of Interventional Radiology, and the guidelines were prepared by them.

'Clinical Practice Guidelines for Vascular Anomalies 2017' were prepared as a revised edition of the 'Clinical Practice Guidelines for Vascular Anomalies 2013'. The organization responsible for preparation was the Health, Labour and Welfare Sciences Research Grants (Research on Policy Planning and Evaluation for Rare and Intractable Diseases), Research Committee for Intractable Vascular Anomalies, and the differences from the previous guidelines are setting the objective at summarizing opinions from related academic societies by inviting many committee members from dermatologists, pediatric surgeons, pediatricians, radiologists (diagnostic radiology), and basic researchers including the pathology, molecular biology, and epidemiology fields, in addition to plastic surgeons and radiologists (interventional radiology). Since the guidelines were prepared following the reformed 'Minds Handbook for Clinical Practice Guideline Development 2014' [4] and 'Minds Manual for Clinical Practice Guideline Development Ver.1.0-2.0' [5, 6], it was fully revised.

The original text of the guidelines (Japanese version) is comprised of Reviews and Clinical Questions (CQs), but only CQs are presented in this report.

Purpose of the guidelines

The objective was to prepare guidelines to perform the current optimum treatment by organizing effective and efficient treatments of hemangiomas and vascular malformations, confirming the safety, and systematizing treatment, employing the EBM techniques and aimed at improvement of the following outcomes: Pain, swelling, esthetic impairment, and functional disorder.

Materials and methods

Organization

For the Guidelines Executive Committee members, representatives of the plastic surgery, dermatology, radiology, pediatric surgery, and basic science fields were selected. The guidelines preparation group and systematic review team for preparation of CQs and recommendations were comprised of 4 groups: groups in charge of arteriovenous malformation (AVM), venous malformation (VM), combined type, and syndrome, in charge of capillary malformation (CM) and infantile hemangioma, in charge of the lymphatic malformation (lymphangioma) (LM), and in charge of the basic field. To the group in charge of AVM, VM, combined type, and syndrome, plastic surgeons and radiologists were mainly assigned. To the group in charge of CM and infantile hemangioma, plastic surgeons and dermatologists were mainly assigned. To the group in charge of the lymphatic system, pediatric surgeons, plastic surgeons, and pediatricians were mainly assigned. The Reviews of the guidelines were also prepared by those selected from each group. Pathologists and molecular biologists were in charge of the Reviews of the basic fields.

Preparation process

The guidelines were revised following the 'Minds Handbook for Clinical Practice Guideline Development 2014' and 'Minds Manual for Clinical Practice Guideline Development Ver.1.0-2.0'.

CQs were decided based on the following important clinical issues: (1) Efficacy of resection, (2) efficacy of sclerotherapy/embolization, (3) efficacy of drug therapy, laser therapy, radiotherapy, and other conservative treatment, (4) differences in appropriate treatment due to the location of lesions, (5) differences in appropriate treatment among symptoms, (6) appropriate timing of treatment and tests, and (7) pathological diagnosis deciding the diagnosis.

For document retrieval, key words for literature searches were set for each CQ and literature published from 1980 to the end of September 2014 was searched in Pubmed, Cochrane Library, and Japana Centra Revuo Medicina (JCRM). Literature search was requested to the Japan Medical Library Association. For decisions on CQs and recommendations lacking evidence or having weak evidence, discussion and agreement in the preparation group were reflected.

The strengths of evidence and recommendations acquired by systematic reviews were determined following the Minds technique as described below and this follows the GRADE guidelines preparation method [7, 8].

Determination of the strength of evidence of the body of evidence (Table 1)

The strength of evidence of the body of evidence was determined according to 'Minds Handbook for Clinical Practice Guideline Development 2014'.

In the case of RCTs, the score "A (strong)" is given at the start of evaluation, and the final score might be downgraded to B, C, or D, according to the results of evaluation of five items, including risk of bias, inconsistency in results, indirectness of evidence, data imprecision, and high possibility of publication bias. In the case of observational studies, the score "C (weak)" is given at the start of evaluation, and five items lowering the strength are evaluated similarly as for RCTs. In addition, three items, including large effect with no confounding factors, dose–response gradient, and possible confounding factors, are weaker than actual effects increasing the strength are evaluated as well.

Presentation of the strength of recommendations (Table 1)

The strength of recommendation was also determined according to 'Minds Handbook for Clinical Practice Guideline Development 2014'.

The strength of recommendations is usually presented in two ways: "1": strongly recommended, and "2": weakly recommended (suggested). If the strength of recommendations cannot be determined by any means, it is occasionally presented as "no definite recommendation can be made". Recommendations will be entered as follows by indicating the strength of evidence (A, B, C, D) with the strength of recommendations "1": strong or "2": weak.

Finalization

Preparation of the draft guidelines was completed in December 2016 and review was requested to the Japanese Society of Plastic and Reconstructive Surgery, Japanese Dermatological Association, Japan Radiology Society, Japanese Society of Interventional Radiology, Japanese Society of Pediatric Surgeons, and Japanese Society of Pathology between December 2016 and January 2017, and corrections were made based on the results of the reviews. In addition, from December 2016 to January 2017, the guidelines were disclosed on the home page of the Research Committee for 'Intractable Vascular Anomalies' and public comments were collected. The draft guidelines were presented to two related patient organizations, 'the Patients Association of Vascular Anomalies' and 'the Patients Association of Combined Vascular Malformations' and comments were received. Based on these, the draft guidelines were revised and CQs, recommendations, and explanations were completed. It was finalized in March 2017.

Table 1 Recommendation grade and definition of the strength of body of evidence in evaluation of systematic review

Recommendation grade
1 strongly recommended
2 weakly recommended (suggested)
Definition of the strength of body of evidence in evaluation of systematic review
A (strong): strongly confident of the estimate of effect
B (moderate): moderately confident of the estimate of effect
C (weak): limited confidence of the estimate of effect
D (very weak): very little confident of the estimate of effect

Results

CQs and recommendations

CQ1: What are the guidelines for the time to begin treatment for AVM?

Recommendation:

It is necessary to judge the time to begin endovascular or surgical treatment for AVM individually by evaluating the stage of symptoms and lesion extent and in consideration of the risk of complications.

Strength of recommendation	2 (weak)
Evidence	D (very weak)

Comments

As a result of primary screening, 92, 3, and 27 papers were extracted from PubMed, JCRM, and Cochrane Library, respectively, and, as a result of secondary screening, 37 and 3 papers were extracted from PubMed and JCRM, respectively. However, as all these references were observational or case series studies, the strength of evidence is rated as "D (very weak)".

There has been no report in which the time to begin treatment for AVM in itself was the endpoint, and only some reports described the view on the time to begin treatment in the discussion. Therefore, as it is difficult to objectively evaluate the validity of the time to begin treatment, we determined whether guidelines can be derived from the patient age, lesion site, symptoms, clinical stage, effectiveness of treatment, frequency of complications in each report.

In the reports [9, 10] on the treatment for AVM, symptomatic AVM is primarily addressed, and treatment can be suspended (follow-up) while the lesion remains asymptomatic. However, as AVM often progresses when left untreated, it is considered important to begin the treatment

at an appropriate time depending on the stage of symptoms. In addition, as there is the tendency that the response rate decreases, and the complication rate increases, with progression of symptoms, some reports from particular pediatric institutions where patients are concentrated recommend early therapeutic intervention in relatively "early" or "mild" stages without waiting for progression of the disease.

Localized lesions may be radically treated by early intervention [11]. Among endovascular procedures, the response (cure) rate tends to be high by ethanol embolization, but as the complication rate is also high [12, 13]. By surgery, localized lesions are unlikely to recur if they are completely resected, although adverse events, such as postoperative cicatrization/deformation or functional impairment, have been seldom discussed [10]. On the other hand, in diffuse lesions, limitations of effectiveness, such as recurrence and persistence and the risk of treatment, are higher by both endovascular treatment and surgery, with the risks outweighing benefits [13]. It should also be considered that children, in particular, are not mentally ready to accept such invasive treatments [14].

As discussed above, it is difficult to give guidelines for the time to begin treatment for AVM at present, and individual judgment is necessary depending on the symptom stage and lesion extent in consideration of the complication risk.

CQ2: Is recurrence (regrowth) after resection of AVM more frequent by wound closure with a skin graft than by reconstruction using a flap?

Recommendation:

Whether recurrence (regrowth) is more frequent by wound closure with a skin graft compared with reconstruction using a flap is unclear.

Strength of recommendation	2 (weak)
Evidence	D (very weak)

Comments

The number of references retrieved by searches using keywords was 40 from JCRM, 75 from PubMed, and 0 from Cochrane, and 39 were extracted by secondary screening. For AVM of a certain size, reconstruction is necessary after resection, and wound closure by skin grafting or reconstruction using a flap is performed according to common reconstruction methods for tissue defects. The reports discussing reconstruction after resection of AVM that we could retrieve were all descriptive studies (case reports or case series studies). Therefore, the evidence level of all these references is D (very weak).

The concept of regulating flap [15, 16], that reconstruction using a free flap controls the recurrence or regrowth after resection of AVM, has been proposed. However, no report has evaluated whether free flaps [16–37] and other flap types [17, 19, 25, 28, 38–49] clearly prevent the recurrence or regrowth compared with skin grafts [21, 23, 50–52].

According to the present knowledge about the recurrence or regrowth after resection of AVM [15, 16, 39, 53], whether AVM can be completely resected is important, and, concerning cases in which complete resection is difficult, it has been reported that the hemodynamics in the residual lesions contributes to the recurrence and regrowth, and that it can be controlled by a flap with rich blood flow.

CQ3: Is proximal ligation/coil embolization of the feeding artery of AVM effective?

Recommendation:

The therapeutic effect of ligation/coil embolization of the feeding artery on the proximal side may be poor, and the possibility of recurrence may be high. In addition, in the event of recurrence, treatment may become difficult due to the development of collateral vessels. Therefore, these procedures are recommended to be avoided, in principle.

Strength of recommendation	2 (weak)
Evidence	D (very weak)

Comments

As a result of secondary screening, 1 and 14 papers were extracted from PubMed and JCRM, respectively, and were reviewed. As a result, all these papers were case reports. In addition, 6 papers retrieved by manual searches were also reviewed, but they were all case series studies at the maximum. Therefore, the strength of evidence as a collection of literature concerning this CQ is D (very weak).

To summarize the evaluation of this collection of papers, AVM was treated by proximal ligation/coil embolization of the feeding artery, but as there have been reports of recurrence following the development of collateral channels (reports of cases of the occurrence of unfavorable situations), the treatment is recommended to be avoided, but the evidence level of this recommendation is low as mentioned above.

The objective of embolization for AVM is obliteration of the nidus, and embolization at or near the nidus is necessary as much as possible. If ligation/coil embolization of the feeding artery is performed on the proximal/central side, the nidus is not obliterated, and the development of several collateral channels is promoted. In many

cases, the collateral channels are thin, complicated, and markedly tortuous, and trans-catheter treatment is often difficult.

Wu et al. [14] performed proximal ligation in 9 of 29 patients treated for AVM of the auricle but that the condition was exacerbated in all patients with 8 requiring auricular resection and 1 requiring additional treatment. They excluded proximal ligation from treatment options for AVM, because it makes subsequent trans-catheter treatments difficult.

Slaba et al. [54] evaluated 25 patients with AVM of the tongue and reported that 3 of the 12 symptomatic patients who underwent ipsilateral external carotid artery ligation at another facility showed marked development of collateral channels.

Other reports include those of a case in which a large number of collateral channels developed as a result of ligation of the feeding artery for AVM of the shoulder with serious complications including high-output heart failure [55], 3 cases in which proximal ligation/embolization was performed for AVM of the limbs and pelvis, collateral vessels developed, but the condition was controlled by multidisciplinary treatment consisting of trans-catheter treatment and direct puncture sclerotherapy [56], and several cases in which external carotid artery ligation was performed for AVM of the head and neck, but the subsequent treatment was difficult.

Suyama et al. [35] reported a case in which AVM of the auricle, treated by proximal embolization using coils and gelatin sponge, recurred and was treated again by ligation at a proximal part of the artery, but the lesion recurred again. Also, Aikawa et al. [57] reported a case of intrapelvic AVM that underwent coil embolization of the left ovarian artery and left internal iliac artery but showed little change in the area of the nidus or the state of arterial or venous dilatation. In addition, Yamamoto et al. [58] reported a case in which TAE was performed for AVM of the mandible via the maxillary artery, facial artery, lingual artery, and ocular artery but was not effective due to the development of collateral channels from the internal carotid artery and vertebral artery.

As observed above, it is recommended not to select proximal/central ligation/coil embolization as a treatment for AVM. However, AV fistulas with direct connection of a large artery and a vessel may be treated by coil embolization if the shunt area is directly accessible with a catheter. Proximal coil embolization may also be accepted as preoperative embolization, but careful evaluation of its indications is necessary, and embolization at a site near the shunt is necessary to leave the room for catheter insertion in the event of future recurrence.

CQ4: What is the appropriate timing for embolization before resection of AVM?

Recommendation:

It is recommended to perform resection within 3 days (72 h) after embolization. If the interval prolongs, the risk of massive intraoperative hemorrhage may increase due to recanalization of the embolized vessel and development of collateral channels. In addition, surgery has been reported to be made difficult by enlargement of the lesion after embolization.

Strength of recommendation	2 (weak)
Evidence	D (very weak)

Comments

While it is difficult to generalize the therapeutic approach as it varies with the affected area and extent of the lesion, there were a few reports that preoperative embolization was useful for the treatment of AVM of the head and neck region.

As a result of secondary screening, 10 and 3 papers from PubMed and JCRM, respectively, were reviewed. All the papers selected by this screening procedure were case reports or case series, and the strength of evidence is "D (very weak)". Mentions about the timing of preoperative embolization and volume of hemorrhage also varied among the papers. Although it is difficult to draw a conclusion, among the papers that mentioned specific timing of preoperative embolization and volume of hemorrhage, Deng et al. [59] performed embolization within 48–72 h before surgery in 16 patients with maxillofacial AVM and reported that the volume of hemorrhage was ≤ 200 mL in all patients and that there were no complications. Erdmann et al. [60] performed embolization within 24 h before surgery in 4 patients with head and neck AVM, and the lesion was resected with hemorrhage of ≤ 100 mL in 3. It is recommended to perform resection within 72 h to prevent increases in difficulty of resection due to inflammation after embolization.

There have also been reports that embolization was performed intraoperatively or within a few days before surgery, resulting in decreases in the volume of hemorrhage or favorable long-term outcomes. Most papers reported no or only mild complications, but as for relatively severe complications, Goldberg et al. [61] reported temporary visual impairment in 2 of the 3 patients with orbital AVM.

Factors that affect the appropriate timing of preoperative embolization include recanalization of the target vessel, development of collateral channels, and swelling and reactive changes after embolization, which make surgery

difficult. To avoid the effects of these phenomena, many papers supported relatively early resection, i.e., within 72 h after embolization. Clinically, also, there is no benefit in taking a long interval, and it is considered valid to recommend resection within 72 h after embolization.

In conclusion, adequate control of hemorrhage may be achieved with fewer complications by performing vascular embolization within a few days before surgery, but no sufficient evidence that support this view has been provided.

CQ5: What treatments are appropriate for the maxillo-mandibular AVM?

Recommendation:

Although surgery alone is not recommended, a combination of surgery with endovascular embolization (including sclerotherapy) can be recommended depending on the case.

Radiotherapy is not recommended.

Endovascular embolization (including sclerotherapy) alone or as a preoperative treatment can be recommended.

Strength of recommendation	2 (weak)
Evidence	D (very weak)

Comments

AVM of the maxilla and mandible is a rare disorder. Most of the literature is reports of a small number of cases except a few case series reported from some special institutions. Only 5 reports [62–66] of a series of 10 or more cases were retrieved by the search of PubMed. Because there is no cohort study or randomized trial comparing various treatments, strong evidence regarding the best treatment is lacking.

Maxillo-mandibular AVM may involve the maxilla, mandible, or both, and it often presents with massive oral hemorrhage around the age of 10 years when milk teeth are lost, but may also be detected due to swelling of the soft tissue.

According to Persky et al. [62], embolization alone resulted in cure in 42%, improvement in 16%, and stabilization of symptoms in 23% of the 26 patients with a maxillo-mandibular AVM. Liu et al. [63] treated 25 patients by transarterial or transvenous embolization alone or in combination with curettage and reported anatomical cure in 14 and clinical cure in 21. Chen et al. [65] treated 15 patients by bone wax packing (BWP) alone in 4, transarterial embolization (TAE) + BWP in 3, TAE + resection in 4, and TAE + radiotherapy + resection in 4 and reported clinical cure in 14.

The following are considered as treatment options for AVM of the maxilla and mandible.

A. Surgical treatment
   - A-1. Resection and reconstruction
   - A-2. Curettage
   - A-3. Bone wax packing
B. Endovascular embolization (including sclerotherapy)
   - B-1. Transarterial embolization
   - B-2. Transvenous embolization
   - B-3. Embolization by direct puncture
C. Combination of A and B
D. Radiotherapy

The literature is mostly about B, i.e., endovascular embolization (including sclerotherapy) alone, or surgical treatment after B. There was no report of case series of surgical treatment alone, but there was only 1 report [65] of case series of surgery + radiotherapy. Surgery alone and radiotherapy are generally not recommended. Endovascular embolization is performed by various approaches including transarterial and transvenous routes and direct puncture, sometimes, in combination. Concerning embolic agents, PVA and Gelfoam® (Pfizer, New York, NY, USA) are used for embolization as an adjuvant therapy immediately before surgery as they allow recanalization. Cyanoacrylate liquid embolic agents are considered effective for embolization performed preoperatively or alone in expectation of a long-term occlusive effect [64, 67, 68]. Coils are often used for transvenous embolization. Recently, there have been reports [69, 70] that favorable outcomes were obtained by TAE using Onyx® (Medtronic, Irvine, CA, USA), a non-adhesive liquid embolic agent. Concerning sclerotherapy, there is a case series study of ethanol sclerotherapy alone, reporting relatively favorable outcomes [71]. Infection and bone necrosis are frequent complications of embolization, and they may occur, when an embolic agent, a foreign body, is injected into lesions that were in contact with the external environment due to direct puncture or hemorrhage. Surgical treatments as listed above are performed primarily after endovascular embolization. Invasive radical resection and reconstruction should be avoided at least as the initial treatment, because many lesions can now be controlled by endovascular embolization alone with the advancement of endovascular technique.

As mentioned above, endovascular embolization is performed using various approaches and embolic agents selected depending on the facility and patient. There are also a wide variety of surgical treatment options. Since the treatment may be performed by combining these options, AVM of the maxilla and mandible should be treated at the institutions where multidisciplinary treatment can be performed by experienced physicians.

CQ6: What treatments are appropriate for AVM of the fingers?

Recommendation:

Although embolization or sclerotherapy is effective as it alleviates symptoms, such as pain, sufficient evaluation is necessary because of the risk of finger necrosis and nerve damage. In surgical resection, total resection is recommended, because partial resection is likely to result in enlargement of the lesion. Occasionally, the disorder results in finger amputation.

Strength of recommendation	2 (weak)
Evidence	D (very weak)

Comments

As a result of primary screening, 38, 16, and 35 papers were retrieved from PubMed, Cochrane Library, and JCRM, respectively. However, during secondary screening, many reports concerned AV shunts in dialysis patients and AVM at sites other than the fingers. Eventually, only 10 papers consisting of 3 case series and 7 case reports remained as references, and the evidence level is extremely low (D: very weak).

AVM of the fingers is often difficult to treat, and treatments are likely to be ineffective, particularly, when the lesion extends from the fingers to the palm. In addition, when AVM is localized in the fingers, complications are likely to occur after treatment [72]. It is recommended to conduct treatment by a team from several departments including the plastic surgery, vascular surgery, and radiology departments [73]. 3D-CTA is useful for preoperative examination [74]. Since complete cure is difficult to obtain by embolization therapy, it is recommended to be performed for alleviation of symptoms such as pain only in symptomatic areas [75]. In addition, as there is the possibility of re-enlargement after embolization, it is recommended to periodically follow-up the condition and repeatedly perform embolization each time symptoms appear [73]. Surgical resection is necessary for permanent cure, and total resection is recommended as there is the possibility of re-enlargement after partial resection [76–78]. Reconstruction is occasionally necessary, but treatment may end in finger amputation. In this event, preoperative embolization or sclerotherapy is effective [79]. The present review has fallen short of clarifying situations in which preoperative embolization is useful in fingers to which a tourniquet can be applied.

CQ7: What treatments are effective for painful VM?

Recommendation:

Sclerotherapy and surgical resection, as well as conservative treatments, such as compression, oral aspirin, and low-molecular-weight heparin, are reported to be effective depending on the site and size of the lesion and symptoms. Endovascular laser treatment, percutaneous cryotherapy, and photodynamic therapy have also been suggested to be effective.

Strength of recommendation	2 (weak)
Evidence	D (very weak)

Comments

As a result of literature search, 54 reports in English and 4 in Japanese were retrieved by primary screening. Of these reports, 39 in English and 4 in Japanese were extracted by secondary screening. Many options were reported as treatments for pain associated with VM, but all these documents were case series or case reports without comparison of treatments. Therefore, the evidence level was rated as "very weak", and the recommendation level as "weak".

Pain is one of the major symptoms of VM. It may respond to conservative treatments that are relatively easy to manage, such as compression and oral aspirin, depending on the site and size of the lesion and symptoms. Particularly, when pain is localized, surgery should also be considered. Relatively novel treatments, such as endovascular laser therapy, percutaneous cryotherapy, and photodynamic therapy, have been reported to be effective for controlling local VM, and they have also been reported to be effective for the control of pain. Limb lesions accompanied by localized intravascular coagulopathy may be indications for low-molecular-weight heparin. Reports on various treatments are mentioned below.

1. Compression

Although there has been no report of comparative evaluation, compression is reportedly effective according to reviews by specialized medical facilities [80–82].

2. Oral aspirin

The literature is also limited, but the treatment has been mentioned in reviews [80–82]. Nguyen et al. [83] reported

that pain was alleviated in 17 (77%) of 22 patients in whom oral aspirin therapy was initiated for pain.

3. Sclerotherapy

Sclerotherapy has often been performed using ethanol or polidocanol. The literature concerning other sclerosing agents is scarce, and their effectiveness remains largely unclear.

Each sclerosing agent is commented below.

i. Ethanol

Shireman et al. [84] reported remission in 6 of 12 patients, and Rimon et al. [85] reported alleviation or remission in 14 patients with painful VM (including 8 with lower limb lesions) except in 4 of those with lower limb lesions. Marrocco-Trischitta et al. [86] reported that pain was resolved in both (100%) of 2 women with external genital lesions.

Concerning the use of ethanol, Suh et al. [87] reported alleviation to 50% or less of the pre-treatment state according to a VAS in 12 (71%) of 17 patients who underwent sclerotherapy using its mixture with lipiodol, and Dompmartin et al. [88] reported 37 patients who underwent sclerotherapy using its mixture with ethylcellulose. According to Schumacher et al. [89], also, 77 patients underwent sclerotherapy using ethylcellulose-ethanol in a multicenter study, and significant improvement compared with the pre-treatment state was observed in all patients.

ii. Polidocanol (including foam sclerotherapy)

Mimura et al. [90] reported remission in 6, alleviation in 4, and no change in 1 of 11 patients with painful VM, and remission in 12 (41%), alleviation in 14 (48%), no change in 2 (7%), and exacerbation in 1 (3%) of 29 patients in another study [91]. Cabrera et al. [92] treated 50 patients (including 15 with Klippel–Trenaunay syndrome) using a foamed sclerosing agent and reported remission in 25 (50%) and alleviation in 14 (28%). Marrocco-Trischitta et al. [86] reported resolution of pain in all 3 women with external genital lesions.

iii. Ethanolamine oleate

Ozaki et al. [93] reported remission in 2 (20%) and alleviation in 8 (80%) of 10 patients.

iv. Sodium tetradecyl sulfate

Krokidis et al. [94] reported alleviation of pain in 4 of 5 women with external genital lesions.

4. Surgical resection

Enjolras et al. [95] performed surgical resection in 7 of 13 patients with VM involving a wide area including the knee joint and reported alleviation of pain in 5 (71%). Steiner et al. [96] reported alleviation to 50% or less of the pre-treatment state by a VAS in 24 (89%) of 27 patients with background pain and 12 (92%) of 13 patients with acute episodic pain. In addition, Noel et al. [97] performed surgical resection and compression therapy for VM of the lower extremities in 20 patients with Klippel–Trenaunay syndrome and reported disappearance of pain in 18 (90%) (mean follow-up period: 63 months).

5. Endovascular laser therapy

Sidhu et al. [98] and Lu et al. [99] reported alleviation of pain in all 8 and 51 lesions in 6 and 33 patients, respectively. Liu et al. [100] also reported marked responses in 46 (35%), responses in 84 (63%), and no change in 3 (2%) of 133 patients.

6. Low-molecular-weight heparin

According to Mazoyer et al. [101], only low-molecular-weight heparin was effective when VM are complicated by localized intravascular coagulation, resulting in disappearance of pain.

7. Percutaneous cryotherapy

Cornelis et al. [102, 103] reported remission of pain in a report of 1 case (observation period: 2 months) and a report of 4 cases (observation period: 6 months).

8. Photodynamic therapy

Betz et al. [104] reported remission in 2 and alleviation in 1 of 3 patients.

CQ8: Is laser therapy effective for VM?

Recommendation:

With appropriate selection of the type of laser according to the site, size, and symptoms of the lesion, laser therapy can be effective for the treatment of VM. It is recommended to evaluate whether the net benefit by laser therapy is worth the cost and resources by comparison with other treatments such as sclerotherapy and surgical resection.

Strength of recommendation	2 (weak)
Evidence	C (weak)

Comments

Venous malformation is a lesion that has been called cavernous hemangioma, and it causes pain, functional impairment, and cosmetic defect depending on the affected site. In addition to conventional resection of the lesion, sclerotherapy has been widely performed in recent years. While reports of laser therapy for VM have increased, there have not been prospective studies comparing the results of laser therapy with those of surgery or sclerotherapy, among types of laser equipment different in wavelength, or using the same equipment type but changing the irradiation method or parameter setting. We analyzed 134 papers extracted by primary screening and 98 papers extracted by secondary screening. Concerning more than 30 cases, the answer to the CQ was based primarily on 7 reports summarizing the methods and sites of treatment and benefits and harms derived from treatment (decrease in size of the lesion, alleviation of symptoms, complications).

In the facial skin, pigmentation and scar formation after irradiation can be serious treatment-related complications compared with unexposed areas. In the airway and digestive tract, the mass effect of the lesion and chronic bleeding from the lesion can be causes of serious symptoms. Thus, as the goal to achieve varies with the anatomical site of the lesion, we reviewed the literature by the anatomical site (the neurosurgery field was excluded). For this reason, we also extracted benefits and harms of treatment from the text of the reports of less than 30 cases. The relevant departments surveyed included ENT, dental and oral surgery, gastrointestinal surgery, ophthalmology, plastic surgery, and dermatology, and secondary screening overviewed laser therapy for VM and vasodilatory lesions.

When a new laser instrument is developed and put into use, reports of therapeutic results using the equipment are presented. The types of laser used for treatment varied widely. The types of laser that have been reported are summarized chronologically in a graph (Fig. 1). While the type of laser with more reports is not necessarily more effective, the graph is considered to reflect tendencies of laser types that are established and gain favorable appraisal or no longer in use.

Since dye laser used for the treatment of port wine stain (wavelength: 595 nm) uses hemoglobin as the observer/heater, photothermal conversion occurs efficiently in the blood vessel, and the thermal energy reaches endothelial cells [105]. However, its optical penetration depth is shallow, being about 1 mm in both the skin and mucosa [105]. However, in Nd:YAG laser with a longer wavelength (1064 nm), the optical penetration depth is about 3 mm in the skin and about 6 mm in the mucosa [105]. Although Nd:YAG laser is advantageous compared with dye laser for the treatment of

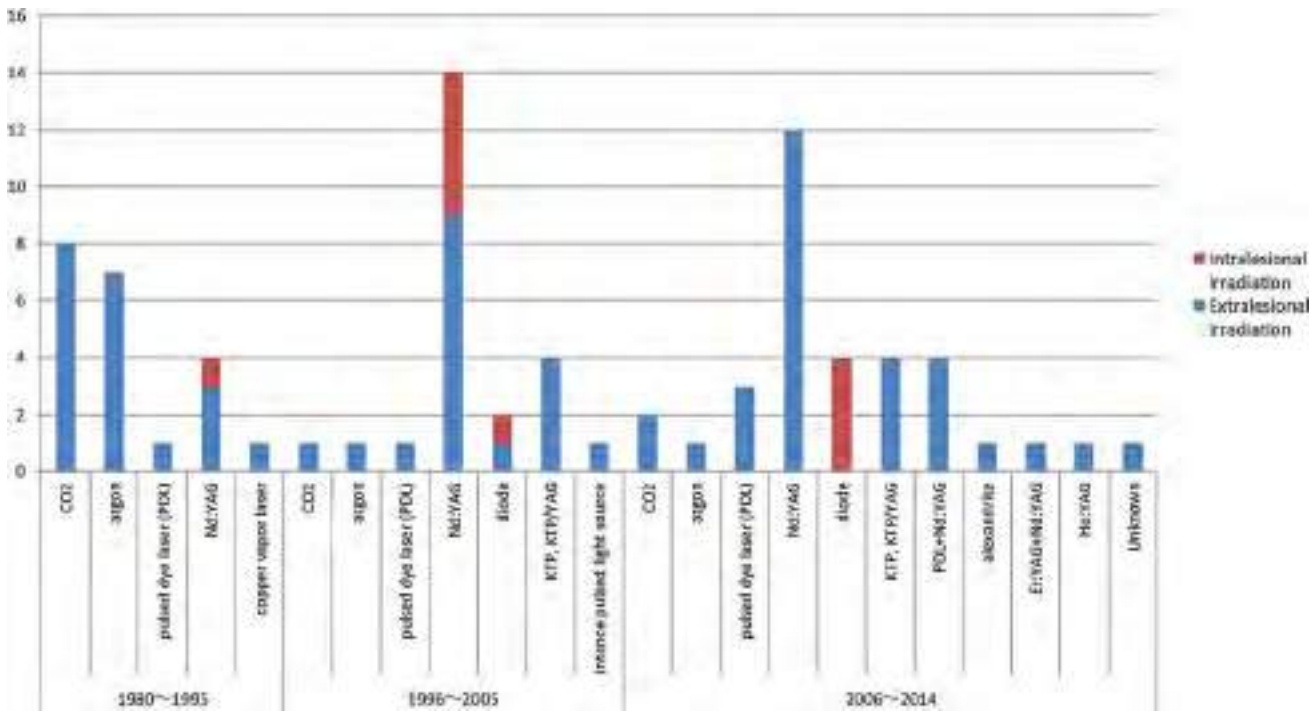

Fig. 1 Reports of laser therapy for hemangiomas/vascular malformations (primarily venous) in various periods and types of laser used in the reports. CO_2; 10 of 11 reports recommend the use for surgical resection. Argon; There are 4 reports of mixed treatments for CM and VM. Nd:YAG; There are 12 reports of its use in combination therapy with surgery, sclerotherapy, or other lasers. Alexandrite; There is only 1 report summarizing cases treated with alexandrite in combination therapy with other lasers

deep lesions, heat is generated also in perivascular tissues, because light is converted to heat as it is absorbed by water contained in the skin and mucosa.

The target of laser treatment for VM is the endothelium of morbidly dilated blood vessels. There is no light that is specifically absorbed by endothelial cells and emits heat. Satisfactory therapeutic results cannot be expected unless treatment is performed by selecting the laser type and modifying the irradiation method based on the understanding of such principles and limitations of phototherapy.

Concerning small VM of the mucosa, tongue, lips, and glans penis, in which scar formation after treatment poses no serious problem, there are a number of reports [106–108] that lesions were resolved by treatment using Nd:YAG laser. There have also been cases in which favorable results were obtained by treatment of anemia due to gastrointestinal bleeding [109] and of symptoms, such as airway obstruction, due to the mass effect of the lesion [110]. While transient purpura and swelling after treatment are unavoidable, they often resolve rapidly [99]. Modifications of the irradiation setting and method are necessary to obtain satisfactory results and avoid serious complications, such as peroneal neuropathy [100] and pigmentation and scar formation of the facial skin [106, 108], and we must learn from the experience of experts.

Nd:YAG laser irradiation by insertion into the lesion under ultrasound guidance has begun to be performed as a treatment to avoid damage of important organs and nerves [98–100], therapeutic experience using this technique has been accumulated, and detailed records and reports have been presented. At present, the results have been satisfactory in terms of safety and efficacy, and standardization of the procedure is anticipated.

CQ9: Is sclerotherapy effective for VM?

Recommendation:

Sclerotherapy for VM is effective for alleviating symptoms and reducing the size of the lesion and is recommended.

Strength of recommendation	2 (weak)
Evidence	D (very weak)

Comments

VM is lesion that used to be called cavernous hemangioma or intramuscular hemangioma and differ from infantile hemangioma. VM poses problems, such as pain, swelling, and functional impairment, and has been treated conventionally by surgical resection. In Western countries, percutaneous sclerotherapy has a long history. In 1989, Yakes et al. [111] reported ethanol sclerotherapy for VM, and the treatment has since been performed worldwide. Recently, sclerotherapy, which is mildly invasive, permits functional and morphological preservation, and can be performed repeatedly, is widely used. However, as of 2016, sclerotherapy is not covered by medical insurance in Japan. In addition, there has been no randomized controlled trial (RCT) on the usefulness of sclerotherapy for VM compared with surgery or placebo.

As a result of secondary screening, 76, 3, and 3 papers were extracted from PubMed, Cochrane, and JCRM, respectively. They include 3 semi-RCTs, but randomization and blinding were insufficient, and their quality as an RCT was low. Also, the theme evaluated by all these RCTs was "comparison of sclerosing agents in sclerotherapy", and none compared sclerotherapy with other treatments. Therefore, control groups related to this CQ were not established, and their contribution as a whole is weak. The other literature was all case reports or case series, and the evidence level is D (very weak). As mentioned above, while the evidence level is low, most of the studies reported alleviation of symptoms and regression of lesions in a high percentage (70–90%) of the patients, suggesting the usefulness of sclerotherapy.

The sclerosing agents used included absolute ethanol, polidocanol, ethanolamine oleate, sodium tetradecyl sulfate (STS), and bleomycin. Polidocanol is approved as a sclerosing agent for lower limb varices and esophageal varices, and ethanolamine oleate as a sclerosing agent for esophageal varices. STS is not marketed in Japan. Each sclerosing agent has characteristic complications. Recently, injection of polidocanol, STS, as a foam by mixing with CO_2 or air has been increasingly performed. Sclerotherapy using ethanol is often performed under general anesthesia, but sclerotherapy using polidocanol or ethanolamine oleate can be performed under local anesthesia.

Three RCTs have been reported as studies that evaluated differences in therapeutic effect according to the sclerosing agent. However, randomization and blinding are insufficient, and their quality as an RCT is low. In addition, the theme evaluated in these RCTs was "comparison of sclerosing agents in sclerotherapy" rather than comparison with other treatments.

Although the evidence level is low, there have been a few case series that reported the usefulness of sclerotherapy, and a wide variety of sclerosing agents including ethanol, polidocanol, ethanolamine oleate, STS, and bleomycin were used. Among studies with a relatively large number of patients, there is a report [112] that sclerotherapy using ethanol in 87 patients with craniofacial VM resulted in a ≥ 75% decrease in size in 23 (32%) and a 25–75% decrease in size in 37 (52%). The results of sclerotherapy using polidocanol in 50 patients with VM were excellent in 19, good in 16,

moderate improvement in 13, and unchanged or worse in 2 [92]. The results of sclerotherapy using ethanolamine oleate performed in 83 patients, who were mostly children, were complete remission of symptoms in 79 lesions and significant alleviation in 6 lesions [113]. Sclerotherapy using STS resulted in subjective improvements in 174 (85.3%) of 204 patients [114]. The results of sclerotherapy using bleomycin were complete cure in 185 of 260 patients, marked improvement in 44, and some improvement or no change in 31 [115]. In addition, regarding the size of the lesion, a very satisfactory decrease was achieved in 104, and a satisfactory decrease was achieved in 10, of 120 patients [116].

Papers that evaluated the types of VM that are likely to respond to sclerotherapy include those by Goyal et al. [117], Yun et al. [118], Mimura et al. [91], Rautio et al. [119], Lee et al. [112], Yamaki et al. [120], and Nagao et al. [121] Types of lesions that were likely to be sclerosed were reported to be well-defined small (≤ 5 cm) lesions by Goyal et al. [117], females, lesions showing no or delayed delineation of the draining vein, and lesions well-defined on MRI by Yun et al. [118], small lesions, well-defined lesions, and lesions that show prolonged drug retention by Mimura et al. [91], localized lesions by Lee et al. [112] and Yamaki et al. [120], and slow flow type lesions by Nagao et al. [121] Nomura et al. [122] evaluated the therapeutic effect according to the degrees of functional and gross improvements and reported that the therapeutic effect was greater in head and neck and trunk lesions than in the upper or lower limb lesions. Moreover, Rautio et al. [119] reported that the treatment-related improvement in the quality of life was higher when the lesion did not involve the muscle or was ≤ 5 cm in size.

Various complications ranging from mild complications, such as transient neuropathy and local inflammation, to serious ones, such as myopathy, skin necrosis, and deep venous thrombosis/pulmonary embolism, have been reported. In sclerotherapy using ethanol or polidocanol, particularly serious life-threatening complications have been reported. Qiu et al. [123] reviewed the literature concerning sclerotherapy for VM and reported that shock and pulmonary embolism occurred in 0.19% each of 522 patients who underwent sclerotherapy using ethanol and that ethanol was used at 1 mL/kg in those who developed shock. They also reported that a decrease in blood pressure/bradycardia was noted in 0.61% of 163 patients who underwent sclerotherapy using polidocanol but that its differentiation from vagus nerve reflex was clinically difficult. Wong et al. [124] reported a case of shock after sclerotherapy using 0.86 g/kg ethanol but could be saved. Tachibana et al. [125] reported that 2 patients (1.1%) developed pulmonary embolism and that the amounts of ethanol used were 0.71 and 0.16 mL/kg. Concerning sclerotherapy using polidocanol, also, cardiac arrest in children has been reported by authors including Marrocco-Trischitta et al. [126] and Shimo et al. [127], who used 4 mL of 1% polidocanol (body weight: 20 kg) and 10 mL of 3% polidocanol (15.6 kg), respectively.

In conclusion, sclerotherapy is generally considered effective for VM, but its problems are that the evidence level is low and that the procedure has not been standardized. In addition, serious complications that are rare but life-threatening have been reported, and caution is needed in deciding the dose of the sclerosing agent.

CQ10: Are clotting abnormalities due to VM an indication for radiotherapy?

Recommendation:

Radiotherapy should not be performed without careful evaluation because malignant neoplasm, growth disorders, and functional impairment have been reported as late complications.

Many reports included both VM and vascular tumors in the subjects, which make it difficult to assess the therapeutic effects of radiotherapy.

Strength of recommendation	2 (weak)
Evidence	D (very weak)

Comments

As a result of primary screening, 6 and 2 documents were retrieved from PubMed and JCRM. However, as a result of secondary screening, liver hemangioma was excluded, and 10 papers including the references from the previous guideline were reviewed. The reviewed papers were case series or case reports, and the evidence level of the literature as a whole is D "very weak".

While there have been reports that radiotherapy was performed for the treatment of vascular tumors and vascular malformations, it is difficult to judge whether the treatment was performed by determining the disorders.

According to many reports [128–132], radiotherapy has been performed to treat Kasabach–Merritt phenomenon. However, while there is no mention about Kasabach–Merritt phenomenon, there is a report [133] of 5 cases in which giant hemangiomas accompanied by clotting disorders, thrombocytopenia, heart failure, and bleeding were controlled by multidisciplinary treatment including radiotherapy.

Vascular tumors that cause Kasabach–Merritt phenomenon are considered to be kaposiform hemangioendothelioma or tufted angioma rather than infantile hemangioma [134]. Because VM and infantile hemangiomas are included in other vascular tumors in the lesions described in these

reports, they are not considered to be indications of radiotherapy for VM or infantile hemangiomas.

Schild et al. [128] reported 13 cases of symptomatic hemangioma (11 of which were pathologically diagnosed as cavernous hemangioma, but as the report is old, vascular tumors and vascular malformations were not distinguished and were probably included). Radiotherapy at 6.25–40 Gy was carried out in these 13 cases. The lesions were located in the limbs in 5, face in 2, vertebral bodies in 3, pituitary fossa in 1, sacrum in 1, and bladder in 1. Note that organs that should be excluded in this CQ were included.

Of these patients, 2 (1 each with a limb and facial lesion) exhibited Kasabach–Merritt phenomenon and showed normalization of clotting disorder (evaluated according to the platelet count and fibrinogen level) after treatment. However, they were aged 3 years and 5 months, and the lesions may not have been VM.

When the subjects were limited to patients with limb or facial lesions, CR was observed in 2, PR in 4, and no response in 1 in terms of decrease in the lesion size, and CR was observed in 4, PR in 1, and no response in 2 in terms of the control of symptoms.

A serious treatment-related complication, which was unilateral visual impairment, was noted in 1 (14 Gy/8 fr) [128]. These problems have been recognized as late complications of radiotherapy for vascular tumors or vascular malformations; malignant neoplasms, such as breast cancer [135], thyroid cancer [136], and vascular sarcoma [137], visual impairment mentioned above [128], shortening of the lower limb, and restriction of the joint motion range [131].

According to Coldwell et al. [137], late complications of radiotherapy for hemangiomas in infancy include bruise and Stewart–Treves syndrome after the patients reach adulthood. Angiosarcoma is also observed. They reported that the median survival period was 24 months, and the 5-year survival rate was about 10%, in those who developed angiosarcoma.

As observed above, the diagnosis was not confirmed in the reports that have suggested the effectiveness of radiotherapy, and its indications have not been specified. In addition, there have been a considerable number of reports of late complications due to radiotherapy. Thus radiotherapy should not be performed without careful evaluation.

CQ11: Is there difference in the effectiveness of dye laser treatment for CM according to the site of the body?

Recommendation:

Dye laser treatment for CM is likely more effective in the face and neck region compared with other sites, and it is more likely to cause complications such as pigmentation in the limbs.

Strength of recommendation	2 (weak)
Evidence	C (weak)

Comments

As a result of literature searches, 176 papers consisting of 139 from PubMed and 37 from JCRM were extracted. They included a few reports that were allegedly RCTs but were not actual RCTs. Therefore, a total of 26 papers consisting of 15 from PubMed and 11 from JCRM including case series with a large number (≥ 100) of relevant cases were selected by secondary screening. In addition, a total of 17 papers were adopted as references for the comments in the guidelines by adding 3 papers in English extracted by manual search to 6 from PubMed and 8 from JCRM considered to be relevant or closely related to the CQ among those selected by secondary screening. Since there was no RCT, the evidence as a whole was rated as C (weak).

Concerning the effect of dye laser treatment for CM, most of the reports were about the effects for hemangioma simplex or port-wine hemangioma in Japan and port-wine stain abroad.

There have been a few papers [138–152] that evaluated the therapeutic results of dye laser treatment according to the site in a small to relatively large number of patients. The laser equipment used varies from early dye laser to pulsed dye laser with adjustable pulse duration with a cooling system, and reports limited to variable-pulse pulsed-dye laser with a cooling system, which is widely used today, are extremely few.

According to many reports [138–149], the response rate is higher in the face and neck region than in the trunk and limbs. In the face, it has been reported that the response rate is higher in the palpebral, forehead and temporal, and lateral buccal regions but is significantly lower in the territory of the 2nd division of the trigeminal nerve (dermatome V2), and that the number of irradiations tends to increase in the midline region, frequently resulting in persistence of redness [150]. There is a report [151] that the response rate did not differ significantly among regions in the lower limb. While the number of patients was small, it has been reported that treatment of the foot involves stronger pain but was less effective than in the face but that the degree of patient satisfaction was relatively high [152].

The incidence of complications of dye laser (bleb formation, depigmentation, pigmentation, scar formation) is reported to be low, being 1.7% in adults, 0.6% in children, and about 1.4% in all patients even when all sites of the body are included, and no significant difference has been reported

in the age at the beginning of treatment, Fitzpatrick skin type [153], site, number of treatments, or irradiation energy between those who developed complications and those who did not, but complications may occur more frequently in the lower limbs [154]. Moreover, there is a report [152] that complications, such as pigmentation, depigmentation, and atrophic scar, were observed more frequently in the lower limbs.

CQ12: Do CM recur after dye laser treatment?

Recommendation:

Although the effectiveness of dye laser treatment for capillary malformations is established, the recurrence rate may increase with time after treatment.

Strength of recommendation	2 (weak)
Evidence	C (weak)

Comments

As a result of literature searches, a total of 211 papers consisting of 149 from PubMed, 53 from Cochrane, and 9 from JCRM were retrieved. They did not include RCTs, and a total of 30 papers consisting of 23 from PubMed and 7 from Cochrane, which were mostly case reports and case series studies, were extracted by secondary screening. In addition, a total of 10 papers that were relevant and closely related to the CQ (including 8 case series) consisting of 7 from PubMed, 2 from Cochrane, and 1 in English retrieved by manual search were adopted as references for the guidelines. Since there was no RCT, the strength of evidence of the group of literature concerning this CQ is C "weak".

Concerning papers that referred to "whether CM recur after dye laser treatment", there are 4 retrospective studies [155–158] after treatment by pulsed dye laser (wavelength: 585 nm) with a cooling system, and the recurrence rate was 15.9–35%. Also, there is a report [155] that the recurrence rate increased with time after treatment and was 3.1% after 1 year, 20.8% after 2 years, 40% after 3 years, and 50% after 4 years. Therefore, it is necessary to treat CM with the recurrence after dye laser treatment in mind.

It is difficult to strictly distinguish whether the recurrence is generation of new dilated vessels after laser therapy or it is regeneration of blood vessels damaged due to treatment or re-proliferation of remaining vessels. However, there have been reports that, in an experiment using mice, angiogenesis occurred in the process of wound healing at the site of irradiation in early recurrence [159] and that, in an experiment using hamsters, complete treatment was difficult, and morbid vessels persisted, because coagulation was difficult to induce by dye laser irradiation in vessels ≤ 2–16 μm in diameter [160]. While there is a report [161] that genes affected by dye laser therapy early after treatment were identified, further evaluation is necessary to clarify their relationships with the recurrence.

Concerning the prevention of recurrence, there is a report [162] that the recurrence-free period was long in the patients treated with a variable-pulse pulsed-dye laser with a cooling system (wavelength: 595 nm), which is widely used today, and they were treated within 6 months after birth. In addition, there have been reports of animal experiments using Rapamycin, which inhibits angiogenesis after laser irradiation [159, 163], and of prospective RCT using imiquimod [164, 165], and these treatments were considered effective for the prevention of recurrence. However, careful evaluation by large-scale investigations, including the assessment of the safety concerning drugs, is considered necessary.

CQ13: Is dye laser irradiation for CM more effective as it is initiated at a younger age?

Recommendation:

Laser therapy before the age of 1 year may be effective, and the earliest possible initiation of treatment is recommended as an option.

Strength of recommendation	2 (weak)
Evidence	D (very weak)

Comments

Concerning the timing of treatment for CM, there is the opinion that early initiation of treatment is recommended, because, in young children, the skin is thinner, so the depth of penetration is larger, the vascular wall is also immature, cure after laser irradiation is better, pigmentation is less, and the irradiation area is small, so the treatment efficiency is higher. However, there is still controversy. As a result of secondary screening of past reports, 6 and 1 were extracted from PubMed and JCRM, respectively. While the papers selected by these screening procedures include 2 papers on prospective studies as described below, their conclusions differed, and the evidence level is considered to decline when these references are reviewed together.

Oguri et al. [138] performed a non-randomized controlled trial by dividing children into those aged 0–12 months, 13–24 months, and 25–36 months and observed significant differences in the response rate combining 'markedly effective' and 'effective' among the groups. They also compared

the response rate according to the age in months at the beginning of treatment in the 0-year-old group and reported that the response rate was higher as the treatment was initiated earlier. Furthermore, Nguyen et al. [166] divided their patients into those aged less than 1 year, those aged 1–6 years, and those aged 6 or more years and investigated the correlation between treatment response and age. They reported that those aged less than 1 year and lesions with a size of less than 20 cm^2 located in the center of the face showed the best treatment response.

Among reports suggesting no difference in the therapeutic effect according to the age at the beginning of treatment, van der Horst et al. [167] studied 100 patients with untreated CM of the head and neck region prospectively and concluded from the results of colorimetry and clinical evaluation that there was no significant difference in the therapeutic effect of pulsed dye laser among the 4 groups in which the treatment was started at the age of 0–5, 6–11, 12–17, and 18–31 years. In the retrospective study of Katugampola et al. [140], also, comparison of 4 groups in which treatment was started at the age of 0–5, 6–12, 13–50, and 50 + years showed no significant difference in the therapeutic effect.

Among the above reports, those did not affirm the usefulness of early laser treatment were relatively old. Also, reports of Oguri et al. [138] and Nguyen et al. [166] indicated laser therapy may be more effective in those aged less than 1 year. In addition, the effectiveness of laser clearly declines when the lesion is elevated or thickens with time. In consideration of "benefits" of early laser treatment and "harms", which include the occasional necessity of general anesthesia for laser treatment around the eye in small children, the recommendation level was rated as 2D based on the consensus of this guidelines drafting committee.

CQ14: Is propranolol safe and effective for infantile hemangiomas?

Recommendation:

If administered under careful monitoring, oral propranolol therapy may be the first choice for the treatment of infantile hemangioma.

Strength of recommendation	1 (strong)
Evidence	A (strong)

Comments

(1) Effectiveness: There was the serendipity that regression of hemangioma was induced in a child under steroid therapy with a giant infantile hemangioma by propranolol administered for obstructive hypertrophic cardiomyopathy in 2008 [168]. Based on this report, oral propranolol therapy began to be used for the treatment of infantile hemangioma, and its high efficacy against alarming hemangioma/life-threatening hemangioma in the proliferating phase and in patients with cosmetic problems, such as giant lesions in the face, those with ulcerated and hemorrhagic lesions, and those who may develop functional impairment, has been demonstrated, resulting in its use (Hemangiol®, Pierre Fabre Dermatologie, Boulogne, France) as the first choice in Western countries. In addition, its effectiveness for the treatment of hemangiomas after the proliferating phase was also described. Moreover, a group of physicians used propranolol earlier due to cosmetic significance and at the request of the family even in cases of small or localized lesions, and it is also effective in such cases.

A total of 131 papers consisting of 25 from JCRM, 106 from PubMed, and 0 from Cochrane Library were extracted as related to the CQ, "Is propranolol safe and effective for infantile hemangioma?", and they were subjected to primary and secondary screenings with reduction of hemangioma (effectiveness of propranolol) and treatment-related complications (adverse effects) as outcomes. Twenty-six papers [169–194], most of which were RCTs or observational studies, were adopted.

For example, Hogeling et al. [180] administered placebo or propranolol at 2 mg/kg/day for 6 months with randomization to 40 patients aged 9 weeks–5 years with infantile hemangiomas in the face or sites with the potential for disfigurement. They reported significant improvements in size, redness, and elevation in the propranolol group. Elevated lesions disappeared in 4 of the 19 patients in the propranolol group but none of the 18 patients in the placebo group. As for adverse events, the trial was interrupted in 1 patient due to upper respiratory tract infection, and conditions including bronchiolitis, gastroenteritis, streptococcal infection, cool extremities, dental caries, and sleep disturbance were observed.

Zaher et al. [181] observed 45 patients by randomly dividing them into 15 each treated by oral administration, topical application, and intralesional injection of propranolol. Responses were observed in 60% in the oral group, 20% in the topical ointment group, and 13.3% in the injection group. No major adverse events were noted, and the trial was discontinued in 1 in the oral group and 3 in the injection group due to inconvenience or pain of the treatment.

Malik et al. [182] randomly allotted 30 patients aged 1 week–8 months to propranolol alone, prednisolone alone, or both propranolol and prednisolone. They found that the mean initial response times were lower in the propranolol group than in the prednisolone group but that there was no clear difference between the propranolol + prednisolone group and propranolol alone group. All 10 patients in the propranolol group and 9 patients in the corticosteroid group

responded to the 3-month treatment. However, adverse events were observed in 2 of the 10 patients in the propranolol group (asymptomatic hypoglycemia, insomnia) and 9 of the 10 patients in the steroid group (cushingoid appearance, gastrointestinal upset), and were more frequently in the latter group.

Bauman et al. [183] performed a phase 2, investigator-blinded, multi-center RCT in 44 patients aged 2 weeks-6 months. Propranolol or prednisolone (2 mg/kg/day) was administered orally until halted due to toxic effects or clinical response. During 4-months treatment, no significant difference was observed between the two groups, for example, with regression of 5 of the 6 tumors in the corticosteroid group and 9 of the 10 tumors in the propranolol group. For long-term analyses, the effect of prednisolone appeared earlier. While the incidence of adverse events as a whole did not differ between the two groups, severe adverse events were observed in 1 of the 11 patients in the propranolol group but 5 of the 7 patients in the prednisolone group, being significantly more frequently in the latter group.

Léauté-Labrèze et al. [184] carried out an RCT in patients aged less than 4 months by comparing 7 administered and 7 not administered propranolol. Since color changes and softening were observed within 24 h, and the thickness and size of the lesions decreased within 4 weeks in the propranolol group, the treatment was considered useful for the prevention of scarring. No serious adverse effect was observed except asymptomatic mild decreases in heart rate and diastolic blood pressure.

There have also been comparisons between atenolol and propranolol and between laser and laser plus topical propranolol [185, 186]. In 2015, the largest RCT was published in the New England Journal of Medicine, also reporting that propranolol was significantly effective for hemangioma compared with placebo [187]. Hemangioma showed complete or nearly complete resolution after 6-month treatment in 2 (4%) of 55 patients in the placebo group and 61 (60%) of 101 patients in the 3 mg/kg/day propranolol group.

Furthermore, there have also been a few systematic reviews and meta-analyses primarily of observational studies. Menezes et al. [188] reviewed 49 English papers published between June 2008 and September 2010, and summarized 6 studies with 10 or more patients administered propranolol (totally 154 patients). Propranolol was administered to infants with a mean age of 4.5 months at a dose of 2 mg/kg/day in 65% and 3 mg/kg/day in 25.3%. Two-thirds of the patients were treated with propranolol alone. Recurrence was observed in 21% after treatment for a mean of 4.3 months, and adverse events including hypotension, somnolence, wheezing, insomnia, agitation, nightmare, cool hands, night sweat, gastroesophageal reflux disease, and psoriasiform rash appeared in 18.1%.

Marqueling et al. [189] reviewed the therapeutic results in 1264 patients (including 806 girls) in 41 reports published from 2008 to 2012 retrieved from Medline and Cochrane database. The treatment was initiated at a mean age of 6.6 months at 2.1 mg/kg/day and continued for a mean of 6.4 months. The overall response rate was 98%, and the treatment was also effective in clinically problematic areas such as the face (100%), airway (100%), periorbital (98%), head and neck region (97%), and parotid gland (82%). However, recurrence was observed in 17% after treatment. Adverse effects were noted in 371 of 1189 patients. Changes in sleep (136 patients) and acrocyanosis (61) were the most frequent among them, and hypotension was observed in 44, bradycardia in 9, and hypoglycemia in 4 as serious complications. In conclusion, the grade of recommendation was 1, quality of evidence is A, and propranolol was recommended as the first-line drug for complicated infantile hemangiomas. Regarding adverse effects, the grade of recommendation was 1, quality of evidence was A or B. while serious adverse effects may be observed, their frequency is low, and they can be usually avoided by proper monitoring at initiation of treatment.

Xu et al. [190], on the other hand, evaluated volume changes, improvement in overall appearance, visual function, and adverse effects using 15 online databases. The data of 419 cases were analyzed, but meta-analysis was not performed because of the wide differences among studies. Some studies showed superiority of propranolol compared with corticosteroid in reducing volume and improving the overall appearance. No marked difference was noted in adverse effects or visual function.

In addition, in meta-analysis of 16 studies (2629 cases) and 25 studies (795) published in 1965–2012, 69% of the patients responded to 12-month corticosteroid therapy, but the response rate to propranolol was 97% with a significant difference [191].

In periorbital hemangiomas, the response rate to propranolol was found to be significantly higher than that to corticosteroid by meta-analysis of papers published before 2013 [192], and propranolol showed the strongest effect against airway hemangiomas compared with steroid, CO_2 laser, and vincristine on meta-analysis [193, 194].

From these observations, we concluded that propranolol was significantly more effective than placebo and to be similarly effective compared with corticosteroid. Concerning the safety, propranolol is considered to have significantly fewer adverse effects than corticosteroid. Since there have been several RCTs and systematic reviews or meta-analyses directly related to this CQ, the evidence level is considered to be extremely high.

(2) Meta-analysis: Regarding the effectiveness and adverse effects of propranolol, a large number of systematic reviews and meta-analyses based on observational studies

are already present in the above 26 papers. We, therefore, used only 4 reports [180, 182, 183, 187] on interventional studies for meta-analysis.

As a result of meta-analysis, regarding "tumor reduction", it was found that propranolol had significantly stronger reducing effects than placebo and that it had a stronger reducing effect, which, however, was not significant, compared with corticosteroid. Concerning "complications", propranolol was compared with steroid and was shown by 2 RCTs to have significantly fewer adverse events than corticosteroid. Since this meta-analysis found significantly stronger reducing effect of propranolol compared with placebo and in fewer complications compared with steroid, and since our results were similar to those of systematic reviews of many existing observational studies considered to have high-quality evidence, we considered that there was a major tendency in this CQ and judged the evidence level as A.

(3) Estimated action mechanism: Beta blockers have a wide range of actions on the blood vessels and vascular endothelium, and have diverse actions on cell proliferation and vascular remodeling. Thus, the action mechanism of propranolol on infantile hemangiomas is still unclear. In vascular endothelial cells, propranolol is considered to induce vascular contraction by suppressing NO production, inhibit renin production, control angiogenesis by regulating the expression of VEGF•bFGF•MMP2/MMP9, and induce apoptosis, but it may also affect pericytes and hemangioma stem cells [195–197].

(4) Adverse events associated with propranolol in children

In conducting propranolol therapy, it is necessary to have knowledge about possible adverse effects, their symptoms, and their management. In addition, as there are also preventive measures for, and points of attention about, adverse effects and the timing for discontinuation of propranolol, sufficient explanation to the patients and their families is essential.

Adverse events that have been reported include sleep disorders, peripheral cyanosis, hypotension (symptomatic, asymptomatic), bradycardia (symptomatic, asymptomatic), hypoglycemia, respiratory disorders, gastrointestinal disorders, and mental disorders. Severe cases that require interruption of treatment are few, but particular caution is needed regarding the following points [189, 196–200].

(a) Since there is the risk of hypoglycemia, the patient should be fed before and after propranolol administration. If the patient cannot be fed, or is vomiting, for some reason, the administration should be suspended.
(b) Since propranolol has cardiovascular adverse effects, such as hypotension and bradycardia, interviewing for the past history and familial history, examination, and electrocardiography are recommended before treatment. Even if no abnormality is noted on these examinations, hypotension, and bradycardia may occur during treatment. In such cases, interruption of the administration is necessary.
(c) Propranolol is contraindicated for bronchial asthma as it causes bronchial contraction due to its β2-blocking action. Caution is also necessary in patients who have been suspected to have bronchial asthma.

CQ15: What treatments are effective for ulcer formation in infantile hemangioma?

1. Propranolol

Recommendation:
The administration of propranolol is recommended for ulcer formation.

Strength of recommendation	2 (weak)
Evidence	C (weak)

2. Topical administration of antibiotics

Recommendation:
Topical and systemic administration of antibiotics is recommended for ulcer formation.

Strength of recommendation	2 (weak)
Evidence	D (very weak)

3. Dressings

Recommendation:
The use of dressings is recommended for ulcer formation.

Strength of recommendation	2 (weak)
Evidence	D (very weak)

4. Laser therapy

Recommendation:
Although laser therapy may be effective in some patients with ulcer formation, the evidence is not considered sufficient at present.

Strength of recommendation	2 (weak)

Evidence	D (very weak)

5. Systemic administration of steroid

Recommendation:

Systemic administration of steroid is recommended not to be performed for ulcer formation.

Strength of recommendation	2 (weak)
Evidence	D (very weak)

6. Platelet-derived growth factor preparations

Recommendation:

The accumulation of cases is insufficient for the judgment of the recommendability of the use of platelet-derived growth factor preparations for ulcer formation.

Strength of recommendation	No recommendation
Evidence	D (very weak)

Comments

Concerning this CQ, 42 papers in Japanese and 156 in English were retrieved. As a result of their primary screening, 47 papers were submitted to secondary screening for this CQ. None of them were about studies with a high level of evidence, such as RCT, and they were all retrospective studies, case series, or case reports.

As a result, 15 papers in English were adopted, and the evidence level was C for propranolol alone, because of the presence of a prospective controlled trial, but D for other treatments, because the related papers were case reports or case series.

According to cross-sectional analysis in a multicenter prospective cohort study in 1096 cases of infantile hemangioma by Chamlin et al. [201], it was complicated by ulcer, which was or was not bleeding, in 173 (15.8%), the median age of the patients was 4.0 months (SD = 8.5, mean = 6.6 months), and the age at the first examination was significantly lower in patients with ulcerated hemangioma (median = 3.5 months, mean = 3.98 months) than in those with non-ulcerated hemangioma.

By the site, ulcer formation was observed in 21 (30%) of 71 patients in the lower lip, 25 (25%) of 100 patients in the neck, and 46 (50%) of 93 patients in the perianal/perigenital area, and the frequency was statistically lowest in the upper eyelid ($p = 0.0140$).

Ulcer formation was observed more frequently in mixed or segmental hemangiomas. Bleeding was noted in 78 lesions (41%) and was mild in 56 (29%), moderate in 11 (6%), and severe in 4 (2%). Severe bleeding occurred in 3 lesions in the limbs and 1 lesion in the face, and bleeding occurred in 2 cases at home. Two cases required blood transfusion by hospitalization, because they showed symptoms due to serious bleeding. Of the ulcerated hemangiomas, 67 (35%) were in the proliferating phase.

Ulcerated hemangiomas required treatment (odds ratio (OR) = 6.86, 95% CI = 3.70–12.71, $p < 0.0001$), and non-ulcerated hemangiomas were observed (OR = 19.01, 95% CI = 11.23–28.88, $p < 0.0001$). Ulcerated hemangiomas tended to be treated by conventional wound care and pulsed dye lase (OR = 2.03, 95% CI = 1.19–3.46, $p < 0.0091$), and non-ulcerated hemangiomas were treated by topical glucocorticoid administration (OR = 2.57, 95% CI = 1.49–4.43, $p < 0.0007$) and surgical resection (OR = 2.04, 95% CI = 1.08–3.86, $p < 0.0286$).

However, propranolol has recently been suggested to be effective regardless of the presence or absence of ulcer formation, and as it has few adverse effects, it is expected to become the first choice treatment in the future.

[Treatments]

1. Oral propranolol

Hermans et al. [172] treated 20 previously treated patients with ulcerated infantile hemangioma using propranolol and compared them with 36 patients treated without propranolol. The administration was initiated by hospitalization, and the dose was increased from 0.7–1.0 to 2.0–2.5 mg/kg/day in 3 divided doses at an interval of at least 3 days. The blood pressure, heart rate, and blood sugar level were monitored during the initial administration period, and the administration was continued on an outpatient basis until the age of 1 year. The mean age at the beginning of propranolol administration was 3.5 months, and the mean duration of administration was 9.1 months. Not only the color and elevation of the lesion but also pain was reduced from early after the beginning of administration. The administration was concluded before the age of 1 year in 19 patients, and no recurrence of ulcer was noted in any of these patients except that some reactivation (enlargement) of hemangioma was observed after the discontinuation in 4 of these patients.

The mean time until complete cure of ulcer was 8.7 weeks, and those in whom the administration was initiated later (> 3.5 months) tended to require a longer time until cure than those in whom the administration was initiated earlier ($p = 0.025$). Also, analysis using the *t* test showed a significant difference in the time until disappearance of the tumor, which was 8.7 and 22.4 weeks ($t = 2.6$, $df = 38$, $p = 0.012$, 95% CI = 3.2-24.2) in the treated and control groups, respectively. Temporary sleepiness/malaise was observed in 6 patients, irritable before falling asleep in 2

patients, coldness of the limbs in 6 patients, anorexia in 2 patients, and gastrointestinal disorders (diarrhea, vomiting) in 1 patient, but no adverse event was noted in 9 patients.

Vercellino et al. [202], who started the administration at 1 mg/kg/day and increased to 2 mg/kg/day, and Sadykov et al. [203], who started the administration at 2 mg/kg/day, also reported that propranolol was effective.

2. Topical and/or systemic administration of antibiotics

Kim et al. [204] topically administered antibiotics in 40 patients with ulcerated hemangioma and reported that the results were better in 37 patients (92.5%), worse in none, and no change in 3 patients (7.5%). They also systemically administered antibiotics in 26 patients and reported that the results were better in 24 patients (92.3%), worse in 2 patients (7.7%), and no change in 0 patient.

Wananukul et al. [205] topically and/or systemically administered antibiotics in 41 patients with ulcerated hemangioma and reported improvement in 19 patients (46%).

Pandey et al. [206] treated 608 patients showing ulcer formation with an ointment containing an antibiotic (mupirocin, sodium fusidate, sisomicin, or metronidazole) combined with systemic administration of an antibiotic (amoxiclav at 20–40 mg/kg/day) in those with ulcers with an area of > 10 cm^2 and examined the effectiveness of treatment according to the time until cure. The time until cure was 32.63 ± 13.06 days in superficial lesions, 42.89 ± 19.89 days in mixed lesions, and 57.03 ± 16.12 days in extensive lesions, with a mean of 40.09 ± 19.41 days in all lesions combined, showing significant differences among the 3 groups ($p < 0.05$). They also reported that the time until cure was significantly longer in larger (> 10 cm^2) than smaller ulcers ($p < 0.05$).

3. Dressings

Kim et al. [204] treated 25 patients using dressings and reported that the results were better in 23 patients (92%), and no change in 2 patients (8%). Oranje et al. [207] applied polyurethane film and reported rapid relief of pain and cure of ulcer in 1–2 months. In addition, Bauland et al. [208] treated 41 patients using a non-adhering dressing containing an antibiotic and reported that the results were good in 26 patients (63.4%), moderate in 5 patients (12.2%), and little change in 10 patients (24.4%).

4. Laser therapy

In the 1980–1990s, there were reports [209, 210] of argon, Nd YAG, and KTP, but recent reports [211, 212] are primarily about treatment using dye laser. Morelli et al. [209] treated 37 patients with ulcerated hemangioma by dye laser irradiation (SPTL1b® (Candela Corporation, Wyland, MA, USA), wavelength: 585 nm, spot size: 5–7 mm, irradiation power: 5–6.8 J/cm^2, pulse width: 0.45 ms) and reported that the number of irradiations until cure was 1 in 26 patients (68%) and 2 in 8 patients (21%) and that the mean period from the first treatment until cure of ulcer was 2.84 ± 0.22 weeks. Lacour et al. [210] irradiated 8 patients with ulcerated hemangioma that resisted conventional treatments using the same equipment and reported acceleration of cure. David et al. [211] performed dye laser irradiation (PhotoGenica V® (Cynosure, Westford, MA, USA), wavelength: 585 nm, spot size: 5–7 mm, irradiation power: 5–6.8 J/cm^2, pulse width: 0.3–0.5 ms) in 78 patients and reported the effectiveness of laser therapy alone in 72 (92.3%). Also, Michel [212] performed 1 or 2 irradiations using Dermobeam 2000® (Deka MELA, Calenzano, Italy) with a cooling system 595 nm (2 pulsed irradiations with a 10% overlap, spot size: 7 mm, irradiation power: 4–8 J/cm^2) and reported resolution of pain in 10 of the 12 patients. Moreover, Di Maio et al. [213] performed laser treatment in 65 patients with hemangioma with ulcer and reported that the effect was excellent and that no clear adverse events were observed, because scarring, which was noted in a few patients, did not differ markedly compared with scarring that occurs after conventional treatments.

However, Kim et al. [204] treated 22 patients with pulsed dye laser and reported that the results were better in 11 patients (50%), worse in 1 patient (4.5%), and no change in 4 patients (18.2%), but warned that 5 patients in the proliferating phase showed ulcer formation after irradiation.

As observed above, although there have been several reports of the effectiveness of laser therapy against ulcer as factors of "benefit", many reports are relatively old and lack controls, and the evidence is not considered sufficient. Further accumulation of cases is necessary. Laser may be effective in limited patients, but as there is the risk of ulcer formation as an adverse effect of laser irradiation of infantile non-ulcerated hemangioma, greater caution is needed in treating already ulcerated lesions.

5. Steroids

There have been few reports on steroid therapy focusing on ulcer. Kim et al. [204] treated 7 patients by local steroid injections and reported that the results were better in 4 patients (57.1%), worse in 1 patient (14.3%), and no change in 1 patient (14.3%). They also systemically administered steroid to 22 patients and reported that the results were better in 16 patients (72.7%), worse in 1 patient (4.5%), and no change in 5 patients (22.7%). Based on these results, they considered that the treatment was effective for reducing the

lesion size, and there are few other reports suggesting the effectiveness of steroid. Considering that the patients are infants and that there are other treatment options, steroid cannot be recommended at present.

6. Topical preparations of recombinant human platelet-derived growth factor

0.01% becaplermin (Regranex® (Ortho-McNeil Pharmaceutical, Raritan, NJ, USA)) is a preparation for diabetic foot ulcer approved by the FDA in 1997. Sugarman et al. [214] and Metz et al. [215] reported its effectiveness for the treatment of ulcerated hemangioma in 1 and 8 patients, respectively, but its effectiveness cannot be appraised at present because of the small number of cases.

CQ16: Is intralesional corticosteroid injection more effective than systemic administration for infantile hemangioma?

Recommendation:

Treatment using corticosteroid is effective for inducing early regression of hemangioma. While no significant difference is observed in the effectiveness between intralesional injection and systemic administration, attention to complications including those at the administration site, such as the periocular region, on local injection and those, such as hypertension and growth retardation, on systemic administration is necessary.

Strength of recommendation	2 (wean)
Evidence	B (moderate)

Comments

As a result of primary screening, 99, 9, and 35 papers were extracted from PubMed, Cochrane, and JCRM, respectively, and 4 papers in English were subjected to secondary screening for this CQ. There was 1 report of an RCT, but the other reports were about case series while they evaluated a large number of cases. In addition, 2 papers on complications considered important in relation to intralesional corticosteroid injection for periocular lesions were added by manual search. Since there is a report of an RCT, and since other case series studies with a large number of subjects presented the results that there was no significant difference in the effectiveness of corticosteroid depending on the administration method, the strength of evidence was rated as "B".

There was 1 report [216] of an RCT focusing on "Is intralesional corticosteroid injection more effective than systemic administration for infantile hemangioma?". In this trial, the subjects were divided into control, oral administration (prednisolone at 2 mg/kg/day every other day for 6 weeks), and intralesional injection (triamcinolone at 1-5 mg/kg with a maximum of 30 mg once a month for 6 months) groups, and the lesion size was significantly reduced in the treated groups compared with the control group. While no significant difference was noted between the oral administration and the intralesional injection groups, the reduction rate tended to be larger in the local injection group, and local injection was concluded to be slightly superior [216].

There were reports [217, 218] of case series with more than 1000 subjects, but the findings were not statistically analyzed. Although both intralesional injection and oral administration were effective, there was also a mixed group of intralesional injection and oral administration, the condition of patients varied among the 3 groups (intralesional injection, oral administration, mixed), and the effectiveness according to the administration method was not shown. Regarding complications, systemic symptoms, such as hypertension, retarded body weight gains, and cushingoid appearance, were reported to be more frequent on oral administration than intralesional injection [217, 218]. Moreover, concerning complications, in one report [219], periocular lesions were excluded from the targets of intralesional injection to avoid its effect on visual function. Indeed, there have also been case reports [220, 221] that visual impairment was caused by occlusion of the retinal artery after intralesional corticosteroid injection for periocular hemangiomas. Currently, in Japan, intralesional corticosteroid injection is a treatment unapproved by the national health insurance system.

CQ17: Is topical therapy effective for infantile hemangioma?

Recommendation:

Although it must be noted that there are no reports of comparison with placebo and that the degree of improvement is smaller compared with systemically administered drugs, topical medication can be an option for the treatment of infantile hemangioma with no risk of complications if drugs with milder adverse effects are selected.

Strength of recommendation	2 (weak)
Evidence	C (weak)

Comments

As a result of literature searches, a total of 111 papers consisting of 70, 7, and 34 papers from PubMed, Cochrane, and JCRM, respectively, were extracted. They included 1

RCT study. Including this RCT, 48 papers were extracted by secondary screening. In addition to the papers selected by secondary screening as closely related to the CQ, a total of 47 papers obtained by manual search were adopted as reference for the preparation of guidelines. There was 1 RCT, and comparative studies of therapeutic results by topical therapy and case series studies with a relatively large number of subjects were adopted as papers of relatively high quality, the strength of evidence was rated as C "weak".

In the reports related to the CQ:

(1) Drug type: The drugs were classified into imiquimod, timolol, propranolol, corticosteroid, and others [215, 222–225].

(2) Drug concentration and dosage form: Imiquimod was used as a 5% cream [222, 226–233], timolol as 0.5% ophthalmic solution or gel [222, 223, 232, 234–243], propranolol as 1% ointment [181, 234, 241, 244, 245], and corticosteroid were often used as ointments of agents ranked as relatively strong such as clobetasol propionate, halobetasol propionate, and betamethasone dipropionate [246, 247].

(3) Methods for topical application: Frequent administration methods were once a day every other day for imiquimod, 2 times a day every day at 1–2 drops each time for timolol, 2 times a day every day for propranolol, and 2 times a day every day for corticosteroid.

(4) Methods for efficacy evaluation: Comparison of gross findings and photographs were adopted in all papers. The area was compared using photographs in one report [227]. There was also a report [228] of half-side test for a control.

(5) Adverse effects: No systemic adverse effect was reported, and most adverse effects were local. Imiquimod caused pain, flare, and erosion relatively frequently [231, 233]. Few local adverse effects were reported for timolol and propranolol [232, 234, 241, 242, 245]. No local adverse effects were reported also by corticosteroid [246, 247].

(6) Relative advantages of drugs Imiquimod has been reported to have usefulness comparable to that of topical beta blockers, but it is not considered superior in terms of adverse effects [226, 228, 230, 232].

Corticosteroid was not shown to be superior in efficacy compared with beta blockers.

There was also one RCT study [181] concerning the CQ, which is related to topical propranolol concerning drugs. In this RCT, 15 each of a total of 45 subjects were allotted to oral (propranolol at 2 mg/kg/day, 2 times a day), topical (1% propranolol water soluble ointment, applied 2 times a day), and local injection (1 mg/1 mL, 0.2 mL/1 cm in diameter, 1 mL/injection at the maximum, 1 time/week) groups. Ten patients (66.7%) in the topical group responded, but they were fewer than 13 (86.7%) in the oral group. The time until the appearance of the effect and time until complete cure were also longer in the topical group than in the oral group. Concerning complications, none was observed in the topical group, but 1 patient in the oral group showed unexplained syncope as an adverse effect and was excluded. While decreases in the heart rate and blood pressure were observed in 3 in the oral group, they did not necessitate interruption of the study. In the local injection group, 8 (53.3%) responded, but 3 were lost due to pain. From these results, the study concluded that topical therapy is an option to be evaluated for patients with a risk of adverse reactions to oral medication. While there were no reports of comparison under the same conditions, comparative studies of therapeutic results by topical therapy and case series studies with a relatively large number were adopted as relatively high-quality papers. In all these reports, topical therapy of beta blockers (propranolol, timolol) was effective to an extent with no serious complications.

Thus, topical therapy, particularly, of beta blockers is considered generally useful, but there has not been a report of its comparison with placebo, and further accumulation of cases is necessary.

Research by comparison between dye laser treatment and topical beta blocker therapy is considered to be necessary.

CQ18: Is compression therapy effective for infantile hemangioma?

Recommendation:

Although appropriate compression method must be performed for individual patients, compression therapy may be regarded as an option on condition that the therapy is carried out by a skilled physician. Sufficient attention to skin abnormalities and local/neighboring growth disturbance due to the compression are needed.

Strength of recommendation	2 (weak)
Evidence	D (very weak)

Comments

While 23, 1, and 14 papers were extracted from PubMed, Cochrane, and JCRM, respectively, only 3 case reports remained to be reviewed as a result of primary and secondary screening. Thus, the evidence level is very low at D (very weak).

According to a case report of ulcerated infantile hemangiomas of the limbs by Kaplan et al. [248], the ulcers of most patients showed rapid improvements and cured within 2 weeks by compression therapy using the self-adherent wrap Coban® (3M, St. Paul, MN, USA) combined with topical treatment with an antibiotic ointment (or early systemic antibiotic administration when secondary infection was apparent). They concluded that, compared with antibiotic

ointment alone, its combination with compression therapy was more effective, and is a safe and easy treatment that promotes regression of hemangiomas.

Ochi et al. [249] reported 12 cases of infantile hemangioma (9 girls and 3 boys with a mean age of 8.4 months; sites of the lesion: limbs in 6, head and neck in 5, and trunk in 1). By treatment using elastic bandages (5 patients), Presnet® (ALCARE, Tokyo, Japan) (4), supporter (1), or Elatex® (ALCARE, Tokyo, Japan) and cryotherapy (2), the hemangiomas disappeared or decreased in size in 11 of the 12 patients, with only 1 (head and neck) showing no improvement. The time until the disappearance of the lesion in the 11 responders was 2 months to 3 years (mean: 19.5 months), no complications associated with compression therapy were noted, and the authors recommended early initiation of compression therapy if the site of the lesion can be compressed.

Totsuka et al. [250] treated 3 girls with parotid gland hemangiomas (mean age: 4.3 months) by splinting using a resin plate and compression using a handmade cap. The mean duration of treatment was 13 months (8–16 months), and the patients were followed up until a mean age of 4.6 years (2–7 years), resulting in clinical and echographic disappearance of hemangioma in all 3. Since infantile hemangiomas often regress spontaneously, it is impossible to conclude that they regressed due to compression therapy, but they reported the therapy to be safe and effective.

Thus, concerning factors related to "benefits" of compression therapy, there are reports that suggest the effectiveness of compression methods appropriate for sites (elastic bandages, Present, splinting with a resin plate). However, it must be noted that they are all old reports. Concerning factors related to "harm", while compression is a relatively safe and simple method without reports of serious complications, the occurrence of dermatitis and growth disturbance at the site of compression or surrounding areas is considered possible. The recommendation level was set at 2D with consensus of the present guidelines preparation committee on condition that the treatment is performed carefully by a skilled physician in consideration of these points. The present guidelines do not exclude compression therapy, but it is necessary to consider oral propranolol, oral administration or local injection of steroid, and laser therapy first for infantile hemangiomas that need treatment.

CQ19: Is glucose transporter 1 (GLUT-1) immunostaining useful for the diagnosis of infantile hemangioma?

Recommendation:

Immunostaining for GLUT-1 is positive in the proliferating, involuting, and involuted phases, shows high sensitivity and specificity, and is useful for the diagnosis of infantile hemangiomas if the clinical diagnosis is difficult.

Strength of recommendation	2 (weak)
Evidence	C (weak)

Comments

To evaluate whether GLUT-1 immunostaining is useful for the diagnosis of infantile hemangiomas, the literature was searched first for the following key words.

Infantile OR juvenile AND hemangioma AND marker AND immunohistochemistry

The search of JCRM resulted in 26 hits, but none of them performed analysis of GLUT-1 or evaluated its usefulness by comparing infantile hemangioma with other hemangiomas/vascular malformations even if GLUT-1 was analyzed. The search of PubMed resulted in 182 hits. From these papers, those that deserved detailed analysis were selected according to the following criteria.

(1) Those in which GLUT-1 immunostaining was performed for infantile hemangioma or other hemangiomas/vascular malformations.

(2) Those that were retrospective epidemiological studies rather than reports of one case.

Fifteen research papers selected by these criteria were analyzed in detail.

In 7 of these reports [251–257], infantile hemangiomas were stained using GLUT-1 simultaneously with other hemangiomas/vascular malformations, and differences in positive/negative results were evaluated. Of all cases reported in the 7 papers, GLUT-1 was positive in 268 of the 273 cases of infantile hemangioma and negative in 244 of the 247 cases of lesions other than infantile hemangioma. There were also 4 papers [258–261] in which GLUT-1 staining was performed for clinically typical infantile hemangiomas and hemangiomas that need to be differentiated from infantile hemangioma although they were not simultaneously stained in the same paper. When the 4 papers were combined, GLUT-1 was positive in all 8 cases of infantile hemangioma and negative in all 49 cases of non-infantile hemangioma. When the above cases are totaled, GLUT-1 was positive in 276 of the 281 cases of infantile hemangioma and negative in 293 of the 296 cases of non-infantile hemangioma, and the sensitivity and specificity of GLUT-1 positivity for infantile hemangioma were 98.2 and 99.0%, respectively.

The usefulness of GLUT-1 staining has also been confirmed by re-evaluation of cases that were initially examined by hematoxylin–eosin staining alone [262–265]. There have been 4 papers in which cases were re-evaluated using GLUT-1

staining, and 1 paper reported that the diagnosis was impossible by HE staining alone in 18% of the cases [262].

CQ20: What gastrointestinal examinations are useful for children suspected to have blue rubber bleb nevus syndrome? When should the examinations be started?

Recommendation:

It is recommended to start screening by examinations including blood tests and fecal occult blood test as early as possible. In children suspected to have gastrointestinal bleeding, the usefulness of endoscopic examination, red blood cell scintigraphy (99mTc-labeled red blood cells), and single photon emission computed tomography-CT (SPECT-CT) has been reported for the identification of the source of bleeding. If no abnormality is detected by screening, and search for gastrointestinal lesions needs to be performed to diagnose this disease or evaluate the future risk of bleeding, there is no standard for its timing. Among the examinations that led to the detection of gastrointestinal lesions in past reports, CT and MRI can be performed with relatively mild invasion and from an early stage.

Strength of recommendation	2 (weak)
Evidence	D (very weak)

Comments

Gastrointestinal lesions of blue rubber bleb nevus syndrome (bean syndrome) are observed in the entire digestive tract, but they frequently appear, particularly, in the small intestine. Since it is an extremely rare disease, the literature is primarily case reports and reviews, and there have been no reports of clinical studies of many cases that are relevant for the CQ. Therefore, we investigated examinations that were useful for the detection of gastrointestinal lesions in reports, primarily, of child cases. Lesions in the small intestine are difficult to observe by conventional endoscopy, but techniques such as double-balloon endoscopy, capsule endoscopy, CT enterography, CT, and MRI as well as upper and lower gastrointestinal endoscopy have been reported to be useful [266–276].

As a result of database searching, 11 papers in English were adopted through primary and secondary screening. All papers selected by these screening processes were case reports or case series, and the strength of evidence is “D (very weak)”.

There is no clear standard as to when the examinations should be initiated. However, neonates who developed gastrointestinal bleeding shortly after birth have been reported [270], and the earliest possible examinations are necessary if this disease is suspected. Invasive examinations are difficult to perform in small children, but blood tests (presence or absence of anemia or consumption coagulopathy) and fecal occult blood tests can be performed. If gastrointestinal bleeding is suspected, procedures such as endoscopy, particularly, double-balloon endoscopy and capsule endoscopy, 99mTc-labeled red blood cell scintigraphy, and 99mTc-labeled red blood cell SPECT-CT have been reported to be useful for the determination of the source of bleeding [266, 268, 271, 275].

If no abnormality has been detected by screening tests, and if search for gastrointestinal lesions needs to be performed non-emergently to diagnose this disease or evaluate the future risk of bleeding, there is no standard for the timing, which may vary among facilities. Among the above examinations, CT and MRI can be performed earlier and with relatively milder invasion, and are worth attempting if this disease is suspected. The necessity of the other examinations for the gastrointestinal lesions mentioned above should be considered when the patient reaches the age that tolerates the examinations.

CQ21: How are limb overgrowths to be managed in vascular malformations and syndromes?

Recommendation:

If leg-length inequality is insignificant, shoe lift is recommended. As significant inequality causes gait disturbance complicated with scoliosis, surgical treatment aimed to arrest epiphyseal growth is performed in the growth period. Shortening of the femur or tibia may be performed as an additional treatment. Bone elongation of the intact side is considered effective for the correction of leg-length inequality.

Strength of recommendation	2 (weak)
Evidence	D (very weak)

Comments

As a result of literature searches, 40 papers in English and 4 papers in Japanese were retrieved by primary screening. Of these papers, 17 in English and 4 in Japanese were extracted by secondary screening. As for the control of overgrowth of limbs, measures against leg-length inequality and soft tissue hypertrophy are separately discussed and regarded as effective, but these papers were all classified either as case reports or as general discussions. Therefore, the evidence

level is rated as "very weak", and the recommendation level as "weak".

In vascular malformations, typical disorders with hypertrophy of the affected limbs are Klippel–Trenaunay syndrome and Parkes Weber syndrome and most of the papers refer to the management of limb overgrowth due to vascular malformations were written about these disorders. The literature regarding lesions at different sites is commented on below.

Lower limbs

In most reports, treatment for the overgrowth of the lower limbs were aimed to prevent physical disorders caused by leg-length inequality. Some reports particularly mentioned treatment for foot lesions.

1. Correction of leg-length inequality

If the leg-length inequality is ≤ 2 cm, the management of leg-length difference and accompanying scoliosis is considered possible by the use of shoe lift [277–281]. If the leg-length inequality is ≥ 2 cm, significant gait disturbance, postural abnormalities, and compensatory changes in the contralateral limb are likely to develop, and before consequent unphysiological gait leads to irreversible impairment, surgical treatment to correct the leg-length inequality should be considered [277–281]. Long-leg radiography is useful for determining the best time for surgery [282], and the measurement of the leg-length by long-leg radiography or CT is reported to be effective [278]. Surgical treatment reported in the papers are as follows.

Treatment for overgrown limbs affected by vascular malformations

Jacob et al. [277] performed epiphysiodesis in 41 patients with a leg-length inequality of ≥ 2 cm among 252 patients with Klippel–Trenaunay syndrome and reported improvement in more than 90% of the patients. The effectiveness of this surgery is also confirmed by other review articles [277–281]. The effectiveness of shortening of the femur and tibia was reported in the review by Capraro et al. [278] The fixation period is considered to be shortened as a whole by simultaneously performing femoral or tibial shortening in addition to epiphysiodesis. Redondo et al. [280] recommended endoscopic growth control of the epiphyseal plate in the distal end of the femur for patients with a leg-length inequality of ≥ 2 cm. Capraro et al. [278] did not recommend growth control with the epiphyseal stapling because of the unpredictability of the results and high frequency of complications. The appropriate time for surgical intervention on affected limbs is reported to be around the age of 11 years [280].

Elongation of the intact leg

Tanaka et al. [283] performed bone elongation of the intact limbs using an external fixator in adult patients with mild structural scoliosis and reported that the procedure was effective for correcting the leg-length inequality and scoliosis. Jacob et al. [277] also recommended bone elongation of the intact limb using Ilizarov external fixation apparatus in their review.

Popliteal vein ligation

Servelle [284] hypothesized that elongation of the affected limbs was due to a high venous pressure and performed ligation of the popliteal vein of the intact limb in 48 children, and they reported significant improvement in leg-length inequality. However, there are also negative views, saying its effectiveness is uncertain [278].

2. Foot lesions

Redondo et al. [280] recommended resection of the toes (ray resection) and debulking for wearing shoes and cosmetic improvement. Gates et al. [285] notably reported that compared with ray resection, wound healing of the stumps was poor after major resection.

Upper limbs

Asymmetry due to hypertrophy of the upper limb less frequently causes impairment of ADL than that of the lower limb. In one article, resection in patients with functional impairment due to marked finger deformities is reported [282], but articles reporting treatment for upper limb overgrowth are very few. While debulking has been reported to be advantageous from the cosmetic viewpoint [279], it has also been reported to induce exacerbate of edema of the affected limb [284], causing complications including cicatricial contracture, recurrence of the lesion, and refractory ulcer [278], and sufficient caution is necessary.

CQ22: Is surgical resection effective for soft tissue/superficial LM?

Recommendation:

Although surgical resection is an effective treatment, it should be performed after comprehensive evaluation of

cosmetic aspects, prognosis, functional prognosis, resectability, and possibility of recurrence/complications.

Strength of recommendation	2 (weak)
Evidence	D (very weak)

Comments

[Process of preparation of recommendation]

Surgical resection is one of the major treatment options performed for LM. Although LM can be cured by total resection, the objective of treatment is not necessarily total resection, because the disease is not malignant, and surgical resection is often carried out for cosmetic, functional, and symptomatic improvements. Cosmetic problems are considered to be particularly serious if the lesion is located in superficial areas such as the body surface and soft tissue. However, surgical resection has been known to cause complications including hemorrhage, infection, deformation, and nerve paralysis.

In evaluating whether resection is effective, the balance between its positive aspects and negative aspects, such as complications, is important. For soft tissue/superficial LM, in which cosmetic improvement is important, problems including in what situations resection can be performed, whether there are criteria for the selection of resection, and, as there are differences in the incidence of complications, cure rate, and recurrence rate depending on the circumstances, whether its indications should be evaluated under different conditions are unclear. Therefore, the CQ, "Is surgical resection effective for soft tissue/superficial LM effective?", was formulated, and the current knowledge was summarized.

<Literature search and screening>

As a result of literature search, 105 papers in Japanese and 348 papers in English were subjected to primary screening. Of these papers, 5 in Japanese and 42 in English were subjected to secondary screening concerning this CQ. They did not include papers with a high level of evidence, such as a systematic review and RCT, and all of them were case series or case reports. As a result, in the evaluation of this CQ, the results and discussion in each case series were integrated.

<Review of observational studies (case series)>

The effectiveness of resection of LM was evaluated from the following 5 viewpoints: (1) Effectiveness regarding the prognosis (mortality), (2) resection rate of the lesions (resectability), (3) functional outcome after resection (function), (4) recurrence rate (recurrence), and (5) complications.

Results of review

Generally, the rate of successful surgical resection is high, and ≥ 90% resection is reported to be possible in 60% or more of the patients [286–288]. This also applies to the head and neck region, which is the frequent site of the lesion [286]. However, the percentage of resectable lesions decreases from the cystic to mixed and to cavernous type [286]. Since many LM are distributed diffusely in the skin and subcutaneous adipose tissue and around structures including muscles, blood vessels, and nerves, resection of the lesion involves resection of normal tissues in varying degrees. In lesions that show complicated distribution in the head and neck region, complications after surgical resection are observed relatively frequently. Serious complications including nerve paralysis, hematoma, local necrosis, sepsis, deformation, salivary fistula, hoarseness, airway obstruction, and malocclusion have been reported [286, 287, 289–297], and facial nerve paralysis is likely to result from resection, particularly, of LM infiltrating the parotid region [289]. By the site, the incidence of complications increases as the area of involvement widens from unilateral to bilateral, from below to above the lingual bone, both sides, and both above and below the lingual bone [293, 296]. Postoperative death may occur in patients with a severe neck lesion, but the extent of the effect of surgical resection is unclear [287, 288, 298]. Postoperative recurrence is closely related to the resectability of the lesion depending on its distribution, and lesions that are difficult to resect due to a wide area of involvement and a strong tendency of infiltration have been reported to be associated with recurrence [296].

Limitations

Indications for surgical resection vary among papers, and differences in the patient background must be considered in the evaluation of the effectiveness of resection. While there were many reports that surgical resection was performed in combination with sclerotherapy, and resection is considered to have been performed when more favorable results were expected from resection rather than sclerotherapy, criteria for their selection are unclear. Therefore, there is certainly the large bias of individual variation in the circumstances, and it was clearly impossible to conclude that resection is uniformly effective.

<Summary>

While the effectiveness of surgical resection for soft tissue/superficial LM was evaluated, there was no literature with a high level of evidence. One of the major reasons is the diversity of the lesion type (cystic or cavernous), area of involvement, and history of other treatments. Because of this diversity, the condition of patients is considered to show an

extremely wide variation, and their generalization is impossible. However, if conditions, such as the type of the lesion (cystic or cavernous), site of origin, and relationship with other treatments are restricted, tendencies were observed in functional prognosis, recurrence rate, and contents and incidence of complications.

While the resection rate of lesions by surgical treatment was suggested to be generally high, selection criteria for resection were unclear. Therefore, it is speculated that resection was performed for patients clinically judged to be treated more effectively by surgery. However, since there were some serious complications of surgical resection that persist as sequelae, their possibility should be evaluated carefully in performing surgical resection. The risk of resection has been suggested to vary with conditions of the lesion. The functional outcome is poor, and the recurrence rate and incidence of complications after resection are high, in those that occupy a wide area and those that are accompanied by symptoms such as airway obstruction.

From these observations, we propose at present, "While surgical resection is often effective, it must be selected in consideration of cosmetic aspects, prognosis, functional prognosis, resectability, and possibility of recurrence and complications.", despite limited scientific grounds. If complete resection of the lesion is possible, surgical resection may be performed as the first-line treatment, but the possibility of other treatments including sclerotherapy, in particular, should be evaluated according to the diverse conditions of individual patients, and surgical resection should be performed when other treatments are ineffective or when surgical resection is considered clearly superior.

CQ23: What is the optimal timing of surgery for soft tissue/superficial LM?

Recommendation:

It is impossible to recommend optimal timing of surgery, and judgments according to the condition of each case are necessary.

Strength of recommendation	2 (weak)
Evidence	D (very weak)

Comments

[Process of preparation of recommendation]

Soft tissue/superficial LM are not malignant lesions. Emergent treatment may be necessitated by life-threatening symptoms, such as airway obstruction, but the initiation of treatment immediately after the diagnosis is generally considered unnecessary. The natural course of the disease differs considerably among individuals, particularly, in infancy, and the lesions may show a tendency of spontaneous regression but may also cause various functional problems due to rapid enlargement. Moreover, there are cosmetic problems characteristic of this disease in addition to functional problems, and early therapeutic effects are necessary to make social life comfortable. For these reasons, the selection of optimal timing of treatment, surgery in particular, is a major issue.

For the selection of the timing of surgical resection, conditions to obtain the best results as well as indications for resection must be evaluated, and sufficient consideration of the balance between merits and demerits depending on the timing of resection is necessary. Therefore, in this CQ, we attempted to summarize the presently available knowledge about "What is the optimal timing of surgery for soft tissue/superficial lesions?".

<Literature search and screening>

As a result of literature search, 67 papers in Japanese and 231 papers in English were subjected to primary screening. Of these papers 5 in Japanese and 42 in English were subjected to secondary screening for this CQ. They included none with a high level of evidence, such as a systematic review and RCT, and all papers were case series or case reports. Therefore, the results and discussion in each case series were integrated in the evaluation of this CQ.

<Review of observational studies (case series)>

Defining "the optimal timing of surgery" mentioned in the CQ as "the timing of surgery at which good results can be obtained", we aimed to evaluate the timing of surgery at which resection is effective, problems, such as complications are few, and, i.e., "the best results" can be obtained as a whole. Conditions must be evaluated on the basis of the timing in addition to the effectiveness of surgery, but objective judgments were considered difficult in this evaluation. However, as it was considered possible to obtain information about the age and time of surgery from the literature reviewed in the previous CQs concerning the effectiveness, papers that evaluated the age at surgery were searched.

Results of review

Despite a careful review of the literature by secondary screening, there was no paper that analyzed cases from the viewpoint of optimal timing of surgery. There was information concerning the age at surgery, but its appropriateness was not evaluated. Papers that mentioned the timing of surgery are shown below.

Concerning the timing (age) of surgery, unless the size of the lesion is small or there are symptoms that require urgent treatment, such as respiratory disturbance, it is recommended to delay surgery until the age of 3 years by

expecting spontaneous regression or for the ease of identification of surrounding structures during surgery, ease of control of bleeding, and less problems with postoperative management [294]. There was also a paper [295] that suggested the necessity of the determination of the time of surgery in consideration of problems that change with age including the priority of securing the airway and appropriate nutritional management in neonates with head and neck and giant lesions, control of hemorrhage and infection and measures to prevent dysarthria and dental problems in infants, and skeletal and cosmetic problems in school-age children, although it did not mention the optimal timing of surgery.

However, there was no paper that positively recommended resection without considering the time after the diagnosis or grounds for such a recommendation.

<Summary>

As a result of literature search for evaluating the CQ, "What is the optimal timing of surgery for soft tissue/superficial LM", there were papers that mentioned the timing of surgery, but none of them objectively evaluated its appropriateness. Therefore, no suggestion about the appropriate timing of surgery was obtained from the literature available at present, but there were a few papers suggesting that the decision to perform surgery should be made carefully.

Similar to the previous CQ, soft tissue/superficial LM of which the background vary in individual cases, and it is difficult to uniformly evaluate the effectiveness of resection. In clinical practice, in addition to medical reasons, social reasons including school attendance are considered to largely influence the decision of the time of resection. The results of RCTs are necessary to obtain objective data, but it is practically very difficult to arrange an RCT fulfilling the above conditions.

While this CQ is a very important issue for patients and families as well as clinicians, there has not been objective evaluation of the optimal timing of surgery in the past. Presently, as quick decisions to perform surgery should be avoided, this guideline proposes, "The optimal timing of surgery cannot be decided in general, and judgments according to the condition of each case are necessary."

CQ24: Is sclerotherapy effective for facial microcystic LM?

Recommendation:

A wide range of drugs are used for sclerotherapy. Although comparison among drugs has not been made, and consensus regarding the methods or frequency of their administration has not been reached, improvements are observed after sclerotherapy in various symptomatic, functional, and cosmetic (esthetic) aspects. However, complications including functional impairment have also been reported.

Strength of recommendation	2 (weak)
Evidence	D (very weak)

Comments

[Process of preparation of recommendation]

[Literature search and screening]

Concerning this CQ, 35 papers in Japanese and 92 papers in English (60 from PubMed, 32 from Cochrane) were retrieved. After their primary screening, 6 in Japanese and 18 in English were subjected to secondary screening concerning this CQ. Although they included 3 RCTs, many of the other papers were case series or case reports. Therefore, in the evaluation of the draft recommendation concerning this CQ, the results and discussion in each RCT and case series were integrated. While the evidence is scarce, the papers judged to be useful for the preparation of the draft recommendation are presented as review data.

[Review of case series]

As a result of literature screening, it was found that the effectiveness of sclerotherapy for facial microcystic LM has been evaluated from the following viewpoints.

1. Treatment responses
   A. Size
   B. Symptoms
   C. Functions
   D. Cosmetics
2. Complications

The contents of the accounts concerning the effectiveness of sclerotherapy are summarized according to these viewpoints.

However, there were few reports that exclusively analyzed facial (and microcystic) LM, and lesions of the neck and other regions as well as the face were evaluated or different types of LM, such as cystic and mixed types, were reported together. In addition, the definition of the cavernous type and standard procedure of sclerotherapy (method and number of administrations) varied among reports, and these differences in the background should be considered in the evaluation of the effectiveness of sclerotherapy.

The sclerosing agents used for the literature search ranged widely from OK-432, bleomycin, ethanol, doxycycline, and sodium tetradecyl sulfate (STS). However, as none of the papers reviewed for the preparation of these guidelines evaluated differences in the effectiveness for facial microcystic

lesions among drugs or the method or number of administrations of each drug, these evaluation items were excluded in discussing this CQ.

1. Responses

A. Size

Many of the papers that referred to the regression rate of the lesion classified the responses into (1) excellent or complete (regression rate ≥ 90%), (2) good or substantial (regression rate ≥ 50% and < 90%), (3) fair or intermediate (regression rate ≥ 20% and < 50%), and (4) poor or none (regression rate < 20%).

Although there was no paper that collected cases of facial lesions alone, Yang et al. [299] reported that the regression rate after sclerotherapy was ≥ 90% in 19 (63%) of the 30 patients with head and neck lesions and ≥ 50% in 10 (33%). In addition, the regression rate was reported to be ≥ 50% in 18 (85.7%) of the 21 patients with head and neck lesions by Alomari et al. [300] and in 30 of the 31 patients to be ≥ 50%, who included those with mixed type lesions, by Chaudry et al. [301]

Smith et al. [302] reported that none showed a response (complete or substantial) in 17 patients who underwent sclerotherapy, some of whom had mediastinal lesions. Giguere et al. [303] also reported that all 5 patients with head and neck lesions showed no response (poor) to the therapy. While these studies were RCTs evaluating the time of sclerotherapy, the results suggest that sclerotherapy is not effective for microcystic lesions regardless of the time of treatment.

There was no paper that compared sclerotherapy and resection for facial microcystic LM.

B. Symptoms

There is no literature that evaluated this item based on objective data, and few reports referred to symptoms themselves. The information was limited to the report by Chaudry et al. [301] that symptoms disappeared after sclerotherapy using bleomycin in 75% of the patients who complained of pain and a few case reports [304, 305] that symptoms, such as hemorrhage and respiratory impairment, were relieved after sclerotherapy.

C. Functions

Ravindranathan et al. [306] performed sclerotherapy in 3 patients with diffuse microcystic lesions extending from the face to the tongue and pharynx and reported that respiratory impairment and swallowing disorder due to airway obstruction observed before treatment were mitigated. Poonyathalang et al. [307] administered STS to a patient with orbital lesions primarily complaining of visual defect and reduced visual acuity due to retrobulbar hemorrhage and reported alleviation of the symptoms, but relevant literature was scarce similar to that concerning symptoms.

D. Cosmetic aspects

Cosmetic improvements are difficult to evaluate objectively. Poonyathalang et al. [307] administered STS to 3 patients with orbital lesions with exophthalmos as the primary symptom and reported improvement by measuring the degree of protrusion before and after the treatment. There have also been reports of objective assessment based on the degree of satisfaction in the patients' families. According to Chaudry et al. [301], all patients with head and neck lesions (9 with microcystic lesions, 22 with mixed lesions) and their families reported improvements in the size and appearance of the lesions. In addition, Alomari et al. [300] treated 32 patients with mostly microcystic but including some cystic LM of the head and neck region by sclerotherapy and reported improvements compared with the condition before treatment by the families of 26 patients (81.3%).

2. Complications

As complications in the facial region, there are a large number of reports [299, 301, 307–312] of transient complications associated with sclerotherapy, such as fever, local swelling and pain, intracystic hemorrhage, and infection, although the lesions were poorly characterized in some reports. In addition, complications considered to have been caused by the effect of treatment, such as ulcer of the oral mucosa and tongue, facial nerve paralysis, leakage of saliva, and respiratory insufficiency due to airway obstruction, have been occasionally reported [303, 306, 307]. There have also been reports [307, 313, 314] of an elevation of the intraorbital pressure, exophthalmos, intraorbital hemorrhage, corneal damage, and external ocular muscle paralysis due to enlargement of the mass after sclerotherapy for ocular LM. There was also no literature showing the incidence of complications in facial microcystic LM.

As complications caused by sclerosing agents, skin ulcer and necrosis and nerve damage due to ethanol leakage, hypotension during anhydrous ethanol injection, and epidermal detachment due to doxycycline have been reported [300, 315]. However, there was no report of serious complications due to OK-432. Pulmonary fibrosis is widely known to be a complication of bleomycin, but, according to Chaudry et al. [301] and Yang et al. [299], impairment of respiratory function does not occur at a dose routinely employed for sclerotherapy.

[Summary]

In evaluating the CQ, "Is sclerotherapy effective for facial microcystic LM?", analysis was performed from

the viewpoints of responses to the treatment in terms of symptoms, functions, and cosmetic (esthetic) aspects and complications, but few papers with a high level of evidence were found. While the degree of regression of the lesions by sclerotherapy varied widely, the size-reducing effect of the therapy was consistently small unlike that in cystic lesions. Some papers referred to symptoms, functional outcome, and cosmetic improvement, but they were insufficient for general discussion of sclerotherapy for facial microcystic LM. As complications characteristic of sclerotherapy, serious impairment may be caused by leakage of the sclerosing agent (ethanol, in particular), and this point needs attention. Based on the above observations, it is difficult at present to evaluate indications for sclerotherapy against microcystic LM by formulating criteria. Therefore, for the future, it is considered necessary to evaluate the usefulness of sclerotherapy addressed by this CQ by designs such as RCT.

CQ25: Is sclerotherapy effective for intra-abdominal LM?

Recommendation:

Although there are many reports that sclerotherapy is useful, there is the risk of complications, and careful judgments about matters including the resectability of the lesion and selection of the sclerosing agent are necessary.

Strength of recommendation	2 (weak)
Evidence	D (very weak)

Comments

[Process of preparation of recommendation]

LM is the most frequent lymphatic vessel disorder of the abdomen. Intra-abdominal lesions are estimated to account for 10–20% of all LM, and the selection of treatment is difficult depending on the site of the lesion. While surgical resection is expected to be effective, less invasive treatments are considered necessary in view of stress to the patient and the possibility of severe complications such as lymphatic fluid leakage and bowel obstruction. Sclerotherapy, which is a major treatment for LM, is considered to be less invasive than surgery. Although positive therapeutic effects are expected, sclerotherapy is known to induce marked inflammation. Whether it can be performed safely without negative effects including complications and its long-term effects are major clinical concerns. In addition, what therapeutic effects are expected or what complications should be anticipated after sclerotherapy for the intra-abdominal lesion is also unclear. Therefore, the CQ, "Is sclerotherapy effective for intra-abdominal LM?", was formulated, and knowledge available at present was compiled.

<Literature search and screening>

As a result of literature search, 19 papers in Japanese and 38 papers in English (32 from PubMed, 6 from Cochrane) were subjected to primary screening. Of these papers, 2 in Japanese and 9 in English were subjected to secondary screening concerning this CQ. They included no papers with a high level of evidence, such as systematic reviews and RCTs, and all were case series or case reports. Consequently, the results and discussion in each case series were integrated in the evaluation of this CQ.

<Review of observational studies (case series)>

The literature concerning the effectiveness of sclerotherapy for intra-abdominal LM was reviewed from the viewpoints of (1) therapeutic effects (decrease in lesion size, symptoms) and (2) complications.

The drugs used for sclerotherapy ranged widely from OK-432 to bleomycin, ethanol, doxycycline, STS, acetic acid, steroid/tetracycline, and 50% glucose solution. According to our review, there was no paper that evaluated the differences in effectiveness of sclerotherapy in the abdomen according to the drug type or administration method or number of administrations of each drug.

Results of review

1. Therapeutic effects

A. Regression rate of the lesion

Regression of lesions of intra-abdominal LM by sclerotherapy was mentioned in 5 papers [288, 316–319]. According to the report by Chaudry et al. [316], the reduction rate was ≥ 90% in 7 and ≥ 20% in 1 of the 10 patients with LM of the mesentery and retroperitoneum treated with doxycycline, and evaluation using imaging examination was not performed in 2 cases. The patient who showed a low regression rate had a mixed type of cystic and cavernous lymphangiomas, and the other patients had cystic lesions. Oliveira et al. [317] reported that the lesion regressed by 70% in 1 of the 2 patients with cystic lymphangiomas treated with OK-432. Won et al. [318] reported 1 patient who showed complete disappearance of cystic retroperitoneal lesions after sclerotherapy using acetic acid. Shiels et al. [319] reported that cystic lesions responded to sclerotherapy using STS and ethanol in 2 patients, but there was no mention about the reduction rate. However, according to Alqahtani et al. [288], no effect was observed in 10 patients who underwent sclerotherapy using steroid/tetracycline or 50% glucose solution.

B. Symptoms

There were 3 papers that referred to symptoms of patients treated by sclerotherapy for intra-abdominal LM [316, 317].

According to Chaudry et al. [316], of the 10 patients who underwent sclerotherapy, 3 had chronic abdominal pain, 3 had acute abdominal pain, 1 had fever/chill, 1 had anemia, and 2 had palpable masses, but the symptoms were alleviated by treatment in all patients, and no recurrence was noted.

Oliveira et al. [317] reported that sclerotherapy was performed in a patient with a palpable mass and in 1 with a palpable mass, abdominal compartment syndrome, and a poor general condition. While the condition was alleviated in the patient who only showed a palpable mass after 2 courses of OK-432 sclerotherapy, but the treatment was changed to surgery in the patient who had abdominal compartment syndrome because of enlargement of the mass due to intracystic hemorrhage.

2. Complications

Three papers specifically mentioned complications of sclerotherapy for intra-abdominal LM. There was no report of deaths due to treatment-related complications. Oliveira et al. [317] treated 3 patients by sclerotherapy using OK-432 and reported that one of them developed subbowel obstruction after the treatment and another required emergency surgery due to exacerbation of abdominal compartment syndrome induced by intracystic hemorrhage. Chaudry et al. [316] reported that doxycycline used for sclerotherapy leaked into the retroperitoneal space in 1 of the 10 patients but that the lesion regressed without any particular problem. Won et al. [318] performed sclerotherapy using acetic acid in 1 patient with retroperitoneal cystic lymphangioma. Although pain and hematuria were observed, they concluded that the relationship of hematuria with the therapy was unclear, because it was observed during menstruation.

Limitations

Sclerotherapy was often performed before, after, or during surgical resection, and papers that reported the results of sclerotherapy alone were few. There was no paper that directly compared observation without treatment, sclerotherapy, and surgical resection. Few papers analyzed intra-abdominal lesions alone, and many papers included lesions in other areas or evaluated lesions in different intra-abdominal regions including the mesentery, retroperitoneum, and viscera collectively.

Moreover, differences in properties of LM, such as cystic, cavernous, and mixed types, their definitions, criteria for the selection of sclerotherapy (combination with surgery, types of sclerosing agents and methods of their use, number of administrations) varied among papers, and few papers evaluated these matters separately.

Such differences in the patient background and contents of treatment must be considered in evaluating the effectiveness of sclerotherapy. In evaluating this CQ, particularly, differences in morphology of LM and sclerosing agents were excluded.

<Summary>

The CQ, "Is sclerotherapy effective for intra-abdominal LM?" was evaluated from the viewpoints of therapeutic effect, symptoms/functions, and complications, but no paper with a high level of evidence was found. While sufficient regression of the lesion and alleviation of symptoms were achieved by sclerotherapy in some patients, the response rate varied among reports, and information was insufficient for general discussion of sclerotherapy. Concerning treatment-related complications, there have been reports of bowel obstruction associated with sclerotherapy, and attention to this condition as well as intracystic hemorrhage is considered necessary. However, there was no report of chylorrhea, which was reportedly caused by surgery.

Based on the above observations, it is presently difficult to determine indications for sclerotherapy in intra-abdominal LM by setting up criteria, but as there was no literature that strongly ruled out intra-abdominal LM as indications of sclerotherapy, these guidelines propose, "Although there are many reports that sclerotherapy is useful, there is the risk of complications, and careful judgments about matters including the resectability of the lesion and selection of the sclerosing agent are necessary." For the future evaluation of this CQ, validation by a design with a high level of evidence, such as RCT, is considered necessary.

CQ26: Are patients with scarcely symptomatic intra-abdominal LM candidates for treatment?

Recommendation:

Since there is risk of treatment-related complications, it is proposed to consider therapeutic intervention when the lesion tends to enlarge or has become symptomatic.

Strength of recommendation	2 (weak)
Evidence	D (very weak)

Comments

[Process of preparation of recommendation]

Intra-abdominal LM occasionally presents with severe symptoms, such as abdominal pain, giant mass, and bowel

obstruction, but may also be asymptomatic and detected incidentally. Lesions may gradually enlarge and cause serious symptoms due to infection and intraluminal hemorrhage.

Under such circumstances, whether patients with nearly asymptomatic intra-abdominal LM should be aggressively treated, or when intervention should be optimally performed during their long follow-up period are major problems that pose clinical dilemma. Therefore, the CQ, "Are patients with scarcely symptomatic intra-abdominal LM candidates for treatment?", was formulated, and knowledge available at present was summarized.

<Literature search and screening>

As a result of literature search, 206 papers in Japanese and 237 papers in English (230 from PubMed, 7 from Cochrane) were subjected to primary screening. Of these papers, 6 in Japanese and 9 in English were subjected to secondary screening concerning CQ 26. They included no papers with a high level of evidence, such as a systematic review or RCT, and many of them were case series or case reports. Since 7 papers among them described asymptomatic LM, their results and discussions were integrated to answer the CQ.

<Review of observational studies (case series)>

Seven papers [316, 317, 320–324] among reviewed literature described asymptomatic LM. Fifteen cases reported in these papers were considered to have actually presented few symptom (including asymptomatic patients who were incidentally detected by imaging studies to have intra-abdominal masses at the sites as greater omentum, mesentery and retroperitoneum).

The literature was screened, and papers addressing issues concerning therapeutic intervention for scarcely symptomatic intra-abdominal LM including "What symptoms they may present with if they are left untreated?", "By what studies and how often should they be examined?", and "What other treatments are available and how serious are complications or risk of each treatment?" were reviewed.

Results of review

From the literature reviewed, symptoms of intra-abdominal LM (abdominal pain, bowel obstruction, torsion, infection, hemorrhage, vomiting/sucking difficulty, frequent urination and abdominal mass [320–326]) are considered to be dependent on factors such as site, size and age. It is necessary to determine risk factors by stratification of these factors in the future [320, 322, 325].

Reported complications in treated cases include recurrence that required re-treatment [321], bowel obstruction [317, 323, 324], chylous ascites [324, 326], embolism [317], hemorrhage [317] and wound infection. Embolism of the inferior vena cava after surgery [317] and abdominal compartment syndrome after adhesion therapy [317] were reported as severe complications. It deserves special attention that, if surgical resection is performed for mesenteric LM, the intestine may have to be resected with the lesion [326].

While there have been reports [320, 322] that intra-abdominal LM with few clinical symptoms regressed during follow-up, they may become symptomatic later (as observed in many case reports). For that reason, the opinion that intervention should not been chosen during the follow-up until the lesion enlarges or new symptoms appear was frequently described.

Limitations

It should be noted that many asymptomatic cases may be left unreported and some asymptomatic lesions that had been detected were treated. There is no study with a high level of evidence indicating explicit criteria concerning the age, site or situation about whether intervention should be made for asymptomatic intra-abdominal LM.

<Summary>

The necessity of treatment of a patient with intra-abdominal LM with few symptoms should be determined after evaluating the balance between the risk of treatment and non-treatment considering its site and size as well as patient age. However, since research on indications for treatments has been insufficient so far and serious complications after treatment have been reported, deliberate evaluation for each patient is mandatory. When observation is selected, periodic imaging studies are recommended to optimize therapeutic intervention by detecting enlargement of the lesion. Also if any symptom has developed during follow-up, intervention should be considered. For these reasons, the recommendation, "Since there is risk of treatment-related complications, it is proposed to consider therapeutic intervention when the lesion tends to enlarge or has become symptomatic." was adopted.

CQ27: What treatments are effective for refractory chylous ascites?

Recommendation:

Conservative treatments, such as fasting, high-calorie infusion, and medium chain triglyceride (MCT), should be performed first, but, if they are ineffective, drug treatment, sclerotherapy, and surgery may also be considered.

Strength of recommendation 2 (weak)

Evidence D (very weak)

Comments

[Process of preparation of recommendation]

Refractory chylous ascites causes loss of large amounts of protein and lymphocytes, decreases in the blood lipid levels, and abdominal pain, unpleasantness, and dyspnea due to abdominal distention and markedly reduces the quality of life. The cause of ascites often remains unknown. Treatment of chylous ascites may require drainage to avoid abdominal distention. It is a very important point for clinicians to make proper judgments by understanding treatments and their effects and demerits. Therefore, it is considered beneficial to collect information about chylous ascites over a long period and compile guidelines. For this purpose, the presently available knowledge was collected by formulating the CQ, "What treatments are effective for refractory chylous ascites?"

<Literature search and screening>

As a result of search, 161 papers in Japanese and 728 papers in English (564 from PubMed, 164 from Cochrane) were subjected to primary screening. Of these papers, 15 in Japanese and 12 in English were subjected to secondary screening for CQ 27. They included none with a high level of evidence, such as systematic reviews and RCTs, and consisted of 1 multicenter and 2 single-center case series and case reports. Consequently, we used the results and discussion of 27 papers judged for the preparation of the draft recommendation were integrated although evidence was insufficient for the evaluation of this CQ.

<Review of observational studies (case series)>

As for causes of chylous ascites, congenital chylous ascites [327–342], idiopathic chylous ascites [328], chylous ascites after laparotomy [343–346], protein-losing enteropathy [345], LM [347, 348], lymphangiectasis [349, 350], lymphangiomatosis [351, 352], and lymphatic dysplasia [353] were reported. None of the papers evaluated treatments according to the cause.

When treatments are categorized, conservative treatments (fasting, high-calorie infusion, MCT), drug treatments, sclerotherapy, and surgical treatment were performed.

Results of review

The results of review are presented below according to the treatment.

1. Conservative treatments

Whether the amount of ascites changes by fasting should be checked first.

High-calorie infusion is often used with fasting, and since there was no report that ascites increased under the effect of high-calorie infusion according to our review, it is recommended for nutritional support during fasting. In the multicenter case series reported by Bellini et al. [327], high-calorie infusion/total parenteral nutrition was performed in 15 patients without adverse effects.

Medium chain triglyceride was used before, after, and during treatment [327, 328, 330–335, 337, 339–341, 343, 345, 346, 348–352]. In the multicenter case series by Bellini et al. [327], MCT was reportedly performed in 14 patients without adverse effects.

2. Drug treatments

In drug therapy for chylous ascites, primarily octreotide (a long-acting somatostatin analogue) was used, and no report that discussed the effectiveness of other drug therapies was found by the present literature search.

In the multicenter case series by Bellini et al. [327], octreotide was administered to 6 of the 16 patients with chylous ascites for 8–38 days, and a decrease in chylous ascites was reported in all of them. In the single-center case series by Huang et al. [344], 2 of the 4 patients with chylous ascites treated by high-calorie infusion and octreotide administration were reported to have shown a decrease in ascites within 10 days. However, there has been a report [330] that no effect was observed despite the administration of octreotide for 3 weeks. Concerning the dose of octreotide, it was administered at 1 μg/kg/h [327], at 3 μg/kg/h [332], began to be administered at 0.5 μg/kg/h and increased to 10 μg/kg/h by 1 μg/kg/h [329], administered by continuous intravenous infusion at 0.5–2.0 μg/kg/h [333], and began to be administered by subcutaneous injection at 2.5 μg/kg 2 times/day and increased every 2 days to 8 μg/kg 2 times/day [330]. Regarding the time of the beginning of administration, the administration was started as no improvement was observed in chylous ascites after conservative treatments for 2 weeks [330, 334], and as chylous ascites was alleviated by conservative treatments but was exacerbated again [333]. No adverse effects of octreotide administration were noted in the present review of the literature. Thus, no control study that evaluated the effect of octreotide on chylous ascites was found by the present literature search, and the level of evidence concerning the efficacy is low, but as there are case series and many case reports that chylous ascites was reduced by octreotide administration, it appears reasonable to consider drug treatment using octreotide for chylous ascites that does not respond to conservative treatments.

3. Sclerotherapy

Sclerotherapy was performed in 6 patients in 5 case reports [339, 347, 349, 351, 352]. The sclerosing agent was OK-432 in 5 of the 6 patients and was Beta-Isodona-solution® (MUNDIPHARMA GmbH, Cambridge, UK) in 1 [349]. OK-432 was locally injected into the lesion in 4 [347, 351, 352], administered intraperitoneally in 1 [352], and administered via the drain in 2 [347, 352]. Concerning sclerotherapy, the number of reported cases that were reviewed was limited, and further accumulation of cases is considered necessary to establish its usefulness.

4. Abdominal drainage, abdominal puncture, and surgical treatment

Abdominal drainage and abdominal puncture are performed when organ compression symptoms (compartment syndrome and respiratory insufficiency) due to abdominal distention are present or possible or when the drain is inserted postoperatively. However, drainage itself cannot improve chylous ascites, and treatments, such as infusion, blood preparations, and blood transfusion, are necessary to supplement the ascites lost due to drainage [327, 330–333, 337–340, 343, 345–347, 349, 351, 352].

Surgical treatment is reported to be frequently performed after conservative or drug treatments. According to the single-center case series by Zeidan et al. [343], surgical treatment was performed in patients who responded poorly to conservative treatments for over a mean of 25.3 days. In other reports, surgical treatment was performed after conservative treatments for 1–3 months [328, 329] and in patients with congenital chylous ascites 1–4 months after birth [330, 334, 350]. Since it is often impossible to identify the leakage site of chylous ascites [330], attempts to identify the leakage site by orally administering a lipophilic dye (Sudan black, Sudan III) before operation. [328, 329, 336, 343] When the leakage site can be identified, ligation, suturing, clipping, and cauterization have been performed [328, 334, 336, 343, 350]. In addition to reports of the usefulness of techniques to stop leakage, such as applying or sprinkling fibrin glue at the leakage site of chylous ascites or over the surrounding retroperitoneum [329, 331, 343, 350] and applying a patch of oxidized cellulose/resorbable local hemostatic agent [331, 343], there have also been reports of peritoneovenous shunting [349, 353] and peritoneoamniotic shunting for fetal cases [338].

There was no large clinical study in the past literature. Therefore, although the level of evidence is low, we consider that surgical treatment is recommendable for chylous ascites that does not respond to conservative or drug treatments, because it has been performed in case series and case reports for chylous ascites that did not respond to conservative or drug treatments for over about 1 month. Although techniques to enhance the response rate of surgical treatment, such as identifying the leakage site by using a lipophilic dye and applying fibrin glue or a patch of oxidized cellulose/resorbable local hemostatic agent, have been attempted, there are only case series and case reports, and none of the papers retrieved by the present literature search evaluated their usefulness.

Limitations

There was no literature that defined refractory chylous ascites based on the duration of illness or treatment responses. Therefore, we extracted and summarized factors that were considered to contribute to clinical refractoriness, such as the duration of illness and treatment responses, in each paper related to the treatment for chylous ascites. Also, as the cause of chylous ascites varies widely, the therapeutic effect is expected to differ depending on the cause, but no paper that was reviewed evaluated treatments according to the cause. Therefore, in the present evaluation, the statements are limited to treatments and their effects regardless of the cause.

<Summary>

It was difficult to comprehensively discuss treatments, because its cause varied widely, and treatments for various causes were performed. Therefore, treatments were classified into conservative treatments (fasting, high-calorie infusion, MCT), drug treatments (octreotide), sclerotherapy, abdominal drainage, abdominal puncture, and surgical treatment, and the effects of each treatment were evaluated.

Treatments effective for refractory chylous ascites can be summarized as follows with the understanding that they may depend on the cause and that the level of evidence of the available reports concerning treatments and their effects is low. Conservative treatments, such as fasting, high-calorie infusion, and MCT, should be performed first because of the rareness of adverse effects. In patients who respond insufficiently to conservative treatments, drug treatments using octreotide can be considered as there have been case series and many case reports. Concerning sclerotherapy, the number of reported cases is small, and further large clinical studies will be needed to confirm its usefulness. Abdominal paracentesis and surgical treatments may be considered for chylous ascites that does not response to conservative or drug treatments for about 1 month.

Thus, the draft recommendation is “Conservative treatments, such as fasting, high-calorie infusion, and MCT, should be performed first, and, if they are ineffective, drug treatments, sclerotherapy, and surgical treatments may be considered”. However, evaluation of this CQ by a design with a higher level of evidence, such as RCT, is considered necessary for the future.

CQ28: What kinds of complications are associated with treatments for intra-abdominal LM?

Recommendation:

Complications associated with sclerotherapy for intra-abdominal LM include bowel obstruction, hemorrhage, pain, hematuria and chylous ascites. Surgical treatment of the disease can be associated with serious complications such as occlusion of the inferior vena cava and massive resection of the intestine as well as more common, wound infection, bowel obstruction, hemorrhage and chylous ascites.

Strength of recommendation	No recommendation
Evidence	D (very weak)

Comments

[Process of preparation of recommendation]

Patients with intra-abdominal LM are treated with various modalities from non-surgical therapy to surgical procedures. Treatment modality is selected depending on the patient's state. Therefore, it is necessary for the clinician, patient, and family to share information concerning complications that may be associated with treatments for implementing them smoothly. However, there are no resources that give a clear answer to this problem, and both clinicians and patients may become disconcerted. Therefore, the CQ "What kinds of complications are associated with treatments for intra-abdominal LM?" was formulated, and information available at present was accumulated and integrated for the answer.

<Literature search and screening>

As a result of literature search, 203 papers in Japanese and 602 papers in English (593 from PubMed, 9 from Cochrane) were subjected to primary screening. Of these papers, 23 in Japanese and 27 in English were subjected to secondary screening concerning this CQ. They included no papers with a high level of evidence, such as systematic reviews or RCTs, and all of them were case series or case reports. To answer CQ 28, the results and discussion in each case series were integrated.

<Review of observational studies (case series)>

Complications in the CQ were evaluated by defining them as those encountered when patients with intra-abdominal LM were treated, and reports on sclerotherapy and surgery were reviewed.

Results of review

1. Complications associated with sclerotherapy

Sclerotherapy using OK-432 was reported to be associated with bowel obstruction and hemorrhage for mesenteric LM [317], and chylous ascites for retroperitoneal LM [326]. Sclerotherapy using acetic acid was reported to be associated with pain and hematuria in patients with retroperitoneal LM [318].

2. Complications associated with surgical procedures

Complete resection of both mesenteric and retroperitoneal LM by laparotomy was reported to be associated with wound infection [324, 354] and bowel obstruction [323, 354, 355] as common complications. There were reports of serious complications such as occlusion of the inferior vena cava [317] and massive resection of the intestine was necessary due to diffuse infiltration of the LM tissue to the intestinal wall [356].

In a report [357] about complications associated with complete laparoscopic resection of intra-abdominal LM by Tran et al., resection was attempted in 47 patients, and conversion to laparotomy was necessary in 3 (6.4%) due to tight adhesion in 2 and intraoperative hemorrhage in 1.

Partial resection by laparotomy was reported to be associated with persistent ascites over a long period that was refractory to the treatment [355].

Limitations

Patients with intra-abdominal LM are treated with various modalities including sclerotherapy and surgical procedures. Modalities were combined in many cases, and complications are often reported as those of entire treatment without more detail information about those associated with individual treatment.

<Summary>

For answering the CQ, "What kinds of complications are associated with treatments for intra-abdominal LM?", no literature with a high level of evidence was found, but foreseeable complications were listed from many case reports. Bowel obstruction, hemorrhage, pain, hematuria, and chylous ascites were reported as complications of sclerotherapy. Serious conditions, such as occlusion of the inferior vena cava and massive resection of the intestine, as well as common complications, such as wound infection, bowel obstruction, hemorrhage and chylous ascites were reported as complications after surgical procedures.

Although the incidences and differences in complications in respect of the site and histological type are not shown in the literature, each patient with intra-abdominal

LM should be treated with sufficient evaluation of the site, size and symptoms. In addition, treatment must be implemented with sufficient understanding of the possible complications.

Thus, we propose "Complications associated with sclerotherapy for intra-abdominal LM include bowel obstruction, hemorrhage, pain, hematuria, and chylous ascites. Surgical treatment of the disease can be associated with serious complications such as occlusion of the inferior vena cava and massive resection of the intestine as well as more common, wound infection, bowel obstruction, hemorrhage and chylous ascites." as a recommendation draft.

CQ29: What treatments are effective for LM causing airway obstruction in the mediastinum?

Recommendation:

Sclerotherapy is effective for macrocystic lesions, and surgical resection is effective for microcystic lesions. However, as the complication rate is relatively high, treatments should be selected according to the condition of each case.

Strength of recommendation	2 (weak)
Evidence	D (very weak)

Comments

[Process of preparation of recommendation]

Among LM, those that may cause airway obstruction due to their sites are life-threatening. Lesions in the mediastinum cause respiratory disorders if they physically compress the trachea or bronchi and obstruction the airway or markedly protrude into the thoracic cavity and narrow it.

In such situations, aggressive and effective treatment is necessary, but the therapeutic approach must be selected carefully in consideration of the relationship of the lesion with the important organs around it such as the large cardiac vessels, mediastinal nerve, and thoracic duct. However, the judgment is often difficult in clinical settings.

Therefore, the CQ, "What treatments are effective for LM causing airway obstruction in the mediastinum?" was formulated, and the presently available knowledge concerning matters including the risk of complications and prognosis of treatments, such as surgical resection and sclerotherapy, was summarized.

<Literature search and screening>

As a result of literature search, 134 papers in Japanese and 227 in English (226 from PubMed, 1 from Cochrane) were subjected to primary screening. Of these papers, 5 in Japanese and 16 in English were subjected to secondary screening concerning this CQ. Since they included none with a high level of evidence, such as a systematic review or RCT, and all were case series or case reports, the results and discussion in each case series were integrated.

<Review of observational studies (case series)>

By screening of the literature, the following approaches were found for the treatment of LM in the mediastinum.

Therapeutic options are surgical resection, puncture and drainage, sclerotherapy (OK-432, bleomycin, ethiblock, anhydrous ethanol), drug treatments (Chinese herbal medicines such as *eppikajutsuto* and *ogikenchuto*), and no treatment. Of these approaches, surgical resection and sclerotherapy using OK-432 have been evaluated in a relatively large number of cases, and reports of other therapy had extremely limited number of cases, e.g., reports of only 1 case.

Results of review

Boardman et al. [358] reported that, of the 97 patients with LM of the head and neck region, surgical treatments were necessary in 6 of the 12 patients with mediastinal lesions, that complications of surgery occurred in 4 of the 6 patients, and that long-term nerve damage was observed in 3 of them. In addition, they reported that management by tracheotomy was necessary in 15% of all patients. Complete or nearly complete remission was observed in 92% of the patients, but they suggested that surgical treatments should be indicated only when there is airway obstruction or there is the risk of it, because surgical treatment of mediastinal lesions frequently causes complications.

Park et al. [359] reported that they surgically resected mediastinal LM in 12 patients. Seven of them had dyspnea, and 3 were asymptomatic, but they were all judged to have indications for surgery due to symptoms or the tendency of the lesions to enlarge. A total of 5 recurrences were observed in 4 patients (33%) during a mean period of 3.6 years after the initial surgery, and all underwent by re-resection. No perioperative death was observed, and, in a total of 25 cases including past cases, the overall survival was not different compared with that in healthy individuals over a follow-up period of 11.5 years.

Smith et al. [302] performed local injection of OK-432 in 16 patients with mediastinal LM and reported ≥ 60% regression of the lesion in 13 (81%). They also mentioned treatment responses according to the histological types and, by reporting responses (complete or nearly complete remission) in 94% of those with macrocystic lesions, 63% of those with mixed lesions, but 0% in those with microcystic lesions, suggested a macrocystic lesion to be a good indication for sclerotherapy using OK-432. Although not from the viewpoint

of airway obstruction, they reported that treatment using OK-432 was more effective than surgical resection and less frequently caused serious complications.

Limitations

There have been no papers that directly analyzed treatments effective for mediastinal lesions expected to cause airway obstruction, and many papers reported cases of mediastinal lesions that responded to treatments. Therefore, we simply extracted matters relevant to this CQ from these reports.

<Summary>

There was no literature with a high level of evidence concerning effective treatments for LM in the mediastinum causing airway obstruction. A few case reports that referred to the effects of surgery and sclerotherapy were observed, but it was difficult to present objective and specific figures concerning their effectiveness or safety. However, according to the available information, it should be noted that favorable responses have been obtained by OK-432 local injection in macrocystic lesions and that complications due to surgical resection are likely to occur relatively frequently.

From these observations, we consider the following to be a therapeutic approach that can be proposed: "Sclerotherapy, such as that by local injection of OK-432, should be considered for macrocystic lesions, and, for lesions that are technically difficult to treat by sclerotherapy or microcystic lesions, surgical resection should be considered with attention to complications. In addition, it is necessary to pay attention to the appearance of respiratory disturbances before and after these treatments and to constantly evaluate indications for securing the airway by intratracheal intubation or tracheostomy." Therefore, at present, we recommend, "Sclerotherapy is effective for macrocystic lesions, and surgical resection is effective for microcystic lesions. However, as the complication rate is relatively high, treatments should be selected according to the condition of each case."

CQ30: Should sclerotherapy be performed in infancy for a patient with head and neck LM affecting the airway?

Recommendation:

In a patient with LM around the airway, there is risk of respiratory distress in infancy, while airway obstruction is likely to be exacerbated by sclerotherapy. Particularly, when risk of airway obstruction is judged to be high or when the patient has already presented symptoms, it is proposed to perform sclerotherapy with sufficient preparations including airway management.

Strength of recommendation	2 (weak)
Evidence	D (very weak)

Comments

[Process of preparing recommendation]

LM of the neck, which are located in an exposed part of the body, may cause cosmetic problems that are important, but airway obstruction can particularly be a serious problem in some cases.

Sclerotherapy, which is one of the major treatment modalities, is most effective in patients with cystic LM, but swelling of the treated portion after the therapy may cause or exacerbate airway obstruction symptoms especially in neonates. The upper airway will become less vulnerable to obstruction because it becomes less frail and wider as patients grow and respiratory distress tends to be unlikely. Therefore, it is occasionally difficult to determine how a patient who does not present any obstructive symptom should be treated in infancy.

Thus, we evaluated this problem by formulating the CQ, "Should sclerotherapy be performed in infancy for a patient with the neck LM affecting airway?"

<Literature search and screening>

As a result of search, 86 papers in Japanese and 135 papers in English (130 from PubMed, 5 from Cochrane) were subjected to primary screening. Of these papers, 6 in Japanese and 20 in English were subjected to secondary screening concerning this CQ. They included 1 systematic review (SR), 1 RCT, 2 prospective studies (PS) and 1 retrospective cohort study, but all the others were case series or case reports. Therefore, the results and discussion, primarily, in these SR, RCT, PS, and retrospective cohort study, but also in other case series were integrated.

<Review of observational studies>

The literature concerning the effectiveness of sclerotherapy for head and neck LM in infancy was reviewed from the viewpoints of responses (prognosis (survival rate or mortality), size, symptoms, and cosmetic improvement) and complications.

Sclerosing agents used as keywords for the present literature search varied widely and included OK-432, bleomycin, ethanol, doxycycline, STS and fibrin glue. No paper evaluated differences in effectiveness of various agents due to their methods of administrations for lesions around the neck affecting airway. Therefore, differences among agents were excluded from the evaluation of this CQ.

Results of review

1. Responses

A. Prognosis (survival rate or mortality)

According to the SR by Adams et al. [360], the mortality was 4.7% in 277 cases with head and neck LM. Since lesions around the airway were not the only target, and since sclerotherapy was not the only treatment modality, the paper has not quite rightly answered to the CQ. However, since patients who died were all before one year of age and their causes of death are considered to have been mostly airway problems, such as airway obstruction and aspiration due to vocal cord paralysis in 8, and as at least 1 patient is judged to have died due to complications of invasive treatment, the paper is considered to indicate the risk of this disorder during infancy.

B. Size

Many of the papers that referred to the size regression evaluated it by four categories; (1) excellent or complete (≥90% regression), (2) good or substantial (≥50% and <90% regression), (3) fair or intermediate (≥20% and <50% regression), (4) and poor or none (≤20% regression).

Ravindranathan et al. [306] treated 5 patients (aged 4–19 months) with cervicofacial LM by sclerotherapy using OK-432 (in addition to Fibrovein® (STD Pharmaceutical Products Ltd, Hereford, UK) in 2) and reported that the responses were good in 1 (20%) (cystic), partial in 1 (20%) (cavernous), and poor in 3 (60%) (2 with cavernous lesions that required tracheotomy and 1 with cystic lesions in whom the condition improved to good after surgical resection). However, they did not mention the evaluation criteria for good, partial, and poor.

According to the report of 8 cases with head and neck LM by Leung et al. [361], all patients underwent sclerotherapy, ≥50% regression was observed in all patients with complete regression in 2. However, the patient age varied from 2 months to 11 years, and the types of LM were not mentioned.

Ogawa et al. [362] reported 9 patients (including 5 preschoolers and toddlers, 2 school children, and 2 adults) who underwent OK-432 sclerotherapy for the neck LM and evaluated it to be markedly effective in 8, in whom the lesions mostly disappeared, and effective in 1, who showed a ≥50% regression. Eight patients in whom the treatment was markedly effective consisted of 1 with mixed and 7 with cystic lesions, and the one in whom the treatment was effective had a mixed type.

Cahill et al. [315] reported doxycycline sclerotherapy in 17 patients with head and neck LM (cystic in 10, mixed in 7 (3 required tracheotomy)), and its size regression was reported to be >90% in 7 (41.2%) (cystic in 6, mixed in 1), 75–89% in 4 (23.5%) (cystic in 2, mixed in 2), 51–74% in 4 (23.5%) (cystic in 1, mixed in 3), and 25–50% in 2 (11.8%) (mixed in 2).

Nehra et al. [311] reported doxycycline sclerotherapy in 11 patients with head and neck LM (cystic in 7, mixed in 4; aged 2 days–21 months) (later combined with surgical resection in 3). The treatment results were excellent in 5 (45.5% of all patients) and satisfactory in 2 (18.2% of all patients) among 7 patients with cystic lesions but poor in all 4 patients with mixed type lesions (36.4% of all patients). Particularly, 3 of the 4 patients with mixed type lesions required tracheal intubation shortly after birth and underwent sclerotherapy while intubated, but the effects were poor in all of them. Surgical resection was added in 1 and was under consideration in another.

C. Symptoms

According to Ravindranathan et al. [306] who reported 5 patients with cervicofacial LM (aged 4–19 months) treated with sclerotherapy using OK-432 (in addition to Fibrovein® (STD Pharmaceutical Products Ltd, Hereford, UK) in 2), 4 exhibited symptoms of airway obstruction before treatment. Symptoms included dysphagia in 2 and dyspnea (including croup-like symptoms) in 4 (some both). Symptoms were alleviated by sclerotherapy in 2 out of 4 (cystic 1, cavernous 1), but tracheotomy was necessary in the remaining 2 (cavernous in both) without improvement.

In the report of 8 patients with head and neck LM and 5 patients with VM (aged 2 months–11 years) by Leung et al. [361], their symptoms noted before treatment were mass or swelling [10 patients (77%)], pain after hemorrhage [2 patients (15%)], skin discoloration (blue) [1 patient (8%)], obstructive airway symptoms [6 patients (46%)], and swallowing difficulty [1 patient, (8%)]. All symptoms were alleviated by sclerotherapy (doxycycline for LM, STS foam for VM).

Arimoto et al. [363] reported a patient with cystic LM in the neck presented 3 months after birth. The patient presented with respiratory distress at the age of 10 months due to enlargement of the LM following upper respiratory infection. While left vocal cord fixation due to the mass was confirmed by ultrasonography before treatment, aspiration of the cyst and steroid administration resulted in opening of the glottic area and regression of the mass with relief of wheezing and distress. Since they underwent sclerotherapy 2 months after the disappearance of symptoms, aspiration of internal fluid and steroid administration rather than sclerotherapy were directly effective for the alleviation of symptoms.

Kitagawa et al. [364] reported a patient with giant LM of the neck which had been prenatally diagnosed and was treated under ex utero intrapartum treatment (EXIT) by tracheal intubation after aspiration of the cyst. The lesion was reported to be refractive to subsequent sclerotherapy and tracheotomy was eventually needed.

Nehra et al. [311] reported that, among 11 patients with head and neck LM (cystic type in 7 and mixed type of

cystic + cavernous in 4; aged 2 days–21 months), 3 out of 4 with mixed LM presented respiratory distress soon after birth and were managed by intubation, but that all were extubated after sclerotherapy using doxycycline (1–3 times, median: 1.6 times).

D. Cosmetic improvements

No paper has reported cosmetic results in detail. Only sporadically they mentioned about surgery for redundant skin after regression of cystic lesions by sclerotherapy.

4. Complications

Complications associated with treatment for LM around the airway have been reported in many papers. They include temporary conditions caused by sclerotherapy such as fever [292, 303, 312, 362, 365–371], local swelling [303, 312, 365, 367, 368, 370, 371] pain [288, 312, 362, 367, 370–372], hemorrhage into the cyst [288, 303, 312, 368], and infection [288, 292, 303, 310, 312, 360, 365, 372]. There also reported complications as the effects of treatment for head and neck lesions such as respiratory distress due to airway obstruction [292, 303, 306, 312, 362, 365, 366], as well as nerve palsy [288, 292, 312, 360, 365].

According to a systematic review about head and neck LM by Adams et al. [360], both nerve damage due to sclerotherapy and post-therapeutic infection were reported in 1 (0.8%) out of 123 patients. Since nerve damage and infection after surgery were observed in 12 (10.2%) and 7 (5.9%) out of 118 patients, respectively, the complication rate would be lower by sclerotherapy than by surgery.

Ogawa et al. [362] reported a 1-year- and-5-month-old patient who developed airway edema after OK-432 sclerotherapy for the cystic neck LM and necessitated tracheal intubation for 3 days and cautioned against sclerotherapy for LM around the airway in young children (particularly, those less than 2 years old).

Kudo et al. [369] also reported 2 patients aged 11 months and 1 year and 11 months who were treated with OK-432 sclerotherapy intubated in advance for fear of airway obstruction due to post-therapeutic swelling. Tomemori et al. [373] also cautioned against sclerotherapy for LM in children aged less than 2 years as in the report by Ogawa et al. [362]

On the other hand, Kudo et al. [369] reported 2 cases whose neck LM having been enlarged rapidly after suffering from measles or upper respiratory tract infection (URTI). Arimoto et al. [363] also reported a patient with cystic LM of the neck 3 months after birth, who developed dyspnea due to enlargement of the lesion after URTI at 10 months and was about to be intubated.

Regarding complications due to sclerosing agents, Cahill et al. [315] reported those by doxycycline, STS and absolute ethanol. They reported delayed complications, such as Horner's syndrome, transient left lip weakness, right facial nerve palsy, and transient left hemidiaphragm paralysis, in addition to peri-procedural complications such as hemolytic anemia after doxycycline injection in 2 patients, hypoglycemic and metabolic acidosis in 3 neonates, transient hypotension during absolute alcohol instillation and self-limiting skin excoriation secondary to peri-catheter leakage of doxycycline. Other reported complications include permanent vocal cord paralysis after local ethanol injection [374], serious complications after OK-432 injection such as death due to pulmonary embolism [375], deaths due to pulmonary complications after treatment using bleomycin [376, 377] and leukocytopenia due to bleomycin [368].

Limitations

There are few papers that solely analyzed LM around the cervical airway. Most papers included lesions involving not only the neck but also the craniofacial and other parts of the body and reported LM with different properties such as cystic and mixed types. In addition, definition of cavernous lesions and methods of sclerotherapy (injection techniques, number of injections) were not similar among papers, and differences in these backgrounds must be taken into consideration to evaluate the effectiveness of sclerotherapy.

<Summary>

The CQ, "Should sclerotherapy be performed in infancy for a patient with head and neck LM affecting the airway?", was evaluated from the viewpoints of responses (prognosis (survival rate or mortality), decrease in size, symptoms, cosmetic improvements) and complications. Since there have been some reports on the risk of respiratory distress due to LM around the airway in infants, and therapeutic intervention is necessary even in infants when the risk is high or they have already developed symptoms. Such intervention is made by sclerotherapy or surgery, and as surgical resection is associated with the risk of more serious complications than sclerotherapy, intervention by less invasive sclerotherapy is recommended. Sclerotherapy is considered to be very effective because of high regression rate of the lesion and symptom/function-improving effect. However, its effect varies depending on the disease type, somewhat less effective in the cavernous and mixed types than in the cystic type. Furthermore, when it was performed for the lesions around the airway, it may be associated with the risk of exacerbation of airway obstruction symptoms due to reactive enlargement of the lesion. Thus, we formulated the recommendation, "In LM around the airway, there is the risk of respiratory disturbances from infancy, but airway obstruction is likely

to be exacerbated by sclerotherapy. Particularly, when the risk of airway obstruction is judged to be high or when symptoms have appeared, it is proposed to perform sclerotherapy with sufficient preparations including securing the airway."

CQ31: Is surgical resection effective for LM of the tongue?

Recommendation:

Surgical resection is effective for reducing the size of the lesion and alleviating symptoms and functional impairment. However, total resection is often difficult, and careful decision is required in consideration of the possibility of complications and recurrence.

Strength of recommendation	2 (weak)
Evidence	D (very weak)

Comments

[Process of preparation of recommendation]

While the tongue is one of the frequent sites of LM, the lesion is often distributed widely over the neck rather than is localized in the tongue. LM of the tongue not only cause cosmetic problems, such as protrusion from the mouth and bleeding, but also readily occupy the oropharyngeal cavity and cause functional problems such as disorder of mouth closing, difficulty in speaking, respiratory disturbances, and impairment of oral food intake. These conditions are treated at departments including plastic surgery, oral surgery, otorhinolaryngology, and pediatric surgery. LM of the tongue are treated by surgical resection or sclerotherapy, but comprehensive evaluation of the condition of individual cases including the distribution of the lesion in the tongue, involvement of other areas and cyst components, and vascular distribution in addition to general information, such as the risk of complications and recurrence in each treatment, is necessary.

Therefore, the CQ, "Is surgical resection effective for LM of the tongue?" was formulated, and the present knowledge about the effectiveness of surgical resection of the lesion, particularly, by partial glossectomy was summarized.

<Literature search and screening>

As a result of search, 29 papers in Japanese and 76 papers in English (75 from PubMed, 1 from Cochrane) were subjected to primary screening. Of these papers, 2 in Japanese and 10 in English were subjected to secondary screening concerning this CQ. They included 1 retrospective cohort study, but most other papers were case series or case reports. Consequently, in the evaluation of this CQ, the results and discussion of the cohort study and each case series were integrated.

<Review of observational studies (case series)>

The effectiveness of surgical resection of LM of the tongue was evaluated from the viewpoints of resectability of the lesion, symptoms, function, and cosmetic improvements as elements of responses as well as complications and recurrence.

Results of review

1. Responses

A. Resectability of the lesion

Twenty-four cases of tongue lesions treated by surgical resection alone were reported in 4 papers. Catalfamo et al. [378] performed surgical resection of localized masses including normal structures with a margin of 1 cm in the horizontal direction and reported that the size of tongue lesions was reduced in 8 (88.9%) of the 9 patients.

Concerning large lesions impossible to resect totally, Boardman et al. [358] reported 13 cases of partial surgical resection, but several operations were often necessary to reduce lesion size. A total of 2 case have been reported [379, 380], and the lesion size was reduced in both. Although differences were observed in re-enlargement after surgery, they are discussed in detail in "(2) Complications".

In 1 case report, sclerotherapy was performed 15 times, but the lesion size could not be reduced, and surgical resection was performed, eventually resulting in a favorable outcome without recurrence [381].

According to a report of 89 cases of head and neck LM by Lei et al. [291], the outcome was excellent in 73 (82%) and good in 16 (18%) although it was not a report of cases of tongue lesions alone. They included 43 cases of tongue lesions.

In addition, a few papers [382–385] that suggested the effectiveness of combinations of surgical resection with sclerotherapy and laser therapy were observed. Wiegand et al. [383] classified the disease into 4 stages according to the area of involvement and reported that the stage can be a prognostic factor. Surgery was effective, and complications were rare, when the lesion was localized in the superficial layer and part of the muscle layer. Surgical resection can also be effective, but complete resection is difficult, when the lesion extends over the entire muscle layer or to the tongue base and neck. Therefore, partial resection is often repeated and combined with laser therapy and sclerotherapy, but the recurrence is observed very frequently,

and the results did not contradict the reports mentioned below in the section of the recurrence rate [291, 358].

B. Symptoms

A wide variety of symptoms have been reported depending on the site of the mass, and they include tongue discomfort, bleeding, pain, and difficulty in oral feeding [386]. Roy et al. [387] reported that bleeding from the tongue surface, pain, and eating difficulty were alleviated by cauterization.

C. Functions

In most patients who exhibited functional impairment, the lesions were so extended that they were no longer indications for one-time surgical resection. Large masses located at sites such as the tongue base cause respiratory disturbances, swallowing disorders, and difficulty in speech. According to the report by Azizkhan et al. [385], oral intake of normally cooked food became possible in 14, and normal vocalization became possible in 8, of the 21 patients with tongue base lesions. In addition, 5 of the 17 patients who needed tracheotomy were weaned.

D. Cosmetic improvements

Objective evaluation of cosmetic effects is also difficult.

Azizkhan et al. [385] reported that, of the 20 patients, excluding 1 with severe deformity who died, deformity of structures around the tongue, such as the mandible and maxilla, was mild in 6, moderate in 5, and severe in 9. There have been a few reports that cosmetic improvements were also observed in patients who showed a reduction of the tongue size by surgical resection, but objective evaluation is insufficient.

2. Complications

Although the properties of the lesions are unclear in some papers, facial nerve paralysis, vagus nerve paralysis, infection, hematoma, seroma, salivary leakage, ruptured suture, and skin flap necrosis have been reported as complications of the facial region. There have also been reports of temporary complications such as pain and hemorrhage.

3. Recurrence

There have been a few postoperative evaluations reporting that no reactivation that clinically required treatment was observed. Lei et al. [291] reported greater details: Recurrence was observed in 21 (23.6%) of 89 patients and was more frequent in those aged less than 1 year, those with lesions in the oral cavity/face, those with lesions at 3 or more sites, and those with microcystic lesions. According to Boardman et al. [358], LM of the tongue recurred in 12 (48%) of 28 patients, more often than other head and neck lesions. As factors related to this more frequent recurrence of lingual LM, more frequent involvement of other regions, such as the floor of mouth, and a high percentage of microcystic lesions (70%) have been suggested. Of the 2 patients treated by surgical resection alone, 1 who underwent resection of the middle part of the tongue showed no re-enlargement for 1 year or longer after surgery [379], but surgery was repeated 3 times in the 1 who underwent marginal resection [380]. This patient who underwent repeated resections also showed no re-enlargement although the time of the last resection is unclear.

Limitations

In some papers, surgical resection was combined with other treatments [381–385, 387], lesions in other areas such as the neck were included [291], and the lesion types were unknown. The lack of standardization of subjects and uniformity of the definition or time of recurrence must be considered in the evaluation of the effectiveness of surgical resection.

<Summary>

Many papers suggest that surgical resection is effective for reducing the size of lingual LM. However, in patients with large lesions, lesions extending to structures other than the tongue, and microcystic lesions, several resections or combination of resection with other treatments such as sclerotherapy and laser therapy were necessary, and the recurrence rate tended to be higher. While a few papers referred to symptoms, functional outcome, and cosmetic improvements, none showed a high level of evidence, and the evidence was insufficient for general discussion of the effectiveness of surgical resection.

Therefore, concerning the effectiveness of surgical resection for LM of the tongue, "Surgical resection is effective for reducing the size of the lesion and alleviating symptoms and functional impairment. However, total resection is often difficult depending on the distribution of the lesion, and careful decision is required in consideration of the possibility of complications and recurrence." was proposed as a draft recommendation.

CQ32: Is aggressive surgical intervention effective for chylous pleural effusion in the neonatal period?

Recommendation:

For chylous pleural effusion refractory to conservative treatments, surgical procedures, such as pleurodesis, ligation of the thoracic duct, and pleuroperitoneal shunting, may be effective.

Strength of recommendation	2 (weak)
Evidence	D (very weak)

Comments

[Process of determining recommendation]

Primary chylous pleural effusion during the neonatal period is often refractory and can be fatal. Thoracic drainage is performed for respiratory insufficiency due to accumulation of pleural effusion, followed by conservative treatments, such as nutritional therapy, steroid, and octreotide therapy, conducted primarily by neonatologist until resolution of chylous pleural effusion.

In refractory cases that do not respond to these conservative therapies, surgical intervention, such as ligation of the thoracic duct and pleurodesis, may be performed. However, no sufficient consensus has been obtained concerning their effects. To evaluate problems, such as at what point surgical intervention should be made and whether aggressive surgical intervention is effective for such a condition, the CQ, "Is aggressive surgical intervention effective for chylous pleural effusion in the neonatal period?", was formulated, and the knowledge available at present was summarized.

<Literature search and screening>

As a result of search, 98 papers in Japanese and 264 papers in English (262 from PubMed, 2 from Cochrane) were subjected to primary screening. Of these papers, 8 in Japanese and 9 in English were subjected to secondary screening concerning this CQ. They included none with a high level of evidence, such as a systematic review or RCT that evaluated surgical treatment, and all papers were case series or case reports. Consequently, the results and discussion in each of the case series judged to be useful for the preparation of the draft recommendation were integrated although they were weak as the evidence for the evaluation of this CQ.

<Review of observational studies (case series)>

The literature concerning the effectiveness of surgical treatment for chylous pleural effusion in the neonatal period was reviewed from the viewpoints of responses and complications.

Results of review

1. Responses

Surgical treatment for neonatal chylothorax is performed in patients who respond insufficiently even to thoracic drainage in addition to nutritional therapy using MCT milk or total parenteral nutrition or drug treatment such as octreotide administration.

The methods for surgical intervention found by the present literature review included ligation of the thoracic duct and pleuroperitoneal shunting as well as pleurodesis with OK-432 administration, intrathoracic infusion of fibrin, and povidone-iodine administration, and some patients diagnosed in utero underwent pleuro-amniotic shunting. Cases in which mildly invasive treatments, such as thoracoscopic ligation of the thoracic duct and intrathoracic fibrin application, have been reported in addition to those who underwent thoracic duct ligation by thoracotomy.

Treatments that were performed before surgery and their periods were not uniform. In addition, since there are cases that developed chylous pleural effusion after surgery and those of congenital chylothorax, the diversity of the patient background must be taken into consideration in the efficacy evaluation.

Among the surgically treated cases, those in whom chylous plural effusion disappeared, respiratory symptoms were alleviated, and weaning from the respirator became possible have been reported [388, 389]. In addition, the absence of recurrence or reactivation is considered to be a point. [388–391] There were reports that chylous pleural effusion after thoracic surgery was resolved by drainage alone. Cleveland et al. [392] considered conservative treatments, such as total parenteral nutrition, octreotide, and diuretic administration, to be the best and, observing that, of the poor responders, the mortality was 80% in 5 who continued to be managed by conservative treatments but 0% in 4 who underwent additional surgery, reported that surgical treatment contributed to the reduction of the mortality. According to the guidelines for the treatment of chylous thoracic effusion by Buttiker et al. [393], conservative treatment should be continuing for about 3 weeks but should be abandoned thereafter because of the risk of nutritional disturbance, increased susceptibility to infection, and liver disorders. However, Kaji et al. [394] reported that it is difficult to set a clear period of conservative therapy, because the effectiveness and success rate of surgical treatment are unclear.

2. Complications

As complications due to sclerosing agents, fever and increased inflammatory reaction due to the administration of OK-432 as well as pulmonary abscess and temporary flaccidity and protrusion of the upper abdominal region considered to have been due to intercostal nerve damage have been reported. While chyle leakage in the abdominal cavity was

noted in a patient who underwent pleuroperitoneal shunting, there were no reports of fatal complications.

Limitations

Surgical treatment was performed in most reported cases when responses to conservative therapy were not obtained. Therefore, it must be assumed that the results of evaluation of this CQ are based on data concerning the effectiveness of surgery performed with conservative therapy.

<Summary>

The literature was reviewed concerning the effectiveness of aggressive surgical intervention for neonatal chylous thoracic effusion from the viewpoints of responses and complications, but no objective study with a high level of evidence was found. In most reported cases, surgical treatment was performed when responses to conservative treatments were poor. Therefore, it is difficult to compare surgery with other therapies, and the evaluation of the period of conservative treatment before surgery remains insufficient. However, there was a paper that proposed surgical intervention after attempting conservative treatments for 3 weeks as a standard.

Thus, surgical intervention for neonatal chylous pleural effusion is characterized at present as an approach that may be effective but should be evaluated when the condition is not improved by other treatments, and "Surgical procedures, such as pleurodesis, ligation of the thoracic duct, and pleuroperitoneal shunting, may be effective for chylous pleural effusion refractory to conservative treatments." is proposed as a draft recommendation.

CQ33: What treatments are effective for refractory chylous pleural, and pericardial effusion and respiratory disturbances of the patients with generalized lymphatic anomaly (GLA) and Gorham-Stout disease (GSD)?

Recommendation:

While treatments including surgery, sclerotherapy, radiotherapy, nutritional therapy, and drug therapy are conducted, there is presently no effective treatment with a high level of evidence. Treatments should be selected in consideration of complications and adverse effects according to individual symptoms.

Strength of recommendation	2 (weak)
Evidence	D (very weak)

Comments

[Process of preparation of recommendation]

GLA and GSD are refractory diseases that cause a wide variety of symptoms in the entire body and are difficult to diagnose and treat. The investigation by the Health and Labour Sciences Research group (Ozeki group) carried out by 2013 showed that the mortality is particularly high when the patients had thoracic lesions.

Among the thoracic symptoms, chylous pleural effusion/pericardial effusion are often refractory and occasionally fatal. While information about the disease is extremely limited because of its rareness, case reports are being globally accumulated as chronic cases are managed on an outpatient basis, and as severe cases are treated intensively.

Presently, no radical treatment for these refractory diseases is known, but the CQ, "What treatments are effective for refractory chylous pleural, and pericardial effusion and respiratory disturbances of the patients with GLA and GSD?" was formulated to compile the knowledge about what treatments are effective as it is a problem of clinical importance.

<Literature search and screening>

As a result of search, 208 papers in Japanese and 617 papers in English (598 from PubMed, 19 from Cochrane) were subjected to primary screening. Of these papers, 2 in Japanese and 25 in English were subjected to secondary screening concerning CQ 37. They included no studies with a high level of evidence, such as a systematic review and RCT, and all were reports of 1-2 cases. Therefore, the evaluation of this CQ was performed by integrating the results and discussion in case series judged to be useful for the preparation of the draft recommendation despite the lack of evidence.

<Review of observational studies (case series)>

The effectiveness of various treatments for refractory GLA and GSD was evaluated according to the prognosis and the presence or absence of improvement in imaging findings, improvement in symptoms, improvement in airway obstruction, enlargement of the lesion, regression, treatment-related complications, recurrence, and reactivation.

Conditions of patients

The cause of chylous pleural and pericardial effusion is lymphorrhea from lymphatic vessel tissue lesions that have primarily invaded the mediastinum and pleura, and lymphorrhea from osteolytic lesions of the ribs and vertebrae was also observed. Respiratory disturbances were caused by

pleural effusion, chylous pleural effusion, pericardial effusion, and direct invasion of the mediastinum and lungs.

Results of review

As surgical treatments for chylous pleural effusion, procedures, such as thoracentesis, thoracic drainage, ligation of the thoracic duct, and pleural decortication, have been performed, and local lesions were surgically resected. In most cases, thoracentesis and thoracic drainage were performed, but chyle leakage was not resolved. As for complications, there were patients who developed hypovolemic shock and required blood transfusion and catecholamine administration or supplementation of albumin, immunoglobulin, and clotting factors [395–397]. While chylous pleural effusion was controlled in some patients who underwent ligation of the thoracic duct [397–408], the treatment was performed in combination with other surgical procedure or radiotherapy in all cases [400, 402, 408]. There was 1 case that showed improvement in respiratory disturbance [406]. As complications of ligation of the thoracic duct, splenomegaly and lymphorrhea [405] and left-sided pleural effusion [397, 405] have been reported. In the patients who showed marked improvements in chylous pleural effusion [395, 405, 408] after pleural decortication [395, 396, 401, 403–405, 408, 409], the procedure was performed in combination with other surgical treatments or sclerotherapy, and there was no mention about complications. There were cases that showed marked improvements in chylous pleural effusion [396, 400, 405, 408] among those who underwent surgical resection of local lesions including splenectomy [396, 397, 400, 405, 408, 410–412], but the procedure was performed in combination with other surgical treatments in most of them. Hemorrhage was reported as a complication [410]. Among other treatments, pleuroperitoneal shunting [403] and lung transplantation [413] were performed, and alleviation of respiratory disturbance was noted in the patient who underwent lung transplantation.

As a surgical treatment for pericardial effusion, pericardiocentesis was performed [396, 414–416], and pericardial fenestration was performed when pericardial effusion could not be controlled by pericariocentesis [396, 416]. There was no mention about complications.

As sclerotherapy, pleurodesis was performed using OK-432, talc, and minocycline [395, 397–399, 404, 408, 411, 416–418]. There were patients who responded markedly to sclerotherapy alone and sclerotherapy combined with surgical procedures such as pleural decortication or local radiotherapy. There was no mention about complications of sclerotherapy.

There have also been reports [399, 400, 402–404, 410–412, 415, 416, 418–420] on local (e.g., lesion area, thoracic duct region) and thoracic radiotherapy for chylous pleural effusion and local lesions, and marked responses of chylous pleural effusion and responses of respiratory symptoms were noted, but other treatments were performed concomitantly in some patients. Radiation pneumonitis has been reported as a complication [416].

Concerning nutritional therapy, fasting, high-calorie infusion, and MCT diet have been performed alone or in combinations, but few cases that showed alleviation of chylous pleural effusion were observed [395, 396, 398–400, 403, 405, 408, 421].

For drug therapy against chylous pleural effusion, drugs including interferon α, propranolol, anticancer agents (e.g., vincristine), bisphosphonate, octreotide, steroid, sirolimus, and low-molecular-weight heparin were used. Interferon α was used most frequently [395–398, 400, 401, 403, 415, 421], and marked improvement in chylothorax was reported in 5 cases. Of these cases, interferon α was used with propranolol in 1 [395] and with low-molecular-weight heparin and local radiotherapy (15 Gy) in 1 [400]. As for complications of drug therapy using interferon α, there were reports of fever, nausea, and headache [421] and thrombocytopenia and hepatic toxicity [397]. There was no report of improvement in chylous pleural effusion by the use of steroid [395, 399, 403, 415] or octreotide [395, 397, 398, 400, 403, 405] alone. Concerning other drug therapies, only a few cases have been reported with no improvement in chylous pleural effusion. One case that showed regression of mediastinal invasion of GLA and alleviation of respiratory disturbance by sirolimus treatment has been reported [414], and hypertension was noted as a complication. In drug therapy for pericardial effusion, diuretics were used for conservative therapy [400].

Limitations

Although cases that responded to various therapies have been reported, treatments are often performed in combinations, and the evaluation of the effectiveness of each treatment alone is difficult at this point.

<Summary>

Treatments effective for GLA and GSD presenting with refractory chylous pleural effusion, pericardial effusion, and respiratory disturbances were evaluated by a review of the literature, which was primarily case reports. Various treatments, such as surgery, sclerotherapy, radiotherapy, nutritional therapy, and drug therapy, have been performed, but, there was no study with a sufficient number of cases and a high level of evidence because of the rareness of the disease and diversity of symptoms. Although cases that responded to various treatments have been reported, treatments are frequently performed in combinations, and

the evaluation of the effectiveness of individual therapies is difficult at present. Sirolimus (a mTOR inhibitor) is considered promising as a drug for this disease, and some clinical trials are currently under way in Japan and abroad.

In clinical situations, these diseases are not recognized as indications of various drug therapies by the Japanese health insurance system, and the therapeutic effects of other treatments are also uncertain. Therefore, the above treatments cannot be recommended, but we propose that treatments "should be selected in consideration of complications and adverse effects according to individual symptoms". It is necessary to evaluate the invasiveness, complications, and adverse effects, and select the treatments judged to be appropriate for each case.

Conclusion

The practice guidelines for vascular anomalies have been prepared as the evidence-based guidelines for the management of vascular anomalies.

Acknowledgements We thank all members of the systematic review team as follows. Tomoko Izaki, Ryohei Ishiura, Yohei Iwata, Tatsuo Ueda, Naoki Okura, Sachiyo Osawa, Jun Otaka, Kuniaki Ohara, Shinya Ogishima, Takuro Kazama, Motoi Kato, Takahide Kaneko, Motohiro Kano, Tamihiro Kawakami, Tatsuki Kono, Eisuke Shibata, Yohsuke Suyama, Kazuhiro Takahashi, Yuichi Takama, Takaya Takeguchi, Kensuke Tashiro, Masashi Tamura, Atsushi Tamura, Masato Tsuchiya, Kyoichi Deie, Toshihide Tokuda, Asami Tozawa, Fumio Nagai, Michiko Nagahama, Yasuhiro Nakamura, Akifumi Nozawa, Naoki Hashizume, Takuya Hara, Koji Higuchi, Masahito Hibi, Takaya Fukumoto, Shinji Fujizuka, Megumi Furuya, Seiji Houbara, Kyoko Hoshino, Tomohiro Hori, Takanobu Maekawa, Junko Miyata, Kenji Murakami, Kiichiro Yaguchi, Daisuke Yasui, Kentaro Yamada, Yohei Yamada, Yuki Yamamoto, and Azusa Watanabe.

Funding The funding for preparation of the Japanese Clinical Practice Guidelines for Vascular Anomalies 2017 was from Health, Labour and Welfare Sciences Research Grants (Research on Policy Planning and Evaluation for Rare and Intractable Diseases) provided to 'Japanese Research Committees for Intractable Vascular Anomalies' (main funding source), 'Japanese Study Group for Intractable Diseases of Pediatric Gastrointestinal Tract', and 'Japanese Research Committees for Survey and Establishment of Guidelines for Pediatric Respiratory Dysplastic/hypoplastic Disease'. No financial support was received from any other organization or corporation.

Compliance with ethical standards

Conflict of interest Conflict of interest of the guidelines preparation organization was managed by the Guidelines Executive Committee. The following corporations were disclosed by self-declaration of the Guidelines Committee members in the 3 year-period before 1 April 2017. Japan Pharmaceuticals and Medical Devices Agency (PMDA), Mitsubishi Foundation, Rohto Pharmaceutical Co., Ltd., Mitsubishi Tanabe Pharma Corporation, and Shionogi & Co., Ltd.

Open Access This article is licensed under a Creative Commons Attribution 4.0 International License, which permits use, sharing, adaptation, distribution and reproduction in any medium or format, as long as you give appropriate credit to the original author(s) and the source, provide a link to the Creative Commons licence, and indicate if changes were made. The images or other third party material in this article are included in the article's Creative Commons licence, unless indicated otherwise in a credit line to the material. If material is not included in the article's Creative Commons licence and your intended use is not permitted by statutory regulation or exceeds the permitted use, you will need to obtain permission directly from the copyright holder. To view a copy of this licence, visit http://creativecommons.org/licenses/by/4.0/.

References

1. ISSVA Classification of Vascular Anomalies© 2014 International Society for the Study of Vascular Anomalies. http://www.issva.org/classification. Accessed Apr 2014.
2. Wassef M, Blei F, Adams D, Alomari A, Baselga E, Berenstein A, et al. Vascular anomalies classification: recommendations from the international society for the study of vascular anomalies. Pediatrics. 2015;136:e203–14.
3. Clinical practice guidelines for vascular anomalies. The Research Committee of Intractable Vascular Anomalies, Research on Measures for Intractable Diseases, Health, Labour and Welfare Sciences Research Grants, the Ministry of Health, Labour and Welfare, Japan. 2013. http://www.marianna-u.ac.jp/va/files/vascular%20anomalies%20practice%20guideline%202013.pdf. Accessed 29 Mar 2013 **(Japanese)**.
4. Fukui T, Yamaguchi N, Morizane T, Yoshida M, Kojimahara N (eds). Minds handbook for clinical practice guideline development 2014. Ver 1.0, Tokyo: Minds Guideline Center, Japan Council for Quality Health Care. 2014. http://minds4.jcqhc.or.jp/minds/guideline/pdf/MindsHB2014.pdf. Accessed 1 Feb 2015.
5. Morizane T, Yoshida M (eds). Minds manual for guideline development Ver. 1.0. Tokyo: Japan Council for Quality Health Care. Accessed 31 Mar 2014 **(Japanese)**.
6. Kojimahara N, Nakayama T, Morizane T, Yamaguchi N, Yoshida M (eds). Minds manual for guideline development Ver. 2.0, Tokyo: Japan Council for Quality Health Care. http://minds4.jcqhc.or.jp/minds/guideline/pdf/manual_all_2.0.pdf. Accessed 15 Mar 2016 **(Japanese)**.
7. Balshem H, Helfand M, Schunemann HJ, Oxman AD, Kunz R, Brozek J, et al. GRADE guidelines: 3. Rating the quality of evidence. J Clin Epidemiol. 2011;64:401–6.
8. Andrews J, Guyatt G, Oxman AD, Alderson P, Dahm P, Falck-Ytter Y, et al. GRADE guidelines: 14. Going from evidence to recommendations: the significance and presentation of recommendations. J Clin Epidemiol. 2013;66:719–25.
9. Liu AS, Mulliken JB, Zurakowski D, Fishman SJ, Greene AK. Extracranial arteriovenous malformations: natural progression and recurrence after treatment. Plast Reconstr Surg. 2010;125:1185–94.
10. Kohout MP, Hansen M, Pribaz JJ, Mulliken JB. Arteriovenous malformations of the head and neck: natural history and management. Plast Reconstr Surg. 1998;102:643–54.
11. Richter GT, Suen J, North PE, James CA, Waner M, Buckmiller LM. Arteriovenous malformations of the tongue: a spectrum of disease. Laryngoscope. 2007;117:328–35.
12. Hyun D, Do YS, Park KB, Kim DI, Kim YW, Park HS, et al. Ethanol embolotherapy of foot arteriovenous malformations. J Vasc Surg. 2013;58:1619–26.
13. Park KB, Do YS, Kim DI, Kim YW, Shin BS, Park HS, et al. Predictive factors for response of peripheral arteriovenous

malformations to embolization therapy: analysis of clinical data and imaging findings. J Vasc Interv Radiol. 2012;23:1478–86.
14. Wu JK, Bisdorff A, Gelbert F, Enjolras O, Burrows PE, Mulliken JB. Auricular arteriovenous malformation: evaluation, management, and outcome. Plast Reconstr Surg. 2005;115:985–95.
15. DesPrez JD, Kiehn CL, Vlastou C, Bonstelle C. Congenital arteriovenous malformation of the head and neck. Am J Surg. 1978;136:424–9.
16. Dompmartin A, Labbé D, Barrellier MT, Théron J. Use of a regulating flap in the treatment of a large arteriovenous malformation of the scalp. Br J Plast Surg. 1998;51:561–3.
17. Yamamoto Y, Ohura T, Minakawa H, Sugihara T, Yoshida T, Nohira K, et al. Experience with arteriovenous malformations treated with flap coverage. Plast Reconstr Surg. 1994;94:476–82.
18. Hartzell LD, Stack BC Jr, Yuen J, Vural E, Suen JY. Free tissue reconstruction following excision of head and neck arteriovenous malformations. Arch Facial Plast Surg. 2009;11:171–7.
19. Visser A, FitzJohn T, Tan ST. Surgical management of arteriovenous malformation. J Plast Reconstr Aesthet Surg. 2011;64:283–91.
20. Hong JP, Choi JW, Chang H, Lee TJ. Reconstruction of the face after resection of arteriovenous malformations using anterolateral thigh perforator flap. J Craniofac Surg. 2005;16:851–5.
21. Koshima I, Takahashi Y, Namba Y, Inagawa K, Oka H, Moriguchi T, et al. Treatment for arteriovenous malformation. Keisei Geka. 2001;44:665–73 **(Japanese)**.
22. Toh S, Tsubo K, Arai H, Harata S. Vascularized free flaps for reconstruction after resection of congenital arteriovenous malformations of the hand. J Reconstr Microsurg. 2000;16:511–7.
23. Yokoo K, Nishihori K, Kono A, Ishiguchi T, Ohta T. Surgical treatment of arteriovenous malformations in the head and neck combined with antecedent embolization. Keisei Geka. 2009;52:1201–8 **(Japanese)**.
24. Koshima I, Nanba Y, Tsutsui T, Takahashi Y, Watanabe A, Ishii R. Free perforator flap for the treatment of defects after resection of huge arteriovenous malformations in the head and neck regions. Ann Plast Surg. 2003;51:194–9.
25. Kajitani N, Ikuta Y, Ishida O, Mochizuki Y, Kimori K. Surgical treatment of arteriovenous fistula of the hand. Nihon Te No Geka Gakkai Zasshi. 1999;15:758–61 **(Japanese)**.
26. Minami A, Kato H, Hirachi K. Complete removal plus dorsalis pedis flap for arteriovenous malformation in the hypothenar region. J Reconstr Microsurg. 1998;14:439–43.
27. Koshima I, Soeda S, Murashita T. Extended wrap-around flap for reconstruction of the finger with recurrent arteriovenous malformation. Plast Reconstr Surg. 1993;91:1140–4.
28. Wojcicki P, Wojcicka K. The treatment of extensive arteriovenous malformations in the head. Pol Przegl Chir. 2013;85:83–9.
29. Ermer MA, Gutwald R, Schumacher M, Schmelzeisen R, Taschner C. Use of the radial forearm artery for secondary embolization of an extensive life-threatening arteriovenous malformation of the mid-face and anterior skull base—a case report. J Craniomaxillofac Surg. 2013;41:258–64.
30. Ueda K, Oba S, Nakai K, Okada M, Kurokawa N, Nuri T. Functional reconstruction of the upper and lower lips and commissure with a forearm flap combined with a free gracilis muscle transfer. J Plast Reconstr Aesthet Surg. 2009;62:e337–40.
31. Ninkovic M, Sucur D, Starovic B, Markovic S. Arteriovenous fistulae after free flap surgery in a replanted hand. J Hand Surg Br. 1992;17:657–9.
32. Bit N, Vidyasagaran T, Amalorpavanathan J, Balakrishnan TM, Sritharan N. Management of a challenging arteriovenous malformation of the scalp and orbit in a patient with polycystic kidney disease. Ann Vasc Surg. 2012;26(1129):e9–11.
33. Righi PD, Bade MA, Coleman JJ 3rd, Allen M. Arteriovenous malformation of the base of tongue: case report and literature review. Microsurgery. 1996;17:706–9.
34. Minagawa T, Itaya Y, Furukawa H. Resection of an arteriovenous malformation of the scalp using a modified tumescent technique. Nihon Keisei Geka Gakkai Kaishi. 2010;30:87–9.
35. Suyama Y, Nakayama B, Fukuoka K, Takeuchi E, Hashimoto M, Kaminou T, et al. Auricular reconstruction with a free radial forearm flap for necrotized ear after sclerotherapy for arteriovenous malformation: a case report. Nihon Maikuro Sajari Gakkai Kaishi. 2010;23:311–5 **(Japanese)**.
36. Urayama H, Harada T, Kawase H, Watanabe Y. Surgical management of soft tissue arteriovenous malformations and hemangiomas. Shoni Geka. 1993;25:415–9 **(Japanese)**.
37. Yamamoto Y, Sugihara T, Minakawa H, Ohkubo Y, Hayashi T. Surgical treatment of massive arteriovenous malformation with application of hypothermia and cardiopulmonary bypass. Nihon Keisei Geka Gakkai Kaishi. 1996;16:863–71 **(Japanese)**.
38. Hormozi AK, Shafii MR. Supraclavicular flap: reconstructive strategy for massive facial arteriovenous malformations. J Craniofac Surg. 2011;22:931–6.
39. Hurwitz DJ, Kerber CW. Hemodynamic considerations in the treatment of arteriovenous malformations of the face and scalp. Plast Reconstr Surg. 1981;67:421–34.
40. Kiyokawa K, Takagi M, Fukushima J, Kizuka Y, Inoue Y, Tai Y. Surgical treatment following huge arteriovenous malformation extending from the lower lip to the chin: combination of embolization, total resection, and a double cross lip flap. J Craniofac Surg. 2005;16:443–8.
41. Thomas WO. Facial arteriovenous malformation managed with ablative surgery and dual rotational flap reconstruction. South Med J. 1994;87:1178–82.
42. Warwick DJ, Milling MA. Growth of a vascular malformation into a cross-finger flap. Br J Clin Pract. 1993;47:48.
43. Agir H, Sen C, Onyedi M. Extended lateral supramalleolar flap for very distal foot coverage: a case with arteriovenous malformation. J Foot Ankle Surg. 2007;46:310–3.
44. Sakurai H, Nozaki M, Sasaki K, Yamaki T, Aiba H, Tohda J, et al. Successful management of a giant arteriovenous fistula with a combination of selective embolization and excision: report of a case. Surg Today. 2002;32:189–93.
45. Watanabe T, Asato H, Umekawa K, Nomura H, Suzuki Y. Resurfacing the index finger after resection of an arteriovenous malformation using a reverse forearm flap combined with additional venous anastomosis: a case report. Nihon Keisei Geka Gakkai Kaishi. 2012;32:335–9 **(Japanese)**.
46. Ishisaka T, Naitoh H, Akiyama K, Shigeyoshi N. A case of lower lip arteriovenous malformation with verrucous carcinoma. Nihon Keisei Geka Gakkai Kaishi. 2009;29:7–11 **(Japanese)**.
47. Kitagawa S, Kizaki K, Yajima H, Mii Y, Tamai S. Treatment of hemangiomas associated with arteriovenous fistulae in a family. Chubu Nihon Seikei Geka Saigai Geka Gakkai Zasshi. 1997;40:331–2 **(Japanese)**.
48. Gunji H, Suda K, Ono I, Ariga T, Kaneko F. Arteriovenous fistula of auricle treated with a temporoparietal fascial flap: a case report. Nihon Keisei Geka Gakkai Kaishi. 1993;13:221–7 **(Japanese)**.
49. Fujita A, Asada M, Saitoh M, Nakamura H, Hanagaki H, Ban M, et al. A case of congenital arteriovenous malformation of the scalp treated with rotation flap. No Shinkei Geka Janaru. 2000;9:86–91 **(Japanese)**.
50. Nakamura E, Suzuki S, Imagawa K, Akamatsu T, Miyasaka M. Experience of two patients with auricular arteriovenous malformation. Skin Surg. 2014;23:73–8 **(Japanese)**.

51. Yoshimura Y, Mizuno M, Kobayashi T, Oishi K, Maeda S, Hirano T, et al. Case reports: extracranial arteriovenous malformation. Hifuka No Rinsho. 2014;56:1180–3 **(Japanese)**.
52. Matsuzaki K, Nakamura T, Tahara T, Kashiwa H, Oshima H, Souzumi T. Congenital arteriovenous malformation of the auricle. Jibi Inkoka Tokeibu Geka. 1995;67:337–41 **(Japanese)**.
53. Schultz RC, Hermosillo CX. Congenital arteriovenous malformation of the face and scalp. Plast Reconstr Surg. 1980;65:496–501.
54. Slaba S, Herbreteau D, Jhaveri HS, Casasco A, Aymard A, Houdart E, et al. Therapeutic approach to arteriovenous malformations of the tongue. Eur Radiol. 1998;8:280–5.
55. Toker ME, Eren E, Akbayrak H, Numan F, Guler M, Balkanay M, et al. Combined approach to a peripheral congenital arteriovenous malformation: surgery and embolization. Heart Vessels. 2006;21:127–30.
56. Doppman JL, Pevsner P. Embolization of arteriovenous malformations by direct percutaneous puncture. AJR Am J Roentgenol. 1983;140:773–8.
57. Aikawa H, Okino Y, Yamada Y, Tomonari K, Gotoh T, Gotoh Y, et al. A review of embolization for arteriovenous malformations (fistulae). Oita Kenritsu Byoin Igaku Zasshi. 1997;26:77–82 **(Japanese)**.
58. Yamamoto T, Kanamura N, Tsukitani K, Hori N, Iehara T, Fukushima Y, et al. Direct embolization for a life-threatening mandibular arteriovenous malformation by means of hypothermic cardio-pulmonary arrest. Kyoto Furitsu Ika Daigaku Zasshi. 1999;108:981–94.
59. Deng W, Huang D, Chen S, Zhang X, Li X, Li J, et al. Management of high-flow arteriovenous malformation in the maxillofacial region. J Craniofac Surg. 2010;21:916–9.
60. Erdmann MW, Jackson JE, Davies DM, Allison DJ. Multidisciplinary approach to the management of head and neck arteriovenous malformations. Ann R Coll Surg Engl. 1995;77:53–9.
61. Goldberg RA, Garcia GH, Duckwiler GR. Combined embolization and surgical treatment of arteriovenous malformation of the orbit. Am J Ophthalmol. 1993;116:17–25.
62. Persky MS, Yoo HJ, Berenstein A. Management of vascular malformations of the mandible and maxilla. Laryngoscope. 2003;113:1885–92.
63. Liu DG, Ma XC, Zhao FY, Zhang JG. A preliminary study of angiographic classification and its correlation to treatment of central arteriovenous malformation in the jaw. Oral Surg Oral Med Oral Pathol Oral Radiol Endod. 2005;100:473–80.
64. Rodesch G, Soupre V, Vazquez MP, Alvarez H, Lasjaunias P. Arteriovenous malformations of the dental arcades. The place of endovascular therapy: results in 12 cases are presented. J Craniomaxillofac Surg. 1998;26:306–13.
65. Chen W, Wang J, Li J, Xu L. Comprehensive treatment of arteriovenous malformations in the oral and maxillofacial region. J Oral Maxillofac Surg. 2005;63:1484–8.
66. Chen WL, Ye JT, Xu LF, Huang ZQ, Zhang DM. A multidisciplinary approach to treating maxillofacial arteriovenous malformations in children. Oral Surg Oral Med Oral Pathol Oral Radiol Endod. 2009;108:41–7.
67. Churojana A, Khumtong R, Songsaeng D, Chongkolwatana C, Suthipongchai S. Life-threatening arteriovenous malformation of the maxillomandibular region and treatment outcomes. Interv Neuroradiol. 2012;18:49–59.
68. Liu D, Ma XC. Clinical study of embolization of arteriovenous malformation in the oral and maxillofacial region. Chin J Dent Res. 2000;3:63–70.
69. Chandra RV, Leslie-Mazwi TM, Orbach DB, Kaban LB, Rabinov JD. Transarterial embolization of mandibular arteriovenous malformations using ONYX. J Oral Maxillofac Surg. 2014;72:1504–10.
70. Fifi J, Niimi Y, Berenstein A. Onyx embolization of an extensive mandibular arteriovenous malformation via a dual lumen balloon catheter: a technical case report. J Neurointerv Surg. 2013;5:e5.
71. Fan XD, Su LX, Zheng JW, Zheng LZ, Zhang ZY. Ethanol embolization of arteriovenous malformations of the mandible. AJNR Am J Neuroradiol. 2009;30:1178–83.
72. Park HS, Do YS, Park KB, Kim DI, Kim YW, Kim MJ, et al. Ethanol embolotherapy of hand arteriovenous malformations. J Vasc Surg. 2011;53:725–31.
73. Park UJ, Do YS, Park KB, Park HS, Kim YW, Lee BB, et al. Treatment of arteriovenous malformations involving the hand. Ann Vasc Surg. 2012;26:643–8.
74. Hibino N, Hamada Y, Goda Y, Endo K, Yasui N, Kasai T, et al. Arterial graft for reconstruction after complete removal of the arteriovenous malformation. Nihon Maikuro Sajari Gakkai Kaishi. 2005;18:78–82.
75. Widlus DM, Murray RR, White RI Jr, Osterman FA Jr, Schreiber ER, Satre RW, et al. Congenital arteriovenous malformations: tailored embolotherapy. Radiology. 1988;169:511–6.
76. Hattori Y, Doi K, Kawakami F, Watanabe M. Extended wrap-around flap for thumb reconstruction following radical excision of a congenital arteriovenous fistula. J Hand Surg Br. 1998;23:72–5.
77. Sugioka T, Sunagawa T, Suzuki O, Kijima Y, Ochi M. Surgical treatment for arteriovenous malformation involving the hand and forearm. Nihon Te No Geka Gakkai Zasshi. 2008;24:940–3 **(Japanese)**.
78. Furuya T, Nakazawa T. Congenital arteriovenous malformation of the index finger: a case report. Myakkangaku. 2009;49:430–3 **(Japanese)**.
79. Moore JR, Weiland AJ. Embolotherapy in the treatment of congenital arteriovenous malformations of the hand: a case report. J Hand Surg Am. 1985;10:135–9.
80. Arneja JS, Gosain AK. Vascular malformations. Plast Reconstr Surg. 2008;121:195e–206e.
81. Hein KD, Mulliken JB, Kozakewich HP, Upton J, Burrows PE. Venous malformations of skeletal muscle. Plast Reconstr Surg. 2002;110:1625–35.
82. Marler JJ, Mulliken JB. Current management of hemangiomas and vascular malformations. Clin Plast Surg. 2005;32:99–116 **(ix)**.
83. Nguyen JT, Koerper MA, Hess CP, Dowd CF, Hoffman WY, Dickman M, et al. Aspirin therapy in venous malformation: a retrospective cohort study of benefits, side effects, and patient experiences. Pediatr Dermatol. 2014;31:556–60.
84. Shireman PK, McCarthy WJ, Yao JS, Vogelzang RL. Treatment of venous malformations by direct injection with ethanol. J Vasc Surg. 1997;26:838–44.
85. Rimon U, Garniek A, Galili Y, Golan G, Bensaid P, Morag B. Ethanol sclerotherapy of peripheral venous malformations. Eur J Radiol. 2004;52:283–7.
86. Marrocco-Trischitta MM, Nicodemi EM, Nater C, Stillo F. Management of congenital venous malformations of the vulva. Obstet Gynecol. 2001;98:789–93.
87. Suh JS, Shin KH, Na JB, Won JY, Hahn SB. Venous malformations: sclerotherapy with a mixture of ethanol and lipiodol. Cardiovasc Intervent Radiol. 1997;20:268–73.
88. Dompmartin A, Blaizot X, Théron J, Hammer F, Chene Y, Labbé D, et al. Radio-opaque ethylcellulose-ethanol is a safe and efficient sclerosing agent for venous malformations. Eur Radiol. 2011;21:2647–56.
89. Schumacher M, Dupuy P, Bartoli JM, Ernemann U, Herbreteau D, Ghienne C, et al. Treatment of venous malformations: first experience with a new sclerosing agent—a multicenter study. Eur J Radiol. 2011;80:e366–72.

90. Mimura H, Kanazawa S, Yasui K, Fujiwara H, Hyodo T, Mukai T, et al. Percutaneous sclerotherapy for venous malformations using polidocanol under fluoroscopy. Acta Med Okayama. 2003;57:227–34.
91. Mimura H, Fujiwara H, Hiraki T, Gobara H, Mukai T, Hyodo T, et al. Polidocanol sclerotherapy for painful venous malformations: evaluation of safety and efficacy in pain relief. Eur Radiol. 2009;19:2474–80.
92. Cabrera J, Cabrera J Jr, Garcia-Olmedo MA, Redondo P. Treatment of venous malformations with sclerosant in microfoam form. Arch Dermatol. 2003;139:1409–16.
93. Ozaki M, Kurita M, Kaji N, Fujino T, Narushima M, Takushima A, et al. Efficacy and evaluation of safety of sclerosants for intramuscular venous malformations: clinical and experimental studies. Scand J Plast Reconstr Surg Hand Surg. 2010;44:75–87.
94. Krokidis M, Venetucci P, Hatzidakis A, Iaccarino V. Sodium tetradecyl sulphate direct intralesional sclerotherapy of venous malformations of the vulva and vagina: report of five cases. Cardiovasc Intervent Radiol. 2011;34(Suppl 2):S228–31.
95. Enjolras O, Ciabrini D, Mazoyer E, Laurian C, Herbreteau D. Extensive pure venous malformations in the upper or lower limb: a review of 27 cases. J Am Acad Dermatol. 1997;36:219–25.
96. Steiner F, FitzJohn T, Tan ST. Surgical treatment for venous malformation. J Plast Reconstr Aesthet Surg. 2013;66:1741–9.
97. Noel AA, Gloviczki P, Cherry KJ Jr, Rooke TW, Stanson AW, Driscoll DJ. Surgical treatment of venous malformations in Klippel-Trenaunay syndrome. J Vasc Surg. 2000;32:840–7.
98. Sidhu MK, Perkins JA, Shaw DW, Bittles MA, Andrews RT. Ultrasound-guided endovenous diode laser in the treatment of congenital venous malformations: preliminary experience. J Vasc Interv Radiol. 2005;16:879–84.
99. Lu X, Ye K, Shi H, Li W, Huang Y, Huang X, et al. Percutaneous endovenous treatment of congenital extratruncular venous malformations with an ultrasound-guided and 810-nm diode laser. J Vasc Surg. 2011;54:139–45.
100. Liu G, Liu X, Li W, Shi H, Ye K, Yin M, et al. Ultrasound-guided intralesional diode laser treatment of congenital extratruncular venous malformations: mid-term results. Eur J Vasc Endovasc Surg. 2014;47:558–64.
101. Mazoyer E, Enjolras O, Laurian C, Houdart E, Drouet L. Coagulation abnormalities associated with extensive venous malformations of the limbs: differentiation from Kasabach-Merritt syndrome. Clin Lab Haematol. 2002;24:243–51.
102. Cornelis F, Neuville A, Labreze C, Kind M, Bui B, Midy D, et al. Percutaneous cryotherapy of vascular malformation: initial experience. Cardiovasc Intervent Radiol. 2013;36:853–6.
103. Cornelis F, Havez M, Labreze C, Taieb A, Bui BN, Midy D, et al. Percutaneous cryoablation of symptomatic localized venous malformations: preliminary short-term results. J Vasc Interv Radiol. 2013;24:823–7.
104. Betz CS, Jager HR, Brookes JA, Richards R, Leunig A, Hopper C. Interstitial photodynamic therapy for a symptom-targeted treatment of complex vascular malformations in the head and neck region. Lasers Surg Med. 2007;39:571–82.
105. Bashkatov AN, Genina EA, Kochubey VI, Tuchin VV. Optical properties of human skin, subcutaneous and mucous tissues in the wavelength range from 400 to 2000 nm. J Phys D Appl Phys. 2005;38:2543–55.
106. Sarig O, Kimel S, Orenstein A. Laser treatment of venous malformations. Ann Plast Surg. 2006;57:20–4.
107. Vesnaver A, Dovsak DA. Treatment of vascular lesions in the head and neck using Nd:YAG laser. J Craniomaxillofac Surg. 2006;34:17–24.
108. Asai T, Suzuki H, Enomoto Y, Shigeoka M, Matsumoto K, Takeuchi J, et al. Clinical evaluation of 74 vascular malformations of the oral region treated by photocoagulation with an Nd:YAG laser. Nihon Reza Shigakkaishi. 2013;24:3–9 **(Japanese)**.
109. Ng EK, Cheung FK, Chiu PW. Blue rubber bleb nevus syndrome: treatment of multiple gastrointestinal hemangiomas with argon plasma coagulator. Dig Endosc. 2009;21:40–2.
110. Cholewa D, Waldschmidt J. Laser treatment of hemangiomas of the larynx and trachea. Lasers Surg Med. 1998;23:221–32.
111. Yakes WF, Haas DK, Parker SH, Gibson MD, Hopper KD, Mulligan JS, et al. Symptomatic vascular malformations: ethanol embolotherapy. Radiology. 1989;170:1059–66.
112. Lee IH, Kim KH, Jeon P, Byun HS, Kim HJ, Kim ST, et al. Ethanol sclerotherapy for the management of craniofacial venous malformations: the interim results. Korean J Radiol. 2009;10:269–76.
113. Hoque S, Das BK. Treatment of venous malformations with ethanolamine oleate: a descriptive study of 83 cases. Pediatr Surg Int. 2011;27:527–31.
114. Stuart S, Barnacle AM, Smith G, Pitt M, Roebuck DJ. Neuropathy after sodium tetradecyl sulfate sclerotherapy of venous malformations in children. Radiology. 2015;274:897–905.
115. Zhao JH, Zhang WF, Zhao YF. Sclerotherapy of oral and facial venous malformations with use of pingyangmycin and/or sodium morrhuate. Int J Oral Maxillofac Surg. 2004;33:463–6.
116. Bai N, Chen YZ, Fu YJ, Wu P, Zhang WN. A clinical study of pingyangmycin sclerotherapy for venous malformation: an evaluation of 281 consecutive patients. J Clin Pharm Ther. 2014;39:521–6.
117. Goyal M, Causer PA, Armstrong D. Venous vascular malformations in pediatric patients: comparison of results of alcohol sclerotherapy with proposed MR imaging classification. Radiology. 2002;223:639–44.
118. Yun WS, Kim YW, Lee KB, Kim DI, Park KB, Kim KH, et al. Predictors of response to percutaneous ethanol sclerotherapy (PES) in patients with venous malformations: analysis of patient self-assessment and imaging. J Vasc Surg. 2009;50:581–9 **(9 e1)**.
119. Rautio R, Saarinen J, Laranne J, Salenius JP, Keski-Nisula L. Endovascular treatment of venous malformations in extremities: results of sclerotherapy and the quality of life after treatment. Acta Radiol. 2004;45:397–403.
120. Yamaki T, Nozaki M, Sakurai H, Takeuchi M, Soejima K, Kono T. Prospective randomized efficacy of ultrasound-guided foam sclerotherapy compared with ultrasound-guided liquid sclerotherapy in the treatment of symptomatic venous malformations. J Vasc Surg. 2008;47:578–84.
121. Nagao M, Sasaki S, Furukawa H, Saito N, Yamamoto Y. A clinical study of sclerotherapy for venous malformation of an upper extremity. Nihon Keisei Geka Gakkai Kaishi. 2012;32:463–8 **(Japanese)**.
122. Nomura T, Sakurai A, Nagata I, Terashi H, Tahara S. Our strategy for the treatment of venous malformations. Jomyakugaku. 2008;19:161–8 **(Japanese)**.
123. Qiu Y, Chen H, Lin X, Hu X, Jin Y, Ma G. Outcomes and complications of sclerotherapy for venous malformations. Vasc Endovascular Surg. 2013;47:454–61.
124. Wong GA, Armstrong DC, Robertson JM. Cardiovascular collapse during ethanol sclerotherapy in a pediatric patient. Paediatr Anaesth. 2006;16:343–6.
125. Tachibana K, Kobayashi S, Kojima T, Kaseno S, Kemmotsu O. Pulmonary emboli in sclerotherapy for peripheral vascular malformations under general anesthesia; a report of two cases. Masui. 2004;53:645–9 **(Japanese)**.
126. Marrocco-Trischitta MM, Guerrini P, Abeni D, Stillo F. Reversible cardiac arrest after polidocanol sclerotherapy of peripheral venous malformation. Dermatol Surg. 2002;28:153–5.

127. Shimo T, Hidaka K, Yanagawa S, Kadota W, Kawakami S, Tsuchida H. Two episodes of cardiac arrest in a boy receiving sclerotherapy with polydocanol—a case report. Masui. 2005;54:57–9 **(Japanese)**.
128. Schild SE, Buskirk SJ, Frick LM, Cupps RE. Radiotherapy for large symptomatic hemangiomas. Int J Radiat Oncol Biol Phys. 1991;21:729–35.
129. Mitsuhashi N, Furuta M, Sakurai H, Takahashi T, Kato S, Nozaki M, et al. Outcome of radiation therapy for patients with Kasabach-Merritt syndrome. Int J Radiat Oncol Biol Phys. 1997;39:467–73.
130. Ogino I, Torikai K, Kobayasi S, Aida N, Hata M, Kigasawa H. Radiation therapy for life- or function-threatening infant hemangioma. Radiology. 2001;218:834–9.
131. Miller JG, Orton CI. Long term follow-up of a case of Kasabach-Merritt syndrome successfully treated with radiotherapy and corticosteroids. Br J Plast Surg. 1992;45:559–61.
132. Frevel T, Rabe H, Uckert F, Harms E. Giant cavernous haemangioma with Kasabach-Merritt syndrome: a case report and review. Eur J Pediatr. 2002;161:243–6.
133. Stringel G, Mercer S. Giant hemangioma in the newborn and infant. Complications and management. Clin Pediatr (Phila). 1984;23:498–502.
134. Enjolras O, Wassef M, Mazoyer E, Frieden IJ, Rieu PN, Drouet L, et al. Infants with Kasabach-Merritt syndrome do not have "true" hemangiomas. J Pediatr. 1997;130:631–40.
135. Lundell M, Mattsson A, Hakulinen T, Holm LE. Breast cancer after radiotherapy for skin hemangioma in infancy. Radiat Res. 1996;145:225–30.
136. Haddy N, Andriamboavonjy T, Paoletti C, Dondon MG, Mousannif A, Shamsaldin A, et al. Thyroid adenomas and carcinomas following radiotherapy for a hemangioma during infancy. Radiother Oncol. 2009;93:377–82.
137. Caldwell JB, Ryan MT, Benson PM, James WD. Cutaneous angiosarcoma arising in the radiation site of a congenital hemangioma. J Am Acad Dermatol. 1995;33:865–70.
138. Oguri A, Oda M, Yokoo K. The relation between age and the effectiveness of laser treatment for capillary malformation. Nihon Keisei Geka Gakkai Kaishi. 2009;29:407–11 **(Japanese)**.
139. Reynolds N, Exley J, Hills S, Falder S, Duff C, Kenealy J. The role of the Lumina intense pulsed light system in the treatment of port wine stains—a case controlled study. Br J Plast Surg. 2005;58:968–80.
140. Katugampola GA, Lanigan SW. Five years' experience of treating port wine stains with the flashlamp-pumped pulsed dye laser. Br J Dermatol. 1997;137:750–4.
141. Minato S. Comparison between results of treatment with dye laser and argon laser in cases of hemangioma simplex. Iwate Igaku Zasshi. 1997;49:299–302.
142. Ryuzaki K, Tamura A, Amano H, Takeuchi Y, Ishikawa O, Miyachi Y. An overview of dye laser treatment for superficial hemangiomas at the Department of Dermatology, Gunma University. Hifuka Kiyo. 1996;91:41–6 **(Japanese)**.
143. Matsumoto T. Comparative study in laser treatment of portwine stains with dye and argon lasers. Part 2: statistical study of clinical effects. Nihon Keisei Geka Gakkai Kaishi. 1996;16:246–59 **(Japanese)**.
144. Fitzpatrick RE, Lowe NJ, Goldman MP, Borden H, Behr KL, Ruiz-Esparza J. Flashlamp-pumped pulsed dye laser treatment of port-wine stains. J Dermatol Surg Oncol. 1994;20:743–8.
145. Morikawa K, Yamauchi K, Saheki M, Tezuka T. Treatment of portwine stain using pulsed dye laser: comparison of effectiveness with location of lesion, age and wavelength. Hifu. 1994;36:514–21 **(Japanese)**.
146. Matsushita Y, Suzuki S, Koyama H, Akamatsu J, Kawata Y, Kawai K. Treatment of portwine stains with dye lasers. Hifuka Kiyo. 1994;89:205–10 **(Japanese)**.
147. Namba Y, Mae O, Nagase Y, Ao M, Hamaya K, Nose S. Dye laser treatment of cutaneous simple hemangioma. Okayama Saiseikai Sogo Byoin Zasshi. 1991;22:1–10 **(Japanese)**.
148. Bandoh Y, Yanai A, Tsuzuki K. Dye laser treatment of port-wine stains. Aesthetic Plast Surg. 1990;14:287–91.
149. Bandoh Y. Pulsed dye laser treatment for port-wine stains. Rinsho Hifuka. 1989;43:1337–40 **(Japanese)**.
150. Renfro L, Geronemus RG. Anatomical differences of port-wine stains in response to treatment with the pulsed dye laser. Arch Dermatol. 1993;129:182–8.
151. Lanigan SW. Port wine stains on the lower limb: response to pulsed dye laser therapy. Clin Exp Dermatol. 1996;21:88–92.
152. Sommer S, Seukeran DC, Sheehan-Dare RA. Efficacy of pulsed dye laser treatment of port wine stain malformations of the lower limb. Br J Dermatol. 2003;149:770–5.
153. Fitzpatrick TB. The validity and practicality of sun-reactive skin types I through VI. Arch Dermatol. 1988;124:869–71.
154. Wareham WJ, Cole RP, Royston SL, Wright PA. Adverse effects reported in pulsed dye laser treatment for port wine stains. Lasers Med Sci. 2009;24:241–6.
155. Orten SS, Waner M, Flock S, Roberson PK, Kincannon J. Portwine stains. An assessment of 5 years of treatment. Arch Otolaryngol Head Neck Surg. 1996;122:1174–9.
156. Michel S, Landthaler M, Hohenleutner U. Recurrence of portwine stains after treatment with the flashlamp-pumped pulsed dye laser. Br J Dermatol. 2000;143:1230–4.
157. Soueid A, Waters R. Re-emergence of port wine stains following treatment with flashlamp-pumped dye laser 585 nm. Ann Plast Surg. 2006;57:260–3.
158. Huikeshoven M, Koster PH, de Borgie CA, Beek JF, van Gemert MJ, van der Horst CM. Redarkening of port-wine stains 10 years after pulsed-dye-laser treatment. N Engl J Med. 2007;356:1235–40.
159. Phung TL, Oble DA, Jia W, Benjamin LE, Mihm MC Jr, Nelson JS. Can the wound healing response of human skin be modulated after laser treatment and the effects of exposure extended? Implications on the combined use of the pulsed dye laser and a topical angiogenesis inhibitor for treatment of port wine stain birthmarks. Lasers Surg Med. 2008;40:1–5.
160. Babilas P, Shafirstein G, Bäumler W, Baier J, Landthaler M, Szeimies RM, et al. Selective photothermolysis of blood vessels following flashlamp-pumped pulsed dye laser irradiation: in vivo results and mathematical modelling are in agreement. J Invest Dermatol. 2005;125:343–52.
161. Laquer VT, Hevezi PA, Albrecht H, Chen TS, Zlotnik A, Kelly KM. Microarray analysis of port wine stains before and after pulsed dye laser treatment. Lasers Surg Med. 2013;45:67–75.
162. Chapas AM, Eickhorst K, Geronemus RG. Efficacy of early treatment of facial port wine stains in newborns: a review of 49 cases. Lasers Surg Med. 2007;39:563–8.
163. Jia W, Sun V, Tran N, Choi B, Liu SW, Mihm MC Jr, et al. Long-term blood vessel removal with combined laser and topical rapamycin antiangiogenic therapy: implications for effective port wine stain treatment. Lasers Surg Med. 2010;42:105–12.
164. Chang CJ, Hsiao YC, Mihm MC Jr, Nelson JS. Pilot study examining the combined use of pulsed dye laser and topical Imiquimod versus laser alone for treatment of port wine stain birthmarks. Lasers Surg Med. 2008;40:605–10.
165. Tremaine AM, Armstrong J, Huang YC, Elkeeb L, Ortiz A, Harris R, et al. Enhanced port-wine stain lightening achieved with combined treatment of selective photothermolysis and imiquimod. J Am Acad Dermatol. 2012;66:634–41.

166. Nguyen CM, Yohn JJ, Huff C, Weston WL, Morelli JG. Facial port wine stains in childhood: prediction of the rate of improvement as a function of the age of the patient, size and location of the port wine stain and the number of treatments with the pulsed dye (585 nm) laser. Br J Dermatol. 1998;138:821–5.
167. van der Horst CM, Koster PH, de Borgie CA, Bossuyt PM, van Gemert MJ. Effect of the timing of treatment of port-wine stains with the flash-lamp-pumped pulsed-dye laser. N Engl J Med. 1998;338:1028–33.
168. Léauté-Labrèze C, Dumas de la Roque E, Hubiche T, Boralevi F, Thambo JB, Taïeb A. Propranolol for severe hemangiomas of infancy. N Engl J Med. 2008;358:2649–51.
169. Broeks IJ, Hermans DJ, Dassel AC, van der Vleuten CJ, van Beynum IM. Propranolol treatment in life-threatening airway hemangiomas: a case series and review of literature. Int J Pediatr Otorhinolaryngol. 2013;77:1791–800.
170. Sharma VK, Fraulin FO, Dumestre DO, Walker L, Harrop AR. Beta-blockers for the treatment of problematic hemangiomas. Can J Plast Surg. 2013;21:23–8.
171. Zvulunov A, McCuaig C, Frieden IJ, Mancini AJ, Puttgen KB, Dohil M, et al. Oral propranolol therapy for infantile hemangiomas beyond the proliferation phase: a multicenter retrospective study. Pediatr Dermatol. 2011;28:94–8.
172. Hermans DJ, van Beynum IM, Schultze Kool LJ, van de Kerkhof PC, Wijnen MH, van der Vleuten CJ. Propranolol, a very promising treatment for ulceration in infantile hemangiomas: a study of 20 cases with matched historical controls. J Am Acad Dermatol. 2011;64:833–8.
173. Saint-Jean M, Léauté-Labrèze C, Mazereeuw-Hautier J, Bodak N, Hamel-Teillac D, Kupfer-Bessaguet I, et al. Propranolol for treatment of ulcerated infantile hemangiomas. J Am Acad Dermatol. 2011;64:827–32.
174. Caussé S, Aubert H, Saint-Jean M, Puzenat E, Bursztejn AC, Eschard C, et al. Propranolol-resistant infantile haemangiomas. Br J Dermatol. 2013;169:125–9.
175. Vassallo P, Forte R, Di Mezza A, Magli A. Treatment of infantile capillary hemangioma of the eyelid with systemic propranolol. Am J Ophthalmol. 2013;155(165–70):e2.
176. Lynch M, Lenane P, O'Donnell BF. Propranolol for the treatment of infantile haemangiomas: our experience with 44 patients. Clin Exp Dermatol. 2014;39:142–5.
177. Price CJ, Lattouf C, Baum B, McLeod M, Schachner LA, Duarte AM, et al. Propranolol vs corticosteroids for infantile hemangiomas: a multicenter retrospective analysis. Arch Dermatol. 2011;147:1371–6.
178. Hermans DJ, Bauland CG, Zweegers J, van Beynum IM, van der Vleuten CJ. Propranolol in a case series of 174 patients with complicated infantile haemangioma: indications, safety and future directions. Br J Dermatol. 2013;168:837–43.
179. de Graaf M, Breur J, Raphael MF, Vos M, Breugem CC, Pasmans S. Adverse effects of propranolol when used in the treatment of hemangiomas: a case series of 28 infants. J Am Acad Dermatol. 2011;65:320–7.
180. Hogeling M, Adams S, Wargon O. A randomized controlled trial of propranolol for infantile hemangiomas. Pediatrics. 2011;128:e259–66.
181. Zaher H, Rasheed H, Esmat S, Hegazy RA, Gawdat HI, Hegazy RA, et al. Propranolol and infantile hemangiomas: different routes of administration, a randomized clinical trial. Eur J Dermatol. 2013;23:646–52.
182. Malik MA, Menon P, Rao KL, Samujh R. Effect of propranolol vs prednisolone vs propranolol with prednisolone in the management of infantile hemangioma: a randomized controlled study. J Pediatr Surg. 2013;48:2453–9.
183. Bauman NM, McCarter RJ, Guzzetta PC, Shin JJ, Oh AK, Preciado DA, et al. Propranolol vs prednisolone for symptomatic proliferating infantile hemangiomas: a randomized clinical trial. JAMA Otolaryngol Head Neck Surg. 2014;140:323–30.
184. Léauté-Labrèze C, Dumas de la Roque E, Nacka F, Abouelfath A, Grenier N, Rebola M, et al. Double-blind randomized pilot trial evaluating the efficacy of oral propranolol on infantile haemangiomas in infants < 4 months of age. Br J Dermatol. 2013;169:181–3.
185. Abarzúa-Araya A, Navarrete-Dechent CP, Heusser F, Retamal J, Zegpi-Trueba MS. Atenolol versus propranolol for the treatment of infantile hemangiomas: a randomized controlled study. J Am Acad Dermatol. 2014;70:1045–9.
186. Ehsani AH, Noormohammadpoor P, Abdolreza M, Balighi K, Arianian Z, Daklan S. Combination therapy of infantile hemangioma with pulsed dye laser with topical propranolol: a randomized clinical trial. Arch Iran Med. 2014;17:657–60.
187. Léauté-Labrèze C, Hoeger P, Mazereeuw-Hautier J, Guibaud L, Baselga E, Posiunas G, et al. A randomized, controlled trial of oral propranolol in infantile hemangioma. N Engl J Med. 2015;372:735–46.
188. Menezes MD, McCarter R, Greene EA, Bauman NM. Status of propranolol for treatment of infantile hemangioma and description of a randomized clinical trial. Ann Otol Rhinol Laryngol. 2011;120:686–95.
189. Marqueling AL, Oza V, Frieden IJ, Puttgen KB. Propranolol and infantile hemangiomas four years later: a systematic review. Pediatr Dermatol. 2013;30:182–91.
190. Xu SQ, Jia RB, Zhang W, Zhu H, Ge SF, Fan XQ. Beta-blockers versus corticosteroids in the treatment of infantile hemangioma: an evidence-based systematic review. World J Pediatr. 2013;9:221–9.
191. Izadpanah A, Izadpanah A, Kanevsky J, Belzile E, Schwarz K. Propranolol versus corticosteroids in the treatment of infantile hemangioma: a systematic review and meta-analysis. Plast Reconstr Surg. 2013;131:601–13.
192. Xu S, Jia R, Ge S, Lin M, Fan X. Treatment of periorbital infantile haemangiomas: a systematic literature review on propranolol or steroids. J Paediatr Child Health. 2014;50:271–9.
193. Peridis S, Pilgrim G, Athanasopoulos I, Parpounas K. A meta-analysis on the effectiveness of propranolol for the treatment of infantile airway haemangiomas. Int J Pediatr Otorhinolaryngol. 2011;75:455–60.
194. Vlastarakos PV, Papacharalampous GX, Chrysostomou M, Tavoulari EF, Delidis A, Protopapas D, et al. Propranolol is an effective treatment for airway haemangiomas: a critical analysis and meta-analysis of published interventional studies. Acta Otorhinolaryngol Ital. 2012;32:213–21.
195. Storch CH, Hoeger PH. Propranolol for infantile haemangiomas: insights into the molecular mechanisms of action. Br J Dermatol. 2010;163:269–74.
196. Drolet BA, Frommelt PC, Chamlin SL, Haggstrom A, Bauman NM, Chiu YE, et al. Initiation and use of propranolol for infantile hemangioma: report of a consensus conference. Pediatrics. 2013;131:128–40.
197. Kum JJ, Khan ZA. Mechanisms of propranolol action in infantile hemangioma. Dermatoendocrinology. 2014;6:e979699.
198. Horev A, Haim A, Zvulunov A. Propranolol induced hypoglycemia. Pediatr Endocrinol Rev. 2015;12:308–10.
199. Blei F, McElhinney DB, Guarini A, Presti S. Cardiac screening in infants with infantile hemangiomas before propranolol treatment. Pediatr Dermatol. 2014;31:465–70.
200. Raphael MF, Breugem CC, Vlasveld FA, de Graaf M, Slieker MG, Pasmans SG, et al. Is cardiovascular evaluation necessary prior to and during beta-blocker therapy for infantile hemangiomas?: a cohort study. J Am Acad Dermatol. 2015;72:465–72.

201. Chamlin SL, Haggstrom AN, Drolet BA, Baselga E, Frieden IJ, Garzon MC, et al. Multicenter prospective study of ulcerated hemangiomas. J Pediatr. 2007;151:684–9 (**9 e1**).
202. Vercellino N, Romanini MV, Pelegrini M, Rimini A, Occella C, Dalmonte P. The use of propranolol for complicated infantile hemangiomas. Int J Dermatol. 2013;52:1140–6.
203. Sadykov RR, Podmelle F, Sadykov RA, Kasimova KR, Metellmann HR. Use of propranolol for the treatment infantile hemangiomas in the maxillofacial region. Int J Oral Maxillofac Surg. 2013;42:863–7.
204. Kim HJ, Colombo M, Frieden IJ. Ulcerated hemangiomas: clinical characteristics and response to therapy. J Am Acad Dermatol. 2001;44:962–72.
205. Wananukul S, Chatproedprai S. Ulcerated hemangiomas: clinical features and management. J Med Assoc Thai. 2002;85:1220–5.
206. Pandey A, Gangopadhyay AN, Sharma SP, Kumar V, Gopal SC, Gupta DK. Conservative management of ulcerated haemangioma—twenty years experience. Int Wound J. 2009;6:59–62.
207. Oranje AP, de Waard-van der Spek FB, Devillers AC, de Laat PC, Madern GC. Treatment and pain relief of ulcerative hemangiomas with a polyurethane film. Dermatology. 2000;200:31–4.
208. Bauland CG, Smit JM, Ketelaars R, Rieu PN, Spauwen PH. Management of haemangiomas of infancy: a retrospective analysis and a treatment protocol. Scand J Plast Reconstr Surg Hand Surg. 2008;42:86–91.
209. Morelli JG, Tan OT, Yohn JJ, Weston WL. Treatment of ulcerated hemangiomas infancy. Arch Pediatr Adolesc Med. 1994;148:1104–5.
210. Lacour M, Syed S, Linward J, Harper JI. Role of the pulsed dye laser in the management of ulcerated capillary haemangiomas. Arch Dis Child. 1996;74:161–3.
211. David LR, Malek MM, Argenta LC. Efficacy of pulse dye laser therapy for the treatment of ulcerated haemangiomas: a review of 78 patients. Br J Plast Surg. 2003;56:317–27.
212. Michel JL. Treatment of hemangiomas with 595 nm pulsed dye laser dermobeam. Eur J Dermatol. 2003;13:136–41.
213. Di Maio L, Baldi A, Dimaio V, Barzi A. Use of flashlamp-pumped pulsed dye laser in the treatment of superficial vascular malformations and ulcerated hemangiomas. In Vivo. 2011;25:117–23.
214. Sugarman JL, Mauro TM, Frieden IJ. Treatment of an ulcerated hemangioma with recombinant platelet-derived growth factor. Arch Dermatol. 2002;138:314–6.
215. Metz BJ, Rubenstein MC, Levy ML, Metry DW. Response of ulcerated perineal hemangiomas of infancy to becaplermin gel, a recombinant human platelet-derived growth factor. Arch Dermatol. 2004;140:867–70.
216. Jalil S, Akhtar J, Ahmed S. Corticosteroids therapy in the management of infantile cutaneous hemangiomas. J Coll Physicians Surg Pak. 2006;16:662–5.
217. Gangopadhyay AN, Sinha CK, Gopal SC, Gupta DK, Sahoo SP, Ahmad M. Role of steroid in childhood haemangioma: a 10 years review. Int Surg. 1997;82:49–51.
218. Pandey A, Gangopadhyay AN, Gopal SC, Kumar V, Sharma SP, Gupta DK, et al. Twenty years' experience of steroids in infantile hemangioma—a developing country's perspective. J Pediatr Surg. 2009;44:688–94.
219. Tan BH, Leadbitter PH, Aburn NH, Tan ST. Steroid therapy for problematic proliferating haemangioma. N Z Med J. 2011;124:57–65.
220. Ruttum MS, Abrams GW, Harris GJ, Ellis MK. Bilateral retinal embolization associated with intralesional corticosteroid injection for capillary hemangioma of infancy. J Pediatr Ophthalmol Strabismus. 1993;30:4–7.
221. Egbert JE, Schwartz GS, Walsh AW. Diagnosis and treatment of an ophthalmic artery occlusion during an intralesional injection of corticosteroid into an eyelid capillary hemangioma. Am J Ophthalmol. 1996;121:638–42.
222. Craiglow BG, Antaya RJ. Management of infantile hemangiomas: current and potential pharmacotherapeutic approaches. Paediatr Drugs. 2013;15:133–8.
223. Ni N, Langer P, Wagner R, Guo S. Topical timolol for periocular hemangioma: report of further study. Arch Ophthalmol. 2011;129:377–9.
224. Elsas FJ, Lewis AR. Topical treatment of periocular capillary hemangioma. J Pediatr Ophthalmol Strabismus. 1994;31:153–6.
225. Lapidoth M, Ben-Amitai D, Bhandarkar S, Fried L, Arbiser JL. Efficacy of topical application of eosin for ulcerated hemangiomas. J Am Acad Dermatol. 2009;60:350–1.
226. Barry RB, Hughes BR, Cook LJ. Involution of infantile haemangiomas after imiquimod 5% cream. Clin Exp Dermatol. 2008;33:446–9.
227. Ho NT, Lansang P, Pope E. Topical imiquimod in the treatment of infantile hemangiomas: a retrospective study. J Am Acad Dermatol. 2007;56:63–8.
228. Jiang C, Hu X, Ma G, Chen D, Jin Y, Chen H, et al. A prospective self-controlled phase II study of imiquimod 5% cream in the treatment of infantile hemangioma. Pediatr Dermatol. 2011;28:259–66.
229. Mao XH, Wang JY, Yan JL. Topical imiquimod treatment of cutaneous vascular disorders in pediatric patients: clinical evaluation on the efficacy and safety. J Zhejiang Univ Sci B. 2012;13:745–50.
230. McCuaig CC, Dubois J, Powell J, Belleville C, David M, Rousseau E, et al. A phase II, open-label study of the efficacy and safety of imiquimod in the treatment of superficial and mixed infantile hemangioma. Pediatr Dermatol. 2009;26:203–12.
231. Qiu Y, Ma G, Lin X, Jin Y, Chen H, Hu X. Treating protruding infantile hemangiomas with topical imiquimod 5% cream caused severe local reactions and disfiguring scars. Pediatr Dermatol. 2013;30:342–7.
232. Qiu Y, Ma G, Yang J, Hu X, Chen H, Jin Y, et al. Imiquimod 5% cream versus timolol 0.5% ophthalmic solution for treating superficial proliferating infantile haemangiomas: a retrospective study. Clin Exp Dermatol. 2013;38:845–50.
233. Welsh O, Olazaran Z, Gomez M, Salas J, Berman B. Treatment of infantile hemangiomas with short-term application of imiquimod 5% cream. J Am Acad Dermatol. 2004;51:639–42.
234. Blatt J, Morrell DS, Buck S, Zdanski C, Gold S, Stavas J, et al. β-blockers for infantile hemangiomas: a single-institution experience. Clin Pediatr (Phila). 2011;50:757–63.
235. Cante V, Pham-Ledard A, Imbert E, Ezzedine K, Léauté-Labrèze C. First report of topical timolol treatment in primarily ulcerated perineal haemangioma. Arch Dis Child Fetal Neonatal Ed. 2012;97:F155–6.
236. Chakkittakandiyil A, Phillips R, Frieden IJ, Siegfried E, Lara-Corrales I, Lam J, et al. Timolol maleate 0.5% or 0.1% gel-forming solution for infantile hemangiomas: a retrospective, multicenter, cohort study. Pediatr Dermatol. 2012;29:28–31.
237. Chambers CB, Katowitz WR, Katowitz JA, Binenbaum G. A controlled study of topical 0.25% timolol maleate gel for the treatment of cutaneous infantile capillary hemangiomas. Ophthalmic Plast Reconstr Surg. 2012;28:103–6.
238. Khunger N, Pahwa M. Dramatic response to topical timolol lotion of a large hemifacial infantile haemangioma associated with PHACE syndrome. Br J Dermatol. 2011;164:886–8.
239. Ma G, Wu P, Lin X, Chen H, Hu X, Jin Y, et al. Fractional carbon dioxide laser-assisted drug delivery of topical timolol solution for the treatment of deep infantile hemangioma: a pilot study. Pediatr Dermatol. 2014;31:286–91.

240. Moehrle M, Léauté-Labrèze C, Schmidt V, Röcken M, Poets CF, Goelz R. Topical timolol for small hemangiomas of infancy. Pediatr Dermatol. 2013;30:245–9.
241. Ni N, Guo S, Langer P. Current concepts in the management of periocular infantile (capillary) hemangioma. Curr Opin Ophthalmol. 2011;22:419–25.
242. Oranje AP, Janmohamed SR, Madern GC, de Laat PC. Treatment of small superficial haemangioma with timolol 0.5% ophthalmic solution: a series of 20 cases. Dermatology. 2011;223:330–4.
243. Pope E, Chakkittakandiyil A. Topical timolol gel for infantile hemangiomas: a pilot study. Arch Dermatol. 2010;146:564–5.
244. Kunzi-Rapp K. Topical propranolol therapy for infantile hemangiomas. Pediatr Dermatol. 2012;29:154–9.
245. Xu G, Lv R, Zhao Z, Huo R. Topical propranolol for treatment of superficial infantile hemangiomas. J Am Acad Dermatol. 2012;67:1210–3.
246. Garzon MC, Lucky AW, Hawrot A, Frieden IJ. Ultrapotent topical corticosteroid treatment of hemangiomas of infancy. J Am Acad Dermatol. 2005;52:281–6.
247. Pandey A, Gangopadhyay AN, Sharma SP, Kumar V, Gupta DK, Gopal SC. Evaluation of topical steroids in the treatment of superficial hemangioma. Skinmed. 2010;8:9–11.
248. Kaplan M, Paller AS. Clinical pearl: use of self-adhesive, compressive wraps in the treatment of limb hemangiomas. J Am Acad Dermatol. 1995;32:117–8.
249. Ochi G, Ohkawa H, Kaneko M, Hori T, Shinoda M, Kojima M, et al. Compression therapy and cryosurgery for hemangiomas in childhood. Shoni Geka. 1992;24:539–47 **(Japanese)**.
250. Totsuka Y, Fukuda H, Tomita K. Compression therapy for parotid haemangioma in infants. A report of three cases. J Craniomaxillofac Surg. 1988;16:366–70.
251. Osaki TH, Jakobiec FA, Mendoza PR, Lee Y, Fay AM. Immunohistochemical investigations of orbital infantile hemangiomas and adult encapsulated cavernous venous lesions (malformation versus hemangioma). Ophthalmic Plast Reconstr Surg. 2013;29:183–95.
252. Laing EL, Brasch HD, Steel R, Jia J, Itinteang T, Tan ST, et al. Verrucous hemangioma expresses primitive markers. J Cutan Pathol. 2013;40:391–6.
253. North PE, Waner M, James CA, Mizeracki A, Frieden IJ, Mihm MC Jr. Congenital nonprogressive hemangioma: a distinct clinicopathologic entity unlike infantile hemangioma. Arch Dermatol. 2001;137:1607–20.
254. North PE, Waner M, Mizeracki A, Mihm MC Jr. GLUT1: a newly discovered immunohistochemical marker for juvenile hemangiomas. Hum Pathol. 2000;31:11–22.
255. North PE, Waner M, Mizeracki A, Mrak RE, Nicholas R, Kincannon J, et al. A unique microvascular phenotype shared by juvenile hemangiomas and human placenta. Arch Dermatol. 2001;137:559–70.
256. Leon-Villapalos J, Wolfe K, Kangesu L. GLUT-1: an extra diagnostic tool to differentiate between haemangiomas and vascular malformations. Br J Plast Surg. 2005;58:348–52.
257. Ahrens WA, Ridenour RV 3rd, Caron BL, Miller DV, Folpe AL. GLUT-1 expression in mesenchymal tumors: an immunohistochemical study of 247 soft tissue and bone neoplasms. Hum Pathol. 2008;39:1519–26.
258. Trindade F, Kutzner H, Requena L, Tellechea O, Colmenero I. Microvenular hemangioma—an immunohistochemical study of 9 cases. Am J Dermatopathol. 2012;34:810–2.
259. Sadeghpour M, Antaya RJ, Lazova R, Ko CJ. Dilated lymphatic vessels in tufted angioma: a potential source of diagnostic confusion. Am J Dermatopathol. 2012;34:400–3.
260. Drut RM, Drut R. Extracutaneous infantile haemangioma is also Glut1 positive. J Clin Pathol. 2004;57:1197–200.
261. Lyons LL, North PE, Mac-Moune Lai F, Stoler MH, Folpe AL, Weiss SW. Kaposiform hemangioendothelioma: a study of 33 cases emphasizing its pathologic, immunophenotypic, and biologic uniqueness from juvenile hemangioma. Am J Surg Pathol. 2004;28:559–68.
262. Al-Adnani M, Williams S, Rampling D, Ashworth M, Malone M, Sebire NJ. Histopathological reporting of paediatric cutaneous vascular anomalies in relation to proposed multidisciplinary classification system. J Clin Pathol. 2006;59:1278–82.
263. Badi AN, Kerschner JE, North PE, Drolet BA, Messner A, Perkins JA. Histopathologic and immunophenotypic profile of subglottic hemangioma: multicenter study. Int J Pediatr Otorhinolaryngol. 2009;73:1187–91.
264. Hernandez F, Navarro M, Encinas JL, Lopez Gutierrez JC, Lopez Santamaria M, Leal N, et al. The role of GLUT1 immunostaining in the diagnosis and classification of liver vascular tumors in children. J Pediatr Surg. 2005;40:801–4.
265. Mo JQ, Dimashkieh HH, Bove KE. GLUT1 endothelial reactivity distinguishes hepatic infantile hemangioma from congenital hepatic vascular malformation with associated capillary proliferation. Hum Pathol. 2004;35:200–9.
266. Das KJ, Sharma P, Naswa N, Soundararajan R, Kumar R, Bal C, et al. Hybrid SPECT-CT with 99 mTc-labeled red blood cell in a case of blue rubber bleb nevus syndrome: added value over planar scintigraphy. Diagn Interv Radiol. 2013;19:41–3.
267. Senturk S, Bilici A, Miroglu TC, Bilek SU. Blue rubber bleb nevus syndrome: imaging of small bowel lesions with peroral CT enterography. Abdom Imaging. 2011;36:520–3.
268. Thomson M, Venkatesh K, Elmalik K, van der Veer W, Jaacobs M. Double balloon enteroscopy in children: diagnosis, treatment, and safety. World J Gastroenterol. 2010;16:56–62.
269. Agnese M, Cipolletta L, Bianco MA, Quitadamo P, Miele E, Staiano A. Blue rubber bleb nevus syndrome. Acta Paediatr. 2010;99:632–5.
270. Hansen LF, Wewer V, Pedersen SA, Matzen P, Paerregaard A. Severe blue rubber bleb nevus syndrome in a neonate. Eur J Pediatr Surg. 2009;19:47–9.
271. Yarlagadda R, Menda Y, Graham MM. Tc-99m red blood cell imaging in a patient with blue rubber bleb nevus syndrome. Clin Nucl Med. 2008;33:374–6.
272. Mechri M, Soyer P, Boudiaf M, Duchat F, Hamzi L, Rymer R. Small bowel involvement in blue rubber bleb nevus syndrome: MR imaging features. Abdom Imaging. 2009;34:448–51.
273. Certo M, Lopes L, Ramada J. Blue rubber bleb nevus syndrome: manifestations at computed tomography. Acta Radiol. 2007;48:962–6.
274. Kopacova M, Tacheci I, Koudelka J, Kralova M, Rejchrt S, Bures J. A new approach to blue rubber bleb nevus syndrome: the role of capsule endoscopy and intra-operative enteroscopy. Pediatr Surg Int. 2007;23:693–7.
275. De Bona M, Bellumat A, De Boni M. Capsule endoscopy for the diagnosis and follow-up of blue rubber bleb nevus syndrome. Dig Liver Dis. 2005;37:451–3.
276. Place RJ. Blue rubber bleb nevus syndrome: a case report with long-term follow-up. Mil Med. 2001;166:728–30.
277. Jacob AG, Driscoll DJ, Shaughnessy WJ, Stanson AW, Clay RP, Gloviczki P. Klippel-Trenaunay syndrome: spectrum and management. Mayo Clin Proc. 1998;73:28–36.
278. Capraro PA, Fisher J, Hammond DC, Grossman JA. Klippel-Trenaunay syndrome. Plast Reconstr Surg. 2002;109:2052–60 **(quiz 61–2)**.
279. Meine JG, Schwartz RA, Janniger CK. Klippel-Trenaunay-Weber syndrome. Cutis. 1997;60:127–32.
280. Redondo P, Aguado L, Martinez-Cuesta A. Diagnosis and management of extensive vascular malformations of the lower

limb: part II Systemic repercussions [corrected], diagnosis, and treatment. J Am Acad Dermatol. 2011;65:909–23 **(quiz 24)**.
281. Gloviczki P, Hollier LH, Telander RL, Kaufman B, Bianco AJ, Stickler GB. Surgical implications of Klippel-Trenaunay syndrome. Ann Surg. 1983;197:353–62.
282. McGrory BJ, Amadio PC. Klippel-Trenaunay syndrome: orthopaedic considerations. Orthop Rev. 1993;22:41–50.
283. Takata M, Watanabe K, Matsubara H, Takato K, Nomura I, Tsuchiya H. Lengthening of the normal tibia in a patient with hemihypertrophy caused by Klippel-Trenaunay-Weber syndrome: a case report. J Orthop Surg (Hong Kong). 2011;19:359–63.
284. Servelle M. Klippel and Trenaunay's syndrome. 768 operated cases. Ann Surg. 1985;201:365–73.
285. Gates PE, Drvaric DM, Kruger L. Wound healing in orthopaedic procedures for Klippel-Trenaunay syndrome. J Pediatr Orthop. 1996;16:723–6.
286. Bajaj Y, Hewitt R, Ifeacho S, Hartley BE. Surgical excision as primary treatment modality for extensive cervicofacial lymphatic malformations in children. Int J Pediatr Otorhinolaryngol. 2011;75:673–7.
287. Orvidas LJ, Kasperbauer JL. Pediatric lymphangiomas of the head and neck. Ann Otol Rhinol Laryngol. 2000;109:411–21.
288. Alqahtani A, Nguyen LT, Flageole H, Shaw K, Laberge JM. 25 years' experience with lymphangiomas in children. J Pediatr Surg. 1999;34:1164–8.
289. Wiegand S, Zimmermann AP, Eivazi B, Sesterhenn AM, Werner JA. Lymphatic malformations involving the parotid gland. Eur J Pediatr Surg. 2011;21:242–5.
290. Chen WL, Zhang B, Wang JG, Ye HS, Zhang DM, Huang ZQ. Surgical excision of cervicofacial giant macrocystic lymphatic malformations in infants and children. Int J Pediatr Otorhinolaryngol. 2009;73:833–7.
291. Lei ZM, Huang XX, Sun ZJ, Zhang WF, Zhao YF. Surgery of lymphatic malformations in oral and cervicofacial regions in children. Oral Surg Oral Med Oral Pathol Oral Radiol Endod. 2007;104:338–44.
292. Okazaki T, Iwatani S, Yanai T, Kobayashi H, Kato Y, Marusasa T, et al. Treatment of lymphangioma in children: our experience of 128 cases. J Pediatr Surg. 2007;42:386–9.
293. Hamoir M, Plouin-Gaudon I, Rombaux P, Francois G, Cornu AS, Desuter G, et al. Lymphatic malformations of the head and neck: a retrospective review and a support for staging. Head Neck. 2001;23:326–37.
294. Fageeh N, Manoukian J, Tewfik T, Schloss M, Williams HB, Gaskin D. Management of head and neck lymphatic malformations in children. J Otolaryngol. 1997;26:253–8.
295. Padwa BL, Hayward PG, Ferraro NF, Mulliken JB. Cervicofacial lymphatic malformation: clinical course, surgical intervention, and pathogenesis of skeletal hypertrophy. Plast Reconstr Surg. 1995;95:951–60.
296. de Serres LM, Sie KC, Richardson MA. Lymphatic malformations of the head and neck. A proposal for staging. Arch Otolaryngol Head Neck Surg. 1995;121:577–82.
297. Riechelmann H, Muehlfay G, Keck T, Mattfeldt T, Rettinger G. Total, subtotal, and partial surgical removal of cervicofacial lymphangiomas. Arch Otolaryngol Head Neck Surg. 1999;125:643–8.
298. Greinwald J Jr, Cohen AP, Hemanackah S, Azizkhan RG. Massive lymphatic malformations of the head, neck, and chest. J Otolaryngol Head Neck Surg. 2008;37:169–73.
299. Yang Y, Sun M, Ma Q, Cheng X, Ao J, Tian L, et al. Bleomycin A5 sclerotherapy for cervicofacial lymphatic malformations. J Vasc Surg. 2011;53:150–5.
300. Alomari AI, Karian VE, Lord DJ, Padua HM, Burrows PE. Percutaneous sclerotherapy for lymphatic malformations: a retrospective analysis of patient-evaluated improvement. J Vasc Interv Radiol. 2006;17:1639–48.
301. Chaudry G, Guevara CJ, Rialon KL, Kerr C, Mulliken JB, Greene AK, et al. Safety and efficacy of bleomycin sclerotherapy for microcystic lymphatic malformation. Cardiovasc Intervent Radiol. 2014;37:1476–81.
302. Smith MC, Zimmerman MB, Burke DK, Bauman NM, Sato Y, Smith RJ, et al. Efficacy and safety of OK-432 immunotherapy of lymphatic malformations. Laryngoscope. 2009;119:107–15.
303. Giguère CM, Bauman NM, Sato Y, Burke DK, Greinwald JH, Pransky S, et al. Treatment of lymphangiomas with OK-432 (Picibanil) sclerotherapy: a prospective multi-institutional trial. Arch Otolaryngol Head Neck Surg. 2002;128:1137–44.
304. Udagawa A, Yoshimoto S, Matumoto F, Ishii K, Nakajima Y, Hasegawa M, et al. A case of facial cavernous lymphangioma: observation from infancy to adulthood. Nihon Togai Gaku Ganmen Geka Gakkaishi. 2005;21:302–9.
305. Nagao M, Sasaki S, Furukawa H, Uchiyama E, Yamamoto Y. Treatments for huge lymphatic malformations of cheek, oral cavity and neck. Nihon Keisei Geka Gakkai Kaishi. 2007;27:779–82 **(Japanese)**.
306. Ravindranathan H, Gillis J, Lord DJ. Intensive care experience with sclerotherapy for cervicofacial lymphatic malformations. Pediatr Crit Care Med. 2008;9:304–9.
307. Poonyathalang A, Preechawat P, Jiarakongmun P, Pongpech S. Sclerosing therapy for orbital lymphangioma using sodium tetradecyl sulfate. Jpn J Ophthalmol. 2008;52:298–304.
308. Emran MA, Dubois J, Laberge L, Al-Jazaeri A, Butter A, Yazbeck S. Alcoholic solution of zein (Ethibloc) sclerotherapy for treatment of lymphangiomas in children. J Pediatr Surg. 2006;41:975–9.
309. Bai Y, Jia J, Huang XX, Alsharif MJ, Zhao JH, Zhao YF. Sclerotherapy of microcystic lymphatic malformations in oral and facial regions. J Oral Maxillofac Surg. 2009;67:251–6.
310. Shiels WE 2nd, Kang DR, Murakami JW, Hogan MJ, Wiet GJ. Percutaneous treatment of lymphatic malformations. Otolaryngol Head Neck Surg. 2009;141:219–24.
311. Nehra D, Jacobson L, Barnes P, Mallory B, Albanese CT, Sylvester KG. Doxycycline sclerotherapy as primary treatment of head and neck lymphatic malformations in children. J Pediatr Surg. 2008;43:451–60.
312. Asonuma K, Inomata Y. Current strategy and outcome of treatment of lymphangioma in children: the analysis of a survey in the Kyushu and Okinawa area. Nihon Shoni Geka Gakkai Zasshi. 2006;42:215–21 **(Japanese)**.
313. Schwarcz RM, Ben Simon GJ, Cook T, Goldberg RA. Sclerosing therapy as first line treatment for low flow vascular lesions of the orbit. Am J Ophthalmol. 2006;141:333–9.
314. Oyama T, Eguchi K, Cho H, Abe H. A variety of orbital lymphangioma treatments: one case treated with orbital decompression therapy and the other case with intralesional injection of OK-432 therapy. Nihon Ganka Gakkai Zasshi. 2009;113:732–40 **(Japanese)**.
315. Cahill AM, Nijs E, Ballah D, Rabinowitz D, Thompson L, Rintoul N, et al. Percutaneous sclerotherapy in neonatal and infant head and neck lymphatic malformations: a single center experience. J Pediatr Surg. 2011;46:2083–95.
316. Chaudry G, Burrows PE, Padua HM, Dillon BJ, Fishman SJ, Alomari AI. Sclerotherapy of abdominal lymphatic malformations with doxycycline. J Vasc Interv Radiol. 2011;22:1431–5.
317. Oliveira C, Sacher P, Meuli M. Management of prenatally diagnosed abdominal lymphatic malformations. Eur J Pediatr Surg. 2010;20:302–6.
318. Won JH, Kim BM, Kim CH, Park SW, Kim MD. Percutaneous sclerotherapy of lymphangiomas with acetic acid. J Vasc Interv Radiol. 2004;15:595–600.

319. Shiels WE 2nd, Kenney BD, Caniano DA, Besner GE. Definitive percutaneous treatment of lymphatic malformations of the trunk and extremities. J Pediatr Surg. 2008;43:136–9 **(discussion 40)**.
320. Chiappinelli A, Forgues D, Galifer RB. Congenital abdominal cystic lymphangiomas: what is the correct management? J Matern Fetal Neonatal Med. 2012;25:915–9.
321. Muraoka A, Suzuki N, Niwa Y, Komatsu Y, Tagami K. A case report of an asymptomatic giant retroperitoneal lymphangioma pointed out at a physical examination. Nihon Rinsho Geka Gakkai Zasshi. 2009;70:899–905 **(Japanese)**.
322. Oyachi N, Iwashita K, Kubo M. Diagnosis and management of mesenteric lymphangioma: comparison of prenatal and school-age diagnosed cases. Nihon Shoni Geka Gakkai Zasshi. 2008;44:33–7 **(Japanese)**.
323. Mendez-Gallart R, Bautista A, Estevez E, Rodriguez-Barca P. Abdominal cystic lymphangiomas in pediatrics: surgical approach and outcomes. Acta Chir Belg. 2011;111:374–7.
324. Ikeda T, Asai Y, Nango Y, Hoshino M, Ohashi K, Inoue M, et al. Childhood abdominal cystic lymphangioma. Nihon Shoni Geka Gakkai Zasshi. 2008;44:959–64 **(Japanese)**.
325. Losanoff JE, Kjossev KT. Mesenteric cystic lymphangioma: unusual cause of intra-abdominal catastrophe in an adult. Int J Clin Pract. 2005;59:986–7.
326. Uchiyama M, Murata H, Ohtaki M. Acute abdomen by inflammatory infiltration of retroperitoneal lymphangioma to the duodenum: report of a case and review of cases in childhood. Nihon Shoni Geka Gakkai Zasshi. 2007;43:938–44 **(Japanese)**.
327. Bellini C, Ergaz Z, Radicioni M, Forner-Cordero I, Witte M, Perotti G, et al. Congenital fetal and neonatal visceral chylous effusions: neonatal chylothorax and chylous ascites revisited. A multicenter retrospective study. Lymphology. 2012;45:91–102.
328. Matsuo Y, Okada A. The role and use of Sudan Black in the surgical treatment of chylothorax and chylous ascites. Shoni Geka. 2001;33:186–90 **(Japanese)**.
329. Spagnol L, Conforti A, Valfre L, Morini F, Bagolan P. Preoperative administration of Sudan III and successful treatment of persistent chylous ascites in a neonate. J Pediatr Surg. 2011;46:994–7.
330. Joe K, Kemmotsu H, Mori T, Goto C, Ohkawa H. Treatment of idiopathic chylous ascites in infants. Shoni Geka. 2001;33:134–40 **(Japanese)**.
331. Moreira Dde A, Santos MM, Tannuri AC, Tannuri U. Congenital chylous ascites: a report of a case treated with hemostatic cellulose and fibrin glue. J Pediatr Surg. 2013;48:e17–9.
332. Olivieri C, Nanni L, Masini L, Pintus C. Successful management of congenital chylous ascites with early octreotide and total parenteral nutrition in a newborn. BMJ Case Rep. 2012;2012:bcr2012006196.
333. Huang Y, Zhuang S, Li Y, Liu M, Chen H, Du M. Successful management of congenital chylous ascites in a premature infant using somatostatin analogue. Indian J Pediatr. 2011;78:345–7.
334. Melo-Filho AA, Souza IJ, Leite CA, Leite RD, Colares JH, Correia JM. Refractory congenital chylous ascites. Indian J Pediatr. 2010;77:1335–7.
335. Karagol BS, Zenciroglu A, Gokce S, Kundak AA, Ipek MS. Therapeutic management of neonatal chylous ascites: report of a case and review of the literature. Acta Paediatr. 2010;99:1307–10.
336. Kuroiwa M, Toki F, Suzuki M, Suzuki N. Successful laparoscopic ligation of the lymphatic trunk for refractory chylous ascites. J Pediatr Surg. 2007;42:E15–8.
337. Antao B, Croaker D, Squire R. Successful management of congenital chyloperitoneum with fibrin glue. J Pediatr Surg. 2003;38:E7–8.
338. Nakagawa J, Nakabayashi M, Kikuchi M, Sato C, Kido M, Kasai Y, et al. A case of congenital chyloperitoneum improved by prenatal treatment. Nihon Sanka Fujinka Gakkai Tokyo Chiho Bukai Kaishi. 2002;51:399–403 **(Japanese)**.
339. Wakisaka M, Kitagawa H, Satoh Y, Nakada K. Congenital chyloascites treated by laparotomy and OK-432 injection. Shoni Geka. 2001;33:196–200 **(Japanese)**.
340. Sato H, Okamatsu T, Yatsuzuka M, Gomi A, Suzuki J, Suzuki K, et al. Chylous ascites resolved by exploratory laparotomy. Shoni Geka. 2001;33:191–5 **(Japanese)**.
341. Takahashi A, Suzuki N, Kuwano H. Neonatal chylous ascites. Shoni Geka. 2001;33:144–7 **(Japanese)**.
342. Komuro H. Endoscopic surgery for chylothorax and chylous ascites. Shoni Geka. 2010;42:805–8 **(Japanese)**.
343. Zeidan S, Delarue A, Rome A, Roquelaure B. Fibrin glue application in the management of refractory chylous ascites in children. J Pediatr Gastroenterol Nutr. 2008;46:478–81.
344. Huang Q, Jiang ZW, Jiang J, Li N, Li JS. Chylous ascites: treated with total parenteral nutrition and somatostatin. World J Gastroenterol. 2004;10:2588–91.
345. Nemoto T, Tsuchiya H, Nagashima K. Clinical and experimental analysis for chylothorax and chylous ascites. Shoni Geka. 2001;33:119–22 **(Japanese)**.
346. Ohtsu K, Ueda Y, Kurihara S, Kawashima M. Intractable chylous ascites. Shoni Geka. 2011;43:747–50 **(Japanese)**.
347. Ono S, Iwai N, Chiba F, Furukawa T, Fumino S. OK-432 therapy for chylous pleural effusion or ascites associated with lymphatic malformations. J Pediatr Surg. 2010;45:e7–10.
348. Tanaka M, Yokomori K, Kamii Y. Chylous ascites caused by a retroperitoneal lymphangioma: a case report. Shoni Geka. 2001;33:163–7 **(Japanese)**.
349. Siebert S, Helbling C, Wolff M, Franz A, Müller A, Kau N, et al. Peritoneovenous shunting as palliative treatment in an infant with chylous ascites due to generalised congenital lymphangiectasia. Klin Padiatr. 2010;222:317–8.
350. Densupsoontorn N, Jirapinyo P, Aanpreung P, Laohapensang M, Parichatikanond P. Congenital chylous ascites: the roles of fibrin glue and CD31. Acta Paediatr. 2009;98:1847–9.
351. Guvenc BH, Ekingen G, Tuzlaci A, Senel U. Diffuse neonatal abdominal lymphangiomatosis: management by limited surgical excision and sclerotherapy. Pediatr Surg Int. 2005;21:595–8.
352. Kotera A, Kamagata S, Hirobe S, Shimono R, Fuchimoto Y, Sakuma T, et al. A case of diffuse lymphangiomatosis with chylothorax and chylous ascites. Shoni Geka. 2001;33:128–33 **(Japanese)**.
353. Horisawa M, Nishimoto K, Ogura Y, Tainaka T, Matsunaga K, Niinomi N. Generalized lymphatic dysplasia with intermittent chylous discharge from the scrotum: a case report. Shoni Geka. 2001;33:180–5 **(Japanese)**.
354. Katz MS, Finck CM, Schwartz MZ, Moront ML, Prasad R, Timmapuri SJ, et al. Vacuum-assisted closure in the treatment of extensive lymphangiomas in children. J Pediatr Surg. 2012;47:367–70.
355. Sugito K, Ikeda T, Hagiwara N, Goto H, Endo K, Tanaka M, et al. A case of large mesenteric cyst with inflammatry reaction. Shoni Geka. 2001;33:1017–20 **(Japanese)**.
356. Chang TS, Ricketts R, Abramowsky CR, Cotter BD, Steelman CK, Husain A, et al. Mesenteric cystic masses: a series of 21 pediatric cases and review of the literature. Fetal Pediatr Pathol. 2011;30:40–4.
357. Tran NS, Nguyen TL. Laparoscopic management of abdominal lymphatic cyst in children. J Laparoendosc Adv Surg Tech A. 2012;22:505–7.
358. Boardman SJ, Cochrane LA, Roebuck D, Elliott MJ, Hartley BE. Multimodality treatment of pediatric lymphatic malformations of the head and neck using surgery and sclerotherapy. Arch Otolaryngol Head Neck Surg. 2010;136:270–6.

359. Park JG, Aubry MC, Godfrey JA, Midthun DE. Mediastinal lymphangioma: Mayo Clinic experience of 25 cases. Mayo Clin Proc. 2006;81:1197–203.
360. Adams MT, Saltzman B, Perkins JA. Head and neck lymphatic malformation treatment: a systematic review. Otolaryngol Head Neck Surg. 2012;147:627–39.
361. Leung M, Leung L, Fung D, Poon WL, Liu C, Chung K, et al. Management of the low-flow head and neck vascular malformations in children: the sclerotherapy protocol. Eur J Pediatr Surg. 2014;24:97–101.
362. Ogawa T, Shibayama M, Shimizu T. Clinical analysis of lymphangioma in the neck: the effects of local OK-432 injection therapy. Jibi Inkoka Rinsho. 2010;103:249–55 **(Japanese)**.
363. Arimoto Y, Kudo F, Suzuki H. Usefulness of ultrasonography in the differential diagnosis of respiratory distress disorders including infantile paresis of the vocal cords. Shoni Jibi Inkoka. 2005;26:37–42 **(Japanese)**.
364. Kitagawa H, Kawase H, Wakisaka M, Satou Y, Satou H, Furuta S, et al. Six cases of children with a benign cervical tumor who required tracheostomy. Pediatr Surg Int. 2004;20:51–4.
365. Hiki S, Yamataka A, Kobayashi H, Okada Y, Miyano T. Treatment of lymphangioma in children. A report of 105 cases. Juntendo Igaku. 2003;48:476–83 **(Japanese)**.
366. Desir A, Ghaye B, Duysinx B, Dondelinger RF. Percutaneous sclerotherapy of a giant mediastinal lymphangioma. Eur Respir J. 2008;32:804–6.
367. Kim DW. OK-432 sclerotherapy of lymphatic malformation in the head and neck: factors related to outcome. Pediatr Radiol. 2014;44:857–62.
368. Niramis R, Watanatittan S, Rattanasuwan T. Treatment of cystic hygroma by intralesional bleomycin injection: experience in 70 patients. Eur J Pediatr Surg. 2010;20:178–82.
369. Kudo F, Arimoto Y, Nakano A. Sclerosing therapy for cystic hygroma in infants: intracystic injection of OK-432. Tokeibu Geka. 2008;18:71–5 **(Japanese)**.
370. Kim MG, Kim SG, Lee JH, Eun YG, Yeo SG. The therapeutic effect of OK-432 (picibanil) sclerotherapy for benign neck cysts. Laryngoscope. 2008;118:2177–81.
371. Baskota DK, Singh BB, Sinha BK. OK-432: an effective sclerosing agent for the treatment of lymphangiomas of head and neck. Kathmandu Univ Med J (KUMJ). 2007;5:312–7.
372. Jamal N, Ahmed S, Miller T, Bent J, Brook A, Parikh S, et al. Doxycycline sclerotherapy for pediatric head and neck macrocystic lymphatic malformations: a case series and review of the literature. Int J Pediatr Otorhinolaryngol. 2012;76:1127–31.
373. Tomemori T, Kudo F, Sasamura Y, Numata T. Cystic hygroma in infants. Tokeibu Shuyo. 2003;29:58–63 **(Japanese)**.
374. Dasgupta R, Adams D, Elluru R, Wentzel MS, Azizkhan RG. Noninterventional treatment of selected head and neck lymphatic malformations. J Pediatr Surg. 2008;43:869–73.
375. Hogeling M, Adams S, Law J, Wargon O. Lymphatic malformations: clinical course and management in 64 cases. Australas J Dermatol. 2011;52:186–90.
376. Acevedo JL, Shah RK, Brietzke SE. Nonsurgical therapies for lymphangiomas: a systematic review. Otolaryngol Head Neck Surg. 2008;138:418–24.
377. Kim KH, Sung MW, Roh JL, Han MH. Sclerotherapy for congenital lesions in the head and neck. Otolaryngol Head Neck Surg. 2004;131:307–16.
378. Catalfamo L, Nava C, Lombardo G, Iudicello V, Siniscalchi EN, de Saverio PF. Tongue lymphangioma in adult. J Craniofac Surg. 2012;23:1920–2.
379. Magoshi S, Okada M, Shigematsu H, Suzuki S, Kusama K, Sakashita H. A case of hemangio-lymphangioma of the tongue. Nihon Koku Shindan Gakkai Zasshi. 2003;16:250–2 **(Japanese)**.
380. Ogiuchi H, Yamazaki T, Yamamura T, Kuwazawa T, Ogiuchi H. A long-term follow-up, case of lymphangioma of tongue and floor of the mouth. Shoni Koku Geka. 2003;13:17–20 **(Japanese)**.
381. Rowley H, Perez-Atayde AR, Burrows PE, Rahbar R. Management of a giant lymphatic malformation of the tongue. Arch Otolaryngol Head Neck Surg. 2002;128:190–4.
382. Chakravarti A, Bhargava R. Lymphangioma circumscriptum of the tongue in children: successful treatment using intralesional bleomycin. Int J Pediatr Otorhinolaryngol. 2013;77:1367–9.
383. Wiegand S, Eivazi B, Zimmermann AP, Neff A, Barth PJ, Sesterhenn AM, et al. Microcystic lymphatic malformations of the tongue: diagnosis, classification, and treatment. Arch Otolaryngol Head Neck Surg. 2009;135:976–83.
384. Hong JP, Lee MY, Kim EK, Seo DH. Giant lymphangioma of the tongue. J Craniofac Surg. 2009;20:252–4.
385. Azizkhan RG, Rutter MJ, Cotton RT, Lim LH, Cohen AP, Mason JL. Lymphatic malformations of the tongue base. J Pediatr Surg. 2006;41:1279–84.
386. Ogawa-Ochiai K, Sekiya N, Kasahara Y, Chino A, Ueda K, Kimata Y, et al. A case of mediastinal lymphangioma successfully treated with Kampo medicine. J Altern Complement Med. 2011;17:563–5.
387. Roy S, Reyes S, Smith LP. Bipolar radiofrequency plasma ablation (Coblation) of lymphatic malformations of the tongue. Int J Pediatr Otorhinolaryngol. 2009;73:289–93.
388. Kemmotsu T, Takeda Y, Nakamura K, Tateishi I. A case of congenital chylothorax requiring early OK-432 pleurodesis. Nihon Shusanki Shinseiji Igakkai Zasshi. 2012;48:945–50 **(Japanese)**.
389. Tani G, Okuyama H, Kubota A, Kawahara H. Thoracoscopic thoracic duct ligation in a premature infant with congenital chylothorax. Nihon Shoni Geka Gakkai Zasshi. 2011;47:844–7 **(Japanese)**.
390. Miura K, Yoshizawa K, Tamaki M, Okumura K, Okada M. Congenital chylothorax treated with video-assisted thoracic surgery. Kyobu Geka. 2008;61:1149–51 **(Japanese)**.
391. Amagai T, Nakamura H, Kaneko M, Sugiura M, Hamada H. Use and problems of pleuro-peritoneal shunting tube for neonatal chylothorax. Shoni Geka. 2001;33:201–7 **(Japanese)**.
392. Cleveland K, Zook D, Harvey K, Woods RK. Massive chylothorax in small babies. J Pediatr Surg. 2009;44:546–50.
393. Buttiker V, Fanconi S, Burger R. Chylothorax in children: guidelines for diagnosis and management. Chest. 1999;116:682–7.
394. Kaji M, Sakauchi M, Yoshii K, Seki A, Tani Y, Kishi T, et al. A case of chylothorax treated effectively with surgery. Tokyo Joshi Ika Daigaku Zasshi. 2013;83:E366–70 **(Japanese)**.
395. Haga T, Toida C, Muguruma T, Fujino A. Two cases of mediastinal lymphangiomatosis that required intensive care management. Nihon Shonika Gakkai Zasshi. 2013;117:1483–8 **(Japanese)**.
396. Chen YL, Lee CC, Yeh ML, Lee JS, Sung TC. Generalized lymphangiomatosis presenting as cardiomegaly. J Formos Med Assoc. 2007;106:S10–4.
397. Pfleger A, Schwinger W, Maier A, Tauss J, Popper HH, Zach MS. Gorham-Stout syndrome in a male adolescent-case report and review of the literature. J Pediatr Hematol Oncol. 2006;28:231–3.
398. Noda M, Endo C, Hoshikawa Y, Ishibashi N, Suzuki T, Okada Y, et al. Successful management of intractable chylothorax in Gorham-Stout disease by awake thoracoscopic surgery. Gen Thorac Cardiovasc Surg. 2013;61:356–8.
399. Fukahori S, Tsuru T, Asagiri K, Nakamizo H, Asakawa T, Tanaka H, et al. Thoracic lymphangiomatosis with massive chylothorax after a tumor biopsy and with disseminated intravenous coagulation–lymphoscintigraphy, an alternative minimally invasive imaging technique: report of a case. Surg Today. 2011;41:978–82.

400. Brodszki N, Lansberg JK, Dictor M, Gyllstedt E, Ewers SB, Larsson MK, et al. A novel treatment approach for paediatric Gorham-Stout syndrome with chylothorax. Acta Paediatr. 2011;100:1448–53.
401. Deveci M, Inan N, Corapcioglu F, Ekingen G. Gorham-Stout syndrome with chylothorax in a six-year-old boy. Indian J Pediatr. 2011;78:737–9.
402. Seok YK, Cho S, Lee E. Early surgical management of chylothorax complicated by Gorham's disease. Thorac Cardiovasc Surg. 2010;58:492–3.
403. Kose M, Pekcan S, Dogru D, Akyuz C, Ozcelik U, Ozsurekci Y, et al. Gorham-Stout Syndrome with chylothorax: successful remission by interferon alpha-2b. Pediatr Pulmonol. 2009;44:613–5.
404. Boyle MJ, Alison P, Taylor G, Lightbourne BA. A case of Gorham's disease complicated by bilateral chylothorax. Heart Lung Circ. 2008;17:64–6.
405. Burgess S, Harris M, Dakin C, Borzi P, Ryan C, Cooper D. Successful management of lymphangiomatosis and chylothorax in a 7-month-old infant. J Paediatr Child Health. 2006;42:560–2.
406. Underwood J, Buckley J, Manning B. Gorham disease: an intraoperative case study. AANA J. 2006;74:45–8.
407. Fujiu K, Kanno R, Suzuki H, Nakamura N, Gotoh M. Chylothorax associated with massive osteolysis (Gorham's syndrome). Ann Thorac Surg. 2002;73:1956–7.
408. Chavanis N, Chaffanjon P, Frey G, Vottero G, Brichon PY. Chylothorax complicating Gorham's disease. Ann Thorac Surg. 2001;72:937–9.
409. Konez O, Vyas PK, Goyal M. Disseminated lymphangiomatosis presenting with massive chylothorax. Pediatr Radiol. 2000;30:35–7.
410. Morita K, Fukumoto K, Mitsunaga M, Yamoto M, Nouso H, Miyake H, et al. A case of thoracic lymphangiomatosis causing difficulty in treatment due to dyspnea and hemorrhage. Nihon Shoni Ketsueki Gan Gakkai Zasshi. 2013;50:644–9 **(Japanese)**.
411. Kitami A, Suzuki T, Suzuki S, Usuda R, Kamio Y, Kadokura M. Gorham's disease complicated by chyloma of the chest wall. Jpn J Thorac Cardiovasc Surg. 2006;54:311–3.
412. Lee S, Finn L, Sze RW, Perkins JA, Sie KC. Gorham Stout syndrome (disappearing bone disease): two additional case reports and a review of the literature. Arch Otolaryngol Head Neck Surg. 2003;129:1340–3.
413. Reinglas J, Ramphal R, Bromwich M. The successful management of diffuse lymphangiomatosis using sirolimus: a case report. Laryngoscope. 2011;121:1851–4.
414. Tamay Z, Saribeyoglu E, Ones U, Anak S, Guler N, Bilgic B, et al. Diffuse thoracic lymphangiomatosis with disseminated intravascular coagulation in a child. J Pediatr Hematol Oncol. 2005;27:685–7.
415. Duffy BM, Manon R, Patel RR, Welsh JS. A case of Gorham's disease with chylothorax treated curatively with radiation therapy. Clin Med Res. 2005;3:83–6.
416. Kinnier CV, Eu JP, Davis RD, Howell DN, Sheets J, Palmer SM. Successful bilateral lung transplantation for lymphangiomatosis. Am J Transplant. 2008;8:1946–50.
417. Huang SY, Lee YM, Tzeng ST, Su CP, Huang SF, Wu YK, et al. Gorham syndrome with postoperative respiratory failure and requiring prolonged mechanical ventilation. Respir Care. 2013;58:e144–8.
418. Lee WS, Kim SH, Kim I, Kim HK, Lee KS, Lee SY, et al. Chylothorax in Gorham's disease. J Korean Med Sci. 2002;17:826–9.
419. Fontanesi J. Radiation therapy in the treatment of Gorham disease. J Pediatr Hematol Oncol. 2003;25:816–7.
420. Yoo SY, Goo JM, Im JG. Mediastinal lymphangioma and chylothorax: thoracic involvement of Gorham's disease. Korean J Radiol. 2002;3:130–2.
421. Timke C, Krause MF, Oppermann HC, Leuschner I, Claviez A. Interferon alpha 2b treatment in an eleven-year-old boy with disseminated lymphangiomatosis. Pediatr Blood Cancer. 2007;48:108–11.

Publisher's Note Springer Nature remains neutral with regard to jurisdictional claims in published maps and institutional affiliations.

Affiliations

Hidefumi Mimura[1] · Sadanori Akita[2] · Akihiro Fujino[3] · Masatoshi Jinnin[4] · Mine Ozaki[5] · Keigo Osuga[6] · Hiroki Nakaoka[7] · Eiichi Morii[8] · Akira Kuramochi[9] · Yoko Aoki[10] · Yasunori Arai[1] · Noriko Aramaki[11] · Masanori Inoue[12] · Yuki Iwashina[5] · Tadashi Iwanaka[13] · Shigeru Ueno[14] · Akihiro Umezawa[15] · Michio Ozeki[16] · Junko Ochi[17] · Yoshiaki Kinoshita[18] · Masakazu Kurita[19] · Shien Seike[20] · Nobuyuki Takakura[21] · Masataka Takahashi[15] · Takao Tachibana[22] · Kumiko Chuman[23] · Shuji Nagata[24] · Mitsunaga Narushima[25] · Yasunari Niimi[26] · Shunsuke Nosaka[27] · Taiki Nozaki[28] · Kazuki Hashimoto[1] · Ayato Hayashi[29] · Satoshi Hirakawa[30] · Atsuko Fujikawa[1] · Yumiko Hori[8] · Kentaro Matsuoka[31] · Hideki Mori[7] · Yuki Yamamoto[4] · Shunsuke Yuzuriha[32] · Naoaki Rikihisa[33] · Shoji Watanabe[34] · Shinichi Watanabe[35] · Tatsuo Kuroda[36] · Shunsuke Sugawara[37] · Kosuke Ishikawa[38] · Satoru Sasaki[39]

Sadanori Akita
akitas@hf.rim.or.jp

Akihiro Fujino
fujino-a@ncchd.go.jp

Masatoshi Jinnin
mjin@wakayama-med.ac.jp

Mine Ozaki
zakimin@nifty.com

Keigo Osuga
osuga@radiol.med.osaka-u.ac.jp

Hiroki Nakaoka
hirok@m.ehime-u.ac.jp

Eiichi Morii
morii@molpath.med.osaka-u.ac.jp

Akira Kuramochi
aquirax@saitama-med.ac.jp

Yoko Aoki
aokiy@med.tohoku.ac.jp

Yasunori Arai
yarai1976@gmail.com

Noriko Aramaki
nonken@2001.jukuin.keio.ac.jp

Masanori Inoue
Inomasa1130@gmail.com

Yuki Iwashina
yuki19841226@gmail.com

Tadashi Iwanaka
iwanaka-tky@umin.ac.jp

Shigeru Ueno
ps_uenos@is.icc.u-tokai.ac.jp

Akihiro Umezawa
umezawa-a@ncchd.go.jp

Michio Ozeki
michioo@gifu-u.ac.jp

Junko Ochi
ochijun1213@gmail.com

Yoshiaki Kinoshita
kinoppy@med.niigata-u.ac.jp

Masakazu Kurita
masakazukurita122@gmail.com

Shien Seike
seikeshien@gmail.com

Nobuyuki Takakura
ntakaku@biken.osaka-u.ac.jp

Masataka Takahashi
takahashi-mst@ncchd.go.jp

Takao Tachibana
takao@kuhp.kyoto-u.ac.jp

Kumiko Chuman
koro5122@yahoo.co.jp

Shuji Nagata
sn4735@med.kurume-u.ac.jp

Mitsunaga Narushima
sancho-ps@clin.medic.mie-u.ac.jp

Yasunari Niimi
yasunm@luke.ac.jp

Shunsuke Nosaka
nosaka-s@ncchd.go.jp

Taiki Nozaki
nojyakki@gmail.com

Kazuki Hashimoto
kazkik1980@marianna-u.ac.jp

Ayato Hayashi
ayhayasi@juntendo.ac.jp

Satoshi Hirakawa
hirakawa@hama-med.ac.jp

Atsuko Fujikawa
a2fujikawa@marianna-u.ac.jp

Yumiko Hori
yumiko-hori@molpath.med.osaka-u.ac.jp

Kentaro Matsuoka
kenta-ma@dokkyomed.ac.jp

Hideki Mori
hanakuro@m.ehime-u.ac.jp

Yuki Yamamoto
yukiy@wakayama-med.ac.jp

Shunsuke Yuzuriha
yuzuriha@shinshu-u.ac.jp

Naoaki Rikihisa
rikihisa@faculty.chiba-u.jp

Shoji Watanabe
watanabe.shoji@scmc.pref.saitama.jp

Shinichi Watanabe
watanabe@med.teikyo-u.ac.jp

Tatsuo Kuroda
kuroda-t@z8.keio.jp

Shunsuke Sugawara
sugasuga_shun@yahoo.co.jp

Kosuke Ishikawa
kishikawa-hok@umin.org

Satoru Sasaki
satoru-s@tonan.gr.jp

[1] Department of Radiology, St. Marianna University School of Medicine, 2-16-1, Sugao, Miyamae, Kawasaki, Kanagawa 216-8511, Japan

[2] Department of Plastic Surgery, Wound Repair and Regeneration, Fukuoka University, School of Medicine, Fukuoka, Japan

[3] Division of Surgery, National Center for Child Health and Development, Tokyo, Japan

[4] Department of Dermatology, Wakayama Medical University, Wakayama, Japan

[5] Department of Plastic and Reconstructive, Aesthetic Surgery, Kyorin University School of Medicine, Mitaka, Japan

[6] Department of Diagnostic and Interventional Radiology, Osaka University Graduate School of Medicine, Suita, Japan

[7] Department of Plastic Surgery, Ehime University Hospital, Toon, Japan

[8] Department of Pathology, Osaka University Graduate School of Medicine, Suita, Japan

[9] Department of Dermatology, Saitama Medical University, Irumagun, Japan

[10] Department of Medical Genetics, Tohoku University School of Medicine, Sendai, Japan

[11] Department of Plastic and Reconstructive Surgery, Keio University School of Medicine, Tokyo, Japan

[12] Department of Radiology, Keio University School of Medicine, Tokyo, Japan

[13] Department of Pediatric Surgery, The University of Tokyo Hospital, Tokyo, Japan

[14] Department of Pediatric Surgery, Tokai University School of Medicine, Isehara, Japan

[15] Department of Reproductive Biology, Center for Regenerative Medicine, National Center for Child Health and Development, Tokyo, Japan

[16] Department of Pediatrics, Gifu University Graduate School of Medicine, Gifu, Japan

[17] Department of Diagnostic Radiology, Tohoku University, Sendai, Japan

[18] Department of Pediatric Surgery, Niigata University Graduate School of Medical and Dental Sciences, Niigata, Japan

[19] Department of Plastic and Reconstructive Surgery, The University of Tokyo Hospital, Tokyo, Japan

[20] Department of Plastic Surgery, Osaka University Graduate School of Medicine, Suita, Japan

[21] Department of Signal Transduction, Research Institute for Microbial Diseases, Osaka University, Suita, Japan

[22] Department of Dermatology, Osaka Red Cross Hospital, Osaka, Japan

[23] Department of Dermatology, Kanto Central Hospital, Tokyo, Japan

[24] Department of Radiology, Kurume University School of Medicine, Kurume, Japan

[25] Department of Plastic and Reconstructive Surgery, Graduate School of Medicine, Mie University, Tsu, Japan

[26] Department of Neuroendovascular Therapy, St. Luke's International Hospital, Tokyo, Japan

[27] Division of Radiology, National Center for Child Health and Development, Tokyo, Japan

[28] Department of Radiology, St Luke's International Hospital, Tokyo, Japan

[29] Department of Plastic and Reconstructive Surgery, Juntendo University Urayasu Hospital, Urayasu, Japan

[30] Department of Dermatology, Hamamatsu University School of Medicine, Hamamatsu, Japan

[31] Department of Pathology, Dokkyo Medical University, Saitama Medical Center, Koshigaya, Japan

[32] Department of Plastic and Reconstructive Surgery, Shinshu University School of Medicine, Matsumoto, Japan

[33] Department of Plastic and Reconstructive Surgery, Oyumino Central Hospital, Chiba, Japan

[34] Department of Plastic and Reconstructive Surgery, Saitama Children's Medical Center, Saitama, Japan

[35] Department of Dermatology, Teikyo University School of Medicine, Tokyo, Japan

[36] Department of Pediatric Surgery, Keio University School of Medicine, Tokyo, Japan

[37] Department of Diagnostic Radiology, National Cancer Center Hospital, Tokyo, Japan

[38] Department of Plastic and Reconstructive Surgery, Faculty of Medicine and Graduate School of Medicine, Hokkaido University, Sapporo, Japan

[39] Department of Plastic and Reconstructive Surgery, Center for Vascular Anomalies, Tonan Hospital, Sapporo, Japan

Resistance Mutations of Hepatitis B Virus in Entecavir-Refractory Patients

Norie Yamada,[1,2] Ryuichi Sugiyama,[1] Sayuri Nitta,[1,3] Asako Murayama,[1] Minoru Kobayashi,[2] Chiaki Okuse,[4] Michihiro Suzuki,[4] Kiyomi Yasuda,[2] Hiroshi Yotsuyanagi,[5] Kyoji Moriya,[6] Kazuhiko Koike,[7] Takaji Wakita,[1] and Takanobu Kato[1]

The emergence of resistance mutations in the reverse transcriptase gene of hepatitis B virus (HBV) is associated with treatment failure. Entecavir (ETV) is one of the most potent anti-HBV reagents; it has a very low resistance rate and is used as the first-line treatment for chronic hepatitis B. In this study, we isolated HBVs in 4 ETV-refractory patients (2 with viral breakthrough, 1 with partial virological response, and 1 with flare-up) and assessed ETV resistance using replication-competent 1.38-fold HBV genome-length molecular clones. The full genome sequences of infected HBVs in ETV-refractory patients were determined. The HBV molecular clones were generated with the patient-derived sequences. After transfection of these molecular clones into HepG2 cells, viral replications and ETV susceptibilities were evaluated by measuring the amount of intracellular core-particle-associated HBV DNA using Southern blotting and real-time polymerase chain reaction. Among these cases, ETV-resistant variants were detected in 2 patients with viral breakthrough and responsible amino acid mutations in reverse transcriptase were successfully identified in these variants. No ETV-resistant mutation was detected in the other cases. The identified ETV-resistant mutations did not confer resistance to tenofovir disoproxil fumarate. *Conclusion:* The HBV replication model with patient-derived sequences is useful for assessing replication efficiency, susceptibility to anti-HBV reagents, and responsible resistance mutations and can aid in choosing the appropriate treatment strategy for treatment-failure cases of chronic hepatitis B. (*Hepatology Communications* 2017;1:110-121)

Introduction

Hepatitis B virus (HBV), a member of the Hepadnaviridae family, has a partially double-stranded 3.2-kb DNA genome and comprises four open reading frames coding for hepatitis B surface antigen (HBsAg), core protein/hepatitis B e antigen (HBeAg), viral polymerase, and X protein.[1,2] Infection with this virus causes severe liver diseases, including acute, chronic, and fulminant hepatitis; cirrhosis; and hepatocellular carcinoma (HCC).[3] Although effective vaccines against HBV are available in many countries, chronic hepatitis B (CHB) infection remains a significant global health problem. The World Health Organization estimates that approximately 240 million people are afflicted with CHB infections, and these people are at risk for cirrhosis and HCC.[4,5] Currently, two classes of anti-HBV reagents are clinically available: interferon-α and nucleos(t)ide analogues (NAs). Interferon treatment can reduce HBeAg and HBsAg through a combination of direct antiviral and immunomodulatory effects,[6] but it is associated with unfavorable side effects. NAs target the step of reverse transcription and inhibit the production

Abbreviations: CI, confidence interval; EC_{50}, effective concentration required to inhibit 50%; ETV, entecavir; HBeAg, hepatitis B e antigen; HBsAg, hepatitis B surface antigen; HBV, hepatitis B virus; HCC, hepatocellular carcinoma; HLA, human leucocyte antigen; LAM, lamivudine; NA, nucleos(t)ide analogue; PCR, polymerase chain reaction; RT, reverse transcriptase; TDF, tenofovir disoproxil fumarate; VBT, viral breakthrough.

Received October 26, 2016; accepted February 8, 2017.

Supported by grants for Research Programs on Hepatitis (16fk0310050j0005 and 16fk0310059j0105) from the Japan Agency for Medical Research and Development. The funders had no role in the study design, data collection and interpretation, or the decision to submit the work for publication.

The nucleotide sequences in this paper will appear in the DDBJ/EMBL/GenBank with accession numbers LC170474-LC170477.

Additional Supporting Information may be found at onlinelibrary.wiley.com/doi/10.1002/hep4.1022/suppinfo.

Copyright © 2017 The Authors. Hepatology Communications published by Wiley Periodicals, Inc., on behalf of the American Association for the Study of Liver Diseases. This is an open access article under the terms of the Creative Commons Attribution-NonCommercial-NoDerivs License, which permits use and distribution in any medium, provided the original work is properly cited, the use is non-commercial and no modifications or adaptations are made.

View this article online at wileyonlinelibrary.com.

DOI 10.1002/hep4.1022

Potential conflict of interest: K.K. received honoraria for lectures from Bristol-Meyers Squibb. The other authors have nothing to disclose.

of HBV DNA from pregenomic RNA. Although these reagents ameliorate liver diseases and prevent disease progression to HCC, such long-term treatment often causes the emergence of resistance mutations. In Japan, NAs of lamivudine (LAM), adefovir dipivoxil (ADV), entecavir (ETV), and tenofovir disoproxil fumarate (TDF) have been approved. Because these NAs share a common target for the viral reverse transcriptase (RT), resistance mutations to these reagents have been reported only in RT domains. Among these NAs, ETV is one of the most potent anti-HBV reagents; it has a very low resistance rate in treatment-naive patients[7-11] and has long been used as a first-line reagent. To date, a limited number of ETV-resistant mutations have been reported. They include the LAM-resistant-associated amino acid mutations at rt180 and rt204 and require additional mutations at rt169, rt184, rt202, or rt250.[8,12] Mutations of rtI163V and rtA186T in addition to the LAM-resistant mutations have been reported to confer ETV resistance.[13]

In this study, we isolated HBVs from four ETV-refractory cases (2 viral breakthrough [VBT] patients, 1 partial virological response patient, and 1 flare-up patient) and generated replication-competent 1.38-fold HBV genome-length molecular clones with patient-derived sequences. After transfection of these molecular clones into HepG2 cells, viral replication and ETV susceptibility were evaluated by measuring the amount of intracellular core-particle-associated HBV DNA using Southern blotting and real-time polymerase chain reaction (PCR).

Materials and Methods

PATIENTS

We performed a retrospective analysis of 70 patients with CHB (male/female, 53/17; mean age, 46.6 ± 8.9 years) who received ETV treatment at Seizankai Kiyokawa Hospital, Tokyo, Japan, from December 2006 to May 2016. All patients were clinically diagnosed with chronic hepatitis and were HBsAg-positive and HBV DNA-positive for at least 6 months prior to the start of treatment. None were diagnosed with cirrhosis or HCC. All patients received 0.5 mg ETV for more than 1 year, and no patient had received other NAs. This study was approved by the Ethics Committees of our institutions (approval numbers 246 from Seizankai Kiyokawa Hospital and 377 from the National Institute of Infectious Diseases), and written informed consent was obtained from each patient. Of the 70 patients with CHB treated with ETV, four cases appeared to be refractory (Table 1). These four subjects were male, positive for HBsAg and HBeAg, and infected with HBV genotype C. Their ages ranged from 40 to 59 years, and all were negative for serological markers of hepatitis C virus and human immunodeficiency virus infections. Profiles of the 4 ETV-refractory patients are as follows: Case A (40-year-old male; Fig. 1A): The administration of ETV (0.5 mg daily) was started in August 2007. Serum HBV DNA became undetectable after 3 years of ETV treatment but re-emerged after 3.3 years of treatment. The HBV DNA titer was 8.0 log copies/mL at that time. The increased dosage of ETV (1.0 mg daily) was not effective. This case was diagnosed as a VBT case. HBV was isolated from serum samples collected at two time points, at the beginning of treatment (time point 1) and at VBT (time point 2) (Fig. 1A). The isolated HBVs were named clones A1 and A2, respectively. The entire genomes of the isolated HBVs were sequenced, and the deduced amino acids in the RT region were aligned and compared with the genotype C consensus sequence (Supporting Fig. S1). The known resistance mutation to NAs was not detected in

ARTICLE INFORMATION:

From the [1]Department of Virology II, National Institute of Infectious Diseases, Tokyo, Japan; [2]Department of Internal Medicine, Center for Liver Diseases, Seizankai Kiyokawa Hospital, Tokyo, Japan; [3]Department of Gastroenterology and Hepatology, Tokyo Medical and Dental University, Tokyo, Japan; [4]Department of Internal Medicine, Division of Gastroenterology and Hepatology, St. Marianna University School of Medicine, Kanagawa, Japan; [5]Division of Infectious Diseases, Advanced Clinical Research Center, Institute of Medical Science; [6]Department of Infection Control and Prevention, Graduate School of Medicine; [7]Department of Gastroenterology, Graduate School of Medicine, The University of Tokyo, Tokyo, Japan.

ADDRESS CORRESPONDENCE AND REPRINT REQUESTS TO:

Takanobu Kato, M.D., Ph.D.
Toyama 1-23-1, Shinjuku-ku
Tokyo 162-8640, Japan

E-mail: takato@nih.go.jp
Tel.: +81-3-5285-1111

TABLE 1. PROFILES OF ETV-REFRACTORY CASES

Patients	Case A	Case B	Case C	Case D
Sex	male	male	male	male
Age* (year)	40	43	59	53
ALT* (IU/mL)	312	211	291	309
HBV genotype	C	C	C	C
HBeAg	positive	positive	positive	positive
Core promoter (nt 1762/1764)	mutant/mutant	mutant/mutant	wild/wild	mutant/mutant
Precore(nt 1896)	wild	wild	wild	wild
HBV DNA*(log copy/mL)	7.6	8.6	9.1	8.7

*Values at the beginning of ETV treatment.

clone A1. However, reported LAM-resistant mutations of rtV173L/L180M/M204V emerged in clone A2. Case B (43-year-old male; Fig. 1B): The administration of ETV (0.5 mg daily) was started in April 2007. Serum HBV DNA was undetectable after 2.5 years of ETV treatment and remained undetectable until 6.8 years from the start of ETV when HBV DNA re-emerged and reached 8.3 log copies/mL. This case was also diagnosed as a VBT case. HBVs isolated at the beginning of treatment (time point 1) and at VBT (time point 2) were sequenced (Fig. 1B). As in the HBVs isolated in case A, no resistance mutation was detected in clone B1. However, mutations of rtN238H/L269I accompanied by LAM-resistant mutations of rtL180Q/M204V emerged in clone B2. Case C (59-year-old male; Fig. 1C): The administration of ETV (0.5 mg daily) was started in June 2010. Serum HBV DNA was 9.1 log copies/mL before treatment and decreased to 5.0 log copies/mL soon after starting ETV; however, HBV DNA remained positive for 1.5 years of ETV treatment. This case was considered to be a partial virological response case. HBV isolated from serum samples at multiple time points (time points 1-3 in Fig. 1C) were sequenced. Of these HBV clones, the deduced amino acid sequences in the RT region were identical but had several

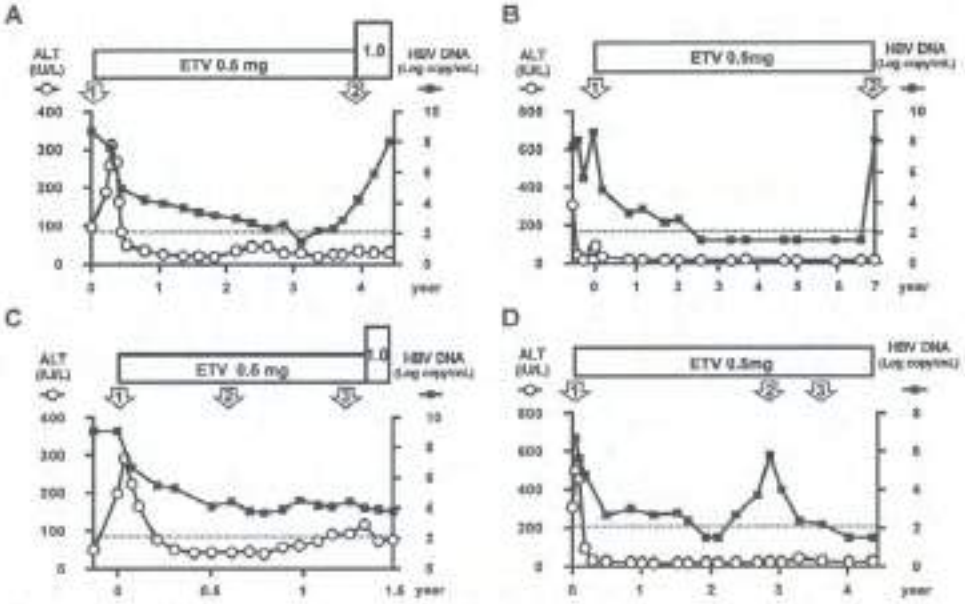

FIG. 1. Clinical courses of 4 ETV-refractory patients (A: Case A with VBT, B: Case B with VBT, C: Case C with partial virological response, D: Case D with flare-up). Serum HBV DNA titers (solid squares) and ALT levels (open circles) are indicated. The lower detection limit of HBV DNA is indicated by the dotted line. The serum samples were collected at the time points indicated by open arrows with numbers, and the sequences of infected HBV were analyzed. Abbreviation: ALT, alanine aminotransferase.

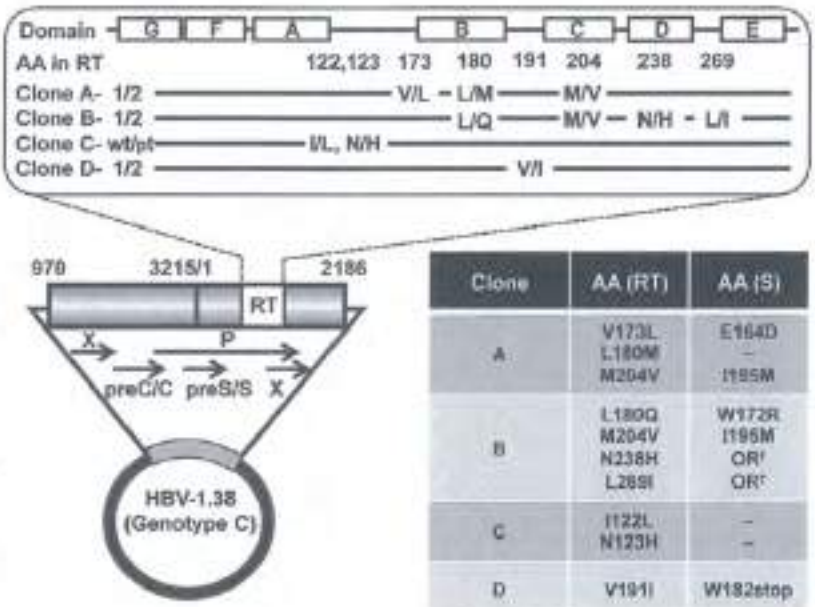

Clone	AA (RT)	AA (S)
A	V173L L180M M204V	E164D – I195M
B	L180Q M204V N238H L269I	W172R I195M OR[1] OR[1]
C	I122L N123H	– –
D	V191I	W182stop

FIG. 2. Construction of replication-competent 1.38-fold HBV genome length molecular clone. The schema of the constructed replication-competent 1.38-fold HBV genome is indicated. This construct contains 4,432 bp of HBV genome and covers all four open reading frames. The upper panel shows the domain of RT and the introduced amino acid mutations in each clone. The lower panel indicates amino acid mutations in the RT region and the corresponding surface gene. Abbreviations: OR, out of region of the surface gene; AA, amino acid; preC/C, precore/core region; X, X gene of HBV; P, polymerase gene of HBV; preS/S, preS/S region; S, surface gene of HBV.

differences compared with the genotype C consensus sequence. Case D (53-year-old male; Fig. 1D): The administration of ETV (0.5 mg daily) was started in June 2007. After 2 years of treatment with ETV, serum HBV DNA became undetectable. After 3 years from the start of ETV treatment, HBV DNA suddenly flared up. This flare-up of HBV DNA was transient and decreased to an undetectable level without additional treatment. Therefore, this case was defined as a flare-up case. HBV was isolated at three time points: the beginning of treatment (time point 1), the flare-up point (time point 2), and the subsided point (time point 3) (Fig. 1D). The deduced amino acid sequences in the RT region were identical in clones D1 and D3 and an amino acid substitution of V191I was detected in clone D2. All four patients were treatment naive and confirmed their medication adherence.

VIROLOGICAL MARKERS FOR HBV

HBsAg and HBeAg were measured by chemiluminescent immunoassay using a commercial assay kit (Abbott Japan Co., Ltd., Tokyo, Japan). The HBV genotype was determined by enzyme immunoassay (IMMUNIS HBV Genotype EIA; Institute of Immunology Co., Ltd., Tokyo, Japan). HBV DNA titer was determined by the COBAS TaqMan HBV test ver. 2.0 (Roche Diagnostics K.K., Tokyo, Japan) or the Amplicor HBV Monitor assay (Roche Diagnostics K.K.); the lower detection limits of these assays were 2.1 and 2.6 log copies/mL, respectively.

SEQUENCE ANALYSIS OF HBV

Total DNA was isolated from 200 μL of patient serum collected at the indicated time points in Fig. 1 using the QIAamp Blood Mini Kit (Qiagen K.K., Tokyo, Japan). The entire genome of HBV was amplified by PCR using primers as described.[14] Amplified fragments were sequenced directly with an automated DNA sequencer (3500 Genetic Analyzer; Applied Biosystems, Foster City, CA).

CONSTRUCTION OF REPLICATION-COMPETENT MOLECULAR CLONES

PCR-amplified fragments were inserted into the pGEM-T Easy Vector system (Promega, Madison, WI). At least five clones of each fragment were sequenced, and the consensus sequence was determined. Using the obtained clones as templates, two material fragments (fragment 1, nucleotide [nt] 970-3215/1-178

and fragment 2, nt 178-2186; the number of nucleotides was referred from the genotype C prototype clone [accession number AB246344, https://www.ncbi.nlm.nih.gov/nuccore/AB246344]) with consensus sequences for construction generated using the fusion PCR technique. The replication-competent HBV molecules with 1.38-fold genome length were constructed by ligation of two material fragments (Fig. 2). The intended mutations were introduced by site-directed PCR and fragment swap. Established molecular clones were sequenced and confirmed to be correctly constructed.

TRANSFECTION INTO HepG2 CELLS

HepG2 cells were obtained from the European Collection of Authenticated Cell Cultures (Salisbury, UK, https://www.phe-culturecollections.org.uk/collections/ecacc.aspx) and cultured at 37°C in a 5% CO_2 environment in complete growth medium. HepG2 cells at 80%-90% confluence in 100-mm dishes were transfected with 2.5 μg of HBV molecular clones using Lipofectamine 3000 Reagent (Thermo Fisher Scientific, Waltham, MA) according to the manufacturer's instructions. Twenty-four hours after transfection, cells were washed and the medium was changed to fresh medium with or without reagents. The transfected cells were harvested at 3 days after transfection. The anti-HBV reagents of ETV and TDF were purchased from LKT Laboratories, Inc. (St. Paul, MN) and Selleck Chemicals (Houston, TX), respectively.

ISOLATION OF CORE-PARTICLE-ASSOCIATED HBV DNA

Isolation of intracellular core-particle-associated HBV DNA was accomplished as described by Günther et al. with some modifications.[15] Briefly, cells were suspended in 500 μL of lysis buffer (100 mM Tris-HCl pH 8.0, 0.2% Nonidet P40), and nuclei were pelleted by centrifugation. The supernatant was transferred and treated with DNase (RQ1 RNase-free DNase; Promega) and RNase (RNase A; Qiagen K.K.). Then, proteinase K, 500 mM ethylene diamine tetraacetic acid, 5 M NaCl, and 10% sodium dodecyl sulfate were added and the samples were incubated at 55°C for 1 hour. HBV DNA was then recovered by phenol–chloroform (1:1) extraction and 2-propanol precipitation.

SOUTHERN BLOT HYBRIDIZATION OF HBV DNA

The isolated core-particle-associated HBV DNA was separated on a 1.0% agarose gel and transferred to a nylon membrane (positively charged; Roche Diagnostics, Penzberg, Germany). The transferred membrane was immobilized by an ultraviolet crosslinker and hybridized by an alkaline- phosphatase-labeled probe of a full-length HBV DNA fragment (accession number AB246344, https://www.ncbi.nlm.nih.gov/nuccore/AB246344) generated with the Gene Images AlkPhos Direct labeling system (DIG-High Prime DNA Labeling and Detection Starter Kit II; Roche Diagnostics). Chemiluminescent detection was performed with CDP-Star (DIG-High Prime DNA Labeling and Detection Starter Kit II) and analyzed using an LAS4000 image analyzer (Fuji Photo Film, Tokyo, Japan).

QUANTIFICATION OF HBV DNA BY REAL-TIME PCR

The titer of core-particle-associated HBV DNA was also evaluated by real-time PCR with the TaqMan Fast Universal PCR Master Mix (Applied Biosystems, Foster City, CA). The sequences of primers and probe used have been described.[16] Amplification and detection were performed with StepOnePlus Real-Time PCR Systems (Applied Biosystems).

CALCULATION OF 50% EFFECTIVE CONCENTRATION VALUE AND FIT MODEL

Dose-response curves were drawn using GraphPad Prism 6 software (GraphPad Software, Inc., La Jolla, CA). The effective concentrations required to inhibit 50% (EC_{50}) values were calculated with data obtained by real-time PCR. The following model was used to draw the dose-response curve: $Y = \text{Bottom} + (\text{Top} - \text{Bottom})/(1 + 10\text{^}((X - \text{logEC50})))$, where X is the concentration of the reagent, Y is the response expressed as the percentage of core-particle-associated HBV DNA related to the corresponding control, logEC50 represents the log EC_{50} control, and Top and Bottom represent the Y values at the top and bottom plateau of the fitted curve, respectively.

STATISTICAL ANALYSIS

Statistical analysis was performed using an unpaired two-tailed Student t test with Welch's correction. P values < 0.05 were considered statistically significant.

Results

CONSTRUCTION OF HBV MOLECULAR CLONES

Using the full genome sequence of HBV isolated at the beginning of treatment in each case, we constructed replication-competent 1.38-fold HBV genome-length molecular clones. These molecular clones contain the 4,432 bp of HBV genome covering all four open reading frames (Fig. 2). In cases A, B, and D, mutations that emerged during ETV treatment were introduced into the prototype clone (clones A1, B1, and D1) of each case and generated clones A2, B2, and D2, respectively (upper panel of Fig. 2; Supporting Fig. S1). Some of these mutations in RT were accompanied by amino acid mutations of overlapping surface genes, as indicated in the lower panel of Fig. 2. In case C, all isolated clones have identical amino acids in the RT region but have several differences in comparison with the genotype C consensus sequence. We selected the amino acid substitution of I122L/N123H detected between the RT domains of B and C. We introduced these mutations into a patient-isolated clone, clone C-pt, and generated clone C-wt. These mutations do not affect amino acids in the surface gene.

ANALYSIS FOR SUSCEPTIBILITIES TO ETV

Using these generated HBV molecular clones, we assessed the replication efficiencies and susceptibilities to ETV in culture cells. Plasmids of HBV clones were transfected into HepG2 cells, and ETV was administered to the transfected cells at concentrations of 500, 50, 5, and 0.5 nM. After 3 days of treatment with ETV, the cells were harvested and intracellular core-particle-associated HBV DNA was extracted. The amounts of core-particle-associated HBV DNA were assessed by Southern blotting and real-time PCR. All patient-derived HBV molecules were replicable in HepG2 cells, and by administration of ETV, HBV replication was reduced in a dose-dependent manner (Fig. 3). These reductions of HBV replication were similarly observed by both Southern blotting and real-time PCR. To assess the susceptibility to ETV, the EC_{50} values were determined by drawing the dose-response curves with data obtained by real-time PCR (Fig. 4; Table 2).

In assessments of HBV clones isolated from patients A and B, HBV DNA titers without ETV treatment were significantly lower ($P < 0.05$) in clones of A2 and B2 in comparison with the prototype clones of A1 and B1 (0.494-fold and 0.247-fold, respectively), suggesting lower replication efficiencies of emerged clones during ETV treatment (Table 2). The mutation-introduced clones of A2 and B2 exhibited significantly lower susceptibility to ETV in comparison with the prototype clones (clones A1 and B1). The calculated EC_{50} values of clones A2 and B2 were 99.3-fold and 63.9-fold higher than that of clones A1 and B1, respectively. In assessments of HBV clones isolated from patient C, HBV DNA titers of clone C-pt without ETV treatment were similar to clone C-wt. However, in assessments of HBV clones isolated from patient D, HBV DNA titers of clone D2 without ETV treatment were significantly higher (1.94-fold) than that of clone D1. The EC_{50} values of clone C-pt and D2 were comparable to those of clones C-wt and D1, respectively.

IDENTIFICATION OF RESPONSIBLE MUTATIONS OF ETV RESISTANCE

In our assessment with patient-derived HBV molecular clones, the clones of A2 and B2 were revealed to be resistant to ETV. Both clones have key LAM-resistant mutations plus one or two additional mutations (Fig. 2). To identify the mutation responsible for ETV resistance, we performed a mapping study by generating additional clones as follows: Clone A2 has the mutation rtV173L with the key LAM-resistant mutations rtL180M/M204V. We generated a clone that has only the LAM-resistant mutations rtL180M/M204V and named the clone A1+MV. Clone B2 has the mutations rtN238H/L269I accompanied by the LAM-resistant mutations rtL180Q/M204V. Thus, we generated three clones as follows: clone B1+QV (introduced only the LAM-resistant mutations rtL180Q/M204V to clone A1), clone B1+QVH (introduced rtL180Q/M204V plus rtN238H to clone A1), and clone B1+QVI (introduced rtL180Q/M204V plus rtL269I to clone A1).

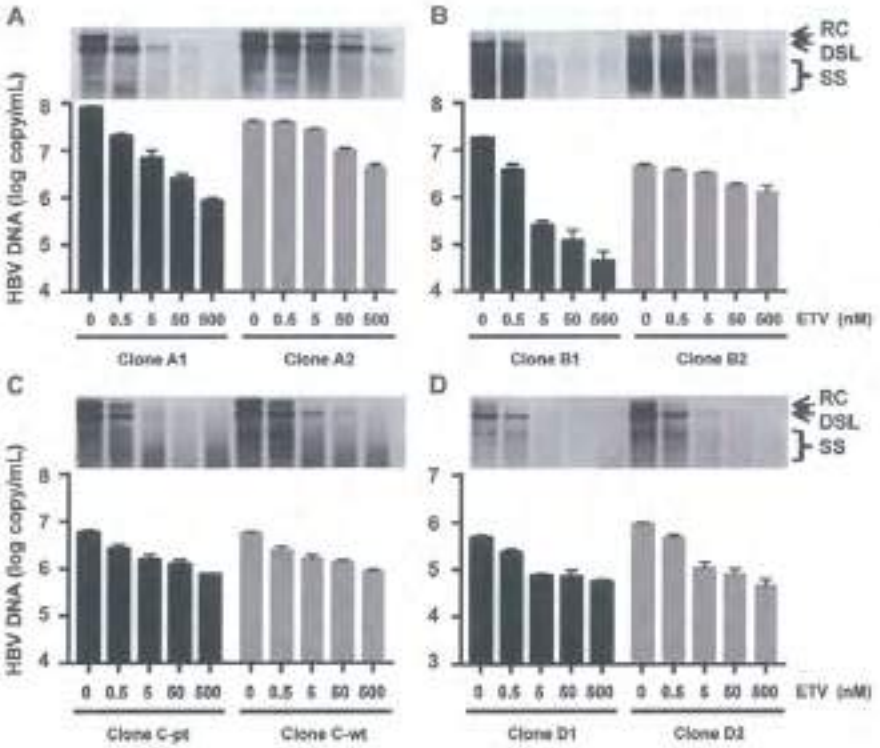

FIG. 3. Replication of patient-derived HBV molecular clones and susceptibility to ETV (A: Case A with VBT, B: Case B with VBT, C: Case C with partial virological response, D: Case D with flare-up). HBV molecular clones were transfected into HepG2 cells, and ETV was administered to the transfected cells at the indicated concentrations. HBV replication and its reduction by ETV administration were assessed by measuring the intracellular core-particle-associated HBV DNA using Southern blotting (upper panel) and real-time PCR (lower panel). The results are shown as the means ± SD. Abbreviations: DSL, double-stranded liner HBV DNA; RC, related circular HBV DNA; SS, single-stranded HBV DNA.

Using these additional clones, we compared the replication efficiencies and susceptibilities to ETV with the prototype of each clone (Fig. 4; Supporting Fig. S2). In comparison with clone A1, clone A1+MV exhibited resistance to ETV. The EC_{50} value of clone A1+MV was 115-fold higher than that of clone A1 and was comparable to clone A2 (Table 2). On the other hand, the replication efficiency of clone A1+MV was substantially lower. The HBV DNA titer of clone A1+MV without ETV treatment was 0.0651-fold lower than that of clone A1. These data indicate that the introduction of the additional mutation of rtV173L rescued the replication efficiency to 0.494-fold of clone A1. In the case of clone B, the clone with the LAM-resistant mutations rtL180Q/M204V (clone B1+QV) exhibited slightly reduced susceptibility to ETV. The EC_{50} value of this clone was 3.92-fold higher than that of clone B1. The addition of rtN238H to this clone (clone B1+QVH) did not enhance the ETV resistance. However, the addition of the mutation rtL269I (clone B1+QVI) caused severe deterioration of ETV susceptibility. The EC_{50} value of clone B1+QVI was 84.6-fold higher than that of clone B1 and was comparable to clone B2. The replication levels of clones B1+QV, B1+QVH, and B1+QVI were almost identical; however, when these mutations were combined (clone B2), the replication efficiency was enhanced to 0.247-fold of clone B1. We also analyzed the effect of mutation rtL269I alone. The EC_{50} value of clone B1+I was 0.472 nM (95% confidence interval [CI], 0.318-0.699) and was 3.50-fold higher than that of clone B1.

ANALYSIS FOR SUSCEPTIBILITIES TO TDF OF ETV-RESISTANT CLONES

To assess the susceptibility to TDF of these ETV-resistant clones, the clones were transfected into HepG2 cells and treated with TDF at concentrations of 500, 50, 5, and 0.5 nM. The replication of these HBV clones was similarly inhibited by TDF treatment in a dose-dependent manner (Fig. 5). The EC_{50} values of clones A1 and A2 were 10.5 nM (95% CI, 6.65-16.6) and 10.7 nM (95% CI, 6.41-17.8), respectively. The EC_{50} values of clones B1 and B2 were 11.4 nM

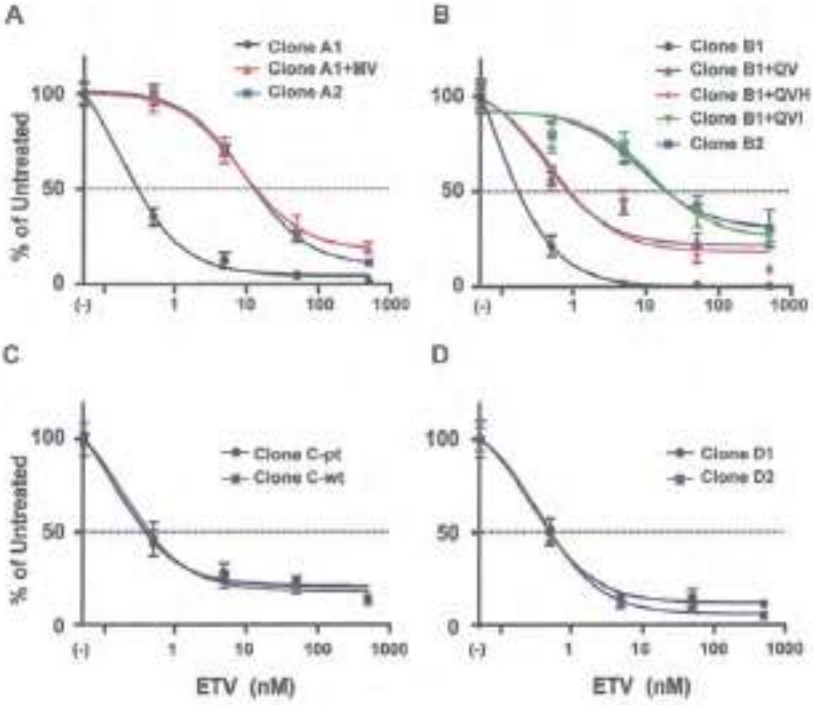

FIG. 4. Dose-response curve analysis of susceptibilities of patient-derived and identified mutation-introduced HBV clones (A: Case A with VBT, B: Case B with VBT, C: Case C with partial virological response, D: Case D with flare-up). The dose-response curves were drawn with data obtained by real-time PCR described in Fig. 3 and Supporting Fig. S2. The amount of core-particle-associated HBV DNA without ETV treatment was defined as the untreated control, and percentages of the amount of core-particle-associated HBV DNA at the indicated concentration of ETV were calculated. The results are shown as the means ± SD.

(95% CI, 5.45-23.9) and 10.5 nM (95% CI, 3.46-32.1), respectively. These data indicate that the ETV-resistant mutations identified in this study do not confer resistance to TDF.

Discussion

HBV is a significant human pathogen that is spread worldwide. Approximately 240 million people globally have CHB infection.[4] Although advances have been made in anti-HBV therapy with NAs, patients infected with this virus still need many years of treatment or lifelong treatment.[17] Even in treatment with ETV, one of the most potent anti-HBV reagents with a very low resistance rate, long-term administration of this reagent is required, and it often leads to emergence of resistance-associated variants in refractory cases. Therefore, the analysis of resistance-associated variants

TABLE 2. REPLICATION EFFICIENCY AND EC_{50} VALUES FOR ETV OF HBV CLONES

	Replication Efficiency		ETV Resistance	
Clones	HBV DNA (copy/mL)	Fold	EC_{50} in nM (95% CI)	Fold Resistance
Clone A1	$8.06 \times 10^7 \pm 5.06 \times 10^6$	1	0.0866 (0.0633-0.141)	1
Clone A2	$3.98 \times 10^7 \pm 2.32 \times 10^{6*}$	0.494	8.60 (5.66-13.0)	99.3
Clone A1+MV	$5.24 \times 10^6 \pm 2.78 \times 10^{5*}$	0.0651	9.95 (7.39-13.4)	115
Clone B1	$1.80 \times 10^7 \pm 1.10 \times 10^6$	1	0.135 (0.0999-0.182)	1
Clone B2	$4.44 \times 10^6 \pm 3.89 \times 10^{5*}$	0.247	8.63 (3.26-22.8)	63.9
Clone B1+QV	$1.22 \times 10^6 \pm 1.14 \times 10^{5*}$	0.0675	0.530 (0.244-1.15)	3.92
Clone B1+QVH	$8.37 \times 10^5 \pm 3.17 \times 10^{4*}$	0.0465	0.670 (0.286-1.57)	4.96
Clone B1+QVI	$1.54 \times 10^6 \pm 1.15 \times 10^{5*}$	0.0855	11.4 (4.30-30.4)	84.6
Clone C-pt	$5.86 \times 10^6 \pm 1.93 \times 10^5$	1	0.271 (0.153-0.480)	1
Clone C-wt	$5.88 \times 10^6 \pm 5.40 \times 10^5$	1.00	0.215 (0.132-0.350)	0.794
Clone D1	$4.84 \times 10^5 \pm 4.74 \times 10^4$	1	0.377 (0.257-0.552)	1
Clone D2	$9.37 \times 10^5 \pm 5.83 \times 10^{4*}$	1.94	0.454 (0.351-0.587)	1.21

*$P < 0.05$ in comparison with the prototype of each clone.

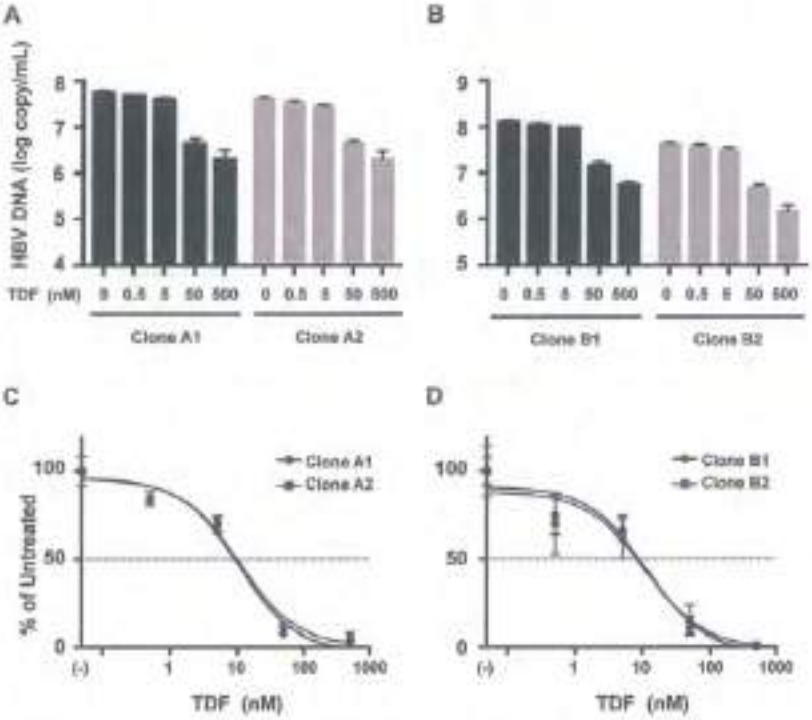

FIG. 5. Susceptibilities to TDF of ETV-resistant clones identified in this study. HBV molecular clones derived from patients A and B were transfected into HepG2 cells, and TDF was administered to the transfected cells at the indicated concentrations. (A, B) HBV replication and its reduction by TDF administration were assessed by measuring the intracellular core-particle-associated HBV DNA using real-time PCR. (C, D) Dose-response curves were drawn with the obtained data. The amount of core-particle-associated HBV DNA without TDF treatment was defined as the untreated control, and percentages of the amount of core-particle-associated HBV DNA at the indicated concentrations of TDF were calculated. The results are shown as the means ± SD.

in such cases is indispensable. In this study, to assess ETV-resistant mutations, we generated replication-competent HBV molecular clones using sequences from four ETV-refractory cases and assessed the resistance to NAs, ETV, and TDF after transient transfection into HepG2 cells. We evaluated the replication abilities and susceptibilities of these clones by Southern blotting and found that they could be quantified by real-time PCR for core-particle-associated HBV DNA. We used the 1.38-fold-genome length molecular clone, which contains two copies of the X region (Fig. 2) and therefore has some advantages in replication efficiencies in comparison with the minimum-length molecular clones.[18] We considered it preferable to obtain sufficient replication efficiency of the HBV molecular clones with patient-derived sequences. Among the four ETV-refractory cases, we detected the ETV-resistant variants in two VBT patients (cases A and B). The HBV clones isolated from other cases exhibited susceptibilities to ETV.

ETV-resistant variants were detected in VBT cases, and the responsible mutations were identified in both clones. In case A, emerged HBV at VBT (clone A2) had three mutations compared with the prototype clone A1 that was isolated at the beginning of treatment. The identified mutations, rtV173L/L180M/M204V, are known to be LAM resistant.[19] Among these, rtL180M/M204V have been reported previously to confer LAM resistance associated with a decline in replication efficiency.[20] The rtV173L mutation did not affect susceptibility to LAM but instead enhanced viral replication.[19] Similarly, the introduction of the rtL180M/M204V mutations in clone A1 could confer ETV resistance. The EC_{50} value of the clone with these mutations was 99.3-fold higher than that of the prototype clone and was not affected by the introduction of the additional mutation of rtV173L. On the other hand, the replication efficiency was strongly reduced by mutations of rtL180M/M204V but rescued by rtV173L. These observations of compensation by rtV173L were analogous with the case of LAM resistance,[19] and we could clarify that these mutations are also associated with ETV resistance. The ETV-resistant level of clone A1+MV seemed to be high, although the essential role of LAM-resistant mutations to ETV is well known. Moreover, rtL180M/M204V-associated high-level resistance to ETV has been reported in patient-derived strains but not laboratory strains.[21] Such high-level ETV resistance attributable to these

mutations may be peculiar to the ETV refractory patient-derived clone, and other amino acid residues in the RT region or other regions may be associated with this ETV resistance. These data suggest that the switch to or add-on of ETV to LAM treatment-failure patients described in reports was not recommended.[22,23]

In case B, clone B2 with the four mutations rtL180Q/M204V/N238H/L269I emerged during ETV treatment. The mapping study of these mutations revealed that the key LAM-resistant mutations rtL180Q/M204V could confer ETV resistance, similar to the HBV isolated in case A, but the extent of resistance was not high. The EC_{50} value was 3.92-fold higher than that of the prototype clone. This lower contribution of these mutations to ETV resistance may be attributed to the difference of the mutations at rt180; M or Q_4 or to the genetic backgrounds of strains in other regions. By the addition of rtL269I to clone B1+QV, ETV resistance was enhanced and EC_{50} was increased to a level similar to clone B2, although the addition of the rtN238H mutation had minimal effects on ETV resistance. The rtN238H mutation was sometimes detected in NA-treated patients and has been reported not to influence the susceptibilities to LAM, ADV, or other NAs.[24-26] The rtL269I mutation was also detected in NA treatment-failure patients. This mutation has been reported to enhance the replication efficiency and to be associated with enhanced replication efficiency when combined with the rtM204I mutation, although rtL269I alone did not alter susceptibilities to NAs.[25,27] In our experiment, rtL269I but not rtN238H could enhance ETV resistance when combined with rtL180Q/M204V, which is consistent with previous data.[27,28]

In this study, we detected two ETV-resistant variants, clones A2 and B2. Clone A2 comprised LAM-resistant mutations, and clone B2 harbored novel ETV-resistant mutations. Both clones were isolated at VBT and exhibited 99.3-fold and 63.9-fold resistance, respectively, compared with the prototype. In such clinical situations, selection and administration of other appropriate NAs will be required. We assessed the susceptibilities to TDF of these ETV-resistant variants and found that the replication of these variants was efficiently suppressed. EC_{50} values were similar to those of prototype clones. In fact, the patient of case B was treated with 300 mg TDF daily after VBT and achieved sufficient reduction of HBV DNA and HBsAg levels (data not shown). Thus, the HBV replication system will be useful to determine effective reagents for treatment-failure cases.

On the other hand, we did not detect ETV-resistant variants in cases of partial virological response (case C) and flare-up (case D). We found that the HBV strain in case C was constant. We selected the amino acid substitutions in comparison with the genotype C consensus sequence and assessed the effects on susceptibility to ETV by introducing these mutations. However, no remarkable difference in replication efficiency or susceptibility was detected. Thus, in this case, other factors for resistance, such as host factors associated with antiviral responses, were considerable. Genome-wide association studies have indicated that genetic variants in the human leucocyte antigen (HLA)-DP and HLA-DQ are associated with the risk of persistent infection with HBV.[29,30] The polymorphisms in HLA-DP were also reported to be associated with clearance of HBV by LAM treatment.[31] Such genetic variations might be related to the partial virological response to ETV administration observed in case C, although these variations have not been investigated.

We detected one amino acid mutation, V191I, in the RT region of HBV isolated at the time point of flare-up in case D. In our *in vitro* assessment with this mutation-introduced clone, we could not detect any effect on susceptibility to ETV. rtA181T mutation-associated ADV resistance has been reported.[28,32-34] This mutation is often associated with a stop codon at the overlapping surface gene, and the sW172stop mutation impairs HBsAg secretion by generating a truncated protein and also causes the susceptibility to ADV to deteriorate. The rtV191I mutation is also associated with a stop codon of the surface gene (sW182stop), but its influence on ETV resistance was not confirmed. Instead, we found that this mutation had an effect on replication efficiency. The introduction of this mutation into the prototype clone enhanced replication 1.94-fold. This enhanced replication might be associated with HBV DNA-titer flare-up in this case. This mutation is also detected in ADV-resistant cases,[35,36] although *in vitro* analysis revealed that this mutation is not associated with ADV resistance.

In this study, to evaluate the resistance to NAs, we used replication-competent HBV molecular clones. The full genome sequence of infected HBV in each patient was determined and exploited to make molecular clones. Using this strategy, we found that the contribution of mutations to ETV resistance was clone

dependent. The introduction of similar mutations at positions 180 and 204 in the RT region into the A1 and B1 clones resulted in different resistance levels. Therefore, the use of patient-derived HBV clones is important to determine the correct resistance level of infected HBV in patients.

In conclusion, using the HBV replication model with patient-derived sequences, we identified ETV-resistant mutations. The system used in this study is useful for assessing replication efficiency, susceptibility to anti-HBV reagents, and responsible resistance mutations. Such evaluation can provide worthwhile information when choosing the appropriate treatment strategy for treatment-failure cases of CHB.

Acknowledgment: We thank Ms. Nao Sugiyama for laboratory work and support.

REFERENCES

1) Ghany M, Liang TJ. Drug targets and molecular mechanisms of drug resistance in chronic hepatitis B. Gastroenterology 2007; 132:1574–1585.
2) Michailidis E, Kirby KA, Hachiya A, Yoo W, Hong SP, Kim SO, et al. Antiviral therapies: focus on hepatitis B reverse transcriptase. Int J Biochem Cell Biol 2012;44:1060-1071.
3) Beasley RP, Hwang LY, Lin CC, Chien CS. Hepatocellular carcinoma and hepatitis B virus. A prospective study of 22 707 men in Taiwan. Lancet 1981;2:1129-1133.
4) Ott JJ, Stevens GA, Groeger J, Wiersma ST. Global epidemiology of hepatitis B virus infection: new estimates of age-specific HBsAg seroprevalence and endemicity. Vaccine 2012;30:2212-2219.
5) Liang TJ, Block TM, McMahon BJ, Ghany MG, Urban S, Guo JT, et al. Present and future therapies of hepatitis B: from discovery to cure. Hepatology 2015;62:1893-1908.
6) Suzuki F, Arase Y, Suzuki Y, Akuta N, Sezaki H, Seko Y, et al. Long-term efficacy of interferon therapy in patients with chronic hepatitis B virus infection in Japan. J Gastroenterol 2012;47:834-822.
7) Colonno RJ, Rose R, Baldick CJ, Levine S, Pokornowski K, Yu CF, et al. Entecavir resistance is rare in nucleoside naive patients with hepatitis B. Hepatology 2006;44:1656-1665.
8) Baldick CJ, Tenney DJ, Mazzucco CE, Eggers BJ, Rose RE, Pokornowski KA, et al. Comprehensive evaluation of hepatitis B virus reverse transcriptase substitutions associated with entecavir resistance. Hepatology 2008;47:1473-1482.
9) Tenney DJ, Rose RE, Baldick CJ, Pokornowski KA, Eggers BJ, Fang J, et al. Long-term monitoring shows hepatitis B virus resistance to entecavir in nucleoside-naive patients is rare through 5 years of therapy. Hepatology 2009;49:1503-1514.
10) Yuen MF, Seto WK, Fung J, Wong DK, Yuen JC, Lai CL. Three years of continuous entecavir therapy in treatment-naive chronic hepatitis B patients: VIRAL suppression, viral resistance, and clinical safety. Am J Gastroenterol 2011;106:1264-1271.
11) Zoutendijk R, Reijnders JG, Brown A, Zondervan E, Mutimer D, Deterding K, et al. Entecavir treatment for chronic hepatitis B: adaptation is not needed for the majority of naive patients with a partial virological response. Hepatology 2011;54:443-451.
12) Tenney DJ, Levine SM, Rose RE, Walsh AW, Weinheimer SP, Discotto L, et al. Clinical emergence of entecavir-resistant hepatitis B virus requires additional substitutions in virus already resistant to Lamivudine. Antimicrob Agents Chemother 2004; 48:3498-3507.
13) Hayashi S, Murakami S, Omagari K, Matsui T, Iio E, Isogawa M, et al. Characterization of novel entecavir resistance mutations. J Hepatol 2015;63:546-553.
14) Yamada N, Shigefuku R, Sugiyama R, Kobayashi M, Ikeda H, Takahashi H, et al. Acute hepatitis B of genotype H resulting in persistent infection. World J Gastroenterol 2014;20:3044-3049.
15) Guetter S, Li BC, Miska S, Kruger DH, Meisel H, Will H. A novel method for efficient amplification of whole hepatitis B virus genomes permits rapid functional analysis and reveals deletion mutants in immunosuppressed patients. J Virol 1995;69: 5437-5444.
16) Abe A, Inoue K, Tanaka T, Kato J, Kajiyama N, Kawaguchi R, et al. Quantitation of hepatitis B virus genomic DNA by real-time detection PCR. J Clin Microbiol 1999;37:2899-2903.
17) Chotiyaputta W, Peterson C, Ditah FA, Goodwin D, Lok AS. Persistence and adherence to nucleos(t)ide analogue treatment for chronic hepatitis B. J Hepatol 2011;54:12-18.
18) Sugiyama M, Tanaka Y, Kato T, Orito E, Ito K, Acharya SK, et al. Influence of hepatitis B virus genotypes on the intra- and extracellular expression of viral DNA and antigens. Hepatology 2006;44:915-924.
19) Delaney WE, Yang H, Westland CE, Das K, Arnold E, Gibbs CS, et al. The hepatitis B virus polymerase mutation rtV173L is selected during lamivudine therapy and enhances viral replication in vitro. J Virol 2003;77:11833-11841.
20) Allen MI, Deslauriers M, Andrews CW, Tipples GA, Walters KA, Tyrrell DL, et al. Identification and characterization of mutations in hepatitis B virus resistant to lamivudine. Lamivudine Clinical Investigation Group. Hepatology 1998;27:1670-1677.
21) Brunelle MN, Lucifora J, Neyts J, Villet S, Holy A, Trepo C, et al. In vitro activity of 2,4-diamino-6-[2-(phosphonomethoxy) ethoxy]-pyrimidine against multidrug-resistant hepatitis B virus mutants. Antimicrob Agents Chemother 2007;51: 2240-2243.
22) Chang TT, Gish RG, Hadziyannis SJ, Cianciara J, Rizzetto M, Schiff ER, et al. A dose-ranging study of the efficacy and tolerability of entecavir in Lamivudine-refractory chronic hepatitis B patients. Gastroenterology 2005;129:1198-1209.
23) Sherman M, Yurdaydin C, Sollano J, Silva M, Liaw YF, Cianciara J, et al. Entecavir for treatment of lamivudine-refractory, HBeAg-positive chronic hepatitis B. Gastroenterology 2006;130:2039-2049.
24) Angus P, Vaughan R, Xiong S, Yang H, Delaney W, Gibbs C, et al. Resistance to adefovir dipivoxil therapy associated with the selection of a novel mutation in the HBV polymerase. Gastroenterology 2003;125:292-297.
25) **Kwon SY, Park YK**, Ahn SH, Cho ES, Choe WH, Lee CH, et al. Identification and characterization of clevudine-resistant mutants of hepatitis B virus isolated from chronic hepatitis B patients. J Virol 2010;84:4494-4503.
26) Zhong Y, Lv J, Li J, Xing X, Zhu H, Su H, et al. Prevalence, virology and antiviral drugs susceptibility of hepatitis B virus rtN236T polymerase mutation from 1865 Chinese patients with chronic hepatitis B. Antiviral Res 2012;93:185-190.

27) Ahn SH, Kim DH, Lee AR, Kim BK, Park YK, Park ES, Ahn SH, et al. Substitution at rt269 in hepatitis B virus polymerase is a compensatory mutation associated with multi-drug resistance. PLoS One 2015;10:e0136728.
28) Ahn SH, Park YK, Park ES, Kim JH, Kim DH, Lim KH, et al. The impact of the hepatitis B virus polymerase rtA181T mutation on replication and drug resistance is potentially affected by overlapping changes in surface gene. J Virol 2014;88:6805-6818.
29) Kamatani Y, Wattanapokayakit S, Ochi H, Kawaguchi T, Takahashi A, Hosono N, et al. A genome-wide association study identifies variants in the HLA-DP locus associated with chronic hepatitis B in Asians. Nat Genet 2009;41:591-595.
30) Mbarek H, Ochi H, Urabe Y, Kumar V, Kubo M, Hosono N, et al. A genome-wide association study of chronic hepatitis B identified novel risk locus in a Japanese population. Hum Mol Genet 2011;20:3884-3892.
31) Honda T, Suzuki F, Kobayashi M, Fukushima T, Kawamura Y, Sezaki H, et al. HLA-DP genes polymorphisms associate with hepatitis B surface antigen kinetics and seroclearance during nucleos(t)ide analogue therapy. Liver Int 2015;35:1290-1302.
32) Warner N, Locarnini S. The antiviral drug selected hepatitis B virus rtA181T/sW172* mutant has a dominant negative secretion defect and alters the typical profile of viral rebound. Hepatology 2008;48:88-98.
33) Villet S, Pichoud C, Billioud G, Barraud L, Durantel S, Trepo C, et al. Impact of hepatitis B virus rtA181V/T mutants on hepatitis B treatment failure. J Hepatol 2008;48:747-755.
34) Dai J, Chen EQ, Bai L, Gong DY, Zhou QL, Cheng X, Huang FJ, et al. Biological characteristics of the rtA181T/sW172* mutant strain of Hepatitis B virus in animal model. Virol J 2012;9:280.
35) Yang H, Westland CE, Delaney WE, Heathcote EJ, Ho V, Fry J, et al. Resistance surveillance in chronic hepatitis B patients treated with adefovir dipivoxil for up to 60 weeks. Hepatology 2002;36:464-473.
36) Sheldon J, Rodes B, Zoulim F, Bartholomeusz A, Soriano V. Mutations affecting the replication capacity of the hepatitis B virus. J Viral Hepat 2006;13:427-434.

Author names in bold designate shared co-first authorship.

Supporting Information

Additional Supporting Information may be found at onlinelibrary.wiley.com/doi/10.1002/hep4.1022/suppinfo.

IJC
International Journal of Cancer

Identification of human papillomavirus (HPV) 16 DNA integration and the ensuing patterns of methylation in HPV-associated head and neck squamous cell carcinoma cell lines

Takashi Hatano[1], Daisuke Sano[1,2], Hideaki Takahashi[1,3], Hiroshi Hyakusoku[1], Yasuhiro Isono[1], Shoko Shimada[1], Kae Sawakuma[1], Kentaro Takada[1], Ritsuko Oikawa[4], Yoshiyuki Watanabe[4], Hiroyuki Yamamoto[4], Fumio Itoh[4], Jeffrey N. Myers[3] and Nobuhiko Oridate[1,2]

[1] Department of Biology and Function in Head and Neck, Yokohama City University Graduate School of Medicine, Yokohama, Japan
[2] Department of Otorhinolaryngology – Head and Neck Surgery, Yokohama City University, School of Medicine, Yokohama, Japan
[3] Department of Head and Neck Surgery, The University of Texas MD Anderson Cancer Center, Houston, TX
[4] Division of Gastroenterology and Hepatology, Department of Internal Medicine, St. Marianna University School of Medicine, Kawasaki, Japan

Cancer Genetics and Epigenetics

Recent studies showed that human papillomavirus (HPV) integration contributes to the genomic instability seen in HPV-associated head and neck squamous cell carcinoma (HPV-HNSCC). However, the epigenetic alterations induced after HPV integration remains unclear. To identify the molecular details of HPV16 DNA integration and the ensuing patterns of methylation in HNSCC, we performed next-generation sequencing using a target-enrichment method for the effective identification of HPV16 integration breakpoints as well as the characterization of genomic sequences adjacent to HPV16 integration breakpoints with three HPV16-related HNSCC cell lines. The DNA methylation levels of the integrated HPV16 genome and that of the adjacent human genome were also analyzed by bisulfite pyrosequencing. We found various integration loci, including novel integration sites. Integration loci were located predominantly in the intergenic region, with a significant enrichment of the microhomologous sequences between the human and HPV16 genomes at the integration breakpoints. Furthermore, various levels of methylation within both the human genome and the integrated HPV genome at the integration breakpoints in each integrant were observed. Allele-specific methylation analysis suggested that the HPV16 integrants remained hypomethylated when the flanking host genome was hypomethylated. After integration into highly methylated human genome regions, however, the HPV16 DNA became methylated. In conclusion, we found novel integration sites and methylation patterns in HPV-HNSCC using our unique method. These findings may provide insights into understanding of viral integration mechanism and virus-associated carcinogenesis of HPV-HNSCC.

Introduction

Head and neck squamous cell carcinoma (HNSCC) is the sixth most common cancer worldwide, accounting for 3–5% of all cancers.[1] Recently, the incidence of oropharyngeal cancer (OPC) has been reported to be increasing markedly. This is mainly because the number of human papillomavirus (HPV)-related oropharyngeal cancers (HPV-OPC) has risen globally,[2] while the incidence of HNSCC associated with the use of tobacco and alcohol use has remained constant or decreased.

The tumor biology and clinical characteristics of HPV-OPC differ from those of HPV-negative HNSCCs, which are mainly alcohol- and smoking-related HNSCCs.[3] Most patients with HPV-OPC present with advanced nodal stage, and tend to be younger than patients with non-HPV-associated tumors. Furthermore, HPV-OPC is associated with better response rates to treatment, and overall better prognosis when compared to non-HPV HNSCC. Therefore, the presence of HPV is now one of the most important prognostic factors in OPC patients.[2]

While there are 15 high-risk subtypes of HPV with carcinogenic potential in humans, the vast majority of HPV-OPC is associated with HPV16.[4,5] High-risk HPV infection of mucosal epithelia leads to the expression of viral E6 and E7 oncoproteins inducing the inactivation of both the p53 and the retinoblastoma (Rb) tumor suppressive proteins, which contribute to the malignant formation of HPV-related

Key words: human papillomavirus (HPV), DNA integration, epigenome, head and neck squamous cell carcinoma (HNSCC)
Additional Supporting Information may be found in the online version of this article.
Grant sponsor: Grant-in-Aid for Scientific Research; **Grant numbers:** 16K11240 (PI: DS) and 16K11242 (PI: HT)
DOI: 10.1002/ijc.30589
History: Received 15 Aug 2016; Accepted 13 Dec 2016; Online 22 Dec 2016
Correspondence to: Daisuke Sano, Department of Otorhinolaryngology – Head and Neck Surgery, Yokohama City University, School of Medicine, 3-9 Fukuura, Kanazawa-ku, Yokohama 236-0004, Japan, E-mail: dsano@yokohama-cu.ac.jp; Tel: +81 45 787 2687

What's new?

Human papillomavirus (HPV) integration into the human genome induces genomic instability in HPV-associated squamous cell carcinoma; however, the details of the epigenetic alterations after HPV integration remain unclear. Here, the authors identified HPV16 integration breakpoints by next-generation sequencing using a target-enrichment method. Moreover, they observed that the methylation levels of the HPV16 integrants were associated with the methylation status of the flanking host genome using bisulfite pyrosequencing. The findings provide insights into the mechanisms for viral integration and carcinogenesis of HPV-associated head and neck squamous cell carcinoma and suggest that epigenetic alterations might provide candidate biochemical markers for precancerous stage.

cancers. In addition, immune escape, genomic instability, HPV DNA integration and epigenetic alterations are also important for HPV-related cancer progression.[6] In fact, high-risk HPV integration is now known to be associated with the progression from low- to high-grade cervical intraepithelial neoplasia.[7] Many epigenetic alterations have also been reported during the process of cervical carcinogenesis in both the HPV and human genomes.[8] The mechanisms of these factors affecting HPV-induced cervical carcinogenesis have been thus well studied.

In HNSCC, a recent study using deep sequencing of HPV-HNSCC cell lines and HNSCC samples concluded that HPV16 integration itself directly promotes genomic instability and is important for carcinogenesis.[9] Park *et al.* have shown that hypomethylation status within the viral genome, especially in the long control region (LCR) including E2 binding sites (E2BSs), was related to E6 and E7 expression in HPV-related HNSCC.[10] On the other hand, several articles have also reported that hypermethylation status in the E2BSs might cause deregulated E6 and E7 expression.[11,12] Thus, the roles of altered methylation status of HPV during HPV-HNSCC development remain unclear. Therefore, the HPV methylation status, including the association of epigenetic alterations in HPV integrants and the flanking host genomes, requires further characterization to allow us a better understanding of the detailed mechanisms of the viral integration and carcinogenesis of HPV-HNSCC.

In our study, we identified the molecular details of HPV16 DNA integration and the ensuing patterns of methylation in HPV-HNSCC with a previously reported[13] next-generation sequencing (NGS)-based method for methylation analysis of integrated viral genomes (G-NaVI) using 3 HPV-related HNSCC cell lines to reveal the association of epigenetic alterations in HPV integrants and the flanking host genomes.

Materials and Methods

Cell lines

The UPCI:SCC090, UPCI:SCC152 and UPCI:SCC154 cell lines were kindly provided by Dr Susanne M. Gollin, University of Pittsburgh. The clinicopathological data for the patients and tumors from which the cell lines were derived are shown in Table 1. Cell lines were maintained in appropriate media containing 10% fetal bovine serum in plastic culture plates. Adherent monolayer cultures were maintained on plastic and incubated at 37°C in 5% CO_2 and 95% air. The integrity of each maintained cell line was clearly established by comparing the results from short tandem repeat profiling[14] with that reported for the original stock.[15] The cultures were free of *Mycoplasma* species and were maintained for no longer than 12 weeks after recovery from frozen stocks.

Analysis of HPV16 integration site sequences using next-generation sequencing (NGS)

Genomic DNA was extracted from cultured cells using the QIAamp DNA Mini Kit (Qiagen, Valencia, CA) according to the manufacturer's instructions. The concentration and quantity of extracted DNA were measured using a NanoDrop spectrophotometer (Nano Drop Technologies, Wilmington, DE). A total of 427 custom-made RNA probes covering the entire HPV16 DNA sequences were designed using the Agilent SureSelect Target Enrichment System, a highly efficient hybrid selection technique for optimizing NGS. After capture and amplification, the templates were sequenced using the GS FLX Titanium system (Roche, Basel, Switzerland). Reads that aligned perfectly with the human (GRCh37/hg19) or HPV16 (KO2718) genome were removed. Reads that aligned partially with the human genome and HPV16 genome were reserved. PCR and Sanger sequencing were used to verify the selected HPV integration breakpoints. PCR primers were designed to amplify the integrated HPV and the flanking human genome. As a template, 1 μL of genomic DNA solution was used in the subsequent PCR. Touchdown PCR was used for most of the assays. All PCR assays included a denaturation step at 95°C for 30 s, followed by an annealing step at various temperatures for 30 s, and an extension step at 72°C for 30 s. PCR products were analyzed using electrophoresis through 2% agarose gels.

Genomic elements around the integration positions

Genomic elements around the integration sites were analyzed using the RepeatMasker from the UCSC genome browser (https://genome.ucsc.edu/index.html). Each integration site was compared to previously reported integration and fragile sites.[16,17] HPV16 breakpoints were mapped to the HPV16

Table 1. Primary site and source of tumors used to derive the 3 HPV-HNSCC cell lines

Cell line	UPCI:SCC090	UPCI:SCC152	UPCI:SCC154
Sex	Male	Male	Male
Age at surgery	46	47	54
Smoking	Yes	Yes	Yes
Alcohol	Yes	Yes	Yes
Primary tumor site	Base of tongue	Hypopharynx	Tongue
TNM classification	T2N0	Recurrence	T4N2
Degree of differentiation	Poorly to moderately	Moderately	NA

genome, and the distribution of the integration sites was analyzed.

Microhomology (MH) calculation at the HPV16 genome integration sites

Bilateral sequences from the human and HPV16 genomes were extracted and the paired sequences were compared base by base to count the same sequences. The contiguous identical bases that could not be extended were defined as MH units and the MH lengths at the integration sites were also calculated.

DNA methylation analysis of the integrated HPV genome as well as the adjacent human genome

DNA methylation was analyzed using bisulfite pyrosequencing. Bisulfite PCR was performed according to the manufacturer's protocol. One microliter of bisulfite-treated DNA, prepared using an EpiTect Bisulfite Kit (Qiagen), was used as a template. The primers used for amplifying the CpG sequences in the given sequence are described in Supplementary Table 1. After PCR, the biotinylated strand was captured on streptavidin-coated beads (Amersham Bioscience, Uppsala, Sweden) and incubated with sequencing primers (Supplementary Table 1). The pyrosequencing reactions were performed using the PyroMark Q24 Advanced (Qiagen) with the 3 HPV-HNSCC cell lines. Primers for the methylation analysis of integration sites in the UPCI:SCC090 line are shown in Supplementary Table 1.

DNA fragments, including 150 bp of the integrated HPV DNA and 150 bp of the human genome around the boundary, were then analyzed for average methylation to examine the correlation between the methylation pattern of the integrated HPV DNA and that of the human genome.

Lastly, allele-specific DNA methylation of both the integrated HPV genome and adjacent human genome was analyzed as described previously.[18] For this analysis, the pyrosequencing reactions were performed using the PyroMark Q24 Advanced (Qiagen).

LINE1 methylation analysis

To quantify the relatively high LINE1 methylation levels, pyrosequencing technology was again used as described previously.[19] Briefly, PCR and the subsequent pyrosequencing for LINE1 were performed using the PyroMark kit (Qiagen). This assay amplifies a region of the LINE1 elements that includes 3 CpG sites. PCR was conducted as follows: 45 cycles at 95°C for 20 s, 50°C for 20 s and 72°C for 20 s, followed by 72°C for 5 min. The biotinylated PCR product was purified and converted to single strands to serve as a template for the pyrosequencing reaction using the Pyrosequencing Vacuum Prep Tool (Qiagen). The pyrosequencing reactions were performed using the PyroMark Q24 (Qiagen). The percentage of Cs relative to the total sum of the Cs and Ts at each CpG site was calculated. The average of the percentages of Cs at the 3 CpG sites was used to represent the overall LINE1 methylation level in each cell line.

Statistical analysis

The Spearman correlation coefficient was used to assess correlations between the average methylation of the HPV DNA and that of the human genome. Randomly selected breakpoints across the human genome were used to compare the observed and expected integration results. The χ^2 test was used for statistical analyses to compare variables between two groups. Statistical analyses were performed using GraphPad Prism Version 6.05 (GraphPad Software, La Jolla, CA) and IBM SPSS Statistics for Windows Version 22.0 (IBM Corp., Armonk, NY). A p-values of <0.05 was considered statistically significant.

Results

NGS analysis of HPV16 DNA integration site sequences

To detect the HPV16 integration sites effectively, we designed a target-enrichment technique using NGS analysis (Supplementary Fig. 1) with a total of 427 custom RNA probes to specifically target the HPV genome. The average read length was 414.18 bp, and the average read quality was 31.30 with >99.9% accuracy. The genome wide map of HPV16 integration sites is shown in (Fig. 1). The HPV integrants were mapped to chromosomes 2q23, 3p12, 6p21 and 9q22 in UPCI:SCC090, chromosomes 2q23, 3p12, 9q22 and 9q31 in UPCI:SCC152, and chromosome 21q21 in UPCI:SCC154. Integration sites were mainly located in the intergenic regions, and no integration sites were observed in the promoter or exon region (Fig. 1). The UPCI:SCC090 and UPCI:SCC152 cell lines, derived from a recurrent tumor from the same patient, showed almost identical integration

Cancer Genetics and Epigenetics

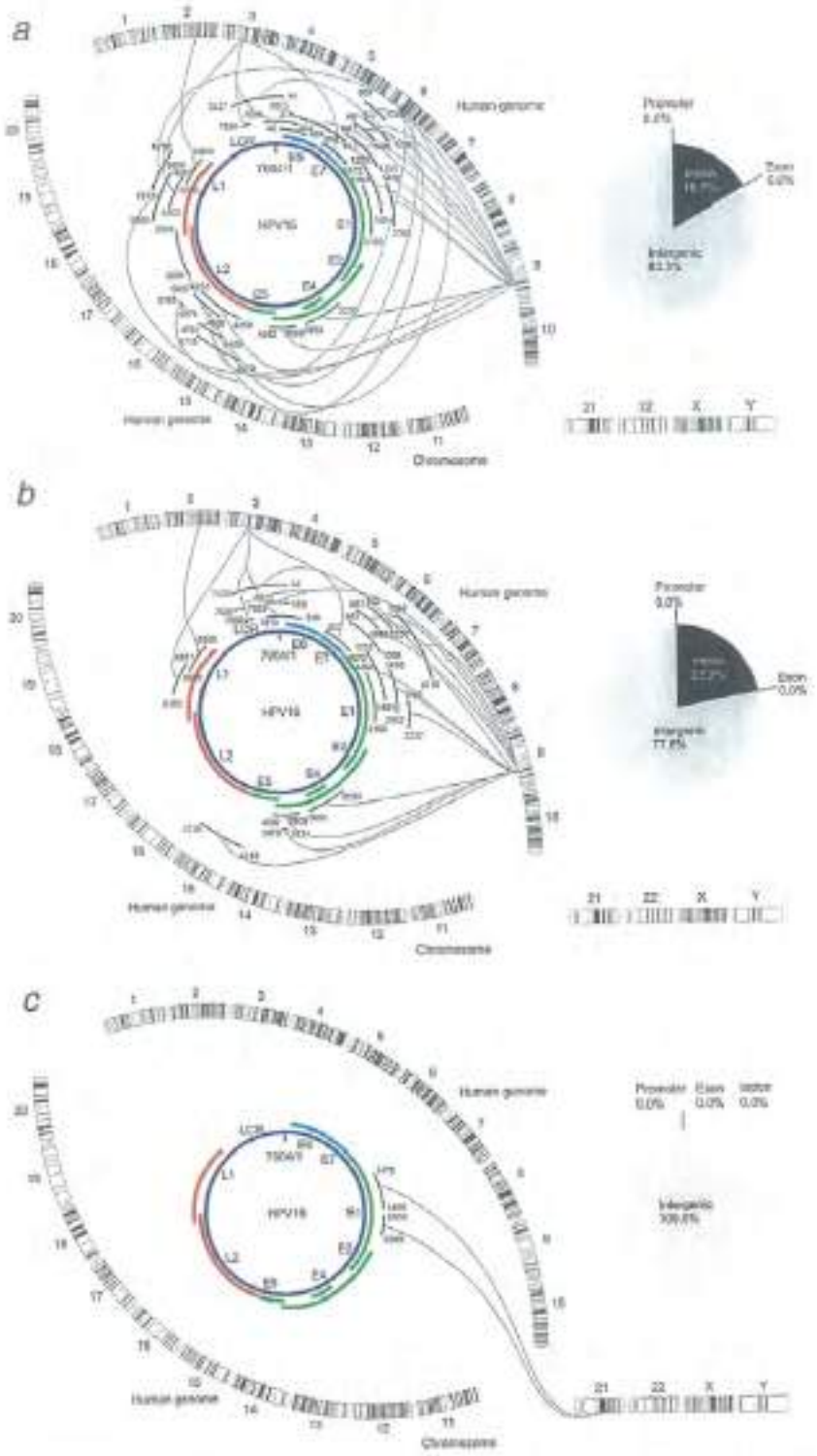

Figure 1. Distribution of integration breakpoints in the human chromosomes and HPV16 genome represented by Circos plots of (a) the UCSC:SCC090 genome, (b) the UCSC:SCC152 genome and (c) the UCSC:SCC154 genome. [Color figure can be viewed at wileyonlinelibrary.com]

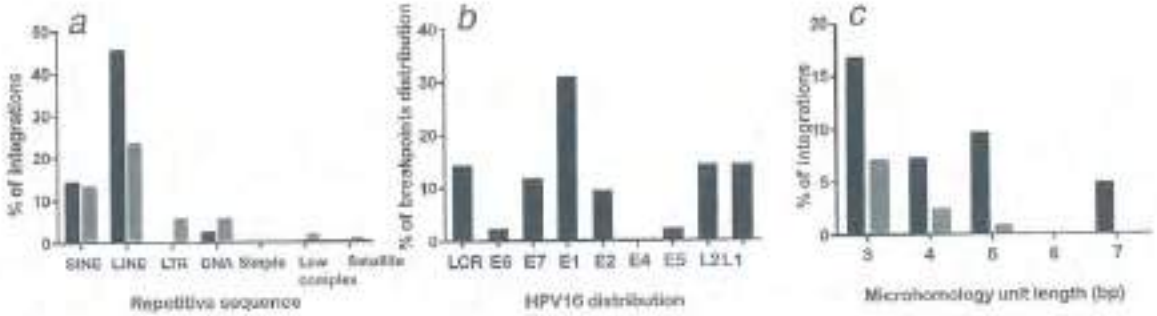

Figure 2. Analysis of the HPV16 integration sites. (*a*) Repetitive elements analysis at integration breakpoints in the human genome, compared to expected the results. (*b*) The percentage of breakpoints distribution in the HPV16 genome. (*c*) Comparison between observed and expected integrations harboring MHs of different sizes at the integration sites.

sites, although a lack of integration in chromosome 6 was observed in UPCI:SCC152. Our mapping of the HPV16 integration sites provided greater detail than a previous report using FISH and APOT- and DIPS- PCR analysis in UPCI:SCC090 and UPCI:SCC152 cells.[20] Furthermore, our results for the UPCI:SCC090 cell line was consistent with those of a previous report based on the whole genome sequence (WGS).[9] In addition, we found some new HPV integration sites in our study.

Characterization of genomic sequences adjacent to HPV16 integration breakpoints

To validate whether the HPV integrants in HNSCC target common fragile sites (CFSs) as reported previously in cervical cancers,[21] we compared the observed integration breakpoints in 3 cell lines with previously reported fragile sites.[16] We confirmed that these integration breakpoints are not only at or near CFSs but also at rare fragile sites (RFSs) in the UPCI:SCC090 and UPCI:SCC152 cell lines. Integration breakpoints in the UPCI:SCC154 cell line were detected at chromosome 21q21. This site was neither a CFS nor a RFS, however, it had previously been reported as one of the integration breakpoints in cervical cancer.[17] In addition, repetitive sequences at the integration sites were analyzed using RepeatMasker (http://www.repeatmasker.org/). Our results showed that 26/42 of the integration sites were distributed in repeating elements throughout the human genome. The number of integrations in long interspersed nuclear element (LINE) repeats (19/42) was found to be significantly larger than that of the expected occurrences by χ^2 test (Fig. 2*a*, $p = 0.006$).

HPV16 integration sites were distributed across almost the whole genome except for E4. Breakpoints were prone to occur in E1 13/42 (Fig. 2*b*), which is consistent with previous reports.[22,23]

Distinct categories of viral-host sequence at the HPV16 integration breakpoints

Furthermore, viral-host junctional sequences were analyzed to reveal the existence of three distinct categories as reported previously.[24,25] The first category was defined as a seamless transition from one sequence to the next with a clearly defined breakpoint, as shown in Figure 3*a* and 3*d* (4/42). The second category 15/42 was defined as the presence of short inserted sequences at the breakpoint that match neither reference sequence (Fig. 3*b* and 3*d*, 15/42). The final category, which includes the majority of tumors 23/42, characterized by breakpoint microhomology was defined as the presence of several base of pairs of sequence homology at the breakpoint junction that could be assigned to either genome (Fig. 3*c* and 3*d*, 23/42). In our samples, the breakpoint microhomology ranged from 1 to 7 bp in length. Furthermore, there was a significant enrichment of MHs when the MH length was 7 bp between the human genome and the HPV genome at or near integration breakpoints compared to the expected integration ($p = 0.002$). When MH lengths were 3, 4 or 5 bp in length, the observed integrations tended to have more MHs than did the expected integrations; however, the differences were not significant ($p = 0.054$, 0.17 and 0.21, respectively, Fig. 2*c*).

Correlation between the methylation pattern of the integrated HPV16 DNA and the human genome DNA

To reveal the association between the epigenetic alterations in HPV integrants and the flanking host genomes, we first evaluated DNA methylation of the human genome at the HPV16 integration breakpoints by bisulfite pyrosequencing. We detected varying levels of methylation of the human genome at the HPV16 integration breakpoints in the genome of UPCI:SCC090, UPCI:SCC152 and UPCI:SCC154 cells as shown in Figure 4*b* and Supplementary Figure 2. However, no association was observed between the presence of integration occurrence and methylation level of the human genome.

We then evaluated DNA methylation of the integrated HPV16 genome by bisulfite pyrosequencing. We also found varying levels of methylation of the HPV16 sequences integrated into the genome of UPCI:SCC090, UPCI:SCC152 and UPCI:SCC154 cells. In addition, each integrant with the same viral gene showed differing methylation levels (Fig. 4*b* and Supplementary Fig. 2).

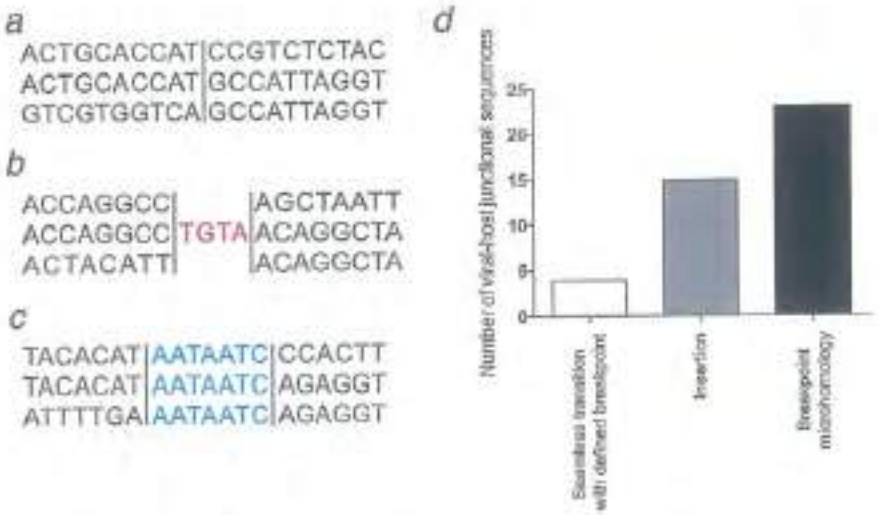

Figure 3. Categories of viral-host breakpoints. (Gray in b) Nucleotides that align to neither reference genome (insertions); (Gray in c) nucleotides that align to both reference genome (microhomology). (a) Seamless transition with defined breakpoint. (b) Insertion. (c) Breakpoint microhomology. (d) The number of viral-host junctional sequences. [Color figure can be viewed at wileyonlinelibrary.com]

To evaluate if the levels of methylation in the HPV16 DNA were associated with that of human genome, DNA fragments including the 150 bp of the HPV16 DNA and 150 bp of the human genome around the boundary were analyzed for average methylation. A statistically significant correlation was observed between the average methylation of the HPV16 and that of the human genome in all 3 cell lines (Figs. 5a and 5b).

These results suggested that the DNA methylation status of the integrated HPV16 genome was affected by the methylation status of the human genome flanking integration breakpoints. As our previous report also showed that methylation of the integrated HBV DNA is related to the methylation status of the flanking human genome,[15] we therefore hypothesized that DNA methylation in the integrated HPV16 genome is related to the methylation status of the integration sites within the host genome.

Allele-specific DNA methylation analysis of the HPV16 genome

To confirm our hypothesis, we further characterized the methylation status of the HPV genome and human genome by allele-specific DNA methylation analysis (Fig. 4a). We confirmed that the HPV genome was often highly methylated when integrated into highly methylated sites in the host genome, while the HPV16 genome remained largely unmethylated when integrated into unmethylated regions (Fig. 5c). Our results thus suggested that the HPV16 integrants became hypomethylated when the flanking host genomes were hypomethylated.

LINE1 methylation analysis

Despite the fact that integration mainly occurs in intergenic regions, which are usually considered to be highly methylated, we found varying levels of methylation in the human genome at the HPV16 integration breakpoints. Therefore, we planned to evaluate the global methylation levels of these cell lines. As LINE1 methylation level has been reported to be a good indicator of the global DNA methylation level,[26–28] we performed LINE1 methylation analysis in these cell lines. We found hypomethylation status of LINE1 in all of 3 cell lines as shown in Figure 4c. These results indicate that global hypomethylation occurred in all 3 cell lines, consistent with the varying levels of methylation in intergenic regions observed in our study.

Discussion

In our study, we revealed the detailed association between the epigenetic alterations in HPV integrants and the flanking host genomes in 3 HPV-related HNSCC cell lines using our novel approach with an NGS-based method for the structural methylation analysis of integrated viral genomes. Our NGS-based method using unique probes enabled us to identify some previously unreported integrants and that the HPV genome is often highly methylated when integrated into highly methylated sites in the host genome, while HPV16 integrants remained hypomethylated when the flanking host genome was hypomethylated.

The methylation of viral DNA integrated into the human genome has been studied over the past decade[29] and in general it has been found that the local pattern of DNA methylation gradually spreads to involve the integrated viral genome.[30] Our study showed a statistically significant correlation between the average methylation level of the HPV16 DNA and that of the flanking host genome in 3 HPV-HNSCC cell lines. This correlation may be explained by our previous observation, indicating that the HBV genome often became significantly methylated when integrated into highly

Figure 4. Allele-specific methylation analysis of 3 cell lines. (A) A schema of the allele-specific methylation analysis. (B) Methylation levels of the HPV16 and human genomes for the integrated and unintegrated alleles. Detailed results of the HPV16 integrants (LCR, E6, E7, E1, E2, E4, E5, L2, L1) and flanking host genomes (chromosome and location of the genome) are shown. DNA methylation of the integrated HPV16 genomes as well as the flanking human genome was examined by allele-specific DNA methylation analysis using bisulfite pyrosequencing. (C) The results of LINE1 methylation analysis.

methylated host sites.[25] To the best of our knowledge, this is the first report to show a relationship between DNA methylation in the integrated HPV16 genome and the methylation status of the flanking host genome at the integration breakpoints in HPV-HNSCC.

The methylation of viral DNA in the virus-integrated cells has the potential to alter the expression levels of the viral genome.[31] A previous report showed a causal relationship between the demethylation of gene bodies and altered expression of the associated genes in cancer.[32] Our current and previous results thus suggested that the HPV integrants might be inactivated by methylation when integrated into a highly methylated human genome, while the HPV integrants could remain unmethylated after integrated into an unmethylated host genome, leading to tumorigenesis. However, there remains possibility that some alterations of methylation status of the HPV genome are occurred before the HPV integration into the human genome, as several publications have reported the hypothesis indicating that differential methylation of the E2BSs is related to the activation of both viral oncogene expression and the viral genome remains in the episomal state.[12,33] In this case, the methylation status of the

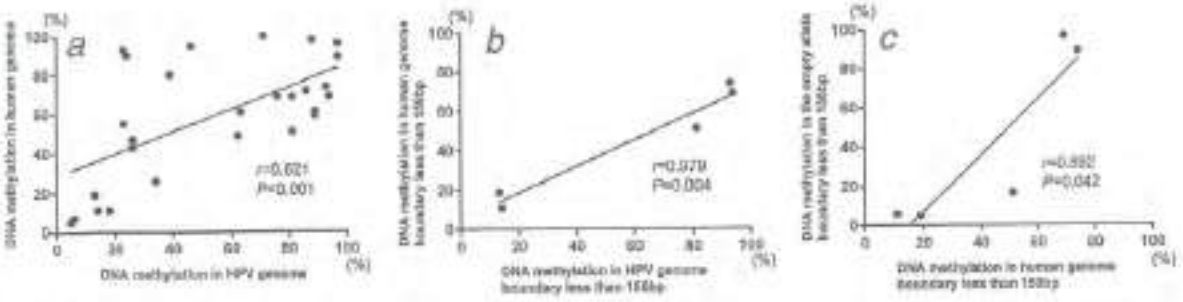

Figure 5. Correlation analysis between the methylation pattern of the integrated HPV16 DNA and that of the human genome. DNA fragments, including 150 bp of the HPV16 DNA and 150 bp of the human genome around the boundary, were analyzed for average methylation. (A) Correlation for total integration sites between the methylation levels of the HPV16 DNA and that of the human genome in the 3 cell lines. (B) Correlation between 150 bp of the HPV16 DNA and 150 bp of the human genome around the boundary analyzed for average methylation. (C) Correlation between 150 bp of the human genome and 150 bp of the empty allele around the boundary analyzed for average methylation. Correlations were analyzed with Pearson's correlation coefficients, and *p*-values were computed for the two-tailed test.

human genome might be affected by the methylation status of the HPV genome, as there were a couple of areas showing that the methylation status of human genome was not correlated with the methylation status of the HPV genome in our study. The biological impact of methylation on viral function needs to be further addressed. Since HPV integrations were mainly observed in non-coding regions in our study, the association of epigenetic alteration with non-coding RNAs, including miRNA and long non-coding RNA, might be related to these epigenetic alterations.

In addition, the hypomethylation of LINE1 was also observed in all 3 cell lines, indicating that global hypomethylation could occur in HPV-HNSCC. Global hypomethylation of DNA sequences is often observed, not only during the early stage of tumorigenesis or in abnormal non-neoplastic tissues, but also on tumor progression.[34] As the degree of DNA hypomethylation increases with the grade of cervical neoplasia,[35] the DNA hypomethylation status might serve as oropharyngeal precancerous marker, since HPV-induced precancerous lesions, such as cervical intraepithelial neoplasias, have yet to be noted.

Recent genome-wide profiling of HPV integration in cervical cancer has shown that breakpoints could occur in any region of the viral genome, in contrast to the previously commonly held idea that integrated HPV16 would retain intact oncogene E6 and E7 with the long control region (LCR).[23] Our results in HPV-HNSCC cells were consistent with these previous results. In our study, the UPCI:SCC152 cell line, derived from a recurrent tumor in the patient from whom the UPCI:SCC090 cell line was derived, showed almost identical integration sites to UPCI:SCC090, which is consistent with a previous report that these cell lines have clonal expansion.[20] Interestingly, a lack of integration in chromosome 6 was observed only in the UPCI:SCC152 line. Further analysis would be required if this integration event itself caused genomic instability or the HPV integration tended to occur in the instable human genome regions.

There are several mechanisms for DNA repair, including non-homologous end joining (NHEJ), non-allelic homologous recombination (NAHR), fork stalling and template switching (FoSTeS),[36] and microhomology-mediated break-induced replication (MMBIR).[37] A recent report indicated that these mixed DNA-repair pathways participate in viral integration at genomic instability-related genomic elements.[23] The characteristics of the boundary including insertion and microhomology in our study were consistent with this idea. In addition, a previous report showed that microhomology occurred not only at the breakpoint but also near the breakpoint, which was called flanking microhomology.[24] This phenomenon was also reported in association with HPV genome integration in cervical carcinoma.[23] This mechanism was also observed in HBV integration,[23] indicating that both breakpoint and flanking microhomology might be a common mechanism for dsDNA virus integration. As several definitions exist for breakpoint and flanking microhomology,[23,24] we only analyzed breakpoint microhomology in our study. Recently, Akagi *et al.* proposed a "looping model" to explain HPV integrant-mediated DNA replication and recombination leading to disruption of the expression and structure of neighboring genes.[9] Although our methodology was not able to examine the presence of this phenomenon, analysis around the boundary is thus important to understand molecular mechanism of HPV integration.

One of the main limitations in our study was that only 3 cell lines were analyzed. A larger cohort, including clinical samples, should be analyzed to confirm our findings and to fully understand the pattern of methylation in the carcinogenesis of HPV-HNSCC. Other limitations might exist regarding the method itself using bisulfite pyrosequencing analysis with limited sequencing length from the boundary in our study. Particularly, the association between the methylation levels and transcription levels of the integrants in HPV-HNSCC cells could not be clarified in our study, since multiple HPV16 integration sites were present in the analyzed

samples. We therefore have performed Amplification of Papillomavirus Oncogene Transcripts PCR (APOT-PCR) assay as described before[38] to detect both integrated and episomal state of HPV. This PCR-based assay showed that all of 3 cell lines had the integration pattern and two of 3 cell lines had the episomal pattern (data not shown). Thus, the observed association between the methylation of the HPV integrants and the flanking host genome probably needs to be clarified as sequencing technology advances in the future. Lastly, while our results for the UPCI:SCC090 cell line were consistent with those of a previous report using WGS[9] with some additional integration sites identified, there were also several integration sites identified by Akagi *et al.*[9] which we could not observe in our study. These small discrepancies could also be clarified with further advances in RNA sequencing technology. Despite these limitations, our results suggested that our G-NaVI method was a robust tool for the analysis of not only genomic sequences but also epigenetic alterations around integration breakpoints.

In conclusion, we here presented the molecular details of HPV16 DNA integration and various patterns of methylation in HPV-HNSCC using G-NaVI with 3 HPV-related HNSCC cell lines to reveal the association between epigenetic alterations in HPV integrants and the flanking host genomes. These results provided insights into the understanding of HPV integration in HNSCC with regard to HPV-related tumor progression, and also suggested that epigenetic alterations might provide candidate biochemical markers for establishing the precancerous stage in head and neck neoplasms. Together with previous reports on the whole genome and deep sequencing analysis,[9,22] the detailed analysis performed in our study can help us understand the mechanisms for the viral integration and carcinogenesis of HPV-HNSCC.

Acknowledgements

We thank Mari Mitsuka (Department of Biology and Function in head and Neck, Yokohama City University Graduate School of Medicine, Yokohama, Japan) for her excellent technical assistance, and Dr Jun Nakabayashi (Advanced medical research center bioinformatics laboratory, Yokohama City University Graduate School of Medicine, Yokohama, Japan) for his professional advice with regard to the statistical analysis.

Accession Numbers

All raw sequence data for our study have been submitted to the DNA Data Bank of Japan (DDB); http://biosciencedbc.jp/en/) under the accession number DRA004152.

Disclosure of Potential Conflicts of Interest

The authors have no competing interests to disclose.

References

1. Ferlay J, Shin HR, Bray F, et al. Estimates of worldwide burden of cancer in 2008: GLOBOCAN 2008. *Int J Cancer* 2010;127:2893–917.
2. Ang KK, Harris J, Wheeler R, et al. Human papillomavirus and survival of patients with oropharyngeal cancer. *N Engl J Med* 2010;363:24–35.
3. Marur S, D'Souza G, Westra WH, et al. HPV-associated head and neck cancer: a virus-related cancer epidemic. *Lancet Oncol* 2010;11:781–9.
4. Gillison ML, Koch WM, Capone RB, et al. Evidence for a causal association between human papillomavirus and a subset of head and neck cancers. *J Natl Cancer Inst* 2000;92:709–20.
5. Ndiaye C, Mena M, Alemany L, et al. HPV DNA, E6/E7 mRNA, and p16INK4a detection in head and neck cancers: a systematic review and meta-analysis. *Lancet Oncol* 2014;15:1319–31.
6. Sano D, Oridate N. The molecular mechanism of human papillomavirus-induced carcinogenesis in head and neck squamous cell carcinoma. *Int J Clin Oncol* 2016;21:819–26.
7. Arias-Pulido H, Peyton CL, Joste NE, et al. Human papillomavirus type 16 integration in cervical carcinoma in situ and in invasive cervical cancer. *J Clin Microbiol* 2006;44:1755–62.
8. Duenas-Gonzalez A, Lizano M, Candelaria M, et al. Epigenetics of cervical cancer. An overview and therapeutic perspectives. *Mol Cancer* 2005;4:38.
9. Akagi K, Li J, Broutian TR, et al. Genome-wide analysis of HPV integration in human cancers reveals recurrent, focal genomic instability. *Genome Res* 2014;24:185–99.
10. Park IS, Chang X, Lopez M, et al. Characterization of the methylation patterns in human papillomavirus type 16 viral DNA in head and neck cancers. *Cancer Prev Res (Phila)* 2011;4:207–17.
11. Vinokurova S, von Knebel Doeberitz M. Differential methylation of the HPV 16 upstream regulatory region during epithelial differentiation and neoplastic transformation. *PLoS One* 2011;6:e24451.
12. Rauschenbach M, Hoehbert CU, Prigge ES, et al. Methylation status of HPV16 E2-binding sites classifies subtypes of HPV-associated oropharyngeal cancers. *Cancer* 2015;121:1966–76.
13. Watanabe T, Yamamoto H, Oikawa R, et al. DNA methylation at hepatitis B viral integrants is associated with methylation at flanking human genomic sequences. *Genome Res* 2015;25:328–37.
14. Masters JR, Thomson JA, Daly-Burns B, et al. Short tandem repeat profiling provides an international reference standard for human cell lines. *Proc Natl Acad Sci USA* 2001;98:8012–7.
15. Zhao M, Sano D, Pickering CR, et al. Assembly and initial characterization of a panel of 85 genomically validated cell lines from diverse head and neck tumor sites. *Clin Cancer Res* 2011;17:7265–68.
16. Lakshmi T, Pryde JF. Human chromosome fragility. *Biochim Biophys Acta* 2008;1779:3–16.
17. Wentzensen N, Ridder R, Klaes R, et al. Characterization of viral-cellular fusion transcripts in a large series of HPV16 and 18 positive genomically lesions. *Oncogene* 2002;21:419–26.
18. Yamada Y, Ito T. Highly efficient PCR assay to discriminate allelic DNA methylation status using whole genome amplification. *BMC Res Notes* 2011;4:179.
19. Igarashi S, Suzuki H, Niinuma T, et al. A novel correlation between LINE-1 hypomethylation and the malignancy of gastrointestinal stromal tumors. *Clin Cancer Res* 2010;16:5114–23.
20. Olthof NC, Huibers CU, Kolligs J, et al. Viral load, gene expression and mapping of viral integration sites in HPV16-associated HNSCC cell lines. *Int J Cancer* 2015;136:E207–E18.
21. Thorland EC, Myers SL, Gostout BS, et al. Common fragile sites are preferential targets for HPV16 integrations in cervical tumors. *Oncogene* 2003;22:1225–37.
22. Parfenov M, Pedamallu CS, Gehlenborg N, et al. Characterization of HPV and host genome interactions in primary head and neck cancers. *Proc Natl Acad Sci USA* 2014;111:15544–9.
23. Hu Z, Zhu D, Wang W, et al. Genome-wide profiling of HPV integration in cervical cancer identifies clustered genomic hot spots and a potential microhomology-mediated integration mechanism. *Nat Genet* 2015;47:158–63.
24. Lawrence AB, Hindley GF, Fischer T, et al. RAF gene fusion breakpoints in pediatric brain tumors are characterized by significant enrichment of sequence microhomology. *Genome Res* 2011;21:305–14.
25. Liu Y, Lu Z, Ma R, et al. Comprehensive mapping of the human papillomavirus (HPV) DNA integration sites in cervical carcinomas by HPV capture technology. *Oncotarget* 2016;7:3852–64.
26. Yang AS, Estecio MR, Doshi K, et al. A simple method for estimating global DNA methylation using bisulfite PCR of repetitive DNA elements. *Nucleic Acids Res* 2004;32:e76.
27. Weisenberger DJ, Campan M, Long TI, et al. Analysis of repetitive element DNA methylation by MethyLight. *Nucleic Acids Res* 2005;33:6823–36.
28. Yang AS, Doshi KD, Choi SW, et al. DNA methylation changes after 5-aza-2'-deoxycytidine therapy in patients with leukemia. *Cancer Res* 2006;66:5495–503.

29. Doerfler W, Remus R, Muller K, et al. The fate of foreign DNA in mammalian cells and organisms. *Dev Biol (Basel)* 2001;106:88–97; discussion 143–60.
30. Oesterl G, Kohlmann I, Doerfler W. Spreading of DNA methylation across integrated foreign (adenovirus type 12) genomes in mammalian cells. *J Virol* 1991;65:4301–8.
31. Fernandez AF, Rosales C, Lopez-Nieva P, et al. The dynamic DNA methylomes of double-stranded DNA viruses associated with human cancer. *Genome Res* 2009;19:438–51.
32. Yang X, Han H, De Carvalho DD, et al. Gene body methylation can alter gene expression and is a therapeutic target in cancer. *Cancer Cell* 2014;26:577–90.
33. Chatwinghori A, Vinokurova S, Pfeifer G, et al. Differential methylation of E2 binding sites in episomal and integrated HPV 16 genomes in preinvasive and invasive cervical lesions. *Int J Cancer* 2013;132:2087–94.
34. Ehrlich M. DNA hypomethylation in cancer cells. *Epigenomics* 2009;1:239–59.
35. Kim YI, Giuliano A, Hatch KD, et al. Global DNA hypomethylation increases progressively in cervical dysplasia and carcinoma. *Cancer* 1994;74:893–9.
36. Lee JA, Carvalho CM, Lupski JR. A DNA replication mechanism for generating nonrecurrent rearrangements associated with genomic disorders. *Cell* 2007;131:1235–47.
37. Hastings PJ, Ira G, Lupski JR. A microhomology-mediated break-induced replication model for the origin of human copy number variation. *PLoS Genet* 2009;5:e1000327.
38. Klaes R, Woerner SM, Ridder R, et al. Detection of high-risk cervical intraepithelial neoplasia and cervical cancer by amplification of transcripts derived from integrated papillomavirus oncogenes. *Cancer Res* 1999;59:6133–6.

Cancer Genetics and Epigenetics

Cancer Science
Japanese Cancer Association JCA
Open Access

Serum monomeric laminin-γ2 as a novel biomarker for hepatocellular carcinoma

Hirofumi Kiyokawa,[1] Hiroshi Yasuda,[1] Ritsuko Oikawa,[1] Chiaki Okuse,[1] Nobuyuki Matsumoto,[1] Hiroki Ikeda,[1] Tsunamasa Watanabe,[1] Hiroyuki Yamamoto,[1] Fumio Itoh,[1] Takehito Otsubo,[2] Toru Yoshimura,[3] Eisaku Yoshida,[3] Masatoshi Nakagawa,[3] Naohiko Koshikawa[4,5] and Motoharu Seiki[5]

[1]Division of Gastroenterology and Hepatology; [2]Department of Surgery, St. Marianna University School of Medicine, Kawasaki; [3]Diagnostics Division, Abbott Japan Co. Ltd., Chiba; [4]Division of Cancer Cell Research, Kanagawa Cancer Center Research Institute, Yokohama; [5]Division of Cancer Cell Research, Institute of Medical Science, University of Tokyo, Tokyo, Japan

Key words
Biomarker, des-gamma-carboxy prothrombin, hepatocellular carcinoma, laminin-γ2, surveillance

Correspondence
Hiroshi Yasuda, Division of Gastroenterology and Hepatology, St. Marianna University School of Medicine, 2-16-1 Sugao, Kawasaki 216-8511, Japan.
Tel: +81-44-977-8111; Fax: +81-44-976-5805;
E-mail: hyasuda@marianna-u.ac.jp

Funding Information
N. Koshikawa received research funding from Abbott Laboratories (Chicago, IL, USA). This work was supported in part by a Grant-in-Aid for Scientific Research from the Ministry of Education, Culture, Sports, Science, and Technology of Japan (H. Yasuda), a Medical Research and Development Programs Focused on Technology Transfer: Adaptable and Seamless Technology Transfer Program through Target-Driven Research and Development (A-STEP) (T. Yoshimura, E. Yoshida, M. Nakagawa, N. Koshikawa and M. Seiki), and a Project for Development of Innovative Research on Cancer Therapeutics (P-DIRECT) (N. Koshikawa) from The Japan Agency for Medical Research and Development (AMED).

Received January 10, 2017; Revised April 6, 2017; Accepted April 8, 2017

Cancer Sci 108 (2017) 1432–1439

doi: 10.1111/cas.13261

The diagnosis of hepatocellular carcinoma (HCC) in the early stages is important for successful clinical management. Laminin (Ln)-γ2 expression has been reported in various types of malignant carcinomas. We recently developed a highly sensitive method to measure serum monomeric Ln-γ2 levels using a fully automated chemiluminescent immunoassay (CLIA). Using our CLIA, we evaluated its diagnostic value in sera from patients with chronic liver disease (CLD) and patients with hepatocellular carcinoma (HCC). Serum alpha-fetoprotein (AFP) and des-gamma-carboxy prothrombin (DCP) were also examined in these subjects. Median levels of Ln-γ2 were significantly higher in patients with HCC (173.2 pg/mL; range: 39.5–986 pg/mL) compared with patients with CLD (76.7 pg/mL; range: 38.7–215.9 pg/mL) and with healthy volunteers (41.1 pg/mL; range: 10.9–79.0 pg/mL). The optimal cutoff value for Ln-γ2 that allowed us to distinguish between HCC and nonmalignant CLD was 116.6 pg/mL. Elevated Ln-γ2 levels were observed in 0% of healthy volunteers, 17% of patients with CLD, and 63% of patients with HCC. The positivity rate in patients with HCC for the combination of Ln-γ2 and DCP was 89.5%, which was better than that for either of the two markers alone (63% and 68%, respectively). Among patients with early-stage HCC (T1 or T2), the positivity rates for monomeric Ln-γ2, AFP and DCP were 61%, 39% and 57%, respectively. Serum Ln-γ2 may be a potential biomarker for HCC surveillance. The combination of Ln-γ2 and DCP may be more sensitive for laboratory diagnosis of HCC than the combination of AFP and DCP.

Primary liver cancer is the second most common cancer-related death worldwide, estimated to be responsible for nearly 746 000 deaths in 2012 (9.1% of total deaths from cancer). The prognosis for primary liver cancer is very poor (overall ratio of mortality to incidence: 0.95).[1] Hepatocellular carcinoma (HCC) accounts for approximately 90% of primary liver cancers and generally occurs in patients with underlying chronic liver disease (CLD), such as viral hepatitis, alcoholic liver disease, nonalcoholic steatohepatitis (NASH), autoimmune hepatitis and primary biliary cirrhosis.[2] Surveillance of patients with the highest risk for developing HCC is important.[3–6] Alpha-fetoprotein (AFP) and des-gamma-carboxy prothrombin (DCP) are the most commonly used biomarkers for HCC.[3–7] Thus, the Japan Society of Hepatology recommends surveillance with ultrasonography and multiple biomarkers for early detection of HCC in patients with CLD.[8] However, recent studies show that the diagnostic accuracy of these biomarkers is not fully satisfactory in terms of sensitivity and specificity for effective surveillance.[9] Accordingly, the American Association for the Study of Liver Diseases Practice Guidelines Committee recommended the use of ultrasound alone, without AFP, for HCC surveillance in patients with cirrhosis.[10] However, ultrasonography is operator-dependent, and several factors are known to affect the degree of reliability of ultrasonographic findings, including patient obesity, liver atrophy, and coarseness of the liver parenchyma.[11] Hence, a novel noninvasive diagnostic method for early detection of HCC is needed.

Laminins (Lns) are a family of basement membrane (BM) proteins associated with cell adhesion, differentiation, proliferation and migration.[12] Lns are heterotrimeric glycoproteins composed of three polypeptide chains designated as α, β and γ, linked by disulfide bonds to form a cross-shaped structure. A separate gene encodes each polypeptide chain, and different combinations of these chains lead to 16 different Ln isoforms. Ln-332 (former name: Ln-5) consists of α3, β3 and

© 2017 The Authors. *Cancer Science* published by John Wiley & Sons Australia, Ltd on behalf of Japanese Cancer Association.
This is an open access article under the terms of the Creative Commons Attribution-NonCommercial License, which permits use, distribution and reproduction in any medium, provided the original work is properly cited and is not used for commercial purposes.

γ2 chains, which are encoded by three distinct genes (*LAMA3*, *LAMB3* and *LAMC2*, respectively).[13] Ln-332 mediates epithelial cell adhesion to the BM. In particular, Ln-γ2, a component of Ln-332, is frequently expressed as a monomer in several types of malignant cancer cells and tissues without simultaneous expression of Ln-α3 and Ln-β3 chains.[14] Ln-γ2 expression has been immunohistochemically detected in various malignant carcinomas (stomach, esophageal, colon, biliary and pancreatic tumors) in areas where Ln-α3 and Ln-β3 are not expressed, indicating that Ln-γ2 as a monomer might be a specific marker of invasion.[15–18] Although Ln-332 is widely expressed in human tissues, it is not detected in the normal liver.[16] Interestingly, several reports indicated that the γ2 chain of Ln-332 is expressed in HCC tissues.[17,19] Therefore, the presence of monomeric Ln-γ2 in the serum may be useful as a biomarker for HCC. In an earlier study, we developed a monoclonal antibody that preferentially recognizes the monomeric form of Ln-γ2[20] and used it for ELISA to detect the Ln-γ2 chain.[21] We also developed a fully automated highly sensitive detection method for serum monomeric Ln-γ2 based on a chemiluminescent immunoassay (CLIA). With this method, a linear calibration curve was obtained in the range of 10 000–20 000 pg/mL and serum monomeric Ln-γ2 could be stably measured within 20 min (Nakagawa M, manuscript in preparation). In the present study, we used CLIA to evaluate the diagnostic value of monomeric Ln-γ2 in sera from patients with CLD and patients with HCC.

Patients and Methods

Patients. Study subjects were enrolled from the liver clinic at the St. Marianna University School of Medicine Hospital (Kanagawa, Japan) between January 2007 and April 2015. The study protocol was approved by the institutional review boards of St. Marianna University School of Medicine (Res-2302), the Institute of Medical Science, University of Tokyo (24-44-1017), the Kanagawa Cancer Center (Res-24) and Abbott Japan (OSE2014-006). Written informed consent was obtained from each patient. Demographic and clinical information was collected from each subject. Healthy volunteers with no history of liver disease, alcohol consumption of less than 40 g/week, and no risk factors for viral hepatitis were recruited among the hospital staff and were used as controls (Table 1). The etiology of the underlying liver disease was attributed to hepatitis C virus (HCV) based on the detection of HCV antibody/HCV RNA in the serum, to hepatitis B virus (HBV) based on the detection of hepatitis B surface antigen in the serum, or to alcohol based on a daily alcohol intake of more than 40 g/ethanol per day for more than 15 years. The CLD group consisted of patients with no evidence of hepatic mass lesions suspicious for HCC on ultrasound, computed tomography (CT) or magnetic resonance imaging (MRI). To establish the diagnosis of HCC, at least two liver imaging results indicating a mass lesion with characteristics resembling an HCC (arterial enhancement ± washout on CT with contrast medium, MRI and/or hepatic angiography) were required.[22] Typical HCC shows hypervascularity in the arterial phase and washout of contrast medium in the portal venous phase. For few cases, in which the diagnosis of HCC was still equivocal despite liver imaging studies, percutaneous liver biopsy was performed. Tumors were staged based on the General Rules for the Clinical and Pathological Study of Primary Liver Cancer (Liver Cancer Study Group of Japan).[23] In this classification, the T factor includes three criteria: solitary tumor, maximum tumor diameter <2 cm and no vascular invasion. Tumor stage T1 meets all the three criteria, T2 meets two of the three criteria, T3 meets one of the three criteria, and T4 does not meet any of the criteria. Serum samples were stored at −80°C until analysis.

Table 1. Demographic information and etiology of liver diseases

	Healthy control (n = 52)	Chronic liver disease (n = 24)	Hepatocellular carcinoma (n = 57)
Gender			
M:F	32/20	11/13	38/19
Age (y)	33 (25–58)	59 (35–74)	71 (49–80)
Etiology (%)			
HCV		20 (83)	30 (52)
HBV		3 (13)	8 (14)
HBV+HCV			1 (2)
Alcohol			12 (21)
NBNCNAL		1 (4)	5 (9)
Autoimmune			1 (2)

All data are expressed as median (range).

Antibodies and antigens. Recombinant monomeric Ln-γ2 protein was purified from the culture medium of Madin-Darby canine kidney cell transfectants, as described previously (Nakagawa M *et al.*, manuscript in preparation).[24] Recombinant heterotrimeric Ln-332 was purchased from Oriental Yeast (Tokyo, Japan). For CLIA and western blotting, a monoclonal anti–Ln-γ2 antibody (2H2) and a polyclonal anti–Ln-γ2 domain III antibody were prepared in our laboratory, as described previously.[24] A monoclonal anti–Ln-α3 antibody was purchased from Oriental Yeast.

Laminin-γ2 chain immunohistochemistry. For immunohistochemical analysis, archival formalin-fixed, paraffin-embedded tissues from 10 patients who had undergone surgical excision of HCC were used. For immunostaining of Ln-α3 and Ln-γ2, sections were analyzed by immunohistochemistry to characterize the tumor cells. Sections were deparaffinized with xylene, treated with 0.05% protease XXIV (Sigma, St Louis, MO, USA) in 50 mM Tris–HCl (pH 7.5) for 5 min followed by washing with PBS to retrieve the antigen, then treated by microwaving in 10 mM citrate buffer (pH 6.0). Sections were incubated with each primary antibody overnight (anti-Ln-α3 antibody, 1/500 dilution; anti-Ln-γ2 domain III polyclonal antibody, 1/1000 dilution). Then, they were incubated for 30 min with avidin-biotinyl-peroxidase complex with a Vectastain ABC kit (Vector Laboratories, Burlingame, CA, USA) and subjected to the peroxidase reaction.

Western blot. Cells and tissues were lysed on ice in buffer containing 20 mmol/L Tris-HCl (pH 7.5), 1% CHAPS, 0.005% (w/v) Brij-35 and 0.5 M NaCl, and precleared by centrifugation at 18 870 *g* for 20 min at 4°C. Lysates were sonicated for 20 s on ice and centrifuged at 18 870 *g* for 10 min. Proteins (10 μg/lane) were separated by using 6% (w/v) or 10% (w/v) SDS-PAGE under reducing or nonreducing conditions and then transferred to nitrocellulose membranes. The membranes were incubated with primary antibodies overnight at 4°C. Immunoreactive proteins were visualized by using an enhanced chemiluminescence (ECL) detection system (Amersham Pharmacia Biotech UK, Little Chalfont, Buckinghamshire, UK).

Fully automated chemiluminescent immunoassay. Human monomeric Ln-γ2 protein concentration was measured by a

© 2017 The Authors. Cancer Science published by John Wiley & Sons Australia, Ltd on behalf of Japanese Cancer Association.

two-step sandwich assay using paramagnetic microparticles coated with 2H2 antibody (Nakagawa M *et al.*, manuscript in preparation) and rabbit polyclonal antibody labeled with acridinium. The procedure was adjusted to be applied to a fully automated detection machine (ARCHITECT of Abbott Laboratories, Chicago, IL, USA).

Analysis of tumor markers for hepatocellular carcinoma. Serum AFP levels were measured by using the ARCHITECT system, and DCP levels were measured by using LUMIPULSE (Fujirebio, Tokyo, Japan) in SRL Tokyo Laboratories (Tokyo, Japan).

Statistical analysis. Serum monomeric Ln-γ2 levels were reported as mean ± SD and median (and range). Serum AFP and DCP levels were reported as median: range. Log transformation was used on the AFP and DCP values to account for the large range of values for both markers among patients with HCC. Continuous variables were compared between the two groups using the Mann–Whitney *U*-test and Student's *t*-test; *P* -values less than 0.05 were considered significant. GraphPad Prism 6 Software (San Diego, CA, USA) was used to generate all scatter plots, receiver operating characteristic (ROC) curves, and the calculation of the area under the ROC (AUC) curves. The optimal cutoff point included the point on the ROC curve closest to the (0, 1).

Results

Detection of Ln-γ2 expression in hepatocellular carcinoma tissues. To investigate the expression of Ln-γ2 in HCC, immunohistochemical analyses were performed. In accordance with previous reports,[17,19] cytoplasmic staining of Ln-γ2 was observed in 5/10 of surgically-removed HCC nodules (Fig. 1a). Ln-γ2 immunoreactivites were observed in marginal, poorly differentiated parts of the tumor nodules in most of cases (Fig. 1a), but not in well-differentiated parts of HCC and adjacent normal tissues . Moreover, expression of Ln-α3 was not observed in HCC nodules (Fig. 1b) and their adjacent normal tissues. To further identify the molecular composition of Ln-γ2 in HCC, Ln-γ2 protein was detected by western blotting using HCC tissue lysates from patients. When purified monomeric Ln-γ2 was electrophoresed on SDS-PAGE under nonreducing conditions, two proteolytic fragments (140 and 100 kDa) were detected by an anti–Ln-γ2 polyclonal antibody that detects both Ln-γ2 isoforms (Fig. 2a). Ln-γ2 is known to be processed by metalloproteinases, such as MMP2 and MT1-MMP, and two different fragments (named γ2′ of 140 kDa, and γ2× of 100 kDa, under nonreducing conditions) have been previously described.[24] In contrast, recombinant Ln-332 was detected as a large 450-kDa band, which corresponds to a complex of three polypeptide chains cross-linked by disulfide bonds. Western blotting under reducing conditions indicated that Ln-332 was the source of monomeric Ln-γ2 and of the proteolytic fragment(s) (Fig. 2b). Two HCC cell lines, Alexander and HepG2, also expressed both forms of monomeric Ln-γ2 fragments (Fig. 2c). Then, we examined Ln-γ2 in tissues from surgically-removed HCC nodules. Similar to HCC cell lines, HCC tissue lysates also contained both forms of monomeric Ln-γ2 (Fig. 2d). Heterotrimeric Ln-332-γ2 was undetectable in HCC cell lines or surgically-removed HCC nodules (Fig. 2c,d). Ln-α3 was not detected in HCC cell lines or surgically-removed HCC nodules (data not shown). Taken together, our immunohistochemical and western blotting studies indicate that monomeric, but not heterotrimeric, Ln-γ2 was expressed in HCC nodules.

Monomeric Ln-γ2, alpha-fetoprotein and des-gamma-carboxy prothrombin levels among healthy volunteers, patients with chronic liver disease, and patients with hepatocellular carcinoma. Because monomeric Ln-γ2 rather than heterotrimeric Ln-γ2 was expressed preferentially in HCC nodules, the

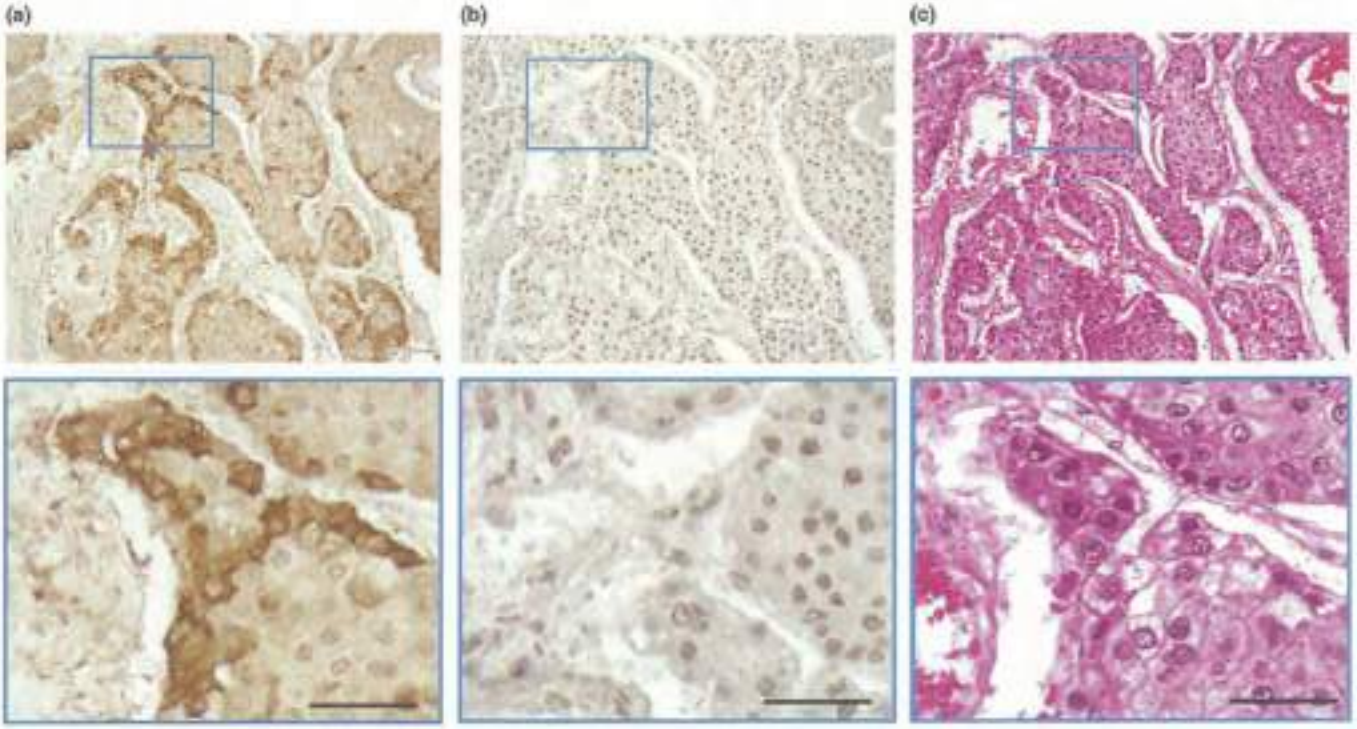

Fig. 1. Immunohistochemical staining for Ln-γ2 and Ln-α3 in hepatocellular carcinoma (HCC). (a) A representative example of positive staining for Ln-γ2. Cytoplasmic staining of Ln-γ2 was observed in 5/10 of surgical resected HCC nodules. (b) Expression of Ln-α3 was not observed in HCC nodules. (c) HE staining. Scale bars, 50 μm.

© 2017 The Authors. Cancer Science published by John Wiley & Sons Australia, Ltd on behalf of Japanese Cancer Association.

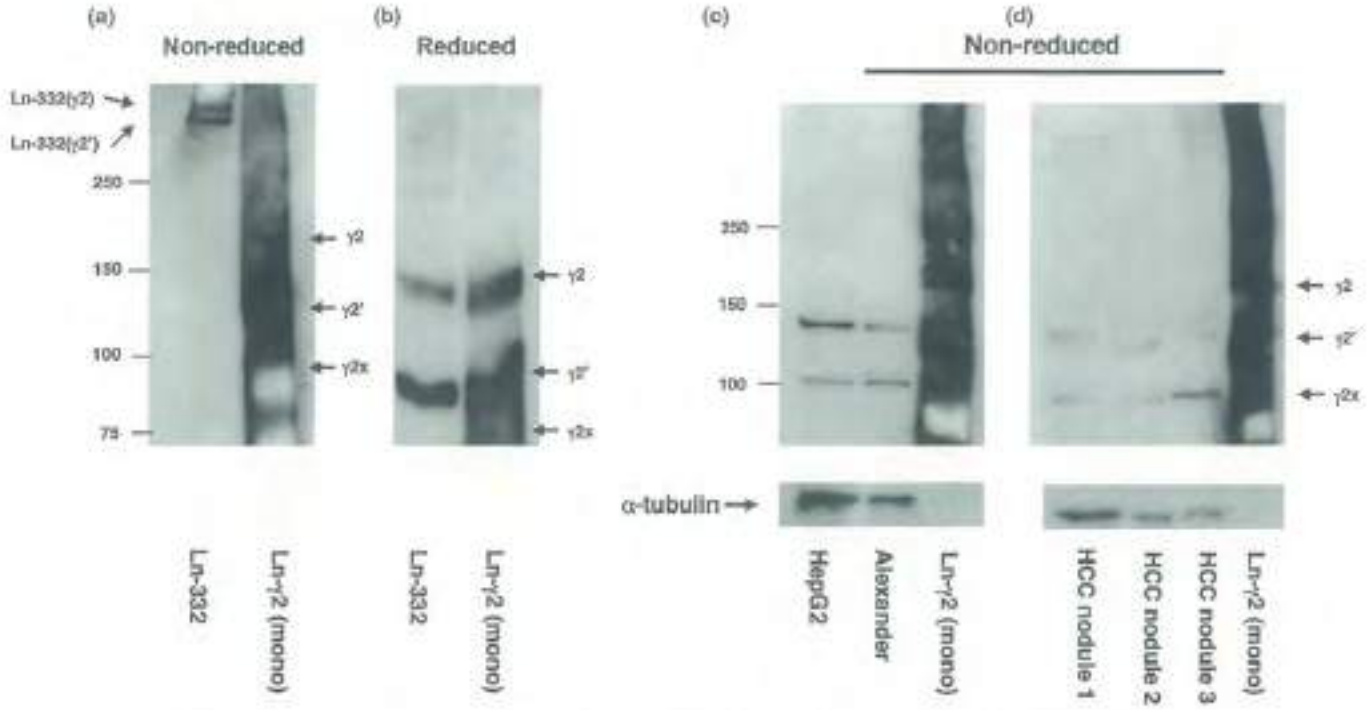

Fig. 2. Western blot analysis using an anti-Ln-γ2 antibody. Purified Ln-332 and Ln-γ2 were separated by 6% SDS-PAGE under nonreducing (a) or reducing (b) conditions and blotted. The expression of Ln-γ2 in hepatocellular carcinoma (HCC) cell lines and surgically-removed HCC nodules was assessed. Cell lysates prepared from HepG2 or Alexander cells (c) and tissue lysates from surgically-removed HCC nodules of three different patients (HCC nodule 1–3; d) were separated by 6% SDS-PAGE under nonreducing conditions and blotted. Arrows, Ln-332 heterodimer (Ln-332), two different processed fragments of the Ln-γ2 monomer, named γ2' (140 kDa) and γ2x (100 kDa).

diagnostic value of monomeric Ln-γ2 was evaluated in sera from patients with HCC and CLD using the automated CLIA. To establish the cutoff value for Ln-γ2, control sera from 52 healthy Japanese volunteers were analyzed. Demographic and clinical characteristics of healthy volunteers and patients with CLD or HCC are shown in Table 1. Child–Pugh scores of patients with HCC are shown in Table 2. Clinical characteristics of patients with HCC are presented in Table 3.

The mean and median serum monomeric Ln-γ2 levels of healthy volunteers were 44.3 ± 17.6 pg/mL (mean ± SD) and 41.1 pg/mL (range: 10.9–79.0 pg/mL), respectively.

Serum monomeric Ln-γ2 levels were measured in 24 patients with CLD and 57 patients with HCC (Fig. 3a). Infection with HCV was the most common etiologic factor between the two groups of subjects with liver disease. The median monomeric Ln-γ2 concentrations were 76.7 pg/mL, with a range between 38.7 and 215.9 pg/mL (patients with CLD) and 173.2 pg/mL, with a range between 32.4 and 986 pg/mL (patients with HCC). A significant increase in monomeric Ln-γ2 levels was observed in patients with HCC when compared with patients with CLD and healthy volunteers ($P < 0.01$). ROC curves were plotted to identify cutoff values for serum monomeric Ln-γ2 to distinguish between patients with HCC and healthy controls (Fig. 3b). When the cutoff value was set at 75.9 pg/mL, the sensitivity and specificity were 86% (95% confidence interval [CI], 74–94%) and 98% (95% CI, 90–99%), respectively. The discriminative ability of monomeric Ln-γ2 (ROC curve AUC = 0.952; 95% CI, 91–99%) significantly surpassed that of DCP (ROC curve AUC = 0.825; 95% CI, 73–92%, $P < 0.05$) and it was as effective as AFP (ROC curve AUC = 0.929; 95% CI, 88–98%) when comparing healthy volunteers and patients with HCC. When healthy volunteers were compared with patients with nonmalignant CLD, this cutoff value yielded a discriminative ability for monomeric Ln-γ2 (ROC curve AUC = 0.819; 95% CI, 72–92%), with a sensitivity of 50% (95% CI, 29–71%) and specificity 96% (95% CI, 87–99%). With this cutoff value, monomeric Ln-γ2 positivity was found in 1 (2%), 12 (50%) and 50 (86%) subjects among healthy volunteers, patients with CLD, and patients with HCC, respectively. These results indicate that this cutoff value (>75.9 pg/mL) is useful to discriminate patients with CLD, with or without HCC, from healthy subjects.

Receiver operating characteristic curves were plotted to evaluate the cutoff value for monomeric Ln-γ2 that would distinguish between patients with HCC and patients with CLD. The optimal cutoff value was 116.6 pg/mL (Fig. 3c), with a sensitivity of 63% (95% CI, 49–76%) and a specificity of 83% (95% CI, 63–95%). When discriminating patients with CLD from those with HCC, DCP (ROC curve AUC = 0.845; 95% CI, 76–93%) outperformed monomeric Ln-γ2 (ROC curve AUC = 0.793; 95% CI, 69–89%; differences were not statistically significant) and AFP (ROC curve AUC = 0.788; 95% CI,

Table 2. Child–Pugh scores of patients with hepatocellular carcinoma

	n
CH	3
Child-Pugh A	34
Child-Pugh B	16
Child-Pugh C	4

Numbers of chronic hepatitis (CH)/cirrhosis (Child–Pugh A/B/C) are presented.

© 2017 The Authors. Cancer Science published by John Wiley & Sons Australia, Ltd on behalf of Japanese Cancer Association.

Table 3. Clinical characteristics of patients with hepatocellular carcinoma

	n	Numbers of tumors	Diameter of largest tumor	AFP	DCP
TNM I	10	1 (1)	15.0 ± 3.1 (15; 10–19)	12.3 ± 15.6 (5.3; 2.2–44.6)	97 ± 110 (55; 14–302)
TNM II	18	4.9 ± 12 (2; 1–52)	25.9 ± 10.0 (26.5; 13–44)	98.7 ± 211.8 (16.2; 1.5–899)	483 ± 1417 (47.5; 13–5380)
TNM III	21	23 ± 32 (5; 1–113)	36.9 ± 18.0 (32.5; 21–85)	345.9 ± 598.7 (72.5; 3.2–2364)	1842 ± 5487 (162; 11–20 779)
TNM IV	8	58 ± 89 (14; 1–225)	51 ± 20.0 (48.0; 26–82)	54 209 ± 146 719 (1116; 5.3–417 198)	18 400 ± 29 309 (683; 32–75 000)
TNM IVA	5	42 ± 76 (6; 2–177)	50.0 ± 17.3 (46; 33–71)	86 583 ± 146 719 (1522; 5.3–417 198)	29 152 ± 33 435 (17 300; 32–75 000)
TNM IV B	3	86 ± 122 (31; 1–225)	52.7 ± 28.1 (50; 26–82)	919 ± 1278 (371.9; 5.3–2379)	481 ± 362 (589; 78–777)
					Mean ± SD (median; range)

Numbers of TNM stages (I/II/III/IV-A/IV-B), numbers of tumors (mean ± SD, median; range), largest tumor diameter (mean ± SD, median; range), AFP (mean ± SD, median; range) and DCP (mean ± SD, median; range) are presented. AFP, alpha-fetoprotein; DCP, des-gamma-carboxy prothrombin.

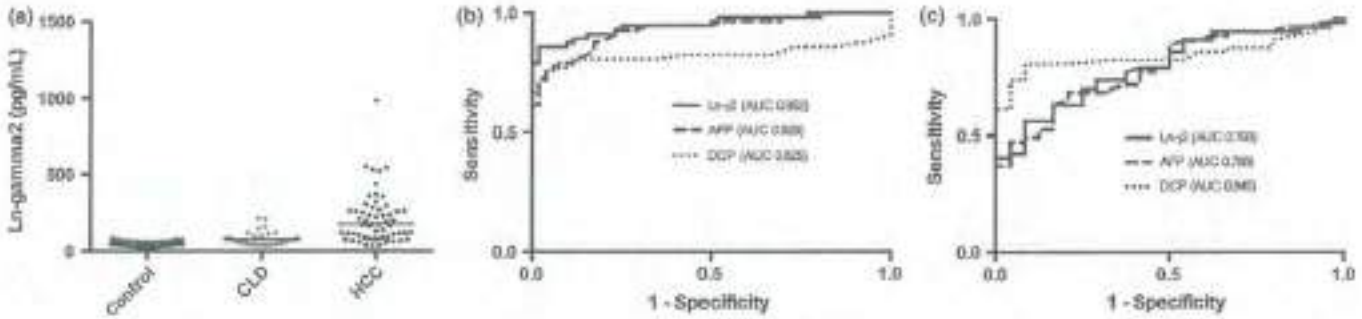

Fig. 3. (a) Scatter plot of Ln-γ2 concentrations determined in serum samples from healthy subjects ($n = 52$), patients with chronic liver disease (CLD) ($n = 24$), and patients with hepatocellular carcinoma (HCC) ($n = 57$). The horizontal lines represent median concentrations. (b) ROC curves comparing Ln-γ2, alpha-fetoprotein (AFP) and des-gamma-carboxy prothrombin (DCP) in patients with HCC versus healthy volunteers. (c) ROC curves comparing Ln-γ2, AFP, and DCP in patients with HCC versus patients with CLD.

69–89%). Monomeric Ln-γ2 positivity (>116.6 pg/mL) was observed in 0/52 (0%), 4/24 (17%) and 36/57 (63%) subjects among healthy volunteers, patients with CLD, and patients with HCC, respectively. AFP positivity (>20 ng/mL; the upper normal limit reported in Japanese subjects)[7] was observed in 0/52 (0%), 4/24 (17%) and 30/57 (53%) subjects among healthy volunteers, patients with CLD, and patients with HCC, respectively. The median concentrations (range) of AFP were 2.3 ng/mL (healthy controls, range: 0.9–8.2 ng/mL), 3.8 ng/mL (patients with CLD, range: 1.2–109.7 ng/mL), and 24.4 ng/mL (patients with HCC, range: 1.5–417 199 ng/mL) (Fig. 4a). DCP positivity (>40 mAU/mL, the upper normal limit reported in Japanese subjects)[7] was observed in 1/52 (1.9%), 1/24 (4.2%) and 39/57 (68%) subjects among healthy volunteers, patients with CLD, and patients with HCC, respectively. The median concentrations (range) of DCP were 24.5 mAU/mL (healthy controls, range: 15.0–45.0 mAU/mL), 21.0 mAU/mL (patients with CLD, range: 12.0–58.0 mAU/mL) and 103 mAU/mL (patients with HCC, range: 11.0–75 000 mAU/mL) (Fig. 4b). Monomeric Ln-γ2, AFP and DCP levels were found to be significantly elevated ($P < 0.001$) in sera from patients with HCC compared with sera from both healthy volunteers and patients with CLD. Moreover, Ln-γ2 and AFP levels were found to be significantly elevated ($P < 0.01$) in sera from patients with CLD compared with sera from healthy volunteers. When Ln-γ2 levels of patients with HCC were compared with log-transformed AFP or DCP levels of those patients, significant positive correlation was observed between Ln-γ2 and AFP ($r = 0.41$; $P = 0.0015$).

We also evaluated whether a combination of monomeric Ln-γ2 (>116.6 pg/mL) and AFP (>20 ng/mL) or DCP (>40 mAU/mL) could improve the diagnostic efficacy for HCC (Fig. 5). Monomeric Ln-γ2 and DCP were detected in 51/57 patients (89.5%), monomeric Ln-γ2 and AFP in 46/57 (80.7%), and DCP and AFP in 47/57 (82.5%). The combination of all three markers was detected in 54/57 patients (94.7%). Interestingly, 67% (12/18) of patients who were negative for DCP were positive for Ln-γ2.

Monomeric Ln-γ2, alpha-fetoprotein and des-gamma-carboxy prothrombin values according to tumor staging. According to the TNM classification, 10 patients were diagnosed with stage I, 18 with stage II, 21 with stage III and 8 with stage IV tumors. Monomeric Ln-γ2 levels increased from stage I to stage IV with median levels (range) of 114.3 pg/mL (range: 65.3–323.6 pg/mL), 184.3 pg/mL (range: 39.5–549.1 pg/mL), 174.6 pg/mL (range: 32.4–985.8 pg/mL) and 248.1 pg/mL (range: 59.8–529.4 pg/mL), respectively (Fig. 6a). The AFP values were 5.3 ng/mL (range: 2.2–44.6 ng/mL), 16.2 ng/mL (range: 1.5–899 ng/mL), 72.5 ng/mL (range: 3.2–2364 ng/mL) and 1116 ng/mL (range: 5.3–417198 ng/mL) for stage I, II, III and IV HCC, respectively (Fig. 6b). The DCP values were 55.0 mAU/mL (range: 14.0–302 mAU/mL), 47.5 mAU/mL (range: 13.0–5380), 162 mAU/mL (range: 11.0–20 779), and 683 mAU/mL (range: 32.0–75 000 mAU/mL) for stage I, II, III and IV HCC, respectively (Fig. 6c). Among patients with early-stage HCC (T1 or T2), the positivity rates for monomeric Ln-γ2, AFP and DCP were 17/28 (61%), 11/28 (39%) and 16/28 (57%), respectively.

Discussion

In our study, the clinicopathological significance of monomeric Ln-γ2 levels in the serum of patients with HCC was

© 2017 The Authors. Cancer Science published by John Wiley & Sons Australia, Ltd on behalf of Japanese Cancer Association.

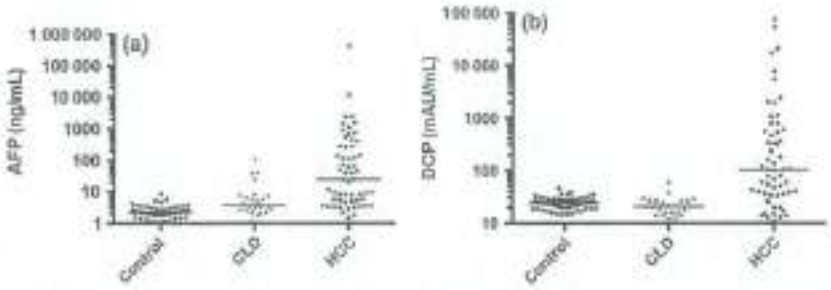

Fig. 4. (a) Scatter plot of alpha-fetoprotein (AFP) concentrations determined in serum samples from healthy subjects ($n = 52$), patients with chronic liver disease (CLD) ($n = 24$), and patients with hepatocellular carcinoma (HCC) ($n = 57$). (b) Scatter plot of des-gamma-carboxy prothrombin (DCP) concentrations determined in serum samples from healthy subjects (healthy) ($n = 52$), patients with CLD ($n = 24$), and patients with HCC ($n = 57$). The horizontal lines represent median concentrations.

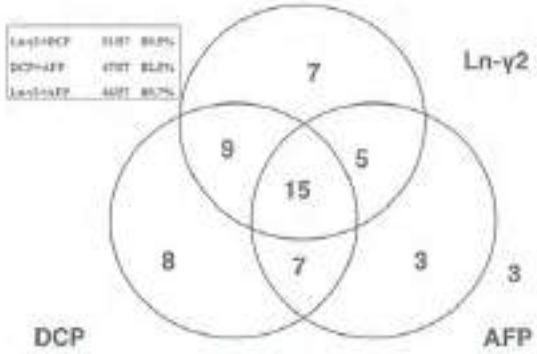

Fig. 5. Comparison of hepatocellular carcinoma (HCC) positive rates obtained when combining two biomarkers. Three patients were negative for all three biomarkers. The HCC detection rates of the combination of Ln-γ2 and DCP, Ln-γ2 and alpha-fetoprotein (AFP), and des-gamma-carboxy prothrombin (DCP) and AFP were 89.5% (51/57), 82.5% (47/57) and 80.7% (46/57), respectively.

investigated. By using a fully automated CLIA, a significant increase in serum monomeric Ln-γ2 levels was observed in patients with HCC when compared with patients with CLD and healthy volunteers. Our results indicate the potential efficacy of serum monomeric Ln-γ2 levels as a marker for HCC surveillance.

Although trimeric Ln-332 is absent in the normal liver tissue,[16] increased expression of Ln-γ2 has been reported in metastatic and primary HCC nodules.[17] Recent reports showed that the γ2 chain of Ln-332 was highly expressed in HCC expressing the biliary marker keratin 19.[18] In our study, western blot analysis indicated that monomeric Ln-γ2 was predominantly expressed in surgically removed HCC nodules and HCC cell lines. Notably, using a CLIA, we observed a significant increase in serum monomeric Ln-γ2 levels in patients with HCC when compared with patients with CLD and healthy volunteers. Aberrant activation of Wnt/β-catenin signaling is a common genetic abnormality in human HCC.[25] Accordingly, β-catenin targets *LAMC2* through T-cell factor-binding elements,[18] thus supporting our data showing that serum and cytoplasmic expression of monomeric Ln-γ2 levels in HCC patients were increased. Etiologies of HCC in patients with elevated serum monomeric Ln-γ2 levels include HBV and HCV, but also alcoholic liver disease, NASH and autoimmune hepatitis. We also observed that monomeric Ln-γ2 levels increased according to the stepwise progression of liver disease (i.e. from chronic hepatitis to HCC) and according to tumor stages. We observed a modest increase in serum monomeric Ln-γ2 levels in patients with CLD without HCC. The ROC curve indicated a cutoff value for monomeric Ln-γ2 of 75.9 pg/mL for discriminating patients with HCC from healthy controls. A value of 116.6 pg/mL for monomeric Ln-γ2 yielded the best sensitivity and specificity for differentiating patients with HCC from those with CLD. Of the patients with CLD without HCC, four (16.7%) had elevated monomeric Ln-γ2 levels (>116.6 pg/mL). They also showed elevated AFP (>20 ng/mL, three of them) or DCP (>40 mAU/mL, one of them) levels. Increased levels of monomeric Ln-γ2 in such patients may reflect the hepatocellular regeneration that occurs during chronic liver injury, a mechanism suggested by other biomarkers.

AFP and DCP are the two most commonly used biomarkers for HCC.[7] Several studies indicate that each of these biomarkers alone is not sufficient for HCC surveillance.[9] We found that serum monomeric Ln-γ2 appeared to be more effective than AFP in differentiating patients with HCC from those

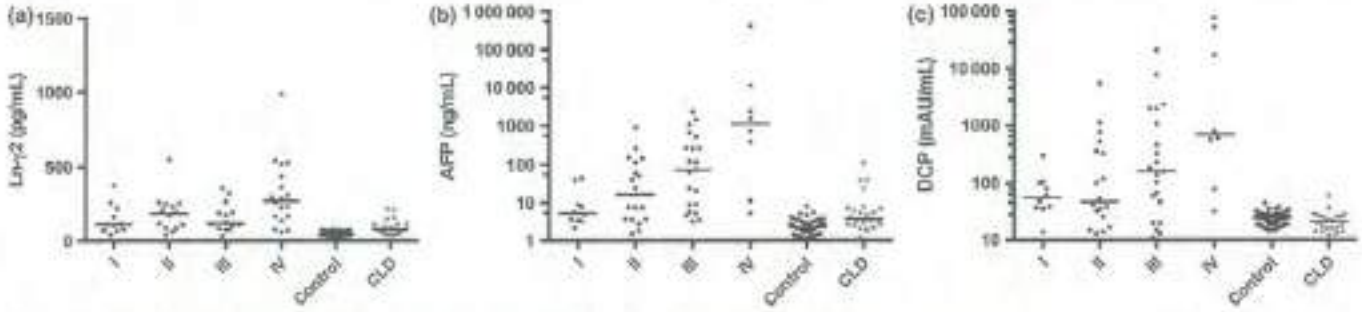

Fig. 6. Ln-γ2 (a), alpha-fetoprotein (AFP) (b) and des-gamma-carboxy prothrombin (DCP) (c) values according to tumor staging based on the TNM classification. The horizontal lines represent median concentrations.

© 2017 The Authors. Cancer Science published by John Wiley & Sons Australia, Ltd on behalf of Japanese Cancer Association.

with nonmalignant CLD. Among patients with early-stage HCC (T1 or T2), positivity rates for monomeric Ln-γ2 (>116.6 pg/mL), DCP and AFP were 61%, 57% and 39%, respectively. These results indicate that serum monomeric Ln-γ2 is potentially a useful biomarker to detect early-stage HCC. The combination of DCP and AFP has been reported to be useful for the early detection of HCC in patients with CLD.[26] Accordingly, the Asian Pacific Association for the Study of the Liver stated that the simultaneous measurement of AFP and DCP for the diagnosis of HCC provides higher sensitivity without decreasing specificity.[27] Interestingly, the positivity rate for the combination of monomeric Ln-γ2 and DCP was higher (89.5%) than that of either of the markers alone (63% and 68%, respectively, $P < 0.02$) or of the combination of DCP and AFP (80.7%).

In addition to HCC, monomeric Ln-γ2 is also involved in a number of other malignancies. Several immunohistochemical studies indicated that Ln-γ2 is expressed in various malignant carcinomas.[13–19] Our preliminary results indicated that elevated serum monomeric Ln-γ2 levels could be observed in patients with various malignancies, such as pancreatic adenocarcinoma (data not shown) and bladder carcinoma.[21] Although further analysis is required, serum monomeric Ln-γ2 is a potentially useful biomarker for the screening of cancer in various organs, similar to the carcinoembryonic antigen.

The higher diagnostic positive rate shown by the combination of serum monomeric Ln-γ2 with DCP may improve the efficiency of surveillance programs for HCC. Approximately 75–80% of HCC cases are attributable to persistent HBV or HCV infections. While the rate of patients with HCC with viral infection has been decreasing, the rate and number of cases of patients with non-B non-C (NBNC)-HCC have been increasing, during the last two decades.[2] Most NBNC-HCC cases tend to be discovered in advanced stages when compared with patients with HBV-HCC and HCV-HCC, because patients with NBNC-HCC (i.e. patients who do not have viral hepatitis) do not receive regular HCC surveillance, whereas patients with HBV or HCV receive regular HCC surveillance. Accordingly, monomeric Ln-γ2 is potentially a useful biomarker for HCC surveillance in patients who are less likely to benefit from regular ultrasound screening, such as patients with metabolic syndrome and/or alcoholic liver disease.

Our results are very encouraging despite several limitations. First, because this was a single-center observational study, multi-center prospective studies are needed to evaluate the usefulness of serum monomeric Ln-γ2 for HCC surveillance in patients with CLD. Second, blood samples were collected only at one time point before treatment for HCC. However, despite the limitations, the use of serum monomeric Ln-γ2 as a biomarker to monitor therapeutic effects is of particular interest.

In conclusion, serum monomeric Ln-γ2 levels significantly increased in patients with HCC when compared with patients with CLD and healthy volunteers. The diagnostic value of the combination of monomeric Ln-γ2 with DCP levels was better than that of either of these markers alone, suggesting the potential usefulness of serum monomeric Ln-γ2 in HCC surveillance.

Acknowledgments

This work was supported in part by a Grant-in-Aid for Scientific Research from the Ministry of Education, Culture, Sports, Science, and Technology of Japan (H. Yasuda), a Medical Research and Development Programs Focused on Technology Transfer: Adaptable and Seamless Technology Transfer Program through Target-Driven Research and Development (A-STEP) (T. Yoshimura, E. Yoshida, M. Nakagawa, N. Koshikawa and M. Seiki), and a Project for Development of Innovative Research on Cancer Therapeutics (P-DIRECT) (N. Koshikawa) from The Japan Agency for Medical Research and Development (AMED), and by Abbott Laboratories (N. Koshikawa and M. Seiki).

Disclosure Statement

N. Koshikawa received research funding from Abbott Laboratories (Chicago, IL, USA). T. Yoshimura, E. Yoshida and M. Nakagawa are employees of Abbott Japan Co., Ltd. No potential competing interests were disclosed by other authors.

References

1 World Health Organization, International Agency for Research on Cancer. GLOBOCAN, 2012. Available from URL: http://globocan.iarc.fr.
2 El-Serag HB. Hepatocellular carcinoma. *N Engl J Med* 2011; **365**: 1118–27.
3 Bolondi L, Sofia S, Siringo S *et al.* Surveillance programme of cirrhotic patients for early diagnosis and treatment of hepatocellular carcinoma: a cost effectiveness analysis. *Gut* 2001; **48**: 251–9.
4 Chen JG, Parkin DM, Chen QG *et al.* Screening for liver cancer: results of a randomized controlled trial in Qidong, China. *J Med Screen* 2003; **10**: 204–9.
5 McMahon BJ, Bulkow L, Harpster A *et al.* Screening for hepatocellular carcinoma in Alaska natives infected with chronic hepatitis B: a 16-year population-based study. *Hepatology* 2000; **32**: 842–6.
6 Zhang BH, Yang BH, Tang ZY. Randomized controlled trial of screening for hepatocellular carcinoma. *J Cancer Res Clin Oncol* 2004; **130**: 417–22.
7 Mita Y, Aoyagi Y, Yanagi M *et al.* The usefulness of determining des-gamma-carboxy prothrombin by sensitive enzyme immunoassay in the early diagnosis of patients with hepatocellular carcinoma. *Cancer* 1998; **82**: 1643–8.
8 Arii S, Sata M, Sakamoto M *et al.* Management of hepatocellular carcinoma: report of Consensus Meeting in the 45th Annual Meeting of the Japan Society of Hepatology (2009). *Hepatol Res* 2010; **40**: 667–85.
9 Sterling RK, Wright EC, Morgan TR *et al.* Frequency of elevated hepatocellular carcinoma (HCC) biomarkers in patients with advanced hepatitis C. *Am J Gastroenterol* 2012; **107**: 64–74.
10 Bruix J, Sherman M. Management of hepatocellular carcinoma: an update. *Hepatology* 2011; **53**: 1020–2.
11 Mikami S, Tateishi R, Hagiwara S *et al.* Tumor markers are more useful in patients undergoing surveillance for hepatocellular carcinoma with unreliable results by ultrasonography. *Hepatol Res* 2015; **45**: 415–22.
12 Miyazaki K. Laminin-5 (laminin-332): unique biological activity and role in tumor growth and invasion. *Cancer Sci* 2006; **97**: 91–8.
13 Domogatskaya A, Rodin S, Tryggvason K. Functional diversity of laminins. *Annu Rev Cell Dev Biol* 2012; **28**: 523–53.
14 Koshikawa N, Moriyama K, Takamura H *et al.* Overexpression of laminin γ2 chain monomer in invading gastric carcinoma cells. *Cancer Res* 1999; **59**: 5596–601.
15 Soini Y, Mäkinen M, Salo S *et al.* Expression of the laminin γ2 chain in pancreatic adenocarcinoma. *J Pathol* 1996; **180**: 290–4.
16 Mizushima H, Koshikawa N, Moriyama K *et al.* Wide distribution of laminin-5 γ2 chain in basement membranes of various human tissues. *Hor Res* 1998; **50**(Suppl. 2): 7–14.
17 Giannelli G, Fransvea E, Bergamini C *et al.* Laminin-5 chains are expressed differentially in metastatic and nonmetastatic hepatocellular carcinoma. *Clin Cancer Res* 2003; **9**: 3684–91.
18 Hlubek F, Jung A, Kotzor N *et al.* Expression of the invasion factor laminin gamma2 in colorectal carcinomas is regulated by beta-catenin. *Cancer Res* 2001; **61**: 8089–93.
19 Govaere O, Wouters J, Petz M *et al.* Laminin-332 sustains chemoresistance and quiescence as part of the human hepatic cancer stem cell niche. *J Hepatol* 2016; **64**: 609–17.
20 Koshikawa N, Mizegishi T, Nabeshima K *et al.* Development of a new tracking tool for the human monomeric laminin-γ2 chain *in vitro* and *in vivo*. *Cancer Res* 2008; **68**: 530–6.

© 2017 The Authors. Cancer Science published by John Wiley & Sons Australia, Ltd on behalf of Japanese Cancer Association.

21 Kamada M, Koshikawa N, Minegishi T *et al.* Urinary laminin-γ2 is a novel biomarker of non-muscle invasive urothelial carcinoma. *Cancer Sci* 2015; **106**: 1730–7.
22 Baron RL, Oliver JH III, Dodd GD III *et al.* Hepatocellular carcinoma: evaluation with biphasic, contrast-enhanced helical CT. *Radiology* 1996; **199**: 505–11.
23 Liver Cancer Study Group of Japan. *General Rules for the Clinical and Pathological Study of Primary Liver Cancer*, 5th edn. Tokyo: Kanehara & Co., Ltd., 2010.
24 Koshikawa N, Minegishi T, Sharabi A *et al.* Membrane-type matrix metalloproteinase-1 (MT1-MMP) is a processing enzyme for human laminin γ2 chain. *J Biol Chem* 2005; **280**: 88–93.
25 Fujimoto A, Furuta M, Totoki Y *et al.* Whole-genome mutational landscape and characterization of noncoding and structural mutations in liver cancer. *Nat Genet* 2016; **48**: 500–9.
26 Ishii M, Gama H, Chida N *et al.* Simultaneous measurements of serum alpha-fetoprotein and protein induced by vitamin K absence for detecting hepatocellular carcinoma. South Tohoku District Study Group. *Am J Gastroenterol* 2000; **95**: 1036–40.
27 Omata M, Lesmana LA, Tateishi R *et al.* Asian Pacific Association for the Study of the Liver consensus recommendations on hepatocellular carcinoma. *Hepatol Int* 2010; **4**: 439–74.

© 2017 The Authors. Cancer Science published by John Wiley & Sons Australia, Ltd on behalf of Japanese Cancer Association.

J Gastroenterol
DOI 10.1007/s00535-017-1316-3

The Japanese Society of Gastroenterology

ORIGINAL ARTICLE—LIVER, PANCREAS, AND BILIARY TRACT

Effects of vaccine-acquired polyclonal anti-HBs antibodies on the prevention of HBV infection of non-vaccine genotypes

Masaki Kato[1,2] · Susumu Hamada-Tsutsumi[3] · Chiaki Okuse[4] · Aiko Sakai[5] · Nobuyuki Matsumoto[2] · Masaaki Sato[6] · Toshiyuki Sato[6] · Mitsumi Arito[6] · Kazuki Omoteyama[6] · Naoya Suematsu[6] · Kazuki Okamoto[6] · Takanobu Kato[7] · Fumio Itoh[2] · Ryo Sumazaki[5] · Yasuhito Tanaka[3] · Hiroshi Yotsuyanagi[8] · Tomohiro Kato[6] · Manae Suzuki Kurokawa[1]

Received: 8 November 2016 / Accepted: 31 January 2017
© Japanese Society of Gastroenterology 2017

Abstract

Background In universal hepatitis B (HB) vaccination, single vaccine-derived polyclonal anti-HBs antibodies (anti-HBs) need to inhibit infection of HB viruses (HBV) of non-vaccine genotypes. We experimentally addressed this issue.

Methods Anti-HBs-positive sera were obtained by vaccination with genotype A- or C-derived HBs antigen (HBsAg, gtA-sera or gtC-sera). Their reactivity to genotype A- and C-derived HBsAg (gtA-Ag and gtC-Ag) was measured by ELISA. The capacity of sera to neutralize HBV was evaluated using an in vitro infection model.

Results Of 135 anti-gtA-Ag-reactive gtA-sera, 134 (99.3%) were anti-gtC-Ag-reactive. All (100%) 120 anti-gtC-Ag-reactive gtC-sera were anti-gtA-Ag-reactive. The reactivity to gtA-Ag was strongly correlated with that to gtC-Ag (gtA-sera, $\rho = 0.989$; gtC-sera, $\rho = 0.953$; $p < 0.01$). In gtA-sera ($n = 10$), anti-HBs to gtA-Ag were less completely absorbed with gtC-Ag (96.4%) than with gtA-Ag (100%, $p < 0.05$). Similarly, in gtC-sera ($n = 10$), anti-HBs to gtC-Ag were less completely absorbed with gtA-Ag (96.0%) than with gtC-Ag (100%, $p < 0.01$). Thus, 3.6 and 4.0% of anti-HBs in gtA-sera and gtC-sera were vaccine genotype HBsAg-specific, respectively. In the neutralization test, gtA-sera ($n = 4$) and gtC-sera ($n = 3$) with anti-HBs titers adjusted to 100 mIU/mL equally inhibited genotype C HBV infection (92.8 vs. 95.4%, $p = 0.44$). However, at 30 mIU/mL, the gtA-sera less effectively inhibited infection than the gtC-sera (60.2 vs. 90.2%, $p < 0.05$).

Conclusions Vaccination with genotype A- or C-derived HBsAg provided polyclonal anti-HBs that sufficiently bound to non-vaccine genotype HBsAg. However, a small portion of anti-HBs were specific to the vaccine genotype HBsAg. High anti-HBs titers would be required to prevent HBV infection of non-vaccine genotypes. *UMIN/CTR* UMIN000014363.

Keywords Hepatitis B virus · Genotypes · Universal vaccination · Polyclonal anti-HBs antibodies

Abbreviations

Anti-HBs	Anti-hepatitis B surface antibodies
DNA	Deoxyribonucleic acid
ELISA	Enzyme-linked immunosorbent assay

Electronic supplementary material The online version of this article (doi:10.1007/s00535-017-1316-3) contains supplementary material, which is available to authorized users.

✉ Manae Suzuki Kurokawa
manae@marianna-u.ac.jp

[1] Disease Biomarker Analysis and Molecular Regulation, St. Marianna University Graduate School of Medicine, 2-16-1, Sugao, Miyamae-Ku, Kawasaki 216-8511, Japan

[2] Division of Gastroenterology and Hepatology, Department of Internal Medicine, St. Marianna University School of Medicine, Kawasaki, Japan

[3] Department of Virology and Liver Unit, Nagoya City University Graduate School of Medical Sciences, Nagoya, Japan

[4] Division of Gastroenterology and Hepatology, Kawasaki Municipal Tama Hospital, Kawasaki, Japan

[5] Department of Child Health, Faculty of Medicine, University of Tsukuba, Tsukuba, Japan

[6] Clinical Proteomics and Molecular Medicine, St. Marianna University Graduate School of Medicine, Kawasaki, Japan

[7] Department of Virology II, National Institute of Infectious Diseases, Tokyo, Japan

[8] Department of Infectious Diseases, Graduate School of Medicine, The University of Tokyo, Tokyo, Japan

Published online: 14 February 2017

F	Female
HB	Hepatitis B
HBIG	Immunoglobulins containing high-titer antibodies against HBsAg
HBsAg	Hepatitis B surface antigen
HBV	Hepatitis B virus
HCC	Hepatocellular carcinoma
gtA-Ag	Genotype A-derived hepatitis B surface antigen
gtC-Ag	Genotype C-derived hepatitis B surface antigen
gtA-sera	Anti-HBs-antibody-positive sera from Heptavax-II-immunized individuals
gtC-sera	Anti-HBs-antibody-positive sera from Bimmugen-immunized individuals
M	Male
NC	Negative control
NI-sera	Anti-HBs-negative sera from HB vaccine-non-immunized individuals
OD	Optical density
PCR	Polymerase chain reaction
SD	Standard deviation

Introduction

Hepatitis B virus (HBV) infection is an important public health problem worldwide, leading to chronic hepatitis, liver cirrhosis, and hepatocellular carcinoma (HCC) [1, 2]. Approximately 248 million individuals were estimated to be HBs antigen (HBsAg)-positive globally in 2010 [3], and more than 600,000 individuals die annually due to liver cirrhosis and cancer [4]. The prevention of HBV infection by vaccination is crucial for eradicating HBV-associated life-threatening diseases, as well as for treating infection with anti-viral drugs.

Safe and effective universal vaccination against HBV infection has been available since 1981 [1, 5]. By 2014, 184 countries had introduced childhood vaccination against HBV including birth dose vaccination [6]. Ten HBV genotypes (A-J) have been identified at present and are an important factor for developing strategies to prevent HBV infection [7, 8]. Infection of various genotypes of HBV has been found in most countries [9]. HB vaccines, most of which are derived from genotype A HBV, have an excellent record of effectiveness, reducing the rate of chronic infection in children from 8–15% to less than 1% [6]. This result indicates that HB vaccines made from a single genotype-derived HBsAg are capable of neutralizing HBV of non-vaccine genotypes [9]. For example, although almost all HBV infection in Taiwan were caused by genotypes B and C [10], systematic vaccination using a genotype A-derived vaccine decreased the HBsAg seropositivity in children from 9.8 to 1.3% by 10 years after the start of vaccination [11]. Furthermore, the HBsAg seropositivity and HCC incidence in Thailand, where genotype B and C were dominant, were markedly reduced in cohorts immunized with a genotype A-derived vaccine [12, 13]. These observations also indicate that single genotype-derived HB vaccines are largely effective in neutralizing HBV of non-vaccine genotypes.

However, whether single genotype-derived HB vaccines prevent infection of non-vaccine genotype HBV as effectively as they do vaccine genotype HBV remains unclear. Interestingly, surveillance of blood donors in the United States detected nine HBV-seronegative but HBV-DNA-positive donors, six of whom had received a genotype A2-vaccine and showed low or undetectable levels of anti-HBs antibody (anti-HBs) titers [14]. The infecting genotypes were significantly different between the vaccinated and unvaccinated donors: five out of the six vaccinated donors were exclusively or predominantly infected with non-A2 strains, while the remaining one vaccinated and the three unvaccinated donors were infected with A2 strain. We also reported that an anti-HBs monoclonal antibody derived from a recipient of a genotype C-derived vaccine efficiently neutralized genotype C HBV, however, it failed to neutralize genotype A HBV at a low anti-HBs titer [15]. These studies indicate an insufficient capacity of single genotype-derived HB vaccines to prevent infection of non-vaccine genotype HBV. However, no experimental study has examined the capacity of vaccine-acquired polyclonal anti-HBs to bind to and neutralize non-vaccine genotype HBV.

In Japan, universal vaccination against HBV launched in October 2016. Japan had already introduced HB vaccination for infants born to HBV-infected mothers in combination with hepatitis B immunoglobulin approximately 30 years before this launch [16]. This strategy was found to be very effective, reducing the rate of HBsAg-positivity in children from 0.75 to 0.04%. However, recently, HBV infection in children via their fathers and unknown origins has been shown to be a relatively common cause of chronic hepatitis B [17, 18]. In Japan, 82% and 14% of HBV-infected individuals are infected with genotypes C and B, respectively [19, 20]. Recently, the rate of infection with genotype A HBV has been increasing, especially among young individuals [21, 22]. Indeed, in 52% of patients with acute hepatitis B, the hepatitis was caused by genotype A HBV [22]. Therefore, universal HB vaccination in Japan needs to mainly prevent infection of genotype C HBV in children as well as infection of genotype A HBV in adults. In this regard, it is important to evaluate whether single genotype-derived HB vaccines sufficiently prevent infection of non-vaccine genotype HBVs. At present, two kinds of HB vaccines of recombinant small S antigens are available in Japan: genotype A2 HBV-derived Heptavax-II,

which is commonly used worldwide, and genotype C-derived Bimmugen, which is generated in Japan.

In this study, we examined whether polyclonal anti-HBs generated by genotype A-derived HBsAg vaccination bound to genotype C-derived HBsAg and vice versa. Both Heptavax-II and Bimmugen vaccinations provided polyclonal anti-HBs that bound to HBsAgs of the other genotypes. However, a small portion of the polyclonal anti-HBs repertoire did not bind to HBsAgs of the other genotypes. Heptavax-II vaccination-derived anti-HBs as well as Bimmugen vaccination-derived anti-HBs neutralized genotype C HBV at a high anti-HBs titer, whereas the former neutralized genotype C HBV less effectively than the latter at a low titer. Our data suggested that high titers of anti-HBs should be maintained for the prevention of non-vaccine genotype HBV infection.

Materials and methods

Subjects and serum samples

The subjects were medical students and health care providers ≥18 years of age who needed to be immunized with HB vaccines for their future work. Subjects with a fever or acute diseases were excluded from the vaccination. In total, 474 subjects were enrolled in this study at St. Marianna University School of Medicine (including its branch, Kawasaki Municipal Tama Hospital) and University of Tsukuba. Of these, 196 subjects were vaccinated with Heptavax-II (MSD, Kenilworth, NJ, USA) (genotype A-derived vaccine). The anti-HBs titers were evaluated by Stacia (LSI Medience, Tokyo, Japan) or Architect (Abbott, Abbott Park, IL, USA). Anti-HBs-positive sera (≥10 mIU/mL) were selected as genotype A-derived vaccine-immunized sera (gtA-sera). A total of 150 gtA-sera with low-to-high anti-HBs titers, obtained 3–52 months after the last vaccination, were subjected to our analyses. Another gtA-serum, the anti-HBs titer of which was 842.7 mIU/mL measured by Stacia, was used as an internal control serum sample. Similarly, 148 subjects were vaccinated with Bimmugen (Kaketsuken, Kumamoto, Japan). Their anti-HBs titers were evaluated by Stacia or Architect. Anti-HBs-positive sera (≥10 mIU/mL) were selected as genotype C-derived vaccine-immunized sera (gtC-sera). A total of 124 gtC-sera with low-to-high anti-HBs titers, obtained 1–2 months after the last vaccination, were subjected to our analyses. The anti-HBs titers were evaluated by Stacia in 130 university freshmen, 101 of whom were anti-HBs-negative and had no experience of HB vaccination. Sera from these 101 students were subjected to our analyses as HB vaccine-non-immunized sera (NI-sera). The age and sex of the subjects were as follows: 150 gtA-sera providers, mean ± standard deviation (SD) of age 22.7 ± 2.9 years, male (M)/female (F) ratio 67/83; 124 gtC-sera providers, age 20.0 ± 2.7 years, M/F 31/93; 101 NI-sera providers, age 20.3 ± 3.3 years, M/F 60/41. The protocol of this clinical study, which conformed to the provisions of the 1964 Declaration of Helsinki and its later amendments, was approved by the ethics committees of St. Marianna University School of Medicine and University of Tsukuba (UMIN000014363). All of the subjects gave their informed consent prior to their inclusion in this study.

Sandwich ELISA for genotype A- and C-derived HBsAg

Genotype A2-derived HBs small Ag (gtA-Ag) was purchased (adw2; Abcam, Cambridge, UK), and genotype C-derived HBs small Ag (gtC-Ag) was kindly provided by Kaketsuken (Bimmugen, adrq+). A total of 5 μg/mL of each antigen was immobilized onto 8-well strips (Immobilizer amino F8 module; Thermo Fisher Scientific, Waltham, MA, USA) for 2 h at room temperature. The sera and peroxidase-conjugated HBsAg (ad + ay, Enzygnost Anti-HBs II; Siemens, München, Germany) were added and incubated for 1 h at 37 °C. The reactivity was developed in accordance with the protocol of Enzygnost Anti-HBs II. When the sera showed optical density (OD) values exceeding 1.5, they were diluted until their OD values fell into the range of 0.25–1.5; the obtained OD values were then multiplied by the serum dilutions. The multiplied values were compensated by the OD value of the internal control serum sample in each experiment, and the compensated values were shown as reactivity specific to gtA- and gtC-Ag.

Alternatively, the reactivity of some gtA- and gtC-sera were absorbed with serially diluted soluble gtA- and gtC-Ags, and the resultant reactivity to the HBsAgs of the vaccine genotypes was measured. The absorption ratios with HBsAgs of non-vaccine genotypes were calculated using the following formula: (OD values without absorption—OD values absorbed with the non-vaccine genotype-derived HBsAg)/(OD values without absorption—OD values absorbed with the vaccine genotype-derived HBsAg).

HBV-neutralization

Genotype C HBVs (7×10^5 copies) were suspended in 90 μL of dHCGM medium [15]. gtA- and gtC-sera were serially diluted with the negative control (NC) serum (Enzygnost Anti-HBs II) to adjust their anti-HBs titers to 100, 200, 300, 500, 1,000, and 10,000 mIU/mL. The anti-HBs titers of the diluted sera were confirmed by measurement using Enzygnost Anti-HBs II. Three NI sera (no dilution) and immunoglobulins containing high-titer

antibodies against HBsAg (HBIG) (Hebsbulin, Japan Blood Products Organization, Tokyo, Japan), anti-HBs titers of which were adjusted to 10, 100, 1,000 and 10,000 mIU/mL, were also prepared. Each serum sample or HBIG (10 μL) was added to 90 μL of the virus-suspended medium, and incubated at 37 °C for 2 h. After the incubation, primary human hepatocytes (PhoenixBio, Higashi-hiroshima, Japan), seeded at 7.0×10^4 cells/well, were cultured in 100 μL of the medium containing the HBV and the serum sample above (Day 0). On Days 2 and 3, the culture supernatants of mock wells (10 μL of dHCGM was added in place of sera) were recovered, and the supernatants of the other wells were discarded. The cells were washed in 100 μL of DMEM 3 times and again cultured in 100 μL of fresh dHCGM. On Day 7, the culture supernatants of each well were replaced with 100 μL of fresh dHCGM. On Days 12, 17, and 22, the culture supernatants were recovered. On Days 12 and 17, 100 μL of fresh dHCGM was added to each well. HBV genomic DNA was extracted using Smitest (Medical Biology, Nagoya, Japan) from the supernatants on Day 17.

The extracted HBV-DNA was quantified by real-time polymerase chain reaction (PCR) using Eagle Taq Universal Master Mix (Roche Diagnostics, Basel, Switzerland). The sequences of the primers and probes were as follows: forward, 5′-CACATCAGGATTCCTAGGACC-3′; reverse, 5′-AGGTTGGTGAGTGATTGGAG-3′; probe, 5′-CAGAGTCTAGACTCGTGGTGGACTTC-3′. Serially diluted pHBV/Aa-1.24, in which the whole genome of HBV was sub-cloned, was used as the template for the standard samples. The amplification program was performed as follows using a StepOne Plus PCR system (Thermo Fisher Scientific): 50 °C for 2 min, 95 °C for 10 min, and (95 °C for 15 s and 60 °C for 1 min) for 45 cycles.

Statistical analyses

The significance of differences in the reactivity between gtA- and gtC-sera was calculated using Wilcoxon's signed-rank test (Fig. 1a, b) and Student's *t* test (Fig. 2c). The correlations between the reactivity to gtA-Ag and that to gtC-Ag were calculated using Spearman's rank correlation coefficient (Fig. 2a, b). The significance of differences in the absorption ratios between sera absorbed with vaccine genotype HBsAg and those absorbed with the non-vaccine genotype HBsAg was calculated by Wilcoxon's signed-rank test (Fig. 3a, b). The significance of differences in the absorption ratios between a serum sample absorbed with the vaccine genotype HBsAg and that absorbed with the non-vaccine genotype HBsAg was calculated using Student's *t* test (Fig. 3c–e). The significance of differences in the HBV neutralization levels between gtA- and gtC-sera was also calculated using Student's *t* test (Fig. 4b, d).

Results

gtA-sera were cross-reactive to gtC-Ag and gtC-sera were cross-reactive to gtA-Ag

First, we examined whether gtA-sera (anti-HBs-positive sera from Heptavax-II-immunized individuals) were reactive to gtC-Ag and whether gtC-sera (anti-HBs-positive sera from Bimmugen-immunized individuals) were reactive to gtA-Ag. The reactivity of 147 gtA-sera, 120 gtC-sera, and 101 NI-sera (anti-HBs-negative sera from HB vaccine-non-immunized individuals) to gtA- and gtC-Ag was measured by sandwich ELISA (Fig. 1a, b). The mean + 2SD of the OD values of the NI-sera were set as the cut-off values to determine whether the examined gtA- and gtC-sera were anti-HBs-positive or -negative (0.067 AU in gtA-Ag ELISA, and 0.078 AU in gtC-Ag ELISA) (Fig. 1a, b, broken lines).

We found that 135 out of the 147 gtA-sera (91.8%) were positive for anti-gtA-Ag (2.94 ± 4.04 AU), and 134 out of the 135 anti-gtA-Ag-positive sera (99.3%) were also positive for anti-gtC-Ag (4.54 ± 6.21 AU) (Fig. 1a–c). The titer of the remaining 1 gtA-serum sample, A56, was 0.085 AU to gtA-Ag and 0.075 AU to gtC-Ag, which were close to the cutoff values (Table 1). All of the examined 120 gtC-sera (100%) were positive for anti-gtC-Ag (38.4 ± 49.4 AU) as well as anti-gtA-Ag (19.5 ± 28.9 AU) (Fig. 1a–c). Thus, almost all of the anti-HBs-positive sera obtained by vaccination with Heptavax-II and Bimmugen were found to be cross-reactive to gtC-Ag and gtA-Ag, respectively.

We found 13 gtA-sera that were not reactive to gtA- or gtC-Ag (Fig. 1a–c; Table 1). Eleven of these 13 gtA-sera were both anti-gtA-Ag- and anti-gtC-Ag-negative. Regarding the remaining two sera, the results of one A56 were described above; the other sample (A142) was anti-gtA-Ag-negative but anti-gtC-Ag-positive (Table 1).

In addition, the 120 gtC-sera showed significantly higher reactivity to both gtA-Ag and gtC-Ag than the 147 gtA-sera (gtA-sera vs. gtC-sera: 2.70 ± 3.95 vs. 19.5 ± 28.9 AU to gtA-Ag, $p < 0.001$; 4.15 ± 6.06 vs. 38.4 ± 49.4 AU to gtC-Ag, $p < 0.001$) (Fig. 1a, b).

gtC-sera bound more strongly to gtC-Ag than to gtA-Ag compared to gtA-sera, and vice versa for gtA-sera

We compared the reactivity to gtA-Ag with that to gtC-Ag in the 135 anti-gtA-Ag-positive gtA-sera and the 120 anti-

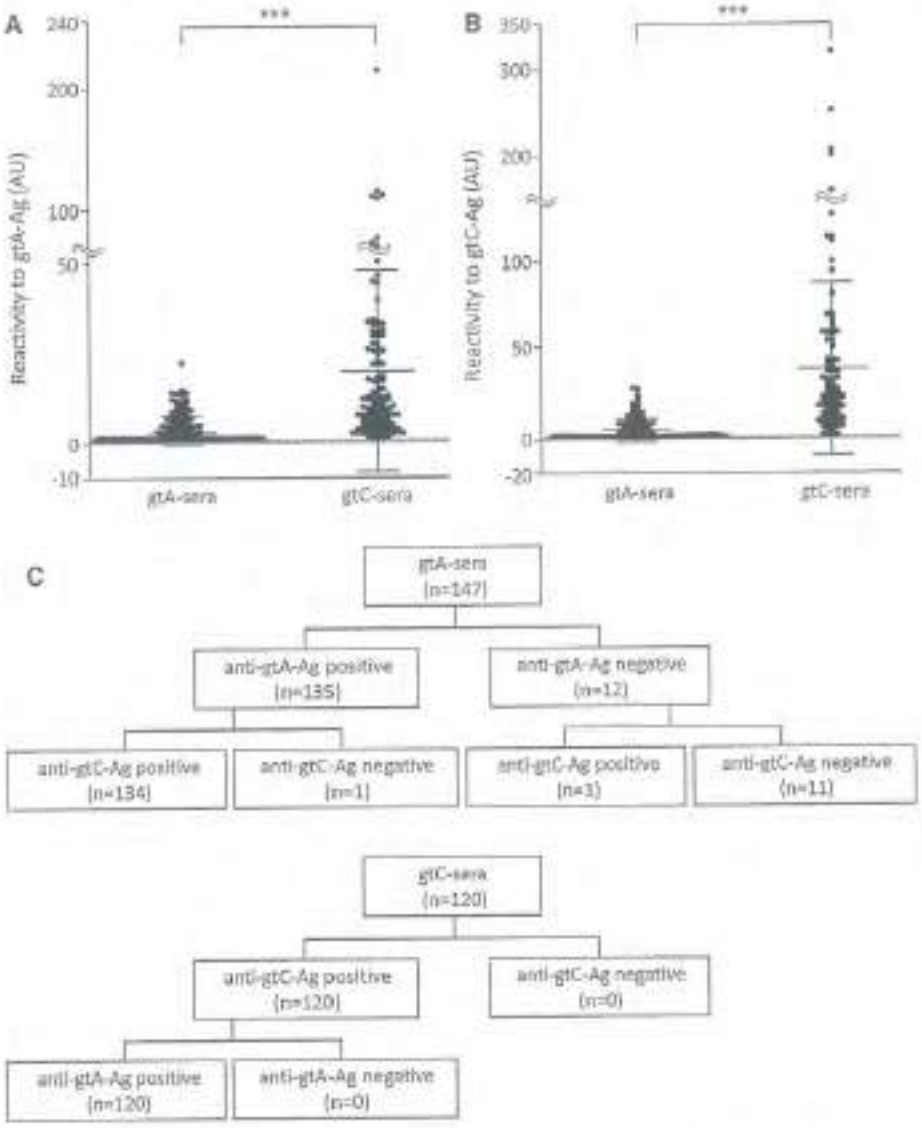

Fig. 1 Reactivity of gtA-sera to gtC-Ag and that of gtC-sera to gtA-Ag. A total of 147 gtA-sera and 120 gtC-sera, determined as anti-HBs-positive by clinical examinations, were measured for their reactivity to gtA-Ag and gtC-Ag by respective sandwich ELISAs. The resultant OD values were compensated using the OD values of an internal control serum in every ELISA experiment, and the compensated values are shown as the reactivity. The cut-off values were determined as the mean + 2SD of 101 NI-sera (*broken lines*). The results of gtA-Ag (a) and gtC-Ag (b) are shown. A summary of the results is shown (c).
$^{***}p < 0.001$

gtC-Ag-positive gtC-sera. We examined the correlation between the gtA-serum reactivity to gtA-Ag and that to gtC-Ag, and the correlation between the gtC-serum reactivity to gtA-Ag and that to gtC-Ag. In the 135 gtA-sera, the reactivity to gtA-Ag and that to gtC-Ag showed a strong positive correlation ($\rho = 0.989$, $p < 0.01$) (Fig. 2a). In the 120 gtC-sera, the reactivity to gtA-Ag and that to gtC-Ag also showed a strong positive correlation ($\rho = 0.953$, $p < 0.01$) (Fig. 2b).

We next examined the difference between the serum reactivity to vaccine genotype HBsAg and that to non-vaccine genotype HBsAg. To analyze the difference, we calculated the ratio of "the reactivity to gtC-Ag/the reactivity to gtA-Ag" (y/x in Fig. 2a, b). Interestingly, the ratio was higher in gtC-sera than in gtA-sera (2.40 ± 0.80 vs. 1.54 ± 0.42, $p < 0.001$) (Fig. 2a, b). To demonstrate the different reactivity between gtA- and gtC-sera more clearly, we calculated the normalized ratio of "the reactivity to gtC-Ag/the reactivity to gtA-Ag" by setting the average ratio of the total samples as 1.0. gtC-sera showed an average normalized ratio of more than 1.0, while gtA-sera showed an average normalized ratio of less than 1.0 (1.23 [−7.41 to 3.03] vs. −1.25 [−2.64 to 2.00], $p < 0.001$) (Fig. 2c). These results suggested that the gtC-sera were more strongly reactive to gtC-Ag than to gtA-Ag and that the gtA-sera were more strongly reactive to gtA-Ag than to gtC-Ag.

A small fraction of polyclonal anti-HBs was vaccine genotype HBsAg-specific

Next, we investigated whether vaccine genotype-specific anti-HBs fractions were present in gtA- and gtC-sera by

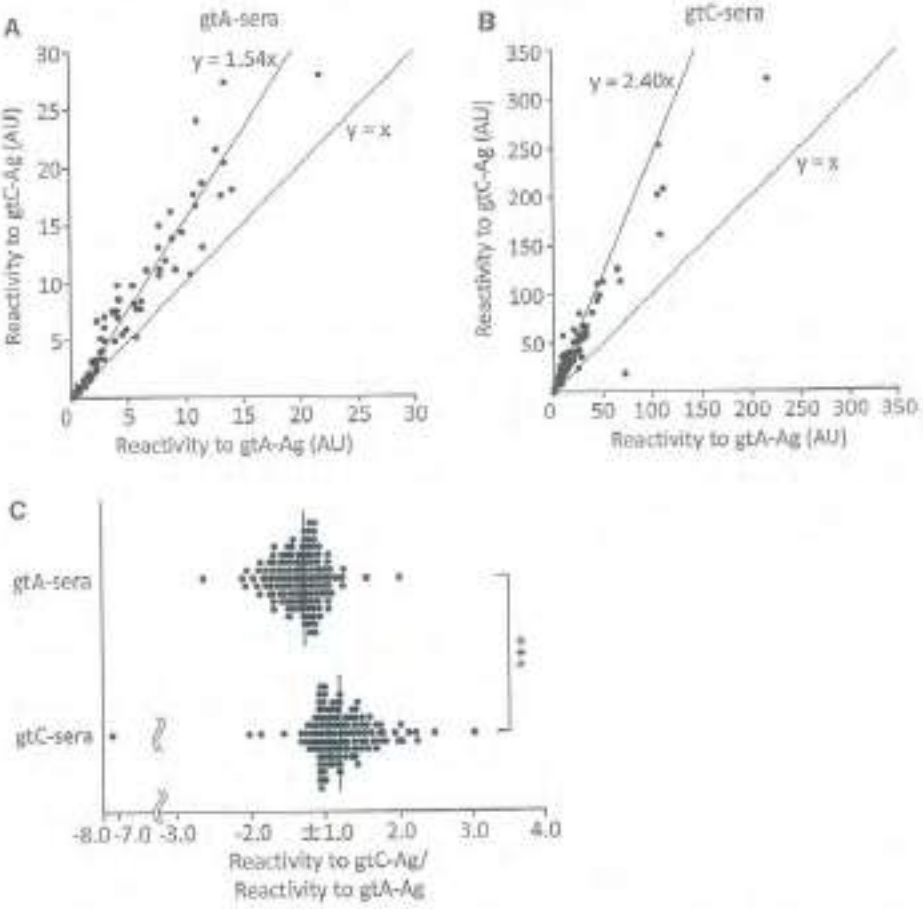

Fig. 2 The correlations of gtA- and gtC-serum reactivity to gtA-Ag and gtC-Ag. **a**, **b** The correlations of gtA- and gtC-serum reactivity to gtA-Ag and gtC-Ag were examined. The results of 135 gtA-sera (**a**, $\rho = 0.989$, $p < 0.01$) and 120 gtC-sera (**b**, $\rho = 0.953$, $p < 0.01$) are shown. **c** The difference in the reactivity between gtA- and gtC-sera was examined by calculating the ratio of "the reactivity to gtC-Ag/the reactivity to gtA-Ag." The ratios were normalized as the average of all examined sera as 1.0. "-x" indicates "1/x". ***$p < 0.001$

an antibody-absorption test using gtA- and gtC-Ag. Ten samples each of gtA- and gtC-sera adjusted to show anti-HBs values of approximately 1.0 OD were absorbed with serial concentrations of soluble gtA- and gtC-Ag, respectively (Table 2). The reactivity of the absorbed gtA-sera to gtA-Ag, and that of the absorbed gtC-sera to gtC-Ag was measured by ELISA. In all 10 examined gtA-sera, the reactivity to gtA-Ag was completely (100%) absorbed with 5 μg/mL gtA-Ag (data not shown). Similarly, in all 10 examined gtC-sera, the reactivity to gtC-Ag was completely (100%) absorbed with 5 μg/mL gtC-Ag (data not shown). Given these results, we determined the concentration of soluble antigens for the absorption as 5 μg/mL.

We then measured the absorption ratios of the OD-adjusted gtA-sera and gtC-sera absorbed with 5 μg/mL gtC-Ag and gtA-Ag, respectively. On average, 96.4 ± 6.5% of the reactivity of gtA-sera to gtA-Ag was absorbed with gtC-Ag ($p < 0.01$) (Table 2; Fig. 3a). Similarly, 96.0 ± 2.6% of the reactivity of gtC-sera to gtC-Ag was absorbed with gtA-Ag ($p < 0.001$) (Table 2; Fig. 3b). Thus, 3.6 and 4.0% anti-HBs in gtA- and gtC-sera were not absorbed with gtC- and gtA-Ag, respectively. Sixteen of the 20 sera showed 91.1–99.8% absorption ratios (Table 2, a representative case of C24 is shown in Fig. 3c). Three gtA-sera (A74, A75, and A93) showed 100% absorption with gtC-Ag (Table 2; Fig. 3d). Interestingly, in 1 gtA-serum sample, A72, only 79.2% of the reactivity to gtA-Ag was absorbed with gtC-Ag (Table 2; Fig. 3e). Collectively, almost all of the examined gtA- and gtC-sera showed identical or slightly less reactivity to non-vaccine genotype HBsAg than to the vaccine genotype HBsAg. In each anti-HBs-positive serum, most polyclonal anti-HBs were cross-reactive to non-vaccine genotype HBsAg, however, a small fraction of the anti-HBs was vaccine genotype HBsAg-specific.

gtA- and gtC-sera with a high anti-HBs titer effectively neutralized genotype C HBV

Finally, we examined whether or not the genotype C HBV-neutralization levels were different between gtA-sera ($n = 4$) and gtC-sera ($n = 3$) (Table 3). The sera were serially diluted to show anti-HBs titers of 100–10,000 mIU/mL. The resultant titers of the diluted sera were confirmed to be within ±20% of each titer (data

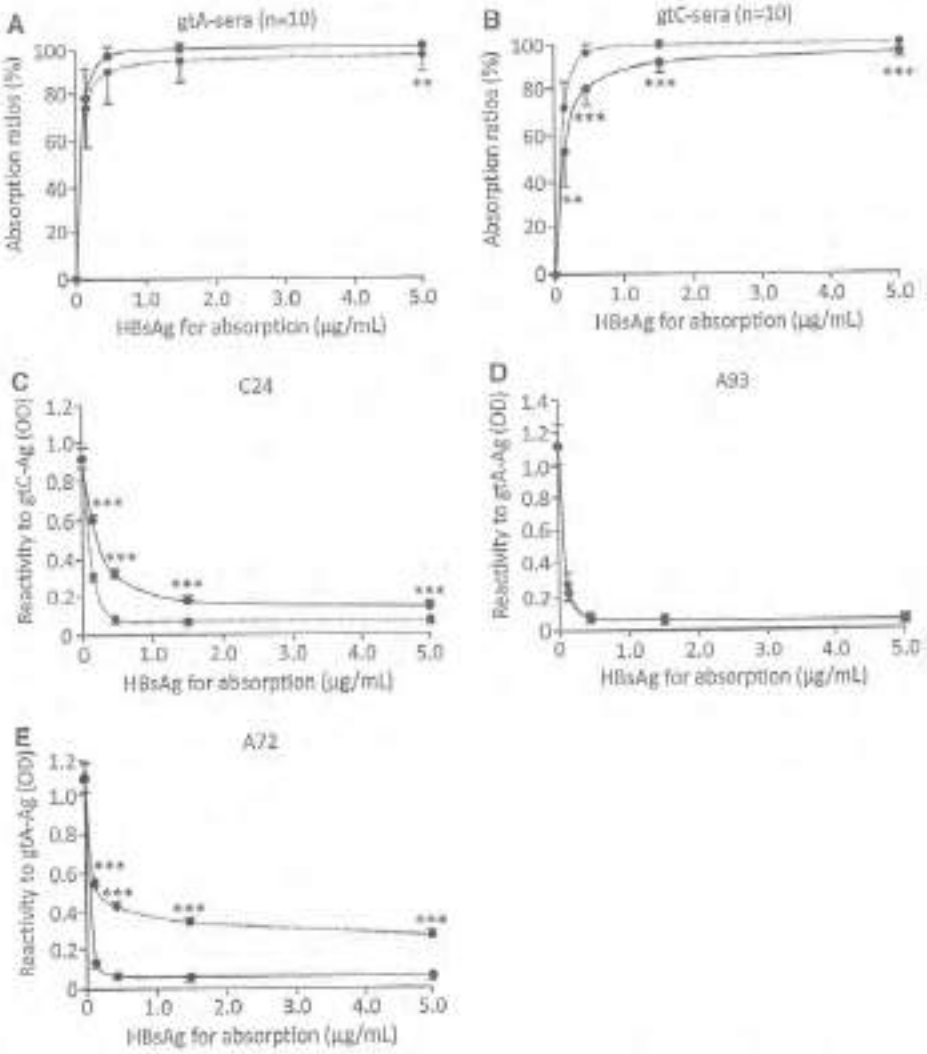

Fig. 3 gtA-serum reactivity absorbed with gtC-Ag and gtC-serum reactivity absorbed with gtA-Ag. A total of 10 gtA-sera and 10 gtC-sera (Table 2) were absorbed with serially diluted gtA-Ag and gtC-Ag. The resultant reactivity of the gtA-sera was measured by gtA-ELISA, and that of the gtC-sera was measured by gtC-ELISA. When the gtA-sera absorbed with gtA-Ag and the gtC-sera absorbed with gtC-Ag showed the same or lower reactivity than the reactivity of anti-HBs-negative control serum (NC serum in Enzygnost anti-HBs II), we determined that those sera had been completely absorbed. The averages of the absorption ratios of gtA-sera (a) and gtC-sera (b), and the representative results of 3 sera (the absorption ratios with the non-vaccine genotype HBsAg were 91.1%, c; 100%, d; and 79.2%, e) are shown. *Solid lines*, absorption with gtA-Ag; *dotted lines*, absorption with gtC-Ag. $^{**}p < 0.01$, $^{***}p < 0.001$

not shown). We then mixed the diluted sera with HBV-suspended culture media to obtain final anti-HBs titers at 1/10 of the adjusted titers (10–1,000 mIU/mL) (Fig. 4a).

First, we tried to determine the anti-HBs titers of HBIG and gtC-sera that sufficiently neutralized HBV in this experiment. We found that 100 and 1,000 mIU/mL HBIG sufficiently neutralized the genotype C HBV (the extracellular HBV-DNA, 7.1 and 4.3 copies, respectively) (Fig. 4a). Similarly, 100 and 1,000 mIU/mL gtC-sera sufficiently neutralized the genotype C HBV (6.5 ± 7.4 and 4.6 ± 5.9 copies, respectively). In contrast, 10 mIU/mL HBIG was insufficient for the neutralization (405.5 copies) (Fig. 4a), showing a level similar to that of anti-HBs-negative sera (NI 1–3 and NC, 309.3 ± 115.1 copies).

In this condition, the gtA-sera sufficiently neutralized genotype C HBV at an anti-HBs titer of 100 mIU/mL (10.7 ± 5.5 copies) (Fig. 4a). The gtA-sera showed inhibition ratios similar to those of the gtC-sera at 100 mIU/mL (92.8 ± 3.7 vs. 95.4 ± 4.8%, $p = 0.44$) (Fig. 4b). The A72 serum sample that showed low absorption with gtC-Ag (79.2%, Fig. 3e) provided an inhibition ratio similar to those of the other three gtA-sera at 100 mIU/mL anti-HBs (92.0 vs. 93.0 ± 4.5%) (Fig. 4a, b).

Interestingly, the inhibition ratios at a relatively low anti-HBs titer of 30 mIU/mL were significantly lower in the gtA-sera than the gtC-sera (60.2 ± 17.0 vs. 90.2 ± 8.2%, $p < 0.05$) (Fig. 4b). To compare the genotype C HBV-neutralizing capacity between the gtA- and gtC-sera, we compared the anti-HBs titers of those sera that showed an inhibition ratio of 87.0% (Fig. 4c, broken line). This ratio, which was equal to that of 92.2 mIU/mL HBIG, was selected because all 7 sera were able to be evaluated. As a result, the anti-HBs titers of the gtA-sera that showed an inhibition ratio of 87.0% were significantly higher than those of the gtC-sera (72.8 ± 23.7 vs. 25.6 ± 14.2 mIU/mL, $p < 0.05$) (Fig. 4d). This indicates that the genotype C

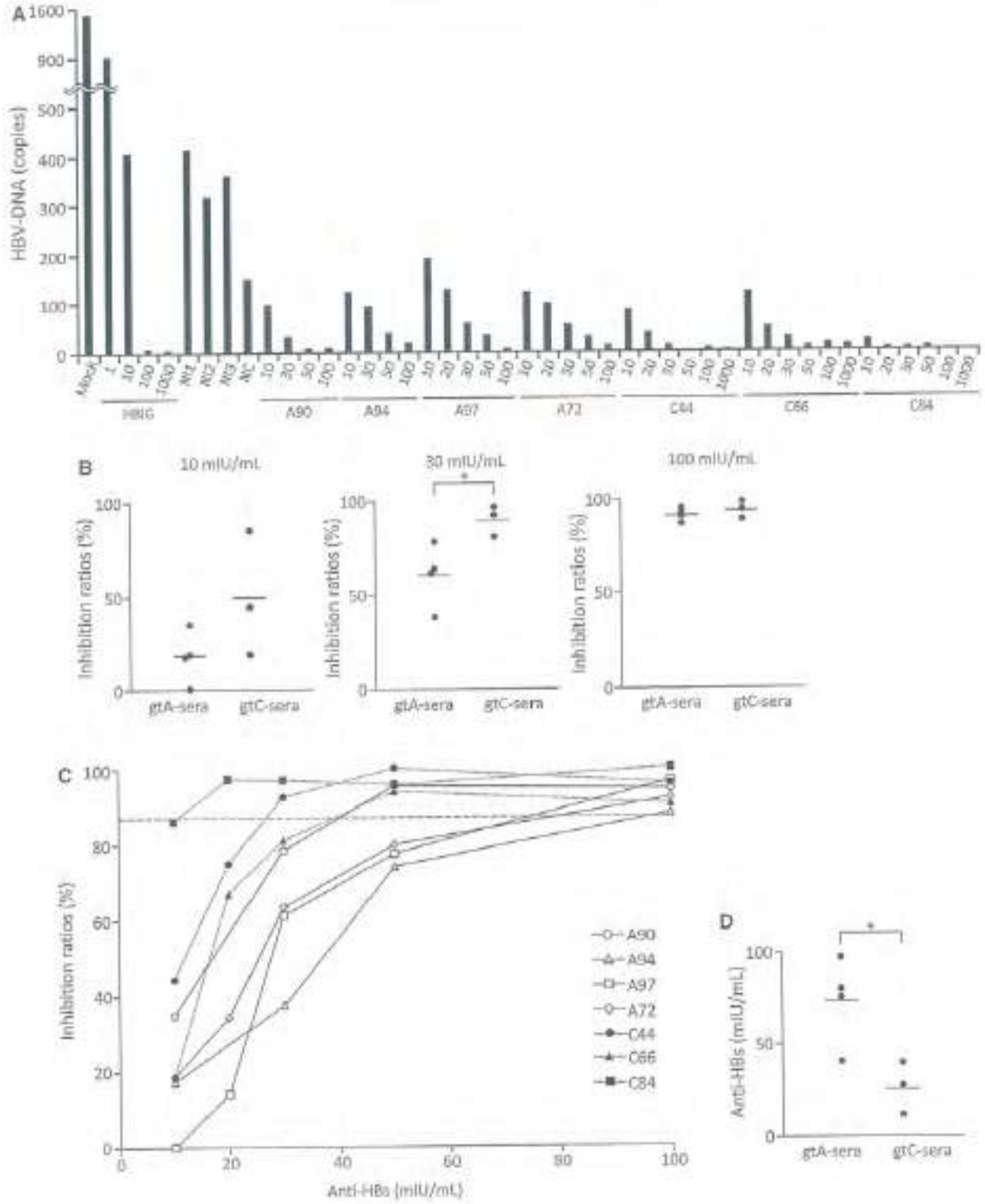
A
HBV-DNA (copies)
HBIG
A90
A94
A97
A72
C44
C66
C84
B
10 mIU/mL
30 mIU/mL
100 mIU/mL
Inhibition ratios (%)
gtA-sera
gtC-sera
C
Inhibition ratios (%)
Anti-HBs (mIU/mL)
A90
A94
A97
A72
C44
C66
C84
D
Anti-HBs (mIU/mL)
gtA-sera
gtC-sera

◀Fig. 4 Genotype C HBV-neutralization by gtA-sera and gtC-sera. a Four gtA-sera and three gtC-sera (Table 3) were diluted until their anti-HBs titers were 100, 200, 300, 500, 1,000, and 10,000 (gtC-sera only) mIU/mL and subsequently mixed with genotype C HBV. The final anti-HBs titers were at 1/10 of the adjusted titers (10–1,000 mIU/mL). The mixture was incubated at 37 °C for 2 h, and infected into primary human hepatocytes. The HBV-DNA copy numbers in the culture supernatants on Day 17 were quantified. HBV-DNA copy numbers of medium-alone wells, in which HBV was not infected, were subtracted from the resultant HBV-DNA copy numbers of all experiments. b Since all of the gtA- and gtC-sera were diluted with NC serum, we calculated the inhibition ratios of the genotype C-HBV infection as 0% inhibition for NC serum (147.45 copies) and as 100% for 0 copies (C44, 50 mIU/mL; C84, 100 and 1,000 mIU/mL). The inhibition ratios of genotype C HBV infection by gtA- and gtC-sera, diluted to anti-HBs titers of 10, 30, and 100 mIU/mL, are shown. c, d The anti-HBs titers of the 4 gtA-sera and the 3 gtC-sera that showed an inhibition ratio of 87.0% (*broken line*, c) were compared. Mock: HBV was infected, and either HBIG or serum was not added. $^{*}p < 0.05$

HBV-neutralizing capacity of the gtA-sera was lower than that of the gtC-sera. In addition, the A72 serum sample showed an anti-HBs titer of 79.5 mIU/mL with over 87.0% inhibition, which was similar to the anti-HBs titers of the other 3 gtA-sera (70.5 ± 28.5 mIU/mL) (Fig. 4c, d).

Discussion

To examine whether or not vaccine-acquired polyclonal anti-HBs effectively bound to the HBsAg of non-vaccine genotypes, we established gtA-Ag ELISA and gtC-Ag ELISA. Of 101 NI sera that were anti-HBs-negative in a clinical examination, 99 (98%) and 94 (93%) samples showed compensated OD values less than the cut-off values of the gtA-Ag ELISA and gtC-Ag ELISA, respectively (data not shown). In contrast, of 147 gtA-sera and 120 gtC-sera that were anti-HBs-positive in clinical examinations, 135 gtA-sera (92%) and all 120 gtC-sera (100%) showed OD values exceeding the cut-off values in the gtA-Ag ELISA and gtC-Ag ELISA, respectively (Fig. 1a–c; Table 1). Collectively, at most 8% of the examined gtA-sera were judged to be anti-HBs-negative in the gtA-Ag ELISA. It was reported that approximately 7% of serum samples showed conflicting results between the 2 established anti-HBs measurement methods [23]. Thus, our ELISAs were considered to be accurate enough to measure the reactivity to single genotype-derived HBsAgs.

Notably, 134 of the 135 gtA-sera (99.3%) and all 120 gtC-sera (100%) were both anti-gtA-Ag-positive and anti-gtC-Ag-positive (Fig. 1a–c). Indeed, gtA- and gtC-sera showed very high correlations between the reactivity to gtA-Ag and that to gtC-Ag (gtA-sera, $\rho = 0.989$, $p < 0.01$; gtC-sera, $\rho = 0.953$, $p < 0.01$) (Fig. 2a, b). Heptavax-II and Bimmugen were therefore concluded to provide polyclonal anti-HBs that bound not only to HBsAgs of the vaccine genotypes but also to those of non-vaccine genotypes. This finding concurs with that from a previous study in Uzbekistan in which both adr- and adw2-type vaccines were reported to provide equally high anti-HBs acquisition ratios [24]. We therefore believe that vaccine recipients who become anti-HBs-positive can still prevent infection

Table 1 gtA-sera not reactive to either or both gtA-Ag or gtC-Ag

Sera	Age (years)	Sex	Anti-HBs* (mIU/mL)	Anti-HBs (AU)**		Duration*** (months)
				gtA-Ag	gtC-Ag	
A56	24	F	*21.0*	*0.085*	0.075	33
A126	22	M	125.6	0.041	0.047	4
A128	20	M	52.0	0.040	0.044	33
A130	22	M	21.5	0.032	0.043	16
A131	20	F	191.8	0.042	0.046	16
A132	20	M	70.6	0.043	0.056	16
A136	22	M	108.2	0.063	0.058	16
A137	21	M	681.5	0.065	0.053	4
A139	22	M	27.9	0.047	0.063	16
A142	22	M	340.2	0.050	*0.114*	4
A143	22	M	24.4	0.040	0.055	33
A144	23	M	15.3	0.039	0.060	16
A147	20	F	21.5	0.042	0.051	33

* The anti-HBs titers of the sera were measured by Architect (A56, italic) or Stacia (others)

** The reactivity to single genotype-derived HBsAg was measured. The cut-off values were 0.067 and 0.078 AU for reactivity to gtA-Ag and gtC-Ag, respectively. A56 was anti-gtA-Ag-positive, whereas A142 was anti-gtC-Ag-positive (italic). The other sera were anti-gtA-Ag-negative and anti-gtC-Ag-negative

*** Duration from the last vaccination to blood sampling

Table 2 gtA-sera and gtC-sera examined by the absorption test

Sera	Age/sex	Anti-HBs* (mIU/mL)	Anti-HBs (AU) to		Absorption (%) with		Duration (months)
			gtA-Ag	gtC-Ag	gtA-Ag	gtC-Ag	
A9	24/F	361.0	13.474	20.340	100	99.2	52
A40	23/F	436.5	11.561	13.062	100	99.8	4
A53	22/M	>1000	11.562	18.632	100	98.4	4
A57	24/F	>1000	9.752	14.369	100	98.9	16
A72	19/F	840.3	4.863	5.996	100	79.2	4
A74	20/F	>1000	10.787	17.663	100	100	16
A75	20/F	>1000	–	–	100	100	4
A80	20/F	847.5	7.730	10.665	100	93.4	4
A93	34/M	>1000	12.785	21.514	100	100	4
A105	21/F	>1000	8.805	16.118	100	96.3	4
C10	19/F	2111.3	72.841	19.197	95.1	100	1
C11	19/F	1415.9	13.473	25.743	99.4	100	1
C13	21/F	1334.2	33.233	63.650	96.2	100	1
C24	20/F	1519.5	29.919	54.688	91.1	100	1
C49	19/F	2990.8	112.926	208.351	96.6	100	2
C56	19/M	1681.1	25.290	50.826	98.1	100	2
C77	19/F	3792.2	45.235	111.681	96.1	100	2
C81	21/F	1379.7	21.172	33.248	95.4	100	2
C91	21/F	17173.6	217.508	320.561	98.8	100	2
C121	19/F	1913.6	–	–	93.0	100	2

* The anti-HBs titers of gtA-sera and gtC-sera were measured by Stacia and Architect, respectively

Table 3 gtA-sera and gtC-sera examined by the neutralization test

Sera	Age (years)	Sex	Anti-HBs* (mIU/mL)	Anti-HBs (AU)		Durations (months)
				gtA-Ag	gtC-Ag	
A72	19	F	840.3	4.863	5.996	4
A90	19	F	>1000	–	–	4
A94	20	F	>1000	21.855	27.878	4
A97	19	M	>1000	–	–	4
C44	19	F	15675.8	–	–	1
C66	19	M	11862.7	–	–	2
C84	21	M	34646.0	–	–	2

* The anti-HBs titers of gtA-sera and gtC-sera were measured by Stacia and Architect, respectively

with a non-vaccine genotype HBV. Our results provide evidence to support efforts to promote universal HB vaccination using single genotype-derived HB vaccines from the viewpoint of anti-HBs values to HBsAg of non-vaccine genotypes. In addition, the gtC-sera showed higher reactivity to both gtA- and gtC-Ag than did gtA-sera (Fig. 1a, b). This would be mainly because the durations from the last vaccination to blood sampling were shorter in the gtC-sera providers (1–2 months) than in the gtA-sera providers (3–52 months) (Supplementary Figures).

We hypothesized that the reactivity of anti-HBs-positive sera to vaccine genotype HBsAg was stronger than that to non-vaccine genotype HBsAg. Since gtC-Ag-ELISA and gtA-Ag-ELISA were two independent assays, the OD values of those ELISAs could not be directly compared. To analyze the difference in the serum reactivity, we calculated the ratio of "the reactivity to gtC-Ag/the reactivity to gtA-Ag". The ratio was higher in gtC-sera than in gtA-sera (2.40 ± 0.80 vs. 1.54 ± 0.42, $p < 0.001$) (Fig. 2a, b), which suggested stronger reactivity of anti-HBs-positive sera to vaccine-genotype HBsAg than to non-vaccine genotype HBsAg. However, it was difficult to comprehend, as both sera showed average "the reactivity to gtC-Ag/the reactivity to gtA-Ag" values exceeding 1.0 (gtA-sera,

1.54 ± 0.42; gtC-sera, 2.40 ± 0.80) (Fig. 2a, b). In other words, anti-HBs values to gtC-Ag were apparently higher than those to gtA-Ag in both gtA- and gtC-sera. Although the possibility that the reactivity to gtC-Ag was really higher than that to gtA-Ag in both sera could not be completely excluded, it was unlikely that most anti-sera (gtA-sera in this case) would show higher reactivity to another antigen than to the immunized antigen. We therefore considered the apparently higher anti-HBs to gtC-Ag than to gtA-Ag to be because of higher sensitivity of gtC-Ag-ELISA than gtA-Ag-ELISA. Indeed, the OD values of anti-HBs showed higher values in gtC-Ag-ELISA than in gtA-Ag-ELISA (gtA-sera, 4.15 ± 6.06 AU to gtC-Ag, 2.70 ± 3.95 AU to gtA-Ag; gtC-sera, 38.4 ± 49.4 AU to gtC-Ag, 19.5 ± 28.9 AU to gtA-Ag) (Fig. 1a, b). To exclude the assay difference from the analysis, we calculated the normalized ratio of "the reactivity to gtC-Ag/the reactivity to gtA-Ag." This normalization suggested that vaccine-acquired polyclonal anti-HBs preferentially recognize vaccine genotype HBsAg compared to non-vaccine genotype HBsAg (gtA-sera, −1.25 [−2.64 to 2.00] vs. gtC-sera, 1.23 [−7.41 to 3.03]; $p < 0.001$) (Fig. 2c).

Consistent with the above result, in the absorption test, almost all of the polyclonal anti-HBs repertoire was absorbed by non-vaccine genotype HBsAg; however, the absorption was not complete (gtA-sera, 96.4%; gtC-sera 96.0%) (Table 2; Fig. 3a, b). The different ratios between the absorption with vaccine genotype HBsAg and that with non-vaccine genotype HBsAg is due to the differences in the HBsAg epitopes covered by polyclonal anti-HBs. Whole HBsAg epitopes of gtA- and gtC-Ag consist of gtA-Ag-specific epitopes, gtC-Ag-specific epitopes, and epitopes common to both. The ratios of absorption with non-vaccine genotype HBsAg indicate the ratios of the common epitope-covering anti-HBs repertoire to the whole anti-HBs repertoire. The common epitopes of gtA-Ag and gtC-Ag include "a"-determinant (aa124-149) and "d" epitope (aa122) but not "w" or "r" epitopes (aa160) [25–27]. Interestingly, among 222 B-cell lines secreting anti-HBs antibodies, established from 34 good responders to HB vaccine, 216 (97.3%) and 5 (2.3%) lines recognized the "a" and "d" epitopes, respectively, whereas only one (0.4%) line recognized "w" epitope [28]. The ratio of 99.6% recognition of "a" and "d" epitopes by the B cell lines was within the range of our non-vaccine genotype HBsAg-absorption ratios of 19 out of the 20 examined sera, 91.1–100% (Table 2). Collectively, more than 90% of the whole anti-HBs repertoire would recognize the common major epitopes in almost all vaccine recipients. This part of the anti-HBs repertoire may contribute to the neutralization of non-vaccine genotype HBV.

We directly assessed the neutralizing capacity and found that the gtA-sera as well as the gtC-sera showed sufficient levels of genotype C HBV-neutralization at a high anti-HBs titer of 100 mIU/mL (92.8 ± 3.7 vs. 95.4 ± 4.8%, $p = 0.44$) (Fig. 4b). Thus, vaccine-acquired polyclonal anti-HBs with high titers would be capable of preventing infection of both vaccine and non-vaccine genotype HBV equally. This result is in accordance with previous epidemiological studies that reported that single genotype-derived HBsAg vaccination effectively decreased multiple genotype HBV infection [9, 11–13]. Our result is also in accordance with our previous in vitro study, where we found that monoclonal anti-HBs prevented HBV infection of non-vaccine genotype at high titers [15]. These findings indicate that the neutralizing capacity through the common major epitopes such as "a"-determinant and C(K/R)TC motif (aa121-124) is critical for preventing HBV infection of multiple genotypes [25, 29].

However, we also found that the gtA-sera showed lower inhibition levels than the gt-C sera at a low anti-HBs titer of 30 mIU/mL (60.2 ± 17.0 vs. 90.2 ± 8.2%, $p < 0.05$) (Fig. 4b). Furthermore, the gtA-sera required higher anti-HBs titers than the gtC-sera to provide a particular inhibition ratio (72.8 ± 23.7 vs. 25.6 ± 14.2 mIU/mL, $p < 0.05$) (Fig. 4c, d). Thus, vaccination with a single genotype HBsAg may be less effective in preventing the infection of non-vaccine genotype HBV than that of vaccine genotype HBV. The neutralizing capacity through genotype-specific epitopes was also important for preventing HBV infection of individual genotypes, as suggested in our previous observation [30]. Taken together, these present and previous findings indicate that high titers of anti-HBs are required to prevent infection with non-vaccine genotype HBV. In addition, we tried to compare the capacity of the gtA- and gtC-sera to neutralize genotype A HBV. However, genotype A HBV available at that time did not sufficiently infect the primary hepatocytes (data not shown). In the near future, we will prepare a new genotype A HBV and attempt to perform the neutralizing study again.

Of the 20 sera examined by the absorption test, 17 showed incomplete absorption with non-vaccine genotype HBsAg (Table 2; Fig. 3c, e). Among these 17 sera, 1 gtA-serum sample (A72) showed a relatively low ratio of absorption with gtC-Ag (79.2%) (Fig. 3e). However, the inhibition ratios of genotype C HBV infection were similar between the A72 serum sample and the other gtA-sera (Fig. 4c). In the polyclonal anti-HBs repertoire of each of the 17 sera, a portion was against the epitopes common to gtA-Ag and gtC-Ag, while another portion was against gtA-Ag- or gtC-Ag-specific epitopes. It is well known that the titers of vaccine-acquired polyclonal anti-HBs decrease over time: indeed, a notable proportion of complete vaccine recipients lost their immune memories 15–18 years

after vaccination [31, 32]. In the above 17 sera, the anti-HBs repertoire that can neutralize non-vaccine genotype HBV is smaller than the anti-HBs repertoire that can neutralize vaccine genotype HBV; as such, the former would be lost earlier than the latter. This speculation is supported by the different neutralization capacities between gtA- and gtC-sera at 30 mIU/mL anti-HBs titer (Fig. 4b). When the anti-HBs titers against the common epitopes drop below the threshold of the minimum necessary titer for HBV neutralization, infection with non-vaccine genotype HBV would preferentially occur compared to infection with vaccine genotype HBV. Stramer et al. reported that a majority of individuals with low anti-HBs titers (5 out of 6 cases), who were found to be HBV-DNA-positive 7–16 years after the vaccination, were exclusively or predominantly infected with non-vaccine genotype HBV [14]. These cases may be examples of vaccine recipients who were infected with non-vaccine genotype HBV due to the time-dependent decrease in the polyclonal anti-HBs. To maintain anti-HBs titers, booster vaccination has been proposed, especially for cohorts with a high risk of HBV infection such as immunocompromised patients and health care providers [33–36]. Taken together, these findings suggested that booster vaccination would be useful for preventing infection of non-vaccine genotype HBV in individuals with low anti-HBs titers.

In conclusion, single genotype HBsAg vaccination with Heptavax-II and Bimmugen provided polyclonal anti-HBs that possessed sufficient capacity to bind to non-vaccine HBsAg. The vaccine-acquired polyclonal anti-HBs sufficiently neutralized non-vaccine genotype HBV at a high anti-HBs titer; however, the neutralization was insufficient at a low anti-HBs titer. It is recommended to maintain high anti-HBs titers to prevent infection of non-vaccine genotype HBV as well as vaccine genotype HBV.

Acknowledgements The authors are indebted to Ms Atsuko Nozawa and Ms Fumiko Oikawa for their technical assistance. The authors are also grateful to Kaketsuken, Abbott, Siemens, Abcam, and Thermo Fisher Scientific for their support for this study. This work was partly supported by a Grant from Ministry of Health, Labour and Welfare.

Compliance with ethical standards

Conflict of interest Chiaki Ohuse received a research grant from Takeda Pharma. Yasuhito Tanaka received lecture fees from Chugai Pharma, Bristol-Myers Squibb, and GlaxoSmithKline. Hiroshi Yotsuyanagi received lecture fees from MSD K.K. and Bristol-Myers Squibb. Tomohiro Kato received a research grant from FUJI OIL.

References

1. Trépo C, Chan HL, Lok A. Hepatitis B virus infection. Lancet. 2014;384:2053–63.
2. Lin CL, Kao JH. Novel therapies for hepatitis B virus cure-advances and perspectives. Aliment Pharmacol Ther. 2016;44:213–22.
3. Schweitzer A, Horn J, Mikolajczyk RT, et al. Estimations of worldwide prevalence of chronic hepatitis B virus infection: a systematic review of data published between 1965 and 2013. Lancet. 2015;386:1546–55.
4. GBD 2013 Mortality and Causes of Death Collaborators. Global, regional, and national age-sex specific all-cause and cause-specific mortality for 240 causes of death, 1990–2013: a systematic analysis for the Global Burden of Disease Study 2013. Lancet. 2015;385:117–71.
5. Zanetti AR, Van Damme P, Shouval D. The global impact of vaccination against hepatitis B: a historical overview. Vaccine. 2008;26:6266–73.
6. World Health Organization. Hepatitis B. 2016. http://www.who.int/mediacentre/factsheets/fs204/en/. Accessed 31 Oct 2016.
7. Norder H, Hammas B, Löfdahl S, et al. Comparison of the amino acid sequences of nine different serotypes of hepatitis B surface antigen and genomic classification of the corresponding hepatitis B virus strains. J Gen Virol. 1992;73:1201–8.
8. Tian Q, Jia J. Hepatitis B virus genotypes: epidemiological and clinical relevance in Asia. Hepatol Int. 2016;10:854–60 (in press).
9. Cassidy A, Mossman S, Olivieri A, et al. Hepatitis B vaccine effectiveness in the face of global HBV genotype diversity. Expert Rev Vaccines. 2011;10:1709–15.
10. Kao JH, Chen PJ, Lai MY, et al. Clinical and virological aspects of blood donors infected with hepatitis B virus genotypes B and C. J Clin Microbiol. 2002;40:22–5.
11. Chen HL, Chang MH, Ni YH, et al. Seroepidemiology of hepatitis B virus infection in children: ten years of mass vaccination in Taiwan. JAMA. 1996;276:906–8.
12. Chongsrisawat V, Poovorawan Y, Theamboonlers A, et al. Hepatitis B seroprevalence in Thailand: 12 years after hepatitis B vaccine integration into the national expanded programme on immunization. Trop Med Int Health. 2006;11:1496–502.
13. Wichajam K, Kosalaraksa P, Wiangnon S. Incidence of hepatocellular carcinoma in children in Khon Kaen before and after national hepatitis B vaccine program. Asian Pac J Cancer Prev. 2008;9:507–9.
14. Stramer SL, Wend U, Candotti D, et al. Nucleic acid testing to detect HBV infection in blood donors. N Engl J Med. 2011;364:236–47.
15. Hamada-Tsutsumi S, Ito E, Watanabe T, et al. Validation of cross-genotype neutralization by hepatitis B virus-specific monoclonal antibodies by in vitro and in vivo infection. PLoS One. 2015;10:e0118062.
16. Koyama T, Matsuda I, Sato S, et al. Prevention of perinatal hepatitis B virus transmission by combined passive–active immunoprophylaxis in Iwate, Japan (1981–1992) and epidemiological evidence for its efficacy. Hepatol Res. 2003;26:287–92.
17. Komatsu H, Inui A, Fujisawa T, et al. Transmission route and genotype of chronic hepatitis B virus infection in children in Japan between 1976 and 2010: A retrospective, multicenter study. Hepatol Res. 2015;45:629–37.
18. Tajiri H, Tanaka Y, Kaginoto S, et al. Molecular evidence of father-to-child transmission of hepatitis B virus. J Med Virol. 2007;79:922–6.
19. Matsuura K, Tanaka Y, Hige S, et al. Distribution of hepatitis B virus genotypes among patients with chronic infection in Japan shifting toward an increase of genotype A. J Clin Microbiol. 2009;47:1476–83.
20. Ito K, Yotsuyanagi H, Sugiyama M, Japanese AHB CHB Study Group, et al. Geographic distribution and characteristics of genotype A hepatitis B virus infection in acute and chronic

hepatitis B patients in Japan. J Gastroenterol Hepatol. 2016;31:190–9.
21. Suzuki Y, Kobayashi M, Ikeda K, et al. Persistence of acute infection with hepatitis B virus genotype A and treatment in Japan. J Med Virol. 2005;76:33–9.
22. Yano K, Tamada Y, Yatsuhashi H, Japan National Hospital Acute Hepatitis Study Group, et al. Dynamic epidemiology of acute viral hepatitis in Japan. Intervirology. 2010;53:70–5.
23. Oono K, Kani S, Ochashi M, et al. Comparative Study for Anti-Hepatitis B Surface Antigen Titers Based on Two Measurement Methods: Using Monoclonal Antibodies Isolated from Hepatitis B Vaccinated Recipients. Rinsho Byori. 2015;63:907–12.
24. Avazova D, Kurbanov F, Tanaka Y, et al. Hepatitis B virus transmission pattern and vaccination efficiency in Uzbekistan. J Med Virol. 2008;80:217–24.
25. Romanò L, Paladini S, Galli C, et al. Hepatitis B vaccination. Hum Vaccin Immunother. 2015;11:53–7.
26. Okamoto H, Imai M, Tsuda F, et al. Point mutation in the S gene of hepatitis B virus for a d/y or w/r subtypic change in two blood donors carrying a surface antigen of compound subtype adyr or adwr. J Virol. 1987;61:3030–4.
27. Kay A, Zoulim F. Hepatitis B virus genetic variability and evolution. Virus Res. 2007;127:164–76.
28. Shokrgozar MA, Shokri F. Subtype specificity of anti-HBs antibodies produced by human B-cell lines isolated from normal individuals vaccinated with recombinant hepatitis B vaccine. Vaccine. 2002;20:2215–20.
29. Qin X, Schroeder P, Bridon D. Identification and characterization of a C (K/R) TC motif as a common epitope present in all subtypes of hepatitis B surface antigen. J Immunol. 1996;156:3350–6.
30. Aono J, Yotsuyanagi H, Miyoshi H, et al. Amino acid substitutions in the S region of hepatitis B virus in sera from patients with acute hepatitis. Hepatol Res. 2007;37:731–9.
31. Lu CY, Ni YH, Chiang BL, et al. Humoral and cellular immune responses to a hepatitis B vaccine booster 15–18 years after neonatal immunization. J Infect Dis. 2008;197:1419–26.
32. Wu TW, Lin HH, Wang LY. Chronic hepatitis B infection in adolescents who received primary infantile vaccination. Hepatology. 2013;57:38–45.
33. European Consensus Group on Hepatitis B Immunity. Are booster immunisations needed for lifelong hepatitis B immunity? Lancet. 2000;355:561–5.
34. Chaves SS, Fischer G, Groeger J, et al. Persistence of long-term immunity to hepatitis B among adolescents immunized at birth. Vaccine. 2012;30:1644–9.
35. Tajiri K, Shimizu Y. Unsolved problems and future perspectives of hepatitis B virus vaccination. World J Gastroenterol. 2015;21:7074–83.
36. Hahné S, van Houdt R, Koedijk F, et al. Selective hepatitis B virus vaccination has reduced hepatitis B virus transmission in the Netherlands. PLoS One. 2013;8:e67866.

Check for updates

Original Article

Tumor Biology

Tumor Biology
October 2017: 1–7
© The Author(s) 2017
Reprints and permissions:
sagepub.co.uk/journals/Permissions.nav
DOI: 10.1177/1010428317734865
journals.sagepub.com/home/tub
SAGE

Enrichment of *Helicobacter pylori* mutant strains after eradication therapy analyzed by gastric wash–based quantitative pyrosequencing

Ritsuko Oikawa[1], Yoshiyuki Watanabe[1,2], Shuichi Miyamoto[3], Yoshinori Sato[1], Shoko Ono[4], Katsuhiro Mabe[5], Hiroyuki Yamamoto[1], Mototsugu Kato[5] and Fumio Itoh[1]

Abstract

The eradication of *Helicobacter pylori* reduces the risk of gastric cancer. A clear understanding of the factors underlying mixed infection with multiple clarithromycin-susceptible and clarithromycin-resistant *H. pylori* strains is necessary to design more effective therapies against *H. pylori*. We aimed to assess how the abundance and prevalence of *H. pylori* strains vary after clarithromycin-based eradication therapy. Using gastric wash samples, which represent the entire stomach, we sequentially analyzed the abundance and prevalence of *H. pylori* DNA by 23S ribosomal RNA pyrosequencing before and 1, 2, and 3 years after eradication therapy. Low levels of *H. pylori* DNA were still detectable at the first-year follow-up in all samples with negative post-treatment urea breath test results. The abundance of *H. pylori* DNA decreased significantly until the 2-year follow-up, but it switched to an increase at the 3-year follow-up. Importantly, the ratio of the prevalence of mutant strains to the prevalence of wild-type strains had already increased at the first-year follow-up and continued to increase, suggesting the selection and growth of clarithromycin-resistant strains during the follow-up periods. Being sensitive and representative, our assay will be useful in effectively addressing gastric cancer development by enhancing the long-term success of intervention strategies and consecutive surveillance for *H. pylori* eradication.

Keywords

Helicobacter pylori, mixed infection, gastric wash, 23S ribosomal RNA, pyrosequencing

Date received: 22 August 2017; accepted: 12 September 2017

Introduction

The eradication of *Helicobacter pylori* infection reduces the risk of recurrent peptic ulcer diseases and the development of gastric adenocarcinoma.[1–6] It is now widely accepted that clarithromycin (CAM) resistance among *H. pylori* strains has been increasing worldwide and is the most important factor responsible for the failure of *H. pylori* eradication.[6–18] Various molecular methods have been developed to detect CAM resistance in *H. pylori* isolates in clinical specimens, such as biopsy samples and

[1]Division of Gastroenterology and Hepatology, Department of Internal Medicine, St. Marianna University School of Medicine, Kawasaki, Japan
[2]Department of Internal Medicine, Kawasaki Rinko General Hospital, Kawasaki, Japan
[3]Department of Gastroenterology and Hepatology, Hokkaido University Graduate School of Medicine, Sapporo, Japan
[4]Division of Endoscopy, Hokkaido University Hospital, Sapporo, Japan
[5]Department of Gastroenterology, National Hospital Organization Hakodate Hospital, Hakodate, Japan

Corresponding author:
Hiroyuki Yamamoto, Division of Gastroenterology and Hepatology, Department of Internal Medicine, St. Marianna University School of Medicine, 2-16-1 Sugao, Miyamae-ku, Kawasaki 216-8511, Kanagawa, Japan.
Email: h-yama@marianna-u.ac.jp

Creative Commons Non Commercial CC BY-NC: This article is distributed under the terms of the Creative Commons Attribution-NonCommercial 4.0 License (http://www.creativecommons.org/licenses/by-nc/4.0/) which permits non-commercial use, reproduction and distribution of the work without further permission provided the original work is attributed as specified on the SAGE and Open Access pages (https://us.sagepub.com/en-us/nam/open-access-at-sage).

feces.[12,15,16] These assays for detecting CAM resistance in *H. pylori* are based on the detection of mutations in the 23S ribosomal RNA (rRNA) gene.

In an earlier study, 39% of patients with CAM-resistant *H. pylori* were reported to be infected with both CAM-resistant and CAM-susceptible *H. pylori*.[20] Frequent mixed infections with multiple *H. pylori* strains in the human stomach have also been reported.[21–25] Because mixed infections are common and one of the reasons for unsuccessful therapy, an accurate quantitative test for the presence of CAM-resistant *H. pylori* is necessary for successful eradication therapy. However, gastric biopsy is a topical procedure in which only a small portion of tissue is excised during endoscopy. One study showed two different *H. pylori* strains to have variable distribution among biopsy sites in a *H. pylori*-infected individual,[22] which indicates that biopsy-based analysis might underestimate mixed infection detection.

In contrast, gastric wash samples are collected from the whole stomach using saline during endoscopy.[26] Because abundant cells are exfoliated from the gastric mucosa during washing, undamaged human and *H. pylori* DNA can be recovered from the wash and be assayed by sensitive quantitative techniques.[26–28] We recently developed a pyrosequencing-based method for the quantification of *H. pylori* genotypes using gastric washes and found that many patients carried mixed infection with CAM-susceptible (wild-type) and CAM-resistant (A2143G or A2144G mutant) *H. pylori*.[29] These data suggest that our method can detect mixed infections with higher sensitivity than biopsy-based methods, because *H. pylori* DNA can be extracted from gastric washes, which reflect the whole stomach.

In the case of mixed infections, CAM-resistant *H. pylori* may be selected for survival after CAM-based eradication therapy, which might result in the failure of therapy. However, it remains unknown how the abundance and prevalence of *H. pylori* strains vary after eradication therapy. A better understanding of mixed infection with multiple *H. pylori* strains is necessary to design more effective therapies against *H. pylori*. In this prospective study, using gastric wash samples from patients with early gastric cancer who had undergone endoscopic resection, we sequentially analyzed the abundance and prevalence of *H. pylori* DNA by 23S rRNA pyrosequencing before and 1, 2, and 3 years after CAM-based triple eradication therapy.

Materials and methods

Clinical samples

In this prospective study, 19 patients with early gastric cancer who had undergone endoscopic resection were diagnosed with *H. pylori* infection at the time of endoscopic resection. All the patients (13 males and 6 females) were diagnosed as *H. pylori* infection–positive by the *H. pylori* IgG assay, rapid urease test, or urea breath test (UBT). The patients received CAM-based triple eradication therapy. Successful eradication was confirmed by negative results of the UBT 1 month or more after the eradication. Patients were followed-up annually by endoscopic evaluation and collection of gastric wash samples at 1 ($n=14$), 2 ($n=14$), and 3 ($n=13$) years after endoscopic resection and *H. pylori* eradication therapy. Several patients could not be followed-up annually by endoscopic evaluation at all three timepoints because of non-medical reasons or medical reasons other than gastrointestinal disease. Samples were immediately frozen at −80°C and DNA was extracted as previously reported. The study was conducted in accordance with all the rules and regulations of the St. Marianna University School of Medicine Institutional Review Board (#1929), and written informed consent was obtained from each patient (Table 1).

Sample collection of gastric washes

Approximately 10 min prior to endoscopy, patients were asked to swallow 100 mL water containing 80 mg dimethylpolysiloxane (GASCON; Kissei Pharmaceutical Co., Ltd., Matsumoto, Japan), 1 g sodium bicarbonate, and 20,000 units pronase (Pronase MS; Kaken Pharmaceutical Co., Ltd., Tokyo, Japan). Gastric washes were collected in specimen containers (No. 111219; Forte Grow Medical, Tochigi, Japan), which were directly fitted to the endoscope modulator. Gastric washes were manually aspirated under vacuum through the suction channel of the endoscope and centrifuged immediately, and resulting pellets were frozen at −80°C. Disposable sample collection tubes, connector tubes, and other endoscopic devices were used. The endoscope was washed after each procedure according to the guidelines, using 0.55% DISOPA (Johnson and Johnson, Langhorne, PA, USA) and an automatic washing machine.

DNA extraction

DNA was extracted from gastric wash samples by phenol chloroform. Briefly, frozen pellets from gastric washes were resuspended in 10% sodium dodecyl sulfate (SDS) and proteinase K, mixed vigorously, and incubated at 37°C for 6 h. Samples were then mixed vigorously for approximately 30 s with one volume of 25:24:1 phenol: chloroform:isoamyl alcohol and centrifuged at room temperature for 5 min at 16,000×g. The aqueous layer was then transferred to a fresh tube and extracted in the same manner another two times. Final extracts were then mixed with 100% ethanol, centrifuged at 4°C for 5 min at 16,000×g, and stored at −20°C overnight to precipitate DNA. Precipitates were collected by centrifugation, washed with 70% ethanol, and centrifuged at 4°C for 2 min at 16,000×g. As much of the supernatant was removed as

Table 1. Clinical characteristics of gastric cancer patients and time course of mixed Helicobacter *pylori* infection.

No.	Age	Sex	Pre HP-IgG	Pre RUT	Pre UBT	Post UBT	Histology[a]	Smoking	2143G[b] (%) Pre	1 year	2 years	3 years	2144G[b] (%) Pre	1 year	2 years	3 years
1	73	M	64			0.5	M/M	+	0	24	24	27	1	26	28	30
2	79	M	36			0.3	M/M	+	0	23			1	27		
3	76	F	28			0.1	M/M	N/A	0	27	32	25	1	35	45	36
4	72	M	12			2.1	M/M	+	14		30		18		41	
5	80	F	18			1.3	M/M	−	0	32	31		1	34	39	
6	67	M	43			0.0	M/M	−	0	35	38		1	50	38	
7	69	M	15			1.6	M/M	+	0	22	31	30	2	22	46	37
8	62	M	80			0.4	M/M	+	69	34			94	60		
9	72	M			17.3	1.7	M/M	+	0		48	45	12		82	73
10	75	M		+		0.2	M/M	+	10	53	40		35	89	70	
11	74	F	30			1.3	M/M	−	49	61		50	85	91		79
12	51	M	18			0.7	M/M	−	0	40	55	52	7	75	89	83
13	78	M		+		0.5	M/M	−	5		57	59	30		84	83
14	70	F	>100			0.7	M/M	+	0		61	62	11		91	90
15	69	M	69			0.0	M/M	+	19	57	61	61	78	87	85	84
16	68	M	19			0.3	M/M	+	31	64	65	61	63	65	93	94
17	60	F	54			0.4	M/M	−	60	63		56	90	90		81
18	69	F	13			1	M/M	−	21		60	62	54		95	92
19	73	M	22			1.5	M/M	+	41	66		68	74	90		96

M: male; F: female; HP-IgG: *H. pylori* immunoglobulin G; RUT: rapid urease test; UBT: urea breath test.
[a]Histology (Pre/Post): marked/marked inflammation.
[b]Time course of the ratio of the prevalence of A2143G or A2144G to that of wild-type *H. pylori*.

possible, and pellets were resuspended in 500 µL Tris-EDTA buffer. Final DNA concentration and quality were measured on a ND-1000 spectrophotometer (NanoDrop Technologies, Wilmington, DE, USA).

Abundance of H. pylori 23S rRNA in gastric wash samples

We analyzed gastric wash DNA samples by SYBR Green real-time polymerase chain reaction (PCR), with *H. pylori* 23S rRNA as target and human *GAPDH* as reference. It was necessary to normalize abundance of *H. pylori* 23S rRNA gene using total volume of gastric washes. However, it was difficult to accurately quantify total volume of gastric washes obtained in each endoscopy. Alternatively, the amounts of DNA of human cells exfoliated from the gastric mucosa during washing reflect total volume of gastric washes.[26,29] Therefore, we normalized abundance of *H. pylori* 23S rRNA gene using human *GAPDH* gene instead of other bacterial gene. *H. pylori* 23S rRNA was amplified with sense primer "acgagatgggagctgtctcaacc" and antisense primer "agcattgtcctgcctgtggataac," while human *GAPDH* was amplified with sense primer "cgagatcccctccaaaatcaa" and antisense primer "ctgcaaatgagcctacagca." Reactions were performed on an ABI 7500 Real-Time PCR System (Applied Biosystems, Foster City, CA, USA) according to the manufacturer's instructions. Data were analyzed in SDS2.1 by comparative cycle threshold (ΔCt).

Quantitative pyrosequencing analysis of multiple H. pylori strains

Pyrosequencing enables quantitative analysis of the abundance of polymorphisms at a given site. 23S rRNA was amplified and biotinylated by nested PCR from gastric wash samples. In the first reaction, a 255 bp fragment was amplified with sense primer "acgagatgggagctgtctcaacc" and antisense primer "agcattgtcctgcctgtggataac." Amplification products were then used as a template in the second reaction to amplify a 90 bp fragment with sense primer "gaggtgaaaattcctcctacccgcg" and antisense primer "gcgcatgatattcccattagcagtgc." Reactions consisted of touchdown PCR with denaturation at 95°C for 30 s, annealing at appropriate temperatures for 30 s, and extension at 72°C for 30 s. Finally, amplification products were analyzed by pyrosequencing on a Pyromark Q24 (QIAGEN, Valencia, CA, USA) using primer "acccgcggcaagacg." Sequence to analyze A2143V is "GVAAGACCCCGTGG ACCTTTACTACAA" and A2144R "RAGACCCCGTGG ACCTT TACTACAAC."

Results

H. pylori abundance in gastric wash samples

We clinically diagnosed 19 patients in whom *H. pylori* had been "successfully eradicated" on the basis of the UBT, because all results showed values below the cutoff line

(<2.5‰; Table 1). Interestingly, the values showed some variance among patients, although they were below the cutoff line (0.0‰–2.1‰, mean 0.77‰±0.64‰). We used real-time PCR to estimate the abundance of *H. pylori* DNA in gastric wash samples, as measured by the abundance of 23S rRNA gene relative to the abundance of human *GAPDH* gene. Abundance of *H. pylori* 23S rRNA gene significantly decreased 1 year after *H. pylori* eradication, but none of the samples showed a value of 0 (1242.0±1313.0 to 367.6±467.2, $p=0.02$; Figure 1). The abundance of *H. pylori* DNA was the lowest at the 2-year follow-up, but it was found to have increased at the 3-year follow-up.

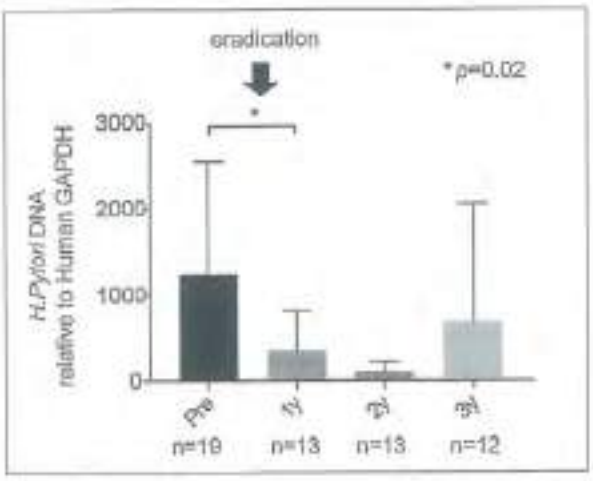

Figure 1. Time course of the abundance of *Helicobacter pylori* DNA at four timepoints. The *H. pylori* 23S rRNA gene and human *GAPDH* gene were analyzed as the target and housekeeping reference genes, respectively.

Measurement of the ratio of H. pylori strains before and after eradication therapy

Representative pyrograms were shown in Figure 2. The frequencies of the A2143G, A2143C, and A2144G mutant *H. pylori* strains were examined using gastric wash samples at four timepoints (Table 1, Figure 3(a) and (b)). None of the samples showed the A2143C mutant, whereas both A2143G and A2144G mutant strains were detected before eradication therapy. The prevalence of the A2143G and A2144G mutants increased after eradication therapy, and the prevalence at 3 years was significantly higher than that before treatment (16.8%±22.6% to 50.6%±14.6% for A2143G, $p=0.0001$; 34.6%±35.4% to 73.7%±23.4% for A2144G, $p=0.002$). Moreover, there was a significant correlation between the frequencies of A2143G and A2144G mutants at the timepoint of 3 years ($r=0.96$, $p=0.0001$; Figure 3(c)).

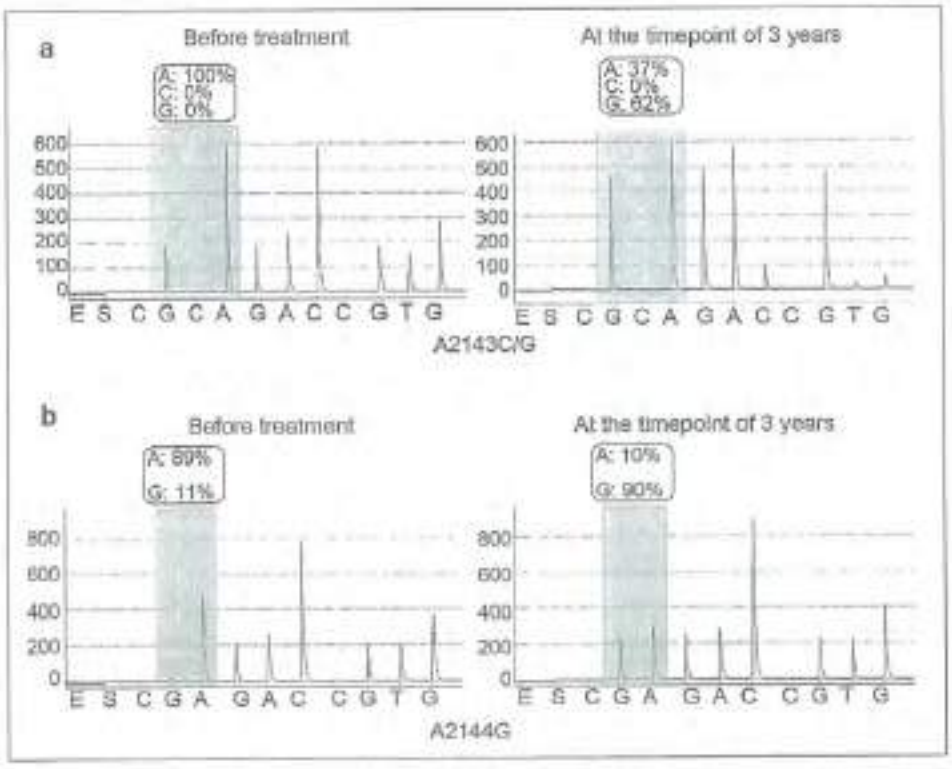

Figure 2. Representative pyrograms of positions 2143 and 2144 of the 23S rRNA gene (a) before treatment and (b) at the timepoint of 3 years in case no. 14.

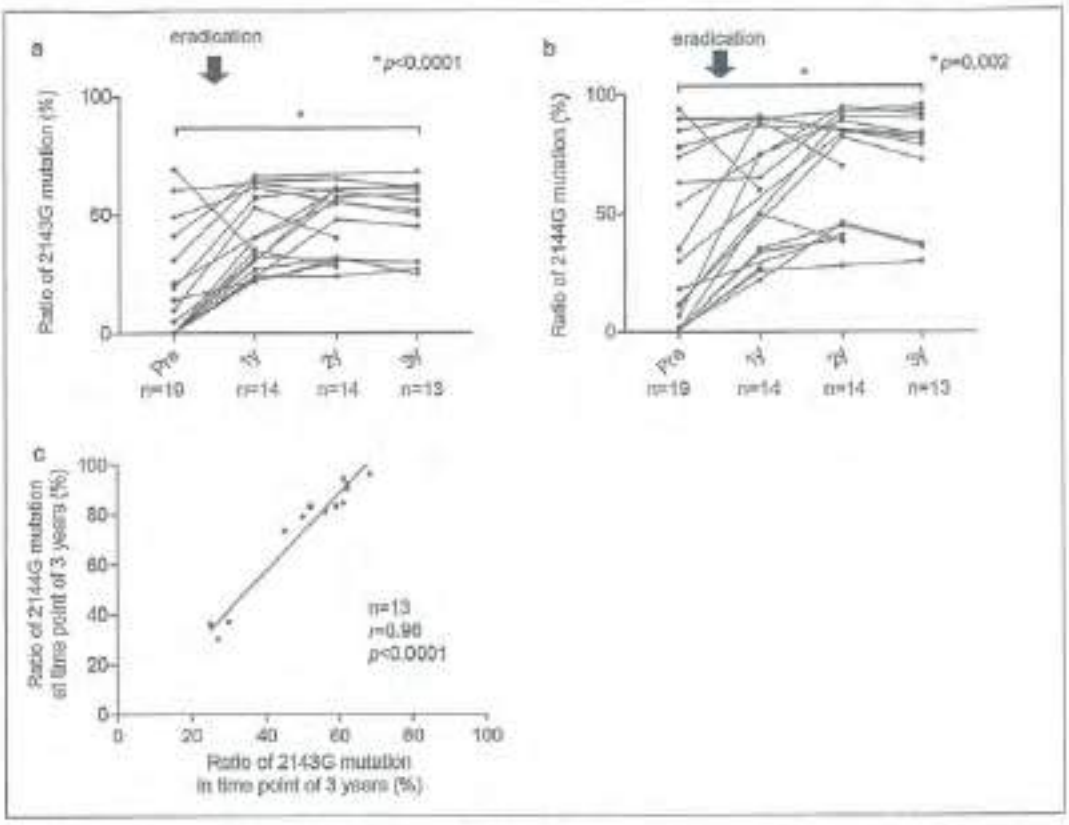

Figure 3. (a) Time course of the ratio of the prevalence of A2143G to that of wild-type Helicobacter *pylori* at four timepoints. (b) Time course of the prevalence of A2144G to that of wild-type *H. pylori* at four timepoints. (c) Significant correlation of the ratio of A2143G prevalence to that of A2144G at the timepoint of 3 years.

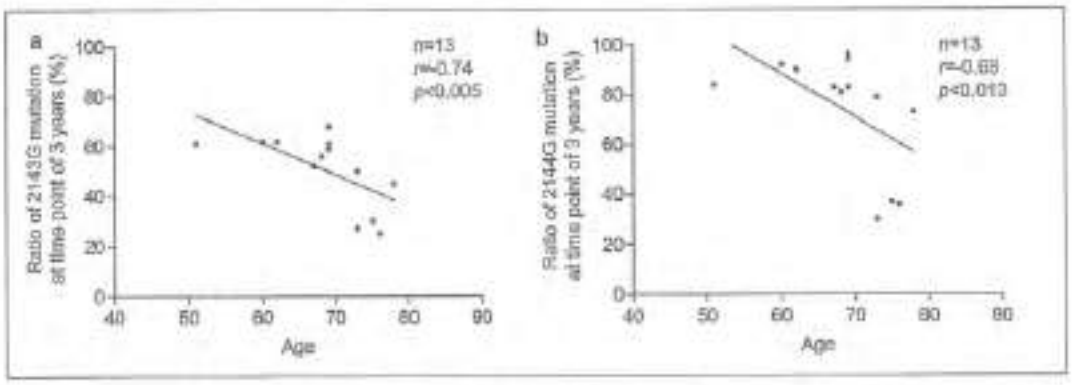

Figure 4. Significant inverse correlation of the frequency of (a) A2143G and (b) A2144G with age at the timepoint of 3 years.

Mutant H. pylori strains were inversely correlated with age

Both mutant strains A2143G and A2144G were inversely correlated with age at the timepoint of 3 years (A2143G, $r=-0.74$, $p=0.005$; A2144G, $r=-0.68$, $p=0.013$; Figure 4(a) and (b)).

Discussion

Using gastric wash DNA, we obtained a quantitative time-course analysis of the abundance and prevalence of *H. pylori* genotypes before and after CAM-based eradication therapy (Figure 5). Low levels of *H. pylori* DNA were still detectable at the first-year follow-up in all samples with

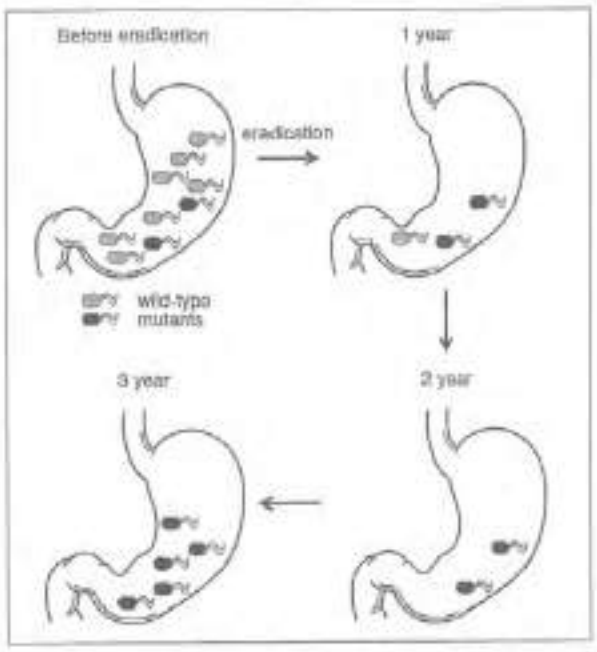

Figure 5. The illustration of time course of mixed *Helicobacter pylori* infection analyzed by 23S rRNA pyrosequencing at four timepoints. The abundance of *H. pylori* DNA decreased significantly until the 2-year follow-up, but it had increased at the 3-year follow-up. Although the abundance of CAM-resistant strains was low after eradication therapy, these strains increased and were found to be enriched in the follow-up period, leading to persistent *H. pylori* infection and eventually to the recrudescence (clinically detectable recurrence) of *H. pylori* infection after successful eradication therapy.

negative post-treatment UBT results. The abundance of *H. pylori* DNA decreased significantly until the 2-year follow-up, but it had increased at the 3-year follow-up. These results suggest that our PCR assay is more sensitive than conventional methods and that it is necessary to monitor the impact of treatments in the follow-up period even if *H. pylori* is found to be successfully eradicated in patients on the basis of conventional tests after eradication therapy.

Both A2143G and A2144G mutant strains were detected before CAM-based eradication therapy. Moreover, the ratio of the prevalence of mutant strains to that of the wild-type strain was found to have already increased significantly 1 year after eradication therapy and continued to increase, suggesting that CAM-resistant strains survived more easily after treatment. Although the abundance of CAM-resistant strains was low after eradication therapy, these strains increased and were found to be enriched in the follow-up period, leading to persistent *H. pylori* infection and eventually to the recrudescence (clinically detectable recurrence) of *H. pylori* infection after successful eradication therapy. In an earlier qualitative study, Matsuoka et al.[21] suggested that a small number of CAM-resistant strains could emerge spontaneously in the stomach and that resistant strains are not formed but selected by CAM administration.

Both the mutant *H. pylori* strains A2143G and A2144G were inversely correlated with age at the timepoint of 3 years, indicating that the prevalence of CAM-resistant strains is on the rise in patients of younger age. This might be attributed to the overuse of macrolides in Japan. In fact, in Europe, the use of macrolides for various infections over the past 2 decades, especially long-standing macrolides, has contributed to the selection of resistant *H. pylori* strains.[30]

Our assay enables the detection of *H. pylori* DNA at a higher sensitivity than that of conventional tests, and it can quantify multiple genotypes. Failure of *H. pylori* eradication is one of the independent risk factors for recurrent neoplasia after endoscopic resection of early gastric cancer.[31] Hence, our assay is useful to (1) diagnose *H. pylori* infection, including mixed infections; (2) choose personalized treatment strategies; and (3) monitor the impact of the treatment in the follow-up period, especially for high-risk patients.

Our assay has several advantages, such as being simple and safe because it circumvents the need for biopsy, as well as being quantitative, rapid, economical, and representative of the whole stomach. Moreover, it is possible to analyze gastric wash DNA for both *H. pylori* genotypes and human cancer-related genes.[26–29] Therefore, our assay is feasible for clinical application and should thus be validated in large-scale clinical trials. We believe that the long-term success of preventing gastric cancer development lies in effective *H. pylori* eradication interventions and consecutive surveillance, which can be facilitated by the application of sensitive and accurate detection techniques.

Acknowledgements

R.O., Y.W., and H.Y. conceived the study, designed and executed experiments, analyzed data, prepared figures and tables, and wrote the manuscript. S.M., S. O., and Y.S. obtained clinical samples and analyzed data. K.M., M.K., and F.I. provided intellectual support. H.Y. supervised all aspects of the study. R.O. and Y.W. share co-first authorship.

Declaration of conflicting interests

The author(s) declared no potential conflicts of interest with respect to the research, authorship, and/or publication of this article.

Ethical approval

The study was conducted in accordance with all rules and regulations of the St. Marianna University School of Medicine Institutional Review Board (#1929), and written informed consent was obtained from each patient.

Funding

The author(s) disclosed receipt of the following financial support for the research, authorship, and/or publication of this article:

This work was supported by JSPS KAKENHI Grant (JP25460937 and JP16K09295) to Y.W.

Guarantor

Hiroyuki Yamamoto.

References

1. Rugge M, Genta RM, Di Mario F, et al. Gastric cancer as preventable disease. *Clin Gastroenterol Hepatol*. Epub ahead of print 19 May 2017. DOI: 10.1016/j.cgh.2017.05.023.
2. Miftahussurur M, Yamaoka Y and Graham DY. *Helicobacter pylori* as an oncogenic pathogen, revisited. *Expert Rev Mol Med* 2017; 19: e4.
3. Lee YC, Chiang TH, Chou CK, et al. Association between *Helicobacter pylori* eradication and gastric cancer incidence: a systematic review and meta-analysis. *Gastroenterology* 2016; 150: 1113–1124.
4. Asaka M, Mabe K, Matsushima R, et al. *Helicobacter pylori* eradication to eliminate gastric cancer: the Japanese strategy. *Gastroenterol Clin North Am* 2015; 44: 639–648.
5. Fukase K, Kato M, Kikuchi S, et al.; Japan Gast Study Group. Effect of eradication of *Helicobacter pylori* on incidence of metachronous gastric carcinoma after endoscopic resection of early gastric cancer: an open-label, randomised controlled trial. *Lancet* 2008; 372: 392–397.
6. Hooi JKY, Lai WY, Ng WK, et al. Global prevalence of *Helicobacter pylori* infection: systematic review and meta-analysis. *Gastroenterology* 2017; 153: 420–429.
7. Sugano K, Tack J, Kuipers EJ, et al. Kyoto global consensus report on *Helicobacter pylori* gastritis. *Gut* 2015; 64: 1353–1367.
8. Graham DY and Dore MP. Helicobacter pylori therapy: a paradigm shift. *Expert Rev Anti Infect Ther* 2016; 14: 577–585.
9. Shiotani A, Lu H, Dore MP, et al. Treating *Helicobacter pylori* effectively while minimizing misuse of antibiotics. *Cleve Clin J Med* 2017; 84: 310–318.
10. Dang BN and Graham DY. *Helicobacter pylori* infection and antibiotic resistance: a WHO high priority? *Nat Rev Gastroenterol Hepatol* 2017; 14: 383–384.
11. O'Connor A, Fischbach W, Gisbert JP, et al. Treatment of *Helicobacter pylori* infection 2016. *Helicobacter* 2016; 21(suppl. 1): 55–61.
12. Gisbert JP and McNicholl AG. Optimization strategies aimed to increase the efficacy of *H. pylori* eradication therapies. *Helicobacter* 2017; 22: e12392.
13. Thung I, Aramin H, Vavinskaya V, et al. Review article: the global emergence of *Helicobacter pylori* antibiotic resistance. *Aliment Pharmacol Ther* 2016; 43: 514–533.
14. Kawai T, Takahashi S, Suzuki H, et al. Changes in the first line *Helicobacter pylori* eradication rates using the triple therapy—a multicenter study in the Tokyo metropolitan area (Tokyo *Helicobacter pylori* study group). *J Gastroenterol Hepatol* 2014; 29(suppl. 4): 29–32.
15. Nishizawa T and Suzuki H. Mechanisms of *Helicobacter pylori* antibiotic resistance and molecular testing. *Front Mol Biosci* 2014; 1: 19.
16. Xuan SH, Wu LP, Zhou YG, et al. Detection of clarithromycin-resistant *Helicobacter pylori* in clinical specimens by molecular methods: a review. *J Glob Antimicrob Resist* 2016; 4: 35–41.
17. Chey WD, Leontiadis GI, Howden CW, et al. ACG clinical guideline: treatment of *Helicobacter pylori* infection. *Am J Gastroenterol* 2017; 112: 212–239.
18. Malfertheiner P, Megraud F, O'Morain CA, et al.; European *Helicobacter* and Microbiota Study Group and Consensus panel. Management of Helicobacter pylori infection—the Maastricht V/Florence consensus report. *Gut* 2017; 66: 6–30.
19. Yeo YH, Shiu SI, Ho HJ, et al. Taiwan Gastrointestinal Disease and *Helicobacter* Consortium. First-line *Helicobacter pylori* eradication therapies in countries with high and low clarithromycin resistance: a systematic review and network meta-analysis. *Gut*. Epub ahead of print 26 September 2016. DOI: 10.1136/gutjnl-2016-311868.
20. Rimbara E, Noguchi N, Tanabe M, et al. Susceptibilities to clarithromycin, amoxycillin and metronidazole of *Helicobacter pylori* isolates from the antrum and corpus in Tokyo, Japan, 1995–2001. *Clin Microbiol Infect* 2005; 11: 307–311.
21. Matsuoka M, Yoshida Y, Hayakawa K, et al. Simultaneous colonisation of *Helicobacter pylori* with and without mutations in the 23S rRNA gene in patients with no history of clarithromycin exposure. *Gut* 1999; 45: 503–507.
22. Yakoob J, Fan XG, Hu GL, et al. Polycolonization of *Helicobacter pylori* among Chinese subjects. *Clin Microbiol Infect* 2000; 7: 187–192.
23. Noguchi N, Rimbara E, Kato A, et al. Detection of mixed clarithromycin-resistant and -susceptible *Helicobacter pylori* using nested PCR and direct sequencing of DNA extracted from faeces. *J Med Microbiol* 2007; 56: 1174–1180.
24. Selgrad M, Tammer I, Langner C, et al. Different antibiotic susceptibility between antrum and corpus of the stomach, a possible reason for treatment failure of *Helicobacter pylori* infection. *World J Gastroenterol* 2014; 20: 16245–16251.
25. Cao Q, Dédelot X, Wu Z, et al. Progressive genomic convergence of two *Helicobacter pylori* strains during mixed infection of a patient with chronic gastritis. *Gut* 2015; 64: 554–561.
26. Watanabe Y, Kim HS, Castoro RJ, et al. Sensitive and specific detection of early gastric cancer with DNA methylation analysis of gastric washes. *Gastroenterology* 2009; 136: 2149–2158.
27. Baba S, Oishi Y, Watanabe Y, et al. Gastric wash-based molecular testing for antibiotic resistance in *Helicobacter pylori*. *Digestion* 2011; 84: 299–305.
28. Yamamoto H, Watanabe Y, Oikawa R, et al. *BARHL2* methylation using gastric wash DNA or gastric juice exosomal DNA is a useful marker for early detection of gastric cancer in an *H. pylori*-independent manner. *Clin Transl Gastroenterol* 2016; 7: e184.
29. Miyamoto S, Watanabe Y, Oikawa R, et al. Analysis of *Helicobacter pylori* genotypes in clinical gastric wash samples. *Tumour Biol* 2016; 37: 10123–10132.
30. Megraud F, Coenen S, Versporten A, et al.; Study Group participants. *Helicobacter pylori* resistance to antibiotics in Europe and its relationship to antibiotic consumption. *Gut* 2013; 62: 34–42.
31. Kwon YH, Heo J, Lee HS, et al. Failure of *Helicobacter pylori* eradication and age are independent risk factors for recurrent neoplasia after endoscopic resection of early gastric cancer in 283 patients. *Aliment Pharmacol Ther* 2014; 39: 609–618.

Anaerobe 48 (2017) 144–146

Contents lists available at ScienceDirect

Anaerobe

journal homepage: www.elsevier.com/locate/anaerobe

Case report

Fusobacterium nucleatum detected simultaneously in a pyogenic liver abscess and advanced sigmoid colon cancer

Ryuta Shigefuku [a, 1], Tsunamasa Watanabe [a, 1], Yuki Kanno [a], Hiroki Ikeda [a], Hiroyasu Nakano [a], Nobuhiro Hattori [a], Kotaro Matsunaga [a], Nobuyuki Matsumoto [a], Shin-ichi Kanno [b], Katsuhiko Nosho [b], Atsuko Hachiya [c], Yasumasa Iwatani [c], Tomoko Matsumori [d], Satoshi Tsukikawa [d], Ryoji Makizumi [d], Takehito Otsubo [d], Hiroyuki Yamamoto [a, *], Fumio Itoh [a]

[a] Division of Gastroenterology and Hepatology, Department of Internal Medicine, St. Marianna University School of Medicine, Kawasaki, Japan
[b] Department of Gastroenterology, Sapporo Medical University School of Medicine, Japan
[c] Department of Infectious Diseases and Immunology, Clinical Research Center, National Hospital Organization Nagoya Medical Center, Japan
[d] Division of Gastroenterological and General Surgery, St. Marianna University School of Medicine, Kawasaki, Japan

ARTICLE INFO

Article history:
Received 18 April 2017
Received in revised form
6 July 2017
Accepted 15 August 2017
Available online 16 August 2017

Handling Editor: Hanna Fitzsch

Keywords:
Fusobacterium nucleatum
Pyogenic liver abscess
Colon cancer
Metagenome analysis
Microbial FISH

ABSTRACT

Fusobacterium nucleatum is an invasive, adherent, and pro-inflammatory anaerobic bacterium involved in various infections and colorectal cancer. We report a case with pyogenic liver abscess, diagnosed with advanced sigmoid colon cancer, in whom *F. nucleatum* was simultaneously detected. In this patient, *F. nucleatum* was systematically analyzed using the molecular biological techniques of metagenome analysis, conventional PCR, and microbial fluorescence in situ hybridization.

© 2017 Elsevier Ltd. All rights reserved.

1. Introduction

Fusobacterium nucleatum (*F. nucleatum*) is an invasive, adherent, and pro-inflammatory anaerobic bacterium. It is common in dental plaque, and there is an association between *F. nucleatum* and disorders such as periodontitis, cerebral abscess, pericarditis, and acute appendicitis [1,2]. Moreover, *F. nucleatum* reportedly not only localizes to and is enriched in colorectal cancer but may also play a role in tumor growth and survival [1–4]. *F. nucleatum* has also been reported to be a rare cause of pyogenic liver abscess (PLA) [5]. Importantly, patients with PLA has been shown to have high incidence of colorectal cancer [6]. The association and mechanism between abscess formation diseases and colorectal cancer have been reported [7–10]. Destruction of the colonic mucosal barrier and the bacterial translocation are considered as one of the mechanisms. We present findings from a patient with PLA, diagnosed with advanced sigmoid colon cancer, in whom *F. nucleatum* was detected in both the colon cancer and the PLA.

2. Case report

A 78-year-old man with sub-acute subjective fever with chills, diarrhea, and lower abdominal pain was referred to our hospital. Physical examination revealed no abnormal findings. Abdominal contrast-enhanced computed tomography images showed a low-density mass in the right liver lobe (Fig. 1A). This lesion was recognized as a relatively ill-defined hypoechoic nodule by abdominal ultrasonography. We diagnosed this lesion as a liver

* Corresponding author. Division of Gastroenterology and Hepatology, Department of Internal Medicine, St. Marianna University School of Medicine, 2-16-1 Sugao, Miyamae-ku, Kawasaki, Kanagawa, Japan.
E-mail address: h-yama@marianna-u.ac.jp (H. Yamamoto).
[1] Authors share co-first authorship.

http://dx.doi.org/10.1016/j.anaerobe.2017.08.010
1075-9964/© 2017 Elsevier Ltd. All rights reserved.

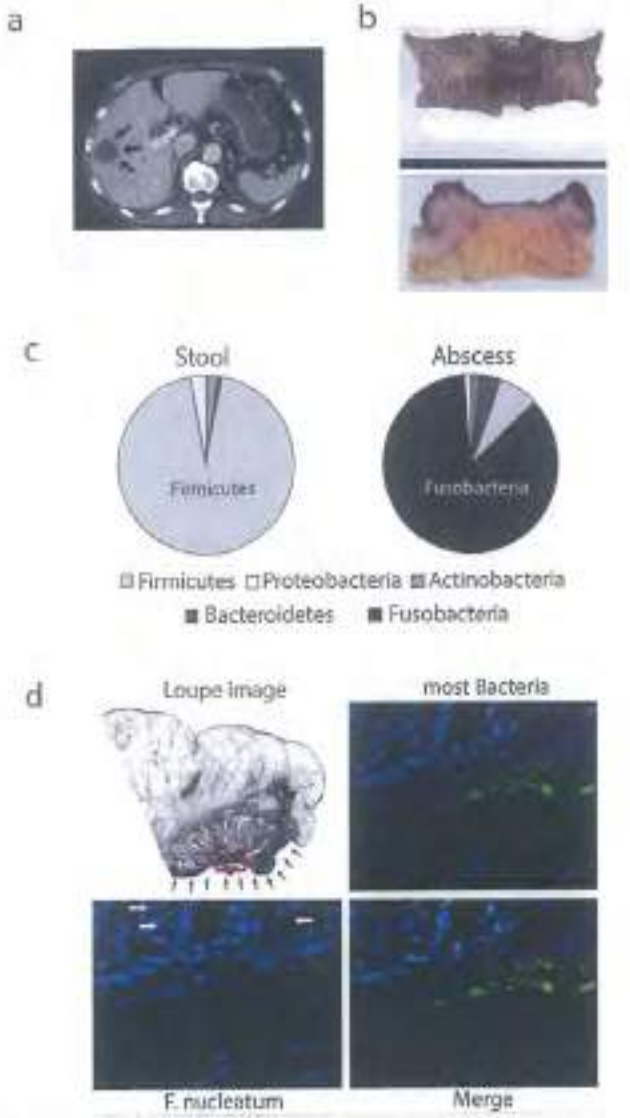

Fig. 1. (A) Abdominal contrast-enhanced computed tomography image showing a low-density mass in the right liver lobe. (B) Resected specimen showing a mass in the sigmoid colon. Cut surface of colonic carcinoma extending into the subserosa. (C) Bacterial composition in feces and liver abscess. DNA was isolated from liquid cultures by applying the bead beating technique to samples. The V3-V4 region of the 16S rRNA gene was amplified via PCR using barcoded primers, 5′-TCG TCG GCA GCG TCA GAT GTG TAT AAG AGA CAG CCT ACG GGN GGC WGC AG-3′ (forward) and 5′-GTC TCG TGG GCT CGG AGA TGT GTA TAA GAG ACA GGA CTA CHV GGG TAT CTA ATC C-3′ (reverse) [11]. PCR products were sequenced using the paired-end technique (Illumina MiSeq platform), as previously described [11]. Sequencing data were then processed, and diversity trends were analyzed using QIIME v1.8.0 [12]. (D) Loupe image of detected *F. nucleatum* in colon cancer tissues and microbial FISH analysis using the universal bacterial probe EUB338 (Cy3 labeled, 5′-GCT GCC TCC CGT AGG AGT-3′) and *F. nucleatum*-targeted probe FUS664 (FITC labeled, 5′-CTT GTA GTT CCG C(C/T) TAC CTC-3′).

abscess. Percutaneous drainage of the liver abscess and intravenous infusion of piperacillin/tazobactam were initiated and continued. After starting treatment, he showed significant clinical improvement. Blood and abscess aspirates were cultured aerobically and anaerobically. Fresh bacterial cultures were grown for 48 h on Schaedler agar at 35 °C in an anaerobic atmosphere for control of viability, inoculum concentration and confirmation of identification by matrix assisted laser desorption/ionisation time of flight mass spectrometry (MALDI-TOF MS). The isolates were identified by MALDI-TOF MS using Remel RapID (Thermo Fisher Scientific, Waltham, MA, USA) and Bruker microflex LT system (Bruker Daltonics, Bremen, Germany). The final report from the abscess culture indicated positivity for *F. nucleatum*. This identification was proven using the genomic DNA amplification via PCR.

Oral examination including inspection, palpitation, and X-ray examination revealed no dental caries or poor oral hygiene. Colonoscopy showed an encircling type 2 advanced cancer of the sigmoid colon. Sigmoidectomy was performed (Fig. 1B) and histopathological findings of the resected specimen indicated moderately differentiated adenocarcinoma with subserosal and venous invasion.

Using DNA extracted from feces and the liver abscess, we performed a metagenome analysis. DNA was isolated from liquid cultures by applying the bead beating technique to samples. The V3-V4 region of the 16S rRNA gene was amplified via PCR using barcoded primers, 5′-TCG TCG GCA GCG TCA GAT GTG TAT AAG AGA CAG CCT ACG GGN GGC WGC AG-3′ (forward) and 5′-GTC TCG TGG GCT CGG AGA TGT GTA TAA GAG ACA GGA CTA CHV GGG TAT CTA ATC C-3′ (reverse) [11]. PCR products were sequenced using the paired-end technique (Illumina MiSeq platform), as previously described [11]. Sequencing data were then processed, and diversity trends were analyzed using QIIME v1.8.0 [12]. *Streptococcus* (74.1%) and *Fusobacterium* (86.2%) were the most common species of bacterium in feces and liver abscess, respectively (Fig. 1C).

Conventional polymerase chain reaction (PCR) using primers targeting *F. nucleatum* (5′-CAA CCA TTA CTT TAA CTC TAC CAT GTT CA-3′ and 5′-GTT GAC TTT ACA GAA GGA GAT TAT GTA AAA ATC-3′) was done [2]. The analysis detected amplification of *F. nucleatum* in the liver abscess but not in feces (data not shown). Microbial fluorescence in situ hybridization (FISH) analysis using the "universal bacterial" probe, EUB338 (Cy3 labeled, 5′-GCT GCC TCC CGT AGG AGT-3′) and the Fn-targeted probe, FUS664 (FITC labeled, 5′-CTT GTA GTT CCG C(C/T) TAC CTC-3′) was done [4]. The analysis detected invasive *F. nucleatum* in the cancer tissue but not in the adjacent normal colonic mucosa (Fig. 1D). Finally, Sanger sequencing using primers targeting *F. nucleatum* (5′-CAA CCA TTA CTT TAA CTC TAC CAT GTT CA-3′ and 5′-GTT GAC TTT ACA GAA GGA GAT TAT GTA AAA ATC-3′) [2] confirmed detection of the *F. nucleatum* sequence in the surgically resected cancer tissues (data not shown).

3. Discussion

Our case demonstrates a patient with PLA coincident with advanced sigmoid colon cancer, in which *F. nucleatum* was detected in both specimens. This is the first report in which *F. nucleatum* was systematically analyzed using the molecular biological techniques of metagenome analysis, conventional PCR, and microbial FISH. The results suggest that *F. nucleatum* was specifically localized in the colon cancer, which was the possible source of PLA. Clonality studies between *F. nucleatum* strains isolated from both sites are necessary to further address the issue.

F. nucleatum reportedly not only localizes to and is enriched in colorectal cancer but may also play a role in tumor growth and survival [1–4]. It has been reported that *F. nucleatum*-bound colon cancer cells and *F. nucleatum*-containing cancers inhibited natural killer cell cytotoxicity and tumor infiltrating lymphocyte cell activity via the interaction of the *F. nucleatum* protein Fap2 with human TIGIT [13].

The major mechanisms leading to PLA include ascending infection from the biliary and pancreatic ducts and hematogenous spread from organs of the portal system caused by digestive tract

diseases, including neoplasms, with mucosal defects or an impaired mucosal barrier [6]. The association and mechanism between abscess formation diseases and colorectal cancer have been reported [7–10]. Destruction of the colonic mucosal barrier and the bacterial translocation are considered as one of the mechanisms. Because the sigmoid colon cancer showed subserosal and venous invasion, the translocation of *F. nucleatum* from the colon to the liver in this case is most likely due to hematogenous spread.

Carbohydrate moiety Gal-GalNAc is reportedly involved in host-pathogen interaction during *Entamoeba histolytica*-induced liver abscess [14]. Interestingly, Fap2 has been shown to play a critical role in mediating fusobacterial enrichment in colorectal cancer by binding to the Gal-GalNAc, which is overexpressed in human colorectal cancer and metastases [3]. Factors involved in the specific interaction between *F. nucleatum* and the liver deserves further investigation. Awareness of PLA complication for colon cancer with *F. nucleatum* infection should be emphasized to physicians.

Conflict of interest

Authors declare no conflict of interest.

Acknowledgements

This work was supported by the Research Program on Hepatitis and Research Program on HIV/AIDS research from the Japan Agency for Medical Research and Development, AMED (17fk0410205j0002), and by a grant-in-aid from the Ministry of Education, Culture, Sports, Science and Technology, Japan (16K09379 and 16K19371).

References

[1] A.D. Kostic, D. Gevers, C.S. Pedamallu, M. Michaud, F. Duke, A.M. Earl, et al., Genomic analysis identifies association of *Fusobacterium* with colorectal carcinoma, Genome Res. 22 (2012) 292–298.
[2] M. Castellarin, R.L. Warren, J.D. Freeman, L. Dreolini, M. Krzywinski, J. Strauss, et al., *Fusobacterium nucleatum* infection is prevalent in human colorectal carcinoma, Genome Res. 22 (2012) 299–306.
[3] J. Abed, J.E. Emgård, G. Zamir, M. Faroja, G. Almogy, A. Grenov, et al., Fap2 mediates *Fusobacterium nucleatum* colorectal adenocarcinoma enrichment by binding to tumor-expressed Gal-GalNAc, Cell Host Microbe 20 (2016) 215–225.
[4] J. Yu, Y. Chen, X. Fu, X. Zhou, Y. Peng, L. Shi, et al., Invasive *Fusobacterium nucleatum* may play a role in the carcinogenesis of proximal colon cancer through the serrated neoplasia pathway, Int. J. Cancer 139 (2016) 1318–1326.
[5] K. Wijampreecha, N. Yukhyava, S. Sompram, C. Hyman, *Fusobacterium nucleatum*: atypical organism of pyogenic liver abscess might be related to sigmoid diverticulitis, N. Am. J. Med. Sci. 8 (2016) 197–199.
[6] H.C. Lai, C.C. Lin, K.S. Cheng, J.T. Kao, J.W. Chou, C.Y. Peng, et al., Increased incidence of gastrointestinal cancers among patients with pyogenic liver abscess: a population-based cohort study, Gastroenterology 146 (2014) 129–137.
[7] S. Teitz, A. Guidetti-Sharon, H. Manor, A. Halevy, Pyogenic liver abscess: warning indicator of silent colonic cancer. Report of a case and review of the literature, Dis. Colon Rectum 38 (1995) 1220–1223.
[8] K. Qu, C. Liu, Z.X. Wang, F. Tian, J.C. Wei, M.H. Tai, et al., Pyogenic liver abscesses associated with nonmetastatic colorectal cancers: an increasing problem in Eastern Asia, World J. Gastroenterol. 18 (2012) 2948–2955.
[9] T. Tajima, M. Mokai, S. Hasegawa, S. Yamamoto, E. Nomura, T. Tajiri, et al., Early rectal cancer accompanied by multiple systemic abscesses: a case report, Oncol. Lett. 10 (2015) 3219–3222.
[10] M.G. Mavilia, M. Molina, G.Y. Wu, The evolving nature of hepatic abscess: a review, J. Clin. Transl. Hepatol. 4 (2016) 158–168.
[11] A. Klindworth, E. Pruesse, T. Schweer, J. Peplies, C. Quast, M. Horn, et al., Evaluation of general 16S ribosomal RNA gene PCR primers for classical and next-generation sequencing-based diversity studies, Nucleic Acids Res. 41 (2013) e1.
[12] J. Kuczynski, J. Stombaugh, W.A. Walters, A. González, J.G. Caporaso, R. Knight, Using QIIME to analyze 16S rRNA gene sequences from microbial communities, Curr. Protoc. Microbiol. (2012) (Chapter 1): Unit 1E.5, doi: http://dx.doi.org/10.1002/9780471729259.mc01e05s27.
[13] C. Gur, Y. Ibrahim, B. Isaacson, R. Yamin, J. Abed, M. Gamliel, et al., Binding of the Fap2 protein of *Fusobacterium nucleatum* to human inhibitory receptor TIGIT protects tumors from immune cell attack, Immunity 42 (2015) 344–355.
[14] D.M. Faust, J. Marquay Markiewicz, J. Santi-Rocca, N. Guillen, New insights into host-pathogen interactions during Entamoeba histolytica liver infection, Eur. J. Microbiol. Immunol. 1 (2011) 10–18.

Digestive Endoscopy 2018; **30**: 5–19 doi: 10.1111/den.12964

Special Report

Design paper: Japan Endoscopy Database (JED): A prospective, large database project related to gastroenterological endoscopy in Japan

Koji Matsuda,[1,2] Kiyohito Tanaka,[1,2] Mitsuhiro Fujishiro,[1,2] Yutaka Saito,[1,2] Kazuo Ohtsuka,[1] Ichiro Oda,[1] Chikatoshi Katada,[1] Masayuki Kato,[1] Mitsuhiro Kida,[1] Kiyonori Kobayashi,[1] Shu Hoteya,[1] Takahiro Horimatsu,[1] Shinya Kodashima,[1] Takahisa Matsuda,[1] Manabu Muto,[1] Hironori Yamamoto,[1] Shomei Ryozawa,[1] Ryuichi Iwakiri,[2] Hiromu Kutsumi,[2] Hiroaki Miyata,[2] Mototsugu Kato,[2] Ken Haruma,[2] Kazuma Fujimoto,[2] Naomi Uemura,[2] Michio Kaminishi[2] and Hisao Tajiri[2]

[1]*MSED-J (Minimal Standard Endoscopic Database) Creation Subcommittee, and* [2]*JED (Japan Endoscopy Database) Project Committee, JGES, Japan*

The advent of electronic medical records brought image filing systems to many hospitals, as well as electronic endoscopic medical records. However, data integration among multiple different vendors has not yet been accomplished. We start the Japan Endoscopic Database (JED) Project endorsed by Japan Gastroenterological Endoscopy Society (JGES) from January 2015. The purposes of this project are as follows: (i) developing the world's largest endoscopic database generated from daily use of the reporting system; (ii) capturing the actual performance of endoscopic practice in Japan; and (iii) standardizing the terminology and fundamental items for registry of clinical studies. Moreover, the JED project has the potential to automatically collect data about adverse events, competency and evaluation of residents, and actual numbers of procedures on a nationwide scale, certification for the specialty board system, and so on. We believe that this design paper will be helpful not only for future nationwide research but also for international research (UMIN000016093).

Key words: database, diagnosis, endoscopy, therapy

INTRODUCTION

IN JAPAN, MANY hospitals use electronic medical record systems with their own endoscopic database. All the same, no nationwide data collection for gastroenterological endoscopy in Japan has been accomplished, although one of the largest endoscopic databases known as CORI (Clinical Outcomes Research Initiative) project has been developed in the USA (Clinical Outcomes Research Initiative http://www.cori.org) and these data have been effectively used for much clinical research to contribute to evidence-based medicine. The great demands of nationwide data collection of an endoscopic database are desired.

This project aims to contribute to the improvement of quality of medical care and to provide patients with the best medical care, by registering, aggregating and analyzing information concerning procedures and treatment related to endoscopy throughout Japan. This type of accumulation of information concerning endoscopic procedures on a nationwide scale is the first attempt, and this surely brings significant benefits not only to patients but also to healthcare providers.

Corresponding: Koji Matsuda, St. Marianna University School of Medicine, Yokohama City Seibu Hospital, Gastroenterology and Endoscopy, 1197-1 Yasashi-cho, Asahi-ku, Yokohama, 241-0811, Japan. Email: euskoji@gmail.com
Received 17 May 2017; accepted 5 September 2017.

OBJECTIVE

ANALYZING DATA COLLECTED through this project mainly sheds light on the following:

- Characteristics of clinical departments of institutes where endoscopic procedures are carried out
- Assessment of medical level
- Proper allocation of gastrointestinal endoscopy specialists and other health-care professionals such as gastrointestinal endoscopy technicians and nurses
- Accurate information concerning registration of early-stage cancer cases
- Prognosis of patients who received endoscopic examination or treatment
- Information concerning endoscopic examination and treatment from a medical economy point of view and

© 2017 Japan Gastroenterological Endoscopy Society

- Information for those who intend to receive endoscopy procedures including their risk of death and complications.

This enables each institute to clearly understand its own characteristics and issues and, based on such understanding, make efforts to improve its condition. By demonstrating medical level of not only each institute but also each medical region, local area and the entire nation, comparison between regions and countries becomes possible. Furthermore, with the understanding of risks associated with endoscopic procedures, physicians are able to work together with their patients and patients' family to make a policy decision on surgery and treatment.

Japan Gastroenterological Endoscopy Society (JGES) has been conducting a nationwide survey on adverse events related to gastroenterological endoscopy every 5 years since 1983 and has published the results five times in the past. However, through the creation of a nationwide database, accurate information would be readily available without conducting this type of individual sequential survey.

In addition, the database will provide information necessary to determine proper remuneration for medical services, and serve as basic data to verify a better specialist system to enable everyone throughout the nation to receive endoscopic examination and treatment without undue worries, and further, by operating the database in collaboration with various study projects, better health-care services are provided at clinical sites, which consequently assists health-care professionals to work toward new medical services.

PROJECT DESIGN, SUBJECTS, INSTITUTES AND DATA COLLECTION

AS THIS IS a large-scale project, subject institutes and the period during which information is to be collected are divided into several phases, and information is collected in a phased manner. The planned period and subjects in each phase are changeable according to the state of progress of phases and outcomes obtained by a prior phase. The study in this project is conducted as an observational study using database shared by multiple institutes (UMIN000016093). Collection of information for the project does not interfere with the endoscopic procedures.

Phase 1: Feasibility study

The period during which data are collected and subjects are all cases of gastroenterological endoscopic examination and treatment carried out in one year from 1 January 2015 to 31 December 2015. Subject institutes are the following eight collaborating institutes selected by the Committee (Japan Endoscopy Database [JED] Project Committee): The University of Tokyo Hospital; National Cancer Center Hospital; Kitasato University Hospital; Toranomon Hospital; Kyoto University Hospital; Tokyo Medical and Dental University, University Hospital of Medicine; The Jikei University Katsushika Medical Center; Saitama Medical University International Medical Center.

The items separately specified are output and collected from the endoscopy database of the above eight subject institutes. During Phase 1, data in a Comma Separated Value (CSV) file are anonymized with Hash process at each institute, and collected offline using USB memory sticks or any other media, without using the Internet. Media used must be purchased brand new media, which is not used at any place other than the institute used at the time of collection. In consideration of the risk of loss of media, media with a security function for which a password can be set is used. Identifiable information is securely stored at each institute. Patient personal information including patient IDs and their names in Kanji and Katakana is deleted and anonymized in the output data from the institutes.

Collected data are stored in the server installed in the JGES headquarters, cleaned, and converted to an analyzable format. For the purpose of data cleansing, data for one month (January 2015) are collected from eight institutes as the initial data collection and, thereafter, data are collected sequentially, at intervals of three months or so. When conducting the second and subsequent data collection, consideration is made to the confidentiality of patient personal information as in the case of the initial collection. Data collection during Phase 1 also aims to establish a more effective data submission method that can be used for data collection in Phase 2 and later.

Furthermore, current items of data to be collected are reviewed throughout Phase 1, and the items finally selected are published as JGES specifications for the data to be submitted, which are widely available to the endoscopy filing system and endoscopy database producers, to achieve simple processing by each vendor. If patient IDs can be anonymized within the system in the endoscopy department of each institute, individual registration by each institute becomes easier from Phase 2. Therefore, specifications containing this point are prepared.

Phase 2: Safety/efficacy analysis

Data of all cases of gastroenterological endoscopic examination and treatment from 1 January 2016 to 31 December 2018 are collected from the guiding institutes recognized by JGES and institutes that are able to provide data for this study. Phase 1 institutes automatically move to Phase 2 if their consents and the approval of their Ethics Committees are obtained.

© 2017 Japan Gastroenterological Endoscopy Society

Table 1 Head and neck procedures

Head and Neck
Procedure
No
Yes
Biopsy
Polypectomy
EMR
ESD
No. specimens
En bloc
Piecemeal
Input no.
Evaluation of endoscopic resection
Complete
Incomplete
Duration of procedure (min)
Device used for procedure
None
Snare
IT knife
Dual knife
IT nano
Flex knife
Hook knife
Flush knife
Clutch cutter
Hemostatic
Other
Injection
None
Hyaluronic acid
Glycerol
Normal saline
Other
Marking
Successful
Unsuccessful
ELPS
Successful
Unsuccessful
Ablation (includes APC)
Successful
Unsuccessful
Hemostasis (includes preventive measures)
Successful
Unsuccessful
Dilation
Successful
Unsuccessful
Stent placement
Successful
Unsuccessful
Removal of foreign object
Successful
Unsuccessful
Other
Successful
Unsuccessful
†Pathological diagnosis
Size of resected specimen
Major axis
Minor axis
NA
Size of lesion
Major axis
NA
Pathological/Morphological
0-Ip
0-Is
0-IIa
0-IIb
0-IIc
0-III
NA
Pathological depth
Intraepithelial
Subepithelial
≥Muscularis propria
NA
Primary histological type
Low-grade intraepithelial neoplasia
High-grade intraepithelial neoplasia
Mild dysplasia
Moderate dysplasia
Severe dysplasia
Squamous cell carcinoma
NA
Description
Lymphatic invasion
ly0
ly1
NA
Venous invasion
ly0
ly1
NA
Horizontal margin
HM0
HM1
HMX
Vertical margin
VM0
VM1
VMX

APC, argon plasma coagulation; ELPS, Endoscopic laryngo-pharyngeal surgery; EMR, endoscopic mucosal resection; ESD, endoscopic submucosal dissection; NA, not applicable.

© 2017 Japan Gastroenterological Endoscopy Society

Table 2 Esophageal procedures

Esophagus
Procedure
No
Yes
Biopsy
Polypectomy
EMR
ESD
No. specimens
En bloc
Piecemeal
Input no.
Evaluation of endoscopic resection
Complete
Incomplete
Duration of procedure (min)
Device used for procedure
None
Snare
IT knife
Dual knife
IT nano
Flex knife
Hook knife
Flush knife
Clutch cutter
Hemostatic
Other
Injection
None
Hyaluronic acid
Glycerol
Normal saline
Other
Marking
Successful
Unsuccessful
PDT
Successful
Unsuccessful
Ablation (includes APC)
Successful
Unsuccessful
EVL
Successful
Unsuccessful
EIS
Successful
Unsuccessful
Dilation
Successful
Unsuccessful

Table 2 (Continued)

RIC
Successful
Unsuccessful
Stent placement
Successful
Unsuccessful
PTEG
Successful
Unsuccessful
Removal of foreign object
Successful
Unsuccessful
Other
Successful
Unsuccessful
†Pathological diagnosis
Size of resected specimen
Major axis
Minor axis
NA
Size of lesion
Major axis
NA
Pathological/Morphological type
0-Ip
0-Is
0-IIa
0-IIb
0-IIc
0-III
NA
Pathological depth
EP
LPM
MM
SM1
>SM2
NA
Primary histological type
Low-grade intraepithelial neoplasia
High-grade intraepithelial neoplasia
Squamous cell carcinoma
Adenocarcinoma
NA
Lymphatic invasion
ly0
ly1
NA
Venous invasion
ly0
ly1
NA

© 2017 Japan Gastroenterological Endoscopy Society

Table 2 (*Continued*)

Horizontal margin
HM0
HM1
HMX
Vertical margin
VM0
VM1
VMX

APC, argon plasma coagulation; EIS, Endoscopic injection sclerotherapy; EMR, endoscopic mucosal resection; ESD, endoscopic submucosal dissection; EVL, Endoscopic varicoal ligation; NA, not applicable; PDT, Photodynamic therapy; PTEG, Percutaneous transesophageal gastro-tubing; RIC, Radial incision and cutting.

Table 3 Gastric procedures

Stomach
Procedure
No
Yes
Biopsy
Polypectomy
EMR
ESD
No. specimens
En bloc
Piecemeal
Input no.
Evaluation of endoscopic resection
Complete
Incomplete
Duration of procedure (min)
Device used for procedure
None
Snare
IT knife
Dual knife
IT nano
Flex knife
Hook knife
Flush knife
Clutch cutter
Hemostatic forceps
Other
Injection
None
Hyaluronic acid
Glycerol
Normal saline
Other
Marking
Successful
Unsuccessful

Table 3 (*Continued*)

PDT
Successful
Unsuccessful
Ablation (includes APC)
Successful
Unsuccessful
EVL
Successful
Unsuccessful
EIS
Successful
Unsuccessful
Dilation
Successful
Unsuccessful
Stent placement
Successful
Unsuccessful
Removal of foreign object
Successful
Unsuccessful
PEG
Successful
Unsuccessful
Other
Successful
Unsuccessful
†Pathological diagnosis
Size of resected specimen
Major axis
Minor axis
NA
Size of lesion
Major axis
NA
Pathological/Morphological type
0-I
0-IIa
0-IIb
0-IIc
0-III
NA
Pathological depth
M
SM1
>SM2
NA
UL
Yes
No
NA
Primary histological type
tub1
tub2

© 2017 Japan Gastroenterological Endoscopy Society

Table 3 (Continued)

pap
sig
por
muc
Other
NA
Adenoma
Secondary histological type
tub1
tub2
pap
sig
por
muc
Other
Adenoma
Lymphatic invasion
Yes
No
NA
Venous invasion
Yes
No
NA
Horizontal margin
HM0
HM1
HMX
Vertical margin
VM0
VM1
VMX

APC, argon plasma coagulation; EIS, Endoscopic injection sclerotherapy; EMR, endoscopic mucosal resection; ESD, endoscopic submucosal dissection; EVL, Endoscopic vericeal ligation; NA, not applicable; PDT, Photodynamic therapy; PEG, Percutaneous endoscopic gastrostomy; UL, Ulcerative findings.

In addition to the data collection method used for Phase 1; that is, a person in charge visits each institute and collects data, the following data submission/collection method is used: the representative of each institute who attends the general meetings of JGES held in Spring and Fall brings password locked media containing password locked files to the front desk of the general meeting. A secure online collection method is also currently positively considered, and when a method that guarantees quick deliverability is established, registration through secure data transfer via the Internet will be implemented.

However, the intention of each institute as to whether or not it wishes to provide data is respected as much as possible, and the number of institutes which provide data sequentially increase. A system to check online errors in the

Table 4 Duodenal procedures

Duodenum
Procedure
No
Yes
Biopsy
Polypectomy
EMR
ESD
No. specimens
En bloc
Piecemeal
Input no.
Evaluation of endoscopic resection
Complete
Incomplete
Duration of procedure (min)
Device used for procedure
None
Snare
IT knife
Dual knife
IT nano
Flex knife
Hook knife
Flush knife
Clutch cutter
Hemostatic forceps
Other
Injection
None
Hyaluronic acid
Glycerol
Normal saline
Other
Marking
Successful
Unsuccessful
Hemostasis of varices (includes preventive measures)
Successful
Unsuccessful
Hemostasis of other hemorrhage (includes preventive measures)
Successful
Unsuccessful
Dilation
Successful
Unsuccessful
Stent placement
Successful
Unsuccessful
Removal of foreign object
Successful
Unsuccessful

© 2017 Japan Gastroenterological Endoscopy Society

Table 4 (*Continued*)

Other
Successful
Unsuccessful
†Pathological diagnosis
Size of resected specimen
Major axis
Minor axis
NA
Size of lesion
Major axis
NA
Pathological/Morphological type
0-I
0-IIa
0-IIb
0-IIc
0-III
NA
Pathological depth
M
SM1
>SM2
NA
Primary histological type
tub1
tub2
pap
sig
por
muc
Other
NA
Adenoma
Secondary histological type
tub1
tub2
pap
sig
por
muc
Other
Adenoma
Lymphatic invasion
Yes
No
NA
Venous invasion
Yes
No
NA
Horizontal margin
HM0
HM1
HMX

Table 4 (*Continued*)

Vertical margin
VM0
VM1
VMX

EMR, endoscopic mucosal resection; ESD, endoscopic submucosal dissection; NA, not applicable.

data registered by each institute is established, if possible. At the same time, anonymized patient IDs are further encrypted to achieve unlinkability and anonymity of data.

A review on the current items of information to be collected has been made based on the data collected during Phase 1, and the items finally selected have been published as JEGS specifications for data submission. This allows each filing system and endoscopy database producer to have easy access to data and to conduct simple processing of data.

Phase 3: Nationwide distribution for all guiding institutes

After finishing the feasibility study and Safety/efficacy analysis, we will start to distribute this scheme to all guiding institutes endorsed by JGES.

Through the data collected by this project, information on the numbers of physicians who actually carried out endoscopy, attending physicians who provided advice, and support staff is also collected. Registration of medical performance records of endoscopists becomes possible using these data. Currently, when submitting an application for qualification of candidacy for specialist examination, screening can only be made based on self-reported information and far from accurate information is currently being collected. However, if this JED project expands to all guiding institutes, the data can be used as information needed for the application for qualification of candidacy for specialist examination.

Although details of the new specialist system are still not clear, all institutes participating in this project are requested to record the names of physicians who carried out endoscopy and attending physicians, to enable physicians who intend to become specialists, specialists who wish to renew their license, and physicians who intend to obtain a license as attending physician, to report their performance records. It is undeniable that specialists and attending physicians are subject to severe future scrutiny. The data also provides information on the actual medical performance records of endoscopists.

PATIENTS' CONSENT AND ETHICS REGULATIONS

THIS PROJECT IS conducted in compliance with the spirit of 'Declaration of Helsinki, Ethical Principles for

© 2017 Japan Gastroenterological Endoscopy Society

Table 5 Small bowel procedures

Small intestine
Procedure
No
Yes
Biopsy
EMR
No. specimens
En bloc
Piecemeal
Input no.
Polypectomy
Evaluation of endoscopic resection
Complete
Incomplete
Duration of procedure (min)
Ablation
Successful
Unsuccessful
Hemostasis
Successful
Unsuccessful
Balloon dilation
Successful
Unsuccessful
Removal of foreign object
Successful
Unsuccessful
EUS
Other
†Pathological diagnosis
Size of resected specimen
Major axis
Minor axis
NA
Size of lesion
Major axis
NA
Pathological/Morphological type
0-I
0-IIa
0-IIb
0-IIc
0-III
NA
Pathological depth
M
SM1
>SM2
NA
Primary histological type
tub1
tub2
pap
sig
por
muc
Other
NA
Adenoma
Secondary histological type
tub1
tub2
pap
sig
por
muc
Other
Adenoma
Lymphatic invasion
Yes
No
NA
Venous invasion
Yes
No
NA
Horizontal margin
HM0
HM1
HMX
Vertical margin
VM0
VM1
VMX

EMR, endoscopic mucosal resection; EUS, endoscopic ultrasonography; NA, not applicable.

Medical Research Involving Human Subjects' (as amended in Fortaleza, October 2013).[1] Furthermore, the project is also conducted in compliance with 'Ethical Guidelines for Medical and Health Research involving Human Subjects'.[2]

The clinical study carried out in this project is a prospective observational study, and does not involve any risk that exceeds the minimum risk to study subjects. In addition, this study is considered to serve the interests of the public; we do not intend to obtain separate consent from the subjects. Consent of subjects for gastroenterological endoscopic examination, procedure and treatment carried out at each institute is obtained through explaining the meaning, objective and adverse events of the examination within the scope of regular medical care. Information concerning the implementation of this project including the objective of this study should be disclosed to the public and, thus, information concerning the study is disclosed by, among other means, posting the documents for which approval of disclosure from the Ethics Review Committee has

© 2017 Japan Gastroenterological Endoscopy Society

Table 6 Colon procedures

Colon
Procedure
- No
- Yes
- Biopsy
- Cold forceps polypectomy
- Hot biopsy
- Cold snare polypectomy
- Polypectomy
- EMR (en bloc)
- EMR (piecemeal <5 pieces)
- EMR (piecemeal ≥5 pieces)
- ESMR-L
- EMR-C
- ESD (en bloc)
- ESD (piecemeal)
  - Device
  - IT knife
  - B knife
  - IB knife
  - Jet knife
  - IT nano
  - Flex knife
  - Hook knife
  - Flush knife
  - Clutch cutter
  - Dual knife
  - Other
- Injection
  - Hyaluronic acid
  - Glycerol
  - Normal saline
  - Other
- UL
  - (+) Advanced
  - (+) Intermediate
  - (+) Mild
  - (–)
- Non-lifting sign
  - (+)
  - (±)
  - (–)
- Ablation
  - Successful
  - Unsuccessful
- Endoscopic hemostasis
  - Successful
  - Unsuccessful
- Endoscopic balloon dilation
  - Successful
  - Unsuccessful
- Endoscopic stent placement
  - Successful
  - Unsuccessful

Table 6 (Continued)

- Transanal ileus tube insertion
  - Successful
  - Unsuccessful
- Marking
  - Successful
  - Unsuccessful
- Other
  - Successful
  - Unsuccessful

†Pathological diagnosis
- Primary histological type
  - tub1
  - tub2
  - pap
  - sig
  - por
  - muc
  - Adenoma
  - TSA
  - Hyper
  - SSA/P
  - Other
  - NA
- Secondary histological type (mixed types only)
  - tub1
  - tub2
  - pap
  - sig
  - por
  - muc
  - Adenoma
  - TSA
  - Hyper
  - SSA/P
  - Other
  - NA
- Pathological depth
  - M (TIs)
  - SM (T1a)
  - SM (T1b)
  - NA
  - ≥MP
- Lymphatic invasion
  - Yes
  - No
  - NA
- Venous invasion
  - Yes
  - No
  - NA
- Budding
  - G1
  - G2

© 2017 Japan Gastroenterological Endoscopy Society

Table 6 (Continued)

G3
Horizontal margin
HM0
HM1
HMX
Vertical margin
VM0
VM1
VMX

†Pathological diagnosis required. (For ESD lesions, input of 'Primary histological type' to 'vertical margin' is mandatory. For others, input of 'Primary histological type' only is sufficient.)
EMR, endoscopic mucosal resection; EMR-C, endoscopic mucosal resection using a cap-fitted endoscope; ESD, endoscopic submucosal dissection; ESMR-L, endoscopic submucosal resection with a ligation device; NA, not applicable; TSA, traditional serrated adenoma; UL, ulcer.

been obtained on the participating institutes' websites or public spaces. Study subjects who wish to retract information are asked to notify such a request within one month after the completion of the endoscopic examination, procedure or treatment. Documents to be publicly disclosed contain the following information:

- Objective (meaning), subjects and method (information used) of the project
- Names of the participating institutions, the persons responsible for these institutions and contact information
- How personal information is handled and
- Matters concerning non-participation in the study.

ITEMS OF INFORMATION TO BE COLLECTED

AS FOR THE items of information to be collected, the terms to be used are standardized and stratified. This basically allows participants to input data by selecting applicable items. By doing so, variation of data input in each item is limited. In accordance with classification of upper gastrointestinal endoscopy, lower gastrointestinal endoscopy and endoscopic retrograde cholangiopancreatography (ERCP) procedure, Minimal Standard Endoscopic Database (MSED-J) Creation Subcommittee defined terms that are deemed necessary for stating findings of gastrointestinal endoscopy for each organ.

The following items of information are collected for both gastrointestinal endoscopic examination and therapeutic findings:

Items of information to be collected that are common to all upper gastrointestinal endoscopy are as follows:

- Patient's basic information
  Examination date, age, sex, American Society of Anesthesiologists (ASA) grade, antithrombotic agents (including details of use, suspension of use and replacement), smoker/non-smoker, drinking history and drinking condition, family history of cancer, previous history of other organ cancer, *Helicobacter pylori* and infection state
- Information to be requested
  Predictability, outpatient/inpatient, purpose of examination and purpose of treatment
- Drugs
  Status of use of antispasmodic agents and matters concerning sedation, analgesia and anesthesia
- Insertion route
- Scope of use
- Type of air/gas
- Special observation method
- Scope of observation
- Starting and ending time of procedure
- Adverse events during procedure
- Adverse events after procedure
- Death within 30 days
- Name of performing physician (physician's registration number).

(Full names of physician and assistant physician carrying out endoscopy. When obtaining physician's registration number, whether or not the physician accepts to be registered as a sub-investigator of this study [study investigator] is confirmed with the physician)

- Name of assistant physician carrying out endoscopy (physician's registration number)
- Names of endoscopy nurses and technicians (When obtaining the names of endoscopy nurses and technicians, consent of the patient is also mandatory and, if consent is not obtained, only the number of persons involved in the examination is stated).

In addition to the information to be collected that is common to all upper gastrointestinal endoscopies, three items (previous record of abdominal surgeries, life history of colonoscopy, and bowel preparation: excellent, good, fair, poor, based on modified Aronchick Bowel Preparation Score [ABPS])[3] and five items (extent of contrast radiography, cannulation, bile duct and pancreas duct diameter, degree of difficulty of cannulation, method to approach to bile duct) are collected as common items in all lower gastrointestinal endoscopies and in all ERCP-related procedures, respectively. *Helicobacter pylori* and infection state is not collected in these procedures instead.

© 2017 Japan Gastroenterological Endoscopy Society

Table 7 Endoscopic retrograde cholangiopancreatography procedures of the papilla, bile duct, and pancreatic duct

- Major papilla
  - No
  - Yes
    - Biopsy
      - Fluoroscopy assisted
        - Yes
        - No
    - Cytology
      - Suction
      - Brushing
      - Both
    - EST (endoscopic sphincterotomy)
      - Large size
      - Middle size
      - Small size
      - Successful
      - Unsuccessful
    - Papillectomy
      - Type of treatment
        - Specify
      - Successful
      - Unsuccessful
    - EPBD (endoscopic papillary balloon dilation)
      - Balloon size (mm)
      - Successful
      - Unsuccessful
    - EPLBD (endoscopic papillary large balloon dilation)
      - Balloon size (mm)
      - Successful
      - Unsuccessful
    - Biliary stent placement
      - Type of stent
      - Stent size (Fr)
      - Stent length (cm)
      - Successful
      - Unsuccessful
    - Pancreatic stent placement
      - Type of stent
      - Stent size (Fr)
      - Stent length (cm)
      - Successful
      - Unsuccessful
    - Ablation
      - Devices (specify)
      - Successful
      - Unsuccessful
    - Hemostasis
      - Devices (specify)
      - Successful
      - Unsuccessful
    - Other
      - (specify)
      - Successful
      - Unsuccessful

Table 7 *(Continued)*

- Minor papilla
  - No
  - Yes
    - Biopsy
      - Fluoroscopy assisted
        - Yes
        - No
    - Cytology
      - Suction
      - Brushing
      - Both
    - EPST (endoscopic pancreatic sphincterotomy)
      - Large size
      - Middle size
      - Small size
      - Successful
      - Unsuccessful
    - Papillectomy
      - Type of treatment
        - Specify
      - Successful
      - Unsuccessful
    - EPBD (endoscopic papillary balloon dilation)
      - Balloon size (mm)
      - Successful
      - Unsuccessful
    - EPLBD (endoscopic papillary large balloon dilation)
      - Balloon size (mm)
      - Successful
      - Unsuccessful
    - Pancreatic stent placement
      - Type of stent
      - Stent size (Fr)
      - Stent length (cm)
      - Successful
      - Unsuccessful
    - Ablation
      - Devices (specify)
      - Successful
      - Unsuccessful
    - Hemostasis
      - Devices (specify)
      - Successful
      - Unsuccessful
    - Other
      - Successful
      - Unsuccessful
- Bile duct
  - No
  - Yes
    - Biopsy
      - Fluoroscopy assisted
        - Yes
        - No
    - Cholangioscopy guided

© 2017 Japan Gastroenterological Endoscopy Society

Table 7 (Continued)

- Yes
- No
- Cytology
  - Suction
  - Brushing
  - Both
- EST (endoscopic sphincterotomy)
  - Large size
  - Middle size
  - Small size
  - Successful
  - Unsuccessful
- EPBD (endoscopic papillary balloon dilation)
  - Balloon size (mm)
  - Successful
  - Unsuccessful
- EPLBD (endoscopic papillary large balloon dilation)
  - Balloon size (mm)
  - Successful
  - Unsuccessful
- Balloon dilation for stricture
  - Type of device
  - Size (mm)
  - Successful
  - Unsuccessful
- Biliary stent placement
  - Type of stent
  - Stent size (Fr)
  - Stent length (cm)
  - Successful
  - Unsuccessful
- Stone extraction
  - Maximum size of stone
  - No. stones
  - Balloon
  - Basket
  - Duct cleared
  - Partially cleared
  - Successful
  - Unsuccessful
- Mechanical lithotripsy
  - Maximum size of stone
  - No. stones
  - Successful
  - Unsuccessful
- Ablation
  - Devices (specify)
  - Successful
  - Unsuccessful
- Other
  - (specify)
  - Successful
  - Unsuccessful

Pancreatic duct

- No

Table 7 (Continued)

- Yes
  - Biopsy
    - Fluoroscopy assisted
      - Yes
      - No
    - Pancreatoscopy guided
      - Yes
      - No
  - Cytology
    - Suction
    - Brushing
    - Both
  - EPST (endoscopic pancreatic sphincterotomy)
    - Successful
    - Unsuccessful
  - EPBD (endoscopic papillary balloon dilation)
    - Balloon size (mm)
    - Successful
    - Unsuccessful
  - EPLBD (endoscopic papillary large balloon dilation)
    - Balloon size (mm)
    - Successful
    - Unsuccessful
  - Balloon dilation for stricture
    - Type of device
    - Size (mm)
    - Successful
    - Unsuccessful
  - Pancreatic stent placement
    - Type of stent
    - Stent size (Fr)
    - Stent length (cm)
    - Successful
    - Unsuccessful
  - Stone extraction
    - Maximum size of stone
    - No. stones
    - Balloon
    - Basket
    - Duct cleared
    - Partially cleared
    - Successful
    - Unsuccessful
  - Mechanical lithotripsy
    - Maximum size of stone
    - No. stones
    - Successful
    - Unsuccessful
  - Ablation
    - Devices (specify)
    - Successful
    - Unsuccessful
  - Other
    - (specify)
    - Successful
    - Unsuccessful

© 2017 Japan Gastroenterological Endoscopy Society

Table 8 Endoscopic retrograde cholangiopancreatography (ERCP) procedures: Major measurements in ERCP

Total procedure time (minute(s))		
Time to access the major papilla or anastomosis (minute(s))		
Fluoroscopy time (minute(s))		
Extent of opacification of biliary duct		
Up to intrahepatic duct		
Up to hilum		
Up to upper common bile duct		
Up to middle common bile duct		
Up to lower common bile duct		
None		
Extent of opacification of pancreatic duct		
Up to head		
Up to body		
Up to tail		
None		
Cannulation for biliary duct		
Successful		
Partially successful		
Unsuccessful		
Cannulation for pancreatic duct		
Successful		
Partially successful		
Unsuccessful		
Size of common bile duct (upper : middle : lower) (mm)		
Size of pancreatic duct (head : body : tail) (mm)		
Grading the difficulty of ERCP†	Based on modified Schutz	
	Diagnostic	Therapeutic
Grade 1 standard	Selective deep cannulation	Biliary sphincterotomy
	Biopsy and cytology	Stones ≤10 mm
		Stents for biliary leaks
		Stents for lower tumors
		Prophylactic small pancreatic stent
Grade 2 advanced	Billroth II diagnostic	Stones >10 mm
	Minor papilla cannulation	Hilar tumor stent placement
		Benign biliary strictures
Grade 3 tertiary	Sphincter manometry	Billroth II therapeutics
	Whipple/Roux-en-Y	Intrahepatic stones
	Intraductal endoscopy	Pancreatic therapies
		Ampullectomy
		Pseudocyst drainage
Prior endoscopic intervention	None	
	Biliary EST	
	EST for major pancreatic duct	
	EST for minor pancreatic duct	
	Biliary stent	
	Pancreatic stent	
	EPBD for common bile duct	

© 2017 Japan Gastroenterological Endoscopy Society

Table 8 (Continued)

	EPLBD for common bile duct EPBD for major pancreatic duct EPBD for minor pancreatic duct
Method for first biliary attempt	Cannula + contrast agent Cannula + guidewire Cannula + guidewire + contrast agent Papillotomy knife + guidewire EUS-guided Other (specify) Unsuccessful Not for biliary purpose
Number of attempts for deep biliary cannulation	1, 2, 3, 4, 5 or more, none
Method for final biliary access	Cannula + contrast agent Cannula + guidewire Cannula + guidewire + contrast agent Papillotomy knife + contrast agent Papillotomy knife + guidewire Papillotomy knife + guidewire + contrast agent Guidewire placement for major pancreatic duct Access sphincterotomy Double guidewire method EUS-guided Other (specify) Unsuccessful Not for biliary purpose

†Add X after grade if the previous procedure was unsuccessful (e.g. Grade 1X)
EPBD, endoscopic papillary balloon dilation; EPLBD, endoscopic papillary large balloon dilation; EST, endoscopic sphincterotomy; EUS, endoscopic ultrasonography.

For findings of gastroenterological endoscopic examination, contents of diagnosis and treatment and pathological diagnosis, input is made using the terms separately defined for each organ (Tables 1–8).

ASSESSMENT

DATA ARE ANALYZED and the following feedback is provided to the members of the Society. Data accumulated at each institute may be used as data from a prospective clinical study approved by the ethical committee of each institute. Representative feedback to the Society member institutes which are available is:

- Feedback related to endoscopic diagnosis
  - Detailed disease statistics
  - Prevalence rate by age and sex of patients who received endoscopic procedure
  - Prevalence rate in the entire endoscopic examination cases
- Feedback related to endoscopic treatment and treatment outcome
  - Data related to the certainty of treatment
  - Comparison between the number of surgical treatment cases and the number of endoscopic treatment cases
- Feedback related to complications
  - Incidence of complications that is more accurate and detailed than that obtained through current questionnaire survey.

MATTERS PERTAINING TO STABILIZATION OF PROJECT AND ASSURANCE OF SAFETY

AS THIS PROJECT is carried out within the scope of regular medical care, no disadvantage or risk would occur to any individual as a result of this project. However, if any health hazards or adverse events occur, the person

© 2017 Japan Gastroenterological Endoscopy Society

responsible for the institute promptly and properly provides best possible treatment.

A safety threat in this project is leakage of data. To deal with this threat:

- Data server is established within the headquarters and
- Any person other than the data manager and data analyst is prohibited access to the data server.

Measures to maintain backup of data stored in the data server are in place. Furthermore, once it is confirmed that security is guaranteed, backup in an external data center is considered upon approval of JGES.

PUBLIC DISCLOSURE AND STORAGE

EFFORTS ARE MADE to disclose or announce to the member institutes each item listed in the 'Assessment' section over the Internet. When announcing or disclosing the results of data analysis, privacy of patients as well as the institutes which provided data and each municipality must be taken into consideration and, thus, an organization to deliberate issues related to announcement and disclosure has been established. JGES has established a Committee on the Uses of JED which discusses the future uses of outcomes obtained from the study. The outcomes are finally deliberated at the JGES Executive Committee and used after obtaining member consent.

CONFLICTS OF INTEREST

THIS PROJECT IS fully supported by JGES and public funds would be obtained to proceed in addition to JGES's own funds. There is no 'possible conflicts of interest (possibility that interests, positions etc. of individual researchers affect the fairness of the study, impartiality of plan, implementation and report)' which may affect the outcome or interpretation of the studies obtained from this project in planning, implementing and reporting. Furthermore, the implementation of this project does not adversely affect the rights and interests of subjects.

REFERENCES

1 World Medical Association. WMA Declaration of Helsinki: ethical principles for medical research involving human subjects. Adopted by the 18th WMA General Assembly, Helsinki, Finland, June 1964, and last amended by the 64th WMA General Assembly, Fortaleza, Brazil, October 2013. [Cited 2 Nov 2017.] Available from URL: http://www.wma.net/en/30publications/10policies/b3/index.html.

2 Ministry of Education, Culture, Sports, Science and Technology and Ministry of Education, Culture, Sports, Science and Technology. Ethical Guidelines for Medical and Health Research involving Human Subjects (in Japanese). [Cited 2 Nov 2017.] Available from URL: http://www.mext.go.jp/b_menu/hondou/26/12/__icsFiles/afieldfile/2014/12/22/1354186_1.pdf

3 Aronchick CA, Lipshutz WH, Wright H. Validation of an instrument to assess colon cleansing. *Am. J. Gastroenterol.* 1999; **94**: 2667.

© 2017 Japan Gastroenterological Endoscopy Society

J Gastroenterol (2018) 53:247–257
https://doi.org/10.1007/s00535-017-1360-z

The Japanese Society of Gastroenterology

ORIGINAL ARTICLE—LIVER, PANCREAS, AND BILIARY TRACT

Combinational use of hepatitis B viral antigens predicts responses to nucleos(t)ide analogue/peg-interferon sequential therapy

Akihiro Matsumoto[1] · Shuhei Nishiguchi[2] · Hirayuki Enomoto[2] · Jong-Hon Kang[3] · Yasuhito Tanaka[4] · Noboru Shinkai[4] · Masayuki Kurosaki[5] · Masaru Enomoto[6] · Tatsuo Kanda[7] · Osamu Yokosuka[7] · Hiroshi Yatsuhashi[8] · Shinya Nagaoka[8] · Chiaki Okuse[9] · Tatehiro Kagawa[10] · Tetsuya Mine[10] · Koichi Takaguchi[11] · Satoru Saito[12] · Keisuke Hino[13] · Fusao Ikeda[14] · Shotaro Sakisaka[15] · Daisuke Morihara[15] · Shiho Miyase[16] · Masataka Tsuge[17] · Kazuaki Chayama[17] · Naoki Hiramatsu[18] · Yoshiyuki Suzuki[19] · Kazumoto Murata[20,21] · Eiji Tanaka[1]

Received: 18 April 2017 / Accepted: 4 June 2017 / Published online: 20 June 2017
© Japanese Society of Gastroenterology 2017

Abstract

Background This prospective cohort study searched for factors associated with a response to nucleos(t)ide analogue/peg-interferon (NUC/peg-IFN) sequential therapy.

Methods A total of 95 patients with chronic hepatitis B being treated with NUCs were enrolled. Immediately following NUC cessation, peg-IFN was administered at 180 μg/dose weekly for 48 weeks.

Results Twenty-six patients (27%) were judged to be responders at 48 weeks after the completion of peg-IFN. Analysis of baseline factors revealed that hepatitis B surface antigen (HBsAg) <3.1 log IU/ml and HB core-related antigen (HBcrAg) <3.9 log U/ml were significant indicators of a treatment response. The levels of the markers decreased in both responders and non-responders during peg-IFN therapy but continued falling in responders only after halting peg-IFN. Lower HBsAg (<2.0 log IU/ml) and HBcrAg (<3.8 log U/ml) levels at the time of response judgment were also significantly associated with a favorable response. While lower HBcrAg at baseline was the sole predictor of decreased HBcrAg levels at judgment, lower HBsAg, lower HBcrAg, and the use of adefovir dipivoxil at baseline predicted decreased HBsAg levels at the study endpoint. The use of adefovir dipivoxil was also associated with higher serum IFN-λ3, which might have contributed to the reduction in patient HBsAg levels.

Conclusions The combinational use of HBsAg and HBcrAg levels at baseline and their changes throughout sequential therapy may be useful for predicting a response to NUC/peg-IFN sequential therapy.

✉ Eiji Tanaka
etanaka@shinshu-u.ac.jp

1 Department of Medicine, Shinshu University School of Medicine, Asahi 3-1-1, Matsumoto 390-8621, Japan

2 Division of Hepatobiliary and Pancreatic Disease, Department of Internal Medicine, Hyogo College of Medicine, Nishinomiya, Japan

3 Center for Gastroenterology, Teine Keijinkai Hospital, Sapporo, Japan

4 Department of Virology and Liver Unit, Nagoya City University Graduate School of Medical Sciences, Nagoya, Japan

5 Department of Gastroenterology and Hepatology, Musashino Red Cross Hospital, Tokyo, Japan

6 Department of Hepatology, Osaka City University Medical School, Osaka, Japan

7 Department of Gastroenterology and Nephrology, Graduate School of Medicine, Chiba University, Chiba, Japan

8 The Clinical Research Center, National Hospital Organization Nagasaki Medical Center, Omura, Japan

9 Division of Gastroenterology and Hepatology, Department of Internal Medicine, St. Marianna University School of Medicine, Kawasaki, Japan

10 Division of Gastroenterology, Department of Internal Medicine, Tokai University School of Medicine, Isehara, Japan

11 Department of Hepatology, Kagawa Prefectural Central Hospital, Takamatsu, Japan

12 Department of Gastroenterology and Hepatology, Yokohama City University School of Medicine, Yokohama, Japan

13 Department of Hepatology and Pancreatology, Kawasaki Medical School, Kurashiki, Japan

14 Department of Gastroenterology and Hepatology, Okayama University Graduate School of Medicine, Dentistry, and Pharmaceutical Sciences, Okayama, Japan

Keywords Hepatitis B surface antigen · Hepatitis B core-related antigen · Covalently closed circular DNA · Chronic hepatitis · Anti-viral therapy

Abbreviations

HBV	Hepatitis B virus
HCC	Hepatocellular carcinoma
NUCs	Nucleos(t)ide analogues
IFN	Interferon-alpha
LAM	Lamivudine
ADV	Adefovir dipivoxil
ETV	Entecavir
TDF	Tenofovir disoproxil fumarate
HBsAg	Hepatitis B surface antigen
HBcrAg	Hepatitis B core-related antigen
peg-IFN	Peg-IFN-alpha 2a
ALT	Alanine transaminase
HBeAg	Hepatitis B e antigen
CLEIA	Chemiluminescence enzyme immunoassay
cccDNA	Covalently closed circular DNA
IFN-λ	Interferon-lambda
ROC	Receiver operating characteristic curve
AUC	Area under the curve
PPV	Positive predictive value
NPV	Negative predictive value
CI	Confidence interval

Introduction

With an estimated 350 million carriers worldwide, hepatitis B virus (HBV) infection is a widespread health problem that frequently causes chronic hepatitis and eventual liver cirrhosis and hepatocellular carcinoma (HCC) [1–3]. The majority of HBV carriers in Japan have genotype C and become infected perinatally or during early childhood. Response rates to antiviral therapies are lower in the Japanese as compared with Caucasian patients because of suspected differences in the main mode of transmission and genotype [4].

Currently available antiviral agents for hepatitis B include nucleos(t)ide analogues (NUCs) and interferon-alpha (IFN). NUCs are orally administered and associated with low rates of adverse effects. Although treatment with such NUCs as lamivudine (LAM), adefovir dipivoxil (ADV), entecavir (ETV), and tenofovir disoproxil fumarate (TDF) induces virological and biochemical responses in most patients, NUC therapy also carries the risk of drug resistance. Furthermore, patients with hepatitis B are required to undergo extended treatment with NUCs since early discontinuance often leads to relapse. In contrast, the remission of chronic hepatitis B by IFN is prolonged but achieved only in a small percentage of patients. Combination therapy with NUCs and IFN may therefore confer additive or synergistic antiviral effects. Serfaty et al. [5] conducted a pilot study on sequential therapy using LAM and IFN and suggested a cooperative effect of the antiviral agents. However, ensuing reports [6–10] have been unable to confirm this.

We previously evaluated 50 patients with chronic hepatitis B who underwent 24 weeks of sequential IFN therapy for the cessation of NUCs and concluded that the combinational use of hepatitis B surface antigen (HBsAg) and hepatitis B core-related antigen (HBcrAg) levels [11, 12] might be useful in predicting the 24-month outcome. Since the study was retrospective and the number of patients was small, the present prospective cohort investigation of sequential therapy, in which 48 weeks of peg-IFN alpha 2a (peg-IFN) was administered subsequently to NUCs, was undertaken to clarify the factors associated with the effects of NUC/peg-IFN sequential therapy.

Patients and methods

Study design

A prospective cohort study entitled "Study on usefulness of PEG-IFN alpha-2a administration to discontinue nucleos(t)ide analogue treatment in patients with chronic hepatitis B" was registered at the University Hospital Medical Information Network Center of Japan on January 10, 2012 (UMIN 000007045). The investigation originally consisted of three non-randomized arms with different procedures aiming at the discontinuation of NUCs. In the present study, we analyzed one of the three arms in which patients with NUC/peg-IFN sequential therapy were enrolled. We consider that such selection causes minimum bias because each arm proceeds independently.

[15] Department of Gastroenterology and Medicine, Fukuoka University Faculty of Medicine, Fukuoka, Japan

[16] Department of Gastroenterology and Hepatology, Kumamoto Shinto General Hospital, Kumamoto, Japan

[17] Department of Gastroenterology and Metabolism, Applied Life Sciences, Institute of Biomedical and Health Sciences, Hiroshima University, Hiroshima, Japan

[18] Department of Gastroenterology, Osaka Rosai Hospital, Sakai, Japan

[19] Department of Hepatology, Toranomon Hospital, Tokyo, Japan

[20] The Research Center for Hepatitis and Immunology, National Center for Global Health and Medicine, Ichikawa, Japan

[21] Department of Gastroenterology, Graduate School of Medical Sciences, International University of Health and Welfare, Narita, Japan

Patients with chronic hepatitis B who had been receiving NUCs for at least 1 year were recruited. Immediately after stopping NUCs, peg-IFN (Chugai Pharmaceutical Co., Ltd., Tokyo, Japan) was administered at 180 μg/dose once weekly for 48 weeks. The dose of peg-IFN could be reduced to 90 μg during exceptional circumstances, such as side effects. Patients were followed for 48 weeks after completing peg-IFN administration, at which time the treatment response was judged.

Patients who met the following conditions were classified as responders according to the guidelines of the Japan Society of Hepatology: alanine transaminase (ALT) <31 IU/l, negative result for HBeAg, HBV DNA <4.0 log copies/ml, and no recommencement of NUCs [13]. Patients who did not meet all of these criteria were recorded as non-responders.

Patients

A total of 95 patients with chronic hepatitis B who had been receiving NUC therapy were prospectively enrolled in the present study between February 2012 and December 2013. The cohort included 68 men and 27 women of a median age of 45 years (range, 27–87 years) at peg-IFN commencement. HBe antigen was positive in 33 (35%) patients. HBV genotype was A in seven (7%) patients, B in four (4%) patients, C in 77 (82%) patients, other in three (3%) patients, and undetermined in four (4%) patients. Genotype C was predominant as previously reported in Japan [14]. The NUCs at cessation were ETV in 58 (61%) patients, ETV + ADV in 12 (13%) patients, LAM in two (2%) patients, and LAM + ADV in 23 (24%) patients. The median duration of NUC administration was 4.9 years (range, 1.0–12.3 years).

HBsAg was confirmed to be positive on a minimum of two occasions at least 6 months apart in all patients before NUC treatment. Tests for hepatitis C and human immunodeficiency virus antibodies were negative. Patients complicated with HCC or signs of hepatic failure at the cessation of NUC administration were excluded from the study, as were patients with contraindications for peg-IFN therapy. HBsAg level, HBcrAg level, hepatitis B e antigen (HBeAg) status, NUCs used, and HBV genotype were not considered during patient recruitment. With few exceptions, subjects were seen at least once a month during peg-IFN therapy and at least once every 3 months afterwards. No patient developed HCC or hepatic failure during the follow-up period. Stored serum samples were kept frozen at −20 °C or below until assayed.

This study was approved by the Ethics Committees of all participating institutions (approval references 1906 and 353 for Shinshu University, 1172 and 92 for Hyogo College of Medicine, 184 and 125 for Musashino Red Cross Hospital, 45-11-0028 and 67 for Nagoya City University Graduate School of Medical Sciences, 2272 for Osaka City University Graduate School of Medicine, 639 and 379 for Chiba University, 2089 and 91 for St. Marianna University School of Medicine, 2485 and 23020 for National Hospital Organization Nagasaki Medical Center, 121-27 and 2086 for Tokai University School of Medicine, 1170 for Kawasaki Medical School, 1326 for Okayama University Graduate School of Medicine, B120705027 for Yokohama City University Graduate School of Medicine, 411 for Kumamoto Shinto General Hospital, and "Study on usefulness of Peg-IFN alpha 2a administration to discontinue NUC treatment in patients with chronic hepatitis B" for Teine Keijinkai Hospital and Kagawa Prefectural Central Hospital).

Hepatitis B viral markers

Serological markers for HBV, including HBsAg, HBeAg, and antibody to HBeAg, were tested using commercially available enzyme immunoassay kits (Abbott Japan Co., Ltd., Tokyo, Japan). HBsAg was quantitatively measured using a chemiluminescence enzyme immunoassay (CLEIA)-based ARCHITECT HBsAg QT assay manufactured by Abbott Japan Co., Ltd. [15] with a quantitative range of 0.05–250 IU/ml (−1.3 to 2.4 log IU/ml). End titer was determined by diluting samples according to the manufacturer's instructions when initial results exceeded the upper limit of the assay range.

Serum HBcrAg levels were measured using a CLEIA HBcrAg assay kit with a fully automated Lumipulse System analyzer (Fujirebio Inc., Tokyo, Japan) as described previously [16]. The HBcrAg assay measures all antigens transcribed and translated from the pre-core and core genes of the HBV genome, which include hepatitis B e, core, and p22cr antigens [12, 16]. HBcrAg concentration was calculated based on a standard curve generated using recombinant pro-HBeAg. The immunoreactivity of pro-HBeAg at 10 fg/ml was defined as 1 U/ml. We expressed HBcrAg in terms of log U/ml, with a quantitative range set at 3.0–6.8 log U/ml.

Serum HBV DNA was determined using a COBAS TaqMan HBV kit (Roche, Tokyo, Japan) with a quantitative range of 2.1–9.0 log copies/ml [17]. According to the manufacturer's instructions, detection of a positive signal below the quantitative range was described as <2.1 log copies/ml and no signal detection was regarded as negative. Six HBV genotypes (A–F) were evaluated according to the restriction patterns of DNA fragments from the method reported by Mizokami et al. [18].

Intrahepatic HBV covalently closed circular DNA (cccDNA) was measured based on the method reported by Suzuki et al. [19]. Briefly, liver biopsy specimens were

obtained and stored at −80 °C until DNA extraction, after which the concentration of extracted HBV DNA was determined according to absorbance at 260 nm. Two oligonucleotide primers, cccF2 (nucleotides 1424–1444) and cccR4 (nucleotides 1755–1737), and a cccP2 probe (nucleotides 1672–1655) were designed to flank the direct repeat region between the hepatitis B core and the polymerase gene. The use of cccF2 and cccR4 oligonucleotide primers spanning the direct repeat region of the HBV genome enabled the polymerase chain reaction of native viral DNA in the Dane particle to block the amplification of products since the partially double-stranded HBV DNA was disrupted in the direct repeat region [20]. Twenty-five microliters of the extracted DNA (0.5 μg) was analyzed with a sequence detector system (SRL Inc., Tokyo, Japan). The concentration of HBV cccDNA was expressed as the log copy number per 1 μg of total DNA extracted from the liver tissue at a lower quantitative limit of 1.7 log copies/μg. Detection of a positive signal below the quantitative threshold was described as <1.7 log copies/μg and no signal detection was regarded as negative. Measurement of intrahepatic HBV cccDNA was not considered essential since the study protocol permitted liver biopsy histology samples obtained within 1 year before starting peg-IFN therapy.

Interleukin-28B (IL28B) genotyping and serum IFN-λ3 level

Patients were evaluated for single-nucleotide polymorphisms near IL28B (rs8099917) using the Invader Plus assay (Invader Chemistry, Madison, WI, USA), as previously reported [21]. We did not investigate the polymorphism of rs12979860 because rs8099917 and rs12979860 have shown strong linkage disequilibrium in Japanese patients. Written informed consent was obtained from each patient.

Serum levels of IFN-λ3 were evaluated by a recently introduced CLEIA [22–24] that enabled the quantification of serum IFN-λ3 without any overlap of IFN-λ1 or IFN-λ2. The measurement range for this assay was 0.1–10,000 pg/ml.

Liver histological examination

Histological examination of liver samples was performed in 85 (89%) of the 95 patients within 1 year before starting peg-IFN. Histological findings were assessed according to the new Inuyama classification system [25]. Briefly, staging of liver fibrosis was classified as F0 (no fibrosis), F1 (mild fibrosis), F2 (moderate fibrosis), F3 (severe fibrosis), or F4 (liver cirrhosis). Grading of liver inflammation was classified as A0 (no activity), A1 (mild activity), A2 (moderate activity), or A3 (severe activity).

Statistical analyses

The Fisher's exact and Pearson's Chi-square tests were adopted to test for differences between patient subgroups. The Mann–Whitney U test was employed to compare continuous data. The Friedman test with Bonferroni correction was used to assess changes in HBsAg and HBcrAg levels. Multivariate analysis was performed with a logistic model for the 48-week response to NUC/peg-IFN sequential therapy using factors whose p value was less than 0.2 in univariate analysis. All continuous data values were translated into categorical data and divided by the cut-off value decided by Youden's index using receiver operating characteristic (ROC) curve analysis. A value of 0.5 was substituted for any missing values. Correlations between the levels of HBsAg, HBcrAg, and cccDNA were calculated using the Spearman's rank correction correlation coefficient test.

All tests were performed using the IBM SPSS Statistics Desktop for Japan ver. 23.0 (IBM Japan Inc., Tokyo, Japan). p values of less than 0.05 were considered to be statistically significant.

Results

Of the 95 patients enrolled, 75 (79%) completed peg-IFN therapy without dose reduction, 15 (16%) completed it with a necessary dose reduction, and the remaining five (5%) discontinued treatment due to side effects of epilepsy (15 weeks after starting peg-IFN), ALT elevation up to 937 IU/ml (16 weeks), interstitial pneumonia (17 weeks), retinal hemorrhage (42 weeks), or chronic thyroiditis (43 weeks). Five (5%) patients were lost to follow-up during the 48 weeks subsequent to peg-IFN completion.

All patients requiring re-administration of NUCs after stopping peg-IFN had ALT >80 IU/l and/or HBV DNA >5.8 log copies/ml at or just before the point of NUC resumption that fulfilled the established requirements for restarting NUCs [11, 12, 26]. Under these conditions, NUCs were recommenced in 37 (39%) of the 95 patients prior to the study endpoint.

Twenty-six (27%) of the 95 patients were judged as responders to NUC/peg-IFN sequential therapy and the remaining 69 (73%) were determined to be non-responders. The reasons for a non-response were lost to follow-up in five (7%) patients, high ALT in five (7%) patients, high HBV DNA in nine (13%) patients, high ALT and HBV DNA in 13 (19%) patients, and recommencement of NUCs in 37 (54%) patients.

Table 1 Comparison of clinical background, laboratory data, and viral markers at start of peg-IFN between responders and non-responders

Factor	Responders ($n = 26$)	Non-responders ($n = 69$)	p value
Age (years)[a]	50 (33 to 87)	43 (27 to 72)	0.085
Male gender[b]	20 (77%)	48 (70%)	>0.2
Past history of hepatocellular carcinoma[b]	1 (4%)	3 (4%)	>0.2
Past history of blood transfusion[b]	1 (4%)	2 (3%)	>0.2
Past history of IFN therapy[b]	1 (4%)	2 (3%)	>0.2
Family history of hepatitis B[b]	10 (38%)	30 (43%)	>0.2
Body mass index (kg/m^2)[a]	22.9 (18.7 to 20.7)	23.6 (17.3 to 30.6)	>0.2
Genotype[b]			>0.2
A	2 (8%)	5 (7%)	
B	1 (4%)	3 (4%)	
C	21 (81%)	56 (81%)	
Other	0 (0%)	3 (4%)	
Undetermined	2 (8%)	2 (3%)	
NUCs used just prior to peg-IFN[b]			0.103
ETV	15 (58%)	43 (61%)	
ETV + ADV	2 (8%)	10 (14%)	
LAM	2 (8%)	0 (0%)	
LAM + ADV	7 (27%)	16 (23%)	
Duration of NUC administration (years)[a]	5.0 (1.0 to 12.3)	4.7 (1.0 to 12.1)	
Liver histology stage[b]			>0.2
F0	2 (8%)	3 (4%)	
F1	8 (31%)	32 (47%)	
F2	9 (34%)	16 (23%)	
F3	5 (19%)	10 (14%)	
F4	0 (0%)	0 (0%)	
Undetermined	2 (8%)	8 (12%)	
Liver histology grade[b]			>0.2
A0	3 (12%)	9 (13%)	
A1	11 (41%)	32 (46%)	
A2	9 (35%)	13 (19%)	
A3	1 (4%)	7 (10%)	
Undetermined	2 (8%)	8 (12%)	
Peg-IFN treatment[b]			>0.2
Completed 48 weeks without dose reduction	20 (77%)	55 (80%)	
Completed 48 weeks with dose reduction	6 (23%)	10 (14%)	
Discontinued before 48 weeks	0 (0%)	4 (6%)	
IL28B genotype[b]			>0.2
Major	18 (69%)	46 (66%)	
Minor	3 (12%)	15 (22%)	
Undetermined	5 (19%)	8 (12%)	
Laboratory data[a]			
White blood cell count (/μl)	5220 (2900 to 11,200)	4900 (2000 to 10,780)	>0.2
Red blood cell count (×10^6/μl)	4.67 (3.79 to 5.51)	4.84 (3.67 to 5.61)	>0.2
Hemoglobin (g/dl)	15.0 (12.4 to 16.7)	14.9 (9.5 to 17.1)	>0.2
Platelet count (×10^3/μl)	165 (104 to 298)	181 (65 to 297)	>0.2
Total bilirubin (g/dl)	0.8 (0.3 to 2.3)	0.7 (0.3 to 1.7)	>0.2
Aspartate transaminase (IU/l)	23 (14 to 46)	22 (11 to 63)	0.060
Alanine transaminase (IU/l)	18 (6 to 45)	19 (6 to 83)	>0.2

Table 1 continued

Factor	Responders ($n = 26$)	Non-responders ($n = 69$)	p value
Alpha fetoprotein (ng/ml)	2.4 (1.7 to 5.0)	2.5 (0.5 to 7.5)	>0.2
Viral markers			
HBeAg positive[b]	5 (19%)	28 (41%)	0.057
HBV DNA (log copies/ml)[a]	<2.1 (neg. −3.1)	<2.1 (neg. −6.2)	>0.2
HBsAg (log IU/ml)[a]	2.9 (1.1 to 4.3)	3.4 (1.7 to 4.4)	0.001
HBcrAg (log U/ml)[a]	3.7 (<3.0 to 6.0)	4.6 (<3.0 to >6.8)	0.005

[a] Data are expressed as the median (range)

[b] Data are expressed as a positive number (percentage)

Table 2 Multivariate analysis of factors at start of peg-IFN associated with NUC/peg-IFN sequential therapy responders

Factor	Odds ratio	95% CI	p value
HBcrAg <3.9 log U/ml	4.3	1.5–11.9	0.006
HBsAg <3.1 log IU/ml	3.2	1.2–8.9	0.023

Clinical background, laboratory data, and viral markers are compared between the 26 responders and 69 non-responders in Table 1. Age distribution tended to be higher in responders, while gender and history were similar between the groups. Genotype C was over 80% in both groups. Approximately 60% of patients were treated with ETV alone and 35% were treated with regimens that included ADV just prior to starting peg-IFN in both groups. Histological liver staging and grading were comparable between the groups, as was the frequency of peg-IFN administration completion. The distribution of the major and minor IL28B genotypes was similar among the 82 (86%) of 95 patients tested. Laboratory data, including blood cell count and transaminase enzyme levels, were similar between the groups and HBV DNA levels were comparably low, possibly reflecting the effects of NUCs. HBeAg positivity tended to be lower in responders than in non-responders, while levels of HBsAg and HBcrAg were significantly lower in this group. Median HBV cccDNA level was lower in responders ($n = 6$, median 2.5 log copies/μg, range: negative result −4.0 log copies/μg) than in non-responders ($n = 22$, median 3.6 log copies/μg, range: negative result −8.1 log copies/μg), but this difference was not statistically significant ($p = 0.158$) likely due to the small number of patients analyzed.

Multivariate analysis of factors associated with a response to NUC/peg-IFN sequential therapy at peg-IFN initiation revealed that lower levels of HBsAg and HBcrAg were significantly associated with responders (Table 2). The area under the curve (AUC) to predict responders was 0.748 ($p < 0.001$) for HBsAg and 0.692 ($p = 0.005$) for HBcrAg according to ROC analysis. The calculated threshold to predict responders was 3.1 log IU/ml for HBsAg [sensitivity: 64.0%, specificity: 67.1%, positive predictive value (PPV): 41.0%, negative predictive value (NPV): 83.9%, accuracy: 66.3%] and 3.9 log U/ml for HBcrAg (sensitivity: 62.5%, specificity: 73.5%, PPV: 45.5%, NPV: 84.7%, accuracy: 70.8%). Figure 1a shows the distribution of responders and non-responders according to HBsAg and HBcrAg level at the start of peg-IFN. The response rate was highest (56%) when both HBsAg and HBcrAg levels were low and was lowest (6%) when both levels were high ($p = 0.003$). The maximum response rate (56%) was 10–15% higher than those predicted using low levels of HBsAg (41.0%) or HBcrAg (45.5%) separately. The minimum response rate (6%) was approximately 10% lower than those predicted using high levels of HBsAg (16.1%) or HBcrAg (15.3%) separately.

The changes in HBsAg and HBcrAg levels during peg-IFN therapy and the ensuing follow-up period are compared between responders and non-responders in Fig. 2. Median antigen levels were significantly lower in responders at all three points examined for both HBsAg and HBcrAg. Median HBsAg levels decreased during peg-IFN administration in responders (from 2.9 to 2.1 IU/ml) and non-responders (from 3.4 to 3.1 IU/ml). However, antigen levels subsequently decreased in responders (from 2.1 to 2.0 IU/ml) but increased in non-responders (from 3.1 to 3.2 IU/ml) during follow-up after peg-IFN therapy. Similarly, median HBcrAg levels decreased during peg-IFN administration in responders (from 3.7 to 3.4 U/ml) and non-responders (from 4.6 to 4.0 U/ml) but decreased in responders (from 3.4 to <3.0 U/ml) and increased in non-responders (from 4.0 to 4.4 U/ml) during post-peg-IFN therapy follow-up.

Lower levels of HBsAg [odds ratio 3.1, 95% confidence interval (CI) 1.0–9.2, $p = 0.041$] and HBcrAg (odds ratio 8.8, 95% CI 2.3–33.3, $p = 0.001$) at 48 weeks after completing peg-IFN administration were also significantly associated with a favorable response to sequential therapy. The AUC to predict responders was 0.748 ($p < 0.001$) for HBsAg and 0.692 ($p = 0.005$) for HBcrAg at 48 weeks after completing peg-IFN administration according to ROC analysis. The threshold to predict responders was

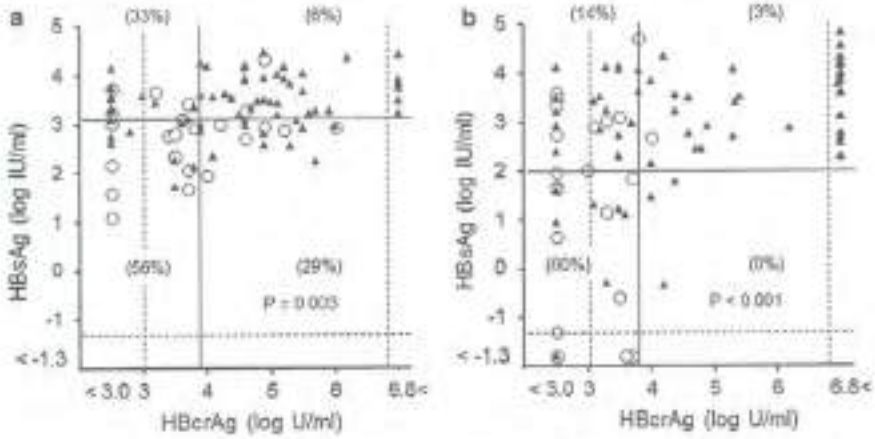

Fig. 1 Distribution of responders and non-responders according to serum levels of HBsAg and HBcrAg. **a** Antigen levels at the start of peg-IFN therapy. **b** Antigen levels at 48 weeks after stopping peg-IFN therapy. Figures are divided into four areas according to quantitative thresholds. The *vertical dashed lines* delineate the upper and lower detection limits of HBcrAg. The *horizontal dashed line* indicates the lower detection limit of HBsAg. The percentage in each area represents the responder rate. Differences in responder rates among areas were analyzed by the Mantel–Haenszel test

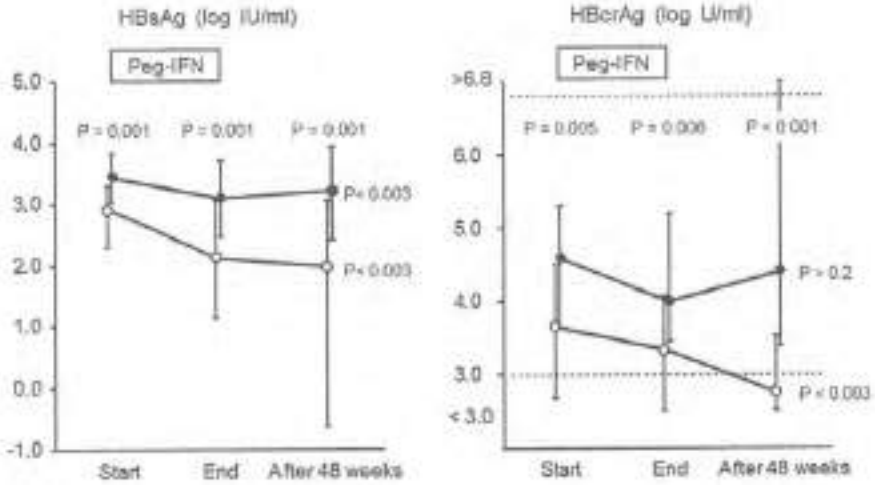

Fig. 2 Comparison of changes in HBsAg and HBcrAg levels during peg-IFN administration and follow-up of 48 weeks afterwards. Data are expressed as the median and 25–75% range. *Open circles* indicate responders and *closed circles* indicate non-responders. The *horizontal dashed lines* in the *right figure* delineate the upper and lower quantitative ranges of HBcrAg. Changes in the antigen levels of responders and non-responders were analyzed by the Friedman test with Bonferroni correction

2.0 log IU/ml for HBsAg (sensitivity: 64.0%, specificity: 67.1%, PPV: 41.0%, NPV: 83.9%, accuracy: 66.3%) and 3.8 log U/ml for HBcrAg (sensitivity: 62.5%, specificity: 73.5%, PPV: 45.5%, NPV: 84.7%, accuracy: 70.8%). Figure 1b presents the distribution of responders and non-responders according to HBsAg and HBcrAg levels at 48 weeks after completing peg-IFN. The response rate was high (60%) only when both levels were low ($p < 0.001$).

Multivariate analysis revealed that lower levels of HBsAg and HBcrAg at the initiation of peg-IFN and the use of ADV before peg-IFN therapy were significant factors associated with lower HBsAg levels (<2.0 log IU/ml) at 48 weeks after peg-IFN therapy (Table 3). Thresholds to predict lower HBsAg were 3.0 log IU/ml for HBsAg (AUC 0.872, $p < 0.001$), 4.0 U/ml for HBcrAg (AUC 0.703, $p = 0.008$), and ADV use (AUC 0.643, $p < 0.061$). The only factor associated with decreased HBcrAg (<3.8 log U/ml) levels at the study endpoint was itself at 4.8 log IU/ml (AUC 0.852, $p < 0.001$) (Table 3).

IFN-λ3 levels at peg-IFN commencement were measured in 80 (84%) of the 95 patients. Median IFN-λ3 was roughly ten times higher ($p < 0.001$) in the 29 patients who received ADV (median 18.4, range 1.2–118.6 pg/ml) than in the 51 patients who did not (median 1.4, range 0.3–23.0 pg/ml). On the other hand, IFN-λ3 level did not differ ($p = 0.706$) between patients with the IL28B-SNP major type ($n = 16$, median 19.4 pg/ml, range 1.2–55.6 pg/ml) and those with the minor type ($n = 10$, median 24.2 pg/ml, range 2.9–118.6 pg/ml) in subjects receiving ADV. Similarly, IFN-λ3 level did not differ ($p = 0.708$) between patients with the IL28B-SNP major type ($n = 39$, median 1.4 pg/ml, range 0.3–23.0 pg/ml) and those with the minor type ($n = 6$,

Table 3 Multivariate analysis of factors at start of peg-IFN associated with low levels of HBsAg (<2.0 log IU/ml) and HBcrAg (<3.8 log U/ml) at 48 weeks after stopping peg-IFN

Factor	Odds ratio	95% CI	*p* value
HBsAg <2.0 log IU/ml at 48 weeks after stopping peg-IFN			
HBsAg <3.0 log IU/ml	9.7	2.9–32.7	<0.001
HBcrAg <4.0 log U/ml	8.1	2.2–30.3	0.002
Use of ADV before peg-IFN administration	3.6	1.0–12.5	0.046
HBcrAg <3.8 log U/ml at 48 weeks after stopping peg-IFN			
HBcrAg <4.8 log U/ml	12.8	4.3–37.7	<0.001

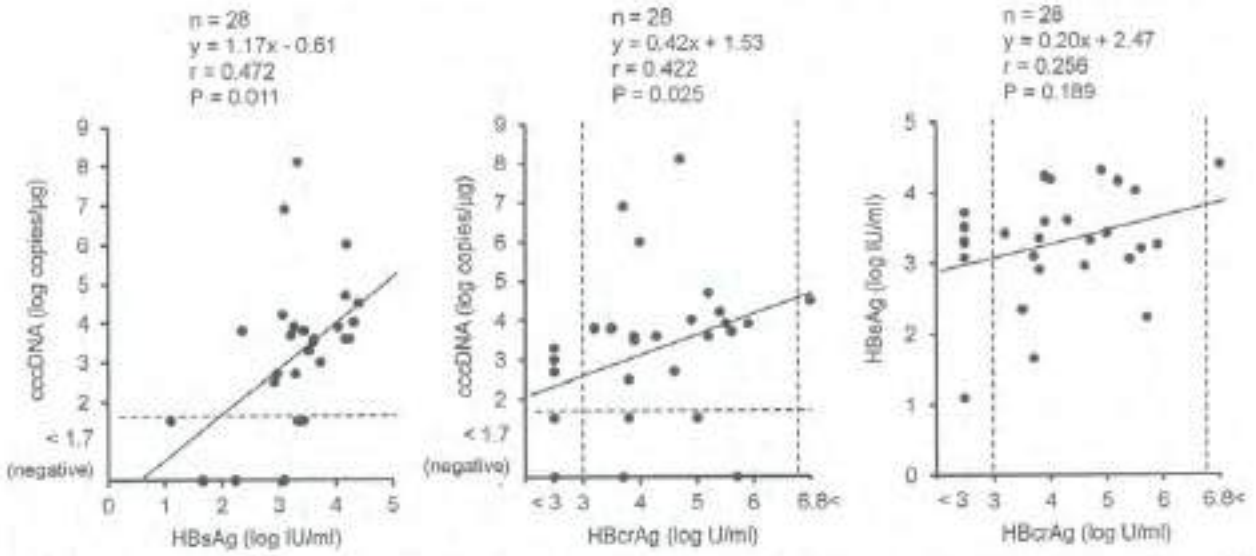

Fig. 3 Correlations among serum HBsAg, serum HBcrAg, and intrahepatic HBV cccDNA in 28 patients undergoing NUC therapy. The *vertical dashed lines* delineate the upper and lower quantitative ranges of HBcrAg. The *horizontal dashed line* indicates the lower quantitative range of HBV cccDNA

median 1.8 pg/ml, range 0.3–7.5 pg/ml) in subjects not receiving ADV. These findings were in agreement with the results described by Murata et al. [24].

Figure 3 assessed for correlations among serum HBsAg, serum HBcrAg, and intrahepatic HBV cccDNA in 28 patients receiving NUC therapy. Serum HBV DNA was suppressed to the level of signal-positive or negative in 26 (93%) patients. HBsAg and HBcrAg were both significantly correlated with HBV cccDNA, but only weakly with each other.

Discussion

NUCs and IFN are commonly used anti-HBV agents worldwide. NUCs induce a rapid reduction in serum HBV DNA and hepatitis remission in many cases. They also produce histological improvement resulting in a diminished occurrence of HCC [27]. However, it is difficult to eradicate the virus completely, and NUCs face such complications as the emergence of resistant strains and hepatitis relapse following treatment discontinuation. One reason for these problems is that while NUCs can efficiently reduce serum HBV DNA, they have virtually no effect on HBV cccDNA levels in hepatocyte nuclei, which are the origin of HBV replication. Based on this fact, the simple discontinuation of NUCs is discouraged. On the other hand, the duration of peg-IFN therapy is usually limited to 48 weeks [28, 29] and a sustained off-treatment response can be expected in some patients. Thus, the sequential administration of peg-IFN after NUCs may be useful to successfully halt NUC treatment [30]. In this context, we analyzed the efficacy of NUC/peg-IFN sequential therapy in patients with chronic hepatitis B who were treated with NUCs and searched for factors associated with a favorable response.

Responders were defined as patients who fulfilled the conditions of inactive HBV carriers with a generally benign clinical course [1, 26]. A considerable fraction of non-responders required re-administration of NUCs during follow-up after completing peg-IFN therapy. NUC resumption was decided by physicians only when the patient satisfied the established requirements [11, 12, 26], which indicated that individuals with ALT >80 IU/l and/or

HBV DNA >5.8 log copies/ml after stopping peg-IFN were likely to be non-responders. The percentage of responders was 27.4% by intention-to-treat analysis in the present study. Although this figure seems relatively low, it is noteworthy that over 80% of patients with genotype C are reported to be mostly resistant to interferon therapy [31].

Among various factors at the start of peg-IFN, lower levels of HBcrAg and HBsAg were determined as associated with a response to NUC/peg-IFN sequential therapy. HBsAg has been reported to closely relate to peg-IFN therapy outcome [32–35]. Moucari et al. analyzed HBeAg-negative hepatitis B patients who had been treated with peg-IFN for 48 weeks and concluded that an early serum HBsAg drop was strongly predictive of a sustained virological response [34]. Sonneveld et al. assessed HBeAg-positive hepatitis B patients who had received peg-IFN with or without LAM for 52 weeks and observed that patients experiencing no decline in HBsAg level from baseline at week 12 had little chance of achieving a sustained response and no possibility of an HBsAg loss [32]. HBcrAg includes antigens that are transcribed and translated from pre-core and core genes of the HBV genome, and HBeAg is a primary component of these antigens [16]. HBcrAg levels have been reported to predict the risk of hepatitis relapse after NUC discontinuation [12, 36] as well as the likelihood of developing HCC in patients under NUC therapy [37, 38]. We previously described that a combinational use of HBsAg and HBcrAg levels was useful to predict the 24-month outcome of NUC/IFN sequential therapy [39]. Martinot-Peignoux et al. also reported that HBsAg and HBcrAg levels either separately or in combination could estimate the response to peg-IFN-based precision therapy [40]. However, the above studies suffered from a retrospective design and relatively small number of patients. It was therefore meaningful that the present prospective cohort study confirmed the ability of combined HBsAg and HBcrAg levels for predicting a response to NUC/peg-IFN sequential therapy.

We witnessed that levels of both HBsAg and HBcrAg were significantly associated with that of HBV cccDNA in the liver, even under the sufficient suppression of HBV replication by NUCs. Intrahepatic HBV cccDNA is a key molecule in HBV replication whose amount is closely related to viral activity. Several reports have shown that HBV cccDNA is associated with the response to antiviral therapies using peg-IFN and NUCs [35, 41, 42]. Sung et al. analyzed HBeAg-positive hepatitis B patients who had been treated with either LAM monotherapy or a combination of peg-IFN and LAM and concluded that intrahepatic HBV cccDNA level at the end of therapy was superior to serum HBV DNA in predicting a sustained virological response [41]. Serum HBV DNA is correlated with intrahepatic HBV cccDNA and is widely used as an indicator of HBV replication activity. However, such associations may be incompatible with antiviral therapies, and especially NUC treatment, since the drugs directly hamper production of the HBV virion by inhibiting reverse transcription of pre-genomic RNA without affecting HBV cccDNA directly. As levels of serum HBsAg and HBcrAg are easier to measure than that of intrahepatic HBV cccDNA, these assays may be more suitable as surrogate markers of HBV replication activity in patients undergoing antiviral therapy. It is possible that HBsAg and HBcrAg have complimentary roles in monitoring antiviral effects because their production is regulated by alternative enhancer-promoter systems in the HBV genome. Accordingly, the levels of the two antigens showed a weak, non-significant correlation in the present study.

HBsAg and HBcrAg levels decreased in both responders and non-responders during peg-IFN administration but continued falling in responders only after stopping peg-IFN. Consequently, we presumed that the levels of HBsAg and HBcrAg at the treatment response judgment point of 48 weeks after peg-IFN cessation were closely associated with therapy response. Analysis of baseline parameters associated with low HBcrAg levels (<3.8 log U/ml) at response judgment revealed lower HBcrAg to be the sole significant factor. On the other hand, lower HBsAg, lower HBcrAg, and the use of ADV were significant baseline factors predicting decreased HBsAg levels (<2.0 log IU/ml) at response judgment. Murata et al. reported that serum IFN-λ3 level increased during ADV and TDF administration but did not with LAM and ETV in patients with chronic hepatitis B. They also showed that ADV and TDF exerted the additional pharmacological effect of IFN-λ3 upregulation, which further induced IFN-stimulated genes and resulted in a reduction of HBsAg production in a cell culture system [24]. IFN-λ3 levels at baseline were approximately ten times higher in patients with ADV treatment than in those without in our cohort. It is therefore plausible that the administration of ADV is related to HBsAg level reduction during sequential therapy. Further studies are required to clarify this notion.

In conclusion, the combinational use of HBsAg and HBcrAg levels was able to predict the response to NUC/peg-IFN sequential therapy. Decreases in these antigens during and after peg-IFN administration were closely associated with a favorable response. The use of ADV was related to higher serum IFN-λ3 and suspected to be linked to a rapid decrease in HBsAg level during sequential therapy.

Acknowledgements We thank Ms. Hiroe Banno for her secretarial assistance and Mr. Trevor Ralph for his English editorial assistance. This research is partially supported by the Research Program on

Hepatitis and the Program for Basic and Clinical Research on Hepatitis from the Ministry of Health, Labor, and Welfare of Japan as well as by the Japan Agency for Medical Research and Development (AMED).

Compliance with ethical standards

Conflict of interest Dr. Nishiguchi S. received lecture fees from Gilead Sciences and MSD; Dr. Tanaka Y. received honoraria from Bristol-Myers Squibb, FUJIREBIO, Chugai, and Glaxo Smith Kline; Dr. Kanda T. received a research Grant from MSD, AbbVie and Chugai; Dr. Okuse C. received honoraria from AbbVie, and Otsuka; Dr. Takaguchi K. received lecture fees from Bristol Meyer Squib, AbbVie, and Astra Zeneca; Dr. Hino K. received lecture fees from Bristol Meyers Squibb, Otsuka, MSD, Dainippon Sumitomo, and Gilead Sciences. Dr. Hino K. also received a research grant from Bristol Meyers Squibb; Dr. Tsuge M. received Grant/Research Support from Bristol-Myers Squibb; Dr. Chayama K. received honoraria from Dainippon Sumitomo, Otsuka, Gilead, Bristol-Myers Squibb, AbbVie, MSD, Ajinomoto, Eisai, Toray, Tanabe Mitsubishi, Chugai, Daiichi Sankyo, Takeda, and Nihon Kayaku. Dr. Chayama K. also received commercial research funding from Bristol-Myers Squibb, AbbVie, Toray, and Dainippon Sumitomo; Dr. Suzuki Y. received lecture fees from AbbVie, GK, and Bristol-Myers Squibb; Dr. Tanaka E. received honoraria from Chugai, Bristol-Myers Squibb, Glaxo Smith Kline, and Gilead Sciences.

References

1. Hoofnagle JH, Doo E, Liang TJ, et al. Management of hepatitis B: summary of a clinical research workshop. Hepatology. 2007;45:1056–75.
2. Lee WM. Hepatitis B virus infection. N Engl J Med. 1997;337:1733–45.
3. Lok AS, McMahon BJ. Chronic hepatitis B. Hepatology. 2007;45:507–39.
4. Okanoue T, Minami M. Update of research and management of hepatitis B. J Gastroenterol. 2006;41:107–18.
5. Serfaty L, Thabut D, Zoulim F, et al. Sequential treatment with lamivudine and interferon monotherapies in patients with chronic hepatitis B not responding to interferon alone: results of a pilot study. Hepatology. 2001;34:573–7.
6. Shi M, Wang RS, Zhang H, et al. Sequential treatment with lamivudine and interferon-alpha monotherapies in hepatitis B e antigen-negative Chinese patients and its suppression of lamivudine-resistant mutations. J Antimicrob Chemother. 2006;58:1031–5.
7. Manesis EK, Papatheodoridis GV, Hadziyannis SJ. A partially overlapping treatment course with lamivudine and interferon in hepatitis B e antigen-negative chronic hepatitis B. Aliment Pharmacol Ther. 2006;23:99–106.
8. Enomoto M, Nishiguchi S, Tamori A, et al. Entecavir and interferon-alpha sequential therapy in Japanese patients with hepatitis B e antigen-positive chronic hepatitis B. J Gastroenterol. 2013;48:397–404.
9. Enomoto M, Tamori A, Nishiguchi S, et al. Combination therapy with a nucleos(t)ide analogue and interferon for chronic hepatitis B: simultaneous or sequential. J Gastroenterol. 2013;48:999–1005.
10. Minami M, Okanoue T. Management of HBV infection in Japan. Hepatol Res. 2007;37:S79–82.
11. Matsumoto A, Tanaka E, Suzuki Y, et al. Combination of hepatitis B viral antigens and DNA for prediction of relapse after discontinuation of nucleos(t)ide analogs in patients with chronic hepatitis B. Hepatol Res. 2012;42:139–49.
12. Tanaka E, Matsumoto A. Guidelines for avoiding risks resulting from discontinuation of nucleoside/nucleotide analogs in patients with chronic hepatitis B. Hepatol Res. 2014;44:1–8.
13. Kumada H, Okanoue T, Onji M, et al. Guidelines for the treatment of chronic hepatitis and cirrhosis due to hepatitis B virus infection for the fiscal year 2008 in Japan. Hepatol Res. 2010;40:1–7.
14. Orito E, Ichida T, Sakugawa H, et al. Geographic distribution of hepatitis B virus (HBV) genotype in patients with chronic HBV infection in Japan. Hepatology. 2001;34:590–4.
15. Schüttler CG, Wend UC, Faupel FM, et al. Antigenic and physicochemical characterization of the 2nd International Standard for hepatitis B virus surface antigen (HBsAg). J Clin Virol. 2010;47:238–42.
16. Kimura T, Rokuhara A, Sakamoto Y, et al. Sensitive enzyme immunoassay for hepatitis B virus core-related antigens and their correlation to virus load. J Clin Microbiol. 2002;40:439–45.
17. Rossin C, Pillet A, Bali C, et al. Evaluation of the COBAS AmpliPrep-total nucleic acid isolation-COBAS TaqMan hepatitis B virus (HBV) quantitative test and comparison to the VERSANT HBV DNA 3.0 assay. J Clin Microbiol. 2006;44:1390–9.
18. Mizokami M, Nakano T, Orito E, et al. Hepatitis B virus genotype assignment using restriction fragment length polymorphism patterns. FEBS Lett. 1999;450:66–71.
19. Suzuki F, Miyakoshi H, Kobayashi M, et al. Correlation between serum hepatitis B virus core-related antigen and intrahepatic covalently closed circular DNA in chronic hepatitis B patients. J Med Virol. 2009;81:27–33.
20. Mason AL, Xu L, Guo L, et al. Molecular basis for persistent hepatitis B virus infection in the liver after clearance of serum hepatitis B surface antigen. Hepatology. 1998;27:1736–42.
21. Ito K, Higami K, Masaki N, et al. The rs8099917 polymorphism, when determined by a suitable genotyping method, is a better predictor for response to pegylated alpha interferon/ribavirin therapy in Japanese patients than other single nucleotide polymorphisms associated with interleukin-28B. J Clin Microbiol. 2011;49:1853–60.
22. Aoki Y, Sugiyama M, Murata K, et al. Association of serum IFN-lambda3 with inflammatory and fibrosis markers in patients with chronic hepatitis C virus infection. J Gastroenterol. 2015;50:894–902.
23. Sugiyama M, Kimura T, Naito S, et al. Development of specific and quantitative real-time detection PCR and immunoassays for lambda3-interferon. Hepatol Res. 2012;42:1089–99.
24. Murata K, Asano M, Matsumoto A, et al. Induction of IFN-lambda3 as an additional effect of nucleotide, not nucleoside, analogues: a new potential target for HBV infection. Gut. 2017 (**In press**).
25. Ichida F, Tsuji T, Omata M, et al. New Inuyama classification; new criteria for histological assessment of chronic hepatitis. Int Hepatol Commun. 1996;6:112–9.
26. Drafting Committee for Hepatitis Management Guidelines and the Japan Society of Hepatology. JSH guidelines for the management of hepatitis B virus infection. Hepatol Res. 2014;44(Suppl S1):1–58.
27. Papatheodoridis GV, Lampertico P, Manolakopoulos S, et al. Incidence of hepatocellular carcinoma in chronic hepatitis B patients receiving nucleos(t)ide therapy: a systematic review. J Hepatol. 2010;53:348–56.
28. Marcellin P, Lau GK, Bonino F, et al. Peginterferon alfa-2a alone, lamivudine alone, and the two in combination in patients with HBeAg-negative chronic hepatitis B. N Engl J Med. 2004;351:1206–17.
29. Lau GK, Piratvisuth T, Luo KX, et al. Peginterferon alfa-2a, lamivudine, and the combination for HBeAg-positive chronic hepatitis B. N Engl J Med. 2005;352:2682–95.

30. Kim V, Ahrens RM, Nakagawa DM, et al. Pegylated interferon alfa for chronic hepatitis B: systematic review and meta-analysis. J Viral Hepat. 2016;23:154–69.
31. Shi YH. Correlation between hepatitis B virus genotypes and clinical outcomes. Jpn J Infect Dis. 2012;65:476–82.
32. Sonneveld MJ, Rijckborst V, Boucher CA, et al. Prediction of sustained response to peginterferon alfa-2b for hepatitis B e antigen-positive chronic hepatitis B using on-treatment hepatitis B surface antigen decline. Hepatology. 2010;52:1251–7.
33. Brunetto MR, Moriconi F, Bonino F, et al. Hepatitis B virus surface antigen levels: a guide to sustained response to peginterferon alfa-2a in HBeAg-negative chronic hepatitis B. Hepatology. 2009;49:1141–50.
34. Moucari R, Mackiewicz V, Lada O, et al. Early serum HBsAg drop: a strong predictor of sustained virological response to pegylated interferon alfa-2a in HBeAg-negative patients. Hepatology. 2009;49:1151–7.
35. Chan HL, Wong VW, Tse AM, et al. Serum hepatitis B surface antigen quantitation can reflect hepatitis B virus in the liver and predict treatment response. Clin Gastroenterol Hepatol. 2007;5:1462–8.
36. Matsumoto A, Tanaka E, Minami M, et al. Low serum level of hepatitis B core-related antigen indicates unlikely reactivation of hepatitis after cessation of lamivudine therapy. Hepatol Res. 2007;37:661–6.
37. Hosaka T, Suzuki F, Kobayashi M, et al. HBcrAg is a predictor of post-treatment recurrence of hepatocellular carcinoma during antiviral therapy. Liver Int. 2010;30:1461–70.
38. Kumada T, Toyoda H, Tada T, et al. Effect of nucleos(t)ide analogue therapy on hepatocarcinogenesis in chronic hepatitis B patients: a propensity score analysis. J Hepatol. 2013;58:427–35.
39. Matsumoto A, Yotsuhashi H, Nagaoka S, et al. Factors associated with the effect of interferon-alpha sequential therapy in order to discontinue nucleoside/nucleotide analog treatment in patients with chronic hepatitis B. Hepatol Res. 2015;45:1195–202.
40. Martinot-Peignoux M, Lapalus M, Maylin S, et al. Baseline HBsAg and HBcrAg titres allow peginterferon-based 'precision medicine' in HBeAg-negative chronic hepatitis B patients. J Viral Hepat. 2016;23:905–11.
41. Sung JJ, Wong ML, Bowden S, et al. Intrahepatic hepatitis B virus covalently closed circular DNA can be a predictor of sustained response to therapy. Gastroenterology. 2005;128:1890–7.
42. Wursthorn K, Lutgehetmann M, Dandri M, et al. Peginterferon alpha-2b plus adefovir induce strong cccDNA decline and HBsAg reduction in patients with chronic hepatitis B. Hepatology. 2006;44:675–84.

Advertisement

Cochrane Colloquium Toronto 4-7 Oct Toront

Rapid-learning Health Systems

The Journal of Dermatology / Volume 44, Issue 11

Concise Communication

Nerve conduction study of lower extremities in cutaneous arteritis patients with neurological manifestations

Kenji Isahaya, Tamihiro Kawakami, Makoto Shiraishi, Hisanao Akiyama, Yasuhiro Hasegawa

First published:30 June 2017
https://doi.org/10.1111/1346-8138.13946

St.marianna@FullText

Abstract

Some patients originally diagnosed with cutaneous arteritis (CA) could develop additional disease manifestations, including peripheral neurological involvement. We evaluated the biological neurological parameters among CA patients who underwent nerve conduction studies for neurological involvement in the lower extremities. We reviewed 164 patients who were originally diagnosed with CA at our dermatology department between 2004 and 2015. Seventeen (10.4%) of the CA patients underwent further nerve conduction studies to determine their peripheral neurological manifestations, primarily in the lower extremities, in our neurology division. The frequency of low compound muscle action potential (CMAP) was significantly higher compared with that of delayed latency in both the peroneal nerve and sural nerve based on nerve conduction studies. The frequency of low CMAP was significantly higher compared with that of prolonged distal latency in both the peroneal and sural nerves. We suggest that impairment of the nerve axon pathways in the peroneal and sural nerves could result in the peripheral neurological manifestations in the lower extremities in CA patients.

Introduction

Cutaneous arteritis (CA) is a new classification under the description of single-organ vasculitis, as adopted by the 2012 Chapel Hill consensus conference.1 CA is a necrotizing vasculitis of medium-sized arteries within the skin, without the involvement of internal organs.2, 3 However, some patients originally diagnosed with CA could develop additional disease manifestations such as peripheral neurological involvement.

Polyarteritis nodosa (PAN) is a multisystem necrotizing vasculitis of medium-sized arteries characterized by involvement of the renal and visceral arteries. In PAN, very high morbidity and mortality rates characterized by fulminant deterioration or by relentless progression are associated with intermittent acute exacerbations. CA is considered as a form of PAN that is restricted to the skin, which shows a chronic relapsing benign course.[4-6] However, the definition remains controversial.

In an effort to clarify the clinical significance of neurological involvement, we evaluated the biological neurological parameters seen in nerve conduction studies among CA patients who underwent nerve conduction studies of the clinical presence of neurological involvement in their lower extremities.

Case Report

Patients

We reviewed 164 patients (48 men, 116 women; age range, 12–86 years [mean, 46.5]) seen at the Department of Dermatology, St Marianna University School of Medicine between 2004 and 2015, who were originally diagnosed with CA. These patients were diagnosed according to the Japanese criteria[3] and KAWAKAMI algorithm.[7] A diagnosis of vasculitis requires the presence of necrotizing vasculitis including fibrinoid degeneration, nuclear dust, neutrophilic infiltration and erythrocyte extravasation using skin biopsies. Antineutrophil cytoplasmic autoantibodies, including antibodies to myeloperoxidase and proteinase 3, were negative. Furthermore, none of the patients demonstrated any evidence of a coexisting malignancy, other autoimmune diseases or viral hepatitis, neither were any of the patients positive for mixed cryoglobulinemia. Some patients complained of peripheral neurological manifestations and wished to visit the Division of Neurology.

Nerve conduction studies

Skin temperatures were kept to range between 32°C and 34°C. Compound muscle action potential (CMAP) from the peroneal nerve was recorded at the extensor digitorum brevis muscle with stimulation at the ankle and knee. CMAP from the tibial nerve was recorded at the abductor hallucis muscle with stimulation at the ankle and popliteal. Sensory action potential (SNAP) from the sural nerve was recorded at the lateral malleolus with stimulation at the posterolateral side of the calf.

Statistical analysis

Differences among quantitative parameters between groups were assessed using the Mann–Whitney *U*-test. Differences among qualitative results were compared using a paired *t*-test. $P < 0.05$ was considered statistically significant. All data are expressed as means ± standard deviation.

Clinical and serological findings in 17 patients with CA who underwent nerve conduction studies

Seventeen patients with CA (six men, 11 women; mean age, 49.5 ± 13.6 years) underwent nerve conduction studies for their peripheral neurological manifestations, primarily of their lower extremities, in the Division of Neurology, St Marianna University School of Medicine. The clinical and nerve conduction study findings can be seen in Table 1. Mean onset time from cutaneous biopsy to the appearance of neurological symptoms was 38.2 ± 52.8 months. We did not find any correlation between the location of peripheral neurological manifestations and skin ulcers. Eight (47.1%) of the CA patients who underwent nerve conduction studies had skin ulcers. There was no significant clinical and neurological difference between those patients with skin ulcers and those without. We diagnosed seven (41.2%) of the CA patients who underwent nerve conduction studies with mononeuritis multiplex. There were no significant clinical or neurological differences between those seven patients and the others. Neurological symptoms in the 17 patients with CA consisted of 14 (82.4%) patients with sensory dominant abnormal sensation in the extremities and three (17.6%) with both motor and sensory dominant abnormal sensations in the extremities. There were no significant clinical and neurological differences between the sensory sensation patients only and the motor and sensory sensation patients.

Table 1. Clinical and nerve conduction study findings in 17 patients with CA

Age	Sex	Onset of neurological symptoms (months)	Presence of skin ulcer	Peripheral neurological manifestations	Presence of mononeuritis multiplex	Motor or sensory	Nerve conduction nerve)	
							CMAP (right)	CMAP (left)
							Normal; ≥2.9 mV	Normal ≥2.9 m\
49	M	48	Skin ulcer	Numbness of lower limbs and sole	None	Sensory	**0**	**0.16**
65	M	120	Skin ulcer	Irritability of lower limbs	None	Sensory	3.8	4.1
45	F	12	x	Numbness of lower limbs and sole	None	Sensory	4.6	**2.7**
61	M	60				Sensory	**1.71**	**1.6**

Bold number indicates abnormal. CA, cutaneous arteritis; CMAP, compound muscle action potential; ND, not detected; SNAP, sensory action potential.

Correlation among mediators on nerve conduction studies in the CA patients with peripheral neurological manifestations

Fifteen (88.2%) of the 17 CA patients showed low CMAP in the peroneal nerve based on nerve conduction studies. On the other hand, six (35.3%) of the 17 CA patients had a prolonged distal latency period in the peroneal nerve. The frequency of low CMAP was significantly higher compared with the frequency of prolonged distal latency in the peroneal nerve (P = 0.00062).

Among the 17 CA patients, CMAP could not be determined by nerve conduction studies for the tibial nerve due to skin ulcer in the lower extremities of one patient. We could only measure the prolonged distal latency period of the left tibial nerve but not the right tibial nerve. Four (25.0%) of the other 16 CA patients in whom the CMAP could be measured in nerve conduction studies for the tibial nerve revealed low CMAP in the tibial nerve. On the other hand, two (11.8%) of the 17 CA patients had prolonged distal latency in the tibial nerve. We found that the frequency of low CMAP was not significantly higher compared with frequency of prolonged distal latency of the tibial nerve.

In the 17 CA patients, two patients could not undergo nerve conduction studies for the sural nerve due to skin ulcers in their lower extremities. Fourteen (93.3%) of 15 CA patients who could undergo nerve conduction studies for the sural nerve showed low SNAP of the sural nerve. On the other hand, seven (46.7%) of the 15 CA patients had prolonged distal latency of the sural nerve. The frequency of low SNAP was significantly higher compared with the frequency of prolonged distal latency in the sural nerve (P = 0.0035).

We found a significantly higher frequency of low CMAP in the peroneal nerve compared with frequency in the tibial nerve (P = 0.0011). Similar trends were seen with respect to the relationship between the tibial nerve and sural nerve. The frequency of low CMAP in the sural nerve was significantly higher compared with that in the tibial nerve (P = 0.00032). There was no significant relationship associated with prolonged distal latency among the peroneal nerve, tibial nerve and sural nerve.

Discussion

Among CA patients with peripheral neurological manifestations, we found that the frequency of low CMAP and low SNAP was significantly higher compared with that of prolonged distal latency in both the peroneal nerve and sural nerve based on nerve conduction studies of the lower extremities, respectively. The low CMAP and SNAP seen in the nerve conduction

studies reflect nerve axonal degeneration and the prolonged distal latency seen is consistent with the myelin sheath pathways under nerve conduction studies. Mimouni *et al.*8 suggested that patients with medium-sized vasculitis characteristically show axonal neuropathy with spontaneous activity consistent with mononeuritis multiplex. In the present study, we found that CA patients with peripheral neurological manifestations suffered significantly damaged peroneal nerves and sural nerves in the lower extremities. Based on these findings, we suggest that impairment of the nerve axonal degeneration in the peroneal and sural nerves could produce the peripheral neurological manifestations in the lower extremities of our CA patients. Vasculitis affecting the peripheral nerves predominantly manifests as subacute and progressive mononeuritis multiplex. It is important for clinicians to recognize these findings in nerve conduction studies for earlier detection of peripheral nerve impairment and earlier neurological treatment for CA patients.

The diagnosis is often problematic because the skin manifestations and histological findings in systemic PAN and CA are identical. For many years, the question of whether CA could be seen as a distinct clinical entity or merely as an early stage of systemic PAN has remained unanswered.9 We investigated 17 (10.4%) of 164 patients with CA, and they underwent nerve conduction studies to determine the clinical presence of peripheral neurological involvement among them. The presence of nerve conduction studies for peripheral neurological manifestations may be useful for distinguishing between the two diseases. In contrast, Daoud *et al.*10 evaluated 79 patients with CA, but did not observe progression to PAN. We previously suggested the presence of antibodies against the CA-specific phosphatidylserine–prothrombin complex.11 Even with the present data, we believe that the distinction between PAN and CA could not be clearly made.

Conflict of Interest

None declared.

References

1 Jennette JC, Falk RJ, Bacon PA*et al.* 2012 revised international Chapel Hill consensus conference nomenclature of vasculitides. *Arthritis Rheum*2013; **65**: 1– 11.
Wiley Online Library | CAS | PubMed | Web of Science® | Google Scholar | St.marianna@FullText

2 Moreland LW, Ball GV. Cutaneous polyarteritis nodosa. *Am J Med*1991; **88**: 426– 430.
Crossref | PubMed | Web of Science® | Google Scholar | St.marianna@FullText

3 Nakamura T, Kanazawa N, Ikeda T*et al.* Cutaneous polyarteritis nodosa: revisiting its definition and diagnostic criteria. *Arch Dermatol Res*2009; **301**: 117– 121.
Crossref | PubMed | Web of Science® | Google Scholar | St.marianna@FullText

4 Borrie P. Cutaneous polyarteritis nodosa. *Br J Dermatol*1972; **87**: 87– 95.
Wiley Online Library | CAS | PubMed | Web of Science® | Google Scholar | St.marianna@FullText

5 Dewar CL, Bellamy N. Necrotizing mesenteric vasculitis after longstanding cutaneous polyarteritis nodosa. *J Rheumatol*1992; **19**: 1308– 1311.
CAS | PubMed | Web of Science® | Google Scholar | St.marianna@FullText

6 Thomas RH, Black MM. The wide clinical spectrum of polyarteritis nodosa with cutaneous involvement. *Clin Exp Dermatol*1983; **8**: 47– 59.
Wiley Online Library | CAS | PubMed | Web of Science® | Google Scholar | St.marianna@FullText

7 Kawakami T. New algorithm (KAWAKAMI algorithm) to diagnose primary cutaneous vasculitis. *J Dermatol*2010; **37**: 113– 124.
Wiley Online Library | CAS | PubMed | Web of Science® | Google Scholar | St.marianna@FullText

8 Mimouni D, Ng PP, Rencic *Aet al*. Cutaneous polyarteritis nodosa in patients presenting with atrophie blanche. *Br J Dermatol*2003; **148**: 789– 794.
Wiley Online Library | CAS | PubMed | Web of Science® | Google Scholar | St.marianna@FullText

9 Criado PR, Marques GF, Morita TC, de Carvalho JF. *Autoimmun Rev*2016; **15**: 558– 563.
Crossref | PubMed | Web of Science® | Google Scholar | St.marianna@FullText

10 Daoud MS, Hutton KP, Gibson LE. Cutaneous periarteritis nodosa: a clinicopathological study of 79 cases. *Br J Dermatol*1997; **136**: 706– 713.
Wiley Online Library | CAS | PubMed | Web of Science® | Google Scholar | St.marianna@FullText

11 Kawakami T, Yamazaki M, Mizoguchi M*et al*. High titer of anti-phosphatidylserine-prothrombin complex antibodies in patients with cutaneous polyarteritis nodosa. *Arthritis Rheum*2007; **57**: 1507–1513.
Wiley Online Library | CAS | PubMed | Web of Science® | Google Scholar | St.marianna@FullText

About Wiley Online Library

Privacy Policy
Terms of Use
Cookies

Sasaki et al. Cerebellum & Ataxias (2017) 4:9
DOI 10.1186/s40673-017-0068-4

Cerebellum & Ataxias

RESEARCH Open Access

Stratification of disease progression in a broad spectrum of degenerative cerebellar ataxias with a clustering method using MRI-based atrophy rates of brain structures

Rie Sasaki[†], Futaba Maki[*†], Daisuke Hara, Shigeaki Tanaka and Yasuhiro Hasegawa

Abstract

Background: The rate of disease progression differs among patients with degenerative cerebellar ataxia. The uncertain natural course in individual patients hinders clinical trials of promising treatments. In this study, we analyzed atrophy changes in brain structures with cluster analysis to find sub-groups of patients with homogenous symptom progression in a broad spectrum of degenerative cerebellar ataxias.

Methods: We examined 48 patients including 21 cases of spinocerebellar ataxia (SCA), 17 cases of the cerebellar type of multiple system atrophy (MSA-C), and 10 cases of cortical cerebellar ataxia (CCA). In all patients, at least two sets of evaluations including magnetic resonance imaging (MRI) and the International Cooperative Ataxia Rating Scale (ICARS) scoring were performed. The median number (min-max) of follow-up studies in each patient was three (2–6), and the mean follow-up period was 3.1 ± 1.6 years. The area of the corpus callosum on midsagittal images and the cerebellar volume were measured using MRI, and these values were divided by the cranial antero-posterior diameter of each patient to correct for individual head size differences as an area index (Adx) and a volume index (Vdx), respectively. The annual changes in Adx, Vdx, and ICARS score were calculated in each patient, and atrophy patterns in patients were categorized with cluster analysis.

Results: The annual atrophy rates for the corpus callosum (Adx) and cerebellum (Vdx) and symptom progression differed significantly by subtype of cerebellar ataxia ($p = 0.026$, 0.019, and 0.021, respectively). However, neither the annual atrophy rate of Adx nor Vdx was significantly correlated with the annual increase in the ICARS score. When the patients were categorized into three clusters based on the annual changes in Adx and Vdx, the annual increase in the ICARS score was significantly different among clusters (2.9 ± 1.7/year in Cluster 1, 4.8 ± 3.2/year in Cluster 2, and 8.7 ± 6.1/year in Cluster 3; $p = 0.014$).

Conclusions: The annual increase in the ICARS score can be stratified by cluster analysis based on the atrophy rates of the corpus callosum and cerebellum. Further studies are warranted to explore whether these simple MRI methods could be used for random allocation of a broad spectrum of patients with degenerative cerebellar ataxia in clinical trials.

Keywords: MRI, Cerebellar volume, Spinocerebellar degeneration, Multiple system atrophy, Corpus callosum, Spinocerebellar ataxia, Cluster analysis

* Correspondence: f2maki@marianna-u.ac.jp
[†]Equal contributors
Department of Internal Medicine, Division of Neurology, St. Marianna University School of Medicine, 2-16-1 Sugao, Miyamae, Kawasaki, Kanagawa 216-8511, Japan

BioMed Central

© The Author(s). 2017 **Open Access** This article is distributed under the terms of the Creative Commons Attribution 4.0 International License (http://creativecommons.org/licenses/by/4.0/), which permits unrestricted use, distribution, and reproduction in any medium, provided you give appropriate credit to the original author(s) and the source, provide a link to the Creative Commons license, and indicate if changes were made. The Creative Commons Public Domain Dedication waiver (http://creativecommons.org/publicdomain/zero/1.0/) applies to the data made available in this article, unless otherwise stated.

Background

Degenerative cerebellar ataxia comprises heterogeneous diseases that mainly affect the cerebellum with various degrees of pathological changes in other brain structures. Many types of neurodegenerative ataxia are inherited as autosomal dominant traits and have been named spinocerebellar ataxia (SCA) [1]. The current molecular classification of SCAs corresponds to the order in which the responsible genes were described, and more than 30 types of SCAs have been identified [2–5]. Genetic testing is available for several types of SCAs in routine clinical practice, but 10–20% of cases of dominant SCA are due to unknown mutations [6]. Moreover, the rate of progression may vary, even in patients with the same genotype [7]. Among subtypes of degenerative cerebellar ataxia, the sporadic form is the most common form in Japan (67.2%) and includes cortical cerebellar ataxia (CCA) [7, 8] and the cerebellar type of multiple system atrophy (MSA-C) [9]. A nationwide registry system of 'intractable diseases' in Japan demonstrated the prevalence of CCA in Japan has reached about 9000 [6, 7]. CCA is nearly synonymous with sporadic adult-onset ataxia of unknown origin [10] and idiopathic cerebellar ataxia [11] in Western countries. The concept of CCA as a disease is somewhat ambiguous, because the diagnosis is made by ruling out acquired and genetic causes of ataxia, as well as MSA. CCA may not be necessarily sporadic, and the differential diagnosis from MSA-C in the early stages is difficult [8].CCA may be a mixed disease entity with recessive inheritance or dominant inheritance with very low penetrance [8]. Differential diagnosis of degenerative cerebellar ataxia in the early stage remains challenging.

Since Sobue et al. reported that intravenous administration of taltirelin hydrate, a synthetic thyrotropin-releasing hormone analogue, improves ataxia in these diseases in 1983 [12], taltirelin hydrate has been the most widely used drug in Japan for the treatment of neurodegenerative ataxia. Although several drugs have been tested in randomized controlled trials, including lithium [13] and varenicline [14] in patients with SCA3 and riluzole [15] in patients with a broad spectrum of neurodegenerative ataxias, no new treatments have been approved in over 40 years. The uncertainty of the natural course in individual patients confounds determination of the most appropriate study design to verify the efficacy of promising drugs [16–18].

Cerebellar volume measurement using magnetic resonance imaging (MRI) could be used as an imaging biomarker to predict progression rates in individual patients with these diseases [1, 19–21]. We demonstrated that the cerebellar volume obtained from MRI correlates well with the International Cooperative Ataxia Rating Scale (ICARS) score in a broad spectrum of degenerative cerebellar ataxias [22]. We also confirmed that the annual atrophy rate of the cerebellar volume and the annual progression of the ICARS score were significantly different among subtypes of cerebellar degeneration [23]. However, categorizing individual symptom progression only by the atrophy rate of the cerebellum is not feasible. Atrophy of the corpus callosum, the quantitative evaluation of which is easy on midsagittal MR images, has been used as an indirect but sensitive index of cortical neuronal loss [24, 25]. Cluster analysis has been used to identify phenotypes that exhibit differences in clinical response to treatment algorithms [26–29]. The clustering method is a multivariate statistical procedure used to create homogenous groups of subjects as suggested by the data, but not defined prior to analysis. In this study, we investigated whether categorization by cluster analysis using atrophy rates of the corpus callosum and cerebellum could be used as an imaging biomarker to predict gross neurological deterioration as evaluated by ICARS.

Methods

Patients

We retrospectively analyzed a database of patients with degenerative cerebellar ataxia who were treated in our hospital from January 2004 to April 2013. A total of 111 patients were followed using a standardized follow-up protocol including MRI and neurological examination with ICARS. To determine the annual atrophy rates of the cerebellum and corpus callosum, we chose 48 patients (24 males; mean age 60.5 ± 11.3 years) from our data set using the following inclusion criteria: 1) at least two sets of evaluations including MRI and ICARS scoring were performed, 2) at least one follow-up study was performed after 18 months (allowance, ±6 months), and 3) ICARS scoring was performed on the same day of MRI examination (allowance, ±45 days).

Diagnosis of MSA-C was made in accordance with the second consensus statement including MRI findings [9]. Patients with a family history suggestive of dominant inheritance were diagnosed with SCA. After obtaining informed consent for genetic testing, patients were screened for SCA1, SCA2, SCA3, and SCA6. Further screening for SCA7, SCA8, SCA17, and SCA31 was performed in patients in whom the first screening was negative. When the other rare SCAs were suggested, further studies were performed according to the flow chart suggested by the Study Group on Ataxic Diseases and supported by the Ministry of Health, Labour and Welfare of Japan [6]. Patients with autosomal recessive cerebellar ataxia, such as Friedreich ataxia, ataxia-telangiectasia, ataxia with vitamin E deficiency, etc. were excluded. The diagnosis of CCA was made based on the following criteria: progressive ataxia; disease onset after 20 years of age; no acute or subacute disease onset; informative and

negative family history or no evidence of a causative gene mutation, at least the negative results for screening test of SCA1, SCA2, SCA3 and SCA6; no established symptomatic cause; and no possible or probable MSA [8]. For the subtype categorization of patients, we adopted their final diagnosis.

This study was conducted in a single hospital. The study protocol was approved by the St. Marianna University Bioethics Committee, and written informed consent was obtained from normal volunteers. Written informed consent from patients was waived because of the retrospective analysis of anonymized data.

Measurements of brain structures

Brain MRI was performed in all patients using a 1.5-T scanner (EXCELART®, Toshiba Medical Systems Co., Ltd., Tokyo, Japan; Achieva Nova-Dual®, Philips Electronics, Tokyo, Japan). Morphometric analyses of brain structures were performed with an image analyzer (TRI/3D–VOL; Ratoc System Engineering, Tokyo, Japan) using Digital Imaging and Communications in Medicine data from T1-weighted sagittal images (repetition time, 520 ms; echo time, 15 ms; repetition time, 520 ms; slice thickness, 4 mm; matrix, 272 × 256 sagittal sections). The corpus callosum on midsagittal images was extracted using the automated segmentation tool in the imaging analyzer (Fig. 1a), and we measured the total area (mm^2).

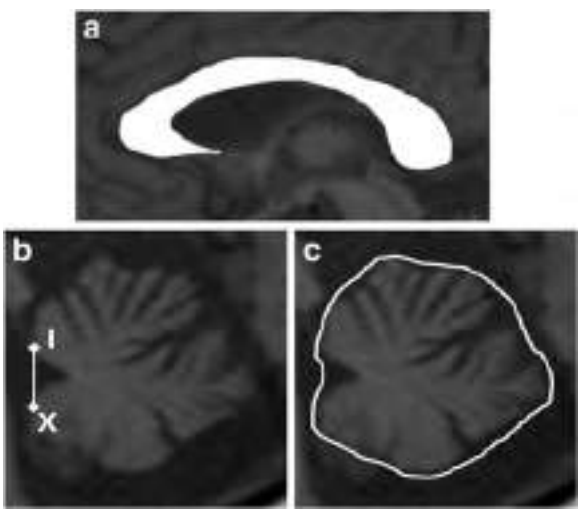

Fig. 1 Segmentation of the corpus callosum and the cerebellum on MR images**.** The corpus callosum on a midsagittal T1-weighted image was extracted with the automated segmentation tool (**a**). The total area of the corpus callosum (mm^2) was divided by the individual cranial AP diameter to correct for the individual head size differences as an area index (Adx). The cerebellum was defined as the area lateral to the line connecting the anterior lobe of the cerebellum (I segment) and cerebellar flocculus (X segment) (**b**). On the central slice, the fourth ventricle and surrounding cerebellar tissue were selected, and the cerebellum was automatically extracted using the imaging analyzer (**c**)

Cerebellar volume was measured as described elsewhere [22, 23]. Briefly, the cerebellum was defined as the area lateral to the line connecting the anterior lobe of the cerebellum and cerebellar flocculus. On the central slice, the fourth ventricle and surrounding cerebellar tissue were selected, and the cerebellum was automatically extracted using the imaging analyzer (Fig. 1b, c). The ventricle around the cerebellum, with a pixel number different than the cerebellar tissue, was separated from the cerebellum. Cerebellar volume was determined by linear interpolation from the automatically extracted cerebellar tissue area and slice thickness. In all patients, cranial antero-posterior (AP) diameter, which was defined as the distance between two points at which the skull and the anterior commissure – posterior commissure (AC-PC) line intersected, was measured. For statistical analysis, the area of the corpus callosum and the volume of the cerebellum of all patients were divided by each cranial AP diameter to correct for the individual head size differences as an area index (Adx) and a volume index (Vdx), respectively. Representative images of the cerebellum are shown in Fig. 2.

The normal values for Adx and Vdx in 30 healthy adults (mean age, 64.2 ± 18.7 years, cranial AP diameter, 18.2 ± 1.1 cm, body height, 163.5 ± 6.7 cm) were 3.80 ± 0.50 mm^2/mm and 0.65 ± 0.06 cm^3/mm, respectively. Inter-rater variability and test-retest reliability for the MRI-based morphometry were calculated using 12 randomly selected patients from our data set. Adx and Vdx were measured three times by three experienced neurologists who were blinded to the patient's clinical information. The intraclass correlation coefficients for Vdx were 0.988 for inter-rater variability and 0.994 for test-retest reliability. The annual atrophy volume and the annual progression as measured with the ICARS score were calculated using a linear regression model in each patient.

Statistical analyses

Hierarchical cluster analysis was used to define three homogeneous groups of individuals based on the annual atrophy changes in the corpus callosum (Adx) and cerebellum (Vdx) irrespective of etiology. Ward's minimum-variance clustering method was used to create the best set of clusters for each possible number of clusters. Hierarchical clustering methods were first used to assign each individual to his or her own cluster. Then, the most similar pairs of clusters (in terms of the chosen distance metric) were merged into a new cluster, resulting in one less cluster.

Data are presented as the means and standard deviation (SD), unless otherwise indicated. In each patient, Adx and Vdx at the last follow-up visit were subtracted from the initial values, and these subtracted values were divided by

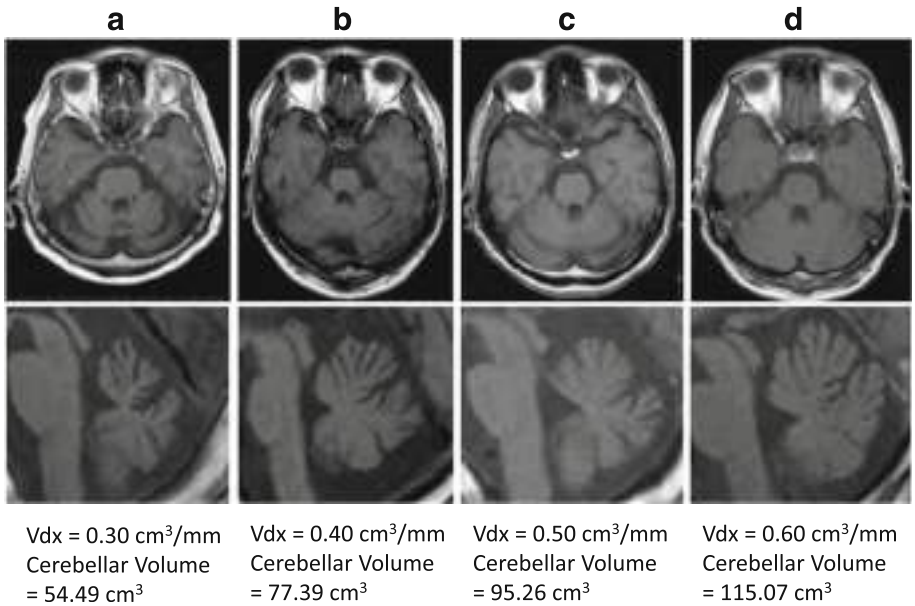

Fig. 2 Representative images of cerebellar atrophy (T1-weighted image) and Vdx (**a**-**d**). Vdx is the cerebellar volume index (Vdx = cerebellar volume/cranial AP diameter). The mean Vdx value in normal adults (mean age, 64.2 ± 18.7 years; cranial AP diameter, 18.2 ± 1.1 cm) is 0.65 ± 0.06 cm^3/mm. Vdx can be used to quantify the decrease in volume due to cerebellar atrophy, which is difficult to evaluate with visual qualitative assessment alone

the follow-up periods between the first and the last evaluation. Thus, the annual atrophy area in Adx and the annual atrophy volume in Vdx were calculated for each patient. The annual progression in the ICARS score was calculated by using the initial and last ICARS scores. Comparisons among three subgroups were made using ANOVA and the post-hoc Dunnett's test. Values of $p < 0.05$ were considered significant. All statistical analyses were performed using SPSS version 22 (IBM SPSS Statistics for Windows; IBM Corp, Armonk, NY).

Results

We examined 48 patients including 21 patients with SCA (six with SCA6, four with SCA3, three with SCA2, three with SCA1, one with SCA31, and four for whom the type of SCA was unknown), 17 patients with MSA-C, and 10 patients with CCA. Patient characteristics and annual changes in Adx, Vdx, and the ICARS score are shown in Table 1. A total of 169 follow-up studies were performed in these patients. The median number (min-max) of follow-up studies was three (2–6). The mean follow-up period (min-max) was 3.1 ± 1.6 (1.25–7.58) years. The mean age at symptom onset and the age at entry into the study were younger for SCA than the other types (p = 0.005 and 0.046, respectively). The mean interval between onset and study entry for MSA-C was the shortest (p = 0.004). We found no significant difference in the ICARS score at the first evaluation among patients with SCA, MSA-C, and CCA. Both the annual atrophy of the corpus callosum area (Adx) and the cerebellar volume (Vdx) were highest in MSA-C (p = 0.026 and 0.019, respectively). The annual increase in the ICARS score was also highest in MSA-C (9.8 ± 6.1 points/year, p = 0.021). Serial changes in the ICARS score of individual patients were plotted against years after symptom onset in Fig. 3. Neither the annual atrophy rate of Adx nor Vdx was significantly correlated with the annual increase in the ICARS score.

The annual callosal (Adx) atrophy was plotted against the annual cerebellar volume (Vdx) atrophy as a scattergram in Fig. 4. Based on these variables, 48 patients were categorized into three clusters with cluster analysis. Patient characteristics according to these clusters are shown in Table 2. The mean age at entry was similar among clusters. Frequencies of SCA, MSA-C, and CCA were significantly different among clusters (p = 0.007). The percent of patients with MSA-C was higher in Clusters 2 and 3. The annual atrophy of the corpus callosum (Adx) and cerebellum (Vdx) were significantly different among clusters (p = 0.001 for both; Table 2). The annual increases in the ICARS score were 2.9 ± 1.7 in Cluster 1, 4.8 ± 3.2 in Cluster 2, and 8.7 ± 6.1 in Cluster 3 (p = 0.014, Fig. 4).

Discussion

Designing clinical trials to treat degenerative cerebellar ataxia has been challenging because differential diagnosis is usually difficult in the early stage when treatment would be most effective, and the rate of progression may vary, even in patients with the same clinical subtype or the same genotype [7]. Our study demonstrated that symptom progression significantly differed by subtype of

Table 1 Patient characteristics and annual atrophy changes in the corpus callosum and cerebellum

	Total (n = 48)	SCA (n = 21)	MSA-C (n = 17)	CCA (n = 10)	p value
Age at onset (years)	52.6 ± 12.5	46.2 ± 13.1*	57.5 ± 10.0	57.6 ± 9.2	0.005
Age at study entry (years)	60.5 ± 11.3	56.6 ± 12.5*	61.4 ± 9.4	67.1 ± 9.0	0.046
Male (%)	50%	62%	47%	30%	0.241
Body height (cm)	159.3 ± 9.0	160.3 ± 9.2	163.0 ± 8.0	154.7 ± 8.2	0.124
AP diameter of the cranium (mm)	181.4 ± 8.6	180.6 ± 8.4	185.0 ± 6.3	177.2 ± 10.7	0.061
Follow-up period (years)	3.1 ± 1.6	3.1 ± 1.7	2.7 ± 1.1	3.6 ± 1.8	0.522
Follow-up period (min-max)	(1.25–7.58)	(1.50–7.58)	(1.25–4.67)	(1.25–6.00)	
Number of follow-up studies, median (min-max)	3 (2–6)	3 (2–6)	3 (2–6)	4 (2–6)	0.083
Interval between onset and the first evaluation (years)	8.0 ± 6.4	10.4 ± 7.3	4.0 ± 3.3*	9.4 ± 5.3	0.004
Interval between the first and last evaluation (years)	2.6 ± 1.5	2.6 ± 1.6	2.2 ± 1.3	3.1 ± 1.6	0.308
ICARS score at the first visit	35.5 ± 16.5	36.7 ± 12.9	35.8 ± 23.0	33.2 ± 14.0	0.871
Initial corpus callosum area (mm^2)	598.2 ± 79.2	575.2 ± 80.6	657.9 ± 84.9	587.0 ± 47.8	0.042
Initial corpus callosum area index (Adx)	3.38 ± 0.45	3.33 ± 0.50	3.46 ± 0.47	3.32 ± 0.26	0.622
Annual atrophy area in Adx	−0.11 ± 0.08	−0.09 ± 0.07	−0.15 ± 0.10	−0.08 ± 0.05	0.026
Initial cerebellar volume (cm^3)	84.9 ± 13.7	88.1 ± 12.7	85.5 ± 8.8	78.4 ± 17.9	0.276
Initial cerebellar volume index (Vdx)	0.47 ± 0.09	0.48 ± 0.08	0.45 ± 0.09	0.47 ± 0.11	0.725
Annual atrophy volume in Vdx	−0.04 ± 0.02	−0.02 ± 0.02	−0.04 ± 0.02†	−0.01 ± 0.03	0.019
Annual increase in ICARS score	4.4 ± 4.5	3.5 ± 2.9	9.8 ± 6.1*	2.9 ± 2.8	0.021

*$p < 0.05$ vs. the other two subtypes (post-hoc analysis), †$p < 0.05$ vs. CCA (post-hoc analysis)

cerebellar ataxia, especially both the annual cerebellar/corpus callosum atrophy rating and increase in ICARS score were highest in MSA-C patients. However, the standard deviations for these values were relatively large, even in the same subtype. Schmitz-Hubsch et al. reported that 250 patients per group were required to detect a 50% reduction in disease progression as evaluated with the Scale for Assessment and Rating of Ataxia (SARA) in a two-arm trial with the outcome measured within 1 year, implying that the sample size estimate was still large, even in patients with genetically proven etiology [30]. Detailed characterization of phenotypes of

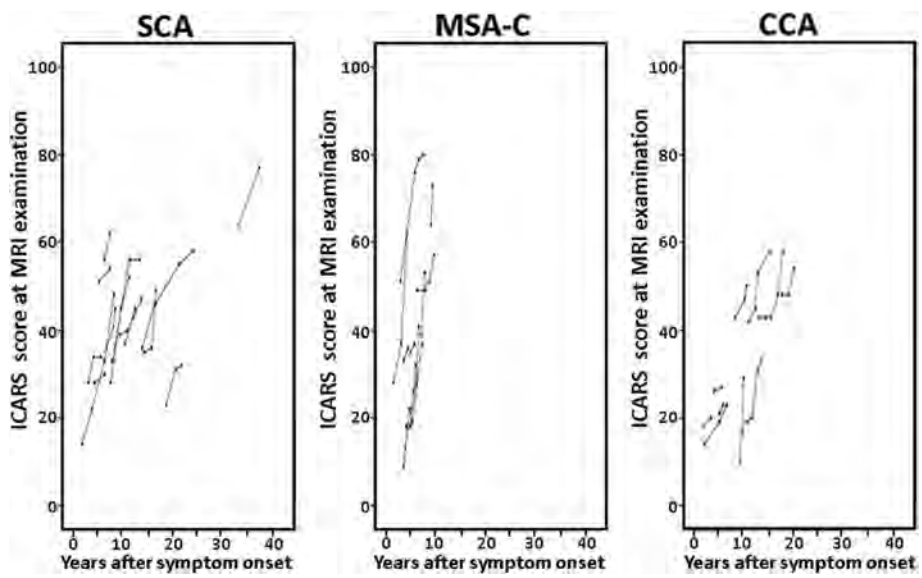

Fig. 3 Serial changes in the ICARS score of individual patients by subtype of degenerative cerebellar ataxia. The median number (min-max) of follow-up studies was three (2–6). The mean follow-up period (min-max) was 3.1 ± 1.6 (1.25–7.58) years

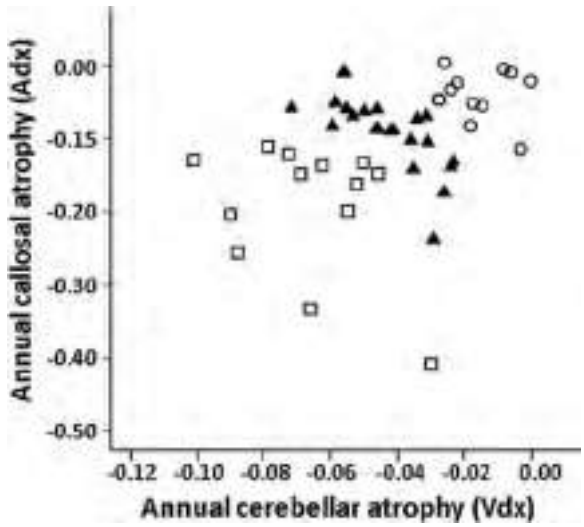

Fig. 4 Categorization of patients by cluster analysis. Based on the annual atrophy rates of corpus callosum (Adx) and cerebellum (Vdx), patients were classified into three clusters (○: cluster 1, ▲: cluster 2, □: cluster 3)

degenerative cerebellar ataxia is essential for identification of responder populations to allow medical intervention. Our study is the first to explore different subtypes of disease progression through cluster analysis in an attempt to overcome this sample size problem.

MRI-based cerebellar volume measurement has been proposed as an imaging biomarker to predict differences in progression rates in these diseases [1, 19–21]. The relationship between MRI-based cerebellar volume measurements and the SARA score has been extensively studied in several types of SCA [1]. However, MRI-based cerebellar volume measurements have never been established as a stratification tool to categorize disease progression. Recently, we demonstrated that the annual atrophy rate of the cerebellar volume and the annual progression of the ICARS score are significantly different among subtypes of cerebellar degeneration, but categorizing individual symptom progression only with the atrophy rate of the cerebellum is not feasible [22, 23]. Our current study demonstrated that cluster analysis based on the annual atrophy rates of the corpus callosum and cerebellum successfully categorized the difference in disease progression in a broad spectrum of degenerative cerebellar ataxias. This simple MRI method may be useful as a stratification tool during the run-in period of clinical trials.

Table 2 Patient characteristics by clusters

	Total (n = 48)	Cluster 1 (n = 12)	Cluster 2 (n = 22)	Cluster 3 (n = 14)	p value
Age at the first MRI (years)	60.5 ± 11.3	66.3 ± 8.5	60.4 ± 12.0	56.0 ± 10.6	0.088
Sex (Male/Female)	24/24	7/5	8/14	9/5	0.211
Diagnosis					
SCA, n (%)	21 (43.8)	6 (50.0)	11 (50)	4 (28.6)	0.007
SCA1	3	0	3	0	
SCA2	3	1	1	1	
SCA3	4	0	1	3	
SCA6	6	2	4	0	
SCA31	1	1	0	0	
SCA (unknown)	4	2	2	0	
MSA-C, n (%)	17 (35.4)	0 (0.0)	9 (40.9)	8 (57.1)	
CCA, n (%)	10 (20.8)	6 (50.0)	2 (9.1)	2 (14.3)	
ICARS score at the first visit	35.5 ± 16.5	39.1 ± 7.4	35.2 ± 22.2	30.0 ± 16.1	0.464
Initial cerebellar volume index (Vdx)	0.47 ± 0.09	0.45 ± 0.08	0.45 ± 0.10	0.50 ± 0.07	0.275
Annual atrophy volume in Vdx	−0.04 ± 0.02	0.02 ± 0.01*	−0.04 ± 0.01	−0.07 ± 0.02	0.001
Initial callosal area index (Adx)	3.38 ± 0.45	3.13 ± 0.39	3.53 ± 0.37‡	3.28 ± 0.46	0.011
Annual atrophy area in Adx	−0.11 ± 0.08	−0.04 ± 0.03†	−0.10 ± 0.05†	−0.19 ± 0.09†	0.001
Annual increase in ICARS score	4.4 ± 4.5	2.9 ± 1.7	4.8 ± 3.2	8.7 ± 6.1	0.014

Vdx cerebellar volume index, *ICARS* International Cooperative Ataxia Rating Scale
*Cluster 1 vs. Cluster 2, $p < 0.05$, Cluster 1 vs. Cluster 3, $p < 0.05$
‡Cluster 1 vs. Cluster 2, $p < 0.05$
†Cluster 1 vs. Cluster 2, $p < 0.05$, Cluster 1 vs. Cluster 3, $p < 0.05$, Cluster 2 vs. Cluster 3, $p < 0.05$ (post-hoc Dunnett's test)

We adopted the ICARS scoring system, a validated, 100-point ordinal scale (higher scores indicate greater ataxia). ICARS scoring is sensitive across a range of ataxia severities, from very mild to severe, and the inter-rater reliability is very high [31]. However, ceiling effects have been reported in more advanced stages of disability with an ICARS sum score above 60 [32]. As shown in Fig. 3, the ICARS score was similarly increased in all patients, and an initial ICARS score above 60 was found only in two patients. A strength of our study was the long follow-up period. Because of the gradual progression of this disease, cluster analysis may not sensitive enough to detect the difference in progression speed in a short period. Our study suggests that follow-up of around 18 months may be feasible for stratifying patients with different progression speeds.

Our study has some limitations. First, our study was a retrospective analysis using longitudinal follow-up data. Brain MRI and ICARS scores were assessed around the same time, but the study period was not established beforehand, and no prospective data were collected. Therefore, the follow-up periods and number of examinations differed among patients. Second, we did not use the initial diagnosis but the final diagnosis, and the age of onset was based on the medical history given by each patient. Third, we retrospectively analyzed 2D MRI data with 4-mm slice thickness obtained by routine examination. Nowadays, high-resolution 3D MR imaging can be easily performed, and several sophisticated MRI methods have been developed for the measurement of cerebellar volume [33–35]. In designing clinical trials, much more sensitive MRI methods than used in this study could be selected to detect changes in atrophy.

Conclusions

Our study is the first to demonstrate the utility of cluster analysis based on the atrophy rates of the corpus callosum and cerebellum to categorize gross neurological deterioration as evaluated by ICARS. Further studies are warranted to explore whether these simple MRI methods could be used for random allocation of patients with a broad spectrum of degenerative cerebellar ataxias in clinical trials, for example, by setting up a run-in phase.

Abbreviations

AC-PC line: Anterior commissure-posterior commissure line; AP: Antero-posterior; CCA: Cortical cerebellar atrophy; ICARS: International cooperative ataxia rating scale; MRI: Magnetic resonance imaging; MSA: Multiple system atrophy; MSA-C: Multiple system atrophy, especially the cerebellar type; SARA: Scale for the assessment and rating of ataxia; SCA: Spinocerebellar ataxia

Acknowledgements

None.

Funding

The authors declare that they have no financial competing interests.

Availability of data and materials

The datasets analyzed for the current study are available from the corresponding author upon reasonable request.

Authors' contributions

SR and FM contributed to collection and analysis of data and drafted the manuscript. FM, DH, and ST contributed to measurement of the MRI-based length, area, and volume of intracranial structures. YH contributed to revision of the manuscript and supervised this. All authors have read and approved the final manuscript.

Ethics approval and consent to participate

The study protocol was approved by the St. Marianna University Bioethics Committee (committee's reference number: 2816), and written informed consent was obtained from normal volunteers. Written informed consent from patients was waived because of the retrospective analysis of anonymized data.

Consent for publication

Not applicable.

Competing interests

The authors declare that they have no competing interests.

Publisher's Note

Springer Nature remains neutral with regard to jurisdictional claims in published maps and institutional affiliations.

Received: 17 May 2017 Accepted: 21 June 2017
Published online: 29 June 2017

References

1. Reetz K, Costa AS, Mirzazade S, Lehmann A, Juzek A, Rakowicz M, et al. Genotype-specific patterns of atrophy progression are more sensitive than clinical decline in SCA1, SCA3 and SCA6. Brain. 2013;136:905–17.
2. Kawaguchi Y, Okamoto T, Taniwaki M, Aizawa M, Inoue M, Katayama S, et al. CAG expansions in a novel gene for Machado-Joseph disease at chromosome 14q32.1. Nat Genet. 1994;8:221–8.
3. Paulson HL. The spinocerebellar ataxias. J Neuroophthalmol. 2009;29:227–37.
4. Riess O, Schols L, Bottger H, Nolte D, Vieira-Saecker AM, Schimming C, et al. SCA6 is caused by moderate CAG expansion in the alpha1A-voltage-dependent calcium channel gene. Hum Mol Genet. 1997;6:1289–93.
5. Schols L, Bauer P, Schmidt T, Schulte T, Riess O. Autosomal dominant cerebellar ataxias: clinical features, genetics, and pathogenesis. Lancet Neurol. 2004;3:291–304.
6. Japan intractable disease information center. http://www.nanbyou.or.jp/. Accessed 10 May 2017.
7. Tsuji S, Onodera O, Goto J, Nishizawa M. Sporadic ataxias in Japan–a population-based epidemiological study. Cerebellum. 2008;7:189–97.
8. Klockgether T. Sporadic adult-onset ataxia of unknown etiology. In: Subramony SH, Dürr A, editors. Handbook of clinical neurology, ataxic disorders, vol. 3rd. 103rd ed. Edinburgh: Elsevier; 2012. p. 253–62.
9. Gilman S, Wenning GK, Low PA, Brooks DJ, Mathias CJ, Trojanowski JQ, et al. Second consensus statement on the diagnosis of multiple system atrophy. Neurology. 2008;71:670–6.
10. Abele M, Bürk K, Schöls L, Schwartz S, Besenthal I, Dichgans J, et al. The aetiology of sporadic adult-onset ataxia. Brain. 2002;125:961–8.
11. Burk K, Globas C, Wahl T, Buhring U, Dietz K, Zuhlke C, et al. MRI-based volumetric differentiation of sporadic cerebellar ataxia. Brain. 2004;127:175–81.
12. Sobue I, Takayanagi T, Nakanishi T, Tsubaki T, Uono M, Kinoshita M, et al. Controlled trial of thyrotropin releasing hormone tartrate in ataxia of spinocerebellar degenerations. J Neurol Sci. 1983;61:235–48.
13. Saute JA, de Castilhos RM, Monte TL, Schumacher-Schuh AF, Donis KC, D'Avila R, et al. A randomized, phase 2 clinical trial of lithium carbonate in Machado-Joseph disease. Mov Disord. 2014;29:568–73.
14. Zesiewicz TA, Greenstein PE, Sullivan KL, Wecker L, Miller A, Jahan I, et al. A randomized trial of varenicline (Chantix) for the treatment of spinocerebellar ataxia type 3. Neurology. 2012;78:545–50.
15. Ristori G, Romano S, Visconti A, Cannoni S, Spadaro M, Frontali M, et al. Riluzole in cerebellar ataxia: a randomized, double-blind, placebo-controlled pilot trial. Neurology. 2010;74:839–45.

16. Biaggioni I, Freeman R, Mathias CJ, Low P, Hewitt LA, Kaufmann H. Randomized withdrawal study of patients with symptomatic neurogenic orthostatic hypotension responsive to droxidopa. Hypertension. 2015;65:101–7.
17. Poewe W, Seppi K, Fitzer-Attas CJ, Wenning GK, Gilman S, Low PA, et al. Efficacy of rasagiline in patients with the parkinsonian variant of multiple system atrophy: a randomised, placebo-controlled trial. Lancet Neurol. 2015; 14:145–52.
18. Lee PH, Lee JE, Kim HS, Song SK, Lee HS, Nam HS, et al. A randomized trial of mesenchymal stem cells in multiple system atrophy. Ann Neurol. 2012;72:32–40.
19. Klockgether T, Skalej M, Wedekind D, Luft AR, Welte D, Schulz JB, et al. Autosomal dominant cerebellar ataxia type I. MRI-based volumetry of posterior fossa structures and basal ganglia in spinocerebellar ataxia types 1, 2 and 3. Brain. 1998;121:1687–93.
20. Eichler L, Bellenberg B, Hahn HK, Koster O, Schols L, Lukas C. Quantitative assessment of brain stem and cerebellar atrophy in spinocerebellar ataxia types 3 and 6: impact on clinical status. AJNR Am J Neuroradiol. 2011;32: 890–7.
21. Schulz JB, Skalej M, Wedekind D, Luft AR, Abele M, Voigt K, et al. Magnetic resonance imaging-based volumetry differentiates idiopathic Parkinson's syndrome from multiple system atrophy and progressive supranuclear palsy. Ann Neurol. 1999;45:65–74.
22. Hara D, Maki F, Tanaka S, Sasaki R, Hasegawa Y. MRI-based cerebellar volume measurements correlate with the International cooperative ataxia rating scale score in patients with spinocerebellar degeneration or multiple system atrophy. Cerebellum Ataxias. 2016;3:14.
23. Tanaka S, Maki F, Hara D, Sasaki R, Hasegawa Y. MRI-based annual Cerebellar volume atrophy rate as a biomarker of disease progression in patient with Cerebellar degeneration. J St Marianna Univ. 2016;7:117–24.
24. Di Paola M, Spalletta G, Caltagirone C. In vivo structural neuroanatomy of corpus callosum in Alzheimer's disease and mild cognitive impairment using different MRI techniques: a review. J Alzheimers Dis. 2010;20:67–95.
25. Yamauchi H, Fukuyama H, Nagahama Y, Katsumi Y, Hayashi T, Oyanagi C, et al. Comparison of the pattern of atrophy of the corpus callosum in frontotemporal dementia, progressive supranuclear palsy, and Alzheimer's disease. J Neurol Neurosurg Psychiatry. 2000;69:623–9.
26. Feighner JP, Sverdlov L, Nicolau G, Noble JF. Cluster analysis of clinical data to identify subtypes within a study population following treatment with a new pentapeptide antidepressant. Int J Neuropsychopharmacol. 2000;3:237–42.
27. Ortega H, Li H, Suruki R, Albers F, Gordon D, Yancey S. Cluster analysis and characterization of response to mepolizumab. A step closer to personalized medicine for patients with severe asthma. Ann Am Thorac Soc. 2014;11: 1011–7.
28. Vollert J, Maier C, Attal N, Bennett DLH, Bouhassira D, Enax-Krumova EK, et al. Stratifying patients with peripheral neuropathic pain based on sensory profiles: algorithm and sample size recommendations. Pain. 2017;7 [Epub ahead of print]
29. Ilmarinen P, Tuomisto LE, Niemelä O, Tommola M, Haanpää J, Kankaanranta H. Cluster analysis on longitudinal data of patients with adult-onset asthma. J Allergy Clin Immunol Pract. 2017; doi:10.1016/j.jaip.2017.01.027.
30. Schmitz-Hubsch T, du Montcel ST, Baliko L, Berciano J, Boesch S, Depondt C, et al. Scale for the assessment and rating of ataxia: development of a new clinical scale. Neurology. 2006;66:1717–20.
31. Storey E, Tuck K, Hester R, Hughes A, Churchyard A. Inter-rater reliability of the International cooperative ataxia rating scale (ICARS). Mov Disord. 2004; 19:190–2.
32. Metz G, Coppard N, Cooper JM, Delatycki MB, Durr A, Di Prospero NA, et al. Rating disease progression of Friedreich's ataxia by the International cooperative ataxia rating scale: analysis of a 603-patient database. Brain. 2013;136:259–68.
33. Kamitani T, Kuroiwa Y, Wang L, Li M, Suzuki Y, Takahashi T, et al. Visual event-related potential changes in two subtypes of multiple system atrophy, MSA-C and MSA-P. J Neurol. 2002;249:975–82.
34. Papp MI, Lantos PL. The distribution of oligodendroglial inclusions in multiple system atrophy and its relevance to clinical symptomatology. Brain. 1994;117:235–43.
35. Hauser TK, Luft A, Skalej M, Nagele T, Kircher TT, Leube DT, et al. Visualization and quantification of disease progression in multiple system atrophy. Mov Disord. 2006;21:1674–81.

Submit your next manuscript to BioMed Central and we will help you at every step:

- We accept pre-submission inquiries
- Our selector tool helps you to find the most relevant journal
- We provide round the clock customer support
- Convenient online submission
- Thorough peer review
- Inclusion in PubMed and all major indexing services
- Maximum visibility for your research

Submit your manuscript at
www.biomedcentral.com/submit

BioMed Central

J Med Ultrasonics (2017) 44:207–210
DOI 10.1007/s10396-016-0747-4

CASE REPORT

A case in which contrast-enhanced transoral carotid ultrasonography was useful for pre- and post-procedural evaluation in carotid artery stenting

Yuta Hagiwara[1] · Tomohide Yoshie[2] · Takahiro Shimizu[1] · Hana Ogura[1] · Takayuki Fukano[2] · Tatsuro Takada[2] · Toshihiro Ueda[2] · Yasuhiro Hasegawa[1]

Received: 19 May 2016 / Accepted: 2 September 2016 / Published online: 11 October 2016
© The Japan Society of Ultrasonics in Medicine 2016

Abstract Contrast-enhanced transoral carotid ultrasonography (CETOCU) is a novel examination modality that is superior to other modalities in the cases of pseudo-occlusion with severe arteriosclerotic stenosis of the distal internal carotid artery (ICA), and is also useful for noninvasively evaluating changes over time in the vessel distal to the stent following carotid artery stenting (CAS). We report a case of a patient who we evaluated with CETOCU for a pseudo-occlusive ICA before and after CAS.

Keywords Contrast-enhanced transoral carotid ultrasonography · Carotid artery stenting · ICA pseudo-occlusion

Introduction

Transoral carotid ultrasonography (TOCU) is a modality proposed by Yasaka et al. for imaging the extracranial internal carotid artery (ICA), which is not possible with the conventional carotid ultrasonography [1]. In TOCU, a probe intended for transrectal or transvaginal use is inserted into the mouth and pressed against the wall of the left or right pharynx to image the distal ICA. As imaging to the second cervical vertebra is possible, TOCU is useful for evaluating ICA dissection and other extensive lesions of the ICAs [2, 3]. We herein report our use of contrast-enhanced TOCU (CETOCU) with the contrast agent Sonazoid® for the assessment of the extracranial ICA before and after carotid artery stenting (CAS). CETOCU was found to be useful for diagnosing pseudo-occlusion and for evaluation distal to the stent, which is difficult with other modalities.

Case report

Patient

A 72-year-old man.

Medical history

Hypertension, diabetes mellitus, dyslipidemia.

Course

The patient presented cerebral infarcts caused by complete occlusion of the right ICA. In the absence of sequelae, the patient was sent home and followed up on an outpatient basis. However, magnetic resonance angiography performed 2 months later revealed recanalization of the right ICA. The patient was admitted for CAS of the affected area.

Carotid ultrasonography showed severe stenosis of the right ICA (85 % according to North American Symptomatic Carotid Endarterectomy Trials method) with flow of 450 cm/s in the most constricted area. Cerebral

Electronic supplementary material The online version of this article (doi:10.1007/s10396-016-0747-4) contains supplementary material, which is available to authorized users.

✉ Yuta Hagiwara
shinnai@marianna-u.ac.jp

[1] Division of Neurology, Department of Internal Medicine, St. Marianna University School of Medicine, 2-16-1, Sugao, Miyamae, Kawasaki 216-8511, Japan

[2] Department of Strokology, Stroke Center, St. Marianna University Toyoko Hospital, Kawasaki, Japan

angiography showed severe stenosis at the origin of the right ICA, with distal imaging showing a flow delay suggestive of pseudo-occlusion (Fig. 1a). We performed TOCU, because cerebral angiography was unable to clarify whether the distal end of the stenosis represented an elongated arteriosclerotic lesion or vascular collapse. However, we were unable to evaluate either the inside of the vessel lumen in detail on B-mode TOCU (Fig. 2a, b), or the flow of ICA on color Doppler TOCU because of the extremely slow flow through the narrowed, collapsed vessel. Subsequent intravenous injection of Sonazoid® contrast agent allowed clear imaging of the ICA. This contrast-enhanced TOCU showed, in addition to ICA collapse due to vessel narrowing, that plaque stenosis extended further than indicated on cerebral angiography (Fig. 3a).

We performed CAS using the Parodi anti-embolic system, placing a stent (Precise 7 × 30 mm; Johnson & Johnson, Cordis, Miami, FL) after balloon predilation. We did not perform postdilation. As pre-stenting CETOCU showed the diameter of the distal ICA to be much narrower than that of the common carotid artery, we deployed and placed the stent so as to cover only the ICA. The procedure was uneventful and resulted in a small amount of debris, but post-procedural angiography showed the step between the distal end of the stent and the de-collapsed vessel (Fig. 1b). No further procedures were performed, because distal flow was considered to have improved sufficiently after stenting.

CETOCU was again performed post-procedurally to closely evaluate the vessel distal to the stent. As a result of de-collapsing, the diameter of the ICA distal to the stented region was increased compared to preoperatively, and no flow problems were apparent. Although no protrusions were present within the stent, a step at the stent-vessel border indicated the presence of remnant plaque around the vessel (Fig. 3b). Pre-stenting CETOCU (Fig. 3a) had shown plaque in this area. The selected stent was clearly too short to cover the entire lesion, but we decided against further intervention, because the stenosis of less than 50 % and satisfactory intraluminal flow indicated a low risk of obstruction.

Discussion

The ability of TOCU to image the extracranial ICA to a degree not possible with the conventional carotid ultrasonography makes this modality useful for diagnosing and following extracranial ICA dissection [2, 3] and for perioperative evaluation of carotid endarterectomy (CEA) [4–6]. TOCU allows the evaluation of the extracranial ICA, which is not possible on the conventional carotid artery ultrasonography. CETOCU, which is essentially TOCU performed with the ultrasonography contrast agent Sonazoid®, produces clearer intraluminal imaging, as the contrast agent flows through the lumen. CETOCU is also

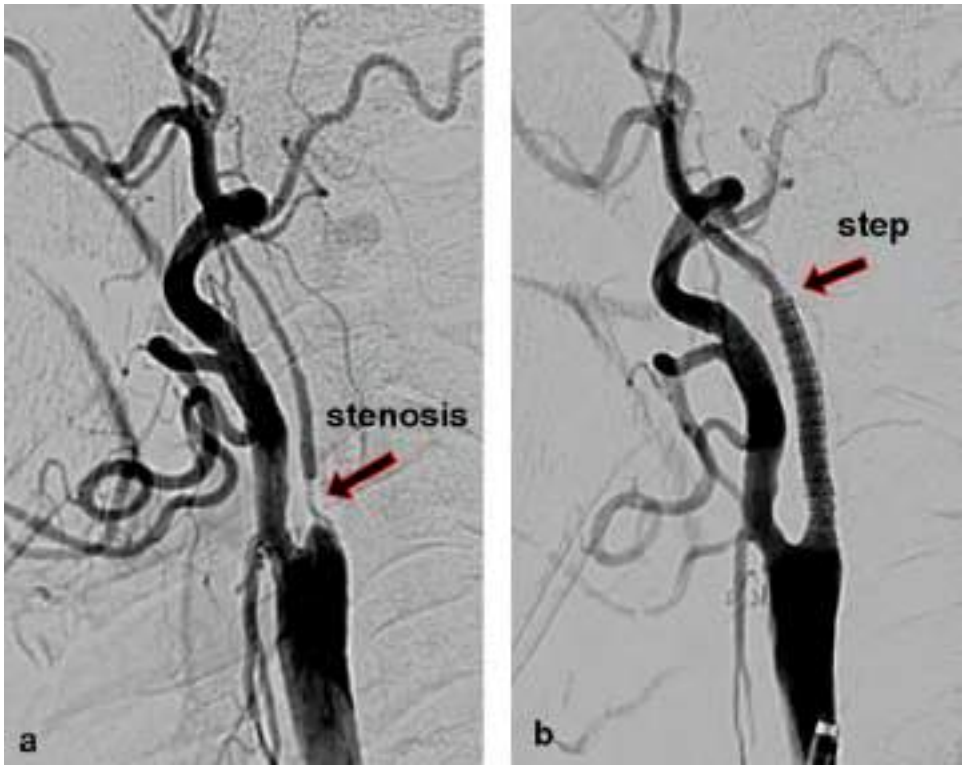

Fig. 1 **a** Right carotid angiography before carotid stenting. Severe stenosis is present at the origin of the right ICA. The distal vessel is collapsed and shows delayed blood flow, representing pseudo-occlusion. **b** Right carotid angiography after carotid stenting. Stenting has expanded the stenosis at the origin of the right ICA, but a step is evident between the collapsed distal ICA and stent. The diameter of the previously collapsed distal ICA is relatively large, but remains too small for the collapse to be completely corrected at this stage

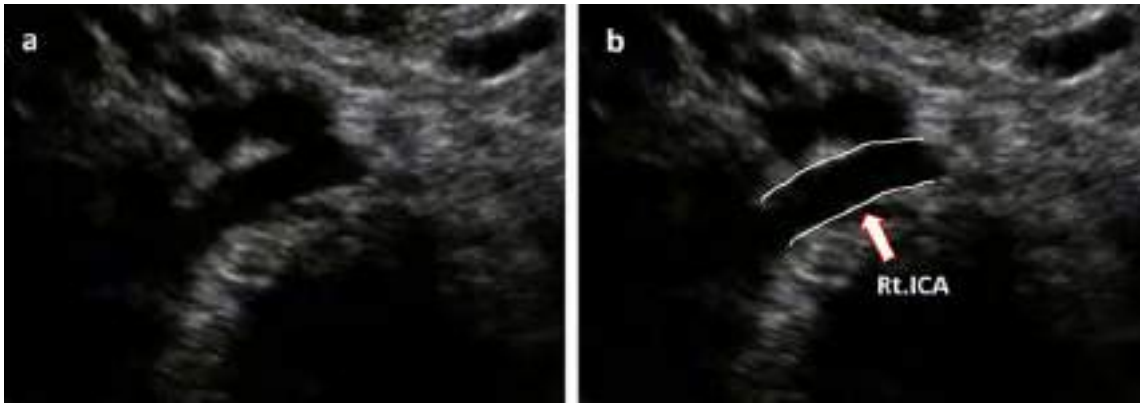

Fig. 2 **a** Conventional transoral carotid ultrasonography (TOCU) before carotid stenting. TOCU shows a collapsed ICA, but the plaque in the vascular lumen is not evident. **b** The schematic image of **a**

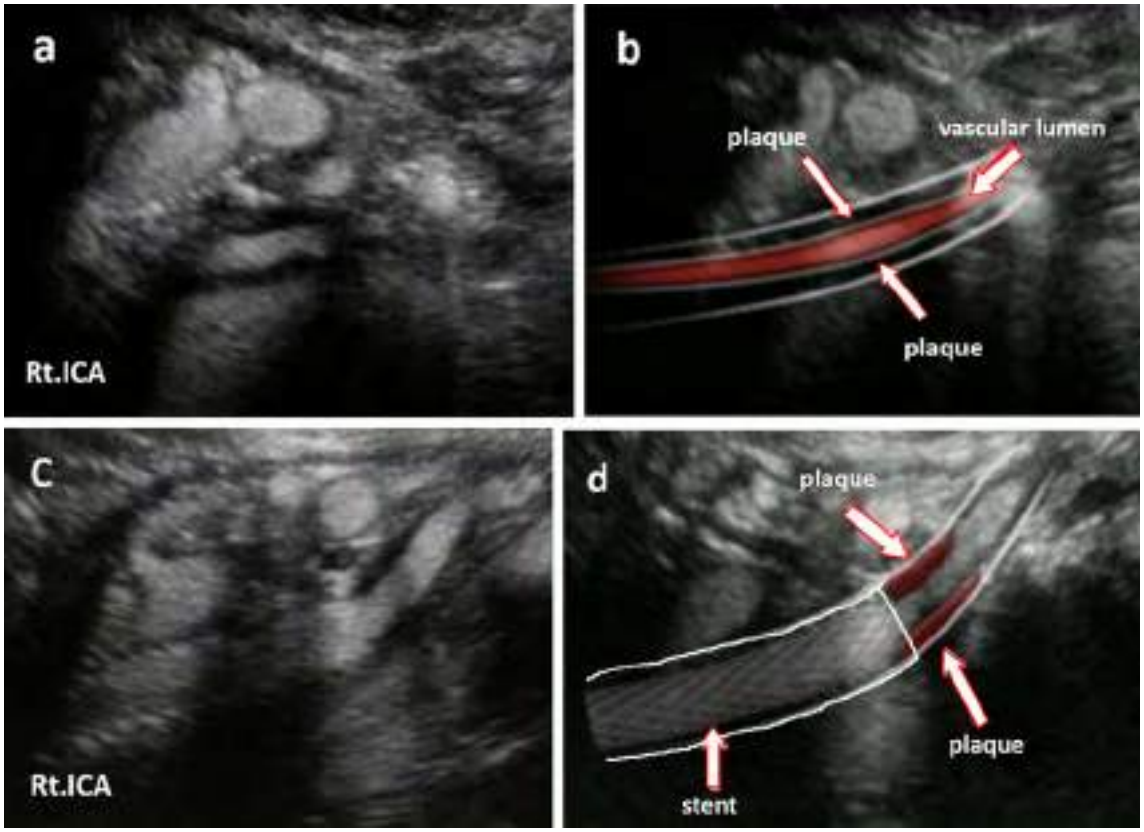

Fig. 3 Contrast-enhanced transoral carotid ultrasonography (CETOCU) was performed using a Xario system (Toshiba Medical Systems, Tokyo, Japan) equipped with a PVT-661VT 3–9 MHz endovaginal probe (Toshiba Medical Systems). The mechanical index was set at 0.9. **a** CETOCU before carotid stenting. **b** *Right* figure is a schematic representation of **a**. Sonazoid reveals the distal end of the collapsed ICA. Imaging shows a narrowed ICA with surrounding the plaque. Although the vascular lumen is collapsed, the extent of the plaque is apparent. **c** CETOCU after carotid stenting. **d** *Right* figure is a schematic representation of **c**. Stenosis caused by remnant plaque is evident at the distal end of the stent. The step observed on angiography between the stent and vessel is attributable to the plaque

suited to evaluating peripheral tissues and plaque status. Unlike CT angiography and cerebral angiography, CETOCU enables imaging for 5–10 min after contrast agent injection, and thus allows focused evaluation of the region of interest. Since Sonazoid is not nephrotoxic, this agent can be used safely and repeatedly in patients with renal impairment [7, 8]. The most important advantage of CETOCU over TOCU is availability to evaluate the vessel in the cases of ICA pseudo-occlusion. Differentiation of pseudo-occlusion from stenosis caused by elongated

arteriosclerotic lesions is difficult with angiography, and TOCU, which provides information on the periphery of the vascular lumen at the site of stenosis, is useful. However, identifying the ICA is extremely difficult when flow is extremely slow in a collapsed vessel, even using color Doppler TOCU. As long as some blood flow is present, CETOCU reveals collapsed vessels when Sonazoid passes through. This modality can thus better depict the extent of ICA stenosis in patients with pseudo-occlusion, enabling selection of the appropriate stent length for CAS. Confirmation of the lesion extent also allows medical personnel to judge how difficult CEA will be. Although the use of cerebral angiography alone in patients with pseudo-occlusion does not enable identification of the extent of stenosis and is not conducive to preoperative determination of the appropriate stent length, angiography paired with CETOCU provides relevant information for stent length and procedure selection. Evidence is building that plaques apparent on contrast-enhanced ultrasonography may be unstable [7, 8]. If this hypothesis is borne out, CETOCU is also expected to allow the evaluation of plaque status.

Angiography of the present patient just after stenting revealed a step between the distal edge of the stent and the vessel, suggesting the possibility of plaque protrusion or dissection. CETOCU suggested that the step represented remnant plaque not covered by the stent, because pre-stenting CETOCU had shown plaque in the same region. The stent selected for the procedure was too short to cover the entire lesion. TOCU without an ultrasonography contrast agent does not show echolucent plaques, such as in the present patient. Such plaques within a stent and before and after stenting are generally difficult to visualize on color Doppler ultrasonography, making CETOCU useful for post-stenting evaluation. Providing detailed information about the extracranial ICA, noninvasive CETOCU can be repeatedly performed at the bedside for perioperative CAS evaluation. Our hope is that CETOCU, which is not yet supported in the literature, will become more widely used.

Compliance with ethical standards

Ethical statements All procedures followed were approved by the St. Marianna University Bioethics Committee and performed in accordance with the Helsinki Declaration of 1964 and later versions.

Informed consent Informed consent was obtained from the patient for inclusion in this study.

Conflict of interest The authors have no conflicts of interest to declare.

References

1. Yasaka M, Kimura K, Otsubo R, et al. Transoral carotid ultrasonography. Stroke. 1998;29:1383–8.
2. Mori M, Yasaka M, Sakima H, et al. A case of the spontaneous dissection of the bilateral internal carotid arteries diagnosed by the transoral carotid ultrasonography (TOCU). Rinsho Shinkeigaku. 2007;47:217–21.
3. Suzuki R, Koga M, Toyoda K, et al. Identification of internal carotid artery dissection by transoral carotid ultrasonography. Cerebrovasc Dis. 2012;33:369–77.
4. Kamouchi M, Kishikawa K, Okada Y, et al. Transoral ultrasonographic evaluation of carotid flow in predicting cerebral hemodynamics after carotid endarterectomy. AJNR Am J Neuroradiol. 2006;27:1295–9.
5. Kishikawa K, Kamouchi M, Okada Y, et al. Transoral carotid ultrasonography as a diagnostic aid in patients with severe carotid stenosis. Cerebrovasc Dis. 2004;17:106–10.
6. Kishikawa K, Kamouchi M, Okada Y, et al. Evaluation of distal extracranial internal carotid artery by transoral carotid ultrasonography in patients with severe carotid stenosis. AJNR Am J Neuroradiol. 2002;23:924–8.
7. Matsumoto N, Kimura K, Uno M, et al. Enhanced carotid plaque on contrast-enhanced ultrasound is associated with plaque instability and rupture. Int J Stroke. 2012;7:E12.
8. Faggioli GL, Pini R, Mauro R, et al. Identification of carotid vulnerable plaque by contrast-enhanced ultrasonography: correlation with plaque histology, symptoms and cerebral computed tomography. Eur J Vasc Endovasc Surg. 2010;41:238–48.

INTERNAL MEDICINE

□ CASE REPORT □

Reversible Cerebral Vasoconstriction Syndrome Presenting with Transient Global Amnesia

Kenji Isahaya, Kensuke Shinohara, Masashi Akamatu, Takahiro Shimizu, Kenzo Sakurai, Makoto Shiraishi, Hisanao Akiyama and Yasuhiro Hasegawa

Abstract

A 65-year-old man who had been diagnosed with transient global amnesia (TGA) 15 years previously was admitted to hospital with complaints of amnesia and headache. His symptoms improved on day-2. The initial brain MRI and electroencephalography findings were normal. He was diagnosed with a recurrence of TGA and discharged. However, he returned with right leg weakness and complained of a thunderclap headache. MRI demonstrated subarachnoid hemorrhage and multifocal segmental narrowing of the left posterior cerebral artery (PCA) and large intracranial arteries, and he was diagnosed with reversible cerebral vasoconstriction syndrome (RCVS). He was discharged on day-30 without any neurological deficits. This case suggested that TGA should be interpreted as one of the symptoms of RCVS or a prodromal symptom of RCVS.

Key words: reversible cerebral vasoconstriction syndrome, transient global amnesia, subarachnoid hemorrhage, thunderclap headache

(Intern Med 56: 1569-1573, 2017)
(DOI: 10.2169/internalmedicine.56.7460)

Introduction

Reversible cerebral vasoconstriction syndrome (RCVS) is characterized by severe headache and reversible vasoconstriction of the cerebral arteries with or without cortical subarachnoid hemorrhage, infarction or intracerebral hemorrhage. Thunderclap headache, seizures and focal neurological deficits are commonly observed, but amnesia is rare. We herein report the case of a 65-year-old patient with a history of transient global amnesia (TGA) 15 years prior to his presentation, who was admitted with typical symptoms of TGA and who was subsequently diagnosed with RVCS - implying a causal relationship between RVCS and TGA.

Case Report

A 65-year-old man was admitted to our hospital with a complaint of amnesia. After returning home on the day of admission, he could not remember what he had done all day. He remained confused and kept asking repetitive questions. He had no seizure activity or palsy. Fifteen years prior to his presentation he had experienced TGA. When he was 50 years of age, his wife noticed that his memory was severely disturbed: when she talked with him at home, he repeatedly asked the same questions. He was admitted to hospital by ambulance. His memory disturbance continued for approximately 12 hours and then completely normalized. He had not experienced any headache during the course of TGA and his MRI findings were normal. He was diagnosed with TGA. He was not a smoker, but had a history of hypertension and spinal stenosis. He had no history of surgery and no family history of neurological disease. Two weeks before the onset of symptoms, hydrochlorothiazide (4 mg), reserpine (0.1 mg), and carbazochrome (5 mg) were added to his medications.

A general physical examination revealed that his blood pressure was 161/84 mmHg, his heart rate was 68 beats per minute, and his temperature was 36.7ºC. He was alert and oriented to person and place but not to time. He had anterograde amnesia; his cognitive impairment was limited to amnesia. He had no other neurological symptoms or signs. Laboratory investigations revealed a normal complete blood count and chemistry panel. Lumbar puncture was not per-

Department of Neurology, St. Marianna University School of Medicine, Japan
Received for publication April 9, 2016; Accepted for publication October 16, 2016
Correspondence to Dr. Kenji Isahaya, isahaya_kenji@marianna-u.ac.jp

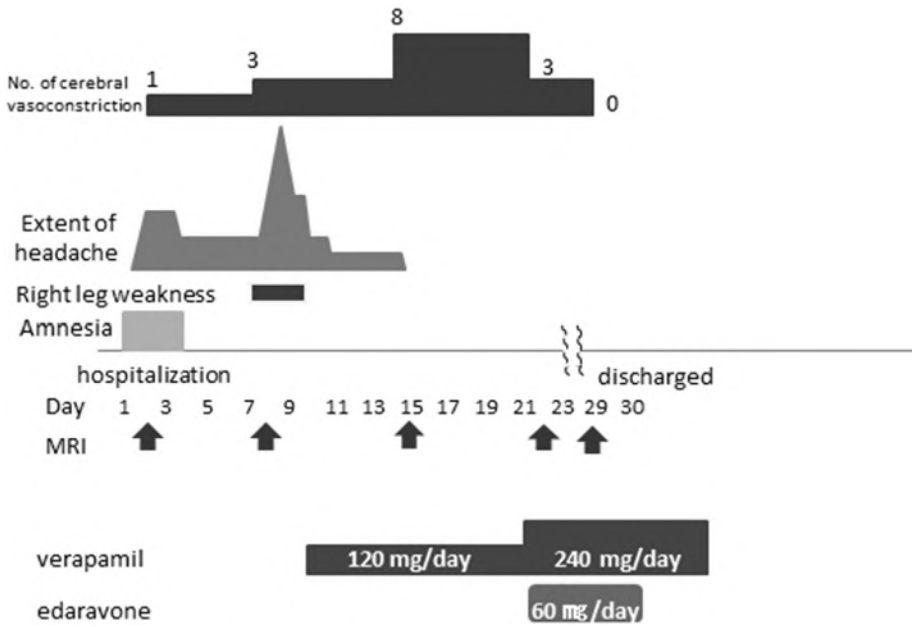

Figure 1. Clinical course. The patient complained of amnesia and headache on admission and subsequently a thunderclap headache on day 9. His headache disappeared on day 13, but a brain MRI on day 14 showed segmental vasoconstriction of the cerebral arteries. A brain MRI on day 21 showed new areas of infarction, and he was started on oral verapamil 240 mg/day and edaravone 60 mg/day. A brain MRI on day 29 showed resolution of the segmental vasoconstriction. He was discharged directly home on oral verapamil on day 30.

formed. An electrocardiogram demonstrated normal sinus rhythm. Magnetic resonance imaging (MRI) of the brain showed no acute findings, while magnetic resonance angiography (MRA) of the brain showed mild stenosis in the left posterior cerebral artery.

His clinical course is shown in Fig. 1. His Mini Mental State Examination (MMSE) score on day-1 was 27, the subtest scores were as follows: temporal orientation (5 points), spatial orientation (5 points), immediate memory (3 points), attention/concentration (5 points), delayed recall (no points), naming (2 points), verbal repetition (1 points), verbal comprehension (3 points), writing (1 points), reading a sentence (1 points), and constructional praxis (1 points). His amnesia began to improve on day-2 (MMSE total score; 30) and disappeared by day-4.

Because of his history of TGA, his amnestic episode was diagnosed as a recurrence of TGA according to the diagnostic criteria of Hodges and Warlow (1), and he was discharged from the hospital on day-7. However, he developed right leg weakness and returned to the hospital on the evening of the same day. In the emergency room, his NIH stroke scale score was 2. MRI and MRA were performed; however, he complained of a thunderclap headache in the gantry. We could complete almost entire protocol, and the MRI findings were normal. However MRA revealed multifocal segmental narrowing of the right vertebral artery (VA), bilateral posterior cerebral artery (PCA), bilateral middle cerebral artery (MCA) and left anterior cerebral artery (ACA) (Fig. 2A). Brain computed tomography (CT) scanning on day-9 demonstrated a subarachnoid hemorrhage over the left frontal convexity (Fig. 3A) and CT angiography demonstrated no improvement of the segmental stenosis. He was diagnosed with RCVS and was started on oral verapamil (120 mg/day).

His right leg weakness improved and eventually disappeared. On day-15, his headache had disappeared; however, follow-up brain MRI showed new areas of ischemia in the left upper occipital region (Fig. 3B-D). MRA showed persistent multifocal irregular stenosis of the right VA, bilateral PCA, bilateral MCA and left ACA, which was consistent with vasoconstriction (Fig. 2B). He was started on oral verapamil (240 mg/day) and edaravone (60 mg/day). He did not experience any other neurological symptoms and made a full neurological recovery. On day-22, brain MRA showed the resolution of the segmental vasoconstriction (Fig. 2C). Brain MRI on day-29 showed no new areas of infarction and the resolution of the segmental vasoconstriction. On day-30, he was discharged directly to his home (NIH Stroke scale score, 0; modified Rankin scale score, 0) on oral verapamil.

Discussion

The proposed diagnostic criteria for RCVS (2-4) are as follows: (a) acute and severe headache (often thunderclap) with or without focal deficits or seizures, (b) a uniphasic course without new symptoms for more than 1 month after the clinical onset, (c) segmental vasoconstriction of the cerebral arteries on indirect (e.g., MRI or CT) or direct catheter angiography, (d) no evidence of aneurysmal subarachnoid hemorrhage, (e) normal or near-normal CSF levels (protein

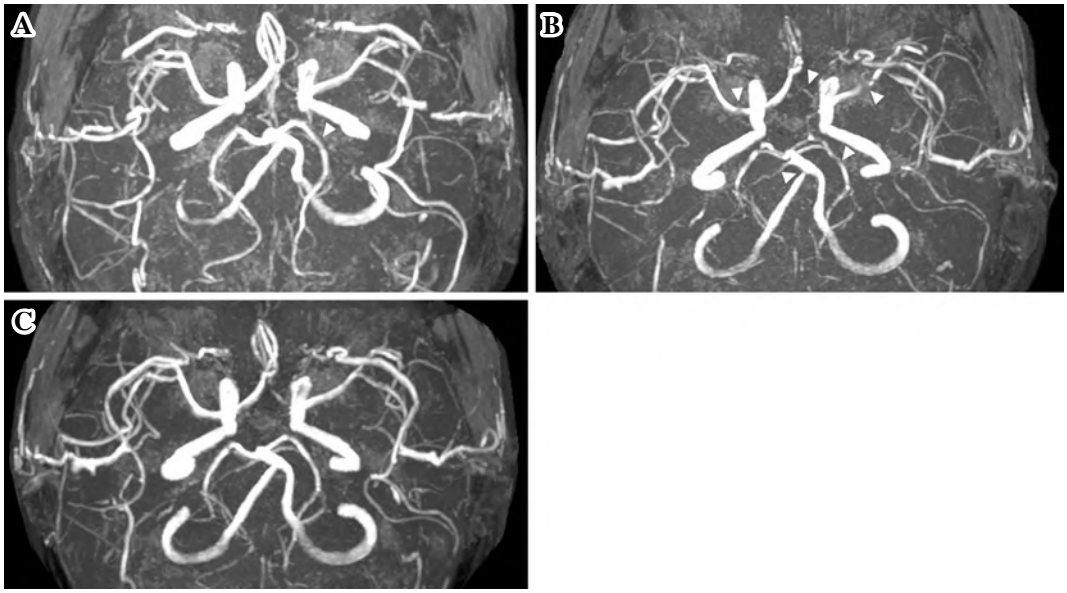

Figure 2. Brain magnetic resonance angiography. (A) Magnetic resonance angiography (MRA) of a 65-year-old man with reversible cerebral vasoconstriction syndrome on day 2 showing segmental constriction of the right posterior cerebral artery (PCA) (arrow head). (B) MRA showing segmental constriction of the right vertebral artery (VA), bilateral PCA, bilateral middle cerebral artery (MCA) and left anterior cerebral artery (ACA) (arrow heads) on day 15. (C) MRA showing resolution of the segmental vasoconstriction on day 22.

concentration <100 mg /dL, <15 white blood cells per μL), and (f) the complete or substantial normalization of arteries shown by follow-up indirect or direct angiography within 12 weeks of the clinical onset. This case was diagnosed according to the above-mentioned criteria. The patient in the present case satisfied criteria (a), (b), (c) and (f), and was therefore diagnosed with RCVS.

Headache is the main symptom of RCVS. Thunderclap headache is reported in 85% of RCVS cases. Recurrent thunderclap headache is reported in 82% of cases of RCVS and occurs at 3-12 days after the onset of the initial thunderclap headache (5). In this case, the patient presented with headache on admission, while thunderclap headache developed on day-8.

Subarachnoid hemorrhage (SAH), cerebral hemorrhage, seizures and posterior reversible encephalopathy syndrome (PRES) are reported in 22%, 6%, 3% and 9% of patients, respectively, during the acute phase of RCVS (≤1 week after onset). Transient ischemic attack (TIA) and cerebral infarction are reported in 16% and 4% of patients, respectively, during the late phase (>1 week after onset) (6). In the present case, SAH occurred on day-7 and cerebral infarction occurred on day-15. The entire clinical course of the present case is consistent with RCVS.

Several mechanisms of TGA have been proposed. These include vascular (venous congestion or arterial ischemia), epileptic, or migraine related mechanisms. The venous congestion theory may be supported by the DWI abnormalities in the hippocampus that are observed in TGA patients with internal jugular vein valve incompetence (7-10). Arterial vasoconstriction, which might cause TGA, is usually precipitated by emotional stress or the Valsalva maneuver (11, 12). A case of Takotsubo cardiomyopathy with TGA, in which both coronary and cerebral arterial vasoconstriction were suggested, has also been reported (13). However, no signs of intracranial arterial vasoconstriction were demonstrated in a case-control study using transcranial arterial echo-color Doppler sonography (14). Although RCVS is one of the forms of arterial vasoconstriction, the relationship between TGA and vasoconstriction has been a matter of speculation. This case is clinically important because the patient had a history of TGA and because typical symptoms of TGA were observed during his initial presentation during the development of RCVS. Although persistent neurological deficits such as hemiplegia, aphasia, hemianopia and cortical blindness have been reported in patients with RCVS (4), there have been no reports of amnesia. This case suggested that TGA should be interpreted as one of the symptoms of RCVS or a prodromal symptom of RCVS.

Several causes of RCVS have been reported, including postpartum, hypercalcemia, porphyria, cerebral venous thrombosis, vasoactive drugs (serotonergic and adrenergic drugs, cannabis, cocaine, ergot alkaloid derivatives and triptans) (4), and herbal medicines containing ginseng and ephedra (15). A combination tablet (hydrochlorothiazide, reserpine, and carbazochrome) had been prescribed to the present patient two weeks before his admission. Although these substances have not been reported as precipitants of RCVS, reserpine has been known to cause amnesia (16). Thus, we stopped the administration of the combination tablet after admission. Although severe headache-induced delirium and/or drug-induced consciousness disturbance (e.g., hydrochlo-

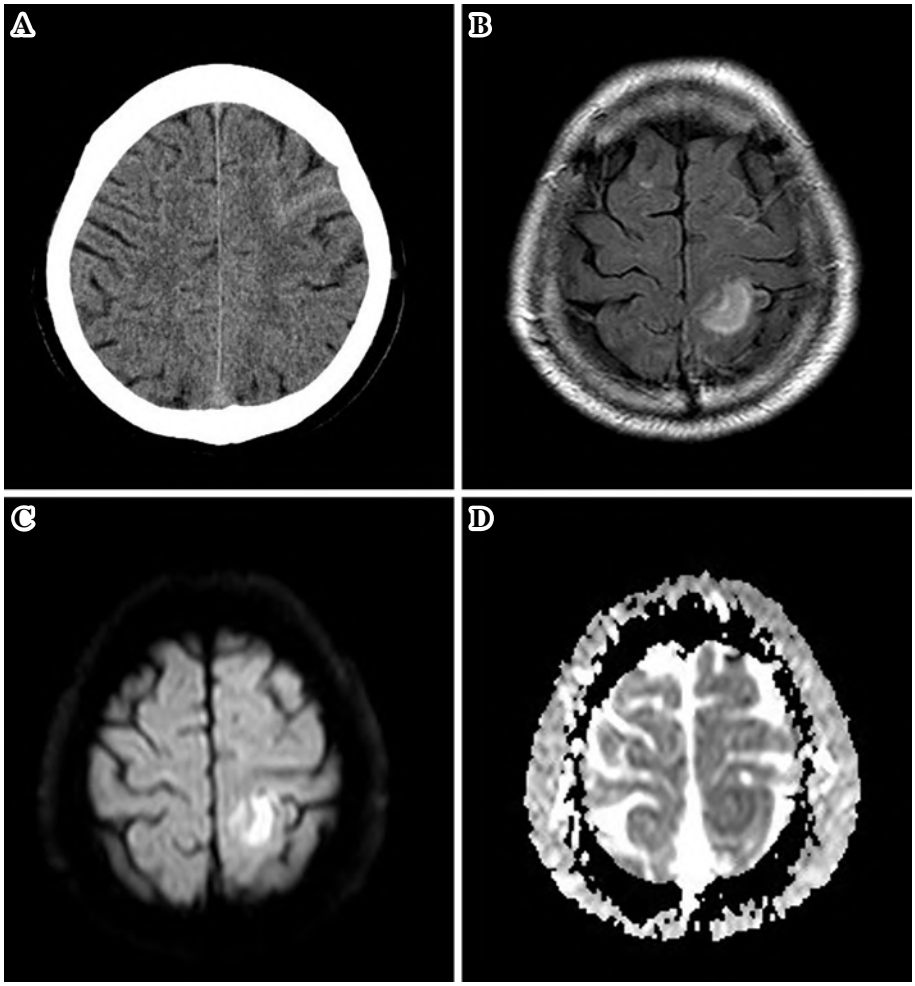

Figure 3. Computed tomography (CT) on day 9 and magnetic resonance imaging (MRI) on day 21. (A) On day 9, CT showing left frontal subarachnoid hemorrhage. (B) On day 21, Fluid Attenuated Inversion Recovery (FLAIR), (C) diffusion-weighted MRI, and (D) apparent diffusion coefficient maps revealed lesions in the left parietal lobe consistent with infarction.

rothiazide, reserpine) can cause amnesia-like symptoms, his consciousness - as evaluated by awareness and responsiveness - was normal throughout the period of amnesia, implying that it was quite unlikely that the patient's amnesia-like symptoms were associated with consciousness disturbance.

The hippocampal body is perfused by the anterior hippocampal artery and the middle hippocampal artery and the posterior hippocampal artery branches from the proximal portion of the PCA. The hippocampal head is perfused by the anterior choroidal artery (AChA), which is supplied by the internal carotid artery (ICA). Amnesia may be associated with infarctions of the PCA and AChA (17). It has been suggested that the vasoconstriction of the cerebral arteries in RCVS progresses from the distal portion of the arteries to the more proximal arteries, such as the branches of the circle of Willis (6). When our patient's amnestic symptoms occurred, the proximal portion of his left PCA showed stenosis on MRA, suggesting that transient ischemia in the hippocampal artery territory might have resulted in the symptoms of transient amnesia. Unfortunately, we did not have the chance to perform brain SPECT imaging to demonstrate cerebral blood flow abnormalities in the PCA area, because his amnesia resolved within a few days. Furthermore, we did not perform serial CT angiography to demonstrate the time-course of the resolution of vasoconstriction, because the use of contrast material for conventional cerebral angiography or CT angiography is known to be a risk factor for RCVS (18). Although calcium antagonists do not affect the period of cerebral vasospasm, they have been used to relieve arterial narrowing (6, 15, 18). In the present case, oral verapamil (120 mg/day) was found to be effective in relieving the patient's vasoconstriction.

To the best of our knowledge, this is the first case suggesting a causal relationship between TGA and RCVS. TGA could be a prodromal symptom of RCVS. Although RCVS is relatively uncommon, it should be considered in the differential diagnosis of patients presenting with TGA.

The authors state that they have no Conflict of Interest (COI).

References

1. Hodges JR, Warlow CP. Syndromes of transient amnesia: towards a classification. A study of 153 cases. J Neurol Neurosurg Psychiatry **53**: 834-843, 1990.
2. Headache Classification Subcommittee of the International Headache Society. The international classification of headache disorders. Cephalalgia **24** Suppl 1: 1-160, 2004.
3. Calabrese LH, Dodick DW, Schwedt TJ, Singhal AB. Narrative review: reversible cerebral vasoconstriction syndromes. Ann Intern Med **146**: 34-44, 2007.
4. Ducros A. Reversible cerebral vasoconstriction syndrome. Lancet Neurol **11**: 906-917, 2012.
5. Chen SP, Fuh JL, Lirng JF, Chang FC, Wang SJ. Recurrent primary thunderclap headache and benign CNS angiopathy: spectra of the same disorder? Neurology **67**: 2164-2169, 2006.
6. Ducros A, Boukobza M, Porcher R, Sarov M, Valade D, Bousser MG. The clinical and radiological spectrum of reversible cerebral vasoconstriction syndrome. A prospective series of 67 patients. Brain **130**: 3091-3101, 2007.
7. Cejas C, Cisneros LF, Lagos R, Zuk C, Ameriso SF. Internal jugular vein valve incompetence is highly prevalent in transient global amnesia. Stroke **41**: 67-71, 2010.
8. Yang Y, Kim S, Kim JH. Ischemic evidence of transient global amnesia: location of the lesion in the hippocampus. J Clin Neurol **4**: 59-66, 2008.
9. Schreiber SJ, Doepp F, Klingebiel R, Valdueza JM. Internal jugular vein valve incompetence and intracranial venous anatomy in transient global amnesia. J Neurol Neurosurg Psychiatry **76**: 509-513, 2005.
10. Nedelmann M, Eicke BM, Dieterich M. Increased incidence of jugular valve insufficiency in patients with transient global amnesia. J Neurol **252**: 1482-1486, 2005.
11. Kaida T, Nakano H, Watanabe I, et al. A unique case of Takotsubo cardiomyopathy with transient global amnesia which might be caused by simultaneous and multiple vasospasms. J Cardiac Failure **15** Suppl: S159, 2009.
12. Caplan LR. Transient global amnesia and jugular vein incompetence. Stroke **41**: e568, 2010.
13. Pantoni L, Lamassa M, Inzitari D. Transient global amnesia: a review emphasizing pathogenic aspects. Acta Neurol Scand **102**: 275-283, 2000.
14. Baracchini C, Farina F, Ballotta E, Meneghetti G, Manara R. No signs of intracranial arterial vasoconstriction in transient global amnesia. J Neuroimaging **25**: 92-96, 2014.
15. Ichiki M, Watanabe O, Okamoto Y, Ikeda K, Takashima H, Arimura K. A case of reversible cerebral vasoconstriction syndrome (RCVS) triggered by a Chinese herbal medicine. Rinsho Shinkeigaku (Clin Neurol) **48**: 267-270, 2008 (in Japanese).
16. Alves CS, Andreatini R, da Cunha C, Tufik S, Vital MA. Phosphatidylserine reverses reserpine-induced amnesia. Eur J Pharmacol **404**: 161-167, 2000.
17. Ott BR, Saver JL. Unilateral amnesic stroke. Six new cases and a review of the literature. Stroke **24**: 1033-1042, 1993.
18. Chen SP, Fuh JL, Wang SJ, et al. Magnetic resonance angiography in reversible cerebral vasoconstriction syndromes. Ann Neurol **67**: 648-656, 2010.

The Internal Medicine is an Open Access article distributed under the Creative Commons Attribution-NonCommercial-NoDerivatives 4.0 International License. To view the details of this license, please visit (https://creativecommons.org/licenses/by-nc-nd/4.0/).

© 2017 The Japanese Society of Internal Medicine
http://www.naika.or.jp/imonline/index.html

Clinical Case Report

Medicine®

OPEN

Utility of osteosclerotic lesion biopsy in diagnosis of POEMS syndrome

A case report

Daisuke Hara, MD, PhD[a], Hisanao Akiyama, MD, PhD[a,*], Saki Nukui, MD[a], Takahiro Shimizu, MD, PhD[a], Masahiro Hoshikawa, MD, PhD[b], Yasuhiro Hasegawa, MD, PhD[a]

Abstract

Rationale: We report a case of successful diagnosis of POEMS (polyneuropathy, organomegaly, endocrinopathy, monoclonal gammopathy, and skin changes) syndrome based on monoclonality that was confirmed by an osteosclerotic lesion biopsy in a patient without pathognomonic symptoms or monoclonal gammopathy, probably because of comorbidities, which included systemic lupus erythematosus, rheumatoid arthritis, and Sjögren syndrome.

Patient concerns: A 57-year-old woman presented with an approximately 2-year history of numbness in the toes that had gradually spread, along with muscle weakness in both arms and legs. She had been receiving immunosuppressant and corticosteroid therapy since being diagnosed with systemic lupus erythematosus and Sjögren syndrome at the age of 31 years and rheumatoid arthritis at the age of 44 years. Neurological examination revealed predominantly distal hypoesthesia and weakness in a typical stocking-and-glove pattern. Immunoelectrophoresis revealed elevated polyclonal immunoglobulin, which was attributed to her known underlying disease.

Diagnoses: Biopsy of an osteosclerotic lesion confirmed proliferation of monoclonal plasma cells, leading to a diagnosis of POEMS syndrome.

Interventions and outcomes: Lenalidomide therapy was started after the diagnosis and the patient had a favorable outcome.

Lessons: Osteosclerotic lesion biopsy can be useful for diagnosis of POEMS syndrome in difficult cases.

Abbreviations: CT = computed tomography, FLC = free light chain, MRI = magnetic resonance imaging, POEMS = polyneuropathy, organomegaly, endocrinopathy, monoclonal gammopathy, and skin changes, RA = rheumatoid arthritis, SLE = systemic lupus erythematosus, SS = Sjögren syndrome, VEGF = vascular endothelial growth factor.

Keywords: osteosclerotic lesion, POEMS syndrome, rheumatoid arthritis, Sjögren syndrome, systemic lupus erythematosus

Editor: Zelena Dora.

Authorship: DH, HA, SN, and TS examined the patient, drafted the manuscript, and created the figures. MH performed the pathological examination. YH helped draft the manuscript. All authors read and approved the final manuscript.

The Human Research Ethics Committee of St. Marianna University Hospital provided a waiver considering that approval is not necessary for a single case report. Written informed consent was obtained from the patient.

The patient provided written informed consent for publication of clinical details and images. A copy of the consent form is available for review by the journal editor.

All relevant data are contained in the manuscript.

The authors declare that they have no competing interests.

[a] Department of Internal Medicine, Division of Neurology, [b] Department of Diagnostic Pathology, Division of Diagnostic Pathology, St. Marianna University School of Medicine, Kawasaki, Kanagawa, Japan.

[*] Correspondence: Hisanao Akiyama, Department of Internal Medicine, Division of Neurology, St. Marianna University School of Medicine, 2-16-1 Sugao, Miyamae-ku, Kawasaki, Kanagawa, Japan (e-mail: h2akiyama@marianna-u.ac.jp).

Copyright © 2017 the Author(s). Published by Wolters Kluwer Health, Inc. This is an open access article distributed under the terms of the Creative Commons Attribution-Non Commercial-No Derivatives License 4.0 (CCBY-NC-ND), where it is permissible to download and share the work provided it is properly cited. The work cannot be changed in any way or used commercially without permission from the journal.

Medicine (2017) 96:41(e8188)

Received: 20 June 2017 / Received in final form: 24 August 2017 / Accepted: 8 September 2017

http://dx.doi.org/10.1097/MD.0000000000008188

1. Introduction

POEMS (polyneuropathy, organomegaly, endocrinopathy, monoclonal gammopathy, and skin changes) syndrome is a rare disorder with signs and symptoms that vary from one body site to another.[1] There are about 340 people with POEMS syndrome in Japan, indicating a prevalence of approximately 0.3 per hundred thousand population.[2] Furthermore, there is a few cases frequency of POEMS syndrome with collagen disease.[3–5] Proliferation of monoclonal plasma cells within an intramedullary plasmacytoma likely contributes to the pathology of POEMS syndrome. The condition is characterized by increased production of M-protein to a detectable level, an abnormal λ/κ free light chain (FLC) ratio, and obvious monoclonality (monoclonal gammopathy confirmed by immunoelectrophoresis).[1] Painless osteosclerotic lesions that are visible on plain skeletal radiography are also characteristic of POEMS syndrome. We report here a case of successful diagnosis of POEMS syndrome based on monoclonality (proliferation of monoclonal plasma cells) that was confirmed by an osteosclerotic lesion biopsy in a patient without pathognomonic symptoms or monoclonal gammopathy, probably because of comorbidities, which included systemic lupus erythematosus (SLE), rheumatoid arthritis (RA), and Sjögren syndrome (SS). Lenalidomide therapy was started after the diagnosis and the patient had a favorable outcome.

Table 1

Laboratory data on admission.

Hematological Data		K	4.9 mEq/L	KL-6	377 U/mL
WBC	5100/μL	Cl	102 mEq/L	β2-MG	3.7 mg/L
Neut	50.5 %	Ca	8.6 mg/dL	IL-6	3.5 pg/mL
Lym	39.6 %	UN	14.7 mg/dL	VEGF (plasma)	879 pg/mL
Mono	8.9 %	Cre	0.85 mg/dL	ANA	(−)
Eo	1.5 %	CRP	0.11 mg/dL	MAG	(−)
Ba	6.0 %	CK	11 U/L	ACE	6.1 U/L
RBC	38.3×10^5/μL	Glucose	110 mg/dL	Free T_3	1.2 pg/mL
Hb	12.2 g/dL	BNP	25.9 pg/mL	Free T_4	9.8 pg/mL
Hct	36.5 %	FLC		PTH-intact	59.0 pmol/L
Plt	44.6×10^3/μL	κ chain	77.6 mg/L	LH	29.6 mIU/mL
Biochemical and Serological Data		λ chain	60.5 mg/L	FSH	65.7 mIU/mL
TP	6.0 g/dL	κ/λ ratio	1.28	PRL	22.5 ng/mL
Protein fraction		IgG	1408 mg/dL	**Urinalysis**	
alb	54.6 %	IgA	471 mg/dL	B-J protein	(−)
α1-globulin	2.9 %	IgM	64 mg/dL	Total protein	345 mg/day
α2-globulin	8.0 %	IgD	2.5 mg/dL	Total Alb	102 mg/day
β-globulin	10.8 %	M protein	(−)	Ccr 24 h	70.2 mL/min
γ-globulin	23.7 %	MMP-3	156.6 ng/mL	**CSF Data Analysis**	
Alb	3.2 g/dL	SS-A	2 ×	Initial pressure	120 mmH_20
AST	15 U/L	SS-B	4 ×	Cell	4/μL (mono)
ALT	17 U/L	IgG4	98 mg/dL	Protein	210 mg/dL
LDH	112 U/L	CH 50	40.2 U/mL	Alb	135 mg/dL
ALP	234 U/L	ds-DNA-IgG	9.6 IU/mL	Glucose	57 mg/dL
Na	144 mEq/L	sIL-2R	380 U/mL	IgG index	0.65

β2 MG = β2 microglobulin, ACE = angiotensin-converting enzyme, ANA = anti-nuclear antibody, B-J protein = Bence–Jones protein, Ccr 24 h = 24-hour creatine clearance, CSF = cerebrospinal fluid, ds-DNA-IgG = anti-double stranded DNA antibody, FLC = free light chain, FSH=follicle stimulating hormone, IL-6=interleukin-6, LH=luteinizing hormone, MAG = anti-myelin associated glycoprotein antibody, MMP-3 = matrix metalloproteinase-3, PRL = prolactin, PTH = parathyroid hormone, sIL-2R = soluble interleukin-2 receptor, SS-A = anti-Sjögren syndrome related antigen type A, SS-B = anti-Sjögren syndrome related antigen type B, VEGF = vascular endothelial growth factor.

2. Case report

A 57-year-old right-handed woman was admitted to our department of neurology with numbness and weakness of both arms and legs. Her past medical history included SLE and SS diagnosed at the age of 31 years, RA diagnosed at the age of 44 years, atherothrombotic brain infarction (with no sequelae), aortic valve stenosis, and spinal canal stenosis (L4/5) diagnosed at the age of 56 years, and right-sided deep vein thrombosis diagnosed at the age of 57 years. She reported drinking socially and denied smoking. Her family history was unremarkable. She was taking prednisolone 7 mg, azathioprine 75 mg, aspirin 100 mg, edoxaban 30 mg, lansoprazole 15 mg, polaprezinc 150 mg, pregabalin 100 mg, and eldecalcitol 0.75 μg daily.

She had noticed episodes of numbness in the toes on both sides that started in around May 2014, but did not seek treatment because she suspected they were attributable to her known pre-existing disease. The numbness then spread to the ankles and by late October 2015 was accompanied by pain in the soles of both feet. By late January 2016, the numbness extended to below the knees and involved the area distal to the wrists; plantar flexion and dorsiflexion of the right ankle became difficult. This progressed to difficulty in plantar flexion and dorsiflexion of the left ankle joint and in palmar flexion and extension of both wrists in February 2016. The patient then developed edema in the lower extremities bilaterally and was admitted to our hospital for further examination and treatment in April 2016.

On admission, height was 158 cm, body weight was 42 kg, blood pressure was 126/86 mm Hg, pulse rate was regular at 86 beats/min, body temperature was 36.8°C, and respiratory rate was 16 breaths/min. Physical examination revealed a systolic murmur (Levine grade IV/VI) in the second intercostal space at the right sternal border, edema in the lower extremities bilaterally, finger joint deformities, and angiomas on the chest and back. The patient was lucid and neurological examination revealed no cranial nerve abnormalities. Motor system examination confirmed distal muscle weakness in all extremities (upper and lower extremity strength score by manual muscle testing 5-/4 and 2/1, respectively; right and left grip strength, 12 and 8 kg, respectively). Tendon reflexes were absent in all extremities and pathological reflexes were negative. Sensory system examination revealed numbness in the areas distal to both wrists and knees, pain in the areas distal to the ankles bilaterally, and superficial and deep sensory impairment in the affected areas, particularly in the lower extremities. The patient could stand briefly but with considerable unsteadiness and could not walk unaided. There were no autonomic disorders, such as urinary disorder or orthostatic hypotension. Overall Neuropathy Limitation Scale[6] score was 8.

Laboratory data on admission (Table 1) revealed elevated platelet count (446,000/μL), but the coagulation profile was normal. Total serum protein, albumin, and γ-globulin levels were normal (except for a slight increase in immunoglobulin A); antinuclear, anti-SS-A, and anti-SS-B antibody titers were increased 320-fold, 2-fold, and 4-fold, respectively. Serum matrix metalloproteinase-3 was 156.6 ng/mL (normal range 17.3–59.7 ng/mL) and immunofixation for M-protein was negative. Polyclonal gammopathy was confirmed by immunoelectrophoresis. Her κ and λ FLC levels were 77.6 mg/L (normal range 2.42–18.92 mg/L) and 60.5 mg/L (normal range 4.44–26.18 mg/L), respectively, and the κ/λ ratio was 1.28 (normal range 0.248–1.804). Metabolic and endocrine data and tumor

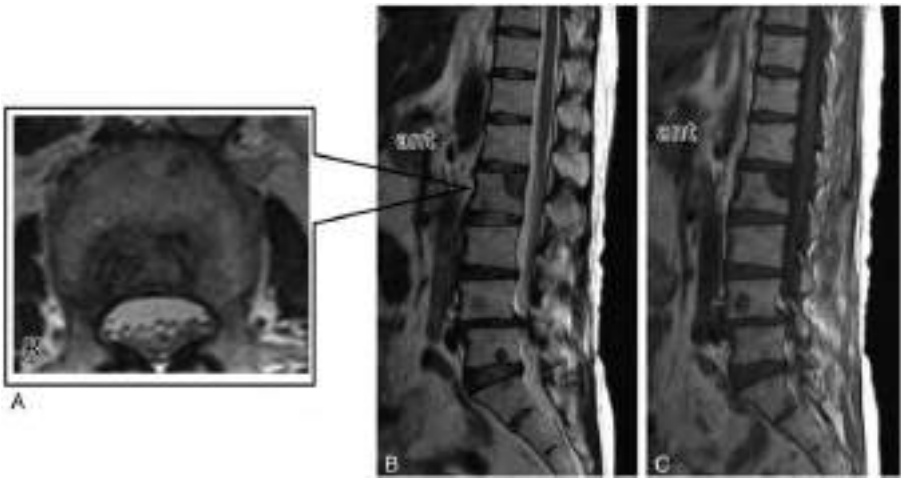

Figure 1. Spinal cord magnetic resonance image on admission. (A) Axial T2-weighted image of the second lumbar vertebra (1.5 T; 3250 ms, echo time 90 ms) showing osteosclerotic lesions with high-density signals surrounded by low-density signals. (B) Sagittal T2-weighted image (1.5 T; 456 ms, echo time 10 ms) of the lumbar vertebra showing multiple osteosclerotic lesions. (C) Sagittal T1-weighted image of the lumbar vertebra (1.5 T; 519 ms, echo time 15 ms) showing multiple osteosclerotic lesions. ant = anterior, R = right.

marker levels were normal. Protein in cerebrospinal fluid had increased to 135.4 mg/dL.

Electrocardiography showed sinus rhythm, heart rate of 86 beats/min, and normal R-R interval variability. Schellong test was negative. Plain chest radiography revealed no abnormalities and there were no acute lesions on plain magnetic resonance imaging (MRI) of the head. MRI of the lumbar spine showed forward slipping of the body of L4, spinal stenosis at L4/5, and osteosclerotic lesions in the bodies of L2, L4, L5, and S1 (low on T1-weighted and T2-weighted images and high on short-tau inversion recovery images; Fig. 1). Thoracoabdominal contrast computed tomography (CT) showed osteosclerotic lesions in the ribs, vertebral bodies, clavicles, and pelvis, and positron emission tomography-CT showed tracer accumulation in the area corresponding to an osteosclerotic lesion in the body of L2. There was mild pericardial effusion but no lymphadenopathy, hepatosplenomegaly, or accumulation of thoracoabdominal fluid. Bone scintigraphy demonstrated increased accumulation in the ribs on both sides and at several spinal levels. Transthoracic echocardiography revealed severe aortic valve stenosis with calcification and diffuse left ventricular hypertrophy, in good agreement with previous findings. Nerve conduction studies showed mildly decreased motor nerve conduction velocity and temporal dispersion in the upper extremities, with considerably decreased compound muscle action potential amplitude and motor nerve conduction velocity in the lower extremities (Table 2). Sensory nerve conduction velocity was markedly decreased and sensory nerve action potential amplitude was also considerably decreased in the lower extremities (Table 2). In short, the electrophysiological findings indicated polyneuropathy with demyelination in the upper extremities and both demyelination and axonopathy in the lower extremities. Furthermore, the terminal latency index[7] was high in the median nerve bilaterally (0.44 on the right, 0.47 on the left). Needle electromyography showed no clear neurogenic pattern, but revealed fibrillation potentials at rest in the tibialis anterior and gastrocnemius muscles bilaterally. The patient declined a nerve biopsy.

The clinical course is shown in Fig. 2. CT-guided biopsy of a lesion in the L2 vertebra performed 12 days after hospitalization showed a marked increase in strongly CD138-positive plasma cells with clonality skewed toward λ light chains rather than κ light chains (Fig. 3). A repeat plasma vascular endothelial growth

Table 2

Nerve conduction study.

		DL (ms)	CMAP (mV)	MCV (m/s)	SNAP (μV)	SCV (m/s)
Median Nerve	R	4.2	6.9	38.8	12.0	42.1
	L	3.8	6.8	41.9	21.4	50.8
	Normal values	< 4.2	> 3.5	> 48.0	> 10.0	> 49.8
Peroneal Nerve	R	6.4	0.092	34.8		
	L	5.5	0.300	32.8		
	Normal values	< 5.5	> 2.5	> 40.0		
Tibial Nerve	R	10.1	0.053	28.5		
	L	7.3	0.170	27.6		
	Normal values	< 6.0	> 2.9	> 41.0		
Sural Nerve	R				3.1	36.5
	L				5.5	33.3
	Normal values				> 10.5	> 45.2

CMAP = compound muscle action potential, DL = distal latency, L = left, MCV = motor conduction velocity, R = right, SCV = sensory conduction velocity, SNAP = sensory nerve action potential.

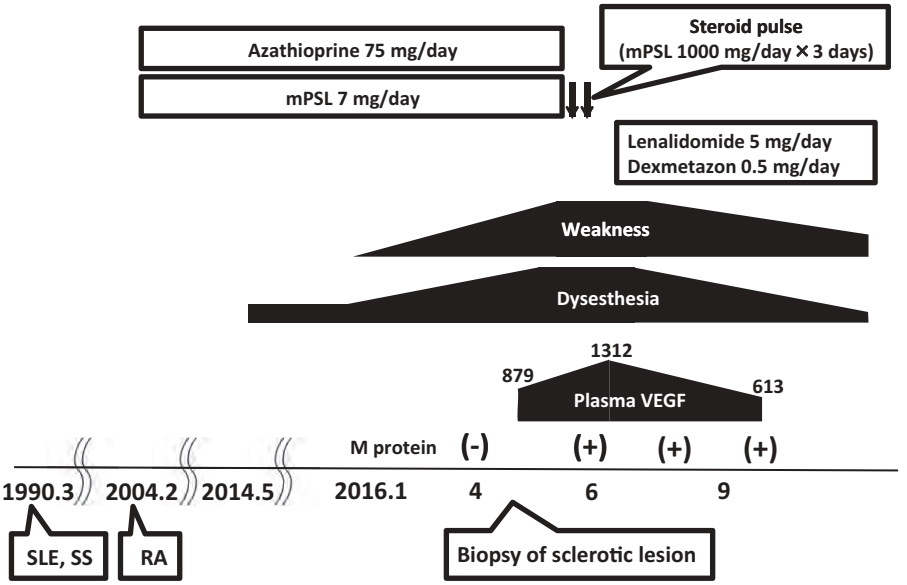

Figure 2. Clinical course. After treatment with lenalidomide and dexamethasone, her numbness, paresthesia, and weakness gradually improved and her serum VEGF level decreased. mPSL = methylprednisolone, RA = rheumatoid arthritis, SLE = systemic lupus erythematosus, SS = Sjögren syndrome.

factor (VEGF) level measured on day 25 of hospitalization showed elevation to 879 pg/mL (normal level <38.7 pg/mL). Fulfillment of the diagnostic criteria together with other findings prompted the diagnosis of POEMS syndrome. Two cycles of pulse corticosteroid therapy (methylprednisolone 1000 mg/day) started 45 days after hospitalization did not alleviate the patient's neurological symptoms. Her plasma VEGF increased further to 1312 pg/mL and M-protein (IgG λ) became positive 57 days after hospitalization. Oral azathioprine was withdrawn and new treatment comprising lenalidomide 5 mg/day and dexamethasone 0.5 mg/day was started 64 days after hospitalization. The patient was discharged home after 76 days in hospital. The same treatment was continued after discharge. Her Overall Neuropathy Limitation Scale score improved from 8 to 3, the edema in her

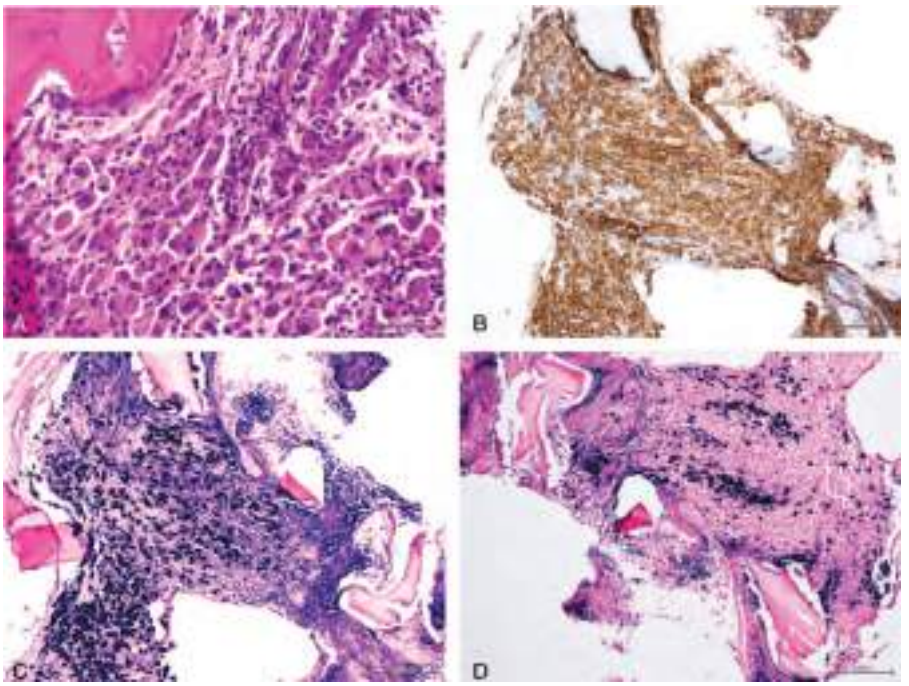

Figure 3. Biopsy specimen of a sclerotic lesion in the L2 vertebra. The specimen was obtained by computed tomography-guided needle biopsy of the lesion. (A) Sheets of mature-appearing plasma cells (hematoxylin-eosin staining, bar = 50 μm). (B) Plasma cells strongly positive for the plasma cell marker CD138 (bar = 200 μm). (C) In situ hybridization showing only rare plasma cells are positive for immunoglobulin λ light chain (bar = 200 μm). (D) In situ hybridization showing that plasma cells are rarely positive for immunoglobulin κ light chain (bar = 200 μm).

lower extremities resolved, and her plasma VEGF improved to 613 pg/mL. She is currently continuing the same treatment.

3. Discussion

Patients with POEMS syndrome present with various symptoms at different sites of the body. All patients with POEMS syndrome develop polyneuropathy, but organomegaly, endocrinopathy, monoclonal gammopathy, and skin changes have been reported to occur in 45% to 85%, 67% to 84%, 24% to 54%, and 46% to 93% of patients, respectively.[1] A diagnosis of POEMS syndrome requires fulfillment of 2 mandatory criteria, at least one of 3 other major criteria, and at least one of 6 minor criteria. The major mandatory criteria are plasma cell dyscrasia and polyneuropathy, and other major criteria include Castleman disease, sclerotic bone lesions, and elevated VEGF. Minor criteria include organomegaly, extravascular volume overload, endocrinopathy, skin changes, papilledema, and thrombocytosis/polycythemia.[1] The mandatory major criteria of plasma cell dyscrasia and polyneuropathy, other major criteria of sclerotic bone lesions and elevated VEGF, and minor criteria of skin changes, extravascular volume overload, and thrombocytosis were fulfilled in this case. However, characteristic symptoms are often absent in the early stages, and subsequent delays in diagnosis and treatment can result in a poor prognosis. POEMS syndrome was not easily diagnosed in our case for the following reasons. First, the patient had multiple comorbidities (SLE, RA, SS, aortic stenosis, and deep vein thrombosis), symptoms of which overlap with the characteristic symptoms of POEMS syndrome (such as polyneuropathy, edema, and skin disorders). Second, M-protein, which is indicative of increased monoclonal immunoglobulin levels, was not detected, the λ/κ FLC ratio was normal, and immunoelectrophoresis did not indicate monoclonal gammopathy. Polyneuropathy, chronic inflammatory demyelinating polyneuropathy, amyloid neuropathies, diabetic polyneuropathy, connective tissue-related peripheral neuropathy, paraneoplastic syndrome, alcoholic neuropathy, celiac disease, neuropathy related to human immunodeficiency virus or hepatitis C virus infection, various drugs, thyroid disorders, paraproteinemia, sarcoid polyneuropathy, vitamin B12 deficiency, and hereditary diseases (e.g., Fabry disease and hereditary sensory autonomic neuropathy) were excluded by various laboratory findings. However, chronic inflammatory demyelinating polyneuropathy and connective tissue related peripheral neuropathy remained in the differential diagnosis. Ultimately, these neuropathies were ruled out by a high terminal latency index value[7] on nerve conduction studies as well as the therapeutic effect of lenalidomide.

Proliferation of monoclonal plasma cells is usually evident in protein fractions recovered from patients with POEMS syndrome,[8] but our initial findings of immunoelectrophoresis, FLC analysis, and M-protein detection did not support this. Aggarwal et al[9] reported higher levels of both λ and κ FLC in patients with SLE or RA than in normal controls, and that testing for FLC in addition to testing C3, C4, and anti-ds-DNA antibody levels is useful for assessing disease activity in SLE. Similarly, the underlying SLE and RA in our patient might have caused the increase in polyclonal immunoglobulins, thereby masking apparent monoclonality. Therefore, osteosclerotic lesion biopsy to confirm abnormal proliferation of plasma cells with a predominance of monoclonal λ chains was critical in reaching the diagnosis of POEMS syndrome in this case. There have been a few previous reports of a patient with POEMS syndrome also having SLE, SS, and RA,[3–5] so the present case is valuable in demonstrating the utility of a diagnostic osteosclerotic lesion biopsy when immunoelectrophoresis for monoclonality is inconclusive. M-protein level is not very high in patients with POEMS syndrome, with a positive rate of only 24% to 54%,[1] so the undetectable level of M-protein in our patient does not conflict with a diagnosis of POEMS syndrome.

Serum and plasma VEGF levels increase in POEMS syndrome, suggesting its usefulness in diagnosis and assessment of disease activity. D'Souza et al[10] showed that a serum VEGF threshold of 200 pg/mL had a specificity of 95% and a sensitivity of 63% for differentiating POEMS syndrome from other diseases that also include elevated serum VEGF, such as RA, SLE, chronic inflammatory demyelinating polyradiculoneuropathy, and multiple myeloma. Plasma cells and platelets both secrete VEGF in POEMS syndrome, and serum levels are reportedly 10 to 50 times higher than plasma levels.[11] The abnormally high plasma VEGF level in our patient supports a diagnosis of POEMS syndrome. Nevertheless, because there have been no prior reports of plasma VEGF levels in patients with POEMS syndrome and multiple underlying diseases such as SLE and RA, diagnostic osteosclerotic lesion biopsy was essential in diagnosing POEMS syndrome in the present case.

Standard treatment for POEMS syndrome has not yet been established, so we opted for lenalidomide because autologous stem cell transplantation and long-term thalidomide therapy were not realistic options in our patient because of the underlying connective tissue disease and the risk of neurological complications, respectively. A recent study showed that lenalidomide is effective and safe and has some neurological benefit in patients with POEMS syndrome.[1] Indeed, lenalidomide therapy had a favorable outcome in the present case, including alleviation of neurological symptoms and decreased plasma VEGF levels.

POEMS syndrome is a rare disease that requires therapeutic strategies different from those used for other peripheral nerve disorders, and delayed diagnosis and treatment may have severe sequelae. Osteosclerotic lesion biopsy is recommended in the differential diagnosis of POEMS syndrome from other conditions, particularly in a patient with peripheral neuropathy and comorbid connective tissue disease who is unresponsive to treatment and in whom thorough systemic examination reveals an osteosclerotic lesion, but symptoms and investigations are not pathognomonic for POEMS syndrome.

References

[1] Dispenzieri A. POEMS syndrome: 2017 update on diagnosis, risk stratification, and management. Am J Hematol 2017;92:814–29.
[2] Nasu S, Misawa S, Sekiguchi Y, et al. Different neurological and physiological profiles in POEMS syndrome and chronic inflammatory demyelinating polyneuropathy. J Neurol Neurosurg Psychiatr 2012;83:476–9.
[3] Murphy N, Schumacher HRJr. POEMS syndrome in systemic lupus erythematosus. J Rheumatol 1992;19:796–9.
[4] Liang M, Jiang Z, Lin Z, et al. Polyneuropathy as novel initial manifestation in a case of "nonsecretory" POEMS syndrome with Sjögren's syndrome. Case Rep Med 2017;2017:1276759.
[5] Akagi T, Mukai T, Kodama S, et al. POEMS syndrome in a patient with rheumatoid arthritis. BMJ Case Rep 2017;2017:pii: bcr-2017-220875.
[6] Graham RC, Hughes RA. A modified peripheral neuropathy scale: the Overall Neuropathy Limitations Scale. J Neurol Neurosurg Psychiatry 2006;77:973–6.
[7] Mauermann ML, Sorenson EJ, Dispenzieri A, et al. Uniform demyelination and more severe axonal loss distinguish POEMS syndrome from CIDP. J Neurol Neurosurg Psychiatry 2012;83:480–6.

[8] Dispenzieri A, Kyle RA, Lacy MQ, et al. POEMS syndrome: definitions and long-term outcome. Blood 2003;101:2496–506.
[9] Aggarwal R, Sequeira W, Kokebie R, et al. Serum free light chains as biomarkers for systemic lupus erythematosus disease activity. Arthritis Care Res (Hoboken) 2011;63:891–8.
[10] D'Souza A, Hayman SR, Buadi F, et al. The utility of plasma vascular endothelial growth factor levels in the diagnosis and follow-up of patients with POEMS syndrome. Blood 2011;118:4663–5.
[11] Tokashiki T, Hashiguchi T, Arimura K, et al. Predictive value of serial platelet count and VEGF determination for the management of DIC in the Crow-Fukase (POEMS) syndrome. Intern Med 2003;42:1240–3.

DOI: 10.5797/jnet.oa.2017-0044

Original Article

Use of Contrast-enhanced Carotid Ultrasonography in Preoperative Assessment for Carotid Artery Stenting

Yuta Hagiwara,[1] Tatsuro Takada,[2] Takahiro Shimizu,[1] Tomohide Yoshie,[2] Hana Ogura,[1] Toshihiro Ueda,[2] and Yasuhiro Hasegawa[1]

Objective: Contrast-enhanced carotid ultrasonography (CEUS) is a new technique for assessing carotid artery plaques. The present study attempted to demonstrate the association between the findings of CEUS performed prior to carotid artery stenting (CAS) and plaque debris caught during CAS.

Methods: This study was conducted with 16 patients (15 men, 1 woman; mean age: 74.8 years) who had undergone evaluation of carotid plaque vulnerability followed by CAS. The carotid plaque evaluation consisted of CEUS and MRI. The amount of debris retrieved during CAS was semi-quantitatively classified into three grades (large, moderate, and small) by three independent physicians based on inspection of photographs of retrieved debris. The existence of a correlation between CEUS findings and the amount of debris was examined.

Results: Enhanced plaque on CEUS was observed in 7 of 16 patients. A large amount of debris was observed during CAS in four of the seven patients with CEUS-enhanced plaques that were also assessed as unstable on MRI, while two patients had a moderate amount and one patient had a small amount of debris. There were significant correlations between the amount of debris and plaque enhancement on CEUS, unstable plaque on MRI, and enhancement of plaque on CEUS with unstable plaque on MRI ($p = 0.036$, $p = 0.029$, $p = 0.036$, respectively). For the prediction of moderate to large amount of debris occurring in CAS, enhancement of plaque demonstrated by CEUS had a sensitivity of 66.7% and a specificity of 85.7%, unstable plaque determined by MRI had a sensitivity of 100% and a specificity of 42.9%, and enhancement of plaque by CEUS and unstable plaque determined by MRI had a sensitivity of 100% and a specificity of 75%.

Conclusion: Plaque vulnerability assessment using the combination of CEUS and MRI can predict the amount of debris retrieved during CAS, while using CEUS alone proved to be insufficient.

Keywords ▶ contrast-enhanced ultrasonography, carotid ultrasonography, carotid artery stenting

Introduction

In carotid artery stenting (CAS), the occurrence of cerebral embolism due to plaque debris during stent deployment is not uncommon. There is currently no established method for predicting the onset of cerebral embolism due to plaque debris. Assessment of carotid artery plaques prior to CAS is typically done with carotid ultrasonography (US), T1-weighted black-blood MRI (BB-MRI), or time-of-flight MRA (TOF MRA).[1-3] In recent years, however, contrast-enhanced carotid ultrasonography (CEUS) using an ultrasound contrast agent has become a viable modality for diagnosing intra-plaque neovascularization in the carotid artery, and it has attracted attention as a novel plaque imaging technique.[4] In the present study, the validity of CEUS in evaluation of plaque vulnerability was investigated by analyzing the relationship between the findings of preoperative plaque imaging including CEUS and the amount of debris retrieved during CAS.

Materials and Methods

A total of 16 patients (15 men, 1 woman; mean age: 74.8 years) who underwent preoperative assessment

[1]*Department of Internal Medicine, Division of Neurology, St. Marianna University School of Medicine, Kawasaki, Kanagawa, Japan*
[2]*Department of Strokology, Stroke Center, St. Marianna University Toyoko Hospital, Kawasaki, Kanagawa, Japan*

Received: April 8, 2017; Accepted: August 2, 2017
Corresponding author: Yuta Hagiwara, Department of Neurology, St. Marianna University School of Medicine, Sugao, Miyamae-ku, Kawasaki, Kanagawa 216-8511, Japan
Email: y2hagiwara@marianna-u.ac.jp

This work is licensed under a Creative Commons Attribution-NonCommercial-NoDerivatives International License.
©2017 The Japanese Society for Neuroendovascular Therapy

between April 2014 and March 2015 with cerebral angiography, carotid US, carotid plaque MRI, and CEUS prior to CAS to treat severe stenosis of the carotid artery were prospectively enrolled in this study.

The rate of carotid artery stenosis was measured using the North American Symptomatic Carotid Endarterectomy Trial (NASCET) method[5] based on conventional carotid angiography. All patients underwent diagnostic angiography to verify the characteristics of the stenotic lesion. The presence of a stenotic lesion of the internal carotid artery (ICA) responsible for an ipsilateral ischemic stroke was defined as symptomatic ICA stenosis. The aspiration frequency, number of stent placements, and amount and size of debris caught during CAS were recorded and studied for correlations with the preoperative test findings. This study was conducted in a single hospital, and the study protocol was approved by the St. Marianna University Bioethics Committee.

Carotid artery stenting

All procedures were performed via the femoral approach using the Seldinger method. All patients were on long-term antiplatelet therapy using aspirin, clopidogrel, or cilostazol monotherapy or in combination. Unfractionated heparin (10000 units) was administered before starting the procedure. The procedures included proximal balloon protection using Optimo (Tokai Medical Products, Aichi, Japan) and distal balloon protection using Carotid Guardwire PS (Medtronic, Santa Rosa, CA, USA). After predilatation of the stenotic lesion, an appropriate stent for the stenotic lesion was implanted and then dilated. Predilatation was performed in all patients using a balloon catheter, 4 mm or 4.5 mm in diameter. Postdilatation was performed only in patients with placement of a single closed-cell stent using a balloon catheter, 5 mm in diameter.

Debris

After deploying the stent, aspiration of the blood was started while occluding distal blood flow. The debris was removed from the aspirated blood using a filter, and then the blood was returned to the veins via a venous sheath. Aspiration of blood was performed repeatedly using a 20 mL syringe. Visual inspection of the filter was performed at every 4th, 8th, 12th, and 16th aspirations. If any debris was observed at the 16th aspiration, further aspiration was continued until the debris was completely removed. The amount of debris captured by the filter when returning the blood to the veins was also included in the assessment.

All debris was collected in a cell strainer (Medtronic, Minneapolis, MN, USA) and recorded by a digital camera (**Fig. 1**). The size of the debris was classified into three categories, that is, small (<1 mm), medium (≥1 mm and <3 mm), and large (≥3 mm). The amount of debris was classified into three grades based on the amount of small debris, that is, small amount (<10 pieces of debris), medium amount (11–30 pieces of debris), and large amount (>30 pieces of debris). When one medium-sized piece of debris was found, it was counted as three small-sized pieces of debris. Whenever large-sized debris was found, the amount of debris was categorized as a large amount. Based on these definitions, the amount and size of debris were determined by agreement between two neurologists. When there was no agreement, the amount and size were graded by consensus after re-assessment of the photographs.

Ultrasonography

All US examinations were performed by a single doctor qualified by the Japan Academy of Neurosonology. Carotid US with a 7.5-MHz linear probe (SSA-770A Aplio; Toshiba Medical Co., Tokyo, Japan) was used. B-mode imaging and color and power Doppler imaging and CEUS were performed using Sonazoid (perfluorobutane microbubbles; Daiichi Sankyo Pharmaceutical, Tokyo, Japan). A total of 16 μL of Sonazoid were dissolved in 2 mL of water, and an intravenous bolus of 0.15 mL per kg of the contrast agent suspension was injected into the antecubital vein. The acoustic power of the harmonic US was set with a mechanical index (MI) of 0.2–0.3, depth of 3 cm, and focus set at 2.5 cm. The presence of enhanced lesions was identified as the echogenic reflections of microbubbles in the plaque. Carotid plaque was evaluated from the longitudinal and transverse views for about 5 min after contrast injection. The evaluation of enhancement on CEUS was made by two neurologists; the kappa coefficient for diagnostic concordance of plaque enhancement between them was 0.875. According to the echogenicity on B-mode imaging, plaque was categorized as high-echoic, iso-echoic, and low-echoic by the two neurologists. Any sites with variation in plaque echogenicity were regarded as mixed plaques, and they were classified in descending order as having mixed high-, mixed iso-, or mixed hypo-echogenicity.

MRI imaging

Carotid artery BB-MRI was performed with a 1.5 T scanner (Achieva Nova Dual; Philips Healthcare, Best, The Netherlands) using a 16-channel NeuroVascular (NV) coil.

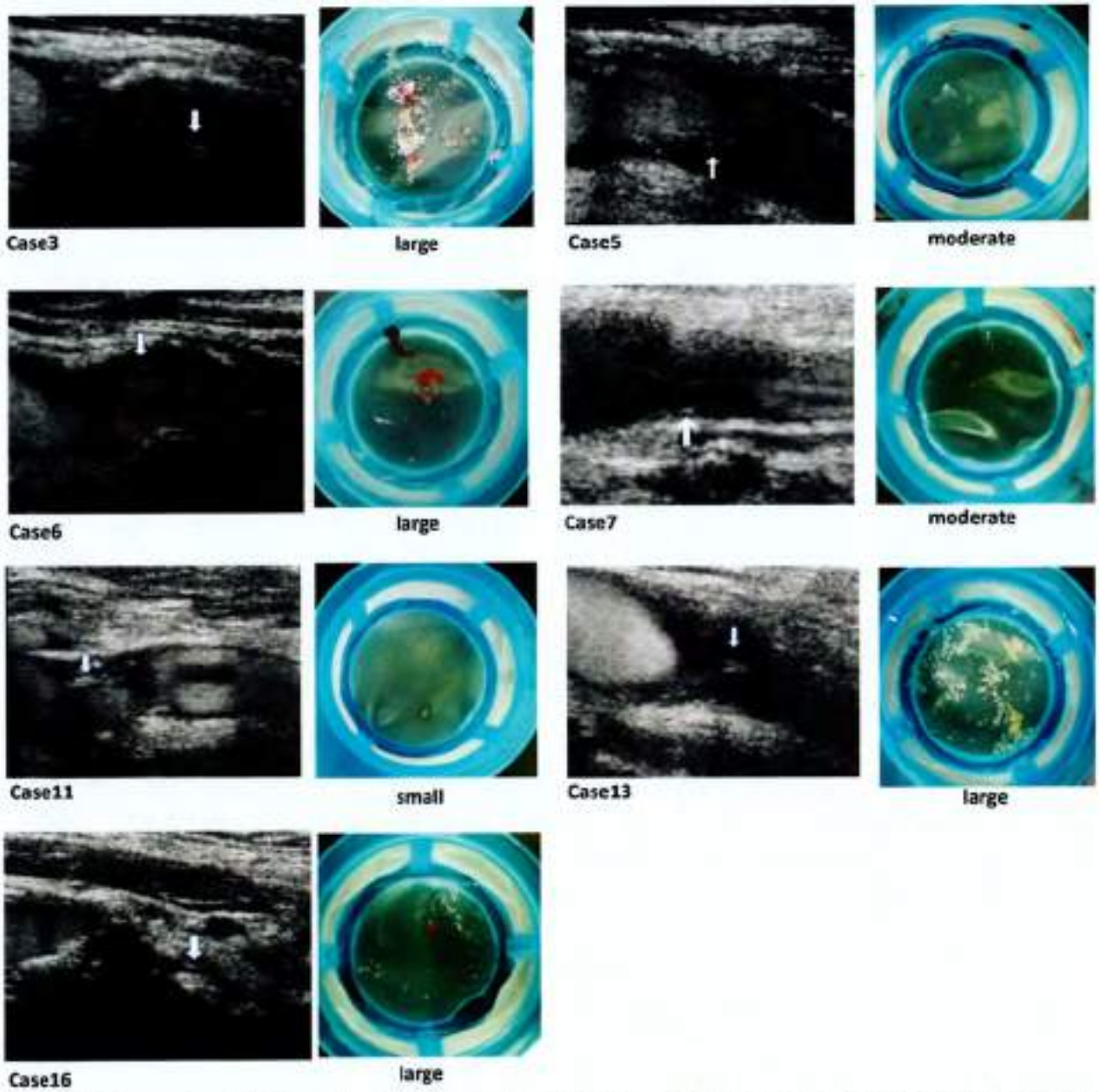

Fig. 1 The left images show the findings of contrast enhancement of carotid plaque, and the right images show debris obtained during carotid artery stenting. The white arrows indicate contrast enhancement of carotid plaque.

For positioning of the greatest wall thickness, a standard imaging protocol was used, that is, TOF, T1-weighted and T2-weighted. For short-axis T1-weighted images (two dimensional [2D] turbo spin echo [TSE]), the parameters were as follows: recovery time (TR) 1 cardiac cycle (1 R-R interval), echo time (TE) 15 ms, matrix 153 × 192, thickness 3 mm, field of view (FOV) 150 mm, number of samples (NSA) 6, and fat saturation (+). For short-axis T2-weighted images (2D-TSE), the parameters were as follows: TR 2 cardiac cycles (2 R-R intervals), TE 80 ms, matrix 153 × 192, thickness 3 mm, FOV 150 mm, NSA 8, and fat saturation (+). For TOF 2D-TSE, the parameters were as follows: TR 23 ms, TE 6.9 ms, matrix 120 × 240, thickness 1.25 mm, number of excitations 1, and fat saturation (+).

For the characterization of carotid plaque, TOF, T1-weighted, and T2-weighted images were used. The signal intensity ratio relative to the ipsilateral sternocleidomastoid muscle, the plaque/muscle ratio (P/M ratio), was calculated, and high intensity was defined as a plaque/muscle ratio >1.5.[6] Unstable plaque was defined as the

presence of a high-intensity signal (HIS) in the carotid plaque on TOF imaging or high intensity of the carotid plaque on T1-weighted imaging.[1,2]

Statistical analyses

The subjects' characteristics are reported as means and standard deviation (SD), unless otherwise indicated. Comparisons between plaque enhancement on CEUS and the amount of debris among large, moderate, and small were performed with chi-squared tests. Comparisons between unstable plaque findings on MRI and the amount of debris among large, moderate, and small were also performed with chi-squared tests for categorical data. A p-value less than 0.05 was considered significant. All statistical analyses were performed using SPSS version 22 (IBM SPSS Statistics for Windows; IBM Corp, Armonk, NY, USA).

Results

Patients' demographics and intraoperative findings are shown in **Table 1**. Plaque enhancement on CEUS was observed in seven patients. **Figure 1** shows the correlation between CEUS findings and the amount of debris in these seven patients with enhanced plaque. Among these seven patients with enhanced plaque, a large amount of debris was observed in four patients, while two patients had a moderate amount, and one patient had a small amount of debris. In the remaining nine patients without plaque enhancement on CEUS (not shown in the figure), the amount of debris was as follows: a large amount in two patients, a moderate amount in one patient, and a small amount in six patients.

For the prediction of a moderate to large amount of debris, enhancement of plaque demonstrated on CEUS had a sensitivity of 66.7% and a specificity of 85.7%. There was a significant association between plaque enhancement on CEUS and the amount of debris (χ^2 test, $p = 0.036$).

In all, 13 patients, including all patients with plaque enhancement on CEUS, were diagnosed as having unstable plaque by carotid plaque MRI. Among these 13 patients with unstable plaque on MRI, a large amount of debris was observed in six patients, while three patients had a moderate amount, and four patients had a small amount of debris. For the prediction of a moderate to large amount of debris, unstable plaque determined by MRI had a sensitivity of 100% and a specificity of 42.9%. There was a significant association between a diagnosis of unstable plaque on MRI and the amount of debris (χ^2 test, $p = 0.029$).

Table 1 Patients' demographics and intraoperative findings

Case	Age (y)	Sex	Symptomatic/ Asymptomatic stenosis	Lesion on DSA (side, %)	Echogenicity of plaque	Sonazoid enhancement	MRI T1-BB P/M ratio	MRI TOF HIS	MRI stability	Debris	Aspiration count (×20 cc)	Stent count
1	71	M	Asymptomatic	L 73	Low	-	0.99	-	Stable	Small	16	1
2	81	M	Asymptomatic	R 70	Mixed iso	-	0.98	+	Unstable	Small	16	1
3	81	M	Symptomatic	L 78	Mixed high	+	1.78	+	Unstable	Large	20	2
4	73	M	Asymptomatic	R 72	Iso	-	0.98	-	Stable	Small	16	2
5	76	M	Asymptomatic	L 65	Low-iso	+	1.83	+	Unstable	Moderate	16	2
6	57	M	Asymptomatic	R 83	Iso	+	2.01	-	Unstable	Large	42	4
7	87	M	Asymptomatic	R 55	Mixed iso	+	1.56	+	Unstable	Moderate	20	1
8	83	M	Asymptomatic	L 60	Mixed iso	-	1.43	+	Unstable	Large	16	2
9	81	M	Symptomatic	R 65	Mixed high	-	0.93	-	Stable	Small	16	1
10	76	M	Symptomatic	R 85	Iso	-	1.46	+	Unstable	Small	16	2
11	77	M	Asymptomatic	L 80	Mixed low	+	0.57	+	Unstable	Small	20	1
12	79	M	Asymptomatic	R 85	Mixed iso	-	1.08	+	Unstable	Large	32	1
13	82	M	Symptomatic	R 95	Low	+	1.81	-	Unstable	Large	62	3
14	70	M	Symptomatic	L 77	Low-iso	-	2.02	+	Unstable	Small	22	1
15	73	F	Asymptomatic	R 72	Mixed high	-	1.88	+	Unstable	Moderate	26	1
16	70	M	Symptomatic	R 80	Mixed high	+	1.76	-	Unstable	Large	40	2

T1-BB P/M ratio: plaque/muscle ratio on T1-black blood; TOF: time-of-flight; HIS: high-intensity signal

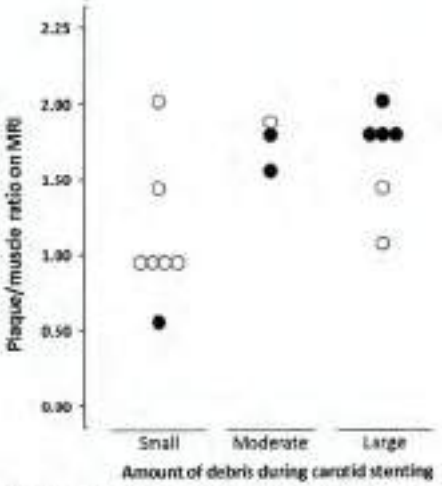

Fig. 2 The plaque characteristics with enhancement of plaque on CEUS and unstable plaque on MRI (plaque/muscle ratio >1.5) is associated with amount of debris. For the prediction of a moderate to large amount of debris had a sensitivity of 100% and a specificity of 75% (χ^2 test, p = 0.036). CEUS: contrast-enhanced carotid ultrasonography, ○: enhancement (−) on CEUS, ●: enhancement (+) on CEUS

All seven patients with plaque enhancement on CEUS showed unstable plaque on MRI. The amount of debris with plaque enhancement on CEUS was as described above. All three patients with no plaque enhancement on CEUS and a diagnosis of stable plaque on MRI had only a small amount of debris.

The scattergram in **Fig. 2** provides the relationship between plaque characteristics and amount of debris during the procedure of CAS. For the prediction of a moderate to large amount of debris, plaque characteristics with enhancement of plaque on CEUS and unstable plaque on MRI had a sensitivity of 100% and a specificity of 75%. There was a significant association between enhancement of plaque on CEUS with unstable plaque on MRI and the amount of debris (χ^2 test, p = 0.036). There was no significant correlation between the number of stents and the amount of debris and between the aspiration count of blood and the amount of debris.

Discussion

Cerebral infarction due to plaque fragmentation and debris during stent deployment is a common occurrence in CAS. This is a major complication, so diagnostic imaging should be used prior to surgery to properly assess plaque stability. Measures to prevent plaque debris from flowing into peripheral regions during surgery include flow reversal using the Parodi Anti-Emboli System[7] and distal protection using balloon occlusion, and predicting the amount of debris likely to be encountered during surgery is a key to selecting the right procedure. Depending on the estimated amount of debris, the surgeon can also decide in advance whether it would be more appropriate to use an open-cell or closed-cell stent.

T1-weighted BB-MRI and TOF MRA have been reported as indicators of plaque stability.[1-3] Unstable findings with high intensity on BB-MRI and TOF MRA were considered to indicate the presence of intra-plaque hemorrhage and neovascularization. Plaque enhancement on CEUS has also been reported as an indicator of intra-plaque neovascularization, fibrous cap degradation, and plaque inflammation, leading to the increased adoption of this new imaging modality in the assessment of plaque stability. CEUS has recently been used to visualize intra-plaque neovascularization as an element of vulnerability.[4,8-12] The source of neovascularization is direct branching from the vasa vasorum or the intimal surface. These areas are very fragile, and plaque hemorrhage can easily occur.[7] Evaluation of neovascularization is therefore important in assessing plaque instability. While CEUS shows neovascularization, intra-plaque hemorrhage and large lipid cores are evaluated as unstable plaque on MRI. Hypo-echoic plaques seen on carotid US are also pathologically associated with large lipid cores and intra-plaque hemorrhage, and they are widely recognized as plaques that confer a high risk of cerebral infarction.[13,14]

The difference between neovascularization and intra-plaque hemorrhage is that neovascularization is a sign of plaque starting to grow; plaque then continues to grow and finally collapses, causing intra-plaque hemorrhage.[15]

Thus, it is considered that CEUS and MRI evaluate different aspects of plaque stability. The difference between these two imaging modalities is considered to be one of the reasons that the combination of these two may allow greater diagnostic accuracy for the prediction of amount of debris.

Six of seven patients with CEUS-enhanced plaque had a moderate to large amount of debris, and there was a significant correlation between plaque enhancement on CEUS and the amount of debris in the present study. Plaque enhancement on CEUS is a potential indicator of the amount of debris during CAS and should therefore be considered prior to surgery.

According to the results of the present study, the sensitivity of plaque enhancement on CEUS was 66.7% and the specificity was 85.7% for a moderate to large amount of debris occurring in CAS. The sensitivity of a diagnosis of unstable plaque

on MRI was 100%, with specificity of 42.9% for a moderate to large amount of debris occurring in CAS.

As a cause of the low sensitivity of CEUS in this study, it is thought that CEUS mainly evaluates neovascularization seen in the early phase of plaque growth. Thus, CEUS may overlook unstable plaque, such as intra-plaque hemorrhage, in the late phase of plaque growth.

As a cause of the low specificity of MRI in this study, the use of cardiac-gated BB-MRI for plaque evaluation may have been involved. Sato et al[16] reported that the plaque/muscle ratio is higher for cardiac-gated BB-MRI than for noncardiac-gated MRI. Therefore, MRI often shows plaque as unstable, which lowers the specificity.

The sensitivity of plaque enhancement on CEUS and unstable plaque determined by BB-MRI was 100%, and the specificity was 75% for a moderate to large amount of debris occurring in CAS. According to the results, the combination of MRI and CEUS can improve both of the sensitivity and specificity.

The present study has some limitations. First, subjective evaluation was used for the categorization of the amount of debris, enhancement on CEUS, and MRI findings. Second, a small number of patients were studied. Third, the technical methods and type of stent were optimized for each patient. These differences might affect the amount of debris. However, the present findings serve for hypothesis generation, and further prospective studies are warranted.

Conclusion

While CEUS alone is currently inadequate for assessing plaque stability prior to CAS, combining this modality with carotid plaque MRI enables a more reliable assessment for the prediction of embolic risk due to debris in CAS. We expect to see an increase in the use of CEUS in the development of therapeutic strategies for CAS in the future.

Disclosure Statement

The authors have no conflicts of interest to declare.

References

1) Qiao Y, Etesami M, Astor BC, et al: Carotid plaque neovascularization and hemorrhage detected by MR imaging are associated with recent cerebrovascular ischemic events. *AJNR Am J Neuroradiol* 2012; 33: 755–760.

2) Yoshimura S, Yamada K, Kawasaki M, et al: High-intensity signal on time-of-flight magnetic resonance angiography indicates carotid plaques at high risk for cerebral embolism during stenting. *Stroke* 2011; 42: 3132–3137.

3) Qiao Y, Etesami M, Malhotra S, et al: Identification of intraplaque hemorrhage on MR angiography images: a comparison of contrast-enhanced mask and time-of-flight techniques. *AJNR Am J Neuroradiol* 2011; 32: 454–459.

4) Mofidi R, Crotty TB, McCarthy P, et al: Association between plaque instability, angiogenesis and symptomatic carotid occlusive disease. *Br J Surg* 2001; 88: 945–950.

5) North American Symptomatic Carotid Endarterectomy Trial. Methods, patient characteristics, and progress. *Stroke* 1991; 22: 711–720.

6) Narumi S, Sasaki M, Natori T, et al: Carotid plaque characterization using 3D T1-weighted MR imaging with histopathologic validation: a comparison with 2D technique. *AJNR Am J Neuroradiol* 2015; 36: 751–756.

7) Parodi JC, Ferreira LM, Sicard G, et al: Cerebral protection during carotid stenting using flow reversal. *J Vasc Surg* 2005; 41: 416–422.

8) Faggioli GL, Pini R, Mauro R, et al: Identification of carotid 'vulnerable plaque' by contrast-enhanced ultrasonography: correlation with plaque histology, symptoms and cerebral computed tomography. *Eur J Vasc Endovasc Surg* 2011; 41: 238–248.

9) Hamada O, Sakata N, Ogata T, et al: Contrast-enhanced ultrasonography for detecting histological carotid plaque rupture: quantitative analysis of ulcer. *Int J Stroke* 2016; 11: 791–798.

10) Saito K, Nagatsuka K, Ishibashi-Ueda H, et al: Contrast-enhanced ultrasound for the evaluation of neovascularization in atherosclerotic carotid artery plaques. *Stroke* 2014; 45: 3073–3075.

11) Deyama J, Nakamura T, Takishima I, et al: Contrast-enhanced ultrasound imaging of carotid plaque neovascularization is useful for identifying high-risk patients with coronary artery disease. *Circ J* 2013; 77: 1499–1507.

12) Alonso A, Artemis D, Hennerici MG: Molecular imaging of carotid plaque vulnerability. *Cerebrovasc Dis* 2015; 39: 5–12.

13) Grønholdt ML, Nordestgaard BG, Schroeder TV, et al: Ultrasonic echolucent carotid plaques predict future strokes. *Circulation* 2001; 104: 68–73.

14) Mathiesen EB, Bønaa KH, Joakimsen O: Echolucent plaques are associated with high risk of ischemic cerebrovascular events in carotid stenosis: the tromsø study. *Circulation* 2001; 103: 2171–2175.

15) Koenig W, Khuseyinova N: Biomarkers of atherosclerotic plaque instability and rupture. *Arterioscler Thromb Vasc Biol* 2007; 27: 15–26.

16) Sato Y, Ogasawara K, Narumi S, et al: Optimal MR plaque imaging for cervical carotid artery stenosis in predicting the development of microembolic signals during exposure of carotid arteries in endarterectomy: comparison of 4 T1-weighted imaging techniques. *AJNR Am J Neuroradiol* 2016; 37: 1146–1154.

PLOS ONE

RESEARCH ARTICLE

Impact of inability to turn in bed assessed by a wearable three-axis accelerometer on patients with Parkinson's disease

Kenji Uchino*☯, Makoto Shiraishi☯, Keita Tanaka☯, Masashi Akamatsu☯, Yasuhiro Hasegawa☯

Department of Neurology, St. Marianna University School of Medicine, Kawasaki, Kanagawa, Japan

☯ These authors contributed equally to this work.
* k2uchino@marianna-u.ac.jp

Check for updates

OPEN ACCESS

Citation: Uchino K, Shiraishi M, Tanaka K, Akamatsu M, Hasegawa Y (2017) Impact of inability to turn in bed assessed by a wearable three-axis accelerometer on patients with Parkinson's disease. PLoS ONE 12(11): e0187616. https://doi.org/10.1371/journal.pone.0187616

Editor: Christian Veauthier, Charite Medical University Berlin, GERMANY

Received: April 5, 2017

Accepted: October 23, 2017

Published: November 9, 2017

Copyright: © 2017 Uchino et al. This is an open access article distributed under the terms of the Creative Commons Attribution License, which permits unrestricted use, distribution, and reproduction in any medium, provided the original author and source are credited.

Data Availability Statement: All relevant data are within the paper.

Funding: This study was supported by internal funds from St. Marianna University School of Medicine. The funder had no role in study design, data collection and analysis, decision to publish, or preparation of the manuscript.

Competing interests: Thw authors have declared that no competing interests exist.

Abstract

Background

Difficulty turning over in bed is a common night-time symptom in Parkinson's disease (PD). We aimed to quantitatively evaluate overnight turnover movements using a three-axis accelerometer and to investigate whether inability to turn in bed is related to daytime sleepiness, sleep quality, and depressive mood in PD patients.

Methods

We examined 64 patients with PD (mean age, 73.3±8.21 years; modified Hoehn-Yahr [mH-Y] stage, 3.0±1.0; disease duration, 7.2±6.3 years; unified Parkinson's disease rating scale [UPDRS], 36.9±18.3). Overnight monitoring of turnover movements using a wearable three-axis accelerometer was performed in all patients. Nocturnal kinetic parameters including total time recumbent, total time supine, number of turnover movements, and mean interval between turnover movements were obtained. Daytime immobility was assessed using the Barthel index (B-I), UPDRS, and mH-Y stage. Patients were also assessed with the Epworth Sleepiness Scale (ESS), Parkinson's Disease Sleep Scale-2 (PDSS-2), and Beck Depression Inventory (BDI).

Results

Number of turnover movements in bed correlated negatively with disease duration ($r = -0.305$; $p<0.05$), L-dopa-equivalent dose ($r = -0.281$; $p<0.05$), mH-Y staging ($r = -0.336$; $p<0.01$), total score of UPDRS ($r = -0.386$; $p<0.01$) and positively with B-I score ($r = 0.365$; $p<0.01$). Number of turnover movements in bed was generally inconsistent with awareness of turnover movement impairment as evaluated by PDSS-2 Item 9 scores, but patients who were never aware of impaired turnover movements showed $\geq$5 turnover movements overnight. Multivariate logistic regression analyses revealed no correlations between number of nocturnal turnover movements in bed and BDI, ESS, or PDSS-2. Use of anti-psychotic

drugs was associated with ESS (p = 0.045). UPDRS was associated with PDSS-2 (p = 0.016).

Conclusion

Decreased number of turnover movements may not be a direct determinant of daytime sleepiness, sleep disorders, or depressive mood in PD patients. Use of anti-psychotic drugs and higher UPDRS score are factors significantly associated with daytime sleepiness and uncomfortable sleep, respectively.

Introduction

Difficulty turning over in bed is one of the motor symptoms of Parkinson's disease (PD), with a prevalence of 45±82% for this subjective complaint [1±4]. Nocturnal movement and sleep disorders such as rapid eye movement sleep behavior disorder in PD patients have been extensively studied using polysomnography [5±7]. Whether this nocturnal motor deficit affects the quality of life of PD patients thus remains unclear. In recent years, the accuracy of three-axis accelerometers has improved together with advances in miniaturization, and wearable accelerometers are now available to analyze kinetic data of overnight movements in PD patients [8±11]. This sensor-based kinetic analysis may shed light on the real clinical impact of difficulty turning over in bed among PD patients. This study set out to objectively assess nocturnal turnover movements in PD patients with overnight monitoring using a wearable three-axis accelerometer to test the hypothesis that inability to turn in bed would negatively impact on daytime sleepiness, sleep quality, and depressive mood in PD patients.

Patients and methods

Study population

We examined PD patients who met the following inclusion criteria: 1) fulfilment of the diagnostic criteria described by the UK Parkinson Disease Society brain bank [12]; 2) age $\geq$18 years; 3) provision of written informed consent to participate in this study; 4) treatment with the same antiparkinsonian drug during the 2 weeks before entry; and 5) ability to comply with the study protocol. We excluded patients with: 1) serious concurrent disease such as severe inflammatory disease (white blood cell count $> 1.0 \times 10^4$ mm^3; C-reactive protein $>$ 3.0 mg/dl); 2) hallucination or delusion; or 3) dementia (Mini-Mental State Examination [MMSE] $<$16). No restrictions were placed on disease duration. This study was conducted in a single hospital, and the study protocol was approved by the St. Marianna University Bioethics Committee (approval no. 2487). All participants provided written informed consent.

Overnight monitoring of turnover movements in bed

We used a published method for assessing turnover movements in bed with the three-axis accelerometer [8]. To state the method in brief, a wearable motion recorder (75 mm × 50 mm × 20 mm, 120 g) equipped with three-axis acceleration sensors (Mimamori-Gait system, MG-M1110-HW; LSI Medience, Tokyo, Japan) was fixed on the center of the abdomen at the navel using a special belt (Fig 1). Three-axis acceleration data were collected at 100 Hz and serially stored in the micro Secure Digital memory card of the recorder through A/D conversion. All patients were monitored for 10 h from 21:00 to 07:00 the next day, and data were analyzed offline using commercially available software (MG-M1100-PC; LSI Medience). The

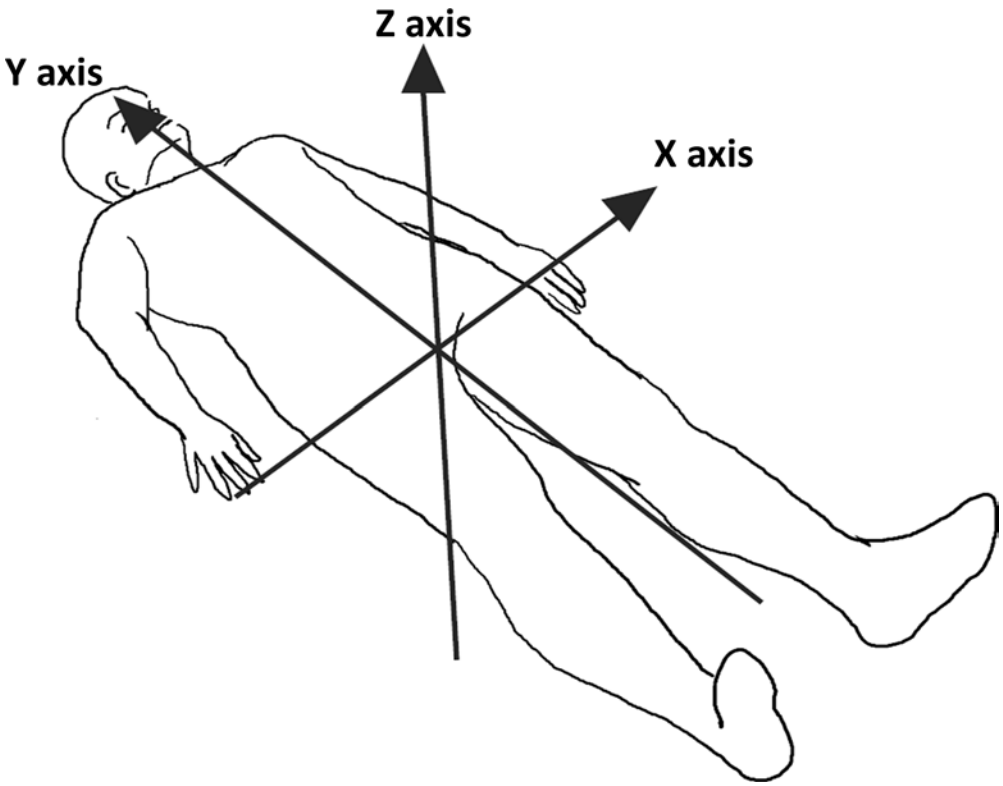

Fig 1. Three-axis accelerometer sensor axes in the recumbent position. X axis: from right to left; Y axis: from caudal to rostral; Z axis: from back to front.

https://doi.org/10.1371/journal.pone.0187616.g001

nocturnal kinetic parameters used in this study were: 1) total time recumbent; 2) total time supine; 3) number of turnover movements; and 4) mean interval between turnover movements.

Typical overnight monitoring charts are shown in Fig 2. Variations in acceleration along the X, Y, and Z axes are represented by red, blue, and green lines, respectively. As a turnover movement in bed is a movement around the Y axis, acceleration in the Y axis direction remains essentially zero (blue lines in Fig 2A and Fig 2B). Turnover movements in bed were defined as movements simultaneously registering acceleration along the three axes as follows: $\geq$0.58 G for the X axis; $\leq$0.32 G for the Y axis; and $\geq$0.20 G for the Z axis. These cut-off values were derived based on a 95% confidence interval to detect patient rotations $\geq$30Êaround the center of the anteroposterior axis as turnover movements in bed [8]. Accordingly, turnover movements with angles of rotation <30Êwere not regarded as turnover movements in bed. Turnover movements in bed can thus be counted based on the typical turnover movements followed by a stable period (Fig 2).

Once a turnover movement occurs, body position remains stable for a variable duration from a few minutes to hours. Evaluating not only the number of turnover movements but also the pattern of appearance of turnover movements is important. Some PD patients showed several clusters of turnover movement with short duration and staying in supine sleep for a long time. We thus introduced the mean interval between turnover movements in this study. The position of the patient (i.e., recumbent, sitting, or standing) based on the waveform of the Y axis is also easy to determine. Total measurement period was 600 min, and the amount of time the patient stayed in an upright position (acceleration on the Y axis $\approx$ 1.0), which was assumed to represent the patient being awake and out of bed, was subtracted from this total

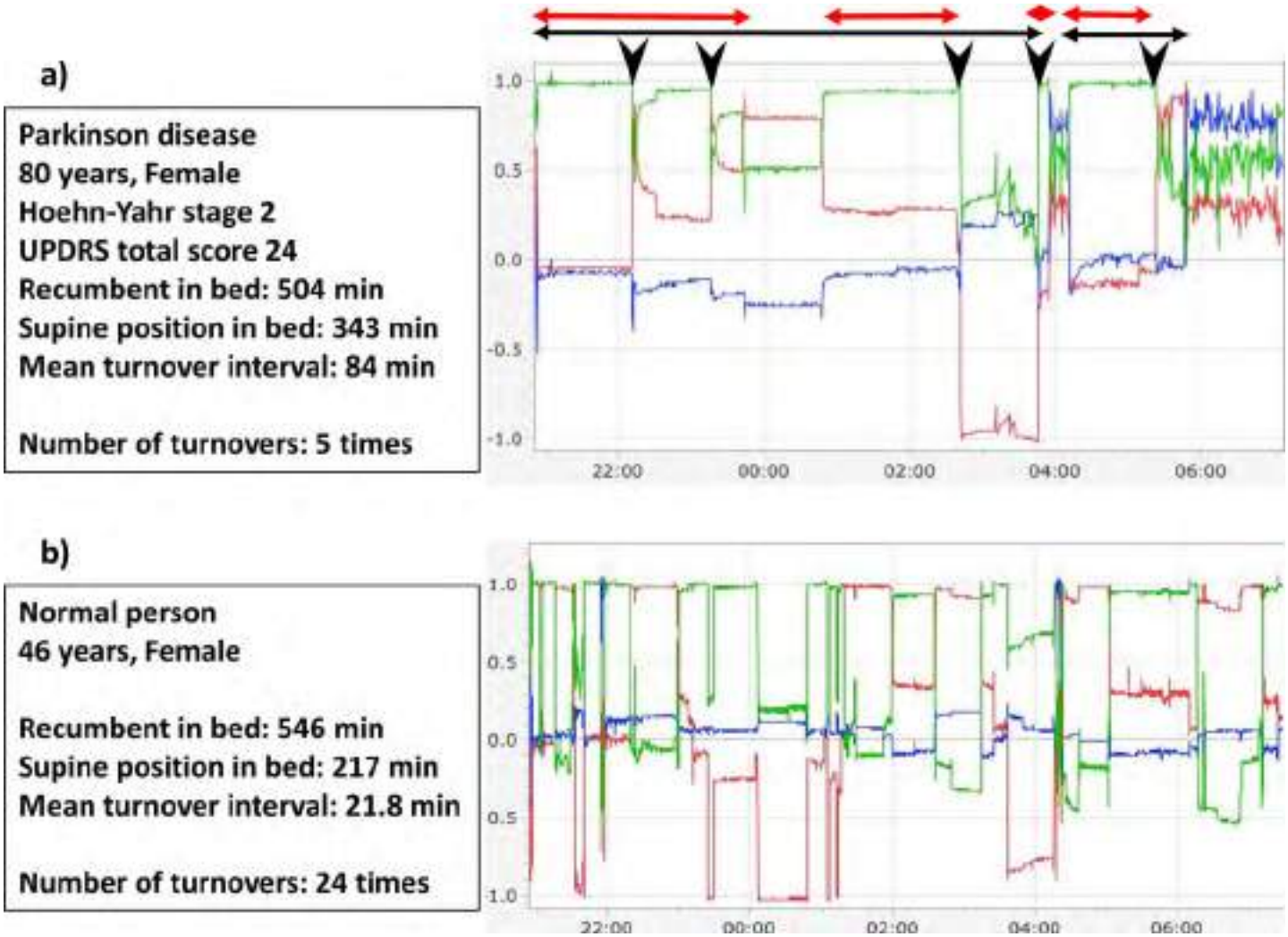

Fig 2. Number of turnover movements in bed in PD patients and healthy subjects. Representative overnight recordings from 21:00 to 07:00 the following day are shown. a) Chart from a PD patient. Arrowhead indicates turnover movement, black lines indicate time recumbent, and red lines indicate time supine. b) Chart from a healthy subject. Variations in acceleration along the X, Y, and Z axes are represented by red, blue, and green lines, respectively.

https://doi.org/10.1371/journal.pone.0187616.g002

measurement period to obtain the duration spent in bed in a recumbent position, i.e., total time recumbent. We also obtained the total time supine, because several studies have shown that the supine sleep of PD patients is associated with increased obstructive sleep apnea, suggesting that for individuals with PD, alleviating the difficulties of turning over in bed might reduce time spent in the supine sleep position and improve sleep-disordered breathing [13].

The reliability of measurement results was verified by overnight monitoring for 11 PD patients (5 men; mean age, 76.1 years; median Hoehn and Yahr (H-Y) scale measurement, 4 [2±5]) twice, at an interval of 2 days. For the number of turnover movements, these measurements yielded an intraclass correlation coefficient of 0.737 ($p = 0.019$).

Clinical data collection

Clinical characteristics of each patient in the study were assessed by a certified neurologist. The clinical background of each patient (age, disease duration, initial presentation, and oral

medication) was checked. The dose of antiparkinsonian drugs (levodopa [L-dopa], dopamine agonists, and catechol-O-methyltransferase [COMT] inhibitors) was converted into an L-dopa-equivalent dose (LED), as necessary [14]. We also established whether patients were taking drugs that could be expected to affect sleep or depression such as sleeping medication, anti-depressants, anti-psychotic drugs, or amantadine. Severity of PD was assessed using a modified H-Y (mH-Y) staging scale [15] and the UPDRS [16]. Activities of daily living were assessed using the Barthel index (B-I) [17]. UPDRS assessments included the total score and sub-scores for Parts 2 and 3.

Sleepiness, awareness of sleep disturbance, and depressive features were assessed with the Epworth Sleepiness Scale (ESS) [18], Parkinson's Disease Sleep Scale-2 (PDSS-2) [19, 20], and the Beck Depression Inventory (BDI) [21], respectively. Subjective awareness of difficulty turning in bed in each patient was classified into five categories from Score 0 to Score 4 using a question in PDSS-2 item 9 ([a]Did you feel uncomfortable at night because you were unable to turn in bed or move due to immobility?[o]). Possible responses to this question were scored as: 0, [a]never[o]; 1, [a]occasionally (1 night/week)[o]; 2, [a]sometimes (2±3 nights/week)[o]; 3, [a]often (4±5 nights/week)[o]; or 4, [a]very often (6±7 nights/week)[o].

Statistical analyses

Characteristics of patients are given as the mean and standard deviation (SD), unless otherwise indicated. Unpaired Student's *t* test was used to compare continuous variables, and χ^2 tests were used for nominal parameters. The Mann-Whitney U test and Kruskal-Wallis test were used for data that did not show normal distributions. Relationships between clinical scales and nocturnal kinetic parameters were investigated using Spearman's rank correlation analysis. Overnight frequency of turnover movement in patients with PD was divided into quartiles and logistic regression models adjusted for potential confounders including age, disease duration, and mH-Y scale score were used to estimate odds ratios with 95% confidence intervals for associations with the first quartile (i.e., lowest frequency group). For logistic regression analysis, ESS scores $\geq$10 were taken to indicate excessive daytime sleepiness [18], PDSS-2 scores $\geq$15 were taken to indicate sleep disturbance [22], and BDI scores $>$20 were taken to indicate moderate to severe depressive features [21]. Two-sided p-values $<$0.05 were considered statistically significant. All statistical analyses were performed using SPSS Statistics for Windows version 21 software (IBM, Armonk, NY).

Results

We examined 65 patients with PD from April 2013 to July 2016. Overnight monitoring of turnover movements was performed in all patients. We excluded 1 patient for whom overnight recordings were discontinued because of hallucinations. A total of 64 patients (35 men; mean age, 73.3±8.21 years) were analyzed. Patient demographic characteristics are shown in Table 1. Daytime assessment results were as follows: B-I, 76.6±27.4; UPDRS, 36.9±18.3 (range, 4±88); BDI, 15.5±12.4 (range, 0±43); ESS, 7.03±4.55 (range, 0±19); and PDSS-2, 19.3±9.96 (range, 1±49). Mean LED for patients was 540±317 mg (range, 0±1265 mg). Thirty-five patients (54.7%) were treated with dopamine agonist, with pramipexole as the most widely used medication (17 patients, 26.6%). Eleven patients were taking anti-psychotic drugs to prevent hallucinations, and eight patients were taking antidepressants.

Turnover movements and severity of PD

Disease duration, LED, mH-Y staging, B-I and UPDRS (total score, Part 2, and Part 3) correlated significantly with nocturnal parameters (Table 2). Number of turnover movements in

Table 1. Patient characteristics.

	Patients with PD n = 64
Age, mean (SD)	73.3 (8.21)
Male sex, n (%)	35 (54.7)
Height, m (SD)	159 (9.77)
Weight, kg (SD)	54.2 (12.2)
BMI, kg/m^2 (SD)	21.2 (3.65)
Age at onset, years (SD)	66.1 (10.1)
Disease duration, years (SD)	7.22 (6.28)
Modified Hoehn-Yahr staging (SD)	3.0 (1.0)
Barthel index (SD)	76.6 (27.4)
Unified Parkinson's Disease Rating Scale	
Total score	36.9 (18.3)
Part 1	2.61 (2.03)
Part 2	10.9 (6.76)
Part 3	19.9 (11.4)
Part 4	2.39 (2.99)
Beck Depression Inventory	15.5 (12.4)
Epworth Sleepiness Scale	7.03 (4.55)
Parkinson's Disease Sleep Scale-2	19.3 (10.0)
LED, mg (SD)	540 (317)
Dopamine agonist, n (%)	35 (54.7)
Pramipexole, n (%)	17 (26.6)
Rotigotine, n (%)	8 (12.5)
Ropinirole, n (%)	11 (17.2)
Ergot, n (%)	1 (1.56)
Amantadine, n (%)	9 (14.1)
Sleeping drug, n (%)	15 (23.4)
Antipsychotic drug, n (%)	11 (17.2)
Antidepressant, n (%)	8 (12.5)

LED, L-dopa-equivalent dose; SD, standard deviation.

https://doi.org/10.1371/journal.pone.0187616.t001

bed correlated negatively with duration of disease (r = -0.305; $p<0.05$), LED (r = -0.281; $p<0.05$), mH-Y staging (r = -0.336; $p<0.01$), total score of UPDRS (r = -0.386; $p<0.01$), UPDRS Part 2 (r = -0.317; $p<0.05$), and UPDRS Part 3 (r = -0.310; $p<0.05$), and positively with B-I score (r = 0.365; $p<0.01$). Higher mH-Y stage and UPDRS score indicate poor function, whereas higher B-I score indicates better activities of daily living. The tendencies of correlation coefficients are thus similar. For total time recumbent, total time supine, and mean interval between turnover movements, tendencies of correlation coefficients were similar; i.e., patients with poor motor activity as indicated by mH-Y, B-I, and UPDRS scores tended to show longer time staying in bed, longer time staying supine, and longer interval between turnover movements. These relationships were similarly observed in disease duration and LED. Correlations between number of turnover movements and patient characteristics are shown in Fig 3.

The frequency of turnover movements in bed for PD patients by quartile was as follows: 0±2 times, n = 17; 3±5 times, n = 16; 6±11 times, n = 16; and ≥12 times, n = 15. Predictive accuracies of mH-Y, B-I, and UPDRS for the 1st quartile (0±2 turnover movements) were obtained from receiver operated characteristics curve (ROC) analysis, with areas under the

Table 2. Correlation coefficients between nocturnal parameters and patient's characteristics.

	Age	Disease duration	LED	mH-Y staging	Barthel index	UPDRS Total	UPDRS Part 1	UPDRS Part 2	UPDRS Part 3	UPDRS Part 4
Number of Turnovers	-.100	**-.305***	**-.281***	**-.336****	**.365****	**-.386****	.019	**-.317***	**-.310***	-.217
Total Time for recumbent position	.039	**.313***	**.311***	**.407****	**-.425****	**.286***	.152	**.307***	.181	.111
Total Time for supine position	.230	**.252***	-.071	**.307***	**-.435****	**.317***	.098	.227	.255	-.005
Mean interval of turnovers	.121	**.350****	**.325****	**.381****	**-.410****	**.412****	.000	**.345***	.334*	.223

Values represent Spearman correlation coefficients.

*p<0.05

**p<0.01.

LED, L-dopa-equivalent dose; mH-Y scale, modified Hoehn-Yahr scale; UPDRS, Unified Parkinson's Disease Rating Scale.

https://doi.org/10.1371/journal.pone.0187616.t002

ROC curves of 0.685 (95% confidence interval (CI), 0.532±0.839), 0.698 (95%CI, 0.553±0.844), and 0.709 (95%CI, 0.559±0.858), respectively.

Awareness of inability to turn in bed and actual number of turnover movements in bed

Relationships between subjective awareness of difficulty turning in bed as categorized by the PDSS-2 item 9 and nocturnal kinetic parameters are shown in Table 3. Although PD patients with a higher score for PDSS-2 item 9 tended to show longer total time recumbent and longer

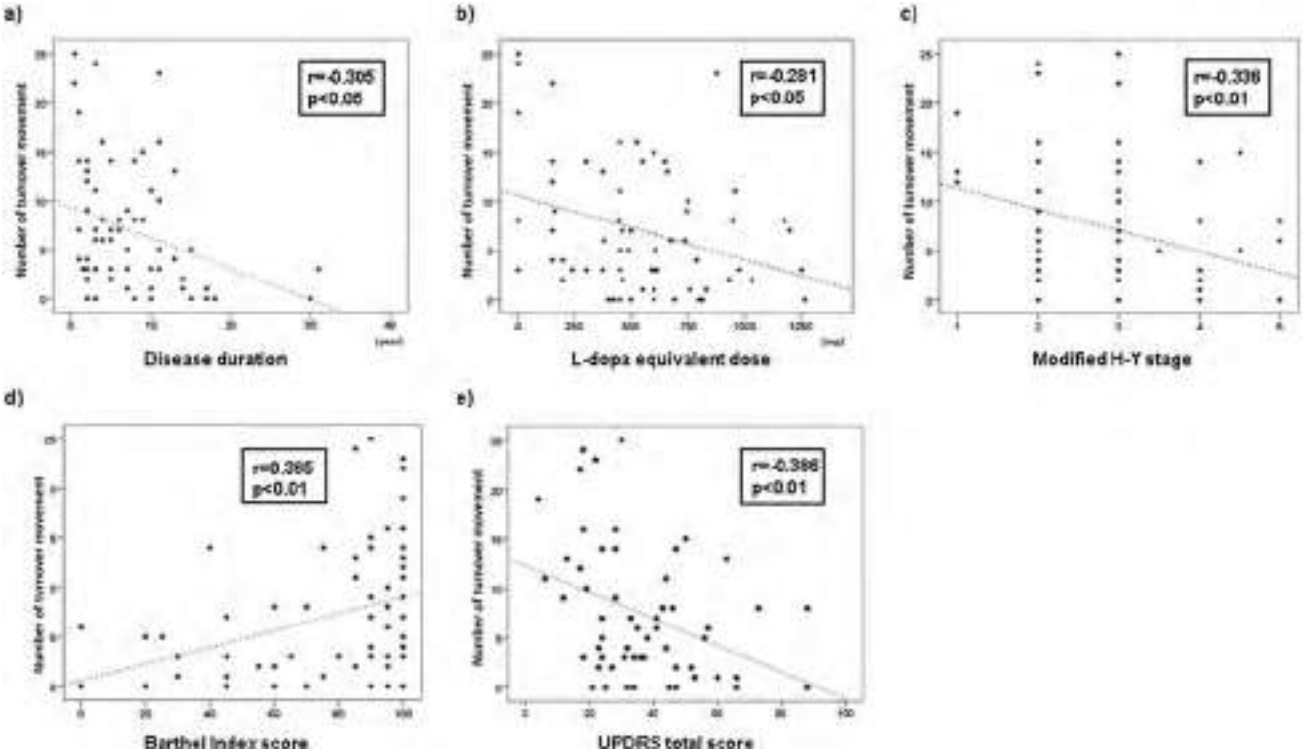

Fig 3. Correlations between number of turnover movements in bed and background factors. Number of turnover movements in bed correlated significantly with disease duration (a), L-dopa equivalent dose (b), modified H-Y stage (c), B-I (d), and total UPDRS score (e).

https://doi.org/10.1371/journal.pone.0187616.g003

Table 3. Subjective awareness of difficulty turning in bed as evaluated by PDSS-2 item 9 and nocturnal kinetic parameters.

	Score 0 (Never)	Score1 (Occasionary)	Score2 (Sometimes)	Score3 (Often)	Score 4 (Very often)	P value
Number of Turnovers, median (min-max)	5 (4±8)	5 (2±13)	6 (1±7)	6 (2±10)	3 (1±12)	0.077
Total Time for recumbent position, mean (SD) minutes	520.4(49.1)	514.4 (47.9)	540.2 (39.0)	489.0 (72.1)	563.2 (36.9)	0.771
Total Time for supine position, mean (SD) minutes	299.1(156.3)	346.0 (141.1)	322.6 (129.9)	337.3 (123.5)	277.0 (158.2)	0.133
Mean interval of turnovers, mean (SD) minutes	45.6 (22.8)	225.1 (204.4)	86.9 (85.6)	153.9 (173.9)	168.4 (205.7)	0.081

https://doi.org/10.1371/journal.pone.0187616.t003

mean interval between turnover movements (p = 0.077 and p = 0.081, respectively), no significant difference was observed among the 5 groups categorized by PDSS-2 item 9 scores.

Scattergrams in Fig 4 show the relationship between number of turnover movements and mean interval between consecutive turnover movements. Visual analysis of data from patients

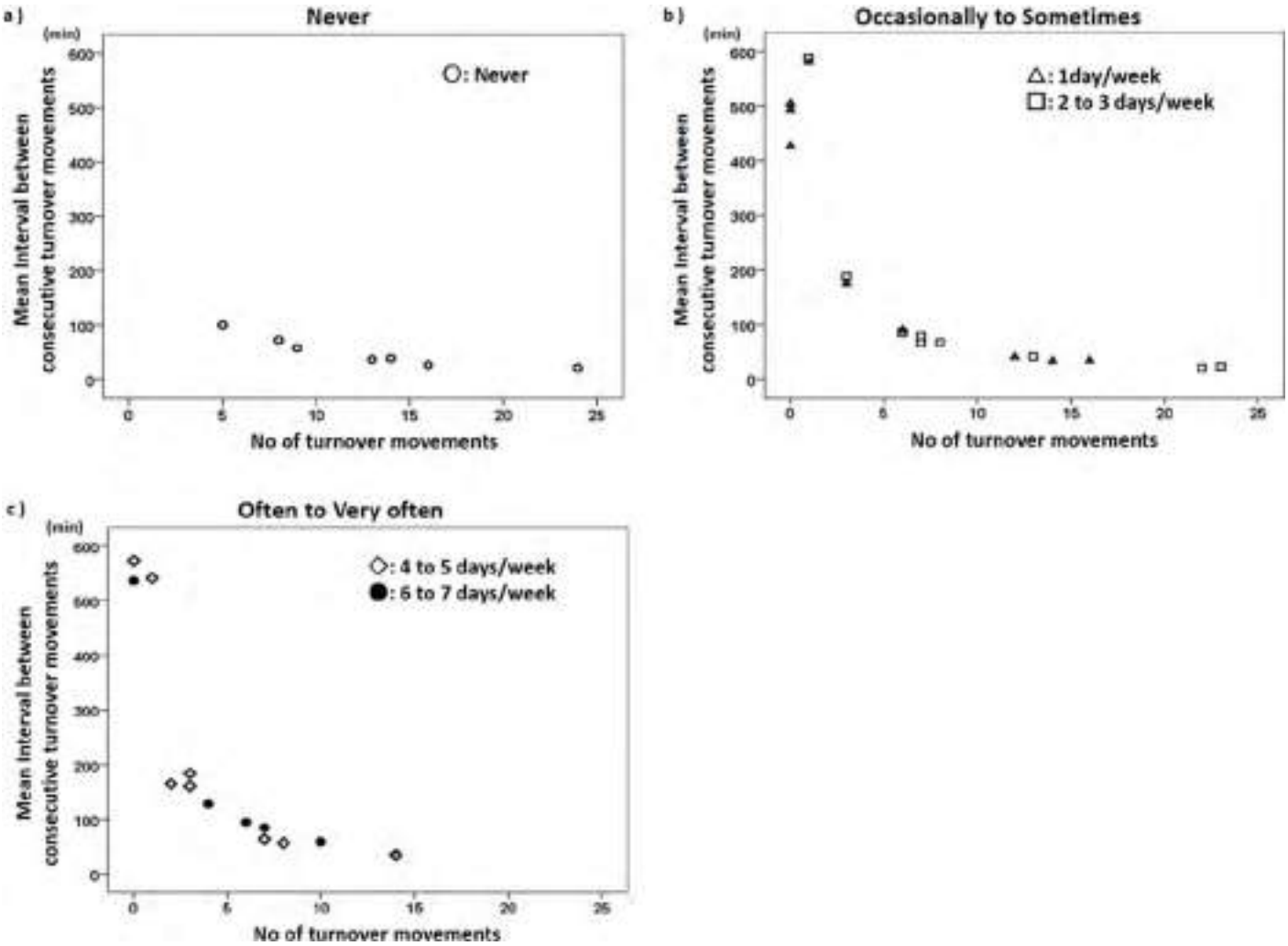

Fig 4. Subjective scoring of discomfort and immobility in bed as evaluated by PDSS-2 Item 9 and objective numbers of overnight turnover movements. Mean interval between consecutive turnover movements (minutes) as plotted against number of turnover movements in scattergrams by subjective scores as evaluated by PDSS-2 item 9: never aware of impairment of turnover movement (a); occasionally to sometimes (b); and often to very often (c). In patients with no subjective complaint, number of turnover movements overnight was ≥5 and mean interval between consecutive turnovers was <100 min (a). Among patients showing >5 turnover movements, various PDSS-2 Item 9 scores ranging from 0 to 4 (ªneverº to ªvery oftenº) were noted.

https://doi.org/10.1371/journal.pone.0187616.g004

who were never aware of impairment of turnover movement (PDSS-2 Item 9 Score = 0) showed ≥5 turnover movements overnight (Fig 4A). Patients who were often or very often aware of impaired turnover movement (PDSS-2 Item 9 Score = 3 or 4) showed a maximum of 15 turnover movements in overnight measurements. However, among patients showing 5±15 turnover movements, various PDSS-2 Item 9 scores ranging from 0 to 4 (ᵃnever° to ᵃvery often°) were noted. The number of turnover movements in bed was thus generally inconsistent with awareness of impaired turnover movement as evaluated by PDSS-2 Item 9 scores.

Correlations between number of turnover movements in bed, sleepiness and depressive features

A total of 58 patients (90.6%) were receiving L-dopa and 6 patients (9.4%) were receiving other drugs. A total of 24 patients (37.5%) were receiving L-dopa alone, and 34 patients (53.1%) were receiving concomitant treatment with L-dopa and dopamine adjuvants. We constructed a model using age, LED, UPDRS, use of sleeping drugs, use of anti-psychotic drugs, use of dopamine agonists, and number of nocturnal turnover movements in bed, and investigated associations between each of these factors and outliers in ESS, PDSS-2, and BDI in multivariate logistic regression analysis (Table 4). Anti-psychotic drug use was significantly associated with ESS scores ≥10, and UPDRS was significantly associated with PDSS-2 scores ≥15. No factors were significantly associated with depressive features as evaluated by BDI score (>20). Number of nocturnal turnover movements in bed was not significantly correlated with BDI, ESS, or PDSS-2 abnormal score.

Discussion

Nocturnal parameters including number of turnover movements, time spent in a recumbent position in bed, time spent in a supine position in bed, and mean interval between consecutive turnover movements correlated significantly with disease duration, LED, mH-Y, UPDRS total score, and B-I (Table 2 and Fig 3). These results suggest that less frequent nocturnal turnover movements and longer period spent recumbent or supine are observed in PD patients showing deterioration in scores reflecting daytime immobility, greater disease duration, and LED. It is reasonable to assume that the degree of daytime immobility is also predictive of night-time motor disability. Our study demonstrated UPDRS total score as the most predictive for turnover movement impairment (area under the ROC curve, 0.709) and the number of turnover movements in bed correlated significantly with mH-Y, B-I, and UPDRS. However, the most

Table 4. Multivariate logistic regression analyses.

	ESS			PDSS-2			BDI		
	OR	(95%CI)	p	OR	(95%CI)	p	OR	(95%CI)	p
Age	0.951	(0.829±1.090)	0.471	0.785	(0.596±1.035)	0.087	1.004	(0.892±1.131)	0.941
LED	1.003	(0.999±1.007)	0.193	0.999	(0.995±1.003)	0.554	1.003	(0.999±1.007)	0.211
UPDRS	1.002	(0.943±1.064)	0.948	1.152	(1.027±1.291)	**0.016**	1.019	(0.967±1.075)	0.476
Sleeping drugs	0.103	(0.005±2.244)	0.148	1.293	(0.140±11.971)	0.821	3.156	(0.475±20.954)	0.232
Antipsychotics	46.183	(1.099±1941.5)	**0.045**	1.941	(0.091±41.363)	0.671	1.920	(0.209±17.648)	0.564
Dopamine agonist	2.442	(0.229±26.00)	0.459	0.599	(0.067±5.384)	0.647	0.833	(0.090±7.728)	0.872
Number of turnovers	1.174	(0.972±1.353)	0.105	1.062	(0.907±1.245)	0.454	0.924	(0.794±1.075)	0.331

ESS, Epworth Sleepiness Scale; PDSS-2, Parkinson's Disease Sleep Scale-2; BDI, Beck Depression Inventory

For logistic regression analysis, ESS score ≥10, PDSS-2 score ≥15, and BDI score >20 were taken to indicate excessive daytime sleepiness, sleep disturbance, and moderate to severe depressive features, respectively.

https://doi.org/10.1371/journal.pone.0187616.t004

significant correlation (UPDRS, -0.386) still yielded a low coefficient. Our study also demonstrated that number of turnover movements in bed was generally inconsistent with awareness of turnover movement impairment as evaluated by PDSS-2 Item 9 score (Fig 4), implying that nocturnal immobility should be assessed objectively with three-axis accelerometers rather than subjectively by self-report.

This study posed the question of whether night-time immobility affects quality of life among PD patients, but multivariate logistic regression analysis failed to demonstrate an association between number of turnover movement and outliers of ESS, PDSS-2, and BDI. Use of anti-psychotic drugs and UPDRS total score appeared to represent major determinants for outliers of ESS and PDSS-2, respectively. No factor, including number of turnover movements in bed, was significantly associated with BDI. We thus conclude that nocturnal immobility may not be a major determinant of daytime sleepiness, nor mood disorders including depressive features in PD patients. However, further studies are needed to answer this question. Bhidayasiri et al. recently demonstrated that nocturnal apomorphine infusion improved nocturnal hypokinesia in PD patients using a wearable three-axis accelerometer [11]. Rotigotine treatment reportedly improved UPDRS Part 2 sub-score and PDSS in a study by Trenkwalder et al. [19]. Prolonged-release ropinirole tablets reportedly improved objective quality of sleep in a study by Dusek et al. [23]. These drugs can be expected to ameliorate nocturnal symptoms. The real clinical significance of nocturnal turnover movement impairment needs to be investigated in further research focusing on how nocturnal turnover movement impairment can be ameliorated with adjustments in dopamine agonist medication and how such treatments can improve quality of life in PD patients. We therefore consider that the method of overnight monitoring with three-axis accelerometers reported in this study has great utility for such therapeutic intervention studies. In such studies, use of antipsychotic drugs and UPDRS score should be considered as important confounders.

A number of limitations need to be considered when interpreting the results of this study. First, we did not perform polysomnographic analysis. Our sensor-based monitoring of nocturnal movement can detect periods of wakefulness based on body position, but sleep stage in the recumbent position in bed cannot be evaluated. In future studies focusing on daytime sleepiness or mood disorders, polysomnography combined with a sensor-based kinetic method may provide comprehensive data. A second limitation concerns the definition of turnover movements in bed for this study, which was based on the method reported by Akamatsu et al. [8]. Sensors were set to pick up movements $\geq$30Êaround the posteroanterior body axis. Accordingly, any effects of movements involving corresponding rotations $<$30Êduring sleep would not have been identified in this study. The third limitation concerned the nature of this research as a cross-sectional, observational study.

Acknowledgments

We wish to thank Professor Koichi Hirata and Keisuke Suzuki from the Department of Neurology, Dokkyo Medical University, for permission to use the Japanese version of the PDSS-2.

Author Contributions

Conceptualization: Kenji Uchino, Makoto Shiraishi, Masashi Akamatsu, Yasuhiro Hasegawa.

Data curation: Kenji Uchino, Makoto Shiraishi, Keita Tanaka, Masashi Akamatsu.

Formal analysis: Kenji Uchino, Makoto Shiraishi.

Investigation: Kenji Uchino, Makoto Shiraishi.

Methodology: Kenji Uchino, Makoto Shiraishi, Keita Tanaka, Masashi Akamatsu.

Software: Makoto Shiraishi.

Supervision: Makoto Shiraishi, Yasuhiro Hasegawa.

Validation: Makoto Shiraishi, Yasuhiro Hasegawa.

Writing ± original draft: Kenji Uchino, Makoto Shiraishi, Yasuhiro Hasegawa.

Writing ± review & editing: Yasuhiro Hasegawa.

References

1. Louter M, Munneke M, Bloem BR, Overeem S. Nocturnal Hypokinesia and Sleep Quality in Parinson's Disease. J Am Geriatr Soc. 2012; 60: 1104±1108. https://doi.org/10.1111/j.1532-5415.2012.03966.x PMID: 22642534
2. Lees AJ, Blackburn NA, Campbell VL. The nighttime problems of Parkinson's disease. Clin Neuropharmacol, 1988; 11: 512±519. PMID: 3233589
3. Stack EL, Ashburn AM. Impaired bed mobility and disordered sleep in Parkinson's disease. Mov Disord. 2006; 21: 1340±1342. https://doi.org/10.1002/mds.20944 PMID: 16773640
4. Gjerstad MD, Wentzel-Larsen T, Aarsland D, Larsen JP. Insomnia in Parkinson's disease: frequency and progression over time. J Neurol Neurosurg Psychiatry. 2007; 78: 476±479. https://doi.org/10.1136/jnnp.2006.100370 PMID: 17098844
5. Yong MH, Fook-Chong S, Pavanni R, Lim LL, Tan EK. Case control polysomnographic studies of sleep disorders in Parkinson's disease. PLoS One. 2011; 6(7): e22511. https://doi.org/10.1371/journal.pone.0022511 PMID: 21799880
6. Bhidayasiri R, Sringean J, Rattanachaisit W, Truong DD. The sleeping brain in Parkinson's disease: A focus on REM sleep behaviour disorder and related parasomnias for practicing neurologists. J Neurol Sci. 2017; 374: 32±37. https://doi.org/10.1016/j.jns.2017.01.018 PMID: 28126342
7. Arnulf I, Neutel D, Herlin B, Golmard JL, Leu-Semenescu S, Cochen de Cock V, et al. Sleepness in Idiopathic REM Sleep Behavior Disorder and Parkinson Disease. Sleep. 2015; 38: 1529±1535. https://doi.org/10.5665/sleep.5040 PMID: 26085299
8. Akamatsu M, Shiraishi M, Uchino K, Maki F, Tsuruoka A, Tanaka S, et al. Overnight monitoring of turnover, movements in Parkinson's disease using a wearable three-axis accelerometer. J Neurol Disord. 2016; 4: 267.
9. Bhidayasiri R, Sringean J, Taechalertpaisarn P, Thanawattano C. Capturing nighttime symptoms in Parkinson disease: Technical development and experimental verification of inertial sensors for nocturnal hypokinesia. J Rehabil Res Dev. 2016; 53: 487±98. https://doi.org/10.1682/JRRD.2015.04.0062 PMID: 27533042
10. Sringean J, Anan C, Thanawattano C, Bhidayasiri R. Time for a strategy in night-time dopaminergic therapy? An objective sensor-based analysis of nocturnal hypokinesia and sleeping positions in Parkinson's disease. J Neurol Sci. 2017; 15: 244±248.
11. Bhidayasiri R, Sringean J, Anan C, Boonpang K, Thanawattano C, Chaudhuri R. Quantitative demonstration of the efficacy of night-time apomorphine infusion to treat nocturnal hypokinesia in Parkinson's disease using wearable sensors. Parkinsonism Relat Disord. 2016; 33: 36±41. https://doi.org/10.1016/j.parkreldis.2016.09.008
12. Gibb WR, Lees AJ. The relevance of the Lewy body to the pathogenesis of idiopathic Parkinson's disease. J Neurol Neurosurg Psychiatry. 1988; 51: 745±752. PMID: 2841426
13. Cochen De Cock V, Benard-Serre N, Driss V, Granier M, Charif M, Carlander B et al. Supine sleep and obstructive sleep apnea syndrome in Parkinson's disease. Sleep Med. 2015; 16: 1497±501. https://doi.org/10.1016/j.sleep.2014.09.014 PMID: 26611947
14. Tomlinson CL, Stowe R, Patel S, Rick C, Gray R, Clarke CE. Systematic review of levodopa dose equivalency reporting in Parkinson's disease. Mov Disord. 2010; 25: 2649±2653. https://doi.org/10.1002/mds.23429 PMID: 21069833
15. Goetz CG, Poewe W, Rascol O, Stebbins GT, Counsell C, Giladi N, et al. Movement Disorder Society Task Force Report on the Hoehn and Yahr Staging Scale: Status and recommendations. Mov Disord. 2004; 19: 1020±1028. https://doi.org/10.1002/mds.20213 PMID: 15372591
16. Fahn S, Elton RL, UPDRS program members. Unified Parkinsons Disease Rating Scale. In: Fahn S, Marsden CD, Goldstein M, Calne DB, editors. Recent developments in Parkinsons disease, vol 2. Florham Park, NJ: Macmillan Healthcare Information; 1987. p 153±163.

17. Mahoney FI, Barthel DW. FUNCTIONAL EVALUATION: THE BARTHEL INDEX. Md State Med J. 1965; 14:61±65.

18. Johns MW. A new Methods for Measuring Daytime Sleepiness: The Epworth Sleepiness Scale. Sleep. 1991; 14: 540±545. PMID: 1798888

19. Suzuki K, Miyamoto M, Miyamoto T, Tatsumoto M, Watanabe Y, Suzuki S, et al. Nocturnal disturbances and restlessness in Parkinson's disease: using the Japanese version of the Parkinson's disease sleep scale-2. J Neurol Sci. 2012; 318:76±81. https://doi.org/10.1016/j.jns.2012.03.022 PMID: 22534309

20. Trenkwalder C, Kies B, Rudzinska M, Fine J, Nikl J, Honczeghy P, et al. Rotigotine effects of on early morning motor function and sleep in Parkinson`s disease: a double-blind, randomized, placebo-controlled study(RECOVER). Mov Disord. 2011; 26: 90±99. https://doi.org/10.1002/mds.23441 PMID: 21322021

21. Wang YP, Gorenstein C. Assessment of depression in medical patients: a systematic review of the utility of the Beck Depression Inventory-II. Clinics. 2013; 68: 1274±1287. https://doi.org/10.6061/clinics/2013(09)15 PMID: 24141845

22. Suzuki K, Miyamoto T, Miyamoto M, Suzuki S, Numao A, Watanabe Y, et al. Evaluation of cutoff scores for the Parkinson's disease sleep scale-2. Acta Neurol Scand. 2015; 131: 426±430. https://doi.org/10.1111/ane.12347 PMID: 25402773

23. Dusek P, Buskova J, Ruzicka E, Majerova V, Srp A, Jech R, et al. Effects of ropinerole prolonged-release on sleep disturbances and daytime sleepiness in Parkinson's disease. Clin Neuropharmacol. 2010; 33: 186±189. https://doi.org/10.1097/WNF.0b013e3181e71166 PMID: 20661025

Akiyama et al. BMC Neurology (2017) 17:148
DOI 10.1186/s12883-017-0926-y

BMC Neurology

CASE REPORT Open Access

Effectiveness of spinal cord stimulation for painful camptocormia with Pisa syndrome in Parkinson's disease: a case report

Hisanao Akiyama[1*], Saki Nukui[1], Masashi Akamatu[1], Yasuhiro Hasegawa[1], Osamu Nishikido[3] and Soichiro Inoue[2]

Abstract

Background: Spinal cord stimulation (SCS) has recently been reported to be effective for truncal postural abnormalities such as camptocormia and Pisa syndrome in Parkinson's disease. In this case report, we describe a case of a woman with Parkinson's disease in whom SCS was effective for painful camptocormia with Pisa syndrome.

Case presentation: A 65-year-old woman was admitted to our hospital because of painful camptocormia. She had noticed resting tremor in the left upper limb and aprosody at 48 years of age. She was diagnosed as having Parkinson's disease (Hoehn & Yahr stage 1) at 53 years of age. Cabergoline was started during that same year, with subsequent addition of selegiline hydrochloride; the symptoms of parkinsonism disappeared. Wearing-off occurred when she was 57 years old, 3 years after starting carbidopa/levodopa, and truncal postural abnormalities—painful camptocormia with Pisa syndrome to the right—appeared at 58 years of age. These symptoms worsened despite adjustment of her oral medications, and deep brain stimulation (DBS) was performed when she was 60 years old. The truncal postural abnormalities improved after DBS, and she could travel abroad at 61 years of age. However, from 62 years of age, painful camptocormia with Pisa syndrome to the right reappeared. The pain was unsuccessfully treated with oral analgesics, radiofrequency coagulation of the dorsal and medial branches of the lumbar spinal nerve, and lumbar epidural block. Finally, SCS was performed for the pain relief. The pain disappeared immediately after SCS and her posture then gradually improved. Unified Parkinson's Disease Rating Scale score improved from 48 to 34 points and Timed Up and Go Test improved from 15 s to 7 s after SCS.

Conclusions: This case suggests that SCS may be effective for improving painful truncal postural abnormalities and motor complications of Parkinson's disease. Pain relief or a direct effect on the central nervous system by SCS was considered to explain the alleviation of these symptoms.

Keywords: Spinal cord stimulation, Parkinson's disease, Painful truncal postural abnormality, Camptocormia, Pisa syndrome

Background

Truncal postural abnormalities such as camptocormia and Pisa syndrome, as well as Parkinson's-related and -unrelated pain, are not uncommon in patients with Parkinson's disease [1, 2], and medical treatment for these symptoms is often difficult. An alternative treatment strategy is spinal cord stimulation (SCS), which was recently reported to be effective for truncal postural abnormalities, chronic pain, and motor symptoms of Parkinson's disease, though the mechanism of SCS remains unclear [3–5].

In this case report, we present a case of painful camptocormia that was effectively treated with SCS in a woman with Parkinson's disease. In addition, we briefly review the past literature.

Case presentation

A 65-year-old woman with Parkinson's disease was admitted to our hospital because of painful camptocormia. She had a past medical history of postoperative adhesive intestinal obstruction after surgery for cancer of the uterine body. She was a housewife and had no significant social history of drinking and smoking. She had noticed resting tremor of the left upper limb and aprosody at 48 years of age. When she was 53 years old, she was diagnosed as

* Correspondence: h2akiyama@marianna-u.ac.jp
[1]Department of Neurology, St. Marianna University School of Medicine, 2-16-1 Sugao, Miyamae-ku, Kawasaki, Kanagawa 216-8511, Japan
Full list of author information is available at the end of the article

BioMed Central

© The Author(s). 2017 **Open Access** This article is distributed under the terms of the Creative Commons Attribution 4.0 International License (http://creativecommons.org/licenses/by/4.0/), which permits unrestricted use, distribution, and reproduction in any medium, provided you give appropriate credit to the original author(s) and the source, provide a link to the Creative Commons license, and indicate if changes were made. The Creative Commons Public Domain Dedication waiver (http://creativecommons.org/publicdomain/zero/1.0/) applies to the data made available in this article, unless otherwise stated.

having Parkinson's disease (Hoehn & Yahr stage 1) according to the UK Parkinson's Disease Society Brain Bank criteria [6]. At the time of diagnosis, magnetic resonance imaging (MRI) of the head showed no abnormality such as bilateral outer layer slit high-intensity lesions on T2-weighted imaging (suggesting putaminal atrophy), hot cross bun sign, and brain stem and cerebellar atrophy. Oral administration of cabergoline and selegiline hydrochloride resulted in improvement in her parkinsonism symptoms, but their effectiveness decreased gradually after 6 months. Subsequently, carbidopa/levodopa 100 mg was started at 54 years of age, and the wearing-off phenomenon occurred when she was 57 years old. Painful camptocormia with Pisa syndrome to the right appeared at the age of 58 years. Despite several adjustments to her medications, such as increasing up to the maximum dose of 400 mg carbidopa/levodopa or decreasing the dose of dopamine agonist, her symptoms worsened. She underwent deep brain stimulation (DBS) at 60 years of age. Model 3387 DBS leads (Medtronic, Inc., Minneapolis, MN; medical device certificate number 20700BZY00880000) were inserted into both subthalamic nuclei and connected to two neurostimulators (Activa SC; Medtronic, Inc., Minneapolis, MN; medical device certificate number 22300BZX00414000). The DBS parameters were as follows. Right internal generator program: anode, contact case; cathode, contacts Nos. 2 and 3; amplitude, 3.5 V; pulse width, 60 μs; frequency, 60 Hz. Left internal generator program: anode, contacts case; cathode, contact Nos. 2 and 3; amplitude, 3.2 V; pulse width, 60 μs; frequency, 60 Hz maximally. By 1 year after commencing DBS, when she was 61 years old, the camptocormia had disappeared completely. As a result, she could travel abroad independently. However, the painful camptocormia with Pisa syndrome reappeared at 62 years of age. Oral administration of analgesics, radiofrequency coagulation of the medial and dorsal branches of the spinal nerves L2/3, 3/4, and 4/5, and lumbar epidural block were administered for the lumbar pain, but were ineffective. At that time, ^{123}I–ioflupane dopamine transporter SPECT (DAT scan) revealed severe hypo-accumulation (right dominant) in both striata; and head CT revealed no brain stem and cerebellar atrophy at 64 years of age. She was hospitalized for SCS in March 2016 because a temporary 1-week testing trial of SCS utilizing a pair of Vectris SureScan® MRI 1 × 8 Compact leads (Medtronic, Inc.; medical device certificate number 22500BZX00346000) and external generator External Stim® (Medtronic, Inc.; medical device certificate number 22100BZX00196000) in February was found to be effective.

On admission, her oral medications were carbidopa/levodopa 800 mg in 4 divided doses (2–2–3–1 tablets), pramipexole 4.5 mg in 3 divided doses, istradefylline 20 mg once daily, midodrine hydrochloride 8 mg in 2 divided doses, limaprost alfadex 15 μg in 3 divided doses, teprenone 150 mg in 3 divided doses, and loxoprofen 180 mg in 3 divided doses. General examination revealed no abnormalities except for the bilateral anterior thoracic DBS generators. On neurological examination she was fully conscious, with aprosody, and masked facies. The cranial nerves, motor system, reflexes, sensory system, coordination, and meningeal signs were all normal, though urinary incontinence was present. Regarding extrapyramidal symptoms, there was no resting tremor or rigidity in the limbs, but bradykinesia, postural instability, and painful camptocormia with Pisa syndrome to the right were observed (Fig. 1, top left). Urinalysis, blood tests, electrocardiogram, and chest X-ray revealed no abnormalities except for mild degenerative lumbar spondylosis on spinal X-ray (Fig. 1, top right). Cardiac metaiodobenzylguanidine scintigraphy and DAT scan were not performed during this admission. The Unified Parkinson's Disease Rating Scale (UPDRS) score was 48 (part I, 4; II, 25; III, 15; IV, 4) and Timed Up and Go Test was 15 s before SCS implantation.

After admission, on 12 May 2016, a PrimeAdvanced SureScan® MRI pulse generator (Medtronic, Inc.; Medical device certificate number 22500BZX00345000) was implanted and a pair of Vectris SureScan® MRI 1 × 8 Compact leads were inserted percutaneously. Skin was punctured at the level of L3 on the right and L4 on the left, and the top of the stimulation points was at the level of Th8 (Fig. 1, bottom) as a result of adjustment to achieve pain relief with mild paresthesia. For the SCS implant, the pulse generator was placed in the subcutaneous pocket of the lower abdomen. SCS parameters were as follows. Program 1: anode, contacts Nos. 2 and 10; cathode, contact Nos. 0, 1, and 8; amplitude, 2.5 V; pulse width, 450 μs; and frequency, 7 Hz. Program 2: anode, contact No. 0; cathode, contact No. 1; amplitude, 3.5 V; pulse width, 250 μs and frequency, 7 Hz.

Pain was markedly improved after SCS implantation, with the visual analog scale score improving from 10 points before SCS to 2 points after SCS on the day of surgery. The camptocormia also improved gradually after SCS (Fig. 2), UPDRS score improved from 48 points (part II, 25) to 33 points (part I, 5; II, 10; III, 15; IV, 3), with a particularly large improvement for part II (which evaluates activities of daily living). The Timed Up and Go Test markedly improved from 15 s before SCS to 8 s on the 11th day after SCS at the same time of day (always measured at 14:00, during the ON period). By the 29th day after SCS, the camptocormia had further improved; the UPDRS score was 34 points (part II, 12), and the Timed Up and Go Test was 7 s during the ON period. In addition, the following improvements were observed in scores for chronic pain, psychiatric symptoms, and disability after SCS: Numerical Rating Scale, 9 to 7; Leeds Assessment of

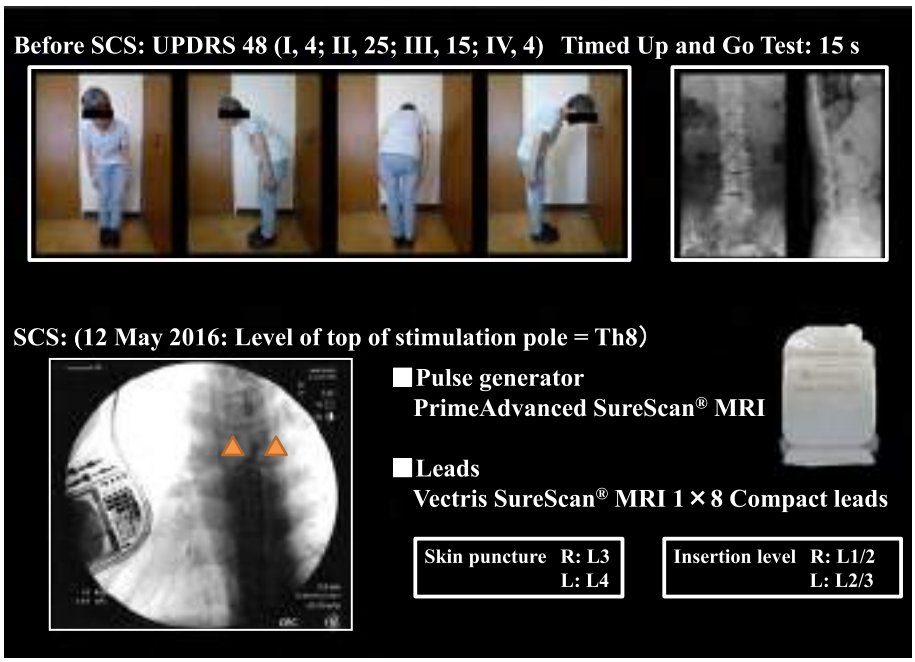

Fig. 1 Painful camptocormia and SCS device. The patient's camptocormia with Pisa syndrome to the right (top *left*). Spinal X-ray revealed mild degenerative lumbar spondylosis (top *right*). For SCS, a PrimeAdvanced SureScan® MRI pulse generator was implanted and a pair of Vectris SureScan® MRI 1 × 8 Compact leads were inserted percutaneously

Neuropathic Symptoms and Signs Pain Scale, 11 to 5; Hospital Anxiety and Depression Scale 4 to 9; EuroQol (EQ-5S), 0.101 to 0.208; and Pain Disability Assessment Scale, 39 to 36. Her general condition has remained satisfactory for 6 months as of this writing.

Discussion

Postural abnormalities such as camptocormia occur with a prevalence of approximately 3.0–12.7% in patients with Parkinson's disease [1]. Camptocormia is one of the motor symptoms that adversely affect activities of daily

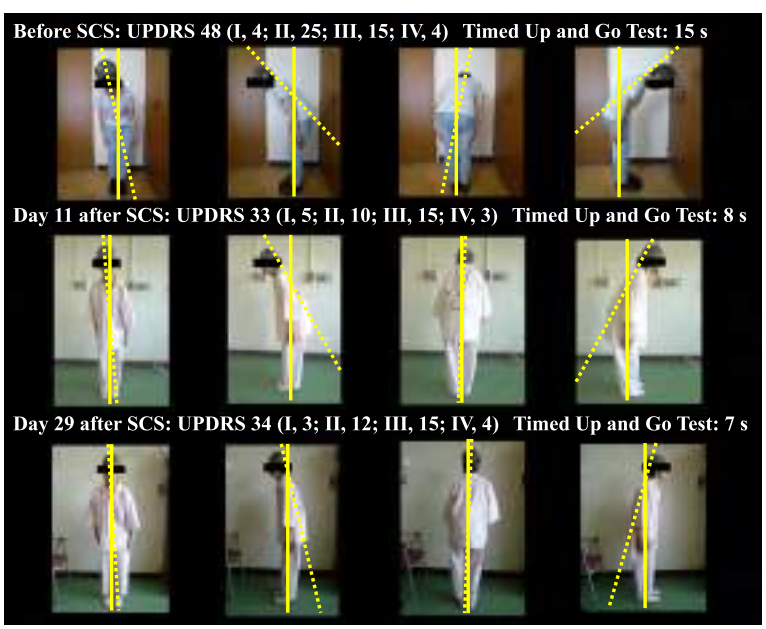

Fig. 2 Improvement of painful camptocormia with Pisa syndrome after SCS. Painful camptocormia and Pisa syndrome to the right improved gradually after SCS

living. Many possible causes of camptocormia have been reported, including muscle rigidity and dystonia in the abdomen, proprioceptive deficits, adverse effects of dopamine agonists, soft tissue imbalance, and fatty degeneration and myopathy in the back muscles, but details remain unclear [7]. Although there is no effective curative therapy, several symptomatic therapies are reported to be effective, including dosage of oral carbidopa/levodopa or dopamine agonists, botulinum toxin injections, and DBS [3, 8–11]. Meanwhile, pain in the low back and legs is common in Parkinson's disease, with a prevalence of approximately 40–85% [3]. Camptocormia occurs with or without pain, and either way, it is an important factor impairing activities of daily living. However, the mechanism underlying the onset of pain is still not known [2]. Pain can be Parkinson's disease-related or -unrelated, but strictly distinguishing between the two types is clinically difficult. Given that drug resistance commonly occurs, SCS has been investigated, which relieves pain by electrically stimulating the posterior funiculus. SCS was recently shown to be particularly effective in patients with Parkinson's disease-unrelated pain and/or postural abnormalities [3–5]. In the present case, SCS therapy was effective for a patient with Parkinson's disease who had camptocormia accompanied by intractable chronic pain in the absence of bone lesions and who had no history of botulinum toxin injection, showed resistance to oral carbidopa/levodopa and dopamine agonists, and had previously experienced transient alleviation of symptoms by DBS.

The mechanism of pain relief by SCS is generally explained by the gate control theory proposed by Melzack and Wall in 1965, but the details remain unclear [12]. Based on the gate control therapy, several mechanisms involved in pain relief by SCS have been proposed. For instance, stimulation of the posterior funiculus by SCS causes excitation of thick Aβ sensory fibers and excitation of thick Aβ fibers leads to suppression of sensory pain C fibers at the spinal dorsal horn. Blockage of pain at the spinal dorsal horn and the spinothalamic tract occurs by retrograde impulse conduction, which activates inhibitory neurons, increases GABA release, and reduces excitatory glutamic acid level. Other mechanisms have also been reported: activation of the descending pain suppression pathway and direct stimulation of the thalamus by SCS ascending impulses, leading to pain relief and improvement of failed sensory modulation action in the basal ganglia [4, 13–19].

In our patient, pain relief was observed immediately after both temporary and permanent placement of the SCS device, followed by gradual improvement in postural abnormalities such as camptocormia with Pisa syndrome. This suggests indirect alleviation of postural abnormalities via pain relief by SCS, as described by Agari et al. [3]. However, the time lag between pain relief (immediately recognized after placement of the SCS device) and alleviation of postural abnormalities (gradually recognized roughly 10 days after placement of the SCS device), and the complete but transient disappearance of camptocormia after DBS, which directly affects the central nervous system (including the subthalamic nucleus or globus pallidus), suggests a pain relief-independent mechanism for the alleviation of camptocormia in our patient, in whom stimulation of the posterior funiculus resulted in improvement, directly alleviating abnormalities of central nerve circuits such as the cortico-basal ganglia-thalamic loop via the medial lemniscus-thalamic system. Such direct effects on the central and peripheral nervous systems have already been confirmed in animal models [20–22], indicating the need for studies investigating the effect of SCS in patients with camptocormia but no pain.

Notably, the scores for UPDRS part II and postural abnormalities were markedly improved in this case. Alleviation of postural abnormalities and improved motor function can be explained by an indirect effect of pain relief due to SCS, but a pain relief-independent explanation, involving direct correction of the trunk posture and consequent adjustment of the dynamic center of body mass, has also been reported [3]. Given the time difference between pain relief and alleviation of camptocormia by SCS observed in our case, neither a direct nor an indirect mechanism can be eliminated in explaining the alleviation of individual symptoms. Furthermore, improvement in activities of daily living indicates the possibility that SCS can also alleviate motor symptoms in patients with parkinsonism and motor dysfunction.

Conclusions

This case suggests that SCS could be effective for improving camptocormia or Pisa syndrome and motor symptoms of Parkinson's disease through pain relief, and is a treatment option for postural abnormalities such as camptocormia and Pisa syndrome and for parkinsonism with Parkinson's-unrelated pain. There is a possibility that SCS works through a mechanism other than pain relief, and further accumulation of cases is needed.

Abbreviations

DAT: dopamine transporter; DBS: deep brain stimulation; MRI: magnetic resonance imaging; SCS: spinal cord stimulation; UPDRS: Unified Parkinson's Disease Rating Scale

Acknowledgements

Not applicable.

Funding

None.

Availability of data and materials

All data contained in the manuscript.

Authors' contributions
HA examined the patient, drafted the manuscript, and created the figs. SN and MA performed the UPDRS test for this patient. YH helped draft the manuscript. ON and SI implanted the SCS device. All authors read and approved the final manuscript.

Ethics approval and consent to participate
The Human Research Ethics Committee of St. Marianna University Hospital provided a waiver considering that approval is not necessary for a single case report. Written informed consent was obtained from the patient.

Consent for publication
Written informed consent for publication of clinical details and images was obtained from the patient. A copy of the consent form is available for review by the journal editor.

Competing interests
The authors declare that they have no competing interests.

Publisher's Note
Springer Nature remains neutral with regard to jurisdictional claims in published maps and institutional affiliations.

Author details
[1]Department of Neurology, St. Marianna University School of Medicine, 2-16-1 Sugao, Miyamae-ku, Kawasaki, Kanagawa 216-8511, Japan. [2]Department of Anesthesiology, St. Marianna University School of Medicine, Kawasaki, Kanagawa, Japan. [3]Department of Palliative Medicine, Showa University Northern Yokohama Hospital, Yokohama, Kanagawa, Japan.

Received: 23 March 2017 Accepted: 18 July 2017
Published online: 17 August 2017

References
1. Seki M, Takahashi K, Koto A, Mihara B, Morita Y, Isozumi K, Ohta K, Muramatsu K, Gotoh J, Yamaguchi K, Tomita Y, Sato H, Nihei Y, Iwasawa S, Suzuki N, on behalf of Keio Parkinson's Disease Database. Camptocormia in Japanese patients with Parkinson's disease: a multicenter study. Mov Disord. 2011;26(14):2567–71.
2. Fil A, Cano-de-la-Cuerda R, Muñoz-Hellín E, Vela L, Ramiro-González M, Fernández-de-Las-Peñas C. Pain in Parkinson disease: a review of the literature. Parkinsonism Relat Disord. 2013;19(3):285–294; discussion 285. doi:10.1016/j.parkreldis.2012.11.009.
3. Agari T, Date I. Spinal cord stimulation for the treatment of abnormal posture and gait disorder in patients with Parkinson's disease. Neurol Med Chir (Tokyo). 2012;52:470–4.
4. Nishioka K, Nakajima M. Beneficial therapeutic effects of spinal cord stimulation in advanced cases of Parkinson's disease with intractable chronic pain: a case series. Neuromodulation. 2015;18:751–3.
5. De Andrade EM, Ghilardi MG, Cury RG, Barbosa ER, Fuentes R, Teixeira MJ, Fonoff ET. Spinal cord stimulation for Parkinson's disease: a systematic review. Neurosurg Rev. 2016 ;39(1):27–35; discussion 35. doi:10.1007/s10143-015-0651-1.
6. Hughes AJ, Daniel SE, Kilford L, Lees AJ. Accuracy of clinical diagnosis of idiopathic Parkinson's disease: a clinic-pathological study of 100 cases. J Neurol Neurosurg Psychiatry. 1992;55:181–4.
7. Doherty KM, van de Warrenburg BP, Peralta MC, Silveria-Moriyama L, Azulay J-P, Gershanik OS, Bloem BR. Postural deformities in Parkinson's disease. Lancet Neurol. 2011;10(6):538–49. doi:10.1016/S1474-4422(11)70067-9.
8. Azher SN, Jankovic J. Camptocormia: pathogenesis, classification, and response to therapy. Neurol. 2005;65(3):355–9.
9. Ho B, Prakash R, Morgan JC, Sethi KD. A case of levodopa-responsive camptocormia associated with advanced Parkinson's disease. Nat Clin Pract Neurol. 2007;3(9):526–30.
10. Finsterer J, Strobl W. Presentation, etiology, diagnosis, and management of camptocormia. Eur Neurol. 2010;64(1):1–8. doi:10.1159/000314897.
11. Fukaya C, Otaka T, Obuchi T, Kano T, Nagaoka T, Kobayashi K, Oshima H, Yamamoto T, Katayama Y. Pallidal high-frequency deep brain stimulation for camptocormia: an experience of three cases. Acta Neurochir Suppl. 2006;99:25–8.
12. Melzack R, Wall PD. Pain mechanisms: a new theory. Science. 1965;150:971–9.
13. Thang TC, Janik JJ, Grill WM. Mechanisms and models of spinal cord stimulation for the treatment of neuropathic pain. Brain Res. 2014;1569:19–31. doi:10.1016/j.brainres.2014.04.039.
14. Larson SJ, Sances A Jr, Riegal DH, Meyer GA, Dallmann DE, Swiontek T. Neurophysiological effects of dorsal column stimulation in man and monkey. J Neurophysiol. 1974;41:217–23.
15. Campbell JN. Examination of possible mechanisms by which stimulation of the spinal cord in man relieves pain. Appl Neurophysiol. 1981;44:181–6.
16. Meyerson BA, Herrregodts P, Linderoth B, Ren B. An experimental animal model of spinal cord stimulation for pain. Stereotact Funct Neurosurg. 1994; 62:256–62.
17. Duggan AW, Foong FW. Bicuculline and spinal inhibition produced by dorsal column stimulation in the cat. Pain. 1985;22:249–59.
18. Stiller CO, Cui JG, O'Connor WT, Brodin E, Meyerson BA, Linderoth B. Release of GABA in the dorsal horn and suppression of tactile allodynia by spinal cord stimulation in mononeuropathic rats. Neurosurgery. 1996;39:367–75.
19. Cui JG, O'Connor WT, Ungerstedt U, Linderoth B, Meyerson BA. Spinal cord stimulation attenuates augmented dorsal horn release of excitatory amino acids in mononeuropathy via a GABAergic mechanism. Pain. 1997;73:87–95.
20. Fuentes R, Petersson P, Nicolelis MA. Restoration of locomotive function in Parkinson's disease by spinal cord stimulation: mechanistic approach. Eur J Neurosci. 2010;32(7):1100–8. doi:10.1111/j.1460-9568.2010.07417.x.
21. Hassan S, Amer S, Alwaki A, Elborno A. A patient with Parkinson's disease benefits from spinal cord stimulation. J Clin Neurosci. 2013 Aug;20(8):1155–6. doi:10.1016/j.jocn.2012.08.018.
22. Brys I, Bobela W, Schneider BL, Aebischer P, Fuentes R. Spinal cord stimulation improves forelimb use in an alpha-synuclein animal model of Parkinson's disease. Int J Neurosci. 2017;127(1):28–36.

Submit your next manuscript to BioMed Central and we will help you at every step:

- We accept pre-submission inquiries
- Our selector tool helps you to find the most relevant journal
- We provide round the clock customer support
- Convenient online submission
- Thorough peer review
- Inclusion in PubMed and all major indexing services
- Maximum visibility for your research

Submit your manuscript at www.biomedcentral.com/submit

BioMed Central

Case Studies

Nonbacterial Thrombotic Endocarditis Complicated by Cerebral Infarction in a Patient with Adenomyosis with High Serum CA125 Level; A Case Report

Kenji Uchino, MD, Takahiro Shimizu, PhD, Heisuke Mizukami, PhD, Kenji Isahaya, PhD, Hana Ogura, PhD, Kensuke Shinohara, PhD, and Yasuhiro Hasegawa, PhD

We report a case of a 48-year-old woman with multiple cerebral infarctions caused by nonbacterial thrombotic endocarditis (NBTE) because of adenomyosis with high serum carbohydrate antigen (CA)125 level. Transesophageal echocardiography (TEE) showed a vegetation, 4 mm in diameter, adjacent to the anterior leaflet of the mitral valve on day 2. Soluble CA125 level was elevated to 901 U/mL. Intravenous infusion of unfractionated heparin sodium was started. On day 35, TEE revealed reduction of the vegetation in size, 2 mm in diameter. On day 38, she was transferred to the hospital for further rehabilitation. CA125 is a transmembrane mucin that contributes to the progression of epithelial ovarian cancer. It is important to keep in mind that adenomyosis with abnormally high serum CA125 level may be at high risk of NBTE. **Key Words:** Cerebral infarction—nonbacterial thrombotic endocarditis—adenomyosis—CA-125—mucin.
© 2018 National Stroke Association. Published by Elsevier Inc. All rights reserved.

Introduction

Nonbacterial thrombotic endocarditis (NBTE) is a well-known form of thromboembolism in which endothelial cells are damaged by immune complexes and hypercoagulability because of malignant tumors and autoimmune disease.[1] NBTE is often associated with malignant tumors such as ovarian, pancreatic, and lung adenocarcinomas, but may on very rare occasions arise as a complication of benign tumor.[2] Here, we report the case of a patient with cerebral infarction because of NBTE caused by adenomyosis with high serum concentrations of carbohydrate antigen (CA)125.

Case Presentation

A 48-year-old woman was admitted to our hospital with right hemiplegia and aphasia. She was a previously healthy woman with no history of vascular risk factors. About 1 month earlier, she had experienced abnormal vaginal bleeding and presented to another hospital, where iron deficiency anemia and adenomyosis were diagnosed.

On presentation, level of consciousness according to the Glasgow Coma Scale was E4V1M5. Body temperature was 37.4°C, blood pressure was 118/67 mm Hg, and heart rate was 80 beats/min. She showed motor aphasia and right hemiplegia, and National Institutes of Health Stroke Scale score was 9.

Initial laboratory examination indicated a hemoglobin level of 8.5 g/dL, and a platelet count of $135 \times 10^3/\mu L$

Received June 11, 2017; revision received September 11, 2017; accepted September 29, 2017.

Conflict of interest: There are no conflicts of interest to disclose with regard to this paper.

Address correspondence to Kenji Uchino, MD, 2-16-1, Sugao, Miyamae-ku, Kawasaki-City 216-8511, Japan. E-mail: k2uchino@marianna-u.ac.jp.

1052-3057/$ - see front matter

© 2018 National Stroke Association. Published by Elsevier Inc. All rights reserved.

https://doi.org/10.1016/j.jstrokecerebrovasdis.2017.09.064

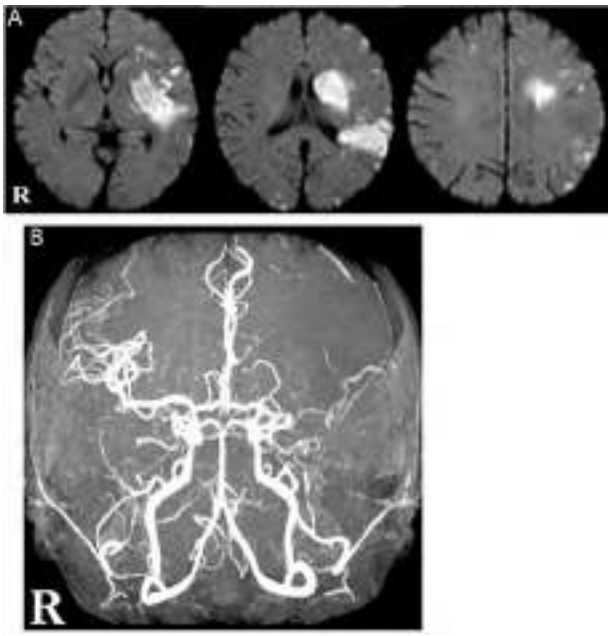

Figure 1. *Head MRI DWI and MRA: (A) Diverse embolic infarction is observed in the left MCA area. Cerebral infarction is also scattered in other areas. (B) Left MCA admits occlusion at M1 origin. Abbreviations: DWI, diffusion-weighted imaging; MCA, middle cerebral artery; MRA, magnetic resonance angiography; MRI, magnetic resonance imaging.*

and slightly elevated C-reactive protein (1.09 mg/dL), D-dimer (1.9 μg/mL), and markedly elevated serum CA125 concentration (901 units/mL; normal range, 0-35 units/mL), and CA19-9 level (1791 units/mL; normal range, 0-37 units/mL). Diffusion-weighted magnetic resonance imaging (MRI) showed high-intensity lesions in the territories of the right and left middle cerebral arteries (Fig 1, A). Magnetic resonance angiography revealed an occluded M1 segment of the left middle cerebral artery (Fig 1, B). Transesophageal echocardiography (TEE) revealed a mobile vegetation on the mitral valve (Fig 2). MRI of the pelvis revealed giant adenomyosis (10 cm × 10 cm) with multiple hemorrhages in the myometrium (Fig 3).

Post-Hospitalization Course

The patient had no history of heart disease or tooth extraction, and 2 sets of blood culture collected on the day of admission remained sterile. Based on the medical history, head MRI or magnetic resonance angiography, and TEE findings, cardiogenic cerebral embolism caused by NBTE was suspected. Continuous infusion of unfractionated heparin at 10,000 units/d was started from the first day of illness. We suspected NBTE associated with malignant tumor, and examined tumor markers,

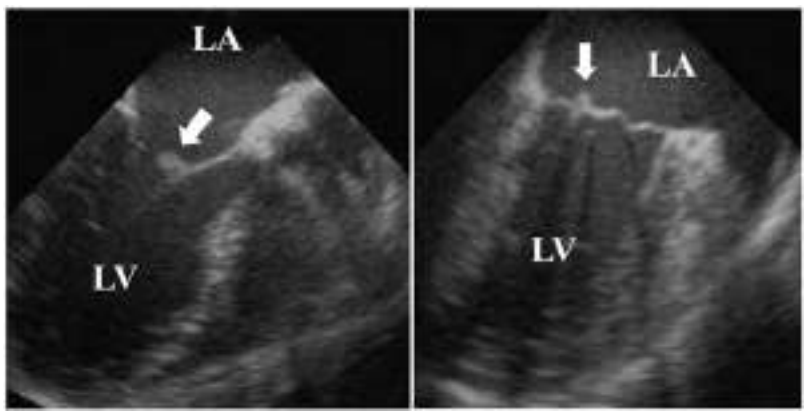

Figure 2. *TEE (day 1): A high echo structure (➡) with a size of about 4 mm movable is attached to the anterior cusp of the mitral valve. Abbreviations; LA, left atrium; LV, left ventricle; TEE, transesophageal echocardiography.*

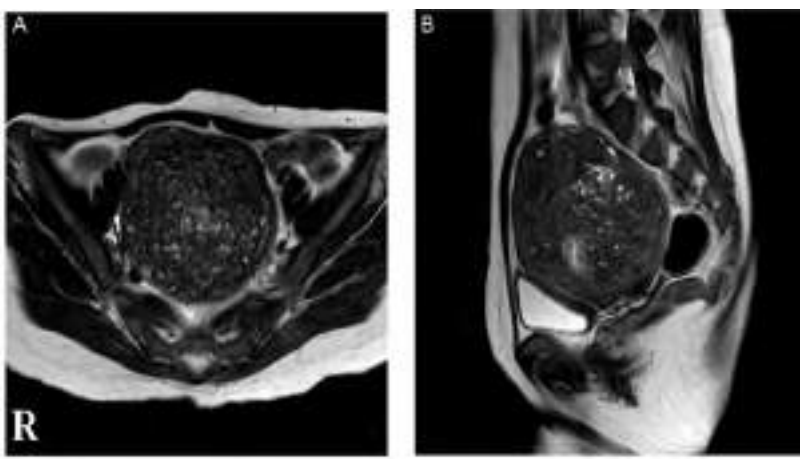

Figure 3. *Lower abdomen MRI T2 highlight image (day 2). 10 × 10 cm uterine adenomyosis with numerous small bleeding inside (A, horizontal cut; B, arrowhead). Abbreviation: MRI, magnetic resonance imaging.*

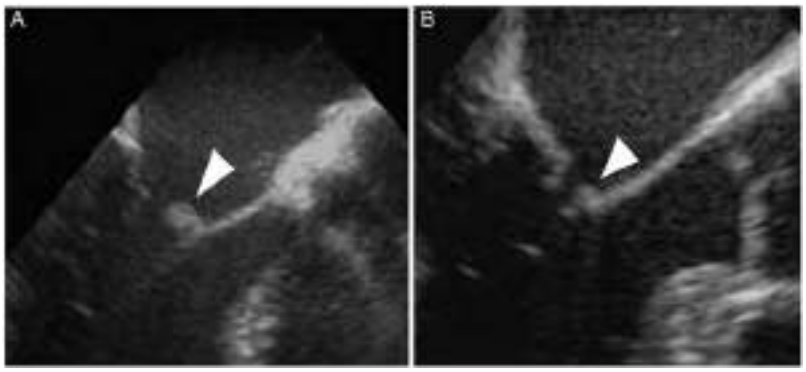

Figure 4. *The 35th disease day shows obvious shrinking (B, about 2 mm × 1 mm) compared with the second disease day (A, about 4 mm × 3 mm).*

performed various ultrasonographic examinations (thyroid gland, mammary gland, hepatobiliary tract, urology), upper gastrointestinal endoscopy, and other examination, but no malignant tumor was observed. During the hospitalization, aphasia and right hemiplegia gradually improved. On day 17, TEE findings did not change, but no new infarcts were evident on MRI. We started oral administration of warfarin. Although no blood transfusion was performed, progression of anemia was not observed only by administration of iron preparation. On day 12, hemoglobin increased to 11.1 mg/dL. Tumor markers were CA125 75 U/mL and CA19-9 576 U/mL on day 12. However, on day 37, CA125 decreased to 357 U/mL and CA19-9 also decreased to 424 U/mL. On day 35, TEE demonstrated a reduction in vegetation size (Fig 4). The patient was transferred to a rehabilitation hospital on day 38. Three months later, she was discharged home from the rehabilitation hospital, and follow-up TEE performed in an outpatient clinic demonstrated disappearance of the vegetation. Total hysterectomy was performed in the department of gynecology, with no complications after surgery. The treatment with warfarin finished in 6 months. After that, we followed up with TEE, but no recurrence of vegetation was observed.

Discussion

NBTE is associated with hypercoagulability caused by malignant tumors, sepsis, autoimmune diseases, and is a disease that forms a sterile mass composed of fibrin and platelets in a healthy heart valve without damage.[1] Malignant tumor is the most common disease underlying NBTE, and malignant tumor is seen as a complication in about 40%-85% of cases. Vascular endothelial damage is caused by cytokines released from monocytes and macrophages coming into contact with cancer cells. In that way, platelet thrombus and fibrin thrombus form on heart valves and endocardium.[2] Histologically, mucin secreted into the blood from adenocarcinoma, especially mucin-producing adenocarcinoma, is associated with hypercoagulability.[3] Mucin is a generic name for macromolecular glycoproteins with a molecular weight ≥200,000, and is a main component of mucus produced and secreted by epithelial cells. There are 2 types: soluble secretory mucin and membrane-bound mucin. The secretory mucin type has a large molecular weight and is produced from organs such as the eyes, gastrointestinal tract, trachea, lungs, bladder, pancreatic duct, gall bladder, and reproductive organs. Membrane-bound mucin is a high molecular weight glycoprotein that is structurally similar to mucin from the stomach, lungs, salivary glands, sweat glands, breast, and cancer cells.[4] Mucin derived from cancer works as a ligand for selectin. Mucin causes L-selectin on the surface of white blood cells and P-selectin interaction on platelet surface, and promotes platelet aggregation.[3] CA125 is a carbohydrate antigen-related tumor marker and is the most relevant marker in gynecologic tumors. In recent years, the characteristics of the CA125 molecule have been elucidated. The CA125 antigenic molecule has been cloned, and is attracting attention as membrane-bound mucin (MUC16).[5] Because CA125 is expressed in the peritoneum, pleura, pericardial membrane, and endometrium, high levels are also seen in pregnancy, menstruation, and endometriosis. In this case, the vegetation was recognized on TEE, but no bacteremia was identified from multiple blood culture tests. Results for infectious endocarditis were thus considered negative, and we diagnosed NBTE. Because results for malignant tumor were negative from blood testing and image examination, NBTE was considered to be associated with endothelial cell damage caused by uterine adenomyosis. Uterine adenomyosis is a benign tumor in which the endometrium proliferates ectopically in the myometrium and results in dysmenorrhea and hypermenstruation. Because of intrauterine infection and increased uterine volume, tissue factor (TF) is generated by vascular endothelial dysfunction and the tissue disorder of uterine myopathy. TF may also cause the development of disseminated intravascular coagulation syndrome.[6] Other reports have described NBTE complicated by cerebral infarction, and TF from microthrombus and necrotic tissue in uterine adenomyosis is speculated to be involved.[7,8] Uterine adenomyosis is not a malignant tumor, but the concentration of CA125 is known to be elevated. CA125

is used to determine disease activity and therapeutic effect. Mogensen reported that CA125 after chemotherapy for ovarian cancer correlates strongly with prognosis. The mortality rate in cases with CA125 ≥100 U/mL is about 6 times higher than that in cases with CA125 ≤ 10 U/mL.[9] In this case, the CA125 value at the time of the visit had increased markedly to 901 U/mL, and abundant membrane-bound mucin was present in the blood. In addition, TF released from the uterine muscles causes vascular endothelial damage by increasing uterine volume and increasing vaginal bleeding. Therefore, it was thought that TF became to form vegetation in a normal heart valve. Following heparin infusion, the vegetation shrank and concentration of CA125 decreased. Because NBTE has not recurred since hysterectomy, this procedure does not appear to represent a contraindication. However, not all cases of endometriosis and uterine adenomyosis accompanied by increased CA125 are necessarily at high risk of developing NBTE, and further cases need to be accumulated to clarify risk factors.

Conclusion

We encountered a 48-year-old woman with NBTE secondary to adenomyosis. Uterine adenomyosis is a benign tumor, but if a case with abnormally high CA125 value shows cerebral infarction, the complication of NBTE should be suspected. Searching for sources of emboli including TEE is important.

References

1. Sutherland DE, Weitz IC, Liebman HA. Thromboembolic complications of cancer: epidemiology, pathogenesis, diagnosis, and treatment. Am J Hematol 2003;72:43-52.
2. Bick RL. Cancer-associated thrombosis. N Engl J Med 2003; 349:109-110.
3. Wahrenbrock M, Borsig L, Le D, et al. Selectin-mucin interactions as a probable molecular explanation for the association of Trousseau syndrome with mucinous adenocarcinomas. J Clin Invest 2003;112:853-862.
4. Shi L. Biomimetic surfaces of biomaterials using mucin-type glycoproteins. Trends Glycosci Glycotech 2000;12:229-239.
5. Yin BW, Lloyd KO. Molecular cloning of the CA125 ovarian cancer antigen: identification as a new mucin, MUC16. J Biol Chem 2001;276:27371-27375.
6. Nakamura Y, Kawamura N, Ishiko O, et al. Acute disseminated intravascular coagulation developed during menstruation in an adenomyosis patient. Arch Gynecol Obstet 2002;267:110-112.
7. Soeda S, Mathuda N, Hashimoto Y, et al. Non-bacterial thrombotic endocarditis with systemic embolic events caused by adenomyosis. J Obstet Gynaecol Res 2011;37: 1838-1841.
8. Tadokoro Y, Sakaguchi M, Yagita Y, et al. Ischemic stroke in patients with solid gynecologic tract tumors and coagulopathy. Eur Neurol 2013;70:304-307.
9. Mogensen O. Prognostic value of CA 125 in advanced ovarian cancer. Gynecol Oncol 1992;44:207-212.

Clinical Case Report

Medicine®

OPEN

A trial case of medical treatment for primary headache using telemedicine

Hisanao Akiyama, MD, PhD*, Yasuhiro Hasegawa, MD, PhD

Abstract

Rationale: Video-based treatment in telemedicine is a potential alternative to face-to-face treatment. We describe our trial use of telemedicine to treat a patient with primary headache.

Patient concerns: A 25-year-old woman visited our branch hospital with a chief complaint of recurrent headache. Our branch hospital had no headache specialist, so a headache specialist at our main hospital provided treatment remotely.

Diagnoses: She was diagnosed with migraine without aura by the headache specialist using telemedicine.

Interventions: The branch hospital physician and the headache specialist used video conferencing to interview and examine the patient and share cranial magnetic resonance imaging (MRI). Audio and camera angle/zoom could be adjusted during interviews, and high-quality video was continuously displayed at both hospitals simultaneously without lag between audio and video. Temporal/spatial resolution was sufficient for proper neurological evaluation. MRI had sufficient image quality and resolution for detailed interpretation. A prescription for medication was issued by the branch hospital physician and confirmed by the headache specialist.

Outcomes: Zolmitriptan was effective in treating her migraine.

Lessons: Telemedicine was useful for treating this primary headache patient and can contribute to regional health care. Future challenges in telemedicine include expanding its use to other areas within the purview of general physicians and headache specialists, covering implementation and maintenance costs, providing adequate explanations to patients and family members, ensuring security of video transmissions, maintaining patient medical records, and supervising treatment.

Abbreviations: CT = computed tomography, EEG = electroencephalogram, ICT = information and telecommunication technology, JHS = Japan Headache Society, MRI = magnetic resonance imaging.

Keywords: face-to-face examination, face-to-face interview, medical treatment, primary headache, telemedicine

1. Introduction

Chronic headache affects around 40 million people in Japan, and headache sufferers experience varying degrees of impairment in daily life and at work.[1] Although a considerable number of chronic (primary) headache patients visit hospitals or clinics attended by headache specialists or general physicians, the "Clinical Practice Guideline for Chronic Headache" published by the Japan Headache Society (JHS) states that only around 50% of patients are accurately diagnosed and properly treated. Several reports in the literature argue that headache specialists play a useful role in the treatment of headache sufferers, and assert that general physicians who lack the equipment to perform cranial imaging such as computed tomography (CT) or magnetic resonance imaging (MRI) and who have trouble diagnosing the cause of the headache should promptly refer the patient to a headache specialist.[2–5] However, the number of headache specialists in Japan with expertise in the treatment of chronic headache is limited, at around 900 specialists in 2017. The development and spread of information and telecommunication technology (ICT) in recent years has created new possibilities for so-called telemedicine, where ICT devices are used to support the delivery of healthcare. There are growing expectations that telemedicine will be used to provide video-based treatment in place of traditional face-to-face treatment, but so far, there has been only limited uptake of telemedicine in the treatment of headache.

In this report, we describe the clinical utility of our attempt to use telemedicine to remotely treat a patient with primary headache via a connection between our branch hospital (which does not have a headache specialist) and our main hospital. In the context of this case, we describe this approach as "doctor-to-patient with doctor" telemedicine.

2. Case study

The patient was a 25-year-old female junior resident/intern with a chief complaint of recurrent headache. She did not have any remarkable past medical history and did not drink or smoke.

Editor: N/A.

Authorship: HA examined the patient by using telemedicine. HA drafted the manuscript and created the figures. YH helped to draft the manuscript. All authors read and approved the final manuscript.

St. Marianna University Hospital Human Research Ethics Committee waived approval because this is a case report.

Written informed consent for publication was obtained from the patient herself. A copy of the consent form is available for review by the Editor of this journal.

The authors declare that they have no competing interests.

Department of Neurology, St. Marianna University School of Medicine, Kawasaki, Kanagawa, Japan.

* Correspondence: Hisanao Akiyama, Department of Neurology, St. Marianna University School of Medicine, 2-16-1 Sugao, Miyamae-ku, Kawasaki, Kanagawa 216-8511, Japan (e-mail: h2akiyama@marianna-u.ac.jp).

Copyright © 2018 the Author(s). Published by Wolters Kluwer Health, Inc. This is an open access article distributed under the terms of the Creative Commons Attribution-Non Commercial-No Derivatives License 4.0 (CCBY-NC-ND), where it is permissible to download and share the work provided it is properly cited. The work cannot be changed in any way or used commercially without permission from the journal.

Medicine (2018) 97:9(e9891)

Received: 5 October 2017 / Received in final form: 14 December 2017 / Accepted: 24 January 2018

http://dx.doi.org/10.1097/MD.0000000000009891

Figure 1. Our telemedicine system and interactive video conferencing system. Top: The telemedicine system operates via a high-speed NTT internet connection between our branch and main hospitals. Bottom: The interactive video conferencing system "Life Size HD Visual Communication System" (Hitachi High Technology Corporation) consists of a 40-inch LCD monitor, camera, remote controller, and MicPod.

From the age of 14 years, she started experiencing headaches in the superior left orbit several times a month. The headaches did not involve any visual aura but manifested as a throbbing sensation that continued for at least half a day with nausea in the absence of medication. She was examined at the internal medicine department of our branch hospital after a typical headache episode while working at the hospital as part of her residency.

Our branch hospital has no headache specialist, so we used the telemedicine system linking our main hospital which does have one, in order to have a face-to-face interview and examine the patient, to perform cranial MRI and electroencephalogram (EEG), to facilitate a discussion between the 2 physicians, and to prescribe medication, all via data and video transmission (Fig. 1-top). Our telemedicine program uses a video conferencing system (Life Size HD Visual Communication System; Hitachi High Technologies Corporation, Tokyo, Japan) comprising a 40-inch LCD monitor (Toshiba, Tokyo, Japan), camera, remote controller, and MicPod. The system enables real-time video-based communication via a high-speed internet connection [Nippon Telegraph and Telephone Corporation (NTT), Tokyo, Japan] between our main hospital and branch hospitals (Fig. 1-bottom).

2.1. Face-to-face interview

In the patient interview using our telemedicine system, we could adjust the audio and camera angle and zoom, and were able to maintain simultaneous video on each hospital's monitor without any disruption in image quality or lag between the audio and video. This setup allowed us to perform a detailed interview of the patient as though we were in the same room. We could also measure the patient's scores on the Migraine Disability Assessment Scale (MIDAS)[6] and Headache Impact Test-6 (HIT-6),[7] which are used to evaluate the extent to which a headache interferes with daily activities (Fig. 2).

2.2. Face-to-face examination

In addition to a physical examination, the physician at our branch hospital performed a neurological examination, including tests of consciousness, higher brain function, cranial nerves, motor system, reflexes, sensory system, and coordination. During these assessments, there was sufficient temporal and spatial resolution on both monitors (Fig. 3-left). In addition, the headache specialist at our main hospital could issue the necessary instructions and obtain clear, close-up images of the patient's eyes allowing us to evaluate the pupillary light reflex findings, which are generally difficult to examine on a monitor (Fig. 3-right).

2.3. Transmission of test results

Image quality and resolution were sufficient to enable detailed interpretation of the cranial MRI and EEG waveforms (Fig. 4-top). No abnormal findings were apparent on these images.

2.4. Diagnosis, explanation to the patient, and medical discussion

The headache specialist had no difficulty explaining the diagnosis and cause of the headache to the patient in real time using diagrams. We could also have a medical discussion in real time between the 2 physicians in front of the monitors (Fig. 4-lower left). The diagnosis reached was migraine without aura.

2.5. Prescription medication

The headache specialist advised the appropriate course of treatment to the branch hospital physician, who then issued a prescription for medication. The specialist was also able to visually confirm the prescription (Fig. 4-lower right). Zolmitriptan was effective in treating her migraine.

Figure 2. Face-to-face interview with the patient using the telemedicine system. We could adjust the audio and camera angle and zoom, and were able to maintain simultaneous video on each hospital's monitor without any disruption in image quality or lag between the audio and video.

3. Discussion

Headache is a common illness among outpatients, and migraine in particular has been identified by the World Health Organization as the 19th highest cause worldwide of years lost to disability. However, despite the fact that headache, particularly primary headache, can cause significant interference in daily life and at work, only a small percentage of headache sufferers visit a clinic or hospital for treatment.[1,8] This situation can be attributed to several factors, including the following: a lack of awareness of headache as a legitimate illness; unwillingness to take time off work to visit the doctor due to feelings of guilt; attempts to remedy headaches with over-the-counter medication due to not knowing which doctor, clinic, or hospital to visit; and the tendency among general practitioners to treat consultations as one-off visits and prescribe analgesics without proper treatment after diagnosing the patient's condition as a simple

Figure 3. Face-to-face examination using the telemedicine system. In addition to a physical examination, the physician at the branch hospital performed a neurological examination, including tests of consciousness, higher brain function, cranial nerves, motor system, sensory system, and coordination. During these assessments, there was sufficient temporal and spatial resolution on both monitors.

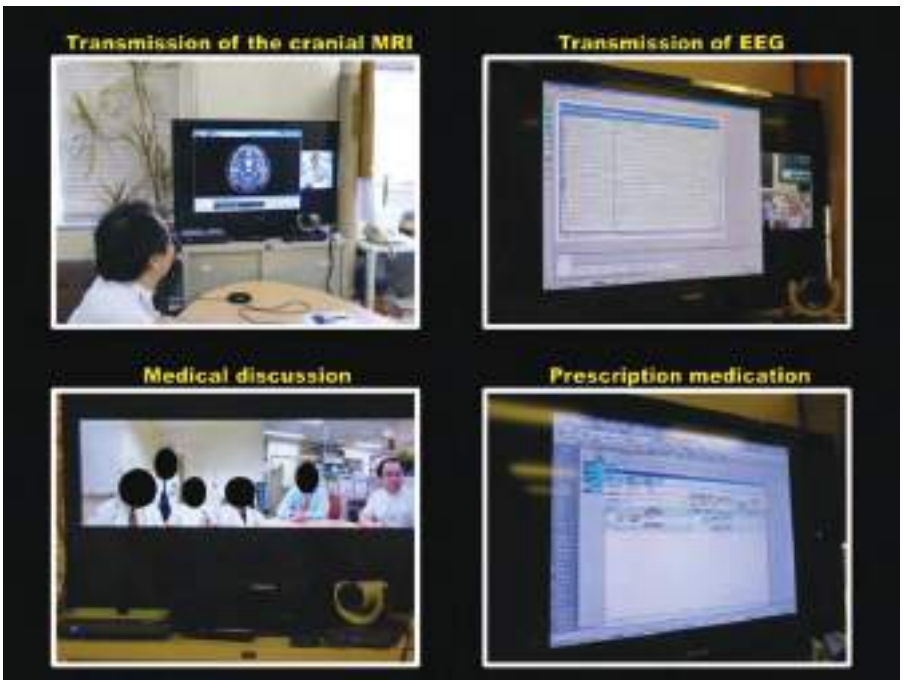

Figure 4. Data transmission, diagnosis, explanation to the patient, and prescription using the telemedicine system. Top: The cranial MRI and EEG also had sufficient image quality and resolution to enable detailed interpretation. Bottom left: We could also have a medical discussion in real time by gathering the physicians from both hospitals in front of the monitors. Bottom right: The headache specialist at the main hospital advised the nonspecialist physician at the branch hospital on the appropriate course of treatment. The branch hospital physician then issued a prescription for medication, which the headache specialist could visually confirm via the video link.

headache while ruling out organic diseases on the basis of image findings. Furthermore, migraine is no longer the primary form of headache in adults alone, it is a serious problem for children as well. In the case of younger children who cannot yet express themselves, a nonspecialist physician may not be able to diagnose migraine. As a result, and despite reports in the literature describing the effectiveness of consulting a headache specialist with expertise in the treatment of chronic headache, as of 2017, there are only 900 headache specialists in Japan who are accredited by the JHS. Given that migraine is estimated to affect around 8.4 million people in Japan,[1] this means that each headache specialist would have to examine around 10,000 migraine patients, which is obviously infeasible. There are also regional disparities between Japan's urban and rural communities, such as a lack of even general practitioners in rural areas, so opportunities to visit headache specialists are obviously limited for patients who would have to travel long distances.

The type of telemedicine that we performed in this case would prove useful for clinics and hospitals without a headache specialist. Patients could overcome the geographical restraints of having to travel long distances to see a specialist and could have a new consultation and receive proper diagnosis and treatment from a facility with a headache specialist without the physical burden associated with an actual visit. Also, the headache specialist can not only diagnose migraine but also advise families of children with migraine by utilizing their knowledge of comorbidities such as low-quality emotional functioning, absenteeism from school, poor academic performance and cognitive functioning,[9,10] motor coordination impairment,[11] and sleep disorders,[12–18] which are common in children affected by migraine. Telemedicine also allowed our headache specialist to issue real-time instructions to the branch hospital physician on the techniques required to examine the patient, such as palpation and auscultation. Moreover, the physicians could consult before deciding on how the test data should be interpreted and which medication could be prescribed. Our experience suggests that this type of telemedicine system is an effective tool in the treatment of headache patients because it enables specialists to transmit the information required to perform a medical intervention. It also allows general practitioners in more remote areas where there is no specialist—especially general practitioners who do not specialize in internal medicine—to examine and treat the patients while receiving instructions from a specialist at a separate geographic location.

In terms of legislation, telemedicine was previously prohibited under Article 20 of the Medical Practitioners Act, which states that "No medical or dental practitioner shall provide medical care without personally performing a face-to-face examination, and telemedicine shall be performed only in a manner that complements face-to-face medical care." However, the practice of telemedicine was legalized in December 1997 following issuance of a notification by the Ministry of Labour, Health and Welfare stating that "The practice of telemedicine does not directly infringe on Article 20 of the Medical Practitioners Act provided that it can be used to obtain useful information on the patient's physical or mental condition to the extent that it can be used as an alternative to face-to-face medical treatment even if it is not equivalent." Indications for telemedicine were rapidly expanded in March 2011 to allow mainly doctor-to-patient treatments of chronic-stage patients who are receiving ongoing therapy and whose recent condition has been stable. These changes have led to the use of telemedicine not only in-home care situations but also on a trial basis in hyperacute stroke patients[19–22] in a doctor-to-patient with doctor setting.

The telemedicine system used by our hospitals' nonspecialist physician and headache specialist to treat the present patient also proved to be effective and appears to share some similarities with telemedicine in other disease areas. However, a number of challenges remain, such as establishing the necessary infrastructure (e.g., communication networks, computer equipment, standardized specifications), covering the costs of implementing and maintaining this equipment, providing adequate explanations to patients and family members, ensuring the security of patient video transmissions, establishing a technique to maintain patient medical records, assigning suitable medical personnel to supervise the treatment, and covering the costs associated with developing financial incentives and remuneration.

It should be noted that certain circumstances in this case likely made our telemedicine approach successful. The telemedicine system used to treat the patient's primary headache made use of an existing high-speed NTT internet connection between our branch and main hospitals, and it had already been used to provide care to hyperacute stroke patients. Moreover, the treatment went smoothly because the patient was a junior resident who consented to participate in the use of telemedicine. Telemedicine performed at a different facility may not proceed as smoothly.

4. Conclusion

Our findings suggest that telemedicine can be used by a general physician and a headache specialist to facilitate treatment of patients with primary headache and can make a meaningful contribution to regional health care in the future. We believe that this case provides valuable insights for the development and spread of telemedicine in Japan. Future challenges to the use of telemedicine include expanding its use to other areas, covering the costs of implementing and maintaining the equipment, providing adequate explanations to patients and family members, ensuring the security of patient video transmissions, establishing a technique to maintain patient medical records, assigning suitable medical personnel to supervise the treatment, and covering the associated costs.

Acknowledgments

We thank Dr Kanako Teramoto and Dr Masahiro Horiuchi from the Department of Internal Medicine, Division of Neurology of Kawasaki Municipal Tama Hospital for the cooperation and participation in this telemedicine trial.

References

[1] Sakai F, Igarashi H. Prevalence of migraine in Japan: a nationwide survey. Cephalalgia 2002;46:343–9.
[2] Lipton RB, Scher AI, Steiner TJ, et al. Patterns of health care utilization for migraine in England and in the United States. Neurology 2003; 60:441–8.
[3] Lipton RB, Stewart WF, Simon D. Medical consultation for migraine: results from the American Migraine Study. Headache 1998;38:87–96.
[4] Bekkelund SI, Salvesen R. Are headache patients who initiate their referral to a neurologist satisfied with the consultation? A population study of 927 patients-the North Norway Headache Study (NNHS). Fam Pract 2001;18:524–7.
[5] Bekkelund SI, Salvesen R. Patients satisfaction with a neurological specialist consultation for headache. Scand J Prim Heath Care 2002; 20:157–60.
[6] Stewart WF, Lipton RB, Kolondner KB, et al. Validity of the migraine disability assessment (MIDAS) score in comparison to a diary-based measure in a population sample of migraine sufferers. Pain 2000;88: 41–52.
[7] Kosinski M, Bayliss MS, Bjorner JB, et al. A six-item short-form survey for measuring headache impact: the HIT-6. Qual Life Res 2003;12: 963–74.
[8] Takashima T, Ishizaki K, Fukuhara Y, et al. Population-based door-to-door survey of migraine in Japan: the Daisen study. Headache 2004; 44:8–19.
[9] Kernick D, Campbell J. Measuring the impact of headache in children: a critical review of the literature. Cephalalgia 2009;29:3–16.
[10] Esposito M, Pascotto A, Gallai B, et al. Can headache impair intellectual abilities in children? An observational study. Neuropsychiatr Dis Treat 2012;8:509–13.
[11] Esposito M, Verrotti A, Gimigliano F, et al. Motor coordination impairment and migraine in children: a new comorbidity? Eur J Pediatr 2012;171:1599–604.
[12] Carotenuto M, Guidetti V, Ruju F, et al. Headache disorders as risk factors for sleep disturbances in school aged children. J Headache Pain 2005;6:268–70.
[13] Vendrame M, Kaleyias J, Valencia I, et al. Polysomnographic findings in children with headaches. Pediatr Neurol 2008;39:6–11.
[14] Carotenuto M, Esposito M, Precenzano F, et al. Cosleeping in childhood migraine. Minerva Pediatr 2011;63:105–9.
[15] Carotenuto M, Esposito M, Pascotto A. Migraine and enuresis in children: an unusual correlation? Med Hypotheses 2010;75:120–2.
[16] Esposito M, Gallai B, Parisi L, et al. Primary nocturnal enuresis as a risk factor for sleep disorders: an observational questionnaire-based multicenter study. Neuropsychiatr Dis Treat 2013;9:437–43.
[17] Esposito M, Roccella M, Parisi L, et al. Hypersomnia in children affected by migraine without aura: a questionnaire-based case-control study. Neuropsychiatr Dis Treat 2013;9:289–94.
[18] Esposito M, Parisi P, Miano S, et al. Migraine and periodic limb movement disorders in sleep in children: a preliminary case-control study. J Headache Pain 2013;14:57.
[19] Schwamm LH, Holloway RG, Amarenco P, et al. A review of the evidence for the use of telemedicine within stroke system of care: a scientific statement from the American Heart Association/American Stroke Association. Stroke 2009;40:2616–34.
[20] Schwamm LH, Audebert HJ, Amarenco P, et al. Recommendations for the implementation of telemedicine within stroke systems of care: a policy statement from the American Heart Association. Stroke 2009; 40:2635–60.
[21] Meyer BC, Lyden PD, Al-Khoury L, et al. Prospective reliability of the STRokE DOC wireless/site independent telemedicine system. Neurology 2005;64:1058–60.
[22] Sakurai K, Imai T, Kato B, et al. Feasibility of NIH stroke scale evaluation and telestroke use via an interactive high-vision videoconferencing system. Jpa J Stroke 2012;34:414–20.

ORIGINAL ARTICLE

Approach for the Derivation of Melanocytes from Induced Pluripotent Stem Cells

Tamihito Kawakami[1], Takuro Okano[1], Sora Takeuchi[1], Kayako Osumi[1], Yoshinao Soma[1], Muneteru Itoh[2], Tomohisa Hirobe[3] and Kowichi Jimbow[4]

Induced pluripotent stem (iPS) cells have the ability to differentiate into multiple cell types in the body and have an unlimited growth potential. However, iPS cell-derived melanocytes produced by existing protocols have significant limitations in developing novel strategies for regenerative medicine and cell therapies of pigmentation disorders in humans because they involve culture in media containing fetal bovine serum and nonphysiological agents. In this study, we established an in vitro approach to generate iPS cell-derived human melanocytes that have higher proliferation rates and increased melanin production compared with melanocytes prepared by previously reported approaches. Importantly, our iPS cell-derived human melanocytes are prepared in fetal bovine serum-free culture conditions that do not contain any non-physiological agents. We designed two original methods, transferring black colonies by pipette and recovering black cell pellets from centrifuged medium, and numerous human iPS cell-derived melanocytes proliferated in gelatinous dishes coated with Matrigel after 12 days. We also succeeded in inducing melanin pigmentation in the nude mouse skin in vivo using those human iPS cell-derived melanocytes. We propose that this method using iPS cells established from T cells in the blood of normal human volunteers could be applied clinically to develop regenerative medicine and cell therapies for various forms of human pigmentation disorders.

Journal of Investigative Dermatology (2018) 138, 150–158; doi:10.1016/j.jid.2017.07.831

INTRODUCTION

Melanocytes in human skin produce melanin pigments that are secreted to surrounding keratinocytes and are responsible not only for protecting the skin from sunlight damage but also cause the majority of pigmentation disorders. Induced pluripotent stem (iPS) cells have the ability to differentiate into multiple cell types in the body and have an unlimited growth potential. To date, human melanocytes derived from iPS cells have been prepared in fetal bovine serum (FBS)-containing cultures supplemented with nonphysiological agents such as 12-O-tetradecanoylphorbol-13-acetate and cholera toxin. Thus, iPS cell-derived human melanocytes produced by existing protocols have significant limitations for developing novel strategies to treat pigmentation disorders in humans (Kunisada et al., 2014; Mica et al., 2013; Nissan et al., 2011; Ohta et al., 2011, 2013; Tsuchiyama et al., 2013).

We have previously shown that a number of growth factors are necessary to regulate the proliferation and differentiation of human epidermal melanocytes in in vitro cultures. They include stem cell factor, Wingless/integrase-1, bone morphogenetic protein 4, ascorbic acid, 1,25-dihydroxyvitamin D_3, α-human melanocyte-stimulating hormone, N6,2′-O-dibutyryladenosine 3′,5′-cyclic monophosphate sodium salt, tyrosine, transferrin, keratinocyte growth factor, granulocyte-macrophage colony stimulating factor, hepatocyte growth factor, basic fibroblast growth factor 2 (FGF2), hydrocortisone, and endothelin 1 (Chang et al., 2014; Hirobe, 2011; Hirobe et al., 2013; Hirobe and Ishikawa, 2015; Kawakami et al., 2008, 2014).

Current approaches for treating congenital and acquired melanin pigmentation disorders of the skin are largely unsatisfactory. Cutaneous pigmentary disorders such as vitiligo and dyschromatosis symmetrica hereditaria result from a loss of functional melanocytes in the affected cutaneous areas. These disorders have often been treated by grafting normal autologous epidermal melanocytes in the hypopigmented lesions, but the efficacy has always been variable (Kawakami et al., 2013).

There is an urgent need to develop an approach for producing human iPS cell-derived melanocytes in large quantities within a short period and to differentiate them with high melanogenic potency in serum-free culture conditions without supplementations by nonphysiological agents. In this study, we established an in vitro approach to generate iPS cell-derived human melanocytes that have high proliferation rates and increased melanin production compared with cells prepared by previously reported approaches (Nissan et al., 2011; Ohta et al., 2011, 2013). Importantly, our iPS

Departments of Dermatology, St. Marianna University School of Medicine, Kawasaki, Kanagawa, Japan; [2]Department of Dermatology, Iwate University School of Medicine, Tokyo, Japan; [3]Department of Molecular Imaging and Dermatology, Sapporo Medical University of Radiological Sciences, Chiba, Japan and [4]Institute of Dermatology, Cutaneous Sciences, Sapporo, Japan

Correspondence: Tamihito Kawakami, Department of Dermatology, St. Marianna University School of Medicine, 2-16-1 Sugao, Miyamae-ku, Kawasaki, Kanagawa 216-8511, Japan. tamih@marianna-u.ac.jp

Abbreviations: FBS, fetal bovine serum; FGF2, fibroblast growth factor 2; iPS cell, induced pluripotent stem cell; iPS-MC, induced pluripotent stem cell-derived melanocyte medium; MC, melanocyte; MEK, mitogen-activated protein kinase/ERK kinase; MITF, microphthalmia-associated transcription factor; ORNA, short interfering RNA; TYRP1, tyrosinase-related protein 1

Received 13 February 2017; revised 14 July 2017; accepted 17 July 2017; accepted manuscript published online 5 September 2017; corrected proof published online 11 November 2017

© 2017 the Authors. Published by Elsevier, Inc. on behalf of the Society for Investigative Dermatology

cell-derived human melanocytes are prepared using FBS free culture conditions that do not contain any non physiological agents. The safety and efficacy of these human iPS cell-derived melanocytes to generate in vivo melanin pigmentation was then successfully tested in the nude mouse skin.

RESULTS

Successful protocol to generate melanocytes derived from human iPS cells

After 20 days of culture in human iPS cell-derived melanocyte medium (iDMM) that includes stem cell factor, Wingless/integrase-3A, bone morphogenetic protein 4, ascorbic acid, 1,25-dihydroxyvitamin D3, α-human melanocyte stimulating hormone, N6,2′-O-dibutyryladenosine 3′,5′-cyclic monophosphate sodium salt, L-tyrosine, transferrin, keratinocyte growth factor, granulocyte-macrophage colony stimulating factor, hepatocyte growth factor, FGF2, hydrocortisone, and endothelin 1, many pigmented cells with black granules were generated from the border of human iPS cell oids or gelatinous dishes coated with Matrigel (Figure 1a and b). These pigmented cells displayed bipolar processes with many pigmented granules that extended from small ovoid cell bodies (Figure 1c). These granules were strongly tyrosinase positive as observed by high magnification confocal immunofluorescence laser microscopy, which suggested that they are mature melanocytes (Figure 1d).

We examined the mRNA expression levels of NANOG, microphthalmia-associated transcription factor (MITF), tyrosinase, and tyrosinase related protein 1 (TYRP1) in the human iPS cell-derived melanocytes using reverse transcription PCR (Figure 1e). The mRNA expression level of the pluripotency marker NANOG in these iPS cell-derived melanocytes was significantly lower than in human iPS cells ($P < 0.0001$). In contrast, mRNA expression levels of three melanocyte-specific markers (MITF, tyrosinase, and TYRP1) in the iPS cell-derived melanocytes were significantly higher than in human iPS cells ($P < 0.0001$). NANOG, MITF, tyrosinase, and TYRP1 mRNA expression levels in the iPS cell-derived melanocytes were similar to the levels found in human epidermal melanocytes (adult-lightly pigmented cells), an established line of normal human melanocytes. Thus, we regard these pigmented cells as human iPS cell-derived melanocytes based on these findings.

Approximately 5 to 6 weeks later, the human iPS cell-derived melanocytes reached confluence in 60-mm-diameter gelatinous dishes coated with Matrigel (Figure 1f). We mechanically isolated human iPS cell-derived melanocyte colonies from these dishes by picking them up gently with a pipette. These mechanically isolated colonies were then transferred to new gelatinous dishes coated with Matrigel and were cultured with human iDMM. Within 2 days, the transferred cell aggregates adhered to the dishes and the melanocytes then proliferated further (Figure 1g). We also removed human iDMM when we changed the medium after 2 days. After centrifugation of these media, black pellets were observed at the bottoms of the tubes and these pellets were directly added to newly prepared human iDMM and were then mixed gently. The medium was then directly added to new gelatinous dishes coated with Matrigel and was cultured with human iDMM. In several days, these melanocytes contained a small number of black pellets that had adhered and were growing with other human iPS cell-derived melanocytes on Matrigel (Figure 1h). Using these two original methods together, that is, plotting the black colonies and adding the black pellets after centrifugation of the iDMM, we found numerous human iPS cell-derived melanocytes in each of the gelatinous dishes coated with Matrigel after 12 days (Figure 1i).

Induction of skin pigmentation by subepidermal inoculation of human iPS cell-derived melanocytes into nude mice

Using these two new methods, we were able to produce approximately 1×10^7 melanocytes in 20 days after differentiation from each 60-mm gelatinous dish (containing confluent iPS cell colonies (approximately 1×10^5 starting iPS cells). The human iPS cell-derived melanocytes were pelleted by centrifugation and the color of the supernatant was black (Figure 2a).

Suspensions of the melanocyte pellets were applied subepidermally into the flank skin of nude mice at various cell concentrations (0, 1×10^5, 1×10^6, or 3×10^6 cells/ml) in isotonic sodium chloride solution. Three days after the inoculation of 1×10^6 or 3×10^6 cells/ml, blue to black pigmented lesions (approximately 5 mm in diameter) on the flank skin of each mouse were seen that were consistent with the inoculation site and the surrounding area (Figure 2b). On day 7 after inoculation, a postmortem examination discloses black masses in the flank of each inoculated nude mouse (Figure 2c). In contrast, even up to day 28 we did not find any pigmentary changes in the flank skin of any mice inoculated with 0 or 1×10^5 cells/ml. The pigmented lesions elicited by inoculation of 1×10^6 or 3×10^6 cells/ml decreased with each passing day and had disappeared by day 21.

Histopathological findings of human iPS cell-derived melanocytes in nude mice

Microscopic examination after Fontana Masson histochemical staining demonstrated the presence of numerous melanocytes with positive black melanin pigment granules in the pigmented lesions after inoculation of cell suspensions with 3×10^6 cells/ml (Figure 2d). Immunohistochemical staining of these sections with melanocyte-specific Melan-A antibodies revealed positive cells with brown to black cytoplasm located consistently at the inoculation sites compared with the negative controls (Figure 2e). The "grafted" melanocytes were largely located in the dermis to subcutaneous fascia, and to some extent, in or close to the epidermis. On the other hand, we found no human iPS cell-derived melanocytes using Fontana-Masson histochemical staining in the epidermis. However, Fontana-Masson-positive cells with brown to black cytoplasm were detected largely in the upper dermis using immunohistochemical staining with anti-Melan-A antibodies (Figure 2f). Importantly, several melanocytes appeared to have migrated from the upper dermis to the epidermis (Figure 2g). An average of two to three melanocytes that had migrated to the epidermis were counted in 10 consecutive high power fields (×200).

DISCUSSION

A number of approaches have been used to establish human iPS cell-derived melanocytes (Nissan et al., 2011; Ohta et al.,

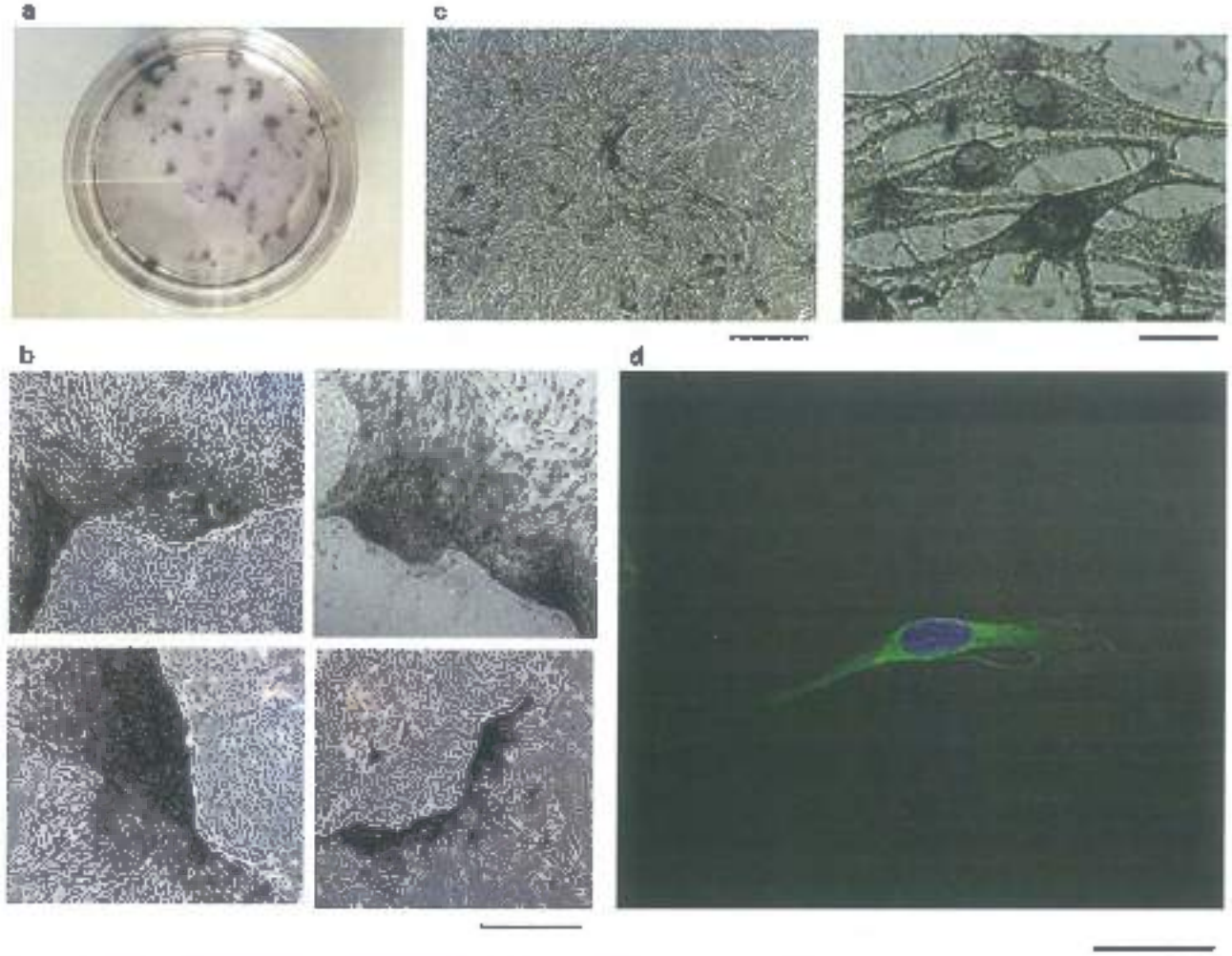

Figure 1. Generation of human epidermal melanocytes derived from human iPS cells. (**a**) Human iPS cell-derived melanocytes appear as black dots and slightly black areas on UDM on 60-mm gelatinous dishes coated with Matrigel. (**b**) High-resolution photomicrographs of mature human iPS cell-derived melanocytes were presented here on the border of human iPS cell colonies. Scale bar = 100 μm. (**c**) Human iPS cell-derived melanocytes contained many melanin granules in the cytoplasm. Scale bar = 100 μm. (**d**, **e**) Human iPS cell-derived melanocytes (red) on coverslips stained with an anti-vesicular antibody (green) and imaged by immunofluorescence microscopy. Scale bar = 20 μm. (**e**) RT-PCR analysis of human iPS cell-derived melanocytes. Bands bars show differences among human cell lines and normal human adult epidermal UEMa-LP melanocytes under various conditions. RT-PCR analysis of human iPS cell-derived melanocytes revealed significantly decreased mRNA levels of the pluripotency gene NANOG, compared with human iPS cells. In contrast, the mRNA expression levels of melanocyte-specific markers (MITF, tyrosinase, and TYRP1) were significantly higher in human iPS cells-derived melanocytes than in human iPS cells. NANOG, MITF, tyrosinase, and TYRP1 mRNA expression levels in human iPS cell-derived melanocytes were similar to UEMa-LP cells. (**f**) Human iPS cell-derived melanocytes cultured overnight in 60-mm gelatinous dishes coated with Matrigel for 8 weeks. We found many colonies and individual cells on the dishes. (**g**) Two-black colonies from confluent photo adhered and were growing in a new human iPS cell-derived melanocyte culture on Matrigel. Melanocytes in (**g**) were picked up from (**f**). The magnifications are shown as enlarged views in the insets. Scale bar = 100 μm. (**h**) Pigmented cells obtained from human iPS cell-derived melanocyte medium adhered and grew to slightly black areas with new human iPS cell-derived melanocytes on Matrigel dish. The presence of human iPS cell-derived melanocytes indicated that pigmented cells in the culture medium were triggered to undergo new melanocyte proliferation from human iPS cells on the gelatinous dishes coated with Matrigel. (**i**) Pigmented cells in the dishes are shown as enlarged views in the insets. (**j**) Human iPS cell-derived melanocyte was cultured for 8 days after removal of the pigmented melanocytes in the medium. Scale bar = 100 μm. (**k**) Numerous human iPS cell-derived melanocytes were seen in culture medium after removal of the cultured cells. Matrigel over 12 days. Five representative clones are containing medium. UEMa-LP human epidermal melanocytes (dark), highly pigmented UDMa iPS cell-derived melanocyte medium. iPS, induced pluripotent stem; MITF, microphthalmia-associated transcription factor; RT-PCR, reverse transcription PCR; TYRP1, tyrosinase-related protein 1.

2011, 2013). Previous approaches to grow and differentiate iPS cells into melanocytes needed first to produce embryoid bodies and then to process them to differentiate into melanocytes (Jores et al., 2013; Ohta et al., 2011), which took approximately 70 days. In contrast, our new approach to utilize a Matrigel coating has shortened this differentiation process from 30 to 20 days in total. In addition, previous studies for growing and differentiating human melanocytes in vitro employed TPA in the culture as well as non-physiological agents such as 12-O-tetradecanoylphorbol-13-acetate and cholera toxin (Ohta et al., 2011; Yamane et al., 1999; Yang et al., 2011). Extending our previous studies (Chang et al., 2014; Hirobe, 2011; Hirobe et al., 2013; Hirobe and Ishikawa, 2013; Kawakami et al., 2008, 2014),

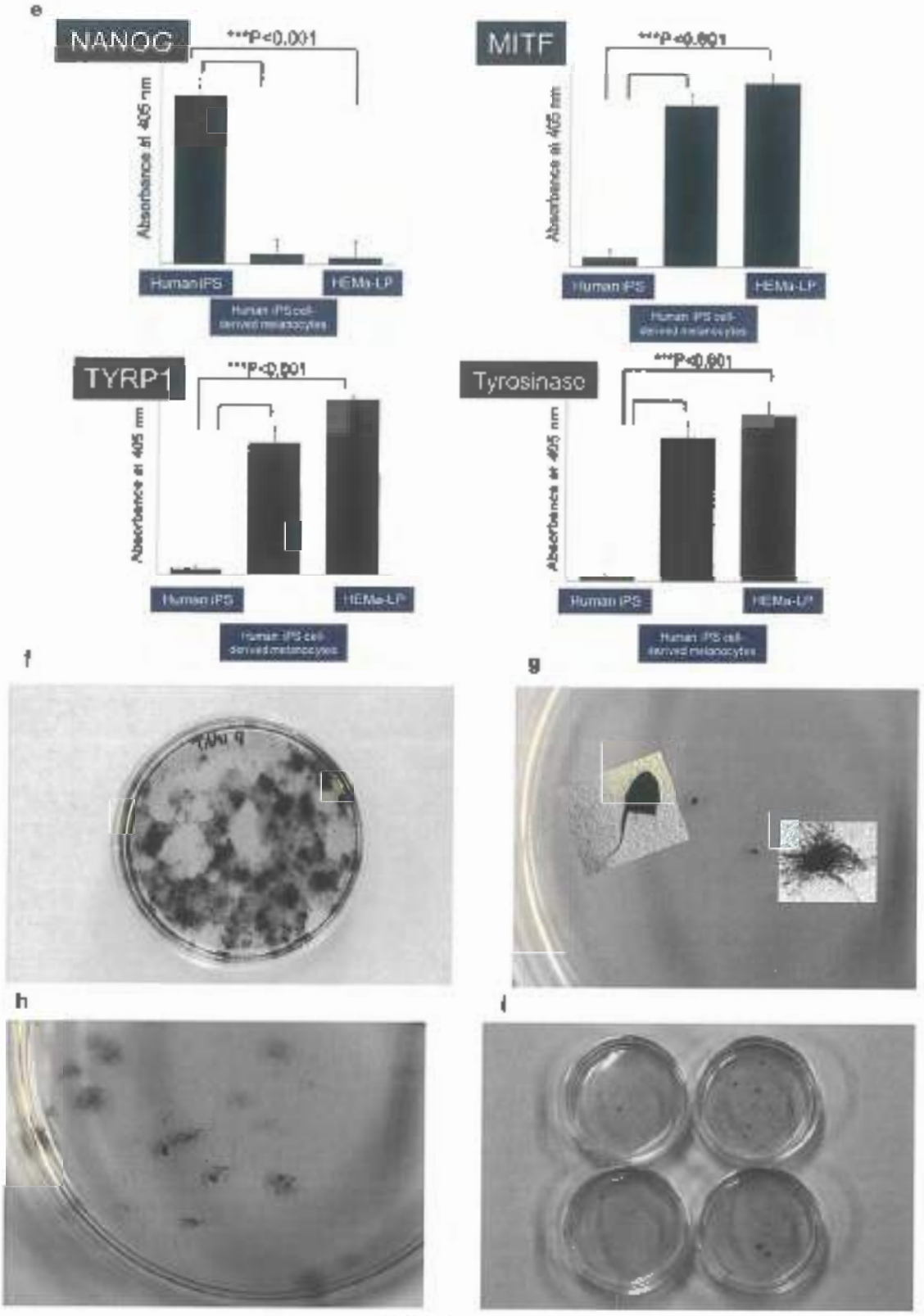

Figure 1. Continued

Figure 2. Pigmentation changes in the nude mouse skin after injection of human melanocytes derived from iPS cells. (**a**) Human iPS cell-derived melanocytes pelleted by centrifugation on the bottom of the tube (left) and in the medium (right). Upper: Dark pigmentation was found in the dorsal skin of nude mouse that was injected with the melanocytes (left) and [illegible] cell suspension (right). Pigmentation disappeared [illegible] in the dorsal skin of the nude mouse consistent with the injection site. (**d**) Fontana-Masson staining revealing melanocyte aggregates in the epidermal layer. Original magnification [illegible] (left) and [illegible] (right). Scale bar = [illegible] μm. (**e**) Melanocyte aggregates in the dermal skin of the inoculated nude mouse were positive for anti-Melan-A immunostaining. Inoculated human iPS cell-derived melanocytes positive for staining with Melan-A antibodies were seen throughout the skin including the dermis and subcutaneous tissue (left), and in the dermal epidermal junction and epidermis (right). Original magnification [illegible] (left) and [illegible] (right). Scale bar = 50 μm. (**f**) Fontana-Masson staining revealed no melanocytes in the inoculation site [illegible]. Immunohistochemical staining with anti-Melan-A antibodies revealed dermal melanocytes at the inoculation site (right). Original magnification [illegible] (left) and [illegible] (right). Scale bar = 50 μm. (**g**) Immunohistochemical staining with anti-Melan-A antibodies showed that the transplanted melanocytes appeared to migrate from the upper dermis to the epidermis. Original magnification [illegible]. Scale bar = 50 μm. iPS, induced pluripotent stem

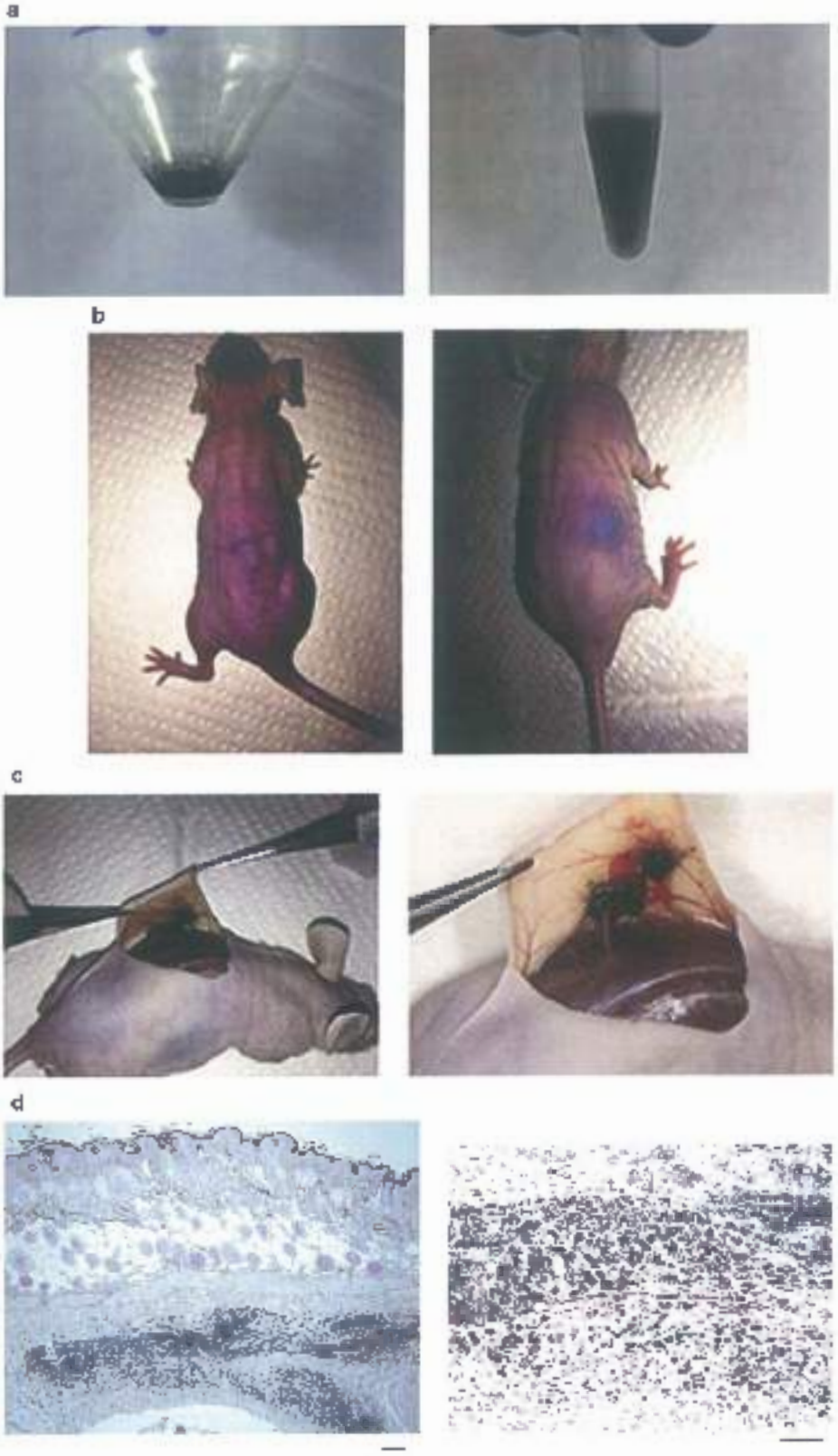

Figure 2. Continued

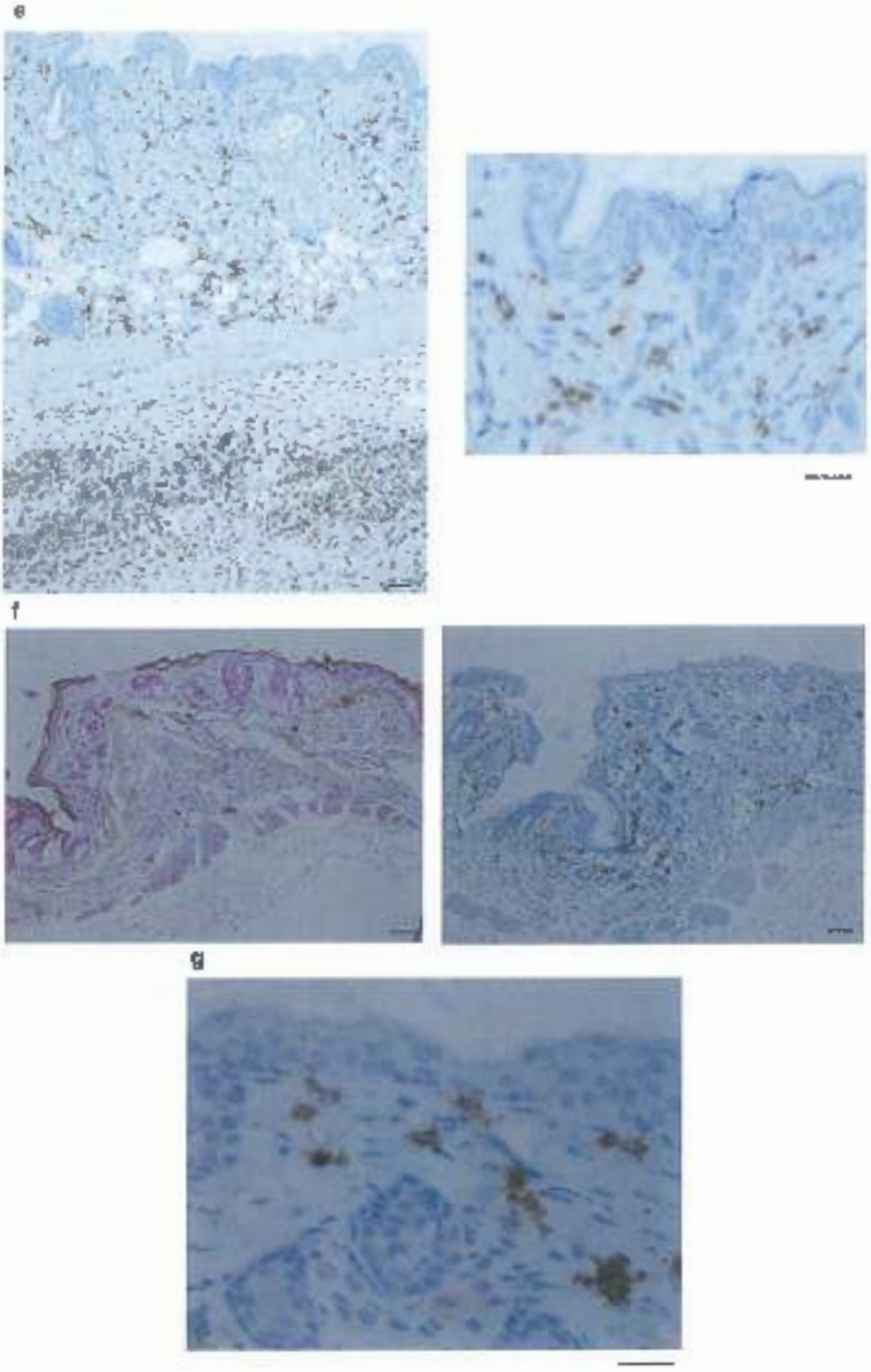

we found that many pigmented cells developed from the border of human iPS cell nests, and that their NANOG mRNA expression level was significantly lower than in human iPS cells. In contrast, MITF, tyrosinase, and TYRP1 mRNA expression levels were similar to those seen in normal human melanocytes, indicating that they are autologous human iPS cell-derived melanocytes. Using our two original methods, we were able to establish a successful approach for the strategies to significantly improve the culture conditions and melanin synthesis during the proliferation and differentiation of in vitro human iPS cell-derived melanocytes under FBS-free culture conditions without supplementation by non-physiological agents, to our knowledge, previously unreported.

We also succeeded in inducing melanin pigmentation in the nude mouse skin in vivo using our human iPS cell-derived

melanocytes. At day 3 after their subepidermal transplantation into the dorsal flanks of nude mice, we found blue to black pigmented lesions that were positive for Fontana-Masson and anti-Melan-A staining in all mice examined, highlighting the reproducibility of the phenotype. Furthermore, we found that a certain number of the subepidermally inoculated human iPS cell-derived melanocytes appeared to migrate upward to the epidermis in the nude mouse skin. On the basis of these findings, we propose that the present method described herein using iPS cells established from T cells in the blood of normal human volunteers could be applied clinically to develop regenerative medicine and cell therapies for various forms of human melanin pigmentation disorders, because of their ability to differentiate into multiple cell types in the body and their unlimited growth potential.

Alterations of human melanocytes have been implicated in the pathogenesis of various pigmentation disorders such as vitiligo and hair graying. Vitiligo is a common disease that affects approximately 1% of the world's population and is associated with high morbidity and psychiatric complications (Alkhateeb et al., 2003; Nissan et al., 2011). Vitiligo is considered to be caused by a loss of functional melanocytes in the skin. Although various methods have been developed to reintroduce cultured melanocytes in vitiliginous skin, their efficacy needs to be improved largely because of the poor proliferation and quality of the autologous melanocytes. Repigmentation of vitiligo requires a numerical increase of functional melanocytes in the depigmented skin (Wu et al., 2004). Our technique makes it possible to produce large numbers of functional melanocytes with active melanin synthesis through the generation of autologous melanocytes derived from human iPS cells established from T cells in the blood and the Sendai virus vector. The utilization of human iPS cell-derived melanocytes may prove invaluable in developing a novel cell therapy for patients with vitiligo. However, in the case of autoimmune nonsegmental/generalized vitiligo (Cavalli et al., 2016; Spritz, 2011), some local immunosuppression may be necessary because the immune system may continue to remove some of the melanocytes. In addition, hair graying could be improved by treatment using human iPS cell-derived melanocytes. The key to understanding the mechanism of melanin production in each hair cycle is the melanocyte stem cell population (Nishimura, 2011).

MATERIALS AND METHODS

Cell culture

Normal human epidermal melanocytes (adult, lightly pigmented cells) were purchased from Invitrogen (Gibco, Carlsbad, CA) and were maintained in melanocyte medium 254CF (Gibco) with human melanocyte growth supplement-2 (Gibco) and 0.2 mM calcium chloride. Human melanocyte growth supplement-2 contained 3 ng/ml FGF2, 0.18 μg/ml hydrocortisone, and 15 nM tetradecanoyl.

KSN/Slc nude mice

Five-week-old male KSN/Slc nude mice were obtained from SLC (Nagoya, Japan). All mice were housed and fed at facilities approved by the Japanese Association for Accreditation of Laboratory Animal Care. The mice were inoculated subepidermally with melanocytes derived from human iPS cells. All animal protocols and procedures were approved by the St. Marianna University Institutional Animal Care and Use Committee. Patient consent for experiments was not required.

Human iPS cell generation and characterization

Expanded T cells obtained from the blood of a healthy 42-year-old Japanese man were reprogrammed using a Sendai virus vector (multiplicity of infection = 2, at 37 °C for 2 hours) expressing four reprogramming factors (OCT3/4, SOX2, c-MYC, and KLF4) (Nishimura et al., 2011). Sendai virus vector was kindly provided by Dr. Mahito Nakanishi (Research Center for Stem Cell Engineering, National Institute of Advanced Industrial Science and Technology). The transfected cells were seeded on X-ray-irradiated mouse embryonic fibroblasts (MEFs) in human T-cell medium (RPMI 1640 with 10% FBS), 1% penicillin-streptomycin (Thermo Fisher Scientific, Waltham, MA) and IL-2 (PeproTech, Rocky Hill, NJ). After 2 days, the medium was changed to primate embryonic stem cell culture medium (ReproCELL, Yokohama, Japan) supplemented with FGF2 (5 ng/ml, R&D Systems, Minneapolis, MN) and was cultured until colonies appeared. Colonies of iPS cells were mechanically picked up and replated on X-ray-irradiated MEFs for expansion and characterization. The established iPS cell line, W1-iPSC1, was maintained in human iPS cell medium, DMEM/F12 (Sigma-Aldrich, Saint Louis, MO), supplemented with 20% knockout serum replacement (Invitrogen), 1% nonessential amino acids (Thermo Fisher Scientific), 0.1 mM 2-mercaptoethanol, 1% penicillin-streptomycin, and 5 ng/ml FGF2. To completely remove Sendai virus vector, a small interfering RNA (siRNA) mixture (40 nM L527s-RNA-1 and 2.5 μl RNAiMAX (Thermo Fisher Scientific) in 500 μl OptiMEM) was added several times into the medium. The following siRNAs were used: L527s-RNA-1, 5′-GCAUUCCAUCAUCAAUUAUGAAGCJ′ and L527s-RNA-2, 5′-UCAUCAUCUUCAUGCCUGAAUCAUU-3′. The authenticity of the iPS cell lines was confirmed in our previous reports (Itoh et al., 2016a, 2016b).

Established iPS cell line, W1-iPSC1

Human iPS cells were seeded on mitomycin C-treated MEFs in human iPS cell medium. Y-27632, a selective inhibitor of p160-Rho-associated coiled-coil kinase, was added to the medium as an effective inhibitor of apoptosis and enhanced the survival of human iPS cells. Before the initiation of melanocyte differentiation, human iPS cells were dissociated into clumps using tissue (Sigma-Aldrich) and were then plated on growth factor reduced BD Matrigel Basement Membrane Matrix (BD Biosciences, Lexington, KY). These cells were cultured in the MEF-conditioned medium for 2 to 3 days.

Melanocyte differentiation from human iPS cells

To induce melanocyte differentiation, human iPS cells were plated on fibrillar gelatinous lenses coated with Matrigel (BD Biosciences) in DMEM/F12. After surrounding human iPS cells in the MEF-conditioned medium on Matrigel for 1 day, these cells were cultured in melanocyte medium 254CF (Gibco) containing human melanocyte growth supplement-2 (Gibco), 0.2 mM calcium chloride, 50 ng/ml stem cell factor (R&D Systems), 50 ng/ml Wnt-3a (R&D Systems), 20 nM human recombinant bone morphogenetic protein 4 (R&D Systems), 0.3 mM ascorbic acid (Sigma-Aldrich), 10⁻⁷ M 1,25-dihydroxyvitamin D₃ (Enzo Life Sciences, Plymouth Meeting, PA), 100 μM 8-bromo-melanocyte stimulating hormone (Sigma-Aldrich), 0.2 mM N,2′-O-dibutyrylcarbosine 3′,5′-cyclic

monophosphate sodium salt (Sigma-Aldrich), 0.1 mM L-tyrosine (Sigma-Aldrich), 100 ng/ml Forskolin (Sigma-Aldrich), 10 ng/ml keratinocyte growth factor (Sigma-Aldrich), 0.1 ng/ml granulocyte-macrophage colony-stimulating factor (Sigma-Aldrich), and 0.1 ng/ml hepatocyte growth factor (Sigma-Aldrich).

Confocal immunofluorescence laser microscopy

Human iPS cell derived melanocytes were fixed on coverslips and were stained with an anti-tyrosinase antibody (ab2418, Abcam, Cambridge, UK). Immunofluorescent images were obtained by confocal laser scanning microscopy using an Axioset (LSM Cal Zeiss, Thornwood, NY) equipped with LSM-510 (Cal Zeiss).

RNA isolation and reverse transcription PCR for human melanocytes derived from iPS cells

RNAs were extracted using an RNeasy Mini Kit (Qiagen, Hilden, Germany), and complementary DNAs were synthesized using 2 μg RNA by Superscript III reverse transcriptase and Oligo-dT primer (Thermo Fisher Scientific) according to the manufacturer's instructions. Quantitative analysis was performed by real-time reverse transcription PCR using the PowerSYBR Green PCR Master Mix (Applied Biosystems, Foster City, CA) and a StepOne Real-Time PCR System (Applied Biosystems). The primers were designed as follows: NANOG: 5′-CAAACGGCAAACAACCAACTT-3′ and 5′-TCTTGCTTGGGATGCCTGAGGTAT-3′, PAX3: 5′-CTGGAACATTTGCTCCAGACT-3′ and 5′-GCTCTTCGTTCTTAGTTCCACA-3′, MITF: 5′-CCGGCTCCAGAATTGTAACTT-3′ and 5′-CCATCAATTTTGGCATTTTGG-3′, TYRP1: 5′-AGCAGTAGTTTGGCTGTTTTGT-3′ and 5′-TCAGTCAGGAGAGGCTGGTTT-3′, and tyrosinase: 5′-TTGTACTCCTTCCTCTGTGTAC-3′ and 5′-TACCAACCTCTCATTGAAAC-3′.

Subepidermal inoculation of nude mice with melanocytes derived from human iPS cells

Melanocytes derived from human iPS cells growing on plastic dishes were dissociated by StemPro Accutase (Gibco), washed and then pelleted by centrifugation. Melanocytes were then resuspended at 0.1×10^6, 1×10^6, or 5×10^6 cells/ml in isotonic sodium chloride solution. Nude mice were anesthetized with diethyl ether. Inoculation of 1 ml of each cell suspension was carried out subepidermally into the dorsal flank. The skin samples of nude mice were fixed in PBS containing 4% formaldehyde and were embedded in paraffin. Formalin-fixed paraffin-embedded tissues of nude mice were sectioned at 4 μm thickness.

Melanocyte-related staining

Formalin-fixed paraffin sections were deparaffinized with Furopa aromatic solvent solution for 10 hours at room temperature following the manufacturer's instructions. The tissue sections were also stained with hematoxylin and eosin for morphological analyses. Human monoclonal anti-Melan-A antibodies (Dako, Santa Clara, CA) were used at a dilution of 1:50. The formalin-fixed paraffin-embedded tissues were incubated with anti-Melan-A antibody at 4°C overnight. The slides were then incubated with a biotinylated secondary antibody, avidin-peroxidase complex (Dako), and the chromogenic substrate diaminobenzidine. Irish-stained saline was used instead of the primary antibody as a negative control.

Statistical analysis

All data are expressed as means ± standard deviation. A P value of less than 0.05 is considered to be statistically significant. Differences among quantitative parameters between groups were assessed using the Mann–Whitney U test.

CONFLICT OF INTEREST

The authors state no conflict of interest.

ACKNOWLEDGMENTS

We are grateful to our colleagues and laboratory staff who helped in several run studies. We are also grateful to Professor Dorothy Bennett, PhD, Molecular & Clinical Sciences Institute, UK, who provided critical comments on manuscript during its preparation. We are indebted to Professor Takahiro Okazaki, Department of Internal Medicine, St. Marianna University School of Medicine, and Professor Hideki Nagasawa, Department of Dermatology, Iwate University School of Medicine. This work was supported by grants from the Scientific Research Fund of the Ministry of Education, Science, Sports and Culture, Japan (Grant-in-Aid for Scientific Research, No. 21591176 and 25591156).

REFERENCES

Alkhateeb A, Fain PR, Thody A, Bennett DC, Spritz RA. Epidemiology of vitiligo and associated autoimmune diseases in Caucasian probands and their families. Pigment Cell Res 2003;16:208–14.

Cavalli G, Hayashi M, Jin Y, Yargov D, Santorico SA, Holcomb C, et al. MHC class II super-enhancer increases surface expression of HLA-DR and HLA-DQ and affects cytokine production in autoimmune vitiligo. Proc Natl Acad Sci USA 2016;113:1363–8.

Chang CH, Tsai RK, Tsai MH, Lin YH, Hirobe T. The roles of Frizzled-3 and Wnt1a on melanocyte development: in vitro studies on neural crest cells and melanocyte precursor cell lines. J Dermatol Sci 2014;75:100–8.

Hirobe T. How are proliferation and differentiation of melanocytes regulated? Pigment Cell Melanoma Res 2011;24:462–78.

Hirobe T, Hosegawa K, Furuya R, Fujiwara R, Sato K. Effects of fibroblast-derived factors on the proliferation and differentiation of human melanocytes in culture. J Dermatol Sci 2013;71:45–57.

Hirobe T, Ishikawa A. L-tyrosine induces melanocyte differentiation in novel pink-eyed dilution castaneus mouse mutant showing age-related pigmentation. J Dermatol Sci 2015;80:203–11.

Itoh M, Kawagoe S, Okano HJ, Nakagawa H. Integration-free T cell-derived human induced pluripotent stem cells (iPSCs) from a healthy individual: WT-iPSC1. Stem Cell Res 2016a;17:22–4.

Itoh M, Kawagoe S, Okano HJ, Nakagawa H. Integration-free T cell-derived human induced pluripotent stem cells (iPSCs) from a healthy individual: WT-iPSC2. Stem Cell Res 2016b;17:16–8.

Jones JC, Sabatini K, Liao X, Tran HT, Lynch CL, Morey RE, et al. Melanocytes derived from transgene-free human induced pluripotent stem cells. J Invest Dermatol 2013;133:2104–8.

Kawakami T, Kimura S, Kawa Y, Kato M, Mizoguchi M, Soma Y. BMP-4 upregulates Kit expression in mouse melanoblasts prior to the Kit-dependent cycle of melanogenesis. J Invest Dermatol 2008;128:1220–6.

Kawakami T, Ohgushi A, Hirobe T, Soma Y. Effects of 1,25-dihydroxyvitamin D3 on human epidermal melanocytes and melanoblasts. J Dermatol Sci 2014;76:72–4.

Kawakami T, Otaguchi R, Kyoya M, Soma Y, Suzuki T. Patient with dyschromatosis symmetrica hereditaria treated with miniature punch grafting, followed by excimer light therapy. J Dermatol 2013;40:771–2.

Kunisada T, Tezuka K, Aoki H, Motohashi T. The stemness of neural crest cells and their derivatives. Birth Defects Res C Embryo Today 2014;102:251–62.

Mica Y, Lee G, Chambers SM, Tomishima MJ, Studer L. Modeling neural crest induction, melanocyte specification, and disease-related pigmentation defects in hESCs and patient-specific iPSCs. Cell Rep 2013;3:1140–52.

Nishimura EK. Melanocyte stem cells: a melanocyte reservoir in hair follicles for hair and skin pigmentation. Pigment Cell Melanoma Res 2011;24:401–10.

Nishimura K, Sano M, Ohtaka M, Furuta B, Umemura Y, Nakajima Y, et al. Development of defective and persistent Sendai virus vector: a unique gene delivery/expression system ideal for cell reprogramming. J Biol Chem 2011;286:4760–71.

Nissan X, Larribere L, Saidani M, Hurbain I, Delevoye C, Feteira J, et al. Functional melanocytes derived from human pluripotent stem cells

engraft into pluristratified epidermis. Proc Natl Acad Sci USA 2011;108:14861–6.

Ohta S, Imaizumi Y, Akamatsu W, Okano H, Kawakami Y. Generation of human melanocytes from induced pluripotent stem cells. Methods Mol Biol 2013;989:193–215.

Ohta S, Imaizumi Y, Okada Y, Akamatsu W, Kuwahara R, Ohyama M, et al. Generation of human melanocytes from induced pluripotent stem cells. PLoS One 2011;6:e16182.

Spritz RA. The genetics of vitiligo. J Invest Dermatol 2011;131:E18–20.

Tauchiyama K, Wakao S, Kuroda Y, Ogura F, Nojima M, Sawaya N, et al. Functional melanocytes are readily reprogrammable from multilineage-differentiating stress-enduring (muse) cells, distinct stem cells in human fibroblasts. J Invest Dermatol 2013;133:2423–35.

Yamane T, Hayashi S, Mizoguchi M, Yamazaki H, Kanisaka T. Derivation of melanocytes from embryonic stem cells in culture. Dev Dyn 1999;216:450–8.

Yang R, Jiang M, Kumar SM, Xu T, Wang F, Xiang L, et al. Generation of melanocytes from induced pluripotent stem cells. J Invest Dermatol 2011;131:2458–66.

Wu CS, Yu CL, Wu CS, Lan CC, Yu HS. Narrow-band ultraviolet-B stimulates proliferation and migration of cultured melanocytes. Exp Dermatol 2004;13:753–63.

Allergology International 66 (2017) 398–403

Contents lists available at ScienceDirect

Allergology International

journal homepage: http://www.elsevier.com/locate/ali

Review article

Atopic dermatitis: immune deviation, barrier dysfunction, IgE autoreactivity and new therapies

Masutaka Furue [a, b, c, *], Takahito Chiba [d], Gaku Tsuji [a, b], Dugarmaa Ulzii [a], Makiko Kido-Nakahara [a], Takeshi Nakahara [a, c], Takafumi Kadono [d]

[a] Department of Dermatology, Kyushu University, Fukuoka, Japan
[b] Research and Clinical Center for Asian-type Atopic Dermatitis, Kyushu University, Fukuoka, Japan
[c] Division of Skin Surface Sensing, Department of Dermatology, Gifu Hi University, Fukuoka, Japan
[d] Department of Dermatology, St. Marianna University School of Medicine, Kawasaki, Japan

ARTICLE INFO

Article history:
Received 8 November 2016
Accepted 18 November 2016
Available online 2 January 2017

Keywords:
Atopic dermatitis
Filaggrin
IgE autoreactivity
Th2
Th22

List of abbreviations:
AD, atopic dermatitis; c-NAC, c-nascent polypeptide associated complex; AHR, aryl hydrocarbon receptor; CLA, cutaneous lymphocyte antigen; FcεRI, high-affinity IgE receptor; FLG, filaggrin; H4R, histamine H4 receptor; IFN, interferon; IL, interleukin; IL22, interleukin-22 producing T; JAK, Janus kinase; Th, T helper; TrkA, tropomyosin receptor kinase A; TSLP, thymic stromal lymphopoietin.

ABSTRACT

Atopic dermatitis (AD) is a chronic or chronically relapsing, eczematous, severely pruritic skin disorder mostly associated with IgE elevation and skin barrier dysfunction due to decreased filaggrin expression. The lesional skin of AD exhibits Th2- and Th22-deviated immune reactions that are progressive during disease chronicity. Th2 and Th22 cytokines further deteriorate the skin barrier by inhibiting filaggrin expression. Some IgEs are reactive to self-antigens. The IgE autoreactivity may explain the chronicity of AD. Upon activation of the ORAI1 calcium channel, atopic epidermis releases large amounts of thymic stromal lymphopoietin (TSLP), which initiates the Th2 and Th22 immune response. Th2-derived interleukin-31 and TSLP induce itch sensation. Taken together, TSLP/Th2/Th22 pathway is a promising target for developing new therapeutics for AD. Enhancing filaggrin expression using ligands for the aryl hydrocarbon receptor may also be an adjunctive measure to restore the disrupted barrier function specifically for AD.

Copyright © 2016 Japanese Society of Allergology. Production and hosting by Elsevier B.V. This is an open access article under the CC BY-NC-ND license (http://creativecommons.org/licenses/by-nc-nd/4.0/).

Introduction

Atopic dermatitis (AD) is a common eczematous skin disorder affecting 2–20% of the general population with age and ethnic differences.[1,2] AD is characterized by chronic cutaneous inflammation and dry skin with epidermal barrier dysfunction.[1–5] Intense pruritus is the major and burdensome symptom of AD.[6,7] Itch-induced scratching appears to exacerbate skin inflammation by accelerating cellular damage in the lesional skin.[8]

Approximately 80% of AD patients exhibit elevated levels of serum IgE.[9,10] In contrast to normal-IgE and non-allergic intrinsic AD patients, extrinsic AD patients with hyper IgE levels are associated with increased disease severity,[11,12] mutations in the *FLG* gene,[13] and impaired skin barrier function.[14,15] Recent genome-wide association studies and immunochip analyses indicate at least 31 significant susceptibility loci for AD, which emphasize the potential engagement of T helper 2 (Th2) cytokines (*IL13/IL4*, *IL4/IL13*), IL-1 family receptors (*IL18R1/IL18RAP*, *IL33R/IL1RL1*) and skin barrier proteins (*FLG*).[16–20]

With regards to immune abnormalities, AD is currently considered as a biphasic T cell-mediated disease. A Th2 signal predominates in the acute phase, whereas a Th2 to Th1 switch promotes disease chronicity.[21,22] However, recent studies have proposed a significant role for interleukin (IL)-22-producing T (Th22)

* Corresponding author. Department of Dermatology, Kyushu University, Maidashi 3-1-1, Higashi-ku, Fukuoka 812-8582, Japan.
E-mail address: furue@dermatol.med.kyushu-u.ac.jp (M. Furue).
Peer review under responsibility of Japanese Society of Allergology.

http://dx.doi.org/10.1016/j.alli.2016.12.002
1323-8930/Copyright © 2016 Japanese Society of Allergology. Production and hosting by Elsevier B.V. This is an open access article under the CC BY-NC-ND license (http://creativecommons.org/licenses/by-nc-nd/4.0/).

cells, and to a less extent IL-17-producing Th17 cells, in the initiation and maintenance of AD.[22–26] Infiltrations of CD4+ T cells, CD1c+ dendritic cells and CD1c+ dendritic cells are accompanied with acute AD, and more intense infiltrations are associated with chronic AD.[22]

In addition to the involvement of cellular immunity towards Th2 and T22 differentiation, elevated IgE is likely to be engaged in the development and severity of AD by manifesting IgE autoreactivity.[27–31] Total IgE levels are strongly correlated with the prevalence of IgE autoreactivity.[28–30] Some reports indicate a correlation between autoreactivity and disease severity in AD.[28,31] In addition, numerous cells infiltrated in the lesional skin of AD are positive for IgE or the high affinity Fc IgE receptor (FcεRI).[24,32,33]

Based on the pathogenetic role of barrier and immune abnormalities in AD, standard therapeutics include topical emollients for barrier dysfunction and topical steroids and calcineurin inhibitors for skin inflammation.[11] These conventional treatments are more or less effective in reducing atopic inflammation and itch; however, patient satisfaction is generally low in daily clinics. Several targeting therapies are now emerging and being assessed in clinical trials.[5]

Immune deviation towards Th2 and T22 expansion in AD

Historically, acute AD lesions have a significantly greater number of Th2 cytokine (IL-4, IL-5 and IL-13) mRNA-expressing cells compared with normal skin or uninvolved AD skin.[6,26] Compared with acute lesions, chronic AD lesions have fewer IL-4 and IL-13 mRNA expressing cells but greater numbers of interferon (IFN)-γ mRNA expressing Th1 cells.[5,26] The Th2 to Th2/Th1 shift is also exemplified in an atopic patch test elicited by house dust mite antigen.[37,38] In addition, the importance of Th2 deviation in AD is evidenced by the fact that the disease severity of AD is significantly correlated with IL-4/IL-13-related molecules, such as CCL17, periostin and galectin-9.[39–41] Although the potential role of IL-17-producing Th17 cells is proposed in AD,[42] controversial results have been reported.[43,44]

In addition to Th2 deviation, a series of recent studies by Guttman-Yassky et al. have stressed a critical role of IL-22-producing T22 cells in AD (Fig. 1).[22,24,45] Unlike murine Th17 cells, which coproduce IL-22, human T cells harbor distinct T22 cells that lack IL-17 expression.[45,46] Nograles et al. first demonstrated a significant accumulation of T22 cells in the lesional skin of AD compared with psoriasis and normal controls.[45] The infiltrated T22 cells included CD4+ helper (Th22) and CD8− cytotoxic (Tc22) cells. Of note, the clinical severity of AD is correlated with the number of Tc22 cells rather than that of Th22 cells.[45] In a study comparing nonlesional skin with acute and chronic lesions in 10 patients with AD, the acute lesions exhibit a striking upregulation of genes related to Th2 (*IL4*, *IL10*, *IL31* and *CCL17*) and T22 (*IL22*, *S100A7*, *S100A8*, *S100A9*, *S100A12* and *IL32*).[22] The increased Th2/T22 signatures in acute AD lesions are further enhanced in chronic lesions intermingled with upregulation of Th1-related genes (*IFNG*, *CXCL9*, *CXCL10* and *CXCL11*).[22] Multicolor flow cytometric analyses have revealed that circulating cutaneous lymphocyte antigen-positive (CLA+; skin homing receptor) Th2 cells are markedly expanded in both children (aged 5–78 months) and adults (aged 18–74 years) with AD compared with normal control subjects.[24] The number of CLA+ Th1 cells is significantly decreased in childhood AD but not adult AD, whereas the number of both CLA+ Th22 and CLA+ Tc22 is significantly increased in adult but not childhood AD patients compared with normal controls.[24] The comparative study enrolling early (aged 0–3 years) and late (aged 5–15 years) childhood AD patients has elucidated a significant elevation of CLA+ Th2 and a significant decrease of CLA+ Th1 population in the early but not in late childhood AD patients compared with normal age-matched control subjects.[47] No significant difference is observed in the number of CLA+ Tc22 cells between AD patients and normal controls in either early or late childhood AD.[47] In parallel with the pivotal participation of Th2/T22 cells, the upregulation of chemokines and

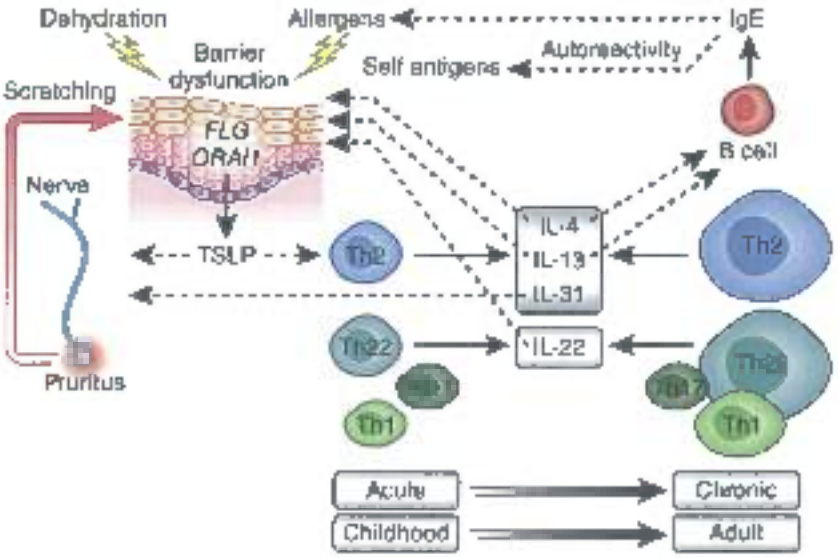

Fig. 1. Pathogenesis of atopic dermatitis (AD). Skin barrier dysfunction and T22/Th22-mediated immune responses are the fundamental abnormality of AD. Genetic mutations in filaggrin (FLG) cause barrier disruption and dehydration, which make the external allergens permeable. The barrier-disrupted epidermis secondary releases thymic stromal lymphopoietin (TSLP), which triggers the Th2/Th22 immune response. The IgE/Th2 deviation is further accelerated during disease progression, for example, from acute to chronic or childhood to adult AD. In addition, Th1 but not Th17 cells seem to participate in the chronic phase of AD. Th2 cytokines (IL-4 and IL-13) enhance production of IgE antibodies to allergens. Some IgEs react to self-antigens. IgE autoreactivity also contributes to disease activity. In addition, IL-4, IL-13 and IL-31 are strong suppressors of SC expression. Pruritus is evoked by TSLP and Th2 cytokines IL-31, and the subsequent scratching further worsens skin barrier dysfunction. The release of TSLP from keratinocytes is dependent on calcium influx regulated by the ORAI1 channel. Targeting TSLP/Th2/Th22 as well as ORAI1 pathways is a promising strategy to overcome atopic inflammation.

chemokine receptors is also an integral component of atopic inflammation, i.e., CCL1, CCL4, CCL13, CCL17, CCL18, CCL20, CCL22, CCL26, CXCL1, CXCL2, CXCL3, CXCL8, CXCL9, CXCL10, CCR1 and CCR7 with increased expression of janus kinases (JAK) 1 and 3.[48–51]

Disruption of barrier proteins by IL-4, IL-13 and IL-22

The epidermal barrier function is formed by coordinated and sequential cross-linking of various barrier proteins, such as filaggrin (FLG) and loricrin (LOR). The majority of human epidermal barrier proteins map to a 2.5-Mbp cluster termed the "epidermal differentiation complex" (EDC) located on chromosome 1q21.[51,52] The expression of barrier protein genes in the EDC locus is up- and downregulated by various external and internal stimuli, including Th2 (IL-4 and IL-13) and T22 (IL-22) cytokines.[41,51–57] Interleukin-4 and IL-13 significantly inhibit FLG and LOR mRNA and protein expression.[53–56] FLG and LOR expression is also markedly downregulated by IL-22 (Fig. 1).[41,57] In accordance with the loss of function mutation of *FLG* in AD,[15,42] the downregulated action of Th2 and T22 cytokines explain the disrupted expression of FLG and LOR in the lesional skin of AD patients, leading to epidermal barrier dysfunction.[10,54,55,58] In contrast to the decreased expression of FLG and LOR, the lesional skin of AD patients exhibited increased expression of S100A7, the gene of which is also located in the EDC locus.[7,45,51,55] Although IL-4 and IL-13 inhibit the expression of S100A7 in keratinocytes, IL-22 is a strong inducer of S100A7 gene expression.[51,45,59]

IgE autoreactivity in AD

The definition of "atopy" is a diathesis to overproduce IgE antibodies or to have a personal and/or family history of asthma, allergic rhinitis, allergic conjunctivitis and AD.[60] With the help of Th2 cytokines, activated B cells undergo IgE production.[61] Diverse activation and differentiation of multiple B cell subsets are indeed reported in AD but not in psoriasis or normal controls, with a significant correlation with circulating IgE levels.[62] Consistent with the preponderant Th2 deviation in early childhood AD,[12,63] elevated levels of total or allergen-specific IgE are noted in infantile and early childhood AD.[50,51,63] IgE levels specific for ovomucoid, wheat and mite allergens are correlated with serum levels of the Th2-related cytokines CCL17 and CCL22.[17,51] The skin barrier dysfunction with FLG mutation and increased *Staphylococcus aureus* colonization contribute to disease progression and aberrant IgE production in AD.[13,64–66]

As previously demonstrated in the autoimmune diseases, such as systemic lupus erythematosus and bullous pemphigoid,[67] IgE autoreactivity is given increasing attention in AD (Fig. 1).[37–37] A positive skin test to human dander and sweat had suggested the presence of IgE autoreactivity to unknown auto-antigens in the 1940s.[67–71] In addition, the fungal protein MGL_1414, which is derived from *Malassezia globosa*, is identified as the major antigen for the sweat targeting IgE antibodies from AD.[72] However, some autoreactive IgE antibodies in AD patients potentially bind to cell membrane and intracellular structures of cultured human keratinocytes.[73] Natter et al., Zelier et al. and other researchers have examined human cDNA clones coding for auto-antigens targeted by IgE autoantibodies from AD patients and have found a variety of plausible self-antigens, including manganese superoxide dismutase, ribosomal P2 protein, profilin 1, cyclophilin B, thioredoxin, α-nascent polypeptide-associated complex (α-NAC), keratin 6A, actin α2 and tubulin α1A, some of which have high homology to environmental allergens.[30,71,72] It is intriguing that the titers of anti-manganese superoxide dismutase IgE autoantibodies correlate with AD disease severity.[74] Some of these auto-antigens activate basophils via FcεRI and induce a positive skin reaction of the immediate or delayed type.[44,6,75]

The transcriptional coactivator α-NAC is an intracellular protein that is involved in sorting of newly synthesized polypeptides without any homology with environmental known allergens.[76] Peripheral blood mononuclear cells (PBMC) from AD patients with anti-α-NAC IgE antibodies produce significantly increased amounts of IL-17, IL-22 and IFN-γ compared with normal control PBMCs in vitro in the presence of α-NAC and IL-2. The cytokine production is cancelled by the depletion of antigen-presenting monocytes from PBMC, demonstrating that the α-NAC self-antigen is presented by monocytes to T cells by the ordinary immune system.[76] The autoreactive T cells specific for α-NAC are CLA+ and CCR4+.[79] Recently, α-NAC-specific autoreactive CD8+ T cells are also detected in AD patients. These α-NAC-specific CD8+ T cells coproduce IL-4 and IFN-γ.[80] These studies highlight the potential role of autoreactive IgE and T cell responses in exacerbating and perpetuating AD disease severity.

New therapies for atopic dermatitis

First-line treatments of AD include the application of emollients for dry skin, topical steroids and tacrolimus for skin inflammation, and oral antihistamines for pruritus, followed by second-line adjunct therapies, such as systemic cyclosporine, short-term oral steroids, and ultraviolet radiation.[10] Although many reports confirm the effects of conventional treatments, the satisfaction and adherence to treatments are typically very low in AD patients.[81] Considering the recent progress in the understanding of the pathomechanisms of AD, there is room for new strategies and therapies in the management of AD.

Dupilumab

Dupilumab is a fully human monoclonal antibody directed against the α subunit of the IL-4 receptors that blocks signaling from both IL-4 and IL-13. In phase I and II studies of adults with moderate-to-severe AD, administration of dupilumab resulted in significant improvements in inflammation and pruritus with no dose-limiting toxicity.[82–84] Significant decrease in mRNA expression of genes related to Th2-associated chemokines (CCL17, CCL18, CCL22 and CCL26) is detected without significant modulation of Th1-associated genes (IFNG).[84] Dupilumab also significantly improves the disturbance of sleep and quality of life at 16 weeks of treatment.[85] These findings indicate that dupilumab is a promising new anti-inflammatory and anti-pruritic treatment for AD.

Anti-IL-31 A receptor antibody (CIM331)

An anti-IL-31 receptor A antibody may be another promising agent to inhibit atopic itch. In humans and mice, IL-31 is predominantly produced by Th2 cells, and its cutaneous injection induces pruritus.[86] A recent clinical trial has revealed that a single injection of an anti-IL-31 receptor A antibody (CIM331) significantly inhibits pruritus in patients with moderate to severe AD for up to 4 weeks after administration without any serious adverse events.[87] CIM331 also increases sleep efficiency and decreases the use of topical hydrocortisone butyrate.[87] Notably, IL-31 receptor A is defined as a downstream molecule of FcεRI activation.[88]

Phosphodiesterase 4 inhibitors

Phosphodiesterase 4 inhibitors exhibit immunosuppressive activity by enhancing the intracellular concentration of cyclic AMP and inhibit IL-4 and tumor necrosis factor α in experimental

animals.[84] In clinical trials, several topical phosphodiesterase 4 inhibitors, including E6005,[87,88] OPA-15406,[89] and crisaborole[90] have demonstrated effectiveness against inflammation and pruritus in AD. Although the oral phosphodiesterase 4 inhibitor apremilast is effective in the treatment of AD and psoriasis, a higher dose may be necessary to obtain significant improvement in AD compared with psoriasis.[91,92]

Histamine H4 receptor antagonist

Based on its anti-pruritic and anti-inflammatory effects in experimental animals, a clinical trial of the oral administration of histamine H4 receptor (H4R) antagonist (JNJ-39758979) was conducted in Japanese patients with AD.[93] Although the H4R antagonist significantly reduced day- and night-time pruritus in AD patients, the clinical study was terminated due to the severe adverse effects of agranulocytosis. In addition to its neural expression,[94] H4R is involved in the CCL17 and CCL22 production from monocyte-derived dendritic cells and the Th2-deviated inflammation in atopic model mice.[95,96]

Janus kinase inhibitor (tofacitinib)

Cytokines exert their effects by activating intracellular signaling pathways, such as the JAK family. Tofacitinib is a pan-JAK inhibitor that preferentially inhibits JAK1 and JAK3, and to a lesser extent, JAK2 and tyrosine kinase 2.[97] Both oral and topical tofacitinib significantly improve the skin inflammation and pruritus of AD.[98,99] The mean percent changes from baseline at week 4 in eczema area and severity index (EASI) score are significantly greater ($p < 0.001$) for topical tofacitinib (−81.7%) vs. vehicle (−29.9%).[100] Significant improvements in EASI are observed by week 1 and pruritus by day 2.[101] Although tofacitinib is a promising agent, its potential adverse events due to immunosuppression should be carefully evaluated in a long-term clinical trial.

Topical tropomyosin receptor kinase A inhibitor

Tropomyosin receptor kinase A (TrkA) is a high-affinity NGF receptor. Nerve fibers positive for TrkA are detected in human epidermis, dermis, and dorsal root ganglion.[102] A recent clinical trial by Rebinger et al. demonstrates that the topical TrkA kinase inhibitor CT327 is an effective treatment for pruritus due to psoriasis.[103] Further trials are necessary to prove the anti-pruritic effects of CT327 in AD.

Conclusion

The expression of FLG is upregulated by the specific activation of aryl hydrocarbon receptor (AHR), which senses various external and internal chemical ligands.[54,55,56] Ligation of AHR by coal tar, soybean tar or certain phytochemicals cancels the inhibitory action of Th2 cytokines on the FLG expression, which may partly account for the medicinal use of these agents to treat inflammatory skin disease.[53,55,56,104] Exploring the safe and effective ligands for AHR is one of the potential methods to develop new adjunctive therapeutics for barrier-disrupted skin diseases. AHR is also a key molecule in establishing the intestinal microbial community by influencing the balance between Th17 cells and regulatory T cells.[105] Therefore, one can also hypothesize that spontaneous regression of infantile AD[106] may be related to the restoration of FLG expression by endogenous and exogenous AHR ligands supplied from skin microbiota[107] together with the normalization of immune deviation.

As revealed in psoriasis,[107] epidermal and immune interactions also play critical roles in the pathogenesis of AD.[108] Thymic stromal lymphopoietin (TSLP) is strongly expressed in the lesional epidermis in AD and acts as a "master" switch that triggers the Th2 and Th22 response (Fig. 1).[109,110] In addition, TSLP directly activates sensory nerves to induce pruritus.[111] The production of TSLP by epidermal keratinocytes is highly dependent on an increase in intracellular Ca^{2+} regulated by the activation of ORAI1, which is the major subunit of a store-operated Ca^{2+} channel in keratinocytes.[112,113] Knockdown of ORAI1 significantly attenuates TSLP release by keratinocytes.[112] Of interest, an ORAI1 genetic polymorphism is associated with the susceptibility of AD in Japanese and Taiwanese populations.[113] Taken together, targeting TSLP/Th2/Th22 as well as ORAI1 pathways is a promising strategy to overcome atopic inflammation.

Conflict of interest

M. Furue is a consultant of P&G and receives research funds from P&G and Sanofi. The rest of the authors have no conflict of interest.

References

1. Takeuchi S, Esaki H, Furue M. Epidemiology of atopic dermatitis in Japan. J Dermatol 2014;41:200–4.
2. Sybilski AJ, Raithaler J, Lipiec A, Lemańska-Żuberska A, Glowacki G, Samel-Kowalik P, et al. Epidemiology of atopic dermatitis in Poland according to the Epidemiology of Allergic Disorders in Poland (ECAP) study. J Dermatol 2015;42:140–7.
3. Park J, Cheon DW, Kim Y, Kim J, Kim M, Park YM. Novel FLG null mutations in Korean patients with atopic dermatitis: comparison of the mutational spectra in Asian populations. J Dermatol 2015;42:567–73.
4. Nakagawa S, Morita M, Ikeya S, Sakane T, Takeuchi Y. Atopic dermatitis presenting as generalized poikiloderma with filaggrin gene mutations. J Dermatol 2014;41:230–1.
5. Lee SC, Committee of Korean Atopic Dermatitis Association for REACH. Various diagnostic criteria for atopic dermatitis (AD): a proposal of Reliable Estimation of Atopic Dermatitis in Childhood (REACH) criteria, a novel questionnaire based diagnostic tool for AD. J Dermatol 2015;43:576–84.
6. Furue M, Kadono T. New therapies for controlling atopic itch. J Dermatol 2015;42:647–50.
7. Tominaga M, Takamori K. Itch and nerve fibers with special reference to atopic dermatitis: therapeutic implications. J Dermatol 2014;41:205–12.
8. Takeuchi S, Nakakawa K, Furue M, Katz SI. Collected mouse model to assess the effects of scratching. J Dermatol Sci 2010;57:44–50.
9. Tokura Y. Extrinsic and intrinsic types of atopic dermatitis. J Dermatol Sci 2010;58:1–7.
10. Martel BC, Esman T, Stahl A, Nomura I, Tsoitis P, Dyring-Andersen B, et al. Distinct molecular signatures of mild non-lesional and extrinsic atopic dermatitis. Exp Dermatol 2016;25:453–9.
11. Bieber-Inkinger FF, Spits PF, Tegetoe CM, Lindebaum R, Smit JH, Bos JD. Clinical differences between atopic and atopiform dermatitis. J Am Acad Dermatol 2008;58:407–14.
12. Kabashima-Kubo R, Nakamura M, Sakabe J, Sugita K, Ohno R, Mori T, et al. A group of atopic dermatitis without IgE elevation or barrier impairment shows a high Th1 frequency: possible immunological state of the intrinsic type. J Dermatol Sci 2012;67:37–43.
13. Weidinger S, Rodriguez E, Stahl C, Wagenpfeil S, Klopp N, Illig T, et al. Filaggrin mutations strongly predispose to early-onset and extrinsic atopic dermatitis. J Invest Dermatol 2007;127:724–6.
14. Mori T, Ikeda K, Matsuyama S, Yamada Y, Inokawa G, Nakashima K, et al. Comparison of skin barrier function and sensory nerve electric current perception threshold between IgE-high extrinsic and IgE-normal intrinsic types of atopic dermatitis. Br J Dermatol 2010;162:82–90.
15. Esparza-Gordillo J, Weidinger S, Fölster-Holst R, Bauerfeind A, Ruschendorf F, Patone G, et al. A common variant on chromosome 11q13 is associated with atopic dermatitis. Nat Genet 2009;41:596–601.
16. Sun LD, Xiao FL, Li Y, Zhou WM, Tang HY, Tang XF, et al. Genome-wide association study identifies two new susceptibility loci for atopic dermatitis in the Chinese Han population. Nat Genet 2011;43:690–4.
17. Paternoster L, Standl M, Chen CM, Ramasamy A, Bonnelykke K, Duffy L, et al. Meta-analysis of genome-wide association studies identifies three new risk loci for atopic dermatitis. Nat Genet 2012;44:187–92.
18. Hirota T, Takahashi A, Kubo M, Tsunoda T, Tomita K, Sakashita M, et al. Genome-wide association study identifies eight new susceptibility loci for atopic dermatitis in the Japanese population. Nat Genet 2012;44:1222–6.
19. Illingham D, Barrett JH, Esparza-Gordillo J, Rodriguez E, Matanovic A, Marenholz I, et al. High-density genotyping study identifies four new susceptibility loci for atopic dermatitis. Nat Genet 2013;45:808–12.

20. Tamari M, Hirota T. Genome-wide association studies of atopic dermatitis. J Dermatol 2014;41:293–20.
21. Leung DY, Boguniewicz M, Howell MD, Nomura I, Hamid QA. New insights into atopic dermatitis. J Clin Invest 2004;113:651–57.
22. Guttman-Yassky E, Diaz A, Pavel AB, Fernandes M, Lefferts AR, Suprun M, Zhang N, Wang C, Li X, Krueger JG, Paller AS. Progressive activation of IL-13/IL-22 cytokines and skin barrier epidermal proteins characterizes acute and chronic atopic dermatitis. J Allergy Clin Immunol 2019;144:1548–1564.
23. Hayashida S, Uchi H, Takeuchi S, Esaki H, Moroi Y, Furue M. Significant correlation of serum IL-22 levels with CCL17 levels in atopic dermatitis. J Dermatol Sci 2011;68:75–79.
24. Czarnowicki T, Esaki H, Gonzalez J, Malajian D, Shemer A, Noda S, et al. Early pediatric atopic dermatitis T cell clusters are characterized by a cutaneous lymphocyte antigen (CLA)+ TH17/TH1 cell imbalance, whereas adults acquire CLA+ TH22/TC22 cell subsets. J Allergy Clin Immunol 2015;136:1641–51.
25. Tang TS, Bieber T, Williams HC. Does "autoeczemas" play a role in atopic dermatitis? J Allergy Clin Immunol 2012;129:1109–115.
26. Cipriani F, Ricci G, Leoni MC, Capra L, Badolato G, Longo G, et al. Autoimmunity in atopic dermatitis: biomarkers in simply erythematous? J Dermatol 2014;41:569–75.
27. Sangani MA, Sagar R, Kulkarni R, Rele et al. IgE in autoimmunity. J Allergy Clin Immunol 2016;137:1651–61.
28. Jeanrod-Grendelmeier P, Flückiger S, Disch R, Trautmann A, Wüthrich B, Blaser K, et al. IgE-mediated and T cell-mediated autoimmunity against manganese superoxide dismutase in atopic dermatitis. J Allergy Clin Immunol 2006;118:1610–7.
29. Altrichter S, Kinshuber E, Moser J, Valenta R, Kopp T, Stingl G. Serum IgE autoantibodies target keratinocytes in patients with atopic dermatitis. J Invest Dermatol 2008;128:2232–8.
30. Zeller S, Kreyner T, Meyer N, Schmid-Grendelmeier P, Akdis CA, Cramer R. Exploring the repertoire of IgE-binding self-antigens associated with atopic eczema. J Allergy Clin Immunol 2009;124:278–87.
31. Kinanian T, Salter S, Kroll H, Stingl G, Valenta R. IgE autoantibodies monitored in a patient with atopic dermatitis under cyclosporin A treatment reflect lower disease. J Allergy Clin Immunol 2012;108:717–9.
32. Bruynzeel-Koomen C, van Wichen D, Toonstra J, Bruynzeel P. The presence of IgE molecules on epidermal Langerhans cells in patients with atopic dermatitis. Arch Dermatol Res 1988;278:399–403.
33. Leung DY, Schneeberger EE, Sreagantan RP, Geha RS, Shan AK. The presence of IgE on macrophages and dendritic cells in normal and atopic skin lesions of atopic dermatitis. Clin Immunol Immunopathol 1987;42:328–37.
34. Stary G, Bergler G, Stingl G, Kopp T. Dendritic cells in atopic dermatitis: expression of Fcε2/CD23 in two distinct inflammation-associated subsets. Arch Allergy Immunol 2005;138:375–90.
35. Tsuri H, Hirokawa Y, Sasaki M. Abundant immunoglobulin E-positive cells in skin lesions support an allergic etiology of atopic dermatitis in the elderly. J Eur Acad Dermatol Venereol 2011;27:943–50.
36. Hamid Q, Boguniewicz M, Leung DY. Differential in situ cytokine gene expression in acute versus chronic atopic dermatitis. J Clin Invest 1994;94:870–6.
37. Grewe M, Walther S, Gyufko K, Czech W, Schopf E, Krutmann J. Analysis of the cytokine pattern expressed in situ in irritant allergic patch test reactions of atopic dermatitis patients. J Invest Dermatol 1995;105:407–10.
38. Jacobsen L, Langeveld-Wildschut EG, Bihari IC, van Wijk RG, van Reijsen FC, Mudde GC, et al. Biphasic response against aeroallergen in atopic dermatitis showing a switch from an initial TH2 response to a TH1 response. A short-term immunocytokinetical study. J Allergy Clin Immunol 1996;97:1476–17.
39. Yamada Y. Thymus and activation regulated chemokine as a clinical biomarker in atopic dermatitis. J Dermatol 2014;41:271–9.
40. Miyoshi M, Shirahi H, Ohta S, Suzuki S, Arima K, Aoki S, et al. Periostin promotes chronic allergic inflammation in response to Th2 cytokines. J Clin Invest 2012;122:2590–600.
41. Nakajima R, Miyagaki T, Oka T, Nakio M, Kawaguchi M, Suga H, et al. Elevated serum galectin-9 levels in patients with atopic dermatitis. J Dermatol 2015;42:723–6.
42. Kuga C, Kabashima K, Sakurai S, Katagiri W, Tsuchiya Y. Pruritic pathogenic role of Th17 cells for atopic dermatitis. J Invest Dermatol 2008;128:2625–30.
43. Negroiu G, Zaha DC, Shemer A, Trautmann-Dumitran J, Czarnowicki T, Kikuchi T, et al. IL-22-producing CD4+ T cells account for upregulated IL-22 in atopic dermatitis despite reduced IL-17-producing TH17 T cells. J Allergy Clin Immunol 2008;123:1244–52.
44. Hayashida S, Uchi H, Moroi Y, Furue M. Decrease in circulating Th17 cells correlates with increased levels of CCL17, IgE and eosinophils in atopic dermatitis. J Dermatol 2010;37:601–6.
45. Nograles KE, Zaba LC, Guttman-Yassky E, Fuentes-Duculan J, Suárez-Fariñas M, Cardinale I, et al. Th17 cytokines interleukin (IL)-17 and IL-22 modulate distinct inflammatory and keratinocyte-response pathways. Br J Dermatol 2008;159:1092–102.
46. Tupin E, Nogueras KL, Kikuchi T, Gonzales J, Carucci JA, Krueger JG. Human T-cell lymphotrophic virus 1-activated CD4+ T cells secreting IL-17 production. Proc Natl Acad Sci USA 2008;105:2175–80.
47. Saeki H, Czarnowicki T, Gonzales J, Ulrich M, Takeuchi S, Baugh L, et al. Accelerated T-cell activation and differentiation of polar subsets characterize early atopic comorbidity development. J Allergy Clin Immunol 2010;138:1474–7.
48. Kaja E, Elyard JA, Ungar B, Rozenblit M, Zheng X, Li L, et al. Identification of novel immune and barrier genes in atopic dermatitis by means of laser capture microdissection. J Allergy Clin Immunol 2015;135:133–63.
49. Sugaya M, Morimura S, Suga H, Kawaguchi M, Miyagaki T, Tamaki K, et al. CCR4+ expressed on infiltrating cells in lesional skin of early mycosis fungoides and atopic dermatitis. J Dermatol 2014;42:617–1.
50. Takahashi S, Esaki H, Furusyo N, Hayashida S, Tsukamoto K, Tsuji G, et al. Incidence, serum IgE and TARC/CCL17 levels in atopic dermatitis associated with other allergic diseases: an update from the Kagoshima cohort. Acta Derm Venereol 2015;95:480–4.
51. Esaki H, Takeuchi S, Furusyo N, Tsukamoto K, Hayashida S, Tsuji G, et al. Levels of immunoglobulin E specific to the major food allergen and chemokine (C-C motif) ligand (CCL) 17/thymus and activation-regulated chemokine and CCL22/macrophage-derived chemokine in infantile atopic dermatitis: an Ishigaki Island cohort. J Dermatol 2016;43:1278–82.
52. Kypriotou M, Huber M, Hohl D. The human epidermal differentiation complex: cornified envelope precursors, S100 proteins, and the 'fused genes' family. Eur Dermatol 2012;21:643–55.
53. Tunge M, Tsuji G, Mizuma C, Nakahara T, Ohba T, Moroi Y, Koga S, et al. Gene regulation of filaggrin and other skin barrier proteins via aryl hydrocarbon receptor. J Dermatol Sci 2015;80:83–5.
54. Howell MD, Kim BE, Gao P, Grant AV, Boguniewicz M, Debenedetto A, et al. Cytokine modulation of atopic dermatitis filaggrin skin expression. J Allergy Clin Immunol 2009;124:500–5.
55. van den Bogaard EH, Bergboer JG, Vonk-Bergers M, van Vlijmen-Willems IM, Hato SV, van der Valk PG, et al. Coal tar induces AHR-dependent skin barrier repair in atopic dermatitis. J Clin Invest 2014;124:3917–27.
56. Tsuji G, Mizuma C, Fujimoto-Kamata A, Uchi H, Takahara M, Tsuji G, et al. Antioxidant soybean lectin glycan structures T-helper-mediated downregulation of filaggrin expression via aryl hydrocarbon receptor. J Dermatol 2015;42:177–90.
57. Gutowska-Owsiak D, Schaupp AL, Salimi M, Taylor S, Ogg GS. Interleukin-22 downregulates filaggrin expression and alters expression of prolitaggrin processing enzymes. Br J Dermatol 2012;165:401–6.
58. Seguchi T, Cui CY, Kusuda S, Takahashi M, Aisu K, Tezuka T. Decreased expression of filaggrin in atopic skin. Arch Dermatol Res 1996;288:442–6.
59. Glover R, Meyer-Hoffert U, Fluhr J, Gunzer J, Wittersheim M, Kuhl-Alova S, et al. The antimicrobial protein psoriasin (S100A7) is upregulated in atopic dermatitis and after experimental skin barrier disruption. J Invest Dermatol 2009;129:641–5.
60. Sasai H, Kasahara T, Tanaka A, Kabashima K, Sugaya M, Murata H, et al. Clinical practice guidelines for the management of atopic dermatitis 2016. J Dermatol 2016;43:1111–49.
61. Poulsen LK, Hummelshoj L. Triggers of IgE class switching and allergy development. Ann Med 2007;39:440–56.
62. Czarnowicki T, Gonzalez J, Bonifacio KM, Shemer A, Xiangyu R, Kanoh H, et al. Diverse activation and differentiation of multiple B-cell subsets in patients with atopic dermatitis but not in patients with psoriasis. J Allergy Clin Immunol 2016;137:118–29.
63. Hamada M, Furusyo N, Doiuchi K, Maeda K, Nakahara J, Kinukawa N, et al. Prevalence of atopic dermatitis and serum IgE values in nursery school children in Ishigaki Island, Okinawa. Jpn J Dermatol 2005;93:749–55.
64. Elias PM, Wakefield JS. Mechanisms of abnormal lamellar body secretion and the dysfunctional skin barrier in patients with atopic dermatitis. J Allergy Clin Immunol 2014;134:781–91.
65. Leung DY, Harbeck R, Bina P, Reiser RF, Yang E, Norris DA, et al. Presence of IgE antibodies to staphylococcal exotoxins on the skin of patients with atopic dermatitis. Evidence for a new group of allergens. J Clin Invest 1993;92:1374–80.
66. Powers CE, Mathias DR, Lilliquist DR, Burchett CN, Murrell DF. Microbiome and peptidome in atopic dermatitis. J Dermatol 2015;42:1137–42.
67. Hampton S, Lister R. The sensitivity of man to human dander, with particular reference to eczema (atopic dermatitis). J Allergy 1941;13:65–75.
68. Sulzberger MB. The allergen of human dander present in skin of the general body surface. J Invest Dermatol 1947;9:379–82.
69. Sulzberger MB. The allergen of human dander: its relative concentration in several skin areas and in appendages, products and secretions of the epidermis. J Invest Dermatol 1948;11:203–7.
70. Adachi K, Aoki T. IgE antibody to wheat in atopic dermatitis. Acta Derm Venereol Suppl (Stockh) 1958;144:83–7.
71. Hide M, Tanaka T, Yamamura Y, Aono D, Yamamoto S. IgE-mediated hypersensitivity against human sweat antigen in patients with atopic dermatitis. Acta Derm Venereol 2003;83:175–80.
72. Hiragun T, Ishii K, Hiragun M, Suzuki H, Kido H, Mitsuda S, et al. Fungal protein MGL_1304 in sweat is an allergen for atopic dermatitis patients. J Allergy Clin Immunol 2011;128:608–15.
73. Nagler S, Seibold S, Huhnagl P, Binder BR, Hirschl AM, Rieg J, et al. Elevation of cDNA clones reactive for IgE autoantigens with serum IgE from atopic dermatitis patients. FASEB J 1998;12:1559–69.
74. Borkiewicz K, Miller DR, Szczepanska T, Dyer DJ, Dikanov S, Grover MC, et al. Comparison of the crystal structures of the human manganese superoxide dismutase and the homologous Aspergillus fumigatus allergen at 2.4 resolution. J Immunol 2002;168:1067–72.
75. Mayer C, Appenzeller U, Seelbach H, Achatz G, Oberkofler H, Hoerenbach M, et al. Humoral and cell-mediated autoimmune reactions in human atopic

ribosomal P2 protein is immunodominant allergen in Aspergillus fumigatus P2 protein. J Exp Med 1995;182:1507–14.

76 Dudler T, Gruber P, Whitley P, Blaser K, Cramer R. Cyclophilins, a new family of cross-reactive allergens. Eur J Immunol 2002;32:1–7.

77 Limacher A, Glaser AG, Meier C, Schmid-Grendelmeier P, Zeller S, Scapozza L, et al. Cross-reactivity and 3-D crystal structure of Malassezia sympodialis thioredoxin (Mala S 3), a member of a new pan-allergen family. J Allergy Clin Immunol 2007;120:1096–103.

78 Hradetzky S, Brewer JM, Salaji H, Heratizadeh A, Mittermann I, Valenta R, et al. Pollution effects induced by the human allergen e-NAC. J Allergy Clin Immunol 2014;134:157–8.

79 Heratizadeh A, Mittermann I, Bilo M, Wichmann K, Niebuhr M, Valenta R, et al. The role of T-cell reactivity towards the allergen e-NAC in atopic dermatitis. Br J Dermatol 2011;164:516–24.

80 Brewer JM, Heratizadeh A, Wichmann K, Mittermann I, Valenta R, Lee-Vesper B, et al. e-NAC specific anergic effector CD4+ T cells in atopic dermatitis are of an effector memory type and secrete IL-4 and IFN-γ. J Immunol 2016;196:3215–53.

81 Muneta H, Tsuchiya S, Sugaya M, Tamaki M, Ohmori K, Higashiura A, et al. Characteristics of anaphylaxis status of Japanese patients with atopic dermatitis showing poor medical adherence and reasons for drug discontinuation. J Dermatol Sci 2015;79:232–83.

82 Hamilton JD, Suárez-Farñas M, Dhingra N, Cardinale I, Li X, Kostic A, et al. Dupilumab suppresses the molecular signature in skin of patients with moderate-to-severe atopic dermatitis. J Allergy Clin Immunol 2014;134:1293–300.

83 Beck LA, Thaçi D, Hamilton JD, Graham NM, Bieber T, Rocklin R, et al. Dupilumab treatment in adults with moderate-to-severe atopic dermatitis. N Engl J Med 2014;371:130–9.

84 Thaçi D, Simpson EL, Beck LA, Bieber T, Blauvelt A, Papp K, et al. Efficacy and safety of dupilumab in adults with moderate-to-severe atopic dermatitis inadequately controlled by topical treatments: a randomized, placebo-controlled, dose-ranging phase 2b trial. Lancet 2016;387:40–52.

85 Simpson EL, Gadkari A, Worm M, Soong W, Blauvelt A, Eckert L, et al. Dupilumab therapy provides clinically meaningful improvement in patient-reported outcomes (PROs): a phase IIb, randomized, placebo-controlled, clinical trial in adult patients with moderate to severe atopic dermatitis (AD). J Am Acad Dermatol 2016;75:488–15.

86 Desilakas E, Wang X, Akiyama T, Kempkes C, Sawinka T, Antel A, et al. A novel non-expressor IL-31 receptor mutation T helper cell dependent IL31 involvement of TSLPR and TRPV1. J Allergy Clin Immunol 2014;134:445–50.

87 Sugimoto D, Furuie M, Nakagawa H, Shiramizu M, Hanada K, Masuda S, et al. The first trial of CM-101, a humanized anti-human interleukin 31 receptor A antibody, in healthy volunteers and patients with atopic dermatitis to evaluate safety, tolerability and pharmacokinetics of a single dose in a randomized, double-blind, placebo-controlled study. Br J Dermatol 2016;174:296–304.

88 Yamaoka K, Okayama Y, Kawakami O, Kayama R, Mori A, Tagum H, et al. Proteomic approach to "epidermal" regulation of signal transduction cascade in human mast cells. Int Arch Allergy Immunol 2006;140(Suppl. 1):1–6.

89 Cortelli DR, Welsh EF, Bolger AM, Gotyal PD, Levendusky PF, Barnette MA, et al. SB 207499 (Apilint), a second generation phosphodiesterase 4 inhibitor, reduces dermal mast cell tryptase, alpha and interleukin-4 production in skin. J Pharmacol Exp Ther 1998;287:705–11.

90 Furue M, Kitahara Y, Akama H, Hori Y, Kawashi N, Nakagawa H, et al. Safety and efficacy of topical E6005, a phosphodiesterase 4 inhibitor, in Japanese adult patients with atopic dermatitis: results of a randomized, vehicle-controlled, multicenter clinical trial. J Dermatol 2014;41:577–85.

91 Nemoto O, Hayashi N, Kitahara Y, Furue M, Hori S, Nomoto M, et al. Effect of topical phosphodiesterase 4 inhibitor E6005 in Japanese children with atopic dermatitis: results of a randomized, vehicle-controlled exploratory trial. J Dermatol 2016;43:363–7.

92 Hanifin JM, Ellis CN, Fleischer JJ, Eliasz-Rubio R, Stein Gold LF, Sevy A, et al. OPA-15406, a novel, topical, nonsteroidal, selective phosphodiesterase-4 (PDE4) inhibitor, in the treatment of adult and adolescent patients with mild to moderate atopic dermatitis (AD): a phase-3, randomized, double-blind, placebo-controlled study. J Am Acad Dermatol 2015;75:247–305.

93 Pafer AS, Tom WL, Lebwohl MG, Blumenthal RL, Boguniewicz M, Call RS, et al. Efficacy and safety of crisaborole ointment, a novel, nonsteroidal phosphodiesterase 4 (PDE4) inhibitor for the topical treatment of atopic dermatitis (AD) in children and adults. J Am Acad Dermatol 2016;75:444–51.

94 Saraceno R, Barry TM, Gooshi R, Simpson EL. A pilot study of an oral phosphodiesterase 4 inhibitor hypersensitivity for atopic dermatitis in adults. Arch Dermatol 2012;148:800–2.

95 Papp K, Cather JC, Rosoph L, Syed H, Langley RG, Mathieson RT, et al. Efficacy of apremilast in the treatment of moderate to severe psoriasis: a randomized controlled trial. Lancet 2012;380:738–46.

96 Murata Y, Ishii M, Kouchi F, Hirohata K, Xu XL, Corrington A, et al. Phase 2a randomized, double-blind, placebo-controlled, multicenter, parallel group study of a TNF-antagonist (JNJ-39758979) in Japanese adults with moderate atopic dermatitis. J Dermatol 2015;42:129–39.

97 Akiyama T, Tavares L, Nagy I. Neural processing in itch. Neuroscience 2017;340:197–214.

98 Miyano K, Matsushita S, Tsuchida T, Nakamura K, Chihiro Y, et al. Inhibitory effect of a histamine 4 receptor antagonist on CCL17 and CCL22 production by monocyte-derived Langerhans cells in patients with atopic dermatitis. J Dermatol 2016;43:1074–6.

99 Rossbach K, Schaper K, Eloit C, Gutmann R, Wedel T, Kretzmann M, et al. Histamine H4 receptor knockout mice display reduced inflammation in a chronic model of atopic dermatitis. Allergy 2016;71:150–57.

100 Di Lernia V, Bardazzi F, Profile of tofacitinib citrate and its potential in the treatment of moderate-to-severe chronic plaque psoriasis. Drug Des Devel Ther 2016;10:543–9.

101 Levy LL, Urban J, King BA. Treatment of refractory atopic dermatitis with the oral Janus kinase inhibitor tofacitinib citrate. J Am Acad Dermatol 2015;73:191–4.

102 Bissonnette R, Papp KA, Poulin Y, Gooderham M, Raman M, Maldonado L, et al. Topical tofacitinib for atopic dermatitis: a phase 2a randomized trial. Br J Dermatol 2016;175:1212–21.

103 Bhatt D, Yeshpowich G, Boyle B, Robinson J, Sandy J, Mahajan V, et al. Topical JAK kinase inhibitor CTP-690 ointment for treatment of pruritus due to psoriasis: results from preclinical studies and efficacy and safety of CTP-690 in a phase 2b trial of adult patients with psoriasis. Acta Derm Venereol 2015;95:542–8.

104 Hou M, Sun R, Hupe M, Xie FL, Park K, Crumrine D, et al. Topical apigenin improves epidermal permeability barrier homeostasis in normal murine skin by divergent mechanisms. Exp Dermatol 2013;22:210–5.

105 Murray IA, Nichols RG, Zhang L, Patterson AD, Perdew GH. Expression of the aryl hydrocarbon receptor contributes to the establishment of intestinal microbial community structure in mice. Sci Rep 2016;6:31994.

106 Aoki T, Fukuzumi T. Atopy-related skin rash in a cohort population of infants, distribution and risks for 50 separate skin regions: cohort study from 4 months to 4.5 years. J Dermatol 2015;42:461–66.

107 Furue M, Kadono T. Psoriasis: behind the scenes. J Dermatol 2016;43:1–8.

108 Jarrett R, Salimi M, Barlow JW, Ogg G, Ono J, Ohtani K, et al. The role of layilin, a lymphocyte-specific, in the immunopathogenesis of atopic dermatitis. Clin Exp Allergy 2011;41:1515–20.

109 Tsogbe D, Fauconnier L, Mazouni F, Marchal T, Chenuet P, Rouxel N, et al. Thymic stromal lymphopoietin enhances T2/T22 and reduces IL-17A in house-dust-mite-induced airways inflammation. Clin Exp Allergy 2011;2011:971016.

110 Wilson SR, The L, Batia LM, Beattie K, Katibah GE, McClain SP, et al. The epithelial cell-derived atopic dermatitis cytokine TSLP activates neurons to induce itch. Cell 2013;155:285–95.

111 Rosado JA, Diez R, Smani T, Jardin I. STIM and Orai1 variants in store-operated calcium entry. Pharmacol Sci 2016;6:325.

112 Vazquez-Hernandez M, Rintoul M, Lehrman G, Sordillo D, Hasbe R, Rotin D, et al. ORAI1 calcium channel orchestrates skin homeostasis. Proc Natl Acad Sci USA 2014;111:14836–38.

113 Chang WC, Lee CH, Hirota T, Wang JF, Tsai S, Miyatake A, et al. CRAC1 genetic polymorphisms associated with the susceptibility of atopic dermatitis in Japanese and Taiwanese populations. Plos One 2012;7:e32087.

REVIEW ARTICLE

Check for updates

Highlighting Interleukin-36 Signalling in Plaque Psoriasis and Pustular Psoriasis

Kazuhisa FURUE[1], Kazuhiko YAMAMURA[1], Gaku TSUJI[2], Chikage MITOMA[1,2], Hiroshi UCHI[1], Takeshi NAKAMARA[1,3], Makiko KIDO-NAKAHARA[1], Takafumi KADONO[1] and Masutaka FURUE[1,4]

[1]Department of Dermatology, [2]Division of Skin Surface Sensing, Department of Dermatology, Kyushu University, [3]Research and Clinical Center for Yusho and Dioxin, Kyushu University Hospital, Kyushu University, Fukuoka, and [4]Department of Dermatology, St Marianna University School of Medicine, Kanagawa, Japan

Plaque psoriasis and pustular psoriasis are overlapping, but distinct, disorders. The therapeutic response to biologics supports the pivotal role of the tumour necrosis alpha (TNF-α)/ interleukin (IL)-23/IL-17/IL-22 axis in the pathogenesis of these disorders. Recently, functional activation of the IL-36 receptor (IL-36R) was discovered to be another driving force in the pathogenesis of psoriasis. This was first highlighted by the discovery that a loss-of-function mutation of the IL-36R antagonist (IL-36Ra) causes pustular psoriasis. Although the TNF-α/IL-23/IL-17/IL-22 axis and the functional activation of IL-36R are fundamentally involved in plaque psoriasis and pustular psoriasis, respectively, the 2 pathways are closely related and mutually reinforced, resulting in full-blown clinical manifestations. This review summarizes current topics on how IL-36 agonists (IL-36α, IL-36β, IL-36γ) signal IL-36R, the pathological expression of IL-36 agonists and IL-36Ra in plaque and pustular psoriatic lesions, and the cross-talk between the TNF-α/IL-23/IL-17/IL-22 axis and the functional activation of IL-36R in the epidermal milieu.

Key words: psoriasis; pustular psoriasis; IL-36; IL-36 receptor; IL-36 receptor antagonist; IL-17; IL-22.

Accepted Oct 2, 2017; Epub ahead of print Oct 2, 2017

Acta Derm Venereol 2018; 98: 5–13.

Corr: Masutaka Furue, Department of Dermatology, Kyushu University, Maidashi 3-1-1, Higashiku, Fukuoka, 812-8582, Japan. E-mail: furue@dermatol.med.kyushu-u.ac.jp

Psoriasis is a common, immune-mediated, chronic inflammatory, erythemato-desquamative skin disease that is characterized by the altered proliferation and differentiation of keratinocytes with infiltration of neutrophils, dendritic cells (DCs) and T cells (1, 2). Psoriasis has shown a diverse prevalence across populations worldwide: 2.5% in Europeans, 0.05–3% in Africans and 0.1–0.5% in Asians (1, 2). Psoriasis is divided into 2 major clinical variants, plaque psoriasis and generalized pustular psoriasis, with shared pathogenetic backgrounds (1–4). Pustule formation of plaque psoriasis is not uncommon in severe cases (1, 4). A recent study revealed that palmoplantar pustulosis, a localized variant of pustular dermatosis, shares a similar pathogenesis with the generalized form (5). The therapeutic guidelines include the use of topical steroids, topical vitamin D, systemic immunosuppressants and various biologics, such as anti-tumour necrosis factor (TNF) α, anti-interleukin (IL)-23 and anti-IL-17 antibodies (6–14). However, treatment adherence and the quality of life of the affected patients are generally very low (1, 15–20). Recent genome-wide association studies have identified many susceptibility loci for psoriasis and pustular psoriasis, including *HLA-C*06:02*, *LCE3D*, *IL23R*, *CARD14* and *IL36RN* (21–24). These susceptibility genes are predominantly related to the innate and adaptive immune systems and to skin barrier functions (1, 25).

Psoriasis often coexists with other systemic diseases, such as arthritis, diabetes mellitus, arterial hypertension, obesity and cardiovascular diseases (the so-called "psoriatic march" or "inflammatory march") (25–30). Psoriasis is also co-morbid with other autoimmune diseases, including Hashimoto's thyroiditis and autoimmune bullous diseases (31–36). The recent therapeutic success of anti-TNF-α, anti-IL-23 and anti-IL-17 antibodies, as well as the diverse action of IL-22, has emphasized the pivotal role of the TNF-α/IL-23/IL-17/IL-22 pathway in the pathogenesis of plaque psoriasis and pustular psoriasis (2, 37, 38). In addition to the TNF-α/IL-23/IL-17/IL-22 pathway, IL-36 and IL-36 receptor antagonist (IL-36Ra/*IL36RN*) are currently the focus of much attention. The gene and immunohistological expression of IL-36 members is upregulated in plaque psoriasis and pustular psoriasis (39–41). Moreover, *IL36RN* deficiency has been associated with the development of generalized pustular psoriasis (23, 42). This review summarizes recent topics on IL-36 signalling with reference to plaque psoriasis and pustular psoriasis.

IL-36 MEMBERS AND THEIR RECEPTOR

Epithelial cells, including keratinocytes, are a good source of the IL-1 family (IL-1F), which is composed of 11 members: IL-1α, IL-1β, IL-1 receptor antagonist (IL-1RN), IL-18, IL-33, IL-36α/IL-1F6, IL-36β/IL-1F8, IL-36γ/IL-1F9, IL-36Ra/IL-1F5, IL-37/IL-1F7 and IL-38/IL-1F10 (43–45). IL-36α, IL-36β, IL-36γ and IL-36Ra use the same receptor, IL-36R (previously called IL-1Rrp2 or IL-1RL2), coupled with the IL-1 receptor accessory protein (IL1RAP), which is a common subunit

This is an open access article under the CC BY-NC license. www.medicaljournals.se/acta
Journal Compilation © 2018 Acta Dermato-Venereologica.

doi: 10.2340/00015555-2808
Acta Derm Venereol 2018; 98: 5–13

shared with IL-1R and IL-33R (40, 44). IL-36α, IL-36β and IL-36γ show similar levels of agonistic activity upon binding to IL-36R (44). However, ligation of IL-36R by IL-36Rα does not induce the recruitment of IL1RAP and therefore does not initiate a signalling response (44, 45).

Like other IL-1 family members, such as IL-1β and IL-18, proteolytic processing is required to unleash the proinflammatory activity of IL-36α, IL-36β and IL-36γ (4, 46). IL-36α, IL-36β and IL-36γ are processed and activated differentially by the neutrophil granule-derived proteases cathepsin G, elastase, and proteinase-3, increasing their biological activity by approximately 500-fold (46). For endogenous processing, caspase 1 is essentially involved in gene expression, and caspase 3 is involved in the release of IL-36γ (47). Other endogenous processing pathways of IL-36α, IL-36β and IL-36γ are not yet fully understood. However, a recent study by Ainscough et al. (48) demonstrated that keratinocyte- or fibroblast-derived cathepsin S is a key skin-resident enzyme that cleaves full-length IL-36γ into the active form IL-36γ-Ser18. It is feasible that IL-36γ-Ser18 *per se* induces hyperkeratosis and CXCL8 (IL-8) production in a skin-equivalent model (48). In addition to CXCL8 production, IL-36γ upregulates the production from human keratinocytes of CXCL1 (Gro1), CXCL10 (IP10) and CCL20 (MIP3A), which is differentially mediated by p38 MAPK, JNK MAPK and NF-κB, respectively (49).

Human keratinocytes apparently express IL-36α, IL-36β, IL-36γ, IL-36Rα and their receptor IL-36R/IL1RAP (4, 50). The treatment of human keratinocytes with IL-36α, IL-36β or IL-36γ upregulates the gene expression of various chemokines for macrophages (*CCL3, CCL4, CCL5, CCL2, CCL17* and *CCL22*), T cells (*CCL20, CCL5, CCL2, CCL17* and *CCL22*), and neutrophils (*CXCL8, CCL20* and *CXCL1*). In addition to keratinocytes, human monocytes and myeloid DCs, but not $CD4^+$ or $CD8^+$ T cells, express IL-36R, while all subsets express IL1RAP. IL-36R was not detected on activated T cells stimulated with anti-CD3/CD28 antibodies. The circulating neutrophils also lacked IL-36R and did not respond to IL-36 treatment (50).

Myeloid DCs express approximately 10 times higher IL-36R levels than monocytes (50). Treatment with IL-36α, IL-36β or IL-36γ significantly enhances the surface expression of CD83, CD86 and HLA-DR, as well as the release of IL-1β and IL-6 in DCs. In addition, the surface expression of IL-36R is augmented during maturation of monocyte-derived DCs cultured with IL-4 and granulocyte-macrophage colony-stimulating factor. IL-36α, IL-36β or IL-36γ further accelerates the phenotypic and functional maturation of monocyte-derived DCs (50). Human M2 macrophages and Langerhans cells are also target cells of IL-36 signalling to produce IL-6 (51). These studies suggested that IL-36 members released from keratinocytes could feasibly induce a plethora of chemokines in keratinocytes in an autocrine fashion, recruiting circulating myeloid DCs, monocytes, T cells and neutrophils to the skin. IL-36 members also support the phenotypic and functional maturation of antigen-presenting cells (DCs and monocytes), which mediate local inflammation.

GENE MUTATION OF IL-36 RECEPTOR ANTAGONIST IN PUSTULAR PSORIASIS

The pathogenetic importance of "functional activation of IL-36R" in psoriasis and pustular psoriasis was first proposed by findings that missense mutations in *IL36RN* were associated with pustular psoriasis (23, 52). Elevated levels of IL-36Rα are believed to counteract the proinflammatory reaction of IL-36 in plaque psoriasis and pustular psoriasis (4, 41). Therefore, loss of function mutation of *IL36RN* exaggerates IL-36 signalling (23, 52). Keratinocytes from patients with *IL36RN* mutation produced higher levels of CXCL8 than keratinocytes from controls in response to IL-36α, IL-36β and IL-36γ, as well as to IL-1β or polyinosinic-polycytidylic acid (poly [I:C]), which is a synthetic ligand specific for Toll-like receptor 3 (TLR3) (23). Mutations in *IL36RN* have been shown to account for 46–82% of cases of pustular psoriasis without associated plaque psoriasis (42, 53). A recent meta-analysis of 233 generalized pustular psoriasis cases revealed that carriage of 1 or 2 *IL36RN* mutant alleles conferred a more severe clinical phenotype with an earlier age of onset and an increased risk of systemic inflammation compared with non-carriage (54). A gene-dosage effect is also apparent because homozygous carriers have an earlier age of onset than heterozygotes (4, 54). These studies have emphasized the importance of gene mutations of *IL36RN* and subsequent "functional activation of IL-36R" in the pathogenesis of pustular psoriasis.

CURRENT PATHOGENESIS OF PLAQUE PSORIASIS

Plaque psoriasis occurs preferentially on areas susceptible to frequent friction or minor trauma, as represented by Koebner's phenomenon (55–58). Cathelicidin (LL-37) is one of the anti-microbial peptides produced by keratinocytes and neutrophils (59). Cutaneous trauma, such as incisional injury, induces the expression of functional cathelicidin at the injured site (59). Human cathelicidin (hCAP18/LL-37) is encoded by the *CAMP* gene, and active LL-37 is released from pro-form hCAP18 via limited proteolysis exerted by proteinase 3 (Fig. 1) (60). An initial trigger of psoriasis is believed to be the activation of plasmacytoid DCs being stimulated by complexes of host DNA and LL-37, which are produced by keratinocytes after minor injuries (37, 38, 61, 62) (Fig. 1). Activated plasmacytoid DCs and damaged keratinocytes produce interferon (IFN)-α, IFN-β and TNF-α, which result in further production of TNF-α and IL-23 by plasmacytoid

ActaDV Acta Dermato-Venereologica ActaDV Advances in dermatology and venereology

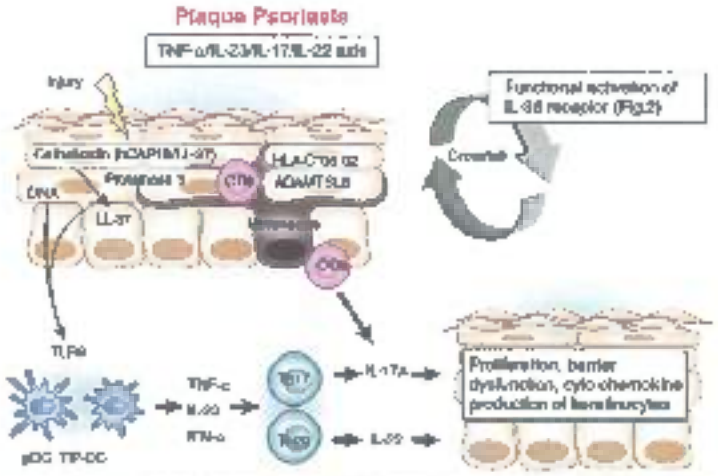

Fig. 1. Pathogenesis of plaque psoriasis. Psoriatic lesions are frequently triggered by minor trauma (Koebner's phenomenon). Skin injury causes dead keratinocytes to release self-DNA and cathelicidin (LL-37). Full-length cathelicidin (hCAP18/LL-37) is cleaved into active form (LL-37) by proteinase 3. Self-DNA and LL-37 complex activate Toll-like receptor 9 (TLR9) in plasmacytoid dendritic cells (pDCs) and tumour necrosis factor (TNF)-α/inducible nitric oxide synthase-producing dendritic cells (TIP-DCs) to produce interferon-α (IFN-α), TNF-α and interleukin (IL)-23. IL-23 facilitates Th17 and Th22 cell proliferation. IL-17A and IL-22 induces the proliferation, barrier dysfunction and diverse cyto-chemokine production of epidermal keratinocytes, leading to epidermal acanthosis, parakeratosis and inflammatory cell infiltration, including neutrophils. The lesional epidermis harbours CD8$^+$ T cells which target ADAMTS-like protein 5 (ADAMTSL5) on melanocytes and produce IL-17A. The "TNF-α/IL-23/IL-17/IL-22 axis" and the "functional activation of IL-36 receptor" (Fig. 2) are closely related to each other.

and recruited inflammatory DCs (TNF/iNOS-producing DCs or TNF-α/inducible nitric oxide synthase, producing dendritic cells [TIP-DCs]) (38, 62–65). IL-23 is critically involved in the generation and activation of IL-17- and IL-22-producing effector Th (Th17 and Th22) cells (38, 66, 67). Th17 cells have been detected in the blood and lesional skin, and they readily produce IL-17A and IL-22 (67, 68). In addition, the pivotal role of intraepidermal CD8$^+$ T cells has been documented in psoriasis (69–71). These intraepidermal CD8$^+$ T cells produce pathogenic IL-17A, and neutralization of CD8$^+$ T cells effectively prevented psoriasis development in xenotransplanted mice model *in vivo* (71). Moreover, a recent study by Arakawa et al. (72) showed that intraepidermal CD8$^+$ T cells recognize ADAMTS-like protein 5 (ADAMTSL5) on melanocytes, in concert with HLA-C*06:02, which is the main psoriasis risk allele.

IL-17A upregulates the proliferation of keratinocytes and downregulates their differentiation (73). IL-22 also drives epidermal hyperplasia, primarily by the downregulation of genes involved in terminal differentiation (74, 75). IL-17A acts on keratinocytes to induce chemokines that lead to neutrophil, TIP-DC, and Th17 cell influx into the skin (76). TIP-DCs produce inducible NO synthase (leading to NO production, which can dilate dermal blood vessels) and secrete TNF-α, IL-20 and IL-23 (63, 77, 78). IL-17A upregulates the production of the neutrophil-attractive chemokines CXCL1, CXCL2 and CXCL8 by keratinocytes (4, 79). IL-17A also promotes the expression of TNF-α by keratinocytes (80), indicating that the aforementioned TNF-α/IL-23/IL-17/IL-22 axis probably forms a vicious cycle in the development of psoriasis lesions (Fig. 1). The mechanistic hypothesis coincides with the remarkable clinical effects of the antibodies against TNF-α, IL-23, IL-17A on both psoriasis and pustular psoriasis (81–83), further emphasizing the canonical role of the TNF-α/IL-23/IL-17/IL-22 axis in psoriatic pathogenesis.

PLAQUE PSORIASIS AND IL-36 MEMBERS

In addition to the TNF-α/IL-23/IL-17/IL-22 axis, the gene expression levels of IL-36α, IL-36β, IL-36γ and IL-36Ra are all significantly elevated in lesional psoriatic skin, compared with normal control skin. However, only IL-36γ and IL-36RN exhibited hierarchical increases in the ascending order of normal < non-lesional psoriatic < lesional psoriatic skin (41, 84, 85). Moreover, treatment using etanercept, a human TNF receptor fusion protein, significantly decreased the lesional gene expression levels of IL-36α, IL-36γ and IL-36Ra (41). Carrier et al. (86) reported that the gene expression levels of IL-36α, IL-36β and IL-36γ were all elevated in the lesional skin of psoriasis and that this increase was strongly correlated with the expression levels of IL-22, IL-17A and TNF-α, respectively, but not of IL-17F. In addition, elevated IFN-γ expression was detected in lesions and was correlated well with the expression of all IL-36 members (86). On immunohistology, upregulated expression of IL-36γ was detected in the increasing order of lesional psoriatic > non-lesional psoriatic > normal control skin (49, 85).

Boutet et al. (39) compared the expression of IL-36 members and IL-36Ra in psoriasis, rheumatoid arthritis and Crohn's disease in humans and in murine models. In an imiquimod-induced murine psoriatic model and in human psoriasis, the expression levels of IL-36α, IL-36γ and IL-36Ra, but not IL-36β, were correlated with IL-1β and Th17-related cytokines (IL-17A, IL-22, IL-23, and CCL20). In mice with collagen-induced arthritis and in the synovium of patients with rheumatoid arthritis, IL-36α, IL-36β, IL-36γ and IL-36Ra were all elevated and were correlated with levels of IL-1β, CCL3, CCL4 and macrophage colony-stimulating factor, but not with Th17-related cytokines. In the colons of mice with dextran sulphate sodium-induced colitis and in patients with Crohn's disease, only IL-36α and IL-36γ were induced at low levels and were correlated with IL-1β and IL-17A. Overall, only a minor subgroup of patients with rheumatoid arthritis (17–29%) or Crohn's disease (25%) has an

ActaDV Acta Dermato-Venereologica ActaDV Advances in dermatology and venereology

elevated IL-36 agonist/receptor antagonist ratio, which is in sharp contrast to its elevation in as many as 93% of patients with plaque psoriasis (39).

These results suggest that IL-36 members are indeed overexpressed in the lesional skin of plaque psoriasis and that the "functional activation of IL-36R" might contribute to the persistence and perpetuation of psoriatic inflammation, together with the TNF-α/IL-23/IL-17/IL-22 axis (Fig. 1). To support this notion, the effectiveness of anti-IL-36R blocking antibody was confirmed in a human psoriatic skin xenotransplantation model (78). SCID mice transplanted with human psoriatic lesional skin were treated with an anti-human IL-36R antibody that blocked the actions of IL-36α, IL-36β and IL-36γ. Anti-IL-36R antibody substantially reduced the epidermal hyperplasia and other skin changes associated with psoriasis as effectively as etanercept (78). The anti-human IL-36R antibody did not cross-react with murine IL-36R, and murine IL-36α, IL-36β and IL-36γ did not signal through human IL-36R (78).

PUSTULAR PSORIASIS AND IL-36 MEMBERS

A different treatment response to biologics indicates that the pathogenesis of plaque psoriasis and pustular psoriasis does not completely overlap (4). The "functional activation of IL-36R" is likely to be more closely associated with pathogenesis in generalized pustular psoriasis, pustule formation of plaque psoriasis and palmoplantar pustulosis than with plaque psoriasis (Fig. 2) (4, 5, 54). The transcriptome of generalized pustular psoriasis shares features of plaque psoriasis, but is skewed toward innate immune inflammation, including IL-1 and IL-36 (4, 5). The expression levels of IL-1β, IL-1RN, IL-36α, IL-36β, IL-36γ and IL-36Ra are significantly increased, both in generalized pustular psoriasis and plaque psoriasis, compared with normal skin, with significantly greater expressions of IL-1β, IL-36α and IL-36γ in generalized pustular psoriasis than in plaque psoriasis (4, 5). In contrast, the expression levels of Th17/Th1-related cytokines, such as IL-17A, IL-22, IL-23p19, IFN-γ and IL-18, are significantly increased in plaque psoriasis compared with the levels observed in generalized pustular psoriasis and in normal skin (4).

In parallel with the augmented IL-1and IL-36 signals in generalized pustular psoriasis compared with plaque psoriasis, the expression levels of neutrophilic chemoattractants, CXCL1, CXCL2 and CXCL8, are also significantly and more abundantly increased in generalized pustular psoriasis than in plaque psoriasis (4). Infiltrated neutrophils were positively stained with cathepsin G, neutrophil elastase and proteinase 3 in the lesional skin of psoriasis and pustular psoriasis. Notably, IL-36α was processed and activated by neutrophil elastase, but not by cathepsin G, and its processing was abrogated by serpin A1, a specific inhibitor of neutrophil elastase. In contrast, IL-36γ was processed and activated by cathepsin G, but not by neutrophil elastase, and its processing was prevented by serpin A3, a specific inhibitor of cathepsin G. Activated IL-36α and IL-36γ were capable of enhancing the expression levels of CXCL1, CXCL2, CXCL8 and CCL20 from keratinocytes (4). Moreover, IL-17A induced IL-36 more potently in human psoriasis-derived keratinocytes than in healthy keratinocytes, while *IL36RN* expression remained unaffected (87).

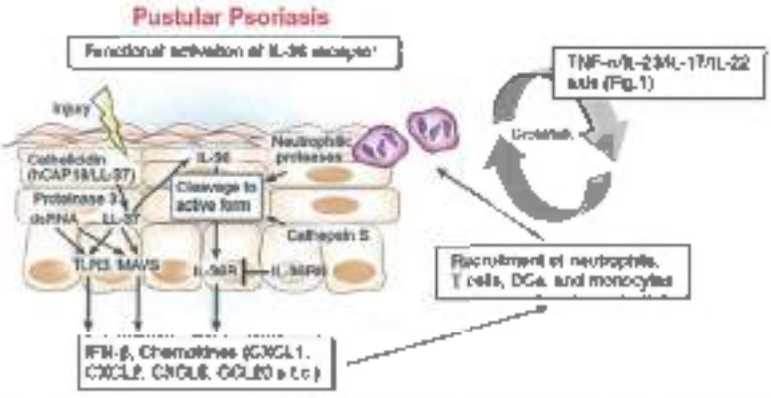

Fig. 2. Pathogenesis of pustular psoriasis. Skin injury causes dead keratinocytes to release double-stranded RNA (dsRNA) and cathelicidin (LL-37). LL-37 or dsRNA (possibly by TLR3 ligation) activates surrounding keratinocytes to produce interleukin (IL)-36 members. LL-37 and dsRNA complex activate mitochondrial antiviral-signaling protein (MAVS) in the surrounding keratinocytes to release interferon (IFN)-β. The ligation of IL-36R by IL-36 enhances the production of diverse chemokines and attractants neutrophils, T cells, dendritic cells (DCs) and monocytes. Full-length IL-36 is processed and activated by neutrophilic proteases, as well as keratinocyte-derived cathepsin S. The IL-36 receptor antagonist (IL-36Ra/IL-36RN) inhibits IL-36R activation by competitive inhibition. The functional activation of IL-36R is preferentially involved in the pathogenesis of pustular psoriasis, and conversely, the TNF-α/IL-23/IL-17/IL-22 axis is driven more efficiently in plaque psoriasis (Fig. 1). However, these 2 pathways are closely related and cross-talk with each other, forming a positive inflammatory loop.

On immunohistology, the expression of IL-36γ was localized in the suprabasal to granular layer of the epidermis (especially peripustular keratinocytes), and staining of the basal layer was minimal in generalized pustular psoriasis and plaque psoriasis (4, 49, 85). The immunohistological expression of IL-36α was also confirmed in the upper spinous layer to granular layer in generalized pustular psoriasis and plaque psoriasis, especially in peripustular keratinocytes (4). Using an *in situ* hybridization technique, the expression of IL-36α was also strongly detected in the superficial layers of the epidermis in the lesional skin of generalized pustular psoriasis and plaque psoriasis, but not in chronic eczema or nummular eczema (88).

In contrast to the high proportion (46–82%) of *IL36RN* mutant carriage in generalized pustular psoriasis (42, 53), it was lower (10–17%) in pustular cases of

plaque psoriasis (54). Transcriptome assay also demonstrated the importance of *IL1A/B*, *IL36A/B/G/RN* and the neutrophil chemokines *CXCL1/CXCL8* in palmoplantar pustulosis (5). However, the *BBS1* and *TWIST1* genes related to limb malformation are specifically linked to palmoplantar pustulosis, but not to generalized pustular psoriasis (5). In addition, *STEAP1* and *STEAP4*, expressed in keratinocytes, are key players for regulating *IL1A/B*, *IL36A/B/G/RN* and *CXCL1/CXCL8* (5).

These results emphasize the critical roles of IL-36/(IL-1β) in the pathogenesis of pustular psoriasis. However, it should be borne in mind that Th17/(Th1) signalling is also an active and common player in both pustular psoriasis and plaque psoriasis (4, 5) (Figs 1 and 2).

MURINE MODELS TARGETING IL-36 SIGNAL

Murine models have shown the diverse action of IL-36 agonists on keratinocytes and immunocytes. Transgenic overexpression of IL-36α (*K14/Il36a* transgenic) in basal keratinocytes in mice resulted in epidermal thickening, hyperkeratosis, mixed inflammatory cell infiltrate (CD205$^+$DCs, CD3$^+$ T cells, macrophages and neutrophils) and elevated chemokine expression (CCL2, CXCL6, CCL7, and CXCL2), manifesting in newborns, while the phenotype is not dependent on mature T cells because it is not cancelled in T-cell deficient *Rag2*$^{-/-}$ mice (88). Backcrossing to an *Il36rn*-deficient mouse augments the IL-36α transgenic phenotype, reflecting the effects of nonsense *IL36RN* mutations in human pustular psoriasis (88). The IL-36α transgenic phenotype is partly cancelled by the neutrophil-depleting antibody or TNF-α-neutralizing antibody, suggesting roles for both neutrophils and TNF-α in IL-36α-induced skin changes (88).

Interestingly, the epidermal and dermal changes in *K14/Il36a* transgenic mice resolve by 3 weeks of age, but reappear at approximately 6 months of age (88). However, the epicutaneous application of 12-O-tetradecanoylphorbol-13-acetate (TPA) to the resolved and phenotypically normal skin of *K14/Il36a* transgenic mice elicited severe skin inflammation, similar to human psoriasis (78). The TPA-treated transgenic skin was reddened, thickened, scaly and crusted with acanthosis, hyperkeratosis, parakeratosis, hypogranulosis and neutrophilic microabscesses in the spinous and cornified layers, a mixed dermal infiltrate containing macrophages/DCs, neutrophils and lymphocytes, and an increase in and dilation of superficial dermal blood vessels (78). Like human psoriasis, IL-17A, IL-22, IL-23 (both p19 and p40 subunits), and the antimicrobial peptides S100A8, S100A9 and β-defensin 4 (an orthologue of human β defensin 2) were significantly upregulated in TPA-treated transgenic skin. IL-1β, a regulator of Th17 differentiation, was also upregulated (78). Notably, psoriasiform eruption in TPA-treated transgenic mice showed significant improvement by injection of anti-TNF-α, anti-IL-12/23p40 or anti-IL-23p19 antibody (78). Intradermal injection of IL-36α into wild-type FVB mice led to substantial increases in IL-36α, IL-17A, IL-23, TNF-α and IFN-γ mRNA. Conversely, intradermal injections of IL-17A, IL-23, TNF-α, IFN-γ, IL-22 or their combination upregulated the mRNA expression of IL-36α, as well as IL-36β and IL-36γ (78).

The skin changes in the *K14/Il36a* transgenic mice were distinct from those generated in *K14/Il1a* and *K5/Il18* transgenic mice. The *K14/Il1a* transgenic mice exhibited marked hair loss without any prominent epidermal acanthosis. The dermal infiltrates were mainly macrophages in the *K14/Il1a* transgenic mice (89). The *K14/Il36a* transgenic mice had increases in epidermal thickness and in the numbers of neutrophils, CD205$^+$ DCs and T cells (88, 89). In contrast, the *K5/Il18* transgenic mice did not have overt macroscopic or microscopic abnormalities in the skin (90). However, the contact hypersensitivity reaction to trinitrochlorobenzene in the *K5/Il18* transgenic mice was significantly intensified compared with wild-type counterparts, resembling atopic dermatitis featuring acanthosis; an infiltrate composed of eosinophils, neutrophils, and mast cells; as well as an increase in serum IgE levels (90).

Intradermal injection of murine IL-36α into CD1 mice every other day for 10 days induced mild epidermal acanthosis and pronounced leukocytic infiltrate without any visible skin changes (50). The infiltrated dermal cells were largely CD11b$^+$ neutrophils with few CD4$^+$CD8$^+$ T cells. The gene expression of the injected skin revealed upregulation of *Ccl3*, *Ccl4*, *Cxcl12*, *Il1b* and *Hbegf* (50).

Imiquimod (TLR7 agonist)-induced skin inflammation is currently well investigated as a murine model for psoriatic inflammation (41, 91). Topical treatment with imiquimod of skin cancer induces psoriasis in susceptible patients (92, 93). The topical application of imiquimod on the ears of C57BL/6 mice induced ear swelling, erythema, skin flaking, acanthosis and hyperkeratosis with dermal infiltration of IL-17A+ γδ T cells, neutrophils, macrophages and IL-23$^+$ DCs (91). These epidermal and dermal features were strongly inhibited in mice deficient in *Il36r* and were augmented in mice lacking *Il36rn* (91). Moreover, imiquimod-induced ear thickness was modestly protected against in *Il17a*$^{-/-}$ and *Il22*$^{-/-}$ mice and was slightly more potently inhibited in *Il23a*$^{-/-}$ mice, probably because IL-23 can induce both IL-17- and IL-22-producing cells. Consistent with this notion, ear thickness and neutrophil infiltrates were further ameliorated in *Il17a*$^{-/-}$ mice when combined with injection of anti-IL-22 neutralizing antibody (91). The IL-23-mediated expansion of IL-17A-producing γδ T cells was reported to depend on IL-1 (94). Nevertheless, IL-1R1 deficiency did not protect mice from imiquimod-induced psoriasiform dermatitis. Ear swelling, acanthosis, and skin flaking were comparable in *Il1r1*$^{-/-}$ and wild-type mice. Only dermal neutrophilia was

suppressed in *Il1r1*$^{-/-}$ mice (91). Among these knockout mice, imiquimod-induced psoriasiform inflammation, including epidermal thickness and dermal neutrophilic infiltration, was most inhibited in *Il36r*$^{-/-}$ mice because: (*i*) IL-36 induces the production of CXCL1 and CCL20 from keratinocytes and fibroblasts and attracts neutrophils and T cells; (*ii*) IL-36 upregulates the expression of the keratinocyte mitogens, such as granulocyte colony-stimulating factor and transforming growth factor α in keratinocytes; and (*iii*) IL-36 induces the production of IL-36 in keratinocytes in an autocrine fashion (91). Because keratinocytes are devoid of TLR7, imiquimod initiates IL-36 production by activating TLR7^{+} CD11c^{+} DCs. The released IL-36 upregulates the production of IL-23 from activated DCs, as well as the proliferation and chemokine induction of keratinocytes. The recruited T cells are directed by IL-23 to produce IL-17A and IL-22, and these Th17 cytokines further accelerate keratinocyte proliferation and neutrophilic infiltration (91). Although the aforementioned murine models were useful in investigating psoriatic inflammation, no animal models exist so far for pustular psoriasis.

CROSS-TALK AMONG IL-36, LL-37, IL-17, IL-22 AND INTERFERON

As demonstrated in the above murine studies *in vivo*, the IL-36 agonists interact with LL-37, IL-17, IL-22 and IFN to enhance the inflammatory response in human keratinocytes *in vitro*, and the cross-talk among these psoriatic factors is important to manifesting clinical psoriasis. In addition to skin injury (55), the administration of type I IFN (IFN-α and IFN-β) exacerbates psoriasis (95). The role of IFN-α or IFN-β in psoriasis has also been reported in mice lacking the type I IFN receptor or in mice treated with IFN-α- or IFN-β-neutralizing antibodies because both systems failed to develop T-cell-mediated skin inflammation (61, 96). LL-37 links skin injury to type I IFN production in human keratinocytes (59, 61, 64, 96). LL-37, together with double-stranded RNA (dsRNA) released from damaged keratinocytes, potently upregulates the production of IFN-β from keratinocytes, indeed promoting the activation and maturation of DCs (64). Human keratinocytes express the highest amounts of mitochondrial antiviral-signalling protein (MAVS) mRNA and moderate mRNA levels of TLR3, while other TLRs, including TLR4, TLR7, TLR8, and TLR9, are barely detectable (64). Poly [I:C] (dsRNA) activates TLR3, but not MAVS and causes keratinocytes to produce IFN-β, while LL-37 and dsRNA complex activate both TLR3 and MAVS and induce higher production of IFN-β (64). Notably, CRAMP, the murine homologue of LL-37, fails to enhance poly [I:C]-induced IFN-β expression, suggesting that the synergistic effect is specific to human LL-37 (64) (Fig. 2). In contrast, plasmacytoid DCs express high levels of TLR7 and TLR9 (64). LL-37 binds to self-DNA, and the LL-37/self-DNA complex induces IFN-α expression in plasmacytoid DCs through TLR9 (Fig. 1) (62).

In the lesional skin of psoriasis, overexpressed LL-37 co-localized with IFN-β expression (64). Notably, upregulated expression of IL-36γ coexists with LL-37 expression in psoriatic lesions (49). LL-37 significantly increases functional IL-36γ expression in both undifferentiated (low calcium) and differentiated (high calcium) keratinocytes, whereas the enhancing effect is stronger in the differentiated condition (49). The IL-36γ-inducible effect of LL-37 is dependent on the Gi protein-coupled receptor and p38 MAPK signalling (49). LL-37 upregulates the production of CXCL1, CXCL8, CXCL10 and CCL20 from human keratinocytes, in part via released IL-36γ (49). In accordance with this notion, LL-37 also enhances IL-36R and IL1RAP (49). These studies emphasize the importance of LL-37 as an injury sensor in the epidermis.

dsRNA could also directly enhance the gene and protein expression levels of IL-36β and IL-36γ in human keratinocytes (47). Human keratinocytes were challenged with a panel of TLR ligands, including poly [I:C] (TLR3 ligand), flagellin (TLR5 ligand), *E. coli* DNA (TLR9 ligand), lipoteichoic acid (TLR2 ligand), lipopolysaccharide (TLR4 ligand) and zymosan (TLR2 ligand) (47). The gene expression levels of IL-1α and IL-1β were upregulated by these ligands at 1, 6 and 24 h, while the robust upregulation of IL-36β and IL-36γ was induced only by poly [I:C] and flagellin at 6 and 24 h after stimulation. Lipopolysaccharide and zymosan weakly upregulated IL-36γ gene expression at 24 h (47). The release of IL-36γ protein was observed only by poly [I:C] but not by flagellin. The extracellular release of IL-36γ was augmented in the presence of 5 mM ATP. The secretion of IL-36β protein was not detected by any stimulation. Poly [I:C], but not flagellin, caused cell death (pyroptosis) of keratinocytes in a caspase-3/7-dependent manner, and caspase-3/7 is a prerequisite for the release of IL-36γ (47). In addition, caspase 1 activation is required for IL-36γ gene expression and caspase 3/7 activation (47). These results also suggest the importance of IL-36γ as an injury sensor in the epidermis.

Both IL-17 and IL-22 and TNF-α are potent inducers of IL-36α, IL-36β and IL-36γ in human keratinocytes (86) (Fig. 1). IL-22, in concert with IL-17 or TNF-α, synergistically or additively enhances the production of IL-36α, IL-36β and IL-36γ from keratinocytes. Although IL-17A and TNF-α induce all 3 IL-36 members in keratinocytes, IL-17A most strongly induces the expression of IL-36α, and TNF-α strongly induces IL-36β. Moreover, the expression levels of IL-36α, IL-36β and IL-36γ are induced by either IL-36, especially in the simultaneous presence of IL-17A, or by TNF-α (86). IL-36α, IL-36β and IL-36γ also upregulate the expression levels of TNF-α, IL-6 and IL-8, respectively, which are further augmented by the simultaneous addition of IL-17A or

ActaDV Acta Dermato-Venereologica ActaDV Advances in dermatology and venereology

TNF-α. IFN-γ selectively activates the expression of IL-36β, but not IL-36α or IL-36γ (86). Johnston et al. (41) reported similar findings that the gene expression of IL-36γ in human keratinocytes was augmented by each of the psoriasis-associated cytokines, i.e. TNF-α, IL-1α and IL-17A. Although IL-22 alone is ineffective to induce IL-36γ gene expression, it synergistically potentiates the upregulatory effects of IL-17A. The synergistic action of IL-36γ induction is evident in combination with IL-1α+ TNF-α or IL-1α+IFN-γ (41). These *in vitro* studies using skin-resident keratinocytes indicated the active and mutual cross-talk of the TNF-α/IL-23/IL-17/IL-22 axis and the functional activation of IL-36R.

CONCLUSION

Psoriasis is considered a human-specific disorder. Unlike human keratinocytes, murine cathelicidin CRAMP fails to activate MAVS in combination with dsRNA (64). Murine keratinocytes do not produce IL-1β (97, 98). The characteristics of human keratinocytes might explain the human-specific enigma. Plaque psoriasis and pustular psoriasis have relevant and partially overlapping, but distinct, clinical features. The TNF-α/IL-23/IL-17/IL-22 axis is the common pathogenetic pathway in these disorders, because blockade of IL-23 by ustekinumab is effective in generalized pustular psoriasis regardless of *IL36RN* mutation status (99). Nevertheless, the functional activation of IL-36R by agonists and the loss of function mutation of its antagonist IL-36Ra are implicated to be key pieces in a pathogenetic jigsaw puzzle. Considering: (*i*) the potent proliferative activity of IL-17 and IL-22 on human keratinocytes; (*ii*) the lack of clubbed regular acanthosis in pustular psoriasis; and (*iii*) the effective chemoattraction of neutrophil by IL-36 agonists; functional IL-36R activation is preferentially involved in the pathogenesis of pustular psoriasis, and conversely, the TNF-α/IL-23/IL-17/IL-22 axis more efficiently drives plaque psoriasis (Figs 1 and 2). Notably, these 2 pathways are closely related and cross-talk with each other, forming a positive inflammatory loop. Although the agonistic activities of IL-36α, IL-36β and IL-36γ on IL-36R are redundant, current studies have supported the importance of IL-36γ (and IL-36α) in human psoriatic inflammation (4, 39, 41, 48, 49, 85, 88). The biological significance of each isoform of IL-36R agonists warrants future investigation.

The authors have no conflicts of interest to declare.

REFERENCES

1. Boehncke WH, Schön MP. Psoriasis. Lancet 2015; 386: 983–994.
2. Furue M, Kadono T. Psoriasis: behind the scenes. J Dermatol 2016; 43: 4–8.
3. Ko H, Cho MH, Kim WJ, Kim JH, Song M, Kim HS, et al. Clinical features and course of generalized pustular psoriasis in Korea. J Dermatol 2015; 42: 674–678.
4. Johnston A, Xing X, Wolterink L, Barnes DH, Yin Z, Reingold L, et al. IL-1 and IL-36 are dominant cytokines in generalized pustular psoriasis. J Allergy Clin Immunol 2017; 140: 109–120.
5. Liang Y, Xing X, Beamer MA, Swindell WR, Sarkar MK, Roberts LW, et al. Six-transmembrane epithelial antigen of the prostate comprises a novel inflammatory nexus in patients with pustular skin disorders. J Allergy Clin Immunol 2017; 139: 1217–1227.
6. Menter A, Korman NJ, Elmets CA, Feldman SR, Gelfand JM, Gordon KB, et al. Guidelines of care for the management of psoriasis and psoriatic arthritis: section 6. Guidelines of care for the treatment of psoriasis and psoriatic arthritis: case-based presentations and evidence-based conclusions. J Am Acad Dermatol 2011; 65: 137–174.
7. Nast A, Gisondi P, Ormerod AD, Saiag P, Smith C, Spuls PI, et al. European S3-Guidelines on the systemic treatment of psoriasis vulgaris – Update 2015 – Short version – EDF in cooperation with EADV and IPC. J Eur Acad Dermatol Venereol 2015; 29: 2277–2294.
8. Bhushan R, Lebwohl MG, Gottlieb AB, Boyer K, Hamerstrom E, Korman NJ, et al. Translating psoriasis guidelines into practice: Important gaps revealed. J Am Acad Dermatol 2016; 74: 544–551.
9. Asahina A, Ohtsuki M, Etoh T, Gu Y, Okun MM, Teixeira HD, et al. Adalimumab treatment optimization for psoriasis: results of a long-term phase 2/3 Japanese study. J Dermatol 2015; 42: 1042–1052.
10. Ito K, Koga M, Shibayama Y, Tatematsu S, Nakayama J, Imafuku S. Proactive treatment with calcipotriol reduces recurrence of plaque psoriasis. J Dermatol 2016; 43: 402–405.
11. Kawakami H, Maeda T, Abe N, Matsumoto Y, Mitsuhashi Y, Tsubo R, et al. Efficacy of adalimumab and methotrexate combination therapy on generalized pustular psoriasis patients unresponsive to infliximab monotherapy due to anti-infliximab antibody development. J Dermatol 2015; 42: 94–95.
12. Kusakari Y, Yamasaki K, Takahashi T, Tsuchiyama K, Shimada-Omori R, Nasu-Tamabuchi M, et al. Successful adalimumab treatment of a psoriasis vulgaris patient with hemodialysis for renal failure: A case report and a review of the previous reports on biologic treatments for psoriasis patients with hemodialysis for renal failure. J Dermatol 2015; 42: 727–730.
13. Hirmanniya K, Tatsishi C, Nizukami Y, Hamamoto Y, Yamada S, Goto H, et al. Successful treatment with ustekinumab of psoriasis vulgaris in a patient undergoing hemodialysis. J Dermatol 2016; 43: 92–94.
14. Asahina A, Torii H, Ohtsuki M, Tokimoto T, Nase H, Tsuchiya T, et al. Safety and efficacy of adalimumab treatment in Japanese patients with psoriasis: results of SALSA study. J Dermatol 2016; 43: 1257–1266.
15. Korman NJ, Zhao Y, Pike J, Roberts J. Relationship between psoriasis severity, clinical symptoms, quality of life and work productivity among patients in the USA. Clin Exp Dermatol 2016; 41: 514–521.
16. Saeki H, Imafuku S, Abe M, Shintani Y, Onozuka D, Hagihara A, et al. Poor adherence to medication as assessed by the Morisky Medication Adherence Scale-8 and low satisfaction with treatment in 237 psoriasis patients. J Dermatol 2015; 42: 367–372.
17. López-Estebaranz JL, Sánchez-Carazo JL, Sulleiro S. Effect of a family history of psoriasis and age on comorbidities and quality of life in patients with moderate to severe psoriasis: results from the ARIZONA study. J Dermatol 2016; 43: 395–401.
18. Ng CY, Yang YW, Du SH, Lu JF, Yang LC, Yang CH, et al. SF-36 healthy survey on psoriasis quality-of-life: a study of 414 Taiwanese patients. J Dermatol 2015; 42: 158–165.
19. Do YK, Lakhani N, Malhotra R, Halstatter R, Thang C, Rathye I. Association between psoriasis and leisure-time physical activity: findings from the National Health and Nutrition Examination Survey. J Dermatol 2015; 42: 148–153.
20. Atakan N, Yazici AC, Özarmağan G, İnaltöz HS, Güner MA, Sabuncu I, et al. TUR-PSO: A cross-sectional study investigating quality of life and treatment status of psoriasis patients in Turkey. J Dermatol 2016; 43: 298–304.
21. Baurecht H, Hotze M, Brand S, Büning C, Cormican P, Corvin A, et al. Genome-wide comparative analysis of atopic dermatitis

and psoriasis gives insight into opposing genetic mechanisms. Am J Hum Genet 2015; 96: 104–120.
22. Feng C, Wang T, Li SJ, Fan YM, Shi G, Zhu KJ. CARD14 gene polymorphism c.C2458T (p.Arg820Trp) is associated with clinical features of psoriasis vulgaris in a Chinese cohort. J Dermatol 2016; 43: 294–297.
23. Marrakchi S, Guigue P, Renshaw BR, Puel A, Pei XY, Fraitag S, et al. Interleukin-36-receptor antagonist deficiency and generalized pustular psoriasis. N Engl J Med 2011; 365: 620–628.
24. Tang H, Jin Y, Li Y, Jiang H, Tang X, Yang K, et al. A large-scale screen for coding variants predisposing to psoriasis. Nat Genet 2014; 46: 45–50.
25. Boehncke WH, Boehncke S, Tobin AM, Kirby B. The 'psoriatic march': a concept of how severe psoriasis may drive cardiovascular comorbidity. Exp Dermatol 2011; 20: 303–307.
26. Torii H, Terui T, Matsukawa M, Takeuchi K, Ohtsuki M, Nakagawa H. Safety profiles and efficacy of infliximab therapy in Japanese patients with plaque psoriasis with or without peripheral arthritis, pustular psoriasis or psoriatic erythroderma: results from the prospective post-marketing surveillance. J Dermatol 2016; 43: 767–778.
27. Takata T, Takahashi A, Taniguchi Y, Tsuda Y, Sano S. Detection of asymptomatic enthesitis in psoriasis patients: an onset of psoriatic arthritis? J Dermatol 2016; 43: 650–654.
28. Youn SW, Kang SY, Kim SA, Park GY, Lee WW. Subclinical systemic and vascular inflammation detected by (18) F-fluorodeoxyglucose positron emission tomography/computed tomography in patients with mild psoriasis. J Dermatol 2015; 42: 559–566.
29. Takeshita J, Grewal S, Langan SM, Mehta NN, Ogdie A, Van Voorhees AS, et al. Psoriasis and comorbid diseases: epidemiology. J Am Acad Dermatol 2017; 76: 377–390.
30. Yamanaka K, Mizutani H. "Inflammatory skin march": IL-1-mediated skin inflammation, atopic dermatitis, and psoriasis to cardiovascular events. J Allergy Clin Immunol 2015; 136: 823–824.
31. Akiyama H, Ueno T, Kanzaki A, Kuwana M, Nagao M, Saeki H. Association of psoriasis with Hashimoto's thyroiditis, Sjögren's syndrome and dermatomyositis. J Dermatol 2016; 43: 711–712.
32. Okahashi K, Otsu N, Ishii N, Uchida S, Matsuda H, Hashimoto T, et al. Bullous pemphigoid associated with psoriasis: a possible example of an inverse intra-molecular epitope-spreading phenomenon. J Dermatol 2015; 42: 758–759.
33. Maki N, Demitsu T, Umemoto N, Nagashima K, Nakamura T, Kakurai M, et al. Possible paraneoplastic syndrome case of bullous pemphigoid with immunoglobulin G anti-BP180 C-terminal domain antibodies associated with psoriasis and primary macroglobulinemia. J Dermatol 2016; 43: 571–574.
34. Imanishi A, Tateishi C, Imanishi K, Sawa-Osako J, Koga H, Tsuruta D, et al. Pemphigoid with antibodies to laminin γ1, BP180 and BP230, associated with psoriasis vulgaris: successful disease control with cyclosporin. J Dermatol 2015; 42: 394–397.
35. Ishida S, Takahashi K, Kanaoka M, Okawa T, Tateishi C, Yasukochi A, et al. Case of subepidermal autoimmune bullous disease with psoriasis vulgaris reacting to both BP180 C-terminal domain and laminin gamma-1. J Dermatol 2015; 42: 391–393.
36. Takahashi H, Sato K, Takagi A, Ikawa S, Ishii K, Hashimoto T, et al. Subepidermal autoimmune blistering lesion in a case of psoriasis successfully treated with cyclosporin. J Dermatol 2015; 42: 1125–1126.
37. Lowes MA, Suárez-Fariñas M, Krueger JG. Immunology of psoriasis. Annu Rev Immunol 2014; 32: 227–255.
38. Teng MW, Bowman EP, McElwee JJ, Smyth MJ, Casanova JL, Cooper AM, et al. IL-12 and IL-23 cytokines: from discovery to targeted therapies for immune-mediated inflammatory diseases. Nat Med 2015; 21: 719–729.
39. Boutet MA, Bart G, Penhoat M, Amraoui Z, Bruin G, Chartier C, et al. Distinct expression of interleukin (IL) 36α, β and γ, their antagonist IL-36Ra and IL-38 in psoriasis, rheumatoid arthritis and Crohn's disease. Clin Exp Immunol 2016; 184: 159–173.
40. Towne JE, Sims JE. IL-36 in psoriasis. Curr Opin Pharmacol 2012; 12: 486–490.
41. Johnston A, Xing X, Guzman AM, Riblett M, Loyd CM, Ward NL, et al. IL-1F5, -F6, -F8, and -F9: a novel IL-1-family signaling system that is active in psoriasis and promotes keratinocyte antimicrobial peptide expression. J Immunol 2011; 186: 2613–2622.
42. Sugiura K, Takemoto A, Yamaguchi M, Takahashi H, Shoda Y, Mitsuma T, et al. The majority of generalized pustular psoriasis without psoriasis vulgaris is caused by deficiency of interleukin-36 receptor antagonist. J Invest Dermatol 2013; 133: 2514–2521.
43. Dinarello C, Arend W, Sims J, Smith D, Blumberg H, O'Neill L, et al. IL-1 family nomenclature. Nat Immunol 2010; 11: 973.
44. Gabay C, Towne JE. Regulation and function of interleukin-36 cytokines in homeostasis and pathological conditions. J Leukoc Biol 2015; 97: 645–652.
45. Sims JE, Smith DE. The IL-1 family: regulators of immunity. Nat Rev Immunol 2010; 10: 89–102.
46. Henry CM, Sullivan GP, Clancy DM, Afonina IS, Kulms D, Martin SJ. Neutrophil-derived proteases escalate inflammation through activation of IL-36 family cytokines. Cell Rep 2016; 14: 708–722.
47. Lian LH, Milora KA, Manupipatpong KK, Jensen LE. The double-stranded RNA analogue polyinosinic-polycytidylic acid induces keratinocyte pyroptosis and release of IL-36γ. J Invest Dermatol 2014; 132: 1346–1353.
48. Ainscough JS, Macleod T, McGonagle D, Brakefield R, Baron JM, Alase A, et al. Cathepsin S is the major activator of the psoriasis-associated proinflammatory cytokine IL-36γ. Proc Natl Acad Sci U S A 2017; 114: E2746–E2757.
49. Li N, Yamasaki K, Saito R, Fukushi-Takahashi S, Shimada-Omori R, Asano M, et al. Alarmin function of cathelicidin antimicrobial peptide LL37 through IL-36γ induction in human epidermal keratinocytes. J Immunol 2014; 193: 5140–5148.
50. Foster AM, Baliwag J, Chen CS, Guzman AM, Stoll SW, Gudjonsson JE, et al. IL-36 promotes myeloid cell infiltration, activation, and inflammatory activity in skin. J Immunol 2014; 192: 6053–6061.
51. Dietrich D, Martin P, Flacher V, Sun Y, Jarrossay D, Brembilla N, et al. Interleukin-36 potently stimulates human M2 macrophages, Langerhans cells and keratinocytes to produce pro-inflammatory cytokines. Cytokine 2016; 84: 88–98.
52. Onoufriadis A, Simpson MA, Pink AE, Di Meglio P, Smith CH, Pullabhatla V, et al. Mutations in IL36RN/IL1F5 are associated with the severe episodic inflammatory skin disease known as generalized pustular psoriasis. Am J Hum Genet 2011; 89: 432–437.
53. Körber A, Mössner R, Renner R, Sticht H, Wilsmann-Theis D, Schulz P, et al. Mutations in IL36RN in patients with generalized pustular psoriasis. J Invest Dermatol 2013; 133: 2634–2637.
54. Hussain S, Berki DM, Choon SE, Burden AD, Allen MH, Arostegui JI, et al. IL36RN mutations define a severe autoinflammatory phenotype of generalized pustular psoriasis. J Allergy Clin Immunol 2015; 135: 1067–1070.e9.
55. Kelekciyan A, Aydemir EH, Kotogyan A. Experimental Koebner phenomenon in patients with psoriasis. Dermatology 2007; 215: 114–117.
56. Yu RX, Hui Y, Li CR. Koebner phenomenon induced by cupping therapy in a psoriasis patient. Dermatol Online J 2013; 19: 18575.
57. Morais P, Oliveira H, Matos J. Stress: a potential precipitating factor for Koebner phenomenon in psoriasis? Dermatol Online J 2013; 19: 18566.
58. Weiss G, Shemer A, Trau H. The Koebner phenomenon: review of the literature. J Eur Acad Dermatol Venereol 2002; 16: 241–248.
59. Dorschner RA, Pestonjamasp VK, Tamakuwala S, Ohtake T, Rudisill J, Nizet V, et al. Cutaneous injury induces the release of cathelicidin anti-microbial peptides active against group A Streptococcus. J Invest Dermatol 2001; 117: 91–97.
60. Sørensen OE, Follin P, Johnsen AH, Calafat J, Tjabringa GS, Hiemstra PS, et al. Human cathelicidin, hCAP-18, is processed to the antimicrobial peptide LL-37 by extracellular cleavage with proteinase 3. Blood 2001; 97: 3951–3959.
61. Nestle FO, Conrad C, Tun-Kyi A, Homey B, Gombert M, Boyman O, et al. Plasmacytoid predendritic cells initiate psoriasis

through interferon-alpha production. J Exp Med 2005; 202: 135–143.
62. Lande R, Gregorio J, Facchinetti V, Chatterjee B, Wang YH, Homey B, et al. Plasmacytoid dendritic cells sense self-DNA coupled with antimicrobial peptide. Nature 2007; 449: 564–569.
63. Lowes MA, Chamian F, Abello MV, Fuentes-Duculan J, Lin SL, Nussbaum R, et al. Increase in TNF-alpha and inducible nitric oxide synthase-expressing dendritic cells in psoriasis and reduction with efalizumab (anti-CD11a). Proc Natl Acad Sci USA 2005; 102: 19057–19062.
64. Zhang LJ, Sen GL, Ward NL, Johnston A, Chun K, Chen Y, et al. Antimicrobial peptide LL37 and MAVS signaling drive interferon-β production by epidermal keratinocytes during skin injury. Immunity 2016; 45: 119–130.
65. Serbina NV, Salazar-Mather TP, Biron CA, Kuziel WA, Pamer EG. TNF/iNOS-producing dendritic cells mediate innate immune defense against bacterial infection. Immunity 2003; 19: 59–70.
66. McGeachy MJ, McSorley SJ. Microbial-induced Th17: superhero or supervillain? J Immunol 2012; 189: 3285–3291.
67. Ramirez-Valle F, Gray EE, Cyster JG. Inflammation induces dermal Vγ4 γδT17 memory-like cells that travel to distant skin and accelerate secondary IL-17-driven responses. Proc Natl Acad Sci USA 2015; 112: 8046–8051.
68. Teunissen MB, Yeremenko NG, Baeten DL, Chaoka S, Spuls PI, de Rie MA, et al. The IL-17A-producing CD8+ T-cell population in psoriatic lesional skin comprises mucosa-associated invariant T cells and conventional T cells. J Invest Dermatol 2014; 134: 2898–2907.
69. Chang JC, Smith LR, Froning KJ, Schwabe BJ, Laker JA, Carelli LL et al. CD8+ T cells in psoriatic lesions preferentially use T-cell receptor V beta 3 and/or V beta 13.1 genes. Proc Natl Acad Sci U S A 1994; 91: 9282–9286.
70. Conrad C, Boyman O, Tonel G, Tun-Kyi A, Laggner U, de Fougerolles A, et al. Alpha1beta1 integrin is crucial for accumulation of epidermal T cells and the development of psoriasis. Nat Med 2007; 13: 836–842.
71. Di Meglio P, Villanova F, Navarini AA, Mylonas A, Tosi I, Nestle FO, et al. Targeting CD8(+) T cells prevents psoriasis development. J Allergy Clin Immunol 2016; 138: 274–276.
72. Arakawa A, Siewert K, Stohr J, Besgen P, Kim SM, Rühl G, et al. Melanocyte antigen triggers autoimmunity in human psoriasis. J Exp Med 2015; 212: 2203–2212.
73. Ha HL, Wang H, Pisitkun P, Kim JC, Tassi I, Tang W, et al. IL-17 drives psoriatic inflammation via distinct, target cell-specific mechanisms. Proc Natl Acad Sci USA 2014; 111: E3422–3431.
74. Boniface K, Bernard FX, Garcia M, Gurney AL, Lecron JC, Morel F. IL-22 inhibits epidermal differentiation and induces proinflammatory gene expression and migration of human keratinocytes. J Immunol 2005; 174: 3695–3702.
75. Sa SM, Valdez PA, Wu J, Jung K, Zhong F, Hall L, et al. The effects of IL-20 subfamily cytokines on reconstituted human epidermis suggest potential roles in cutaneous innate defense and pathogenic adaptive immunity in psoriasis. J Immunol 2007; 178: 2229–2240.
76. Nograles KE, Zaba LC, Guttman-Yassky E, Fuentes-Duculan J, Suárez-Fariñas M, Cardinale I, et al. Th17 cytokines interleukin (IL)-17 and IL-22 modulate distinct inflammatory and keratinocyte-response pathways. Br J Dermatol 2008; 159: 1092–1102.
77. Haider AS, Lowes MA, Suárez-Fariñas M, Zaba LC, Cardinale I, Khatcherian A, et al. Identification of cellular pathways of "type 1," Th17 T cells, and TNF- and inducible nitric oxide synthase-producing dendritic cells in autoimmune inflammation through pharmacogenomic study of cyclosporine A in psoriasis. J Immunol 2008; 180: 1913–1920.
78. Blumberg H, Dinh H, Dean C Jr, Trueblood ES, Bailey K, Shows D, et al. IL-1RL2 and its ligands contribute to the cytokine network in psoriasis. J Immunol 2010; 185: 4354–4362.
79. Reich K, Papp KA, Matheson RT, Tu JH, Bissonnette R, Bourcier M, et al. Evidence that a neutrophil-keratinocyte crosstalk is an early target of IL-17A inhibition in psoriasis. Exp Dermatol 2015; 24: 529–535.
80. Iwakura Y, Ishigame H, Saijo S, Nakae S. Functional specialization of interleukin-17 family members. Immunity 2011; 34: 149–162.
81. Gómez-García F, Epstein D, Isla-Tejera B, Lorente A, Vélez García-Nieto A, Ruano J. Short-term efficacy and safety of new biological agents targeting the interleukin-23-T helper 17 pathway for moderate-to-severe plaque psoriasis: a systematic review and network meta-analysis. Br J Dermatol 2017; 176: 594–603.
82. Imafuku S, Honma M, Okubo Y, Komine M, Ohtsuki M, Morita A, et al. Efficacy and safety of secukinumab in patients with generalized pustular psoriasis: a 52-week analysis from phase III open-label multicenter Japanese study. J Dermatol 2016; 43: 1011–1017.
83. Saikaly SK, Mattes M. Biologics and pediatric generalized pustular psoriasis: an emerging therapeutic trend. Cureus 2016; 8: e652.
84. Zhou X, Krueger JG, Kao MC, Lee E, Du F, Menter A, et al. Novel mechanisms of T-cell and dendritic cell activation revealed by profiling of psoriasis on the 63,100-element oligonucleotide array. Physiol Genomics 2003; 13: 69–78.
85. Keermann M, Kõks S, Reimann E, Abram K, Erm T, Silm H, et al. Expression of IL-36 family cytokines and IL-37 but not IL-38 is altered in psoriatic skin. J Dermatol Sci 2015; 80: 150–152.
86. Carrier Y, Ma HL, Ramon HE, Napierata L, Small C, O'Toole M, et al. Inter-regulation of Th17 cytokines and the IL-36 cytokines in vitro and in vivo: implications in psoriasis pathogenesis. J Invest Dermatol 2011; 131: 2428–2437.
87. Muhr P, Zeitvogel J, Meitland I, Werfel T, Wittmann M. Expression of interleukin (IL)-1 family members upon stimulation with IL-17 differs in keratinocytes derived from patients with psoriasis and healthy donors. Br J Dermatol 2011; 165: 189–193.
88. Blumberg H, Dinh H, Trueblood ES, Pretorius J, Kugler D, Weng N, et al. Opposing activities of two novel members of the IL-1 ligand family regulate skin inflammation. J Exp Med 2007; 204: 2603–2614.
89. Groves RW, Mizutani H, Kieffer JD, Kupper TS. Inflammatory skin disease in transgenic mice that express high levels of interleukin 1 alpha in basal epidermis. Proc Natl Acad Sci U S A 1995; 92: 11874–11878.
90. Kawase Y, Hoshino T, Yokota K, Kuzuhara A, Kiri Y, Nishiwaki E, et al. Exacerbated and prolonged allergic and non-allergic inflammatory cutaneous reaction in mice with targeted interleukin-18 expression in the skin. J Invest Dermatol 2003; 121: 502–509.
91. Tortola L, Rosenwald E, Abel B, Blumberg H, Schäfer M, Coyle AJ, et al. Psoriasiform dermatitis is driven by IL-36-mediated DC-keratinocyte crosstalk. J Clin Invest 2012; 122: 3965–3976.
92. Rajan N, Langley RA. Generalized exacerbation of psoriasis associated with imiquimod cream treatment of superficial basal cell carcinomas. Clin Exp Dermatol 2006; 31: 140–141.
93. Wu JK, Siller G, Strutton G. Psoriasis induced by topical imiquimod. Australas J Dermatol 2004; 45: 47–50.
94. Cai Y, Shen X, Ding C, Qi C, Li K, Li X, et al. Pivotal role of dermal IL-17-producing γδ T cells in skin inflammation. Immunity 2011; 35: 596–610.
95. Funk J, Langeland T, Schrumpf E, Hanssen LE. Psoriasis induced by interferon-alpha. Br J Dermatol 1991; 125: 463–465.
96. Gregorio J, Meller S, Conrad C, Di Nardo A, Homey B, Lauerma A, et al. Plasmacytoid dendritic cells sense skin injury and promote wound healing through type I interferons. J Exp Med 2010; 207: 2921–2930.
97. Shornick LP, Bhanya AK, Chaplin DD. IL-1beta is essential for Langerhans cell activation and antigen delivery to the lymph nodes during contact sensitization: evidence for a dermal source of IL-1beta. Cell Immunol 2001; 211: 105–112.
98. Matsushima H, Ogawa Y, Miyaoki T, Tanaka H, Nishibu A, Takashima A. Intravital imaging of IL-1beta production in skin. J Invest Dermatol 2010; 130: 1571–1580.
99. Arakawa A, Ruzicka T, Prinz JC. Therapeutic efficacy of interleukin 12/interleukin 23 blockade in generalized pustular psoriasis regardless of IL36RN mutation status. JAMA Dermatol 2016; 152: 825–828.

Review Article

Innate Immunity

Innate Immunity
2019, Vol. 25(6) 337–343
© The Author(s) 2019
Article reuse guidelines:
sagepub.com/journals-permissions
DOI: 10.1177/1753425919852156
journals.sagepub.com/home/ini
SAGE

The contribution of IL-17 to the development of autoimmunity in psoriasis

Masutaka Furue[1] and Takafumi Kadono[2]

Abstract

Psoriasis is an (auto)immune-mediated disease that manifests as widespread desquamative erythema. The TNF-α/IL-23/IL-17A axis is crucial to its pathogenesis, which is demonstrated by its excellent therapeutic response to biologics that target this axis. There is a strong association between HLA-C*0602 and psoriasis, and researchers have identified autoantigens that are restricted to this major histocompatibility class I molecule. These auto-Ags include LL-37, A disintegrin and metalloprotease domain containing thrombospondin type I motif-like 5 (ADAMTSL5), and keratin 17. IL-17A-producing T cells have been identified in T cell populations that are reactive to these auto-Ags. In addition, lipid Ags have surfaced as candidate auto-Ags that activate IL-17A-producing T cells in a CD1a-restricted manner. In this article, we review the candidate auto-Ags that may contribute to the activation of the IL-17A-deviated immune response in psoriasis.

Keywords

Psoriasis, autoimmunity, LL-37, A disintegrin and metalloprotease domain containing thrombospondin type I motif-like 5, keratin 17, HLA-C*0602

Date Received: 29 January 2019; revised 24 April 2019; accepted: 30 April 2019

Introduction

Psoriasis is an (auto)immune-mediated disease that manifests as widespread desquamative erythema,[1,2] and occurs in approximately 2% of the general population of North America and Europe.[1,2] Psoriasis patients represent 4.43% of all Japanese dermatological patients,[3] while its prevalence is estimated to be only 0.1% of the general population of Japan.[4] Males are twice as likely to be affected than females.[4,5] The cosmetic disfigurement associated with psoriasis profoundly impairs the patients' quality of life, treatment satisfaction and adherence, and socioeconomic stability.[6–10]

Therapeutic modalities for psoriasis include topical steroids, topical vitamin D3 derivatives, phototherapy, phosphodiesterase-4 inhibitors, cyclosporine, methotrexate, and biologics targeting TNF-α, IL-23, and IL-17A.[11–19] The excellent therapeutic efficacy of anti-TNF-α/IL-23/IL-17A biologics for psoriasis point to a central role of the TNF-α/IL-23/IL-17A axis in its pathogenesis.[20,21] Additionally, genetic and environmental factors are known to be involved in its pathogenesis.[22–25]

The autoimmune nature of psoriasis is exemplified by its high comorbidity with psoriatic arthritis,[1,26] and other autoimmune diseases including autoimmune bullous diseases.[27–31] The onset of psoriasis is commonly observed in patients who are infected with the human immunodeficiency virus or those who are undergoing treatment with immune checkpoint Abs.[32–34] Psoriasis is also comorbid with cardiovascular diseases, metabolic diseases, and renal disorders, which represent a condition known as inflammatory skin march.[35–41]

[1]Department of Dermatology, Kyushu University, Fukuoka, Japan
[2]Department of Dermatology, St. Marianna University School of Medicine, Kawasaki, Japan

Corresponding author:
Masutaka Furue, Department of Dermatology, Graduate School of Medical Sciences, Kyushu University, Maidashi 3-1-1, Higashi-ku, Fukuoka 812-8582, Japan.
Email: furue@dermatol.med.kyushu-u.ac.jp

Creative Commons Non Commercial CC BY-NC: This article is distributed under the terms of the Creative Commons Attribution-NonCommercial 4.0 License (http://www.creativecommons.org/licenses/by-nc/4.0/) which permits non-commercial use, reproduction and distribution of the work without further permission provided the original work is attributed as specified on the SAGE and Open Access pages (https://us.sagepub.com/en-us/nam/open-access-at-sage).

Additionally, biological markers that represent systemic inflammation are elevated in psoriasis patients.[42,43] It has also been shown that the biologics that target the TNF-α/IL-23/IL-17A axis also improve the symptoms of the comorbid diseases and the systemic inflammation.[44,45]

Genetic meta-analyses reveal that HLA-C*0602 is a strong susceptibility allele for psoriasis and that HLA-C*0602-positive patients with psoriasis exhibit a younger age of onset and a more severe phenotype than HLA-C*0602-negative patients.[46,47] As a result, several HLA-C*0602-restricted auto-Ags have been identified.[48–51] Additionally, some lipid auto-Ags are restricted to CD1a.[52] These auto-Ags-reactive T cells produce IL-17 and are considered to be pathogenic in psoriasis.[48–52]

In this review, we summarize the recent advances in the field concerning the pathogenesis of psoriasis with a focus on autoantigens.

The pathogenic role of the TNF-α/IL-23/IL-17A axis in psoriasis

The histopathology of psoriasis is characterized by epidermal acanthosis, accelerated keratinocyte proliferation, and infiltration of neutrophils and T cells (Figure 1).[1] Gene expression of *TNF*, *IL23*, and *IL17A* is up-regulated in the skin lesions of psoriasis.[3,11] Three of the six *IL17* family genes, *IL17A*, *IL17F*, and *IL17C*, are overexpressed in psoriatic lesions, but the pathogenic role of IL-17F and IL-17C remains unclear.[34,35] IL-17A, which is

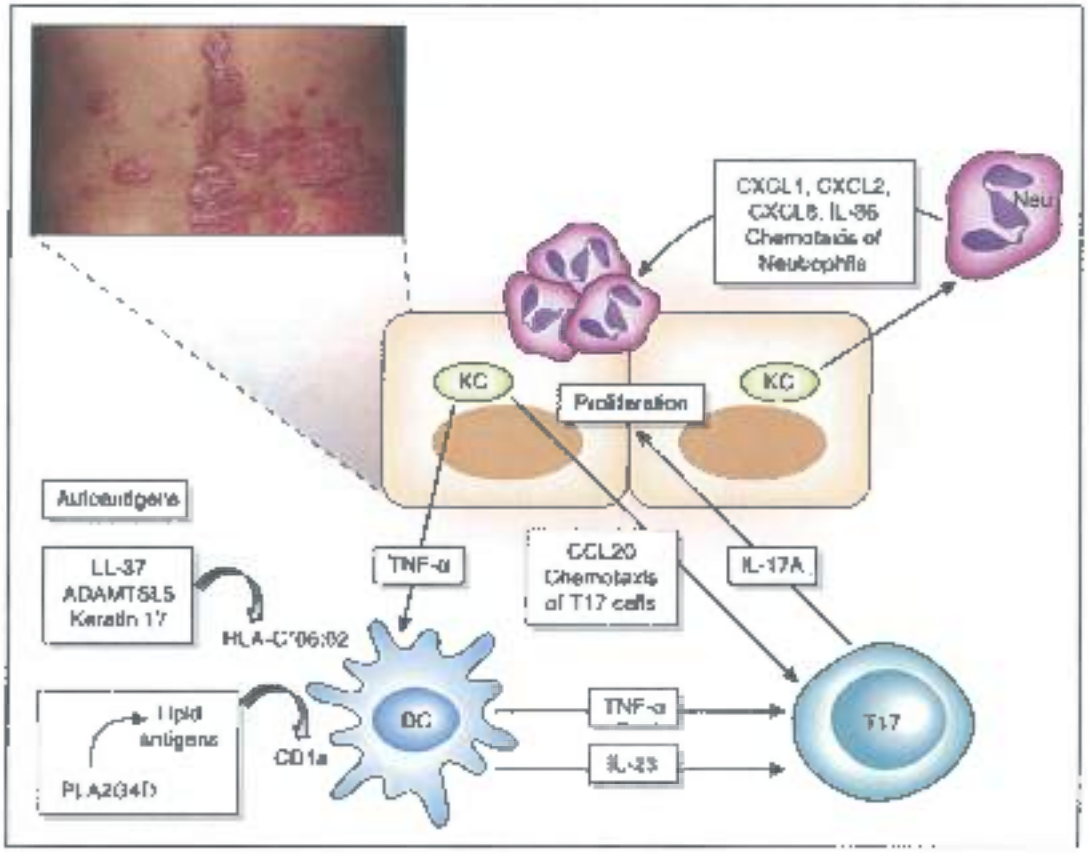

Figure 1. The simplified pathogenesis of psoriasis. Psoriasis is an (auto)immune-mediated inflammatory skin disease. Increased reactivity of T cells against autoantigens has been observed in psoriasis. Dendritic cells (DCs) present auto-Ags such as LL-37, ADAMTSL5, and keratin 17 in association with HLA-C*06:02. The phospholipase A2 group IV D (PLA2G4D) enzyme generates various lipid metabolites. Some lipid Ags are presented by DCs in association with CD1a. TNF-α and IL-23 produced by DCs induce IL-17A-producing T (T17) cells. IL-17A induces the proliferation of keratinocytes. IL-17A also induces the production of CXCL1, CXCL2, CXCL8, and IL-36 in keratinocytes, all of which stimulate neutrophil (Neu) migration into the epidermis. Moreover, IL-17A stimulates keratinocytes to produce CCL20, which recruits T17 cells. The TNF-α/IL-23/IL-17A axis plays a crucial role in the pathogenesis of psoriasis.
ADAMTSL5; A disintegrin and metalloprotease domain containing thrombospondin type 1 motif-like 5

produced by T helper 17 (Th17) cells and T cytotoxic 17 (Tc17) cells, accelerates the proliferation of keratinocytes.[58–61] Additionally, IL-17A stimulates keratinocytes to produce cyto/chemokines that attract neutrophils (CXCL1, CXCL2, CXCL8, and IL-36) and Th17 cells (CCL20).[56–60]

TNF-α and IL-23 are critical for dendritic cells (DCs) to induce and maintain Th17 and Tc17 cells.[61–63] A highly sensitive immunohistological study found that the expression of TNF is confined to the HLA-DR+CD11c+ DCs and the CD163+ macrophages in psoriatic lesions.[64] In the first 48 h after an intravenous administration of the TNF antagonist infliximab, no overt changes in the number of TNF+ cells or signs of apoptosis were observed. However, a rapid decrease in IL-12/IL-23p40, CCL20, and IL-12/IL-23RB1 mRNA levels was detected, which suggests that TNF antagonism efficiently inhibits the activation of Ag-presenting cells.[64] In addition, psoriatic keratinocytes produced larger amounts of TNF-α as well as CXCL8 when compared to keratinocytes from healthy volunteers in *ex vivo* cultures.[65]

IL-23 is composed of two subunits, p19 and p40. While the p19 subunit is an element unique to IL-23, the p40 subunit is shared with IL-12.[66] IL-12 is composed of the p40 and IL-12-specific p35 subunits.[66] IL-23 p40/p19 binds to the IL-23 receptor, which comprises IL-23R and IL-12RB1.[66] Dermal DCs and monocytes are major sources of IL-23 production.[67] At least 10 biologics have been used in clinics or in ongoing clinical trials, including anti-TNF-α (etanercept, infliximab, adalimumab), anti-IL-23 (ustekinumab, guselkumab, tildrakizumab, risankizumab), and anti-IL17 (secukinumab, ixekizumab, brodalumab) Abs.[19] Clinical efficacy is assessed by measuring reductions in the Psoriasis Area and Severity Index (PASI) after 12 or 16 wk of treatment. The PASI90 (the percentage of patients who achieved greater than a 90% reduction in their PASI score) for the anti-TNF-α agents (25.7–54.5%) is similar to or slightly less than the PASI90 for the anti-IL-23 agents (37–77%).[19] The PASI90 for the anti-IL-17 agents (59.2–70.9%) is comparable to the PASI90 for the anti-IL-23 biologics.[19] Thirty-to-forty percent of patients with moderate-to-severe psoriasis experience a clearance of skin lesions in response to treatment with some of these anti-IL-23 or anti-IL-17 biologics.[19] These results indicate a central role of the TNF-α/IL-23/IL-17A axis in the pathogenesis of psoriasis.

Auto-Ags in psoriasis

In psoriasis, IL-17A-producing Th17 cells and Tc17 cells emerge during DC/T cell Ag presentation in a TNF-α/IL-23-dependent fashion.[63,64] As a major histocompatibility Ag, HLA-C*0602 is strongly associated with a genetic predisposition to psoriasis, and several laboratories have focused their attention on autoantigens that are restricted to HLA-C*0602 and induce IL-17, leading to autoimmunity in psoriasis.[48,50] HLA-C*06:02 is present in more than 60% of psoriasis patients and is associated with an 8.9-fold increased risk in heterozygous carriers and a 23.1-fold increased risk in homozygous carriers, as well as an earlier onset of disease and a more severe disease course.[69] Although the auto-Ags that are responsible for the development of psoriasis are not fully understood, at least four have been identified in psoriasis, namely, LL-37 (cathelicidin), A disintegrin and metalloprotease domain containing thrombospondin type I motif-like 5 (ADAMTSL5), keratin 17, and lipid Ags that are generated by phospholipase A2 group IV D (PLA2G4D).[48–52]

LL-37 (cathelicidin)

LL-37 is an anti-microbial peptide of human cathelicidin that is produced when keratinocytes are injured by a broad range of bacteria.[70] The released LL-37 binds to the infiltrated neutrophils.[70] Neutrophils are a rich source of extracellular DNA due to their neutrophil extracellular traps.[71] Upon stimulation with complexes of host DNA and LL-37, plasmacytoid DCs produce large amounts of IFN-α.[72] Notably, LL-37 induces the proliferation of circulating CD3+ T cells in 24 out of 52 psoriasis patients (46%).[50] LL-37-reactive CD3+ T cells include both CD4+ and CD8+ T cells and express the skin-homing receptor cutaneous lymphocyte Ag.[50] LL-37 peptides bind to HLA-DR in DCs and are presented to CD4+ T cells, while LL-37 peptides and HLA-C*0602 complex has been demonstrated to activate CD8+ T cells.[50] The majority of LL-37-reactive CD3+ T cells produce IL-17 and the capacity of their IL-17 production is associated with disease severity. Interestingly, the LL-37-specific IL-17-producing T cells are exclusively CD4+ whereas the LL-37-specific CD8+ T cells do not produce IL-17.[50]

A disintegrin and metalloprotease domain containing thrombospondin type I motif-like 5 (ADAMTSL5)

Intraepidermal CD8+ T cells have been the focus of several research groups in psoriasis.[48,73–75] The intraepidermal CD8+ T cells are oligoclonal and use a restricted set of T cell receptor β chains.[73] The majority of epidermal CD8+ T cells also co-express α1β1 integrin.[74] In a xenotransplantation mouse model, the xenotransplanted nonlesional skin from a psoriasis patient gradually develops psoriatic lesions at 35 d posttransplant. The onset of the psoriatic epidermal changes occurs in parallel with the appearance of epidermal

T cells expressing α1β1 integrin.[74] Additionally, the blockade of α1β1 integrin by specific Abs inhibits the immigration of epidermal T cells and the development of psoriatic lesions in the xenotransplantation model.[74]

A recent study by Arakawa et al. demonstrated that intraepidermal CD8+ T cells recognize ADAMTSL5 on melanocytes in association with HLA-C*06:02.[48] In the epidermis, ADAMTSL5 is only expressed by the melanocytes.[48] Contact is observed between melanocytes and, on average, 37.2% of the intraepidermal CD8+ T cells in psoriasis. A synthetic ADAMTSL5 peptide increases the frequency of CD8+ T cells expressing IL-17A and IFN-γ in the peripheral blood mononuclear cells (PBMCs) in psoriasis patients, but the same effect is not found in healthy individuals.[48] Approximately one-third of psoriasis patients are HLA-C*06:02 negative, yet PBMCs from both HLA-C*06:02-positive and HLA-C*06:02-negative patients react similarly to ADAMTSL5 peptide stimulation, which suggests that HLA class I molecules other than HLA-C*06:02 may present ADAMTSL5 and promote melanocyte-specific autoimmunity.[48]

Keratin 17

The onset of acute guttate psoriasis is frequently associated with throat infections by group A β-hemolytic streptococci.[76] The streptococcal M-protein is a surface molecule of *Streptococcus* that has extensive amino acid sequence homology with human keratin 17.[77] The keratin 17 peptide induces a significantly higher number of IFN-γ-producing T cells in psoriasis patients than it does in healthy controls. This T cell response to the keratin 17 peptide is much stronger than its response to the M-protein peptide.[77] Shen et al. have confirmed that the keratin 17 peptide is a potent stimulator of IFN-γ production in the T cells of psoriasis patients,[78] which further indicates a molecular mimicry of the keratin 17 peptide by the streptococcal M-protein.[79] However, it is still not known if keratin 17-reactive T cells have the ability to produce IL-17A.

Yunushaeva et al. have also demonstrated that the proliferative response to full-length keratin 17 and its peptides is significantly increased in psoriasis patients when compared to healthy controls.[51] In their case series, the positive ratio of the HLA-C*06:02 allele is 53.85% in psoriasis patients and 14.29% in healthy controls. The HLA-C*06:02 allele dose is strongly associated with the T cell proliferative response to keratin 17 peptides.[51] In addition, endogenous proteins other than keratin 17, such as maspin, ezrin, PRDX2, hsp27, and potentially keratin 6 have been previously shown to act as auto-Ags in both the streptococcal-induced autoimmune response and in psoriasis.[80]

Neolipid Ags generated by PLA2G4D

PLA2G4D is found in psoriatic lesions but is absent in normal skin.[81] Mast cells are known to be the primary cellular source of PLA2G4D.[82] In patients who are comorbid with psoriasis and eczema, *PLA2G4D* expression is up-regulated in psoriatic lesions when compared to eczematous lesions.[82] PLA2 contributes to the generation of lipid metabolites such as arachidonic acids.[83] Cutaneous DCs, such as Langerhans cells, express CD1a and present lipid Ags to autoreactive T cells.[84] Bee venoms and house dust mites contain exogenous PLA2 activity and are known to activate CD1a-restricted T cells.[85,86]

In psoriasis, the number of CD1a-restricted autoreactive T cells in the blood is increased when compared to healthy controls.[52] Psoriatic skin lesions harbor increased numbers of these autoreactive T cells compared to nonlesional skin in psoriatic patients and healthy control skin.[52]

These autoreactive T cells respond in CD1a-dependent manner to fatty acids and lysophospholipids, all of which are generated by PLA2G4D.[52] These CD1a-restricted neolipid Ag-reactive T cells produce IL-17A, IFN-γ, and IL-22. Mast cells are the major cellular source of PLA2G4D and mast cell-derived exosomes deliver PLA2G4D to DCs.[37] These results suggest that lipid Ags may also be meaningful auto-Ags in the development of psoriasis

Conclusion

Psoriasis is a TNF-α/IL-23/IL-17A-driven inflammatory skin disease that is significantly affected by genetic (e.g., HLA-C*06:02) and environmental factors.[27] While the antigenic properties that lead to the development of psoriasis remain elusive, auto-Ags such as LL-37, ADAMTSL5, keratin 17, and neolipids are promising candidate molecules. Autoreactive T cells to these self-Ags are partly restricted to HLA-C*06:02 or CD1a. Moreover, the autoreactive T cells appear to include IL-17A-producing T cell clones. In a particular circumstance, the production of IL-17 may possibly occur in the very early post-presentation phases of the Ag and not always under the compulsory influence of IL-23. Considering a diverse plasticity of Th17 cells, the primed Th17 cells may differentiate into other types of helper T cells in different cytokine milieu in autoimmunity.[87] Further studies are required to elucidate the

precise role of these auto-Ags in the pathogenesis of psoriasis.

Declaration of conflicting interests

The author(s) declared no potential conflicts of interest with respect to the research, authorship, and/or publication of this article.

Funding

The author(s) disclosed receipt of the following financial support for the research, authorship, and/or publication of this article: This work was partly supported by grants from The Ministry of Health, Labour, and Welfare, Japan (H30-Shokuhin-Shitei-005) and The Leading Advanced Projects for Medical Innovation, Japan (LEAP).

ORCID iD

Masutaka Furue https://orcid.org/0000-0002-2967-1073

References

1. Boehncke WH and Schön MP. Psoriasis. *Lancet* 2015; 386: 983–994.
2. Krueger JG and Brunner PM. Interleukin-17 alters the biology of many cell types involved in the genesis of psoriasis, systemic inflammation and associated comorbidities. *Exp Dermatol* 2018; 27: 115–123.
3. Furue M, Yamazaki S, Jimbow K, et al. Prevalence of dermatological disorders in Japan: a nationwide, cross-sectional, seasonal, multicenter, hospital-based study. *J Dermatol* 2011; 38: 310–320.
4. Ogawa E, Okuyama R, Seki T, et al. Epidemiological survey of patients with psoriasis in Matsumoto city, Nagano Prefecture, Japan. *J Dermatol* 2018; 45: 314–317.
5. Ito T, Takahashi H, Kawada A, et al. Epidemiological survey from 2009 to 2012 of psoriatic patients in Japanese Society for Psoriasis Research. *J Dermatol* 2018; 45: 293–301.
6. Ichiyama S, Ito M, Funasaka Y, et al. Assessment of medication adherence and treatment satisfaction in Japanese patients with psoriasis of various severities. *J Dermatol* 2018; 45: 727–731.
7. Ergin T, Seckin Ozcoosmanoglu D, Alpsoy E, et al. Efficacy, safety and drug survival of conventional agents in pediatric psoriasis: a multicenter, cohort study. *J Dermatol* 2017; 44: 630–634.
8. Alpsoy E, Polat M, FetlahloGlu-Karaman B, et al. Internalized stigma in psoriasis: a multicenter study. *J Dermatol* 2017; 44: 885–891.
9. Takahashi H, Satoh K, Takagi A, et al. Economic burden of psoriatic patients in Japan: analysis from a single outpatient clinic. *J Dermatol* 2017; 44: 1024–1026.
10. Masaki S, Tatsukawa R, Ifryu M, et al. Treatment satisfaction, willingness to pay and quality of life in Japanese patients with psoriasis. *J Dermatol* 2017; 44: 143–146.
11. Imafuku S, Zheng M, Tada Y, et al. Asian consensus on assessment and management of mild to moderate plaque psoriasis with topical therapy. *J Dermatol* 2018; 45: 805–811.
12. Kishimoto M, Komine M, Hioki T, et al. Real-world use of apremilast for patients with psoriasis in Japan. *J Dermatol* 2018; 45: 1345–1348.
13. Meephansan J, Subpayasarn U, Poomkorn S, et al. Methotrexate, but not narrowband ultraviolet B radiation, suppresses interleukin-33 mRNA levels in psoriatic plaques and protein levels in serum of patients with psoriasis. *J Dermatol* 2018; 45: 322–325.
14. Morita A. Current developments in phototherapy for psoriasis. *J Dermatol* 2018; 45: 287–292.
15. Oh EH, Koh WS, Sim JM, et al. Clinical experience of cyclosporin treatment in patients with psoriasis and psoriatic arthritis. *J Dermatol* 2018; 45: 329–330.
16. Ohtsuki M, Okubo Y, Komine M, et al. Apremilast, an oral phosphodiesterase 4 inhibitor, in the treatment of Japanese patients with moderate to severe plaque psoriasis: efficacy, safety and tolerability results from a phase 2b randomized controlled trial. *J Dermatol* 2017; 44: 873–884.
17. Pongparit K, Chokunjaturmontri L, Limphoka P, et al. Effectiveness of and factors associated with clinical response to methotrexate under daily life conditions in Asian patients with psoriasis: a retrospective cohort study. *J Dermatol* 2018; 45: 540–545.
18. Usui K, Okubo Y, Hirano T, et al. Vitamin D3 derivatives, alone or in combination with glucocorticoids, suppress streptococcal pyrogenic enterotoxin A-stimulated proliferation of peripheral blood mononuclear cells in patients with psoriasis. *J Dermatol* 2017; 44: 567–572.
19. Furue K, Ito T and Furue M. Differential efficacy of biologic treatments targeting the TNF-α/IL-23/IL-17 axis in psoriasis and psoriatic arthritis. *Cytokine* 2018; 111: 182–188.
20. Ogawa E, Sato Y, Minagawa A, et al. Pathogenesis of psoriasis and development of treatment. *J Dermatol* 2018; 45: 264–272.
21. Hawkes JE, Chan TC and Krueger JG. Psoriasis pathogenesis and the development of novel targeted immune therapies. *J Allergy Clin Immunol* 2017; 140: 645–653.
22. Bayram B and Imafuku S. Relationship between environmental factors, age of onset and familial history in Japanese patients with psoriasis. *J Dermatol* 2018; 45: 715–718.
23. Elder JT. Expanded genome-wide association study meta-analysis of psoriasis expands the catalog of common psoriasis-associated variants. *J Investig Dermatol Symp Proc* 2018; 19: S77–S78.
24. Strange A, Capon F, Spencer CC, et al. A genome-wide association study identifies new psoriasis susceptibility loci and an interaction between HLA-C and ERAP1. *Nat Genet* 2010; 42: 985–990.
25. Zeng J, Luo S, Huang Y, et al. Critical role of environmental factors in the pathogenesis of psoriasis. *J Dermatol* 2017; 44: 863–872.

26. Yamamoto T, Ohtsuki M, Sano S, et al. Prevalence and current therapies of psoriatic arthritis in Japan: a survey by the Japanese Society of Psoriasis Research in 2016. *J Dermatol* 2017; 44: e121.
27. Furue K, Ito T, Tsuji G, et al. Autoimmunity and autoinflammatory co-morbidities in psoriasis. *Immunology* 2018; 154: 21–27.
28. Gál B, Dulic S, Kiss M, et al. Increased circulating anti-αvβ-integrin autoantibodies in psoriasis and psoriatic arthritis but not in rheumatoid arthritis. *J Dermatol* 2017; 44: 370–374.
29. Ho PH and Tsai TF. Development of bullous pemphigoid during secukinumab treatment for psoriasis. *J Dermatol* 2017; 44: e220–e221.
30. Matsuo H, Asahina A, Fukuda T, et al. Relapsing polychondritis associated with psoriasis vulgaris successfully treated with adalimumab: a case report with published work review. *J Dermatol* 2017; 44: 826–829.
31. Prinz JC. Autoimmune aspects of psoriasis: heritability and autoantigens. *Autoimmun Rev* 2017; 16: 970–979.
32. Chiyo S, Asahina A, Itoh Y, et al. New onset of psoriasis during nivolumab treatment for lung cancer. *J Dermatol* 2018; 45: e55–e56.
33. Itoi-Ochi S, Hayashi M, Yamaoka T, et al. Occult HIV infection in Japanese rupioid psoriasis. *J Dermatol* 2017; 44: e172–e173.
34. Murata S, Kaneko S, Harada Y, et al. Case of de novo psoriasis possibly triggered by nivolumab. *J Dermatol* 2017; 44: 99–100.
35. Furue M and Kadono T. "Inflammatory skin march" in atopic dermatitis and psoriasis. *Inflamm Res* 2017; 66: 833–842.
36. Guttman-Yassky E, Krueger JG and Lebwohl MG. Systemic immune mechanisms in atopic dermatitis and psoriasis with implications for treatment. *Exp Dermatol* 2018; 27: 409–417.
37. Honma M, Shibuya T, Iwasaki T, et al. Prevalence of coronary artery calcification in Japanese patients with psoriasis: a close correlation with bilateral diagonal earlobe creases. *J Dermatol* 2017; 44: 1122–1128.
38. Honma M, Shibuya T, Honma S, et al. Close correlation of bone mineral density and body mass index in Japanese psoriasis patients. *J Dermatol* 2017; 44: e1–e2.
39. Momose M, Asahina A, Fukuda T, et al. Evaluation of epicardial adipose tissue volume and coronary artery calcification in Japanese patients with psoriasis vulgaris. *J Dermatol* 2018; 45: 1349–1352.
40. Oh EH, Ro YS and Kim JE. Epidemiology and cardiovascular comorbidities in patients with psoriasis: a Korean nationwide population-based cohort study. *J Dermatol* 2017; 44: 621–629.
41. Wang CC, Tang CH, Huang KC, et al. Increased risk of incident psoriasis in end-stage renal disease patients on chronic hemodialysis: a nationwide population-based cohort study. *J Dermatol* 2018; 45: 1063–1070.
42. Asahina A, Kubo N, Umezawa Y, et al. Neutrophil-lymphocyte ratio, platelet-lymphocyte ratio and mean platelet volume in Japanese patients with psoriasis and psoriatic arthritis: response to therapy with biologics. *J Dermatol* 2017; 44: 1112–1121.
43. Minakawa S, Kaneko T, Matsuzaki Y, et al. Psoriasis Area and Severity Index is closely related to serum C-reactive protein level and neutrophil to lymphocyte ratio in Japanese patients. *J Dermatol* 2017; 44: e236–e237.
44. Gkalpakiotis S, Arenbergerova M, Gkalpakioti P, et al. Impact of adalimumab treatment on cardiovascular risk biomarkers in psoriasis: results of a pilot study. *J Dermatol* 2017; 44: 363–369.
45. Takamura S, Takahashi A, Inoue Y, et al. Effects of tumor necrosis factor-α, interleukin-23 and interleukin-17A inhibitors on bodyweight and body mass index in patients with psoriasis. *J Dermatol* 2018; 45: 1130–1134.
46. Fan X, Yang S, Sun LD, et al. Comparison of clinical features of HLA-Cw*0602-positive and -negative psoriasis patients in a Han Chinese population. *Acta Derm Venereol* 2007; 87: 335–340.
47. Wu D, Wu Y, Liu JL, et al. Association between HLA-Cw*0602 polymorphism and psoriasis risk: a meta-analysis. *Genet Mol Res* 2011; 10: 3109–3120.
48. Arakawa A, Siewert K, Stöhr J, et al. Melanocyte antigen triggers autoimmunity in human psoriasis. *J Exp Med* 2015; 212: 2203–2212.
49. Fuentes-Duculan J, Bonifacio KM, Hawkes JE, et al. Autoantigens ADAMTSL5 and LL37 are significantly upregulated in active Psoriasis and localized with keratinocytes, dendritic cells and other leukocytes. *Exp Dermatol* 2017; 26: 1075–1082.
50. Lande R, Botti E, Jandus C, et al. The antimicrobial peptide LL37 is a T-cell autoantigen in psoriasis. *Nat Commun* 2014; 5: 5621.
51. Yunusbaeva M, Valiev R, Bilalov F, et al. Psoriasis patients demonstrate HLA-Cw*06:02 allele dosage-dependent T cell proliferation when treated with hair follicle-derived keratin 17 protein. *Sci Rep* 2018; 8: 6098.
52. Cheung KL, Jarrett R, Subramaniam S, et al. Psoriatic T cells recognize neolipid antigens generated by mast cell phospholipase delivered by exosomes and presented by CD1a. *J Exp Med* 2016; 213: 2399–2412.
53. Lowes MA, Russell CB, Martin DA, et al. The IL-23/T17 pathogenic axis in psoriasis is amplified by keratinocyte responses. *Trends Immunol* 2013; 34: 174–181.
54. Guttman-Yassky E and Krueger JG. IL-17C: a unique epithelial cytokine with potential for targeting across the spectrum of atopic dermatitis and psoriasis. *J Invest Dermatol* 2018; 138: 1467–1469.
55. Papp KA, Merola JF, Gottlieb AB, et al. Dual neutralization of both interleukin 17A and interleukin 17F with bimekizumab in patients with psoriasis: results from BE ABLE 1, a 12-week randomized, double-blinded, placebo-controlled phase 2b trial. *J Am Acad Dermatol* 2018; 79: 277–286.
56. Krueger JG, Fretzin S, Suárez-Fariñas M, et al. IL-17A is essential for cell activation and inflammatory gene circuits in subjects with psoriasis. *J Allergy Clin Immunol* 2012; 130: 145–154.

57. Ha HL, Wang H, Pisitkun P, et al. IL-17 drives psoriatic inflammation via distinct, target cell-specific mechanisms. *Proc Natl Acad Sci USA* 2014; 111: E3422–E3431.
58. Peters JH, Teabridge GS, Fasse E, et al. Co-culture of healthy human keratinocytes and T-cells promotes keratinocyte chemokine production and RORγt-positive IL-17 producing T-cell populations. *J Dermatol Sci* 2013; 69: 44–53.
59. Liu Y, Lagowski JP, Gao S, et al. Regulation of the psoriatic chemokine CCL20 by E3 ligases Trim32 and Pirh2 in keratinocytes. *J Invest Dermatol* 2010; 130: 1384–1390.
60. Nograles KE, Zaba LC, Guttman-Yassky E, et al. Th17 cytokines interleukin (IL)-17 and IL-22 modulate distinct inflammatory and keratinocyte-response pathways. *Br J Dermatol* 2008; 159: 1092–1102.
61. Cheng S, Chen H, Wang A, et al. Blockade of IL-23 ameliorates allergic lung inflammation via decreasing the infiltration of Tc17 cells. *Arch Med Sci* 2016; 12: 1362–1369.
62. Lowes MA, Suárez-Fariñas M and Krueger JG. Immunology of psoriasis. *Annu Rev Immunol* 2014; 32: 227–255.
63. Zaba LC, Cardinale I, Gilleaudeau P, et al. Amelioration of epidermal hyperplasia by TNF inhibition is associated with reduced Th17 responses. *J Exp Med* 2007; 204: 3183–3194.
64. Brunner PM, Koszik F, Reininger B, et al. Infliximab induces downregulation of the IL-12/IL-23 axis in 6-sulfo-LacNac (slan)+-dendritic cells and macrophages. *J Allergy Clin Immunol* 2013; 132: 1184–1193.
65. Martin G, Guérard S, Fortin MM, et al. Pathological crosstalk in vitro between T lymphocytes and lesional keratinocytes in psoriasis: necessity of direct cell-to-cell contact. *Lab Invest* 2012; 92: 1058–1070.
66. Teng MW, Bowman EP, McElwee JJ, et al. IL-12 and IL-23 cytokines: from discovery to targeted therapies for immune-mediated inflammatory diseases. *Nat Med* 2015; 21: 719–729.
67. Lee E, Trepicchio WL, Oestreicher JL, et al. Increased expression of interleukin 23 p19 and p40 in lesional skin of patients with psoriasis vulgaris. *J Exp Med* 2004; 199: 125–130.
68. Lowes MA, Chamian F, Abello MV, et al. Increase in TNF-alpha and inducible nitric oxide synthase-expressing dendritic cells in psoriasis and reduction with efalizumab (anti-CD11a). *Proc Natl Acad Sci USA* 2005; 102: 19057–19062.
69. Gudjonsson JE, Karason A, Antonsdottir A, et al. Psoriasis patients who are homozygous for the HLA-Cw*0602 allele have a 2.5-fold increased risk of developing psoriasis compared with Cw6 heterozygotes. *Br J Dermatol* 2003; 148: 233–235.
70. Dorschner RA, Pestonjamasp VK, Tamakuwala S, et al. Cutaneous injury induces the release of cathelicidin antimicrobial peptides active against group A *Streptococcus*. *J Invest Dermatol* 2001; 117: 91–97.
71. Hu SC, Yu HS, Yen FL, et al. Neutrophil extracellular trap formation is increased in psoriasis and induces human β-defensin-2 production in epidermal keratinocytes. *Sci Rep* 2016; 6: 31119.
72. Lande R, Gregorio J, Facchinetti V, et al. Plasmacytoid dendritic cells sense self-DNA coupled with antimicrobial peptide. *Nature* 2007; 449: 564–569.
73. Chang JC, Smith LR, Froning KJ, et al. CD8+ T cells in psoriatic lesions preferentially use T-cell receptor V beta 3 and/or V beta 13.1 genes. *Proc Natl Acad Sci USA* 1994; 91: 9282–9286.
74. Conrad C, Boyman O, Tonel G, et al. Alpha1beta1 integrin is crucial for accumulation of epidermal T cells and the development of psoriasis. *Nat Med* 2007; 13: 836–842.
75. Di Meglio P, Villanova F, Navarini AA, et al. Targeting CD8(+) T cells prevents psoriasis development. *J Allergy Clin Immunol* 2016; 138: 274–276.
76. Telfer NR, Chalmers RJ, Whale K, et al. The role of streptococcal infection in the initiation of guttate psoriasis. *Arch Dermatol* 1992; 128: 39–42.
77. Gudmundsdottir AS, Sigmundsdottir H, Sigurgeirsson B, et al. Is an epitope on keratin 17 a major target for autoreactive T lymphocytes in psoriasis? *Clin Exp Immunol* 1999; 117: 580–586.
78. Shen Z, Wang G, Fan JY, et al. HLA-DR B1*04, *07-restricted epitopes on keratin 17 for autoreactive T cells in psoriasis. *J Dermatol Sci* 2005; 38: 25–39.
79. Valdimarsson H, Thorleifsdottir RH, Sigurdardottir SL, et al. Psoriasis: as an autoimmune disease caused by molecular mimicry. *Trends Immunol* 2009; 30: 494–501.
80. Besgen P, Trommler P, Vollmer S, et al. Ezrin, maspin, peroxiredoxin 2, and heat shock protein 27: potential targets of a streptococcal-induced autoimmune response in psoriasis. *J Immunol* 2010; 184: 5392–402.
81. Chiba H, Michibata H, Wakimoto K, et al. Cloning of a gene for a novel epithelium-specific cytosolic phospholipase A2, cPLA2delta, induced in psoriatic skin. *J Biol Chem* 2004; 279: 12890–12897.
82. Quaranta M, Knapp B, Garzorz N, et al. Intraindividual genome expression analysis reveals a specific molecular signature of psoriasis and eczema. *Sci Transl Med* 2014; 6: 244ra90.
83. Leslie CC. Regulation of the specific release of arachidonic acid by cytosolic phospholipase A2. *Prostaglandins Leukot Essent Fatty Acids* 2004; 70: 373–376.
84. de Jong A, Peña-Cruz V, Cheng TY, et al. CD1a-autoreactive T cells are a normal component of the human αβ T cell repertoire. *Nat Immunol* 2010; 11: 1102–1109.
85. Bourgeois EA, Subramaniam S, Cheng TY, et al. Bee venom processes human skin lipids for presentation by CD1a. *J Exp Med* 2015; 212: 149–163.
86. Jarrett R, Salio M, Lloyd-Lavery A, et al. Filaggrin inhibits generation of CD1a neolipid antigens by house dust mite-derived phospholipase. *Sci Transl Med* 2016; 8: 325ra18.
87. Stadhouders R, Lubberts E, Hendriks RW. A cellular and molecular view of T helper 17 cell plasticity in autoimmunity. *J Autoimmun* 2018; 87: 1–15.

INTERNAL MEDICINE

REVIEW ARTICLE

Cardiovascular and Metabolic Diseases Comorbid with Psoriasis: Beyond the Skin

Masataka Furue[1], Gaku Tsuji[1], Takahito Chiba[1] and Takafumi Kadono[2]

Abstract

A close association of systemic inflammation with cardiovascular diseases and metabolic syndrome is recently a popular topic in medicine. Psoriasis is a chronic inflammatory skin disease with a prevalence of approximately 0.1-0.5% in Asians. It is characterized by widespread scaly erythematous macules that cause significant physical and psychological burdens for the affected individuals. The accelerated inflammation driven by the TNF-α/IL-23/IL-17A axis is now known to be the major mechanism in the development of psoriasis. Psoriasis is not a mere skin disease; it is significantly associated with cardiovascular diseases and metabolic syndrome, which suggests that the chronic skin inflammation extends the systemic inflammation beyond the skin. In this article, we review the epidemiological and pathological aspects of psoriasis and its comorbidities.

Key words: psoriasis, cardiovascular disease, metabolic syndrome, tumor necrosis factor α, interleukin 23, interleukin 17

(Intern Med 56: 1613-1619, 2017)
(DOI: 10.2169/internalmedicine.56.8209)

Introduction

The close association of systemic inflammation with cardiovascular diseases (CVD) and metabolic syndrome is a recent topic in medicine (1-3). Inflammatory skin diseases such as psoriasis are an integral part of diseases causing systemic inflammation (4). Psoriasis is a common immune-mediated chronic inflammatory skin disease that is characterized by the altered proliferation and differentiation of keratinocytes, vascular remodeling and inflammation in the skin (Figure). Psoriasis shows a diverse prevalence across populations worldwide: 2.5% in Europeans, 0.05-3% in Africans and 0.1-0.5% in Asians (5-8). Psoriasis patients comprise 4.43% of all Japanese dermatological patients (8). Men are likely to experience a higher severity of the disease than women are. Phenotypic heterogeneity of psoriasis has also been reported among ethnic populations. Small plaque psoriasis is specific to Asian populations, while severe psoriasis is more predominant in Western populations (5-8). Recent genome-wide association studies have identified numerous risk-associated variants within 44 susceptibility loci for psoriasis, including *HLA-C*06:02*, *LCE3D*, *IL23R* and *CARD14*. *HLA-C*12:02* may be a susceptibility locus for late-onset psoriasis in the Japanese population (5, 9-11). These susceptibility genes are predominantly related to the innate and adaptive immune systems and skin barrier functions (5, 9).

Pathogenesis of Psoriasis

Like other forms of systemic inflammation, tumor necrosis factor (TNF)-α is a key pro-inflammatory cytokine in psoriasis because its inhibitor significantly improves coronary microvascular dysfunction and levels of highly sensitive C-reactive protein, as well as ameliorates psoriatic symptoms (12). In addition, recent therapeutic success with other biologics seems to have revealed the pivotal role of the TNF-α/interleukin (IL)-23/IL-17 axis in the pathogenesis of psoriasis (Figure). The initial trigger of psoriasis is thought to be the activation of plasmacytoid dendritic cells (DCs) being stimulated by complexes of host DNA and the antimicrobial peptide LL-37 (cathelicidin), which are produced by keratinocytes after minor injuries (8, 13-15). Activated plasmacytoid DCs and damaged keratinocytes produce interferon (IFN)-α and TNF-α, which results in the further

[1]Department of Dermatology, Kyushu University, Japan and [2]Department of Dermatology, St. Marianna University School of Medicine, Japan
Received for publication August 31, 2016; Accepted for publication October 26, 2016
Correspondence to Dr. Masataka Furue, furue@dermatol.med.kyushu-u.ac.jp

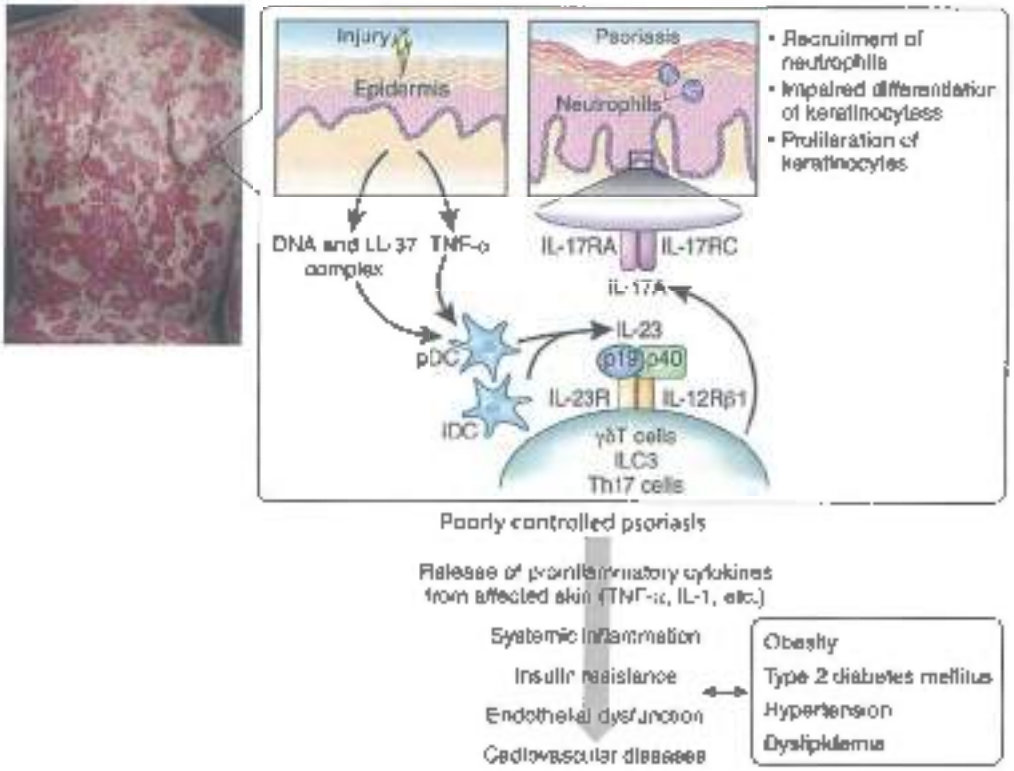

Figure. Pathophysiology of psoriasis and its comorbidities (simplified model modified from references 5, 8 and 47). The initial trigger of psoriasis is thought to be the activation of plasmacytoid dendritic cells (pDCs) by complexes of host DNA and the antimicrobial peptide LL-37 (cathelicidin) produced by keratinocytes after minor injuries. Plasmacytoids and recruited inflammatory DCs (pDCs and iDCs) produce TNF-α, IL-12 and IL-23. IL-23 is critically involved in the generation and activation of IL-17-producing effector cells. In humans and experimental psoriasis models, γδT cells (Vγ9Vδ2 T cells in human), innate lymphoid cells type 3 (ILC3) and Th17 cells are detected in the lesional skin and blood, and these cells readily produce IL-17A. IL-17A binds to the IL-17 receptor (IL-17R), which is composed of IL-17RA and IL-17RC. IL-17A upregulates the proliferation and downregulates the differentiation of keratinocytes and also enhances the recruitment of neutrophils and aids in the crosstalk between neutrophils and keratinocytes. Chronically released proinflammatory cytokines (e.g., TNF-α, IL-1) from poorly controlled psoriatic skin to the circulatory system potentiates and perpetuates the systemic inflammation and induces insulin resistance, endothelial dysfunction and cardiovascular diseases. This systemic inflammation also causes obesity, hypertension, dyslipidemia and type 2 diabetes mellitus. These systemic involvements interact with each other to increase the mortality for psoriatic patients from cardiovascular diseases.

production of TNF-α, IL-12 and IL-23 by plasmacytoids and recruited inflammatory DCs (8, 14, 15) (Figure). IL-12 promotes the differentiation of naive CD4+ T cells into IFN-γ-producing T helper (Th) 1 cells. IL-23 is critically involved in the generation and activation of IL-17-producing effector cells (13, 15, 16) (Figure). In humans and experimental models of psoriasis, γδT cells (Vγ9Vδ2 T cells in human), innate lymphoid cells type 3 (ILC3) and Th17 cells are detected in blood and lesional skin. These cells readily produce IL-17A and IL-22 (8, 17, 18). IL-17A binds to the IL-17 receptor (IL-17R), which is composed of IL-17RA and IL-17RC (19) (Figure). IL-17A upregulates the proliferation of keratinocytes and downregulates its differentiation (20) and also enhances the recruitment of neutrophils and aids in the crosstalk between neutrophils and keratinocytes by upregulating the neutrophil-attractive chemokines CXCL8 and CXCL1 (21). IL-17A promotes the expression of TNF-α by keratinocytes (19), which indicates that the above-mentioned TNF-α/IL-23/IL-17 axis likely forms a vicious loop in the development of psoriasis lesions (Figure). The mechanistic hypothesis coincides with the fact that antibodies against TNF-α, IL-23(p19), IL-23(p40), IL-23R, IL-17A or IL-17RA exert remarkable clinical effects on psoriasis both in Caucasian and Asian ethnicities (8, 22-31). In contrast, the decisive pathogenic roles of IL-12, IFN-γ and IL-22 in psoriasis remain elusive, as clinical trials of the anti-IL-12 p35-p40 antibody (SMART), anti-IFN-γ antibody (HuZAF) and anti-IL-22 antibody (fezakinumab) have been discontinued (8).

Table 1. Comorbidity of Cardiovascular Diseases in Psoriasis.

References	Subjects	Brief description
Ref 41	Meta-analysis of 14 cohorts	Risk ratio relative to general population Cardiovascular disease mortality, 1.37 (95% CI: 1.17-1.60) Myocardial infarction: 3.04 (95% CI 0.65-14.35) Stroke: 1.59 (95% CI 1.34-1.89)
Ref 42	Germany cross-sectional study (n=4,185) German Health Insurance beneficiaries (n=1,811,098)	Adjusted odds ratio Myocardial infarction: 2.26 (95% CI 1.03-4.96)
Ref 43	Control patients (n=586,995) Mild psoriasis (n=127,139) Severe psoriasis (n=3,847)	Adjusted relative risk in a 30-year old patient Myocardial infarction in mild psoriasis: 1.29 (95% CI 1.14-1.46) Myocardial infarction in severe psoriasis: 3.10 (95% CI 1.98-4.86)
Ref 44	Control patients (n=14,370) Severe psoriasis (n=3,503)	Adjusted relative risk in a 40-year old patient Cardiovascular mortality in severe psoriasis: 2.69 (95% CI 1.28-4.69)
Ref 46	Prospective study for 5.2 years follow-up Control patients (n=208,187) Psoriasis (n=48,523)	Fully adjusted hazard ratio Cardiovascular events: 1.02 (95% CI 0.98-1.08)
Ref 47	Hospital-based patients (n=1,3,985)	Adjusted odds ratio Coronary heart disease: 1.27 (95% CI 1.01-1.58) Hypertension: 3.78 (95% CI 2.25-6.35)
Ref 61	Control patients (n=24,283) Psoriasis (n=12,502)	Adjusted odds ratio Hypertension: 1.33 (95% CI 1.24-1.45)

High Clinical Burden in Psoriasis

Both the physical and psychological quality of life are significantly impaired in all populations of psoriasis sufferers (32-35), and patients' adherence to medication regimens and satisfaction with their results are very poor (36). The disease burden of psoriasis is further increased by its association with psoriatic arthritis, which is characterized by seronegative spondyloarthropathies, enthesitis and elevated C-reactive protein levels (5, 37-39). Approximately 15-30% of Caucasians with psoriasis eventually develop psoriatic arthritis (37). Although the prevalence is lower in Asian populations (Chinese 5.3-7.3%, Japanese 10.5% and Korean 11.2%), psoriatic arthritis significantly hampers patients' daily lives (37, 40). Additionally, psoriasis has significant comorbidity with CVD and metabolic syndrome.

Comorbidity with Cardiovascular Diseases

A recent meta-analysis and systematic review of 14 cohorts identified a CVD risk in individuals with severe psoriasis (defined as requiring systemic therapy or hospital admission): the risk ratio relative to the general population was 1.37 [95% confidence interval (CI): 1.17-1.60] for CVD mortality, 3.04 (95% CI: 0.65-14.35) for myocardial infarction and 1.59 (95% CI: 1.34-1.89) for stroke (41) (Table 1). The relative risks of CVD were highest in younger, more severe psoriasis patients [3.10 (95% CI: 1.98-4.86) for myocardial infarction at 30 years of age], and the absolute risks were greatest in older individuals with severe psoriasis (23.2 excess myocardial infarctions per 10,000 person-years at 60 years of age) (41). A German cross-sectional study that included 4,185 patients with psoriasis and a prospective cohort of German Health Insurance beneficiaries (n=1,811,098) showed that psoriasis was significantly associated with myocardial infarction (odds ratio: 2.26; 95% CI: 1.03-4.96) (42). In a longitudinal study, psoriasis slightly increased the incident risk for myocardial infarction (relative risk: 1.14; 95% CI: 1.06-1.22), with the highest risk increments found in systemically treated psoriasis, which accounted for 17 excess cases of myocardial infarctions per 10,000 person-years (42). A significantly higher risk of myocardial infarction has been observed in psoriasis patients in the United Kingdom (43). For example, for a 30-year-old patient with mild or severe psoriasis, the adjusted relative risk of having a myocardial infarction is 1.29 (95% CI: 1.14-1.46) or 3.10 (95% CI: 1.98-4.86), respectively, compared with the control population (43). Furthermore, patients with severe psoriasis have an increased risk of CVD mortality that is independent of traditional CVD risk factors (44, 45). In a prospective cohort study that included 48,523 patients with psoriasis and 208,187 controls in the United Kingdom, 1,257 patients with psoriasis (2.59%) had a major CVD, compared with 4,784 controls (2.30%), during a median follow-up of 5.2 years (46). A multivariable analysis showed that the patients with psoriasis had significantly higher incidence of CVD than did the controls, with a hazard ratio (HR) 1.37 (95% CI: 1.29-1.45) for hypertension, HR 2.74 (95% CI: 2.41-3.12) for transient ischemic attack, HR 1.54 (95% CI: 1.36-1.73) for atrial fibrillation, HR 1.23 (95% CI: 1.05-1.44) for valvular heart disease, HR 1.32 (95% CI: 1.17-1.49) for thromboembolism and HR 1.57 (95% CI: 1.39-1.78) for congestive heart failure. The age- and gender-adjusted HRs of a major CVD for psoriasis were 1.10 (95% CI: 1.04-1.17) and 1.40 (95% CI: 1.07-1.84) for severe psoriasis (46).

A hospital-based study conducted by Shiba et al. in Japan analyzed the prevalence of coronary heart disease (n=5,167, 4.5%), hypertension (n=16,476, 14.5%), dyslipidemia (n=9,236, 8.1%), diabetes mellitus (n=11,555, 10.2%) and peo-

Table 2. Comorbidity of Metabolic Syndrome in Psoriasis.

References	Subjects	Brief description
Ref.42	German cross-sectional study (n=4,185) German Health Insurance beneficiaries (n=1,811,998)	Adjusted odds ratio Diabetes mellitus, 2.36 (95% CI 1.26-4.41)
Ref.48	Control patients (n=14,370) Psoriasis (n=3,603)	Adjusted hazard ratio Mortality from diabetes mellitus, 2.86 (95% CI 1.06-2.96)
Ref.46	Prospective study for 3.2 years follow-up Control patients (n=206,167) Psoriasis (n=49,523)	Adjusted hazard ratio Diabetes mellitus, 1.18 (95% CI 1.06-1.31)
Ref.47	Hospital and clinic patients (n=113,065)	Adjusted odds ratio Diabetes mellitus, 2.86 (95% CI 2.67-3.06) Dyslipidemia, 2.35 (95% CI 2.19-2.52)
Ref.51	Control patients (n=14,095) Severe psoriasis (n=1,954)	Adjusted odds ratio in severe psoriasis Diabetes mellitus, 1.62 (95% CI 1.3-2.02) Obesity, 1.79 (95% CI 1.55-2.06)
Ref.52	Control patients (n=6,543) Psoriasis (n=543)	Adjusted odds ratio Diabetes mellitus: 1.5 (95% CI 1.2-2.0) Dyslipidemia, 1.3 (95% CI 1.0-1.6) Obesity, 1.3 (95% CI 1.0-1.7)
Ref.55	Control patients (n=71,937) Psoriasis (n=36,851)	Adjusted odds ratio Diabetes mellitus, 1.58 (95% CI 1.48-1.68)
Ref.56	Danish population based twin study (n=3,751 pairs)	Odds ratio Diabetes mellitus, 1.53 (95% CI 1.14-2.27) Obesity, 1.81 (95% CI 1.28-2.55)
Ref.57	Control patients (n=16,028) Psoriasis (n=429)	Odds ratio Obesity, 2.25 (95% CI 1.57-3.22)
Ref.60	Control patients (n=22,946) Psoriasis (n=11,669)	Adjusted odds ratio Dyslipidemia, 1.19 (95% CI 1.12-1.26)

riasis (n=1,197, 1.1%) in 113,065 patients (47). Their multivariate analysis showed that psoriasis was an independent variable associated with coronary heart disease (adjusted odds ratio; 1.27; 95% CI; 1.01-1.58; p=0.0404), hypertension (7.78; 95% CI; 7.25-8.36; p<0.0001), dyslipidemia (2.35; 95% CI; 2.19-2.52; p<0.0001) and diabetes (2.86; 95% CI; 2.67-3.06; p<0.0001) (47).

Comorbidity with Metabolic Syndrome

The association of psoriasis with metabolic syndrome (obesity, glucose intolerance, hypertension and dyslipidemia) has also been well documented (48, 49). As Henseler and Christophers reported in an earlier study (50), obesity and type 2 diabetes mellitus are significantly associated with psoriasis in the United Kingdom (51), Israel (52, 53), Italy (54), Germany (55) and Denmark (56) (Table 2). These results have been consistent with those for psoriasis patients in Japan (57), Korea (58) and Thailand (59). Psoriasis is also comorbid with other components of metabolic syndrome, such as dyslipidemia (51, 52, 60) and hypertension (51, 52, 55, 61). Furthermore, a significant association of psoriasis with dyslipidemia (58) and hypertension (59) has been reported in Asian populations. Moreover, patients with severe psoriasis had a higher prevalence of diabetes (51) and obesity (51) than did those with mild psoriasis. In this context, it is intriguing that dipeptidyl peptidase-4 inhibitors, a new class of antidiabetic agents, have been shown to improve skin symptoms in some psoriasis patients (62). Because topical vitamin D3 application is effective in treating psoriasis (63), the vitamin D3 level and bone mineral density have been assessed (64, 65). In those studies, the serum level of vitamin 25(OH)D3 was inversely correlated with the severity of psoriasis (64). Patients with a low bone mineral density showed a statistically significant longer average duration of psoriasis than those with better bone density (65).

Pathophysiology of Comorbidity

As mentioned above, psoriasis is a chronic inflammatory skin disease driven by the TNF-α/IL-23/IL-17 axis (1, 4, 10). This notion is well supported by the high clinical efficacy of biologics against the TNF-α/IL-23/IL-17 pathway (5, 8, 15, 66). The release of excessive amounts of proinflammatory cytokines such as TNF-α and IL-1 may cause chronic low-grade systemic inflammation (67, 68) (Figure). The chronic state of inflammation appears to be a central mechanism underlying the pathophysiology of insulin resistance, visceral adiposity, hypertension and dyslipidemia. All of these conditions increase the risk for the development of type 2 diabetes and cardiovascular disease (67-69) (Figure). Consistent with this hypothesis, subclinical systemic and vascular inflammation have been detected by ^{18}F-fluorodeoxyglucose positron emission tomography/computed tomography in patients with psoriasis (70). In a six-month prospective study, carotid arterial stiffness in patients with psoriasis was significantly improved by anti-

TNF-α therapy (71). In addition, other markers for systemic inflammation such as asymmetric dimethylarginine, red blood cell distribution width, the neutrophil-to-lymphocyte ratio, and the platelet-to-lymphocyte ratio, have proven to be upregulated in psoriatic patients (72-74).

In parallel with the above notions, the blockade of TNF-α by etanercept (anti-TNF-α treatment) improves the glucose tolerance in obese diabetic Zucker rats (75). Anti-TNF-α treatment with etanercept also suppresses cerebral damage caused by middle cerebral artery occlusion/reperfusion in both normal and diabetic rats (76). Furthermore, the inhibition of TNF-α production by a thalidomide analog decreases triglyceride levels and increases high-density lipoprotein levels in rats fed hypercholesterolemic diets (77).

Conclusion

Although the pathomechanisms of psoriasis are not fully understood, increasing research attention is being paid to the cutaneous-to-systemic expansion of the inflammatory process, which is now identified as the "psoriatic march" or "inflammatory skin march" (67, 68). This systemic inflammatory expansion is also seen in patients with severe eczema who have an increased risk for CVD (78). Another important fact related to "inflammatory skin march" is the significant association of psoriasis with other immune-mediated or autoimmune diseases such as inflammatory bowel disease (79, 80), multiple sclerosis (81) and autoimmune hepatitis (82). In addition, frequent comorbidity is noted in psoriasis and autoimmune bullous diseases (83-86). Further immunological studies into the genuine master switch underlying the comorbidity are warranted.

Finally, a disfigured appearance because of psoriasis may affect the psychological stability of patients (89). The cosmetic disfigurement associated with psoriasis increases the risk of depression, anxiety, feeling stigmatized and self-harm ideation, which profoundly impairs their satisfaction and adherence to medical care (36, 89, 90). In addition, internal physicians may hesitate to perform electrocardiogram, echocardiogram and even blood examinations, especially in severe cases with extensive skin eruption. These undesirable factors may delay the correct diagnosis and treatment of comorbid CVD and metabolic syndromes. As anti-TNF-α treatment is feasible for managing both skin lesions and comorbidities in psoriasis (12, 66), the early diagnosis and appropriate intervention by internal physicians in cooperation with dermatologists is required in order to increase the physical and mental quality of life in psoriatic patients.

The authors state that they have no Conflict of Interest (COI).

References

1. Libby P, Nahrendorf M, Swirski FK. Leukocytes link local and systemic inflammation in ischemic cardiovascular disease: an expanded "cardiovascular continuum". J Am Coll Cardiol 67: 1091-1103, 2016.
2. de Souza Bastos A, Graves DT, de Melo Loureiro AP, et al. Diabetes and increased lipid peroxidation are associated with systemic inflammation even in well-controlled patients. J Diabetes Complications 30: 1593-1599, 2016.
3. Herder C, Farch K, Carstensen-Kirberg M, et al. Biomarkers of subclinical inflammation and increases in glycaemia, insulin resistance and beta-cell function in non-diabetic individuals: the Whitehall II study. Eur J Endocrinol 175: 367-377, 2016.
4. Joshi AA, Lerman JB, Aberra TM, et al. GlycA is a novel biomarker of inflammation and subclinical cardiovascular disease in psoriasis. Circ Res pii: CIRCRESAHA.116.309657, 2016.
5. Boehncke WH, Schön MP. Psoriasis. Lancet 386: 983-994, 2015.
6. Yin X, Low HQ, Wang L, et al. Genome-wide meta-analysis identifies multiple novel associations and ethnic heterogeneity of psoriasis susceptibility. Nat Commun 6: 6916, 2015.
7. Kim J, Oh CH, Jeon J, et al. Molecular phenotyping small (Asian) versus large (Western) plaque psoriasis shows common activation of IL-17 pathway genes but different regulatory gene sets. J Invest Dermatol 136: 161-172, 2016.
8. Furue M, Kadono T. Psoriasis: behind the scenes. J Dermatol 43: 4-8, 2016.
9. Bauerchi H, Hoxer M, Brand S, et al. Genome-wide comparative analysis of atopic dermatitis and psoriasis gives insights into opposing genetic mechanisms. Am J Hum Genet 96: 104-120, 2015.
10. Mabuchi T, Ota T, Manabe Y, et al. *HLA-C*12:02* is a susceptibility factor in late-onset type of psoriasis in Japanese. J Dermatol 41: 697-704, 2014.
11. Feng C, Wang T, Li SJ, Fan YM, Shi G, Zhu KJ. *CARD14* gene polymorphism c.C2458T (p.Arg820Trp) is associated with clinical features of psoriasis vulgaris in a Chinese cohort. J Dermatol 43: 294-297, 2016.
12. Piaggio S, Oato B, Famoso G, et al. Treatment with tumor necrosis factor inhibitors restores coronary microvascular function in young patients with severe psoriasis. Atherosclerosis 251: 25-30, 2016.
13. Teng MW, Bowman EP, McElwee JJ, et al. IL-12 and IL-23 cytokines: from discovery to targeted therapies for immune-mediated inflammatory diseases. Nat Med 21: 719-729, 2015.
14. Lande R, Gregorio J, Facchinetti V, et al. Plasmacytoid dendritic cells sense self-DNA coupled with antimicrobial peptide. Nature 449: 564-569, 2007.
15. Lowes MA, Suárez-Fariñas M, Krueger JG. Immunology of psoriasis. Annu Rev Immunol 32: 227-255, 2014.
16. McGeachy MJ, McSorley SJ. Microbial-induced Th17: superhero or supervillain? J Immunol 189: 3285-3291, 2012.
17. Ramírez-Valle F, Gray EE, Cyster JG. Inflammation induces dermal Vγ4+ γδT17 memory-like cells that travel to distant skin and accelerate secondary IL-17-driven responses. Proc Natl Acad Sci USA 112: 8046-8051, 2015.
18. Teunissen MB, Yeremenko NG, Baeten DL, et al. The IL-17A-producing CD8+ T-cell population in psoriatic lesional skin comprises mucosa-associated invariant T cells and conventional T cells. J Invest Dermatol 134: 2898-2907, 2014.
19. Iwakura Y, Ishigame H, Saijo S, Nakae S. Functional specialization of interleukin-17 family members. Immunity 34: 149-162, 2011.
20. Ha HL, Wang H, Pisitkun P, et al. IL-17 drives psoriatic inflammation via distinct, target cell-specific mechanisms. Proc Natl Acad Sci USA 111: E3422-E3431, 2014.
21. Reich K, Papp KA, Matheson RT, et al. Evidence that a neutrophil keratinocyte crosstalk is an early target of IL-17A inhibition in psoriasis. Exp Dermatol 24: 529-533, 2015.
22. Torii H, Terui T, Matsukawa M, et al. Safety profiles and efficacy of infliximab therapy in Japanese patients with plaque psoriasis with or without psoriatic arthritis, pustular psoriasis or psoriatic

erythrodermic results from the prospective post-marketing surveillance. J Dermatol 43: 767-778, 2016.
23. Asahina A, Torii H, Ohtsuki M, et al. Safety and efficacy of adalimumab treatment in Japanese patients with psoriasis: results of SALSA study. J Dermatol 43: 1257-1266, 2016.
24. Asahina A, Ohtsuki M, Etoh T, et al. Adalimumab treatment optimization for psoriasis: results of a long-term phase 2/3 Japanese study. J Dermatol 42: 1042-1052, 2015.
25. Kawakami H, Matsumoto Y, Abe N, et al. Perioperative management of tumor necrosis factor-alpha blocker-treated psoriatic patients: case reports and review. J Dermatol 43: 190-193, 2016.
26. Kawakami H, Maeda T, Abe N, et al. Efficacy of adalimumab and methotrexate combination therapy on generalized pustular psoriasis patients unresponsive to infliximab monotherapy due to anti-infliximab antibody development. J Dermatol 42: 94-95, 2015.
27. Takahashi H, Iirama S, Tsuji H, Honma M, Iizuka H. Biologics are more potent than other treatment modalities for improvement of quality of life in psoriasis patients. J Dermatol 41: 686-689, 2014.
28. Kusakari Y, Yamasaki K, Takahashi T, et al. Successful adalimumab treatment of a psoriasis vulgaris patient with hemodialysis for renal failure: a case report and a review of the previous reports on biologic treatments for psoriasis patients with hemodialysis for renal failure. J Dermatol 42: 727-730, 2015.
29. Umezawa Y, Hayashi M, Kikuchi S, et al. Ustekinumab treatment in patients with psoriasis undergoing hemodialysis. J Dermatol 42: 731-734, 2015.
30. Nunomaniya K, Tsuchiya C, Mizukami Y, et al. Successful treatment with ustekinumab of psoriasis vulgaris in a patient undergoing hemodialysis. J Dermatol 43: 92-94, 2016.
31. Ohtsuki M, Morita A, Abe M, et al. Secukinumab efficacy and safety in Japanese patients with moderate-to-severe plaque psoriasis: subanalysis from ERASURE, a randomized, placebo-controlled, phase 3 study. J Dermatol 41: 1039-1046, 2014.
32. Rapp SR, Feldman SR, Exum ML, Fleischer AB Jr, Rehmusin DM. Psoriasis causes as much disability as other major medical diseases. J Am Acad Dermatol 41: 401-407, 1999.
33. Do YK, Lakhani N, Malhotra R, Halstenter B, Theng C, Okubye T. Associations between psoriasis and leisure-time physical activity: findings from the National Health and Nutrition Examination Survey. J Dermatol 42: 148-153, 2015.
34. Ng CY, Yang YW, Lin SH, et al. SF-36 health survey on psoriasis quality-of-life: a study of 414 Taiwanese patients. J Dermatol 42: 159-165, 2015.
35. Atakan N, Yazici AC, Özarmağan O, et al. TUR-PSO: a cross sectional study investigating quality of life and treatment status of psoriasis patients in Turkey. J Dermatol 43: 298-304, 2016.
36. Saeki H, Imafuku S, Abe M, et al. Poor adherence to medication as assessed by the Morisky Medication Adherence Scale-8 and low satisfaction with treatment in 237 psoriasis patients. J Dermatol 42: 367-372, 2015.
37. Stuart PE, Nair RP, Tejasvi T, et al. Genome-wide association analysis of psoriatic arthritis and cutaneous psoriasis reveals differences in their genetic architecture. Am J Hum Genet 97: 816-830, 2015.
38. Asahina A, Umezawa Y, Yanaba K, Nakagawa H. Serum C-reactive protein levels in Japanese patients with psoriasis and psoriatic arthritis: long-term differential effects of biologics. J Dermatol 43: 779-784, 2016.
39. Takata T, Takahashi A, Taniguchi Y, Terada Y, Sano S. Detection of asymptomatic enthesitis in psoriasis patients: an onset of psoriatic arthritis? J Dermatol 43: 650-654, 2016.
40. Yamamoto T, Ohtsuki M, Sano S, et al. Epidemiological analysis of psoriatic arthritis patients in Japan. J Dermatol 43: 1193-1196, 2016.
41. Samarasekera EJ, Neilson JM, Warren RB, Parnham J, Smith CH. Incidence of cardiovascular disease in individuals with psoriasis: a systematic review and meta-analysis. J Invest Dermatol 133: 2340-2346, 2013.
42. Koch M, Baurecht H, Ried JS, et al. Psoriasis and cardiometabolic traits: modest association but distinct genetic architectures. J Invest Dermatol 135: 1283-1291, 2015.
43. Gelfand JM, Neimann AL, Shin DB, Wang X, Margolis DJ, Troxel AB. Risk of myocardial infarction in patients with psoriasis. JAMA 296: 1735-1741, 2006.
44. Mehta NN, Azfar RS, Shin DB, Neimann AL, Troxel AB, Gelfand JM. Patients with severe psoriasis are at increased risk of cardiovascular mortality: cohort study using the General Practice Research Database. Eur Heart J 31: 1000-1006, 2010.
45. Abuabara K, Azfar RS, Shin DB, Neimann AL, Troxel AB, Gelfand JM. Cause-specific mortality in patients with severe psoriasis: a population-based cohort study in the U.K. Br J Dermatol 163: 586-592, 2010.
46. Parisi R, Rutter MK, Lunt M, et al. Psoriasis and the risk of major cardiovascular events: cohort study using the clinical practice research datalink. J Invest Dermatol 135: 2189-2197, 2015.
47. Shiba M, Kato T, Furusako M, et al. Association between psoriasis vulgaris and coronary heart disease in a hospital-based population in Japan. PLoS One 11: e0149316, 2016.
48. Takahashi H, Iizuka H. Psoriasis and metabolic syndrome. J Dermatol 39: 212-218, 2012.
49. Puig L, Kirby B, Mallbris L, Stocchi R. Psoriasis beyond the skin: a review of the literature on cardiometabolic and psychological comorbidities of psoriasis. Eur J Dermatol 24: 305-311, 2014.
50. Henseler T, Christophers E. Disease concomitance in psoriasis. J Am Acad Dermatol 32: 982-986, 1995.
51. Neimann AL, Shin DB, Wang X, Margolis DJ, Troxel AB, Gelfand JM. Prevalence of cardiovascular risk factors in patients with psoriasis. J Am Acad Dermatol 55: 829-835, 2006.
52. Cohen AD, Gilutz H, Henkin Y, et al. Psoriasis and the metabolic syndrome. Acta Derm Venereol 87: 506-509, 2007.
53. Cohen AD, Dreiher J, Shapiro Y, et al. Psoriasis and diabetes: a population-based cross-sectional study. J Eur Acad Dermatol Venereol 22: 384-389, 2008.
54. Gisondi P, Tessari G, Conti A, et al. Prevalence of metabolic syndrome in patients with psoriasis: a hospital-based case-control study. Br J Dermatol 157: 68-73, 2007.
55. Schwandt A, Bergis D, Digby A, et al. Psoriasis and diabetes: a multicenter study in 222078 type 2 diabetes patients reveals high levels of depression. J Diabetes Res 2015: 792968, 2015.
56. Lønnberg AS, Skov L, Skytthe A, Kyvik KO, Pedersen OB, Thomsen SF. Association of psoriasis with the risk for type 2 diabetes mellitus and obesity. JAMA Dermatol 152: 761-767, 2016.
57. Naito R, Imafuku S. Distinguishing features of body mass index and psoriasis in men and women in Japan: a hospital-based case-control study. J Dermatol 43: 1406-1411, 2016.
58. Choi WJ, Park EJ, Kwon IH, Kim KH, Kim KJ. Association between psoriasis and cardiovascular risk factors in Korean patients. Ann Dermatol 22: 300-306, 2010.
59. Kulprat C, Ankplakorn W, Rajatanavin N. Prevalence and characteristics of metabolic syndrome in South-East Asian psoriatic patients: a case-control study. J Dermatol 41: 898-902, 2014.
60. Dreiher J, Weitzman D, Davidovici B, Shapiro J, Cohen AD. Psoriasis and dyslipidaemia: a population-based study. Acta Derm Venereol 88: 561-565, 2008.
61. Cohen AD, Weitzman D, Dreiher J. Psoriasis and hypertension: a case-control study. Acta Derm Venereol 90: 24-26, 2010.
62. Nagai H, Fujiwara S, Takahashi Y, Nishigori C. Ameliorating effect of the novel dipeptidyl peptidase-4 inhibitor teneligliptin on psoriasis: a report of two cases. J Dermatol 42: 1094-1097, 2015.
63. Mancuso C, Paolino G, Richetta AG, Calvieri S. Psoriasis, vitamin D and the importance of the cutaneous barrier's integrity: an up-

dale. J Dermatol 43: 507-514, 2016.
64. Kincse G, Bíró T, Hendi E, et al. Vitamin D levels and bone mineral density in patients with psoriasis and/or psoriatic arthritis. J Dermatol 42: 679-684, 2015.
65. D'Epiro S, Menocci C, Salvi M, et al. Psoriasis and bone mineral density: implications for long term patients. J Dermatol 41: 783-787, 2014.
66. Imafuku S, Honma M, Okubo Y, et al. Efficacy and safety of secukinumab in patients with generalized pustular psoriasis: a 52-week analysis from phase III open-label multicenter Japanese study. J Dermatol 43: 1011-1017, 2016.
67. Boehncke WH, Boehncke S, Tobin AM, Kirby B. The 'psoriatic march': a concept of how severe psoriasis may drive cardiovascular comorbidity. Exp Dermatol 20: 303-307, 2011.
68. Yamanaka K, Mizutani H. "Inflammatory skin march": IL-1-mediated skin inflammation, atopic dermatitis, and psoriasis to cardiovascular events. J Allergy Clin Immunol 136: 823-824, 2015.
69. Welty FK, Alfaddagh A, Elajami TK. Targeting inflammation in metabolic syndrome. Transl Res 167: 257-280, 2016.
70. Yoon SW, Kang SY, Kim SA, Park CY, Lee WW. Subclinical systemic and vascular inflammation detected by ^{18}F-fluorodeoxyglucose positron emission tomography/computed tomography in patients with mild psoriasis. J Dermatol 42: 559-566, 2015.
71. Pina T, Corrales A, Lopez-Mejias R, et al. Anti tumor necrosis factor-alpha therapy improves endothelial function and arterial stiffness in patients with moderate to severe psoriasis: a 6-month prospective study. J Dermatol 43: 1267-1272, 2016.
72. Pina T, Genre F, Lopez-Mejias R, et al. Asymmetric dimethylarginine but not osteoprotegerin correlates with disease severity in patients with moderate-to-severe psoriasis undergoing anti-tumor necrosis factor-α therapy. J Dermatol 43: 389-394, 2016.
73. Kim DS, Shin D, Jee H, et al. Red blood cell distribution width is increased in patients with psoriasis vulgaris: a retrospective study on 261 patients. J Dermatol 42: 567-571, 2015.
74. Kim DS, Shin D, Lee MS, et al. Assessments of neutrophil to lymphocyte ratio and platelet to lymphocyte ratio in Korean patients with psoriasis vulgaris and psoriatic arthritis. J Dermatol 43: 305-310, 2016.
75. Grauballe MB, Ostergaard JA, Schou S, Flyvbjerg A, Holmstrup P. Effects of TNF-α blocking on experimental periodontitis and type 2 diabetes in obese diabetic Zucker rats. J Clin Periodontol 42: 807-816, 2015.
76. Iwata N, Takayama H, Xuan M, et al. Effects of etanercept against transient cerebral ischemia in diabetic rats. Biomed Res Int 2015: 189292, 2015.
77. Furnian MM, de Mello NA, Maia R, et al. LASSBio-1425, an analog of thalidomide, decreases triglyceride and increases HDL cholesterol levels by inhibition of TNF-α production. Int J Cardiol 202: 497-499, 2016.
78. Silverberg JI, Greenland P. Eczema and cardiovascular risk factors in 2 US adult population studies. J Allergy Clin Immunol 135: 721-728, 2015.
79. Egeberg A, Mallbris L, Warren RB, et al. Association between psoriasis and inflammatory bowel disease: a Danish nationwide cohort study. Br J Dermatol 175: 487-492, 2016.
80. Nakamura K, Asano Y, Shibata S, et al. Case of psoriasis vulgaris developing ulcerative colitis during adalimumab treatment. J Dermatol 42: 1029-1030, 2015.
81. Egeberg A, Mallbris L, Gislason GH, Skov L, Hansen PR. Risk of multiple sclerosis in patients with psoriasis: a Danish nationwide cohort study. J Invest Dermatol 136: 93-98, 2016.
82. Jensen P, Egeberg A, Gislason G, Hansen PR, Thyssen JP, Skov L. Increased risk of autoimmune hepatitis in patients with psoriasis: a Danish nationwide cohort study. J Invest Dermatol 136: 1515-1517, 2016.
83. Takahashi H, Sato K, Takagi A, et al. Subepidermal autoimmune blistering lesion in a case of psoriasis successfully treated with cyclosporin. J Dermatol 42: 1125-1126, 2015.
84. Maki N, Demitsu T, Umemoto N, et al. Possible paraneoplastic syndrome case of bullous pemphigoid with immunoglobulin G anti-BP180 C-terminal domain antibodies associated with psoriasis and primary macroglobulinemia. J Dermatol 43: 571-574, 2016.
85. Okahashi K, Oiso N, Ishii N, et al. Bullous pemphigoid associated with psoriasis: a possible example of an inverse intramolecular epitope-spreading phenomenon. J Dermatol 42: 758-759, 2015.
86. Ishida S, Takahashi K, Kanaoka M, et al. Case of subepidermal autoimmune bullous disease with psoriasis vulgaris reacting to both BP180 C-terminal domain and laminin gamma-1. J Dermatol 42: 391-393, 2015.
87. Imanishi A, Tateishi C, Imanishi H, et al. Pemphigoid with antibodies to laminin γ1, BP180 and BP230, associated with psoriasis vulgaris: successful disease control with cyclosporin. J Dermatol 42: 394-397, 2015.
88. Ansai S, Hashizume S, Kawana S, Tateishi C, Koga H, Hashimoto T. Case of anti-laminin gamma-1 pemphigoid with antibody against C-terminal domain of BP180 in a patient with psoriasis vulgaris. J Dermatol 41: 1031-1033, 2014.
89. Tomas-Aragones L, Marron SE. Body image and body dysmorphic concerns. Acta Derm Venereol 96: 47-50, 2016.
90. Diffinati E, Del Bino D, Prignago F, Tomba E. Discriminating the presence of psychological distress in patients suffering from psoriasis: an application of the clinimetric approach in dermatology. Acta Derm Venereol 96: 69-73, 2016.

The Internal Medicine is an Open Access article distributed under the Creative Commons Attribution-NonCommercial-NoDerivatives 4.0 International License. To view the details of this license, please visit (http://creativecommons.org/licenses/by-nc-nd/4.0/).

© 2017 The Japanese Society of Internal Medicine
http://www.naika.or.jp/imonline/index.html

Australasian Journal of Dermatology

Australasian Journal of Dermatology (2017) 58, 171–175 doi: 10.1111/ajd.12562

REVIEW ARTICLE

Pemphigus, a pathomechanism of acantholysis

Masutaka Furue[1] and Takafumi Kadono[2]

[1]*Department of Dermatology, Kyushu University, Fukuoka, and* [2]*Department of Dermatology, St Marianna University School of Medicine, Kawasaki, Japan*

ABSTRACT

Autoantibodies to the desmosomal proteins desmogleins 1 and 3 cause pemphigus foliaceus and pemphigus vulgaris, which are characterised by keratinocyte dissociation (acantholysis) and intraepidermal blister formation. The passive transfer of pathogenic anti-desmoglein antibodies induces blisters in vivo *in vivo* and the loss of keratinocyte adhesion *in vitro*. The pathogenetic mechanisms of acantholysis due to anti-desmoglein autoantibodies are not fully understood. However, recent studies have revealed that signalling-dependent and signalling-independent pathways are operative in the loss of cell adhesion. In this review, we focus on the pathomechanism of acantholysis due to autoantibodies to desmogleins and recent therapeutic approaches.

Key words: acantholysis, desmoglein, p38 MAPK, pathomechanism, pemphigus.

INTRODUCTION

Desmosomes are intercellular junctional complexes that confer strong cell–cell adhesion in tissue such as epidermis and myocardium, which undergo large amounts of mechanical strain.[1–4] The desmosomes are composed of five major proteins: desmogleins (DSG), desmocollins, desmoplakins, plakoglobin and plakophilins. The epidermal DSG, desmocollins and plakophilins have several isoforms: DSG 1 to 4, desmocollins 1 to 3 and plakophilins 1 to 3.[1,4] These isoforms are differentially expressed as the keratinocytes undergo terminal differentiation (Fig. 1). DSG3 and DSG3 are mainly distributed in the lower layers of the epidermis and mucous membrane, whereas DSG1 is preferentially expressed in the upper layers of the epidermis. DSG4 is primarily expressed in the hair follicle and the granular layer. Desmocollins 2 and 3 are present in the basal and spinous layers, whereas desmocollin 1 is expressed in the granular layer.[1] Plakoglobin, desmoplakin and plakophilin 3 are distributed throughout the epidermis, while plakophilin 1 is compartmentalised in the upper epidermis and plakophilin 2 is preferentially expressed in the lower epidermis (Fig. 1).[1] At the molecular level, the DSG and desmocollins are assumed to form strong extracellular homo (DSG–DSG and desmocollin–desmocollin) and hetero-philic (DSG–desmocollin) bonds and to mediate intercellular adhesion. Intracellularly, their tails interact with plakoglobin and plakophilins, which in turn bind to desmoplakin, whose functions are to anchor keratins and to stabilise desmosomes (Fig. 1).[1–4]

PATHOGENESIS OF ACANTHOLYSIS

Pemphigus is an autoimmune blistering disease in which pathogenic autoantibodies target DSG1 (pemphigus foliaceus [PF]) and DSG1 and DSG3 (pemphigus vulgaris [PV]), leading to acantholysis, a characteristic histological feature.[5,6] In line with the distribution patterns of DSG3 and DSG1, PV affects both the epidermis and mucous membranes with a potentially fatal course, whereas the upper epidermis is the major target for PF. The DSG3:DSG1 ratio in the oral mucosa is higher than that in the epidermis, which explains the preponderant occurrence of oral lesions in PV.[6] Patients with PV possessing both anti-DSG3 and anti-DSG1 autoantibodies tend to manifest extensive mucocutaneous blisters.[5,6] A small percentage of patients with PF manifests mucosal involvement without anti-DSG3 autoantibodies.[7] Characteristic clinical presentation and the heterogeneity of paraneoplastic pemphigus can be accounted for by the presence of a varying range of

Correspondence: Dr Masutaka Furue, Department of Dermatology, Kyushu University, Maidashi 3-1-1, Higashiku, Fukuoka, 812-8582, Japan. E-mail: furue@dermatol.med.kyushu-u.ac.jp

Masutaka Furue, MD, PhD, Takafumi Kadono, MD, PhD.

Conflict of interest: none.

Submitted 24 March 2016; accepted 13 August 2016.

Abbreviations:

DSG	desmoglein
MAPK	mitogen-activated protein kinase
PF	pemphigus foliaceus
PV	pemphigus vulgaris

© 2017 The Australasian College of Dermatologists

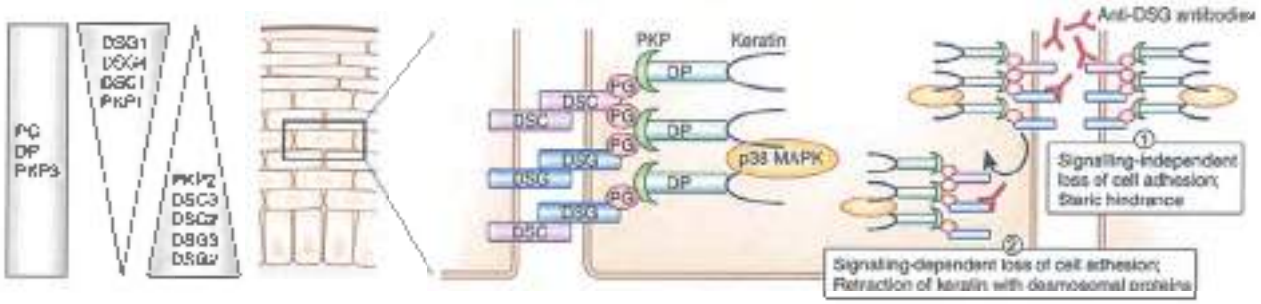

Figure 1 Desmosomal proteins and the pathomechanism of acantholysis (i.e., loss of keratinocyte adhesion) by autoantibodies. Intercellular adhesion of desmosomes is maintained by the homophilic and hetero-philic binding of desmogleins (DSG) and desmocollins (DSC). The intracellular tails of DSG and DSC interact with plakoglobin (PG) and plakophilins (PKP), which, in turn, bind to desmoplakin (DP), whose functions are to anchor keratins and to stabilise desmosomes. DSG, DSC and PKP have several isoforms. PG, DP and PKP3 are distributed evenly in the epidermis, while DSG1, DSG4, DSC1 and PKP1 are localised mainly in the upper dermis. DSG2, DSG3, DSC2, DSC3 and PKP2 are predominantly localised in the lower epidermis. Pathogenic anti-DSG autoantibodies directly bind to the N-terminal extracellular domain 1 (EC1) of DSG. This domain is essential for the adhesive transinteraction of DSG, and autoantibody binding to EC1 results in so-called steric hindrance, leading to keratinocyte dissociation in a signalling independent manner. Moreover, autoantibody binding induces the internalisation of the desmosome complex into the cytoplasm, with inward retraction of keratin fibers via P38 mitogen-activated protein kinase (P38 MAPK) activation (the signalling-dependent pathway). Both the signalling dependent and signalling-independent pathways are operative in inducing acantholysis.

autoantibodies against DSG3, DSG1, envoplakin, periplakin, desmoplakin 1, desmoplakin 2, bullous pemphigoid antigen 1, plectin and a previously unidentified 170-kd protein.[8] Intraepidermal neutrophilic infiltration is usually seen in immunoglobulin (Ig)A pemphigus, which shows IgA autoantibodies targeting desmocollin 1 and unidentified epidermal molecules.[9,10] The acantholysis and dyskeratosis found in Darier disease (mutations of SERCA2 protein encoded by *ATP2A2*) and Hailey-Hailey disease (mutations of SPCA1 protein encoded by *ATP2C1*) are caused by the dysregulation of the calcium pump, as reviewed elsewhere.[11,12]

The passive transfer of anti-DSG autoantibodies into newborn mice causes epidermal blistering.[5,13–15] Pathogenic autoantibodies in PF and PV compromise the adhesion strength of cultured keratinocytes and induce loss of cell adhesion when added to a culture media *in vitro*.[15–17] Recent studies have advanced our understanding of the pathomechanisms leading to the loss of cell adhesion (acantholysis), especially in PV. It is believed that the N-terminal extracellular domain 1 (EC1) of DSG3 is essential for the adhesive transinteraction of DSG3. Mouse monoclonal antibodies targeting this domain are pathogenic and induce experimental PV *in vivo*.[13,15,16] However, the situation in human PV is more complex than that in mouse models. PV patients produce polyclonal antibodies targeting the EC1 epitope, yet non-EC1-targeting polyclonal autoantibodies can also be pathogenic in human PV.[14] Although conflicting results have been reported in these monoclonal and polyclonal anti-DSG3 antibodies,[15–18] Saito and colleagues demonstrated that both signalling-dependent and signalling-independent pathways are operative in acantholysis development.[14] After binding to cell surface DSG3, both EC1-targeting and EC1-nontargeting polyclonal PV autoantibodies induce clustering and endocytosis of DSG3 with P38 mitogen-activated protein kinase (MAPK) activation, leading to collapse of the keratin filaments (i.e., the retraction of keratin filaments from desmosomes to the perinuclear area). DSG3 internalisation correlates with the loss of cell adhesion, whereas p38 MAPK inhibitors prevent the autoantibody-mediated clustering and endocytosis of DSG3 and the collapse of the keratin filaments, along with the loss of cell adhesion (signalling-dependent pathway).[14,15,17] In contrast, the loss of cell adhesion due to monoclonal anti-DSG3 antibodies is not dependent on either p38 MAPK activation, clustering and endocytosis of DSG3 or the collapse of the keratin filaments. Rather, it is likely to be caused by the direct inhibition of monoclonal antibodies against adhesive DSG3 transinteraction (i.e., steric hindrance, signalling-independent pathway).[13–15,17] However, a recent study by Vielmuth and colleagues showed that DSG3 disassembly is not sufficient for keratinocyte dissociation in PV.[19] Another attractive concept is the cholesterol raft theory.[19–21] DSG3 preferentially assemble in the cholesterol rafts on the keratinocyte surface. The binding of PV autoantibodies cause the internalisation of DSG3 by endocytic vesicles with cholesterol rafts, leading to the depletion of cell surface DSG3.[20,21] The pathogenic potency (i.e., the capacity to induce the loss of cell adhesion) of polyclonal PV autoantibodies differs in each PV patient. Patients with low pathogenic anti-DSG3 autoantibodies may lack mucosal lesions.[22] On the other hand, highly pathogenic anti-DSG3 autoantibodies, even at undetectably low levels, can induce mucosal involvement.[23] The assembly of DSG3 and subsequent desmosome formation appears to be calcium dependent.[24] Moreover, autoantibodies targeting calcium-dependent epitopes of DSG3 are more pathogenic.[24]

FUTURE THERAPEUTIC APPROACH

Therapy for pemphigus patients is based on the long-term use of high-dose systemic corticosteroids in combination

© 2017 The Australasian College of Dermatologists

with high dose i.v. immunoglobulin or other immunosuppressants, including azathioprine, mycophenolate, cyclophosphamide and, more recently, rituximab.[24] Due to the frequent occurrence of adverse events in long-term steroid therapy, novel and specific treatment options are greatly anticipated. Based on the above-mentioned pathomechanisms of acantholysis, Spindler and colleagues developed a promising treatment option.[13] Tandem peptide (TP) consists of two connected peptide sequences targeting the DSG1 adhesive interface and is capable of blocking the PV autoantibody-mediated interference of DSG3 transinteraction, as revealed by atomic force microscopy and optical trapping.[13] Both the systemic and topical administration of TP overturns autoantibody-induced skin blistering in mice. Mechanistically, TP promotes desmosomal DSG3 oligomerisation and inhibits the p38 MAPK-induced keratin filament retraction.[13] This preclinical observation may facilitate future drug development.

REFERENCES

1. Delva E, Tucker DK, Kowalczyk AP. The desmosome. *Cold Spring Harb Perspect Biol* 2009; 1: a002543.
2. Thomason HA, Scothern A, McHarg S *et al.* Desmosomes: adhesive strength and signalling in health and disease. *Biochem. J* 2010; 428: 419–55.
3. Brusseard JA, Getsios S, Green KJ. Desmosome regulation and signaling in disease. *Cell Tissue Res.* 2013; 360: 501–12.
4. Osmani N, Labouesse M. Remodeling of keratin-coupled cell adhesion complexes. *Curr. Opin. Cell Biol.* 2015; 33: 50–8.
5. Stanley JR, Amagai M. Pemphigus, bullous impetigo, and the staphylococcal scalded skin syndrome. *N. Engl. J. Med.* 2006; 355: 1800–10.
6. Payne AS, Hanakawa Y, Amagai M *et al.* Desmosomes and disease: pemphigus and bullous impetigo. *Curr. Opin. Cell Biol.* 2004; 16: 536–43.
7. Koga H, Ohyama B, Tsuruta D *et al.* Five Japanese cases of antidesmoglein 1 antibody-positive and antidesmoglein 3 antibody-negative pemphigus with oral lesions. *Br. J. Dermatol.* 2012; 166: 976–80.
8. Yong AS, Tey HL. Paraneoplastic pemphigus. *Australas. J. Dermatol.* 2015; 54: 241–50.
9. Tsuruta D, Ishii N, Hamada T *et al.* IgA pemphigus. *Clin. Dermatol.* 2011; 29: 437–42.
10. Hosoda S, Adachi A, Suzuki M *et al.* Case of pemphigus with immunoglobulin G and A antibodies, binding to both the intercellular spaces and basement membrane zone. *J. Dermatol.* 2016; 43: 194–6.
11. Takagi A, Kamijo M, Ikeda S. Darier disease. *J. Dermatol.* 2016; 43: 375–9.
12. Micaroni M, Giacchetti G, Bertani E *et al.* ATP2C1 gene mutations in Hailey Hailey disease and possible roles of SPCA1 isoforms in membrane trafficking. *Cell Death Dis.* 2016; 7: e2249.
13. Heupel WM, Zillikens D, Drenckhahn D *et al.* Pemphigus vulgaris IgG directly inhibit desmoglein 3-mediated transinteraction. *J. Immunol.* 2008; 181: 1825–34.
14. Salvo M, Stahley SN, Caughman CY *et al.* Signaling dependent and independent mechanisms in pemphigus vulgaris blister formation. *PLoS One* 2012; 7: e50086.
15. Spindler V, Rötzer V, Dehner C *et al.* Peptide-mediated desmoglein 3 crosslinking prevents pemphigus vulgaris autoantibody-induced skin blistering. *J. Clin. Invest.* 2015; 125: 800–11.
16. Spindler V, Endlich A, Hartlieb E *et al.* The extent of desmoglein 3 depletion in pemphigus vulgaris is dependent on Ca (2+)-induced differentiation: a role in suprabasal epidermal skin splitting? *Am. J. Pathol.* 2011; 178: 1005–18.
17. Jennings JM, Tucker DK, Kottke MD *et al.* Desmosome disassembly in response to pemphigus vulgaris IgG occurs in distinct phases and can be reversed by expression of exogenous Dsg3. *J. Invest. Dermatol.* 2011; 131: 206–18.
18. Virchow I, Walschke J, Spindler V. Loss of desmoglein binding is not sufficient for keratinocyte dissociation in pemphigus. *J. Invest. Dermatol.* 2015; 135: 3069–77.
19. Delva E, Jennings JM, Calkins CC *et al.* Pemphigus vulgaris IgG-induced desmoglein-3 endocytosis and desmosomal disassembly are mediated by a clathrin- and dynamin-independent mechanism. *J. Biol. Chem.* 2008; 283: 18505–15.
20. Brennan D, Peltonen S, Dowling P *et al.* Desmosome assembly and cell-cell adhesion are membrane raft-dependent processes. *J. Biol. Chem.* 2011; 286: 1499–507.
21. Stahley SN, Saito M, Faundez V *et al.* Desmosome assembly and disassembly are membrane raft-dependent. *PLoS One* 2014; 9: e87809.
22. Saleh MA, Hashimoto R, Kaur Y *et al.* Low pathogenicity of anti-desmoglein 3 immunoglobulin G autoantibodies contributes to the atypical clinical phenotypes in pemphigus. *J. Dermatol.* 2015; 42: 865–9.
23. Kasuya K, Aoyama Y, Wakasilina C *et al.* Atypical pemphigus with immunoglobulin G autoantibodies against desmoglein 3 and desmocollin 3. *J. Dermatol.* 2016; 43: 429–31.
24. Kasuya K, Aoyama Y, Shirafuji Y *et al.* A higher correlation of the antibody activities against the calcium-dependent epitopes of desmoglein 3 quantified by ethylenediaminetetraacetic acid-treated enzyme-linked immunosorbent assay with clinical disease activities of pemphigus vulgaris. *J. Dermatol. Sci.* 2015; 79: 180–5.
25. Amagai M, Tanikawa A, Shimizu T *et al.* Japanese guidelines for the management of pemphigus. *J. Dermatol.* 2014; 41: 471–86.

© 2017 The Australasian College of Dermatologists

Current Oncology Reports (2018) 20: 29
https://doi.org/10.1007/s11912-018-0676-z

Melanoma and Immune Checkpoint Inhibitors

Masutaka Furue[1] · Takamichi Ito[1] · Naoko Wada[1] · Maiko Wada[1] · Takafumi Kadono[2] · Hiroshi Uchi[1]

© Springer Science+Business Media, LLC, part of Springer Nature 2018

Abstract

Purpose of Review Prognosis of patients with advanced melanoma is dismal with a median overall survival of about 8 months and 5-year overall survival from a diagnosis of metastatic disease of roughly 10%. However, immune checkpoint inhibitors have brought indispensable benefits to melanoma patients. Here we will review the recent clinical efficacy and adverse events of immune checkpoint inhibitors for melanoma patients.

Recent Findings The immune checkpoint inhibitors increase confirmed objective response and prolong progression-free and overall survival of the afflicted patients in association with maintaining their quality of life. Although diverse immune-related adverse events occur, most of them are manageable by appropriate immunomodulating agents. Clinical efficacy of immune checkpoint inhibitors continues even after discontinuation of drugs.

Summary Compared with conventional therapeutic options, the immune checkpoint inhibitors appear to prolong the survival of patients with advanced melanoma. Further clinical trials are warranted to determine whether their combinatory use with other treatment options may augment benefits or not.

Keywords Melanoma · Immune checkpoint inhibitors · Ipilimumab · Nivolumab · Pembrolizumab

Introduction

Incidence of melanoma in most developed countries has risen and the World Health Organization currently estimates that approximately 132,000 people will be diagnosed with melanoma each year and that about 37,000 people will die of the disease annually [1–4]. The average 5-year survival rate is approximately 90, 70, 40, and less than 10% for patients with stage I, II, III, and IV disease, respectively [1–3, 5]. Median progression-free survival is only 1.7 months in stage IV patients [1–3]. Recent advances in skin imaging by dermoscopy help early and correct diagnosis of melanoma [6–12]. Melanoma has four histopathological subtypes, superficial spreading melanoma, nodular melanoma, lentigo maligna melanoma, and acral lentiginous melanoma [13, 14]. Although acral lentiginous melanoma commonly occurs in dark skin population, patients' survival rates are similar between acral lentiginous melanoma and other types of melanoma [13]. Consistently, treatment response of acral lentiginous melanoma to immune checkpoint inhibitor is comparable to that of other types of melanoma [15].

Treatments of melanoma include surgical resection; chemotherapies such as dacarbazine, paclitaxel, and carboplatin; and immunotherapies such as interleukin-2 and interferon-α [16–19]. Recent discoveries regarding the complex networks involved in melanoma proliferation, progression, and survival have created many opportunities for targeted drugs, biomarkers, and new therapeutic approaches for this disease [3, 16, 20–24]. One of the most frequent mutations in melanoma involves the BRAF kinase with *BRAF* gene mutations in approximately 50% of melanomas, leading to constitutive activation of the mitogen-activated protein kinase (MAPK) pathway in affected cells. Vemurafenib and dabrafenib are inhibitors targeting mutated BRAF kinases [3, 16, 25]. Despite a high response rate, the durability of responses is unexpectedly short (usually less than 6 months) mostly due to MAPK reactivation [3, 16, 25]. Therefore, inhibitors for mitogen-activated protein

This article is part of the Topical Collection on *Melanoma*

✉ Masutaka Furue
furue@dermatol.med.kyushu-u.ac.jp

[1] Department of Dermatology, Kyushu University, Maidashi 3-1-1, Higashiku, Fukuoka 812-8582, Japan

[2] Department of Dermatology, St. Marianna University School of Medicine, Kawasaki 216-8511, Japan

Published online: 23 March 2018

kinase kinase (MEK) are developed and combinatorial administration of BRAF inhibitors and MEK inhibitors nearly doubles a progression-free survival and frequently decreases adverse events [2, 16, 25, 26]. However, the therapeutic resistance remains and the majority of patient experiences relapse within 1 year of initiating the combined BRAF and MEK inhibition therapy. In addition, various adverse events occur very frequently [3, 25, 27, 28]. Nonetheless, approximately 20% of patients remain progression free for 3 years [1, 25, 27].

Just overlapping with the development of kinase inhibitors, monoclonal antibodies against immune checkpoint molecules have gained a particular attention. In this article, we summarize recent topics of immune checkpoint inhibitors in melanoma therapy.

Immune Checkpoint Inhibitors

Cellular immune defense against neoplasms begins with the T cell recognition of a tumor antigen presented by antigen-presenting cell. Activated T cells expand and become effector T cells which attack tumor cells bearing tumor antigen. To prevent overactivation of T cells, the immune system possesses a cooling or immune checkpoint system that downregulates the exceeded activation [29–31]. In a simplified description, at least two key immune checkpoints exist in the immune system; one is in the early antigen-recognition phase and the other in the effector phase (Fig. 1). Cytotoxic T lymphocyte antigen 4 (CTLA4) is a coinhibitory molecule on T cells and inhibits the T cell activation upon ligation by CD86 or CD80 on antigen-presenting cells [29–31] (Fig. 1). Programmed death 1 (PD-1) is another key immune checkpoint receptor on T cells and is a potent inhibitor of T cell activation upon ligation by programmed death 1 ligand 1 (PD-L1) and PD-L2 expressed on the tumor cells [29–31]. Since melanoma cells express PD-L1 [32–34], the infiltrated effector T cells are dampened by PD-1/PD-L1 ligation. Anti-PD-1 antibody treatment enhances the overall survival (OS) of melanoma patients and response rates are better in PD-L1-positive patients [33]. The expression intensity of PD-L1 on melanomas correlated with the objective response rate after anti-PD-1 antibody administration [33].

Monoclonal antibodies against CTLA4 (ipilimumab) and PD-1 (nivolumab and pembrolizumab) are currently in clinical use worldwide for melanoma treatment as potent immune checkpoint inhibitors. As CTLA4 and PD-1 are distinct immune checkpoints, combinatory treatment with anti-CTLA-4 and anti-PD-1 antibodies is synergistic and is more effective than their monotherapy in melanoma [30, 35•, 36].

Ipilimumab and Melanoma

Development of ipilimumab preceded that of nivolumab and pembrolizumab (Table 1). Ipilimumab is a fully human IgG1 monoclonal antibody designed to block CTLA-4 [49]. Patients with unresectable stage III or IV melanoma were randomly assigned, in a 3:1:1 ratio, to receive ipilimumab (3 m/kg) plus glycoprotein 100 (gp100) vaccine ($N = 403$), ipilimumab alone ($N = 137$), or gp100 alone ($N = 136$) [49]. The median OS was 10 months among patients receiving ipilimumab plus gp100, as compared with 6.4 months among patients receiving gp100 alone—hazard ratio (HR) for death, 0.68; $P < 0.001$. The median OS with ipilimumab alone was 10.1 months (HR, 0.66; $P = 0.003$) in comparison with gp100 alone. No difference in OS was detected between the ipilimumab groups and ipilimumab plus gp100 (HR, 1.04; $P = 0.76$) [49] (Table 1). This led to FDA approval of ipilimumab in the USA and other regulatory approvals globally.

Patients with previously untreated metastatic melanoma were randomly assigned, in a 1:1 ratio, to ipilimumab (10 m/kg) plus dacarbazine ($N = 250$) or dacarbazine alone ($N = 252$) [48]. The ipilimumab plus dacarbazine group showed a significantly longer median OS (11.2 months; HR, 0.72; $P < 0.001$) than the dacarbazine alone group (9.1 months) [48]. In a maintenance study, ipilimumab (every 12 weeks (q12W)) plus dacarbazine q3W were continued in the former group, and dacarbazine q3W alone in the latter group [50]. Five-year survival rate was 18.2% in the ipilimumab plus dacarbazine group and 8.8% in the dacarbazine alone group ($P = 0.02$) [50].

In an ipilimumab adjuvant trial, patients had undergone complete resection of stage III cutaneous melanoma and were randomly assigned to receive ipilimumab (10 mg/kg) ($N = 475$) or placebo ($N = 476$) [47]. At a median follow-up of 5.3 years, the 5-year rate of recurrence-free survival was 40.8% in the ipilimumab group, as compared with 30.3% in the placebo group (HR, 0.76; $P < 0.001$). The rate of OS at 5 years was 65.4% in the ipilimumab group, as compared with 54.4% in the placebo group (HR, 0.72; $P = 0.001$) [47]. This dataset led to US FDA approval of adjuvant ipilimumab at dose of 10 mg/kg for melanoma.

Patients with unresectable stage III or IV melanomas were randomly treated with 10 or 3 mg/kg administration of ipilimumab. Median OS was 15.7 months for ipilimumab 10 mg/kg compared with 11.5 months for ipilimumab 3 mg/kg (HR, 0.84; $P = 0.04$) [46]. Although these studies

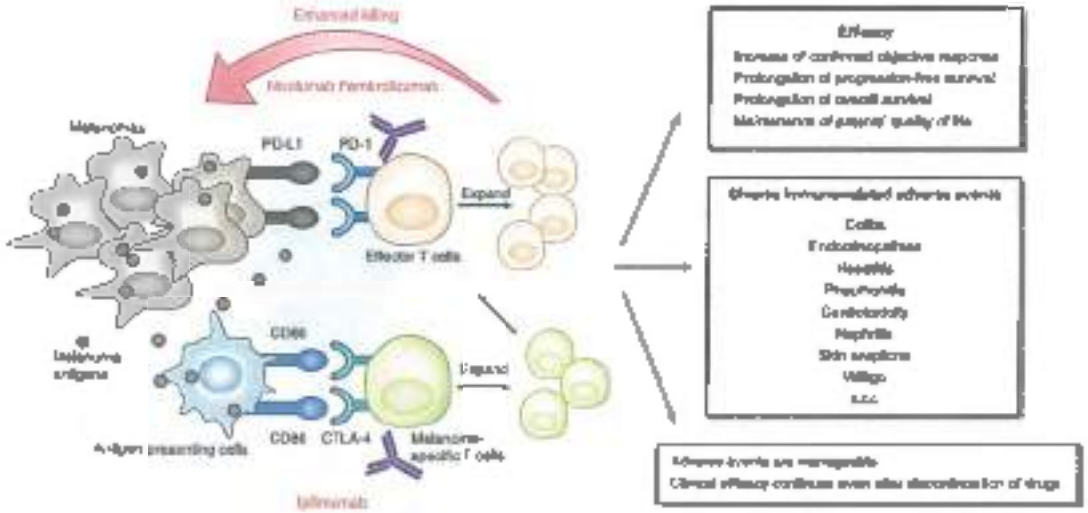

Fig. 1 Melanoma antigens are presented to melanoma-specific T cells with the help of costimulatory molecules CD80 and CD86. CD80 and CD86 also activate coinhibitory molecule CTLA-4 and suppress the activation of T cells. Anti-CTLA-4 antibody ipilimumab dampens CTLA-4 activity and accelerates the activation and expansion of melanoma-specific T cells. Some of these melanoma-specific T cells possess effector and cytotoxic function against melanoma cells. However, melanoma cells express PD-L1 which binds to PD-1 on effector T cells and induces cell death. Anti-PD-1 antibody nivolumab or pembrolizumab inhibits the function of PD-1 and supports the expansion of effector T cells leading to enhancement of melanoma killing

support the clinical effectiveness of ipilimumab in extending the OS of advanced melanoma patients, its potency is minimum and limited.

Nivolumab and Melanoma

Nivolumab is a fully human IgG4 anti-PD-1 antibody that selectively blocks the interaction of PD-1 and PD-L1/PD-L2 [45]. Patients with metastatic melanoma without a BRAF mutation were randomly assigned in a 1:1 ratio to the two treatment groups, the nivolumab (3 mg/kg, q2W) ($N = 210$) and dacarbazine groups ($N = 208$) [45]. At 1 year, the overall rate of survival was 72.9% in the nivolumab group, as compared with 42.1% in the dacarbazine group (HR, 0.42; $P < 0.001$). The median progression-free survival was 5.1 months in the nivolumab group versus 2.2 months in the dacarbazine group (HR, 0.43, $P < 0.001$). The objective response rate was 40% in the nivolumab group versus 13.9% in the dacarbazine group (odds ratio, 4.06; $P < 0.001$) [45] (Table 1). This data led to the US FDA approval of nivolumab for the treatment of advanced melanoma.

Patients with advanced melanoma who progressed after ipilimumab and/or BRAF therapy received 3 mg/kg of nivolumab ($N = 272$) or investigator's choice of chemotherapy (ICC, dacarbazine or paclitaxel plus carboplatin) ($N = 133$) in a randomized, controlled study [44]. In an interim analysis, confirmed objective responses were reported in 38 (31.7%) of the first 120 patients in the nivolumab group versus 5 (10.6%) of 47 patients in the ICC group [44]. Later on, further analysis was reported for this trial [43]. Median OS was 16 months for nivolumab versus 14 months for ICC (HR, 0.95); median progression-free survival was 3.1 months versus 3.7 months, respectively (HR), suggesting that nivolumab does not significantly elongate survival of patients with ipilimumab-refractory metastatic melanoma. However, overall response rate (27 versus 10%) and median duration of response (32 versus 13 months) were higher for nivolumab than ICC [43].

Patients with stage IIIB, IIIC, or IV melanoma following surgical resection received nivolumab ($N = 453$) or ipilimumab as adjuvant therapy ($N = 453$) [42]. At a minimum follow-up of 18 months, the 12-month rate of recurrence-free survival was 70.5% in the nivolumab group and 60.8% in the ipilimumab group (HR, 0.65; $P < 0.001$). Treatment-related grade 3 or 4 adverse events were reported in 14.4% of the patients in the nivolumab group and in 45.9% of those in the ipilimumab group. The adjuvant therapy with nivolumab resulted in significantly longer recurrence-free survival and a lower rate of grade 3 or 4 adverse events than adjuvant therapy with ipilimumab [42]. This data led to the recent US FDA approval of adjuvant nivolumab for the treatment of high-risk melanoma.

Pembrolizumab and Melanoma

Pembrolizumab is a humanized IgG4 monoclonal antibody against PD-1 [41]. Similar to nivolumab, pembrolizumab

Table 1 Efficacy of immune checkpoint inhibitors in clinical trials

Wolchok et al. [in press][5,*]		Median OS (months)
	Nivolumab (1mg/kg) + Ipilimumab (3mg/kg)	Not reached
	vs	vs
	Nivolumab (3mg/kg)	37.6
	vs	vs
	Ipilimumab (3mg/kg)	19.9
		HR=0.55; HR=0.65
Larkin et al. (2015)[39,+]		Median progression-free survival (months)
	Nivolumab (1mg/kg) + Ipilimumab (3mg/kg)	11.5
	vs	vs
	Nivolumab (1mg/kg)	6.9
	vs	vs
	Ipilimumab (3mg/kg)	2.8
		HR=0.42; HR=0.57
Hodi et al. (2016)[42,◊]	Nivolumab (1mg/kg) + Ipilimumab (3mg/kg) vs Ipilimumab (3mg/kg)	Confirmed objective response (%) 58 vs 19, odds ratio=12.2
Postow et al. (2015)[44,◊]	Nivolumab (1mg/kg) + Ipilimumab (3mg/kg) vs Ipilimumab (3mg/kg)	Confirmed objective response (%) 61 vs 11, interim report
Schachter et al. (2017)[48,#]		Median OS (months)
	Pembrolizumab (10mg/kg, q2W)	Not reached
	vs	vs
	Pembrolizumab (10mg/kg, q3W)	Not reached
	vs	vs
	Ipilimumab (3mg/kg)	16.0
		HR=0.68; HR=0.58
Robert et al. (2015)[47,#]		Rate of progression-free survival at 6 months (%)
	Pembrolizumab (10mg/kg, q2W)	47.3
	vs	vs
	Pembrolizumab (10mg/kg, q3W)	46.3
	vs	vs
	Ipilimumab (3mg/kg)	26.5
		HR=0.58; HR=0.58
Ribas et al. (2013)[46]		Rate of progression-free survival at 6 months (%)
	Pembrolizumab (10mg/kg) for ipilimumab-refractory patients	38
	vs	vs
	Pembrolizumab (2mg/kg) for ipilimumab-refractory patients	34
	vs	vs
	ICC for ipilimumab-refractory patients	20
		HR=0.50; HR=0.57
Weber et al. [in press][49]	Nivolumab adjuvant (3mg/kg) vs Ipilimumab adjuvant (10mg/kg)	Recurrence-free survival at 12 months (%) 70.5 vs 50.8, HR=0.65
Larkin et al. (2017)[50,*]	Nivolumab (3mg/kg) vs ICC for ipilimumab-refractory patients	Median OS (months) 16 vs 10, HR=0.80
Weber et al. (2015)[45,*]	Nivolumab (3mg/kg) vs ICC for ipilimumab-refractory patients	Confirmed objective response (%) 33.7 vs 10.6, interim report
Robert et al. (2015)[43]	Nivolumab (3mg/kg) vs Dacarbazine	Overall rate of survival at 1 year (%) 72.9 vs 42.1, HR=0.42
Ascierto et al. (2017)[51]	Ipilimumab (10mg/kg) vs Ipilimumab (3mg/kg)	Median OS (months) 14.6 vs 13.3, HR=0.84
Eggermont et al. (2016)[40]	Ipilimumab (10mg/kg) Adjuvant vs Placebo	Recurrence-free survival (%) 40.9 vs 30.3, HR=0.76
Robert et al. (2011)[38]	Ipilimumab (10mg/kg) + Dacarbazine vs Dacarbazine alone	Median OS (months) 11.2 vs 9.1, HR=0.72
Hodi et al. (2010)[37]		Median OS (months)
	Ipilimumab (3mg/kg) + gp100 vaccination	10.0
	vs	vs
	Ipilimumab (3mg/kg) alone	10.1
	vs	vs
	gp100 vaccination alone	6.4
		HR=0.68; HR=0.66

gp100, glycoprotein 100; ICC, investigator's choice of chemotherapy (dacarbazine or paclitaxel + carboplatin); OS, overall survival. Same clinical trials are indicated by +, ◊, # and *.

gp100, glycoprotein 100; ICC, investigator's choice of chemotherapy (dacarbazine or paclitaxel + carboplatin); OS, overall survival
+,◊,# Same clinical trials

versus ICC was challenged to ipilimumab-refractory melanoma. Patients with advanced melanoma who progressed after ipilimumab and/or BRAF therapy received 10 mg/kg (N = 181) or 2 mg/kg (N = 180) of pembrolizumab or ICC (N =

179) in a randomized, controlled study [41]. Six-month progression-free survival rate was 38% (HR,0.5 versus ICC; $P < 0.0001$) in the pembrolizumab 10 mg/kg group, 34% (HR,0.57 versus ICC; $P < 0.0001$) in the 2 mg/kg group, and 16% in the ICC group [41] (Table 1).

Patients with advanced melanoma were assigned to in a 1:1:1 ratio to pembrolizumab 10 mg/kg q2W ($N = 279$), pembrolizumab 10 mg/kg q3W ($N = 277$), and ipilimumab 3 mg/kg q3W ($N = 278$) [40]. The interim 6-month progression-free survival rates were 47.3% for pembrolizumab q2W (HR, 0.58 versus ipilimumab; $P < 0.001$), 46.4% for pembrolizumab q3W (HR, 0.58 versus ipilimumab; $P < 0.001$), and 26.5% for ipilimumab [40]. In the final survival analysis, median OS was not reached in both pembrolizumab groups, while it was 16 months with ipilimumab (HR, 0.68 for pembrolizumab every q2W versus ipilimumab; $P = 0.0009$, and HR, 0.68 for pembrolizumab q3W versus ipilimumab; $P = 0.0008$) [39•]. Twenty-four-month OS rate was 55% in the q2W group, 55% in the q3W group, and 43% in the ipilimumab group [39•]. In addition to prolonged survival, quality of life of melanoma patients are maintained during the course of nivolumab or pembrolizumab treatment [51, 52]. These datasets led to US FDA approval of pembrolizumab for ipilimumab- and/or BRAF inhibitor-refractory advanced melanoma.

Combined Immune Checkpoint Inhibitors and Melanoma

As mentioned earlier, CTLA-4 and PD-1 are nonredundant T cell inhibitory checkpoint pathways, acting at different stages of the T cell activation. CTLA-4 is primarily involved in the early antigen-recognition stages of T cell activation within the lymph node, whereas the PD-1 pathway acts at late, effector stages of the antitumor immunity within the tumor microenvironment (Fig. 1). Therefore, combined checkpoint inhibitors provide additive or synergistic effects on anti-melanoma immunity [35•, 36] (Table 1).

Patients with previously untreated, unresectable stage III or IV melanomas were assigned in a 1:1:1 ratio to receive nivolumab + ipilimumab ($N = 314$), nivolumab alone ($N = 316$), and ipilimumab alone ($N = 315$) [35•]. The median progression-free survival was 11.5 months in the nivolumab-plus-ipilimumab group, 6.9 months in the nivolumab group, and 2.9 months in the ipilimumab group. Significantly longer progression-free survival was observed in the nivolumab-plus-ipilimumab group than in the ipilimumab group (HR, 0.42; $P < 0.001$) and in the nivolumab group than in the ipilimumab group (HR, 0.57; $P < 0.001$). The HR for the comparison between the nivolumab-plus-ipilimumab group and the nivolumab group was 0.74 [35•]. In patients with tumors positive for the PD-L1, the median progression-free survival was 14 months both in the nivolumab-plus-ipilimumab group and in the nivolumab group. Notably, in patients with PD-L1-negative tumors, the progression-free survival was longer with the combination therapy than with nivolumab monotherapy (11.2 versus 5.3 months) [35•]. At a minimum follow-up of 36 months, the median OS had not been reached in the nivolumab-plus-ipilimumab group and was 37.6 months in the nivolumab group, as compared with 19.9 months in the ipilimumab group (HR for death with nivolumab plus ipilimumab versus ipilimumab, 0.55 [$P < 0.001$]; HR for death with nivolumab versus ipilimumab, 0.65 [$P < 0.001$]) [37•].

Patients with previously untreated, metastatic, *BRAF* wild-type melanomas were enrolled in a 2:1 ratio to receive nivolumab plus ipilimumab ($N = 72$) or ipilimumab alone ($N = 37$) [36]. Patients with *BRAF*-mutated metastatic melanomas were also similarly assigned to receive nivolumab plus ipilimumab ($N = 23$) or ipilimumab alone ($N = 10$) [36]. Among patients with *BRAF* wild-type tumors, the rate of confirmed objective response was 61% (44 of 72 patients) in the ipilimumab and nivolumab combination group versus 11% (4 of 37 patients) in the ipilimumab monotherapy group ($P < 0.001$), with complete responses reported in 16 patients (22%) in the combination group and no patients in the ipilimumab monotherapy group. The median progression-free survival was not reached with the combination therapy and was 4.4 months with ipilimumab monotherapy (HR, 0.40, $P < 0.001$) [36]. Similar results for response rate and progression-free survival were observed in 33 patients with *BRAF* mutation–positive tumors [36]. The above clinical trial was reanalyzed at a median follow-up of 24.5 months [38•]. The rate of objective response in total patients irrespective of *BRAF* mutation was 59% (56 of 95 patients) in the ipilimumab and nivolumab combination group versus 11% (5 of 47 patients) in the ipilimumab monotherapy group ($P < 0.001$) [38•]. Complete responses were reported for 21 (22%) of 95 patients in the combination group and no patients in the ipilimumab group. Progression-free survival at 1 year was 52.5% in the combination group and 16% for ipilimumab alone and seemed to plateau after 12 months; at 2 years, it was 51.3% in the combination group and 12% for ipilimumab monotherapy [38•].

Immune-Related Adverse Events

Despite the fact that immune check point inhibitors are revolutionizing therapy for melanoma, their application is also

associated with diverse immune-related adverse events (irAEs) including colitis, endocrinopathies, hepatitis, pneumonitis, cardiotoxicity, uveitis, skin eruptions, and vitiligo [53–60] (Fig. 1). Interestingly, development of vitiligo predicts a beneficial clinical effects of nivolumab on advanced melanoma patients [55]. Any grade irAEs were observed 90.4% in the ipilimumab group compared to 39.7% in the placebo group [47]. Among them, grade 3 or 4 irAEs were reported 43.6 and 2.7%, respectively [47].

Any grade adverse events for nivolumab monotherapy is 99% (grade 3 or 4; 47%), while those of ICC is 96% (grade 3 or 4; 43%) [43]. Any treatment-related adverse events leading to discontinuation of drug is found in 5% in the nivolumab group but in 11% in the ICC group [43]. Any grade adverse events related to 10 mg/kg pembrolizumab, 2 mg/kg of pembrolizumab, and ICC are 73.7, 67.4, and 80.7%, respectively [41]. Any grade adverse events leading to discontinuation of the drug are 6.7, 2.2, and 5.8%, respectively [41]. Any treatment-related adverse events in nivolumab plus ipilimumab, nivolumab monotherapy, and ipilimumab monotherapy are 95.5, 82.1, and 86.2%, respectively [35•]. Any treatment-related adverse events leading to drug discontinuation are 36.4, 7.7, and 14.8%, respectively [35•]. Combined immune checkpoint inhibitor therapy with ipilimumab and nivolumab is associated with synergistic toxicity.

Importantly, most irAEs resolve or are controlled with immune-modulating agents such as corticosteroid, infliximab, and mycophenolic acid [61]. Recent analysis by Schadendorf et al. shows that median progression-free survival was 8.4 months for patients who discontinued nivolumab plus ipilimumab because of adverse events during the induction phase and 10.8 months for patients who did not discontinue because of adverse events ($P = 0.97$) [62]. The objective response rate was 58.3% for patients who discontinued because of adverse events during the induction phase and 50.2% for patients who did not discontinue. The vast majority of grade 3 or 4 adverse events occur during the induction phase, with most resolving after appropriate management. Therefore, even after discontinuation, many patients continue to derive benefit from combination therapy [62].

Conclusion

The immune checkpoint inhibitors appear open a new era for the treatment of melanoma and other malignant neoplasms. Although they are not almighty, they significantly prolong the survival of patients even in an advanced stage and maintain the patients' quality of life [51, 52]. Diverse irAEs occur but can be manageable by appropriate immunosuppressive agents. The efficacy of immune checkpoint inhibitors is likely to be maintained even in patients who are obliged to discontinue the immune checkpoint inhibitors by adverse events [62]. Additional immunotherapy and radiotherapy may enhance the objective response to immune checkpoint inhibitors [63, 64]. Further long-term follow-up analyses are warranted to delineate and highlight the benefits of immune checkpoint inhibitors.

Compliance with Ethical Standards

Conflict of Interest Masutaka Furue, Takamichi Ito, Naoko Wada, Maiko Wada, Takafumi Kadono, and Hiroshi Uchi declare they have no conflict of interest.

Human and Animal Rights and Informed Consent This article does not contain any studies with human or animal subjects performed by any of the authors.

References

Papers of particular interest, published recently, have been highlighted as:
• Of importance

1. Ernst DS, Petrella T, Joshua AM, Hamou A, Thebaud M, Vaenyheen S, et al. Burden of illness for metastatic melanoma in Canada, 2011-2013. Curr Oncol. 2016;23(6):e563–e70. https://doi.org/10.3747/co.23.3161.
2. Gwadry-Sridhar F, Nikas S, Hanson A, Seung SJ, Perrella T, Joshua AM, et al. Resource utilization and costs of managing patients with advanced melanoma: a Canadian population-based study. Curr Oncol. 2017;24(1):168–73. https://doi.org/10.3747/co.24.2432.
3. Sarangarajan Sloane RA, Gopalakrishnan V, Reddy SM, Zhang X, Reuben A, Wargo JA. Interaction of molecular alterations with immune response in melanoma. Cancer. 2017;123(S11):2130–42. https://doi.org/10.1002/cncr.30681.
4. World Health Organization, International Agency on Cancer Research (iarc). GLOBOCAN 2008. Cancer incidence and mortality worldwide in 2008 [Web resource]. Lyon, France: iarc: 2008. [Current version (2012) available online at: http://globocan.iarc.fr/Default.aspx: cited 5 Mar 2016].
5. Garbe C, Eigentler TK, Keilholz U, Hauschild A, Kirkwood JM. Systematic review of medical treatment in melanoma: current status and future prospects. Oncologist. 2011;16(1):3–24. https://doi.org/10.1634/theoncologist.2010-0190.
6. Furuichi F, Scope A, Coco V, Guida S, Gelmetti AM, Fiorani S, et al. Paradigmatic cases of pigmented lesions: how to not miss melanoma. J Dermatol. 2016;43(12):1433–7. https://doi.org/10.1111/1346-8138.13522.
7. Yamamura K, Otsuka A, Kaku Y, Seidel JA, Nomura M, Nagao H, et al. Dermoscopic changes in malignant melanoma after successful treatment with nivolumab: a case report. J Dermatol. 2017;44(5):547–8. https://doi.org/10.1111/1346-8138.13501.
8. Wolbling N, Schmid-Zalaudek K, Deinlein T, Ramusat K, Hofmann-Wellenhof R, Zalaudek I. Abundance of the benign melanocytic universe: dermoscopic-histopathological correlation in nevi. J Dermatol. 2017;44(5):499–506. https://doi.org/10.1111/1346-8138.13808.
9. Sakai H, Ando Y, Ichinga K, Tanaka M. Estimating melanin location in the pigmented skin lesions by hue-saturation-lightness color space values of dermoscopic images. J Dermatol. 2017;44(5):490–8. https://doi.org/10.1111/1346-8138.13725.

10. Rosato T, Pezzolo V, Fornari G, Agozzino M, Alfieo R, Longo C, et al. Dermoscopy pathology correlation in melanoma. J Dermatol. 2017;44(5):507–14. https://doi.org/10.1111/1346-8138.13629.
11. Florizán Muruzábal U, Gamo Villegas R, Pampín Franco A, Pinedo Moraleda F, Pérez Fernández E, López-Estebaranz JL. Combined in vivo reflectance confocal microscopy and digital dermoscopy for follow up of patients at high risk of malignant melanoma: a prospective case series study. J Dermatol. 2017;44(6):681–9. https://doi.org/10.1111/1346-8138.13743.
12. Asahara M, Hoashi T, Shirakawa N, Matsuo Y, Furusaka Y, Saeki H. Case of nodular melanoma on the upper eyelid dermoscopically mimicking pigmented basal cell carcinoma. J Dermatol. 2017;44(5):543–5. https://doi.org/10.1111/1346-8138.13615.
13. Wada M, Ito T, Tsuji G, Nakahara T, Hagihara A, Furue M, et al. Acral lentiginous melanoma versus other melanoma: a single-centre analysis in Japan. J Dermatol. 2017;44(8):932–8. https://doi.org/10.1111/1346-8138.13834.
14. Hosaka T, Furusaka Y, Shirakawa N, Matsuo Y, Azami SI, Saeki H. Case of subungual malignant melanoma showing the subtle clinical features and unexpected typical histopathological findings of melanoma in situ. J Dermatol. 2016;43(11):1361–2. https://doi.org/10.1111/1346-8138.13397.
15. Shoushtari AN, Munhoz RR, Kuk D, Ott PA, Johnson DB, Tsai KK, et al. The efficacy of anti-PD-1 agents in acral and mucosal melanoma. Cancer. 2016;122(21):3354–62. https://doi.org/10.1002/cncr.30259.
16. Furue M, Kadono T. Melanoma therapy: check the checkpoints. J Dermatol. 2016;43(2):121–4. https://doi.org/10.1111/1346-8138.13257.
17. Achkar T, Tarhini AA. The use of immunotherapy in the treatment of melanoma. J Hematol Oncol. 2017;10(1):88. https://doi.org/10.1186/s13045-017-0458-3.
18. Yamazaki N, Uhara H, Wada H, Matsuda K, Yamamoto K, Shimamoto Y, et al. Phase I study of pegylated interferon-alpha-2b as an adjuvant therapy in Japanese patients with malignant melanoma. J Dermatol. 2016;43(10):1146–53. https://doi.org/10.1111/1346-8138.13338.
19. Rivas-Tolosa K, Ortiz-Brugués A, Toledo-Pastrana T, Hassdenteufel M, Traves V, Sánchez V, et al. Local cryosurgery and imiquimod: a successful combination for the treatment of locoregional cutaneous metastasis of melanoma, a case series. J Dermatol. 2016;43(5):553–6. https://doi.org/10.1111/1346-8138.13297.
20. Shain AH, Yeh I, Kovalyshyn I, Sriharan A, Talevich E, Gagnon A, et al. The genetic evolution of melanoma from precursor lesions. N Engl J Med. 2015;373(20):1926–36. https://doi.org/10.1056/NEJMoa1502583.
21. Tokumaru A, Fukushima S, Miyashita A, Nakahara S, Kubo Y, Yamashita J, et al. Cell division cycle-associated protein 1 as a new melanoma-associated antigen. J Dermatol. 2016;43(12):1399–405. https://doi.org/10.1111/1346-8138.13436.
22. Uenemura H, Yamaoki O, Kaji T, Otsuka M, Asagoe K, Takata M, et al. Usefulness of serum 3-S-cysteinyl-dopa as a biomarker for predicting prognosis and detecting relapse in patients with advanced stage malignant melanoma. J Dermatol. 2017;44(4):449–54. https://doi.org/10.1111/1346-8138.13651.
23. Mori M, Funakoshi T, Kanoyama K, Kawakami Y, Sato E, Nakayama E, et al. Lack of XAGE-1b and NY-ESO-1 in metastatic lymph nodes may predict the potential survival of stage III melanoma patients. J Dermatol. 2017;44(6):671–80. https://doi.org/10.1111/1346-8138.13730.
24. Fukunoto T, Sakaguchi M, Oka M, Nishimura M, Makohara T, Nishigori C. Malignant melanoma with bone marrow involvement diagnosed from hypercalcemia: development of a neural cell adhesion molecule stain. J Dermatol. 2017;44(3):e105–e6. https://doi.org/10.1111/1346-8138.13718.
25. Volpe VO, Klufas DM, Hegde U, Grant-Kels JM. The new paradigm of systemic therapies for metastatic melanoma. J Am Acad Dermatol. 2017;77(2):356–68. https://doi.org/10.1016/j.jaad.2017.04.1126.
26. Furudate S, Fujimura T, Kambayashi Y, Hidaka T, Sato Y, Tsuta K, et al. Keratoacanthoma, palmoplantar keratoderma developing in an advanced melanoma patient treated with vemurafenib regressed by blockade of mitogen-activated protein kinase/kinase signaling. J Dermatol. 2017;44(9):e226–e7. https://doi.org/10.1111/1346-8138.13798.
27. Long GV, Weber JS, Infante JR, Kim KB, Daud A, Gonzalez R, et al. Overall survival and durable responses in patients with BRAF V600-mutant metastatic melanoma receiving dabrafenib combined with trametinib. J Clin Oncol. 2016;34(8):871–8. https://doi.org/10.1200/JCO.2015.62.9345.
28. Leal L, Agüa-Buxaque E, Rumoni J, Safont M, Yebenes M, Saez A, et al. Cutaneous granulomatous paraciliitis and sarcoidal granulomatous papular eruptions in a patient with metastatic melanoma treated with a BRAF inhibitor. J Dermatol. 2016;43(6):715–6. https://doi.org/10.1111/1346-8138.13255.
29. Topalian SL, Drake CG, Pardoll DM. Immune checkpoint blockade: a common denominator approach to cancer therapy. Cancer Cell. 2015;27(4):450–61. https://doi.org/10.1016/j.ccell.2015.03.001.
30. Walker LSK. PD-1 and CTLA4: two checkpoints, one pathway? Sci Immunol. 2017;2(11):eaan3864. https://doi.org/10.1126/sciimmunol.aan3864.
31. Blank C, Brown I, Peterson AC, Spiotto M, Iwai Y, Honjo T, et al. PD-L1/B7H-1 inhibits the effector phase of tumor rejection by T cell receptor (TCR) transgenic CD8+ T cells. Cancer Res. 2004;64(3):1140–5. https://doi.org/10.1158/0008-5472.CAN-03-3259.
32. Oba J, Nakahara T, Abe T, Hagihara A, Morii Y, Furue M. Expression of programmed death receptor ligand 1 in melanoma may indicate tumor progression and poor patient survival. J Am Acad Dermatol. 2014;70(5):954–6. https://doi.org/10.1016/j.jaad.2014.01.880.
33. Daud AI, Wolchok JD, Robert C, Hwu WJ, Weber JS, Ribas A, et al. Programmed death-ligand 1 expression and response to the anti-programmed death 1 antibody pembrolizumab in melanoma. J Clin Oncol. 2016;34(34):4102–9. https://doi.org/10.1200/JCO.2016.67.2477.
34. Kraft S, Fernandez-Figueras MT, Richarz NA, Flaherty KT, Hoang MP. PDL1 expression in desmoplastic melanoma is associated with tumor aggressiveness and progression. J Am Acad Dermatol. 2017;77(3):534–42. https://doi.org/10.1016/j.jaad.2017.05.007.
35.• Larkin J, Chiarion-Sileni V, Gonzalez R, Grob JJ, Cowey CL, Lao CD, et al. Combined nivolumab and ipilimumab or monotherapy in untreated melanoma. N Engl J Med. 2015;373(1):23–34. **This report shows that combinatory nivolumab and ipilimumab treatment prolongs the patient survival than monotherapy.** https://doi.org/10.1056/NEJMoa1504030.
36. Postow MA, Chesney J, Pavlick AC, Robert C, Grossmann K, McDermott D, et al. Nivolumab and ipilimumab versus ipilimumab in untreated melanoma. N Engl J Med. 2015;372(21):2006–17. https://doi.org/10.1056/NEJMoa1414428.
37.• Wolchok JD, Chiarion-Sileni V, Gonzalez R, Rutkowski P, Grob JJ, Cowey CL, et al. Overall survival with combined nivolumab and ipilimumab in advanced melanoma. N Engl J Med. 2017;377(14):1345–56. https://doi.org/10.1056/NEJMoa1709684. **This report shows that combinatory nivolumab and ipilimumab treatment prolongs the patient survival than monotherapy.**
38.• Hodi FS, Chesney J, Pavlick AC, Robert C, Grossmann KF, McDermott DF, et al. Combined nivolumab and ipilimumab versus ipilimumab alone in patients with advanced melanoma: 2-year overall survival outcomes in a multicentre, randomised, controlled,

phase 2 trial. Lancet Oncol. 2016;17(11):1558–68. This report shows that nivolumab prolongs the patient survival more than ipilimumab. https://doi.org/10.1016/S1470-2045(16)30166-7

39.• Schachter J, Ribas A, Long GV, Arance A, Grob JJ, Mortier L, et al. Pembrolizumab versus ipilimumab for advanced melanoma: final overall survival results of a multicentre, randomised, open-label phase 3 study (KEYNOTE-006). Lancet. 2017;390(10105):1854–62. https://doi.org/10.1016/S0140-6736(17)31601-X. This report shows that pembrolizumab prolongs the patient survival more than ipilimumab.

40. Robert C, Schachter J, Long GV, Arance A, Grob JJ, Mortier L, et al. Pembrolizumab versus ipilimumab in advanced melanoma. N Engl J Med. 2015;372(26):2521–32. https://doi.org/10.1056/NEJMoa1503093.

41. Ribas A, Puzanov I, Dummer R, Schadendorf D, Hamid O, Robert C, et al. Pembrolizumab versus investigator-choice chemotherapy for ipilimumab-refractory melanoma (KEYNOTE-002): a randomised, controlled, phase 2 trial. Lancet Oncol. 2015;16(8):908–18. https://doi.org/10.1016/S1470-2045(15)00083-2.

42. Weber J, Mandala M, Del Vecchio M, Gogas HJ, Arance AM, Cowey CL, et al. Adjuvant nivolumab versus ipilimumab in resected stage III or IV melanoma. N Engl J Med. 2017;377(19):1824–35. https://doi.org/10.1056/NEJMoa1709030.

43. Larkin J, Minor D, D'Angelo S, Neyes B, Smylie M, Miller WH Jr, et al. Overall survival in patients with advanced melanoma who received nivolumab versus investigator's choice chemotherapy in CheckMate 037: a randomized, controlled, open-label phase III trial. J Clin Oncol. 2017:JCO2016718023. doi: https://doi.org/10.1200/JCO.2016.71.8023.

44. Weber JS, D'Angelo SP, Minor D, Hodi FS, Gutzmer R, Neyes B, et al. Nivolumab versus chemotherapy in patients with advanced melanoma who progressed after anti-CTLA-4 treatment (CheckMate 037): a randomized, controlled, open-label, phase 3 trial. Lancet Oncol. 2015;16(4):375–84. https://doi.org/10.1016/S1470-2045(15)70076-8.

45. Robert C, Long GV, Brady B, Dutriaux C, Maio M, Mortier L, et al. Nivolumab in previously untreated melanoma without BRAF mutation. N Engl J Med. 2015;372(4):320–30. https://doi.org/10.1056/NEJMoa1412082.

46. Ascierto PA, Del Vecchio M, Robert C, Mackiewicz A, Chiarion-Sileni V, Arance A, et al. Ipilimumab 10 mg/kg versus ipilimumab 3 mg/kg in patients with unresectable or metastatic melanoma: a randomized, double-blind, multicentre, phase 3 trial. Lancet Oncol. 2017;18(5):611–22. https://doi.org/10.1016/S1470-2045(17)30231-0.

47. Eggermont AM, Chiarion-Sileni V, Grob JJ, Dummer R, Wolchok JD, Schmidt H, et al. Prolonged survival in stage III melanoma with ipilimumab adjuvant therapy. N Engl J Med. 2016;375(19):1845–55. https://doi.org/10.1056/NEJMoa1611299.

48. Robert C, Thomas L, Bondarenko I, O'Day S, Weber J, Garbe C, et al. Ipilimumab plus dacarbazine for previously untreated metastatic melanoma. N Engl J Med. 2011;364(26):2517–26. https://doi.org/10.1056/NEJMoa1104621.

49. Hodi FS, O'Day SJ, McDermott DF, Weber RW, Sosman JA, Haanen JB, et al. Improved survival with ipilimumab in patients with metastatic melanoma. N Engl J Med. 2010;363(8):711–23. https://doi.org/10.1056/NEJMoa1003466.

50. Maio M, Grob JJ, Aamdal S, Bondarenko I, Robert C, Thomas L, et al. Five-year survival rates for treatment-naïve patients with advanced melanoma who received ipilimumab plus dacarbazine in a phase III trial. J Clin Oncol. 2015;33(10):1191–6. https://doi.org/10.1200/JCO.2014.56.6018.

51. Long GV, Atkinson V, Ascierto PA, Robert C, Hassel JC, Rutkowski P, et al. Effect of nivolumab on health-related quality of life in patients with treatment-naïve advanced melanoma: results from the phase III CheckMate 066 study. Ann Oncol. 2016;27(10):1940–6. https://doi.org/10.1093/annonc/mdw265.

52. Schadendorf D, Dummer R, Hauschild A, Robert C, Hamid O, Daud A, et al. Health-related quality of life in the randomised KEYNOTE-002 study of pembrolizumab versus chemotherapy in patients with ipilimumab-refractory melanoma. Eur J Cancer. 2016;67:46–54. https://doi.org/10.1016/j.ejca.2016.07.018.

53. De Velasco G, Je Y, Bossé D, Awad MM, Ott PA, Moreira RB, et al. Comprehensive meta-analysis of key immune-related adverse events from CTLA-4 and PD-1/PD-L1 inhibitors in cancer patients. Cancer Immunol Res. 2017;5(4):312–8. https://doi.org/10.1158/2326-6066.CIR-16-0212.

54. Heinzerling L, Ott PA, Hodi FS, Husain AN, Tajmir-Riahi A, Tawbi H, et al. Cardiotoxicity associated with CTLA4 and PD1 blocking immunotherapy. J Immunother Cancer. 2016;4(1):50. https://doi.org/10.1186/s40425-016-0152-y.

55. Nakamura Y, Tanaka R, Asami Y, Teramoto Y, Imamura T, Sato S, et al. Correlation between vitiligo occurrence and clinical benefit in advanced melanoma patients treated with nivolumab: a multi-institutional retrospective study. J Dermatol. 2017;44(2):117–22. https://doi.org/10.1111/1346-8138.13520.

56. Arai T, Harada K, Usui Y, Inaba R, Tsuboi R. Case of acute anterior uveitis and Vogt-Koyanagi-Harada syndrome-like eruptions induced by nivolumab in a melanoma patient. J Dermatol. 2017;44(3):875–6. https://doi.org/10.1111/1346-8138.13612.

57. Fujimura T, Kambayashi Y, Furudate S, Kakizaki A, Hidaka T, Haga T, et al. Isolated adrenocorticotropic hormone deficiency possibly caused by nivolumab in a metastatic melanoma patient. J Dermatol. 2017;44(3):e83–e84. https://doi.org/10.1111/1346-8138.13532.

58. Tsuchiya A, Kimuga K, Kiyohara E, Tanemura A, Watanabe-Kanoda M, Fujimura R, et al. Critical renal adverse event induced by nivolumab therapy in a stage IV melanoma patient. J Dermatol. 2017;44(6):727–8. https://doi.org/10.1111/1346-8138.13538.

59. Teramoto Y, Nakamura Y, Asami Y, Imamura T, Takahira S, Nemoto M, et al. Case of type 1 diabetes associated with long-dose nivolumab therapy in a melanoma patient. J Dermatol. 2017;44(5):605–6. https://doi.org/10.1111/1346-8138.13480.

60. Wada N, Uchi H, Furue M. Case of remitting seronegative symmetrical synovitis with pitting edema (RS3PE) syndrome induced by nivolumab in a patient with advanced malignant melanoma. J Dermatol. 2017;44(8):e196–e7. https://doi.org/10.1111/1346-8138.13840.

61. Weber JS, Hodi FS, Wolchok JD, Topalian SL, Schadendorf D, Larkin J, et al. Safety profile of nivolumab monotherapy: a pooled analysis of patients with advanced melanoma. J Clin Oncol. 2017;35(7):785–92. https://doi.org/10.1200/JCO.2015.66.1389.

62. Schadendorf D, Wolchok JD, Hodi FS, Chiarion-Sileni V, Gonzalez R, Rutkowski P, et al. Efficacy and safety outcomes in patients with advanced melanoma who discontinued treatment with nivolumab and ipilimumab because of adverse events: a pooled analysis of randomized phase II and III trials. J Clin Oncol. 2017:JCO2017732289. doi: https://doi.org/10.1200/JCO.2017.73.2289.

63. Fujimura T, Furudate S, Kakizaki A, Kambayashi Y, Haga T, Hashimoto A, et al. Contact sensitization therapy enhances the therapeutic effects of nivolumab in treating in-transit melanoma: two cases reports. J Dermatol. 2018;43(6):686–9. https://doi.org/10.1111/1346-8138.13229.

64. Fujimura T, Kambayashi Y, Furudate S, Hidaka T, Sato Y, Tanita K, et al. Successful treatment of multiple in-transit melanomas on the leg with intensity-modulated radiotherapy and immune checkpoint inhibitors: report of two cases. J Dermatol. 2017;44(5):592–5. https://doi.org/10.1111/1346-8138.13703.

Elevated levels of serum IgM anti-phosphatidylserine-prothrombin complex antibodies in patients with cancer-associated vasculitis

Cancer-associated vasculitis has been included in the category of vasculitis associated with probable etiology by the CHCC 2012.[1] Among the many clinical manifestations of cancer-associated vasculitis, cutaneous signs represent earlier and informative diagnostic signs.[2] Antiphospholipid (aPL) antibodies are a group of autoantibodies directed against membrane phospholipids such as phospholipid-binding proteins. Our previous studies have suggested that IgM anti-phosphatidylserine-prothrombin complex (aPSPT) antibodies could play a significant role in the pathogenesis of cutaneous vasculitis.[3] We also found that serum IgM aPSPT antibody levels in model rats with cutaneous vasculitis were significantly higher than those of wild-type rats.[4]

We retrospectively investigated three patients with cancer-associated vasculitis in the Department of Dermatology at our university. All patients were diagnosed as having cancer-associated vasculitis according to criteria established by McLean *et al.*[5] aPL antibodies, including aPSPT antibodies, anticardiolipin antibodies, as well as anti-β_2-glycoprotein I-dependent cardiolipin (aβ_2GPI/CL) antibodies, were measured as previously reported.[3]

A 65-year-old woman (Patient 1) had small cell lung carcinoma associated with cutaneous vasculitis. She presented with a mildly painful purpuric rash accompanied by swelling and redness on her lower extremities and swollen ankle joints. A 74-year-old woman (Patient 2) had liver cancer associated with cutaneous vasculitis. She showed diffuse palpable purpuric lesions on her swollen lower extremities (Fig. 1a). A 79-year-old woman (Patient 3) had malignant brain tumor associated with cutaneous vasculitis. She presented with painful purpuric rash and edematous erythema in a livedoid pattern on her lower extremities.

We detected elevated serum IgM aPSPT antibody levels (18 U/ml) in Patient 1. Patient 2 demonstrated elevated serum IgM aPSPT antibodies (35 U/ml). Patient 3 had elevated serum IgM aPSPT antibodies (22 U/ml). No aCL antibodies or aβ_2GPI/CL antibodies were detected in the serum of any of the patients. Antineutrophil cytoplasmic autoantibodies, antinuclear antibody, cryoglobulins, and lupus anticoagulant were negative in all three patients. Complement values were normal in all patients. Histopathological findings of skin biopsies were consistent with necrotizing vasculitis and thrombosis in all patients (Fig. 1b). Direct immunofluorescence studies of skin biopsies revealed IgM deposits within the affected vessel walls of the necrotizing vasculitis (Fig. 1c).

The association between aPLs and cancer has been previously reported.[6] Some of these reports have suggested that phosphatidylserine is segregated to the internal leaflet of the plasma membrane in vascular endothelial cell. Loss of asymmetry has been described under different pathological and physiological conditions, including apoptosis and malignant transformation. In fact, Ran *et al.*[7] demonstrated that anionic phospholipids become exposed on the vascular endothelium of blood vessels in mice bearing malignant tumors. The tumor cells can secrete procoagulants and inhibit anticoagulant properties of endothelial cells. However, it remains unclear whether aPL antibodies, including aPSPT antibodies, have a pathogenic role in the development of thrombosis or, in contrast, these antibodies are an epiphenomenon in cancer patients.

The following etiopathogenic hypotheses of cancer-associated vasculitis have recently been discussed: an immunologic dysregulation with a circulating immune complex, handling, production, or elimination of circulating immune complexes; and an immunogenetic abnormality with autogenes and oncogenes with up- and/or downregulation of cell proliferation through abnormal apoptosis.[8] In our patients, direct immunofluorescence studies revealed IgM deposits within the affected vessel walls of the

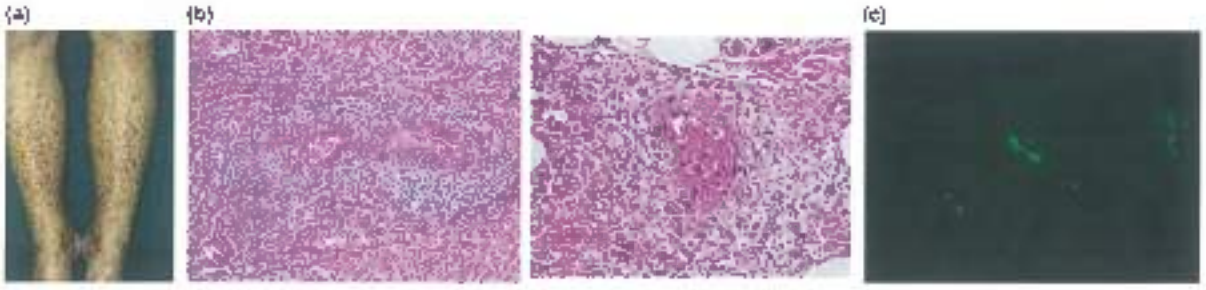

Figure 1 (a) Examination revealed diffuse palpable purpuric lesions on the patient's swollen lower extremities (Patient 2). (b) Histopathology of the cutaneous lesion showed neutrophilic infiltrates and nuclear dust around the vessel walls, indicative of necrotizing vasculitis in the lower dermis to the subcutaneous fat (hematoxylin-eosin stain; original magnification ×200) (Patient 1). In addition, we found thrombosis in the lower dermis to the subcutaneous fat (hematoxylin-eosin stain; original magnification ×400) (Patient 1). (c) Direct immunofluorescence studies revealed IgM depositions within the affected vessels (original magnification ×400) (Patient 3)

© 2017 The International Society of Dermatology

cancer-associated cutaneous vasculitis. We previously proposed that serum IgM aPSPT antibodies should be monitored as an indicator of cutaneous vasculitis activity.[4,5] Based on these findings, we suggested that immune complex-associated mechanisms, including IgM aPSPT antibodies in serum, could play an important role in the formation of cancer-associated vasculitis.

Tamihiro Kawakami, MD, PhD
Sora Takeuchi, MD, PhD
Yoshinao Soma, MD, PhD
Department of Dermatology
St. Marianna University School of Medicine
Kawasaki
Japan
E-mail: tami@marianna-u.ac.jp

Conflicts of interest: None declared
Funding source: None.

References

1 Jennette JC, Falk RJ, Bacon PA, *et al.* 2012 revised International Chapel Hill Consensus Conference nomenclature of vasculitides. *Arthritis Rheum* 2013; 65: 1–11.
2 Bugiani G, Krysenka A, Grazzini M, *et al.* Paraneoplastic vasculitis and paraneoplastic vasculitis syndromes. *Dermatol Ther* 2010; 23: 597–606.
3 Kawakami T, Yamazaki M, Mizoguchi M, *et al.* High titer of serum antiphospholipid antibody levels in adult Henoch-Schönlein purpura and cutaneous leukocytoclastic angiitis. *Arthritis Rheum* 2006; 54: 661–667.
4 Kawakami T, Yoon EY, Takeuchi S, *et al.* Novel monoclonal antibodies that recognize both rat and mouse phosphatidylserine/prothrombin complexes. *Mod Rheumatol* 2015; 29: 1–2.
5 McLean DI. Cutaneous paraneoplastic syndromes. *Arch Dermatol* 1986; 122: 765–767.
6 Gómez-Puerta JA, Cervera R, Espinosa G, *et al.* Antiphospholipid antibodies associated with malignancies: clinical and pathological characteristics of 120 patients. *Semin Arthritis Rheum* 2006; 35: 322–332.
7 Ran S, Downes A, Thorpe PE. Increased exposure of anionic phospholipids on the surface of tumor blood vessels. *Cancer Res* 2002; 62: 6132–6140.
8 Fortin PR. Vasculitides associated with malignancies. *Curr Opin Rheumatol* 1996; 8: 30–33.
9 Kawakami T, Yamazaki M, Mizoguchi M, *et al.* High titer of anti-phosphatidylserine-prothrombin complex antibodies in patients with cutaneous polyarteritis nodosa. *Arthritis Rheum* 2007; 57: 1507–1513.

Bed bug dermatitis: detection dog as a useful survey tool for environmental research of *Cimex lectularius*

Infestation by *Cimex lectularius* L. (Hemiptera: Cimicidae), or bed bug, constitutes an emerging public health problem. It is a wingless, oval-shaped, flat, reddish-brown, and temporary obligate hematophagous insect on humans and other warm-blooded animals.[1] Over the past two decades, an increase in bed bug activity has been reported worldwide because of global dispersion of this insect with international traveling, commerce, and migrations.[2] In addition, alarming resurgence of bed bug infestations has occurred over the last 10 years due to widespread resistance to current chemical insecticides (pyrethroids, carbamates, organophosphates),[3] with medical, epidemiological, and economic implications.

A 35-year-old non-atopic woman, with no significant medical history, was admitted to our outpatient clinic with itchy erythematous-edematous and papular lesions on the neck, arms, back, abdomen, and limbs (Fig. 1a,b), with one month of evolution. Some lesions appeared in a linear sequence, in numbers of three, reminding us of the "breakfast, lunch, and dinner" pattern.[1] A canine olfactory inspection for *Cimex lectularius* was performed using a canine detection unit, previously certified by the Associazione Italiana Cani Anti Cimici (AICA)[4] (Fig. 2a). The detection dog used was a female Malinois (Belgian Shepherd Dog), 36-month-old, led by one handler. The dog located the bed bug infestation in two bed slats within a wood base of a double bed. This positive result obtained from canine inspection was confirmed by a visual inspection of the handler who found at that site some aggregation points of *Cimex lectularius* (Fig. 2b,c). Targeted treatment with nitrogen liquid was performed, allowing eradication of the infestation without insecticides. After this procedure, skin lesions progressively disappeared in 10 days; 1-year follow-up was negative, confirming the etiological role of the bed bug.

Figure 1 Dermatitis with typical "breakfast, lunch, and dinner" arrangement. (a) Erythematous-edematous and excoriated papular lesions on right lower limb and (b) ankle

© 2017 The International Society of Dermatology

Immunology
immunology

IMMUNOLOGY REVIEW ARTICLE

Autoimmunity and autoimmune co-morbidities in psoriasis

Kazuhisa Furue,[1] Takanichi Ito,[1] Gaku Tsuji,[1] Takafumi Kadono,[2] Takeshi Nakahara[1,3] and Masutaka Furue[1,3]

[1]Department of Dermatology, Kyushu University, Fukuoka, Japan, [2]Department of Dermatology, St Marianna University School of Medicine, Kawasaki, Japan and [3]Division of Skin Surface Sensing, Department of Dermatology, Kyushu University, Fukuoka, Japan

doi:10.1111/imm.12893
Received 31 October 2017; revised 18 December 2017; accepted 19 December 2017.

Correspondence: Masutaka Furue, Department of Dermatology, Kyushu University, Maidashi 3-1-1, Higashiku, Fukuoka 812-8582, Japan.
Email: furue@dermatol.med.kyushu-u.ac.jp
Senior author: Masutaka Furue

Summary

Psoriasis is characterized by widespread scaly erythematous plaques that cause significant physical and psychological burdens for the affected individuals. Accelerated inflammation driven by the tumour necrosis factor-α/interleukin-23/interleukin-17 axis is now known to be the major mechanism in the development of psoriasis. In addition, psoriasis has an autoimmune nature that manifests as autoreactive T cells and is co-morbid with other autoimmune diseases, such as autoimmune bullous diseases, vitiligo, alopecia and thyroiditis. In this article, we review the recent topics on autoimmunity and autoimmune co-morbidities in psoriasis.

Keywords: alopecia; autoimmunity; bullous pemphigoid; psoriasis; thyroiditis; vitiligo.

Introduction

Psoriasis is a chronic, immune-mediated, inflammatory skin disorder that affects approximately 0·1–3% of the general population worldwide.[1–3] Given the visible nature of skin lesions, including those on the face, scalp, hands and nails,[4–9] psoriasis is a significant physical and psychological burden to afflicted patients, decreases patient quality of life, and induces feelings of internalized stigma.[8–11]

The disease burden of psoriasis is further increased by its association with psoriatic arthritis, which is characterized by seronegative spondyloarthropathies, enthesitis and elevated C-reactive protein levels.[1,12–16] Approximately 15–30% of Caucasians with psoriasis eventually develop psoriatic arthritis.[17] Although the prevalence is lower in Asian populations (Chinese 5·3–7·3%, Japanese 10·5% and Korean 11·2%), psoriatic arthritis significantly hampers patients' daily lives.[16,17] Additionally, psoriasis has significant co-morbidity with systemic inflammatory diseases, such as cardiovascular diseases and metabolic syndrome, and these conditions are currently receiving increasing attention.[18–27] In parallel, a plethora of inflammatory biomarkers are elevated in psoriasis.[28–32]

In addition to these co-morbid diseases that have a systemic inflammatory nature,[33] psoriasis presents with autoimmune aspects and co-exists with a variety of autoimmune disorders.[34–39] In this article, we summarize recent topics on autoimmunity and autoimmune co-morbidities in psoriasis.

Current pathogenesis of psoriasis and its treatments

Pathogenesis of psoriasis is multifactorial, including environmental,[40–42] genetic[43,44] and immune-related factors.[45–49] Recent genome-wide association studies have identified numerous risk-associated variants within 44 susceptibility loci for psoriasis, including HLA-C*06:02, LCE3D, IL23R and CARD14.[1,43,44,50–52] These susceptibility genes are predominantly related to the innate and adaptive immune system as well as to skin barrier function.[1,43,44]

Cutaneous trauma, such as incisional injury, induces the expression of functional cathelicidin at the injured site.[53] Cathelicidin (LL37) is one of the anti-microbial peptides that are produced by keratinocytes and neutrophils.[53] An initial trigger of psoriasis is believed to involve activation of plasmacytoid dendritic cells (DCs) upon stimulation by complexes of host DNA and LL37.[45–48] Activated plasmacytoid DCs and damaged

keratinocytes produce interferon-α (IFN-α), IFN-β and tumour necrosis factor-α (TNF-α), which result in further production of TNF-α and interleukin-23 (IL-23) by plasmacytoid and recruited inflammatory DCs [TNF/inducible nitric oxide synthase-producing DCs (TIP-DCs)].[45–46] Interleukin-23 is critically involved in the generation and activation of IL-17- and IL-22-producing effector T helper type 17 (Th17) and Th22 cells.[48,49]

Interleukin-17 up-regulates the proliferation of keratinocytes and down-regulates their differentiation.[54] Interleukin-22 also drives epidermal hyperplasia, primarily by down-regulation of genes involved in terminal differentiation.[55,56] Interleukin-17 acts on keratinocytes to induce chemokines that lead to neutrophil, TIP-DC and Th17 cell influx into the skin;[57] and up-regulates production of the neutrophil-attractive chemokines CXCL1, CXCL2 and CXCL8 by keratinocytes.[58–60]

The accelerated TNF-α/IL-23/IL-17 axis coincides with the characteristic histopathology of psoriasis, such as epidermal hyperproliferation, aberrant differentiation and neutrophilic microabscess. Regarding treatments, topical application of steroids and vitamin D3 analogues inhibits psoriatic inflammation and normalizes epidermal differentiation.[61–63] Systemic treatments, such as cyclosporine, methotrexate and the phosphodiesterase 4 inhibitor apremilast, are useful for patients with extensive lesions.[64–68] Clinical trials have demonstrated the efficacy of the oral janus kinase inhibitor tofacitinib for psoriasis.[69,70] Biological agents targeting TNF-α, IL-23 and IL-17 signalling exhibit high efficacy for patients with severe lesions, arthritis or disturbed quality of life.[71–78] However, development of the anti-IL-22 antibody fezakinumab (ILV-094) has been discontinued due to treatment failure, probably because of the redundancy of IL-22 in humans.[80] The biologicals are applicable in both paediatric and elderly patients, in patients undergoing haemodialysis and patients with perioperational circumstances.[80–83] They are also used in pregnant women, although their safety warrants further evaluation.[84,85] Switching of biologicals is recommended for patients with primary failure, secondary failure and infusion reactions.[86]

Genetic backgrounds are also related to the treatment response to biologicals.[87,88] The high cost of biologicals limits access to these medications; however, cost-saving biosimilars are rapidly advancing to the market worldwide.[89–91] Biologicals are effective not only for psoriasis but also for co-morbid cardiovascular and metabolic diseases.[92,93] In addition, monitoring of infection is mandatory to avoid serious consequences.[94–96] The emergence of antidrug antibodies is another important issue that reduces the treatment response and promotes treatment failure during biological therapy.[97,98]

Autoimmunity in psoriasis

In addition to the TNF-α/IL-23/IL-17-shifted immune deviation, psoriasis is likely to be associated with an autoimmune background.[34,35] Several studies have

Figure 1. Based on clear-cut effectiveness of biologicals, the tumour necrosis factor-α (TNF-α)/ interleukin-23 (IL-23)/ IL-17A/ IL-22 axis plays a major role in the pathogenesis of psoriasis. In addition, psoriasis possesses an autoimmune nature manifesting autoreactive T cells that are frequently restricted to HLA-C*06:02. Psoriasis is also co-morbid with other autoimmune diseases, such as bullous pemphigoid, vitiligo, alopecia and thyroiditis.

© 2018 John Wiley & Sons Ltd, Immunology, 154, 21–27

revealed the presence of autoreactive T cells in psoriasis (Fig. 1).[99–102]

Exacerbation of chronic psoriasis can be associated with streptococcal throat infections.[99,100] Lesional skin and tonsils of patients with psoriasis harbour T cells co-reactive to streptococcal M protein and type I keratin.[99,100] Streptococcal M protein exhibits structural homology with type I keratins in epidermal keratinocytes.[100] These co-reactive T cells elicited by molecular mimicry are cutaneous lymphocyte antigen (CLA)$^+$, CD8$^+$ and IL-17 producers.[100] The co-reactive T cells may be pathogenic because tonsillectomy improves clinical symptoms in concert with a significant reduction of this T-cell population.[100] Type I keratin-specific T cells are also reported in psoriasis by another research group.[101]

The antimicrobial peptide LL37 is over-expressed in psoriatic epidermis.[46,101,102] LL37 not only triggers the TNF-α/IL-23/IL-17 axis by activating DCs but also works as an autoantigen to activate the T-cell adaptive immune system.[46,101,103] LL37 is recognized as an autoantigen by circulating T cells in 46% of psoriasis patients and more frequently (75%) in moderate-to-severe psoriasis.[101] In 54% of LL37-responder patients, LL37-specific T cells are exclusively CD4$^+$, 29% are both CD4$^+$ and CD8$^+$, and 17% are exclusively CD8$^+$. These LL37-specific T cells express CLA and produce variable amounts of IFN-γ, IL-17 and IL-22 but not IL-4. The frequency of LL37-specific T cells is significantly correlated with disease severity and is reduced by anti-TNF-α therapy.[102]

The pivotal role of intra-epidermal CD8$^+$ T cells has been documented in psoriasis.[105–106] These intra-epidermal CD8$^+$ T cells produce pathogenic IL-17A, and neutralization of CD8$^+$ T cells effectively prevents psoriasis development in xenotransplanted mice models *in vivo*.[106] Moreover, a recent study by Arakawa *et al.*[106] demonstrated that intraepidermal CD8$^+$ T cells recognize ADAMTS-like protein 5 (ADAMTSL5) on melanocytes in concert with HLA-C*06:02, which is the main psoriasis risk allele. Of note, LL37-specific CD8$^+$ T cells are also restricted to HLAC*06:02.[107]

In addition to the autoreactive T-cell response, several autoantibodies have been demonstrated in patients with psoriasis, including anti-stratum corneum antibody,[107] anti-squamous cell carcinoma antigen[108] and anti-heat-shock protein 65.[109] However, the clinical significance of the autoantibody production remains elusive.

HLA class I and class II polymorphisms are associated with immune-mediated diseases typically in a disease-specific manner.[110,111] Among susceptibility genes in psoriasis, HLAC*06:02 has a fundamental importance and defines familial clustering, early onset and a more severe course of psoriasis.[112,113] The fact that patients with psoriasis harbour autoreactive T cells that are restricted to HLAC*06:02 stress a potential role for these T cells in the development and perpetuation of psoriasis.

Intriguingly, the occurrence of psoriasis is commonly noted in human immunodeficiency virus (HIV) infection.[114–118] Psoriasis with HIV infection may have a more severe course with sudden exacerbations and may be refractory to treatment.[114–118] Paradoxical onset of psoriasis and arthritis is also demonstrated in patients treated with biologicals.[119,120] Anti-TNF-α antibodies frequently induce increased levels of IL-6, which is a serum marker for interstitial pneumonia.[121] In addition, the onset and exacerbation of psoriasis have been reported in melanoma patients treated with the anti-programmed cell death protein 1 antibody nivolumab.[122,123] These phenomena may be related to a disruption in cytokine balance following treatment with biologicals, resulting in the up-regulation of plasmacytoid DCs and the subsequent production of unopposed IFNs, leading to the bypassed IL-17 over production.[124]

Autoimmune diseases co-morbid with psoriasis

Consistent with the autoimmune nature of psoriasis, numerous other autoimmune diseases, including autoimmune bullous diseases,[125] vitiligo,[126] alopecia[127] and thyroiditis,[128] are co-morbid with psoriasis. Among them, autoimmune bullous diseases, such as bullous pemphigoid and anti-laminin γ1 (p200) pemphigoid, are consistently documented.[27,125,129,130] In a nationwide population-based study of 3485 patients with bullous pemphigoid and 17425 matched controls, psoriasis is significantly associated with bullous pemphigoid (odds ratio (OR) 2·02, 95% CI 1·54–2·66).[130] In a case–control study of 287 patients with bullous pemphigoid and 1373 matched controls, the prevalence rate of psoriasis is greater in patients with bullous pemphigoid compared with control subjects (OR 4·4; 95% CI 2·2–8·9).[125] This association is also significant among both sexes.[125] In a case series of coexisting psoriasis and autoimmune bullous diseases, bullous pemphigoid is the most prevalent (63·4%) followed by anti-laminin γ1 pemphigoid (37·2%).[129]

Vitiligo is an autoimmune hypopigmentation disorder that is associated with psoriasis. Arunachalam *et al.*[126] reported that 27 of 463 (5·8%) patients with vitiligo have co-morbid psoriasis. A cross-sectional study of 1925 children and adolescents with psoriasis and 1 194 712 controls without psoriasis reveals a strong association of vitiligo with psoriasis (adjusted OR 4·76; 95% CI 1·71–13·26).[131] A significant association of vitiligo is evident in a nationwide study including 51 800 psoriasis patients with an OR of 5·94 (95% CI 3·79–9·31).[132] In parallel, it is interesting that vitiligo and psoriasis share a common genetic susceptible locus (rs9468925 in *HLA-C/HLA-B*).[133]

Psoriasis is also associated with autoimmune hair loss, namely alopecia areata (OR 4·71; 95% CI 2·98–7·45), in a national database in Taiwan.[133] In a cohort study

including 25 341 patients with psoriasis, a significant association of alopecia areata and psoriasis was also noted (OR 2·5; 95% CI 2·0–3·0).[137]

Hashimoto's thyroiditis and thyroid autoimmunity are frequently observed in the general population.[154] Free thyroxin levels are significantly increased in 105 psoriasis patients without arthritis compared with control 96 patients with tinea pedis.[155] In a hospital-based cross-sectional study of 856 615 patients, 9615 patients were diagnosed with psoriasis, and 1745 patients had Hashimoto's thyroiditis. A significant association exists for psoriasis and Hashimoto's thyroiditis even after adjusting for confounding variables, including gender, age, psoriatic arthropathy and the use of systemic anti-psoriatic agents (OR 2·49; 95% CI 1·79–3·48).[156] However, Vassilatou et al.[156] did not identify any tendency of association between psoriasis and autoimmune thyroiditis in their 314 patients with psoriasis.

Although the precise mechanisms underlying the autoimmune co-morbidities are not completely understood, damage to the basement membrane, melanocytes and hairs by chronic psoriatic inflammation may initiate and accelerate skin-related autoimmune diseases. An association of Crohn's disease and collagen diseases, such as systemic lupus erythematosus, rheumatoid arthritis, Sjögren's syndrome and systemic sclerosis, has been demonstrated in psoriasis patients.[127,157,158] Some patients with psoriasis develop collagen diseases upon treatment with biologicals.[139–141]

Similar to psoriasis, IFNs, DNA–LL37 complex and plasmacytoid DCs play a pivotal role in triggering and perpetuating systemic lupus erythematosus.[142–144] Interferons accelerate the formation of DNA–LL37 complex that activates plasmacytoid DCs to produce high levels of IFNs and IL-23.[142,144] Interleukin-23 induces IL-17 production, which promotes autoimmunity.[145] Crohn's disease is also deeply linked to TNF-α/IL-23 signalling because both anti-TNF-α and anti-IL-23 biologicals are effective in this disease.[145,146] In vitiligo, IFN signature is also involved in the initiation of its immune response with the activation of plasmacytoid DCs.[147] Serum levels of IL-23 are also elevated in vitiligo.[148] These results supports a notion that common pathogenic pathways or shared autoantigens exist in psoriasis and other autoimmune diseases.

Conclusion

Psoriasis is a common chronic inflammatory skin disease that significantly decreases the physical and psychological quality of life of afflicted patients. The underlying inflammatory process results in increased co-morbidity with systemic inflammatory diseases, such as cardiovascular diseases and metabolic syndrome. In addition, numerous pathogenic traits are shared by psoriasis and other autoimmune diseases, such as autoimmune bullous diseases, vitiligo and alopecia areata. Future studies are warranted to explore the distinct pathways that underpin the inflammatory and autoimmune co-morbidity.

Disclosures

The authors declare that they have no conflict of interest.

References

1 Barbalho MH, Silva MF. Psoriasis. Lancet 2015; 386:983–94.
2 Furue M, Kadono T. Psoriatic tetrad on the scalp. J Dermatol 2016; 43:1–4.
3 Furue M, Yamazaki T. "Inflammatory skin march" in atopic dermatitis and psoriasis. Clin Rev Allerg Immunol 2017; 44:189–92.
4 Kim WB, Jerosch-Herold C, Silverwood R, Williams HC, Chalmers JR. Psoriasis Area and Severity Index 7 (PASI 7) and PASI 12 to define treatment response in clinical practice: reliability, validity, responsiveness, and interpretability. J Dermatol 2016; 43:894–8.
5 Chen JW, Chen WB, Lin Y, Chang SW. Interpretation of nail lesions assessed with psoriatic severity. J Dermatol 2017; 44:147–53.
6 Fabbrocini G, Fabbrocini G, Scala E, Cameli N, Occhiuzzo L, Sacco S, De Vincenzo C, et al. Dermoscopy of nail bed and albuginea in the differential diagnosis of nail psoriasis, nail lichen planus and nail rheumatoid arthritis. J Dermatol 2016; 43:1217–20.
7 Errichetti E, Stinco G. Dermoscopy in differential diagnosis of palmar psoriasis and chronic hand eczema. J Dermatol 2016; 43:615–6.
8 Atakan N, Yazici AC, Cosansizgüç G, Inalözü HS, Gürer MA, Sakarya Y, et al. TLQ-PSO: a cross-sectional study investigating quality of life and treatment status of psoriasis patients in Turkey. J Dermatol 2016; 43:799–804.
9 López-Lawrence H, Sandoval-Cruz H, Sullero S. Effect of a family history of psoriasis and age on comorbidities and quality of life in patients with moderate to severe psoriasis: results from the ARIZONA study. J Dermatol 2016; 43:395–401.
10 Alpsoy E, Polat M, Polat-Ozsoy Ö, Karadag AS, Durdu M, Yazici S, et al. Interdisciplinary approach to psoriasis: a multicentre study. J Dermatol 2017; 44:181–6.
11 Hrehorow M, Mössner R, Weiss E, Nakatani R, Takeuchi-Tomozoe A, Kuzuba A, et al. Lesions on the back of hands and family gender predisposes to psoriasis in patients with psoriasis. J Am Acad Dermatol 2013; 74:846–54.
12 Takeshita J, Takeshita R, Ogawa M, Takahara M, Furue M, Okada C, et al. Tendinopathy, enthesitis, malignancy in gay and quality of life in Japanese patients with psoriasis. J Dermatol 2011; 38:109–6.
13 Asahina A, Okamoto T, Tsuboi R, Nakagawa H. Serum C-reactive protein levels in Japanese patients with psoriasis and psoriatic arthritis: long-term differential effects of biologics. J Dermatol 2016; 43:779–84.
14 Takeshita J, Takeshita A, Yanagida S, Terada T, Sano S. Detection of asymptomatic carotid in psoriasis patients: an issue of psoriatic arthritis. J Dermatol 2016; 43:450–4.
15 Yamazaki T, Ohtsuki M, Sano S, Igarashi A, Morita A, Okuyama R, et al. Epidemiological analysis of psoriatic arthritis patients in Japan. J Dermatol 2016; 43:1493–6.
16 Yamazaki T, Ohtsuki M, Sano S, Igarashi A, Morita A, Okuyama R, et al. Prevalence and current therapies of psoriatic arthritis in Japan: a survey by the Japanese Society of Psoriasis Research in 2014. J Dermatol 2017; 44:e121.
17 Stuart PE, Nair RP, Tejasvi T, Chia D, Tejasvi T, Duffin KC, Ellinghaus E, et al. Genome-wide association analysis of psoriatic arthritis and cutaneous psoriasis reveals differences in their genetic architecture. Am J Hum Genet 2015; 97:816–36.
18 Koch M, Baurecht H, Rodriguez E, Rodriguez E, Schlangen C, Weichenthal M, et al. Psoriasis and cardiometabolic traits: modest association but distinct genetic architectures. J Invest Dermatol 2020; 140:1351–61.
19 Parisi R, Rutter MK, Lunt M, Young RG, Symmons DPM, Griffiths CEM, et al. Psoriasis and the risk of major cardiovascular events: cohort study using the General Practice Research Database. J Invest Dermatol 2010; 130:2668–77.
20 Tomalin LE, Shin S, Seyahi E, Kirtsoglou E, Fabrizio CB, Thomson SA. Associations of psoriasis with the risk for type 2 diabetes mellitus and obesity. JAMA Dermatol 2016; 152:761–7.
21 Cohen AD, Drucker J, Shapiro Y, Vidavsky L, Yardy DA, Dreiznik M, et al. Psoriasis and diabetes: a population-based cross-sectional study. J Eur Acad Dermatol Venereol 2008; 22:585–9.
22 Naito T, Imafuku S. Distinguishing features of body mass index and psoriasis in men and women in Japan: a hospital-based case–control study. J Dermatol 2016; 43:1406–11.

[illegible]

[illegible]

[illegible]

Guidelines of care for the treatment of psoriasis and psoriatic arthritis: case-based, presentation and evidence-based conclusions. J Am Acad Dermatol 2011; 65: 137–74.

73 Iskhan-Lopez EE, Yin XYX, Wind V, Eaton LS, Global biologic RWE, Sevenskiery F et al. Characteristics enhancers of biologic therapy agents for psoriasis: a systematic review and network meta-analysis. J Eur Dermatol 2017; 31: 1448–54.

74 Torii H, Nakano M, Fujita T, Kanda F, Katagiri H. Efficacy and safety of dose escalation of infliximab therapy in Japanese patients with psoriasis: results of the SRR-NIS study. J Dermatol 2017; 44:383–9.

75 Torii H, Tatsi T, Matsuhashi M, Takeuchi K, Ohtsuki M, Katagiri H. Safety profiles and efficacy of infliximab therapy in Japanese patients with plaque psoriasis with or without psoriatic arthritis, psoriatic pustulosis or psoriatic erythroderma: results from the prospective post-marketing surveillance. J Dermatol 2014; 41:763–70.

76 Imafuku S, Honma M, Okubo Y, Kawai M, Ohtsuki M, Morita A et al. Efficacy and safety of secukinumab in patients with generalized pustular psoriasis: a 52-week analysis from phase III open-label extension Japanese study. J Dermatol 2016; 43:1011–7.

77 Ando N, Torii H, Okubo H, Tokunaga T, Hino H, Tsuchiya T et al. Safety and efficacy of ustekinumab treatment in Japanese patients with psoriasis: results of 64-52 study. J Dermatol 2016; 43:1257–66.

78 Enoki H, Katagiri H, Kawaji K, Ishii T, Morisaki Y, Ando T et al. Efficacy and safety of ustekinumab treatment for Japanese patients with moderate to severe plaque psoriasis, erythrodermic psoriasis and generalized pustular psoriasis: results from a 52-week, open-label, phase 3 study (UNCOVER-J). J Dermatol 2017; 44:155–62.

79 Takeuchi A, Tsunemi Y, Tsuchiya H, Ohtsuki M, Okubo H, Kawamura T. Secondary seroconversion after infliximab therapy is a successful treatment strategy for generalized pustular psoriasis. J Dermatol 2012; 39:363–4.

80 Zheng H, Yang DW, Kim BR, Yu ZH, Kim T, Kim J, Lee J et al. Clinical factors predicting the therapeutic response to ustekinumab in patients with moderate to severe chronic plaque psoriasis. J Dermatol 2017; 44:560–6.

81 Kawahara Y, Yamamoto K, Takahashi T, Tsujikawa K, Shiraishi Y, Nishi-Tatsumbashi M et al. Successful ustekinumab treatment of a psoriatic vulgaris patient with hemodialysis for renal failure: a case report and a review of the previous reports on biologic treatments for psoriatic patients with hemodialysis for renal failure. J Dermatol 2014; 41:727–30.

82 Nishimatsuya K, Tsuchiya C, Morikawa T, Hirasawa Z, Yamada S, Gotz H et al. Successful treatment with ustekinumab of psoriatic vulgaris in a patient undergoing hemodialysis. J Dermatol 2016; 43:913–4.

83 Kanehiro H, Morisawa T, Abe H, Kawai S, Takahashi F, Tsubo R et al. Perioperative management of clinical uncertain factors of biologic-treated psoriatic patients: case reports and review. J Dermatol 2015; 42:196–3.

84 Morrison M, Ashton A, Hajeski M, Tomko K, Hoertnagel Y, Katagiri H. Biologic treatments for elderly patients with psoriasis. J Dermatol 2017; 44:1023–5.

85 Bechman M, Aguiar E, Anderson M, Arnorsson K, Baker C, Foley P et al. Psoriasis in those planning a family, pregnant or breast-feeding. The Australasian Psoriasis Collaboration. Australas J Dermatol 2017; https://doi.org/10.1111/ajd.12661

86 Adachi A, Kawana M, Hirano T, Tada H, Kanekura M, Murata S et al. Case of generalized pustular psoriasis exacerbated during pregnancy, successfully treated with ustekinumab. J Dermatol 2016; 43:1439–40.

87 Maeda H, Hayama F, Kikuchi A, Yamada K, Fukuchi O, Ito T et al. Switching of biologics in psoriatic patients and results. J Dermatol 2017; 44:16–18.

88 Tejasvi T, Stuart PE, Chandran V, Voorhees JJ, Gladman DD, Rahman P et al. TNFAIP3 gene polymorphisms are associated with response to TNF blockade in psoriasis. J Invest Dermatol 2012; 132:593–600.

89 Nakahara T, Kaga M, Ito T, Ishii T, Horiuchi T, Adachi A et al. Genetic prediction of the effectiveness of biologics for psoriasis treatment. J Dermatol 2015; 42:1375–7.

90 de la Cruz C, de Carvalho AV, Demarchi IG, Cordeiro Garcia AM, Gonzalez C, Maeda M et al. Biosimilars in psoriasis: clinical practice and regulatory perspectives in Latin America. J Dermatol 2017; 44:5–12.

91 Cohen AD, Wu D, Puig L, Chimenti S, Vender R, Papoutsakis M et al. Biosimilars for psoriasis: worldwide overview of regulatory guidelines, uptake and implications for dermatology clinical practice. Br J Dermatol 2017; 177:1496–501.

92 Takeshita H, Saeki K, Tokuyo A, Imura H. Economic burden of psoriatic patients in Japan: analysis from a single outpatient clinic. J Dermatol 2017; 44:1028–8.

93 Chalopatis A, Avramopoulos M, Chalopatis P, Potekhina I, Avramopoulos P, Krunic P. Impact of ustekinumab treatment on cardiovascular risk biomarkers in psoriasis patients: a pilot study. J Dermatol 2017; 44:963–9.

94 Pina T, Corrales A, Lopez-Mesa B, Armesto S, Gonzalez-Lopez MA, Gonzalez-Vela J et al. Anti-tumor necrosis factor α therapy improves endothelial function and arterial stiffness in patients with moderate to severe psoriasis: a 6-month prospective study. J Dermatol 2016; 43:1267–71.

95 Dubreuil P, Farhat B, Daudin M-A, Carretero G, Gottrand M, Vanuchelen F et al. Interleukin 12 inhibition in moderate to severe psoriasis patients treated with biological drugs compared to classic systemic drugs: findings from the BIOSPAM/IHDAB Registry. J Eur Dermatol 2017; 457:513–21.

96 Mizuno H, Nakamura T, Watanabe T, Fujimura MT, Ohkawa S, Watanabe S et al. Loss of recurrent severe cellulitis and cutaneous conditions during psoriasis treatment with guselkumab. J Dermatol 2017; 44:306–7.

97 Schlenger C, Blanchet T, Vanelle cause urine meningitis under ustekinumab because of plaque psoriasis. J Dermatol 2017; 44:704–5.

98 Kim H, Gil H, Gold M, Kim M, Kimball L, Gyulai R. Pharmacokinetic modelling and exposure-response analysis of adalimumab and ustekinumab in patients with psoriasis treated with adalimumab or ustekinumab. J Dermatol 2016; 43:1016–25.

99 Gyldenkerne N, Ferkingstad O, Jensen P, Gudbjartsson H, Stefansdottir L, Sveinbjornsson G et al. Drug-induced gene and multilevel modulation in patients with psoriasis treated with adalimumab or ustekinumab. J Eur Acad Dermatol Venereol 2017; 31:1510–9.

100 DiLuna L, Vollmer S, Bangs P, Elkhart JW, Chiarenza S, Prins K. Identical TCR β-chain rearrangements in oligoclonal expansions and skin lesions of patients with psoriasis vulgaris. J Invest Dermatol 2006; 126:2104–11.

101 Christophidis RH, Sigurdardottir BL, Sigurgeirsson B, Olafsson JH, Sigurdsson MI, Thorleifsdottir RH et al. Improvement of psoriasis after ustekinumab is associated with a decrease in the frequency of circulating T cells that recognize keratinocyte-derived peptides and homologous skin autoantigens. J Invest Dermatol 2012; 132:2148–5.

102 Lande R, Botti E, Jandus C, Dojcinovic D, Fanoni G, Conrad C et al. The antimicrobial peptide LL37 is a T-cell autoantigen in psoriasis. Nat Commun 2014; 5:5621.

103 Lande R, Chamilos G, Ganguly D, Demaria O, Frasca L, Durr S et al. Cationic antimicrobial peptides in psoriatic skin cooperate to break innate tolerance to self-DNA. Eur J Immunol 2015; 45:203–13.

104 Chang K, Smith RB, Jennings JJ, Schwab JH, Lotze JA, Cavalli LL et al. CD4+ T cells in psoriatic lesions preferentially use T-cell receptor Vβ5 and/or Vβ13.1 genes. Proc Natl Acad Sci USA 1994; 91:9183–4.

105 Conrad C, Boyman O, Tonel G, Tun-Kyi A, Laggner C, de Fougerolles A et al. αIIβ3 integrin is crucial for accumulation of epidermal T cells and the development of psoriasis. Nat Med 2007; 13:836–42.

106 Di Meglio P, Villanova F, Nestle FO. Interleukin 17 and psoriasis pathogenesis. J Allergy Clin Immunol 2014; 134:274–6.

107 Sanchez A, Ferrari E, Stifel J, Bogen P, Kim EJ, Rich T et al. Melanocyte antigen triggers autoimmunity to human psoriasis. J Exp Med 2015; 212:2203–12.

108 Jakobsen S, Chandrashekar TP, Brunner EH, Mainieroska P, Jarrett C, Chandrashekar M, Barrett G. Autoimmunity in psoriasis. Relation of disease activity and form of psoriasis to immunopathogenetic findings. Arch Dermatol Res 1978; 261:115–46.

109 El-Rachkidy RG, Young HS, Griffiths CE, Camp RD. Planned treatment response to the squamous cell carcinoma antigen peptide family in psoriasis. J Invest Dermatol 2006; 126:2219–26.

110 Bartholomew A, Qin HY, Weiberg L, Tong X, Mayerich MM, Bos JD. Antibodies to recombinant 45-2D6 heat shock protein and other keratinocyte antigens in patients with psoriasis. J Invest Dermatol 1995; 105:427–9.

111 Stokkan BC, Rollman PM, Tugal GH, van Dommelen EJ, HLA-DR and -DQ phenotypes in erythrodermic forms: a meta-analysis. Gen 1999; 43:395–401.

112 Fernandes MMA, Stevens CR, Walsh EC, De Jager PL, Goyette P, Plenge RM et al. Defining the role of the MHC in autoimmunity: a review and pooled analysis. PLoS Genet 2008; 4:e1000024.

113 Gudjónsson JE, Kárason A, Antonsdóttir AA, Rúnarsdóttir EH, Gudjónsdóttir H, Jonsdóttir I et al. HLA-Cw6-positive and HLA-Cw6-negative patients with Icelandic psoriasis vulgaris have distinct clinical features. J Invest Dermatol 2002; 118:362–5.

114 Gudjónsson JE, Karason A, Antonsdóttir A, Runarsdottir EH, Hallgrimsdottir EB, Gudjónsdóttir H et al. Psoriasis patients who are homozygous for the HLA-Cw*0602 allele have a 2.5-fold increased risk of developing psoriasis compared with carrier heterozygotes. Br J Dermatol 2003; 148:233–5.

115 Drewe E, Johnson TW, Rapini RP, Power T, Barnetson R, Ross A. Acquired immunodeficiency syndrome-associated psoriasis and Reiter's syndrome. Arch Dermatol 1987; 123:1621–22.

116 Olbrich HL, Maurer TA, Becker B, Bergin TG. Psoriasis and human immunodeficiency virus infection. J Am Acad Dermatol 1998; 39:267–71.

117 Tsai TF, Jee SH, Chen JH, Lee TC, Lee CT, Chiang PH et al. HIV infection increases the risk of incident psoriasis: a nationwide population-based cohort study in Taiwan. J Acquir Immune Defic Syndr 2013; 63:493–8.

118 Johnson TW, Drewe M, Rapini RP, Ross A. CD4 lymphocyte phenotype. N Engl J Med 1985; 313:1415.

119 Saeki H, Kiyoshi M, Yamamoto T, Kobayashi K, Ito T, Okumura T et al. Quick, HIV infection in Japanese typical psoriasis. J Dermatol 2017; 44:127–3.

120 Ruiz-Genao D, Perez-Zabala B, Lopez-Estebaranz J, Sebastian J, Garcia-Diez A, Fonseca M et al. Possible periodontal occurrence of inflammatory arthritis in patients with psoriasis treated with biologics: findings in the Biomaterialeria cohort. Br J Dermatol 2013; 176:797–9.

© 2018 John Wiley & Sons Ltd, *Immunology*, 154, 21–27

[illegible]

[illegible]

[illegible]

"Inflammatory skin march" in atopic dermatitis and psoriasis

Masutaka Furue & Takafumi Kadono

Inflammation Research
Official Journal of: The International Association of Inflammation Societies + The European Histamine Research Society

ISSN 1023-3830
Volume 66
Number 10

Inflamm. Res. (2017) 66:833-842
DOI 10.1007/s00011-017-1065-z

Springer

Your article is protected by copyright and all rights are held exclusively by Springer International Publishing AG. This e-offprint is for personal use only and shall not be self-archived in electronic repositories. If you wish to self-archive your article, please use the accepted manuscript version for posting on your own website. You may further deposit the accepted manuscript version in any repository, provided it is only made publicly available 12 months after official publication or later and provided acknowledgement is given to the original source of publication and a link is inserted to the published article on Springer's website. The link must be accompanied by the following text: "The final publication is available at link.springer.com".

Springer

Author's personal copy

Inflamm. Res. (2017) 66:833–842
DOI 10.1007/s00011-017-1065-2

Inflammation Research

"Inflammatory skin march" in atopic dermatitis and psoriasis

Masataka Furue[1] · Takafumi Kadono[2]

Received: 11 May 2017 / Accepted: 8 June 2017 / Published online: 15 June 2017
© Springer International Publishing AG 2017

Abstract

Background Comorbidities of cardiovascular diseases (CVDs), metabolic syndrome and autoimmune diseases with systemic inflammation are recent topics to mediate. Inflammatory skin diseases such as atopic dermatitis and psoriasis are an active source of diverse proinflammatory cytokines and chemokines, which are readily detectable in the circulation and are likely to be involved in developing comorbidities.

Evidence Both atopic dermatitis and psoriasis are frequently comorbid with CVD, metabolic syndrome and autoimmune diseases, the consequence of which is called "inflammatory skin march", "psoriatic march" or "march of psoriasis".

Conclusion In this review, we summarize the epidemiological evidence and pathogenetic concepts regarding inflammatory skin march in atopic dermatitis and psoriasis.

Keywords Atopic dermatitis · Psoriasis · Comorbidity · Systemic inflammation · Proinflammatory cytokines

Responsible Editor: Yoshiya Tanaka

✉ Masataka Furue
furue@dermatol.med.kyushu-u.ac.jp

[1] Department of Dermatology, Kyushu University, Maidashi 3-1-1, Higashi-ku, Fukuoka 812-8582, Japan.

[2] Department of Dermatology, St. Marianna University School of Medicine, Kawasaki, Japan

Introduction

Atopic dermatitis (AD) and psoriasis are common chronic inflammatory skin disorders affecting 2–20% and 0.1–3% of general populations worldwide, respectively [1–4]. Both AD and psoriasis are immune-mediated ailments targeting the skin, but they have distinct pathogenic immune responses [5]; therefore, topical and systemic immunosuppressants with specific biologics are recommended in their therapeutic guidelines [6–13].

Regarding immune abnormalities, AD is currently considered a biphasic or combined T cell-mediated disease. A T helper (Th)2 signal predominates in the acute phase, whereas a Th2/Th1 switch promotes disease chronicity [2, 14]. However, recent studies have proposed a significant role for interleukin (IL)-22-producing T (T22) cells and, to a lesser extent, IL-17-producing Th17 cells, in the initiation and maintenance of AD [14–16]. In addition to the involvement of cellular immunity in Th2 and T22 differentiation, elevated IgE is likely to be engaged in the development and severity of AD by manifesting IgE autoreactivity [2, 5, 17, 18]. Recent genome-wide association studies and immunochip analyses indicate at least 19 significant susceptibility loci for AD, which emphasize the potential engagement of T helper 2 (Th2) cytokines (*IL4RA/IL-4/IL13*), IL-1 family receptors (*IL1R1/IL1R1/IL1RL1/IL1RAP*) and skin barrier proteins (*FLG*) [19, 20].

The psoriatic lesion occurs preferentially on the area susceptible to frequent friction or minor trauma known as Koebner's phenomenon [21]. An initial trigger of psoriasis is thought to be the activation of plasmacytoid dendritic cells (DCs) being stimulated by complexes of host DNA and cathelicidin (LL-37) that are produced by keratinocytes after minor injuries [22–24]. Activated plasmacytoid DCs and damaged keratinocytes produce interferon (IFN)-α,

Author's personal copy

IFN-β and TNF-α, which result in further production of TNF-α, IL-12 and IL-23 by plasmacytoid and recruited inflammatory DCs [22, 23]. IL-12 promotes the differentiation of naïve CD4+ T cells into IFN-γ-producing Th1 cells. IL-23 is critically involved in the generation and activation of IL-17- and IL-22-producing effector Th (Th17 or Th22) cells [23]. IL-17A upregulates the proliferation of keratinocytes and downregulates their differentiation [25]. IL-22 also drives epidermal hyperplasia, primarily by the downregulation of genes involved in terminal differentiation [26]. IL-17A upregulates the production of neutrophil-attractive chemokines CXCL1, CXCL2 and CXCL8 by keratinocytes [27]. IL-17A also promotes the expression of TNF-α by keratinocytes [28], which indicates that the above-mentioned TNF-α/IL-23/IL-17/IL-22 axis likely forms a vicious loop in the development of psoriasis lesions. The mechanistic hypothesis coincides with the fact that antibodies against TNF-α, IL-23, IL-17A exhibit remarkable clinical effects on psoriasis [29–38], which further stress the canonical role of the TNF-α/IL-23/IL-17/IL-22 axis in the psoriatic pathogenesis.

A close association of systemic inflammation with cardiovascular disease (CVD) and metabolic syndrome is one of the recent topics in medicine [39–41]. Inflammatory skin diseases such as AD and psoriasis produce a vast range of proinflammatory cytokines and chemokines not only in the lesional skin but also into the circulation, causing systemic inflammation and comorbidity—the so called "psoriatic march", "march of psoriasis" and "inflammatory skin march" (Fig. 1) [5, 42–45]. In this review, we summarize the epidemiological evidence and pathogenetic concepts regarding inflammatory skin march in AD and psoriasis.

Inflammatory skin march in atopic dermatitis

Intense itch and frequent exacerbations are significant burdens for patients with AD; therefore, their quality of life (QOL) is impaired, especially in patients with extensive lesions [46, 47]. AD is associated with impetigo contagiosum, Kaposi's varicelliform eruption and contact dermatitis [8, 48, 49]. In addition to skin lesions, AD is frequently associated with other atopic disorders such as food allergy in infants, which then progresses to asthma and allergic rhinitis in later childhood or adulthood and has been referred to as "allergic march" or "atopic march" [50, 51]. Ophthalmologic complications such as cataract, keratoconus and retinal detachment are also important associations with AD [52–54]. Moreover, AD is significantly comorbid with systemic disorders such as obesity, CVD, mental problems and autoimmune diseases [8, 45].

Fig. 1 Inflammatory skin March in atopic dermatitis and psoriasis. Simplified model modified from references [42] and [44]. In addition to the disease-specific cytokine milieu in atopic dermatitis (IL-4/IL-22 axis) and psoriasis (TNF-α/IL-23/IL-17/IL-22 axis), the inflammatory skin of both diseases releases a vast range of proinflammatory cytokines such as TNF-α and IL-1 into the circulation and may cause chronic low-grade systemic inflammation. The chronic systemic inflammation induces insulin resistance, endothelial dysfunction and cardiovascular diseases. It also causes obesity, hypertension, dyslipidemia and type 2 diabetes mellitus. These systemic comorbidities further reduce the patients' quality of life

Author's personal copy

Obesity and atopic dermatitis

A retrospective, case–control study randomly sampled 414 patients with childhood and adolescent AD and 828 randomly sampled healthy control subjects and revealed that obesity is associated with increased AD [conditional logistic regression: odds ratio (OR) 2.00, 95% confidence interval (CI) 1.22–3.26; $P = 0.006$] [55]. The AD-predisposing effects are found when obesity starts by less than 2 years of age [adjusted OR (aOR) 15.10; 95% CI 1.51–151.21, $P = 0.02$] and 2–5 years (aOR 2.58; 95% CI 1.24–5.41; $P = 0.01$) but not greater than 5 years (aOR 1.32; 95% CI 0.66–2.64; $P = 0.43$). Obesity is associated with severer AD (ordinal logistic regression: aOR 2.37; 95% CI 1.24–5.37; $P = 0.01$) [55]. Prolonged obesity in early childhood is a risk factor for AD. A recent systematic review and meta-analysis including 30 studies have demonstrated that patients who are overweight or obese have higher odds of AD than do normal weight patients (Cochran Mantel Haenszel OR 1.42; 95% CI 1.34–1.50; random effects OR 1.31; 95% CI 1.16–1.48) [56]. In sensitivity analyses, children who are overweight or obese (random effects OR 1.32; 95% CI 1.15–1.51) and adults who are overweight or obese (random effects OR 1.29; 95% CI 1.05–1.59) have higher odds of AD. The association remains significant in North America and Asia but not Europe [56].

Cardiovascular diseases and atopic dermatitis

In two United States National Health Interview Surveys of adults aged 18–85 years ($n = 27,157$ and 34,525), individuals with eczema had a body mass index of 35 or more (aOR 2.54; 95% CI 1.16–2.05) and higher odds of hypertension (aOR 1.48, 95% CI 1.18–1.85) and lifetime prediabetes (aOR 1.71; 95% CI 1.19–2.45) [57]. Additionally, eczema presenting fatigue, daytime sleepiness, or insomnia is associated with even higher odds of obesity, hypertension, prediabetes, diabetes, and high cholesterol than eczema alone [57]. A consecutive analysis using the abovementioned database demonstrates that eczema is associated with significantly higher odds of coronary artery disease ($P \leq 0.02$), angina ($P \leq 0.02$), heart attack ($P \leq 0.047$), other heart disease ($P \leq 0.0001$), stroke ($P \leq 0.02$), and peripheral vascular disease (≤ 0.0001) in multivariate models [58]. In a National Health and Nutrition Examination Survey ($n = 4970$), flexural eczema in the past year was associated with significantly higher odds of coronary artery disease ($P \leq 0.04$), heart attack ($P \leq 0.01$), and congestive heart failure ($P \leq 0.02$) [58].

Computed tomography angiography of the coronary arteries in 31 AD patients and 33 matched control revealed that the prevalence of a coronary artery calcium score >0 was 45.2% in AD vs. 15.2% in controls ($P = 0.01$) [59]. The presence of plaques in AD patients (48.1%) was also significantly higher than that in controls (21.2%, $P = 0.03$), suggesting that AD is associated with an increased prevalence of coronary artery disease [59].

By contrast, a Danish citizen study including 26,898 patients with mild AD, 2527 patients with severe AD, and 145,372 controls showed no association of AD with myocardial infarction, stroke or cardiovascular death [60]. Notably, the patients with AD had rather significantly decreased odds for myocardial infarction, stroke or cardiovascular death [60]. Thus, the association of AD with CVD remains controversial.

Mental diseases and atopic dermatitis

Intense pruritus is the major and most burdensome symptom of AD [46, 61, 62]. The association between itch and psychological factors has been explored in patients and general populations [63, 64]. In the National Survey of Children's Health, USA ($n = 91,642$, aged 0–17 years), children with AD have a significantly greater prevalence of attention-deficit/hyperactivity disorder (aOR 1.87; 95% CI 1.54–2.27), depression (aOR 1.81; 95% CI 1.33–2.46), anxiety (aOR 1.77, 95% CI 1.36–2.29), conduct disorder (aOR 1.87, 95% CI 1.46–2.39), and autism (aOR 3.04; 95% CI 2.13–4.34) compared with those without AD [65]. A clear dose-dependent relationship has been observed between the prevalence of a mental health disorder and the reported severity of AD [65]. In the National Health and Nutrition Examination Survey ($n = 5555$, ≥18 years), the prevalence of depression was higher in AD patients compared with non-AD controls (17.5 vs. 10.5%, aOR 1.89, 95% CI 1.28–2.77) [66]. Moreover, AD was associated with higher odds of moderate (aOR 2.24; 95% CI 1.20–4.17) and severe (aOR 5.64; 95% CI 2.58–11.07) depression [66]. In the United States National Health Interview Survey ($n = 34,613$), the lifetime prevalence of depression was higher in adults with AD compared with adults who did not have AD (26.9 vs. 13.1%; aOR 2.29, 95% CI 2.02–2.61) [66]. It should be mentioned that some of the mental problems are reversible because successful treatment with anti-IL-4 receptor α antibody dupilumab improves anxiety, depression and QOL in patients with AD [67].

Autoimmune diseases and atopic dermatitis

IgE autoreactivity in AD has been given increasing attention [2, 5, 17, 18]. Some autoreactive IgE antibodies in AD patients potentially bind to cell membrane and intracellular structures of cultured human keratinocytes [68]. Natter et al., Zeller et al. and other researchers have examined

Author's personal copy

human cDNA clones coding for auto-antigens targeted by IgE autoantibodies from AD patients and have found a variety of plausible self-antigens, including manganese superoxide dismutase, ribosomal P2 protein, profilin 1, cyclophilin B, thioredoxin, α-nascent polypeptide-associated complex (α-NAC), keratin 6A, actin α2 and tubulin α1A, some of which have a high homology to environmental allergens [69, 70]. The transcriptional coactivator α-NAC is an intracellular protein that is involved in sorting newly synthesized polypeptides without any homology to environmental known allergens [71]. Peripheral blood mononuclear cells (PBMCs) from AD patients with anti-α-NAC IgE antibodies produce significantly increased amounts of IL-17, IL-22 and IFN-γ compared with normal control PBMCs in vitro in the presence of α-NAC and IL-2. The cytokine production is canceled by the depletion of antigen-presenting monocytes from PBMCs, demonstrating that the α-NAC self-antigen is presented by monocytes to T cells by the ordinary immune system [71]. The autoreactive T cells specific for α-NAC are CLA+ and CCR4+ [72]. Recently, α-NAC-specific autoreactive CD8+ T cells were also detected in AD patients. These α-NAC-specific CD8+ T cells coproduce IL-4 and IFN-γ [73]. These studies highlight the potential role of autoreactive IgE and T cell responses in exacerbating and perpetuating AD disease severity.

In Denmark citizens (6112 patients with AD and 40,560 matched controls), AD is significantly associated with alopecia areata (aOR 26.31; 95% CI 14.46–47.80), vitiligo (aOR 17.98; 95% CI 7.76–42.01), chronic urticaria (aOR 9.92; 95% CI 6.43–15.32), celiac disease (aOR 5.19; 95% CI 2.93–9.20), chronic glomerulonephritis (aOR 4.17; 95% CI 2.16–8.07), Sjögren syndrome (aOR 3.74; 95% CI 2.41–5.82), systemic lupus erythematosus (aOR 2.65; 95% CI 1.62–4.31), ankylosing spondylitis (aOR 2.33, 95% CI 1.42–3.83), Crohn's disease (aOR 2.09; 95% CI 1.52–2.85), ulcerative colitis (aOR 1.64; 95% CI 1.31–2.05), and rheumatoid arthritis (aOR 1.61; 95% CI 1.29–2.01) [74]. No significant associations have been found between AD and autoimmune thyroid diseases, multiple sclerosis, type 1 diabetes, autoimmune hematologic diseases, or pulmonary fibrosis [74]. The incidence of IgA vasculitis (Henoch-Schönlein purpura) was significantly greater, with a hazard ratio (HR) of 1.75 (95% CI 1.27–2.42), in the AD cohort (N = 95,208 children) than in the randomly selected non-AD cohort (N = 190,416 children) in Taiwan [75]. Concurrent allergic rhinitis or asthma does not increase the HR of IgA vasculitis further. The risk of developing IgA vasculitis in the AD cohort was highest within the 1 year after AD diagnosis (HR 3.99, 95% CI 1.61–9.89). The AD cohort with IgA vasculitis had a higher occurrence rate of renal involvement, particularly hematuria, than did the non-AD cohort with IgA vasculitis [75]. In a consecutive study in Taiwan, the incidence of immune thrombocytopenia was 1.72-fold greater in HR (95% CI 1.13–2.62) in the AD children cohort (N = 120,704) than in the randomly selected non-AD cohort (N = 241,408) [76]. The HR of immune thrombocytopenia in AD children increased significantly with the number of AD-related hospital visits (P < 0.001). The risk of developing immune thrombocytopenia in the AD cohort was highest within the first 3 years after the diagnosis of AD (HR 1.78; 95% CI 1.14–2.78) [76]. These studies further stress the autoimmune nature of AD.

Inflammatory skin march in psoriasis

Both the physical and psychological QOL are significantly impacted in all populations of psoriasis sufferers [77–80], and patients' adherence and satisfaction are very poor [81]. The disease burden of psoriasis is further increased by its association with psoriatic arthritis, which is characterized by seronegative spondyloarthropathies, enthesitis and elevated C-reactive protein [1, 82–85]. Approximately 15–30% of Caucasians with psoriasis eventually develop psoriatic arthritis [82]. Although the prevalence is lower in Asian populations (Chinese 5.3–7.3%, Japanese 10.5% and Korean 11.2%), psoriatic arthritis significantly hampers patients' daily lives [82, 85]. Additionally, psoriasis has a significant comorbidity with CVD, metabolic syndrome, and autoimmune diseases [86–89].

Cardiovascular diseases and psoriasis

A recent meta-analysis and systematic review of 14 cohorts identified a CVD risk in individuals with severe psoriasis (defined as requiring systemic therapy or hospital admission): the risk ratio relative to the general population was 1.37 (95% CI 1.17–1.60) for CVD mortality, 3.04 (95% CI 0.65–14.35) for myocardial infarction, and 1.59 (95% CI 1.34–1.89) for stroke [86]. The relative risks of CVD were highest in younger, severe psoriasis patients (e.g., 3.10 (95% CI 1.98–4.86) for 1 at 30 years), and the absolute risks were greatest in older individuals with severe psoriasis (e.g., 23.2 excess myocardial infarctions per 10,000 person-years at 60 years) [86]. A German cross-sectional study that included 4185 patients with psoriasis and a prospective cohort of German Health Insurance beneficiaries (n = 1,811,098) showed that psoriasis was significantly associated with myocardial infarction (OR 2.26; 95% CI 1.03–4.95) [90]. In a longitudinal study, psoriasis slightly increased the incident risk for myocardial infarction (relative risk 1.14; 95% CI 1.06–1.22), with the highest risk increments found in systemically treated psoriasis, which accounted for 17 excess cases of myocardial

Author's personal copy

infarction per 10,000 person-years [90]. A significantly higher risk of myocardial infarction has been observed in psoriasis patients in the USA [91]. For example, for a 30-year-old patient with mild or severe psoriasis, the adjusted relative risk of having a myocardial infarction is 1.29 (95% CI 1.14–1.46) or 3.10 (95% CI 1.98–4.86), respectively, compared with the control population [91]. Moreover, patients with severe psoriasis have an increased risk of CVD mortality that is independent of traditional CVD risk factors [92, 93]. In a prospective cohort study that included 48,523 patients with psoriasis and 208,187 controls in the United Kingdom, 1257 patients with psoriasis (2.59%) had a major CVD, compared with 4784 controls (2.30%), during a median follow-up of 5.2 years [94]. The multivariable analysis showed that the patients with psoriasis had a significantly higher incidence of CVD than did the controls, with an HR of 1.37 (95% CI 1.29–1.45) in hypertension; HR 2.74 (95% CI 2.41–3.12) in transient ischemic attack; HR, 1.54 (95% CI 1.36–1.73) in atrial fibrillation, HR 1.23 (95% CI 1.03–1.44) in valvular heart disease; HR 1.32 (95% CI 1.17–1.49) in thromboembolism; and HR, 1.57 (95% CI 1.39–1.78) in congestive heart failure. The age- and gender-adjusted HRs of a major CVD for psoriasis were 1.10 (95% CI 1.04–1.17) and 1.40 (95% CI 1.07–1.84) for severe psoriasis [94].

A hospital-based study conducted by Shiba et al. in Japan analyzed the prevalence of coronary heart disease ($n = 5167$, 4.5%), hypertension ($n = 16,476$, 14.5%), dyslipidemia ($n = 9236$, 8.1%), diabetes mellitus ($n = 11,555$, 10.2%), and psoriasis ($n = 1197$, 1.1%) in 113,065 patients [95]. Their multivariate analysis showed that psoriasis was an independent variable that was an associated factor for coronary heart disease (aOR 1.27; 95% CI 1.01–1.58; $P = 0.0404$) along with hypertension (aOR 7.78; 95% CI 7.25–8.35; $P < 0.0001$), dyslipidemia (aOR 2.35; 95% CI 2.19–2.52; $P < 0.0001$), and diabetes (aOR 2.80, 95% CI 2.67–2.98, $P < 0.0001$) [95]. Subclinical and vascular inflammation is readily detected by ^{18}F-fluorodeoxyglucose positron emission tomography/computed tomography even in patients with mild psoriasis [96].

Metabolic syndrome and psoriasis

The association of psoriasis with metabolic syndrome (obesity, glucose intolerance, hypertension and dyslipidemia) has also been well documented [97, 98]. As Henseler and Christophers reported in an earlier study [99], obesity and type 2 diabetes mellitus are significantly associated with psoriasis in the USA [87], Israel [100, 101], Italy [102], Germany [103] and Denmark [104]. These results have been consistent with those for psoriasis patients in Japan [105], Korea [106] and Thailand [107, 108]. Psoriasis is also comorbid with other components of metabolic syndrome, such as dyslipidemia [87, 100, 109] and hypertension [87, 100, 103, 110]. Furthermore, a significant association of psoriasis with dyslipidemia [106] and hypertension [107] has been reported in Asian populations. Moreover, patients with severe psoriasis have a higher prevalence of diabetes and obesity than do those with mild psoriasis [87]. In this context, it is intriguing that dipeptidyl peptidase 4 inhibitors, a new class of antidiabetic agents, have been shown to improve skin symptoms in some psoriasis patients [111]. Because topical vitamin D3 application is effective in treating psoriasis [112], vitamin D3 level and bone mineral density have been assessed [113, 114]. In those studies, the serum level of vitamin 25(OH)D3 was inversely correlated with the severity of psoriasis [113, 115]. Patients with a low bone mineral density showed a statistically significant longer average duration of psoriasis [114].

Autoimmune (or autoinflammatory) diseases and psoriasis

Another important fact related to "inflammatory skin march" in psoriasis is the frequent association with other immune-mediated or autoimmune diseases such as inflammatory bowel disease [116, 117], multiple sclerosis [118], autoimmune hepatitis [119] and Hashimoto's thyroiditis [120]. Moreover, frequent comorbidity is noted in psoriasis and autoimmune bullous diseases [121–125]. According to the classification proposed by McGonagle et al. [126, 127], both autoinflammation (dominated by innate immune mechanisms) and autoimmunity (dominated by antigen-specific T- and B-cell driven mechanisms) are intermingled in these psoriasis-associated comorbidities [88]. Although the association of psoriasis and celiac disease or inflammatory bowel diseases is epidemiologically clear, a larger sample investigation is mandatory to prove the definite association of psoriasis with other autoimmune/autoinflammatory diseases [88, 128–130].

Pathophysiology of inflammatory skin march

As mentioned above, AD and psoriasis are chronic inflammatory skin diseases that are driven by the IL-4/IL-22 pathway and the TNF-α/IL-23/IL-17/IL-22 axis, respectively [1, 4, 5, 14, 16, 23]. This notion is well supported by the high clinical efficacy of biologics (anti-IL-4 receptor α antibody for AD and anti-TNF-α, anti-IL-23, and anti-IL-17 antibodies against psoriasis) [1, 4, 23, 30, 67]. In addition, the release of excessive

Author's personal copy

amounts of other proinflammatory cytokines such as TNF-α and IL-1 may cause chronic low-grade systemic inflammation (Fig. 1) [42, 44]. The chronic state of inflammation appears to be a central mechanism underlying the pathophysiology of insulin resistance, visceral adiposity, hypertension and dyslipidemia. All of these conditions increase the risk for the development of type 2 diabetes and cardiovascular disease (Fig. 1) [42, 44, 131]. Consistent with this hypothesis, carotid arterial stiffness in patients with psoriasis was significantly improved by anti-TNF-α therapy in a 6-month prospective study [132]. In addition, other markers for systemic inflammation such as asymmetric dimethylarginine, red blood cell distribution width, neutrophil to lymphocyte ratio, and platelet to lymphocyte ratio, have proved to be upregulated in psoriatic patients [133–135].

The pivotal roles of TNF-α and IL-1 in systemic inflammation have been proved in experimental animals. The blockade of TNF-α by etanercept (anti-TNF-α treatment) improves glucose tolerance in obese diabetic Zucker rats [136]. Anti-TNF-α treatment with etanercept also suppresses cerebral damage caused by middle cerebral artery occlusion/reperfusion in both normal and diabetic rats [137]. Moreover, the inhibition of TNF-α production by a thalidomide analog decreases triglyceride levels and increases high-density lipoprotein levels in rats fed hypercholesterolemic diets [138]. K14/caspase-1 transgenic mice develop skin inflammation gradually spreading across the entire body surface [139]. Notably, they manifest severe systemic cardiovascular diseases and metabolic abnormalities, including aberrant vascular wall remodeling with aortic stenosis, cardiomegaly, impaired limb and tail circulation, fatty tissue loss and systemic amyloid deposition in multiple organs with liver and kidney dysfunction along with a significant increase in plasma levels of IL-1α and IL-1β. These morbid conditions are ameliorated by the simultaneous administration of anti-IL-1α and anti-IL-1β antibodies [139]. These human and murine studies support the essential role of IL-1 and TNF-α in the inflammatory skin march triggered by AD and psoriasis (Fig. 1).

Conclusion

Increasing research attention is being paid to the systemic expansion of the cutaneous inflammatory process, which is now identified as "psoriatic march", "march of psoriasis" and "inflammatory skin march" [5, 42–45]. Similar to AD, a disfigured appearance because of psoriasis may affect the psychological stability of patients [140]. The cosmetic disfigurements associated with psoriasis increase the risk of depression, anxiety, feeling of stigmatization and self-harm ideation, which profoundly impairs their satisfaction and adherence to medical care [81, 140, 141]. In addition, internal physicians may hesitate to perform electrocardiograms, echocardiograms and even blood tests, especially in severe inflammatory skin diseases with extensive skin eruptions. These undesirable factors may delay the correct diagnosis and treatment of comorbid CVD and metabolic syndromes. As anti-TNF-α treatment is feasible to manage both skin lesions and comorbidities in psoriasis [32, 142], early diagnosis and appropriate intervention by internal physicians in cooperation with dermatologists are mandatory to increase the physical and mental quality of life in psoriatic patients. Early and effective treatments may also be beneficial in preventing systemic comorbidity in AD.

Compliance with ethical standards

Conflict of interest: The authors state that they have no conflicts of interest.

References

1. Baeuerle WH, Schon MP: Psoriasis. Lancet. 2005;366:983–94.
2. Furue M, Chiricozzi A, Tsuji G, Ulzii D, Kido-Nakahara M, Nakahara T, et al. Atopic dermatitis: immune deviation, barrier dysfunction, IgE autoreactivity and new therapies. Allergol Int. 2017. doi:10.1016/j.alit.2016.12.002.
3. Sybilski AJ, Raciborski F, Lipiec A, Tomaszewska A, Lusawa A, Samel-Kowalik P, et al. Epidemiology of atopic dermatitis in Poland according to the epidemiology of allergic disorders in Poland (ECAP) study. J Dermatol. 2015;42:240–7.
4. Furue M, Kadono T: Psoriasis: beyond the scales. J Dermatol. 2016;43:4–8.
5. Guttman-Yassky E, Krueger JG, Lebwohl MG: Systemic immune mechanisms in atopic dermatitis and psoriasis with implications for treatment. Exp Dermatol. 2017. doi:10.1111/exd.13336.
6. Saeki H, Kakehara T, Tanaka A, Kabashima K, Sugaya M, Murota H, et al. Clinical practice guidelines for the management of atopic dermatitis 2016. J Dermatol. 2016;43:1117–45.
7. Katayama I, Aihara M, Ohya Y, Saeki H, Shimojo N, Shoji S, et al. Japanese guidelines for atopic dermatitis 2017. Allergol Int. 2017;66:230–47.
8. Sidbury R, Tom WL, Bergman JN, Cooper KD, Silverman RA, Berger TG, et al. Guidelines of care for the management of atopic dermatitis: Section 4. Prevention of disease flares and use of adjunctive therapies and approaches. J Am Acad Dermatol. 2014;71:1218–33.
9. Proudfoot LE, Powell AM, Ayis S, Barbarot S, Rustiga Tunes T, et al. The European treatment of severe atopic eczema in children taskforce (TREAT) survey. Br J Dermatol. 2013;169:901–9.
10. Fujii T, Hirakawa S, Narita M, Nomura I, Matsumoto K, Takaoka Y, et al. Potential preventive effects of prescriber therapy on sensitization in moderate to severe childhood atopic dermatitis: a randomized, investigator-blinded, controlled study. J Dermatol. 2014;41:1263–52.
11. Lee SC, Committee of Korean Atopic Dermatitis Association for REACH: Various diagnostic criteria for atopic dermatitis (ADC): a proposal of reliable estimation of atopic dermatitis in childhood (REACH) criteria, a novel questionnaire-based diagnostic tool for AD. J Dermatol. 2016;43:197–204.

Author's personal copy

12. Nast A, Arsonati P, Ormerod AD, Saing P, Smith C, Spuls PI, et al. European S3-Guidelines on the systemic treatment of psoriasis vulgaris. Update 2013. Short version—EDF in cooperation with EADV and IPC. J Eur Acad Dermatol Venereol. 2015;29:2277–94.
13. Menter A, Korman NJ, Elmets CA, Feldman SR, Gelfand JM, Gordon KB, et al. Guidelines of care for the management of psoriasis and psoriatic arthritis: section 6. Guidelines of care for the treatment of psoriasis and psoriatic arthritis: case-based presentations and evidence-based conclusions. J Am Acad Dermatol. 2011;65:137–74.
14. Geller JK, Shemer A, Suárez-Fariñas M, Fuentes-Duculan J, Gulewicz KJ, Wang CQ, et al. Progressive set cascades of T(H)2/T(H)17/T(H)22 cytokines and selective epidermal proteins characterizes acute and chronic atopic dermatitis. J Allergy Clin Immunol. 2012;130:1344–54.
15. Hayashida S, Uchi H, Takeuchi S, Esaki H, Moroi Y, Furue M. Significant correlation of serum IL-22 levels with CCL17 levels in atopic dermatitis. J Dermatol Sci. 2011;61:78–9.
16. Czarnowicki T, Esaki H, Gonzalez J, Malajian D, Shemer A, Noda S, et al. Early pediatric atopic dermatitis shows only a cutaneous lymphocyte antigen (CLA)(+) TH2/TH1 cell imbalance, whereas adults acquire CLA(+) TH22/TH22 cell subsets. J Allergy Clin Immunol. 2015;136:941–51.
17. Tang TS, Bieber T, Williams HC. Does "atopic march" play a role in atopic dermatitis? J Allergy Clin Immunol. 2012;129:1209–15.
18. Sargent MA, Sugar D, Kolbeck R, Rodriguez-Sanchez J. Molecular mechanisms of IgE-mediated immunity. J Allergy Clin Immunol. 2016;137:1651–61.
19. Tamari M, Hirota T. Genome-wide association studies of atopic dermatitis. J Dermatol. 2014;41:210–20.
20. Park J, Jakhar DW, Kim Y, Kim J, Kim M, Park YM, Sinal FLG null mutations in Korean patients with atopic dermatitis and comparison of the mutational spectra in Asian populations. J Dermatol. 2015;42:567–73.
21. Weiss G, Shemer A, Trau H. The Koebner phenomenon: review of the literature. J Eur Acad Dermatol Venereol. 2002;16:241–8.
22. Lande R, Gregorio J, Facchinetti V, Chatterjee B, Wang YH, Homey B, et al. Plasmacytoid dendritic cells sense self-DNA coupled with antimicrobial peptide. Nature. 2007;449:564–9.
23. Lowes MA, Suárez-Fariñas M, Krueger JG. Immunology of psoriasis. Annu Rev Immunol. 2014;32:227–55.
24. Teng MW, Bowman EP, McElver JJ, Srinivas SR, Gwardyna P, Cornelissen N, Cooper AM, et al. IL-12 and IL-23 cytokines: from discovery to targeted therapies for immune-mediated inflammatory diseases. Nat Med. 2015;21:719–29.
25. Ha HL, Wang H, Pisitkun P, Kim JC, Tassi I, Tang W, et al. IL-17 drives psoriatic inflammation via distinct, target cell-specific mechanisms. Proc Natl Acad Sci USA. 2014;111:E3423–11.
26. Bonifacio K, Bernard FX, Garcia M, Gurney AL, Lecron JC, Morel F. IL-22 inhibits epidermal differentiation and induces proinflammatory gene expression and migration of human keratinocytes. J Immunol. 2005;174:3695–702.
27. Reich K, Papp KA, Matheson RT, Tu JH, Bissonnette R, Bourcier M, et al. Evidence that a neutrophil-keratinocyte crosstalk is an early target of IL-17A inhibition in psoriasis. Exp Dermatol. 2015;24:529–35.
28. Iwakura Y, Ishigame H, Saijo S, Nakae S. Functional specialization of interleukin-17 family members. Immunity. 2011;34:149–62.
29. Gómez-García F, Epstein D, Isla-Tejera B, Lorenzo A, Vélez García-Nieto A, Ruano J. Short-term efficacy and safety of new biological agents targeting the interleukin-23-T helper 17 pathway for moderate to severe plaque psoriasis: a systematic review and network meta-analysis. Br J Dermatol. 2016. doi:10.1111/bjd.14814.
30. Imafuku S, Honma M, Esaki Y, Kimoto M, Ohsaki M, Morita A, et al. Efficacy and safety of secukinumab in patients with generalized pustular psoriasis: a 52-week analysis from phase III open-label multicentre Japanese study. J Dermatol. 2016;43:1011–7.
31. Asahina A, Ohtsuki M, Ito T, Ito Y, Okuno MM, Terui HD, et al. Ustekinumab treatment optimization for psoriasis: results of a long-term phase 2/3 Japanese study. J Dermatol. 2015;42:1042–52.
32. Asahina A, Terui T, Ohtsuki M, Tokimitsu T, Hase H, Tsuchiya T, et al. Safety and efficacy of adalimumab treatment in Japanese patients with psoriasis: results of SALSA study. J Dermatol. 2016;43:1257–65.
33. Kawakami H, Maeda T, Abe N, Matsumoto Y, Matsuhashi Y, Tsuboi R, et al. Efficacy of infliximab and methotrexate combination therapy on generalized pustular psoriasis patients unresponsive to infliximab monotherapy due to anti-infliximab antibody development. J Dermatol. 2015;42:94–5.
34. Kawakami H, Matsumoto Y, Abe N, Kawai Y, Takahashi K, Tsuboi R, et al. Perioperative management of tumor necrosis factor-alpha blocker-treated psoriatic patients: case reports and review. J Dermatol. 2016;43:190–3.
35. Kawakami Y, Yamasaki K, Takahashi T, Tsuchiyama K, Shimada-Omori R, Nasu-Tamabuchi M, et al. Successful adalimumab treatment of a psoriasis vulgaris patient with hemodialysis for renal failure: a case report and a review of the previous reports on biologic treatments for psoriasis patients with hemodialysis for renal failure. J Dermatol. 2015;42:325–30.
36. Dozono Y, Hayashi M, Kikuchi S, Fujiwara O, Yamato K, Lo T, et al. Ustekinumab treatment in patients with psoriasis undergoing hemodialysis. J Dermatol. 2015;42:733–4.
37. Nemmanniya K, Tatsushi C, Mizukawa Y, Hamamoto K, Yamada S, Gota H, et al. Successful treatment with ustekinumab of psoriasis vulgaris in a patient undergoing hemodialysis. J Dermatol. 2016;43:93–4.
38. Terui T, Terui T, Matsukawa M, Takesaki K, Ohsaki M, Nakayama H, Japanese Dermatological Association (JDA) PMS committee. Safety profiles and efficacy of infliximab therapy in Japanese patients with plaque psoriasis with or without psoriatic arthritis, pustular psoriasis or psoriatic erythroderma: results from the prospective post-marketing surveillance. J Dermatol. 2016;43:767–78.
39. Libby P, Nahrendorf M, Swirski FK. Leukocytes link local and systemic inflammation in ischemic cardiovascular disease: an expanded "cardiovascular continuum". J Am Coll Cardiol. 2016;67:1091–103.
40. de Souza Barros A, Graves DT, de Melo Loureiro AP, Junior CR, Corbi SC, Figueiredo F, et al. Diabetes and increased lipid peroxidation are associated with systemic inflammation even in well-controlled patients. J Diabetes Complicat. 2016;30:1593–6.
41. Hooper C, Karch R, Castronovo-Kuhrig M, Lunar ED, Harapanahalli R, Wojtowicz DR, et al. Biomarkers of subclinical inflammation and increases in glycemia, insulin resistance and beta-cell function in non-diabetic individuals: the Whitehall II study. Eur J Endocrinol. 2016;175:469–77.
42. Boehncke WH, Boehncke S, Tobin AM, Kirby B. The 'psoriatic march': a concept of how severe psoriasis may drive cardiovascular comorbidity. Exp Dermatol. 2011;20:303–7.
43. Davidovici BB, Sattar N, Prinz J, Puig L, Emery P, Barker JN, et al. Psoriasis and systemic inflammatory diseases: potential mechanistic links between skin disease and co-morbid conditions. J Invest Dermatol. 2010;130:1785–96.
44. Yamanaka K, Mizutani H. "Inflammatory skin march": IL-1-mediated skin inflammation, atopic dermatitis and psoriasis to-

Author's personal copy

cardiovascular events. J Allergy Clin Immunol. 2015;136:815–4.
45. Brunner PM, Silverberg JI, Guttman-Yassky E, Paller AS, Kabashima K, Amagai M, et al. Increasing comorbidities suggest that atopic dermatitis is a systemic disorder. J Invest Dermatol. 2017;137:18–25.
46. Furue M, Kadono T. New Perspectives for controlling atopic itch. J Dermatol. 2015;42:847–50.
47. Halvorsen JA, Aamot T, Clausen ML, Thomsen SF. Quality of life and disease severity in patients with atopic dermatitis. J Eur Acad Dermatol Venereol. 2016;30:1760–7.
48. Hayashi H, Furusho N, Ujiie H, Miyazaki S, Tsuaku K, Gondo C, et al. Are lifetime prevalence of impetigo, molluscum and herpes infections really increased in children having atopic dermatitis? J Dermatol Sci. 2010;59:172–8.
49. Tamagawa-Mineoka R, Masuda K, Ueda S, Nakamura N, Hojo E, Hatano J, et al. Corneal sensitivity in patients with recalcitrant atopic dermatitis. J Dermatol. 2015;42:226–2.
50. Thomsen SF. Epidemiology and natural history of atopic diseases. Eur Clin Respir J. 2015;2:24642. doi:10.3402/ecrj.v2.24642.
51. Schneider L, Hanifin J, Boguniewicz M, Eichenfield LF, Spergel JM, Dakovic R, et al. Study of the atopic March: development of atopic comorbidities. Pediatr Dermatol. 2016;33:388–98.
52. Bur H, Dodd J, Hedelberg K, Reich K. Cutaneous on atopic dermatitis: a case presentation and review of the literature. Arch Dermatol. 2011;147:385–8.
53. Furue M, Chiba T, Tsuchida S. Current status of atopic dermatitis in Japan. Asia Pac Allergy. 2011;1:64–72.
54. Shajari M, Eberhardt L, Mueller M, Al Khateeb G, Frederich S, Rudy M, et al. Effects of atopic syndrome on keratoconus. Cornea. 2016;35:1416–20.
55. Silverberg JI, Klanderman B, Lee-Chang H, Silverberg NB, Durkin HG, Joks R, et al. Association between obesity and atopic dermatitis in childhood: a case-control study. J Allergy Clin Immunol. 2011;127:1180–6.
56. Zhang A, Silverberg JI. Association of atopic dermatitis with being overweight and obese: a systematic review and meta-analysis. J Am Acad Dermatol. 2015;73:608–15.
57. Silverberg JI. Greenland P. Eczema and cardiovascular risk factors in 2 US adult population studies. J Allergy Clin Immunol. 2015;135:721–8.
58. Silverberg JI. Association between adult atopic dermatitis, cardiovascular disease, and increased heart attacks in three population-based studies. Allergy. 2015;70:1080–8.
59. Hjuler KF, Böttcher M, Vestergaard C, Thielsen M, Rudy L, Becker HE, et al. Increased prevalence of coronary artery disease in severe psoriasis and severe atopic dermatitis. Am J Med. 2015;128:1325–34.
60. Andersen YM, Egeberg A, Gislason GH, Hansen PR, Skov L, Thyssen JP. Risk of myocardial infarction, ischemic stroke, and cardiovascular death in patients with atopic dermatitis. J Allergy Clin Immunol. 2016;138:313–7.
61. Kido-Nakahara M, Furue M, Ito T, Nakahara T. Itch in Atopic Dermatitis. Immunol Allergy Clin N Am. 2017;37:113–22.
62. Takeuchi S, Oba J, Usaki H, Furue M. Practice of patients with atopic dermatitis in daily life and their experience of therapeutic effects: results of a web-based questionnaire survey. Br J Dermatol. 2015;173:259–2.
63. Schneider G, Driesch G, Heuft G, Evers S, Luger TA, Stander S. Psychosomatic co-factors and psychiatric comorbidity in patients with chronic itch. Clin Exp Dermatol. 2006;31:762–7.
64. Halvorsen JA, Dalgard F, Thonesen M, Thonesen M, Bjertness E, Lien L. Itch and mental distress: a cross-sectional study among late adolescents. Acta Derm Venereol. 2009;89:39–44.
65. Yaghmaie P, Koudelka CW, Simpson EL. Mental health comorbidity in patients with atopic dermatitis. J Allergy Clin Immunol. 2013;131:428–33.
66. Yu SH, Silverberg JI. Association between atopic dermatitis and depression in US adults. J Invest Dermatol. 2015;135:3163–6.
67. Simpson EL, Bieber T, Guttman-Yassky E, Beck LA, Blauvelt A, Cork MJ, et al. Two phase 3 trials of dupilumab versus placebo in atopic dermatitis. N Engl J Med. 2016;375:2335–48.
68. Altrichter S, Kriehuber E, Maier J, Valenta R, Kopp T, Stingl G. Serum IgE autoantibodies target keratinocytes in patients with atopic dermatitis. J Invest Dermatol. 2008;128:2352–9.
69. Natter S, Seiberler S, Hofstaetter P, Binder BR, Hirschl AM, King I, et al. Isolation of cDNA clones coding for IgE autoantigens with serum IgE from atopic dermatitis patients. FASEB J. 2998;12:1339–49.
70. Zeller S, Rhyner C, Meyer N, Schmid-Grendelmeier P, Akdis CA, Crameri R. Exploring the repertoire of IgE-binding self-antigens associated with atopic eczema. J Allergy Clin Immunol. 2009;124:278–85.
71. Hudetzky S, Hausser LM, Bilgi H, Herrizadeh A, Mittermann I, Valenta R, et al. Cytokine effects induced by the human autoallergen α-NAC. J Invest Dermatol. 2014;134:1570–8.
72. Herrizadeh A, Mittermann I, Isakson H, Wichmann K, Niebuhr M, Valenta R, et al. The role of T-cell reactivity towards the autoantigen α-NAC in atopic dermatitis. Br J Dermatol. 2011;164:318–24.
73. Reesink HM, Herrizadeh A, Wieschowski S, Mittermann I, Valenta R, Ez-Vesper B, et al. α-NAC-specific autoreactive CD4+ T cells in atopic dermatitis are of an effector memory type and secrete IL-4 and IFN-γ. J Immunol. 2016;196:5245–53.
74. Andersen YM, Egeberg A, Gislason GH, Skov L, Thyssen JP. Autoimmune diseases in adults with atopic dermatitis. J Am Acad Dermatol. 2017;76:274–80.
75. Wei CC, Lin CL, Shen TC, Li TC, Chen AC. Atopic dermatitis and association of risk for henoch-schoenlein purpura (IgA Vasculitis) and renal involvement among children: results from a population-based cohort study in Taiwan. Medicine (Baltimore). 2016;95:e2565.
76. Wei CC, Lin CL, Shen TC, Tsai TD. Atopic dermatitis and association of risk for primary immune thrombocytopenia and autoimmune diseases among children: a nationwide population-based cohort study. Medicine (Baltimore). 2016;95:e2424.
77. Mennan B, Hotwani J, Malpeel B, Tuels A, Jozefiak K, Senechal J. DLQI as a major criterion for introduction of systemic agents in patients with mild psoriasis. J Eur Acad Dermatol Venereol. 2016;30:1061–4.
78. Do YK, Lakhani K, Malhotra R, Holstaner B, Cheng C, Østbye T. Association between psoriasis and leisure-time physical activity: findings from the National Health and Nutrition Examination Survey. J Dermatol. 2015;42:148–53.
79. Ng CY, Yang YW, Liu SH, Lu JF, Yang JC, Yang CH, et al. SF-36 health survey on psoriasis quality-of-life: a study of 414 Taiwanese patients. J Dermatol. 2015;42:159–65.
80. Atakan N, Yalcin AF, Ozarmagan G, Inalozu HS, Akcali MA, Sabancio E, et al. TUR-PSO: a cross-sectional study investigating quality of life and treatment status of psoriasis patients in Turkey. J Dermatol. 2016;43:298–304.
81. Saeki H, Imahata S, Abe M, Shintani Y, Ohtsuka B, Hagihara A, et al. Poor adherence to medication as assessed by the Morisky Medication Adherence Scale 8 and low satisfaction with treatment in 2,97 psoriasis patients. J Dermatol. 2015;42:367–72.
82. Suzuki PF, Nair RP, Tsoi LC, Tejasvi T, Das S, Kang HM, et al. Genome-wide association analysis of psoriatic arthritis and cutaneous psoriasis reveals differences in their genetic architecture. Am J Hum Genet. 2015;97:816–36.

Author's personal copy

83. Asahina A, Umezawa Y, Yanaba K, Nakagawa H, Suzuki T. C-reactive protein levels in Japanese patients with psoriasis and psoriatic arthritis: long-term differential effects of biologics. J Dermatol. 2016;43:779–84.
84. Takeno T, Takahashi A, Tanigawa Y, Terada Y, Sano S. Detection of asymptomatic enthesitis in psoriasis patients at onset of psoriatic arthritis? J Dermatol. 2016;43:650–1.
85. Yamazaki T, Ohtsuki M, Sano S, Igarashi A, Morita A, Okuyama R, et al. Epidemiological analysis of psoriatic arthritis patients in Japan. J Dermatol. 2016;43:1193–6.
86. Samanovich EJ, Nelson JM, Warren RB, Parnham J, Smith CH. Incidence of cardiovascular disease in individuals with psoriasis: a systematic review and meta-analysis. J Invest Dermatol. 2013;133:2340–6.
87. Neimann AL, Shin DB, Wang X, Margolis DJ, Troxel AB, Gelfand JM. Prevalence of cardiovascular risk factors in patients with psoriasis. J Am Acad Dermatol. 2006;55:829–35.
88. Stebbing M. Psoriasis and autoimmunity. Autoimmun Rev. 2016;15:1167–81.
89. Liu HL, Chen Y, Zhou Z, Yang CK, Chen J, Chen HH, et al. Relation between endothelial progenitor cells and arterial stiffness in patients with psoriasis. J Dermatol. 2016;43:888–93.
90. Koch M, Baurecht H, Ruge IE, Rodriguez E, Schlesinger S, Volks N, et al. Psoriasis and cardiometabolic traits: modest association but distinct genetic architectures. J Invest Dermatol. 2015;135:1283–97.
91. Gelfand JM, Neimann AL, Shin DB, Wang X, Margolis DJ, Troxel AB. Risk of myocardial infarction in patients with psoriasis. JAMA. 2006;296:1735–41.
92. Mehta NN, Azfar RS, Shin DB, Neimann AL, Troxel AB, Gelfand JM. Patients with severe psoriasis are at increased risk of cardiovascular mortality: cohort study using the general practice research database. Eur Heart J. 2010;31:1000–6.
93. Abuabara K, Azfar RS, Shin DB, Neimann AL, Troxel AB, Gelfand JM. Cause-specific mortality in patients with severe psoriasis: a population-based cohort study in the UK. Br J Dermatol. 2010;163:586–92.
94. Parisi R, Rutter MK, Lunt M, Young RS, Symmons DP, Griffiths CE, et al. Psoriasis and the risk of major cardiovascular events: cohort study using the clinical practice research datalink. J Invest Dermatol. 2015;135:2183–92.
95. Shiba M, Yano T, Funasako M, Nakane E, Miyamoto N, Izumi T, et al. Association between psoriasis vulgaris and coronary heart disease in a hospital-based population in Japan. PLoS One. 2016;11:e0149516.
96. Yuan SW, Kang SY, Kim SA, Park GY, Lee WW. Subclinical systemic and vascular inflammation detected by (18) F-fluorodeoxyglucose positron emission tomography/computed tomography in patients with mild psoriasis. J Dermatol. 2015;42:591–66.
97. Takahashi H, Iizuka H. Psoriasis and metabolic syndrome. J Dermatol. 2013;39:217–8.
98. Parisi L, Kirby B, Malfeis L, Strohal R. Psoriasis beyond the skin: a review of the literature on cardiometabolic and psychological comorbidities of psoriasis. Eur J Dermatol. 2014;24:395–11.
99. Henseler T, Christophers E. Disease concomitance in psoriasis. J Am Acad Dermatol. 1995;32:982–6.
100. Cohen AD, Gibor H, Harlev Y, Zaheer D, Shapiro J, Bonneh DY, et al. Psoriasis and the metabolic syndrome. Acta Derm Venereol. 2007;87:506–9.
101. Cohen AD, Dreiher J, Shapiro Y, Vidavsky L, Vardy DA, Davidovici B, et al. Psoriasis and diabetes: a population-based cross-sectional study. J Eur Acad Dermatol Venereol. 2008;22:535–9.
102. Gisondi P, Tessari G, Conti A, Piaserico S, Schianchi S, Peserico A, et al. Prevalence of metabolic syndrome in patients with psoriasis: a hospital-based case-control study. Br J Dermatol. 2007;157:68–73.
103. Schwarz A, Berger D, Gupp A, Lehter S, Jehle PM, Kupper S, et al. Psoriasis and diabetes: a multicenter study in 222078 type 2 diabetes patients reveals high levels of depression. J Diabetes Res. 2015;2015:792968.
104. Lønnberg AS, Skov L, Skytthe A, Kyvik KO, Pedersen OB, Thomsen SF. Association of psoriasis with the risk for type 2 diabetes mellitus and obesity. JAMA Dermatol. 2013;149:1362–7.
105. Naito R, Inafuku S. Distinguishing features of body mass index and psoriasis in men and women in Japan: a hospital-based case-control study. J Dermatol. 2016;43:1409–11.
106. Choi WJ, Park HJ, Kwon JH, Kim KH, Kim KJ. Association between psoriasis and cardiovascular risk factors in Korean patients. Ann Dermatol. 2010;22:200–6.
107. Kokpol C, Arbjitsomsir W, Rajatanavin R. Prevalence and characteristics of metabolic syndrome in South-East Asian psoriatic patients: a cross-sectional study. J Dermatol. 2014;41:898–902.
108. Chularojanamontri L, Wongpraparut C, Silpa-Archa N, Chowchuenkhit P. Metabolic syndrome and psoriasis severity in South East Asian patients: an investigation of potential association using current and chronological assessments. J Dermatol. 2011;38:1124–8.
109. Dreiher J, Weitzman D, Davidovici B, Shapiro J, Cohen AD. Psoriasis and dyslipidaemia: a population-based study. Acta Derm Venereol. 2008;88:561–5.
110. Cohen AD, Weitzman D, Dreiher J. Psoriasis and hypertension: a case-control study. Acta Derm Venereol. 2010;90:23–6.
111. Nagai H, Fujiwara S, Takahashi Y, Nishigori C. Ameliorating effect of the novel dipeptidyl peptidase-4 inhibitor teneligliptin on psoriasis: a report of two cases. J Dermatol. 2015;42:1094–7.
112. Mahdavi G, Pashazadeh G, Richette AG, Calvani S. Psoriasis, vitamin D and the importance of the cutaneous barrier's integrity: an update. J Dermatol. 2016;43:507–14.
113. Kinese G, Bhalerao PH, Herédi E, Varga J, Szegedi A, Kéri J, et al. Vitamin D3 levels and bone mineral density in patients with psoriasis and/or psoriatic arthritis. J Dermatol. 2015;42:1079–84.
114. D'Epiro S, Massoni C, Salvi M, Malovzi C, Luci C, Macaluso L, et al. Psoriasis and bone mineral density: implications for long-term patients. J Dermatol. 2014;41:783–7.
115. Ito K, Koga M, Shibayama Y, Tatematsu S, Nakayama J, Inafuku S. Prolonged treatment with calcipotriol reduces recurrence of plaque psoriasis. J Dermatol. 2016;43:502–5.
116. Egeberg A, Mallbris L, Warren RB, Bryldegaard F, Gislason GH, Hansen PR, et al. Association between psoriasis and inflammatory bowel disease: a Danish nationwide cohort study. Br J Dermatol. 2016;175:687–92.
117. Nakamura K, Asado Y, Shibata S, Kakeo M, Shozu R, Takahashi T, et al. Case of psoriasis vulgaris developing ulcerative colitis during adalimumab treatment. J Dermatol. 2015;42:1029–30.
118. Egeberg A, Mallbris L, Gislason GH, Skov L, Hansen PR. Risk of multiple sclerosis in patients with psoriasis: a Danish nationwide cohort study. J Invest Dermatol. 2016;136:95–8.
119. Jensen P, Egeberg A, Gislason G, Hansen PR, Thyssen JP, Skov L. Increased risk of autoimmune hepatitis in patients with psoriasis: a Danish nationwide cohort study. J Invest Dermatol. 2016;136:1515–7.
120. Akiyama M, Ueno T, Kuroki A, Kuwana M, Nagao M, Saeki H. Association of psoriasis with Hashimoto's thyroiditis, Sjögren's syndrome and dermatomyositis. J Dermatol. 2016;43:711–2.

Author's personal copy

121. Takahashi H, Sato K, Takagi A, Ikawa S, Ishii N, Hashimoto T, et al. Subepidermal autoimmune blistering lesion in a case of psoriasis successfully treated with cyclosporin. J Dermatol. 2015;42:1125–6.
122. Maki N, Daikoku T, Okamoto N, Nagashima K, Nakamura T, Kakuta M, et al. Possible paraneoplastic syndrome case of bullous pemphigoid with immunoglobulin G anti-BP180 C-terminal domain antibodies associated with psoriasis and primary macroglobulinemia. J Dermatol. 2016;43:571–4.
123. Okashiro K, Oiwa N, Ishii N, Uehara S, Masuda H, Hashimoto T, et al. Bullous pemphigoid associated with psoriasis: a possible example of an inverse intramolecular epitope-spreading phenomenon. J Dermatol. 2015;42:798–9.
124. Ishida S, Takahashi K, Kaneko M, Ohsawa T, Tacisho C, Yamamoto A, et al. Case of subepidermal autoimmune bullous disease with psoriasis vulgaris reacting to both BP180 C-terminal domain and laminin gamma 1. J Dermatol. 2015;42:491–3.
125. Imanishi A, Tateishi C, Imanishi H, Sawa-Ozaki J, Koga H, Tsuruta D, et al. Pemphigoid with antibodies to laminin γ1, BP180 and BP230, associated with psoriasis vulgaris: successful disease control with cyclosporin. J Dermatol. 2015;42:394–7.
126. Mc Gonagle D, McDermott MF. A proposed classification of the immunological diseases. PLoS Med. 2006;3:e297.
127. Mc Gonagle D, Aydin A, Dickie LJ, McDermott MF. An integrated classification of pediatric inflammatory diseases based on the concepts of systemic autoinflammation and the immunological disease continuum. Pediatr Res. 2009;65:458R–458R.
128. Bokenkamp S, Dreiber I, Weitzman D, Ozen AO. Cluster disease associated with psoriasis. Br J Dermatol. 2009;161:1351–4.
129. Augustin M, Reich K, Glaeske G, Schaefer I, Radtke M. Co-morbidity and age-related prevalence of psoriasis: analysis of health insurance data in Germany. Acta Derm Venereol. 2010;90:47–51.
130. Hui LN, Armstrong AW. Psoriasis and autoimmune disorders: a review of the literature. J Am Acad Dermatol. 2012;67:1036–9.
131. Welty FK, Alfaddagh A, Elajami TK. Targeting inflammation in metabolic syndrome. Transl Res. 2016;167:257–80.
132. Pizzi L, Ocampo A, Lopez-Mejias R, Armesto S, Gonzalez-Lopez MA, Gómez-Arche J, et al. Anti-tumor necrosis factor-alpha therapy improves endothelial function and arterial stiffness in patients with moderate to severe psoriasis: a 6-month prospective study. J Dermatol. 2016;43:367–72.
133. Pina T, Genre F, Lopez-Mejias R, Armesto S, Ubilla B, Mijares V, et al. Asymmetric dimethylarginine but not interleukin-6 correlates with disease severity in patients with moderate-to-severe psoriasis initiating anti-tumor necrosis factor-α therapy. J Dermatol. 2016;43:389–94.
134. Kim DS, Shin D, Jee H, Kim TG, Kim SH, Kim DY, et al. Red blood cell distribution width is increased in patients with psoriasis vulgaris: a retrospective study of 261 patients. J Dermatol. 2015;42:567–71.
135. Kim DS, Shin D, Lee MS, Kim HJ, Kim DY, Kim SM, et al. Assessments of neutrophil to lymphocyte ratio and platelet to lymphocyte ratio in Korean patients with psoriasis vulgaris and pustular subtypes. J Dermatol. 2016;43:406–12.
136. Graubard B, Ostergaard JA, Schou S, Flyvbjerg A, Holmstrup P. Effects of TNF-α blocking on experimental periodontitis and type 2 diabetes in obese diabetic Zucker rats. J Clin Periodontol. 2015;42:807–16.
137. Iwata N, Takayama H, Xuan M, Kaminski S, Matsuzaki H, Okazaki M, et al. Effects of etanercept against transient cerebral ischemia in diabetic rats. Biomed Res Int. 2015;2015:189392.
138. Ferreira MM, de Melo NA, Maia R, Braga CA, Barreto EJ, de Brito FC, LASSBio-1425, an analog of thalidomide, decreases triglyceride and increases HDL cholesterol levels by inhibition of TNF-α production. Int J Cardiol. 2016;202:407–9.
139. Yamanaka K, Nakanishi T, Saito H, Matsuyama J, Ikoda K, Yoneda A, et al. Persistent release of IL-18 from skin is associated with systemic cardiovascular disease, emaciation and systemic amyloidosis: the potential of anti-IL-1 therapy for systemic inflammatory diseases. PLoS One. 2014;9:e104479.
140. Tomas-Aragones L, Marron SE. Body image and body dysmorphic symptoms. Acta Derm Venereol. 2016;96:47–50.
141. Orlandi E, Del Bosco D, Prignano F, Zamba E. Discriminating the presence of psychological distress in patients suffering from psoriasis: an application of the clinimetric approach in dermatology. Acta Derm Venereol. 2016;96:69–72.
142. Piscitelli S, Uslo E, Barisano G, Zanetti L, Lizegari D, Poreba A, et al. Treatment with tumor necrosis factor inhibitors improves coronary microvascular function in young patients with severe psoriasis. Atherosclerosis. 2016;251:35–40.

[10] M. Severa, E.M. Coccia, K.A. Fitzgerald, Toll-like receptor-dependent and -independent viperin gene expression and counter-regulation by PRDI-binding factor-1/BLIMP1, J. Biol. Chem. 281 (2006) 26188–26195.

Hyeon Soo Lee, Ji Hyun Lee, Young Min Park*
Department of Dermatology, Seoul St. Mary's Hospital, College of Medicine, The Catholic University of Korea, 222 Banpo-daero, Seocho-gu, 06591 Seoul, Republic of Korea

* Corresponding author.
E-mail address: yymmpark6301@hotmail.com (Y. Park).

Received 5 November 2016
Received in revised form 1 February 2017
Accepted 7 February 2017

http://dx.doi.org/10.1016/j.jdermsci.2017.02.001

Letter to the Editor

Elevated moesin mRNA level in skin tissue of patients with polyarteritis nodosa based on real time RT-PCR

Polyarteritis nodosa (PAN) is a multisystem necrotizing vasculitis of medium-sized arteries characterized by involvement of the renal and visceral arteries. Cutaneous arteritis (CA) is not associated with systemic manifestation of PAN [1]. Superficial venous thrombosis is inflammation of the superficial veins associated with venous thrombosis, but not histological necrotizing vasculitis [2].

Moesin is an intracellular protein that links the cell membrane and cytoskeleton, mediating the formation of microtubules and cell adhesion sites as well as ruffling of the cell membrane, which is crucial for platelet activation. Some studies have suggested that anti-moesin antibodies are associated with the pathogenesis of active developing vasculitis via neutrophil activation [3–5]. We previously found significant positive correlations between serum anti-moesin antibody levels and clinical Birmingham Vasculitis Activity Scores (BVAS) as vasculitis disease activity in patients with PAN [6]. We used quantitative real time reverse transcription-polymerase chain reaction (RT-PCR) assay to investigate moesin mRNA expression in formalin fixed and paraffin-embedded (FFPE) skin biopsy specimens from PAN, CA, and superficial venous thrombosis patients.

We enrolled seven PAN patients (2 men, 5 women; mean age 56.7 ± 8.56 years) at the Department of Dermatology, St. Mariannia University School of Medicine. PAN was diagnosed according to the American College of Rheumatology Criteria [7]. All seven PAN patients had cutaneous manifestations on their legs and showed the presence of typical histological necrotizing vasculitis in their skin specimens (Fig. 1a). Antineutrophil cytoplasmic autoantibodies (ANCAs), including antibodies to myeloperoxidase (MPO-ANCA) and proteinase 3 (PR3-ANCA), were negative. Furthermore, none of the patients demonstrated any evidence of a co-existing malignancy, other autoimmune diseases or viral hepatitis, nor were any of the patients positive for mixed cryoglobulinemia. In addition, we measured copy numbers of moesin mRNA in three patients (1 man, 2 women; mean age 36.3 ± 7.37 years) who had CA and three persons (3 women; mean age 44.3 ± 21.22 years) who had superficial venous thrombosis except histological necrotizing vasculitis in their skin specimen (Fig. 1b). We examined BVAS in patients with PAN and CA [8].

Copy numbers of moesin mRNA differed significantly between PAN patients (191.5 ± 28.35 copies/ng RNA) and CA patients (201.4 ± 19.42 copies/ng RNA, $p < 0.01$) (Fig. 2a). Similarly, moesin mRNA copy numbers in patients with PAN were significantly higher than in superficial venous thrombosis patients (74.2 ± 13.75 copies/ng RNA, $p < 0.01$). Moesin mRNA copy numbers were not significantly higher in patients with CA than in superficial venous thrombosis. We found a significant positive correlation between moesin mRNA copy numbers and BVAS scores in patients with PAN and CA ($rs = 0.755$, $p = 0.0236$) (Fig. 2b). BVAS reflects clinical disease activity of vasculitis including PAN and CA. Moesin mRNA copy numbers in FFPE skin biopsy specimen showed a positive relationship with clinical disease activity in patients with typical histological necrotizing vasculitis such as PAN and CA.

All enrolled PAN patients showed associated cutaneous manifestations due to typical histological necrotizing vasculitis in their skin biopsy specimens. Using quantitative real-time PCR analysis, we found significantly higher copy numbers of moesin mRNA in FFPE tissues of skin biopsy specimen in PAN patients compared to CA. In addition, our results revealed that the moesin mRNA copy numbers in FFPE skin tissues were significantly correlated with BVAS in patients with PAN and CA. In PAN, very high morbidity and mortality rates characterized by fulminant deterioration or by relentless progression are associated with

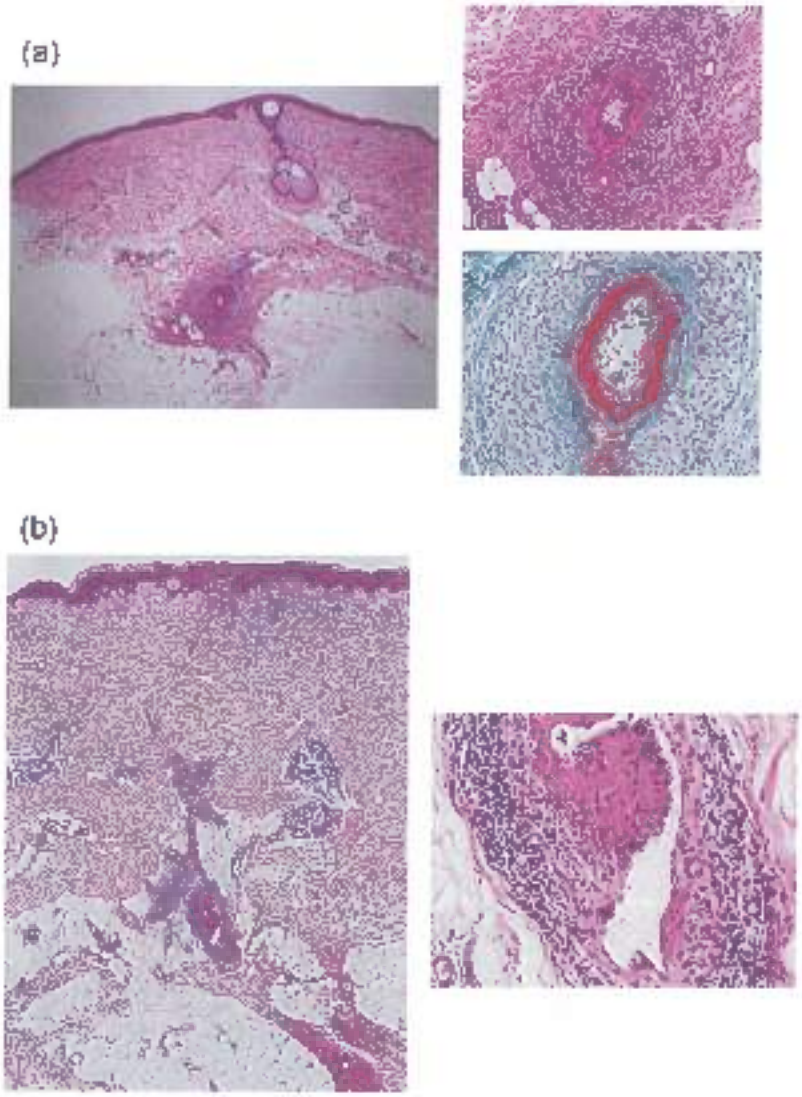

Fig. 1. Pathological cutaneous findings in PAN (a) and superficial venous thrombosis (b).
(a) PAN shows typical histological necrotizing vasculitis such as fibrinoid necrosis and neutrophil infiltration of the affected arteries. Fibrinoid necrosis appears red (Masson trichrome staining).
(b) Superficial venous thrombosis shows mainly lymphocyte infiltration of superficial veins with thrombosis.

intermittent acute exacerbations. Early intervention such as intravenous cyclophosphamide pulse therapy or steroid pulse therapy is indicated for these patients [9]. Very little is known about the events at any particular point in time that trigger the exacerbation in PAN.

CA is characterized by necrotizing vasculitis such as fibrinoid necrosis and neutrophil inflammation of cutaneous arteries. In contrast, superficial venous thrombosis indicates mainly lymphocyte inflammation of cutaneous veins. We found mRNA copy numbers in FFPE skin tissues of patients with CA were not significantly higher compared to that in superficial venous thrombosis. Furthermore, we found copy numbers of moesin mRNA in FFPE skin tissues of patients with PAN were significantly higher than in both CA and superficial venous thrombosis. These findings suggest that the presence of histological necrotizing vasculitis in the skin tissues is not necessarily crucial as a trigger for primed moesin overexpression. In addition, we previously proposed that elevated serum anti-moesin antibodies could play some role in the exacerbation of symptoms in patients with PAN [6]. Based on these findings, we suggest that some immune complexes including moesin and anti-moesin antibodies might be related to active development to systemic PAN.

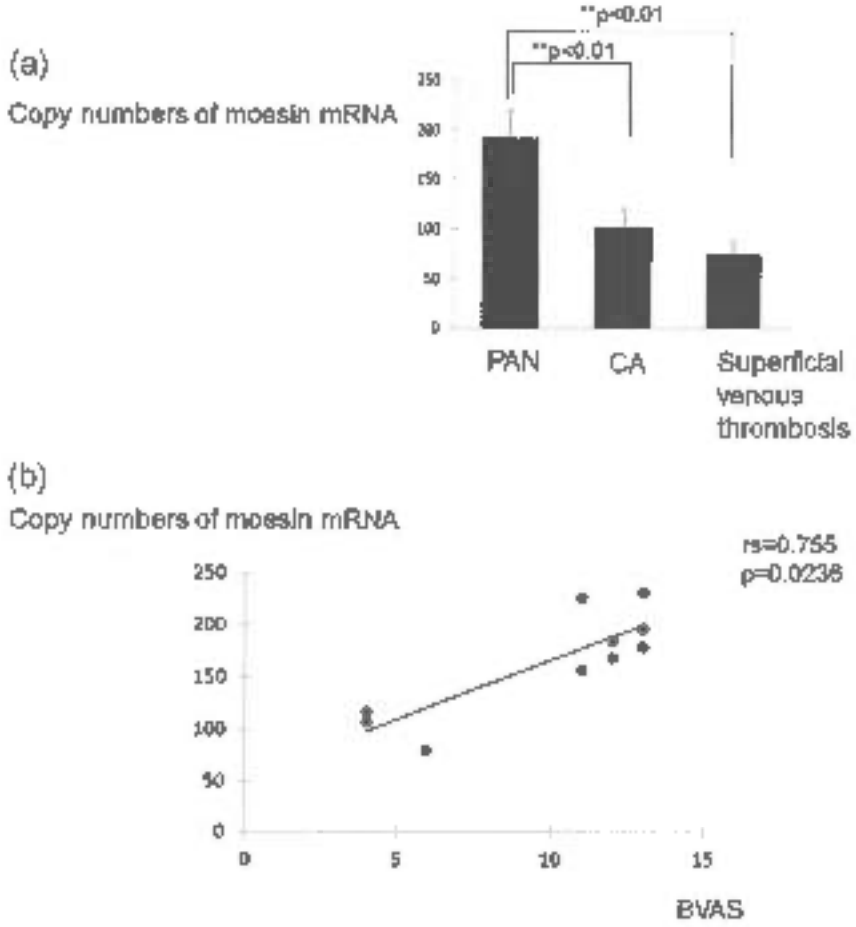

Fig. 2. (a) Differences in moesin mRNA copy numbers in FFPE skin biopsy specimens among PAN, CA, and superficial venous thrombosis.
Moesin mRNA copy numbers in FFPE skin biopsy specimens were measured using quantitative real-time PCR analysis. Copy numbers of moesin mRNA in PAN patients were significantly higher than in both CA and superficial venous thrombosis.
(b) Correlation between moesin mRNA copy numbers in FFPE skin biopsy specimens and BVAS in patients with PAN and CA.
We found significant positive correlation between moesin mRNA copy numbers and BVAS in patients with typical histological necrotizing vasculitis in their skin biopsy specimens ($r_s = 0.755$, $p = 0.0238$).

Funding sources

None.

Conflict of interest disclosure

None declared.

Acknowledgements

This work was supported by grants from the Scientific Research Fund of the Ministry of Health Labour and Welfare, Japan (Grant-in-Aid for Scientific Research, No. 23591658 and 26461734).

Appendix A. Supplementary data

Supplementary data associated with this article can be found in the online version, at http://dx.doi.org/10.1016/j.jdermsci.2017.02.002.

References

[1] J.C. Jennette, R.J. Falk, P.A. Bacon, N. Basu, M.C. Cid, F. Ferrario, et al., 2012 revised international chapel hill consensus conference nomenclature of vasculitides, Arthritis Rheum. 65 (1) (2012) 1–11.
[2] L.D. Hall, S.R. Dalton, E.F. Fillman, E. Dolse, D.M. Elston, Re-examination of features to distinguish polyarteritis nodosa from superficial thrombophlebitis, Am. J. Dermatopathol. 35 (4) (2013) 463–471.
[3] T. Nagao, K. Suzuki, K. Utsunomiya, M. Matsumura, K. Saiga, P.C. Wang, et al., Direct activation of glomerular endothelial cells by anti-moesin activity of anti-myeloperoxidase antibody, Nephrol. Dial. Transplant. 26 (9) (2011) 2752–2760.
[4] K. Suzuki, Neutrophil functions of patients with vasculitis related to myeloperoxidase-specific anti-neutrophil antibody, Int. J. Hematol. 74 (2) (2001) 134–143.
[5] K. Suzuki, T. Nagao, M. Itabashi, Y. Hamano, R. Sugamata, Y. Yamazaki, et al., A novel autoantibody against moesin in the serum of patients with MPO-ANCA-associated vasculitis, Nephrol. Dial. Transplant. 29 (6) (2014) 1168–1177.
[6] T. Okano, S. Takeuchi, Y. Soma, K. Suzuki, S. Tsukita, A. Ishizu, K. Suzuki, T. Kawakami, Presence of anti-phosphatidylserine-prothrombin complex antibodies and anti-moesin antibodies in patients with polyarteritis nodosa, J. Dermatol. (2016), doi:http://dx.doi.org/10.1111/1346-8138.13491.
[7] R.W. Lightfoot Jr., B.A. Michel, D.A. Bloch, G.G. Hunder, N.J. Zvaifler, D.J. McShane, et al., The American College of Rheumatology 1990 criteria for the classification of polyarteritis nodosa, Arthritis Rheum. 33 (8) (1990) 1088–1093.

[8] C. Mukhtyar, R. Lee, D. Brown, D. Carruthers, B. Dasgupta, S. Dubey, et al., Modification and validation of the Birmingham Vasculitis Activity Score (version 3), Ann. Rheum. Dis. 68 (12) (2009) 1827–1832.
[9] M. Fujimoto, Y. Asano, T. Ishii, F. Ogawa, T. Kawakami, M. Kodera, et al., Wound/Burn Guidelines Committee. The wound/burn guidelines-4: guidelines for the management of skin ulcers associated with connective tissue disease/vasculitis, J. Dermatol. 43 (7) (2016) 729–757.

Tomoyuki Kawakami*, Tatsuro Okano, Sora Takeuchi, Yoshinao Soma
Department of Dermatology, St. Marianna University School of Medicine, Kawasaki, Japan

Fuyu Ito
Department of Health Protection, Graduate School of Medicine Tokyo University Asia International Institute of Infectious Disease Control, Japan

Akihiro Ishizu
Department of Pathology/Pathophysiology, Division of Pathophysiological science, Hokkaido University Graduate School of Medicine, Sapporo, Japan

Yoshihiro Arimura
First Department of Internal Medicine, Kyorin University School of Medicine, Tokyo, Japan

Kazuo Suzuki
Department of Health Protection, Graduate School of Medicine, Tokyo University Asia International Institute of Infectious Disease Control, Japan

* Corresponding author at: Department of Dermatology, St. Marianna University School of Medicine, 2-16-1 Sugao, Miyamae-ku, Kawasaki, Kanagawa 216-8511, Japan.
E-mail address: tami@marianna-u.ac.jp (T. Kawakami).

Received 1 November 2016

http://dx.doi.org/10.1016/j.jdermsci.2017.02.002

Journal of Dermatological Science 87 (2017) 46–49

Contents lists available at ScienceDirect

Journal of Dermatological Science

journal homepage: www.jdsjournal.com

Serum peptides as putative modulators of inflammation in psoriasis

Tetsuhiko Matsuura[a], Masaaki Sato[b], Kouhei Nagai[c], Toshiyuki Sato[b], Mitsumi Arita[b], Kazuki Omoteyama[b], Naoya Suematsu[b], Kazuki Okamoto[b], Tomohiro Kato[b], Yoshinari Soma[a], Manae S. Kurokawa[d,*]

[a] Department of Dermatology, St. Marianna University School of Medicine, Japan
[b] Clinical Pathology and Molecular Medicine, St. Marianna University Graduate School of Medicine, Japan
[c] Department of Genetic Engineering, Faculty of Biology-Oriented Science and Technology, Kindai University, Japan
[d] Disease Biomarker Analysis and Molecular Regulation, St. Marianna University Graduate School of Medicine, Japan

ARTICLE INFO

Article history:
Received 28 September 2016
Accepted 21 March 2017

Keywords:
Psoriasis vulgaris
Psoriatic arthritis
Serum peptides
Mass spectrometry
Fibrinogen α chain
Filaggrin

ABSTRACT

Background: Psoriasis is a refractory inflammatory disease, however, its pathophysiology is still not fully understood.

Objective: We tried to identify novel serum peptides associated with the pathophysiology of psoriasis.

Methods: Serum peptides from 24 patients with psoriasis vulgaris (PV), 10 patients with psoriatic arthritis (PsA), 14 patients with atopic dermatitis (AD) and 23 healthy control (HC) subjects were analyzed by mass spectrometry. The effects of some peptides on the secretion of humoral factors from dermal cells were investigated by cytokine arrays and ELISAs.

Results: A total of 95 peptides were detected. 24, 20, 23, and 2 peptides showed at least 1.2-fold difference which in intensity between the psoriasis (PV + PsA) and HC groups, between the PV + PsA and AD groups, between the PV and PsA groups, and between patients with severe to moderate PV (n = 6) and those with mild PV (n = 18), respectively ($p < 0.05$). 13 out of 27 peptides that showed at least 1.5-fold ion intensity difference in the above mentioned 4 comparisons were identified. The parent proteins of the identified peptides included a coagulation factor, proteins involved in the maintenance of skin, and a protein relating to cytoskeleton. We focused on 2 peptides that were increased in the PV + PsA group: a fibrinogen α chain-derived peptide (1462 m/z), the monadic cationic form of which was the tripeptide A-des-alanine (FPAdA), and a filaggrin (FLG)-derived peptide (1977 m/z), a modified form of $FLG_{[2,2,2,2,2,2,2,2]}$ ($Q_{[2,2,2,2,2,2,2,2]}$pE, $Q_{[2,2,2,2,2,2,2,2]}$F, FLG-pEE). FPAdA stimulation increased the secretion of GROs from dermal microvascular endothelial cells (dMVECs) and decreased the secretion of lipocalin-2 from keratinocytes in comparison to FPAdA-sequenced peptide stimulation (GROs: 200.9 ± 7.3 pg/mL vs. 229.6 ± 5.0 pg/mL, $p < 0.001$; lipocalin-2: 27.1 ± 1.1 pg/mL vs. 35.0 ± 1.0 pg/mL, $p < 0.01$). Interestingly, FLG-pEE stimulation decreased the secretion of GROs, IL-8, and MCP-1 from dMVECs in comparison to FLG-derived control peptide stimulation (GROs: 844.3 ± 47.5 pg/mL vs. 1128.5 ± 81.5 pg/mL, $p < 0.05$; IL-8: 2280.1 ± 172.1 pg/mL vs. 3222.8 ± 325.7 pg/mL, $p < 0.05$; MCP-1: 405.8 ± 15.2 pg/mL vs. 461.1 ± 21.4 pg/mL, $p < 0.05$).

Abbreviations: AD, atopic dermatitis; α2HS-GP, alpha-2-HS-glycoprotein; CCL20, C-C motif ligand 20; CCR2, C-C chemokine receptor type 2; CRP, C-reactive protein; CYA, cyclosporine; DC, dendritic cells; Dkk-1, dickkopf-related protein 1; dMVECs, dermal microvascular endothelial cells; E, glutamate; ELISA, enzyme-linked immunosorbent assay; EQ, glutamate-glutamine; FIBA, fibrinogen alpha chain; FIBA-CTC, C-terminal portion of the αC domain of FIBA; FLG, filaggrin; FPA, fibrinopeptide A; FPAdA, fibrinopeptide A des-alanine; GROs, growth regulated oncogene alpha; HC, healthy control; HLA, human leukocyte antigen; HPLC, high-performance liquid chromatography; IL-1ra, interleukin-1 receptor antagonist; IMQ, imiquimod; M, methionine; MALDI-TOF/MS, matrix-assisted laser desorption/ionization time-of-flight mass spectrometry; MCP-1, monocyte chemoattractant protein 1; MIF, macrophage migration inhibitory factor; MMP, matrix metalloproteinase; mPV, mild psoriasis vulgaris; MS, mass spectrometry; MTX, methotrexate; NSAIDs, non-steroidal anti-inflammatory drugs; PASI, Psoriasis Area and Severity Index; pE, pyroglutamate; PsA, psoriatic arthritis; PSL, prednisolone; PV, psoriasis vulgaris; Q, glutamine; SD, standard deviation; sFlt1, soluble fms-like tyrosine kinase-1; sPV, severe-to-moderate psoriasis vulgaris; TGF-α, transforming growth factor alpha; TNF, tumor necrosis factor; VEGF, vascular endothelial growth factor.

* Corresponding author at: Disease Biomarker Analysis and Molecular Regulation, St. Marianna University Graduate School of Medicine, 2-16-1, Sugao, Miyamae-ku, Kawasaki, Japan.
E-mail address: manae@marianna-u.ac.jp (M.S. Kurokawa).

http://dx.doi.org/10.1016/j.jdermsci.2017.03.014
0923-1811/ © 2017 Japanese Society for Investigative Dermatology. Published by Elsevier Ireland Ltd. All rights reserved.

Conclusions: The results suggested that some serum peptides are involved in the pathophysiology of psoriasis, regulating the secretion of inflammatory chemokines and an antimicrobial protein. The modulation of serum peptides may be a potential therapeutic strategy for psoriasis.

© 2017 Japanese Society for Investigative Dermatology. Published by Elsevier Ireland Ltd. All rights reserved.

1. Introduction

Psoriasis is a chronic inflammatory multi-organ disease that mainly manifests in the skin [1,2]. The estimated prevalence of psoriasis is approximately 2% worldwide and 0.34% in Japan [1,3]. The most common type of psoriasis is psoriasis vulgaris (PV), which accounts for approximately 90% of cases [1,4]. The typical lesions are monomorphic and well-demarcated erythematous plaques covered by silvery scales [1,5]. Patients with PV suffer from pain, itching, and bleeding of the skin lesions. Furthermore, patients with psoriasis are at risk of developing other chronic inflammatory diseases such as arthritis (psoriatic arthritis: PsA), metabolic syndrome, cardiovascular disorders, depression, and cancer [1,4,5]. Since the pathophysiology of psoriasis remains unclear, it is imperative to elucidate the pathophysiology in order to establish effective treatments for the disease.

It is widely accepted that aberrant immune responses shifting toward the IL-23/Th17 and Th1 axes play major roles in the pathophysiology of psoriasis [1,5]. IL-17, which is produced by Th17 cells, γδT cells, neutrophils, and mast cells, activates keratinocytes to produce ELR⁺ chemokines such as CROα and IL-8 and CCL20 bringing neutrophils, dendritic cells (DCs), and T cells into the psoriatic lesion [6–10]. IL-22, which is produced by Th17 cells, Th1 cells, and Th22 cells, promotes the proliferation of keratinocytes and hyperkeratosis [6]. The activation of keratinocytes by TGFα, which is overexpressed in psoriatic epidermis, increases the secretion of VEGFs from the cells [11]. VEGFs bind to its receptors, kdr and flt-1, which are expressed by papillary dermal microvascular endothelial cells (dMVECs) to induce hyperpermeability. VEGFs, hypoxia-inducible factors, angiopoietins, and proangiogenic cytokines such as TNF, IL-8, and IL-17, are up-regulated in psoriatic lesions, which increases dermal vascularity [11,12]. On the other hand, keratinocytes overexpress antimicrobial peptides such as LL37 and β defensin 2, which trigger the self nucleic acid-mediating activation of plasmacytoid DCs through toll-like receptor 9 [13,14]. Furthermore, genetic risk factors such as HLA-CwS are associated with the onset [1,15]. Nonetheless, the precise pathophysiology of psoriasis is not fully understood. The identification of novel disease-related molecules will thus be necessary to elucidate of the pathophysiology.

In the present study, we comprehensively analyzed the serum peptides in PV and PsA patients. We found that the serum peptide profiles of psoriasis differed from those of healthy individuals and atopic dermatitis (AD) patients. Some of the peptides that were increased in psoriasis were found to modulate the secretion of inflammatory chemokines from dermal cells. Our data suggested a novel disease mechanism of psoriasis, which involves the degradation of proteins in the skin and blood.

2. Materials and methods

2.1. Patients and serum samples

The diagnosis of PV was clinically made. The diagnoses of PsA and AD were made according to the respective criteria [16,17]. Serum samples were obtained from 24 patients with PV, 10 patients with PsA, 14 patients with AD, and 25 healthy control (HC) subjects after they provided written informed consents (Table 1). The study protocol conformed to the ethical guidelines of the 1964 Declaration of Helsinki and its later amendments and was approved by the ethics committee of St. Marianna University School of Medicine.

Table 1
The clinical information of the subjects.

	PV (n = 24)	PsA (n = 10)	AD (n = 14)	HC (n = 25)
Male/female	15/9	5/5	n.a.	15/8
Age (years)[a]	50.8 ± 18.2	53.1 ± 17.6	38.6 ± 12.7	40.4 ± 15.5
Disease duration (years)[a]	12.1 ± 7.0	6.6 ± 4.7	24.7 ± 10.1	–
PASI[a]	7.0 ± 4.0	3.6 ± 1.5	–	–
BSA (%)[a]	15.8 ± 17.0	6.2 ± 7.4	–	–
CRP (mg/dL)[a,b]	0.20 ± 0.30 (n = 18)	0.33 ± 0.33		
Comorbid diseases[c]	2 HT, 2 HT+DM, 1 HT+DM+CL, 1 HT+CL+DML, 1 DM+HL, 1 HL, 1 DM, 1 CA, 1 PR, 1 PC	2 DM, 1 HL, 1 HT+DM+HL, 1 HT+DM+CL, 1 HT	None	None
Treatment[d]	24 ex: CS/VD3, 3 CYA, 1 ADA, 1 IFX, 1 GST, 1 VA	9 ex: CS/VD3, 1 ex: CS/VD3/ISD, 1 IFX, 1 VA+MTX, 1 VA+UST, 1 ISD+CYA, 1 ISD+CYA+IFX	13 ex: CS, 2 CYA, 1 FK	

PV, psoriasis vulgaris; PsA, psoriatic arthritis; AD, atopic dermatitis; HC, healthy control; PASI, Psoriasis Area and Severity Index; BSA, body surface area; HT, hypertension; DM, diabetes mellitus; CL, cerebral infarction; DL, dyslipidemia; HL, fatty liver; ML, malignant lymphoma; AU, alpecia areata; BD, Basedow's disease; CR, chronic kidney disease; PP, palmoplantar pustulosis; PC, prostatic carcinoma; R, rheumatoid; CYA, cyclosporin; ADA, adalimumab; IFX, infliximab; UST, ustekinumab; VA, vitamin A derivative; MTX, methotrexate; UST, ustekinumab; FK, tacrolimus.

[a] Mean ± standard deviation.

[b] C-reactive protein (CRP) was measured in 18 out of 24 PV patients and in all the 10 PsA patients.

[c] Comorbid diseases such as metabolic diseases, cardiovascular diseases, and other inflammatory diseases are shown.

[d] The external use of corticosteroids (CS), vitamin D3 (VD3), and indomethacin (ISD) were counted independently from other treatments.

The disease severity of PV was estimated according to the Psoriatic Area and Severity Index (PASI) [18,19]. The 24 PV patients were divided into 2 groups according to their PASI values [20]: the severe-to-moderate PV (sPV, PASI > 10) group ($n = 6$, male, $n = 3$, female, $n = 3$; mean ± standard deviation [SD] age, 42.7 ± 15.7 years, disease duration, 10.5 ± 8.6 years; PASI, 14.3 ± 7.8) and the mild PV (mPV, PASI ≤ 10) group ($n = 18$, male, $n = 12$; female, $n = 6$, age, 61.6 ± 16.4 years; disease duration, 9.6 ± 5.7 years; PASI, 4.6 ± 2.4).

To analyze the correlation between peptide ion intensity and treatment, we designed a treatment score in which the treatments for psoriasis in this study were classified into five groups as follows: Score 0 ($n = 0$), no treatment; Score 1 ($n = 10$), external medication and/or oral vitamin A derivative; Score 2 ($n = 3$), non-steroidal anti-inflammatory drugs (NSAIDs), with or without drugs in score 1; Score 3 ($n = 0$), prednisolone (PSL) ≤ 5 mg/day, methotrexate (MTX) ≤ 8 mg/week, cyclosporin (CYA) ≤ 3 mg/kg/day, or maintenance dosages of biological drugs, with or without drugs in scores 1 and 2. Score 4 ($n = 4$), (i) PSL > 5 mg/day, MTX > 8 mg/week, CYA > 3 mg/kg/day, or increased dosages of biological drugs, (ii) at least two of PSL, immunosuppressants (MTX or CYA), and biological drugs, both (i) and (ii) are with or without drugs in scores 1 and 2.

2.2. The comparison of peptide profiles and the identification of peptide sequences

Serum peptides were purified using weak cation exchange chromatography (Bruker Daltonics, Bellingen, Germany). The concentration of each peptide was measured according to the ion intensity on matrix assisted laser desorption/ionization time of flight mass spectrometry (MALDI TOF/MS, Ultraflex, Bruker Daltonics). The ion intensity of the peptides was obtained as the peak heights using ClinProt Tools software program (Bruker Daltonics). The peptides were designated according to the mass to charge ratios (i.e., p1056 indicates a peptide with 1056 m/z).

The amino acid sequences of the peptides were identified by random mass spectrometry using a nano-HPLC system (Eksigent nano-LC400 system, AB sciex, Framingham, MA, USA) connected to a Triple TOF5600 system (AB sciex). The MS and MS/MS spectra that were obtained were used to identify the parent proteins of the peptides by searching the Uniprot protein database using a software (Protein Pilot version 4.0, AB sciex).

2.3. The synthesis of peptides and cell culturing

A peptide corresponding to fibrinopeptide A-des-alanine (FPAdA, N-DSGEGDFLAEGGGVR-C) and a control peptide for FPAdA (FPAdA-Cont) in which the 15 amino acids were randomly resequenced (N-GDRGEGASGELDVFG-C) were synthesized (Eurofins Genomics, Tokyo, Japan). Peptides derived from filaggrin (FLG), $FLG_{2986-2998}$ (N-QSFSTFGQSAIPSTGGHQGSH-C, FLG-Q_2), a modified form of $FLG_{2986-2998}$ ($FLG_{2986-2998}$-Q_{2986}PE-Q_{2998}E, N-pESFSTHGQSAIPSTGGHEGSH-C, FLG-pEF), and a control peptide, $FLG_{2986-2998}$ (N-DMVDVFMDHLHHHNKKIDF-C, FLG-Cont) were similarly synthesized (Eurofins Genomics).

Human dermal FCs and human keratinocytes were purchased (Lonza, Walkersville, MD, USA). To prepare the culture supernatants for cytokine assays, 1×10^5 cells were cultured with FPAdA, FPAdA-Cont or medium alone for 24 h. Similarly, 1×10^5 cells were

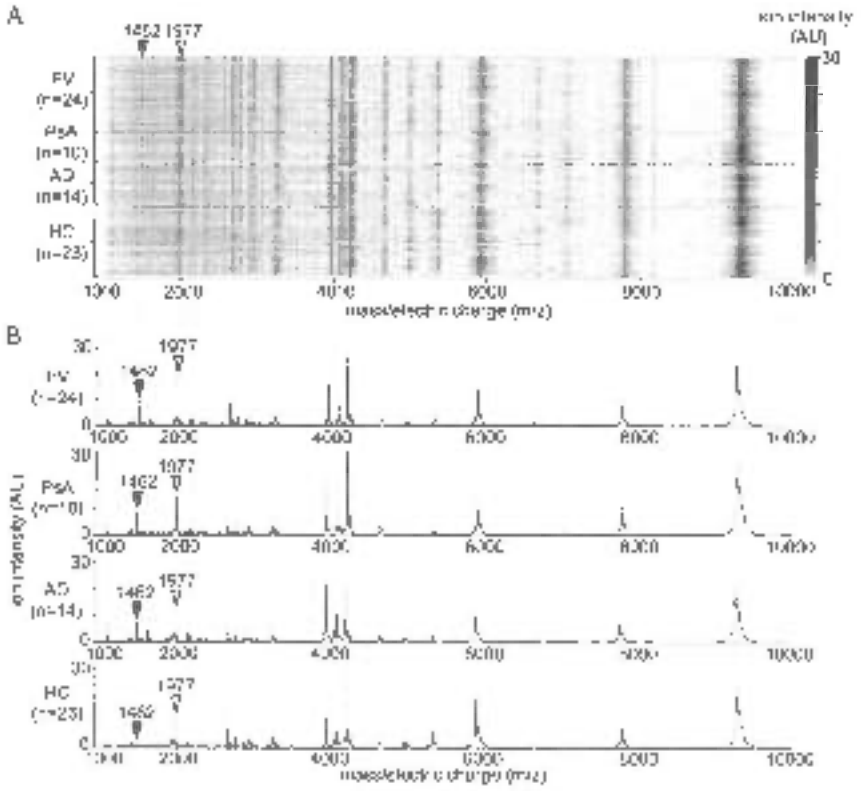

Fig. 1. The serum peptide profile of the psoriasis patients. (A) A gel image of the serum peptides of the detected peptides. The results of each serum sample are vertically aligned. The number of the patients in the PV, PsA, AD and HC groups are shown in the parentheses. The intensity is shown in black-white gradation, as indicated on the right side of the panel. (B) The average ion intensity of the serum peptides in the PV, PsA, AD and HC groups. Black arrowheads show p1452, the ion intensity of which was increased 2.99-fold in the PV + PsA groups in comparison to the HC group. The white arrowheads show p1977, the ion intensity of which was increased 1.64-fold and 1.45-fold in the PV + PsA group in comparison to the HC and AD groups, respectively.

cultured with FLG-pEF, FLG-Q_5, FLG-Cont, or medium-alone for 24 h. The culture supernatants were recovered and stocked at −80 °C until the analysis.

2.4. The analysis of the secretion of humoral factors from dermal cells stimulated with the peptides

Humoral factors including proinflammatory cytokines and chemokines in culture supernatants were measured in duplicate by cytokine arrays (for dMVECs, Human Cytokine Array, R&D Systems, Minneapolis, MN, USA; for keratinocytes, Human XL Cytokine Array kit, R&D Systems). Humoral factors that were detected as specific spots were visualized using ECL Plus (GE Healthcare, Piscataway, NJ, USA) and a LAS-3000 Imager (Fujifilm, Tokyo, Japan). The intensity of each spot, which was measured using the Science Lab 2007 Image Gauge software program (Fujifilm), was normalized based on the intensity of a positive control sample. The humoral factors that were selected by cytokine arrays were measured in triplicate with their respective ELISA kits (R&D Systems).

2.5. Statistical analysis

The significance of the differences in peptide ion intensity among the PV, PsA, AD and HC groups was calculated using Student's t-test. The correlations between the peptide ion intensity and clinical parameters were calculated using Spearman's rank correlation coefficient. The significance of the differences in peptide ion intensity according to the difference in treatment was calculated using Wilcoxon's signed-rank test.

3. Results

3.1. A comparison of the serum peptide profiles among the PV, PsA, AD, and HC groups

To find the serum peptides associated with the pathophysiology of psoriasis (PV + PsA), we comprehensively measured the ion intensity of serum peptides in the PV, PsA, AD, and HC groups. A total of 93 peptide ion peaks were detected (Fig. 1A and B). Among these, we compared the ion intensity between the PV + PsA and HC groups, and between the PV + PsA and AD groups (Table 2). In the PV + PsA group, 18 peptides showed an ion intensity that was at least 1.2-fold higher and 6 peptides showed an ion intensity that was at least 1.3-fold lower in comparison to the HC group ($p < 0.05$). Similarly, in the PV + PsA group, 11 peptides showed an ion intensity that was at least 1.3-fold higher and 4 peptides showed an ion intensity that was at least 1.3-fold lower in comparison to the AD group ($p < 0.05$).

Furthermore, we compared the serum peptide profiles between the subgroups of psoriasis patients. In the PsA group, 7 peptides showed an ion intensity that was at least 1.2-fold higher and 16 peptides showed an ion intensity that was at least 1.3-fold lower in comparison to the PV group ($p < 0.05$) (Table 2). In the sPV group, 2 peptides showed an ion intensity that was at least 1.3-fold lower in comparison to the mPV group ($p < 0.05$).

Collectively, the serum peptide profiles of psoriasis (PV + PsA) patients were found to differ from AD patients and HC subjects. Among the psoriasis patients, there were differences in the peptide profiles of PV and PsA patients, and in the peptide profiles of sPV and mPV patients.

3.2. The identification of the disease-specific peptides in psoriasis

We tried to identify the peptides with an ion intensity that showed a ≥1.5-fold difference in the 4 comparisons (Table 2). Although Table 2 shows 35 of these peptides, the actual number was 27 because some of the peptides overlapped.

We identified 13 out of the 27 peptides and found 4 parent proteins (Table 3). It is noteworthy that 9 of the 13 identified peptides were derived from the fibrinogen alpha chain (FIBA); in the PV + PsA group, the ion intensity of most of these peptides was higher in comparison to the HC and/or AD groups. Two out of the 9 FIBA peptides were derived from FPA; the other 7 were derived from the αC-domain (Fig. 2). In the PV + PsA group, the ion intensity of p1462 derived from FPA was 2.69-fold higher than that in the HC group. p1462 was identified as $FPA_{1-45}S_{epitopes}$ or N-terminal alanine-deletive FPA, FPA_{2-n} (FPAdA) (Table 3).

Interestingly, in the PV + PsA group, the ion intensity of p1977 was 1.44-fold and 1.45-fold higher than that in the HC and AD groups, respectively. p1977 was identified as being derived from FLG, which is involved in the terminal differentiation of mammalian epidermis (Table 3) [21,22]. This peptide included two types of post-translational modifications: the N-terminal (20th Gln) glutamine (Q) was changed to pyroglutamate (pE) and the 17th (21 Gln) Q was deamidated (changed to glutamate). F1 (H_2N-Q_{20}-pE_{21}-Q_{22}-pE_{23}-H_2N-Q_{30}-pE_{31}-H_2N-Q_{40}-pE_{41}-H_2N-Q_{50}-pE_{51}-H_2N-Q_{60}-pE_{61}-H_2N-Q_{70}-pE_{71}-H_2N-Q_{80}-pE_{81}-H_2N-Q_{90}-pE_{91}-H_2N-Q_{100}-pE_{101}-H_2N-Q_{110}-pE_{111}-H_2N-Q_{120}-pE_{121}-H_2N-Q_{130}-pE_{131}-H_2N-Q_{140}-pE_{141}-H_2N-Q_{150}-pE_{151}-H_2N-Q_{160}-pE_{161}-H_2N-Q_{170}-pE_{171}-H_2N-Q_{180}-pE_{181}-H_2N-Q_{190}-pE_{191}-H_2N-Q_{200}-pE_{201}-H_2N-Q_{210}-pE_{211}-H_2N-Q_{220}-pE_{221}-H_2N-Q_{230}-pE_{231}-H_2N-Q_{240}-pE_{241}-H_2N-Q_{250}-pE_{251}-H_2N-Q_{260}-pE_{261}-H_2N-Q_{270}-pE_{271}-H_2N-Q_{280}-pE_{281}-H_2N-Q_{290}-pE_{291}-H_2N-Q_{300}-pE_{301}-H_2N-Q_{310}-pE_{311}-H_2N-Q_{320}-pE_{321}-H_2N-Q_{330}-pE_{331}-H_2N-Q_{340}-pE_{341}-H_2N-Q_{350}-pE_{351}-H_2N-Q_{360}-pE_{361}-H_2N-Q_{370}-pE_{371}-H_2N-Q_{380}-pE_{381}-H_2N-Q_{390}-pE_{391}-H_2N-Q_{400}-pE_{401}-H_2N-Q_{410}-pE_{411}-H_2N-Q_{420}-pE_{421}-H_2N-Q_{430}-pE_{431}-H_2N-Q_{440}-pE_{441}-H_2N-Q_{450}-pE_{451}-H_2N-Q_{460}-pE_{461}-H_2N-Q_{470}-pE_{471}-H_2N-Q_{480}-pE_{481}-H_2N-Q_{490}-pE_{491}-H_2N-Q_{500}-pE_{501}-H_2N-Q_{510}-pE_{511}-H_2N-Q_{520}-pE_{521}-H_2N-Q_{530}-pE_{531}-H_2N-Q_{540}-pE_{541}-H_2N-Q_{550}-pE_{551}-H_2N-Q_{560}-pE_{561}-H_2N-Q_{570}-pE_{571}-H_2N-Q_{580}-pE_{581}-H_2N-Q_{590}-pE_{591}-H_2N-Q_{600}-pE_{601}-H_2N-Q_{610}-pE_{611}-H_2N-Q_{620}-pE_{621}-H_2N-Q_{630}-pE_{631}-H_2N-Q_{640}-pE_{641}-H_2N-Q_{650}-pE_{651}-H_2N-Q_{660}-pE_{661}-H_2N-Q_{670}-pE_{671}-H_2N-Q_{680}-pE_{681}-H_2N-Q_{690}-pE_{691}-H_2N-Q_{700}-pE_{701}-H_2N-Q_{710}-pE_{711}-H_2N-Q_{720}-pE_{721}-H_2N-Q_{730}-pE_{731}-H_2N-Q_{740}-pE_{741}-H_2N-Q_{750}-pE_{751}-H_2N-Q_{760}-pE_{761}-H_2N-Q_{770}-pE_{771}-H_2N-Q_{780}-pE_{781}-H_2N-Q_{790}-pE_{791}-H_2N-Q_{800}-pE_{801}-H_2N-Q_{810}-pE_{811}-H_2N-Q_{820}-pE_{821}-H_2N-Q_{830}-pE_{831}-H_2N-Q_{840}-pE_{841}-H_2N-Q_{850}-pE_{851}-H_2N-Q_{860}-pE_{861}-H_2N-Q_{870}-pE_{871}-H_2N-Q_{880}-pE_{881}-H_2N-Q_{890}-pE_{891}-H_2N-Q_{900}-pE_{901}-H_2N-Q_{910}-pE_{911}-H_2N-Q_{920}-pE_{921}-H_2N-Q_{930}-pE_{931}-H_2N-Q_{940}-pE_{941}-H_2N-Q_{950}-pE_{951}-H_2N-Q_{960}-pE_{961}-H_2N-Q_{970}-pE_{971}-H_2N-Q_{980}-pE_{981}-H_2N-Q_{990}-pE_{991}-H_2N-Q_{1000}-pE_{1001}-H_2N-Q_{1010}-pE_{1011}-H_2N-Q_{1020}-pE_{1021}-H_2N-Q_{1030}-pE_{1031}-H_2N-Q_{1040}-pE_{1041}-H_2N-Q_{1050}-pE_{1051}-H_2N-Q_{1060}-pE_{1061}-H_2N-Q_{1070}-pE_{1071}-H_2N-Q_{1080}-pE_{1081}-H_2N-Q_{1090}-pE_{1091}-H_2N-Q_{1100}-pE_{1101}-H_2N-Q_{1110}-pE_{1111}-H_2N-Q_{1120}-pE_{1121}-H_2N-Q_{1130}-pE_{1131}-H_2N-Q_{1140}-pE_{1141}-H_2N-Q_{1150}-pE_{1151}-H_2N-Q_{1160}-pE_{1161}-H_2N-Q_{1170}-pE_{1171}-H_2N-Q_{1180}-pE_{1181}-H_2N-Q_{1190}-pE_{1191}-H_2N-Q_{1200}-pE_{1201}-H_2N-Q_{1210}-pE_{1211}-H_2N-Q_{1220}-pE_{1221}-H_2N-Q_{1230}-pE_{1231}-H_2N-Q_{1240}-pE_{1241}-H_2N-Q_{1250}-pE_{1251}-H_2N-Q_{1260}-pE_{1261}-H_2N-Q_{1270}-pE_{1271}-H_2N-Q_{1280}-pE_{1281}-H_2N-Q_{1290}-pE_{1291}-H_2N-Q_{1300}-pE_{1301}-H_2N-Q_{1310}-pE_{1311}-H_2N-Q_{1320}-pE_{1321}-H_2N-Q_{1330}-pE_{1331}-H_2N-Q_{1340}-pE_{1341}-H_2N-Q_{1350}-pE_{1351}-H_2N-Q_{1360}-pE_{1361}-H_2N-Q_{1370}-pE_{1371}-H_2N-Q_{1380}-pE_{1381}-H_2N-Q_{1390}-pE_{1391}-H_2N-Q_{1400}-pE_{1401}-H_2N-Q_{1410}-pE_{1411}-H_2N-Q_{1420}-pE_{1421}-H_2N-Q_{1430}-pE_{1431}-H_2N-Q_{1440}-pE_{1441}-H_2N-Q_{1450}-pE_{1451}-H_2N-Q_{1460}-pE_{1461}-H_2N-Q_{1470}-pE_{1471}-H_2N-Q_{1480}-pE_{1481}-H_2N-Q_{1490}-pE_{1491}-H_2N-Q_{1500}-pE_{1501}-H_2N-Q_{1510}-pE_{1511}-H_2N-Q_{1520}-pE_{1521}-H_2N-Q_{1530}-pE_{1531}-H_2N-Q_{1540}-pE_{1541}-H_2N-Q_{1550}-pE_{1551}-H_2N-Q_{1560}-pE_{1561}-H_2N-Q_{1570}-pE_{1571}-H_2N-Q_{1580}-pE_{1581}-H_2N-Q_{1590}-pE_{1591}-H_2N-Q_{1600}-pE_{1601}-H_2N-Q_{1610}-pE_{1611}-H_2N-Q_{1620}-pE_{1621}-H_2N-Q_{1630}-pE_{1631}-H_2N-Q_{1640}-pE_{1641}-H_2N-Q_{1650}-pE_{1651}-H_2N-Q_{1660}-pE_{1661}-H_2N-Q_{1670}-pE_{1671}-H_2N-Q_{1680}-pE_{1681}-H_2N-Q_{1690}-pE_{1691}-H_2N-Q_{1700}-pE_{1701}-H_2N-Q_{1710}-pE_{1711}-H_2N-Q_{1720}-pE_{1721}-H_2N-Q_{1730}-pE_{1731}-H_2N-Q_{1740}-pE_{1741}-H_2N-Q_{1750}-pE_{1751}-H_2N-Q_{1760}-pE_{1761}-H_2N-Q_{1770}-pE_{1771}-H_2N-Q_{1780}-pE_{1781}-H_2N-Q_{1790}-pE_{1791}-H_2N-Q_{1800}-pE_{1801}-H_2N-Q_{1810}-pE_{1811}-H_2N-Q_{1820}-pE_{1821}-H_2N-Q_{1830}-pE_{1831}-H_2N-Q_{1840}-pE_{1841}-H_2N-Q_{1850}-pE_{1851}-H_2N-Q_{1860}-pE_{1861}-H_2N-Q_{1870}-pE_{1871}-H_2N-Q_{1880}-pE_{1881}-H_2N-Q_{1890}-pE_{1891}-H_2N-Q_{1900}-pE_{1901}-H_2N-Q_{1910}-pE_{1911}-H_2N-Q_{1920}-pE_{1921}-H_2N-Q_{1930}-pE_{1931}-H_2N-Q_{1940}-pE_{1941}-H_2N-Q_{1950}-pE_{1951}-H_2N-Q_{1960}-pE_{1961}-H_2N-Q_{1970}-pE_{1971}-H_2N-Q_{1980}-pE_{1981}-H_2N-Q_{1990}-pE_{1991}-H_2N-Q_{2000}-pE_{2001}-H_2N-Q_{2010}-pE_{2011}-H_2N-Q_{2020}-pE_{2021}-H_2N-Q_{2030}-pE_{2031}-H_2N-Q_{2040}-pE_{2041}-H_2N-Q_{2050}-pE_{2051}-H_2N-Q_{2060}-pE_{2061}-H_2N-Q_{2070}-pE_{2071}-H_2N-Q_{2080}-pE_{2081}-H_2N-Q_{2090}-pE_{2091}-H_2N-Q_{2100}-pE_{2101}-H_2N-Q_{2110}-pE_{2111}-H_2N-Q_{2120}-pE_{2121}-H_2N-Q_{2130}-pE_{2131}-H_2N-Q_{2140}-pE_{2141}-H_2N-Q_{2150}-pE_{2151}-H_2N-Q_{2160}-pE_{2161}-H_2N-Q_{2170}-pE_{2171}-H_2N-Q_{2180}-pE_{2181}-H_2N-Q_{2190}-pE_{2191}-H_2N-Q_{2200}-pE_{2201}-H_2N-Q_{2210}-pE_{2211}-H_2N-Q_{2220}-pE_{2221}-H_2N-Q_{2230}-pE_{2231}-H_2N-Q_{2240}-pE_{2241}-H_2N-Q_{2250}-pE_{2251}-H_2N-Q_{2260}-pE_{2261}-H_2N-Q_{2270}-pE_{2271}-H_2N-Q_{2280}-pE_{2281}-H_2N-Q_{2290}-pE_{2291}-H_2N-Q_{2300}-pE_{2301}-H_2N-Q_{2310}-pE_{2311}-H_2N-Q_{2320}-pE_{2321}-H_2N-Q_{2330}-pE_{2331}-H_2N-Q_{2340}-pE_{2341}-H_2N-Q_{2350}-pE_{2351}-H_2N-Q_{2360}-pE_{2361}-H_2N-Q_{2370}-pE_{2371}-H_2N-Q_{2380}-pE_{2381}-H_2N-Q_{2390}-pE_{2391}-H_2N-Q_{2400}-pE_{2401}-H_2N-Q_{2410}-pE_{2411}-H_2N-Q_{2420}-pE_{2421}-H_2N-Q_{2430}-pE_{2431}-H_2N-Q_{2440}-pE_{2441}-H_2N-Q_{2450}-pE_{2451}-H_2N-Q_{2460}-pE_{2461}-H_2N-Q_{2470}-pE_{2471}-H_2N-Q_{2480}-pE_{2481}-H_2N-Q_{2490}-pE_{2491}-H_2N-Q_{2500}-pE_{2501}-H_2N-Q_{2510}-pE_{2511}-H_2N-Q_{2520}-pE_{2521}-H_2N-Q_{2530}-pE_{2531}-H_2N-Q_{2540}-pE_{2541}-H_2N-Q_{2550}-pE_{2551}-H_2N-Q_{2560}-pE_{2561}-H_2N-Q_{2570}-pE_{2571}-H_2N-Q_{2580}-pE_{2581}-H_2N-Q_{2590}-pE_{2591}-H_2N-Q_{2600}-pE_{2601}-H_2N-Q_{2610}-pE_{2611}-H_2N-Q_{2620}-pE_{2621}-H_2N-Q_{2630}-pE_{2631}-H_2N-Q_{2640}-pE_{2641}-H_2N-Q_{2650}-pE_{2651}-H_2N-Q_{2660}-pE_{2661}-H_2N-Q_{2670}-pE_{2671}-H_2N-Q_{2680}-pE_{2681}-H_2N-Q_{2690}-pE_{2691}-H_2N-Q_{2700}-pE_{2701}-H_2N-Q_{2710}-pE_{2711}-H_2N-Q_{2720}-pE_{2721}-H_2N-Q_{2730}-pE_{2731}-H_2N-Q_{2740}-pE_{2741}-H_2N-Q_{2750}-pE_{2751}-H_2N-Q_{2760}-pE_{2761}-H_2N-Q_{2770}-pE_{2771}-H_2N-Q_{2780}-pE_{2781}-H_2N-Q_{2790}-pE_{2791}-H_2N-Q_{2800}-pE_{2801}-H_2N-Q_{2810}-pE_{2811}-H_2N-Q_{2820}-pE_{2821}-H_2N-Q_{2830}-pE_{2831}-H_2N-Q_{2840}-pE_{2841}-H_2N-Q_{2850}-pE_{2851}-H_2N-Q_{2860}-pE_{2861}-H_2N-Q_{2870}-pE_{2871}-H_2N-Q_{2880}-pE_{2881}-H_2N-Q_{2890}-pE_{2891}-H_2N-Q_{2900}-pE_{2901}-H_2N-Q_{2910}-pE_{2911}-H_2N-Q_{2920}-pE_{2921}-H_2N-Q_{2930}-pE_{2931}-H_2N-Q_{2940}-pE_{2941}-H_2N-Q_{2950}-pE_{2951}-H_2N-Q_{2960}-pE_{2961}-H_2N-Q_{2970}-pE_{2971}-H_2N-Q_{2980}-pE_{2981}-H_2N-Q_{2990}-pE_{2991}-H_2N-Q_{3000}-pE_{3001}-H_2N-Q_{3010}-pE_{3011}-H_2N-Q_{3020}-pE_{3021}-H_2N-Q_{3030}-pE_{3031}-H_2N-Q_{3040}-pE_{3041}-H_2N-Q_{3050}-pE_{3051}-H_2N-Q_{3060}-pE_{3061}-H_2N-Q_{3070}-pE_{3071}-H_2N-Q_{3080}-pE_{3081}-H_2N-Q_{3090}-pE_{3091}-H_2N-Q_{3100}-pE_{3101}-H_2N-Q_{3110}-pE_{3111}-H_2N-Q_{3120}-pE_{3121}-H_2N-Q_{3130}-pE_{3131}-H_2N-Q_{3140}-pE_{3141}-H_2N-Q_{3150}-pE_{3151}-H_2N-Q_{3160}-pE_{3161}-H_2N-Q_{3170}-pE_{3171}-H_2N-Q_{3180}-pE_{3181}-H_2N-Q_{3190}-pE_{3191}-H_2N-Q_{3200}-pE_{3201}-H_2N-Q_{3210}-pE_{3211}-H_2N-Q_{3220}-pE_{3221}-H_2N-Q_{3230}-pE_{3231}-H_2N-Q_{3240}-pE_{3241}-H_2N-Q_{3250}-pE_{3251}-H_2N-Q_{3260}-pE_{3261}-H_2N-Q_{3270}-pE_{3271}-H_2N-Q_{3280}-pE_{3281}-H_2N-Q_{3290}-pE_{3291}-H_2N-Q_{3300}-pE_{3301}-H_2N-Q_{3310}-pE_{3311}-H_2N-Q_{3320}-pE_{3321}-H_2N-Q_{3330}-pE_{3331}-H_2N-Q_{3340}-pE_{3341}-H_2N-Q_{3350}-pE_{3351}-H_2N-Q_{3360}-pE_{3361}-H_2N-Q_{3370}-pE_{3371}-H_2N-Q_{3380}-pE_{3381}-H_2N-Q_{3390}-pE_{3391}-H_2N-Q_{3400}-pE_{3401}-H_2N-Q_{3410}-pE_{3411}-H_2N-Q_{3420}-pE_{3421}-H_2N-Q_{3430}-pE_{3431}-H_2N-Q_{3440}-pE_{3441}-H_2N-Q_{3450}-pE_{3451}-H_2N-Q_{3460}-pE_{3461}-H_2N-Q_{3470}-pE_{3471}-H_2N-Q_{3480}-pE_{3481}-H_2N-Q_{3490}-pE_{3491}-H_2N-Q_{3500}-pE_{3501}-H_2N-Q_{3510}-pE_{3511}-H_2N-Q_{3520}-pE_{3521}-H_2N-Q_{3530}-pE_{3531}-H_2N-Q_{3540}-pE_{3541}-H_2N-Q_{3550}-pE_{3551}-H_2N-Q_{3560}-pE_{3561}-H_2N-Q_{3570}-pE_{3571}-H_2N-Q_{3580}-pE_{3581}-H_2N-Q_{3590}-pE_{3591}-H_2N-Q_{3600}-pE_{3601}-H_2N-Q_{3610}-pE_{3611}-H_2N-Q_{3620}-pE_{3621}-H_2N-Q_{3630}-pE_{3631}-H_2N-Q_{3640}-pE_{3641}-H_2N-Q_{3650}-pE_{3651}-H_2N-Q_{3660}-pE_{3661}-H_2N-Q_{3670}-pE_{3671}-H_2N-Q_{3680}-pE_{3681}-H_2N-Q_{3690}-pE_{3691}-H_2N-Q_{3700}-pE_{3701}-H_2N-Q_{3710}-pE_{3711}-H_2N-Q_{3720}-pE_{3721}-H_2N-Q_{3730}-pE_{3731}-H_2N-Q_{3740}-pE_{3741}-H_2N-Q_{3750}-pE_{3751}-H_2N-Q_{3760}-pE_{3761}-H_2N-Q_{3770}-pE_{3771}-H_2N-Q_{3780}-pE_{3781}-H_2N-Q_{3790}-pE_{3791}-H_2N-Q_{3800}-pE_{3801}-H_2N-Q_{3810}-pE_{3811}-H_2N-Q_{3820}-pE_{3821}-H_2N-Q_{3830}-pE_{3831}-H_2N-Q_{3840}-pE_{3841}-H_2N-Q_{3850}-pE_{3851}-H_2N-Q_{3860}-pE_{3861}-H_2N-Q_{3870}-pE_{3871}-H_2N-Q_{3880}-pE_{3881}-H_2N-Q_{3890}-pE_{3891}-H_2N-Q_{3900}-pE_{3901}-H_2N-Q_{3910}-pE_{3911}-H_2N-Q_{3920}-pE_{3921}-H_2N-Q_{3930}-pE_{3931}-H_2N-Q_{3940}-pE_{3941}-H_2N-Q_{3950}-pE_{3951}-H_2N-Q_{3960}-pE_{3961}-H_2N-Q_{3970}-pE_{3971}-H_2N-Q_{3980}-pE_{3981}-H_2N-Q_{3990}-pE_{3991}-H_2N-Q_{4000}-pE_{4001}-H_2N-Q_{4010}-pE_{4011}-H_2N-Q_{4020}-pE_{4021}-H_2N-Q_{4030}-pE_{4031}-H_2N-Q_{4040}-pE_{4041}-H_2N-Q_{4050}-pE_{4051}-H_2N-Q_{4060}-pE_{4061}-H_2N-Q_{4070}-pE_{4071}-H_2N-Q_{4080}-pE_{4081}-H_2N-Q_{4090}-pE_{4091}-H_2N-Q_{4100}-pE_{4101}-H_2N-Q_{4110}-pE_{4111}-H_2N-Q_{4120}-pE_{4121}-H_2N-Q_{4130}-pE_{4131}-H_2N-Q_{4140}-pE_{4141}-H_2N-Q_{4150}-pE_{4151}-H_2N-Q_{4160}-pE_{4161}-H_2N-Q_{4170}-pE_{4171}-H_2N-Q_{4180}-pE_{4181}-H_2N-Q_{4190}-pE_{4191}-H_2N-Q_{4200}-pE_{4201}-H_2N-Q_{4210}-pE_{4211}-H_2N-Q_{4220}-pE_{4221}-H_2N-Q_{4230}-pE_{4231}-H_2N-Q_{4240}-pE_{4241}-H_2N-Q_{4250}-pE_{4251}-H_2N-Q_{4260}-pE_{4261}-H_2N-Q_{4270}-pE_{4271}-H_2N-Q_{4280}-pE_{4281}-H_2N-Q_{4290}-pE_{4291}-H_2N-Q_{4300}-pE_{4301}-H_2N-Q_{4310}-pE_{4311}-H_2N-Q_{4320}-pE_{4321}-H_2N-Q_{4330}-pE_{4331}-H_2N-Q_{4340}-pE_{4341}-H_2N-Q_{4350}-pE_{4351}-H_2N-Q_{4360}-pE_{4361}-H_2N-Q_{4370}-pE_{4371}-H_2N-Q_{4380}-pE_{4381}-H_2N-Q_{4390}-pE_{4391}-H_2N-Q_{4400}-pE_{4401}-H_2N-Q_{4410}-pE_{4411}-H_2N-Q_{4420}-pE_{4421}-H_2N-Q_{4430}-pE_{4431}-H_2N-Q_{4440}-pE_{4441}-H_2N-Q_{4450}-pE_{4451}-H_2N-Q_{4460}-pE_{4461}-H_2N-Q_{4470}-pE_{4471}-H_2N-Q_{4480}-pE_{4481}-H_2N-Q_{4490}-pE_{4491}-H_2N-Q_{4500}-pE_{4501}-H_2N-Q_{4510}-pE_{4511}-H_2N-Q_{4520}-pE_{4521}-H_2N-Q_{4530}-pE_{4531}-H_2N-Q_{4540}-pE_{4541}-H_2N-Q_{4550}-pE_{4551}-H_2N-Q_{4560}-pE_{4561}-H_2N-Q_{4570}-pE_{4571}-H_2N-Q_{4580}-pE_{4581}-H_2N-Q_{4590}-pE_{4591}-H_2N-Q_{4600}-pE_{4601}-H_2N-Q_{4610}-pE_{4611}-H_2N-Q_{4620}-pE_{4621}-H_2N-Q_{4630}-pE_{4631}-H_2N-Q_{4640}-pE_{4641}-H_2N-Q_{4650}-pE_{4651}-H_2N-Q_{4660}-pE_{4661}-H_2N-Q_{4670}-pE_{4671}-H_2N-Q_{4680}-pE_{4681}-H_2N-Q_{4690}-pE_{4691}-H_2N-Q_{4700}-pE_{4701}-H_2N-Q_{4710}-pE_{4711}-H_2N-Q_{4720}-pE_{4721}-H_2N-Q_{4730}-pE_{4731}-H_2N-Q_{4740}-pE_{4741}-H_2N-Q_{4750}-pE_{4751}-H_2N-Q_{4760}-pE_{4761}-H_2N-Q_{4770}-pE_{4771}-H_2N-Q_{4780}-pE_{4781}-H_2N-Q_{4790}-pE_{4791}-H_2N-Q_{4800}-pE_{4801}-H_2N-Q_{4810}-pE_{4811}-H_2N-Q_{4820}-pE_{4821}-H_2N-Q_{4830}-pE_{4831}-H_2N-Q_{4840}-pE_{4841}-H_2N-Q_{4850}-pE_{4851}-H_2N-Q_{4860}-pE_{4861}-H_2N-Q_{4870}-pE_{4871}-H_2N-Q_{4880}-pE_{4881}-H_2N-Q_{4890}-pE_{4891}-H_2N-Q_{4900}-pE_{4901}-H_2N-Q_{4910}-pE_{4911}-H_2N-Q_{4920}-pE_{4921}-H_2N-Q_{4930}-pE_{4931}-H_2N-Q_{4940}-pE_{4941}-H_2N-Q_{4950}-pE_{4951}-H_2N-Q_{4960}-pE_{4961}-H_2N-Q_{4970}-pE_{4971}-H_2N-Q_{4980}-pE_{4981}-H_2N-Q_{4990}-pE_{4991}-H_2N-Q_{5000}-pE_{5001}-H_2N-Q_{5010}-pE_{5011}-H_2N-Q_{5020}-pE_{5021}-H_2N-Q_{5030}-pE_{5031}-H_2N-Q_{5040}-pE_{5041}-H_2N-Q_{5050}-pE_{5051}-H_2N-Q_{5060}-pE_{5061}-H_2N-Q_{5070}-pE_{5071}-H_2N-Q_{5080}-pE_{5081}-H_2N-Q_{5090}-pE_{5091}-H_2N-Q_{5100}-pE_{5101}-H_2N-Q_{5110}-pE_{5111}-H_2N-Q_{5120}-pE_{5121}-H_2N-Q_{5130}-pE_{5131}-H_2N-Q_{5140}-pE_{5141}-H_2N-Q_{5150}-pE_{5151}-H_2N-Q_{5160}-pE_{5161}-H_2N-Q_{5170}-pE_{5171}-H_2N-Q_{5180}-pE_{5181}-H_2N-Q_{5190}-pE_{5191}-H_2N-Q_{5200}-pE_{5201}-H_2N-Q_{5210}-pE_{5211}-H_2N-Q_{5220}-pE_{5221}-H_2N-Q_{5230}-pE_{5231}-H_2N-Q_{5240}-pE_{5241}-H_2N-Q_{5250}-pE_{5251}-H_2N-Q_{5260}-pE_{5261}-H_2N-Q_{5270}-pE_{5271}-H_2N-Q_{5280}-pE_{5281}-H_2N-Q_{5290}-pE_{5291}-H_2N-Q_{5300}-pE_{5301}-H_2N-Q_{5310}-pE_{5311}-H_2N-Q_{5320}-pE_{5321}

Table 3
The identification of the serum peptides in pseudoascitis

m/z	Scores	Protein	Accession ID[a]	Theoretical	Observed	Confidence	Error	Confirmed sequence[b]	Modifications
1055	1.56 (PV + PsA) 2.01	[illegible] alpha-2-HS-glycoprotein	[illegible]	1055.6	1056.2	[illegible]	−1.15E−04	[illegible]	–
1402	2.01 (PV + PsA) HC	Fibrinogen alpha chain	P02671_FIBA_HUMAN	1402.6	1402.5	[illegible]	−1.02E−05	[illegible]	Phosphoserine
		Fibrinogen alpha chain	P02671_FIBA_HUMAN	1461.6	1461.5	[illegible]	−5.30E−05	[illegible]	
1511	1.50 (PV + PsA) HC	Fibrinogen alpha chain	P02671_FIBA_HUMAN	1510.7	1510.5	[illegible]	2.2E−07	[illegible]	Phosphoserine
1572	1.46 (PV + PsA) HC 1.45 (PV + PsA) AD	Fibrinogen	P02671_FIBA_HUMAN	1573.8	1573.0	98.16	[illegible]	[illegible]	Pyro-Glu (N-terminal) Deamidated [illegible]
2038	1.61 (PsA) PV	Fibrinogen alpha chain	P02671_FIBA_HUMAN	2038.2	2038.5	[illegible]	9.86E−04	[illegible]	
2041	1.45 (PV + PsA) AD 1.54 (PsA) PV	Fibrinogen alpha chain	P02671_FIBA_HUMAN	2040.2	2040.8	[illegible]	5.72E−04	[illegible]	–
2052	1.46 (PV + PsA) AD	Fibrinogen alpha chain	P02671_FIBA_HUMAN	2052.2	2054.0	[illegible]	7.05E−04	[illegible]	–
2090	1.46 (PV + PsA) HC 1.41 (PV + PsA) AD 1.35 (PsA) PV	Fibrinogen alpha chain	P02671_FIBA_HUMAN	2090.2	2091.0	[illegible]	−1.15E−01	[illegible]	–
2235	1.55 (PV + PsA) AD 1.57 (PsA) PV 1.51 (Psoriasis)	Fibrinogen alpha chain	P02671_FIBA_HUMAN	2235.3	2243.0	[illegible]	2.00E−04	[illegible]	
4060	2.04 (PV + PsA) HC	Fibrinogen alpha chain	P02671_FIBA_HUMAN	4060.8	4062.0	[illegible]	1.29E−09	[illegible]	–
4964	1.56 (PsA) PV	TMSB4X protein	Q9UNW8_THYM4_HUMAN	4962.5	4963.0	[illegible]	2.72E−04	[illegible]	Protein N-terminal acetylation
4995	1.57 (PsA) PV	TMSB4X protein	Q9UNW8_THYM4_HUMAN	4995.5	4995.0	96.74	2.06E−05	[illegible]	Protein N-terminal acetylation; Serine (S) Oxidation (M)
5037	1.69 (PV + PsA) AD 1.22 (PsA) PV	Fibrinogen alpha chain	P02671_FIBA_HUMAN	5037.3	5038.7	[illegible]	2.46E−05	[illegible]	–

The mass to charge values used for the designation of most ions were obtained by MALDI-TOF/MS, whereas those for "observed" were obtained by LC–MS.
The peptides that showed a >1.5-fold difference in ion abundance between the PV + PsA and HC groups, between the PV + PsA and AD groups, between the PsA and PV groups, and between the sPV and mPV groups were selected for identification.
[a] The positions of amino acids of the HSA-derived peptides are specifically shown as the first amino acid of the mature peptide as 1. The positions of amino acids of the other identified peptides are shown according to the indications in the accession ID data files. TMSB4X, thymosin β4.

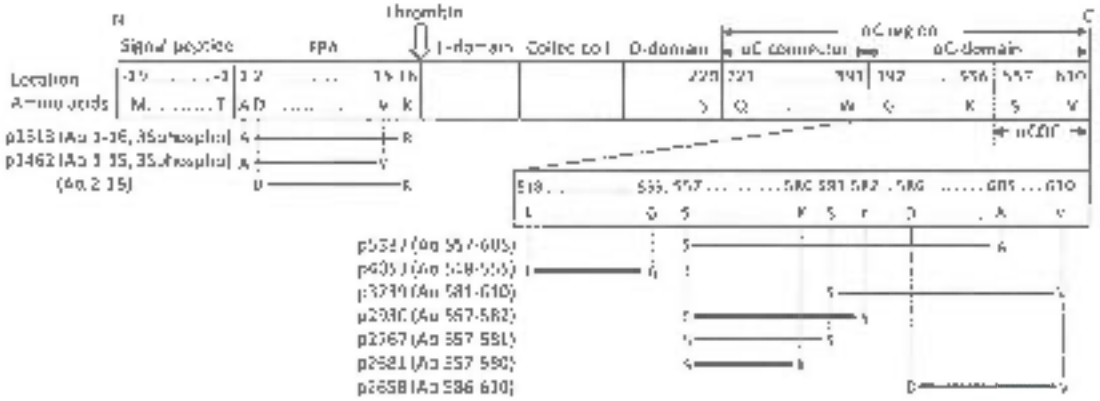

Fig. 2. The intra-molecular locations of the identified FIBA derived peptides. A schematic illustration of the structure of the FibA precursor and the locations of the identified FIBA derived peptides. The mature FibA protein without its signal peptide consists of FPA, the E-domain, the coiled coil region, the D-domain and the αC region. The αC region (Aα 221–610) consists of the αC-connector (Aα 221–391) and the αC-domain (Aα 392–610) [38]. The C-terminal region of the αC-domain (Aα 557–610) was designated as αCDF [29].

lower than their respective ion intensities in the PV group (Table 3). p1056 was derived from a protein that was highly similar to alpha-2-HS-glycoprotein (α2HS-GP), which may be involved in the development and maintenance of skin [24].

3.2. The effect of FPAdA on the secretion of humoral factors

Among the peptides that were identified, we focused on p1462 and p1977 (FLG-pEF), which showed a higher ion intensity in the PV + PsA group than in the HC and/or AD groups (Table 3). We hypothesized that these peptides may function as modulators of the inflammation in psoriasis. We therefore examined whether these peptides stimulated the dermal cells to alter the secretion of inflammatory humoral factors.

We first synthesized FPAdA, the unmodified form of p1462 (Table 3). dMVECs and keratinocytes were stimulated with FPAdA or its re-sequenced control peptide (FPAdA-Cont). The concentration of FPAdA and FPAdA-Cont in the cell culture (1.5 mg/mL) was calculated from the plasma concentration of fibrinogen. At this concentration, the cell viability of both the dMVEC and keratinocyte cultures was >97% (data not shown).

In a cytokine array of dMVEC culture supernatants, spots of GROα, IL-8, MCP-1, MIF, and serpin E1 were detected. FPAdA stimulation caused a >1.2-fold change in the spot intensity of those humoral factors in comparison to non-stimulated dMVECs (Fig. 3A). Among these, GROα, IL-8, and MCP-1 that showed a >1.3-fold change in the spot intensity were subsequently measured by ELISAs.

As a result, the secretion of GROα following FPAdA stimulation (280.9 ± 7.3 pg/mL) was increased 1.20-fold and 1.22-fold in comparison to non-stimulated (234.5 ± 5.3 pg/mL, $p < 0.0001$) and FPAdA-Cont stimulated (229.5 ± 5.0 pg/mL, $p < 0.001$) dMVECs, respectively (Fig. 3B). In contrast, the measured secretion of IL-8 was found to decrease following FPAdA stimulation (679.6 ± 89.3 pg/mL) in comparison to non-stimulated dMVECs (919.2 ± 36.2 pg/mL, $p < 0.05$); this result conflicted with the results of the cytokine array. The secretion of MCP-1 in response to FPAdA stimulation (1404 ± 108 pg/mL) was increased 1.19-fold in comparison to FPAdA-Cont-stimulated dMVECs (1181 ± 47 pg/mL, $p < 0.05$); however, there was no difference in comparison to non-stimulated dMVECs (1368 ± 41 pg/mL, $p = 0.63$) (Fig. 3B).

Next, we analyzed the secretion of humoral factors from keratinocytes in response to FPAdA stimulation. The cytokine array showed that FPAdA stimulation caused a >1.5-fold change in the spot intensities of VEGF, pentraxin-3, MIF, lipocalin-2, osteopontin, and Dkk-1 in comparison to non-stimulated keratinocytes (Fig. 4A). Among these, MIF, lipocalin-2, osteopontin, and Dkk-1 that showed a >1.7-fold change in the spot intensity were subsequently measured by ELISAs.

As a result, the secretion of lipocalin-2 following FPAdA stimulation (273 ± 13 pg/mL) was decreased −1.17-fold and −1.28-fold in comparison to non-stimulated (321 ± 10 pg/mL, $p < 0.01$) and FPAdA-Cont-stimulated (350 ± 10 pg/mL, $p < 0.01$) keratinocytes, respectively (Fig. 4B). The secretion of MIF following FPAdA stimulation (12.0 ± 0.7 pg/mL) was decreased −1.28-fold in comparison to non-stimulated keratinocytes (15.3 ± 3.3 pg/mL, $p < 0.05$), however, no difference was found in the FPAdA-Cont-stimulated keratinocytes (12.5 ± 3.4 pg/mL, $p = 0.501$) (Fig. 4B). The secretion of osteopontin following FPAdA stimulation (1720 ± 27 pg/mL) was increased 1.15-fold in comparison to that in FPAdA-Cont-stimulated keratinocytes (1502 ± 27 pg/mL, $p < 0.001$); however, no difference was found in comparison to non-stimulated keratinocytes (1754 ± 47 pg/mL, $p = 0.47$) (Fig. 4B). After FPAdA stimulation, there were no significant changes in the secretion of Dkk-1 in comparison to FPAdA-Cont-stimulated and non-stimulated keratinocytes.

3.4. The effect of FLG-pEF on humoral factor secretion

We similarly examined the effects of FLG-pEF on the secretion of humoral factors from dMVECs and keratinocytes. The concentrations of FLG-pEF and its control peptides, FLG-Q_2 and FLG-Cont, were determined by examining the cell viability. As a result, 3.4 μg/mL for dMVECs and 1.5 μg/mL for keratinocytes were found to be the highest concentrations to provide >95% cell viability (data not shown).

First, the secretion of humoral factors from dMVECs was analyzed. A cytokine array detected the spots of 5 humoral factors, GROα, IL-8, MCP-1, MIF, and Serpin E1. The spot intensities of GROα, IL-8, and MCP-1 were changed >−1.3-fold by FLG-pEF stimulation in comparison to non-stimulated dMVECs (Fig. 5A). These 3 humoral factors were subsequently measured by ELISAs.

As a result, the secretion of GROα following FLG-pEF stimulation (844.3 ± 47.5 pg/mL) was found to decrease −1.46-fold and −1.23-fold in comparison to non-stimulated dMVECs (1230.9 ± 32.3 pg/mL, $p < 0.001$) and FLG-Cont stimulated dMVECs (1038.5 ± 96.9 pg/mL, $p < 0.05$), respectively (Fig. 5B). However, no difference was found between the secretion of GROα following FLG-pEF stimulation or FLG-Q_2 stimulation (768.2 ± 49.3 pg/mL, $p = 0.13$). The secretion of IL-8 following FLG-pEF stimulation

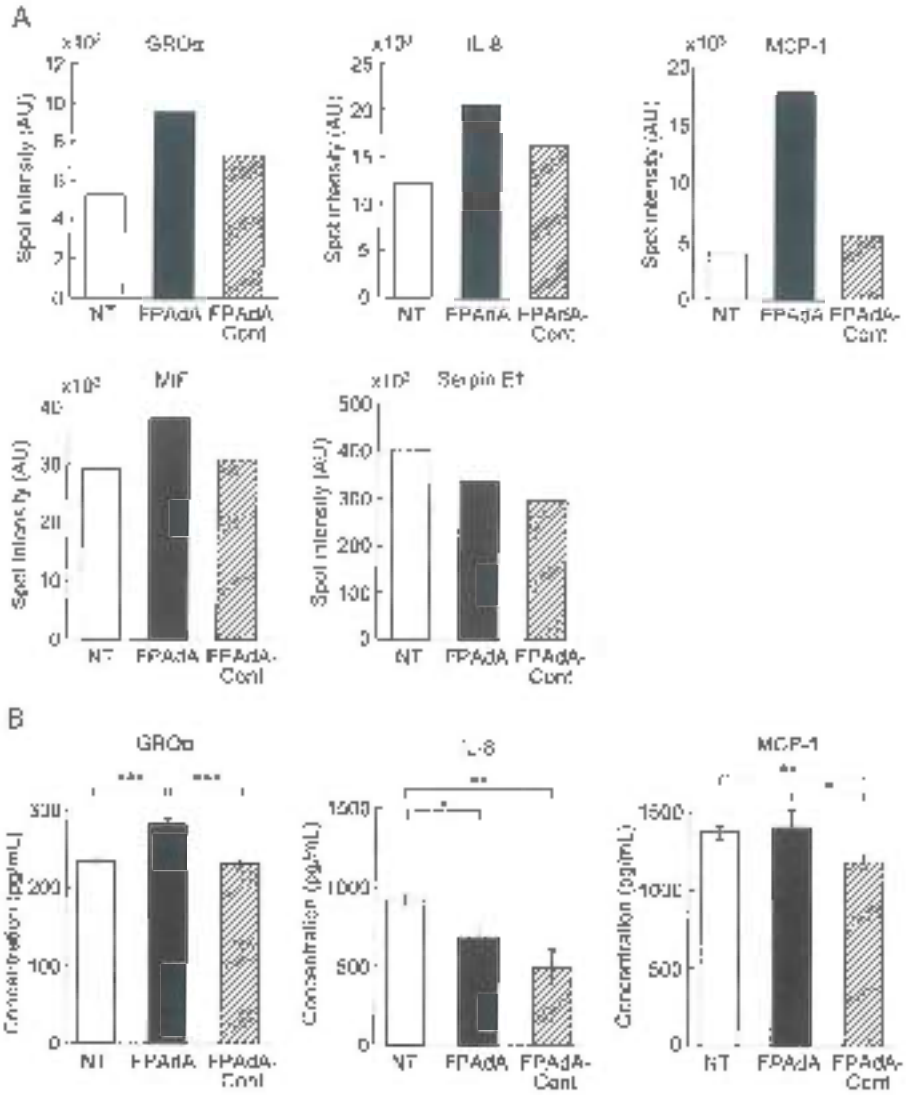

Fig. 3. The secretion of humoral factors from FPAdA-stimulated dMVECs. (A) The secretion of humoral factors from dMVECs cultures with recombinant (no treatment, NT), with FPAdA, and with FPAdA-Cont was assayed using a cytokine array. The spot intensities of GROα, IL-8, MCP-1, MIF, and serpin E1, spots of which were detected in the cytokine array, are shown. (B) The secretion of GROα, IL-8, and MCP-1 from dMVECs which was found to be increased more than 1.5-fold following FPAdA stimulation in comparison to non-stimulated dMVECs in the cytokine array, was measured by ELISAs (*p < 0.05, **p < 0.01, ***p < 0.001).

(22403.1 ± 172.0 pg/mL) decreased 1.35-fold and 1.44-fold in comparison to non-stimulated dMVECs (30193.9 ± 38.4 pg/mL, $p < 0.01$) and FLG-Cont stimulated dMVECs (32219.9 ± 524.7 pg/mL, $p < 0.05$), respectively. However, no difference was found between the secretion of IL-8 following FLG-pEE stimulation or FLG-Q_2 stimulation (1967.8 ± 179.9 pg/mL, $p = 0.05$). Interestingly, the secretion of MCP-1 following FLG-pEE stimulation (4057.8 ± 157.2 pg/mL) decreased 1.23-fold and 1.14-fold in comparison to non-stimulated dMVECs (4989.1 ± 238.7 pg/mL, $p < 0.01$) and FLG-Q_2-stimulated dMVECs (4619.1 ± 213.4 pg/mL, $p < 0.05$), respectively. However, no difference was found between the secretion of MCP-1 following FLG-pEE stimulation or FLG-Cont stimulation (4624.0 ± 424.4 pg/mL, $p = 0.09$) (Fig. 5B).

Next, the secretion of humoral factors from keratinocytes was analyzed after FLG-pEE stimulation. The cytokine array detected the spots of all of the humoral factors except IL-6, IL-1ra, lipocalin-2, MMP-9, and SHBG showed a >1.2 fold change in intensity following FLG-pEE stimulation in comparison to non-stimulated keratinocytes. These 4 humoral factors were subsequently measured by ELISAs (Fig. 6A).

Among the 4 humoral factors, the secretion of lipocalin-2 following FLG-pEE stimulation (648.2 ± 88.3 pg/mL) was increased 1.35-fold in comparison to non-stimulated keratinocytes (480.8 ± 25.5 pg/mL, $p < 0.05$); however, no changes were observed in comparison to FLG-Cont stimulation (643.0 ± 15.0 pg/mL, $p = 0.93$) and FLG-Q_2 stimulation (558.8 ± 3.0 pg/mL, $p = 0.19$) (Fig. 6B). The secretion of IL-1ra and MMP-9 after FLG-pEE stimulation was not significantly different from that in non-stimulated keratinocytes (Fig. 6B). All of the SHBG results were below the detection limits (data not shown).

3.5. Correlation of peptide spot intensity and clinical parameters

To detect the peptides that would be associated with the pathophysiology of psoriasis in another way, we analyzed correlations between intensity of the identified peptides and

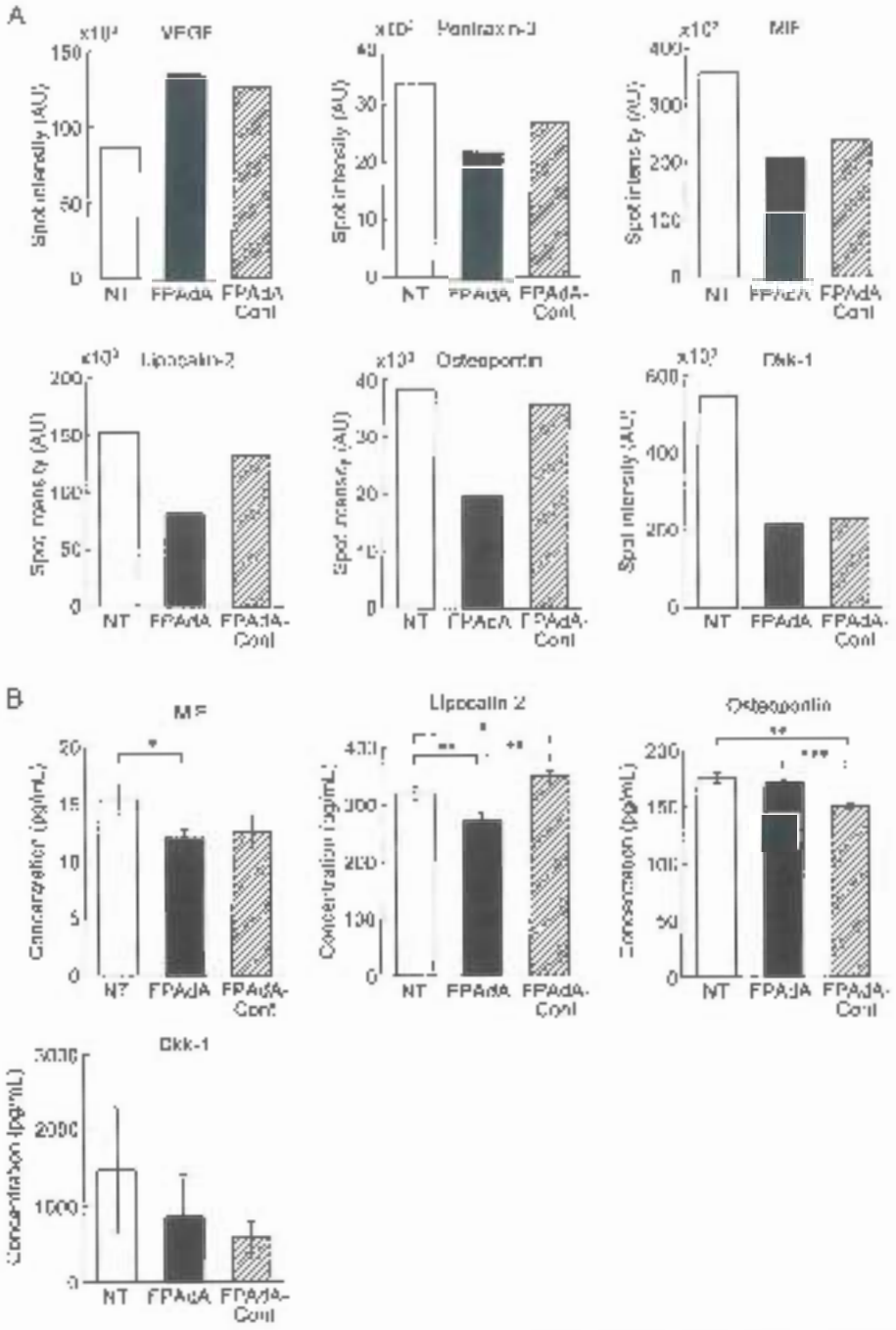

Fig. 4. Protein expression in human keratinocytes from FPAdA-treated keratinocytes. (A) The secretion of human cytokines from keratinocytes cultured with culture medium (NT), with FPAdA, and with FPAdA-Cont was assayed using a cytokine array. The spot intensities of VEGF, pentraxin-3, MIF, lipocalin-2, osteopontin, and Dkk-1, which showed more than 20,000 AU and increased ≥1.5 fold following FPAdA stimulation in comparison to non-stimulated keratinocytes, are shown. (B) The secretion of MIF, lipocalin-2, osteopontin and Dkk-1 from dermal DFCs, which was found to be decreased less than −1.5-fold following FPAdA-stimulation in comparison to non-stimulated keratinocytes. The cytokine array was measured by ELISAs. *p < 0.05, **p < 0.01, ***p < 0.001.

clinical parameters. PASI, C-reactive protein (CRP), and treatment were selected as the clinical parameters because they reflected the disease severity, activity, and demands for the disease control, respectively. To analyze the correlation between peptide ion intensity and treatment, we specifically designed a treatment score in which the treatments for psoriasis in this study were classified into five groups as described in Section 2.

As a result, we found that p3056, derived from a protein highly similar to α2HS-GP, was negatively correlated with PASI ($\rho = -0.481$, $p < 0.01$; Fig. 7A). p2681, an N-terminal peptide of FHA-αCDC (C-terminal portion of the αC-domain of FHA, Fig. 2), was negatively correlated with CRP ($\rho = -0.394$, $p < 0.05$; Fig. 7B). p2930, p3239, and p5337, the relatively long FHA-αCDC-derived peptides, were negatively correlated with the treatment score

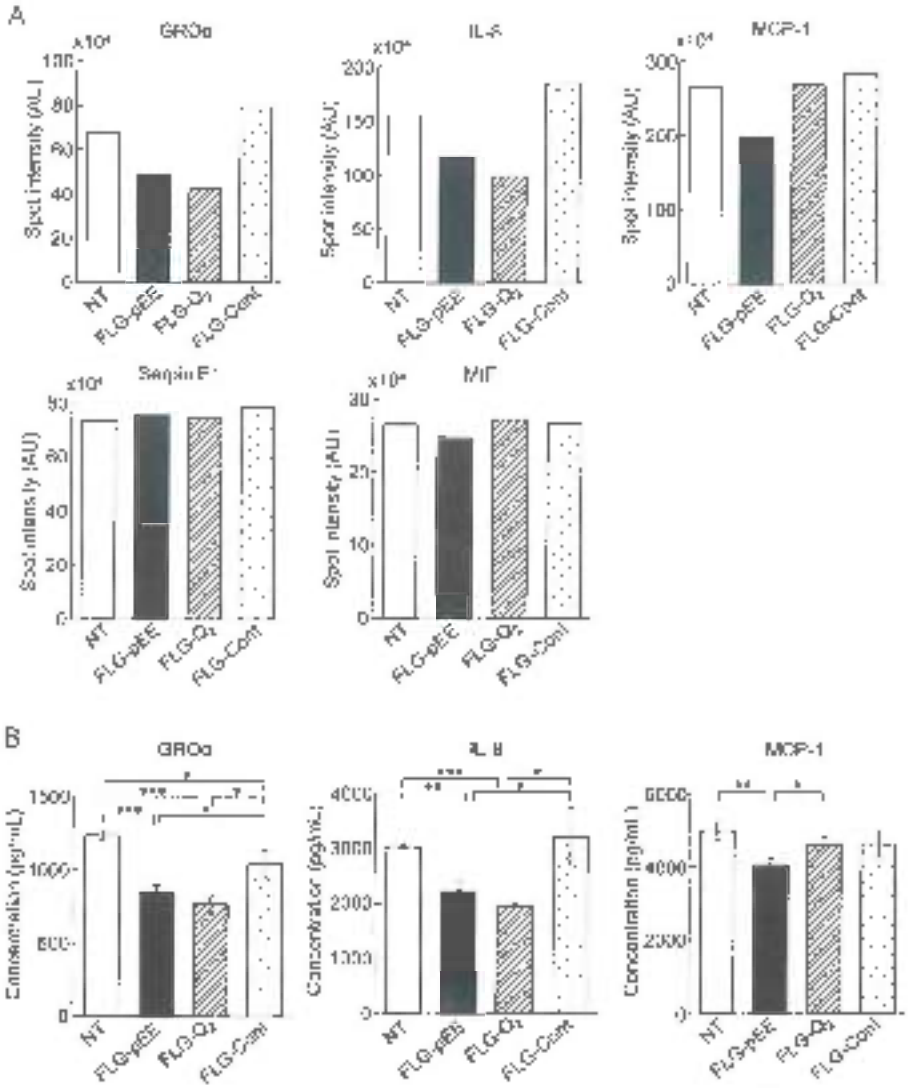

Fig. 5. The secretion of inflammatory factors from dMVECs stimulated with FLG-pEE. (A) The secretion of humoral factors from dMVECs cultured with medium-alone (NT), with FLG-pEE, with FLG-O2, and with FLG-Cont was assayed using a cytokine array. The spot intensities of GROα, MCP-1, IL-8, MIF, and serpin E1, spots of which were detected, are shown. (B) The secretion of GROα, MCP-1, and IL-8 from dMVECs, which were deprived less than 1 h-old following FLG-pEE stimulation in comparison to non-transferred dMVECs in the cytokine array, was measured by ELISAs. *p < 0.05, **p < 0.01, ***p < 0.001.

(p2930, $\rho = -0.531$, $p < 0.01$, Fig. 7C; p3239, $\rho = -0.440$, $p < 0.01$, Fig. 7D; p5337, $\rho = -0.451$, $p < 0.01$, Fig. 7E).

As shown in Fig. 7C–E, psoriasis patients treated with NSAIDs (treatment score 2) showed relatively low ion intensity of the FIBA-derived peptides. We therefore specifically compared ion intensity of all the identified peptides between the psoriasis patients treated with NSAIDs (n = 6) and those treated without NSAIDs (n = 28), between the psoriasis patients treated with immunosuppressants (MTX and CYA) (n = 8) and those treated without immunosuppressants (n = 26), and between the psoriasis patients treated with biological drugs (n = 3) and those treated without biological drugs (n = 31). Interestingly, the ion intensity of p2659, p2681, p2930, and p3239, which are all derived from FIBA-cCDC, was significantly decreased in the NSAID-treated group compared to the NSAID-non-treated group (Fig. 7F–I). The ion intensity of p4979, which is derived from thymosin β4, was also significantly decreased in the NSAID-treated group compared to the NSAID-non-treated group (Fig. 7J). Furthermore, the ion intensity of p2930 was significantly decreased in the immunosuppressant-treated group compared to the immunosuppressant-non-treated group (Fig. 7K). No peptide showed ion intensity difference between the psoriasis patients treated with biological drugs and those treated without biological drugs (data not shown). The production of these peptides and/or their parent proteins may be suppressed by NSAIDs and/or immunosuppressants.

4. Discussion

We analyzed serum peptide profiles to find peptides that are involved in the pathophysiology of psoriasis. The major psoriasis-affected site is the skin, however, the inflammation also affects the joints and other organs such as the eyes, lungs, and heart. To explore novel molecules that are associated with the inflammation in psoriasis, we selected serum peptidome that contained processed proteins as a source of unknown molecules with pathophysiologic effects.

We comprehensively analyzed the serum peptides of PV, PsA, and AD patients and HC subjects and found 93 serum peptides that

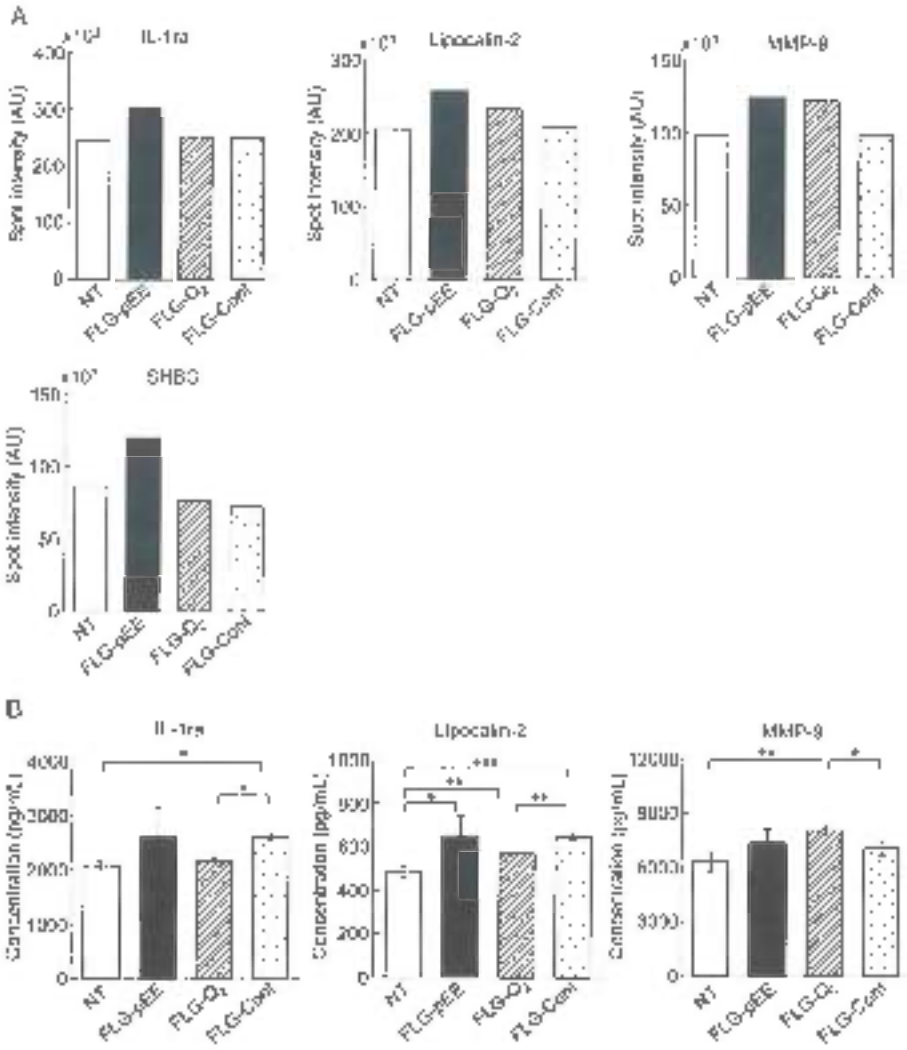

Fig. 6. The secretion of humoral factors from keratinocytes stimulated with FLG-pEE. (A) The secretion of humoral factors from keratinocytes cultured with medium alone (NT), with FLG-pEE, with FLG-Q1, and with FLG-Con was analyzed using a cytokine array. The spot intensities of IL-1ra, lipocalin-2, MMP-9, and SHBG, which increased 1.2-fold following FLG-pEE stimulation in comparison to non-stimulated keratinocytes, are shown. (B) The results of ELISA measuring IL-1ra, lipocalin-2, and MMP-9. *p < 0.05, **p < 0.01, ***p < 0.001.

possibly contained the disease-related peptides (Fig. 1A and B). There were significant differences in the ion intensities of 24 of these peptides between the PV + PsA and HC groups, and 20 of the peptides between the PV + PsA and AD groups ($p < 0.05$) (Table 2). These peptides were considered to be candidates that are involved in the pathophysiology of psoriasis. Interestingly, in the PsA group, the number of peptides for which the ion intensity decreased was greater than the numbers of peptides for which the ion intensity increased in comparison to the PV group; a similar finding was observed in the sPV group in comparison to the mPV group (Table 2). The decrease of serum peptides may be associated with the onset of arthritis and the severity of psoriasis.

None of the 13 identified peptides were FIBA-derived, and were fragments of FPA and the αC-domain (Table 3 and Fig. 2). Physiologically, cleavage of FIBA by thrombin releases FPA and initiates the conversion of fibrinogens to fibrins that polymerize themselves to form fibrin clots [25]. The ion intensity of the FPA-derived peptides, p1462 and p1615, was higher in the PV + PsA group than in the HC group ($p < 0.05$) (Table 3). Fibrinogen and FPA have been reported to be increased in psoriasis patients in comparison to healthy individuals [26,27]. The increase in FPA-derived peptides may reflect the increased expression of the parent protein, suggesting the activation of coagulation due to the microvascular abnormalities of the psoriatic lesion.

On the other hand, 7 FIBA-derived peptides were from the αC-domain, 6 of which were from αCDC, the C-terminal portion of the αC-domain (Fig. 2) [28,29]. The αC-domain is the site at which fibrins interact intermolecularly for the polymerization [30]. The overall results of the ion intensity of αC-domain-derived peptides were as follows: (1) the PV + PsA group > the AD group; (2) the PsA group < the PV group; and (3) the sPV group < the mPV group ($p < 0.05$) (Table 3). Since fibrinogen was reported to be increased in psoriasis patients in comparison to healthy individuals [26], the fragmentation of the αC-domain can be expected to be decreased in psoriasis, especially in PsA and sPV. The decrease of αC-domain-derived peptides may be associated with the onset of arthritis and the severity of psoriasis, which suggests a protective effect of αC-domain fragmentation and/or the αC-domain-derived peptides in

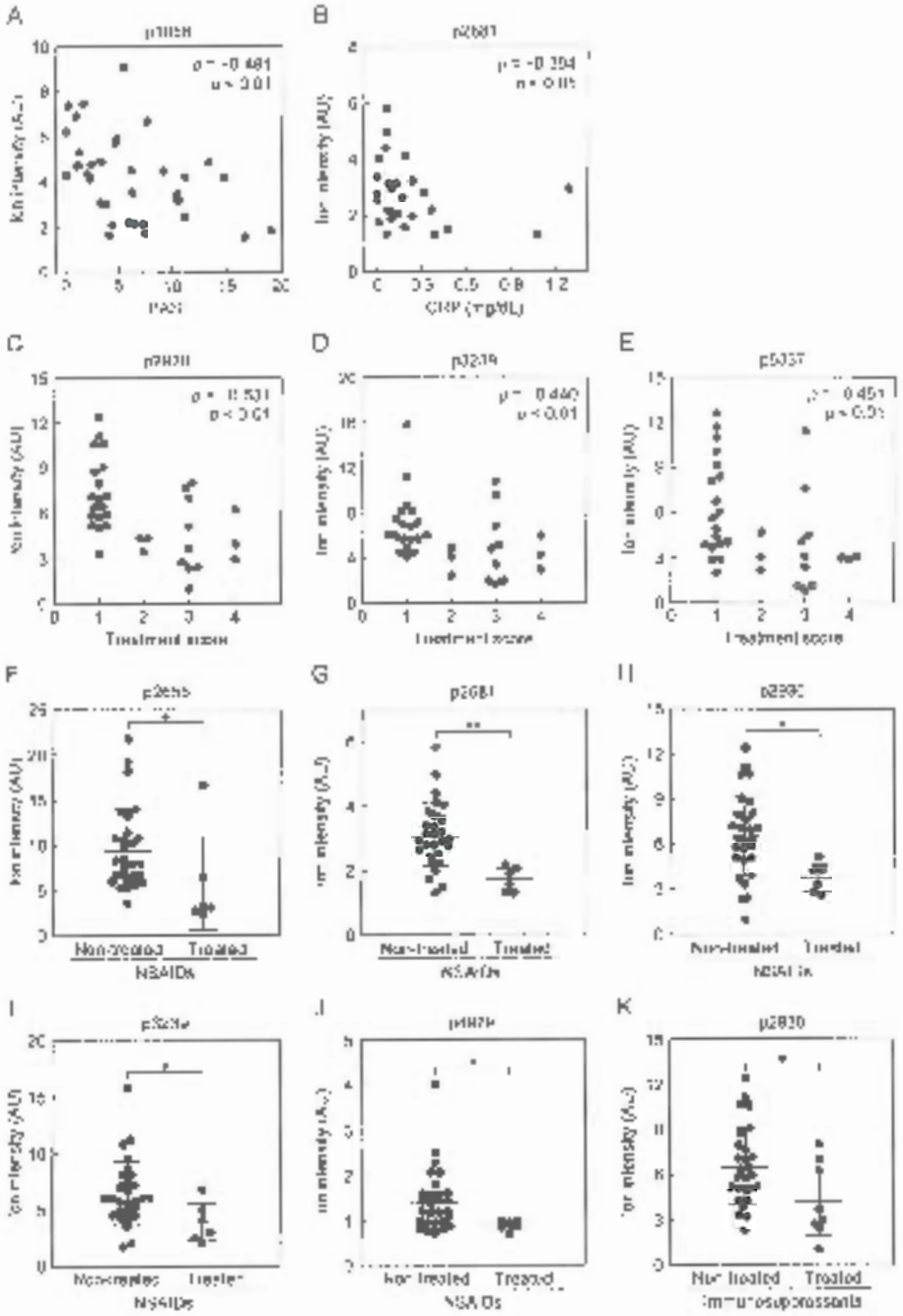

Fig. 7. The correlations between the peptide ion intensities and clinical parameters in psoriatic patients. (A) The correlations between the ion intensities of the 11 citrulline peptides and clinical parameters of PASI (n = 34), CRP (n = 26), and the treatment score (n = 34) were examined in the psoriasis (PsA) patients (Table 1). In the univariate analysis of CRP in PsA patients with malignant lymphoma (ML) and a PsA patient with liver disease (PsA with ML/LD), CRP values of > 2.00 were regarded as 2. The results of the 5 peptides that showed correlations are shown (A–E). The results of the 5 peptides that showed significant differences in ion intensity between the NSAID-treated group (n = 6) and the NSAID-non-treated group (n = 28) and between the immunosuppressant-treated group (n = 6) and the immunosuppressant-non-treated group (n = 26) are also shown (F–K). *p < 0.05, **p < 0.01.

psoriasis. p2681 was negatively correlated with CRP values ($\rho = -0.394$, $p < 0.05$). However, most of the psoriasis patients showed CRP values within normal limits (Table 1 and Fig. 7B). Therefore, this correlation should be confirmed using a large cohort of psoriatic patients that includes a sufficient number of CRP-positive patients. p2930, p3239, and p5337, relatively longer α-CDC-derived peptides, were negatively correlated with the treatment score ($\rho = -0.531$, $\rho = -0.440$, and $\rho = -0.451$; $p < 0.01$) (Fig. 7C–E). These FIBA-derived peptides are expected to be decreased according to the intensity of the treatment. In addition, the ion intensity of p2686, p2681, p2930, and p3239, which are all derived from FIBA-α-CDC, was decreased in the NSAID-treated group compared to the NSAID non-treated group, and the ion intensity of p2930 was also decreased in the immunosuppressant-treated group compared to the immunosuppressant-non-treated group ($p < 0.05$) (Fig. 7F–I and K). Thus, NSAIDs and

immunosuppressants, especially NSAIDs, may effectively suppress the inflammatory process of psoriasis, which results in a decrease in the production of fibrinogen.

It is noteworthy that the ion intensity of p1977 FLG-pEE was higher in the PV + PsA group than in the HC and AD groups ($p < 0.05$) (Table 3). FLG is processed from its large precursor protein, profilaggrin. FLG aggregates the keratin filaments to form tight bundles that promote the flattening of corneocytes [22]. FLG monomers are degraded into free amino acids and further metabolized to constitute natural moisturizing factors. Mutations of FLG cause ichthyosis vulgaris and FLG deficiency is known to contribute to the pathogenesis of AD [22,31]. FLG monomers, FLG1–FLG23, are located in tandem in profilaggrin and FLG-pEE was derived from an intervening sequence located between FLG12 and FLG13 [32]. The expression of FLG has been reported to be decreased in the skin of PV patients in comparison to the skin of healthy individuals and AD patients [33]. Although the mechanism by which FLG-intervening peptides are catabolized is unclear, FLG-pEE may escape from further degradation because of its post-translational modification. p1056, which is decreased in the PV + PsA group in comparison to the AD group, was derived from a protein that is highly similar to α2HS-GP ($p < 0.05$) (Table 3). α2HS-GP is associated with skin development and wound healing [24]. p1056 was also negatively correlated with PASI in psoriasis patients ($\rho = -0.481$, $p < 0.01$) (Fig. 7A). These results suggest that the expression of the parent protein decreased in psoriasis, according to their disease severity, which would also function as a skin-protective protein in a manner similar to α2HS-GP. p1056 may be a candidate biomarker for the severity of psoriasis.

p4964 and p4979, which are derived from thymosin β4 protein, were decreased in the PsA group in comparison to the PV group ($p < 0.05$) (Table 3). Thymosin β4 is one of the regulators of actin polymerization [34]. Thymosin β4 is thought to participate in anti-inflammation and wound healing, through its relationship to the secretion of MMPs and inflammatory cytokines and the upregulation of anti-oxidative enzymes [35–37]. Thus, thymosin β4 may suppress the onset of arthritis in psoriasis. The decrease of thymosin β4-derived peptides suggests the decreased expression of thymosin β4 in PsA. Interestingly, the ion intensity of p4979, the oxidated thymosin β4-derived peptide, was decreased in the NSAID-treated group compared to the NSAID-non-treated group ($p < 0.05$) (Fig. 7J). This suggested that the oxidation at the 32nd methionine (M) was decreased by the treatment with NSAIDs which may be involved in the inflammation of psoriasis (Table 3).

It was noteworthy that FLG-pEE stimulation resulted in the decreased secretion of GROα and IL-8 from dMVECs in comparison to FLG Cont-stimulated and non-stimulated dMVECs ($p < 0.05$) (Fig. 5B). IL-17, a key inflammatory cytokine in psoriasis, is abundantly produced by the Th17 cells, γδT cells, neutrophils and mast cells in psoriatic skin [7,38,39]. IL-17A acts on the keratinocytes to increase the expression of ELR$^+$ chemokines such as GROs and IL-8, recruiting neutrophils and T cells to the lesion sites [39,40]. IL-17 receptors are expressed on vascular endothelial cells [41–43], and human dermal endothelial cells migrated following IL-17A stimulation [44]. Thus, dMVECs as well as keratinocytes could be stimulated by IL-17A. Our data showed that FLG-pEE downregulated the secretion of GROα and IL-8 from dMVECs, which would lead to a reduction of the neutrophil- and T cell-mediated inflammation in psoriasis. FLG-pEE stimulation also led to a decrease in the secretion of MCP-1 from dMVECs in comparison to non-stimulated and IL_{17}-Q_{17}-stimulated dMVECs ($p < 0.05$) (Fig. 5D). In psoriasis, the keratinocytes are known to produce MCP-1 and to recruit CCR2$^+$ and CD163-positive macrophages/monocytes to the skin lesions [45–47]. The injection of MCP-1 together with TNFα induced psoriasiform skin inflammation in a CD18-hypomorphic psoriasis-prone model, thus MCP-1 is considered to be the disease-causing inflammatory chemokine in psoriasis [48]. Our data showed that FLG-pEE stimulation down-regulated the secretion of MCP-1 from dMVECs, which may lead to a reduction in the macrophage-mediated inflammation of psoriasis. Interestingly, this downregulation of MCP-1 was not found after the stimulation with FLG-Q_2 (Fig. 5B). Since N-terminal glutamine ($Q_{2\,pep}$) is spontaneously changed to pyroglutamate (pE) when a peptide is solved, the other post-translational modification, $Q_{2\,pep}$, may be specifically involved in the downregulation of MCP-1 by FLG-pEE.

In contrast, FPAdA-stimulation increased the secretion of GROα from dMVECs in comparison to FPAdA-Cont-stimulated and non-stimulated dMVECs ($p < 0.001$) (Fig. 5B). This result suggested that FPAdA upregulates neutrophil chemotaxis to aggravate the inflammation. On the other hand, FPAdA decreased the secretion of lipocalin-2 from keratinocytes in comparison to FPAdA-Cont-stimulated and non-stimulated keratinocytes ($p < 0.05$) (Fig. 4B). Lipocalin-2 is an antimicrobial protein that is highly expressed in the psoriatic skin [49]. Since the intraperitoneal injection of lipocalin-2 exacerbated erythema and scaling and the neutralization of lipocalin-2 alleviated the epidermal inflammation in a murin model of IMQ treated psoriatic skin, lipocalin-2 has been recognized to contribute to the pathogenesis of psoriasis [49,50]. Because FPAdA downregulated the secretion of lipocalin-2 from keratinocytes, this peptide may reduce inflammation. The elucidation of the overall contribution of FPAdA to inflammation in psoriasis will require further studies.

As a limitation of this study, we analyzed serum but not skin peptide profiles of psoriasis. Analyzing the peptide profiles in skin and comparing them to the profiles in sera would be extremely useful. Peptidomics analyze the native fragmentation of proteins, and clinical peptidomics are generally conducted using body fluids such as plasma/serum and urine, which are uniform and have low protease activity [51–53]. Tissue samples contain a large amount of proteases, which are probably activated during the peptide extraction, resulting in artificial digestion of the parent proteins. Therefore, to reduce protease activity in tissue samples, a number of methods for a variety of tissue have been proposed for sample preparation, such as heat inactivation and the addition of acetone, trichloroacetic acid, and protease inhibitors [54–56]. To the best of our knowledge, however, no method involving a protease activity-reducing treatment has been established in human skin peptidomics. In the near future, we will attempt to establish a novel method for analyzing natively digested peptides to compare the peptide profiles between skin and serum in psoriasis. In addition, most of the psoriasis patients in this study possessed comorbid diseases such as metabolic diseases and cardiovascular diseases, and all of the patients were treated with external and/or internal medication (Table 1). Therefore, production of some peptides has been probably affected by such comorbid diseases as well as treatments as shown in Fig. 7C–K.

It was reported that anti-microbial peptides such as β-defensin 2, LL37, and psoriasin are increased in sera from psoriasis patients compared to those from healthy individuals [57]. However, we did not detect MS peaks for those anti-microbial peptides in our serum peptidomic results (data not shown). This may be due to the differences in the sensitivity between ELISA and peptidomics. The sensitivity of proteomics/peptidomics with standard sample preparation remains in the pg/mL orders [58], which is lower than the sensitivity of ELISA that detects proteins/peptides in the ng/mL to pg/mL orders. Proteomics/peptidomics are useful methods for detecting novel proteins/peptides related to the pathophysiology of targeted diseases, however, already-identified proteins/peptides at low concentrations should be detected and quantified by specific and sensitive methods such as ELISA. If the concentration of the overexpressed anti-microbial peptides in skin

is much higher than in that in sera, they may be detectable via the novel peptidomic strategy that we will try to establish as described above.

In conclusion, serum peptides are thus considered to be involved in the pathophysiology of psoriasis, as well as in the onset of arthritis and the severity of psoriasis. p1056, derived from a protein highly similar to α2HS-GP, may be a candidate biomarker for the severity of psoriasis. If the correlation can be confirmed with a large cohort of psoriasis patients, FLG-pEL may reduce inflammation in psoriasis by downregulating the chemotaxis of neutrophils, T cells, and macrophages. FPMA may aggravate inflammation by inducing neutrophils; however, it may alleviate inflammation by downregulating the anti-microbial activity. Modulating the fragmentation of serum proteins is a potential therapeutic strategy for the treatment of psoriasis.

Funding

This work was partly supported by the Supported Program for the Strategic Research Foundation at Private Universities of Ministry of Education, Culture, Sports, Science and Technology. The other part of this work was supported by St. Marianna University School of Medicine.

Conflict of interest

The authors have no conflict of interest to declare.

Acknowledgements

The authors are indebted to Ms Arsuko Nezawa and Ms Fumiko Ohkawa for their technical assistance.

References

[1] W.H. Boehncke, M.P. Schön, Psoriasis, Lancet 386 (2015) 983–994.
[2] S.K. Raychaudhuri, T. Maverakis, S.P. Raychaudhuri, Diagnosis and classification of psoriasis, Autoimmun. Rev. 13 (2014) 490–495.
[3] K. Kubota, Y. Kamijima, T. Sato, N. Ohtsu, D. Kunii, H. Inoue, H. Nakagawa, Epidemiology of psoriasis and palmoplantar pustulosis: a nationwide study using the Japanese national claims database, BMJ Open 5 (2015) e006450.
[4] C.E.M. Griffiths, J.N.W.N. Barker, Pathogenesis and clinical features of psoriasis, Lancet 370 (2007) 263–271.
[5] I.O. Nestle, D.H. Kaplan, J. Barker, Psoriasis, N. Engl. J. Med. 361 (2009) 496–509.
[6] K.E. Nograles, L.C. Zaba, E. Guttman-Yassky, J. Fuentes-Duculan, M. Suárez-Fariñas, I. Cardinale, A. Khatcherian, et al., Th17 cytokines interleukin (IL)-17 and IL-22 modulate distinct inflammatory and keratinocyte response pathways, Br. J. Dermatol. 159 (2008) 1092–1102.
[7] M.A. Lowes, T. Kikuchi, J. Fuentes-Duculan, I. Cardinale, L.C. Zaba, A.S. Haider, E.P. Bowman, et al., Psoriasis vulgaris lesions contain discrete populations of Th1 and Th17 T cells, J. Invest. Dermatol. 128 (2008) 1207–1211.
[8] Y. Cai, X. Shen, C. Ding, C. Qi, K. Li, X. Li, V.R. Jala, et al., Pivotal role of dermal IL-17-producing γδ T cells in skin inflammation, Immunity 35 (2011) 596–610.
[9] K.P.M.C. Weijers, A.E.M. Hendriks, P.E.J. van Erp, E. van Cranenbroek, P.C.M. van de Kerkhof, R.J.P.M. Koenen, L. Joosten, In vivo induction of cutaneous inflammation results in the accumulation of extracellular trap forming neutrophils expressing RORγt and IL-17, J. Invest. Dermatol. 134 (2014) 2274–2284.
[10] A.M. Lin, C.J. Rubin, R. Khandpur, J.Y. Wang, M. Riblett, S. Yalavarthi, E.C. Villanueva, et al., Mast cells and neutrophils release IL-17 through extracellular trap formation in psoriasis, J. Immunol. 187 (2011) 490–500.
[11] M. Dvorak, S.R. Brown, K.P. Leffler, K.T. Yeo, G. Kocher, R.W. Jackman, H. Berse, et al., Overexpression of vascular permeability factor/vascular endothelial growth factor and its receptors in psoriasis, J. Exp. Med. 185 (1997) 1141–1148.
[12] R. Heidenreich, M. Röcken, K. Ghoreschi, Angiogenesis drives psoriasis pathogenesis, Int. J. Exp. Pathol. 90 (2009) 232–248.
[13] R. Lande, J. Gregorio, V. Facchinetti, B. Chatterjee, Y.H. Wang, B. Homey, W. Cao, et al., Plasmacytoid dendritic cells sense self-DNA coupled with antimicrobial peptide, Nature 449 (2007) 564–569.
[14] R. Lande, G. Chamilos, D. Ganguly, O. Demaria, L. Frasca, S. Durr, C. Conrad, et al., Cationic antimicrobial peptides in psoriatic skin cooperate to break innate tolerance to self-DNA, Eur. J. Immunol. 45 (2015) 203–213.
[15] L. Perg, A. Juhl, S. Murral, The pathogenesis and genetics of psoriasis, Acta Dermatovenerol. 206 (2004) 545–548.
[16] CASPAR Study Group, W. Taylor, D. Gladman, P. Helliwell, A. Marchesoni, P. Mease, H. Mielants, Classification criteria for psoriatic arthritis: development of new criteria from a large international study, Arthritis Rheum. 54 (2006) 2665–2673.
[17] J.M. Hanifin, G. Rajka, Diagnostic features of atopic dermatitis, Acta Dermatovener. (Stockholm) Suppl. 92 (1980) 44–47.
[18] T. Fredriksson, U. Pettersson, Severe psoriasis – oral therapy with a new retinoid, Dermatologica 157 (1978) 238–244.
[19] U. Mrowietz, K. Kragballe, K. Reich, P. Spuls, I.B. Griffiths, A. Nast, J. Franke, et al., Definition of treatment goals for moderate to severe psoriasis: a European consensus, Arch. Dermatol. Res. 303 (2011) 1–10.
[20] A.Y. Finlay, Current severe psoriasis and the rule of tens, Br. J. Dermatol. 152 (2005) 861–867.
[21] J.F. Thyssen, S. Kezic, Causes of epidermal filaggrin reduction and their role in the pathogenesis of atopic dermatitis, J. Allergy Clin. Immunol. 134 (2014) 792–799.
[22] B. Cabanillas, N. Novak, Atopic dermatitis and filaggrin, Curr. Opin. Immunol. 42 (2016) 1–8.
[23] D. Rengaraj, Y.S. Hwang, X.H. Liang, W.B. Deng, Z.M. Yang, J.Y. Han, Comparative expression and regulation of DMRT3 in male reproductive tissues of rats and chickens, J. Exp. Zool. A. Ecol. Genet. Physiol. 319 (2013) 584–595.
[24] G. Nicolas, A.J. Poole, Y. Drazkin, M. Taya, T. Tokas, J.H. Lin, H.N. Kirkeby, Human stem cell-derived skin progenitors produce alpha 2-HS glycoprotein (fetuin), a neurotrophic cosmetic ingredient, J. Drugs Dermatol. 15 (2016) 583–588.
[25] M.W. Mosesson, Fibrinogen and fibrin structure and functions, J. Thromb. Haemost. 3 (2005) 1894–1904.
[26] P. Rocha-Pereira, A. Santos-Silva, I. Rebelo, A. Figueiredo, A. Quintanilha, F. Teixeira, The inflammatory response in nail and in serum psoriasis, Br. J. Dermatol. 150 (2004) 917–928.
[27] F. Marongiu, C.C. Serano, C. Pubba, M.F. Fiorilli, M. Corda, F. Molas, A. Balestrieri, et al., Abnormalities of blood coagulation and fibrinolysis in psoriasis, Dermatology 189 (1994) 32–37.
[28] S. Yakovlev, A. Mikhailenko, G. Zorina, A.M. Nelson, L. Medved, Polymerization of fibrin(ogen) C domains promotes endothelial cell migration and proliferation, Thromb. Haemost. 113 (2015) 1244–1251.
[29] M. Noguchi, T. Sato, K. Nagai, I. Utagawa, I. Suzuki, M. Arito, K. Iizuka, et al., Roles of serum fibrinogen γ chain-derived peptides in Alzheimer's disease, Int. J. Geriatr. Psychiatry 29 (2014) 808–818.
[30] J.W. Weisel, L. Medved, The structure and function of the alpha C domains of fibrinogen, Ann. N. Y. Acad. Sci. 936 (2001) 312–327.
[31] F.J. Smith, A.D. Irvine, A. Terron-Kwiatkowski, A. Sandilands, L.E. Campbell, Y. Zhao, K. Liao, et al., Loss-of-function mutations in the gene encoding filaggrin cause ichthyosis vulgaris, Nat. Genet. 38 (2006) 337–342.
[32] Universal Protein Resource, UniProtKB – P02671 (FIBA_HUMAN) http://www.uniprot.org/uniprot/P02671 (accessed 13.11.16).
[33] T. Wakino, M. Mizawa, T. Yamakoshi, M. Takashi, T. Shimizu, Expression of filaggrin-2 protein in the epidermis of human skin diseases: a comparative analysis with filaggrin, Biochem. Biophys. Res. Commun. 449 (2014) 100–106.
[34] M.F. Sanders, A.L. Gokhgeen, Y.L. Wang, Thymosin beta 4 (Tβ4 peptide) is a potent regulator of actin polymerization in living cells, Proc. Natl. Acad. Sci. U. S. A. 89 (1992) 4678–4682.
[35] H.W. Chu, Y.A. Lee, H.L. Yang, M.L. Yao, K.A. Kim, Increased levels of thymosin β4 in synovial fluid of patients with rheumatoid arthritis: association of thymosin β4 with tumor necrosis factor α and involved in inflammation and bone erosion in joints, Int. J. Rheum. Dis. 14 (2011) 320–324.
[36] D. Philp, B. Schomerus, K.S. Kleiss, M. Zhou, D.L. Dine, M. Nguyen, L. Wahl, et al., Thymosin beta4 promotes matrix metalloproteinase expression during wound repair, J. Cell. Physiol. 208 (2006) 195–200.
[37] J.R. Hu, A.L. Jiang, W.H. Ma, K.B. Chen, H.K. Jer, Y. Su, Thymosin beta-4 up-regulates anti-oxidative enzymes and protects human corneal epithelial cells against oxidative damage, Br. J. Ophthalmol. 92 (2008) 992–997.
[38] S. Pastolpushal, S. Haak, B. Ingold, B. Kurg, F.L. Koppen, A.A. Nanini, B. Becher, Benign mouse lymphocytes and γδ T cells initiate psoriasiform plaque formation in mice, J. Clin. Invest. 122 (2012) 2252–2256.
[39] S. Ciofoaia, U. Wegwerth, C. Pace, Psoriasis: rationale for targeting interleukin-17, Br. J. Dermatol. 167 (2012) 713–714.
[40] K. Reich, X.H. Papp, R.T. Matheson, J.H. Tu, R. Bissonnette, M. Bourcier, D. Gratton, et al., Evidence that a neutrophil-keratinocyte crosstalk is an early target of IL-17A inhibition in psoriasis, Exp. Dermatol. 24 (2015) 529–535.
[41] M.V. Honorati, R. Meliconi, I. Pulsatelli, S. Cane, I. Frizziero, A. Iacchino, High in situ expression of interleukin-17 receptor in synovial endothelial cells and chondrocytes from arthritis patients, Rheumatology (Oxf.) 40 (2001) 522–527.
[42] J.Z. Yang, Y. Li, L.X. Sun, J. Fang, L.J. Kang, J.Q. Zhang, Interleukin-17 receptor expression on vascular endothelial cells of masses of skeletal extramedullary disease in myeloma patients, Pathol. Res. Pract. 210 (2014) 986–990.
[43] K. Fujii, K. Nio, M. Ohba, Y. Tomioka, H. Kitazawa, K. Nagashima, T. Ohno, et al., A distinct regulatory role of Th17 cytokines IL-19 and IL-17F in chemokine secretion from lung microvascular endothelial cells, Inflammation 35 (2012) 1109–1117.
[44] E.M. Moran, M. Connolly, W. Gao, J. McCormack, D. Fearon, D.J. Veale, Fractalkine-17A induction of angiogenesis, cell migration, and cytoskeletal rearrangement, Arthritis Rheum. 63 (2011) 3673–3677.
[45] R. Gilzean, K. Wolff, D. Tosg, C. Müller, T. Yoshimura, A.A. Hartmann, G. Stingl, et al., MCP-1 mRNA expression in basal keratinocytes of psoriatic lesions, J. Invest. Dermatol. 101 (1993) 127–131.

[46] G. Martin, S. Guérard, M.M. Fortin, D. Rusu, J. Soucy, P.E. Poubelle, R. Poulliot, Pathological crosstalk in vitro between T lymphocytes and lesional keratinocytes in psoriasis: necessity of direct cell-to-cell contact, Lab. Invest. 92 (2012) 1058–1070.
[47] C. Vestergaard, H. Just, J. Baumgartner Nielsen, K. Thestrup-Pedersen, M. Deleuran, Expression of CCR2 on monocytes and macrophages in chronically inflamed skin in atopic dermatitis and psoriasis, Acta Derm. Venereol. 84 (2004) 353–358.
[48] H. Wang, T. Peters, D. Kess, A. Sindrilaru, T. Oreshkova, N. Van Rooijen, A. Stratis, et al., Activated macrophages are essential in a murine model for T cell-mediated chronic psoriasiform skin inflammation, J. Clin. Invest. 116 (2006) 2105–2114.
[49] S. Shao, T. Cao, L. Jin, B. Li, H. Fang, J. Zhang, Y. Zhang, et al., Increased lipocalin-2 contributes to the pathogenesis of psoriasis by modulating neutrophil chemotaxis and cytokine secretion, J. Invest. Dermatol. 136 (2016) 1418–1428.
[50] C.S. Han, N. Kanda, Y. Tada, S. Shibata, H. Uozaki, T. Fukusato, S. Sato, et al., Lipocalin-2 exacerbates psoriasiform skin inflammation by augmenting T-helper 17 response, J. Dermatol. 43 (2016) 785–794.
[51] S. Mahboob, A. Mohamedali, S.B. Ahn, P. Schulz-Knappe, E. Nice, M.S. Baker, Is isolation of comprehensive human plasma peptidomes an achievable quest? J. Proteomics 127 (Pt B) (2015) 200–209.
[52] P. Zhu, P. Bowden, D. Zhang, J.G. Marshall, Mass spectrometry of peptides and proteins from human blood, Mass Spectrom. Rev. 30 (2011) 685–732.
[53] A. Albalat, H. Mischak, W. Mullen, Clinical application of urinary proteomics/peptidomics, Expert Rev. Proteomics 8 (2011) 615–629.
[54] D.C. Dallas, A. Guerrero, E.A. Parker, R.C. Robinson, J. Gan, J.B. German, D. Barile, et al., Current peptidomics: applications, purification, identification, quantification, and functional analysis, Proteomics 15 (2015) 1026–1038.
[55] A. Secher, C.D. Kelstrup, K.W. Conde-Frieboes, C. Pyke, K. Raun, B.S. Wulff, J.V. Olsen, Analytic framework for peptidomics applied to large-scale neuropeptide identification, Nat. Commun. 7 (2016) 11436.
[56] A.D. Tinoco, D.M. Tagore, A. Saghatelian, Expanding the dipeptidyl peptidase 4-regulated peptidome via an optimized peptidomics platform, J. Am. Chem. Soc. 132 (2010) 3819–3830.
[57] T. Gambichler, F.G. Bechara, N. Scola, S. Rotterdam, P. Altmeyer, M. Skrygan, Serum levels of antimicrobial peptides and proteins do not correlate with psoriasis severity and are increased after treatment with fumaric acid esters, Arch. Dermatol. Res. 304 (2012) 471–474.
[58] L. Anderson, C.L. Hunter, Quantitative mass spectrometric multiple reaction monitoring assays for major plasma proteins, Mol. Cell. Proteomics 5 (2006) 573–588.
[59] R.I. Litvinov, S. Yakovlev, G. Tsurupa, O.V. Gorkun, L. Medved, J.W. Weisel, Direct evidence for specific interactions of the fibrinogen alphaC-domains with the central E region and with each other, Biochemistry 46 (2007) 9133–9142.

Journal of Dermatological Science 93 (2019) 117–125

Contents lists available at ScienceDirect

Journal of Dermatological Science

journal homepage: www.jdejournal.com

Original Article

The vitamin D_3 analog, maxacalcitol, reduces psoriasiform skin inflammation by inducing regulatory T cells and downregulating IL-23 and IL-17 production

Carren Sy. Hau[a,1], Teruo Shimizu[a,1], Yayoi Tada[a,*,2], Masahiro Kamata[a,*,2], Shintaro Takeoka[a], Sayaka Shibata[b], Aya Mitsui[b], Yoshihide Asano[b], Makoto Sugaya[b], Takafumi Kadono[b], Shinichi Sato[b], Shinichi Watanabe[a]

[a] Department of Dermatology, Tokyo University School of Medicine, Tokyo, Japan
[b] Department of Dermatology, University of Tokyo Faculty of Medicine, Tokyo, Japan

ARTICLE INFO

Article history:
Received 15 October 2017
Received in revised form 27 July 2018
Accepted 29 August 2018

Keywords:
Psoriasis
Imiquimod
Vitamin D
Th17
Treg

ABSTRACT

Background. Psoriasis is a Th1/Th17-mediated inflammatory dermatosis treated with topical corticosteroids and vitamin D_3 analogs (VD3As).

Objective: To compare the effects of a VD3A, maxacalcitol and betamethasone valerate (BV) steroid lotion on topical imiquimod (IMQ)-induced psoriasiform skin inflammation.

Methods: Female BALB/c mice were treated with vehicle, maxacalcitol or BV lotion on the skin for 3 days, and IMQ cream for 6 days. q-PCR, H&E, immunohistochemistry and immunofluorescence studies were performed on skin samples. Additionally, mice were treated with vehicle, maxacalcitol or BV lotions for 3 days, and $CD4^+CD25^+$ regulatory T cells (Tregs) and $CD4^+CD25^-$ cells from each group were isolated from lymph nodes. Adoptive transfer of the cells was performed on recipient mice which were treated with IMQ cream for 6 days, and skin samples were obtained for q-PCR and H&E staining.

Results: Maxacalcitol and BV were comparable in regards clinical improvement, although maxacalcitol reduced the MHC class II inflammatory cell infiltration more than BV in IMQ skin. While both treatments downregulated IL-17A, IL-17F, IL-22, IL-12p40, TNF-α and IL-6 mRNA expression levels, only maxacalcitol downregulated IL-23p19 expression. Significantly increased $Foxp3^+$ cell infiltrations and IL-10 expression were noted in maxacalcitol-treated IMQ skin. Adoptive transfer of Treg cells from maxacalcitol-treated donor mice improved IMQ-induced inflammation clinically and histopathologically more than the recipients of Treg cells from BV-treated donor groups, showing reduced levels of inflammatory cytokines and increased IL-10 expression.

Conclusion: These results indicate that maxacalcitol reduces psoriasiform skin inflammation by inducing Treg cells as well as downregulating IL-23 and IL-17 production.

© 2018 Japanese Society for Investigative Dermatology. Published by Elsevier B.V. All rights reserved.

1. Introduction

Psoriasis is a chronic, helper T (Th)1/Th17-mediated inflammatory autoimmune dermatosis associated with abnormal keratinocyte (KC) differentiation and hyperproliferation, resulting in the appearance of erythematous, scaly plaques. Although of unknown etiology, it is characterized by the presence of helper T (Th)1 cells producing IFN-γ and Th17 cells, which produce interleukin (IL)-17A, IL-17F, or IL-22, infiltrating into the dermis of the psoriatic lesions while prominent neutrophil infiltration can be found in the epidermis [1]. Treatment of mild to moderate psoriasis includes topical corticosteroids as well as vitamin D_3 (VD_3) and its analogs (VD3As).

Known mainly as a central regulator of calcium homeostasis and bone metabolism [2], the therapeutic effects of $1,25(OH)_2D_3$,

Abbreviations: APC, antigen presenting cell; BV, betamethasone valerate; DC, dendritic cell; IL, interleukin; IMQ, imiquimod; KC, keratinocyte; Q-PCR, quantitative real time polymerase chain reaction; Th1, helper T cell; Treg, regulatory T cells; VD_3, vitamin D_3; VD3As, vitamin D_3 analogs.

* Corresponding authors at: Department of Dermatology, Tokyo University School of Medicine, 2-11-1 Kaga, Itabashi-ku, Tokyo, 173-8605, Japan.
E-mail addresses: yytada-tky@umin.ac.jp (Y. Tada), mkamata-tky@umin.ac.jp (M. Kamata).

[1] These authors contributed to this work equally as first authors.
[2] These authors contributed to this work equally as corresponding authors.

https://doi.org/10.1016/j.jdermsci.2018.08.007
0923-1811/© 2018 Japanese Society for Investigative Dermatology. Published by Elsevier B.V. All rights reserved.

the active form of VD_3, or psoriasis have been long recognized although hypercalcemia limited its systemic use. The development of topical VD3As such as maxacalcitol, tacalcitol and calcipotriol has lowered this risk while retaining other vitamin D-mediated cellular events such as normalizing epidermal cell differentiation, inhibiting cell proliferation and angiogenesis, and immunomodulation [3]. Immune cells such as T lymphocytes and antigen presenting cells (APCs) consisting of macrophages and dendritic cells (DCs) express the vitamin D receptor and topical VD3As can directly suppress T cell proliferation and activation, decreasing IL-17, IL-6, IFN-γ, IL-12/23p40, IL-1α, IL-1β and TNF-α expression, and reducing inflammation in psoriatic plaques [4–7]. Furthermore, under appropriate conditions they can shift the immune response to the Th2 pathway [8,9]. Also, VD3As such as calcipotriol suppress the antimicrobial peptides psoriasin (S100A7) and kallikrein (S100A15) which can amplify Th17 induced inflammation in psoriasis [10]. Additionally, DCs treated with VD_3 and VD3As can down-regulate the expression of the costimulatory molecules CD40, CD80, CD86, with decreased IL-12 and enhanced IL-10 and Macrophage Inflammatory Protein-1α production, resulting in the maintenance of an immature state for DCs which induced T cell hyporesponsiveness and regulatory T cell (Treg) generation [2,4,11].

Maxacalcitol (1α, 25-Dihydroxy-22-oxacalcitriol) is a synthetic VD3A that inhibits murine T lymphocyte proliferation in vitro [12] and, together with other topical VD3As, can potently suppress KC proliferation and induce differentiation [13,14]. VD3As are used along with topical corticosteroids for the treatment of mild to moderate psoriasis and are beneficial especially during prolonged topical therapy, with marked persistence of reduced inflammation noted in VD3A treatment compared to corticosteroid preparations [15]. In addition, long term corticosteroid use is associated with adverse effects such as skin atrophy which are absent in non-steroidal VD3As.

In this paper, we further elucidated the effect of maxacalcitol on a commonly used murine model for imiquimod (IMQ) induced psoriasiform skin inflammation [16,17]. Betamethasone valerate (BV), a medium-potency corticosteroid, is selected as comparison for maxacalcitol in our experiments. We have found that maxacalcitol and BV reduce production of Th17-related cytokines but, unlike BV, maxacalcitol induces Tregs through which psoriasiform skin inflammation is suppressed.

2. Materials and methods

2.1. Mice

The experiments were approved by the Animal Research Committee of Teikyo University School of Medicine (Number 15-002). Six to 8-week-old female BALB/c mice were maintained in specific pathogen free conditions at the Animal Facility in Teikyo University School of Medicine.

2.2. Reagents

Vehicle (control) lotion was offered by Maruho Co., LTD. (Osaka, Japan). Commercially available 2.5 μg/g maxacalcitol (Oxarol®) lotion (Maruho Co., LTD.), 5% imiquimod cream (Beselna Cream, Mochida Pharmaceuticals, Tokyo, Japan) and 0.125 betamethasone valerate (Kenderon-V®; Shionogi and Co., Osaka, Japan) lotion were also used. Goat anti-mouse CD3ε (M-20) was obtained from Santa Cruz Biotechnology (Santa Cruz, CA). Rat anti-mouse MHC class (IA/IE) mAb purified, biotinylated or PE conjugated rat anti-mouse, rat Foxp3 mAb and PE conjugated rat IgG antibody were purchased from eBioscience (San Diego, CA). Control goat IgG and rat IgG (Zac) were purchased from BD Biosciences (San Jose, CA). Biotinylated anti-goat IgG was obtained from Vector Laboratories (Burlingame, CA). FITC conjugated anti-mouse CD4, BV-421 conjugated anti-mouse CD25, Alexa-647 conjugated anti-mouse IL-10 and FITC conjugated streptavidin were purchased from BioLegend (San Diego, CA).

2.3. Development of IMQ induced psoriasiform skin inflammation

Psoriasiform skin inflammation using IMQ cream was developed as previously described [16]. Each experiment consisted of 6 groups of mice receiving vehicle, maxacalcitol or BV lotion application on the shaved back skin for 3 consecutive days. Furthermore, one day after the initial intervention, application of IMQ cream was started and scheduled 6 h apart from vehicle, maxacalcitol or BV lotion treatment. Topical IMQ application was continued for 6 consecutive days, and a blinded investigator performed daily evaluations for clinical severity scoring of erythema, scaling, and thickening, based on Psoriasis Area and Severity Index (PASI) scores: 0= none, 1= slight, 2= moderate, 3= marked, 4= very marked. The cumulative score served as a measure of disease severity, with a scale of 0–12 [16].

2.4. Histological analyses and immunofluorescence

Murine skin samples were paraffin-embedded for H&E staining as well as embedded in Optimal Cutting Temperature Compound (Sakura Finetek Japan, Tokyo, Japan) and snap-frozen in liquid nitrogen. For immunohistochemistry, frozen murine skin samples were cut into 5-μm-thick sections, fixed with cold acetone and washed with PBS. Samples were blocked for nonspecific binding and incubated overnight at 4 °C with the primary antibodies or isotype controls. After washing, slides were incubated with the appropriate secondary antibodies for 2 h. The slides were washed again and incubated with an avidin-biotin peroxidase complex followed by diaminobenzidine (brown staining) and counterstained with Mayer hematoxylin. Epidermal thickness was measured using the Olympus cellSense Standard software. Inflammatory cells were counted in 5 random grids per section under 400× high power fields.

For IL-10 and Foxp3 immunofluorescence, frozen skin samples cut into 5-μm-thick sections were air-dried and washed in PBS and blocked with 10% normal goat and mouse serum in PBS for 1 h at room temperature. After PBS washing, they were incubated with biotinylated rat anti-mouse Foxp3 antibodies for 1 h at room temperature. The slides were washed again and incubated with Alexa-647 conjugated anti-mouse IL-10 and FITC conjugated streptavidin for 30 min at room temperature. After washing, nuclei were counterstained with 4,6-diamidino-2-phenylindole (DAPI) for 1 min at room temperature (Dojindo, Kumamoto, Japan). Images were acquired by Olympus BX53 Advanced Research Microscope (Olympus, Tokyo, Japan).

2.5. Quantitative real time PCR (q PCR)

Total RNA was isolated from mouse back skin and inguinal lymph nodes using RNeasy Fibrous Tissue Mini-Kit (Qiagen, Valencia, CA) and cDNA was synthesized using SuperScript First-Strand Synthesis System (Invitrogen Life Technologies). Gene expression in murine skin was quantified using the TaqMan gene expression assay (Applied Biosystems, Warrington, UK). Primers were available from Applied Biosystems. All samples were analyzed in parallel for GAPDH gene expression as an internal control. The relative expression levels of each gene were determined by the $2^{-\Delta\Delta CT}$ method. The timing of harvesting skin or lymph nodes for gene expression assay is written in each figure legend.

2.6. Cell preparation and flow cytometric analysis

Murine inguinal lymph node sample prepared from skin applied with vehicle, Maxacalcitol or BV for 3 days and filtered through 70 μm mesh. Single cell suspensions stain with fixable viability dye (BioLegend, San Diego, CA) and cell surface antibodies, and then fixation/permeabilization using Foxp3/Transcription Factor Staining Buffer Set (eBioscience, San Diego, CA) followed by anti foxp3 antibody staining. Thereafter, the cells were analyzed by FACS Aria III (Flow cytometer) and FlowJo v10 soft. (Becton Dickinson, San Jose, CA).

2.7. CD4+CD25+ Treg cell isolation and adaptive transfer

Mice were non-treated or treated with vehicle, maxacalcitol or BV lotion for 3 days before they were sacrificed, and the inguinal lymph nodes were extracted. Mice receiving no adaptive transfer of Treg cells were also included as controls. Single cell suspensions from the lymph nodes were generated by gentle dissection and the $CD4^+$ T cells were purified, with $CD4^+CD25^+$ cells being subsequently negatively selected, using MACS separation (Miltenyi Biotec, Bisley, Germany). After isolation, 1×10^6 $CD4^+CD25^+$ Treg (+) cells were i.v. injected into BALB/c mice. Adoptive transfer of $CD4^+CD25^-$ Treg (−) cells was also performed on other recipient mice. After two days, IMQ cream was applied on the shaved dorsal murine skin for 6 consecutive days, with daily assessments for clinical severity scoring. mRNA was extracted from the skin of mice at day 1 or 2 of IMQ treatment as described above for q-PCR.

2.8. Statistical analyses

Data obtained were presented as mean ± SE of at least 3 separate experiments. Comparisons were made using one way analysis of variance with Dunnett's multiple comparison test. Values of $P < 0.05$ represent significant differences.

3. Results

3.1. Topical application of maxacalcitol and BV lotions reduced psoriatic skin inflammation clinically and pathologically

To investigate the effects of maxacalcitol on murine psoriasiform inflammation, we topically applied vehicle, maxacalcitol or BV lotion 24 h before beginning IMQ treatment on the shaved dorsal skin of BALB/c mice. Then, 62.5 mg IMQ cream was applied, with vehicle, maxacalcitol or BV lotion applied 6 h after IMQ treatment. Vehicle, maxacalcitol or BV lotion was administered for 3 consecutive days while IMQ was administered for 6 consecutive days. Daily scores for disease severity were collected by a blinded investigator using a clinical scoring system described in method part. Beginning at day 4 and most noticeably by day 6, IMQ significantly increased erythema, scaling and skin thickening, and maxacalcitol or BV treatment apparently reduced the IMQ-induced psoriasiform rash (Fig. 1A). Significant differences in total clinical disease severity were observed between vehicle + IMQ-treated mice and maxacalcitol + IMQ or BV + IMQ-treated mice from day 4 to 6 (Fig. 1B).

Likewise, H&E histology of vehicle + IMQ treated murine skin showed intense inflammatory cell infiltrates which were significantly reduced by maxacalcitol or BV treatment (Fig. 1C, D), and the IMQ-induced increased epidermal thickness was significantly decreased by maxacalcitol + IMQ compared to BV + IMQ (Fig. 1D). We further investigated the inflammatory infiltrates of vehicle + IMQ and found they consisted mostly of $CD3^+$ cells indicating T cells (Fig. 1E) and MHC Class II^+ cells indicating APCs (Fig. 1F), and maxacalcitol or BV treatment significantly reduced these infiltrates. Although $CD3^+$ cell numbers were not significantly different between maxacalcitol and BV (Fig. 1G), maxacalcitol yielded significantly reduced MHC Class II^+ cells infiltration compared to BV (Fig. 1G). These findings indicate that maxacalcitol and BV can suppress IMQ-induced inflammation in murine skin, leading to significantly reduced dermal inflammatory infiltrates in the skin and an improvement in dermatitis clinically and histopathologically, with maxacalcitol being more able to reduce epidermal thickness and MHC Class II^+ cell infiltration compared to BV.

3.2. Maxacalcitol and BV down-regulated Th17-related cytokine gene expression in IMQ-treated murine psoriasiform inflammation

We next studied the effect of maxacalcitol and BV treatment on psoriasis-related cytokine mRNA expression using IMQ-treated murine skin. Topical application of maxacalcitol or BV lotion on IMQ treated murine skin significantly reduced the mRNA levels of Th17 and Th1-related cytokines such as IL-17A, IL-17F, IL-22 and IL-12p40 (Fig. 2A–C, E), along with other proinflammatory cytokines such as TNF-α and IL-6 (Fig. 2F, G), compared to vehicle + IMQ. However, maxacalcitol + IMQ but not BV + IMQ showed significantly reduced mRNA levels of IL-23p19, important for Th17 cell propagation and maintenance (Fig. 2D). Interestingly, compared to vehicle + IMQ, IL-10 expression was significantly increased in maxacalcitol + IMQ and, on the other hand, significantly decreased in BV + IMQ (Fig. 2H). As for EGF-β1 mRNA expression, there was no significant difference among groups (Fig. 2I). Maxacalcitol suppressed IMQ-induced IFN-γ production (Fig. 2J). In order to evaluate impairment of epidermal differentiation by IMQ treatment, expression of loricrin, one of epidermal differentiation markers, was measured. The results showed that it significantly decreased by IMQ application. Maxacalcitol showed a tendency of alleviating loss of loricrin induced by IMQ treatment, but the difference was not significant in statistics (Fig. 2K). Thymic stromal lymphopoietin (TSLP) expression was significantly elevated in the maxacalcitol treated psoriasiform skin induced by IMQ compared to vehicle-treated one (Fig. 2L).

3.3. Treg cells are induced by maxacalcitol in IMQ treated murine skin

In order to study whether increased IL-10 expression in maxacalcitol + IMQ mice skin is due to Treg induction, we examined $Foxp3^+$ Treg cell infiltration in each treatment group. Immunohistochemistry showed that maxacalcitol induced significantly elevated number of $Foxp3^+$ cells in IMQ-treated skin compared to vehicle or BV (Fig. 3A,B). Immunofluorescence showed that these $Foxp3^+$ cells were also IL-10 positive (Fig. 3C). These findings suggested a role for Tregs in the immunosuppressive effect of maxacalcitol.

To investigate further, donor mice were treated with maxacalcitol or BV lotion for 3 consecutive days and we performed adoptive transfers of $CD4^+CD25^-$ Treg (−) and $CD4^+CD25^+$ Treg (+) cells isolated from the inguinal lymph nodes of donor mice to recipient mice which were subsequently treated with IMQ cream for 6 consecutive days. Three consecutive days' application of maxacalcitol did not increase the percentage of Treg cells ($CD25^+Foxp3^+$ cells) in $CD4^+$ cells of lymph nodes, although its percentage in BV-treated mice was significantly lower than that in maxacalcitol-treated group (Fig. 4A, B). However, IL-10 mRNA expression in $CD4^+CD25^+$ Treg (+) cells sorted by MACS separation was significantly higher than those in $CD4^+CD25^-$ Treg (−) cells in lymph node cells of maxacalcitol-treated mice, and maxacalcitol-treatment significantly increased IL-10 production of $CD4^+CD25^+$ Treg (+) cells compared with vehicle or BV treatment (Fig. 4C). As for production of TGF-β1, little difference was seen among groups.

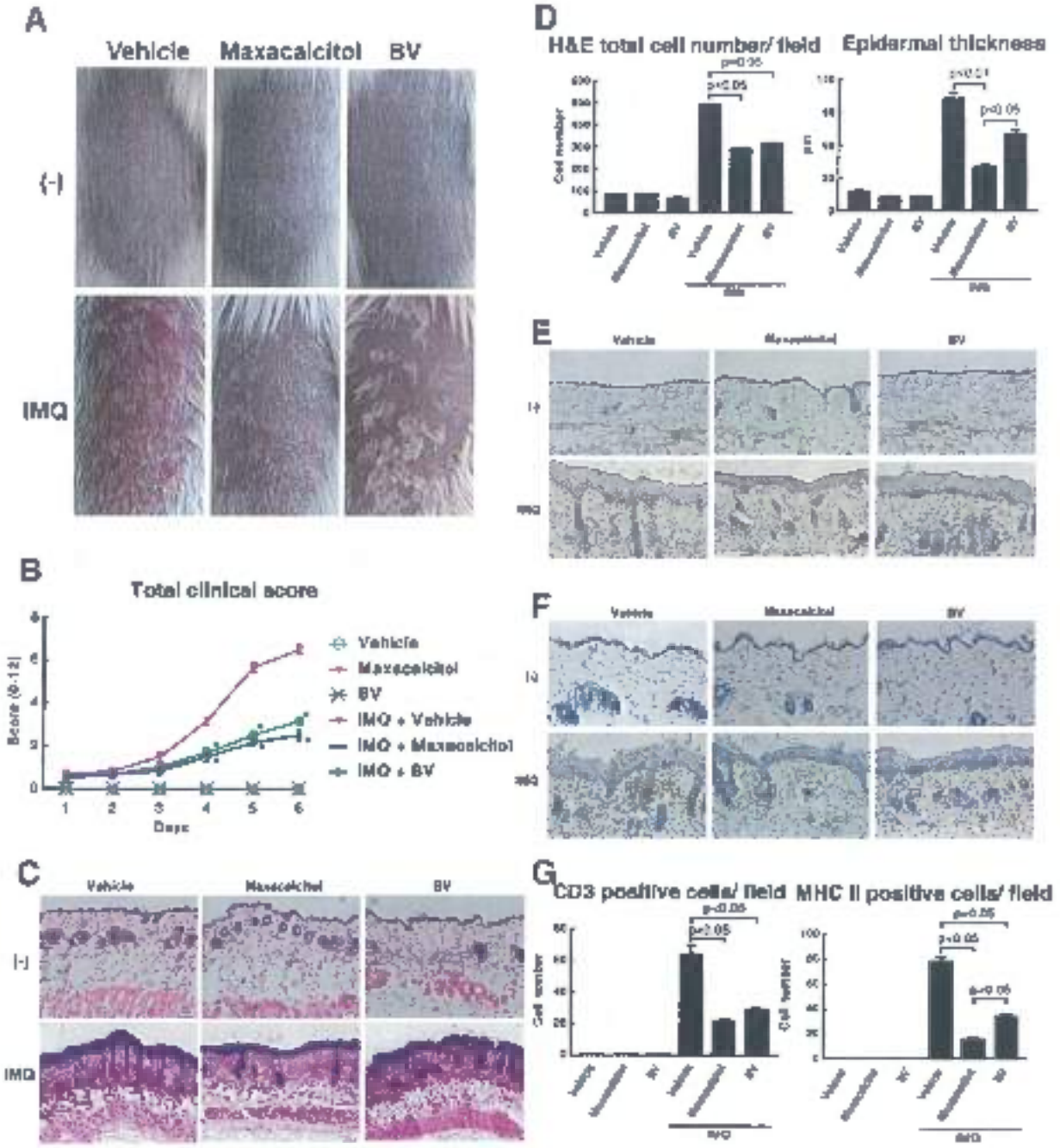

Fig. 1. The clinical effects of maxacalcitol or betamethasone valerate (BV) topical on imiquimod (IMQ)-induced psoriasiform dermatitis. Vehicle, maxacalcitol or BV-treated BALB/c mice were given daily applications of IMQ on the back skin as described in materials and methods (A) Clinical pictures. Among the shaved back skin of mice treated with vehicle, maxacalcitol, BV, vehicle + IMQ, maxacalcitol + IMQ or BV + IMQ. Results are representative of 3 separate experiments. (B) The total clinical scores are shown for each grouped mice. The data are shown as mean ± SE (n = 6). *P < 0.05 versus vehicle + IMQ. (C–D) The histological effects of maxacalcitol or betamethasone valerate (BV) topical on IMQ-induced psoriasiform dermatitis. Vehicle, maxacalcitol or BV-treated mice were given daily applications of IMQ on the back skin as described in materials and methods. (C) Hematoxylin-eosin (H&E) staining was performed on skin sections at Day 6 of IMQ treatment. (D) Dermal inflammatory infiltrates on H&E staining (×200) were counted in 5 random grids per section under 400× high power fields. Epidermal thickness was measured using Olympus cellSens Standard software. (E–G) CD3+ and MHC Class II+ cell infiltration in IMQ induced psoriasis from skin treated with vehicle, maxacalcitol or BV. Vehicle, maxacalcitol or BV-treated mice were given daily applications of IMQ on the back skin as described in materials and methods. Immunohistochemical staining for (E) CD3+ and (F) MHC Class II+ cells were performed on skin sections at Day 6 of IMQ treatment. (G) Dermal inflammatory infiltrates on CD3+ and MHC Class II+ staining (×400) were counted in 5 random grids per section under 400× high-power fields. The results are shown as mean ± SE (n = 6).

Although statistics showed significant difference between CD4+CD25+ Treg (+) cells in maxacalcitol-treated group and those in vehicle treated- or BV treated- group (Fig. 4D). Based on clinical severity scores, recipient mice i.v. injected with CD4+CD25+ cells from donor mice treated with maxacalcitol or BV showed a significant improvement in erythema, scaling and thickening compared to mice i.v. injected with CD4+CD25- cells as well as mice with no adoptive transfer donor or treated with vehicle CD4+CD25

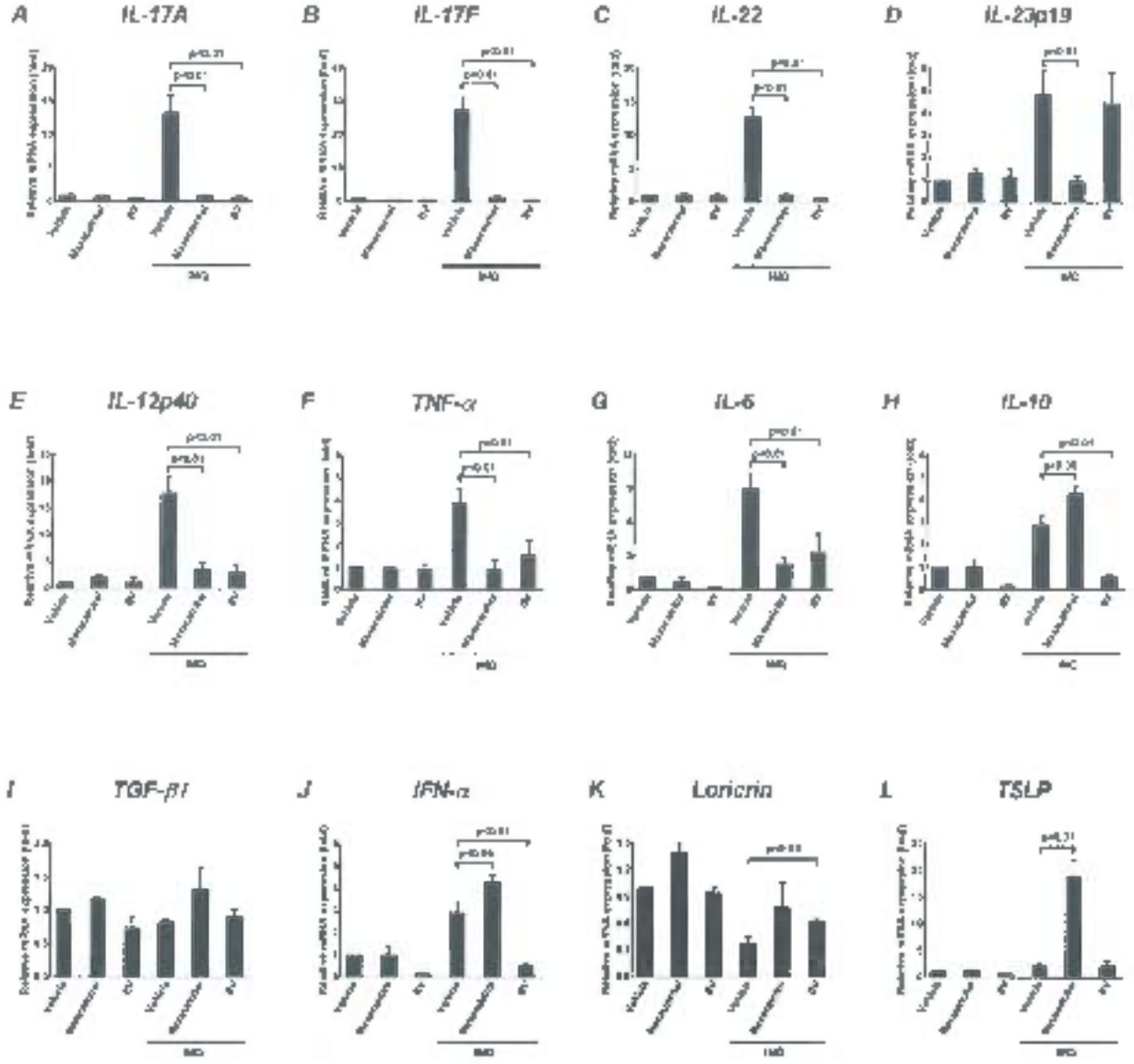

Fig. 2. Quantitative real-time PCR analyses of proinflammatory cytokine and TSLP mRNA levels in IMQ-treated skin treated with vehicle, maxacalitol or BV. Mice (Vehicle, maxacalitol or BV treated) were given daily applications of IMQ on the back skin and mRNA levels were determined at day 4 by quantitative real-time PCR for (A) IL-17A, (B) IL-17F, (C) IL-22, (D) IL-23p19, (E) IL-12p40, (F) TNF-α, (G) IL-6, (H) IL-10, (I) TGF-β1, (J) IFN-α, (K) loricrin, or (L) TSLP normalized to GAPDH, and are expressed as fold induction relative to that of vehicle. The data were obtained from skin samples from 6 mice per group. Values are presented as means ± SE (n = 6).

and CD4⁺CD25⁺ cells (Fig. 5A, B). Among the recipient groups i.v. injected with CD4⁺CD25⁺ cells, those from maxacalitol treated mice more significantly reduced inflammatory cell infiltrates (Fig. 5C, D) and improved epidermal thickness (Fig. 5D) compared to cells from BV treated mice. Adoptive transfer of CD4⁺CD25⁺ cells from donor mice treated with maxacalitol brought significant increase of Foxp3⁺ cells infiltrating an IMQ-induced psoriasiform skin of recipient mice, compared to that of CD4⁺CD25⁻ cells. Among CD4⁺CD25⁺ cells from vehicle-, maxacalitol-, or BV-treated donor mice, recipient mice adoptively transferred with CD4⁺CD25⁺ cells from maxacalitol-treated donor mice demonstrated increased number of Foxp3⁺ cells infiltrating into IMQ-induced psoriasiform skin (Fig. 5E, F).

q PCR showed a significant IL-17A downregulation for maxacalitol or BV treated mice derived CD4⁺CD25⁺ cells i.v. injected group compared to CD4⁺CD25⁻ cells i.v. injected group (Fig. 6A), while significant downregulation of IL-17F, IL-22, IL-23p19, IL-12p40 and IL-6, but not TNF-α, was noted only for the maxacalitol treated mice derived CD4⁺CD25⁺ cells i.v. injected group compared to CD4⁺CD25⁻ cells i.v. injected group (Fig. 6B–G). Consistently, only maxacalitol treated mice derived CD4⁺CD25⁺ cells induced significantly elevated IL-10 expression (Fig. 6H). As for mRNA expression of loricrin, there was no significant difference among groups (Fig. 6I). These results indicated that maxacalitol induced Treg cells possess immunosuppressive effects on psoriasiform inflammation induced by IL-23 and IL-17, and may be responsible for the prolonged immunosuppressive response noted in VDRAs [15].

4. Discussion

In this study, we found that topical maxacalitol, a VDRA, and topical BV, a corticosteroid also commonly used in psoriasis treatment, significantly lowered the total clinical scores of mice

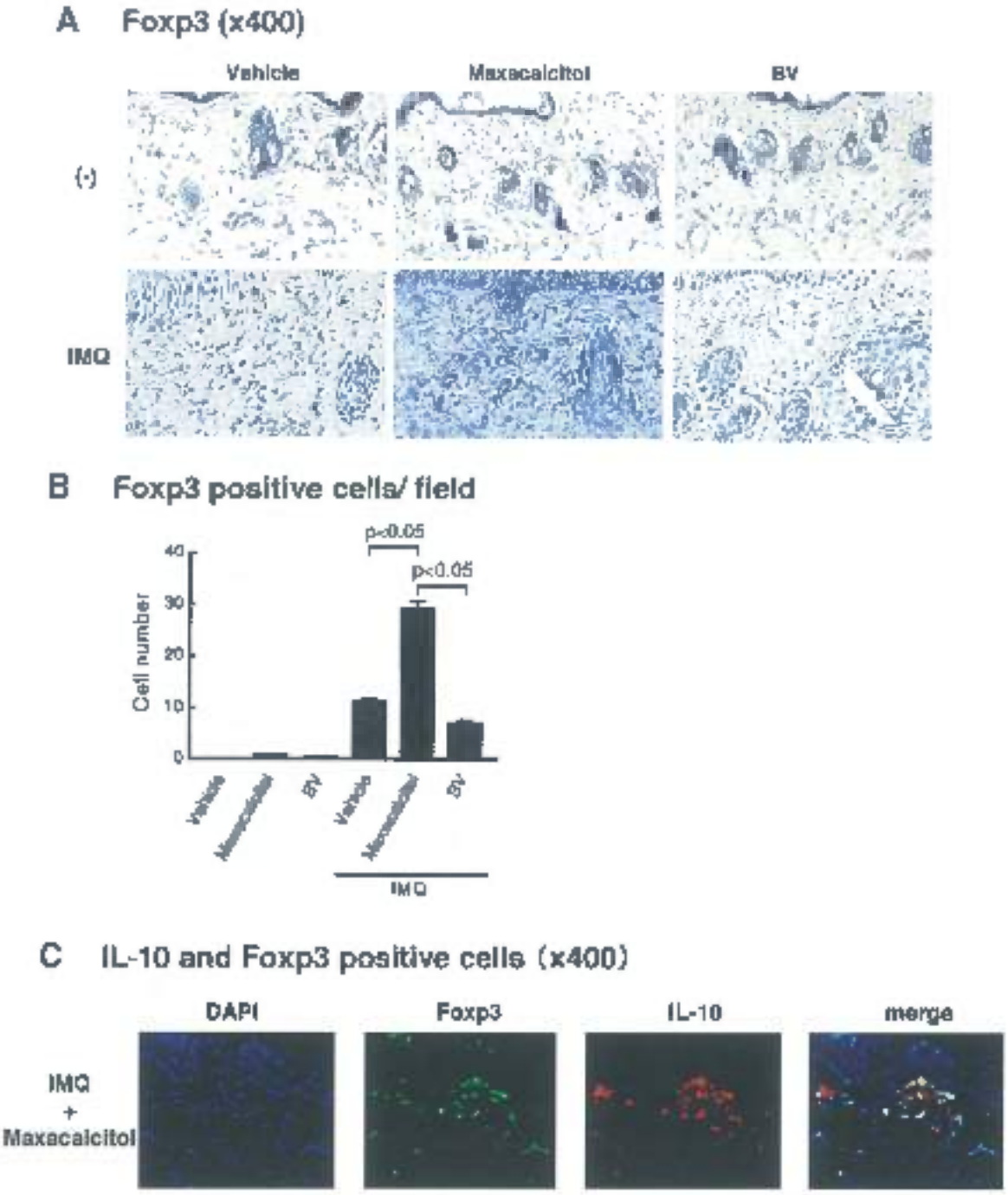

Fig. 3. Foxp3 cell infiltrates in IMQ-induced psoriasiform skin treated with vehicle, maxacalcitol or BV. Vehicle, maxacalcitol or BV-treated mice were given daily topical doses of IMQ on the back skin. (A) Immunohistochemical staining for Foxp3+ cells were performed on skin sections at day 5 of IMQ treatment. (B) The dermal inflammatory infiltrates or Foxp3 immunostaining (×400) were counted in 5 random fields per section under 400× high-power fields. The results are shown as mean ± SD (n = 10). (C) Immunofluorescence imaging of IL-10+ and Foxp3+ cells in a maxacalcitol+IMQ skin section. Results are representative of at least 3 separate experiments.

IMQ-induced psoriasiform skin and histologically, they reduced the number of inflammatory infiltrates, with maxacalcitol significantly reducing MHC Class II+ APC infiltration compared to BV. Based on q-PCR results, treatment with maxacalcitol lotion in IMQ-induced psoriasiform skin significantly lowered the mRNA levels of proinflammatory Th17 cytokines such as IL-17A, IL-17F, IL-22, IL-23p19, IL-12p40, as well as TNF-α and IL-6, while BV lotion also decreased all cytokine levels except IL-23p19, which is mainly produced by APCs such as DCs and is responsible for driving Th17 polarization of T cells and maintenance of Th17 cells [19,20]. Thus, our results indicated that maxacalcitol and BV possess a comparable immunosuppressive effect on psoriasiform inflammation, although we found that they exerted their effects on cells from different immunological backgrounds.

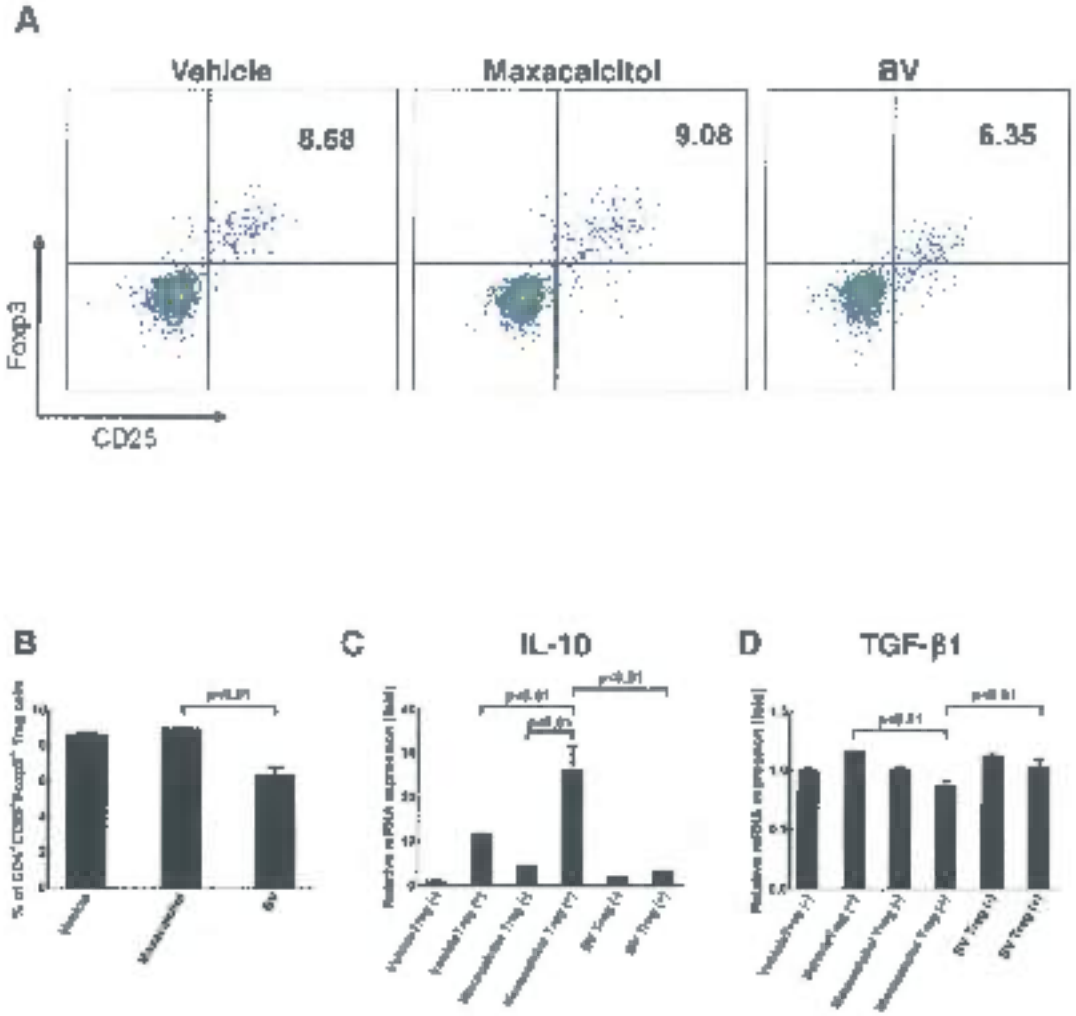

Fig. 4. Characteristics of Treg cells in lymph nodes draining from IMQ-induced mice treated with vehicle, maxacalcitol or BV lotion for 7 days. (A) Representative plots of flow cytometry analysis on lymph nodes single cells. Upper-right quadrant shows CD4, CD25 and Foxp3 Treg cells in pre-gated $CD4^+$ cell populations. (B) The percentage of $CD4^+CD25^+Foxp3^+$ Treg cells in each group (n = 3). (C) IL-10 and (D) TGF-β1 mRNA levels were determined by quantitative real-time PCR in Treg (+) $CD4^+CD25^+$ cells and Treg (−) $CD4^+CD25^-$ cells which were isolated by MACS separation. Values are presented as means ± SE (n = 6).

Aside from its direct effects on T cells as well as its well-known effect of reducing epidermal thickness and improving abnormal epidermal differentiation, VD_3 also exerts indirect effects on T cells through APCs such as DCs. DCs are especially responsive to VD_3, which can alter the cells' phenotype and functionality by inhibiting DC maturation and differentiation in vitro, resulting in a marked decrease in T cell stimulatory capacity [21–23]. Indeed, our results showed a significant reduction of MHC Class II$^+$ cells infiltration in maxacalcitol + IMQ skin compared to vehicle + IMQ and BV + IMQ, although topical steroids are also reported to reduce TNF-α production from epidermal Langerhans cells, which is important for their migration out of the epidermis [24]. As for Th1 or Th17 responses, VD_3 can inhibit DC production of IL-12 and IL-23 which are known as the major cytokines driving Th1-differentiation and Th17-differentiation, respectively, while increasing IL-10 production [19], as also seen in our results.

Another important mechanism of VD_3-mediated suppression is DC priming to induce $CD4^+CD25^+Foxp3^+$ Treg cells that can arrest autoimmune disease development [25–28]. Indeed, we found that maxacalcitol treatment induced elevated mRNA levels of IL-10, an anti-inflammatory cytokine produced by Tregs that can inhibit APC function and cytokine production by inflammatory cells, and is also required in part for the proper functioning of Treg cells [29,30]. On the other hand, BV suppressed IL-10 expression although it did not suppress $Foxp3^+$ cell infiltration, which suggests that BV could inhibit the function of not only T cells producing IL-17 but also Treg cells. This difference could explain why VD_3 is more efficient in maintaining psoriasis remission compared to steroids [15,31]. Immunostaining and immunofluorescence further confirmed the presence of significantly elevated numbers of IL-10 producing $Foxp3^+$ cells in IMQ skin treated with maxacalcitol but not with BV. These results suggest that maxacalcitol, as a VD_3A, can induce peripheral immune tolerance via the recruitment of tolerogenic Treg cells. As for the mechanism of this recruitment of Treg cells by VD_3, it remains to be elucidated. Leichner et al. demonstrated that skin-derived TSLP systemically expanded Treg cells [32]. In our study, when psoriasiform dermatitis was induced by imiquimod, application of maxacalcitol induced TSLP expression shown in Fig. 2L. Considering them together, this increased TSLP expression by maxacalcitol could account for one of the mechanisms of Treg induction. However, we need further investigation in order to unveil the detailed mechanism.

Additionally, it is reported that topically applied VD_3 enhanced $CD4^+CD25^+$ Treg suppressive activity from draining lymph nodes

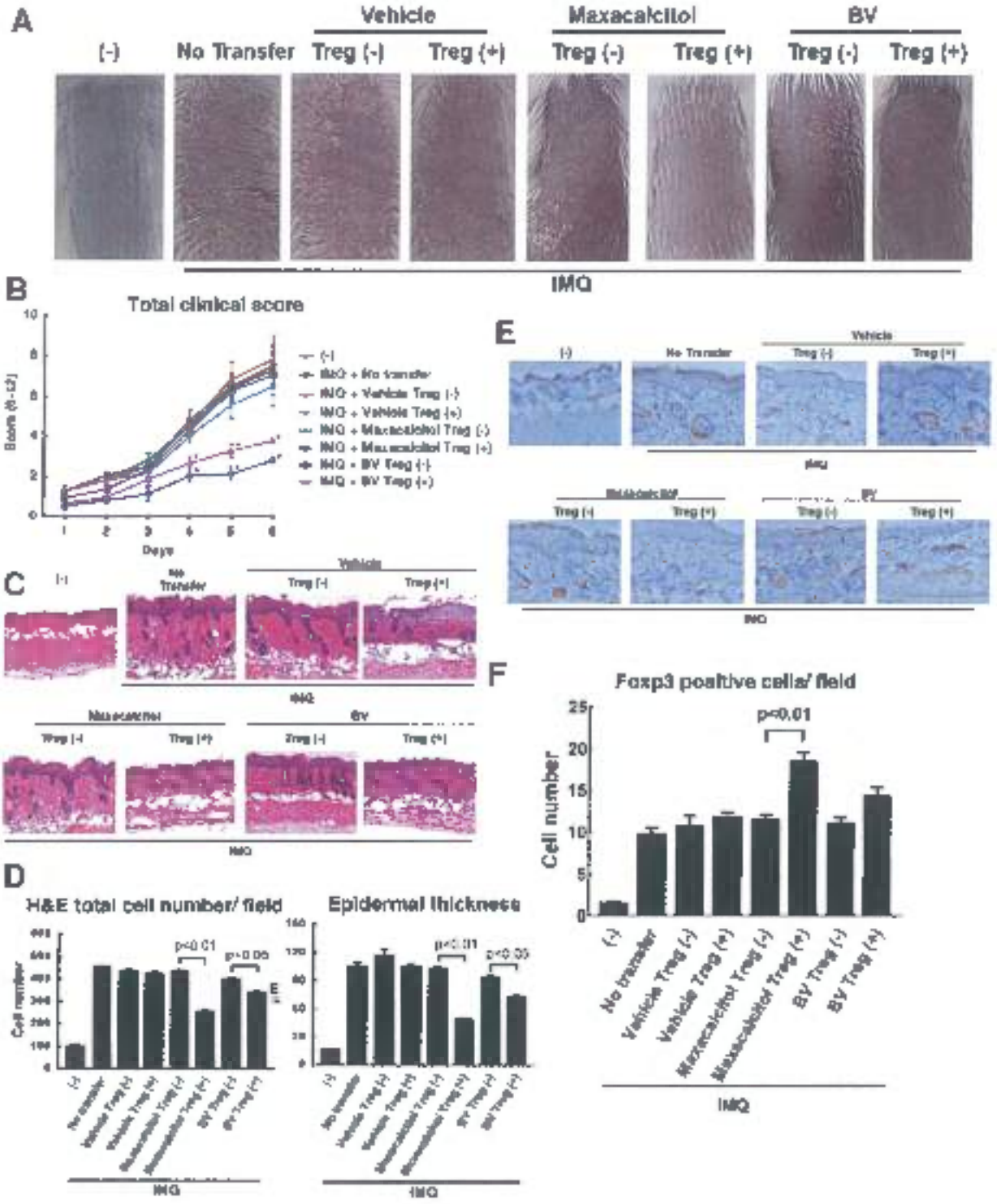

Fig. 5. The clinical effects of vehicle, maxacalcitol, or BV-induced $CD4^+CD25^+$ Treg cells on IMQ-induced psoriaform dermatitis. Balb/c mice were given daily topical application of vehicle, maxacalcitol or BV on the back skin, and adoptive transfer of $CD4^+CD25^-$ cells and $CD4^+CD25^+$ Treg cells from the inguinal lymph nodes from donor mice to recipient mice was performed followed by IMQ treatment on the shaved back skin of non-treated mice and recipient mice. Mice receiving no adoptive transfer were used as control. (A) Clinical pictures showing the shaved back skin of recipient mice treated with IMQ for 6 days. Results are representative of at least 3 separate experiments. (B) The total clinical scores. $^*P < 0.05$ versus control. (C, D) The histological effects of vehicle, maxacalcitol or BV-induced $CD4^+CD25^+$ Treg cells on IMQ-induced psoriaform dermatitis. Balb/c mice were given daily applications of vehicle, maxacalcitol or BV on the back skin, and adoptive transfer of $CD4^+CD25^-$ cells and $CD4^+CD25^+$ Treg cells from the inguinal lymph nodes from donor mice to recipient mice was performed followed by IMQ treatment on the shaved back skin of non-treated mice and recipient mice. Mice receiving no adoptive transfer were used as control. (C) H&E staining of skin sections of recipient mice treated with IMQ for 6 days. Results are representative of at least 3 separate experiments. (D) Dermal inflammatory infiltration on H&E staining (×200) were counted in 5 random grids per section under 400× high-power fields. Epidermal thickness was measured using Olympus cellSens Standard software. (E–F) $Foxp3^+$ cells infiltrate into IMQ-induced psoriaform skin after adoptive transfer. (E) Representative images of immunohistochemical staining for $Foxp3^+$ cells on skin sections at day 6 of IMQ treatment (magnification, ×400). (F) The dermal $Foxp3^+$ cells were counted in 5 random grids per section under 400× high-power fields. The results are shown as mean ± SE (n = 10).

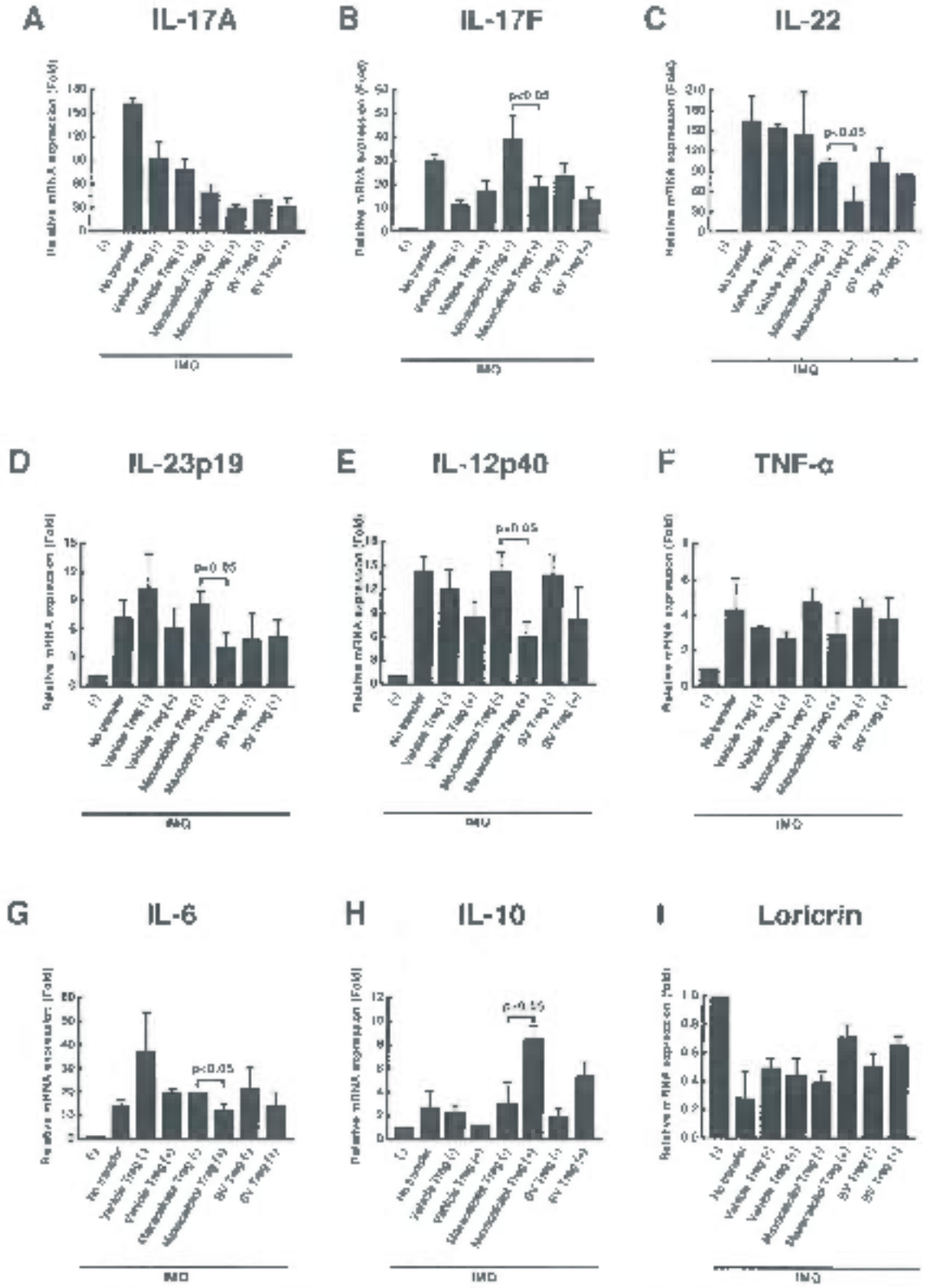

Fig. 4. Quantitative real-time PCR analysis of cytokine mRNA levels in IMQ-treated skin of recipient mice injected with CD4+CD25− or CD4+CD25+ Treg cells from donor mice treated with nasal saline. Relative mRNA levels were determined at day 7 by quantitative real-time PCR for (A) IL-17A, (B) IL-17F, (C) IL-22, (D) IL-23p19, (E) IL-12p40, (F) TNF-α, (G) IL-6, (H) IL-10, and (I) Loricrin, normalized to GAPDH, and are expressed as fold-change relative to vehicle. The data were obtained from skin samples (n = 6 mice per group). Values are presented as mean ± SE (n = 6). Treg (+): CD4+CD25+ cells, Treg (−): CD4+CD25− cells.

and these cells can expand in vivo with antigenic stimulation upon adoptive transfer from donor to recipient mice [33]. Thus, we performed adoptive transfer of CD4+CD25+ Treg cells from the draining lymph nodes of donor mice treated with vehicle, maxacalcitol or BV to recipient mice, which showed that the Treg cells from donor mice pre-treated with maxacalcitol had more potential to produce IL-10 and induced more immunosuppression compared to BV in terms of lowering the mRNA levels of Th17-related cytokines in IMQ-treated skin.

The limitation of this initial study is that we used a prevention model rather than a treatment model. Further studies are needed to assess the effects of maxacalcitol and BV on active, pre-existing psoriasiform inflammation.

5. Conclusion

Our results indicate that the VDRA maxacalcitol improves psoriasiform skin inflammation by possibly modulating Th17 responses and compared to BV, it can better suppress APC infiltration and function, and induce CD4+CD25+ Treg cells which contribute to prolonging its immunosuppressive effect and ability to maintain psoriasis remission.

Funding source

This study was performed through entrusted research agreement between Teikyo University and Maruho Co., LTD. with funding from Maruho Co., LTD.

Acknowledgement

Not applicable.

References

[1] M.A. Lowes, A.M. Bowcock, J.G. Krueger, Pathogenesis and therapy of psoriasis, Nature 445 (2007) 866–873.
[2] F. Baeke, T. Takishima, H. Korf, C. Gysemans, C. Mathieu, Vitamin D: modulator of the immune system, Curr. Opin. Pharmacol. 10 (2010) 482–496.
[3] E.C.M. van de Kerkhof, Biological activity of vitamin D analogues in the skin with special reference to antipsoriatic mechanisms, Br. J. Dermatol. 132 (1995) 675–692.
[4] F. Baeke, H. Korf, L. Overbergh, A. Verstuyf, L. Thorrez, L. Van Lommel, M. Waer, F. Schuit, I. Gysemans, C. Mathieu, The vitamin D analog, TX527, promotes a human CD4+CD25highCD127low regulatory T cell profile and induces a migratory signature specific for homing to sites of inflammation, J. Immunol. 186 (2011) 1332–1342.
[5] T.L. van Belle, A.S. Vanherwegen, D. Feyaerts, F. De Clercq, A. Verstuyf, F. Korf, I. Gysemans, C. Mathieu, 1,25-dihydroxyvitamin D3 and its analog TX527 promote a stable regulatory T cell phenotype in T cells from type 1 diabetic patients, PLoS One (9) (2014) e104394.
[6] J. Tang, R. Zhou, D. Luger, W. Zhu, D.B. Silver, K.S. Grageda, S.K. Su, C.C. Chan, L. Adorini, R.R. Caspi, Calcitriol suppresses antiretinal autoimmunity through inhibitory effects on the Th17 effector response, J. Immunol. 182 (2009) 4624–4632.
[7] F. Sato-Deguchi, S. Imafuku, H. Chen, K. Ishii, K. Hirakawa, J. Nakayama, Topical vitamin D3 analogues induce thymic stromal lymphopoietin and cathelicidin in psoriatic skin lesions, Br. J. Dermatol. 167 (2012) 77–84.
[8] H. Zheng, H. Wu, J. Liu, R. Li, D.Q. Shih, X. Zhang, 1,25-dihydroxyvitamin D3 regulates the development of chronic colitis by modulating both T helper (Th)1 and Th17 activation, APMIS 123 (2015) 490–501.
[9] L. Adorini, S. Amuchastegui, E. Consiglio, G. Laverny, T. Le Meur, C. Penna, Vitamin D receptor agonists as anti-inflammatory agents, Expert Rev. Clin. Immunol. 3 (2007) 477–488.
[10] Z. Szegedi, S. Zwirner, H. Furnik, M. Peter, S. Kaplan, A. Hatyska-Haran, C. Penna, T. Ruzicka, J. Schauber, R. Wolf, Vitamin D analog calcipotriol suppresses the Th17 cytokine-induced proinflammatory S100 "alarmins" psoriasin (S100A7) and koebnerisin (S100A15) in psoriasis, J. Invest. Dermatol. 132 (2012) 1418–1424.
[11] L. Adorini, N. Giarratana, G. Penna, Pharmacological induction of tolerogenic dendritic cells and regulatory T cells, Semin. Immunol. 16 (2004) 127–134.
[12] M. Kosmie, Y. Watabe, S. Shimokawa, K. Sato, K. Kaku, A. Nishima, M. Ohtsuki, H. Nakagawa, K. Tamaki, The action of a novel vitamin D3 analogue, OCT, on immunomodulatory function of keratinocytes and lymphocytes, Arch. Dermatol. Res. 291 (1999) 500–506.
[13] H. Takahashi, M. Ito, M. Iwamoto, A. Ikuta-Yamanouchi, Y. Hashimoto, K. Ikuta, Similarly potent action of 1,25-dihydroxyvitamin D3 and its analogues, tacalcitol, calcipotriol, and maxacalcitol on normal human epidermal keratinocyte proliferation and differentiation, J. Dermatol. Sci. 31 (2003) 21–29.
[14] J.N. Barker, R.C. Ashton, R. Marks, R.I. Harris, J. Barth-Jones, Topical maxacalcitol for the treatment of psoriasis vulgaris: a placebo-controlled, double-blind, dose-finding study with active comparator, Br. J. Dermatol. 141 (2000) 234–238.
[15] J.M. Camarasa, J.P. Ortonne, J. Dubertret, Calcitriol shows greater persistence of treatment effect than betamethasone dipropionate in topical psoriasis therapy, J. Dermatol. Treat. 14 (2003) 8–13.
[16] L. van der Fits, S. Mourits, J.S.A. Voerman, M. Kant, L. Boon, J.D. Laman, F. Cornelissen, A.M. Muis, E. Florencia, E.P. Prens, E. Lubberts, Imiquimod-induced psoriasis-like skin inflammation in mice is mediated via the IL23/IL17 axis, J. Immunol. 182 (2009) 5836–5845.
[17] X. Sun, J. Zhang, P. Hua, T. Zhai, H. Fu, P. Wu, X. Zhu, Z. Zhou, B. Shen, N. Li, Baicalin/baicalein inhibits skin lesions in imiquimod-induced psoriasis-like mice by downregulating inflammation, Int. Immunopharmacol. 24 (2015) 302–309.
[18] S. Shiraishi, Y. Iida, C.A. Han, A. Mitsui, M. Kamata, Y. Asano, M. Nagaya, T. Kadono, Y. Masamoto, M. Kumakiri, T. Yamauchi, N. Kubota, T. Kadowaki, S. Sato, Adiponectin regulates psoriasiform skin inflammation by suppressing IL-17 production from γδ-T cells, Nat. Commun. 6 (2015) 7687.
[19] G. Penna, S. Amuchastegui, N. Giarratana, X.C. Daniel, M. Vulcano, S. Sozzani, L. Adorini, 1,25-dihydroxyvitamin D3 selectively modulates tolerogenic properties in myeloid but not plasmacytoid dendritic cells, J. Immunol. 178 (2007) 145–153.
[20] A. Di Cesare, P. Di Meglio, F.O. Nestle, The IL-23/Th17 axis in the immunopathogenesis of psoriasis, J. Invest. Dermatol. 129 (2009) 1339–1350.
[21] G. Penna, L. Adorini, 1 Alpha,25-dihydroxyvitamin D3 inhibits differentiation, maturation, activation, and survival of dendritic cells leading to impaired alloreactive T cell activation, J. Immunol. 164 (2000) 2405–2411.
[22] M.D. Griffin, W.H. Lutz, V.A. Phan, L.A. Bachman, D.J. McKean, R. Kumar, Potent inhibition of dendritic cell differentiation and maturation by vitamin D analogs, Biochem. Biophys. Res. Commun. 270 (2000) 701–708.
[23] A.C. van Halteren, I. van Etten, P.C. de Jong, N. Roep, D.D. Koep, C. Mathieu, Reduction of human autoreactive T cells upon interaction with dendritic cells modified by TX527, an analog of 1,25 dihydroxyvitamin D(3), Diabetes 51 (2002) 2119–2125.
[24] M.A. Al-S. Thower, S. Hanna, S. Cochran, J. Birchall, F. Wong, C.M. Dayan, D. Talmor, Topical steroid therapy induces pro-tolerogenic changes in Langerhans cells in human skin, Immunology 146 (2015) 411–421.
[25] A.M. van der Aar, D.S. Siberyar, G. Bakdash, T.M. van Capel, H.E. van der Kleij, D.J. Opdenoter, M.B. Teunissen, M.L. Kapsenberg, E.C. de Jong, Vitamin D3 targets epidermal and dermal dendritic cells for induction of distinct regulatory T cells, J. Allergy Clin. Immunol. 127 (2011) 1502–1508.
[26] L. Adorini, 1,25 Dihydroxyvitamin D3 analogs as potential therapies in transplantation, Curr. Opin. Investig. Drugs 9 (2008) 1458–1463.
[27] L. Adorini, G. Penna, Dendritic cell tolerogenicity: a key mechanism in immunomodulation by vitamin D receptor agonists, Hum. Immunol. 70 (2009) 348–352.
[28] M. Chorelsh, S. Bach, J. Ohst, M. Komba, J.C. Fiset, J.P. Burn, Expansion of antigen-specific regulatory T cells with the topical vitamin D analog calcipotriol, J. Immunol. 182 (2009) 6271–6278.
[29] L. Kystalis, S. Kusumakar, S. Boswell, P. Trych, P. Ung, D.F. Richards, T. Adilibi, C. Pridgeon, M. Dallman, T.K. Lim, D.S. Robinson, F.J. Barrat, A. O'Garra, P. Lavender, T.H. Lee, C. Corrigan, C.M. Fazekasova, Reversing the defective induction of IL-10-secreting regulatory T cells in glucocorticoid-resistant asthma patients, J. Clin. Invest. 116 (2006) 146–155.
[30] M. Demirsoy, J.P. Duez, Tolerance induction by transcutaneous immunization through ultraviolet-irradiated skin is transferable through CD4+CD25+ T regulatory cells and is dependent on host-derived IL-10, J. Immunol. 176 (2006) 2635–2644.
[31] M. Lebwohl, A. Weiss, F. Lombardi, W. Lou, Calcipotriene ointment and betamethasone ointment in the long-term treatment of psoriasis: effects on the duration of improvement, J. Am. Acad. Dermatol. 39 (1998) 447–450.
[32] T.M. Leichner, A. Calder, V.L. Harrison, Y. Tanaka, A.S. Archambault, J.S. Kim, M.C. Siracusa, W.J. Leonard, A. Naji, G.E. Wu, D. Aronchik, T. Kambayashi, Skin-derived TSLP systemically expands regulatory T cells, J. Autoimmun. 70 (2016) 39–52.
[33] S. Gorman, L.A. Kuritzky, M.A. Judge, K.M. Dixon, J.P. McGlade, R.S. Mason, H. Finlay-Jones, P.H. Hart, Topically applied 1,25-dihydroxyvitamin D3 enhances the suppressive activity of CD4+CD25+ cells in the draining lymph nodes, J. Immunol. 179 (2007) 6273–6283.

INDEXED BY
INDEX MEDICUS
(MEDLINE)
SCIENCE CITATION INDEX
EXPANDED (ISI)

GIORNALE ITALIANO DI

DERMATOLOGIA E VENEREOLOGIA

OFFICIAL JOURNAL OF THE SOCIETÀ ITALIANA DI DERMATOLOGIA MEDICA, CHIRURGICA, ESTETICA E DELLE MALATTIE SESSUALMENTE TRASMESSE (SIDeMaST)

1885

Società Italiana di Dermatologia
(SIDeMaST)

VOLUME 154 - No. 4 - AUGUST 2019

EDIZIONI MINERVA MEDICA

© 2019 EDIZIONI MINERVA MEDICA
Online version at http://www.minervamedica.it

Giornale Italiano di Dermatologia e Venereologia 2019 August, 154(4):418-24
DOI: 10.23736/S0392-0488.18.06202-8

REVIEW

Psoriasis and the TNF/IL23/IL17 axis

Kazuhiro FURUE [1], Takamichi ITO [1], Gaku TSUJI [1], Takafumi KADONO [2], Masutaka FURUE [1] *

[1]Department of Dermatology, Graduate School of Medical Sciences, Kyushu University, Fukuoka, Japan; [2]Department of Dermatology, St. Mariana University School of Medicine, Kawasaki, Japan

*Corresponding author: Masutaka Furue, Department of Dermatology, Graduate School of Medical Sciences, Kyushu University, Maidashi 3-1-1, Higashi-ku, Fukuoka 812-8582, Japan. E-mail: furue@dermatol.med.kyushu-u.ac.jp

ABSTRACT

The excellent response of psoriasis to anti-TNF-α(TNF)/IL23/IL17A biologics implies a crucial role for the TNF/IL23/IL17 axis in developing psoriasis. In addition to the TNF/IL23/IL17 axis provided by immune cells, current evidence points to an important contribution of TNF, IL23 and IL17C produced from non-hematopoietic keratinocytes. Therefore, crosstalk between immune cells and keratinocytes forms a multilayered feed-forward loop to accelerate the TNF/IL23/IL17A axis. Many biologics have already been licensed or are under clinical trials. Given that the IL-17 signature is more upregulated in the skin than in synovium in psoriatic arthritis, anti-IL-23/IL-17 agents seem to be superior to anti-TNF-α remedies in the treatment of skin lesions. In this review, we summarize recent topics in psoriasis and the TNF/IL23/IL17 axis.

(Cite this article as: Furue K, Ito T, Tsuji G, Kadono T, Furue M. Psoriasis and the TNF/IL23/IL17 axis. G Ital Dermatol Venereol 2019;154:418-24. DOI: 10.23736/S0392-0488.18.06202-8)

Key words: Psoriasis, Tumor necrosis factor-alpha; Interleukin-23, Interleukin-17

Psoriasis is an immune-mediated inflammatory skin disease with an approximate prevalence of 0.1 to 3% in the general population.[1, 2] Psoriasis patients compose 4.43% of all Japanese dermatological patients.[3] Dissemination of desquamative erythema throughout the entire body, including face, scalp, hands and nails, causes significant physical, psychological and economic burdens to the afflicted patients.[4-8] Associations with psoriatic arthritis and other autoimmune diseases further decreases patients' quality of life.[9-13] Psoriasis is also significantly comorbid with cardiovascular and metabolic diseases, a condition known as inflammatory skin march.[2, 14-19]

That the TNF-α(TNF)/IL23/IL17 axis appears to be a major driver in the pathogenesis of psoriasis is underscored by the excellent response of psoriasis to biologics targeting TNF, IL23 and IL17, although a slight difference exists in their efficacy.[3, 20-23] Anti-TNF/IL23/IL17 biologics also successfully improve psoriatic arthritis.[24-27] Reductions in comorbid cardiovascular events and systemic inflammation have also been reported in patients with psoriasis treated with anti-TNF/IL23/IL17 biologics.[15, 28-30] An increased risk of psoriasis has been reported after scabies infection, which is associated with IL17 elevation.[31]

The histopathology of psoriasis is characterized by hyperkeratosis, parakeratosis and epidermal hyperproliferation as well as intraepidermal neutrophilic infiltration.[32-34] The infiltrating dermal immune cells include IL23-positive dendritic cells (DCs) and IL17A-producing T (T17) cells.[34-36] IL17 upregulates the proliferation of keratinocytes and downregulates their differentiation.[37, 38] IL17 also upregulates the production of the neutrophil-attracting cyto/chemokines IL36, CXCL1, CXCL2 and CXCL8 by keratinocytes.[1, 39, 40] IL17 also promotes the expression of TNF by keratinocytes,[41] and TNF synergistically augments the production of neutrophilic chemokines from keratinocytes in the presence of IL17.[40] DC-derived IL23 is essential for the priming and maturation of T17 cells.[42] In addition, recent studies have revealed that keratinocytes are potent IL23 producers upon stimulation with TNF[43] and that IL23 directly modulates the proliferation and differentiation of keratinocytes.[43, 44]

In this article, we review the feed-forward mechanism

operated by the TNF/IL23/IL17 axis between immune cells and keratinocytes that leads to the development of full-blown psoriasis.

The TNF/IL23/IL17 axis in psoriasis pathogenesis

Psoriasis is now recognized as an autoimmune disease driven by the TNF/IL23/IL17 axis.[35, 45] Although autoantigens responsible for the development of psoriasis are not fully understood, at least three autoantigens have been demonstrated in psoriasis, namely, cathelicidin (LL-37),[46] a disintegrin and metalloprotease domain containing thrombospondin type 1 motif-like 5 (ADAMTSL5),[47] and lipid antigens generated by phospholipase A2 group IVD (PLA2G4D).[48] Accordingly, HLA-Cw06 is one of the major susceptibility genes for psoriasis.[49] ADAMTSL5 and LL-37 have been shown to be restricted to HLA-C*06:02 (Figure 1).[39, 46, 47, 50] T cell clones reactive to ADAMTSL5 or LL37 contain IL-17-producing T17 cells.[46, 47] PLA2G4D are known to be recognized by CD1a-restricted T17 cells.[48]

Psoriasis occurs preferentially in areas susceptible to frequent friction or trauma eponymously known as Koebner's phenomenon.[51] An initial trigger for psoriasis is believed to be the activation of DCs stimulated by complexes of host DNA and LL-37, which are produced by keratinocytes after minor injuries.[34, 42, 46, 51, 52] LL-37 is an active anti-microbial peptide of cathelicidin produced by injured keratinocytes.[34] Extracellular DNA has been shown in the psoriatic epidermis in association with neutrophil extracellular traps.[53] Activated DCs produce TNF and IL23, thereby inducing T17 differentiation.[34, 42, 53] Among DCs, TNF/iNOS (inducible NO synthase)-producing DCs (Tip-DCs) are particularly pathogenic because they are high TNF and IL23 producers.[56, 57] TNF is also released from injured keratinocytes and may strengthen the IL23/IL17 axis (Figure 1).[57]

Gene expression of *TNF*, *IL23*, and *IL17A* is upregulated in the lesional skin in psoriasis.[34, 58, 59] Three of six *IL17* family genes, *IL17A*, *IL17F* and *IL17C*, are overexpressed in psoriatic lesions; however, the pathogenic roles of IL17F and IL17C remain unclear.[34, 60, 61] IL17A produced by T17 cells accelerates the proliferation of keratinocytes and induces epidermal acanthosis characteristic of psoriasis.[32, 38, 62] Other elevated cyto/chemokines include *CXCL1*, *CXCL2*, *CXCL8*, *CCL20*, *IL36A*, *IL36B* and *IL36G*.[1, 34, 35, 53, 59] These cyto/chemokines are produced by activated keratinocytes and are potent chemoattractants for neutrophils (CXCL1, CXCL2, CXCL8 and IL36) and T17

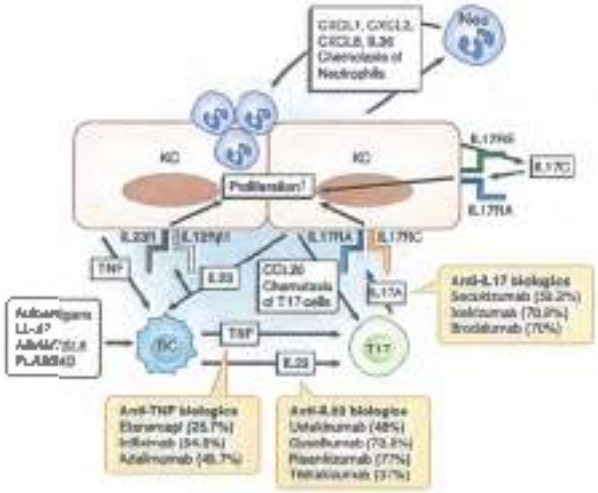

Figure 1.—Pathogenesis of psoriasis and the PASI90 scores of anti-TNF/IL23/IL17 biologics. Upon recognition of autoantigens such as LL-37, ADAMTSL5 and PLA2G4D, dendritic cells (DCs) produce TNF and IL23, which accelerate the differentiation of IL17A-producing T cells (T17s). IL17A binds to its receptor composed of the IL17RA/IL17RC heterodimer and induces the proliferation of keratinocytes (KCs). KCs also produce TNF and IL23 and facilitate DC-T17 interactions. IL23 and IL17C derived from KCs bind to IL23R/IL12Rβ1 and IL17RA/IL17RC, respectively. Both IL23 and IL17C promote the proliferation of KCs in an autocrine mechanism. TNF and IL17A activate KCs to produce the neutrophil (Neu)chemoattractants CXCL1, CXCL2, CXCL8 and IL36. TNF and IL17A also induce CCL20 production by KCs, which recruits T17 cells into the psoriatic lesion. Anti-TNF/IL23/IL17 biologics are listed with their PASI90 score in parenthesis. ADAMTSL5, a disintegrin and metalloprotease domain containing thrombospondin type 1 motif-like 5, PLA2G4D, phospholipase A2 group IVD, PASI90, percentage of responders who achieve a 90% reduction in their Psoriasis Area and Severity Index score (PASI90)

cells (CCL20).[1, 34, 35, 53, 59, 63, 64] Neutrophil-derived proteases are essential for the conversion of immature IL36 to its active form.[65] Therefore, the TNF/IL23/IL17A axis makes a multilayered feed-forward loop between immune cells and keratinocytes in skin that develops a full-fledged psoriatic lesion (Figure 1).

At least 10 biologics have been used in clinics or in ongoing clinical trials, including anti-TNF (etanercept, infliximab, adalimumab), anti-IL23 (ustekinumab, guselkumab, tildrakizumab, risankizumab) and anti-IL17 (secukinumab, ixekizumab, brodalumab) antibodies. Clinical efficacy of the biologics is assessed by reductions in the Psoriasis Area and Severity Index (PASI) after a 12- (or 16-) week treatment. The PASI90 (the percentage of patients who achieved more than a 90% reduction in their PASI score) by anti-TNF-α agents (25.7% to 54.5%) are similar to PASI90 by anti-IL-23 agents (37% to 77%) and anti-IL-17 agents (59.2% to 70.9%) (Fig.1).[66] Thirty to

forty percent of patients with moderate to severe psoriasis experience PASI100 by some of these anti-IL-23 or anti-IL-17 biologics.[66]

TNF and its inhibition

Infiltrating TipDCs in the lesional skin in psoriasis are active producers of TNF.[56] Lesional psoriatic skin overexpresses *TNF* compared to non-lesional psoriatic skin and healthy control skin.[67] The role of TNF in the pathogenesis of psoriasis is likely multifaceted; however, its key actions are to promote DC and T cell interactions and to upregulate IL23 synthesis in DCs for subsequent T17 differentiation.[57, 68] Neutralization of TNF with Etanercept reduced TipDC activity by downregulating iNOS, TNF and IL23 levels within the first 2 weeks of treatment.[57] This early effect paralleled the downregulated expression of activation or costimulatory markers such as HLA-DR, CD40 and CD86 in TipDCs.[57] In contrast, downregulation of the type 1 signature, as assessed by interferon-γ (IFNG) expression, was only observed late at 12 weeks of Etanercept treatment.[57]

A sensitive immunohistological study revealed that the expression of TNF is confined to HLA-DR+CD11c+ DCs and CD163+ macrophages in psoriatic lesions.[69] In the first 48 hours after intravenous administration of the TNF antagonist Infliximab, no overt changes in the number of TNF+ cells or signs of apoptosis were observed. However, a rapid decrease was detected in IL12/IL23p40, CCL20, and IL12/IL23RB1 mRNA levels, suggesting that TNF antagonism efficiently inhibits the activation of antigen-presenting cells.[69]

In addition, psoriatic keratinocytes produced larger amounts of TNF as well as CXCL8 compared with keratinocytes from healthy volunteers in ex vivo cultures.[70] The expression of CXCL1, CXCL2, CXCL8 and IL36 is upregulated in the lesional skin in psoriasis, and all these cyto/chemokines strongly stimulate neutrophil chemotaxis.[59, 71] As TNF is a potent stimulator of the production of CXCL1, CXCL2, CXCL8 and IL36 in keratinocytes,[72, 73] TNF may, at least in part, be responsible for histological intraepidermal neutrophilic accumulation by enhancing the production of these cyto/chemokines.

PASI90 scores for etanercept (human soluble TNF receptor), Infliximab (chimeric anti-TNF antibody) and adalimumab (fully human anti-TNF antibody) were 25.7%, 54.5% and 49.7%, respectively, at 12 or 16 weeks after treatment in representative clinical studies.[74-76]

IL23 and its inhibition

IL23 is composed of two subunits, p19 and p40. While the p19 subunit is an element unique to IL23, the p40 subunit is shared with IL12.[42] IL12 is composed of p40 and IL12-specific p35.[42] IL12 p40/p35 binds to the IL12 receptor, which comprises IL12Rβ1 and IL12Rβ2, while IL23 p40/p19 binds to the IL23 receptor, which comprises IL23R and IL12Rβ1.[42] IL12 promotes the differentiation of IFNG-producing T cells. Functional activation of IL23R/IL12Rβ1 by the IL23 p40/p19 heterodimer is crucial not only for inducing the T17 phenotype but also for enhancing the pathogenicity of T17 cells.[42, 77]

In the lesional skin in psoriasis, both IL23p40 and IL23p19 are upregulated compared to nonlesional skin levels, whereas the IL12p35 subunit remains unchanged.[68] Dermal DCs and monocytes are major sources of IL23 production.[68] Anti-TNF biologics significantly inhibited the expression of IL23p40 and IL23p19 as well as IL17 as early as 1 or 2 weeks after administration.[53, 69] Notably, reductions in IL12p35 and IFNG levels were not observed in the early treatment time course.[57] These results stress an insignificant pathogenic role for the IL12/IFNG pathway in psoriasis. In parallel, blockade of the IL23/IL17 axis successfully improved psoriatic inflammation,[76, 78, 79] while clinical trials using anti-IL12 antibodies and anti-IFNG antibodies have been discontinued.[42, 80]

The PASI90 scores of Ustekinumab (fully human anti-IL-12/23 p40 antibody), Guselkumab (fully human anti-IL23 p19 antibody), Risankizumab (fully human anti-IL23 p19 antibody), and Tildrakizumab (fully human anti-IL-23 p19 antibody) were 48%, 73.3%, 77%, and 37%, respectively, in representative clinical studies.[76, 78, 81, 82] The efficacy of anti-IL23p19 biologics Guselkumab and Risankizumab seems to be higher than that of anti-TNF biologics.

While dermal DCs express IL23p40, immunohistological staining also proves that IL23p40 and IL23p19 are expressed in normal and psoriatic keratinocytes.[57, 68, 83] Moreover, the epidermal expression of IL23p40 and IL23p19 is stronger in psoriasis lesions than in healthy controls.[57, 68, 83] Murine keratinocytes also produce biologically active IL-23.[84] IL-23 can promote keratinocyte growth and histological acanthosis *via* the JAK2/AKT/STAT3/LMO4 signaling pathway.[83] LMO4 is a LIM-domain protein that is known to regulate keratinocyte proliferation and differentiation during embryogenesis.[85] In addition, TNF is an active stimulator of IL23 production from keratinocytes in mice and probably in humans.[84] Thus, anti-IL23 biologics can target IL-23 derived from DCs as well as keratinocytes (Figure 1).

IL17 and its inhibition

The IL17 family plays a critical role in the immune response in infectious, inflammatory and autoimmune disorders.[84, 85] IL17 family members comprise IL17A, IL17B, IL17C, IL17D, IL17E, IL17F and IL17AF.[41, 84, 85] IL17AF is a hybrid heterodimer of IL17A and IL17F. IL17E is also called IL25 and is related to the type 2 immune response and allergy.[41, 84, 86] IL17A is produced from hematopoietic cells, but IL17B, IL17C, and IL17E are preferentially produced from nonhematopoietic cells, including keratinocytes. Both hematopoietic cells and keratinocytes produce IL17F.[41, 84] The IL17 receptor (IL17R) is composed of heterodimeric molecules. IL17A, IL17F and IL17AF share the same IL17R comprising IL17RA and IL17RC. IL17C binds to IL17RA and IL17RE heterodimers.[41, 84, 85]

Although the expression of *IL17A*, *IL17F* and *IL17C* is upregulated in the psoriatic lesional skin,[87-90] IL17A is believed to be the most pathogenetic family member in psoriasis.[91] However, intradermal injection of IL17C induces epidermal thickening and neutrophil infiltration.[91] In addition, the significant efficacy of anti-IL17C antibodies has been recently noted in patients with psoriasis and atopic dermatitis.[92, 93] Commercially available anti-IL17 biologics are Secukinumab (fully human IgG1κ anti-IL17A antibody), Ixekizumab (fully human IgG4 anti-IL17A antibody) and Brodalumab (fully human IgG2 anti-IL17RA antibody). The PASI90 scores of Secukizumab, Ixekizumab and Brodalumab are 59.2%, 70.9% and 70%, respectively, at 12 weeks posttreatment.[73, 93, 94] The clinical efficacy of anti-IL17 biologics is comparable to that of anti-IL23 biologics.

IL17A is an active promoter of keratinocyte proliferation.[32, 38, 47] IL17A stimulates keratinocytes to produce neutrophil-chemoattracting cyto/chemokines such as IL36G, CXCL1 and CXCL8. TNF synergistically or additively augments these IL17A effects on keratinocytes.[64, 95] Autocrine production of IL17A from neutrophils has been stressed,[96] but neutrophils are not the major source of IL17A.[97] CCL20 produced from keratinocytes is a key chemokine in the recruitment of T17 cells and DCs.[98] Both IL17A and TNF potently upregulate the expression of CCL20 in keratinocytes.[65, 99] In parallel, Secukizumab downregulates the lesional expression of CXCL1 and CXCL8 in a dose-dependent manner in patients with psoriasis as early as 2 weeks posttreatment.[96] Ixekizumab also dose-dependently reduces keratinocyte proliferation, hyperplasia, epidermal thickness and infiltration of T cells and DCs into the dermis and epidermis 2 weeks after administration.[62] These results stress a critical role for IL17A as an effector molecule driving the epidermal hyperplasia and intraepidermal neutrophil accumulation that characterize the histopathology of psoriasis.[33]

Conclusions

The TNF/IL23/IL17A axis appears to be a cardinal driving force in developing psoriasis by orchestrating the activities of keratinocytes, DCs, T cells and neutrophils. These players mutually communicate and cooperate to form a multilayered feed-forward loop leading to psoriatic eruption. The autoimmune process is likely to be one of the triggers that initiates the expansion of T17 cells. The pathogenic T cell clones remain in the lesional skin even after the lesion heals with treatment.[36] This fact may explain why psoriasis recurs preferentially in previously afflicted areas.[99]

Biologics targeting the TNF/IL23/IL17A axis are now indispensable therapeutic agents for moderate to severe psoriasis. Representative clinical trials suggest that anti-IL23/IL17 biologics are slightly better for treating psoriatic skin lesions than anti-TNF biologics. Keratinocytes produce a plethora of cyto/chemokines, including IL23, IL17C and IL36, which are overproduced in psoriatic skin. Future clinical studies using anti-IL17C and anti-IL36 antibodies are warranted to elucidate the role of these cytokines in the pathogenesis of psoriasis.

References

1. Furue K, Yamamura K, Tsuji G, Mitoma C, Uchi H, Nakahara T, *et al.* Highlighting interleukin-36 signalling in plaque psoriasis and pustular psoriasis. Acta Derm Venereol 2018;98:5–13.

2. Krueger JG, Brunner PM. Interleukin-17 alters the biology of many cell types involved in the genesis of psoriasis, systemic inflammation and associated comorbidities. Exp Dermatol 2018;27:115–23.

3. Furue M, Yamazaki S, Jimbow K, Tsuchida T, Amagai M, Tanaka T, *et al.* Prevalence of dermatological disorders in Japan: a nationwide, cross-sectional, seasonal, multicenter, hospital-based study. J Dermatol 2011;38:310–20.

4. Alpsoy E, Polat M, FettahlioGlu-Karaman B, Karadag AS, Karal-Durmazlar E, YalCin B, *et al.* Internalized stigma in psoriasis: A multicenter study. J Dermatol 2017;44:885–91.

5. Hawro M, Maurer M, Weller K, Maleszka R, Zalewska-Janowska A, Kaszuba A, *et al.* Lesions on the back of hands and female gender predispose to stigmatization in patients with psoriasis. J Am Acad Dermatol 2017;76:648–654.e2.

6. Ishiyama S, Ito M, Funasaka Y, Abe M, Nishida E, Murasatsu S, *et al.* Assessment of medication adherence and treatment satisfaction in Japanese patients with psoriasis of various severities. J Dermatol 2018;45:727–31.

7. Matsui S, Tatsukawa R, Uryu M, Takahara M, Furue M, Ohata C, *et al.* Treatment satisfaction, willingness to pay and quality of life in Japanese patients with psoriasis. J Dermatol 2017;44:163–6.

8. Takahashi H, Saeki K, Takaya A, Iizuka H. Economic burden of psoriatic patients in Japan: analysis from a single outpatient clinic. J Dermatol 2017;44:1024–6.

9. Furue K, Ito T, Tsuji G, Kadono T, Nakahara T, Furue M. Autoimmunity and autoinflammatory co-morbidities in psoriasis. Immunology 2018;154:21–7.

10. Ito T, Takahashi H, Kawada A, Iizuka H, Nakagawa H, Japanese Society For Psoriasis Research. Epidemiological survey from 2009 to 2012 of psoriatic patients in Japanese Society for Psoriasis Research. J Dermatol 2018;45:293–301.

11. Mercuri SR, Gregorio G, Brunasso P. Quality of life of psoriasis patients measured by the PSOdisk, a new visual method for assessing the impact of the disease. G Ital Dermatol Venereol 2017;152:424–31.

12. Prinz JC. Autoimmune aspects of psoriasis: heritability and autoantigens. Autoimmun Rev 2017;16:970–9.

13. Yamamoto T, Ohtsuki M, Sano S, Igarashi A, Morita A, Okuyama R, *et al.*, Working Group of the Epidemiological Survey in the Japanese Society for Psoriasis Research. Prevalence and current therapies of psoriatic arthritis in Japan: A survey by the Japanese Society of Psoriasis Research in 2016. J Dermatol 2017;44:e121.

14. Furue M, Kadono T. "Inflammatory skin march" in atopic dermatitis and psoriasis. Inflamm Res 2017;66:833–42.

15. Guttman-Yassky E, Krueger JG, Lebwohl MG. Systemic immune mechanisms in atopic dermatitis and psoriasis with implications for treatment. Exp Dermatol 2018;27:409–17.

16. Hamura M, Shibuya T, Inoguchi T, Inoue S, Takahashi N, Kishibe M, *et al.* Prevalence of coronary artery calcification in Japanese patients with psoriasis: A close correlation with bilateral diagonal earlobe creases. J Dermatol 2017;44:1113–8.

17. Kari L, Tiesalin L, Lee J, Fitz LJ, Bonstein O, Costa-da Rosa J, *et al.* Reduction of inflammatory and cardiovascular proteins in the blood of patients with psoriasis: differential responses between infliximab and etanercept after 4 weeks of treatment. J Invest Dermatol 2018;138:275–81.

18. Oh JH, Ro YS, Kim JE. Epidemiology and cardiovascular comorbidities in patients with psoriasis: A Korean nationwide population-based cohort study. J Dermatol 2017;44:621–9.

19. Yamanaka K, Mizutani H. "Inflammatory skin march": IL-1-mediated skin inflammation, atopic dermatitis, and psoriasis to cardiovascular events. J Allergy Clin Immunol 2015;136:823–4.

20. Boutet MA, Nerviani A, Gallo Afflitto G, Pitzalis C. Role of the IL-23/IL-17 axis in psoriasis and psoriatic arthritis: the clinical importance of its divergence in skin and joints. Int J Mol Sci 2018;19:E530.

21. Jabbar-Lopez ZK, Yiu ZZ, Ward V, Exton LS, Mohd Mustapa MF, Samarasekera E, *et al.* Quantitative evaluation of biologic therapy options for psoriasis: A systematic review and network meta-analysis. J Invest Dermatol 2017;137:1646–54.

22. Torii H, Nakano M, Yano T, Kondo K, Nakagawa H, SPREAD Study Group. Efficacy and safety of dose escalation of infliximab therapy in Japanese patients with psoriasis: results of the SPREAD study. J Dermatol 2017;44:552–9.

23. Wu NL, Hsu CJ, Sun PJ, Tsai TF. Efficacy and safety of secukinumab in Taiwanese patients with moderate to severe plaque psoriasis: subanalysis from FIXTURE phase III study. J Dermatol 2017;44:1329–37.

24. Ramanujam A, Raffayova H, Kungurov NV, Kobalava Z, Vergin A, Helmle L, *et al.*; RESPOND investigators. Infliximab plus methotrexate is superior to methotrexate alone in the treatment of psoriatic arthritis in methotrexate-naïve patients: the RESPOND study. Ann Rheum Dis 2012;71:543–8.

25. Kavanaugh A, McInnes IB, Mease PJ, Hall S, Chuney H, Kivitz AJ, *et al.* Efficacy of subcutaneous secukinumab in patients with active psoriatic arthritis stratified by prior tumor necrosis factor inhibitor use: results from the randomized placebo-controlled FUTURE 2 study. J Rheumatol 2016;43:1713–7.

26. McInnes IB, Kavanaugh A, Gottlieb AB, Puig L, Rahman P, Ritchlin C, *et al.*; PSUMMIT 1 Study Group. Efficacy and safety of ustekinumab in patients with active psoriatic arthritis: 1 year results of the phase 3, multicentre, double-blind, placebo-controlled PSUMMIT 1 trial. Lancet 2013;382:780–9.

27. Veale DJ, Fearon U. The pathogenesis of psoriatic arthritis. Lancet 2018;391:2273–84.

28. Asahina A, Kubo N, Umezawa Y, Honda H, Yanaba K, Nakagawa H. Neutrophil-lymphocyte ratio, platelet-lymphocyte ratio and mean platelet volume in Japanese patients with psoriasis and psoriatic arthritis: response to therapy with biologics. J Dermatol 2017;44:1182–23.

29. Gkalpakiotis S, Arenberger P, Arenbergerova M, Gkalpakiotis P, Polochova J, Arenberger P, Kraml P. Impact of adalimumab treatment on cardiovascular risk biomarkers in psoriasis: results of a pilot study. J Dermatol 2017;44:363–9.

30. Gulliver WP, Randell S, Gulliver S, Conners S, Bachelez H, MacDonald D, *et al.* Do biologics protect patients with psoriasis from myocardial infarction? A retrospective cohort. J Cutan Med Surg 2016;20:536–41.

31. Liu JM, Liu CY, Chang FW, Liu YP, Chang CP, Hsu RJ. Increased risk of psoriasis following scabies infection: A nationwide population-based matched-cohort study. J Dermatol 2018;45:302–8.

32. Rechtsche WH, Schön MP. Psoriasis. Lancet 2015;386:983–94.

33. Ferreli C, Pinna AL, Pilloni L, Tomasini CF, Rongioletti F. Histopathological aspects of psoriasis and its uncommon variants. G Ital Dermatol Venereol 2018;153:173–84.

34. Lowes MA, Russell CB, Martin DA, Towne JE, Krueger JG. The IL-23/T17 pathogenic axis in psoriasis is amplified by keratinocyte responses. Trends Immunol 2013;34:174–81.

35. Hawkes JE, Chan TC, Krueger JG. Psoriasis pathogenesis and the development of novel targeted immune therapies. J Allergy Clin Immunol 2017;140:645–53.

36. Matos TR, O'Malley JT, Lowry EL, Hamm D, Kirsch IR, Robins HS, *et al.* Clinically resolved psoriatic lesions contain psoriasis-specific IL-17-producing αβ T cell clones. J Clin Invest 2017;127:4031–41.

37. Ha HL, Wang H, Pisitkun P, Kim JC, Tassi I, Tang W, *et al.* IL-17 drives psoriatic inflammation via distinct, target cell-specific mechanisms. Proc Natl Acad Sci USA 2014;111:E3422–31.

38. Ma WY, Jia K, Zhang Y. IL-17 promotes keratinocyte proliferation via the downregulation of C/EBPα. Exp Ther Med 2016;11:631–6.

39. Muhr P, Zeibregol J, Heitland I, Werfel T, Wittmann M. Expression of interleukin (IL)-1 family members upon stimulation with IL-17 differs in keratinocytes derived from patients with psoriasis and healthy donors. Br J Dermatol 2011;165:889–93.

40. Wang CQ, Akalu YT, Suarez-Farinas M, Gonzalez J, Mitsui H, Lowes MA, *et al.* IL-17 and TNF synergistically modulate cytokine expression while suppressing melanogenesis: potential relevance to psoriasis. J Invest Dermatol 2013;133:2741–52.

41. Iwakura Y, Ishigame H, Saijo S, Nakae S. Functional specialization of interleukin-17 family members. Immunity 2011;34:149–62.

42. Teng MW, Bowman EP, McElwee JJ, Smyth MJ, Casanova JL, Cooper AM, *et al.* IL-12 and IL-23 cytokines: from discovery to targeted therapies for immune-mediated inflammatory diseases. Nat Med 2015;21:719–29.

43. Tu Y, Zhang S, Zhou G, Zhou L, Xiang Q, Chen Q, *et al.* JMJD3 is a disease-provocative transcription coregulator activated by IL-23 in psoriatic keratinocytes. J Invest Dermatol 2014;134:1078–87.

44. Li H, Yao Q, Mariscal AG, Wu X, Hülse J, Pedersen E, *et al.* Epigenetic control of IL-23 expression in keratinocytes is important for chronic skin inflammation. Nat Commun 2014;5:4620.

45. Ogawa E, Sato Y, Minagawa A, Okuyama R. Pathogenesis of psoriasis and development of treatment. J Dermatol 2018;45:264–72.

46. Lande R, Botti E, Jandus C, Dojcinovic D, Fanelli G, Conrad C, *et al.* The antimicrobial peptide LL37 is a T-cell autoantigen in psoriasis. Nat Commun 2014;5:5621.

47. Arakawa A, Siewert K, Stöhr J, Besgen P, Kim SM, Rühl G, *et al.* Melanocyte antigen triggers autoimmunity in human psoriasis. J Exp Med 2015;212:2203–12.

48. Cheung KL, Jarrett R, Subramaniam S, Salimi M, Gutowska-Owsiak D, Chen YL, *et al.* Psoriatic T cells recognize neolipid antigens generated by mast cell phospholipase delivered by exosomes and presented by CD1a. J Exp Med 2016;213:2399–412.

49. Nair RP, Stuart PE, Nistor I, Hiremagalore R, Chia NV, Jenisch S, *et al.* Sequence and haplotype analysis supports HLA-C as the psoriasis susceptibility 1 gene. Am J Hum Genet 2006;78:827–51.

50. Fuentes-Duculan J, Bonifacio KM, Hawkes JE, Kunjravia N, Cueto I, Li X, *et al.* Autoantigens ADAMTSL5 and IL37 are significantly upregulated in active Psoriasis and localized with keratinocytes, dendritic cells and other leukocytes. Exp Dermatol 2017;26:1075–82.

51. Kalayciyan A, Aydemir EH, Karagyan A. Experimental Koebner phenomenon in patients with psoriasis. Dermatology 2007;215:314–7.

52. Lande R, Gregorio J, Facchinetti V, Chatterjee B, Wang YH, Homey B, *et al.* Plasmacytoid dendritic cells sense self-DNA coupled with antimicrobial peptide. Nature 2007;449:564–9.

53. Lowes MA, Suárez-Fariñas M, Krueger JG. Immunology of psoriasis. Annu Rev Immunol 2014;32:227–55.

54. Dorschner RA, Pestonjamasp VK, Tamakuwala S, Ohtake T, Rudisill J, Nizet V, *et al.* Cutaneous injury induces the release of cathelicidin antimicrobial peptides active against group A Streptococcus. J Invest Dermatol 2001;117:91–7.

55. Hu SC, Yu HS, Yen FL, Lin CL, Chen GS, Lan CC. Neutrophil extracellular trap formation is increased in psoriasis and induces human β-defensin-2 production in epidermal keratinocytes. Sci Rep 2016;6:31119.

56. Lowes MA, Chamian F, Abello MV, Fuentes-Duculan J, Lin SL, Nussbaum R, *et al.* Increase in TNF-alpha and inducible nitric oxide synthase-expressing dendritic cells in psoriasis and reduction with efalizumab (anti-CD11a). Proc Natl Acad Sci U S A 2005;102:19057–62.

57. Zaba LC, Cardinale I, Gilleaudeau P, Sullivan-Whalen M, Suárez-Fariñas M, Fuentes-Duculan J, *et al.* Amelioration of epidermal hyperplasia by TNF inhibition is associated with reduced Th17 responses. J Exp Med 2007;204:3183–94.

58. Lu M, Saeki K, Matsuzawa T, Okuno T, Kuga T, Sugimoto Y, *et al.* 12-Hydroxyheptadecatrienoic acid promotes epidermal wound healing by accelerating keratinocyte migration via the BLT2 receptor. J Exp Med 2014;211:1063–78.

59. Johnston A, Xing X, Wolterink L, Barnes DH, Yin Z, Reingold L, *et al.* IL-1 and IL-36 are dominant cytokines in generalized pustular psoriasis. J Allergy Clin Immunol 2017;140:109–20.

60. Guttman-Yassky E, Krueger JG. IL-17C: A Unique epithelial cytokine with potential for targeting across the spectrum of atopic dermatitis and psoriasis. J Invest Dermatol 2018;138:1467–9.

61. Papp KA, Merola JF, Gottlieb AB, Griffiths CE, Cross N, Peterson L, *et al.* Dual neutralization of both interleukin 17A and interleukin 17F with bevekizumab in patients with psoriasis: results from BE ABLE 1, a 12-week randomized, double-blinded, placebo-controlled phase 2b trial. J Am Acad Dermatol 2018;79:277–286.e10.

62. Krueger JG, Fretton S, Suárez-Fariñas M, Haslett PA, Phipps KM, Cameron GS, *et al.* IL-17A is essential for cell activation and inflammatory gene circuits in subjects with psoriasis. J Allergy Clin Immunol 2012;130:145–54.e9.

63. Liu Y, Lagowski JP, Gao S, Raymond JH, White CR, Kulesz-Martin MF. Regulation of the psoriatic chemokine CCL20 by E3 ligases Trim32 and Pias4 in keratinocytes. J Invest Dermatol 2010;130:1384–90.

64. Nograles KE, Zaba LC, Guttman-Yassky E, Fuentes-Duculan J, Suárez-Fariñas M, Cardinale I, *et al.* Th17 cytokines interleukin (IL)-17 and IL-22 modulate distinct inflammatory and keratinocyte-response pathways. Br J Dermatol 2008;159:1092–102.

65. Henry CM, Sullivan GP, Clancy DM, Afonina IS, Kulms D, Martin SJ. Neutrophil-derived proteases escalate inflammation through activation of IL-36 family cytokines. Cell Rep 2016;14:708–22.

66. Furue K, Ito T, Furue M. Differential efficacy of biologic treatments targeting the TNF-α/IL-23/IL-17 axis in psoriasis and psoriatic arthritis. Cytokine 2014;111:182–8.

67. Johansen C, Funding AT, Otkjaer K, Kragballe K, Jensen UB, Madsen M, *et al.* Protein expression of TNF-alpha in psoriatic skin is regulated at a post-transcriptional level by MAPK-activated protein kinase 2. J Immunol 2006;176:1431–8.

68. Lee E, Trepicchio WL, Oestreicher JL, Pittman D, Wang F, Chamian F, *et al.* Increased expression of interleukin 23 p19 and p40 in lesional skin of patients with psoriasis vulgaris. J Exp Med 2004;199:125–30.

69. Brunner PM, Koszik F, Reininger B, Kalb ML, Bauer W, Stingl G. Infliximab induces downregulation of the IL-12/IL-23 axis in 6-sulfo-LacNac (slan)+ dendritic cells and macrophages. J Allergy Clin Immunol 2013;132:1184–1193.e8.

70. Martin G, Guerrard S, Fortin MM, Rusu D, Soucy J, Poubelle PE, *et al.* Pathological crosstalk in vitro between T lymphocytes and keratinocytes in psoriasis: necessity of direct cell-to-cell contact. Lab Invest 2012;92:1056–70.

71. Schröder JM, Gregory H, Young J, Christophers E. Neutrophil-activating proteins in psoriasis. J Invest Dermatol 1992;98:241–7.

72. Bouwma DM, de Haan P, Willemze R, Stoof TJ. Human growth factor (huGRO), interleukin-8 (IL-8) and interferon-gamma-inducible protein (gamma-IP-10) gene expression in cultured normal human keratinocytes. Arch Dermatol Res 1994;286:471–5.

73. Carrier Y, Ma HL, Ramon HE, Napierata L, Small C, O'Toole M, *et al.* Inter-regulation of Th17 cytokines and the IL-36 cytokines in vitro and in vivo: implications in psoriasis pathogenesis. J Invest Dermatol 2011;131:2428–37.

74. Griffiths CE, Reich K, Lebwohl M, van de Kerkhof P, Paul C, Menter A, *et al.* UNCOVER-1 and UNCOVER-3 investigators. Comparison of ixekizumab with etanercept or placebo in moderate-to-severe psoriasis (UNCOVER-2 and UNCOVER-3): results from two phase 3 randomised trials. Lancet 2015;386:541–51.

75. Barker J, Hoffmann M, Wozel G, Ortonne JP, Zheng H, van Hoogstraten H, *et al.* Efficacy and safety of infliximab vs methotrexate in patients with moderate-to-severe plaque psoriasis: results of an open-label, active-controlled, randomized trial (RESTORE1). Br J Dermatol 2011;165:1109–17.

76. Blauvelt A, Papp KA, Griffiths CE, Randazzo B, Wasfi Y, Shen YK, *et al.* Efficacy and safety of guselkumab, an anti-interleukin-23 monoclonal antibody, compared with adalimumab for the continuous treatment of patients with moderate to severe psoriasis: results from the phase III, double-blinded, placebo- and active comparator-controlled VOYAGE 1 trial. J Am Acad Dermatol 2017;76:405–17.

77. Bettelli E, Carrier Y, Gao W, Korn T, Strom TB, Oukka M, *et al.* Reciprocal developmental pathways for the generation of pathogenic effector TH17 and regulatory T cells. Nature 2006;441:235–8.

78. Lebwohl M, Strober B, Menter A, Gordon K, Weglowska J, Puig L, *et al.* Phase 3 studies comparing Brodalumab with Ustekinumab in psoriasis. N Engl J Med 2015;373:1318–28.

79. Ohtsuki M, Morita A, Igarashi A, Imafuku S, Tada Y, Fujita H, *et al.* Secukinumab improves psoriasis symptoms in patients with inadequate response to cyclosporine A: A prospective study to evaluate direct switch. J Dermatol 2017;64:1105–11.

80. Hacker JL, Johnson-Huang LM, Chamian MF, Lee E, Pierce T, Leonardi CL, *et al.* Humanized anti-IFN-γ (HuZAF) in the treatment of psoriasis. J Allergy Clin Immunol 2015;135:553–6.

81. Papp KA, Blauvelt A, Bukhalo M, Gooderham M, Krueger JG, Lacour JP, *et al.* Risankizumab versus ustekinumab for moderate-to-severe plaque psoriasis. N Engl J Med 2017;376:1551–60.

82. Reich K, Papp KA, Blauvelt A, Tyring SK, Sinclair R, Ohtsuki T, *et al.* Tildrakizumab versus placebo or etanercept for chronic plaque psoriasis

(reSURFACE 1 and reSURFACE 2): results from two randomized controlled, phase 3 trials. Lancet 2017;390:276–88.

83. Piskin G, Sylva-Steenland RM, Bos JD, Teunissen MB. In vivo and in situ expression of IL-23 by keratinocytes in healthy skin and psoriasis lesions: enhanced expression in psoriatic skin. J Immunol 2006;176:1908–15.

84. Matsuzaki G, Umemura M. Interleukin-17 family cytokines in protective immunity against infections: role of hematopoietic cell-derived and non-hematopoietic cell-derived interleukin-17s. Microbiol Immunol 2018;62:1–13.

85. Brembilla NC, Senra L, Boehncke WH. The IL-17 family of cytokines in psoriasis: IL-17A and beyond. Front Immunol 2018;9:1682.

86. Akdis MK, Kido-Nakahara M, Fujita M, Nakahara T. Mutual up-regulation of endothelin-1 and IL-25 in atopic dermatitis. Allergy 2015;70:846–54.

87. Blauvelt A, Chiricozzi A. The immunologic role of IL-23 in psoriasis and psoriatic arthritis pathogenesis. Clin Rev Allergy Immunol 2018;55:379–90.

88. Johansen C, Usher PA, Kjellerup RB, Lundgaard D, Iversen L, Kragballe K. Characterization of the interleukin-17 isoforms and receptors in lesional psoriatic skin. Br J Dermatol 2009;160:319–24.

89. Johnston A, Fritz Y, Dawes SM, Diaconu D, Al-Attar PM, Guzman AM, *et al.* Keratinocyte overexpression of IL-17C promotes psoriasiform skin inflammation. J Immunol 2013;190:2252–62.

90. Martin DA, Towne JE, Kricorian G, Klekotka P, Gudjonsson JE, Krueger JG, *et al.* The emerging role of IL-17 in the pathogenesis of psoriasis: preclinical and clinical findings. J Invest Dermatol 2013;133:17–26.

91. Ramirez-Carrozzi V, Sambandam A, Luis E, Lin Z, Jeet S, Lesch J, *et al.* IL-17C regulates the innate immune function of epithelial cells in an autocrine manner. Nat Immunol 2011;12:1159–66.

92. Vandeghinste N, Klattig J, Jagerschmidt C, Lavrozas S, Marsais F, Haas JD, *et al.* Neutralization of IL-17C reduces skin inflammation in mouse models of psoriasis and atopic dermatitis. J Invest Dermatol 2018;138:1555–63.

93. Langley RG, Elewski BE, Lebwohl M, Reich K, Griffiths CE, Papp K, *et al.*; ERASURE Study Group, FIXTURE Study Group. Secukinumab in plaque psoriasis—results of two phase 3 trials. N Engl J Med 2014;371:326–38.

94. Gordon KB, Blauvelt A, Papp KA, Langley RG, Luger T, Ohtsuki M, *et al.*; UNCOVER-1 Study Group, UNCOVER-2 Study Group, UNCOVER-3 Study Group. Phase 3 trials of ixekizumab in moderate-to-severe plaque psoriasis. N Engl J Med 2016;375:345–56.

95. Chiricozzi A, Guttman-Yassky E, Suárez-Fariñas M, Nograles KE, Tian S, Cardinale I, *et al.* Integrative responses to IL-17 and TNF-α in human keratinocytes account for key inflammatory pathogenic circuits in psoriasis. J Invest Dermatol 2011;131:677–87.

96. Reich K, Papp KA, Matheson RT, Tu JH, Bissonnette R, Bourcier M, *et al.* Evidence that a neutrophil-keratinocyte crosstalk is an early target of IL-17A inhibition in psoriasis. Exp Dermatol 2015;24:529–35.

97. Yasunaka K, Yamagata A, Akeda T, Kondo M, Kakeda M, Hahe K, *et al.* Neutrophils are not the dominant interleukin-17 producer in psoriasis. J Dermatol 2017;44:e170–1.

98. Harper EG, Guo C, Rizzo H, Lillis JV, Kurtz SR, Skorchova I, *et al.* Th17 cytokines stimulate CCL20 expression in keratinocytes in vitro and in vivo: implications for psoriasis pathogenesis. J Invest Dermatol 2009;129:2175–83.

99. Ito K, Kaga M, Shibayama Y, Tatematsu S, Nakayama J, Imafuku S. Proactive treatment with calcipotriol reduces recurrence of plaque psoriasis. J Dermatol 2016;43:402–5. https://www.ncbi.nlm.nih.gov/entrez/query.fcgi?cmd=Retrieve&db=PubMed&dopt=Abstract https://doi.org/10.1111/1346-8138.13158

Conflict of interest. The authors certify that there is no conflict of interest with any financial organization regarding the material discussed in the manuscript.

Funding. This work was partly supported by grants from The Ministry of Health, Labour and Welfare, Japan (H27-Shokuhin-Shitei-017), and The Leading Advanced Projects for Medical Innovation, Japan (LEAP).

Article first published online: January 15, 2019 - Manuscript accepted: December 17, 2018 - Manuscript revised: December 6, 2018 - Manuscript received: September 13, 2018

This document is protected by international copyright laws. No additional reproduction is authorized. It is permitted for personal use to download and save only one file and print only one copy of this Article. It is not permitted to make additional copies (either repeatedly or systematically, either printed or electronic) of the Article for any purpose. It is not permitted to distribute the electronic copy of the article through online internet and/or intranet file sharing systems, electronic mailing or any other means which may allow access to the Article. The use of all or any part of the Article for any Commercial Use is not permitted. The creation of derivative works from the Article is not permitted. The creation of reprints by personal or commercial use is not permitted. It is not permitted to remove, cover, overlay, obscure, block, or change any copyright notices or terms of use which the Publisher may post on the Article. It is not permitted to frame or use framing techniques to enclose any trademark, logo, or other proprietary information of the Publisher.

Journal of Dermatological Science 97 (2020) 125–134

Contents lists available at ScienceDirect

Journal of Dermatological Science

journal homepage: www.jdsjournal.com

Original Article

Regulation of skin fibrosis by RALDH1-producing dermal dendritic cells via retinoic acid-mediated regulatory T cell induction: A role in scleroderma

Shunsuke Miura[a], Yoshihide Asano[a,*], Ryosuke Saigusa[a], Takashi Yamashita[a], Takashi Taniguchi[a], Takehiro Takahashi[a], Yohei Ichimura[a], Tetsuo Toyama[a], Ayumi Yoshizaki[a], Shinichi Sato[a], Takafumi Kadono[a,b,**]

[a] Department of Dermatology, University of Tokyo Graduate School of Medicine, Tokyo, Japan
[b] Department of Dermatology, St. Marianna University School of Medicine, Kawasaki, Japan

ARTICLE INFO

Article history:
Received 7 May 2019
Revised in revised form 8 January 2020
Accepted 8 January 2020

Keywords:
Dendritic cell
Treg cells
Systemic sclerosis
Skin fibrosis
Retinoic acid

ABSTRACT

Background: Skin fibrosis of systemic sclerosis (SSc) is believed to be driven by complex processes including injury, vascular abnormalities, but the underlying immune response remains enigmatic. In particular, the role of dermal dendritic cells (DCs) is totally unknown.

Objective: We investigated the impact of CD103 loss on bleomycin-induced skin fibrosis because CD103 is a critical molecule determining DC phenotypes.

Methods: Bleomycin-induced skin fibrosis was generated with Itgae$^{-/-}$ mice. The alterations of tissue fibrosis and related inflammation were investigated by histologic examination, hydroxyproline assay, quantitative reverse transcription PCR and flow cytometry. SSc skin samples were evaluated by immunofluorescence.

Results: CD103 loss decreased bleomycin-induced dermal thickness and collagen contents, along with TGF-β1 and CTGF suppression. Treg proportion was increased, while Th1/Th2/Th17 cell proportions were decreased in the skin of bleomycin-treated Itgae$^{-/-}$ mice. Bleomycin injection enhanced CD11b$^+$CD103$^+$ DC progenitors in wild-type mice, which was further augmented in Itgae$^{-/-}$ mice. Importantly, RALDH1/ALDH1A1, enzyme oxidizing retinaldehyde to retinoic acid, an inducer of Tregs, was preferentially expressed by CD11b$^+$CD103$^+$ DCs and its expression levels were elevated in bleomycin-injected skin lesions, to a greater extent in Itgae$^{-/-}$ mice than in wild-type mice. Importantly, the number of RALDH1-positive DCs was decreased in the lesional skin of SSc patients and tended to inversely correlate with skin fibrosis severity.

Conclusion: This study identified a critical role of dermal DCs as a regulator of Treg development through RALDH1 in bleomycin-treated mice and possibly in human SSc. This finding sheds new light on dermal DCs as a new therapeutic target of SSc.

© 2020 Japanese Society for Investigative Dermatology. Published by Elsevier B.V. All rights reserved.

1. Introduction

Systemic sclerosis (SSc) is a multisystem autoimmune and vascular disease resulting in multiple organ fibrosis [1,2], in which skin fibrosis is caused by the combination of dermal fibroblast activation [3–6], Th2/Th17-skewed immune polarization [7,8], M2 macrophage differentiation [9], aberrant B cell activation [10,11], increased infiltration of plasmacytoid dendritic cells [12], vascular functional and structural abnormalities [13–16] and epithelial cell activation [17–20]. In particular, immune cells seem to play a central role because immunosuppressants and/or corticosteroids are mostly effective for skin fibrosis. Therefore, the characterization of skin fibrosis-related immune responses would be helpful to further understand SSc pathogenesis.

Under a homeostatic condition, dermal immune cells predominantly consist of dendritic cells (DCs) and macrophages. Dermal DCs are classified into several subsets based on their origins and cell surface markers. For instance, conventional DCs (cDCs)

* Corresponding author at: Department of Dermatology, University of Tokyo Graduate School of Medicine, 7-3-1 Hongo, Bunkyo-ku, Tokyo 113-8655, Japan.
** Corresponding author at: Department of Dermatology, St. Marianna University School of Medicine, 2-16-1 Sugao, Miyamae-ku, Kawasaki-shi, Kanagawa, 216-8511, Japan.
E-mail addresses: yasano-tky@umin.ac.jp (Y. Asano), tkadono-tky@umin.ac.jp (T. Kadono).

https://doi.org/10.1016/j.jdermsci.2020.01.002
0923-1811/© 2020 Japanese Society for Investigative Dermatology. Published by Elsevier B.V. All rights reserved.

develop from blood-derived pre-cDC precursors, while monocyte-derived DCs originate from blood Ly6C^{hi} monocytes. cDCs are further stratified into three subsets, such as XCR1^{+} cDCs, CD11b^{+} cDCs and XCR1^{-} CD11b^{-} cDCs [21]. Since cDCs uptake internal and external antigens, migrate to lymph nodes, and present antigens to naïve T cells, cDCs serve as a bridge between innate and adaptive immunity. Under a physiological condition homeostatic maturation continuously occurs in a part of cDCs, which transport cutaneous self antigen to the T cell zones of draining lymph nodes and activate abortive program of autoreactive T cells. In contrast, when exposed to external antigen, cDCs undergo terminal differentiation, migrate to draining lymph nodes, and promote the clonal expansion of naïve antigen-specific T cells and the acquisition of T cell effector functions. The pathological role of dermal DCs has been well studied in sterile inflammation, including contact hypersensitivity (CHS) and psoriasis-like skin inflammation [22,23]. However, the role of dermal DCs in tissue fibrosis remains unknown.

Retinoic acid (RA) is a lipophilic molecule regulating gene expression via binding to nuclear receptors [24], mediating peripheral tolerance through the generation of inducible Foxp3^{+} regulatory T cells (iTregs) from conventional naïve CD4^{+} T cells. RA generation from vitamin A is a sequential step tightly regulated by enzymes, such as alcohol dehydrogenase, retinol dehydrogenase and aldehyde dehydrogenase (RALDH). Although the former two enzymes are widely expressed in various cell types, RALDH is produced exclusively by certain cell types, including DCs. Thus, RA is preferentially produced by DCs and promotes iTreg development which is basically induced by subimmunogenic dose of antigen, low costimulation and high levels of TGF-β. In particular, CD11b^{+}CD103^{+} intestinal DCs and CD11b^{+}CD103^{-} dermal DCs express aldehyde dehydrogenase 2 (RALDH2/ALDH1A2) and promote iTreg development [25–28]. Thus, RA-dependent regulation of iTregs by DCs has drawn attention in peripheral tolerance, but its role in fibrotic diseases remains unexplored.

Although impaired immune system has been well studied in SSc, especially focusing on CD4^{+} T cells [29,30], M2 macrophage [9] and B cells [10,31,32], the role of dermal DCs has been poorly documented. Therefore, we here investigated the role of DCs in SSc skin fibrosis. Given that CD103 is a key marker of RA-producing DCs, we examined bleomycin (BLM)-induced dermal fibrosis in *Cd103*$^{-/-}$ mice. We also assessed the potential contribution of RA-producing DCs to SSc skin fibrosis.

2. Materials and methods

2.1. Ethics statement

This study was approved by the ethical committee and the committee on animal experimentation of The University of Tokyo Graduate School of Medicine and performed according to the Declaration of Helsinki. Written informed consent was obtained from all the participants.

2.2. A BLM-induced murine model of SSc

Wild-type (WT) C57BL/6 and *Cd103*$^{-/-}$ mice were purchased from Japan SLC (Hamamatsu, Japan) and Jackson Laboratory (Bar Harbor, ME, USA), respectively. BLM (Nippon Kayaku, Tokyo, Japan) was dissolved in phosphate buffered saline (PBS) (1 mg/ml) and sterilized by filtration. BLM (200 μg) or PBS was injected subcutaneously into a single location on the shaved backs of mice (female, 6–8 weeks old) with a 27 gauge needle. The injection was conducted consecutively for 1 week or 4 weeks dependent on the purpose of experiments. For gene silencing of *Raldh2*, the mixtures of *Raldh2* siRNA (Santa Cruz Biotechnology, Santa Cruz, CA, USA) or scrambled non-silencing RNA with atelocollagen (Koken, Tokyo, Japan) in a 150 μl volume were administered biweekly subcutaneously into BLM-challenged skin areas before BLM injection until skin samples were taken. Histological assessment, immunohistochemistry, immunofluorescence, hydroxyproline assay, quantitative reverse transcription PCR, flow cytometry and analysis of RALDH activity are described in Supplementary Materials and Methods.

2.3. Statistical analysis

Statistical analysis was carried out using GraphPad Prism. Data are presented as the mean ± SEM. The Mann–Whitney U test was used for two-group comparison and for 4-group multiple comparison with Bonferroni correction. The Kruskal–Wallis test followed by the Dunn's multiple comparison test was used for 3-group multiple comparison. Statistical significance was defined as a P value of <0.05 except for 4-group multiple comparison with Bonferroni correction. In 4-group multiple comparison with Bonferroni correction, P < 0.0083 means a statistical significance and (0.0083 < P < 0.0167) represents a trend toward significance.

3. Results

3.1. CD103 loss attenuates BLM-induced dermal fibrosis

We initially assessed the impact of CD103 loss on BLM-induced dermal fibrosis after confirming no apparent histologic abnormality in the skin of *Cd103*$^{-/-}$ mice under a physiological condition (data not shown). Four-week BLM injection tended to induce less dermal thickness in *Cd103*$^{-/-}$ mice than in WT mice, while dermal thickness was comparable after PBS injection (Fig. 1A). Collagen contents measured by hydroxyproline assay and mRNA levels of *Col1a1*, *Col1a2*, *Col3a1* and *Col5a1* were also decreased in BLM-injected skin of *Cd103*$^{-/-}$ mice compared with that of WT mice (Fig. 1B and C). Furthermore, the expression of fibrosis-related growth factors, such as connective tissue growth factor (CTGF) and transforming growth factor (TGF) β1, was significantly reduced in BLM-injected skin of *Cd103*$^{-/-}$ mice at mRNA and/or protein levels (Fig. 1D and E). These results indicate that the loss of cells expressing CD103 in the absence of the specific subset in the *Cd103*$^{-/-}$ mice plays a vital role in BLM-dependent skin fibrosis.

3.2. CD103 loss suppresses BLM-induced inflammation in the lesional skin

We next assessed the inflammatory aspect in *Cd103*$^{-/-}$ mice treated with BLM for a week when inflammation reaches a peak [33]. Histological analysis failed to detect the difference in the numbers of infiltrating T cells, B cells, macrophages, mast cells and DCs between BLM-treated *Cd103*$^{-/-}$ and WT mice (Fig. 2A). The mRNA expression profiles of several key pro-inflammatory cytokines and chemokines in the lesional skin displayed decreased IL-4 expression and increased IL-10 expression in BLM-treated *Cd103*$^{-/-}$ mice compared with BLM-treated WT mice. On the other hand, the expression levels of IFN-γ, IL-17A and IL-6 were comparable (Fig. 2B). These results indicate that CD103 loss attenuates BLM-induced dermal fibrosis in association with an increase of IL-10.

3.3. CD103 loss increases the proportion of Tregs

Since IL-10 was up-regulated in the lesional skin of BLM-treated *Cd103*$^{-/-}$ mice, we examined Th1/Th2 and Th17/Treg lineage alterations by flow cytometry after 1-week BLM injection. In skin-draining lymph nodes, IFN-γ-, IL-4- and IL-17A-producing CD4^{+} T

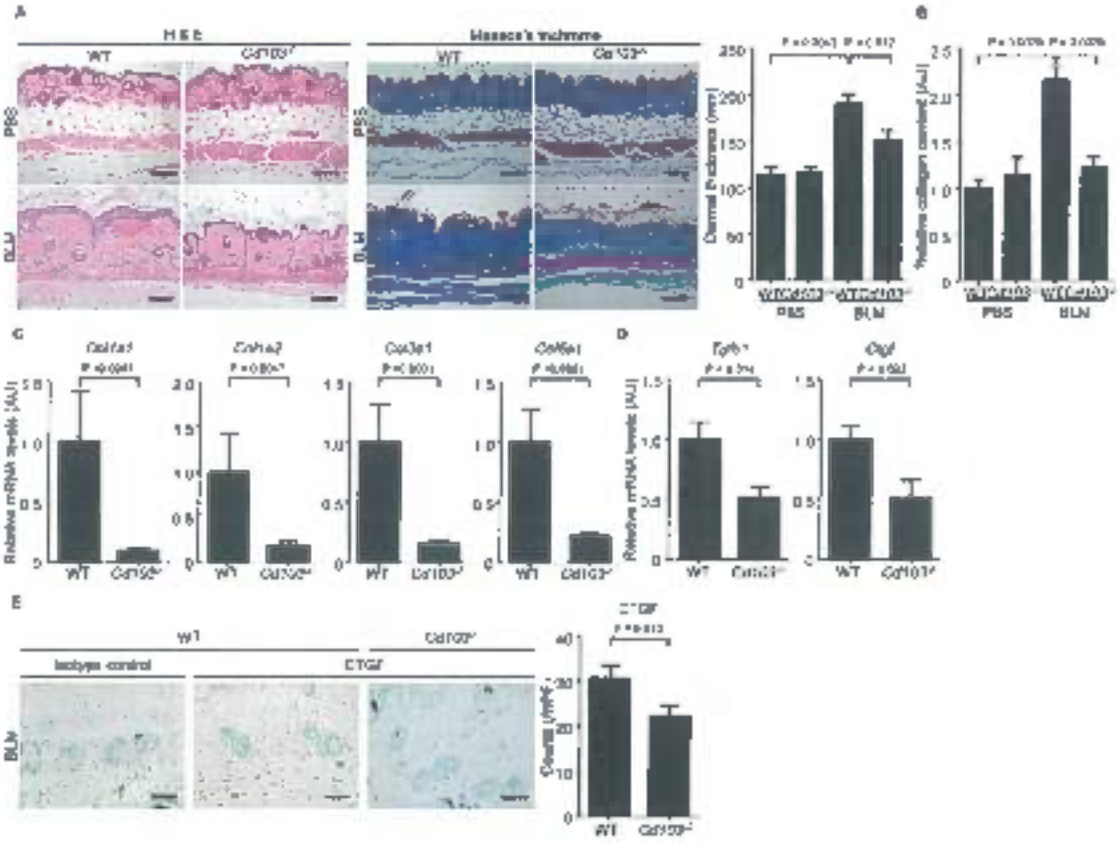

Fig. 1. CD103 loss aggravates BLM-induced dermal fibrosis.
Wild-type (WT) and Cd103⁻/⁻ mice were injected with bleomycin (BLM) in phosphate-buffered saline (PBS) for 4 weeks. A. Skin specimens were subjected to hematoxylin and eosin staining (left panels) or to Masson's trichrome staining (right panels). Dermal thickness in each group of mice was evaluated (n = 5–6 per group; graph). B. Collagen content in each group of mice was measured by hydroxyproline assay (n = 5 per group). C, D. mRNA expression of fibrosis-related molecules (C) and growth factors (D) was assessed in the lesional skin by qRT-PCR (n = 5–10 per group). E. The expression of CTGF was assessed at protein levels by immunohistochemistry. The numbers of CTGF-positive cells were evaluated by counting positive cells in a ×400 high-power field (HPF) (n = 5–7 per group; graph). Each graph indicates mean ± SEM of the indicated parameters. Scale bars are 100 μm for A and 50 μm for E. AU, arbitrary unit.

cell proportions were not altered, while Foxp3⁺CD25⁺CD4⁺ T cell proportion was increased in BLM-treated Cd103⁻/⁻ mice compared with BLM-treated WT mice (Fig. 2C). In dermis, of note, IFN-γ-, IL-4- and IL-17A-producing CD4⁺ T cell proportions were decreased in BLM-treated Cd103⁻/⁻ mice compared with BLM-treated WT mice, while Foxp3⁺CD25⁺CD4⁺ T cell proportion was increased (Fig. 2D). Since CD103 deletion reduces Treg function in some murine disease models [34,35], we further assessed Foxp3 expression levels in Foxp3⁺CD25⁺CD4⁺ T cells because Foxp3 expression correlates with the regulatory activity of Tregs. When evaluated by mean fluorescence intensity, both of skin- and lymph node-derived Tregs showed Foxp3 expression levels comparable between BLM-treated Cd103⁻/⁻ and WT mice (Fig. 2E). These results indicate that CD103 loss increases the proportion of Tregs in the skin of BLM-treated mice without affecting Foxp3 expression. Given that Foxp3 expression is essential but not sufficient to determine the activity of Treg function [36], this result does not draw any definitive conclusion regarding the effect of CD103 loss on Treg function in BLM-treated mice.

3.4. CD11b⁺CD103⁻ DC proportion is remarkably increased in BLM-treated Cd103⁻/⁻ mice compared with BLM-treated WT mice

In general, DCs regulate iTreg development from conventional, naïve CD4⁺ T cells in the secondary lymphoid organs, importantly, CD11b⁺CD103⁻ DCs promote iTreg differentiation through RA production by RALDH2 in the skin [28], while the same effect is owned by CD103⁺ DCs in intestinal mucosa [25], suggesting that DC subsets involved in iTreg induction are different in the context-dependent manner. To evaluate the contribution of DCs to Treg increase in the skin of BLM-treated Cd103⁻/⁻ mice, we looked at the proportions of CD11b⁺CD103⁻, CD11b⁻CD103⁻ and CD11b⁻CD103⁺ DCs in the dermis of mice treated with PBS or BLM for 1 week (Fig. 3A). BLM injection significantly decreased CD11b⁻CD103⁺ DC proportion in WT mice, whereas the proportions of CD11b⁻CD103⁻ DC and CD11b⁺CD103⁻ DC were unchanged. Under CD103 loss, CD11b⁺CD103⁻ DC proportion was remarkably lowered in dermis by BLM injection, while CD11b⁻CD103⁻ DC proportion was significantly enhanced. To evaluate the impact of CD103 loss on CD11b⁻CD103⁺ DCs in dermis, we employed XCR1 as an alternative marker of CD103 because XCR1⁺ DCs are equivalent to CD11b⁻CD103⁺ DCs in dermis [21,37]. BLM injection did not affect the number of XCR1⁺ DCs and XCR1⁻ DCs in dermis of Cd103⁻/⁻ mice (Fig. 3B). These results suggest that CD103 loss affect the proportions of CD11b⁺CD103⁻ DCs and CD11b⁻CD103⁻ DCs in dermis.

We next examined which DC subset migrates from dermis to skin-draining lymph nodes by FITC-induced cutaneous DC migration. When treated with PBS, migrated DCs were mostly CD11b-positive in both Cd103⁻/⁻ and WT mice. After 1-week BLM

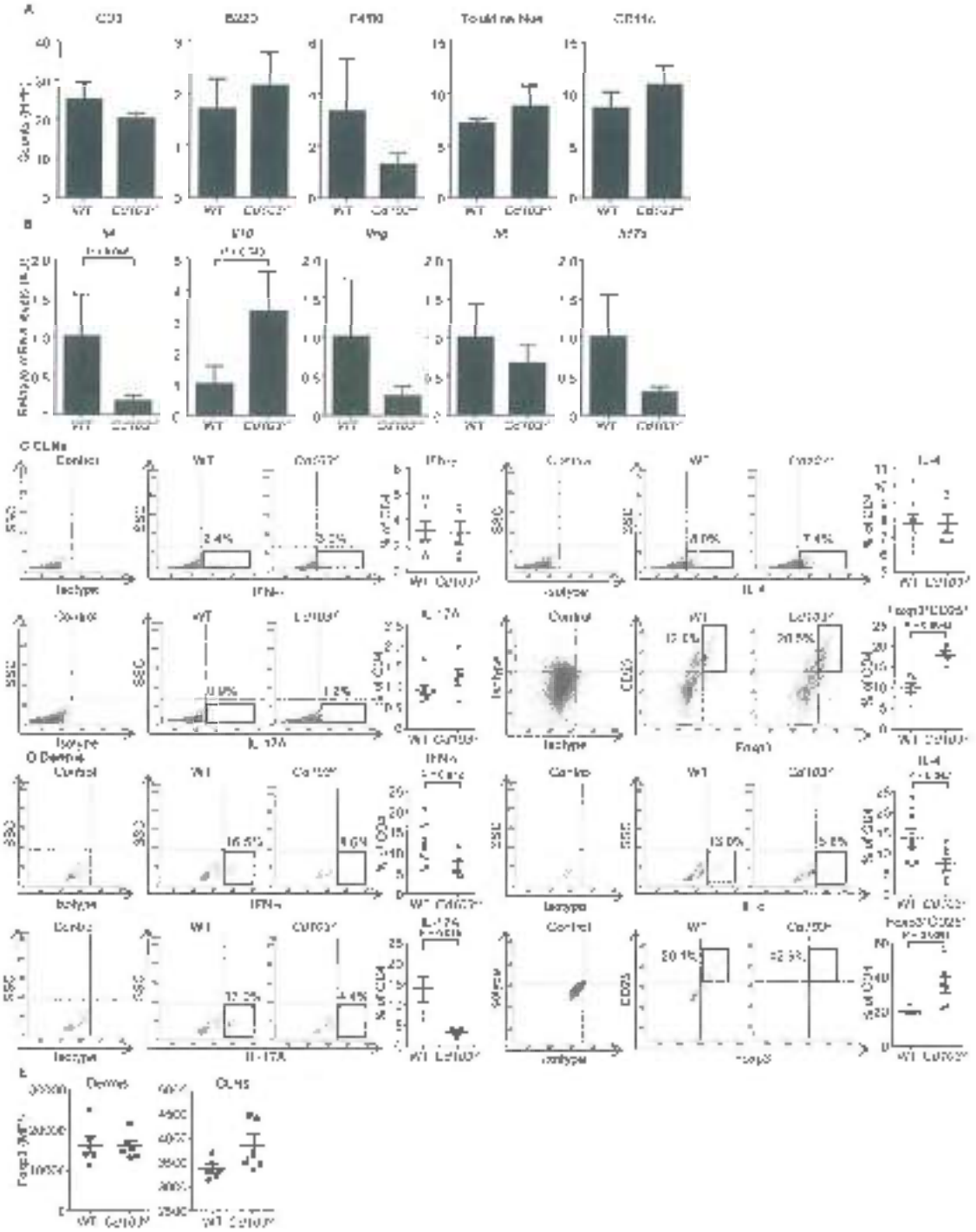

Fig. 2. CD103 loss suppresses IMQ-induced inflammation in the lesional skin via Treg induction.
Wild-type (WT) and Cd103 −/− mice were treated with Imiquimod (IMQ) Cream. A. The numbers of CD3+, B220+, F4/80+ and CD11c+ positive cells and toluidine blue-stained cells in the dermal skin were evaluated by counting positively stained cells (×400 high-power field, HPF; n = 5–10 per group). B, C, D, E, F, G, H, I, J, K, L, M, N, O, P, Q, R, S, T, U, V, W, X, Y, Z, AA, AB, AC, AD, AE, AF, AG, AH, AI, AJ, AK, AL, AM, AN, AO, AP, AQ, AR, AS, AT, AU, AV, AW, AX, AY, AZ, BA, BB, BC, BD, BE, BF, BG, BH, BI, BJ, BK, BL, BM, BN, BO, BP, BQ, BR, BS, BT, BU, BV, BW, BX, BY, BZ, CA, CB, CC, CD, CE, CF, CG, CH, CI, CJ, CK, CL, CM, CN, CO, CP, CQ, CR, CS, CT, CU, CV, CW, CX, CY, CZ, DA, DB, DC, DD, DE, DF, DG, DH, DI, DJ, DK, DL, DM, DN, DO, DP, DQ, DR, DS, DT, DU, DV, DW, DX, DY, DZ, EA, EB, EC, ED, EE, EF, EG, EH, EI, EJ, EK, EL, EM, EN, EO, EP, EQ, ER, ES, ET, EU, EV, EW, EX, EY, EZ, FA, FB, FC, FD, FE, FF, FG, FH, FI, FJ, FK, FL, FM, FN, FO, FP, FQ, FR, FS, FT, FU, FV, FW, FX, FY, FZ, GA, GB, GC, GD, GE, GF, GG, GH, GI, GJ, GK, GL, GM, GN, GO, GP, GQ, GR, GS, GT, GU, GV, GW, GX, GY, GZ, HA, HB, HC, HD, HE, HF, HG, HH, HI, HJ, HK, HL, HM, HN, HO, HP, HQ, HR, HS, HT, HU, HV, HW, HX, HY, HZ, IA, IB, IC, ID, IE, IF, IG, IH, II, IJ, IK, IL, IM, IN, IO, IP, IQ, IR, IS, IT, IU, IV, IW, IX, IY, IZ, JA, JB, JC, JD, JE, JF, JG, JH, JI, JJ, JK, JL, JM, JN, JO, JP, JQ, JR, JS, JT, JU, JV, JW, JX, JY, JZ, KA, KB, KC, KD, KE, KF, KG, KH, KI, KJ, KK, KL, KM, KN, KO, KP, KQ, KR, KS, KT, KU, KV, KW, KX, KY, KZ, LA, LB, LC, LD, LE, LF, LG, LH, LI, LJ, LK, LL, LM, LN, LO, LP, LQ, LR, LS, LT, LU, LV, LW, LX, LY, LZ, MA, MB, MC, MD, ME, MF, MG, MH, MI, MJ, MK, ML, MM, MN, MO, MP, MQ, MR, MS, MT, MU, MV, MW, MX, MY, MZ, NA, NB, NC, ND, NE, NF, NG, NH, NI, NJ, NK, NL, NM, NN, NO, NP, NQ, NR, NS, NT, NU, NV, NW, NX, NY, NZ, OA, OB, OC, OD, OE, OF, OG, OH, OI, OJ, OK, OL, OM, ON, OO, OP, OQ, OR, OS, OT, OU, OV, OW, OX, OY, OZ, PA, PB, PC, PD, PE, PF, PG, PH, PI, PJ, PK, PL, PM, PN, PO, PP, PQ, PR, PS, PT, PU, PV, PW, PX, PY, PZ, QA, QB, QC, QD, QE, QF, QG, QH, QI, QJ, QK, QL, QM, QN, QO, QP, QQ, QR, QS, QT, QU, QV, QW, QX, QY, QZ, RA, RB, RC, RD, RE, RF, RG, RH, RI, RJ, RK, RL, RM, RN, RO, RP, RQ, RR, RS, RT, RU, RV, RW, RX, RY, RZ, SA, SB, SC, SD, SE, SF, SG, SH, SI, SJ, SK, SL, SM, SN, SO, SP, SQ, SR, SS, ST, SU, SV, SW, SX, SY, SZ, TA, TB, TC, TD, TE, TF, TG, TH, TI, TJ, TK, TL, TM, TN, TO, TP, TQ, TR, TS, TT, TU, TV, TW, TX, TY, TZ, UA, UB, UC, UD, UE, UF, UG, UH, UI, UJ, UK, UL, UM, UN, UO, UP, UQ, UR, US, UT, UU, UV, UW, UX, UY, UZ, VA, VB, VC, VD, VE, VF, VG, VH, VI, VJ, VK, VL, VM, VN, VO, VP, VQ, VR, VS, VT, VU, VV, VW, VX, VY, VZ, WA, WB, WC, WD, WE, WF, WG, WH, WI, WJ, WK, WL, WM, WN, WO, WP, WQ, WR, WS, WT, WU, WV, WW, WX, WY, WZ, XA, XB, XC, XD, XE, XF, XG, XH, XI, XJ, XK, XL, XM, XN, XO, XP, XQ, XR, XS, XT, XU, XV, XW, XX, XY, XZ, YA, YB, YC, YD, YE, YF, YG, YH, YI, YJ, YK, YL, YM, YN, YO, YP, YQ, YR, YS, YT, YU, YV, YW, YX, YY, YZ, ZA, ZB, ZC, ZD, ZE, ZF, ZG, ZH, ZI, ZJ, ZK, ZL, ZM, ZN, ZO, ZP, ZQ, ZR, ZS, ZT, ZU, ZV, ZW, ZX, ZY, ZZ

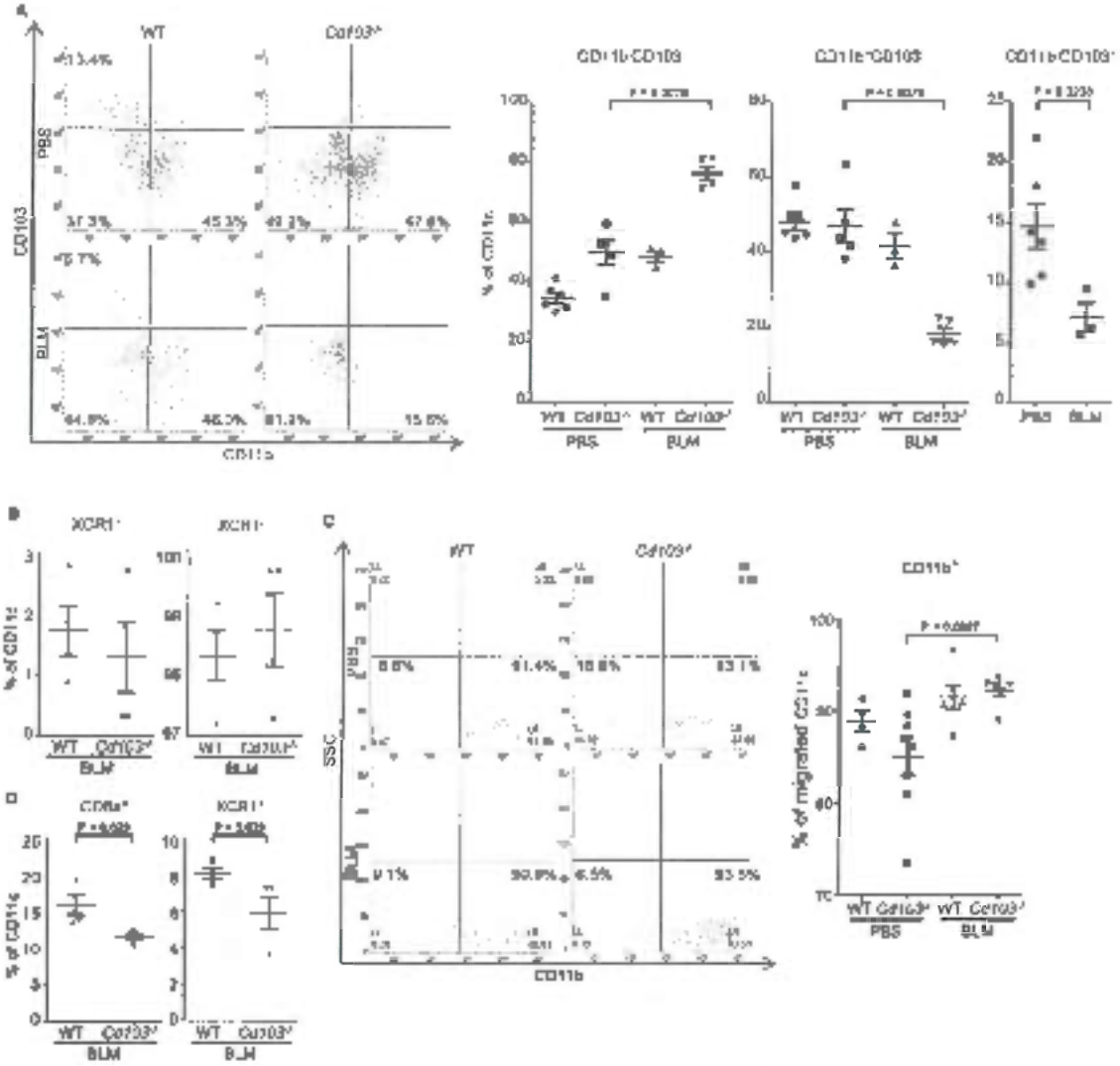

Fig. 3. CD11b CD103 DC proportion is remarkably increased in BLM-treated Cd103 mice compared with WT mice.
Wild type (WT) and Cd103 mice were treated with strumycin (BLM) or phosphate buffered saline (PBS) for a week. A. Representative flow cytometry plots of CD11b and CD103 staining in CD11c cells from skin dermis are shown. The percentages of CD11b+CD103−, CD11b+CD103+ and CD11b−CD103+ cells in CD11c+ cells in WT and Cd103 mice are summarized in graphs. B. The percentages of XCR1+ and XCR1− cells in CD11c+ cells in dermis are shown in graphs. C. Representative flow cytometry plots of CD11b staining in CD11c+CD11b+ cells from skin draining lymph nodes are shown. The percentage of CD11b+ cells in migrated CD11c+ cells are summarized in graph. D. The percentages of CD8α+ and XCR1+ in CD11b+ draining lymph nodes are shown in graphs. Flow cytometry profiles are representative of 3–6 individual animals from at least 2 separate experiments. Bars show the mean ± SEM.

injection. The proportion of CD11b+ cells in migrated DCs was significantly increased in Cd103 mice, while it changed in WT mice (Fig. 3C). Since XCR1+ DCs and CD8α+ DCs are equivalent to CD11b−CD103+ DCs in secondary lymphoid tissues [38,39], we assessed the proportions of XCR1+ or CD8α+ DCs in skin-draining lymph nodes. Relevant to the increased migration of CD11b+ DCs in BLM-treated Cd103 mice, the proportions of XCR1+ DCs and CD8α+ DCs were significantly lower in BLM-treated Cd103 mice than in BLM-treated WT mice (Fig. 3D).

Taken together, these results suggest that CD103 is related to the retention of CD11b+ DCs in dermis, contributing to the increased CD11b+ DC proportion in dermis of BLM-treated Cd103 mice. Since XCR1+ DC proportion was unaffected in dermis by BLM injection, CD11b+ CD103− DC proportion was consequently increased in dermis of BLM-treated Cd103 mice. Given that BLM-treated Cd103 mice showed less dermal fibrosis associated with the increased proportion of Tregs and CD11b+ CD103− DCs in dermis, CD11b+ CD103− DCs may contribute to the attenuation of skin fibrosis by increasing Treg proportion, possibly due to iTreg induction.

3.5. CD11b+ CD103− DCs produce aldehyde dehydrogenase 1 (RALDH1/ALDH1A1) in the skin of BLM-treated mice

To further explore the mechanism by which Tregs are increased in the skin of BLM-treated Cd103 mice, we focused on RALDH because DCs regulate iTreg development by producing RALDH [42]. We investigated the expression of three members of the RALDH family, namely, RALDH1, RALDH2 and aldehyde dehydrogenase 3 (RALDH3/ALDH1A3), in BLM-injected skin. As shown in Fig. 4A, Raldh2 mRNA expression was significantly suppressed by BLM injection in Cd103 mice, while not in WT mice (P = 0.032). On

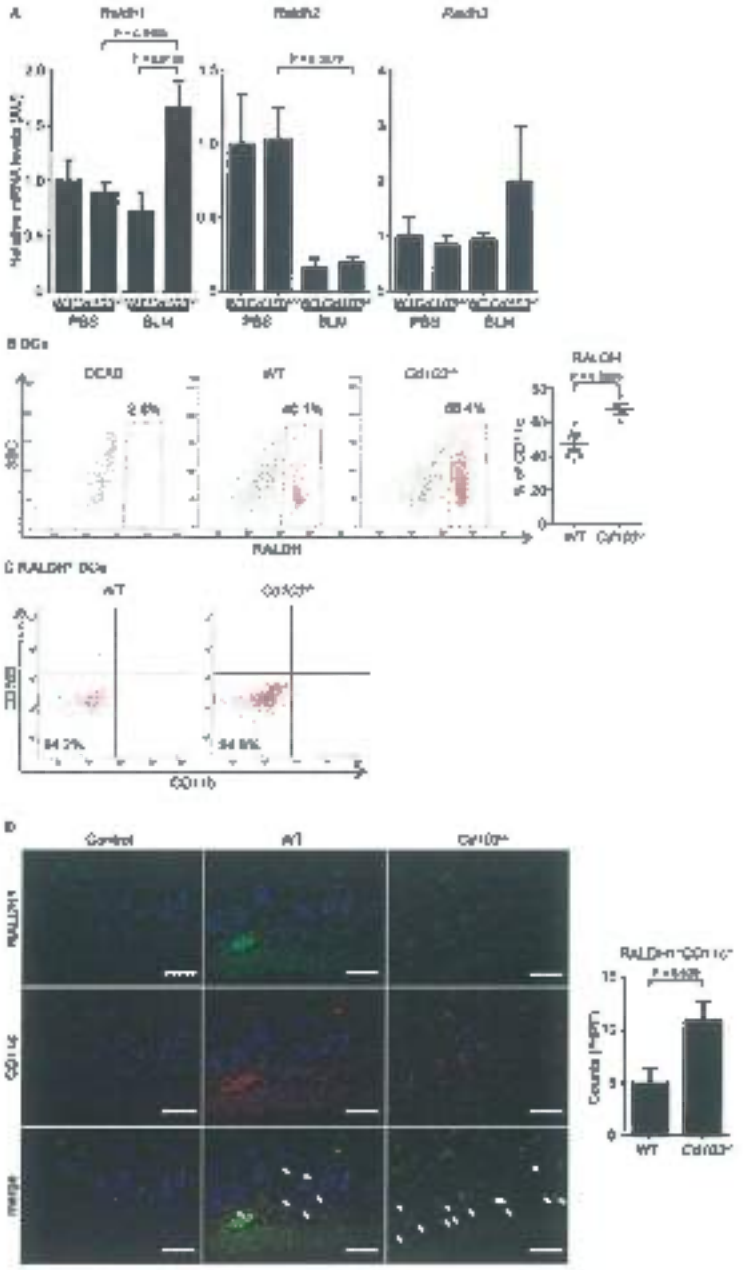

Fig. 4. CD11b$^+$ CD103$^-$ DCs produce RALDH$^+$ in the skin of BLM-treated mice.
Wild-type (WT) and Cd103$^{-/-}$ mice were injected with bleomycin (BLM) or phosphate buffered saline (PBS) for 2 weeks. A. mRNA levels of Raldh1, Raldh2 and Raldh3 in the lesional skin were assessed by qRT-PCR (n = 5 per group). B. Representative flow cytometry plots of RALDH staining in CD11c$^+$ cells from the dermis of BLM-treated WT and Cd103$^{-/-}$ mice are shown (left panel). The cells in the presence of the RALDH substrate dimethylaminobenzaldehyde, which was done simultaneously with the positive staining, was shown as control. The expressions of CD11c$^+$ cells positive for RALDH are summarized in a right graph (n = 4–6 per group). C. Representative flow cytometry plots of CD103 and CD11b staining in RALDH-producing CD11c$^+$ cells from the dermis of BLM-treated WT and Cd103$^{-/-}$ mice are shown (n = 4–6 per group). D. Representative immunofluorescence images of RALDH1/CD11c double staining in skin samples of BLM-treated WT and Cd103$^{-/-}$ mice are displayed. The negative control staining was done simultaneously with the positive staining. Arrows indicate double positive cells. The number of double positive cells was quantified by counting positive cells in a 100 high-power field (HPF) (n = 7 per group, right graph). Each graph indicates mean ± SEM of the indicated parameters. Scale bars are 100 μm. AU, arbitrary unit.

the other hand, *Raldh1* mRNA expression tended to be increased by BLM injection in Cd103$^{-/-}$ mice, while not changed in WT mice. *Raldh2* mRNA expression was not altered by BLM injection in both WT and Cd103$^{-/-}$ mice. These results suggest that RALDH1 is involved in Treg increase possibly through iTreg induction in BLM-injected skin of Cd103$^{-/-}$ mice. Since CD11b$^+$CD103$^-$ DCs were increased in BLM-injected skin of Cd103$^{-/-}$ mice, it was assumed that CD11b$^+$CD103$^-$ DCs are the main source of RALDH1. To address this issue, we evaluated RALDH activity by flow cytometry, in which we can evaluate the sum activities of RALDH1, 2 and 3

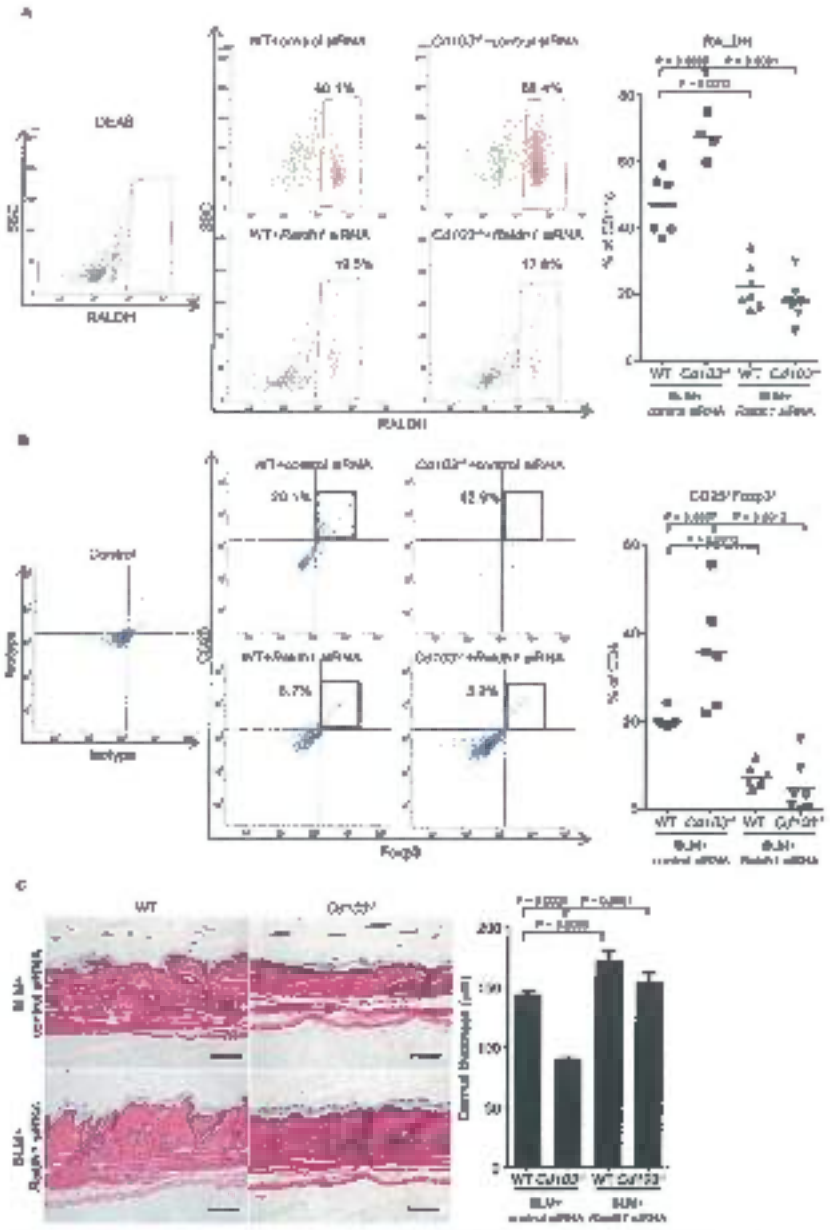

Fig. 5. Raldh1 gene silencing enhances skin fibrosis by preventing the induction of RALDH1 activity and Tregs in BLM-treated Cd103$^{+/-}$ mice.
Wild-type (WT) and Cd103$^{+/-}$ mice were injected with control or Raldh1 siRNA, followed by 3-week and 4-week bleomycin (BLM) challenge. A, B. Representative flow cytometry plots of RALDH staining in CD11c$^+$ cells (A) and Foxp3 and CD25 staining in CD4$^+$ cells (B) from the dermis of BLM-treated WT and Cd103$^{+/-}$ mice treated with control or Raldh1 siRNA are compared (left graphs). The results in the presence of the RALDH inhibitor diethylamino-benzaldehyde (A) and the results of isotype control staining (B) (both of which were done simultaneously with the positive staining) were shown as controls. The percentages of CD11c$^+$ cells positive for RALDH and CD4$^+$ cells positive for CD25$^+$ and Foxp3$^+$ are summarized in right graphs, respectively (n = 4–7 per group). C. After 4-week BLM injection, skin sections were stained with hematoxylin and eosin. Dermal thickness was measured (n = 4–7 per group; right graph). Each graph indicates mean ± SEM of the indicated parameters. Scale bars are 100 μm.

activities. The results showed that DCs with RALDH activity were increased in dermis of BLM-treated Cd103$^{+/-}$ mice compared with BLM-treated WT mice (Fig. 4B), and that more than 90 % of DCs with RALDH activity were CD11c$^+$CD103$^-$ DCs in both statuses (Fig. 4C). Furthermore, an immunohistochemistry with a specific antibody for RALDH1, RALDH1-expressing DCs were increased in BLM injected skin of Cd103$^{+/-}$ mice compared with WT mice (Fig. 4D). These results indicate that CD11b$^+$CD103$^-$ DCs express RALDH1 and subsequently induce Tregs possibly through iTreg development in BLM injected skin.

3.6. Raldh1 gene silencing enhances skin fibrosis by preventing the induction of RALDH1 activity and Tregs in BLM-treated Cd103$^{+/-}$ mice

There are some cell types expressing CD103 other than dermal DCs, including Tregs, CD8$^+$ epithelial T cells, and dendritic epidermal T cells [43]. To further confirm if dermal fibrosis reduction in BLM-treated Cd103$^{+/-}$ mice is primarily owing to dermal DCs, we assessed the effect of Raldh1 siRNA on Tregs in BLM-treated skin of Cd103$^{+/-}$ mice. In response to Raldh1 siRNA, RALDH activity was alleviated significantly in BLM-treated

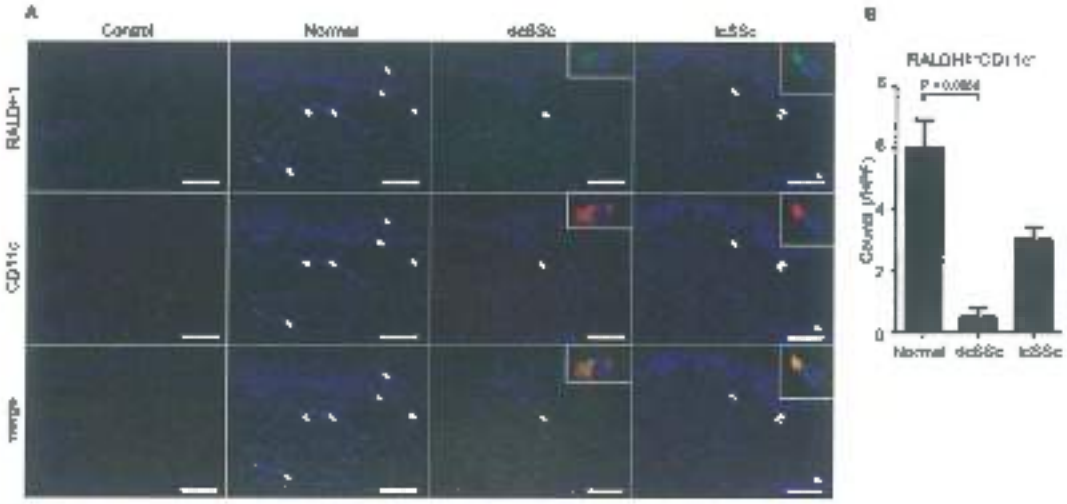

Fig. 6. RALDH1 expression is decreased in dermal DCs of SSc.
A. Representative immunofluorescence images of RALDH1 (red) CD11c (green) double staining in skin samples of control, normal, dcSSc and lcSSc. B. Double positive cells were counted in a ×100 high-power field (HPF) (n = 4 for normal, n = 5, n = 4 for diffuse cutaneous systemic sclerosis [dcSSc], n = 4 for limited cutaneous systemic sclerosis [lcSSc]). A statistical analysis was conducted with the Kruskal–Wallis test followed by the Dunn's multiple comparison test. Graphs represent mean ± SEM. Arrows indicate positive cells. Scale bars are 100 μm.

Cd103$^{-/-}$ mice and with a tendency toward significance in BLM-treated WT mice, indicating that RALDH1 is a main source of RALDH activity in BLM-treated mice (Fig. 5A). More importantly, *Raldh1* siRNA blocked BLM-dependent Treg increase in dermis significantly in BLM-treated *Cd103*$^{-/-}$ and with a trend toward significance in BLM-treated WT mice (Fig. 5B). Consistently, *Raldh1* siRNA enhanced dermal thickness in both BLM-treated *Cd103*$^{-/-}$ and WT mice (Fig. 5C). These results indicate that RALDH1-dependent Treg increase, probably through iTreg induction, plays a critical role in the attenuation of BLM-induced dermal fibrosis in *Cd103*$^{-/-}$ mice.

3.7. RALDH1 expression is decreased in dermal DCs of SSc

Finally, we assessed if these findings are applicable to SSc by double immunofluorescence for RALDH1 and CD11c in skin samples. As shown in Fig. 6, the number of double positive cells was decreased in SSc lesional skin, especially reaching a statistically significant decrease in patients with diffuse cutaneous SSc compared with healthy controls. Given that tissue fibrosis is generally much greater in diffuse cutaneous subtype than in limited cutaneous subtype [43], the number of RALDH1-positive DCs may inversely correlate with the degree of skin fibrosis. These results indicate that RALDH1-dependent Treg regulation is potentially involved in the pathological tissue fibrosis of SSc.

4. Discussion

Supporting the notion that DCs regulate iTreg generation through RALDH1 expression and subsequent RA production [42], our study demonstrated a potent regulatory role of dermal DCs in BLM-induced dermal fibrosis based on the following findings: (i) the proportions of CD11b^{-}CD103^{+} dermal DCs and Tregs were increased in parallel, (ii) CD11b^{-}CD103^{+} dermal DCs produced RALDH1, and (iii) *Raldh1* siRNA suppressed Treg induction and reversed skin fibrosis. Given that CD103^{+} intestinal DCs and CD11b^{+}CD103^{-} dermal DCs serve as regulatory DCs by producing RALDH2 [25,28], the RALDH-dependent regulatory role of DCs seems to be strictly organized in a context-dependent manner.

In the skin, CD103 is expressed by epithelial lymphocytes, such as CD8^{+} epidermal T cells [43] and dendritic epidermal T cells [40], as well as Tregs [44], γδT cells [45] and dermal DCs [46]. Since E-cadherin, a CD103 ligand, is expressed primarily in epithelial cells such as keratinocytes and Langerhans cells, CD103 regulates the retention and function of epithelial lymphocytes by interacting with epithelial cells under a homeostatic condition. In inflammatory skin conditions, a critical role of CD103 has been disclosed so far only in a murine model of CHS [34], in which CD103 loss exacerbates skin inflammation at least by affecting Tregs and dermal DCs. Supporting a significant role of CD103 in inflammatory skin conditions, our current data demonstrated the attenuation of BLM-induced skin fibrosis in *Cd103*$^{-/-}$ mice. Although CD103 loss potentially modulates the behaviors of various cell types expressing this molecule, the altered cytokine profiles, such as IL-4 suppression and IL-10 up-regulation, led us to focus on Tregs and dermal DCs. There remains a possibility that CD103-expressing cells other than Tregs and dermal DCs contribute to the reduced skin fibrosis in BLM-treated *Cd103*$^{-/-}$ mice, but we can plausibly speculate that this possibility is minimal because the adoptive transfer of CD4^{+} splenic T cells isolated from BLM-injected mice is enough to reproduce the BLM-induced pathological feature in recipient mice without BLM challenge [47]. Consistent with the dermal cytokine profiles, Th1, Th2 and Th17 cell proportions were reduced, while Treg proportion was enhanced in BLM-treated skin of *Cd103*$^{-/-}$ mice. Since effector CD4^{+} T cell proportion was not altered in skin-draining lymph nodes of BLM-treated *Cd103*$^{-/-}$ mice, it was assumed that Tregs primarily exert its regulatory role in the skin, but much less in skin-draining lymph nodes. This encouraged us to investigate dermal DCs as an inducer of Tregs in BLM-injected skin.

According to previous data, CD103 regulates the retention and function of Tregs in a context-dependent manner. In the lesional skin of CHS, CD103 expression is required for the retention of Tregs, but not effector T cells. The decreased retention of Tregs due to CD103 loss is likely a major mechanism explaining augmentation of CHS in *Cd103*$^{-/-}$ mice [34]. On the other hand, anti-CD103 antibody has no effect on tumor-infiltrating Treg numbers in several murine cancers [35]. Also, CD103 loss does not affect the number of intestinal homing and retention of Tregs in a murine

colitis model [48,49]. Regarding CD103 impact on Treg function, some evidence has been documented. In murine tumors, CD103 is expressed in 30%–40% of tumor-infiltrating Foxp3+ Tregs and this proportion positively correlates with tumor growth in vivo. Further, in in vitro experiments with CD4+ T cells isolated from tumor-draining lymph nodes, CD103+ Tregs suppress the proliferation and activation of CD4+CD25− effector T cells much greater than CD103− Tregs [35]. In CHS, Foxp3 expression within the cutaneous CD4+CD25+ T cells is higher by ~40 % in WT mice compared with *Cd103*−/− mice, suggesting that impaired regulatory role of Tregs may be involved in exacerbated skin inflammation of *Cd103*−/− mice [34]. In the current study, the inhibition of skin fibrosis was associated with the increased proportion of Tregs and the decreased proportion of effector CD4+ T cells. In addition, Foxp3 expression levels within skin- and lymph node-derived Tregs were not altered. Although only Foxp3 expression is not enough to show the Treg function [36], these current data suggest that the retention and function of Tregs are not impaired in BLM-treated skin of *Cd103*−/− mice. Indeed, this was the second reason why we speculated that dermal DC function is altered in BLM-treated *Cd103*−/− mice.

When looking at dermal DC proportion, we found that the proportions of CD11b+CD103− DCs, CD11b+CD103+ DCs and CD11b−CD103+ DCs were largely modified in dermis and skin-draining lymph nodes of *Cd103*−/− mice. Since Th1, Th2 and Th17 cell proportions were decreased in dermis, but not in skin-draining lymph nodes, we decided to further investigate the phenotypical alteration of dermal DCs in the lesional skin of *Cd103*−/− mice. Through a couple of experiments, we finally concluded that RALDH1 produced by CD11b+CD103+ DCs promotes iTreg differentiation in BLM-injected skin and that the increased proportion of CD11b+CD103+ DCs is a major mechanism underlying reduced skin fibrosis in BLM-treated *Cd103*−/− mice. Although we did not confirm iTreg induction in BLM-injected skin of *Cd103*−/− mice, *Raldh1* siRNA experiments strongly support this idea. Given that the migration of CD11b+ DCs to skin draining-lymph nodes was enhanced in BLM treated *Cd103*−/− mice, it is suggested that CD103 contributes to the retention of CD11b+ DCs in dermis, and that this abnormality is primarily attributable to the increased proportion of CD11b+CD103+ DCs in dermis of BLM treated *Cd103*−/− mice. Until now, CD11b+CD103+ DCs had been nominated as the only regulatory dermal DC subset producing RALDH2 [28]. Since CD11b+CD103+ DC proportion and RALDH2 expression were significantly suppressed in BLM-injected skin irrespective of CD103 loss, the subsets of dermal DCs and RALDH involved in each biological process are totally different. The identification of skin fibrosis-specific regulatory dermal DC subset, namely RALDH1-producing CD11b+CD103+ DCs, would provide us a rationale to develop a new therapy against skin fibrotic disorders.

To translate these findings in mice into humans, we conducted immunostaining with skin samples obtained from SSc patients. Of note, the number of RALDH1-producing dermal DCs was decreased in SSc lesional skin. More importantly, we could see a possible inverse correlation between the number of RALDH1-producing dermal DCs and the severity of tissue fibrosis in SSc patients. Therefore, the RALDH1-producing subset of dermal DCs likely plays a critical regulatory role in skin fibrosis development of this disease.

In flow cytometric analysis with skin samples, it was difficult to obtain a number of CD4+ T cells enough to precisely determine Treg proportion in *Cd103*−/− mice. This is probably because skin inflammation was suppressed in *Cd103*−/− mice by Tregs. Also, flow cytometric analysis with anti XCR1 antibody instead of anti CD103 antibody was more suitable to evaluate CD103+ DC subsets in *Cd103*−/− mice. These were the limitations of this study, but we confirmed the main message of this study in WT mice, namely the identification of a critical regulatory subset of dermal DCs, CD103+CD11b+ cells, producing RALDH1 in BLM-treated mice. This finding further supports the notion that regulatory roles of dermal DCs are complicated and condition-dependent, and sheds new light on dermal DCs as a new therapeutic target of skin fibrotic disorders including SSc.

Funding sources

This study was supported in part by grants from the Ministry of Health, Labor, and Welfare of Japan. The funder had no role in study design, data collection and analysis, decision to publish, or preparation of the manuscript.

Declaration of Competing Interest

The authors have no conflict of interest to declare.

Acknowledgements

The authors thank A. Hatsuta, N. Toda and T. Kaga for tissue processing and staining, and E. Numasaki, H. Inomata, Y. Hakuta and N. Watanabe for technical assistance.

Appendix A. Supplementary data

Supplementary material related to this article can be found, in the online version, at doi:https://doi.org/10.1016/j.jdermsci.2020.01.002.

References

[1] J.H. Distler, C. Feghali-Bostwick, A. Soare, Y. Asano, O. Distler, D.J. Abraham, Review: frontiers of antifibrotic therapy in systemic sclerosis, . 69 (2017) 257–267.
[2] Y. Asano, Systemic sclerosis, J. Dermatol. 45 (2018) 128–138.
[3] S. Bu, Y. Asano, A. Bujor, K. Highland, F. Ilani, M. Trojanowska, Dihydromyriocinsine 1-phosphate has a potent antifibrotic effect in scleroderma fibroblasts via normalization of phosphatase and tensin homolog levels, Arthritis Rheum. 62 (2010) 2117–2126.
[4] H. Jin, K. Yamane, Y. Asano, M. Jinnin, K. Tamaki, Constitutively phosphorylated Smad3 interacts with Sp1 and p300 in scleroderma fibroblasts, Rheumatology (Oxford) 45 (2006) 157–165.
[5] A.M. Bujor, Y. Asano, P. Haines, R. Lafyatis, M. Trojanowska, The c-Abl tyrosine kinase controls protein kinase C6-induced Fli-1 phosphorylation in human dermal fibroblasts, Arthritis Rheum. 63 (2011) 1729–1737.
[6] Y. Asano, H. Ihn, K. Yamane, M. Jinnin, Y. Mimura, K. Tamaki, Involvement of alphavbeta5 integrin-mediated activation of latent transforming growth factor beta1 in autocrine transforming growth factor beta signaling in systemic sclerosis fibroblasts, Arthritis Rheum. 52 (2005) 2897–2905.
[7] R. Saigusa, Y. Asano, T. Taniguchi, M. Hirabayashi, K. Nakamura, S. Miura, et al., Fli1-haploinsufficient dermal fibroblasts promote skin-localized transdifferentiation of Th2-like regulatory T cells, Arthritis Res. Ther. 20 (2018) 23.
[8] R. Saigusa, Y. Asano, K. Nakamura, M. Hirabayashi, S. Miura, T. Yamashita, et al., Systemic sclerosis dermal fibroblasts suppress Th1 cytokine production via Galectin-9 overproduction due to Fli1 deficiency, J. Invest. Dermatol. 137 (2017) 1850–1859.
[9] N. Higashi-Kuwata, M. Jinnin, T. Makino, S. Fukushima, Y. Inoue, E.C. Muchemwa, et al., Characterization of monocyte/macrophage subsets in the skin and peripheral blood derived from patients with systemic sclerosis, Arthritis Res. Ther. 12 (2010) R128.
[10] M. Fujimoto, S. Sato, B. lymphocytes and systemic sclerosis, Curr. Opin. Rheumatol. 17 (2005) 749–751.
[11] T. Taniguchi, T. Miyagawa, S. Toyama, T. Yamashita, K. Nakamura, R. Saigusa, et al., CXCL13 produced by macrophages due to Fli1 deficiency may contribute to the development of tissue fibrosis, vasculopathy and immune activation in systemic sclerosis, Exp. Dermatol. 27 (2018) 1030–1037.
[12] H. Duan, J. Fleming, D.K. Pritchard, L.M. Amon, J. Xue, H.A. Amett, et al., Combined analysis of monocyte and lymphocyte messenger RNA expression with serum protein profiles in patients with scleroderma, Arthritis Rheum. 58 (2008) 1465–1474.
[13] Y. Asano, A.M. Bujor, M. Trojanowska, The impact of Fli1 deficiency on the pathogenesis of systemic sclerosis, J. Dermatol. Sci. 59 (2010) 153–162.
[14] R. Saigusa, Y. Asano, T. Yamashita, T. Taniguchi, T. Takahashi, Y. Ichimura, et al., Fli1 deficiency contributes to the downregulation of endothelial protein C receptor in systemic sclerosis: a possible role in prothrombotic conditions, Br. J. Dermatol. 174 (2016) 338–347.
[15] R. Saigusa, Y. Asano, T. Taniguchi, T. Yamashita, T. Takahashi, Y. Ichimura, et al., A possible contribution of endothelial CCN1 downregulation due to Fli1

deficiency in the development of digital ulcers in systemic sclerosis. Exp Dermatol. 24 (2015) 127–132.
[33] I. Takahashi, Y. Asano, T. Amiya, M. Hazano, Z. Tamaki, M. Takata, et al., Clinical correlation of brachial artery flow-mediated dilation in patients with systemic sclerosis. Mod. Rheumatol. 24 (2014) 106–111.
[34] I. Takahashi, Y. Asano, K. Sugawara, T. Yamashita, R. Nakamura, R. Saigusa, et al., Epithelial FID deficiency drives systemic autoimmunity and fibrosis: possible roles in scleroderma. J. Exp. Med. 214 (2017) 1129–1150.
[35] I. Takahashi, Y. Asano, T. Yamashita, Y. Nakamura, R. Saigusa, S. Miura, et al., A potential contribution of osteopontin to vascular and epithelial abnormalities and inflammation in systemic sclerosis. J. Eur. Acad. Dermatol. Venereol. 32 (2018) 291–297.
[36] R. Saigusa, T. Yamashita, S. Miura, M. Hirabayashi, R. Nakamura, T. Kitagawa, et al., A potential contribution of decreased selectin-7 expression in stratified epithelia to the development of cutaneous and esophageal manifestations in systemic sclerosis. Exp. Dermatol. (2018).
[37] R. Saigusa, Y. Asano, T. Yamashita, T. Takahashi, R. Nakamura, S. Miura, et al., Systemic sclerosis complicated with isolated scleroderma-like lesions induced by Koebner phenomenon. J. Dermatol. Sci. 89 (2018) 262–269.
[38] F. Ginhoux, S. Tamoutounour, S. Florez, The origins and functions of dendritic cells and macrophages in the skin. Nat. Rev. Immunol. 14 (2014) 417–428.
[39] T. Honda, G. Egawa, S. Grabbe, K. Kabashima, Update of immune events in the murine contact hypersensitivity model: toward the understanding of allergic contact dermatitis. J. Invest. Dermatol. 133 (2013) 303–315.
[40] M. Haniffa, M. Collin, L. Ginhoux, Human skin dendritic cells in health and disease. J. Dermatol. Sci. 77 (2015) 85–92.
[41] R. Niedermeiser, P. Dulic, Retinoic acid in development: towards an integrated view. Nat. Rev. Genet. 14 (2013) 541–553.
[42] J.L. Coombes, K.R. Siddiqui, C.V. Arancibia-Carcamo, J. Hall, C.M. Sun, Y. Belkaid, et al., A functionally specialized population of mucosal CD103+ DCs induces Foxp3+ regulatory T cells via a TGF-beta and retinoic acid-dependent mechanism. J. Exp. Med. 204 (2007) 1757–1764.
[43] C.M. Sun, J.A. Hall, R.B. Blank, N. Bouladoux, M. Oukka, J.R. Mora, et al., Small intestine lamina propria dendritic cells promote de novo generation of Foxp3 T cells via retinoic acid. J. Exp. Med. 204 (2007) 1775–1785.
[44] O. Mucida, Y. Park, G. Kim, O. Turovskaya, I. Scott, M. Kronenberg, et al., Recipro cal TH17 and regulatory T cell differentiation mediated by retinoic acid. Science 317 (2007) 256–260.
[45] M. Gallimore, K. Cosset, S. Harris, S. Tamoutounour, F. Garnier, E. Devaux, et al., Skin-draining lymph nodes contain dermis-derived CD103+ dendritic cells that constitutively produce retinoic acid and induce Foxp3+ regulatory T cells. Blood 115 (2010) 1958–1968.
[46] T. Matsushita, M. Hasegawa, Y. Hamaguchi, Y. Takehara, S. Sato, Longitudinal analysis of serum cytokine concentrations in systemic sclerosis: association of interleukin 12 elevation with spontaneous regression of skin sclerosis. J. Rheumatol. 34 (2006) 2275–2284.
[47] M. Muro, M. Fujimoto, T. Matsushita, Y. Hamaguchi, M. Hasegawa, K. Takehara, et al., Clinical association of serum interleukin-17 levels in systemic sclerosis: is systemic sclerosis a Th17 disease? J. Dermatol. Sci. 50 (2008) 240–242.
[48] R. Saigusa, Y. Asano, T. Taniguchi, T. Yamashita, Y. Ichimura, T. Takahashi, et al., Multifaceted contribution of the TLR4-activated IRF5 transcriptome to systemic sclerosis. Proc. Natl. Acad. Sci. U. S. A. 112 (2015) 15136–15141.
[49] S. Noda, Y. Asano, S. Nishimura, T. Taniguchi, K. Fujiu, T. Manabe, et al., Simultaneous downregulation of KLF5 and Fli1 is a key feature underlying systemic sclerosis. Sci. Rep. 5 (2015) 5797.
[50] M. Hasegawa, M. Fujimoto, K. Kikuchi, K. Takehara, Elevated serum levels of interleukin 4 (IL-4), IL-10, and IL-13 in patients with systemic sclerosis. J. Rheumatol. 24 (1997) 328–332.
[51] A. Bauer, N. Deuser, F. Brunssen, V. Schnabel, J.J. Hardenberg, B. Ridder, et al., Integrin alphaE(CD103) is involved in regulatory T-cell function in allergic contact hypersensitivity. J. Invest. Dermatol. 135 (2015) 2982–2991.
[52] D. Aoki, W. Mueller, M. Bolz, W.G. Kunz, M. Rapp, V.H. Koelzer, et al., CD103+ a hallmark of tumor-infiltrating regulatory T cells, Int. J. Cancer. 129 (2011) 2420–2426.
[53] N. Chihara, M. Hamaguchi, H. Morikawa, Y. Suzuma, A. Tanaka, Y. Ito, et al., T cell receptor stimulation-induced epigenetic changes and Foxp3 expression are independent and complementary events required for Treg cell development. Immunity. 37 (2012) 709–719.
[54] A. Bachem, E. Hartung, S. Guttler, A. Mora, X. Zhou, A. Hegenbarth, et al., Expression of IRF8 characterizes the Batf3-dependent lineage of dendritic cells capable of antigen cross-presentation. Front. Immunol. 3 (2012) 214.
[55] M. Collin, V. Bigley, M. Haniffa, S. Hambleton, Human dendritic cell deficiency: the missing ID? Nat. Rev. Immunol. 11 (2011) 575–583.
[56] M. Gallimore, S. Harris, S. Tamoutounour, F. Ardouin, I. Schwartz-Cornil, M. Balad, et al., From skin dendritic cells to a simplified classification of human and mouse dendritic cell subsets. Eur. J. Immunol. 40 (2010) 2084–2094.
[57] M.K. Schon, M. Schon, L.M. Parker, I.R. Williams, Dendritic epidermal T cells (DETC) are diminished in integrin alphaE(CD103) deficient mice. J. Invest. Dermatol. United States (2002) 196–203.
[58] E.C. Lefaty, C. Black, R. Hesselmann, S. Johnsola, I. Wang, T.A. Medsger, et al., Scleroderma (systemic sclerosis): classification, subsets and pathogenesis. J. Rheumatol. 15 (1988) 202–205.
[59] J.L. Coombes, Y. Ma, L. Lauzenanian, S.A. Cauden, W. Dranoff, Regulatory dendritic cells for immunotherapy in immunologic diseases. Front. Immunol. 5 (2014) 7.
[60] Y. Hong, O. Wang, R. Yuan, L.M. Parker, D.L. Farber, S.A. Hadley, CD103 expression is required for destruction of pancreatic islet allografts by CD8(+) T cells. J. Exp. Med. 196 (2002) 877–886.
[61] L. Suffia, S.K. Reckling, G. Salay, Y. Belkaid, A role for CD103 in the retention of CD4+CD25+ Treg and control of Leishmania major infection. J. Immunol. 174 (2005) 5444–5455.
[62] M.L. Thomas, R.A. Badwe, R.K. Deosagunde, D.C. Samant, S.V. Chipalkatti, Role of adhesion molecules in peripheral blood T cells from the peripheral blood to the tumor tissue of esophageal cancer patients. Cancer Immunol. Immunother. 50 (2001) 216–225.
[63] J.C. Miller, B.D. Brown, T. Shay, E.L. Gautier, V. Jojic, A. Cohain, et al., Deciphering the transcriptional network of the dendritic cell lineage. Nat. Immunol. 13 (2012) 888–899.
[64] H. Ishikawa, K. Takeda, A. Okamoto, S. Maruo, K. Kobe, Induction of autoimmunity in a bleomycin-induced murine model of experimental systemic sclerosis: an important role for CD4+ T cells. J. Invest. Dermatol. 129 (2009) 1688–1695.
[65] O. Annacker, J.L. Coombes, V. Malmstrom, H.H. Uhlig, T. Bourne, B. Johansson-Lindbom, et al., Essential role for CD103 in the T cell-mediated regulation of experimental colitis. J. Exp. Med. 202 (2005) 1051–1061.
[66] X. Yuan, M.J. Bee, N.R. Ahmed, T.R. Malek, IL-2Rbeta-dependent signaling and CD103 functionally cooperate to maintain tolerance in the gut mucosa. J. Immunol. 194 (2015) 1174–1186.

Pathogenesis of systemic sclerosis—current concept and emerging treatments

Masutaka Furue, Chikage Mitoma, Hiroki Mitoma, Gaku Tsuji, Takahito Chiba, Takeshi Nakahara, Hiroshi Uchi & Takafumi Kadono

Immunologic Research

ISSN 0257-277X
Volume 65
Number 4

Immunol Res (2017) 65:790-797
DOI 10.1007/s12026-017-8926-y

Springer

Your article is protected by copyright and all rights are held exclusively by Springer Science +Business Media New York. This e-offprint is for personal use only and shall not be self-archived in electronic repositories. If you wish to self-archive your article, please use the accepted manuscript version for posting on your own website. You may further deposit the accepted manuscript version in any repository, provided it is only made publicly available 12 months after official publication or later and provided acknowledgement is given to the original source of publication and a link is inserted to the published article on Springer's website. The link must be accompanied by the following text: "The final publication is available at link.springer.com".

Springer

Author's personal copy

Immunol Res (2017) 65:790–797
DOI 10.1007/s12026-017-8926-y

REVIEW

Pathogenesis of systemic sclerosis—current concept and emerging treatments

Masutaka Furue[1,2,3] · Chikage Mitoma[1,3] · Hiroki Mitoma[4] · Gaku Tsuji[1,3] · Takahito Chiba[1] · Takeshi Nakahara[1,3] · Hiroshi Uchi[1] · Takafumi Kadono[5]

Published online: 9 May 2017
© Springer Science+Business Media New York 2017

Abstract Systemic sclerosis (SSc) is an intractable multifaceted disease with high mortality. Although its pathogenesis is not fully understood, recent studies have advanced our knowledge on SSc. The cardinal pathological features of SSc are autoimmunity, vasculopathy, and fibrosis. The B cells in SSc are constitutively activated and lead to the production of a plethora of autoantibodies, such as anti-topoisomerase I and anti-centromere antibodies. In addition to these autoantibodies, which are valuable for diagnostic criteria or biomarkers, many other autoantibodies targeting endothelial cells, including endothelin type A receptor and angiotensin II type I receptor, are known to be functional and induce activation or apoptosis of endothelial cells. The autoantibody-mediated endothelial cell perturbation facilitates inflammatory cell infiltration, cytokine production, and myofibroblastic transformation of fibroblasts and endothelial cells. Profibrotic cytokines, such as transforming growth factor β, connective tissue growth factor, interleukin 4/interleukin 13, and interleukin 6, play a pivotal role in collagen production from myofibroblasts. Specific treatments targeting these causative molecules may improve the clinical outcomes of patients with SSc. In this review, we summarize recent topics on the pathogenesis (autoantibodies, vasculopathy, and fibrosis), animal models, and emerging treatments for SSc.

Keywords Systemic sclerosis · Autoantibodies · Vasculopathy · Fibrosis

✉ Masutaka Furue
furue@dermatol.med.kyushu-u.ac.jp

1 Department of Dermatology, Kyushu University, Maidashi 3-1-1, Higashiku, Fukuoka 812-8582, Japan

2 Research and Clinical Center for Yusho and Dioxin, Kyushu University, Fukuoka, Japan

3 Division of Skin Surface Sensing, Department of Dermatology, Kyushu University, Fukuoka, Japan

4 Department of Clinical Immunology and Rheumatology/Infectious Disease, Kyushu University, Fukuoka, Japan

5 Department of Dermatology, St. Marianna University School of Medicine, Kawasaki, Japan

Introduction

The prevalence of systemic sclerosis (SSc) ranges from 0.7/100,000 to 53/100,000 depending on the different ethnicities, and there are higher numbers in the USA than in Europe or Japan [1]. In a nationwide, cross-sectional hospital-based study in Japan, patients with SSc comprised 0.92% of dermatological patients [2]. SSc has a high mortality rate due to the development of SSc-associated interstitial lung disease and pulmonary arterial hypertension, which are the most frequent causes of disability and mortality in SSc [3–5].

Depending on the extent of skin involvement, SSc is classified into the following two main subtypes: limited cutaneous SSc and diffuse cutaneous SSc. Given the heterogeneity of clinical symptoms and signs, the American College of Rheumatology/the European League against Rheumatism developed new classification criteria in 2013 [6–8].

SSc is not an inherited disease, therefore, twins show a low disease concordance rate (4.7%) that is similar between monozygotic and dizygotic twin pairs [9]. However, genetic factors contribute to its susceptibility, as shown by a 60-fold higher occurrence of the disease in families compared to the general population [10–12]. Genetic linkage studies and genome-wide association studies have identified many susceptible genes, including the major histocompatibility complex (MHC) class II as well as non-MHC genes related to the metabolism of

Author's personal copy

extracellular matrix molecules, innate immunity, macrophage activation, and T cell functions [10–12].

Systemic sclerosis (SSc) is a multisystem connective tissue disease characterized by three cardinal pathological features, including aberrant immune activation, vasculopathy, and tissue fibrosis with an unknown aetiology [3, 4, 13]. Although its pathogenesis is not fully understood, recent studies have advanced our knowledge on SSc. In this review, we summarize recent topics on the pathogenesis (autoantibodies, vasculopathy, and fibrosis), animal models, and emerging treatments for SSc.

Pathogenesis

Pathogenesis of SSc remains unknown, whereas it is commonly thought that autoimmunity and vasculopathy precede fibroblast activation and interstitial fibrosis [14, 15]. Autoantibodies to endothelial cells, ischemia–reperfusion injury following Raynaud's phenomenon, generation of reactive oxygen species (ROS) with inflammatory cell infiltration, and subsequent cytokine production trigger myofibroblastic transformation of endothelial cells as well as fibroblasts and induce excessive production of collagens and other extracellular matrices [5, 8, 14, 15]. Various profibrotic cytokines, such as transforming growth factor β (TGFβ), interleukin (IL)-4, IL-13, IL-6, and IL-33 are likely to be involved in the development of fibrosis [13, 14, 16–18].

Autoantibody and vasculopathy

The immune system activation is exemplified by the activation of B cells and the production of autoantibodies [19–23]. B cells from patients with SSc overexpress the B cell stimulatory receptor CD19 by 54% in patients with early SSc and by 28% in those with long-standing disease compared to normal controls [22–24]. Notably, a small increase (15–29%) in the CD19 expression of B cells in transgenic mice induced autoantibody production [25]. In contrast, the function of CD22, an inhibitory B cell molecule, is inhibited by anti-CD22 autoantibodies present in patients with SSc [22, 23, 25]. An increased CD19/CD22 ratio may facilitate the sustained activation of B cells and consequent overproduction of various autoantibodies [22, 23, 25, 26].

Anti-nuclear antibodies are found in the sera of the vast majority of SSc patients, and their antigenic specificity significantly correlates with the clinical characteristics of the disease [19–21]. Autoantibodies are currently the most reliable biomarkers for diagnosis, classification, and prediction of specific clinical features of SSc [19–21]. Certain autoantibodies, such as anti-topoisomerase I, anti-centromere, anti-RNAP III, anti-U3 RNP, anti-Th/To, and anti-U1 RNP antibodies, are closely associated with distinct clinical features and disease activities of SSc [19–21, 27, 28] (Fig. 1). Other autoantibodies targeting a variety of cytoplasmic, cell membrane, and extracellular autoantigens were also detected in SSc [21, 23]. Some of them, such as anti-endothelial cell, anti-intercellular adhesion molecule-1 (ICAM-1), anti-endothelin type A receptor (ETAR), and anti-angiotensin II type I receptor (AT1R) antibodies, may be functional and pathogenic [21, 23]. In addition to autoantibodies, a plethora of biomarkers related to immune reactions [29, 30], endothelial cell function [31, 32], and the extracellular matrix [33, 34] have been reported recently [19].

Raynaud's phenomenon and abnormal nailfold capillary changes, which are the representative vascular manifestations of SSc, often appear before the onset of sclerosis [8, 15, 35]. Raynaud's phenomenon is the abnormal thermal regulation of blood flow that is probably triggered by endothelial injury [15]. The skin fibrosis tends to occur on locations, such as fingers, distal extremities, and face, which are frequently exposed to cold temperatures [15]. Nailfold capillaroscopy reveals structural alterations in capillaries that include dilatation, distortion, and microhemorrhages that lead to progressive loss of the capillaries (Fig. 1) [36]. Microscopically, capillary damage of SSc is characterized by endothelial apoptosis, intimal and medial fibrous thickening, and adventitial fibrosis with perivascular infiltration of the macrophages, B cells, and T cells [15]. Precapillary arterioles then show endothelial proliferation and mononuclear inflammatory infiltrates followed by intimal proliferation and luminal narrowing [37]. The origin of the cells that populate the intima and participate in collagen production remains unknown. However, activated resident fibroblasts, circulating fibroblast precursors (fibrocytes), the endothelial cells, and pericytes have all been implicated [15]. In line with these findings, an endothelial cell to mesenchymal transition is shown in the lesional vascular systems in SSc [5].

The endothelial apoptosis or activation is likely mediated by functional autoantibodies [23, 38]. Anti-endothelial cell antibodies cause endothelial cell apoptosis [39]. Anti-ICAM-1 antibodies induce the production of ROS and expression of vascular cell adhesion molecule-1 (VCAM-1) which may facilitate the attachment of immune cells [40]. Anti-ETAR and anti-AT1R autoantibodies, which are detected in most SSc patients, are agonistic antibodies that upregulate the expression of TGF-β, IL-8, and VCAM-1 of endothelial cells and cause fibrosis, vasoconstriction, and recruitment of immune cells [41–43]. Both AT1R and ETAR are expressed on cells of both the vascular and immune system [38]. Angiotensin II increased the production of TGFβ and collagen by fibroblasts via AT1R [44]. Endothelin-1 also induced collagen production and vasoconstriction via ETAR [45]. The expressions of ETAR and AT1R are found to be highest in patients with early SSc [46]. The anti-ETAR and anti-AT1R antibodies from SSc patients induce obliterative vasculopathy when injected into mice [43]. The endothelial cell apoptosis has been demonstrated in the skin lesions of patients with SSc as well as in avian

Author's personal copy

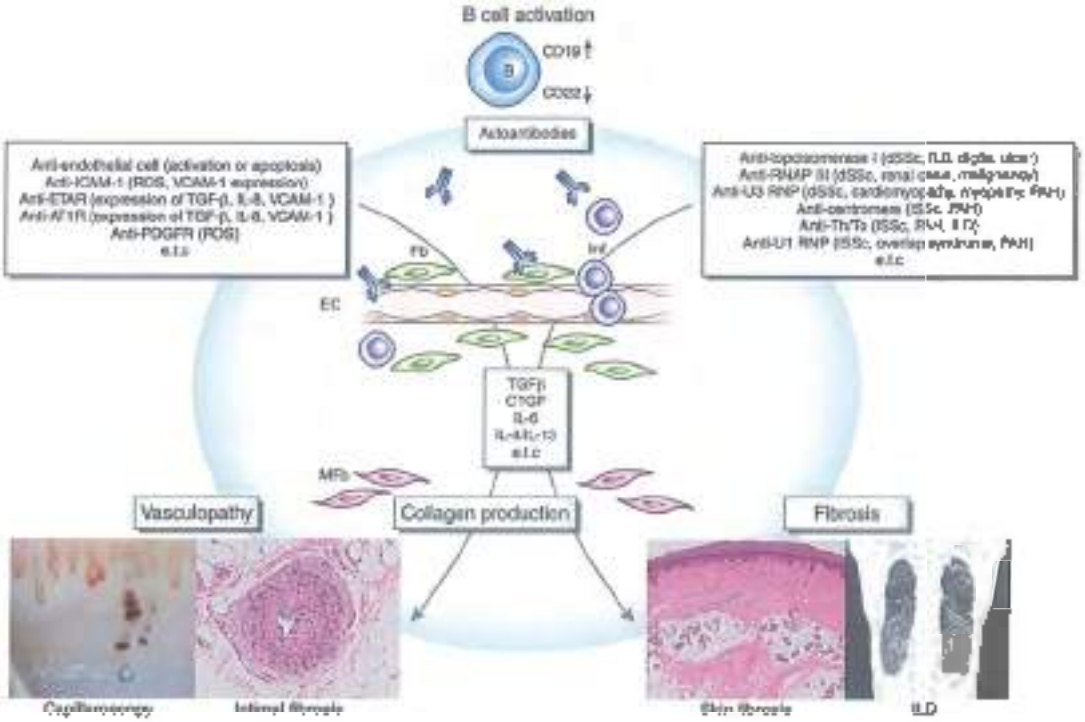

Fig. 1 Pathogenesis of systemic sclerosis. The cardinal pathological features of systemic sclerosis (SSc) are autoantibodies, vasculopathy, and fibrosis. B cells in SSc are constitutively activated with increased CD19 and decreased CD22 expression, which leads to the overproduction of a plethora of autoantibodies, such as anti-topoisomerase I, anti-RNAP III, anti-U3 RNP, anti-centromere, anti-Th/To, and anti-U1 RNP antibodies. These autoantibodies are associated with characteristic clinical features, such as diffuse SSc (dSSc), limited SSc (lSSc), interstitial lung disease (ILD), digital ulcer, renal crisis, malignancy, cardiomyopathy, myopathy, pulmonary artery hypertension (PAH), and overlap syndrome. Many other functional autoantibodies targeting endothelial cells, intercellular adhesion molecule 1 (ICAM-1), endothelin type A receptor (ETAR), and angiotensin II type I receptor (AT1R) as well as platelet-derived growth factor receptor (PDGFR) are known to induce activation or apoptosis of endothelial cell (EC). The stimulated ECs express reactive oxygen species (ROS), transforming growth factor β (TGFβ), interleukin-8 (IL-8), and vascular endothelial cell adhesion molecule 1 (VCAM-1). The autoantibody-mediated endothelial cell perturbation facilitates inflammatory cell (Inf) infiltration, cytokine production, and myofibroblastic transformation of fibroblasts (Fb) and ECs. Profibrotic cytokines, such as TGFβ, connective tissue growth factor (CTGF), IL-6, and IL-4/IL-13, play a pivotal role in collagen production from myofibroblasts (MFb). Perturbation of ECs and consequent profibrotic processes result in vasculopathy (including capillaroscopic abnormalities and intimal fibrosis) and tissue fibrosis (including skin fibrosis and ILD)

SSc models [47]. Moreover, many SSc patients have antibodies against a human cytomegalovirus-derived UL94 protein that shares homology with NAG-2 (tetraspan novel antigen-2), which is expressed on the surface of human endothelial cell and fibroblast [48, 49]. The anti-UL94 peptide antibodies bind to NAG-2 and induce "scleroderma-like" gene expression in endothelial cells and fibroblasts [48, 49]. Thus, the molecular mimicry mechanism links antibodies against the human-cytomegalovirus-derived protein UL94 to the pathogenesis of systemic sclerosis [48, 49].

Fibrosis

The degree of cell infiltration correlates with both the degree and progression of skin thickening, which results from excessive accumulation of type I collagen and extracellular matrix proteins [3, 8, 50, 51]. These infiltrated cells, especially endothelial cells and fibroblasts, are potential candidates for producing various cytokines, chemokines, and growth factors that induce fibrosis [3, 8, 50, 51]. Despite the differences in the extent and distribution of skin involvement, both limited and diffuse type SSc produce marked fibrosis followed by the preceded autoimmunity, vasculopathy, and perivascular inflammatory cell infiltration [8, 50, 51].

Representative profibrotic growth factors and cytokines encompass TGFβ, connective tissue growth factor (CTGF), platelet-derived growth factor (PDGF), IL-6, and IL-4/IL-13 (Fig. 1). After ligation with TGFβ receptor type II (TGFβRII) and TGFβRI, TGFβ induces gene transcription of type I collagen, α smooth muscle actin (αSMA), and CTGF via SMAD2/SMAD3 phosphorylation [3]. An increased TGFβRI/TGFβRII ratio was found in the SSc fibroblasts, which was implicated in the overactivation of TGFβ signaling [52]. The expression of αSMA is a hallmark of myofibroblastic transformation of activated fibroblasts, which is also frequently detected in SSc [53, 54]. CTGF is a cysteine-rich modular protein belonging to the

Author's personal copy

CCN family of matricellular growth factors, all of which function as adaptor molecules connecting the cell surface to the extracellular matrix [3, 55]. The expression of CTGF is induced by TGF-β, ET-1, and hypoxia [3, 55]. The levels of CTGF are markedly elevated in the lesional skin of SSc patients [56] and in mouse models of scleroderma [57].

The expression of PDGF and its receptors is elevated in SSc fibroblasts and in the lesional skin [58]. Antibodies that stimulate the PDGF receptor (PDGFR) were frequently found in SSc patients [59]. The autoantibodies recognize native PDGFR and selectively activate Ha-Ras-ERK1/2 and ROS cascades to induce type I collagen gene expression and myofibroblast phenotype conversion in normal human fibroblasts [59]. The activated B cells secreted IL-6, which directly stimulates fibroblasts [60–62]. IL-6 induces the type I collagen expression via enhancing TGFβ-Smad3 signalling pathway [62]. Both IL-4 and IL-13 likely activate fibroblasts and induce type I collagen synthesis via a TGFβ-independent approach [63–65]. Serum levels of IL-4 and IL-13 were significantly higher in patients with SSc compared to normal controls [66]. It is likely that IL-13, rather than IL-4, plays a more dominant role in fibrosis [17, 67]. Notably, CD8+ T cells producing IL-13 have been shown to have skin-homing receptors in SSc skin and they upregulate type I collagen production when incubated with healthy dermal fibroblasts [68].

Animal models of systemic sclerosis

Inducible fibrotic models

Among inducible animal models, the most widely used and established ones are a bleomycin-induced SSc model and a scleroderma-like graft-versus-host disease model in mice [13, 69–71]. Recently, three new inducible murine models of SSc have been established by utilizing ROS [72], DNA topoisomerase I antigen with complete Freund's adjuvant [73], and angiotensin II [74]. Basically, the focus of these inducible models was put on the induction of fibrosis tissue and, to a lesser extent, on the immunological aspects of SSc, instead of its vascular pathology [13].

Genetic animal models

The best-characterized genetic animal models of SSc are tight skin-1 (Tsk-1) mice, in which an in-frame tandem partial re-duplication of the *Fbn1* gene encoding fibrillin-1, which is a major component of microfibrils mediating elastic fiber assembly, is responsible for the phenotype [75]. Although the Tsk-1 mice exhibit TGFβ upregulation with the aberrant activation of B cells and autoantibody production, the fibrosis of Tsk-1 mice occurs in the hypodermis, which is not observed in human SSc [13]. Mice with constitutively active TGFβRI recapitulate clinical, histological, and biochemical features of human SSc [76]. In addition, mice expressing the *Ccn2* gene in fibroblasts [77] or *Wnt10b* in adipocytes [78] exhibit extensive fibrosis in the dermis and internal organs.

New genetic animal models

Fra-2 is one of the components of Fos (c-Fos, Fra-1, Fra-2, FosB) which dimerize with Jun (c-Jun, JunB, JunD) subunits to make AP-1 transcription factor [13]. The *Fra2* transgenic mice developed dermal and pulmonary fibrosis following the apoptosis of endothelial cells [79, 80]. Urokinase-type plasminogen activator receptor (uPAR) is a glycosylphosphatidylinositol-anchored cell surface receptor expressed by several cell types, including hematopoietic cells, fibroblasts, and endothelial cells [13]. A major role of uPAR is to concentrate its ligand, uPA, at the cell-matrix interface. uPA has a serine protease activity that induces the conversion of plasminogen to plasmin and the activation of growth factors and pro-enzymes, such as matrix metalloproteinases [13]. Interestingly, the cleavage and/or inactivation of uPA/uPAR is associated with the transition of fibroblasts to myofibroblasts and subsequent fibrosis as well as with the functional and structural abnormalities of microvasculature in SSc [81–84]. In line with these findings, uPAR-deficient mice recapitulate the fibrotic and vascular features of SSc [85]. However, both *Fra2* transgenic mice and uPAR-null mice totally lack immunological aspects, specifically autoantibody production, in SSc (Table 1) [13].

In contrast to these animal models, *Ikjs*$^{+/-}$; *Fli1*$^{+/-}$ mice develop immune activation, vasculopathy, and fibrosis, which are the three cardinal features of SSc [13, 86]. Fli1 is a member of the Ets transcription factor family expressed in endothelial and hematopoietic cells under physiological conditions, and to a lesser extent in dermal fibroblasts [13]. Fli1 exerts a potent repressor of the *COL1A1* and *COL1A2* gene expression in dermal fibroblasts [87, 88]. The expression of Fli1 was decreased in dermal fibroblasts, dermal microvascular endothelial cells, and perivascular inflammatory cells in the lesional and non-lesional skin of SSc patients, especially in the lesional skin [88]. Fli1 haploinsufficiency is enough to reduce the

Table 1 Phenotypic differences of new genetic animal models for systemic sclerosis

	Fra2 tg mice	uPAR$^{-/-}$ mice	*Ikjs*$^{+/-}$, *Fli1*$^{+/-}$ mice
Dermal fibrosis	+	+	+
Vasculopathy in the skin	+	+	+
Pulmonary fibrosis	+	+	+
Pulmonary arterial occlusion	+	−	+
Autoantibody production	−	−	+

Author's personal copy

production of type I collagen [87, 88]. However, Fli1 haploinsufficiency had no effect on CTGF expression [86]. Therefore, some additional factors are mandatory to upregulate the CTGF expression that is also the hallmark feature of dermal fibroblasts derived from SSc patients [13, 56]. Kruppel-like factor 5 (KLF5) is a potent repressor of the *Ctgf* gene [86]. Moreover, KLF5 was downregulated in the lesional skin of SSc [89]. Thus, *Kif3*$^{-/-}$; *Fli1*$^{+/-}$ double haploinsufficiency mice spontaneously develop remarkable dermal fibrosis, which is characterized by the increase in dermal thickness, the amount of collagen content, and the mRNA of the *Col1a1*, *Col1a2*, and *Ctgf* genes, at the age of 3 months [86]. In addition, the pathological cascade from vasculopathy (stenosis of arterioles and bushy capillaries) to tissue fibrosis was also present in these mice [86]. Furthermore, the *Kif3*$^{-/-}$; *Fli1*$^{+/-}$ mice mimicked the immunological aspects of human SSc, including increased CD19 expression in B cells, upregulated production of IL-6, and the production of autoantibodies (Table 1) [86].

Treatments and therapeutic perspectives

Although the treatment outcomes are not satisfactory, immunosuppressive agents, such as corticosteroids [8], methotrexate [90, 91], cyclophosphamide [92, 93], mycophenolate mofetil [94, 95], and intravenous immunoglobulin [96, 97], are currently being used [98]. ETAR antagonist and angiotensin-converting enzyme blockade have been used to treat clinical complications related to vasculopathies of patients with SSc [99, 100]. Injection of botulinum toxin is useful for preventing Raynaud's phenomenon [101].

B cell depletion by rituximab (anti-CD20 antibody) improves lung function and skin thickening in patients with SSc [102–104]. Fresolimumab, a neutralizing antibody that targets all three isoforms of TGFβ, also decreases skin fibrosis with histological reduction of dermal myofibroblasts [105]. As for the anti-IL-6 receptor α antibody, a randomized controlled trial revealed that tocilizumab tended to reduce the skin thickening compared to placebo, but not significantly [106, 107]. Rapamycin binds to the FK-506 binding protein 12 and inhibits the function of mammalian target of rapamycin. Rapamycin prevents fibrosis of the skin and lungs as well as autoantibody production in a murine model of SSc [108]. In a phase I, single-blinded, randomized, parallel trial of rapamycin versus methotrexate, rapamycin was just as effective as methotrexate for skin sclerosis [109]. Pirfenidone, a pyridine with a simple chemical structure, is an antifibrotic agent, and it has been approved for the treatment of idiopathic pulmonary fibrosis worldwide [110, 111]. Although the molecular mechanisms underlying the antifibrotic effects of pirfenidone are not completely understood, it is thought to work predominantly by modulating TGFβ and TNFα signaling [9, 112]. Further clinical studies are needed to prove the effectiveness of pirfenidone on the skin and pulmonary fibrosis in SSc.

Conclusion

Pathogenesis of SSc is dominated by complex interactions between vascular, immunological, and fibrotic processes, but it is still poorly understood. SSc is an intractable disease with high mortality. Research efforts towards understanding the cellular and molecular basis of scleroderma have aimed to reveal novel molecular targets and diagnostic agents, which has led to early and accurate diagnosis as well as innovative therapies against this disease [10, 112]. The development of preclinical models, including animal models that accurately recapitulate human disease, will be essential tools for the ultimate goal of finding a cure for this disease. The list of potential molecular targets for the treatment of fibrosis is growing. Several of those studies to target pathogenetic molecules have direct translational implications for treating SSc in the very near future [6, 11, 111].

References

1. Distler O, Cozzio A. Systemic sclerosis and localized scleroderma—current concepts and novel targets for therapy. Semin Immunopathol. 2016;38(1):87–95.
2. Furue M, Yamazaki S, Jimbow K, Tsuchida T, Amagai M, Tanaka T, et al. Prevalence of dermatological disorders in Japan: a nationwide, cross-sectional, seasonal, multicenter, hospital-based study. J Dermatol. 2011;38(4):310–20.
3. Varga J, Abraham D. Systemic sclerosis: a prototypic multisystem fibrotic disorder. J Clin Invest. 2007;117(3):557–67.
4. Denton CC, Cossu P. Systemic sclerosis: an update in 2016. Autoimmun Rev. 2016;15(5):413–26.
5. Jimenez SA, Piera-Velazquez S. Endothelial to mesenchymal transition (EndoMT) in the pathogenesis of systemic sclerosis-associated pulmonary fibrosis and pulmonary arterial hypertension. Myth or reality? Matrix Biol. 2016;51:26–36.
6. van den Hoogen F, Khanna D, Fransen J, Johnson SR, Baron M, Tyndall A, et al. 2013 classification criteria for systemic sclerosis: an American College of Rheumatology/European league against rheumatism collaborative initiative. Arthritis Rheum. 2013;65(11):2737–47.
7. Toki S, Motegi S, Yamada K, Uchiyama A, Kanai S, Yamanaka M, et al. Clinical and laboratory features of systemic sclerosis complicated with localized scleroderma. J Dermatol. 2015;42(3):283–7.
8. Yamada K. Strategy for treatment of fibrosis in systemic sclerosis: present and future. J Dermatol. 2016;43(1):46–55.
9. Feghali-Bostwick C, Medsger TA Jr, Wright TM. Analysis of systemic sclerosis in twins reveals low concordance for disease and high concordance for the presence of autoinfectious antibodies. Arthritis Rheum. 2003;48(7):1956–63.
10. Fuschiotti P. Current perspectives on the immunopathogenesis of systemic sclerosis. Immunotargets Ther. 2016;5:21–33.

Author's personal copy

11. Makino T, Jinnin M. Genetic and epigenetic abnormalities in systemic sclerosis. J Dermatol. 2016;43(1):10–8.
12. Mordaca G, Colombo M, Gulli R, Marfisi R, Puppo F. Genetic factors and systemic sclerosis. Autoimmun Rev. 2016;15(1):427–32.
13. Asano Y. Recent advances in animal models of systemic sclerosis. J Dermatol. 2016;43(1):19–28.
14. Vettori S, Cuomo G, Iudici M, D'Abronzo V, Gracco V, Barra G, et al. Early systemic sclerosis: serum profiling of factors involved in endothelial, T-cell, and fibroblast interplay is marked by elevated interleukin-33 levels. J Clin Immunol. 2014;34(6):663–8.
15. Matucci-Cerinic M, Kahaleh B, Wigley FM. Review: evidence that systemic sclerosis is a vascular disease. Arthritis Rheum. 2013;65(8):1953–62.
16. Denton CP. Advances in pathogenesis and treatment of systemic sclerosis. Clin Med (Lond). 2016;16(1):55–60.
17. O'Reilly S. Role of interleukin-33 in fibrosis, particularly systemic sclerosis. Biofactors. 2013;39(6):593–6.
18. Bergmann C, Distler JH. Canonical Wnt signaling in systemic sclerosis. Lab Investig. 2016;96(2):151–4.
19. Hasegawa M. Biomarkers in systemic sclerosis: their potential to predict clinical courses. J Dermatol. 2016;43(1):29–38.
20. Peretz F, Prete M, Di Lernia G, Ostuni C, Pavesio E, Valentini G. Anti-centromere protein a antibodies in systemic sclerosis: significance and origin. Autoimmun Rev. 2016;15(1):102–9.
21. Günther J, Radermacher J, von Laer JM, Siegert E, Riemekasten G. Functional autoantibodies in systemic sclerosis. Semin Immunopathol. 2015;37(5):529–42.
22. Yoshizaki A. B lymphocytes in systemic sclerosis: abnormalities and therapeutic targets. J Dermatol. 2016;43(1):39–45.
23. Sakkas LI, Bogdanos DP. Systemic sclerosis: new evidence reinforces the role of B cells. Autoimmun Rev. 2016;15(2):155–61.
24. Mavropoulos A, Simopoulou T, Varna A, Liaskos C, Katsiari CG, Bogdanos DP, et al. Breg cells are numerically decreased and functionally impaired in patients with systemic sclerosis. Arthritis Rheumatol. 2016;68(2):494–504.
25. Odaka M, Hasegawa M, Hamaguchi Y, Ishiura N, Kumada S, Matsushita T, et al. Autoantibody-mediated regulation of B cell responses by functional anti-CD22 autoantibodies in patients with systemic sclerosis. Clin Exp Immunol. 2010;159(2):176–84.
26. Sato S, Hasegawa M, Fujimoto M, Tedder TF, Takehara K. Quantitative genetic variation in CD19 expression correlates with autoimmunity. J Immunol. 2000;165(11):6635–43.
27. Saigusa R, Asano Y, Nakamura K, Yamashita T, Ichimura Y, Takahashi T, et al. Association of anti-RNA polymerase III antibody and silicone breast implants in patients with systemic sclerosis. J Dermatol. 2014;41(7):606–10.
28. Saigusa R, Asano Y, Nakamura K, Miura S, Ichimura Y, Takahashi T, et al. Association of anti-RNA polymerase III antibody and malignancy in Japanese patients with systemic sclerosis. J Dermatol. 2015;42(5):524–7.
29. Yanaba K, Hayashi M, Yoshihara Y, Nakagawa H. Serum levels of soluble programmed death-1 and programmed death ligand-1 in systemic sclerosis: association with extent of skin sclerosis. J Dermatol. 2016;43(8):954–7.
30. Nakamura K, Asano Y, Taniguchi T, Minatsuki S, Inabe T, Maki H, et al. Serum levels of interleukin-18-binding protein isoform a: clinical association with inflammation and pulmonary hypertension in systemic sclerosis. J Dermatol. 2014;41(8):912–8.
31. Miura S, Asano Y, Saigusa R, Yamashita T, Taniguchi T, Takahashi T, et al. Serum omentin levels: a possible contribution to vascular involvement in patients with systemic sclerosis. J Dermatol. 2015;42(5):461–6.
32. Miura S, Asano Y, Saigusa R, Yamashita T, Taniguchi T, Takahashi T, et al. Serum vaspin levels: a possible correlation with digital ulcers in patients with systemic sclerosis. J Dermatol. 2015;42(5):528–31.
33. Wu CY, Asano Y, Taniguchi T, Sato S, Yu HS. Serum level of circulating syndecan-1: a possible association with proliferative vasculopathy in systemic sclerosis. J Dermatol. 2016;43(1):63–6.
34. Wu CY, Asano Y, Taniguchi T, Sato S, Yu HS. Serum heparanase levels: a protective marker against digital ulcers in patients with systemic sclerosis. J Dermatol. 2015;42(6):625–8.
35. Campbell PM, LeRoy EC. Pathogenesis of systemic sclerosis: a vascular hypothesis. Semin Arthritis Rheum. 1975;4(4):351–68.
36. Fleischmajer R, Perlish JS. Capillary alterations in scleroderma. J Am Acad Dermatol. 1980;2:161–70.
37. Hunzelmann UF, Hermann K, Böhme HJ. Pathogenesis of progressive systemic sclerosis. Int J Dermatol. 1986;25(5):286–93.
38. Cabral-Marques O, Riemekasten G. Vascular hypothesis revisited: role of stimulating antibodies against angiotensin and endothelin receptors in the pathogenesis of systemic sclerosis. Autoimmun Rev. 2016;15(7):690–4.
39. Bordron A, Dueymes M, Levy Y, Jamin C, Lasry JP, Piette JC, et al. The binding of some human anti-endothelial cell antibodies induces endothelial cell apoptosis. J Clin Invest. 1998;101(10):2029–35.
40. Wolf SI, Howat S, Abraham DJ, Peterson JD, Leskjan C, Agouniti; anti-ICAM-1 antibodies in scleroderma: activation of endothelial pro-inflammatory cascades. Vasc Pharmacol. 2013;59(1–2):19–26.
41. Kill A, Tabeling C, Undeutsch R, Kühl AA, Günther J, Radic M, et al. Autoantibodies to angiotensin and endothelin receptors in systemic sclerosis induce cellular and systemic events associated with disease pathogenesis. Arthritis Res Ther. 2014;16(1):R29. doi:10.1186/ar4457.
42. Xia Y, Kellems RE. Angiotensin receptor agonistic autoantibodies and hypertension: preeclampsia and beyond. Circ Res. 2013;113(1):78–87.
43. Becker MO, Kill A, Kaeche M, Guenther J, Rose A, Tabeling C, et al. Vascular receptor autoantibodies in pulmonary arterial hypertension associated with systemic sclerosis. Am J Respir Crit Care Med. 2014;190(7):808–17.
44. Kawaguchi Y, Takagi K, Hara M, Fukasawa C, Sugiura T, Nishimagi E, et al. Angiotensin II in the lesional skin of systemic sclerosis patients contributes to tissue fibrosis via angiotensin II type 1 receptors. Arthritis Rheum. 2004 Jan;50(1):216–26.
45. Akamata K, Asano Y, Aozasa N, Noda S, Taniguchi T, Takahashi T, et al. Bosentan reverses the pro-fibrotic phenotype of systemic sclerosis dermal fibroblasts via increasing DNA binding ability of transcription factor Fli1. Arthritis Res Ther. 2014;16(2):R36. doi:10.1186/ar4529.
46. Günther J, Kill A, Becker MO, Heidecke H, Radermacher J, Siegert E, et al. Angiotensin receptor type 1 and endothelin receptor type a on immune cells mediate migration and the expression of IL-8 and CCL18 when stimulated by autoantibodies from systemic sclerosis patients. Arthritis Res Ther. 2014;16(2):R65. doi:10.1186/ar4503.
47. Sgonc R, Gruschwitz MS, Dietrich H, Recheis H, Gershwin ME, Wick G. Endothelial cell apoptosis is a primary pathogenetic event underlying skin lesions in avian and human scleroderma. J Clin Invest. 1996;98(3):785–92.
48. Lunardi C, Bason C, Navone R, Millo E, Damonte G, Corrocher R, et al. Systemic sclerosis immunoglobulin G autoantibodies bind the human cytomegalovirus late protein UL94 and induce apoptosis in human endothelial cells. Nat Med. 2000;6(10):1183–6.
49. Lunardi C, Dolcino M, Peterlana D, Bason C, Navone R, Tamassia N, et al. Antibodies against human cytomegalovirus in the pathogenesis of systemic sclerosis: a gene array approach. PLoS Med. 2006;3(1):e2.

Author's personal copy

50. Roumm AD, Whiteside TL, Medsger TA Jr, Rodnan GP. Lymphocytes in the skin of patients with progressive systemic sclerosis. Quantification, subtyping, and clinical correlations. Arthritis Rheum. 1984;27(6):645–53.
51. Gilbane AJ, Denton CP, Holmes AM. Scleroderma pathogenesis: a pivotal role for fibroblasts as effector cells. Arthritis Res Ther. 2013;15(3):215.
52. Penno J, Ouro-Hyor E, Yamamoto M, Smith EA, Robinchik S, Dong JY, et al. An increased transforming growth factor beta receptor type I:type II ratio contributes to elevated collagen protein synthesis that is resistant to inhibition via a kinase-deficient transforming growth factor beta receptor type II in scleroderma. Arthritis Rheum. 2004;50(5):1566–77.
53. Sernali S, Chilli A, Lauricella A, Marghieri F, Giannoni E, Magnelli L, et al. Systemic sclerosis endothelial cells recruit and activate dermal fibroblasts by induction of a connective tissue growth factor (CCN2)/transforming growth factor β-dependent mesenchymal-to-mesenchymal transition. Arthritis Rheum. 2013;65(1):258–69.
54. Leask A. Towards an anti-fibrotic therapy for scleroderma: targeting myofibroblast differentiation and recruitment. Fibrogenesis Tissue Repair. 2010;3:8. doi:10.1186/1755-1536-3-8.
55. Leask A. Getting out of a sticky situation: targeting the myofibroblast in scleroderma. Open Rheumatol J. 2012;6:165–9.
56. Igarashi A, Nashiro K, Kikuchi K, Sato S, Ihn H, Fujimoto M, et al. Connective tissue growth factor gene expression in tissue sections from localized scleroderma, keloid, and other fibrotic skin disorders. J Invest Dermatol. 1996;106(4):729–33.
57. Lakos G, Takagawa S, Chen SJ, Ferreira AM, Han G, Masuda K, et al. Targeted disruption of TGF-beta/Smad3 signaling modulates skin fibrosis in a mouse model of scleroderma. Am J Pathol. 2004;165(1):203–17.
58. Gay S, Jones RE Jr, Huang GQ, Gay RE. Immunohistologic demonstration of platelet-derived growth factor (PDGF) and sis-oncogene expression in scleroderma. J Invest Dermatol. 1989;92(2):301–1.
59. Baroni SS, Santillo M, Bevilacqua F, Luchetti M, Spadoni T, Mancini M, et al. Stimulatory autoantibodies to the PDGF receptor in systemic sclerosis. N Engl J Med. 2006;354(25):2667–76.
60. Hasegawa M, Hamaguchi Y, Yanaba K, Bouaziz JD, Uchida J, Fujimoto M, et al. B-lymphocyte depletion reduces skin fibrosis and autoimmunity in the tight-skin mouse model for systemic sclerosis. Am J Pathol. 2006;169(3):954–66.
61. Castelino FV, Bain G, Pace VA, Black KE, George L, Probst CK, et al. An anastasin-LPA-IL-6 amplification loop drives scleroderma fibrosis. Arthritis Rheumatol. 2014;66(12):2964–74.
62. O'Reilly S, Ciechomska M, Cant R, van Laar JM. Interleukin-6 (IL-6) trans signalling drives a STAT3-dependent pathway that leads to hyperactive transforming growth factor-β (TGF-β) signaling promoting SMAD3 activation and fibrosis via gremlin protein. J Biol Chem. 2014;289(14):9952–60.
63. Postlethwaite AE, Holness MA, Katai H, Raghow R. Human fibroblasts synthesize elevated levels of extracellular matrix proteins in response to interleukin 4. J Clin Invest. 1992;90(4):1479–85.
64. Jinnin M, Ihn H, Yamane K, Tamaki K. Interleukin-13 stimulates the transcription of the human alpha2(I) collagen gene in human dermal fibroblasts. J Biol Chem. 2004;279(40):41783–91.
65. Kavanaugh M, Hesse M, Lemaitre M, Chaver AW, Davey SJ, McKerrow JH, et al. IL-13 activates a mechanism of tissue fibrosis that is completely TGF-beta independent. J Immunol. 2004;173(6):4020–9.
66. Hasegawa M, Fujimoto M, Kikuchi K, Takehara K. Elevated serum levels of interleukin 4 (IL-4), IL-10, and IL-13 in patients with systemic sclerosis. J Rheumatol. 1997;24(2):328–32.
67. Fallon PG, Richardson EJ, McKenzie GJ, McKenzie AN. Schistosome infection of transgenic mice defines distinct and contrasting pathogenic roles for IL-4 and IL-13: IL-13 is a profibrotic agent. J Immunol. 2000;164(5):2585–91.
68. Fuschiotti P, Larregina AT, Ho J, Feghali-Bostwick C, Medsger TA Jr. Interleukin-13-producing CD8+ T cells mediate dermal fibrosis in patients with systemic sclerosis. Arthritis Rheum. 2013;65(1):236–46.
69. Takagawa S, Lakos G, Mori Y, Yamamoto T, Nishioka K, Varga J. Sustained activation of fibroblast transforming growth factor-beta/Smad signaling in a murine model of scleroderma. J Invest Dermatol. 2003;121(1):41–50.
70. Jaffee BD, Claman HN. Chronic graft-versus-host disease (GVHD) as a model for scleroderma. I. Description of model systems. Cell Immunol. 1983;77(1):1–12.
71. Rieck MC, Jin S, Ledbetter S, Richards SM, Garmer RD. A modified model of graft-versus-host-induced systemic sclerosis (scleroderma) exhibits all major aspects of the human disease. Arthritis Rheum. 2004;50(4):1319–31.
72. Servettaz A, Goulvestre C, Kavian N, Nicco C, Guilpain P, Chéreau C, et al. Selective oxidation of DNA topoisomerase 1 induces systemic sclerosis in the mouse. J Immunol. 2009;182(9):5855–64.
73. Yoshizaki A, Yanaba K, Ogawa A, Asano Y, Kadono T, Sato S. Immunization with DNA topoisomerase I and Freund's complete adjuvant induces skin and lung fibrosis and autoimmunity via interleukin-6 signaling. Arthritis Rheum. 2011;63(11):3515–85.
74. Stawski L, Han R, Bujor AM, Trojanowska M. Angiotensin II induces skin fibrosis: a novel mouse model of dermal fibrosis. Arthritis Res Ther. 2012;14(4):R194. doi:10.1186/ar4028.
75. Saracusa LD, McGrath R, Ma Q, Moskow JJ, Manne J, Christner PJ, et al. A tandem duplication within the fibrillin 1 gene is associated with the mouse tight skin mutation. Genome Res. 1996;6(4):300–13.
76. Sonnylal S, Denton CP, Zheng B, Keene DR, He R, Adams HP, et al. Postnatal induction of transforming growth factor beta signaling in fibroblasts of mice recapitulates clinical, histologic, and biochemical features of scleroderma. Arthritis Rheum. 2007;56(1):334–44.
77. Sonnylal S, Shi-Wen X, Leoni P, Naff K, Van Pelt CS, Nakamura H, et al. Selective expression of connective tissue growth factor in fibroblasts in vivo promotes systemic tissue fibrosis. Arthritis Rheum. 2010;62(5):1523–32.
78. Wei J, Melichian D, Komura K, Hinchcliff M, Lam AP, Lafyatis R, et al. Canonical Wnt signaling induces skin fibrosis and subcutaneous lipoatrophy: a novel mouse model for scleroderma? Arthritis Rheum. 2011;63(6):1707–17.
79. Eferl R, Hasselblatt P, Rath M, Popper H, Zenz R, Komnenovic V, et al. Development of pulmonary fibrosis through a pathway involving the transcription factor Fra-2/AP-1. Proc Natl Acad Sci U S A. 2008;105(30):10525–30.
80. Maurer B, Busch N, Jüngel A, Pileckyte M, Gay RE, Michel BA, et al. Transcription factor fos-related antigen-2 induces progressive peripheral vasculopathy in mice closely resembling human systemic sclerosis. Circulation. 2009;120(23):2367–76.
81. Kanno Y, Kanzaki A, Minamiide M, Kanno M, Tomogane K, Takeuchi K, et al. The absence of uPAR is associated with the progression of dermal fibrosis. J Invest Dermatol. 2008;128(12):2792–7.
82. Bernstein AM, Twining SS, Warejcka DJ, Tall E, Masur SK. Urokinase receptor cleavage: a crucial step in fibroblast-to-myofibroblast differentiation. Mol Biol Cell. 2007;18(7):2716–27.
83. D'Alessio S, Fibbi G, Cinelli M, Guiducci S, Del Rosso A, Margheri F, et al. Matrix metalloproteinase 12-dependent cleavage of urokinase receptor in systemic sclerosis microvascular

Author's personal copy

endothelial cells results in impaired angiogenesis. Arthritis Rheum. 2004;50(10):1275–85.

84. Manfioro F, Muneti M, Serrati S, Nosi D, Pucci M, Matucci-Cerinic M, et al. Domain 1 of the urokinase-type plasminogen activator receptor is required for its morphologic and functional beta2 integrin-mediated connection with actin cytoskeleton in human microvascular endothelial cells: failure of association in systemic sclerosis endothelial cells. Arthritis Rheum. 2006;54(12):3926–18.

85. Muneti M, Rossi L, Milia AF, Guiducci S, Carmeliet P, Ibba-Manneschi L, et al. Inactivation of urokinase-type plasminogen activator receptor (uPAR) gene induces dermal and pulmonary fibrosis and peripheral microvasculopathy in mice: a new model of experimental scleroderma? Ann Rheum Dis. 2014;73(9):1700–9.

86. Noda S, Asano Y, Nishimura S, Taniguchi T, Fujiu K, Manabe I, et al. Simultaneous downregulation of KLF5 and Fli1 is a key feature underlying systemic sclerosis. Nat Commun. 2014;5:5797. doi:10.1038/ncomms6797.

87. Czuwara-Ladykowska J, Shirasaki F, Jackers P, Watson DK, Trojanowska M. Fli-1 inhibits collagen type I production in dermal fibroblasts via an Sp1-dependent pathway. J Biol Chem. 2001;276(24):20839–48.

88. Kubo M, Czuwara-Ladykowska J, Moussa O, Markiewicz M, Smith E, Silver RM, et al. Persistent down-regulation of Fli1, a suppressor of collagen transcription, in fibrotic scleroderma skin. Am J Pathol. 2003;163(2):571–81.

89. Whitfield ML, Finlay DR, Murray JI, Troyanskaya OG, Chi JT, Pergamenschikov A, et al. Systemic and cell type-specific gene expression patterns in scleroderma skin. Proc Natl Acad Sci U S A. 2003;100(21):12319–24.

90. van den Hoogen FH, Boerbooms AM, Swaak AJ, Rasker JJ, van Lier HJ, van de Putte LB. Comparison of methotrexate with placebo in the treatment of systemic sclerosis: a 24 week randomized double-blind trial, followed by a 24 week observational trial. Br J Rheumatol. 1996;35(4):364–72.

91. Pope JE, Bellamy N, Seibold JR, Baron M, Ellman M, Carette S, et al. A randomized, controlled trial of methotrexate versus placebo in early diffuse scleroderma. Arthritis Rheum. 2001;44(6):1351–8.

92. Tashkin DP, Elashoff R, Clements PJ, Goldin J, Roth MD, Furst DE, et al. Cyclophosphamide versus placebo in scleroderma lung disease. N Engl J Med. 2006;354(25):2655–66.

93. Hoyles RK, Ellis RW, Wellsbury J, Lees B, Newlands P, Goh NS, et al. A multicenter, prospective, randomized, double-blind, placebo-controlled trial of corticosteroids and intravenous cyclophosphamide followed by oral azathioprine for the treatment of pulmonary fibrosis in scleroderma. Arthritis Rheum. 2006;54(12):3962–70.

94. Koutroumpas A, Ziogas A, Alexiou I, Iliaroula G, Sakkas LI. Mycophenolate mofetil in systemic sclerosis-associated interstitial lung disease. Clin Rheumatol. 2010;29(10):1167–8.

95. Gerbino AJ, Goss CH, Molitor JA. Effect of mycophenolate mofetil on pulmonary function in scleroderma-associated interstitial lung disease. Chest. 2008;133(2):455–60.

96. Poelman CL, Hummers LK, Wigley FM, Anderson C, Boin F, Shah AA. Intravenous immunoglobulin may be an effective therapy for refractory, active diffuse cutaneous systemic sclerosis. J Rheumatol. 2015;42(2):236–42.

97. Takehara K, Ihn H, Sato S. A randomized, double-blind, placebo-controlled trial. Intravenous immunoglobulin treatment in patients with diffuse cutaneous systemic sclerosis. Clin Exp Rheumatol. 2013;31(2 Suppl 76):151–6.

98. Kowal-Bielecka O, Landewé R, Avouac J, Chwiesko S, Miniati I, Czirjak L, et al. EULAR recommendations for the treatment of systemic sclerosis: a report from the EULAR scleroderma trials and research group (EUSTAR). Ann Rheum Dis. 2009;68(5):620–8.

99. Denton CP, Pope JE, Peter HH, Gilleichl A, Bocanegra A, van den Hoogen FH, et al. Long-term effects of bosentan on quality of life, survival, safety and tolerability in pulmonary arterial hypertension related to connective tissue diseases. Ann Rheum Dis. 2008;67(9):1222–8.

100. Lopez-Ovejero JA, Saul SD, D'Angelo WA, Cheigh JS, Stenzel KH, Laragh JH. Reversal of vascular and renal crises of scleroderma by oral angiotensin-converting-enzyme blockade. N Engl J Med. 1979;300(25):1417–9.

101. Motegi S, Yamada K, Toki S, Uchiyama A, Kubota Y, Nakamura T, et al. Beneficial effect of botulinum toxin a on Raynaud's phenomenon in Japanese patients with systemic sclerosis: a prospective, case series study. J Dermatol. 2016;43(1):58–62.

102. Daoussis D, Melissaropoulos K, Sakellaropoulos G, Antonopoulos I, Markatseli TE, Simopoulou T, et al. A multicenter, open-label, comparative study of B-cell depletion therapy with rituximab for systemic sclerosis-associated interstitial lung disease. Semin Arthritis Rheum. 2016; doi:10.1016/j.semarthrit.2016.10.003.

103. Smith V, Piette Y, Butrym A, Decuman S, Brusselle G, De Keyser F, et al. Stabilization of microcirculation in patients with early systemic sclerosis with diffuse skin involvement following rituximab treatment: an open-label study. J Rheumatol. 2016;43(5):995–6.

104. Boselli S, De Santis M, Lama G, Spadi C, Angelucci C, Tolusso B, et al. B cell depletion in diffuse progressive systemic sclerosis: safety, skin score modification and IL-6 modulation in an up to thirty-six months follow-up open-label trial. Arthritis Res Ther. 2010;12(2):R54. doi:10.1186/ar2965.

105. Rice LM, Padilla CM, McLaughlin SR, Mathes A, Ziemek J, Goummih S, et al. Fresolimumab treatment decreases biomarkers and improves clinical symptoms in systemic sclerosis patients. J Clin Invest. 2015;125(7):2795–807.

106. Khanna D, Denton CP, Jahreis A, van Laar JM, Frech TM, Anderson ME, et al. Safety and efficacy of subcutaneous tocilizumab in adults with systemic sclerosis (faSScinate): a phase 2, randomized, controlled trial. Lancet. 2016;387(10038):2630–40.

107. Shima Y, Hosen N, Kimuro T, Arimitsu J, Nishida S, Hagihara K, et al. Expansion of range of joint motion following treatment of systemic sclerosis with tocilizumab. Mod Rheumatol. 2015;25(1):134–7.

108. Yoshizaki A, Yanaba K, Yoshizaki A, Iwata Y, Komura K, Ogawa F, et al. Treatment with rapamycin prevents fibrosis in tight-skin and bleomycin-induced mouse models of systemic sclerosis. Arthritis Rheum. 2010;62(8):2476–87.

109. Su TI, Khanna D, Furst DE, Danoviteh G, Burger C, Maranian P, et al. Rapamycin versus methotrexate in early diffuse systemic sclerosis: results from a randomized, single-blind pilot study. Arthritis Rheum. 2009;60(12):3821–30.

110. Albera C, Costabel U, Fagan EA, Glassberg MK, Gorina E, Lancaster L, et al. Efficacy of pirfenidone in patients with idiopathic pulmonary fibrosis with more preserved lung function. Eur Respir J. 2016;48(3):843–51.

111. Lopez-de la Mora DA, Sanchez-Roque C, Montaya-Buelna M, Sanchez-Enriquez S, Lucano-Landeros S, Macias-Barragan J, et al. Role and new insights of Pirfenidone in fibrotic diseases. Int J Med Sci. 2015;12(11):846–7.

112. Distler JH, Feghali-Bostwick C, Soare A, Asano Y, Distler O, Abraham DJ. Frontiers of antifibrotic therapy in systemic sclerosis. Arthritis Rheumatol. 2017;69(2):257–67.

Expert Opinion on Investigational Drugs

ISSN: 1354-3784 (Print) 1744-7658 (Online) Journal homepage: http://www.tandfonline.com/loi/ieid20

Topical E6005/RVT-501, a novel phosphodiesterase 4 inhibitor, for the treatment of atopic dermatitis

Masutaka Furue, Takafumi Kadono, Gaku Tsuji & Takeshi Nakahara

To cite this article: Masutaka Furue, Takafumi Kadono, Gaku Tsuji & Takeshi Nakahara (2017) Topical E6005/RVT-501, a novel phosphodiesterase 4 inhibitor, for the treatment of atopic dermatitis, Expert Opinion on Investigational Drugs, 26: 12, 1403-1408, DOI: 10.1080/13543784.2017.1397626

To link to this article: http://dx.doi.org/10.1080/13543784.2017.1397626

Accepted author version posted online: 25 Oct 2017.
Published online: 31 Oct 2017.

Submit your article to this journal

Article views: 31

View related articles

View Crossmark data

Full Terms & Conditions of access and use can be found at
http://www.tandfonline.com/action/journalInformation?journalCode=ieid20

Download by: [Kyushu University] Date: 06 November 2017, At: 23:48

EXPERT OPINION ON INVESTIGATIONAL DRUGS, 2017
VOL. 26, NO. 12, 1401–1408
https://doi.org/10.1080/13543784.2017.1397626

Taylor & Francis
Taylor & Francis Group

DRUG EVALUATION

Topical E6005/RVT-501, a novel phosphodiesterase 4 inhibitor, for the treatment of atopic dermatitis

Masutaka Furue[a,b], Takafumi Kadono[d], Gaku Tsuji[c] and Takeshi Nakahara[c]

[a]Department of Dermatology, Kyushu University, Fukuoka, Japan; [b]Division of Skin Surface Sensing, Department of Dermatology, Kyushu University, Fukuoka, Japan; [c]Research and Clinical Center for Yusho and Dioxin, Kyushu University, Fukuoka, Japan; [d]Department of Dermatology, St Marianna University School of Medicine, Kawasaki, Japan

ABSTRACT

Introduction: Local adverse effects of steroid use and the burning sensation of calcineurin inhibitors impair patients' adherence to treatment and decrease the treatment response in atopic dermatitis (AD). Steroid phobia appears to be a psychological problem in patients with AD. Topical non-steroidal remedies are in demand.

Areas covered: This manuscript reviews the current literature on preclinical and clinical studies regarding topical E6005/RVT-501, a novel phosphodiesterase 4 inhibitor. We also discuss the mechanistic background of E6005/RVT-501 in the treatment of AD.

Expert opinion: Topical E6005/RVT-501 improves skin eruption and pruritus of pediatric and adult AD patients without any serious side effects. It is useful for mild to moderate lesions of AD in pediatric and adult patients. Topical E6005/RVT-501 is non-steroidal agent but its potency is equal to that of mild rank topical steroid, therefore, it may fit the demand of patients with steroid phobia. Its steroid-sparing effects may also be investigated in future clinical trials and may minimize the dose and frequency of topical steroids.

ARTICLE HISTORY
Received 26 August 2017
Accepted 24 October 2017

KEYWORDS
Atopic dermatitis; E6005/RVT-501; clinical trial; pathomechanism; steroid phobia

Downloaded by [Kyushu University] at 23:48 06 November 2017

1. Introduction

Atopic dermatitis (AD) is a common eczematous skin disorder affecting between 2% and 20% of the general population across age and ethnic differences [1]. AD is characterized by chronic cutaneous inflammation and dry skin with epidermal barrier dysfunction [1,2,3]. Intense itching and frequent exacerbations are significant burdens for patients with AD, therefore, patient quality of life is impaired, especially in patients with extensive lesions [1,4,5]. Itch-induced scratching appears to exacerbate skin inflammation by accelerating cellular damage in the afflicted skin [6]. Although many reports confirm the anti-pruritic effects of conventional treatments [7], the satisfaction and tolerance to treatments are typically very low in AD patients [8]. Development of new antipruritic agents is currently in demand.

2. Overview of the market

AD is currently considered as a biphasic T cell-mediated disease. A Th2 signal predominates in the acute phase, whereas a Th2 to Th1 switch promotes disease chronicity [9–11]. However, recent studies have proposed a significant role for interleukin (IL)-22 producing T cells (Th22), and to a lesser extent, IL-17 producing Th17 cells in the initiation and maintenance of AD [9,10]. In addition, sustained skin inflammation in AD increases comorbidity risk for systemic disorders such as obesity, cardiovascular diseases, mental problems, and autoimmune diseases, most likely due to enhanced production of IL-1 and tumor necrosis factor α (TNFα) [12,13].

Th2-derived IL-4 and IL-13 are particularly important in promoting atopic inflammation [9,14]. IL-4 and IL-13 also reduce the expression of skin barrier proteins such as filaggrin and exacerbate barrier dysfunction leading to skin irritation and microbial colonization [14–17]. Therefore, injection of anti-IL-4 receptor α antibody dupilumab, which blocks IL-4 and IL-13 signaling, is effective in controlling clinical signs and symptoms of AD [18–21].

Among various pruritogens [22], Th2-derived IL-31 has generated increased attention because the administration of IL-31 induces scratching behavior in rodents, dogs, and monkeys [23]. In line with this notion, injection of the anti-IL-31 receptor A antibody nemolizumab successfully and safely reduces pruritus and skin inflammation in patients with AD [24,25]. Oral administration of histamine H4 receptor antagonist is also potentially useful for reducing atopic itch [26,27].

In addition to targeting the IL-4 receptor, IL-31 receptor, and H4 receptor, several new topical nonsteroidal agents are now in preclinical and clinical trial testing including Janus kinase inhibitors [28,29] and aryl hydrocarbon receptor agonist [30,31]. Topical phosphodiesterase 4 (PDE4) inhibitors are promising new drugs that act to inhibit the inflammation and pruritus of AD. The topical PDE4 inhibitor crisaborole (Eucrisa) has already been approved for the treatment of AD in the

CONTACT Masutaka Furue furue@dermatol.med.kyushu-u.ac.jp Department of Dermatology, Kyushu University, Maidashi 3-1-1, Higashiku, Fukuoka 812-8582, Japan

© 2017 Informa UK Limited, trading as Taylor & Francis Group

Article highlights

- E6005/RVT-501 is a novel phosphodiesterase 4 inhibitor.
- Topical E6005/RVT-501 exhibits anti-inflammatory and anti-pruritic function.
- Topical E6005/RVT-501 is effective for the treatment of infantile and adult atopic dermatitis without any serious adverse events.
- Topical E6005/RVT-501 may satisfy the demand for an effective, non-steroidal topical drug for AD patients and their caregivers.

This box summarizes key points contained in the article

United States [32–34]. In this study, we summarize the preclinical and clinical data on another topical PDE4 inhibitor, E6005/RVT-501 [35,36].

3. Introduction to the compound

The cyclic nucleotide cAMP is a naturally occurring, intracellular, secondary messenger which regulates production and release of various mediators. Adenylyl cyclase induces the production of cAMP, and it is degraded by PDEs [37,38]. Among 11 PDEs, PDE3 and PDE4 predominantly hydrolyze cAMP in most mammalian cells [37,38]. Unlike PDE3, PDE4 is cAMP-specific and the dominant PDE in immune cells [37,38]. PDE4 is also expressed in keratinocytes, vascular endothelial cells, mast cells, and dorsal root ganglion (DRG) neurons [37–40].

PDE4 inhibitor interferes with the degradation of cAMP by inhibiting enzymatic activity of PDE4; therefore, intracellular levels of cAMP increase [38,41]. The elevated cAMP activates protein kinase A and then inhibits the activity of transcription factors NFAT and NFκB, which act to downregulate the production of various cytokines such as TNFα, IL-1, IL-2, IL-4, IL-6, IL-23, IL-31, and interferon-γ (IFNγ) [38,42]. The levels of PDE4 in the peripheral bloods are increased in patients with AD compared to healthy controls, indicating that atopic immune cells retain a pro-inflammatory state [43]. Moreover, the levels of cAMP were downregulated in the lesional skin compared to non-lesional skin in NC/Nga mice with AD like skin lesion [44].

Apremilast is an oral PDE4 inhibitor which has been approved for clinical use for the treatment of psoriasis. Apremilast inhibits a broad spectrum of Th1-, Th2-, and Th17-derived cyto-chemokines and pro-inflammatory cytokines including IL-2, IFNγ, IL-5, IL-13, IL-10, CCL5, IL-17, TNFα, and granulocyte-macrophage colony stimulating factor [38,41,45]. Based on their mild, but broad and consistent immunosuppressive action, both oral apremilast and topical crisaborole are effective in treating psoriasis and AD, respectively [32–34,46–48].

4. Chemistry and preclinical study

E6005 (methyl4-[(3-[6,7-dimethoxy-2-(methylamino)quinazolin-4-yl]phenyl)amino]carbonyl]benzoate) is a novel, selective PDE4 inhibitor which was developed in-house by Eisai's Tsukuba Research Institute and is now called RVT-501 after licensing out to Novant, Switzerland, and is advancing to

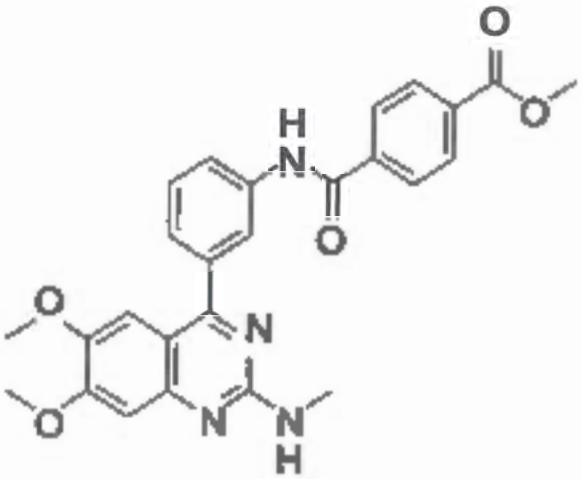

Figure 1. Chemical structure of E6005/RVT-501. https://www.chemspider.com/Chemical-Structure.947620.html

Box 1. Drug summary.

Drug name	E6005/RVT-501
Phase	Phase II
Indication	Atopic dermatitis
Pharmacology description/ mechanism of action	Type 4 cyclic nucleotide phosphodiesterase inhibitor
Route of administration	Topical
Chemical structure	$C_{26}H_{24}N_4O_5$
Pivotal trial(s)	[37]

further clinical trials (https://dermavantsciences.com/category/rvt-501/) [49] (Figure 1) (Box 1). Like other PDE4 inhibitors, E6005/RVT-501 inhibits the production of IL-2, IL-4, IFNγ, TNFα, and IL-12 in human peripheral blood cells (Table 1) [49].

Topical E6005/RVT-501 ameliorates the dermatitis score of chronic murine dermatitis by repeated application of oxazolone, which is associated with a downregulation of IL-1β and IL-4 gene expression [49]. Mite-induced murine dermatitis is also inhibited by topical E6005/RVT-501 [49]. In histology analyses, topical E6005/RVT-501 reduced the epidermal acanthosis both in oxazolone- and mite-induced dermatitis models [49]. Topical application of E6005/RVT-501 does increase and normalize the decreased cAMP levels in murine dermatitis lesions (Table 1) [44].

Interestingly, scratching behaviors are inhibited by E6005/RVT-501 in mice with oxazolone-induced dermatitis and in the mite-infested NC/Nga mice models [44,49]. Likewise, E6005/RVT-501 inhibits the firing spike activity of cutaneous nerves innervating in the area affected by

Table 1. E6005/RVT-501.

Inhibits IL-2, IL-4, IFNγ, TNFα, and IL-12 production [49]
Inhibits oxazolone-induced murine dermatitis [49]
Inhibits mite-induced murine dermatitis [49]
Inhibits scratching behaviors in murine dermatitis [44,49]
Inhibits proteinase-activated receptor 2-mediated scratching [39]
Inhibits firing frequency of murine cutaneous nerve in inflamed skin [39]
Inhibits firing frequency of dorsal root ganglion cells stimulated with capsaicin [49]

Downloaded by [Kyushu University] at 23:48 30 November 2017

dermatitis [44]. Cutaneous levels of nerve growth factor are correlated with dermatitis score and scratching behaviors in the lesions of murine irritated skin model [50]. Topical application of E6005/RVT-501 dose-dependently reduces the cutaneous levels of nerve growth factor [50].

Agonistic stimulation of proteinase-activated receptor 2 (PAR2) induces pruritus [4,5]. Intradermal injection of SLIGRL, a selective agonist for PAR2, evokes scratching behavior in mice [39]. Topical E6005/RVT-501 dose-dependently inhibited the PAR2-mediated scratching in conjunction with a significant reduction in the firing frequency of innervated cutaneous nerves [39]. In the PAR2-injected skin, the cAMP levels are also decreased, but it is recovered or normalized by topical application of E6005/RVT-501 [39]. Regarding the neuronal regulation, E6005/RVT-501 elevates the cAMP levels in the DRG neurons and inhibits their depolarization induced by a transient receptor potential vanilloid 1 activator, capsaicin (Table 1) [40].

These preclinical results indicate the anti-inflammatory and antipruritic potency of topical E6005/RVT-501. Therefore, clinical trials were begun to prove its safety and efficacy in the treatment of AD.

5. Clinical efficacy, pharmacokinetics, and safety

Four reports have been published in the literature [35,36,51,52]. Safety, tolerability, and pharmacokinetics of topical application of E6005/RVT-501 were studied in healthy volunteers ($N = 36$, Study 001) and in patients with AD ($N = 40$, Study 101) by topically applying 0.01–0.2% of E6005/RVT-501 ointment in a randomized, investigator-blind, vehicle-controlled manner [51,52]. Neither skin irritation nor photosensitization was observed with application of E6005/RVT-501 in Study 001. Four subjects receiving E6005/RVT-501 in Study 001 experienced a treatment-emergent adverse event (application site edema, increased alanine aminotransferase or erythema); three of these subjects discontinued the study. Two subjects receiving E6005/RVT-501 in Study 101 experienced an adverse event (gout or enterocolitis); one discontinued the study. Plasma concentrations of E6005/RVT-501 were below the detectable limit of quantification (1 ng/ml) in both studies [51]. These results indicated acceptable safety and tolerability thresholds for E6005/RVT-501 ointment. Systemic exposure was also negligible by topical E6005/RVT-501 application.

In a randomized, investigator-blinded, vehicle-controlled, multiple ascending dose study (Study 101), 40 adult male patients with AD were randomly assigned to 10 days of treatment with either E6005/RVT-501 ointment (0.01%, 0.03%, 0.1%, or 0.2%) or vehicle ointment [52]. One patient receiving 0.03% E6005/RVT-501 treatment discontinued because of acute gout, and one receiving vehicle treatment discontinued because of progression of AD. The targeted lesion severity scores decreased in a concentration-dependent manner in patients treated with E6005. The decrease in severity scores was significant in the 0.2% E6005/RVT-501 ointment treatment group (mean percent change: 54.30%, $p = 0.007$) [52].

In the third clinical trial, a total of 78 adult AD patients were randomized to receive either the 0.2% E6005/RVT-501 ointment or vehicle control at an allocation ratio of 2:1 [35]. A randomization phase of 4 weeks was followed by an extension phase of 8 weeks. In the extension phase, all 67 subjects who completed the randomization phase were treated with 0.2% E6005/RVT-501 ointment. The 12 week application of topical E6005/RVT-501 twice daily was safe and well tolerated. No deaths or other serious adverse effects were observed. Plasma E6005/RVT-501 was undetectable in all subjects at all sampling points, while very low plasma concentrations of an E6005/RVT-501 metabolite were detected in 47% of subjects receiving E6005/RVT-501 treatment. At the end of week 4, Eczema Area and Severity Index (EASI), Severity Scoring Atopic Dermatitis (SCORAD) objective, SCORAD-C (visual analog scales for pruritus and sleep loss), Behavioral Rating Scale for Itch, and the severity of the targeted eczematous lesions in the topical E6005/RVT-501 group showed trends toward improvement compared with those in the vehicle group (not statistically significant). In addition, the group receiving topical E6005/RVT-501 for 12 weeks showed significant score reductions from baselines for EASI ($p = 0.030$), SCORAD objective ($p < 0.001$), and SCORAD-C ($p = 0.038$) [35].

Due to the safety profile and favorable efficacy for adult AD patients, the next clinical trial targeted childhood AD [36]. A randomized, multicenter study was conducted in 62 children with mild-to-moderate AD who were treated with E6005/RVT-501 (0.05% or 0.2%) or vehicle ointment twice daily for 2 weeks [36]. The 2-week application of topical E6005/RVT-501 was safe and well tolerated, with no cutaneous adverse events. The whole blood concentration of E6005/RVT-501 was quantified in only one subject receiving 0.2% E6005/RVT-501 treatment, while its major metabolite was undetectable. The 0.2% E6005/RVT-501 group showed a greater decrease in the severity score as opposed to the vehicle group (−45.94% vs. −32.26%), although this difference was not statistically significant. Similarly, the treatment success rate according to the investigator's global assessment of the total application sites was higher in the 0.2% E6005/RVT-501 group than in the vehicle group (34.4% vs. 20.0%). Moreover, the 0.2% E6005/RVT-501 group showed a greater decrease in the pruritus score than the vehicle group (−37.5% vs. −6.7%) in a predefined subpopulation [36].

These clinical studies suggest that topical 0.2% E6005/RVT-501 treatment is safe, tolerable, and effective in pediatric and adult patients with AD. However, further large confirmatory clinical trials are warranted.

6. Regulatory affairs and conclusion

Since topical E6005/RVT-501 has been licensed out from Eisai to Roivant, clinical trial transiently slows down. However, further global studies are now scheduled by Roivant. In conclusion, topical E6005/RVT-501 is a new, safe, and effective therapeutic agent which may satisfy the unmet needs of patients with pediatric and adult AD.

Downloaded by [Kyushu University] at 23:48 06 November 2017

7. Expert opinion

First-line treatments of AD comprise application of emollients for dry skin, topical steroids, and calcineurin inhibitors for skin inflammation, followed by second-line adjunct therapies such as systemic cyclosporin, short-term oral steroids, and ultraviolet radiation [3,53]. The daily application of emollients is useful for reducing the risk of AD development and has steroid-sparing effects [54–56]. However, moisturizers are not feasible to inhibit ongoing skin inflammation and severe pruritus.

Topical steroids and calcineurin inhibitors, especially by proactive application, are effective in controlling the symptoms and signs of AD [57–59]. However, the main obstacle to use of topical calcineurin inhibitors is its local side effect, a burning sensation, which sometimes leads to discontinuation of treatment [60]. Black-box caution for putative oncogenesis is another obstacle to lower the adherence to topical calcineurin inhibitors. Long-term use of topical steroid induces localized side effects such as skin atrophy [61–63]. It is not uncommon for patients to express irrational fear and anxiety (steroid phobia) about using topical steroids, and this may lead to poor patient adherence and lack of response to treatment [8,61–63]. Steroid phobia is intractable in some patients even after therapeutic patient education [64].

Systemic cyclosporine is useful for the patients with extensive lesions untreatable with topical therapy alone. Physicians must check renal function, hypertension, hepatitis virus infection, and blood sugar in patients treated with systemic cyclosporine. Pituitary-adrenal insufficiency is an unavoidable adverse effect in systemic steroid. These systemic treatments including systemic phototherapy are not usually applicable to pediatric AD [65].

Nonsteroidal topical remedies with minimal side effects are in high demand for pediatric patients and their caregivers. Topical Fe(III)-5/RVT-501 does possess anti-inflammatory function without any serious side effects [35,36,51,52]. Although its anti-inflammatory potency is not strong enough as potent topical steroid, it is useful for mild to moderate lesions of AD in pediatric and adult patients [35,36,51,52]. Its steroid-sparing effects may also be expected to be seen in future clinical trials and it may contribute to lessening patient fear by minimizing the dose and frequency of topical steroids.

Funding

This paper was not funded.

Declaration of interest

Masutaka Furue served as a consultant to Eisai Co., Ltd. The authors have no other relevant affiliations or financial involvement with any organization or entity with a financial interest in or financial conflict with the subject matter or materials discussed in the manuscript apart from those disclosed.

A reviewer on this manuscript has disclosed support from pharmaceutical companies including Pfizer (Eucrisa) and Sanofi/Regeneron (dupilumab). A reviewer on this manuscript has also disclosed that they are a consultant for Otsuka Pharmaceutical Development (OPA-15406).

References

Papers of special note have been highlighted as either of interest (•) or of considerable interest (••) to readers.

1. Furue M, Chiba T, Tsuji G, et al. Atopic dermatitis: immune deviation, barrier dysfunction, IgE autoreactivity and new therapies. Allergol Int. 2017;66(3):389–403.
2. Lee SC. Committee of Korean Atopic Dermatitis Association for REACH. Various diagnostic criteria for atopic dermatitis (AD): a proposal of Reliable Estimation of Atopic Dermatitis in Childhood (REACH) criteria, a novel questionnaire-based diagnostic tool for AD. J Dermatol. 2016;43(1):378–384.
3. Saeki H, Nakahara T, Tanaka A, et al. Clinical practice guidelines for the management of atopic dermatitis. J Dermatol. 2016;43(10):1117–1145.
4. Furue M, Kadono T. New therapies for controlling atopic itch. J Dermatol. 2015;42(9):847–850.
5. Kelly-Rabinowitz M, Furue M, Ulzurrun-de-la-Colina N, et al. In vivo atopic dermatitis immunopathology. Allergy Clin Immunol. 2017;139(1):113–122.
6. Takeuchi S, Yasukawa F, Furue M, et al. Colored mice: a model to assess the effects of scratching. J Dermatol Sci. 2010;57(1):44–50.
7. Sher LG, Chang J, Patel B, et al. Relieving the pruritus of atopic dermatitis: a meta-analysis. Acta Derm Venereol. 2012;92(5):455–461.
8. Minota H, Takeuchi S, Sugaya M, et al. Characterization of socio-economic status of Japanese patients with atopic dermatitis showing poor medical adherence and reasons for drug discontinuation. J Dermatol Sci. 2015;79(3):279–287.
9. Gittler JK, Shemer A, Suárez-Fariñas M, et al. Progressive activation of T(H)2/T(H)22 cytokines and selective epidermal proteins characterizes acute and chronic atopic dermatitis. J Allergy Clin Immunol. 2012;130(5):1344–1354.
10. Czarnowicki T, Esaki H, Gonzalez J, et al. Early pediatric atopic dermatitis shows only a cutaneous lymphocyte antigen (CLA)(+) TH2/TH1 cell imbalance, whereas adults acquire CLA(+) TH22/TC22 cell subsets. J Allergy Clin Immunol. 2015;136(4):941–951.
11. Esaki H, Takeuchi S, Furusyo N, et al. Levels of immunoglobulin E specific to the major food allergen and chemokine (C-C motif) ligand (CCL)17/thymus and activation-regulated chemokine and CCL22/macrophage-derived chemokine in infantile atopic dermatitis on Ishigaki Island. J Dermatol. 2016;43(11):1278–1282.
12. Kanipa R, Aoyama Y, Nicho E, et al. Management of erythematous skin lesions in bullous pemphigoid associated with atopic dermatitis. J Dermatol. 2016;43(9):1102–1103.
13. Furue M, Kadono T. Inflammatory skin match in atopic dermatitis and psoriasis. Inflamm Res. 2017 Jun 15. DOI:10.1007/s00011-017-1065-z.
14. Van Den Bogaard EH, Bergboer JG, Vonk-Bergers M, et al. Coal tar induces AHR-dependent skin barrier repair in atopic dermatitis. J Clin Invest. 2013;123(2):917–927.
15. Tabe K, Mitoma C, Hashimoto-Hachiya A, et al. Antioxidant soybean for Glyteer rescues T-helper-mediated downregulation of filaggrin expression via aryl hydrocarbon receptor. J Dermatol. 2015;43(2):157–163.
16. Park J, Jekal DW, Kim Y, et al. Novel FLG null mutations in Korean patients with atopic dermatitis and comparison of the mutational spectra in Asian populations. J Dermatol. 2015;42(9):867–873.
17. Powers CE, McShane DB, Gilliam AE, et al. Microbiome and pediatric atopic dermatitis. J Dermatol. 2015;42(12):1137–1142.
18. Tsianakas A, Luger TA. The anti-IL-4 receptor alpha antibody dupilumab: facing a new era in treating atopic dermatitis. Expert Opin Biol Ther. 2015;15(11):1657–1666.
19. Simpson EL, Bieber T, Guttman-Yassky E, et al. Two phase 3 trials of dupilumab versus placebo in atopic dermatitis. N Engl J Med. 2016;375(24):2335–2348.
20. Blauvelt A, De Bruin-Weller M, Gooderham M, et al. Long-term management of moderate-to-severe atopic dermatitis with dupilumab and concomitant topical corticosteroids (LIBERTY AD CHRONOS): a 1-year, randomized, double-blinded, placebo-controlled, phase 3 trial. Lancet. 2017;389(10080):2287–2303.

Downloaded by [Kyushu University] at 23:46 06 November 2017

21. Fan Y, Chen Y, Lin X, et al. Efficacy and safety of dupilumab for the treatment of adult atopic dermatitis: A meta-analysis of randomized clinical trials. J Allergy Clin Immunol. 2017 May 4 pii:S0091-6749(17)30687-3. DOI:10.1016/j.jaci.2017.04.015
22. Stull C, Lavery M, Yosipovitch G. Advances in therapeutic strategies for the treatment of pruritus. Expert Opin Pharmacother. 2016;17(5):677–687.
23. Furue M, Yamamura K, Kido Nakahara M, et al. Emerging role of interleukin-31 and interleukin-31 receptor in pruritus in atopic dermatitis. Allergy. 2017 Jul 3. DOI:10.1111/all.13239.
24. Nemoto O, Furue M, Nakagawa H, et al. The first trial of OM-8331, a humanized anti-human interleukin-31 receptor A antibody, in healthy volunteers and patients with atopic dermatitis to evaluate safety, tolerability and pharmacokinetics of a single dose in a randomized, double-blind, placebo-controlled study. Br J Dermatol. 2016;174(2):296–304.
25. Ruzicka T, Hanifin JM, Furue M, et al. Anti-interleukin-31 receptor A antibody for atopic dermatitis. N Engl J Med. 2017;376(826):826–835.
26. Murata Y, Song M, Rikuchi H, et al. Phase 2a, randomized, double-blind, placebo-controlled, multicenter, parallel-group study of a H4R antagonist (JNJ-39758979) in Japanese adults with moderate atopic dermatitis. J Dermatol. 2015;42(2):129–138.
27. Miyano K, Matsushita S, Tsuchida T, et al. Inhibitory effect of a histamine 4 receptor antagonist on CCL17 and CCL22 production by monocyte-derived Langerhans cells in patients with atopic dermatitis. J Dermatol. 2016;43(9):1024–1029.
28. Bissonnette R, Papp KA, Poulin Y, et al. Topical tofacitinib for atopic dermatitis: a phase 1a randomized trial. Br J Dermatol. 2016;175(5):902–911.
29. Tanimoto A, Shimizaki Y, Yamamoto Y, et al. A novel JAK inhibitor TF-052 reduces skin inflammation and ameliorates chronic dermatitis in recent models compared with conventional therapeutic agents. Exp Dermatol. 2017 Apr 19. DOI:10.1111/exd.13379.
30. Bissonnette R, Poulin Y, Zhou Y, et al. Efficacy and safety of topical WBI-1001 in patients with mild to severe atopic dermatitis: results from a 12-week, multicentre, randomized, placebo-controlled double blind trial. Br J Dermatol. 2012;166(4):853–860.
31. Smith SH, Jayawickreme C, Rickard DJ, et al. Tapinarof is a natural AhR agonist that resolves skin inflammation in mice and humans. J Invest Dermatol. 2017 Jun 5 pii: S0022-202X(17)31543-9. DOI:10.1016/j.jid.2017.05.004.
32. Paller AS, Tom WL, Lebwohl MG, et al. Efficacy and safety of crisaborole ointment, a novel nonsteroidal phosphodiesterase 4 (PDE4) inhibitor for the topical treatment of atopic dermatitis (AD) in children and adults. J Am Acad Dermatol. 2016;75(3):494–503.
33. Chamlin SL, Cordoro KM, Lanpher BC, et al. 2-Year assessment of safety results for crisaborole, a novel phosphodiesterase 4 inhibitor for atopic dermatitis. J Dermatol Sci. 2017;87(2):116–122.
34. Chesape AC, Murrell DF. 2% Crisaborole topical ointment for the treatment of mild-to-moderate atopic dermatitis. Expert Rev Clin Immunol. 2017;13(5):415–423.
35. Furue M, Kitahara Y, Akama H, et al. Safety and efficacy of topical E6005, a phosphodiesterase 4 inhibitor, in Japanese adult patients with atopic dermatitis: results of a randomized, vehicle-controlled, multicenter clinical trial. J Dermatol. 2014;41(7):577–585.
   - **Clinical results of topical E6005/RVT-501 for adult atopic dermatitis.**
36. Nemoto O, Hayashi N, Kitahara Y, et al. Effect of topical phosphodiesterase 4 inhibitor E6005 on Japanese children with atopic dermatitis: results from a randomized, vehicle-controlled, exploratory trial. J Dermatol. 2016;43(6):681–687.
   - **Clinical results of topical E6005/RVT-501 for pediatric atopic dermatitis.**
37. Francis SH, Blount MA, Corbin JD. Mammalian cyclic nucleotide phosphodiesterases: molecular mechanisms and physiological functions. Physiol Rev. 2011;91(2):651–690.
38. Schafer PH, Parton A, Capone L, et al. Apremilast is a selective PDE4 inhibitor with regulatory effects on innate immunity. Cell Signal. 2014;26(9):2016–2024.
39. Andoh T, Kuraishi Y. Antipruritic mechanisms of topical OC000, a phosphodiesterase 4 inhibitor: inhibition of responses to protease-activated receptor 2 stimulation mediated by increase in intracellular cyclic AMP. J Dermatol Sci. 2014;76(1):208–213.
40. Wakita H, Ohkuma M, Ishii N, et al. A putative antipruritic mechanism of the phosphodiesterase-4 inhibitor E6005 by attenuating capsaicin-induced depolarization of C-fiber terminals. Exp Dermatol. 2015;24(3):215–216.
41. Zane LT, Chanda S, Jarnagin K, et al. Crisaborole and its potential role in treating atopic dermatitis: overview of early clinical studies. Immunotherapy. 2015;7(8):855–866.
42. Jimenez JL, Iniguez MA, Munoz-Fernandez MA, et al. Effect of phosphodiesterase 4 inhibitors on NFAT-dependent cyclooxygenase 2 expression in human T lymphocytes. Cell Signal. 2004;16(12):1363–1373.
43. Hanifin JM, Chan SC, Cheng JB, et al. Type 4 phosphodiesterase inhibitors have clinical and in vitro anti-inflammatory effects in atopic dermatitis. J Invest Dermatol. 1996;107(1):51–56.
44. Andoh T, Yoshida T, Kuraishi Y. Topical E6005, a novel phosphodiesterase 4 inhibitor, alleviates spontaneous itch-related responses in mice with chronic atopy-like dermatitis. Exp Dermatol. 2014;23(5):359–361.
45. Christopoulos A, Papoutsis D, Gamlidis V, et al. A new therapeutic for the treatment of moderate-to-severe plaque psoriasis: apremilast. Expert Rev Clin Immunol. 2010;12(3):237–243.
46. Chimenti MS, Costanzo T, Sebastiani R, et al. Apremilast for the treatment of psoriasis. Expert Opin Pharmacother. 2015;16(13):2083–2094.
47. Bianchi L, Del Duca E, Bernardelli M, et al. Pharmacodynamic assessment of apremilast for the treatment of moderate-to-severe plaque psoriasis. Expert Opin Drug Metab Toxicol. 2016;12(9):1121–1128.
48. Dattola A, Del Duca E, Saraceno R, et al. Safety evaluation of apremilast for the treatment of psoriasis. Expert Opin Drug Saf. 2017;16(3):381–383.
49. Ishii N, Shinato M, Wakita H, et al. Antipruritic effect of the topical phosphodiesterase 4 inhibitor E6005 ameliorates skin lesions in a mouse atopic dermatitis model. J Pharmacol Exp Ther. 2013;346(1):105–112.
50. Ishii N, Wakita H, Shinato M. Effect of the phosphodiesterase 4 inhibitor OC000 on nerve growth factor elevation in irritated skin of NC/Nga mice. J Dermatol Sci. 2014;76(3):263–264.
51. Ohba F, Nomoto M, Hajo S, et al. Safety, tolerability and pharmacokinetics of a novel phosphodiesterase inhibitor, OB/C5 ointment, in healthy volunteers and in patients with atopic dermatitis. J Dermatolog Treat. 2016;27(3):241–246.
   - **Clinical results of topical E6005/RVT-501 for adult atopic dermatitis and healthy controls.**
52. Ohba F, Watsuzi S, Imayama S, et al. Efficacy of a novel phosphodiesterase inhibitor, E6005, in patients with atopic dermatitis: an investigator-blinded, vehicle-controlled study. J Dermatolog Treat. 2016;27(5):467–472.
   - **Clinical results of topical E6005/RVT-501 for adult atopic dermatitis.**
53. Eichenfield LF, Ahluwalia J, Waldman A, et al. Current guidelines for the evaluation and management of atopic dermatitis: a comparison of the Joint Task Force Practice Parameter and American Academy of Dermatology guidelines. J Allergy Clin Immunol. 2017;139(4):1542–1557.
54. Horimukai K, Morita K, Narita M, et al. Application of moisturizer to neonates prevents development of atopic dermatitis. J Allergy Clin Immunol. 2014;134(4):824–830.
55. Kusunoki K, Morita K, Narita M, et al. Transepidermal water loss measurement during infancy can predict the subsequent development of atopic dermatitis regardless of filaggrin mutations. Allergol Int. 2016;65(1):103–108.

Downloaded by [Kyushu University] at 23:48 06 November 2017

56. Ng JP, Liew HM, Ang SB. Use of emollients in atopic dermatitis. J Eur Acad Dermatol Venereol. 2015;29(5):854–857.
57. Wollenberg A, Barlan I, Proactive therapy of atopic dermatitis—an emerging concept. Allergy. 2009;64(12):276–278.
58. Wollenberg A, Oranje A, Deleuran M, et al. EADV/EAACI Eczema task force 2015 position paper on diagnosis and treatment of atopic dermatitis in adult and pediatric patients. J Eur Acad Dermatol Venereol. 2016;30(5):729–747.
59. Tokura Y, Hirakawa S, Narita M, et al. Potential preventive effects of proactive therapy on sensitization in moderate to severe childhood atopic dermatitis: a randomized, investigator-blinded, controlled study. J Dermatol. 2016;43(11):1293–1297.
60. Seo SH, Lee SG, Lee HJ, et al. Disrupted skin barrier is associated with burning sensation after topical tacrolimus application in atopic dermatitis. Acta Derm Venereol. 2017. May 17. DOI:10.2340/00015555-2699.
61. Furue M, Terao H, Weihse W, et al. Clinical dose and adverse effects of topical steroids in daily management of atopic dermatitis. Br J Dermatol. 2003;148(1):148–153.
62. Charman CR, Morris AD, Williams HC. Topical corticosteroid phobia in parents with atopic eczema. Br J Dermatol. 2000;142(5):931–936.
63. Charman C, Williams H. The use of topical corticosteroids and corticosteroid phobia in atopic dermatitis. Clin Dermatol. 2003;21(3):199–203.
64. Gonzales F, Ramdane M, Delebarre-Sauvage C, et al. Monitoring of topical corticosteroid phobia in a population of patients with children with atopic dermatitis using the TOPICORPH scale: prevalence, risk factors and the impact of therapeutic patient education. J Eur Acad Dermatol Venereol. 2017;31(3):e172–e174.
65. Silverberg NB. Special D-MC considerations for therapy of pediatric atopic dermatitis. Dermatol Clin. 2017;35(3):361–365.

Downloaded by [Kyushu University] at 23:48 04 November 2017

リウマチ膠原病アレルギー内科

著書

1) 柴田朋彦．アナフィラキシー やさしい臨床医学テキスト 第4版 2018;:363-375.
2) 柴田朋彦．薬剤アレルギー・食物アレルギー・消化管アレルギー やさしい臨床医学テキスト 第4版 2018;:375.
3) 柴田朋彦．シェーグレン症候群 やさしい臨床医学テキスト 第4版 2018;:390-391.
4) 川畑仁人．混合性結合組織病 今日の治療指針2018 2018;:847-849.
5) 岡崎貴裕 他．クリオグロブリン血症性血管炎 血管炎症候群の診療ガイドライン(2017年改訂版) 2018;:63-68.

学術論文[和文]

① 原著

1) 佐々木 広和、溝口 史高、川畑 仁人、吉橋 祥子、木村 直樹、上阪 等．多発性筋炎マウスモデルにおいてIFNγは炎症局所で免疫抑制性タンパクPD-L1を誘導する．日本臨床免疫学会会誌 ，2017;40(4)：312.
2) 神谷 麻理、木村 直樹、高村 聡人、溝口 史高、川畑 仁人、上阪 等．多発性筋炎における細胞傷害性T細胞による筋傷害のin vitro解析．日本臨床免疫学会会誌 ，2017;40(4)：302.

② 総説又は症例解説

1) 川畑仁人．T細胞サブセットの作用と役割．分子リウマチ治療 ，2017;10(3)：47-50.
2) 川畑仁人．他科への手紙 リウマチ内科→内科一般へ．日本医事新報 ，2017;4862：47.
3) 永渕裕子．結節性多発動脈炎・顕微鏡的多発血管炎の理解と治療．難病と在宅ケア ，2017;22(3)：35-39.
4) 川畑仁人．制御性T細胞．医学のあゆみ ，2017;別冊：27-31.
5) 花岡洋成．ループス腎炎、NPSLE．分子リウマチ治療 ，2017;10：41-44.
6) 山崎宜興．難治性肺高血圧症診療の経験から学ぶ 強皮症に伴う肺高血圧症治療．Pulmonary Hypertension Update ，2017;13(2)：35-44.
7) 山崎宜興．続発性炎症性筋疾患における自己抗体検査～自己抗体検査のアプローチと測定意義．医学のあゆみ ，2017;263(13)：1197-1202.
8) 山崎宜興．特発性炎症性筋疾患における自己抗体検査．医学のあゆみ ，2017;263(13)：1197-1202.
9) 荻野昇、川畑仁人、花岡亮輔、國松淳和．日本の筋骨格疾患診療のあり方について．内科 ，2018;121(3)：511-519.
10) 川畑仁人．結節性多発動脈炎．診療と治療 ，2018;106(2)：176-180.

③ 症例報告

1) 廣川悠季、北澤智子、松岡摩耶、川上民裕、村上富美子、浅利佑紗．下垂足・下垂手を生じた顕微鏡的多発血管炎の1例．皮膚科の臨床 ，2017;59(5)：559-563.
2) 岡野遼祐、門野岳史、北澤智子、川上民裕、恒馬良直、高桑由希子．ランダム皮膚生検が診断と治療効果判定に有用であったIntravascular Large B-cell Lymphomaの1例．皮膚科の臨床 ，2017;59(8)：1241-1245.

④ その他

1) 永渕裕子．関節リウマチ―病気の理解と生活のポイント―．会報 かながわ ，2017;122：8-11.

学術論文[英文]

① 原著

1) Hanaoka H, Kiyokawa T, Iida H, Ishimori K, Takakuwa Y, Okazaki T, Yamada H, Ichikawa D, Shirai S, Koike J, Ozaki S.. Comparison of renal response to four different induction therapies in Japanese patients with lupus nephritis class III or IV: a single-centre retrospective study. PloS One ，2017;12(4)：0175152.
2) Eri T, Kawahata K, Kanzaki T, Immura M, Michishita K, Akahira L, Bannai E, Yoshikawa N, Kimura Y, Satoh T, Uematsu S, Tanaka H, Yamamoto K.. Intestinal microbiota link lymphopenia to murine autoimmunity via PD-1+CXCR5-/dim B-helper T cell induction. Scientific Reports ，2017;26(7)：46037.
3) Hasegawa H, Kawahata K, Mizoguchi F, Okiyama N, Miyasaki N, Kohsaka H. Direct suppression of autoaggressive CD8+ T cells with CD80/86 blockade in CD8+ T cell-mediated polymyositis models of mice. Clinical and experimental rheumatology ，2017;35(4)：593-597.
4) Toshiki E., Kawahata K., Kanzaki T., Immura M., Michishita K., Akahira L., Bannai E., Kimura Y., Satoh T., Yoshikawa N., Uematsu S., Tanaka H. Yamamoto K.. Intestinal microbiota link lymphopenia to murine autoimmunity via PD-1+CXCR5-/dim B-helper T cell induction. Sci Rep ，2017;7：46037.
5) Ooka Seido, Kurokawa-Suzuki Manne, Yokoyama Michiyo, Arito Mitsusi, Sato Toshiyuki, Sato Masaaki, Takakuwa Yukiko, Omoteyama Kazuki, Suematsu Naoya, Kawahata Kimito, Kato Tomohiro. Effects of iguratimod on protein profiles of chondrosarcoma cells. Integrative Molecular Medicine ，2017;4(6)：1-8.

データ

6) Shinagawa S, Okazaki T, Ikeda M, Yudoh K, Kisanuki Y, Yanagisawa M, Kawahata K, Ozaki S.. T cells upon activation promote endothelin 1 production monocytes via INF-γ and TNF-α. SCIENTIFIC REPORTS ，2017;7(14500)：1-8.

データ

7) Takada H, Kimura N, Yoshihashi-nakazato Y, Kawahata K, Kohsaka H.. Discoid lupus erythematosus complicated with pregnancy-induced hemophagocytic syndrome. Internal Medicine ，2017;56(12)：1581-1583.
8) Umezawa N, Kawahata K, Mizoguchi F, Kimura N, Yoshihashi-Nakazato Y, Miyasaka N, and Kohsaka H.. Interleukin-23 as a therapeutic target for inflammatory myopathy. Sci Rep ，2018;：in press.

② 症例報告

1) Amano H, Matsuda R, Shibata T, Takahashi D, Suzuki S.. Paradoxical SAPHO syndrome observed during anti-TNFα therapy for Crohn's disease. doi: 10.2147/BTT.S134508. eCollection 2017. Biologics ，2017;22(11)：65-69.
2) Kiyokawa T, Hanaoka H, Iida H, Ishimori K, Takakuwa Y, Yamasaki Y, Okazaki T, Ozaki S, Kawahata K.. Syndrome of inappropriate antidiuretic hormonesecretion (SIADH) in a patient with microscopic polyangiitis following low-dose intravenous cyclophosphamide: a possible pathogenic link with disease activity. Modern Rheumatology Case Reports ，2017;2(2)：177-180.

データ

3) Iida H, Hanaoka H, Asari Y, Ishimori K, Kiyokawa T, Takakuwa Y, Yamasaki Y, Yamada H, Okazaki T, Doi M, Ozaki S.. Rhabdomyolysis in a Patient with Polyarteritis Nodosa. Internal Medicine ，2018;57(1)：101-106.
4) Yamasaki Yoshioki, Suzuki Kengo, Kamijima Ryo, Asari Yusa, Tsuchida Kosei, Mizushima Machiko, Okazaki Takahiro, Akashi Yoshihiro, Ozaki Shoichi, Yamada Hideshiro.. Combined disease with pulmonary arterial hypertension and pulmonary venous hypertension revealed after treatment of heart failure with preserved ejection fraction in a case with primary Sjogren syndrome. Modern Rheumatology ，2018;28(1)：193-196.

学会発表

① 国内学会

1) 永渕裕子、尾崎承一．薬剤関連性顎骨壊死をきたした関節リウマチの臨床的特徴．第61回日本リウマチ学会総会・学術集会，2017.
2) ◎水島万智子、鈴木豪、安藤貴泰、飯田春信、品川尚志、石森加奈、清川智史、松下広美、高桑由希子、殿岡久美子、花岡洋成、大岡正道、岡崎貴裕、尾崎承一．リツキシマブで寛解維持が得られた肺アスペルギルス症合併、難治性多発血管炎性肉芽腫症の一例．第61回日本リウマチ学会総会・学術集会，2017.
3) 永渕裕子、浅利佑紗、鈴木豪、岡崎貴裕、尾崎承一．リウマチ性疾患に合併した骨吸収抑制薬関連顎骨壊死７例．第61回日本リウマチ学会総会・学術集会，2017.

今日の治療指針

私はこう治療している

TODAY'S THERAPY 2018

総編集　福井次矢　高木　誠　小室一成

責任編集

赤司　浩一　赤水　尚史　石竹　達也
一瀬　雅夫　金子　一成　上條　吉人
川越　正平　神田　隆　木村　正
久志本成樹　楠田　聡　上阪　等
坂本　泰二　巽　浩一郎　田中　栄
筒井　裕之　戸倉　新樹　永田　真
夏目　長門　丹生　健一　深川　雅史
藤田　次郎　堀江　重郎　丸山　治彦
水野　雅文　持田　智　行岡　哲男
吉岡　成人
（五十音順）

医学書院

[illegible]

[illegible]

- レバチオ錠（20 mg）：1日1～3錠を1～3回に分けて投与
- オプスミット錠（10 mg）：1回1錠，1日1回
- アデムパス錠（1 mg）：1回1錠，1日3回から開始し，血圧低下の有無を確認しつつ最高1日7.5錠まで増量可能
- ウプトラビ錠（0.2 mg）：1回1錠，1日2回から開始し，忍容性を確認しつつ最高1日16錠まで増量可能

5) はプロスタサイクリン系の新規薬剤で，効果が期待されるが実臨床の経験は少ない．

Ⅱ WHO機能分類Ⅳ度の症例

処方例　上記の内服薬併用，もしくは下記1)，2)いずれかの薬剤の持続投与が適応となる．

1) フローラン注：2 ng/kg/分より持続静注を開始し，症状や忍容性を確認しながら逐次増量．投与経路として単独の中心静脈ラインが必要であり，溶液は冷却しておく必要がある．
2) トレプロスト注：1.25 ng/kg/分より持続静注（または持続皮下注）を開始し，症状や忍容性を確認しながら逐次増量．

2) は1) より半減期が長く薬剤調整の負担が少ない．

● 腎クリーゼ

本邦では欧米より発症頻度は低いとされるが，重篤な合併症である．抗RNAポリメラーゼIII抗体陽性やステロイド使用がリスク因子とされる．アンジオテンシン変換酵素（ACE）阻害薬が第1選択である．

処方例

- カプトリル錠（12.5 mg）：1回0.5～1錠，1日3回より開始し，最初の24時間で血圧を収縮期20 mmHg，拡張期10 mmHgずつ低下させ，3日以内に収縮期血圧140 mmHg以下を目指す．

薬剤指導・薬剤情報　大嶋 繁

- PGE_1 注射薬は，高頻度で血管痛がみられるので事前に情報提供をする．
- プレドニンの使用に際しては，必要性ならびに服用量，投与期間について説明する．腎障害の誘発，不眠（夜間使用の場合），感染症の誘発，消化管潰瘍，血糖上昇などの副作用を起こす危険性があるため，それらの初期症状を十分に説明する．
- プロスタサイクリン誘導体製剤ではほてり感，出血傾向に注意する．皮下出血や歯ぐきの出血のほかに，脳出血の初期症状としての急な悪心，頭痛に気づいた場合にはすぐに連絡・受診するよう指導する．
- トラクリア錠では，頭痛が高頻度でみられることを情報提供する．
- レバチオ錠は硝酸薬あるいは一酸化窒素供与薬との併用により過度の血圧下降が起こるため併用薬をチェックする．

混合性結合組織病
mixed connective tissue disease（MCTD）

川畑仁人　聖マリアンナ医科大学教授・リウマチ・膠原病・アレルギー内科

病態と診断

- 混合性結合組織病（MCTD）は，全身性エリテマトーデス（SLE）様，強皮症様，多発性筋炎様の症状が混在し，かつ血清抗U1-RNP抗体が高値である全身性自己免疫疾患である．
- レイノー現象，指ないし手背の腫脹を共通症状とし，他の膠原病と比し高率の肺高血圧症の合併（10～15%）を特徴とする．
- MCTDの診断は，厚生労働省研究班作成のMCTD診断基準（2004年改訂版）を参考にする．
- 肺高血圧症や三叉神経障害，無菌性髄膜炎の合併頻度，HLA解析などより，SLEや強皮症と異なる特徴が報告され，独立疾患として再認識されている．
- 抗U1-RNP抗体の存在はMCTDの疾患概念にかかわる重要所見だが，その産生機序や病態への関与については不明である．

治療方針

患者が呈している全身症状および臓器症状を把握し，各症状に対して可能な非免疫抑制治療があればそれを行いつつ，免疫抑制治療を必要とする場合にはそれらに共通して対応できる治療薬選択と用量設定を行う．最後に患者個々の状況を考慮に入れ方針を決定する．

2011年厚生労働省研究班作成の「混合性結合組織病の診療ガイドライン（改訂第3版）」が参考となる．

Ⓐ 軽症例

発熱，関節炎，倦怠感などの全身症状を認めるものの，他の臓器障害を認めない場合はステロイドの

少量経口投与を行う．

Rp 処方例

プレドニン錠（5 mg） 1日1～3錠を1～3回に分けて投与 食後

関節炎症状に対しては，骨びらんがある場合，抗CCP抗体陽性の場合，少量ステロイドでもコントロールできない場合は，抗リウマチ薬の使用を考慮する．非ステロイド性抗炎症薬（NSAIDs）が使用される場合もあるが，無菌性髄膜炎合併の報告もあり注意して使用する．

B 末梢循環障害

末梢循環障害により指趾のレイノー現象，チアノーゼ，潰瘍，壊死を認める．

レイノー現象を避けるには，保温が重要であり，寒冷刺激を避け体全体が温まるよう日常生活を工夫する．喫煙者は禁煙も重要である．

レイノー現象が強く，潰瘍の危険がある場合は，以下のような薬剤を単独もしくは併用する．潰瘍が生じた場合は，薬物療法と局所処置を行う．

Rp 処方例 下記の薬剤を症状に応じて適宜用いる．

1) ドルナー錠（20 μg） 1回1～2錠 1日3回 保外
2) トラクリア錠（62.5 mg） 1回1～2錠 1日2回
3) ユベラNカプセル（100 mg） 1回1～2カプセル 1日3回 保外
4) アンプラーグ錠（100 mg） 1回1錠 1日3回 保外
5) プレタールOD錠（100 mg） 1回1錠 1日2回 保外
6) アムロジンOD錠（5 mg） 1回1～2錠 1日1回 保外
7) リプル注 1回10 μg 1日1回 ゆっくり静注あるいは点滴静注

C 漿膜炎

心膜炎ではステロイドの中等量投与が基本である．重度の心外膜炎ではプレドニン量を1 mg/kgにする場合やステロイドパルス療法が選択される場合もある．

心嚢液貯留の頻度も高いが，その場合，随伴所見からSLEもしくは強皮症のどちらの要素が強いかを考慮する．強皮症における心嚢液貯留では，ステロイドへの反応性が乏しい．

Rp 処方例

プレドニン錠（5 mg） 1日4～6錠（1日0.5 mg/kg）を3回に分けて投与 毎食後

D 肺高血圧症

MCTDにおける肺高血圧症の機序として，肺動脈の末梢における内腔の狭窄や閉塞，間質性肺炎，慢性肺血栓塞栓症による場合がある．肺静脈閉塞性疾患を伴う場合もある．早期診断，早期治療が重要であり，早期からの定期的なスクリーニングを行う．

肺動脈性肺高血圧症では，以下の治療を行う．

1. 疾患活動性がある場合，もしくは発症早期や進行性の場合

Rp 処方例 下記を併用する．

プレドニン錠（5 mg） 1日8～12錠（1日1 mg/kg）を3回に分けて投与 毎食後

エンドキサン注 1回500～1,000 mg/m² 2～4週に1回 点滴静注

2. 血管拡張薬 3系統（下記のa．およびb．，c．，d．およびe．）の薬剤から複数を早期より併用するupfront combination therapy，および逐次薬剤を追加するsequential combination therapyがある．近年では前者の方法が多く用いられる．なお，a．とb．，d．とe．の併用は禁忌である．

a. プロスタサイクリン誘導体製剤

Rp 処方例 下記のいずれかを用いる．

1) ケアロードLA錠（60 μg） 1回1～3錠 1日2回
2) ベンテイピス吸入液 1回2.5～5.0 μg（成分量として） 1日6～9回 吸入
3) フローラン注 2～10 ng/kg/分で持続静注
4) トレプロスト注 0.625～2.5 ng/kg/分で持続静注または持続皮下注

b. プロスタサイクリン受容体作動薬

Rp 処方例

ウプトラビ錠（0.2・0.4 mg） 1回0.2～1.6 mg 1日2回

c. エンドセリン受容体拮抗薬

Rp 処方例 下記のいずれかを用いる．

1) トラクリア錠（62.5 mg） 1回1～2錠 1日2回
2) ヴォリブリス錠（2.5 mg） 1回2～4錠 1日1回
3) オプスミット錠（10 mg） 1回1錠 1日1回

d. ホスホジエステラーゼ5阻害薬

Rp 処方例 下記のいずれかを用いる．

1) レバチオ錠（20 mg） 1回1錠 1日3回
2) アドシルカ錠（20 mg） 1回2錠 1日1回

- 可溶性グアニル酸シクラーゼ刺激薬

処方例

アデムパス錠（0.5・1.0・2.5 mg）　1回 1.0～2.5 mg　1日3回

❸ 筋炎

「多発性筋炎・皮膚筋炎」の項（⇨842頁）を参照。

❹ 間質性肺炎

進行せず安定化している場合には，積極的な治療の対象とはならない。

処方例　徐々に進行を認める場合には，1）および2）を併用する。慢性型の急性増悪や急性間質性肺炎では，1）とともに5）および6）を併用する。3）および4）は1）の代わりや後の維持療法として用いられることがある。

1）エンドキサン注　1回 500～1,000 mg　2～4週に1回　点滴静注
2）プレドニン錠（5 mg）　1日4～6錠（1日 0.5 mg/kg）を3回に分けて投与　毎食後
3）プログラフカプセル（0.5・1 mg）　1日 0.075 mg/kg を2回に分けて投与　朝・夕食後　トラフは 5～10 ng/mL に調節
4）ネオーラルカプセル（25・50 mg）　1日 3～5 mg/kg を2回に分けて投与　朝・夕食後　トラフは 150～200 ng/mL に調節（保険）
5）ソル・メドロール注　1回 500～1,000 mg＋ソリタ-T 3号注　1回 200 mL　2時間かけて点滴静注　3日間連続
6）プレドニン錠（5 mg）　1日 8～12錠（1日 1 mg/kg）を3回に分けて投与　毎食後

専門医へのコンサルト

- MCTD を疑う場合，また診断確定後も，膠原病専門医へのコンサルトが望ましい。

患者説明のポイント

- 起きうる症状や定期的受診および検査の重要性，治療薬の意義，副作用情報を説明する。
- レイノー現象に対する日常生活での注意および工夫について説明する。

看護・介護のポイント

- 末梢循環障害に対する保温などの日常生活上のケア。
- 筋力低下が著しいときは，良肢位の維持や誤嚥の防止に注意する。

高安動脈炎，巨細胞性動脈炎

Takayasu arteritis, giant cell arteritis

中島亜矢子　三重大学医学部附属病院リウマチ・膠原病センター教授

病態と診断

Ⓐ 病態

- 高安動脈炎（TAK）および巨細胞性動脈炎（GCA）は，大動脈およびその第1分枝に生じる原因不明の肉芽腫性多発血管炎で，全身炎症症状と罹患血管部位に応じた血流障害が生じる。

Ⓑ 診断

- 原因不明の発熱，炎症反応高値などがあるも特異的な所見はない。
- TAK は若年女性に多い，GCA は高齢者に多く，側頭動脈炎やリウマチ性多発筋痛症がみられる。
- 造影 CT による大動脈血管壁の造影効果のある肥厚，進行すると動脈瘤の不整，動脈の拡張・狭窄・途絶を認める。保険適用はないが，PET-CT による動脈炎の検出が診断に有用である。

治療方針

画像診断の進歩により，非特異的炎症の段階で診断・治療することが可能となってきている。日本循環器学会が「血管炎症候群の診療ガイドライン」（2008年）を公開している。

治療方針

Ⓐ 内科的治療

動脈炎を鎮静化させることにより，不可逆的血流障害の出現，進行防止をはかる。

1. 急性期治療

a. ステロイド

処方例　中等症例には下記を用いる。

プレドニン錠（5 mg）　1回 2～3錠　1日3回（1日 30～50 mg 程度）　2～4週間，初期治療として投与

重症例や GCA で眼症状（失明の危険）・中枢神経障害症状がある例ではプレドニン錠 1 mg/kg/日を投与し，ステロイドパルス療法（メチルプレドニゾロン 1 g/日の3日間点滴静注療法）も考慮する。症状や炎症反応の改善が得られたあと，30 mg/日までは1～2週で 5～10 mg ずつ，10 mg/日までは2～4週で 2.5～5 mg ずつ減量する。

b. 免疫抑制薬　禁忌がなければステロイドに併用する。これらの治療を行う際には，専門家にコンサルトする。

処方例　下記のいずれかを用いる。5）は疾患活動性が高くほかの治療薬での制御が困難な場合に

分子リウマチ治療

別　刷

発行：株式会社　先端医学社
〒103-0007 東京都中央区日本橋浜町 2-17-8　浜町平和ビル

免疫学のABC　第4回

T細胞サブセットの作用と役割

川畑仁人

聖マリアンナ医科大学リウマチ・膠原病・アレルギー内科

われわれの免疫系は，微生物などの異物を攻撃する機構を有しながら，自己抗原や食事抗原などの異物には反応しないようにする免疫学的寛容の機構を巧みに共存させている．これには自然免疫と獲得免疫の協調が重要だが，多様なT細胞サブセットを誕生させ，多面的な作用を得ることで達成されている．$CD4^+$ T細胞はMHCクラスII上の抗原を認識し，おもに分泌するサイトカインによって分類されている．IFN-γを産生するTh1細胞，IL-4を産生するTh2細胞，IL-17を産生するTh17細胞，IL-21を産生しB細胞をヘルプするTfh細胞，TGF-βやIL-10を産生し抑制性の機能を有する制御性T細胞などのサブセットの存在が明らかにされている[1]．またT細胞と自己免疫疾患，アレルギー性疾患，腫瘍免疫，移植免疫とのかかわりについても多くの研究がなされており，T細胞サブセットやその機能を標的とする治療も試みられている．

はじめに―T細胞サブセットのはたらき―

私たちの体は，微生物，真菌などさまざまな外敵から身を守るため，免疫という機構を有している．免疫は，外敵の私たちとは異なる構造のパターンを認識し，それを排除するための炎症を惹起する自然免疫と，異物の個々に異なる細かい構造を認識し反応する獲得免疫に分類できる．前者はおもに樹状細胞やマクロファージなどが中心となり，後者はT細胞やB細胞が担っている．われわれは自然免疫とともに，ヘルパーT細胞や細胞障害性T細胞などのT細胞サブセットやB細胞からなる獲得免疫を上手に協調させることにより，外敵を排除しているのである．

しかし，異物に対して攻撃する仕組みだけでは，私たちは生きていくことができない．たとえば，私たちは，植物や動物，魚などの異物を排除するどころか摂取し栄養としているほか，腸内や皮膚には常在菌がいて共存しているのである．さらに，T細胞やB細胞の中で自己に反応する細胞は，各胸腺や骨髄の分化過程で除去される機構になっているほか，末梢の臓器のみにある抗原や，種々の蛋白修飾も存在しているため，末梢においても自己反応性リンパ球が不活化される機構がなければならない．実際に，正常個体の末梢に自己抗原反応性を有するT細胞やB細胞が存在しながら，反応せずに恒常性を保っていることが知られている．この免疫学的寛容の達成や維持には，制御性T細胞とよばれる抑制性の機能を有するT細胞サブセットがかかわっているのである．このように免疫学的寛容を有しながら，異物を攻撃する機構を巧みに共存させるために，免疫系は多様なT細胞サブセットを誕生させ多面的な作用を得ているのである．

これらの機構に障害が生じるとどうなるのであろうか．たとえば，免疫系が，非自己抗原に不適切にもしくは過剰に反応するとアレルギー疾患が生じ，自己に不適切に反応してしまうと組織傷害や機能障害をきたし自己免疫疾患が発症する．T細胞サブセットは，この恒常性

Key Words
$CD4^+$ T細胞，Th1細胞，Th2細胞，Th17細胞，制御性T細胞

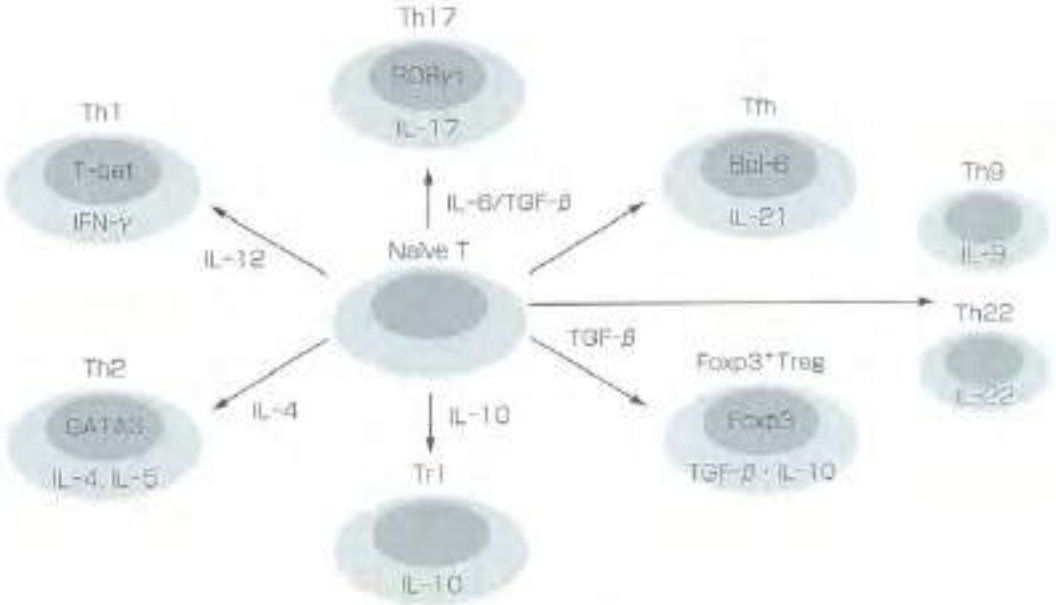

図❶ CD4⁺T細胞サブセット

破綻や病態形成にもかかわることで，疾患でも重要な役割を担っている場合があると考えられている．したがって，特定のT細胞サブセットを標的とする治療は，疾患によっては有効な可能性がある．

おもなT細胞サブセット

T細胞は抗原提示細胞上で自己主要組織適合性抗原（major histocompatibility complex：MHC）分子に結合した抗原を認識するが，この際に用いる受容体がT細胞受容体（T cell receptor：TCR）である．TCRにはα鎖とβ鎖からなるαβ鎖T細胞受容体と，γ鎖とδ鎖からなるγδ鎖T細胞受容体があり，各TCRを有するT細胞がそれぞれαβT細胞とγδT細胞である．さらにαβT細胞はCD4⁺T細胞，CD8⁺T細胞に大別される．前者はMHCクラスII上の抗原を認識する一方，後者はMHCクラスI上の抗原を認識し細胞障害性T細胞として知られている．

CD4⁺T細胞は，さらに，いくつかのヘルパーT細胞サブセットに分類される（**図❶**）．このヘルパーT細胞サブセットの概念は，1986年にMosmannらがマウスT細胞クローン間のサイトカイン分泌パターンによってTh1細胞およびTh2細胞の2つのヘルパーT細胞亜集団に分けられることを示したことに始まる．現在では，CD4⁺T細胞は，ナイーブT細胞，Th1細胞，Th2細胞，Th17細胞，Tfh細胞，制御性T細胞などに分類される．

1）Th1細胞

Th1細胞はIFN-γを産生し細胞性免疫にはたらく．IFN-γはマクロファージを活性化させ，結核菌などの細胞内寄生性病原体の感染防御に重要な役割を担う．一方，関節リウマチをはじめとする自己免疫疾患の病態形成にもかかわっていると考えられている．抗原提示細胞から産生されるIL-12がTh1細胞の分化に必須であり，転写因子ではT-betの発現が必要である．

2）Th2細胞

Th2細胞はIL-4やIL-5を産生し液性免疫にはたらく．これらのサイトカインはB細胞の分化，増殖に作用し，細胞外寄生性病原体の防御に重要な役割を担う．一方，アレルギー疾患の病態形成にもかかわっていると考えられている．自然免疫系によって産生されるIL-4がTh2細胞の分化に必須であり，転写因子ではGATA3の発現が必要である．

3) Th17 細胞

Th17 細胞は IL-17A, IL-17F を産生し炎症惹起にはたらく. G-CSF や CXCL8 の産生などを介して好中球を誘導し, 細胞外寄生性病原体の感染早期の防御機構を担う. 一方, 多発性硬化症や乾癬などの自己免疫疾患の病態形成にもかかわっていると考えられている. TGF-β および IL-6 が Th17 細胞の分化に必要であり, 転写因子では RORγt の発現が必要である. IL-21 や IL-23 は Th17 細胞の増殖を促進する. Th17 は IL-22 も産生するが, IL-17 を産生せず IL-22 を産生する Th22 の存在もヒトで報告されている.

4) Tfh 細胞

Tfh 細胞はリンパ節のリンパ濾胞に存在し CXCR5 を発現している細胞で, IL-21 を産生し, 高親和性抗体産生 B 細胞への分化や記憶 B 細胞の誕生に関与している. 一方, 全身性エリテマトーデスなどの自己免疫疾患の病態形成にもかかわっていると考えられている. 転写因子では Bcl-6 の発現が必要である.

5) Tr1 細胞

Tr1 細胞は, IL-10 存在下に T 細胞受容体からの刺激で誘導されおもに IL-10 産生により抑制的に機能する誘導性の制御性 T 細胞として知られてきた. 現在では, LAG3 および CD49b の共発現 $CD4^+$ T 細胞として同定され, CD25 や Foxp3 は発現せず, 刺激により大量の IL-10 および TGF-β を分泌する細胞であることが知られている. この細胞群に発現する転写因子として, c-Maf や AhR, Egr-2 などが報告されている.

実際の自己免疫疾患, 移植免疫, 腫瘍免疫における Tr1 細胞の役割もしくは治療への応用についてはまだ不明な点が多い. 重症複合免疫不全マウスに $CD4^+$ $CD45RB^{high}$ T 細胞を移入し生じる腸炎モデルや移植片対宿主病モデルにおける Tr1 細胞の抑制効果, 頭頸部扁平上皮細胞癌患者における Tr1 細胞の存在などが示されている.

6) $Foxp3^+$ 制御性 T 細胞

$Foxp3^+$ 制御性 T 細胞は, CD25 を発現する一方で, IL-7Rα 鎖である CD127 の発現を欠き, 転写因子 Foxp3 をマスター遺伝子とする抑制細胞集団として知られている. $CD4^+CD25^+$ 制御性 T 細胞の分化や機能に中心的役割を担う転写因子である *Foxp3* 遺伝子に異常があり制御性 T 細胞を欠くため, 種々の臓器特異的自己免疫疾患を呈する. Scurfy マウスやヒトの疾患である IPEX (immune dysregulation, polyendocrinopathy, enteropathy, and X-linked inheritance) 症候群の存在が知られており, この T 細胞サブセットの重要性が明らかになっている.

マウスでは, $CD4^+$ T 細胞の 5～10% に CD25 が発現しており, その大部分が制御性 T 細胞であるが, ヒト末梢血では, 単に $CD4^+CD25^+$ T 細胞を分離しただけで十分な抑制能は得られず, CD25 を高発現している 1～3% 程度の $CD4^+CD25^{high}$ T 細胞に存在していることが示されている. $CD4^+CD25^-$ T 細胞にも少数ながら Foxp3 発現細胞がある. 胸腺ではわれわれ[2]や海外からの研究により, 自己抗原へのアフィニティが強い $CD4^+$ T 細胞から分化することが示されている. 末梢では, TGF-β や未成熟樹状細胞とともに $CD4^+$ T 細胞が T 細胞受容体刺激を受けた際に, $Foxp3^+$ T 細胞に分化することも報告されている.

自己免疫疾患における $Foxp3^+$ 制御性 T 細胞の役割については不明な点が多い. 一方で本細胞群を標的とする治療は, 実際の移植や自己免疫疾患でも報告されている. 低用量 IL-2 投与によるヒト重症複合免疫不全治療の報告では, 制御性 T 細胞の増加とともに臨床的な効果を認め, 2 年にわたる長期経過でも有効性と安全性が確認されている.

7) その他

$CD8^+$ T 細胞は, 標的細胞上の MHC クラス I 分子に結合した抗原を認識する. 活性化した $CD8^+$ T 細胞は抗原を提示した標的細胞を, パーフォリンやグランザイムを介して, または Fas/Fas-L を介して傷害する. γδT 細胞は αβT 細胞にくらべて T 細胞受容体の多様性は少な

い細胞だが，$\alpha\beta$T 細胞と同様に多様な機能を有している．皮膚や腸管などの上皮間に多く存在し，非ペプチド抗原を認識する細胞も存在している．NKT 細胞（Natural Killer T cells：NKT cells）は，$CD4^-CD8^-$または$CD4^+CD8^-$のT細胞で，マウスでは単一のVα14-Jα18鎖と限られたVβからなるT細胞受容体を発現している．ヒトではVα24/Vβ11 T細胞がこれに相当する．CD1d分子に提示された微生物および自己由来の糖脂質を認識している．MAIT細胞（Mucosal-associated invariant T cells：MAIT cells）はマウスではVα19-Jα33，ヒトではVα7.2を発現する細胞で，MR1によって選択される．MAIT細胞はヒト末梢血のT細胞の1−8%を占め，腸管粘膜や腸間膜リンパ節に豊富に存在する．

ヘルパーT細胞においても，さらにいくつかのサブセットが報告されている．IL-9を専ら産生するTh9細胞や，ごく最近，われわれ[3]や海外[4]からの研究によりマウス自己免疫モデルやヒト関節リウマチで存在が示されたIL-21産生$CXCR5^-PD\text{-}1^+CD4^+$T細胞〔$T_{PH}$細胞（peripheral helper T cells）ともよばれている〕なども注目されている．

おわりに

自己免疫疾患の病態形成や制御におけるT細胞の役割は，従来の細胞免疫学的アプローチだけではなく，疾患感受性遺伝子解析や実際のヒトにおける免疫チェックポイント阻害療法の効果と副作用など多面的な観点からも明らかにされつつある．これらの知見が統合され，自己免疫，感染免疫，腫瘍免疫，移植免疫など，多様な免疫病態の克服につながる治療法の開発が望まれる．

文献

1) Hirahara K *et al*：CD4+ T-cell subsets in inflammatory diseases：beyond the Th1/Th2 paradigm. *Int Immunol* **28**：163-171, 2016
2) Kawahata K *et al*：Generation of CD4（+）CD25（+）regulatory T cells from autoreactive T cells simultaneously with their negative selection in the thymus and from nonautoreactive T cells by endogenous TCR expression. *J Immunol* **168**：4399-4405, 2002
3) Eri T *et al*：Intestinal microbiota link lymphopenia to murine autoimmunity via PD-1+CXCR5−/dim B-helper T cell induction. *Sci Rep* **7**：46037, 2017
4) Rao DA *et al*：Pathologically expanded peripheral T helper cell subset drives B cells in rheumatoid arthritis. *Nature* **542**：110-114, 2017

別冊・医学のあゆみ

自己免疫疾患

——Preclinical Stateから発症・早期診断まで

編集　熊谷俊一　神鋼記念病院膠原病リウマチセンター

病因にせまる

自己免疫疾患の病因研究としてのゲノム研究
——疾患ゲノム研究の次世代シークエンシングによる変化
自己免疫疾患の発症関連環境要因
腸内細菌と免疫疾患
自己免疫疾患のエピジェネティクス
制御性T細胞

全身性自己免疫疾患

関節リウマチのpreclinical state
全身性エリテマトーデスの病因　ゲノム解析からの知見
慢性筋炎合併皮膚筋炎
強皮症の自然歴と早期診断
ANCA関連血管炎
ベーチェット病
成人Still病の病態と診断のポイント
シェーグレン症候群
脊椎関節炎
　体軸性脊椎関節炎のpreclinical stateから発症・早期診断まで
高安動脈炎の発症機序におけるHLAとサイトカインの寄与
小児リウマチ性疾患

臓器特異的自己免疫疾患

炎症性腸疾患の初期病変
多発性硬化症と腸内細菌叢異常
成人1型糖尿病
乾癬のpreclinical stageから発症まで

医歯薬出版株式会社
http://www.ishiyaku.co.jp/

制御性T細胞

Regulatory T cells

川畑仁人
Kimito Kawahata
聖マリアンナ大学リウマチ・膠原病・アレルギー内科

○抑制機能を有するT細胞として，胸腺あるいは末梢で分化し，転写因子Foxp3や表面分子CD25を発現するFoxp3$^+$制御性T細胞(Treg)や，末梢で分化し，転写因子c-MafやAhR，Egr-2，表面分子LAG3およびCD49bを発現し，刺激によりIL-10およびTGF-βを分泌するTr1細胞などの制御性T細胞が知られている．これらの細胞群は自己免疫だけではなく，腫瘍免疫や移植免疫などにおいても病態形成や治療における役割が検討されている．また，Foxp3$^+$制御性T細胞からTh17細胞への変化など制御性T細胞の安定性にかかわる現象が明らかになっており，Foxp3や抑制機能の維持に関するエピジェネティックスや翻訳後修飾などの観点からの研究も進んでいる．

Key word　関節リウマチ(RA)，制御性T細胞(Treg)，Foxp3，Tr1細胞

生体はさまざまな外来抗原への反応を可能にするために，多様なT細胞受容体およびB細胞受容体をつくりだしているが，そのことにより同時に自己反応性リンパ球が出現する可能性が生じている．実際に膠原病のなかには，自己抗原に反応性を有するB細胞やT細胞が存在していることが示されている疾患がある．全身性エリテマトーデスや混合性結合組織病などの全身性自己免疫疾患は，抗核抗体の出現を特徴としているが，この出現には核抗原反応性B細胞のほか，核抗原反応性T細胞の関与が示唆されている．さらに，正常個体においても自己抗原反応性を有する自己反応性T細胞やB細胞が存在していることが示されているが，免疫系における制御機構により自己免疫疾患発症が抑制されている．

トレランス(免疫学的寛容)とは，T細胞やB細胞のような抗原特異的認識系を有する獲得免疫系が，ある抗原に特異的に無応答になることであり，とくに自己抗原に対して反応しなくなる状態をセルフトレランスとよぶ．自己抗原の免疫系への曝露が自己反応性リンパ球活性化の閾値以下のため，これらの細胞が自己反応性を有しながらも自己抗原とは反応しない免疫学的無視の状態となっている場合もあるが，このトレランスを誘導し維持する種々の機構により自己反応性リンパ球の除去あるいは機能的不活化が生じ，膠原病の発症が抑制されていると考えられている．種々の遺伝要因や環境要因によりトレランスの破綻や免疫学的無視の状態が解除されると，免疫系による自己組織に対する過剰な，あるいは不適切な免疫応答が生じ，組織傷害や機能障害をきたし膠原病の発症に至ると考えられている．

このトレランスの成立・維持機構において重要な役割を担っていると考えられている細胞群のひとつに，制御性T細胞(regulatory T cell：Treg)があげられる．この細胞群については自己免疫だけではなく，腫瘍免疫や移植免疫における役割や病的な意義，治療への応用など多面的な研究がなされている．

本稿では，Tregの全体像に触れた後，おもにFoxp3$^+$Tregにかかわる研究の進展を紹介したい．

制御性T細胞(Treg)

トレランスには，その誘導される時期により，リンパ球の産生や分化が起こる一次リンパ組織で未熟リンパ球に誘導される中枢性トレランスと，リンパ球が免疫応答を生じる二次リンパ組織で成熟リンパ球に誘導される末梢性トレランスに大別される．この末梢性トレランスは自己反応性リンパ球の除去だけではなく，抗原提示細胞または他の細胞の膜型あるいは分泌型の抑制性分子により，積極的に自己反応性リンパ球の機能や増殖を阻害する場合がある．とくに抑制機能を有する細胞群は制御性細胞として知られ，マクロファージや樹状細胞，B細胞，T細胞など種々の細胞がある状況下で制御性細胞として機能する場合が知られている．誘導により誕生するTregとして，IL-10存在下にT細胞受容体からの刺激で誘導されおもにIL-10産生により抑制的に機能するTr1細胞や，経口免疫寛容で誘導されるTGF-βを産生するTh3細胞などが報告されてきた．しかし，もっともよく研究されているのは，すくなくともマウスからヒトまで存在し，胸腺あるいは末梢で誕生し，転写因子Foxp3や表面分子CD25やCD4を発現する抑制性細胞集団，Foxp3$^+$Tregであろう．この細胞群については後で詳述することとし，その他のサブセットについて最初に簡単に触れておきたい．

1. Tr1細胞

Tr1細胞は，IL-10存在下にT細胞受容体からの刺激で誘導されおもにIL-10産生により抑制的に機能する誘導性のTregとして知られてきた．現在ではLAG3およびCD49bの共発現CD4$^+$T細胞として同定され，CD25やFoxp3は発現せず，刺激により大量のIL-10およびTGF-βを分泌する細胞であることが知られている[1]．この細胞群に発現する転写因子として，c-MafやAhR，Egr-2などが報告されている．機能として，IL-10やTGF-βによるT細胞やB細胞，抗原提示細胞の抑制，LAG3による抗原提示細胞機能調節，perforin，granzyme Bによる細胞死誘導，CD39およびCD72のエクト酵素による細胞外アデノシン産生，そのほか細胞表面分子を介した細胞間接触による抑制などがあげられている．

実際の自己免疫疾患，移植免疫，腫瘍免疫におけるTr1細胞の役割あるいは治療への応用についてはまだ不明な点が多い．SCIDマウスにCD4$^+$CD45RB^{high}T細胞を移入し生じる腸炎モデルやGVHDモデルにおけるTr1細胞の抑制効果，頭頸部扁平上皮細胞癌患者におけるTr1細胞の存在などが示されている．

2. CD8$^+$Treg

CD4$^+$T細胞では，IL-2受容体α鎖CD25を発現している細胞にFoxp3$^+$T細胞として抑制機能を有している細胞群が存在しているが，CD8$^+$T細胞ではIL-2受容体β鎖CD122を発現するT細胞に抑制性機能を有する細胞が含まれていることが報告されている．CD8$^+$CD122$^+$T細胞は，IL-10やTGF-β，IFN-γやそのほかの作用により抑制能を発揮すると考えられているが，不明な点も多い．さらに，CD4$^+$T細胞と同様にCD8$^+$T細胞でも，転写因子Foxp3を発現するCD8$^+$CD25$^+$Foxp3$^+$T細胞が抑制機能を有しているとの研究がある．マウスおよびヒトで，末梢T細胞の0.1～0.4%にCD8$^+$CD25$^+$Foxp3$^+$T細胞が存在しT細胞を抑制する機能を有している．CD8$^+$CD25$^+$Foxp3$^+$T細胞に関しても，その分化や抑制機序は今後の課題であろう．

Foxp3$^+$Treg

1. 概要

Foxp3$^+$TregはCD25を発現する一方で，IL-7Rα鎖であるCD127の発現を欠き，転写因子Foxp3をマスター遺伝子とする抑制細胞集団として知られている．

この細胞群は坂口らの先駆的な一連の研究により，その存在や機能，発現分子などの解明が進んだ．CD4$^+$CD25$^+$T細胞が生体で臓器特異的自己免疫疾患を抑制していることは，T細胞を欠損しているヌードマウスにCD4$^+$CD25$^+$T細胞を移入すると胃炎や腸炎，卵巣炎，甲状腺炎などが生じるが，胸腺や末梢CD4$^+$CD25$^+$T細胞も同時に移入するとこれらの自己免疫疾患が生じないことなどの研究により示されている．このように，CD4$^+$CD25$^+$Tregには，臓器特異的自己抗原反応性T細胞を抑制する役割を担っていると考えら

れるが，さらにこの細胞群を欠くマウスやヒトの解析により，その生体における重要性が確認されている．CD4$^+$CD25$^+$Tregの分化や機能に中心的役割を担う転写因子であるFoxp3遺伝子に異常がありTregを欠くため，種々の臓器特異的自己免疫疾患を呈するScurfyマウスや，ヒトの疾患であるimmune dysregulation, polyendocrinopathy, enteropathy, and X-linked inheritance (IPEX)症候群の存在が知られている．Scurfyマウスは，下痢や貧血，血小板減少症，白血球増多症，リンパ節腫大，肝脾腫などを認め，3〜4週で死亡し，病理では脾やリンパ節をはじめとする多臓器に活性化T細胞の浸潤を認める．ヒト疾患であるIPEX症候群は，下痢やI型糖尿病，甲状腺機能低下症，溶血性貧血，血小板減少症，リンパ節腫大，肝脾腫などを認め，湿疹や易感染性も出現する疾患である．

マウスではCD4$^+$T細胞の5〜10%にCD25が発現しており，その大部分がTregであるが，ヒト末梢血では単にCD4$^+$CD25$^+$T細胞を分離しただけで十分な抑制能は得られず，CD25を高発現している1〜3%程度のCD4$^+$CD25^{hi}T細胞に存在していることが示されている．このことは，CD4$^+$CD25$^+$Tregにおける主要転写因子であるFoxp3の発現とも一致している．また，ヒトではCD4$^+$CD25$^-$T細胞刺激後Foxp3発現を一時的に認めることも報告されている．一方，Foxp3発現の観点からみるとCD4$^+$CD25$^-$T細胞にも少数ながらFoxp3発現細胞がある．

2. 分化

Foxp3$^+$Tregは胸腺に由来するtTreg(あるいはnTreg)および末梢で誘導されるpTreg(あるいはiTreg)に分類されることが多い．胸腺では，著者ら[2]や海外からの研究により，自己抗原へのアフィニティが強いCD4$^+$T細胞から分化することが示されている．つまり自己反応性T細胞は，細胞除去あるいはFoxp3$^+$Tregに分化することで中枢性トレランスが維持されるうえ，末梢性トレランスも維持されているのである．一方，末梢ではTGF-βや未成熟樹状細胞とともにCD4$^+$T細胞がT細胞受容体刺激を受けた際に，Foxp3$^+$T細胞に分化することも報告されている．とくに樹状細胞からの刺激により，アナジーT細胞，Tr1，Foxp3$^+$Treg，Th1・Th2・Th7細胞への振分けがいかになされるのかは重要な問題であるが，樹状細胞の成熟度だけでなく，樹状細胞サブセット，たとえばlymphoid-resident dendritic cellsおよびmigratory dendritic cells，および細胞の状態，たとえばsteady stateなのか炎症下なのかなど，種々の要因が関係しており，今後の課題となっている．

3. 機能

抑制機能の発現にはいくつかの機序が報告されている．IL-2受容体を構成するCD25によりIL-2を，CTLA-4により抗原提示細胞上のCD80/86を，通常のT細胞(Tconv)と競合することによりTconvの活性化を抑制する機序や，抑制性サイトカインであるTGF-βやIL-10，IL-35，エクト酵素であるCD39を介したATPからのアデノシン産生，perforinやgranzymeによる細胞傷害などが報告されている．

4. 維持および安定性，可塑性

Foxp3$^+$Tregの維持には，IL-2が重要な役割を担っている．Foxp3$^+$T細胞はIL-2受容体を構成するCD25の発現が特徴であるが，機能面でも重要な働きをしている．たとえば，IL-2欠損マウスやIL-2中和抗体を投与された野生型マウスではTregが減少し，自己免疫疾患を発症する．

Foxp3$^+$TregにおけるFoxp3発現は，つねに安定的ではなく，その発現を失いIL-17およびIFN-γを発現するエフェクターT細胞に分化しうることも報告されている．このようなT細胞はexTreg細胞やexFoxp3細胞などといわれ，たとえば関節炎モデルにおいて局所の滑膜線維芽細胞が産生するIL-6によりexFoxp3 Th17細胞が誘導され，通常のTh17細胞と遺伝子発現プロファイルが異なる，より破骨細胞の分化を促進する細胞に分化していることが示されている[3]．

このようなFoxp3発現を失うTregの由来についても，興味深い研究がなされている．ある研究では種々の炎症下でもFoxp3発現を失うFoxp3$^+$Tregは5%以下であること，また別のグループからはCD25^{low}Foxp3$^+$T細胞がおもにFoxp3の発現を失うことなどの報告がなされている．一方，

Foxp3陽性細胞からの一過性のFoxp3発現も知られている．Foxp3レポーターマウスの解析では，Foxp3-CD4$^+$T細胞を *in vitro* で活性化すると，TGF-βの非存在下においても約10%にFoxp3を発現するが，Foxp3$^+$T細胞とは異なり活性化Foxp3-T細胞と同様の遺伝子発現プロファイルで抑制機能ももたず，再刺激によりFoxp3発現を容易に失うことが示されている．また，このことはマウスと比べヒトでより生じやすいと考えられている．さらに，ヒトではCD25^{high}Foxp3$^+$T細胞からでも，また炎症性サイトカインがなくともT細胞受容体刺激によりTh17細胞に分化しうることが報告されている．

ヒトでもマウスでも，ともにFoxp3の持続的発現にはエピジェネティックスおよび翻訳後の調節が重要であることが示されている．Foxp3遺伝子発現に影響を与えるnon-coding sequenceとして，CNS1，CNS2，CNS3が同定されているが，とくにCNS2がFoxp3の発現量や安定性にかかわっている．tTregではこの部位の脱メチル化によりオープンなクロマチン構造となっているが，pTregでは脱メチル化が生じずクローズドな構造となっている．このTreg特異的脱メチル化領域であるCNS2に，Foxp3およびRUNX1-CBF-β complexが結合することで，Foxp3の発現が維持される．CNS1およびCNS3はFoxp3発現誘導に重要であり，CNS1には転写因子Smad 3やNFATc2が結合しTGF-βセンサーとなっている．CNS3にはc-Relが結合する．これらの領域におけるヒストンアセチル化状態が，転写因子の結合に影響している[6]．

Foxp3の翻訳後の調節としては，アセチル化やユビキチン化，リン酸化が知られている．アセチル化はFoxp3のクロマチンとの結合において重要な役割を担っており，p300によるアセチル化，SIRT1による脱アセチル化などが作用している．また，Foxp3の蛋白分解はユビキチン/プロテアソーム系が作用しているが，ここにE3ユビキチンリガーゼであるSTUB1，脱ユビキチン化酵素であるUSP7などが関与している．リン酸化はFoxp3の抑制能に関与しており，TNF-αの作用によりTregの抑制機能が減弱し，TNF-α阻害薬によりこの機能が復活することが報告されているが，おそらくこの過程にTNF-αにより誘導されたprotein phosphatase 1(PP1)がFoxp3のSer418を脱リン酸化することで抑制機能の低下に至っていると考えられる．

5. 自己免疫疾患におけるFoxp3$^+$Treg

種々の自己免疫疾患でFoxp3$^+$Tregの関与について検討がなされているが，ここでは報告が多い関節リウマチ(rheumatoid arthritis：RA)での研究を紹介したい．RA患者末梢血液中でのTregに関しては，減少の報告や不変とする報告がある．また，一部の報告では増加とするものもある．この報告間の差は，CD4$^+$CD25^{high}T細胞やFoxp3$^+$細胞などのTregの検出方法の違いや，疾患のステージ，治療薬が影響しているのかもしれない．一方，関節液内のTregに関しては，増加しているとする報告が多い．これに関しては末梢血液中と比較し，関節局所におけるエフェクターT細胞はTregによる抑制を受けにくいことが報告されており，局所のTreg増加にもかかわらず疾患が持続している理由のひとつと考えられている．エフェクターT細胞のTregによる抑制への抵抗性獲得に関しては，IL-6，IL-7，IL-21などによる作用が示唆されている．

RAにおけるTregの機能に関しては，関節液内では抑制能を有しているとする報告の一方で，末梢血液中では正常の抑制能を有するとするものや，エフェクターT細胞の増殖は抑制するが，IFN-γやTNF-αなどのT細胞や単球からのサイトカイン産生に対する抑制能は低下しているとする報告など，異なる結果が示されている．このような違いが生じる原因として，やはり細胞群の同定方法や，治療や経過などが影響していると考えられる．

RAの病因としてのTregの役割については不明な点が多い．RAでは胸腺や骨髄機能の異常が指摘されており，早くにT細胞をはじめとする骨髄由来細胞のテロメア短縮・老化，胸腺からのT細胞産生減少などが生じることが知られている．このことが，末梢におけるT細胞のレパトワに影響を及ぼし，自己反応性T細胞の増加やTregの選択維持の障害にかかわっている可能性が指摘さ

れている．ヒト胸腺では，ハッサル小体という構造が知られており，Tregの選択に重要な場となっている．この部分の上皮細胞に，RAの自己抗原として重要なフィラグリンやgp39が発現されていることから，胸腺機能の低下がTregの数や機能，特異性に影響し，関節炎発症に関与する可能性が示唆されている．しかし，IPEX症候群では関節炎の頻度は少ないとされることから，病態形成は別として病因としての$Foxp3^+$Tregの意義は大きくないであろう．

6. 治療への応用

自己免疫や移植免疫における治療では，寛容誘導が腫瘍免疫では逆に抑制能の解除が求められている．したがって，Tregを標的とすると，前者ではTregの移入や誘導，機能増強や維持を誘導する薬剤が，後者では$Foxp3^+$Tregの数や可塑性に作用する薬剤，たとえばFoxp3発現を阻害する薬剤や分解を促進する薬剤，抑制機能解除に作用する薬剤，が適している．具体的には，$Foxp3^+$Tregの増加を狙った低用量IL-2投与や，メチル化やアセチル化，ユビキチン化にかかわる薬剤などが候補となっている．とくに低用量IL-2投与に関してはヒトGVHD治療に用いられた結果が報告されており，Tregの増加とともに臨床的な効果を認め，2年にわたる長期経過でも有効性と安全性が報告されている．さらに，全身性エリテマトーデスやI型糖尿病患者に対する低用量IL-2投与の報告も出てきているほか，食物アレルギーに対しては動物モデルでの検討がなされている．

おわりに

近年，腫瘍治療における免疫チェックポイント阻害療法の効果と副作用が明らかになり，生体の恒常性維持におけるT細胞の役割があらためて注目されている．Tregについても低用量IL-2投与の臨床試験の結果はあらたな治療標的としての可能性を示している．一方で，Tregの可塑性に関する研究からは，疾患制御においてもTregの誘導だけではなく安定性や維持といった多面的な検討が必要であろう．また，多くのTregに関する研究がなされているが，今後抑制という機能だけではとらえがたい他の機能の同定が，さらなる病態理解や疾患制御の開発には有用かもしれない．

文献

1) Zeng, H. et al.：Type 1 regulatory T cells：a new mechanism of peripheral immune tolerance. *Cell Mol. Immunol.*, **12**：566-571, 2015.
2) Kawahata, K. et al.：Generation of CD4(+)CD25(+)regulatory T cells from autoreactive T cells simultaneously with their negative selection in the thymus and from nonautoreactive T cells by endogenous TCR expression. *J. Immunol.*, **168**：4399-4405, 2002.
3) Komatsu, N. et al.：Pathogenic conversion of Foxp3+ T cells into TH17 cells in autoimmune arthritis. *Nat. Med.*, **20**：62-68, 2014.
4) Li, Z. et al.：FOXP3+ regulatory T cells and their functional regulation. *Cell Mol. Immunol.*, **12**：558-565, 2015.

第121巻 第3号 2018年3月1日発行（毎月1回1日発行）［1914年6月5日第3種郵便物認可］
ISSN 0020-1991 NAIKA

内科

Internal Medicine

3 臨床雑誌
Vol.121 No.3
2018
南江堂

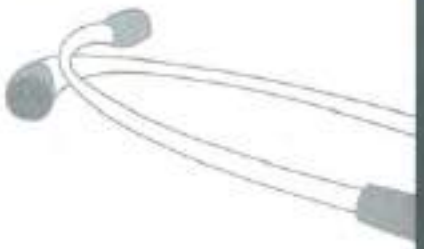

特集

内科医が診る 関節痛・腰痛

リウマチ学の原点に戻る

- 局所症候へのアプローチ
- 筋骨格疾患へのアプローチ
- 筋骨格症状をみる・なおす

〔企画〕萩野　昇

連載

- ～キホンをシンプルに考える～ 体液・電解質・酸塩基平衡異常のとらえ方
- 明日から使える！ 臨床英語論文の書き方，書かせ方
- 呼吸器内科 ×○○科で語る！ Comorbidity 患者さんの診かた
- 教えて！レントゲン 胸部単純 X 線の㊙目付けポイント
- 未来は明るい！明日を担う女性医師の活躍

Focus On

座談会

日本の筋骨格疾患診療のあり方について

[司会]
萩野　昇 氏
帝京大学ちば総合医療センター
第三内科学講座

川畑仁人 氏
聖マリアンナ医科大学内科学
(リウマチ・膠原病・アレルギー内科)

花岡亮輔 氏
上都賀総合病院
リウマチ膠原病内科

國松淳和 氏
国立国際医療研究センター病院
総合診療科

萩野　本日は,「日本の筋骨格疾患診療のあり方について」という，若干大上段に振りかぶったタイトルですが，川畑仁人先生，花岡亮輔先生，國松淳和先生の３名をお迎えしました．

まず，川畑先生は，聖マリアンナ医科大学リウマチ・膠原病・アレルギー内科の教授に着任されたばかりで，基礎免疫学・臨床が高いレベルでバランスのとれた，僕のメンターに当たる先生です．本日は卒前・卒後教育についてもお話を伺いたいと思います．

花岡先生は，栃木県北部の上都賀総合病院で何でも診療しておられます．上都賀総合病院がカバーする人々は，高齢者が多く，必然的にしばしば「高齢＝痛い」状態です．そういった方に花岡先生がどのようにアプローチしているかお話しいただきたいと思います．

國松先生は，国立国際医療研究センター病院の総合診療科にいらっしゃいます．自称「臓器不定科」と言っておられて，非常にいいネーミングだなと(笑)．あと，國松先生は『ニッチなディジーズ』や，『外来で診る不明熱』という素晴らしい書籍を出しておられます．臓器不定科として，現在の日本の筋骨格診療のあり方についてお話しいただきたいと思います．

萩野　昇 氏 | Nobori HAGINO

2000年東京大学医学部卒．横須賀海軍病院，都立駒込病院などでの内科研修を経て2006年より東京大学医学部アレルギー・リウマチ科．2011年より帝京大学ちば総合医療センター第三内科学講座講師．「リウマチ膠原病セミナー」を年4回開催し若手の教育にも努める．『ロジックで進めるリウマチ・膠原病診療』(医学書院)が近日刊行予定．「"痛み"で悩める患者さんに寄り添う先生方の一助となるような特集であれば幸甚です」と語る，本特集企画者．

診断：本邦のunmet needs

1．卒前・卒後医学教育における運動器診療の教育の現状と問題点

萩野　まずは，卒前・卒後の医学教育における運動器診療についてです．

関節痛の患者さんへのアプローチ方法は，内科診断学のなかで時間をとって教育されていないという印象があります．場合によっては，指導する立場の医師が，「腰痛や関節痛は整形外科」という指導をしていたりもします．一方で，『ハリソン内科学』には筋骨格の診療のやり方，肩の痛み・腰の痛みへのアプローチに1章を割いてあります．全身が痛いという患者さんをみていくうえで内科医としてどうあるべきか，川畑先生にお聞きしたいと思います．

川畑　大学教育を考えてみると，中枢から筋が神経内科，筋から関節はリウマチ内科で分け合っているのが現状だと思います．ところが，運動器として機能する，また痛みを感じる皮膚までと考えると基本的には中枢から末梢まで通して考えるべきです．その意味では，現状の教育は非効率だと思います．

卒前では，系統立った考え方，たとえば中枢か末梢か，筋腱か関節あるいは滑膜かを，運動系だとどういう仕組みで見分けるかなどの基本的な考え方を身につけて，まだ専門家になっていない時期に症例を通してみていくのが大事だと思っています．

卒後は，リウマチ科，神経内科も含めて，それぞれ補わなければならない点があると思っていますが，折に触れて患者さんを若手と一緒にみる場面をつくって足りないところを是正しているのが現状です．

萩野　園松先生，臓器不定科としての工夫がありましたらお聞かせください．

園松　「臓器不定科」は完全に私が自称しているだけで，病院でまったくオフィシャルにされていません．でも，それが現状を物語っている気がします．腎臓や循環器などのわかりやすい臓器はそれなりの教育が確立していると思いますが，筋骨格・皮膚軟部組織をひと固まりで教えようという機運やシステムがないし，気概のある先生もいないので，「誰がそれを教えるか」というのが問題です．当院がうまくやっているかというと，そうはでないという現状です．

私は総合診療科にいるので，その立場を活かしたいと思っています．たとえば痛風発作をどの科がみるかという問題も，本当に困れば整形外科の先生が助けてくれますから，まずは総合診療科がさわやかにみる．われわれはファーストタッチを専門と自称して，一般内科医でも関節や筋肉を触ってマネジメントするという姿を研修医にみせたいわけです．

萩野　そうですよね．まず触っている姿を指

導医がみせたい.

國松　「何もせずに，これは整形外科」という姿だけはみせないようにしていこうかなと，それをまとめるスローガンとして，『THE 整形内科』という本が出て，その「整形内科」という言葉がよいと思っているのです．臓器不定科というと，何でもみるということでちょっと重荷になるので，運動器を内科医が総合的にみる「整形内科」という言葉がちょうどよいのかなと思っています．

萩野　あの言葉は本当にいいですね．

國松　若者を巻き込むというのが教育の肝だと思うので，若者に対してわかりやすいスローガンですよね．

萩野　大学から研修医を受けておられる花岡先生はいかがですか．

花岡　当院でも受け入れますし，他大学に指導に行くこともあるのですが，それぞれの医療機関において教育内容が標準化されていない気がします．

あと，ナンバー内科の時代は，内科医であれば内科全領域を何でも扱う必要がありました．ところが今は，リウマチ科の医師であれば関節のことしかわからなくなっていて，若い先生たちの内科学全体に関する知識の統合性が失われている感じです．それぞれの臓器やシステムの関連を統合して考えられない．

川畑　多臓器の関連，神経筋骨格系の統合は重要な問題だと思います．

花岡　卒前・卒後教育の大きな問題だと思うのですが，教える側も臓器別医療のなかで育てられ，内科医としての知識の統合性が失われた世代になっていることも結構大きいのではないかと思います．

萩野　人は臓器の集合体ではないので，それが総合診療科あるいは総合内科になるのかはわかりませんが，大きなスパンではもう一度統合の動きがあると思います．

川畑仁人 氏 | Kimito KAWABATA

1992年東京大学医学部卒．東京大学医学部附属病院，東京医科歯科大学膠原病・リウマチ内科などを経て，2017年より聖マリアンナ医科大学内科学(リウマチ・膠原病・アレルギー内科)教授．趣味は野球，将棋の観戦．「リウマチ・膠原病診療に携わる先生には(臨床)免疫学への関心を，免疫学に興味をもつ人には，リウマチ・膠原病診療への関心をもつことをお勧めします．診察では，所見のパターン化と鑑別疾患検討の前に，所見を適切に表現することを意識しています」と語る．

2．超高齢化社会における筋骨格疾患診療

萩野　花岡先生の患者さんは，高齢者が多いと思うのですがいかがですか．

花岡　鹿沼という医療圏は，山に囲まれていて，ほかに出ようがないのです．ほかの場所に行けないので，その場所で生まれて，働いて，死んでいく，という場所です．実際，コホート研究をしてもほとんど脱落がないです．

國松　それはすごいですね(笑)．

花岡　ですので，人口構成を如実に反映した疾患構造になっていると思います．

萩野　痛みを訴える高齢者は多いので，内科の先生が外来フォロー中に，患者さんが首，肩，腰，足が痛くなってきて，「整形外科に行って」ということはよくあるのではないかと思います．実際どういった疾患が問題になりますか．

花岡亮輔 氏 | Ryosuke HANAOKA
1997年昭和大学医学部卒．都立駒込病院，昭和大学などを経て，2008年より上都賀総合病院リウマチ膠原病内科医長，2010年より同部長．「リウマチ膠原病内科は，"自己免疫疾患，リウマチ性疾患をもった人々の総合診療科"です．この理念を実現するためには，総合診療科のマインドを学びつつ，同時に専門領域の研修を行うべきで，当科の若手には，あえて専門領域以外の患者さんも受けもち，広い視野を養ってもらっています」と語る．

花岡　高齢者なら，偽痛風じゃないでしょうか．それこそ一般内科医が最初につまずく筋骨格疾患は，偽痛風だと思うのです．たとえば毎日のように，誤嚥性肺炎の患者さんが入院してきます．でも，これを惰性的に診療してはいけない．多くのまれな疾患は「誤嚥性肺炎」と間違えられたまま入院してはじめて判明することが多いのです．

國松　本当にそう思います．

花岡　「誤嚥性肺炎だと思って，meropenemもvancomycinも使ったのに，CRPが下がりません」と相談されて，膝をみたら真っ赤で，偽痛風ですべてが解決する．入院する必要すらなかったのではという症例は，本当に多いですね．

萩野　花岡先生のご指摘のとおり，結晶性関節炎はたくさん見逃されていると思います．結晶性関節炎は何がしか全身性のプレゼンテーションをきたしうるというのは，大事な視点です．

花岡　高齢者が偽痛風になると，実はそれだけで衰弱して命の危機になります．内科医が深く考えずに整形外科に紹介し，整形外科の先生は偽痛風のために全身が衰弱しているとはまったく考えずに関節だけをみる．でも，実際には転科した時点でもう偽痛風だけでは済まなくなっていて，肺水腫になっていたり，それこそ本当に誤嚥性肺炎になっている．

萩野　本当にご指摘のとおりです．患者さんからみたら内科も整形外科も片手落ちの診療ということが多い疾患ですね．

川畑　筋骨格疾患には行き場のない患者さんが多くいらっしゃいますよね．

萩野　作家の橋本治さんが，顕微鏡的多発血管炎を発症して，病院でさまざまな診療科に回されたことを書いておられました．正直，われわれにはよくある風景ですけれども，やっぱりこれは改善が必要だなと思いますね．

花岡　神経系とか免疫系などの，目にみえないシステムの病気について，内科医がすごく弱くなっているなと思うのです．みえないものを洞察するということが忘れられてきていますね．

川畑　たとえば，ある異常所見をバラバラに考えて，まったく統一感のない鑑別疾患が出されることもしばしば目にします．みえないシステムを洞察するとか全体像をみる力が必要であることを実感します．

3. 検査モダリティの進歩と位置づけ

萩野　國松先生の施設はFDG-PETの報告がよく出されていますが，コメントをいただけますか．

國松　関節炎とわかっている人よりは，不明熱・不明炎症という状況で，多少当たりはついていたとしても，やむをえずにやるという状況が多いと聞いています．

そこで明るみになる具体的なリウマチ性疾患は，PMR（リウマチ性多発筋痛症），脊椎関節炎，高齢者発症の血清陰性の関節炎，鼻や耳に炎症がない気管軟骨に割と限局したわかりづらいRP（再発性多発軟骨炎），あとは高安病とか大血管炎です．PETで一気に診断できているさまをたくさんみていると，若者が「おお！」という感じですごく引きつけられるので，若者を引きつけるデバイスという一面もあります．

萩野　強力なモダリティであることは間違いないですね．ただ，適切な位置づけはまだまだ難しそうですね．

國松　PETを撮って肝臓に妙な集積があるけれど，それが結果的には生理的なものだったりして，かえって現場が混乱している姿をみることもあるので，PETを撮る前の鑑別診断がきわめて大事だと思います．

萩野　私は意地が悪いので（笑），PETの「空振り症例」を集めていて，やはり管腔臓器が圧倒的に苦手だと思います．それから，悪性腫瘍に全然集積しないこともあります．cytologyが陽性で明らかに肺がんなのに，腫脹した縦隔リンパ節に全然FDGの集積がない．足元をすくわれる可能性が常にあると思います．

川畑　使うからには限界を知るということですね．

花岡　以前に，前立腺がんがPETの読影で見落とされていた症例をみたことがあります．不明熱として紹介された方で，PET-CTでも有意な所見がないとされていたのですが，骨髄生検をしたら前立腺由来の腫瘍細胞が多数浸潤していました．組織をとれるのだったら組織のほうがずっと診断的意義が高いので，PETなどの画像診断が，侵襲的な検査を避けるためのエクスキューズになってはいけないなと思います．

國松　本当にそう思います．

萩野　結局，tissue is the issueというところに落ちつきそうですね．

國松淳和 氏 | Junwa KUNIMATSU
2003年日本医科大学卒．日本医科大学付属病院，国立国際医療研究センター国府台病院などを経て，2011年より国立国際医療研究センター病院総合診療科．専門は一般内科診療のほか不明熱・不明炎症診療，自己炎症性疾患で，不明熱外来を開設している．主な著書に『外来で診る不明熱』（中山書店），『ニッチなディジーズ』（金原出版），『はじめての学会発表 症例報告』（中山書店）など多数．

治療：進歩と課題

1．CSA，生命予後

萩野　治療の進歩と課題ということですが，この分野は間違いなく生物学的製剤の恩恵を受けて分野自体が拡大したと思います．ただ一方で，大きな課題を残したままになっているとも思うのです．たとえば，よりいっそう早く関節炎をみつけようということで，欧州では，破壊性関節炎を発症するリスクが高い人たちを集めるclinically suspect arthralgia（CSA）といった方向に行き，早期関節炎クリニックをつくっていますが，日本にはありません．逆にリウマチ診療に熱心な専門施設が，生物学的製剤などの治療が不要な患者さんに対しては冷たい，ということがあります．川畑先生からお話しいただければと思います．

川畑　CSAは注目すべき今後の課題だと思っています．ただし，早期所見ということになると，関節の部位とか，リスクファクターとか，家族歴などを取り込まないと診断もしくは特定しにくくなっているので，実際に関節リウマチに移行する人がどれだけ含まれているかなど明らかにすべき問題も多いと思います．あと，CSAがわかることで，どのような介入が有効でその人の予後を変えられるのか，そこも明らかにする必要があると思います．CSAを実臨床でどう生かすかはこれからの問題だと思います．

このCSAの考え方は開業医の先生方と密接な関係があります．たとえば関節炎所見はなく関節痛を訴える患者さんがこられて，リウマトイド因子と抗CCP抗体をみて，「陽性じゃないから大丈夫でしょう」とか，逆にリウマトイド因子や抗CCP抗体が陽性であることで，「すぐに紹介しよう」など，それぞれ実際の臨床では起きていることだと思いますが，そういう実際の対応がCSAの特定によってより適切に修正される可能性があることも注目だと思っています．

萩野　花岡先生はいかがでしょうか．

花岡　われわれがリウマチ医になったころは，生物学的製剤なんかもちろんなく，治療薬自体たいしたものがなかったので，関節は壊れてしまっても，せめて患者さんが亡くなるのは防ぎたいというのがすごく大きなテーマだったと思うのです．今はそれが忘れられてしまっているのではないか．それこそ積み残された課題になっていると思うのです．

ごく最近になって，リウマチの生命予後がずいぶん改善してきたと報告されるようになりましたが，ごく最近まで，死亡率は2倍，生命予後は10年短いという状況は変わっていませんでした．にもかかわらず生命予後を改善しようという積極的な取り組みは非常に乏しかったと思うのです．

たとえば，有害作用を恐れて生物学的製剤を拒否しているリウマチ患者さんに，「治療によって，あなたが今，潜在的に抱えている死亡リスクを改善することができる」とアピールしなければ，本当に説得力のある治療のオファーにはならないのではないかと思います．CSAに関しても同じで，「CSAは，経過によってはあなたの命に関係する問題なのだよ」とアピールしなければ，患者さんの問題意識はかなり軽くなってしまうのではないでしょうか．

萩野　大事なテーマをご提起いただきました．生命予後をよくしないといけないということも考えて，20歳代の関節リウマチの患者さん，50歳代の患者さん，80歳代の患者さんで，同じような症状でも治療は別々の比重の置き方があるでしょう，という話を私は後期研修医によくします．80歳代の患者さんは，極端な話，長期の関節予後をそれほど重視しなくてもよいので，痛みがなく元気で長生きしてほしいということになります．20歳代の方だったら，その後，60～70年と関節を使うので，なるべく関節破壊を抑えることを，本人の自覚症状とはある程度独立に考えないといけません．

2．非専門医がどこまで治療してよいのか

萩野　非専門医からよく聞かれるのは，非専門医が関節リウマチをどこまでやってよいのかということです．疑った時点で専門医に紹介してもらうといっても，専門医のいない地域に住んでいる場合や，MTX（methotrexate）や生物学的製剤は使いこなせるべきなのか，など難しいと思うのです．川畑先生は，非専門医からの相談にどうお答えしていますか．

川畑　これはなかなか難しくて，個人的にどういう先生かということにもよります．顔がみえてわかっている関係だと相互にやりやすいです．一般的には，squeeze test（bilateral compression test）や血清学的な所見の解釈の段階で自信がない先生は専門科にご紹介いただければと思います．

私は，神奈川に移り，地域医療の観点で東京と違う状況なのがわかりましたので，近隣の先生ごとにMTXや生物学的製剤など，どの薬剤までの治療に対応していただけるかのリストをいただきました．相互にわかるにつれて患者さんの診療をより適切だと思う医療機関に移行していくための参考リストです．

萩野　なるほど．

花岡　あと，地域連携において，専門医が紹介状にきちんとした返事を出すことはとても大事だと思います．学会や講演会にきてくださる先生は熱心に勉強されるのですが，その場にいらっしゃらない先生にも情報を提供することが必要です．開業の先生方は，紹介状への返事をとても楽しみにされているので，できるかぎり詳しく，アカデミックなバックグラウンドの解説も含めてお返事すると喜んでいただけますし，次もご紹介いただけます．また，そのうちにご自身でも頑張ってみてくれるようになることが多いです．

川畑　2回目の返書が大事ですね．

花岡　「こんな所見が認められたため，こんなふうにしました」と書くことですね．

当院は，私が赴任してから，「リウマチ因子だけではなく，抗CCP抗体というのもあります．そして，リウマチは左右対称性に多発する末梢優位の関節炎ですよ」ということを常に紹介状の返事に書くようにしていたら，典型的なリウマチが紹介されることはかなり減り，むしろ乾癬性関節炎など，血清反応陰性で，診断が難しい症例が紹介されることが増えてきました．診断が容易な症例であればご自身で診療されるケースが増えたのでしょう．すごくいい形になったと思います．

川畑　私は近隣の開業の先生に，抗CCP抗体やリウマチ因子が陽性でなくても手足の指や小さい関節にいくつも痛みが持続する方はご紹介ください，とお話ししています．

萩野　私も当院に赴任したときに周りの先生方へのご挨拶に「リウマトイド因子と抗CCP抗体を調べて，どちらかが陽性だったら紹介してください」，「どちらも陰性であっても，約2週間，対症療法でNSAIDなどを処方しても，よくならないときにはご紹介ください」という形にして，それで紹介されるようになりました．

川畑　やはり抗体検査は大事ですが，陰性の方への指針を示すことも重要ですね．

花岡　リウマチ医がそんなに多くいるわけではないので，地域の医師全体のレベルを引き上げる努力を専門医がするべきだし，地域の医師会の講演会などに出ていくことも必要だと思います．

萩野　私がいる千葉内房地域に，もともと小児科でしたが小児科・内科として開業されて，「関節リウマチの方をぜひ逆紹介してください．あと何例かみたらわかりそうな気がするので」という熱心な先生がいらっしゃいます．こういった先生が地域医療を守っていると実感しました．

3. 乾癬性関節炎

萩野　最近，乾癬性関節炎の新規薬剤が次々出てきています．乾癬性関節炎は，皮膚科の先生がみていたり，皮膚科と整形外科で連携していたり，あるいはリウマチ科がみたり，いろいろなパターンがあると思いますけれども，川畑先生，現状はいかがでしょうか．

川畑　最近の薬剤の進歩で認識されてきた影響か，紹介される患者さんが昔より増えている気がします．問題は，OA（変形性関節炎）との鑑別です．erosive OAと乾癬性関節炎に関しては，鑑別に困られている医師も多いのではないかと思います．

あと，乾癬の治療体系も変わってきているので，われわれはapremilastなどの乾癬の治療についてもキャッチアップしないといけないと思っています．

花岡　当院は，皮膚科の先生と相談して，当

科と両方でみています．乾癬の患者さんは，生活習慣病も多いので，そちらも一緒に僕らが管理しますよと言うと，喜ばれますね．

萩野　米国では「乾癬は心血管系リスクだから，皮膚科で乾癬と診断されたら，一度総合内科で心血管リスクの評価を受けるべきだ」とされています．花岡先生のところは理想的な連携ですね．

川畑　私は，乾癬の紹介を受けて，逆にOAにとても興味をもちました．かなりDIPが腫れてくると局所の血流障害などが起きたりしますので，OAでも爪の所見が出てきます．そのような鑑別が難しい例に当たることで興味深くなってきました．

萩野　OAは興味深いですね．本当に勉強することがまだまだいっぱいあると再認識します．

4．リウマチ性多発筋痛症（PMR）

萩野　國松先生にPMRについて伺いたいと思います．先生のところは膠原病科がありますが，全身が痛いという高齢者はどちらでみていますか．

國松　診断がついていなければまずはこっちにきます．かつ，私は自分たちでみたいという気概でやっているので，PMRはほとんど自己完結できています．

萩野　それがまた難しくて，プライマリー・ケア医がPMRを自己完結してよいのかという話になるわけです．私は「してよい」派ですが．

國松　私も「してよい」派なのですが，私がリウマチ・膠原病を教わった三森明夫先生は，「プライマリー・ケア医はPMRという病気を知らなくてよい」と言われました．リウマチ専門医はPMRをある程度特異的に診断できる．でも，非専門医は除外診断という位置づけなので，あまり知らなくてよい．そういうことを一言で遠慮に言った表現なのですが．

萩野　65歳以上の約2%の有病率ですよね．

國松　きわめてcommonな病気です．

萩野　commonですし，場合によっては，CPPD沈着症によって偽PMRみたいな病態が起きて難しいということもありますし．

國松　PMRは高齢者を総合的にみることになるので，内科医やプライマリー・ケア医にとってすごくやりがいがあると私は思うのです．指導的な方がプライマリー・ケア医を啓発する必要はあると思うのですが，基本的なことを教わるか学ぶかして，このcommon diseaseを特殊な状況にならない限りはみる．どちらかというとそのほうがよいのではないかと思っています．

萩野　実際，プライマリー・ケア医で勉強熱心な先生は完全に範疇と考えていて「これはPMRにしてはちょっとおかしい」といってご相談いただくことがあります．

花岡　その一方で，「リウマチ因子陰性で痛かったらPMR」と短絡的に診療されている事例もときどき見受けられます．取り落としができるだけ少なくなるようなシステムを構築する必要があるので，地域によって，1回はリウマチ科医がみるようにするのもありかなと思います．

萩野　プライマリー・ケア医は，PMRがcommon diseaseだという意識があるので鑑別にあがるのです．一方，ピットフォールになるのがリウマチ科医のいない中規模から大規模の病院です．そういう病院に全身が痛くて炎症がある患者さんが入ったら，言葉は悪いですけれども，たらい回しが始まって何ヶ月も診断がつかないということがあったりします．

川畑　線維筋痛症疑いになっていたり，五十肩と診断されていることもあります．

萩野　首・肩・腰・脚に症状が出て，でも炎症反応が上がる以外に特異的な所見がない場合には，可能ならば専門の医師あるいは経験数の多い医師がみることが望ましいですね．

今後の展望

萩野　今後の超高齢化社会における筋骨格疾患ということで，花岡先生のお考えをお聞かせください．

花岡　私は，「筋骨格疾患を，あくまで内科の一領域として診療してほしい．他臓器から切り離された，排他的な一領域であるかのごとく考えないでほしい」と思っています．筋骨格疾患は，生理学的にも，免疫学的にも，他臓器との緊密な連関をもっています．それらの諸臓器への影響も加味した，総合的な視点を養って欲しい．さらに，その人の社会的な背景や予後なども考慮しなければいけないと思います．つまるところ全人的な診療をしようということです．

萩野　全体を考慮しないと検査値異常の原因をすべて正す，みたいなことになってしまいますね．

花岡　そうです．今の内科のシステムは自然発生的に専門分化されていったので，各科の守備範囲にすき間が空いていたり，重複したりしています．科と科のすき間に患者さんが落ち込んでいる場合がすごく多いと思うのです．それを防ぐために「内科全般をみるけれども，とくにリウマチが好きだよ」という医師をたくさんつくりたいと思っています．

萩野　私も，rheumatology in general practice（RiGP）をかけ声にしてやっていければと思います．まさにそういう存在である國松先生に，これから総合診療科を率いていくに当たっての抱負をお願いしたいと思います．

國松　総合内科という看板をあえて利用して，rheumatologist にとっては基本である，皮膚をみて，軟部組織をみて，脂肪織をみて，筋肉をみて，筋膜を想像して，滑膜をみて，関節をみてという診療を内科医がカッコよくやっているのを見せたい．不明熱をみる際にもそういった運動器を想定する必要があることを，あえて声高にやっていけばよいと思いますね．

萩野　日本の内科でピットフォールになりがちなのは，耳鼻咽喉，筋骨格，軟部組織，それから泌尿・生殖器系だと思いますので，ぜひ臓器不定科として取り組んでもらいたいです．

最後に，川畑先生に「今後の展望」ということで締めていただければと思います．

川畑　患者さんの置かれている状況を正確に表現できる，記載できることが大事だと思っています．プロフェッショナルとしてすでに確立している先生方だったら，病名を思い浮かべるというのはよいと思うのですが，自分の拙い知識で自分の領域だと思い込んでいる病気に無理やり当てはまるという考え方で，患者さんを記載してはいけないと思っています．実際に何が起きているのか，起きていることを正確に記載して，それから患者背景を改めて考えて，病気を考える，そういったトレーニングが必要だと思っています．

萩野　図らずも「リウマチ学の原点に戻る」という特集のサブタイトルに戻るかたちになりましたけれども，正確な記載というのは重要な論点です．ぜひ若い先生方にリウマチ学の原点に戻る大切さを川畑先生からご教育いただければと思います．

本日はここまでとさせていただきます．どうもありがとうございました．

昭和19年12月21日第3種郵便物認可　毎月1回1日発行（1267冊）　2018年2月1日発行　ISSN 0370-999 X

診断と治療 2

Diagnosis and Treatment

2018
Vol.106
No.2

特集

血管の炎症を俯瞰する

一般診療で押さえておきたい"血管の炎症"の
知識・最新の話題をこの1冊で網羅!!

連載

症例を俯瞰する総合診療医の眼
黒色嘔吐を主訴に来院した85歳女性

人気の診療科紹介
横浜労災病院内分泌・糖尿病センター

注目の新薬
ナルデメジン（スインプロイク®，
経口末梢性μオピオイド受容体拮抗薬）

診断と治療社

血管炎

結節性多発動脈炎

Author 川畑仁人 聖マリアンナ医科大学内科学(リウマチ・膠原病・アレルギー内科)

KeyWords ○結節性多発動脈炎 ○抗好中球細胞質抗体 ○壊死性血管炎 ○血管造影 ○免疫抑制薬

Headline

1 結節性多発動脈炎は中小動脈の壊死性血管炎であり，細小動脈・毛細血管・細小静脈の血管炎を伴わず，抗好中球細胞質抗体は陰性である．

2 診断に際しては，病理による中型血管炎の存在や血管造影による小動脈瘤の証明，ANCA 陰性，小型血管である細小動静脈・毛細血管の病変を含まないことの確認を行う．

3 寛解導入療法および寛解維持療法からなる治療をすすめていく．ステロイド治療が中心だが，予後不良因子や進行性，治療反応性，患者背景を考慮しながら，免疫抑制薬の併用を検討する．

疾患概念

結節性多発動脈炎(polyarteritis nodosa：PAN)は，最新の血管炎分類である Chapell Hill Consensus Conference 2012(CHCC2012)[1]では，「中型血管炎」に分類され，中小動脈の壊死性血管炎で，細小動脈・毛細血管・細小静脈の血管炎を伴わず抗好中球細胞質抗体(anti-neutrophil cytoplasmic antibody：ANCA)と関連のない疾患として定義されている．

さらにこの分類では，従来から PAN の原因の一つとしてあげられてきた HBV に関連する場合については，「病因が判明している血管炎」の HBV 関連血管炎に分離された．

また，従来からの皮膚型結節性多発動脈炎に関しては，「単一臓器を侵す血管炎」の皮膚動脈炎のなかに含まれる．

用語

1866 年内科医 Kussmaul と病理学者 Maier が，原因不明の発熱，体重減少，腹痛，末梢神経障害を呈した 27 歳男性患者の剖検報告を，結節性多発動脈周囲炎(periarteritis nodosa)として発表したのが本疾患の最初である．現在では，本疾患では動脈全層の炎症が生じ，全身性に侵されうることから，polyarteritis nodosa という名称で 1903 年の Ferrari による発表以降用いられるようになっている．その後，この名称でよばれる疾患に，中型血管だけではなく顕微鏡的検討が必要な小型血管も侵される場合があるとして，小型血管炎の認識が 1923 年の Wohlwill や 1930 年の Arkin らによってなされた．その後，この小型血管炎のタイプは，1948 年の Davson による microscopic form of PAN，1985 年の Savage による microscopic polyarteritis として，classic PAN と区別して報告されるようになってきたのである．これらの疾患の多くは，現在の顕微鏡的多発血管炎(microscopic polyangiitis：MPA)と考えられ，その他の代表的小型血管炎である多発血管炎性肉芽腫症は 1936 年の Wegener により，現在の好酸球性多発血管炎性肉芽腫症は 1951 年の Churg と Strauss により報告されている．

しかし，1990 年の Lightfoot らによる米国リウマチ学会からの PAN 分類基準では[2]，この小型血管炎を PAN から分けることは想定されておらず，1994 年の Jennette らによる CHCC 1994

0370-999X/18/¥100/頁/JCOPY

で[1]，あらためて polyarteritis nodosa から小型血管炎を除かれ，中型血管炎として分類された．したがって，1994 年以前の PAN の報告には現在の小型血管炎も含まれており，それらの報告の解釈には十分注意が必要である．

疫学

PAN は現在，小型血管炎が除かれていることから，かなり頻度の低い疾患と考えられている．欧米では有病率は 100 万人あたり 2～33 人，罹患率は 2～9 人程度と考えられている．日本では，全国の患者数は 1,400 人程度，罹患率は全国で 100 万人あたり一人程度と推定されている．平均発症年齢は 55 歳で，男女比は報告により異なるが 1～3:1 とやや男性に多い傾向がある．

病因と病態

従来の PAN では B 型肝炎ウイルスが病因の一つとしてあげられていたが，現在では原因の明らかな血管炎は別に分類され，病因が不明のものが PAN とされている．B 型肝炎ウイルスのほか，C 型肝炎ウイルス，小児における連鎖球菌感染，B 型肝炎ウイルスワクチンなどをきっかけに生じた例もこれまで報告されてきたことから，何らかの感染も示唆されるが，明らかになっているものはない．Hairy cell leukemia で生じた例も報告されているが，機序は不明である．

中型筋性動脈血管壁の炎症と壊死が病変の主体であり，血管壁では内弾性板の断裂と炎症細胞浸潤，フィブリノイド壊死を認める．病変部位の壁内でもしばしば均質ではなく非対称性の分布を示すほか，病変部位と正常部位に挟まれるように存在し，活動性部位と非活動性部位も同時に存在する．病変の巣状分節性，不均一性がある．微小血管瘤も特徴的であり，剖検や画像では認められることがある．浸潤細胞は，顆粒球中心ではなく，マクロファージや CD4 陽性 T 細胞も多く含んでいるといわれている．

症状

PAN の症状は，発熱，体重減少，倦怠感などの全身症状(80%)と臓器虚血症状に分類できる．関節痛や筋痛(60%)を認めるほか，皮膚症状(50%)では，紫斑や潰瘍，結節，梗塞，網状皮疹などを認め，手指，下腿や足部に認めることが多い．末梢神経障害(75%)では，運動感覚神経障害を呈する多発単神経炎や単神経炎を認める．腎動脈およびその分枝の病変から生じる症状(50%)では，腎血管性高血圧や腎出血によるショックを呈することがある．腸間膜動脈などの腹部血管病変(40%)では，腹痛や下血，下痢を認めることがある．脳血管病変(20%)では意識障害やけいれん，脳出血や梗塞を起こすことがある．この他，心血管病変(20%)では心筋梗塞や伝導障害，心膜炎が生じる．

また，精巣や前立腺，子宮，胆嚢，虫垂，肺腹部の血管炎による各部位の疼痛を認めることがある．これらは単一臓器の血管炎として単独で認めることもある．

検査

血液検査では CRP 上昇や赤沈亢進などの炎症所見を認める．ANCA は陰性である．HBV，HCV のスクリーニングも行う．HIV やパルボウイルス B19 に関連した血管炎の報告もあり，症例により確認の必要性を検討する．

腎血管病変を有する例では，血清クレアチニンの上昇や尿蛋白・潜血陽性を認めることがある．ただし，尿所見は軽微なことが多く，赤血球円柱はほとんど認めない．

腹部血管病変を有する例では，消化管出血を伴う場合，内視鏡で血管露出性の潰瘍病変を認めることがある．症状の有無にかかわらず，腹部血管造影で腸間膜動脈や腎動脈などに小動脈瘤を認めることがあり，本疾患を疑うも生検による中型血管炎の証明ができない場合には有力な検査となる．1 mm 程度の小動脈瘤をも明ら

かにするためには，以前は造影CTではなく腹部血管造影が必須と考えられてきたが，近年は空間分解能の進歩によりCTでも発見される例も出てきている．また，腎血管病変を疑う例では，出血のリスクも考慮し腎生検から始めるのではなく，腹部血管造影から検討を開始するのがよい．

末梢神経障害を呈する例では，神経伝導速度検査は非常に重要な検査であり，血管炎では神経束ごとに虚血の影響が異なることを反映して，早期には速度は正常，振幅が低下する例が多いことを確認する．さらに障害神経の分布を検討することで多発単神経炎を証明できれば，糖尿病を伴う場合，血管炎を考えることは妥当である．腓腹神経障害を認める場合は，腓腹神経生検および短腓骨筋生検の同時生検により感度を高める方法もとられている．

皮膚潰瘍の場合の病理検査では，皮膚潰瘍の中枢側の部位を選択し，中型血管を確認するために皮下脂肪織まで検討できる深さで生検を行う．

診断

PANの診断に際しては，病理による中型血管炎の証明や，血管造影による小動脈瘤の確認を行うとともに，ANCA陰性および小型血管である細小動静脈・毛細血管の病変を含まないことを確認する．

1990年米国リウマチ学会が発表したACR-PAN分類基準に関しては，体重減少や筋痛など非特異的項目があるため診断には不向きであり，かつHBV感染も一項目に含まれていることから，日常診療における診断にこれを用いることは注意しなければならない．

細小動静脈・毛細血管病変を含まないことを示すには，病変部位の病理で確認ができるときはそれを行い，臨床的には小型血管炎を示す糸球体腎炎や肺胞出血を示さず，ANCA陰性であることを確認する．

病理では，血管壁における内弾性板の断裂と炎症細胞浸潤，フィブリノイド壊死が重要所見だが，関節リウマチや全身性エリテマトーデスなどの二次性血管炎でも類似した所見を呈することがあるほか，小型血管炎を呈する疾患でも中型血管の病変を合併することもあり，臨床症状も含めた全体像の把握が重要である．一方，臨床症状や画像所見だけでは，線維筋性異形成やアテローム塞栓，心房粘液腫塞栓など血管炎類似の所見を呈する疾患があることに注意しなければならない．

病変分布の性質から，生検では血管壁に異常所見を認めない場合もあるが，腓腹神経生検では血管壁所見がなくとも，障害神経の生検である以上，軸索変性所見と神経束毎の神経線維の障害度の差異は期待される所見として確認する必要がある．

PANでは肉芽腫はほとんど認めないが，その存在だけで本疾患を除外することはできない．腎では糸球体腎炎は認めないが，細動脈までの病変は認めうる．MPAが分離される前には肺血管系も侵されるとされてきたが，現在では侵されにくいと考えられている．ただし，5%程度で認めるとする報告もあり，その存在だけでは本疾患は除外できない．

また，本疾患は指定難病になっており，その際に用いられる診断基準，重症度分類を各々，表1，表2に示す．

治療

他の原発性血管炎と同様に，寛解導入療法および寛解維持療法からなる治療をすすめていく．ただし，治療方針の根拠となる研究には乏しく，これまでANCA関連血管炎とPANを含んだ患者コホート研究が治療研究の中心となってきた．予後不良因子は，これまで，旧Five Factor Score(FFS)として，クレアチニン>1.58 mg/dL，尿蛋白>1 g/日，心症状，重症消化器症状(消化管出血，穿孔，膵炎)，中枢神経症

表1　結節性多発動脈炎の診断基準

Definite，Probable を対象とする．

【主要項目】

(1)主要症候

①発熱(38℃以上，2週以上)と体重減少(6か月以内に6kg以上)

②高血圧

③急速に進行する腎不全，腎梗塞

④脳出血，脳梗塞

⑤心筋梗塞，虚血性心疾患，心膜炎，心不全

⑥胸膜炎

⑦消化管出血，腸閉塞

⑧多発性単神経炎

⑨皮下結節，皮膚潰瘍，壊疽，紫斑

⑩各関節痛(炎)，筋痛(炎)，筋力低下

(2)組織所見

中・小動脈のフィブリノイド壊死性血管炎の存在

(3)血管造影所見

腹部大動脈分枝(特に腎内小動脈)の多発小動脈瘤と狭窄・閉塞

(4)診断のカテゴリー

①Definite

主要症候2項目以上と組織所見のある例

②Probable

(a)主要症候2項目以上と血管造影所見の存在する例

(b)主要症候のうち①を含む6項目以上存在する例

(5)参考となる検査所見

①白血球増加(10,000/μL以上)

②血小板増加(400,000/μL以上)

③赤沈亢進

④CRP陽性

(6)鑑別診断

①顕微鏡的多発血管炎

②多発血管炎性肉芽腫症(旧称：Wegener肉芽腫症)

③好酸球性多発血管炎性肉芽腫症(旧称：アレルギー性肉芽腫性血管炎)

④川崎病動脈炎

⑤膠原病(全身性エリテマトーデス(SLE)，関節リウマチ(RA)など)

⑥IgA血管炎(旧称：紫斑病性血管炎)

【参考事項】

1　組織学的にI期変性期，II期急性炎症期，III期肉芽期，IV期瘢痕期の四つの病期に分類される．

2　臨床的にI，II病期は全身の血管の高度の炎症を反映する症候，III，IV病期変は侵された臓器の虚血を反映する症候を呈する．

3　除外項目の鑑疾患は壊死性血管炎を呈するが，特徴的な症候と検査所見から鑑別できる．

※診断基準および重症度分類の適応における留意事項

1　病名診断に用いる臨床症状，検査所見等に関して，診断基準上に特段の規定がない場合には，いずれの時期のものを用いても差し支えない(ただし，当該疾病の経過を示す臨床症状等であって，確認可能なものに限る)．

2　治療開始後における重症度分類については，適切な医学的管理の下で治療が行われている状態であって，直近6か月間で最も悪い状態を医師が判断することとする．

3　なお，症状の程度が上記の重症度分類等で一定以上に該当しない者であるが，高額な医療を継続することが必要なものについては，医療費助成の対象とする．

(難治性血管炎に関する調査研究班：結節性多発動脈炎(指定難病42)，難病情報センター，2017［http://www.nanbyou.or.jp/entry/244］より)

状があげられ，これらの一項目でもある場合はステロイドに免疫抑制薬を併用し治療を進めていくことで予後が改善されるとされてきた[1]．ただし，多発単神経炎では予後不良因子には入らずとも機能障害を考えると予後不良因子と同様に考慮してもよいと考える．さらに，旧FFS＝0であっても，ステロイド単剤治療では再燃が多く，免疫抑制薬併用が有効とする研究もあることから，寛解維持ではより広く免疫抑制薬の併用を考えることが多い．

1．寛解導入療法

経口プレドニゾロン1 mg/kgで治療を開始し，重要臓器病変を認める場合はメチルプレドニゾロン大量点滴静注療法(ステロイドパルス

表2 結節性多発動脈炎の重症度分類

結節性多発動脈炎の重症度分類において，3度以上を対象とする．

1度	ステロイドを含む免疫抑制薬の維持量ないしは投薬なしで1年以上病状が安定し，臓器病変および合併症を認めず日常生活に支障なく寛解状態にある患者(血管拡張剤，降圧剤，抗凝固剤などによる治療は行ってもよい)．
2度	ステロイドを含む免疫抑制療法の治療と定期的外来通院を必要とするも， 臓器病変と合併症は併存しても軽微であり，介助なしで日常生活に支障のない患者．
3度	機能不全に至る臓器病変(腎，肺，心，精神・神経，消化管など)ないし合併症(感染症，圧迫骨折，消化管潰瘍，糖尿病など)を有し，しばしば再燃により入院又は入院に準じた免疫抑制療法ないし合併症に対する治療を必要とし，日常生活に支障をきたしている患者．臓器病変の程度は注1のa～hのいずれかを認める．
4度	臓器の機能と生命予後に深く関わる臓器病変(腎不全，呼吸不全，消化管出血，中枢神経障害，運動障害を伴う末梢神経障害，四肢壊死など)ないしは合併症(重症感染症など)が認められ，免疫抑制療法を含む厳重な治療管理ないし合併症に対する治療を必要とし，少なからず入院治療，時に一部介助を要し，日常生活に支障のある患者．臓器病変の程度は注2のa～hのいずれかを認める．
5度	重篤な不可逆性臓器機能不全(腎不全，心不全，呼吸不全，意識障害・認知障害，消化管手術，消化・吸収障害，肝不全など)と重篤な合併症(重症感染症，DICなど)を伴い，入院を含む厳重な治療管理と少なからず介助を必要とし，日常生活が著しく支障をきたしている患者．これには，人工透析，在宅酸素療法，経管栄養などの治療を要する患者も含まれる．臓器病変の程度は注3のa～hのいずれかを認める．

注1：以下のいずれかを認めること
- a．肺線維症により軽度の呼吸不全を認め，PaO2が60～70 Torr．
- b．NYHA 2度の心不全徴候を認め，心電図上陳旧性心筋梗塞，心房細動(粗動)，期外収縮あるいはST低下(0.2 mV以上)の一つ以上認める．
- c．血清クレアチニン値が2.5～4.9 mg/dLの腎不全．
- d．両眼の視力の和が0.09～0.2の視力障害．
- e．手指を含む2関節以上の指・趾切断．
- f．末梢神経障害による1肢の機能障害(筋力3)．
- g．脳血管障害による軽度の片麻痺(筋力4)．
- h．血管炎による便潜血反応中等度以上陽性，コーヒー残渣物の嘔吐．

注2：以下のいずれかを認めること
- a．肺線維症により中等度の呼吸不全を認め，PaO2が50～59 Torr．
- b．NYHA 3度の心不全徴候を認め，胸部X線上CTR 60%以上，心電図上陳旧性心筋梗塞，脚ブロック，2度以上の房室ブロック，心房細動(粗動)，人口ペースメーカーの装着，のいずれかを認める．
- c．血清クレアチニン値が5.0～7.9 mg/dLの腎不全．
- d．両眼の視力の和が0.02～0.08の視力障害．
- e．1肢以上の手・足関節より中枢側における切断．
- f．末梢神経障害による2肢の機能障害(筋力3)．
- g．脳血管障害による著しい片麻痺(筋力3)．
- h．血管炎による顕著な下血，嘔吐を認める．

注3：以下のいずれかを認めること
- a．肺線維症により高度の呼吸不全を認め，PaO2が50 Torr未満．
- b．NYHA4度の心不全徴候を認め，胸部X線上CTR 60%以上，心電図上陳旧性心筋梗塞，脚ブロック，2度以上の房室ブロック，心房細動(粗動)，人口ペースメーカーの装着のいずれか2以上を認める．
- c．血清クレアチニン値が8.0 mg/dLの腎不全．
- d．眼の視力の和が0.01以下の視力障害．
- e．2肢以上の手・足関節より中枢側の切断．
- f．末梢神経障害による3肢以上の機能障害(筋力3)，又は1肢以上の筋力全麻痺(筋力2以下)．
- g．脳血管障害による完全片麻痺(筋力2以下)．
- h．血管炎による消化管切除術を施行．

※診断基準および重症度分類の適応における留意事項
1. 病名診断に用いる臨床症状，検査所見等に関して，診断基準上に特段の規定がない場合には，いずれの時期のものを用いても差し支えない(ただし，当該疾病の経過を示す臨床症状等であって，確認可能なものに限る)．
2. 治療開始後における重症度分類については，適切な医学的管理の下で治療が行われている状態であって，直近6か月間で最も悪い状態を医師が判断することとする．
3. なお，症状の程度が上記の重症度分類等で一定以上に該当しない者であるが，高額な医療を継続することが必要なものについては，医療費助成の対象とする．

(難治性血管炎に関する調査研究班：結節性多発動脈炎(指定難病42)，難病情報センター，2017 [http://www.nanbyou.or.jp/entry/244] より)

療法：メチルプレドニゾロン500 mg～1,000 mg/日の点滴3日間連続)からスタートし経口ステロイド治療に移行する．

旧FFS≧1もしくはそれに準じて予後不良と考えられる場合には，シクロホスファミド間欠的大量静注療法(intermittent pulse intravenous

cyclophosphamide therapy：IVCY〉を併用する．IVCYの回数を6回と12回で比較した研究があり，12回の方が再燃は少なかったとする結果もあるが，実臨床では前者も多いものと思われる．

2．寛解維持療法

プレドニゾロンは徐々に減量し，できるだけ少量での維持を目指す．維持療法で用いる免疫抑制薬としてはアザチオプリンが最も多く用いられている．

3．対症療法

高血圧や虚血がある場合は，それぞれ降圧薬や循環改善薬による治療を行い，末梢神経障害がある場合はそれに対する対症療法を行う．ステロイド副作用の予防にもつとめる．

無治療では1年生存率50%，5年生存率13%と予後であったが，近年は治療が進歩し，ステロイドと免疫抑制薬併用により5年生存率は約80%となっている．

文　献

1) Jennette JC, et al.：2012 revised International Chapel Hill Consensus Conference Nomenclature of Vasculitides. Arthritis Rheum 65：1-11, 2013
2) Lightfoot RW Jr, et al. The American College of Rheumatology 1990 criteria for the classification of polyarteritis nodosa. Arthritis Rheum 33：1088-1093, 1990
3) Jennette JC, et al.：Nomenclature of systemic vasculitides. Proposal of an international consensus conference. Arthritis Rheum 37：187-192, 1994
4) Guillevin L, et al.：Prognostic factors in polyarteritis nodosa and Churg-Strauss syndrome. A prospective study in 342 patients. Medicine（Baltimore）75：17-28, 1996

保険診療におけるカルテ記載のあり方
（改訂第4版）

元杏林大学医学部総合医療学講師　高木　泰　著

●A5判・112頁・定価（本体2,800円+税）ISBN978-4-7878-2188-1

●保険診療におけるカルテの記載要件はより細分化，複雑化する一方，診療報酬事業の厳密化，第三者への開示に対応するためにも，適切なカルテ記載のあり方が求められている．本書では，実際に書く際の考え方，やってはいけない点など，具体的な事例を紹介しながら，カルテの適切な書き方，留意点等についてわかりやすく解説している．改訂第4版では，具体的事例を追加するとともに，算定要件としてのカルテの記載事項を充実した．

診断と治療社

〒100-0014　東京都千代田区永田町2-14-2山王グランドビル4F
電話 03(3580)2770　FAX 03(3580)2776
http://www.shindan.co.jp/　E-mail:eigyobu@shindan.co.jp

Integrative Molecular Medicine

Review Article ISSN: 2056-6360

Effects of iguratimod on protein profiles of chondrosarcoma cells

Seido Ooka[1*], Manae S Kurokawa[2], Michiyo Yokoyama[1], Mitsumi Arito[1], Toshiyuki Sato[1], Masaaki Sato[1], Yukiko Takakuwa[1], Kazuki Omoteyama[3], Naoya Suematsu[1], Kimito Kawahata[1] and Tomohiro Kato[1]

[1]Division of Rheumatology and Allergy, Department of Internal Medicine, St. Marianna University School of Medicine, Kawasaki, Japan

[2]Disease Biomarker Analysis and Molecular Medicine, St. Marianna University Graduate School of Medicine, Kawasaki, Japan

[3]Clinical Proteomics and Molecular Medicine, St. Marianna University Graduate School of Medicine, Kawasaki, Japan

Abstract

Objective: To explore novel mechanisms for the effect of iguratimod (IGU) on rheumatoid arthritis (RA), we analyzed protein profile changes caused by IGU using chondrosarcoma cells. Methods: OUMS-27 cells were cultured in the presence or absence of 100 μM IGU. Proteins were extracted and separated by 2 dimensional-differential image gel electrophoresis (2D-DIGE). Protein spots of interest were identified by mass spectrometry. Results: 776 and 803 protein spots were detected in the 2D-DIGE results of 24 hour- and 6 day-treatment with IGU, respectively. In the 6 day-treatment, 22 protein spots showed 1.3-fold or higher intensity by IGU-treatment than no-treatment, whereas 15 spots showed -1.3 (1/1.3) -fold or lower intensity ($p<0.05$). We identified 15 out of the 37 spots, which included proteins involved in packaging and splicing of pre-mRNA, regulation of signaling pathways/protein folding, innate immunity and inflammation, transcription, ATP synthesis, cytoprotection, and cytoskeleton organization. Interestingly, intensity of multiple spots of heterogenous nuclear ribonucleoprotein (hnRNP) A2/B1 and A1 was decreased by the IGU treatment, which are highly expressed in synovia of RA and/or its animal model. Specifically, hnRNP A2/B1 are known as autoantigens in RA and also as proinflammatory activators for NF-κB, the target of IGU. Conclusion: IGU affected protein profiles of chondrosarcoma cells. The decreased expression of hnRNPs suggests novel mechanisms for anti-rheumatic effects of IGU.

Introduction

Rheumatoid arthritis (RA) is a systemic inflammatory disease that causes progressive joint destruction and functional loss [1]. Although its etiology remains unknown, early diagnosis and a treat-to-target approach are recommended as standard care to achieve the remission [2]. Developments of biologics and small-molecule immunosuppressive disease-modifying anti-rheumatic drugs (DMARDs) such as methotrexate and janus kinase inhibitors have enabled this strategy [1, 2]. Nonetheless, it is difficult to use the immunosuppressive drugs in a considerable portion of RA patients with comorbidities such as malignant tumors and chronic infection. Furthermore, for RA patients that achieved the remission, application of treatments with immunomodulatory drugs should be considered.

From these points of view, the role of conventional disease-modifying anti-rheumatic drugs (cDMARDs) is important in RA treatment. The immunomodulatory cDMARDs include salazosulfapyridine and bucillamine which are recommended as alternatives for methotrexate-intolerant patients by RA treatment guidelines [3, 4]. The immunomodulatory cDMARDs can be used in the patients with malignancy and infection. Iguratimod (IGU), a novel immunomodulatory cDMARD developed in Japan, inhibits the production of immunoglobulins and proinflammatory cytokines such as TNFα, IL-1β, and IL-6 [5-8]. IGU has been considered to exhibit its anti-rheumatic effects through suppression of NF-κB, by the inhibition of phosphorylation and nuclear translocation of RelA/p65 without interfering with IκB [6, 7, 9]. IGU also suppresses ERK and NF-κB pathways in RANKL-induced osteoclast differentiation [9-11]. Recently, IGU was found to block IL-17 signaling in a murine arthritis model, targeting an IL-17 receptor adaptor protein, Act-1 [12]. However, mechanisms of the effects of IGU, especially those on chondrocytes, are still obscured.

In this study, we comprehensively analyzed changes of protein expression of chondrosarcoma cells caused by IGU. We found that IGU affected the protein profile of chondrosarcoma cells. Interestingly, IGU suppressed expression of heterogenous nuclear protein (hnRNP) A2/B1 and A1. Specifically, hnRNP A2/B1 play roles as autoantigens and proinflammatory regulators in RA and also as coactivators for NF-κB, the target of IGU. Our findings suggested novel mechanisms of the effect of IGU on RA treatment.

Methods

Cell culture

A chondrosarcoma cell line, OUMS-27 (C-2012-1583, Human Science Research Resources Bank, Sennan, Osaka, Japan) [13], was cultured in DMEM (Sigma-Aldrich, St. Louis, MO, USA) and 10% FBS

Correspondence to: Seido Ooka, MD, PhD, Division of Rheumatology and Allergy, Department of Internal Medicine, St. Marianna University School of Medicine, 2-16-1, Sugao, Miyamae-ku, Kawasaki, 216-8511, Japan, Tel: 81-44-977-8111; Fax: 81-44-976-7553; E-mail: ooka@marianna-u.ac.jp

Key words: *chondrosarcoma cells, iguratimod, mass spectrometry, proteomics, rheumatoid arthritis*

Received: November 20, 2017; **Accepted:** December 11, 2017; **Published:** December 14, 2017

(Hyclone, South Logan, Utah, USA) in type I collagen-coated dishes (AGC techno glass, Haibara-gun, Shizuoka, Japan). To analyze effects of IGU (Tokyo chemical industry, Chuo-ku, Tokyo, Japan) on the cell viability and growth, $1.5x10^5$ of OUMS-27 cells were seeded and cultured for 24 hours in the presence or absence of 10-300 μM of IGU. Similarly, to analyze a longer term (6 days) effect, $1.5x10^5$ of the cells were seeded and 100 μM IGU was added three times every 48 hours. The cells were harvested after 48 hours from the last treatment. All the experiments were performed in triplicates.

Two dimensional-differential image gel electrophoresis (2D-DIGE)

Proteins, extracted from the OUMS-27 cells, were analyzed by 2D-DIGE as previously described [14]. Briefly, an equal weight of proteins taken from six lysates from the 24 hour-cultured cell samples (three of 100 μM IGU-treated and three non-treated) were mixed and labeled with Cyanine dye 3 (Cy3, Cy Dye DIGE Saturation dye, GE Healthcare, Piscataway, NJ, USA) for preparation of an internal control "standard sample". Each of the six samples was labeled with Cyanine dye 5 (Cy5, GE Healthcare). 2.5 μg of the individual Cy5-labeled samples were mixed with 2.5 μg of the Cy3-labeled standard sample. Then each of the mixed protein sample was applied to an isoelectric focusing (IEF) gel strip (Immobiline Drystrip pH 3-11, 24 cm, non-linear, GE Healthcare). After the proteins were separated by IEF, they were further separated by sodium dodecyl sulfate-polyacrylamide gel electrophoresis. The resultant protein spots were scanned using an image analyzer (Typhoon 9400 Imager, GE Healthcare). The Cy5-fluorescent intensity of each protein spot was normalized by the Cy3-fluorescent intensity of an identical spot by using a quantitative analysis program (Progenesis, Nonlinear Dynamics, Newcastle, UK). The normalized Cy5-intensity was compared between the IGU-treated and non-treated protein samples using Progenesis. Similarly, protein profiles of the 6 day-cultured cells were compared between the IGU-treated and non-treated OUMS-27 cells.

Identification of proteins

Proteins were identified by mass spectrometry (MS) [14]. In brief, 50 μg of proteins was separated by 2-dimensional electrophoresis. Gel specimens corresponding to protein spots of interest were recovered. Then proteins in the gel fragments were digested with trypsin. Peptides produced by the digestion were analyzed using a matrix-assisted laser desorption/ionization time of flight mass spectrometer (MALDI-TOF/MS) (Ultraflex, Bruker Daltonics, Ettlingen, Germany). Based on the mass spectra, some peptides were selected for MS/MS analysis. The obtained MS and MS/MS spectra were used to identify the proteins by database searching (Mascot, http://www.matrixscience.com) against the Swiss Prot human protein sequence database. Protein identification was accepted when MASCOT search results delivered significant MOWSE scores ($p<0.05$).

Analysis of protein interaction

Interactions among the identified proteins were searched by Ingenuity Pathway Analysis (IPA) (Qiagen, Venlo, NLD). Core analysis was performed using names and the fold differences (IGU/Control) of all the identified proteins and information of all the cells in all the species in IPA database.

Statistical analysis

Significance of differences of cell viability, cell growth, and protein spot intensity in 2D-DIGE was calculated by Student's t-test.

Results

Effects of 24 hour-treatment by IGU on OUMS-27 cells

We first treated OUMS-27 cells for 24 hours with 0-300 μM IGU to examine its effect on viability and growth of the cells. OUMS-27 cells showed viability of more than 94% in the presence of 10-300 μM IGU as well as in the absence of IGU (100%). The cell growth in all the conditions was also at similar levels (0.95- to 1.05-fold) except that in the presence of 300 μM iguratimod (0.84-fold), which showed slightly lower level ($p<0.05$). Thus, we determined the concentration of IGU as 100 μM and analyzed protein profile of OUMS-27 cells at this condition.

We compared protein profiles of OUMS-27 cells between the 100 μM IGU-treatment and no-treatment by 2D-DIGE. We found 776 protein spots in total (Figure 1A, B). In the 776 protein spots, 41 protein spots showed different intensity between the two conditions ($p<0.05$) (Table 1). Among the 41 protein spots, 11 protein spots showed 1.3-fold or higher intensity in the IGU-treated cells compared to the non-treated cells. In contrast, 5 spots showed -1.3 (1/1.3)-fold or lower intensity in the IGU-treated cells compared to the non-treated cells. It was shown that IGU affected the protein profile of OUMS-27 cells.

Effects of 6 day-treatment by IGU on OUMS-27 cells

Next, we treated OUMS-27 cells for a longer term of 6 days with 100 μM IGU. The levels of cell viability and growth were high enough and at similar levels at 6 days between the IGU-treated and non-treated cells (100 μM; cell viability, 100.1 %, $p=0.92$; cell growth, 1.05-fold, $p=0.64$). Thus, we performed 2D-DIGE using those cell lysates.

In total, 803 protein spots were detected in the 2D-DIGE results (Figure 1C, D). In the 803 protein spots, 150 protein spots showed different intensity between the IGU-treated and non-treated cells ($p<0.05$, Table 1). Among the 150 protein spots, 22 protein spots showed 1.3-fold or higher intensity in the IGU-treated cells compared to the non-treated cells. On the other hand, 15 spots showed -1.3-fold or lower intensity in the IGU-treated cells compared to the non-treated cells. Protein spots that changed to ±1.3-fold or more in the 6-day treatment (150 spots) showed 3.7-fold in number compared to those in the 24-hour treatment (41 spots) (Table 1).

To follow a time course of the protein expression, we observed intensity change of the protein spots that showed ±1.3-fold or more change by the 24 hour-treatment with IGU. In the case of 9 intensity-increased spots, intensity of almost all the spots were decreased in the 6 day-treatment (Figure 2A). Similarly, in the case of 4 intensity-

Table 1. Change of the OUMS-27 protein profile by the treatment with IGU

Culture periods	Total number of detected protein spots	Number of protein spots with different intensity ($p<0.05$)	Fold difference, IGU/Control	Number of the protein spots
24 hours	776	41	$x \geq 1.5$	2
			$1.5 > x \geq 1.3$	9
			$1.3 > x \geq -1.3$	25
			$-1.3 > x \geq -1.5$	3
			$-1.5 \geq x$	2
6 days	803	150	$x \geq 1.5$	7
			$1.5 > x \geq 1.3$	15
			$1.3 > x \geq -1.3$	113
			$-1.3 > x \geq -1.5$	11
			$-1.5 \geq x$	4

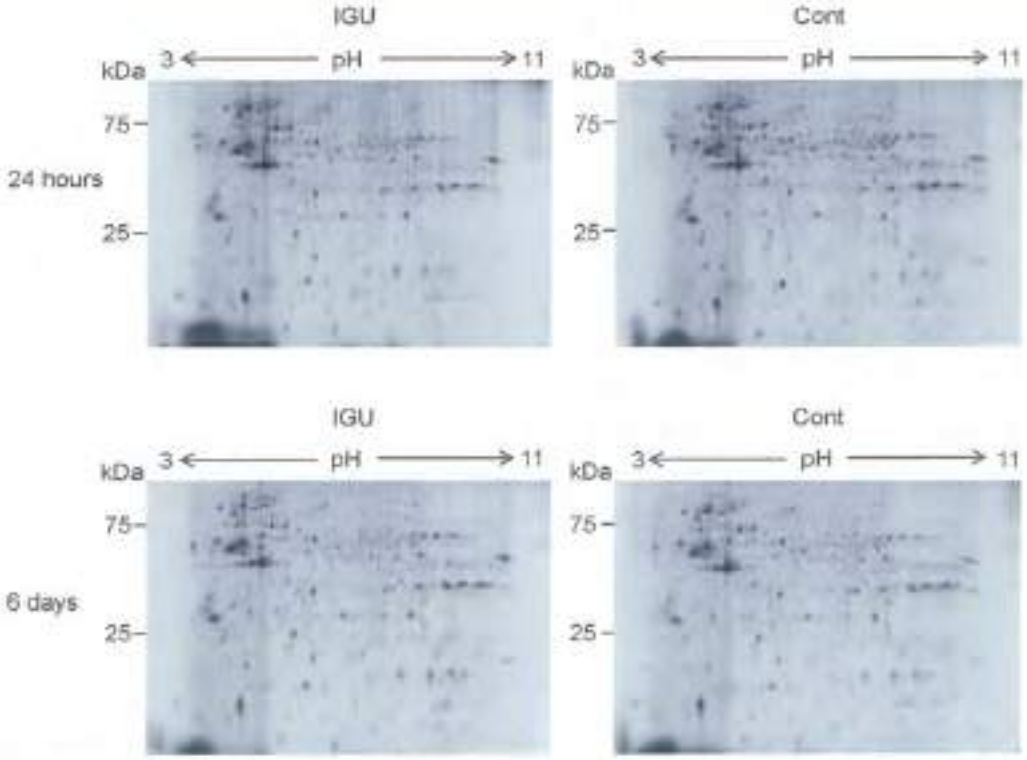

Figure 1. Protein profiles of OUMS-27 cells treated with IGU. Representative results of 2D-DIGE of proteins from OUMS-27 cells cultured in the presence (left upper) or absence (right upper) of 100 μM IGU for 24 hours are shown. Similarly, those cultured in the presence (left lower) or absence (right lower) of 100 μM IGU for 6 days are shown.

decreased spots, intensity of 3 spots were increased in the 6 day-treatment (Figure 2B). The effect of the 24 hour-treatment on OUMS-27 cells was tentative. In contrast, when we observed intensity of the protein spots that showed ±1.3-fold or more change in the 6 day-treatment, almost all the spots of the 22 intensity-increased spots and the 15 intensity-decreased spots similarly increased and decreased in the 24 hour-treatment, respectively (Figure 2C, D). The 6 day-treatment was considered to reflect a long term effect of IGU on OUMS-27 cells.

Identification of the proteins expression of which was changed by IGU

We tried to identify the proteins in the spots intensity of which was changed by the 6 day-treatment with IGU. 37 protein spots that showed ±1.3-fold or more intensity change by the treatment were subjected to the identification. As a result, 14 proteins were identified from 15 out of the 37 spots (Figure 3, 4 and Table 2).

Seven proteins were identified from the 7 spots intensity of which was increased by the treatment with IGU. They were 1) proteins involved in splicing of pre-mRNA (cyclin L1 [CCLN1]; and tuftelin-interacting protein 11 [TFIP11]), 2) proteins that regulate signaling pathways and protein folding (14-3-3 protein epsilon, tyrosine 3-monooxygenase/tryptophan 5-monooxygenase activation protein epsilon [YWHAE]; and cyclophilin A, peptidyl-prolyl cis-trans isomerase A [PPIA]), 3) a protein involved in innate immunity and inflammation (NACHT, LRR and PYD domains-containing protein 3 [NLRP3]), 4) a transcription factor (human immunodeficiency virus type 1 enhancer-binding protein 2 [HIVEP2]), and 5) a protein with unknown function (transmembrane protein 95 [TMM95]).

The other 7 proteins were included in the 8 spots intensity of which was decreased by the treatment with IGU. They were 1) proteins involved

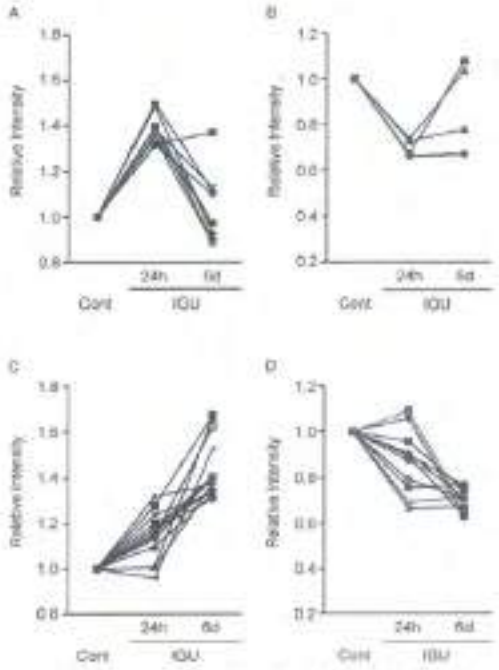

Figure 2. Time course of each protein expression of OUMS-27 cells in the presence of IGU. A, B. Nine out of the 11 protein spots and 4 out of the 5 protein spots, intensity of which were increased to 1.3-fold or more (A) and decreased to -1.3-fold or less (B) in the 24 hour-treatment, respectively (Table 1), were detected both in the 24 hour- and 6 day-treatments and applied for time course analysis. C, D. 14 out of the 22 protein spots and 11 out of the 15 protein spots, intensity of which were increased to 1.3-fold or more (C) and decreased to -1.3-fold or less (D) in the 6 day-treatment, respectively (Table 1), were detected both in the 24 hour- and 6 day-treatments and applied for time course analysis. Control samples (Cont) were proteins from OUMS-27 cells cultured without IGU for 24 hours (A, B) and 6 days (C, D).

Table 2. Identification of protein spots, intensity of which was changed by the treatment with IGU

Spot ID	Difference (folds)	Proteins	Accession ID	MW (kDa) Theorei	MW (kDa) Observed	pI Theorei	pI Observed	Mascot scores	Coverage (%)	Confirmed sequences (Mascot ion scores)
1072	1.67	NACHT, LRR and PYD domains-containing protein 3 (NLRP3)	NLRP3_HUMAN	118.1	23	6.22	6.1	71	13	[1]MDHMVSSFCIENCHR[17] (11)
487	1.53	Cyclin-L1 (CCNL1)	CCNL1_HUMAN	39.6	60	10.7	6.2	75	18	[9]LPQVAM*ATGQVLFHR[11] (21)
1033	1.50	Transmembrane protein 95 (TMM95)	TMM95_HUMAN	19.6	24	8.98	7.8	57	37	[11]LARLCSQMEAR[21] (2) [28]EAVSSLPSYWSWLRK[39] (3)
763	1.40	Transcription factor HIVEP2 (HIVEP2)	ZEP2_HUMAN	228.9	41	6.5	5.8	65	8	[1]NALSVTTTSQERAAM*GR[13] (11)
445	1.37	Tuftelin-interacting protein 11 (TFIP11)	TFP11_HUMAN	96.8	64	5.45	5.8	61	12	[60]ELSQVKVIDMTGR[73] (25) [77]M*QPDCSNPLTLDECAR[92] (7)
924	1.34	14-3-3 protein epsilon (YWHAE)	1433E_HUMAN	29.2	29	4.63	4.5	189	18	[1]YLAEFATGNDR[10] (54) [7]YLAEFATGNDRK[18] (16) [19]AASDIAMTELPPTHPIR[35] (77) [36]DSTLIMQLLR[45] (18)
1107	1.34	Cyclophilin A (PPIA)	PPIA_HUMAN	18.0	21	7.68	8.0	74	10	[1]VNPTVFFDIAVDGEPLGR[18] (66)
87	−1.35	Hypoxia up-regulated protein 1 (HYOU1)	HYOU1_HUMAN	111.3	98	5.16	5.3	66	12	[1]DAVVYPILVEFTR[13] (24)
599	−1.34	ATP synthase subunit alpha, mitochondrial (ATP5A1)	ATPA_HUMAN	59.7	53	9.16	8.0	185	11	[1]TGAIVDVPVGEELLGR[16] (72) [43]EAYPGDVFYLHSR[54] (72) [46]GIRPAINVGLSVSR[61] (15)
376	−1.49	Keratin, type II cytoskeletal 1, (KRT1)	K2C1_HUMAN	66.0	69	8.15	6.9	166	9	[17]YEELQITAGR[26] (78)
		Keratin, type II cytoskeletal 6B (K2C6B)	K2C6B_HUMAN	66.0		8.09		82	1	[16]YEELQITAGR[25] (78)
784	−1.31	Heterogenous nuclear ribonucleoproteins A2/B1 (hnRNP A2/B1)	ROA2_HUMAN	37.4	39	8.97	9.5	99	8	[1]LFIGGLSFETTEESLR[16] (38) [21]GGGGNFGPGPGSNFR[35] (46)
797	−1.35	Heterogenous nuclear ribonucleoproteins A2/B1 (hnRNP A2/B1)	ROA2_HUMAN	37.4	38	8.97	8.8	256	23	[1]LFIGGLSFETTEESLR[16] (52) [15]GFGFVTFDDHDPVDK[30] (85) [21]GGGGNFGPGPGSNFR[35] (64)
794	−1.42	Heterogenous nuclear ribonucleoproteins A2/B1 (hnRNP A2/B1)	ROA2_HUMAN	37.4	38	8.97	8.7	129	13	[1]LFIGGLSFETTEESLR[16] (47) [21]GGGGNFGPGPGSNFR[35] (60)
773	−1.52	Heterogenous nuclear ribonucleoproteins A1 (hnRNP A1)	ROA1_HUMAN	38.7	40	9.17	9.2	77	24	[19]LFIGGLSFETTDESLR[33] (9) [37]SSGFYGGGGQYFAKPR[52] (5)
		Heterogenous nuclear ribonucleoproteins A1-like 2 (hnRNP A1L2)	RA1L2_HUMAN	34.2		9.08		61	23	[19]LFIGGLSFETTDESLR[33] (9)
775	−1.60	Heterogenous nuclear ribonucleoproteins A1 (hnRNP A1)	ROA1_HUMAN	38.7	39	9.17	8.8	62	8	[19]KLFIGGLSFETTDESLR[34] (15) [19]LFIGGLSFETTDESLR[33] (25)

37 protein spots, intensity of which changed to ±1.3-fold or more by the 6 day-treatment with IGU, were selected for the protein identification. Proteins of 15 out of the 37 spots were identified. MW, molecular weights.
*Oxidation of methionine.

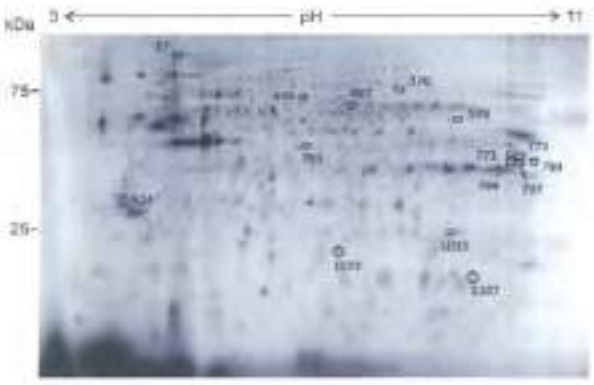

Figure 3. Locations of the identified protein spots on a 2D-DIGE gel. Proteins included in 15 spots out of the 37 spots that showed ±1.3-fold or more change in intensity by the 6 day-treatment with IGU were identified. A representative result of the standard sample is shown.

in packaging of pre-mRNA (heterogenous nuclear ribonucleoproteins A2/B1 [hnRNP A2/B1]; heterogenous nuclear ribonucleoproteins A1 [hnRNP A1]; and heterogenous nuclear ribonucleoproteins A1-like 2 [hnRNP A1L2]), 2) a cytoprotective protein from hypoxia (hypoxia up-regulated protein 1 [HYOU1]), 3) an ATP synthase (ATP synthase subunit alpha, mitochondrial [ATP5A1]), and 4) Cytoskeletal proteins (keratin, type II cytoskeletal 1 [KRT1]; and keratin, type II cytoskeletal 6B [K2C6B]).

Interestingly, hnRNP A2/B1 was identified in 3 protein spots (spot ID 784, 794, and 797) (Table 2). Similarly, hnRNP A1 was identified in 2 protein spots (spot ID 773 and 775). In spot ID 773, only hnRNP A1 or both hnRNP A1 and hnRNP A1L2 were considered to be included. Spot ID 376 included KRT1 and/or K2C6B. The observed molecular weights of TFIP11 in the spot ID 445, HIVEP2 in the spot ID 763, and NLRP3 in the spot ID 1072 were smaller than their theoretical weights, indicating that the detected proteins were fragments of those

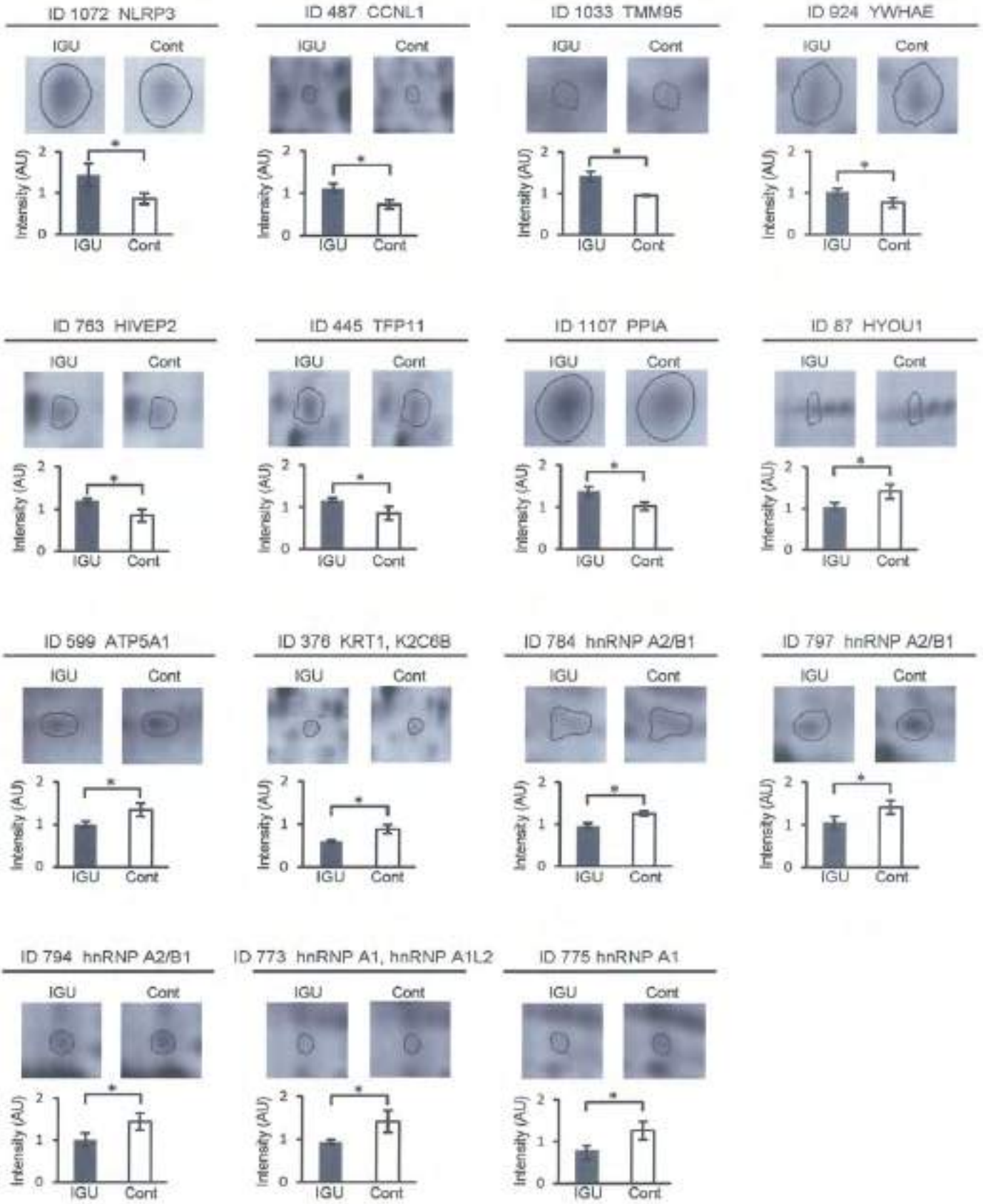

Figure 4. Comparisons of spot intensity of the identified proteins between IGU-treated and non-treated conditions. Representative results of the identified 15 protein spots and intensity difference of these spots between the IGU-treated and non-treated (control) cells are shown. Error bars, standard deviations, *p<0.05.

proteins. The pathway analysis showed deduced interactions of 11 out of the 14 identified proteins (Figure 5). hnRNP A2/B1, hnRNP A1 and their complex located at the center of the network. Of note, NF-κB, Akt, and p53 (encoded by TP53 gene) appeared as relay points of the network. These proteins would directly and/or indirectly interact with the identified proteins.

Discussion

We compared protein profiles of a chondrosarcoma cell line OUMS-27 cells between the presence and absence of IGU. Although the maximal plasma concentration after repetitive administration of 50 mg/day IGU for 14 days was 5 μM, the concentration is ununiform in vivo and would reach much higher levels in tissue such as RA-affected joints [15]. Treatment with 100 μM IGU caused significant changes in protein profiles of OUMS-27 cells, that is, intensity of 41 and 150 protein spots was changed by the 24 hour- and 6 day-treatment, respectively ($p<0.05$) (Table 1). When we examined time courses, intensity of most of the examined spots was much increased or decreased at 6 days compared to that at 24 hours (Figure 2C, D). Continuous treatment with IGU would augment its effect on protein expression.

The 6-day treatment changed intensity of 37 protein spots by 1.3-fold or more (Table 1). Such change levels of protein expression were considered to affect the function of proteins. Among the 14 identified proteins, we focused on three proteins, hnRNP A2/B1, hnRNP A1, and PPIA (Table 2, Figure 4, 5). Of note, intensity of multiple spots of hnRNP A2/B1 and hnRNP A1 was decreased by IGU (Table 2). This indicated that total expression of these proteins would be decreased by IGU regardless of differences of isoforms and/or post-translational modifications.

The main function of hnRNP A/B proteins, components of hnRNP particles, is to package pre-mRNA into hnRNP particles [16]. hnRNP A/B also play roles in telomere maintenance, transcription, pre-mRNA splicing, mRNA nucleo-cytoplasmic export, mRNA stability, and translation. Interestingly, high expression of hnRNP A2/B1 and A1 has been found in inflamed joints of RA patients and/or arthritis models [17-19]. Autoantibodies and autoreactive T cells against hnRNP A2/B1 have been detected in approximately 30% and 60% of RA patients, respectively [17, 20, 21]. Since depletion of hnRNP A2/B1 almost completely blocked development of arthritis both in collagen-induced arthritis (CIA) and K/BxN serum-transfer arthritis, hnRNP A2/B1 was considered to play a crucial role in the pathogenesis of inflammatory arthritis [22]. Besides their role as autoantigens in arthritis, hnRNP A2/B1 act as proinflammatory regulators. hnRNP A2 activates the Raf-MEK-ERK signaling pathway, located at the upstream of NF-κB, by elevating full length A-Raf transcription and reducing production of short dominant-negative isoform of A-Raf [23]. Furthermore, hnRNP A2, phosphorylated and activated by the serine/threonine kinase Akt1, also functions as a transcriptional coactivator for NF-κB c-Rel [24, 25].

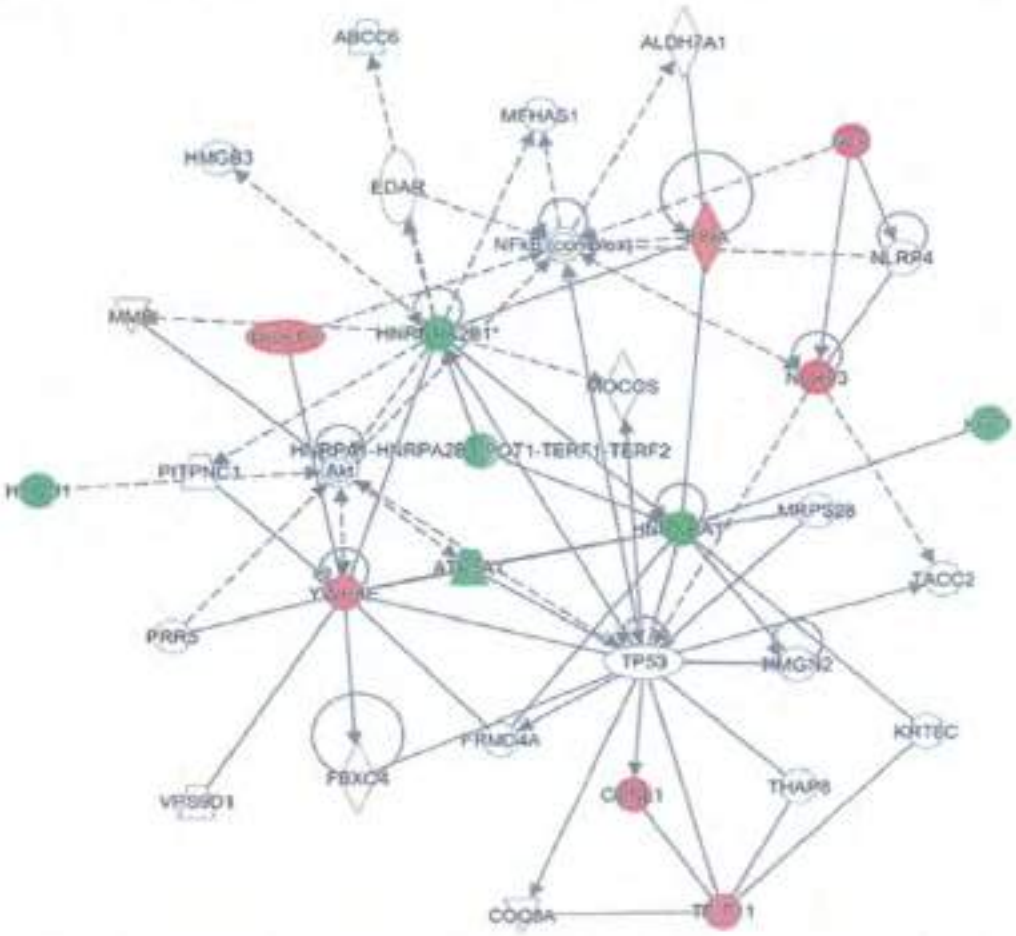

Figure 5. Interaction of the identified proteins. Result of a pathway analysis. Symbols in red and green show the identified proteins intensity of which were increased and decreased by the IGU-treatment, respectively. Solid lines and dotted lines show direct and indirect interactions, respectively. Arrows indicate activation.

NF-κB p65 and p50 are known to be targets of IGU [6, 7, 9, 11]. Thus, NF-κB c-Rel activated by hnRNP A2 would be also a target of IGU. Moreover, depletion of hnRNP A2/B1 almost completely inhibited bone erosion in RA models [22]. Since IGU suppresses bone erosion via RANKL- and ERK-mediating pathways [9, 11, 26, 27], its effect to suppress bone erosion may be also associated with the decrease of hnRNP A2/B1.

Our IPA result indicated that both hnRNP A2/B1 and hnRNP A1 could interact with p53 (Figure 5). However, p53 of OUMS-27 cells as well as that of most cancer cells is a mutant-type and thus does not function as a tumor suppressor [13]. Interestingly, suppression of hnRNP A1/A2 induces apoptosis in a variety of human cancer cells irrespective of p53 expression [28]. This was considered because hnRNP A1/A2 have a capping function of telomeres as G-tail binding proteins in cancer cells [28]. Suppression of hnRNPs may inhibit the tumorigenic growth of RA synovial cells.

The other protein of interest, PPIA, was increased by IGU, which has dual function as a chaperone and a signal transducer (Table 2, Figure 4, 5) [29]. Interestingly, PPIA was highly expressed in RA and CIA synovia [30]. PPIA aggravated the arthritis by polarizing macrophages toward proinflammatory M1 phenotypes that produced IL-1β, IL-6, MMP-2, and MMP-9 [30, 31]. The polarization was dependent on the activation of ERK-NF-κB p65 pathway and also on the PPIase activity [30, 32]. On the other hand, in concert with NF-κB p65, PPIA mediates BMP-2-induced Sox9 production and regulation of chondrogenesis signaling [33]. These processes may contribute to repairment of destructed cartilage in RA. Since IGU targets NF-κB, PPIA may be increased to recover the reduced functions of NF-κB.

In conclusion, we found that IGU affected protein profiles of OUMS-27 cells. IGU specifically decreased expression of hnRNP A2/B1 and A1, which are highly expressed in synovia of RA and its arthritis model. Since hnRNP A2/B1 are autoantigens in RA and activators for NF-κB, the decrease of hnRNPs would downregulate the autoimmune responses and also be involved in the NF-κB-targeting mechanism of IGU. The reduction of hnRNP A2/B1 may be further associated with the inhibition of bone erosion by IGU. The present data should be validated using RA chondrocytes and synovial cells in near future. Our results suggest novel mechanisms of the effect of IGU.

Acknowledgement

The authors indebted Ms Kumi Aso for her technical assistance.

Conflict of interest

Kimito Kawahata received research grants from Astellas, Eli lilly, Chugai Pharma, and Pfizer, and a personal fee from Ono Pharma.

References

1. McInnes IB, Schett G (2017) Pathogenetic insights from the treatment of rheumatoid arthritis. *Lancet* 389: 2328-2337. [Crossref]
2. Burmester GR, Pope JE (2017) Novel treatment strategies in rheumatoid arthritis. *Lancet* 389: 2338-2348. [Crossref]
3. Liu CS, Chia F, Harrison A, Hsieh TY, Jain R, et al. (2015) APLAR rheumatoid arthritis treatment recommendations. *Int J Rheum Dis* 18: 685-713. [Crossref]
4. Gaujoux-Viala C, Gossec L, Cantagrel A, Dougados M, Fautrel B, et al. (2014) Recommendations of the French Society for Rheumatology for managing rheumatoid arthritis. *Joint Bone Spine* 81: 287-297. [Crossref]
5. Tanaka K, Aikawa Y, Kawasaki H, Asaoka K, Isaka T, et al. (1992) Pharmacological studies on 3-formylamino-7-methylsulfonylamino-6-phenoxy-4H-1-benzopyran-4-one (T-614), a novel anti-inflammatory agent. 4th communication: inhibitory effect on the production of interleukin-1 and interleukin-6. *J Pharmacobiodyn* 15: 649-655. [Crossref]
6. Kobno M, Aikawa Y, Tsubouchi Y, Hashiramoto A, Yamada R, et al. (2001) Inhibitory effect of T-614 on tumor necrosis factor-alpha induced cytokine production and nuclear factor-kappaB activation in cultured human synovial cells. *J Rheumatol* 28: 2591-2596. [Crossref]
7. Aikawa Y, Yamamoto M, Yamamoto T, Morimoto K, Tanaka K (2002) An anti-rheumatic agent T-614 inhibits NF-kappaB activation in LPS- and TNF-alpha-stimulated THP-1 cells without interfering with IkappaBalpha degradation. *Inflamm Res* 51: 188-194. [Crossref]
8. Tanaka K, Yamamoto T, Aikawa Y, Kizawa K, Muramoto K, et al. (2002) Inhibitory effects of an anti-rheumatic agent T-614 on immunoglobulin production by cultured B cells and rheumatoid synovial tissues engrafted into SCID mice. *Rheumatology* 42: 1365-1371. [Crossref]
9. Gan K, Yang L, Xu L, Feng X, Zhang Q, et al. (2016) Iguratimod (T-614) suppresses RANKL-induced osteoclast differentiation and migration in RAW264.7 cells via NF-κB and MAPK pathways. *Int Immunopharmacol* 35: 294-300. [Crossref]
10. Sun Y, Ye DW, Zhang P, Wu YX, Wang BY, et al. (2016) Anti-rheumatic drug iguratimod (T-614) alleviates cancer-induced bone destruction via down-regulating interleukin-6 production in a nuclear factor-κB-dependent manner. *J Huazhong Univ Sci Technolog Med Sci* 36: 691-699. [Crossref]
11. Wei Y, Sun X, Hua M, Tan W, Wang F, et al. (2015) Inhibitory Effect of a Novel Antirheumatic Drug T-614 on the IL-6-Induced RANKL/OPG, IL-17, and MMP-3 Expression in Synovial Fibroblasts from Rheumatoid Arthritis Patients. *Biomed Res Int* 2015: 214683. [Crossref]
12. Lee Q, Sun Y, Liu W, Qian C, Jin B, et al. (2013) A novel disease-modifying antirheumatic drug, iguratimod, ameliorates murine arthritis by blocking IL-17 signaling, distinct from methotrexate and leflunomide. *J Immunol* 191: 4969-4978. [Crossref]
13. Katano M, Kurokawa MS, Matsui K, Masuko K, et al. (2017) Phosphoproteome analysis of synoviocytes from patients with rheumatoid arthritis. *Int J Rheum Dis* 20: 708-721. [Crossref]
14. Fiehn C (2010) Methotrexate transport mechanisms: the basis for targeted drug delivery and ß-folate-receptor-specific treatment. *Clin Exp Rheumatol* 28: S40-45. [Crossref]
15. He Y, Smith R (2009) Nuclear functions of heterogeneous nuclear ribonucleoproteins A/B. *Cell Mol Life Sci* 66: 1239-1256. [Crossref]
16. Fritsch R, Eichhöck D, Skriner K, Jahn-Schmid B, Scheinecker C, et al. (2002) Characterization of autoreactive T cells to the autoantigen heterogeneous nuclear ribonucleoprotein A2 (RA33) and filaggrin in patients with rheumatoid arthritis. *J Immunol* 169: 1068-1076. [Crossref]
17. Hayer S, Tohidast-Akrad M, Hainfarnbour S, Jahn-Schmid B, Skriner K, et al. (2005) Aberrant expression of the autoantigen heterogeneous nuclear ribonucleoprotein-A2 (RA33) and spontaneous formation of rheumatoid arthritis-associated anti-RA33 autoantibodies in TNF-alpha transgenic mice. *J Immunol* 175: 8327-8336. [Crossref]
18. Hoffmann MH, Tuncel J, Skriner K, Tohidast-Akrad M, Türk B, et al. (2007) The rheumatoid arthritis-associated autoantigen hnRNP-A2 (RA33) is a major stimulator of autoimmunity in rats with pristane-induced arthritis. *J Immunol* 179: 7568-7576. [Crossref]
19. Nell VP, Machold KP, Stamm TA, Eberl G, Heinzl H, et al. (2005) Autoantibody profiling as early diagnostic and prognostic tool for rheumatoid arthritis. *Ann Rheum Dis* 64: 1731-1736. [Crossref]
20. Steiner G (2007) Auto-antibodies and autoreactive T-cells in rheumatoid arthritis: pathogenetic players and diagnostic tools. *Clin Rev Allergy Immunol* 32: 23-36. [Crossref]
21. Herman S, Fischer A, Prommaz J, Hoffmann M, Kocoders ML, et al. (2015) Inhibition of inflammation and bone erosion by RNA interference-mediated silencing of heterogeneous nuclear RNP A2/B1 in two experimental models of rheumatoid arthritis. *Arthritis Rheumatol* 67: 2536-2546. [Crossref]
22. Shilo A, Ben Hur V, Denichenko P, Stein I, Pikarsky E, et al. (2014) Splicing factor hnRNP A2 activates the Ras-MAPK-ERK pathway by controlling A-Raf splicing in hepatocellular carcinoma development. *RNA* 20: 505-515. [Crossref]
23. Guha M, Tang W, Sondheimer N, Avadhani NG (2010) Role of calcineurin, hnRNPA2 and Akt in mitochondrial respiratory stress-mediated transcription activation of nuclear gene targets. *Biochim Biophys Acta* 1797: 1055-1065. [Crossref]
24. Guha M, Fang JK, Monks R, Birnbaum MJ, Avadhani NG (2010) Activation of Akt is essential for the propagation of mitochondrial respiratory stress signaling and activation of the transcriptional coactivator heterogeneous ribonucleoprotein A2. *Mol Biol Cell* 21: 3578-3589. [Crossref]
25. Sun Y, Wu YX, Zhang P, Peng G, Yu SY (2017) Anti-rheumatic drug iguratimod protects against cancer-induced bone pain and bone destruction in a rat model. *Oncol Lett* 13: 4849-4856. [Crossref]

26. Wu YX, Sun Y, Ye YP, Zhang P, Guo JC, et al. (2017) Iguratimod prevents ovariectomy-induced bone loss and suppresses osteoclastogenesis via inhibition of peroxisome proliferator-activated receptor-γ. *Mol Med Rep* 16: 8200-8208. [Crossref]

27. Kunisada T, Miyazaki M, Mihara K, Gao C, Kawai A, et al. (1998) A new human chondrosarcoma cell line (OUMS-27) that maintains chondrocytic differentiation. *Int J Cancer* 77: 854-859. [Crossref]

28. Patry C, Bouchard L, Labrecque P, Gendron D, Lemieux B, et al. (2003) Small interfering RNA-mediated reduction in heterogeneous nuclear ribonucleoparticle A1/A2 proteins induces apoptosis in human cancer cells but not in normal mortal cell lines. *Cancer Res* 63: 7679-7688. [Crossref]

29. Fischer G, Aumüller T (2003) Regulation of peptide bond cis/trans isomerization by enzyme catalysis and its implication in physiological processes. *Rev Physiol Biochem Pharmacol* 148: 105-150. [Crossref]

30. Dongsheng Z, Zhiguang F, Junfeng J, Zifan L, Li W (2010) Cyclophilin A Aggravates Collagen-Induced Arthritis via Promoting Classically Activated Macrophages. *Inflammation* 40: 1761-1772. [Crossref]

31. Wang L, Wang CH, Jin JF, Ma XK, Li Y, et al. (2010) Contribution of cyclophilin A to the regulation of inflammatory processes in rheumatoid arthritis. *J Clin Immunol* 30: 24-33. [Crossref]

32. Wang L, Jia J, Wang C, Ma X, Liao C, et al. (2013) Inhibition of synovitis and joint destruction by a new single domain antibody specific for cyclophilin A in two different murine models of rheumatoid arthritis. *Arthritis Res Ther* 15: R208. [Crossref]

33. Guo M, Shen J, Kwak JH, Choi B, Lee M, et al. (2015) Novel role for cyclophilin A in regulation of chondrogenic commitment and endochondral ossification. *Mol Cell Biol* 35:2119-2130. [Crossref]

Copyright: ©2017 Ooka S. This is an open-access article distributed under the terms of the Creative Commons Attribution License, which permits unrestricted use, distribution, and reproduction in any medium, provided the original author and source are credited.

SCIENTIFIC REPORTS

OPEN

T cells upon activation promote endothelin 1 production in monocytes via IFN-γ and TNF-α

Received: 16 May 2017
Accepted: 6 October 2017
Published online: 03 November 2017

Shoshi Shinagawa[1], Takahiro Okazaki[1], Mari Ikeda[1], Kazuo Yudoh[2], Yaz Y. Kisanuki[3], Masashi Yanagisawa[4], Kimito Kawahata[1] & Shoichi Ozaki[1]

Endothelin 1 (ET-1), mainly produced from vascular endothelial cells, induces vasoconstriction in physiological conditions. The endothelin receptor antagonist is among the most effective agents for pulmonary hypertension. However, little is known about the production source of ET-1 in inflammation and immunity. Here, we studied whether T cell-mediated ET-1 production system exists and operates independent of the production system in vascular endothelial cells. ET-1 production was readily detectable in the culture supernatant of human PBMCs and murine spleen cells stimulated with anti-CD3 antibody. Immunocytostaining showed that ET-1-producing cells emerged only in PBMCs stimulated with anti-CD3 antibody. Using the Transwell system, both murine and human monocytes sorted with magnetic beads in the inner chamber produced ET-1 when T cells were activated with antigen or anti-CD3 antibody in the outer chamber. This ET-1 production was inhibited by anti-IFN-γ and/or TNF-α antibody. Furthermore, monocytes purified from $ET^{flox/flox}$;Tie2-Cre(+) mice, which conditionally lack ET-1 in hematopoietic stem cells and vascular endothelial cells, did not produce ET-1 even when stimulated by antigen-specific T cell activation. This study demonstrates the existence of an immune-mediated ET-1 production induced by T cells upon activation through IFN-γ and TNF-α.

A prominent role for the endothelin (ET) system in the physiological regulation of blood pressure has been long recognized[1]. Endothelin 1 (ET-1) is a major factor that induces vasoconstriction and is mainly produced by vascular endothelial cells, the primary source of ET-1 in physiological conditions[1,2]. Binding of ET-1 to the endothelin type A receptor (ETa) results in vasoconstriction, growth, and remodeling effects[1,3]. Focusing on this mechanism, endothelin receptor antagonists were developed and have proven to be among the most effective therapeutic agents, especially for controlling pulmonary hypertension[1,4].

Recently, in addition to regulation of the circulatory system through ET-1 from vascular endothelial cells, an increasing body of evidence suggests that the ET-1 system may play a role in some experimental models of inflammation[5–11]. Although the ET-1 production system has been well investigated in normal physiology in vascular endothelial cells, whether a specific ET-1 production system works in inflammatory conditions remains to be determined. Some investigators have suggested that immune cells such as macrophages[12–15] and dendritic cells synthesize ET-1[16]. Production of ET-1 from these cells may occur via lipopolysaccharide stimulation[14] or an autocrine loop mechanism[16]. However, immune-mediated ET-1 producing system other than LPS-triggering ET-1 production remains to be determined.

For this reason, we postulate the possible relationship between T cells and ET-1 producing cells in an immune-mediated ET-1 production system. In our current study, we explored the existence of an ET-1 production and induction system that is related to the immune system, and demonstrate a newly discovered T cell-mediated vascular endothelial cell-independent ET-1 production system by using human and murine immune cells.

[1]Division of Rheumatology and Allergology, Department of Internal Medicine, St. Marianna University School of Medicine, Kawasaki, Japan. [2]Department of Frontier Medicine, Institute of Medical Science, St. Marianna University School of Medicine, Kawasaki, Japan. [3]Department of Neurology, Division of Neurogenetics, The Ohio State University Wexner Medical Center, Columbus, Ohio, USA. [4]International Institute for Integrative Sleep Medicine (WPI-IIIS), University of Tsukuba, Tsukuba, Japan. Correspondence and requests for materials should be addressed to T.O. (email: okazakit@marianna-u.ac.jp)

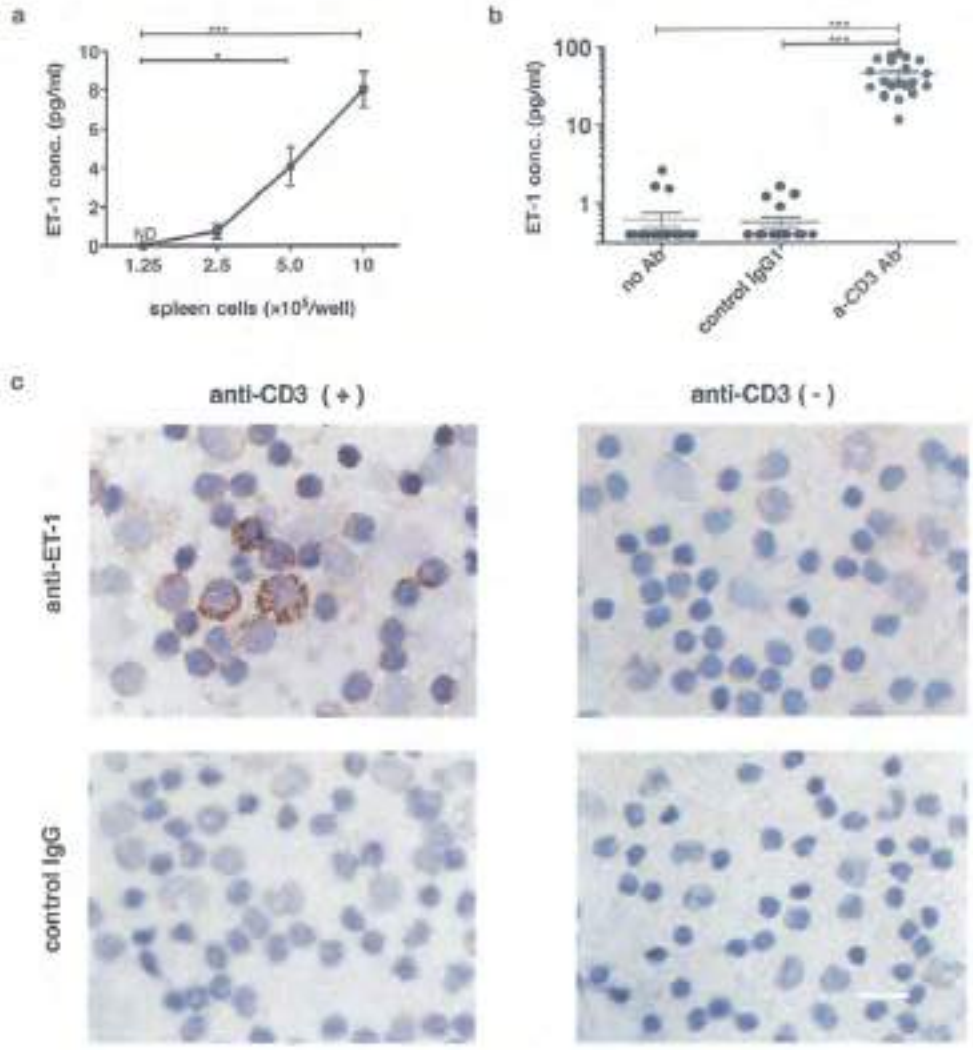

Figure 1. ET-1 production by immune cells following anti-CD3 Ab-mediated activation of T cells in murine spleen cells and human PBMCs. ET-1 production in the culture supernatant of 1×10^6 cells/well of (**a**) murine spleen cells (**b**) human PBMCs from 20 healthy donors cultured for 24 h with or without stimulation with 10 μg/ml immobilized anti-human CD3 Ab or control IgG1. The value under the limit of detection (0.39 pg/ml) with ET-1 ELISA assay was defined as 0.39 pg/ml. The assays were performed in triplicate wells. Data are expressed as the mean ± SEM. $^*p < 0.05$, $^{***}p < 0.001$ as compared with negative control by (**a**) one-way ANOVA followed by post-hoc Tukey's multiple comparison test and (**b**) Kruskal-Wallis followed by post-hoc Dunn's multiple comparison test. (**c**) Representative images of immunocytochemical staining of human PBMCs with anti-human ET1 mAb. PBMCs were cultured in the presence or absence of immobilized anti-human CD3 Ab for 28 h. Brefeldin A (10 μg/ml) was added to the culture for the last 4 h. After fixation with 4% paraformaldehyde and methanol, DAB staining was performed using anti-hET1 Ab (TR.ET.48.5) or control IgG. Scale bar represents 20 μm. Similar results (**a**) and images (**c**) were obtained in 3 different experiments.

Results

ET-1 production by human PBMCs and murine spleen cells following activation of T cells. T cells express receptors for some vasoconstriction factors such as angiotensin and 5-hydroxytryptamine[17,18]. Some investigators have used RT-PCR and flow cytometric analysis, and reported that endothelin receptors are expressed in human peripheral T cells[19,20]. Considering that ET-1 may work in an autocrine or paracrine manner, the T cells themselves or adjacent immunocompetent cells could produce ET-1 and stimulate endothelin receptors on activated T cells during inflammation. We investigated whether murine immune spleen cells stimulated with immobilized anti-CD3 Ab can produce ET-1 and observed that such cells produced ET-1 in a cell number-dependent manner (Fig. 1a). Based on this fact, we also tested whether T cell activation could promote PBMCs from 20 healthy donors to produce ET-1. This human *in vitro* study also clearly showed that PBMCs, independent of vascular endothelial cells, produced ET-1 in a manner that was dependent only on the activation of T cells (Fig. 1b). Furthermore, immunocytochemistry showed that cells that produced ET-1 were present among PBMCs activated by immobilized anti-CD3 Ab (Fig. 1c).

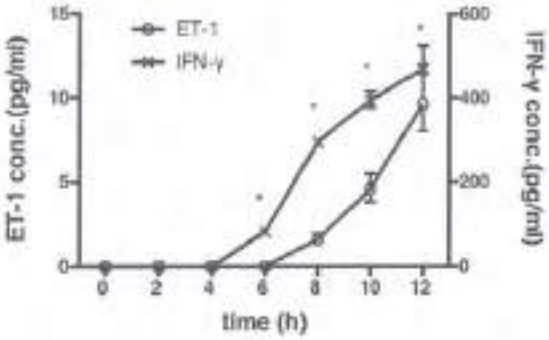

Figure 2. Comparison of the production kinetics between IFN-γ and ET-1 in the culture supernatant of PBMCs stimulated with immobilized anti-CD3 Ab. ET1 production in the culture supernatant of 1×10^6 cells/well of human PBMCs from a healthy donor cultured with 10μg/ml immobilized anti-human CD3 Ab. The culture supernatants at appropriate times were collected and measured by ET-1 or IFN-γ ELISA. Assays were performed in triplicate wells, and data represent means ± SEM. ND = not detected. $^*P < 0.001$ as calculated compared with negative control (Time 0) by two-way ANOVA followed by post-hoc Sediak's multiple comparison test. Similar results were obtained in 3 different experiments.

ET-1 production from monocytes induced by activated T cells via IFN-γ and TNF-α. To investigate how ET-1 is produced from PBMCs induced by activated T cells, we compared the production kinetics of IFN-γ and ET-1 from activated T cell-induced PBMCs. The kinetics of ET-1 production was clearly later than that of IFN-γ for activation of T cells, suggesting that T cells may induce other immune cells to produce ET-1 in PBMCs (Fig. 2).

Based on previous reports showing that ET-1 is synthesized by macrophages and dendritic cells[12–16], we focused on monocytes as candidates for the source of ET-1 production. T cells and monocytes were purified from PBMCs with magnetic beads and separated with a porous membrane (0.4 μm) using the Transwell system. Purified monocytes in the inner chamber did not produce ET-1 without activated T cells induced by immobilized anti-CD3 Ab in the outer chamber (see Supplementary Fig. S1). Activation of T cells with immobilized anti-CD3 Ab in the outer chamber induced ET-1 production only by monocytes, and not by T cells, in the inner chamber (Fig. 3a). Furthermore, ET-1 production was strongly detected in purified monocytes separated with a porous membrane in the inner chamber by immunofluorescent staining only when T cells were activated with immobilized anti-CD3 Ab in the outer chamber (Fig. 3d). These results indicated that T cells induced monocytes to produce ET-1, possibly via soluble factors released by T cells upon activation. TNF-α is a key cytokine that induces ET-1 production from vascular endothelial cells[21,22]. On the other hands, the cytokines produced by T cells that give rise to macrophages with a phenotype that is distinct from monocytes are IFN-γ, TNF-α, IL-4, and IL-10[23,24]. We next examined the effect of blocking Abs for these cytokines on this T cell-mediated ET-1 production system from monocytes. In the inhibition assay using the double chamber system, Abs against TNF-α and IFN-γ partially inhibited ET-1 production from monocytes, whereas Abs against IL-4 and IL-10 did not (Fig. 3b). Moreover, addition of both Abs blocking IFN-γ and TNF-α completely abolished this ET-1 production from monocytes (Fig. 3c). These findings demonstrated that IFN-γ and TNF-α released from activated T cells induced monocytes to produce ET-1 in human PBMCs.

ET-1 production from monocytes induced by murine antigen-specific CTL activation. Stimulation by immobilized anti-CD3 Ab induces canonical T-cell receptor signaling, which may not reflect natural T cell activation. Therefore, we next examined whether antigen-specific T cell activation could induce ET-1 production from monocytes in mice. The tax-specific CTL line we developed recognizes a specific antigen, Tax11-19 peptide of HTLV-1 restricted with HLA-A2, upon activation in HLA-A2 transgenic HHD mice[25,26]. Tax-specific CTLs and mitomicyn C-treated syngeneic spleen cells from HHD mice were used as antigen-specific T cells and antigen-presenting cells, respectively. Using magnetic beads, murine monocytes were purified from bone marrow cells in HHD mice. Bone marrow-derived monocytes in the inner chamber produced ET-1 only in the presence of antigen-specific activation of CTLs in the outer chamber (Fig. 4a). Furthermore, ET-1 production from monocytes induced by antigen-specific activation of CTLs was also inhibited by anti-IFN-γ and anti-TNF-α Abs (Fig. 4a). Furthermore, from another point of view, to determine whether monocytes can produce ET-1, we used cells from Tie2-Cre;$ET^{flox/flox}$ mice that allow conditional deletion of ET-1 using the Cre-loxP system[27]. Because Tie2 is expressed in endothelial cells and hematopoietic stem cells[28], bone marrow-derived monocytes purified from Tie2-Cre(+);$ET^{flox/flox}$ mice should not be able to produce ET-1. Antigen-specific activation of murine CTLs in the outer chamber induced the bone marrow-derived monocytes purified from Tie2-Cre(−);$ET^{flox/flox}$ mice, which do not harbor the Tie2 promotor, to produce ET-1 in the upper chamber. However, ET-1 production was abolished when using cells from Tie2-Cre(+);$ET^{flox/flox}$ mice in the inner chamber (Fig. 4b). All these findings clearly demonstrated that T cells, upon activation in an antigen-specific manner, promoted monocytes to produce ET-1 via the soluble factors of IFN-γ and TNF-α.

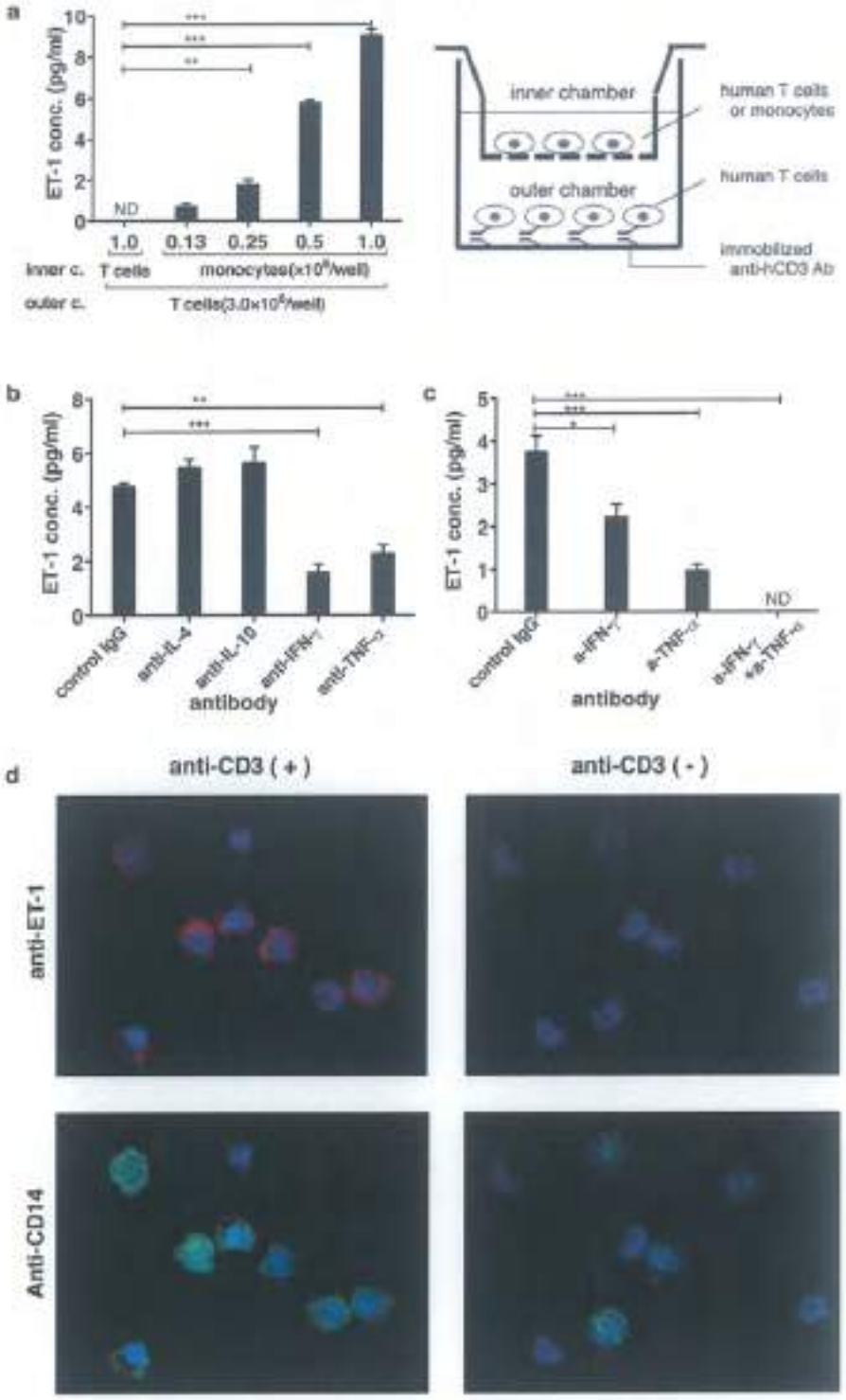

Figure 3. The relationship between T cells and monocytes in ET-1 induction with the double chamber system using human cells. After PBMCs were prepared from 100 ml of whole blood of a volunteer, T cells and monocytes were purified from human PBMCs with Mini-MACS, respectively. Three million T cells were stimulated with immobilized anti-CD3 Ab in the outer chamber of the Transwell system (See the schema on the right of Fig. 3a.). In the inner chamber (**a**), the number of purified T cells or monocytes with magnetic beads is shown on the x axis. For panels (**b**) and (**c**), 1.5×10^6 purified human monocytes were cultured for 24 h. The ET-1 concentration in the supernatant of each culture was measured using ELISA. The concentration of each blocking Ab used was 30 μg/ml. ND = not detected. The assays were performed in triplicate wells. Data are expressed as the mean ± SEM. $^*p < 0.05$, $^{**}p < 0.01$, $^{***}p < 0.001$ as compared with negative control with T cells in the inner chamber (**a**) or positive control (**b**,**c**) by one-way ANOVA followed by post-hoc Tukey's multiple comparison test. (**d**) Images of the detection of ET-1 production from monocytes purified from PBMCs in the inner chamber. The monocytes in the inner chamber were cultured with T cells in the

outer chamber in the presence or absence of immobilized anti-human CD3 Ab for 28 h. Brefeldin A (10 μg/ml) was added to the culture for the last 4 h. After fixation with 4% paraformaldehyde and 0.5% Triton X-100, immunofluorescent staining was performed using anti-ET-1 Ab (TR.ET.48.5) with anti-polyclonal mouse IgG(H + L) conjugated with Alexa Fluor 594 (Red) and anti-human CD14 (1:25 dilution) conjugated with Alexa Fluor 488 (Green). Nuclei were visualized with DAPI (Blue). Similar results and images were obtained in at least 3 different experiments (**a–d**).

Discussion

ET-1 is a vasoconstriction factor producing powerful contraction of a range of mammalian blood vessel *in vitro*, including human arteries and veins[1]. In physiological condition, ET-1 synthesized in vascular endothelial cells plays a role in regulating vascular tones by affecting vascular smooth muscles. On the other hand, with the implementation of endothelin receptor antagonist in experimental studies, the blockade of ET-1 mediated signaling with endothelin receptor antagonists reduces the level of inflammation in some animal models of LPS-induced lung inflammation[5], allograft rejection[6], antigen-induced arthritis[7,8], antigen-induced allergic rhinitis[10] and monocrotaline-induced pulmonary artery hypertension[11]. However, how ET-1 is produced and works in such inflammation models other than LPS-induced inflammation remains unknown. Especially in allograft rejection, antigen-induced inflammation and monocrotaline-induced pulmonary artery hypertension models, T cells play a pivotal role in initiating the adaptive immune response[29–32]. In clinical studies, immunosuppressive therapy is effective in some cases of connective tissue disease-related pulmonary artery hypertension (PAH), and ET-1 could play a key role in its pathogenesis[33–38]. In idiopathic and connective tissue disease-associated PAH, the existence of perivascular infiltrates and lymphoid follicles that include adaptive immune cells around pulmonary arteries is a pathological finding of pulmonary hypertension[37–39]. Although these experimental, clinical and pathological studies suggest that the ET-1 production system may be modulated by immune cells, the results are conflicting, and evidence for such actions is largely indirect. Thus, we hypothesized that T cells might induce ET-1 production in immune cells. The present study provides clear evidence regarding a potential role for activated T cells to induce the production of ET-1 as a pressor factor from monocytes in both humans and mice.

Endothelin receptors were expressed in T cells[40]. Because ET-1 is considered to act in an autocrine/paracrine manner, endothelin receptors on T cells could be affected by T cells themselves or adjacent immune cells. ET-1 was not detected in the culture supernatant of immobilized anti-CD3 Ab-stimulated T cells (Fig. 3a), whereas both human PBMCs and murine spleen cells stimulated with immobilized anti-CD3 Ab produced significant levels of ET-1 (Fig. 1a,b). Using immunocytochemistry, we also confirmed the existence of ET-1-producing cells among PBMCs stimulated with immobilized anti-CD3 Ab (Fig. 1c). These results indicated that a vascular endothelial cell-independent ET-1 production system can emerge following activation of T cells in human PBMCs and murine spleen cells. Although the primary source of ET-1 synthesis is regarded as vascular endothelial cells, the peptide is produced by other cell types including epithelial cells in the lung, kidney, and colon[1,40–42] and the choroid plexus and reactive glial cells in the brain[43,44]. Among immune cells, ET-1 synthesis is detected in macrophages[12–14] and dendritic cells[16]. However, little is known about the induction mechanism of ET-1 production by immune cells other than the lipopolysaccharides-activation system of macrophages[12] and the putative autocrine loop mechanism in dendritic cells[16]. To determine how activated T cells could induce immune cells to produce ET-1, we focused on monocytes as a candidate cell type for ET-1-producing immune cells and purified each population of T cells and monocytes with magnetic beads from human PBMCs or murine bone marrow cells. Using the Transwell system, purified T cells, upon activation with immobilized anti-CD3 Ab in the outer chamber, induced monocytes in the inner chamber to produce ET-1 (Fig. 3a, Supplementary Figure S1). Induction of ET-1 production in this noncontact system indicates the existence of soluble mediator molecules between T cells and monocytes. Monocytes/macrophages are highly plastic cells that adopt a variety of activation states. They are broadly divided into classically activated, wound healing, and regulatory macrophages. The important inducers are IFN-γ and TNF-α, IL-4 and IL-10, respectively[23,24]. Assays using Abs that inhibit these cytokines demonstrated that IFN-γ and TNF-α may be key cytokines for directing monocytes to produce ET-1 as well as induction of classically activated macrophages (Fig. 3b,c, Fig. 4a). Furthermore, in addition to artificial stimulation with immobilized anti-CD3 Ab, antigen-specific activation of cytotoxic T cells led to induction of ET-1 production from bone marrow-derived monocytes in mice, and this induction was blocked by anti-IFN-γ and anti-TNF-α Abs in the Transwell system (Fig. 4a). Since IFN-γ and TNF-α are cytokines produced from CTLs or Th1 cells, we suggest that ET-1 is usually produced during Th1 inflammation and adaptive immunity.

Tie2 is a critical molecule in the development of endothelial cells and hematopoietic stem cells[26]. $ET1^{flox/flox}$;Tie2-Cre mice, which harbor the Tie2 promotor, are conditionally deficient in ET-1 production in endothelial cells and immune cells derived from hematopoietic stem cells[27]. The monocytes purified from bone marrow cells in $ET1^{flox/flox}$;Tie2-Cre mice lost the ability to produce ET-1, but this was not seen in $ET1^{flox/+}$;Tie2-Cre and $ET1^{flox/flox}$;Tie2-Cre(−) mice (Fig. 4b). These results also provide evidence for the existence of an ET-1 production system in monocytes induced by T cells upon activation.

The current study suggests that not only acquired immunity may have a potential to directly affect the circulatory system with the newly discovered T cell-mediated ET-1 production mechanism, but also the signal transfer via IFN-γ and TNF-α from T cells to monocytes could play a key role in the regulation of such an immune-mediated ET-1 production system.

In the final part of our study, we focused on the relationship between T cell activation and ET-1 in humans and mice. However, the details of how and where ET-1 is released from monocytes in the immune system are unclear. Further studies will be needed to clarify the physiological and pathological role of the T cell-induced ET-1 production system within the immune system.

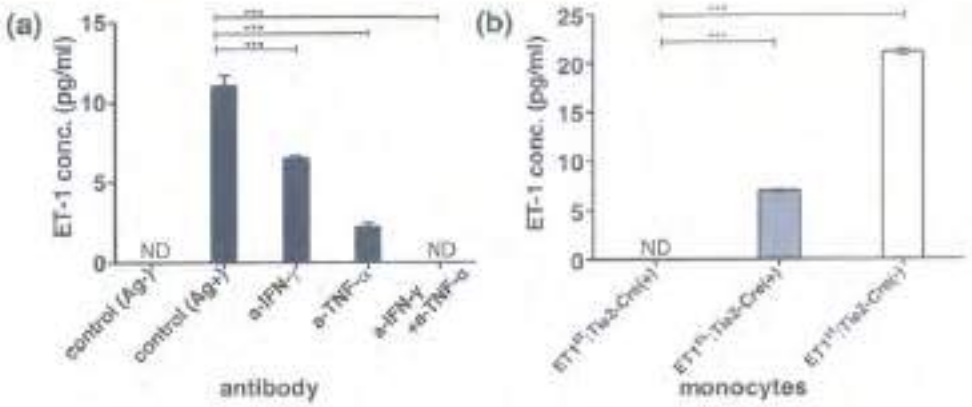

Figure 4. Effect of antigen-specific activation of T cells on monocytes in mice. Three million Tax11-19-specific CTLs were stimulated with 4×10^6 mitomycin C-treated syngeneic spleen cells from HHD mice in the presence or absence of 0.1 μM Tax11-19 peptide as an antigen (Ag) in the outer chamber. In the inner chamber, after bone marrow cells were prepared from 4 mice of femurs in each strain, 1.5×10^6 /well of monocytes purified with Mini-MACS from bone marrow cells of (**a**) HHD mice and (**b**) $ET1^{flox/flox}$;Tie2-Cre(+), $ET1^{flox/+}$;Tie2-Cre(+), and $ET1^{flox/flox}$;Tie2-Cre(−) mice were cultured for 24 h. The concentration of each blocking Ab used was 30 μg/ml. ND = not detected. The assays were performed in triplicate wells. Data are expressed as the mean ± SEM. ***$p < 0.001$ as compared with positive (**a**) or negative (**b**) control by one-way ANOVA followed by post-hoc Tukey's multiple comparison test. Similar results were obtained in two experiments (**a**,**b**).

Materials and Methods

Mice. Transgenic HHD-2 mice (gift from Dr. François Lemonnier, Institute Pasteur, Paris, France) were bred in our colony at the Institute of Experimental Animals at St. Marianna University. HHD-2 mice are characterized by knock-out of the murine β_2-microglobulin gene, as well as murine H-$2D^b$, plus transgenic expression of human HLA-A2.1 with covalently linked human β_2-microglobulin and a murine D^b-derived α3 domain to allow interaction with mouse CD8[26]. A tax-specific cytotoxic T lymphocyte (CTL) line was developed from HHD mice. Antigen-specific CTLs recognize the specific antigen of the Tax11-19 peptide of HTLV-1, LLFGYPVYV[25].

Generation of tyrosine kinase with immunoglobulin and epidermal growth factor homology domains-2 (Tie2)-Cre(+);$ET^{flox/flox}$ mice. B6.Cg-Edn1 <tm1Ywa> ($ET^{flox/flox}$ transgenic) mice harbor a transgene with loxP sites flanking exon 2 of the ET1 gene[26]. B6.Cg-Tg(Tek-cre)1Ywa (Tie2-Cre transgenic) mice express the Cre recombinase gene under the control of the mouse Tek(Tie2) promoter[26]. Both mouse strains were provided by RIKEN Bioresource Center (Tsukuba, Japan). Tie2-Cre(+);$ET^{flox/flox}$ mice were obtained from crossbreeding these two transgenic lines. To confirm establishment of Tie2-Cre(+);$ET^{flox/flox}$ mice, genomic DNA was prepared from earlobe biopsies from postnatal day 21 mice and used for genotyping with PCR analysis[27].

Murine spleen cells and bone marrow cells. All animal studies were approved by the Institute of Experimental Animals Committee at St. Marianna University and the methods in these studies were carried out in accordance with the approved guideline. The murine spleen was removed, the tissue was disrupted, red blood cells were lysed with osmotic lysis, and the single cell suspension was passed through a 70-μm sterile cell strainer. Murine bone marrow cells were obtained from the femur by flushing the shaft with buffer using a syringe with a 25 G needle. After obtaining a single-cell suspension by gently pipetting several times, the cells were passed through a cell strainer to remove cell clumps that may clog the column. Cells were washed with PBS (300 × *g* for 10 minutes) three times.

Human peripheral blood mononuclear cells (PBMCs). Peripheral blood samples from 20 healthy volunteers who provided informed and written consent following permission from the institutional review board at St. Marianna University were used for preparation of PBMCs, which were isolated using Lympholyte-H (CEDARLANE, Canada). All methods using PBMCs in human studies were carried out in accordance with the approved guidelines.

Cell separation. Immune cells including both human and murine total T cells and monocytes were sorted by negative selection on a Mini-MACS with a cell isolation kit (Miltenyi Biotec, Bergisch Gladbach, Germany) according to the manufacturer's instructions. The efficiency of cell purification was ~95% confirmed by flow-cytometric analysis in each cell purification kit.

IFN-γ and ET-1 ELISA. IFN-γ and ET-1 in the culture supernatant that was harvested at appropriate times were determined using an ELISA kit (R&D, Minneapolis, MN) according to the manufacturer's instructions. Values of all samples were expressed as means ± SEM of triplicate measurements.

Antibodies. Anti-human cytokine blocking Abs were purchased as follows: IFN-γ and tumor necrosis factor-alpha (TNF-α) from eBioscience Inc. (San Diego, CA), interleukin (IL)-4 from U-cytech (Utrecht, Netherland), and IL-10 from Diaclone (Besançon Cedex, France). Anti-murine IFN-γ and TNF-α blocking Abs were purchased from Thermo Scientific (Waltham, MA) and R&D Systems, respectively.

Immunocytochemistry. ET-1 expression was assessed with immunocytochemistry. PBMCs collected from the culture were prepared on cytospin slides. After fixation with 4% paraformaldehyde and methanol, immunocytochemistry staining was carried out. After blocking with 10% human serum in Block Ace (DS Pharma Biomedical, Osaka, Japan), PBMCs were incubated with diluted primary Abs (anti-ET1 mAb (TR.ET.48.5) 1:200) overnight at 4 °C. Immunodetection was performed using diluted secondary anti-mouse IgG1 Ab conjugated to horseradish peroxidase (1:1,000, Bethyl Laboratories, Montgomery, TX). Visualization was carried out with the Liquid DAB + Substrate Chromogen System (DAKO, Santa Clara, CA). Images were taken using a BZ-9000 fluorescence microscope (KEYENCE, Osaka, Japan).

In the study using Transwell system, after co-cultured with T cells with or without immobilized anti-CD3 Ab in the outer chamber, monocytes collected from the inner chamber were prepared on cytospin slide. After fixation with 4% paraformaldehyde and 0.5% Triton X-100, immunofluorescence was performed using the following antibodies: anti-ET1 mAb (TR.ET.48.5, 1:400 dilution) and Alexa Fluor 594-conjugated anti-mouse IgG(H + L) (1:500 dilution) (Jackson ImmunoReseach Inc., West Grove, PA). Cells were incubated in primary antibody diluted in Can Get Signal immunostain (TOYOBO, Osaka, Japan) at 4 °C overnight. After rinsing thrice with PBS(−), Alexa Fluor 594-conjugated secondary antibody was used for detection. Alexa Fluor 488-conjugated anti-human CD14 (1: 25 dilution) (BioLegend, San Diego, CA) was subsequently used for double staining. After four additional PBS washes, cells were stained with 4′,6-diamidino-2-phenylindole (DAPI) (Sigma-Aldrich, St. Louis, MO). Images were taken using a BZ-9000 fluorescence microscope (KEYENCE, Osaka, Japan).

Statistical analysis. All of the detection experiments using ELISA were performed in triplicate, and the data were expressed as the mean ± SEM and were analyzed using Graph Pad Prism V.6.0 (San Diego, CA). We used one-way ANOVA followed by *post-hoc* Tukey's multiple comparison test in Figs 1a, 3a,b, 4a and b. In Fig. 1b, based on the result by D'Agostino & Pearson omnibus normality test, we used Kruskal–Wallis followed by *post-hoc* Dunn's multiple comparison test. Two-way ANOVA was performed in Fig. 2. Significance was accepted as $p < 0.05$.

References

1. Davenport, A. P. *et al.* Endothelin. *Pharmacological reviews* **68**, 357–418, https://doi.org/10.1124/pr.115.011833 (2016).
2. Yanagisawa, M. *et al.* A novel potent vasoconstrictor peptide produced by vascular endothelial cells. *Nature* **332**, 411–415 (1988).
3. Kedzierski, R. M. & Yanagisawa, M. Endothelin system: the double-edged sword in health and disease. *Annu Rev Pharmacol Toxicol* **41**, 851–876 (2001).
4. Maguire, J. J. & Davenport, A. P. Endothelin receptors and their antagonists. *Seminars in nephrology* **35**, 125–136, https://doi.org/10.1016/j.semnephrol.2015.02.002 (2015).
5. Santiago, A. L., Rae, G. A. & Henriques, M. Effects of endothelin ETA receptor antagonism on granulocyte and lymphocyte accumulation in LPS-induced inflammation. *J Leukoc Biol* **76**, 210–216 (2004).
6. Lattmann, T. *et al.* Activation of pro-inflammatory and anti-inflammatory cytokines in host organs during chronic allograft rejection: role of endothelin receptor signaling. *Am J Transplant* **5**, 1042–1049 (2005).
7. Imhof, A. K. *et al.* Potent anti-inflammatory and antinociceptive activity of the endothelin receptor antagonist bosentan in monoarthritic mice. *Arthritis Res Ther* **13**, R97 (2011).
8. Dorsate, P. B. *et al.* Bosentan, an endothelin receptor antagonist, ameliorates collagen-induced arthritis: the role of TNF-alpha in the induction of endothelin system genes. *Inflammation research: official journal of the European Histamine Research Society. [et al.]* **61**, 337–348, https://doi.org/10.1007/s00011-011-0415-9 (2012).
9. Guo, Y. *et al.* Endothelin-1 overexpression exacerbate experimental allergic encephalomyelitis. *Journal of neuroimmunology* **276**, 64–70, https://doi.org/10.1016/j.jneuroim.2014.08.616 (2014).
10. Tatar, A. *et al.* The role of endothelin-1 and endothelin receptor antagonists in allergic rhinitis inflammation: ovalbumin-induced rat model. *Rhinology*, doi:https://doi.org/10.4193/Rhin15.059 (2016).
11. Fontoura, D. *et al.* Myocardial and anti-inflammatory effects of chronic bosentan therapy in monocrotaline-induced pulmonary hypertension. *Revista portuguesa de cardiologia: orgao oficial da Sociedade Portuguesa de Cardiologia = Portuguese journal of cardiology: an official journal of the Portuguese Society of Cardiology* **33**, 213–222, https://doi.org/10.1016/j.repc.2013.09.016 (2014).
12. Ehrenreich, H. *et al.* Endothelins, peptides with potent vasoactive properties, are produced by human macrophages. *The Journal of experimental medicine* **172**, 1741–1748 (1990).
13. Wahl, L. R. *et al.* Murine macrophages produce endothelin-1 after microbial stimulation. *Experimental biology and medicine (Maywood, N.J.)* **230**, 652–658 (2005).
14. McKenna, S. *et al.* Endotoxemia Induces IkappaBbeta/NF-kappaB-Dependent Endothelin-1 Expression in Hepatic Macrophages. *J Immunol* **195**, 3866–3879, https://doi.org/10.4049/jimmunol.1501017 (2015).
15. Sun, G. *et al.* Functional analysis of the preproendothelin-1 gene promoter in pulmonary epithelial cells and monocytes. *Biochemical and biophysical research communications* **221**, 647–652, https://doi.org/10.1006/bbrc.1996.0650 (1996).
16. Gurulli, G. *et al.* Function and survival of dendritic cells depend on endothelin-1 and endothelin receptor autocrine loops. *Blood* **104**, 2107–2115, https://doi.org/10.1182/blood-2003-10-3559 (2004).
17. Maeda, A. *et al.* Immunosuppressive effect of angiotensin receptor blocker on stimulation of mice CTLs by angiotensin II. *Int Immunopharmacol* **9**, 1183–1188 (2009).
18. Inoue, M. *et al.* Regulation of antigen-specific CTL and Th1 cell activation through 5-Hydroxytryptamine 2A receptor. *Int Immunopharmacol* **11**, 67–73 (2011).
19. Gunther, J. *et al.* Angiotensin receptor type 1 and endothelin receptor type A on immune cells mediate migration and the expression of IL-8 and CCL18 when stimulated by autoantibodies from systemic sclerosis patients. *Arthritis Res Ther* **16**, R65, https://doi.org/10.1186/ar4503 (2014).
20. Elisa, T. *et al.* Endothelin Receptors Expressed by Immune Cells Are Involved in Modulation of Inflammation and in Fibrosis: Relevance to the Pathogenesis of Systemic Sclerosis. *Journal of immunology research* **2015**, 147616, https://doi.org/10.1155/2015/147616 (2015).
21. Corder, R., Carrier, M., Khan, N., Klemm, P. & Vane, J. R. Cytokine regulation of endothelin-1 release from bovine aortic endothelial cells. *Journal of cardiovascular pharmacology* **26**(Suppl 3), 556–58 (1995).
22. Kalaleh, M. B. & Fan, P. S. Effect of cytokines on the production of endothelin by endothelial cells. *Clinical and experimental rheumatology* **15**, 163–167 (1997).
23. Mosser, D. M. & Edwards, J. P. Exploring the full spectrum of macrophage activation. *Nature reviews. Immunology* **8**, 958–969, https://doi.org/10.1038/nri2448 (2008).
24. Wynn, T. A., Chawla, A. & Pollard, J. W. Macrophage biology in development, homeostasis and disease. *Nature* **496**, 445–455, https://doi.org/10.1038/nature12034 (2013).

25. Kitazono, T. *et al.* Advantage of higher-avidity CTL specific for Tax against human T-lymphotropic virus-1 infected cells and tumors. *Cell Immunol* **272**, 11–17 (2011).
26. Pascolo, S. *et al.* HLA-A2.1-restricted education and cytolytic activity of CD8(+) T lymphocytes from beta2 microglobulin (beta2m) HLA-A2.1 monochain transgenic H-2Db beta2m double knockout mice. *The Journal of experimental medicine* **185**, 2043–2051 (1997).
27. Kisanuki, Y. Y. *et al.* Low blood pressure in endothelial cell-specific endothelin 1 knockout mice. *Hypertension* **56**, 121–128, https://doi.org/10.1161/HYPERTENSIONAHA.109.138701 (2010).
28. Takakura, N. *et al.* Critical role of the TIE2 endothelial cell receptor in the development of definitive hematopoiesis. *Immunity* **9**, 677–686 (1998).
29. Marino, J., Paster, J. & Benichou, G. Allorecognition by T Lymphocytes and Allograft Rejection. *Frontiers in immunology* **7**, 582, https://doi.org/10.3389/fimmu.2016.00582 (2016).
30. Andersson, S. E., Lexmuller, K., Alving, K. & Ekstrom, G. M. Periarticular tissue levels of cytokine- and endothelin-1-like immunoreactivity during the course of antigen-induced arthritis in the rat. *Inflammation research: official journal of the European Histamine Research Society… [et al.]* **48**, 491–496, https://doi.org/10.1007/s000110050492 (1999).
31. Guo, C., Chen, G. & Ge, R. IL-23, rather than IL-17, is crucial for the development of ovalbumin-induced allergic rhinitis. *Molecular immunology* **67**, 436–443, https://doi.org/10.1016/j.molimm.2015.07.009 (2015).
32. Cuttica, M. J. *et al.* Perivascular T-cell infiltration leads to sustained pulmonary artery remodeling after endothelial cell damage. *American journal of respiratory cell and molecular biology* **45**, 62–71, https://doi.org/10.1165/rcmb.2009-0365OC (2011).
33. Giaid, A. *et al.* Expression of endothelin-1 in the lungs of patients with pulmonary hypertension. *The New England journal of medicine* **328**, 1732–1739 (1993).
34. Sanchez, O., Sitbon, O., Jais, X., Simonneau, G. & Humbert, M. Immunosuppressive therapy in connective tissue diseases-associated pulmonary arterial hypertension. *Chest* **130**, 182–189, https://doi.org/10.1378/chest.130.1.182 (2006).
35. Jais, X. *et al.* Immunosuppressive therapy in lupus- and mixed connective tissue disease-associated pulmonary arterial hypertension: a retrospective analysis of twenty-three cases. *Arthritis Rheum* **58**, 521–531, https://doi.org/10.1002/art.23303 (2008).
36. Miyamichi-Yamamoto, S. *et al.* Intensive immunosuppressive therapy improves pulmonary hemodynamics and long-term prognosis in patients with pulmonary arterial hypertension associated with connective tissue disease. *Circulation journal: official journal of the Japanese Circulation Society* **75**, 2668–2674 (2011).
37. Stacher, E. *et al.* Modern age pathology of pulmonary arterial hypertension. *Am J Respir Crit Care Med* **186**, 261–272, https://doi.org/10.1164/rccm.201201-0164OC (2012).
38. Rabinovitch, M., Guignabert, C., Humbert, M. & Nicolls, M. R. Inflammation and immunity in the pathogenesis of pulmonary arterial hypertension. *Circ Res* **115**, 165–175, https://doi.org/10.1161/circresaha.113.301141 (2014).
39. Perros, F. *et al.* Pulmonary lymphoid neogenesis in idiopathic pulmonary arterial hypertension. *Am J Respir Crit Care Med* **185**, 311–321, https://doi.org/10.1164/rccm.201105-0927OC (2012).
40. Rozengurt, N., Springall, D. R. & Polak, J. M. Localization of endothelin-like immunoreactivity in airway epithelium of rats and mice. *The Journal of pathology* **160**, 5–8, https://doi.org/10.1002/path.1711600104 (1990).
41. Zeidel, M. L., Brady, H. R., Kone, B. C., Gullans, S. R. & Brenner, B. M. Endothelin, a peptide inhibitor of Na(+)-K(+)-ATPase in intact renal tubular epithelial cells. *The American journal of physiology* **257**, C1101–1107 (1989).
42. Takahashi, K. *et al.* Endothelin in the gastrointestinal tract. Presence of endothelinlike immunoreactivity, endothelin-1 messenger RNA, endothelin receptors, and pharmacological effect. *Gastroenterology* **99**, 1660–1667 (1990).
43. Jiang, M. H., Eriksson, L. & Olsson, Y. Immunohistochemical evidence of endothelin-1 in human choroid plexus. *Acta neuropathologica* **84**, 457–460 (1992).
44. MacCumber, M. W., Ross, C. A. & Snyder, S. H. Endothelin in brain: receptors, mitogenesis, and biosynthesis in glial cells. *Proc Natl Acad Sci USA* **87**, 2359–2363 (1990).
45. Shohet, R. V. *et al.* Mice with cardiomyocyte-specific disruption of the endothelin-1 gene are resistant to hyperthyroid cardiac hypertrophy. *Proc Natl Acad Sci USA* **101**, 2088–2093, https://doi.org/10.1073/pnas.0307159101 (2004).
46. Kisanuki, Y. Y. *et al.* Tie2-Cre transgenic mice: a new model for endothelial cell-lineage analysis in vivo. *Developmental biology* **230**, 230–242, https://doi.org/10.1006/dbio.2000.0106 (2001).

Acknowledgements

This study was supported in part by a grant-in-aid from the Ministry of Health, Labor, and Welfare of Japan. We would like to thank Toshiko Sato and Mayumi Tamaki for technical assistance provided during the study.

Author Contributions

S.S. and M.I. performed data analysis and prepared manuscript. T.O. helped prepare the manuscript, managed data collection. K.Y. assisted in analysis and interpretation. Y.Y.K. and M.Y. assisted the development of conditional knockout mice. T.O., K.K. and S.O. conceived of and designed the study. All authors reviewed and contributed to the manuscript.

Additional Information

Supplementary information accompanies this paper at https://doi.org/10.1038/s41598-017-14202-5.

Competing Interests: The authors declare that they have no competing interests.

Publisher's note: Springer Nature remains neutral with regard to jurisdictional claims in published maps and institutional affiliations.

Open Access This article is licensed under a Creative Commons Attribution 4.0 International License, which permits use, sharing, adaptation, distribution and reproduction in any medium or format, as long as you give appropriate credit to the original author(s) and the source, provide a link to the Creative Commons license, and indicate if changes were made. The images or other third party material in this article are included in the article's Creative Commons license, unless indicated otherwise in a credit line to the material. If material is not included in the article's Creative Commons license and your intended use is not permitted by statutory regulation or exceeds the permitted use, you will need to obtain permission directly from the copyright holder. To view a copy of this license, visit http://creativecommons.org/licenses/by/4.0/.

© The Author(s) 2017

MODERN RHEUMATOLOGY CASE REPORTS, 2017
https://doi.org/10.1080/24725625.2017.1414913

Taylor & Francis
Taylor & Francis Group

CASE REPORT

Syndrome of inappropriate antidiuretic hormone secretion (SIADH) in a patient with microscopic polyangiitis following low-dose intravenous cyclophosphamide: a possible pathogenic link with disease activity

Tomofumi Kiyokawa, Hironari Hanaoka, Harunobu Iida, Kana Ishimori, Yukiko Takakuwa, Yoshioki Yamasaki, Takahiro Okazaki, Shoichi Ozaki and Kimito Kawahata

Division of Rheumatology and Allergology, Department of Internal Medicine, St. Marianna University School of Medicine, Kanagawa, Japan

ABSTRACT

Syndrome of inappropriate antidiuretic hormone secretion (SIADH) induced by cyclophosphamide (CY) in rheumatology has been rarely described. Most reported cases developed SIADH at the first administration of high-dose CY. We report the case of a 76-year-old female with microscopic polyangiitis (MPA) who developed SIADH during the seventh course of low-dose intravenous cyclophosphamide (IVCY). Our report suggested that SIADH may be developed at any course of IVCY treatment and a process other than CY toxicity may be involved. An exacerbation of interstitial lung disease (ILD) and overexpression of inflammatory cytokines may have contributed to the development of SIADH in this case. Since the active phase of MPA might be a risk factor for SIADH, MPA patients should be evaluated for subclinical SIADH.

ARTICLE HISTORY
Received 5 September 2017
Accepted 5 December 2017

KEYWORDS
Syndrome of inappropriate antidiuretic hormone secretion; cyclophosphamide; vasculitis; interstitial lung disease; hyponatremia

Introduction

Cyclophosphamide (CY) is an alkylating agent widely used in rheumatology, particularly for patients with antineutrophil cytoplasmic antibody (ANCA)-associated small-vessel vasculitis [1]. The introduction of CY has greatly improved patient prognosis [2]. The recent European Vasculitis Study Group (EUVAS) recommendations for management of ANCA-associated small-vessel vasculitis [3] suggest that patients with serum creatinine levels <5.7 mg/dL should be treated with prednisone and IVCY for 3–6 months. The therapeutic protocol consists of three pulses of 15 mg/kg IVCY administered two weeks apart, followed by pulses at 3-week intervals. Severe hyponatremia, secondary to SIADH, has been reported in patients with malignant disease who were treated with high-dose IVCY (40 mg/kg), primarily at the first infusion [4–6]. Experience of SIADH in patients with hematological disorders including hematopoietic stem cell transplantation has been frequently reported [7]. Mechanisms underlying hyponatremia may involve the antidiuretic effect of an active alkylating metabolite of CY [8]. ADH release has also been demonstrated with ifosfamide, a close structural analogue of CY [9].

Here, we report the case of a patient with MPA with diffuse cutaneous systemic sclerosis (dcSSc) who developed severe hyponatremia from SIADH following her seventh pulse of IVCY.

Case presentation

One year before presentation, a 76-year-old woman was diagnosed with dcSSc by the following clinical findings: sclerodactyly to the metacarpophalangeal joint, Raynaud phenomenon, positive for anti-topoisomerase I (anti-Topo-1) antibody, and pulmonary fibrosis. Four months before presentation, she developed a fever (>38 °C) that was not resolved by antibiotics. A high titer of myeloperoxidase (MPO)-ANCA was detected and she was hospitalized.

Physical examination revealed fine crackles in the lower lungs and sensory disturbance in her extremities. Laboratory findings on admission included: WBC count of 16100/μL, Hb 11.2 g/dL, Plt 519 × 10^3/μL, serum protein 7.1 g/dL, serum albumin 3.2 g/dL, AST 14 IU/L, ALT 15 IU/L, LDH 176 IU/L, ALP 207 IU/L, γ-GTP 32 IU/L, Cr 0.51 mg/dL, eGFR 86.4 mL/min, BUN 15.5 mg/dL, uric acid 2.9 mg/dL, serum Na 135 mEq/L, serum K 4.3 mEq/L, serum Cl 98 mEq/L, C-reactive protein (CRP) 10.56 mg/dL, Krebs von den Lungen-6 (KL-6) 568 U/mL, hemolytic complement (CH50) 57.3 U/mL, IgA 320 mg/dL, IgG 1903 mg/dL, IgM 147 mg/dL, and MPO-ANCA 216.0 U/mL. Indirect immunofluorescence testing for ANCA revealed a

CONTACT Hironari Hanaoka hhanaoka@marianna-u-ac.jp Division of Rheumatology and Allergology, Department of Internal Medicine, St. Marianna University School of Medicine, Sugao, Miyamae, Kawasaki, 216-8511, Japan

© 2017 Japan College of Rheumatology

perinuclear pattern. Urinalysis showed a specific gravity of 1.024; pH 6.0; protein 1+; occult blood 1+; WBC 1-4/HPF; and RBC 20–29/HPF. Computed tomography (CT) showed pulmonary fibrosis. Electromyography showed a neurogenic pattern in the lower limbs while brain magnetic resonance imaging (MRI) demonstrated no significant findings. Comparing with the data obtained when the patient was diagnosed with SSc, pulmonary function test values at diagnosed as MPA were decreased from 78.5 to 64.4 in forced vital capacity (FVC) and from 69.5 to 46.3 in diffusing capacity of the lung for carbon monoxide (DLCO).

These findings led to the diagnosis of MPA with dcSSc. She was treated with prednisolone 40 mg/day (1 mg/kg/day) followed by IVCY therapy. The IVCY protocol consisted of three 400-mg pulses given 2 weeks apart, followed by three pulses at 3-week intervals, as recommended [3]. Although MPO-ANCA titers serially decreased from 216 to 4.6 IU/L and FVC improved from 64.4% to 68.2% after the sixth infusion of IVCY, CRP levels were persistently high (1.93 mg/dL) and KL-6 levels increased from 568 to 886 U/mL. Chest X-ray and CT showed persistent bilateral reticular shadows and ground-glass opacities in the lower lungs with no improvement (Figure 1(A,B)). She was hospitalized and treated with a 500-mg pulse of IVCY. About 12 h after the administration, she vomited and experienced a sudden seizure complicated by sustained loss of consciousness. Head CT revealed no evidence of acute haemorrhage or brain tumour. The patient was noted to be hyponatremic (116 mEq/L) and hypoosmolar (244 mOsm/kg water), but her serum antidiuretic hormone (ADH) level was within the normal range (3.35 pg/mL; normal range 0.3–4.2 pg/mL). Additionally, her urine osmolarity was high at 426 mOsm/kg water, as was her urine sodium at 129 mEq/L, which are consistent with SIADH. Renal dysfunction was ruled out based on normal serum creatinine (0.43 mg/dL). Her serum adrenocorticotropic hormone (ACTH) was normal (24.5 μg/dL; normal range 7.2–63.3), and her cortisol was increased (37.5 μg/dL; normal range 4.0–23.3), which ruled out the possibility of adrenal dysfunction. Furosemide 20 mg and 3% NaCl were intravenously administered with restriction of water intake and she recovered consciousness 3 days after the seizure.

Discussion

We present the case of an elderly woman with ANCA-associated small vessel vasculitis who developed severe hyponatremia from SIADH following seventh low-dose of IVCY.

To our knowledge, there have been nine reported cases of patients with connective tissue disease that

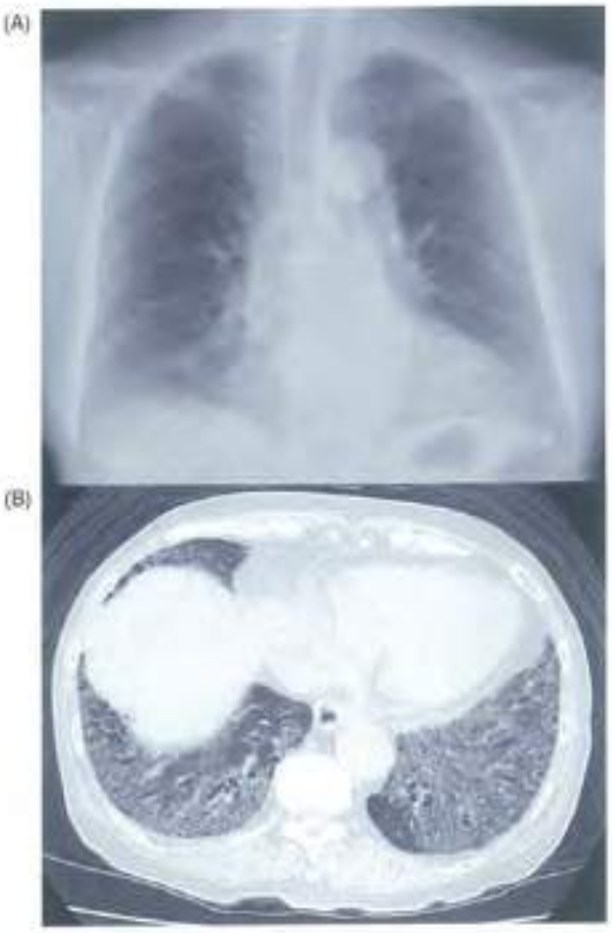

Figure 1. Chest X-ray and CT before the seventh infusion of IVCY. The chest X-ray (A) and CT (B) showed bilateral reticular and ground glass opacities in the lower lungs.

developed severe symptomatic hyponatremia following low-dose CY (<15 mg/kg) [10–17] (Table 1). SIADH occurred at the first infusion of IVCY in all cases. The authors of some of these studies have proposed potential mechanisms for SIADH caused by CY. Buckner et al. suggested that the antidiuretic effect of an active alkylating metabolite of CY may induce hyponatremia [8]. De Fronzo et al. further suggested that the alkylating metabolite of CY may act on the kidneys to enhance permeability of the distal tubules to water [4]. Kirch et al. investigated ADH release following treatment with ifosfamide, a close structural analogue to CY, which led to the development of SIADH after administration of CY [9]. In all of these cases, SIADH was induced by the first infusion of high-dose IVCY. In our case, SIADH occurred after a seventh low-dose IVCY administration. In addition to IVCY, other factors may have caused hyponatremia in this patient. First, her ILD was exacerbated when the seventh IVCY pulse was administered. As lung fibrosis proceeds, reduction of the alveolar capillary bed volume may be induced. This process consequently leads to loss of venous return volume, resulting in hyperstimulation of the baroreceptors followed by ADH oversecretion. Furthermore, water intake or pneumonia has been

Table 1. Case reports of patients with connective tissue disease developing severe symptomatic hyponatraemia.

	Our case	Biessler (1985) [10]	McCarron (1995) [11]	Spizal (1997) [12]	Salido (2003) [13]	Salido (2003) [13]	Koo (2007) [14]	Kato (2008) [15]	Jayachandran (2009) [16]	Park (2011) [17]
Age	76	54	59	57	48	53	27	70	49	68
Sex	F	F	F	F	F	F	F	F	F	F
Disease	MPA, SSc, ILD, GN	SLE, LN	SLE	SS	SLE, LN	SLE, LN, SS	SLE	MPA, GN	SSc, ILD	MPA, GN
Injection method	IV	IV	IV	IV	IV	IV	IV	PO	IV	PO
Cyclophosphamide dose	500 mg (10 mg/kg)	750 mg (20 mg/kg)	10 mg/kg	780 mg	750 mg (12.5 mg/kg)	500 mg	750 mg (15 mg/kg)	50 mg/day	500 mg	100 mg/day
Time	Seventh	First	First	First	First	First	First		Second	
Outcome	Recovered	Recovered	Recovered	Recovered	Recovered	Recovered	Recovered	Recovered	CPM	Recovered

F: female; GN: glomerulonephritis; SLE: systemic lupus erythematosus; LN: lupus nephritis; SS: Sjögren syndrome; IV: intravenous; PO: per os; CPM: central pontine myelinolysis.

reported to directly stimulate ADH secretion [18,19]. Second, overexpression of inflammatory cytokines may contribute to the development of SIADH. A previous study reported that various inflammatory cytokines are up-regulated in the active phase of ANCA-associated small-vessel vasculitis [20]. Among these, IL-6 plays a pivotal role in the disease process, with administration of tocilizumab, an anti-IL-6 receptor antibody, effectively modifying the disease course [20]. Further, there has been evidence that IL-6 directly stimulates ADH secretion [21,22]. ANCA-associated small vessel vasculitides in the active phase, especially in patients with ILD, may confer risk of SIADH development even with low-dose IVCY administration. Finally, dcSSc may contribute to ADH secretion by promoting IL-6 production or as a result of its associated pulmonary fibrosis [23].

In summary, we present the case of an elderly woman with MPA who developed severe hyponatremia following her seventh low-dose IVCY administration. Our report suggested that SIADH might be developed at any course of IVCY treatment. A possible mechanism other than IVCY toxicity for SIADH development in ANCA-associated small vessel vasculitis may be involved. More cases and further studies are required to confirm our hypothesis.

Conflict of interest

None

Patient consent

Written informed consent for publication of the clinical details and clinical images was obtained from the patient.

References

[1] Schena FP. Survey of the Italian registry of renal biopsies. Frequency of the renal diseases for 7 consecutive years. The Italian group of renal immunopathology. Nephrol Dial Transplant. 1997;12:418–426.

[2] de Lind van Wijngaarden RA, Hauer HA, Wolterbeek R, et al. Clinical and histologic determinants of renal outcome in ANCA-associated vasculitis: a prospective analysis of 100 patients with severe renal involvement. J Am Soc Nephrol. 2006;17:2264–2274.

[3] de Groot K, Harper L, Jayne DR, et al. European Vasculitis Study Group (EUVAS). Pulse versus daily oral cyclophosphamide for induction of remission in antineutrophil cytoplasmic antibody-associated vasculitis: a randomized trial. Ann Intern Med. 2009;150:670–680.

[4] DeFronzo RA, Colvin OM, Braine H, et al. Proceedings: cyclophosphamide and the kidney. Cancer. 1974;33:483–491.

[5] Baker M, Markman M, Niu J. Cyclophosphamide-induced severe acute hyponatremic encephalopathy

in patients with breast cancer: report of two cases. Case Rep Oncol. 2014;7:550–554.

[6] Shepshelovich D, Schechter A, Calvarysky B, et al. Medication-induced SIADH: distribution and characterization according to medication class. Br J Clin Pharmacol. 2017;83:1801–1807.

[7] Festuccia F, Polci R, Pugliese F, et al. Syndrome of inappropriate ADH secretion: a late complication of hematopoietic stem cell allograft. G Ital Nefrol. 2002;19:353–360.

[8] Buckner C, Rudolph R, Fefer A, et al. High-dose cyclophosphamide therapy for malignant disease. Toxicity, tumor response, and the effects of stored autologous marrow. Cancer. 1972;29:357–365.

[9] Kirch C, Gachot B, Germann N, et al. Recurrent ifosfamide-induced hyponatraemia. Eur J Cancer. 1997;33:2438–2439.

[10] Bressler RB, Huston DP. Water intoxication following moderate-dose intravenous cyclophosphamide. Arch Intern Med. 1985;145:548–549.

[11] McCarron M, Wright GD, Roberts SD. Water intoxication after low dose cyclophosphamide. BMJ. 1995; 311:292.

[12] Spital A, Ristow S. Cyclophosphamide induced water intoxication in a woman with Sjögren's syndrome. J Rheumatol. 1997;24:2473–2475.

[13] Salido M, Macarron P, Hernandez-Garcia C, et al. Water intoxication induced by low-dose cyclophosphamide in two patients with systemic lupus erythematosus. Lupus. 2003;12:636–639.

[14] Koo TY, Bae SC, Park JS, et al. Water intoxication following low-dose intravenous cyclophosphamide. Electrolyte Blood Press. 2007;5:50–54.

[15] Kato A, Sugiura T, Yamamoto T, et al. Water intoxication induced by low-dose oral cyclophosphamide in a patient with anti-neutrophil cytoplasmic antibody-related glomerulonephritis. NDT Plus. 2008;1:286–288.

[16] Jayachandran NV, Chandrasekhara PK, Thomas J, et al. Cyclophosphamide-associated complications: we need to be aware of SIADH and central pontine myelinolysis. Rheumatology. 2009;48:89–90.

[17] Park S, Kim W, Choi HY, et al. Severe symptomatic hyponatremia caused by low dose oral cyclophosphamide: a case report. Korean J Nephrol. 2011;30: 647–650.

[18] Madero M, Monares E, Dominguez AM, et al. Acute symptomatic hyponatremia in a flight attendant. Clin Nephrol. 2015;84:108–110.

[19] Corona G, Giuliani C, Parenti G, et al. Moderate hyponatremia is associated with increased risk of mortality: evidence from a meta-analysis. PLoS One. 2013;8:e80451.

[20] Sakai R, Kondo T, Kikuchi J, et al. Corticosteroid-free treatment of tocilizumab monotherapy for microscopic polyangiitis: a single-arm, single-center, clinical trial. Mod Rheumatol. 2016;26:900–907.

[21] Mastorakos G, Weber JS, Magiakou MA, et al. Hypothalamic-pituitary-adrenal axis activation and stimulation of systemic vasopressin secretion by recombinant interleukin-6 in humans: potential implications for the syndrome of inappropriate vasopressin secretion. J Clin Endocrinol Metab. 1994; 79:934–939.

[22] Tabata C, Kubo H, Tabata R, et al. All-trans retinoic acid modulates radiation-induced proliferation of lung fibroblasts via IL-6/IL-6R system. Am J Physiol Lung Cell Mol Physiol. 2006;290:597–606.

[23] Khanna D, Denton CP, Jahreis A, et al. Safety and efficacy of subcutaneous tocilizumab in adults with systemic sclerosis (faSSclinate): a phase 2, randomised, controlled trial. Lancet. 2016;387:2630–2640.

Effect of Optimizing Guideline-Directed Medical Therapy Before Discharge on Mortality and Heart Failure Readmission in Patients Hospitalized With Heart Failure With Reduced Ejection Fraction

Tetsuo Yamaguchi, MD, PhD[a,*], Takeshi Kitai, MD, PhD[b,c], Takamichi Miyamoto, MD[c], Nobuyuki Kagiyama, MD[d], Takahiro Okumura, MD, PhD[e], Keisuke Kida, MD, PhD[f], Shogo Oishi, MD[g], Eiichi Akiyama, MD[h], Satoshi Suzuki, MD, PhD[i], Masayoshi Yamamoto, MD, PhD[j], Junji Yamaguchi, MD[a], Takamasa Iwai, MD[a], Sadahiro Hijikata, MD[a], Ryo Masuda, MD[a], Ryoichi Miyazaki, MD[a], Nobuhiro Hara, MD[a], Yasutoshi Nagata, MD[a], Toshihiro Nozato, MD[a], and Yuya Matsue, MD, PhD[k,l,m]

Guideline-directed medical therapy (GDMT) is recommended for patients with heart failure with reduced ejection fraction (HFrEF). However, the prognostic impact of medication optimization at the time of discharge in patients hospitalized with heart failure (HF) is unclear. We analyzed 534 patients (73 ± 13 years old) with HFrEF. The status of GDMT at the time of discharge (prescription of angiotensin converting enzyme inhibitor [ACE-I]/angiotensin receptor blocker [ARB] and β blocker [BB]) and its association with 1-year all-cause mortality and HF readmission were investigated. Patients were divided into 3 groups: those treated with both ACE-I/ARB and BB (Both group: n = 332, 62%), either ACE-I/ARB or BB (Either group: n = 169, 32%), and neither ACE-I/ARB nor BB (None group: n = 33, 6%), respectively. One-year mortality, but not 1-year HF readmission rate, was significantly different in the 3 groups, in favor of the Either and Both groups. A favorable impact of being on GDMT at the time of discharge on 1-year mortality was retained even after adjustment for covariates (Either group: hazard ratio [HR] 0.44, 95% confidence interval [CI] 0.21 to 0.90, p = 0.025 and Both group: HR 0.29, 95% CI 0.13–0.65, p = 0.002, vs None group). For 1-year HF readmission, no such association was found. In conclusion, optimization of GDMT before the time of discharge was associated with a lower 1-year mortality, but not with HF readmission rate, in patients hospitalized with HFrEF. **© 2018 Elsevier Inc. All rights reserved.** **(Am J Cardiol 2018;121:969–974)**

Heart failure (HF) is associated with high morbidity and mortality.[1] To improve patient outcome, current guidelines[2,3] recommend guideline-directed medical therapy (GDMT), including angiotensin-converting enzyme inhibitors (ACE-I) or angiotensin II receptor blockers (ARB) and β blockers (BB) for HF with reduced ejection fraction (HFrEF), defined as left ventricular ejection fraction (LVEF) ≤ 40%. Previous studies have demonstrated that administration of ACE-I/ARB[4–7] or BB[8–11] reduces mortality and HF hospitalization in patients with HFrEF. However, the current guidelines[2,3] do not provide specific recommendations on appropriate timing of initiation of GDMT in patients hospitalized with HF in the absence of acute myocardial infarction. The aim of the present study was to assess the status of GDMT at the time of discharge in patients hospitalized with acute HF and to evaluate its association with all-cause mortality and HF

[a]Department of Cardiology, Japanese Red Cross Musashino Hospital, Tokyo, Japan; [b]Department of Cardiovascular Medicine, Kobe City Medical Center General Hospital, Kobe, Japan; [c]Department of Cardiovascular Medicine, Heart and Vascular Institute, Cleveland Clinic, Cleveland, Ohio; [d]Division of Cardiology, Washington University in St. Louis, Washington, District of Columbia; [e]Department of Cardiology, Nagoya University Graduate School of Medicine, Nagoya, Japan; [f]Department of Cardiology, St. Marianna University School of Medicine, Kawasaki, Japan; [g]Department of Cardiology, Himeji Cardiovascular Center, Himeji, Japan; [h]Division of Cardiology, Yokohama City University Medical Center, Yokohama, Japan; [i]Department of Cardiovascular Medicine, Fukushima Medical University, Fukushima, Japan; [j]Cardiovascular Division, Faculty of Medicine, University of Tsukuba, Tsukuba, Japan; [k]Department of Cardiology, Kameda Medical Center, Chiba, Japan; [l]Department of Cardiology, University of Groningen, University Medical Center Groningen, Groningen, The Netherlands; and [m]Department of Cardiovascular Medicine, Juntendo University School of Medicine, Tokyo, Japan. Manuscript received September 26, 2017; revised manuscript received and accepted January 2, 2018.

RELIEF-AHF was funded by The Cardiovascular Research Fund, Tokyo, Japan.

Authors' contributions: Drs. Yamaguchi and Matsue were involved in conception and design of the study, data analysis, interpretation of data analysis, manuscript drafting, and manuscript review. Drs. Kagiyama, Miyamoto, Okumura, Kida, Oishi, and Akiyama, in study conception and design and data analysis. Drs. Suzuki, Yamamoto, Yamaguchi, Iwai, and Hijikata, in manuscript critical review. Drs. Masuda, Miyazaki, Hara, Nagata, and Nozato, in final approval of the manuscript.

See page 973 for disclosure information.

*Corresponding author: Tel: +81 422 32 3111; fax: +81 422 32 3430.
E-mail address: tetsu@musashino.jrc.or.jp (T. Yamaguchi).

0002-9149/© 2018 Elsevier Inc. All rights reserved.
https://doi.org/10.1016/j.amjcard.2018.01.005

readmission, using real-world multicenter prospective registry data.

Methods

We performed a post hoc analysis of the Registry Focused on Very Early Presentation and Treatment in Emergency Department of Acute Heart Failure (REALITY-AHF) data, in which 1,682 consecutive patients hospitalized with acute HF were prospectively registered from 20 hospitals in Japan. The main objective for REALITY-AHF was to study the prognostic impact of time to treatment for acute HF performed in the acute phase. Details of the study were published elsewhere.[12] Shortly, all consecutive patients aged ≥ 20 years old with a primary diagnosis of acute HF hospitalized through the emergency department at participating hospitals were enrolled upon the initial hospital admission and were followed-up. Acute HF diagnosis was made based on the Framingham criteria.[13] Estimated glomerular filtration rate (ml/min/1.73 m^2) was calculated using Chronic Kidney Disease Epidemiology Collaboration equation.[14] All participants were notified regarding their participation in the study and it was explained that they were free to opt out of participation at any time. Our study complies with the Declaration of Helsinki and Japanese Ethical Guideline for Medical and Health Research involving Human Subjects. The study protocol was approved by the ethics committee of each participating hospital. Study information including objectives, inclusion and exclusion criteria, and the names of participating hospitals were published in the publicly available University Hospital Information Network (UMIN-CTR, unique identifier: UMIN000014105) before the first patient was enrolled.

Patient information at the time of discharge and prognosis within 1 year of discharge was prospectively collected. Data were collected up to December 2016. End points of this study were all-cause death and HF readmission within 1 year of discharge. After discharge, most patients were followed up in outpatient clinics. We prospectively followed up all patients at least every 3 months after discharge. Additionally, patients were followed up in each outpatient clinic according to their medical needs. For those without follow-up in clinics, prognostic data were obtained from telephone interviews with the medical records department of other medical facilities that took care of the patient or with the family. The causes of death were classified according to RELAX-AHF classification.[15] Also, readmission event was defined as HF readmission only if criteria for HF readmission described in the American College of Cardiology/American Heart Association Key Data Elements and Definitions for Cardiovascular Endpoint Events in Clinical Trials were fulfilled.[16]

Echocardiography was performed when the patients became hemodynamically stable, and we defined HFrEF as LVEF ≤ 40% according to the international guidelines.[11] Patients were divided into 3 groups according to the status of GDMT at discharge, both ACE-I/ARB and BB (Both group), either ACE-I/ARB or BB (Either group), and neither ACE-I/ARB nor BB (None group), respectively. Additionally, we performed 4-group analyses: None, Only ACE-I/ARB at discharge, Only BB at discharge, or Both to investigate whether there is a difference in the effects of ACE-I/ARB and BB.

Data are expressed as mean and standard deviation for normally distributed variables, and as median with interquartile range (IQR) for non-normally distributed data. Categorical data are expressed as numbers and percentages. The correlation between baseline characteristics and each group was compared using the one-way analyses of variance test, Kruskal-Wallis test, or chi-square tests, where appropriate. When necessary, variables were transformed for further analyses. Cumulative incidence curves for all-cause death stratified by GDMT group were calculated using Kaplan-Meier estimates, and were analyzed using the log-rank test. Regarding HF readmission, cumulative incidence curves for HF readmission stratified by GDMT group were constructed reflecting time to death due to non-HF causes and time to HF readmission as competing risks, and compared through the Gray test.[17] For prognostic analysis, the hazard ratio (HR) of being in the Either or Both group versus the None group was adjusted for Meta-Analysis Global Group in Chronic Heart Failure (MAGGIC) risk score in the Cox regression model.[18] The MAGGIC risk score is the score based on 13 independent predictors of long-term mortality including age, gender, systolic blood pressure, LVEF, body mass index, creatinine level, New York Heart Association class, diabetes mellitus, chronic obstructive pulmonary disease, current smoker, diagnosis of HF in the past 18 months, and not taking BB, ACE-I, or ARB. We used the MAGGIC risk score modifying by excluding BB and ACE-I/ARB factors as an adjustment variable in a multivariable prognostic model for 1-year mortality, and discrimination and calibration of this MAGGIC score was evaluated with a receiver operator characteristics curve and Hosmer-Lemeshow test. As for outcome of HF readmission, we selected variables of age, gender, history of HF, chronic obstructive pulmonary disease, diabetes mellitus, body mass index, systolic blood pressure, creatinine level, hemoglobin, serum sodium level, and New York Heart Association III/IV at discharge as adjustment variables in a multivariable model. We selected these variables according to their clinical importance and based on previous studies.[19,20] Statistical analyses were performed using R version 3.1.2 (R Foundation for Statistical Computing, Vienna, Austria; ISBN 3-900051-07-0, http://www.R-project.org). A 2-sided p value < 0.05 was considered statistically significant.

Results

In 1,682 patients, 556 were diagnosed with HFrEF. We excluded 13 patients (2.3%) with in-hospital death and 9 patients (1.7%) with missing data on GDMT at discharge. The remaining 534 patients were enrolled in this study (Figure 1). Baseline characteristics of the Both group (n = 332), Either group (n = 169), and None group (n = 33) are listed in Table 1.

In this study, we found that 83.7% of patients were receiving BB at discharge, whereas 72.5% of patients were receiving ACE-I/ARB at discharge. At 1 year after discharge, 70 patients had died and 142 patients had experienced HF readmission. The 1-year mortality was significantly different in the 3 groups (Both: 7.8% vs Either: 19.6% vs None 34.4%) and there was a significant difference in survival curves on Kaplan-Meier analysis (Log-rank: p < 0.001) (Figure 2). In contrast, 1-year HF readmission rate was similar between groups (Both: 25.3% vs Either: 30.4% vs None 21.9%) and Fine and Gray model analyses showed that there was no statistically significant difference in groups when accounting for death as a competing risk (Gray test: p = 0.48) (Figure 2)

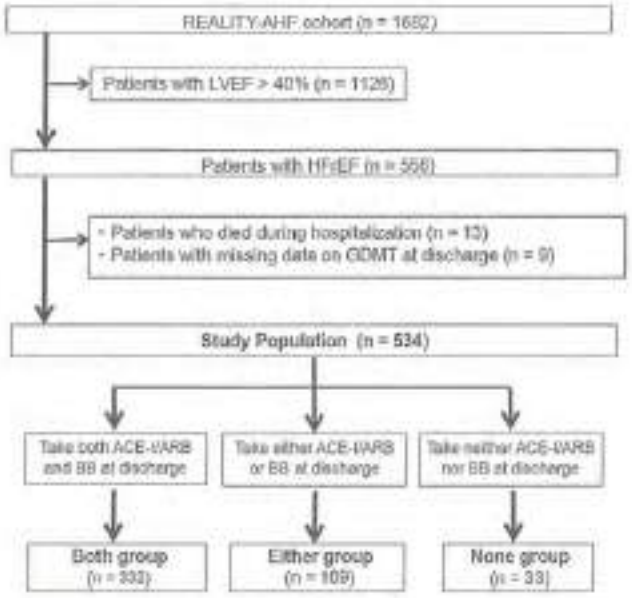

Figure 1. Study flow chart.

Table 2 lists the results of univariate and multivariable Cox proportional hazard model analyses. We checked discrimination and calibration of the modified MAGGIC score. The area under the curve of the modified MAGGIC score in the receiver operator characteristics curve was 0.70 (95% confidence interval [CI]: 0.66 to 0.81), and the Hosmer-Lemeshow test showed no problem with calibration ($p = 0.28$). The MAGGIC score showed a 14% increase in 1-year mortality as a 1-point increase (HR 1.14, 95% CI 1.10 to 1.19, $p < 0.001$). In multivariate analyses, the status of GDMT prescribed before discharge was significantly associated with lower 1-year mortality, even after adjustment for the modified MAGGIC risk score (Table 2). However, prescription of GDMT before discharge was not significantly associated with 1-year HF readmission rates (Table 2). We also evaluated for interaction between age over 80 years old, de novo HF, and GDMT groups on prognosis and found nonsignificant p values for interaction (p value > 0.3 for all).

Thereafter, we compared the prognosis of 4 groups: None, Only ACE-I/ARB at discharge, Only BB at discharge, and Both groups. The results showed that there was a significant difference with respect to 1-year mortality in the 4 groups; the Only ACE-I/ARB group, Only BB group, and Both group showed significantly lower HR compared with the None group even after adjustment for MAGGIC risk score (Supplementary Figure 1 and Supplementary Table 1). However, there was no statistically significant difference in patients in the Only ACE-I/ARB group and Only BB group in the multivariable Cox model ($p = 0.65$). As for 1-year HF readmission, there was no significant difference in the 4 groups in 1-year HF readmission based on Fine and Gray model analyses (Supplementary Figure 1 and Supplementary Table 1).

Discussion

In the present study, we investigated the status of GDMT prescribed at the time of discharge in patients hospitalized with AHF and its association with 1-year all-cause mortality and HF readmission. The main finding of this study was that prescription of GDMT before discharge was significantly associated with a lower 1-year mortality, even after adjustment for covariates. However, there was no significant association between GDMT at discharge and HF readmission when death was accounted for as a competing risk.

International guidelines[2,3] recommend that GDMT should be started as soon as the diagnosis of HFrEF is made. However, there have been no specific recommendations on whether GDMT should be started before discharge for patients hospitalized with acute HF. In the current study, the initiation of either ACE-I/ARB or BB before discharge was significantly associated with lower 1-year mortality than in patients discharged with neither of them. Moreover, patients on both ACE-I/ARB and BB at discharge showed more favorable 1-year survival than patients on either ACE-I/ARB or BB. These results are clinically important because they imply that the hospitalization is an important time to optimize HF medication for patients with HF.

Unlike the results of previous studies[6-11] cited in the guidelines, prescription of ACE-I/ARB or BB was not associated with reduced HF readmission in this study. This difference could be explained by the differences in patients' background, concomitant medical therapy, and study designs. For example, in the Studies of Left Ventricular Dysfunction (SOLVD) Treatment Trial,[7] only 6.4% of all identified patients with HFrEF (LVEF < 35%) were enrolled because of the strict exclusion criteria. The MERIT-HF study[10] investigated patients with chronic, stabilized HF (not acute HF) with LVEF ≤ 40%. The mean age of patients in these studies[6-11] was 10 years younger than that of the current study. Moreover, in most studies, including recent studies describing the favorable impact of BB on 30-day HF readmission rate after hospitalized HF,[21,22] HF hospitalization was analyzed as a composite end point of death or HF hospitalization or was analyzed without considering death as a competing risk. Given that a substantial number of deaths attributable to non–HF-related causes occur in patients with HF, neglecting competing risk would lead to severely biased results. A recent study using a competing risk analysis for evaluating effect of ACE-I/ARB prescription at discharge on HF readmission showed that there was no difference in 1-year readmission rates regardless of the prescription status.[23]

It should be acknowledged that we were not able to evaluate the reason for not receiving GDMT at the time of discharge. In this study, however, systolic blood pressure at discharge was similar in the 3 groups, and was not so low that physicians would be reluctant to start these medications. Heart rate at discharge was significantly higher in the None and Either groups than that in the Both group. Although estimated glomerular filtration rate at discharge was significantly lower in the None group compared with the Both group, it was not so low to prevent prescription of ACE-I/ARB, given the guideline recommendations on serum creatinine levels requiring caution. Serum potassium levels were also similar in the 3 groups. These results may indicate that in the None group, GDMT was not prescribed, not because of low systolic blood pressure, low heart rate, or contraindications according to current guidelines. Previous studies showed that elderly patients

Table 1
Patients' baseline characteristics at discharge

Variable	Both (n = 332)	Either (n = 169)	None (n = 33)	p value
Age (years)	70.4 ± 13.6	77.7 ± 11.2	76.9 ± 12.7	<0.001
Men	257 (77.4%)	110 (65.1%)	22 (66.7%)	0.010
Body Mass Index (Kg/m^2)	22 [19–24]	20 [18–23]	18 [16–21]	<0.001
Systolic Blood Pressure (mmHg)	111 ± 17	110 ± 17	111 ± 22	0.50
Diastolic Blood Pressure (mmHg)	63 ± 12	62 ± 12	65 ± 14	0.34
Heart Rate (bpm)	71 ± 12	74 ± 14	78 ± 19	0.002
Sinus Rhythm	185 (56.2%)	92 (54.4%)	22 (66.7%)	0.75
Atrial Fibrillation	108 (32.8%)	58 (34.3%)	7 (21.2%)	
Others	36 (10.9%)	19 (11.2%)	4 (12.1%)	
New York Heart Association III/IV at Discharge	22 (6.6%)	22 (13.1%)	8 (24.2%)	0.010
Left Ventricular Ejection Fraction (%)	29.7 ± 6.8	29.8 ± 7.2	30.8 ± 5.8	0.65
Heart Failure	160 (48.2%)	92 (54.4%)	15 (45.5%)	0.36
Hypertension	212 (64.0%)	113 (66.9%)	13 (39.4%)	0.010
Diabetes Mellitus	138 (41.6%)	53 (31.4%)	13 (39.4%)	0.084
Coronary Artery Disease	101 (30.4%)	60 (35.5%)	9 (27.3%)	0.43
Chronic Obstructive Pulmonary Disease	23 (6.9%)	18 (10.7%)	4 (12.1%)	0.27
Smoker	164 (49.5%)	68 (40.5%)	14 (42.4%)	0.14
White Blood Cell Count (×10^3/L)	5750 [4500–7108]	5700 [4000–7300]	5600 [3900–6300]	0.57
Haemoglobin (g/dL)	12.7 ± 2.5	11.7 ± 2.1	11.3 ± 2.7	<0.001
Creatinine (mg/dL)	1.4 ± 0.90	1.7 ± 1.4	1.7 ± 1.2	0.011
Blood Urea Nitrogen (mg/dL)	23 [18–34]	31 [22–45]	32 [20–46]	<0.001
Estimated Glomerular Filtration Rate (mL/min/1.73 m^2)	62 [44–84]	50 [29–76]	55 [25–77]	<0.001
Sodium (mEq/L)	139 ± 4	139 ± 4	137 ± 5	0.061
Potassium (mEq/L)	4.5 ± 1.9	4.3 ± 0.5	4.3 ± 0.6	0.33
Brain Natriuretic Peptide (pg/mL)	287 [158–530]	467 [302–731]	358 [203–517]	<0.001
Medication at Discharge				
Loop diuretics	271 (81.6%)	153 (90.5%)	29 (87.9%)	0.028
Angiotensin Converting Enzyme Inhibitor	216 (65.1%)	33 (19.5%)	0 (0.0%)	<0.001
Angiotensin II Receptor Blocker	121 (36.4%)	22 (13.0%)	0 (0.0%)	<0.001
Beta-Blocker	332 (100.0%)	115 (68.0%)	0 (0.0%)	<0.001
Aldosterone Blocker	189 (56.9%)	84 (49.7%)	17 (51.5%)	0.29
Meta-Analysis Global Group in Chronic Heart Failure (MAGGIC) score	23 [19–28]	29 [25–34]	33 [28–37]	<0.001
Length of hospital stay (days)	17 [11–27]	18 [11–27]	16 [10–31]	0.96

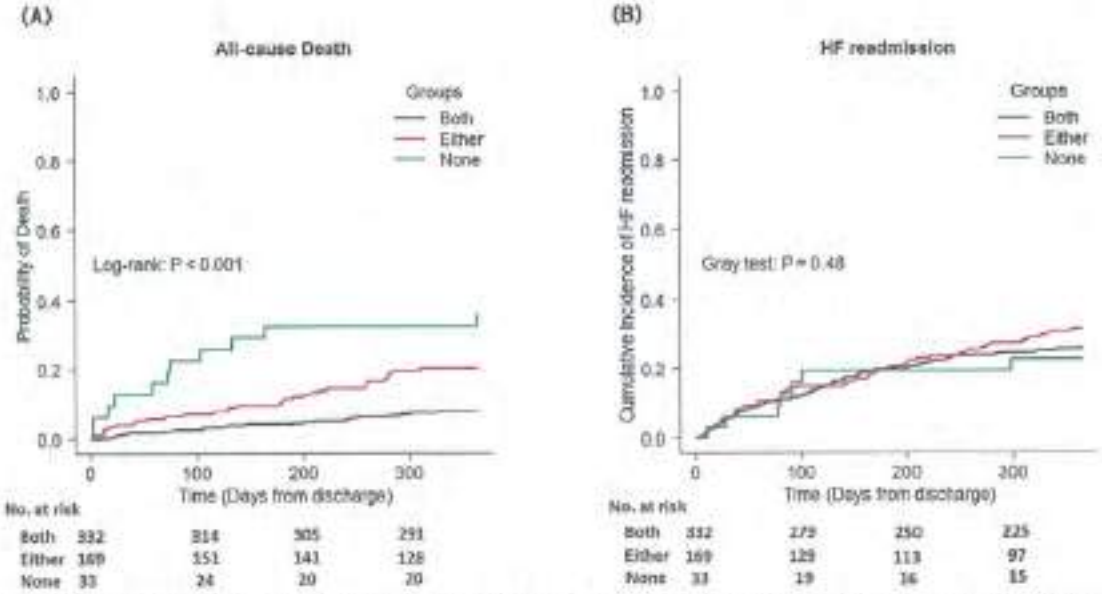

Figure 2. (A) Kaplan-Meier cumulative incidence of all-cause death. (B) Fine and Gray model analyses of heart failure readmission in the 3 groups.

Table 2
Cox proportional hazard models comparing the Both group, the Either group, and the None group in relation to 1-year mortality and 1-year readmission rate for heart failure

Groups	1-year death						1-year heart failure readmission					
	Univariate			Multivariable*			Univariate			Multivariable†		
	HR	95% CI	p value	HR	95% CI	p value	HR	95% CI	p value	HR	95% CI	p value
None		1 (Reference)			1 (Reference)			1 (Reference)			1 (Reference)	
Either	0.48	0.24–0.94	<0.001	0.42	0.21–0.85	0.016	1.39	0.62–3.08	0.42	1.51	0.61–3.73	0.37
Both	0.18	0.09–0.36	<0.001	0.25	0.12–0.51	<0.001	1.14	0.52–2.50	0.74	1.53	0.61–3.84	0.36

* Adjusted for modified Meta-Analysis Global Group in Chronic Heart Failure score.

† Adjusted for age, gender, history of heart failure, chronic obstructive pulmonary disease, diabetes mellitus, body mass index, systolic blood pressure, creatinine, haemoglobin, sodium, and New York Heart Association III/IV at discharge.

HR = hazard ratio; CI = confidence interval.

with HF are less likely to receive GDMT.[24,25] These study results are in line with ours, and older age is one of the most plausible main drivers of low GDMT prescription rate in this study. It should be noted that there is no clear data on effectiveness of GDMT in elderly patients with HF; however, our study also showed that compared with the None group, the Both and Either groups showed significantly favorable survival independent of age. Indeed, our finding was consistent even in very elderly patients over 80 years old.

Our study results should be interpreted in the context of its limitations. This study was a post hoc analysis of an observational study. Although we attempted to adjust for confounders as much as possible by using a risk score that comprised 11 important predictors that were well performing in our dataset, unadjusted confounding factors may affect our results. It should also be acknowledged that although drugs were prescribed at hospital discharge, there were no data collected to substantiate whether prescriptions were filled and medications were taken. The small sample size of our study and small number of events may be another possible limitation. However, we used data from our real-world registry with very few exclusion criteria in which an almost equal number of university and nonuniversity hospitals participated, and this would not mitigate the implication of our study.

In the patients hospitalized with acute HFrEF, GDMT prescription before discharge might lead to a lower 1-year mortality than in those discharged with neither. However, GDMT was not associated with a lower HF readmission rate when accounting for death as a competing risk.

Disclosures

Dr. Yuya Matsue is supported by JSPS (Japan Society for the Promotion of Science) Postdoctoral Fellowships for Research Abroad, and received an honorarium from Otsuka Pharmaceutical Co. Dr. Takahiro Okumura has received grants from Ono, Bayer, Daiichi-Sankyo, and Tanabe-Mitsubishi, outside the submitted work.

Supplementary Data

Supplementary data associated with this article can be found, in the online version, https://doi.org/10.1016/j.amjcard.2018.01.006.

1. Sato N, Kajimoto K, Keida T, Minami M, Minami Y, Yumino D, Asai K, Murai K, Munakata R, Aokage T, Sakata Y, Minino K, Takano T, Investigators TEND. Clinical features and outcome in hospitalized heart failure in Japan (from the ATTEND Registry). *Circ J* 2013;77:944–951.
2. Yancy CW, Jessup M, Bozkurt B, Butler J, Casey DE Jr, Drazner MH, Fonarow GC, Geraci SA, Horwich T, Januzzi JL, Johnson MR, Kasper EK, Levy WC, Masoudi FA, McBride PE, McMurray JJ, Mitchell JE, Peterson PN, Riegel B, Sam F, Stevenson LW, Tang WH, Tsai EJ, Wilkoff BL, American College of Cardiology Foundation, American Heart Association Task Force on Practice Guidelines. 2013 ACCF/AHA guideline for the management of heart failure. *Circulation* 2013;128:e240–e327.
3. Ponikowski P, Voors AA, Anker SD, Bueno H, Cleland JG, Coats AJ, Falk V, González-Juanatey JR, Harjola VP, Jankowska EA, Jessup M, Linde C, Nihoyannopoulos P, Parissis JT, Pieske B, Riley JP, Rosano GM, Ruilope LM, Ruschitzka F, Rutten FH, van der Meer P. Authors/Task Force Members; Document Reviewers. 2016 ESC guidelines for the diagnosis and treatment of acute and chronic heart failure. *Eur Heart J* 2016;37:2129–2200.
4. The CONSENSUS Trial Study Group. Effects of enalapril on mortality in severe congestive heart failure. Results of the Cooperative North Scandinavian Enalapril Survival Study (CONSENSUS). *N Engl J Med* 1987;316:1429–1435.
5. Garg R, Yusuf S. Overview of randomized trials of angiotensin-converting enzyme inhibitors on mortality and morbidity in patients with heart failure. *JAMA* 1995;273:1450–1456.
6. Pitt B, Segal R, Martinez FA, Meinertz G, Cowley AJ, Thomas I, Deedwania PC, Ney DE, Snavely DB, Chang PI. Randomised trial of losartan versus captopril in patients over 65 with heart failure (Evaluation of Losartan in the Elderly Study, ELITE). *Lancet* 1997;349:747–752.
7. SOLVD Investigators. Effect of enalapril on survival in patients with reduced left ventricular ejection fractions and congestive heart failure. *N Engl J Med* 1991;325:293–302.
8. Packer M, Bristow MR, Cohn JN, Colucci WS, Fowler MB, Gilbert EM, Shusterman NH. The effect of carvedilol on morbidity and mortality in patients with chronic heart failure. *N Engl J Med* 1996;334:1349–1355.
9. CIBIS-II Investigators and Committees. The Cardiac Insufficiency Bisoprolol Study II (CIBIS II): a randomized trial. *Lancet* 1999;353:9–13.
10. MERIT-HF Study Group. Effect of metoprolol CR/XL in chronic heart failure: metoprolol CR/XL Randomised Intervention Trial in Congestive Heart Failure (MERIT-HF). *Lancet* 1999;353:2001–2007.
11. Hjalmarson A, Goldstein S, Fagerberg B, Wedel H, Waagstein F, Kjekshus J, Wikstrand J, El Allaf D, Vítovec J, Aldershvile J, Halinen M, Dietz R, Neuhaus KL, Jánosi A, Thorgeirsson G, Dunselman PH, Gullestad L, Kuch J, Herlitz J, Rickenbacher P, Ball S, Gottlieb S, Deedwania P. Effects of controlled-release metoprolol on total mortality, hospitalizations, and well-being in patients with heart failure: the Metoprolol CR/XL Randomized Intervention Trial in congestive heart failure (MERIT-HF). MERIT-HF Study Group. *JAMA* 2000;283:1295–1302.

12. Matsue Y, Damman K, Voors A, Kagiyama N, Yamaguchi T, Okumura T, Kida K, Mizuno A, Oishi S, Inuzuka Y, Akiyama E, Matsukawa R, Kato K, Suzuki S, Naruke T, Yoshioka K, Miyoshi T, Baba Y, Yamamoto M, Murai K, Mizutani K, Yoshida K, Kimi T. Time-to-furosemide treatment and mortality in patients hospitalized with acute heart failure. *J Am Coll Cardiol* 2017;69:3042–3051.
13. Ho KK, Anderson KM, Kannel WB, Grossman W, Levy D. Survival after the onset of congestive heart failure in Framingham Heart Study subjects. *Circulation* 1993;88:107–115.
14. Levey AS, Stevens LA, Schmid CH, Zhang YL, Castro AF 3rd, Feldman HI, Kusek JW, Eggers P, Van Lente F, Greene T, Coresh J; CKD-EPI (Chronic Kidney Disease Epidemiology Collaboration). A new equation to estimate glomerular filtration rate. *Ann Intern Med* 2009;150:604–612.
15. Felker GM, Teerlink JR, Butler J, Hernandez AF, Miller AB, Cotter G, Davison BA, Filippatos G, Greenberg BH, Ponikowski P, Voors AA, Hua TA, Severin TM, Unemori E, Metra M. Effect of serelaxin on mode of death in acute heart failure: results from the RELAX-AHF study. *J Am Coll Cardiol* 2014;64:1591–1598.
16. Hicks KA, Tcheng JE, Bozkurt B, Chaitman BR, Cutlip DE, Farb A, Fonarow GC, Jacobs JP, Jaff MR, Lichtman JH, Limacher MC, Mahaffey KW, Mehran R, Nissen SE, Smith EE, Targum SL. 2014 ACC/AHA key data elements and definitions for cardiovascular endpoint events in clinical trials: a report of the American College of Cardiology/American Heart Association Task Force on Clinical Data Standards (writing committee to develop cardiovascular endpoints data standards). *J Am Coll Cardiol* 2015;66:403–469.
17. Gray RJ. A class of K-sample tests for comparing the cumulative incidence of a competing risk. *Ann Stat* 1988;16:1141–1154.
18. Pocock SJ, Ariti CA, McMurray JJ, Maggioni A, Köber L, Squire IB, Swedberg K, Dobson J, Poppe KK, Whalley GA, Doughty RN, Meta-Analysis Global Group in Chronic Heart Failure. Predicting survival in heart failure: a risk score based on 39 372 patients from 30 studies. *Eur Heart J* 2013;34:1404–1413.
19. O'Connor CM, Miller AB, Blair JE, Konstam MA, Wedge P, Bahit MC, Carson P, Haass M, Hauptman PJ, Metra M, Oren RM, Patten R, Pina I, Roth S, Sackner-Bernstein JD, Traver B, Cook T, Gheorghiade M, Efficacy of Vasopressin Antagonism in heart Failure Outcome Study with Tolvaptan (EVEREST) Investigators. Causes of death and rehospitalization in patients hospitalized with worsening heart failure and reduced left ventricular ejection fraction: results from efficacy of vasopressin antagonism in heart failure outcome study with tolvaptan (EVEREST) program. *Am Heart J* 2010;159:841–849.
20. Saito M, Negishi K, Marwick TH. Meta-analysis of risks for short-term readmission in patients with heart failure. *Am J Cardiol* 2016;117:626–632.
21. Leong KT, Wong LY, Ang KC, Macdonald M, Cao Y, Lee S, Chow WL, Doddamani S, Richards AM. Risk stratification model for 30-day heart failure readmission in a multiethnic South East Asian community. *Am J Cardiol* 2017;119:1428–1432.
22. Hernandez AF, Fonarow GC, Liang L, Heidenreich PA, Yancy C, Peterson ED. The need for multiple measures of hospital quality: results from the Get with the Guidelines-Heart Failure Registry of the American Heart Association. *Circulation* 2011;124:712–719.
23. Gilstrap LG, Fonarow GC, Desai AS, Liang L, Matsouaka R, DeVore AD, Smith EE, Heidenreich P, Hernandez AF, Yancy CW, Bhatt DL. Initiation, Continuation, or Withdrawal of Angiotensin-Converting Enzyme Inhibitors/Angiotensin Receptor Blockers and Outcomes in Patients Hospitalized With Heart Failure With Reduced Ejection Fraction. *J Am Heart Assoc* 2017;6:e004675.
24. Hatsuguchi S, Kinugawa S, Goto D, Tsuchihashi-Makaya M, Yokota T, Yamada S, Yokoshiki H, Takeshita A, Tsutsui H, JCARE-CARD Investigators. Predictors of long-term adverse outcomes in elderly patients over 80 years hospitalized with heart failure. *Circ J* 2011;75:2403–2410.
25. Akita K, Kohno T, Kohsaka S, Shiraishi Y, Nagatomo Y, Izumi Y, Goda A, Mizuno A, Sawano M, Inohara T, Fukuda K, Yoshikawa T; West Tokyo Heart Failure Registry Investigators. Current use of guideline-based medical therapy in elderly patients admitted with acute heart failure with reduced ejection fraction and its impact on event-free survival. *Int J Cardiol* 2017;235:162–168.

VIA MEDICA

ORIGINAL ARTICLE

Cardiology Journal
2018, Vol. 25, No. 2, 179–187
DOI: 10.5603/CJ.a2017.0097
Copyright © 2018 Via Medica
ISSN 1897–5593

Left atrial appendage closure for "primary primary" prevention during percutaneous closure of septal defects in patients with large atria but no atrial fibrillation

Shingo Kuwata[1], Juliane Vierecke[2], Steffen Gloekler[2], Francesco Maisano[1], Bernhard Meier[2], Fabian Nietlispach[1]

[1]University Heart Center, Zurich, Switzerland
[2]University Hospital Bern, Bern, Switzerland
[3]Cardiology, Schwarzwald-Baar Klinikum, Villingen-Schwenningen, Germany

Abstract

Background: *Percutaneous atrial septal defect (ASD) closure is a routine procedure to prevent right ventricular failure, pulmonary hypertension, or paradoxical embolism. The latter is the typical reason for percutaneous patent foramen ovale (PFO) closure. Atrial enlargement represents a risk for developing atrial fibrillation (AF). Percutaneous left atrial appendage (LAA) closure is emerging as a preventive therapy for patients in AF who suffered from a previous stroke or bleeding (secondary prevention) or patients without previous stroke or bleeding (primary prevention). Percutaneous septal closure, particularly that of large ASDs, may inhibit future percutaneous left atrial access when required for LAA closure. Reported herein is the feasibility and safety of concomitant percutaneous closure of the LAA and a septal shunt, mostly large ASDs, in patients without AF, in the sense of "primary primary" preventive LAA closure. The first "primary" relates to "in anticipation of AF" and potentially also for "for prevention of AF". The second "primary" relates to "prevention of stroke or bleeding".*

Methods: *Thirteen consecutive patients, older than 40 years without any clinical or electrocardiographic evidence of AF, underwent percutaneous closure of large ASDs or PFOs in the presence of enlarged atria at the university hospitals of Bern and Zurich between April 2013 and June 2015. They concomitantly received "primary primary" preventive LAA closure after informed consent.*

Results *Mean patient age was 58 ± 9 years (46% male). Procedural success was achieved in all patients and no major adverse events occurred acutely or during the following 2.0 ± 0.8 years. No patient developed AF.*

Conclusions: *Concomitant closure of ASD or PFO in the presence of enlarged atria and LAA for "primary primary" prevention appears feasible and safe but has yet to prove its justification.* (Cardiol J 2018; 25, 2: 179–187)

Key words: atrial fibrillation, atrial septal defect closure, patent foramen ovale closure, left atrial appendage closure

Address for correspondence: Fabian Nietlispach, MD, PhD, University Heart Center, University Hospital of Zurich, Rämistrasse 100, CH-8091 Zürich, Switzerland, tel: +41 44 255 32 98, fax: +41 44 255 44 46, e-mail: Fabian.Nietlispach@usz.ch

Received: 26.06.2017 Accepted: 22.08.2017

Introduction

Atrial septal defect (ASD) is one of the most frequent congenital heart defects [1]. While the only risk of small ASDs is paradoxical embolism, sequelae of larger ASDs comprise pulmonary hypertension, congestive heart failure, and atrial arrhythmia, in particular atrial fibrillation (AF) [2–5]. Percutaneous ASD closure is the treatment of choice for ASDs to prevent such adverse outcome and to improve exertional dyspnea [6–8]. Percutaneous ASD closure is an overall safe procedure but it carries a potential risk for developing AF by device irritation of the septum [9–11]. Although such new onset AF typically occurs only in the first few weeks after device implantation [9, 12], patients undergoing percutaneous closure of large ASDs are temporarily at a double risk for developing AF, 1) due to septal device irritation and 2) due to the preexisting atrial enlargement. Subsequent reduction of atrial diameters after shunt elimination reduces the risk for AF. A net benefit in that respect can be expected but the overall risk for AF of such patients remains elevated. The situation is similar for patients with a patent foramen ovale (PFO) and enlarged atria.

In AF, left atrial appendage (LAA) closure has emerged as an alternative to medical therapy in the form of chronic oral anticoagulation (COA) for stroke or bleeding prevention. While closure of the LAA comes at the price of 2–7% procedural adverse events, it shows a significant reduction in major bleeding events at a similar stroke rate compared to COA [13–16]. After 4 years of follow-up, closure of the LAA even showed significantly improved survival in randomized comparisons [17, 18].

Closure of the LAA so far has been exclusively performed in patients with documented AF, either for primary prevention (patients with AF without previous embolic ischemic event or bleeding) or secondary prevention (patients with AF with a previous embolic ischemic event or bleeding).

Percutaneous closure of septal defects, particularly large ASDs, hinders future percutaneous transseptal left atrial access although it remains possible at least in the case of smaller ASD [19] or PFO devices [20]. Even if such patients never had AF, their risk for developing AF during follow-up is 2-fold higher after ASD closure than that of the general population [21] and also increased after PFO closure in the presence of enlarged atria.

Herein reported is the first experience with concomitant percutaneous closure of LAA at the time of closure of ASDs or PFOs in the presence of enlarged atria in patients without history of AF. They were considered at increased risk for later AF, particularly in the initial phase after septal shunt closure due to septal device irritation while atrial dimensions have not yet shrunk after volume unload. It is referred to in this procedure as "primary primary" preventive LAA closure, i.e., LAA closure for primary prevention (in anticipation of AF or even preventing AF) and for primary prevention of stroke or bleeding, should AF occur.

Methods

Population

This is a retrospective study of consecutive patients (≥ 40 years) undergoing percutaneous closure of a large ASD (≥ 20 mm) or a PFO with large atria (left atrium [LA] ≥ 40 mm, parasternal long axis) and at the same time of the LAA. Patients neither had clinical or electrocardiographic signs of prior AF nor an AF associated embolic ischemic or bleeding event. In the patients with prior ischemic events, AF had been excluded by long-term electrocardiogram (ECG). Patients consented to both procedures (ASD closure and LAA closure) separately and also to data collection. The potential benefits and risks of "primary primary" preventive LAA closure was discussed extensively with the patients. The local institutional review boards approved data collection of clinically indicated investigations during follow-up. The procedures were performed at the university hospitals of Bern and Zurich. Demographic and clinical characteristics, including risk for stroke and major bleeding (CHA_2DS_2-VASc score, HAS-BLED score), procedural data, and outcome data of in-hospital and follow-up periods were captured from medical records and patient contact.

Procedure

All procedures were performed under fluoroscopy guidance without echocardiography [15, 22, 23]. All patients had had transesophageal echocardiography (TEE) during their workups. Computer tomography was not used. Oral antibiotics (2–3 doses) were given before and after the procedure and all patients received 5000 units of intravenous heparin at the beginning of the procedure. All procedures were done using Amplatzer devices (Amplatzer Cardiac Plug (ACP), Amplatzer Amulet Occluder, Amplatzer Septal Occluder (ASO), Amplatzer Cribriform Occluder, or Amplatzer PFO Occluder, Abbott, St. Paul, MN, USA). Figures 1–4 provide examples. LAA closure

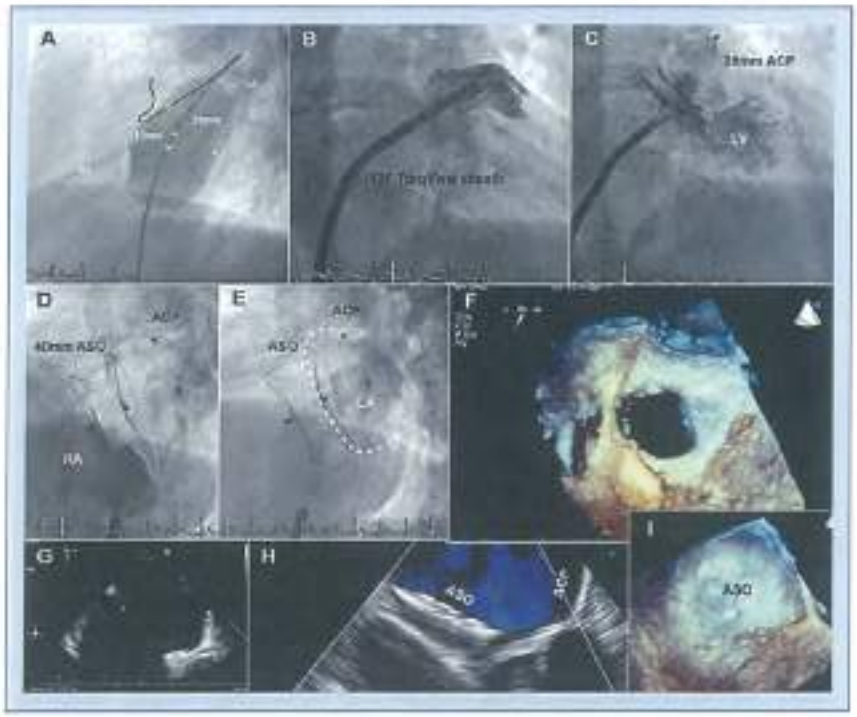

Figure 1. Simultaneous closure of the left atrial appendage (LAA) and an atrial septal defect (ASD) in a 55-year-old male with exertional dyspnea and a newly detected large ASD secundum but no history of atrial fibrillation. **A.** Overinflated 34 mm Amplatzer sizing balloon in ASD, measuring 38 mm at the waist representing the ASD; **B.** Contrast medium injection into the LAA through a 13 French (F) TorqView sheath in a right anterior oblique projection; **C.** Implantation of a 28 mm Amplatzer Cardiac Plug (ACP) through this sheath; **D.** Implantation of a 40 mm Amplatzer Septal Occluder (ASO) through the same sheath in a left anterior oblique projection. The right atrium (RA) is filled with contrast medium; **E.** Same view during the levophase with the left atrium (LA) delineated (dotted line) by contrast medium; **F.** Three-dimensional (3D) transesophageal echocardiography (TEE) before the procedure depicting the ASD; **G.** Two-dimensional (2D) TEE before the procedure indicating an ASD diameter of 28 mm; **H.** 2D TEE at 11-month follow-up depicting the ASD and LAA occluders; **I.** 3D TEE at 11-month follow-up. The ASO occludes the ASD completely without evidence of thrombus.

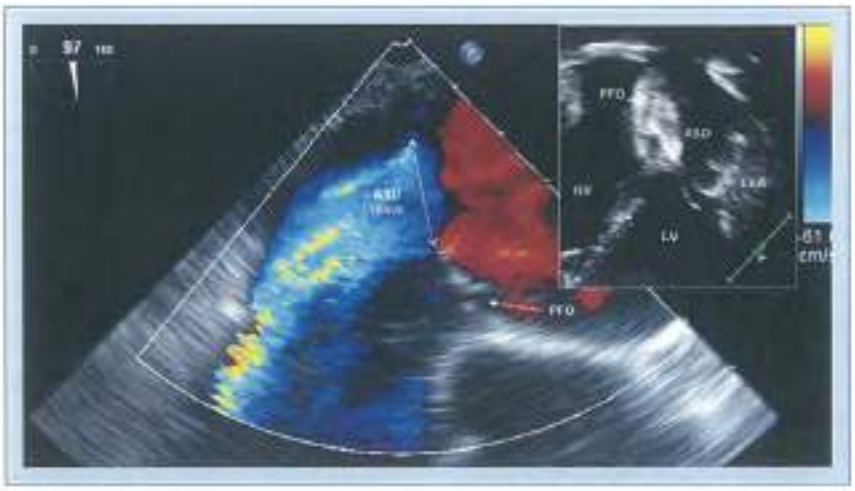

Figure 2. Transesophageal echocardiography of a 53-year-old woman with exertional dyspnea and chest pain and a newly detected secundum atrial septal defect (ASD) as well as a patent foramen ovale (PFO) but no history of atrial fibrillation. The coronary arteries were normal on the incidental angiogram. The insert shows the result after simultaneous device closure of ASD (26 mm Amplatzer Septal Occluder), PFO (30 mm Amplatzer Cribriform Occluder), and left atrial appendage (LAA, 22 mm Amplatzer Amulet) Occluder; LV — left ventricle; RV — right ventricle.

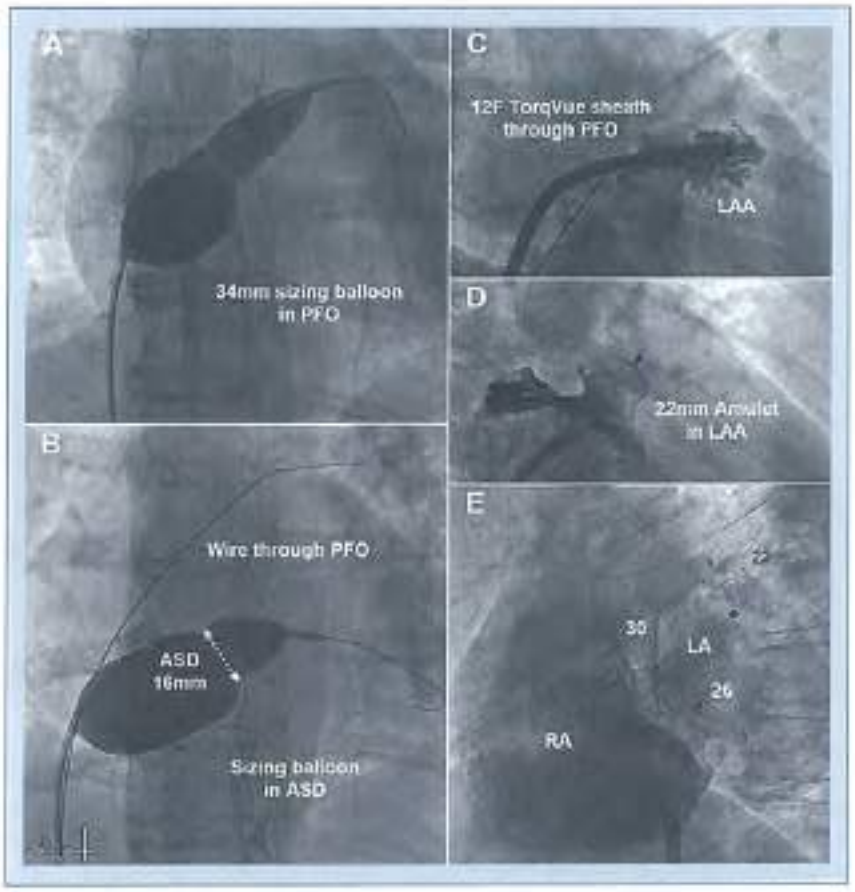

Figure 3. Simultaneous closure of patent foramen ovale (PFO), atrial septal defect (ASD), and left atrial appendage (LAA) in patient of Figure 2; **A.** Sizing balloon in PFO; **B.** Sizing balloon in ASD, wire through PFO; **C.** Contrast medium injection into LAA through 12 French (F) TorqVue sheath in a right anterior oblique projection; **D.** LAA occluded (with 22 mm Amplatzer Amulet Occluder); **E.** Final result: LAA occluded with 22 mm Amplatzer Amulet Occluder (22), then PFO occluded with 30 mm Amplatzer Cribriform Occluder (30), and finally ASD occluded with 26 mm Amplatzer Septal Occluder (26). Left anterior oblique projection; LA — left atrium; RA — right atrium.

was performed before septal closure. After crossing the septal defect from the right femoral vein, a 0.035" Backup wire (Boston Scientific, Natick, MA, USA) was placed in the LA. A 34 mm Amplatzer sizing balloon was placed across ASDs and inflated to aid eyeball sizing of the defect. The balloon was removed. Over the Backup wire, the 14 French (F) 45° × 45° Amplatzer TorqVue delivery sheath was introduced. The LAA was engaged in a right anterior oblique (RAO) view and contrast injections were performed in RAO caudal and cranial views. Sizing was done by eyeballing the outer diameter of the delivery sheath (12 F: 4.5 mm, 13 F: 5.0 mm, and 14 F: 5.5 mm) served as reference. About 20–50% oversizing was the rule [15]. Stability of the device was assessed by a tug test and by angiographic imaging with contrast medium injections in 2 views showing the device in profile without overlap of the 2 device components. After release of the LAA occluder, the TorqVue sheath was left in the LA and the appropriately sized septal occluder (aiming for at least 30% oversizing in ASDs) was attached to the same delivery cable and introduced through the sheath. In case of ASDs, the left atrial disc was fully and the right atrial disc partially deployed in the LA. This technique forces the ASO to self-center in the defect. The pulling of the right disc trough, the defect was observed based on the migrating of the lower device indentation in a left anterior oblique (LAO) projection before the right atrial disc was fully deployed. Correct device position was confirmed by LAO contrast medium injections and a robust wiggle of the device. The sheath was removed and the puncture site was manually compressed by the patient unless a simultaneous arterial puncture mandated compression

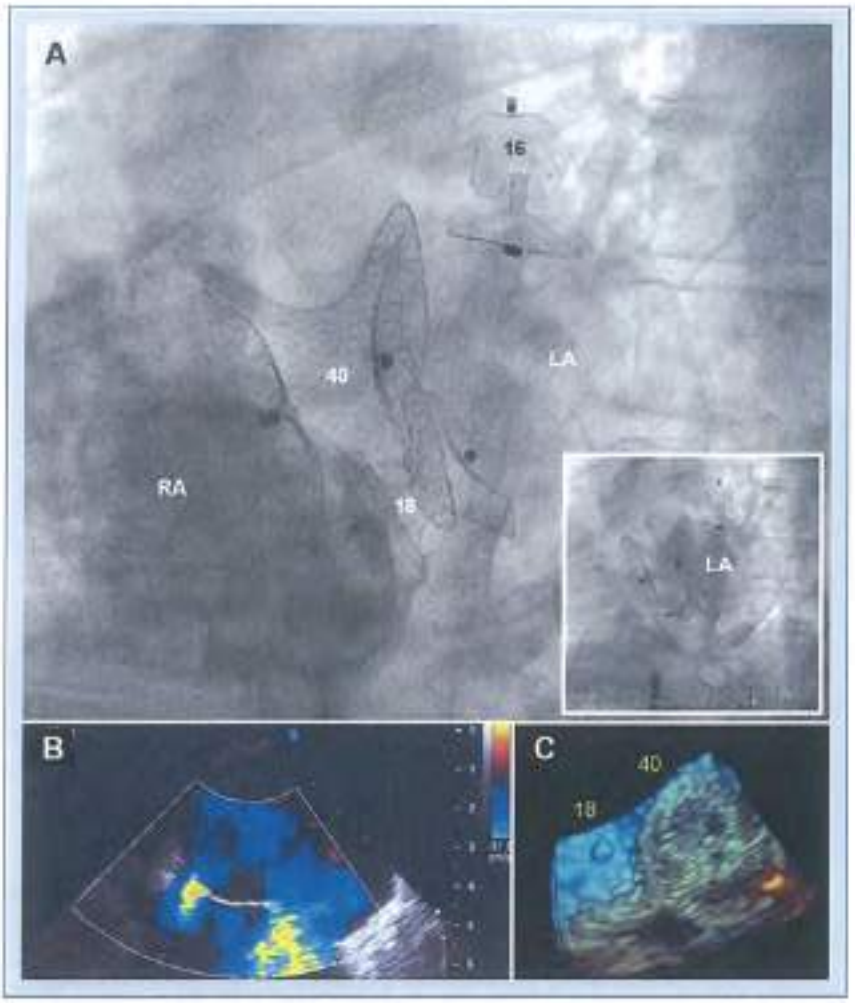

Figure 4. Simultaneous closure of the left atrial appendage (LAA) and a newly detected double atrial septal defect (ASD) in a 64-year-old male with dyspnea but no atrial fibrillation. All devices were implanted through the same 14 French TorqVue sheath; **A.** 40 mm Amplatzer Septal Occluder (ASO, 40), 18 mm ASO (18), and 16 mm Amplatzer Amulet Occluder (16) depicted in a in a left anterior oblique projection. The right atrium (RA) and in the insert the left atrium (LA) are filled with contrast medium; **B.** Double ASD in a transesophageal echocardiography (TEE) before the intervention; **C.** Double ASD in a three-dimensional TEE 4 months after the intervention with the two ASOs in place.

by a medical person. Before discharge the same or the following day, transthoracic echocardiography was performed to assure the correct position of the devices and to exclude pericardial effusion. There were no recommendations for physical restrictions of any sort.

Post interventional antithrombotic regimen comprised clopidogrel 75 mg for 1–3 months and acetylsalicylic acid 100 mg for 5–6 months. Control TEE was recommended after 3–6 months to assess for device thrombi and residual shunts or leaks.

Outcome

The composite endpoint was defined according to Valve Academic Research Consortium (VARC)-2 criteria [24]. The primary safety endpoint was defined as death related to closure of the LAA, procedure-related ischemic stroke, hemorrhagic stroke, cardiac tamponade, need for urgent surgery (e.g., due to embolization of the device, repair of procedure-related injury, or bleeding) and major or life-threatening bleeding (according to VARC-2 criteria). The primary efficacy endpoint was defined as stroke (non-disabling, disabling, ischemic, or hemorrhagic), systemic embolization, or cardiovascular or unexplained death. New-onset of AF was looked for clinically and by (24-h) ECG. Clinical follow-up data were obtained reviewing medical records and by contacting patients.

Table 1. Baseline characteristics (n = 13).

Characteristics	
Age [years]	58.2 ± 9.1
Body mass index [kg/m²]	27.0 ± 4.4
Women	7 (54%)
$CHADS_2$ score	1.2 ± 1.3
CHA_2DS_2-VASc score	1.92 ± 1.7
HAS-BLED score	0.85 ± 1.1
Atrial rhythm (including history)	
Atrial fibrillation (paroxysmal or permanent)	0 (0%)
Atrial flutter	0 (0%)
Clinical features	
Prior ischemic stroke	3 (23%)
Coronary artery disease	0 (0%)
Valvular heart disease	0 (0%)
Renal function (mean eGFR, in mL/min/1.73 m²)	97 ± 24
Anti-thrombotic therapy prior to Iaac	
Acetylsalicylic acid	3 (23%)
Platelet inibitors other than acetylsalicylic acid	0 (0%)
Chronic oral anticoagulation	0 (0%)
Echocardiographic data	
Systolic left ventricular ejection fraction [%]	65 ± 2
Left atrial diameter (PLAX echo, mm)	42 ± 5

Values are number (%) or mean ± standard deviation; eGFR — estimated glomerular filtration rate; PLAX — parasternal long axis

Table 2. Intervention (n = 13).

Procedural characteristics	
Flouroscopy time [min]	16 ± 8
Amplatzer Cardiac Plug	6 (20 ± 3, 16–24 mm)
Amplatzer Amulet Occluder	7 (21 ± 4, 16–25 mm)
Amplatzer Septal Occluder	10 (34 ± 6, 24–40 mm)
Amplatzer Cribriform Occluder	1 (30 mm)
Amplatzer PFO Occluder	2 (25 mm)
Implantation attempts	1.0 ± 0.0
Concomittant procedures	
Coronary angiography	12 (92%)
Perirocedural success and adverse events	
Procedural success	13 (100%)
Combined safety endpoint*	0 (0%)

*Composite of death, stroke, clinically relevant pericardial effusion, VARC-2 life-threatening or major bleeding, VARC-2 major access vessel complication, device embolization, VARC-2 severe kidney injury, or bailout surgery. Values are number (%) or mean ± standard deviation; PFO — patent foramen ovale; VARC — Valve Academic Research Consortium

Statistical analysis

Data are expressed as mean and standard deviation for continuous variables and as number and percentage for categorical variables. Analysis was performed using a standard statistical software program (SPSS, version 23; IBM, Armonk, NY, USA).

Results

Baseline characteristics

Thirteen patients were included between April 2013 and June 2015. Patients were 58 ± 9 years old (54% women). Baseline characteristics are described in Table 1. No patient had any history of AF. Three patients had a previous history of ischemic cerebrovascular events. The total procedural fluoroscopy time was 16 ± 8 min (Table 2).

Device success

In all patients ASD or PFO and LAA closures were successful. In 1 patient, 2 ASDs and in 1 patient, a PFO in addition to an ASD were present and closed with 2 separate devices (Figs. 2, 3). No periprocedural complications occurred (Table 2).

Clinical follow-up

Length of hospital stay was 1 night in 9 patients and the remaining 4 patients were discharged the same day. TEE follow-up was available after 6.7 ± 2.0 months in 10 patients. No device-related complications occurred (Table 3). One patient needed a re-intervention because of 2 residual ASD shunts at follow up. Re-intervention was successfully performed under fluoroscopy only using a 25 mm and a 18 mm PFO Occluder at 6 months after initial procedure. At clinical follow-up of 2.0 ± 0.8 years, no adverse events had occurred, no patient had reached a primary safety or efficacy endpoint, and at latest contact 91% of patients were on no anticoagulant or antiplatelet medication and 9% still acetylsalicylic acid (Table 4). The patients were asked for clinical symptoms of AF and all postinterventional ECGs were screened for AF. No patient had developed AF.

Discussion

Atrial fibrillation is the most common sustained cardiac arrhythmia [25] and is associated with substantial mortality and morbidity, particularly due to stroke [26]. ASD closure is advocated for prevention of stroke (paradoxical or secondary to AF) or heart failure due to volume overload. PFO closure is used for prevention of paradoxical

Table 3. Postprocedural data and follow-up transesophageal echocardiography (TEE).

Post procedure in-hospital (n = 13)	
Hospital stay (days)	0.8 ± 0.4
Same day discharge	4 (31%)
Pericardial effusion	0 (0%)
Antithrombotic therapy (n = 13)	
Acetylsalicylic acid	12 (92%)
Platelet inibitors other than acetylsalicylic acid	12 (92%)
Dual antiplatelet therapy	12 (92%)
Vitamin K antagonists	0 (0%)
Non vitamin K dependant oral anticoagulants	0 (0%)
TEE (n = 10)	
Duration from intervention (months)	6.7 ± 2.0
All devices in correct position	10 (100%)
Late pericardial effusion	0 (0%)
Late device embolization	0 (0%)
Device thrombus (any)	0 (0%)
Procedural success at TEE follow-up	8 (100%)
Shunt or leak > 5 mm	1 (10%)
Shunt or leak < 5 mm	2 (20%)

Values are number (%) or mean ± standard deviation.

Table 4. Clinical follow-up (n = 13).

Long-term clinical follow-up	13 (100%)
Duration from procedure (years)	2.0 ± 0.8
Antithrombotic therapy	
Acetylsalicylic acid	1 (9%)
Other platelet inibitors	0 (0%)
Dual antiplatelet therapy	0 (0%)
Vitamin K antagonists	0 (0%)
Non vitamin K dependant oral anticoagulants	0 (0%)
Clinical outcome	
All-cause death	0 (0%)
All-cause stroke	0 (0%)
All-cause transient ischemic attack	0 (0%)
Myocardial infarction	0 (0%)
Systemic embolism	0 (0%)
Venous thrombosis/ /pulmonary embolism	0 (0%)
Fatal, lifethreatening, or major bleeding	0 (0%)
Hospitalization	0 (0%)
Primary safety endpoint	0 (0%)
Primary efficacy endpoint	0 (0%)

Values are number (%) or mean ± standard deviation.

stroke. LAA closure is indicated for prevention of stroke or bleeding in patients with AF [13–18].

The present study reports the feasibility and safety of "primary primary" preventive LAA closure during percutaneous ASD or PFO closure in patients with enlarged atria but no AF. It proved technically successful and safe but efficacy of our approach cannot be determined. No patient developed AF and therefore the potential of preventing embolic ischemia or bleeding because of the obviated need for oral anticoagulation remains unknown.

A large nationwide study of Nyboe et al. [21] included 1168 patients with ASD who were followed-up over a long-term period. The risk of developing AF was up to 10-fold in comparison to the general population. In case of conservative management, the stroke risk was 2.6-fold. In case of ASD closure, the stroke risk was reduced to 2-fold. This can be due to both, the elimination of paradoxical embolism and the reduction of atrial sizes. Yet, the risk of AF-associated stroke remains elelvated [21].

Atrial fibrillation with the need for COA is expected to occur with a certain frequency in patients at some point in time after septal defect closure while they were still in sinus rhythm [9, 27]. Age > 40 years is a well-known risk factor for AF after ASD closure [28]. Moreover, ASD closure devices can trigger new-onset AF in the early phase. In the later phase they may reduce the risk of AF as the atria shrink after elimination of the shunt [10, 11]. Large devices in the interatrial septum may render percutaneous LAA closure intricate or downright impossible.

Chronic oral anticoagulation has been proven to effectively prevent thromboembolic strokes but there is a risk of serious bleeding which deters many patients from taking this therapy [29]. Therefore, alternative treatment options for stroke prevention in patients with AF with increased stroke risk are needed. Closure of the LAA has emerged as promising [13, 30].

Left atrial appendage closure in the sense of "primary primary" prevention has the potential to avoid future strokes in case new-onset AF goes undetected on top of the potential to avoid major bleeding in case a patient requires COA for AF during follow-up. However as is inherent to every preventive intervention, the risk and cost of the combined and partially preventive intervention may become unjustified, in case AF never develops during follow-up. This concern is alleviated by the safety of such an approach which is apparent from these data.

Limitations of the study

The study has several limitations. It is a retrospective study and not a randomized trial and therefore selection bias is evident. The sample size is small. Furthermore, none of these patients developed AF during the relatively short observation period. More patients and longer follow-up are required to derive a clinically important message.

Conclusions

This study demonstrates feasibility of "primary primary" preventive LAA closure during percutaneous closure of large ASDs or PFOs with atrial enlargement in patients without AF. In this series no adverse safety events occurred. The idea is to prepare such patients for the likely event of later AF. ASD closure alone with a large septal device renders it difficult if not impossible to later perform a transseptal puncture for LAA closure.

Conflict of interest: S. Gloekler — grant from the Swiss Heart Foundation; F. Maisano — consultant for Abbott, Edwards, and Medtronic, and cofounder and shareholder of 4Tech Cardio and receiver of royalties from Edwards; B. Meier — speaker fees of Abbott; F. Nietlispach — consultant for Abbott, Edwards, and Medtronic, and shareholder of Edwards.

References

1. Hoffman J, Kaplan S. The incidence of congenital heart disease. J Am Coll of Cardiol. 2002; 39(12): 1890–1900, doi: 10.1016/s0735-1097(02)01886-7, indexed in Pubmed: 12084585.
2. Gatzoulis MA, Freeman MA, Siu SC, et al. Atrial arrhythmia after surgical closure of atrial septal defects in adults. N Engl J Med. 1999; 340: 839–846, doi: 10.1056/nejm199903183401103, indexed in Pubmed: 10080846.
3. Konstantinides S, Geibel A, Olschewski M, et al. A comparison of surgical and medical therapy for atrial septal defect in adults. N Engl J Med. 1995; 333(8): 469–473, doi: 10.1056/nejm199508243330801, indexed in Pubmed: 7623878.
4. Gatzoulis M, Redington A, Somerville J, et al. Should atrial septal defects in adults be closed? Ann Thorac Surg. 1996; 61(2): 657–659, doi:10.1016/0003-4975(95)01043-2, indexed in Pubmed: 8572783.
5. Akula V, Durgaprasad R, Velan V, et al. Right ventricle before and after atrial septal defect device closure. Echocardiography. 2016; 33(9): 1381–1388, doi: 10.1111/echo.13250, indexed in Pubmed: 27109837.
6. Du ZD, Hijazi Z, Kleinman C, et al. Comparison between transcatheter and surgical closure of secundum atrial septal defect in children and adults: results of a multicenter nonrandomized trial. J Am Coll Cardiol. 2002; 39(11): 1836–1844, doi: 10.1016/s0735-1097(02)01862-4, indexed in Pubmed:12039580.
7. Fischer G, Stieh J, Uebing A, et al. Experience with transcatheter closure of secundum atrial septal defects using the Amplatzer septal occluder: a single centre study in 230 consecutive patients. Heart. 2003; 89(2): 199–204, doi: 10.1136/heart.89.2.199, indexed in Pubmed: 12527678.
8. Omeish A, Hijazi Z. Transcatheter closure of atrial septal defects in children & adults using the Amplatzer Septal Occluder. J Interv Cardiol. 2001; 14(1): 37–44, doi: 10.1111/j.1540-8183.2001.tb00709.x, indexed in Pubmed: 12053325.
9. Spies C, Khandelwal A, Timmermanns I, et al. Incidence of atrial fibrillation following transcatheter closure of atrial septal defects in adults. Am J Cardiol. 2008; 102(7): 902–906, doi: 10.1016/j.amjcard.2008.05.045, indexed in Pubmed: 18805119.
10. Wagdi P. Incidence and predictors of atrial fibrillation following transcatheter closure of interatrial septal communications using contemporary devices. Clin Res Cardiol. 2010; 99(8): 507–510, doi: 10.1007/s00392-010-0149-3, indexed in Pubmed: 20352436.
11. Schneeberger Y, Schneider A, Conradi L, et al. Minimally invasive endoscopic surgery versus catheter-based device occlusion for atrial septal defects in adults: reconsideration of the standard of care. Interact Cardiovasc Thorac Surg. 2016; ivw366, doi: 10.1093/icvts/ivw366, indexed in Pubmed:28040751.
12. Bunyw A, Schwerzmann M, Wallmann D, et al. Atrial fibrillation following device closure of patent foramen ovale. Cardiology. 2008; 111(1): 47–50, doi:10.1159/000113427, indexed in Pubmed: 18239392.
13. Holmes D, Reddy V, Turi Z, et al. Percutaneous closure of the left atrial appendage versus warfarin therapy for prevention of stroke in patients with atrial fibrillation: a randomised non-inferiority trial. Lancet. 2009; 374(9689): 534–542, doi: 10.1016/s0140-6736(09)61343-x, indexed in Pubmed: 19683039.
14. Tzikas A, Shakir S, Gafoor S, et al. Left atrial appendage occlusion for stroke prevention in atrial fibrillation: multicentre experience with the AMPLATZER Cardiac Plug. EuroIntervention. 2016; 11(10): 1170–1179, doi: 10.4244/eijy15m01_06, indexed in Pubmed: 25604089.
15. Nietlispach F, Gloekler S, Krause R, et al. Amplatzer left atrial appendage occlusion: Single center 10-year experience. Catheter Cardiovasc Interv. 2013; 82(2): 283–289, doi: 10.1002/ccd.24872, indexed in Pubmed: 23412815.
16. Ghanti RA, Obeid S, Maisano F, et al. The evolving role of left atrial appendage occlusion: a high-volume single-centre experience. Cardiovasc Med. 2016; 19(11): 288–296, doi: 10.4414/cvm.2016.00437.
17. Holmes D, Doshi S, Kar S, et al. Left atrial appendage closure as an alternative to warfarin for stroke prevention in atrial fibrillation. J Am Coll Cardiol. 2015; 65(24): 2614–2623, doi: 10.1016/j.jacc.2015.04.025, indexed in Pubmed: 26088300.
18. Reddy V, Sievert H, Halperin J, et al. Percutaneous left atrial appendage closure vs warfarin for atrial fibrillation. JAMA. 2014; 312(19): 1988–1996, doi:10.1001/jama.2014.15192, indexed in Pubmed: 25399274.
19. Wagdi P, Alkadhi H. Can computer tomography help predict feasibility of transseptal puncture after percutaneous closure of an interatrial septal communication? J Interv Card Electrophysiol. 2012; 34(2): 167–172, doi: 10.1007/s10840-011-9625-6, indexed in Pubmed: 22314668.
20. Zeher-Shahrak R, Meier B. Transseptal puncture for catheter ablation of atrial fibrillation after device closure of patent foramen ovale. Catheter Cardiovasc Interv. 2008; 71(4): 551–553, doi: 10.1002/ccd.21363, indexed in Pubmed: 18307237.
21. Nyboe C, Olsen MS, Nielsen-Kudsk JE, et al. Atrial fibrillation and stroke in adult patients with atrial septal defect and the long-

term effect of closure. Heart. 2015; 101(9): 706–711, doi: 10.1136/heartjnl-2014-306552, indexed in Pubmed: 25691512.

22. Praz F, Wahl A, Schmutz M, et al. Safety, feasibility, and long-term results of percutaneous closure of atrial septal defects using the Amplatzer septal occluder without periprocedural echocardiography. J Invasive Cardiol. 2015; 27(3): 157–162, indexed in Pubmed: 25740969.
23. Meier B, Blaauw Y, Khattab AA, et al. EHRA/EAPCI expert consensus statement on catheter-based left atrial appendage occlusion. Europace. 2014; 16(10): 1397–1416, doi: 10.1093/europace/euu174, indexed in Pubmed: 25160595.
24. Kappetein AP, Head SJ, Généreux P, et al. Updated standardized endpoint definitions for transcatheter aortic valve implantation: the Valve Academic Research Consortium-2 consensus document. J Am Coll Cardiol. 2012; 60: 1438–1454, doi: 10.4244/EIJV8I7A121, indexed in Pubmed: 23022744.
25. Go A, Hylek E, Phillips K, et al. Prevalence of diagnosed atrial fibrillation in adults: national implications for rhythm management and stroke prevention: the AnTicoagulation and Risk Factors in Atrial Fibrillation (ATRIA) Study. JAMA. 2001; 285(18): 2370–2375, doi: 10.1001/jama.285.18.2370, indexed in Pubmed: 11343485.
26. De Backer O, Arnous S, Inlemann N, et al. Percutaneous left atrial appendage occlusion for stroke prevention in atrial fibrillation: an update. Open Heart. 2014; 1(1): e000020, doi: 10.1136/openhrt-2013-000020, indexed in Pubmed: 25332785.
27. Rigatelli G, Pedon L, Zecchel R, et al. Long-term outcomes and complications of intracardiac echocardiography-assisted patent foramen ovale closure in 1,000 consecutive patients. J Interv Cardiol. 2016; 29(5): 530–538, doi: 10.1111/joic.12325, indexed in Pubmed: 27500752.
28. Giardini A, Donti A, Sciarra F, et al. Long-term incidence of atrial fibrillation and flutter after transcatheter atrial septal defect closure in adults. Int J Cardiol. 2009; 134(1): 47–51, doi: 10.1016/j.ijcard.2008.02.003, indexed in Pubmed: 18396341.
29. Landmesser U, Holmes DR. Left atrial appendage closure: a percutaneous transcatheter approach for stroke prevention in atrial fibrillation. Eur Heart J. 2012; 33(6): 696–704, indexed in Pubmed: 22041550.
30. Fountain R, Holmes D, Chandrasekaran K, et al. The PROTECT AF (WATCHMAN Left atrial appendage system for embolic PROTECTion in patients with atrial fibrillation) trial. Am Heart J. 2006; 151(5): 956–961, doi: 10.1016/j.ahj.2006.02.005, indexed in Pubmed: 16644311.

ESC HEART FAILURE
ESC Heart Failure 2018; 5: 297–305
Published online 21 October 2017 in Wiley Online Library (wileyonlinelibrary.com) DOI: 10.1002/ehf2.12228

ORIGINAL RESEARCH ARTICLE

Chronic obstructive pulmonary disease and β-blocker treatment in Asian patients with heart failure

Yoshiaki Kubota[1*], Wan Ting Tay[2], Kuniya Asai[1], Koji Murai[1], Ikutaro Nakajima[3], Nobuhisa Hagiwara[4], Takanori Ikeda[5], Takashi Kurita[6], Tiew-Hwa Katherine Teng[2,7], Inder Anand[8], Carolyn S.P. Lam[2,9,10], Wataru Shimizu[1] and on behalf of the ASIA-HF Study Investigators[†]

[1]Department of Cardiovascular Medicine, Nippon Medical School, Bunkyō, Tokyo, Japan; [2]National Heart Centre Singapore, Singapore, Singapore; [3]Division of Cardiology, Department of Internal Medicine, National Cerebral and Cardiovascular Center Hospital, Suita, Osaka, Japan; [4]Department of Cardiology, School of Medicine, Tokyo Women's Medical University, Shinjuku, Tokyo, Japan; [5]Division of Cardiovascular Medicine, Department of Internal Medicine, Toho University Ohashi Hospital, Meguro, Tokyo, Japan; [6]Division of Cardiology, Department of Internal Medicine, Aiseikai University School of Medicine, Higashinari-ku, Osaka, Japan; [7]School of Population Health, University of Western Australia, Perth, WA, Australia; [8]VA Medical Center, University of Minnesota, Minneapolis, MN, USA; [9]Cardiovascular Research Institute, National University Heart Centre, Singapore, Singapore; [10]Duke-National University of Singapore, Singapore, Singapore

Abstract

Aims Chronic obstructive pulmonary disease (COPD) and heart failure (HF) are increasingly frequent in Asia and commonly coexist in patients. However, the prevalence of COPD among Asian patients with HF and its impact on HF treatment are unclear.

Methods and results We compared clinical characteristics and treatment approaches between patients with or without a history of COPD, before and after 1:2 propensity matching (for age, sex, geographical region, income level, and ethnic group). In 5232 prospectively recruited patients with HF and reduced ejection fraction (HFrEF, <40%) from 11 Asian regions (Northeast Asia: South Korea, Japan, Taiwan, Hong Kong, and China; South Asia: India; Southeast Asia: Thailand, Malaysia, Philippines, Indonesia, and Singapore). Among the 5232 patients with HFrEF, a history of COPD was present in 8.3% ($n = 434$), with significant variation in geography (11.0% in Northeast Asia vs. 4.7% in South Asia), regional income level (9.7% in high income vs. 5.8% in low income), and ethnicity (17.0% in Filipinos vs. 5.2% in Indians) (all $P < 0.05$). Use of mineralocorticoid receptor antagonists and diuretics was similar between groups, while usage of all β-blockers was lower in the COPD group than in the non-COPD group in the overall (66.3% vs. 79.9%) and propensity-matched cohorts (66.3% vs. 81.7%) (all $P < 0.05$). A striking exception was the Japanese cohort in which β-blocker use was high in COPD and non-COPD patients (95.2% vs. 91.2%).

Conclusions The prevalence of COPD in HFrEF varied across Asia and was related to underuse of β-blockers, except in Japan.

Keywords Chronic obstructive pulmonary disease; Heart failure; β-Blocker

Received: 6 June 2017; Revised: 21 August 2017; Accepted: 1 September 2017
*Correspondence to: Wataru Shimizu, Department of Cardiovascular Medicine, Nippon Medical School, 1-1-5, Sendagi, Bunkyō, Tokyo 113-8622, Japan.
Tel: +81- 3- 3822- 2131; Fax: +81- 3- 3814- 6850; Email: wshimizu@nms.ac.jp
†A list of investigators is provided in the Acknowledgements.

Introduction

Chronic obstructive pulmonary disease (COPD) is present in approximately one-third of patients with heart failure (HF) and reduced ejection fraction (HFrEF).[1] Because of concern regarding respiratory deterioration, COPD is an important cause of underuse and underdosing of β-blockers.[1–4] The mechanistic relationship between COPD and HFrEF is complex, multifactorial, and not fully understood. Hyperinflation and greater changes in intrathoracic pressure during respiration might enhance ventricular pre-load and afterload, resulting in left ventricular (LV) dysfunction and HF.[5] Despite increasing evidence that β-blockers are safe and beneficial in patients with COPD,[6,7] they are often underused in this group worldwide.[8] The reason is most likely related to concerns that β-blockers may induce bronchospasm in COPD patients. The National Institute for Health and Care Excellence and European Society of Cardiology guidelines state that COPD is not a contraindication for the use of β-blockers, and mild deterioration in pulmonary

© 2017 The Authors. ESC Heart Failure published by John Wiley & Sons Ltd on behalf of the European Society of Cardiology.
This is an open access article under the terms of the Creative Commons Attribution-NonCommercial License, which permits use, distribution and reproduction in any medium, provided the original work is properly cited and is not used for commercial purposes.

function and symptoms should not indicate the necessity for prompt discontinuation.[9,10] Nonetheless, low-dose initiation and gradual uptitration are recommended in the guidelines.[9,10] In Asia, ageing populations and large increases in cardiovascular risk factors have contributed to a high burden of HF.[11] Patients with HFrEF from Asia may differ in clinical characteristics from patients elsewhere.[12,13] The Asian Sudden Cardiac Death in Heart Failure (ASIAN-HF) registry was established to bridge the knowledge gap regarding the burden associated with chronic HF in Asian patients. In the present study, we report data on co-morbidities of Asian patients with HFrEF enrolled from 1 October 2012 to 31 December 2015, with special reference to COPD and its treatment.[14,15]

Methods

Study design

The ASIAN-HF registry was a prospective observational registry of symptomatic patients with HFrEF from 44 centres in 11 Asian regions (China, Hong Kong, India, Indonesia, Japan, South Korea, Malaysia, Philippines, Singapore, Taiwan, and Thailand) that enrolled patients between 2010 and 2015. Detailed methods have been previously published.[14] HFrEF was defined as patients >18 years of age with symptomatic HF (at least one episode of decompensated HF in the previous 6 months that resulted in a hospital admission or was treated in an outpatient clinic) and LV systolic dysfunction (ejection fraction ≤40% on baseline echocardiography).[14] Ethics approval was obtained from the local institutional review board of each participating centre, and the study complied with the Declaration of Helsinki.

For this study, patients from the ASIAN-HF registry with both HF and COPD were identified, and health data including vital signs and other diagnosed illnesses were analysed. Heart rate was measured at rest using electrocardiography. Hypertension was defined as the presence of a clinical diagnosis of hypertension (blood pressure ≥ 140/90 mmHg) or treatment with anti-hypertensive medications. Diabetes was defined as the presence of a clinical diagnosis of diabetes (fasting plasma glucose ≥ 7 mmol/L or random plasma glucose ≥ 11.1 mmol/L or HbA1C ≥ 6.5%) or treatment with anti-diabetic therapy. COPD was diagnosed in accordance with the Global Initiative for Chronic Obstructive Lung Disease criteria.[16] The usage of β-blocker was defined at first visit.

Statistical analyses

The primary analysis compared the clinical characteristics of HF patients with or without COPD in the overall cohort. Secondary analyses were conducted in a 1:2 propensity-matched cohort and the Japanese cohort separately. Propensity matching for age, sex, geographical region, income level, and ethnic group was performed to produce the matched cohort (with a ratio of COPD to non-COPD patients of 1:2). Patients were categorized on the basis of geographic region of recruitment, income level, and ethnic group, with groups defined as follows:

(1) Geographic region (by United Nations; Northeast Asia: South Korea, Japan, Taiwan, Hong Kong, and China; South Asia: India; Southeast Asia: Thailand, Malaysia, Philippines, Indonesia, Singapore)
(2) Income level (by World Health Organization; high: Japan, Singapore, Hong Kong, Taiwan, South Korea; middle: China, Malaysia, Thailand; low: Philippines, Indonesia, India)
(3) Ethnicity (Chinese, Indian, Malay, Japanese, Korean, Thai, and Indigenous Southeast Asians)

Continuous variables were expressed as mean ± standard deviation, while categorical variables were expressed as number (percentage). To compare baseline characteristics in HF patients with or without COPD, χ^2 tests and independent *t*-tests were used for categorical and continuous variables, respectively. Multivariable logistic regression to assess those factors associated with the diagnosis of COPD, including variables with *P*-values <0.10 in univariable analysis as well as clinical and demographic variables from a prior knowledge. A *P*-value ≤0.05 was considered statistically significant. Stata software version 14 (StataCorp., TX) was used for statistical analyses.

Results

Baseline characteristics of the overall population

In the overall HFrEF cohort, 434 (8.3%) patients had a diagnosis of COPD, whereas 4798 (91.7%) did not. *Table 1* shows the clinical characteristics of the groups categorized by the presence or absence of COPD. There was signification variation in the prevalence of COPD by geographical region and income level (all $P < 0.05$). The highest prevalence of COPD was found in Northeast Asians (11.0%), who were significantly older than patients in other areas (mean age: 62 ± 14 years vs. 58 ± 12 years in other regions), while COPD prevalence was lowest in South Asians (4.7%) (*Table S1*). COPD was also more prevalent in high- and middle-income regions than in low-income regions (*Table S1*). The prevalence of COPD varied widely among ethnicities, ranging from 17.0% in Filipinos to 5.2% in Indians (*Table S2*). Overall, the COPD group was significantly older, had a greater severity of HF as assessed with the New York Heart Association

Table 1 Baseline characteristics of heart failure patients with and without chronic obstructive pulmonary disease

	Overall cohort			1:2 matched† cohort			Japanese cohort		
	With COPD	Without COPD	*P*-value	With COPD	Without COPD	*P*-value	With COPD	Without COPD	*P*-value
N	434 (8.3%)	4798 (91.7%)		410	820		63 (11.8%)	471 (88.2%)	
Demographics									
Age (years)	63.9 ± 13.7	59.3 ± 12.9	<0.001	63.9 ± 13.7	64.2 ± 12.7	0.666	68.5 ± 12.6	64.6 ± 13.7	0.033
Male	347 (80.0)	3742 (78.0)	0.343	330 (80.5)	666 (81.2)	0.758	50 (79.4)	363 (77.1)	0.683
Geographical region			<0.001			0.556			
Northeast Asia	181 (41.7)	1471 (30.7)		175 (42.7)	360 (43.9)				
South Asia	68 (15.7)	1368 (28.5)		60 (14.6)	134 (16.3)				
Southeast Asia	185 (42.6)	1959 (40.8)		175 (42.7)	326 (39.8)				
Income level			<0.001			0.547			
High income	218 (50.2)	2020 (42.1)		214 (52.2)	444 (54.2)				
Middle income	111 (25.6)	1077 (22.5)		103 (25.1)	183 (22.3)				
Low income	105 (24.2)	1701 (35.4)		93 (22.7)	193 (23.5)				
Presenting characteristics									
NYHA class, VII/III/IV (%)	11/45/33/11	13/53/28/6	<0.001	12/44/33/11	13/52/30/5	0.001	8/67/23/2	6/73/18/3	0.621
Shortness of breath on exertion	349 (80.4)	3567 (74.4)	0.005	328 (80.0)	608 (74.2)	0.023	45 (71.4)	343 (72.8)	0.815
Shortness of breath at rest	104 (24.0)	860 (17.9)	0.002	95 (23.2)	151 (18.4)	0.049	9 (14.3)	59 (12.5)	0.694
Reduction in exercise tolerance	318 (73.3)	3346 (69.8)	0.128	301 (73.4)	553 (67.5)	0.034	38 (60.3)	311 (66.0)	0.371
Nocturnal cough	115 (26.5)	841 (17.5)	<0.001	109 (26.6)	136 (16.6)	<0.001	5 (7.9)	22 (4.7)	0.267
Orthopnoea	137 (31.6)	1046 (21.8)	<0.001	132 (32.2)	174 (21.2)	<0.001	3 (4.8)	28 (5.9)	0.706
Paroxysmal nocturnal dyspnoea	116 (26.7)	878 (18.3)	<0.001	112 (27.3)	156 (19.0)	0.001	3 (4.8)	21 (4.5)	0.913
Angina	67 (15.5)	530 (11.1)	0.006	62 (15.2)	93 (11.3)	0.057	2 (3.2)	6 (1.3)	0.243
Systolic blood pressure (mmHg)	119.4 ± 19.0	118.3 ± 20.3	0.317	119.3 ± 18.8	119.8 ± 19.9	0.688	114.2 ± 18.3	112.7 ± 19.7	0.571
Diastolic blood pressure (mmHg)	71.4 ± 12.1	72.5 ± 12.6	0.087	71.2 ± 12.1	71.7 ± 12.3	0.545	66.7 ± 11.3	66.1 ± 12.9	0.708
Heart rate (b.p.m.)	80.5 ± 15.0	79.6 ± 16.3	0.275	80.2 ± 14.9	77.9 ± 15.5	0.015	72.5 ± 10.7	72.6 ± 14.5	0.937
Body mass index (kg/m^2)	24.8 ± 6.2	24.9 ± 5.0	0.709	24.8 ± 6.0	24.5 ± 4.9	0.403	23.4 ± 3.9	22.8 ± 4.2	0.255
eGFR (mL/min/1.73 m^2)	63.8 ± 19.8	65.1 ± 28.6	0.403	64.1 ± 30.4	63.1 ± 27.9	0.610	67.1 ± 32.9	65.0 ± 28.8	0.603
LVEF (%)	27.8 ± 7.2	27.3 ± 7.0	0.207	27.8 ± 7.1	28.2 ± 6.6	0.305	28.6 ± 7.5	27.9 ± 7.6	0.542
Medical history									
Aetiology HF, ischaemic	213 (49.1)	2245 (46.8)	0.389	201 (49.0)	418 (51.0)	0.734	16 (25.4)	129 (27.4)	0.373
Ventricular tachycardia/fibrillation	44 (10.1)	362 (7.5)	0.053	40 (9.8)	70 (8.6)	0.484	18 (28.6)	115 (24.4)	0.474
Coronary artery disease	214 (49.3)	2411 (50.3)	0.698	200 (48.8)	457 (55.8)	0.020	23 (36.5)	172 (36.5)	0.999
Atrial fibrillation/flutter	83 (19.1)	851 (17.7)	0.472	79 (19.3)	188 (23.0)	0.139	22 (34.9)	183 (38.9)	0.547
Hypertension	236 (54.4)	2475 (51.6)	0.274	227 (55.4)	467 (57.0)	0.581	31 (49.2)	226 (48.0)	0.855
Diabetes	167 (38.5)	1948 (40.6)	0.383	158 (38.5)	374 (45.7)	0.017	13 (20.6)	156 (33.1)	0.045
Stroke	31 (7.1)	305 (6.4)	0.522	30 (7.3)	58 (7.1)	0.880	7 (11.1)	51 (10.8)	0.946
Peripheral arterial vascular disease	26 (6.0)	152 (3.2)	0.002	25 (6.1)	55 (5.4)	0.606	3 (4.8)	17 (3.6)	0.651
Renal artery stenosis	10 (2.3)	36 (0.8)	0.001	10 (2.4)	8 (0.1)	0.044	2 (3.2)	3 (0.6)	0.050
Smoking, current or ex	261 (60.1)	2093 (43.7)	< 0.001	254 (62.0)	388 (47.4)	< 0.001	38 (60.3)	252 (53.6)	0.316
Alcohol, current or ex	153 (35.3)	1359 (28.4)	0.001	156 (38.1)	234 (28.6)	0.001	31 (49.2)	200 (42.6)	0.317
12-lead ECG									
ECG rhythm, SR/AF/others or unknown (%)	64/11/25	70/12/18	< 0.001	64/12/24	66/15/19	0.057	32/11/57	41/15/44	0.172
ECG heart rate (b.p.m.)	83.3 ± 18.9	81.3 ± 19.0	0.048	83.3 ± 19.1	80.1 ± 18.8	0.007	74.7 ± 18.1	73.6 ± 15.9	0.616
Left bundle branch block	63 (15.0)	628 (13.8)	0.732	58 (14.6)	97 (12.5)	0.516	9 (14.8)	38 (8.1)	0.086
Right bundle branch block	39 (10.5)	350 (8.7)	0.247	35 (10.0)	60 (8.9)	0.566	6 (9.7)	41 (8.0)	0.811
QRS duration (ms)	117.6 ± 32.2	115.1 ± 32.4	0.138	117.6 ± 32.0	116.8 ± 32.4	0.684	136.9 ± 37.4	128.3 ± 34.3	0.069

(Continued)

ESC Heart Failure 2018; 5: 297–309
DOI: 10.1002/ehf2.12288

https://onlinelibrary.wiley.com/doi/10.1002/ehf2.12288, Wiley Online Library on [07/07/2023]

Table 1 (continued)

	Overall cohort			1:2 matched* cohort			Japanese cohort		
	With COPD	Without COPD	*P*-value	With COPD	Without COPD	*P*-value	With COPD	Without COPD	*P*-value
Echocardiography									
LV end diastolic volume (mL)	182.9 ± 78.0	179.7 ± 67.2	0.460	182.1 ± 77.4	178.8 ± 66.1	0.538	202.0 ± 88.2	203.1 ± 72.7	0.916
LV end systolic volume (mL)	133.5 ± 67.1	130.4 ± 57.4	0.392	133.0 ± 67.0	126.4 ± 55.7	0.140	147.7 ± 80.2	141.6 ± 66.0	0.545
LA volume (mL)	75.1 ± 35.8	70.8 ± 42.3	0.135	75.4 ± 36.0	78.8 ± 54.9	0.411	97.0 ± 42.9	96.4 ± 66.4	0.954
ICD and medications									
ICD/pacemaker/CRT	87 (20.1)	661 (13.8)	<0.001	83 (20.2)	154 (18.8)	0.546	42 (66.7)	242 (51.4)	0.022
ICD/CRT	66 (15.2)	502 (10.6)	0.003	62 (15.1)	119 (14.5)	0.782	33 (52.4)	220 (46.7)	0.397
Pacemaker	21 (4.8)	154 (3.2)	0.071	21 (5.1)	35 (4.3)	0.501	9 (14.3)	22 (4.7)	0.002
ACE-I or ARB	292 (70.9)	3503 (75.8)	0.028	292 (71.2)	605 (73.8)	0.341	48 (77.4)	386 (83.0)	0.278
β-blockers	273 (66.3)	3692 (79.9)	< 0.001	272 (66.3)	670 (81.7)	< 0.001	59 (95.2)	423 (91.2)	0.287
Diuretics	330 (80.1)	3772 (81.6)	0.454	328 (80.0)	658 (80.2)	0.919	40 (64.5)	340 (73.1)	0.156
Aldosterone antagonists	240 (58.3)	2751 (59.5)	0.619	239 (58.3)	479 (58.4)	0.967	34 (54.8)	270 (58.1)	0.829

ACE-I, angiotensin-converting enzyme inhibitor; AF, atrial fibrillation; ARB, angiotensin II receptor blocker; COPD, chronic obstructive pulmonary disease; CRT, cardiac resynchronization therapy; ECG, electrocardiogram; eGFR, estimated glomerular filtration rate; HF, heart failure; ICD, implantable cardioverter defibrillator; LVEF, left ventricular ejection fraction; NYHA, New York Heart Association; SR, sinus rhythm. Mean ± standard deviation.
*Propensity matched for age, sex, geographical region, income level, and ethnic group.

(NYHA) classification, and had higher prevalence of renal artery stenosis and smoking than the non-COPD group (all $P < 0.05$). The most common presenting symptoms in the COPD group were breathlessness on exertion, orthopnoea, and paroxysmal nocturnal dyspnoea. No significant differences were found between the COPD and non-COPD groups for body mass index, ischaemic aetiology, or the prevalence of hypertension, diabetes mellitus, and atrial fibrillation/flutter or echo parameters, including LV ejection fraction, LV end diastolic volume, LV end systolic volume, and left atrium volume. The average heart rate on electrocardiogram of the COPD group (83 ± 19 b.p.m.) was significantly higher than that of the non-COPD group (81 ± 19 b.p.m.; $P = 0.048$). HF medications were significantly underused in the COPD group. Angiotensin-converting enzyme inhibitor (ACE-I) or angiotensin receptor blockers (ARB) were used in 70.9% and 75.8% of patients in the COPD and non-COPD groups, respectively ($P = 0.028$). Similarly, β-blockers were used in 66.3% and 79.9% of patients in the COPD and non-COPD groups, respectively ($P < 0.001$). Conversely, the use of mineralocorticoid receptor antagonists and diuretics was approximately the same between the two groups. HF device therapy (defibrillator, pacemaker, or cardiac resynchronization therapy) was more frequently employed in the COPD group than in the non-COPD group (20.1% vs. 13.8%, respectively, $P < 0.001$), which might be attributed to a more severe HF condition assessed by the NYHA classification in the COPD group.

Independent correlates of chronic obstructive pulmonary disease

Table 2 shows the multivariable associations with COPD after adjustment for the variables listed. Compared with low-income regions, the middle- and high-income regions had 1.81 [95% confidence interval (CI), 1.33–2.47] and 1.82 (95% CI, 1.30–2.54) times higher odds of having COPD, respectively (*Table 2*). COPD was significantly associated with older age, high NYHA classification, renal artery stenosis, smoking, and a high average heart rate on electrocardiography. The prevalence of COPD might lead to the underuse of β-blockers in the overall cohort, but not in the Japanese cohort.

Propensity-matched and Japanese cohorts

Because of significant differences in the baseline characteristics, HFrEF patients were 1:2 matched into a COPD group (n = 410) and non-COPD group (n = 820) using propensity matching for age, sex, geographical region, income level, and ethnic group as a secondary analysis (*Table 1*). As noted

ESC Heart Failure 2019; 6: 297–306
DOI: 10.1002/ehf2.12228

Table 2 Multivariable associations with chronic obstructive pulmonary disease

	Whole cohort		Japanese cohort	
Characteristics	Adjusted odds ratio (95% confidence intervals)	*P*-value	Adjusted odds ratio (95% confidence intervals)	*P*-value
Age (years)	1.031 (1.021, 1.040)	<0.001	1.025 (1.003, 1.047)	0.026
Income level				
High income	1.82 (1.30, 2.54)	<0.001		
Middle income	1.81 (1.33, 2.47)	<0.001		
Low income	Reference			
NYHA				
Class III/IV	1.37 (1.08, 1.74)	0.010		
Class III	Reference			
Diabetes	0.79 (0.62, 1.00)	0.054	0.50 (0.26, 0.96)	0.038
Renal artery stenosis	3.49 (1.60, 7.66)	0.002	6.12 (0.86, 43.44)	0.070
Smoking, current or ex	2.27 (1.75, 2.95)	<0.001	1.29 (0.74, 2.26)	0.370
ECG heart rate (b.p.m.)	1.007 (1.001, 1.013)	0.016		
ACE-I or ARB	0.93 (0.72, 1.20)	0.594		
β-Blockers	0.47 (0.37, 0.61)	<0.001	2.12 (0.63, 7.14)	0.228

ACE-I, angiotensin-converting enzyme inhibitor; ARB, angiotensin II receptor blocker; COPD, chronic obstructive pulmonary disease; ECG, electrocardiogram; NYHA, New York Heart Association.
Adjusted for female, nocturnal cough, ventricular tachycardia/fibrillation, coronary artery disease, and variables listed.

In the overall cohort, the COPD group had a higher average heart rate and lower usage of β-blockers than the non-COPD group (83 ± 19 b.p.m. vs. 80 ± 19 b.p.m., $P = 0.007$; and 66.3% vs. 81.7%, $P < 0.001$).

Among the Japanese cohort, usage of β-blockers was remarkably high (COPD group: 95.2% vs. non-COPD group: 91.2%, $P = 0.287$) and the average heart rate (COPD group: 75 ± 18 b.p.m. vs. non-COPD group: 74 ± 16 b.p.m., $P = 0.616$) was lower than other cohort data (*Table 1*). No significant differences were found between the COPD and non-COPD groups with respect to other parameters in this cohort.

Proportion of cardioselective and non-cardioselective β-blocker treatment

Table 3 shows usage of cardioselective and non-cardioselective β-blocker treatment for the COPD and non-COPD groups. In all cohorts, the non-COPD group had a higher usage of carvedilol, a non-cardioselective β-blocker, than the COPD group. Whereas in the overall cohort and 1:2 matched cohort, cardioselective β-blockers were used equally in the COPD and non-COPD groups, in the Japanese cohort, the usage of cardioselective β-blockers was twofold higher in the COPD group as compared with the non-COPD group.

Discussion

This analysis of the multi-national ASIAN-HF registry shows that a history of COPD was present in only 8.3% of the overall cohort, with significant variation in geography, regional income level, and ethnicity. The COPD group was significantly older, had higher NYHA classification scores, had higher average heart rate, and had a greater rate of HF device therapy than the non-COPD group in the overall and matched cohorts. Furthermore, β-blockers were significantly underused

Table 3 Proportion of cardioselective and non-cardioselective β-blocker treatment for heart failure patients with and without chronic obstructive pulmonary disease

	Overall cohort			1:2 matched[a] cohort			Japanese cohort		
	With COPD	Without COPD	*P*-value	With COPD	Without COPD	*P*-value	With COPD	Without COPD	*P*-value
N	434 (8.3%)	4798 (91.7%)		410	820		63 (11.8%)	471 (88.2%)	
Any β-blockers	273 (66.3)	3692 (79.9)	<0.001	272 (66.3)	669 (81.7)	<0.001	59 (95.2)	423 (91.2)	0.287
HF guidelines β-blockers[b]	236 (57.3)	3200 (69.2)	<0.001	235 (57.3)	569 (69.5)	<0.001	59 (95.2)	419 (90.1)	0.198
Any cardioselective β-blockers[c]	153 (37.1)	1696 (36.7)	0.849	152 (37.1)	311 (38.0)	0.759	30 (48.4)	108 (23.2)	<0.001
HF guidelines cardioselective β-blockers[d]	149 (36.2)	1651 (35.7)	0.854	148 (36.1)	305 (37.2)	0.695	30 (48.4)	108 (23.2)	<0.001
Carvedilol only	89 (21.6)	1605 (34.7)	<0.001	89 (21.7)	277 (33.8)	<0.001	30 (48.4)	319 (68.6)	0.002

[a]Propensity matched for age, sex, geographical region, income level, and ethnic group.
[b]Bisoprolol, metoprolol, nebivolol, and carvedilol.
[c]Bisoprolol, metoprolol, nebivolol, and atenolol.
[d]Bisoprolol, metoprolol, and nebivolol.

Provided by National Taiwan University - Taiwan, 2.32.38.68 - 4/16/2020 2:21:11 PM
TEMPO/OVID IB 2020/04/16 14:10 Page 11 of 20

in the COPD group when compared with the non-COPD group in both the overall and propensity-matched cohorts. COPD was significantly correlated with the lower usage of β-blockers in the overall and matched cohorts, but not in the Japanese cohort. The presence of COPD influenced the use of cardioselective β-blockers in the Japanese cohort, with usage being twofold higher in COPD patients than in non-COPD patients.

The high prevalence of smoking, coupled with an ageing population, threatens to further increase the burden of COPD. In addition, a previous report in Japan suggested that COPD is underdiagnosed.[17] The ASIAN-HF registry found a lower rate of COPD diagnosis in the HF cohort than in other studies such as the Acute Decompensated Heart Failure National Registry[18] (27%), Get with the Guidelines registry[19] (26.7%), United States Veterans[20] (26.6%), and Olmsted County[21] (30%). Whether COPD is being underdiagnosed in these countries is unclear, but the findings suggest the need for enhanced screening efforts for COPD in Asians with HF.

COPD is a systemic inflammatory disease characterized by airflow limitation that is not fully reversible.[22] Up to one-third of all deaths in patients with COPD can be attributed to cardiovascular disease, and for every 10% decrease in the forced expiratory volume in 1 s, the risk of cardiovascular mortality reportedly increases by 28%.[23] COPD is a key cause of β-blocker underuse, largely owing to concerns regarding the precipitation of respiratory deterioration in HF patients.[4] Indeed, results from this contemporary study of the ASIAN-HF registry showed significant underuse of β-blockers in HF patients with COPD compared with those without COPD. Furthermore, the mean heart rate of COPD patients was significantly higher than that of non-COPD patients. It is also possible that the relatively high heart rate observed in the COPD group was reflective of increased HF severity, as indicated by more severe NYHA classification relative to the non-COPD group. Importantly, heart rate is directly related to overall risk of death, risk of cardiovascular death, and hospitalization risk in patients with HF,[24] while heart rate reduction is associated with improved outcomes.[25]

In the past, β-blockers were thought to be potentially harmful in patients with COPD. However, several recent studies have demonstrated significant benefits of the use of β-blockers in COPD patients.[26,27] One of these studies showed that β-blockers might reduce the risk of mortality and respiratory exacerbation in patients with COPD.[28] Similarly, a systematic review and meta-analysis of nine retrospective cohort studies reported a reduction in COPD-related mortality of 31% with β-blocker use.[29] Another study clearly demonstrated the safety of β-blockers during COPD exacerbation.[8] Furthermore, the use of β-blockers when started either at the time of hospital admission for myocardial infarction or before myocardial infarction has been shown to be associated with improved survival after myocardial infarction in patients with COPD.[30] We have also reported on the effectiveness of β-blockers in Japanese HF patients with COPD.[31]

The ACE-I or ARB was significantly underused in the COPD group in the overall cohort. The use of ACE-I or ARB might be influenced by the discretion of the treating physicians, because the renal artery stenosis was significantly higher in the COPD group than in the non-COPD group.

Evaluating prospective multi-national data from the ASIAN-HF registry has shown the important influence of both ethnicity and regional income level on the characteristics of HF patients with COPD. Our data suggest that the very high use of β-blockers in Japanese HFrEF patients with COPD shows that these agents may be used safely in Asian patients with these two conditions. Further studies should evaluate long-term data from the ASIAN-HF registry for patients with COPD.

Study limitations

Several limitations associated with the present study warrant consideration. These baseline registry data were cross-sectional in nature, and we were unable to exclude the possibility of selection bias. Bias is inevitable in the selection of sites in each region, and the willingness of patients to participate in a prospective protocol influences enrolment. In previous objective data on the prevalence of COPD in Asia, the COPD prevalence rates were 6.3%.[31] According to the Global Burden of Disease Study, not only each region but also multi-ethnicity in the same country influenced the prevalence rates of COPD.[32] Our results may therefore still underestimate the true burden of HF with COPD in Asia. Furthermore, the use of β-blockers was left to the discretion of the treating physicians in each nation, and the β-blocker doses and COPD grades were unclear. The usage rate of β-blockers in each region might be influenced by different understanding of the safety and usefulness of the β-blockers. This study cohort comprised only HFrEF patients in the ASIAN-HF registry. Owing to the specificity of this population, β-blockers should be considered as standard therapy. However, in patients with severe COPD, low-dose initiation and gradual uptitration are recommended. In the overall cohort, the number of patients with COPD was relatively small. We therefore confirmed the results observed in the overall cohort using the propensity-matched cohort as a way of minimizing confounding factors. It is noted that the prevalence of COPD in the Japanese cohort was low.

Conclusions

In the Asian HF registry, COPD prevalence showed significant variation according to geography, regional income level, and

Wiley Online Library for rules of use; OA articles are governed by the applicable Creative Commons License

https://onlinelibrary.wiley.com/reader/content/10.1002/ehf2.12228/format/pdf/OEBP 2020/04/27

ethnicity. The prevalence of COPD was strongly related to the underuse of β-blockers, in patients with both HF and COPD.

Acknowledgements

Current site investigators of the ASIAN-HF study are as follows.

China

Ruijin Hospital, Shanghai Jiao Tong University School of Medicine: Lijun Wu. Fuwai Hospital: Shu Zhang. Jiangsu Province People's Hospital: Xinli Li. Zhongshan Hospital Fudan University: Yangang Su.

Hong Kong

The Chinese University of Hong Kong: Cheuk Man Yu.

India

Sir Ganga Ram Hospital: Jitendra Sawhney. West Fort Hi-Tech Hospital Ltd: Mohanan Padinhare Purayil. Dayanand Medical College and Hospital: Gurpreet Singh Wander. Medanta The Medicity: Vijay Chopra. Care Institute of Medical Sciences: Ajay Naik. Care Hospital: Narasimhan Calambur.

Indonesia

Rumah Sakit Khusus Jantung Binawaluya: Muhammad Munawar. Rumah Sakit Hasan Sadikin: Pintoko Tedjokusumo. Harapan Kita National Cardiovascular Center: Bambang Budi Siswanto. Siloam Karawaci Hospital: Antonia A. Lukito.

South Korea

Korea University Anam Hospital: Jaemin Shim. Korea University Guro Hospital: Jin Oh Na. Severance Hospital, Yonsei University Health System: Boyoung Joung. Chonnam National University Hospital: Hyung-Wook Park. Hyewon Medical Foundation Sejong General Hospital: Suk Keun Hong. Korea University Ansan Hospital: Seong Hwan Kim.

Malaysia

Institut Jantung Negara: Razali Omar. University Malaya Medical Centre: Imran Zainal Abidin. Hospital Queen Elizabeth II: Houng Bang Liew. Sarawak General Hospital: Tiong Kiam Ong.

Philippines

Philippine Heart Center: Eleanor Lopez. Makati Medical Center: Raul Lapitan. Manila Doctors Hospital: Eugenio Reyes.

Singapore

National Heart Centre: Kheng Leng David Sim. Tan Tock Seng Hospital: Poh Shwan Daniel Yeo. Changi General Hospital-Parent: Kui Toh Gerard Leong. Singapore General Hospital-Parent: Fazlur Rehman Jaufeerally. Khoo Teck Puat Hospital: Hean Yee Ong.

Taiwan

Mackay Memorial Hospital: Chung-Lieh Hung. National Taiwan University Hospital: Juey-Jen Hwang. Taipei Veterans General Hospital: Wen-Chung Yu. China Medical University Hospital: Hsin-Yueh Liang.

Thailand

Phramongkutklao Hospital: Waraporn Tiyanon. Maharaj Nakorn Chiang Mai Hospital: Wanwarang Wongcharoen. Ramathibodi Hospital: Tachapong Ngarmukos.

Japan

National Cerebral and Cardiovascular Center: Takashi Noda, Mitsuru Wada, Kohei Ishibashi. Tokyo Women's Medical University: Atsushi Suzuki, Takeshi Suzuki. Kinki University: Ryoichiro Yasuoka. Toho University Omori Medical Center: Sinji Hisatake, Shunsuke Kuchi, Takayuki Kabuki. Nippon Medical School Hospital: Yuki Izumi.

Conflict of interest

None declared.

Funding

The ASIAN-HF study is funded by the Investigator-Sponsored Research Program of Boston Scientific, via a competitive grant for investigator-initiated studies awarded to the Cardiovascular Research Institute, Singapore. Recruitment of

Downloaded from https://onlinelibrary.wiley.com/doi/10.1002/ehf2.12228 by Nanyang Technological Univ, Wiley Online Library on [22/04/2020]. See the Terms and Conditions (https://onlinelibrary.wiley.com/terms-and-conditions) on Wiley Online Library for rules of use; OA articles are governed by the applicable Creative Commons License

https://onlinelibrary.wiley.com/reader/content/10.1002/ehf2.12228/format/pdf/OERP 2020/04/27

patients in Singapore is partially supported by the Singapore Heart Failure Outcomes and Phenotypes study, funded by the National Medical Research Council of Singapore [centre grant principal investigator (PI): A.M.R, theme PI: C.S.P.L]. C.S.P.L is supported by a Clinician Scientist Award from the National Medical Research Council.

Supporting information

Additional Supporting Information may be found online in the supporting information tab for this article.

Table S1. Prevalence of COPD and usage of β-blockers by region and stage of economic development.
Table S2. Prevalence of COPD and usage of β-blockers by ethnicity.

References

1. Lelonek M, Cleland JG, Leizen MJ, Pollock F, Komajda M, Swedberg K. International variations in the treatment and co-morbidity of left ventricular systolic dysfunction: data from the EuroHeart Failure Survey. *Eur J Heart Fail* 2007; 9: 392–399.
2. Sin DD, McAlister FA. The effects of beta-blockers on morbidity and mortality in a population-based cohort of 11,942 elderly patients with heart failure. *Am J Med* 2002; 113: 650–656.
3. Komajda M, Pollock F, Swedberg K, Cleland J, Aguilar JC, Cohen-Solal A, Dietz R, Gavazzi A, Van Gilst WH, Hobbs R, Korewicki J, Madeira HC, Moiseyev VS, Preda I, Widimsky J, Freemantle N, Eastaugh J, Mason J. The EuroHeart Failure Survey programme—a survey on the quality of care among patients with heart failure in Europe. Part 2: treatment. *Eur Heart J* 2003; 24: 464–474.
4. Hawkins NM, Petrie MC, Jhund PS, Chalmers GW, Dunn FG, McMurray JJ. Heart failure and chronic obstructive pulmonary disease: diagnostic pitfalls and epidemiology. *Eur J Heart Fail* 2009; 11: 130–139.
5. Holguin F, Folch E, Redd SC, Mannino DM. Comorbidity and mortality in COPD-related hospitalizations in the United States, 1979 to 2001. *Chest* 2005; 128: 2005–2011.
6. Dransfield MT, Rowe SM, Johnson JE, Bailey WC, Gerald LB. Use of beta blockers and the risk of death in hospitalized patients with acute exacerbations of COPD. *Thorax* 2008; 63: 301–305.
7. Short PM, Lipworth SI, Elder DH, Schembri S, Lipworth BJ. Effect of beta blockers in treatment of chronic obstructive pulmonary disease: a retrospective cohort study. *BMJ* 2011; 342: d2549.
8. Stefan MS, Rothberg MB, Priya A, Priore PS, Au DH, Lindenauer PK. Association between β-blocker therapy and outcomes in patients hospitalized with acute exacerbations of chronic obstructive lung disease with underlying ischaemic heart disease, heart failure or hypertension. *Thorax* 2012; 67: 977–984.
9. Dickstein K, Cohen-Solal A, Filippatos G, McMurray JJ, Ponikowski P, Poole-Wilson PA, Strömberg A, van Veldhuisen DJ, Atar D, Hoes AW, Keren A, Mebazaa A, Nieminen M, Priori SG, Swedberg K. ESC Guidelines for the diagnosis and treatment of acute and chronic heart failure 2008: the Task Force for the Diagnosis and Treatment of Acute and Chronic Heart Failure 2008 of the European Society of Cardiology. Developed in collaboration with the Heart Failure Association of the ESC (HFA) and endorsed by the European Society of Intensive Care Medicine (ESICM). *Eur Heart J* 2008; 29: 2388–2442.
10. Al-Mohammad A, Mant J. The diagnosis and management of chronic heart failure: review following the publication of the NICE guidelines. *Heart* 2011; 97: 411–416.
11. Shimokawa H, Miura M, Nochioka K, Sakata Y. Heart failure as a general pandemic in Asia. *Eur J Heart Fail* 2015; 17: 884–892.
12. Atherton JJ, Hayward CS, Wan Ahmad WA, Kwok B, Jorge J, Hernandez AF, Liang L, Kodol RD, Krum H. Patient characteristics from a regional multicenter database of acute decompensated heart failure in Asia Pacific (ADHERE International-Asia Pacific). *J Card Fail* 2012; 18: 82–88.
13. Mentz RJ, Roessig L, Greenberg BH, Sato N, Shitagawa K, Yeo D, Kwok BW, Reyes EB, Krum H, Pieske B, Greene SJ, Anthony AP, Kelly JP, Zannad F, Pitt B, Lam CS. Heart failure clinical trials in East and Southeast Asia: understanding the importance and defining the next steps. *JACC Heart Fail* 2016; 4: 419–427.
14. Lam CS, Anand I, Zhang S, Shimizu W, Narasimhan C, Park SW, Yu CM, Ngarmukos T, Omar R, Reyes EB, Siswanto B, Ling LH, Richards AM. Asian Sudden Cardiac Death in Heart Failure (ASIAN-HF) registry. *Eur J Heart Fail* 2013; 15: 928–936.
15. Lam CS, Teng TK, Tay WT, Anand I, Zhang S, Shimizu W, Narasimhan C, Park SW, Yu CM, Ngarmukos T, Omar R, Reyes EB, Siswanto BB, Hung CL, Ling LH, Yap J, MacDonald M, Richards AM. Regional and ethnic differences among patients with heart failure in Asia: the Asian Sudden Cardiac Death in Heart Failure registry. *Eur Heart J* 2016; 37: 3141–3153.
16. Vestbo J, Hurd SS, Agusti AG, Jones PW, Vogelmeier C, Anzueto A, Barnes PJ, Fabbri LM, Martinez FJ, Nishimura M, Stockley RA, Sin DD, Rodriguez-Roisin R. Global strategy for the diagnosis, management, and prevention of chronic obstructive pulmonary disease: GOLD executive summary. *Am J Respir Crit Care Med* 2013; 187: 347–365.
17. Fukuchi Y, Nishimura M, Ichinose M, Adachi M, Nagai A, Kuriyama T, Takahashi K, Nishimura K, Ishioka S, Aizawa H, Zaher C. COPD in Japan: the Nippon COPD Epidemiology study. *Respirology* 2004; 9: 458–465.
18. Yancy CW, Lopatin M, Stevenson LW, De Marco T, Fonarow GC. ADHERE Scientific Advisory Committee and Investigators. Clinical presentation, management, and in-hospital outcomes of patients admitted with acute decompensated heart failure with preserved systolic function: a report from the Acute Decompensated Heart Failure National Registry (ADHERE) Database. *J Am Coll Cardiol* 2006; 47: 76–84.
19. Cheng RK, Cox M, Neely ML, Heidenreich PA, Bhatt DL, Eapen ZJ, Hernandez AF, Butler J, Yancy CW, Fonarow GC. Outcomes in patients with heart failure with preserved, borderline, and reduced ejection fraction in the Medicare population. *Am Heart J* 2014; 168: 721–730.
20. Alter S, Chan W, Bozkurt B, Aguilar D, Ramasubbu K, Zachariah AA, Wilson JM, Deswal A. Impact of noncardiac comorbidities on morbidity and mortality in a predominantly male population with heart failure and preserved versus reduced ejection fraction. *J Am Coll Cardiol* 2012; 59: 998–1005.
21. Borel F, Weston SA, Redfield MM, Jacobsen SJ, Pakhomov S, Nkomo VT, Meverden RA, Roger VL. Systolic and

© 2018 The Authors. ESC Heart Failure published by John Wiley & Sons Ltd and the European Society of Cardiology. All rights reserved.

diastolic heart failure in the community. JAMA 2006; 296: 2209–2216.
22. Fabbri LM, Luppi F, Beghé B, Rabe KF. Complex chronic comorbidities of COPD. Eur Respir J 2008; 31: 204–212.
23. Mannino DM, Thorn D, Swensen A, Holguin F. Prevalence and outcomes of diabetes, hypertension and cardiovascular disease in COPD. Eur Respir J 2008; 32: 962–969.
24. Potash SJ, Wang D, Pfeffer MA, Yusuf S, McMurray JJ, Swedberg KB, Ostergren J, Michelson EL, Pieper KS, Granger CB. Predictors of mortality and morbidity in patients with chronic heart failure. Eur Heart J 2006; 27: 65–75.
25. Flannery G, Gehrig-Mills R, Billah B, Krum H. Analysis of randomized controlled trials on the effect of magnitude of heart rate reduction on clinical outcomes in patients with systolic chronic heart failure receiving beta-blockers. Am J Cardiol 2009; 103: 865–869.
26. Rutten FH, Zuithoff NP, Hak E, Grobbee DE, Hoes AW. Beta-blockers may reduce mortality and risk of exacerbations in patients with chronic obstructive pulmonary disease. Arch Intern Med 2010; 170: 880–887.
27. Du Q, Sun Y, Ding N, Lai L, Chen Y. Beta-blockers reduced the risk of mortality and exacerbation in patients with COPD: a meta-analysis of observational studies. PLoS One 2014; 9: e113048.
28. Ernstzen M, Jafari S, Carlsten B, FitzGerald JM. Beta-blocker use and COPD mortality: a systematic review and meta-analysis. BMC Pulm Med 2012; 12: 48.
29. Quinn JK, Hersey E, Bhatnagar K, Timmis A, Hemingway H, Wedzicha JA, Smeeth L. Effect of beta blockers on mortality after myocardial infarction in adults with COPD: population based cohort study of UK electronic healthcare records. BMJ 2013; 347: f6660.
30. Kubota Y, Asai K, Furuse E, Nakamura S, Murai K, Tsukada YT, Shimizu W. Impact of beta-blocker selectivity on long-term outcomes in congestive heart failure patients with chronic obstructive pulmonary disease. Int J Chron Obstruct Pulmon Dis 2015; 10: 515–523.
31. Regional COPD Working Group. COPD prevalence in 12 Asia-Pacific countries and regions: projections based on the COPD prevalence estimation model. Respirology 2003; 8: 192–198.
32. Murray CJ, Lopez AD. Alternative projections of mortality and disability by cause 1990–2020: global burden of disease study. Lancet 1997; 349: 1498–1150.

ESC Heart Failure 2016; 3: 297–305
DOI: 10.1002/ehf2.12128

https://onlinelibrary.wiley.com/reader/content/10.1002/ehf2.12228/format/pdf/OEBP 2020/04/27

Circ J 2018; 82: 1666–1674
doi:10.1253/circj.CJ-17-1275

ORIGINAL ARTICLE
Ischemic Heart Disease

Rural-Urban Disparity in Emergency Care for Acute Myocardial Infarction in Japan

Jun Masuda, MD, PhD; Mikio Kishi, MD; Naoto Kumagai, MD, PhD; Toru Yamazaki, PhD; Kenji Sakata, MD, PhD; Takumi Higuma, MD, PhD; Akiyoshi Ogimoto, MD, PhD; Kaoru Dohi, MD, PhD; Takashi Tanigawa, MD, PhD; Hiroyuki Hanada, MD, PhD; Mashio Nakamura, MD, PhD; Shigeru Sokejima, MD, PhD; Morimasa Takayama, MD, PhD; Jitsuo Higaki, MD, PhD; Masakazu Yamagishi, MD, PhD; Ken Okumura, MD, PhD; Masaaki Ito, MD, PhD

Background: There are few reports examining regional differences between rural prefectures and metropolitan areas in the management of acute myocardial infarction (AMI) in Japan.

Methods and Results: In the Rural AMI registry, a prospective, multi-prefectural registry of AMI in 4 rural prefectures (Ishikawa, Aomori, Ehime and Mie), a total of 1,695 consecutive AMI patients were registered in 2013. Among them, 1,313 patients who underwent primary percutaneous coronary intervention (PPCI) within 24 h of onset were enrolled in this study (Rural group), and compared with the cohort data from the Tokyo CCU Network registry for AMI in the same period (Metropolitan group, 2,075 patients). The prevalence of direct ambulance transport to PCI-capable facilities in the Rural group was significantly lower than that in the Metropolitan group (43.8% vs. 60.3%, P<0.01), which resulted in a longer onset-to-balloon time (OTB: 225 vs. 210 min, P=0.02) and lower prevalence of PPCI in a timely fashion (OTB ≤2h: 11.5% vs. 20.7%, P<0.01) in the Rural group. Multivariate analysis revealed that direct ambulance transport was the strongest predictor for PPCI in a timely fashion (odds ratio=4.13, P<0.001).

Conclusions: AMI patients in rural areas were less likely to be transported directly to PCI-capable facilities, resulting in time delay to PPCI compared with those in metropolitan areas.

Key Words: Acute myocardial infarction; Direct ambulance transport; Emergency care; Onset-to-balloon time; Rural vs. metropolitan

Acute myocardial infarction (AMI) is a major cause of morbidity and mortality in Japan and other foreign countries. Primary percutaneous coronary intervention (PPCI) in a timely fashion is the preferred treatment strategy for AMI patients, and current guidelines suggest that the total ischemic time should not exceed 120 min, especially in patients with ST elevation MI (STEMI).[1-3] A large number of hospitals can perform PPCI in Japan, but it is unclear if there are regional differences between rural and urban areas in the rate of PPCI performed in such a timely fashion. In addition, there are no reports on whether these rural-urban disparities, if present, are associated with regional differences in patient characteristics, including life style and traffic patterns, or prehospital and hospital emergency medical service (EMS) systems between rural and urban areas.

Accordingly, the purpose of the present study was to describe the regional differences in the current state of emergency care for AMI between rural prefectures and Tokyo metropolitan areas regarding the following aspects: (1) transportation status from symptom onset to hospital arrival, (2) patient characteristics and therapeutic strategies, and (3) time delay to reperfusion therapy, and to clarify the contributing factors to the differences in the time delay to reperfusion by comparing the Rural AMI registry data with the Tokyo CCU Network registry database in Japan.

Received November 21, 2017; revised manuscript received January 27, 2018; accepted February 15, 2018; released online March 27, 2018 Time for primary review: 20 days

Department of Cardiology and Nephrology (J.M., K.D., M.I.), Department of Public Health and Occupational Medicine (T.Y., S.S.), Mie University Graduate School of Medicine, Mie; Tokyo CCU Network Scientific Committee, Tokyo (M.K., M.T.); Mie CCU Network, Mie (N.K., T.T., M.N.); Department of Cardiovascular and Internal Medicine, Kanazawa University Graduate School of Medicine, Ishikawa (K.S., M.Y.); Department of Cardiology, Respiratory Medicine and Nephrology, Hirosaki University Graduate School of Medicine, Aomori (T.H., H.H.); Department of Integrated Medicine and Informatics, Ehime University Graduate School of Medicine, Ehime (A.O., J.H.); and Division of Cardiology, Saiseikai Kumamoto Hospital, Kumamoto (K.O.), Japan

Mailing address: Masaaki Ito, MD, PhD, Department of Cardiology and Nephrology, Mie University Graduate School of Medicine, 2-174 Edobashi, Tsu, Mie 514-8507, Japan. E-mail: mitoka@clin.medic.mie-u.ac.jp

ISSN-1346-9843 All rights are reserved to the Japanese Circulation Society. For permissions, please e-mail: cj@j-circ.or.jp

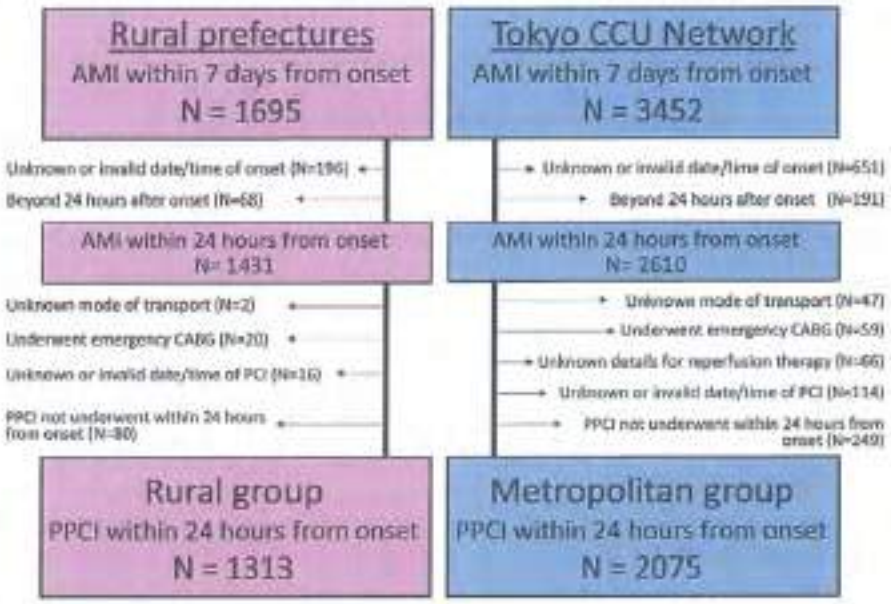

Figure 1. Flow chart for selection of study population. AMI, acute myocardial infarction; CABG, coronary artery bypass graft; PCI, percutaneous coronary intervention; PPCI, primary PCI.

Methods

Study Design

The Rural AMI registry study is a prospective, multicenter, multi-prefectural, observational study of AMI in 4 rural prefectures (Aomori, Ishikawa, Ehime and Mie) with a population size of less than 2 million in Japan. This study enrolled patients with AMI hospitalized within 7 days from symptom onset between January 2013 and December 2013 in Aomori, Ehime and Mie prefectures, and between April 2013 and March 2014 in Ishikawa prefecture because of the delay of the final ethical approval. In these 4 rural prefectures, there are a total of 57 hospitals that have cardiac catheterization facilities for emergency PCI. Among them, 41 hospitals participated in the Rural AMI registry study, and were encouraged to enroll consecutive AMI patients. We aimed to compare the effects of prehospital- and hospital-EMS systems on the probability of survival of AMI patients between urban and rural areas, with special reference to the difference between the Rural AMI registry study and the Tokyo CCU Network registry database. Therefore, the Rural registry used the same registration form as the Tokyo CCU Network registry for AMI. Data collection was performed via individual chart review by trained data collection personnel at each collaborating hospital, and all data were anonymized and transmitted to the data collection center at the Department of Cardiology and Nephrology, Mie University Graduate School of Medicine, Tsu, Japan for processing and analysis.

The following data were collected: the date and time of symptom onset, patient characteristics, history of cardiovascular disease, Killip classification, prehospital management (e.g., transport pathway, transport mode, time interval from the onset of symptoms to coronary revascularization), laboratory data, angiographic data and PCI procedure, duration of hospitalization and in-hospital death.

The data for AMI patients in Tokyo metropolitan areas were obtained from the cohort registered in the Tokyo CCU Network during the same periods. Details of the Tokyo CCU Network registry have been described previously.[4] In brief, the Tokyo CCU Network is a well-organized cardiovascular care network covering more than 90% of all AMI patients in the Tokyo metropolitan area. The Tokyo CCU Network registry is an ongoing multicenter registry that prospectively collects information from both EMS (Tokyo Metropolitan EMS) and investigators at participating hospitals on emergency admission to acute cardiac facilities. In 2013, among all 71 hospitals participating in the Tokyo CCU Network, patient data were enrolled to the registry database from 61 hospitals. Individual clinical information is recorded into the database by network members at each institution, and the final datasets are collected by the Tokyo CCU Network Scientific Committee under anonymity, according to the ethical guidelines on epidemiological surveys released from the Japanese Ministry of Health, Labour, and Welfare.

The diagnosis of and therapeutic strategies for AMI were decided by the cardiologists in each hospital, and all patients were treated according to the Japanese Circulation Society, ESC and ACCF/AHA guidelines for the diagnosis and treatment of AMI.[1-3,5,6] This study was conducted in accordance with the Declaration of Helsinki. The protocol was approved by the institutional review board or ethics committee of Mie University Graduate School of Medicine, Kanazawa University Graduate School of Medicine, Hirosaki University Graduate School of Medicine, Ehime University Graduate School of Medicine, and Tokyo CCU Network Scientific Committee. Obtaining written informed consent from the patients was not required because all collected data were anonymized and it was a

Table 1. Baseline Clinical Characteristics

	Rural group (n=1,313)	Metropolitan group (n=2,075)	P value
Baseline characteristics			
Age, years	67.9±13.0	67.1±13.2	0.099
≥80 years, n (%)	276 (20.9)	409 (19.7)	0.355
Male, n (%)	1,017 (77.5)	1,593 (76.8)	0.644
BMI, kg/m²	23.8±3.6	23.9±3.9	0.249
Hypertension, n (%)	860 (65.5)	1,250 (60.8)	0.006
Diabetes, n (%)	451 (34.3)	648 (31.4)	0.078
Dyslipidemia, n (%)	594 (45.2)	842 (41.8)	0.032
Current smoking, n (%)	470 (35.8)	746 (36.2)	0.789
Previous stroke, n (%)	72 (5.5)	116 (5.6)	0.843
PAD, n (%)	32 (2.4)	20 (1.0)	0.001
Previous MI, n (%)	102 (7.8)	330 (16.0)	<0.001
Previous PCI, n (%)	107 (8.1)	205 (10.0)	0.075
Previous CABG, n (%)	8 (0.6)	26 (1.3)	0.063
Hemodialysis, n (%)	13 (1.0)	40 (1.9)	0.030
Presentation			
Chest pain as chief complaint, n (%)	1,156 (88.0)	1,799 (86.8)	0.284
Killip class 1, n (%)	984 (74.9)	1,515 (75.2)	
Killip class 2, n (%)	154 (11.7)	253 (12.6)	0.606
Killip class 3, n (%)	77 (5.9)	99 (4.9)	
Killip class 4, n (%)	98 (7.5)	147 (7.3)	
STEMI, n (%)	1,113 (84.8)	1,722 (84.2)	0.625

Data are expressed as n (%) for categorical variables and as mean±standard deviation or median (interquartile range) for continuous variables unless otherwise specified. For each variable with missing values, data are expressed as the number (valid percentage). BMI, body mass index; CABG, coronary artery bypass grafting; MI, myocardial infarction; PAD, peripheral artery disease; PCI, percutaneous coronary intervention; STEMI, ST elevation MI.

noninvasive observational study.

Data Analysis and Definitions

The diagnosis of AMI was based on the 3rd universal definition of myocardial infarction.[7] In brief, AMI was diagnosed by a detection of a rise and/or fall in cardiac biomarker values (preferably cardiac troponin: cTn), with at least 1 value above the 99th percentile of the upper reference limit observed together with evidence of myocardial ischemia with at least 1 of the following: symptoms of ischemia, ECG changes indicative of new ischemia, development of pathological Q waves on ECG, or imaging evidence of new loss of viable myocardium or new regional wall motion abnormalities.

Direct ambulance transport was defined as direct transport from the field to the PCI-capable hospital by EMS. Inter-facility transport was defined as indirect transport via family physician offices or non-PCI-capable hospitals to the PCI-capable hospital. Self-transport was defined as direct visit to the PCI-capable hospital by walking or by using public/private vehicles.

Onset-to-balloon (OTB) time was defined as the interval from the onset of symptoms of ischemia to the first device use or balloon inflation. Door time was defined as the arrival time at the emergency department where emergency catheterization was performed (not the arrival time at the referral hospital or clinic for transferred patients). In the multivariate analysis of associated factors for time delay to reperfusion, we selected a cutoff point of 2h for delayed OTB time based on recommendations by several Western and Japanese guidelines.[1-3]

Statistical Analysis

Continuous variables are presented as mean and standard deviation or median and interquartile range (IQR), and categorical variables as numbers and percentages. We compared categorical variables with the chi-square test or Fisher's exact test, and continuous variables with Student's t-test or the Mann-Whitney U test on the basis of the distribution. In the chi-square analyses involving variables with more than 2 coding categories, adjusted standardized residuals were used to identify the contribution of different cells to the significance of the chi squares.

Comparison of the peak CPK levels or duration of hospital stay between rural and metropolitan groups were analyzed using analysis of covariance (ANCOVA) after logarithmic transformation, with the following covariates as potential confounders: age, sex, mode of transport, hypertension, diabetes mellitus, dyslipidemia, current smoker, previous PCI, previous MI, Killip classification at presentation, STEMI, multivessel disease and left anterior descending coronary artery (LAD) lesion as culprit. Multivariate analysis was used to clarify the independent predictors of final Thrombolysis in Myocardial Infarction (TIMI) flow grade 3, OTB time ≤2h and for not using direct ambulance transport. A logistic regression model was constructed by adjusting for clinically relevant variables, and factors that were significantly different between rural and metropolitan groups (P<0.1) were included in the multivariate analysis with the stepwise backward elimination procedure. We also conducted a sensitivity analysis using a simple imputation method (regression imputation) to examine the effects of missing data. A Cox proportional hazard model was used to investigate the predictors of in-

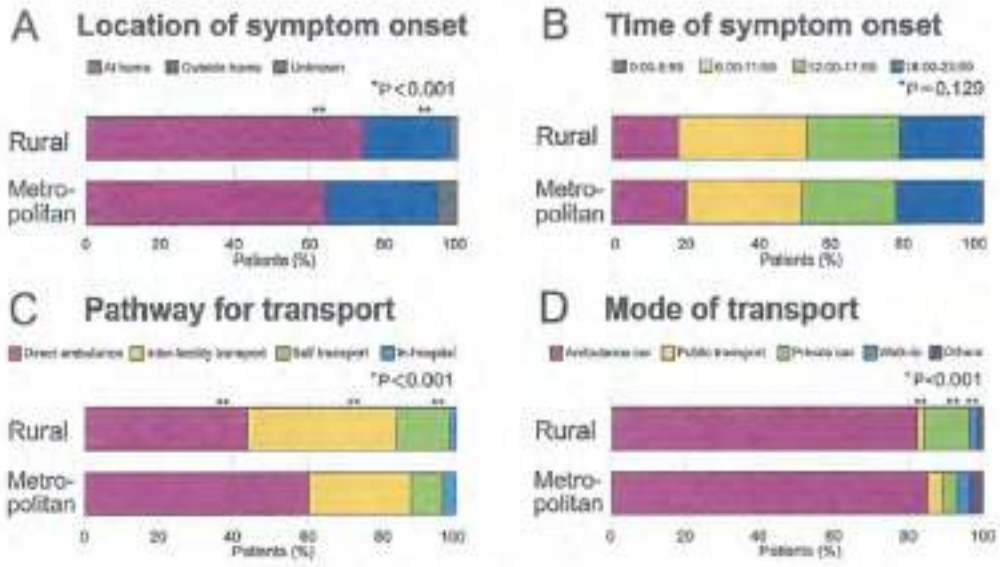

Figure 2. Comparison of situation at symptom onset and pathway or mode of transport. (**A**) Location of symptom onset. (**B**) Time of symptom onset. (**C**) Pathway of transport to the PCI-capable hospital. (**D**) Mode of transport to the PCI-capable hospital. *P value for the chi-square test. **P value <0.01 for analysis of the adjusted standardized residuals. PCI, percutaneous coronary intervention.

hospital death. The variables with a univariate P-value <0.1 were selected for entry into the multivariate analysis using the Cox proportional hazard model. For all analyses, two-tailed probability values of <0.05 were considered significant, and all statistical analyses were supported by specialists in biostatistics at the Department of Public Health and Occupational Medicine, Mie University Graduate School of Medicine, Mie, Japan, using the SPSS version 20 software (SPSS, Inc., IL, USA).

Results

Patient Population

The following numbers of patients hospitalized within 7 days from onset of AMI were registered in each registry: 1,695 in the Rural AMI registry and 3,452 in the Tokyo CCU Network registry. Among them, the following patients in the Rural AMI registry and the Tokyo CCU Network registry, respectively, were excluded from the analysis: 196 and 651 patients with missing information about date/time of symptom onset; 68 and 191 patients who were admitted >24h after symptom onset; 2 and 47 patients with missing information about the mode and pathway of emergency transport; 20 and 59 patients treated by coronary artery bypass grafting (CABG) surgery; 0 and 66 patients with missing information about whether the reperfusion therapy succeeded or failed; 16 and 114 patients with missing information about date/time of PCI; and 80 patients and 249 patients who did not undergo PCI within 24h from symptom onset (**Figure 1**). Therefore, the population of this study consisted of a total of 3,388 AMI patients who underwent PPCI within 24h of symptom onset: 1,313 patients from the Rural AMI registry cohort (Rural group) and 2,075 patients from the Tokyo CCU Network registry cohort (Metropolitan group).

Baseline Clinical Characteristics

Baseline characteristics were different in several aspects between the Rural and Metropolitan groups (**Table 1**). The Rural group had a significantly higher prevalence of hypertension, dyslipidemia and peripheral artery disease (PAD), whereas the metropolitan group had a higher prevalence of previous MI and hemodialysis. There were no significant differences in Killip classification or the prevalence of patients with STEMI. The mean percentage of missing data among variables in **Table 1** was 0.7% in the Rural group and 1.4% in the Metropolitan group; the highest proportion of missing data was for body mass index (11.7% and 8.6%), followed by Killip class (0% and 2.9%) and ST elevation MI (0.1% and 1.4%), respectively.

Situation at Onset of AMI, Pathway and Mode of Transport

The situation at onset of AMI, and pathway and mode of transport to the PCI-capable hospitals are summarized in **Figure 2**. The Rural group included a higher proportion of patients who developed AMI symptoms at home than in the Metropolitan group (74% vs. 64%, P<0.001) (**Figure 2A**). Circadian distribution of AMI onset was similar in the 2 groups, occurring most frequently between 06:00 and 11:59 hours (**Figure 2B**). Regarding the pathway of transport to the PCI-capable hospital, patients in the Rural group were less likely to be transported by direct ambulance than those in the Metropolitan group, but more likely to be transported by inter-facility transport or self-transport (44% vs. 60%, 40% vs. 28%, 15% vs. 9%, P<0.001, respectively, **Figure 2C**). Regarding the mode of transport, both groups included a high proportion of patients who were transported by ambulance to the PCI-capable hospitals (82% vs. 85%), but the Rural group had a higher proportion of patients who were transported by private cars than the Metropolitan group (**Figure 2D**).

Table 2. Angiographic, Procedural Characteristics and In-Hospital Outcome

	Rural group (n=1,313)	Metropolitan group (n=2,075)	P value
Infarct-related artery			
RCA, n (%)	509 (38.8)	812 (39.1)	
Left main trunk, n (%)	37 (2.8)	35 (1.7)	0.120
LAD, n (%)	610 (46.5)	943 (45.4)	
Left circumflex, n (%)	154 (11.7)	280 (13.5)	
Undefined, n (%)	3 (0.2)	6 (0.3)	
Multivessel disease, n (%)	636 (48.5)	953 (46.2)	0.187
Initial TIMI flow grade 0, n (%)	850 (65.3)	1,203 (60.7)	0.002
Revascularization			
Aspiration thrombectomy, n (%)	963 (77.3)	1,539 (74.4)	0.064
Distal protection device, n (%)	141 (11.5)	212 (10.3)	0.285
Stent implantation, n (%)	1,206 (92.0)	1,855 (90.1)	0.069
Drug-eluting stent, n (%)	815 (62.2)	1,256 (61.0)	0.509
Final TIMI flow grade 3, n (%)	1,084 (88.8)	1,901 (93.6)	<0.001
PCI <12h of onset, n (%)	1,185 (90.2)	1,841 (88.7)	0.161
Door-to-balloon time, min	75 (54, 108)	68 (47, 97)	<0.001
Level of peak CPK, IU/L	2,208 (1,051, 4,225)	1,893 (677, 3,061)	<0.001
Duration of hospital stay, days	14 (11, 19)	12 (8, 16)	0.001
In-hospital all-cause death	86 (6.6)	105 (5.1)	0.066

Data are expressed as n (%) for categorical variables and as mean±standard deviation or median (interquartile range) for continuous variables unless otherwise specified. For each variable with missing values, data are expressed as the number (valid percentage). CPK, creatine phosphokinase; LAD, left anterior descending artery; RCA, right coronary artery; TIMI, Thrombolysis in Myocardial Infarction.

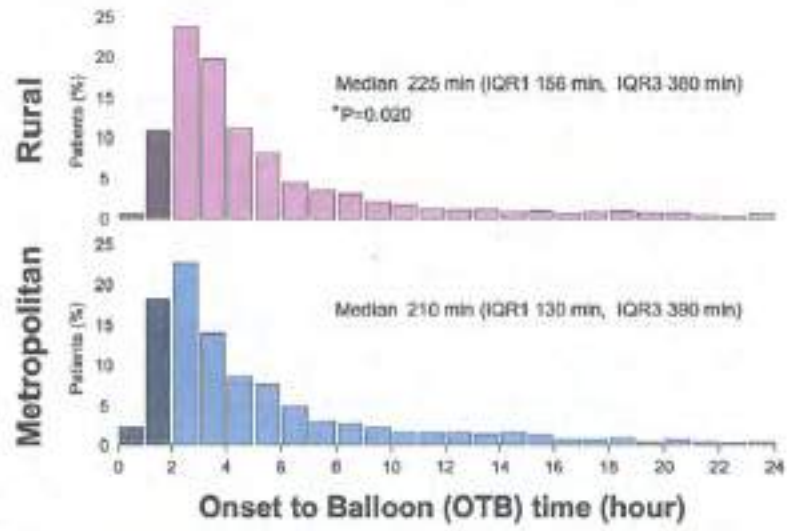

Figure 3. Median onset-to-balloon (OTB) time in the Rural group (**Top**) and Metropolitan group (**Bottom**). The shaded areas indicate the percentage of patients with OTB time delay of ≤2 h, which was significantly lower in the Rural group than in the Metropolitan group (11.5% vs. 20.7%, P<0.01).*P value for the difference between the Rural group and the Metropolitan group by Mann-Whitney U-test.

Angiographic and Procedural Characteristics

The distribution of the infarct-related arteries and prevalence of multivessel disease were similar between the 2 groups (**Table 2**). Initial TIMI flow grade 0 was more prevalent in the Rural group than in the Metropolitan group. Although the use of distal protection device, aspiration thrombectomy and stent implantation were similar between groups, the attainment rate of final TIMI flow grade 3 was significantly lower in the Rural group than in the Metropolitan group. The prevalence of PPCI within 12 h of symptom onset was similar between the 2 groups: 90.2% in the Rural group and 88.7% in the Metropolitan group (P=0.161). The Rural group had significantly higher levels of peak CPK and longer hospital stay than the Metropolitan group, even after adjustment for potential confounders. In-hospital all-cause death tended to be higher in the Rural group, but not significantly (6.6% vs. 5.1%, P=0.066, respectively). The mean percentage of missing data among variables shown in **Table 2** was 1.5% in the Rural group and 3.6% in the Metropolitan group; the respective highest proportions were for door-to-balloon time (0.1% and 31.0%), followed by final TIMI flow grade 3 (7.0% and 2.1%), distal protection device (6.4% and 0.6%) and initial TIMI flow grade (0.8% and 4.4%).

Table 2. Comparison of Time Delay to Reperfusion With Each Transport Pathway (Direct Ambulance Transport or Inter-Facility/Self-Transport)

	Rural group	Metropolitan group	P value
Direct ambulance transport			
Onset to EMS call, min	41 (15, 105)	37 (13, 112)	0.283
EMS call to arrival at scene, min	7 (5, 10)	8 (6, 10)	<0.001
On-scene time, min	10 (7, 15)	16 (13, 20)	<0.001
Transport time, min	12 (8, 19)	9 (6, 12)	<0.001
Onset-to-door time, min	78 (50, 146)	76 (48, 151)	0.639
Onset-to-balloon time, min	178 (134, 267)	170 (120, 282)	0.080
Inter-facility or self-transport			
Onset-to-door time, min	198 (120, 388)	204 (108, 432)	0.554
Onset-to-balloon time, min	286 (195, 494)	285 (180, 522)	0.516

Data are expressed as median (interquartile range) for continuous variables. EMS, emergency medical services.

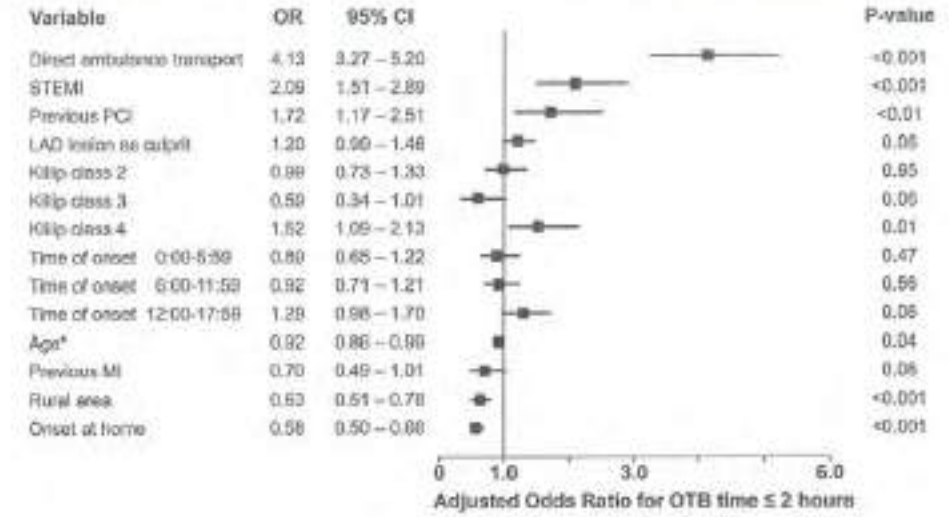

Figure 4. Factors associated with onset to balloon (OTB) time ≤2 h. Adjusted odds ratio (OR) and 95% confidence intervals (CI) indicate likelihood of OTB time ≤2h from logistic regression analysis. OR >1 indicates increased odds of OTB time ≤2h. Respective reference categories: transportation other than direct ambulance transport, non-STEMI, absence of selected medical history variables, other vessels as culprit, Killip class 1, symptom onset between 18:00–23:59 hours, metropolitan area, onset outside home. *OR and CI were reported for a 10-U incremental change. Covariates: age, sex, pathway for transport, hypertension, diabetes mellitus, dyslipidemia, current smoker, previous PCI, previous MI, previous CABG, time of onset, location of onset, rural vs. Tokyo, Killip classification at presentation, STEMI and LAD lesion as culprit. CABG, coronary artery bypass graft; LAD, left anterior descending artery; MI, myocardial infarction; PCI, percutaneous coronary intervention; STEMI, ST elevation MI.

Comparison of Time Delay to Reperfusion

The distribution of OTB time in the 2 groups is shown in **Figure 3**. The median OTB time in the Rural group was significantly longer than that in the Metropolitan group (225 [IQR, 156–380] vs. 210 [IQR, 130–390] min, P=0.02). The rate of achievement of OTB ≤2 h (shaded area in **Figure 3**), which is recommended in Japanese and international guidelines,[1-3] was significantly lower in the Rural group than in the Metropolitan group (11.5% vs. 20.7%, P<0.01).

Table 3 shows the comparison of time delay to reperfusion with each transport pathway (direct ambulance transport or inter-facility/self-transport). Among patients with direct ambulance transport, time from symptom onset to EMS call was comparable in both groups. Time from EMS call to arrival at scene and on-scene time were significantly shorter in the Rural group than in the Metropolitan group, but the transport time was significantly longer in the Rural group than in the Metropolitan group. In total, onset-to-door (OTD) time was comparable between the 2 groups (78 [IQR, 50–146] min for the Rural group vs. 76 [IQR, 48–151] min for the Metropolitan group, P=0.64). OTB time was also comparable (178 [IQR, 134–267] vs. 170 [IQR, 120–282] min, respectively, P=0.08). Similarly, among patients with inter-facility or self-transport, the OTD and OTB times were comparable in the 2 groups (198 [IQR, 120–388] vs. 204 [IQR, 108–432] min, P=0.55; 286 [IQR, 195–494] vs. 285 [IQR, 180–522] min, P=0.52). In addition, no significant differences were observed between the Rural and Metropolitan groups for in-hospital deaths (7.7% vs. 5.7%, P=0.08 among patients with direct ambulance transport; 4.6% vs. 3.5%, P=0.26 among patients with inter-

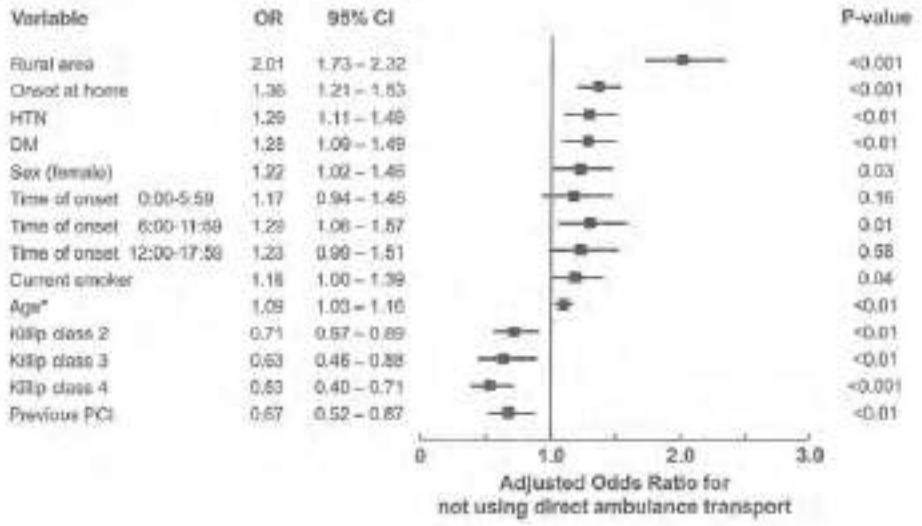

Figure 5. Factors associated with not using direct ambulance transport. Adjusted OR and 95% CI indicate likelihood of not using direct ambulance transport from the logistic regression analysis. OR >1 indicates increased odds of not using direct ambulance transport. Respective reference categories=Tokyo, onset outside home, absence of selected medical history variables, sex (male), symptom onset between 18:00–23:59 hours, Killip class 1. *OR and CI were reported for a 10-U incremental change. Covariates: age, sex, hypertension, diabetes mellitus, dyslipidemia, current smoker, previous PCI, previous MI, previous CABG, time of onset, location of onset, rural vs. Tokyo, Killip classification at presentation, STEMI and chest pain as a chief complaint. Abbreviations as in Figure 4.

facility or self-transport, respectively).

Factors Associated With Time Delay to Reperfusion

Figure 4 shows the factors associated with OTB time ≤2h assessed with a multiple logistic regression model. Direct ambulance transport, STEMI, previous PCI and Killip class IV at hospital presentation were independent positive predictive factors for OTB time ≤2h. On the other hand, onset at home, rural area and older patients were independent negative predictive factors for OTB time ≤2h. In particular, direct ambulance transport was the strongest positive predictive factor for OTB time ≤2h (odds ratio (OR): 4.13, 95% confidence interval (CI): 3.27–5.20, P<0.001). We also evaluated factors associated with not using direct ambulance transport (**Figure 5**). Rural area, onset at home, coexistence of hypertension and diabetes, female sex, onset at 06:00–11:59 hours, current smoker and older age were significantly associated with not using direct ambulance transport. On the other hand, Killip classes II–IV and previous PCI were associated with the use of direct ambulance transport. In particular, the Rural group had the least use of direct ambulance transport. In each multiple logistic regression model, sensitivity analyses for imputation procedure were performed, but the results did not differ from the main results (data not shown).

Factors Associated With Final TIMI Flow Grade and In-Hospital Death

We analyzed the factors associated with final TIMI flow grade 3 by multivariate logistic regression analysis (**Figure S1**). Stent implantation, previous MI and direct ambulance transport were independently associated with a higher probability of achieving final TIMI flow grade 3 (OR: 4.58, 95% CI: 3.29–6.38, P<0.001; OR: 1.58, 95% CI: 1.02–2.44, P=0.04; OR: 1.38, 95% CI: 1.04–1.84, P=0.03, respectively). Multivariate analysis by the Cox proportional hazard model revealed that age, previous CABG, high Killip class at presentation, multivessel disease and attainment of final TIMI flow grade 3, but not direct ambulance transport, were the independent predictors of in-hospital death (**Table S1**).

Discussion

The major findings of this study were: (1) AMI patients in the rural prefectures were less likely to be transported directly by EMS to PPCI-capable facilities than those in the metropolitan areas, and (2) this low frequency of direct transportation for patients in the rural prefectures was directly correlated with the low frequency of PPCI within 2h from onset. To the best of our knowledge, this is the first prospective, multicenter, multi-prefectural observational study to demonstrate the regional differences in the current status of emergency care for AMI between rural prefectures and Tokyo metropolitan areas in contemporary Japanese clinical practice.

Most of the previous registry studies of AMI included only patients who were transported by EMS, whereas the present study also included self-transported patients to reflect real-world clinical practice in Japan. The frequency of inter-facility transport was 27.6% in the Metropolitan area in the present study, which was comparable with previous studies in urban areas (23–30%),[8,9] but was as high as 39.9% in the Rural group.

Previous studies of STEMI have reported that inter-facility transfer for PPCI was found to be associated with longer OTB times, and poorer short- and long-term clinical outcomes than direct transfer.[8,10,11] The Rural group

had a significantly longer OTB time and lower prevalence of OTB ≤2h than the Metropolitan group in the present study, and direct ambulance transport was the strongest predictive factor for OTB time ≤2h. However, when patients were assessed independently on the basis of the transport pathway, there were no significant differences in either OTD time or OTB time between the Rural and Metropolitan groups for both patients with direct ambulance transport or inter-facility/self- transport. Thus, the low frequency of direct ambulance transport in the rural prefectures was considered to be one of the major factors that caused prolonged OTB time.

The Rural group had a similar prevalence of PPCI within 12h from onset, distal protection, aspiration thrombectomy and stent implantation compared with the Metropolitan group. However, the Rural group had a significantly lower attainment rate of final TIMI flow grade 3 and significantly higher peak CPK levels even after adjusting for confounding factors. Several previous studies reported that indirect transfer patients had a significantly increased risk of less satisfactory reperfusion flow after PPCI, determined as TIMI flow grade <3 or blush score <3 than direct transfer patients.[8,12] Consistent with those previous studies, direct ambulance transport was independently associated with a higher probability of achieving final TIMI flow grade 3 in the present study. In general, prolonged ischemic time leads to disruption of the microvascular bed and edema in distal capillary beds, which leads to the no-reflow phenomenon, and low TIMI flow grade and myocardial blush score.[13-15] Early studies also found that myocardial salvage and recovery of left ventricular function are greatest when reperfusion is achieved at <2h.[16,17] Therefore, the lower attainment rate of final TIMI flow grade 3 and higher peak CPK levels in the Rural group of the present study may be attributed to the lower likelihood of undergoing PPCI in a timely manner.

As described, the importance of rapid transport and minimizing the time delay to treatment has been confirmed for STEMI patients, but it is also beneficial for non-STEMI (NSTEMI) patients. The latest ESC guidelines for the management of NSTEMI recommended that very-high-risk patients should undergo angioplasty within 2h, high-risk patients within 24h and intermediate-risk patients within 72h.[18]

In the present study, the Rural group had significantly lower use of direct ambulance transport than the Metropolitan group. In general, PPCI-capable facilities in rural areas cover a wider area, including regions with difficult geographical accessibility than those in metropolitan areas because of the wider dispersion of the population and medical facilities. Therefore, such geographic differences can influence the prevalence of direct ambulance transport to PCI-capable facilities. On the other hand, continuous long-term efforts in the metropolitan area may have contributed to this result. In the Tokyo metropolitan district, the Tokyo CCU Network was established in 1978 and has continuously attempted to (1) operate the emergency medical network with the help of the Tokyo Fire Department and local medical associations in order to directly transport patients with suspected acute coronary syndrome (ACS) to the nearby PCI-capable hospitals with CCU and (2) hold public health educational campaigns for both the general population and health care workers.[19] The differences between areas with and without such long-term efforts may have been reflected in the present results.

The present study was unable to show the beneficial association between direct ambulance transport and in-hospital death. The Cox proportional hazard model analysis demonstrated that direct ambulance transport was not a significant predictor of in-hospital death. Patients with direct ambulance transport had a higher in-hospital mortality rate than those with inter-facility or self-transport in both the Rural group (7.7% vs. 4.6%) and the Metropolitan group (5.7% vs. 3.5%), presumably because patients who were transported by direct ambulance had much more serious conditions at presentation than those who were not. Indeed, patients transported directly by ambulance comprised a higher proportion of Killip class III or IV than those with inter-facility or self-transport (data not shown). These results suggest that severe cardiac conditions on hospital presentation can mask and even surpass the beneficial effects of direct ambulance transport on in-hospital death. On the other hand, as several previous studies have reported the beneficial effect of direct ambulance transport on mid- and long-term death,[8,10,11] a longer follow-up duration may have been required in the present study to evaluate the association between the regional differences in the prevalence of direct ambulance transport and death.

Clinical Implications

Our data suggested that in order to improve EMS to ensure timely transport of AMI patients directly to PCI-capable hospitals in the rural prefectures the following specific steps should be taken: (1) hold frequent public health education campaigns for the general population to better understand AMI symptoms and the importance of direct ambulance transport to PCI-capable facilities for early reperfusion, and (2) coordinate the regional emergency medical network systems in order to transport directly to nearby PCI-capable facilities for patients with suggestive symptoms of ACS. Use of prehospital 12-lead ECG may contribute to an increased rate of direct transfer and to a shorter delay in reperfusion.[20]

Study Limitations

There are several limitations. First, it was not a randomized trial, and it is possible that unappreciated or unmeasurable confounding variables altered the results. Second, the present study included only patients who underwent PPCI at participating hospitals within 24h of onset from among 4 rural prefectures in the Rural group; therefore, there may have been some selection bias for enrollment, which may make it difficult to apply the present results to all AMI patients in Japan. Third, we did not have detailed data on inter-facility transfer patients, including the initial mode of transport to the referral facilities and door-in to door-out (DIDO) time. Thus, we did not distinguish whether those patients were transferred to the PCI-incapable referral hospital regardless of EMS call at onset or whether they directly went to the PCI-incapable referral hospital or clinic. Fourth, there was no information regarding medications before onset, which may affect patient prognosis. Fifth, there were no data on prognosis after hospital discharge. Sixth, we were unable to adjust for differences in social structural factors between rural and metropolitan areas, such as composition or density of regional population, economic status, traffic networks, scale or density of PPCI-capable facilities, and numbers of physicians, which may have affected our results. Additional detailed nationwide observational studies with long-term follow-up are

needed for further evaluation.

Conclusions

Direct ambulance transport was the strongest independent predictor for PPCI in a timely fashion within 2h of onset. In rural prefectures, however, AMI patients were less likely to be transported directly by EMS to PPCI-capable facilities, resulting in significant longer OTB times, and lower prevalence of PPCI in a timely manner. In the rural prefectures, further effort is needed to promote widespread awareness of the importance of direct ambulance transport to PCI-capable facilities in order to minimize time delay to reperfusion in patients with AMI.

Acknowledgments

We thank all the collaborators in the Rural AMI registry and Tokyo CCU Network. All hospitals participating in this study are listed in "**Appendix S1**". This study was supported by the MHLW KAKENHI Grant Numbers H24-Shinkin-Ippan-002.

Disclosures

M.I. received departmental research grant support equal to or more than 1,000,000 yen from Pfizer Japan Inc., Daiichi Sankyo Company Limited, Shionogi & Co., Ltd., Sumitomo Dainippon Pharma Co., Ltd., MSD K.K., Astellas Pharma Inc., Takeda Pharmaceutical Company Limited, and Nippon Boehringer Ingelheim Co., Ltd. in 2016. M.I. received lecture fees equal to or more than 500,000 yen from Daiichi Sankyo Company Limited, Mitsubishi Tanabe Pharma Corporation, and Bayer Holding Ltd. in 2016. K.O. received lecture fees equal to or more than 500,000 yen from Johnson & Johnson K.K., Nippon Boehringer Ingelheim Co., Ltd., Bayer Healthcare, and Daiichi Sankyo Company Limited in 2016. J.H. received departmental research grant support equal to or more than 1,000,000 yen from Takeda Pharmaceutical Company Limited, Nippon Beringer-Ingelheim Co., Ltd., Astellas Pharma Ltd., Daiichi Sankyo Company Limited, Pfizer Healthcare Ltd., Teijin-Pharma Ltd., MSD K.K., Abbott Vascular Japan Co., Ltd., Mochida Pharmaceutical Co., Ltd., and Mitsubishi Tanabe Pharma Corporation, and received remuneration equal to or more than 500,000 yen from Takeda Pharmaceutical Company Limited, Nippon Beringer-Ingelheim Co., Ltd., Astellas Pharma Ltd., and Daiichi Sankyo Company Limited in 2016. M.N. received lecture fees equal to or more than 500,000 yen from Daiichi Sankyo Company Limited, Bayer Holding Ltd., Pfizer Japan Inc., and Bristol-Myers Squibb K.K. K.D. received lecture fees equal to or more than 500,000 yen from Otsuka Pharma Inc. in 2016. T.H. belongs to the endowed department from Abbott vascular Japan Co., Ltd. S.S. received research funding from Ministry of Health Labour and Welfare and OKASAN-KATO foundation. The other authors declare no conflicts of interest relevant to this article.

References

1. Japan Resuscitation Council. JRC resuscitation guideline 2015 for ACS. http://www.japanresuscitationcouncil.org/wp-content/uploads/2016/04/4f63e3aa0fcd083d92435f391d343f16.pdf (in Japanese) (accessed May 10, 2017).
2. Japanese Circulation Society. 2013 Guidelines for the management of patients with ST-elevation acute myocardial infarction. http://www.j-circ.or.jp/guideline/pdf/JCS2013_kimura_h.pdf (in Japanese) (accessed May 10, 2017).
3. American College of Emergency Physicians; Society for Cardiovascular Angiography and Interventions, O'Gara PT, Kushner FG, Ascheim DD, Casey DE Jr, Chung MK, de Lemos JA, et al. 2013 ACCF/AHA guideline for the management of ST-elevation myocardial infarction: A report of the American College of Cardiology Foundation/American Heart Association Task Force on Practice Guidelines. *J Am Coll Cardiol* 2013; **61**: e78–e140.
4. Miyachi H, Takagi A, Miyauchi K, Yamasaki M, Tanaka H, Yoshikawa M, et al. Current characteristics and management of ST elevation and non-ST elevation myocardial infarction in the Tokyo metropolitan area: From the Tokyo CCU network registered cohort. *Heart Vessels* 2016; **31**: 1740–1751.
5. Hamm CW, Bassand JP, Agewall S, Bax J, Boersma E, Bueno H, et al. ESC Guidelines for the management of acute coronary syndromes in patients presenting without persistent ST-segment elevation: The Task Force for the management of acute coronary syndromes (ACS) in patients presenting without persistent ST-segment elevatio. *Eur Heart J* 2011; **32**: 2999–3054.
6. Steg PG, James SK, Atar D, Badano LP, Lundqvist CB, Borger MA, et al. ESC Guidelines for the management of acute myocardial infarction in patients presenting with ST-segment elevation. *Eur Heart J* 2012; **33**: 2569–2619.
7. Thygesen K, Alpert JS, Jaffe AS, Simoons ML, Chaitman BR, White HD, et al. Third universal definition of myocardial infarction. *Eur Heart J* 2012; **33**: 2551–2567.
8. Imori Y, Akasaka T, Shishido K, Ochiai T, Tobita K, Yamanaka F, et al. Prehospital transfer pathway and mortality in patients undergoing primary percutaneous coronary intervention. *Circ J* 2015; **79**: 2000–2008.
9. Nakayama N, Kimura K, Endo T, Fukui K, Himeno H, Iwasawa Y, et al. Current status of emergency care for ST-elevation myocardial infarction in an urban setting in Japan. *Circ J* 2009; **73**: 484–489.
10. Nakatsuma K, Shiomi H, Morimoto T, Furukawa Y, Nakagawa Y, Ando K, et al. Inter-facility transfer vs. direct admission of patients with ST-segment elevation acute myocardial infarction undergoing primary percutaneous coronary intervention. *Circ J* 2016; **80**: 1764–1772.
11. Pedersen SH, Galatius S, Hansen PR, Mogelvang R, Abildstrom SZ, Sorensen R, et al. Field triage reduces treatment delay and improves long-term clinical outcome in patients with acute ST-segment elevation myocardial infarction treated with primary percutaneous coronary intervention. *J Am Coll Cardiol* 2009; **54**: 2296–2302.
12. Brodie BR, Stone GW, Cox DA, Stuckey TD, Turco M, Tcheng JE, et al. Impact of treatment delays on outcomes of primary percutaneous coronary intervention for acute myocardial infarction: Analysis from the CADILLAC trial. *Am Heart J* 2006; **151**: 1231–1238.
13. De Luca G, Suryapranata H, Zijlstra F, Van't Hof AWJ, Hoorntje JCA, Gosselink ATM, et al. Symptom-onset-to-balloon time and mortality in patients with acute myocardial infarction treated by primary angioplasty. *J Am Coll Cardiol* 2003; **42**: 991–997.
14. Ali A, Cox D, Dib N, Brodie B, Berman D, Gupta N, et al. Rheolytic thrombectomy with percutaneous coronary intervention for infarct size reduction in acute myocardial infarction: 30-day results from a multicenter randomized study. *J Am Coll Cardiol* 2006; **48**: 244–252.
15. Zhou H, He X, Zhuang S, Wang J, Lai Y, Qi W, et al. Clinical and procedural predictors of no-reflow in patients with acute myocardial infarction after primary percutaneous coronary intervention. *World J Emerg Med* 2014; **5**: 96–102.
16. Brodie BR, Stuckey TD, Wall TC, Kissling G, Hansen CJ, Muncy DB, et al. Importance of time to reperfusion for 30-day and late survival and recovery of left ventricular function after primary angioplasty for acute myocardial infarction. *J Am Coll Cardiol* 1998; **32**: 1312–1319.
17. Milavetz JJ, Giebel DW, Christian TF, Schwartz RS, Holmes DR, Gibbons RJ. Time to therapy and salvage in myocardial infarction. *J Am Coll Cardiol* 1998; **31**: 1246–1251.
18. Roffi M, Patrono C, Collet JP, Mueller C, Valgimigli M, Andreotti F, et al. 2015 ESC Guidelines for the management of acute coronary syndromes in patients presenting without persistent ST-segment elevation. *Eur Heart J* 2016; **37**: 267–315.
19. Yamamoto T, Takayama M. Tokyo CCU Network. *J Japanese Coron Assoc* 2015; **21**: 132–136 (in Japanese).
20. Kawakami S, Tahara Y, Noguchi T, Yagi N, Kataoka Y, Asaumi Y, et al. Time to reperfusion in ST-segment elevation myocardial infarction patients with vs. without pre-hospital mobile telemedicine 12-lead electrocardiogram transmission. *Circ J* 2016; **80**: 1624–1633.

Supplementary Files

Supplementary File 1

Appendix S1. Participating Enrolling Facilities by Prefecture

Figure S1. Factors associated with attainment of final Thrombolysis in Myocardial Infarction (TIMI) flow grade 3.

Table S1. Factors associated with in-hospital death

Please find supplementary file(s);
http://dx.doi.org/10.1253/circj.CJ-17-1275

Circ J 2018; 82: 1546–1551
doi:10.1253/circj.CJ-17-1001

ORIGINAL ARTICLE
Arrhythmia/Electrophysiology

Safety and Efficacy of Subcutaneous Cardioverter Defibrillator in Patients at High Risk of Sudden Cardiac Death

— Primary Japanese Experience —

Shingo Sasaki, MD, PhD; Hirofumi Tomita, MD, PhD; Takuo Tsurugi, MD; Yuji Ishida, MD, PhD; Yoshihiro Shoji, MD; Kimitaka Nishizaki, MD, PhD; Takahiko Kinjo, MD, PhD; Tomohide Endo, MD, PhD; Fumie Nishizaki, MD, PhD; Kenji Hanada, MD, PhD; Kenichi Sasaki, MD, PhD; Daisuke Horiuchi, MD, PhD; Masaomi Kimura, MD, PhD; Takumi Higuma, MD, PhD; Hideharu Okamatsu, MD; Yasuaki Tanaka, MD; Junjiroh Koyama, MD; Ken Okumura, MD, PhD

Background: The entirely subcutaneous implantable cardioverter defibrillator (S-ICD) was introduced as a new alternative to conventional transvenous ICD (TV-ICD) in Japan in February 2016, but its safety and efficacy are unclear.

Methods and Results: A total of 60 patients (48 men, median age, 60 years; IQR, 44–67 years; primary prevention, n=24) underwent S-ICD implantation between February 2016 and August 2017. The device pocket was formed in the intermuscular space between the serratus anterior muscle and the latissimus dorsi muscle, and the parasternal S-ICD lead was placed according to pre-implant screening. Defibrillation test was performed in 56 patients (93%). Ventricular fibrillation (VF) was induced in 55 patients and terminated by a single 65-J shock in all patients. The median time to shock therapy was 13.4 s (IQR, 12.1–14.9 s) and the median post-shock impedance of the S-ICD lead was 64 Ω (IQR, 58–77 Ω). There were no operation-related complications or subsequent infectious complications. During follow-up (median, 275 days; IQR, 107–421 days), 1 patient (1.7%) had appropriate shock for VF with successful termination, whereas 5 patients (8.3%) had inappropriate shock due to oversensing of myopotential (n=3) or T-wave (n=1), and detection of supraventricular tachycardia (n=1).

Conclusions: S-ICD is a safe and effective alternative to conventional TV-ICD. The long-term safety and efficacy of the S-ICD need further investigation.

Key Words: Subcutaneous cardioverter defibrillator; Sudden cardiac death; Transvenous implantable cardioverter defibrillator

The entirely subcutaneous cardioverter defibrillator (EMBLEM S-ICD; A209, Boston Scientific, USA) was introduced as a new alternative to the conventional transvenous ICD (TV-ICD) and has been expected to reduce device-related complications such as lead failure, venous obstruction, and systemic infection.[1,2] The 2-year follow-up results from a pooled analysis of the IDE study and EFFORTLESS registry suggested the efficacy and safety of the S-ICD system,[3] and a recently reported complete dataset of the EFFORTLESS registry further confirmed its usefulness.[4] The S-ICD has been available in Japan since February 2016, and a small single-center study in Japan has been reported.[5] The efficacy and safety in Japanese patients at high risk of sudden cardiac death (SCD), however, are largely unclear. Here, we report our primary experience of S-ICD use in the 60 consecutive patients treated in 2 Japanese institutions.

Methods

Patients

Sixty consecutive patients who underwent S-ICD implantation between February 2016 and August 2017 at Hirosaki University Hospital (n=38) and Saiseikai Kumamoto Hospital (n=22) were enrolled in the present study. S-ICD was selected as an alternative to TV-ICD because these patients had an indication for ICD but none of them required pacing therapy, such as bradycardia, cardiac

Received September 21, 2017; revised manuscript received January 10, 2018; accepted January 16, 2018; released online April 11, 2018 Time for primary review: 31 days

Department of Advanced Management of Cardiac Arrhythmias (S.S., D.H.), Department of Cardiology (H.T., Y.I., Y.S., K.N., T.K., T.E., F.N., K.H., K.S., M.K., T.H.), Hirosaki University Graduate School of Medicine, Hirosaki; Advanced Arrhythmia Therapeutic Branch, Division of Cardiology, Saiseikai Kumamoto Hospital Cardiovascular Center, Kumamoto (T.T., H.O., Y.T., J.K., K.O.), Japan

Mailing address: Hirofumi Tomita, MD, PhD, Department of Cardiology, Hirosaki University Graduate School of Medicine, 5 Zaifu-cho, Hirosaki 036-8562, Japan. E-mail: tomitah@hirosaki-u.ac.jp

ISSN-1346-9843 All rights are reserved to the Japanese Circulation Society. For permissions, please e-mail: cj@j-circ.or.jp

Table 1. Clinical Characteristics vs. Device Status

	S-ICD (n=60)	TV-ICD (n=47)	P-value
Age (years)	60 (44–67)	69 (58–79)	0.0001
Male gender	48 (80)	35 (74)	0.64
BMI (kg/m²)	24.4 (20.9–27.0)	23.5 (22.1–26.6)	0.98
Device infection or lead failure	9 (15)	0	0.004
Atrial fibrillation	4 (7)	8 (17)	0.12
LVEF (%)	58 (39–66)	35 (28–57)	0.0003
≤35	14 (23)	23 (49)	0.004
≥50	31 (52)	14 (30)	0.004
History of VT/VF			
Primary prevention	24 (40)	26 (55)	0.12
Secondary prevention	36 (60)	21 (45)	

Data given as median (IQR) or n (%). BMI, body mass index; LVEF, left ventricular ejection fraction; S-ICD, subcutaneous implantable cardioverter defibrillator; TV-ICD, transvenous implantable cardioverter defibrillator; VF, ventricular fibrillation; VT, ventricular tachycardia.

resynchronization therapy (CRT), and anti-tachycardia pacing (ATP). Particularly, S-ICD was selected in those patients in whom venous access was difficult or TV-ICD was removed for device infection, or in young patients with a necessity for long-term ICD therapy. All of them were screened for potential T-wave oversensing utilizing a manufacturer-provided tool that analyzes surface electrocardiogram (ECG) recordings taken during lying down, standing, and immediately after exercise test. Screening was deemed successful if a single ECG vector passed during both lying down and standing. If patients passed screening, they were offered the S-ICD therapy.

During the same study period, 47 patients were treated with TV-ICD at the 2 hospitals. Their clinical characteristics were also evaluated.

The present data were retrospectively collected. The study was approved by the Ethics Committee of Hirosaki University and Saiseikai Kumamoto Hospital.

S-ICD Implantation

S-ICD implantation was performed under conscious sedation using continuous i.v. infusion of midazolam or dexmedetomidine hydrochloride with intermittent i.v. fentanyl, and local anesthesia, except for 7 initial patients who had general anesthesia. Vital signs were monitored continuously during the procedure. Respiratory care was performed using adaptive-servo ventilator to prevent respiratory depression and decompensation of heart failure in patients with low left ventricular ejection fraction (LVEF). Implantation of the S-ICD was performed using a 2- or 3-incision approach. The 3-incision approach is a standard implantation technique, the details of which have been described elsewhere.[1] Forty-three patients underwent S-ICD implantation with the 3-incision approach. The remaining 17 patients (23%) underwent S-ICD implantation by the 2-incision approach. The 2-incision approach has been developed and applied in hundreds of patients.[6] This approach does not require a parasternal incision, and a standard 11-Fr peel-away sheath is used to deliver the lead from the xiphoid incision in a cephalad direction parallel to the sternum. The pulse generator is placed in the intermuscular space between the serratus anterior muscle and the latissimus dorsi muscle via a lateral submammary incision in all patients.[7] After the S-ICD system is placed, the S-ICD assesses the optimal vector for sensing, and the vector with the greatest distinction between the QRS and the T-wave is chosen. Defibrillation test was performed subsequently and we confirmed termination of ventricular fibrillation (VF) by a 65-J shock delivered by the S-ICD. When this 65-J shock was not effective, the defibrillation energy was increased to 80 J and applied. If these 2 shocks failed to terminate VF, external defibrillation using 200 J of biphasic energy was planned. After defibrillation test, the S-ICD was programmed with 2 zones of tachycardia detection: a conditional shock zone and a non-conditional (shock) zone. In the present case, threshold heart rate for the conditional shock zone and non-conditional shock zone was programmed at 190 beats/min and 240 beats/min respectively. Shock energy was set to 80 J for both tachycardia detection zones.

Statistical Analysis

Data are expressed as median (IQR) or n (%). Continuous data were compared using Mann-Whitney U-test. Categorical variables are summarized as frequencies and percentages and compared using Fisher's exact test. Rates of freedom from appropriate shock and inappropriate shock were analyzed using the Kaplan-Meier method. Statistical analysis was performed using JMP 13 (SAS, Cary, NC, USA).

Results

Clinical Characteristics

To clarify the characteristics of the patients who were eligible for S-ICD, we compared the clinical characteristics between S-ICD and TV-ICD patients treated in the 2 hospitals from February 2016 to August 2017 (**Table 1**). Of the 107 consecutive patients, 60 were treated with S-ICD (56%) and the other 47 were treated with TV-ICD (44%). Median age was significantly younger in the S-ICD group than in the TV-ICD group (60 years; IQR, 44–67 years vs. 69 years; IQR, 58–79 years, P=0.0001). Approximately 70–80% were male in both groups. The median body mass index (BMI) in S-ICD patients was 24.4 kg/m² (IQR, 20.9–27.0 kg/m²) with the lowest of 14.3 kg/m² and highest of 42.5 kg/m², and there was no difference between the 2 groups. Median LVEF on echocardiography was significantly

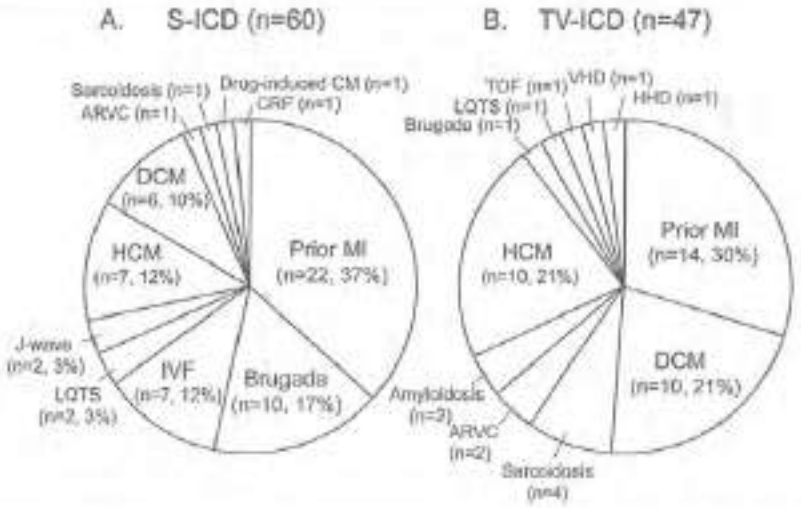

Figure 1. Underlying heart disease in (**A**) subcutaneous implantable cardioverter defibrillator (S-ICD) patients and (**B**) transvenous implantable cardioverter defibrillator (TV-ICD) patients. ARVC, arrhythmogenic right ventricular cardiomyopathy; CRF, chronic renal failure; DCM, dilated cardiomyopathy; HCM, hypertrophic cardiomyopathy; HHD, hypertensive heart disease; IVF, idiopathic ventricular fibrillation; LQTS, long QT syndrome; MI, myocardial infarction; TOF, tetralogy of Fallot; VHD, valvular heart disease.

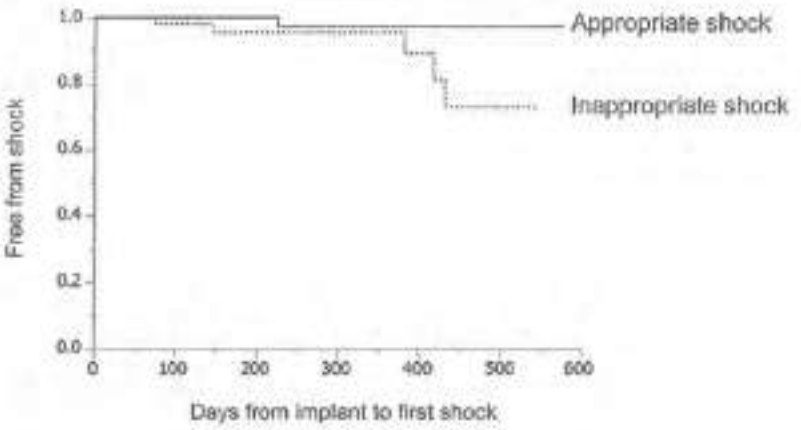

Figure 2. Kaplan-Meier estimates of appropriate and inappropriate shocks in subcutaneous implantable cardioverter defibrillator patients.

higher in S-ICD patients than in TV-ICD patients (58%; IQR, 39–66% vs. 35%, IQR, 28–57%, P=0.0003). More patients had low LVEF (≤35%) in the TV-ICD group compared with the S-ICD group (n=23; 49% vs. n=14; 23%, P=0.004). Notably, 9 patients (15%), who had previous TV-ICD infection or TV-ICD lead failure, were converted to S-ICD implantation. Of all S-ICD patients, 36 (60%) had recent sudden cardiac arrest due to ventricular tachycardia (VT) or VF and were treated as a secondary prevention. Underlying heart disease in the S-ICD group was prior myocardial infarction (MI) in 22 patients (37%); Brugada syndrome in 10 (17%); idiopathic VF in 7 (12%); long QT syndrome in 2 (3%); J-wave syndrome in 2 (3%); hypertrophic cardiomyopathy (HCM) in 7 (12%); dilated cardiomyopathy (DCM) in 6 (10%); and arrhythmogenic right ventricular cardiomyopathy (ARVC), cardiac sarcoidosis; drug-induced cardiomyopathy; and reduced LVEF with chronic renal failure in 1 each (**Figure 1A**). The underlying heart diseases in the TV-ICD group are shown in **Figure 1B**. Compared with the TV-ICD group, the S-ICD group had a higher prevalence of inherited heart disease. All patients were at risk for SCD based on the 2011 Japanese Circulation Society Guidelines,[8] and the S-ICD patients did not need pacing therapy, CRT, or ATP.

Defibrillation Test

Defibrillation test was performed in 56 patients (56/60; 93%) during the procedure. Three patients did not undergo defibrillation test because of the presence of intracardiac thrombi, which were detected in the left atrial appendage (LAA) due to long-standing atrial fibrillation (AF) in 2 patients and in the left ventricular apex due to prior MI in 1 patient. Defibrillation test was avoided due to low LVEF in the remaining 1 patient. VF was induced in 55 patients during the procedure and successfully terminated by a single 65-J shock in all patients. Induced VF was detected appropriately by the S-ICD and no external defibrillation was needed. The median time to shock therapy was 13.4 s (IQR, 12.1–14.9 s) and the median post-shock impedance of the S-ICD lead was 64 Ω (IQR, 58–77 Ω). None of them

Table 2. Inappropriate Shock: Patient Characteristics

Patient age (years)/ Sex	Primary heart disease	Days from implant	Reason for inappropriate shock	Situation at the time of shock	Sensing vector at the time of shock
69/M	Prior MI	416	T-wave oversensing	Sleeping	Primary
46/M	BrS	76	Myopotential	Doing yard work	Secondary
56/M	Prior MI	147	Myopotential	Upper limb lifting work	Secondary
34/M	BrS	430	SVT	Shampooing hair	Secondary
17/M	IVF	381	Myopotential	Shampooing hair	Alternate

BrS, Brugada syndrome; IVF, idiopathic ventricular fibrillation; MI, myocardial infarction; SVT, supraventricular tachycardia.

Figure 3. Representative example of subcutaneous implantable cardioverter defibrillator (S-ICD) electrocardiogram in a patient with inappropriate shock. The secondary sensing vector was automatically chosen as the optimal sensing vector by the S-ICD at implantation. Periodic interference of myopotentials was followed by detection in the ventricular fibrillation zone. Black arrow, shock (80-J) delivery by S-ICD. Oversensing of myopotentials caused inappropriate shock delivery. C, charging; N, noisy beat; S, sensed beat; T, tachy detection.

required revision of position of the pulse generator or parasternal tunneling after defibrillation test.

Implantation-Related Complications and Follow-up

There were no implantation-related complications such as infection, pocket erosion, hematoma, or inadequate/prolonged healing of incision site, although 32 patients (53%) were on anti-thrombotic medication. There was no suboptimal position of pulse generator and/or parasternal S-ICD lead requiring re-implantation.

During a median follow-up of 275 days (IQR, 107–421 days), 1 patient (1.7%) with chronic renal failure (male, 66 years old) had appropriate shock for VF and it was successfully terminated, whereas 5 patients (8.3%) had inappropriate shock. The median time from S-ICD implantation to first inappropriate shock was 381 days (IQR, 112–423 days). The Kaplan-Meier estimates of appropriate and inappropriate shocks are shown in **Figure 2**. In 4 of the 5 patients, inappropriate shock was caused by oversensing of myopotential (n=3) and T-wave (n=1; **Table 2**). A representative example of inappropriate shock is given in **Figure 3**. After inappropriate shock occurred, 4 patients were forced to change a sensing vector from the initial sensing vector to another vector that did not detect the myopotential during exercise test, and there was no recurrence of inappropriate shock after this change. In the remaining 1 patient, inappropriate shock was caused by supraventricular tachycardia (SVT), the average ventricular rate of which exceeded the detection rate of VF. For this patient, radiofrequency catheter ablation was performed and then there was no recurrence of inappropriate shock.

Discussion

Major Findings

In the present study, we have provided information on S-ICD use in Japanese patients who were all indicative of ICD implantation and not of either pacing therapy or CRT indication. There were no implantation-related complications nor subsequent infectious complication. VF

was induced in 55 patients during the procedure and successfully terminated by a single 65-J shock in all patients. One patient had appropriate shock therapy for VF and it was successfully terminated by first shock therapy, whereas 5 patients had inappropriate shocks due to oversensing of myopotential or T-wave and detection of SVT. This study has shown that S-ICD is a safe and an effective alternative to TV-ICD for Japanese patients at high risk of SCD.

S-ICD Use in Japan: Patient Characteristics

The safety and effectiveness of the S-ICD has been established in Europe and the USA.[3,9] A pooled analysis of the IDE study and EFFORTLESS registry include a wide variety of younger patients (median age, 50 years), 70% of whom had primary prevention indication. This tendency was also seen in the S-ICD Post-Approval Study, which enrolled 1,637 patients who underwent S-ICD implantation at 86 US centers.[10] In contrast, the majority (60%) of the present patients had a secondary prevention indication for TV-ICD and had preserved LVEF, characteristic of the present report compared with reports from Western countries. This suggests a Japanese trend in patient selection for S-ICD toward resuscitated patients with inherited disease and normal LV function, such as Brugada syndrome, long-QT syndrome, idiopathic VF, and HCM.

In the present study, 14 patients with reduced LVEF (≤35%) who underwent S-ICD implantation also met the indication for conventional TV-ICD implantation. The majority of these patients (n=9, 64%) did not have a history of sudden cardiac arrest due to VT/VF and underwent S-ICD implantation for primary prevention. Underlying heart disease was prior MI in 10 patients (71%), DCM in 3 patients, and drug-induced cardiomyopathy. Although optimal pharmacological therapy including β-blocker has been achieved in all patients, none of them met the indications of pacing for bradycardia at the time of S-ICD implantation.

Safety and Efficacy of S-ICD

One of the greatest advantages of the S-ICD system is avoidance of TV-ICD lead complications, such as lead failure and venous obstruction. With regard to S-ICD implantation, the most common complications were infection requiring device removal and skin erosion, which accounted for 4.1% in total, followed by other procedural complications, which accounted for 1.1%.[4] In the present study, none of the 60 patients had implantation-related complications or suboptimal positioning of pulse generator and/or parasternal S-ICD lead requiring re-implantation. Although the present follow-up period was short, these results suggest the safety of S-ICD implantation with intermuscular pocket formation.

In the present study, only 1 patient (1.7%) had appropriate shock for VF during follow-up. The possible reasons for the low incidence of appropriate shock in the present study are as follows. First, the follow-up period was short. The median follow-up period of 275 days is shorter than that of recent S-ICD cohorts/trials. Another reason related to the primary heart disease. Approximately 60% of eligible patients in the present study had prior MI, and S-ICD was for secondary prevention of SCD. Because only 1 patient had appropriate shock during follow-up, the confirmation of defibrillation efficacy of the S-ICD system was successful defibrillation rate on defibrillation test. In the present study, VF was induced in 93% of patients during the procedure and successfully terminated by a single 65-J shock in all patients.

Furthermore, given that the S-ICD provides a higher current across the left atrium at the time of defibrillation compared with the TV-ICD, it may be more likely to terminate AF. On defibrillation test, however, 2 long-standing AF patients without intracardiac thrombi had failure to terminate AF in the present study. Further studies are needed to clarify the efficacy of S-ICD for termination of AF. Although defibrillation test was not performed in 2 AF patients with thrombus in the LAA, these patients may be at risk for thromboembolism or development of sick sinus syndrome after possible termination of AF by S-ICD shock therapy. Careful attention should be paid in such cases.

S-ICD Inappropriate Shock

The potential limitation of the S-ICD system is the need for pre-implantation screening to prevent double-counting of QRS complexes or T-wave oversensing. The inappropriate shock rate ranges from 5% to 15%.[3,11-14] In the present study, 5 patients (8.3%) had inappropriate shock during follow-up. In 4 of these patients, inappropriate shock was caused by interference of myopotential during daily life movement or T-wave oversensing at rest. Olde Nordkamp et al reported the incidence of inappropriate shocks in the EFFORTLES S-ICD Registry.[15] During a follow-up period of 21±13 months, 101 inappropriate shocks were detected in 48 of 581 patients (8.3%). The most common cause was cardiac signal oversensing (73%) such as T-wave oversensing, followed by SVT in 18% and non-cardiac oversensing such as myopotential oversensing in 9%. Although the incidence of inappropriate shock (5/60; 8.3%) in the present study is similar to that in the EFFORTLES S-ICD Registry, the incidence of inappropriate shock due to myopotential oversensing was unexpectedly higher (3/5; 60%). One reason is the small number of patients. Another possible reason seems to be the relative change of position of the S-ICD pulse generator to the thorax. All inappropriate shocks due to myopotential oversensing were caused by interference of myopotential during daily life movement. Two patients had shock therapy while raising the left upper extremity upward periodically, and the secondary sensing vector was chosen in both patients at the time of inappropriate shock. This suggests that such a movement causes shifting of the S-ICD generator to the former upper part of the thorax, which may be related to the interference of myopotential. In the remaining 1 patient, sequential decrease of QRS amplitude was found in both surface ECG and subcutaneous ECG in association with progression of the underlying heart disease. Such changes on subcutaneous ECG may make it impossible to differentiate tachycardia from myopotential, leading to inappropriate shock. Although inappropriate shock was able to be avoided in that patient by changing a sensing vector from the initial vector to another, the QRS amplitude in the selected vector was still low and the risk of recurrent inappropriate shock remained. The experience of this patient suggests that there may be a potential limitation of S-ICD indication in patients with progressive heart diseases such as ARVC.

Notably, the majority of inappropriate shocks occurred ≥1 year after S-ICD implantation. These patients also passed a usual pre-implantation screening that included treadmill exercise test. This suggests that the conventional exercise test such as treadmill exercise test may be insufficient

to ensure optimal selection of patients suitable for S-ICD. A novel algorithm (SMART Pass algorithm) designed to reduce oversensing in the S-ICD, has recently been developed. This algorithm uses a high-pass filter (9 Hz) to sense and estimate heart rate more precisely. Therefore, the algorithm is expected to reduce inappropriate shock due to T-wave oversensing. We added this algorithm to all S-ICD in the present study, except in 1 patient, for whom the SMART Pass algorithm was not added to the S-ICD due to the limitation of QRS morphology in the selected vector. This patient had inappropriate shock due to T-wave oversensing. Inappropriate shock due to interference of myopotential, however, was caused in 3 of 5 patients, and this new algorithm had been added for 2 of them. Although the number of patients was small, this suggests that there might be a limitation in preventing interference of myopotential by the SMART Pass algorithm. A new screening system that is capable of avoiding inappropriate shock, is warranted.

Study Limitations

There were several limitations in the present study. First, this was a retrospective observational study and therefore generalization of the results may be limited. We, however, studied consecutive patients admitted during the study period, which seems to have minimized the bias caused by the study design. Second, this was a multicenter study, but only 2 hospitals participated and the number of patients was relatively small. Finally, the follow-up period may not have been sufficiently long to provide evidence. A further large-scale prospective study across the whole of Japan is required to confirm the present results.

Conclusions

The S-ICD as a viable alternative to conventional TV-ICD. The long-term safety and efficacy of the S-ICD need further investigation.

Acknowledgments

We gratefully thank Mrs. Takeshi Goto and Eiichi Tomita in the Department of Clinical Engineering, Hirosaki University Hospital, and Yoshiro Sakai in the Department of Clinical Engineering, Saiseikai Kumamoto Hospital, for their excellent technical support.

Disclosures

S.S. and D.H. have received research grant support from Medtronic Japan Co., Ltd. and Fukuda Denshi Kitajonhoku Hanbai Co., Ltd. K.O. and M.K. have received speaker honoraria from Johnson & Johnson K.K. and Medtronic Japan Co., Ltd. The other authors declare no conflicts of interest.

References

1. Bardy GH, Smith WM, Hood MA, Crozier IG, Melton IC, Jordaens L, et al. An entirely subcutaneous implantable cardioverter-defibrillator. *N Engl J Med* 2010; **363:** 36–44.
2. Lambiase PD, Barr C, Theuns DA, Knops R, Neuzil P, Johansen JB, et al. Worldwide experience with a totally subcutaneous implantable defibrillator: Early results from the EFFORTLESS S-ICD Registry. *Eur Heart J* 2014; **35:** 1657–1665.
3. Burke MC, Gold MR, Knight BP, Barr CS, Theuns DA, Boersma LV, et al. Safety and efficacy of the totally subcutaneous implantable defibrillator: 2-year results from a pooled analysis of the IDE study and EFFORTLESS registry. *J Am Coll Cardiol* 2015; **65:** 1605–1615.
4. Boersma L, Barr C, Knops R, Theuns D, Eckardt L, Neuzil P, et al. Implant and midterm outcomes of the Subcutaneous Implantable Cardioverter-Defibrillator Registry: The EFFORTLESS Study. *J Am Coll Cardiol* 2017; **70:** 830–841.
5. Nishii N, Tachibana M, Morimoto Y, Kawada S, Miyoshi A, Sugiyama H, et al. Initial experience with the subcutaneous implantable cardioverter-defibrillator in a single Japanese center. *J Arrhythm* 2017; **33:** 338–341.
6. Knops RE, Olde Nordkamp LR, de Groot JR, Wilde AA. Two-incision technique for implantation of the subcutaneous implantable cardioverter-defibrillator. *Heart Rhythm* 2013; **10:** 1340–1343.
7. Ferrari P, Giofré F, Filippo P. Intermuscular pocket for subcutaneous implantable cardioverter defibrillator: Single-center experience. *J Arrhythm* 2016; **32:** 223–226.
8. JCS Joint Working Group. Guidelines for non-pharmacotherapy of cardiac arrhythmias (JCS 2011): Digest version. *Circ J* 2013; **77:** 249–274.
9. Weiss R, Knight BP, Gold MR, Leon AR, Herre JM, Hood M, et al. Safety and efficacy of a totally subcutaneous implantable-cardioverter defibrillator. *Circulation* 2013; **128:** 944–953.
10. Gold MR, Aasbo JD, El-Chami MF, Niebauer M, Herre J, Pratkin JM, et al. Subcutaneous implantable cardioverter-defibrillator Post-Approval Study: Clinical characteristics and perioperative results. *Heart Rhythm* 2017; **14:** 1456–1463.
11. Jarman JW, Todd DM. United Kingdom national experience of entirely subcutaneous implantable cardioverter defibrillator technology. Important lessons to learn. *Europace* 2013; **15:** 1158–1165.
12. Olde Nordkamp LR, Dabiri Abkenari L, Boersma LV, Maass AH, de Groot JR, van Gostrom AJ, et al. The entirely subcutaneous implantable cardioverter-defibrillator: Initial clinical experience in a large Dutch cohort. *J Am Coll Cardiol* 2012; **60:** 1933–1939.
13. Aydin A, Hartel F, Schlüter M, Bunter C, Köbe J, Seifert M, et al. Shock efficacy of subcutaneous implantable cardioverter-defibrillator for prevention of sudden cardiac death: Initial multicenter experience. *Circ Arrhythm Electrophysiol* 2012; **5:** 913–919.
14. Köbe J, Reinke F, Meyer C, Shin DI, Martens E, Kähb S, et al. Implantation and follow-up of totally subcutaneous versus conventional implantable cardioverter-defibrillators: A multicenter case-control study. *Heart Rhythm* 2013; **10:** 29–36.
15. Olde Nordkamp LR, Brouwer TF, Barr C, Theuns DA, Boersma LV, Johansen JB, et al. Inappropriate shocks in the subcutaneous ICD: Incidence, predictors and management. *Int J Cardiol* 2015; **195:** 126–133.

Received 9 February 2017 | Revised 21 February 2017 | Accepted 20 July 2017
DOI: 10.1002/ccd.27343

ORIGINAL STUDIES

WILEY

Visual estimation versus different quantitative coronary angiography methods to assess lesion severity in bifurcation lesions

Maik J. Grundeken, MD, PhD[1] | Carlos Collet, MD[1] | Yuki Ishibashi, MD, PhD[2] | Philippe Généreux, MD[3,4,5,6] | Takashi Muramatsu, MD, PhD[7] | Laura LaSalle, MPH[3] | Aaron V. Kaplan, MD[8] | Joanna J. Wykrzykowska, MD, PhD[1] | Marie-angèle Morel, BsC[9] | Jan G. Tijssen, PhD[1,9] | Robbert J. de Winter, MD, PhD[1] | Yoshinobu Onuma, MD, PhD[2,9] | Martin B. Leon, MD[3,4] | Patrick W. Serruys, MD, PhD[10]

[1]Amsterdam Heart Center, Academic Medical Center, Amsterdam, The Netherlands
[2]Thoraxcenter, Erasmus Medical Center, Rotterdam, The Netherlands
[3]Cardiovascular Research Foundation, New York
[4]Columbia University Medical Center, New York
[5]Morristown Medical Center, Morristown, New Jersey
[6]Hôpital du Sacre-Coeur de Montréal, Université de Montréal, Montréal, Québec, Canada
[7]Department of Cardiology, Fujita Health University Hospital, Toyoake, Japan
[8]Geisel School of Medicine/Dartmouth Hitchcock Medical Center, New Hampshire, Lebanon
[9]Cardialysis B.V, Rotterdam, The Netherlands
[10]International Centre for Circulatory Health, NHLI, Imperial College London, United Kingdom

Correspondence
Patrick W. Serruys, MD, PhD, International Centre for Circulatory Health, NHLI, Imperial College London, London, The United Kingdom (or) P.O. Box 2125, 3000 CC Rotterdam, The Netherlands.
Email: patrick.w.j.c.serruys@gmail.com

Abstract

Objectives: To compare visual estimation with different quantitative coronary angiography (QCA) methods (single-vessel versus bifurcation software) to assess coronary bifurcation lesions.

Background: QCA has been developed to overcome the limitations of visual estimation. Conventional QCA however, developed in "straight vessels," has proved to be inaccurate in bifurcation lesions. Therefore, bifurcation QCA was developed. However, the impact of these different modalities on bifurcation lesion severity classification is yet unknown.

Methods: From a randomized controlled trial investigating a novel bifurcation stent (Clinicaltrials.gov NCT01589721) patients with baseline assessment of lesion severity by means of visual estimation, single-vessel QCA, 2D bifurcation QCA and 3D bifurcation QCA were included. We included 113 bifurcations lesions in which all 5 modalities were assessed. The primary end-point was to evaluate how the different modalities affected the classification of bifurcation lesion severity and extent of disease.

Results: On visual estimation, 100% of lesions had side-branch diameter stenosis (%DS) >50%, whereas in 83% with single-vessel QCA, 27% with 2D bifurcation QCA and 26% with 3D bifurcation QCA a side-branch %DS >50% was found (P < 0.0001). With regard to the percentage of "true" bifurcation lesions, there was a significant difference between visual estimate (100%), single-vessel QCA (73%) and bifurcation QCA (17% with 2D bifurcation software and 13% with 3D bifurcation software, P < 0.0001).

Conclusions: Our study showed that bifurcation lesion complexity was significantly affected when more advanced bifurcation QCA software were used. "True" bifurcation lesion rate was 100% on visual estimation, but as low as 13% when analyzed with dedicated bifurcation QCA software.

KEYWORDS
angiography, coronary, bifurcation lesion, bifurcation quantitative coronary angiography, coronary artery disease, interventional devices/innovation, medical, percutaneous coronary intervention, percutaneous coronary intervention complex PCI, quantitative coronary angiography, visual estimation

 © 2017 Wiley Periodicals, Inc.

1 | INTRODUCTION

Ever since the introduction of coronary angiography, it has been recognized that visual estimation is inaccurate to quantify coronary stenosis severity [1,2]. This seems to be particularly true for the side branch stenosis in bifurcation lesions, even for experts in the field of bifurcations [3]. Conventional quantitative coronary angiography (QCA) software, developed to objectively quantify lesion severity in "straight" vessel segments without side branches, also have been shown to be inaccurate in bifurcation lesions due to the natural fractal geometry of the coronary tree, with a "step-down" in diameter at each branching point (i.e., coronary bifurcation), overestimating the reference vessel diameter (and thus diameter stenosis) of the distal main branch and side branch [4–6]. Dedicated bifurcation QCA software packages were developed and have proved, in a bifurcation phantom model, to be accurate and reproducible for the quantification of bifurcation stenosis severity [4].

However, to date no study has been performed to investigate the impact of the use of bifurcation QCA when compared with conventional "straight" vessel QCA or visual estimation in patients with coronary artery disease involving a bifurcation. This is of particular importance for several reasons: (i) side branch involvement (i.e., presence or absence of side branch stenosis) represents a major inclusion criterion for clinical trials assessing treatment strategy of true bifurcation lesions [7], (ii) it is used by operators as guidance to select the most appropriate treatment strategy, with a tendency to select more complex (2-stent) approaches when the side branch is involved [8–10] and (iii) it is associated with a worse prognosis [11]. We therefore investigated how the use of different modalities (visual estimation, "straight vessel" QCA, and bifurcation QCA) affected the classification of bifurcation lesion severity and extent of disease.

2 | METHODS

2.1 | Setting

For this study, coronary angiographies were used from a randomized controlled trial investigating a novel dedicated bifurcation stent [7]. The institutional review board at each participating site approved the trial, and all patients provided written informed consent before inclusion in the trial. Angiographic inclusion criteria were based on visual estimation. The key angiographic inclusion criteria were the presence of >50% stenosis in both the main branch and side branch in a native coronary artery with side branch diameters from ≥2.5 to ≤3.5 mm and main branch diameters from ≥2.5 to ≤4.0 mm [7]. All baseline angiographies were collected and sent to two independent core laboratories [The Cardiovascular Research Foundation (CRF, NY) and Cardialysis B. V. (Rotterdam, The Netherlands)] for further offline QCA analysis [5].

2.2 | Modalities to assess bifurcation lesion severity

Visual estimation of lesion severity was reported by investigators in the electronic case report form using the Medina score. The Medina score indicates for each of the three bifurcation segments separately whether a ≥50% stenosis is present (as "1") or absent (as "0") in the following order: proximal main branch, distal main branch, and side branch, resulting in scores ranging from Medina 0.0.0 to Medina 1.1.1 [12].

Baseline QCA were performed by both core labs using different methodologies [5]. CRF corelab applied a conventional single vessel QCA algorithm for their analyses (QAngio XA, version 7.2.24, Medis Medical Imaging Systems, Leiden, The Netherlands) [5]. For each bifurcation, two separate analyses were performed: one for the main branch and one for the side branch (Figures 1 and 2) [5]. First, calibration was performed before each analysis. Then, for the main branch the "region of interest" was determined manually from the proximal to the distal main branch [5]. For the side branch, the region of interest was set in two different ways. In the first method, the region of interest was set from the proximal main branch to the side branch (see Figures 1 and 2). In the alternative method, the region of interest for the side branch was set from the side branch ostium to distally in the side branch (see Figures 1 and 2). Then, the QCA software automatically detected the vessel contours [13]. The main branch reference vessel diameter (RVD), used to calculate diameter stenosis, was determined by the average between the proximal main branch and distal main branch reference diameter. For the side branch, the RVD was determined in two different ways. In the first methodology, the average between the proximal main branch diameter and the side branch diameter was chosen (in case the region of interest was set from the proximal main branch to the side branch). Alternatively, the diameter of a "healthy" part distally in the side branch was taken as reference diameter (in case the region of interest was from the side branch ostium to distally in the side branch). Diameter stenoses were calculated as follows: [(RVD−minimal lumen diameter (MLD)/RVD)] [5].

Cardialysis corelab used a bifurcation QCA software package for their analyses (Coronary Angiography Analysis System (CAAS), version 5.10, Pie Medical Imaging, Maastricht, The Netherlands) [5]. For each bifurcation, only one analysis was performed in which the "region of interest" included all three bifurcation segments: the proximal main branch, distal main branch and side branch. The software automatically detected the vessel contours and the percentage diameter stenosis was automatically calculated using an interpolated RVD at the MLD site of each of the three bifurcation segments separately [5]. The analyses were performed both in a two-dimensional (2D) as in a three-dimensional (3D) fashion, as previously described [14]. Two angiographic images separated by a viewing angle of ≥ 30° were selected for the 3D analysis [14]. After contour detection of two angiographic images, a common image point (CIP) was defined to correct for the distortion introduced by the isocenter offset. Subsequently, the centre line of the main branch and the side branch were reconstructed based on the adaptive 3-D epipolar geometry algorithm. A 3D model of the bifurcated vessel assuming elliptical cross-section was constructed. In the central bifurcation area, defined as the polygon of confluence the cross sectional area was defined by using the "minimum energy" cross-section, that is, the smoothest possible surface that spans the lumen at each centre line position. MLD was derived from the absolute minimal lumen area using the previously described "equivalent diameters" methodology [14,15].

https://onlinelibrary.wiley.com/doi/10.1002/ccd.27243/format/pdf/QERPS/ 2020/04/27

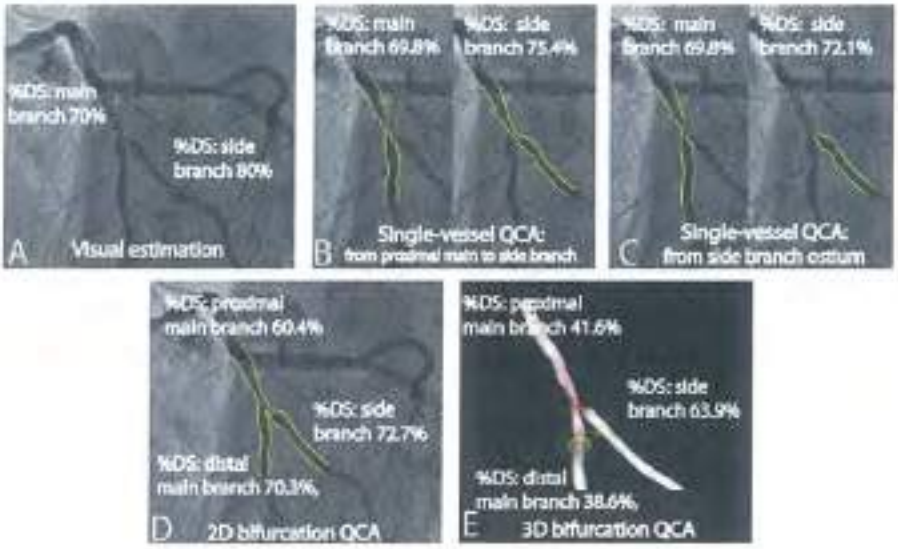

FIGURE 1 **Different modalities to assess bifurcation lesion severity.** A, Coronary bifurcation lesion of the left anterior descending and diagonal branch. Panel A represents the visual estimation of lesion severity, without additional help from software. B, single-vessel QCA applied to a bifurcation lesion. The left panel represents QCA of the (proximal and distal) main branch, whereas the right panel represents QCA of the side branch with the region of interest taken from the proximal main branch to the side branch. C, single-vessel QCA applied to a bifurcation lesion. The left panel again represents QCA of the main branch, similar to the left panel in B. The right panel represents QCA of the side branch with the region of interest taken from the side branch ostium to distally in the side branch. D, 2D bifurcation QCA in which the region of interest includes all three segments (proximal main branch, distal main branch and side branch) of the bifurcation. E, 3D bifurcation QCA in which a 3D image was reconstructed from two different angiographic views [Color figure can be viewed at wileyonlinelibrary.com]

2.3 | Statistical analysis

For the current analysis, only those baseline angiograms were used in which all used modalities (i.e., visual estimation, single-vessel QCA (two different methodologies for the side branch), 2D bifurcation QCA and 3D bifurcation QCA) were available. Presence of a stenosis on QCA was defined as a percentage diameter stenosis of ≥50%. For the 2D and 3D bifurcation QCA analysis, Medina scores were derived using the calculated percentage diameter stenosis of each bifurcation segment, in a similar fashion as the Medina scores assessed by visual estimate by the investigators. This was not possible for the single-vessel QCA because there was only one value calculated for the main branch (i.e., not for the proximal and distal main branch separately).

Furthermore, bifurcation lesions were divided according to the following categories:

- "True" bifurcation lesions, with ≥50% stenosis in both the main branch and the side branch;
- "Nontrue" bifurcation lesions, with ≥50% stenosis in the main branch, but <50% stenosis in the side branch;
- "Side branch lesion only," with ≥50% stenosis in the side branch, but <50% stenosis in the main branch;
- "No lesion," defined as <50% stenosis in the main branch and side branch.

Finally, bifurcation lesions were dichotomized according to "side branch involvement" (i.e., all bifurcation lesions with ≥50% stenosis of side branch) or "no side branch involvement" (i.e., all the remainder bifurcation lesions with <50% stenosis of the side branch).

Categorical variables were presented as frequencies and percentages, and comparisons were made using chi-square. All statistical analysis were performed using the SPSS software package (version 19.0, IBM, Chicago, IL).

To evaluate whether morphological characteristics of the bifurcation lesions influence bifurcation lesion severity assessment, all analyses were repeated for side branch reference diameters <2.00 mm versus ≥2.00 mm on 3D bifurcation QCA (based on the median of 1.96 mm), and for distal bifurcation angles <60° versus ≥60° on 3D bifurcation QCA (based on the median of 59.14°).

3 | RESULTS

There were in total 113 baseline angiographies in which all 5 modalities were available. Table 1 shows the extent of disease in the bifurcation lesions according to the different modalities. On visual estimate all lesions were scored as either Medina 0,1,1, 1,0,1, or 1,1,1.

With regard to the percentage of "true" bifurcation lesions (i.e., bifurcations in which both main and side branch had ≥ 50% stenosis), there was a significant difference between visual estimate (100%),

https://onlinelibrary.wiley.com/reader/content/10.1002/ccd.27243/format/pdf/OFRPS/ 2020/04/27

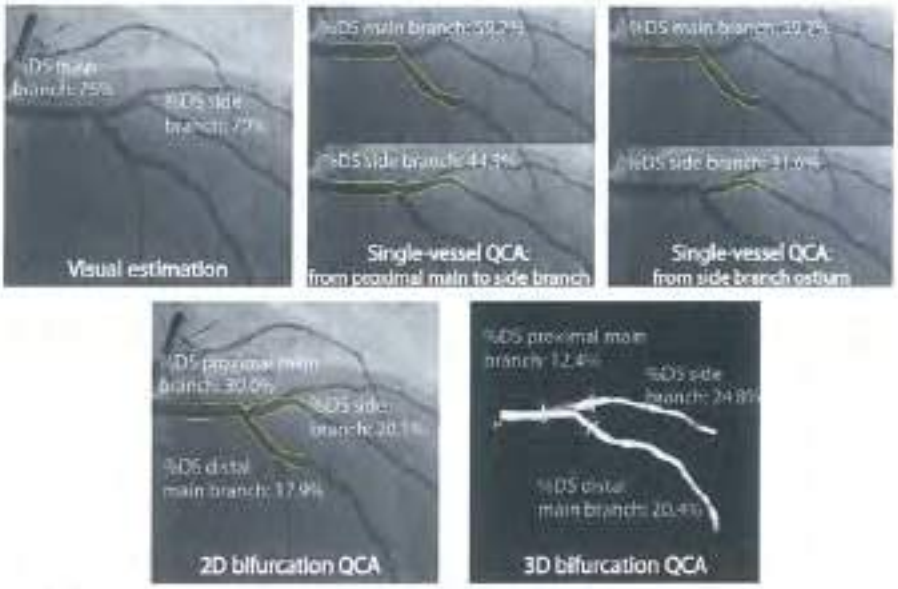

FIGURE 2 Different modalities to assess bifurcation lesion severity. A second case example in which all modalities were used to assess bifurcation lesions. Panels as in Figure 1. A, represents the visual estimation. B, single-vessel QCA applied to a bifurcation lesion. The upper panel represents QCA of the (proximal and distal) main branch, whereas the lower panel represents QCA of the side branch with the region of interest taken from the proximal main branch to the side branch. C, single-vessel QCA with the side branch region of interest taken from the side branch ostium to distally in the side branch. D, 2D bifurcation QCA in which the region of interest includes all three segments (proximal main branch, distal main branch and side branch) of the bifurcation. E, 3D bifurcation QCA in which a 3D image was reconstructed from two different angiographic views [Color figure can be viewed at wileyonlinelibrary.com]

single-vessel QCA (75 or 56%, depending on the methodology) and bifurcation QCA (17% with 2D bifurcation software and 13% with 3D bifurcation software, $P < 0.0001$). Moreover, there was a significant difference in percentage of bifurcations without any stenosis > 50%: 0% with visual estimation, 1 or 4% with single vessel QCA, 33% with 2D bifurcation QCA, and even 45% with 3D bifurcation QCA (Table 1).

The percentage of bifurcation lesions with side branch involvement (i.e., the presence of >50% stenosis in the side branch) was 100% on visual estimate. However, this percentage was significantly lower when single-vessel QCA was used, and further reduced when bifurcation QCA was used (only 27% (2D bifurcation QCA) and 26% (3D bifurcation QCA) of lesions had side branch involvement with bifurcation QCA) (Table 1).

Findings were similar in small (<2.00 mm) and "large" (≥2.00 mm) side branches and in narrow (<60°) and large (≥60°) distal bifurcation angles.

4 | DISCUSSION

The main findings of our study are: (1) the rate of "true" bifurcation lesions (i.e., bifurcation lesions with ≥ 50% stenosis in both main and side branch), a major inclusion criterion of the trial, was 100% on visual estimation, and 13% when dedicated bifurcation QCA software was used; (2) When dedicated bifurcation software was used, 33% (2D bifurcation QCA) or even 45% (3D bifurcation QCA) of the bifurcation lesions did not have any stenosis ≥ 50% in any of the bifurcation segments.

This is the first study with a head-to-head comparison between visual estimation, single-vessel QCA and bifurcation QCA to assess coronary bifurcation lesions. Within this study, no "true value" could be established. However, previous studies on precision phantom bifurcation models, made from Plexiglas with a tolerance <10 μm, have shown that visual estimates of diameter stenoses by experts in the field of bifurcations were inaccurate and highly variable [3]. This seemed to be particularly true for the side branch ostium. An explanation for this might be that the experienced interventional cardiologists intuitively interpreted the side branch stenosis by using the reference diameter of the proximal main branch. However, due to the fractal geometry of the coronary tree with its natural step-down in diameter at each branching point, the reference diameter of the side branch is per definition smaller than the reference diameter of the proximal main branch, hence overestimating diameter stenosis of the side branch [3,6,16,17].

Another study on the same precision phantom bifurcation models, comparing single-vessel QCA with 2D bifurcation QCA, have shown that the accuracy and precision of single-vessel QCA was very poor [4]. Single-vessel QCA systematically overestimated the RVD (and thus percent diameter stenosis) of the side branch [4]. The same study

https://onlinelibrary.wiley.com/reader/content/10.1002/ccd.27243/format/pdf/OERPS/ 2020/04/27

TABLE 1 Impact of different modalities on classification of bifurcation lesion severity

	Visual estimate by investigators (n = 113)	QCA with single-vessel software (SB RVD based on prox. and dist. ref.) (n = 113)	QCA with single-vessel software (SB RVD based on distal ref.) (n = 113)	QCA with 2D bifurcation software (n = 113)	QCA with 3D bifurcation software (n = 113)	P-value
Medina score						<0.0001
1,1,1	77 (68%)	NA	NA	6 (5%)	0 (-)	
1,0,1	12 (11%)	NA	NA	5 (4%)	7 (6%)	
0,1,1	24 (21%)	NA	NA	8 (7%)	8 (7%)	
1,1,0	0 (-)	NA	NA	5 (4%)	4 (4%)	
1,0,0	0 (-)	NA	NA	24 (21%)	14 (12%)	
0,1,0	0 (-)	NA	NA	17 (15%)	15 (13%)	
0,0,1	0 (-)	NA	NA	11 (10%)	14 (12%)	
0,0,0	0 (-)	NA	NA	37 (33%)	51 (45%)	
Bifurcation type						<0.0001
"True" (>50% stenosis in both MB and SB)	113 (100%)	85 (75%)	63 (56%)	19 (17%)	15 (13%)	
"Nontrue" (MB stenosis >50%, SB stenosis <50%)	0 (-)	18 (16%)	40 (35%)	46 (41%)	33 (29%)	
"SB only" (MB stenosis <50%, SB stenosis >50%)	0 (-)	9 (8%)	5 (4%)	11 (10%)	14 (12%)	
"No lesion" (<50% stenosis in both MB and SB)	0 (-)	1 (1%)	5 (4%)	37 (33%)	51 (45%)	
SB involvement						<0.0001
SB involvement	113 (100%)	94 (83%)	68 (60%)	30 (27%)	29 (26%)	
No SB involvement	0 (-)	19 (17%)	45 (40%)	83 (73%)	84(74%)	
Diameter stenosis side branch (%)	72.5 ± 12.5	60.2 ± 11.0	53.2 ± 12.7	38.5 ± 14.7	40.0 ± 15.6	<0.0001

Abbreviations: MB, main branch; NA, not available; RVD, reference vessel diameter; SB, side branch.

showed that dedicated bifurcation QCA, either CAAS software (CAAS, Pie Medical Imaging, Maastricht, the Netherlands) or QAngio XA software (Medis Medical Imaging Systems, Leiden, The Netherlands), were both accurate and precise and therefore suitable for quantification of stenosis in bifurcation lesions [4].

The data from this study, paired with the previous work on the precision phantom models, suggests that the human eye is unreliable to quantify bifurcation lesions, overestimating side branch stenosis. On visual estimate, all bifurcation lesions included had a ≥ 50% side branch stenosis, while with the more sophisticated 2D bifurcation QCA methodology, 27% of bifurcations had side branch involvement. Our study also showed that single-vessel QCA, especially when the side branch reference diameter was derived based on the proximal main branch and side branch reference diameters, does not overcome the limitations of the human eye. These findings might have important implications for the following reasons:

1. First, when inclusion criteria of trials are based on visual estimation of side branch stenosis, this will lead to over exaggeration of side branch lesion severity and overtreatment of insignificant stenosis. This is important because more complex lesion treatment strategies, including the use of two stents with or without the use of dedicated bifurcation stents, are not expected to confer any incremental benefit compared with provisional single stent strategy when used in less complex bifurcation lesions without significant side branch stenosis. The use of single-vessel QCA will not overcome this problem because it will still lead to overestimation of side branch stenosis as has been shown in the phantom study [4]. Major bifurcation randomized trials such as BBC ONE, CACTUS, the Thoeringer bifurcation study and the Tryton IDE trial in which two-stent techniques (with or without a bifurcation stent) were compared with the provisional single-stent approach have used single-vessel QCA analysis for their baseline analysis [7,18–20]. Mandatory preprocedural lesion assessment with bifurcation QCA might have resulted in inclusion of truly significant side branch stenosis, which could have showed the clinical benefit of the two-stent approach. The European Bifurcation Club recommends the use of bifurcation QCA [9,21].

2. Second, in trials with a repeat angiography, overestimation of side branch stenosis during repeat angiography might result in increased rates of clinically indicated target lesion revascularization. As defined by the Academic Research Consortium, revascularizations are considered clinically indicated if the lesion is >70, or >50% stenosis with additional evidence of ischemia [22]. Use of single-vessel QCA during repeat angiographic follow-up might therefore influence event adjudication.

The additional advantage of 3D bifurcation software over 2D bifurcation software in terms of assessing stenosis severity are yet to be determined. A validation study using the above mentioned precision phantom bifurcation models have showed that 3D bifurcation software being accurate, precise and reproducible [23]. However, a head-to-head study comparing 2D with 3D bifurcation software in this phantom model is lacking. The potential benefits of 3D over 2D bifurcation software is difficult to demonstrate in this model for the following reasons: (1) in the phantom model, stenoses are shaped concentric, while advantage of 3D are expected to be more pronounced when stenoses are elliptically shaped; (2) the phantom model is constructed in a horizontal plane, while in-vivo the coronary arteries are curved around the heart, which would result in an expected benefit of 3D QCA over 2D QCA in terms of less foreshortening of the curved arteries; (3) in the bifurcation model the most optimal view, perpendicular to the bifurcation, is easily to obtain, while it has been shown in-vivo that the optimal viewing angle for bifurcation lesions cannot be obtained in almost half of the cases, hampering accurate 2D bifurcation QCA assessment while this optimal view can be reconstructed with 3D bifurcation QCA software [24].

A previous study by Samo et al. comparing single vessel versus 2D bifurcation QCA against invasive fractional flow reserve (FFR) in bifurcation lesions has shown a higher correlation between anatomic severity (i.e., diameter stenosis) and functional significance (FFR < 0.80) with dedicated bifurcation software. These finding seem to be particularly more pronounced when assessing side-branch stenosis, which can be overestimated when using single vessel QCA [25]. In addition, Yong et al. has shown that 3D QCA luminal measurements had a better correlation with invasive FFR measurements than 2D QCA derived parameters [26]. This suggests a more accurate assessment of luminal dimensions with 3D than with 2D QCA, although this needs further research including a head-to-head comparison in an appropriate phantom model. In addition to luminal dimensions measurements, the true advantage of 3D bifurcation QCA seems to be the superiority of 3D QCA modalities to assess (lesion) length, overcoming the disadvantage of length measurements in 2D caused by foreshortening [27]. Another potential advantage of 3D over 2D bifurcation software is its ability to perform analysis in the (reconstructed) most optimal viewing angle, even when it is not possible to obtain this viewing angle during angiography [24].

Further study will be required to understand if these algorithms, when compared with visual estimation, better characterize the risk of procedural complications (abrupt closure/bailout stenting), stent thrombosis and restenosis.

5 | LIMITATIONS

A true 'gold standard' was lacking in this study. However, previous studies have shown the superiority of bifurcation QCA over visual estimate and over single-vessel QCA in assessing lesion severity in bifurcation lesions. The potential benefit of 3D bifurcation QCA compared to 2D bifurcation QCA software in terms of assessment of luminal dimensions is still uncertain. Nevertheless, we showed that the assessment of bifurcation lesion complexity (i.e., involvement with >50% stenosis of the different bifurcation segments) is strongly affected when more advanced bifurcation QCA techniques were used. 3D QCA analysis depend on the acquisition of two views, obtained more than 30° apart. If only 1 view was available 3D QCA analyses could not be performed, which might have introduced a selection bias.

6 | CONCLUSIONS

Our study showed that characterization of bifurcation lesion complexity was significantly affected when more advanced bifurcation QCA software was used. "True bifurcation lesion" (i.e., bifurcation lesions with ≥50% stenosis in both main and side branch) rate was 100% on visual estimation, but as low as 13% when dedicated bifurcation QCA software was used. Side branch involvement (defined as >50% stenosis of the side branch) was found in 100% of the cases on visual estimation and in only 27% of the cases when 2D bifurcation QCA software was used. Furthermore, when dedicated bifurcation software was used, 33% (2D bifurcation QCA) or even 45% (3D bifurcation QCA) of the bifurcation lesions did not have any stenosis ≥50% in any of the bifurcation segments.

CONFLICTS OF INTEREST

Philippe Généreux received speaker fees from Abbott Vascular, Cardiovascular System Inc., Tryton Medical, Edwards Lifesciences, and Astra Zeneca. Research grant from Boston Scientific and Cardiovascular System Inc.; is a consultant for Cardiovascular System Inc. and Soundbite Medical Solutions Inc., and is equity holder of Soundbite Medical Solutions Inc. Joanna Aaron V. Kaplan is a Founder and Director of Tryton Medical, Inc. J. Wykrzykowska: Receives speaker and consultancy fees from Abbott, Tryton Medical, and Stentys. Martin B. Leon is member of the Scientific Advisory Board for Abbott Vascular, Boston Scientific, and Medtronic; and he is the Principal Investigator of the Tryton Bifurcation Study. The other authors have nothing to disclose.

ORCID

Maik J. Grundeken MD, PhD http://orcid.org/0000-0003-2068-3833
Patrick W. Serruys MD, PhD http://orcid.org/0000-0002-9636-1104

REFERENCES

[1] Zir LM, Miller SW, Dinsmore RE, Gilbert JP, Harthorne JW. Interobserver variability in coronary angiography. Circulation 1976;53:627-632.

[2] Galbraith JE, Murphy ML, de Soyza N. Coronary angiogram interpretation. Interobserver variability. JAMA 1978;240:2053–2056.

[3] Girasis C, Onuma Y, Schuurbiers JC, Morel MA, van Es GA, van Geuns RJ, Wentzel JJ, Serruys PW. 5th meeting of the European Bifurcation C. Validity and variability in visual assessment of stenosis severity in phantom bifurcation lesions: a survey in experts during the fifth meeting of the European Bifurcation Club. Catheter Cardiovasc Interv 2012;79:561–568.

[4] Ishibashi Y, Grundeken MJ, Nakatani S, Iqbal J, Morel MA, Generaux P, Girasis C, Wentzel JJ, Garcia-Garcia HM, Onuma Y, Serruys PW. In vitro validation and comparison of different software packages or algorithms for coronary bifurcation analysis using calibrated phantoms: Implications for clinical practice and research of bifurcation stenting. Catheter Cardiovasc Interv 2015;85:554–563.

[5] Grundeken MJ, Ishibashi Y, Generaux P, LaSalle L, Iqbal J, Wykrzykowska JJ, Morel MA, Tijssen JG, de Winter RJ, Girasis C, Garcia-Garcia HM, Onuma Y, Leon MB, Serruys PW. Inter-core lab variability in analyzing quantitative coronary angiography for bifurcation lesions: A post-hoc analysis of. A Randomized Trial. JACC Cardiovasc Interv 2015;8:305–314.

[6] Grundeken MJ, Ishibashi Y, Ramchandar S, Tuinenburg JC, Reiber JH, Tu S, Aben JP, Girasis C, Wykrzykowska JJ, Onuma Y, Serruys PW. The need for dedicated bifurcation quantitative coronary angiography (QCA) software algorithms to evaluate bifurcation lesions. EuroIntervention 2015;11Suppl V:V44–V49.

[7] Generaux P, Kumars I, Lesiak M, Kini A, Fontes G, Slagboom T, Urgi J, Metzger DC, Wykrzykowska JJ, Stella PR, Bartorelli AL, Fearon WF, Lefevre T, Feldman RL, LaSalle L, Francese DP, Onuma Y, Grundeken MJ, Garcia-Garcia HM, Lask LL, Costa DE, Kaplan AV, Serruys PW, Leon MB. A randomized trial of a dedicated bifurcation stent versus provisional stenting in the treatment of coronary bifurcation lesions. J Am Coll Cardiol 2015;65:533–543.

[8] Ziomek DM, Ramanath VS, Brown JR, Kaplan AV. Classification and treatment of coronary artery bifurcation lesions: Putting the Medina classification to the test. Cardiovasc Revasc Med 2012;13:228–233.

[9] Lassen JF, Holm NR, Stankovic G, Lefevre T, Chieffo A, Hildick-Smith D, Pan M, Darmoni O, Albiero R, Ferenc M, Louvard Y. Percutaneous coronary intervention for coronary bifurcation disease: consensus from the first 10 years of the European Bifurcation Club meetings. EuroIntervention 2014;10:545–560.

[10] Levine GN, Bates ER, Blankenship JC, Bailey SR, Bittl JA, Cercek B, Chambers CE, Ellis SG, Guyton RA, Hollenberg SM, Khot UN, Lange RA, Mauri L, Mehran R, Moussa ID, Mukherjee D, Nallamothu BK, Ting HH. ACCF/AHA/SCAI 2011 Guideline for Percutaneous Coronary Intervention. A report of the American College of Cardiology Foundation/American Heart Association Task Force on Practice Guidelines and the Society for Cardiovascular Angiography and Interventions. J Am Coll Cardiol 2011;58:e44–122.

[11] Chen SL, Sheiban I, Xu B, Jepson N, Paiboon C, Zhang JJ, Ye F, Sansoto T, Kwan TW, Lee M, Han YL, Lv SZ, Wen SY, Zhang Q, Wang HC, Jiang TM, Wang Y, Chen LL, Tian NL, Cao F, Qiu CG, Zhang YJ, Leon MB. Impact of the complexity of bifurcation lesions treated with drug-eluting stents: the DEFINITION study [Definitions and impact of complEx bifurcation lesions on clinical outcomes after percutaNeous coronary IntervenTIOn using drug-eluting stentS]. JACC Cardiovasc Interv 2014;7:1266–1276.

[12] Medina A, Suarez de Lezo J, Pan M. [A new classification of coronary bifurcation lesions]. Rev Esp Cardiol 2006;59:183.

[13] Reiber JH, Serruys PW, Kooijman CJ, Wijns W, Slager CJ, Gerbrands JJ, Schuurbiers JC, den Boer A, Hugenholtz PG. Assessment of short-, medium-, and long-term variations in arterial dimensions from computer-assisted quantification of coronary cineangiograms. Circulation 1985;71:280–288.

[14] Muramatsu T, Grundeken MJ, Ishibashi Y, Nakatani S, Girasis C, Campos CM, Morel MA, Joster H, de Winter RJ, Wykrzykowska JJ, Garcia-Garcia HM, Leon MB, Serruys PW, Onuma Y; Investigators TPICBT. Comparison between two- and three-dimensional quantitative coronary angiography bifurcation analysis for the assessment of bifurcation lesions: A subanalysis of the TRYTON pivotal IDE coronary bifurcation trial. Catheter Cardiovasc Interv 2015;86:E140–E149.

[15] Onuma Y, Girasis C, Aben JP, Serruys G, Piazza N, Lokkerbol C, Morel MA, Serruys PW. A novel dedicated 3-dimensional quantitative coronary analysis methodology for bifurcation lesions. EuroIntervention 2011;7:629–635.

[16] Kassab GS, Fixel G. Anatomy and function relation in the coronary tree: From bifurcations to myocardial flow and mass. EuroIntervention 2015;11Suppl V:V13–V17.

[17] Kassab GS, Rider CA, Tang NJ, Fung YC. Morphometry of pig coronary arterial trees. Am J Physiol 1993;265:H350–H365.

[18] Hildick-Smith D, de Belder AJ, Cooter N, Curzen NP, Clayton TC, Oldroyd KG, Bennett L, Holmberg S, Cotton JM, Glennon PE, Thomas MR, Marcantoni PA, Bavinbach A, Mulvihill NT, Henderson RA, Rothwood SR, Starkey IR, Stables RH. Randomized trial of simple versus complex drug-eluting stenting for bifurcation lesions: the British Bifurcation Coronary Study: Old, new, and evolving strategies. Circulation 2010;121:1235–1245.

[19] Colombo A, Bramucci E, Saccà S, Violini R, Lettieri C, Zanini R, Sheiban I, Paloscia L, Grube E, Schofer J, Bolognese L, Orlandi M, Niccoli G, Latib A, Airoldi F. Randomized study of the crush technique versus provisional side-branch stenting in true coronary bifurcations: The CACTUS (Coronary Bifurcations: Application of the Crushing Technique Using Sirolimus-Eluting Stents) Study. Circulation 2009;119:71–78.

[20] Kim HV, Yu J, Ohlow MA, Huegl B, Schulte W, Wagner A, Wassmer G, Gruene S, Petek O, Laun B. Interventional therapy of bifurcation lesions: A TIMI flow-guided concept to treat side branches in bifurcation lesions-a prospective randomized clinical study (Thuringer bifurcation study, THUERIS study as pilot trial). Circ Cardiovasc Interv 2009;2:535–542.

[21] Lansky A, Tuinenburg J, Costa M, Maeng M, Koning G, Popma J, Cristea E, Govil L, Costa R, Rares A, Van Es GA, Lefevre T, Reiber H, Louvard Y, Morice MC: European Bifurcation Angiographic S-C. Quantitative angiographic methods for bifurcation lesions: A consensus statement from the European Bifurcation Group. Catheter Cardiovasc Interv 2009;73:258–266.

[22] Cutlip DE, Windecker S, Mehran R, Boam A, Cohen DJ, van Es GA, Steg PG, Morel MA, Mauri L, Vranckx P, McFadden E, Lansky A, Hamon M, Krucoff MW, Serruys PW; Academic Research C. Clinical end points in coronary stent trials: a case for standardized definitions. Circulation 2007;115:2344–2351.

[23] Girasis C, Schuurbiers JC, Muramatsu T, Aben JP, Onuma Y, Soekhradj S, Morel MA, van Geuns RJ, Wentzel JJ, Serruys PW. Advanced three-dimensional quantitative coronary angiographic assessment of bifurcation lesions: Methodology and phantom validation. EuroIntervention 2013;8:1451–1460.

[24] Tu S, Jing J, Holm NR, Onsea K, Zhang T, Adriaenssens T, Dubois C, Desmet W, Thuesen L, Chen Y, Reiber JH. In vivo assessment of bifurcation optimal viewing angles and bifurcation angles by three-dimensional (3D) quantitative coronary angiography. Int J Cardiovasc Imaging 2012;28:1617–1625.

[25] Sarno G, Garg S, Onuma Y, Girasis C, Tonino P, Morel MA, van Es GA, Pijls N, Serruys PW. Bifurcation lesions: Functional assessment by fractional flow reserve vs. anatomical assessment using conventional and dedicated bifurcation quantitative coronary angiograms. Catheter Cardiovasc Interv 2010;76:817–823.

[26] Yong AS, Ng AC, Brieger D, Lowe HC, Ng MK, Kritharides L. Three-dimensional and two-dimensional quantitative coronary angiography, and their prediction of reduced fractional flow reserve. Eur Heart J 2011;32:345–353.

[27] Meerkin D, Maroni H, Cohen-Bitan O, Elnar S. Three-dimensional vessel analyses provide more accurate length estimations than the gold standard QCA. J Interv Cardiol 2010;23:152–159.

SUPPORTING INFORMATION

Additional Supporting Information may be found online in the supporting information tab for this article.

How to cite this article: Grundeken MJ, Collet C, Ishibashi Y, et al. Visual estimation versus different quantitative coronary angiography methods to assess lesion severity in bifurcation lesions. Catheter Cardiovasc Interv. 2018;91:1263–1270. https://doi.org/10.1002/ccd.27243

https://onlinelibrary.wiley.com/reader/content/10.1002/ccd.27243/format/pdf/OFRPS/ 2020/04/27

https://onlinelibrary.wiley.com/reader/content/10.1002/ccd.27243/format/pdf/QRPRS/ 2020/04/27

ESC European Society of Cardiology
European Heart Journal (2018) 39, 2032–2046
doi:10.1093/eurheartj/ehy076

CONSENSUS PAPER

International Expert Consensus Document on Takotsubo Syndrome (Part I): Clinical Characteristics, Diagnostic Criteria, and Pathophysiology

Jelena-Rima Ghadri[1], Ilan Shor Wittstein[2], Abhiram Prasad[3], Scott Sharkey[4], Keigo Dote[5], Yoshihiro John Akashi[6], Victoria Lucia Cammann[1], Filippo Crea[7], Leonarda Galiuto[7], Walter Desmet[8,9], Tetsuro Yoshida[10], Roberto Manfredini[11], Ingo Eitel[12], Masami Kosuge[13], Holger M. Nef[14], Abhishek Deshmukh[3], Amir Lerman[3], Eduardo Bossone[15], Rodolfo Citro[15], Takashi Ueyama[16†] Domenico Corrado[17], Satoshi Kurisu[18], Frank Ruschitzka[1], David Winchester[19], Alexander R. Lyon[20,21], Elmir Omerovic[22,23], Jeroen J. Bax[24], Patrick Meimoun[25], Guiseppe Tarantini[17], Charanjit Rihal[3], Shams Y.-Hassan[26], Federico Migliore[17], John D. Horowitz[27], Hiroaki Shimokawa[28], Thomas Felix Lüscher[29,30], and Christian Templin[1*]

International Experts: Jeroen J. Bax, Eduardo Bossone, Victoria Lucia Cammann, Rodolfo Citro, Domenico Corrado, Filippo Crea, Walter Desmet, Ingo Eitel, Leonarda Galiuto, Jelena-Rima Ghadri, Thomas Felix Lüscher, Alexander R. Lyon, Roberto Manfredini, Patrick Meimoun, Federico Migliore, Holger M. Nef, Elmir Omerovic, Frank Ruschitzka, Guiseppe Tarantini, Christian Templin, Shams Y-Hassan (European sites); Abhishek Deshmukh, Amir Lerman, Abhiram Prasad, Charanjit Rihal, Scott Sharkey, David Winchester, Ilan Shor Wittstein (USA sites); Yoshihiro John Akashi, Keigo Dote, Masami Kosuge, Satoshi Kurisu, Hiroaki Shimokawa, Takashi Ueyama, Tetsuro Yoshida (Asian sites); John D. Horowitz (Australian site)

[1]University Heart Center, Department of Cardiology, University Hospital Zurich, Zurich, Switzerland; [2]Department of Medicine, Johns Hopkins University School of Medicine, Baltimore, MD, USA; [3]Division of Cardiovascular Diseases Mayo Clinic, Rochester, MN, USA; [4]Cardiovascular Research Division, Minneapolis Heart Institute Foundation, Minneapolis, MN, USA; [5]Department of Cardiology, Hiroshima City Asa Hospital, Hiroshima, Japan; [6]Division of Cardiology, Department of Internal Medicine, St. Marianna University School of Medicine, Kawasaki, Japan; [7]Department of Cardiovascular Sciences, Catholic University of the Sacred Heart, Rome, Italy; [8]Department of Cardiovascular Medicine, University Hospitals Leuven, Leuven, Belgium; [9]Department of Cardiovascular Sciences, University of Leuven, Leuven, Belgium; [10]Department of Cardiovascular

The opinions expressed in this article are not necessarily those of the Editors of the European Heart Journal or of the European Society of Cardiology.

This paper was guest edited by Bernard J. Gersh (Mayo Clinic, gersh.bernard@mayo.edu).

* Corresponding author. Tel: +41 44 255 9585, Fax: +41 44 255 4401, Email: christian.templin@usz.ch

† Deceased.

© The Author(s) 2018. Published by Oxford University Press on behalf of the European Society of Cardiology.
This is an Open Access article distributed under the terms of the Creative Commons Attribution Non-Commercial License (http://creativecommons.org/licenses/by-nc/4.0/), which permits non-commercial re-use, distribution, and reproduction in any medium, provided the original work is properly cited. For commercial re-use, please contact journals.permissions@oup.com

Downloaded from https://academic.oup.com/eurheartj/article-abstract/39/22/2032/5025412 by EndocrineSociety Admin user on 27 April 2020

Medicine, Ongo Nakama Medical Association Ongo Hospital, Fukuoka, Japan; [11]Clinica Medica, Department of Medical Sciences, University of Ferrara, Ferrara, Italy; [12]University Heart Center Luebeck, Medical Clinic II, Department of Cardiology, Angiology and Intensive Care Medicine, University of Luebeck, Luebeck, Germany; [13]Division of Cardiology, Yokohama City University Medical Center, Yokohama, Japan; [14]Department of Cardiology, University Hospital Giessen, Giessen, Germany; [15]Heart Department, University Hospital "San Giovanni di Dio e Ruggi d'Aragona", Salerno, Italy; [16]Department of Anatomy and Cell Biology, Wakayama Medical University School of Medicine, Wakayama, Japan; [17]Department of Cardiac, Thoracic, and Vascular Sciences, University of Padua Medical School, Padova, Italy; [18]Department of Cardiovascular Medicine, Hiroshima University Graduate School of Biomedical and Health Sciences, Hiroshima, Japan; [19]Division of Cardiovascular Disease, Department of Medicine, University of Florida, Gainesville, FL, USA; [20]NIHR Cardiovascular Biomedical Research Unit, Royal Brompton Hospital, London, UK; [21]National Heart and Lung Institute, Imperial College, London, UK; [22]Department of Cardiology, Sahlgrenska University Hospital, Gothenburg, Sweden; [23]Department of Molecular and Clinical Medicine, Institute of Medicine, Sahlgrenska Academy, Gothenburg University, Gothenburg, Sweden; [24]Department of Cardiology, Leiden University Medical Center, Leiden, The Netherlands; [25]Department of Cardiology and Intensive Care, Centre Hospitalier de Compiegne, Compiegne, France; [26]Department of Cardiology, Karolinska University Hospital, Huddinge, Stockholm, Sweden; [27]Department of Cardiology, Basil Hetzel Institute, Queen Elizabeth Hospital, University of Adelaide, Adelaide, Australia; [28]Department of Cardiovascular Medicine, Tohoku University Graduate School of Medicine, Sendai, Japan; [29]Center for Molecular Cardiology, Schlieren Campus, University of Zurich, Zurich, Switzerland; and [30]Department of Cardiology, Royal Brompton & Harefield Hospital and Imperial College, London, UK.

Received 2 June 2017; revised 23 November 2017; editorial decision 30 January 2018; accepted 17 April 2018; online publish-ahead-of-print 29 May 2018

Takotsubo syndrome (TTS) is a poorly recognized heart disease that was initially regarded as a benign condition. Recently, it has been shown that TTS may be associated with severe clinical complications including death and that its prevalence is probably underestimated. Since current guidelines on TTS are lacking, it appears timely and important to provide an expert consensus statement on TTS. The clinical expert consensus document part I summarizes the current state of knowledge on clinical presentation and characteristics of TTS and agrees on controversies surrounding TTS such as nomenclature, different TTS types, role of coronary artery disease, and etiology. This consensus also proposes new diagnostic criteria based on current knowledge to improve diagnostic accuracy.

Keywords Takotsubo syndrome • Broken heart syndrome • Takotsubo definition • Acute heart failure • Consensus statement • InterTAK Diagnostic Criteria

Outline

History ... 2033
Nomenclature ... 2033
Epidemiology ... 2034
Symptoms and signs ... 2035
Diagnostic criteria ... 2035
Pathophysiology ... 2036
Sympathetic stimulation ... 2036
Potential pathophysiological effects of enhanced sympathetic stimulation ... 2036
Plaque rupture ... 2036
Multi-vessel epicardial spasm ... 2036
Microcirculatory dysfunction ... 2036
Catecholamine toxicity on cardiomyocytes ... 2037
Activation of myocardial survival pathways ... 2037
Predisposition and risk factors ... 2038
Hormonal factors ... 2038
Genetic factors ... 2038
Psychiatric and neurologic disorders ... 2038
Triggers ... 2039
Emotional stressors ... 2039
Physical stressors ... 2039
Absence of identifiable causes ... 2039
Types of takotsubo syndrome ... 2039
Chronobiology ... 2042
References ... 2042

History

The term takotsubo syndrome (TTS) was first introduced when Sato et al.[1] published their report of five cases in a Japanese medical textbook in 1990. The first TTS case of this series was managed in 1983 in the Hiroshima City Hospital (Figure 1). A 64-year-old female presented with acute chest pain consistent with acute myocardial infarction (AMI), typical electrocardiographic (ECG) changes, but normal coronary arteries and an unusual appearance of the left ventricle (LV) with a narrow neck and apical ballooning during systole. Interestingly, the marked wall motion abnormalities on left ventriculography disappeared after 2 weeks. Over time TTS was more frequently diagnosed in Japan. Therefore, it was first assumed that this disorder only affected people of Asian descent, as TTS was completely unknown to the Western world until the first cases were published from French and American research groups in the late 1990s.[2,3] Desmet et al.[4] introduced the first patient case series in Caucasians using the term 'takotsubo'.

Takotsubo syndrome gained international awareness among researcher and physicians when Wittstein et al.[5] reported their findings in the *New England Journal of Medicine* in 2005. Since then TTS has been more frequently recognized worldwide but still remains an underappreciated and often misdiagnosed disorder.[6,7]

Nomenclature

Takotsubo syndrome derived its name from the Japanese word for octopus trap, due to the shape of the LV at the end of systole and has been described under a remarkable number of different names in the literature including 'broken heart syndrome', 'stress cardiomyopathy', and 'apical ballooning syndrome'.[8] No single term precisely describes the heterogeneous ventricular appearance with which this syndrome can occur. To date, consensus has not been reached on the nomenclature. The term 'takotsubo' is widely used in acknowledgement of the

Downloaded from https://academic.oup.com/eurheartj/article-abstract/39/22/2033/5025412 by EndocrineSociety Admin user on 27 April 2020

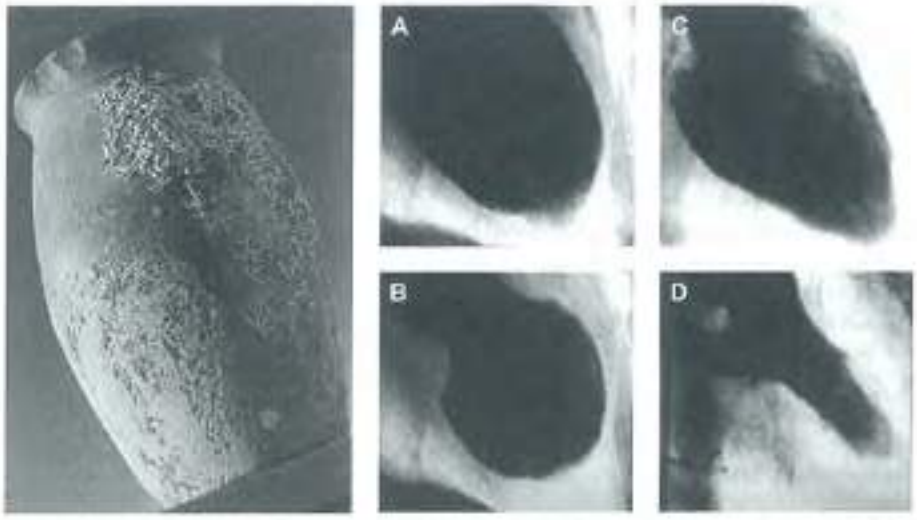

Figure 1 Historical Japanese octopus trap (left). Courtesy of Dr Templin, University Hospital Zurich, Zurich, Switzerland. Left ventriculogram of the first reported case of takotsubo syndrome. Diastole (A) and systole (B) during the acute phase of takotsubo syndrome. Recovery of left ventricular wall motion abnormality two weeks after the event (C and D). Courtesy of Dr Dote, Hiroshima City Asa Hospital, Hiroshima, Japan.

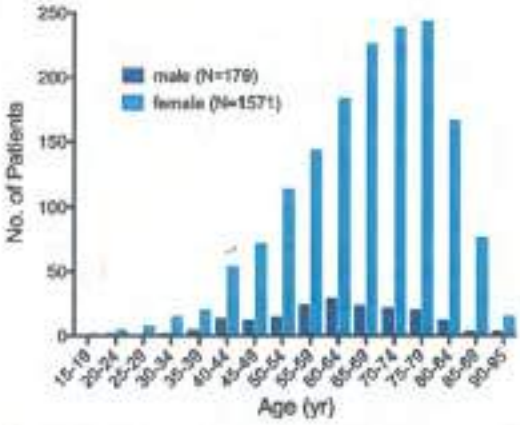

Figure 2 Age and sex distribution of patients with takotsubo syndrome. Reprinted with permission from Templin et al.[16]

Japanese physicians who initially described this disorder.[1] However, in contrast to other cardiomyopathies that are usually not transient in nature, TTS is characterized by a temporary wall motion abnormality of the LV and shares common features with acute coronary syndrome (ACS) [similar symptoms at presentation, ECG abnormalities, elevated cardiac biomarkers as well as a comparable in-hospital mortality with ST-segment elevation myocardial infarction (STEMI) and non-STEMI] specifically in terms of a microvascular ACS form.[9] Among different etiologies of heart failure such as coronary artery disease (CAD), tachyarrhythmias etc. TTS includes a wide spectrum of emotional or physical triggers resulting also in left ventricular dysfunction. Therefore, it is best described as a 'syndrome' and the term 'takotsubo syndrome' seems most appropriate.[9,10,11]

Epidemiology

Since the initial report by Japanese cardiologists 25 years ago, TTS has been increasingly recognized in diverse countries across six continents. Takotsubo syndrome is estimated to represent approximately 1–3%[12,13] of all and 5–6%[14] of female patients presenting with suspected STEMI. The Nationwide Inpatient Sample discharge records from 2008 using the International Classification of Diseases revealed that TTS accounts for 0.02% of hospitalizations in the United States.[15] Recurrence rate of TTS is estimated to be 1.8% per-patient year.[16] Based on the published literature about 90%[16,17] of TTS patients are women with a mean age of 67–70 years,[16,18] and around 80% are older than 50 years (Figure 2).[16] Women older than 55 years have a five-fold greater risk of developing TTS than women younger than 55 years and a 10-fold greater risk than men.[15] With growing awareness of TTS, male patients are diagnosed more often, especially after a physical triggering event.[19] TTS has also been described in children[20,21] with the youngest reported TTS patient being a premature neonate born in the 28th gestational week.[22] Current data on racial differences are inconsistent and large-scale studies are lacking. However, it has been reported that TTS seems to be uncommon in African-Americans and Hispanics,[23] while most of the cases reported in the United States have been Caucasians.[13,24] Furthermore, it has been reported that patients of African-American descent have more in-hospital complications such as respiratory failure, stroke and require more frequently mechanical ventilation compared to Caucasians and Hispanics.[25] With regard to ECG differences, it has been shown that QT prolongation as well as T-wave inversion are more often reported in African-American women with TTS.[26] Of note, regarding gender differences the TTS prevalence in men appears to be higher in Japan.[19] The prevalence of TTS appears to be higher in patients with non-emotional triggers admitted to intensive care units.[27] Moreover, it is likely that

Downloaded from https://academic.oup.com/eurheartjarticle-abstract/39/22/2032/5024412 by EndocrineSociety Admin user on 27 April 2020

Table 1 International Takotsubo Diagnostic Criteria (InterTAK Diagnostic Criteria)

1. Patients show transient[a] left ventricular dysfunction (hypokinesis, akinesia, or dyskinesia) presenting as apical ballooning or midventricular, basal, or focal wall motion abnormalities. Right ventricular involvement can be present. Besides these regional wall motion patterns, transitions between all types can exist. The regional wall motion abnormality usually extends beyond a single epicardial vascular distribution; however, rare cases can exist where the regional wall motion abnormality is present in the subtended myocardial territory of a single coronary artery (local TTS).[b]
2. An emotional, physical, or combined trigger can precede the takotsubo syndrome event, but this is not obligatory.
3. Neurologic disorders (e.g. subarachnoid haemorrhage, stroke/transient ischaemic attack, or seizures) as well as pheochromocytoma may serve as triggers for takotsubo syndrome.
4. New ECG abnormalities are present (ST-segment elevation, ST-segment depression, T-wave inversion, and QTc prolongation); however, rare cases exist without any ECG changes.
5. Levels of cardiac biomarkers (troponin and creatine kinase) are moderately elevated in most cases; significant elevation of brain natriuretic peptide is common.
6. Significant coronary artery disease is not a contradiction in takotsubo syndrome.
7. Patients have no evidence of infectious myocarditis.[b]
8. Postmenopausal women are predominantly affected.

[a]Wall motion abnormalities may remain for a prolonged period of time or documentation of recovery may not be possible. For example, death before evidence of recovery is captured.
[b]Cardiac magnetic resonance imaging is recommended to exclude infectious myocarditis and diagnosis confirmation of takotsubo syndrome.

subclinical TTS cases remain undetected, especially in non-percutaneous coronary intervention centres.[28]

Symptoms and signs

The most common symptoms of TTS are acute chest pain, dyspnoea, or syncope and thus indistinguishable from AMI at the first glance.[16] However, in some patients, TTS may be diagnosed incidentally by new ECG changes or a sudden elevation of cardiac biomarkers. Clinical manifestation of TTS induced by severe physical stress may be dominated by the manifestation of the underlying acute illness. In this regard, patients with ischaemic stroke or seizure-triggered, TTS had less frequent chest pain,[29,30] which could be explained by impaired consciousness, neurologic complications, or a sudden haemodynamic deterioration. In contrast, patients with emotional stress factors had a higher prevalence of chest pain and palpitations.[31] Importantly, a subset of TTS patients may present with symptoms arising from its complications, e.g. heart failure, pulmonary oedema, stroke, cardiogenic shock, or cardiac arrest.

Diagnostic criteria

The diagnosis of TTS is often challenging because its clinical phenotype may closely resemble AMI regarding ECG abnormalities and biomarkers.[32] While a widely established non-invasive tool allowing a rapid and reliable diagnosis of TTS is currently lacking, coronary angiography with left ventriculography is considered the gold standard diagnostic tool to exclude or confirm TTS.

Abe *et al.*[33] introduced the first diagnostic criteria for TTS in 2003. One year later, a dedicated group of cardiologists from the Mayo Clinic proposed their diagnostic criteria.[34] In 2006, the American College of Cardiology and American Heart Association classified TTS as a primary acquired cardiomyopathy.[35] In 2008, the revised version of the Mayo Clinic Diagnostic Criteria was published incorporating neurogenic stunned myocardium.[32] Furthermore, the authors defined different TTS sub-types and highlighted that obstructive coronary lesions may occasionally be present concomitantly.[32] The Mayo Clinic Diagnostic Criteria are the most widely known, but exceptions to the rule [e.g. the presence of CAD] are poorly appreciated among physicians and cardiologists. More recently, other research groups have proposed slightly different criteria for TTS, i.e. the Japanese Guidelines,[36] the Gothenburg criteria,[37] the Johns Hopkins criteria,[38] the Tako-tsubo Italian Network proposal,[39] the criteria of the Heart Failure Association (HFA) TTS Taskforce of the European Society of Cardiology (ESC),[10] as well as the criteria recommended by Madias.[40] Thus, there is a lack of a worldwide consensus.[41] Based on current knowledge, we have developed new international diagnostic criteria (InterTAK Diagnostic Criteria, *Table 1*) for the diagnosis of TTS that may help to improve identification and stratification of TTS. The most important changes with accompanying rationale include:

(i) Pheochromocytoma is a neuroendocrine tumour derived from enterochromaffin cells of the adrenal gland that may lead to a 'catecholamine storm' with LV dysfunction, ECG abnormalities, and increased biomarkers as well as hypercontraction of sarcomeres and contraction band necrosis indistinguishable from TTS.[42]

Notwithstanding, most of the diagnostic criteria have excluded pheochromocytoma as a specific cause of TTS.[32–34,36,37,40] The Japanese criteria emphasize that pheochromocytoma is a TTS-like myocardial dysfunction.[36] Pheochromocytoma is also included as a secondary cause of TTS in the diagnostic criteria of the HFA of the ESC.[10]

(ii) Concomitant CAD is reported with a prevalence ranging from 10–29%.[16,43,44] In this regard, patients with TTS and obstructive CAD are often misdiagnosed as classical ACS and differentiation can be challenging.[45] Therefore, the presence of CAD should not be considered as an exclusion criterion as acknowledged by the modified

Downloaded from https://academic.oup.com/eurheartj/article-abstract/36/22/2032/2025412 by EndocrineSociety Admin user on 27 April 2020

Mayo Clinic Diagnostic Criteria.[32] In such patients, the wall motion abnormalities usually extend beyond the territory of the involved coronary artery. Furthermore, TTS may co-exist with ACS[46] and it has been reported that ACS itself may trigger TTS.[47–50]

(iii) There are rare cases in which the regional wall motion abnormality corresponds to the distribution of a single coronary artery.[16,32,51] This holds true for the focal TTS type mostly involving an anterolateral segment.[16,51] Therefore, the criteria should not exclude cases in which the wall motion abnormalities are restricted to the distribution of a single coronary artery. In this situation, a clear differentiation of TTS, ACS, or myocarditis requires cardiac magnetic resonance imaging demonstrating myocardial oedema rather than late gadolinium enhancement in case of TTS.[52]

Pathophysiology

Sympathetic stimulation

The precise pathophysiological mechanisms of TTS are incompletely understood, but there is considerable evidence that sympathetic stimulation is central to its pathogenesis. An identifiable emotionally or physically triggering event precipitates the syndrome in most cases,[16] and TTS has been associated with conditions of catecholamine excess (e.g. pheochromocytoma,[53] central nervous system disorders[54]) and activated specific cerebral regions.[55] Clinical features of TTS and the various ballooning patterns can be caused by intravenous administration of catecholamines and beta-agonists.[56] Although it has been shown that patients with TTS triggered by emotional stress have markedly elevated levels of catecholamines compared to patients with Killip Class III myocardial infarction,[5] others[57] could not replicate this finding most likely due to methodological issues. In line with a sympathetic stimulation, elevated norepinephrine levels in the coronary sinus have been found in TTS patients, suggesting an increase in the local release of myocardial catecholamines.[58] Accordingly, analyses of heart rate variability have also demonstrated a sympathetic predominance and marked depression of parasympathetic activity during the acute phase.[59] Microneurographic studies confirmed increased muscle sympathetic nerve activity and decreased spontaneous baroreflex control of sympathetic tone in some TTS patients,[60] as did myocardial scintigraphy using ^{123}I-metaiodobenzylguanidine.[61] Furthermore, abnormalities in myocardial sympathetic function can persist for months after recovery of LV systolic function.[62] These abnormalities appear to induce an interstitial mononuclear inflammatory response and occasionally contraction band necrosis.[5]

Several animal models have also supported the central role of adrenergic stimulation in TTS.[63–65] In rats, LV apical ballooning can be provoked by immobilization stress and attenuated by alpha- and beta-receptor blockade.[66] Furthermore, in a more recent and novel rat model, it was possible to demonstrate that the administration of different catecholamines instigates the various ventricular ballooning patterns by an afterload-dependent mechanism.[67]

Potential pathophysiological effects of enhanced sympathetic stimulation

Although enhanced sympathetic stimulation is central to TTS, the mechanism by which catecholamine excess precipitates myocardial stunning in the variety of regional ballooning patterns that characterize this syndrome is unknown. Several hypotheses have been proposed as follows:

Plaque rupture

It has been suggested that transient ischaemia induced by plaque rupture followed by rapid lysis may cause myocardial stunning in patients with apparent non-obstructed CAD at angiography. Indeed, eccentric atherosclerotic plaques in the mid-portion of the left anterior descending (LAD) coronary artery have been reported, but intravascular ultrasound and optical coherence tomography have failed to identify ruptured plaques in the vast majority of TTS patients.[68–70] Furthermore, this explanation is very unlikely as patients with TTS exhibit wall motion abnormalities extending beyond single coronary vascular territories and also sometimes include the right ventricle. In addition, the apical ballooning phenotype is known to occur in the absence of a wraparound LAD and this coronary anatomical variant is not more prevalent in TTS than in the control group.[71]

Multi-vessel epicardial spasm

Sympathetically mediated epicardial spasm has been proposed as a potential cause in TTS. Takotsubo syndrome may be associated with endothelial dysfunction and other conditions of abnormal vasomotor function such as migraine or Raynaud's phenomenon.[72] Similarly, endothelium-dependent dilation is reduced after emotional stress and prevented by endothelin antagonists.[73] At presentation, patients with TTS have marked impairment in brachial artery flow-mediated dilation compared to those with infarction or healthy controls, which gradually improves over several weeks.[74] In the early recovery period, predisposition to coronary vasospasm using intracoronary acetylcholine was demonstrated in some, but not all TTS patients.[75] Furthermore, it has been suggested that the pattern of LV dysfunction in patients with TTS may require involvement of specific coronary side branches.[76] Similarly, myocardial bridging in the LAD has been considered.[77] Although epicardial coronary vasoconstriction may contribute to TTS in a subset of patients,[1,78] the vast majority of patients do not show any evidence of epicardial spasm even with use of provocative agents.

Furthermore, endothelial dysfunction is often associated with oxidative stress, and studies suggest that this may play a role in myocardial dysfunction in TTS. A recent study by Zhang et al.[79] found that hydrogen sulfide relieved cardiac dysfunction in animal models by decreasing oxidative stress. It has been reported that the level of oxidative stress correlates to the extent of myocardial dysfunction in TTS patients in the acute recovery phase. Nanno et al.[80] measured 8-hydroxy-2′-deoxyguanosine (8-OHdG) and norepinephrine levels in TTS patients compared with AMI patients. They found that 8-OHdG levels changed proportionately with wall motion score and plasma levels of norepinephrine were twice as high in TTS patients as in AMI patients.

Microcirculatory dysfunction

Catecholamines and endothelin exert their vasoconstrictor effects primarily in the coronary microvasculature where α_1-receptors[81] and endothelin receptor type A predominate suggesting that acute microcirculatory dysfunction may have a central role in TTS.

Downloaded from https://academic.oup.com/eurheartj/article-abstract/38/22/2032/5025412 by EndocrineSociety Admin user on 27 April 2020

Furthermore, acutely TTS exhibits decreased microRNA (miRNA) 125a-5p as well as increased plasma levels of its target endothelin-1 in line with the microvascular spasms hypothesis.[82] Microvascular blood flow may be reduced in the acute phase of TTS as is coronary flow reserve.[83–87] Similarly, increased thrombolysis in myocardial infarction (TIMI) frame counts and abnormal grades of TIMI myocardial perfusion have been noted.[11,88]

In the acute phase, intravenous administration of adenosine has been shown to transiently improve myocardial perfusion, wall motion score index, and left ventricular ejection fraction (LVEF) in TTS, suggesting that intense microvascular constriction plays a major role in the pathophysiology.[89] In addition, the notion of acute microcirculatory dysfunction in TTS as a contributing pathophysiological factor secondary to enhanced sympathetic stimulation is supported by endomyocardial biopsies revealing apoptosis of microvascular endothelial cells.[90] Microcirculatory dysfunction in the acute phase of TTS is transient and its recovery appears to correlate with improved myocardial function.

Cold pressor testing 1–3 years after the acute episode results in an elevation of catecholamines and transient apical and mid-LV wall motion abnormalities.[91] Mental stress or reactive hyperaemia result in lower vasomotor responses, but higher catecholamine levels in women with TTS compatible with impaired vascular reactivity and endothelial function.[92] Similarly, in women with a history of TTS coronary vasomotion to acetylcholine is impaired.[93] Impaired microvascular endothelial function was observed in virtually all patients with TTS.

Catecholamine toxicity on cardiomyocytes

Transient LV dysfunction in TTS could also result from direct effects of catecholamines on cardiomyocytes. Endomyocardial biopsies revealed occasional contraction band necrosis, which is generally observed in clinical settings of extreme catecholamine production such as pheochromocytoma or subarachnoid haemorrhage, associated with hypercontracted sarcomeres, dense eosinophilic transverse bands, and interstitial mononuclear inflammation as a reflection of myocyte injury.[28] Catecholamines can decrease myocyte viability through cyclic adenosine monophosphate (cAMP) mediated Ca^{2+} overload as it may occur in TTS. Sarcoplasmic-Ca^{2+}-adenosine-triphosphatase (SERCA2a) gene expression is downregulated and that of sarcolipin upregulated, while phospholamban is dephosphorylated in TTS.[94] Thus, an increased phospholamban/SERCA2a ratio could result in contractile dysfunction due to decreased Ca^{2+}-affinity.[95] Indeed, intense G-protein stimulated β_1-adrenergic receptor signalling modulates gene expression via the cAMP responsive element binding protein-1 and nuclear factor of activated T-cells signalling pathways.[95]

In rodent heart failure models, administration of isoproterenol yields apical fibrosis,[96] and abnormalities of apical contraction and metabolism,[97] features known to occur in dysfunctional apical segments during the acute phase in TTS using fludeoxyglucose-positron emission tomographic studies.[98,99] In animal models, intracellular lipid droplets accumulate in cardiomyocytes in response to high doses of catecholamines[100] as in endomyocardial biopsies of TTS patients during the acute phase, but not after recovery.[101] In a rat model of TTS myocardial perfusion in dysfunctional segments appears preserved, challenging microvascular spasm as a primary mediator.[102]

In the mammalian LV β-adrenergic receptor density is highest in the apex, while sympathetic innervation is the lowest[63,103–105] suggesting that it may be more sensitive to high levels of catecholamines which may reduce not only coronary blood flow, but at high levels paradoxically also exert negative inotropic effects[63,104] due to a 'molecular switch' of the β_2-adrenergic receptor from the positive inotropic G_s to the negatively inotropic G_i pathway.[106–108] Since the β_2-adrenoceptor is linked via G_i activation to stimulation of endothelial nitric oxide (NO) synthase, it seems possible, that peroxynitrate mediated nitrosative stress could lead to negative inotropy and inflammation in TTS. Indeed, TTS patients have markers of increased NO signalling[109] and post-mortem hearts of TTS patients also demonstrate markers of increased nitrosative stress.[110] Peroxynitrite release would also result in activation of poly(ADP-ribose)-transferase-1, which might contribute to the myocardial energetic impairment, which has recently been reported in patients with TTS.[111] Endomyocardial biopsies in patients with TTS further suggest that these anti-apoptotic pathways are activated acutely.[112] A polymorphism of the G-protein receptor kinase 5 (GRK5) gene L41Q that blunts β_2-G_i trafficking appears common in TTS.[113] On the other hand, a larger study failed to support the conclusions of this study.[114]

In summary, current evidence suggests that TTS is caused by an acute release of catecholamines from either sympathetic nerves, the adrenal medulla, or as drug therapy and occurs primarily in subjects with increased susceptibility of the coronary microcirculation and of cardiac myocytes to the stress hormones leading to prolonged but transient LV dysfunction with secondary myocardial inflammation.

Activation of myocardial survival pathways

The severe wall motion abnormalities seen in TTS are transient suggesting that protective mechanisms are likely to operate to preserve myocardial integrity. Two different mechanisms might elicit myocardial protection. The first one is represented by adrenoceptor-related protective mechanisms. Indeed, supra-physiological levels of epinephrine trigger β_2-adrenoceptor to switch from G_s to G_i coupling, thus causing a negative inotropic response, which limits the degree of acute myocardial injury in response to the catecholamine surge.[107] The second mechanism is represented by the phosphoinositide 3-kinase/protein kinase B (AKT) survival pathway, which has been found to be transiently activated during the acute phase of TTS.[112] AKT is critical for postnatal cardiac growth and coronary angiogenesis. Also, its downstream targets, especially the mechanistic target of rapamycin and glycogen synthase kinase 3 (GSK3), are well-established regulators of metabolism, proliferation, and cell survival. Cell survival is achieved through various mechanisms: (i) direct inhibition of apoptosis, (ii) inhibition of proapoptotic transcriptional factors, (iii) enhancement of anti-apoptotic transcriptional factors, and (iv) enhancement of cell metabolism by inhibition of the GSK3.

The demonstration that down-regulation of myocardial function is a protective mechanism caused by a severe reduction of perfusion is confirmed by several clinical studies showing 'inverse perfusion-metabolism mismatch,' which is typically observed during myocardial stunning.[115]

Downloaded from https://academic.oup.com/eurheartj/article-abstract/34/27/2037/1502412 by EndocrinoSocietyAdmin user on 27 April 2020

Predisposition and risk factors

Psychological and physical stressors are universal and affect virtually all individuals throughout their life. However, very few people develop TTS and even fewer experience recurrent episodes. These observations support the existence of risk factors that may make certain individuals more susceptible to TTS. Predisposition and risk factors for TTS are reviewed below:

Hormonal factors

The striking preponderance of postmenopausal females suggests a hormonal influence. Potentially, declining oestrogen levels after menopause increase the susceptibility to TTS in women.[116] Indeed, women older than 55 years have an almost five-fold risk of developing TTS compared to those younger than 55 years.[15] Oestrogens can influence vasomotor tone via up-regulation of endothelial NO synthase.[117] Also, there is evidence that oestrogens can attenuate catecholamine-mediated vasoconstriction and decrease the sympathetic response to mental stress in perimenopausal women.[118,119] In women with subarachnoid haemorrhage, low levels of oestradiol have been associated with an increased risk of LV wall motion abnormalities.[120] In ovariectomized rats subjected to immobilization stress, ECG and contractile abnormalities can be induced and attenuated with oestrogen supplementation.[121] However, systematic data demonstrating a clear link between oestrogen levels and the development of TTS are lacking so far.

Genetic factors

A genetic predisposition to TTS has been suggested by a report of five cases of familial TTS, two in mother-daughter pairs[122,123] and three in pairs of sisters.[124–126] Takotsubo syndrome does not appear to have a multigenerational Mendelian inheritance pattern. Hence, it is likely that a genetic predisposition (if present) may interact with environmental factors, polygenic aetiology and/or recessive susceptibility alleles. Polymorphisms in adrenergic genes indeed affect receptor function and downstream signaling,[127] and this raises the possibility that their distribution may differ in TTS patients. Indeed, functional variants of adrenergic receptor genes have been associated with the magnitude of cardiac dysfunction in patients with subarachnoid haemorrhage[128] and pheochromocytoma,[129] conditions which can trigger TTS.

β_1-adrenergic receptor (amino acid position 389) and β_2-adrenergic receptor (amino acid position 27) variants were associated with a greater release of troponin I and α_2-adrenergic receptor deletion (del322–325) with reduced LVEF.[128] However, α_{2c}-adrenergic receptor and β_1-adrenergic receptor polymorphisms do not seem to differ between TTS and controls.[130] In contrast, a different distribution of β_1-receptor polymorphisms Arg389Gly [homozygous arginine (Arg)/Arg] is more frequently found in TTS, while β_2-receptor polymorphisms Gln27Glu [homozygous glutamine (Gln)/Gln] were found more frequently in healthy controls, and no difference was observed in the β_2-receptor Arg16Gly variant between groups.[131] Furthermore, similar genetic polymorphisms in the β_1-adrenergic receptor and the β_3-adrenergic receptor were noted in TTS and controls, while a higher frequency of rs17098707 polymorphism in the GRK5 gene was found in TTS patients.[132] Unfortunately, these studies provide conflicting results and are limited in their gene-targeted approach and incomplete in genetic characterization of the complex adrenergic signalling network. Whole-exome sequencing in 28 TTS subjects revealed no difference in allele frequency or burden between TTS subjects and population controls.[132] As such, these data do not provide strong evidence for a genetic predisposition in TTS, but lend support to genetic heterogeneity and a potential polygenic susceptibility conferring a cumulative effect on dysregulation of adrenergic pathways. Most of the published studies were conducted in small cohorts and much larger cohorts are required to evaluate the genetics of TTS comprehensively.

Borchert et al.[133] have investigated a genetic predisposition for TTS by creating the first 'takotsubo in a dish' model by using TTS-specific induced pluripotent stem cell-derived cardiomyocytes (iPSC-CMs). This model recapitulates some of the pathophysiology observed in patients during the acute phase of TTS allowing further exploration of underlying mechanisms.[134] They found an overactive β-adrenergic pathway and higher sensitivity of catecholamines in TTS iPSC-CMs and TTS engineered heart muscle.[133] Interestingly, receptor desensitization and different β_1/β_2-adrenoreceptor responses shed further light on the mechanisms of TTS. Based on this TTS-model future treatment targets should be identified to rescue patients with TTS.[133,134]

Psychiatric and neurologic disorders

A high prevalence of psychiatric and neurologic disorders has been reported in patients with TTS. In an age- and sex-matched comparison between patients with TTS and ACS, rates of psychiatric or neurologic disorders were substantially higher in TTS.[16] In this regard, 27% had an acute, former, or chronic history of neurologic disorders and 42% had a psychiatric diagnosis with half of them suffering from depression.[16] Indeed, anxiety and depression appear more common in TTS than in patients with STEMI or healthy controls[135] and in a prospective study, the prevalence of depression and anxiety was 78%, much higher than in patients with ACS.[136] Patients with TTS also appear to have a high prevalence of type-D-personality, which is characterized by negative emotions and social inhibition, and which has been associated with an increased cardiovascular risk.[137] However, another study found no difference in the personality profile and stress coping skills between TTS patients and population controls.[138,139] Interestingly, in a recent study comparing the signature of circulating miRNAs in TTS and STEMI, miR-16 and miR-26a, known to be associated with neuropsychiatric conditions, were significantly upregulated in TTS.[87] Psychological disorders may thus have a pathogenic role. Of note, depressed patients have an exaggerated norepinephrine response to emotional stress,[140] and a subset of patients has an increased spillover and decreased reuptake of norepinephrine. Similarly, patients with panic disorder and anxiety have a decreased catecholamine reuptake due to impairment of norepinephrine reuptake transporters.[141] On the other hand, antidepressants, e.g. selective norepinephrine reuptake inhibitors, may facilitate myocardial stunning by increasing local levels of catecholamines.[142] This increased sympathetic response to acute stress combined with greater cardiac sympathetic sensitivity may make patients with mood disorders and anxiety susceptible to stress-related cardiac dysfunction.

Takotsubo syndrome has been reported to occur after neurologic disorders especially stroke,[143] subarachnoid haemorrhage,[144] and seizures.[29] Histopathological findings of autopsied patients with sudden unexpected death in epilepsy revealed contraction band

Downloaded from https://academic.oup.com/eurheartj/article-abstract/39/22/2032/5029412 by EndocrineSociety Admin user on 27 April 2020

necrosis,[145] abnormalities also found in autopsied patients with TTS.[146] It has been demonstrated that regions of the insular or posterior fossa are mainly affected in patients with ischaemic stroke and epileptic events.[147] This suggests that neurologic or psychiatric conditions may serve as predisposing factors for the development of TTS. Furthermore, a heart-brain interaction has been proposed in TTS. In this regard, substantial structural differences between TTS and healthy controls have been shown including the limbic network comprising the insula, amygdala, cingulate cortex, and hippocampus, all of which are strongly involved in the control of emotional processing, cognition, and the autonomic nervous system.[148]

Triggers

A hallmark of TTS is its association with a preceding stressful event. Initially, most reported triggers involved an emotional trauma.[1] As TTS became more known, an association with physical stressors was also noted as well as TTS cases that occur in the absence of an evident stressor.[16,149] A systematic illustration of preceding emotional and physical stressors is shown in *Figure 3*.

Physical triggers are more common than emotional stress factors.[16] Interestingly, male patients are more often affected from a physical stressful event, while in women an emotional trigger can be more frequently observed.[16] Of note, precipitating triggers may represent a combination of emotional and physical issues[19] (e.g. panic attack during a medical procedure), as well as environmental triggers such as long-term exposure to aircraft noise[150]. On the other hand, about one-third of patients presents without evidence of an identifiable preceding stressful event.[151]

In hospitalized patients, TTS may have an atypical presentation and manifest itself by tachycardia, hypotension, heart failure, elevation of cardiac biomarkers, or ECG abnormalities. It has been reported that patients with in-hospital TTS are more frequently males and have a higher prevalence of in-hospital death compared to patients with out-of-hospital TTS.[152] This suggests that out-of-hospital TTS often occurs in the absence of a critical medical problem, while in-hospital TTS is preceded mainly by chronic comorbidities or acute medical illnesses.

Emotional stressors

Psychological triggers represent a range of traumatic emotions including grief (e.g. death of a family member, friend, or pet), interpersonal conflicts (e.g. divorce or family estrangement), fear and panic (e.g. robbery, assault, or public speaking), anger (e.g. argument with a family member or landlord), anxiety (e.g. personal illness, childcare, or homelessness), financial or employment problems (e.g. gambling loss, business failure, or job loss), or embarrassment (e.g. legal proceedings, infidelity, incarceration of family member, defeat in a competitive event).[149] Natural disasters such as earthquakes[153,154] and floods[155] are also associated with an increase in TTS events. However, emotional triggers are not always negative as positive emotional events can also provoke TTS (e.g. surprise birthday party, winning a jackpot, and positive job interview)[156] as shown in *Figure 3*. This entity has been described as the 'happy heart syndrome.'[156]

Physical stressors

Physical stressors may be related to physical activities (for instance heavy gardening[157] or sports[158]), medical conditions, or procedures such as acute respiratory failure (e.g. asthma,[159] end-stage chronic obstructive lung disease[160]), pancreatitis,[161] cholecystitis,[162] pneumothorax,[163] traumatic injury,[164] sepsis,[165] thyrotoxicosis,[166] malignancy also including chemotherapy[167] and radiotherapy,[168] pregnancy,[169] Caesarean section,[170] lightning strike,[171] near drowning,[172] hypothermia,[173] cocaine,[174] alcohol[175] or opiate withdrawal,[176] and carbon-monoxide poisoning.[177] Exogenous drugs in terms of catecholamines[56,178] and sympathomimetic drugs[56,179] may also act as triggers for TTS including dobutamine stress testing,[180] electrophysiological testing[181] (with isoproterenol or epinephrine) and beta-agonists for asthma or chronic obstructive lung disease.[179,182] Also, acute coronary artery obstruction might act also as a trigger for TTS.[47]

Nervous system conditions (e.g. stroke,[142] head trauma,[183] migraine[77], intracerebral haemorrhage,[184] or seizures[75]) also represent an important trigger in the acute onset of TTS.

Endogenous catecholamine spillover related to pheochromocytoma serves as a distinct physical trigger.

Absence of identifiable causes

Recognition that TTS may occur spontaneously has demonstrated the inappropriateness of the term 'stress cardiomyopathy' to describe the entire spectrum of TTS. Whether the clinical course differs for this subset is unknown, and levels of catecholamines and related hormones have not been reported.

Types of takotsubo syndrome

Although several anatomical TTS variants have been described four major types can be differentiated based on the distribution of regional wall motion abnormalities as shown in *Figure 4*.[16,51] The most common TTS type and widely recognized form is the (i) apical ballooning type also known as the typical TTS form, which occurs in the majority of cases.[16,51] Over the past years, atypical TTS types have been increasingly recognized.[51] These include the (ii) midventricular, (iii) basal, and (iv) focal wall motion patterns.[51] Recently, it has been demonstrated that patients suffering from atypical TTS have a different clinical phenotype.[51] These patients are younger, suffer more often from neurologic comorbidities, have lower brain natriuretic peptide values, a less impaired LVEF, and more frequent ST-segment depression compared to typical TTS.[51,185] In-hospital complication rate is similar between typical and atypical types, while 1-year mortality is higher in typical TTS.[51] After adjustment for confounders, LVEF <45%, atrial fibrillation, neurologic disorders but not TTS phenotype were independent predictors of death.[51] Beyond 1-year, long-term mortality is similar in typical and atypical TTS phenotypes, therefore, patients should be equally monitored and treated.[51] The basal phenotype has been reported to be associated with the presence of pheochromocytoma,[186] epinephrine-induced TTS,[178] or subarachnoid haemorrhage[187] consequently, these conditions should be considered in this particular setting.

Besides the four major TTS types, other morphological variants have been described including the biventricular (apical type and right

Downloaded from https://academic.oup.com/eurheartj/article-abstract/38/22/2032/5025412 by Endocrina Society Admin user on 27 April 2020

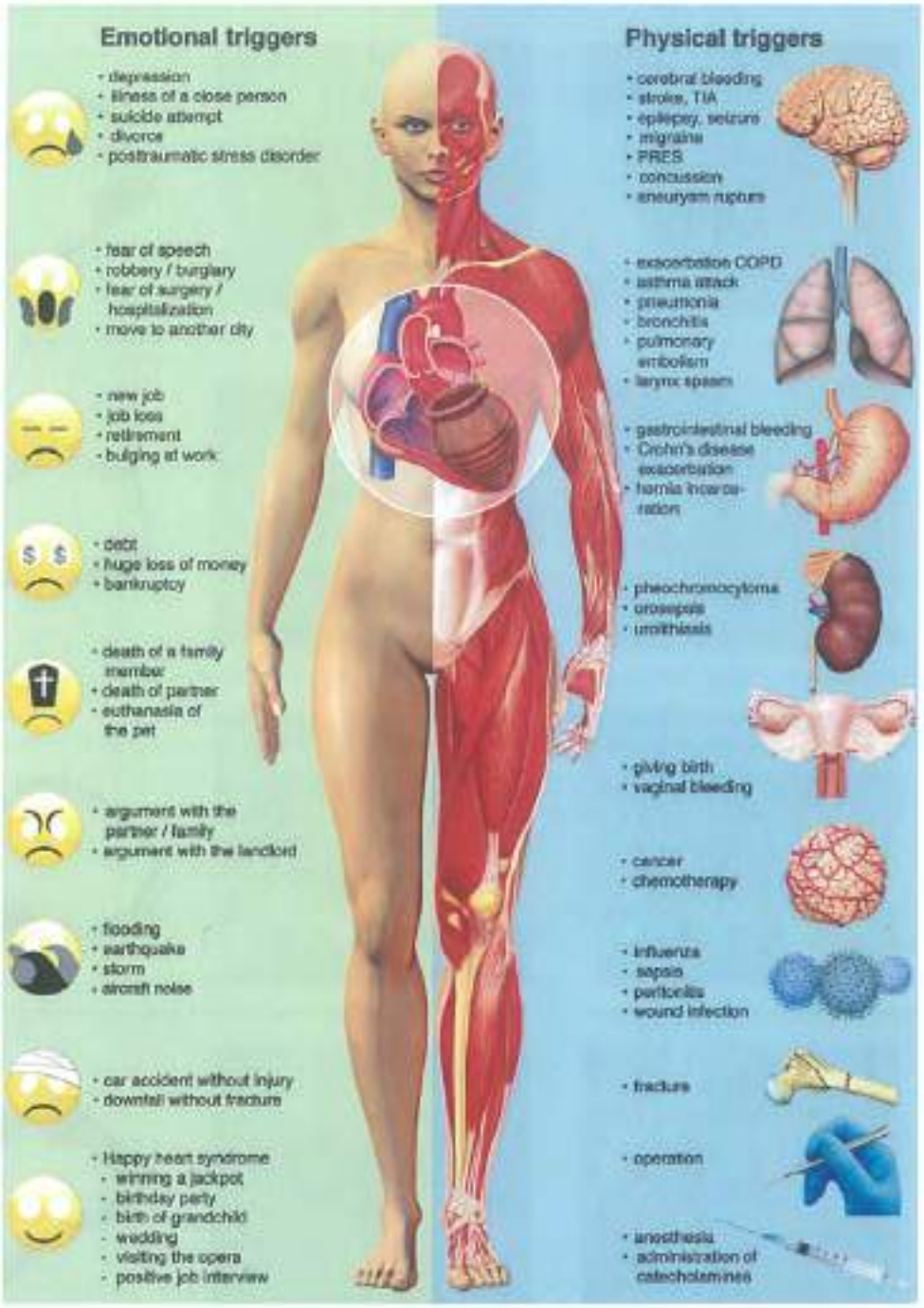

Figure 3 Emotional and physical stress factors precipitating takotsubo syndrome. Reprinted, modified, and translated with permission from Schlosshauer et al.[7] COPD, chronic obstructive pulmonary disease; PRES, posterior reversible encephalopathy syndrome; TIA, transient ischaemic attack.

ventricular involvement),[19] isolated right ventricular,[188,189] and global form.[190] Global hypokinesia as a manifestation of TTS is difficult to prove given the very broad differential diagnoses including conditions such as tachycardia-induced cardiomyopathy. Right ventricular involvement is present in about one-third of TTS patients and may be a predictor for worse outcome.[191] The true prevalence of the isolated right ventricular form is unknown since little attention is paid to the right ventricle in daily clinical echo routine.

Downloaded from https://academic.oup.com/eurheartj/article-abstract/39/22/2032/5025412 by EndocrineSociety Admin user on 27 April 2020

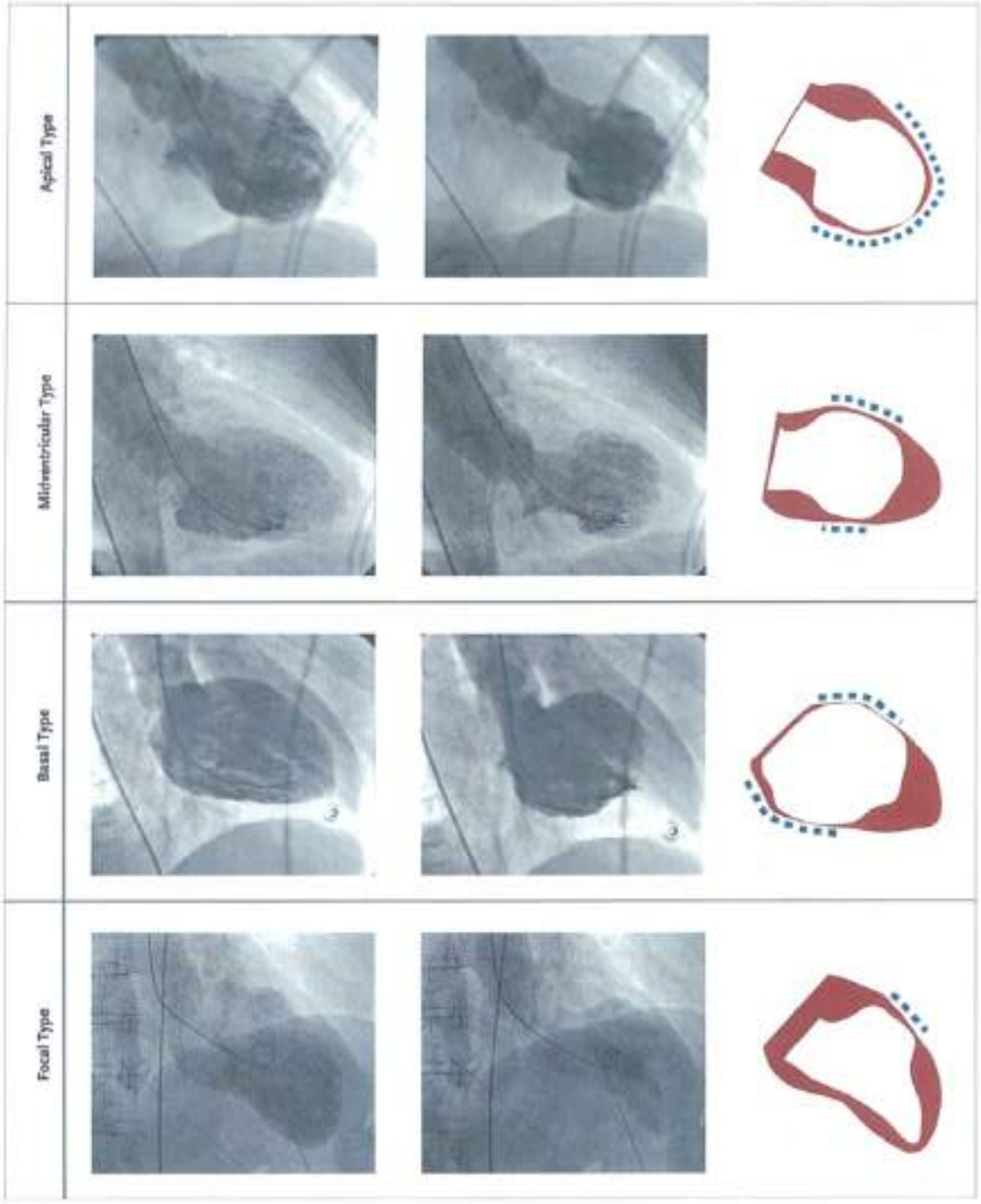

Figure 4 The four different types of takotsubo syndrome during diastole (left column) and systole (middle column). The right column depicts diastole in red and systole in white. The blue dashed lines demonstrate the region of the wall motion abnormality. Reprinted and modified with permission from Templin et al.[14]

Downloaded from https://academic.oup.com/eurheartj/article-abstract/39/22/2032/5025412 by EndocrineSociety Admin user on 27 April 2020

Patients with recurrent TTS can demonstrate different wall motion patterns at each event,[192,193] suggesting that left ventricular adrenergic receptor distribution does not explain different TTS types.

Chronobiology

A growing body of evidence reveals that acute cardiovascular events are not distributed randomly over time, but instead depend on the time of day, day of the week, and months/season of the year.[194–197] Several studies have investigated chronobiological features of TTS. Two studies reported a peak in the morning[198,199] and afternoon hours,[200] while others failed to show a statistically significant temporal pattern.[201] Two studies observed the highest frequency on Monday[196,202] and a third investigation has not found a weekly variation.[198] Most conducted studies reported a summer preference for TTS,[24,203] while one study reported a winter peak.[204] Hence, conflicting results about the chronobiological pattern of TTS exist.

Funding

J.R.G. has received a research grant "Filling the gap" from the University of Zurich.

Conflict of Interest: none declared.

References

1. Sato H. Tako-tsubo-like left ventricular dysfunction due to multivessel coronary spasm. In: K Kodama, K, Haze M Hori, eds. *Clinical Aspect of Myocardial Injury: From Ischemia to Heart Failure*. Tokyo: Kagakuhyoronsha Publishing Co; 1990. p56–64; (Article in Japanese).
2. Pavin D, Le Breton H, Daubert C. Human stress cardiomyopathy mimicking acute myocardial syndrome. *Heart* 1997;**78**:509–511.
3. Sharkey SW, Shear W, Hodges M, Hertog CA. Reversible myocardial contraction abnormalities in patients with an acute noncardiac illness. *Chest* 1998;**114**: 98–105.
4. Desmet WJ, Adriaenssens BF, Dens JA. Apical ballooning of the left ventricle: first series in white patients. *Heart* 2003;**89**:1027–1031.
5. Wittstein IS, Thiemann DR, Lima JA, Baughman KL, Schulman SP, Gerstenblith G, Wu KC, Rade JJ, Bivalacqua TJ, Champion HC. Neurohumoral features of myocardial stunning due to sudden emotional stress. *N Engl J Med* 2005;**352**: 539–548.
6. Templin C, Napp LC, Ghadri JR. Takotsubo syndrome: underdiagnosed, underestimated, but understood? *J Am Coll Cardiol* 2016;**67**:1937–1940.
7. Schlossbauer SA, Ghadri JR, Templin C. Takotsubo-Syndrom—ein häufig verkanntes Krankheitsbild. *Praxis (Bern 1994)* 2016;**105**:1185–1192.
8. Sharkey SW, Lesser JR, Maron MS, Maron BJ. Why not just call it tako-tsubo cardiomyopathy: a discussion of nomenclature. *J Am Coll Cardiol* 2011;**57**: 1496–1497.
9. Lüscher TF, Templin C. Is takotsubo syndrome a microvascular acute coronary syndrome? Towards of a new definition. *Eur Heart J* 2016;**37**:2816–2820.
10. Lyon AR, Bossone E, Schneider B, Sechtem U, Citro R, Underwood SR, Sheppard MN, Figtree GA, Parodi G, Akashi YJ, Ruschitzka F, Filippatos G, Mebazaa A, Omerovic E. Current state of knowledge on takotsubo syndrome: a position statement from the taskforce on takotsubo syndrome of the heart failure Association of the European Society of Cardiology. *Eur J Heart Fail* 2016; **18**:8–27.
11. Pelliccia F, Sinagra G, Elliott P, Parodi G, Basso C, Camici PG. Takotsubo is not a cardiomyopathy. *Int J Cardiol* 2018;**254**:250–253.
12. Prasad A, Dangas G, Srinivasan M, Yu J, Gersh BJ, Mehran R, Stone GW. Incidence and angiographic characteristics of patients with apical ballooning syndrome (takotsubo/stress cardiomyopathy) in the HORIZONS-AMI trial: an analysis from a multicenter, international study of ST-elevation myocardial infarction. *Catheter Cardiovasc Interv* 2014;**83**:343–348.
13. Bybee KA, Prasad A, Barsness GW, Lerman A, Jaffe AS, Murphy JG, Wright RS, Rihal CS. Clinical characteristics and thrombolysis in myocardial infarction frame counts in women with transient left ventricular apical ballooning syndrome. *Am J Cardiol* 2004;**94**:343–346.
14. Redfors B, Vedad R, Angerås O, Ramunddal T, Petursson P, Haraldsson I, Ali A, Dworeck C, Odenstedt J, Ioanes D, Libungan B, Shao Y, Albertsson P, Stone GW, Omerovic E. Mortality in takotsubo syndrome is similar to mortality in myocardial infarction—a report from the SWEDEHEART registry. *Int J Cardiol* 2015;**185**:282–289.
15. Deshmukh A, Kumar G, Pant S, Rihal C, Murugiah K, Mehta JL. Prevalence of Takotsubo cardiomyopathy in the United States. *Am Heart J* 2012;**164**: 66–71 e1.
16. Templin C, Ghadri JR, Diekmann J, Napp LC, Bataiosu DR, Jaguszewski M, Cammann VL, Sarcon A, Geyer V, Neumann CA, Seifert B, Hellermann J, Schwyzer M, Eisenhardt K, Jenewein J, Franke J, Katus HA, Burgdorf C, Schunkert H, Moeller C, Thiele H, Bauersachs J, Tschöpe C, Schultheiss HP, Laney CA, Rajan L, Michels G, Pfister R, Ukena C, Böhm M, Erbel R, Cuneo A, Kuck K-H, Jacobshagen C, Hauerfuss G, Karakas M, Koenig W, Rottbauer W, Said SM, Braun-Dullaeus RC, Cuculi F, Banning A, Fischer TA, Vasankari T, Airaksinen KEJ, Fijalkowski M, Rynkiewicz A, Pawlak M, Opolski G, Dworakowski R, MacCarthy P, Kaiser C, Osswald S, Galiuto L, Crea F, Dichtl W, Franz WM, Empen K, Felix SB, Delmas C, Lairez O, Erne P, Bax JJ, Ford I, Ruschitzka F, Prasad A, Lüscher TF. Clinical features and outcomes of takotsubo (stress) cardiomyopathy. *N Engl J Med* 2015;**373**:929–938.
17. Schneider B, Athanasiadis A, Stollberger C, Pistner W, Schwab J, Gottwald U, Schoeller R, Gerecke B, Hoffmann E, Wagner C, Sechtem U. Gender differences in the manifestation of tako-tsubo cardiomyopathy. *Int J Cardiol* 2013;**166**: 584–588.
18. Rorhamamir S, Showkathali R. Takotsubo cardiomyopathy a short review. *Curr Cardiol Rev* 2013;**9**:191–196.
19. Akawa K, Suzuki T. Takotsubo cardiomyopathy: Japanese perspective. *Heart Fail Clin* 2013;**9**:243–247.
20. Berton E, Vitali-Serdoz L, Vallon P, Mauchlo M, Gortani G, Benettoni A. Young girl with apical ballooning heart syndrome. *Int J Cardiol* 2012;**161**:e4–e6.
21. Ostlio JK, Harris JK, Tauri R. A 6-year-old girl with undiagnosed hemophagocytic lymphohistiocytosis and takotsubo cardiomyopathy, a case report and review of the literature. *Pediatr Emerg Care* 2014;**30**:561–565.
22. Rozema T, Klein LR. Takotsubo cardiomyopathy: a case report and literature review. *Cardiol Young* 2016;**26**:406–409.
23. Nascimento FO, Larrauri-Reyes MC, Santana O, Pérez-Carrero M, Lama GA. Comparison of stress cardiomyopathy in hispanic and non-hispanic patients. *Rev Esp Cardiol (Engl Ed)* 2013;**66**:67–68.
24. Ragnatte RA, Zusek RW, Weinsier SB, Latif SR, Lindy RA, Ahmed HN, Sadiq I. Clinical characteristics and four-year outcomes of patients in the Rhode Island Takotsubo Cardiomyopathy Registry. *Am J Cardiol* 2009;**103**:1015–1019.
25. Franco E, Dias A, Koshkelashvili N, Pressman GS, Hebert K, Figueredo VM. Distinctive electrocardiographic features in African Americans diagnosed with takotsubo cardiomyopathy. *Ann Noninvasive Electrocardiol* 2016;**21**:486–492.
26. Qaqa A, Dasko J, Jallad N, Abuismeh O, Goldfarb I, Shamoon F. Takotsubo syndrome in African American vs. non-African American women. *West J Emerg Med* 2011;**12**:218–223.
27. Park JH, Kang SJ, Song JK, Kim HK, Lim CM, Kang DH, Koh Y. Left ventricular apical ballooning due to severe physical stress in patients admitted to the medical ICU. *Chest* 2005;**128**:296–302.
28. Ghadri JR, Ruschitzka F, Luscher TF, Templin C. Takotsubo cardiomyopathy: still much more to learn. *Heart* 2014;**100**:1804–1812.
29. Stollberger C, Wegner C, Finsterer J. Seizure-associated Takotsubo cardiomyopathy. *Epilepsia* 2011;**52**:e160–e167.
30. Jung JM, Kim JG, Kim JB, Cho KH, Yu S, Oh K, Kim YH, Choi JY, Seo WK. Takotsubo-like myocardial dysfunction in ischemic stroke: a hospital-based registry and systematic literature review. *Stroke* 2016;**47**:2729–2736.
31. Song BG, Yang HS, Hwang HK, Kang GH, Park YH, Chun WJ, Oh JH. The impact of stressor patterns on clinical features in patients with tako-tsubo cardiomyopathy: experiences of two tertiary cardiovascular centers. *Clin Cardiol* 2012; **35**:E6–E13.
32. Prasad A, Lerman A, Rihal CS. Apical ballooning syndrome (tako-tsubo or stress cardiomyopathy): a mimic of acute myocardial infarction. *Am Heart J* 2008;**155**:408–417.
33. Abe Y, Kondo M, Matsuoka R, Araki M, Dohyama K, Tanio H. Assessment of clinical features in transient left ventricular apical ballooning. *J Am Coll Cardiol* 2003;**41**:737–742.
34. Bybee KA, Kara T, Prasad A, Lerman A, Barsness GW, Wright RS, Rihal CS. Systematic review: transient left ventricular apical ballooning: a syndrome that mimics ST-segment elevation myocardial infarction. *Ann Intern Med* 2004;**141**: 858–865.
35. Maron BJ, Towbin JA, Thiene G, Antzelevitch C, Corrado D, Arnett D, Moss AJ, Seldman CE, Young JB, American Heart Association; Council on Clinical Cardiology, Heart Failure and Transplantation Committee; Quality of Care and

Downloaded from https://academic.oup.com/eurheartjournal/article-abstract/39/22/2032/5025412 by Endocrine Society Admin user on 27 April 2020

Outcomes Research and Functional Genomics and Translational Biology Interdisciplinary Working Groups; Council on Epidemiology and Prevention. Contemporary definitions and classification of the cardiomyopathies: an American Heart Association Scientific Statement from the Council on Clinical Cardiology, Heart Failure and Transplantation Committee; Quality of Care and Outcomes Research and Functional Genomics and Translational Biology Interdisciplinary Working Groups; and Council on Epidemiology and Prevention. *Circulation* 2006;**113**:1807–1816.
36. Kawai S, Kitabatake A, Tomoike H. Guidelines for diagnosis of takotsubo (ampulla) cardiomyopathy. *Circ J* 2007;**71**:990–992.
37. Schultz T, Shao Y, Redfors B, Svensdottir YB, Ramunddal T, Albertsson P, Matejka G, Omerovic E. Stress-induced cardiomyopathy in Sweden: evidence for different ethnic predisposition and altered cardio-circulatory status. *Cardiology* 2012;**122**:180–186.
38. Wittstein IS. Stress cardiomyopathy: a syndrome of catecholamine-mediated myocardial stunning? *Cell Mol Neurobiol* 2012;**32**:847–857.
39. Parodi G, Citro R, Bellandi B, Provenza G, Marrani M, Bossone E; Tako-Tsubo Italian Network. Revised clinical diagnostic criteria for tako-tsubo syndrome: the Tako-tsubo Italian Network proposal. *Int J Cardiol* 2014;**172**:282–283.
40. Madias JE. Why the current diagnostic criteria of takotsubo syndrome are outmoded: a proposal for new criteria. *Int J Cardiol* 2014;**174**:468–470.
41. Scantlebury DC, Prasad A. Diagnosis of takotsubo cardiomyopathy. *Circ J* 2014; **78**:2139–2139.
42. Samuels MA. The brain-heart connection. *Circulation* 2007;**116**:77–84.
43. Winchester DE, Ragosta M, Taylor AM. Concurrence of angiographic coronary artery disease in patients with apical ballooning syndrome (tako-tsubo cardiomyopathy). *Catheter Cardiovasc Interv* 2008;**72**:612–616.
44. Kurisu S, Inoue I, Kawagoe T, Ishihara M, Shimatani Y, Nakama Y, Maruhashi T, Kagawa E, Dai K, Matsushita J, Ikenaga H. Prevalence of incidental coronary artery disease in tako-tsubo cardiomyopathy. *Genin Arterio Dis* 2009;**20**:214–218.
45. Napp LC, Ghadri JR, Bauersachs J, Templin C. Acute coronary syndrome or takotsubo cardiomyopathy: the suspect may not always be the culprit. *Int J Cardiol* 2015;**187**:116–119.
46. Haghi D, Papavassiliu T, Hamm K, Kaden JJ, Borggrefe M, Suselbeck T. Coronary artery disease in takotsubo cardiomyopathy. *Circ J* 2007;**71**: 1092–1094.
47. Y-Hassan S. Takotsubo syndrome triggered by acute coronary syndrome in a cohort of 20 patients: an often missed diagnosis. *Int J Cardiol Res* 2015;**02**:28–33.
48. Y-Hassan S, Böhm F. The causal link between spontaneous coronary artery dissection and takotsubo syndrome: a case presented with both conditions. *Int J Cardiol* 2016;**203**:828–831.
49. Redfors B, Ramunddal T, Shao Y, Omerovic E. Takotsubo triggered by acute myocardial infarction: a common but overlooked syndrome? *J Geriatr Cardiol* 2014;**11**:171–173.
50. Napp LC, Ghadri JR, Cammann VL, Bauersachs J, Templin C. Takotsubo cardiomyopathy: completely simple but not so easy. *Int J Cardiol* 2015;**197**:257–259.
51. Ghadri JR, Cammann VL, Napp LC, Jurisic S, Diekmann J, Bacolod DR, Seifert B, Jaguszewski M, Sarcon A, Neumann CA, Geyer V, Prasad A, Bax JJ, Ruschitzka F, Luscher TF, Templin C; International Takotsubo Registry. Differences in the clinical profile and outcomes of typical and atypical takotsubo syndrome: data from the International Takotsubo Registry. *JAMA Cardiol* 2016;**1**: 335–340.
52. Kato K, Kitahara H, Fujimoto Y, Sakai Y, Ishibashi I, Hirai T, Kobayashi Y. Prevalence and clinical features of focal takotsubo cardiomyopathy. *Circ J* 2016; **80**:1824–1829.
53. Giavarini A, Chedid A, Bobrie G, Plouin PF, Hagege A, Amar L. Acute catecholamine cardiomyopathy in patients with pheochromocytoma or functional paraganglioma. *Heart* 2013;**99**:1438–1444.
54. Finsterer J, Wahbi K. CNS disease triggering Takotsubo stress cardiomyopathy. *Int J Cardiol* 2014;**177**:322–329.
55. Suzuki H, Matsumoto Y, Kaneta T, Sugimura K, Takahashi J, Fukumoto Y, Takahashi S, Shimokawa H. Evidence for brain activation in patients with takotsubo cardiomyopathy. *Circ J* 2014;**78**:256–258.
56. Abraham J, Mudd JO, Kapur NK, Klein K, Champion HC, Wittstein IS. Stress cardiomyopathy after intravenous administration of catecholamines and beta-receptor agonists. *J Am Coll Cardiol* 2009;**53**:1320–1325.
57. Y-Hassan S, Henareh L. Plasma catecholamine levels in patients with takotsubo syndrome: implications for the pathogenesis of the disease. *Int J Cardiol* 2015; **181**:35–38.
58. Kume T, Kawamoto T, Okura H, Toyota E, Neishi Y, Watanabe N, Hayashida A, Okahashi N, Yoshimura Y, Saito K, Nezuo S, Yamada R, Yoshida K. Local release of catecholamines from the hearts of patients with tako-tsubo-like left ventricular dysfunction. *Circ J* 2008;**72**:106–108.
59. Ortak J, Khattab K, Barantke M, Wiegand UK, Bansch D, Ince H, Nienaber CA, Bonnemeier H. Evolution of cardiac autonomic nervous activity indices in patients presenting with transient left ventricular apical ballooning. *Pacing Clin Electrophysiol* 2009;**32**:521–525.
60. Vaccaro A, Despas F, Delmas C, Lairez O, Lambert E, Lambert G, Labrunee M, Guiraud T, Esler M, Galinier M, Senard JM, Pathak A. Direct evidences for sympathetic hyperactivity and baroreflex impairment in Tako Tsubo cardiopathy. *PLoS One* 2014;**9**:e93378.
61. Burgdorf C, von Hof K, Schunkert H, Kurowski V. Regional alterations in myocardial sympathetic innervation in patients with transient left ventricular apical ballooning (Tako-Tsubo cardiomyopathy). *J Nucl Cardiol* 2008;**15**:65–72.
62. Verberne HJ, van der Heijden DJ, van Eck-Smit BL, Somsen GA. Persisting myocardial sympathetic dysfunction in takotsubo cardiomyopathy. *J Nucl Cardiol* 2009;**16**:321–324.
63. Paur H, Wright PT, Sikkel MB, Tranter MH, Mansfield C, O'Gara P, Stuckey DJ, Nikolaev VO, Diakonov I, Pannell L, Gong H, Sun H, Peters NS, Petrou M, Zhang Z, Gorelik J, Lyon AR, Harding SE. High levels of circulating epinephrine trigger apical cardiodepression in a β2-adrenergic receptor/Gi-dependent manner: a new model of Takotsubo cardiomyopathy. *Circulation* 2012;**126**:697–706.
64. Shao Y, Redfors B, Scharin Tang M, Mollmann H, Troidl C, Szardien S, Hamm C, Nef H, Boren J, Omerovic E. Novel rat model reveals important roles of beta-adrenoreceptors in stress-induced cardiomyopathy. *Int J Cardiol* 2013;**168**: 1943–1950.
65. Sachdeva J, Dai W, Kloner RA. Functional and histological assessment of an experimental model of Takotsubo's cardiomyopathy. *J Am Heart Assoc* 2014;**3**: e000921.
66. Ueyama T, Kasamatsu K, Hano T, Yamamoto K, Tsuruo Y, Nishio I. Emotional stress induces transient left ventricular hypocontraction in the rat via activation of cardiac adrenoceptors: a possible animal model of 'tako-tsubo' cardiomyopathy. *Circ J* 2002;**66**:712–713.
67. Redfors B, Ali A, Shao Y, Lundgren J, Gan LM, Omerovic E. Different catecholamines induce different patterns of takotsubo-like cardiac dysfunction in an apparently afterload dependent manner. *Int J Cardiol* 2014;**174**:330–336.
68. Delgado GA, Truesdell AG, Kirchner RM, Zvarek RW, Pomerantzev EV, Gordon PC, Regunta RA. An angiographic and intravascular ultrasound study of the left anterior descending coronary artery in takotsubo cardiomyopathy. *Am J Cardiol* 2011;**108**:888–891.
69. Pawlowski T, Mintz GS, Kubawik T, Gil RJ. Virtual histology intravascular ultrasound evaluation of the left anterior descending coronary artery in patients with transient left ventricular ballooning syndrome. *Kardiol Pol* 2010;**68**: 1093–1098.
70. Eitel I, Stiermaier T, Graf T, Mollar C, Rommel KP, Eitel C, Schuler G, Thiele H, Desch S. Optical coherence tomography to evaluate plaque burden and morphology in patients with Takotsubo syndrome. *J Am Heart Assoc* 2016;**5**.
71. Hoye J, Lerman A, Lennon RJ, Rihal CS, Prasad A. Left anterior descending artery length and coronary atherosclerosis in apical ballooning syndrome (Takotsubo/stress induced cardiomyopathy). *Int J Cardiol* 2010;**145**:112–115.
72. Scantlebury DC, Prasad A, Rabinstein AA, Best PJ. Prevalence of migraine and Raynaud phenomenon in women with apical ballooning syndrome (Takotsubo or stress cardiomyopathy). *Am J Cardiol* 2013;**111**:1284–1288.
73. Spieker LE, Hurlimann D, Ruschitzka F, Corti R, Enseleit F, Shaw S, Hayoz D, Deanfield JE, Luscher TF, Noll G. Mental stress induces prolonged endothelial dysfunction via endothelin-A receptors. *Circulation* 2002;**105**:2817–2820.
74. Vasileva E, Vorobyeva I, Lebedeva A, Urazovskaya I, Kalinskaya A, Skrypnik D, Shpektor A. Brachial artery flow-mediated dilation in patients with tako-tsubo cardiomyopathy. *Am J Med* 2011;**124**:1176–1179.
75. Tsuchihashi K, Ueshima K, Uchida T, Oh-Mura N, Kimura K, Owa M, Yoshiyama M, Miyazaki S, Haze K, Ogawa H, Honda T, Hase M, Kai R, Morii I; Angina Pectoris-Myocardial Infarction Investigations in Japan. Transient left ventricular apical ballooning without coronary artery stenosis: a novel heart syndrome mimicking acute myocardial infarction. Angina Pectoris-Myocardial Infarction Investigations in Japan. *J Am Coll Cardiol* 2001;**38**:11–18.
76. Angelini P, Monge J, Simpson L. Biventricular takotsubo cardiomyopathy: case report and general discussion. *Tex Heart Inst J* 2013;**40**:312–315.
77. Migione F, Maffei E, Perazzolo Marra M, Bilato C, Napodano M, Corbetti F, Zorzi A, Andres AL, Sarais C, Cacciavillani L, Favaretto E, Martini C, Seitun S, Cademartiri F, Corrado D, Iliceto S, Tarantini G. LAD coronary artery myocardial bridging and apical ballooning syndrome. *JACC Cardiovasc Imaging* 2013;**6**: 32–41.
78. Fiol M, Carrillo A, Rodriguez A, Herrero J, Garcia-Niebla J. Left ventricular ballooning syndrome due to vasospasm of the middle portion of the left anterior descending coronary artery. *Cardiol J* 2012;**19**:314–316.
79. Zhang Z, Jin S, Teng X, Duan X, Chen Y, Wu Y. Hydrogen sulfide attenuates cardiac injury in takotsubo cardiomyopathy by alleviating oxidative stress. *Nitric Oxide* 2017;**67**:10–25.
80. Nanno T, Kobayashi Y, Oda S, Ishiguchi H, Myoren T, Miyazaki Y, Suetomi T, Ono M, Mochizuki M, Oda T, Okuda S, Yamada J, Okamura T, Yano M. A

Downloaded from https://academic.oup.com/eurheartjpublications-abstract/39/22/2032/5025412 by EndocrineSociety Admin user on 27 April 2020

Marked increase in myocardial oxidative stress associated with sympathetic hyperactivity is related to transient myocardial dysfunction in patients with takotsubo cardiomyopathy. *Circulation* 2015;**132**:A14124.
81. Cohen RA, Shepherd JT, Vanhoutte PM. Prejunctional and postjunctional actions of endogenous norepinephrine at the sympathetic neuroeffector junction in canine coronary arteries. *Circ Res* 1983;**52**:16–25.
82. Jaguszewski M, Osipova J, Ghadri JR, Napp LC, Widera C, Franke J, Fijalkowski M, Nowalany-Kozielska E, Fijalkowska M, Vollmann I, Katus HA, Wollert KC, Bauersachs J, Erne P, Luscher TF, Thum T, Templin C. A signature of circulating microRNAs differentiates takotsubo cardiomyopathy from acute myocardial infarction. *Eur Heart J* 2014;**35**:999–1006.
83. Ghadri JR, Dougoud S, Maier W, Kaufmann PA, Gaemperli O, Prasad A, Luscher TF, Templin C. A PET/CT-follow-up imaging study to differentiate takotsubo cardiomyopathy from acute myocardial infarction. *Int J Cardiovasc Imaging* 2014;**30**:207–209.
84. Meimoun P, Malaquin D, Sayah S, Benali T, Luyce-Bore A, Levy F, Zemir H, Tribouilloy C. The coronary flow reserve is transiently impaired in tako-tsubo cardiomyopathy: a prospective study using serial Doppler transthoracic echocardiography. *J Am Soc Echocardiogr* 2008;**21**:72–77.
85. Rigo F, Sicari R, Citro R, Ossena G, Buja P, Picano E. Diffuse, marked, reversible impairment in coronary microcirculation in stress cardiomyopathy: a Doppler transthoracic echo study. *Ann Med* 2009;**41**:462–470.
86. Kume T, Akasaka T, Kawamoto T, Yoshitani H, Watanabe N, Neishi Y, Wada N, Yoshida K. Assessment of coronary microcirculation in patients with takotsubo-like left ventricular dysfunction. *Circ J* 2005;**69**:934–939.
87. Cuisset T, Quilici J, Pankert M, Fourcade L, Poyet R, Lambert M, Bonnet JL. Usefulness of index of microcirculatory resistance to detect microvascular dysfunction as a potential mechanism of stress-induced cardiomyopathy (Takotsubo syndrome). *Int J Cardiol* 2011;**153**:e51–e53.
88. Elesber A, Lerman A, Bybee KA, Murphy JG, Barsness G, Singh M, Rihal CS, Prasad A. Myocardial perfusion in apical ballooning syndrome correlate of myocardial injury. *Am Heart J* 2006;**152**:469 e9–413.
89. Galiuto L, De Caterina AR, Porfidia A, Paraggio L, Barchetta S, Loconsolo G, Rebuzzi AG, Crea F. Reversible coronary microvascular dysfunction: a common pathogenetic mechanism in apical ballooning or tako-tsubo syndrome. *Eur Heart J* 2010;**31**:1319–1327.
90. Uchida Y, Egami H, Uchida Y, Sakurai T, Kanai M, Shirai S, Nakagawa O, Ochima T. Possible participation of endothelial cell apoptosis of coronary microvessels in the genesis of Takotsubo cardiomyopathy. *Clin Cardiol* 2010;**33**: 371–377.
91. Barletta G, Del Pace S, Boddi M, Del Bene R, Salvadori C, Bellandi B, Coppo M, Saletti E, Gensini GF. Abnormal coronary reserve and left ventricular wall motion during cold pressor test in patients with previous left ventricular ballooning syndrome. *Eur Heart J* 2009;**30**:3007–3014.
92. Martin EA, Prasad A, Rihal CS, Lerman LO, Lerman A. Endothelial function and vascular response to mental stress are impaired in patients with apical ballooning syndrome. *J Am Coll Cardiol* 2010;**56**:1840–1846.
93. Patel SM, Lerman A, Lennon RJ, Prasad A. Impaired coronary microvascular reactivity in women with apical ballooning syndrome (takotsubo/stress cardiomyopathy). *Eur Heart J Acute Cardiovasc Care* 2013;**2**:147–152.
94. Nef HM, Mollmann H, Troidl C, Kostin S, Voss S, Hilpert P, Behrens CB, Rolf A, Rixe J, Weber M, Hamm CW, Elsasser A. Abnormalities in intracellular Ca2+ regulation contribute to the pathomechanism of tako-tsubo cardiomyopathy. *Eur Heart J* 2009;**30**:2155–2164.
95. Nef HM, Mollmann H, Akashi YJ, Hamm CW. Mechanisms of stress (Takotsubo) cardiomyopathy. *Nat Rev Cardiol* 2010;**7**:187–193.
96. Rona G. Catecholamine cardiotoxicity. *J Mol Cell Cardiol* 1985;**17**:291–306.
97. Heather LC, Catchpole AF, Stuckey DJ, Cole MA, Carr CA, Clarke K. Isoproterenol induces in vivo functional and metabolic abnormalities similar to those found in the infarcted rat heart. *J Physiol Pharmacol* 2009;**60**:31–39.
98. Christensen TE, Bang LE, Holmvang L, Gholbi AA, Lassen ML, Andersen F, Ribemann N, Andersson H, Grande P, Kjaer A, Hasbak P. Cardiac (99)(99m)Tc sestamibi SPECT and (11)(18)F FDG PET as viability markers in takotsubo cardiomyopathy. *Int J Cardiovasc Imaging* 2014;**30**:1407–1416.
99. Rendl G, Rettenbacher L, Kolesnik P, Abenberger J, Schuler J, Heigert H, Pichler M, Pirich C. Different pattern of regional metabolic abnormalities in takotsubo cardiomyopathy as evidenced by F-18 FDG PET-CT. *Wiener Klin Wochenschr* 2010;**122**:184–185.
100. Shao Y, Redfors B, Stahlman M, Tang MS, Miljanovic A, Mollmann H, Troidl C, Szardien S, Hamm C, Nef H, Boren J, Omerovic E. A mouse model reveals an important role for catecholamine-induced lipotoxicity in the pathogenesis of stress-induced cardiomyopathy. *Eur J Heart Fail* 2013;**15**:9–22.
101. Nef HM, Mollmann H, Kostin S, Troidl C, Voss S, Weber M, Dill T, Rolf A, Brandt R, Hamm CW, Elsasser A. Tako-Tsubo cardiomyopathy: intraindividual structural analysis in the acute phase and after functional recovery. *Eur Heart J* 2007;**28**:2456–2464.
102. Redfors B, Shao Y, Wikstrom J, Lyon AR, Oldfors A, Gan LM, Omerovic E. Contrast echocardiography reveals apparently normal coronary perfusion in a rat model of stress-induced (Takotsubo) cardiomyopathy. *Eur Heart J Cardiovasc Imaging* 2014;**15**:152–157.
103. Kawano H, Okada R, Yano K. Histological study on the distribution of autonomic nerves in the human heart. *Heart Vessels* 2003;**18**:32–39.
104. Lyon AR, Rees PS, Prasad S, Poole-Wilson PA, Harding SE. Stress (Takotsubo) cardiomyopathy—a novel pathophysiological hypothesis to explain catecholamine-induced acute myocardial stunning. *Nat Clin Pract Cardiovasc Med* 2008;**5**:22–29.
105. Mori H, Ishikawa S, Kojima S, Hayashi J, Watanabe Y, Hoffman JI, Okino H. Increased responsiveness of left ventricular apical myocardium to adrenergic stimuli. *Cardiovasc Res* 1993;**27**:192–198.
106. Communal C, Colucci WS, Singh K. p38 mitogen-activated protein kinase pathway protects adult rat ventricular myocytes against beta-adrenergic receptor-stimulated apoptosis. Evidence for Gi-dependent activation. *J Biol Chem* 2000; **275**:19395–19400.
107. Heubach JF, Ravens U, Kaumann AJ. Epinephrine activates both Gs and Gi pathways, but norepinephrine activates only the Gs pathway through human beta2-adrenoceptors overexpressed in mouse heart. *Mol Pharmacol* 2004;**65**: 1313–1322.
108. Zhu WZ, Zheng M, Koch WJ, Lefkowitz RJ, Kobilka BK, Xiao RP. Dual modulation of cell survival and cell death by beta(2)-adrenergic signaling in adult mouse cardiac myocytes. *Proc Natl Acad Sci U S A* 2001;**98**:1607–1612.
109. Nguyen TH, Neil CJ, Sverdlov AL, Ngo DT, Chan WP, Horowitz T, Chirkov YY, Takas D, Frenneaux MP, Horowitz JD. Enhanced NO signaling in patients with Takotsubo cardiomyopathy: short-term pain, long-term gain? *Cardiovasc Drugs Ther* 2012;**27**:541–547.
110. Sunkaw SY, Raman B, Licari J, Singh K, Nguyen TH, Horowitz JD. Evidence of nitrosative stress within hearts of patients dying of Tako-tsubo cardiomyopathy. *Int J Cardiol* 2015;**189**:112–114.
111. Dawson DK, Neil CJ, Henning A, Cameron D, Jagpal B, Bruce M, Horowitz J, Frenneaux MP. Tako-Tsubo cardiomyopathy: a heart stressed out of energy? *JACC Cardiovasc Imaging* 2015;**8**:985–987.
112. Nef HM, Mollmann H, Hilpert P, Troidl C, Voss S, Rolf A, Behrens CB, Weber M, Hamm CW, Elsasser A. Activated cell survival cascade protects cardiomyocytes from cell death in Tako-Tsubo cardiomyopathy. *Eur J Heart Fail* 2009;**11**: 758–764.
113. Spinelli L, Trimarco V, Di Marino S, Marino M, Iaccarino G, Trimarco B. L41Q polymorphism of the G protein coupled receptor kinase 5 is associated with left ventricular apical ballooning syndrome. *Eur J Heart Fail* 2010;**12**:13–16.
114. Figtree GA, Bagnall RD, Abdulla J, Buchholz S, Gallaugher KK, Yan W, Tan T, Neil C, Horowitz JD, Semsarian C, Ward ML. No association of G-protein-coupled receptor kinase 5 or beta-adrenergic receptor polymorphisms with Takotsubo cardiomyopathy in a large Australian cohort. *Eur J Heart Fail* 2013; **15**:730–733.
115. Vitale C, Rosano GM, Kaski JC. Role of coronary microvascular dysfunction in takotsubo cardiomyopathy. *Circ J* 2016;**80**:299–305.
116. Ueyama T, Kasamatsu K, Hano T, Tsuruo Y, Ishikura F. Catecholamines and estrogen are involved in the pathogenesis of emotional stress-induced acute heart attack. *Ann N Y Acad Sci* 2008;**1148**:479–485.
117. Sader MA, Celermajer DS. Endothelial function, vascular reactivity and gender differences in the cardiovascular system. *Cardiovasc Res* 2002;**53**:597–604.
118. Komesaroff PA, Esler MD, Sudhir K. Estrogen supplementation attenuates glucocorticoid and catecholamine responses to mental stress in perimenopausal women. *J Clin Endocrinol Metab* 1999;**84**:606–610.
119. Sung BH, Ching M, Izzo JL Jr, Dandona P, Wilson MF. Estrogen improves abnormal norepinephrine-induced vasoconstriction in postmenopausal women. *J Hypertens* 1999;**17**:523–528.
120. Sugimoto K, Inamasu J, Hirose Y, Kato Y, Ito K, Iwase M, Sugimoto K, Watanabe E, Takahashi A, Ozaki Y. The role of norepinephrine and estradiol in the pathogenesis of cardiac wall motion abnormality associated with subarachnoid hemorrhage. *Stroke* 2012;**43**:1897–1903.
121. Ueyama T, Ishikura F, Matsuda A, Asanuma T, Ueda K, Ichinose M, Kasamatsu K, Hano T, Akasaka T, Tsuruo Y, Morimoto K, Beppu S. Chronic estrogen supplementation following ovariectomy improves the emotional stress-induced cardiovascular responses by indirect action on the nervous system and by direct action on the heart. *Circ J* 2007;**71**:565–573.
122. Cherian J, Angelis D, Filiberti A, Saperia G. Can takotsubo cardiomyopathy be familial? *Int J Cardiol* 2007;**121**:74–75.
123. Kumar G, Holmes DR Jr, Prasad A. "Familial" apical ballooning syndrome (Takotsubo cardiomyopathy). *Int J Cardiol* 2010;**144**:444–445.
124. Ikutomi M, Yamasaki M, Matsuzaki M, Watari Y, Arashi H, Endo G, Yamaguchi JI, Ohnishi S. Takotsubo cardiomyopathy in siblings. *Heart Vessels* 2014;**29**: 119–122.

Downloaded from https://academic.oup.com/eurheartjournal/article-abstract/39/22/2032/4602841 2 by EndocrineSociety Admin user on 27 April 2020

125. Pison L, De Vusser P, Mullens W. Apical ballooning in relatives. *Heart* 2004;**90**:e67.
126. Caretta G, Robba D, Vizzardi E, Bonadei I, Raddino R, Metra M. Takо-tsubo cardiomyopathy in two sisters: a chance finding or familial predisposition? *Clin Res Cardiol* 2013;**104**:614–616.
127. Dorn GW 2nd. Adrenergic signaling polymorphisms and their impact on cardiovascular disease. *Physiol Rev* 2010;**90**:1013–1062.
128. Zaroff JG, Pawlikowska L, Miss JC, Yarbagadda S, Ha C, Achrol A, Kwok PY, McCulloch CE, Lawton MT, Ko N, Smith W, Young WL. Adrenoceptor polymorphisms and the risk of cardiac injury and dysfunction after subarachnoid hemorrhage. *Stroke* 2006;**37**:1680–1685.
129. Guja KR, Adam AF, Priman V, Tejani F, Vasavada B. Initial presentation of pheochromocytoma with Takotsubo cardiomyopathy: a brief review of literature. *J Cardiovasc Med* 2010;**11**:49–52.
130. Shirley SW, Maron BJ, Nelson P, Porpart M, Maron MS, Bristow MR. Adrenergic receptor polymorphisms in patients with stress (tako-tsubo) cardiomyopathy. *J Cardiol* 2009;**53**:53–57.
131. Vitz O, Minisini R, Citro R, Guerra V, Zito C, De Luca G, Pavan D, Pirisi M, Limongelli G, Bossone E. Analysis of beta1 and beta2-adrenergic receptors polymorphism in patients with apical ballooning cardiomyopathy. *Acta Cardiol* 2011;**66**:787–790.
132. Goodloe AH, Evans JM, Middha S, Prasad A, Olson TM. Characterizing genetic variation of adrenergic signaling pathways in Takotsubo (stress) cardiomyopathy exomes. *Eur J Heart Fail* 2014;**16**:942–949.
133. Borchert T, Hübscher D, Guessoum CI, Lam T-DD, Ghadri JR, Schellinger IN, Tiburcy M, Liaw NY, Li Y, Haas J, Sossalla S, Huber MA, Cyganek L, Jacobshagen C, Dressel R, Rast U, Nikolaev VO, Guan K, Thiele H, Meder B, Wollnik B, Zimmermann W-H, Lüscher TF, Hasenfuss G, Templin C, Streckfuss-Bömeke K. Catecholamine-dependent beta-adrenergic signaling in a pluripotent stem cell model of Takotsubo cardiomyopathy. *J Am Coll Cardiol* 2017;**70**:975–991.
134. Lyon A. Stress in a dish: exploring the mechanisms of Takotsubo syndrome. *J Am Coll Cardiol* 2017;**70**:992–995.
135. Summers MR, Lennon RJ, Prasad A. Pre-morbid psychiatric and cardiovascular diseases in apical ballooning syndrome (tako-tsubo/stress-induced cardiomyopathy): potential pre-disposing factors? *J Am Coll Cardiol* 2010;**55**:700–701.
136. Delmas C, Lairez O, Malin E, Delmas T, Boudou N, Dumontell N, Blondel-Picquet C, Roncalli J, Elbaz M, Galinier M, Carrié D. Anxiodepressive disorders and chronic psychological stress are associated with Tako-Tsubo cardiomyopathy-new physiopathological hypothesis. *Circ J* 2013;**77**:175–180.
137. Compare A, Bigi R, Orrego PS, Proietti R, Grossi E, Steptoe A. Type D personality is associated with the development of stress cardiomyopathy following emotional triggers. *Ann Behav Med* 2013;**45**:299–307.
138. Scantlebury DC, Rohe DE, Bell PJ, Lennon RJ, Lerman A, Prasad A. Stress-coping skills and neuroticism in apical ballooning syndrome (Takotsubo/stress cardiomyopathy). *Open Heart* 2016;**3**:e000313.
139. Summers MR, Dib C, Prasad A. Chronobiology of Tako-tsubo cardiomyopathy (apical ballooning syndrome). *J Am Geriatr Soc* 2010;**58**:805–806.
140. Mausbach BT, Dimsdale JE, Ziegler MG, Mills PJ, Ancoli-Israel S, Patterson TL, Grant I. Depressive symptoms predict norepinephrine response to a psychological stressor task in Alzheimer's caregivers. *Psychosom Med* 2005;**67**:638–642.
141. Alvarenga ME, Richards JC, Lambert G, Esler MD. Psychophysiological mechanisms in panic disorder: a correlative analysis of noradrenaline spillover, neuronal noradrenaline reuptake, power spectral analysis of heart rate variability, and psychological variables. *Psychosom Med* 2006;**68**:8–16.
142. Neil CJ, Chong CR, Nguyen TH, Horowitz JD. Occurrence of Tako-Tsubo cardiomyopathy in association with ingestion of serotonin/noradrenaline reuptake inhibitors. *Heart Lung Circ* 2012;**21**:203–205.
143. Scheitz JF, Mochmann HC, Witzenbichler B, Fiebach JB, Audebert HJ, Nolte CH. Takotsubo cardiomyopathy following ischemic stroke: a cause of troponin elevation. *J Neurol* 2012;**259**:189–190.
144. Inamasu J, Guiraha T, Nakai S, Ohmi T, Watakiri A, Tanaka R, Kuwahara K, Kogame H, Kawazoe Y, Kumai T, Hayakawa M, Hirose Y. Therapeutic outcomes for patients with aneurysmal subarachnoid hemorrhage complicated by Takotsubo cardiomyopathy. *Acta Neurochir (Wien)* 2016;**158**:885–893.
145. Natelson BH, Suarez RV, Terrence CF, Turizo R. Patients with epilepsy who die suddenly have cardiac disease. *Arch Neurol* 1998;**55**:857–860.
146. Yoshida T, Hibino T, Kako N, Murai S, Oguri M, Kato K, Yajima K, Ohta N, Yokoi K, Kimura G. A pathophysiologic study of tako-tsubo cardiomyopathy with F-18 fluorodeoxyglucose positron emission tomography. *Eur Heart J* 2007;**28**:2598–2604.
147. Blanc C, Zeller M, Cottin Y, Daubail B, Viaboe AL, Giroud M, Bejot Y. Takotsubo cardiomyopathy following acute cerebral events. *Eur Neurol* 2015;**74**:163–168.
148. Hiestand T, Hänggi J, Klein C, Topka MS, Jaguszewski M, Ghadri JR, Lüscher TF, Jäncke L, Templin C. Takotsubo Syndrome Associated With Structural Brain Alterations of the Limbic System. *J Am Coll Cardiol* 2018;**71**:809–811.
149. Sharkey SW, Windenburg DC, Lesser JR, Maron MS, Hauser RG, Lesser JN, Haas TS, Hodges JS, Maron BJ. Natural history and expansive clinical profile of stress (tako-tsubo) cardiomyopathy. *J Am Coll Cardiol* 2010;**55**:333–341.
150. Münzel T, Knorr M, Schmidt F, von Bardeleben S, Gori T, Schulz E. Airborne disease: a case of a Takotsubo cardiomyopathic as a consequence of nightime aircraft noise exposure. *Eur Heart J*. 2016;**37**:2844 [Epub 19 July 2016].
151. Gianni M, Dentali F, Grandi AM, Sumner G, Hiralal R, Lonn E. Apical ballooning syndrome or takotsubo cardiomyopathy: a systematic review. *Eur Heart J* 2006;**27**:1523–1529.
152. Isogai T, Yasunaga H, Matsui H, Tanaka H, Ueda T, Horiguchi H, Fushimi K. Out-of-hospital versus in-hospital Takotsubo cardiomyopathy: analysis of 3719 patients in the Diagnosis Procedure Combination database in Japan. *Int J Cardiol* 2014;**176**:413–417.
153. Tagawa M, Nakamura Y, Ishiguro H, Satoh K, Chinushi M, Kodama M, Aizawa Y. Transient left ventricular apical ballooning developing after the Central Niigata Prefecture Earthquake: two case reports. *J Cardiol* 2006;**48**:153–158.
154. Chan C, Elliott J, Troughton R, Frampton C, Smyth D, Crozier I, Bridgman P. Acute myocardial infarction and stress cardiomyopathy following the Christchurch earthquakes. *PloS One* 2013;**8**:e68504.
155. Butterly SJ, Inderjith M, Garnaby P, Ng AC, Gould PA, Wang WY. Stress-induced takotsubo cardiomyopathy in survivors of the 2011 Queensland floods. *Med J Aust* 2013;**198**:109–110.
156. Ghadri JR, Sarcon A, Diekmann J, Bataiosu DR, Cammann VL, Jurisic S, Napp LC, Jaguszewski M, Scherff F, Brugger P, Jäncke L, Seifert B, Bax JJ, Ruschitzka F, Lüscher TF, Templin C; InterTAK Co-investigators. Happy heart syndrome: role of positive emotional stress in takotsubo syndrome. *Eur Heart J* 2016;**37**:2823–2829.
157. Lousinha A, Gilkeson R, Bezerra H. Left ventricular outflow tract obstruction and Takotsubo syndrome. *Rev Port Cardiol* 2012;**31**:49–51.
158. Berry M, Roncalli J, Lairez O, Elbaz M, Carrie D, Galinier M. Takotsubo cardiomyopathy in a squash player. *Cardiol Res Pract* 2009;**2009**:351621.
159. Kostiou OS, Douras A, Makris D, Mpaka N, Gourgoulianis KI. Takotsubo cardiomyopathy: a known unknown foe of asthma. *J Asthma* 2017;**54**:880–886.
160. Ghadri JR, Bataiosu RD, Diekmann J, Lüscher TF, Templin C. First case of atypical takotsubo cardiomyopathy in a bilateral lung-transplanted patient due to acute respiratory failure. *Eur Heart J Acute Cardiovasc Care* 2015;**4**:482–485.
161. Rajani R, Przedlacka A, Saha M, de Belder A. Pancreatitis and the broken heart. *Eur J Emerg Med* 2010;**17**:27–29.
162. Aggarwal V, Krantz MJ. Migratory takotsubo cardiomyopathy in the setting of cholecystitis. *Am J Med* 2012;**125**:e5–e6.
163. Gale M, Loarte P, Mirner B, Mallet T, Salciodoli L, Petrie A, Cohen R. Takotsubo cardiomyopathy in the setting of tension pneumothorax. *Case Rep Crit Care* 2015;**2015**:536931.
164. Elikowski W, Kudlicki B, Malek-Elikowska M, Forenski-Ickik J, Baszko A, Skrzywanek P. [Takotsubo cardiomyopathy in a young woman after a traffic accident with blunt chest trauma]. *Pol Merkur Lekarski* 2016;**40**:373–376.
165. Y-Hassan S, Settergren M, Henareh L. Sepsis-induced myocardial depression and takotsubo syndrome. *Acute Cardiac Care* 2014;**16**:102–109.
166. Elades M, El-Masoudie D, Choudhary C, Zimmerster B, Burman KD. Takotsubo cardiomyopathy associated with thyrotoxicosis: a case report and review of the literature. *Thyroid* 2014;**24**:383–389.
167. Smith SA, Auseon AJ. Chemotherapy-induced takotsubo cardiomyopathy. *Heart Fail Clin* 2013;**9**:233–242, x.
168. Modi S, Baig W. Radiotherapy-induced Tako-tsubo cardiomyopathy. *Clin Oncol (R Coll Radiol)* 2009;**21**:361–362.
169. Brezina P, Isler CM. Takotsubo cardiomyopathy in pregnancy. *Obstet Gynecol* 2008;**112**:450–453.
170. Citro R, Lyon A, Arbustini E, Bossone E, Piccione F, Templin C, Narula J. Takotsubo syndrome after cesarean section: rare but possible. *J Am Coll Cardiol* 2018;**71**:1838–1839.
171. Dundas BK, Pari R, Leong DP, Worthley MI. Takotsubo cardiomyopathy following lightning strike. *Emerg Med J* 2008;**25**:460–461.
172. Citro R, Patella MM, Bossone E, Malone A, Provenza G, Gregorio G, Near-drowning syndrome: a possible trigger of tako-tsubo cardiomyopathy. *J Cardiovasc Med* 2008;**9**:501–505.
173. Davis L, Legrand V, Legrand D. A frozen heart. *Eur Heart J* 2009;**30**:1837.
174. Arora S, Albayrami F, Srinivasan V. Transient left ventricular apical ballooning after cocaine use: is catecholamine cardiotoxicity the pathologic link? *Mayo Clin Proc* 2006;**81**:829–832.
175. Stout BJ, Hoskins R, Vincent DS. Takotsubo cardiomyopathy in the setting of acute alcohol withdrawal. *Hawaii J Med Public Health* 2012;**71**:193–194.

Downloaded from https://academic.oup.com/eurheartj/article-abstract/39/22/2032/5025412 by EndocrinoSociety Admin user on 27 April 2020

176. Sarson A, Ghadri JR, Wong G, Luscher TF, Templin C, Amsterdam E. Takotsubo cardiomyopathy associated with opiate withdrawal. QJM 2014;107:301–302.
177. Jung YS, Lee JS, Min YG, Park JS, Jeon WC, Park EJ, Shin JH, Oh S, Choi SC. Carbon monoxide-induced cardiomyopathy. Clin J 2014;78:1437–1444.
178. Y-Hassan S. Clinical features and outcome of epinephrine-induced takotsubo syndrome: analysis of 33 published cases. Cardiovasc Revasc Med 2016;17:450–455.
179. Mendoza I, Novaro GM. Repeat recurrence of takotsubo cardiomyopathy related to inhaled beta-2-adrenoceptor agonists. World J Cardiol 2012;4:211–213.
180. Margey R, Diamond P, McCann H, Sugrue D. Dobutamine stress echo-induced apical ballooning (Takotsubo) syndrome. Eur J Echocardiogr 2009;10:395–399.
181. Collet J, Bimson W, Devine P. A variant of Takotsubo cardiomyopathy: a rare complication in the electrophysiology lab. J Invasive Cardiol 2008;20:E310–E313.
182. Patel B, Assad D, Wiemann C, Zughaib M. Repeated use of albuterol inhaler as a potential cause of Takotsubo cardiomyopathy. Am J Case Rep 2014;15:221–225.
183. Riera M, Llompart-Pou JA, Carrillo A, Blanco C. Head injury and inverted Takotsubo cardiomyopathy. J Trauma 2010;68:E13–E15.
184. Hjalmarsson C, Oras J, Rodfors B. A case of intracerebral hemorrhage and apical ballooning: an important differential diagnosis in ST-segment elevation. Int J Cardiol 2015;186:90–92.
185. Stiermaier T, Moeller C, Oehler K, Desch S, Graf T, Eitel C, Vordhein R, Schuler G, Thiele H, Eitel I. Long-term excess mortality in takotsubo cardiomyopathy: predictors, causes and clinical consequences. Eur J Heart Fail 2016;18:650–656.
186. Y-Hassan S. Clinical features and outcome of pheochromocytoma-induced Takotsubo syndrome: analysis of 80 published cases. Am J Cardiol 2016;117:1836–1844.
187. Shoukat S, Assad A, Nam DK, Hoskins MH, Samuels O, Higginson J, Clamanta SD Jr. Cardiomyopathy with inverted Tako-Tsubo pattern in the setting of subarachnoid hemorrhage: a series of four cases. Neurocrit Care 2013;18:257–260.
188. Kagiyama N, Okura H, Kume T, Hayashida A, Yoshida K. Isolated right ventricular takotsubo cardiomyopathy. Eur Heart J Cardiovasc Imaging 2015;16:205.
189. Stahli BE, Ruschitzka F, Enseleit F. Isolated right ventricular ballooning syndrome: a new variant of transient cardiomyopathy. Eur Heart J 2011;32:1821.
190. Elikowski W, Malek M, Lanocha M, Wroblewski D, Angerer D, Kurosz J, Rachyta K. [Reversible dilated cardiomyopathy as an atypical form of takotsubo cardiomyopathy]. Pol Merkur Lekarski 2013;34:219–223.
191. Eitel I, von Knobelsdorff-Brenkenhoff F, Bernhardt P, Carbone I, Muellerleile K, Aldrovandi A, Francone M, Desch S, Gutberlet M, Strohm O, Schuler G, Schulz-Menger J, Thiele H, Friedrich MG. Clinical characteristics and cardiovascular magnetic resonance findings in stress (takotsubo) cardiomyopathy. JAMA 2011;306:277–286.
192. Ghadri JR, Jaguszewski M, Corti R, Luscher TF, Templin C. Different wall motion patterns of three consecutive episodes of takotsubo cardiomyopathy in the same patient. Int J Cardiol 2012;160:e25–e27.
193. Hurst RT, Prasad A, Askew JW, Sengupta PP, Tajik AJ. Takotsubo cardiomyopathy: a unique cardiomyopathy with variable ventricular morphology. JACC Cardiovasc Imaging 2010;3:641–649.
194. Muller JE, Stone PH, Turi ZG, Rutherford JD, Czeisler CA, Parker C, Poole WK, Passamani E, Roberts R, Robertson T, Sobel BE, Wilkerson JT, Braunwald E. Circadian variation in the frequency of onset of acute myocardial infarction. N Engl J Med 1985;313:1315–1322.
195. Manfredini R, Portaluppi F, Zamboni P, Salmi R, Gallerani M. Circadian variation in spontaneous rupture of abdominal aorta. Lancet 1999;353:643–644.
196. Manfredini R, Manfredini F, Boari B, Bergami E, Mari E, Gamberini S, Salmi R, Gallerani M. Seasonal and weekly patterns of hospital admissions for nonfatal and fatal myocardial infarction. Am J Emerg Med 2009;27:1097–1103.
197. Willich SN, Lowel H, Lewis M, Hornmann A, Arntz HR, Keil U. Weekly variation of acute myocardial infarction. Increased Monday risk in the working population. Circulation 1994;90:87–93.
198. Song BG, Oh JH, Kim HJ, Kim SH, Chung SM, Lee H, Kang GH, Park YH, Chun WJ. Chronobiological variation in the occurrence of Tako-tsubo cardiomyopathy: experiences of two tertiary cardiovascular centers. Heart Lung 2013;42:43–47.
199. Citro R, Previtali M, Bovelli D, Vriz O, Astarita C, Patella MM, Provenza G, Armentano C, Ciampi Q, Gregorio G, Piepoli M, Bossone E, Manfredini R. Chronobiological patterns of onset of Tako-Tsubo cardiomyopathy: a multicenter Italian study. J Am Coll Cardiol 2009;54:180–181.
200. Sharkey SW, Lesser JR, Garberich RF, Park VR, Maron MS, Maron BJ. Comparison of circadian rhythm patterns in Tako-tsubo cardiomyopathy versus ST-segment elevation myocardial infarction. Am J Cardiol 2012;110:795–799.
201. Abdolla I, Kay S, Mussap C, Nelson GL, Rasmussen HH, Hansen PS, Ward MR. Apical sparing in tako-tsubo cardiomyopathy. Intern Med J 2006;36:414–418.
202. Manfredini R, Citro R, Previtali M, Vriz O, Ciampi Q, Pascotto M, Tagliamonte E, Provenza G, Manfredini F, Bossone E. Takotsubo Italian Network Investigators. Monday preference in onset of takotsubo cardiomyopathy. Am J Emerg Med 2010;28:715–719.
203. Aryal MR, Pathak R, Karmacharya P, Donato AA. Seasonal and regional variation in Takotsubo cardiomyopathy. Am J Cardiol 2014;113:1592.
204. Eshtehardi P, Koestner SC, Adorjan P, Windecker S, Meier B, Hess OM, Wahl A, Cook S. Transient apical ballooning syndrome–clinical characteristics, ballooning pattern, and long-term follow-up in a Swiss population. Int J Cardiol 2009;135:370–375.

Downloaded from https://academic.oup.com/eurheartjournal/article-abstract/39/22/2032/5029412 by EndocrineSociety Admin user on 27 April 2020

ESC European Society of Cardiology
European Heart Journal (2018) 39, 2047–2062
doi:10.1093/eurheartj/ehy077

CONSENSUS PAPER

International Expert Consensus Document on Takotsubo Syndrome (Part II): Diagnostic Workup, Outcome, and Management

Jelena-Rima Ghadri[1], Ilan Shor Wittstein[2], Abhiram Prasad[3], Scott Sharkey[4], Keigo Dote[5], Yoshihiro John Akashi[6], Victoria Lucia Cammann[1], Filippo Crea[7], Leonarda Galiuto[7], Walter Desmet[8,9], Tetsuro Yoshida[10], Roberto Manfredini[11], Ingo Eitel[12], Masami Kosuge[13], Holger M. Nef[14], Abhishek Deshmukh[3], Amir Lerman[3], Eduardo Bossone[15], Rodolfo Citro[15], Takashi Ueyama[16†], Domenico Corrado[17], Satoshi Kurisu[18], Frank Ruschitzka[1], David Winchester[19], Alexander R. Lyon[20,21], Elmir Omerovic[22,23], Jeroen J. Bax[24], Patrick Meimoun[25], Guiseppe Tarantini[17], Charanjit Rihal[3], Shams Y.-Hassan[26], Federico Migliore[17], John D. Horowitz[27], Hiroaki Shimokawa[28], Thomas Felix Lüscher[29,30], and Christian Templin[1*]

International Experts: Jeroen J. Bax, Eduardo Bossone, Victoria Lucia Cammann, Rodolfo Citro, Domenico Corrado, Filippo Crea, Walter Desmet, Ingo Eitel, Leonarda Galiuto, Jelena-Rima Ghadri, Thomas Felix Lüscher, Alexander R. Lyon, Roberto Manfredini, Patrick Meimoun, Federico Migliore, Holger M. Nef, Elmir Omerovic, Frank Ruschitzka, Guiseppe Tarantini, Christian Templin, Shams Y-Hassan (European sites); Abhishek Deshmukh, Amir Lerman, Abhiram Prasad, Charanjit Rihal, Scott Sharkey, David Winchester, Ilan Shor Wittstein (USA sites); Yoshihiro John Akashi, Keigo Dote, Masami Kosuge, Satoshi Kurisu, Hiroaki Shimokawa, Takashi Ueyama, Tetsuro Yoshida (Asian sites); John D. Horowitz (Australian site)

[1]University Heart Center, Department of Cardiology, University Hospital Zurich, Zurich, Switzerland; [2]Department of Medicine, Johns Hopkins University School of Medicine, Baltimore, MD, USA; [3]Division of Cardiovascular Diseases Mayo Clinic, Rochester, MN, USA; [4]Cardiovascular Research Division, Minneapolis Heart Institute Foundation, Minneapolis, MN, USA; [5]Department of Cardiology, Hiroshima City Asa Hospital, Hiroshima, Japan; [6]Division of Cardiology, Department of Internal Medicine, St. Marianna University School of Medicine, Kawasaki, Japan; [7]Department of Cardiovascular Sciences, Catholic University of the Sacred Heart, Rome, Italy; [8]Department of Cardiovascular Medicine, University Hospitals Leuven, Leuven, Belgium; [9]Department of Cardiovascular Sciences, University of Leuven, Leuven, Belgium; [10]Department of Cardiovascular Medicine, Oita Nakama Medical Association Oita Hospital, Fukuoka, Japan; [11]Clinica Medica, Department of Medical Sciences, University of Ferrara, Ferrara, Italy; [12]University Heart Center Luebeck, Medical Clinic II, Department of Cardiology, Angiology and Intensive Care Medicine, University of Luebeck, Luebeck, Germany; [13]Division of Cardiology, Yokohama City University Medical Center, Yokohama, Japan; [14]Department of Cardiology, University Hospital Giessen, Giessen, Germany; [15]Heart Department, University Hospital "San Giovanni di Dio e Ruggi d'Aragona", Salerno, Italy; [16]Department of Anatomy and Cell Biology, Wakayama Medical University School of Medicine, Wakayama,

The opinions expressed in this article are not necessarily those of the Editors of the European Heart Journal or of the European Society of Cardiology.

This paper was guest edited by Bernard J. Gersh (Mayo Clinic, gersh.bernard@mayo.edu).

* Corresponding author. Tel: +41 44 255 9585, Fax: +41 44 255 4401, Email: christian.templin@usz.ch

† Deceased.

© The Author(s) 2018. Published by Oxford University Press on behalf of the European Society of Cardiology.
This is an Open Access article distributed under the terms of the Creative Commons Attribution Non-Commercial License (http://creativecommons.org/licenses/by-nc/4.0/), which permits non-commercial re-use, distribution, and reproduction in any medium, provided the original work is properly cited. For commercial re-use, please contact journals.permissions@oup.com

Downloaded from https://academic.oup.com/eurheartj/article-abstract/39/22/2047/4025411 by EndocrineSociety Admin user on 27 April 2020

Japan; [17]Department of Cardiac, Thoracic, and Vascular Sciences, University of Padua Medical School, Padova, Italy; [18]Department of Cardiovascular Medicine, Hiroshima University Graduate School of Biomedical and Health Sciences, Hiroshima, Japan; [19]Division of Cardiovascular Disease, Department of Medicine, University of Florida, Gainesville, FL, USA; [20]NIHR Cardiovascular Biomedical Research Unit, Royal Brompton Hospital, London, UK; [21]National Heart and Lung Institute, Imperial College, London, UK; [22]Department of Cardiology, Sahlgrenska University Hospital, Gothenburg, Sweden; [23]Department of Molecular and Clinical Medicine, Institute of Medicine, Sahlgrenska Academy, Gothenburg University, Gothenburg, Sweden; [24]Department of Cardiology, Leiden University Medical Center, Leiden, The Netherlands; [25]Department of Cardiology and Intensive Care, Centre Hospitalier de Compiegne, Compiegne, France; [26]Department of Cardiology, Karolinska University Hospital, Huddinge, Stockholm, Sweden; [27]Department of Cardiology, Royal Hezel Institute, Queen Elizabeth Hospital, University of Adelaide, Adelaide, Australia; [28]Department of Cardiovascular Medicine, Tohoku University Graduate School of Medicine, Sendai, Japan; [29]Center for Molecular Cardiology, Schlieren Campus, University of Zurich, Zurich, Switzerland; and [30]Department of Cardiology, Royal Brompton & Harefield Hospital and Imperial College, London, UK

Received 1 June 2017; revised 23 November 2017; editorial decision 30 January 2018; accepted 11 April 2018; online publish-ahead-of-print 29 May 2018

The clinical expert consensus statement on takotsubo syndrome (TTS) part II focuses on the diagnostic workup, outcome, and management. The recommendations are based on interpretation of the limited clinical trial data currently available and experience of international TTS experts. It summarizes the diagnostic approach, which may facilitate correct and timely diagnosis. Furthermore, the document covers areas where controversies still exist in risk stratification and management of TTS. Based on available data the document provides recommendations on optimal care of such patients for practising physicians.

Keywords Takotsubo syndrome • Broken heart syndrome • Acute heart failure • Consensus statement • Diagnostic algorithm

Outline

Diagnostic workup 2048
Electrocardiogram 2048
ST-segment elevation 2049
T-wave inversion and QT interval prolongation 2049
Other electrocardiographic findings 2050
InterTAK Diagnostic Score 2050
Biomarkers 2051
Markers of myocardial necrosis 2051
B-type natriuretic peptide and N-terminal prohormone of brain natriuretic peptide 2051
Other potential biomarkers 2051
Imaging 2051
Coronary angiography and ventriculography 2051
Echocardiography 2051
Cardiac computed tomography angiography 2052
Cardiac magnetic resonance imaging 2053
Cardiac nuclear imaging 2053
Perfusion imaging 2053
Metabolic imaging 2053
Sympathetic nervous imaging 2053
Complications and outcomes 2053
Arrhythmias 2055
Ventricular arrhythmias 2055
Other cardiac arrhythmias 2055
Recurrence 2055
Therapeutic management 2056
Pre-hospital treatment 2056
Acute treatment 2056
Long-term treatment 2057
Future directions 2058
Key questions 2058
Prospective approaches 2058
References 2058

Diagnostic workup

A diagnostic algorithm for takotsubo syndrome (TTS) is proposed by the expert committee (*Figure 1*). Patients presenting with ST-segment elevation should undergo urgent coronary angiography (CAG) with left ventriculography to exclude acute myocardial infarction (AMI). In patients with non ST-segment elevation the InterTAK Diagnostic Score can be considered. While an InterTAK Score ≤70 points suggests a low to intermediate probability of TTS, a score ≥70 indicates a high probability for the presence of TTS. Patients with a low probability should undergo CAG with left ventriculography, while in patients with a high score transthoracic echocardiography (TTE) should be considered. In the absence of a circumferential ballooning pattern CAG is recommended. In stable patients with circumferential ballooning pattern coronary computed tomography angiography (CCTA) is favoured to exclude coronary artery disease (CAD). In unstable patients, typical complications of TTS such as left ventricular outflow tract obstruction (LVOTO) should be determined with TTE and CAG to safely rule out AMI. In patients with normal coronaries on CCTA or CAG and typical ballooning patterns without 'red flags' of acute infectious myocarditis TTS is the most likely diagnosis and can be confirmed after follow-up echocardiography. In case of positive 'red flags' of acute infectious myocarditis cardiac magnetic resonance (CMR) should be performed to confirm the diagnosis.

Electrocardiogram

The initial electrocardiogram (ECG) is abnormal in most patients with TTS usually demonstrating ischaemic ST-segment elevation, T-wave inversion, or both.[1–4] In the InterTAK Registry, ST-segment elevation was present in 44%, ST-segment depression in 8%, T-wave inversion in 41%, and left bundle branch block in 5%.[2] As in acute coronary syndrome (ACS), the ECG in TTS demonstrates temporal evolution typically with resolution of initial ST-segment elevation (if present), followed by progressive T-wave inversion and QT interval prolongation

Downloaded from https://academic.oup.com/eurheartj/article-abstract/39/22/2047/5025411 by EndocrineSociety Admin user on 27 April 2020

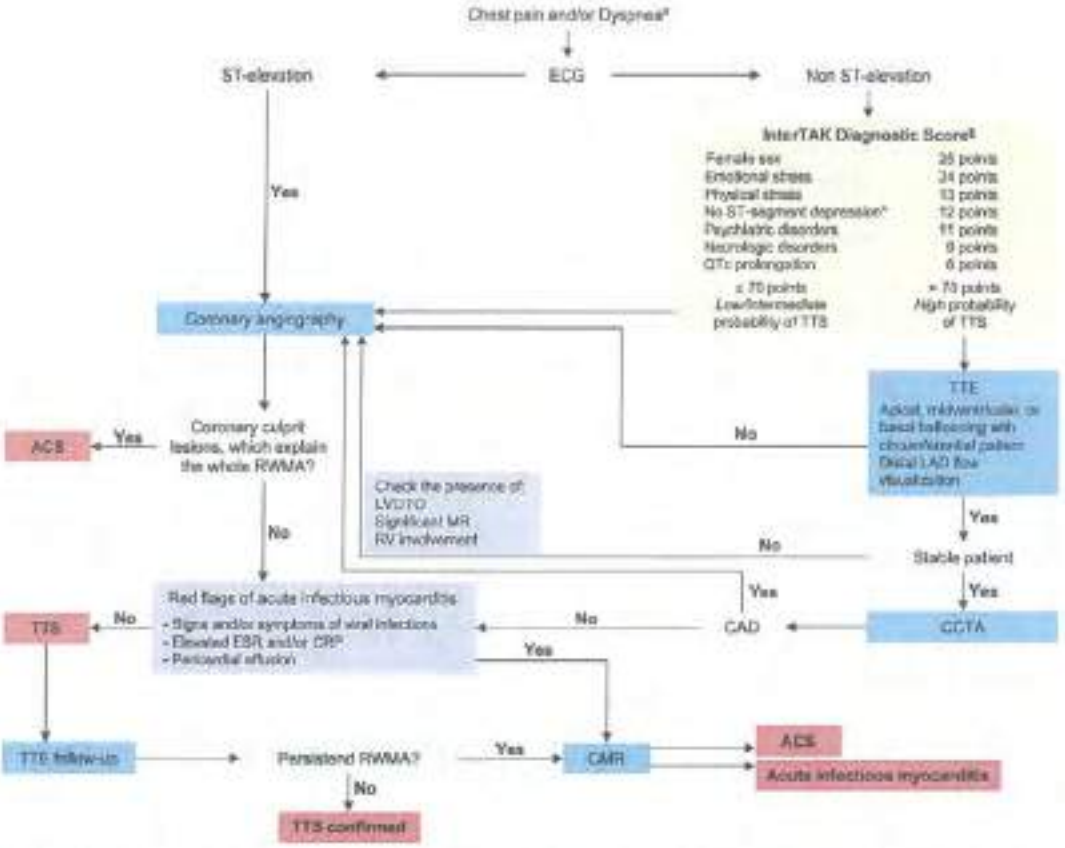

Figure 1 Diagnostic algorithm of takotsubo syndrome. *Applied to patients who are seeking medical emergency departments with e.g. chest pain and/or dyspnoea. §The InterTAK Diagnostic Score did not include patients with pheochromocytoma induced takotsubo syndrome in which atypical pattern are more frequently noted. *Except in lead aVR. ACS, acute coronary syndrome; CAD, coronary artery disease; CCTA, coronary computed tomography angiography; CMR, cardiac magnetic resonance; CRP, c-reactive protein; ECG, electrocardiogram; ESR, erythrocyte sedimentation rate; InterTAK, International Takotsubo Registry; LAD, left anterior descending coronary artery; LVOTO, left ventricular outflow tract obstruction; MR, mitral regurgitation; QTc, QT-time corrected for heart rate; RV, right ventricle; RWMA, regional wall motion abnormality; TTE, transthoracic echocardiography; TTS, takotsubo syndrome.

over several days, with subsequent gradual resolution of T-wave inversion and QT interval prolongation over days to weeks.[5–8] The initial and subsequent ECG findings are influenced by several variables, including the geographic pattern of left ventricular (LV) ballooning, presence or absence of right ventricular (RV) ballooning, time from symptom onset to presentation, presence of myocardial oedema, and recovery rate of myocardial cellular function.

ST-segment elevation

As with ST-segment elevation myocardial infarction (STEMI), the location and extent of ST-segment elevation in TTS corresponds to the anatomic location of myocardial injury, most often the mid and apical LV segments.[7] Consequently, ST-segment elevation usually involves precordial, lateral, and apical ECG leads, closely resembling that of anterior STEMI due to left anterior descending coronary occlusion.[9,10] Lead -aVR (inverse of aVR) representing +30° in the frontal plane is generally aligned with the LV apex, and can be assembled with other leads to create an 'ECG map', useful in comparing the ST-segment elevation pattern of TTS with that of anterior STEMI.[3,9,11,12] ST-segment elevation in TTS is centred on precordial leads V2–V5 and limb leads II and aVR, whereas in anterior STEMI the ST-segment elevation centres on precordial leads V1–V4 and limb leads I and aVL. Several ECG criteria with high sensitivity and specificity have been proposed to reliably distinguish TTS from anterior STEMI.[3,12–14] Most focus on ST-segment elevation in the precordial leads, particularly lead V1, as ST-segment elevation in this lead is less pronounced in TTS than in anterior STEMI.[9,10,13] ST-segment elevation limited to the inferior leads (II, III, aVF) is distinctly uncommon in TTS. Despite these differences, overlap exists and an urgent coronary angiogram is necessary to differentiate TTS from STEMI with certainty.[9–11]

T-wave inversion and QT interval prolongation

Progressive T-wave inversion and QT interval prolongation is a common ECG finding in TTS. In patients with delayed presentation, these

Downloaded from https://academic.oup.com/eurheartj/article-abstract/39/22/2047/5025411 by EndocrineSociety Admin user on 27 April 2020

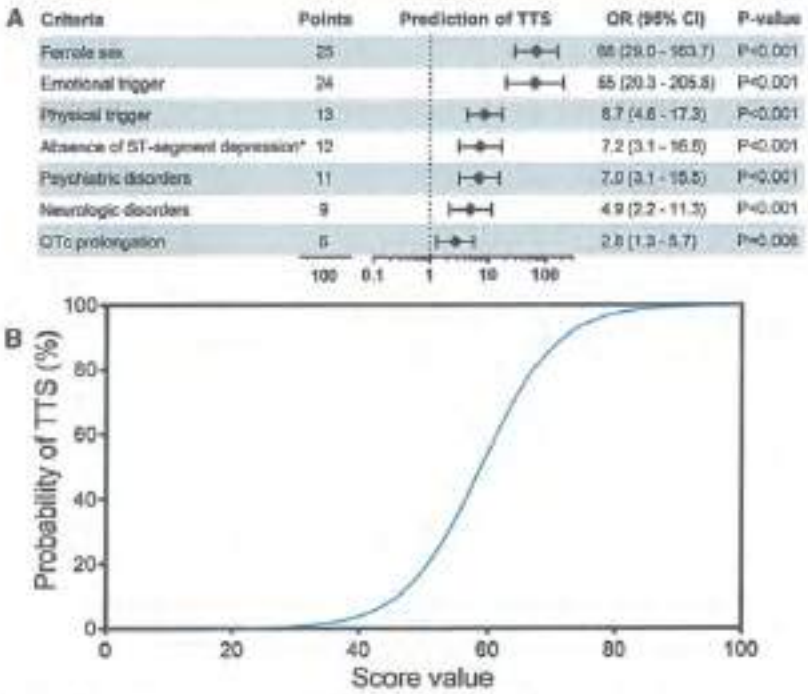

Figure 2 InterTAK Diagnostic Score. Predictors for diagnosing takotsubo syndrome by multiple logistic regression analysis. Odds ratios of the parameters female sex, emotional trigger, physical trigger, absence of ST-segment depression, psychiatric disorders, neurologic disorders, and QTc prolongation, which were chosen to build the InterTAK Diagnostic Score. *Except in lead aVR (A). Sigmoid curve shows the estimated prevalence of takotsubo syndrome in clinical practice (B). Modified and reprinted with permission from Ghadri *et al.*[24]. CI, confidence interval; OR, odds ratio; QTc, QT-time corrected for heart rate; TTS, takotsubo syndrome.

changes may be present on admission in the absence of ST-segment elevation, and can be the only detectable ECG changes and therefore important for the diagnosis. The geographic distribution of T-wave inversion closely parallels that of ST-segment elevation and may be an electrophysiological manifestation of myocardial stunning. In TTS, T-wave inversion is often more prominent and more broadly distributed than in ACS. Furthermore, T-wave inversion is associated with presence of myocardial oedema, and may persist for several months even after LV contractile recovery, thus leaving an electrophysiological footprint of the TTS event.[5,13–19] QT interval prolongation provides a substrate for torsades de pointes ventricular tachycardia and may be a prognostic marker for sudden cardiac death.[16,17]

Other electrocardiogram findings

Anterior Q-waves (or poor R-wave progression) without accompanying ST-segment elevation or T-wave inversion, a pattern sometimes referred to as 'anterior infarction, age indeterminate' occurs with some frequency in TTS. Pathologic Q-waves are less frequently encountered in TTS than anterior STEMI (15% vs. 69%).[14] In TTS, as in anterior STEMI, Q-waves may occur in the acute phase, and regress rapidly with R-wave re-appearance, consistent with electrical stunning.[20,21] Both J-wave and/or fragmented QRS complexes have been reported acutely, the former associated with death from cardiac causes and/or ventricular tachyarrhythmia.[22] Low QRS voltage likely representing myocardial oedema is prevalent in TTS.[23] Left bundle branch block is present in around 5% of patients.[2] ST-segment depression is uncommon, occurring in fewer than 10% of TTS patients but in over 30% of ACS patients,[2] therefore, the presence of ST-segment depression may suggest ACS.

InterTAK Diagnostic Score

The InterTAK Diagnostic Score was developed by the International Takotsubo Registry to provide clinicians a model to assess the likelihood of TTS diagnosis. The criteria that make up the InterTAK Diagnostic Score are based on clinical features and ECG to predict the probability of the presence of TTS and to distinguish TTS from ACS (*Figure 1, Figure 2A*).[24] The InterTAK Diagnostic Score comprises seven parameters [female sex, emotional trigger, physical trigger, absence of ST-segment depression (except in lead aVR), psychiatric disorders, neurologic disorders, and QT prolongation] ranked by their diagnostic importance with a maximum attainable score of 100 points (*Figure 2A*).[24] All parameters can be easily obtained in the emergency department and do not require an imaging modality.[24]

Depending on the disease prevalence this means that patients with 30 score points have a predicted probability of <1%, while patients with 50 points have a probability of 18%, and patients with a score value >70 points have a probability of ~90% of suffering from TTS (*Figure 2B*).[24]

Downloaded from https://academic.oup.com/eurheartj/article-abstract/39/22/2047/5026411 by EndocrineSociety Admin user on 27 April 2020

Biomarkers

Markers of myocardial necrosis

Virtually all cases of TTS exhibit evidence of myocardial necrosis. On admission, troponin values are usually equally elevated compared to ACS, however, peak values are substantially lower compared to the classical ACS.[2] High admission troponin levels are a predictor for a worse in-hospital outcome.[3] Typically, there is only a slight increase in creatine kinase.[2] The extent of LV regional wall motion impairment generally greatly exceeds that of associated myocardial necrosis biomarkers, likely reflecting a large mass of reversibly injured (stunned) myocardium.

B-type natriuretic peptide and N-terminal prohormone of brain natriuretic peptide

Takotsubo syndrome is frequently associated with a substantial increase in the plasma levels of B-type natriuretic peptide (BNP) and N-terminal prohormone of brain natriuretic peptide (NT-proBNP) reaching its peak approximately 24–48 h after symptom onset[25,26] as a reflection of regional LV dysfunction. A gradual return of BNP/NT-proBNP towards normal levels occurs within the next few months after presentation.[27]

The degree of NT-proBNP elevation appears directly related to: (i) the degree of sympathetic overactivation (as reflected by normetanephrine concentrations), (ii) peak C-reactive protein concentrations (suggesting that BNP release might be at least in part of inflammatory origin), and (iii) systolic LV dysfunction [as measured by wall motion score index (WMSI)].[25] Peak NT-proBNP levels also vary with the extent of LV oedema as measured by CMR.[28]

Other potential biomarkers

Interleukin (IL)-6 levels appear less elevated while those of IL-7 are more elevated in TTS compared with AMI.[29] However, differences between groups were small and unlikely to be of diagnostic utility.

Two recently published studies focused on the potential utility of the release and circulation of certain microRNAs (miRNAs) in association with TTS onset.[30,31] Kuwabara *et al.*[30] noted that elevation of circulating miR-133a appeared to represent an early consequence of myocardial injury, including TTS and AMI. However, subsequent analyses of cases of TTS ($N = 36$) and evolving STEMI ($N = 27$) suggested that the elevation of miR-133a was more marked in STEMI than in TTS. Furthermore, Jaguszewski *et al.* demonstrated that a unique signature including miR-1, miR-16, miR-26a, and miR-133a represents a robust biomarker on admission and can be used to differentiate TTS from STEMI patients.[31] Furthermore, the up-regulation of miR-16 and miR-26a is known to be associated with stress- and affective disorders.[32–34]

Especially in patients with biventricular involvement, it has been shown that plasma concentrations of the stress-responsive cytokine growth differentiation factor-15 increased more rapidly after the onset of TTS.[35]

Imaging

Coronary angiography and ventriculography

Although non-invasive imaging modalities are useful in the workup of patients with TTS, final differential diagnosis from ACS requires coronary angiogram, which is performed in the context of ST-elevation in primary percutaneous coronary intervention service. In case of suspected TTS with coexisting and significant CAD, careful comparison of CAG and biplane ventriculography in similar views is mandatory to search for a perfusion-contraction mismatch.[36,37] This comparison is essential for distinguishing TTS from classical AMI in patients with wall motion abnormalities and obstructive CAD. In this regard, it has been reported that approximately one-third of patients with the classical apical ballooning show a small zone with preserved contractility in the most distal portion of the apex, which is described as the 'apical nipple sign'.[38] Furthermore, as LVOTO occurs in approximately 20% of patients with TTS,[39] haemodynamic assessment for the presence of a pressure-gradient in the outflow tract as well as assessment of left ventricular end-diastolic pressure are recommended. Figure 3A demonstrates apical ballooning pattern on left ventriculography.

Echocardiography

Echocardiography is the most used imaging tool to assess changes in LV function such as symmetric regional wall motion abnormalities (RWMAs).[4] Different variants can be identified with echocardiography which include:

(1) Apical ballooning, hypo-, a-, or dyskinesia of mid-apical myocardial segments is typical, sometimes associated with hypokinetic mid-segments.[2,40] The anterior or entire interventricular septum, inferior or midventricular anterolateral wall may also be involved.[41,42] LV twisting on 2D speckle-tracking imaging is reduced or reversed to clockwise apical rotation and the rate of untwisting (a sensitive index of regional diastolic dysfunction) is reduced in the acute phase.[43]

(2) Midventricular TTS featured by hypo-, a-, or dyskinesia of midventricular segments, most often resembling a cuff.[2,40,44,45]

(3) Basal forms where only basal segments are involved[2,45]. This phenotype is rare and appears commonly in patients with subarachnoid haemorrhage,[46] epinephrine-induced TTS[47] or phaeochromocytoma.[48]

(4) Focal TTS mostly involving an anterolateral segment has been described.[2,40] Differentiating this unusual TTS type from ACS or myocarditis requires CMR.[49]

Right ventricular involvement is characterized by RV dilatation with hypo- to akinesia of the free wall and apex in its isolated form.[50,51]

In TTS, LV wall motion abnormalities extend beyond the distribution of a single coronary artery territory, therefore systolic dysfunction appears 'circular' at speckle-tracking echocardiography.[52] A WMSI ≥1.75 with more than four dysfunctional segments identifies TTS with 83% sensitivity and 100% specificity.[53] Doppler estimation of coronary artery flow ameliorates the diagnostic accuracy of wall motion abnormalities,[54] whereas adenosine may lead to dramatic improvements of global and regional LV function.[47]

Intravenous ultrasound contrast agents facilitate wall motion assessment especially at the apex[55] and constitute a useful method especially in patients in whom CAG is not performed, mainly due to active bleeding or other comorbid conditions that may imbalance the risk-benefit ratio of CAG (see Cardiac computed tomography angiography section). Myocardial opacification is reduced within dysfunctional segments with the transmural perfusion defects being more evident early after TTS onset.[55] Coronary flow reserve, assessed by transthoracic Doppler echocardiography, is reduced to 1.6–2.6 at the levels of the right and left coronary arteries[56,57] and correlates with indices of LV systolic but not diastolic function.[58] In contrast to ischaemic cardiomyopathy, myocardial contraction does not improve with low-dose dobutamine at the early stages.[59,60] However, it has also been demonstrated that low dose dobutamine stress echocardiography improved

Downloaded from https://academic.oup.com/eurheartj/article-abstract/39/22/2047/5025411 by EndocrineSociety Admin user on 27 April 2020

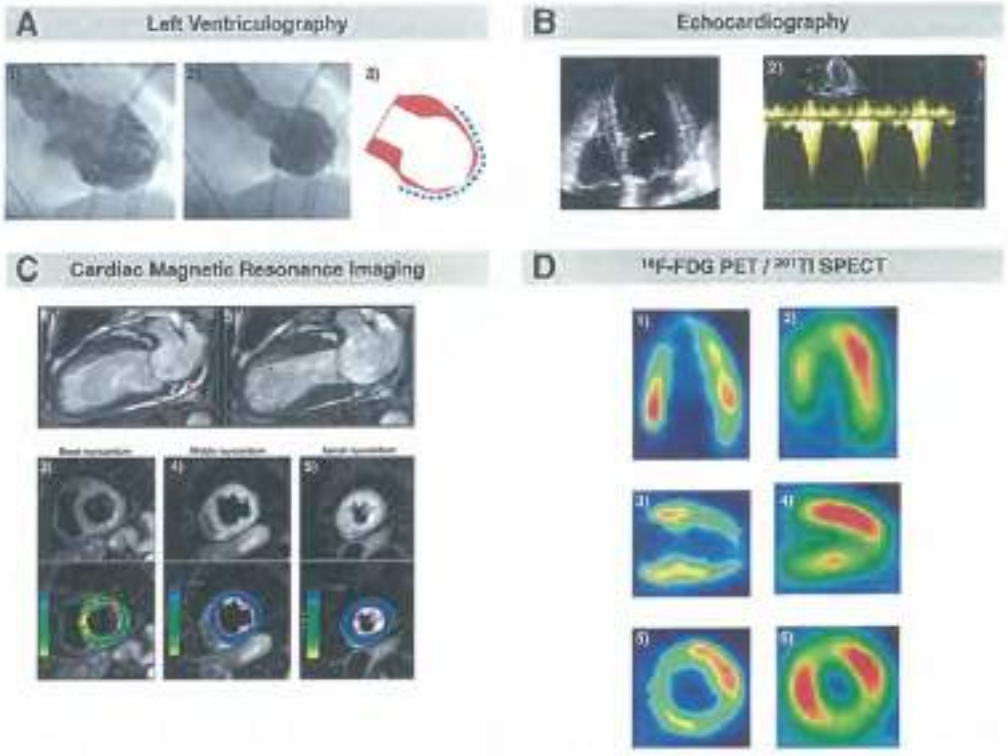

Figure 3 Apical ballooning illustrated by different imaging modalities. Typical takotsubo type with apical ballooning pattern during diastole (*A.1*) and systole (*A.2*) on left ventriculography. Dashed lines indicate extent of wall motion abnormality (*A.3*). Modified and reprinted with permission from Templin et al.[5] Apical four-chamber view obtained by echocardiography showing apical ballooning and left ventricular cavity with bulging of the basal interventricular septum (white arrow) (*B.1*). *B.2* reveals left ventricular outflow tract obstruction by pulsed-wave Doppler interrogation. Modified and reprinted with permission from Merli et al.[100] Apical ballooning as illustrated by cardiac magnetic resonance imaging. The asterisks indicate pericardial effusion (*C.1*) and yellow arrows (*C.2*) shows the region of akinesia. T2-weighted images on short-axis view demonstrates normal signal intensity of the basal myocardium (*C.3*) and global oedema of the mid and apical myocardium (*C.4* and *C.5*). Modified and reprinted with permission from Eitel et al.[92] Metabolic imaging with positron emission tomography and ¹⁸F-fluorodeoxyglucose (*D.1*, *D.3*, *D.5*) demonstrates decreased uptake in the apex and midventricular segments. Perfusion imaging using single photon emission computed tomography with ²⁰¹thallium chloride (*D.2*, *D.4*, *D.6*) shows a smaller perfusion defect in the apex and midventricular segments. Reprinted with permission from Yoshida et al.[98]

systolic left ventricular function by normalizing or improving the hypokinetic segments.[61] Moreover, in STEMI, viable myocardial segments exhibit longitudinal shortening, while in TTS systolic lengthening (passive motion) is present initially and resolves at follow-up.[62]

Importantly, echocardiography allows detection of all acute TTS complications. In LV apical ballooning, basal segments are hyperkinetic and may cause dynamic LVOTO,[63] mainly in patients with pre-existing septal bulge[64] which further reduces stroke volume and is associated with mitral regurgitation (MR) due to systolic anterior motion of the mitral leaflet (Figure 3B).[63,65] Severe MR may also result from leaflet tethering by displacement or dysfunction of papillary muscles. Mitral regurgitation is estimated to be present in 14–25% of TTS patients.[66]

Advanced echocardiographic techniques such as speckle-tracking imaging which reveals a paradoxical (dyskinetic) positive longitudinal systolic strain of biventricular mid-apical segments.[67] Echocardiography also identifies covered rupture of the LV free wall[68] as well as thrombus formation within a dysfunctional LV apex[69] or within left-atrial appendage even in the absence of atrial fibrillation.[70] Independent predictors of adverse outcomes include low left ventricular ejection fraction (LVEF), increased LV filling pressure, and moderate-to-severe MR at 4–6 weeks.[71,72]

At peak, apical and anteroseptal akinesis with basal hypercontractility produces near-cavity obliteration.[73]

Typically, LV contractility recovers completely in 4–8 weeks.[2,74] Some segments of the LV recover earlier than others, displaying increased apical rotation, LV twisting and untwisting and recovered global longitudinal strain.[42,75] Resolution of LVOTO and MR[76] occurs in parallel with myocardial functional recovery. During TTS recurrence, the LV ballooning pattern may resemble the initial event[77] or alternatively, manifest as other variants.[78]

Cardiac computed tomography angiography

In the presence of life-threatening comorbid conditions such as terminal malignancy, intracranial bleeding, advanced age with frailty and bleeding diathesis, invasive CAG may pose a considerable risk for complications. In a recent study by Murugiah et al.,[79] a substantial proportion of patients with TTS as a secondary diagnosis code did not undergo CAG. The reasons for not performing CAG were not

Downloaded from https://academic.oup.com/eurheartj/article-abstract/39/22/2047/5023411 by EndocrineSociety Admin user on 27 April 2020

described but likely included the mentioned life-threatening comorbid conditions. In such patients, non-invasive CCTA may be an appropriate alternative to CAG. Coronary computed tomography angiography provides information on both coronary artery anatomy and regional LV contraction. Assessment of LV contraction by CCTA requires image acquisition throughout the cardiac cycle and thus higher radiation exposure. In patients with suspected recurrent TTS and a previous CAG, CCTA may be a diagnostic alternative. Furthermore, CCTA may be considered instead of CAG in the following circumstances: in stable patients with low suspicion of ACS, suspected recurrent TTS, and patients with elevation of cardiac biomarkers or ECG changes in association with acute critical illnesses such as sepsis, intracranial disease (e.g. subarachnoid haemorrhage, ischaemic stroke), and other critical conditions known to be complicated by TTS.

Cardiac magnetic resonance imaging

Cardiac magnetic resonance imaging cannot be used easily in the acute setting of TTS, but is very useful in the subacute phase. In addition to identification of typical RWMAs, CMR allows precise quantification of RV and LV function, assessment of additional abnormalities/complications (i.e. pericardial and/or pleural effusion, LV and RV thrombi), and characterization of myocardial tissue (i.e. oedema, inflammation, necrosis/fibrosis) (*Figure 3C*).[80,81] Recently, specific CMR criteria for TTS diagnosis at the time of acute presentation were established which include the combination of typical RWMAs, oedema, and the absence of evidence of irreversible tissue injury [late gadolinium enhancement (LGE)].[82] While LGE is usually absent and predicts complete normalization of LV function, subtle fibrosis may be present and a sign of worse outcomes.[83–85] In most TTS patients, myocardial oedema is present in regions with abnormal systolic function possibly due to inflammation, increased wall stress and/or transient ischemia[82] and indicative of the extent and severity of tissue injury.[86] CMR is superior to echocardiography for detection of RV involvement[82] including isolated RV TTS[87] which may negatively impact outcome.[88] Importantly, absence of LGE in dysfunctional LV regions allows distinction between TTS and other conditions including ACS (subendocardial or transmural LGE corresponding to a vascular territory) and many cases of acute myocarditis (frequent, but not universal presence of epicardial or 'patchy' LGE). Therefore, CMR provides incremental value for the differential diagnosis, and therapeutic decision-making in patients with suspected TTS.[89]

Cardiac nuclear imaging

Both single photon emission computed tomography (SPECT, using ^{201}thallium chloride or ^{99m}technetium sestamibi) which provides semi-quantitative information and position emission tomography (PET, using ^{13}N-ammonia, ^{82}Rubidium) which offers quantitative measurements, have been used in TTS for assessment of perfusion, metabolism, and innervation.

Perfusion imaging

Mild reduction of perfusion in dysfunctional segments using myocardial perfusion scintigraphy has been noted in some studies, while others reported normal perfusion.[90–94] However, 'myocardial thinning' in involved segments during the acute phase of TTS may lead to a reduction in isotope counts because of the partial volume effect, which may mimic reduction of perfusion on SPECT, but following correction for this factor on PET, blood flow in the thinned regions (typically in the apex) is indeed maintained, while the normally functioning (basal) segments show hyper-perfusion.[95]

Metabolic imaging

The role of metabolic imaging in the clinical setting has not been determined and it has been performed mainly for research purpose of investigating the pathophysiology of TTS, although it can provide additional information about the diseased myocardium. Both SPECT using ^{123}I-β-methyl-iodophenyl pentadecanoic acid (which reflects fatty-acid) and PET using ^{18}F-flourodeoxyglucose (which reflect glucose utilization) often show reduced metabolic activity in the impaired regions, while myocardial perfusion is often (near) normal.[96,97] An example with apical TTS is shown in *Figure 3D*, revealing severely reduced ^{18}F-flourodeoxyglucose uptake in the apex despite only slightly reduced perfusion as assessed with ^{201}thallium chloride.[98] Possibly, glucose utilization is disturbed due to insulin resistance as a consequence of high levels of circulating catecholamines.[99]

Sympathetic nervous imaging

Myocardial uptake of ^{123}I-metaiodobenzylguanidine (^{123}I-MIBG, imaged with SPECT) reflects myocardial sympathetic innervation. ^{123}I-MIBG is reduced for months in dysfunctional segments whereas perfusion is almost normal, consistent with regional disturbance of sympathetic neuronal activity.[101] In the subacute phase of TTS, ^{123}I-MIBG SPECT can be combined with SPECT perfusion imaging to exclude ACS where both perfusion and innervation are reduced. Position emission tomography imaging has also been used in TTS for assessment of cardiac innervation with the use 11C hydroxyephedrine.[102]

Complications and outcomes

Although TTS is generally considered a benign disease, contemporary observations show that rates of cardiogenic shock and death are comparable to ACS patients treated according to current guidelines.[2,103–108] While TTS is a reversible condition, hemodynamic and electrical instability during the acute phase expose patients to the risk of serious adverse in-hospital events which occur in approximately one-fifth of TTS patients (*Figure 4*).[2] This substantial incidence of life-threatening complications necessitates close monitoring and early intervention in unstable TTS patients with risk stratification at diagnosis allowing triage to appropriate care.[66] Parameters predicting adverse in-hospital outcome include: physical trigger, acute neurologic or psychiatric diseases, initial troponin >10× upper reference limit, and admission LVEF <45%.[2] Furthermore, male patients have an up to three-fold increased rate of death and major adverse cardiac and cerebrovascular events (MACCE)[109] and more often had an underlying critical illness, further contributing to the higher mortality.[2] Sobue et al.[110] demonstrated that physical triggers and male gender are independent risk factors of in-hospital mortality in TTS. Data from the Tokyo Coronary Care Unit Network revealed that high values of BNP and white blood cell counts were also linked to higher rates of in-hospital complications.[111] Complications included cardiac death, pump failure (Killip grade ≥II), sustained ventricular tachycardia or ventricular fibrillation (VT/VF), and advanced atrioventricular block

Downloaded from https://academic.oup.com/eurheartj/article-abstract/38/22/2047/5025411 by EndocrineSociety Admin user on 27 April 2020

Figure 4 Overview of in-hospital complications according to their prevalence. AV, atrioventricular block; LV, left ventricle; LVOTO, left ventricular outflow tract obstruction.

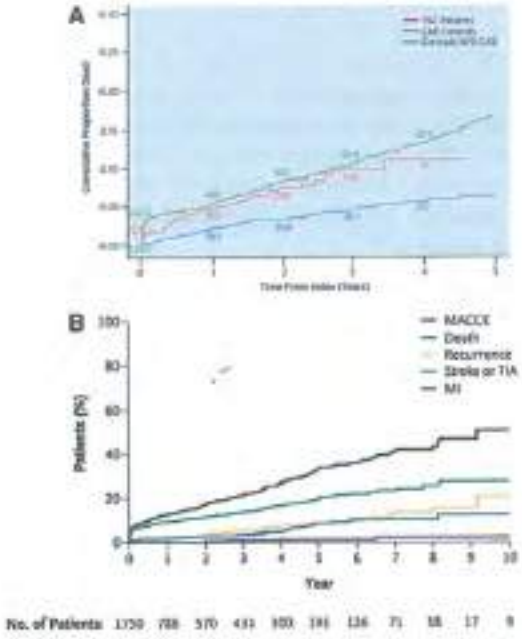

Figure 5 Long-term outcome (5-years) of patients with TTS compared to patients with and without CAD (A). Long-term outcome (10-years) of patients with TTS (B). MACCE refers to a composite of death from any cause, recurrence of takotsubo syndrome, stroke or transient ischaemic attack, or myocardial infarction. CAD, coronary artery disease; MACCE, major adverse cardiac and cerebrovascular event; MI, myocardial infarction; TIA, transient ischaemic attack; TSC, takotsubo stress cardiomyopathy. Reprinted with permission from Tornvall *et al.*[101] and Templin *et al.*[2]

(AV-block). In the study by Takashio *et al.*[113] the magnitude and extent of ST-segment elevation with ECG were found to be independent predictors of in-hospital adverse events. However, those findings were not confirmed by others. Common in-hospital complications include cardiac arrhythmias,[113] LVOTO,[64] cardiogenic shock,[2] ventricular thrombus,[114] pulmonary oedema,[115] ventricular septal defect,[116] and free wall rupture.[117] In addition, to the demographic parameter of age ≥75, echocardiographic parameters that predict adverse in-hospital outcome (acute heart failure, cardiogenic shock, and in-hospital mortality) include LVEF, *E/e'* ratio, and reversible moderate to severe MR. However, only reversible moderate to severe MR was an independent predictor when considering cardiogenic shock and death as the composite outcome in this study, in addition to heart rate. Moreover, it has been demonstrated that high heart rate and low systolic blood pressure are associated with increased mortality in TTS.[118] Along with the Charlson comorbidity index and systolic pulmonary artery pressure, RV involvement is an independent predictor of acute heart failure and of a composite endpoint including adverse events, such as acute heart failure, cardiogenic shock, and in-hospital mortality.[119]

Data on long-term survival are scarce. In 2007, Elesber *et al.*[120] reported that long-term mortality did not differ between a TTS population and an age-, gender-, birth-, year-, and race-matched population. While Sharkey *et al.*[121] found that all-cause mortality during follow-up exceeded a matched general population with most deaths occurring in the first year. More recently, it has been reported that long-term mortality of patients with TTS[122] is similar to (*Figure 5A*) patients with CAD.[103] TTS patient data from the Swedish Angiography and Angioplasty Registry (SCAAR) from 2009 to 2013 were compared to data from patients with and without CAD, and demonstrated that mortality rates for TTS were worse than in patients without CAD and comparable to those of patients with CAD.[103] In the largest TTS registry to date, death rates are estimated to be 5.6% and rate of MACCE 9.9% per-patient year (*Figure 5B*),[2] suggesting that TTS is not a benign disease. A recent study found that patients with the typical TTS type have a comparable outcome to patients presenting with the atypical type even after adjustment for confounders, suggesting that both patient groups should be equally monitored in the long-term.[40] On the other hand, 1-year mortality differs between the two groups, as it is driven by clinical factors including atrial fibrillation, LVEF on admission <45%, and neurologic disorders, rather than by

Downloaded from https://academic.oup.com/eurheartj/article-abstract/39/22/2047/5012411 by EndocrineSociety Admin user on 27 April 2020

Figure 6 Arrhythmic complication in takotsubo syndrome. Left ventriculography (antero-posterior view) showing the typical apical ballooning pattern with akinesia of the mid-apical segments and hyperkinesia of the basal segment (*A*). A 12-lead electrocardiogram recorded at the third day of hospitalization showing giant negative T-waves in leads aVL, L1, L2, aVF and V4–V6, marked QT prolongation (QTc = 552 ms) and 'R on T' premature ventricular beats (*B*). Telemetry recording of a pause-dependent ('long-short sequence') torsade-de-pointes/ventricular fibrillation, which required electrical cardioversion (*C*). Reprinted with permission from Migliore *et al.*[130]

TTS type.[40] In a smaller study, predictive factors of long-term mortality in TTS were male sex, Killip class III/IV, and diabetes mellitus.[122] The prognostic role of diabetes mellitus is controversial, as it is postulated that it may exert a protective effect in TTS, given that the prevalence of diabetes mellitus in TTS is lower than expected for an age- and sex-matched population.[123] Some studies, though limited by their population size and experimental design, suggest that patients with diabetes mellitus have a more favourable in-hospital and 1-year outcome.[124,125]

Arrhythmias

Cardiac arrhythmias are important determinants of short-term clinical outcome.

Ventricular arrhythmias

Life-threatening ventricular arrhythmias, such as torsades de pointes, VT, or VF occur in 3.0–8.6% and are a frequent cause of death.[3,126–128] Life-threatening ventricular arrhythmias occur most often in the subacute phase (i.e. hospital days 2–4) and coincide with anterolateral T-wave inversion and QT-interval prolongation.[127] QTc prolongation at admission occurs in up to half of the patients.[2] Most malignant arrhythmic episodes are associated with a QTc >500 ms, with pause-dependent torsades de pointes degenerating into VF.[127,128,130] Figure 6 shows a patient with apical ballooning (*A*). On the third day of hospitalization giant negative T-waves, marked QT prolongation, and 'R on T' premature ventricular beats were noted on ECG (*B*). Furthermore, pause-dependent ('long-short sequence') torsade-de-pointes/ventricular fibrillation requiring electrical cardioversion were recorded by telemetry (*C*).[130] Accordingly, TTS should be regarded as a type of acquired long QT syndrome with risk for malignant arrhythmic events.[128,130]

Cardiac magnetic resonance findings reveal an association between transient myocardial oedema, as evidenced by T2-weighted sequences, and dynamic T-wave inversion and QT prolongation.[131,132] Thus, myocardial oedema may contribute to transmural or regional (i.e. from the apex to the base of the LV) repolarization inhomogeneity. QT prolongation thus reflects the delayed and dispersed ventricular repolarisation that predisposes to local re-excitation and eventually to torsade de pointes or VF.[131–133]

Rarely, cardiac arrest is the initial presentation of TTS unrelated to QT interval prolongation. The mechanism of these potentially lethal arrhythmias is probably distinct from that encountered during the subacute phase where acute catecholamine toxicity and/or myocardial ischaemia play a primary role. In some cases, TTS may not represent the trigger for tachyarrhythmias, but rather the consequence of the stress of cardiac arrest and/or resuscitation, which may include administration of epinephrine.[134]

Other cardiac arrhythmias

New-onset paroxysmal or persistent atrial fibrillation occurs in 4.7%, sinus-node dysfunction in 1.3%, and AV-block in 2.9%, most likely due to neuro-autonomic imbalance, catecholamine stress, and increased vagal tone.[127,130,134]

Recurrence

Patients who survive the initial event have a second event in approximately 5% of cases, mostly occurring 3 weeks to 3.8 years after the first event.[135] Recurrent TTS afflicts men and women and may occur

Downloaded from https://academic.oup.com/eurheartj/article-abstract/36/22/2047/2025411 by EndocrineSociety Admin user on 27 April 2020

at any age including in childhood.[70,136,137] Both the triggering event and the ballooning pattern may differ during recurrent events.[78] Some have postulated that an index TTS event may protect the affected LV regions from recurrent involvement through a mechanism akin to ischaemic 'pre-conditioning'.[138] However, detailed review of published cases and clinical experience suggest that there are frequent examples of recurrence in which the ballooning pattern is similar between episodes, thereby making this hypothesis unlikely.

Therapeutic management

Guidelines regarding TTS management are lacking as no prospective randomized clinical trials have been performed in this patient population. Therapeutic strategies are therefore based on clinical experience and expert consensus (evidence level C). *Table 1* reviews current data on medical management of TTS patients[139] based of retrospective analysis,[3,140,141] meta-analysis,[142,144] and case series.[143] *Figure 7* summarizes a proposed therapeutic management approach for patients with TTS.

Pre-hospital treatment

As TTS is clinically difficult to distinguish from ACS, upon first presentation patients should be transferred to a cardiology unit with imaging capabilities and a cardiac catheterization laboratory and receive guideline based treatment of ACS,[105–108] in particular aspirin, heparin, and if required morphine and oxygen. Patients with cardiogenic shock or post cardiac arrest require intensive care. Electrocardiogram monitoring is essential as a prolonged QT-interval may trigger malignant ventricular arrhythmias (torsades de pointes) and AV-block may occur.

Acute treatment

Takotsubo syndrome patients with cardiogenic shock, in particular those with apical ballooning should be promptly evaluated for the presence of LVOTO, which occurs in about 20% of cases.[29] This should be performed during angiography with LV pressure recording during careful retraction of the pigtail catheter from the LV apex beyond the aortic valve. Similarly, a pressure gradient can be detected and quantified using Doppler echocardiography using continuous wave Doppler.[145] Particularly, when using catecholamines serial Doppler studies should be considered to detect an evolving pressure gradient. In TTS patients treated with catecholamine drugs a 20% mortality has been reported[81]; although this may represent a selection bias due to the initial presentation of the patients. Recently, it has been suggested that the Ca^{2+}-sensitizer levosimendan could be used safely and effectively in TTS as an alternative inotrope to catecholamine agents.[143] Furthermore, beta-blockers may improve LVOTO, but are contraindicated in acute and severe heart failure with low LVEF, hypotension, and in those with bradycardia. Although evidence is unproven, TTS patients with LVOTO may benefit from the I$_f$ channel inhibitor ivabradine.[146,147]

As catecholamine levels are elevated in TTS, beta-blockers seem to be reasonable until full recovery of LVEF, but trials supporting this hypothesis are lacking. Animal experiments have shown that apical ballooning is attenuated after administration of drugs with both alpha- and beta-adrenoceptor blocking properties.[148] In an animal model, intravenous metoprolol improved epinephrine-induced apical ballooning.[149] However, due to the potential risk of pause-dependent torsades de pointes, beta-blockers should be used cautiously, especially in patients with bradycardia and QTc >500 ms. Angiotensin-converting-enzyme inhibitors (ACEI) or angiotensin II receptor blockers (ARB) may potentially facilitate LV recovery. Diuretics are indicated in patients with pulmonary oedema. In addition, nitroglycerin is useful to reduce LV and RV filling pressures and afterload in

Table 1 Overview of retrospective analyses, meta-analyses, and case series of medical management for takotsubo syndrome[a]

Authors	Study design	No. of patients	Outcome measures	Follow-up time	Medication	Effect
Santoro et al.[143]	Case series	13	Adverse events	During hospitalization	Levosimendan	Probably beneficial
Isogai et al.[140]	Retrospective	2110	Mortality	30 days	β-Blockers	Not beneficial
Dias et al.[141]	Retrospective	206	MACE	During hospitalization	Antiplatelet	Beneficial
					β-Blockers	Not beneficial
					Statins	Not beneficial
					ACEI	Not beneficial
Templin et al.[3]	Retrospective	1118	Mortality	1 year	β-Blockers	Not beneficial
					ACEI/ARB	Beneficial
Santoro et al.[142]	Meta-analysis	511	Recurrence	24–60 months	β-Blockers	Not beneficial
					ACEI/ARB	Not beneficial
					Aspirin	Not beneficial
					Statins	Not beneficial
Singh et al.[144]	Meta-analysis	847	Recurrence	19–33 months	β-Blockers	Not beneficial
					ACEI/ARB	Beneficial

[a]Reprinted with permission from Kato et al.[139]
ACEI, angiotensin-converting-enzyme inhibitor; ARB, angiotensin-receptor blocker; MACE, major adverse cardiac event.

Downloaded from https://academic.oup.com/eurheartj/article-abstract/35/22/2047/502541 by EndocrineSociety Admin user on 27 April 2020

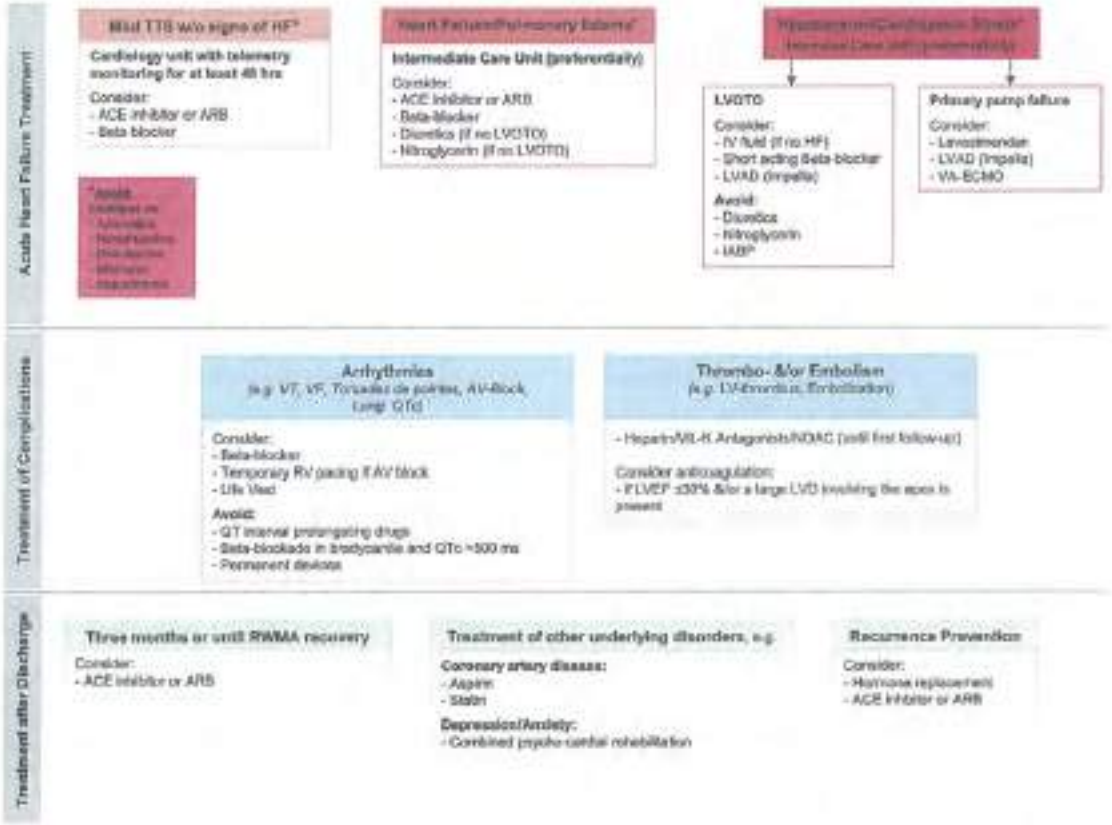

Figure 7 Management of takotsubo syndrome. ACE, angiotensin-converting-enzyme; ARB, angiotensin-receptor blocker; AV-block, atrioventricular block; HF, heart failure; IABP, intra-aortic balloon pump; IV, intravenous; LV, left ventricle; LVAD, left ventricular assist device; LVD, left ventricular dysfunction; LVEF, left ventricular ejection fraction; LVOTO, left ventricular outflow tract obstruction; NOAC, novel oral anticoagulant; QTc, QT-time corrected for heart rate; RV, right ventricle; TTS, takotsubo syndrome; VA-ECMO, venoarterial extracorporeal membrane oxygenation; VF, ventricular fibrillation; VT, ventricular tachycardia.

the case of acute heart failure; however, the administration of nitroglycerin in the presence of LVOTO has been found to worsen the pressure gradient and therefore should be avoided in this scenario (see Figure 7).

QT-interval prolonging drugs should be used cautiously in the acute phase because of the risk to induce torsades de pointes or ventricular tachycardia and fibrillation.

Severe LV dysfunction with extended apical ballooning entails the risk of an LV thrombus and subsequent systemic embolism. Although evidence is lacking, anticoagulation with intravenous/subcutaneous heparin would appear to be appropriate in such patients and post-discharge oral anticoagulation or antiplatelet therapy may be considered on an individual, per-patient basis. As LV dysfunction and ECG abnormalities are reversible, an implantable cardioverter-defibrillator for primary or secondary prevention is of uncertain value in TTS patients experiencing malignant ventricular arrhythmias.[130,150] In case of excessive prolongation of the QT interval or life-threatening ventricular arrhythmias a wearable defibrillator (life vest) could be considered.[151] The residual risk of malignant arrhythmic events after recovery from TTS is unknown. A temporary transvenous pacemaker is appropriate for those with haemodynamically significant bradycardia.

Long-term treatment

The use of ACEi or ARB was associated with improved survival at 1-year follow-up even after propensity matching.[2] In contrast, there was no evidence of any survival benefit for the use of beta-blockers.[2] Moreover, one-third of patients experienced a TTS recurrence during beta-blockade[2] suggesting that other receptors such as alpha-receptors, that are more prevalent in the coronary microcirculation, might be involved.

The prevalence of recurrent TTS is relatively low, consequently conducting randomised trials of pharmacological agents to prevent recurrence is challenging. Beta-blocker therapy after hospital discharge does not appear to prevent recurrence,[2,144] whereas ACEi or ARB are associated with a lower prevalence of recurrence. The significance of this observation remains uncertain and requires validation in other cohorts.

If concomitant coronary atherosclerosis is present, aspirin and statins are appropriate. As TTS mainly occurs in postmenopausal

Downloaded from https://academic.oup.com/eurheartj/article-abstract/39/22/2047/5025411 by EndocrineSociety Admin user on 27 April 2020

women oestrogen supplementation in those with recurrence is questionable. In an animal model oestrogen supplementation partially attenuated TTS,[152] and chronic oestrogen supplementation after oophorectomy improved the condition.[153]

Psychiatric disorders (e.g. depression, anxiety) are common in TTS patients[2,154] and those might benefit from a combined psychocardiologic rehabilitation.[155] Whether anti-depressants or other psychiatric drugs might provide clinical benefit in such patients is controversial.

Future directions

Over recent years research has shown that TTS is a much more heterogeneous condition than previously thought. Originally believed to be a benign disease, studies have shown that TTS has morbidity and mortality rates that are comparable to those of ACS.[2,100] TTS can affect many others aside from postmenopausal women with an emotional trigger,[2,1,15] as originally described, and can present as an atypical type rather than apical ballooning.[40] Still, there is much more to be uncovered surrounding TTS and the underlying pathophysiology of the syndrome.[156]

Key questions

Many questions need further investigation: Why are women affected predominantly? What is the role of triggering factors in stress responses of the heart? Why do different TTS phenotypes exist? Which patients are vulnerable to TTS or prone to recurrence? Is there a genetic predisposition to TTS? What is the exact pathogenesis of TTS? Are there specific treatment options in the acute stage of this life-threatening syndrome or to prevent recurrence? Additional research needs to be conducted to answer these important questions.

Prospective approaches

The link between the brain and heart seems to play a key role in TTS. Additionally, studies on circulating miRNAs suggest there could be a genetic aspect to the pathophysiology of TTS, and the predominance of female patients suggests that TTS could be related to sex hormones and the endocrine system. Takotsubo syndrome is more than a cardiac disease, and it requires a new and interdisciplinary approach to increase awareness among not only cardiologists, but physicians at large. To establish evidence based strategies for effective TTS treatment, randomized prospective trials will be necessary utilizing a large number of patients from multicentre international consortia.

Funding

J.R.G. has received a research grant "Filling the gap" from the University of Zurich.

Conflict of interest: none declared.

References

1. Gianni M, Dentali F, Grandi AM, Sumner G, Hiralal R, Lonn E. Apical ballooning syndrome or Takotsubo cardiomyopathy: a systematic review. *Eur Heart J* 2006; **27**:1523–1529.
2. Templin C, Ghadri JR, Diekmann J, Napp LC, Bataiosu DR, Jaguszewski M, Cammann VL, Sarcon A, Geyer V, Neumann CA, Seifert B, Hellermann J, Schwyzer M, Eisenhardt K, Jenewein J, Franke J, Katus HA, Burgdorf C, Schunkert H, Moeller C, Thiele H, Bauersachs J, Tschöpe C, Schultheiss H-P, Laney CA, Rajan L, Michels G, Pfister R, Ukena C, Böhm M, Erbel R, Cuneo A, Kuck K-H, Jacobshagen C, Hasenfuss G, Karakas M, Koenig W, Rottbauer W, Said SM, Braun-Dullaeus RC, Cuculi F, Banning A, Fischer TA, Vasankari T, Airaksinen KEJ, Fijałkowski M, Rynkiewicz A, Pawlak M, Opolski G, Dworakowski R, MacCarthy P, Kaiser C, Osswald S, Galiuto L, Crea F, Dichtl W, Franz WM, Empen K, Felix SB, Delmas C, Lairez O, Erne P, Bax JJ, Ford I, Ruschitzka F, Prasad A, Lüscher TF. Clinical Features and Outcomes of Takotsubo (Stress) Cardiomyopathy. *N Engl J Med* 2015;**373**:929–938.
3. Frangieh AH, Obeid S, Ghadri JR, Imori Y, D'Ascenzo F, Kovac M, Ruschitzka F, Lüscher TF, Duru F, Templin C, Inter TAKC. ECG criteria to differentiate between Takotsubo (Stress) cardiomyopathy and myocardial infarction. *J Am Heart Assoc* 2016;**5**:e003418.
4. Prasad A, Lerman A, Rihal CS. Apical ballooning syndrome (Tako-Tsubo or stress cardiomyopathy): a mimic of acute myocardial infarction. *Am Heart J* 2008;**155**:408–417.
5. Bennett J, Ferdinande B, Kayaert P, Waynne S, Goetschalckx K, Dubois C, Sinnaeve P, Adriaenssens T, Coosemans M, Desmet W. Time course of electrocardiographic changes in transient left ventricular ballooning syndrome. *Int J Cardiol* 2013;**169**:276–280.
6. Mitsuma W, Kodama M, Ito M, Tanaka K, Yanagawa T, Ikarashi N, Sugiura K, Kimura S, Yaghara N, Kashimura T, Fuse K, Hirono S, Okura Y, Aizawa Y. Serial electrocardiographic findings in women with Takotsubo cardiomyopathy. *Am J Cardiol* 2007;**100**:106–109.
7. Kurisu S, Inoue I, Kawagoe T, Ishihara M, Shimatani Y, Nakamura S, Yoshida M, Mitsuba N, Hata T, Sato H. Time course of electrocardiographic changes in patients with Tako-Tsubo syndrome: comparison with acute myocardial infarction with minimal enzymatic release. *Circ J* 2004;**68**:77–81.
8. Kosuge M, Kimura K. Electrocardiographic findings of Takotsubo cardiomyopathy as compared with those of anterior acute myocardial infarction. *J Electrocardiol* 2014;**47**:684–689.
9. Sharkey SW. Electrocardiogram mimics of acute ST-segment elevation myocardial infarction: insights from cardiac magnetic resonance imaging in patients with Tako-Tsubo (stress) cardiomyopathy. *J Electrocardiol* 2008;**41**:621–625.
10. Bybee KA, Motiei A, Syed IS, Kara T, Prasad A, Lennon RJ, Murphy JG, Hammill SC, Rihal CS, Wright RS. Electrocardiography cannot reliably differentiate transient left ventricular apical ballooning syndrome from anterior ST-segment elevation myocardial infarction. *J Electrocardiol* 2007;**40**:38.e1–6.
11. Chao T, Lindsay J, Collins S, Woldeyes L, Joshi SB, Steinberg DH, Safer LF, Kent KM, Suddath WO, Pichard AD, Wakman R. Can acute occlusion of the left anterior descending coronary artery produce a typical 'Takotsubo' left ventricular contraction pattern? *Am J Cardiol* 2009;**104**:202–204.
12. Kosuge M, Ebina T, Hibi K, Morita S, Okuda J, Iwahashi N, Tsukahara K, Nakachi T, Kiyokuni M, Ishikawa T, Umemura S, Kimura K. Simple and accurate electrocardiographic criteria to differentiate Takotsubo cardiomyopathy from anterior acute myocardial infarction. *J Am Coll Cardiol* 2010;**55**:2514–2516.
13. Tamura A, Watanabe T, Ishihara M, Ando S, Naono S, Zaiken H, Abe Y, Yano S, Shinozaki K, Kosaku M, Momii H, Kadokami T, Kadota J. A new electrocardiographic criterion to differentiate between Takotsubo cardiomyopathy and anterior wall ST-segment elevation acute myocardial infarction. *Am J Cardiol* 2011;**108**:630–633.
14. Ogura R, Hiasa Y, Takahashi T, Yamaguchi K, Fujiwara K, Ohara Y, Nada T, Ogata T, Kusunoki K, Yuba K, Hosokawa S, Kishi K, Ohtani R. Specific findings of the standard 12-lead ECG in patients with 'Takotsubo' cardiomyopathy: comparison with the findings of acute anterior myocardial infarction. *Circ J* 2003;**67**:687–690.
15. Kosuge M, Ebina T, Hibi K, Iwahashi N, Tsukahara K, Endo M, Maejima N, Nagashima Z, Suzuki H, Morita S, Umemura S, Kimura K. Differences in negative T waves between Takotsubo cardiomyopathy and reperfused anterior acute myocardial infarction. *Circ J* 2012;**76**:462–468.
16. Behr ER, Mahida S. Takotsubo cardiomyopathy and the long-QT syndrome: an insult to repolarization reserve. *Europace* 2009;**11**:697–700.
17. Matsuoka K, Okubo S, Fujii E, Uchida F, Kasai A, Aoki T, Makino K, Omichi C, Fujimoto N, Ohta S, Sawai T, Nakano T. Evaluation of the arrhythmogenicity of stress-induced 'Takotsubo cardiomyopathy' from the time course of the 12-lead surface electrocardiogram. *Am J Cardiol* 2003;**92**:230–233.
18. Migliore F, Zorzi A, Marra MP, Basso C, Corbetti F, De Lazzari M, Tarantini G, Rizzi P, Lacognata C, Thiene G, Corrado D, Bisiato S. Myocardial edema underlies dynamic T-wave inversion (Wellens' ECG pattern) in patients with reversible left ventricular dysfunction. *Heart Rhythm* 2011;**8**:1629–1634.
19. Migliore F, Zorzi A, Perazzolo Marra M, Bisiato S, Corrado D. Myocardial edema as a substrate of electrocardiographic abnormalities and life-threatening arrhythmias in reversible ventricular dysfunction of Takotsubo cardiomyopathy: imaging evidence, presumed mechanisms, and implications for therapy. *Heart Rhythm* 2015;**12**:1867–1877.

Downloaded from https://academic.oup.com/eurheartj/article-abstract/39/22/2047/5025411 by EndocrineSocietyAdmin user on 27 April 2020

20. Sclarovsky S, Nikus K. The electrocardiographic paradox of Tako-Tsubo cardiomyopathy-comparison with acute ischemic syndromes and consideration of molecular biology and electrophysiology to understand the electrical-mechanical mismatching. *J Electrocardiol* 2010;**43**:173–176.
21. Namgung J. Electrocardiographic findings in Takotsubo cardiomyopathy: ECG evolution and its difference from the ECG of acute coronary syndrome. *Clin Med Insights Cardiol* 2014;**8**:29–34.
22. Shimizu M, Nishizaki M, Yamawaki N, Fujii H, Sakonda H, Inoue M, Hiraoka M. J wave and fragmented QRS formation during the hyperacute phase in Takotsubo cardiomyopathy. *Circ J* 2014;**78**:943–949.
23. Madias JE. Transient attenuation of the amplitude of the QRS complexes in the diagnosis of Takotsubo syndrome. *Eur Heart J Acute Cardiovasc Care* 2014;**3**:28–36.
24. Ghadri JR, Cammann VL, Jurisic S, Seifert B, Napp LC, Diekmann J, Bataiosu DR, D'Ascenzo F, Ding KJ, Sarcon A, Kazzam E, Birri T, Ruschitzka F, Luscher TF, Templin C; InterTAK co-investigators. A novel clinical score (InterTAK Diagnostic Score) to differentiate Takotsubo syndrome from acute coronary syndrome: results from the International Takotsubo Registry. *Eur J Heart Fail* 2017;**19**:1036–42.
25. Nguyen TH, Neil CJ, Sverdlov AL, Mahadavan G, Chirkov YY, Kucia AM, Standfourth J, Beltrame JF, Selvanayagam JB, Zeitz CJ, Struthers AD, Frenneaux MP, Horowitz JD. N-terminal pro-brain natriuretic protein levels in Takotsubo cardiomyopathy. *Am J Cardiol* 2011;**108**:1316–1321.
26. Morita E, Yasue H, Yoshimura M, Ogawa H, Jougasaki M, Matsumura T, Mukoyama M, Nakao K. Increased plasma levels of brain natriuretic peptide in patients with acute myocardial infarction. *Circulation* 1993;**88**:82–91.
27. Akashi YJ, Musha H, Nakazawa K, Miyake F. Plasma brain natriuretic peptide in Takotsubo cardiomyopathy. *QJM* 2004;**97**:599–607.
28. Neil C, Nguyen TH, Kucia A, Crouch B, Sverdlov A, Chirkov Y, Mahadavan G, Selvanayagam J, Dawson D, Beltrame J, Zeitz C, Unger S, Redpath T, Frenneaux M, Horowitz J. Slowly resolving global myocardial inflammation/oedema in Tako-Tsubo cardiomyopathy: evidence from T2-weighted cardiac MRI. *Heart* 2012;**98**:1278–1284.
29. Pirzer R, Elmas E, Haghi D, Lippert C, Kralev S, Lang S, Borggrefe M, Kalsch T. Platelet and monocyte activity markers and mediators of inflammation in Takotsubo cardiomyopathy. *Heart Vessels* 2012;**27**:186–192.
30. Kuwabara Y, Ono K, Horie T, Nishi H, Nagao K, Kinoshita M, Watanabe S, Baba O, Kojima Y, Shizuta S, Imai M, Tamura T, Kita T, Kimura T. Increased microRNA-1 and microRNA-133a levels in serum of patients with cardiovascular disease indicate myocardial damage. *Circ Cardiovasc Genet* 2011;**4**:446–454.
31. Jagusztowski M, Osipova J, Ghadri JR, Napp LC, Widera C, Franke J, Fijalkowski M, Nowak R, Fijalkowska M, Vollmann I, Katus HA, Wollert KC, Bauersachs J, Erne P, Luscher TF, Thum T, Templin C. A signature of circulating microRNAs differentiates Takotsubo cardiomyopathy from acute myocardial infarction. *Eur Heart J* 2014;**35**:999–1006.
32. Rinaldi A, Vincenti S, De Vito F, Bozzoni I, Oliverio A, Presutti C, Fragapane P, Mele A. Stress induces region specific alterations in microRNAs expression in mice. *Behav Brain Res* 2010;**208**:265–269.
33. Dwivedi Y. Evidence demonstrating role of microRNAs in the etiopathology of major depression. *J Chem Neuroanat* 2011;**42**:142–156.
34. Baudry A, Mouillet-Richard S, Schneider B, Launay JM, Kellermann O. miR-16 targets the serotonin transporter: a new facet for adaptive responses to antidepressants. *Science* 2010;**329**:1537–1541.
35. Stermeier T, Adams V, Just H, Blazek S, Deich S, Schuler G, Thiele H, Eitel I. Growth differentiation factor-15 in Takotsubo cardiomyopathy: diagnostic and prognostic value. *Int J Cardiol* 2014;**173**:424–429.
36. Napp LC, Ghadri JR, Bauersachs J, Templin C. Acute coronary syndrome or Takotsubo cardiomyopathy: the suspect may not always be the culprit. *Int J Cardiol* 2015;**187**:116–119.
37. Patel SM, Lennon RJ, Prasad A. Regional wall motion abnormality in apical ballooning syndrome (Takotsubo/stress cardiomyopathy): importance of biplane left ventriculography for differentiating from spontaneously aborted anterior myocardial infarction. *Int J Cardiovasc Imaging* 2012;**28**:687–694.
38. Desmet W, Bennett J, Ferdinande B, De Cock D, Adriaenssens T, Coosemans M, Sinnaeve P, Kayaert P, Dubois C. The apical ripple sign: a useful tool for discriminating between anterior infarction and transient left ventricular ballooning syndrome. *Eur Heart J Acute Cardiovasc Care* 2014;**3**:264–267.
39. De Backer O, Debonnaire P, Gevaert S, Missault L, Gheeraert P, Muyldermans L. Prevalence, associated factors and management implications of left ventricular outflow tract obstruction in Takotsubo cardiomyopathy: a two-year, two-center experience. *BMC Cardiovasc Disord* 2014;**14**:147.
40. Ghadri JR, Cammann VL, Napp LC, Jurisic S, Diekmann J, Bataiosu DR, Seifert B, Jagusztowski M, Sarcon A, Neumann CA, Geyer V, Prasad A, Bax JJ, Ruschitzka F, Luscher TF, Templin C; International Takotsubo Registry. Differences in the clinical profile and outcomes of typical and atypical Takotsubo syndrome: data from the International Takotsubo Registry. *JAMA Cardiol* 2016;**1**:335–340.
41. Galiuto L, De Catarina AR, Porfida A, Paraggio L, Barchetta S, Locorotondo G, Rebuzzi AG, Crea F. Reversible coronary microvascular dysfunction: a common pathogenetic mechanism in Apical Ballooning or Tako-Tsubo Syndrome. *Eur Heart J* 2010;**31**:1319–1327.
42. Dewachter P, Tanaka C, Levesque E, Nicaise-Roland P, Cholet-Martin S, Mouton-Faivre C, Benhamou D. Apical ballooning syndrome following perioperative anaphylaxis is likely related to high doses of epinephrine. *J Anesth* 2011;**25**:383–385.
43. Meimoun P, Passos P, Benali T, Boulanger J, Elmkies F, Zemir H, Clerc J, Luycx-Bore A. Assessment of left ventricular twist mechanics in Tako-tsubo cardiomyopathy by two-dimensional speckle-tracking echocardiography. *Eur J Echocardiogr* 2011;**12**:931–939.
44. Haghi D, Papavassiliu T, Fluchter S, Kaden J, Poimer T, Borggrefe M, Suselbeck T. Variant form of the acute apical ballooning syndrome (Takotsubo cardiomyopathy): observations on a novel entity. *Heart* 2006;**92**:392–394.
45. Hurst RT, Askew JW, Reeves CS, Lee RW, Sweeney JP, Fortuin FD, Oh JK, Tajik AJ. Transient midventricular ballooning syndrome: a new variant. *J Am Coll Cardiol* 2006;**48**:579–583.
46. Shoukat S, Awad A, Nam DK, Hoskins MH, Samuels O, Higginson J, Clements SD Jr. Cardiomyopathy with inverted Tako-Tsubo pattern in the setting of subarachnoid hemorrhage: a series of four cases. *Neurocrit Care* 2013;**18**:257–260.
47. Y-Hassan S. Clinical features and outcome of epinephrine-induced takotsubo syndrome: Analysis of 33 published cases. *Cardiovasc Revasc Med* 2016;**17**:450–455.
48. Naderi N, Amin A, Setayesh A, Pourdalebar H, Mozaffari K, Maleki M. Pheochromocytoma-induced reverse Tako-Tsubo with rapid recovery of left ventricular function. *Cardiol J* 2012;**19**:527–531.
49. Kato K, Kitahara H, Fujimoto Y, Sakai Y, Ishibashi I, Hirai T, Kobayashi Y. Prevalence and clinical features of focal Takotsubo cardiomyopathy. *Circ J* 2016;**80**:1824–1829.
50. Haghi D, Athanasiadis A, Papavassiliu T, Suselbeck T, Fluechter S, Mahrholdt H, Borggrefe M, Sechtem U. Right ventricular involvement in Takotsubo cardiomyopathy. *Eur Heart J* 2006;**27**:2433–2439.
51. Burgdorf C, Hunold P, Radke PW, Schunkert H, Kurowski V. Isolated right ventricular stress-induced ('Tako-Tsubo') cardiomyopathy. *Clin Res Cardiol* 2011;**100**:617–619.
52. Maraencal N, Pellerin D, Lamar A, Beauchet A, El Mahmoud R, Pillière R, McKenna WJ, Duboeuf O. Diagnostic value of contrast echocardiography in Tako-Tsubo cardiomyopathy. *Arch Cardiovasc Dis* 2010;**103**:447–453.
53. Citro R, Rigo F, Ciampi Q, D'Andrea A, Provenza G, Mirra M, Giudice R, Silvestri F, Di Benedetto G, Bossone E. Echocardiographic assessment of regional left ventricular wall motion abnormalities in patients with Tako-Tsubo cardiomyopathy: comparison with anterior myocardial infarction. *Eur J Echocardiogr* 2011;**12**:542–549.
54. Meimoun P, Clerc J, Vincent C, Flahaut P, Germain AL, Elmkies F, Zemir H, Luycx-Bore A. Non-invasive detection of Tako-Tsubo cardiomyopathy vs. acute anterior myocardial infarction by transthoracic Doppler echocardiography. *Eur Heart J Cardiovasc Imaging* 2013;**14**:464–470.
55. Abdelmoneim SS, Mankad SV, Bernier M, Dhoble A, Hagen ME, Ness SA, Chandrasekaran K, Pellikka PA, Oh JK, Mulvagh SL. Microvascular function in Takotsubo cardiomyopathy with contrast echocardiography: prospective evaluation and review of literature. *J Am Soc Echocardiogr* 2009;**22**:1249–1255.
56. Meimoun P, Malaquin D, Sayah S, Benali T, Luycx-Bore A, Levy F, Zemir H, Tribouilloy C. The coronary flow reserve is transiently impaired in Tako-Tsubo cardiomyopathy: a prospective study using serial Doppler transthoracic echocardiography. *J Am Soc Echocardiogr* 2008;**21**:72–77.
57. Rigo F, Sicari R, Citro R, Ossena G, Buja P, Picano E. Diffuse, marked, reversible impairment in coronary microcirculation in stress cardiomyopathy: a Doppler transthoracic echo study. *Ann Med* 2009;**41**:462–470.
58. Meimoun P, Malaquin D, Benali T, Boulanger J, Zemir H, Tribouilloy C. Transient impairment of coronary flow reserve in Tako-Tsubo cardiomyopathy is related to left ventricular systolic parameters. *Eur J Echocardiogr* 2008;**10**:265–270.
59. Fujiwara S, Takeishi Y, Isayama S, Aono G, Takizawa K, Honda H, Otomo T, Mitsuoka M, Itoh Y, Terashima M, Kubota I, Meguro T. Responsiveness to dobutamine stimulation in patients with left ventricular apical ballooning syndrome. *Am J Cardiol* 2007;**100**:1600–1603.
60. Pérrand L, Picano E. Myocardial viability. In E Picano, ed. *Stress Echocardiography: Fifth, Completely Revised and Updated Edition*. Berlin, Heidelberg: Springer Berlin Heidelberg; 2009, pp. 273–294.
61. Umanska B, Plewka M, Wierzbowska-Drabik K, Chrzanowski L, Kasprzak JD. Early prediction of ventricular recovery in Takotsubo syndrome using stress and contrast echocardiography. *Med Sci Monit* 2009;**15**:CS89–CS94.

Downloaded from https://academic.oup.com/eurheartj/article-abstract/36/22/2047/2025411 by Endocrine Society Admin user on 27 April 2020

62. Meimoun P, Abouth S, Boulanger J, Luycx-Bore A, Martis S, Clerc J. Relationship between acute strain pattern and recovery in Tako-Tsubo cardiomyopathy and acute anterior myocardial infarction: a comparative study using two-dimensional longitudinal strain. *Int J Cardiovasc Imaging* 2014;**30**:1491–1500.
63. Chandrasegaram MD, Celermajer DS, Wilson MK. Apical ballooning syndrome complicated by acute severe mitral regurgitation with left ventricular outflow obstruction–case report. *J Cardiothorac Surg* 2007;**2**:14.
64. El Mahmoud R, Mansencal N, Pilliere R, Leyer F, Abbou N, Michaud P, Nallet O, Digne F, Lacombe P, Cattan S, Dubourg O. Prevalence and characteristics of left ventricular outflow tract obstruction in Tako-Tsubo syndrome. *Am Heart J* 2008;**156**:543–548.
65. Parodi G, Del Pace S, Salvadori C, Carrabba N, Olivotto I, Gensini GF; Tuscany Registry of Tako-Tsubo Cardiomyopathy. Left ventricular apical ballooning syndrome as a novel cause of acute mitral regurgitation. *J Am Coll Cardiol* 2007;**50**:647–649.
66. Lyon AR, Bossone E, Schneider B, Sechtem U, Citro R, Underwood SR, Sheppard MN, Figtree GA, Parodi G, Akashi YJ, Ruschitzka F, Filippatos G, Mebazaa A, Omerovic E. Current state of knowledge on Takotsubo syndrome: a Position Statement from the Taskforce on Takotsubo Syndrome of the Heart Failure Association of the European Society of Cardiology. *Eur J Heart Fail* 2016;**18**:8–27.
67. Vizzardi E, Bonadei I, Rovanelli B, Bugatti S, D'Aloia A, Biventricular Tako-Tsubo cardiomyopathy: usefulness of 2D speckle tracking strain echocardiography. *J Clin Ultrasound* 2014;**42**:131–134.
68. Ishida T, Yasu T, Arao K, Kawakami M, Saito M. Images in cardiovascular medicine. Bedside diagnosis of cardiac rupture by contrast echocardiography. *Circulation* 2005;**112**:e354–e355.
69. Haghi D, Papavassiliu T, Heggemann F, Kaden J, Borggrefe M, Suselbeck T. Incidence and clinical significance of left ventricular thrombus in Tako-Tsubo cardiomyopathy assessed with echocardiography. *QJM* 2008;**101**:381–386.
70. Buchholz S, Ward MR, Bhindi R, Nelson GI, Figtree GA, Grieve SM. Cardiac thrombi in stress (Tako-Tsubo) cardiomyopathy: more than an apical issue! *Mayo Clin Proc* 2010;**85**:863–864.
71. Citro R, Rigo F, D'Andrea A, Ciampi Q, Parodi G, Provenza G, Piccolo R, Mirra M, Zito C, Giudice R, Patella MM, Antonini-Canterin F, Bossone E, Piscione F, Salerno-Uriarte J; Tako-Tsubo Italian Network Investigators. Echocardiographic correlates of acute heart failure, cardiogenic shock, and in-hospital mortality in Tako-Tsubo cardiomyopathy. *JACC Cardiovasc Imaging* 2014;**7**:119–129.
72. Tsuchihashi K, Ueshima K, Uchida T, Oh-Mura N, Kimura K, Owa M, Yoshiyama M, Miyazaki S, Haze K, Ogawa H, Honda T, Hase H, Kai R, Morii I; Angina Pectoris-Myocardial Infarction Investigations in Japan. Transient left ventricular apical ballooning without coronary artery stenosis: a novel heart syndrome mimicking acute myocardial infarction. Angina Pectoris-Myocardial Infarction Investigations in Japan. *J Am Coll Cardiol* 2001;**38**:11–18.
73. Margey R, Diamond P, McCann H, Sugrue D. Dobutamine stress echo-induced apical ballooning (Takotsubo) syndrome. *Eur J Echocardiography* 2009;**10**:395–399.
74. Wittstein IS, Thiemann DR, Lima JA, Baughman KL, Schulman SP, Gerstenblith G, Wu KC, Rade JJ, Bivalacqua TJ, Champion HC. Neurohumoral features of myocardial stunning due to sudden emotional stress. *N Engl J Med* 2005;**352**:539–548.
75. Champ-Rigot L, Alexandre J, Grollier G, Millier P. Atypical Tako-tsubo syndrome: a morphologic variant or a step towards recovery? *Int J Cardiol* 2011;**146**:256–258.
76. Brunetti ND, Iera R, Rossi G, Barone N, De Gennaro L, Pellegrino PL, Mawlio G, Cuccolo A, Di Biase M. Ventricular outflow tract obstruction, systolic anterior motion and acute mitral regurgitation in Tako-Tsubo syndrome. *Int J Cardiol* 2008;**127**:e152–e157.
77. Gogas BD, Antoniadis AG, Zacharoulis AA, Kolokathis F, Lekakis J, Kremastinos DT. Recurrent apical ballooning syndrome: 'The masquerading acute cardiac syndrome'. *Int J Cardiol* 2011;**150**:e17–e19.
78. Ghadri JR, Jaguszewski M, Corti R, Luscher TF, Templin C. Different wall motion patterns of three consecutive episodes of Takotsubo cardiomyopathy in the same patient. *Int J Cardiol* 2012;**160**:e25–e27.
79. Murugiah K, Wang Y, Desai NR, Spatz ES, Nuti SV, Dreyer RP, Krumholz HM. Trends in short- and long-term outcomes for Takotsubo cardiomyopathy among medicare fee-for-service beneficiaries, 2007 to 2012. *JACC Heart Fail* 2016;**4**:197–205.
80. Athanasiadis A, Schneider B, Sechtem U. Role of cardiovascular magnetic resonance in Takotsubo cardiomyopathy. *Heart Fail Clin* 2013;**9**:167–176, viii.
81. Templin C, Ghadri JR, Napp LC. Takotsubo (Stress) Cardiomyopathy. *N Engl J Med* 2015;**373**:2689–2691.
82. Eitel I, von Knobelsdorff-Brenkenhoff F, Bernhardt P, Carbone I, Muellerleile K, Aldrovandi A, Francone M, Desch S, Gutberlet M, Strohm O, Schuler G, Schulz-Menger J, Thiele H, Friedrich MG. Clinical characteristics and cardiovascular magnetic resonance findings in stress (Takotsubo) cardiomyopathy. *JAMA* 2011;**306**:277–286.
83. Wu KC, Weiss RG, Thiemann DR, Kitagawa K, Schmidt A, Dalal D, Lai S, Bluemke DA, Gerstenblith G, Marban E, Tomaselli GF, Lima JA. Late gadolinium enhancement by cardiovascular magnetic resonance heralds an adverse prognosis in nonischemic cardiomyopathy. *J Am Coll Cardiol* 2008;**51**:2414–2421.
84. Rolf A, Nef HM, Mollmann H, Troidl C, Voss S, Conradi G, Rixe J, Steiger H, Belling K, Hamm CW, Dill T. Immunohistological basis of the late gadolinium enhancement phenomenon in Tako-Tsubo cardiomyopathy. *Eur Heart J* 2009;**30**:1635–1642.
85. Heidary S, Patel H, Chung J, Yokota H, Gupta SN, Bennett MV, Katikireddy C, Nguyen P, Pauly JM, Terashima M, McConnell MV, Yang PC. Quantitative tissue characterization of infarct core and border zone in patients with ischemic cardiomyopathy by magnetic resonance is associated with future cardiovascular events. *J Am Coll Cardiol* 2010;**55**:2762–2768.
86. Eitel I, Friedrich MG. T2-weighted cardiovascular magnetic resonance in acute cardiac disease. *J Cardiovasc Magn Reson* 2011;**13**:13.
87. Stahli BE, Ruschitzka F, Enseleit F. Isolated right ventricular ballooning syndrome: a new variant of transient cardiomyopathy. *Eur Heart J* 2011;**32**:1821.
88. Kagiyama N, Okura H, Tamada T, Imai K, Yamada R, Kume T, Hayashida A, Neishi Y, Kawamoto T, Yoshida K. Impact of right ventricular involvement on the prognosis of Takotsubo cardiomyopathy. *Eur Heart J Cardiovasc Imaging* 2016;**17**:210–216.
89. Eitel I, Behrendt F, Schindler K, Kivelitz D, Gutberlet M, Schuler G, Thiele H. Differential diagnosis of suspected apical ballooning syndrome using contrast-enhanced magnetic resonance imaging. *Eur Heart J* 2008;**29**:2651–2659.
90. Abe Y, Kondo M, Matsuoka R, Araki M, Dohyama K, Tanio H. Assessment of clinical features in transient left ventricular apical ballooning. *J Am Coll Cardiol* 2003;**41**:737–742.
91. Ghadri JR, Dougoud S, Maier W, Kaufmann PA, Gaemperli O, Prasad A, Luscher TF, Templin C. A PET/CT-follow-up imaging study to differentiate Takotsubo cardiomyopathy from acute myocardial infarction. *Int J Cardiovasc Imaging* 2014;**30**:207–209.
92. Ito K, Sugihara H, Kawasaki T, Yuba T, Doue T, Tanabe T, Adachi Y, Katoh S, Azuma A, Nakagawa M. Assessment of ampulla (Takotsubo) cardiomyopathy with coronary angiography, two-dimensional echocardiography and 99mTc-tetrofosmin myocardial single photon emission computed tomography. *Ann Nucl Med* 2001;**15**:351–355.
93. Cimarelli S, Imperiale A, Ben-Sellem D, Rischner J, Detour J, Morel O, Ohlmann P, Constantinesco A. Nuclear medicine imaging of Takotsubo cardiomyopathy: typical form and midventricular ballooning syndrome. *J Nucl Cardiol* 2008;**15**:137–141.
94. Cimarelli S, Sauer F, Morel O, Ohlmann P, Constantinesco A, Imperiale A. Transient left ventricular dysfunction syndrome: patho-physiological bases through nuclear medicine imaging. *Int J Cardiol* 2010;**144**:212–218.
95. Christensen TE, Abdiovski KA, Berg LE, Holmvang L, Sakalis H, Ghotbi AA, Andersson H, Vejlstrup N, Iversen K, Engstroem T, Kjaer A, Haslak P. Basal hyperaemia is the primary abnormality of perfusion in Takotsubo cardiomyopathy: a quantitative cardiac perfusion positron emission tomography study. *Eur Heart J Cardiovasc Imaging* 2015;**16**:1162–1169.
96. Kurisu S, Inoue I, Kawagoe T, Ishihara M, Shimatani Y, Nishioka K, Umemura T, Nakamura S, Yoshida M, Sato H. Myocardial perfusion and fatty acid metabolism in patients with Tako-Tsubo-like left ventricular dysfunction. *J Am Coll Cardiol* 2003;**41**:743–748.
97. Matsuo S, Nakajima K, Kiuya S, Yamashi M. Diagnostic utility of 123-BMIPP imaging in patients with Takotsubo cardiomyopathy. *J Cardiol* 2014;**64**:49–54.
98. Yoshida T, Hibino T, Kako N, Murai S, Oguri M, Kato K, Yajima K, Otsu N, Yokoi K, Kimura G. A pathophysiologic study of Tako-Tsubo cardiomyopathy with F-18 fluorodeoxyglucose positron emission tomography. *Eur Heart J* 2007;**28**:3598–3604.
99. Dorfman TA, Iskandrian AE. Takotsubo cardiomyopathy: state-of-the-art review. *J Nucl Cardiol* 2009;**16**:123–134.
100. Merli E, Sutcliffe S, Gori M, Sutherland GG. Tako-Tsubo cardiomyopathy: new insights into the possible underlying pathophysiology. *Eur J Echocardiogr* 2006;**7**:53–61.
101. Akashi YJ, Nakazawa K, Sakakibara M, Miyake F, Musha H, Sasaka K. ^{123}I-MIBG myocardial scintigraphy in patients with 'Takotsubo' cardiomyopathy. *J Nucl Med* 2004;**45**:1123–1127.
102. Prasad A, Madhavan M, Choreonthalawee P. Cardiac sympathetic activity in stress-induced (Takotsubo) cardiomyopathy. *Nat Rev Cardiol* 2009;**6**:430–434.
103. Tornvall P, Collste O, Ehrenborg E, Jambert-Petterson H. A case-control study of risk markers and mortality in Takotsubo stress cardiomyopathy. *J Am Coll Cardiol* 2016;**67**:1931–1936.
104. Stiermaier T, Eitel C, Desch S, Fuernau G, Schuler G, Thiele H, Eitel I. Incidence, determinants and prognostic relevance of cardiogenic shock in patients with Takotsubo cardiomyopathy. *Eur Heart J Acute Cardiovasc Care* 2016;**5**:489–496.

Downloaded from https://academic.oup.com/eurheartj/article-abstract/39/22/2047/5072411 by EndocrineSociety Admin user on 27 April 2020

105. Roffi M, Patrono C, Collet JP, Mueller C, Valgimigli M, Andreotti F, Bax JJ, Borger MA, Brotons C, Chew DP, Gencer B, Hasenfuss G, Kjeldsen K, Lancellotti P, Landmesser U, Mehilli J, Mukherjee D, Storey RF, Windecker S, Baumgartner H, Gaemperli O, Achenbach S, Agewall S, Badimon L, Baigent C, Bueno H, Bugiardini R, Carerj S, Casselman F, Cuisset T, Erol C, Fitzsimons D, Halle M, Haven C, Hildick-Smith D, Huber K, Iliodromitis E, James S, Lewis BS, Lip GY, Piepoli MF, Richter D, Rosemann T, Sechtem U, Steg PG, Vrints C, Luis Zamorano J; Management of Acute Coronary Syndromes in Patients Presenting without Persistent ST-Segment Elevation of the European Society of Cardiology. 2015 ESC Guidelines for the management of acute coronary syndromes in patients presenting without persistent ST-segment elevation: task Force for the Management of Acute Coronary Syndromes in Patients Presenting without Persistent ST-Segment Elevation of the European Society of Cardiology (ESC). *Eur Heart J* 2016;**37**:267–315.
106. Task Force on the management of ST-segment elevation acute myocardial infarction of the European Society of Cardiology (ESC), Steg PG, James SK, Atar D, Badano LP, Blomstrom-Lundqvist C, Borger MA, Mario, C, D Dickstein, K Ducrocq, G Fernandez-Aviles, F Gershlick, AH Giannuzzi, P Halvorsen, S Huber, K Juni, P Kastrati, A Knuuti, J Lenzen, MJ Mahaffey, KW Valgimigli, M van 't Hof, A Widimsky P, Zahger, D. ESC Guidelines for the management of acute myocardial infarction in patients presenting with ST-segment elevation. *Eur Heart J* 2012;**33**:2569–2619.
107. Amsterdam EA, Wenger NK, Brindis RG, Casey DE Jr, Ganiats TG, Holmes DR Jr, Jaffe AS, Jneid H, Kelly RF, Kontos MC, Levine GN, Liebson PR, Mukherjee D, Peterson ED, Sabatine MS, Smalling RW, Zieman SJ; American College of C, American Heart Association Task Force on Practice G, Society for Cardiovascular A, Interventions, Society of Thoracic S, American Association for Clinical C. 2014 AHA/ACC Guideline for the Management of Patients with Non-ST-Elevation Acute Coronary Syndromes: a report of the American College of Cardiology/American Heart Association Task Force on Practice Guidelines. *J Am Coll Cardiol* 2014;**64**:e139–e228.
108. O'Gara PT, Kushner FG, Ascheim DD, Casey DE Jr, Chung MK, de Lemos JA, Ettinger SM, Fang JC, Fesmire FM, Franklin BA, Granger CB, Krumholz HM, Linderbaum JA, Morrow DA, Newby LK, Ornato JP, Ou N, Radford MJ, Tamis-Holland JE, Tommaso CL, Tracy CM, Woo YJ, Zhao DX, Anderson JL, Jacobs AK, Halperin JL, Albert NM, Brindis RG, Creager MA, DeMets D, Guyton RA, Hochman JS, Kovacs RJ, Kushner FG, Ohman EM, Stevenson WG, Yancy CW; American College of Cardiology Foundation/American Heart Association Task Force on Practice G. 2013 ACCF/AHA guideline for the management of ST-elevation myocardial infarction: a report of the American College of Cardiology Foundation/American Heart Association Task Force on Practice Guidelines. *Circulation* 2013;**127**:e362–e425.
109. Brinjikji W, El-Sayed AM, Salka S. In-hospital mortality among patients with Takotsubo cardiomyopathy: a study of the National Inpatient Sample 2008 to 2009. *Am Heart J* 2012;**164**:215–221.
110. Sobue Y, Watanabe E, Ichikawa T, Koshikawa M, Yamamoto M, Harada M, Ozaki Y. Physically triggered Takotsubo cardiomyopathy has a higher in-hospital mortality rate. *Int J Cardiol* 2017;**235**:87–91.
111. Murakami T, Yoshikawa T, Maekawa Y, Ueda T, Isogai T, Koreishi Y, Sakata K, Nagai K, Yamamoto T, Takayama M; Committee CCUNS. Characterization of predictors of in-hospital cardiac complications of Takotsubo cardiomyopathy: multi-center registry from Tokyo CCU Network. *J Cardiol* 2014;**63**:269–273.
112. Takashio S, Yamamoto M, Kojima S, Izumiya Y, Kakita K, Hokimoto S, Sugiyama S, Tsunoda R, Nakao K, Ogawa H. Usefulness of SUM of ST-segment elevation on electrocardiograms (limb leads) for predicting in-hospital complications in patients with stress (Takotsubo) cardiomyopathy. *Am J Cardiol* 2012;**109**:1651–1656.
113. Steinmaier T, Eitel C, Denef S, Desch S, Schuler G, Thiele H, Eitel I. Significance of life-threatening arrhythmias in takotsubo cardiomyopathy. *J Am Coll Cardiol* 2015;**65**:2148–2150.
114. Ili A, Akilli H, Kayrak M, Arikan A, Ozdemir K. Short-term warfarin treatment for apical thrombus in a patient with Takotsubo cardiomyopathy. *Cardiovasc J Afr* 2016;**27**:e12–e13.
115. Bharathi KS, Kulkarni S, Sadananda KS, Gunadan CL. Takotsubo cardiomyopathy precipitated by negative pressure pulmonary oedema following total thyroidectomy. *Indian J Anaesth* 2016;**60**:202–205.
116. Lu DY, Caplow J, Quatromoni N, Forde-McLean R, Owens AT. Ventricular septal defect from Takotsubo syndrome. *Case Rep Cardiol* 2016;**2016**:2693062.
117. Jagiszewski M, Fijałkowski M, Nowak R, Czapiewski P, Ghadri JR, Templin C, Rynkiewicz A. Ventricular rupture in Takotsubo cardiomyopathy. *Eur Heart J* 2012;**33**:1027.
118. Böhm M, Cammann VL, Ghadri JR, Ukena C, Gili S, Di Vece D, Kato K, Deng KJ, Szawan KA, Minai J, Jurisic S, D'Ascenzo F, Frangieh AH, Rechsteiner D, Seifert B, Ruschitzka F, Lüscher T, Templin C; InterTAK Collaborators. Interaction of systolic blood pressure and resting heart rate with clinical outcomes in takotsubo syndrome: insights from the International Takotsubo Registry. *Eur J Heart Fail* 2018; doi: 10.1002/ejhf.1162.
119. Citro R, Bossone E, Parodi G, Rigo F, Nardi F, Primverata G, Zito C, Novo G, Vitale G, Prota C, Silverio A, Vriz O, D'andrea A, Antonini-Canterin F, Salerno-Uriarte J, Piscione F; Tako-tsubo Italian Network Investigators. Independent impact of RV involvement on in-hospital outcome of patients with Takotsubo syndrome. *JACC Cardiovasc Imaging* 2016;**9**:894–895.
120. Bleiber AA, Prasad A, Lennon RJ, Wright RS, Lerman A, Rihal CS. Four-year recurrence rate and prognosis of the apical ballooning syndrome. *J Am Coll Cardiol* 2007;**50**:448–452.
121. Sharkey SW, Pink VR, Lesser JR, Garberich RF, Maron MS, Maron BJ. Clinical profile of patients with high-risk Tako-Tsubo cardiomyopathy. *Am J Cardiol* 2015;**116**:765–772.
122. Stiermaier T, Moeller C, Oehler K, Desch S, Graf T, Eitel C, Vonthein R, Schuler G, Thiele H, Eitel I. Long-term excess mortality in Takotsubo cardiomyopathy: predictors, causes and clinical consequences. *Eur J Heart Fail* 2016;**18**:650–656.
123. Madias JE. Low prevalence of diabetes mellitus in patients with Takotsubo syndrome: a plausible 'protective' effect with pathophysiologic connotations. *Eur Heart J Acute Cardiovasc Care* 2016;**5**:164–170.
124. Bill V, El-Battrawy I, Behnes M, Baumann S, Becher T, Elmas E, Hoffmann U, Hagli D, Fastner C, Kuschyk J, Papavassiliu T, Borggrefe M, Akin I. 'Diabetes paradox' in Takotsubo Cardiomyopathy. *Int J Cardiol* 2016;**224**:88–89.
125. Dias A, Franco E, Rubio M, Koshkelashvili N, Bhalla V, Amanullah S, Hebert K, Figueredo VM. Takotsubo Syndrome: does it matter if you have diabetes mellitus? *Int J Cardiol* 2016;**224**:398–399.
126. Bonello L, Com O, Ait-Moktar O, Theron A, Moro PJ, Salem A, Sbraga F, Paganelli F. Ventricular arrhythmias during Tako-tsubo syndrome. *Int J Cardiol* 2008;**128**:e50–e53.
127. Syed FF, Asirvatham SJ, Francis J. Arrhythmia occurrence with Takotsubo cardiomyopathy: a literature review. *Europace* 2011;**13**:780–788.
128. Madias C, Fitzgibbons TP, Alsheikh-Ali AA, Bouchard JL, Kalamith B, Garlitski AC, Tighe DA, Estes NA 3rd, Aurigemma GP, Link MS. Acquired long QT syndrome from stress cardiomyopathy is associated with ventricular arrhythmias and torsades de pointes. *Heart Rhythm* 2011;**8**:555–561.
129. Brown KH, Trohman RG, Madias C. Arrhythmias in Takotsubo cardiomyopathy. *Card Electrophysiol Clin* 2015;**7**:331–340.
130. Migliore F, Zorzi A, Perazza F, Perazzolo Marra M, Tarantini G, Iliceto S, Corrado D. Incidence and management of life-threatening arrhythmias in Takotsubo syndrome. *Int J Cardiol* 2013;**166**:261–263.
131. Perazzolo Marra M, Zorzi A, Corbetti F, De Lazzari M, Migliore F, Tona F, Tarantini G, Iliceto S, Corrado D. Apicobasal gradient of left ventricular myocardial edema underlies transient T-wave inversion and QT interval prolongation (Wellens' ECG pattern) in Tako-Tsubo cardiomyopathy. *Heart Rhythm* 2013;**10**:70–77.
132. Gasparetto N, Zorzi A, Perazzolo Marra M, Migliore F, Napodano M, Corrado D, Iliceto S, Cacciavillani L. Atypical (mid-ventricular) Takotsubo syndrome in a survival of out-of-hospital ventricular fibrillation: cause or consequence? *Int J Cardiol* 2014;**172**:e51–e53.
133. Zorzi A, Perazzolo Marra M, Migliore F, De Lazzari M, Tarantini G, Iliceto S, Corrado D. Relationship between repolarization abnormalities and myocardial edema in atypical Tako-Tsubo syndrome. *J Electrocardiol* 2013;**46**:349–351.
134. Ohkubo K, Watanabe I, Okumura Y, Ashino S, Kofune M, Nagashima K, Nakai T, Kasamaki Y, Hirayama A. Functional atrioventricular conduction block in an elderly patient with acquired long QT syndrome: elucidation of the mechanism of block. *J Electrocardiol* 2011;**44**:353–356.
135. Sharkey SW, Windenburg DC, Lesser JR, Maron MS, Hauser RG, Lesser JN, Haas TS, Hodges JS, Maron BJ. Natural history and expansive clinical profile of stress (Tako-Tsubo) cardiomyopathy. *J Am Coll Cardiol* 2010;**55**:333–341.
136. Cattinen M, Moccetti M, Pasotti E, Faletra F, Porretta AP, Kobza R, Gallino A. Three recurrent episodes of apical-ballooning Takotsubo cardiomyopathy in a man. *Circulation* 2015;**132**:e377–e379.
137. Srivastava NT, Parent JJ, Hurwitz RA. Recurrent Takotsubo cardiomyopathy in a child. *Cardiol Young* 2016;**26**:410–412.
138. Xu B, Williams PD, Brown M, Macisaac A. Takotsubo cardiomyopathy: does recurrence tend to occur in a previously unaffected ventricular wall region? *Circulation* 2014;**129**:e339–e340.
139. Kato K, Lyon AR, Ghadri JR, Templin C. Takotsubo syndrome: aetiology, presentation and treatment. *Heart* 2017;**103**:1461–1469.
140. Isogai T, Matsui H, Tanaka H, Fushimi K, Yasunaga H. Early β-blocker use and in-hospital mortality in patients with takotsubo cardiomyopathy. *Heart* 2016;**102**:1029–1035.
141. Dias A, Franco E, Koshkelashvili N, Bhalla V, Preuman GS, Hebert K, Figueredo VM. Antiplatelet therapy in Takotsubo cardiomyopathy: does it improve cardiovascular outcomes during index event? *Heart Vessels* 2016;**31**:1285–1290.

Downloaded from https://academic.oup.com/eurheartj/article-abstract/36/22/2047/1502411 by Endocrine Society Admin user on 27 April 2020

143. Santoro F, Ieva R, Musaico F, Ferranetti A, Triggiani G, Tarantino N, Di Biase M, Brunetti ND. Lack of efficacy of drug therapy in preventing takotsubo cardiomyopathy recurrence: a meta-analysis. *Clin Cardiol* 2014;**37**:434–439.
143. Santoro F, Ieva R, Ferranetti A, Ienco V, Carpagnano G, Lodispoto M, Di Biase L, Di Biase M, Brunetti ND. Safety and feasibility of levosimendan administration in Takotsubo cardiomyopathy: a case series. *Cardiovasc Ther* 2013;**31**: e133–e137.
144. Singh K, Carson K, Usmani Z, Sawhney G, Shah R, Horowitz J. Systematic review and meta-analysis of incidence and correlates of recurrence of Takotsubo cardiomyopathy. *Int J Cardiol* 2014;**174**:696–701.
145. Citro R, Lyon AR, Meimoun P, Omerovic E, Redfors B, Buck T, Larskis S, Parodi G, Silverio A, Etsl I, Schneider B, Prasad A, Bossone E. Standard and advanced echocardiography in Takotsubo (stress) cardiomyopathy: clinical and prognostic implications. *J Am Soc Echocardiogr* 2015;**28**:57–74.
146. Munzel T, Knorr M, Schmidt F, von Bardeleben S, Gori T, Schulz E. Airborne disease: a case of a Takotsubo cardiomyopathie as a consequence of nighttime aircraft noise exposure. *Eur Heart J* 2016;**37**:2844.
147. Madias JE. If channel blocker ivabradine vs. beta-blockers for sinus tachycardia in patients with Takotsubo syndrome. *Int J Cardiol* 2016;**223**:877–878.
148. Ueyama T, Kasamatsu K, Hano T, Yamamoto K, Tsuruo Y, Nishio I. Emotional stress induces transient left ventricular hypocontraction in the rat via activation of cardiac adrenoceptors: a possible animal model of 'Tako-Tsubo' cardiomyopathy. *Circ J* 2002;**66**:712–713.
149. Izumi Y, Okatani H, Shiota M, Nakao T, Ise R, Kito G, Miura K, Iwao H. Effects of metoprolol on epinephrine-induced Takotsubo-like left ventricular dysfunction in nonhuman primates. *Hypertens Res* 2009;**32**:339–346.
150. Stiermaier T, Rommel KP, Bitel C, Moller C, Graf T, Desch S, Thiele H, Eitel I. Management of arrhythmias in patients with Takotsubo cardiomyopathy: is the implantation of permanent devices necessary? *Heart Rhythm* 2016;**13**: 1979–1986.
151. Peters S, Klein HU. WCD LifeVest: risk stratification in a case of Tako-Tsubo cardiomyopathy with QT interval prolongation. *Herz* 2012;**37**:219–221.
152. Ueyama T, Kasamatsu K, Hano T, Tsuruo Y, Ishikura F. Catecholamines and estrogen are involved in the pathogenesis of emotional stress-induced acute heart attack. *Ann N Y Acad Sci* 2008;**1148**:479–485.
153. Ueyama T, Ishikura F, Matsuda A, Asanuma T, Ueda K, Ichinose M, Kasamatsu K, Hano T, Akasaka T, Tsuruo Y, Morimoto K, Beppu S. Chronic estrogen supplementation following ovariectomy improves the emotional stress-induced cardiovascular responses by indirect action on the nervous system and by direct action on the heart. *Circ J* 2007;**71**:565–573.
154. Deleuze C, Lainez O, Hulin E, Delmas T, Baudou N, Dumonteil N, Blondel-Picquet C, Roncalli J, Elbaz M, Galinier M, Carrié D. Amiodepressive disorders and chronic psychological stress are associated with Tako-Tsubo cardiomyopathy—new physiopathological hypothesis. *Circ J* 2013;**77**: 175–180.
155. Mayer KN, Ghadri J-R, Jagusiewski M, Scherff F, Saguner AM, Kazemian E, Baumann CR, Jenewein J, Traikins M, Lüscher TF, Brugger P, Templin C. Takotsubo syndrome—a close connection to the brain; a prospective study investigating neuropsychiatric traits. *JCE Metab Endocr* 2016;**12**: 36–41.
156. Ghadri JR, Ruschitzka F, Luscher TF, Templin C. Takotsubo cardiomyopathy: still much more to learn. *Heart* 2014;**100**:1804–1812.

Downloaded from https://academic.oup.com/eurheartj/article-abstract/38/27/2047/5025411 by EndocrineSociety Admin user on 27 April 2020

Internal Medicine
The Japanese Society of Internal Medicine

doi: 10.2169/internalmedicine.0029-17
Intern Med 57: 1553-1559, 2018
http://internmed.jp

[ORIGINAL ARTICLE]

The Factors Affecting the Non-dipper Pattern in Japanese Patients with Severe Obstructive Sleep Apnea

Hiromitsu Sekizuka[1,2], Naohiko Osada[1] and Yoshihiro J Akashi[1]

Abstract:

Objective Obstructive sleep apnea (OSA) is assumed to influence the circadian blood pressure (BP) fluctuation, particularly causing nocturnal hypertension and changing the dipping pattern of nocturnal BP. This study aimed to clarify the triggers of the non-dipper pattern in nocturnal BP in Japanese patients with severe OSA (the apnea-hypopnea index ≥30/h).

Methods Of 541 patients with OSA diagnosed using polysomnography (PSG) and ambulatory BP monitoring (ABPM), 163 patients <60 years of age (Younger group) and 101 patients ≥60 years of age (Older group) were stratified into the dipper or non-dipper pattern groups.

Results A logistic regression analysis was performed using a non-dipper pattern as a dependent variable. A multivariate analysis demonstrated that the cumulative percentage of time at saturation below 90% was the only independent risk factor for the non-dipper and riser patterns in the Younger group (odds ratio, 1.022; 95% confidence interval, 1.001-1.044; p=0.035), whereas slow-wave sleep (odds ratio, 0.941; 95% confidence interval, 0.891-0.990; p=0.019) and the use of angiotensin-converting enzyme inhibitors or angiotensin II receptor blockers (odds ratio, 2.589; 95% confidence interval, 1.051-6.848; p=0.039) were risk factors in the Older group.

Conclusion These findings suggested that the degree of desaturation in young OSA patients and sleep quality in old OSA patients might influence the dipping patterns in nocturnal BP.

Key words: ambulatory blood pressure monitoring, circadian rhythm, nocturnal blood pressure, polysomnography, sleep-disordered breathing

(Intern Med 57: 1553-1559, 2018)
(DOI: 10.2169/internalmedicine.0029-17)

Introduction

Obstructive sleep apnea (OSA) is assumed to influence the development of hypertension (1) and circadian blood pressure (BP) fluctuation patterns (1-3). OSA is well known to elevate the nocturnal BP, which is characterized as non-dipper and riser patterns, and to cause organ damage (4, 5).

This study aimed to clarify the triggers of non-dipper and riser patterns in nocturnal BP in Japanese patients with severe OSA.

Materials and Methods

Subjects

A total of 541 Japanese patients who visited the Sleep Apnea Syndrome Outpatient Department in the St. Marianna University School of Medicine Hospital between February 2004 and March 2013 and underwent polysomnography for suspected sleep-disordered breathing (SDB) and ambulatory BP monitoring (ABPM) for investigating abnormal circadian BP rhythm within 2 months of polysomnography (PSG) were selected (Figure). Of these, 304 patients whose apnea hypopnea index (AHI) was ≥30/h were investigated for their

[1]Division of Cardiology, Department of Internal Medicine, St. Marianna University School of Medicine, Japan and [2]Department of Internal Medicine, Fujitsu Clinic, Japan
Received: August 4, 2017; Accepted: September 19, 2017; Advance Publication by J-STAGE: January 11, 2018
Correspondence to Dr. Hiromitsu Sekizuka, sekimal@marianna-u.ac.jp

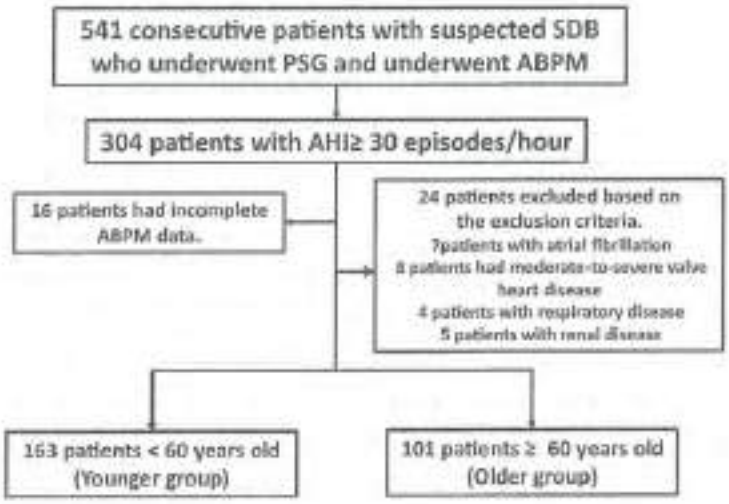

Figure. Patients inclusion flowchart.

gender, age, height, weight, body mass index (BMI), and the use or non-use of antihypertensive agents, diabetes drugs, including insulin, and lipid metabolism disorder drugs at the first visit. Daytime sleepiness was also assessed using the Epworth Sleepiness Scale (ESS), Japanese version (6).

The patients with atrial fibrillation, those with moderate-to-severe heart valve disease, those with respiratory disease, those with renal disease, those <18 years of age and those with insufficient data were excluded from this study (n=40). Ultimately, 264 Japanese patients were enrolled into this study.

All patients diagnosed with SDB had OSA and had not previously received OSA treatment. Based on the results of an earlier study demonstrating the association of SDB with hypertension in patients <60 years of age (7), our study patients were stratified into the following groups: patients <60 years of age (Younger group, n=163) and those ≥60 years of age (Older group, n=101).

The present study was performed in accordance with the ethical principles set forth in the Declaration of Helsinki. The study protocol was reviewed and approved by the Institutional Review Board of the St. Marianna University School of Medicine and implemented in compliance with the Personal Information Protection Law (Ethical Committee Approval Nos. 1142 and 1603).

Blood parameters

Blood samples were collected for measuring the serum concentration of fasting plasma glucose, glycosylated hemoglobin, triglyceride, high-density lipoprotein cholesterol, low-density lipoprotein cholesterol and creatinine in the fasting state at the first examination. Diabetes mellitus was defined as glucose ≥126 mg/dL in the fasting state or glycosylated hemoglobin ≥6.5% according to the National Glycohemoglobin Standardization Program. Patients with low-density lipoprotein cholesterol ≥140 mg/dL, high-density lipoprotein cholesterol <40 mg/dL or triglyceride ≥150 mg/dL and those who were receiving lipid metabolism disorder treatment were defined as having dyslipidemia. According to the recommendation of the Japanese Society of Nephrology, the estimated glomerular filtration rate (eGFR) was calculated as follows: eGFR (mL/min/1.73 m^2) = 194× $Cr^{-1.094}$ × $age^{-0.287}$ (×0.739 for women) (8).

Evaluation of sleep-disordered breathing

Polysomnography (SleepWatcher®, Compumedics, Abbotsford, Australia; or Polymate®, Miyuki Giken, Tokyo, Japan) was employed to evaluate SDB. A nasal cannula was placed at the nares to measure the respiratory airflow using a disposable airflow sensor; a strain gauge sensor monitored respiratory movements of the chest and abdominal walls. Arterial oxygen saturation (SpO_2) was measured with a pulse oximeter detecting the percentage of oxygenated hemoglobin in arterial blood by two wavelengths of light transmitted to the finger to extract the pulse wave component according to the heart beat (9, 10). The results obtained during sleep were manually analyzed by laboratory technician specialists using the Rechtschaffen and Kales criteria (11); breathing events and cessation of airflow for 10 seconds or longer were recognized as apnea. Hypopnea was defined as an obvious reduction in airflow (less than 50%) for 10 seconds or longer compared with stable breathing before and after an event and decrease in oxygen saturation of 3% from the baseline or when the event is associated with arousal (12). AHI is defined as the frequency of apnea/hypopnea per hour. Low-oxygen exposure was defined as SpO_2 <90% and the rate of SpO_2 <90% (cumulative percentage of time at saturation below 90%, CT90%). The non-REM sleep stages 3 and 4 was defined as slow-wave sleep (SWS) in the present study.

Blood pressure measurement in a doctor's office

Each patient sat in a backed chair in the doctor's office without crossing their legs for a few minutes. BP was then measured using the brachial artery by physicians with electric automated manometers (Omron Healthcare, Kyoto, Ja-

Table 1. Patient Background Data.

Group	All patients	Younger group	Older group	p value
Number of patients	264	163	101	/
Male sex no. (%)	219 (83)	151 (93)	68 (67)	<0.001
Age (years)	54.8±12.9	46.7±9.0	67.9±5.1	<0.001
BMI (kg/m²)	28.1±5.5	29.1±5.8	26.6±4.7	<0.001
ESS	8.9±5.9	10.0±5.9	7.3±5.4	<0.001
Heart diseses and/or cerebrovascular diseases no. (%)	43 (16)	19 (12)	24 (24)	0.010
Antihypertensive agents use no. (%)	93 (35)	43 (26)	50 (50)	<0.001
Calcium-channel blocker	62 (23)	32 (20)	30 (30)	0.060
ACE-I/ARB	66 (25)	30 (18)	36 (36)	0.002
Diuretic	23 (9)	7 (4)	16 (16)	0.001
β blocker	15 (6)	9 (6)	6 (6)	0.886
α blocker	6 (2)	3 (2)	3 (3)	0.549
Aldosterone blocker	5 (2)	0 (0)	5(5)	0.004
Diabetes mellitus no. (%)	57 (22)	28 (17)	29 (28)	0.027
Dyslipidemia no. (%)	152 (58)	96 (59)	56 (55)	0.581
Creatinine (mg/dL)	0.93±0.63	0.86±0.19	1.04±0.98	0.022
eGFR (mL/min/1.73m²)	71.8±19.5	78.2±17.3	61.4±18.4	<0.001
24-h Systolic blood pressure (mmHg)	133.2±11.7	132.9±11.4	133.6±12.3	0.653
AHI (/h)	54.1±17.4	55.7±17.3	51.5±17.2	0.054

BMI: body mass index, ESS: Epworth sleepiness scale, ACE-I: angiotensin-converting enzyme inhibitor, ARB: angiotensin II receptor blocker, eGFR: estimated glomerular filtration rate, AHI: apnea-hypopnea index

The values are presented as the mean±s.d.

pan; or Terumo, Tokyo, Japan); its accuracy was comparable to the BP measured with the auscultatory method using a mercury manometer. BP was measured during the usual outpatient consultation time between 1 PM and 5 PM after adjusting the height of the measuring table in order to keep the position of the cuff at heart level; the upper arm was then wrapped with a tourniquet (width, 13 cm; length, 22 cm). Two stable measurements were used for the average BP calculation. The BP at the first visit was evaluated.

24-h ABPM

Non-invasive ABPM was performed for 24 hours using an FM-800 (Fukuda Denshi, Tokyo, Japan) at 30-minute intervals (2). ABPM and PSG were assessed on two different days. The BP was measured by the oscilloscopic method with an automated BP cuff or by the Korotkoff method. The ABPM data were analyzed based on the method described by Kario et al. (13). The following systolic BP (SBP) and diastolic BP (DBP) were measured: 24-hour BP, the average BP during the recording day; awake BP, the average BP during the rest of the day; and sleep BP, the average BP during sleep at night. The non-dipping BP pattern (ND pattern) was defined when the reduction in the awake SBP was <10% of the sleep SBP, whereas the dipping BP pattern (D pattern) was defined when the reduction in the awake SBP was ≥10% of the sleep SBP (14, 15).

Statistical analyses

All measurements were indicated as mean ± standard deviation. The Mann-Whitney's U-test and Pearson's χ^2 test were used for comparisons between the D and ND patterns in the Younger and Older groups. Univariate and multiple logistic regression analyses were performed to determine the factors related to the ND pattern. Since there were significant differences between the D and ND patterns in the Younger and Older groups, the determinant factors for the ND pattern were analyzed in the BMI and CT90% in the Younger group and the use or non-use of angiotensin-converting enzyme inhibitors (ACE-I) or angiotensin II receptor blockers (ARB) and the rate of SWS and REM in the Older group. Statistical analyses were conducted using the JMP® software program for Windows® (version 10.0; SAS Institute, Cary, USA). Significant difference was set at a p value of <0.05 for the hazard ratio.

Results

Patients' characteristics (Table 1-3)

The patients' background characteristics are summarized in Tables 1 and 2. Significant differences in the BMI in the Younger group (p=0.026) and the use of ACE-I/ARB in the Older group (p=0.034) were found between the D and ND patterns (Table 2). Table 3 shows the obtained sleep and BP data in the two groups.

Evaluation of the ND pattern for each factor Table 4

A logistic regression analysis was performed using the ND pattern as a dependent variable (Table 4). The parameters demonstrating significant differences between the D and ND patterns in the Younger and Older groups were evaluated. The results of a univariate analysis indicated a signifi-

Table 2. Patient Background Data.

Group	Younger group (n=163)			Older group (n=101)		
	D pattern	ND pattern	p value	D pattern	ND pattern	p value
Number of patients	85	78	/	39	62	/
Dipping status (%)	+10.2 – +33.5	-9.2 – +9.9	/	+10.4 – +22.0	-28.1 – +9.9	/
Male sex no. (%)	77 (91)	74 (95)	0.295	27 (69)	41 (66)	0.746
Age (years)	46.4±9.9	47.1±7.9	0.595	67.3±4.8	68.3±5.3	0.309
BMI (kg/m^2)	28.1±5.3	30.1±6.2	0.026	26.6±3.3	26.7±5.4	0.911
ESS	10.1±5.5	9.8±6.4	0.770	7.3±6.1	7.2±4.9	0.923
Heart diseses and/or cerebrovascular diseases no. (%)	11 (13)	8 (10)	0.594	8 (21)	16 (26)	0.543
Antihypertensive agents use no. (%)	24 (28)	19 (24)	0.575	17 (44)	33 (53)	0.346
Calcium-channel blocker	18 (21)	14 (18)	0.604	9 (23)	21 (34)	0.248
ACE-I/ARB	19 (22)	11 (14)	0.175	9 (23)	27 (44)	0.034
Diuretic	4 (5)	3 (4)	0.775	6 (15)	10 (16)	0.821
β blocker	5 (6)	4 (5)	0.833	1 (3)	5 (8)	0.254
α blocker	2 (2)	1 (1)	0.611	0 (0)	3 (5)	0.163
Aldosterone blocker	0 (0)	0 (0)	/	2 (5)	3 (5)	0.948
Diabetes mellitus no. (%)	16 (19)	12 (15)	0.561	18 (29)	11 (28)	0.929
Dyslipidemia no. (%)	45 (53)	51 (65)	0.107	23 (59)	33 (53)	0.572
Creatinine (mg/dL)	0.86±0.21	0.86±0.17	0.957	1.19±1.51	0.95±0.38	0.240
eGFR (mL/min/1.73m^2)	78.5±17.5	78.0±17.1	0.860	60.7±19.1	61.8±19.1	0.771

BMI: body mass index, ESS: Epworth sleepiness scale, ACE-I: angiotensin-converting enzyme inhibitor, ARB: angiotensin II receptor blocker, eGFR: estimated glomerular filtration rate

The values are presented as the mean±s.d.

Table 3. Sleep and Blood Pressure Data.

ABPM		Younger group				Older group			
Period	Blood pressure (mmHg)	All patients (n=163)	D pattern (n=85)	ND pattern (n=78)	p value	All patients (n=101)	D pattern (n=39)	ND pattern (n=62)	p value
24-h	Systole	133±11	132±11	135±12	0.105	134±12	133±11	134±13	0.457
	Diastole	88±9	87±9	89±9	0.071	82±9	82±9	82±9	0.817
Awake	Systole	138±11	138±11	137±12	0.359	137±13	140±11	136±13	0.118
	Diastole	91±9	91±9	91±9	0.929	84±9	87±9	83±9	0.057
Sleep	Systole	123±14	117±11	130±12	<0.001	127±14	118±12	130±13	<0.001
	Diastole	81±10	77±9	85±9	<0.001	77±10	73±10	79±10	<0.001
Dipping status (%)		11.0±7	15.7±4.5	4.9±4.6	<0.010	7.3±8	14.6±3.3	2.7±5.5	<0.001

Polysmonography	All patients	D pattern	ND pattern	p value	All patients	D pattern	ND pattern	p value
AHI (/h)	55.7±17.3	53.7±16.9	58.0±17.6	0.110	51.5±17.2	48.1±15.1	53.7±18.2	0.115
AI (/h)	30.3±23.2	30.1±22.5	30.6±24.0	0.875	24.2±16.2	23.7±16.6	24.5±16.1	0.806
OA (/h)	27.5±22.5	26.9±22.1	28.2±23.1	0.715	18.8±15.6	18.4±17.0	19.1±14.8	0.831
CA (/h)	1.1±1.9	1.3±2.3	0.8±1.2	0.628	3.1±5.9	2.7±4.8	3.3±6.6	0.626
CT90% (%)	15.6±19.3	11.4±12.5	20.1±24.0	0.004	10.9±14.2	8.8±12.1	12.3±15.4	0.230
Lowest oxygen saturation (%)	73.7±8.6	74.9±11.0	72.3±8.7	0.058	76.0±9.2	76.6±10.0	75.5±8.7	0.572
SWS (%)	10.3±8.8	9.5±7.9	11.1±9.7	0.237	11.2±8.5	13.7±8.9	9.6±7.8	0.017
Arousal index (/h)	50.4±20.2	49.4±19.8	51.1±20.8	0.636	46.9±19.3	43.9±14.3	48.7±21.8	0.217

ABPM: ambulatory blood pressure monitoring, AHI: apnea-hypopnea index, AI: apnea index, OA: obstructive apnea, CA: central apnea, ODI: oxygen desaturation index, CT90%: cumulative percentages of time at saturation below 90%, SWS: slow wave sleep

The values are presented as the mean±s.d.

cant relationship between the occurrence of the ND pattern, the BMI and the CT90% in the Younger group and between the use of ACE-I/ARB and SWS in the Older group. The multivariate analysis demonstrated that CT90% was the only independent risk factor in the Younger group [odds ratio, 1.022; 95% confidence interval (CI), 1.001-1.044; p=0.035];

Table 4. Results of Logistic Regression Analyses to Determine Factors Affecting the Non-dipping Blood Pressure Pattern.

Younger group	ND pattern			Younger group	ND pattern		
Univariate analysis	Odds ratio	95%CI	p value	Multiple analysis	Odds ratio	95% CI	p value
BMI (kg/m²)	1.065	1.008-1.131	0.024	BMI	1.033	0.969-1.104	0.318
CT90% (%)	1.026	1.008-1.047	0.004	CT90%	1.022	1.001-1.044	0.035

Older group	ND pattern			Older group	ND pattern		
Univariate analysis	Odds ratio	95%CI	p value	Multiple analysis	Odds ratio	95%CI	p value
ACE-I/ARB (0=no, 1=yes)	2.570	1.075-6.576	0.034	ACE-I/ARB	2.589	1.051-6.848	0.039
SWS (%)	0.943	0.895-0.990	0.017	SWS	0.941	0.891-0.990	0.019

95% CI: 95% confidence interval, BMI: body mass index, CT90%: cumulative percentages of time at saturation below 90%, ACE-I: angiotensin-converting enzyme inhibitor, ARB: angiotensin II receptor blocker, SWS: slow wave sleep

whereas SWS (odds ratio, 0.941; 95% CI, 0.891-0.990; p=0.019) and the use of ACE-I or ARB (odds ratio, 2.589; 95% CI, 1.051-6.848; p=0.039) were risk factors in the Older group.

Discussion

OSA is a known cause of nocturnal hypertension and a non-dipper or riser pattern (1-3). To our knowledge, only a handful of study reports have discussed the factors determining nocturnal BP fluctuation patterns in patients with OSA (16). Analyzing the factors affecting nocturnal BP fluctuation patterns and providing appropriate therapeutic intervention will probably improve nocturnal BP fluctuation and prevent subsequent organ damage in patients with OSA. Several epidemiological studies have reported that the factors of OSA associated with the onset of hypertension vary among age groups (7, 17). Therefore, in the present study, we divided OSA patients into two groups (patients <60 and ≥60 years of age) and then divided those two groups into two subgroups among patients in whom the mean 24-hour BP was nearly equal (no significant differences observed in the mean value) but the nocturnal BP fluctuation patterns were different (D pattern vs. ND pattern). We then analyzed the factors influencing nocturnal BP dipping patterns. In particular, we selected those patients with severe OSA to clarify the possible influence of OSA.

Differences between young and old OSA patients

The BMI and the degree of sleepiness were greater in the Younger group than in the Older group even though the 24-hour SBP and AHI were similar (Table 1). Significant differences were found in the morbidity of cardiovascular diseases, diabetes mellitus and renal dysfunction and in the use of antihypertensive agents. These findings are often seen in older SDB patients in the clinical setting (18). In the younger generation, OSA is considered an independent factor for developing hypertension. However, some reports have suggested that OSA may independently trigger hypertension in individuals ≥60 years of age (7, 17). The possible reasons behind this difference are as follows: 1) the factors associated with the onset of OSA vary by age; and 2) the influence of OSA on human bodies also differs by age (7). There are some factors associated with the onset of OSA due to age, such as the degree of obesity, the structure and function of the upper respiratory tract and the respiratory control function (7). In general, older patients with OSA tend to have less obesity and a lower prevalence of hypoxemia than younger patients, even if their AHIs are similar (19). Indeed, the patient background in the present study showed that the older patients with severe OSA tended to have less obesity and lower oxygen desaturation (CT90% and lowest oxygen saturation) than the younger patients with severe OSA.

Factors associated with the non-dipper pattern in severe OSA patients

- **Younger group**

Our multivariate analysis demonstrated that CT90% was the only independent factor determining the non-dipper and riser patterns (ND group). Previous studies on OSA patients have shown that CT90% was associated with the onset of left ventricular hypertrophy (20) and CT90%, a parameter of SDB, was the only factor associated with brain natriuretic peptide in patients with chronic heart failure (21). Other studies have also reported that OSA patients with a higher degree of obesity had a higher level of oxygen desaturation (22, 23). Similarly, a correlation was confirmed between the BMI and CT90% in the present study (Younger group, R=0.502 and p<0.001; Older group, R=0.513 and p<0.001). OSA causes negative intrathoracic pressure, hypersensitivity of the carotid body chemoreflex, hypoxemia and microarousal; these changes induced OSA-related nocturnal hypertension (24). Accordingly, younger OSA patients who tend to have a higher degree of obesity (higher BMI) may be affected more profoundly by oxygen desaturation due to OSA than older OSA patients. The data obtained from the Younger group suggested that the depth and length of oxygen desaturation, represented by CT90%, might trigger a fall in nocturnal BP and lower nocturnal BP variability.

• **Older group**

The rate of SWS is an independent factor influencing the ND pattern. During non-rapid eye movement (NREM) sleep, sympathetic nervous activity decreases, BP declines, and BP drops as the sleep stages deepen (25). The results of a multivariate analysis in the present study showed that a decrease in the rate of SWS during NREM sleep was an independent trigger of the ND pattern. In one study conducted in healthy subjects, the deprivation of SWS resulted in a lesser extent of nocturnal reduction (26). Decreased SWS might influence nocturnal BP fluctuations. In patients ≥65 years of age, decreased SWS was identified as a predictor for the onset of hypertension during the average follow-up period of 3.4 years (27). The results of our study also support those of the earlier studies and suggest that a reduction in SWS may affect nocturnal BP fluctuations in older OSA patients.

The use of ACE-I or ARB was an independent risk factor in the occurrence of the ND pattern. In the present study, many older patients received ACE-I/ARB; of these, some additionally took other antihypertensive agents. These antihypertensive effects might have persisted in the daytime and ceased at night. Consequently, the 24-hour BP and awake BP in these OSA patients using ACE-I/ARB were relatively well-controlled, whereas the sleep BP was not well-controlled (28).

Clinical implications of the results of this study

In severe OSA patients, the impact of OSA on the nocturnal BP fluctuation may differ by age. That is, even if the severity of OSA based on AHI is similar between younger and older patients, the degree of obesity and the level of hypoxemia differ between the two groups. This difference affects the nocturnal BP in OSA differently.

In clinical practice, continuous positive airway pressure (CPAP) therapy should be actively promoted in younger patients with severe OSA in order to improve desaturation caused by OSA. CPAP therapy improves the nocturnal BP fluctuation patterns and eventually contributes to the prevention of cardiovascular disease. However, whether or not OSA is a trigger for reducing SWS and shortening the duration of SWS in older OSA patients with an ND pattern remains unclear. Physiologically, SWS is known to decrease by age (29); however, one study indicated that CPAP therapy increased SWS (30). Accordingly, CPAP therapy should be considered as a therapeutic option for older patients with severe OSA.

Study limitations

This study was a small, retrospective, single-center and cross-sectional. As such, a prospective study is needed. The disease duration of OSA was not considered in this study. The prognosis of the patients in this study was not investigated. ABPM has poor reproducibility, so whether or not ABPM data accurately reflect the original BP is debatable (31).

The authors state that they have no Conflict of Interest (COI).

References

1. Kario K. Obstructive sleep apnea syndrome and hypertension: ambulatory blood pressure. Hypertens Res **32**: 428-432, 2009.
2. Sekizuka H, Kida K, Akashi YJ, et al. Relationship between sleep apnea syndrome and sleep blood pressure in patients without hypertension. J Cardiol **55**: 92-98, 2010.
3. Sekizuka H, Osada N, Kida K, Yoneyama K, Eguchi Y, Miyake F. Relationship between chronic kidney disease and sleep blood pressure in patients with sleep apnea syndrome. Hypertens Res **33**: 1278-1282, 2010.
4. Kario K, Pickering TG, Matsuo T, Hoshide S, Schwartz JE, Shimada K. Stroke prognosis and abnormal nocturnal blood pressure falls in older hypertensives. Hypertension **38**: 852-857, 2001.
5. Ohkubo T, Hozawa A, Yamaguchi J, et al. Prognostic significance of the nocturnal decline in blood pressure in individuals with and without high 24-h blood pressure: the Ohasama study. J Hypertens **20**: 2183-2189, 2002.
6. John MW. A new method for measuring daytime sleepiness: the Epworth sleepiness scale. Sleep **14**: 540-545, 1991.
7. Haas DC, Foster GL, Nieto FJ, et al. Age-dependent associations between sleep-disordered breathing and hypertension: importance of discriminating between systolic/diastolic hypertension and isolated systolic hypertension in the Sleep Heart Health Study. Circulation **11**: 614-621, 2005.
8. Matsuo S, Imai E, Horio M, et al. Revised equations for estimated GFR from serum creatinine in Japan. Am J Kidney Dis **53**: 932-935, 2009.
9. Chesson AL Jr, Berry RB, Pack A. Practice parameters for the use of portable monitoring devices in the investigation of suspected obstructive sleep apnea in adults. Sleep **26**: 907-913, 2003.
10. Flemons WW, Littner MR, Rowley JA, et al. Home diagnosis of sleep apnea: a systematic review of the literature. Chest **124**: 1543-1579, 2003.
11. Rechtschaffen A, Kales A. Manual of standardized technology, techniques and scoring system for sleep stage of human subjects. Brain Information Service, Brain Research Institute, UCLA, Los Angeles, 1968.
12. American Academy of Sleep Medicine Task Force. Sleep-related breathing disorders in adults: recommendations for syndrome definition and measurement techniques in clinical research. Sleep **22**: 667-689, 1999.
13. Kario K, Pickering TG, Umeda Y, et al. Morning surge in blood pressure as a predictor of silent and clinical cerebrovascular disease in elderly hypertensives: a prospective study. Circulation **107**: 1401-1406, 2003.
14. Shimamoto K, Ando K, Fujita T, et al. The Japanese Society of Hypertension Guidelines for the Management of Hypertension (JSH 2014). Hypertens Res **37**: 253-392, 2014.
15. Hoshide S, Kario K, Hoshide Y, et al. Associations between nondipping of nocturnal blood pressure decrease and cardiovascular target organ damage in strictly selected community-dwelling normotensives. Am J Hypertens **16**: 434-438, 2003.
16. Sasaki N, Ozono R, Yamanchi R, et al. Age-related differences in the mechanism of nondipping among patients with obstructive sleep apnea syndrome. Clin Exp Hypertens **34**: 270-277, 2012.
17. Nieto FJ, Young TB, Lind BK, et al. Association of sleep-disordered breathing, sleep apnea, and hypertension in a large community-based study. Sleep Heart Health Study. JAMA **283**: 1829-1836, 2000.
18. Teramoto S, Inoue Y, Ouchi Y. Clinical significance of geriatric sleep apnea syndrome. Geriatr Gerontol Int **2**: 163-171, 2002.
19. Bixler EO, Vgontzas AN, Ten Have T, Tyson K, Kales A. Effects of age on sleep apnea in men: I. Prevalence and severity. Am J

Respir Crit Care Med **157**: 144-148, 1998.

20. Chami HA, Devereux RB, Gottdiener JS, et al. Left ventricular morphology and systolic function in sleepdisordered breathing: the Sleep Heart Health Study. Circulation **117**: 2599-2607, 2008.
21. Gottlieb JD, Schwartz AR, Marshall J, et al. Hypoxia, not the frequency of sleep apnea, induces acute hemodynamic stress in patients with chronic heart failure. J Am Coll Cardiol **54**: 1706-1712, 2009.
22. Ernst G, Bosio M, Salvado A, Dibur E, Nigro C, Borsini E. Difference between apnea-hypopnea index (AHI) and oxygen desaturation index (ODI): proportional increase associated with degree of obesity. Sleep Breath **20**: 1175-1183, 2016.
23. Kendzerska T, Leung RS, Gershon AS, Tomlinson G, Ayas N. The interaction of obesity and nocturnal hypoxemia on cardiovascular consequences in adults with suspected obstructive sleep apnea. A historical observational study. Ann Am Thorac Soc **13**: 2234-2241, 2016.
24. Kario K. Obstructive sleep apnea syndrome and hypertension: mechanism of the linkage and 24-h blood pressure control. Hypertens Res **32**: 537-541, 2009.
25. Snyder F, Hobson JA, Morrison DF, Goldfrank F. Changes in respiration heart rate and systolic blood pressure in human sleep. J Appl Physiol **19**: 417-422, 1964.
26. Sayk F, Teckentrup C, Becker C, et al. Effects of selective slow-wave sleep deprivation on nocturnal blood pressure dipping and daytime blood pressure regulation. Am J Physiol Regul Integr Comp Physiol **298**: R191-R197, 2010.
27. Fung MM, Peters K, Redline S, et al. Decreased slow wave sleep increases risk of developing hypertension in elderly men.; Osteoporotic Fractures in Men Research Group. Hypertension **58**: 596-603, 2011.
28. Peltari LH, Hietanen EK, Salo TT, Kataja MJ, Kantola IM. Little effect of ordinary antihypertensive therapyon nocturnal high blood pressure in patients with sleep disordered breathing. Am J Hypertens **11**: 272-279, 1998.
29. Wolkove N, Elkholy O, Baltzan M, Palayew M. Sleep and aging: 1. Sleep disorders commonly found in older people. CMAJ **176**: 1299-1304, 2007.
30. Heinzer R, Gaudreau H, Décary A, et al. Slow-wave activity in sleep apnea patients before and after continuous positive airway pressure treatment: contribution to daytime sleepiness. Chest **119**: 1807-1813, 2001.
31. Mochizuki Y, Okutani M, Donfeng Y, et al. Limited reproducibility of circadian variation in blood pressure dippers and non-dippers. Am J Hypertens **11**: 403-409, 1998.

The Internal Medicine is an Open Access article distributed under the Creative Commons Attribution-NonCommercial-NoDerivatives 4.0 International License. To view the details of this license, please visit (https://creativecommons.org/licenses/by-nc-nd/4.0/).

© 2018 The Japanese Society of Internal Medicine

JACC: CARDIOVASCULAR INTERVENTIONS
© 2018 BY THE AMERICAN COLLEGE OF CARDIOLOGY FOUNDATION
PUBLISHED BY ELSEVIER

VOL. 11, NO. 12, 2018

IMAGES IN INTERVENTION

Transcatheter Mitral Annuloplasty in Barlow's Mitral Regurgitation With Deep Cleft

Shingo Kuwata, MD, PhD, Michel Zuber, MD, Fabian Nietlispach, MD, PhD, Maurizio Taramasso, MD, PhD, Francesco Maisano, MD

Barlow's valve is a clinically important etiology of degenerative mitral regurgitation (MR). In addition, abnormal, deep, cleft-like indentations make mitral valve (MV) repair much more complex (1).

An 80-year-old woman (EuroSCORE II 4.05%, STS score 5.6%) was admitted due to heart failure 10 months before. Two- and 3-dimensional transesophageal echocardiography revealed severe MR (**Figure 1A**) (effective regurgitant orifice area 0.7 cm^2) due to bileaflet prolapse with dilated annulus (**Figure 1B**) and a deep, cleft-like indentation in the P2 segment of the posterior leaflet (**Figure 1C**) without significant trans-MV mean pressure gradient (1 mm Hg) (Online Video 1). The patient was considered eligible for transcatheter MV annuloplasty using a Cardioband (Edwards Lifesciences, Irvine, California). The anchors were implanted from the anterolateral commissure,

FIGURE 1 Pathophysiology of MR

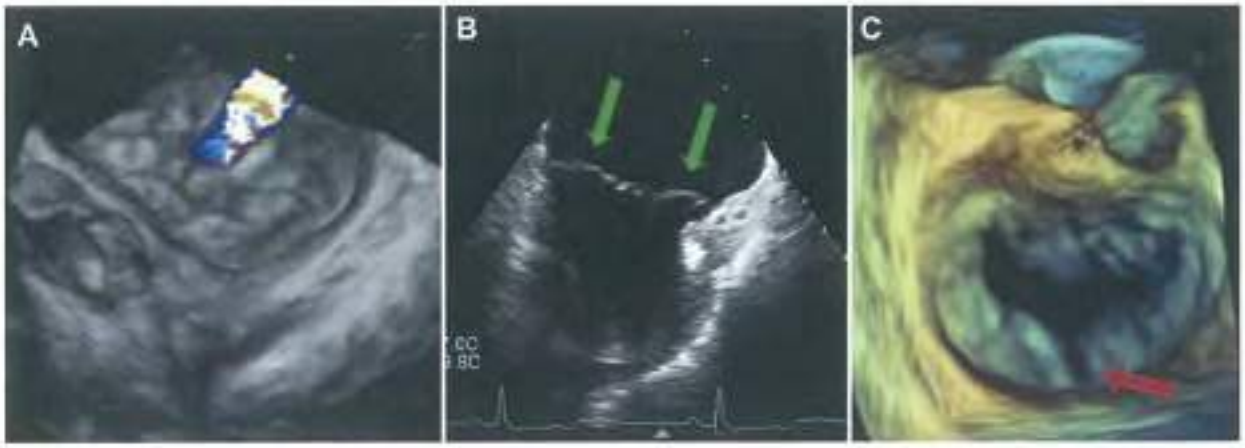

Severe mitral regurgitation (MR) **(A)** was due to bileaflet prolapse with dilated annulus **(green arrows in B)** and a deep, cleft-like indentation in the P2 segment of the posterior leaflet **(red arrow in C)** assessed by transesophageal echocardiography (Online Video 1).

From the University Heart Center Zurich, University Hospital Zurich, Zurich, Switzerland. Dr. Nietlispach is a consultant for Abbott, Medtronic, and Edwards Lifesciences. Dr. Taramasso is a consultant for Abbott Vascular and 4Tech. Dr. Maisano is a consultant for Edwards Lifesciences and Valtech Cardio; and receives royalties from Edwards Lifesciences. All other authors have reported that they have no relationships relevant to the contents of this paper to disclose.

Manuscript received November 30, 2017; revised manuscript received December 18, 2017, accepted January 2, 2018.

ISSN 1936-8798/$36.00

https://doi.org/10.1016/j.jcin.2018.01.229

JACC: CARDIOVASCULAR INTERVENTIONS VOL. 11, NO. 12, 2018
JUNE 25, 2018:e87–8

FIGURE 2 Cardioband Implantation

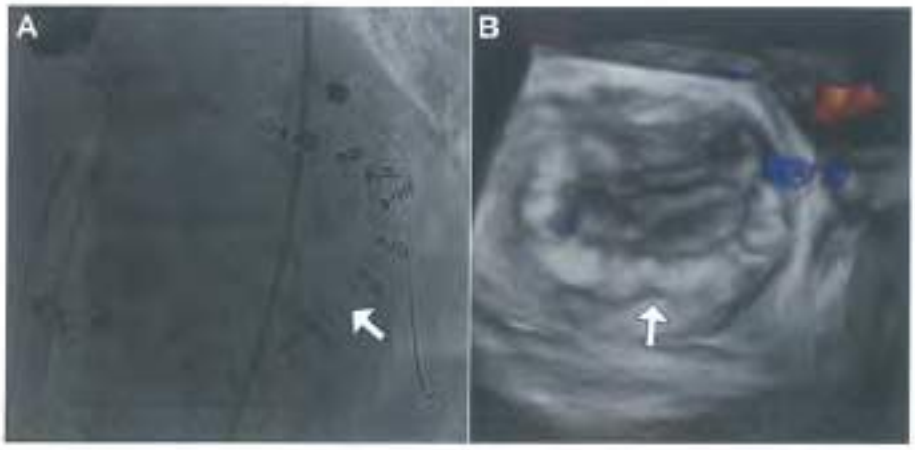

(A) Fluoroscopic image. (B) 3-dimensional transesophageal echocardiographic image. An anchor at the point of the cleft was skipped to deploy the device (**white arrows**) (Online Video 2).

through the posterior annulus, to the posteromedial commissure (**Figure 2A**). The Dacron band was then adjusted with cinching to 4.5 cm. With annular size reduction from 9.1 cm^2 to 4.5 cm^2, bileaflet prolapse was corrected, and MR disappeared (**Figure 2B**) without a significant trans-MV mean pressure gradient (1 mm Hg). In addition, with better coaptation, the deep cleft was closed after the procedure as well (Online Video 2). The solution to the larger difference between the 2 anchors beside the cleft was to close the gap with cinching (**Figure 2**).

Barlow's disease can be treated by surgical mitral annuloplasty (2). Transcatheter direct annuloplasty may be an ideal alternative option to treat Barlow's MR with additional abnormal, deep, cleft-like indentations.

ADDRESS FOR CORRESPONDENCE: Dr. Shingo Kuwata, University Heart Center Zurich, Rämistrasse 100, CH-8091 Zürich, Switzerland. E-mail: shingo.k.571019@gmail.com.

REFERENCES

1. Taramasso M, Maisano F. Challenging mitral clefts with MitraClip: the convergent clips strategy. EuroIntervention 2016;13:e1071.

2. De Paulis R, Maselli D, Salica A, et al. Mitral repair with the sole use of a semi-rigid band in a sub-population of patients with Barlow's disease: a 4-year follow-up with stress echocardiography. Interact Cardiovasc Thorac Surg 2015;21:316–21.

KEY WORDS annuloplasty, cardioband, degenerative MR, transcatheter mitral valve repair

APPENDIX For supplemental videos, please see the online version of this paper.

Journal of Human Hypertension (2018) 32:432–439
https://doi.org/10.1038/s41371-018-0060-3

ARTICLE

Maximum home blood pressure readings are associated with left atrial diameter in essential hypertensives

Toshiki Kaihara[1,2] · Yuki Imaizumi[2] · Kazuo Eguchi[2] · Kazuomi Kario[2]

Received: 29 November 2017 / Revised: 27 February 2018 / Accepted: 5 March 2018 / Published online: 1 May 2018
© Macmillan Publishers Limited, part of Springer Nature 2018

Abstract

We tested the hypothesis that the maximum value of home systolic BP (MSBP) is a marker of hypertensive target organ damage (TOD). We conducted a cross-sectional study of 220 hypertensives. The subjects performed HBP monitoring using a telemonitoring system and measured their HBP for 7 days. Mean, maximum, standard deviation, and coefficient of variation of SBPs were used as independent variables. Brachial–ankle pulse wave velocity, left ventricular mass index (LVMI), mean carotid intima–media thickness, and left atrial diameter index (LADI) were used as dependent variables. Mean and maximum SBPs were significantly associated with each TOD marker. MSBP showed a significantly stronger association with LADI compared to mean SBP ($p = 0.0012$) and a significant relationship with LADI independent of LVMI ($p = 0.024$). Our findings suggest that MSBP is associated with TOD measures, similar to mean SBP. These results may indicate that MSBP could be a target of intervention for patients with atrial fibrillation.

Introduction

The self-monitoring of home blood pressure (HBP) has become one of the standard methods of BP monitoring. The examination of HBP is useful for the diagnosis of hypertension, especially of white-coat hypertension or masked hypertension [1]. HBP data are also useful when evaluating the efficacy of antihypertensive medications [2]. Although HBP monitoring is known to be a valuable method, it has been shown that patients' logbooks of their HBP readings can include "under-reporting" (deleting a BP record as extremely high BP) and "phantom records" (writing false records) [3]. By contrast, an HBP telemonitoring system [4], with which all of a patient's HBP readings are recorded and automatically transmitted to a physician's PC via a cell-phone network, has been shown to be useful and accurate. With such a system, patients' remarkably high or low home systolic BP readings are recorded and not missed.

The clinical significance of day-to-day variability in HBP (HBPV) has been established [5]. Day-to-day HBPV is evaluated by determining the variation of day-to-day home systolic blood pressure (SBP) values using the standard deviation (SD) [6], coefficient of variation (CV) of HBP [7], or variation independent of the mean (VIM) [8]. We have also made an attempt to evaluate day-to-day HBPV by analyzing single maximum HBP readings [9]. HBPV has been reported to be associated with target organ damage (TOD) [9, 10] and cardiovascular prognoses [5, 11]. However, the application of HBPV to clinical practice has not yet been established. It is also not clear whether maximum home BP readings are a clinically significant phenomenon or just noise [9].

A patient's left atrial diameter (LAD) can be used as one of the markers of TOD. Left atrial (LA) dilatation is also one of the risks of atrial fibrillation (AF) and a marker of dilatation disorder. LAD reflects the duration and severity of elevated left atrial pressure [12], and dilatation of LAD is an early stage of arterial hypertension [13]. Thus, the early detection and treatment of LA dilatation are extremely important.

The left atrium is directly influenced by the left ventricle (LV) filling pressure, and the relationship between LA

Electronic supplementary material The online version of this article (https://doi.org/10.1038/s41371-018-0060-3) contains supplementary material, which is available to authorized users.

✉ Toshiki Kaihara
m030146k@jichi.ac.jp

1 Department of Cardiology, Tokyo Metropolitan Hiroo Hospital, Tokyo, Japan

2 Division of Cardiovascular Medicine, Department of Medicine, Jichi Medical University School of Medicine, Tochigi, Japan

dilatation and increased LV-filling pressure has been described in individuals without mitral valve disease [14]. In 4403 Framingham Offspring Study participants (among whom those with AF were excluded), higher BP was shown to be one of the risk factors for LA enlargement [15]. It was also reported that the relationship between BPV and LA enlargement seemed to be significant after controlling the direct effect of BP itself [16]. Although BPV, one of the BP components, is an important factor for LA enlargement, there are few reports about the correlation between home BPV and LA enlargement. In the present study, we tested the hypothesis that HBPV—especially maximum home SBP—is associated with LA enlargement.

Study population and methods

Study population and study design

Between October 2015 and January 2017, 220 subjects were enrolled from among the populations of Shikine-jima Island, Niijima-mura, Tokyo prefecture, and Kotake Town, Fukuoka prefecture, Japan in the Real-BP study, which is ongoing. The Real-BP study was a prospective, multicenter, cross-sectional study. The protocol of the study has been registered on the University Hospital Medical Information Network Clinical Trials Registry (UMIN-CTR) website under the trial no. UMIN000019582.

All subjects over 20 years of age who had hypertension or suspected hypertension were recruited in the Real-BP study. Hypertension is defined as office SBP >140 mmHg or office diastolic BP (DBP) >90 mmHg, or treated hypertension. The exclusion criteria in the Real-BP study were (1) residents of places other than the above-mentioned regions; (2) those with secondary hypertension; (3) patients with ischemic heart disease, stroke, aortic dissection, chronic artery obstruction, or heart failure with hospitalization <6 months prior to enrollment; (4) individuals undergoing hemodialysis treatment; (5) those with AF and multiple ventricular contraction; and (6) individuals who were physically unable to walk unassisted, measure their HBP, or fill out a questionnaire. We defined chronic kidney disease (CKD) as the estimated glomerular filtration rate <60 mL/min/1.73 m^2. The institutional review board of Jichi Medical University School of Medicine approved this study (Clinical category #15-008), and written informed consent was obtained from all subjects of the present study.

One subject was excluded from the present study because a medical history of AF was revealed after enrollment. Thus, a total of 219 subjects completed the study protocol.

Measurements

Home BP

Self-measured HBP readings were obtained by each subject with the use of a validated upper-arm cuff oscillometric device (HEM-7252G-HP; Omron Healthcare, Kyoto, Japan) [17]. The HEM-7252G-HP receives the subject's acquired physiological data (SBP, DBP, and pulse rate) wirelessly and transmits the values immediately to the central web server via a 3G network. We were thus able to check the data of each subject in real time.

The subjects measured their HBP consecutively three times at approximately 15-s intervals in the morning and evening. They measured their HBP while seated within 1 h. After waking up (after urination and breakfast, and before taking medicine) in the morning, they measured their HBP while seated before going to bed in the evening after resting for 1–2 min, following the Japanese Society of Hypertension (JSH) guidelines [18]. Thus, three HBP readings were taken at 15-s intervals in a sitting position, both in the morning and evening for 7 consecutive days. As the measures of home BP variability, we defined the highest SBP value during the 7-day period as the "maximum home SBP" and also calculated the mean, SD, and CV of the SBP (42 values of SBP for 7 days). These were used as independent variables.

Ultrasonography

Echocardiography and carotid ultrasonography were performed at each institution (Nemio XG SSA-580A®, Toshiba, Tokyo [at the Niijima-mura National Health Insurance Shikine-jima Clinic]; Hi VISION Preirus®, Hitachi, Tokyo [at Kotake Town Hospital]). The two-dimensional M-mode or B-mode image was recorded with the ultrasound machine, following the guidelines of the American Society of Echocardiography (ASE) [19]. Left ventricular mass (LVM) (g) was calculated with the formula validated by the ASE: LVM $= 0.8 \times (1.04 \times ([\text{LVEDD} + \text{PWTD} + \text{IVSTD}]^3 - [\text{LVEDD}]^3)) + 0.6$, in which IVSTD (mm) is the interventricular septum thickness in diastole, LVEDD (mm) is the LV end-diastolic diameter, and PWTD (mm) is the posterior wall thickness in diastole. Left ventricular mass index (LVMI) (g/m^2) was calculated as LVM (g)/body surface area (BSA) (m^2) [20]. LAD (mm) was also checked, and LAD index (LADI) (mm/m^2) was defined as LAD (mm)/BSA (m^2) [21]. The carotid intima–media thickness (CIMT) (cm) was calculated by carotid ultrasonography. The CIMT was measured at the bulbus and at 1 cm and 2 cm proximal to the bulbus. We calculated the mean of these three CIMT values. All of these parameters were measured within 7 days during the study period.

Brachial–ankle pulse wave velocity

The brachial–ankle pulse wave velocity (baPWV) can be used as a predictor of cardiovascular events and is a validated marker of cardiovascular disease [22]. It is also an independent predictor of the risk of cardiovascular diseases in Japanese [23]. In the present study's subjects, the baPWV (cm/s) was measured by a volume-plethysmographic device with four cuffs fitted with oscillometric sensors (Form BP-203RPE*; Omron Colin, Tokyo). It was measured within 7 days during the study period.

Outcomes

The primary outcome was the determination of whether maximum home SBP could be one of the markers of TOD, as mean home SBP is. The secondary outcome was the relationship between day-to-day HBPV and the markers of TOD.

Statistical analysis

All statistical analyses were carried out with SPSS/Windows, ver. 19.0 (SPSS, Chicago, IL). Data are presented as the mean (±SD) or as percentages. The χ^2 test was used to calculate proportions. A two-tailed $p < 0.05$ was considered significant. Pearson's correlation for parametric and Spearman's correlation for nonparametric data were used to analyze the relationship between maximum, mean, SD, and CV of HBP and the TOD parameters. The performance of the predictive measures was assessed by the area under the receiver-operating characteristic curve (ROC).

Results

The characteristics of the subjects in this study are summarized in Table 1. Among the 219 subjects, 84% were hypertensive; 59% were treated with a calcium-channel blocker; 64% were treated with a renin–angiotensin system (RAS) inhibitor; 4% were treated with a beta-blocker; and 13% were treated with diuretics.

Relationships between maximum home SBP and TOD markers

The relationships between maximum home SBP and TOD markers (i.e., baPWV, LVMI, CIMT, and LADI) are illustrated in Fig. 1. Significant correlations were revealed between maximum home SBP and all of the following TOD markers: baPWV ($r = 0.34$, $p < 0.001$), LVMI ($r = 0.32$, $p < 0.001$), CIMT ($r = 0.23$, $p < 0.001$), and LADI ($r = 0.26$, $p < 0.001$). A multiple linear-regression analysis adjusted for patient age, sex, smoking, dyslipidemia, diabetes mellitus (DM), and body mass index (BMI) demonstrated significant associations between maximum home SBP and baPWV ($\beta = 0.21$, $p < 0.001$), LVMI ($\beta = 0.23$, $p < 0.001$), CIMT ($\beta = 0.19$, $p = 0.003$), and LADI ($\beta = 0.23$, $p < 0.001$) (Table 2).

Table 1 Baseline characteristics of the 219 subjects

Age, yrs	70
Male sex, no. (%)	123 (56)
BMI, kg/m^2	23.5
Hypertension, %	84
Duration of hypertension, yrs	11
Current smoking, %	16
Habitual drinking, %	43
Dyslipidemia, %	72
Chronic kidney disease, %	35
Diabetes mellitus, %	40
Calcium-channel blockers, %	59
RAS inhibitors[a], %	64
Beta-blockers, %	4
Diuretics, %	13

Values are expressed as the mean number (percentage) unless otherwise indicated

BMI body mass index

[a] RAS inhibitors: either angiotensin-converting enzyme or angiotensin-II receptor blockers

Relationships between mean home SBP and TOD markers

The relationships between mean home SBP and TOD markers baPWV, LVMI, CIMT, and LADI are illustrated in Fig. 2. Significant correlations were shown between mean home SBP and all four TOD markers: baPWV ($r = 0.31$, $p < 0.001$), LVMI ($r = 0.35$, $p < 0.001$), CIMT ($r = 0.22$, $p = 0.001$), and LADI ($r = 0.19$, $p = 0.005$). In the multiple linear-regression analyses adjusted for the same covariates as those listed above, significant associations were revealed between mean home SBP and all four TOD markers: baPWV ($\beta = 0.23$, $p < 0.001$), LVMI ($\beta = 0.24$, $p < 0.001$), CIMT ($\beta = 0.23$, $p < 0.001$), and LADI ($\beta = 0.16$, $p = 0.012$) (Table 2). The relationships between the SD and the CV of home SBP and the four TOD markers, respectively, are also shown in Table 2.

Correlation between maximum home SBP and LADI

By Z-test, the extent of the correlations between maximum home SBP and three of the TOD measures (baPWV, CIMT, and LVMI) and between mean home SBP and TOD

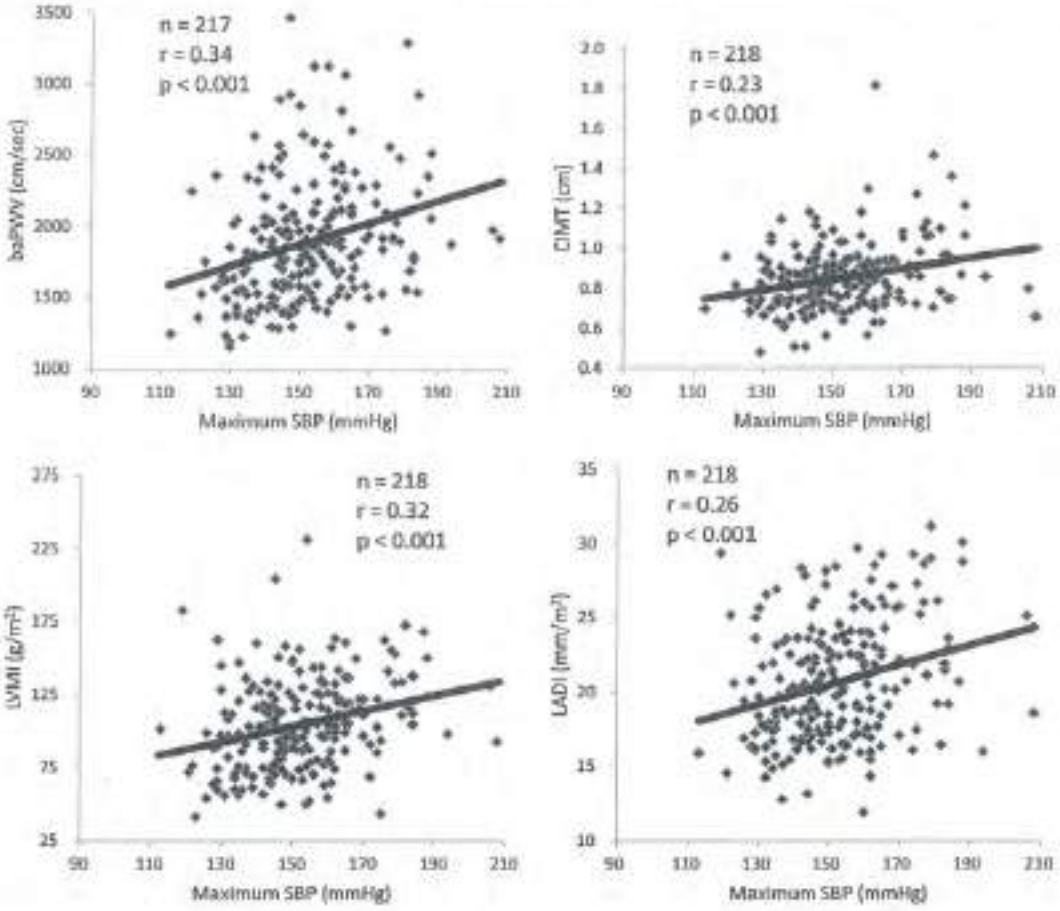

Fig. 1 Relationship of maximum home SBP and TOD markers. SBP systolic blood pressure, TOD tissue organ damage, baPWV brachial–ankle pulse wave velocity, LVMI left ventricular mass index, CIMT carotid intima–media thickness, LADI left atrial diameter index

measures was not significantly different ($p = 0.31$ in baPWV, $p = 0.67$ in CIMT, and $p = 0.31$ in LVMI). However, regarding LADI, the association between maximum home SBP and LADI was significantly stronger than that between mean home SBP and LADI ($p = 0.024$).

We then performed a multiple linear-regression analysis examining maximum, mean, SD, and CV of home SBP and three TOD measures (baPWV, CIMT, and LADI) adjusted for age, sex, smoking, dyslipidemia, DM, BMI, and LVMI. The results show that there are also significant associations between maximum home SBP and baPWV ($\beta = 0.21$, $p < 0.001$), CIMT ($\beta = 0.13$, $p = 0.04$), and LADI ($\beta = 0.14$, $p = 0.024$), and between mean home SBP and baPWV ($\beta = 0.23$, $p < 0.001$) and CIMT ($\beta = 0.17$, $p = 0.008$). However, there was no significant association between mean home SBP and LADI ($\beta = 0.06$, $p = 0.302$) (Table 3). The relationships between the SD and CV of home SBP and the TOD markers are also shown in Table 3. Furthermore, we analyzed subjects without CKD. The results were almost similar with the above results, and it is possible to show that the presence or absence of CKD does not alter the whole results (supplementary Table 1, 2).

Finally, we explored whether maximum home SBP could be a surrogate measure of LA dilatation. Based on a previous study, LA dilatation was defined as LADI > 24 mm/m^2 [19]. The area under the curve (AUC) was 0.62 ($p = 0.008$), and the cutoff maximum home SBP was 155.5 mmHg by the Youden index (Fig. 3). Other TOD parameters were also shown in ROC curve analyses in supplementary Table 3. Thresholds of high baPWV, LVMI, and CIMT were defined as 1800 m/s [24], 115 g/m^2 [19], and 1.0 mm [25].

Discussion

Our analyses demonstrated that exaggerated HBPV—especially maximum home SBP—is significantly associated

Table 2 Relationships among maximum, mean, SD, and CV of home SBP and TOD measures in the multivariate analysis[a]

TOD measures	Maximum home SBP		Mean home SBP		SD of home SBP		CV of home SBP	
	β	p	β	p	β	p	β	p
baPWV	0.21	<0.001	0.23	<0.001	0.12	0.04	0.05	0.414
LVMI	0.23	<0.001	0.24	<0.001	0.18	0.007	0.11	0.094
CIMT	0.19	0.003	0.23	<0.001	0.03	0.693	−0.04	0.555
LADI	0.23	<0.001[b]	0.16	0.012	0.21	0.002	0.16	0.013

All TOD measures were analyzed one by one

SD standard deviation, *CV* coefficient of variation, *SBP* systolic blood pressure, *baPWV* brachial–ankle pulse wave velocity, *LVMI* left ventricular mass index, *CIMT* carotid intima–media thickness, *LADI* left atrial diameter index, *TOD* target organ damage, *BMI* body mass index

[a] Multiple-regression analysis adjusting for age, sex, smoking, dyslipidemia, diabetes mellitus, and BMI was performed

[b] $p = 0.024$ vs. mean SBP by Z-test ($n = 218$)

with LA dilatation. This study highlights the pathophysiological role of home BPV in cardiovascular damage, which deserves further discussion.

Relationships between maximum systolic HBP and TOD markers

Our findings revealed that increased maximum home SBP is correlated with increased baPWV, LVMI, CIMT, and LADI. The extent of the correlations between maximum home SBP and TOD measures and the extent of the correlations between mean home SBP and TOD measures were similar (Table 2). The clinical significance of day-to-day HBPV was shown in 2455 Japanese [5] and 1866 Finnish general population subjects [11]. Several studies have shown relationships between HBPV and TOD measures. Maximum systolic HBP readings, one of the markers of HBPV, were independently associated with CIMT and the urinary albumin creatinine ratio in 356 subjects with untreated hypertension [9]. We also reported that systolic HBPV (SD) and maximum SBP were associated with urinary albumin excretion in 310 hypertensive patients [26]. The results of the present study are in agreement with those results, and confirmed that home BPV is associated with TOD markers similarly to mean home BP.

Relationship between maximum systolic HBP and LA dilatation

Our present investigation demonstrated that increased maximum home SBP was significantly correlated with greater LADI, and the extent of correlation was significantly stronger than that between mean home SBP and LADI. Moreover, the correlation was significant even after adjusting for LVMI (Table 3). There are two possible explanations for the relationship between home BPV and LA enlargement. First, BPV indices evaluated by ABPM were shown to be positively associated with LAVI independent of LVMI in 164 untreated hypertensive subjects [27]. The left atrial ejection fraction (LAEF) and the total LA longitudinal strain were negatively associated with LAVI in the same population [27]. Decreased LAEF and LA longitudinal strain indicated the deterioration of LA reservoir function. Therefore, BPV could be associated with impaired LA reservoir function and consequently cause LA enlargement.

Second, BPV may induce the early enlargement of LA diameter via mechanical stress. The relationship between BPV and LA diameter was reported in a study of 167 newly diagnosed untreated hypertensive patients [16]. The study showed that increasing BPV influenced the early enlargement of the thin atrial wall more so than it influenced the thicker LV myocardium. Our present findings are consistent with those data, and showed that maximum systolic HBP was more important to LA enlargement than the more commonly used parameter of mean systolic HBP.

Study strengths and limitations

One of the strengths of the present study is that it was undertaken as a multicenter trial. Kotake Town is an inland farming town and Shikine-jima Island is surrounded by sea. Consequently, living and environment conditions are different between two regions. Therefore, further studies are required to know whether our findings can be generalized to other populations.

The study is also unusual that it examined subjects in primary care, in clinics of two remote locations, with HBP measured by a telemonitoring system, the precision of which is verified and based on clinical practice.

There are two limitations in this study. First, the sample size ($n = 219$) is relatively small. Second, the cardiac and carotid echocardiography were performed at different sites. However, we tried to rigorously standardize the procedures according to the protocols described in the ASE guidelines.

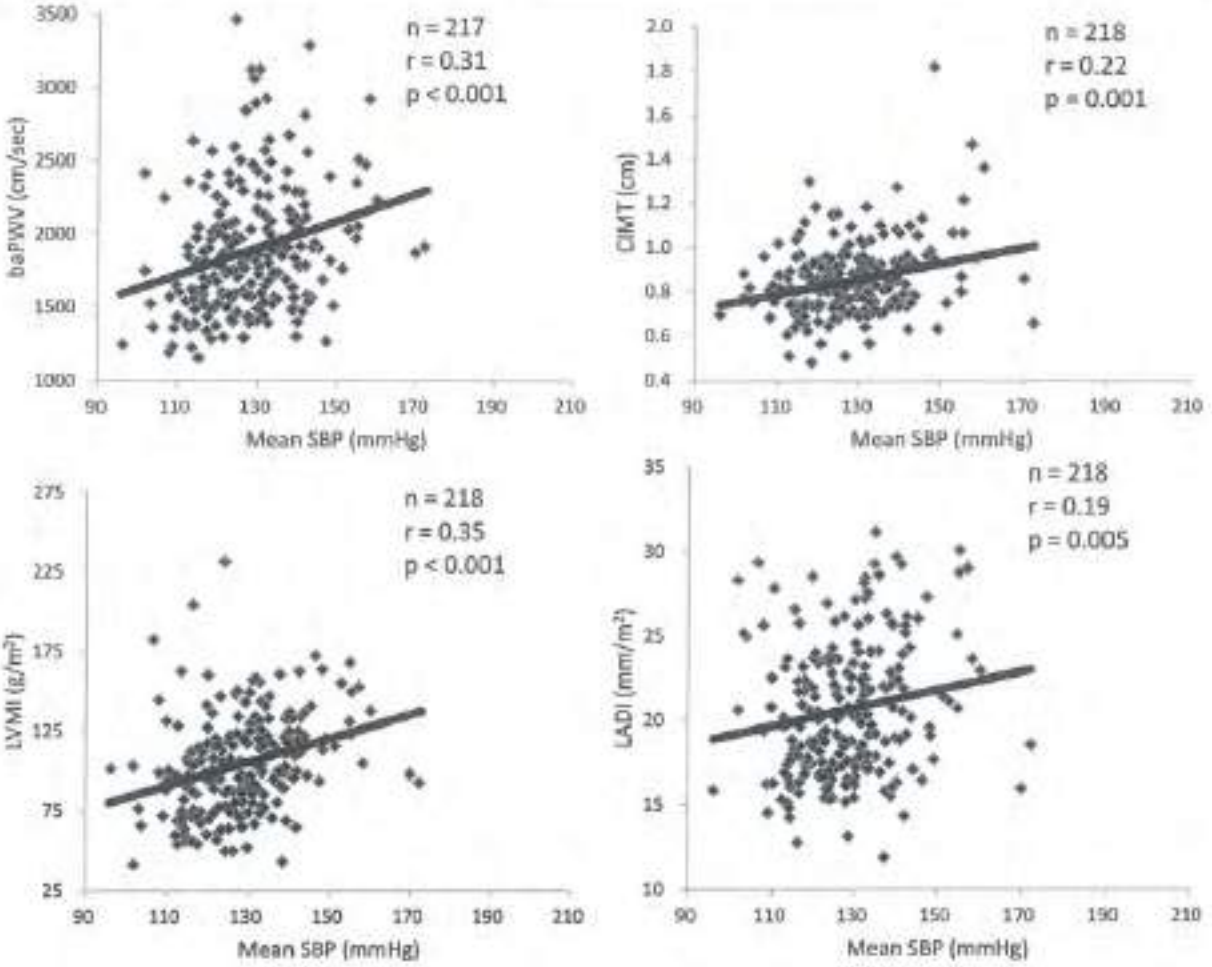

Fig. 2 Relationships between mean home SBP and TOD markers

Conclusions

Maximum and mean home BP reflect the extent of classical hypertensive TOD equivalently. However, compared to mean home BP, maximum home BP is more closely associated with the left atrial diameter, an under-reported marker of hypertensive TOD. It is a well-established fact that the left atrial diameter is strongly correlated with atrial fibrillation. Thus, the clinical significance of maximum home BP shown here merits its measurement in addition to mean home BP.

Summary Table

What is known about the topic?

- The self-monitoring of home blood pressure (HBP) has become one of the standard methods of blood pressure monitoring and is useful for the management of hypertension.
- The clinical significance of day-to-day variability in HBP has been established and reported to be associated with target organ damage (TOD).
- A patient's left atrial diameter can be used as one of the TOD markers. Dilatation of left atrial diameter (LAD) is an early stage of arterial hypertension, and its early detection and treatment are extremely important.

What this study adds?

- The extent of correlations between maximum systolic HBP, one of the markers of HBP variability, and TOD measures was similar to the extent of correlations between mean systolic HBP and TOD markers.

Table 3 Relationships between maximum, mean, SD, and CV of home SBP and TOD measures in multivariate analysis[a]

TOD measures	Maximum home SBP		Mean home SBP		SD of home SBP		CV of home SBP	
	β	p	β	p	β	p	β	p
baPWV	0.21	<0.001	0.23	<0.001	0.11	0.066	0.04	0.532
CIMT	0.13	0.04	0.17	0.008	−0.03	0.656	−0.07	0.247
LADI	0.14	0.024[b]	0.06	0.302	0.13	0.029	0.12	0.053

All TOD measures were analyzed one by one

SD standard deviation, *CV* coefficient of variation, *SBP* systolic blood pressure, *baPWV* brachial–ankle pulse wave velocity, *LVMI* left ventricular mass index, *CIMT* carotid intima–media thickness, *LADI* left atrial diameter index, *TOD* target organ damage, *BMI* body mass index

[a] Multiple-regression analysis adjusting for age, sex, smoking, dyslipidemia, diabetes mellitus, BMI, and LVMI was performed

[b] $p = 0.024$ vs. mean SBP by Z-test ($n = 218$)

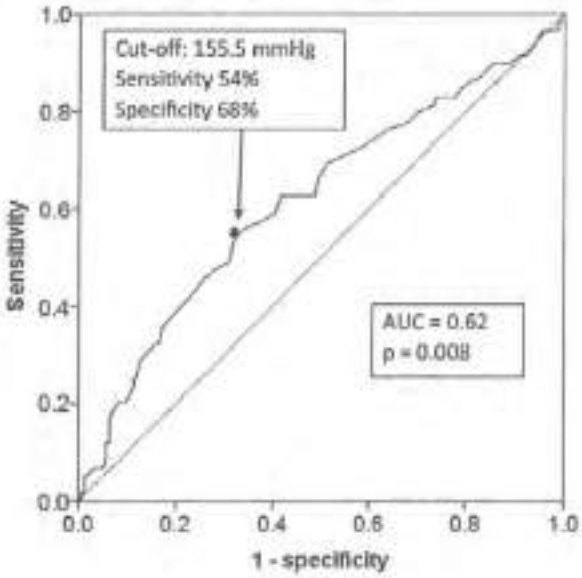

Fig. 3 ROC analysis of maximum home SBP for left atrial dilatation. AUC area under the curve

- The extent of correlations between maximum systolic HBP and LAD index was significantly stronger than that between mean systolic HBP and LAD index.
- The clinical significance of maximum systolic HBP merits its measurement in addition to mean systolic HBP.

Acknowledgements We gratefully acknowledge Ms. Matsumoto, Ms. Okura, and Ms. Ochiai for their coordination and data management of this study and editorial assistance.

Funding This work was supported by the Japanese Study Group for the Physiology and Management of Blood Pressure by Omron Healthcare Co., Ltd.

Compliance with ethical standards

Conflict of interest The authors declare that they have no conflict of interest.

References

1. Bobrie G, Chatellier G, Genes N, Clerson P, Vaur L, Vaisse B, et al. Cardiovascular prognosis of "masked hypertension" detected by blood pressure self-measurement in elderly treated hypertensive patients. JAMA. 2004;291:1342–9.
2. Imai Y, Ohkubo T, Hozawa A, Tsuji I, Matsubara M, Araki T, et al. Usefulness of home blood pressure measurements in assessing the effect of treatment in a single-blind placebo-controlled open trial. J Hypertens. 2001;19:179–85.
3. Mengden T, Hernandez Medina RM, Beltrna B, Alvarez E, Kraft K, Vetter H. Reliability of reporting self-measured blood pressure values by hypertensive patients. Am J Hypertens. 1998;11:1413–7.
4. Kaihara T, Eguchi K, Kario K. Home BP monitoring using a telemonitoring system is effective for controlling BP in a remote island in Japan. J Clin Hypertens. 2014;16:814–9.
5. Kikuya M, Ohkubo T, Metoki H, Asayama K, Hara A, Ohara T, et al. Day-by-day variability of blood pressure and heart rate at home as a novel predictor of prognosis: the Ohasama study. Hypertension. 2008;52:1045–50.
6. Hansen TW, Thijs L, Li Y, Boggia J, Kikuya M, Björklund-Bodegård K, et al. International database on ambulatory blood pressure in relation to cardiovascular outcomes investigators. Prognostic value of reading-to-reading blood pressure variability over 24h in 8938 subjects from 11 populations. Hypertension. 2010;55:1049–57.
7. Rothwell PM, Howard SC, Dolan E, O'Brien E, Dobson JE, Dahlöf B, et al. Prognostic significance of visit-to-visit variability, maximum systolic blood pressure, and episodic hypertension. Lancet. 2010;375:895–905.
8. Dolan E, O'Brien E. Blood pressure variability: clarity for clinical practice. Hypertension. 2010;56:179–81.
9. Matsui Y, Ishikawa J, Eguchi K, Shibasaki S, Shimada K, Kario K. Maximum value of home blood pressure: a novel indicator of target organ damage in hypertension. Hypertension. 2011;57:1087–93.
10. Fukui M, Ushigome E, Tanaka M, Hamaguchi M, Tanaka T, Atsuta H, et al. Home blood pressure variability on one occasion is a novel factor associated with arterial stiffness in patients with type 2 diabetes. Hypertens Res. 2013;36:219–25.
11. Johansson JK, Niiranen TJ, Puukka PJ, Jula AM. Prognostic value of the variability in home-measured blood pressure and heart rate: the Finn-Home study. Hypertension. 2012;59:212–8.
12. Lee SE, Youn JC, Lee HS, Park S, Lee SH, Cho JJ, et al. Left atrial volume index is an independent predictor of hypertensive response to exercise in patients with hypertension. Hypertens Res. 2015;38:137–42.

13. Su G, Cao H, Xu S, Lu Y, Shuai X, Sun Y, et al. Left atrial enlargement in the early stage of hypertensive heart disease: a common but ignored condition. J Clin Hypertens. 2014;16:192–7.
14. Appleton CP, Galloway JM, Gonzalez MS, Gaballa M, Basnight MA. Estimation of left ventricular filling pressures using two-dimensional and Doppler echocardiography in adult patients with cardiac disease. Additional value of analyzing left atrial size, left atrial ejection fraction and the difference in duration of pulmonary venous and mitral flow velocity at atrial contraction. J Am Coll Cardiol. 1993;22:1972–82.
15. McManus DD, Xanthakis V, Sullivan LM, Zacharish J, Aragam J, Larson MG, et al. Longitudinal tracking of left atrial diameter over the adult life course: clinical correlates in the community. Circulation. 2010;121:667–74.
16. Cipollini F, Arcangeli E, Seghieri G. Left atrial dimension is related to blood pressure variability in newly diagnosed untreated hypertensive patients. Hypertens Res. 2016;39:583–7.
17. dabl® Educational Trust. Devices for blood pressure measurement. http://www.dableducational.com. Accessed July 2017.
18. Imai Y, Otsuka K, Kawano Y, Shimada K, Hayashi H, Tochikubo O, et al. Japanese Society of Hypertension (JSH) Guidelines for Self-monitoring of Blood Pressure at Home. Hypertens Res. 2003;26:771–82.
19. Lang RM, Badano LP, Mor-Avi V, Afilalo J, Armstrong A, Ernande L, et al. Recommendations for cardiac chamber quantification by echocardiography in adults: an update from the American Society of Echocardiography and the European Association of Cardiovascular Imaging. J Am Soc Echocardiogr. 2015;28:1–39.
20. Ferrara LA, Vaccaro O, Cardoni O, Laurenzi M, Mancini M, Zanchetti A. Indexation criteria of ventricular mass and predictive role of blood pressure and body composition. Am J Hypertens. 2005;18:1282–7.
21. Pritchett AM, Jacobsen SJ, Mahoney DW, et al. Left atrial volume as an index of left atrial size: a population-based study. J Am Coll Cardiol. 2003;41:1036–43.
22. Tomiyama H, Matsumoto C, Shiina K, Yamashina A. Brachial-ankle PWV: current status and future directions as a useful marker in the management of cardiovascular disease and/or cardiovascular risk factors. J Atheroscler Thromb. 2016;23:128–46.
23. Ohkuma T, Ninomiya T, Tomiyama H, Kario K, Hoshide S, Kita Y, et al. Brachial-ankle pulse wave velocity and the risk prediction of cardiovascular disease: an individual participant data meta-analysis. Hypertension. 2017;69:1045–52.
24. Takashima N, Turin TC, Matsui K, Rumana N, Nakamura Y, Kadota A, et al. The relationship of brachial-ankle pulse wave velocity to future cardiovascular disease events in the general Japanese population: the Takashima Study. J Hum Hypertens. 2014;28:323–7.
25. The Joint Committee of the Japan Academy of Neurosonology and the Japan Society of Embolus Detection and Treatment on Guideline for Neurosonology. Carotid Ultrasound Examination. Neurosonology 2006;19:49–67.
26. Hoshide S, Yano Y, Shimizu M, Eguchi K, Ishikawa J, Kario K. Is home blood pressure variability itself an interventional target beyond lowering mean home blood pressure during antihypertensive treatment? Hypertens Res. 2012;35:862–6.
27. Tadic M, Cuspidi C, Ilic I, Suzic-Lazić J, Zivanovic V, Jozika L, et al. The relationship between blood pressure variability, obesity and left atrial phasic function in hypertensive population. Int J Cardiovasc Imaging. 2016;32:603–12.

Journal of Cardiology 72 (2018) 74–80

Contents lists available at ScienceDirect

Journal of Cardiology

Journal homepage: www.elsevier.com/locate/jjcc

Original article

Reduced variability of visual left ventricular ejection fraction assessment with reference images: The Japanese Association of Young Echocardiography Fellows multicenter study☆☆

Kenya Kusunose (MD, PhD)[a,*], Kentaro Shibayama (MD, PhD)[b], Hiroyuki Iwano (MD, PhD, FJCC)[c], Masaki Izumo (MD, PhD)[d], Nobuyuki Kagiyama (MD)[e], Koji Kurosawa (MD, PhD)[f], Hirotsugu Mihara (MD)[g], Hiroki Oe (MD, PhD)[h], Tetsuari Onishi (MD, PhD)[i], Toshinari Onishi (MD)[j], Mitsuhiko Ota (MD)[k], Shunsuke Sasaki (MD, PhD)[l], Yumi Shiina (MD, FJCC)[m], Hikaru Tsuruta (MD)[n], Hidekazu Tanaka (MD, PhD, FJCC)[o] on behalf of the JAYEF Investigators

[a] Department of Cardiovascular Medicine, Tokushima University Hospital, Tokushima, Japan
[b] Heart Center, Tokyo Bay Urayasu Ichikawa Medical Center, Urayasu, Japan
[c] Department of Cardiovascular Medicine, Faculty of Medicine and Graduate School of Medicine, Hokkaido University, Sapporo, Japan
[d] Division of Cardiology, Department of Internal Medicine, St. Marianna University School of Medicine, Kawasaki, Japan
[e] Cardiovascular Medicine, The Sakakibara Heart Institute of Okayama, Okayama, Japan
[f] Department of Clinical Laboratory Center, Gunma University Hospital, Maebashi, Japan
[g] Department of Cardiovascular Medicine, Yokkaichi Municipal Hospital, Yokkaichi, Japan
[h] Center of Ultrasonic Diagnostics, Okayama University Hospital, Okayama, Japan
[i] Department of Cardiology, Himeji Cardiovascular Center, Himeji, Japan
[j] Department of Cardiovascular Medicine, Osaka University Graduate School of Medicine, Osaka, Japan
[k] Department of Cardiovascular Medicine, Kobe City Medical Center General Hospital, Kobe, Japan
[l] Department of Cardiology, Teine Keijinkai Hospital, Sapporo, Japan
[m] Division of Cardiovascular Centre, St. Luke's International Hospital, Tokyo, Japan
[n] Department of Cardiology, Keio University School of Medicine, Tokyo, Japan
[o] Division of Cardiovascular Medicine, Department of Internal Medicine, Kobe University Graduate School of Medicine, Kobe, Japan

ARTICLE INFO

Article history:
Received 22 November 2017
Received in revised form 20 December 2017
Accepted 6 January 2018
Available online 19 February 2018

Keywords:
Quality control
Ejection fraction
Learning session

ABSTRACT

Background: Visual estimation of left ventricular ejection fraction (LVEF) is widely applied to confirm quantitative EF. However, visual assessment is subjective, and variability may be influenced by observer experience. We hypothesized that a learning session might reduce the misclassification rate.

Methods: Protocol 1: Visual LVEFs for 30 cases were measured by 79 readers from 13 cardiovascular tertiary care centers. Readers were divided into 3 groups by their experience: limited (1–5 years, n = 28), intermediate (6–11 years, n = 26), and highly experienced (12-years, n = 25). Protocol 2: All readers were randomized to assess the effect of a learning session with reference images only or feedback plus reference images. After the session, 20 new cases were shown to all readers following the same methodology. To assess the concordance and accuracy pre- and post-intervention, each visual LVEF measurement was compared to overall average values as a reference.

Results: Experience affected the concordance in visual EF values among the readers. Groups with intermediate and high experience showed significantly better mean difference (MD), standard deviation (SD), and coefficient of variation (CV) than those with limited experience at baseline. The learning session with reference image reduced the MD, SD, and CV in readers with limited experience. The learning session with reference images plus feedback also reduced proportional bias. Importantly, the misclassification rate for mid-range EF cases was reduced regardless of experience.

☆☆ This work was partially supported by JSPS Kakenhi Grants (Number 17K09506 to K. Kusunose).

* Corresponding author at: Department of Cardiovascular Medicine, Tokushima University Hospital, 2-50-1 Kuramoto, 770-0042 Tokushima, Japan.
E-mail address: kusunosek@tokushima-u.ac.jp (K. Kusunose).

https://doi.org/10.1016/j.jjcc.2018.01.007
0914-5087/© 2018 Japanese College of Cardiology. Published by Elsevier Ltd. All rights reserved.

Conclusion: This large multicenter study suggested that a simple learning session with reference images can successfully reduce the misclassification rate for LVEF assessment.
© 2018 Japanese College of Cardiology. Published by Elsevier Ltd. All rights reserved.

Introduction

Precise and reliable echocardiographic assessment of left ventricular ejection fraction (LVEF) is needed for clinical decision-making. Echocardiographic guidelines recommend that EF be assessed by the biplane method of disks or 3-dimensional echocardiographic method, and then the measurement confirmed by visual estimation [1,2]. Even if the guidelines showed that we should be using measured EF, visual estimation of LVEF is widely applied to confirm quantitative EF in daily clinical work. Visual estimation of LVEF is an important component of determining LV function in all institutes.

Originally, visual assessment was subjective, and variability could be influenced from observer experience. Several institutes had various readers with a wide range of experience levels. Because a large variability in LVEF measurements can occur at different centers, therapies may be confounded when decisions are made on the basis of LVEF [3,4]. There might be a fundamental problem with interinstitutional agreement regarding LVEF in both clinical and research fields. An effective intervention for reduction in variability in LVEF is needed [5,6]. In this paper, we present a simple approach to assessing and improving the quality of visual estimation of LVEF in a large group of echocardiographic laboratories. We hypothesized that the degree of experience affects the variability of visual LVEF assessment and that a learning session might reduce the misclassification rate. Our aim of this study was to compare the inter-observer variability among the groups with a wide range of experience, and assess the utility of the learning sessions to reduce the misclassification rate.

Methods

Patient population

Pre- and post-learning session assessments and analysis were performed in this study (Fig. 1). A total of 13 cardiovascular tertiary care centers participated. Of the 79 voluntary observers participating in the full exercise, 45 sonographers and 34 cardiologists with various levels of echocardiographic experience were included. All participants were blinded to each other's interpretation. Datasets were blinded, stored digitally, and contained apical 4-chamber, 2-chamber, and long-axis views of patients who had undergone clinically-indicated standard transthoracic echocardiography using commercially available machines (iE33; Philips Healthcare, Amsterdam, The Netherlands, and Vivid E9; GE Healthcare, Waukesha, WI, USA). We have selected three apical views for this study. A total of 50 datasets from patients in sinus rhythm were included in the analysis. There were 20 cases with ischemic cardiomyopathy, 20 cases with non-ischemic cardiomyopathy, and 10 cases with hypertension or diabetes. All images were scored for image quality on the basis of visualization of the LV walls and endocardium: 1 = excellent acoustic detail, 2 = good acoustic detail, 3 = adequate acoustic detail, and 4 = technically difficult study with poor or inadequate visualization of LV walls and/or endocardium. To avoid any bias, no clinical data about the cases were provided. Readers were required to provide visual estimates of LVEF as single integers and were blinded to one another's interpretations. All data were collected on an identified answer sheet with each case coded separately. The investigation conformed to the principles outlined in the Declaration of Helsinki, and each participating center conformed to local ethical regulations. The Institutional Review Board of the center of this study (Tokushima University Hospital) approved this study protocol.

Protocol 1. Visual LVEF for 30 cases was estimated by 79 readers from 13 tertiary care centers. Readers were divided into three groups by tertile experience: limited (1–5 years, $n = 28$), intermediate (6–11 years, $n = 26$), and highly experienced (12-years, $n = 25$). All readers interpreted at least 200 transthoracic echocardiography cases/year. Averaged visual LVEF measurement was calculated from 13 highly experienced readers of each center among 79 readers as a reference value in each case. These reference values were compared with each visual LVEF measurement from 3 different experience groups for the assessment of concordance and accuracy.

Protocol 2. After the first session of baseline assessment, two types of learning interventions were conducted. Each participant was randomized into either reference images alone or feedback plus reference images groups using a computer generated random sequence by Microsoft Excel. The learning session with reference images alone consisted of presentation of 6 selected reference cases, which were examples of LV function with actual values (LVEFs equal to 20%, 30%, 40%, 50%, 60%, and 70%). There was no focal asynergy of the LV in the reference images. The values of 6 selected reference cases were determined by the averaged visual LVEF values of 13 highly experienced readers from each center. The reference values were confirmed using cardiac magnetic resonance imaging by one experienced reader. The learning session with feedback plus reference images consisted of presentation of reference cases and self-learning sending the specific feedback sheets to individual participants (Supplement Fig. 1). The specific feedback sheet was a summary of their LVEF estimates compared to the reference values using Bland–Altman plots including mean

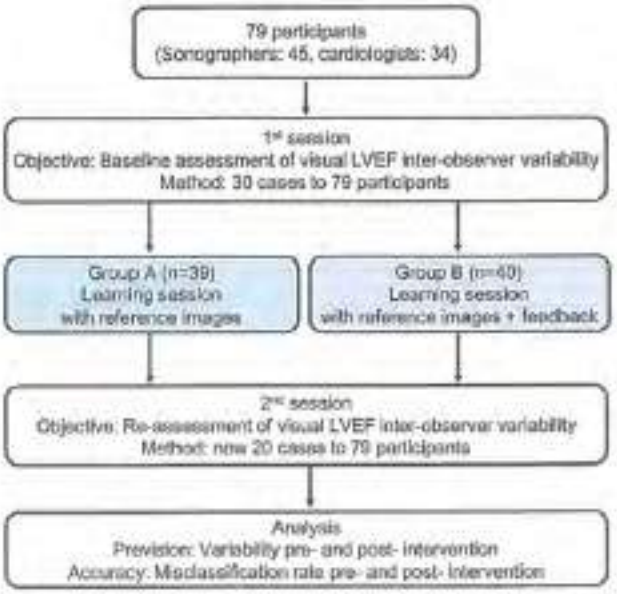

Fig. 1. Study design flowchart for the assessment of visual left ventricular ejection fraction (LVEF).

difference (MD), mean standard deviation (SD), and proportional bias. There was no difference between two groups for readers' experience (9 ± 6 years vs. 10 ± 7 years, $p = 0.17$).

Within two months following the end of the learning session, 20 new cases were shown to all readers following the same methodology described for the baseline assessment. The cases were selected to have similar etiologies, image quality, and range of EF as those of the baseline assessment. For each case, individual visual estimates of LVEF were compared with the reference values. The change of variability after the learning session was calculated. A disagreement between these 2 measures was termed a misclassification. When a visual EF was estimated, many readers tended to visual EF in increments of 5%. In these cases, 5% error may be acceptable. Thus, we defined disagreement between the visual estimate and reference EF when it differed by an EF of more than ±5%. Finally, to assess the interinstitutional variability, individual visual estimates of LVEF from each laboratory by experienced observers were compared with the reference values.

Statistical analysis

The absolute difference in LVEF between each reader and the reference values was calculated. MD was the average of the absolute differences over a single reviewer and then across groups. SD, and coefficient of variation (CV), and intraclass correlation coefficient (ICC) were calculated in a similar way. ICC of visual LVEF was used to determine concordance and improvement. The existence of proportional bias was detected from the regression line of Bland–Altman plots using the *t*-value of the slope. Student *t*-test and paired *t*-tests were used to compare continuous variables when appropriate. One-way analysis of variance analysis for repeated measures was used to compare parameters between groups. Bonferroni's correction was used for post hoc analysis of significant results. Statistical analysis was performed using standard statistical software (SPSS software 21.0, SPSS Inc., Chicago, IL, USA; MedCalc Software 15.8, Mariakerke, Belgium; and R 3.3.3, R Foundation for Statistical Computing, Vienna, Austria) and statistical significance was defined by $p < 0.05$.

Results

Cases and participants

Among the 79 participants, 45 were sonographers and 34 were cardiologists. The median duration of experience was 8 years (range: 1–32 years). All participants had subspecialty echocardiography training. The used 50 images had adequate (protocol 1: $n = 8$, protocol 2: $n = 6$), good (protocol 1: $n = 15$, protocol 2: $n = 10$), or excellent (protocol 1: $n = 7$, protocol 2: $n = 4$) image quality. There were a total of 2370 visual EF responses before the intervention and 1580 responses after the intervention. Averaged visual LVEF values of the cases are summarized for pre- and post-intervention in Supplement Fig. 2. The EF range of the cases was similar at both time points (median value: 44% vs. 43%).

Impact of experience in visual LVEF

Using ICC, good correlations were found between visually estimated LVEF and reference LVEF (ICC: 0.947 ± 0.06). The ICC in the limited experience group was relatively worse than that in the intermediate and high experience groups (0.918 ± 0.09 vs. 0.963 ± 0.03 vs. 0.962 ± 0.02, both $p = 0.02$). The MD, SD, and CV in the limited experience group were higher than those in the intermediate and high experience groups (Fig. 2). There was no difference of *t*-value as a proportional bias among the three groups.

Effect of the learning session with reference images

The ICC of visual LVEF from the second measurement was similar to the first measurement (ICC: 0.947 ± 0.06 vs. 0.948 ± 0.06, $p = 0.78$). The change of ICC in the limited experience group was better than that of the intermediate and high experience groups (0.03 ± 0.10 vs. −0.01 ± 0.02 vs. −0.01 ± 0.03, $p = 0.04$ vs. intermediate, $p = 0.03$ vs. high). After the learning session with reference images, MD, SD, and CV were not significantly changed (MD: 3.3 ± 2.8 vs. 3.1 ± 2.9, $p = 0.66$, SD: 4.8 ± 2.1 vs. 4.4 ± 1.7, $p = 0.09$, CV: 10.5 ± 5.1 vs. 10.1 ± 4.5, $p = 0.78$). The changes in these values in the limited experience group were higher than those in

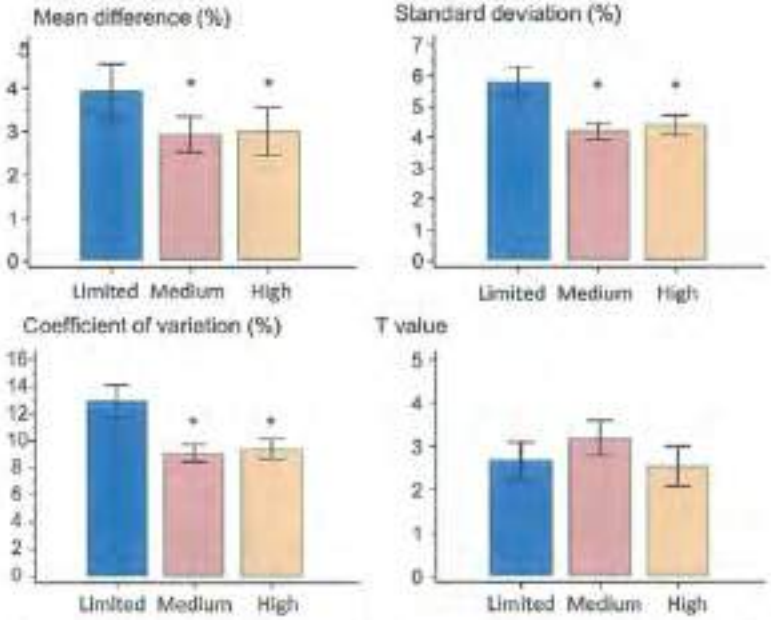

Fig. 2. Impact of experience on visual left ventricular ejection fraction measurements. The *t*-value is a marker of proportional bias.

the intermediate and high experience groups (Fig. 3). Thus, the benefit of intervention with reference images was in improving concordance especially in the limited experience group. There was no difference in the change of t-value as a proportional bias among groups.

Effect of the learning session with feedback

After the intervention, ΔMD, ΔSD, and ΔCV in the group with feedback plus reference images were similar to those in the group with reference images alone. In addition, the change in t-value in the group with feedback plus reference images was better than that in the group with reference images alone (Fig. 4). Therefore, personal feedback may reduce proportional bias for visual LVEF.

Assessment of misclassification

A disagreement between 2 measures was termed a misclassification. A response was considered misclassified if the visually estimated EF differed by more than ±5% from the reference values.

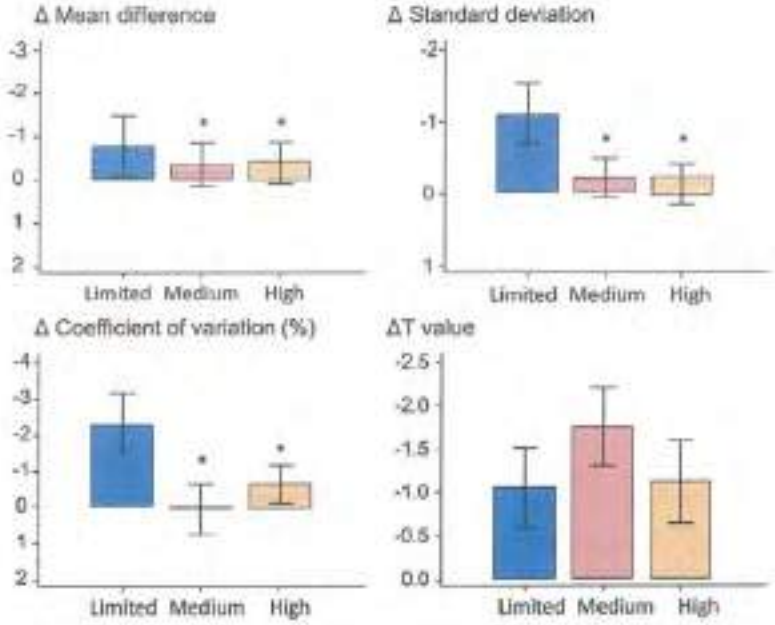

Fig. 3. Impact of experience on changes in variability pre- and post-intervention with reference image.

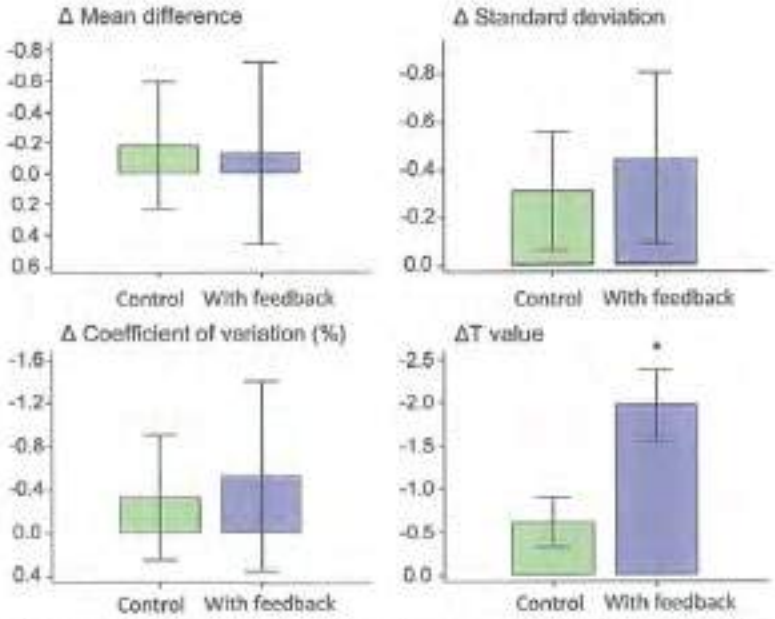

Fig. 4. Impact of intervention on changes in variability pre- and post-intervention with feedback.

The misclassification rate was determined from the 2370 responses pre-intervention and from 1580 responses post-intervention. We defined a category of LVEF (mildly impaired: 40–55%, moderately impaired 30–39%, severely impaired < 30%, and normal > 55%) in all cases. Table 1 lists the misclassification rate for each session. From the mid-range EF cases (mild to moderately impaired EF 30% to 55%, pre-intervention: 891 responses and post-intervention: 790 responses), the misclassification rate was significantly reduced regardless of experience (all $p < 0.05$). Importantly, from the mid-range EF cases, the misclassification rate was also significantly reduced regardless of image quality and professions (all $p < 0.05$). From all range EF cases, the misclassification rate was reduced, especially in the limited experience group, adequate image quality, and cardiologists (all $p < 0.05$).

Interinstitutional variability

Before the intervention, 6 laboratories overestimated visual EF, and 7 laboratories underestimated visual EF compared with reference values (Fig. 5). In particular, two laboratories modestly overestimated (the mean differences were +3% and +4%) and three laboratories modestly underestimated (the mean differences were −3%, −3%, and −5%). After the intervention, there was no laboratory of significant overestimation or underestimation (within 2%). Thus, this intervention may improve the interinstitutional variability.

Discussion

Echocardiography has an important role for diagnosis and guiding clinical interventions. Visual assessment of LVEF is one of the most common parameters. Precise and reliable assessment of visual LVEF is necessary for both clinical and research fields. However, quality control programs are challenging. This large multicenter study showed that: (1) Experience affects the concordance in visual LVEF among readers; (2) A simple learning session with reference images can reduce inter-observer variability for the visual LVEF, especially in limited experience readers; (3) Additional feedback may improve in proportional bias, but not in inter-observer variability; (4) The learning session also resulted in less misclassification of LVEF, especially in the mild to moderately impaired LVEF regardless of experience. These results suggest that a simple learning session with reference images can minimize the inter-observer variability and misclassification in practitioners with a wide range of experience.

Experience in visual LVEF

At baseline, the ICC of the limited experience group was good, and that of the intermediate and high experience group was excellent. There were no differences in ICC between the intermediate and high experience groups. This result suggests that not only knowledge but also experience in visually estimated LVEF are required for better concordance at baseline.

Intervention with reference images in visual LVEF

Several papers have reported a quality assessment program in a clinical setting [7,8]. The investigators used reference cases as a standard to reduce inter-observer variability. Reference LVEFs were provided by radionuclide imaging, cardiac magnetic resonance imaging, and/or echocardiographic expert reviews. In these previous studies, intervention with reference images could improve reproducibility of visually estimated LVEF [7,9,10]. The results of our multicenter study are consistent with previous work linking intervention with reduction of variability for visually estimated LVEF. Moreover, the intervention with reference images was a simple and effective method especially in the limited experience group. Readers with limited experience should undertake a quality control process of visual LVEF before participation in both clinical and research work. We also noted that misclassification reduced in the mid-range of LVEF (as an important range in the clinical setting) in the readers of all experience levels after the intervention. This suggests that even experienced readers can benefit from using the learning session with reference images. In addition, even if the image quality is relatively low, the misclassification rate was also significantly reduced. Visual estimation can be useful as a niche procedure when images are poor.

Intervention with feedback in visual LVEF

Some previous investigators provided not only reference images but also individual feedback identifying the error of estimated LVEF. In these papers, individual feedback improved the correlation between echocardiographic LVEF and the other imaging-based LVEF [11,12]. Our paper is the first study to assess the utility of feedback compared with a control group. As in our results, there was no difference in reproducibility between the reference images alone and the feedback plus reference images group in our cohort. This type of feedback may not be really necessary to improve reproducibility. However, feedback can improve the proportional bias. The feedback session may be useful to assess and standardize the actual value of visually estimated LVEF.

Clinical implications

The variability of echocardiographic assessment and trials depends on quality control between institutes. This multicenter

Table 1
Misclassification rates of individual visual estimates of LVEF compared with reference LVEF for all cases and cases with mid-range EF.

	Misclassification rates (%)							
	Experience			Image quality			Professions	
	Limited	Medium	High	Excellent	Good	Adequate	Sonographer	Cardiologist
Pre-intervention								
All cases	22.3	16.9	17.5	17.8	15.0	24.2	17	21.7
Cases with mid-range EF (EF: 0.30–0.55)	26.6	33.8	26.3	32.5	24.4	30.2	27.9	28.9
Post-intervention								
All cases	**16.8***	15	17.3	17.9	13.9	**19.9***	16.8	**15.9***
Cases with mid-range EF (EF: 0.30–0.55)	**16.4***	**11.6***	**13.5***	**9.4***	**12.2***	**23.4***	**15.6***	**11.8***

* $p < 0.05$ vs. pre-intervention.
LVEF, left ventricular ejection fraction.

Fig. 5. Over and under estimation of visual left ventricular ejection fraction between laboratories in Japan.

study proposed a simple tool with reference images to improve the concordance and accuracy of visually estimated LVEF in readers at various institutes and experience levels. The readers in the limited experience group should have a learning session to improve their reproducibility for visual LVEF, and the readers in the intermediate and high experience group also need to have a learning session to reduce misclassification.

Limitations

The major limitation is the lack of an independent truth standard. The reference values were based on averaged visual LVEF, and did not include other imaging modalities. We have checked the accuracy of 10 visual estimated LVEF reference values using the biplane method of discs from one experienced observer. The reference values were similar to the values by the biplane method of discs (bias: +1% and limit of agreement: ±1.4%). Even if the reference value was calculated from over 10 experienced observers' responses of tertiary care centers, this value is not the truth standard of the world consensus. However, our main purpose was to assess the utility of learning sessions with reference images and feedback. Based on our results, we hope that the Cardiovascular Committee of the American, European, and Asian Societies will develop reference images as a truth standard with specific LVEF, and recommend usage of the reference image to improve reproducibility [13]. In this multi-center study, because we would like to make up the simple intervention, three apical views were used. However, although the apical bi-plane method of discs is used to measure LVEF, the experienced observer considers all available views to assess the estimated LVEF. When we asked to provide a visual EF estimate, many readers tended to visual EF in increments of 5%. This may be a contributor to error in the estimation of accuracy. However, because our pre- and post-intervention EF estimations were done by the same rule, this should not have affected the comparison of change. We also had a smaller number of cases in the post-intervention assessment than at baseline. However, the averaged EF and the EF range were similar at both time points. We assessed reduction in variability and accuracy within two months after the intervention, so the long-term effect of this intervention is not well described. Atrial fibrillation has been excluded because the beat-to-beat variability is too high for the impact assessment of learning interventions. Finally, we did not have data on other types of interventions (e.g. group learning sessions).

Conclusions

This large multicenter study suggested that a simple learning intervention can successfully reduce the variability of LVEF assessment especially in readers with limited experience. These results provide an idea of standardized protocol in LVEF assessment in multicenter studies.

Conflicts of interest

The authors declare that there is no conflict of interest.

Acknowledgments

The authors acknowledge the JAYEF Investigators: Masaru Obokata, MD, Mayo Clinic, Rochester, MN, USA, Misako Toki, BS, The Sakakibara Heart Institute of Okayama, Okayama, Japan, Satoshi Yuda, MD, PhD, Teine Keijinkai Hospital, Sapporo, Japan, Satoshi Ichimiya, MD, PhD, Yokkaichi Municipal Hospital, Yokkaichi, Japan, Satoshi Yamada, MD, PhD, Hokkaido University, Sapporo, Japan, Hiroya Kawai MD, PhD, Himeji Cardiovascular Center, Himeji, Japan, Yoshihiro J Akashi, MD, PhD, St. Marianna University School of Medicine, Kanagawa, Japan, Hiroyuki Watanabe, MD, PhD, Tokyo Bay Urayasu Ichikawa Medical Center, Urayasu, Japan, Satoshi Nakatani, MD, PhD, Osaka University Graduate School of Medicine, Osaka, Japan, Mitsushige Murata, MD, PhD, Keio University School of Medicine, Tokyo, Japan, Hirotsugu Yamada, MD, PhD, Tokushima University Hospital, Tokushima, Japan.

Appendix A. Supplementary data

Supplementary data associated with this article can be found, in the online version, at doi:10.1016/j.jjcc.2018.01.007.

References

[1] Lang RM, Badano LP, Mor-Avi V, Afilalo J, Armstrong A, Ernande L, et al. Recommendations for cardiac chamber quantification by echocardiography in adults: an update from the American Society of Echocardiography and the European Association of Cardiovascular Imaging. Eur Heart J Cardiovasc Imaging 2015;16:233–70.
[2] Enomoto M, Ishizu T, Seo Y, Kameda Y, Suzuki H, Shimano H, et al. Myocardial dysfunction identified by three-dimensional speckle tracking echocardiography in type 2 diabetes patients relates to complications of microangiopathy. J Cardiol 2016;68:282–7.
[3] Kaufmann BA, Min SY, Goetschalckx K, Bernheim AM, Buser PT, Pfisterer ME, et al. How reliable are left ventricular ejection fraction cut offs assessed by echocardiography for clinical decision making in patients with heart failure? Int J Cardiovasc Imaging 2013;29:581–8.
[4] Okuma H, Noto N, Tanikawa S, Kanezawa K, Hirai M, Shimozawa K, et al. Impact of persistent left ventricular regional wall motion abnormalities in childhood cancer survivors after anthracycline therapy: assessment of global left ventricular myocardial performance by 3D speckle-tracking echocardiography. J Cardiol 2017;70:396–401.
[5] Goldberg JS, Bednarz J, Devereux R, Gardin J, Klein A, Manning WJ, et al. American Society of Echocardiography recommendations for use of echocardiography in clinical trials. J Am Soc Echocardiogr 2004;17:1086–119.
[6] Bhattacharyya S, Lloyd G. Improving appropriateness and quality in cardiovascular imaging. Circ Cardiovasc Imaging 2015;8:e003988.

[7] Jobri AM, Picard MH, Newell J, Marshall JE, King MEE, Hung J. Can a teaching intervention reduce interobserver variability in LVEF assessment. JACC: Cardiovasc Imaging 2011;4:821–9.
[8] Wu W-CH, Filikha Z, Girerd N, Huttin O, Courand PY, Bozec E, et al. Reproducibility in echocardiographic assessment of diastolic function in a population based study (the STANISLAS cohort study). PLOS ONE 2015; 10:e0122336.
[9] Akinboboye O, Sommer J, Gopal A, Ring D, Shen Z, Bardfeld P, et al. Visual estimation of ejection fraction by two-dimensional echocardiography: the learning curve. Clin Cardiol 1995;18:726–9.
[10] Thavendiranathan P, Popović ZB, Flamm SD, Dahiya A, Grimm RA, Marwick TH. Improved interobserver variability and accuracy of echocardiographic visual left ventricular ejection fraction assessment through a self-directed learning program using cardiac magnetic resonance images. J Am Soc Echocardiogr 2013;26:1267–73.
[11] Duehert MA, Yow E, Barnhart HX, Rabineau D, Crowley AL, Douglas PS. Quality improvement implementation: improving reproducibility in the echocardiography laboratory. J Am Soc Echocardiogr 2015;28:959–68.
[12] Fanari Z, Choudhry UI, Reddy VK, Eze-Nliam C, Hammami S, Kolm P, et al. The value of quality improvement process in the detection and correction of common errors in echocardiographic hemodynamic parameters in a busy echocardiography laboratory. Echocardiography 2015;32:1778–89.
[13] Douglas P, Iskandrian AE, Krumholz HM, Gillam L, Hendel R, Jollis J, et al. Achieving quality in cardiovascular imaging: proceedings from the American College of Cardiology-Duke University Medical Center Think Tank on Quality in Cardiovascular Imaging. J Am Coll Cardiol 2006;48:2141–51.

Yoneyama et al. Journal of Cardiovascular Magnetic Resonance (2018) 20:53
https://doi.org/10.1186/s12968-018-0472-9

Journal of Cardiovascular Magnetic Resonance

RESEARCH

Open Access

Diabetes mellitus and insulin resistance associate with left ventricular shape and torsion by cardiovascular magnetic resonance imaging in asymptomatic individuals from the multi-ethnic study of atherosclerosis

Kihei Yoneyama[1,5], Bharath A. Venkatesh[1], Colin O. Wu[2], Nathan Mewton[1], Ola Gjesdal[1], Satoru Kishi[1], Robyn L. McClelland[3], David A. Bluemke[4] and João A. C. Lima[1,6*]

Abstract

Background: Although diabetes mellitus (DM) and insulin resistance associate with adverse cardiac events, the associations of left ventricular (LV) remodeling and function with compromised glucose metabolism have not been fully evaluated in a general population. We used cardiovascular magnetic resonance (CMR) to evaluate how CMR indices are associated with DM or insulin resistance among participants before developing cardiac events.

Methods: We studied 1476 participants who were free of clinical cardiovascular disease and who underwent tagged CMR in the Multi-Ethnic Study of Atherosclerosis (MESA). LV shape and longitudinal myocardial shortening and torsion were assessed by CMR. A higher sphericity index represents a more spherical LV shape. Multivariable linear regression was used to evaluate the associations of DM or homeostasis model assessment-estimated insulin resistance (HOMA-IR) with CMR indices.

Results: In multiple linear regression, longitudinal shortening was lower in impaired fasting glucose than normal fasting glucose (NFG) (0.36% lower vs. NFG, $p < 0.05$); torsion was greater in treated DM (0.24 °/cm greater vs. NFG, $p < 0.05$) after full adjustments. Among participants without DM, greater log-HOMA-IR was correlated with greater LV mass (3.92 g/index, $p < 0.05$) and LV mass-to-volume ratio (0.05 /index, $p < 0.01$), and lower sphericity index (−1.26/index, $p < 0.01$). Greater log-HOMA-IR was associated with lower longitudinal shortening (−0.26%/index, $p < 0.05$) and circumferential shortening (−0.30%/index, $p < 0.05$). Torsion was positively correlated with log-HOMA-IR until 1.5 of log-HOMA-IR (0.16 °/cm/index, $p = 0.030$)), and tended to fall once above 1.5 of log-HOMA-IR (−0.50 °/cm/index, $p = 0.203$). The sphericity index was associated negatively with LV mass-to-volume ratio (−0.02/%, $p < 0.001$) and torsion (−0.03°/cm/%, $p < 0.001$).

(Continued on next page)

* Correspondence: jlima@jhmi.edu
[1]Department of Cardiology, Johns Hopkins University, Baltimore, MD, USA
[6]Radiology and Epidemiology, Johns Hopkins University, Blalock 524D1, Johns Hopkins Hospital, 600 North Wolfe Street, Baltimore, MD 21287, USA
Full list of author information is available at the end of the article

BMC

© The Author(s) 2018 **Open Access** This article is distributed under the terms of the Creative Commons Attribution 4.0 International License (http://creativecommons.org/licenses/by/4.0/), which permits unrestricted use, distribution, and reproduction in any medium, provided you give appropriate credit to the original author(s) and the source, provide a link to the Creative Commons license, and indicate if changes were made. The Creative Commons Public Domain Dedication waiver (http://creativecommons.org/publicdomain/zero/1.0/) applies to the data made available in this article, unless otherwise stated.

(Continued from previous page)

Conclusions: Glucose metabolism disorders are associated with LV concentric remodeling, less spherical shape, and reduced systolic myocardial shortening in the general population. Although torsion is higher in participants who are treated for DM and impaired insulin resistance, myocardial shortening was progressively decreased with higher HOMA-IR and torsion was increased only with less severe insulin resistance.

Clinical trial registration: Multi-Ethnic Study of Atherosclerosis (MESA): A full list of participating MESA investigators and institutions can be found at http://www.mesa-nhlbi.org/. Study Start Date: January 1999 (NCT00005487).

Keywords: Glucose tolerance, Heart failure, Metabolic disease, Obesity, Strain

Background

Type 2 diabetes mellitus (DM) is a group of metabolic diseases; insulin resistance is a condition characterized by the failure to respond appropriately to insulin. Chronic hyperglycemia may impair myocardial energy metabolism, induces cardiomyocyte systolic dysfunction and eventually cell death [1, 2]. Epidemiological studies have demonstrated that DM and insulin resistance are related to cardiovascular disease and heart failure [3–5].

Left ventricular (LV) structure, shape and myocardial shortening (myocardial strain) have been shown to have incremental predictive value for cardiovascular events beyond the traditional LV ejection fraction measures [6–10]. Although DM and insulin resistance associate with adverse cardiac events, the associations of LV remodeling and function with compromised glucose metabolism have not been fully evaluated in a general population. We hypothesized that DM or insulin resistance might associate with LV remodeling and systolic function before developing cardiac events.

The Multi-Ethnic Study of Atherosclerosis (MESA)—a prospective study sponsored by the National Heart Lung and Blood Institute (NHLBI) of the National Institutes of Health—is a large cohort study of ethnically diverse individuals free of cardiovascular disease at baseline, and was primarily designed to study the progression of subclinical cardiovascular disease [11]. MESA is the largest cardiovascular magnetic resonance (CMR) tagging study to allow unique investigation of cardiac mechanics at the population level. To test the hypothesis, we used MESA CMR tagging examination to evaluate how CMR indices are associated with DM or insulin resistance among participants free of clinical cardiovascular disease.

Methods

Participants

MESA evaluated the mechanisms that underlie the development and progression of subclinical cardiovascular diseases among asymptomatic individuals. Details of the MESA study design have been previously described [11]. In brief, between July 2000 and August 2002, 6814 men and women—who identified themselves as Caucasian, African American, Hispanic, or Chinese and were 45–84 years of age and free of clinically apparent cardiovascular disease—were recruited. CMR was performed in 5004 participants as part of the baseline examination. In an ancillary study, 1773 consecutive participants underwent tagged CMR studies at enrollment in six centers: Wake Forest University, Columbia University, Johns Hopkins University, the University of Minnesota, Northwestern University, and the University of California. Of these, torsion data were available for 1478 participants as previously described [12]; of those, two cases were excluded because of lack of clinical information. A total of 1476 participants were thus enrolled in the study. None of those were known type 1 DM. All participants gave informed consent, and the study protocol was approved by the institutional review board at each site.

Cine CMR data analysis

LV end-systolic volume and end-diastolic volume (LVEDV), LV mass, and LV ejection fraction were obtained (Additional file 1) [6, 13]. LV mass-to-volume ratio was calculated as LV mass divided by LVEDV. LV length at end-diastole was calculated as the average distance from the epicardial apex to the mitral valve insertion as measured from the 2 and 4 chamber views. The LV sphericity index at end-diastole was calculated as the percentage of the LVEDV relative to the volume of a calculated sphere with the LV length [14]. A higher index represents a more spherical shape of the ventricle and a lower reduced sperricity. LV longitudinal shortening (long-axis fractional shortening) was calculated as (LV length at diastole − LV length at systole)/LV length at diastole*100 (%) [15]. A higher value represents an increased shortening of the ventricle.

Tagged CMR was performed using a segmented k-space electrocardiogram (ECG)-gated fast low angle shot pulse sequence (Additional file 1). Circumferential shortening was represented by the absolute peak strain. Positive numbers of shortening represent more contraction. Torsion (°/cm) was calculated by dividing the peak systolic twist by the inter-slice distance. CMR indices are dysplayed in Additional file 1.

Risk factor measures

Risk factors measures are provided in Additional file 1. Body mass index (BMI) was calculated as weight over

height squared. Untreated DM was defined as fasting glucose ≥126 mg/dl without any use of hypoglycemic medication or insulin. Treated DM was defined as use of hypoglycemic medication or insulin. Impaired fasting glucose (IFG) was defined as fasting glucose levels between 100 mg/dl and 125 mg/dl. All other participants were defined as having normal fasting glucose (NFG). Serum insulin was determined by a radioimmunoassay method using the Linco Human Insulin-Specific RIA kit (MilliporeSigma, Burlington, Massachusetts, USA.). Homeostasis model assessment-estimated insulin resistance (HOMA-IR) was calculated as insulin (mU/l) × (glucose [mg/dl] × 0.055)/22.5 [16, 17]. Participants with DM were excluded from the HOMA-IR calculation.

Statistical analysis

Summary statistics were presented using median (interquartile range; 25 to 75%) for continuous variables, and percent for categorical variables. The chi-square test was used for comparison of categorical variables. Wilcoxon's rank-sum test was used to test the differences to compare each DM fasting glucose state. Multivariable linear regression models were used to compare CMR indices by DM fasting glucose criteria. We also used

Table 1 Baseline demographic characteristics according to DM state (n = 1476)

	DM state*			
Variable	NFG (n = 1004)	IFG (n = 262)	Untreated DM (n = 47)	Treated DM (n = 163)
Age, year	65 (56 to 72)	67 (61 to 72)†	66 (58 to 72)	68 (64 to 75)†
Male sex, %‡	509 (50.7)	158 (60.3)	35 (74.5)	90 (55.2)
Ethnic, n (%)§				
Caucasian	336 (33)	65 (25)	12 (26)	24 (15)
Black	124 (12)	51 (19)	7 (15)	26 (16)
Hispanic	271 (27)	66 (25)	16 (34)	56 (34)
Chinese	273 (27)	80 (31)	12 (26)	57 (35)
Smoking status, n (%)				
Never	513 (51)	142 (54)	22 (47)	88 (54)
Former	376 (38)	87 (33)	20 (43)	54 (33)
Current	109 (11)	32 (12)	5 (11)	20 (12)
Alcohol status, n (%)§				
Never	195 (20)	47 (18)	8 (17)	44 (27)
Former	240 (24)	61 (23)	9 (20)	56 (35)
Current	558 (56)	152 (58)	29 (63)	61 (38)
Body mass index, kg/m^2	27 (24 to 30)	29 (26 to 32)†	28 (25 to 32)	29 (26 to 32)†
Systolic BP, mmHg	124 (111 to 139)	131 (118 to 145)†	125 (115 to 145)	132 (120 to 146)†
Diastolic BP, mmHg	72 (65 to 78)	74 (67 to 82)†	73 (68 to 85)	70 (64 to 77)†
Resting heart rate, bpm	60 (55 to 67)	64 (58 to 71)†	66 (60 to 71)†	66 (58 to 73)†
Hypertension, n (%)§	417 (42)	145 (55)	23 (49)	120 (74)
Current smoker, n (%)	109 (11)	32 (12)	5 (11)	20 (12)
Total-cholesterol, mg/dl	193 (172 to 215)	185 (170 to 220)	200 (170 to 218)	184 (161 to 205)
HDL-cholesterol, mg/dl	50 (42 to 60)	45 (38 to 53)†	42 (33 to 54)†	44 (38 to 54)†
Triglyceride, mg/dl	104 (74 to 150)	125 (86 to 186)†	128 (79 to 233)	128 (83 to 202)†
Lipid-lowering medication, n (%)§	160 (16)	53 (20)	12 (26)	53 (33)
Anti-hypertensive medication, n (%)§	337 (34)	128 (49)	16 (35)	122 (75)
eGFR, mL/min	76 (66 to 87)	76 (64 to 88)	83 (66 to 97)	77 (63 to 91)
Walking, MET-min/week	945 (360 to 1920)	788 (315 to 1770)	1240 (315 to 1995)	2243 (735 to 3750)

Values are median (interquartile range). BP, blood pressure; DM, diabetes mellitus; eGFR, estimated glomerular filtration rate
HDL, high-density lipoprotein; IFG, impaired fasting glucose; NFG, normal fasting glucose
*DM was defined as fasting glucose ≥126 mg/dl or use of hypoglycemic medication or insulin; IFG was defined as fasting glucose levels between 100 mg/dl and 125 mg/dl; all other participants were defined as having NFG
†p < 0.0125 vs. NFG in in Wilcoxon test, ‡p < 0.0125 vs. untreated DM in Wilcoxon test, §p < 0.05 in chi-square

Table 2 Association of CMR LV indices by DM state ($n = 1476$)

Dependent variables (LV indices)	Multivariable linear regression; coefficients			
	IFG (vs. NFG)	Untreated DM (vs. NFG)	Treated DM (vs. NFG)	R^2
End-diastolic volume, ml	−1.86 (1.81)	2.89 (3.82)	0.17 (2.26)	0.41
Mass, g	3.64 (2.00)	5.01 (4.22)	4.42 (2.50)*	0.55
Mass-to-volume	0.04 (0.02)†	0.01 (0.04)	0.04 (0.02)*	0.19
Sphericity index, %	−0.44 (0.43)	0.94 (0.90)	−0.27 (0.54)	0.10
Ejection fraction, %	−0.33 (0.51)	−1.27 (1.06)	0.76 (0.64)	0.19
Longitudinal shortening, %	−0.36 (0.17)†	−0.63 (0.37)*	−0.17 (0.22)	0.17
Circumferential shortening, %	−0.03 (0.18)	−0.43 (0.39)	−0.17 (0.23)	0.15
Torsion, °/cm	0.13 (0.08)	−0.25 (0.18)	0.24 (0.11)†	0.18

Coefficients (standard errors) represents the difference in depend variables compared to NFG as a reference in DM testing glucose criteria. Model include age, gender, race, height, obesity (BMI ≥ 30 kg/m²), smoking status (non, former, and current), heart rate, systolic blood pressure, total cholesterol, use of medication for hypertension and dyslipidemia, estimated glomerular filtration rate, walking in METs per week, and alcoholic status (non-drinker, former, or current)
Abbreviations and definition of DM state at in Table 1
* $p < 0.1$, † $p < 0.05$

multivariable linear regression to evaluate the associations of HOMA-IR with CMR indices. Potential covariates included age, gender, race, height, obesity (BMI ≥ 30 kg/m²), smoking status (never, former, or current), heart rate, systolic blood pressure, total cholesterol, use of medication for hypertension and dyslipidemia, estimated glomerular filtration rate, walking in METs per week, and alcoholic status (non-drinker, former, or current). Significant nonlinearity was present between the torsion and HOMA-IR with a knot at 1.5 of log-HOMA-IR. Therefore, we used a linear spline model to estimate the relationship as a piecewise linear function with adjustments for the same covariates, as described above. Standardized values were defined by dividing the differences between the observed values and the sample means by the corresponding standard deviations. Statistical

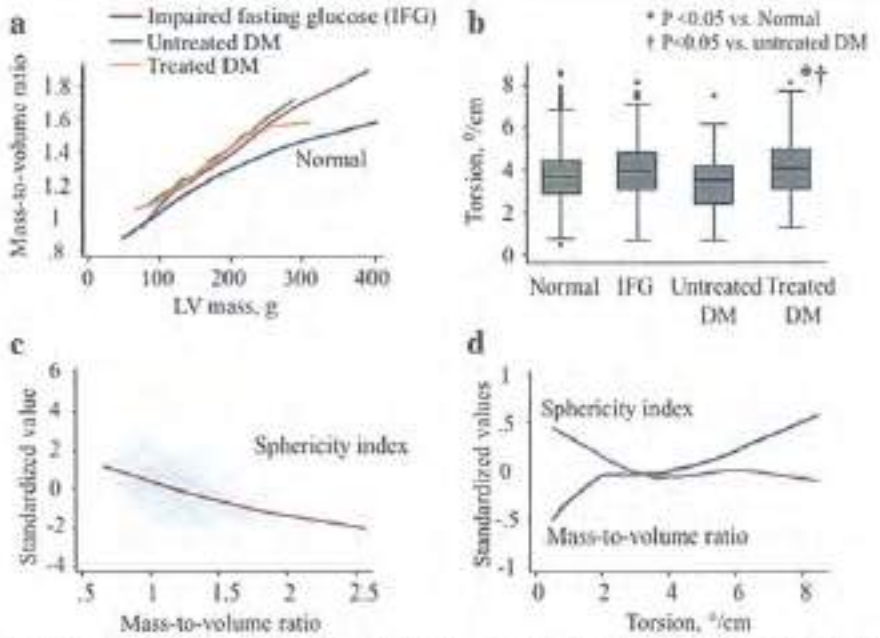

Fig. 1 Associations of diabetes mellitus (DM) status with left ventricular (LV) indices ($n = 1476$). LV mass-to-volume ratio was higher in impaired fasting glucose and DM group than normal at any level of LV mass (**a**). Torsion was greater in treated DM than normal and untreated DM (**b**). The sphericity index was correlated negatively with the mass-to-volume ratio (**c**). Torsion was positively correlated with mass-to-volume ratio, and negatively with shericity index (**d**)

analyses were performed using the Stata statistical software package (Version 14, College Station, Texas, USA). A two-sided p-value < 0.05 was considered statistically significant.

Results

Of the total 1476 participants population, 210 (14%) had DM and 262 (18%) had IFG.

Baseline characteristics according to DM fasting glucose criteria are shown in Table 1. Age and systolic blood pressure were higher in the IFG group and in the Treated DM group than in the NFG group. Diastolic blood pressure was greater in the IFG group and lower in the treated DM group than in the NFG group. Hypertension was common in treated DM (NFG; 42%, IFG; 55%, untreated DM; 49%, treated DM; 74%, $p < 0.05$). Use of lipid-lowering medication was common in treated DM (NFG; 16%, IFG; 20%, untreated DM; 26%, treated DM; 33%, $p < 0.05$).

Differences in LV structure and function in DM fasting glucose criteria compared to NFG

The median LV ejection fraction was 70% interquartile range (64, 74%) in the whole study population, and did not differ among DM fasting glucose criteria. Compared to NFG, treated DM tended to have greater LV mass (4.4 g greater vs. NFG, $p = 0.077$) and mass-to-volume ratio (0.04 greater vs. NFG, $p < 0.05$) with a lower longitudinal shortening (0.36% lower vs. NFG, $p < 0.05$) after adjustments for all prespecified confounders (Table 2). But torsion was greater in treated DM (0.24°/cm greater vs. NFG, $p < 0.05$) than NFG after full adjustments (Fig. 1). Circumferential shortening did not differ in DM status compared to NFG. The association of LV shape with concentric remodeling and torsion are shown in Fig. 1. In multiple linear regression, the sphericity index was associated negatively with LV mass-to-volume ratio (−0.02/%, $p < 0.001$) and torsion (−0.03°/cm/%, $p < 0.001$) after full adjustments (models included as in Table 2).

LV structure and function with serum fasting glucose, insulin, and HOMA-IR

Multivariable linear regression models in Table 3 indicate that greater log-transformed HOMA-IR was associated with greater LV mass (3.9 g/index, $p < 0.05$) and mass-to-volume ratio (0.05 /index, $p < 0.01$), and with lower sphericity index (−1.26/index, $p < 0.01$) after full adjustments. Greater log-HOMA IR associated with lower longitudinal shortening (−0.26%/index, $p < 0.05$) and circumferential shortening (−0.30%/index, $p < 0.05$) after adjustments. These relationships were confounded by hypertension (systolic blood pressure, and use of anti-hypertensive medication) and obesity. The

Table 3 Association of LV remodeling and function by HOMA-IR among participants without diabetes mellitus ($n = 1266$)*

Dependent variables (LV indices)	Multivariable linear regression coefficients	
	Log-HOMA-IR	R^2
End-diastolic volume, ml		
Model 1	2.66 (1.40)	0.36
Model 2	−2.53 (1.48)	0.41
Mass, g		
Model 1	11.58 (1.58)‡	0.49
Model 2	3.92 (1.61)†	0.56
Mass-to-volume		
Model 1	0.07 (0.01)‡	0.18
Model 2	0.05 (0.01)†	0.28
Sphericity index, %		
Model 1	−1.06 (0.33)‡	0.11
Model 2	−1.26 (0.35)‡	0.11
Ejection fraction, %		
Model 1	0.15 (0.38)	0.18
Model 2	0.25 (0.41)	0.18
Longitudinal shortening, %		
Model 1	−0.26 (0.13)†	0.16
Model 2	−0.22 (0.14)	0.17
Circumferential shortening, %		
Model 1	−0.30 (0.14)†	0.13
Model 2	−0.08 (0.15)	0.14
Torsion, °/cm		
Model 1	0.13 (0.06)†	0.16
Model 2	0.11 (0.07)	0.17

Coefficients (standard error) represents the change in dependent variables corresponds to 1 unit increase in independent variables. Model 1 included age, gender, race, height, smoking status(never, former, or current), heart rate, hypertension, total cholesterol, use of medication for dyslipidemia, estimated glomerular filtration rate, walking in METs per week, and alcohol status (non-drinker, former, or current). Model 2 included systolic blood pressure, and hypertensive medication use, and obesity (BMI ≥ 30 kg/m^2) in addition to Model 1

Homeostasis model assessment-estimated insulin resistance (HOMA-IR) was calculated as insulin (mIU/l) × glucose (mg/dl) × 0.0551/22.5. [16, 17]

*Participants with diabetes mellitus were excluded because participants with DM were excluded from the HOMA-IR calculation

†$p < 0.05$, ‡$p < 0.01$

association between torsion and HOMA-IR was nonlinear (Fig. 2 and Table 4). Torsion was correlated positively with log-HOMA-IR until 1.5 of log-HOMA-IR (0.16 °/cm/index, $p = 0.030$), and tended to fall once above 1.5 of log-HOMA-IR (−0.50 °/cm/index, $p = 0.203$) after full adjustments (models included as in Table 2).

Discussion

DM and insulin resistance are two of the most powerful risk factors for cardiovascular disease; however, the

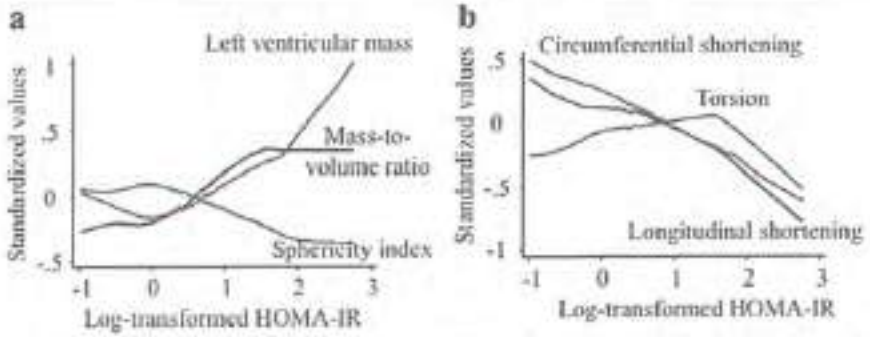

Fig. 2 Associations of HOMA-IR with left ventricular indices among participants without diabees mellitus (n = 1266). Higher HOMA-IR was positively correlated with mass, and inversely with sphericity index (a) and myocardial shortening (b). The mass-to-volume ratio was flatten at the same point where the torsion reduces. Myocardial shortening was progressively decreased with higher IR. Torsion was increased only with less severe insulin resistance. Locally weighted smoothing curve (LOWESS) using unadjusted standardized values are displayed. HOMA-IR, homeostasis model assessment-estimated insulin resistance

mechanisms of adaptation that alter the cardiovascular system in subjects with glucose metabolism disorders remain largely unknown. In MESA participants without known heart disease or clinical evidence of coronary artery disease at inclusion, we found the following: (1) participants with treated DM had greater LV concentric remodeling and greater torsion compared to participants with normal fasting glucose (NFG); (2) insulin resistance (non-DM) was related to a more conical LV shape and concentric remodeling with impaired systolic longitudinal myocardial shortening, but torsion was higher in advance with insulin resistance and was mirrored in a somewhat parallel manner with higher LV mass-to-volume ratio and conical shape. These observations suggest that DM or impaired insulin resistance are associated with adverse LV concentric remodeling, conical LV shape, and impaired systolic function. Increased torsion may be a key compensation mechanism to maintain global systolic function despite the alteration of myocardial shortening and structure due to compromised glucose metabolism in the general population (Fig. 3).

In the present study, subjects with treated DM had a more concentric LV than those with NFG subjects. In the Strong Heart Study, DM patients had increased LV mass and wall thickness by conventional echocardiography than normal glucose tolerance [18]. According to data from the Diabetes Control and Complication Trial/Epidemiology of Diabetes Intervention and Complications (DCC/EDIC) study, the mean Hemoglobin A1c levels are correlated positively with increased concentric remodeling defined by CMR among type 1 DM patients [19]. Our results are consistent with observations of previous large studies. We also found that higher HOMA-IR, a pre-diabetic status, was associated with concentric remodeling. The following studies also support our results: (a) in the Framingham Heart Study, LV mass and wall thickness by echocardiography were positively associated with an increase in HOMA-IR despite the relations being attenuated by BMI [20]; (b) in the Strong Heart Study, echocardiography indices demonstrated that insulin glucose tolerance was associated with higher LV mass and relative wall thickness [21]; (c) in the Coronary Artery Risk Development in Young Adults (CARDIA) study, high insulin resistance was associated with worse relative wall thickness [22]; (d) in a recent report from our study, central obesity and HOMA-IR were also associated with concentric remodeling [23].

Table 4 Association of left ventricular torsion with HOMA-IR (n = 1266)*

	Multivariable spline liner regression		
Depend variable	Log HOMA-IR < 1.5 mg/dl	Log HOMA-IR > 1.5 mg/dl	R^2
Torsion, °/cm			
Model 1	0.16 (0.07)†	−0.51 (.40)	0.15
Model 2	0.16 (0.08)†	−0.50 (0.40)	0.17

Coefficients (standard error) represents the change in torsion corresponds to 1 units increase in log-HOMA-IR
Model 1 included age, gender, race and height
Model 2 included age, gender, race, height, obesity (BMI ≥ 30 kg/m2), smoking status (non, former, and current), heart rate, systolic blood pressure, total cholesterol, use of medication for hypertension and dyslipidemia, estimated glomerular filtration rate, walking in METs per week, and alcoholic status (non-drinker, former, or current) as in Table 3
*Participants with diabetes mellitus were excluded as in Table 3
† $P < 0.05$

Fig. 3 Summary of cardiovascular magnetic resonance (CMR) imaging in asymptomatic individuals. DM or impaired insulin resistance are associated with adverse LV concentric remodeling, less spherical shape, and impaired systolic myocardial shortening in the general population. Torsion, however, is higher in participants who are treated for DM and impaired insulin resistance

Although the effect of LV sphericity shape has been described in LV severe systolic dysfunction [24] or in women's hearts [12], we found that higher HOMA-IR was related to lower LV sphericity (reduced spericity). Since the more conical the LV becomes, the more the relative wall thickness increases, there might be a link between LV conical shape and torsion with respect to the lever-arm theory. In this theory, a greater radius difference between the endocardium and the epicardium would result in increased torsion (Fig. 4). Another mechanism of enhanced torsion in DM could be altered myocardial perfusion by subclinical coronary artery atherosclerosis or by coronary microvascular disease [25]. It has been reported that the apical rotation angle

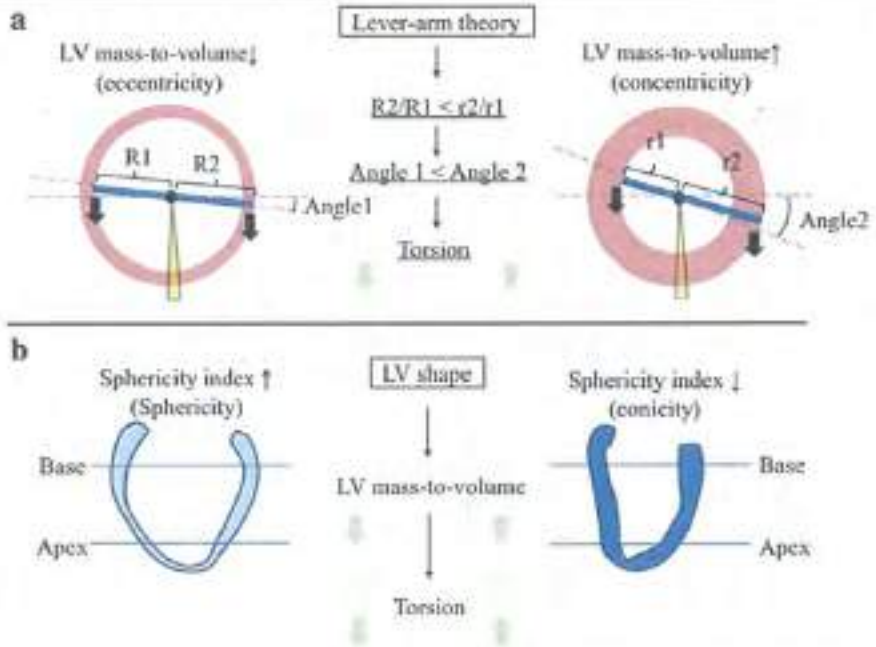

Fig. 4 Illustrations of torsion on LV remodelling and shape geometry. **a** A greater radius difference between the endocardium and epicardium (r2/r1 > R2/R1) would result in an increased rotation angle with respect to the lever-arm theory (α1 > α2). The left arm represents the radius from center to endocardium (R1 or r1), and the right arm center to the epicardium (R2 or r2). Black arrows represent force (myocardial contraction). Dot-line represents rotation angle change. **b** Less spherical shape would result in increased LV mass-to-volume ratio, and would then influence torsion

is internally increased by coronary occlusion in an early phase of myocardial ischemia [26], but the angle might be decreased by long-standing coronary occlusion. Shivu et al. [27] reported that enhanced torsion was associated with lower myocardial perfusion reserve assessed by adenosine stress CMR among type 1 DM patients. Since the structure of the endocardium and epicardium are oriented in different directions, reduced subendocardial function may alter the balance between the opposing rotational forces and thus result in increased torsion [28].

In the present study, torsion was not enhanced in the untreated DM group. It has been noticed in a clinical practice that the direct pathway from DM to dilated cardiac failure (increased LV sphericity and eccentricity change) can occur without a myocardial infarction [29]. Chronic exposure to disturbances of glucose metabolism in DM might negatively affect LV mechanics through myocardial fibrosis and microvascular disease [29, 30]. The spherical and eccentricity change in LV wall could attenuate enhanced torsion.

In our data, longitudinal and circumferential shortening were impaired with insulin resistance despite the relations being confounded by obesity and hypertension. In the Strong Heart Study, DM had lower fractional shortening by echocardiography than normal glucose tolerance [18]. Others have reported alterations in longitudinal and circumferential shortening by cine DENSE and 3D tag analysis in type 2 DM with small sample sizes [31, 32]. Their results agree to the current study, in that circumferential and longitudinal shortening were reduced but torsion increased, with increased mass to volume ratio. High glucose level induces an increased oxidative stress that facilitates cardiomyocyte damage and hypertrophy, and interstitial fibrosis [2]. This is in accordance with our results that reduced longitudinal and circumferential shortening are associated with increased HOMA-IR. In contrast, the data from the Framingham study of fractional shortening by M-mode did not correlate with HOMA-IR [20]. Type-1 DM with normoalbuminuria have longitudinal shortening similar to healthy control subjects [33]. Other studies have found that type-1 DM with mean hemoglobin A1c of 6.8%, had no difference in longitudinal and circumferential shortening, but torsion was increased [34]. The relatively preserved myocardial shortening in DM or insulin resistance may be partly compensated for by increased torsion. Indeed, torsion reflects the circumferential-longitudinal (CL) shear direction of the LV; therefore, the increase in torsion compensates the decrease in longitudinal and circumferential contractility.

LV torsion and myocardial strain are a principle for quantification of LV function which is also feasible with speckle-tracking echocardiography. Global LV torsion may be used to identify subclinical systolic dysfunction in patients with DM in addition to myocardial shortening. Although LV torsion has yet not been included in clinical practice guidelines, it is likely to become a useful application when evaluating patients with heart failure symptoms. Therefore, future studies should investigate if LV torsion may be useful marker of the predicting heart failure.

Our study has several limitations. First, because of the cross-sectional design, we cannot establish causal relations between glucose metabolism disorders and LV indices; however, MESA is the largest CMR tagging study to evaluate these associations so far, allowing unique investigation of cardiac mechanics at the population level. Second, the small number of untreated DM participants affects the power to detect differences in LV indices compared to NFG. This might be a factor explaining why torsion was not increased in the untreated DM group.

Although some investigators have also expressed torsion as the representing the shear deformation angle, wich torsion normalized by twist angle and LV radius [35], we did not assess the torsional shear angle.

Conclusions

Glucose metabolism disorders are associated with LV concentric remodeling, less spherical shape, and reduced systolic myocardial shortening in the general population. Although torsion is higher in participants who are treated for DM and impaired insulin resistance, torsion was increased only with less severe insulin resistance. Increased torsion may be a key compensation mechanism to maintain global systolic function despite impaired myocardial shortening, and be explained by the changes in LV concentric remodeling with less spherical shape due to compromised glucose metabolism.

Additional file

Additional file 1: Methods; CINE Cardiovascular magnetic resonance/ Torsion and Myocardial Strain Analysis/ Left ventricular indices/ Risk factor measures. (DOCX 636 kB)

Abbreviations

BMI: Body mass index; CMR: Cardiovascular magnetic resonance; DM: Diabetes mellitus; ECG: Electrocardiogram; HOMA-IR: Homeostasis model assessment-estimated insulin resistance; IFG: Impaired fasting glucose; LV: Left ventricle/left ventricular; LVEDV: Left ventricular end-diastolic volume; NFG: Normal fasting glucose; MESA: Multi-Ethnic Study of Atherosclerosis

Acknowledgements

The authors thank the other investigators, staff, and participants of the MESA study for their valuable contributions. A full list of participating MESA investigators and institutions can be found at http://www.mesa-nhlbi.org.

Ethics approval and concent to participate

This study was approved by the institutional review boards of each of the participating field sites in the United States, and all participants provided written informed consent.

Funding

This research was supported by contracts N01-HC-95159 through N01-HC-95160, N01-HC-95161, N01-HC-95162, N01-HC-95163, N01-HC-95164, N01-HC-

95165, N01-HC-95166, N01-HC-95167, N01-HC-95168, and N01-HC-95169 from the National Heart, Lung, and Blood Institute and by grants UL1-TR-000040 and UL1-TR-001079 from NCRR.

Availability of data and materials
The datasets analyzed during the current study are available from the corresponding author upon reasonable request.

Declarations
The views expressed in this manuscript are those of the authors and do not necessarily represent the views of the National Heart, Lung, and Blood Institute; the National Institutes of Health; or the U.S. Department of Health and Human Services.

Authors' contributions
KY, BAV, NM, OG, SK, and JACL all made all made substantial contributions to conception and design of the study. KY, NM, and OG analyzed and interpreted the data. KY, BAV, NM, and OG drafted the manuscript. CDW, RLM, DAB, and JACL edited the manuscript. All authors revised the manuscript critically for important intellectual content. All authors read and approved the final manuscript.

Consent for publication
Not applicable.

Competing interests
The authors declare that they have no competing interests.

Publisher's Note
Springer Nature remains neutral with regard to jurisdictional claims in published maps and institutional affiliations.

Author details
[1]Department of Cardiology, Johns Hopkins University, Baltimore, MD, USA. [2]Offices of Biostatistics Research, National Heart, Lung, and Blood Institute, Bethesda, MD, USA. [3]Department of Biostatistics, University of Washington, Seattle, WA, USA. [4]National Institute of Biomedical Imaging and Bioengineering, National Institutes of Health Clinical Center, Bethesda, MD, USA. [5]St. Marianna University School of Medicine, Kawasaki, Japan. [6]Radiology and Epidemiology, Johns Hopkins University, Blalock 524D1, Johns Hopkins Hospital, 600 North Wolfe Street, Baltimore, MD 21287, USA.

Received: 14 August 2017 Accepted: 20 June 2018
Published online: 30 July 2018

References

1. Ren J, Davidoff AJ. Diabetes rapidly induces contractile dysfunctions in isolated ventricular myocytes. Am J Phys. 1997;272:H148–58.
2. Montaigne F, Chakrabarti S. Glucose-induced cell signaling in the pathogenesis of diabetic cardiomyopathy. Heart Fail Rev. 2014;19:75–86.
3. Kannel WB, McGee DL. Diabetes and cardiovascular disease. The Framingham study. JAMA. 1979;241:2035–8.
4. Chahal H, Bluemke DA, Wu CO, et al. Heart failure risk prediction in the multi-ethnic study of atherosclerosis. Heart. 2015;101:58–64.
5. Ingelsson E, Sundström J, Arnlöv J, et al. Insulin resistance and risk of congestive heart failure. JAMA. 2005;294:334–41.
6. Bluemke DA, Kronmal RA, Lima JA, et al. The relationship of left ventricular mass and geometry to incident cardiovascular events: the MESA (multi-ethnic study of atherosclerosis) study. J Am Coll Cardiol. 2008;52:2148–55.
7. McMurray JJ, Adamopoulos S, Anker SD, et al. ESC Guidelines for the diagnosis and treatment of acute and chronic heart failure 2012: The Task Force for the Diagnosis and Treatment of Acute and Chronic Heart Failure 2012 of the European Society of Cardiology. Developed in collaboration with the Heart Failure Association (HFA) of the ESC. Eur Heart J. 2012;33:1787–847.
8. Choi EY, Rosen BD, Fernandes VR, et al. Prognostic value of myocardial circumferential strain for incident heart failure and cardiovascular events in asymptomatic individuals: the multi-ethnic study of atherosclerosis. Eur Heart J. 2013;34:3954–61.
9. Yoneyama K, Venkatesh BA, Bluemke DA, et al. Cardiovascular magnetic resonance in an adult human population: serial observations from the multi-ethnic study of atherosclerosis. J Cardiovasc Magn Reson. 2017;19:52.
10. Ambale-Venkatesh B, Yoneyama K, Sharma RK, et al. Left ventricular shape predicts different types of cardiovascular events in the general population. Heart. 2017;103:499–507.
11. Bild DE, Bluemke DA, Burke GL, et al. Multi-ethnic study of atherosclerosis: objectives and design. Am J Epidemiol. 2002;156:871–81.
12. Yoneyama K, Gjesdal O, Choi EY, et al. Age, sex, and hypertension-related remodeling influences left ventricular torsion assessed by tagged cardiac magnetic resonance in asymptomatic individuals: the multi-ethnic study of atherosclerosis. Circulation. 2012;126:2481–90.
13. Natori S, Lai S, Finn JP, et al. Cardiovascular function in multi-ethnic study of atherosclerosis: normal values by age, sex, and ethnicity. AJR Am J Roentgenol. 2006;186:S357–65.
14. Lamas GA, Vaughan DE, Pfeffer AF, et al. Effects of left ventricular shape and captopril therapy on exercise capacity after anterior wall acute myocardial infarction. Am J Cardiol. 1989;63:1167–73.
15. Gjesdal O, Yoneyama K, Newton N, et al. Reduced long axis strain is associated with heart failure and cardiovascular events in the multi-ethnic study of atherosclerosis. J Magn Reson Imaging. 2016;44:178–85.
16. Matthews DR, Hosker JP, Rudenski AS, et al. Homeostasis model assessment: insulin resistance and beta-cell function from fasting plasma glucose and insulin concentrations in man. Diabetologia. 1985;28:412–9.
17. Bertoni AG, Wong ND, Shea S, et al. Insulin resistance, metabolic syndrome, and subclinical atherosclerosis: the multi-ethnic study of atherosclerosis (MESA). Diabetes Care. 2007;30:2951–6.
18. Devereux RB, Roman MJ, Paranicas M, et al. Impact of diabetes on cardiac structure and function: the strong heart study. Circulation. 2000;101:2271–6.
19. Turkbey EB, Backlund JY, Genuth S, et al. Myocardial structure, function, and scar in patients with type 1 diabetes mellitus. Circulation. 2011;124:1737–46.
20. Rutter MK, Parise H, Benjamin EJ, et al. Impact of glucose intolerance and insulin resistance on cardiac structure and function: sex-related differences in the Framingham heart study. Circulation. 2003;107:448–54.
21. Bercoff A, Devereux RB, Roman ML, et al. Relationship of impaired glucose tolerance to left ventricular structure and function: the strong heart study. Am Heart J. 2001;141:992–8.
22. Kishi S, Gidding SS, Reis JP, et al. Association of Insulin Resistance and Glycemic Metabolic Abnormalities with LV structure and function in middle age: The CARDIA Study. JACC Cardiovasc Imaging. 2017;10:105–14.
23. Shah RV, Abbasi SA, Heydari B, et al. Insulin resistance, subclinical left ventricular remodeling, and the obesity paradox: MESA (multi-ethnic study of atherosclerosis). J Am Coll Cardiol. 2013;61:1698–706.
24. Hung J, Papakostas L, Tahta SA, et al. Mechanism of recurrent ischemic mitral regurgitation after annuloplasty: continued LV remodeling as a moving target. Circulation. 2004;110:885–90.
25. Budoff MJ, Raggi P, Beller GA, et al. Noninvasive cardiovascular risk assessment of the asymptomatic diabetic patient: The Imaging Council of the American College of Cardiology. JACC Cardiovasc Imaging. 2016;9:176–92.
26. Kroeker CA, Tyberg JV, Beyar R. Effects of ischemia on left ventricular apex rotation. An experimental study in anesthetized dogs. Circulation. 1995;92:3539–48.
27. Shivu GN, Abozguia K, Phan TT, et al. Increased left ventricular torsion in uncomplicated type 1 diabetic patients: the role of coronary microvascular function. Diabetes Care. 2009;32:1710–2.
28. Claus P, Omar AM, Pedrizzetti G, et al. Tissue tracking Technology for Assessing Cardiac Mechanics: principles, normal values, and Clinical Applications. JACC Cardiovasc Imaging. 2015;8:1444–60.
29. Coughlin SS, Pearle DL, Baughman KL, et al. Diabetes mellitus and risk of idiopathic dilated cardiomyopathy. The Washington, DC dilated cardiomyopathy study. Ann Epidemiol. 1994;4:67–74.
30. Ohkubo Y, Kishikawa H, Araki E, et al. Intensive insulin therapy prevents the progression of diabetic microvascular complications in Japanese patients with non-insulin-dependent diabetes mellitus: a randomized prospective 6-year study. Diabetes Res Clin Pract. 1995;28:103–17.
31. Emanuel L, Thibault H, Bergerot C, et al. Systolic myocardial dysfunction in patients with type 2 diabetes mellitus: identification at MR imaging with cine displacement encoding with stimulated echoes. Radiology. 2012;265:402–9.
32. Fonseca CG, Dissanayake AM, Doughty RN, et al. Three-dimensional assessment of left ventricular systolic strain in patients with type 2 diabetes.

mellitus, diastolic dysfunction, and normal ejection fraction. Am J Cardiol. 2004;94:1191–5.
33. Jensen MT, Sogaard P, Andersen HU, et al. Global longitudinal strain is not impaired in type 1 diabetes patients without albuminuria: the thousand & 1 study. JACC Cardiovasc Imaging. 2015;8:400–10.
34. Chung J, Abrossevitl P, Yu X, et al. Paradoxical increase in ventricular torsion and systolic torsion rate in type I diabetic patients under tight glycemic control. J Am Coll Cardiol. 2006;47:984–90.
35. Young AA, Cowan BR. Evaluation of left ventricular torsion by cardiovascular magnetic resonance. J Cardiovasc Magn Reson. 2012;14:49.

Ready to submit your research? Choose BMC and benefit from:

- fast, convenient online submission
- thorough peer review by experienced researchers in your field
- rapid publication on acceptance
- support for research data, including large and complex data types
- gold Open Access which fosters wider collaboration and increased citations
- maximum visibility for your research: over 100M website views per year

At BMC, research is always in progress.

Learn more biomedcentral.com/submissions

BMC

Circulation: Cardiovascular Interventions
Volume 11, Issue 8, August 2018
https://doi.org/10.1161/CIRCINTERVENTIONS.117.005935

ORIGINAL ARTICLE

Clinical Outcomes of Drug-Eluting Balloon for In-Stent Restenosis Based on the Number of Metallic Layers

The New Tokyo Registry

See Editorial by Alfonso and Cuesta

Hiroto Yabushita, MD, Hiroyoshi Kawamoto, MD, Yusuke Fujino, MD, PhD, Satoko Tahara, MD, PhD, Takeo Horikoshi, MD, Miho Tada, MD, Tatsuya Amano, MD, Hirokazu Onishi, MD, Akihiro Nakajima, MD, Takayuki Warisawa, MD, Yusuke Watanabe, MD, Toru Yoshizaki, MD, Satoru Mitomo, MD, Tomohiko Sato, MD, Toru Naganuma, MD, Hisaaki Ishiguro, MD, PhD, Naoyuki Kurita, MD, Shotarou Nakamura, MD, Koji Hozawa, MD, and Sunao Nakamura, MD, PhD

BACKGROUND: This study assesses clinical outcomes after drug-eluting balloon treatment for recurrent in-stent restenosis lesions based on the number of metallic layers.

METHODS AND RESULTS: We enrolled 304 consecutive patients (333 lesions) treated with percutaneous coronary intervention using drug-eluting balloon for in-stent restenosis lesions between March 2014 and June 2015. Per the number of stent layers previously implanted to the lesion, the patients were categorized into 3 groups, 1 stent layer (1L), 166 patients; 2 stent layers (2L), 87 patients; and ≥3 stent layers (≥3L), 51 patients. The end points were major adverse cardiovascular events (MACE), including cardiac death, target lesion revascularization, myocardial infarction, and definite or probable stent thrombosis. No significant differences were observed in patients' baseline characteristics among the groups. The 1-year MACE and target lesion revascularization rates were significantly higher in the ≥3L group than those in the 1L and 2L groups (MACE: 1L, 16.9%; 2L, 16.1%; and ≥3L, 43.1%, $P<0.01$; target lesion revascularization: 1L, 14.5%; 2L, 14.9%; and ≥3L, 41.2%, $P<0.01$). The multivariable Cox regression analysis revealed that the number of metallic layers (≥3L compared with 1L; hazard ratio, 3.17; [95% CI, 1.75–5.76]; $P<0.01$ and hemodialysis [hazard ratio, 2.21; (95% CI, 1.12–4.36); $P=0.02$]) were independent predictors for MACE. No significant differences were observed in the occurrence of cardiac death among the groups ($P=0.34$).

CONCLUSIONS: Seemingly, drug-eluting balloon is less effective for ≥3L in-stent restenosis lesions. Hemodialysis and in-stent restenosis with the number of metallic layers are independent predictors for MACE.

Key Words: drug-eluting stents ■ incidence ■ myocardial infarction ■ percutaneous coronary intervention ■ thrombosis

© 2018 American Heart Association, Inc.

WHAT IS KNOWN

- Previous studies have reported that drug-eluting balloon was not inferior to treat recurrent multilayered-metal in-stent restenosis (including drug-eluting stent and in-stent restenosis).

WHAT THE STUDY ADDS

- Drug-eluting balloon seems to be less effective for ≥3 stent layer in-stent restenosis lesions. More treatment options should be considered with first and second restenoses, and the operator should unfavorably consider making multiple metallic layers (particularly with ≥3 stent layer).

Compared with plain old balloon angioplasty, coronary stent implantation decreases the frequency of restenosis after percutaneous coronary intervention (PCI) by preventing elastic recoil and constrictive remodeling. PCI with drug-eluting stents (DES) has decreased the rate of in-stent restenosis (ISR) remarkably.[1] Although the incidence of ISR is low (<5% at 1 year) with the current generation DES, it remains a primary concern, especially in some populations (ie, patients with diabetes mellitus, renal dysfunction, or presenting complex coronary artery lesions). Several studies have reported repeated DES implantation to treat ISR lesions as better than plain old balloon angioplasty.[2–5] Hence, in the clinical setting, ISR lesions have been treated with additional stent implantation. Currently, drug-eluting balloon (DEB) is considered an attractive option in the management of the bare-metal stent (BMS) ISR lesion compared with plain old balloon angioplasty[6–8] and has been extensively used in this setting. However, recurrent multimetallic-layered ISR has been reported to be associated with unfavorable clinical outcomes,[9] and DEB can prevent the requirement for additional metallic layers, which is estimated to decrease the risk of future stent thrombosis or bleeding because of the requirement for prolonged dual antiplatelet therapy. A study reported that DEB was not inferior in treating recurrent ISR with multimetallic layers compared with another DES deployment.[10]

Owing to the limited data available about the utility of DEB for recurrent ISR lesions with the number of metallic layers, this study aims to investigate clinical outcomes after the DEB treatment in this setting.

METHODS

The data, analytic methods, and study materials will be available to other researchers for reproducing the results or replicating the procedure. We examined 2652 patients treated with PCI at our hospital between March 2014 and June 2015. Of these, we

retrospectively evaluated 304 consecutive patients (333 ISR lesions) treated with DEB. All the patients were categorized into the following 3 groups based on the number of stent layers previously implanted to the lesion: 1 stent layer (1L), 166 patients (180 ISR lesions); 2 stent layers (2L), 87 patients (90 ISR lesions); and ≥3 stent layers (≥3L), 51 patients (63 ISR lesions). Figure 1 shows the study flow. If multiple ISR lesions of 1 patient were treated during the follow-up period, the patient was counted per ISR lesions comprising a different number of stents. Conversely, the patient was not repeatedly counted per ISR lesions, whereas ISR lesion comprising the same number of stents was treated. Of 304 patients, 18 were treated in not only the single ISR group, but also the 1L, 2L, or ≥3L ISR groups. All the clinical follow-ups in this study were conducted by hospital visits or telephonic consultations. This study had already passed New Tokyo Hospital Institutional Review Board approval. We obtained written informed consent from each patient for data collection and analysis in accordance with the Declaration of Helsinki.

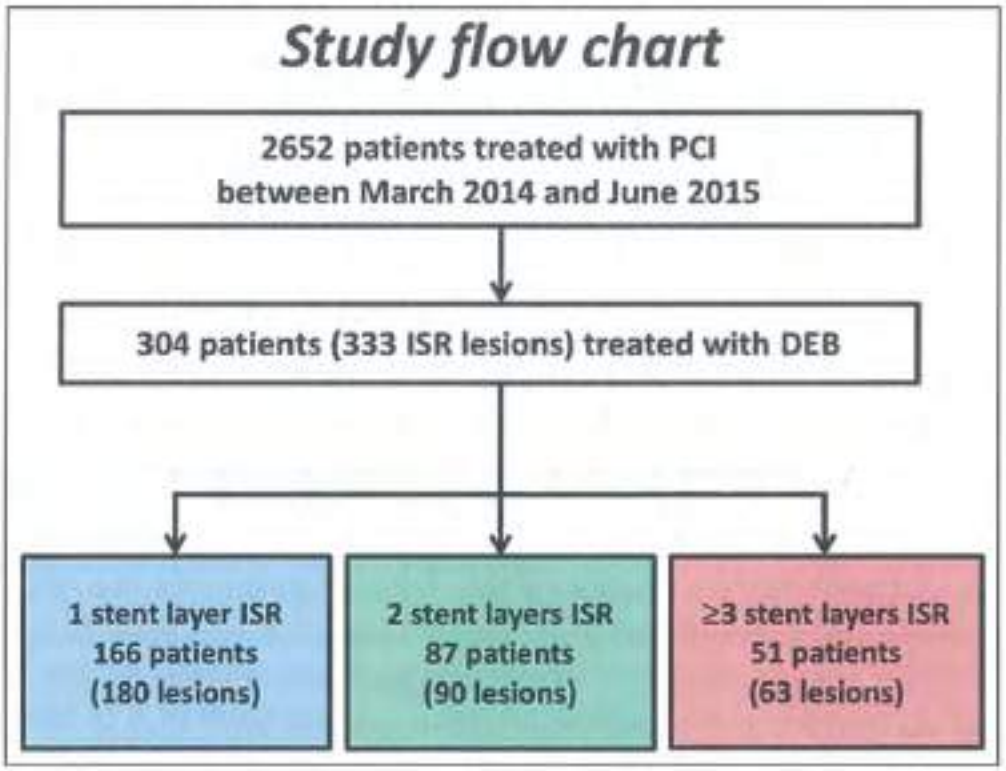

Figure 1. Study population. We examined 2652 patients treated with percutaneous coronary intervention (PCI) at our hospital between March 2014 and June 2015. Of these, we retrospectively evaluated 304 consecutive patients (333 in-stent restenosis [ISR] lesions) treated with drug-eluting balloon (DEB). All the patients were categorized into the following 3 groups based on the number of stent layers previously implanted to the lesion: 1 stent layer, 166 patients (180 ISR lesions); 2 stent layers, 87 patients (90 ISR lesions); and ≥3 stent layers, 51 patients (63 ISR lesions).

In this study, all the patients were treated by predilation with noncompliant balloons or scoring balloons before the DEB treatment. Most of the patients had acceptable angiographic results after predilation,[11] and DEB was inflated at a nominal pressure for a minimum of 30 to 60 seconds to assist drug delivery to the vessel wall. In addition, all the patients were administered dual antiplatelet therapy (200-mg ticlopidine twice daily or

75-mg clopidogrel daily besides low-dose aspirin), at least, 1 month after PCI and advised life-long low-dose aspirin. In cases of ISR within 1 year after DES implantation, the duration of the dual antiplatelet therapy administration depended on the date of the previous BMS or DES implantation.

We defined the 1L ISR, known as the culprit lesion, as a single metallic layer including BMS, first-generation DES (1G-DES), and second-generation DES (2G-DES). In addition, the 2L ISR was defined as double metallic layers, including BMS+BMS, BMS+1G-DES, BMS+2G-DES, 1G-DES+1G-DES, 1G-DES+2G-DES, and 2G-DES+2G-DES. Furthermore, we defined the ≥3L ISR as >3 metallic layers regardless of the initial and last deployed stent type.

The ISR type was classified based on the Mehran classification.[12] If a Mehran type 1A lesion was treated, it was counted as 1L ISR. The ISR lesion covered a broad range, including 1L, 2L, or ≥3L ISR; we counted the most number of stent layers at the DEB treatment lesion. When treating patients with ≥3L ISR, although they were already implanted with multiple stents that resulted in longer ISR lesions (including 4 or 5 longitudinal or layered stents), we focused on the part of the stent layers in this study. Furthermore, we included the stent layers comprising the full cover layers and partial layers and determined the number of layers comprising culprit lesions.

Of the 304 patients, 249 (278 lesions: 1L, 149 lesions; 2L, 73 lesions; and ≥3 L, 56 lesions) underwent an angiographic follow-up scheduled between 6 and 12 months or sooner if the noninvasive evaluation or clinical presentation suggested the presence of ischemia.

Study End Points

In this study, the primary end points were major adverse cardiovascular events (MACE), defined as a composite of target lesion revascularization (TLR), myocardial infarction, definite or probable stent thrombosis, or cardiac death at the 1-year follow-up. TLR was defined as repeated PCI or coronary artery bypass grafting for the lesion in the previously treated ISR segment with DEB or in the adjacent 5 mm. Stent thrombosis was defined per the Academic Research Consortium classification.[13] We defined myocardial infarction as an elevation in the creatine kinase-myocardial band level to >2× the upper limit of normal.[14] Furthermore, a combination with, at least, one of the following: ischemic symptoms, electrocardiographic changes indicative of new ischemia, development of new pathological Q waves on the ECG, imaging evidence of a new loss of viable myocardium or new regional wall motion abnormality, or identification of an intracoronary thrombus by angiography or autopsy.[15] In addition, the quantitative coronary angiographic analysis was performed per the current guidelines.[16] Quantitative coronary angiographic analysis was performed 3× per patient (one immediately before the intervention, one immediately after the intervention, and one at the follow-up), except in patients who did not undergo follow-up coronary angiography. Quantitative coronary angiographic analysis was performed using a validated edge detection system (Cardiovascular Angiography Analysis System, version 2.0; Pie Medical Imaging, the Netherlands). Moreover, angiographic measurements were obtained from matched

orthogonal views before and after each procedure following the administration of intracoronary nitrate. The catheter calibration was based on dimensions of the catheters filled with a contrast medium. In addition, an experienced cardiologist blinded to the clinical procedure analyzed the reference vessel diameter, minimum lumen diameter (MLD), lesion length, and percentage diameter stenosis. Reference vessel diameter was the diameter obtained by an interpolated method, and the lesion length was defined by the curvature analysis. Finally, percentage diameter stenosis was defined as the MLD within the stent associated with the interpolated diameter measured over the length of the stent.

Statistical Analysis

For continuous variables, we used ANOVA to test the difference in the means between the layers and trend of the means by adjusting overlapping a patient among the layers. For binominal variables, we tested the difference in the proportions among the layers and trend using the Cochran-Mantel-Haenszel general association test and correlation test.

In Table 1, the means are expressed as mean (95% CI, lower–upper). The mixed effects models were used for the analysis, with the layer as a fixed effect, and subject as a random effect. In addition, we used the generalized linear mixed effects models for binary response variables, with the layer as a fixed effect, subject as a random effect, and using the logistic link function with the binominal distribution.

Table 1. Baseline Lesion and Procedural Characteristics (Table view)

	1 Layer ISR, 180 Lesions	2 Layers ISR, 90 Lesions	≥3 Layers ISR, 63 Lesions	*P* Value
Lesion characteristics				
RCA	61 (33.9)	37 (41.1)	24 (38.1)	0.50
LAD	81 (45.0)	36 (40.0)	30 (47.6)	0.62
LCX	43 (23.9)	20 (22.2)	12 (19.0)	0.75
Bifurcation	54 (30.0)	18 (20.0)	16 (25.4)	0.14
LMT bifurcation	23 (12.8)	7 (7.8)	9 (14.3)	<0.01
CTO	17 (9.4)	13 (14.4)	12 (19.0)	<0.01
Mehran classification				
	2 (1.1)	0 (0)	0 (0)	0.71

	1 Layer ISR, 180 Lesions	2 Layers ISR, 90 Lesions	≥3 Layers ISR, 63 Lesions	*P* Value
Mehran 1A				
Mehran 1B	9 (5.0)	3 (3.3)	0 (0)	0.19
Mehran 1C	114 (63.3)	48 (53.3)	35 (55.6)	0.25
Mehran 1D	1 (0.6)	3 (3.3)	3 (4.8)	<0.01
Mehran 2	28 (15.6)	19 (21.1)	12 (19.0)	0.12
Mehran 3	10 (5.6)	4 (4.4)	2 (3.2)	0.84
Mehran 4	16 (8.9)	13 (14.4)	12 (19.0)	<0.01
Procedural characteristics				
DEB size, mm	2.91 (2.85–2.98)	2.99 (2.89–3.08)	3.04 (2.93–3.16)	0.12
DEB length, mm*	23.8 (22.1–25.7)	29.0 (26.1–32.3)	32.5 (28.6–37.0)	<0.01
No. of DEB*	1.16 (1.09–1.23)	1.34 (1.23–1.45)	1.54 (1.39–1.70)	<0.01
Usage of scoring balloon	93 (51.7)	40 (44.4)	34 (54.0)	0.61
Rotational atherectomy	11 (6.1)	7 (7.8)	5 (7.9)	0.19
IVUS	44 (24.4)	30 (33.3)	12 (19.0)	0.05

	1 Layer ISR, 180 Lesions	2 Layers ISR, 90 Lesions	≥3 Layers ISR, 63 Lesions	*P* Value
OCT	70 (38.9)	22 (24.4)	15 (23.8)	0.05
Periprocedural MI	2 (1.1)	3 (3.3)	1 (1.6)	0.40

CTO indicates chronic total occlusion; DEB, drug-eluting balloon; ISR, in-stent restenosis; IVUS, intravascular ultrasound; LAD, left anterior descending artery; LCX, left circumflex artery; LMT, left main trunk; MI, myocardial infarction; OCT, optical coherence tomography; and RCA, right coronary artery.
* The distribution lesion length was skewed. Thus, we used log transformation of the values for analysis.

In Table 2, we used the mixed effects models to analyze the MLD, reference vessel diameter, and % diameter stenosis, with the follow-up period, layer, and the interaction of layer by the follow-up period as fixed effects, and subject and lesion within the subject as random effects. In addition, the mixed effects models were used for the analysis of lesion length, with the layer as a fixed effect, and subject as a random effect.

Table 2. Quantitative Coronary Angiographic Analysis (Table view)

	1 Layer ISR	2 Layers ISR	≥3 Layers ISR	*P* Value
	180 Lesions	90 Lesions	63 Lesions	
Baseline				
MLD, mm	0.79 (0.71–0.88)	0.69 (0.57–0.81)	0.74 (0.60–0.88)	0.34
RVD, mm	2.42 (2.28–2.56)	2.49 (2.30–2.69)	2.68 (2.44–2.92)	0.17
% diameter stenosis	65.7 (62.9–68.6)	71.6 (67.5–75.7)	71.3 (66.5–76.2)	0.03
Lesion length, mm*	18.8 (17.5–20.3)	22.3 (20.1–24.8)	25.1 (22.1–28.4)	<0.01
Postprocedural				

	1 Layer ISR	2 Layers ISR	≥3 Layers ISR	*P* Value
	180 Lesions	90 Lesions	63 Lesions	
MLD, mm	1.90 (1.82–1.99)	1.92 (1.80–2.03)	1.95 (1.81–2.09)	0.83
RVD, mm	2.49 (2.35–2.63)	2.80 (2.61–3.00)	2.62 (2.39–2.86)	0.04
% diameter stenosis	22.7 (19.8–25.6)	24.6 (20.5–28.6)	25.8 (20.9–30.7)	0.51
Follow-up	149 lesions	73 lesions	56 lesions	
MLD, mm	1.56 (1.47–1.65)	1.53 (1.40–1.66)	1.18 (1.04–1.33)	<0.01
RVD, mm	2.43 (2.28–2.59)	2.44 (2.23–2.66)	2.59 (2.34–2.84)	0.53
% diameter stenosis	35.7 (32.5–38.8)	37.5 (33.0–42.0)	54.3 (49.1–59.4)	<0.01

ISR indicates in-stent restenosis; MLD, minimum lumen diameter; and RVD, reference vessel diameter.
* The distribution lesion length was skewed. Thus, we used log transformation of the values for analysis.

Furthermore, the distribution lesion length was skewed. Thus, we used log transformation of the values was used for analysis in Tables 1, 2, and 3.

Table 3. Univariable and Multivariable Analyses of MACE (Table view)

Predictor of MACE, n=64	n	MACE	Incidence, %	Univariable			Multivariable		
				Hazard Ratio	95% CI	*P* Value	Hazard Ratio	95% CI	*P* Value
HT									
No	41	9	22.0						

Predictor of MACE, n=64	n	MACE	Incidence, %	Univariable Hazard Ratio	Univariable 95% CI	Univariable *P* Value	Multivariable Hazard Ratio	Multivariable 95% CI	Multivariable *P* Value
Yes	263	55	20.9	0.86	0.42–1.77	0.68			
DM									
No	155	29	18.7						
Yes	149	35	23.5	1.08	0.65–1.79	0.76	0.93	0.55–1.56	0.77
CKD (/eGFR>60)									
eGFR>60	127	28	22.0						
CKD (30<eGFR<60)	118	21	17.8	0.83	0.46–1.50	0.54			
CKD (eGFR<30, non-HD)	12	0	0	0.00	0.00–0.00	<0.01			
HD									
No	257	49	19.1						
Yes	47	15	31.9	2.25	1.23–4.10	<0.01	2.21	1.12–4.36	0.02
CTO									
No	266	55	20.7						
Yes	38	9	23.7	1.19	0.58–2.45	0.63	0.94	0.41–2.12	0.87

Predictor of MACE, n=64	n	MACE	Incidence, %	Univariable			Multivariable		
				Hazard Ratio	95% CI	*P* Value	Hazard Ratio	95% CI	*P* Value
Bifurcation									
No	227	42	18.5						
Yes	77	22	28.6	1.68	1.01–2.81	0.05	1.54	0.85–2.80	0.15
LMT bifurcation									
No	271	55	20.3						
Yes	33	9	27.3	1.42	0.66–3.06	0.37			
Lesion length, mm*									
Continuous	304	64	21.1	1.14	0.82–1.58	0.45	1.06	0.74–1.53	0.74
No. of layers (/1 layer)									
1 layer	166	28	16.9						
2 layers	87	14	16.1	0.84	0.45–1.55	0.57	0.89	0.46–1.75	0.74
≥3 layers	51	22	43.1	2.96	1.69–5.19	<0.01	3.17	1.75–5.76	<0.01
Last deployed stent									
BMS	25	3	12						
1G-DES	89	14	15.7	1.25	0.36–4.31	0.72			
	186	46	24.7	2.21		0.18			

Predictor of MACE, n=64	n	MACE	Incidence, %	Univariable			Multivariable		
				Hazard Ratio	95% CI	*P* Value	Hazard Ratio	95% CI	*P* Value
2G-DES					0.69 –7.06				

Cox proportional hazard models for adjusting overlapping a patient among the layers were used. 1G-DES indicates first-generation drug-eluting stent; 2G-DES, second-generation drug-eluting stent; BMS, bare-metal stent; CKD, chronic kidney disease; CTO, chronic total occlusion; DM, diabetes mellitus; eGFR, estimated glomerular filtration rate; HD, hemodialysis; HT, hypertension; LMT, left main trunk; and MACE, major adverse cardiovascular events.
* The distribution lesion length was skewed. Thus, we used log transformation of the values for analysis.

A follow-up was censored at the date of the last follow-up or after 1 year. The time until the event was calculated using the Kaplan-Meier analysis. The log-rank test was used to compare the event-free survival was compared among the 3 groups. In addition, we performed the multivariable Cox regression analysis to determine the independent risk factors for MACE and used the Cox proportional hazard models for adjusting overlapping patients among the layers. All the variables with $P<0.10$ at the univariable analysis and those determined to be clinically significant were included in the final model. The number of variables used for the final model was limited to 1 for every 8 to 10 events to avoid overfitting. Of note, all the reported *P* values in this study are 2-sided, and we considered $P<0.05$ as statistically significant. All the statistical analyses were conducted using the SPSS software (SPSS version 22.0; IBM, NY) and SAS software (SAS version 9.4; SAS Institute Inc).

RESULTS

No significant differences were observed in the patients' baseline characteristics among the 3 groups (Table 4). The prevalence of diabetes mellitus was 49.4%, 42.5%, and 58.8% ($P=0.18$). The patients with chronic kidney disease or hemodialysis were comparable among the 3 groups. Table 1 presents the lesion and procedural characteristics. The mean DEB size was 2.91, 2.99, and 3.04 mm ($P=0.12$), and the mean DEB length was 23.8, 29.0, and 32.5 mm ($P<0.01$) in the 1L, 2L, and ≥3L ISR groups, respectively. In the procedural characteristics, the number of DEB was observed frequently in the ≥3L group ($P<0.01$). In addition, the lesion length, vessel diameter, and plaque imaging were assessed by intravascular ultrasound or by optical coherence tomography in more than half of patients.

Table 4. Baseline Patients' Characteristics (Table view)

	1 Layer ISR, 166 Patients (180 Lesions)	2 Layers ISR, 87 Patients (90 Lesions)	≥3 Layers ISR, 51 Patients (63 Lesions)	*P* Value
Age	69.8±9.9	72.6±8.8	69.5±10.8	0.08
Male	128 (77.1)	68 (78.2)	40 (78.4)	0.97
HT	141 (84.9)	75 (86.2)	47 (92.2)	0.42
DL	121 (72.9)	71 (81.6)	40 (78.4)	0.28
DM	82 (49.4)	37 (42.5)	30 (58.8)	0.18
eGFR>60	69 (41.6)	35 (40.2)	20 (39.2)	0.95
CKD (30<eGFR<60)	60 (36.1)	38 (43.7)	19 (37.3)	0.50
CKD (eGFR<30, non-HD)	7 (4.2)	2 (2.3)	3 (5.9)	0.56
HD	27 (16.3)	12 (13.8)	8 (15.7)	0.87
Previous MI	95 (57.2)	59 (67.8)	34 (66.7)	0.19
PAD	15 (9.1)	14 (16.1)	10 (19.6)	0.08
Pretreated CABG	13 (7.8)	7 (8.0)	9 (17.6)	0.10
LVEF, %*	56.0±10.5	56.0±11.2	50.9±13.5	0.07

CABG indicates coronary artery bypass grafting; CKD, chronic kidney disease; DL, dyslipidemia; DM, diabetes mellitus; eGFR, estimated glomerular filtration rate; HD, hemodialysis; HT, hypertension; ISR, in-stent restenosis; LVEF, left ventricular ejection fraction; MI, myocardial infarction; and PAD, peripheral artery disease.

* For continuous variables, we used ANOVA to test the difference in the means among the layers and trend of the means by adjusting overlapping a patient among the layers. For binominal variables, we tested the difference in the proportions among the layers and trend using the Cochran-Mantel-Haenszel general association test and correlation test.

Table 2 presents the quantitative coronary angiographic analysis results. The lesion length was longer in the ≥3L group compared with that in the other groups (18.8, 22.3, and 25.1 mm; $P<0.01$). Significant percentage diameter stenosis existed in the ≥3L group compared with that in the other groups during the follow-up period ($P<0.01$). In all, 5 patients required additional stent implantation (4 patients, DES; 1 patient, BMS) after

the DEB treatment, and 1 of these 5 patients experienced underexpansion after predilation and DEB. Table 5 describes the reasons for the additional stent implantation in the 5 patients.

Table 5. Patients' List of Required Additional Stent Implantation After Drug-Eluting Balloon Treatment (Table view)

No.	The Reason of Required Additional Stent Implantation	Age	EF, %	Lesion	Additional Stent	Pre-MLD, mm	Postpr MLD, mm
1	Dissection after DEB inflation	65	64.6	LCX	Xience	0.65	1.59
2	Dissection after DEB inflation	67	38.7	RCA	Resolute	0.58	2.4
3	Underexpansion (after predilation+DEB)	66	42.4	RCA	Integrity (BMS)	0.29	2.78
4	Plaque shift to distal vessel	46	52.2	RCA	Resolute	0 (total occlusion)	1.66
5	Dissection after DEB inflation	65	61.1	LAD	Xience	0.39	1.2

BMS indicates bare-metal stent; DEB, drug-eluting balloon; EF, ejection fraction; LAD, left anterior descending artery; LCX, left circumflex artery; MLD, minimum lumen diameter; and RCA, right coronary artery.

Table 6 presents the clinical outcomes at 1 year using the survival analysis. Both the MACE and TLR rates at 1 year were significantly higher in the ≥3L group compared with that in the other 2 groups (P<0.01; Figure 2). However, no significant differences were observed in other clinical outcomes.

Table 6. Clinical Outcomes at 1 Year (Table view)

	1 Layer ISR, 166 Patients	2 Layers ISR, 87 Patients	≥3 Layers ISR, 51 Patients	*P* Value
MACE	28 (16.9)	14 (16.1)	22 (43.1)	<0.01
TLR	24 (14.5)	13 (14.9)	21 (41.2)	<0.01
All death	7 (4.2)	3 (3.4)	1 (2.0)	0.73
Cardiac death	4 (2.4)	0 (0)	1 (2.0)	0.34
MI (after DEB)	3 (1.8)	0 (0)	2 (3.9)	0.21
Stent thrombosis	3 (1.8)	0 (0)	1 (2.0)	0.43

DEB indicates drug-eluting balloon; ISR, in-stent restenosis; MACE, major adverse cardiovascular events; MI, myocardial infarction; and TLR, target lesion revascularization.

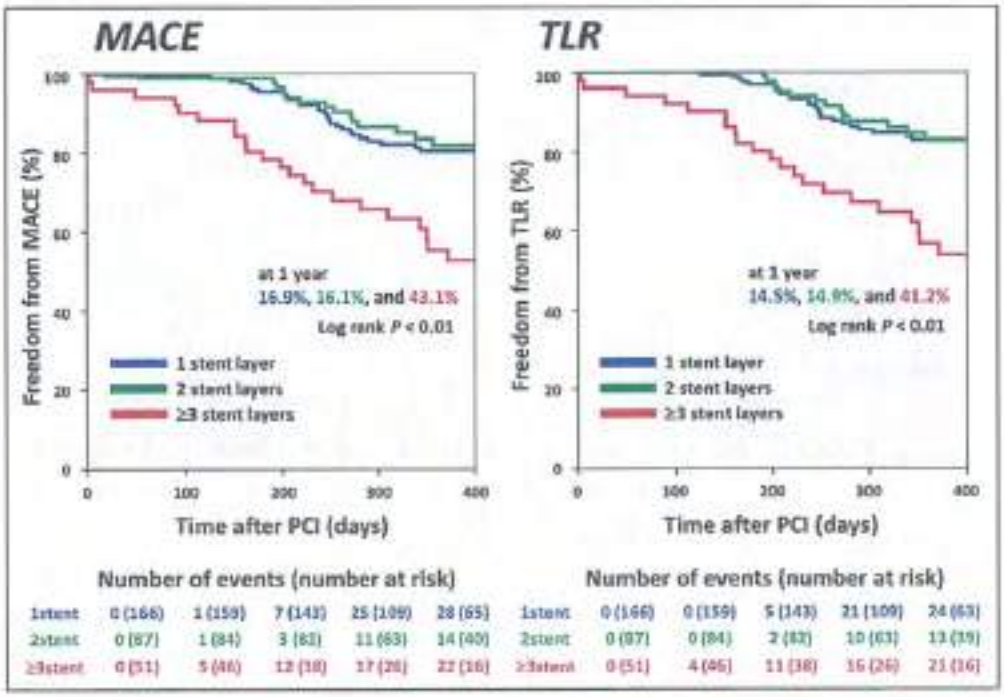

Figure 2. **Kaplan-Meier curves of major adverse cardiac events (MACE) and target lesion revascularization (TLR).** MACE and TLR rates at 1 year were significantly higher in the ≥3 stent layer

group compared with that in the other 2 groups ($P<0.01$). PCI indicates percutaneous coronary intervention.

Table 3 presents univariable and multivariable analyses. We included hemodialysis, bifurcation lesions, and the number of layers to the final multivariable model because of $P<0.10$. In addition, we included diabetes mellitus, chronic total occlusion, and the lesion length to the final multivariable model because these factors were considered to be clinically important (finally, 6 factors were included). In contrast, other factors were not included in the final multivariable model. The multivariable analysis revealed that the following were risk factors of MACE: the number of metallic layers previously implanted (≥3L compared with 1L; hazard ratio, 3.17; [95% CI, 1.75–5.76]; $P<0.01$ and hemodialysis [hazard ratio, 2.21; (95% CI, 1.12–4.36); $P=0.02$]). Furthermore, the univariable and multivariable analyses revealed that the lesion length was not a predictor for MACE (univariable: hazard ratio, 1.14; [95% CI, 0.82–1.58], $P=0.45$; multivariable: hazard ratio, 1.06; [95% CI, 0.74–1.53], $P=0.74$).

DISCUSSION

The primary findings of this study are as follows:

1. DEB for ISR lesions with more than triple metallic layers resulted in a higher incidence of MACE compared with those with single or double metallic layers.
2. MACE were mainly driven by TLR.
3. Hemodialysis and ISR with the number of metallic layers were independent predictors for MACE.

Several randomized and observational studies have reported the post-treatment clinical outcomes after treatment of ISR.[5,17–20] Although DEB has been currently considered as an alternative option for DES-ISR,[6,7,21] its efficacy for recurrent multimetallic-layered ISR remains unclear. Some studies have investigated the efficacy of DEB in patients classified by the previously implanted number of stents. Kawamoto et al[10] reported that DEB was not inferior to treat recurrent multilayered-metallic ISR compared with the DES treatment, and Rittger et al[22] reported that DEB was effective for both DES-ISR with single-layer stent and multiple stent layers (>2 stents). Thus, we evaluated the impact of recurrent restenosis with multimetallic layers, particularly ≥3L ISR, when treated with DEB.

In addition, previous studies have reported that DEB was effective for both BMS-ISR and DES-ISR compared with the 2G-DES implantation.[7,8,17] These studies demonstrated the comparable late luminal loss between the DEB and DES treatment. This study demonstrated that MLD was smaller in the multilayered ISR groups compared with that in the single-layered ISR group, irrespective of the comparable acute gain among all the groups. Kang et al[23] reported that stent underexpansion was observed in 35% of lesions treated with long DES, although neointimal hyperplasia was the dominant mechanism of ISR. Perhaps, stent underexpansion or stent fractures with multimetallic layers could be

more difficult to correct than that with single-metal–layered ISR, resulting in worse clinical outcomes.

The ISAR-DESIRE 4 (Intracoronary Stenting and Angiographic Results: Optimizing Treatment of Drug Eluting Stent In-Stent Restenosis 4) trial reported that the plaque modification using a scoring balloon resulted in less in-stent diameter stenosis at the 6- to 8-month follow-up compared with conventional treatment.[24] However, no differences existed in clinical outcomes between the groups. In this study, the scoring balloon was used in 50.2% (1L, 51.7%; 2L, 44.4%; and ≥3L, 54.0%; P=0.61). The liberal use of scoring balloons could be beneficial in terms of restenosis rates.

In this study, hemodialysis and ISR with multimetallic layers were independent predictors for MACE. In line with previous studies, the lesion length and ISR recurrence within 1 year were independent predictors for TLR.[10] In addition, early recurrence (within 1 year) of ISR could be a consequence of the plaque characteristics of the neointima.[25] Previously, a diffuse ISR pattern has been reported as a predictor of recurrent restenosis.[21,26,27] However, we could not determine predictors for TLR because some patients had multiple ISR lesions treated with DEB.

However, Lee et al[28] reported that DEB is not effective in hemodialysis patients, both BMS-ISR and DES-ISR, compared with nonhemodialysis patients; in line with this study, our results revealed that hemodialysis was an independent predictor for MACE, which could be attributed to the severity of coronary calcification. A study reported severe calcification and resultant stent recoil in patients with hemodialysis, as well as episodic increases in serum Ca level, as observed during hemodialysis or with the use of vitamin D analogs or Ca-based P binders, which potentially could affect vascular calcification in these patients.[29] Furthermore, hemodialysis typically presents concomitantly with systematic diseases, such as diabetes mellitus and hypertension, which cause the progression of in-stent neointimal hyperplasia because of inflammatory responses.

Thus, a dedicated follow-up is required, especially for patients with hemodialysis and patients treated with multimetallic layers. If recurrent ISR is observed in these patients, we should not hesitate to perform appropriate treatment, except for DEB that requires medical treatment, further DES implantation, or coronary artery bypass grafting.

Limitations

This study has some limitations. First, the small cohort of patients and the lack of randomization. However, it should be noted that a randomized study is theoretically impossible to demonstrate the impact of multimetallic layers ISR on clinical outcomes. In addition, a larger study sample with an extended follow-up is required to elucidate the efficacy of PCI using DEB in these populations.

Second, this study enrolled patients treated only with DEB or with DEB and additional DES. Thus, we assessed the lesion treated only with DEB irrespective of the additional stent treatment; however, the procedure described in this study was not always consistent. The use of DEB or DES was at the discretion of each operator in this retrospective study. Hence, the exact number of patients on whom the operator initially planned to use DEB remains unclear because of the retrospective nature of this study.

Finally, the details of restenosis (eg, stent underexpansion or neointimal hyperplasia) could not be assessed in this study because of the limited usage (40% to 50%) of intravascular imaging (intravascular ultrasound or optical coherence tomography). Moreover, intravascular imaging after the DEB treatment was available only for 20% to 30% of patients, which was not adequate to guarantee the optimal expansion and precisely evaluate MLD or reference vessel diameter at the site of the ISR. Furthermore, systematic intravascular ultrasound or optical coherence tomography follow-up was not performed in this study. Hence, we could not assess the impact of plaque characteristics inside of the stents treated with DEB, which may affect clinical outcomes.

Conclusions

DEB seems to be less effective for ≥3L ISR lesions. Hence, more treatment options should be considered with first and second restenoses, and the operator should unfavorably consider making multiple metallic layers (particularly with ≥3L). Furthermore, hemodialysis and ISR with the number of metallic layers were independent predictors for MACE.

ARTICLE INFORMATION

Received 6 September 2017; accepted 21 June 2018.
https://www.ahajournals.org/journal/circinterventions

Correspondence

Hiroto Yabushita, MD, Interventional Cardiology Unit, New Tokyo Hospital, 1271 Wanagaya, Matsudo, Chiba 270-2232, Japan. Email hiroto19841017@gmail.com

Affiliations

Interventional Cardiology Unit, New Tokyo Hospital, Chiba, Japan.

Disclosures

None.

REFERENCES

1. Stone, GW, Ellis, SG, Cannon, L, Mann, JT, Greenberg, JD, Spriggs, D, O'Shaughnessy, CD, DeMaio, S, Hall, P, Popma, JJ, Koglin, J, Russell, ME; TAXUS V Investigators. Comparison of a polymer-based paclitaxel-eluting stent with a bare metal stent in patients with complex coronary artery disease: a randomized controlled trial. *JAMA*. 2005;294:1215–1223. doi: 10.1001/jama.294.10.1215 Crossref. PubMed.
2. Abe, M, Kimura, T, Morimoto, T, Taniguchi, T, Yamanaka, F, Nakao, K, Yagi, N, Kokubu, N, Kasahara, Y, Kataoka, Y, Otsuka, Y, Kawamura, A, Miyazaki, S, Nakao, K, Horiuchi, K, Ito, A, Hoshizaki, H, Kawaguchi, R, Setoguchi, M, Inada, T, Kishi, K, Sakamoto, H, Morioka, N, Imai, M, Shiomi, H, Nonogi, H, Mitsudo, K; j-Cypher Registry Investigators. Sirolimus-eluting stent versus balloon angioplasty for sirolimus-eluting stent restenosis: insights from the j-Cypher Registry. *Circulation*. 2010;122:42–51. doi: 10.1161/CIRCULATIONAHA.109.905802 Crossref. PubMed.
3. Kim, YH, Lee, BK, Park, DW, Park, KH, Choi, BR, Lee, CW, Hong, MK, Kim, JJ, Park, SW, Park, SJ. Comparison with conventional therapies of repeated sirolimus-eluting stent

implantation for the treatment of drug-eluting coronary stent restenosis. *Am J Cardiol*. 2006;98:1451–1454. doi: 10.1016/j.amjcard.2006.07.027 Crossref. PubMed.

4. Kitahara, H, Kobayashi, Y, Takebayashi, H, Fujimoto, Y, Nakamura, Y, Kuroda, N, Himi, T, Miyazaki, A, Haruta, S, Komuro, I. Re-restenosis and target lesion revascularization after treatment of sirolimus-eluting stent restenosis: retrospective analysis of 4 Japanese hospitals. *Circ J*. 2009;73:867–871. Crossref. PubMed.
5. Ko, YG, Kim, JS, Kim, BK, Choi, D, Hong, MK, Jeon, DW, Yang, JY, Ahn, YK, Jeong, MH, Yu, CW, Yun, KH, Lim, DS, Jang, Y; KISS Investigators. Efficacy of drug-eluting stents for treating in-stent restenosis of drug-eluting stents (from the Korean DES ISR multicenter registry study [KISS]). *Am J Cardiol*. 2012;109:607–613. doi: 10.1016/j.amjcard.2011.10.014 Crossref. PubMed.
6. Habara, S, Mitsudo, K, Kadota, K, Goto, T, Fujii, S, Yamamoto, H, Katoh, H, Oka, N, Fuku, Y, Hosogi, S, Hirono, A, Maruo, T, Tanaka, H, Shigemoto, Y, Hasegawa, D, Tasaka, H, Kusunose, M, Otsuru, S, Okamoto, Y, Saito, N, Tsujimoto, Y, Eguchi, H, Miyake, K, Yoshino, M. Effectiveness of paclitaxel-eluting balloon catheter in patients with sirolimus-eluting stent restenosis. *JACC Cardiovasc Interv*. 2011;4:149–154. doi: 10.1016/j.jcin.2010.10.012 Crossref. PubMed.
7. Rittger, H, Brachmann, J, Sinha, AM, Waliszewski, M, Ohlow, M, Brugger, A, Thiele, H, Birkemeyer, R, Kurowski, V, Breithardt, OA, Schmidt, M, Zimmermann, S, Lonke, S, von Cranach, M, Nguyen, TV, Daniel, WG, Wöhrle, J. A randomized, multicenter, single-blinded trial comparing paclitaxel-coated balloon angioplasty with plain balloon angioplasty in drug-eluting stent restenosis: the PEPCAD-DES study. *J Am Coll Cardiol*. 2012;59:1377–1382. doi: 10.1016/j.jacc.2012.01.015 Crossref. PubMed.
8. Scheller, B, Hehrlein, C, Bocksch, W, Rutsch, W, Haghi, D, Dietz, U, Böhm, M, Speck, U. Treatment of coronary in-stent restenosis with a paclitaxel-coated balloon catheter. *N Engl J Med*. 2006;355:2113–2124. doi: 10.1056/NEJMoa061254 Crossref. PubMed.
9. Alfonso, F, García, J, Pérez-Vizcayno, MJ, Hernando, L, Hernandez, R, Escaned, J, Jiménez-Quevedo, P, Bañuelos, C, Macaya, C. New stent implantation for recurrences after stenting for in-stent restenosis: implications of a third metal layer in human coronary arteries. *J Am Coll Cardiol*. 2009;54:1036–1038. doi: 10.1016/j.jacc.2009.04.082 Crossref. PubMed.
10. Kawamoto, H, Ruparelia, N, Latib, A, Miyazaki, T, Sato, K, Mangieri, A, Contri, R, Stella, S, Figini, F, Chieffo, A, Carlino, M, Montorfano, M, Colombo, A. Drug- coated balloons versus second-generation drug-eluting stents for the management of recurrent multimetal-layered in-stent restenosis. *JACC Cardiovasc Interv*. 2015;8:1586–1594. doi: 10.1016/j.jcin.2015.04.032 Crossref. PubMed.
11. Kleber, FX, Rittger, H, Bonaventura, K, Zeymer, U, Wöhrle, J, Jeger, R, Levenson, B, Möbius-Winkler, S, Bruch, L, Fischer, D, Hengstenberg, C, Pörner, T, Mathey, D, Scheller, B. Drug-coated balloons for treatment of coronary artery disease: updated recommendations from a consensus group. *Clin Res Cardiol*. 2013;102:785–797. doi: 10.1007/s00392-013-0609-7 Crossref. PubMed.
12. Mehran, R, Dangas, G, Abizaid, AS, Mintz, GS, Lansky, AJ, Satler, LF, Pichard, AD, Kent, KM, Stone, GW, Leon, MB. Angiographic patterns of in-stent restenosis: classification and implications for long-term outcome. *Circulation*. 1999;100:1872–1878. Crossref. PubMed.
13. Laskey, WK, Yancy, CW, Maisel, WH. Thrombosis in coronary drug-eluting stents: report from the meeting of the circulatory system medical devices advisory panel of the food and drug

administration center for devices and radiologic health, December 7-8, 2006. *Circulation*. 2007;115:2352–2357. doi: 10.1161/CIRCULATIONAHA.107.688416 Crossref. PubMed.

14. Thygesen, K, Alpert, JS, White, HD; Joint ESC/ACCF/AHA/WHF Task Force for the Redefinition of Myocardial Infarction. Universal definition of myocardial infarction. *J Am Coll Cardiol*. 2007;50:2173–2195. doi: 10.1016/j.jacc.2007.09.011 Crossref. PubMed.

15. Thygesen, K, Alpert, JS, Jaffe, AS, Simoons, ML, Chaitman, BR, White, HD, Thygesen, K, Alpert, JS, White, HD, Jaffe, AS, Katus, HA, Apple, FS, Lindahl, B, Morrow, DA, Chaitman, BR, Clemmensen, PM, Johanson, P, Hod, H, Underwood, R, Bax, JJ, Bonow, JJ, Pinto, F, Gibbons, RJ, Fox, KA, Atar, D, Newby, LK, Galvani, M, Hamm, CW, Uretsky, BF, Steg, PG, Wijns, W, Bassand, JP, Menasche, P, Ravkilde, J, Ohman, EM, Antman, EM, Wallentin, LC, Armstrong, PW, Simoons, ML, Januzzi, JL, Nieminen, MS, Gheorghiade, M, Filippatos, G, Luepker, RV, Fortmann, SP, Rosamond, WD, Levy, D, Wood, D, Smith, SC, Hu, D, Lopez-Sendon, JL, Robertson, RM, Weaver, D, Tendera, M, Bove, AA, Parkhomenko, AN, Vasilieva, EJ, Mendis, S, Bax, JJ, Baumgartner, H, Ceconi, C, Dean, V, Deaton, C, Fagard, R, Funck-Brentano, C, Hasdai, D, Hoes, A, Kirchhof, P, Knuuti, J, Kolh, P, McDonagh, T, Moulin, C, Popescu, BA, Reiner, Z, Sechtem, U, Sirnes, PA, Tendera, M, Torbicki, A, Vahanian, A, Windecker, S, Morais, J, Aguiar, C, Almahmeed, W, Arnar, DO, Barili, F, Bloch, KD, Bolger, AF, Botker, HE, Bozkurt, B, Bugiardini, R, Cannon, C, de Lemos, J, Eberli, FR, Escobar, E, Hlatky, M, James, S, Kern, KB, Moliterno, DJ, Mueller, C, Neskovic, AN, Pieske, BM, Schulman, SP, Storey, RF, Taubert, KA, Vranckx, P, Wagner, DR; Joint ESC/ACCF/AHA/WHF Task Force for Universal Definition of Myocardial Infarction; Authors/Task Force Members Chairpersons; Biomarker Subcommittee; ECG Subcommittee; Imaging Subcommittee; Classification Subcommittee; Intervention Subcommittee; Trials & Registries Subcommittee; Trials & Registries Subcommittee; Trials & Registries Subcommittee; Trials & Registries Subcommittee; ESC Committee for Practice Guidelines (CPG); Document Reviewers. Third universal definition of myocardial infarction. *J Am Coll Cardiol*. 2012;60:1581–1598. doi: 10.1016/j.jacc.2012.08.001. Crossref. PubMed.

16. Serruys, PW, Kay, IP, Disco, C, Deshpande, NV, de Feyter, PJ. Periprocedural quantitative coronary angiography after Palmaz-Schatz stent implantation predicts the restenosis rate at six months: results of a meta-analysis of the Belgian Netherlands Stent study (BENESTENT) I, BENESTENT II Pilot, BENESTENT II and MUSIC trials. Multicenter ultrasound stent in coronaries. *J Am Coll Cardiol*. 1999;34:1067–1074. PubMed.

17. Alfonso, F, Pérez-Vizcayno, MJ, Cárdenas, A, García Del Blanco, B, Seidelberger, B, Iñiguez, A, Gómez-Recio, M, Masotti, M, Velázquez, MT, Sanchís, J, García-Touchard, A, Zueco, J, Bethencourt, A, Melgares, R, Cequier, A, Dominguez, A, Mainar, V, López-Mínguez, JR, Moreu, J, Martí, V, Moreno, R, Jiménez-Quevedo, P, Gonzalo, N, Fernández, C, Macaya, C; RIBS V Study Investigators, under the auspices of the Working Group on Interventional Cardiology of the Spanish Society of Cardiology. A randomized comparison of drug-eluting balloon versus everolimus-eluting stent in patients with bare-metal stent-in-stent restenosis: the RIBS V Clinical Trial (Restenosis Intra-stent of Bare Metal Stents: paclitaxel-eluting balloon vs. everolimus-eluting stent). *J Am Coll Cardiol*. 2014;63:1378–1386. doi: 10.1016/j.jacc.2013.12.006 PubMed.

18. Alfonso, F, Pérez-Vizcayno, MJ, Hernández, R, Bethencourt, A, Martí, V, López-Mínguez, JR, Angel, J, Iñiguez, A, Morís, C, Cequier, A, Sabaté, M, Escaned, J, Jiménez-Quevedo, P, Bañuelos, C, Suárez, A, Macaya, C; RIBS-II Investigators. Long-term clinical benefit of sirolimus-eluting stents in patients with in-stent restenosis results of the RIBS-II (Restenosis

Intra-stent: Balloon angioplasty vs. elective sirolimus-eluting Stenting) study. *J Am Coll Cardiol*. 2008;52:1621–1627. doi: 10.1016/j.jacc.2008.08.025 Crossref. PubMed.

19. Mehilli, J, Byrne, RA, Tiroch, K, Pinieck, S, Schulz, S, Kufner, S, Massberg, S, Laugwitz, KL, Schömig, A, Kastrati, A; ISAR-DESIRE 2 Investigators. Randomized trial of paclitaxel- versus sirolimus-eluting stents for treatment of coronary restenosis in sirolimus-eluting stents: the ISAR-DESIRE 2 (Intracoronary Stenting and Angiographic Results: Drug Eluting Stents for In-Stent Restenosis 2) study. *J Am Coll Cardiol*. 2010;55:2710–2716. doi: 10.1016/j.jacc.2010.02.009 Crossref. PubMed.
20. Unverdorben, M, Vallbracht, C, Cremers, B, Heuer, H, Hengstenberg, C, Maikowski, C, Werner, GS, Antoni, D, Kleber, FX, Bocksch, W, Leschke, M, Ackermann, H, Boxberger, M, Speck, U, Degenhardt, R, Scheller, B. Paclitaxel-coated balloon catheter versus paclitaxel-coated stent for the treatment of coronary in-stent restenosis. *Circulation*. 2009;119:2986–2994. doi: 10.1161/CIRCULATIONAHA.108.839282 Crossref. PubMed.
21. Cosgrave, J, Melzi, G, Biondi-Zoccai, GG, Airoldi, F, Chieffo, A, Sangiorgi, GM, Montorfano, M, Michev, I, Carlino, M, Bonizzoni, E, Colombo, A. Drug-eluting stent restenosis the pattern predicts the outcome. *J Am Coll Cardiol*. 2006;47:2399–2404. doi: 10.1016/j.jacc.2006.02.046 Crossref. PubMed.
22. Rittger, H, Wöhrle, J, Brachmann, J, Hohenforst-Schmidt, W, Schlundt, C, Lonke, S, von Cranach, M, Markovic, S, Achenbach, S, Waliszewski, M. Angiographic patterns of drug-eluting stent restenosis after treatment with drug-coated balloon versus balloon angioplasty: late lumen loss subgroup analyses of the PEPCAD-DES study. *Catheter Cardiovasc Interv*. 2016;88:529–534. doi: 10.1002/ccd.26451 Crossref. PubMed.
23. Kang, SJ, Mintz, GS, Park, DW, Lee, SW, Kim, YH, Whan Lee, C, Han, KH, Kim, JJ, Park, SW, Park, SJ. Mechanisms of in-stent restenosis after drug-eluting stent implantation: intravascular ultrasound analysis. *Circ Cardiovasc Interv*. 2011;4:9–14. doi: 10.1161/CIRCINTERVENTIONS.110.940320 Crossref. PubMed.
24. Kufner, S, Joner, M, Schneider, S, Tölg, R, Zrenner, B, Repp, J, Starkmann, A, Xhepa, E, Ibrahim, T, Cassese, S, Fusaro, M, Ott, I, Hengstenberg, C, Schunkert, H, Abdel-Wahab, M, Laugwitz, KL, Kastrati, A, Byrne, RA; ISAR-DESIRE 4 Investigators. Neointimal modification with scoring balloon and efficacy of drug-coated balloon therapy in patients with restenosis in drug-eluting coronary stents: a randomized controlled trial. *JACC Cardiovasc Interv*. 2017;10:1332–1340. doi: 10.1016/j.jcin.2017.04.024 Crossref. PubMed.
25. Habara, M, Terashima, M, Nasu, K, Kaneda, H, Yokota, D, Ito, T, Kurita, T, Teramoto, T, Kimura, M, Kinoshita, Y, Tsuchikane, E, Asakura, Y, Suzuki, T. Morphological differences of tissue characteristics between early, late, and very late restenosis lesions after first generation drug-eluting stent implantation: an optical coherence tomography study. *Eur Heart J Cardiovasc Imaging*. 2013;14:276–284. doi: 10.1093/ehjci/jes183 Crossref. PubMed.
26. Kubo, S, Kadota, K, Otsuru, S, Hasegawa, D, Shigemoto, Y, Habara, S, Tada, T, Tanaka, H, Fuku, Y, Katoh, H, Goto, T, Mitsudo, K. Optimal treatment of recurrent restenosis lesions after drug-eluting stent implantation for in-stent restenosis lesions. *EuroIntervention*. 2013;9:788–796. doi: 10.4244/EIJV9I7A131 Crossref. PubMed.
27. Latib, A, Mussardo, M, Ielasi, A, Tarsia, G, Godino, C, Al-Lamee, R, Chieffo, A, Airoldi, F, Carlino, M, Montorfano, M, Colombo, A. Long-term outcomes after the percutaneous treatment of drug-eluting stent restenosis. *JACC Cardiovasc Interv*. 2011;4:155–164. doi: 10.1016/j.jcin.2010.09.027 Crossref. PubMed.

28. Lee, WC, Fang, YN, Fang, CY, Chen, CJ, Yang, CH, Yip, HK, Hang, CL, Wu, CJ, Fang, HY. Comparison of clinical results following the use of drug-eluting balloons for a bare-metal stent and drug-eluting stent instent restenosis. *J Interv Cardiol.* 2016;29:469–479. doi: 10.1111/joic.12327 Crossref. PubMed.

29. Tanabe, K, Kishi, S, Aoki, J, Tanimoto, S, Onuma, Y, Yachi, S, Taniwaki, M, Nakajima, Y, Nakajima, H, Hara, K, Isobe, M. Impact of coronary calcium on outcome following sirolimus-eluting stent implantation. *Am J Cardiol.* 2011;108:514–517. doi: 10.1016/j.amjcard.2011.03.075 Crossref. PubMed.

Heart and Vessels (2018) 33:837–845
https://doi.org/10.1007/s00380-018-1131-7

ORIGINAL ARTICLE

Vascular response to biolimus A-9 eluting stent in patients with shorter and prolonged dual antiplatelet therapy: optical coherence tomography sub-study of the NIPPON trial

Koji Kuroda[1] · Toshiro Shinke[1] · Hiromasa Otake[1] · Hiroto Kinutani[1] · Raisuke Iijima[2] · Junya Ako[3] · Hisayuki Okada[4] · Yoshiaki Ito[5] · Kenji Ando[6] · Hitoshi Anzai[7] · Hiroyuki Tanaka[8] · Yasunori Ueda[9] · Shin Takiuchi[10] · Yasunori Nishida[11] · Hiroshi Ohira[12] · Katsuhiro Kawaguchi[13] · Makoto Kadotani[14] · Hiroyuki Niinuma[15] · Kazuto Omiya[16] · Takashi Morita[17] · Kan Zen[18] · Yoshinori Yasaka[19] · Kenji Inoue[20] · Sugao Ishiwata[21] · Masahiko Ochiai[22] · Toshimitsu Hamasaki[23] · Kazushi Urasawa[24] · Toru Kataoka[25] · Minoru Yoshiyama[26] · Kenshi Fujii[27] · Takumi Inoue[28] · Masahito Kawata[29] · Hiroyoshi Yokoi[30] · Masato Nakamura[2] · On behalf of the NIPPON Investigators

Received: 28 November 2017 / Accepted: 26 January 2018 / Published online: 20 February 2018
© The Author(s) 2018. This article is an open access publication

Abstract

Dual antiplatelet therapy (DAPT) with thienopyridine and aspirin is the standard care for the prevention of stent thrombosis. However, the optimal duration and effect of the duration of DAPT on intra-stent thrombus (IS-Th) formation are unknown. The NIPPON study (Nobori Dual Antiplatelet Therapy as Appropriate Duration) was an open label, randomized multicenter, assessor-blinded, trial designed to demonstrate the non-inferiority of shorter (6-month) DAPT to prolonged (18-month) DAPT, after biolimus A9 eluting stent implantation in 3773 patients at 130 sites in Japan. Among them, 101 patients were randomly allocated for an optical coherence tomography (OCT) sub-study to assess the difference of local IS-Th formation between the two groups. In addition to standard OCT parameters, the number of IS-Th formed was counted in each target stent at 8 months. Baseline patient characteristics were not different between the 6- and 18-month groups. IS-Th was detected in 9.8% of the cases and the presence of IS-Th was not significantly different between the two groups (10.9% in 6-month vs. 9.1% in 12-month, $P = 0.76$). Furthermore, the number of IS-Th formed was not significantly different between the two groups. This OCT sub-study was in line with the main NIPPON study which demonstrated the non-inferiority of 6-month DAPT to 18-month DAPT. Shorter DAPT duration did not promote progressive IS-Th formation at the mid-term time point.

Keywords Optical coherence tomography · Dual antiplatelet therapy · Biolimus A9 eluting stent · Intra-stent thrombus

Introduction

Dual antiplatelet therapy (DAPT) with thienopyridine and aspirin is the standard of care for prevention of stent thrombosis [1]. Previous guidelines recommended that DAPT should be continued for at least 12 months in all patients undergoing drug-eluting stent (DES) implantation [2]. However, recent studies have reported that stopping DAPT earlier in selected patients with DES was as safe and efficient as prolonged DAPT [3–8]. Thus, the optimal duration of DAPT remains controversial and the impact of DAPT duration on local vascular reaction has not been elucidated.

NIPPON (Nobori Dual Antiplatelet Therapy as Appropriate Duration) is an open label, randomized multicenter, assessor-blinded, trial designed to demonstrate the non-inferiority of shorter (6-month) DAPT to prolonged (18-month) DAPT after biolimus A9 eluting stent (BES) implantation. This NIPPON main study demonstrated that 6 months of DAPT was not inferior to 18 months of DAPT following implantation of BES in terms of net adverse clinical and cerebrovascular events (all-cause mortality, myocardial infarction, stroke, and major bleeding) [9]. Among the enrolled

Electronic supplementary material The online version of this article (https://doi.org/10.1007/s00380-018-1131-7) contains supplementary material, which is available to authorized users.

✉ Toshiro Shinke
shinke@med.kobe-u.ac.jp

Extended author information available on the last page of the article

patients, 101 patients were randomly allocated for an optical coherence tomography (OCT) sub-study to assess the local vascular responses to BES implantation. The aim of this study was to compare local vessel healing and in-stent thrombus formation between patients with shorter (6-month) and prolonged (18-month) DAPT.

Materials and methods

Patient population

NIPPON is an open-label, randomized, multicenter, assessor-blinded trial designed to demonstrate the non-inferiority of shorter (6-month) DAPT to prolonged (18-month) DAPT after NOBORI stent implantation in patients with coronary artery disease from December 2011 to June 2015 at 130 Japanese institutions (supplementary Appendix 1). Nobori (Terumo Corporation, Tokyo, Japan) is a biolimus A9-eluting stent (BES) with an abluminal-side biodegradable polymer coating that degrades 6–9 months after stent implantation [10]. During hospitalization for percutaneous coronary intervention (PCI), the patients were assigned to 6 or 18 months of DAPT at a 1:1 ratio by central randomization using an interactive web-based system. This study was designed to approximate an all-comers trial with broad inclusion criteria to reflect the real-world clinical setting, and patients with acute myocardial infarction (MI) were also enrolled. The extremely limited exclusion criteria were in-stent restenosis (bare metal stent or DES) and index PCI for saphenous vein graft disease or unprotected left main trunk disease. The inclusion and exclusion criteria are detailed in supplementary Appendix 2. The study protocol was approved by the institutional review board at each participating center. Written informed consent was obtained from all patients. The study was conducted in accordance with the Declaration of Helsinki and was registered at Clinical Trial Registration (NCT.01514227). A total of 3773 patients were enrolled to NIPPON trial. Among them, 101 patients at 14 Japanese institutions (supplementary Appendix 3) were randomly allocated for OCT sub-study to assess deference of local in-stent thrombus (IS-Th) formation between two groups at 8–12 months after BES implantation.

Dual antiplatelet therapy

All patients were receiving aspirin (81–162 mg/day). Patients also received ticlopidine (200 mg/day) or clopidogrel (75 mg/day) for the assigned duration after PCI. The allowance of DAPT duration in the two groups was defined as NIPPON trial protocol. The following per-protocol analysis was performed in this OCT sub-study: patients in the 6-month DAPT group were referred for analysis when the DAPT had been stopped until at least 1 month before the follow-up OCT procedure. In the 18-month DAPT group, DAPT had been continued at the time of the OCT follow-up procedure.

OCT examination

The follow-up OCT examination was performed 8–12 months after BES implantation. The frequency-domain OCT system (C7 Dragonfly™ or C8 Dragonfly™; St. Jude Medical, St. Paul, MN, USA) was used in the present study. OCT examination was performed, as previously reported [11]. In the use of the frequency-domain OCT system, a 0.014-inch standard guide wire was positioned distally in the target vessel and the frequency OCT catheter was advanced to the distal end of the target lesion. The entire length of the region of interest was scanned using the integrated automated pullback device at 10 or 20 mm/s. For image acquisition, blood in the coronary artery was replaced with iodine contrast media and continuously flushed.

OCT analysis

Off-line OCT analysis was performed using a dedicated software (LightLab Imaging, Westford, MA, USA). All images were analyzed at every frame in stents by independent investigators, who were blinded to the angiographic and clinical findings. For quantitative analysis, cross-section OCT images were analyzed at 1-mm intervals. As qualitative analysis, IS-Th was defined as a mass protruding beyond the stent strut into the lumen, with significant attenuation behind the mass with a height greater than 250 μm [12, 13] (Fig. 1). In this present study, we additionally counted the mass with a height of 100–250 μm as micro-in-stent thrombus (MIS-Th) for the detailed assessment of small IS-Th (Fig. 1). Stent struts were classified as uncovered if any part of the strut was visibly exposed to the lumen or covered if a layer of tissue was visible all over the reflecting surfaces. Neointimal thickness was measured from the center reflection of the stent strut to the vessel-lumen border (neointimal surface or strut surface if uncovered) for each stent strut. An uncovered strut was defined as a strut with a neointimal thickness equal to 0 μm [14]. The frequency of covered and uncovered struts was calculated as the number of those struts divided by the total number of struts for each stent. A malapposed strut was defined as a distance greater than 140 μm between the center reflection of the strut to the vessel wall [15]. The presence of peri-strut low-intensity area (PLIA) was counted per stent. PLIA was defined as a region around stent struts with a homogeneous lower-intensity appearance than surrounding tissue without significant signal attenuation behind the area [16].

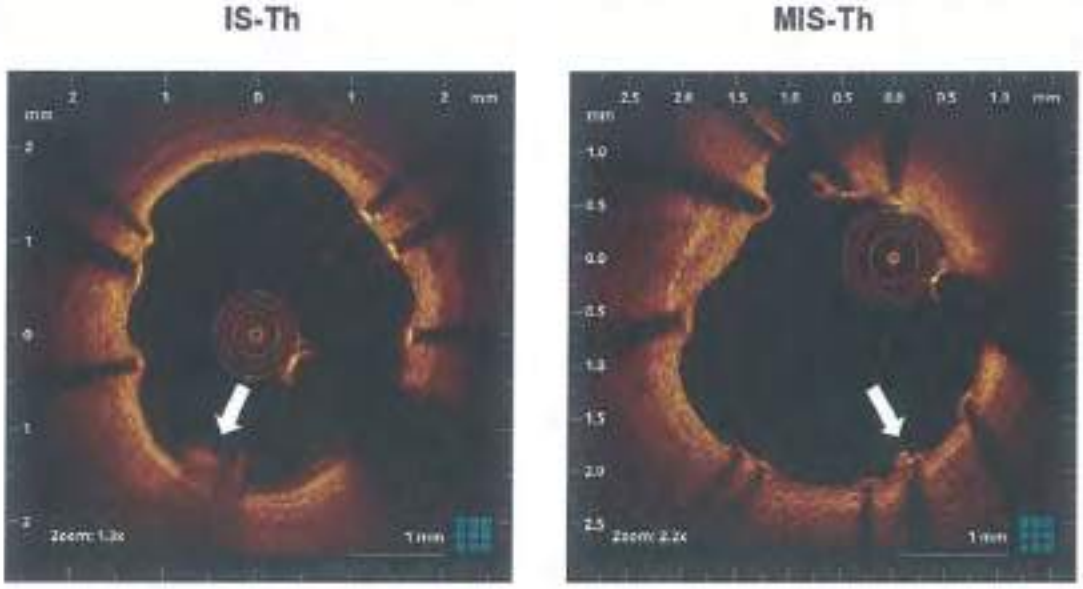

Fig. 1 Representative optical coherence tomographic images of IS-Th and MIS-Th (arrow). IS-Th was defined as a mass protruding beyond the stent strut into the lumen, with significant attenuation behind the mass with a height over 250 μm. MIS-Th was defined as a mass with a height of 100–250 μm. *IS-Th* in-stent thrombus, *MIS-Th* micro in-stent thrombus

Statistical analysis

Continuous variables were shown as mean ± SD and comparisons between two groups were performed using two-sample *t* test or Wilcoxon rank sum test. Discrete variables were presented as frequencies and percentages, and comparisons were performed by Chi-square test or Fisher's exact test. All *P* values were 2-sided, and $P < 0.05$ was considered to indicate statistical significance. The statistical analysis was conducted using the commercially available SPSS software version 23 (SPSS, Chicago, IL, USA).

Statistical sample size calculation was not done for this sub-study. This is because there was no past report assessing the difference of local IS-Th formation between shorter and prolonged DAPT duration. We enrolled the largest possible number of cases into the OCT sub-study from NIPPON study enrollment.

Results

Patient and lesion characteristics

Among 101 patients (135 lesions), 12 patients (23 lesions) were excluded [7 patients (10 lesions), due to deviation from assigned DAPT duration; 5 patients (13 lesions), due to incomplete OCT examination]. Therefore, 89 patients (112 lesions) were enrolled. A total of 41 patients (46 lesions) and 48 patients (66 lesions) were assigned to the 6- and 18-month groups, respectively (Fig. 2). There were no significant differences between the two groups in terms in patient, medication, laboratory data, and lesion characteristics at the OCT follow-up (Tables 1, 2).

OCT characteristics

Stent, lumen, and neointimal characteristics had no significant difference between the two groups in OCT findings. Except in stent struts characteristics, the percentage of uncovered struts was significantly higher in the 6-month group (Table 3).

Fig. 2 Study population

Table 1 Baseline clinical characteristics

Variable	6-month ($n = 41$)	18-month ($n = 48$)	*P* value
Clinical characteristics			
Age (years)	67.1 ± 10.1	66.6 ± 9.0	0.86
Male	27 (65.9)	36 (75.0)	0.34
Diabetes mellitus	16 (39.0)	23 (47.9)	0.40
Hypertension	34 (82.9)	31 (64.6)	0.052
Dyslipidemia	28 (68.3)	32 (66.7)	0.87
Current smoker	10 (24.4)	13 (27.1)	0.77
Angina status			0.97
STEMI	4 (9.8)	4 (8.3)	1.00
Stable AP	21 (51.2)	23 (47.9)	0.76
Unstable AP	9 (22.0)	13 (27.1)	0.58
SMI	6 (14.6)	7 (14.6)	0.99
Past medical history			
PCI history	11 (26.8)	9 (18.8)	0.36
BMS implantation	8 (19.5)	6 (12.5)	0.37
DES implantation	4 (9.8)	3 (6.3)	0.70
CABG history	0 (0.0)	2 (4.2)	0.50
Cerebral infarction	0 (0.0)	1 (2.1)	1.00
TIA	1 (2.4)	0 (0.0)	0.46
Intracranial bleeding	0 (0.0)	0 (0.0)	–
Gastric ulcer bleeding	1 (2.4)	1 (2.1)	1.00
Atrial fibrillation	0 (0.0)	1 (2.1)	1.00
PAD	3 (7.3)	0 (0.0)	0.09
Medication			
NSAIDs	1 (2.4)	2 (4.2)	1.00
Beta blocker	16 (39.0)	13 (27.1)	0.23
ARB	20 (48.8)	25 (52.1)	0.76
ACE-I	6 (14.6)	2 (4.2)	0.14
Ethyl icosapentate	1 (2.4)	2 (4.2)	1.00
PPI	24 (58.5)	31 (64.6)	0.56
Steroid	1 (2.4)	0 (0.0)	0.46
Statin	32 (78.0)	40 (83.3)	0.53
Laboratory data			
Total cholesterol (mg/dL)	173.0 ± 30.2	167.4 ± 31.2	0.44
HDL-cholesterol (mg/dL)	54.0 ± 12.0	52.9 ± 15.6	0.72
LDL-cholesterol (mg/dL)	96.1 ± 24.5	95.1 ± 23.3	0.86
Hb_{A1C} (%)	6.09 ± 0.63	6.50 ± 1.39	0.06
Creatinine (mg/dL)	0.85 ± 0.18	0.83 ± 0.22	0.76

Values are presented as mean ± SD or absolute numbers (%)

ACE-I angiotensin converting enzyme inhibitor, *AP* angina pectoris, *ARB* angiotensin receptor blocker, *BMS* bare metal stent, *CABG* coronary artery bypass graft, *DES* drug-eluting stent, *NSAIDs* nonsteroidal anti-inflammatory drugs, *PAD* peripheral artery disease, *PCI* percutaneous coronary intervention, *PPI* proton pump inhibitor, *SMI* silent myocardial ischemia, *STEMI* ST elevation myocardial infarction, *TIA* transient ischemic attack

IS-Th characteristics

Among 89 patients (112 lesions), IS-Th was identified in 11 lesions (9.8%). The presence and number of IS-Th had no significant difference between the two groups. In addition, the presence and number of MIS-Th had no significant difference between the two groups (Table 4, Figs. 3, 4).

Table 2 Baseline lesion characteristics

Variable	6-month ($n = 46$)	18-month ($n = 66$)	P value
Duration between PCI and OCT follow-up (days)	293.2 ± 49.9	278.6 ± 41.4	0.093
Lesion location			0.35
Left anterior descending artery	30 (65.2)	34 (51.5)	
Left circumflex artery	7 (15.2)	13 (19.7)	
Right coronary artery	9 (19.6)	19 (28.8)	
Stent size (mm)	3.04 ± 0.40	3.08 ± 0.34	0.55
Stent length (mm)	23.4 ± 12.7	26.6 ± 14.9	0.24

Values are presented as mean ± SD or absolute numbers (%)

OCT optical coherence tomography, *PCI* percutaneous coronary intervention

Table 3 Optical coherence tomography findings

Variable	6-month ($n = 46$)	18-month ($n = 66$)	P value
Stent characteristics			
Average stent area (mm^2)	7.29 ± 2.97	7.46 ± 2.56	0.75
Minimum stent area (mm^2)	5.89 ± 2.50	5.67 ± 2.30	0.63
Maximum stent area (mm^2)	8.82 ± 3.60	9.16 ± 3.01	0.60
Average stent diameter (mm)	2.98 ± 0.58	3.03 ± 0.51	0.67
Minimum stent diameter (mm)	2.49 ± 0.54	2.43 ± 0.52	0.52
Maximum stent diameter (mm)	3.51 ± 0.74	3.64 ± 0.65	0.33
Lumen characteristics			
Average lumen area (mm^2)	6.84 ± 2.94	6.85 ± 2.54	0.99
Minimum lumen area (mm^2)	5.27 ± 2.60	5.03 ± 2.37	0.61
Maximum lumen area (mm^2)	8.61 ± 3.51	8.69 ± 2.97	0.89
Ratio (min/max lumen area)	0.61 ± 0.15	0.58 ± 0.15	0.33
Neointimal characteristics			
Average neointimal area (mm^2)	0.50 ± 0.33	0.63 ± 0.36	0.06
% neointimal area (%)	7.97 ± 6.22	9.41 ± 5.35	0.19
Average neointimal thickness (mm)	0.08 ± 0.03	0.09 ± 0.03	0.40
Peri-strut low intensity area (%)	19 (41.3)	37 (56.1)	0.12
Stent struts characteristics			
Total no of cross sections (n)	25.0 ± 12.8	27.3 ± 13.7	0.38
Total no of struts (n)	252.4 ± 138.7	277.1 ± 187.2	0.45
No of uncovered struts (n)	11.57 ± 12.71	8.36 ± 14.85	0.24
% of uncovered struts (%)	4.70 ± 4.92	2.59 ± 2.45	0.009
No of malapposed struts (n)	1.13 ± 3.38	0.42 ± 1.27	0.18
% of malapposed struts (%)	0.44 ± 1.20	0.13 ± 0.39	0.10

Values are presented as mean ± SD or absolute numbers (%)

Discussion

The NIPPON OCT sub-study was a multicenter, randomized control trial to evaluate the difference of IS-Th formation between shorter and prolonged DAPT duration after BES implantation and was first to demonstrate that the incidence of IS-Th formation at mid-term follow-up was equivalent between the two groups. BES has an abluminal-side biodegradable polymer coating that degrades 6–9 months after stent implantation [10]. Several studies reported that BES had similar stent coverage and apposition and low rate of stent thrombosis as compared to everolimus-eluting stent at mid-term after stent implantation [17, 18].

The frequency of IS-Th at mid-term OCT findings after BES implantation was reported in several studies. The range of the frequency was 7–10% in those studies [19, 20]. In the current study, 11 lesions (9.8%) had IS-Th, and the rate corresponded to these previous studies. This

Table 4 IS-Th characteristics

Variable	6-month ($n = 46$)	18-month ($n = 66$)	*P* value
IS-Th			
The presence of thrombus	5 (10.9)	6 (9.1)	0.76
The number of thrombi			0.70
0	41 (89.1)	61 (92.4)	
1	4 (8.7)	5 (7.6)	
2	1 (2.2)	0 (0.0)	
MIS-Th			
The presence of thrombus	8 (17.4)	10 (15.2)	0.75
The number of thrombi			0.085
0	38 (82.6)	56 (84.8)	
1	3 (6.5)	9 (13.6)	
2	4 (8.7)	1 (1.5)	
3	1 (2.2)	0 (0.0)	

Values are presented as absolute numbers (%)

IS-Th in-stent thrombus, *MIS-Th* micro in-stent thrombus

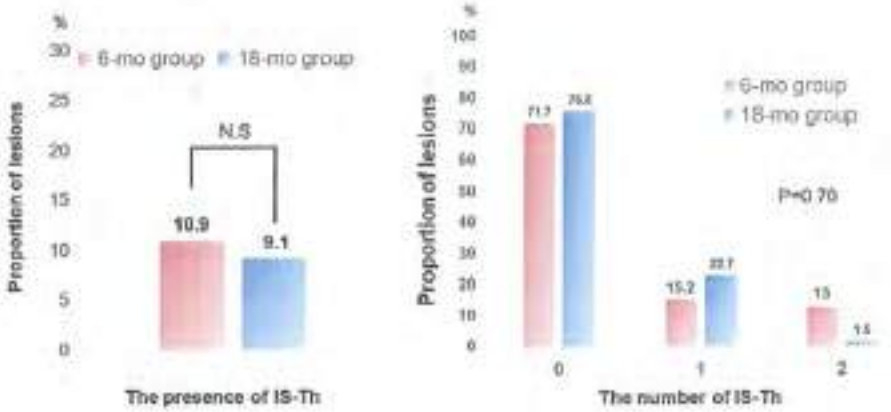

Fig. 3 Association between dual antiplatelet therapy duration and in-stent thrombus formation

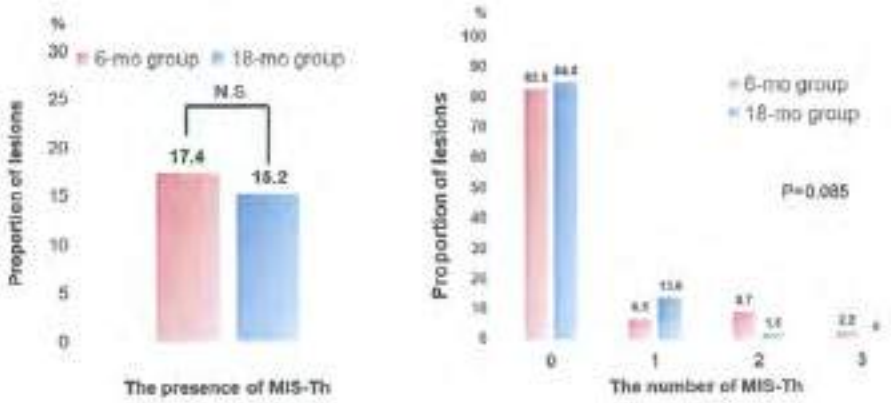

Fig. 4 Association between dual antiplatelet therapy duration and micro in-stent thrombus formation

study also showed that the presence and number of IS-Th had no significant difference between the two groups. This result may support previous studies that demonstrated the non-inferiority of short-term DAPT [3–8]. Konishi et al. [19], has reported that patients with BES implantation achieved favorable vessel healing at 6 months without delayed adverse reaction for up to 12 months.

In the current study, uncovered strut was incidentally higher in the 6-month group than in the 18-month group, but the percentage of malapposed strut was not different. A previous autopsy study evaluating first-generation DESs have shown that an uncovered strut could be a substrate for thrombus formation, which can potentially lead to a thrombotic event [21]. However, a recent clinical trial using OCT for assessing vascular response to DESs has suggested that an uncovered strut, as marker of incomplete vessel healing, may not be directly associated with adverse clinical outcome in second-generation DESs [20]. Regarding BES, stopping DAPT at 6 months does not appear to pose a high risk of provoking IS-Th due to favorable vessel healing during the early phase after stent implantation.

The latest American College of Cardiology/American Heart Association guideline, which is focused on the update on duration of DAPT in patients with coronary artery disease, recommends that patients with stable ischemic heart disease (SIHD) treated with DAPT after DES implantation should undergo P2Y12 inhibitor therapy with clopidogrel for at least 6 months [22]. Identically, European Society of Cardiology guidelines described that DAPT is indicated for 6 months after DES implantation in patients with SIHD [23]. The present study supports these criteria from the viewpoint of local thrombus formation at mid-term OCT findings.

Limitations

This study has several limitations. First, this was not a double-blind trial; thus, selection bias cannot be excluded. Second, the present study may be not adequately powered to calculate the difference of IS-Th formation due to limited sample size. Despite our plan to enroll 100 patients undergoing DAPT, only 89 patients were finally enrolled in the present study. This is because of the reduced number of patients and the small difference in the primary end-point between the two DAPT groups in the main NIPPON trial. Third, antiplatelet therapy was limited to clopidogrel and ticlopidine in our study; thus, the use of more potent antiplatelet agents may have led to different conclusions. Fourth, in the present study, follow-up OCT was performed at 8–12 months after stent implantation. Therefore, there was only 2–6 months deference of the DAPT duration between the two groups. Longer duration after the cessation or continuation of DAPT may be required to estimate the impact of DAPT duration on IS-Th formation. Fifth, the result of the present study suggested that shorter DAPT duration did not provoke IS-Th formation, however, this study was underpowered to show the association between IS-Th formation and clinical events due to small sample size. Finally, vascular healing response depends on the underlying plaque morphology before stenting [24]. More specifically, vulnerable plaque characteristics in ACS can significantly influence vascular healing after BES implantation. More information regarding plaque morphology at the index procedure should be required.

Conclusions

This NIPPON OCT sub-study suggested that a shortened DAPT duration does not appear to provoke IS-Th formation after cessation of one antiplatelet regimen at mid-term OCT follow-up. These results were in line with the main NIPPON study which demonstrated the non-inferiority of 6-month DAPT compared with 18-month DAPT.

Acknowledgements All the authors have participated in the conceptual formulation of the study, data collection, and manuscript preparation. Drs. Nakamura, Tijma, Ako, Shinke, and Yokoi established the study design and conception and interpreted the data. Dr. Kuroda drafted the manuscript, and Dr Shinke contributed to revising it critically for important intellectual content. Dr Hamasaki contributed to the statistical analysis.

Funding This research was supported by the Associations for Establishment of Evidence in Interventions (2-5-3 New-Hamamatsu building, Hamamatsucho, Minato-ku, Tokyo 105-0013, Japan).

Compliance with ethical standards

Conflict of Interest Dr. Nakamura has received research grant support and honoraria from Terumo Corp, Sanofi, and Daiichi Sankyo. Dr Shinke has received research grant support from Terumo Corp and honoraria from Terumo Corp, Daiichi Sankyo, and Sanofi. Dr. Otake has received research grant support and honoraria from Terumo Corp Dr Yokoi received honoraria from Terumo and Daiichi Sankyo. Dr Ochiai has received expert witness fee from Terumo Corp. Dr Kawagachi received honoraria from Terumo Corp. All authors have no commercial associations that might pose a conflict of interest in connection with the manuscript.

Open Access This article is distributed under the terms of the Creative Commons Attribution 4.0 International License (http://creativecommons.org/licenses/by/4.0/), which permits unrestricted use, distribution, and reproduction in any medium, provided you give appropriate credit to the original author(s) and the source, provide a link to the Creative Commons license, and indicate if changes were made.

References

1. King SB 3rd, Smith SC Jr., Hirshfeld JW Jr., Jacobs AK, Morrison DA, Williams DO, 2005 WRITING COMMITTEE MEMBERS, Feldman TE, Kern MJ, O'Neill WW, Schaff HV, Whitlow PL, Adams CD, Anderson JL, Buller CE, Creager MA, Ettinger SM, Halperin JL, Hunt SA, Kramholz HM, Kushner FG, Lytle BW, Nishimura R, Page RL, Riegel B, Tarkington LG, Yancy CW (2008) 2007 Focused Update of the ACC/AHA/SCAI 2005 Guideline Update for Percutaneous Coronary Intervention: a report of the American College of Cardiology/American Heart Association Task Force on Practice Guidelines: 2007 Writing

Group to Review New Evidence and Update the ACC/AHA/SCAI 2005 Guideline Update for Percutaneous Coronary Intervention, Writing on Behalf of the 2005 Writing Committee. Circulation 117:261–295
2. Levine GN, Bates ER, Blankenship JC, Bailey SR, Bittl JA, Cercek B, Chambers CE, Ellis SG, Guyton RA, Hollenberg SM, Khot UN, Lange RA, Mauri L, Mehran R, Moussa ID, Mukherjee D, Nallamothu BK, Ting HH (2011) 2011 ACCF/AHA/SCAI Guideline for Percutaneous Coronary Intervention: executive summary: a report of the American College of Cardiology Foundation/American Heart Association Task Force on Practice Guidelines and the Society for Cardiovascular Angiography and Interventions. Circulation 124:2574–2609
3. Gwon HC, Hahn JY, Park KW, Song YB, Chae IH, Lim DS, Han KR, Choi JH, Hoi SH, Kang HJ, Koo BK, Ahn T, Yoon JH, Jeong MH, Hong TJ, Chung WY, Choi YJ, Hur SH, Kwon HM, Jeon DW, Kim BO, Park SH, Lee NH, Jeon HK, Jang Y, Kim HS (2012) Six-month versus 12-month dual antiplatelet therapy after implantation of drug-eluting stents: the efficacy of xience/promus versus cypher to reduce late loss after stenting (EXCELLENT) randomized, multicenter study. Circulation 125:505–513
4. Kim BK, Hong MK, Shin DH, Nam CM, Kim JS, Ko YG, Choi D, Kang TS, Park BE, Kang WC, Lee SH, Yoon JH, Hong BK, Kwon HM, Jang Y (2012) A new strategy for discontinuation of dual antiplatelet therapy: the RESET Trial (REal Safety and Efficacy of 3-month dual antiplatelet Therapy following endeavor zotarolimus-eluting stent implantation). J Am Coll Cardiol 60:1340–1348
5. Valgimigli M, Campo G, Monti M, Vranckx P, Percoco G, Tumscitz C, Castriota F, Colombo F, Tebaldi M, Fuca G, Kubbajeh M, Cangiano E, Minarelli M, Scalone A, Cavazza C, Frangione A, Borghesi M, Marchesini J, Parrinello G, Ferrari R (2012) Short- versus long-term duration of dual-antiplatelet therapy after coronary stenting: a randomized multicenter trial. Circulation 125:2015–2026
6. Feres F, Costa RA, Abizaid A, Leon MB, Marin-Neto JA, Botelho RV, King SB 3rd, Negoita Liu M, de Paula JE, Mangione JA, Meireles GX, Castello HJ Jr, Nicolela EL Jr, Perin MA, Devito FS, Labrunie A, Salvadori D Jr, Guimaro M, Staico R, Costa JR Jr, de Castro JP, Abizaid AS, Bhatt DL (2013) Three vs twelve months of dual antiplatelet therapy after zotarolimus-eluting stents: the OPTIMIZE randomized trial. JAMA 310:2510–2522
7. Colombo A, Chieffo A, Frasheri A, Garbo R, Masotti-Censi M, Salvatella N, Oteo Dominguez JF, Steffanon L, Tarantini G, Presbitero P, Menozzi A, Pucci E, Mauri J, Cesana BM, Giustino G, Sardella G (2014) Second-generation drug-eluting stent implantation followed by 6- versus 12-month dual antiplatelet therapy: the SECURITY randomized clinical trial. J Am Coll Cardiol 64:2086–2097
8. Schulz-Schupke S, Byrne RA, Ten Berg JM, Neumann FJ, Han Y, Adriaenssens T, Tolg R, Seyfarth M, Maeng M, Zrenner B, Jacobshagen C, Mudra H, von Hodenberg E, Wohrle J, Angiolillo DJ, von Merzljak B, Rifatow N, Kufner S, Morath T, Fenchtenberger A, Ibrahim T, Janssen PW, Valina C, Li Y, Desmet W, Abdel-Wahab M, Tiroch K, Hengstenberg C, Bernlochner I, Fischer M, Schunkert H, Laugwitz KL, Schomig A, Mehilli J, Kastrati A (2015) ISAR-SAFE: a randomized, double-blind, placebo-controlled trial of 6 vs. 12 months of clopidogrel therapy after drug-eluting stenting. Eur Heart J 36:1252–1263
9. Nakamura M, Iijima R, Ako J, Shinke T, Okada H, Ito Y, Ando K, Anzai H, Tanaka H, Ueda Y, Takiuchi S, Nishida Y, Ohira H, Kawaguchi K, Kadotani M, Niinuma H, Omiya K, Morita T, Zen K, Yasaka Y, Inoue K, Ishiwata S, Ochiai M, Hamasaki T, Yokoi H (2017) Dual antiplatelet therapy for 6 versus 18 months after biodegradable polymer drug-eluting stent implantation. JACC Cardiovasc Interv 10:1189–1198
10. Chevalier B, Silber S, Park SJ, Garcia E, Schuler G, Suryapranata H, Koolen J, Hauptmann KE, Wijns W, Morice MC, Carrie D, van Es GA, Nagai H, Deriege D, Pannovic D, Serruys PW (2009) Randomized comparison of the Nobori Biolimus A9-eluting coronary stent with the Taxus Liberte paclitaxel-eluting coronary stent in patients with stenosis in native coronary arteries: the NOBORI 1 trial—Phase 2. Circ Cardiovasc Interv 2:188–195
11. Matsumoto D, Shite J, Shinke T, Otake H, Tanino Y, Ogasawara D, Sawada T, Paredes OL, Hirata K, Yokoyama M (2007) Neointimal coverage of sirolimus-eluting stents at 6-month follow-up: evaluated by optical coherence tomography. Eur Heart J 28:961–967
12. Kume T, Akasaka T, Kawamoto T, Ogasawara Y, Watanabe N, Toyota E, Neishi Y, Sukmawan R, Sadahira Y, Yoshida K (2006) Assessment of coronary arterial thrombus by optical coherence tomography. Am J Cardiol 97:1713–1717
13. Jang IK, Tearney GJ, MacNeill B, Takano M, Moselewski F, Iftima N, Shishkov M, Houser S, Aretz HT, Halpern EF, Bouma BE (2005) In vivo characterization of coronary atherosclerotic plaque by use of optical coherence tomography. Circulation 111:1551–1555
14. Otake H, Shite J, Ako J, Shinke T, Tanino Y, Ogasawara D, Sawada T, Miyoshi N, Kato H, Koo BK, Honda Y, Fitzgerald PJ, Hirata K (2009) Local determinants of thrombus formation following sirolimus-eluting stent implantation assessed by optical coherence tomography. JACC Cardiovasc Interv 2:459–466
15. Konishi A, Shinke T, Otake H, Takaya T, Osue T, Kinutani H, Kuroda M, Takahashi H, Terashita D, Shite J, Hirata K (2015) Serial optical coherence tomography evaluation at 6, 12, and 24 months after biolimus A9-eluting biodegradable polymer-coated stent implantation. Can J Cardiol 31:980–988
16. Otake H, Shite J, Ikeno F, Shinke T, Teramoto T, Miyoshi N, Ako J, Honda Y, Fitzgerald PJ, Hirata K (2012) Evaluation of the peri-strut low intensity area following sirolimus- and paclitaxel-eluting stents implantation: insights from an optical coherence tomography study in humans. Int J Cardiol 157:38–42
17. Natsuaki M, Kozuma K, Morimoto T, Kadota K, Muramatsu T, Nakagawa Y, Akasaka T, Igarashi K, Tanabe K, Morino Y, Ishikawa T, Nishikawa H, Awata M, Abe M, Okada H, Takatsu Y, Ogata N, Kimura K, Urasawa K, Tarutani Y, Shiode N, Kimura T (2013) Biodegradable polymer biolimus-eluting stent versus durable polymer everolimus-eluting stent: a randomized, controlled, noninferiority trial. J Am Coll Cardiol 62:181–190
18. Tada T, Kastrati A, Byrne RA, Schuster T, Cassese S, Joner M, Pache J, Massberg S, Schomig A, Mehilli J (2014) Randomized comparison of biolimus-eluting stents with biodegradable polymer versus everolimus-eluting stents with permanent polymer coatings assessed by optical coherence tomography. Int J Cardiovasc Imaging 30:495–504
19. Konishi A, Shinke T, Otake H, Takaya T, Nakagawa M, Inoue T, Hariki H, Osue T, Taniguchi Y, Iwasaki M, Nishio R, Hiraoka N, Kinutani H, Kuroda M, Takahashi H, Terashita D, Shite J, Hirata K (2014) Favorable vessel healing after nobori biolimus A9-eluting stent implantation-6- and 12-month follow-up by optical coherence tomography. Circ J 78:1882–1890
20. Kubo T, Akasaka T, Kozuma K, Kimura K, Fusazaki T, Okura H, Shinke T, Ino Y, Hasegawa T, Takashima H, Takamisawa I, Yamaguchi H, Igarashi K, Kadota K, Tanabe K, Nakagawa Y, Muramatsu T, Morino Y, Kimura T (2014) Vascular response to drug-eluting stent with biodegradable vs. durable polymer. Optical coherence tomography substudy of the NEXT. Circ J 78:2408–2414
21. Finn AV, Joner M, Nakazawa G, Kolodgie F, Newell J, John MC, Gold HK, Virmani R (2007) Pathological correlates of late drug-eluting stent thrombosis: strut coverage as a marker of endothelialization. Circulation 115:2435–2441

22. Levine GN, Bates ER, Bittl JA, Brindis RG, Fihn SD, Fleisher LA, Granger CB, Lange RA, Mack MJ, Mauri L, Mehran R, Mukherjee D, Newby LK, O'Gara PT, Sabatine MS, Smith PK, Smith SC Jr (2016) 2016 ACC/AHA Guideline Focused Update on duration of dual antiplatelet therapy in patients with coronary artery disease: a Report of the American College of Cardiology/American Heart Association Task Force on Clinical Practice Guidelines. J Am Coll Cardiol 68(10):1082–1115
23. Windecker S, Kolh P, Alfonso F, Collet JP, Cremer J, Falk V, Filippatos G, Hamm C, Head SJ, Juni P, Kappetein AP, Kastrati A, Knuuti J, Landmesser U, Laufer G, Neumann FJ, Richter DJ, Schauerte P, Sousa Uva M, Stefanini GG, Taggart DP, Torracca L, Valgimigli M, Wijns W, Witkowski A (2014) 2014 ESC/EACTS Guidelines on myocardial revascularization: the Task Force on Myocardial Revascularization of the European Society of Cardiology (ESC) and the European Association for Cardio-Thoracic Surgery (EACTS) Developed with the special contribution of the European Association of Percutaneous Cardiovascular Interventions (EAPCI). Eur Heart J 35:2541–2619
24. Nakazawa G, Finn AV, Joner M, Ladich E, Kutys R, Mont EK, Gold HK, Burke AP, Kolodgie FD, Virmani R (2008) Delayed arterial healing and increased late stent thrombosis at culprit sites after drug-eluting stent placement for acute myocardial infarction patients: an autopsy study. Circulation 118:1138–1145

Affiliations

Koji Kuroda[1] · Toshiro Shinke[1] · Hiromasa Otake[1] · Hiroto Kinutani[1] · Raisuke Ijima[2] · Junya Ako[3] · Hisayuki Okada[4] · Yoshiaki Ito[5] · Kenji Ando[6] · Hitoshi Anzai[7] · Hiroyuki Tanaka[8] · Yasunori Ueda[9] · Shin Takiuchi[10] · Yasunori Nishida[11] · Hiroshi Ohira[12] · Katsuhiro Kawaguchi[13] · Makoto Kadotani[14] · Hiroyuki Niinuma[15] · Kazuto Omiya[16] · Takashi Morita[17] · Kan Zen[18] · Yoshinori Yasaka[19] · Kenji Inoue[20] · Sugao Ishiwata[21] · Masahiko Ochiai[22] · Toshimitsu Hamasaki[23] · Kazushi Urasawa[24] · Toru Kataoka[25] · Minoru Yoshiyama[26] · Kenshi Fujii[27] · Takumi Inoue[28] · Masahito Kawata[29] · Hiroyoshi Yokoi[30] · Masato Nakamura[2] · On behalf of the NIPPON investigators

1. Division of Cardiovascular, Department of Cardiology, Kobe University Graduate School of Medicine, 7-5-1 Kusunoki-cho, Chuo-ku, Kobe, Hyogo 650-0017, Japan
2. Division of Cardiovascular Medicine, Toho University Ohashi Medical Center, Tokyo, Japan
3. Department of Cardiovascular Medicine, Kitasato University Hospital, Sagamihara, Japan
4. Department of Cardiology, Seirei Hamamatsu General Hospital, Hamamatsu, Japan
5. Division of Cardiology, Saiseikai Yokohama-City Eastern Hospital, Yokohama, Japan
6. Department of Cardiology, Kokura Memorial Hospital, Kitakyushu, Japan
7. Cardiology Department, Ota Memorial Hospital, Ota, Japan
8. Department of Cardiology, Tokyo Metropolitan Tama Medical Center, Tokyo, Japan
9. Cardiovascular Division, National Hospital Organization Osaka National Hospital, Osaka, Japan
10. Department of Cardiology, Higashi Takarazuka Satoh Hospital, Takarazuka, Japan
11. Department of Cardiovascular Medicine, Takai Hospital, Tenri, Japan
12. Department of Cardiology, Edogawa Hospital, Tokyo, Japan
13. Department of Cardiology, Komaki City Hospital, Komaki, Japan
14. Department of Cardiology, Kakogawa Central City Hospital, Kakogawa, Japan
15. Department of Cardiology, St. Luke's International Hospital, Tokyo, Japan
16. Division of Cardiology, St. Marianna University School of Medicine Yokohama City Seiko Hospital, Yokohama, Japan
17. Division of Cardiology, Osaka General Medical Center, Osaka, Japan
18. Department of Cardiovascular Medicine, Omihachiman Community Medical Center, Omihachiman, Japan
19. Department of Cardiology, Hyogo Brain and Heart Center, Himeji, Japan
20. Department of Cardiology, Juntendo University Nerima Hospital, Tokyo, Japan
21. Division of Cardiovascular Center, Toranomon Hospital, Tokyo, Japan
22. Division of Cardiology and Cardiac Catheterization Laboratories, Showa University Northern Yokohama Hospital, Yokohama, Japan
23. Department of Data Science, National Cerebral and Cardiovascular Center, Suita, Japan
24. Cardiovascular Center, Tokeidai Memorial Hospital, Sapporo, Japan
25. Department of Cardiovascular Medicine, Bell Land General Hospital, Kyoto, Japan
26. Cardiovascular Medicine, Osaka City University Hospital, Osaka, Japan
27. Cardiovascular Center, Sakurabashi Watanabe Hospital, Osaka, Japan
28. Department of Cardiology, Hyogo Prefectural Awaji Medical Center, Sumoto, Japan
29. Department of Cardiology, Akashi Medical Center, Akashi, Japan
30. Department of Cardiovascular Medicine Center, Fukuoka Sanno Hospital, Fukuoka, Japan

JACC: CARDIOVASCULAR IMAGING
© 2018 BY THE AMERICAN COLLEGE OF CARDIOLOGY FOUNDATION
PUBLISHED BY ELSEVIER

VOL. 11, NO. 8, 2018

Single Versus Standard Multiview Assessment of Global Longitudinal Strain for the Diagnosis of Cardiotoxicity During Cancer Therapy

Paaladinesh Thavendiranathan, MD, SM,[a] Tomoko Negishi, MD,[b] Marc-Andre Cotè, MD,[c] Martin Penicka, MD,[d] Richard Massey, BS,[e] Goo-Yeong Cho, MD,[f] Krassimira Hristova, MD,[g] Dragos Vinereanu, MD,[h] Bogdan A. Popescu, MD,[h] Masaki Izumo, MD,[i] Kazuaki Negishi, MD, PhD,[b] Thomas H. Marwick, MBBS, PhD, MPH,[b,j] on behalf of the SUCCOUR Investigators

ABSTRACT

OBJECTIVES The goal of this study was to compare echocardiographic measurements of global longitudinal strain (GLS) (using 3 apical views) with single-view longitudinal strain (LS, 4- or 2-chamber [4CV_LS and 2CV_LS, respectively]) for detection of cancer-therapy related cardiotoxicity.

BACKGROUND GLS is useful for the detection of cardiotoxicity, but the need for repeated measurements poses a significant burden on busy echocardiography laboratories. A single-view LS measurement, possibly at point of care, could improve efficiency.

METHODS Seventeen international centers prospectively recruited 108 patients (mean age 54 ± 13 years) at high risk for cardiotoxicity as part of the ongoing SUCCOUR (Strain Surveillance for Improving Cardiovascular Outcomes During Chemotherapy) randomized controlled trial. Echocardiography performed at baseline and follow-up were analyzed in a core laboratory setting blinded to clinical information. Peak systolic GLS and LS were measured from raw data. Cardiotoxicity was defined by reduction in left ventricular ejection fraction >0.10 to <0.55 or a relative drop in GLS by ≥12%.

RESULTS Cardiotoxicity developed in 46 patients by either criteria. Baseline and follow-up 2-dimensional left ventricular ejection fraction were 61 ± 4% and 58 ± 5%, respectively ($p < 0.001$). The baseline GLS (−20.9 ± 2.4%) was not different from 4CV_LS (−20.7 ± 2.5%; $p = 0.09$) or 2CV_LS (−21.1 ± 3.1%; $p = 0.25$). The follow-up GLS (−19.5 ± 2.4%) was also similar to 4CV_LS (−19.5 ± 2.6%; $p = 0.80$) and 2CV_LS (−19.7 ± 3.1%; $p = 0.19$). There was good correlation between GLS and 4CV_LS at baseline ($r = 0.86$; $p < 0.001$) and follow-up ($r = 0.89$; $p < 0.001$) and with 2CV_LS at baseline ($r = 0.87$; $p < 0.001$) and follow-up ($r = 0.88$; $p < 0.001$). However, there was 15% to 22% disagreement between GLS and 4CV_LS or 2CV_LS for the detection of cardiotoxicity. The interobserver and intraobserver reproducibility was higher for GLS (intraclass correlation: 0.93 to 0.95; coefficient of variance: 2.9% to 3.7%) compared with either single-chamber-based LS measurement (intraclass correlation: 0.85 to 0.91; coefficient of variance: 4.1% to 4.8%).

CONCLUSIONS Although there was good correlation between GLS and single-view LS measurements, single-view LS measurement led to disagreement in the diagnosis of cardiotoxicity in up to 22% of patients. GLS measurements were more reproducible than single-view LS. GLS based on 3 apical views should remain the preferred technique for detection of cardiotoxicity. (Strain Surveillance for Improving Cardiovascular Outcomes During Chemotherapy [SUCCOUR]; ACTRN12614000341628) (J Am Coll Cardiol Img 2018;11:1109–18) © 2018 by the American College of Cardiology Foundation.

From the [a]Toronto General Hospital, Ted Rogers Program in Cardiotoxicity Prevention, Peter Munk Cardiac Center, University of Toronto, Toronto, Canada; [b]Menzies Institute for Medical Research, University of Tasmania, Hobart, Australia; [c]Centre de recherche du CHU de Québec, Québec, Canada; [d]Cardiovascular Center Aalst, OLV Clinic, Belgium, Aalst, Belgium; [e]Oslo University Hospital, Oslo, Norway; [f]Seoul National University, Bundang Hospital, Seoul, Republic of Korea; [g]National Heart Hospital, Sofia, Bulgaria; [h]University of Medicine and Pharmacy Carol Davila, Bucharest, Romania; [i]St. Marianna University School of Medicine, Kawasaki, Japan; and the [j]Baker Heart & Diabetes Institute, Melbourne, Australia. The SUCCOUR trial is supported in

ISSN 1936-878X/$36.00 https://doi.org/10.1016/j.jcmg.2018.03.003

JACC: CARDIOVASCULAR IMAGING, VOL. 11, NO. 8, 2018
AUGUST 2018:1109–19

ABBREVIATIONS AND ACRONYMS

2CV = 2-chamber view

4CV = 4-chamber view

AUC = area under the curve

CI = confidence interval

GLS = global longitudinal strain (using 3 apical views)

LVEF = left ventricular ejection fraction

LS = single-view longitudinal strain (4- or 2-chamber)

Peak systolic global longitudinal strain (GLS) measured using echocardiography has emerged as a sensitive marker of left ventricular systolic dysfunction. Its use has gained particular interest in the field of "cardio-oncology" to facilitate detection of early cardiotoxicity (1). A 10% to 15% relative drop in GLS early during cancer therapy identifies patients at risk of later reduction in left ventricular ejection fraction (LVEF) or development of congestive heart failure (2–4).

SEE PAGE 1119

Standard GLS is calculated from 3 apical images. This method requires careful attention to optimizing 3 views, ensuring consistent heart rate and frame rate during acquisition, and post-processing of 3 datasets. In most cancers, patients receiving cancer therapy require repeated testing to identify cardiotoxicity. There is evidence that reversibility of left ventricular dysfunction is associated with early initiation of heart failure therapy after the onset of cardiotoxicity (5). A single long-axis view could improve efficiency and promote uptake of this technique in busy echocardiography laboratories, or even be applied to imaging approaches at point of care (6), allowing prompt detection of cardiotoxicity (7). Moreover, because cardiotoxicity is believed to be a diffuse process, longitudinal strain (LS) measurements from a single 4-chamber (4CV_LS) or 2-chamber (2CV_LS) view GLS could substitute for traditional GLS measurements. Using such an approach would enable LS measurements to be gathered easily as part of the routine evaluation after each round of chemotherapy, with a higher likelihood of rapid recognition of cardiotoxicity. We hypothesized that single-view LS measurements correlate with GLS, have acceptable measurement reproducibility, and could be used as an alternative to GLS in the detection of cardiotoxicity.

METHODS

PATIENTS. The study cohort consisted of patients recruited to the SUCCOUR (Strain Surveillance During Chemotherapy for Improving Cardiovascular Outcomes) trial. SUCCOUR is a multicenter, international, randomized controlled trial comparing the use of GLS versus LVEF by echocardiography for early detection and management of cardiotoxicity in patients receiving potentially cardiotoxic cancer treatment. Those who have an absolute reduction in LVEF (>0.10 reduction to <0.55) or a relative reduction in GLS (≥12% relative) in the strain arm are treated with a combination of angiotensin-converting enzyme inhibitors and beta-blockers. The primary outcome is a change in LVEF between baseline and the end of 3-year follow-up.

In this baseline substudy, we examined the first 108 patients (enrolled between January 2014 and September 2016), without reference to the outcome standard in the study, and with no knowledge about the patient's randomization status. The measurements in this study were obtained from the core laboratory, which are independent of the GLS or EF analysis being done to guide management in the clinical trial, which are local to the sites. Core laboratory measurements are not sent back to local sites and do not influence clinical management.

ECHOCARDIOGRAPHY. Transthoracic echocardiography was performed before initiation of cancer therapy and repeated every 3 months during treatment. For patients receiving anthracycline-based therapy, the baseline study was performed at the time of initiation of anthracycline; in those receiving anthracycline followed by trastuzumab, the baseline study was performed before trastuzumab initiation but after anthracycline completion. All studies were performed on standard, commercially available echocardiographic systems (Vivid 7 and E9, GE Medical, Milwaukee, Wisconsin).

Apical 2- and 4-chamber views were obtained for calculation of LVEF using the biplane Simpson method. Three long-axis images were recorded with the optimal frame rate (55 to 80 frames/s), stored in raw data format and transferred to the central core laboratory for analysis. Before the start of the study all involved centers participated in a calibration session to ensure uniform technique in image acquisition for strain and EF measurements (8). For this

part by a project grant (1119555) from the National Health and Medical Research Council, Canberra, Australia, and received software and core laboratory support from GE Medical Systems. Dr. Thavendiranathan is supported by the Canadian Institutes of Health Research New Investigator Award (FRN 147854). Dr. Popescu has received research support and lecture honoraria from GE Healthcare. Dr. Marwick has received research grant support from GE Medical Systems for the SUCCOUR study. All other authors have reported that they have no relationships relevant to the contents of this paper to disclose. Drs. Thavendiranathan and Negishi contributed equally to this work and are joint first authors. Rory Senior, MD, served as the Guest Editor for this paper.

Manuscript received December 11, 2017; revised manuscript received March 1, 2018, accepted March 5, 2018.

TABLE 1 Baseline Characteristics of the Included Patients (N = 108)

Age, yrs	54 ± 13
Female	101 (93.5)
Breast cancer	95 (88.0)
Acute myelogenous leukemia	2 (1.9)
Non-Hodgkin's lymphoma	11 (10.2)
Cancer treatment	
Anthracyclines	108 (100.0)
Trastuzumab	79 (73.1)
Chest radiation therapy	30 (27.8)
Cardiac risk factors	
Diabetes	11 (10.2)
Hypertension	37 (34.3)
Dyslipidemia	22 (20.4)
Smoking	37 (34.3)
History of cardiovascular disease	13 (12.0)
Cardiac medications	
Beta-blockers	8 (7.4)
ACE inhibitors/ARBs	19 (17.6)
Statins	14 (13.0)
Systolic blood pressure, mm Hg	125 ± 15
Diastolic blood pressure, mm Hg	78 ± 15
Heart rate, beats/min	78 ± 10
Left ventricular ejection fraction, %	61.0 ± 3.6
Global longitudinal strain, %	−20.9 ± 2.4

Values are mean ± SD or n (%).
ACE = angiotensin-converting enzyme; ARB = angiotensin receptor blocker.

study, the baseline echocardiography study (before any cancer treatment or before trastuzumab) and a subsequent study at the time of cardiotoxicity diagnosis (between visits 3 and 6) or the final study during treatment in those without cardiotoxicity were chosen for analysis. All analyses of LVEF (biplane Simpson method), GLS 4CV_LS, and 2CV_LS were performed by an experienced cardiologist (T.N.) in a core laboratory setting at baseline and follow-up, blinded to all patient data and imaging time point. For the analysis of 4CV_LS and 2CV_LS alone, the measurements obtained as part of the GLS measurements by the same observer were used. Strain analysis was performed using EchoPac version 13.0.0 or 201 (GE Healthcare, Milwaukee, Wisconsin).

CARDIOTOXICITY. Cardiotoxicity was defined as an absolute decrease in 2-dimensional EF >0.10 from baseline to <0.55 or a relative GLS decrease by ≥12% consistent with the definition used in the ongoing SUCCOUR randomized controlled trial. The 2-dimensional EF criterion was used to be consistent with all previous publications examining the value of echocardiography to define cardiotoxicity (1,2,9). In addition, 2 sensitivity analyses with different definitions of cardiotoxicity were performed: 1) absolute LVEF decrease >0.10 from baseline to <0.53 and a relative GLS decrease of >15% (to follow the recent American Society of Echocardiography recommendations) (7); and 2) isolated relative reduction in GLS by ≥12% or >15%.

REPRODUCIBILITY. Interobserver and intraobserver reproducibilities of the strain measurements were performed for GLS, 4CV_LS, and 2CV_LS in 20 independent studies. Strain measurements were performed by 2 experienced analysts (T.N. and P.T.) blinded to each other's measurement. The same measurements were repeated by one analyst (T.N.) blinded to previous measurements.

STATISTICAL ANALYSIS. Data are summarized as mean ± SD or median (interquartile range) as appropriate. All data were first assessed for normality based on skewness, kurtosis, and the Kolmogorov-Smirnov test. Relationships between continuous parameters were assessed using Pearson correlation. Independent sample Student's *t*-test or paired *t*-tests were used to compare continuous variables as appropriate. A Bland-Altman plot was used to examine agreement between techniques. In addition, the Cohen kappa value was calculated to assess agreement between GLS and 4CV_LS or 2CV_LS for the development of cardiotoxicity defined based on reductions in strain alone. Diagnostic accuracy was calculated as ([true positive + true negative]/[true positive + false positive + true negative + false negative]). Receiver-operating curves were generated to identify the threshold changes in single-view LS that had the best accuracy for discriminating cardiotoxicity defined using GLS changes alone. Areas under the curve (AUC) were compared using the Hanley and McNeil method. Interobserver and intraobserver reproducibility of the strain measurements are reported as intraclass correlation and coefficient of variation. Statistical analyses were performed with IBM SPSS statistics version 20.0.0 (IBM SPSS Statistics, IBM Corporation, Armonk, New York) and MedCalc version 11.4.2.0 (MedCalc, Mariakerke, Belgium). All p values are based on 2-sided tests, with a p value <0.05 considered statistically significant.

RESULTS

PATIENTS. A total of 108 patients, predominantly women and mostly with a history of breast cancer (Table 1), were included. All patients received anthracycline-based therapy; their high-risk status was mostly attributable to trastuzumab therapy.

JACC: CARDIOVASCULAR IMAGING, VOL. 11, NO. 8, 2018
AUGUST 2018:1108–18

FIGURE 1 Comparison of GLS and 4CV_LS at Baseline and Follow-Up

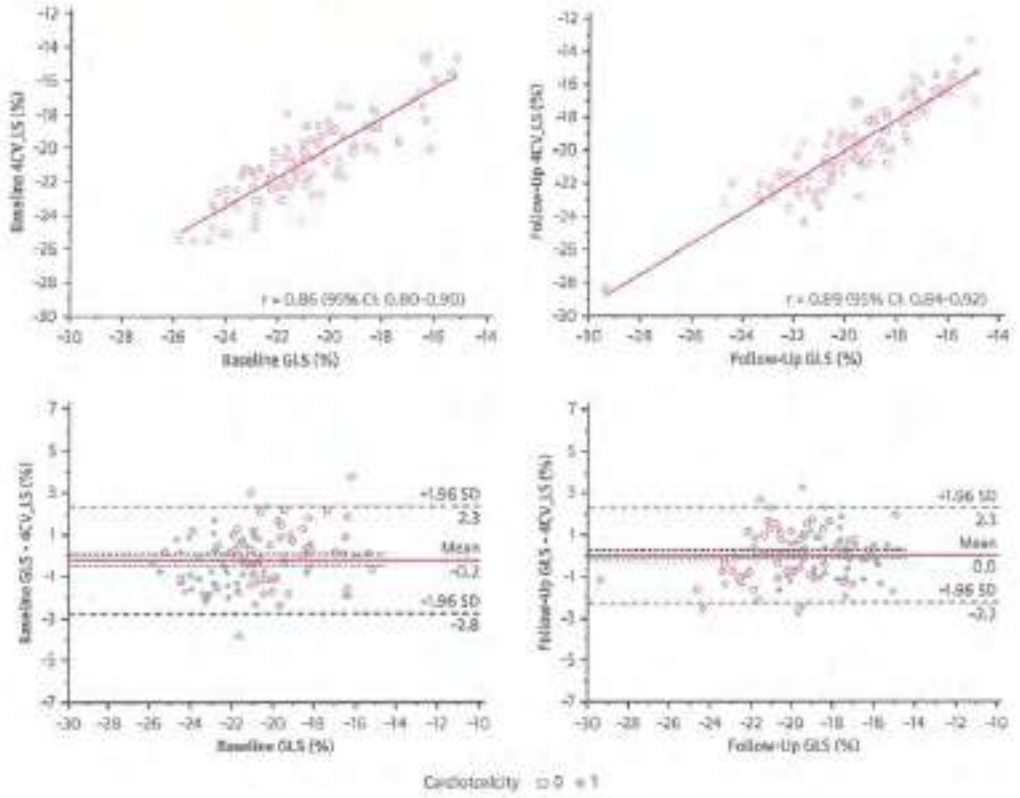

The **top 2 panels** demonstrate linear regression curves comparing baseline **(left panel)** global longitudinal strain (GLS) versus 4-chamber view longitudinal (4CV_LS) strain and follow-up **(right panel)** GLS versus follow-up 4CV_LS. The **bottom 2 panels** are the respective Bland-Altman plots. CI = confidence interval.

STRAIN AGREEMENT. The mean time period between baseline and follow-up imaging was 5.2 ± 2.6 months. Baseline and follow-up LVEF were 61 ± 4% and 58 ± 5%, respectively ($p < 0.001$). The baseline GLS (-20.9 ± 2.4%) was not different from 4CV_LS (-20.7 ± 2.5%; $p = 0.09$) or 2CV_LS (-21.1 ± 3.1%; $p = 0.25$). The follow-up GLS (-19.5 ± 2.4%) was also not significantly different from the follow-up 4CV_LS (-19.5 ± 2.6%; $p = 0.80$) or 2CV_LS (-19.7 ± 3.1%; $p = 0.19$). The changes in strain from baseline to follow-up were significant by all 3 methods ($p < 0.001$ for all).

There was good correlation between GLS and 4CV_LS at baseline ($r = 0.86$; $p < 0.001$) and follow-up ($r = 0.89$; $p < 0.001$) (**Figure 1**). Bland-Altman plots demonstrated minimal bias (0.2% at baseline; 0.0% at follow-up) with modest limits of agreement (2.5% and 2.2%, respectively). There was also good correlation between GLS and 2CV_LS at baseline ($r = 0.87$; $p < 0.001$) and follow-up ($r = 0.88$; $p < 0.001$) (**Figure 2**). Bland-Altman plots demonstrated minimal bias (0.2% at baseline; 0.2% at follow-up) with modest limits of agreement (3.0% and 3.0%).

CARDIOTOXICITY. Three criteria were used for cardiotoxicity. First, using the primary definition (EF >0.10 from baseline to <0.55 or a relative GLS decrease by ≥12%), 46 patients developed cardiotoxicity. Comparing a ≥12% relative change in 4CV_LS versus GLS between baseline and follow-up yielded 15 (14%) false-negative findings and 9 (8%) false-positive findings, resulting in a discordance rate of 22% (**Figure 3A**), and a diagnostic accuracy of 78%. Comparing 2CV_LS versus the GLS change of ≥12% yielded 13 (12%) false-negative findings and 9 (8%) false-positive findings, resulting in a discordance rate of 20% (**Figure 3B**) and a diagnostic accuracy of 80%.

Second, using the American Society of Echocardiography suggested definition (absolute LVEF

FIGURE 1 Comparison of GLS and 2CV_LS at Baseline and Follow-Up

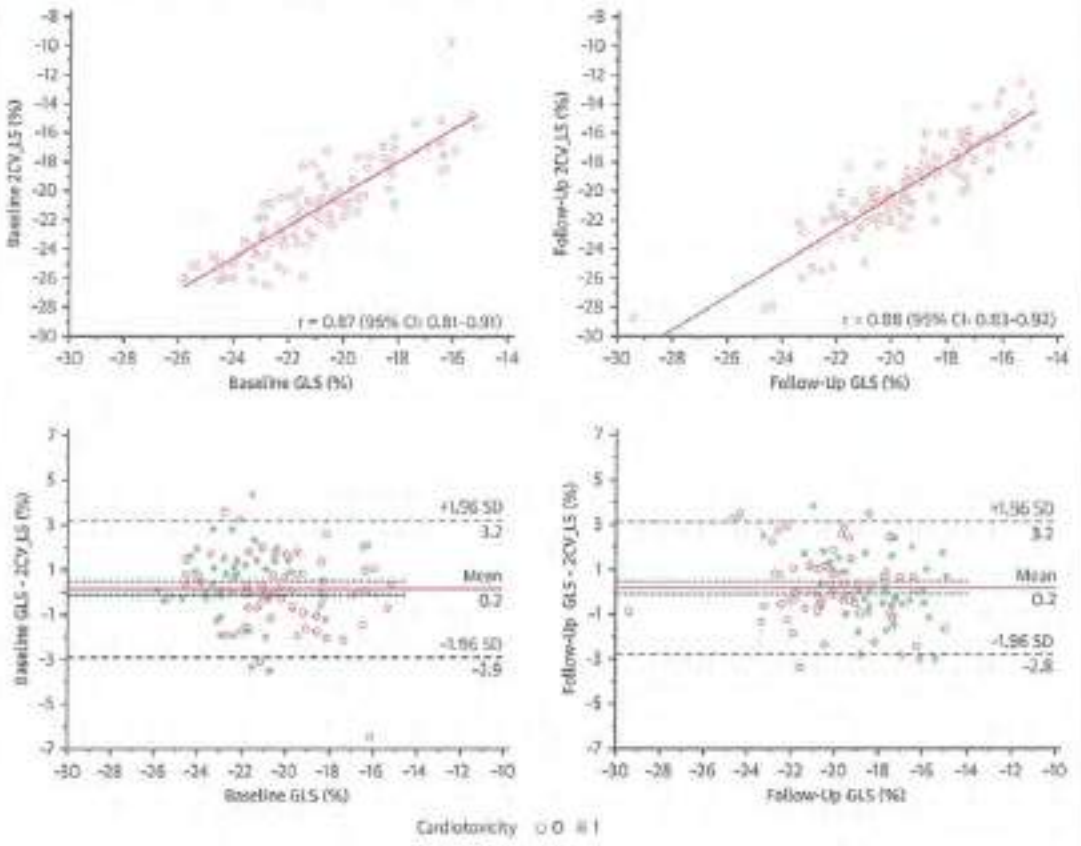

The **top 2 panels** demonstrate linear regression curves comparing baseline **(left panel)** GLS versus the 2-chamber view longitudinal (2CV_LS) strain and follow-up **(right panel)** GLS versus follow-up 2CV_LS. The **bottom 2 panels** are the respective Bland-Altman plots. Abbreviations as in **Figure 1**.

decrease >0.10 from baseline to <0.53 or a relative GLS decrease of >15%) (7), 28 patients developed cardiotoxicity. Comparing a >15% relative change in 4CV_LS versus GLS yielded 5 (5%) false-negative findings and 7 (6%) false-positive findings, resulting in a discordance rate of 11% and a diagnostic accuracy of 89% (**Figure 2**). Comparing a >15% relative change in 2CV_LS versus GLS yielded 6 (6%) false-negative findings and 10 (9%) false-positive findings, resulting in a discordance rate of 15% (**Figure 2**) and a diagnostic accuracy of 85%.

The third criterion involved using only a relative GLS reduction of ≥12% without the LVEF criterion or >15% without the LVEF criterion; 42 and 26 patients, respectively, met these criteria for cardiotoxicity (**Figures 3 and 4**). Agreement for detection of cardiotoxicity using a relative change in GLS ≥12%, and the same change with 4CV_LS and 2CV_LS as determined by the kappa statistic, was 0.52 (95% confidence interval [CI]: 0.35 to 0.69) and 0.56 (95% CI: 0.40 to 0.73). Similarly, for the >15% threshold it was 0.70 (95% CI: 0.55 to 0.86) and 0.62 (95% CI: 0.45 to 0.79). Using receiver-operating curve analysis, we examined the threshold relative changes in single-chamber LS values that would have the best balance of sensitivity and specificity to detect cardiotoxicity using the GLS thresholds of 12% and 15%. A 4CV_LS change of 10.7% (AUC: 0.88; 95% CI: 0.80 to 0.93; sensitivity of 74%; specificity of 86%) and a 2CV_LS change of 10.9% (AUC: 0.90; 95% CI: 0.83 to 0.95; sensitivity of 83%; specificity of 86%) had the best discrimination for a GLS change ≥12%. Similarly, a 4CV_LS change of 16.3% (AUC: 0.95; 95% CI: 0.89 to 0.98; sensitivity of 81%; specificity of 95%) and a

FIGURE 3 Comparison of Differences Between Measurements of GLS and LS

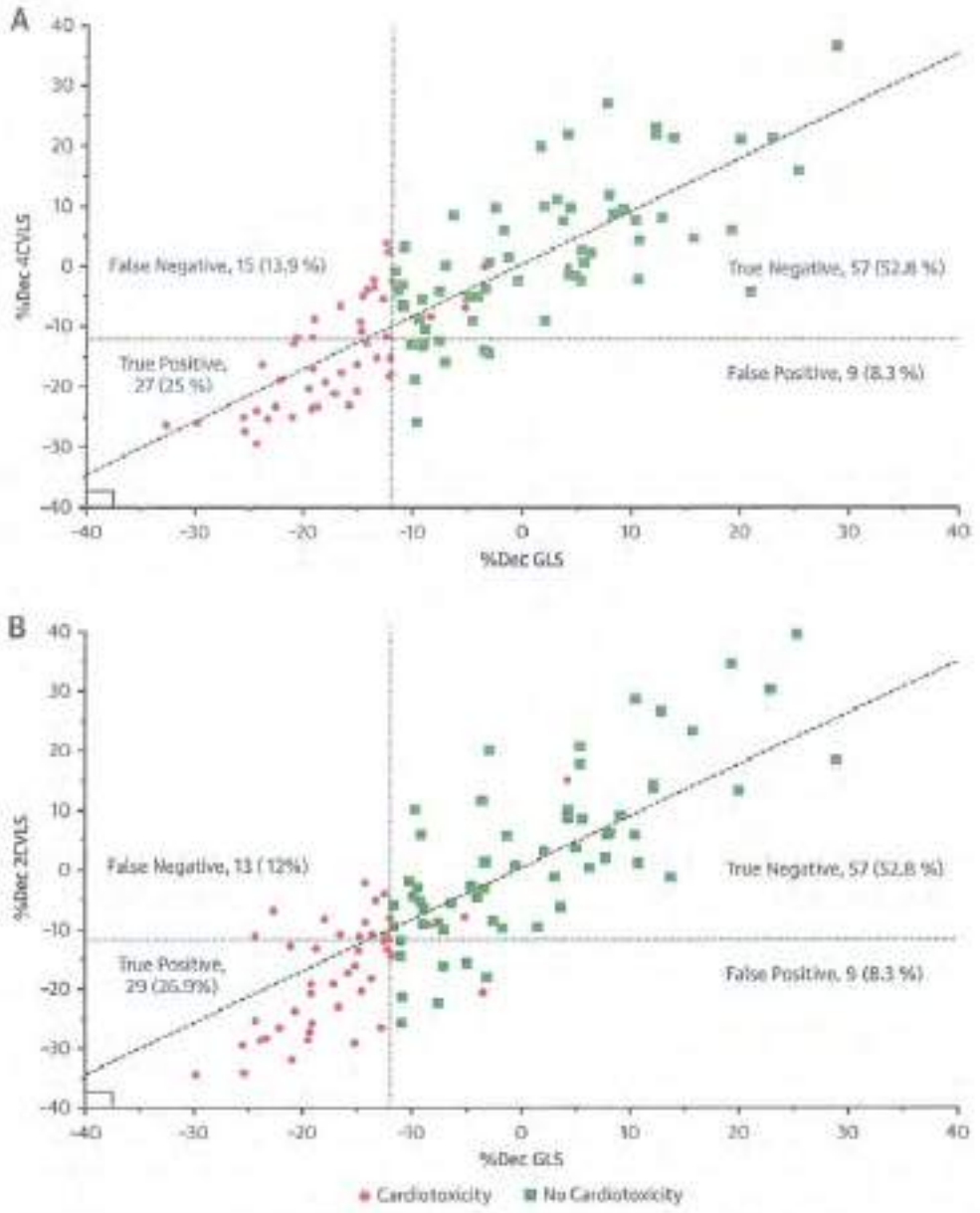

(A) Single-view LS measurement using 4CV_LS and (B) 2CV_LS. Cardiotoxicity is defined based on a drop in strain ≥12% or reduction in left ventricular ejection fraction by >0.10 to <0.55. Abbreviations as in Figures 1 and 2.

2CV_LS change of 11.0% (AUC: 0.92; 95% CI: 0.86 to 0.97; sensitivity of 92%; specificity of 77%) had the best discrimination for a relative GLS change >15%. There was no statistically significant difference in the AUC for the 4CV_LS and 2CV_LS to discriminate cardiotoxicity based on GLS threshold of ≥12% and >15% (Figure 5).

REPRODUCIBILITY. Interobserver and intraobserver reproducibility for GLS, 4CV_LS, and 2CV_LS assessed by using intraclass correlation and coefficients of variation are summarized in Table 2. GLS measurements had better interobserver and intraobserver reproducibility than individual-view based LS measurements.

FIGURE 4 Comparison of Strain Changes Between Measurements of GLS and LS

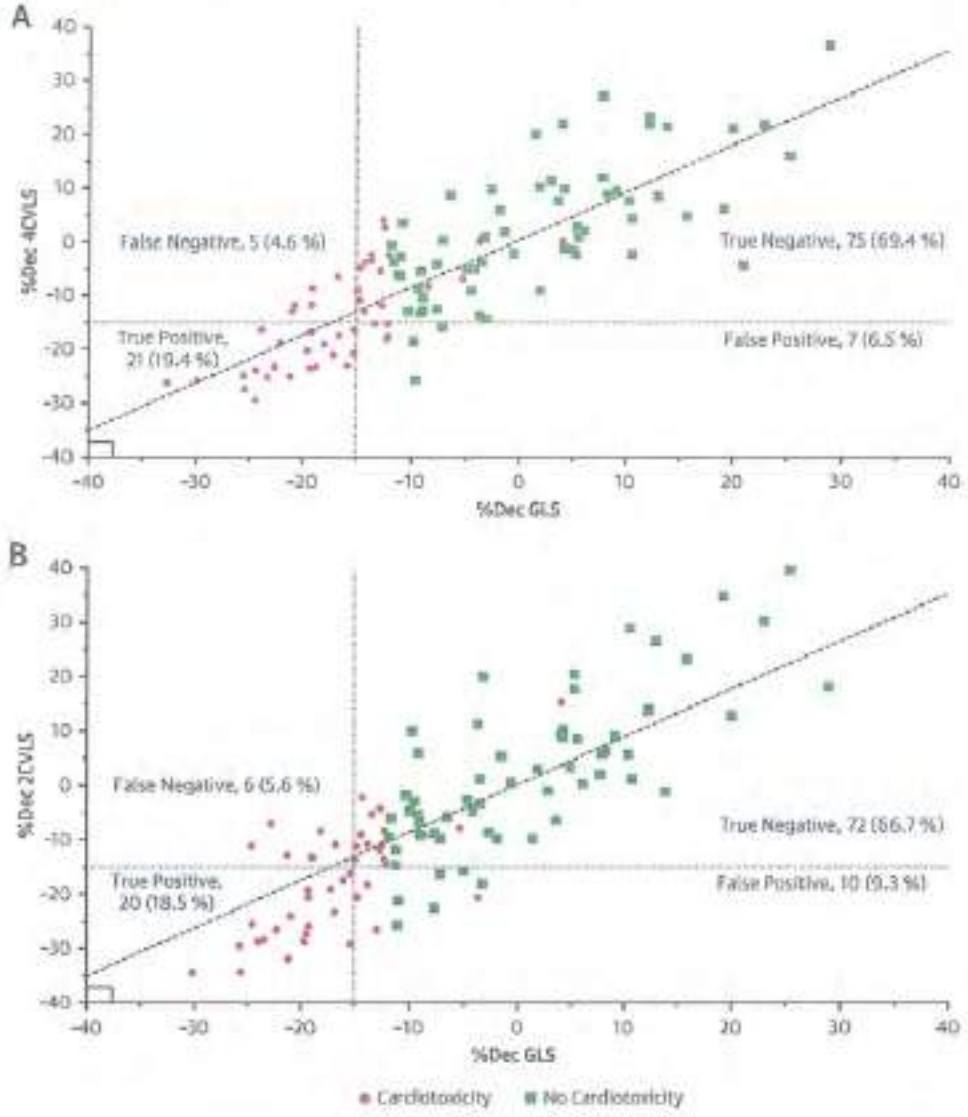

(A) Single-view LS measurement using 4CV_LS and (B) 2CV_LS. Cardiotoxicity is defined based on a relative fall in strain >15% or a reduction in left ventricular ejection fraction by >0.10 to <0.53. Abbreviations as in Figures 1 and 2.

DISCUSSION

The development of a new measurement warrants consideration of 3 relevant parameters: concordance with existing measures, reproducibility, and accuracy. In patients receiving cancer therapy for breast or hematological malignancies, this study showed that measurement of LS using a single 4- or 2-chamber view has good correlation, minimal bias, and modest level of agreement with GLS measurements obtained from the average of 3 long-axis views. However, for the detection of cardiotoxicity, the use of the 4CV_LS or 2CV_LS alone resulted in discordance of 11% to 22% depending on the definition used. When defining cardiotoxicity based on a relative drop in GLS alone, the agreement between 4CV_LS or 2CV_LS and GLS was modest, with kappa values ranging from 0.52 to 0.70. Moreover, the reproducibility of strain measurements was superior for GLS compared with the single-view LS measurements.

JACC: CARDIOVASCULAR IMAGING, VOL. 11, NO. 8, 2018
AUGUST 2018:1108–16

FIGURE 3 Comparison of 4CV_LS and 2CV_LS Measurements to Discriminate a GLS Reduction

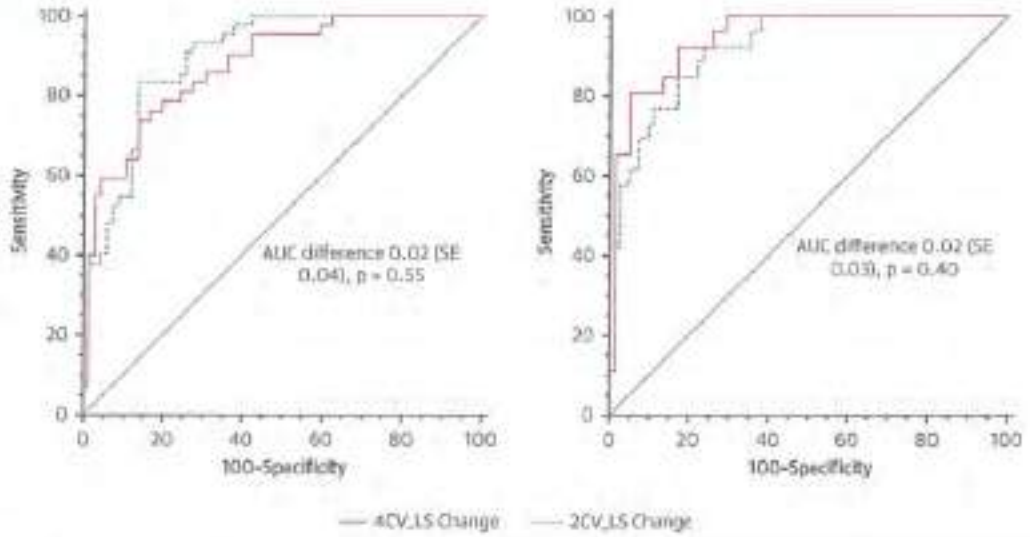

Panels show a relative GLS drop of ≥12% **(left)** and >15% **(right)**, respectively. There were no statistically significant differences between the 2 methods for both definitions. AUC = area under the curve.

GLS AND CARDIOTOXICITY DETECTION. A threshold change in LVEF during cancer therapy has been the most common method used to identify the onset of cardiotoxicity. However, several studies, especially with anthracycline treatment, have shown that once LVEF drops, complete recovery occurs in <25% of the patients despite appropriate heart failure therapy (10). Patients with incomplete recovery are at a higher risk of developing subsequent adverse cardiac events (5,10). Therefore, there has been ongoing interest in early markers of myocardial dysfunction. Echocardiographic GLS has consistently emerged as an imaging technique that identifies subclinical myocardial dysfunction during cancer therapy (1). A >10% to 15% fall, relative to baseline GLS, seems to predict a subsequent significant reduction in LVEF or development of congestive heart failure. Therefore, GLS measurement provides an opportunity to initiate cardioprotective treatments (e.g., beta-blockers) to prevent reduction in LVEF or development of congestive heart failure (11). This approach is the focus of ongoing studies such as the SUCCOUR randomized controlled trial. Subsequent studies may also compare an absolute change versus relative change in GLS; currently, there is no evidence to show that one is superior to the other.

TABLE 2 Interobserver and Intraobserver Variability of Strain Measurements

	Intraobserver		Interobserver	
	ICC	COV	ICC	COV
GLS	0.96 (0.88–0.98)	2.9 (2.1–3.8)	0.93 (0.82–0.97)	3.7 (2.7–4.7)
4CV_LS	0.81 (0.77–0.86)	4.1 (2.8–5.4)	0.85 (0.62–0.94)	4.4 (2.9–6.0)
2CV_LS	0.88 (0.71–0.95)	4.2 (2.0–6.4)	0.87 (0.68–0.95)	4.8 (3.0–6.6)

GLS = global longitudinal strain measured using 3 apical long-axis views; COV = coefficient of variance; ICC = intraclass correlation; 2CV_LS = 2-chamber view longitudinal strain; 4CV_LS = 4-chamber view longitudinal strain.

GLOBAL VERSUS SINGLE-PLANE STRAIN. Given the promising diagnostic and prognostic data with GLS, there has been interest in promoting the uptake of GLS measurements in routine echocardiography. This approach has included standardization of strain measurements between vendors, automated contour detection, and user-friendly strain quantification algorithms. GLS is a reproducible parameter with a relatively short learning curve (8), and its automation might enable access to this measurement at point of care (6). The latter step might improve the workflow for strain imaging in busy echocardiography laboratories, especially in the context of repeated clinic visits.

Further improvement in the speed and feasibility of strain measurements in cardio-oncology and the potential to use strain at point of care may be achieved using a single-view LS as an alternative to GLS. However, despite good correlation and agreement between GLS and single-view LS, there were disagreements in the recognition of threshold

changes in strain used to define cardiotoxicity, with generally more false-negative findings with the single-view LS. The disagreement was lower when using higher strain cutoff values. However, the agreements were still modest at best (kappa of 0.7). In addition, there was no difference in the discriminatory value of 4CV_LS and 2CV_LS for GLS-based definitions of cardiotoxicity. Our findings therefore suggest that GLS and single-view LS measurements are not interchangeable. Different threshold changes in single-view LS can be used to define cardiotoxicity; however, whether these changes have the same prognostic value needs to be defined prospectively.

The existing published data supports the prognostic value of GLS (1), and this measurement should remain the primary method to monitor for cardiotoxicity. This approach is further supported by the fact that GLS measurements had better interobserver and intraobserver variability than individual-view LS measurements. The latter is likely a reflection of the fact that GLS is measured as an average of multiple views and multiple segments, hence reducing overall variability.

IMPROVING WORKFLOW FOR GLS MEASUREMENTS. Given that GLS measurements remain the method of choice to manage patients during cancer therapy, several workflow methods can improve the efficiency of strain measurements in an echocardiography laboratory. First, standard protocols should be implemented for strain measurements. It is helpful to identify a small group of sonographers who are dedicated to performing strain measurements. This group should first become familiar with a single vendor for a prolonged period of time before learning other vendors. This approach provides an opportunity to gain focused expertise in the acquisition, post-processing, and interpretation of the images and to increase the comfort level and speed of measurements. These sonographers could also learn to recognize patients in whom strain measurements would not be useful, as in cases of poor image quality, significant arrhythmia, or foreshortened images. Other sonographers can be educated on the techniques to improve strain acquisition and analysis (12). There should also be a move toward using automated methods for endocardial contouring for strain measurements. Collaboration between vendors is necessary to ensure that strain tracking adequacy can be visualized on all reporting systems for the reporting physician to verify the accuracy of the strain values. In addition, methods to automatically include previous strain values in the report with calculation of relative changes will enhance the utility of GLS in clinical practice.

STUDY LIMITATIONS. Because we do not have an external reference standard, we were only able to compare agreement between GLS and single-chamber LS measurements as opposed to accuracy relative to EF change, for example. However, changes in GLS based on 3 apical views have been shown to have prognostic value in multiple studies of patients receiving cancer therapy, whereas there are currently no prognostic data with single-chamber LS measurements. Therefore, comparing single-chamber LS versus GLS provides a fair comparison of agreement. We were also unable to compare the predictive ability of GLS versus single-view LS for the subsequent reduction in LVEF or congestive heart failure; this information will become available when patients have completed the ongoing trial. We used 2-dimensional LVEF instead of 3-dimensional LVEF as part of the definition of cardiotoxicity to be consistent with the existing published data that has shown the prognostic value of GLS in cardio-oncology. Also, the focus of this study was not on the recognition of cardiotoxicity based on LVEF but rather based on GLS. Our sensitivity analysis excluding LVEF measurements did not reveal any differences in our conclusions.

Although we included patients with breast and hematological malignancies in our study, the common factor in all these patients was the fact that they received anthracycline-based therapy and were deemed to be at elevated risk for cardiotoxicity.

CONCLUSIONS

Our findings show that GLS measured using 3 apical long-axis views has good correlation with LS measured from apical 4- or 2-chamber views alone. However, for the definition of cardiotoxicity based on strain values, these measurements are not interchangeable, with discordance ranging from 11% to 22%. Standard (3 view based) GLS is more reproducible than single-view LS measurements. Therefore, GLS from multiple apical views should remain the preferred method to manage patients during cancer therapy to detect cardiotoxicity.

ADDRESS FOR CORRESPONDENCE: Dr. Thomas H. Marwick, Baker Heart & Diabetes Institute, 75 Commercial Road, Melbourne, Victoria 3004, Australia. E-mail: tom.marwick@bakeridi.edu.au.

PERSPECTIVES

COMPETENCY IN MEDICAL KNOWLEDGE: Although the use of a single-view apical 4- or 2-chamber echocardiography image-based LS measurement could improve workflow in echocardiography laboratories, it was founded to have a 15% to 22% discrepancy compared with GLS for the detection of cardiotoxicity. Measurements of GLS had better interobserver and intraobserver variability than single-view LS measurements.

TRANSLATIONAL OUTLOOK: Echocardiography-measured GLS should remain the method of choice for early detection of cardiotoxicity. Protocols to improve the rapidity and reliability of GLS measurements should be implemented in echocardiography laboratories.

REFERENCES

1. Thavendiranathan P, Poulin F, Lim KD, Plana JC, Woo A, Marwick TH. Use of myocardial strain imaging by echocardiography for the early detection of cardiotoxicity in patients during and after cancer chemotherapy: a systematic review. J Am Coll Cardiol 2014;63:2751–68.

2. Narayan HK, Finkelman B, French B, et al. Detailed echocardiographic phenotyping in breast cancer patients: associations with ejection fraction decline, recovery, and heart failure symptoms over 3 years of follow-up. Circulation 2017;135:1397–412.

3. Negishi K, Negishi T, Hare JL, Haluska BA, Plana JC, Marwick TH. Independent and incremental value of deformation indices for prediction of trastuzumab-induced cardiotoxicity. J Am Soc Echocardiogr 2013;26:493–8.

4. Sawaya H, Sebag IA, Plana JC, et al. Assessment of echocardiography and biomarkers for the extended prediction of cardiotoxicity in patients treated with anthracyclines, taxanes, and trastuzumab. Circ Cardiovasc Imaging 2012;5:596–603.

5. Cardinale D, Colombo A, Lamantia G, et al. Anthracycline-induced cardiomyopathy: clinical relevance and response to pharmacologic therapy. J Am Coll Cardiol 2010;55:213–20.

6. Favot M, Gowland L, Ehrman R, et al. Point-of-care strain echocardiography in acute heart failure. Am J Emerg Med 2016;34:2234–6.

7. Plana JC, Galderisi M, Barac A, et al. Expert consensus for multimodality imaging evaluation of adult patients during and after cancer therapy: a report from the American Society of Echocardiography and the European Association of Cardiovascular Imaging. J Am Soc Echocardiogr 2014;27:911–39.

8. Negishi T, Negishi K, Thavendiranathan P, et al. Effect of experience and training on the concordance and precision of strain measurements. J Am Coll Cardiol Img 2017;10:518–22.

9. Narayan HK, French B, Khan AM, et al. Noninvasive measures of ventricular-arterial coupling and circumferential strain predict cancer therapeutics-related cardiac dysfunction. J Am Coll Cardiol Img 2016;9:1131–41.

10. Cardinale D, Colombo A, Bacchiani G, et al. Early detection of anthracycline cardiotoxicity and improvement with heart failure therapy. Circulation 2015;131:1981–8.

11. Negishi K, Negishi T, Haluska BA, Hare JL, Plana JC, Marwick TH. Use of speckle strain to assess left ventricular responses to cardiotoxic chemotherapy and cardioprotection. Eur Heart J Cardiovasc Imaging 2014;15:324–31.

12. Negishi K, Negishi T, Kurosawa K, et al. Practical guidance in echocardiographic assessment of global longitudinal strain. J Am Coll Cardiol Img 2015;8:489–92.

KEY WORDS cancer therapeutics-related cardiac dysfunction, cardiotoxicity, global longitudinal strain, single-view longitudinal strain

APPENDIX For a list of the SUCCOUR investigators, please see the online version of this paper.

Gender Differences Among Patients With Acute Pulmonary Embolism

Yasuhiro Tanabe, MD, PhD[a,b,*], Takeshi Yamamoto, MD, PhD[a], Teppei Murata, MD[a], Kei Mabuchi, MD[a], Nobuhiro Hara, MD[a], Atsushi Mizuno, MD[a], Toshihiro Nozato, MD[a], Shinji Hisatake, MD[a], Toru Obayashi, MD, PhD[a], Morimasa Takayama, MD, PhD[a], and Ken Nagao, MD, PhD[a]

Gender differences in patients with acute pulmonary embolism (APE) remain unclear and controversial. We aimed to understand the gender differences in patients with APE treated in the cardiovascular care units. The registry database of 1,428 patients with APE treated at the Tokyo cardiovascular care unit Network institutions from 2010 to 2014 was retrieved for analysis. In all, 795 women (55.7%) and 633 men (44.3%) were included in this study. The women were older than men (68.0 ± 16.1 vs 60.9 ± 15.6 years, p <0.0001). Compared with men, women had more complaints of dyspnea and disturbed consciousness, lesser complaints of leg symptoms, and chest pain. Pulmonary arterial systolic pressure (51.5 ± 22.2 mm Hg vs 47.4 ± 22.4 mm Hg, p = 0.012) and the serum B-type natriuretic peptide level (180.4 [50.7 to 526.1] pg/ml vs 107.0 [25.0 to 306.8] pg/ml, p <0.0001) on admission, was higher in women than in men. Severe cases with massive embolism were seen more in women compared with men (14.6% vs 9.2%, p = 0.0002). The use of inferior vena cava filters were lower in women than in men (31.9% vs 37.3%, p = 0.029). Furthermore, 30-day PE-related mortality was higher in women than in men significantly (5.0% vs 2.8%, p = 0.043). In conclusion, women APE patients were older with higher severity than men APE patients, resulting in poor prognosis. **© 2018 Elsevier Inc. All rights reserved.** **(Am J Cardiol 2018;122:1079–1084)**

Acute pulmonary embolism (APE) is a common clinical problem and remains a major health issue that affects an increasing number of patients each year.[1–5] Therefore, under such circumstances the dire need for an appropriate and efficient management is necessary. APE appears to indiscriminately affect patients regardless of sex, age, or race. However, to this date the validity of this assumption remains unclear. In contrast, early studies conducted from 1970 to 2000 revealed that males consistently demonstrated poorer prognosis than females in all racial and age strata,[6–10] while in contrast other separate studies showed opposing results. A Taiwanese study concluded that no difference could be noted between both genders while 2 recent studies conducted in developed countries, concluded that APE female patients had a poorer prognosis.[11–15]

Nevertheless, such results still require further investigation to formulate a clear concept of APE's influence on various races and genders. To this end, in this study we set out to determine whether APE influenced the gender distribution in Asian patients.

Methods

The Tokyo cardiovascular care unit (CCU) Network was established in 1978 and operates through 72 affiliated hospitals with the assistance of ambulance units through the control room of the Tokyo Fire Department to deliver prompt and rapid care to cardiac emergency patients. All patients treated within the CCU network affiliated hospitals are enrolled within the registry and the data obtained are analyzed by the Tokyo CCU Network Scientific Committee.[16] Between 2010 and 2014, we conducted a retrospective cohort study in which a total of 1,492 consecutive APE patients enrolled in the CCU network registry survey forms which included symptoms, vital signs, blood examinations, imaging data, treatment, and prognosis. In the total 1,492 APE patients enrolled, the exclusion criteria was: patients with insufficient data (n = 59), APE of nonthrombus origin (n = 5; fat or tumor emboli). The remaining 1,428 subjects consisting of 633 men and 795 women were enrolled in this study. The diagnosis of APE was confirmed by enhanced computed tomography (CT) (n = 1323), pulmonary scintigraphy (n = 28), pulmonary angiography (n = 21), autopsy (n = 1), whereas the remaining 55 subjects could not be definitively confirmed.

Pulmonary embolism (PE) severity was categorized by physicians at each institution based on blood pressure, echocardiography, and CT findings. Severity was defined as: (1) nonmassive (not accompanied by right heart dysfunction); (2) submassive (right heart dysfunction was present, but circulatory dynamics were stable); and (3) massive (right heart dysfunction was present with vital signs indicative of shock, or systolic blood pressure at rest decreased

[a]Tokyo CCU Network Scientific Committee, Tokyo, Japan; and [b]Division of Cardiology, Department of Internal Medicine, St. Marianna University School of Medicine, Kawasaki-City, Kanagawa Japan. Manuscript received February 4, 2018; revised manuscript received and accepted May 21, 2018.

See page 1079 for disclosure information.

*Corresponding author: Tel: +81-44-977-8111; fax: +81-44-976-7093.
E-mail address: y-tanabe@muj.biglobe.ne.jp (Y. Tanabe).

0002-9149/© 2018 Elsevier Inc. All rights reserved.
https://doi.org/10.1016/j.amjcard.2018.05.042

Table 1
Patients' characteristics

Variable	Men n = 633	Women n = 795	p value
Age	60.9 ± 15.6	68.0 ± 16.1	p <0.0001
Height (cm)	168.3 ± 8.1	153.3 ± 7.3	p <0.0001
Body weight (kg)	70.6 ± 16.6	55.4 ± 12.1	p <0.0001
Body mass index (kg/m^2)	24.9 ± 4.7	23.5 ± 4.5	p <0.0001
Nosocomial case	86 (13.6%)	160 (20.1%)	p = 0.0002
Hypertension	231 (36.5%)	317 (39.9%)	p = 0.21
Hyperlipidemia	109 (17.2%)	143 (18.0%)	p = 0.73
Diabetes mellitus	90 (14.2%)	90 (11.3%)	p = 0.11
Active cancer	30 (4.7%)	46 (5.8%)	p = 0.41
Ischemic heart disease	29 (4.6%)	31 (3.9%)	p = 0.60
Cerebrovascular disease	42 (6.6%)	51 (6.4%)	p = 0.91
Smoker	186 (29.4%)	70 (8.8%)	p <0.0001
Vital signs at first contact			
Body temperature (°C)	36.3 ± 2.7	36.1 ± 3.1	p = 0.19
Systolic blood pressure (mm Hg)	130.6 ± 24.7	126.9 ± 27.8	p = 0.011
Diastolic blood pressure (mm Hg)	81.5 ± 15.8	77.1 ± 18.2	p <0.0001
Heart rate(/min)	91.9 ± 21.8	93.1 ± 21.0	p = 0.31
Respiratory rate(/min)	20.6 ± 6.0	21.6 ± 5.9	p = 0.011
SpO_2 (%) room air oxygen administration	91.5 ± 8.0, 95.3±4.6	91.3 ± 8.4, 94.9 ± 5.6	p = 0.79, p = 0.20

by >40 mm Hg), based on the guidelines of the Japanese Circulation Society.[4] Echocardiographic criteria of right heart dysfunction include right ventricular (RV) dilation and/or an increased end-diastolic right ventricle (RV) to left ventricle (LV) diameter ratio (the threshold value was 0.9 or 1.0); hypokinesia of the free RV wall; increased velocity of the tricuspid regurgitation jet; or combinations of the above. Finally, on CT findings, right heart dysfunction was defined as an increased RV/LV diameter ratio (with a threshold of 0.9 or 1.0). Treatment decisions such as thrombolysis, catheter treatment, and inferior vena cava (IVC) filter insertion were at the discretion of the attending physicians. The gender differences were extracted from the survey forms.

Parametric variables were reported as mean ±1 standard deviations and nonparametric variables were reported as median (25th to 75th interquartile range). PASW Statistics ver. 18 (SPSS Inc., Chicago, Illinois) was used to compare means between 2 groups with the Student's *t* test. For nonparametrically distributed data, Mann-Whitney U test was used. Statistical comparisons of dichotomous variables were carried out using the chi-square test or Fisher's exact test, as appropriate. Statistical significance and tendency were set at p <0.05 and p <0.10. Several potential predictors for PE-related 30-day mortality were also identified on single predictor analysis. Of these, the risk factors with p value <0.10 on univariate analysis were evaluated on multivariate regression analysis.

Results

Patients' characteristics are shown in Table 1. Female patients were significantly older and suffered from a higher percentage of nosocomial diseases than their male counterparts. The female subjects also demonstrated a lower average blood pressure and higher respiratory rate. The differences of clinical symptoms are shown in Table 2.

Table 2
Clinical signs and symptoms

Variable	Men (n = 633)	Women (n = 795)	p value
Dyspnea	354 (55.9%)	487 (61.3%)	p = 0.045
Chest pain	111 (17.5%)	107 (13.5%)	p = 0.038
Consciousness disturbance	27 (4.3%)	58 (7.3%)	p = 0.024
Palpitation	22 (3.5%)	37 (4.7%)	p = 0.29
Leg symptom	112 (17.7%)	102 (12.8%)	p = 0.011
General fatigue	10 (1.6%)	19 (2.4%)	p = 0.35
No symptom	13 (2.1%)	10 (1.3%)	p = 0.29

The results of the blood examinations and the cardiac ultrasound are shown in Table 3. The serum levels of brain natriuretic peptide and the pulmonary arterial pressures estimated by ultrasound cardiography were higher in female patients than those of male patients. The gender differences with respect to APE severity are shown in Figure 1 and clearly shows a higher degree of severity in the female population (p = 0.0002).

The treatment approaches are shown in Figure 2. The proportion of invasive therapies such as thrombolysis, catheter treatment, and surgery was lower in female patients although it was not statistically significant (p = 0.147, Figure 2). Additionally, the rate of insertion of IVC filters was significantly lower in female than in male patients (p = 0.029, Figure 2).

The 30-day prognosis is shown in Figure 3. Although there was no significant difference, women reported a 30-day mortality (all reasons included) rate of 6.2% whereas men reported a lower rate of 4.3%. In all causes of death, we defined recurrence of PE, shock, multiple organ failure, pulmonary hypertension, cardiac arrest, and heart failure as PE-related deaths. The female population demonstrated a significantly higher 30-day PE mortality than that of the male population (5.0% vs 2.8%, p = 0.043). The PE-related

Table 3
Blood examinations and estimated pulmonary arterial pressure

Variable	Men (n = 633)	Women (n = 795)	p value
Blood examination			
White blood cell (/μL)	9346 ± 6100	8987 ± 4722	p = 0.23
Hemoglobin (g/dl)	13.9 ± 2.3	12.1 ± 2.0	p <0.0001
Creatinine (mg/dl)	0.99 ± 0.39	0.82 ± 0.53	p <0.0001
Uric acid (mg/dl)	6.5 ± 2.2	5.7 ± 2.3	p <0.0001
Creatine kinase (IU/dl)	95.5 (60.0~139.8)	71.0 (47.5~105.0)	p <0.0001
Total cholesterol (mg/dl)	179.9 ± 45.3	183.1 ± 42.8	p = 0.37
Triglyceride (mg/dl)	131.2 ± 106.5	112.0 ± 63.3	p = 0.006
High-density lipoprotein (mg/dl)	45.8 ± 16.0	51.4 ± 20.9	p = 0.00015
Low-density lipoprotein (mg/dl)	110.7 ± 37.2	112.9 ± 35.3	p = 0.43
C-reactive protein (mg/dl)	1.60 (0.61 ~ 3.88)	0.96 (0.30 ~ 2.74)	p <0.0001
Glucose (mg/dl)	147.2 ± 80.0	155.5 ± 81.5	p = 0.084
Brain natriuretic peptide (pg/dl)	107.0 (25.6~306.8)	180.4 (50.7~526.1)	p <0.0001
Positive Troponin	252 (39.8%)	371 (46.7%)	p = 0.079
Estimated systolic pulmonary arterial pressure			
Acute phase (mm Hg)	47.4 ± 22.4 (n = 313)	51.5 ± 22.2 (n = 465)	p = 0.012
Subacute phase (mm Hg)	32.3 ± 17.8 (n = 108)	37.9 ± 19.8 (n = 142)	p = 0.021

mortality was consequently evaluated according to age and gender (Figure 4), and showed that women had a higher incidence of PE-related mortality for all ages above 40s and also demonstrated statistical tendencies in patients in the age of 50s and 60s (p = 0.073, 0.095).

Clinical predictors for PE-related 30-day mortality were assessed by multivariate regression analysis (Table 4) and indicated that advanced age, lower blood pressure and higher pulmonary arterial pressure remained significant factors affecting patient mortality but did not display any gender differences.

Discussion

This report is to the best of our knowledge, the first study demonstrating that Asian female APE patients have a poorer prognosis than their male counterparts. Interestingly, the gender distribution of APE patients in this study did not coincide with previous studies conducted in Western countries[7,11–14] but in contrast, its results concurred with several studies from Asian countries demonstrating a higher proportion of female subjects with APE as opposed to males.[5,10,14,16] From these results, we could presume that the APE gender distribution might vary according to the patients' ethnicity.

This study also suggests that in APE, women may tend to experience more severe clinical presentations than men and that the elevated PE-related mortality in female subjects could be attributed to specific parameters that were more commonly found in female subjects such as older age, severe degree of disease, and different treatment strategies. It should be noted however, that older age is not the sole defining element as other parameters increased the PE-related mortality in women of almost all age groups (Figure 4). Recent North American and European landmark registry studies displayed similar results to the present study.[11,12]

Over the course of the last few decades, there appears to have been a considerable change in the gender differences in APE patients. Interestingly, initially it was reported that men had poorer prognosis than women, in both Western and Japanese studies conducted between the 1980s and 1990s. A notable study conducted from 1979 to 1996 in the USA demonstrated that the PE-related mortality was still higher in men than in women, but every year, witnessed a progressive decrease in PE-related mortality in both sexes

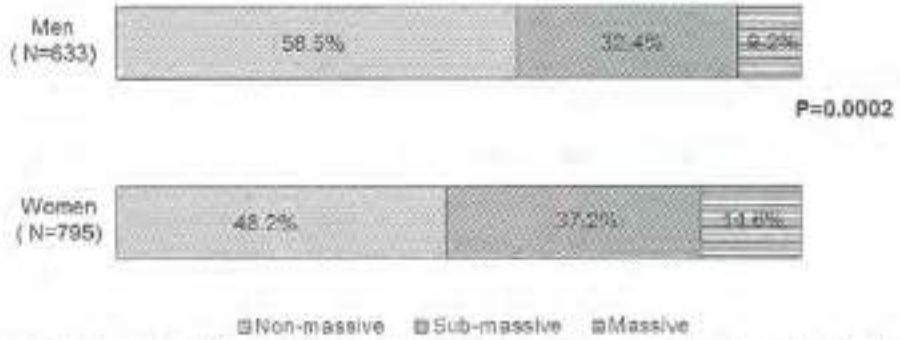

Figure 1. The gender difference in APE severity. The female patients had more disease severity than the male patients did (p = 0.0002).

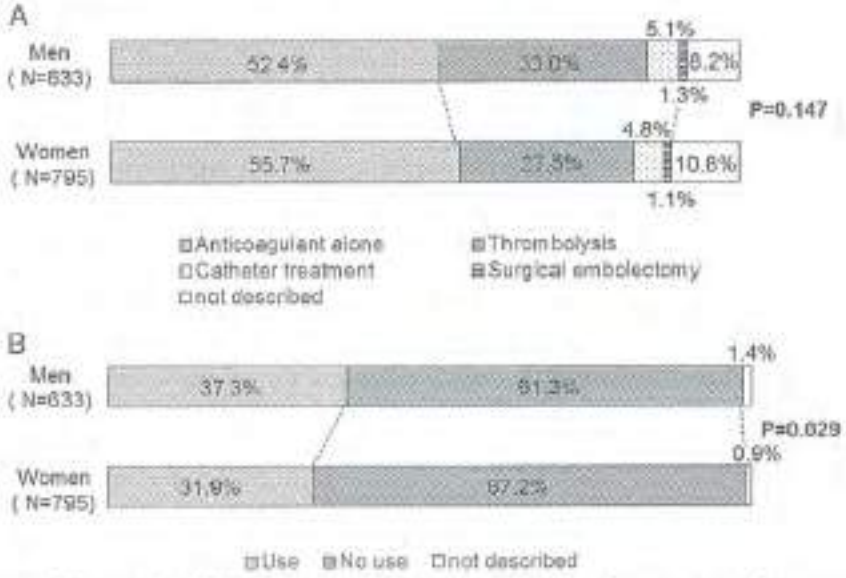

Figure 2. (A) Treatment strategy. The proportion of the invasive therapies such as thrombolysis, catheter treatment and surgery was lower in females than in males, although it was not statistically significant. (B) Usage rate of IVC filter. The use of inferior vena cava filters was significantly lower in women than in men ($p = 0.029$).

in all races. However, the degree of decrease was less in women than in men,[8] which could signify that female APE patients might benefit less from the improved PE diagnostic and management techniques. This trend has been ongoing and the rates of mortality between genders have now reversed as demonstrated by Western studies,[11,12] and the present study. Previous reports regarding gender difference in PE and venous thromboembolism are summarized in Table 5. The reasons for lower decrease rate in PE-related mortality in women could be multifactorial. Compared with men, women had a higher incidence of bleeding complications[12,17] and blood transfusions[11] during the antithrombotic therapy. Besides, the rate of IVC filter use was lower in women.[11] The bleeding complications could not be evaluated in the present study; however, the use of IVC filter was significantly lower in women than in men, which might indicate that clinicians preferred a less aggressive therapy for female patients. Thus, female patients seemed to receive fewer benefits from the advances in treatment such as antithrombolytics and IVC filter.

The female subjects were older and had a higher degree of APE severity than males. A possible reason for the severe clinical presentation might be the longer life expectancy in women and that APE appears to occur more commonly during the postmenopausal period and peaks during older age. The reduced physical ability and the higher incidence of concomitant diseases in elder patients may contribute in the increased severity of APE presentation. However, the poor prognosis for female with APE cannot be solely attributed to old age since women PE-related mortality was higher than men over a wide age range (Figure 4). Symptoms in genders indicated in Table 2 might indicate

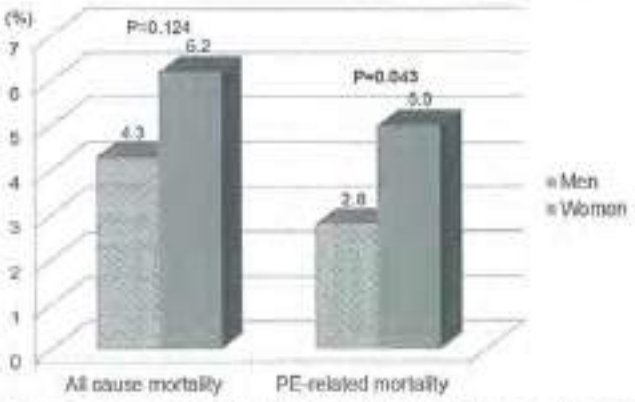

Figure 3. 30-day prognosis. All cause 30-day mortality in women was 6.2%, which was higher than that in men (4.3%) although it was not significant ($p = 0.124$). PE-related 30-day mortality in women was higher than that in men significantly (5.0% vs 2.8%, $p = 0.043$).

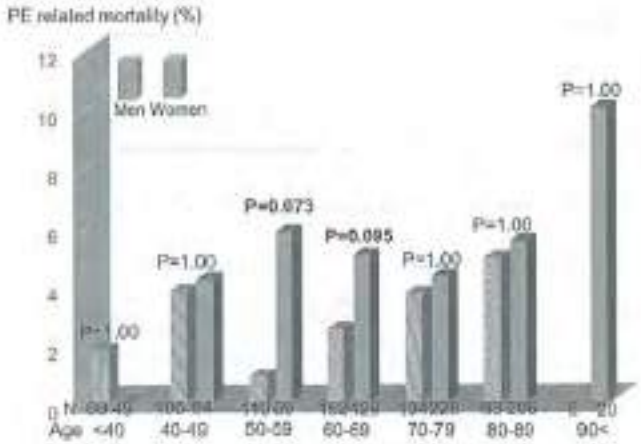

Figure 4. PE-related mortality according to the age and gender. PE-related mortality of women was higher than that of men in the all ages above 40s and the statistical tendencies were seen in 50s and 60s ($p = 0.073, 0.095$).

Table 4
Clinical predictors for PE-related 30-day mortality

	Odds ratio	95% Confidence interval	p value
Age	1.121	1.025–1.227	0.013
Women	2.289	0.325–16.133	0.41
Systolic blood pressure	0.951	0.925–0.979	0.00056
Systolic pulmonary arterial pressure	1.057	1.023–1.092	0.00080
Brain natriuretic peptide	1.000	0.999–1.001	0.83
Inferior vena cave filter use	0.462	0.067–3.176	0.43

that the pathophysiology and behavior from onset to hospital arrival were different between the sexes. The renowned higher pain tolerance in women, could result in delayed primary medical care which could subsequently lead to a poor prognosis. In fact, it has been reported that women tend to have longer delays from symptom onset to emergency department arrival, gravely affecting treatment choices and outcomes in acute ischemic stroke and acute myocardial infarction.[18,19] Female patients in this study might be unaware of any lower limb symptoms, chest pains which led to delayed primary medical care hence causing undesired progression of the disease. Additionally, the response to therapies might differ between the 2 genders. The estimated systolic pulmonary arterial pressure of male patients was normalized in the subacute phase, however, it remained higher than normal limits in female patients (Table 3). An echocardiographic study also revealed that the right heart dysfunction due to PE was recovered at predischarge follow-up in male patients, whereas it remained in female patients.[20] Gender difference of the pathophysiology and response to treatment might play a role in the higher incidence of chronic thromboembolic pulmonary hypertension in women in Japanese population.[21]

There were some limitations in this study. First, we evaluated the APE patients treated at the CCUs whereas the less severe cases treated in general wards were not included in this study. Second, our data did not include nor contained sufficient information in regard to bleeding complications which particularly affected acute mortality rates. However, the population sample size of this study was large enough to provide relevant results concerning the gender differences in APE patients.

In conclusion, APE female patients were in general older than male patients and demonstrated more severe clinical manifestations. They might have received less intensive treatment which could have possibly led to poorer prognosis.

Further investigations are warranted to improve the prognosis of APE female patients.

Table 5
Previous studies describing the gender difference in patients affected by pulmonary embolism and venous thromboembolism

Studies	Study population	Severity of pulmonary embolism	Results
Heelander KT, 2003[9]	Death certificates between 1979 and 1998 in the United States.	Not described	Age-adjusted mortality rate per million in 1979 and 1998; 232, 103 in males and 163, 88 in females.
SiddiqueRM, 1998[7]	Cohort of Medicare patients in 1984 with pulmonary embolism in the United States.	Not described	Median suvival time; Black males 2.5years, Black females 5.2 years, White males 4.3 years, White females 5.9 years.
Lilienfeld DE, 2000[8]	Death certificates between 1979 and 1996 in the United States.	Not described	Age-adjusted mortality rate per 100,000 in 1996 were 2.7 among males and 2.6 among females.
Heit JA, 1999[10]	Cohort of patients with venous thromboembolism between 1966 and 1990 in the United States.	Not described	Males had a significant risk for acute and long-term mortality but the values were not described.
Nakamura M, 2001[16]	Registry data of patients with pulmonary embolism between 1994 and 1997 in Japan.	The patients with shock vital were 36% of all patients.	Males had a significant risk for in-hospital mortality but the values were not described.
Lee CH, 2011[14]	National Health Insurance medical claims databases of patients with venous thromboembolism between 2001and 2003 in Taiwan.	Not described	No difference between sexes but the values were not described.
Agarwal S, 2015[11]	Nationwide Inpatient Sample (NIS) database of patients with pulmonary embolism between 2003 and 2011 in the United States.	Not described	In-hospital mortality rate was 3.19% in males and 3.50% in females.
Blanco-Molina A, 2014[17]	Registry data of patients with venous thromboembolism between 2001 and 2013 in Europe	The patients with unstable hemodynamics were 8.6% in females and 7.4% in males.	30-days and 1-year PE-related mortality were 0.92%, 1.03% in males and 1.13% and 1.22% in females.
The present study, 2018	Registry data of patients with pulmonary embolism treated at cardiovascular care units between 2010 and 2014 in Japan.	The patients with unstable hemodynamics were 14.6% in females and 9.2% in males.	30-days PE-related mortality was 2.8% in males and 5.0% in females.

Acknowledgment

The authors would like to thank Professor Yoshihiro J. Akashi of the Division of Cardiology, Department of Internal Medicine, St Marianna University School of Medicine, for his excellent technical assistance. We would also like to thank Editage (www.editage.jp) and Brandon Lohman, MD for English language editing.

Disclosures

The authors have no conflicts of interest to disclose.

1. Anderson FA, Zayaruzny M, Heit JA, Fidan D, Cohen AT. Estimated annual numbers of US acute-care hospital patients at risk for venous thromboembolism. *Am J Hematol* 2007;82:777–782.
2. Cohen AT, Agnelli G, Anderson FA, Arcelus JI, Bergqvist D, Brecht JG, Greer IA, Heit JA, Hutchinson JL, Kakkar AK, Mottier D, Oger E, Samama MM, Spiezia M. VTE Impact Assessment Group in Europe (VITAE). Venous thromboembolism (VTE) in Europe. The number of VTE events and associated morbidity and mortality. *Thromb Haemost* 2007;98:756–764.
3. Liao S, Woulfe T, Hyder S, Merriman E, Simpson D, Chunilal S. Incidence of venous thromboembolism in different ethnic groups: a regional direct comparison study. *J Thromb Haemost* 2014;12:214–219.
4. JCS Joint Working Group. Guidelines for the diagnosis, treatment and prevention of pulmonary thromboembolism and deep vein thrombosis (JCS2009). *Circ J* 2011;75:1258–1281.
5. Nakamura M, Miyata T, Ozeki Y, Takayama M, Komori K, Yamada N, Origasa H, Satokawa H, Maeda H, Tanabe N, Unno N, Shibuya T, Tanemoto K, Kondo K, Kojima T. Current venous thromboembolism management and outcomes in Japan. *Circ J* 2014;78:708–717.
6. Horlander KT, Mannino DM, Leeper KV. Pulmonary embolism mortality in the United States, 1979–1998: an analysis using multiple-cause mortality data. *Arch Intern Med* 2003;163:1711–1717.
7. Siddique RM, Amini SB, Jr Connors AF, Rinaldi AA. Race and sex differences in long-term survival rates for elderly patients with pulmonary embolism. *Am J Public Health* 1998;88:1476–1480.
8. Lilienfeld DE. Decreasing mortality from pulmonary embolism in the United States, 1979–1996. *Int J Epidemiol* 2000;29:465–469.
9. Heit JA, Silverstein MD, Mohr DN, Petterson TM, O'Fallon WM, Melton 3rd LJ. Predictors of survival after deep vein thrombosis and pulmonary embolism: a population-based, cohort study. *Arch Intern Med* 1999;159:445–453.
10. Nakamura M, Fujioka H, Yamada N, Sakuma M, Okada O, Nakanishi N, Miyahara Y, Koriyama T, Konieda T, Sugimoto T, Nakano T. Clinical characteristics of acute pulmonary thromboembolism in Japan: results of a multicenter registry in the Japanese Society of Pulmonary Embolism Research. *Clin Cardiol* 2001;24:132–138.
11. Agarwal S, Clark 3rd D, Sud K, Isher WA, Cho L, Menon V. Gender disparities in outcomes and resource utilization for acute pulmonary embolism hospitalizations in the United States. *Am J Cardiol* 2015;116:1270–1276.
12. Blanco-Molina A, Enea I, Gadelha T, Tufano A, Bura-Riviere A, Di Micco P, Bounameaux H, Gonzalez J, Villalta J, Monreal M. RIETE Investigators. Sex differences in patients receiving anticoagulant therapy for venous thromboembolism. *Medicine* 2014;93:309–317.
13. Lagorte S, Mismetti P, Décousus H, Uresandi F, Otero R, Lobo JL, Monreal M. RIETE Investigators. Clinical predictors for fatal pulmonary embolism in 15,520 patients with venous thromboembolism: findings from the Registro Informatizado de la Enfermedad TromboEmbolica venosa (RIETE) Registry. *Circulation* 2008;117:1711–1716.
14. Lee CH, Cheng CL, Lin LJ, Tsai LM, Yang YH. Epidemiology and predictors of short-term mortality in symptomatic venous thromboembolism. *Circ J* 2011;75:1998–2004.
15. White RH. The epidemiology of venous thromboembolism. *Circulation* 2003;107:14–18.
16. Tanabe Y, Obayashi T, Yamamoto T, Takayama M, Nagao K. Predictive value of biomarkers for the prognosis of acute pulmonary embolism in Japanese patients: results of the Tokyo CCU Network registry. *J Cardiol* 2015;66:460–465.
17. Loffredo L, Violi F, Perri L. Sex related differences in patients with acute venous thromboembolism treated with new oral anticoagulants. A meta-analysis of the interventional trials. *Int J Cardiol* 2016;212:255–258.
18. Pancholy SB, Shandhu GP, Patel T, Cheskin LJ. Sex differences in short-term and long-term all-cause mortality among patients with ST-segment elevation myocardial infarction treated by primary percutaneous intervention: a meta-analysis. *JAMA Intern Med* 2014;174:1822–1830.
19. Towfighi A, Markovic D, Ovbiagele B. Sex differences in revascularization interventions after acute ischemic stroke. *J Stroke Cerebrovasc Dis* 2013;22:e347–e353.
20. Jenab Y, Ghaffari-Marandi N, Safir A, Ejmalian G, Zoroufian A, Jalali A, Sabeljam M. Sex-related changes in tissue Doppler imaging parameters among patients with acute pulmonary thromboembolism. *J Ultrasound Med* 2013;32:1997–2005.
21. Tanabe N, Sugimura T, Tatsumi K. Recent progress in the diagnosis and management of chronic thromboembolic pulmonary hypertension. *Respir Investig* 2013;51:134–146.

JACC: CLINICAL ELECTROPHYSIOLOGY
© 2018 BY THE AMERICAN COLLEGE OF CARDIOLOGY FOUNDATION
PUBLISHED BY ELSEVIER

VOL. 4, NO. 9, 2018

NEW RESEARCH PAPERS

Development of Heart Failure From Transient Atrial Fibrillation Attacks in Responders to Cardiac Resynchronization Therapy

Ikutaro Nakajima, MD,[a,b] Takashi Noda, MD, PhD,[a] Hideaki Kanzaki, MD, PhD,[a] Tsukasa Kamakura, MD, PhD,[a] Mitsuru Wada, MD,[a] Kohei Ishibashi, MD, PhD,[a] Yuko Inoue, MD, PhD,[a] Koji Miyamoto, MD, PhD,[a] Hideo Okamura, MD, PhD,[a] Satoshi Nagase, MD, PhD,[a] Takeshi Aiba, MD, PhD,[a] Shiro Kamakura, MD, PhD,[a] Teruo Noguchi, MD, PhD,[a] Satoshi Yasuda, MD, PhD,[a] Yoshihiro J. Akashi, MD, PhD,[b] Kengo F. Kusano, MD, PhD[a]

ABSTRACT

OBJECTIVES This study aimed to clarify the clinical impact of transient atrial fibrillation (AF) attacks themselves and the efficacy of cardiac resynchronization therapy (CRT) in patients with intermittent AF.

BACKGROUND The benefit of CRT in patients with intermittent AF, especially the effect of the AF attacks themselves, remains unclear.

METHODS Among our cohort of 269 consecutive CRT patients, we compared the percent of biventricular pacing (BIVP%) and other clinical characteristics between patients with intermittent AF and those with sinus rhythm (SR).

RESULTS During a median follow-up of 942 days (interquartile range: 379 to 1,464 days) a total of 22 patients, including 59% of CRT responders, developed heart failure (HF) due to a transient AF attack itself, and that accounted for 21% of all HF events. The BIVP% during the AF attacks was significantly lower than that during SR ($p < 0.05$). When compared to the SR groups, patients with intermittent AF had a significantly higher risk of developing HF or death (hazard ratio: 2.2; 95% confidence interval: 1.3 to 3.8). However, the patients who received a BIVP% of >90% during AF attacks were comparable to those with SR (hazard ratio: 1.2; 95% confidence interval: 0.4 to 3.0).

CONCLUSIONS A substantial number of patients developed HF due to transient AF attacks themselves even in the CRT responders, and the reason was mainly due to the loss of the BIVP%. (J Am Coll Cardiol EP 2018;4:1227–34) © 2018 by the American College of Cardiology Foundation.

Atrial fibrillation (AF) is a common comorbidity among heart failure (HF) patients with a reduced left ventricular (LV) systolic function and is associated with significant morbidity and mortality specifically in those patients (1–3). Cardiac resynchronization therapy (CRT) has been proven to significantly improve the prognosis in selected patients with sinus rhythm (SR) (4,5), however, the

From the [a]Division of Cardiology, National Cerebral and Cardiovascular Center Japan, Suita Osaka, Japan; and the [b]Division of Cardiology, Department of Internal Medicine, St. Marianna University School of Medicine, Kawasaki, Japan. This study was supported by the intramural research fund (25-4-7, Dr. Kusano) for cardiovascular diseases of the National Cerebral and Cardiovascular Center, and trust research and joint research funds of Medtronic Japan Co., Ltd. Drs. Noda and Kusano have received personal fees from Medtronic Japan Co., Ltd. All other authors have reported that they have no relationships relevant to the contents of this paper to disclose.

All authors attest they are in compliance with human studies committees and animal welfare regulations of the authors' institutions and Food and Drug Administration guidelines, including patient consent where appropriate. For more information, visit the JACC: Clinical Electrophysiology author instructions page.

Manuscript received February 26, 2018; revised manuscript received May 31, 2018, accepted June 7, 2018.

ISSN 2405-500X/$36.00 https://doi.org/10.1016/j.jacep.2018.06.010

JACC: CLINICAL ELECTROPHYSIOLOGY VOL. 4, NO. 9, 2018
SEPTEMBER 2018:1227–34

ABBREVIATIONS AND ACRONYMS

ADHF = acute decompensated heart failure

AF = atrial fibrillation

AVJA = atrioventricular junction ablation

BIVP% = biventricular pacing percentage

CRT = cardiac resynchronization therapy

HF = heart failure

ICD = implantable cardioverter defibrillator

LV = left ventricle/ventricular

NYHA = New York Heart Association

SR = sinus rhythm

benefit of CRT seems to be attenuated in patients with AF based on the recent clinical trials (6,7).

The current guidelines do not distinguish between paroxysmal or permanent AF, and it remains unclear whether patients with intermittent atrial tachyarrhythmias could gain similar beneficial effects from CRT as patients with SR. Recently, by using device detection algorithms, relevant studies have revealed that even in patients with a small AF burden or new-onset AF after CRT, intermittent atrial tachyarrhythmias have been observed to be associated with a worse prognosis than in patients with SR (8-10).

The majority of the studies referring to AF in patients with CRT have focused on the prevalence and prognostic implications, and only limited studies have investigated how intermittent atrial tachyarrhythmias, including paroxysmal and persistent AF themselves, affect the hemodynamics and attenuate the clinical benefit of CRT.

Accordingly, the present study was designed 2-fold. First, we assessed whether the AF attack itself directly caused HF events and clarified how the AF attack affected CRT patients. Second, we evaluated the impact of intermittent AF on the mortality and morbidity after CRT implantations during the long-term follow-up.

SEE PAGE 1228

TABLE 1 Baseline Characteristics

	All Patients (N = 243)	Sinus Rhythm (n = 120)	Intermittent AF (n = 72)	Permanent AF (n = 51)
Age (yrs)	65 ± 13	65 ± 14	65 ± 13	68 ± 10
Male	192 (79)	89 (74)	57 (79)	46 (90)*
Ischemic heart disease	54 (22)	28 (23)	19 (26)	7 (14)
NYHA functional class				
II	65 (27)	34 (28)	17 (24)	14 (27)
III	149 (61)	75 (63)	41 (57)	33 (65)
IV	29 (12)	11 (9)	14 (19)*	4 (8)
CRT-P/CRT-D	38 (16) / 205 (84)	22 (18) / 98 (82)	4 (6) / 68 (94)	7 (14) / 44 (86)
Primary prevention	141 (69)	60 (65)	46 (68)	34 (77)
Creatinine ≥1.4 mg/dl	67 (28)	31 (26)	19 (26)	17 (33)
Diabetes	65 (27)	30 (25)	21 (29)	14 (27)
Electrocardiographic characteristics				
QRS duration (ms)	166 ± 39	170 ± 37	160 ± 36	167 ± 44
LBBB	170 (70)	85 (71)	48 (67)	37 (73)
Echocardiography characteristics				
LVEF (%)	25 ± 9	24 ± 7	25 ± 10	28 ± 9
LVEDV (ml)	267 ± 116	280 ± 101	260 ± 100	241 ± 114
LVESV (ml)	205 ± 109	219 ± 96	199 ± 90	172 ± 106
Left atrial volume (ml)	103 ± 48	94 ± 30	99 ± 39	148 ± 68*
Medications				
Beta-blocker	208 (86)	107 (89)	62 (86)	39 (76)*
ACE inhibitor or ARB	205 (84)	99 (83)	64 (89)	42 (82)
Diuretic agents	222 (91)	108 (90)	64 (89)	50 (98)
Amiodarone	109 (45)	53 (44)	36 (50)	20 (39)
Digoxin	45 (20)	22 (18)	21 (29)	6 (12)

Values are mean ± SD or n (%). *p < 0.05: all compared with the sinus rhythm group.

ACE = angiotensin-converting enzyme; AF = atrial fibrillation; ARB = angiotensin-receptor blocker; CRT-D = cardiac resynchronization therapy with defibrillator; CRT-P = cardiac resynchronization therapy pacemaker; LBBB = left bundle branch block; LVEF = left ventricular ejection fraction; LVEDV = left ventricular end-diastolic volume; LVESV = left ventricular end-systolic volume; NYHA = New York Heart Association.

METHODS

PATIENTS AND STUDY PROTOCOL. All patients receiving CRT at the National Cerebral and Cardiovascular Center Japan between 2009 to 2014 were prospectively registered. The eligibility for CRT was based on the international guidelines (11,12), including advanced HF (New York Heart Association [NYHA] functional class II, III, or IV), a depressed LV function (LV ejection fraction ≤ 35%), and a wide QRS complex (>120 ms). The characteristics at baseline, data of the implant procedure, data of all follow-up visits, and data through remote telemetry were recorded. No patients with an atrioventricular junction ablation (AVJA) during the perioperative period of the CRT were included in the present study.

CLINICAL ASSESSMENT AND FOLLOW-UP. The first evaluation with a device interrogation was held 1 month after CRT implantation. Sequentially, the patients underwent a clinical assessment and device interrogation every 3 to 6 months. The assessment included an evaluation of the NYHA functional class, electrocardiogram, and echocardiogram, of which the parameters were assessed according to the Simpson's biplane method: LV ejection fraction (LVEF), LV end-systolic volume, LV end-diastolic volume, and left atrial volume. The CRT responders were defined as having a reduction in the LV end-systolic volume of >15% at the 6-month follow-up compared to that at baseline. Patients who died before 6 months were considered nonresponders.

DIAGNOSTICS OF AF AND BIVENTRICULAR PACING. We analyzed the continuous monitoring by using an AF detection algorithm via implantable devices and AF was defined as high-rate atrial episodes (≥180 beats per min) lasting for at least 10 min (13). According to the AF guidelines, the type of AF was defined as follows: 1) permanent AF indicated a daily mean AF burden of ≥23 h over the evaluation period; 2) persistent AF indicated ≥7 consecutive days of AF of ≥23 h/day; 3) paroxysmal AF: ≥1 d of AF of ≥6 h,

FIGURE 1 Flowchart of Atrial Fibrillation and Sequential HF Events

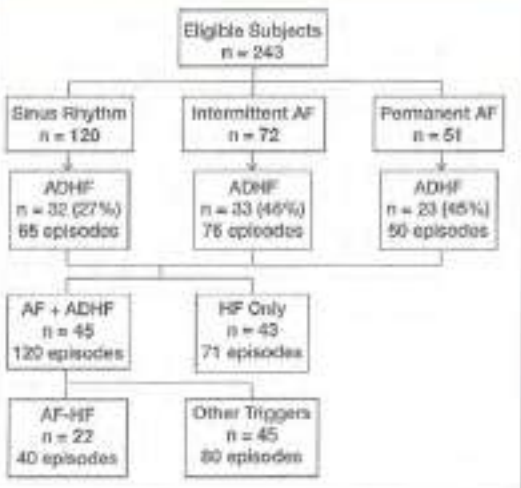

ADHF = acute decompensated heart failure; AF = atrial fibrillation; AF-HF = atrial fibrillation induced heart failure.

TABLE 3 Characteristics of the Patients With AF Induced HF (N = 22)

Baseline characteristics	
Age (yrs)	61 ± 19
Male	17 (77)
Ischemic heart disease	6 (27)
NYHA functional class (II/III/IV) (%)	9 / 59 / 32
QRS duration (ms)	157 ± 42
LVEF (%)	26 ± 9
Beta-blockers	20 (91)
Amiodarone	12 (55)
AF ablation before CRT	4 (18)
AF classification	
Sinus Rhythm	1 (5)
Paroxysmal AF	14 (64)
Persistent AF	7 (32)
Changes after CRT	
ΔNYHA functional class	−0.7 ± 1.0
ΔLVEF (%)	2.5 ± 9.2
ΔLVESV (ml)	−21 ± 42
Δ left atrial volume (ml)	8.0 ± 31
Responder	13 (59)
AF-induced HF events	
Repeated AF-HF	7 (32)
Incidence (/person)	1.8
Inappropriate ICD therapy due to AF	5 (23)
Onset of AF to HF (days)	3.2
Treatments after first AF-HF events	
AF ablation	5 (23)
AV junction ablation	2 (9)
Additional medications	14 (64)

Values are mean ± SD, n (%), unless otherwise noted.
AV = atrioventricular; ICD = implantable cardioverter defibrillator; other abbreviations as in Table 1.

and 4) SR indicated all other patients (14). Intermittent AF was defined as paroxysmal AF and persistent AF in this study.

The type of AF was assessed during the first 3 months post-implantation excluding the first month as the blanking period and the longest AF burden of a single event was accepted. The percentage of biventricular pacing (BIVP%) was calculated as the number of paced or sensed ventricular beats over a given period. The BIVP% was estimated during the total lifetime, AF periods, non-AF periods, and HF events that developed. Premature ventricular contractions were also recorded by the devices. Further, the algorithm, ventricular triggered LV or biventricular pacing, was defined as captured biventricular pacing in this study.

CLINICAL OUTCOMES. The clinical outcomes including all-cause deaths, decompensated HF, and appropriate or inappropriate implantable cardioverter-defibrillator (ICD) shocks were monitored. On the basis of a review of the medical records and information of the device interrogation, the date of the onset was assigned for all AF episodes, HF events, and ICD shock events.

The onset of HF was defined as the initial day of developing HF symptoms or signs including exacerbation of the dyspnea on exertion, orthopnea, paroxysmal nocturnal dyspnea, general fatigue, weight gain, or edema based on the medical history. Although we used the objective nature of the definition of the onset of AF using the device detection algorithm, it was difficult to distinguish the symptoms of HF from AF in some patients if the patients presented with supposed HF symptoms on the same day as the onset of AF. In such cases, the onset of HF was separately defined as the day of the physician's objective diagnosis of acute decompensated heart failure (ADHF).

To clarify AF induced adverse events, the episodes of all HF events with concurrent AF episodes were extracted. AF induced HF (AF-HF) was defined as an event involving decompensated HF preceding the onset of AF within 7 days before the onset of HF, and without any other triggering factors including acute ischemia, infections, anemia, or breaking life restrictions.

STATISTICAL ANALYSIS. The continuous data are expressed as the mean ± SD for a normal distribution, or the median (25th and 75th percentiles) for a skewed distribution. Dichotomous data are presented as numbers and percentages. The proportions were compared with the chi-square test or Fisher exact

JACC: CLINICAL ELECTROPHYSIOLOGY VOL. 4, NO. 9, 2018
SEPTEMBER 2018:1227–34

FIGURE 2 Impact of AF Classification and HF Events on the BIVP%

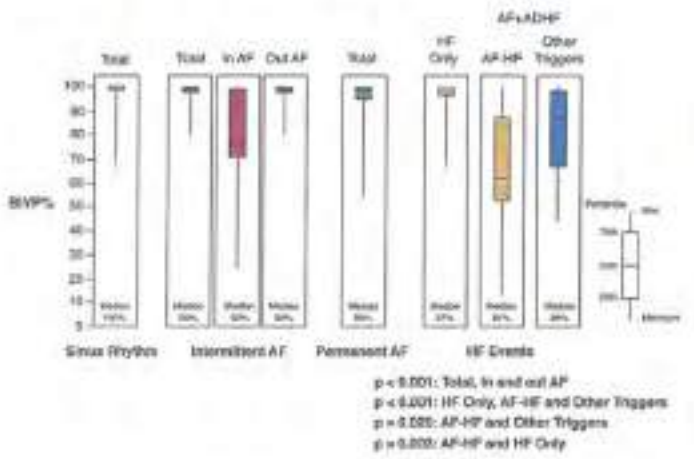

(Gray) Patients with sinus rhythm. (Red) Patients with intermittent AF. (Green) Patients with permanent AF. (Yellow) HF without AF. (Orange) AF induced HF. (Blue) Comorbid condition of AF and ADHF with other triggers except AF. BIVP% = biventricular pacing rate; HF = heart failure; other abbreviations as in Figure 1.

test, as appropriate. A comparison of the continuous data was performed with the Student *t* test for paired and unpaired data. Nonparametric data were compared using the Wilcoxon rank sum test.

The cumulative event rates (HF hospitalization, death, ICD shocks) were analyzed by the Kaplan-Meier method. Those analyses were started at the time of the AF designation and only included patients without events during the first 90 days after CRT implantation. A Cox proportional hazards model was used to assess the impact of intermittent AF at baseline and the BIVP% during AF on the clinical events. We adjusted for any relevant variables including the age, sex, NYHA functional class, proportion of a left bundle branch block morphology, LVEF, QRS duration, left atrial volume, serum creatinine ≥1.4 mg/dl, and use of beta-blockers. Hazard ratios (HRs) with 95% confidence intervals (CIs) and 2-sided p values were reported. A 2-tailed p value of <0.05 was considered statistically significant. All statistical analyses were performed with JMP 12 software (SAS Institute, Inc., Cary, North Carolina).

RESULTS

BASELINE CHARACTERISTICS. The data from 269 consecutive patients receiving a CRT device with the intent to perform BIVP were collected. Of those, 26 were excluded for various reasons, including loss to follow-up, death within 1 month, an LV lead malfunction, lack of an atrial lead, or an extremely low value of the BIVP% (<50%). The remaining 243 CRT recipients were included in the analysis. The median follow-up time was 942 days (interquartile range: 379 to 1,464 days). The baseline characteristics are summarized in Table 1.

Approximately one-half (49%) of our cohort had no history of AF (SR group), 60 (25%) patients had a history of paroxysmal AF, 12 (5%) had a history of developing persistent AF, and the remaining 51 (21%) had permanent AF during the initial 3-month diagnostic phase. According to our definition, 72 (30%) patients were classified as having intermittent AF. As shown in Table 1, when compared with the patients with SR, the patients with intermittent AF contained a higher rate of NYHA functional class IV patients and the patients with persistent AF had a larger left atrial volume.

AF AND SEQUENTIAL HF EVENTS. During the follow-up, 88 (36%) of the eligible patients developed ADHF with a total of 191 episodes. A total of 43 patients (71 episodes) developed ADHF without any AF (HF only) and 45 participants (120 episodes) developed both AF and ADHF. Of those, 22 patients (40 episodes) developed AF-HF based on the definition, and the last 80 episodes had other triggers (Figure 1). Notably, 71% of the total HF events were due to temporal AF attacks.

The clinical characteristics and follow-up data of the patients with AF-HF are shown in Table 2. More than one-half (55%) of the patients with AF-HF were prescribed amiodarone and 4 (18%) subjects underwent radiofrequency catheter ablation of AF before the CRT implantation. After initiating the CRT, the mean NYHA functional class improved from 3.2 ± 0.6 to 2.5 ± 1.0 (p < 0.01) and 13 (59%) patients were responders. The mean time from the onset of AF to developing HF was 3.2 days. After the first AF-HF event, 96% of the patients were administered further treatments, including radiofrequency catheter ablation of AF (23%) and additional medications (64%); however, nearly one-third (32%) of the patients developed repeated episodes of AF-HF.

IMPACT ON THE BIVP% FROM AF EPISODES AND HF EVENTS. When outside the AF period, the BIVP% was maintained at a similarly high level in the patients with SR and intermittent AF. The BIVP% was also high (median 99%) in patients with permanent AF during their constant AF. On the other hand, the BIVP% significantly dropped and varied temporarily during the AF periods in the patients with intermittent AF (p < 0.001) and the BIVP% decreased an average of 16 ± 22% from SR (Figure 2).

FIGURE 3 Risk of HF/Death and ICD Shock

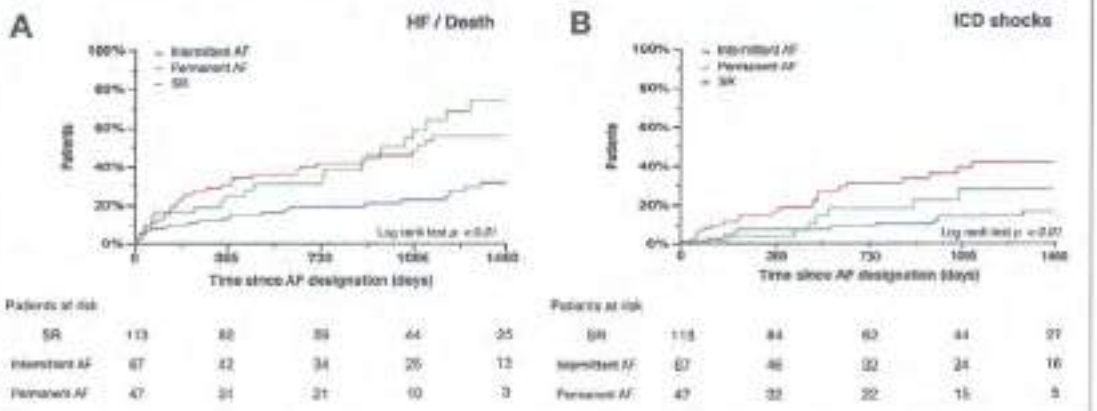

(A) A Kaplan-Meier curve for HF or death in patients with sinus rhythm (SR), intermittent AF, or permanent AF. (B) A Kaplan-Meier curve for all implantable cardioverter defibrillator (ICD) shocks in patients with SR, intermittent AF, or permanent AF. Other abbreviations as in Figures 1 and 2.

Regarding the HF episodes, the BIVP% was held at a high level (median 97%) during the episodes with ADHF without AF (Figure 2, "HF Only") and it was significantly higher when compared to that of the ADHF episodes with AF (Figure 2, "AF + ADHF") ($p = 0.01$). Among the episodes of AF + ADHF, despite the better BIVP% during AF + ADHF episodes with other triggers except AF (Figure 2, "Other Triggers"), there was a smaller BIVP% and greater variation compared with the episodes with HF only ($p = 0.03$). In contrast, the BIVP% during the AF-HF episodes decreased remarkably and 82% of the AF-HF patients had a BIVP% <90%. Moreover, the BIVP% during AF-HF was significantly lower compared to that both during the episodes with HF only ($p = 0.003$) and other triggers ($p = 0.02$). On the other hand, among the patients who developed AF-HF, 18% of them could maintain a BIVP% of >98% during the HF episodes; however, all those patients had recurrences whenever AF temporally occurred again.

MORTALITY AND MORBIDITY. The 4-year cumulative event rates of HF or death were 21% for SR, 46% for intermittent AF, and 47% for permanent AF (Figure 3A). Regarding the SR group, patients with intermittent AF had more than double the risk of HF/death (adjusted HR: 2.2; 95% CI: 1.3 to 3.8; $p = 0.005$), and similarly those with permanent AF had a higher risk (adjusted HR: 2.7; 95% CI: 1.5 to 5.0; $p = 0.002$) as well.

In addition, the 4-year cumulative event rates for all ICD shocks including both appropriate and inappropriate device shocks were 11% for SR, 31% for intermittent AF, and 15% for permanent AF (Figure 3B). Compared to the SR group, the intermittent AF group had greater than double the risk of all ICD shocks (adjusted HR: 2.9; 95% CI: 1.4 to 6.1; $p = 0.004$) and they had a higher risk of both appropriate (adjusted HR: 3.5; 95% CI: 1.7 to 7.9; $p = 0.001$) and inappropriate device shocks (adjusted HR: 7.9; 95% CI: 2.5 to 35.0; $p < 0.001$). The results of the

TABLE 5 Adjusted Hazard Ratios for the Multivariate Analysis

	Sinus Rhythm (n = 113)	Intermittent AF (n = 67)	HR (95% CI)	Adjusted HR (95% CI)	Permanent AF (n = 47)	HR (95% CI)	Adjusted HR (95% CI)*
HF/death	24 (21)	31 (46)	2.4 (1.4–4.1)	2.2 (1.3–3.8)	22 (47)	3.8 (1.5–5.0)	2.7 (1.5–5.0)
All-cause mortality	15 (13)	10 (15)	1.0 (0.4–2.2)	1.0 (0.4–2.2)	6 (13)	1.0 (0.3–2.4)	0.9 (0.3–2.3)
HF hospitalization	23 (20)	28 (42)	2.2 (1.3–3.9)	2.3 (1.3–3.7)	22 (47)	3.0 (1.6–5.3)	2.8 (1.5–5.1)
All ICD shock	12 (11)	22 (33)	3.9 (1.9–8.7)	2.9 (1.4–6.1)	7 (15)	1.5 (0.5–4.3)	1.6 (0.6–4.1)
Appropriate shock	10 (9)	22 (33)	3.9 (1.9–8.7)	3.5 (1.7–7.9)	6 (13)	1.5 (0.5–4.0)	1.5 (0.5–4.3)
Inappropriate shock	3 (3)	16 (24)	9.1 (3.0–35.0)	7.9 (2.5–35.0)	1 (2)	0.8 (0.1–6.2)	0.7 (0.1–6.3)

Values are n (%) unless otherwise noted. *HR adjusted for the age, sex, NYHA functional class, proportion of an LBBB morphology, LVEF, QRS duration, left atrial volume, serum creatinine ≥ 1.4 mg/dL, and use of beta-blockers.

CI = confidence interval; HR = hazard ratio; other abbreviations as in Tables 1 and 2.

JACC: CLINICAL ELECTROPHYSIOLOGY VOL. 4, NO. 9, 2018
SEPTEMBER 2018:1227–37

FIGURE 4 Risk of HF/Death in Patients With SR and Intermittent AF Based on the BIVP% Inside the AF Period

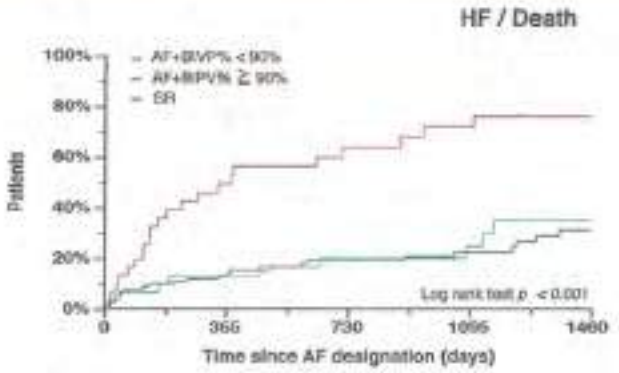

Patients at risk

SR	113	82	59	44	25
AF+BIVP% ≥ 90%	35	26	23	18	8
AF+BIVP% < 90%	32	17	12	8	5

A Kaplan-Meier curve for HF/deaths for the 3 patients groups: SR, patients with a BIVP% inside the AF period for more than 90% of the time (AF + BIVP% ≥ 90%) or patients with a BIVP% inside the AF period for <90% (AF + BIVP% < 90%). Abbreviations as in Figures 1 to 3.

multivariate time-dependent Cox regression analysis for each clinical outcome are shown in Table 3.

To clarify the influence of the BIVP% during AF on the clinical outcome, we divided the patients with intermittent AF into 2 groups depending on whether their BIVP% during AF periods was more than 90% (AF + BIVP% ≥ 90%) or not (AF + BIVP% < 90%), and then compared them to the patients with SR. Based on the Kaplan-Meier analysis, the incidence of HF/death was similar between the patients with AF + BIVP% ≥ 90% and patients with SR ($p = 0.77$). In contrast, the patients with an AF + BIVP% < 90% had a higher incidence of HF/death than both the patients with an AF + BIVP% ≥ 90% and those with SR ($p = 0.004$, $p < 0.0001$; respectively) (Figure 4). In the multivariable analysis, the patients with an AF + BIVP% ≥ 90% had a similar risk for the incidence of HF/death as the patients with SR (adjusted HR: 1.2; 95% CI: 0.4 to 3.0; $p = 0.74$). However, the patients with an AF + BIVP% < 90% had a higher risk (adjusted HR: 3.3; 95% CI: 1.4 to 7.9) than both the patients with an AF + BIVP% ≥ 90% and those with SR (all $p < 0.01$).

DISCUSSION

The main findings of our study on the clinical significance of intermittent AF in CRT patients can be summarized as follows: 1) a significant portion of the patients developed AF-HF, even CRT responders; 2) the BIVP% decreased and varied significantly during AF periods; 3) the BIVP% remarkably decreased when AF-HF occurred; 4) both the patients with intermittent AF and permanent AF had a worse clinical outcome after BIVP than the patients with SR; and 5) the patients with a higher BIVP% during temporary AF periods had a similar clinical outcome as those with SR. In the present study, we showed how intermittent atrial tachyarrhythmias themselves participated in the adverse events and attenuated the clinical benefit from the CRT.

AF-HF EVENTS. We provided new information regarding the incidence of HF subsequent to temporal AF attacks among patients with CRT and also showed the direct relationship to the reduction in the BIVP%. The reasons why AF affects the hemodynamics may be due to tachycardia-related contractile dysfunction, a loss of atrial systole, and an irregular ventricular rhythm. Above all, an uncontrolled tachycardia with a loss of the BIVP% may indicate a strong exacerbation factor of HF.

A higher BIVP% was observed during HF with other triggers even with a comorbidity of AF as compared to AF-HF episodes. This finding may indicate that the greater loss of the BIVP% was 1 of the main reasons why AF itself directly caused HF. Several possible explanations could account for the fact that the BIVP% notably decreased when AF-HF occurred. One possibility is that the patients who developed AF-HF may have easily lost their BIVP% during AF, and the other is that a decreasing BIVP% may have induced hemodynamic deterioration, and the latter may have directly predisposed to the former.

Importantly, a significant proportion of patients recurrently developed similar episodes of AF-HF even among the CRT responders, once AF occurred. Gasparini et al. (15) showed that CRT patients with permanent AF who received AVJA had a significantly better outcome than the patients with drug-treated AF, and a similar long-term survival to the patients with SR. Our findings suggest that AVJA even for the patients with intermittent AF may be reasonable to improve their outcomes. Conversely, several recent reports have shown the effectiveness of biventricular pacing fusion with the intrinsic activation (16,17). Sweeney et al. (16) reported that the QRS fusion complex, representing wavefront interference during biventricular pacing, predicts reverse remodeling during CRT in the patients with left bundle branch block. Van Gelder et al. (17) also showed that the hemodynamic maximal benefit was obtained when LV pacing fusion with intrinsic conduction over the

present right bundle occurred. Thus, intrinsic atrioventricular conduction is preferable for some specific patients and the decision to perform AVJA for intermittent patients with AF remains controversial.

Presumably, catheter ablation of AF is thought to be another option for a solution. Marrouche et al. (18) reported the efficacy of AF ablation in HF patients with systolic dysfunction. According to the report, catheter ablation of AF was associated with lower rates of mortality or HF hospitalization along with reducing the AF burden and improving the LVEF. However, this trial included a relatively small number of patients with CRT and could not show the benefit of AF ablation for these patients based on the subgroup analysis. In fact, some portion of the patients in our cohort underwent AF ablation before or after the CRT; however, most of the patients developed AF again even after the AF ablation. Further studies are needed to clarify the efficacy of AF ablation for CRT patients.

INTERMITTENT AF AND CLINICAL OUTCOMES. Our study found that adverse cardiac events including HF/death and delivered device shocks were more common in patients with intermittent AF than in those with SR. Several clinical trials have shown a worse prognosis in patients with a small AF burden and those results support our findings (8–10). Development of AF itself has been considered to indicate a marker of a potentially worse cardiac status. Thus, we speculated that the difference in the clinical outcome was mainly due to the difference in the underlying substrate. However, our present results indicated the strong factor for a worsening clinical outcome was a decreasing BIVP% due to the AF attack itself. Conversely, the clinical outcome after CRT for patients with intermittent AF whose BIVP% was maintained highly during temporal AF periods could have been similar to that for patients with SR.

In the past study regarding ICD patients, patients with intermittent AF had a significantly increased risk only for inappropriate shocks (19). Differing from general ICD patients, our finding suggested that CRT patients with intermittent AF may have a prognostic implication for both appropriate and inappropriate shocks.

STUDY LIMITATIONS. A potential weakness of this study was that the patients with intermittent AF included those with more severe HF as compared to those with SR, and the influence of this factor regarding the response to CRT could not be ruled out. Furthermore, it is important to emphasize that some of the patients might have had unrecognized common modifying factors that affected both the AF and HF, which made it difficult to clearly distinguish whether they were AF triggering events or not. Finally, the BIVP% investigated in this analysis was based on a device-measured BIVP% and it may have included ineffective complete and consistent BIVP capture. Thus, the actual effective BIVP capture may have been overestimated.

CONCLUSIONS

Among the patients with CRT, intermittent AF has prognostic implications for HF and delivering device shocks. A significant proportion of the patients developed HF due to a temporal AF attack itself even among CRT responders. Once AF occurred, the BIVP% significantly decreased and the patients with a lower BIVP% during temporal AF periods exhibited a worse clinical outcome. These temporal AF episodes with a significant decrease in the BIVP% could be relate to the attenuation of the CRT benefit in patients with intermittent AF.

ADDRESS FOR CORRESPONDENCE: Dr. Takashi Noda, Division of Cardiology, National Cerebral and Cardiovascular Center Japan, 5-7-1 Fujishiro-dai, Suita, Osaka-to 565-8565, Japan. E-mail: tnoda@ncvc.go.jp.

PERSPECTIVES

COMPETENCY IN MEDICAL KNOWLEDGE: The clinical benefit of CRT in patients with intermittent AF is attenuated by the temporal atrial tachyarrhythmia attack itself. AF-HF has unignorable impacts on their worsened clinical outcomes and those patients have a high possibility of recurrences whenever AF temporally occurs again. A significant decrease in the BIVP% during temporal AF periods was related to a poor prognosis, thus maintaining a high BIVP% level during AF periods may have prognostic implication. Hence, controlling AF itself or attempting to achieve a higher BIVP% during AF is a critical issue for patients with intermittent AF.

TRANSLATIONAL OUTLOOK: Additional studies are needed to directly evaluate the hemodynamics during temporal AF periods in patients with CRT. From the viewpoint of understanding the pure influence of uncaptured BIVP during AF, the protocol excluding the effects of tachycardia-related contractile dysfunction, a loss of atrial systole, and an irregular ventricular rhythm should be discovered. Clinically, further studies concerning the effects of atrioventricular junction ablation in CRT patients with intermittent AF are necessary.

REFERENCES

1. The CONSENSUS Trial Study Group. Effects of enalapril on mortality in severe congestive heart failure. Results of the Cooperative North Scandinavian Enalapril Survival Study (CONSENSUS). N Engl J Med 1987;316:1429–35.

2. Benjamin EJ, Wolf PA, D'Agostino RB, Silbershatz H, Kannel WB, Levy D. Impact of atrial fibrillation on the risk of death: the Framingham Heart Study. Circulation 1998;98:946–52.

3. Wang TJ, Larson MG, Levy D, et al. Temporal relations of atrial fibrillation and congestive heart failure and their joint influence on mortality: the Framingham Heart Study. Circulation 2003;107:2920–5.

4. Cleland JG, Daubert JC, Erdmann E, et al. The effect of cardiac resynchronization on morbidity and mortality in heart failure. N Engl J Med 2005;352:1539–49.

5. Moss AJ, Hall WJ, Cannom DS, et al. Cardiac-resynchronization therapy for the prevention of heart-failure events. N Engl J Med 2009;361:1329–38.

6. Gasparini M, Steinberg JS, Arshad A, et al. Resumption of sinus rhythm in patients with heart failure and permanent atrial fibrillation undergoing cardiac resynchronization therapy: a longitudinal observational study. Eur Heart J 2010;31:976–83.

7. Witten SR, Leung AA, Ghali WA, Faris P, Exner DV. Outcomes of cardiac resynchronization therapy in patients with versus those without atrial fibrillation: a systematic review and meta-analysis. Heart Rhythm 2011;8:1088–94.

8. Santini M, Gasparini M, Landolina M, et al. Device-detected atrial tachyarrhythmias predict adverse outcome in real-world patients with implantable biventricular defibrillators. J Am Coll Cardiol 2011;57:167–72.

9. Ousdigian KT, Borek PP, Koehler JL, Heywood JT, Ziegler PD, Wilkoff BL. The epidemic of inadequate biventricular pacing in patients with persistent or permanent atrial fibrillation and its association with mortality. Circ Arrhythm Electrophysiol 2014;7:370–6.

10. Kalscheur MM, Saxon LA, Lee BK, et al. Outcomes of cardiac resynchronization therapy in patients with intermittent atrial fibrillation or atrial flutter in the COMPANION trial. Heart Rhythm 2017;14:858–65.

11. Epstein AE, DiMarco JP, Ellenbogen KA, et al. ACCF/AHA/HRS 2008 guidelines for device-based therapy of cardiac rhythm abnormalities-executive summary: a report of the American College of Cardiology/American Heart Association Task Force on Practice Guidelines. J Am Coll Cardiol 2008;51:2085–105.

12. Epstein AE, DiMarco JP, Ellenbogen KA, et al. 2012 ACCF/AHA/HRS focused update incorporated into the ACCF/AHA/HRS 2008 guidelines for device-based therapy of cardiac rhythm abnormalities: a report of the American College of Cardiology Foundation/American Heart Association Task Force on Practice Guidelines and the Heart Rhythm Society. J Am Coll Cardiol 2013;61:e6–75.

13. Hoppe UC, Casares JM, Eiskjaer H, et al. Effect of cardiac resynchronization on the incidence of atrial fibrillation in patients with severe heart failure. Circulation 2006;114:18–25.

14. Fuster V, Rydén LE, Cannom DS, et al. ACC/AHA/ESC 2006 Guidelines for the Management of Patients with Atrial Fibrillation: a report of the American College of Cardiology/American Heart Association Task Force on Practice Guidelines and the European Society of Cardiology Committee for Practice Guidelines (Writing Committee to Revise the 2001 Guidelines for the Management of Patients With Atrial Fibrillation): developed in collaboration with the European Heart Rhythm Association and the Heart Rhythm Society. J Am Coll Cardiol 2006;48:854–906.

15. Gasparini M, Leclercq C, Lunati M, et al. Cardiac resynchronization therapy in patients with atrial fibrillation: the CERTIFY study (Cardiac Resynchronization Therapy in Atrial Fibrillation Patients Multinational Registry). J Am Coll Cardiol HF 2013;1:500–7.

16. Sweeney MO, Hellkamp AS, van Bommel RJ, Schalij MJ, Borleffs CJ, Bax JJ. QRS fusion complex analysis using wave interference to predict reverse remodeling during cardiac resynchronization therapy. Heart Rhythm 2014;11:806–13.

17. van Gelder BM, Bracke FA, Meijer A, Pijls NH. The hemodynamic effect of intrinsic conduction during left ventricular pacing as compared to biventricular pacing. J Am Coll Cardiol 2005;45:2905–10.

18. Marrouche NF, Brachmann J, Andresen D, et al. Catheter ablation for atrial fibrillation with heart failure. N Engl J Med 2018;378:417–27.

19. Borleffs CJ, van Rees JB, van Welsenes G, et al. Prognostic importance of atrial fibrillation in implantable cardioverter-defibrillator patients. J Am Coll Cardiol 2010;55:879–85.

KEY WORDS atrial fibrillation, biventricular pacing rate, cardiac resynchronization therapy, clinical outcome, heart failure

Journal of Echocardiography (2018) 16:105–129
https://doi.org/10.1007/s12574-018-0382-8

SPECIAL ARTICLE

Practical guidance for the implementation of stress echocardiography

Kengo Suzuki[1] · Yutaka Hirano[2] · Hirotsugu Yamada[3] · Mitsushige Murata[4] · Masao Daimon[5] · Masaaki Takeuchi[6] · Yoshihiro Seo[7] · Chisato Izumi[8] · Makoto Akaishi[9]

Received: 3 April 2018 / Revised: 7 May 2018 / Accepted: 16 May 2018 / Published online: 6 June 2018
© The Author(s) 2018

Abstract

Exercise stress testing has been widely undertaken for the diagnosis of heart diseases. The accurate assessment of clinical conditions can be conducted by comparing the findings obtained from the results of stress echocardiography with the changes in the blood/heart rate and electrocardiograms. Numerous overseas studies have reported the utility of stress echocardiography in diagnosing myocardial ischemia; in Japan, the use of this modality for this purpose was included in the national health insurance reimbursable list in 2012. Nevertheless, stress echocardiography is far from being a widespread practice in Japan. This might be due to insufficient equipment (e.g., ergometers, space for test implementation) at each medical institution, shortage of technicians and sonographers who are well experienced and who are responsible for obtaining images during stress testing. The other possible reasons include the limited evidence available in Japan and the lack of a standardized testing protocol. Further dissemination of the practice of exercise stress echocardiography in this country is deemed necessary to establish satisfactory evidence for the use of stress echocardiography in the Japanese population. To this end, efforts are underway to develop a standardized protocol and report format to be adopted throughout Japan. We here present a guideline created by the Guideline Development Committee of the Japanese Society of Echocardiography that describes safe and effective stress echocardiography protocols and report formats. The readers are encouraged to perform exercise stress echocardiography using the proposed template for consensus document and report attached to this guideline.

Keywords Peak oxygen uptake · METS (metabolic equivalents) · Ischemic heart disease · Valvular heart disease · Cardiomyopathy · Dobutamine · Stress echocardiography

✉ Makoto Akaishi
akaishim@tokai.ac.jp

1 Division of Cardiology, St. Marianna University School of Medicine, Kawasaki, Japan

2 Division of Cardiology, Department of Medicine, Faculty of Medicine, Kindai University, Osakasayama, Japan

3 Department of Cardiology, Tokushima University Hospital, Tokushima, Japan

4 Department of Laboratory Medicine, School of Medicine, Keio University, Tokyo, Japan

5 Department of Clinical Laboratory, Faculty of Medicine, The University of Tokyo, Tokyo, Japan

6 Department of Laboratory and Transfusion Medicine, Hospital of the University of Occupational and Environmental Health, Kitakyushu, Japan

7 Cardiovascular Division, Faculty of Medicine, University of Tsukuba, Tsukuba, Japan

8 National Cerebral and Cardiovascular Center, Suita, Japan

9 Tokai University Tokyo Hospital, 1-2-5 Yoyogi Shibuya-ku, Tokyo, Japan

Introduction

During exercise to sustain the increased metabolic demand of the tissues, increased oxygen and nutrient delivery are accomplished by increasing cardiac output (CO) and blood flow to the microvascular surface area, in addition to increased O_2 extraction in the active muscles (heart, respiratory, abdominal and skeletal muscles).

Furthermore exercise-associated tachycardia and blood pressure elevation lead to valvular regurgitation and increased myocardial oxygen consumption. Examining cardiac function during exercise as well as at rest is thus important for selecting suitable therapy for heart disease. Exercise stress testing has been widely undertaken for the diagnosis of heart diseases [1, 2]. In the circumstances where exercise stress cannot be performed, detailed evaluations under drug stimulation have been carried out to make an assessment of cardiac reserve. The accurate assessment of clinical conditions can be conducted by comparing the findings obtained

Table 1 Stressing methods for stress echocardiography

	Exercise	Pharmacological	Others
Stressing methods	Treadmill	Dobutamine	Pacing
	Ergometer	Dipyridamole	Hyperventilation/cold pressor
	Handgrip	Adenosine	Leg raising
Type of stress	Physiological	Nonphysiological	Nonphysiological
Heart rates	Increased	Increased	Vary depending on stress
Blood pressures	Increased	Not necessarily increased	Vary depending on stress
Image quality	Can be unassessable	Adequate for assessment in many cases	Adequate for assessment in many cases
Venous route	Not needed	Needed	Needed/not needed
Other	In patients capable of performing exercise, objective exercise tolerance and relationship to symptoms can be assessed	Cardiac stress can be imposed in the patients incapable of performing exercise	Leg raising is a simple technique to increase preload

from the results of stress echocardiography with the changes in the blood/heart rate and electrocardiograms (ECGs). Numerous overseas studies have reported the utility of stress echocardiography in diagnosing myocardial ischemia; [3] in Japan, and the use of this modality for this purpose was included in the national health insurance reimbursable list in 2012.

Nevertheless, stress echocardiography is far from being a widespread practice in Japan. This might be due to insufficient equipment (e.g., ergometers, space for test implementation) at each medical institution, shortage of technicians and sonographers who are well experienced and who are responsible for obtaining images during stress testing. The other possible reasons include the limited evidence available in Japan and the lack of a standardized testing protocol. Further dissemination of the practice of exercise test echocardiography in this country is deemed necessary to establish satisfactory evidence for the use of stress echocardiography in the Japanese population. To this end, efforts are underway to develop a standardized protocol and report format to be adopted throughout Japan. We here present a guideline created by the Guideline Development Committee of the Japanese Society of Echocardiography that describes safe and effective stress echocardiography protocols and report formats.

Overview

Stressing methods for stress echocardiography

Stress echocardiography is mainly conducted during exercise or under drug stimulation. For the pharmacological stress testing, adenosine was once administered. At present, dobutamine is the only drug used for this purpose (dobutamine stress testing is described below for reference purposes). The other stressing methods include pacing, hyperventilation, and the use of a cold pressor (Table 1); they are employed only under special circumstances.

Exercise stress testing methods

Exercise stress testing can be performed with isometric (e.g., handgrip) or isotonic (e.g., treadmill, ergometer) exercise. To evaluate the cardiac pumping capacity, we need to increase CO by raising oxygen consumption in the peripheral tissues. When we intend to induce myocardial ischemia by elevating myocardial oxygen consumption, myocardial oxygen demand needs to be raised. Myocardial oxygen consumption largely depends on left ventricular (LV) wall stress and heart rate rather than CO; therefore, to evoke myocardial ischemia, it is necessary to increase LV wall stress and heart rate, i.e., to achieve higher blood pressure and heart rate via exercise. While the cardiac pumping capacity is assessed, it is essential to raise CO.

Generally, an isometric exercise is characterized by smaller increases in heart rate, compared with the magnitude of increases in systolic blood pressure, at higher exercise intensity. In an isotonic exercise, greater exercise intensity is associated with greater CO; both blood pressure and heart rate typically show a linear increase in proportion to exercise intensity. In principle, venous return is increased, resulting chiefly in ventricular expansion. This venous return increase is more conspicuous when the subject is in a recumbent position than on standing.

Isometric exercise stress, which is associated with greater blood pressure elevation than with isotonic stress, may allow improved detection rates for wall motion abnormalities since such abnormalities are more readily visualized in the presence of elevated LV wall stress, as well as ischemia, which can be induced with isometric exercise by increasing myocardial oxygen demand.

To evaluate pumping ability of the heart, an increase in stroke volume (SV) should be monitored. In the exercise

stress testing for aortic stenosis (AS), elevation in pressure gradient and change in valve area resulting from increased SV are examined; therefore, the type of stress that raises SV (e.g., stress on recumbent exercise) is more desirable than the type that merely raises heart rate (e.g., pacing).

On the other hand, in the stress testing for mitral stenosis (MS), where the diastolic period is markedly shortened with increased heart rate, the magnitude of the effect of shortened diastolic period exceeds that of stress from CO increase, resulting in a greater left atrioventricular pressure gradient. In other words, the stress testing for MS is for the assessment of cardiac capacity under the conditions of elevated heart rate.

Mitral regurgitation (MR) can have an organic or functional cause, and how imposed stress will interact with such causes is unpredictable. In this context, it may be best to apply types of stress closest to those encountered in daily activities (e.g., stress that raises cardiac output) in evaluating patients' symptoms.

In many cases, stress testing for myocardial disease is conducted to assess the contractile reserve of the myocardium itself. Pharmacological stress testing with low-dose catecholamines is therefore desirable.

Physiology of exercise stress

During exercise, depending on its intensity, the volume of oxygen uptake (VO_2) increases. The VO_2 at the time when the target heart rate is reached in symptom-limited stress testing is called the peak VO_2. The highest VO_2 achieved with exercise of increasing intensity (plateau VO_2) is called the maximal VO_2.

Peak VO_2 is determined by the maximum oxygen transport capability and the maximum oxygen utilization capability during exercise. The maximum oxygen transport capability depends on the vasodilatory ability and the ability to efficiently perfuse the skeletal muscles with blood, in addition to CO reserve. The maximum oxygen utilization capability relies on the ability of the active muscles to take up oxygen effectively. Possible mechanisms for a decrease in peak VO_2 in patients with heart failure thus include: lower CO, lower blood pressure, reduced vasodilation due to endothelial dysfunction, decreased muscle volume due to restriction of physical activity and disuse atrophy, skeletal mitochondrial change due to chronic hypoperfusion, and decreased activity of enzymes, such as the enzymes of oxidative phosphorylation, which are involved in muscular energy metabolism.

Stress testing should be performed using a method suitable for the purpose of testing, selected based on predicted changes in variables in response to a given stress. In selecting the testing method, it is imperative to give top priority to the safety of the patient, taking into consideration his/her condition. For the elderly, cycle ergometer exercise is recommended as falls are unlikely, rather than a treadmill exercise, which in the elderly is associated with a risk of falls and possibly excessive workload in terms of oxygen consumption.

Ergometer and treadmill exercise tests achieve similar heart rate and ventilation at the highest exercise intensity, but the peak VO_2 at that point is generally 5–11% higher with treadmill exercise [4]. In other words, the peak VO_2 determined using ergometer exercise is lower than that obtained from the results of a treadmill. These two stressing methods also differ in terms of the effect of the subject's body weight on VO_2 per unit weight. With treadmill exercise, workload is produced by walking; that is, the patient does work by shifting his/her weight. The workload is thus expressed by 'work rate', i.e., body weight × walking velocity. The heavier the subject, the greater is the workload. When the incline and walking speed are changed, the VO_2 per weight (METS; metabolic equivalents) changes, while the relationship between the workload and VO_2 remains the same regardless of subject's body weight. Meanwhile, using cycle ergometer exercise, where the subject pedals in a sitting position, the relationship between the workload and VO_2 per body weight varies depending on the body weight: VO_2 per weight becomes smaller at greater weights [5].

When treadmill exercise is used for echocardiography, the patient moves to the testing bed and receives echocardiography after finishing the exercise; the data obtained are thus post-exercise echocardiograms. With supine ergometer exercise, stress testing echocardiograms can be acquired during exercise, a distinct feature of this test.

Objectives of exercise stress echocardiography

Ischemic heart disease[1]

1. The diagnosis of coronary artery disease

   Patients in whom echocardiographic assessment is less reliable when detecting ischemia: in those administered with digoxin, those with pre-excitation (Wolff–Parkinson–White) syndrome and those with complete left bundle-branch block.

[1] Statement on exercise echocardiography for ischemic heart disease from the American Heart Association (AHA) Guideline.

The 2003 AHA guideline [6] includes a new Class I recommendation: Exercise echocardiography for diagnosis of myocardial ischemia in intermediate-risk patients on digoxin, with LV hypertrophy, or with more than 1 mm ST depression at rest on the baseline electrocardiographic assessment; and patients with Wolff–Parkinson–White syndrome or a conduction disturbance such as left bundle-branch block. Namely, exercise echocardiography combined with wall motion assessment should be performed in patients showing abnormal waveforms on the 12-lead electrocardiogram at rest.

Table 2 Diagnostic accuracy of various stress echocardiographic modalities

	Number of studies	Sensitivity (%) (95% confidence interval)	Specificity (%) (95% confidence interval)
Exercise stress	55	82.7 (80.2–85.2)	84.0 (80.4–87.6)
Adenosine	11	79.2 (72.1–86.3)	91.5 (87.3–95.7)
Dipyridamole	58	71.9 (68.6–75.2)	94.6 (92.9–96.3)
Dobutamine	102	81.0 (79.1–82.9)	84.1 (82.0–86.1)

The meta-analysis results are available for diagnostic accuracy of exercise echocardiography for identifying coronary artery disease [7–9] The sensitivity and specificity were reported to be 87 and 72%, respectively, in the meta-analysis by de Jong et al. [8] and 82.7 and 84.0%, respectively, by Heijenbrok-Kal et al. [9]. Table 2 summarizes the findings on the diagnostic accuracy of different stress echocardiographic modalities [9].

2. Prognosis and risk assessment.

   In several studies published to date on the use of exercise stress echocardiography for the assessment of prognosis and risk, this modality has been reported to be useful in assessing numerous diseases. Negative results on exercise stress echocardiography predict favorable patient outcomes [10]. Exercise stress testing has also been found to be of prognostic value for women; [11] the elderly; [12] patients with diabetes mellitus [13]; angina pectoris [14], or acute myocardial infarction; [15–17] and in patients who have undergone coronary artery bypass grafting (CABG) [18]. Monitoring such subpopulation for abnormal wall motion with exercise stress echocardiography is useful for predicting cardiovascular events.

3. Preoperative evaluation for cardiovascular surgery and other major surgery.

   Stress echocardiography has been reported to be useful for preoperative risk assessment prior to cardiovascular surgery [19, 20] and other major surgery [21, 22].

4. Assessment of residual myocardial ischemia after a revascularization procedure such as percutaneous coronary intervention and CABG.

   Exercise stress echocardiography has been reported to be useful in evaluating residual myocardial ischemia in patients following revascularization such as percutaneous coronary intervention [23] and CABG [24].

5. Diagnosis of the location of myocardial ischemia.

   In identifying the location of myocardial ischemia, the utility of exercise stress echocardiography and coronary arteriography has been compared, and it has been concluded that the former is very useful, with a high consistency shown between myocardial ischemia location and coronary lesion [25].

6. Assessment of myocardial viability.

   Regarding myocardial viability assessment, several studies found that low-dose dobutamine stress testing was useful [26]. Some studies reported that myocardial viability can be evaluated based on wall motion assessment performed during low-level ergometer exercise [27, 28].

7. Relationship with chest symptoms on exertion.

   Exercise echocardiography is useful for the diagnosis of patients with dyspnea on exertion and can predict outcomes of patients with dyspnea [29].

Cardiomyopathy

1. *Dilated cardiomyopathy* Evaluation of contractile reserve, exercise-induced dyssynchrony, MR, and pulmonary hypertension (PH).[2]
2. *Hypertrophic cardiomyopathy* Evaluation of exercise-induced LV outflow tract (LVOT) obstruction, MR, PH,[2] and regional wall motion.
3. Relationship with symptoms on exertion.

Valvular heart disease

1. *MR* Assessment of exercise-induced changes in MR and PH.[2] Prediction of postoperative LV function.
2. *MS* Assessment of left atrioventricular pressure gradient in patients who show findings on resting echocardiograms that are disproportionate to symptoms; and assessment of PH.
3. *AS* Risk assessment for asymptomatic, severe AS.
4. *Aortic regurgitation (AR)* Assessment of contractile reserve and prediction of decline in cardiac function after aortic valve replacement.
5. Relationship to symptoms on exertion.

Pulmonary hypertension

1. *PH* Diagnosis of exercise-induced PH,[2] prediction of prognosis, and assessment of treatment effect.
2. Relationship to symptoms on exertion.

Ensuring safety in exercise stress echocardiography

The safety of exercise stress echocardiography has been established. The incidence rate of serious complications (e.g., serious arrhythmias, myocardial infarction) has been

[2] As the tricuspid regurgitation pressure gradient increases during exercise with age, even in healthy individuals, caution is required for the interpretation of the results of evaluation, especially in the elderly [30].

Fig. 1 Stress Echo Room (US Center, St. Marianna University School of Medicine). Exercise stress testing should be performed in a sufficiently spacious room with the following equipment readily available: an emergency cart with emergency drugs and airway management devices, exercise stress monitoring system (automated sphygmomanometer, 12-lead ECG monitor), defibrillator, and oxygen tanks

reported to be 0.04% during stress exercise testing, 0.01% after stress exercise testing, and ≤0.2% for overall complications [7]. Particular attention should be paid to ensure the safety in patients who are unable to perform exercise stress testing for physical reasons, since they are at higher risk of developing serious complications. For such patients, we recommend that the testing is performed in a sufficiently spacious room with the following equipment readily available: an emergency cart with emergency drugs and airway management devices, exercise stress monitoring system (automated sphygmomanometer, 12-lead ECG monitor), defibrillator, and oxygen tanks (Fig. 1).

Contraindications for exercise stress echocardiography

To perform exercise stress testing safely and acquire the data useful for diagnosis, it is important to predetermine if the patient is eligible for stress testing. Patients with the conditions listed below are at high risk of stress-induced cardiac events; in such patients stress testing is contraindicated as a rule.

1. Acute coronary syndrome within 48 h of onset.
2. Poorly controlled heart failure/dyspnea.
3. Poorly controlled hypertension.
4. Symptomatic severe AS.[3]
5. Severe obstructive hypertrophic cardiomyopathy (LVOT pressure gradient > 90 mmHg).
6. Life-threatening arrhythmias.
7. Acute phase of acute aortic dissection, aortic aneurysm with threatened rupture.
8. Inability to exercise.[4]
9. Without prior written consent to undergo the exercise stress testing.
10. Any other patients who are identified as ineligible by their attending physicians.

Implementation of exercise stress testing

Before exercise stress testing

1. General precautions.

   Before stress testing, the clinical diagnosis, purpose of the test, medical history, and the patient's current medications should be confirmed. Prior written consent must be obtained after an explanation of the specific stress testing method and possible side effects should be fully explained. Prior to implementation of exercise stress testing, the physician in charge must ask the patient's clinical course including recent chest symptoms and the frequency of such symptoms. As a rule, a symptom-limited exercise stress test (e.g., leg exhaustion, dyspnea, chest pain) should be performed. The patients are advised to wear comfortable pants and a patient's gown for quick recording of echocardiograms.
2. Measurements of vital signs.

   If the patient suffers from tachycardia or presents blood pressure that differs from his/her normal level, its cause should be investigated and a decision should be made whether exercise stress testing may or may not be performed.

[3] Exercise stress testing is contraindicated in patients with symptomatic severe AS. The patient diagnosed as asymptomatic at the time of appointment for the test may present with symptoms at the time of testing. It is imperative to reconfirm the absence of symptoms immediately before testing. Pharmacological stress should be selected for patients incapable of performing exercise stress testing because of concomitant peripheral blood, orthopedic, or neurological disease. Patients incapable of understanding the explanation on giving consent to testing because of dementia or other reasons should be excluded from exercise stress echocardiography.

[4] In treadmill exercise stress testing, patients may not be able to keep up with the machine's walking speed. With elderly patients, due caution should be exercised to avoid the risk of falls, while ensuring that the treadmill belt velocities to be used are suitable for the patient and are reset if necessary before testing.

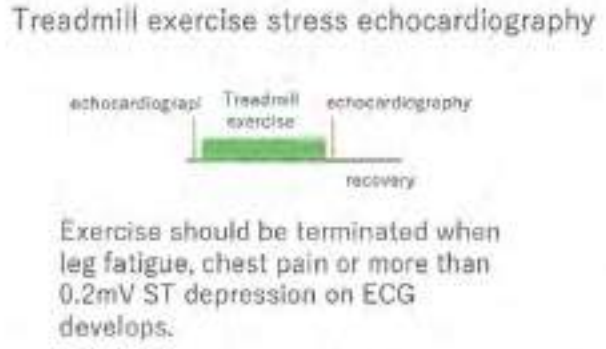

Fig. 2 Exercise stress testing protocol (treadmill). The echocardiograms are obtained before and after the multistage stress test (Bruce protocol)

3. To make it clear whether the patients correctly understood the purpose of testing and procedure.

   It is indispensable to provide special care for patients undergoing the testing to relieve their anxieties.
4. To confirm the accuracy of echocardiographic images.

   You should confirm the chest areas where the transducer is to be properly placed to obtain ultrasound views and check that the chest ECG electrodes will not interfere with the manipulation of the transducer.

Stress testing procedures

Treadmill exercise stress

1. Instruct the patient to stand on the belt and then commence the stress test.
2. Increase the workload in a stepwise manner according to the Bruce protocol or another appropriate protocol. The Bruce protocol, which is originally intended to induce ischemia in patients with heart disease, gradually increases the workload in large increments. It should be noted that in the first step, the patient is required to walk at a rate of 1.7 miles/h (2.7 km/h) at a 10% incline, which is equivalent to a workload of approximately 17–18 mL/min/kg body weight of oxygen consumption (approximately, 5 METS) for the elderly.
3. Monitor the patient's ST-T changes and arrhythmias throughout exercise using an ultrasound monitor and measure blood pressure frequently.
4. Terminate exercise when the patient reaches the target heart rate or when any termination criterion is met; otherwise, continue up to the limit of tolerance of the patient.
5. Place the patient in the left lateral decubitus position immediately after exercise and record post-stress echocardiograms.
6. To obtain better quality images, it is desirable that whenever it is possible, the images should be recorded while the patient is holding his/her breath, although it may be quite difficult for the patient to do so because of post-exercise breathing difficulties.
7. It is desirable to complete echocardiographic recording within 2 min after the completion of exercise (Fig. 2).
8. For several minutes after the completion of treadmill exercise, the patient will experience breathing difficulties, making clear imaging nearly impossible. The patient should be instructed in advance to exhale for as long as possible and inhale as briefly as possible immediately after the completion of exercise. The quality of ECGs can be improved by recording them during prolonged expiration by the patient. The ultrasound images are generally observable during exhalation by the patient, but not during inhalation. Concentrate on recording during exhalation because it is important to collect good-quality images; there is little value in attempting to acquire quality images while the patient is inhaling. If they cannot obtain adequate images despite the above effort, the attending staff may instruct the patient to hold his/her breath briefly. Limit recording of each view to 10 s or less and obtain images in multiple views within a short interval. Struggling with one view that cannot be visualized will lead to losing all recordings in the other views. It is recommended to complete all image recordings within 2 min after exercise. You need to quickly complete the procedure to acquire high-quality images that are adequate for the assessment, and this cannot be achieved without the patient's co-operation.

Supine ergometer exercise stress

1. If the echo bed can be tilted laterally, place the patient in a slightly left lateral decubitus position and raise the upper portion so that the patient will assume a half-sitting position.
2. Record resting echocardiography, blood pressure, and ECGs.
3. Instruct the patient to place his/her feet on the pedals and commence the exercise. The pedaling rate should be set at 50–60 revolutions/min.
4. The workload is generally increased by 25 W every 3 min (Fig. 3a).
5. For the elderly with remarkable leg muscle weakness, a protocol using a 3-min warm-up at 10 W followed by 10 W increments every 3 min may be used (Fig. 3b).
6. Monitor the patient's ST-T changes and arrhythmias throughout exercise using an ultrasound monitor and record an ECG and blood pressure every minute.

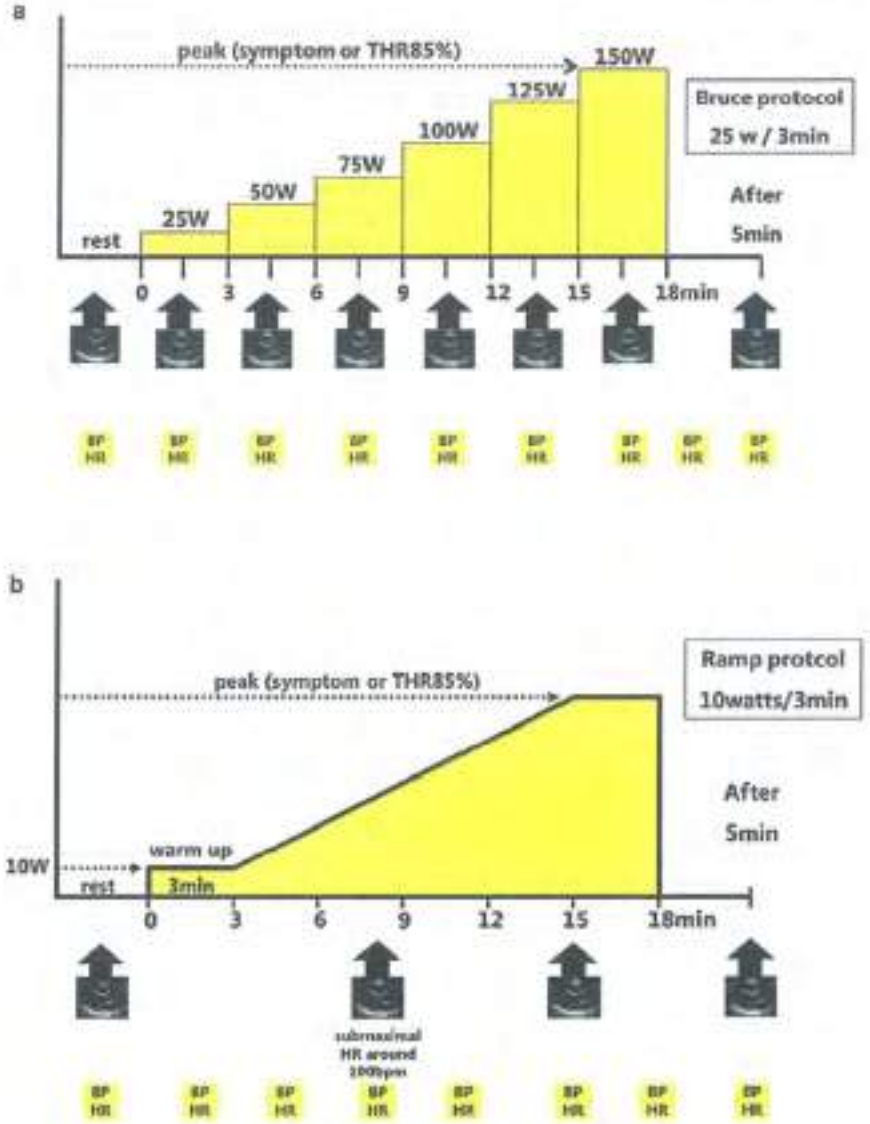

Fig. 3 Exercise stress protocol (ergometer). **a** Multistage protocol: the workload is increased at 25-W increments every 3 min. **b** Ramp protocol: For the elderly with remarkable leg muscle weakness, a protocol with a 3-min warm-up at 10 W, followed by exercise with a 10-W increment every 3 min may be used. *BP* Blood pressure, *HR* heart rate, *THR* target heart rate

7. Terminate the exercise when the patient reaches the target heart rate, or when any termination criterion is met; otherwise, continue up to the limit of tolerance of the patient.
8. In the supine ergometer exercise stress testing echocardiography, echocardiographic assessment during exercise can be performed.
9. In the supine ergometer exercise stress testing, the images should be obtained with the patient placed in the left lateral decubitus position. Some of the authors experienced the following failures to acquire good-quality images at baseline; the improved data can be obtained once the test is commenced, i.e., after the patient starts pedaling with his/her feet on the pedals (with the feet raised). It is necessary to obtain data in the same views as those acquired at baseline. During the treadmill exercise testing, instruct the patient to exhale longer and inhale shorter than usual, and the operator should record as many images as possible during exhalation. In treadmill exercise echocardiography, image recording is commenced on completion of exercise after the patient is placed on the bed in a supine position. Stress-induced changes may resolve before being visualized unless imaging is done promptly; that is, image recording is under time constraints. On the other hand, in the supine ergometer exercise testing, the images can be recorded during exercise, which enables data collection over a longer period.

Handgrip exercise stress

Handgrip exercise is an isometric exercise that imposes a pressure load primarily on the left ventricle. Increasing exercise intensity markedly raises systolic pressure, while it only modestly affects heart rate. Numerous studies used a protocol with a 5-min sustained handgrip at 50% of the maximum voluntary contraction [31, 32]. Kerber et al. performed a handgrip exercise test and a treadmill exercise test in 90 patients with coronary artery disease to evaluate the ability of these tests to detect ischemia. During the treadmill testing, ST segment depression was observed in 25 patients, in contrast with just 3 patients with sustained handgrip exercise. The heart rate–systolic pressure product was 223 ($\times 10^2$) for the former and small at 150 ($\times 10^2$) for the latter, diastolic pressure was 93 mmHg for the latter versus 81 mmHg for the former [33]. The difference between the two modalities of exercise may be explained by the insufficient increase myocardial oxygen demand (less increase in heart rate) and the more coronary perfusion (due to increased diastolic blood pressure) in handgrip exercise. It was reported that the sensitivity of adenosine stress increased with handgrip exercise [34] and that strain evaluation of pre- and post-handgrip exercise images was useful in the diagnosis of myocardial ischemia [35].

Hyperventilation

Hyperventilation (30 bpm) is sustained for 6 min to induce coronary artery spasm [36].

Leg raising

Cardiac preload can be increased with leg raising during echocardiographic assessment. The patient is positioned supine with the leg raised at approximately 45° with the support of a third person or an object (e.g., chair) placed under the feet [37, 38]. In healthy individuals, leg raising increases the SV with a slight change in blood pressure. As an alternative to leg raising, the leg positive pressure method is available, in which the patient's legs are pressurized by inflating cuffs placed around the legs using an automated air pump [39, 40].

Stress test cessation criteria

Patient condition and blood pressure must be monitored while using ECG and during exercise. The test must be terminated immediately in the event of a remarkable increase or decrease in blood pressure or significant arrhythmias and appropriate measures should be taken. The criteria for terminating the testing based on the safety of patient are as follows:

1. Achievement of the target heart rate ([220 − patient's age] × 0.85).
2. Excessive increase in blood pressure (systolic ≥ 220 mmHg, diastolic ≥ 120 mmHg).
3. Decrease in blood pressure (fall of ≥ 10 mmHg during exercise or no increase with continued exercise).
4. Manifestation of sustained tachyarrhythmia.
5. Manifestation of akinesis-like decrease in the wall motion or of wall motion decrease over a broad range involving the territory of more than one coronary artery.
6. ST segment depression of ≥ 0.2 mV on ECG.
7. Development or exacerbation of chest pain.
8. Leg exhaustion.
9. Development of any other symptoms that make continuation of exercise impossible.

What to assess

The assessments are made at rest, during exercise, and post-exercise. Some parameters are unassessable during exercise. Attempts should be made to assess such parameters as promptly as possible after exercise. For items assessed during exercise, there is no consensus regarding when to make an assessment. We usually start echocardiographic observation immediately after the initiation of exercise and continue monitoring until a change can be observed, as the workload is gradually increased.

1. ECG and blood pressure.
2. Echocardiographic assessment.
   (a) In the parasternal long- and short-axis views (at the levels of the mitral valve, papillary muscles, and apex of the heart).
   (b) In the apical 4-chamber, 2-chamber, and long-axis views.
   (c) Of the LV inflow velocity patterns, mitral annular velocity patterns.
   (d) IOf the LVOT velocity patterns.
   (e) Of the tricuspid regurgitation (TR) velocity.
   (f) Severity assessments for each valvular disease.

Precautions for implementation of exercise stress echocardiography

1. For the treadmill exercise testing, arrange the treadmill, a bed, and a compact echocardiographic system so that post-exercise imaging can be initiated as quickly as possible (Fig. 4).
2. Parasternal short-axis view, which contains the perfusion territories of all three coronary arteries, is critical in the exercise stress echocardiographic assessment of the wall motion; yet, oblique sections can be a cause of

Fig. 4 Treadmill exercise testing room (Kindai University Hospital). The treadmill, bed, and echocardiographic system should be arranged as compact as possible

false-positive or false-negative results. An example: in the case of a long-axis view obtained by directing the beam through a lower intercostal space (Fig. 5a), the short-axis view gained by rotating this long-axis view by 90° results in an oblique section (Fig. 5b). In this section, the anteroseptal region is visualized close to the apex and the posterior wall more basally. Hence on visualizing the posterior wall, because of the influence of the mitral annulus, the inferior wall area may be misinterpreted as a site where there is decreased regional wall motion (arrow, Fig. 5c).

3. Exercise stress echocardiography is contraindicated in patients with unstable angina pectoris or symptomatic severe AS. The outpatient diagnosed as asymptomatic at the time of appointment for the test may possibly become symptomatic by the time of the test. It is important to reconfirm the absence of symptoms immediately before starting the test.
4. The examiner should be careful not to concentrate excessively on visualizing the structures, but to keep monitoring the symptoms, blood pressure, heart rate, and ECG of the patient during exercise to minimize the risk of cardiac events.
5. In the supine ergometer testing, the patient may suddenly become unable to pedal because of leg exhaustion at the peak load. Instruct the patient to tell the examiner at the timing when the exercise is becoming too hard to continue before starting the peak load stage; the examiner should start imaging slightly before the peak load stage. It is recommended, whenever possible, to monitor the rate of perceived exertion using the Borg Scale or another appropriate rating scale. If the patient has become completely unable to pedal, assistance may be provided. (It is more practical to commence imaging immediately after ergometer exercise is started and to continue the exercise test while changes in parameters are monitored.)
6. Care should be taken to perform imaging in coordination with the patient's breathing. Although it may be

Fig. 5 An example of an oblique view. **a** A long-axis view obtained by directing the beam through a lower intercostal space; **b** a short-axis view gained by rotating this long-axis view by 90°; **c** the resulting short-axis view is an oblique view with the anteroseptal region visualized close to the apex and the posterior wall more basally (arrow)

difficult for the patient to hold a breath at peak load, attempts should be made to acquire the images while the patient is holding a breath whenever possible (forcing the patient to do so must be avoided). Regardless of such effort, images taken at peak load may not be of sufficient quality. Echocardiograms taken at a submaximal level (i.e., heart rate: approximately 100 bpm) may be used as a substitute for images at peak load.

7. The Images that can be obtained at peak load are limited. The examiner and the physician need to determine which images should be acquired at the peak load (e.g., transmitral and transtricuspid regurgitant flow velocity patterns, LVOT velocity patterns, images for wall motion assessment).

Exercise stress echocardiographic measurements for heart diseases

Ischemic heart disease

1. Wall motion.

   The assessment should be performed by reviewing the images at rest and exercise aligned side by side.

   The use of a 16-segment model of the left ventricle recommended by the American Society of Echocardiography [41]. Evaluate semiquantitatively and score the wall motion of each segment (see the Ischemic Heart Disease Report [appendix]). Grade the wall motion as normokinesis, hypokinesis, akinesis, or dyskinesis. Using too many grades should be avoided since it will lead to greater interobserver variability and decreased assessment objectivity. The wall motion assessment should be based on not only left endocardial excursion, but also changes in the wall thickening. The data from the systolic wall motion alone should be examined so as not to be misled by the diastolic wall motion. Normally, exercise stress increases the systolic wall motion and left ventricular (LV) wall thickness. With stress, the absence of an increase in wall motion or wall thickening is assessed as abnormal. Exacerbation of wall motion of a normal or hypokinetic wall segment by one grade indicates a positive result for ischemia. The sufficient echocardiogram qualities facilitate diagnosis and contribute to the diagnostic accuracy. Constant effort is required to achieve the best possible imaging quality, using optimal gain and slice plane selection.

Valvular heart disease

Mitral stenosis

Exercise stress echocardiography is employed in cases where resting echocardiographic data are not commensurate with the severity of symptoms, i.e., asymptomatic MS despite severe stenosis, or symptomatic MS despite mild to moderate disease.

1. Transmitral pressure gradient.

   A mean pressure gradient is assessed based on mitral flow velocity at rest and exercise. An estimated mean pressure gradient of ≥ 15 mmHg during exercise indicates severe MS [42].
2. Exercise-induced PH.

   Transtricuspid pressure gradient is assessed at rest and during exercise. An estimated systolic pulmonary artery pressure (PAP) of ≥ 60 mmHg during exercise indicates severe MS [42].

Mitral regurgitation

1. Severity of MR.

   Changes in MR are assessed quantitatively or semiquantitatively, comparing rest and exercise. It has been shown that worsening MR with exercise stress is associated with a poor prognosis [43]. The assessment of MR severity has been reported to be impossible in patients with heart rate ≥ 115 bpm [44].
2. Exercise-induced PH.

   Transtricuspid pressure gradient at rest and exercise is assessed. An estimated systolic pulmonary artery pressure of ≥ 60 mmHg during exercise suggests exercise-induced PH [45].
3. Contractile reserve.

   A decline in LV reserve (a change in LVEF during exercise $\leq 5\%$ [46] or a change in the global longitudinal strain $\leq 2\%$ [47]) and reduction in right ventricular systolic function (tricuspid annular plane systolic excursion < 18 mm [48]) have been reported to be predictors of a poor prognosis and of decreased cardiac function following mitral valve surgery.

Aortic stenosis

1. Aortic flow velocity and mean pressure gradient.

   Changes in the aortic flow velocity, mean pressure gradient, and CO (or pulsed Doppler time–velocity integral across the LVOT as a surrogate) are assessed, comparing at rest and exercise. A ≥ 18 mmHg increase in the mean pressure gradient at exercise has been reported to be associated with a poor prognosis, showing the useful-

ness of this evaluation in risk stratification of asymptomatic patients with AS [49].

2. Aortic valve area.

   The aortic valve area (AVA) is assessed under conditions of increased CO with stress.

3. Exercise-induced PH.

   Transtricuspid pressure gradient is assessed at rest and during exercise. An estimated systolic PAP of ≥60 mmHg during exercise suggests exercise-induced PH [50].

Aortic regurgitation (AR)

1. Contractile reserve.

   In patients with asymptomatic severe AR, reduced contractile reserve (increase in LVEF during exercise ≤5%) has been reported to be a predictor of future cardiac functional deterioration and of postoperative cardiac function [51].

Cardiomyopathy

Dilated cardiomyopathy

1. Contractile reserve.

   Contractile reserve has been reported to well predict prognosis and beta blockers response in dilated cardiomyopathy. The stress protocols and assessment methods vary from study to study. Contractile reserve can be assessed based on low-dose (10–20 μg/kg/min) dobutamine-induced changes in LVEF [52], LV volume [53], and strain [54] from the resting state.

2. Functional MR.

   Functional MR at rest and exercise is assessed visually, or if possible, quantitatively. An increase in functional MR with stress (effective regurgitant orifice ≥13 mm^2) has been reported to predict a poor prognosis [55].

3. Exercise-induced PH.

   Transtricuspid pressure gradient is assessed at rest and exercise. An increase in estimated systolic PAP of ≥60 mmHg with exercise has been reported to indicate a poor prognosis [56].

4. Prediction of cardiac resynchronization therapy (CRT).

   LVEF response to low-dose dobutamine infusion (10 μg/kg/min, LVEF ≥7.5%) has been reported to be useful in the prediction of responders to CRT [57].

Hypertrophic cardiomyopathy

1. LVOT obstruction.

   LVOT obstruction may appear at exercise, but not at rest in some patients (exercise-induced LVOT obstruction; maximum LVOT gradient ≥50 mmHg). Exercise stress echocardiography is indicated in the diagnosis of such patients [58].

2. Wall motion assessment.

   Patients without significant coronary stenosis may have relative subendocardial ischemia in the hypertrophic myocardium, and in such patients wall motion abnormalities may be induced by exercise stress. LV wall motion abnormalities with exercise have been reported to indicate a poor prognosis in hypertrophic cardiomyopathy [59].

3. MR.

   Changes in MR that are associated with systolic anterior motion of the mitral valve are also assessed [60].

4. Exercise-induced PH.

   Exercise-induced PH, which is often a complication of LV diastolic dysfunction, is assessed [61].

Ph

1. Exercise-induced PH.

   Transtricuspid pressure gradient at rest and exercise is assessed. An estimated systolic PAP of ≥40–50 mmHg, depending on the exercise stress testing method used, indicating exercise-induced PH [62].

2. CO.

   Since PAP depends on CO, CO is evaluated at rest and exercise. An increase by 3.0 mmHg/L/min in mean PAP (mPAP) as a function of CO (ΔmPAP/ΔCO) in healthy subjects has been reported [63].[5]

Dobutamine stress echocardiography (for reference)

Introduction

Currently, dobutamine echocardiography is not covered by the national health insurance in Japan, whereas in actual clinical settings there are numerous patients, including the elderly, who are unable to perform exercise stress testing and for whom pharmacological stress echocardiography is deemed necessary. In addition, for diagnosis of ischemic heart disease (IHD), pharmacological stress echocardiography is less costly than radionuclide scanning and can be conducted, unlike contrast-enhanced computed tomography or magnetic resonance imaging, in patients with renal dysfunction, bronchial asthma, or hypersensitivity to contrast media. Although this guideline focuses on exercise stress

[5] mPAP was estimated as mPAP = 0.6 × estimated systolic PAP + 2 (mmHg) [64].

echocardiography, dobutamine stress echocardiography is also described herein for reference, considering the clinical utility of this modality.

Objectives of dobutamine stress echocardiography

A considerable number of elderly patients and patients with orthopedic or neurological disease are unable to perform exercise stress testing of sufficient intensity. In such cases, dobutamine echocardiography is indicated. This modality, which permits stable tomographic image recording during stress, allows for more detailed assessment of LV wall motion, compared with exercise stress echocardiography. Dobutamine stress echocardiography is useful not only in the evaluation of myocardial ischemia, but also in the assessment of myocardial viability and contractile reserve in people following myocardial infarction or those with chronic IHD. Furthermore, in distinguishing true, severe AS from 'pseudo-severe' AS in those with low-flow, low-gradient severe AS with reduced LVEF.

Safety of dobutamine stress echocardiography

The most commonly reported complications of dobutamine stress echocardiography include decreased blood pressure (1.7%), supraventricular tachycardia (1.3%), increased blood pressure (1.3%), atrial fibrillation (0.9%), atrioventricular block (0.23%), ventricular tachycardia (0.15%), coronary artery spasm (0.14%), ventricular fibrillation (0.04%), myocardial infarction (0.02%), cerebrovascular disorder (0.005%), and cardiac rupture (0.002%) [65, 66]. In performing dobutamine stress echocardiography, we recommend equipping the testing room with an emergency cart with supplies ready for use, to enable the attending staff to take necessary measures promptly when any of these complications occur. Palpitations, sensation of warmth, and voiding sensation are relatively frequently observed, but rapidly subside when dobutamine infusion is terminated. If any of these symptoms develop during testing, the attending staff should explain this to the patient and continue the test providing the event is deemed to be tolerable. Other possible complications include bradycardia and a decline in blood pressure due to vagal reflexes; in the event of these complications, if discussion or handgrip exercise does not improve the situation, atropine should be administered. In addition, it is recommended to keep the patient at rest and observe his/her clinical course for at least 30 min post-stress.

Implementation of dobutamine stress echocardiography

Dobutamine infusion in patients with IHD should be initiated at 5 μg/kg/min, with an increment to 10, 20, 30, and 40 μg/kg/min at 5-min intervals. In cases where dobutamine doses up to 40 μg/kg/min neither achieve the target heart rate nor meet any cessation criterion, the dose should be increased to 50 μg/kg/min, or 0.25 mg of atropine should be administered every minute up to 2 mg at maximum. It is also helpful to add a handgrip exercise stress. Low-dose dobutamine stress testing for assessment of myocardial viability or AS should be initiated at 5 μg/kg/min, with a 5-μg increment every 5 min to 10, 15, and 20 μg/kg/min.

Criteria for dobutamine stress test termination include the following:

1. The target heart rate of $(220 - \text{age}) \times 0.85$ (bpm) has been reached.
2. A significant decrease in blood pressure (systolic: ≤ 80 mmHg) or significant increase (systolic: ≥ 220 mmHg).
3. Manifestation of a significant tachyarrhythmia.
4. Manifestation of intolerable chest pain, nausea, headache, urge to void, etc.
5. Manifestation of severe myocardial ischemia, such as a new akinesis-like decrease in wall motion and deteriorating wall motion over a broad area involving the territory of more than one coronary artery.
6. ST segment depression of ≥ 0.2 mV on ECG.

Dobutamine echocardiographic measurements for heart diseases

Ischemic heart disease

Wall motion As in the case of exercise stress echocardiography, wall motion is graded as normokinesis, hypokinesis, akinesis, or dyskinesis. Responses to dobutamine stress are categorized into the following four types: (1) improvement: wall motion improves with low-dose dobutamine as well as with high doses; (2) biphasic: wall motion improves with low-dose dobutamine but worsens with high doses; (3) worsening: wall motion decreases with low-dose stress and worsens with high doses; and (4) fixed: wall motion remains unchanged with dobutamine stress. Improvement indicates myocardial viability without ischemia. The biphasic or worsening responses are seen in the presence of both myocardial viability and ischemia. The fixed type, where wall motion remains akinetic during low- and high-dose dobutamine stress, indicates a lack of myocardial viability.

AS

The peak velocity and pressure gradient of aortic flow depend on the flow rate, i.e., the volume of blood that flows past the aortic orifice per unit time. The flow rate is obtained from stroke volume (SV) divided by ejection

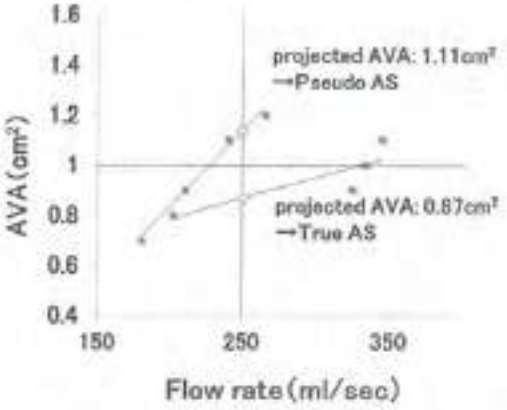

Fig. 6 Calculation of the projected AVA. AVA (cm^2) is plotted against flow rate (mL/s) at four stages (at rest and with dobutamine stress at 5, 10, and 20 μg/kg/min) to generate a linear regression formula. The AVA at flow rate of 250 mL/s is obtained from this formula as the projected AVA. If this value is < 1.0 cm^2, true severe AS is diagnosed

time. Generally, an indexed SV (SV divided by the body surface area) < 35 mL/m^2 is defined as 'low flow,' and a mean aortic pressure gradient < 40 mmHg as 'low gradient'. Low-flow, low-gradient severe AS despite the aortic valve area (AVA) satisfying the diagnostic criteria for severe AS suggests either decreased LVEF or decreased stroke volume due to small LV end-diastolic volume with normal LVEF in the absence of significant MR. The former is referred to as classical low-flow low-gradient severe AS, and the latter as paradoxical low-flow low-gradient severe AS.

Classical low-flow low-gradient severe AS can be divided into two clinical states: true, severe AS and 'pseudo-severe' AS, where complete opening of the aortic valve is hindered, despite AS of intermediate or mild intensity, by decreased LVEF. Dobutamine echography is useful in differentiating between these two states.

In other words, where complete valve opening appears to occur with increased CO, this is diagnosed as 'pseudo-severe' AS.

Cases showing an insufficient (< 20%) SV increase with dobutamine stress are considered to lack LV contractile reserve, and in these circumstances, differentiation between true and pseudo-severe AS is impossible. Patients lacking LV contractile reserve have been reported to be at higher risk of operational death compared to those with reserve, but to be associated with a better prognosis following aortic valve replacement surgery than with medical treatment [68]. In addition to the above semiquantitative assessment method, a method based on the projected AVA [69] is available. AVA (cm^2) is plotted against flow rate (mL/s) at four stages (at rest and with dobutamine stress at 5, 10, and 20 μg/kg/min) to generate a linear regression formula, and using this formula the AVA at a flow rate of 250 mL/s is calculated as the projected AVA. AS is diagnosed as truly severe if the projected AVA is less than 1.0 cm^2 (Fig. 6).

Compliance with ethical standards

Conflict of interest Kengo Suzuki, Yusuke Hirano, Hirotsugu Yamada, Mitsuhiro Murata, Masao Daimon, Masaaki Takenchi, Yoshihiro Seo, Chisato Izumi, and Makoto Akashi declare that they have no conflict of interest.

Open Access This article is distributed under the terms of the Creative Commons Attribution 4.0 International License (http://creativecommons.org/licenses/by/4.0/), which permits unrestricted use, distribution, and reproduction in any medium, provided you give appropriate credit to the original author(s) and the source, provide a link to the Creative Commons license, and indicate if changes were made.

Explanation and consent form for stress echocardiography

Explanation and Consent Form for Stress Echocardiography

ID number _____ Name _____

Date of birth _____

True, severe AS is defined by an AVA ≤ 1.0 cm^2 with a peak aortic valve velocity ≥ 4.0 m/s and a mean aortic valve gradient 40 mmHg [67].

Pibarot et al. [68], define 'true severe AS' using the following criteria, in addition to ≥ 20% increase in SV with 20 μg/kg/min dobutamine infusion; all other AS cases are considered 'pseudo-severe.'

1. An increase in mean pressure gradient to > 30 mmHg.
2. Peak-stress effective orifice area ≤ 1.0 cm^2 or < 1.2 cm^2, depending on testing conditions.
3. An increase in effective orifice area of < 0.3 cm^2.

Why we need to test your heart

Stress echocardiography by putting stress on your heart is required to uncover hidden conditions that are not detectable with resting echocardiography, to allow more detailed assessment of how sick you are.

Objectives of testing

The objectives differ depending on the type of heart disease you have.

1. *Coronary artery disease* To see whether left ventricular wall motion abnormalities appear with stress and to assess whether blood supply from the arteries of the heart to the heart muscle is sufficient.
2. *Valvular heart disease* To diagnose how heart function changes during exercise and to decide whether surgery is necessary or not.
3. *Cardiomyopathy* To detect heart reserve and changes in blood flow during exercise, and to select medications and treatment of the condition

Testing methods

We put stress on the heart using either exercise or drug stimulation. For exercise stress testing, the various methods are shown below. Electrocardiograms (ECGs) will be obtained before stress and during or after stress. A cardiologist will be present during the tests to ensure your safety and monitor your clinical condition. Your ECGs and blood pressure will be recorded. In the testing room, emergency equipment and drugs are readily available for the staff to provide urgent measures when any undesirable event occurs.

- Exercise stress echocardiography.
  - Treadmill.
  - Cycle ergometer (sitting, lying).
  - Handgrip.
  - Six-minute walk.
  - Master step test.
- Pharmacological (dobutamine) stress echocardiography.

Explanation of each method

Treadmill exercise stress test

You will be asked to walk on a moving belt, which looks like a conveyor belt, at a speed set by the machine. The grade and speed will gradually be increased every 2–3 min. A cardiologist will be supervising the test for your safety and from time to time may ask you how you are feeling. Your ECG and blood pressure will be monitored and recorded during the test. The test will be stopped if your heart rate has reached the target level, or if you no longer feel able to exercise because of breathlessness, chest pain, or any other reason, or if any abnormality is found on your ECG. Echocardiography will be performed before and after exercise.

Ergometer stress test

You will be asked to pedal in a sitting or lying position at a constant rate. The pedaling rate suitable for you will be determined for the test. The resistance you will feel will be mild in the beginning and will increase gradually, but you are asked to continue pedaling at the same rate. A cardiologist will supervise the test for your safety and from time to time may ask you how you are feeling. Your ECG and blood pressure will be monitored and recorded during the test. The test will be stopped if your heart rate has reached the target level, or if you no longer feel able to exercise because of breathlessness, chest pain, or any other reason, or if any abnormality is found on your ECG. Echocardiography will be performed before and and during after exercise.

Handgrip exercise stress test

You will be asked to continue grasping a handgrip for 4–5 min at about half of your maximum grip strength. If you notice any symptoms during the exercise, please let the attending staffs know. If you no longer feel able to continue the exercise, the test will be stopped at that point. Echocardiography will be performed before, and during or after exercise.

Six-minute walk test

You will be asked to walk for 6 min at your own pace on a predetermined course with an attending examiner, who will check on you if you are short of breath or have chest pain along the way. Echocardiography will be performed before and after exercise.

Master step test

This is an exercise test where you step up and down, and continue this for either ninety seconds or three minutes, as predetermined by a cardiologist. The number of steps to be used depends on your age and gender. You will be instructed to step up and down the Master step. The test will be stopped if you no longer feel able to continue the exercise because of breathlessness or chest pain, or if any abnormality is noted on your ECG. Echocardiography will be performed before and after exercise.

Pharmacological (dobutamine) stress echocardiography

This is a test to diagnose your heart reserve by imposing stress on your heart with drug infusion. Dobutamine (a drug that stimulates the heart muscle) is used. Symptoms such as a rapid heartbeat and flushing of the face are expected to occur but will disappear within 10 min after the end of the infusion.

Risks, complications, and side effects

There are small risks associated with exercise stress echocardiography. Specifically, these risks include lowering or raising of blood pressure, dizziness, an irregular pulse, fainting, and chest discomfort. Stress imposed on the heart for diagnostic purposes may cause lengthy angina pain, or even myocardial infarction or arrhythmias but serious complications are rare. In the event of a side effect, emergency measures including urgent hospitalization may be required (urgent hospitalization is needed in one in about 43,000 tests; death can occur once in about 264,000 tests [source: Japanese Society of Electrocardiography])—medical costs will then need to be borne by the patient, as is usually the case with our healthcare services. During treadmill stress testing, a fall and resulting bone fracture may occur. If the patient's legs have become very tired during the exercise, the examiner may stop the machine right away to prevent accidents such as falling off the treadmill.

Pharmacological stress testing is also reported to be associated with complications, as is the case with exercise stress testing. Stress testing with drug stimulation is not necessarily safer.

Being a test that imposes stress on the heart, stress echocardiography might result in the development of heart attack or arrhythmias, or very rarely, death. Rates of occurrence of emergency hospitalization or serious but non-fatal complications such as myocardial infarction are estimated at 0.2% or less.

I have received an explanation of the testing described above and satisfactory answers to the questions I have asked; I agree to engage in a stress test.

(I understand that this consent can be withdrawn at any time.)

Date of consent:

Patient or proxy (Relationship with the patient)

Signature

Parent/guardian of minor patient (Relationship with the patient)

Signature

(Relationship with the patient)

Signature

Exercise Stress Echocardiography Report

Patient ID		Referring department	Referring physician
Patient name		Outpatient / Inpatient / Ward	
		Date of test	
		Test number	
Date of birth		Equipment used	
Gender	Age	Test performed by	Technologist: Physician:
Height cm	Weight kg		

Clinical diagnosis: ( )

Objective of the test	Ischemic heart disease workup
	Cardiomyopathy workup (DCM / HCM / other ( )
	Valvular heart disease workup (AS / AR / MS / MR / other ( )
	Pulmonary hypertension workup
	Other ( )
Coronary risk factors	☐ Hypertension ☐ Diabetes mellitus ☐ Hyperlipidemia ☐ Smoking
	☐ Other ( )
Underlying disease information	☐ Old myocardial infarction ☐ Chronic heart failure ☐ CKD ☐ COPD
	☐ Atrial fibrillation ☐ Pacing ☐ Post AVR / MVR ☐ Post CABG
Medication	☐ Beta blocker (/ mg)
	☐ Continued / withheld for 24 h / withheld for 48 h
	☐ ACE-I/ARB ☐ Calcium antagonist ☐ Antiplatelet drug ☐ Other ( )
Special instruction	( )
Post exercise	%THR %
	Test goal achievement (Achieved / Not achieved/Insufficient workload)
Cause of test cessation	Leg exhaustion / Dyspnea / Ischemic changes
	Target heart rate reached(%THR %) / Events
Adverse events	☐ None ☐ Chest pain (Nitroglycerin given / not given)
	☐ ST-T change ( )
	☐ Arrhythmias (PVC / PAF / NSVT / VT /)
	☐ Vagal reflex ☐ Fall/trauma ☐ Other ( )

Treadmill Exercise Stress Test Data Record (Bruce Protocol)

Time started		:				
Stage		SBP / DBP	HR	ST change	Arrhyth-mias	Symptoms
Pre	Cumu-lative time (min)	/				
Stage 1	1	/				
	2	/				
	3	/				
Stage 2	4	/				
	5	/				
	6	/				
Stage 3	7	/				
	8	/				
	9	/				
Stage 4	10	/				
	11	/				
	12	/				
Post Exercise	1	/				
	2	/				
	3	/				
	4	/				
	5	/				

Ergometer Multistep Exercise Stress Test Data Record

Time started						
Stage		SBP (mmHg) / DBP (mmHg)	HR (bpm/beats)	ST change	Arrhyth-mias	Symptoms
Pre	Cumulative time (min)	/				
Exercise 25watt	1	/				
	2	/				
	3	/				
Exercise 50watt	4	/				
	5	/				
	6	/				
Exercise 75watt	7	/				
	8	/				
	9	/				
Exercise 100watt	10	/				
	11	/				
	12	/				
Exercise 125watt	13	/				
	14	/				
	15	/				
Exercise 150watt	16	/				
	17	/				
	18	/				
Post Exercise	1	/				
	2	/				
	3	/				
	4	/				
	5	/				

Ergometer Multistage Exercise Stress Test Data Record

Time started		:				
Stage		SBP (mmHg) / DBP (mmHg)	HR (bpm)	ST change	Arrhythmias	Symptoms
Pre	Cumulative time (min)	/				
Exercise 25 W	1	/				
	2	/				
	3	/				
Exercise 50 W	4	/				
	5	/				
	6	/				
Exercise 75 W	7	/				
	8	/				
	9	/				
Exercise 100 W	10	/				
	11	/				
	12	/				
Exercise 125 W	13	/				
	14	/				
	15	/				
Exercise 150 W	16	/				
	17	/				
	18	/				
Post Exercise	1	/				
	2	/				
	3	/				
	4	/				
	5	/				

Left cardiac system standard measurements

	Rest	Sub maximal	Peak	Post Ex
Heart rate	/min	/min	/min	/min
LAD	mm	mm	mm	mm
LVDd	mm	mm	mm	mm
LVDd index	mm/m²	mm/m²	mm/m²	mm/m²
LVDs	mm	mm	mm	mm
LVDs index	mm/m²	mm/m²	mm/m²	mm/m²
%FS	%	%	%	%
LA volume index	ml/m²	ml/m²	ml/m²	ml/m²
LVEDV biplane	ml	ml	ml	ml
LVESV biplane	ml	ml	ml	ml
SV biplane	ml	ml	ml	ml
EF biplane	%	%	%	%

Doppler measurements

	Rest	Sub maximal	Peak	Post Ex
Heart rate	/min	/min	/min	/min
E wave velocity	cm/s	cm/s	cm/s	cm/s
DcT	ms	ms	ms	ms
E/A				
E' sep	cm/s	cm/s	cm/s	cm/s
S' sep	cm/s	cm/s	cm/s	cm/s
E' lat	cm/s	cm/s	cm/s	cm/s
S' lat	cm/s	cm/s	cm/s	cm/s
E' average	cm/s	cm/s	cm/s	cm/s
E/E' average				

Right cardiac system standard measurements

	Rest	Sub maximal	Peak	Post Ex
Heart rate	/min	/min	/min	/min
RV EDA	cm²	cm²	cm²	cm²
RV ESA	cm²	cm²	cm²	cm²
FAC	%	%	%	%
E' RV	cm/s	cm/s	cm/s	cm/s
S' RV	cm/s	cm/s	cm/s	cm/s
TAPSE	mm	mm	mm	mm
TRPG	mmHg	mmHg	mmHg	mmHg

Ischemic Heart Disease Report

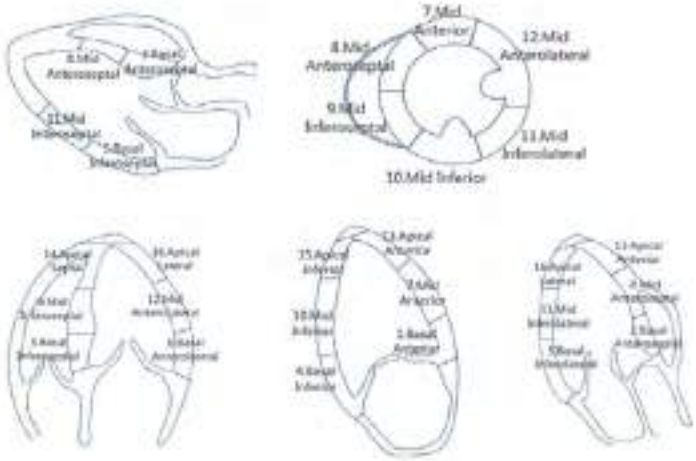

All models			16-17 segment model
1.	Basal anterior	7. Mid anterior	13. Apical anterior
2.	Basal anteroseptal	8. Mid anteroseptal	14. Apical septal
3.	Basal inferoseptal	9. Mid inferoseptal	15. Apical inferior
4.	Basal inferior	10. Mid inferior	16. Apical lateral
5.	Basal inferolateral	11. Mid inferolateral	
6.	Basal anterolateral	12. Mid anterolateral	

Wall motion	score index
Poor image	x
Normal	1
Hypokinesis	2
Akinesis	3
Dyskinesis	4

Stress Echocardiographic Wall Motion Assessment Data Record

Pre-stress

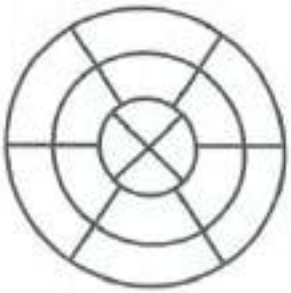

During stress

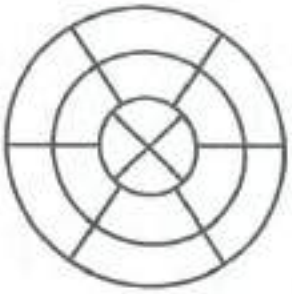

Post-stress

Wall motion	Score
Poorly imaged	0
Normal	1
Hypokinetic	2
Akinetic	3
Dyskinetic	4

Valvular heart disease report

MS	Rest	Sub maximal	Peak	Post Ex
HR	bpm	bpm	bpm	bpm
MV area CW	cm^2	cm^2	cm^2	cm^2
Peak velocity	cm/s	cm/s	cm/s	cm/s
Max PG	mmHG	mmHG	mmHG	mmHG
Mean PG	mmHG	mmHG	mmHG	mmHG
PHT	ms	ms	ms	ms

MR	Rest	Sub maximal	Peak	Post Ex
MR RV (volumetric)	ml	ml	ml	ml
MR RF	%	%	%	%
MR ERO (volumetric)	cm^2	cm^2	cm^2	cm^2
MR RV (PISA)	ml	ml	ml	ml
MR ERO (PISA)	cm^2	cm^2	cm^2	cm^2
Vena contracta	mm	mm	mm	mm
PHT	ms	ms	ms	ms

AS	Rest	Sub maximal	Peak	Post Ex
AVA	cm^2	cm^2	cm^2	cm^2
AVAi	cm^2/m^2	cm^2/m^2	cm^2/m^2	cm^2/m^2
VTI AV	cm	cm	cm	cm
VTI ration (AV/LVOT)				
HR	/min	/min	/min	/min
Ejection time	ms	ms	ms	ms
Peak velocity	cm/s	cm/s	cm/s	cm/s
Mean PG	mmHG	mmHG	mmHG	mmHG

AR	Rest	Sub maximal	Peak	Post Ex
AR RV (volumetric)	ml	ml	ml	ml
AR RF	%	%	%	%
AR ERO (volumetric)	cm^2	cm^2	cm^2	cm^2
AR RV (PISA)	ml	ml	ml	ml
AR ERO (PISA)	cm^2	cm^2	cm^2	cm^2
Vena contracta	mm	mm	mm	mm
PHT	ms	ms	ms	ms

Pulmonary hypertension report

	Rest	Sub maximal	Peak	Post Ex
BP	mmHG	mmHG	mmHG	mmHG
HR	/min	/min	/min	/min
TR peak velocity	cm/s	cm/s	cm/s	cm/s
TRPG	mmHG	mmHG	mmHG	mmHG
RVSP	mmHG	mmHG	mmHG	mmHG
LVOT diameter	mm			
LVOT TVI	cm	cm	cm	cm
HR	/min	/min	/min	/min
Cardiac output	l/min	l/min	l/min	l/min
Stroke volume	ml	ml	ml	ml
RVOT diameter	mm	mm	mm	mm
RVOT TVI	cm	cm	cm	cm
HR	/min	/min	/min	/min
RV cardiac output	l/min	l/min	l/min	l/min
RV stroke volume	$l/min/m^2$	$l/min/m^2$	$l/min/m^2$	$l/min/m^2$

References

1. Pellikka PA, Nagueh SF, Elhendy AA, et al. American Society of Echocardiography recommendations for performance, interpretation, and application of stress echocardiography. J Am Soc Echocardiogr. 2007;20:1021–41.
2. Lancellotti P, Pellikka PA, Budts W, et al. The clinical use of stress echocardiography in non-ischaemic heart disease: recommendations from the European Association of Cardiovascular Imaging and the American Society of Echocardiography. Eur Heart J Cardiovasc Imaging. 2016;17(11):1191–1229.
3. Schinkel A, Bax JJ, Geleijnse ML, et al. Noninvasive evaluation of ischaemic heart disease: myocardial perfusion imaging or stress echocardiography? Eur Heart J. 2003;24:789–800.
4. Hansen JE. Exercise instruments, schemes, and protocols for evaluating the dyspneic patient. Am Rev Respir Dis. 1984;129(suppl):S25–7.
5. Myers J, Arena R, Franklin B, et al. Recommendations for clinical exercise laboratories: a scientific statement from the American Heart Association. Circulation. 2009;119:3144–61.
6. Cheitlin MD, et al. ACC/AHA/ASE 2003 guideline update for the clinical application of echocardiography: summary article: a report of the American College of Cardiology/American Heart Association Task Force on Practice Guidelines (ACC/AHA/ASE Committee to Update the 1997 Guidelines for the Clinical Application of Echocardiography). Circulation. 2003;108:1146–62.
7. Banerjee A, Newman DR, Van den Bruel A, et al. Diagnostic accuracy of exercise stress testing for coronary artery disease: a systematic review and meta-analysis of prospective studies. Int J Clin Pract. 2012;66:477–92.
8. de Jong MC, Genders TS, van Geuns RJ, et al. Diagnostic performance of stress myocardial perfusion imaging for coronary artery disease: a systematic review and meta-analysis. Eur Radiol. 2012;22:1881–95.
9. Heijenbrok-Kal MH, Fleischmann KE, Hunink MG. Stress echocardiography, stress single-photon-emission computed tomography and electron beam computed tomography for the assessment of coronary artery disease: a meta-analysis of diagnostic performance. Am Heart J. 2007;154(3):415–23.
10. Metz LD, Beattie M, Hom R, et al. The prognostic value of normal exercise myocardial perfusion imaging and exercise echocardiography: a meta-analysis. J Am Coll Cardiol. 2007;49:227–37.
11. Roger VL, Pellikka PA, Bell MR, et al. Sex and test verification bias: impact on the diagnostic value of exercise echocardiography. Circulation. 1997;95:405–10.
12. Arruda A, Das F, Roger R, et al. Prognostic value of exercise echocardiography in 2632 patients 65 years of age. J Am Coll Cardiol. 2001;37:1036–41.
13. Garrido IP, Pereiro I, Garcia-Lara J, et al. Prognostic value of exercise echocardiography in patients with diabetes mellitus and known or suspected coronary artery disease. Am J Cardiol. 2005;96:9–12.
14. Elhendy A, Mahoney DW, Burger KN, et al. Prognostic value of exercise echocardiography in patients with classic angina pectoris. Am J Cardiol. 2004;94:559–63.

15. Ryan T, Armstrong WF, O'Donnel JA, et al. Risk stratification following acute myocardial infarction during exercise two-dimensional echocardiography. Am Heart J. 1987;14:1305–16.
16. Quintana M, Lindvall K, Ryden L, et al. Prognostic value of predischarge exercise stress echocardiography after acute myocardial infarction. Am J Cardiol. 1995;76:1115–21.
17. Peteiro J, Monserrat L, Vazquez E, et al. Comparison of exercise echocardiography to exercise electrocardiographic testing added to echocardiography at rest for risk stratification after uncomplicated acute myocardial infarction. Am J Cardiol. 2003;92:373–6.
18. Arruda A, McCully R, Oh J, et al. Prognostic value of exercise echocardiography in patients after coronary artery bypass surgery. Am J Cardiol. 2001;87:1069–73.
19. Shaw LJ, Eagle KA, Gersh BJ, et al. Meta-analysis of intravenous dipyridamole-thallium-201 imaging (1985–1994) and dobutamine echocardiography (1991–1994) for risk stratification before vascular imaging. J Am Coll Cardiol. 1996;27:787–98.
20. Lalka SG, Sawada SG, Dalsing MC, et al. Dobutamine stress echocardiography as a predictor of cardiac events associated with aortic surgery. J Vasc Surg. 1992;15:831–42.
21. Lane RT, Sawada SG, Segar DS, et al. Dobutamine stress echocardiography for assessment of cardiac risk before noncardiac surgery. Am J Cardiol. 1991;68:976–7.
22. Eichelberger JP, Schwarz KQ, Black ER, et al. Predictive value of dobutamine echocardiography just before noncardiac vascular surgery. Am J Cardiol. 1993;72:602–7.
23. Hecht H, DeBord L, Shaw R, et al. Usefulness of supine bicycle stress echocardiography for detection of restenosis after percutaneous transluminal coronary angioplasty. Am J Cardiol. 1993;71:293–6.
24. Kafka H, Leach A, Fitzgibbon G. Exercise echocardiography after coronary artery bypass surgery: correlation with coronary angiography. J Am Coll Cardiol. 1995;25:1019–23.
25. Hecht HS, DeBord L, Sotomayor N, et al. Supine bicycle stress echocardiography: peak exercise imaging is superior to postexercise imaging. J Am Soc Echocardiogr. 1993;6:265–71.
26. Pierard LA, De Landsheere CM, Berthe C, et al. Identification of viable myocardium by echocardiography during dobutamine infusion in patients with myocardial infarction after thrombolytic therapy: comparison with positron emission tomography. J Am Coll Cardiol. 1990;15:1021–31.
27. Applegate RJ, Dell'Italia LJ, Crawford MH. Usefulness of two dimensional echocardiography during low-level exercise testing early after uncomplicated myocardial infarction. Am J Cardiol. 1987;60:10–4.
28. Lancellotti P, Hoffer EP, Pierard LA. Detection and clinical usefulness of a biphasic response during exercise echocardiography early after myocardial infarction. J Am Coll Cardiol. 2003;41:1142–7.
29. Bergeron S, Ommen S, Bailey K, et al. Exercise echocardiographic findings and outcome of patients referred for evaluation of dyspnea. J Am Coll Cardiol. 2004;43:2242–6.
30. Kovacs G, Berghold A, Scheidl S, et al. Pulmonary arterial pressure during rest and exercise in healthy subjects: a systematic review. Eur Respir J. 2009;34:888–94.
31. Voci P, Testa G, Pizzuto G, et al. Coronary Doppler intensity changes during handgrip: a new method to detect coronary vasomotor tone in coronary artery disease. J Am Coll Cardiol. 1999;34:428–34.
32. Kivowitz C, Parmley WW, Donoso R, et al. Effects of isometric exercise on cardiac performance. The grip test. Circulation. 1971;41:994–1002.
33. Kerber RE, Miller RA, Najjar SM. Myocardial ischemic effects of isometric, dynamic and combined exercise in coronary artery disease. Chest. 1975;67:388–94.
34. Tawa CB, Baker WB, Kleiman NS, et al. Comparison of adenosine echocardiography, with and without isometric handgrip, to exercise echocardiography in the detection of ischaemia in patients with coronary artery disease. J Am Soc Echocardiogr. 1996;9:33–43.
35. Ryo K, Tanaka H, Kaneko A, et al. Efficacy of longitudinal speckle tracking strain in conjunction with isometric handgrip stress test for detection of ischemic myocardial segments. Echocardiography. 2012;29:411–8.
36. Hirano Y, Ozasa Y, Yamamoto T, et al. Hyperventilation and cold-pressor stress echocardiography for noninvasive diagnosis of coronary artery spasm. J Am Soc Echocardiogr. 2001;14:626–33.
37. Pozzoli M, Traversi E, Cioffi G, et al. Loading manipulations improve the prognostic value of Doppler evaluation of mitral flow in patients with chronic heart failure. Circulation. 1997;95:1222–30.
38. Ishizu T, Seo Y, Kawano S, et al. Stratification of impaired relaxation filling patterns by passive leg lifting in patients with preserved left ventricular ejection fraction. Eur J Heart Fail. 2008;10:1094–101.
39. Yamada H, Oki T, Tabata T, et al. Differences in transmitral flow velocity pattern during increase in preload in patients with abnormal left ventricular relaxation. Cardiology. 1998;89:152–8.
40. Yamada H, Kusunose K, Nishio S, et al. Pre-load stress echocardiography for predicting the prognosis in mild heart failure. JACC Cardiovasc Imaging. 2014;7:641–97.
41. Lang RM, Badano LP, Mor-Avi V, et al. Recommendations for cardiac chamber quantification by echocardiography in adults: an update from the American Society of Echocardiography and the European Association of Cardiovascular Imaging. J Am Soc Echocardiogr. 2015;28(1):1–39.
42. Brochet E, Detaint D, Fondard O, et al. Early hemodynamic changes versus peak values: what is more useful to predict occurrence of dyspnea during stress echocardiography in patients with asymptomatic mitral stenosis? J Am Soc Echocardiogr. 2011;24:392–8.
43. Magne J, Lancellotti P, Pierard LA. Exercise-induced changes in degenerative mitral regurgitation. J Am Coll Cardiol. 2010;56:300–9.
44. Lancellotti P, Magne J. Stress echocardiography in regurgitant valve disease. Circ Cardiovasc Imaging. 2013;6:840–9.
45. Magne J, Lancellotti P, Pierard LA. Exercise pulmonary hypertension in asymptomatic degenerative mitral regurgitation. Circulation. 2010;122:33–41.
46. Haluska BA, Short L, Marwick TH. Relationship of ventricular longitudinal function to contractile reserve in patients with mitral regurgitation. Am Heart J. 2003;146:183–8.
47. Magne J, Mahjoub H, Dulgheru R, et al. Left ventricular contractile reserve in asymptomatic primary mitral regurgitation. Eur Heart J. 2014;35:1608–16.
48. Kusunose K, Popovic ZB, Motoki H, et al. Prognostic significance of exercise-induced right ventricular dysfunction in asymptomatic degenerative mitral regurgitation. Circ Cardiovasc Imaging. 2013;6:167–76.
49. Lancellotti P, Lebois F, Simon M, et al. Prognostic importance of quantitative exercise Doppler echocardiography in asymptomatic valvular aortic stenosis. Circulation. 2005;112:1377–82.
50. Lancellotti P, Lebois F, Simon M, et al. Determinants and prognostic significance of exercise pulmonary hypertension in asymptomatic severe aortic stenosis. Circulation. 2012;126:851–9.
51. Bonow RO, Lakatos E, Maron BJ, et al. Serial long-term assessment of the natural history of asymptomatic patients with chronic aortic regurgitation and normal left ventricular systolic function. Circulation. 1991;84:1625–35.
52. Lee K, Daimon M, Kawahara Y, et al. Prediction of the response to beta-blocker therapy in patients with dilated cardiomyopathy:

comparison of 123I-MIBG scintigraphy and low-dose dobutamine stress echocardiography. J Echocardiogr. 2009;7:74–9.
53. Scrutinio D, Napoli V, Passantino A, et al. Low-dose dobutamine responsiveness in idiopathic dilated cardiomyopathy: relation to exercise capacity and clinical outcome. Eur Heart J. 2000;21:927–34.
54. Matsumoto K, Tanaka H, Kaneko A, et al. Contractile reserve assessed by three-dimensional global circumferential strain as a predictor of cardiovascular events in patients with idiopathic dilated cardiomyopathy. J Am Soc Echocardiogr. 2012;25:1299–308.
55. Lancellotti P, Lebrun F, Pierard LA. Determinants of exercise-induced changes in mitral regurgitation in patients with coronary artery disease and left ventricular dysfunction. J Am Coll Cardiol. 2003;42:1921–8.
56. Lancellotti P, Magne J, Dulgheru R, et al. Clinical significance of exercise pulmonary hypertension in secondary mitral regurgitation. Am J Cardiol. 2015;115:1454–61.
57. Ypenburg C, Sieders A, Bleeker GB, et al. Myocardial contractile reserve predicts improvement in left ventricular function after cardiac resynchronization therapy. Am Heart J. 2007;154:1160–5.
58. Elliott PM, Anastasakis A, Borger MA, et al. 2014 ESC Guidelines on diagnosis and management of hypertrophic cardiomyopathy: the task force for the diagnosis and management of hypertrophic cardiomyopathy of the European Society of Cardiology (ESC). Eur Heart J. 2014;35:2733–79.
59. Peteiro J, Bouzas-Mosquera A, Fernandez X, et al. Prognostic value of exercise echocardiography in patients with hypertrophic cardiomyopathy. J Am Soc Echocardiogr. 2012;25:182–9.
60. Yu EH, Omran AS, Wigle ED, et al. Mitral regurgitation in hypertrophic obstructive cardiomyopathy: relationship to obstruction and relief with myectomy. J Am Coll Cardiol. 2000;36:2219–25.
61. Nagueh SF, Smiseth OA, Appleton CP, et al. Recommendations for the evaluation of left ventricular diastolic function by echocardiography: an update from the American Society of Echocardiography and the European Association of Cardiovascular Imaging. J Am Soc Echocardiogr. 2016;29:277–314.
62. Bossone E, D'Andrea A, D'Alto M, et al. Echocardiography in pulmonary arterial hypertension: from diagnosis to prognosis. J Am Soc Echocardiogr. 2013;26:1–14.
63. Naeije R, Vanderpool R, Dhakal BP, et al. Exercise-induced pulmonary hypertension: physiological basis and methodological concerns. Am J Respir Crit Care Med. 2013;187:576–83.
64. Argiento P, Chesler N, Mulè M, D'Alto M, Bossone E, Unger P, Naeije R. Exercise stress echocardiography for the study of the pulmonary circulation. Eur Respir J. 2010;35:1273–8.
65. Kane GC, Hepinstall MJ, Kidd GM, et al. Safety of stress echocardiography supervised by registered nurses: results of a 2-year audit of 15,404 patients. J Am Soc Echocardiogr. 2008;21:337–41.
66. Geleijnse ML, Krenning BJ, Nemes A, et al. Incidence, pathophysiology, and treatment of complications during dobutamine-atropine stress echocardiography. Circulation. 2010;121:1756–67.
67. Nishimura RA, Otto CM, Bonow RO, et al. 2014 AHA/ACC guideline for the management of patients with valvular heart disease: executive summary a report of the American College of Cardiology/American Heart Association Task Force on Practice Guidelines. Circulation. 2014;129:e521–643.
68. Pibarot P, Jean G, Dumesnil JG. New concepts in valvular hemodynamics: implications for diagnosis and treatment of aortic stenosis. Can J Cardiol. 2007;23:40B–7B.
69. Tribouilloy C, Lévy F, Rusinaru D, et al. Outcome after aortic valve replacement for low-flow/low-gradient aortic stenosis without contractile reserve on dobutamine stress echocardiography. J Am Coll Cardiol. 2009;53:1865–73.

SpringerLink

Search Log in
Menu

Images in Cardiovascular Intervention | Published: 17 October 2017

Optimizing echo guidance during MitraClip using fluoroscopy: how to see better!

Hector Rodriguez Cetina Biefer, Maurizio Taramasso, Shingo Kuwata, Fabian Nietlispach, Michel Zuber & Francesco Maisano

Cardiovascular Intervention and Therapeutics **33**, 398–399(2018) | Cite this article

169 Accesses | Metrics

This is a preview of subscription content, log in to check access.

Access options

Buy article PDF

¥ 4,750,92

Price **includes VAT** for Japan

Instant access to the full article PDF.

Rent this article via DeepDyve.

Buy journal subscription

¥ 9,167

Price **includes VAT** for Japan

Immediate online access to all issues from 2019. Subscription will auto renew annually.

Learn more about Institutional subscriptions

Author information

Affiliations

Division of Cardiovascular Surgery, University Hospital Zurich, Rämistrasse 100, 8091, Zurich, Switzerland
Hector Rodriguez Cetina Biefer, Maurizio Taramasso, Shingo Kuwata & Francesco Maisano

Division of Cardiology, University Hospital Zurich, Zurich, Switzerland
Fabian Nietlispach & Michel Zuber

Corresponding author

Correspondence to Hector Rodriguez Cetina Biefer.

Ethics declarations

Conflict of interest

F.M. is a consultant for Abbott MitraClip. The other authors have no conflict of interest.

Ethical approval

All procedures performed in this study involving human participants were in accordance with the ethical standards of the institutional and/or national research committee and with the 1964 Helsinki declaration and its later amendments or comparable ethical standards.

About this article

Check for updates

Cite this article

Rodriguez Cetina Biefer, H., Taramasso, M., Kuwata, S. *et al.* Optimizing echo guidance during MitraClip using fluoroscopy: how to see better!. *Cardiovasc Interv and Ther* **33**, 398–399 (2018).
https://doi.org/10.1007/s12928-017-0494-5

Download citation

Received	Accepted
27 April 2017	23 September 2017

Access options

Buy article PDF

¥ 4,750,92

Price **includes VAT** for Japan

Instant access to the full article PDF.

Buy journal subscription

¥ 9,167

Price **includes VAT** for Japan

Immediate online access to all issues from 2019.
Subscription will auto renew annually.

Rent this article via DeepDyve.

Learn more about Institutional subscriptions

Sections Figures

Author information

Ethics declarations

About this article

Over 10 million scientific documents at your fingertips

Academic Edition Corporate Edition

Home Impressum Legal information Privacy statement How we use cookies
Accessibility Contact us

Not logged in - 202.209.68.3
St. Marianna University School of Medicine (3000160972) - Justice Consortium (3000675571)
SPRINGER NATURE

© 2020 Springer Nature Switzerland AG. Part of Springer Nature.

Circ J 2018; 82: 2845–2851
doi:10.1253/circj.CJ-18-0487

ORIGINAL ARTICLE
Ischemic Heart Disease

Number of Board-Certified Cardiologists and Acute Myocardial Infarction-Related Mortality in Japan
— JROAD and JROAD-DPC Registry Analysis —

Koshiro Kanaoka, MD; Satoshi Okayama, MD; Kihei Yoneyama, MD, PhD; Michikazu Nakai, PhD; Kunihiro Nishimura, MD, PhD; Hiroyuki Kawata, MD, PhD; Manabu Horii, MD, PhD; Rika Kawakami, MD, PhD; Hiroyuki Okura, MD, PhD; Yoshihiro Miyamoto, MD, PhD; Yoshihiro Akashi, MD, PhD; Yoshihiko Saito, MD, PhD

Background: The appropriate number of board-certified cardiologists (BCC) for the treatment of acute myocardial infarction (AMI) has not been thoroughly examined in Japan. This study investigated whether the number of BCC/50 cardiovascular beds affects acute outcome in AMI treatment.

Methods and Results: Data on 751 board-certified teaching hospitals and 63,603 patients with AMI were obtained from the Japanese Registry Of All cardiac and vascular Diseases (JROAD) and JROAD Diagnosis Procedure Combination (JROAD-DPC) databases between 1 April 2012 and 31 March 2014. The hospitals were categorized into 3 groups based on the median number of BCC/50 cardiovascular beds: first tertile, 5.0 (IQR, 4.0–5.7); second, 8.3 (IQR, 7.4–9.8); third, 15.3 (IQR, 12.5–22.7), and the patients with AMI admitted to the categorized hospitals were compared (first tertile, 12,002 patients; second, 23,930; third, 27,671). On hierarchical logistic modeling, the adjusted OR for 30-day mortality were 0.86 (95% CI: 0.74–1.00) for the second tertile and 0.75 (95% CI: 0.65–0.88) for the third tertile.

Conclusions: Patients with AMI admitted to hospitals with a large number of BCC/50 cardiovascular beds had a lower 30-day mortality rate. This tendency was independent of patient and hospital characteristics. This is the first study to provide new information on the association between the number of BCC and in-hospital AMI-related mortality in Japan.

Key Words: Acute myocardial infarction; Cardiologist; Diagnosis Procedure Combination (DPC); Japanese Registry Of All cardiac and vascular Diseases (JROAD); Mortality

Reduction of mortality in acute myocardial infarction (AMI) has been an important issue for cardiologists. The age-standardized mortality rate of AMI has been gradually decreasing over the past 3 decades in several countries,[1,2] which is probably due to the development of emergency medical network systems, and the carrying out of reperfusion therapy and optimal medical therapy.[3,4] AMI, however, remains one of the most common causes of death.[1,5]

In 2016, 68,907 patients in Japan were hospitalized because of AMI, and the in-hospital mortality rate was 8.2%, which has not improved in recent years despite the advancements in medical technology.[6,7] Thus, to further improve the acute outcome of AMI treatment, structural and clinical properties of the hospital, including the quality and quantity of medical staff, require more attention.

The aim of this study was to determine whether or not the number of cardiovascular specialists affects the acute mortality of AMI. The Japanese Circulation Society (JCS) launched the board of cardiovascular specialist system in 1989.[8] There were 6,568 JCS board-certified cardiologists (BCC) working full time in 1,612 hospitals in 2012, which included almost all cardiovascular beds in Japan. All hospitals with cardiovascular beds were divided into different classes: class A hospitals have >2 BCC and >30 cardiovascular beds; class B hospitals have >1 BCC and >15 cardiovascular beds, and class C hospitals do not have BCC or they have <15 cardiovascular beds. The number of BCC per hospital in classes A and B widely varied from 1 to 87, and whether this current status is appropriate or

Received May 16, 2018; revised manuscript received July 22, 2018; accepted July 28, 2018; released online September 12, 2018
Time for primary review: 16 days
Department of Cardiovascular Medicine, Nara Medical University, Kashihara (K.K., S.O., H.K., R.K., H.O., Y.S.); Division of Cardiology, Department of Internal Medicine, St Marianna University School of Medicine, Kawasaki (K.Y., Y.A.); Center for Cerebral and Cardiovascular Disease Information, National Cerebral and Cardiovascular Center, Suita (M.N., K.N., Y.M.); and Department of Cardiovascular Medicine, Nara City Hospital, Nara (K.K., M.H.), Japan
Mailing address: Yoshihiko Saito, MD, PhD, Department of Cardiovascular Medicine, Nara Medical University, 840 Shijo-cho, Kashihara 634-8522, Japan. E-mail: yssaito@naramed-u.ac.jp
ISSN-1346-9843 All rights are reserved to the Japanese Circulation Society. For permissions, please e-mail: cj@j-circ.or.jp

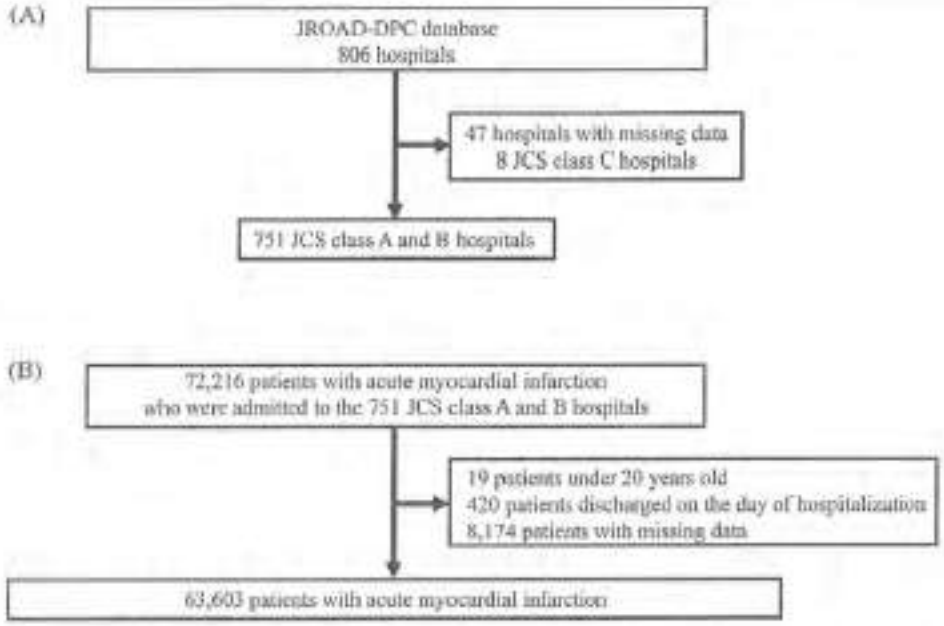

Figure 1. Study flow chart. (**A**) Flow chart for hospital selection, (**B**) flow chart for patient selection class A hospitals need more than 2 BCC and 30 cardiovascular beds, class B hospitals need more than 1 BCC and 15 cardiovascular beds. DPC, Diagnosis Procedure Combination; JCS, Japanese Circulation Society; JROAD, Japanese Registry Of All cardiac and vascular Diseases.

not for the treatment of AMI remains unknown, especially given that available related studies in Japan are limited.

The aim of this study was therefore to clarify the associations between the number of BCC/50 cardiovascular beds and 30-day AMI mortality.

Methods

Patients

This was a cross-sectional study, and we used the Japanese Registry Of All cardiac and vascular Diseases (JROAD) database and Diagnosis Procedure Combination (DPC) discharge database from 2012 to 2014. JROAD is conducted by JCS, and the data were collected from almost all teaching hospitals with cardiovascular beds, except for stroke.[9,10] Of 1,613 hospitals included in the JROAD, 806 provided DPC data to JCS.

We obtained the following data on JCS-certified class A and B teaching hospitals: number of hospital beds and cardiologists; presence or absence of cardiac surgery division and coronary care unit; hospital teaching status (teaching hospitals are defined as JCS-certified cardiovascular specialist training facilities with >2 BCC and >30 cardiovascular beds); and annual number of percutaneous coronary interventions (PCI) and coronary artery bypass grafts (CABG). Consequently, 751 hospitals were enrolled in this study (**Figure 1A**).

Subsequently, we collected data for 72,216 patients from the 751 hospitals based on the following inclusion criteria: (1) hospitalized because of AMI between 1 April 2012 and 31 March 2014; and (2) diagnosis of AMI based on the International Classification of Diseases (ICD-10) codes for AMI (I21.0, I21.1, I21.2, I21.3, I21.4, and I21.9). We excluded 19 patients <20 years old, 420 patients discharged on the day of hospitalization, and 8,174 patients with insufficient data. Consequently, we analyzed 63,603 patients in 751 hospitals (**Figure 1B**).

We categorized the 751 hospitals into 3 groups according to the number of BCC/50 cardiovascular beds and compared the groups of patients admitted to the categorized hospitals. In the subanalysis, we divided the 63,603 patients with AMI into 2 groups according to Killip classification on admission: not severe (Killip I and II) or severe (Killip III and IV).

Ethics

The ethics committees at both JCS and Nara Medical University, which waived the requirement for individual informed consent because no information specifying individuals was included, approved the study protocol. The original DPC data were anonymized using the code change equations, and were then sent to the Ministry of Health, Labor, and Welfare.

Statistical Analysis

Data are presented as mean±SD for normally distributed data, and as median (IQR) for asymmetrically distributed data, or absolute number (proportion) for categorical data. The differences between tertiles were compared using analysis of variance for continuous variables and the chi-squared test with Bonferroni correction for non-continuous and categorical variables. The main outcome measure was in-hospital or 30-day mortality. The tendency for tertile 30-day mortality was analyzed using the Cochran-Armitage trend test. The association between the number of BCC/50 cardiovascular beds and 30-day mortality was

Table 1. Hospital Characteristics vs. No. JCS Board-Certified Cardiologists

	Total	First tertile	Second tertile	Third tertile	P-value
JCS BCC/50 CV beds (range)	0.63–76.58	0.63–6.58	6.63–10.98	11.05–75.58	
No. hospitals[a]	751	238	282	231	
Hospital beds	444 (300–558)	317 (230–400)	406 (307–500)	621 (441–735)	<0.001†
CV beds	38 (30–46)	39 (30–48)	37 (30–42)	39 (28–46)	0.005†
JCS BCC/50 CV beds	8.3 (5.3–13.2)	5.0 (4.0–5.7)	8.3 (7.4–9.8)	15.3 (12.5–22.7)	<0.001†
JCS BCC/hospital	5.4 (3–6)	2.8 (2–3)	4.2 (3–5)	9.4 (5–12)	<0.001†
JCS BCC and non-JCS BCC/hospital	8.3 (4–9)	3.7 (3–5)	6.2 (4–7)	15.8 (8–19)	<0.001†
Cardiac intensive care units	85	71	87	96	<0.001†
Coronary angiography/year	444 (182–595)	247 (107–328)	434 (193–547)	636 (383–807)	<0.001†
Emergency PCI for AMI/year	49 (20–69)	29 (10–40)	49 (23–64)	68 (38–94)	<0.001†
Cardiac surgery	61	42	57	87	<0.001‡
No. CABG/year	31 (13–40)	16 (2–23)	27 (8–38)	41 (19–54)	<0.001†
Hospital teaching status	94	82	95	99	<0.001‡

Data given as median (IQR), n[a] or %. †Kruskal-Wallis test; ‡χ^2 test with Bonferroni correction. AMI, acute myocardial infarction; BCC, board-certified cardiologists; CABG, coronary artery bypass graft; CV, cardiovascular; JCS, Japanese Circulation Society; PCI, percutaneous coronary intervention.

analyzed using multilevel mixed-effect logistics regression, with hospital characteristics at the first level and patient characteristics at the second. The number of BCC/50 cardiovascular beds was analyzed as a continuous variable and as a categorical variable (first, second, and third tertile). The models were adjusted for the following covariates based on previous reports: age; gender; Charlson comorbidity index; comorbidity (hypertension, dyslipidemia, diabetes mellitus, chronic kidney disease, and atrial fibrillation); presence of cardiac surgery division and coronary care unit; hospital teaching status; use of ambulance; and Killip classification. Stepwise analysis was performed to determine whether any combination of clinical findings was associated with 30-day mortality. In addition, propensity score analysis was conducted to evaluate the robustness of the results. We performed one-to-one propensity score matching between the 2 groups by the number of cardiologists. The cut-off for the number of cardiologists was 10.0, which was determined on receiver operating characteristic analysis. Propensity scores were estimated using a logistic regression model with independent variables selected on stepwise analysis. A caliper of 0.001-fold the SD was used.

In the sub-analysis, we performed stratified analysis according to AMI severity to ascertain whether the effect of the number of BCC/50 cardiovascular beds on 30-day mortality is dependent on AMI severity. Biological interaction between the number of BCC/50 cardiovascular beds and AMI severity was evaluated by calculating the relative excess risk.[11-13] STATA (version 14, Stata Corp., College Station, TX, USA) was used for the analysis.

Results

Hospital Characteristics

The median number of BCC/50 cardiovascular beds was 5.0 (IQR, 4.0–5.7) in the first tertile hospitals, 8.3 (IQR, 7.4–9.8) in the second, and 15.3 (IQR, 12.5–22.7) in the third. As the number of BCC/50 cardiovascular beds increased, the following variables also increased: number of hospital beds and cardiologists; presence of cardiac surgery division and coronary care unit; hospital teaching status; and annual number of PCI and CABG (**Table 1**).

Patient Characteristics

Approximately 82% of the patients were admitted to the second or third tertile hospitals. Sex, age, Charlson comorbidity index, Killip classification, comorbidity, ambulance use, and medication were similar between the 3 groups, whereas the use of circulation devices, such as intra-aortic balloon pump (IABP) and percutaneous cardiopulmonary support system (PCPS), increased and the length of hospital stay decreased as the number of BCC/50 cardiovascular beds increased (**Table 2**).

Crude in-hospital mortality was 11.5% for the first tertile, 10.0% for the second, and 8.3% for the third, which all decreased as the number of BCC/50 cardiovascular beds increased.

No. BCC/50 Cardiovascular Beds and 30-Day Mortality

On multilevel mixed-effect logistics regression analysis of the number of BCC/50 cardiovascular beds as a continuous variable, the OR for 30-day mortality was 0.987 (95% CI: 0.982–0.994, P<0.01), and the adjusted OR (AOR) for 30-day mortality was 0.988 (95% CI: 0.982–0.995, P<0.01).

On tertile analysis of the number of BCC/50 cardiovascular beds, unadjusted OR for 30-day mortality was significantly lower in the second tertile (OR, 0.81; 95% CI: 0.71–0.92, P<0.001) and third tertile (OR, 0.66; 95% CI: 0.58–0.76, P<0.001) than in the first tertile. Moreover, inverse trends in 30-day mortality were observed between the tertiles (trend test P<0.01). The AOR for 30-day mortality was 0.88 (95% CI: 0.75–1.03, P=0.10) for the second tertile and 0.77 (95% CI: 0.65–0.92, P<0.001) for the third tertile. The number of BCC remained an independent risk factor after stepwise analysis. On stepwise analysis, the AOR for 30-day mortality was 0.86 (95% CI: 0.74–1.00, P=0.05) in the second tertile and 0.75 (95% CI: 0.65–0.88, P<0.01) in the third tertile (**Table 3**). The OR for the large BCC group vs. the small BCC group was 0.87 (95% CI: 0.78–0.98, P=0.019) after propensity score matching (**Table S1**).

Table 2. Patient Characteristics vs. No. JCS Board-Certified Cardiologists

	Total	First tertile	Second tertile	Third tertile	P-value
JCS BCC/50 CV beds (range)	0.63–75.58	0.63–6.58	6.63–10.98	11.05–75.58	
Patients	63,603 (100)	12,002 (19)	23,930 (38)	27,671 (44)	
Age (years)	69±13	70±13	69±13	69±13	<0.001*
Male	73	71	73	74	<0.001†
Charlson comorbidity index	2 (1–3)	2 (1–3)	2 (1–3)	2 (1–3)	<0.001†
Killip classification					
I	30,336 (48)	5,028 (42)	11,658 (49)	13,650 (49)	<0.001‡
II	18,521 (29)	3,910 (33)	6,514 (27)	8,097 (29)	
III	5,561 (9)	1,187 (10)	2,098 (9)	2,266 (8)	
IV	9,185 (14)	1,867 (16)	3,660 (15)	3,658 (13)	
Comorbidities					
Hypertension	62	61	61	63	<0.001‡
Diabetes mellitus	29	29	28	29	<0.001‡
Dyslipidemia	56	55	55	58	<0.001‡
CKD	4.2	3.7	4	4.5	<0.001‡
Atrial fibrillation	5.0	5.8	5.2	4.7	<0.001‡
Ambulance use	69	59	64	66	<0.001‡
Medication					
ACEI or ARB	86	85	87	89	<0.001‡
β-blockers	58	61	60	56	<0.001‡
Antiplatelets	98	98	98	99	<0.001‡
CCB	63	65	64	60	<0.001‡
Statins	91	89	90	92	<0.001‡
Oral anti-diabetic drugs	64	67	66	62	<0.001‡
Device					
IABP	15	12	15	17	<0.001‡
PCPS	2.3	1.5	2	2.8	<0.001‡
LVAD	0.01	0.00	0.02	0.01	0.96§
CRRT	1.1	0.9	0.9	1.3	<0.001‡
Respirator	18	17	17	18	<0.001‡
LOHS (days)	17 (9–20)	18 (10–22)	17 (10–20)	16 (9–19)	<0.001†
30-day mortality	9.6	11.5	10.0	8.3	<0.001*

Data given as mean ± SD, median (IQR), n (%) or %. *ANOVA; †Kruskal-Wallis rank sum test; ‡χ^2 test with Bonferroni correction. ACEI, angiotensin-converting enzyme inhibitor; ARB, angiotensin II receptor blocker; CCB, calcium channel blockers; CKD, chronic kidney disease; CRRT, continuous renal replacement therapy; IABP, intra-aortic balloon pumping; LOHS, length of hospital stay; LVAD, left ventricular assist device; PCPS, percutaneous cardiopulmonary support. Other abbreviations as in Table 1.

Table 3. No. JCS BCC/50 CV Beds and 30-Day Mortality

	No. JCS BCC/50 CV beds (range)	n	Unadjusted analysis			Multivariate analysis			Stepwise analysis		
			OR	95% CI	P-value	AOR	95% CI	P-value	AOR	95% CI	P-value
First tertile	0.63–6.58	12,002	Ref.			Ref.			Ref.		
Second tertile	6.63–10.98	23,930	0.81	0.71–0.92	<0.001	0.88	0.75–1.03	0.10	0.86	0.74–1.00	0.05
Third tertile	11.05–75.58	27,671	0.66	0.58–0.76	<0.001	0.77	0.65–0.92	<0.001	0.75	0.66–0.88	<0.001

The model includes age (per 10 years), gender, Charlson comorbidity index, Killip classification, hypertension, hyperlipidemia, diabetes, CKD, atrial fibrillation, cardiac surgery, ambulance use, coronary care unit, hospital teaching status, and JCS BCC/50 CV beds. Stepwise analysis includes age (per 10 years), gender, Charlson comorbidity index, Killip classification, hypertension, hyperlipidemia, diabetes, CKD, atrial fibrillation, and ambulance use. AOR, adjusted OR. Other abbreviations as in Tables 1,2.

Patient Characteristics and AMI Severity

To investigate whether AMI severity affects the association between the number of BCC/50 cardiovascular beds and 30-day mortality, we performed a stratified analysis according to AMI severity. Similar tendencies were observed in both the not-severe and severe groups. The number of patients and the use of circulation devices increased as the number of BCC/50 cardiovascular beds increased, whereas patient characteristics and medication remained almost unchanged. The length of hospital stay and the crude 30-day mortality decreased as the number of BCC/50 cardiovascular beds increased (**Table 4**).

Table 4. Patient Characteristics vs. AMI Severity and Cardiologist Tertile

	Not-severe					Severe				
	Total	First tertile	Second tertile	Third tertile	P-value	Total	First tertile	Second tertile	Third tertile	P-value
JCS BCC/50 CV beds (range)	0.63–75.58	0.63–6.58	6.63–10.98	11.05–75.58		0.63–75.58	0.63–6.58	6.63–10.98	11.05–75.58	
Patients	46,857 (100)	8,938 (18)	18,172 (37)	21,747 (45)		14,746 (100)	3,064 (21)	5,758 (39)	5,924 (40)	
Age (years)	68±13	69±13	68±13	67±13	<0.001†	72±13	74±13	73±13	72±13	<0.001†
Male	75	73	74	75	<0.001‡	68	66	68	70	<0.001‡
Charlson comorbidity index	2 (1–3)	2 (1–3)	2 (1–2)	2 (1–3)	<0.001†	2 (1–3)	2 (1–3)	2 (1–3)	2 (1–3)	<0.001†
Comorbidities										
Hypertension	68	67	67	69	<0.001‡	43	42	43	45	<0.001‡
Diabetes mellitus	29	30	29	30	<0.001‡	26	28	25	27	<0.001‡
Dyslipidemia	63	62	61	66	<0.001‡	34	33	34	36	0.077‡
CKD	3.5	2.9	3.4	3.7	<0.001‡	6.5	5.7	6	7.4	<0.001‡
Atrial fibrillation	4.8	5.5	5	4.5	<0.001‡	5.7	5.9	5.8	5.4	<0.001‡
Ambulance use	61	56	61	62	<0.001‡	75	70	74	78	<0.001‡
Medication										
ACEI or ARB	87	86	87	88	<0.001‡	88	87	88	89	0.04‡
β-blockers	56	58	57	54	<0.001‡	68	68	69	66	<0.001‡
Antiplatelets	99	99	99	99	<0.001‡	97	96	97	98	<0.001‡
CCB	60	64	62	56	<0.001‡	72	73	73	71	0.08‡
Statins	91	90	91	92	<0.001‡	89	87	89	90	<0.001‡
Oral anti-diabetic drugs	61	64	62	59	<0.001‡	76	75	77	76	<0.001‡
Device										
IABP	8.9	6.6	9.2	9.6	<0.001‡	37	29	34	44	<0.001‡
PCPS	0.4	0.2	0.4	0.6	<0.001‡	8.3	5.2	7.1	11	<0.001‡
LVAD	0	0	0	0	<0.001‡	0.05	0	0.07	0.05	0.36‡
CRRT	0.7	0.6	0.6	0.8	0.05‡	2.6	1.9	2	3.6	<0.001‡
Respirator	7.7	7.2	7.5	8	0.05‡	50	47	47	54	<0.001‡
LOHS (days)	16 (10–19)	17 (11–21)	16 (10–19)	15 (9–17)	<0.001‡	20 (5–26)	22 (3–26)	19 (4–25)	21 (7–26)	<0.001‡

Data given as mean±SD, median (IQR), n (%) or (%). †ANOVA; ‡Kruskal-Wallis rank sum test; ‡χ^2 test with Bonferroni correction. Abbreviations as in Tables 1,2.

Prognosis and AMI Severity

In the not-severe group, the AOR for 30-day mortality was 0.87 (95% CI: 0.70–1.05, P=0.15) in the second tertile and 0.81 (95% CI: 0.67–0.97, P=0.02) in the third tertile, and an inverse trend for 30-day mortality was observed between the tertiles (trend test P<0.01). In the severe group, the AOR was 0.86 (95% CI: 0.71–1.03, P=0.10) in the second tertile and 0.71 (95% CI: 0.59–0.85, P<0.001) in the third tertile, and an inverse trend for 30-day mortality was observed between the tertiles (trend test P<0.01). No interaction effect between the number of BCC/50 cardiovascular beds and AMI severity was seen on interaction analysis (**Figure 2; Table 5**).

Discussion

In this study, we demonstrated that the number of BCC/50 cardiovascular beds is associated with 30-day in-hospital AMI mortality. In addition, after adjustment for patient and hospital baseline characteristics, we showed that the hospital 30-day mortality rate in the third tertile hospitals is significantly lower than that in the first tertile hospitals. Moreover, this tendency was independent of AMI severity.

The present results are generally consistent with previous studies. O'Neill et al compared 30-day mortality in acute coronary syndrome (ACS) patients between those admitted to non-cardiology services and those admitted to cardiology services. Patients with ACS who were admitted to cardiology services more commonly underwent cardiac catheterization and evidence-based pharmacotherapy and had a significantly lower 30-day mortality than those admitted to non-cardiology services.[14] Badheka et al found that a large operator volume is associated with reduced mortality in patients undergoing PCI.[15] Their study included angina pectoris and AMI,[15] whereas the present study focused on patients with AMI and investigated the number of cardiologists/50 cardiovascular beds, which in turn is considered new.

We infer that the decreased 30-day mortality with the increase in the number of BCC/50 cardiovascular beds could be attributed to the following: (1) increased annual number of coronary angiography, emergency PCI, and CABG per hospital; moreover, the use of circulation devices, such as IABP and PCPS, increased as the number of BCC/50 cardiovascular beds increased, which in turn suggests that the treatment options for AMI are wide and varied and AMI could be treated quickly; and (2) the total number of hospital beds was greater in hospitals with a large number

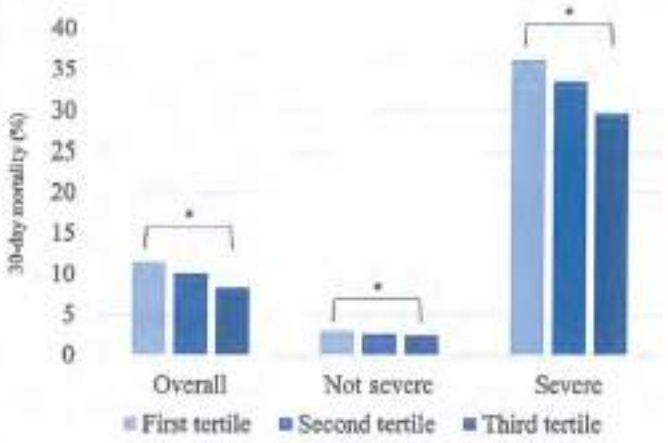

Figure 2. In-hospital 30-day mortality vs. severity of acute myocardial infarction and tertile of number of board-certified cardiologists/50 cardiovascular beds in Japan. *P<0.01.

Table 5. AOR and 95% CI for 30-Day Mortality vs. AMI Severity and Cardiologist Tertile

	No. JCS BCC/ 50 CV beds (range)	Not severe				Severe			
		n	AOR	95% CI	P-value	n	AOR	95% CI	P-value
First tertile	0.63–6.58	8,938	Ref.			3,064	Ref.		
Second tertile	6.63–10.98	18,172	0.87	0.70–1.05	0.15	5,758	0.86	0.71–1.03	0.10
Third tertile	11.05–75.58	21,747	0.81	0.67–0.97	0.02	5,924	0.71	0.59–0.85	<0.001

The model includes age (per 10 years), gender, Charlson comorbidity index, Killip classification, hypertension, hyperlipidemia, diabetes, CKD, atrial fibrillation, and ambulance use. Abbreviations as in Tables 1–3.

of BCC/50 cardiovascular beds than in those with a low number of BCC/50 cardiovascular beds, with the former having several medical staff working and sufficient facilities, and thus cardiologists would more likely receive the needed assistance and cooperation from other departments and medical staff when they encounter problems.

Improvement in the prognosis of AMI requires adherence to treatment guidelines.[16] Differences in the adherence to treatment guidelines for AMI between cardiologists and non-cardiologists exist.[17,18] In the present study, significant differences in the use of medications, such as angiotensin-converting enzyme inhibitors, angiotensin II receptor blocker, β-blockers, and antiplatelets, between tertiles were not found.

New approaches to further improve the acute outcome of AMI treatment are warranted. This study suggests that one of the methods to improve outcome in Japan is to transport patients with AMI to third tertile hospitals. Furthermore, increasing physician volume may be needed to improve treatment outcome.

Study Limitations

This study had several limitations. First, this was an observational study using the JROAD-DPC database, which included approximately 50% of JCS-certified hospitals and 29% of all hospital beds in Japan.[11] Second, the accuracy of the diagnoses and procedures in the DPC database is unclear. Third, the present study could not include some important confounding factors such as door-to-balloon time. Finally, we could not calculate the appropriate number of cardiologists to ensure the best outcome.

Conclusions

Patients with AMI who are admitted to hospitals with a large number of cardiologists/50 cardiovascular beds have a lower 30-day mortality rate. This tendency was independent of patient and hospital characteristics and AMI severity. This study is the first to provide new information about the relationship between the number of BCC and in-hospital AMI-related mortality in Japan.

Acknowledgment

We would like to express our gratitude to Ms Sumita for preparing the data of the JROAD and JROAD-DPC study.

Disclosures

The authors declare no conflicts of interest.

References

1. Hartley A, Marshall DC, Salciccioli JD, Sikkel MB, Maruthappu M, Shalhoub J. Trends in mortality from ischemic heart disease and cerebrovascular disease in Europe: 1980 to 2009. *Circulation* 2016; **133**: 1916–1926.
2. McGovern PG, Jacobs DR Jr, Shahar E, Arnett DK, Folsom AR, Blackburn H, et al. Trends in acute coronary heart disease mortality, morbidity, and medical care from 1985 through 1997: The Minnesota heart survey. *Circulation* 2001; **104**: 19–24.
3. Ministry of Health, Labour and Welfare. Statistics 2015. http://www.mhlw.go.jp/toukei_hakusho/toukei/index.html (accessed January 1, 2018).
4. Puymirat E, Simon T, Steg PG, Schiele F, Guéret P, Blanchard D, et al. Association of changes in clinical characteristics and management with improvement in survival among patients with ST-elevation myocardial infarction. *JAMA* 2012; **308**: 998–1006.
5. Mozaffarian D, Benjamin EJ, Go AS, Arnett DK, Blaha MJ,

Cushman M, et al. Heart disease and stroke statistics–2015 update: A report from the American Heart Association. *Circulation* 2015; **131**: e29–e322.
6. Japanese Registry Of All cardiac and vascular Diseases (JROAD). Survey on medical cardiovascular disease 2016. http://www.j-circ.or.jp/jittai_chosa/jittai_chosa2016web (accessed February 2, 2018).
7. Cui Y, Hao K, Takahashi J, Miyata S, Shindo T, Nishiniya K, et al. Age-specific trends in the incidence and in-hospital mortality of acute myocardial infarction over 30 years in Japan: Report from the Miyagi AMI Registry Study. *Circ J* 2017; **81**: 520–528.
8. The Japanese Circulation Society. Cardiovascular specialist and membership directry. http://www.j-circ.or.jp/ (accessed February 2, 2018).
9. Tomoike H, Yokoyama H, Sumita Y, Hanai S, Kada A, Okamura T, et al. Nationwide distribution of cardiovascular practice in Japan: Results of Japanese Circulation Society 2010 annual survey. *Circ J* 2015; **79**: 1058–1067.
10. Yasuda S, Nakao K, Nishimura K, Miyamoto Y, Sumita Y, Shishido T, et al. The current status of cardiovascular medicine in Japan: Analysis of a large number of health records from a nationwide claim-based database, JROAD-DPC. *Circ J* 2016; **80**: 2327–2335.
11. Rothman K. Epidemiology: An introduction. New York: Oxford University Press, 2002.
12. Andersson T, Alfredsson L, Kallberg H, Zdravkovic S, Ahlbom A. Calculating measures of biological interaction. *Eur J Epidemiol* 2005; **20**: 575–579.
13. VanderWeele TJ, Tchetgen Tchetgen EJ. Attributing effects to interactions. *Epidemiology* 2014; **25**: 711–722.
14. O'Neill DE, Southern DA, Norris CM, O'Neill BJ, Curran HJ, Graham MM. Acute coronary syndrome patients admitted to a cardiology vs non-cardiology service: Variations in treatment and outcome. *BMC Health Serv Res* 2017; **17**: 354.
15. Badheka AO, Patel NJ, Grover P, Singh V, Patel N, Arora S, et al. Impact of annual operator and institutional volume on percutaneous coronary intervention outcomes: A 5-year United States experience (2005–2009). *Circulation* 2014; **130**: 1392–1406.
16. Drozda J Jr, Messer JV, Spertus J, Abramowitz B, Alexander K, Beam CT, et al. ACCF/AHA/AMA-PCPI 2011 performance measures for adults with coronary artery disease and hypertension: A report of the American College of Cardiology Foundation/American Heart Association Task Force on Performance Measures and the American Medical Association-Physician Consortium for Performance Improvement. *J Am Coll Cardiol* 2011; **58**: 316–336.
17. Ayanian JZ, Hauptman PJ, Guadagnoli E, Antman EM, Pashos CL, McNeil BJ. Knowledge and practices of generalist and specialist physicians regarding drug therapy for acute myocardial infarction. *N Engl J Med* 1994; **331**: 1136–1142.
18. Hickson RP, Robinson JG, Annis IE, Killeya-Jones LA, Korhonen MJ, Cole AL, et al. Changes in statin adherence following an acute myocardial infarction among older adults: Patient predictors and the association with follow-up with primary care providers and/or cardiologists. *J Am Heart Assoc* 2017; **6**: e007106.

Supplementary Files

Supplementary File 1

Table S1. No. JCS BCC/50 CV beds and 30-day AMI mortality with PSM

Please find supplementary file(s):
http://dx.doi.org/10.1253/circj.CJ-18-0487

Direct Comparison of Severity Grading Assessed by Two-Dimensional, Three-Dimensional, and Doppler Echocardiography for Predicting Prognosis in Asymptomatic Aortic Stenosis

Yosuke Nabeshima, MD, Yasufumi Nagata, MD, PhD, Kazuaki Negishi, MD, PhD, Yoshihiro Seo, MD, PhD, Tomoko Ishizu, MD, PhD, Kimi Sato, MD, Kazutaka Aonuma, MD, PhD, Dan Koto, MD, Masaki Izumo, MD, PhD, Yoshihiro J. Akashi, MD, PhD, Eiji Yamashita, MD, Shigeru Oshima, MD, PhD, Yutaka Otsuji, MD, PhD, and Masaaki Takeuchi, MD, PhD, FASE, FESC, FJCC, *Kitakyushu, Tsukuba, Kawasaki, and Maebashi, Japan; and Tasmania, Australia*

Background: Reliable assessment of aortic stenosis (AS) severity relies on stroke volume (SV) determination using Doppler echocardiography, but it can also be estimated with two-dimensional/three dimensional echocardiography (2DE/3DE). The aim of this study was to compare SV measurements and AS subgroup classifications among the three modalities and determine their prognostic strength in asymptomatic AS.

Methods: We prospectively enrolled 359 patients with asymptomatic AS. SV was determined using three methods, and the patients were divided into four AS subgroups according to indexed aortic valve area (iAVA) and SV index (SVI) determined by each method and mean pressure gradient. The primary end point was major adverse cardiovascular events (MACEs), which included cardiac death, ventricular fibrillation, heart failure, and aortic valve replacement. We also assessed the presence or absence of upper septal hypertrophy.

Results: Doppler-derived SVI was significantly larger than that derived from 2DE/3DE with modest correlations (r = 0.33 and 0.47). Thus, group classification varied substantially by modality. During the median follow-up period of 17 months, 112 patients developed a major adverse cardiovascular event. Although iAVA assessed by Doppler echocardiography had a significantly better net reclassification improvement compared with iAVA by 2DE or 3DE, prognostic values were nearly identical among the three methods. Ventricular septal geometry affected the accuracy of risk stratification.

Conclusions: AS severity grading varied considerably according to the methods applied for calculating SV. Thus, SV measurements are not interchangeable, even though their prognostic power is similar. Hence, examiners should select one of the three methods to assess AS severity and should use the same method in longitudinal examinations. (J Am Soc Echocardiogr 2018;31:1080-90.)

Keywords: Aortic stenosis, Asymptomatic, Prognosis, Comparison, Echocardiography

The accurate determination of aortic stenosis (AS) severity and subgroup relies on stroke volume (SV) measurement across the left ventricular outflow tract (LVOT), in addition to accurately obtaining the highest jet velocity across the aortic valve using multiple transducer positions.[1,2] The guidelines set forth by the American Society of Echocardiography and the European Association of Cardiovascular Imaging recommend using Doppler-derived SV to determine AS severity.[1] However, the geometry and flow profile across the LVOT

From the Second Department of Internal Medicine (Y.N., Y.N., Y.O.), and Department of Laboratory and Transfusion Medicine (M.T.), University of Occupational and Environmental Health, School of Medicine, Kitakyushu; Cardiovascular Division, University of Tsukuba, Tsukuba (Y.S., T.I., K.S., K.A.); Division of Cardiology, Department of Internal Medicine, St. Marianna University School of Medicine, Kawasaki (D.K., M.I., Y.J.A.); Department of Cardiology, Gunma Prefectural Cardiovascular Center, Maebashi (E.Y., S.O.), Japan; and Menzies Institute for Medical Research, University of Tasmania, Tasmania, Australia (K.N.).

Dr. Takeuchi received an equipment grant from TomTec Imaging Systems.

Conflicts of Interest: None.

Reprint requests: Masaaki Takeuchi, MD, PhD, FASE, FESC, FJCC, Department of Laboratory and Transfusion Medicine, University of Occupational and Environmental Hospital, 1-1 Iseigaoka, Yahatanishi-ku, Kitakyushu 807-8556, Japan (E-mail: takeuchi@med.uoeh-u.ac.jp).

0894-7317/$36.00

Copyright 2018 by the American Society of Echocardiography.

https://doi.org/10.1016/j.echo.2018.05.006

Abbreviations

2D = Two-dimensional

2DE = Two-dimensional echocardiography

3D = Three-dimensional

3DE = Three-dimensional echocardiography

AS = Aortic stenosis

AUC = Area under the curve

AVA = Aortic valve area

AVR = Aortic valve replacement

BSA = Body surface area

CMR = Cardiac magnetic resonance

HPG-SAS = High-pressure-gradient severe aortic stenosis

HR = Hazard ratio

IAVA = Indexed aortic valve area

ICC = Intraclass correlation coefficient

LFLPG-SAS = Low-flow/low-pressure-gradient severe aortic stenosis

LV = Left ventricular

LVEF = Left ventricular ejection fraction

LVOT = Left ventricular outflow tract

MACE = Major adverse cardiac event

MAS = Mild-to-moderate aortic stenosis

NFLPG-SAS = Normal-flow/low-pressure-gradient severe aortic stenosis

NRI = Net reclassification improvement

ROC = Receiver operating characteristic

SV = Stroke volume

SVI = Stroke volume index

USH = Upper septal hypertrophy

Zva = Valvulo-arterial impedance

can cause over- or underestimated SV values.[4-6] Measuring SV with two-dimensional echocardiography (2DE) also has well-known limitations due to malalignment or foreshortened 2D cut planes, which leads to underestimations in ventricular volumes, leading to errors in the calculation of SV.[7] However, due to continuous advances in ultrasound imaging quality, reliable SV measurements could be obtained by an experienced user using the biplane Simpson's method. Additionally, three-dimensional echocardiography (3DE) has been proposed as an accurate and reliable modality for quantifying left ventricular (LV) volumes and deformation parameters.[7-10] To the best of our knowledge, no study has directly compared AS severity classification among these three modalities for predicting future adverse outcomes.

Accordingly, this study aimed to (1) compare SV measurements assessed by 2DE, 3DE, and Doppler echocardiography and (2) determine their prognostic strength in a relatively large number of patients with asymptomatic AS.

METHODS

Study Subjects

This study was part of a recently conducted multicenter study (Japanese Multicenter Aortic Stenosis Study, prospective registry). We prospectively enrolled patients with AS (peak velocity across the aortic valve >2.5 m/sec) who underwent comprehensive echocardiography examination in four Japanese cardiovascular centers (University of Occupational and Environmental Health, University of Tsukuba, St. Marianna University, and Gunma Prefectural Cardiovascular Center) from April 2012 to December 2014. The exclusion criteria for the study enrollment were more than mild mitral regurgitation and very poor image quality. Of the 707 echocardiography examinations performed for enrolled patients with AS, 61 examinations were excluded because they were repeat examinations of the same patient. We further excluded 287 patients because they had AS-related symptoms ($n = 261$), inappropriate data acquisition ($n = 4$), and <1-month follow-up ($n = 22$). Thus, a total of 359 patients with asymptomatic AS with any severity were included in the study. The study protocol was approved by the Ethics Committee in each hospital, and informed consent was obtained from all patients. A part of the study population ($n = 87$) was also used in a previous publication.[10] All echocardiography image data were sent to the core laboratory where all SV measurements were performed.

Clinical Characteristics

During the echocardiography examination, the cardiologist directly asked the patient about risk factors, history of any cardiovascular disease, and symptomatic status. AS-related symptoms (dyspnea, chest pain, and syncope) were carefully checked. Brachial blood pressure and heart rate were also measured.

Two-/Three-Dimensional and Doppler Echocardiography

A standard echocardiography examination was performed using a commercially available ultrasound machine and equipment by a sonographer or cardiologist specially trained in echocardiography. Image acquisition was systematically conducted based on the American Society of Echocardiography guideline. On 2DE, LV end-diastolic and end-systolic volumes were measured using the biplane Simpson's formula in the apical four- and two-chamber views at end diastole and end systole, and LV ejection fraction (LVEF) was obtained from a standard formula. The 2DE-derived SV was measured by LV end-diastolic volume − LV end-systolic volume. LV mass was determined using the Devereux formula. Maximum and minimum left atrial volumes were also measured using the biplane Simpson's formula.[11] Volume and mass were indexed by body surface area (BSA). The Mosteller formula was used to calculate BSA. Upper septal hypertrophy (USH) was evaluated from the angle between the interventricular septum and ascending aorta and the thickness of the upper septum according to a previous publication.[12] LV inflow velocity was obtained at the level of the mitral leaflet tips. Mitral annular velocity (e') was measured at the septal corner of the mitral annulus. Pulse wave LVOT velocity was obtained with the sample volume just below the aortic valve, and LVOT diameter was measured at the level of the aortic valve annulus using zoom mode. Peak aortic valve jet velocity was obtained from multiple echocardiography windows yielding the highest velocity signal. Doppler-derived SV was determined by $\pi \times (\text{LVOT diameter}/2)^2 \times$ velocity-time integral of the pulse-wave LVOT velocity. In patients who had tricuspid regurgitation, systolic pulmonary arterial pressure was measured ($4 \times (\text{peak velocity})^2$ + right atrial pressure). Right atrial pressure was estimated based on the inferior vena cava diameter and its change during respiration.[13]

Full-volume 3DE data sets with multibeat (4 or 6 beats) acquisition were acquired using an apical approach by a commercial ultrasound machine and fully sampled matrix array transducers (iE33 with X5-1 or X3-1, Philips Medical Systems, Andover, MA; Vivid 7/E9 with 4V, GE Healthcare, Horten, Norway). We insured that

HIGHLIGHTS

- Doppler-derived SV was larger than SV by 2D and 3D echocardiography.
- AS severity group classification among the three methods was significantly different.
- The prognostic value of AS severity grading among the three methods was identical.
- The prognosis of asymptomatic paradoxical LF/LG severe AS was intermediate.

the scan plane encompassed the entire left ventricle with the highest volume rate possible. All echocardiography images were stored on a hard drive, and all data were sent to the core laboratory for analysis.

We also calculated valvulo-arterial impedance (Zva), which was defined as (systolic blood pressure + mean PG)/SV index (SVI) obtained in each method.

3DE Speckle-Tracking Analysis

The 3DE-derived LV parameters were measured by an experienced investigator using vendor-independent 3D speckle-tracking software (4D LV analysis version 3.1.2, TomTec Imaging Systems, Unterschleissheim, Germany). The methods have been described in detail in a previous publication.[13] Briefly, end-diastolic apical four-, two-, and three-chamber views and optional levels of short-axis views were extracted from the full-volume 3DE data sets. After making specific landmark points (center point between both sides of the mitral annuli and apex), the software automatically delineated the LV endocardial border line in each view. Manual adjustment of the endocardial border was performed as needed. The same procedure was performed at the end-systolic frame. Once the tracing line was confirmed, the software performed a 3D speckle-tracking analysis on a frame-by-frame basis in a single cardiac cycle and generated time domain LV volume curves, from which LV end-diastolic volume, systolic volume, SV, and LVEF were calculated. The accuracy of this software to measure LV volumes has been validated in the previous publication.[14] A similar comparison was performed in a small group of the current patients who had cardiac magnetic resonance (CMR) imaging (Supplemental Table 1, available at www.onlinejase.com). Comparison of this vendor-independent software with the vendor-specific software showed no significant difference in measurements (Supplemental Table 2, available at www.onlinejase.com). For 3DE LV mass calculation, the epicardial contour was traced at the end-diastolic frame and adjusted in multiple 2D views extracted from the 3DE data sets. LV mass was calculated as follows: (LV epicardial volume − LV endocardial volume) × 1.05.[14]

AS Severity Grading

AS was classified based on valve area, flow, and pressure. The aortic valve area (AVA) was defined as the SV measured by each method divided by the velocity-time integral of the peak aortic jet velocity and indexed by BSA (indexed AVA [iAVA]). Severe AS (SAS) was defined as iAVA < 0.6 cm^2/m^2, and mild-to-moderate AS (MAS) was defined as iAVA ≥ 0.6 cm^2/m^2. According to flow (SVI ≥ or <35 mL/m^2) and pressure gradient (mean pressure gradient ≥ or <40 mm Hg), SAS patients were further divided into three groups, including high-pressure-gradient SAS (HPG-SAS), low-flow/low-pressure-gradient SAS (LFLPG-SAS), and normal-flow/low-pressure-gradient SAS (NFLPG-SAS).[15,16] Thus, the patients were classified into one of four AS grades using each method: MAS, LFLPG-SAS, NFLPG-SAS, and HPG-SAS.

Follow-Up

Patients were followed up regularly in an outpatient clinic. Patients, physicians, and next of kin were contacted by telephone if patients had been treated in other hospitals. Final follow-up data were obtained from January 2016 to May 2016. The primary end point was major adverse cardiovascular events (MACEs), which included cardiac death, ventricular fibrillation/tachycardia, heart failure exacerbation that required hospitalization, and surgical or transcatheter aortic valve replacement (AVR).

Reliability of SV Measurements

Intraobserver variability was assessed in 20 randomly selected patients by having the observer repeat the SV measurement with three methods 2 weeks apart. Interobserver variability was determined by having a second observer perform these measurements in the same 20 patients. The intra- and interobserver variability values were calculated as the absolute differences between the corresponding two measurements in percentages of their mean and intraclass correlation coefficient (ICC).

Statistical Analysis

Continuous data are presented as mean ± SD or median and interquartile interval (25th to 75th percentile) according to the data distribution. Categorical data are expressed as numbers or percentages. A *t*-test or the Wilcoxon sum rank test was used to compare continuous variables between the two groups. One-way analysis of variance or Friedman's analysis was performed to compare three imaging modalities or the four AS subgroups. Categorical variables were compared using Fisher's exact test or the χ^2-test, as appropriate. Survival analysis was performed using the Kaplan-Meier method, and group differences were determined with the log-rank test. A Cox proportional hazards regression analysis was used to calculate the hazard ratios (HRs) and 95% CIs. The prognostic value of the echocardiography parameters was determined using univariate Cox proportional hazards regression analysis. Prognostic power was compared by χ^2 values. To compare the predictive strength of iAVA among the three modalities, we generated receiver operating characteristic (ROC) curves for MACEs. We conducted a pairwise comparison of the areas under the curve (AUCs). We also performed net reclassification improvement (NRI) analysis to compare the predictive ability of iAVA assessed by 2DE/3DE and iAVA by Doppler echocardiography.[17] A two-sided *P* value < .05 was considered statistically significant. All statistical analyses were performed using commercial software (JMP version 13.1.0, SAS Institute, Cary, NC; SPSS version 24, Chicago, IL; R version 3.4.3, The R Foundation for Statistical Computing, Vienna, Austria; and Prism 7, GraphPad Software, Inc., La Jolla, CA).

Table 1 Clinical characteristics in study population

Variables	N = 359
Age, years	76 ± 10
Male (%)	173 (48)
BSA, per m^2	1.53 ± 0.20
Body mass index, kg/m^2	22.6 ± 3.6
USH (%)	113 (31)
Hypertension (%)	260 (73)
Diabetes (%)	93 (26)
Hypercholesterolemia (%)	141 (39)
Chronic kidney disease (%)	156 (44)
Coronary artery disease (%)	70 (20)
Atrial fibrillation (%)	50 (14)
Heart rate, bpm	67 ± 14
Systolic blood pressure, mm Hg	140 ± 25
Diastolic blood pressure, mm Hg	72 ± 14
Beta blocker (%)	76 (21)
Angiotensin converting enzyme inhibitor/angiotensin receptor blocker (%)	174 (48)
Ca antagonists (%)	159 (44)
Diuretics (%)	73 (22)
Statin (%)	118 (33)
Estimated glomerular filtration rate, mL/min/1.73 m^2	58.4 (39.3-71.7)
Brain natriuretic peptide, pg/mL	107 (52-220)
Image quality: good/fair/poor (%)	103 (29)/159 (44)/97 (27)
2D LV end-diastolic volume index, mL/m^2	58 (48-73)
2D LV end-systolic volume index, mL/m^2	21 (16-30)
2D LVEF, %	63 (56-69)
Number of patients with 2D LVEF < 50% (%)	33/359 (9)
2D LV mass index, g/m^2	105 (85-129)
3D LV end-diastolic volume index, mL/m^2	62 (53-74)
3D LV end-systolic volume index, mL/m^2	25 (20-32)
3D LVEF, %	59 (54-64)
Number of patients with 3D LVEF < 50% (%)	35/350 (10)
3D LV mass index, g/m^2	79 (67-94)
Maximum left atrial volume index, mL/m^2	41 (31-53)
Minimum left atrial volume index, mL/m^2	23 (15-34)
E wave velocity, cm/sec	76 (60-96)
A wave velocity, cm/sec	101 (85-120)
E/A	0.70 (0.59-0.86)
e', cm/sec	4.4 (3.8-5.6)
E/e'	16.7 (12.6-22.3)

(Continued)

Table 1 (Continued)

Variables	N = 359
Systolic pulmonary arterial pressure, mm Hg	31 (27-36)
Peak aortic valve jet velocity, m/sec	3.4 (2.8-4.1)
Aortic valve mean pressure gradient, mm Hg	25 (16-38)

Continuous data are expressed as mean ± SD or median (25th to 75th percentile).

RESULTS

The clinical characteristics of the study population are shown in Table 1. Figure 1 shows SV measurements by three imaging modalities. A video of 3DE speckle-tracking analysis in a representative patient is also provided (Video 1).

Comparison of SV Measurements among the Three Methods

SV was measured in 359 (100%), 350 (97%), and 354 (99%) patients using 2DE, 3DE, and Doppler echocardiography, respectively. Among the 345 patients who underwent SV measurements with all three methods, the Doppler-derived SVI (median, 44.1 mL/m^2, 25-75 percentiles; 37.6-53.3 mL/m^2) was significantly larger than the SVIs measured using 2DE (36.4 mL/m^2 [30.6-43.5 mL/m^2]; $P < .001$) and 3DE (36.1 mL/m^2 [30.7-42.1 mL/m^2]; $P < .001$). No significant differences in SVI were noted between 2DE and 3DE measurements ($P = .341$). Figure 2 shows the linear correlation and Bland-Altman analysis of the SVI as assessed by the three methods. Although there was a significant correlation for SVI between the paired comparisons, the Bland-Altman analysis revealed a wide 95% CI, especially between 2DE and Doppler echocardiography. The impact of USH on the differences in SVI and iAVA calculated by each method is shown in Table 2. Patients with USH ($n = 113$) had significantly larger differences in SVI and iAVA between 2DE/3DE and Doppler echocardiographic measurements than those without USH ($n = 246$).

AS Group Classification among the Three Methods

Using 2DE-derived SVI, the prevalence of MAS, LFLPG-SAS, NFLPG-SAS, and HPG-SAS was 112 (31%), 107 (30%), 65 (18%), and 74 (21%), respectively. The corresponding values for 3DE were 101 (29%), 102 (29%), 73 (21%), and 73 (21%), respectively, and those for Doppler echocardiography were 179 (50%), 37 (10%), 69 (20%), and 69 (20%), respectively. Significant differences in group classification were noted in all paired comparisons. The agreement of group classification between 3DE and 2DE was 254 of 349 patients (73%). The corresponding value between 2DE and Doppler echocardiography and that between 3DE and Doppler echocardiography were 61% (217/354) and 63% (218/345), respectively. Table 3 shows the echocardiography parameters among the four AS subgroups stratified by 2DE, 3DE, and Doppler echocardiography. All variables were significantly different among the four subgroups, if either method was used for group classification.

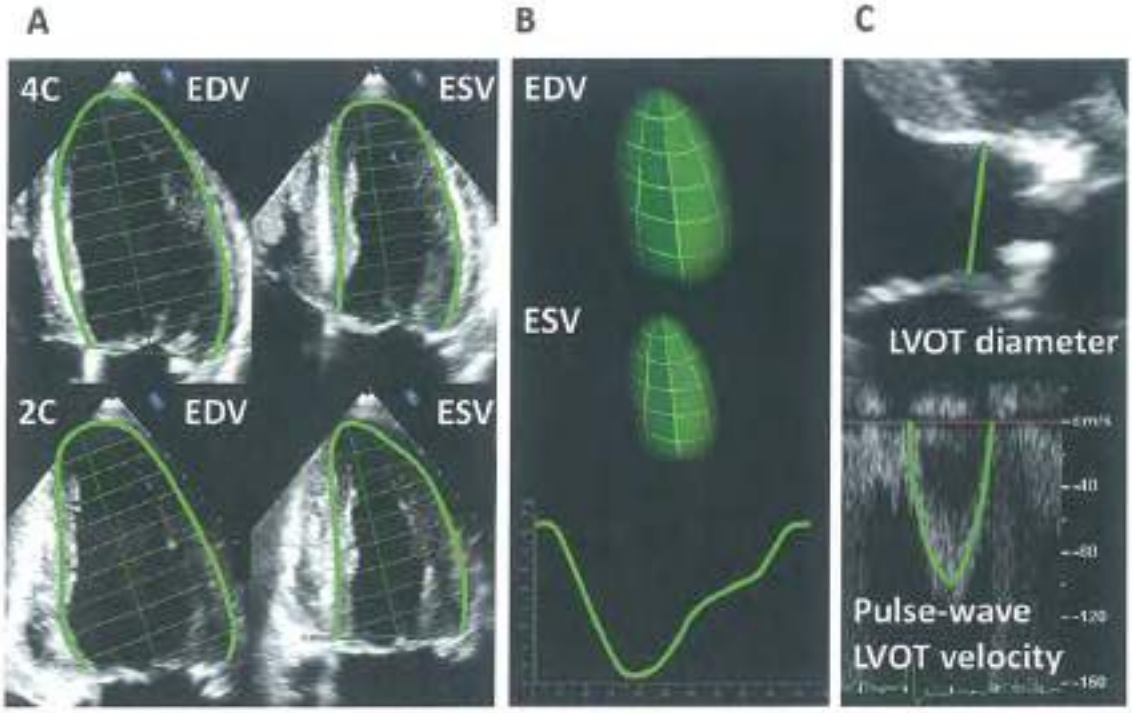

Figure 1 SV measurements by three methods. **(A)** 2S LV end-diastolic and end-systolic volumes (LVEDV, LVESV) were obtained by biplane Simpson's method. SV was determined by LVEDV - LVESV. **(B)** Three-dimensional LVEDV and LVESV were obtained by 3D speckle-tracking analysis. SV was determined by LVEDV – LVESV. **(C)** Doppler echocardiography-derived SV was measured by time-velocity integral of the LVOT profile times LVOT area. *2C*, Apical two-chamber view; *4C*, apical four-chamber view, *EDV*, end-diastolic volume; *ESV*, end-systolic volume.

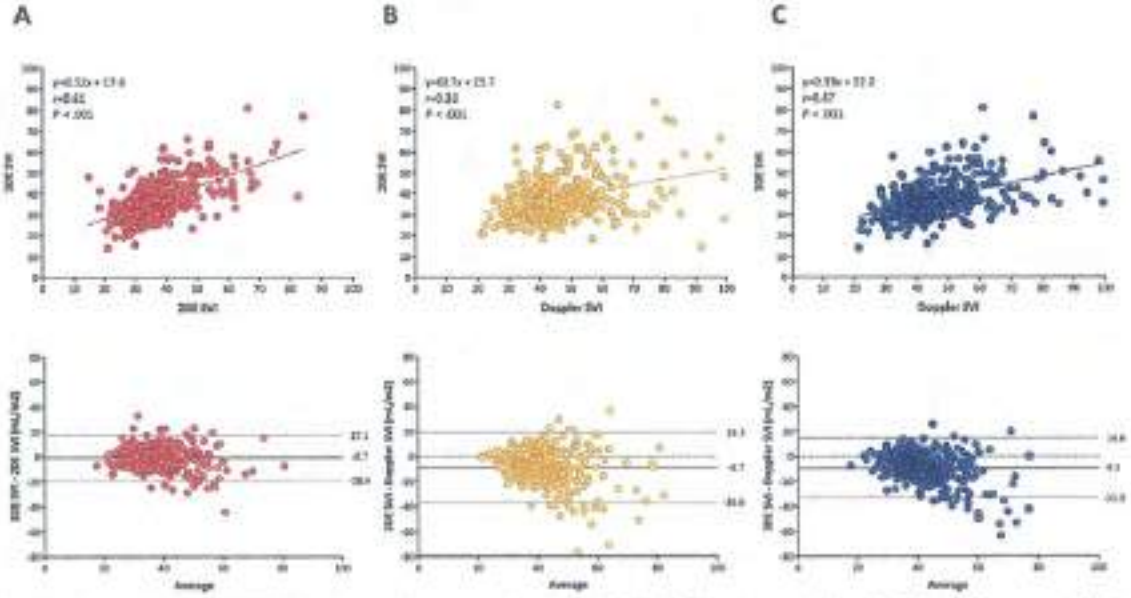

Figure 2 Linear correlation of the SVI between the two methods and Bland-Altman analysis. On Bland-Altman analysis, bias and 95% limit of agreements are shown on the plots. **(A)** 2DE vs 3DE; **(B)** 2DE vs Doppler echocardiography; **(C)** 3DE vs Doppler echocardiography.

Follow-Up

During a median follow-up of 17.0 months (8.5-25.0 months), 112 patients developed 122 MACEs, including 11 cardiac deaths, one myocardial infarction, three ventricular tachycardia/fibrillations, and 29 heart failures requiring hospitalization. Seventy-eight patients had AVR. Figure 3 shows the MACE-free rates among the four AS

Table 2 Impact of USH on the differences of SVI and iAVA among the three modalities

Comparison of methods	Bias of SV			Bias of iAVA		
	USH			USH		
	Yes (n = 113)	No (n = 246)	P value	Yes (n = 113)	No (n = 246)	P value
3DE - Doppler	−11.0 (−17.6 to −4.3)	−7.0 (−14.5 to 0.1)	.0005	−0.14 (−0.28 to −0.04)	−0.09 (−0.19 to 0)	.0127
2DE - Doppler	−10.7 (−20.8 to −1.7)	−6.3 (−12.9 to 1.8)	<.0001	−0.13 (−0.28 to 0)	−0.08 (−0.29 to 0.03)	.0022
3DE - 2DE	0.4 (−4.1 to 5.4)	−1.0 (−6.8 to 4.7)	.1916	0 (−0.06 to 0.07)	−0.01 (−0.10 to 0.06)	.1812

Data are expressed as median (25th to 75th percentile).

Table 3 Characteristics of AS subtype according to the classification by 2D, 3D, and Doppler echocardiography

	All	MAS	LFLPG-SAS	NFLPG-SAS	HPG-SAS	P
2DE:						
Number (%)	358 (100)	112 (31)	107 (30)	65 (18)	74 (21)	
SVI, mL/m²	36 (31-43)	42 (35-52)	29 (26-32)	40 (37-42)	40 (31-47)	<.001
iAVA, cm²/m²	0.48 (0.40-0.64)	0.75 (0.64-0.93)	0.44 (0.38-0.50)	0.49 (0.43-0.55)	0.36 (0.30-0.41)	<.001
Zva, mm Hg/mL/m²	4.60 (3.78-5.47)	3.81 (3.06-4.61)	5.53 (4.86-6.44)	4.31 (3.85-4.64)	4.81 (3.79-5.99)	<.001
LV mass index, g/m²	105 (85-129)	103 (85-135)	96 (80-113)	108 (89-130)	126 (102-146)	<.001
3DE:						
Number (%)	349 (97)	101 (29)	102 (29)	73 (21)	73 (21)	
SVI, mL/m²	36 (31-42)	41 (36-47)	29 (27-32)	37 (36-42)	39 (35-49)	<.001
iAVA, cm²/m²	0.50 (0.39-0.63)	0.73 (0.65-0.89)	0.43 (0.36-0.51)	0.51 (0.45-0.56)	0.36 (0.30-0.41)	<.001
Zva, mm Hg/mL/m²	4.60 (3.87-5.37)	4.03 (3.30-4.63)	5.47 (4.84-6.29)	4.27 (3.82-4.82)	4.75 (3.98-5.78)	<.001
LV mass index, g/m²	79 (67-94)	80 (68-94)	70 (58-81)	81 (72-97)	90 (73-108)	<.001
Doppler echocardiography:						
Number (%)	354 (99)	179 (51)	37 (11)	69 (19)	69 (19)	
SVI, mL/m²	44 (37-53)	49 (41-57)	31 (28-34)	41 (38-45)	47 (41-54)	<.001
iAVA, cm²/m²	0.60 (0.46-0.80)	0.79 (0.68-0.97)	0.44 (0.40-0.54)	0.62 (0.45-0.56)	0.42 (0.36-0.48)	<.001
Zva, mm Hg/mL/m²	3.73 (3.11-4.48)	3.30 (2.86-3.83)	5.20 (4.37-5.92)	4.02 (3.67-4.53)	4.06 (3.34-4.74)	<.001

Data are expressed by median (25th to 75th percentile).

subgroups according to 2DE (A), 3DE (B), and Doppler classifications (C). All group classifications using the three different methods had a significant predictive power for future MACEs among the four AS subgroups, showing that HPG-SAS had the worst prognosis, followed by NFLPG-SAS. Subgroup analysis revealed all group classification worked well in patients with preserved LVEF (≥50%) as well as in those with impaired LVEF (<50%; Supplemental Figure 1, available at www.onlinejase.com). The impacts of USH and image quality on the risk stratification among AS groups by each method are shown in Figure 4. Poor image quality attenuated the predictive power in 2D/3D echocardiographic assessments. In contrast, the presence of USH diminished the utility of Doppler echocardiographic assessment in the risk stratification.

The univariate echocardiographic parameters related to SVI for predicting MACE are shown in Table 4. This analysis revealed that only iAVA was a significant predictor on 2DE and 3DE. In Doppler echocardiography, iAVA, SVI, and Zva were significant predictors for future MACEs.

The ROC analysis revealed that the best cutoff iAVA values using 2DE, 3DE, and Doppler echocardiography for predicting MACEs were 0.48, 0.47, and 0.56 cm²/m², respectively. Comparison of the paired AUCs showed that the AUC of Doppler echocardiography (0.78) was significantly larger than the AUC of 2DE (0.73, $P = .035$), but it was not different from that of 3DE (0.75, $P = .084$; Figure 5). In patients with USH, a different trend in AUC was observed, although the difference did not reach significance: the value by 2DE (AUC = 0.73) and 3DE (AUC = 0.73) was higher than that by Doppler echocardiography (AUC = 0.69; Supplemental Figure 2, available at www.onlinejase.com).

NRI analysis revealed that iAVA by Doppler echocardiography had a significant improvement of classification for the outcome compared with iAVA by 2DE (NRI = 0.294; $P < .001$) and iAVA by 3DE (NRI = 0.224; $P = .003$).

Reliability of SV Measurements among the Three Methods

The intraobserver variability values and ICC for the measurements of 2DE SV, 3DE SV, and Doppler SV were 3.1% ± 2.3%, 5.9% ± 7.6%, and 9.7% ± 7.1% and 0.95, 0.95, and 0.84, respectively. The corresponding interobserver variability values and ICC were 10.7% ± 9.1%, 8.2% ± 10.5%, and 11.3% ± 7.3% and 0.73, 0.84, and 0.82, respectively.

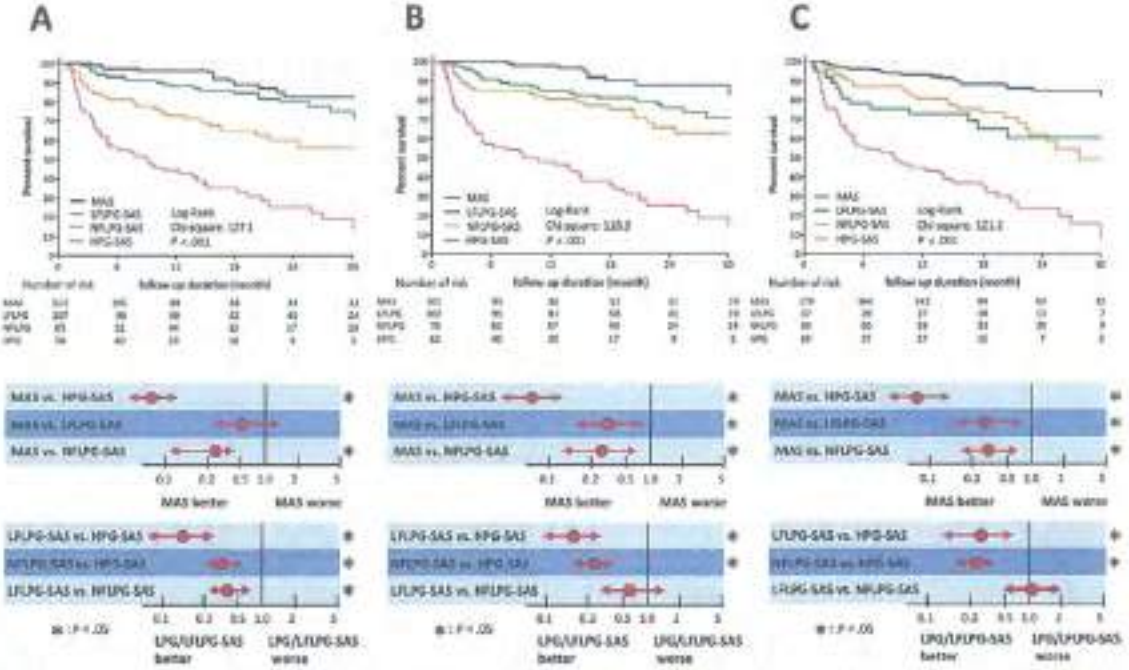

Figure 3 Kaplan-Meier analysis for MACEs among the four AS subtypes according to 2DE (A), 3DE (B), and Doppler echocardiography (C). *Lower panels* show the forest plot depicting the HR (*red dot*) and 95% CI (*arrows*).

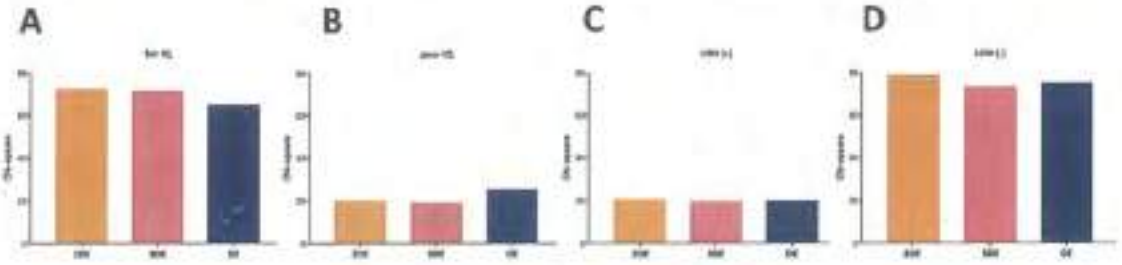

A: fair IQ, n=257

	2DE	3DE	Doppler
	HR (95% CI)	HR (95% CI)	HR (95% CI)
LFLPG	1.71 (0.76-4.09)	3.16 (1.31-8.34)*	3.58 (1.55-7.74)*
NFLPG	4.48 (2.11-10.3)*	5.13 (2.29-13.0)*	3.28 (1.73-6.23)*
HPG	11.2 (5.70-24.6)*	15.5 (7.35-37.9)*	8.65 (5.05-15.4)*

B: poor IQ, n=101

	2DE	3DE	Doppler
type	HR (95% CI)	HR (95% CI)	HR (95% CI)
LFLPG	1.85 (0.49-8.78)	1.37 (0.30-7.69)	3.13 (0.74-13.3)
NFLPG	2.54 (0.56-12.9)	0.63 (0.08-5.29)	2.51 (0.66-10.1)
HPG	11.6 (3.60-51.6)*	7.00 (1.86-45.5)*	18.0 (5.91-66.3)*

C: USH (+), n=113

	2DE	3DE	Doppler
type	HR (95% CI)	HR (95% CI)	HR (95% CI)
LFLPG	2.05 (0.56-9.52)	3.52 (0.88-23.3)	1.35 (0.21-5.14)
NFLPG	4.21 (1.10-20.0)*	2.91 (0.63-20.4)	2.83 (0.86-8.36)
HPG	9.06 (3.00-39.1)*	11.5 (3.26-72.7)*	6.83 (2.95-16.6)*

D: USH (-), n=246

	2DE	3DE	Doppler
type	HR (95% CI)	HR (95% CI)	HR (95% CI)
LFLPG	1.63 (0.72-3.92)	2.01 (0.85-5.28)	4.11 (1.80-9.20)*
NFLPG	4.00 (1.86-9.28)*	3.85 (1.67-9.90)*	3.39 (1.69-7.02)*
HPG	13.9 (7.00-30.8)*	15.7 (7.38-38.6)*	13.6 (7.35-26.7)*

Figure 4 Impact of image quality and USH on the prognostic predictive power of AS classification in univariate Cox proportional hazards analysis. (A) Good or fair image quality; (B) poor image quality; (C) USH; (D) no USH. *Bottom* tables show the HRs of each subgroup against MAS. *Asterisk* indicates significant difference. *IQ*, Image quality.

Table 4 Univariate Cox proportional hazard analysis for predicting MACE among the three methods

	2DE		3DE		Doppler echocardiography	
	HR (95% CI)	P	HR (95% CI)	P	HR (95% CI)	P
iAVA	0.022 (0.006-0.080)	<.0001	0.007 (0.001-0.028)	<.0001	0.009 (0.003-0.030)	<.0001
SVI	1.012 (0.995-1.029)	.1527	1.019 (0.999-1.039)	.0683	0.985 (0.970-0.999)	.0412
Zva	1.006 (0.883-1.136)	.9225	1.109 (0.949-1.285)	.1887	1.358 (1.159-1.576)	.0002

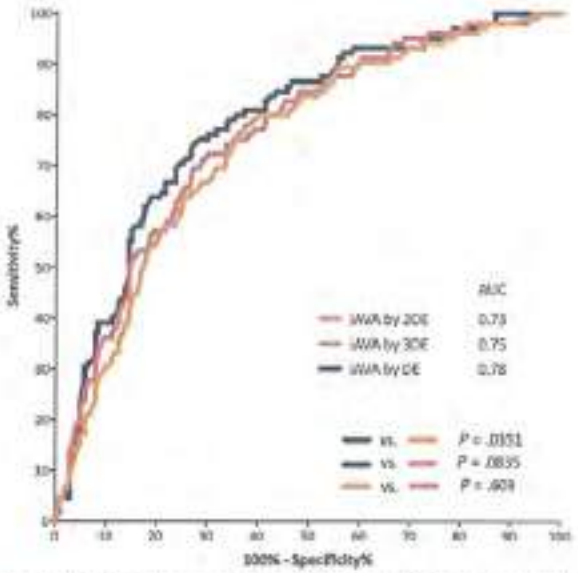

Figure 5 Comparison of the AUC of iAVA measured by 2DE/3DE and Doppler echocardiography. *DE*, Doppler echocardiography.

DISCUSSION

The major findings of this study are summarized as follows: (1) SV assessed using Doppler echocardiography was significantly larger than that measured using 2DE and 3DE, and any paired comparisons showed a modest correlation at best; (2) group classification among the three methods was significantly different (i.e., the Doppler approach had a higher prevalence of MAS and a lower prevalence of LFLPG-SAS); (3) the prognostic strength of AS severity grading among the three methods was nearly identical for predicting MACEs; and (4) the prognosis of LFLPG-SAS was intermediate between MAS and NFLPG-SAS, regardless of the method we used in our cohort of patients with asymptomatic AS.

Previous Studies

An accurate estimation of AS severity is of paramount importance for managing patients with asymptomatic AS. Doppler echocardiography is the primary imaging modality used to calculate AVA.[1,2] In addition to recording the highest aortic valve jet velocity signal, it requires two reliable measurements, the LVOT velocity and LVOT diameter, both of which pose a risk of measurement errors. Subtle changes in the sampling point on the pulsed-wave Doppler examination across the LVOT produce alterations in the velocity that are not clinically negligible, especially in patients who have a distorted LVOT shape, such as USH, which is commonly seen in elderly patients with AS.[5,12] LVOT diameter determination is most vulnerable to measurement error, because it is squared in the continuity equation.[2,18] The continuity equation assumes that the LVOT cross-sectional area is circular, whereas several recent studies have demonstrated that the LVOT cross-sectional area is not circular but rather ellipsoid in most patients with AS.[5,19,20] The LVOT diameter measured using 2DE approximately corresponds to the minor axis of this ellipsoid. Furthermore, the shape of the LVOT is not homogenous during the cardiac cycle, even if patients do not have LVOT obstruction.[21] Hence, Doppler estimation of SV has a risk of both over- and underestimation.

The 2DE determination of SV using the biplane Simpson's formula is seldom used to assess the severity of AS because of the belief that 2DE often underestimates LV volumes due to malalignment of the 2DE cutting plane.[7] With the steady improvement in temporal and spatial resolutions of 2DE image quality, confidence in tracing the endocardial border is much more enhanced compared with earlier, when several publications revealed that 2DE underestimated LV volumes against cardiovascular magnetic resonance as a reference.[7] Thus, it is worth reevaluating 2DE-determined SV to assess the severity of AS.

Theoretically, 3DE-determined LV volumes are more accurate than 2DE-derived LV volumes, because 3DE data sets encompass the whole part of the left ventricle, and 3DE measurements of LV volumes do not require any geometric assumptions. Some studies have sought to establish the accuracy and reliability of 3DE measurements of the left and right heart chambers.[7,9] However, 2DE image quality extracted from the 3DE data sets is still inferior to the corresponding image quality obtained by 2DE, even for those obtained using the latest 3DE scanners, and this limitation could adversely affect the measurement of SV. Thus, all three modalities used to evaluate AS severity have their important shortcomings.

Current Study

Doppler-derived SV was significantly larger than 2DE- or 3DE-derived SV in a large number of patients with asymptomatic AS. It is important to note that any paired comparison had weak to modest correlations. Thus, differences in SV between the two modalities are not predictable. Particularly, larger differences in SVI and iAVA between 2DE/3DE and Doppler echocardiography were observed in patients with USH than in patients without USH. This finding was in agreement with a previous study.[12] The differences in SVI also affected AS severity grading. Although the prevalences of HPG-SAS and NFLPG-SAS were similar among the three methods, the frequencies of the other two AS subgroups were quite different between 2DE/3DE and Doppler echocardiography, with the Doppler approach characterizing a higher percentage of MAS and a lower

percentage of LFLPG-SAS, in contrast to the lower prevalence of MAS and a relatively higher prevalence of LFLPG-SAS assessed using 2DE/3DE methods. Since all methods have some shortcomings, this suggests that the 2DE and 3DE methods were underestimating SV and markedly misclassifying these cases that were actually MAS or that the Doppler method was overestimating SV and misclassifying some cases that were actually LFLPG-SAS. This finding has significant practical implications for AS subgroup classifications performed according to flow and pressure gradient status.

We are reassured that the survival analysis among the four AS grades as assessed using 2DE, 3DE, and Doppler echocardiography revealed similar event-free curves with equivalent statistical power in patients with asymptomatic AS. When we used 3DE or Doppler criteria, asymptomatic MAS had a significantly better survival than the other three subtypes of asymptomatic SAS. Low-pressure-gradient asymptomatic SAS irrespective of flow status had a significantly better MACE-free survival than asymptomatic HPG-SAS, consistent with some previous studies[22-24] but contrary to others.[16] Overall, the same trend was also observed in the use of the 2DE criteria. Regarding LFLPG-SAS, there is a growing consensus that patients with symptomatic paradoxical LFLPG-SAS have a poor prognosis and should be recommended for AVR.[22,25-28] However, clinically important issues regarding the prognosis of asymptomatic paradoxical LFLPG-SAS remain to be settled. Our study demonstrated that the prognosis of asymptomatic paradoxical LFLPG-SAS patients was roughly intermediate regardless of the method used and provides helpful information to facilitate discussion about this clinical issue. Another notable finding was that the event rate of patients with asymptomatic MAS classified by the Doppler method was higher than that of those classified by 3DE (1-year event rate, 7% for Doppler method vs 2% for 3DE). This indicates that the Doppler method may overestimate SV in some cases, which misclassifies SAS as MAS, resulting in the worse prognosis compared with the 3DE method. These findings were in agreement with the previous study where we reported the usefulness of additional classification by 3DE to discriminate patients with a poor prognosis among patients initially classified as MAS by Doppler methods.[17] Gutierrez-Chico *et al*[29] demonstrated, with the use of cardiac catheterization, that the accuracy of AVA calculated by 3DE was sustained irrespective of AS grade, while that obtained by Doppler echocardiography and 2DE was reduced according to increased AVA. Our study may support this finding from the perspective of prognosis. In addition to these findings regarding AS classification and risk stratification among the three approaches, our study showed that image quality and USH may affect the reliability of risk stratification. Together, our results suggest that all three modalities work very well in predicting future cardiovascular events in patients with asymptomatic AS, although several noteworthy advantages and shortcomings exist for each approach.

Indexed AVA was a significant parameter in predicting MACEs in all three methods. Interestingly, the cutoff value of iAVA for MACEs was 0.56 cm^2/m^2 on Doppler echocardiography, which is quite similar to the current cutoff value of iAVA used to define SAS. In contrast, the cutoff iAVA values of 0.48 and 0.46 cm^2/m^2 derived from the 2DE/3DE approaches raise concern regarding the establishment of new cutoff values for iAVA used to define severe AS, when SV is measured using 2DE or 3DE in the clinical setting.

NRI analysis revealed that Doppler echocardiography-determined iAVA had a significantly better improvement of classification for the outcome than iAVA assessed by 2DE or 3DE. Specifically, compared with 2DE-derived iAVA, Doppler echocardiography-derived iAVA improved reclassification for those with MACEs by 15.2% and for those without MACEs by 14.2%, resulting in a significantly improved NRI of 29.4%. Compared with 3DE-derived iAVA, Doppler echocardiography-derived iAVA improved reclassification for those with events by 16.2% and for those without events by 6.2%, resulting in a significantly improved NRI of 22.4%. The results support the continued use of Doppler echocardiography to assess flow status and AS severity in patients with asymptomatic AS. However, 2DE and 3DE predicted outcome better than Doppler echocardiography in patients with USH, although there was no statistical significance. Since USH is not rare in patients with AS, further study is required to clarify this point.

Clinical Implications

Since SV assessed using three modalities (2DE, 3DE, and Doppler echocardiography) usually differs, resulting in a different prevalence of AS severity grades, each modality is not interchangeable for the assessment of AS severity. The selection of one modality is reliant upon the preference of the examiner and local availability of 3DE, because the prognostic power was similar among all three modalities in patients with asymptomatic AS. Hence, when the examiner selects one of the three approaches to assess patients with AS at the first presentation, the advantages and limitations of each approach, such as feasibility, reliability, and effect of image quality, as well as LV geometry, should be taken into consideration. Lastly, the same approach should consistently be used to evaluate AS severity in the same patient in longitudinal examinations.

Study Limitations

This study had several limitations. First, although we directly asked the patients about their symptomatic status during the echocardiography examination, it is possible that not all patients may be truly asymptomatic, given that limited exercise capacity due to advanced aging and comorbidities could mask their symptoms. Second, 3DE has also been used to improve the accuracy of the continuity equation for AVA calculations by facilitating direct planimetry of the LVOT area rather than deriving this from 2DE. We did not incorporate this approach, because the suboptimal image quality with transthoracic 3DE may limit the accuracy of the LVOT area measurement and transesophageal 3DE is usually required for accurate measurements.[19,20] Third, the presence of mitral regurgitation may affect the SV differences between 2DE/3DE and Doppler echocardiography. The fact that Doppler SVI was larger than 3DE or 2DE SVI confirms that significant mitral regurgitation was not present in our patients as the total SV measured by imaging did not exceed the forward SV measured by Doppler, and if significant mitral regurgitation was present the total SV would be expected to be higher than forward SV. Fourth, we used 3DE speckle-tracking software to obtain LV volumes. Thus, our results could not be extrapolated when we use vendor-specific 3D volumetric tool. Fifth, there was no reference standard to determine the accuracy of echocardiography-determined SV. Thus, this study did not provide any information regarding which method was the most accurate for SV measurements. Furthermore, for the acquisition of 2DE/3DE data sets, we used two different ultrasound machines; hence, a risk of intervendor variability of LV parameters exists, although we used vendor-independent 3DE speckle-tracking software.

CONCLUSION

SV, as measured using 2DE, 3DE, and Doppler echocardiography, was significantly different, and the findings profoundly affected AS severity classification in patients with asymptomatic AS. Although AS classification changed depending on the method used for SV assessment, all of the approaches were similar in the assessment of prognosis in these asymptomatic patients. Since there is no gold standard imaging modality for quantitating AS severity, examiners should select one of the three methods while taking into consideration the characteristics of the patients with AS and familiarity of the specific method. One should use the same method to perform longitudinal examinations in the same patient.

ACKNOWLEDGMENTS

The authors thank Drs. Kyoko Otani, Yuichiro Kado, and Tomofumi Nakatsukasa for preparing the patient data.

SUPPLEMENTARY DATA

Supplementary data related to this article can be found at https://doi.org/10.1016/j.echo.2018.05.006.

REFERENCES

1. Baumgartner H, Hung J, Bermejo J, Chambers JB, Edvardsen T, Goldstein S, et al. Recommendations on the echocardiographic assessment of aortic valve stenosis: a focused update from the European Association of Cardiovascular Imaging and the American Society of Echocardiography. J Am Soc Echocardiogr 2017;30:372-92.
2. Pibarot P, Clavel MA. Doppler echocardiographic quantitation of aortic valve stenosis: a science in constant evolution. J Am Soc Echocardiogr 2016;29:1019-22.
3. Caballero L, Saura D, Oliva-Sandoval MJ, Gonzalez-Carrillo J, Espinosa MD, Garcia-Navarro M, et al. Three-dimensional morphology of the left ventricular outflow tract: impact on grading aortic stenosis severity. J Am Soc Echocardiogr 2017;30:28-35.
4. Montealegre-Gallegos M, Matyal R, Khabbaz KR, Owais K, Maslow A, Hess P, et al. Heterogeneity in the structure of the left ventricular outflow tract: a 3-dimensional transesophageal echocardiographic study. Anesth Analg 2016;123:290-6.
5. Pibarot P, Clavel MA. Left ventricular outflow tract geometry and dynamics in aortic stenosis: implications for the echocardiographic assessment of aortic valve area. J Am Soc Echocardiogr 2015;28:1267-9.
6. Hahn RT, Pibarot P. Accurate measurement of left ventricular outflow tract diameter: Comment on the updated recommendations for the echocardiographic assessment of aortic valve stenosis. J Am Soc Echocardiogr 2017;30:1038-41.
7. Mor-Avi V, Sugeng L, Weinert L, MacEneaney P, Caiani EG, Koch R, et al. Fast measurement of left ventricular mass with real-time three-dimensional echocardiography: comparison with magnetic resonance imaging. Circulation 2004;110:1814-8.
8. Mor-Avi V, Sugeng L, Lang RM. Real-time 3-dimensional echocardiography: an integral component of the routine echocardiographic examination in adult patients? Circulation 2009;119:314-29.
9. Sugeng L, Mor-Avi V, Weinert L, Niel J, Ebner C, Steringer-Mascherbauer R, et al. Multimodality comparison of quantitative volumetric analysis of the right ventricle. J Am Coll Cardiol Imaging 2010;3:10-8.
10. Nagata Y, Takeuchi M, Wu VC, Izumo M, Suzuki K, Sato K, et al. Prognostic value of LV deformation parameters using 2D and 3D speckle-tracking echocardiography in asymptomatic patients with severe aortic stenosis and preserved LV ejection fraction. J Am Coll Cardiol Imaging 2015;8:235-45.
11. Lang RM, Badano LP, Mor-Avi V, Afilalo J, Armstrong A, Ernande L, et al. Recommendations for cardiac chamber quantification by echocardiography in adults: an update from the American Society of Echocardiography and the European Association of Cardiovascular Imaging. J Am Soc Echocardiogr 2015;28:1-39.e14.
12. Sato K, Seo Y, Ishizu T, Nakajima H, Takeuchi M, Izumo M, et al. Reliability of aortic stenosis severity classified by 3-dimensional echocardiography in the prediction of cardiovascular events. Am J Cardiol 2016;118:410-7.
13. Rudski LG, Lai WW, Afilalo J, Hua L, Handschumacher MD, Chandrasekaran K, et al. Guidelines for the echocardiographic assessment of the right heart in adults: a report from the American Society of Echocardiography endorsed by the European Association of Echocardiography, a registered branch of the European Society of Cardiology, and the Canadian Society of Echocardiography. J Am Soc Echocardiogr 2010;23:685-713.
14. Mizukoshi K, Takeuchi M, Nagata Y, Addetia K, Lang RM, Akashi YJ, et al. Normal values of left ventricular mass index assessed by transthoracic three-dimensional echocardiography. J Am Soc Echocardiogr 2016;29:51-61.
15. Dumesnil JG, Pibarot P, Carabello B. Paradoxical low flow and/or low gradient severe aortic stenosis despite preserved left ventricular ejection fraction: implications for diagnosis and treatment. Eur Heart J 2010;31:281-9.
16. Bavishi C, Balasundaram K, Argulian E. Integration of flow-gradient patterns into clinical decision making for patients with suspected severe aortic stenosis and preserved LVEF: a systematic review of evidence and meta-analysis. J Am Coll Cardiol Imaging 2016;9:1255-63.
17. Pencina MJ, D'Agostino Sr RB, D'Agostino RB Jr, Vasan RS. Evaluating the added predictive ability of a new marker: from area under the ROC curve to reclassification and beyond. Stat Med 2007;27:157-72.
18. Michelena HI, Margaryan E, Miller FA, Eleid M, Maalouf J, Suri R, et al. Inconsistent echocardiographic grading of aortic stenosis: is the left ventricular outflow tract important? Heart 2013;99:921-31.
19. Otani K, Takeuchi M, Kaku K, Sugeng L, Yoshitani H, Haruki N, et al. Assessment of the aortic root using real-time 3D transesophageal echocardiography. Circ J 2010;74:2649-57.
20. Saitoh T, Shiota M, Izumo M, Gurudevan SV, Tolstrup K, Siegel RJ, et al. Comparison of left ventricular outflow geometry and aortic valve area in patients with aortic stenosis by 2-dimensional versus 3-dimensional echocardiography. Am J Cardiol 2012;109:1626-31.
21. Halpern EJ, Gupta S, Halpern DJ, Wiener DH, Owen AN. Characterization and normal measurements of the left ventricular outflow tract by ECG-gated cardiac CT: implications for disorders of the outflow tract and aortic valve. Acad Radiol 2012;19:1252-9.
22. Maes F, Boulif J, Pierard S, de Meester C, Melchior J, Gerber B, et al. Natural history of paradoxical low-gradient severe aortic stenosis. Circ Cardiovasc Imaging 2014;7:714-22.
23. Yamashita E, Takeuchi M, Seo Y, Izumo M, Ishizu T, Sato K, et al. Prognostic value of paradoxical low-gradient severe aortic stenosis in Japan: Japanese Multicenter Aortic Stenosis Study, Retrospective (JUST-R) Registry. J Cardiol 2015;65:360-8.
24. Jander N, Minners J, Holme I, Gerdts E, Boman K, Brudi P, et al. Outcome of patients with low-gradient "severe" aortic stenosis and preserved ejection fraction. Circulation 2011;123:887-95.
25. Cassiano R, Teixeira RR, Vieira MJ, Goçalves L. Paradoxical aortic stenosis: A systematic review. Rev Port Cardiol 2017;36:287-305.
26. Dayan V, Vignolo G, Magne J, Clavel MA, Mohty D, Pibarot P. Outcome and impact of aortic valve replacement in patients with preserved LVEF and low-gradient aortic stenosis. J Am Coll Cardiol 2015;66:2594-603.
27. Pibarot P, Clavel MA. Management of paradoxical low-flow, low-gradient aortic stenosis: need for an integrated approach, including assessment of

symptoms, hypertension, and stenosis severity. J Am Coll Cardiol 2015; 65:67-71.

28. Bonow RO, Brown AS, Gillam LD, Kapadia SR, Kavinsky CJ, Lindman BR, et al. ACC/AATS/AHA/ASE/EACTS/HVS/SCA/SCAI/SCCT/SCMR/STS 2017 appropriate use criteria for the treatment of patients with severe aortic stenosis: A report of the American College of Cardiology Appropriate Use Criteria Task Force, American Association for Thoracic Surgery, American Heart Association, American Society of Echocardiography, European Association for Cardio-Thoracic Surgery, Heart Valve Society, Society of Cardiovascular Anesthesiologists, Society for Cardiovascular Angiography and Interventions, Society of Cardiovascular Computed Tomography, Society for Cardiovascular Magnetic Resonance, and Society of Thoracic Surgeons. J Am Coll Cardiol 2017;70:2566-98.

29. Gutierrez-Chico JL, Zamorano JL, Prieto-Moriche E, Hernandez-Antolin RA, Bravo-Amaro M, Perez de Isla L, et al. Real-time three-dimensional echocardiography in aortic stenosis: A novel, simple, and reliable method to improve accuracy in area calculation. Eur Heart J 2008;29:1296-306.

SUPPLEMENTARY MATERIAL

Among 359 study patients in this study, 28 patients had undergone both CMR and 2DE/3DE and Doppler echocardiography (DE) on the same day. CMR LV volumes were measured from multiple short-axis steady state fully precession images using an analytical software (Segment v2.0, Medviso, Lund, Sweden), and the disk summation method was used for the calculation of the LV end-diastolic and end-systolic volume (LVEDV, LVESV). We compared SV assessed by 2DE, 3DE, and DE in 28 patients. Results are shown in Supplemental Table 1.

Although there was a good correlation of SV between 2DE/3DE and CMR ($r = 0.85$ and 0.89), 2DE/3DE-derived SV was significantly smaller than that measured by CMR. Doppler-derived SV was not different to that measured by CMR with modest correlation ($r = 0.69$).

We also compared LV volumes, LVEF, and SV assessed using the vendor-independent software (TomTec) and the vendor-specific software (Philips, QLAB, 3DQ adv; GE, EchoPac PC, 4D AutoLVQ) using the same 3DE data sets in 50 study patients (36 Philips data sets and 14 GE data sets). Results are shown in Supplemental Table 2. The results suggest that the TomTec software provided similar values of LV volumes, LVEF, and SV compared with the vendor-specific software.

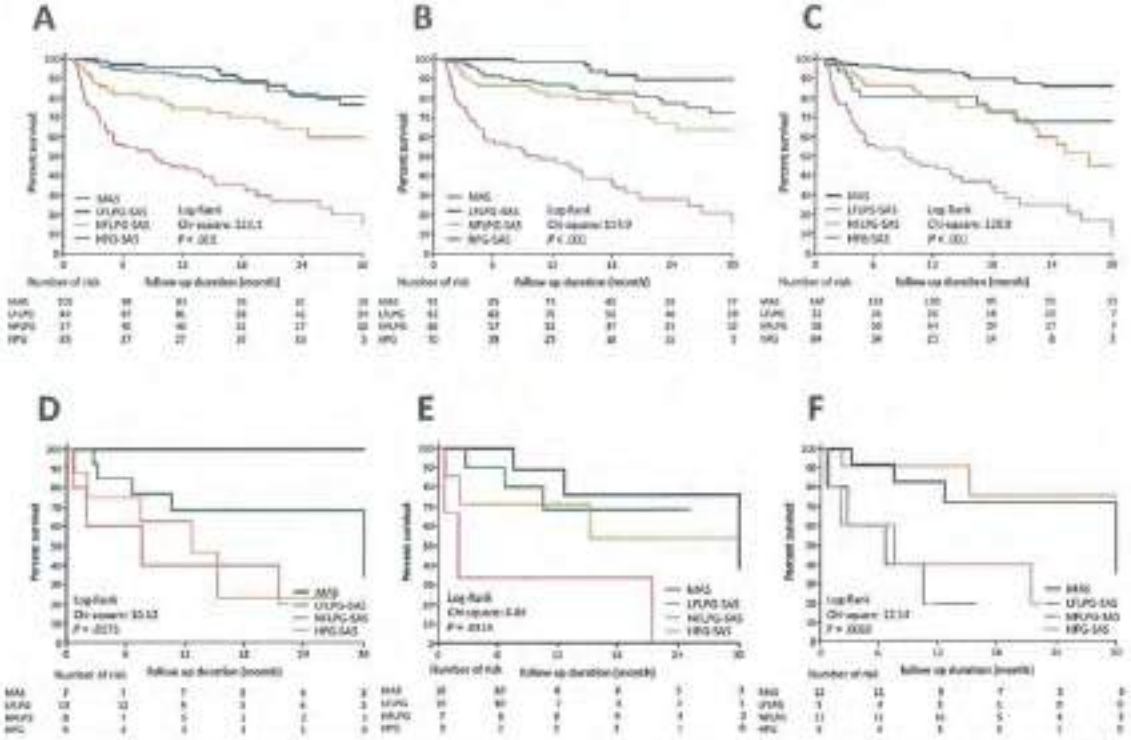

Supplemental Figure 1 Kaplan-Meier analysis for MACEs in patients with preserved LVEF (*upper panel*) and those with impaired LVEF (*lower panel*) according to 2DE (**A** and **D**), 3DE (**B** and **E**), and Doppler echocardiography (**C** and **F**).

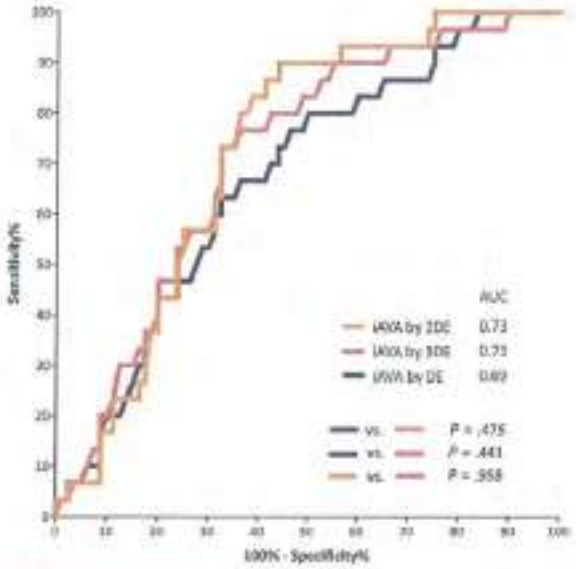

Supplemental Figure 2 Impact of USH on the AUC of iAVA assessed by three methods. The figure shows ROC curves of the three methods in asymptomatic patients with AS who had USH. *DE*, Doppler echocardiography.

Supplemental Table 1 Comparison of LV volumes and ejection fraction analysis among three methods against CMR imaging as a reference ($N = 28$)

	CMR	2DE	3DE	Doppler echocardiography
LV end-diastolic volume, mL	120 ± 37	105 ± 32	106 ± 37	
P (vs CMR)		<.001	<.001	
r		0.93	0.95	
Bias (95% LOA)		−15 (±22)	−14 (±19)	
LV end-systolic volume, mL	51 ± 32	44 ± 21	46 ± 25	
P (vs CMR)		.007	.008	
r		0.97	0.97	
Bias (95% LOA)		−7 (±21)	−6 (±17)	
LVEF, %	60 ± 15	59 ± 11	59 ± 11	
P (vs CMR)		.487	.571	
r		0.93	0.95	
Bias (95% LOA)		−0.8 (±7.1)	−0.6 (±9.4)	
SV, mL	69 ± 20	61 ± 19	61 ± 19	74 ± 24
P (vs CMR)		.001	<.001	.092
r		0.85	0.89	0.69
Bias (95% LOA)		−8 (±13)	−8 (±13)	6 (±26)

LOA, Limit of agreement.

Supplemental Table 2 Comparison of LV volumes, ejection fraction, and SV measured by Vendor-Independent Software and Vendor-Specific Software ($N = 50$)

	TomTec	Philips/GE	*P*	Bias	ICC
LV end-diastolic volume, mL	116 ± 34	115 ± 34	.5284	−1 ± 11	0.95
LV end-systolic volume, mL	52 ± 24	52 ± 24	.6891	0 ± 7	0.95
LVEF, %	57 ± 9	56 ± 9	.0652	-1 ± 4	0.91
SV, mL	64 ± 15	63 ± 17	.1453	-1 ± 6	0.92

Keynote Lecture Series

Transcatheter mitral valve chord repair

Vedran Savic[1#], Alberto Pozzoli[1#], Gökhan Gülmez[1], Halil Demir[1], Nikola Batinkov[1], Shingo Kuwata[1], Alberto Weber[2], Rolf Vogel[3], Felix Tanner[1], Michel Zuber[1], Francesco Maisano[1], Maurizio Taramasso[1]

[1]Heart Valve Clinic, University Hospital of Zürich, University of Zürich, Zürich, Switzerland; [2]Heart Surgery, HerzZentrum Hirslanden Zürich, Zürich, Switzerland; [3]Department of Cardiology, Bürgerspital Solothurn, Solothurn, Switzerland

[#]These authors contributed equally to this work.

Correspondence to: Maurizio Taramasso. University Hospital of Zurich, Rämistrasse, 100 Zurich, Switzerland. Email: Maurizio.Taramasso@usz.ch.

The field of mitral valve disease diagnosis and management is rapidly evolving. New understanding of pathophysiology and improvements in the adoption of sophisticated multimodality imaging modalities have led to early diagnosis and to more complex treatment. The most common cause of mitral regurgitation (MR) in the western world is in the primary alteration of the valve, which leads to degenerative leaflet prolapse due to chordal elongation or rupture and annular dilatation. Untreated, significant MR has a negative impact prognosis, leading to reduction of survival. In the setting of degenerative MR, surgical repair currently represents the standard of care. Treatment of asymptomatic patients with severe MR in the Valve Center of Excellence, in which successful repair reaches more than 95% and surgical mortality less than 1%, symbolizes the direction for the next years. Transcatheter mitral valve repair with different devices, more recently the chordal replacement ones, is providing good outcomes and became a therapeutic option in high-risk patients with degenerative MR. In the future, more advances are expected from further development of interventional techniques, careful evaluation and better patient selection. This review will focus on long-term surgical outcomes of mitral valve repair with artificial chordae and on the emerging transcatheter chordal repair devices as therapeutic options for degenerative MR patients.

Keywords: Mitral valve (MV); transcatheter; chordal repair; mitral regurgitation (MR)

Submitted Feb 27, 2018. Accepted for publication Jul 27, 2018.
doi: 10.21037/acs.2018.09.09
View this article at: http://dx.doi.org/10.21037/acs.2018.09.09

Introduction

One of the most common valvular disorders is mitral regurgitation (MR), which has a prevalence of 2% in the general population and is present in 7% of the population 75 years of age or older (1,2). The most frequent cause of MR in the developed countries is degenerative mitral valve (MV) disease, in which there is myxomatous degeneration of the MV leaflets, elongation and redundant chordal apparatus (3). Thickened redundant leaflets will prolapse back into the left atrium causing malcoaptation of leaflet edges and subsequent regurgitation (*Figure 1*). Rupture of chordae is not uncommon in older patients with MR, which will then cause a further increase in the severity of MR because of unsupported segments of the MV leaflets (*Figure 2*). Patients presenting with severe primary MR has a negative prognostic impact, which also decreases the survival (mortality rate more than 6.3% per year compared with the expected survival rate) (4).

The current standard of care in this setting is surgical repair (1). Treatment of asymptomatic patients with severe MR in Valve Center of Excellence, in which successful repair reaches more than 95% and surgical mortality less than 1%, represents the ideal setting to manage this disease in the next 5 years. Transcatheter MV devices for chordal replacement are emerging therapies with very satisfactory outcomes. Interventional techniques, better patient selection and intraoperative imaging guidance are certainly expected to advance in the near future. In this review, the primary focus will be on the surgical outcomes of chordal repair—as a conventional method of care—and transcatheter chordal repair as an alternative, equivalent therapeutic option.

© Annals of Cardiothoracic Surgery. All rights reserved.

Figure 1 Echo view of a prolapse without flail of the posterior mitral leaflet (central segment). The three panels show, from top to bottom, the morphologic transoesophageal 2D echo aspect of a posterior prolapse, the color-Doppler analysis showing an eccentric jet causing severe regurgitation and a 3D en face view from the left atrium of the mitral leaflet (with the prolapse of P2).

MV anatomy and prevalence of mitral leaflet prolapse

The MV consists of two leaflets, separated by two commissures, a fibrous annulus, a subvalvular apparatus with chordae tendineae and two groups of papillary muscles attached to the left ventricle (5). The two leaflets are connected by chordae tendineae to the anterolateral and to the posteromedial papillary muscles. Three different types of chordae tendineae can be described: marginal or primary chordae (inserted into the free margin of the leaflets), basal or secondary chordae (insert near the annular attachment) and tertiary chordae (insert into the central part of the leaflets). The length of chordae regulates overall chordae tension, mitral haemodynamics and the coaptation area of the mitral leaflets. It has been shown that the chordae which are 10% longer than normal double the chordal tension, but do not make the MV incompetent, which proves that even minor changes in the length can have significant effects on the tension of the chordae.

The prevalence of mitral prolapse is 2–3% and its most common complication is MR (6). The most common etiology of mitral prolapse derives from the myxomatous degeneration, which is an intermediate form of disease which ranges from fibroelastic deficiency with limited prolapse, to more severe forms of multiple bileaflet prolapse with excessive tissue, such as Barlow's disease (7). A severe form is represented by leaflet flail, where no coaptation can be detected during systole. Most commonly, the posterior leaflet is affected by this condition and is associated with torn chordae, or even worse, ruptured papillary muscle.

Preoperative and intraoperative imaging guidance

Two-dimensional and Doppler echocardiography have become standard for the assessment of patients presenting with degenerative MR. Echocardiography is a diagnostic gold standard to identify mitral valve prolapse (MVP) with flail leaflet, determination of the severity of MR and planning. Transthoracic echocardiography (TTE) and transesophageal echocardiography (TEE) are complementary imaging methods, with the latter fundamental for intraprocedural guidance of these transcatheter chordal repairs. Heart multislice computed tomography (MSCT) and cardiac magnetic resonance imaging (MRI) offer complementary information during preoperative planning. MSCT is very useful for those therapies targeting the annulus, to evaluate annular structure and dimensions, quality and amount of annular tissue and its relationship with the left circumflex coronary artery. The MRI allows better visualization of the dynamic MV anatomy throughout the cardiac cycle, although it has no role during MV interventions. It has been proven to be a useful tool in both the preoperative and follow-up phase with a quantitative assessment of MR severity and its impact on left ventricular (LV) volumes and systolic function. In the near future, more sophisticated multimodality imaging software will shape and improve the management of transcatheter mitral repair therapies.

© Annals of Cardiothoracic Surgery. All rights reserved.

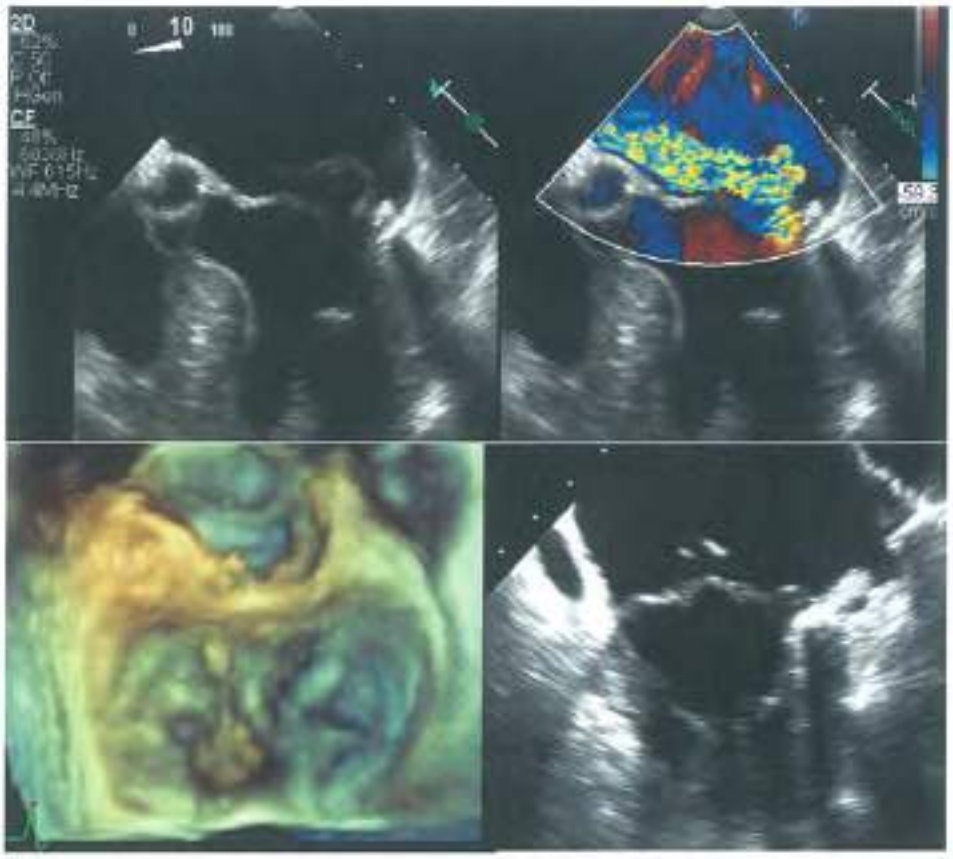

Figure 2 Transesophageal echo view of a prolapse with flail of the posterior mitral leaflet due to chordal rupture. The four-panel image depicts, from the top to the bottom and from left to right, the transoesophageal echo of the two mitral leaflets. Morphologic 2D with color-Doppler analysis show severe mitral regurgitation, with an eccentric jet. The 3D echo, en face view of the mitral leaflets, depicts the chordal rupture which is moving free in the left atrium during the systole. Last, the prolapse flail with bulging of the posterior leaflet in the central and medial segment can be appreciated in the 2D echo intercommissural morphologic view.

Surgical outcomes

Surgical repair is the preferred treatment for patients with primary MR and is associated with better outcomes than mitral replacement (8-10). MR can usually be repaired by either resection of the flail and prolapsing leaflet segment or by reconstructive techniques using artificial polytetrafluoroethylene (PTFE) chords (11). The techniques mainly adopted vary according to the center and the preference and/or experience of the surgeons, but the principal ones are the Von Oppel and Mohr's "loop technique", the simple chordae placement with atrial side knots and the David's multiple interdependent loop technique (12). Posterior leaflet prolapse is the most common pathology, causing severe MR and has higher success of durable repair than anterior leaflet disease or severe bileaflet disease (13). Artificial chordae with PTFE is a popular technique that can enhance the zone of coaptation of the MV when compared with leaflet resection, enhancing the valve performance. Currently, artificial chordae with PTFE is the technique perhaps the most adopted to correct anterior leaflet prolapse. Originally described by Frater and Zussa, this technique has grown in popularity over the past several years (14-17).

Artificial chordae insertion without leaflet resection can repair all prolapsing valves, independent of which leaflet is involved, and is ideal for minimally invasive approaches. One of the advantages of artificial chordae is

© Annals of Cardiothoracic Surgery. All rights reserved.

their versatility, considering that chordae elongation is a major cause of MR in degenerative pathology. They can be applied to almost any pathology including systolic anterior motion (SAM), Barlow's disease, anterior and posterior mitral leaflet pathology, pediatric and adult populations, hypertrophic cardiomyopathy and others (12).

One the largest series of patients was described by Salvador, reporting an operative mortality of <1% in a cohort of 608 patients undergoing MV repairs using artificial chordae. Survival was 84% at 15 years (16). Similar early mortality rates have been described by other series, ranging from 0% to 4.2%. Perier *et al.* report a 10-year survival of 84% in a cohort of 225 patients following chordae implantation (15). These outcomes have been validated by comparison to classical techniques, in both children and adults and in robotic approaches. Falk *et al.* (18) compared Carpentier resection with artificial chordae insertion (using the "loop technique") for the repair of the MV (see later). Only 2 peri-operative deaths, both in the loop group, were reported, without late mortality. Seeburger *et al.* showed that there was 96.6% survival at 5 years in 317 patients undergoing artificial chordae loop insertion (11).

These results validated artificial chordae mortality outcomes as comparable with classical techniques in the long term (12). A seminal paper from David *et al.*, reporting the results with PTFE chordae repair, showed that MV function remains stable in most patients during the first twenty years after operation. At 18 years follow-up, the freedom from reoperation on the MV was 90.2%±2.4%, the freedom from recurrent severe MR was 91.0%±2.7%, while the freedom from moderate or severe MR was 67.5%±4.2%. Cox regression analysis illustrated that isolated prolapse of the anterior leaflet was predictive of MV reoperation. Older age, hypertension and LV ejection fraction less than 40% were predictive of recurrent moderate or severe MR (19). Tabata *et al.* from Tokyo also reported the long-term results of their "tourniquet technique" chordal MV repair (700 patients with anterior, posterior and bileaflet prolapse). Again, the incidence of recurrent MR was higher in the anterior leaflet prolapse group, together with absence of an annuloplasty ring or band (20).

The biggest issue with chordal repair is adequate length determination and fixation during cardioplegic arrest, which can be particularly challenging on the anterior leaflet. The use of preformed, fixed-length chordae loops may be helpful in this regard. As a general rule, it is recommended that for posterior prolapse and chordal rupture, artificial chordae with a length of 12–14 mm are employed, while for the anterior leaflet their length should be 20–22 mm.

Last, the development of artificial chordae techniques, accelerated in part due to their proposed applications in the setting of minimally invasive MV repair. In this setting, there is a large but mixed experience available in literature. Despite the heterogeneity of these studies, it is possible to conclude that the outcomes with artificial chordae implantation using minimally invasive approach offers the same risk and efficacy profile of conventional MV surgery (12).

Transcatheter mitral chordal repair

A great effort has been made in the development of catheter-based techniques for mitral chordae repair. This method applies all the basic steps of the conventional surgery on the beating-heart without the use of the cardiopulmonary bypass and follows the established doctrine of MV repair "respect rather than resect" (21). The first pioneering pre-clinical experiences of transcatheter neochordae implantation was performed by Maisano *et al.*, in which delivery and adjustment of chordal length, after implantation, was done on the beating heart.

By using this feature, the surgeon could correct neochordal length under physiologic conditions, on the beating heart to reach prolapse correction (22,23). Nowadays, there are three devices that enable transcatheter mitral chordae implantation. In terms of number of patients treated, the first and most known device is the NeoChord System (Neochord, Inc., Minnetonka, Minnesota), which received the CE Mark in 2013 and is based on a transapical approach. Second, the Harpoon Mitral Valve Repair System (H-MVRS, Harpoon Medical, Inc., Baltimore, MD, USA), which did not receive the CE Mark, but also works transapically. Finally, the ChordArt system (CoreMedic, Germany), which is based on a fully transcatheter approach (*Table 1*).

NeoChord DS 1000 (Neochord, USA)

NeoChord DS1000 is based on a solid surgical background and its catheter-based technique of implantation of neochordae presents an appealing treatment of degenerative MR (*Figure 3*). According to the mode of application, it is a minimally invasive system with adjustable PTFE sutures (24-26). It is implanted through a small incision on the beating heart with the transapical approach. The procedure is carried out under echocardiographic guidance. An anchor is placed on the leaflet on one side and on the LV

© Annals of Cardiothoracic Surgery. All rights reserved.

Table 1 Characteristics of the transcatheter mitral valve chord repair devices

Device	Advantages	Limitations	Trial	Results
NeoChord System	Minimally invasive system	Complexity of the lesion is affecting the reduction of MR and outcomes	TACT trial	30 patients at 7 centers
	Implantation without the use of CPB	Residual leaflet prolapse in complex anatomy	Multicenter, nonrandomized, prospective study	At 30 days, 17 patients (59%) achieved MR grade ≤2+0.36
	Is carried out under echocardiographic guidance	Long learning curve		More than 500 patients treated worldwide
Harpoon Mitral Valve Repair System	Leaflet anchoring is carried out with a preformed knot instead of free-edge leaflet fixation	Fixation of the neochord far from the free edge of the leaflet	TRACER trial	30 patients at 6 centers
	Smaller introducer sheath on the LV apex enables easier and repeated access	Residual leaflet prolapse in complex anatomy	Multicenter, nonrandomized, prospective study	At 1 month in 89% of patients, MR was mild
				At 6 months in 85% of patients, mild MR was stable
ChordArt	Implantation of premeasured neochordae	Residual leaflet prolapse in complex anatomy	CHAGALL trial	-
	Simple anchoring system, with which the distal chord is applied in its anatomical position, directly to the papillary muscle	Complexity of the lesion is affecting the reduction of MR and outcomes	Multi-center, nonrandomized, prospective study	

CPB, cardiopulmonary bypass; MR, mitral regurgitation; LV, left ventricular.

Figure 3 The NeoChord DS 1000 System. Courtesy of NeoChord (NeoChord, USA).

myocardium on the other side. Neochordae is then secured under the proper tension in order to adjust the artificial chordal length. The device obtained the CE Mark in 2012, after the initial results were reported in the feasibility TACT trial, where an overall reduction of MR to ≤2+ in 86.7% among 30 patients has been described. So far, the device has been used in nearly 1,000 patients.

A multicenter study conducted in Europe showed excellent results with the reduction of MR to mild or less residual in 96.7% of patients who received ≥2 neochordae. Further, a 98% survival at 1-year follow-up and 84% freedom from major cardiac adverse events were observed (26). The complexity of the lesion is clearly affecting the reduction of MR. For example, a treatment of isolated P2 segment flail or prolapse with NeoChord DS 1000, 1-year freedom from MR recurrence, mitral surgery, mortality, rehospitalisation and stroke was 94%. However, in the presence of more complex anatomy (bileaflet or commissural involvement) or treatment of multiple posterior leaflet segments with prolapse or flail freedom from the composite endpoint was 63% and 82%, respectively. There has also been a learning curve effect

© Annals of Cardiothoracic Surgery. All rights reserved.

observed (24).

As the approach with NeoChord is becoming more appealing, a need for a better patient selection has arisen and even the patients in early stages of MR without annulus dilatation have become appropriate candidates for this type of the intervention (27).

There is currently an ongoing clinical investigation of NeoChord in a randomized trial in the United States, "Randomized trial of the NeoChord DS1000 system versus open surgical repair" (RECHORD). The greatest limitations of the current generation of the device lies in its transapical access. The device requires multiple entries and exits through the apex and is delivered sheathless. In the treatment of multi-segment disease, or when there is a need for multiple chordae, there is also an increased risk of bleeding. Nevertheless, NeoChord implantation has been shown as a safe and feasible procedure that shortens the time of operation in comparison to open-heart MV repair.

Figure 4 The Harpoon TSD-5 System_ Courtesy of Harpoon (Edwards Lifescience, USA).

Harpoon TSD-5 (Edwards Lifescience, USA)

In an early feasibility trial in patients with degenerative MR and posterior leaflet prolapse, the Harpoon device has been investigated (28). The Harpoon TSD-5 (Edwards Lifesciences, Irvine, USA) device is a 14F system designed for transapical multiple PTFE implantation. Unlike the NeoChord procedure, where the surgical approach is rather lateral, the apex is reached through a more anterior incision, and the device is inserted into the ventricle more closely to the left anterior descending coronary artery. Selection of the entry site of the left ventricle and navigation towards the MV apparatus is performed using a biplane view at mid-commissural and long-axis views. After identification of the target site on the prolapsing leaflet, the device is stabilized by applying gentle pressure on the ventricular side of the leaflet with the end effector. Further confirmation of the correct position of the device can be obtained using the 3D view from both ventricular and atrial sides, adopting different levels of ultrasound depth that are represented by specific colors. At this point, the device is activated by pushing the handle fire button and a specially designed 21-gauge needle wrapped with 50 coils of ePTFE in a preformed knot configuration perforates the leaflet (*Figures 4,5*). After needle retrieval, a double-helix ePTFE knot is formed on the atrial side of the leaflet, securing the associated pair of artificial ePTFE chords to the leaflet. The major difference from the NeoChord is in the mechanism of leaflet engagement. What should be investigated at long-

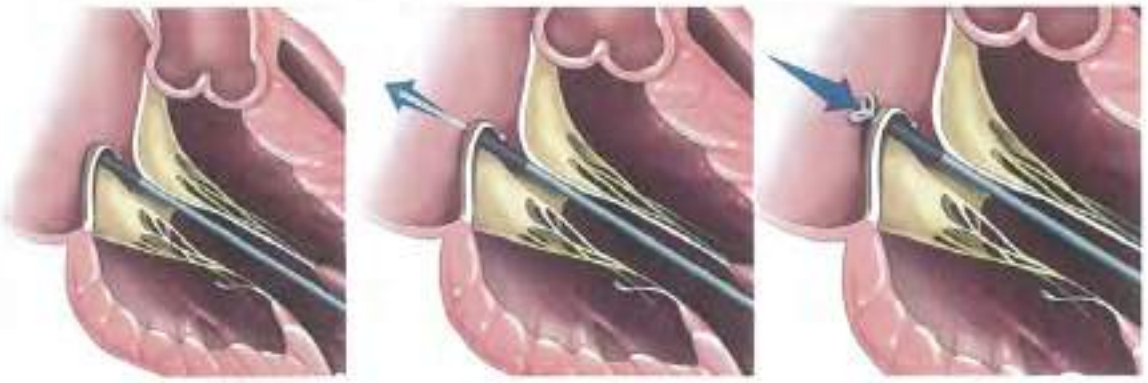

Figure 5 The Harpoon TSD-5 System during the different phases of the chordal implantation_ Courtesy of Harpoon (Edwards Lifescience, USA).

© Annals of Cardiothoracic Surgery. All rights reserved.

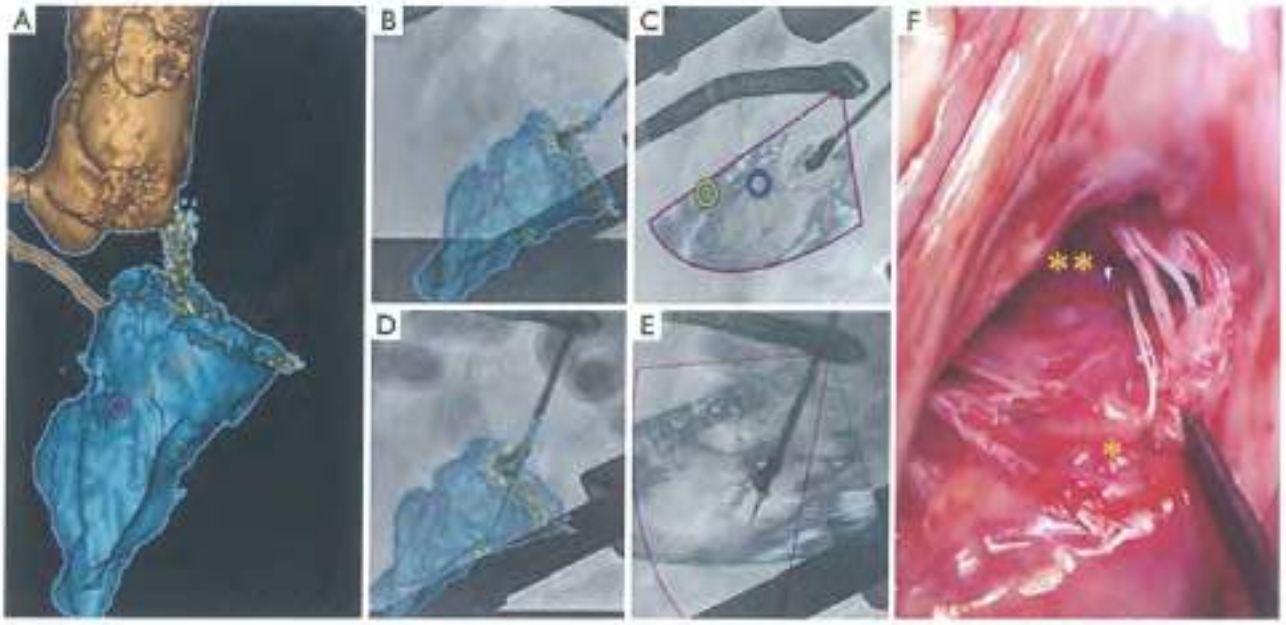

Figure 6 Intraprocedural guidance with multimodality fusion imaging during preclinical experience with Chordart device, using the EchoNavigator®-system (Philips Healthcare, Best, The Netherlands) side-by-side with the HeartNavigator®-system (Philips Healthcare), which enables CT planning and CT-fluoroscopy overlay. Using the HeartNavigator, the optimal trajectory of the device from the tip of the target papillary muscles through the corresponding MV leaflet, to define the coaxial entry point into the left atrium, was assessed (A). Grasping of P2 segment with HeartNavigator (B), EchoNavigator (C) and TEE guidance in real-time. Finally, Chordart implant with HeartNavigator (D) and EchoNavigator (E) guidance [F; Leaflet side of Chordart (*) papillary muscle side of Chordart (**)]. MV, mitral valve; CT, computed tomography; TEE, transesophageal echocardiography.

term follow-up should be the fixation of chordae far from the free edge of the leaflet.

The results of the initial feasibility trial evaluating Harpoon TSD-5 device showed that among 30 patients, 3 patients required conversion to open mitral surgery. Neither major adverse events nor deaths occurred during the study. At 1 month in 24 out of 27 patients (89%), MR was mild or even smaller and in three out off 27 patients (11%), moderate. At 6 months, MR was mild or smaller in 22 out of 26 patients (85%), moderate in two out of 26 patients (8%) and severe in two out of 26 patients (8%). During the investigation at 6 months, favourable cardiac remodeling, decrease of LV and left atrial (LA) volumes and as well as mitral annulus diameter reduction were reported (28).

Crucial patient selection is the critical point to both chordal implantation devices. Preferable pathology of the MV for a successful and durable repair is a mono-segmental pathology, limited LV dilatation and without or with mild annular dilatation. Furthermore, what is different from the surgical chordal repair is that the distal extremity of the PTFE suture is not fixed to the papillary muscles, as in native anatomy, but it is fixed to the apical access. The consequences of this should be investigated at long-term follow-up.

ChordArt (CoreMedic, Germany)

The ChordArt System has been designed to implant premeasured neochordae in order to overcome some of the limitations of the previously mentioned devices. Transatrial or transseptal antegrade approaches are used to place the neochordae. The anchoring system is simple, with which the distal chord is applied in its anatomical position, directly to the papillary muscle. For this type of therapy, multimodality imaging guidance could theoretically play a central role, integrating echo- and computed tomography-fluoro fusion imaging to determine trajectories and orientation (*Figure 6*). With preoperative echo or with CT, the size of the

© Annals of Cardiothoracic Surgery. All rights reserved.

Figure 7 Leaflet-to-Annulus Index <1.4, defined as the ratio between the sum of anterior leaflet length and posterior leaflet length over antero-posterior length, can be used as reliable predictor to identify patients without annular dilatation. Courtesy of NeoChord (NeoChord, USA) (30,31). AML, anterior mitral leaflet; PML, posterior mitral leaflet; AP, antero-posterior diameter.

implant can be determined. Preclinical validation has been done and first-in-human implants with surgical direct implantation of the device has been recently announced, reporting good outcomes (29). The Chagall trial will be the prospective, multicenter study which will establish the safety and the effectiveness of the Chordart system (30).

Role of concomitant annuloplasty to artificial chordae

The progress of transcatheter therapies and in particular, of the implantation of mitral chordae, is constant and in continuous evolution. The major limitation lies in the absence of combined treatment of mitral annulus dilatation, a condition associated in most patients with degenerative mitral pathology. The surgical results of mitral repair without annuloplasty are unsatisfactory in the long term and the initial experience with NeoChord also disadvantages the latter subgroup (26,31). A critical factor is therefore the selection and early treatment of the patient in a phase of disease in which prolapse and/or flail is still the prevalent pathology, whilst in the absence or near-annular dilation. Nowadays, early referral allows treating patients with only leaflet disease and preserved LV volumes and not dilated annuluses, questioning the need for a ring and confirming the rationale behind the transcatheter chordal repair alone.

The Leaflet-to-Annulus Index (LAI) <1.4, defined as the ratio between the sum of anterior leaflet length and posterior leaflet length over antero-posterior length, can be used as reliable predictor to identify patients without annular dilatation (32,33). The LAI identifies the quantity of overlapping leaflet tissue that will represent the potential coaptation surface after the correction (*Figure 7*). This excess of leaflet tissue will constitute the potential coaptation surface after an effective restoration of the posterior leaflet movement, e.g., using the NeoChord repair system. In the near future, with increasing clinical evidence, improvements in multimodality imaging guidance and clearer indications, it will be conceivable to combine in most cases the treatment of leaflets (e.g., chordae, edge to edge) with direct mitral annuloplasty, whenever the latter is needed (34).

Conclusions

In primary MR, surgical repair with artificial chordae, often through a minimally invasive approach, provides excellent outcomes. Transcatheter mitral chordal devices enabled targeted and less invasive repair, providing promising initial results. These therapies have the potential to simplify and increase the quality and rates of mitral repair and decrease the morbidity associated with conventional open cardiac mitral operations. As these devices are in the early phases of clinical experience, further investigation with longer-term follow-up and direct comparison with conventional MV surgery is necessary to validate the role of transcatheter chordae in the armamentarium of multidisciplinary valveMV therapies.

Acknowledgements

None.

Footnote

Conflicts of Interest: The authors have no conflicts of interest to declare.

References

1. Baumgartner H, Falk V, Bax JJ, et al. 2017 ESC/EACTS Guidelines for the management of valvular heart disease. Eur Heart J 2017;38:2739-91.
2. Mirabel M, Iung B, Baron G, et al. What are the characteristics of patients with severe, symptomatic, mitral regurgitation who are denied surgery? Eur Heart J

© Annals of Cardiothoracic Surgery. All rights reserved.

2007;28:1358-65.
3. Olson LJ, Subramanian R, Ackermann DM, et al. Surgical pathology of the mitral valve: a study of 712 cases spanning 21 years. Mayo Clin Proc 1987;62:22-34.
4. Carabello BA. Mitral regurgation: basic pathophysiologic principles. Mod Concepts Cardiovasc Dis 1988;57:53-8.
5. Taramasso M, Pozzoli A, Basso C, et al. Compare and contrast tricuspid and mitral valve anatomy: interventional perspectives for transcatheter tricuspid valve therapies. EuroIntervention 2018;13:1889-98.
6. Delling FN, Vasan RS. Epidemiology and pathophysiology of mitral valve prolapse: new insights into disease progression, genetics and molecular basis. Circulation 2014;129:2158-70.
7. Adams DH, Rosenhek R, Falk V. Degenerative mitral valve regurgitation: best practice revolution. Eur Heart J 2010;31:1958-66.
8. Enriquez-Sarano M, Schaff HV, Orszulak TA, et al. Valve repair improves the outcome of surgery for mitral regurgitation. A multivariate analysis. Circulation 1995;91:1022-8.
9. Jokinen JJ, Hippelainen MJ, Pitkanen OA, et al. Mitral valve replacement versus repair: propensity-adjusted survival and quality-of-life analysis. Ann Thorac Surg 2007;84:451-8.
10. Moss RR, Humphries KH, Gao M, et al. Outcome of mitral valve repair or replacement: a comparison by propensity score analysis. Circulation 2003;108 Suppl 1:II90-7.
11. Seeburger J, Falk V, Borger MA, et al. Chordae replacement versus resection for repair of isolated posterior mitral leafl et prolapse: a egalite. Ann Thorac Surg 2009;87:1715-20.
12. Ibrahim M, Rao C, Savvopoulou M, et al. Outcomes of mitral valve repair using artificial chordae. Eur J Cardiothorac Surg 2014;45:593-601.
13. Suri RM, Clavel MA, Schaff HV, et al. Effect of recurrent mitral regurgitation following degenerative mitral valve repair: long-term analysis of competing outcomes. J Am Coll Cardiol 2016;67:488-98.
14. Frater RW, Vetter HO, Zussa C, et al. Chordal replacement in mitral valve repair. Circulation 1990;82:IV125-30.
15. Perier P, Hohenberger W, Lakew F, et al. Toward a new paradigm for the reconstruction of posterior leaflet prolapse: midterm results of the "respect rather than resect" approach. Ann Thorac Surg 2008;86:718-25; discussion 718-25.
16. Salvador L, Mirone S, Bianchini R, et al. A 20-year experience with mitral valve repair with artificial chordae in 608 patients. J Thorac Cardiovasc Surg 2008;135:1280-7.
17. Padala M, Powell SN, Croft LR, et al. Mitral valve hemodynamics after repair of acute posterior leaflet prolapse: quadrangular resection versus triangular resection versus neochordoplasty. J Thorac Cardiovasc Surg 2009;138:309-15.
18. Falk V, Seeburger J, Czesla M, et al. How does the use of polytetrafluoroethylene neochordae for posterior mitral valve prolapse (loop technique) compare with leaflet resection? A prospective randomized trial. J Thorac Cardiovasc Surg 2008;136:1205; discussion 1205-6.
19. David TE, Armstrong S, Ivanov J. Chordal replacement with polytetrafluoroethylene sutures for mitral valve repair: a 25-year experience. J Thorac Cardiovasc Surg 2013;145:1563-9.
20. Tabata M, Kasegawa H, Fukui T, et al. Long-term outcomes of artificial chordal replacement with tourniquet technique in mitral valve repair: a single-center experience of 700 cases. J Thorac Cardiovasc Surg 2014;148:2033-2038.e1.
21. Espirito D, Onohara D, Kalra K, et al. transcatheter mitral valve repair therapies: evolution, status and challenges. Ann Biomed Eng 2017;45:332-59.
22. Maisano F, Cioni M, Seeburger J, et al. Beating-heart implantation of adjustable length mitral valve chordae:acute and chronic experience in an animal model. Eur J Cardiothorac Surg 2011;40:840-7.
23. Maisano F, Michev I, Rowe S, et al. Transapical endovascular implantation of neochordae using a suction and suture device. Eur J Cardiothorac Surg 2009;36:118-22.
24. Seeburger J, Rinaldi M, Nielsen SL, et al. Off-pump transapical implantation of artificial neo-chordae to correct mitral regurgitation: the TACT Trial (Transapical Artificial Chordae Tendinae) proof of concept. J Am Coll Cardiol 2014;63:914-9.
25. Colli A, Bagozzi L, Bauchelli E, et al. Learning curve analysis of transapical NeoChord mitral valve repair. Eur J Cardiothorac Surg 2018;54:273-80.
26. Colli A, Manzan E, Aidietis A, et al. An early European experience with transapical off-pump mitral valve repair with NeoChord implantation. Eur J Cardiothorac Surg 2018;54:460-6.
27. Suri RM, Vanoverschelde JL, Grigioni F, et al. Association between early surgical intervention vs watchful waiting and outcomes for mitral regurgitation due to flail mitral valve leaflets. JAMA 2013;310:609-16.

© Annals of Cardiothoracic Surgery. All rights reserved.

28. Gammie JS, Bartus K, Gackowski A, et al. Beating-Heart Mitral Valve Repair Using a Novel ePTFE Cordal Implantation Device: A Prospective Trial. J Am Coll Cardiol 2018;71:25-36.
29. First patient treated in first-in-man study of ChordArt mitral valve repair system. Available online: https://cardiovascularnews.com/first-patient-treated-in-first-in-man-study-of-chordart-mitral-valve-repair-system
30. Weber A. Changing the Way of Treating Mitral Valve Prolapse: A Sutureless Neochordal Replacement. TCT 2016, Washington. Available online: https://www.tctmd.com/slide/changing-way-treating-mitral-valve-prolapse-sutureless-neochordal-replacement
31. De Bonis M, Lapenna E, Maisano F, et al. Long-term results (≤18 years) of the edge-to-edge mitral valve repair without annuloplasty in degenerative mitral regurgitation: implications for the percutaneous approach. Circulation 2014;130:S19-24.
32. Maisano F, La Canna G, Grimaldi A, et al. Annular-to-leaflet mismatch and the need for reductive annuloplasty in patients undergoing mitral repair for chronic mitral regurgitation due to mitral valve prolapse. Am J Cardiol 2007;99:1434-9.
33. Colli A, Besola L, Montagner M, et al. Prognostic impact of leaflet-to-annulus index in patients treated with transapical off-pump echo-guided mitral valve repair with NeoChord implantation. Int J Cardiol 2018;257:235-7.
34. von Bardeleben RS, Colli A, Sebula E, et al. First in human transcatheter COMBO mitral valve repair with direct ring annuloplasty and neochord leaflet implantation to treat degenerative mitral regurgitation: feasibility of the simultaneous toolbox concept guided by 3D echo and computed tomography fusion imaging. Eur Heart J 2018;39:1314-5.

Cite this article as: Savic V, Puzzoli A, Gülmez G, Demir H, Batinkov N, Kuwata S, Weber A, Vogel R, Tanner F, Zuber M, Maisano F, Taramasso M. Transcatheter mitral valve chord repair. Ann Cardiothorac Surg 2018;7(6):731-740. doi: 10.21037/acs.2018.09.09

© Annals of Cardiothoracic Surgery. All rights reserved.

Clinical and Experimental Nephrology (2018) 22:1395–1403
https://doi.org/10.1007/s10157-018-1603-1

ORIGINAL ARTICLE

Comparison of the effects of tolvaptan and furosemide on renal water and sodium excretion in patients with heart failure and advanced chronic kidney disease: a subanalysis of the K-STAR study

Naoto Tominaga[1] · Keisuke Kida[2] · Takayuki Inomata[3] · Naoki Sato[4] · Tohru Izumi[3] · Yoshihiro J. Akashi[2] · Yugo Shibagaki[1]

Received: 28 October 2017 / Accepted: 12 June 2018 / Published online: 22 June 2018
© Japanese Society of Nephrology 2018

Abstract

Background Tolvaptan (TLV) is known to increase electrolyte-free water clearance. However, TLV actions on renal electrolytes including urine sodium (uNa) excretion and its consequences are less well understood. This subanalysis investigated the effect of add-on TLV compared to increased furosemide (FUR) on both electrolyte-free water and electrolyte clearance in patients with congestive heart failure (CHF) complicated by advanced chronic kidney disease (CKD).

Methods The Kanagawa Aquaresis Investigators Trial of TLV on HF Patients with Renal Impairment (K-STAR) was a multicenter, open-labeled, randomized, and controlled prospective clinical study. Eighty-one Japanese patients with CHF and residual signs of congestion despite oral FUR treatment (≥ 40 mg/day) were recruited and randomly assigned to a 7-day add-on treatment with either ≤ 40 mg/day FUR or ≤ 15 mg/day TLV. Electrolyte-free water clearance, electrolyte osmolar clearance and electrolyte excretion were compared between the two groups before and after therapy.

Results The change (Δ) in electrolyte-free water clearance was significantly higher in the add-on TLV group than in the add-on FUR group. However, Δelectrolyte osmolar clearance was also higher in the add-on TLV group than in the increased FUR group. This was primarily because ΔuNa excretion was significantly higher in the add-on TLV group than in the increased FUR group, since Δurine potassium excretion was significantly lower in the add-on TLV group than in the increased FUR group.

Conclusions Add-on TLV may increase both renal water and Na excretion in CHF patients with advanced CKD to a greater degree than increased FUR.

Keywords CKD · CHF · Vasopressin V2 receptor antagonist · Renal water excretion · Renal solute excretion

Introduction

Loop diuretics, such as furosemide (FUR), have long been used to treat fluid overload in patients with congestive heart failure (CHF). However, they have numerous adverse effects, including low blood pressure (BP), electrolyte disorders

Electronic supplementary material The online version of this article (https://doi.org/10.1007/s10157-018-1603-1) contains supplementary material, which is available to authorized users.

✉ Naoto Tominaga
tominaga1213@kbd.biglobe.ne.jp

[1] Division of Nephrology and Hypertension, Department of Internal Medicine, St. Marianna University School of Medicine, 2-16-1, Sugao, Miyamae-ku, Kawasaki, Kanagawa 216-8511, Japan

[2] Division of Cardiology, Department of Internal Medicine, St. Marianna University School of Medicine, 2-16-1, Sugao, Miyamae-ku, Kawasaki, Kanagawa 216-8511, Japan

[3] Department of Cardiovascular Medicine, Kitasato University School of Medicine, 1-15-1, Kitasato, Minami-Ku, Sagamihara, Kanagawa 252-0374, Japan

[4] Division of Cardiology, Department of Internal Medicine, Nippon Medical School Musashi-Kosugi Hospital, 1-396, Kosugi-cho, Nakahara-ku, Kawasaki, Kanagawa 211-8533, Japan

(e.g., hyponatremia), worsening renal function (WRF), and worsening nitrogen metabolism [1–3]. Vasopressin (AVP) V2 receptor (V2R) antagonists, such as tolvaptan (TLV), can be administered adjunctively with loop diuretics. TLV binds to AVP receptors in the collecting duct, thereby blocking water reabsorption and promoting electrolyte-free water excretion (aquaresis) [4]. It has been reported that add-on TLV did not affect urine solute excretion in a rat [4] and a CHF dog model [5]; however, its effects have not been fully investigated in patients with CHF and advanced chronic kidney disease (CKD). Therefore, the urine solute profiles of TLV as add-on therapy to FUR in patients with CHF and advanced CKD were determined in a subanalysis of the K-STAR study.

Methods

The Kanagawa Aquaresis Investigators Trial of TLV on Heart Failure (HF) Patients with Renal Impairment (K-STAR) was a multicenter, open-labeled, randomized, and controlled prospective clinical study that evaluated the efficacy and safety of add-on TLV therapy for HF. The main analysis [6] analyzed data from 81 Japanese patients with CHF complicated by advanced CKD [estimated glomerular filtration rate (eGFR) < 45 mL/min/1.73 m^2]. Dialysis patients were not included. These patients had residual signs of congestion (e.g., pedal edema, pulmonary congestion, or distention of the jugular vein) despite oral FUR treatment (≥ 40 mg/day). Each was randomly assigned to 7 days of treatment with either ≤ 15 mg/day of add-on TLV or ≤ 40 mg/day of increased FUR.

Patients

Patients were excluded if they met any of the following criteria: use of assisted circulation devices; hypersensitivity to TLV or a similar drug; anuria; lack of thirst; inability to ingest water or oral medication; increase in serum sodium concentration (s[Na^+]) by ≥ 12 mEq/L/24 h, or above the upper limits provided by the guidelines of medical institute; pregnancy or suspicion of pregnancy; use of TLV at inclusion; acute coronary syndrome and/or an elective percutaneous coronary intervention therapy during the study period; malignancy; or otherwise deemed unfit to participate in the study by a physician. Written informed consent was obtained from all patients before enrollment in the study. During the study, the administration of human atrial natriuretic peptides, phosphodiesterase III inhibitors, catecholamines, colforsin, and changing doses of all diuretics except FUR or TLV were prohibited. Other therapeutics were not restricted. Fifty patients completed the K-STAR study. However, there were data missing for 16 patients, resulting in 17 patients in each group in this subanalysis.

Procedures

The study design of K-STAR is shown in Fig. 1. A screening test was performed first for each participant in the study. Before the administration of either increased FUR or add-on TLV, all participants received a constant dose of FUR during a three-day run-in period (days −2–0). Subsequently, all participants received either ≤ 15 mg/day add-on TLV or ≤ 40 mg/day increased FUR orally for the next 7 days (days 1–7). The patients were hospitalized for at least 4 days before treatment and 2 days after treatment (days 8 and 9). Water intake was not limited for the patients who were assigned for the add-on TLV group during the study because fluid restriction during the therapy with TLV may increase the likelihood of overly rapid correction of s[Na^+] and should generally be avoided.

The study was discontinued for any of the following reasons: (1) early termination, owing to complete or partial improvement of HF; (2) the stop criteria, (a) the patient no longer participated or withdrew consent, (b) adverse events that prevent continued treatment, (c) s[Na^+] was either higher than 12 mEq/L within 24 h or above the upper limits permitted by medical institute after administration, or (d) recommendation by a physician; (3) the event criteria, (a) the need to use higher than regulated doses, (b) the need to add other drugs for HF, or (c) the need to use non-pharmacological therapies (e.g., positive pressure respiration therapeutic device).

Assessments

For this subanalysis, the patients were assessed for serum and urine chemistry, BP, heart rate, daily urine volume (UV), and water intake were also measured (days 1–9). Measurements taken before first dosing of treatment on day 1 were used as baseline values. Measurements of serum and urine

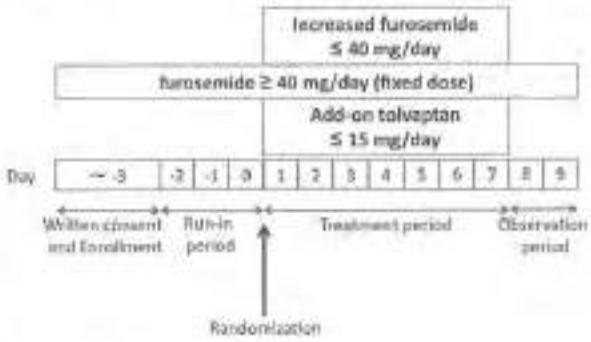

Fig. 1 Study design

chemistry, BP and heart rate taken before the first dosing on day 1, and that of daily UV and water intake taken between day 0 and the first dosing on day 1 were used as baseline values.

Serum levels of sodium (s[Na^+]), potassium (s[K^+]), chloride (s[Cl^-]), urea nitrogen (sUN), and creatinine (sCr) were measured on day 1, 3, and 8. In addition, on day 1 and 8, urine sodium (uNa), urine potassium (uK), urine urea nitrogen (uUN), urine creatinine (uCr), urinary osmolality (uOsm), and serum osmolality (sOsm) were measured. The eGFR was calculated using a slightly modified equation for the Japanese population with renal disease: eGFR (mL/min/1.73 m^2) = $194 \times sCr^{-1.094} \times age^{-0.287}$ (if female, multiply by 0.739) [7]. The electrolyte osmolar clearance (E-C_{Osm}) was calculated using the following equation: E-C_{Osm} (mL/min) = (uNa + uK) × UV/s[Na^+]. The electrolyte-free water clearance (E-C_{H2O}) was calculated using the following equation: E-C_{H2O} (mL/min) = UV−E-C_{Osm} [8]. Pre-treatment values (day 1) were used as baseline values.

Statistical analyses

Changes in the serum chemistry values and the urine sample data obtained from the baseline values for patients in the same group were tested for statistical significance using the Wilcoxon signed rank test, whereas statistically significant changes between the two groups were determined using the Mann–Whitney test. For discrete variables, statistical significance between the two groups was determined using Fisher's exact test. Statistical analyses were performed using Stata version 14 (StataCorp). Statistical significance was defined as $P < 0.05$.

Results

Between October 2012 and August 2014, 81 adult patients (49–93 years old) with CHF and advanced CKD with an eGFR less than 45 mL/min/1.73 m^2) were recruited for the study and randomly assigned into two groups, namely, the increased FUR group (FUR group, $n = 41$) and the add-on TLV group (TLV group, $n = 40$). During the study period, 31 patients dropped out. In the FUR group, patients dropped out for the following reasons: symptom improvement ($n = 4$), WRF ($n = 3$), hypernatremia ($n = 2$), higher dose requirement ($n = 2$), and addition of other drug(s) for HF treatment ($n = 1$). Similarly, in the TLV group, patients dropped out for the following reasons: symptom improvement ($n = 10$), WRF ($n = 1$), hypernatremia ($n = 3$), impaired consciousness ($n = 1$), withdrawn consent ($n = 2$), and the need for higher doses ($n = 2$). The remaining 50 patients (29 in the FUR group and 21 in the TLV group) completed the study (Fig. 2). However, there were data missing for 16 patients (12 in the FUR group and 4 in the TLV group) for this

Fig. 2 Participant flow diagram

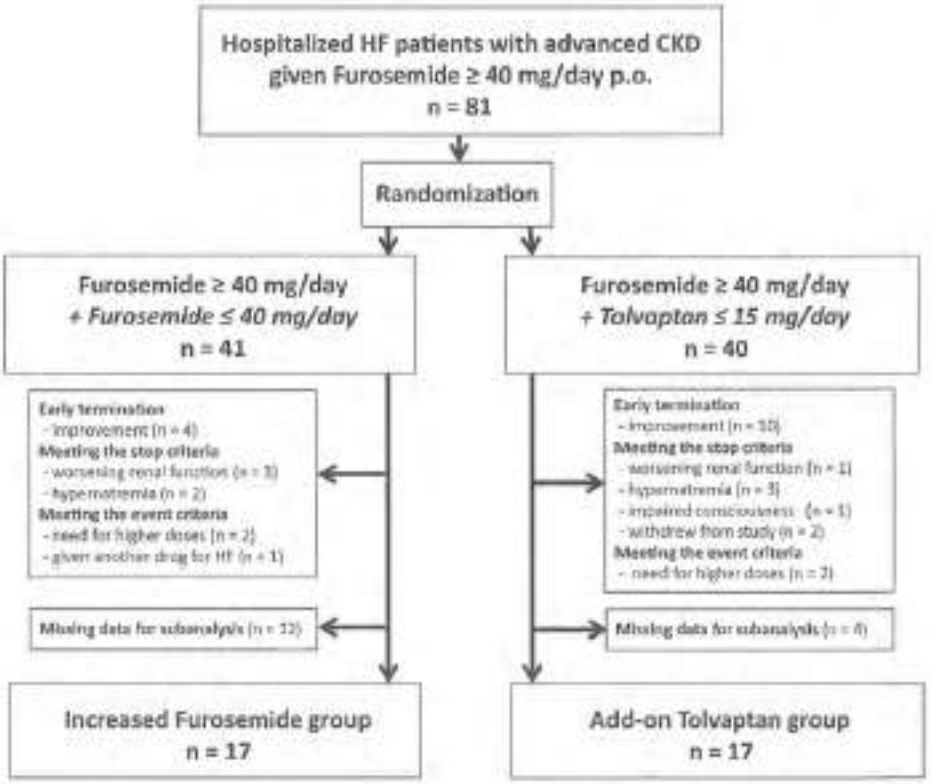

subanalysis. The baseline characteristics of the remaining 34 patients (17 in the FUR group and 17 in the TLV group) in this subanalysis are summarized in Table 1.

FUR doses at baseline were not significantly different between the two groups. At the end of day 7, the mean increased FUR dose was 31.8 ± 2.5 mg/day in the FUR group and the mean add-on TLV dose was 9.3 ± 0.8 mg/day in the TLV group. Therefore, the mean total FUR dose was 87.1 ± 7.4 mg/day in the FUR group and 50.0 ± 5.6 mg/day in the TLV group ($P < 0.001$, Table 2).

The change (Δ) in UV (between day 0 and 1 (before treatment), and between day 7 and day 8) was significantly higher in the TLV group than the FUR group [mean (SE): 450.6 (171.7) mL/day vs. − 121.3 (90.4) mL/min ($P = 0.002$)] (Fig. 3); however, Δwater intake (between day 0 and day 1 (before treatment), and between day 7 and 8) was not significantly different between the TLV group and the FUR group [mean (SE): 120.6 (103.7) mL/day vs. 110.6 (45.5) mL/day ($P = 0.637$)] (Fig. 3). ΔuOsm (from day 1 to 8) was greater in the TLV group than the FUR group [mean (SE): − 72.5 (15.8) mOsm/kg vs. -33.6 (14.6) mOsm/kg ($P = 0.095$)] (Fig. 4). $\Delta E\text{-}C_{H2O}$ (from day 1 to 8) was significantly higher in the TLV group than the FUR group [mean (SE): 0.25 (0.07) mL/min vs. − 0.01 (0.04) mL/min ($P = 0.001$)] (Fig. 5). In addition, $\Delta E\text{-}C_{Osm}$ (from day 1 to 8) was higher in the TLV group than the FUR group [mean (SE): 0.06 (0.06) mL/min vs. − 0.08 (0.07) mL/min ($P = 0.185$)] (Fig. 5). Similarly, ΔuNa excretion (from day 1 to 8) was significantly higher in the TLV group than in the FUR group [mean (SE): 13.8 (10.9) mEq/day vs. − 16.2 (12.0) mEq/day, $P = 0.040$] and ΔuK excretion (from day 1 to 8) was significantly lower in the TLV group than in the FUR group [mean (SE): − 6.7 (2.4) mEq/day vs. 0.8 (1.2) mEq/day, $P = 0.014$] (Fig. 6). However, ΔuUN excretion was not significantly different between the TLV group and the FUR group [mean (SE): 58.8 (73.1) mg/day vs. − 86.0 (34.5) mg/day, $P = 0.134$].

The mean plasma renin activity (PRA) [mean (SE): 4.9 (1.3) ng/mL/h vs. 6.2 (1.4) ng/mL/h, $P = 0.033$] on day 8 was significantly higher than that on day 1 only in the FUR group.

Discussion

AVP-mediated activation of V2R in the collecting ducts stimulates the cAMP-dependent trafficking of aquaporin 2 (AQP2) water channels to the luminal membranes of the principal cells. It allows the diffusion of water along a solute concentration gradient. In contrast to loop diuretics, TLV promotes excretion of electrolyte-free water. It inhibits the trafficking of AQP2 to the luminal membranes of principal cells by blocking the action of AVP on V2R in the renal collecting duct, which leads to inhibition of water reabsorption [4]. Therefore, TLV seems to have no effect on urine solute excretion. As expected, in this study, not only $\Delta E\text{-}C_{H2O}$ but also ΔUV were significantly greater in the add-on TLV group than in the increased FUR group, despite an insignificant difference in Δwater intake between the groups; however, $\Delta E\text{-}C_{Osm}$ was also greater in the add-on TLV group than in the increased FUR group (Figs. 3, 5). This was primarily because ΔuNa excretion was significantly higher in the add-on TLV group than in the increased FUR group (13.8 ± 10.9 vs. −16.2 ± 12.0 mEq/day, $P = 0.040$), since ΔuK excretion was significantly lower in the add-on TLV group than in the increased FUR group (− 6.7 ± 2.4 vs. 0.8 ± 1.2 mEq/day, $P = 0.014$) (Fig. 6). Ecelbarger et al. reported that AVP upregulated epithelial Na channels (ENaC) in the rat kidney [9]. In addition, a study by Bankir et al. [10] indicated the potent V2-dependent antinatriuretic effect of AVP in humans. Whether desmopressin (dDAVP), an AVP agonist, reduced uNa excretion was evaluated in healthy individuals and patients with central diabetes insipidus (CDI) or nephrogenic diabetes insipidus (NDI) owing to mutations of either the aquaporin 2 (AQP2) gene or V2R. dDAVP was found to reduce uNa excretion in healthy individuals and CDI and AQP2-mutated NDI patients, but not in V2R-mutated NDI patients [10]. Stockand also reported that AVP modulated discretionary Na reabsorption across principal cells mediated by ENaC via V2R [11]. There are some other possible reasons for the rise in uNa excretion induced by TLV. First is an influence of endogenous AVP mediated by V1a receptor (V1aR) [12]. By blocking V2R-mediated effects, TLV induces a secondary increase in endogenous AVP secretion, and thus likely more intense effects on V1aR. It has been well demonstrated that V1aR mediate a natriuretic response [13, 14]. This influence is even more marked in patients with chronic renal failure [15]. Second, Mori et al. speculated from the results of Cowley [16] that TLV stimulated natriuresis owing to increased renal blood flow (RBF) [17]. They also suggested that TLV improved FUR delivery due to increased RBF, which reduced FUR resistance. Moreover, congestion in the kidney has recently been focused on in the aspect of diuretic resistance. In 2016, Mori et al. reported that long-term TLV use decreased intracellular fluid and extracellular fluid in patients who underwent peritoneal dialysis with bioimpedance monitoring [18]. The authors also reported that TLV can improve left ventricular diastolic dysfunction. This was demonstrated by the ratio of transmitral Doppler early filling velocity to tissue Doppler early diastolic mitral annular velocity (E/e') of cardiac ultrasound, especially in patients with E/e' greater than 15. Mori et al. have shown a suggestive speculation regarding renal congestion [19]. Renal interstitial fluid flows from the medulla to the cortex [20], and water reabsorbed in the collecting ducts also flows from the medulla to the cortex.

Table 1 Baseline characteristics

Variables	Total ($n=34$)	PUR group ($n=17$)	TLV group ($n=17$)	*P* value
Demographics				
Age (years)	75.2 ± 1.4	71.2 ± 2.2	79.1 ± 1.3	0.002
Gender (% male)	64.7	70.6	58.8	0.473
Measurements				
Systolic BP (mmHg)	117.6 ± 3.6	120.1 ± 6.0	115.2 ± 4.3	0.667
Diastolic BP (mmHg)	61.2 ± 2.0	62.4 ± 3.2	60.1 ± 2.4	0.680
Pulse rate (bpm)	69.4 ± 2.7	68.9 ± 3.6	69.8 ± 4.1	0.943
Weight (kg)	61.1 ± 2.3	64.1 ± 3.2	58.2 ± 3.2	0.221
BMI (kg/m^2)	23.8 ± 0.8	24.0 ± 1.0	23.7 ± 1.2	0.986
Urine volume (mL/day)	1286.4 ± 78.0	1361.5 ± 126.9	1211.4 ± 91.0	0.379
Water intake (mL/day)	732.9 ± 68.6	598.8 ± 77.8	875.3 ± 106.1	0.035
Laboratory				
Serum Alb (g/dL)	3.3 ± 0.1	3.2 ± 0.2	3.5 ± 0.1	0.269
Serum UN (mg/dL)	36.6 ± 2.6	33.2 ± 4.3	40.1 ± 2.7	0.071
Serum Cr (mg/dL)	1.9 ± 0.1	1.9 ± 0.2	1.8 ± 0.2	0.570
eGFR (mL/min/1.73 m^2)	29.6 ± 1.7	29.1 ± 2.3	30.0 ± 2.7	0.918
Serum Na (mEq/L)	138.0 ± 0.9	139.1 ± 1.3	136.9 ± 1.2	0.116
Serum K (mEq/L)	4.2 ± 0.1	4.2 ± 0.1	4.2 ± 0.2	0.876
Serum osmolality (mOsm/kg H_2O)	292.1 ± 2.0	291.5 ± 3.4	292.7 ± 2.4	0.904
BNP (pg/mL)	570.5 ± 73.2	686.0 ± 95.3	445.1 ± 106.6	0.076
PRA (ng/mL/h)	7.7 ± 2.0	4.9 ± 1.3	10.6 ± 3.8	0.208
Urine UN (mg/day)	487.0 ± 36.5	436.1 ± 46.3	537.9 ± 55.1	0.163
Urine Na (mEq/day)	87.7 ± 7.0	102.8 ± 11.1	72.6 ± 7.1	0.024
Urine K (mEq/day)	22.7 ± 1.9	19.8 ± 1.9	25.6 ± 3.2	0.185
Urine osmolality (mOsm/kg H_2O)	349.9 ± 15.5	339.2 ± 19.4	360.5 ± 24.5	0.744
E-C_{H_2O} (mL/min)	0.57 ± 0.04	0.31 ± 0.06	0.33 ± 0.06	0.667
E-C_{Osm} (mL/min)	0.32 ± 0.04	0.63 ± 0.06	0.51 ± 0.04	0.052
Medical history (%)				
Hypertension	70.6	64.7	76.5	0.452
Diabetes mellitus	79.4	82.4	76.5	0.671
Dyslipidemia	55.9	58.8	52.9	0.730
Medications				
ACEI or ARB (%)	70.6	64.7	76.5	0.452
Beta-blocker (%)	61.8	70.6	52.9	0.290
Aldosterone blocker (%)	47.1	35.3	58.8	0.169
Digoxin (%)	11.8	23.5	0	0.033
Ca antagonist (%)	35.3	29.4	41.2	0.473
Thiazide (%)	5.9	5.9	5.9	1.000
Furosemide (mg/day)	52.6 ± 4.6	55.3 ± 7.4	50.0 ± 5.6	0.363
CXR image				
CTR (%)	60.9 ± 1.4	59.8 ± 1.7	61.9 ± 2.3	0.654
Lung congestion (% patients)	73.5	82.4	64.7	0.244

BP blood pressure, *BMI* body mass index, *Alb* albumin, *UN* urea nitrogen, *Cr* creatinine, *eGFR* estimated glomerular filtration rate, *BNP* brain natriuretic peptide, *PRA* plasma renin activity, E-C_{H_2O} electrolyte-free water clearance, E-C_{Osm} electrolyte osmolar clearance, *ACEI* angiotensin-converting enzyme inhibitor, *ARB* angiotensin II receptor blocker, *CXR* chest X-ray, *CTR* cardiothoracic ratio

All values are presented as mean ± SE

Statistical significance was defined as $P < 0.05$

Table 2 Protocol treatments (increased FUR or added TLV)

Variables	FUR group ($n=17$)	TLV group ($n=17$)	*P* value
FUR at baseline (mg/day)	55.5 ± 7.4	50.0 ± 5.6	0.363
Increased FUR or Add-on TLV (mg/day)	31.8 ± 2.5	9.3 ± 0.8	–
Total FUR (mg/day)	87.1 ± 7.4	50.0 ± 5.6	< 0.001

FUR furosemide, *TLV* tolvaptan

All values are presented as mean ± SE

Statistical significance was defined as $P < 0.05$

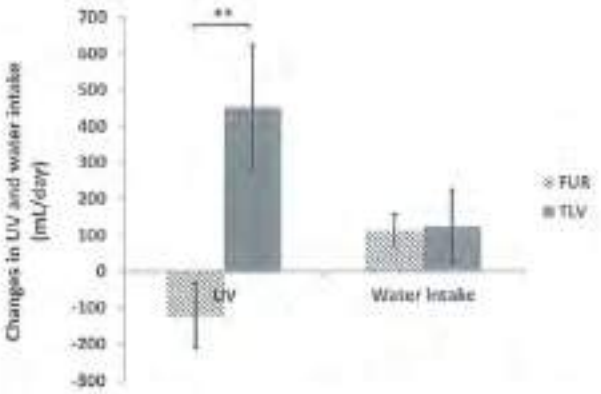

Fig. 3 Changes in daily urine volume (UV) and water intake between day 0 and day 1 (before treatment) and day 7 and day 8 in each group. $^{**}P < 0.01$ between the groups. All values are presented as mean ± SE

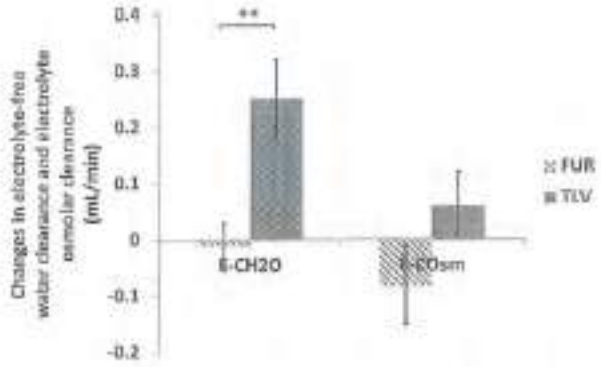

Fig. 5 Changes in electrolyte-free water clearance ($E\text{-}C_{H2O}$) and electrolyte osmolar clearance ($E\text{-}C_{Osm}$) per the measurements taken before the first dosing on day 1 and that on day 8. $^{**}P < 0.01$ between the groups. All values are presented as mean ± SE

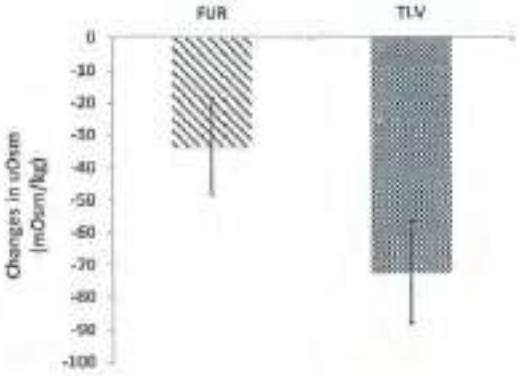

Fig. 4 Changes in urine osmolality (uOsm) per the measurements taken before the first dosing on day 1 and that on day 8 in each group. All values are presented as mean ± SE

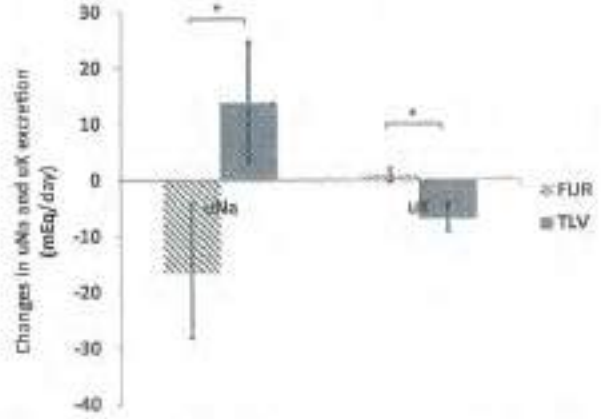

Fig. 6 Changes in urine sodium (uNa) and potassium (uK) excretion per the measurements taken before the first dosing on day 1 and that on day 8 in each group. $^{*}P < 0.05$ between the groups. All values are presented as mean ± SE

If renal venous pressure increases due to a congestive disorder, such as heart failure, renal interstitial pressure also increases [19]. This may result in Na retention via a reduction of renal medullary blood flow. TLV can improve renal congestion by blocking water reabsorption, and may increase renal Na excretion. Third, Shoaf et al. showed that TLV did not increase PRA; however, FUR increased PRA in healthy white men [21]. In this subanalysis, PRA was significantly increased only in the increased FUR group, although ΔBP over the study period (data not shown) and the percentage of patients who received renin–angiotensin–aldosterone system

(RAS) inhibitors (Table 1) were not significantly different between the two groups. The significant increase in PRA could have caused the decrease in uNa excretion in the FUR group (Fig. 5). Generally, FUR increases urine solute excretion mainly by increasing uNa excretion; therefore, based on the results of this subanalysis, the FUR group might become more resistant to FUR.

Because TLV does not decrease RBF or GFR in patients with CHF [22], co-administration of TLV and FUR in CHF patients promoted diuresis at reduced FUR doses. In addition to this, compromised drug absorption in the intestine is observed in patients with CHF due to congestion [23]. Therefore, in this subanalysis, it was also possible for add-on TLV treatment to improve the bioavailability of FUR by reducing edema of the gastrointestinal tract. Thereby, resistance to FUR could also be reduced. However, in this subanalysis, Δbody weight, brain natriuretic peptide, left ventricular ejection fraction, early-to-late diastolic transmitral flow velocity of cardiac ultrasound, and cardiothoracic ratio of chest X-ray were not significantly different between the groups. It should be noted that ΔIn-Out balance between day 1 and 8 was significantly larger in the TLV group than in the FUR group ($P = 0.015$) (Supplementary Table 2). Based on the results of this subanalysis, some factors other than decongestion might contribute to the increase in UV in the TLV group. In fact, ΔuK excretion was significantly lower in the add-on TLV group than in the increased FUR group (Fig. 6). Field et al. reported that AVP stimulated uK secretion independent of urine flow rate, which suggested that AVP increased Na^+/K^+ exchange to prevent K retention during antidiuresis [24]. Blanchard et al. [25] investigated changes in urine in response to dDAVP administered alone (control period) or after 7-day pretreatment with amiloride (amiloride period) in healthy human subjects on a high Na/low K diet to suppress aldosterone secretion. In the control period, the uNa/K ratio decreased and the transtubular potassium gradient (TTKG) increased, suggesting that uK secretion was stimulated by dDAVP in the distal nephron, on which aldosterone acts. However, after 7-day pretreatment with amiloride, the uNa/K ratio significantly increased and TTKG significantly decreased, suggesting that amiloride prevented the effects of dDAVP on TTKG [25]. Udelson et al. investigated the efficacy of TLV monotherapy compared to FUR monotherapy and the combination of TLV and FUR in patients complicated by HF and systolic dysfunction with normal kidney function [26]. Compared with baseline uNa excretion values obtained after diuretic withdrawal, there were no significant differences in ΔuNa excretion from baseline during TLV therapy without a loop diuretic. The result of a significant reduction in aldosterone levels during TLV therapy [26] suggested that diuresis during TLV therapy may not occur simply by aquaresis, but rather may be partly due to no upregulatory effect of TLV on RAS. Therefore, according to the findings of this subanalysis, TLV probably increases uNa excretion and decreases uK excretion, and thus directly overcomes FUR resistance.

In addition to stimulating AQP2 expression in both the inner and outer medulla, AVP also stimulated the expression of urea transporters (UT-A1 and UT-A3) in the inner medulla [27, 28]. Urea transporters rapidly reabsorb urea, a process that is regulated by AVP. It is important to maintain a high urea concentration and to set up the osmotic gradient in the inner medullary interstitium [29]. Therefore, TLV should theoretically increase uUN excretion. Recently, in fact, a screening study was performed in rodents to identify UT-A1-selective inhibitors with suitable pharmacological properties [30]. Owing to their unique mechanism of action on the renal countercurrent mechanisms, UT-A1 inhibitors can increase urine volume by solute diuresis [31]. Mori et al. [17] conducted a study in patients undergoing peritoneal dialysis who were administered FUR. The study indicated that the responders to TLV (increased UV > 400 mL/day) had an increased uUN excretion, but the non-responders had a decreased uUN excretion. However, assessment of the actual uUN excretion was difficult due to a shift of UN between sUN and UN in the peritoneal dialysate. In this subanalysis, ΔuUN excretion was greater in the add-on TLV group than in the increased FUR group, but the difference was not significant.

UV is directly related to the total number of osmoles excreted in a day. Solutes responsible for driving water excretion could be electrolytes, such as Na and K, or urea [32]; therefore if uOsm decreases because of TLV, UV necessarily increases. Potential natriuresis may be less effective than aquaresis because the uOsm was decreased in the TLV group (Fig. 4). It may be difficult to identify whether TLV stimulated uNa excretion, based only on uOsm, not only because the aquaretic effect was stronger than that of osmotic diuresis, but also because the decrease in the osmotic gradient between the collecting duct and interstitium can make reabsorption of water in the inner medulla difficult. The augmented aquaretic effect and potential natriuretic effect of TLV may increase UV.

To the best of our knowledge, this is the first report of the urine solute excretion profiles of TLV as add-on therapy to FUR in patients with CHF complicated by advanced CKD (not including dialysis patients); however, it had several potential limitations. First, 31 patients did not complete the study; therefore, the remaining 50 patients might be the patients who had mild-to-moderate effects. In those patients, 16 patients had missing data, making the number of patients in each group of this subanalysis relatively small. Specifically, the FUR group had a large proportion of missing data. Mean sCr was significantly lower in the missing data subgroup ($n = 12$) than in the subgroup analysis ($n = 17$) ($P = 0.040$) (Supplementary Table 1). Therefore, the lower sCr in the missing data

subgroup may have contributed to a more diuretic effect, especially natriuretic effect which was proved by higher E-C_{Osm} consisted of higher uNa excretion in the FUR group if the subgroup was included in the analysis because furosemide generally has a less natriuretic effect in patients with more advanced CKD. Second, the urine solutes were not measured every day, meaning detailed changes were not known. Third, data for dietary factors which could have affected the uNa and uK excretion were not evaluated due to the nature of the acute treatment phase of CHF. Fourth, the plasma aldosterone concentration was not determined, which may have limited the ability of this study to determine the influence of the increased FUR and add-on TLV.

Conclusion

Administration of TLV as an add-on therapy to FUR increased renal water and Na excretion more than increased FUR in patients with CHF complicated by advanced CKD.

Acknowledgements Portions of this work were presented at the Annual Meeting of the American Society of Nephrology in Chicago, Illinois, in November 2016. We are thankful to Ms. Kazuko Nakamura for managing this study as a data and financial manager. We also greatly benefited from the expertise of Editage (http://www.editage.jp) with regard to English language editing.

Funding The K-STAR study was supported by The Kidney Foundation, Japan.

Compliance with ethical standards

Conflict of interest Naoto Tominaga, Takayuki Inomata, Naoki Sato, and Yugo Shibagaki received lecture fees from Otsuka Pharmaceutical Co., Ltd. Yugo Shibagaki received research grants from Otsuka Pharmaceutical Co., Ltd.

Ethical approval All procedures performed in studies involving human participants were in accordance with the ethical standards of the institutional research committee at which the studies were conducted (IRB approval number 2301) and with the 1964 Helsinki declaration and its later amendments or comparable ethical standards.

Registration of clinical trials The original trial of this subanalysis [The Kanagawa Aquaresis Investigators Trial of TLV on Heart Failure (HF) Patients with Renal Impairment (K-STAR)] was registered with the University Hospital Medical Information Network (UMIN ID 000009201).

Informed consent Informed consent was obtained from all individual participants included in the study.

References

1. Greenberg A. Diuretic complications. Am J Med Sci. 2000;319:10–24.
2. Wilcox CS. Metabolic and adverse effects of diuretics. Semin Nephrol. 1999;19:557–68.
3. Sarafidis PA, Georgianos PI, Lasaridis AN. Diuretics in clinical practice. Part II: electrolyte and acid-base disorders complicating diuretic therapy. Expert Opin Drug Saf. 2010;9:259–73.
4. Yamamura Y, Nakamura S, Itoh S, et al. OPC-41061, a highly potent human vasopressin V2-receptor antagonist: pharmacological profile and aquaretic effect by single and multiple oral dosing in rats. J Pharmacol Exp Ther. 1998;287:860–7.
5. Onogawa T, Sakamoto Y, Nakamura S, Nakayama S, Fujiki H, Yamamura Y. Effects of tolvaptan on systemic and renal hemodynamic function in dogs with congestive heart failure. Cardiovasc Drugs Ther. 2011;25(Suppl 1):S67–76.
6. Inomata T, Ikeda Y, Kida K, et al. Effects of additive tolvaptan versus increased furosemide on heart failure with diuretic resistance and renal impairment: results from the K-STAR study. Circ J 2017; 82:159–167.
7. Matsuo S, Imai E, Horio M, et al. Revised equations for estimated GFR from serum creatinine in Japan. Am J Kidney Dis. 2009;53:982–92.
8. Shimizu K, Karosawa T, Sanjo T, Hoshino M, Nonaka T. Solute-free versus electrolyte-free water clearance in the analysis of osmoregulation. Nephron. 2002;91:51–7.
9. Ecelbarger CA, Kim GH, Masilamani S, et al. Vasopressin-mediated regulation of epithelial sodium channel abundance in rat kidney. Am J Physiol Renal Physiol. 2000;279:F46–53.
10. Bankir L, Fernandes S, Bardoux P, Bouby N, Bichet DG. Vasopressin-V2 receptor stimulation reduces sodium excretion in healthy humans. J Am Soc Nephrol. 2005;16:1920–8.
11. Stockand JD. Vasopressin regulation of renal sodium excretion. Kidney Int. 2010;78(9):849–56.
12. Goldsmith SR, Gheorghiade M. Vasopressin antagonism in heart failure. J Am Coll Cardiol. 2005;46:1785–91.
13. Musabayane CT, Forsling ML, Balment RJ. Arginine vasopressin increases renal sodium excretion in the anesthetized rat through V1 receptors. Ren Fail. 1997;19:23–32.
14. Perucca J, Bichet DG, Bardoux P, Bouby N, Bankir L. Sodium excretion in response to vasopressin and selective vasopressin receptor antagonists. J Am Soc Nephrol. 2008;19:1721–31.
15. Nonoguchi H, Takayama M, Owada A, et al. Role of urinary arginine vasopressin in the sodium excretion in patients with chronic renal failure. Am J Med Sci. 1996;312:195–201.
16. Cowley AW Jr. Role of the renal medulla in volume and arterial pressure regulation. Am J Physiol. 1997;273(1 Pt 2):R1–15.
17. Mori T, Oba I, Koizumi K, et al. Beneficial role of tolvaptan in the control of body fluids without reductions in residual renal function in patients undergoing peritoneal dialysis. Adv Perit Dial. 2013;29:33–7.
18. Mori T, Kurasawa N, Ohsaki Y, et al. Role of chronic use of tolvaptan in patients with heart failure undergoing peritoneal dialysis. Adv Perit Dial. 2016;32:39–43.
19. Mori T, Ohsaki Y, Oba-Yabana I, Ito S. Diuretic usage for protection against end-organ damage in liver cirrhosis and heart failure. Hepatol Res. 2017;47:11–22.
20. Cowley AW, Roman RJ, Fenoy FJ, Mattson DL. Effect of renal medullary circulation on arterial pressure. J Hypertens Suppl. 1992;10:S187–S193.
21. Shoaf SE, Beamer SL, Bricmont P, et al. Pharmacokinetic and pharmacodynamic interaction between tolvaptan, a non-peptide AVP antagonist, and furosemide or hydrochlorothiazide. J Cardiovasc Pharmacol. 2007;50:213–22.
22. Costello-Boerrigter LC, Smith WB, Boerrigter G, et al. Vasopressin-2-receptor antagonism augments water excretion without changes in renal hemodynamics or sodium and potassium excretion in human heart failure. Am J Physiol Renal Physiol. 2006;290:F273–278.

23. Inomata T, Izumi T, Matsuzaki M, Hori M, Hirayama A. Phase III clinical pharmacology study of tolvaptan. Cardiovasc Drugs Ther. 2011;25(Suppl 1):S57–63.
24. Field MJ, Stanton BA, Giebisch GH. Influence of ADH on renal potassium handling: a micropuncture and microperfusion study. Kidney Int. 1984;25:502–11.
25. Blanchard A, Frank M, Waerzner G, et al. Antinatriuretic effect of vasopressin in humans is amiloride sensitive, thus ENaC dependent. Clin J Am Soc Nephrol. 2011;6:753–9.
26. Udelson JE, Bilsker M, Hauptman PJ, et al. A multicenter, randomized, double-blind, placebo-controlled study of tolvaptan monotherapy compared to furosemide and the combination of tolvaptan and furosemide in patients with heart failure and systolic dysfunction. J Card Fail. 2011;17:973–81.
27. Bankir LT, Trinh-Trang-Tan MM. Renal urea transporters. Direct and indirect regulation by vasopressin. Exp Physiol 2000; 85 Spec No:243S–252S.
28. Cai Q, Nelson SK, McReynolds MR, Diamond-Stanic MK, Elliott D, Brooks HL. Vasopressin increases expression of UT-A1, UT-A3, and ER chaperone GRP78 in the renal medulla of mice with a urinary concentrating defect. Am J Physiol Renal Physiol. 2010;299:F712–F719.
29. Fenton RA, Chou CL, Stewart GS, et al. Urinary concentrating defect in mice with selective deletion of phloretin-sensitive urea transporters in the renal collecting duct. Proc Natl Acad Sci USA. 2004;101:7469–74.
30. Esteva-Font C, Cil O, Phuan PW, et al. Diuresis and reduced urinary osmolality in rats produced by small-molecule UT-A-selective urea transport inhibitors. FASEB J. 2014;28:3878–90.
31. Esteva-Font C, Anderson MO, Verkman AS. Urea transporter proteins as targets for small-molecule diuretics. Nat Rev Nephrol. 2015;11:113–23.
32. Levin A, Klassen J, Halperin ML. Challenging consults: application of principles of physiology and biochemistry to the bedside. Osmotic diuresis: the importance of counting the number of osmoles excreted. Clin Invest Med. 1995;18:401–5.

Clinical Rheumatology (2018) 37:3373–3380
https://doi.org/10.1007/s10067-018-4142-y

ORIGINAL ARTICLE

Hemodynamic heterogeneity of connective tissue disease patients with borderline mean pulmonary artery pressure and its distinctive characters from those with normal pulmonary artery pressure: a retrospective study

Yusa Asari[1] · Yoshioki Yamasaki[1] · Kosei Tsuchida[1] · Kengo Suzuki[2] · Yoshihiro J. Akashi[2] · Takahiro Okazaki[1] · Shoichi Ozaki[1] · Hidehiro Yamada[3] · Kimito Kawahata[1]

Received: 20 February 2018 / Revised: 2 May 2018 / Accepted: 8 May 2018 / Published online: 18 May 2018
© International League of Associations for Rheumatology (ILAR) 2018

Abstract

To clarify whether patients with connective tissue disease (CTD)-associated borderline mean pulmonary artery pressure (mPAP) have distinctive hemodynamic characteristics from those with normal mPAP and whether pathogenesis is as heterogeneous as manifest pulmonary hypertension (PH). Seventy-five CTD patients who underwent right heart catheterization (RHC) from 2008 through 2016 were retrospectively analyzed. We compared between-group differences in clinical and hemodynamic findings: normal mPAP ($n = 35$), borderline mPAP ($n = 15$), and PH ($n = 25$). A therapeutic intervention trial based on RHC results was performed in nine patients. The values of tricuspid regurgitation pressure gradient (TRPG) in patients with borderline mPAP were comparable at rest but became higher after exercise compared to those with a normal mPAP ($P = 0.01$). Pulmonary artery wedge pressure in patients with borderline mPAP was higher than in those with normal mPAP ($P < 0.0001$) and comparable to those with PH. Each of the three patients was treated for pre-capillary and post-capillary disease and two for interstitial lung disease (ILD). During the mean follow-up period of 40 months, mPAP or TRPG normalized in all patients treated for pre-capillary and post-capillary disease. One patient with severe ILD developed to PH and died from it. CTD patients with borderline mPAP, the underlining pathogenesis of which is heterogeneous as PH, have distinctive hemodynamic characteristics from those with normal mPAP. Whether a specific treatment targeting the inflammatory process or local hemodynamics may alter the clinical course to PH is a topic for future research.

Keywords Borderline mean pulmonary artery pressure · Connective tissue diseases · Left heart disease · Pulmonary arterial hypertension

✉ Yoshioki Yamasaki
yams@marianna-u.ac.jp

[1] Division of Rheumatology and Allergology, Department of Internal Medicine, St. Marianna University School of Medicine, 2-16-1, Sugao, Miyamae, Kawasaki City, Kanagawa 216-8511, Japan

[2] Division of Cardiology, Department of Internal Medicine, St. Marianna University School of Medicine, 2-16-1, Sugao, Miyamae, Kawasaki City, Kanagawa 216-8511, Japan

[3] Medical Center for Rheumatic Diseases, Seirei Yokohama Hospital, 215, Iwaicho, Hodogaya, Yokohama City, Kanagawa 240-8521, Japan

Introduction

Pulmonary hypertension (PH) is defined as a mean pulmonary artery pressure (PAP) ≥ 25 mmHg, measured by right heart catheterization (RHC) at rest [1]. PH is a severe and fatal complication of connective tissue diseases (CTDs), such as systemic sclerosis (SSc) [2]. Early identification of PH is associated with improved long-term survival in patients with CTD-associated PH (CTD-PH) [3, 4].

Borderline mean PAP (mPAP), defined by values of 21–24 mmHg, may comprise a transition phase from a normal pulmonary hemodynamic condition to pulmonary arterial hypertension (PAH), with this range of pressures possibly being representative of the early stage of PAH [5, 6]. Though early

therapeutic intervention with pulmonary vasodilators is needed to improve the survival of patients with PAH [4], the accumulated evidence is not currently sufficient to conclude that treatment for PAH improves clinical outcomes when pulmonary vasodilators are initiated before developing PAH. In addition, CTD-PH is caused by various cardiopulmonary comorbidities. Therefore, it is possible that borderline mPAP, like overt PH, is caused not only by pulmonary vasculopathy but also by cardiac and pulmonary complications [7].

In this study, we compared clinical and hemodynamic characteristics between patients with normal mPAP, borderline mPAP, and overt PH using RHC and exercise echocardiography, and evaluated how pulmonary vascular damage and left heart disease contribute to PAP elevation in patients with borderline mPAP. Furthermore, we retrospectively evaluated if provision of treatment, based on appropriate hemodynamic assessments prevents the development of overt PH.

Material and methods

Patients

We conducted a retrospective analysis of 75 patients with CTDs who underwent RHC for suspected PH at the St. Marianna University Hospital, Kawasaki, Japan, from January 2008 to March 2016. Of these patients, 51 underwent exercise echocardiography using the Master's double two-step exercise test [8]. The diagnosis of SSc [9] and systemic lupus erythematosus (SLE) [10] was based on the criteria of the American College of Rheumatology. The diagnosis of mixed connective tissue disease (MCTD) [11] and polymyositis/dermatomyositis [12] were based on the criteria of Kasukawa and the criteria of Bohan and Peter, respectively. The study protocol conformed to the Declaration of Helsinki and was approved by the Institutional Review Board of the St. Marianna University School of Medicine (No. 3172).

Definition and classification of PH

PH was classified, according to the Nice classification in 2013 [1], as a mPAP ≥ 25 mmHg, with the five PH groups defined as follows: groups 1 and 2 PH were defined as a pulmonary artery wedge pressure (PAWP) of ≤ and > 15 mmHg, respectively; group 3 PH was defined as PH with a percent predicted forced vital capacity (%FVC) of ≤ 70%, in combination with evidence of interstitial lung disease (ILD) on high-resolution computed tomography; group 4 PH was defined as PH with the presence of chronic pulmonary thromboembolism on perfusion/ventilation scintigraphy; and group 5 PH was defined as PH with uncertain causes or multiple factors. For example, blood diseases, systemic diseases, metabolic diseases, and other rare diseases are causes. Borderline mean PAP was defined as mPAP of 21–24 mmHg.

Data regarding the assessment of left heart disease or pulmonary disease using myocardial scintigraphy, cardiac magnetic resonance imaging (MRI), and pulmonary function test were also included in the analysis.

Resting and exercise echocardiography

The Master's double two-step exercise [13] was used for exercise echocardiography. This exercise testing protocol is generally used in Japan because of its simplicity and convenience [8]. Our procedures were based on previously reported methodology for the test [8]. The tricuspid regurgitation pressure gradient (TRPG) was measured during echocardiography [8] performed with patients lying supine on a bed. Measurements were obtained at four time-points: prior to the exercise test, immediately after the exercise test, and at 3- and 5-min post-test. The following measurements were obtained: left atrial dimension, the average ratio of early diastolic trans-mitral flow velocity and diastolic mitral annular velocity (E/e'), left atrial volume index, and the ejection fraction (EF).

RHC

All RHCs were performed by cardiologists using a Swan-Ganz catheter as described previously [8]. PAP was monitored and averaged over several respiratory cycles during spontaneous breathing. Systolic PAP, diastolic PAP, mPAP, and PAWP were measured. Cardiac output (CO) was measured according to the thermodilution technique, using an analog computer system [8].

Treatment

Based on the assessment, treatment for pre-capillary vasculopathy (pulmonary vasodilators) and left heart disease (angiotensin II receptor blocker, calcium channel blocker, β-blocker, and diuretics) were introduced. Therapeutic strategies for ILD were decided based on each CTD. Immunosuppressants were used in the presence of accompanying disease activity, such as SLE, MCTD, and Takayasu arteritis (TA). Because this is a retrospective study, treatment selection was at the discretion of individual physicians.

Follow-up data

We investigated the clinical course in nine patients with borderline mPAP whom we could follow up. Data on treatment, repeated RHC, and rest/exercise echocardiography, performed for the evaluation of the treatment, were collected. We defined "improvement" as a normalization of the mPAP (< 25 mmHg) or TRPG (< 40 mmHg) on follow-up RHC or echocardiography.

We defined "deterioration" as the development of manifest PH during the observation period.

Statistical analysis

Statistical analysis was performed using Prism 4.0c for Macintosh (GraphPad Software Inc., San Diego, CA, USA) and SPSS 17.0 for Macintosh (SPSS Inc., Chicago, IL, USA). Fisher's exact test was used for comparisons involving binary data, and the Mann-Whitney *U* test was used for comparisons involving continuous data. Receiver operating characteristic (ROC) curve analysis was performed to determine the optimal cut-off value of TRPG obtained from exercise echocardiography to distinguish patients with borderline mPAP from those with normal mPAP. Kaplan-Meier analysis was used for survival analysis.

Results

Of the 75 patients enrolled in the study, 25 (33%) had PH. Of these 25 patients, 13 (52%) were classified as having group 1 PH, 5 (20%) as group 2 PH, and 7 (28%) as group 3 PH. Fifteen patients (20%) had borderline mPAP, and the remaining 35 patients (47%) had normal mPAP. No patients with group 4 PH were identified.

Baseline characteristics of the patients enrolled in the study are reported in Table 1. The groups were comparable with regard to the distribution of age and sex. SSc was the most common diagnosis among enrolled patients (61%), followed by MCTD (16%). Although 47% of the patients with borderline mPAP had a WHO Functional Class (WHO-FC) I, only two patients with manifest PH had a WHO-FC I ($P = 0.01$). Anti-centromere antibodies were identified in about 30–40% of patients in all three PH groups, and these were the most frequently detected autoantibodies. The values of brain natriuretic peptide (BNP) in patients with borderline mPAP, which is widely used for screening of PH, were lower than those with PH but they were comparable to those with normal mPAP. Percent-predicted diffusion capacity of the lungs for carbon monoxide (%DL_{CO}) tended to be low in patients with borderline mPAP compared with those with normal mPAP ($P = 0.06$). ILD frequency was not significantly different among the three PH groups.

Echocardiography parameters, measured at rest and post-exercise, are shown in Table 2. The value of TRPG in patients with borderline mPAP was comparable to that in patients with normal mPAP. After exercise, however, a higher increase in TRPG was observed in patients with borderline mPAP compared to those with normal mPAP. A higher TRPG was observed, not only immediately after exercise ($P = 0.02$), but also at 3 min ($P = 0.02$) and 5 min after exercise ($P = 0.01$). ROC analysis was performed to determine the cut-off value of TRPG at 5 min after exercise. The value of it could differentiate patients with borderline mPAP from those with normal mPAP, with a sensitivity of 81%, and a specificity of 56%, was achieved at a cut-off TRPG value of 34 mmHg (area under the curve = 0.75). E/e', which is used to identify diastolic left ventricular dysfunction, was increased in patients with borderline mPAP ($P = 0.01$). No difference in EF was identified between patients with borderline and normal mean PAP.

RHC data from patients with borderline mPAP, normal mPAP, and overt PH were compared (Table 3). Parameters indicative of pre-capillary disease, such as the pulmonary vascular resistance (PVR) and the transpulmonary gradient (TPG), were increased in patients with borderline mPAP compared to those with normal mPAP ($P = 0.03$ in PVR, $P = 0.03$ in TPG), though these values were lower than those in patients with PH ($P = 0.0001$ in PVR, $P = 0.0002$ in TPG). In addition, the PAW*P* value was higher among patients with borderline mPAP than in those with normal mPAP ($P < 0.0001$), but comparable to those with PH ($P = 0.84$). Therefore, there was heterogeneity in the cause of borderline mPAP in our patients with CTDs, which was associated with either pre-capillary or post-capillary disease. Cardiac function, including the CO and the cardiac index, were well preserved among patients with borderline mPAP (not significant between normal mPAP vs. borderline mPAP).

Figure 1 shows the PVR and PAWP values in 15 patients with borderline mPAP. Patients with borderline mPAP exhibited an elevation of either PVR or PAWP, suggestive of underlying pre-capillary or post-capillary disease, respectively (Fig. 1). The underlying pathogenesis in patients with intermediate values was difficult to evaluate using this approach.

We reviewed the long-term clinical course of the 15 patients. Mean follow-up was 99 ± 40 months. The 5- and 10-year survival was 100 and 75%, respectively. Repeated data on RHC or echocardiography were available in 9 of 15 patients with borderline mPAP (Table 4). Hemodynamics was monitored after treatment for a mean period of 40 ± 20 months by using repeated RHC or echocardiography.

Three of the patients (cases 1–3) were diagnosed with pulmonary vasculopathy based on a lower PAWP value on RHC and a normal E/e' on echocardiography. Three patients (cases 4–6) were diagnosed with left heart disease, with an elevation in PAWP (≥ 15 mmHg) in two cases (5 and 6), with left heart abnormalities identified on cardiac MRI in two cases (4 and 6). The disease status could not be clearly classified into pre-capillary or post-capillary disease in one patient with TA (case 9). All the three patients diagnosed (cases 1-3) as having pulmonary vasculopathy were treated with pulmonary vasodilators.

Case 1 developed dyspnea after 23 months of lupus-associated pericardial effusion, which was treated with prednisolone (30 mg) and azathioprine (50 mg). Borderline mPAP was diagnosed by RHC. Because there were no serological

Table 1 Baseline characteristics of patients with normal mPAP, borderline mPAP, and PH

	Borderline mPAP (n = 15)	Normal mPAP (n = 35)	PH (n = 25)
Age (± SD)	60 (± 19)	60 (± 15)	59 (± 15)
Sex, males/females (female, %)	4/11 (73)	4/31 (89)	3/22 (88)
CTDs			
Lc-SSc, n (%)/Dc-SSc, n (%)	7 (47)/3 (20)	15 (43)/8 (23)	10 (40)/3 (12)
SLE, n (%)	2 (13)	2 (6)	4 (16)
MCTD, n (%)	2 (13)	6 (17)	4 (16)
PM/DM, n (%)	0 (0)	2 (6)	1 (4)
Others, n (%)	1 (7)	2 (6)	3 (12)
Smokers, n (%)	3 (20)	11 (31)	4 (16)
Hypertension, n (%)	5 (33)	11 (31)	3 (12)
Diabetes mellitus, n (%)	0 (0)	0 (0)	0 (0)
Raynaud phenomenon, n (%)	9 (60)	19 (54)	17 (24)
Telangiectasia, n (%)	1 (7)	3 (9)	3 (13)
ILD, n (%)	10 (67)	17 (49)	13 (41)
WHO-FC I/II (n/n)	7[a]/6	19/16	2/8
WHO-FC III/IV (n/n)	1/1[b]	0/0	1/14
Autoantibodies			
Anti-centromere, n (%)	6 (40)	11 (31)	8 (32)
Anti-Scl-70, n (%)	2 (13)	6 (17)	1 (4)
Anti-dsDNA, n (%)	3 (20)	2 (5)	3 (12)
Anti-RNP, n (%)	3 (20)	7 (20)	7 (28)
Anti-SSA, n (%)	4 (27)	9 (26)	9 (36)
BNP (IQR) (pg/mL)	57 (27–198)[c]	65 (31–114)	169 (50–585)
%FVC (± SD)	85.2 (± 23.5)	91.4 (± 20.8)	78.7 (± 16.3)
$\%DL_{CO}$ (± SD)	42.8 (± 16.5)[d]	54.4 (± 20.3)	49.4 (± 25.2)
KL-6 (± SD) (U/ml)	687 (± 641)	571 (± 472)	702 (± 544)

[a] $P = 0.01$ vs. PH

[b] $P = 0.002$ vs. PH

[c] $P = 0.02$ vs. PH

[d] $P = 0.06$ vs. normal mPAP

mPAP mean pulmonary artery pressure, *PH* pulmonary hypertension, *CTDs* connective tissue diseases, *Lc-SSc* limited cutaneous systemic sclerosis, *Dc-SSc* diffuse cutaneous systemic sclerosis, *SLE* systemic lupus erythematosus, *MCTD* mixed connective tissue disease, *PM/DM* polymyositis/dermatomyositis, *ILD* interstitial lung disease, *BNP* brain natriuretic peptide, *IQR* interquartile range, *%FVC* percent predicted forced vital capacity, $\%DL_{CO}$ percent predicted diffusion capacity of the lungs for carbon monoxide

markers of SLE disease activity, bosentan (125 mg) and beraprost (120 μg) were added. mPAP was normalized on repeated RHC, performed 9 months after the first one.

Case 2 was diagnosed as MCTD 13 months before the diagnosis of borderline mPAP. Initially, she was treated with pulse corticosteroid therapy with methylprednisolone, followed by 60 mg of prednisolone for fever and thrombocytopenia. When prednisolone was tapered to 15 mg, the patient reported increasing fatigue. Borderline mPAP was suspected on exercise echocardiography and diagnosed by RHC. Azathioprine (50 mg), used in combination with pulmonary vasodilators, such as sildenafil (40 mg), bosentan (250 mg), and beraprost (60 μg), was added, which resulted in normalization of TRPG after exercise.

Case 3, a patient with limited cutaneous SSc carrying anti-centromere antibody, developed borderline mPAP, 29 months from the onset. Treatment with bosentan (250 mg) and tadarafil (40 mg) was initiated. Normalized mPAP was identified on repeated RHC performed 10 months after the first one.

Treatment for left heart disease was introduced in three patients (cases 4–6). Case 4, a patient with limited cutaneous SSc carrying anti-centromere antibody, was diagnosed as having borderline mPAP. Although she did not have any symptoms associated with PH, an elevation of TRPG was identified by exercise echocardiography on routine screening. She developed hypertension and was treated with candesartan (8 mg) and nifedipine (40 mg), introduced at 24 and 36 months,

Table 2 Echocardiography parameters obtained at rest and after exercise in patients with borderline and normal mPAP

	Borderline mPAP ($n = 15$)	Normal mPAP ($n = 35$)	*P* value
Rest TRPG (± SD) (mmHg)	31.2 (± 8.0)	28.3 (± 6.9)	0.17
Post-exercise TRPG (± SD) (mmHg)	58.4 (± 11.6)	49.0 (± 11.6)	0.02
Post 3 min. TRPG (± SD) (mmHg)	47.4 (± 9.1)	39.6 (± 9.4)	0.02
Post 5 min. TRPG (± SD) (mmHg)	40.0 (± 7.6)	32.8 (± 7.4)	0.01
LAD (± SD) (mm)	33.4 (± 6.7)	34.4 (± 5.2)	0.67
E/e' (± SD)	11.3 (± 4.2)	8.3 (± 1.9)	0.01
LAVI (± SD) (mL/m^2)	31.8 (± 16.2)	31.2 (± 10.9)	0.80
EF (± SD) (%)	70.8 (± 9.1)	69.0 (± 6.2)	0.34

mPAP mean pulmonary artery pressure, *TRPG* tricuspid regurgitation pressure gradient, *LAD* left atrial dimension, *E/e'* the average ratio of early diastolic transmitral flow velocity and diastolic mitral annular velocity, *LAVI* left atrial volume index, *EF* ejection fraction

respectively, from the time of diagnosis. Since myocardial scintigraphy showed evidence of cardiomyopathy, left heart disease-associated borderline mPAP was considered. Treatment with candesartan (8 mg) and nifedipine (40 mg) was continued. The value of TRPG after 5 min of exercise improved at 60 months after the first RHC.

Case 5, a patient with SLE, developed dyspnea on effort 154 months after the onset of lupus, with borderline mPAP diagnosed by RHC. Although PAWP was >15 mmHg, she was initially treated with a low dose of bosentan (62.5 mg), and this treatment was discontinued due to an elevation of TRPG. We re-evaluated the cause of borderline mPAP and administered bisoprolol fumarate (1.25 mg), a β-blocker, for the treatment of left heart disease. A normal range of mPAP was identified on repeated RHC, performed 53 months after the first RHC.

Case 6 was diagnosed as MCTD. Degradation of Raynaud's phenomenon and dyspnea during exercise worsened and RHC was performed. With evidence of an elevated PAWP (>15 mmHg), myocarditis on MRI and myocardial scintigraphy, furosemide (20 mg) was started. Pulmonary vasodilators, including bosentan (125 mg) and sildenafil (60 mg) were also initiated. A normal range of mPAP was identified on repeated RHC and performed 12 months after the first RHC. Since we evaluated the cause of borderline mPAP as left heart disease, bosentan treatment was terminated. On the third RHC, performed 43 months after the second RHC, showed a normalized PA and PAWP.

Two patients were diagnosed with ILD (cases 7 and 8), based on a low %FVC of 53% (case 7) or 60% (case 8), and were followed without specific treatment. Case 7 was diagnosed with diffuse cutaneous SSc, with anti-Scl-70 antibody. In case 7, although there was no rapid progression of ILD, no improvement in hemodynamics was observed over the course of 14 months.

Case 8 was diagnosed with limited cutaneous SSc with anti-centromere antibody. She progressed to ILD-associated

Table 3 Comparison of RHC results in patients with borderline and normal mPAP and those with manifest PH

	Borderline mPAP ($n = 15$)	Normal ($n = 35$)	PH ($n = 25$)	*P* value (borderline mPAP vs. normal)	*P* value (borderline mPAP vs. PH)
sPAP (± SD) (mmHg)	35.2 (± 3.4)	26.6 (± 4.4)	55.2 (± 14)	< 0.0001	< 0.0001
dPAP (± SD) (mmHg)	12.5 (± 1.8)	7.1 (± 3.2)	21.0 (± 7.6)	< 0.0001	< 0.0001
mPAP (± SD) (mmHg)	22.3 (± 1.3)	15.1 (± 2.9)	36.1 (± 8.6)	< 0.0001	< 0.0001
PAWP (± SD) (mmHg)	12.1 (± 3.4)	7.2 (± 2.6)	13.7 (± 7.1)	< 0.0001	0.84
CI (± SD) (l/min/m^2)	4.0 (± 0.6)	4.2 (± 0.9)	3.6 (± 0.9)	0.62	0.13
CO (± SD) (l/min)	5.6 (± 0.9)	5.9 (± 1.4)	5.3 (± 1.7)	0.58	0.36
PVR (± SD) (WU)	1.9 (± 0.7)	1.4 (± 0.5)	4.8 (± 3.3)	0.03	0.0001
TPG (± SD) (mmHg)	10.2 (± 3.5)	7.9 (± 2.4)	22.4 (± 11.2)	0.03	0.0002
DPG (± SD) (mmHg)	0.3 (± 3.5)	−0.1 (± 2.5)	7.3 (± 11.4)	0.87	0.01

RHC right heart catheterization, *mPAP* mean pulmonary artery pressure, *PH* pulmonary hypertension, *sPAP* systolic pulmonary artery pressure, *dPAP* diastolic pulmonary artery pressure, *PAWP* pulmonary artery wedge pressure, *CI* cardiac index, *CO* cardiac output, *PVR* pulmonary vascular resistance, *TPG* (= mPAP − PAWP) transpulmonary pressure gradient, *DPG* (= dPAP − PAWP) diastolic pulmonary vascular pressure gradient

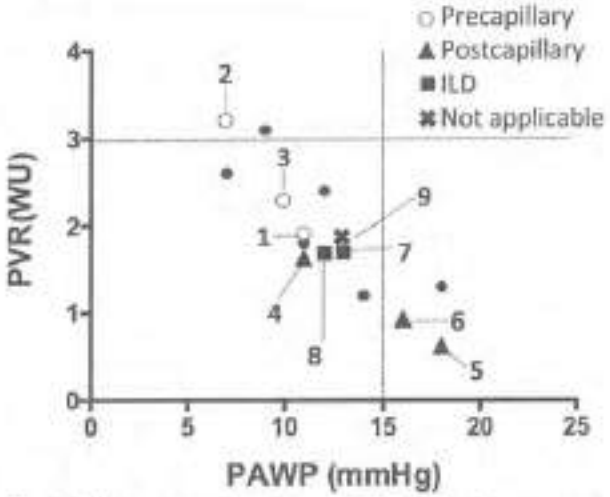

Fig. 1 Pulmonary vascular resistance (PVR) and pulmonary artery wedge pressure (PAWP) in patients with borderline mean PAP

PH and treatment, using domiciliary oxygen therapy, was initiated, 21 months after RHC; but the patient died from respiratory failure, 59 months after diagnosis.

Case 9 was diagnosed with TA and was treated only with prednisolone (50 mg), with the patient's condition improving with immunosuppressive therapy alone.

Discussion

PH is one of the critical organ involvements associated with CTDs [2]. As substantial numbers of patients with CTDs are regularly followed up by their physician, early stage of pulmonary vasculopathy, including borderline mPAP that may represent the early stage of PAH [5, 6], could be detected by routine screening. However, it has not been determined whether treatment of borderline PH [6] could improve survival of patients with CTDs.

Pulmonary vascular disease can be well compensated, with resting PAP increasing with an obstruction of pulmonary circulation of > 50% [14]. Hence, it seems reasonable to consider that early therapeutic intervention for PAH may contribute to improving survival. A previous study provided evidence that the use of pulmonary vasodilators, such as bosentan, could improve the clinical course of patients with SSc presenting with hemodynamic characteristics of borderline PH [15].

Nevertheless, it is important to consider that CTDs are associated with a variety of cardiopulmonary comorbidities, which may contribute to borderline mean PAP [7]. Among patients with PH in our study, as many as 20% of our patients had post-capillary PH, whereas 52% had pre-capillary PH and 28% had ILD-PH. This distribution was consistent with a previous study [16]. It is important to note that post-capillary

Table 4 Follow-up and outcomes in patients with borderline mPAP

Cases	CTDs	Suspected underlining cause/treatment	Outcome (follow-up, months)
1. 58 y/o, female	SLE	Pulmonary vasculopathy/Immunosuppressants (prednisolone 30 mg and azathioprine 50 mg) and pulmonary vasodilators (bosentan 125 mg and beraprost 120 μg)	Improved to normal mPAP (15 mmHg) by RHC (9)
2. 23 y/o, female	MCTD	Pulmonary vasculopathy/Immunosuppressants (pulse IV methy/prednisolone 1000 mg ×3, prednisolone 15 mg, and azathioprine 50 mg) and pulmonary vasodilators (sildenafil 40 mg, bosentan 250 mg, and beraprost 60 μg)	Improved to TRPG (5) (18 mmHg) by echocardiography (55)
3. 78 y/o, male	Lc-SSc	Pulmonary vasculopathy/Pulmonary vasodilators (bosentan 250 mg and tadalafil 40 mg)	Improved to normal mPAP (14 mmHg) by RHC (10)
4. 68 y/o, female	Lc-SSc	Left heart diseases/Candesartan 8 mg and nifedipine 40 mg	Improved to normal TRPG (5) (30 mmHg) by echocardiography (60)
5. 68 y/o, female	SLE	Left heart diseases/Bisoprolol fumarate 1.25 mg (Bosentan was temporality used.)	Improved to normal mPAP (14 mmHg) and PAWP (4 mmHg) by RHC (53)
6. 44 y/o, female	MCTD	Left heart diseases/Furosemide 20 mg (Bosentan was temporality used. Low dose of sildenafil 40 mg was used at 3rd RHC.)	Improved to normal mPAP (12 mmHg/13 mmHg) and PAWP (5 mmHg/4 mmHg) by RHC (2nd/3rd RHC, 12/55).
7. 64 y/o, female	Dc-SSc	ILD/None	Not improved by echocardiography (14)
8. 67 y/o, female	Lc-SSc	ILD/Oxygen	Deteriorated to PH (mPAP 27 mmHg) (21), and died (59)
9. 19 y/o, male	TA	Unknown/Immunosuppressants (prednisolone 50 mg)	Improved to normal TRPG (5) (25 mmHg) by echocardiography (27)

mPAP mean pulmonary artery pressure, *y/o* years old, *CTDs* connective tissue diseases, *SLE* systemic lupus erythematosus, *MCTD* mixed connective tissue disease, *Lc-SSc* limited cutaneous systemic sclerosis, *Dc-SSc* diffuse cutaneous systemic sclerosis, *TA* Takayasu arteritis, *IV* intravenous, *RHC* right heart catheterization, *ILD* interstitial lung disease, *TRPG (5)* tricuspid regurgitation pressure gradient at 5-min post-exercise, *PAWP* pulmonary artery wedge pressure, *PH* pulmonary hypertension

PH in patients with SSc may be revealed only by fluid challenge during RHC [17]. Using fluid challenge, Fox et al. [17] identified overt or occult post-capillary PH in two thirds of patients with PH.

Furthermore, it should be noted that a patient with CTD might share multiple cardiopulmonary involvements associated with PH [18]. The assessment and the management of patients with this condition are difficult, and the introduction of PAH treatments, such as the use of endothelin receptor antagonists [19] and prostaglandins [20], occasionally results in the deterioration of underlying left heart disease. The value of PAWP was significantly elevated in patients with borderline mPAP compared to the PAWP of patients with a normal mPAP and was comparable to the PAWP in patients with overt PH. These results indicate that therapeutic intervention in patients with borderline mPAP, if indicated, should be carefully assessed and monitored. Further studies are needed to evaluate the effects of treatment on the natural course of borderline mPAP. Based on our observation of the clinical course of nine patients with borderline mPAP, we propose that careful assessment and therapeutic intervention, based on the underlying pathogenesis, could result in a favorable outcome. However, in some patients with borderline mPAP, hemodynamic assessment may be difficult or the condition may deteriorate with therapeutic intervention. In these cases, a cautionary approach should be adopted, delaying treatment until hemodynamic assessment and an appropriate diagnosis has been established.

Borderline mPAP progressed to overt PH in one patient in our study group who had a diagnosis of severe ILD. The patient died from respiratory failure 59 months after RHC. Patients with ILD-PH have a lower survival rate than those with isolated PAH, and no treatment has yet been established for this clinical population [21]. A mild elevation in PAP to borderline mPAP may be indicative of a severe stage of PH if it is caused by lung disease or hypoxia. Therefore, identifying a definitive treatment for CTD-associated ILD seems necessary.

The Master's double two-step exercise test is useful to distinguish patients with borderline mPAP from those with normal PAP, although RHC is mandatory to determine the underlying causes of elevated mPAP. Our observation suggests that patients with borderline mPAP already had abnormalities contributing to the increase in PAP, which was clearly distinguished only after the exercise echocardiography.

This study has several limitations. Foremost, the sample size was small, and the outcomes were based on a retrospective analysis of hemodynamic measures. The clinical course of patients with borderline mPAP was not compared to that of a control group. Lastly, the follow-up period was not sufficient to evaluate long-term clinical outcomes. Additionally, there were patients who were lacking hemodynamics data or were lost to follow up, and therefore the study may have observation bias. Longitudinal studies with substantial numbers of patients with CTDs are required in the future. In addition, existence of latent pulmonary veno-occlusive disease, which may be associated or coexisting with PH in patients with CTDs, such as SSc [22], may be underestimated in our study.

In conclusion, since the cause of borderline mPAP in patients with CTDs is heterogeneous, therapeutic intervention should be considered after careful evaluation of the underlying pathogenesis of elevated mPAP in patients with CTDs. Whether a specific treatment targeting the inflammatory process or local hemodynamics may alter the clinical course to PH is a topic for future research. Exercise echocardiography may be useful for identifying patients with borderline mPAP.

Acknowledgments We would like to thank Miss Sakiko Kimura, Mr. Motoki Miyauchi, and the technicians in the Ultrasound center of St. Marianna University Hospital for their assistance. We also appreciate advice from Mr. Takahiko Ueno on statistical analysis.

Compliance with ethical standards

Conflict of interest Yamasaki Y and Hidehiro Y have received speaking fees from Actelion pharmaceuticals Japan Co., Ltd., Nihon Shinyaku Co., Ltd., Pfizer Japan Inc., GlaxoSmithKline K.K., and Bayer Yakuhin, Ltd. The other authors have disclosed no conflicts of interest.

Ethical standards The study protocol conformed to the Declaration of Helsinki, and the study protocol was approved by the Institutional Review Board of the St. Marianna University School of Medicine (No. 3172).

References

1. Simonneau G, Gatzoulis MA, Adatia I, Celermajer D, Denton C, Ghofrani A, Gomez Sanchez MA, Krishna Kumar R, Landzberg M, Machado RF, Olschewski H, Robbins IM, Souza R (2013) Updated clinical classification of pulmonary hypertension. J Am Coll Cardiol 62:D34–D41
2. Shirai Y, Yasuoka H, Okano Y, Takeuchi T, Satoh T, Kuwana M (2012) Clinical characteristics and survival of Japanese patients with connective tissue disease and pulmonary arterial hypertension: a single-center cohort. Rheumatology (Oxford) 51:1846–1854
3. Kahn KP, Byrne DW, Arbogast PG, Doyle TP, Loyd JE, Robbins IM (2003) Outcome in 91 consecutive patients with pulmonary arterial hypertension receiving epoprostenol. Am J Respir Crit Care Med 167:580–586
4. Condliffe R, Kiely DG, Peacock AJ, Corris PA, Gibbs JSR, Vnpi F, Das C, Elliot CA, Johnson M, DeSoyza J, Torpy C, Goldsmith K, Hodgkins D, Hughes RJ, Pepke-Zaba J, Coghlan JG (2009) Connective tissue disease-associated pulmonary arterial hypertension in the modern treatment era. Am J Respir Crit Care Med 179: 151–157
5. Kovacs G, Olschewski H (2015) Borderline pulmonary pressures in scleroderma—a "pre-pulmonary arterial hypertension" condition? Arthritis Res Ther 17:123
6. Valerio CJ, Schreiber BE, Handler CE, Denton CP, Coghlan JG (2013) Borderline mean pulmonary artery pressure in patients with systemic sclerosis: transpulmonary gradient predicts risk of developing pulmonary hypertension. Arthritis Rheum 65:1074–1084

7. Kovacs G, Avian A, Tscherner M, Foris V, Bachmaier G, Olschewski A, Olschewski H (2014) Characterization of patients with borderline pulmonary arterial pressure. Chest 146:1486–1493
8. Suzuki K, Akashi YJ, Manabe M, Mizukoshi K, Kanujima R, Kou S, Takai M, Izumo M, Kida K, Yoneyama K, Omiya K, Yamasaki Y, Yamada H, Nohuoka S, Miyake F (2013) Simple exercise echocardiography using a Master's two-step test for early detection of pulmonary arterial hypertension. J Cardiol 62:176–182
9. Subcommittee for scleroderma criteria of the American rheumatism association diagnostic and therapeutic criteria committee (1980) Preliminary criteria for the classification of systemic sclerosis (scleroderma). Arthritis Rheum 23:581–590
10. Tan EM, Cohen AS, Fries JF, Masi AT, Mcshane DJ, Rothfield NF, Schaller JG, Talal N, Winchester RJ (1982) The 1982 revised criteria for the classification of systemic lupus erythematosus. Arthritis Rheum 25:1271–1277
11. Kasukawa R, Tojo T, Miyawaki S (1987) Preliminary diagnostic criteria for classification of mixed connective tissue disease. In: Kasukawa R, Sharp GC (eds) Mixed connective tissue disease and antinuclear antibodies. Elsevier, Amsterdam, pp 41–47
12. Bohan A, Peter JB (1975) Polymyositis and dermatomyositis (first of two parts). N Engl J Med 292:344–347
13. Master AM (1968) The Master two-step test. Am Heart J 75:809–837
14. Lau EM, Manes A, Celermajer DS, Galie N (2011) Early detection of pulmonary vascular disease in pulmonary arterial hypertension: time to move forward. Eur Heart J 32:2489–2498
15. Kovacs G, Maier R, Aberer E, Brodmann M, Graninger W, Kqiku X, Scheidl S, Tröster N, Hesse C, Rubin L, Olschewski H (2012) Pulmonary arterial hypertension therapy may be safe and effective in patients with systemic sclerosis and borderline pulmonary artery pressure. Arthritis Rheum 64:1257–1262
16. Avouac J, Airo P, Meune C et al (2010) Prevalence of pulmonary hypertension in systemic sclerosis in European Caucasians and metaanalysis of 5 studies. J Rheumatol 37:2290–2298
17. Fox BD, Shimony A, Langleben D, Hirsch A, Rudski L, Schlesinger R, Eisenberg MJ, Joyal D, Hudson M, Boutet K, Serban A, Masetto A, Baron M (2013) High prevalence of occult left heart disease in scleroderma-pulmonary hypertension. Eur Respir J 42:1083–1091
18. Tsuchida K, Yamada H, Yamasaki Y, Suzuki K, Kongoji K, Akashi Y, Ozaki S (2015) Left heart abnormalities in connective tissue disease patients with pre-capillary pulmonary hypertension as well as borderline mean pulmonary arterial pressure. Mod Rheumatol 25:744–747
19. Anand I, McMurray J, Cohn JN, Konstam MA, Notter T, Quitzau K, Ruschitzka F, Lüscher TF (2004) Long-term effects of darusentan on left-ventricular remodelling and clinical outcomes in the endothelin a receptor antagonist trial in heart failure (EARTH): randomised, double-blind, placebo-controlled trial. Lancet 364:347–354
20. Califf RM, Adams KF, McKenna WJ et al (1997) A randomized controlled trial of epoprostenol therapy for severe congestive heart failure: the Flolan international randomized survival trial (FIRST). Am Heart J 134:44–54
21. Mathai SC, Hummers LK, Champion HC, Wigley FM, Zaiman A, Hassoun PM, Girgis RE (2009) Survival in pulmonary hypertension associated with the scleroderma spectrum of diseases: impact of interstitial lung disease. Arthritis Rheum 60: 569–577
22. Johnson SR, Patsios D, Hwang DM, Granton JT (2006) Pulmonary veno-occlusive disease and scleroderma associated pulmonary hypertension. J Rheumatol 33:2347–2350

Prasugrel versus clopidogrel for residual thrombus burden in patients with ST-segment elevation myocardial infarction

an optical coherence tomography study

Yokota, Takashi[a,b]; Higuma, Takumi[b]; Endo, Tomohide[a]; Nishizaki, Fumie[a]; Hanada, Kenji[a]; Yokoyama, Hiroaki[a]; Yamada, Masahiro[a]; Okumura, Ken[c]; Tomita, Hirofumi[a,b]

Author Information

[a]Department of Cardiology

[b]Department of Advanced Cardiovascular Therapeutics, Hirosaki University Graduate School of Medicine, Hirosaki

[c]Division of Cardiology, Saiseikai Kumamoto Hospital, Kumamoto, Japan

Correspondence to Hirofumi Tomita, MD, PhD, Department of Cardiology, Hirosaki University Graduate School of Medicine, 5 Zaifu-cho, Hirosaki 036-8092, Japan Tel: +81 172 395 057; fax: +81 172 359 190; e-mail: tomitah@hirosaki-u.ac.jp

Received May 23, 2018

Accepted September 2, 2018

Coronary Artery Disease: December 2018 - Volume 29 - Issue 8 - p 663-669
doi: 10.1097/MCA.0000000000000663

• Buy

Metrics

Abstract

Background

Prasugrel was shown to inhibit platelet activity more rapidly and consistently than clopidogrel. We compared the effects of prasugrel and clopidogrel on residual thrombus burden assessed by optical coherence tomography after stent implantation in patients with ST-segment elevation myocardial infarction (STEMI).

Patients and methods

A total of 76 patients with STEMI undergoing percutaneous coronary intervention (PCI) within 12 h after the onset were retrospectively enrolled. Of them, 34 patients were treated with prasugrel (loading dose, 20 mg) and the remaining 42 with clopidogrel (loading dose, 300 mg). Stent volume and in-stent thrombus volume were assessed by post-PCI optical coherence tomography.

Results

Baseline clinical characteristics, angiographic findings, and PCI procedure did not differ between the two groups. There was no difference in in-stent volume between patients with prasugrel and clopidogrel [169 (134–214) versus 166 (128–210) mm^3, $P=0.83$]. Patients with prasugrel had a significantly reduced in-stent thrombus volume compared with those with clopidogrel [0.59 (0.16–1.09) vs. 1.08 (0.32–2.30) mm^3, $P=0.03$]. The mean area and maximum area of in-stent thrombus were also significantly smaller in prasugrel than in clopidogrel group [0.03 (0.01–0.05) vs. 0.05 (0.01–0.10) mm^2, $P=0.04$, and 0.45 (0.27–0.75) vs. 0.77 (0.34–1.23) mm^2, $P=0.03$, respectively].

Conclusion

Prasugrel more effectively reduced residual thrombus burden after stent implantation in patients with STEMI, indicating a faster and more potent platelet inhibitory effect of prasugrel compared with clopidogrel.

Copyright © 2018 Wolters Kluwer Health, Inc. All rights reserved.

^Back to Top

Coronary Artery Disease

Never Miss an Issue

Get new journal Tables of Contents sent right to your email inbox Type your email

Get New Issue Alerts

Browse Journal Content

- Most Popular
- Current Issue
- Past Issues
- For Authors
- About the Journal
- Register on the website
- Subscribe
- Get eTOC Alerts

For Journal Authors

- Submit an article
- How to publish with us

Customer Service

- Activate your journal subscription
- Activate Journal Subscription
- Browse the help center
- Help
- Contact us at:
  - EMAIL:
    customerservice@lww.com
  - TEL: (USA):
    TEL: (Int'l):
    800-638-3030 (within USA)
    301-223-2300 (international)
-
- Privacy Policy (Updated March 30, 2020)
- Legal Disclaimer
- Terms of Use
- Open Access Policy
- Sitemap
- RSS Feeds
- LWW Journals

- Copyright © 2020
- Wolters Kluwer Health, Inc. All rights reserved.

Journal of Echocardiography (2018) 16:162–172
https://doi.org/10.1007/s12574-018-0383-7

ORIGINAL INVESTIGATION

Geometry of the left ventricular outflow tract assessed by 3D TEE in patients with aortic stenosis: impact of upper septal hypertrophy on measurements of Doppler-derived left ventricular stroke volume

Dan Koto[1] · Masaki Izumo[1] · Takafumi Machida[2] · Kengo Suzuki[1] · Kihei Yoneyama[1] · Tomomi Suzuki[1] · Ryo Kamijima[1] · Yasuyuki Kobayashi[3] · Tomoo Harada[1] · Yoshihiro J. Akashi[1]

Received: 25 December 2017 / Revised: 14 May 2018 / Accepted: 19 May 2018 / Published online: 24 May 2018
© Japanese Society of Echocardiography 2018

Abstract

Background It is unclear how upper septal hypertrophy (USH) affects Doppler-derived left ventricular stroke volume (SV) in patients with AS. The aims of this study were to: (1) validate the accuracy of 3D transesophageal echocardiography (TEE) measurements of the left ventricular outflow tract (LVOT), (2) evaluate the differences in LVOT geometry between AS patients with and without USH, and (3) assess the impact of USH on measurement of SV.

Methods In protocol 1, both 3D TEE and multi-detector computed tomography were performed in 20 patients with AS [aortic valve area (AVA) ≤ 1.5 cm^2]. Multiplanar reconstruction was used to measure the LVOT short and long diameters in four parts from the tip of the septum to the annulus. In protocol 2, the same 3D TEE measurements were performed in AS patients (AVA ≤ 1.5 cm^2, $n = 129$) and controls ($n = 30$). We also performed 2D and 3D transthoracic echocardiography in all patients.

Results In protocol 1, excellent correlations of LVOT parameters were found between the two modalities. In protocol 2, the USH group had smaller LVOT short and long diameters than the non-USH group. Although no differences in mean pressure gradient, or SV calculated with the 3D method existed between the two groups, the USH group had greater SV calculated with the Doppler method (73 ± 15 vs. 66 ± 15 ml) and aortic valve area (0.89 ± 0.26 vs. 0.73 ± 0.24 cm^2) than the non-USH group.

Conclusions 3D TEE can provide a precise assessment of the LVOT in AS. USH affects the LVOT geometry in patients with AS, which might lead to inaccurate assessments of disease severity.

Keywords Aortic valve stenosis · Echocardiography · Three-dimensional echocardiography · Transesophageal echocardiography

Introduction

From a public health perspective, valvular heart disease, which has a poor prognosis, affects entire communities, and presents an important public health problem in developed countries [1]. Aortic stenosis (AS) is the most common form of valvular heart disease in developed countries and its prevalence is increasing along with the aging population [1–4]. AS is detected in 2–7% of adults aged 65 years and older and characterized by degenerative calcification and congenital valvular defects [1–4]. The accurate assessment of disease severity is critical for the appropriate treatment of patients with AS. Conventional two-dimensional (2D) transthoracic echocardiography (TTE) is the standard approach for evaluating aortic valve area (AVA) calculated by the continuity equation method. AVA derived from continuity equation method relies on geometric assumptions of the left ventricular (LV) outflow tract (LVOT) area, which can amplify errors, particularly in the presence of upper septal hypertrophy (USH). USH, which increases the LVOT velocity, is relatively common in the elderly. However, it is not clear how USH can affect continuity-equation-derived AVA from TTE results in patients with AS. The recently

✉ Masaki Izumo
heartizumo@yahoo.co.jp

[1] Division of Cardiology, Department of Internal Medicine, St. Marianna University School of Medicine, 2-16-1 Sugao, Miyamae-ku, Kawasaki 216-8511, Japan

[2] Department of Pharmacology, St. Marianna University School of Medicine, Kawasaki, Japan

[3] Department of Radiology, St. Marianna University School of Medicine, Kawasaki, Japan

developed three-dimensional (3D) transesophageal echocardiography (TEE) has been a preferred method for the evaluation of aortic root geometry because of its greater accuracy than two-dimensional (2D) TTE and 2D TEE. Earlier studies evaluated the geometry of the aortic root from the aortic annulus to the sinotubular junction; however, the LVOT geometry was not fully elucidated [5–10]. We hypothesized that AS patients with USH have a greater stroke volume (SV) due to increased LVOT velocity despite less LVOT velocity of 1.5 m/s than the AS patients without USH and that this leads to the overestimation of AVA calculated using the continuity equation.

The aims of this study were to: (1) validate the accuracy of 3D TEE measurements of LVOT against multi-detector computed tomography (MDCT) measurements as a reference, (2) evaluate the geometric differences in LVOT geometry between AS patients with and without USH, and (3) assess the impact of USH on the measurement of SV.

Methods

Study population

In protocol 1, 20 patients with AS (AVA $\leq$ 1.5 cm^2) who underwent both MDCT and 3D TEE within 1 month were retrospectively enrolled. Patients allergic to iodine contrast agents and those at high risk for contrast nephropathy were excluded from the analysis. In protocol 2, a total of 152 patients with more-than-moderate AS measured using continuity equation method (AVA < 1.5 cm^2), who underwent TEE between November 2011 and April 2014 and 30 controls were prospectively enrolled. Patients with poor quality images (n = 5, 3.3%), atrial fibrillation (n = 16, 10.5%), moderate or severe mitral regurgitation (n = 0, 0%), and high LVOT velocity (> 1.5 m/s; n = 2, 1.3%) were excluded from the study population. Finally, 129 AS patients and 30 controls were enrolled. The inclusion criteria for the controls in this study were: (1) no significant valvular heart disease, (2) preserved LVEF ($\geq$ 60%), (3) no left ventricular wall motion abnormalities, and (4) no dilated left ventricle. This group was identified from the patients undergoing clinically indicated TEE for investigating a cardioembolic source of stroke. This study was approved by the institutional review board at St. Marianna University School of Medicine. All patients gave their written informed consent before study enrollment.

MDCT

Twenty patients underwent retrospective electrocardiographically gated conventional scans with tube current dose modulation using an MDCT scanner (Aquilion ONE ViSION Edition, Toshiba Medical Systems, Odawara, Japan). This system was equipped with 320-row detector arrays. Computed tomography was performed with a slice thickness of 0.5 mm, tube voltage of 120 kV, and maximum tube current of 580 mA with a gantry rotation time of 275 ms. The voltage was occasionally reduced to 100 kV in patients with thin chests. All patients with heart rates > 65 beats per minute received 10 mg propranolol hydrochloride or 0.125 mg/kg landiolol hydrochloride.

2D and 3D TEE

TEE was performed using an iE33 ultrasound imaging system (Philips Medical Systems, Andover, MA) equipped with a fully sampled matrix array TEE transducer that can display both 2D and live 3D images. After the application of topical anesthetics in the pharynx and intravenous sedation (propofol), the probe was advanced into the esophagus. The aortic valve was visualized from the mid-esophageal position in the zoomed 2D long-axis view (approximately 135°). The 3D full-volume mode of the entire left ventricle, including the aortic root, was then acquired in four consecutive cardiac cycles (frame rate, 23 ± 5 frame/s; range 16–34 frame/s) and stored digitally. The acquisition was triggered with an electrocardiogram R-wave.

MDCT measurements of LVOT

The standard orthogonal axial and sagittal views were used for the initial orientation of the LVOT. The LVOT short and long diameters and areas were analyzed in the coronal, sagittal, and double-oblique transverse views (Fig. 1a). Image reconstruction was performed in 5% intervals from R-wave to R-wave; all 20 phases were loaded into an external workstation. For the LVOT measurements, mid-systolic data sets (20 or 30% of the RR interval) were used. The LVOT from the tip of the septum to the aortic annulus was equally sliced into four parts and each parameter was measured (LVOT 1 = tip of the septum, LVOT 4 = the aortic annulus). These measurements were performed using commercial software (zioTerm2009; Ziosoft Inc, Tokyo, Japan).

3D TEE measurements of LVOT

From the full-volume mode 3D data sets, the two orthogonal long-axis views of LVOT were extracted. A third plane, which was perpendicular to the two long-axis planes, was shifted to adjust the orthogonal 2D cutting plane of the LVOT with quantitative software (QLAB cardiac 3DQ, Philips Medical Systems, Andover, MA, USA). After selecting the mid-systolic frame in which maximal LVOT was visualized, the multiplanar reconstruction planes were aligned at each level of the LVOT to measure the LVOT short and

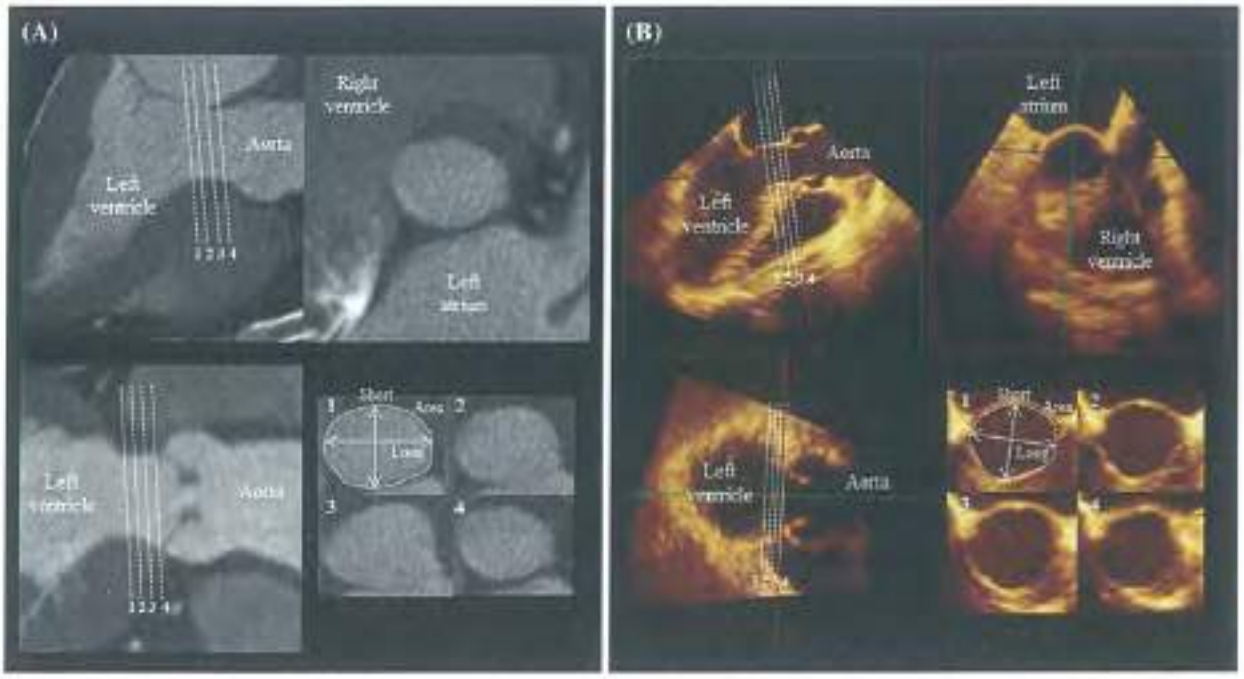

Fig. 1 Left ventricular outflow tract (LVOT) assessed using (a) multi-detector computed tomography (MDCT) and b three-dimensional (3D) transesophageal echocardiography (TEE)

long axis diameters and areas (LVOT 1 = tip of the septum, LVOT 4 = the aortic annulus, Fig. 1b). The LVOT sphericity index (shot/long diameter) was also assessed.

2D TTE

Comprehensive TTE, including 2D and Doppler echocardiography, was performed using commercially available ultrasound equipment according to the American Society of Echocardiography guidelines within 1 week before and after TEE [11]. The aortic valve jet velocity was recorded from the multiple acoustic windows to obtain the highest velocity signal. The AVA was calculated using the time–velocity integral of the aortic valve (AV) and LVOT spectral curves in the standard continuity equation. SV was determined using the velocity–time integral (VTI) from pulsed wave Doppler echocardiography at the LVOT × LV outflow area, which was determined using the following formula: $3.14 \times (\text{LVOT diameter}/2)^2$. The LVOT diameters were measured carefully using the zoom mode of the parasternal long-axis view in mid-systole from the black-and-white interface at the level of the aortic annulus [12]. LVOT velocity was recorded with pulsed Doppler using an apical approach in the 5-chamber view or in the apical long-axis view. The pulsed Doppler sample volume was positioned just proximal to the aortic valve with a length of 3–5 mm. The relative wall thickness was estimated as 2 × (diastolic LV posterior wall thickness)/LV end-diastolic diameter [13]. The LV mass was calculated using linear measurement. The maximum left atrial volume was measured according to the biplane Simpson's method and indexed to the body surface area. The peak early and late diastolic velocities of LV inflow (E and A velocity), deceleration time of early diastolic velocity, and peak early diastolic velocity on the septal corner of the mitral annulus ($E^{\prime}$) were measured in the apical four-chamber view. The ratio of the upper septal wall thickness to the mid-septum wall thickness in diastole was measured to determine the degree of USH. USH was defined according to the following criteria: (1) upper septum knuckle evaluated by visual assessment, (2) upper interventricular septum thickness ≥ 1.4 cm, and (3) ratio of upper septal wall thickness to mid-septal wall thickness ≥ 1.3 (Fig. 2) [14, 15].

3D TTE

3D TTE was also performed using an iE33 scanner (Philips Medical Systems) equipped with fully sampled matrix-array transducer (X3-1) for 3D data acquisition in AS patients and controls. Full-volume data sets were acquired from the apical transducer position during held respiration. To ensure the inclusion of the entire LV volumes within the pyramidal scan volume with a relatively higher volume rate, data sets throughout one cardiac cycle were acquired using the wide-angle mode, wherein four wedge-shaped sub-volumes were

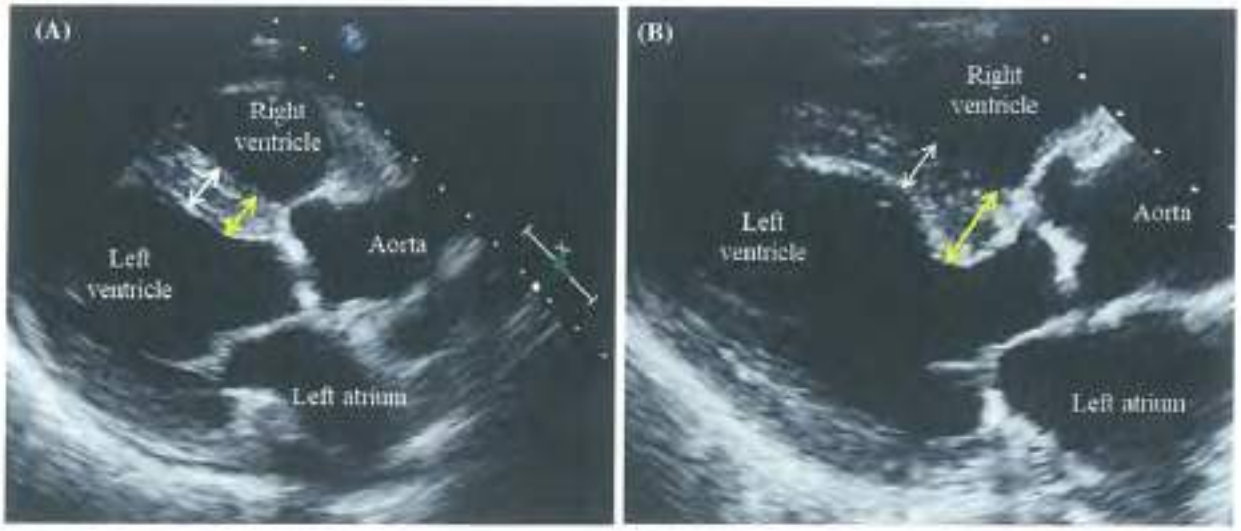

Fig. 2 Example cases of non-upper septal hypertrophy (a) and upper septal hypertrophy (b) in aortic stenosis. Case A met none of the following USH criteria: (1) upper septum knuckle evaluated with visual assessment, (2) upper interventricular septum thickness of ≥ 1.4 cm (1.1 cm), and (3) ratio of upper septal wall thickness to mid-septal wall thickness of ≥ 1.3 (1.0). Case B met all the following USH criteria: (1) upper septum knuckle evaluated with visual assessment, (2) upper interventricular septum thickness of ≥ 1.4 cm (1.5 cm), and 3) ratio of upper septal wall thickness to mid-septal wall thickness of ≥ 1.3 (1.4). White arrow: mid-septal wall thickness. Yellow arrow: upper septal wall thickness

acquired with electrocardiographic gating during a single 5–7-s breath hold. A 3D volumetric assessment of LV was performed according to the biplane Simpson's method using data extracted from 3D data sets with commercially available quantitative software (3DQ, QLAB, version 9.0, Philips Medical Systems, Andover, MA).

Statistical analysis

The results are expressed as mean ± standard deviation (SD) or percentage unless otherwise specified. Data for the USH and non-USH groups were compared using Student's *t* test, Chi-squared test, or Fisher's exact test as appropriate. Differences were considered significant if $P < 0.05$. Pearson's correlation coefficient was used to evaluate the correlation between two parameters. Bland–Altman plots were used to evaluate differences in LVOT areas using 3D TEE and MDCT. The mean differences and limits of agreement were reported. Bland–Altman plots were also used to evaluate differences in SV between Doppler and 3D methods. Both the interobserver and intraobserver variabilities for LVOT areas measured with 3D TEE and MDCT were obtained according to blinded analysis of 10 random images by two independent observers at two different time points. The results were analyzed using both an intraclass correlation coefficient for absolute agreement (ICCa) and the Bland–Altman method. Statistical analyses were performed with SPSS 22.0 software (SPSS, Inc, Chicago, IL, USA).

Results

Protocol 1

The LVOT parameters were successfully measured on MDCT and 3D TEE in all patients. Baseline and echocardiographic findings in this protocol are summarized in Table 1. Figure 3 shows the linear correlation and Bland–Altman plot between MDCT and 3D TEE measurements in each LVOT area. All LVOT areas measured using 3D TEE were slightly, but significantly smaller than those measured using MDCT; however, a favorable correlation was found between the two imaging modalities (Fig. 3, $r = 0.846$–0.941).

Protocol 2

Comparisons in LVOT geometry between the three groups

The baseline characteristics are summarized in Table 2. Of the study patients, 64 were men (49.6%). The mean age of patients was 75 ± 9 years (range, 55–89 years), and 41 of them had USH (31.8%). No differences in the demographic findings without the prevalence of coronary artery disease were found between the USH and non-USH groups. Moreover, no differences in the prevalence of left ventricular asynergy or scar in antero-septal area were found between the two groups (6.8 vs. 4.9%, $P = 0.523$). The LVOT geometries in the three groups are shown in Table 3. No differences in LVOT short and long

Table 1 Baseline and echocardiographic characteristics in protocol 1 ($n=20$)

Variable	($N=20$)
Clinical characteristics	
Age (years)	80 ± 8
Male (%)	51
Height (cm)	154 ± 10
Body weight (kg)	54 ± 10
BSA (m^2)	1.51 ± 0.18
Systolic BP (mmHg)	120 ± 31
Diastolic BP (mmHg)	70 ± 19
HR (bpm)	72 ± 15
Echocardiographic findings	
AVA (cm^2)	0.68 ± 0.26
Indexed AVA (cm^2/m^2)	0.45 ± 0.16
Peak velocity (m/s)	4.0 ± 1.2
Mean PG (mm Hg)	44 ± 32
Severe (AVA ≤ 1.0 cm^2) *n* (%)	18 (90%)
SV_{Dopp} (ml)	67 ± 20
SVI_{Dopp} (ml/m^2)	44 ± 13
LVMI (g/m^2)	117 ± 33
LVDd (mm)	47 ± 7
LVDs (mm)	30 ± 7
EDV (ml)	96 ± 34
ESV (ml)	43 ± 31
LVEF (%)	62 ± 15
RVSP (mm Hg)	37 ± 16
E/A	0.94 ± 0.96
E/E'	17.0 ± 9.6

BP blood pressure; *HR* heart rate; *AVA* aortic valve area; *PG* pressure gradient; *SV* stroke volume; *SVI* stroke volume index; *LVMI* left ventricular mass index; *LVDd* left ventricular end-diastolic diameter; *LVDs* left ventricular end-systolic diameter; *EDV* end-systolic volume; *ESV* end-systolic volume; *RVSP* right ventricular systolic pressure

diameters, area or shape were found between the non-USH group and controls. Although the USH group had smaller short and long diameters, smaller LVOT area, and lower sphericity index than the non-USH group at LVOT 1, the tip of the septum, and LVOT 2, no significant differences in LVOT area and the sphericity index at LVOT-3 and -4 or the aortic annulus were observed between the two groups. The valve annulus of peripheral side (LVOT-3 or -4) was larger than that of the left ventricle central side (LVOT-1 or -2) in the controls and non-USH group, whereas the left ventricle side was smaller than the valve annulus in the USH group. The representative cases are shown in Fig. 4.

Impact of USH on measurement of left ventricular SV and AVA

The results of standard 2D TTE are shown in Table 2. No significant difference in the measured SV was found between Doppler echocardiography and 3D TTE in the controls (58 ± 9 vs. 55 ± 16 ml, $P=0.314$) and the non-USH group (56 ± 15 vs. 56 ± 16 ml, $P=0.264$; Fig. 5). However, the USH group revealed a significantly greater SV calculated with the Doppler method than that obtained with the 3D TTE method (Fig. 5). Moreover, no differences in peak velocity or mean pressure gradient between the USH and the non-USH groups were found; however, the USH group had greater AVA than the non-USH group (0.89 ± 0.26 vs. 0.73 ± 0.24 cm^2, $P=0.002$).

Reproducibility

The intraobserver variabilities assessed using the ICCs were 0.89–0.93 for LVOT areas measured with 3D TEE and 0.90–0.94 for LVOT areas measured with MDCT. The interobserver variabilities were 0.87–0.92 for LVOT areas measured with 3D TEE and 0.88–0.93 for LVOT areas measured with MDCT. The Bland–Altman method showed that interobserver and intraobserver variabilities were 0.32 ± 0.10 and 0.34 ± 0.11 cm^2 for the LVOT areas measured with 3D TEE, and 0.30 ± 0.11 and 0.32 ± 0.10 cm^2 for the LVOT areas measured with MDCT, respectively.

Discussion

The main findings of this study were as follows: (1) the LVOT parameters obtained by 3D TEE were well-correlated with those by MDCT, (2) more than 30% AS patients had USH, (3) USH affected not distal, but proximal LVOT geometry, and (4) the Doppler method overestimated SV in AS patients with USH, which might lead to an underestimation of the AS severity.

Comparison of LVOT morphology between the USH and non-USH groups

The evaluation of aortic root geometry is increasingly important for decision-making in patients with AS and usually performed using MDCT [6–10, 16]. The earlier studies defined the aortic root from the aortic annulus to the sinotubular junction, not including LVOT [5–10]. 3D imaging techniques have provided the unique anatomic views of cardiac structures and improved the definitions of spatial relation in complex abnormalities. To the best of our knowledge, this study first reports the use of 3D TEE to compare the LVOT geometry in AS patients with and without

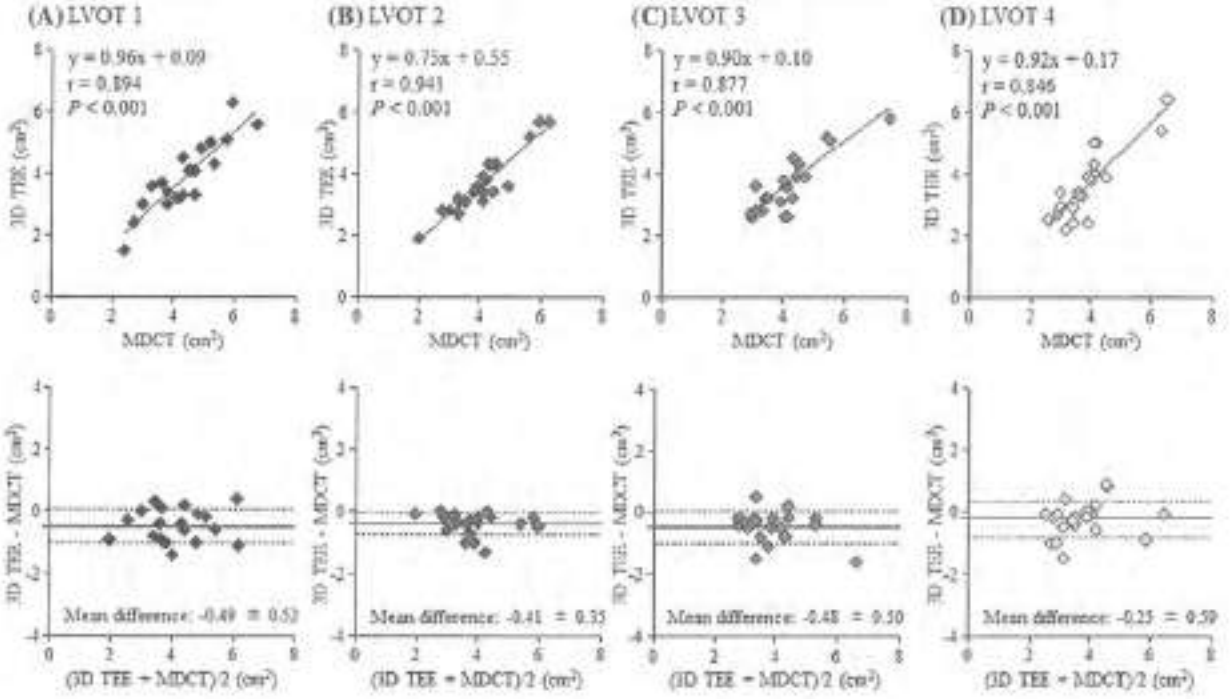

Fig. 3 Linear correlations (upper panel) and Bland–Altman analysis (lower panel) of LVOT parameters on MDCT and 3D TEE. **a** LVOT 1, **b** LVOT 2, **c** LVOT 3, and **d** LVOT 4

USH as well as controls. The LVOT areas measured with 3D TEE were slightly, but significantly smaller than those with MDCT; the results of our study consisted with those of earlier studies [6–10, 16]. This underestimation might be related with lower temporal resolution of 3D TEE images. The presence of calcification might also affect smaller 3D TEE planimetric measurements. The USH group revealed shorter LVOT short diameters and smaller areas at the tip of the septum than the non-USH group, resulting in a more elliptical LVOT shape. Our study result was consistent with the result of an earlier study demonstrating an association between the sigmoid-shaped septum versus the left ventricle and the ascending aorta, which might lead to shorter anterior–posterior diameters (short-diameter) and more elliptical shape of the LVOT [15].

Associations between LVOT geometry and Doppler-derived SV

The primary parameters proposed for the clinical evaluation of AS severity are: (1) peak velocity, (2) mean pressure gradient, and (3) AVA calculated with the continuity equation. Some recent studies have reported decreased peak velocity and mean pressure gradient regardless of ejection fraction [17–19]; thus, AVA calculated by the continuity equation is vital in the assessment of disease severity. The calculation of the valve area by the continuity equation requires three measurements as follows: (1) AS jet velocity evaluated with continuous wave Doppler, (2) LVOT diameters for the calculation of a circular cross-sectional area, and (3) LVOT velocity recorded with pulsed Doppler echocardiography. Its pitfalls are well-known due to inherent assumptions and simplifications. Some studies demonstrated that the calculations of continuity equation-derived AVA using 2D TTE underestimated AVA because of the elliptical shape of LVOT with its shorter anteroposterior diameters [20, 21]. Garcia, et al. conducted a subsequent assessment study using multimodal imaging and reported that the underestimation of LVOT area with TTE was compensated by the overestimation of LVOT VTI, thereby resulting in a good concordance between TTE and cardiac magnetic resonance for the estimation of AVA [22]. In our study, no difference in SV was found between the Doppler and 3D TTE methods in the non-USH group; however, the USH group had greater SV calculated by Doppler echocardiography than 3D TTE because of the greater VTI in this group. This difference is assumed not due to an oval-shaped LVOT, but faster blood flow in the USH group. Figure 6 shows the prevalence of a low-flow status (SV index, ≤ 35 ml/m^2) in the non-USH and USH groups. No significant differences in the prevalence of the low-flow status between the two methods were found in the non-USH group (19.5 vs. 23.7%, $P = 0.624$); however,

Table 2 Baseline characteristics

	Controls ($N=30$)	Non-USH ($N=88$)	USH ($N=41$)	P value non-USH versus USH	P value non-USH versus controls	P value USH versus controls
Clinical characteristics						
Age (years)	61±13	74±10	76±9	0.214	< 0.001	< 0.001
Male n (%)	22 (54)	47 (53)	17 (42)	0.174	0.519	0.321
BSA (m^2)	1.65±0.18	1.53±0.17	1.54±0.19	0.889	0.022	0.016
Systolic BP (mmHg)	128±26	129±20	136±24	0.927	0.928	0.137
Diastolic BP (mmHg)	75±15	74±15	73±15	0.911	0.133	0.414
Heart rate (bpm)	70±14	73±20	70±12	0.912	0.718	0.882
Hemoglobin (g/dl)	13.6±6.6	13.7±6.5	14.8±4.3	0.567	0.933	0.213
Medical history n (%)						
Hypertension	–	52 (59)	30 (73)	0.128	–	–
Dyslipidemia	–	23 (34)	15 (37)	0.913	–	–
Diabetes mellitus	–	25 (28)	12 (29)	0.788	–	–
Coronary artery disease	–	29 (33)	6 (15)	0.009	–	–
Chronic kidney disease	–	27 (31)	15 (37)	0.824	–	–
2D transthoracic echocardiographic findings						
AVA (cm^2)	–	0.73±0.24	0.89±0.26	0.002	–	–
Indexed AVA (cm^2/m^2)	–	0.46±0.21	0.58±0.15	0.003	–	–
Peak velocity (m/s)	–	4.0±1.1	4.1±0.9	0.172	–	–
Mean PG (mm Hg)	–	39±25	33±18	0.115	–	–
Severe (AVA ≤ 1.0 cm^2) n (%)	–	76 (86)	34 (83)	0.821	–	–
LVOT VTI (cm)	18±6	20±3	23±4	0.001	0.003	< 0.001
LVOT peak velocity (cm/s)	82±24	86±16	101±43	0.028	0.072	0.014
SV_{Dopp} (ml)	58±9	56±15	73±15	0.027	0.103	0.012
SVI_{Dopp} (ml/m^2)	35±10	36±15	47±12	0.016	0.007	0.001
$SV_{Simpson}$ (ml)	57±15	61±14	57±11	0.239	0.284	0.434
LVMI (g/m^2)	72±21	115±31	113±29	0.933	< 0.001	< 0.001
Aortic annulus diameter (cm)	2.0±0.3	2.0±0.2	2.0±0.2	0.462	0.762	0.323
LVDd (mm)	45±4	47±6	46±5	0.190	0.053	0.434
LVDs (mm)	29±4	31±7	28±5	0.014	0.052	0.822
EDV (mL)	90±20	100±30	87±22	0.047	0.053	0.821
ESV (mL)	33±11	39±21	30±11	0.022	0.034	0.391
LVEF (%)	63±6	61±8	68±8	0.043	0.651	0.201
RVSP (mm Hg)	25±4	31±10	31±11	0.726	0.001	0.002
E/A	0.97±0.42	0.94±0.64	0.78±0.33	0.216	0.283	0.101
E/E'	7.3±2.0	17±9	15±7	0.014	<0.001	0.004
3D transthoracic echocardiography						
EDV (ml)	91±22	100±31	93±30	0.028	0.041	0.202
ESV (ml)	36±10	44±14	32±16	0.001	0.001	0.121
SV (ml)	55±16	56±16	60±18	0.340	0.433	0.225
SVI (ml/m^2)	33±11	37±12	39±10	0.328	0.243	0.101
EF (%)	60±5	56±9	65±9	0.018	0.092	0.081

USH upper septal hypertrophy; *LVOT* left ventricular outflow tract; *VTI* velocity–time integral; the other abbreviations are shown in Table 1

the USH group had a lower prevalence rate of low-flow status calculated using the Doppler method than 3D TTE method (7.3 vs. 18.4%, $P<0.001$). In addition, measurement errors of SV directly affected AVA estimation calculated using a continuity equation as the gold standard method. Therefore, the continuity equation based on the 2D Doppler method may underestimate AS severity, especially in AS patients with USH. Figure 7 presents the association between VTI and SVs calculated with Doppler echocardiography and 3D TTE. A positive correlation was recognized

Table 3 LVOT geometry in each group

	Controls ($N=30$)	Non-USH ($N=88$)	USH ($N=41$)	P value (non-USH vs. USH)
LVOT 1 short (cm)	2.08 ± 0.37	2.02 ± 0.30	1.66 ± 0.35[a]	< 0.001
Long (cm)	2.76 ± 0.54	2.73 ± 0.50	2.45 ± 0.37	0.013
area (cm^2)	4.64 ± 1.65	4.32 ± 1.26	3.25 ± 1.05[a]	< 0.001
Sphericity index	0.76 ± 0.09	0.74 ± 0.11	0.68 ± 0.12[a]	< 0.001
LVOT 2 short (cm)	1.98 ± 0.30	1.96 ± 0.28	1.67 ± 0.29[a]	< 0.001
Long (cm)	2.51 ± 0.48	2.52 ± 0.45	2.35 ± 0.34	0.245
Area (cm^2)	3.97 ± 1.28	3.89 ± 1.2	3.16 ± 0.87[b]	< 0.001
Sphericity index	0.79 ± 0.1	0.79 ± 0.12	0.71 ± 0.11[a]	0.002
LVOT 3 short (cm)	1.98 ± 0.26	1.93 ± 0.27	1.81 ± 0.28	0.081
Long (cm)	2.27 ± 0.38	2.37 ± 0.37	2.29 ± 0.40	0.438
Area (cm^2)	3.59 ± 0.99	3.59 ± 1.0	3.29 ± 0.90	0.239
Sphericity index	0.88 ± 0.12	0.82 ± 0.13	0.80 ± 0.12[b]	0.524
LVOT 4 short (cm)	1.97 ± 0.23	1.92 ± 0.27	1.90 ± 0.27	0.889
Long (cm)	2.22 ± 0.36	2.25 ± 0.41	2.26 ± 0.38	0.924
Area (cm^2)	3.49 ± 0.88	3.41 ± 1.1	3.41 ± 0.97	0.842
Sphericity index	0.89 ± 0.1	0.86 ± 0.13	0.86 ± 0.13	0.924

Abbreviations are shown in Table 2

[a] $P < 0.01$ versus controls

[b] $P < 0.05$ versus controls

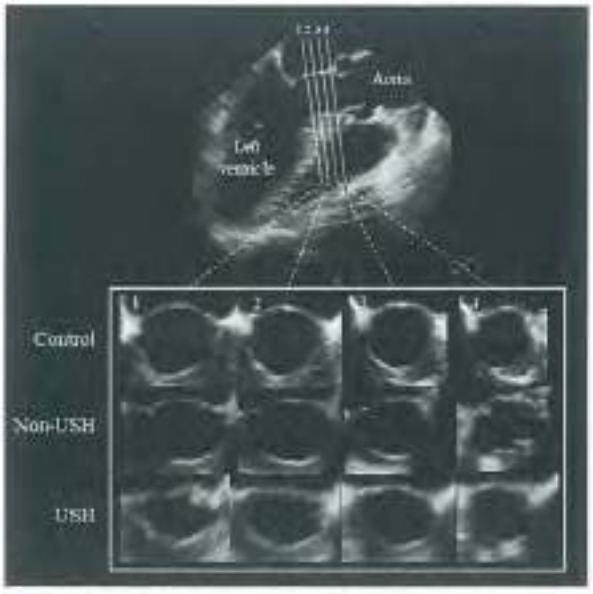

Fig. 4 Examples of LVOT in each group

between VTI and difference in SVs (Dopppler-3D). At the approximately 20 cm VTI, the SV calculated with Doppler echocardiography was consistent with that calculated with 3D TTE; in such cases, many patients in the USH group had VTI > 25 cm. Figure 8 shows the representative LVOT VTI in patients with USH and non-USH. The results of our study supported that of Garcia et al. because the mean VTI was 21 cm in their study. However, the USH group had higher VTI than the non-USH group, which might lead to the overestimation of SV [22]. Currently, flow-pressure status is considered crucial in the prognostic assessment [17–19, 23, 24] and it remains uncertain why normal-flow and low-gradient can be observed. A recent meta-analysis conducted by Dayan V et al. has reported that AS patients with normal-flow and low-gradient despite preserved ejection fraction have similar outcomes to those with normal-flow and high-gradient [25]. Their study discussed that the measurement error of SV might be the reason why AS patients with normal-flow low-gradient had similar outcomes to those with normal-flow high-gradient. This study suggested that the SV derived from the Doppler method should be overestimated rather than showing the real transvalvular flow in the USH group, which might be associated with errors in the measurement of SV. Of the patients in the USH group, 15% patients might be underestimated as having low-flow (SV index ≤ 35 ml/m^2, Fig. 7). In such cases, 3D assessment of SV might be crucial for evaluating disease severity in patients with AS [26–28].

Study limitations

Our study has several limitations. First, the study population consisted entirely of Japanese patients, and the relevance of this study to patients of other ethnicities needs to be confirmed with future research. Second, the MDCT and TEE evaluations were not performed on the same day. Third,

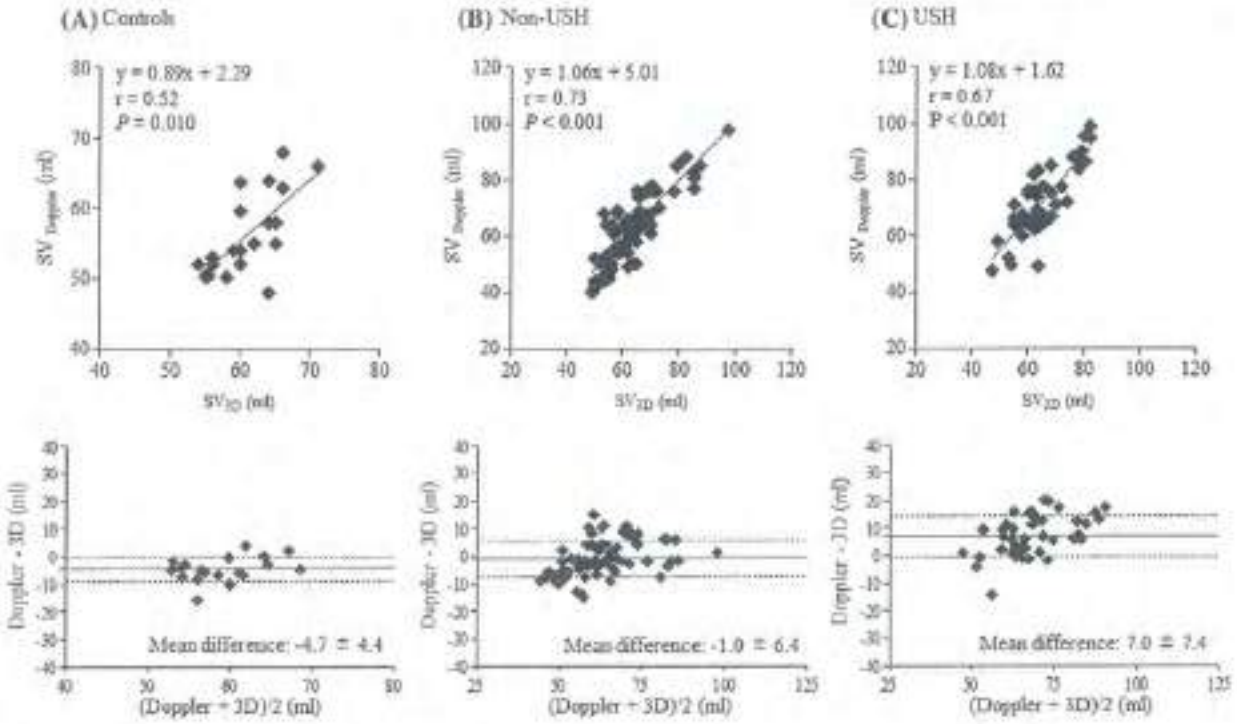

Fig. 5 Linear correlations (upper panel) and Bland–Altman scatter plot (lower panel) determining the agreement in the measurement of left ventricular stroke volume (SV) calculated by Doppler echocardiography and 3D TTE as a gold standard. SV was underestimated by Doppler echocardiography compared with 3D TTE in the controls (a) and the non-USH group (b); however, SV was overestimated by Doppler echocardiography compared with 3D TTE in the USH group (c)

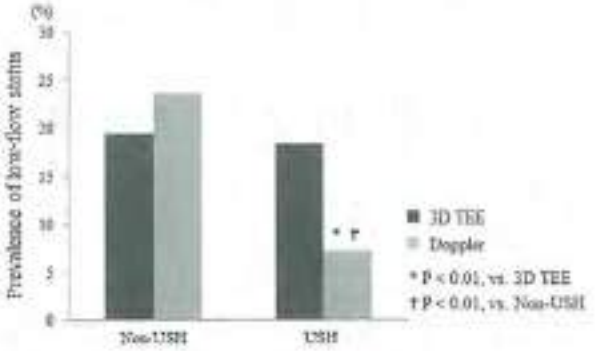

Fig. 6 Prevalence of low-flow status (SV index ≤ 35 ml/m²) in the non-USH group (left) and the USH group (right). No significant differences in the prevalence of low-flow status between the two methods were observed in the non-USH group (19.5 vs. 23.7%, $P = 0.624$); however, the USH group had the lower prevalence rate of low-flow status calculated using the Doppler method than 3D TTE method (7.3 vs. 18.4%, $P < 0.001$)

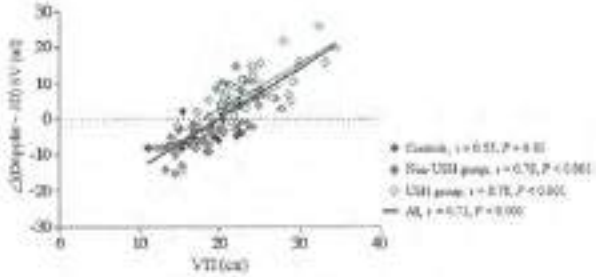

Fig. 7 Linear correlation between velocity–time integral and Δ(Doppler—3D) SV

the anesthetics used during TEE and the β-blockers used during MDCT might have affected the loading conditions. Forth, because of the differences in heart rate and frame rate between the MDCT and 3D TEE studies, the measurements were not performed at exactly the same point during the cardiac cycle. Fifth, this study employed 3D TTE which was thought to be superior to two-dimensional echocardiography and regarded as a gold standard to compare SV evaluated by Doppler echocardiography between the USH and non-USH groups, we did not have invasive measurements. Sixth, the control group in protocol 2 was not a strict representation of controls because the patients had some comorbidities affecting the LVOT geometry. However, the control group in earlier MDCT and TEE studies on aortic root geometry including the LVOT also had the same prevalence of those

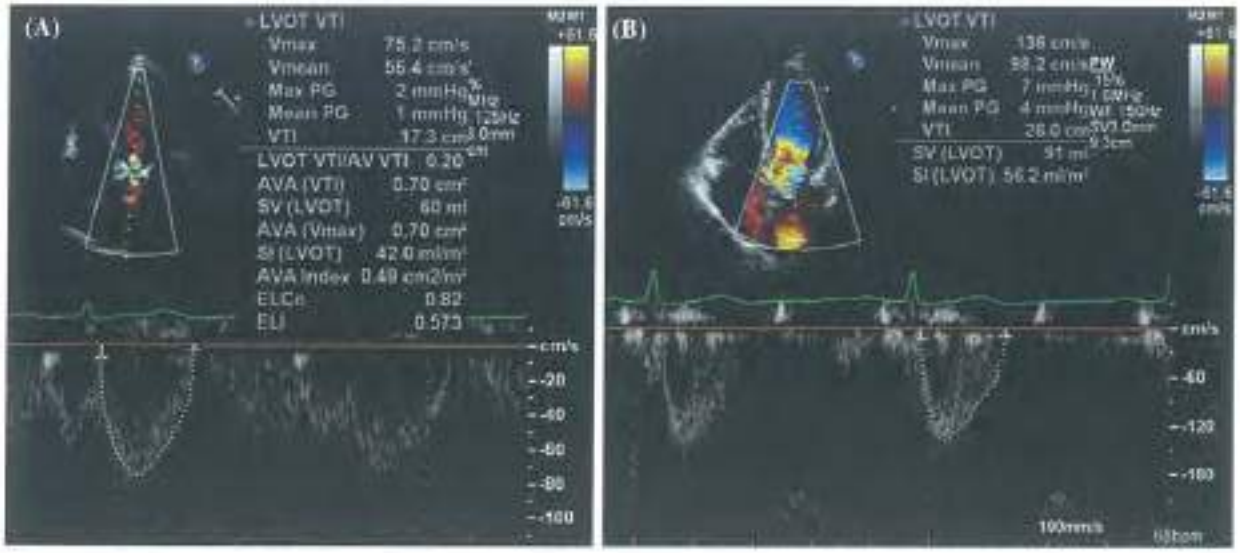

Fig. 8 Examples of LVOT VTI in each group (a non-USH, b USH)

comorbidities [7–10]. Finally, this study included only AS patients; however, we found USH in not only AS patients, but also in the other population. Further investigation with a larger population is warranted

Conclusions

3D TEE can provide a precise assessment of LVOT geometry in patients with AS. USH affects the LVOT geometry, which might lead to inaccurate assessments of AS severity.

Compliance with Ethical Standards

Conflict of interest Dan Koin, Masaki Izumo, Takafumi Machida, Kihei Yoneyama, Tomomi Suzuki, Ryo Kamijima, Yasuyuki Kobayashi, Tomoo Harada, and Yoshihiro J. Akashi declare that they have no conflicts of interest.

Human rights statements and informed consent All procedure followed were in accordance with the ethical standards of the responsible committee on human experimentation (institutional and national) and with the Helsinki Declaration of 1964 and later revisions. The participants were well-informed prior to the test; written informed consent was obtained before enrollment.

References

1. Nkomo VT, Gardin JM, Skelton TN, et al. Burden of valvular heart diseases: a population-based study. Lancet. 2006;368:1005–11.
2. Carabello BA, Paulus WJ. Aortic stenosis. Lancet. 2009;373:956–66.
3. Carabello BA. Clinical practice. Aortic stenosis. N Engl J Med. 2002;346:677–82.
4. Suikrishnan N, Kumar G, Sawaya FJ, et al. Accurate assessment of aortic stenosis: a review of diagnostic modalities and hemodynamics. Circulation. 2014;129:244–53.
5. Delgado V, Ng AC, Schuijf JD, et al. Automated assessment of the aortic root dimensions with multidetector row computed tomography. Ann Thorac Surg. 2011;91:716–23.
6. Tops LF, Wood DA, Delgado V, et al. Noninvasive evaluation of the aortic root with multislice computed tomography implications for transcatheter aortic valve replacement. J Am Coll Cardiol Img. 2008;1:321–30.
7. Akhtar M, Tuzcu EM, Kapadia SR, et al. Aortic root morphology in patients undergoing percutaneous aortic valve replacement: evidence of aortic root remodeling. J Thorac Cardiovasc Surg. 2009;137:950–6.
8. Stolzmann P, Knight J, Desbiolles L, et al. Remodelling of the aortic root in severe tricuspid aortic stenosis: implications for transcatheter aortic valve implantation. Eur Radiol. 2009;19:1316–23.
9. Otani K, Takeuchi M, Kaku K, et al. Assessment of the aortic root using real-time 3D transesophageal echocardiography. Circ J. 2010;74:2649–57.
10. Wu VC, Kaku K, Takeuchi M, et al. Aortic root geometry in patients with aortic stenosis assessed by real-time three-dimensional transesophageal echocardiography. J Am Soc Echocardiogr. 2014;27:32–41.
11. Lang RM, Bierig M, Devereux RB, et al. Chamber Quantification Writing Group; American Society of Echocardiography's Guidelines and Standards Committee; European Association of Echocardiography. Recommendations for chamber quantification: a report from the American Society of Echocardiography's Guidelines and Standards Committee and the Chamber Quantification Writing Group, developed in conjunction with the European Association of Echocardiography, a branch of the European Society of Cardiology. J Am Soc Echocardiogr. 2005;18:1440–63.
12. Pibarot P, Clavel MA. Left ventricular outflow tract geometry and dynamics in aortic stenosis: Implications for the echocardiographic assessment of aortic valve area. J Am Soc Echocardiogr. 2015;28:1267–9.

13. Gore D, Lillehei W, Edwards JE. The "sigmoid septum" variation in the contour of the left ventricular outlet. AJR Am J Roentgenol. 1969;107:366–76.
14. Diaz T, Pencina MJ, Benjamin EJ, et al. Prevalence, clinical correlates, and prognosis of discrete upper septal thickening on echocardiography: the Framingham Heart Study. Echocardiography. 2009;26:247–53.
15. Funabashi N, Umezome T, Takaoka H, et al. Sigmoid shaped interventricular septum exhibit normal myocardial characteristics and has a relationship with aging, ascending aortic sclerosis and its tilt to left ventricle. Int J Cardiol. 2013;168:4484–8.
16. Jilaihawi H, Kashif M, Fontana G, et al. Cross-sectional computed tomographic assessment improves accuracy of aortic annular sizing for transcatheter aortic valve replacement and reduces the incidence of paravalvular aortic regurgitation. J Am Coll Cardiol. 2012;59:1275–86.
17. Hachicha Z, Dumesnil JG, Bogaty P, et al. Paradoxical low-flow, low-gradient severe aortic stenosis despite preserved ejection fraction is associated with higher afterload and reduced survival. Circulation. 2007;115:2856–64.
18. Lancellotti P, Magne J, Donal E, et al. Clinical outcome in asymptomatic severe aortic stenosis: insights from the new proposed aortic stenosis grading classification. J Am Coll Cardiol. 2012;59:235–43.
19. Ozkan A, Hachamovitch R, Kapadia SR, et al. Impact of aortic valve replacement on outcome of symptomatic patients with severe aortic stenosis with low gradient and preserved left ventricular ejection fraction. Circulation. 2013;128:622–31.
20. Doddamani S, Grushko MJ, Makaryus AN, et al. Demonstration of left ventricular outflow tract eccentricity by 64-slice multidetector CT. Int J Cardiovasc Imaging. 2009;25:175–81.
21. Saitoh T, Shiota M, Izumo M, et al. Comparison of left ventricular outflow geometry and aortic valve area in patients with aortic stenosis by 2-dimensional versus 3-dimensional echocardiography. Am J Cardiol. 2012;109:1626–31.
22. Garcia J, Kadem L, Larose E, et al. Comparison between cardiovascular magnetic resonance and transthoracic Doppler echocardiography for the estimation of effective orifice area in aortic stenosis. J Cardiovasc Magn Reson. 2011;13:25.
23. Le Ven F, Freeman M, Webb J, et al. Impact of low flow on the outcome of high-risk patients undergoing transcatheter aortic valve replacement. J Am Coll Cardiol. 2013;62:782–8.
24. Clavel MA, Berthelot-Richer M, Le Ven F, et al. Impact of classic and paradoxical low flow on survival after aortic valve replacement for severe aortic stenosis. J Am Coll Cardiol. 2015;65:645–53.
25. Dayan V, Vignolo G, Magne J, et al. Outcome and impact of aortic valve replacement in patients with preserved LVEF and low-gradient aortic stenosis. J Am Coll Cardiol. 2015;66:2594–603.
26. Poh KK, Levine RA, Solis J, et al. Assessing aortic valve area in aortic stenosis by continuity equation: a novel approach using real-time three-dimensional echocardiography. Eur Heart J. 2008;29:2526–35.
27. Mehrotra P, Flynn AW, Jansen K, et al. Differential left ventricular outflow tract remodeling and dynamics in aortic stenosis. J Am Soc Echocardiogr. 2015;28:1259–66.
28. Sato K, Seo Y, Ishizu T, et al. Reliability of aortic stenosis severity classified by 3-dimensional echocardiography in the prediction of cardiovascular events. Am J Cardiol. 2016;118:410–7.

Original Article

J. St. Marianna Univ.
Vol. 9, pp. 53–62, 2018

The Impact of In-stent Restenosis Detected upon Routine Follow-up Angiography after Percutaneous Coronary Intervention with Metallic Stent

Nozomi Kotoku[1], Yuki Ishibashi[1], Takumi Higuma[1], Kihei Yoneyama[1,2], Hiroshi Yamazaki[1,3], Shingo Kuwata[1,4], Kazuaki Okuyama[1], Takanobu Mitarai[1], Kenichi Chatani[1,3], Yasuhiro Tanabe[1], Tomoo Harada[1], and Yoshihiro J Akashi[1]

(Received for Publication: August 20, 2018)

Abstract

Aims: The prognostic impact of in-stent restenosis (ISR) detected upon routine follow-up coronary angiography (RFU-CAG) after percutaneous coronary intervention (PCI) has been unclear. The aim of our study was to compare the clinical outcomes after RFU-CAG between patients with and without ISR detected upon RFU-CAG.

Methods and results: A total of 824 patients who underwent PCI and RFU-CAG were analysed. Patients were divided into two groups: those with ISR (n=112) and those without (n=712). Outcomes were compared between patients with ISR and those without detected upon RFU-CAG. The study patients were followed up for a median of 1,323 (709 to 2,130) days. The incidence of a major adverse cardiac event (MACE), defined as all-cause death, any myocardial infarction, stroke, revascularisation for de novo lesion(s) or hospitalisation for heart failure was significantly higher in patients with ISR than in those without (45.5% vs. 24.4%, respectively; p<0.01). Specifically, patients with ISR had a higher incidence of all-cause death (16.1% vs. 6.2%, respectively; p<0.01) and revascularisation for de novo lesion(s) (28.6% vs. 16.2%, respectively; p<0.01). Even after adjustment for possible confounders, ISR detected upon RFU-CAG was an independent predictor for MACE (Hazard ratio: 2.13; 95% confidence interval: 1.55 to 2.92: p<0.01)

Conclusions: ISR detected upon RFU-CAG were independently associated with an increased MACE, which was mainly driven by an increased incidence of all-cause death and revascularisation for de novo lesion(s).

Key words

Routine follow-up coronary angiography, in-stent restenosis, prognosis

Abbreviation

RFU-CAG = routine follow-up coronary angiography ISR = in-stent restenosis PCI = percutaneous coronary intervention MI = myocardial infarction MACE = major adverse cardiac event CKD = chronic kidney disease eGFR = estimated glomerular filtration rate ACS = acute coronary syndrome BMI = body mass index LDL-C = low-density lipoprotein cholesterol HDL-C = high-density lipoprotein cholesterol DM = diabetes mellitus BNP = brain natriuretic peptide AMI = acute myocardial infarction BMS = bare metal

1 Division of Cardiology, Department of Internal Medicine, St. Marianna University School of Medicine, Kawasaki, Kanagawa, Japan
2 Division of Cardiology, Department of Internal Medicine, St. Marianna University School of Medicine, Cardiac Center, Toyoko Hospital, Kawasaki, Kanagawa, Japan
3 Division of Cardiology, Department of Internal Medicine, St. Marianna University School of Medicine, Kawasaki Municipal Tama Hospital, Kawasaki, Kanagawa, Japan
4 Division of Cardiology, Department of Internal Medicine, St. Marianna University School of Medicine, Yokohama City Seibu Hospital, Yokohama, Kanagawa, Japan

Conflict of interest statement: The authors have no conflict of interest to declare.

stent G1 DES = first-generation drug-eluting stent G2 DES = second-generation drug-eluting stent ACEI = angiotensin-converting enzyme inhibitor ARB = angiotensin receptor blocker HRs = hazard ratios 95% CIs = 95% confidence intervals TLR = target lesion revascularisation TVR = target vessel revascularisation

Introduction

Routine follow-up coronary angiography (RFU-CAG) is often performed to assess in- stent restenosis (ISR) after percutaneous coronary intervention (PCI). Although the clinical benefit of RFU-CAG remains a matter of debate due to lack of scientific data, prior studies have shown a reduction in the incidence of post-PCI myocardial infarction (MI)[1,2]. A matter of concern, however, is physician susceptibility to the so-called oculostenotic reflex, i.e., the tendency for interventionists to perform repeat revascularisation in the absence of symptoms of ischemia when regional stenosis is detected upon RFU-CAG[3-6]. However, the prognostic impact of restenosis detected upon post-PCI RFU-CAG has been unknown. The aim of this study was to evaluate the significance of ISR detected upon RFU-CAG on long-term outcomes among patients with coronary artery disease treated with PCI with metallic stent(s) for de novo lesion(s).

Methods

STUDY DESIGN AND STUDY PATIENTS

The overall study group comprised 824 patients who had undergone RFU-CAG after successful PCI involving implantation of metallic stent(s) for de novo lesion(s). Our hospital conventionally performed RFU-CAG once about 6 to 9 months after PCI for all patients who had undergone PCI except exceptions. The 824 patients were identified from 917 patients who had undergone PCI at St. Marianna University Hospital between March 2006 and December 2014. Seventy-one of the 917 patients were excluded from the study because they had not received a metallic stent (n=37), PCI had been performed for ISR (n=23), PCI had been performed for bypass graft failure (n=7) or PCI was not successful (n=4). Twenty-two of the 917 patients were excluded because CAG had been performed before RFU-CAG (n=17) or RFU-CAG had not been performed (n=5). We divided the 824 study patients into two groups: those with ISR detected upon RFU-CAG (ISR group, n=112) and those without (non-ISR group, n=712) for comparison of clinical outcomes. The study procedures were approved by the ethics committee at St. Marianna University school of Medicine, Japan (approval number 3904).

DEFINITIONS AND END POINTS

The primary clinical outcome of interest was a major adverse cardiac event (MACE), defined as all-cause death, any MI (spontaneous MI, as defined by the Academic Research Consortium)[7], stroke (neurological dysfunction caused by an ischemic or hemorrhagic cerebrovascular accident requiring hospitalisation with symptoms persisting >24 hours or until death)[8], revascularisation for de novo lesion(s), or hospitalisation for heart failure.

Cardiac death was defined as death due to a proximate cardiac cause (e.g., MI, low-output heart failure, life-threatening arrhythmia). Chronic kidney disease (CKD) categories G3b-G5 was defined as an estimated glomerular filtration rate (eGFR) <45 mL/min/1.73 mm^2. In the patients with multivessel desease, target vessel location was defined as vessel that initially performed PCI (e.g. acute coronary syndrome; ACS).

Restenosis was defined as diameter stenosis >50% in the in-segment area (including the stented segment and the 5-mm segments proximal and distal to the edges of the stent). ISR was assessed on at least two different angiography projections by three experienced cardiologists, and ISR was diagnosed by consensus.

STATISTICAL ANALYSES

Data are shown as median (and interquartile range), mean±SD, or the number (and percentage) of patients. Variables were compared between the two study groups, and differences were analysed by Student's t test, chi-square test, or Fisher's exact test, as appropriate. Kaplan-Meier curves were drawn for time to MACEs. To determine independent predictors of MACEs, univariate logistic regression models were constructed for the following clinical variables: age at the time of PCI; male sex; body mass index (BMI); hypertension requiring medication; dyslipidemia requiring medication; low-density lipoprotein cholesterol (LDL-C) concentration; high-density lipoprotein cholesterol (HDL-C) concentration; diabetes mellitus (DM) requiring medication; insulin use; HbA1c; CKD categories G3b-G5; hemodialysis; cur-

rent smoking; never smoked; brain natriuretic peptide (BNP) concentration; emergency PCI; ACS; acute MI (AMI); use of a bare metal stent (BMS), first-generation drug-eluting stent (G1 DES) or second-generation drug-eluting stent (G2 DES); use of β-blocker, statin, angiotensin-converting enzyme inhibitor (ACEI), or angiotensin receptor blocker (ARB); and restenosis. Variables shown to be significant by univariate analysis were then entered into a multivariable logistic regression model. Hazard ratios (HRs) with 95% confidence intervals (95% CIs) were computed for all variables entered into the multivariable regression model. All statistical analysis were performed with SPSS 24.0 for Mac (IBM, Chicago, IL, USA). All tests were two-sided, and $p<0.05$ was regarded as significant.

Results

RFU-CAG was performed at a median of 187 (182 to 203) days after the index PCI, and the study patients were followed up for a median of 1,323 (709 to 2,130) days after RFU-CAG.

The 112 patients in the ISR group represented 13.6% of the total study patients. Clinical and lesion characteristics of the study patients at the time of PCI are shown per ISR group and non-ISR group on **Table 1**. Only BMI (23.4±3.0 kg/m^2 vs. 24.3±3.7 kg/m^2, respectively; $p<0.01$), use of medication for dyslipidemia (39.3% vs. 59.7%, respectively; $p<0.01$) and BNP (242±304 ng/mL vs. 142±400 ng/mL, respectively; $p<0.01$) differed significantly between the two groups. Lesion characteristics did not differ significantly between the two groups, but ACS was more prevalent in the ISR group than in the non-ISR group (64.3% vs. 41.6%, respectively; $p<0.01$).

Angiographic and procedural details are shown per group in **Table 2**. Emergency PCI (61.6% vs. 36.4%, $p<0.01$), use of manual aspiration (44.6% vs. 27.9%, $p<0.01$), minimum stent diameter at the target lesion (2.5±0.5 mm vs. 2.8±0.5 mm, $p < 0.01$) and use of BMS(s) (53.6% vs. 34.3%, $p<0.01$) were significantly more common in the ISR group than in the non-ISR group. β-blocker use was significantly more common in the ISR group than in the non-ISR group, as shown in **Table 3** (75.0% vs. 63.8%, respectively; $p=0.02$).

Of the 112 patients in the ISR group, 83 (74.1%) underwent PCI for the ISR, 11 (9.8%) underwent bypass surgery, and 18 (16.1%) were treated medically.

MACEs occurred at significantly higher incidence in the ISR group than in the non-ISR group (45.5% vs. 24.4%, $p<0.01$) (**Figure 1**). Specifically, the incidences of all-cause death (16.1% vs. 6.2%, $p<0.01$) and revascularisation for de novo lesion(s) (28.6% vs. 16.2%, $p<0.01$) were significantly higher in the ISR group than in the non-ISR group (**Figure 2**). As shown in **Table 4**, cardiac death (2.6% vs. 1.0%, $p=0.14$) was similar between the two groups. Multivariable logistic regression analysis showed independent determinants of MACEs to be DM requiring medication (HR: 1.53, 95% CI: 1.17 to 2.00; $p=0.02$), CKD categories G3b-G5 (HR: 1.94, 95% CI: 1.29 to 2.92; $p=0.01$), and restenosis (HR: 2.13, 95% CI: 1.55 to 2.92; $p<0.01$) (**Table 5**), whereas use of statins was shown to be protective (HR: 0.71, 95% CI: 0.51 to 0.97; $p=0.03$).

Discussion

In summary, our study yielded three main findings. First, the incidence of MACEs, a study endpoint, was significantly higher in the ISR group than in the non-ISR group, and we believe this was driven mainly by the significantly higher rate at which revascularisation was performed for de novo lesion(s) following RFU-CAG in this group. Second, despite the similarity in the rate of cardiac death, the incidence of all-cause death was significantly higher in the ISR group than in the non-ISR group. Third, restenosis (HR: 2.13, 95% CI: 1.55 to 2.92, $p<0.01$), DM requiring medication (HR: 1.53, 95% CI: 1.17 to 2.00, $p<0.01$), and CKD categories G3b-G5 (HR: 1.94, 95% CI: 1.29 to 2.92, $p<0.01$) were shown to be independent predictors of MACEs, whereas statin use was shown to be protective (HR: 0.71, 95% CI: 0.51 to 0.97; $p=0.03$). Despite numerous advances regarding evidence-based medical therapy and invasive treatment such as PCI, patients with ISR remain at a high risk for MACEs. Our present findings seem to be useful for identifying those patients requiring more aggressive therapy and management.

THE OCULOSTENOTIC REFLEX PHENOMENON

Although we found ISR to be associated with the overall incidence of MACEs, cardiac death, any MI, and hospitalisation for heart failure in particular occurred at similar frequencies between our ISR group and non-ISR group. As noted above, revascularisation for de novo lesion(s) was performed at a higher rate among patients in the ISR group than among patients in the non-ISR group, and this was the result of post-PCI RFU-CAG. Detection of ISR

Table 1. Clinical and Lesion Characteristics, Per Study Group

	ISR group (n=112)	Non-ISR group (n=712)	p Value	
Age, years	67±10	66±11	0.34	
Sex, male	88 (78.6)	572 (80.3)	0.70	
Body mass index, kg/m^2	23.4±3.0	24.3±3.7	< 0.01	*
Diabetes requiring medication	32 (28.6)	215 (30.2)	0.82	
Insulin use	9 (8.0)	80 (11.2)	0.41	
Hypertension requiring medication	67 (59.8)	466 (65.4)	0.24	
Dyslipidemia requiring medication	44 (39.3)	425 (59.7)	< 0.01	*
CKD G3b-G5 (GFR < 45 mL/min/1.73m^2)	14 (12.5)	59 (8.3)	0.15	
Hemodialysis	10 (8.9)	33 (4.6)	0.06	
HbA1c, %	6.0±1.3	5.9±1.0	0.40	
LDL-cholesterol, mg/dL	104±30	103±29	0.59	
HDL-cholesterol, mg/dL	44±12	45±12	0.64	
BNP, pg/mL	242±304	142±400	< 0.01	*
Smoking				
Current	51 (45.5)	278 (39.0)	0.21	
Past	25 (22.3)	206 (28.9)	0.17	
Never	36 (32.1)	228 (32.0)	1.00	
Diagnosis				
ACS	72 (64.3)	296 (41.6)	< 0.01	*
AMI	48 (42.9)	186 (26.1)	< 0.01	*
UAP	24 (21.4)	110 (15.4)	0.13	
RMI	5 (4.5)	28 (3.9)	0.80	
EAP	28 (25.0)	279 (39.2)	< 0.01	*
SMI	7 (6.3)	109 (15.3)	< 0.01	*
Target vessel location				
RCA	40 (35.7)	230 (32.3)	0.52	
LMT	1 (0.9)	12 (1.7)	1.00	
LAD	54 (48.2)	366 (51.4)	0.54	
LCX	17 (15.2)	104 (14.6)	0.89	

Mean±SD values or number (and percentage) of patients are shown.

* $p < 0.05$

ISR = in-stent restenosis; CKD = chronic kidney disease; GFR = glomerular filtration rate; BNP = brain natriuretic peptide; ACS = acute coronary syndrome; AMI = acute myocardial infarction; UAP = unstable angina pectoris; RMI = recent myocardial infarction; EAP = effort angina pectoris; SMI = silent myocardial ischemia; RCA = right coronary artery; LMT = left main trunk; LAD = left anterior descending; LCX = left circumflex.

Table 2. Angiographic and Procedural Details, Per Study Group

	ISR group (n=112)	Non-ISR group (n=712)	p Value	
Emergency PCI	69 (61.6)	259 (36.4)	< 0.01	*
Calcification	57 (50.9)	353 (49.6)	0.85	
Use of manual aspiration	50 (44.6)	199 (27.9)	< 0.01	*
Nominal stent size, mm	3.0±0.4	3.2±0.7	0.03	*
Stent length, mm	23±11	23±11	0.84	
Overlapping	15 (13.4)	80 (11.2)	0.46	
MSD, mm	2.5±0.5	2.8±0.5	< 0.01	*
Residual stenosis, %	11±15	7±12	0.01	*
Stent				
BMS	60 (53.6)	244 (34.3)	< 0.01	*
G1 DES	11 (9.8)	98 (13.8)	0.30	
G2 DES	41 (36.6)	370 (52.0)	< 0.01	*

Mean ± SD values or number (and percentage) of patients are shown.

* $p < 0.05$

ISR = in-stent restenosis; PCI = percutaneous coronary intervention; MSD = minimum stent diameter; BMS = bare metal stent; G1 DES = first-generation drug eluting stent; G2 DES = second-generation drug eluting stent.

Table 3. Use of Medications, Per Study Group

	ISR group (n=112)	Non-ISR group (n=712)	p Value	
β-blocker	84 (75.0)	454 (63.8)	0.02	*
Statin	92 (82.1)	582 (81.7)	1.00	
ACEI or ARB	89 (79.5)	511 (71.8)	0.10	

Number (and percentage) of patients are shown.

* $p < 0.05$

ISR = in-stent restenosis; ACEI = angiotensin converting enzyme inhibitor; ARB = angiotensin receptor blocker.

upon RFU-CAG led to subsequent target lesion revascularisation (TLR). That is, the so-called oculostenotic reflex came into play[4-6,9]. According to previously reported studies, RFU-CAG might result in the oculostenotic reflex but no improvement in prognosis[10,11].

LESSONS LEARNED FROM THE PATIENTS IN THE ISR GROUP

We found that the ISR group had a higher incidence of all-cause and non-cardiac mortality compared with the non-ISR group. The frequencies of ACS and use of BMS(s) were significantly greater in our ISR group than in our non-ISR group. In previously reported study of the EXAMINATION (clinical Evaluation of the Xience-V stent in Acute Myocardial INfArcTION), all-cause and non-cardiac 5-year mortality rate was significantly higher in the BMS group than in the everolimus-eluting stent (EES) group, and most common cause of non-cardiac death was cancer[12]. We could hypothesize that background or complications of ACS and use of BMS(s) might have lead to worsened long-term outcomes. This finding is consistent with our results (malignant tu-

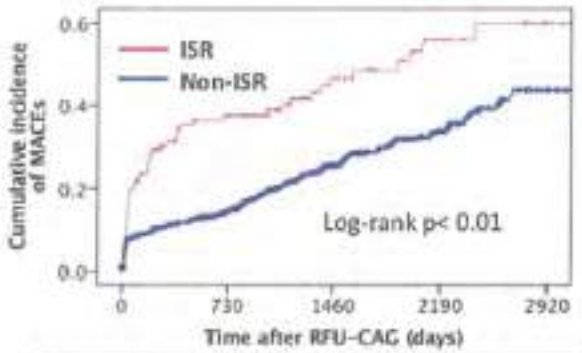

Follow-up time	0 day	1 year	2 years	4 years	8 years
Number at risk					
ISR group	112	66	58	30	4
Non-ISR group	708	522	464	253	27

Figure 1. Cumulative incidence of major adverse cardiac events (MACEs) in patients with and without in-stent restenosis (ISR). The Kaplan-Meier estimated incidence of MACEs was significantly higher in the ISR group than in the non-ISR group (45.5% vs. 24.4%, respectively; p<0.01 by log-rank test).

mor 5.4% vs. 1.7%, p<0.01). Progression of ISR might be associated with mechanism for highly relevance with malignant tumor in clinical events. More studies are needed to evaluate this issue.

IS REVASCULARISATION FOR ISR NECESSARY?

Whether medical treatment for ISR increases the incidence and therefore the risk of cardiac death remains controversial. As noted above, among patients in our ISR group, TLR was performed by means of PCI in 74.1% of patients and by means of bypass surgery in 9.8%. We performed an additional analysis by dividing patients into two groups: those in whom ISR was treated medically (n=18) and those in whom ISR was treated by TLR (n=94). The overall incidence of MACEs was similar between these two groups (33.3% vs. 27.4%, p=0.99 by log-rank test), however, the incidence of any MI, a specific MACE, was significantly higher in the first group than in the second group (11.1% vs. 1.7%, p<0.01 by log-rank test). In previously reported substudies of the BAAS (Balloon Angioplasty and Anticoagulation Study) and TAXUS-IV trial, MI occurred at a higher rate among patients in whom RFU-CAG was not performed than among those in whom RFU-CAG was performed, but with no between-group difference in mortality[1,2,4]. Previous studies and our current study indicated that revascularisation for ISR might protect against the occurrence of future MI.

With respect to mortality associated with target vessel revascularisation (TVR) in patients with ISR, Cassese et al. showed restenosis at the time of RFU-CAG to be predictive of 4-year mortality in large cohort of patients who had undergone coronary stenting[3]. However, performance of TVR for restenosis was shown not to influence 4-year mortality.

In future studies, a question to explore would be whether TLR or TVR can be optimised to further improve clinical outcomes.

WHAT IS THE POTENTIAL ROLE OF FOLLOW-UP CAG?

We found that the frequencies of ACS, emergency PCI and use of BMS(s) and the percentage of relatively small minimum stent diameters were significantly greater in ISR group than in non-ISR group. In previous studies, DM, a complex lesion (B2/C), a relatively small reference vessel diameter, multiple stents, relatively long stents and a relatively small minimal stent diameter immediately after stenting have been shown to be predictors of restenosis[13-15]. Our study data show clearly that follow-up CAG should be seriously considered in patients who present with ACS treated with small BMS(s).

Our study did not aim to examine the effect of RFU-CAG on clinical outcomes, but rather to investigate the significance of ISR detected upon RFU-CAG. A recent guidelines and clinical studies show that follow-up angiography can no longer be recommended as routine strategy in patients with treated with current metal stent(s). However, our results indicated that patients with ISR detected upon RFU-CAG are at high risk for future MACE and require more aggressive therapy and intensive clinical management.

Limitations

Our study was subject to the usual limitations of a retrospective study. In addition, the overall study group was not large and was derived from a single center.

Conclusions

We conclude that ISR detected upon RFU-CAG were independently associated with an increased MACE, which was mainly driven by an increased incidence of all-cause death and revascularisation for de novo lesion(s).

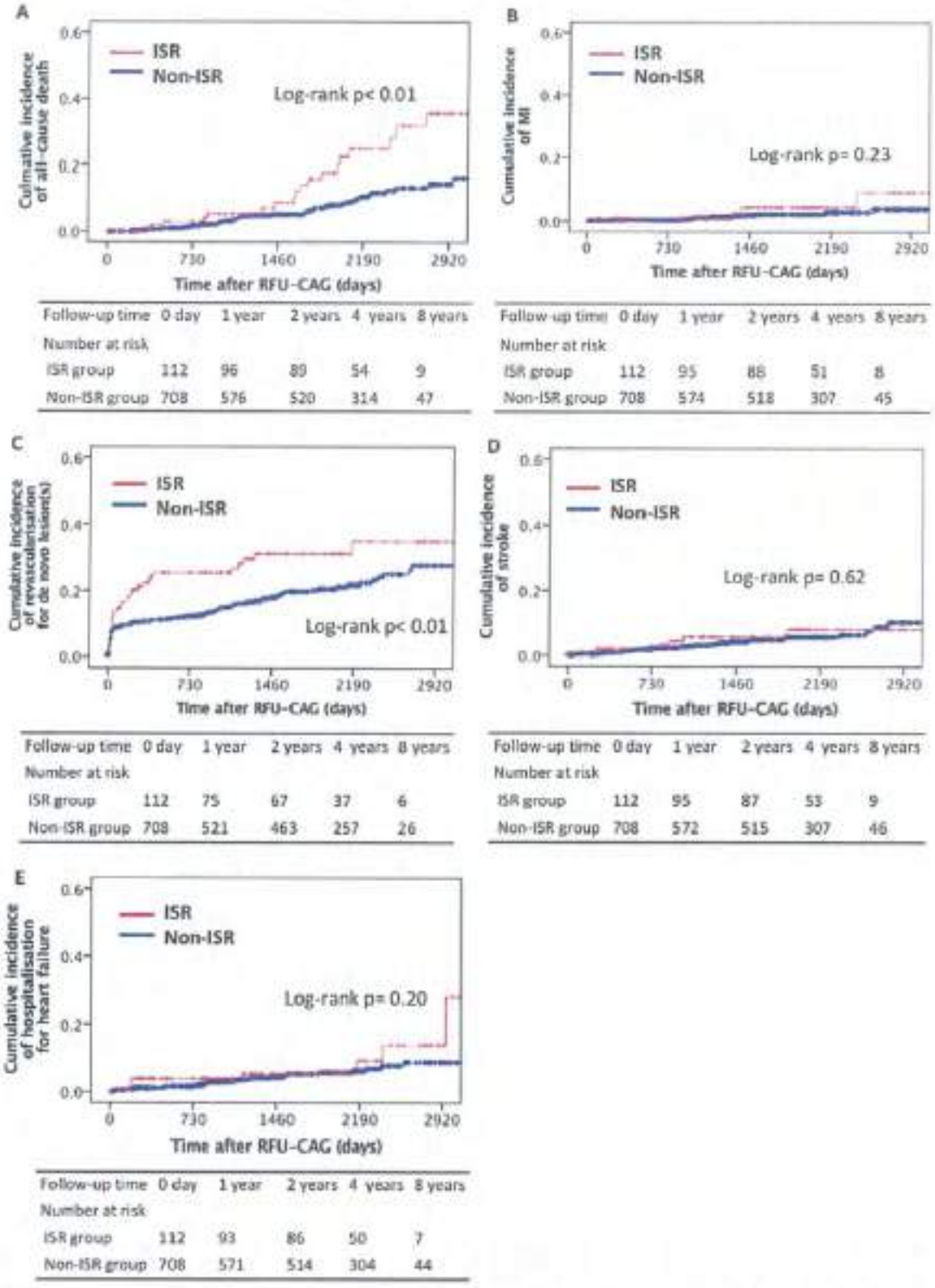

Figure 2. Kaplan-Meier time-to-event curves for (A) all-cause death, (B) any myocardial infarction (MI), (C) revascularisation for de novo lesion(s), (D) stroke, and (E) hospitalisation for heart failure in patients with and without in-stent restenosis (ISR).

The incidences of all-cause death and revascularisation for de novo lesion were significantly higher in the ISR group than in the non-ISR group (16.1% vs. 6.2%, respectively; p <0.01 by log-rank test, 28.6% vs. 16.2%, respectively; p<0.01 by log-rank test).

Table 4. Deaths and Causes of Death, Per Study Group

	ISR group (n=112)	Non-ISR group (n=712)	p Value	
All-cause death	18 (16.1)	44 (6.2)	< 0.01	*
Cardiac death	3 (2.6)	7 (1.0)	0.14	
Non-cardiac death	14 (12.5)	25 (3.5)	< 0.01	*
Cerebral hemorrhage	0 (0)	3 (0.4)	1.00	
Gastrointestinal bleeding	1 (0.9)	0 (0)	0.13	
Malignant tumor	6 (5.4)	12 (1.7)	0.02	*
Unknown	1	12	–	

Number (and percentage) of patients are shown.

* $p < 0.05$

ISR = in-stent restenosis.

Acknowledgements

The authors would like to thank Hiroko Tina Tajima for editorial support of this manuscript and Junko Ueno for assisting in date collection.

References

1) ten Berg JM, Kelder JC, Suttorp MJ, Verheugt FWA, Thijs Plokker HW. Influence of planned six-month follow-up angiography on late outcome after percutaneous coronary intervention. J Am Coll Cardiol 2001; 38: 1061–1069.
2) Pinto DS, Stone GW, Ellis SG, Cox DA, Hermiller J, O'Shaughnessy C, Mann JT, Mehran R, Na Y, Turco M, Caputo R, Popma JJ, Cutlip DE, Russell ME, Cohen DJ. Impact of routine angiographic follow-up on the clinical benefits of paclitaxel-eluting stents: results from the TAXUS-IV trial. J Am Coll Cardiol 2006; 48: 32–36.
3) Choi S, Mun HS, Kang MK, Cho JR, Han SW, Lee N. Clinical impact of routine follow-up coronary angiography after second- or third-generation drug-eluting stent insertion in clinically stable patients. Korean J Intern Med 2015; 30: 49–55.
4) Shiomi H, Morimoto T, Kitaguchi S, Nakagawa Y, Ishii K, Haruna Y, Takamisawa I, Motooka M, Nakao K, Matsuda S, Mimoto S, Aoyama Y, Takeda T, Murata K, Akao M, Inada T, Eizawa H, Hyakuna E, Awano K, Shirotani M, Furukawa Y, Kadota K, Miyauchi K, Tanaka M, Noguchi Y, Nakamura S, Yasuda S, Miyazaki S, Daida H, Kimura K, Ikari Y, Hirayama H, Sumiyoshi T, Kimura T. The ReACT Trial: Randomized Evaluation of Routine Follow-up Coronary Angiography After Percutaneous Coronary Intervention Trial. JACC Cardiovasc Interv 2017; 10: 109–117.
5) Uchida T, Popma J, Stone GW, Ellis SG, Turco MA, Ormiston JA, Muramatsu T, Nakamura M, Nanto S, Yokoi H, Baim DS. The clinical impact of routine angiographic follow-up in randomized trials of drug-eluting stents: a critical assessment of "oculostenotic" reintervention in patients with intermediate lesions. JACC Cardiovasc Interv 2010; 3: 403–411.
6) Mindrescu C, Brener SJ, Guerchicoff A, Fahy M, Parise H, Mehran R, Stone GW. Impact of scheduled angiographic follow-up in patients treated with primary percutaneous coronary intervention for ST-segment elevation myocardial infarction. J Interv Cardiol 2013; 26: 319–324.
7) Cutlip DE, Windecker S, Mehran R, Boam A, Cohen DJ, van Es GA, Steg PG, Morel MA, Mauri L, Vranckx P, McFadden E, Lansky A, Hamon M, Krucoff MW, Serruys PW. Clinical end points in coronary stent trials: a case for standardized definitions. Circulation 2007; 115: 2344–2351.
8) Sacco RL, Kasner SE, Broderick JP, Caplan LR, Connors JJ, Culebras A, Steg PG, Morel MA, Mauri L, Vranckx P, McFadden E, Lansky A, Hamon M, Krucoff MW, Serruys PW. An updated definition of stroke for the 21st century: a statement for healthcare professionals from the American Heart Association/American Stroke Association. Stroke 2013; 44: 2064–2089.

Table 5. Results of Univariate and Multivariable Analysis of MACEs

	Univariate analysis					Multivariable analysis		
	MACE+ (n=227)	MACE− (n=597)	HR (95% CI)	p Value		HR (95% CI)	p Value	
Age, years	68±10	66±11	1.01 (1.00-1.02)	0.05	*	1.00 (0.99-1.02)	0.15	
Male sex	182 (80.2)	478 (80.1)	0.99 (0.71-1.37)	0.95		-	-	
BMI, kg/m2	24.2±3.8	24.2±3.5	0.99 (0.95-1.03)	0.69		-	-	
HTN requiring medication	161 (70.9)	372 (62.3)	1.44 (1.08-1.91)	0.01	*	1.29 (0.95-1.74)	0.09	
DLP requiring medication	126 (55.5)	343 (57.5)	0.85 (0.66-1.11)	0.24		-	-	
LDL-C, mg/dL	101±27	103±30	0.99 (0.99-1.00)	0.25		-	-	
HDL-C, mg/dL	45±13	45±11	1.00 (0.99-1.01)	0.71		-	-	
DM requiring medication	88 (38.8)	159 (26.6)	1.53 (1.17-2.00)	0.02	*	1.53 (1.17-2.00)	0.02	*
Insulin use	41 (18.1)	48 (8.0)	1.80 (1.28-2.53)	0.01	*	-	-	
HbA1c, %	6.0±1.2	5.9±1.0	1.17 (1.04-1.30)	0.05	*	-	-	
CKD (Stb-G5 (GFR<45)	33 (14.5)	40 (6.7)	2.34 (1.62-3.38)	< 0.01	*	1.94 (1.29-2.92)	0.01	*
Hemodialysis	23 (10.1)	20 (3.4)	2.89 (1.89-4.43)	< 0.01	*	-	-	
Current smoking	88 (38.8)	241 (40.4)	0.98 (0.75-1.28)	0.92		-	-	
Never smoked	76 (33.5)	188 (31.5)	1.08 (0.82-1.42)	0.56		-	-	
BNP, pg/mL	187±286	144±422	1.00 (1.00-1.00)	0.05	*	1.00 (1.00-1.00)	0.80	
Emergency PCI	85 (37.4)	243 (40.7)	0.99 (0.76-1.30)	0.96		-	-	
ACS	93 (41.0)	275 (46.1)	0.92 (0.73-1.20)	0.56		-	-	
AMI	60 (26.4)	174 (29.1)	0.97 (0.72-1.30)	0.84		-	-	
BMS	79 (34.8)	225 (37.7)	0.85 (0.64-1.11)	0.24		-	-	
G1 DES	44 (19.4)	65 (10.9)	1.21 (0.86-1.69)	0.28		-	-	
G2 DES	104 (45.8)	307 (51.4)	1.04 (0.79-1.36)	0.75		-	-	
β-blocker	142 (62.6)	396 (66.3)	0.98 (0.75-1.28)	0.89		-	-	
Statin	172 (75.8)	503 (83.9)	0.63 (0.47-0.86)	< 0.01	*	0.71 (0.51-0.97)	0.03	*
ACEI or ARB	168 (74.0)	432 (72.4)	1.05 (0.78-1.41)	0.74		-	-	
Restenosis	50 (22.0)	62 (10.4)	2.05 (1.50-2.80)	< 0.01	*	2.13 (1.55-2.92)	< 0.01	*

Mean±SD values or number (and percentage) of patients are shown.

* $p < 0.05$

MACE = major adverse cardiac event; HR = hazard ratio; CI = confidence interval; BMI = body mass index; HTN = hypertension; DLP = dyslipidemia; LDL-C = low-density lipoprotein cholesterol; HDL-C = high-density lipoprotein cholesterol; DM = diabetes mellitus; CKD = chronic kidney disease; BNP = brain natriuretic peptide; PCI = percutaneous coronary intervention; ACS = acute coronary syndrome; AMI = acute myocardial infarction; BMS = bare metal stent; G1 DES = first-generation drug eluting stent; G2 DES = second-generation drug eluting stent; ACEI = angiotensin converting enzyme inhibitor; ARB = angiotensin receptor blocker.

9) Ruygrok PN, Melkert R, Morel M-AM, Ormiston JA, Bär FW, Fernandez-AF, Suryapranata H, Dawkins KD, Hanet C, Serruys PW. Does angiography six months after coronary intervention influence management and outcome? J Am Coll Cardiol 1999; 34: 1507–1511.

10) Lansky AJ, Brar SS, Yaqub M, Sood P, Applegate RJ, Lazar D, Jankovic I, Hermille J B, Koo K, Sudhir K, Stone GW. Impact of routine angiographic follow-up after percutaneous coro-

nary intervention with drug-eluting stents in the SPIRIT III randomized trial at three years. Am J Cardiol 2012; 110: 21–29.

11) Stone GW, Parise H, Witzenbichler B, Kirtane A, Guagliumi G, Peruga JZ, Brodie BR, Dudek D, Mockel M, Lansky AJ, Mehran R. Selection criteria for drug-eluting versus bare-metal stents and the impact of routine angiographic follow-up: 2-year insights from the HORIZONS-AMI (Harmonizing Outcomes With Revascularization and Stents in Acute Myocardial Infarction) trial. J Am Coll Cardiol 2010; 56: 1597–1604.

12) Sabaté M, Brugaletta S, Cequier A, Iñiguez A, Serra A, Jiménez-Quevedo P, Mainar V, Campo G, Tespili M, den Heijier P, Bethencourt A, Vazquez N, van Es GA, Backx B, Valgimigli M, Serruys PW. Clinical outcomes in patients with ST-segment elevation myocardial infarction treated with everolimus-eluting stents versus bare-metal stents (EXAMINATION): 5-year results of a randomised trial. The Lancet 2016; 387: 357–366.

13) Cassese S, Byrne RA, Schulz S, Hoppman P, Kreutzer J, Feuchtenberger A, Ibrahim T, Ott I, Fusaro M, Schunkert H, Laugwitz KL, Kastrati A. Prognostic role of restenosis in 10 004 patients undergoing routine control angiography after coronary stenting. Eur Heart J 2015; 36: 94–99.

14) Lee MS, Banka G. In-stent restenosis. Interven Cardiol Clin 2016; 5: 211–220.

15) Kastrati A, Schömig A, Elezi S, Schühlen H, Dirschinger J, Hadamitzky M, Wehinger A, Hausleiter J, Walter H, Neumann FJ. Predictive factors of restenosis after coronary stent placement. J Am Coll Cardiol 1997; 30: 1428–1436.

JACC: CARDIOVASCULAR INTERVENTIONS
VOL. 12, NO. 2, 2019
© 2019 BY THE AMERICAN COLLEGE OF CARDIOLOGY FOUNDATION
PUBLISHED BY ELSEVIER

Predictors of Left Ventricular Outflow Tract Obstruction After Transcatheter Mitral Valve Replacement

Sung-Han Yoon, MD,[a] Sabine Bleiziffer, MD,[b,c] Azeem Latib, MD,[d] Lena Eschenbach, MD,[b,c] Marco Ancona, MD,[d] Flavien Vincent, MD,[e] Won-Keun Kim, MD,[f] Axel Unbehaum, MD,[g] Masahiko Asami, MD,[h] Abhijeet Dhoble, MD,[i] Miriam Silaschi, MD,[j] Antonio H. Frangieh, MD,[k] Verena Veulemans, MD,[l] Gilbert H.L. Tang, MD,[m] Shingo Kuwata, MD,[n] Rajiv Rampat, MD,[o] Tobias Schmidt, MD,[p] Amisha J. Patel, MD,[q] Pedro Felipe Gomez Nicz, MD,[r] Luis Nombela-Franco, MD,[s] Annapoorna Kini, MD,[t] Mitsunobu Kitamura, MD,[p] Rahul Sharma, MD,[u] Tarun Chakravarty, MD,[a] David Hildick-Smith, MD,[v] Martin Arnold, MD,[w] Fabio Sandoli de Brito, Jr, MD,[x] Christoph Jensen, MD,[w] Christian Jung, MD,[j] Hasan Jilaihawi, MD,[y] Richard W. Smalling, MD,[j] Francesco Maisano, MD,[z] Albert Markus Kasel, MD,[k] Hendrik Treede, MD,[j] Joerg Kempfert, MD,[g] Thomas Pilgrim, MD,[h] Saibal Kar, MD,[a] Vinayak Bapat, MD,[a] Brian K. Whisenant, MD,[y] Eric Van Belle, MD,[e] Victoria Delgado, MD,[r] Thomas Modine, MD,[e] Jeroen J. Bax, MD,[r] Raj R. Makkar, MD[a]

ABSTRACT

OBJECTIVES The aim of this study was to evaluate the predictors of left ventricular outflow tract (LVOT) obstruction after transcatheter mitral valve replacement (TMVR).

BACKGROUND LVOT obstruction is a major concern with TMVR, but limited data exist regarding its predictors and impact on outcomes.

METHODS Patients with pre-procedural multidetector row computed tomography (MDCT) undergoing TMVR for failed mitral bioprosthetic valves (valve-in-valve), annuloplasty rings (valve-in-ring), and mitral annular calcification (valve-in-MAC) were included in this study. Echocardiographic and procedural characteristics were recorded, and comprehensive assessment with MDCT was performed to identify the predictors of LVOT obstruction (defined as an increment of mean LVOT gradient ≥10 mm Hg from baseline). The new LVOT (neo-LVOT) area left after TMVR was estimated by embedding a virtual valve into the mitral annulus on MDCT, simulating the procedure.

RESULTS Among 194 patients with pre-procedural MDCT undergoing TMVR (valve-in-valve, 107 patients; valve-in-ring, 50 patients; valve-in-MAC, 37 patients), LVOT obstruction was observed in 26 patients (13.4%), with a higher rate after valve-in-MAC than valve-in-ring and valve-in-valve (54.1% vs. 8.0% vs. 1.9%; $p < 0.001$). Patients with LVOT obstruction had significantly higher procedural mortality compared with those without LVOT obstruction (34.6% vs. 2.4%; $p < 0.001$). Receiver-operating characteristic curve analysis showed that an estimated neo-LVOT area ≤1.7 cm^2 predicted LVOT obstruction with sensitivity of 96.2% and specificity of 92.3%.

CONCLUSIONS LVOT obstruction after TMVR was associated with higher procedural mortality. A small estimated neo-LVOT area was significantly associated with LVOT obstruction after TMVR and may help identify patients at high risk for LVOT obstruction. (J Am Coll Cardiol Intv 2019;12:182–93) © 2019 by the American College of Cardiology Foundation.

From the [a]Department of Interventional Cardiology, Cedars-Sinai Heart Institute, Los Angeles, California; [b]Department of Cardiovascular Surgery, German Heart Center Munich, Technische Universität, Munich, Germany; [c]Innere (Institute for Translational Cardiac Surgery), Department of Cardiovascular Surgery, German Heart Center Munich, Technische Universität München, Munich, Germany; [d]Interventional Cardiology Unit, EMO-GVM Centro Cuore Columbus & San Raffaele Scientific Institute, Milan, Italy San Raffaele Hospital, Milan, Italy; [e]Department of Cardiology/Cardiac Surgery, CHU Lille, Inserm, U1011, University of Lille, Lille, France; [f]Herzkhoff Heart and Thorax Center, Department of Cardiology/Cardiac Surgery, Bad Nauheim, Germany; [g]Department of Cardiothoracic and Vascular Surgery, Deutsches Herzzentrum, Berlin, Germany; [h]Department of Cardiology, Bern University Hospital, Bern, Switzerland; [i]Department of Cardiology, University of Texas Health Science Center, Houston, Texas; [j]Department of Cardiac Surgery, University of Halle, Halle, Germany; [k]Deutsches Herzzentrum München, Technische Universität München, Munich, Germany; [l]Division of Cardiology, Pulmonology, and Vascular Medicine, University Hospital Duesseldorf, Duesseldorf, Germany; [m]Department of Cardiovascular Surgery, Mount Sinai Health System, New York, New York; [n]University Heart Center, University Hospital Zurich, Zurich, Switzerland; [o]Sussex Cardiac Centre, Brighton and Sussex University Hospitals

ISSN 1936-8798/$36.00
https://doi.org/10.1016/j.jcin.2018.12.001

Transcatheter mitral valve replacement (TMVR) is an emerging treatment for patients with severe mitral valve disease at high risk for conventional mitral valve surgery. Recent studies showed the efficacy and safety of TMVR in degenerated bioprostheses, failed annuloplasty rings, mitral annular calcification (MAC) and functional severe mitral regurgitation (1–4). However, because of the complexity of the mitral valve apparatus, TMVR poses unique and potentially fatal complications, such as left ventricular outflow tract (LVOT) obstruction.

SEE PAGE 184

Imaging modalities such as 3-dimensional multidetector row computed tomography (MDCT) have contributed to the evolution of transcatheter treatments, providing a deeper understanding of valve anatomy and prediction of complications. Recently, several anatomic and procedural factors associated with LVOT obstruction after TMVR have been proposed (1,5,6). Particularly, the pre-existing native LVOT elongates into the left ventricle after TMVR, creating a new LVOT (neo-LVOT) with permanent displacement of surgical or native mitral anterior leaflet toward the interventricular septum (IVS), and the estimation of the neo-LVOT area with pre-procedural MDCT would help predict LVOT obstruction. Furthermore, the geometry and functions of the left ventricle as well as the mitral and aortic valves may affect the LVOT obstruction. However, previous studies have been limited in sample size to gain a comprehensive understanding of anatomic and functional factors associated with LVOT obstruction after TMVR. In this international multicenter registry of patients treated with TMVR who underwent pre-procedural MDCT, the predictors of LVOT obstruction after TMVR and its impact on outcomes were evaluated.

METHODS

STUDY DESIGN AND PATIENT POPULATION. The TMVR registry is an international, multicenter, observational study that enrolled consecutive patients undergoing TMVR for mitral degenerated bioprostheses (valve-in-valve [ViV]), failed annuloplasty rings (valve-in-ring [ViR]) or MAC (valve-in-MAC [ViMAC]). For the purpose of this study, patients with pre-procedural MDCT were included, and those with suboptimal images were excluded from the analysis. Patients were considered candidates for the procedure if they had significant dysfunction (stenosis, regurgitation, or both) of bioprosthetic mitral valve, annuloplasty ring, or calcified mitral annulus, with comorbid conditions that would preclude a conventional mitral valve surgery. Data collection included baseline

ABBREVIATIONS AND ACRONYMS

IQR = interquartile range

IVS = interventricular septum

LVEDD = left ventricular end-diastolic diameter

LVOT = left ventricular outflow tract

MAC = mitral annular calcification

MDCT = multidetector row computed tomography

TMVR = transcatheter mitral valve replacement

ViMAC = valve-in-mitral annular calcification

ViR = valve-in-ring

ViV = valve-in-valve

NHS Trust, Brighton, United Kingdom; [2]Department of Cardiology, Asklepios Klinik St. Georg, Hamburg, Germany; [3]Columbia University Medical Center/New York Presbyterian Hospital, New York, New York; [4]Department of Cardiology, Hospital Sao Camilo, Sao Paulo, Brazil; [5]Division of Cardiology, Hospital Clinico San Carlos, Madrid, Spain; [6]Division of Cardiology, Mount Sinai Medical Center, New York, New York; [7]Department of Cardiology, University Hospital Erlangen, Erlangen, Germany; [8]Heart Institute of University of Sao Paulo Medical School, Sao Paulo, Brazil; [9]Contilia Heart and Vascular Centre, Elisabeth Krankenhaus Essen, Essen, Germany; [10]Department of Cardiology and Cardiothoracic Surgery, NYU Langone Medical Center, New York, New York; [11]Division of Cardiovascular Diseases, Intermountain Heart Institute, Salt Lake City, Utah; and the [12]Department of Cardiology, Leiden University Medical Center, Leiden, the Netherlands. The Department of Cardiology of the Leiden University Medical Center received unrestricted research grants from Edwards Lifesciences, Biotronik, Medtronic, and Boston Scientific. Dr. Bleiziffer has served as a consultant to Medtronic; has served as a proctor for Medtronic and JenaValve; and has received travel compensation from Edwards Lifesciences, Medtronic, and Johnson & Johnson. Dr. Latib has served on an advisory board for Medtronic; and has served as a consultant for Direct Flow Medical. Dr. Kim has served as a proctor for Symmetis and St. Jude Medical. Dr. Eltchaninoff has served as a proctor for Edwards Lifesciences; and has served as a consultant for St. Jude Medical. Dr. Tang has served as a proctor for Edwards Lifesciences. Dr. Smith has served as a proctor for Medtronic and Boston Scientific. Dr. Arnold has received travel compensation from Edwards Lifesciences; has served as a proctor for Edwards Lifesciences; has served as a proctor and consultant for St. Jude Medical; and has received speaking honoraria from JenaValve. Dr. Blatchford has served as a consultant for Edwards Lifesciences, St. Jude Medical, and Venus Medtech. Dr. Strollig has received consulting fees and research support from St. Jude and Edwards Lifesciences. Dr. Maisano has served as a consultant for Edwards Lifesciences, Medtronic, St. Jude Medical, Abbott Vascular, and Velotech; and has received royalties from Edwards Lifesciences. Dr. Kasel has served as a consultant for Edwards Lifesciences and received research support from Edwards Lifesciences. Dr. Treede has served as a proctor and consultant for Edwards Lifesciences. Dr. Pilgrim has received speaking fees from Biotronik and Medtronic; and has received travel honoraria from Biotronik and Edwards Lifesciences. Dr. Kempfert has served as a proctor for Edwards Lifesciences, Abbott Vascular, Medtronic, and Biotronik. Dr. Ilar has served as a consultant for Abbott Vascular and Boston Scientific. Dr. Bapat has served as a consultant for Edwards Lifesciences, Medtronic, Abbott Vascular, Boston Scientific, and 4Tech. Dr. Whitlenant has served as a consultant for Edwards Lifesciences and Boston Scientific. Dr. Delgado has received speaking fees from Abbott Vascular. Dr. Modine has served as a consultant for Boston Scientific. Dr. Makkar has received grants from Edwards Lifesciences; and has received personal fees from St. Jude Medical and Medtronic. All other authors have reported that they have no relationship relevant to the contents of this paper to disclose.

Manuscript received September 28, 2018; revised manuscript received November 18, 2018, accepted December 4, 2018.

JACC: CARDIOVASCULAR INTERVENTIONS VOL. 12, NO. 1, 2019
JANUARY 28, 2019:181–92

clinical, echocardiographic, and procedural data as well as multidetector row computed tomographic images. All data provided by each institution were anonymized and centrally collected, and all inconsistencies were resolved directly with local investigators. This study was approved by the Institutional Review Board of each institution when required; however, in some countries, for retrospective analysis of clinically acquired and anonymized data, the Institutional Review Board waived the need for written patient informed consent.

STUDY DEVICES AND TMVR PROCEDURE. Patients were selected for TMVR at the institutional level after discussions by the multidisciplinary heart team, and device type and access site were determined thereafter. Device size was selected on the basis of a combination of the manufacture's reported internal diameter and true internal diameter as well as measurements on MDCT and transesophageal echocardiography (7-9). In addition, the Valve in Valve Mitral app was used to ensure the proper device size selection (http://www.uhqo.com/vivmitral). All TMVR procedures were conducted in accordance with local guidelines using standard techniques via transseptal, transapical, or transatrial access, and balloon-expandable transcatheter valves (the SAPIEN, SAPIEN XT, or SAPIEN 3 [Edwards Lifesciences, Irvine, California] and Melody [Medtronic, Minneapolis, Minnesota]) or other transcatheter valves (Lotus [Boston Scientific, Natick, Massachusetts] and Direct Flow [Direct Flow Medical, Santa Rosa, California]) were implanted (10-15). The sizes of transcatheter valves were categorized accordingly: 1) small for balloon-expandable valves with 22 or 23 mm, and Direct Flow with 25 mm; 2) medium for balloon-expandable valves with 26 mm, Lotus with 25 mm, and Direct Flow with 27 mm; and 3) large for balloon-expandable valves with 29 mm, Lotus with 27 mm, and Direct Flow with 29 mm.

ASSESSMENT OF LVOT OBSTRUCTION AND STUDY ENDPOINTS. Echocardiographic studies were performed using commercially available ultrasound systems. LVOT gradient was assessed using continuous-wave Doppler echocardiography before discharge under resting and hemodynamically stable conditions. All echocardiographic, procedural, and clinical data were assessed at each institution according to the Mitral Valve Academic Research Consortium criteria (16,17). LVOT obstruction was defined as follows: 1) acute hemodynamic deterioration immediately after TMVR with intraprocedural transesophageal echocardiographic images showing displacement of prosthetic or anterior native mitral valve leaflet obstructing LVOT; and 2) an increment in mean LVOT gradient ≥10 mm Hg from baseline according to the Mitral Valve Academic Research Consortium criteria (17). Relative wall thickness was defined as the ratio between the posterior wall thickness and the left ventricular end-diastolic diameter (LVEDD).

MITRAL VALVE ASSESSMENT ON MDCT. Protocols for MDCT were applied according to each center's standard practice. Scans were performed using several different scanners, 64-slice or higher, with electrocardiography-synchronized data acquisition. Images were post-processed offline retrospectively in the Cedars-Sinai Heart Institute core laboratory, using dedicated TMVR planning software (3mensio Structural Heart software version 9.0, 3mensio Medical Imaging BV, Bilthoven, the Netherlands). The dimensions of the mitral valve and native LVOT were measured, and the severity of MAC was qualitatively assessed as previously described (18-20).

Neo-LVOT ANALYSIS. For the segmentation and planimetry assessment of the neo-LVOT cross-sectional area, mid to late systolic image reconstructions were used. The neo-LVOT was assessed by embedding a virtual valve according to the pre-procedural mitral valve status and type of transcatheter valves actually implanted (**Figure 1**, Online Figure 1). After adjustment of centerline, the minimal value of estimated neo-LVOT during mid to late systole was assessed by planimetry on cross-sectional images and indexed to body surface area (**Figure 2**). Additionally, the distance between the mitral annulus and the IVS was measured. To assess the temporal changes of estimated neo-LVOT area and other multidetector row computed tomographic parameters, computed tomography data from 38 randomly selected patients (16 patients with VIV, 12 patients with ViR, and 10 patients with ViMAC) were reconstructed in 10% steps throughout the cardiac cycle. In patients with post-procedural MDCT, the neo-LVOT area was assessed similarly to the pre-procedural multidetector row computed tomographic analysis. The details of the neo-LVOT assessment are described in the Online Appendix.

STATISTICAL ANALYSIS. Patients were stratified according to the pre-procedural status of the mitral valve (VIV, VIR, or VIMAC). Dichotomous variables are presented as counts or percentages and were compared using the chi-square or Fisher exact test. Continuous variables are presented as median (interquartile range [IQR]) and compared using the Mann-Whitney *U* test. Comparisons of continuous variables among 3 groups were performed using the

FIGURE 1 Recommendation for Multidetector Row Computed Tomography Analysis Before Transcatheter Mitral Valve Replacement

Recommendation for MDCT Analysis Before TMVR

Cardiac Cycle	Mid-end systole	
Position of Virtual Valve	Valve-in-Valve with Sapien valves	Pericardial surgical valve: ventricular end of stent-post Porcine surgical valve: 4 mm atrial side from stent-post
	Valve-in-Valve with other devices*	Ventricular end of stent-post
	Valve-in-Ring	30 : 70 (atrial : ventricular)
	Valve-in-MAC	30 : 70 (atrial : ventricular)
Direction of Virtual Valve	Perpendicular to mitral annulus	
Size of Virtual Valve	Size of used transcatheter valve	
Neo-LVOT Assessment	Lowest value during mid-end systole	

* Other devices include Lotus, Melody, Direct Flow and other valves without open stent frame

The recommendation for multidetector row computed tomographic analysis before transcatheter mitral valve replacement. LVOT = left ventricular outflow tract; MAC = mitral annular calcification.

FIGURE 2 Assessment of the Neo-Left Ventricular Outflow Tract

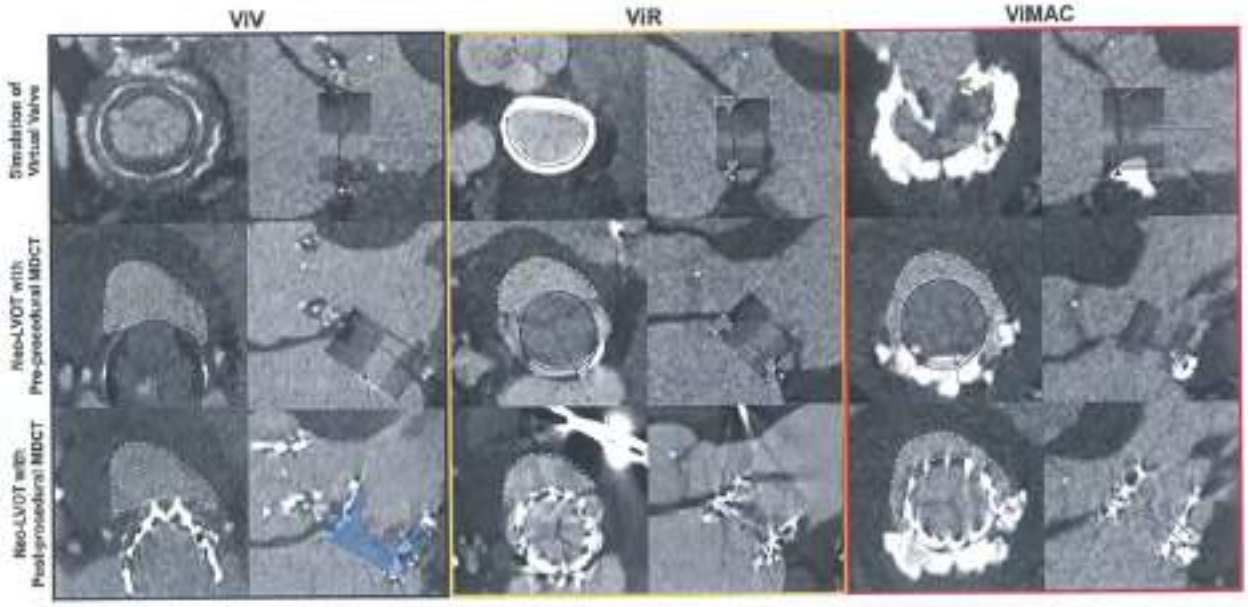

Segmentation of the mitral annulus and embedding virtual valve for valve-in-valve (VIV), valve-in-ring (VIR) and valve-in-mitral annular calcification (VIMAC) **(top)**. With reformatting centerline **(yellow dotted line)** and slicing of cross-sectional view **(blue line)**, cross-sectional image showing minimal area of neo-left ventricular outflow tract (LVOT) was found with pre- and post-procedural MDCT **(middle and bottom)**. **Purple line** indicates outer edges of virtual valve at the level of cross section. The minimal neo-LVOT area was measured by planimetry **(white dotted lines)**. Distance between mitral annulus and interventricular septum was measured **(orange line)**. **Asterisk** and **arrowhead** indicate aortic valve and mitral annulus, respectively.

JACC: CARDIOVASCULAR INTERVENTIONS VOL. 12, NO. 2, 2019
JANUARY 28, 2019:183–93

TABLE 1 Baseline Characteristics

	Overall (N = 194)	ViV (n = 107)	ViR (n = 50)	ViMAC (n = 37)	p Value
Age, yrs	76.0 (69.0–81.0)	77.0 (69.0–83.0)	74.0 (68.0–78.0)	77.0 (66.0–85.0)	0.03
Female	105 (54.1)	63 (58.9)	13 (26.0)	29 (78.4)	<0.001
Body surface area, m²	1.75 (1.63–1.91)	1.70 (1.62–1.90)	1.82 (1.71–1.96)	1.70 (1.57–1.81)	0.005
NYHA functional class III or IV	166 (85.6)	92 (86.0)	43 (86.0)	31 (83.8)	0.96
STS score, %	7.4 (5.1–11.8)	7.3 (5.1–11.9)	6.2 (4.5–9.8)	8.8 (6.8–14.2)	0.015
Diabetes mellitus	47 (24.2)	21 (19.6)	13 (26.0)	13 (35.1)	0.16
Creatinine, mg/dl	1.2 (0.9–1.6)	1.1 (0.9–1.4)	1.2 (1.0–1.9)	1.3 (0.9–1.9)	0.012
Hypertension	150 (77.3)	83 (77.6)	37 (74.0)	30 (81.1)	0.74
Peripheral vascular disease	26 (13.4)	13 (12.1)	8 (16.0)	5 (13.5)	0.82
Prior cerebrovascular accident	32 (16.5)	21 (19.6)	7 (14.0)	4 (10.8)	0.42
Chronic pulmonary disease	60 (30.9)	33 (30.8)	11 (22.0)	16 (43.2)	0.11
Prior myocardial infarction	31 (16.0)	14 (13.1)	12 (24.0)	5 (13.5)	0.21
Prior CABG	63 (32.5)	32 (28.9)	22 (44.0)	9 (24.3)	0.11
Echocardiographic findings					
LVEF, %	55.0 (41.8–62.0)	60.0 (50.0–65.0)	35.0 (25.0–55.0)	60.0 (55.0–63.8)	<0.001
LVEDD, mm	48.0 (42.0–55.4)	46.5 (41.5–51.0)	57.7 (50.8–65.0)	43.0 (38.0–46.3)	<0.001
Interventricular septal wall, cm	1.1 (0.9–1.2)	1.1 (0.9–1.2)	1.0 (0.9–1.2)	1.1 (1.0–1.3)	0.35
LV posterior wall, cm	1.0 (0.9–1.2)	1.0 (0.9–1.2)	1.0 (0.8–1.1)	1.2 (1.0–1.2)	0.07
Relative wall thickness	0.43 (0.34–0.52)	0.44 (0.37–0.53)	0.34 (0.27–0.43)	0.52 (0.42–0.61)	<0.001
LV mass, g	195.3 (139.9–253.6)	185.7 (134.6–224.5)	227.0 (188.8–306.2)	180.5 (115.0–219.9)	<0.001
LV mass index, g/m²	109.3 (86.5–135.1)	109.3 (82.2–141.2)	105.3 (80.1–139.5)	114.1 (96.3–129.4)	0.75
Aortic valve mean gradient, mm Hg	7.0 (3.0–11.0)	7.0 (3.0–12.0)	3.0 (1.0–6.0)	10.0 (7.0–12.0)	0.001
Mitral valve mean gradient, mm Hg	10.0 (6.0–14.0)	11.0 (7.0–15.0)	4.5 (3.0–7.1)	12.0 (7.0–15.0)	<0.001
Anterior mitral leaflet length, mm	23.0 (18.6–26.1)	–	23.0 (18.6–26.1)	–	–
Mechanism of failure					
Regurgitation	73 (37.6)	30 (28.0)	38 (76.0)	5 (13.5)	<0.001
Stenosis	59 (30.4)	38 (35.5)	7 (14.0)	14 (37.8)	
Combined	62 (32.0)	39 (36.4)	5 (10.0)	18 (48.6)	

Values are median (interquartile range) or n (%).

CABG = coronary artery bypass graft surgery; LV = left ventricular; LVEDD = left ventricular end-diastolic diameter; LVEF = left ventricular ejection fraction; NYHA = New York Heart Association; STS = Society of Thoracic Surgeons; ViMAC = valve-in-mitral annular calcification; ViR = valve-in-ring; ViV = valve-in-valve.

Kruskal-Wallis test. Receiver-operating characteristic curve analysis was performed and areas under the curve were calculated to assess the discriminative power of multidetector row computed tomography and echocardiographic parameters for LVOT obstruction. Pearson correlation was used to assess the relationship between 2 continuous variables. All statistical analyses were performed using SPSS software version 24.0 (SPSS, Chicago, Illinois) or MedCalc (MedCalc Software, Mariakerke, Belgium). A 2-sided p value of <0.05 was considered to indicate statistical significance.

RESULTS

BASELINE CHARACTERISTICS. Between February 2009 and January 2018, 211 patients with available pre-procedural MDCT underwent TMVR for degenerated bioprostheses, failed annuloplasty rings, or severely calcified mitral annulus across 22 participating centers. After excluding 17 patients with suboptimal multidetector row computed tomographic images, 194 patients were finally included in the present study: 107 (55.2%) with ViV, 50 (25.8%) with ViR, and 37 (19.1%) with ViMAC. The majority of patients were deemed at high surgical risk with a median Society of Thoracic Surgeons score of 7.4% (IQR: 5.1% to 11.8%), significantly higher in the ViMAC group compared with the ViV and ViR groups (8.8% vs. 7.3% vs. 6.2%; p = 0.015).

The baseline echocardiographic characteristics of the study population varied across the 3 groups: the ViMAC group had smaller LVEDD but larger relative wall thickness, whereas the ViR group had larger LVEDD with lower ejection fraction, and mitral regurgitation was the most frequent form of valve dysfunction (**Table 1**). Although left ventricular mass index was not significantly different across the 3

TABLE 2 Pre-Procedural Multidetector Row Computed Tomographic Data

	Overall (N = 194)	ViV (n = 107)	ViR (n = 50)	ViMAC (n = 37)	p Value
Mitral annular dimensions					
Annular area, cm^2	5.1 (4.1–6.2)	4.9 (4.3–5.6)	4.1 (3.6–5.2)	9.8 (8.3–11.2)	<0.001
Projected perimeter, mm	80.4 (73.4–88.8)	78.4 (73.6–84.1)	74.0 (69.6–82.6)	113.5 (108.0–123.8)	<0.001
Trigone-to-trigone distance, mm	–	–	–	25.8 (22.7–30.6)	–
Intercommissural diameter, mm	26.4 (24.4–28.8)	25.2 (23.4–27.0)	26.6 (24.6–28.7)	35.1 (30.9–37.0)	<0.001
Septolateral diameter, mm	24.4 (21.6–27.3)	24.9 (22.9–26.4)	19.4 (17.5–22.5)	35.4 (31.8–40.8)	<0.001
Native LVOT dimensions					
Minimal diameter, mm	19.8 (17.6–21.5)	19.5 (17.6–21.4)	21.5 (20.0–23.9)	17.6 (16.2–19.6)	<0.001
Maximal diameter, mm	27.4 (25.6–29.8)	27.0 (25.7–29.6)	29.2 (27.1–31.1)	26.1 (23.0–28.4)	<0.001
Area, cm^2	4.3 (3.6–5.0)	4.2 (3.6–4.8)	5.0 (4.3–5.8)	3.7 (3.0–4.3)	<0.001
Perimeter, mm	76.1 (70.3–81.7)	74.9 (70.1–80.6)	80.5 (75.6–87.3)	71.0 (64.1–76.3)	<0.001
Aortomitral angle	58.2 (52.2–66.3)	59.6 (53.0–66.6)	55.6 (50.3–64.0)	57.0 (52.0–66.9)	0.21
Mitral annulus-to-IVS distance, mm	22.9 (20.1–26.4)	23.1 (21.2–26.4)	25.2 (22.5–29.2)	16.4 (14.3–19.0)	<0.001
Neo-LVOT area, cm^2	2.7 (1.9–4.3)	3.0 (2.2–4.3)	3.7 (2.4–5.2)	1.5 (0.5–2.4)	<0.001
Indexed neo-LVOT area, cm^2/m^2	1.6 (1.1–2.4)	1.7 (1.2–2.3)	2.0 (1.3–2.9)	0.9 (0.3–1.3)	<0.001

Values are median (interquartile range).
IVS = interventricular septum; LVOT = left ventricular outflow tract; other abbreviations as in Table 1.

groups, aortic and mitral valve gradient were higher in the ViMAC group.

MULTIDETECTOR ROW COMPUTED TOMOGRAPHIC DATA. The pre-procedural multidetector row computed tomographic data are shown in **Table 2**. Compared with the ViV and ViR group, the ViMAC group showed larger mitral annular dimensions but smaller native LVOT dimensions and mitral annulus-to-IVS distance. However, aortomitral angles were similar among the 3 groups. With simulation of virtual valve implantation, the estimated neo-LVOT area was the smallest in the ViMAC group, followed by the ViV and ViR groups (median area 1.5 cm^2 [IQR: 0.5 to 2.4 cm^2] vs. 3.0 cm^2 [IQR: 2.2 to 4.3 cm^2] vs. 3.7 cm^2 [IQR: 2.4 to 5.2 cm^2]; $p < 0.001$). The indexed neo-LVOT area followed a similar pattern (median area 0.9 cm^2 [IQR: 0.3 to 1.3 cm^2] vs. 1.7 cm^2 [IQR: 1.2 to 2.3 cm^2] vs. 2.0 cm^2 [IQR: 1.3 to 2.9 cm^2]; $p < 0.001$). In the ViMAC group, 43.2% and 86.5% of patients had significant calcification at the anterior and posterior leaflets, respectively. From a repeated measurement for a subset of 12 randomly selected patients, intra-observer and interobserver variability for neo-LVOT area was satisfactory (intraobserver intraclass correlation coefficient = 0.99; $p < 0.001$; interobserver intraclass correlation coefficient = 0.92; $p < 0.001$).

PROCEDURAL DATA. The transseptal approach was used in approximately one-half of the patients, without significant differences among the 3 groups, and balloon-expandable valves were used in the majority of patients (89.7%) (**Table 3**). Procedural death

TABLE 3 Procedural Data

	Overall (N = 194)	ViV (n = 107)	ViR (n = 50)	ViMAC (n = 37)	p Value
Procedural data					
Access site					
Transseptal access	93 (47.9)	47 (43.9)	23 (46.0)	23 (62.2)	0.28
Transapical access	100 (51.5)	59 (55.1)	27 (54.0)	14 (37.8)	
Transatrial access	1 (0.5)	1 (0.9)	0 (0.0)	0 (0.0)	
Device type					0.36
Balloon-expandable valves	174 (89.7)	99 (92.5)	44 (88.0)	31 (83.8)	0.15*
SAPIEN	4 (2.3)	3 (2.8)	1 (2.0)	0 (0.0)	
SAPIEN XT	40 (20.6)	29 (27.1)	8 (16.0)	3 (8.1)	
SAPIEN 3	129 (66.5)	66 (61.7)	35 (70.0)	28 (75.7)	
Melody	1 (0.5)	1 (0.9)	0 (0.0)	0 (0.0)	
Lotus	15 (7.7)	5 (4.7)	5 (10.0)	5 (13.5)	
Direct Flow	5 (2.6)	3 (2.8)	1 (2.0)	1 (2.7)	
Device size					0.16
Small	11 (5.7)	6 (5.6)	5 (10.0)	0 (0.0)	
Medium	75 (38.7)	44 (41.1)	20 (40.0)	11 (29.7)	
Large	108 (55.7)	57 (53.3)	25 (50.0)	26 (70.3)	
Planned concomitant TAVR	9 (4.6)	6 (5.6)	0 (0.0)	3 (8.1)	0.11
Outcomes					
Procedural death	13 (6.7)	2 (1.9)	1 (2.0)	10 (27.0)	<0.001
Conversion to surgery	8 (4.1)	1 (0.9)	3 (6.0)	4 (10.8)	0.015
LVOT obstruction	26 (13.4)	2 (1.9)	4 (8.0)	20 (54.1)	<0.001
Treatment strategy					0.801†
Medical	11 (42.3)	1 (50.0)	1 (25.0)	9 (45.0)	
Emergent surgery	5 (19.2)	0 (0.0)	2 (50.0)	3 (15.0)	
Emergent TAVR	2 (7.7)	0 (0.0)	0 (0.0)	2 (10.0)	
Alcohol septal ablation	8 (30.8)	1 (50.0)	1 (25.0)	6 (30.0)	
Technical success	158 (81.4)	101 (94.4)	37 (74.0)	20 (54.1)	<0.001

Values are n (%). *p value for comparison of the balloon-expandable valve subtypes. †P value for comparison of treatment strategies for LVOT obstruction.
TAVR = transcatheter aortic valve replacement; other abbreviation as in Tables 1 and 2.

JACC: CARDIOVASCULAR INTERVENTIONS VOL. 12, NO. 2, 2019
JANUARY 28, 2019:183–93

FIGURE 3 Procedural Outcomes and Left Ventricular Outflow Tract Obstruction

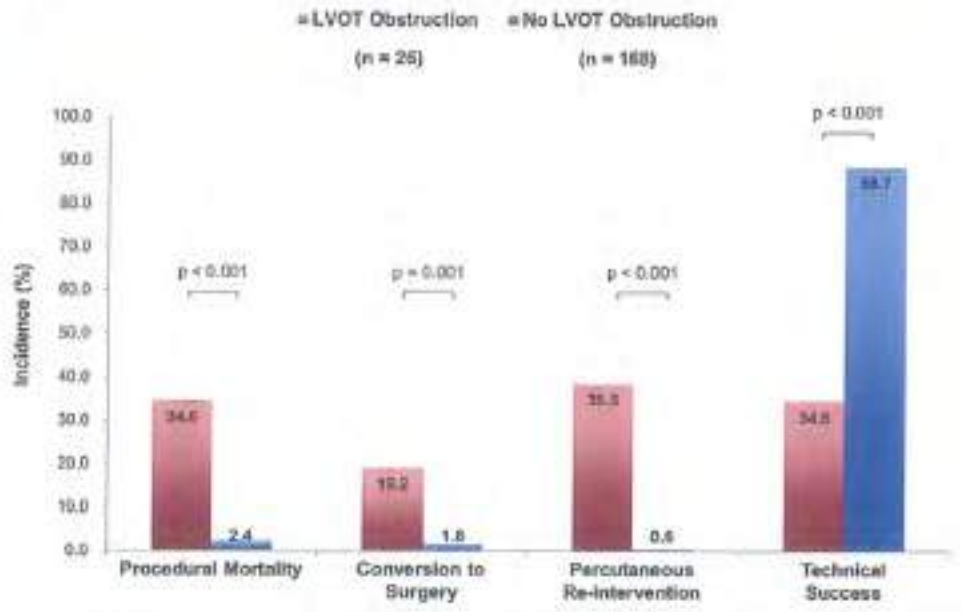

Incidences of procedure-related death, conversion to conventional surgery, emergent percutaneous reintervention, and technical success in patients with and without left ventricular outflow tract (LVOT) obstruction.

and conversion to surgery were observed in 13 (6.7%) and 8 (4.1%) patients, respectively. LVOT obstruction occurred in 26 patients (13.4%), with a significantly higher rate in the ViMAC group compared with the ViR and ViV groups (54.1% vs. 8.0% vs. 1.9%; $p < 0.001$). The rates of LVOT obstruction were similar for the different types of transcatheter valves (balloon-expandable valves vs. the other type of valves, 12.6% vs. 20.0%; $p = 0.32$), for the different sizes of transcatheter valves (small vs. medium vs. large, 0.0% vs. 12.0% vs. 15.7%; $p = 0.31$), and for access site (transseptal access vs. transapical access, 17.2% vs. 10.0%; $p = 0.14$). The technical success rate was 81.4% overall and significantly lower in the ViMAC group compared with the ViR and ViV group (54.1% vs. 74.0% vs. 94.4%; $p < 0.001$).

FIGURE 4 Neo-Left Ventricular Outflow Tract Area Throughout the Cardiac Cycle

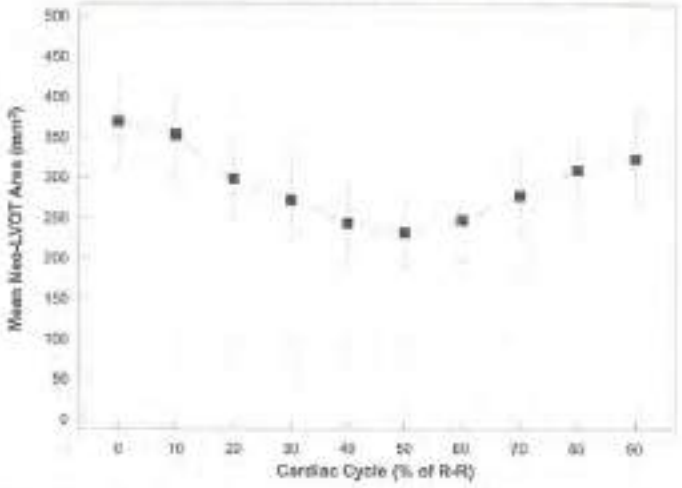

The mean estimated neo-left ventricular outflow tract (LVOT) area decreases during early systole and reaches its nadir at end-systole. **Vertical bars** indicate SD of measurements in 38 patients.

Compared with patients without LVOT obstruction, those with LVOT obstruction had higher rates of procedural adverse events, including procedure-related death (34.6% vs. 2.4%; $p < 0.001$), conversion to surgery (19.2% vs. 1.8%; $p = 0.001$), and emergent percutaneous reintervention (38.5% vs. 0.6%; $p = 0.001$), leading to significantly lower technical success (34.6% vs. 88.7%; $p < 0.001$) (**Figure 3**).

Among those who experienced LVOT obstruction, 15 patients (57.7%) underwent intervention (5 patients [19.2%] underwent emergent surgery, 2 patients [7.7%] were treated with transcatheter aortic valve replacement, and 8 patients [30.8%] were treated with alcohol septal ablation), whereas the remainder received medical therapy. Nine patients

FIGURE 5 Estimated Neo-Left Ventricular Outflow Tract Area and Left Ventricular Outflow Tract Gradient

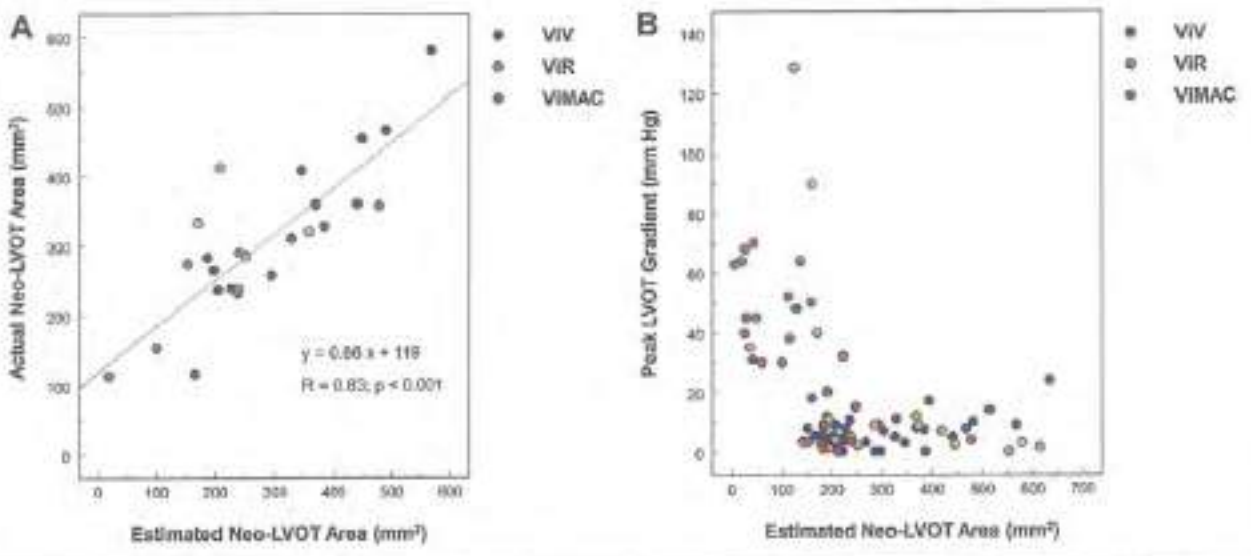

(A) Scatterplot of estimated neo-left ventricular outflow tract (LVOT) area with pre-procedural MDCT (x-axis) and actual neo-LVOT area with post-procedural multidetector row computed tomography (MDCT) (y-axis). (B) Scatterplot of estimated neo-LVOT area with pre-procedural MDCT (x-axis) and peak LVOT pressure gradient at post-procedure (y-axis). **Blue, yellow, and red dots** indicate valve-in-valve (ViV), valve-in-ring (ViR), and valve-in-mitral annular calcification (ViMAC) cases, respectively).

(34.6%) died subsequently. Procedural mortality after LVOT obstruction was 0% in the ViV and ViR groups but 45% in the ViMAC group ($p = 0.26$). Approximately one-half of the patients experiencing LVOT obstruction died when treated with medical therapy, surgery, or transcatheter aortic valve replacement. In contrast, all patients treated with alcohol septal ablation survived (Online Figure 2).

Neo-LVOT AREA AND POST-PROCEDURAL MDCT. Estimated neo-LVOT area, mitral annulus-to-IVS distance, and aortomitral angle varied throughout the cardiac cycle (**Figure 4**, Online Figure 3). In the overall group, minimal neo-LVOT area and mitral annulus-to-IVS distance decreased during systole, reaching a minimum at a median 50% of the R-R interval. Post-procedural assessment by MDCT in 26 patients showed that the mean atrioventricular ratios of implanted transcatheter valves were 29:71 in overall, 24:76 for ViV, 34:66 for ViR, and 34:66 for ViMAC, respectively. There was excellent correlation between the estimated neo-LVOT area with pre-procedural multidetector row computed tomographic and actual neo-LVOT area with post-procedural MDCT (Pearson correlation coefficient = 0.83, $p < 0.001$) (**Figure 5A**). Furthermore, peak LVOT gradient after TMVR and estimated neo-LVOT area on pre-procedural MDCT in 79 patients showed an inverse correlation ($p < 0.001$) (**Figure 5B**).

LVOT OBSTRUCTION AND ANATOMIC PARAMETERS. Multidetector row computed tomographic and echocardiographic measurements were compared between patients with and those without LVOT obstruction in general and within the 3 groups, respectively (**Figure 6**, Online Figure 4). The estimated neo-LVOT area and indexed neo-LVOT area were smaller in patients with LVOT obstruction compared with those without LVOT obstruction in the overall population (median neo-LVOT area 0.6 cm^2 [IQR: 0.3 to 1.3 cm^2] vs. 3.2 cm^2 [IQR: 2.3 to 4.5 cm^2]; $p < 0.001$; median indexed neo-LVOT area 0.4 cm^2 [IQR: 0.2 to 0.8 cm^2] vs. 1.8 cm^2 [IQR: 1.3 to 2.3 cm^2]; $p < 0.001$) and across the 3 groups of treatment. Compared with those without LVOT obstruction, patients with LVOT obstruction had smaller mitral annulus-to-IVS distance and smaller LVEDD as well as larger relative wall thickness. Among patients without planned concomitant transcatheter aortic valve replacement, the aortic valve mean gradient tended to be higher in patients with LVOT obstruction compared with those without LVOT obstruction

JACC: CARDIOVASCULAR INTERVENTIONS VOL. 12, NO. 2, 2019
JANUARY 28, 2019:182–93

FIGURE 6 Neo-Left Ventricular Outflow Tract Area and Left Ventricular Outflow Tract Obstruction

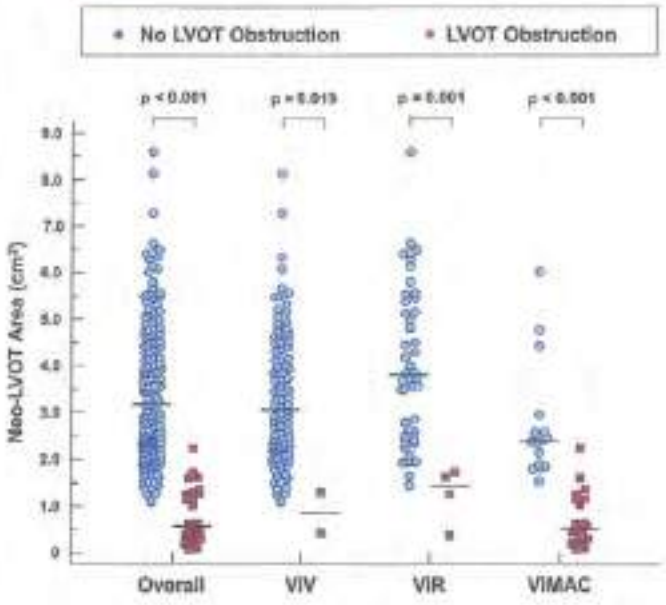

	No LVOT Obstruction	LVOT Obstruction
Overall	3.2 (2.3 – 4.5)	0.6 (0.3 – 1.3)
ViV	3.0 (2.2 – 4.3)	0.8 (0.4 – 1.2)
ViR	3.6 (2.6 – 5.4)	1.4 (0.8 – 1.7)
ViMAC	2.4 (1.9 – 2.8)	0.5 (0.2 – 1.1)

Scatterplot of the estimated neo-left ventricular outflow tract (LVOT) area with pre-procedural multidetector row computed tomography between patients with and without LVOT obstruction in overall, valve-in-valve (ViV), valve-in-ring (ViR), and valve-in-mitral annular calcification (ViMAC) groups, respectively. **Blue dots and red squares** indicate patients with no LVOT obstruction and those with LVOT obstruction, respectively. **Horizontal lines** indicate median values.

(9.0 mm Hg [IQR: 4.0 to 11.0 mm Hg] vs. 5.0 mm Hg [IQR: 2.0 to 10.0 mm Hg]; p = 0.06). There were no significant differences in left ventricular mass index and aortomitral angle between those with and those without LVOT obstruction. In the ViR group, the anterior mitral leaflet tended to be longer in patients with LVOT obstruction compared with those without LVOT obstruction (26.5 mm [IQR: 21.9 to 30.0 mm] vs. 22.8 mm [IQR: 18.0 to 25.5 mm]; p = 0.07). In the ViMAC group, there was no significant difference in severity of MAC between patients with and without LVOT obstruction (Online Table 1).

RECEIVER-OPERATING CHARACTERISTIC CURVE ANALYSES FOR PREDICTION OF LVOT OBSTRUCTION. Multiple pre-procedural multidetector row computed tomographic and echocardiographic variables were evaluated for their predictive value of LVOT obstruction. In the overall cohort, the estimated neo-LVOT area and indexed neo-LVOT area showed greatest discriminatory value for LVOT obstruction, with cutoff values of 1.7 cm^2 and 0.92 cm^2/m^2, respectively (**Figure 7**, Online Figure 5). With the use of cutoff values of neo-LVOT area, the incidence of LVOT obstruction was significantly lower in patients with neo-LVOT area >1.7 cm^2 compared with those with neo-LVOT area ≤1.7 cm^2 (0.6% vs. 65.8%; p < 0.001) (**Figure 8**).

DISCUSSION

In the present study we evaluated predictors and procedural outcomes of LVOT obstruction after TMVR. The major findings of the present study are as follows: 1) LVOT obstruction occurred more frequently after ViMAC compared with ViR and ViV and was associated with higher rates of procedural adverse events; and 2) although cardiac geometry and function differed according to the mitral valve status, a smaller neo-LVOT area assessed using pre-procedural MDCT was significantly associated with LVOT obstruction after TMVR for degenerated bio-prostheses, failed annuloplasty rings, and calcified mitral annulus.

In the present study, 26 patients had LVOT obstruction after TMVR, resulting in procedure-related death in 9 patients and need for surgical or transcatheter intervention in 15 patients. Compared with patients without LVOT obstruction, those with LVOT obstruction had significantly higher rates of adverse events, including procedural death, which confirmed the importance of identifying the significant factors associated with LVOT obstruction. The rates of LVOT obstruction and subsequent mortality after ViMAC were high in the present study but reflect real-world practice and the challenges of predicting this complication. This contrasts with the rate of LVOT obstruction in a previous study (11.2% from the global registry), in which patient selection was probably more restrictive on the basis of pre-procedural MDCT (21). Higher mortality after LVOT obstruction in the ViMAC group was probably due to the severity of hemodynamic deterioration as well as baseline comorbidities, highlighting the importance of careful screening with echocardiography and MDCT prior to TMVR procedures.

As LVOT obstruction after TMVR has gained more attention, the concept of the neo-LVOT has been recently introduced, with expectation to predict this fatal complication (22). The present study showed the dynamic change of the estimated neo-LVOT area throughout the cardiac cycle. The estimated neo-LVOT area decreased during systole, reaching minimum at end-systole. Considering that LVOT obstruction occurs during mid- to end-systole, assessing minimal neo-LVOT area at mid- to end-systole is clinically relevant. The estimated neo-LVOT area with pre-procedural MDCT showed an inverse correlation with peak LVOT gradient and a strong linear correlation with actual neo-LVOT area as assessed with post-procedural multidetector row computed tomographic measurements, indicating that the methodology to assess the neo-LVOT area was robust in the present study. In addition, mitral annulus-to-IVS distance showed excellent predictive value in predicting LVOT obstruction. This measurement is simple and easily performed by echocardiography without simulating the TMVR procedure, providing potential adjunctive role to MDCT.

In our study, a decreased estimated neo-LVOT area assessed using MDCT was significantly associated with LVOT obstruction after TMVR. It should be noted that the dimensions of the neo-LVOT were influenced by the anatomic relationship between the mitral valve, the left ventricle, and the aortic valve: a small size of the native LVOT and left ventricular cavity as well as a hypertrophic left ventricle may affect the neo-LVOT dimensions; the surgical mitral valve leaflet is placed anteriorly after ViV within the stent frame of surgical bioprostheses, whereas redundant or severely calcified anterior mitral leaflet may further reduce the neo-LVOT; procedural factors including dimensions of transcatheter valves and the implantation position may be associated with a small neo-LVOT area: larger and longer transcatheter valves deployed deeper into the LVOT would decrease the neo-LVOT area (23).

The present study emphasizes the importance of careful screening with echocardiography and MDCT before TMVR, particularly ViMAC. The cutoff value of neo-LVOT area in the present study (1.7 cm^2) was similar to previous work (24) and may support the cutoff values currently used in other TMVR studies (NHLBI DIR LAMPOON [Intentional Laceration of the Anterior Mitral Leaflet to Prevent Left Ventricular Outflow Tract Obstruction During Transcatheter Mitral Valve Implantation] [NCT03015194] using 2.0 cm^2 and the Intrepid TMVR pivotal trial using 1.3 cm^2) (2). Estimation of neo-LVOT area may help identify patients at high risk for LVOT obstruction, in whom prophylactic alcohol septal ablation, percutaneous laceration of the anterior mitral leaflet, or resection of the anterior mitral leaflet via the transatrial approach may be needed (25–27). Nevertheless, the performance of the cutoff value of neo-LVOT area proposed in this study to predict the risk for LVOT obstruction in other clinical scenarios such as functional mitral regurgitation needs to be evaluated in future studies.

FIGURE 7 Receiver-Operating Characteristic Curves for Prediction of Left Ventricular Outflow Tract Obstruction

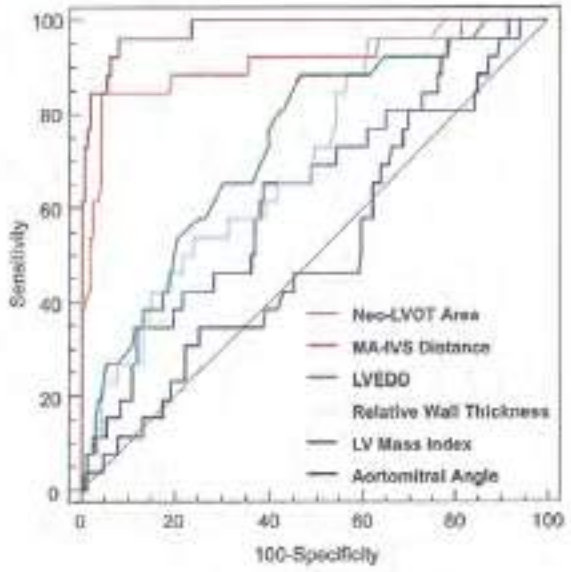

	AUC	Cutoff value	p value	Sensitivity	Specificity
Neo-LVOT Area	0.98	1.7	< 0.001	96.2	92.3
MA-IVS Distance	0.91	17.8	< 0.001	84.6	95.8
LVEDD	0.74	48	< 0.001	88.5	53.3
Relative Wall Thickness	0.70	0.38	0.001	96.2	38.9
LV Mass Index	0.64	105	0.02	65.4	61.1
Aortomitral Angle	0.51	–	0.92	46.2	41.1

Receiver-operating characteristic curve analyses for prediction of left ventricular outflow tract (LVOT) obstruction by multidetector row computed tomographic and echocardiographic parameters. IVS = interventricular septum; LV = left ventricular; LVEDD = left ventricular end-diastolic diameter; MA = mitral annulus.

STUDY LIMITATIONS. First, this study was an observational study, including patients with pre-procedural MDCT undergoing TMVR, leading to potential selection bias. Second, only patients with degenerated bioprostheses, failed annuloplasty rings,

JACC: CARDIOVASCULAR INTERVENTIONS VOL. 12, NO. 2, 2019
JANUARY 28, 2019:182–93

FIGURE 8 Frequencies of Left Ventricular Outflow Tract Obstruction According to Neo-Left Ventricular Outflow Tract Area

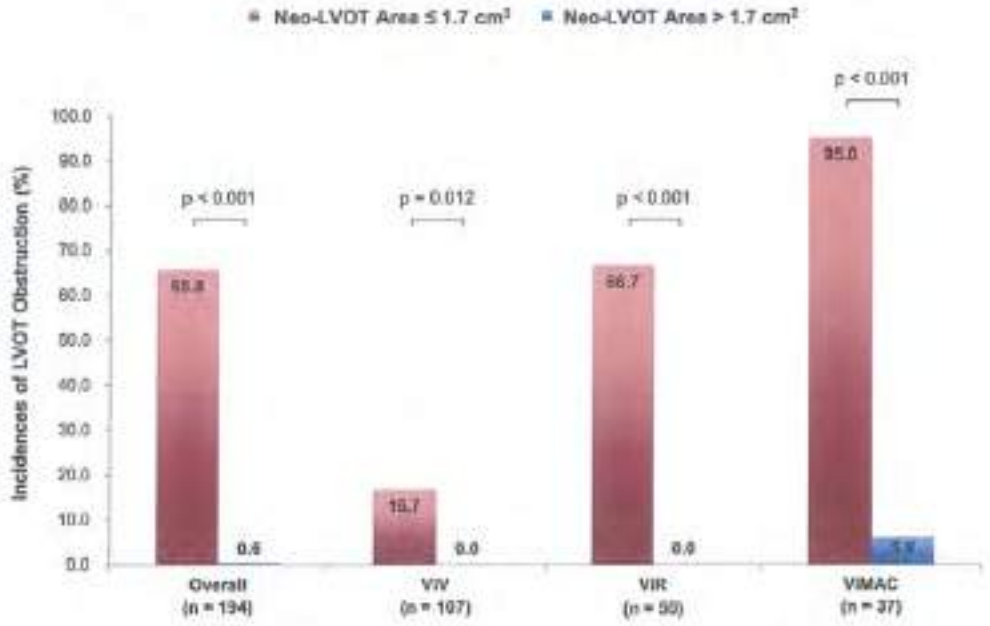

Frequencies of left ventricular outflow tract (LVOT) obstruction according to estimated neo-LVOT area with pre-procedural multidetector row computed tomography for overall, valve-in-valve (VIV), valve-in-ring (VIR), and valve-in-mitral annular calcification (VIMAC) groups, respectively.

or severely calcified mitral annuli were included. Moreover, device position was empirically decided on the basis of the post-procedural findings on MDCT.

CONCLUSIONS

LVOT obstruction occurred more frequently after VIMAC compared with VIR and VIV and was associated with higher rates of procedural adverse events. A small estimated neo-LVOT area was significantly associated with LVOT obstruction after TMVR and may help identify patients at high risk for LVOT obstruction.

ADDRESS FOR CORRESPONDENCE: Dr. Raj Makkar, Cedars-Sinai Heart Institute, 8700 Beverly Boulevard, Los Angeles, California 90048. E-mail: raj.makkar@cshs.org.

PERSPECTIVES

WHAT IS KNOWN? LVOT obstruction is a major concern with TMVR, but limited data exist regarding its predictors.

WHAT IS NEW? Among multidetector row computed tomographic and echocardiographic parameters, neo-LVOT area showed the greatest discriminatory value for predicting LVOT obstruction after TMVR, with a cutoff value of 1.7 cm².

WHAT IS NEXT? The performance of the cutoff value of neo-LVOT area proposed in this study to predict the risk for LVOT obstruction in other clinical scenarios such as functional mitral regurgitation needs to be evaluated in future studies.

REFERENCES

1. Mauer DW, Farivar RS, Jonsz P, et al. Transcatheter Mitral valve replacement for patients with symptomatic mitral regurgitation: a global feasibility trial. J Am Coll Cardiol 2017;69:381–91.

2. Bapat V, Rajagopal V, Meduri C, et al. Early experience with new transcatheter mitral valve replacement. J Am Coll Cardiol 2018;71:12–21.

3. Yoon SH, Whisenant BK, Bleiziffer S, et al. Transcatheter mitral valve replacement for degenerated bioprosthetic valves and failed annuloplasty rings. J Am Coll Cardiol 2017;70:971–31.

4. Guerrero M, Dvir D, Himbert D, et al. Transcatheter mitral valve replacement in native mitral valve disease with severe mitral annular calcification: results from the first multicenter global registry. J Am Coll Cardiol Intv 2016;9:1361–71.

5. Bapat V, Pirone F, Kapetanakis S, Rajani R, Nadeem S. Factors influencing left ventricular outflow tract obstruction following a mitral valve-in-valve or valve-in-ring procedure, part 1. Catheter Cardiovasc Interv 2015;86:747–60.

6. Wang DD, Eng M, Greenbaum A, et al. Predicting LVOT obstruction after TMVR. J Am Coll Cardiol Img 2016;9:1349–52.

7. Bapat V, Mylotte J, Chadalavada S, Tehrani H, Attia R, Thomas M. A guide to fluoroscopic identification and design of bioprosthetic valves: a reference for valve-in-valve procedures. Catheter Cardiovasc Interv 2013;81:853–61.

8. Hamid NB, Khalique OK, Monaghan MJ, et al. Transcatheter valve implantation in failed surgically inserted bioprosthesis: review and practical guide to echocardiographic imaging in valve-in-valve procedures. J Am Coll Cardiol Img 2015;8:960–79.

9. Cheung A, Webb JG, Barbanti M, et al. 5-Year experience with transcatheter transapical mitral valve-in-valve implantation for bioprosthetic valve dysfunction. J Am Coll Cardiol 2013;61:1759–66.

10. Cribier A, Eltchaninoff H, Tron C, et al. Treatment of calcific aortic stenosis with the percutaneous heart valve: mid-term follow-up from the initial feasibility studies: the French experience. J Am Coll Cardiol 2006;47:1214–23.

11. Webb JG, Pasupati S, Humphries K, et al. Percutaneous transarterial aortic valve replacement in selected high-risk patients with aortic stenosis. Circulation 2007;116:755–63.

12. Ye J, Cheung A, Lichtenstein SV, et al. Transapical transcatheter aortic valve implantation: 1-year outcome in 26 patients. J Thorac Cardiovasc Surg 2006;131:167–73.

13. Meredith Am IT, Walters DL, Dumonteil N, et al. Transcatheter aortic valve replacement for severe symptomatic aortic stenosis using a repositionable valve system: 30-day primary endpoint results from the REPRISE II study. J Am Coll Cardiol 2014;64:1339–48.

14. Schofer J, Colombo A, Hugman S, et al. Prospective multicenter evaluation of the direct flow medical transcatheter aortic valve. J Am Coll Cardiol 2014;63:763–8.

15. Zahn EM, Hellenbrand WE, Lock JE, McElhinney DB. Implantation of the melody transcatheter pulmonary valve in patients with a dysfunctional right ventricular outflow tract conduit: early results from the U.S. clinical trial. J Am Coll Cardiol 2009;54:1722–9.

16. Stone GW, Vahanian AS, Adams DH, et al. Clinical trial design principles and endpoint definitions for transcatheter mitral valve repair and replacement: part 1: clinical trial design principles: a consensus document from the Mitral Valve Academic Research Consortium. J Am Coll Cardiol 2015;66:278–307.

17. Stone GW, Adams DH, Abraham WT, et al. Clinical trial design principles and endpoint definitions for transcatheter mitral valve repair and replacement: part 2: endpoint definitions: a consensus document from the Mitral Valve Academic Research Consortium. J Am Coll Cardiol 2015;66:308–21.

18. Blanke P, Dvir D, Cheung A, et al. A simplified D-shaped model of the mitral annulus to facilitate CT-based sizing before transcatheter mitral valve implantation. J Cardiovasc Comput Tomogr 2014;8:459–67.

19. Blanke P, Dvir D, Cheung A, et al. Mitral annular evaluation with CT in the context of transcatheter mitral valve replacement. J Am Coll Cardiol Img 2015;8:672–5.

20. Abramowitz Y, Kazuno Y, Chakravarty T, et al. Concomitant mitral annular calcification and severe aortic stenosis: prevalence, characteristics and outcome following transcatheter aortic valve replacement. Eur Heart J 2017;38:1194–203.

21. Guerrero M, Urena M, Himbert D, et al. 1-Year outcomes of transcatheter mitral valve replacement in patients with severe mitral annular calcification. J Am Coll Cardiol 2018;71:1841–53.

22. Blanke P, Naoum C, Dvir D, et al. Predicting LVOT obstruction in transcatheter mitral valve implantation: concept of the Neo-LVOT. J Am Coll Cardiol Img 2017;10:482–5.

23. Murphy DJ, Ge Y, Dion CW, et al. Use of cardiac computerized tomography to predict neo-left ventricular outflow tract obstruction before transcatheter mitral valve replacement. J Am Heart Assoc 2017;6:e007333.

24. Wang DD, Eng MH, Greenbaum AB, et al. Validating a prediction modeling tool for left ventricular outflow tract (LVOT) obstruction after transcatheter mitral valve replacement (TMVR). Catheter Cardiovasc Interv 2018;92:379–87.

25. Dehero P, Urena M, Himbert D, et al. Bail-out alcohol septal ablation for left ventricular outflow tract obstruction after transcatheter mitral valve replacement. J Am Coll Cardiol Intv 2016;9:e73–6.

26. Babaliaros VC, Greenbaum AB, Khan JM, et al. Intentional percutaneous laceration of the anterior mitral leaflet to prevent outflow obstruction during transcatheter mitral valve replacement: first-in-human experience. J Am Coll Cardiol Intv 2017;10:798–809.

27. Russell HM, Guerrero ME, Salinger MH, et al. Open atrial transcatheter mitral valve replacement in patients with mitral annular calcification. J Am Coll Cardiol 2018;72:437–48.

KEY WORDS annuloplasty ring, degenerated bioprosthesis, left ventricular outflow tract obstruction, mitral annular calcification, mitral valve, transcatheter valve implantation

APPENDIX For a supplemental methods section, table, and figures, please see the online version of this paper.

JACC: CARDIOVASCULAR INTERVENTIONS
© 2019 BY THE AMERICAN COLLEGE OF CARDIOLOGY FOUNDATION
PUBLISHED BY ELSEVIER

VOL. 12, NO. 1, 2019

FOCUS ON MITRAL AND TRICUSPID VALVE INTERVENTIONS

Continuous Direct Left Atrial Pressure

Intraprocedural Measurement Predicts Clinical Response Following MitraClip Therapy

Shingo Kuwata, MD, PhD,[a] Maurizio Taramasso, MD, PhD,[a] Albert Czopak, MD,[a] Marco Luciani, MD, PhD,[a] Alberto Pozzoli, MD,[a] Edwin Ho, MD,[a] Adolfo Ferrero Guadagnoli, MD,[a] Matteo Saccocci, MD,[a] Oliver Gaemperli, MD,[a] Fabian Nietlispach, MD, PhD,[a] Michel Zuber, MD,[a] Ted Feldman, MD,[b] Francesco Maisano, MD[a]

ABSTRACT

OBJECTIVES The aim of this study was to assess the additional utility of measuring left atrial (LA) pressure as a complement to transesophageal echocardiography (TEE) and Doppler imaging.

BACKGROUND The efficacy of the MitraClip (MC) is assessed intraoperatively by TEE. However, TEE measures are operator dependent and can be influenced by left ventricular (LV) function and changes in LA compliance.

METHODS Fifty patients undergoing MC therapy with continuous left-sided heart pressure measurements were analyzed. LA V-wave pressure (LAvP), LA mean pressure (LAmP), LV systolic pressure, and LV end-diastolic pressure were measured continuously. LA pressures were indexed to LV pressures to account for changes in afterload during the procedure.

RESULTS Most patients (70%) had degenerative mitral regurgitation (MR). TEE MR grade decreased from 3+ to 0+. LAvP ($p < 0.001$), LAmP ($p = 0.007$), LV end-diastolic pressure ($p = 0.001$), LAvP index ($p < 0.001$), and LAmP index ($p = 0.001$) decreased significantly, and LV systolic pressure($p = 0.009$) significantly increased after MC therapy. In multivariate Cox regression analysis, intraprocedural increase of LAmP index, but not post-MC ≥2+ residual MR, was significantly associated with rehospitalization due to heart failure (hazard ratio: 3.377; 95% CI: 3.180 to 3.585; $p = 0.007$) and with New York Heart Association functional class III to IV (hazard ratio: 1.497; 95% CI: 1.006 to 2.102; $p = 0.005$) in the follow-up period.

CONCLUSIONS This study demonstrates the value of real-time monitoring of LA pressure during MC therapy to predict clinical outcomes. An increase in LAmP was a predictive of worse clinical outcomes at short-term follow-up, independent from echocardiographic findings. (J Am Coll Cardiol Intv 2019;12:127-36)
© 2019 by the American College of Cardiology Foundation.

MitraClip (MC) therapy (Abbott Vascular, Abbott Park, Illinois) has been proven to be effective in reducing mitral regurgitation (MR) (1,2). As residual MR after MC has been associated with suboptimal outcomes and increased mortality (3), the goal of the procedure is to reduce as much as possible. Implantation of multiple clips is often necessary. However, multiple clip implantation is associated with reduction of mitral valve opening area and increased transmitral pressure gradient (PG). Therefore, procedural outcome is defined by an acceptable compromise between improved MR grade and reduction of valve area.

From the [a]University Heart Center Zürich, University Hospital of Zurich, Zurich, Switzerland, and the [b]Department of Medicine, Division of Cardiology, North Shore University Health System, Evanston Hospital, Evanston, Illinois. Dr. Taramasso has served as a consultant for Abbott Vascular. Dr. Nietlispach has served as a consultant for Abbott Vascular, Edwards Lifesciences, and Medtronic. Dr. Feldman has served as a consultant for and has received research grant support from Abbott Vascular, Boston Scientific, Edwards Lifesciences, and Gore Medical. Dr. Maisano has served as a consultant for and received research grant support from Abbott Vascular. All other authors have reported that they have no relationships relevant to the contents of this paper to disclose.

Manuscript received April 11, 2018; revised manuscript received July 16, 2018, accepted July 31, 2018.

ISSN 1936-8798/$36.00 https://doi.org/10.1016/j.jcin.2018.07.051

JACC: CARDIOVASCULAR INTERVENTIONS VOL. 12, NO. 2, 2019
JANUARY 28, 2019:127–36

ABBREVIATIONS AND ACRONYMS

CI = confidence interval

HF = heart failure

LAmP = left atrial mean pressure

LAmPI = left atrial mean pressure index

LAvP = left atrial V-wave pressure

LVEDP = left ventricular end-diastolic pressure

LVEF = left ventricular ejection fraction

LVSP = left ventricular systolic pressure

MR = mitral regurgitation

NYHA = New York Heart Association

TEE = transesophageal echocardiography

TR = tricuspid regurgitation

Standard intraprocedural MC guidance is based on transesophageal echocardiography (TEE). Color Doppler is used to assess residual MR, and Doppler to evaluate the transmitral gradient. However, the Doppler-derived measures are operator dependent (4) and there is no single echocardiographic parameter for accurate assessment of the severity of MR, especially in a double-orifice valve (5).

As an adjunct to Doppler-derived assessment, previous studies have demonstrated feasibility of continuous LA pressure monitoring during MC therapy (6,7). We prospectively used continuous real-time direct measurement of LA pressure and left ventricular (LV) pressure, during MC therapy.

The prognostic impact of intraprocedural invasive left-sided heart pressures on functional outcomes has not been well known. The aim of this study is to assess the additional benefit of measuring left-sided heart pressures as a complement to echocardiographic assessment during MC therapy and to assess the prognostic impact of LA hemodynamics on clinical outcome at short-term follow-up.

SEE PAGE 137

METHODS

POPULATION. Patients who had MC therapy with continuous left-sided (atrial and ventricular) heart pressure monitoring were enrolled prospectively. The decision to perform MC therapy was based on multidisciplinary heart team discussion. Demographic and clinical characteristics, procedural data, and outcome data of in-hospital and follow-up periods were captured within the MitraSwiss registry. The MitraSwiss registry was approved by the local ethics committee. All patients gave written informed consent. Patients with missing or inaccurate measurements of left heart pressures were excluded from this cohort.

CONTINUOUS LA PRESSURE MONITORING DURING MC IMPLANT. MC therapy was performed using MC or MC NT system under general anesthesia with TEE and fluoroscopic guidance. To measure LA and LV pressures during the procedure we developed the following standardized technique: after transseptal puncture, before MC guide catheter insertion, we advanced 2 guidewires through the transseptal sheath into the left upper pulmonary vein, 1 floppy and 1 super stiff. On the floppy wire, a 5-F pigtail diagnostic catheter was advanced into the LA, while over the super-stiff wire, the steerable MC guiding catheter was advanced in parallel into the LA. A figure-of-8 suture at the groin puncture site was used to control local bleeding due to the passage of both catheters through the same venous puncture. Left atrial V-wave pressure (LAvP) and LA mean pressure (LAmP) were continuously measured by pigtail catheter (Figure 1). In addition, the LV pressure was measured by a second 5-F pigtail diagnostic catheter inserted retrograde in LV by the transfemoral arterial approach. Left ventricular systolic pressure (LVSP) and left ventricular end-diastolic pressure (LVEDP) were recorded simultaneously with the LA pressures. Mitral valve hemodynamic mean PG (invasive mean PG) was obtained by averaging values of 5 heart cycles from the invasive pressure measurements (CardWorks, Schwarzer Cardiotek GmbH, Heilbronn, Germany).

LA pressures were indexed to LVSPs for comparison of hemodynamics in case of changes in afterload during the procedure. The V-wave indexed pressure was calculated as LAvP index = LAvP / LVSP, and the indexed mean LA pressure was calculated as: LAmP index (LAmPI) = LAmP / LVSP. In addition, the differential pressure was calculated as: LA V-wave height = LAvP − LA minimum pressure, which was used to quantify the reduction of LAvP.

All parameters were measured continuously, recorded before clip implant and immediately after grasping the leaflets before retrieval of the clip, and are reported as the percentage change as compared with baseline (reduction rate of invasive hemodynamic parameters = post-procedural value / pre-procedural value × 100).

INTRAOPERATIVE TEE. MR grade with intraoperative TEE were assessed by at least 2 physicians during the MC procedure. The severity of the MR was defined as none or trace (0/4+), mild (1+/4+), moderate (2+/4+), moderate to severe (3+/4+), and severe (4+/4+) using the American Society of Echocardiography guidelines for an integrative approach (8,9). Mitral valve area was calculated using the diastolic transmitral mean PG from the continuous Doppler waveform before and after each clip deployment.

OUTCOMES. Acute outcome was assessed as technical success based on Mitral Valve Academic Research Consortium criteria (10). The technical success was defined as all of the following must be present: 1) absence of procedural mortality; 2) successful access, delivery, and retrieval of the device delivery system; 3) successful deployment and correct positioning of the first intended device; and 4) freedom from emergency surgery or reintervention related to the device or access procedure.

The baseline and follow-up functional status was assessed according to the New York Heart Association (NYHA) criteria.

FIGURE 1 Method for Measurement of Continuous Left-Sided Heart Pressure Monitoring

A 5-F pigtail catheter was inserted into the left atrium via the same transseptal puncture site of the MitraClip (Abbott Vascular, Abbott Park, Illinois) system. The second pigtail catheter is located in the left ventricle for simultaneous pressure monitoring. The **single asterisk** indicates the pigtail catheter in the left atrium; the **double asterisk** indicates the pigtail catheter in left ventricle.

TABLE 1 Baseline Characteristics (N = 50)

Age, yrs	78.7 (73.6–84.4)
Female	20 (40)
Body mass index, kg/m^2	24.6 (22.8–27.0)
Patient history	
Previous congestive heart failure	21 (42)
Previous myocardial infarction	5 (10)
Previous coronary artery bypass graft	5 (10)
Previous valve surgery	2 (4)
Previous percutaneous intervention	13 (26)
Previous cerebral disease	7 (14)
Comorbidities	
Hypercholesterolemia	19 (38)
Hypertension	42 (84)
Diabetes mellitus	3 (6)
COPD	9 (18)
Previous coronary artery disease	19 (38)
Atrial fibrillation	33 (66)
eGFR, ml/min/1.73 m^2	47.5 (34.0–62.0)
Patient status	
NYHA functional class	
I	7 (14)
II	9 (18)
III	27 (54)
IV	7 (14)
STS risk score, %	2.8 (1.4–4.1)
Pre-procedural echo data	
Degenerative MR	35 (70)
MR grade	
III	6 (12)
IV	44 (88)
More than moderate tricuspid regurgitation	16 (32)
LVEF, %	60.0 (48.8–63.0)
LAVI, ml/m^2	72.9 (50.8–92.0)

Values are median (interquartile range) or n (%).

BNP = brain natriuretic peptide; COPD = chronic obstructive pulmonary disease; eGFR = estimated glomerular filtration rate; LAVI, left atrial volume index; LVEF = left ventricle ejection fraction; NYHA = New York Heart Association; STS, Society of Thoracic Surgeons.

The primary clinical outcome endpoints were NYHA functional class ≥III and rehospitalization due to heart failure (HF) at last follow-up (median 112 and maximum 192 days).

STATISTICAL ANALYSIS. Data were expressed as a median (interquartile range [IQR] for continuous variables and as a percentage for categorical variables. The Student's *t*-test was used for continuous variables, and the chi-square test was used for categorical variables. The Wilcoxon test, Mann-Whitney *U* test or analysis of Spearman for correlations coefficient was performed, where appropriate. To test the association of pressure between baseline and after each clip, the nonparametric Jonckheere-Terpstra trend test was performed. The ability of invasive left-sided heart pressures during MC therapy to predict residual symptoms after the procedure (NYHA functional class ≥III at 30 days) were tested by evaluating the area under the curve in the analysis of its receiver-operating characteristic curve. Univariate Cox regression analysis was used to examine potential relationships between variables and outcomes. In multivariate Cox regression analysis were entered variables with a probability value of <0.05 at univariate logistic regression analysis; hazard ratio (HR) was adjusted for etiology of MR, pre-procedural NYHA functional class, ≥2+ residual MR, pre-procedural LV ejection fraction (LVEF) and pre-procedural tricuspid regurgitation (TR). The freedom rate of rehospitalization due to HF was evaluated using Kaplan-Meier analysis and the log-rank-test for overall significance. A probability value of <0.05 was considered to indicate statistical significance. Analysis was performed using a standard statistical software program (SPSS version 23, IBM Corporation, Armonk, New York).

RESULTS

Of 66 consecutive patients undergoing MC therapy, 16 were excluded due to not available or not reliable invasive measurements of left-sided heart pressures

JACC: CARDIOVASCULAR INTERVENTIONS VOL. 12, NO. 2, 2019
JANUARY 28, 2019:327–36

TABLE 2 Periprocedural Characteristics (N = 50)

Duration of procedural time, min	75.0 (60.0–97.0)
Clip implantations	2.0 (1.0–2.0)
Combined with LAAO	8 (16)
Length of stay hospital after procedure, days	4.0 (3.0–5.3)
Technical success	50 (100)
Conversion to surgery	0 (0)
Major bleeding	0 (0)
Major vascular complication	0 (0)
Infection	0 (0)
Greater or equal to moderate residual MR at intraprocedural assessment	3 (6)
Greater or equal to moderate residual MR at discharge	4 (8)

Values are median (interquartile range) or n (%).
LAAO = left atrial appendage occlusion; MR = mitral regurgitation.

(5 with mechanical aortic valve replacement, 4 with imprecise zeroing, 4 with missing recordings, 1 prior LV thrombus, 1 prior MC therapy, 1 chronic aorta disease). The remaining 50 patients undergoing MC therapy with continuous left-sided heart pressure measurements were enrolled. Baseline features of the patients are summarized in **Table 1**. A total of 70% had degenerative MR, and 30% had functional MR. Median patient age was 78.7 years (IQR: 73.6 to 84.4 years) and LVEF was 60.0% (IQR: 48.8% to 63.0%). Sixteen patients were treated using 1 clip, 23 patients received 2, 9 patients had 3, 1 patient had 4, and 1 patient had 5 clips. All patients experienced technical success according to the Mitral Valve Academic Research Consortium criteria (10) (**Table 2**). There were no major vascular complications, but 1 patient had atrial hematoma requiring conservative therapy after procedure. One patient who underwent combined MC therapy and left appendage closure had cardiac tamponade requiring percutaneous pericardiocentesis.

TABLE 3 Invasive Hemodynamic Parameters

	Baseline	Post-Procedure	p Value
LAvP, mm Hg	18.0 (13.0–27.5)	14.0 (10.0–21.0)	<0.001
LAmP, mm Hg	11.0 (9.0–17.3)	10.0 (7.8–14.3)	0.007
LVSP, mm Hg	107.0 (90.0–125.0)	112.0 (102.0–131.0)	0.009
LVEDP, mm Hg	11.0 (9.0–15.0)	10.0 (7.0–13.0)	0.001
LA V-wave height, mm Hg	14.0 (10.0–24.0)	8.0 (5.8–14.0)	<0.001
LAvPI	0.16 (0.12–0.26)	0.12 (0.09–0.19)	<0.001
LAmPI	0.10 (0.08–0.15)	0.09 (0.06–0.13)	0.001
Invasive mPG, mm Hg	4.4 (2.4–7.5)	5.0 (3.0–6.6)	0.401

Values are median (interquartile range).
LAmP = left atrial mean pressure; LAmPI = left atrial mean pressure index; LAvP = left atrial V-wave pressure; LAvPI = left atrial V-wave pressure index; LVEDP = left ventricular end-diastolic pressure; LVSP = left ventricular systolic pressure; mPG = mean pressure gradient.

CONTINUOUS INVASIVE LEFT-SIDED HEART PRESSURE. Overall, LAvP ($p < 0.001$), LAmP ($p = 0.007$), LVEDP ($p = 0.001$), LAvP index ($p < 0.001$), and LAmPI ($p = 0.001$) decreased significantly, and LVSP ($p = 0.009$) significantly increased after MC therapy (**Table 3**).

In patients using 2 clips, there was a trend of decreasing LAvP ($p = 0.04$), LAvP index ($p = 0.005$), and LAmPI ($p = 0.031$). In patients using 3 clips, there was a significant decrease of LVEDP ($p = 0.044$) (Online Tables 1 to 5).

INTRAOPERATIVE TEE ASSESSMENT. All but 3 (94%) patients achieved residual MR ≤1+ after MC implant at intraprocedural assessment (**Table 2**). As a result, MR grade was significantly improved ($p < 0.001$). Excluding the patient who had 5 clips, MR grade assessed by TEE showed a trend to improve after each clip (patients with 1 clip: $p < 0.001$; patients with 2 clips: $p < 0.001$; patients with 3 clips: $p < 0.001$; patients with 4 clips: p for trend = 0.037) (Online Tables 1 to 5).

The intraprocedural noninvasive mean PG increased from 2 (range 1 to 3) mm Hg to 3 (range 2 to 4) mm Hg after MC implantation ($p = 0.001$). In patients using 2 clips, noninvasive mean PG ($p = 0.018$) showed a significant trend of increasing gradients.

All but 4 patients (92%) achieved residual MR ≤1+ at discharge (**Table 2**). The discharge MR grade in these 4 patients was still severe (not specified exactly in **Table 2**).

Transmitral mean PG by transthoracic echocardiography was significantly increased at discharge ($p < 0.001$; 4 [IQR: 3 to 5] mm Hg) and follow-up ($p = 0.001$; 4 [IQR: 3 to 6] mm Hg) compared with the intraprocedural one by TEE assessment (2 [IQR: 1 to 3] mm Hg).

CLINICAL FOLLOW-UP. The median duration of follow-up after MC therapy was 112 (IQR: 49 to 192 days) days (total of 15.5 patient-years), during which 3 (6%) patients died, and 6 (12%) patients were rehospitalized due to HF. Within the follow-up period, MR was improved at least 1 grade from baseline in 95% of patients.

In univariate cox regression analysis, post-implant increases of LAmPI (HR: 1.984; 95% CI: 1.651 to 2.384; $p = 0.044$) were significantly associated with HF rehospitalization at follow-up. In multivariate Cox regression analysis, intraprocedural increase of

TABLE 4 Relationship Between the Intraprocedural Parameters and Rehospitalization Due to HF at Follow-Up Period

	Cox Regression Model			
	Univariate Analysis		Multivariate Stepwise Analysis*	
	Hazard Ratio (95% Confidence Interval)	p Value	Hazard Ratio (95% Confidence Interval)	p Value
Pre-procedural invasive hemodynamic parameters				
LAvP	0.932 (0.833–1.042)	0.214	-	
LAmP	0.936 (0.799–1.096)	0.411	-	
LVSP	0.992 (0.953–1.033)	0.708	-	
LVEDP	0.950 (0.801–1.127)	0.556	-	
LAv height	0.861 (0.715–1.036)	0.113	-	
LAvPI	0.003 (0.000–74.228)	0.263	-	
LAmPI	0.005 (0.000–36,952,256)	0.489	-	
Invasive mPG	1.010 (0.861–1.184)	0.904	-	
Pre-procedural TEE parameters				
MR grade	0.230 (0.041–1.287)	0.094	-	
Noninvasive mPG	1.062 (0.616–1.833)	0.828	-	
Post-procedural invasive hemodynamic parameters				
LAvP	1.009 (0.914–1.115)	0.853	-	
LAmP	1.047 (0.908–1.208)	0.526	-	
LVSP	0.964 (0.913–1.018)	0.185	-	
LVEDP	0.929 (0.758–1.138)	0.475	-	
LAv height	0.954 (0.819–1.112)	0.548	-	
LAvPI	21.744 (0.002–265,080.711)	0.521	-	
LAmPI	1,262.111 (0.004–4,520,000)	0.274	-	
Invasive mPG	1.024 (0.875–1.198)	0.770	-	
Post-procedural TEE parameters				
MR grade ≥1+	7.695 (0.895–66.163)	0.063	-	
Noninvasive mPG	1.030 (0.611–1.734)	0.912	-	
Reduction rate of invasive hemodynamic parameters				
LAvP	1.140 (0.985–1.319)	0.080	-	
LAmP	1.280 (0.970–1.690)	0.081	-	
LVSP	0.977 (0.937–1.019)	0.272	-	
LVEDP	1.010 (0.838–1.216)	0.920	-	
LAv height	1.109 (0.974–1.262)	0.119	-	
LAvPI	2,604,342 (0.014–4,780,000)	0.203	-	
LAmPI	1.984 (1.651–2.384)	0.044	3.377 (3.180–3.585)	0.007
Invasive mPG	1.190 (0.880–1.608)	0.259	-	

*Hazard ratio was adjusted for etiology of mitral regurgitation (MR), pre-procedural New York Heart Association (NYHA) class, greater or equal to moderate residual MR, pre-procedural left ventricular ejection fraction (LVEF), and tricuspid regurgitation (TR).

HF = heart failure; LAv = left atrial V-wave; TEE = transesophageal echocardiography; other abbreviations as in Table 3.

LAmPI (HR: 3.377; 95% CI: 3.180 to 3.585; p = 0.007) was significantly associated with HF rehospitalization at follow-up period after adjustment for etiology of MR, pre-procedural NYHA functional class, residual MR ≥2+, pre-procedural LVEF, and TR (Table 4). In the same population, final LAmP as measured at the end of the procedure, following all clip deployment was not a predicting factor for clinical outcomes.

Figure 2 shows the Kaplan-Meier curves for rehospitalization due to HF according to intraprocedural variation of LAmP and LAmPI. Increased LAmPI after MC therapy (log-rank p = 0.001) was significantly associated with higher rate of HF rehospitalization.

Overall, at latest follow-up, 83% of patient were in NYHA functional class I to II. At univariate Cox regression analysis, pre-procedural MR grade by TEE (HR: 0.143; 95% CI: 0.031 to 0.659; p = 0.013), intraprocedural increase of LAmP (HR: 1.295; 95% CI: 1.010 to 1.659; p = 0.041), and intraprocedural increase of LAmPI (HR: 16.55; 95% CI: 8.546 to 32.034; p = 0.027) were significantly associated with NYHA functional class III to IV at follow-up. In multivariate Cox regression analysis, pre-procedural MR grade by TEE (HR: 0.072; 95% CI: 0.011 to 0.473; p = 0.006), increased (as compared with baseline) LAmP (HR: 1.612; 95% CI: 1.109 to 2.345; p = 0.012), and LAmPI (HR: 1.497; 95% CI: 1.006 to 2.102; p = 0.005) were significant prognostic factors for NYHA functional class III to IV at follow-up period after adjustment for etiology of MR, pre-procedural NYHA functional class, residual MR ≥2+, pre-procedural LVEF, and TR (Table 5). Post-procedural MR grade by TEE was not a predictor of clinical events.

JACC: CARDIOVASCULAR INTERVENTIONS VOL. 12, NO. 2, 2019
JANUARY 28, 2019:127–36

FIGURE 2 Freedom From Rehospitalization Due to HF According to Hemodynamic Changes

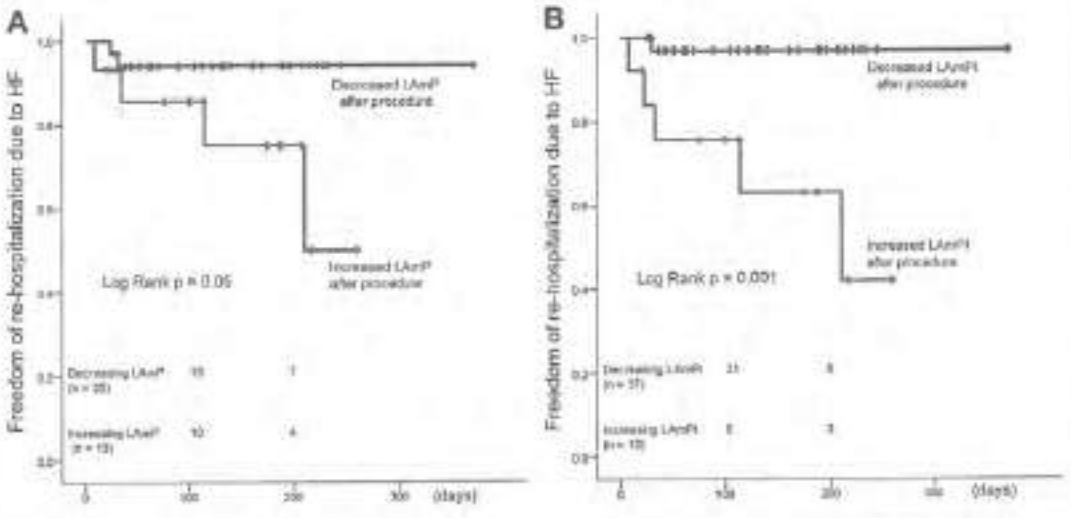

(A) Kaplan-Meier curves for rehospitalization due to heart failure (HF) according to trend of left atrial mean pressure (LAmP). (B) Kaplan-Meier curves for rehospitalization due to HF according to trend of LAmP index (LAmPI).

Figure 3 shows the receiver-operating characteristic curves using intraprocedural changes of LAvP, LAmP, and LAmPI for predicting NYHA functional class III to IV at the follow-up period. Intraprocedural increase of LAmPI (area under the curve: 0.806; 95% CI: 0.674 to 0.939; cutoff value 92% [sensitivity 0.88, specificity 0.70]) had the largest area under the curve.

DISCUSSION

This study provides evidence for an adjunctive value of real-time monitoring of left heart hemodynamics during MC therapy in predicting clinical outcomes. Although overall MC therapy is associated with improved hemodynamics, in a small proportion of patients, LA hemodynamics worsened, with an increase of LAmP and LAmPI, despite improved echocardiographic MR grade. This unfavorable change in LA dynamics was a prognostic factor for negative clinical outcomes at short-term follow-up, independently from echocardiographic findings. The addition of arterial access to the procedure may contribute to vascular complications. Any additional morbidity such as hematomas or transfusions could be encountered during arterial access for LV pressures measurements. In this cohort, there were no major vascular complications but 1 patient had arterial hematoma requiring conservative therapy after procedure. A consideration for a dual-lumen pigtail across the transseptal puncture to measure both LA and LV pressures might eliminate the need for any arterial access.

Interpretation of hemodynamics during MC therapy is a key to guiding the intraprocedural decision-making process. In fact, in case of residual MR, operators have to take immediate action by either repositioning a clip, retrieving it, or implanting an additional one, as they face the dilemma of increasing valvular gradient or accepting some degree of residual MR. Transcatheter edge-to-edge repair is affected by the intrinsic limitation that while MR is treated, the effective orifice area is reduced, thereby increasing the risk of inducing transmitral gradients. Compared with mitral valve surgery, MC therapy has the advantage to allow real-time evaluation of MR and hemodynamics during the procedure by TEE, under more physiologic conditions in the beating heart. Current intraprocedural decisions are mainly based on TEE and Doppler-derived measurement of hemodynamics. However, Doppler measurements are operator dependent and strongly influenced by LV function, LA compliance, and loading conditions (11). In addition, Doppler echocardiographic methods have not been adequately validated in a double-orifice valve model (12). The creation of high-velocity regurgitant jets on either side of the clip may overestimate the appearance of significant residual MR, even if the actual backward volume is low (13,14). On the other hand, even if the actual regurgitant volume

TABLE 5 Relationship Between the Intraprocedural Parameters and NYHA Functional Class III to IV at Follow-Up

	Cox Regression Model			
	Univariate Analysis		Multivariate Stepwise Analysis*	
	Hazard Ratio (95% Confidence Interval)	p Value	Hazard Ratio (95% Confidence Interval)	p Value
Pre-procedural invasive hemodynamic parameters				
LAvP	0.966 (0.898–1.038)	0.345	–	
LAmP	0.962 (0.839–1.103)	0.578	–	
LVSP	1.007 (0.978–1.037)	0.652	–	
LVEDP	1.018 (0.916–1.133)	0.744	–	
LAv height	0.963 (0.897–1.035)	0.307		
LAvPI	0.022 (0.000–29.314)	0.290	–	
LAmPI	0.002 (0.000–3,849.356)	0.410	–	
Invasive mPG	1.026 (0.883–1.192)	0.735	–	
Pre-procedural TEE parameters				
MR grade	0.343 (0.031–0.659)	0.013	0.072 (0.011–0.473)	0.006
Noninvasive mPG	0.838 (0.468–1.501)	0.553	–	
Post-procedural invasive hemodynamic parameters				
LAvP	1.050 (0.871–1.136)	0.220	–	
LAmP	1.086 (0.963–1.226)	0.181	–	
LVSP	1.004 (0.965–1.044)	0.846	–	
LVEDP	1.053 (0.918–1.208)	0.461	–	
LAv height	1.037 (0.933–1.153)	0.497		
LAvPI	68.740 (0.026–178,746.038)	0.292	–	
LAmPI	899.515 (0.007–114,700,000)	0.257	–	
Invasive mPG	1.030 (0.900–1.179)	0.668	–	
Post-procedural TEE parameters				
MR grade ≥1+	4.332 (0.869–21.594)	0.074	–	
Noninvasive mPG	0.867 (0.532–1.413)	0.568	–	
Reduction rate of invasive hemodynamic parameters				
LAvP	1.142 (0.999–1.307)	0.052	–	
LAmP	1.295 (1.010–1.659)	0.041	1.612 (1.109–2.345)	0.012
LVSP	0.991 (0.959–1.024)	0.585	–	
LVEDP	1.025 (0.873–1.204)	0.762	–	
LAv height	1.076 (0.968–1.196)	0.173		
LAvPI	1,925.773 (0.039–96,303,422.34)	0.171	–	
LAmPI	16.55 (8.546–32.034)	0.027	1.487 (1.006–2.102)	0.005
Invasive mPG	1.065 (0.839–1.353)	0.604	–	

*Hazard ratio was adjusted for etiology of MR, pre-procedural NYHA functional class, greater or equal to moderate residual MR, pre-procedural LVEF, and TR.
Abbreviations as in Tables 3 and 4.

is high, eccentric jets after MC therapy may be underestimated.

Under these limitations, the evaluation of directly measured hemodynamic changes immediately after clipping can support decision making. The previous report has demonstrated the feasibility of real-time continuous LA pressure monitoring during MitraClip procedure (15). Reduction of LA pressure while maintaining or improving forward stroke volume is the ultimate goal of mitral repair and the usual result when repair is successful. LA dynamics are strongly influenced by loading conditions and the shape and function of both the LA and LV. As a result, absolute LA pressure changes are not reliable for interpretation. It is common to observe discrepant hemodynamic and echocardiographic findings during MC therapy. Patients with severe MR on TEE may have low LA pressures and minimal V waves, and vice versa. Long-standing MR may modify the mechanical characteristics of the LA and a normal LA pressure cannot exclude the presence of severe MR (16). Conversely, giant V waves may be seen in the absence of any MR, due to poor LA compliance (17). However, it has been shown that the absence of prominent pulmonary capillary wedge pressure V waves is relatively specific for the absence of moderate or severe MR (18). In the present study, pre-procedural LA volume index was not correlated with pre-procedural LAvP (correlation coefficient, 0.070; $p = 0.660$). In light of this result, LAvP could not be correlated with LA remodeling in this population.

Our finding is in line with a prior report that has described overall significantly reduced LVEDP, mean pulmonary capillary wedge pressure, and pulmonary capillary wedge pressure V-wave, and increased mean arterial pressure after MC therapy (19).

JACC: CARDIOVASCULAR INTERVENTIONS VOL. 12, NO. 2, 2019
JANUARY 28, 2019:127–38

FIGURE 3 Receiver-Operating Characteristic Curves of the Value of the Reduction Rate of LAvP, LAmP, and LAmPI to Predict New York Heart Association Functional Class III of IV at Follow-Up

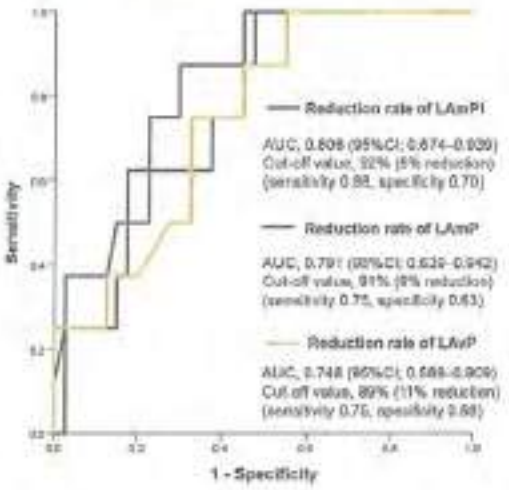

The **red line** refers to the area under the curve (AUC) of the reduction rate of LAmPI (0.808; 95% confidence interval [CI]: 0.674 to 0.939), the **green line** refers to the AUC of reduction rate of LAmP (0.791; 95% CI: 0.639 to 0.942), and the **yellow line** refers to the AUC of reduction rate of LA V-wave pressure (LAvP) (0.748; 95% CI: 0.588 to 0.909). Abbreviations as in Figure 2.

A successful MC therapy results in an acute increase in forward flow and a decrease in preload, as shown herein with increased LVSP and decreased LA pressure and LVEDP, respectively.

Although the rise of LV afterload can potentially create a mismatch, we observed that LA pressures adjusted to LV pressures (LAvP index and LAmPI) were significantly decreased in the current study. These results may indicate that greater effects can be achieved by decreasing LV preload rather than increasing LV afterload.

LA and LV pressures are involved in the symptoms of HF independent from LVEF (20). In the present study, baseline LVEF was not correlated with pre-procedural LAmP (correlation coefficient 0.063; $p = 0.662$), both in patients with degenerative MR (correlation coefficient 0.086; $p = 0.625$) and functional MR (correlation coefficient 0.114; $p = 0.687$).

LA DYNAMICS AS A PROGNOSTIC FACTOR FOR SYMPTOMATIC IMPROVEMENTS. Steady state hemodynamics may be influenced by a number of confounding factors. We focused on trends and intraprocedural changes immediately after the implant of each clip. We have shown that improvement in hemodynamics (reduction of LAmP and V-wave, while increasing LVSP) can be associated with improved clinical outcomes.

The present study highlights the role of relative changes of LA dynamics as a result of clip implantation. Intraprocedural decrease of LA pressure was associated with better outcomes while increase of LAmPI (HR: 3.377; 95% CI: 3.180 to 3.585; $p = 0.007$) was a significant predictor of HF rehospitalization at follow-up. In Kaplan-Meier curves, patients who experienced increased LAmPI after MC therapy (log-rank $p = 0.001$) had a significantly higher rate of rehospitalization due to HF.

The benefit from MR reduction can be counterbalanced by the induction of different degrees of mitral stenosis. Monitoring LA dynamics can be the unifying measure of this balance as trends in pressure can be more informative and carry a greater predictive value than either absolute pressure or TEE measures. As we have mentioned in Tables 4 and 5, increasing transmitral mean gradient per se was associated with neither rehospitalization due to HF (HR: 1.190; 95% CI: 0.880 to 1.608; $p = 0.259$) nor NYHA functional class III to IV at follow-up (HR: 1.065; 95% CI: 0.839 to 1.353; $p = 0.604$).

Improvement of LA dynamics is crucial to achieve symptomatic benefit. The extent of secondary pulmonary hypertension can be a determinant of morbidity and mortality in patients with chronic HF (21,22). Hospitalization rates for HF are increased in patients with echocardiographic evidence of pulmonary hypertension following MC therapy (23). Previous studies showed that a decrease in pulmonary capillary wedge pressure V-wave, mean pulmonary capillary wedge pressure and mean pulmonary artery pressure after MC therapy are predictive of a favorable cardiac outcomes (24). Another previous study has mentioned that acute changes in LA pressure after MC therapy are associated with clinical improvement as measured by 6-min walk test (25). There was no mention of patients with increased LA pressures post-procedure in this particular study. To the contrary, our study documented that increased LA pressure can be adjusted with systolic LV pressure as a measure of afterload to better characterize the impact of MC implantation.

This is the first demonstration that patients who develop increased LAmP (HR: 1.612; 95% CI: 1.109 to 2.345; $p = 0.012$), and LAmPI (HR: 1.497; 95% CI: 1.006 to 2.102; $p = 0.005$), regardless of MR reduction by TEE, have an increased likelihood to remain symptomatic (NYHA functional class III to IV at follow-up). This finding was independent from etiology of MR, pre-procedural NYHA functional class, pre-procedural LVEF, TR, and, interestingly, from residual MR after

FIGURE 4 Continuous Monitoring of Left-Sided Pressure Measurements During MitraClip Therapy

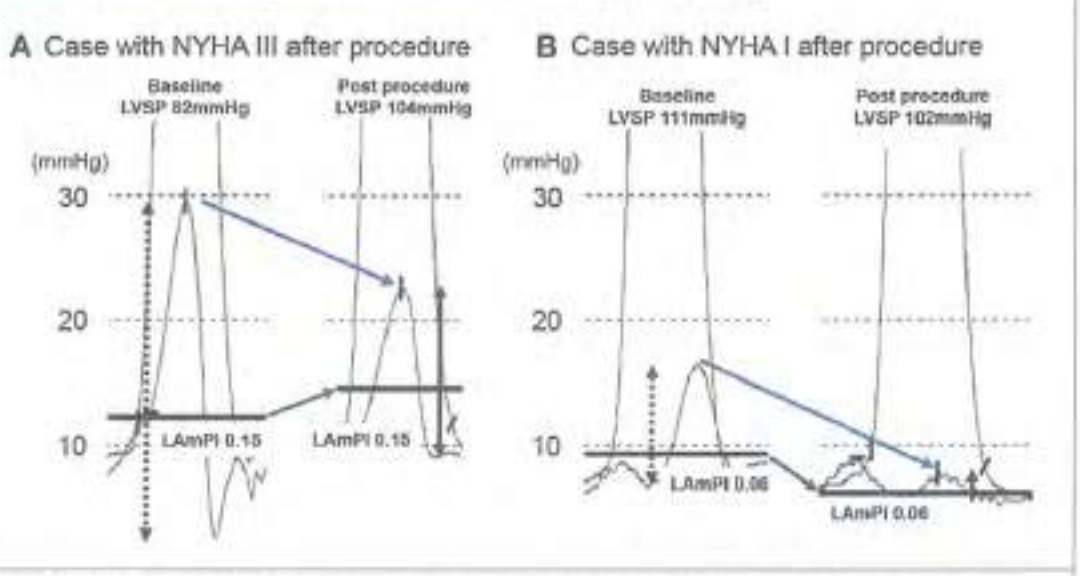

In both cases were LAvP **(blue arrows)** and LA V-wave height **(dot to solid deep red arrows)** decreased. **(A)** The LAmP **(black line, green arrows)** increased 25% as compared with baseline. In addition, the LAmPI was not decreased after MitraClip (Abbott Vascular, Abbott Park, Illinois) therapy. This patient is in New York Heart Association (NYHA) functional class III at follow-up. **(B)** The LAmP **(black line, green arrows)** decreased 33% as compared with baseline, and the LAmPI decreased 25% as compared with baseline. This patient is in NYHA functional class I at follow-up. This example underlines the importance of analyzing the full hemodynamic dataset, not only the decrease in the LAvP. LVSP = left ventricular systolic pressure; other abbreviations as in Figures 2 and 3.

MC. Intraprocedural trend of increasing LAmPI (area under the curve: 0.806; 95% CI: 0.674 to 0.939; cutoff value -8% [sensitivity 0.88, specificity 0.70]) had the largest area under the curve. Conversely, decreasing LAmPI can be best procedural indicator to predict improvements in functional status.

Another interesting finding in our experience is the central role played by the LA mean pressure. Using continuous measuring of the LA pressure, it is possible to monitor the V-wave behavior during clipping. In most cases, a successful grasping in the area of the regurgitant jet is associated with reduction in the amplitude of the V-wave. The absolute peak, or visual effect, of V-wave amplitude might lead to erroneous conclusions as this event is not always coupled with a reduction of LA mean pressure. In contrast to the V-wave, LAmP may be a better measure for predicting functional outcomes. Figure 4 shows 2 representative cases. In both cases, LAvPs and LA V-wave heights (differential pressure) decreased after MC implant, but LAmP increased in 1 case and decreased in the other. Patients with increased LAmP tend to remain in NYHA functional class IV at follow-up.

STUDY LIMITATIONS. There was no established protocol for fluid infusions or the use of pressors to elevate systemic arterial pressure, which might affect LA or LV pressure and influence measures in the present study. This is a single-center study and the sample size was small, which limits comparability. Furthermore, this study focuses on short-term results. Properly designed trials with longer-term follow-up and more patients are required to confirm these initial results.

CONCLUSIONS

An overall improvement in hemodynamics profile measured by direct left-sided heart continuous pressure is observed immediately after MC therapy. Acute increase of LAmPI is a strong prognostic factor for recurrent HF rehospitalization and persistent HF symptoms. Continuous left-sided heart pressure measurements may be complementary to the standard use of Doppler findings during MC procedures. The association between hemodynamic and clinical improvements was independent from residual MR as assessed by echocardiography. As a consequence, even in presence of residual MR, a positive outcome can be expected if hemodynamic improvements are.

ADDRESS FOR CORRESPONDENCE: Dr. Francesco Maisano, University Heart Center Zurich, Rämistrasse 100, CH-8091 Zürich, Switzerland. E-mail: francesco.maisano@usz.ch.

JACC: CARDIOVASCULAR INTERVENTIONS VOL. 12, NO. 2, 2019
JANUARY 28, 2019:127–36

PERSPECTIVES

WHAT IS KNOWN? Efficacy of the MC is assessed intraoperatively by TEE. However, TEE measures are operator dependent and can be influenced by LV function.

WHAT IS NEW? LA hemodynamics worsened as the result of therapy, with an increase of LAmP and LAmPI. This unfavorable change in LA dynamics was a prognostic factor for negative clinical outcomes at short-term follow-up, independently from echocardiographic findings.

WHAT IS NEXT? The present study consists of small sample size and focuses on short-term results. Properly designed trials with longer-term follow-up and more patients are required to confirm these initial results.

REFERENCES

1. Maisano F, Franzen O, Baldus S, et al. Percutaneous mitral valve interventions in the real world: early and 1-year results from the ACCESS-EU, a prospective, multicenter, nonrandomized post-approval study of the MitraClip therapy in Europe. J Am Coll Cardiol 2013;62:1052–61.

2. Glower DD, Kar S, Trento A, et al. Percutaneous mitral valve repair for mitral regurgitation in high-risk patients: results of the EVEREST II study. J Am Coll Cardiol 2014;64:172–81.

3. Siegel P, Vemulapalli S, Feldman T, et al. Outcomes with transcatheter mitral valve repair in the United States. J Am Coll Cardiol 2017;70:2315–27.

4. Zoghbi WA, Enriquez-Sarano M, Foster E, et al. Recommendations for evaluation of the severity of native valvular regurgitation with 2-dimensional and Doppler echocardiography. J Am Soc Echocardiogr 2003;16:777–802.

5. Grayburn PA, Roberts BJ, Aston S, et al. Mechanism and severity of mitral regurgitation by transesophageal echocardiography in patients referred for percutaneous valve repair. Am J Cardiol 2011;108:882–7.

6. Eleid MF, Sanon S, Reeder GS, Suri RM, Rihal CS. Continuous left atrial pressure monitoring during MitraClip: assessing the immediate hemodynamic response. J Am Coll Cardiol Intv 2015;8:e117–9.

7. Hunkulle J, Kloeser C, Beucher H, Schwarzlaender E, von Bardeleben RS, Boekstegers P. Intraprocedural assessment of mitral regurgitation during the mitraclip procedure: Impact of continuous left atrial pressure monitoring. Catheter Cardiovasc Interv 2016;88:1134–43.

8. Zoghbi WA, Adams D, Bonow RO, et al. Recommendations for Noninvasive Evaluation of Native Valvular Regurgitation: a report from the American Society of Echocardiography Developed in Collaboration with the Society for Cardiovascular Magnetic Resonance. J Am Soc Echocardiogr 2017;30:303–71.

9. Lancellotti P, Tribouilloy C, Hagendorff A, et al. Recommendations for the echocardiographic assessment of native valvular regurgitation: an executive summary from the European Association of Cardiovascular Imaging. Eur Heart J Cardiovasc Imaging 2013;14:611–44.

10. Stone GW, Adams DH, Abraham WT, et al. Clinical Trial Design Principles and Endpoint Definitions for Transcatheter Mitral Valve Repair and Replacement: Part 2: Endpoint Definitions. A Consensus Document From the Mitral Valve Academic Research Consortium. J Am Coll Cardiol 2015;66:308–21.

11. Kang WS, Choi JW, Kang JE, Chung JW, Kim SH. Determination of mitral valve area with echocardiography, using intra-operative 3-dimensional versus intra- & post-operative pressure half-time technique in mitral valve repair surgery. J Cardiothorac Surg 2013;8:98.

12. Kar S, Sharma R. Current assessment of mitral regurgitation: not making the grade. J Am Coll Cardiol 2015;65:1089–91.

13. Grayburn PA, Foster E, Sangli C, et al. Relationship between the magnitude of reduction in mitral regurgitation severity and left ventricular and left atrial reverse remodeling after MitraClip therapy. Circulation 2013;128:1667–74.

14. Lin BA, Forouhar AS, Pahlevan NM, et al. Color Doppler jet area overestimates regurgitant volume when multiple jets are present. J Am Soc Echocardiogr 2010;23:993–1000.

15. Gaijar M, Yadlapati A, Van Assche LMR, et al. Real-time continuous left atrial pressure monitoring during mitral valve repair using the MitraClip NT system: a feasibility study. J Am Coll Cardiol Intv 2017;10:1466–7.

16. Braunwald E, Awe WC. The syndrome of severe mitral regurgitation with normal left atrial pressure. Circulation 1963;27:29–35.

17. Syed Z, Salinger MH, Feldman T. Alterations in left atrial pressure and compliance during balloon mitral valvuloplasty. Catheter Cardiovasc Interv 2004;61:571–9.

18. Snyder RW 2nd, Glansam CB, Lange RA, et al. Predictive value of prominent pulmonary arterial wedge V waves in assessing the presence and severity of mitral regurgitation. Am J Cardiol 1994;73:568–70.

19. Geuzebroek G, Biaggi P, Guggenbuhl R, et al. Real-time left ventricular pressure-volume loops during percutaneous mitral valve repair with the MitraClip system. Circulation 2013;127:1018–27.

20. Owan TE, Hodge DO, Herges RM, Jacobsen SJ, Roger VL, Redfield MM. Trends in prevalence and outcome of heart failure with preserved ejection fraction. N Engl J Med 2006;355:251–9.

21. Moraes DL, Colucci WS, Givertz MM. Secondary pulmonary hypertension in chronic heart failure: the role of the endothelium in pathophysiology and management. Circulation 2000;102:1718–23.

22. Costard-Jackle A, Fowler MB. Influence of preoperative pulmonary artery pressure on mortality after heart transplantation: testing of potential reversibility of pulmonary hypertension with nitroprusside is useful in defining a high risk group. J Am Coll Cardiol 1992;19:48–54.

23. Abramson SV, Burke JF, Kelly JJ Jr, et al. Pulmonary hypertension predicts mortality and morbidity in patients with dilated cardiomyopathy. Ann Intern Med 1992;116:888–95.

24. Guerpioli G, Moccetti M, Sinder D, et al. Acute haemodynamic changes after percutaneous mitral valve repair: relation to mid-term outcomes. Heart 2012;98:126–33.

25. Maor E, Raphael CE, Pereich SS, et al. Acute changes in left atrial pressure after MitraClip are associated with improvement in 6-minute walk distance. Circ Cardiovasc Interv 2017;10:e004856.

KEY WORDS MitraClip, mitral regurgitation, mitral valve, transcatheter mitral valve repair

APPENDIX For supplemental tables, please see the online version of this paper.

ESC European Society of Cardiology
European Heart Journal (2019) 40, 441–451
doi:10.1093/eurheartj/ehy590

FASTTRACK CLINICAL RESEARCH
Interventional cardiology

Outcomes of transcatheter mitral valve replacement for degenerated bioprostheses, failed annuloplasty rings, and mitral annular calcification

Sung-Han Yoon[1], Brian K. Whisenant[2], Sabine Bleiziffer[3], Victoria Delgado[4], Abhijeet Dhoble[5], Niklas Schofer[6], Lena Eschenbach[3], Eric Bansal[7], Dale J. Murdoch[8], Marco Ancona[9], Tobias Schmidt[10], Ermela Yzeiraj[11], Flavien Vincent[12], Hiroki Niikura[13], Won-Keun Kim[14], Masahiko Asami[15], Axel Unbehaun[16], Sameer Hirji[17], Buntaro Fujita[18], Miriam Silaschi[19], Gilbert H.L. Tang[20], Shingo Kuwata[21], S. Chiu Wong[22], Antonio H. Frangieh[23], Colin M. Barker[24], James E. Davies[25], Alexander Lauten[26], Florian Deuschl[6], Luis Nombela-Franco[27], Rajiv Rampat[28], Pedro Felipe Gomes Nicz[29], Jean-Bernard Masson[30], Harindra C. Wijeysundera[31], Horst Sievert[32], Daniel J. Blackman[33], Enrique Gutierrez-Ibanes[34], Daisuke Sugiyama[35], Tarun Chakravarty[1], David Hildick-Smith[28], Fabio Sandoli de Brito Jr[36], Christoph Jensen[37], Christian Jung[38], Richard W. Smalling[5], Martin Arnold[39], Simon Redwood[40], Albert Markus Kasel[23], Francesco Maisano[21], Hendrik Treede[19], Stephan M. Ensminger[18], Saibal Kar[1], Tsuyoshi Kaneko[17], Thomas Pilgrim[15], Paul Sorajja[13], Eric Van Belle[12], Bernard D. Prendergast[40], Vinayak Bapat[41], Thomas Modine[12], Joachim Schofer[11], Christian Frerker[10], Joerg Kempfert[16], Guilherme F. Attizzani[7], Azeem Latib[9], Ulrich Schaefer[6], John G. Webb[8], Jeroen J. Bax[4], and Raj R. Makkar[1]*

[1]Department of Interventional Cardiology, Cedars-Sinai Heart Institute, 8700 Beverly Blvd, Los Angeles, CA 90048, USA; [2]Division of Cardiovascular Diseases, Intermountain Heart Institute, Salt Lake City, UT 84107, USA; [3]Department of Cardiovascular Surgery, German Heart Center Munich, Munich, Germany; [4]Department of Cardiology, Leiden University Medical Center, Albinusdreef 2, 2300 RC Leiden, The Netherlands; [5]Department of Cardiology, University of Texas Health Science Center, 6431 Fannin St., MSB 1.224, Houston, TX 77030, USA; [6]Department of General and Interventional Cardiology, University Heart Center, 20246 Hamburg, Germany; [7]The Valve and Structural Heart Interventional Center, University Hospitals Case Medical Center, Cleveland, OH, USA; [8]Department of Cardiology, St Paul's Hospital, University of British Columbia, 1081 Burrard Street, Vancouver, BC V6Z 1Y6, Canada; [9]Interventional Cardiology Unit, EMO-GVM Centro Cuore Columbus & San Raffaele Scientific Institute, San Raffaele Hospital, Milan, Italy; [10]Department of Cardiology, Asklepios Klinik St. Georg, Lohmuehlenstrasse 5, 20099 Hamburg, Germany; [11]Hamburg University Cardiovascular Center, Hamburg, Germany; [12]Department of Cardiology/Cardiac Surgery, CHU Lille, INSERM U1011-EGID, Institut Pasteur de Lille, Lille, France; [13]Valve Science Center, Minneapolis Heart Institute Foundation, Abbott Northwestern Hospital, 800 East 28th St, Minneapolis, MN 55407, USA; [14]Department of Cardiology/Cardiac Surgery, Kardiohelf Heart and Thorax Center, Benekestr. 2-8, D-61231 Bad Nauheim, Germany; [15]Department of Cardiology, Swiss Cardiovascular Center, Bern University Hospital, CH-3010 Bern, Switzerland; [16]Department of Cardiothoracic and Vascular Surgery, German Heart Center Berlin, 13353 Berlin, Augustenburger Platz 1, and DZHK (German Center for Cardiovascular Research), partner site Berlin, Germany; [17]Division of Cardiac Surgery, Brigham and Women's Hospital, 15 Francis Street, Boston, MA 02115, USA; [18]Department of Thoracic and Cardiovascular Surgery, Heart and Diabetes Center NRW, Ruhr-University Bochum, Bad Oeynhausen, Germany; [19]Department of Cardiac Surgery, University Hospital Halle, Ernst-Grube Str. 40, 06120 Halle, Germany; [20]Department of Cardiovascular Surgery, Mount Sinai Health System, 1190 Fifth Avenue, GP2W, Box 1028, New York, NY 10029, USA; [21]University Heart Center, University Hospital Zurich, Rämistrasse 100, 8091 Zurich, Switzerland; [22]Greenberg Division of Cardiology, New York-Presbyterian Hospital, Weil Cornell Medicine, New York, NY, USA; [23]Department of Cardiology, Deutsches Herzzentrum München, Technische Universität München, Lazarettstrasse 36, 80636 Munich, Germany; [24]Department of Cardiology, Houston Methodist Hospital, Smith 1901, 6550 Fannin Street, Houston, TX 77030, USA; [25]Division of Cardiac and Thoracic Surgery, University of Alabama-Birmingham, Birmingham, AL, USA; [26]Department of Cardiology, Charité-Universitätsmedizin Berlin; DZHK (German Centre for Cardiovascular Research), partner site Berlin, Germany; [27]Cardiovascular Institute, Hospital Clinico San Carlos, IdISSC, Profesor Martin Lagos s/n, 28040 Madrid, Spain; [28]Sussex Cardiac Centre, Brighton and Sussex University Hospitals NHS Trust, Brighton, UK; [29]Department of Cardiology, Hospital Sao Camilo, Av. Pompeia 1178,

* Corresponding author. Tel: +1 310 423 3977, Fax: +1 310 423 0106, Email: raj.makkar@cshs.org

Published on behalf of the European Society of Cardiology. All rights reserved. © The Author(s) 2018. For permissions, please email: journals.permissions@oup.com.

Downloaded from https://academic.oup.com/eurheartj/article-abstract/40/5/441/5143983 by ST MARIANNA UNIV user on 27 April 2020

São Paulo 05022-001, Brazil; [30]Division of Cardiology, Centre Hospitalier de l'Université de Montreal, 1051 Sanguinet, Montreal, Quebec H2X 3E4, Canada; [31]Division of Cardiology, Sunnybrook Health Science Centre, 2075 Bayview Avenue, Suite A202 Toronto, ON, Canada; [32]CardioVascular Center, Frankfurt, Germany; [33]Department of Cardiology, Leeds Teaching Hospital, Leeds, UK; [34]Instituto de Investigación Sanitaria Gregorio Marañón, Calle Dr Esquerdo 46, 28007 Madrid, CIBER CV, Spain; [35]Department of Preventive Medicine and Public Health, Keio University School of Medicine, Tokyo, Japan; [36]Heart Institute of University of Sao Paulo Medical School, Av. Dr. Enéas Carvalho de Aguiar 44, São Paulo 05403-000, Brazil; [37]Cardio Heart and Vascular Centre, Elisabeth Krankenhaus Essen, Essen, Germany; [38]Division of Cardiology, Pulmonology and Vascular Medicine, Medical Faculty, Heinrich-Heine-University, Moorenstraße 5, 40225 Düsseldorf, Germany; [39]Department of Cardiology, University Hospital Erlangen, Erlangen, Germany; [40]Cardiothoracic Department, St Thomas Hospital, Westminster Bridge Rd, London SE1 7EH, UK; and [41]Columbia University Medical Center/New York Presbyterian Hospital, New York, NY, USA

Received 7 August 2018; revised 23 August 2018; editorial decision 25 August 2018; accepted 6 September 2018; online publish-ahead-of-print 23 October 2018

See page 452 for the editorial comment on this article (doi: 10.1093/eurheartj/ehy725)

Aims We sought to evaluate the outcomes of transcatheter mitral valve replacement (TMVR) for patients with degenerated bioprostheses [valve-in-valve (ViV)], failed annuloplasty rings [valve-in-ring (ViR)], and severe mitral annular calcification [valve-in-mitral annular calcification (ViMAC)].

Methods and results From the TMVR multicentre registry, procedural and clinical outcomes of ViV, ViR, and ViMAC were compared according to Mitral Valve Academic Research Consortium (MVARC) criteria. A total of 521 patients with mean Society of Thoracic Surgeons score of 9.0 ± 7.0% underwent TMVR (322 patients with ViV, 141 with ViR, and 58 with ViMAC). Trans-septal access and the Sapien valves were used in 39.5% and 90.0%, respectively. Overall technical success was excellent at 87.1%. However, left ventricular outflow tract obstruction occurred more frequently after ViMAC compared with ViR and ViV (39.7% vs. 5.0% vs. 2.2%; $P < 0.001$), whereas second valve implantation was more frequent in ViR compared with ViMAC and ViV (12.1% vs. 5.2% vs. 2.5%; $P < 0.001$). Accordingly, technical success rate was higher after ViV compared with ViR and ViMAC (94.4% vs. 80.9% vs. 62.1%; $P < 0.001$). Compared with ViMAC and ViV groups, ViR group had more frequent post-procedural mitral regurgitation ≥moderate (18.4% vs. 13.8% vs. 5.6%; $P < 0.001$) and subsequent paravalvular leak closure (7.8% vs. 0.0% vs. 2.2%; $P = 0.006$). All-cause mortality was higher after ViMAC compared with ViR and ViV at 30 days (34.5% vs. 9.9% vs. 6.2%; log-rank $P < 0.001$) and 1 year (62.8% vs. 30.6% vs. 14.0%; log-rank $P < 0.001$). On multivariable analysis, patients with failed annuloplasty rings and severe MAC were at increased risk of mortality after TMVR [ViR vs. ViV, hazard ratio (HR) 1.99, 95% confidence interval (CI) 1.27–3.12; $P = 0.003$; ViMAC vs. ViV, HR 5.29, 95% CI 3.29–8.51; $P < 0.001$].

Conclusion The TMVR provided excellent outcomes for patients with degenerated bioprostheses despite high surgical risk. However, ViR and ViMAC were associated with higher rates of adverse events and mid-term mortality compared with ViV.

Keywords Mitral valve • Transcatheter valve implantation • Degenerated bioprostheses • Annuloplasty ring • Mitral annular calcification

Introduction

Mitral valve disease is the most common valvular disease in the developed countries and surgery is the gold standard treatment.[1,2] Due to a massive shift from mechanical to bioprosthetic valves with finite longevity, increasing numbers of patients are presenting with bioprosthetic mitral valve degeneration.[3] Recurrent mitral regurgitation (MR) is frequent after mitral valve repair, particularly in the setting of functional MR.[4] Mitral valve reoperation often entails high risk due to age, multiple comorbidities, and hostile anatomy. In addition, patients with severe mitral annular calcification (MAC) associated with mitral valve disease are considered as poor candidates for traditional surgery due to technical challenges and high perioperative mortality.[5]

Transcatheter mitral valve replacement (TMVR) is an emerging treatment for patients with severe mitral valve disease at high risk for conventional mitral valve surgery. Recent studies have demonstrated the efficacy and safety of TMVR for patients with degenerated bioprostheses, failed annuloplasty repair, and severe MAC.[6,7] Nevertheless, currently used devices were designed for the aortic position and TMVR requires invasive transapical or complex trans-septal approaches. Furthermore, the anatomical differences between mitral bioprosthetic valves, annuloplasty rings, and severely calcified mitral annulus lead to specific procedural challenges for each unique TMVR procedure. Identifying the predictors of adverse outcomes is essential as patients are selected and counselled regarding competing surgical and transcatheter options. In addition, the risk of bioprosthetic valve thrombosis is being increasingly recognized but limited data exists about thrombosis after TMVR. The lack of randomized trial data in this field highlights the importance of reporting outcomes from large-sample registries. Therefore, we created an international multicentre registry of TMVR to evaluate and compare TMVR associated procedural events and clinical outcomes.

Methods

Study design and patient population

The TMVR registry is an international, multicentre, observational study that enrolled consecutive patients undergoing TMVR for mitral degenerated bioprostheses [valve-in-valve (ViV)], failed annuloplasty rings [valve-

Downloaded from https://academic.oup.com/eurheartj/article-abstract/40/15/1441/5143863 by ST MARIANNA UNIV user on 27 April 2020

in-ring (VIR)], or severe MAC [valve-in-mitral annular calcification (VIMAC)]. The registry included 40 European and American centres and was initiated in November 2015. Patients were considered TMVR candidates if they had significant dysfunction (either stenosis, regurgitation, or both) of a bioprosthetic mitral valve, annuloplasty ring, or a calcified mitral annulus, with comorbid conditions that would preclude a conventional mitral valve surgery. The study was approved by the institutional review board of each institution when required; however, in some countries, for retrospective analysis of clinically acquired and anonymized data, the institutional review board waived the need for written patient informed consent.

Study devices and transcatheter mitral valve replacement procedures

Patients were selected for TMVR at the institutional level after discussions by the multidisciplinary heart team, and device type and access site were determined thereafter. Device size was selected based on a combination of the manufacture's reported diameter as well as multidetector row computed tomography and transoesophageal echocardiographic measurements.[8–10] The VIV software application was used to guide the proper device size selection (B.V. Valve in Valve Mitral app, http://www.ubqo.com/vivmitral). All TMVR procedures were conducted in accordance with local guidelines using standard techniques via trans-septal, transapical, or transatrial access. Balloon-expandable transcatheter valves [the Sapien, Sapien XT, Sapien 3 (Edwards Lifesciences, Irvine, CA, USA), and Melody (Medtronic, Minneapolis, MN)] or other transcatheter valves [Lotus (Boston Scientific, Natick, MA, USA) and Direct Flow (Direct Flow Medical Inc., Santa Rosa, CA, USA)] were implanted.[11–13] The sizes of transcatheter valves were categorized as previously described.[8]

Endpoints and definitions

The primary endpoints were all-cause mortality at 30 days and 1 year. Secondary endpoints were technical, device and procedural success, and other major clinical endpoints defined according to the Mitral Valve Academic Research Consortium (MVARC) criteria.[14] In the present study, we used modified criteria for significant mitral stenosis (MS) defined as a mean transmitral gradient ≥10 mmHg and/or an effective orifice area ≤1.0 cm^2 as previously described.[8] Bioprosthetic valve thrombosis was defined as valve dysfunction (mean transvalvular gradient ≥10 mmHg and/or restricted leaflet motion with echocardiography) secondary to thrombosis diagnosed on the basis of response to anticoagulation or surgical findings.

Data collection

Data collection included baseline clinical, echocardiographic and procedural characteristics, and clinical follow-up data, at pre-specified time points (1, 6, and 12 months and yearly thereafter). Follow-up was obtained by clinical visits and/or through telephone contacts. Referring cardiologists, general practitioners, and patients were contacted whenever necessary for further information. All data provided by each institution were anonymized and centrally collected, and all inconsistencies were resolved directly with local investigators.

Statistical analysis

Patients were stratified according to the type of TMVR procedures (VIV, VIR, or VIMAC). Dichotomous variables are presented as counts or percentages and compared using the χ^2 or Fisher exact test. Continuous variables are presented as mean with standard deviation. Comparisons of continuous variables among three groups were performed with the Analysis of Variance (ANOVA) or Kruskal–Wallis test as appropriate. Tukey test for multiple comparisons was used if statistical significance was achieved (see Supplementary material online, *Tables S1–S3*). Comparisons of continuous variables between two groups were performed using the Student's *t*-test or Mann–Whitney *U*-test. Cumulative rates of death, stroke, bleeding, major vascular complication, acute kidney injury, or valve thrombosis were calculated by using the Kaplan–Meier survival analysis, and the log-rank test was used for comparison across the groups. Univariable Cox regression models were used to evaluate potential predictors of all-cause mortality. Statistically significant variables with a *P*-value <0.10 by univariable analysis were included in the multivariable model. The final model was determined by backward elimination procedures with a threshold *P*-value <0.10. The proportional hazard assumption was confirmed by examination of log [-log (survival)] curves and by testing of partial (Schoenfeld) residuals, and no relevant violations were found. The estimated hazard ratio (HR) with 95% confidence interval (CI) was provided by the Cox model. All statistical analyses were performed using SPSS software (version 24.0, SPSS, Inc., Armonk, NY, USA). A two-sided *P*-value of <0.05 was considered to be statistically significant.

Results

Baseline characteristics

A total of 521 patients underwent TMVR across 40 participating centres between February 2009 and April 2018. Of the study population, 322 patients (61.8%) had TMVR for degenerated mitral bioprosthetic valves (VIV), 141 patients (27.1%) for failed annuloplasty rings (VIR), and 58 patients (11.1%) for degenerated mitral valve with severe MAC (VIMAC). The majority of patients were deemed at high risk for conventional surgery with a mean Society of Thoracic Surgeons (STS) score of 9.0% without significant difference across the three groups (VIV vs. VIR vs. VIMAC: 9.2 ± 7.2% vs. 8.1 ± 6.4% vs. 10.1 ± 6.9%; *P* = 0.12) (*Table 1*). However, baseline characteristics significantly differed across the three groups: The patients in VIMAC group were more likely to be female and have New York Heart Association functional Class IV heart failure symptoms and chronic pulmonary disease, whereas patients in VIR group were more likely to have prior coronary artery bypass graft surgery (CABG) and myocardial infarction with lower left ventricular ejection fraction (LVEF). The predominant mechanism of failure was MR in the VIR group but MS was the most frequent form of valve dysfunction in the VIMAC group.

Procedural data

Procedural details are summarized in *Table 2*. The majority of patients were treated via transapical access (59.5%) with the balloon-expandable Sapien valves (90.0%). The Sapien valves were more frequently used in the VIV group, whereas the large size device was more frequently used in the VIMAC group compared with VIV and VIR groups. Planned concomitant aortic valve replacement was performed in 20 patients (3.8%), more frequently with VIMAC compared with VIV and VIR (12.1% vs. 3.7% vs. 0.7%; *P* = 0.001). Balloon pre- and post-dilatation were more frequently performed in the VIMAC group compared with VIV and VIR groups. Contrast dose was the larger in the VIMAC group compared with the other two groups (64.8 ± 55.7 mL vs. 45.9 ± 66.5 mL vs. 36.5 ± 51.5 mL; *P* = 0.01), whereas fluoroscopic time was similar across the three groups.

Procedural outcomes

Procedural and 30-day outcomes are summarized in *Table 3*. Procedural complications varied significantly between the three

Downloaded from https://academic.oup.com/eurheartj/article-abstract/40/5/441/5143863 by ST MARIANNA UNIV user on 27 April 2020

Table 1 Baseline characteristics

	Overall (n = 521)	VIV (n = 322)	ViR (n = 141)	ViMAC (n = 58)	P-value
Age (years)	72.6 ± 11.9	72.6 ± 12.9	71.7 ± 9.7	74.7 ± 10.8	0.28
Female	282 (54.1)	189 (58.7)	52 (36.9)	41 (70.7)	<0.001[b,c]
NYHA functional Class III or IV	461 (88.5)	282 (87.6)	126 (89.4)	53 (91.4)	0.66
NYHA functional Class IV	167 (32.1)	104 (32.3)	36 (25.5)	27 (46.6)	0.015[b,c]
STS score (%)	9.0 ± 7.0	9.2 ± 7.2	8.1 ± 6.4	10.1 ± 6.9	0.12
Diabetes mellitus	124 (23.8)	75 (23.3)	30 (21.3)	19 (32.8)	0.21
Creatinine (mmol/L)	137 ± 114	130 ± 113	145 ± 104	158 ± 139	0.16
Hypertension	368 (70.6)	224 (69.6)	97 (68.8)	47 (81.0)	0.18
Peripheral vascular disease	59 (11.3)	37 (11.5)	15 (10.6)	7 (12.1)	0.95
Prior cerebrovascular accident	82 (15.7)	57 (17.7)	17 (12.1)	8 (13.8)	0.28
Chronic pulmonary disease	156 (29.9)	92 (28.6)	38 (27.0)	26 (44.8)	0.03[b,c]
Prior PCI	94 (18.0)	50 (15.5)	32 (22.7)	12 (20.7)	0.16
Prior CABG	173 (33.2)	93 (28.9)	69 (48.9)	11 (19.0)	<0.001[a,c]
Prior myocardial infarction	82 (15.7)	39 (12.1)	36 (25.5)	7 (12.1)	0.001[a,c]
Echocardiographic findings					
LVEF (%)	52.6 ± 13.7	55.3 ± 11.5	44.3 ± 15.7	57.7 ± 10.7	<0.001[a,c]
Mitral valve mean gradient (mmHg)	10.9 ± 5.9	12.1 ± 5.9	7.1 ± 4.8	11.8 ± 4.8	<0.001[a,c]
Mechanism of failure					
Regurgitation	238 (45.7)	118 (36.6)	109 (77.3)	11 (19.0)	<0.001[a,b,c]
Stenosis	173 (33.2)	131 (40.7)	9 (6.4)	33 (56.9)	
Combined	110 (21.1)	73 (22.7)	23 (16.3)	14 (24.1)	

CABG, coronary artery bypass graft surgery; LVEF, left ventricular ejection fraction; NYHA, New York Heart Association; PCI, percutaneous coronary intervention; STS, society of thoracic surgeons; ViMAC, valve in mitral annular calcification; ViR, valve in ring; ViV, valve in valve.
[a]P < 0.05 for ViV vs. ViR.
[b]P < 0.05 for ViV vs. ViMAC.
[c]P < 0.05 for ViR vs. ViMAC.

groups. Conversion to surgery and valve embolization were observed in 12 (2.3%) and nine patients overall (1.7%), more frequently after ViMAC compared with ViR and ViV. Left ventricular perforation was observed only after ViV (1.2%), whereas second valve implantation was more frequently performed in ViR group compared with ViMAC and ViV groups (12.1% vs. 5.2% vs. 2.5%; $P < 0.001$). Left ventricular outflow tract (LVOT) obstruction was observed in 37 patients (7.1%), with a significantly higher rate after ViMAC compared with ViR and ViV procedures (39.7% vs. 5.0% vs. 2.2%; $P < 0.001$). Technical success was achieved in 87.1% of the entire cohort, with a higher rate after ViV compared with ViR and ViMAC (94.4% vs. 80.9% vs. 62.1%; $P < 0.001$). Paravalvular leak closure was more frequently performed in the ViR group compared with ViV and ViMAC groups (7.8% vs. 2.2% vs. 0.0%; $P = 0.006$), whereas alcohol septal ablation was more frequently performed in the ViMAC group than ViV and ViR groups (12.1% vs. 0.6% vs. 0.7%; $P < 0.001$). There were no significant differences in atrial septal defect closure and surgical mitral valve replacement between the three groups.

Post-procedural LVEF remained lowest in the ViR group compared with ViV and ViMAC groups. Significant MS was only observed in seven patients (1.3%) of the entire cohort. Post-procedural MR ≥moderate was more frequently observed in the ViR group compared with ViMAC and ViV groups (18.4% vs. 13.8% vs. 5.6%; $P < 0.001$). Following the paravalvular leak closure, the rates of MR ≥moderate at 30 days remained higher in ViMAC and ViR groups than the ViV group (13.2% vs. 12.6% vs. 3.3%; $P < 0.001$) (see Supplementary material online, *Figure S1*). Device success was the highest in the ViV group followed by ViR and ViMAC groups (84.8% vs. 69.5% vs. 53.4%; $P < 0.001$).

Clinical outcomes

All-cause 30-day mortality was the highest in the ViMAC group followed by the ViR and ViV groups (34.5% vs. 9.9% vs. 6.2%; $P < 0.001$). There were no significant differences in stroke and major or extensive bleeding between the three groups. Life-threatening or fatal bleeding tended to be more frequent in the ViR group, whereas major vascular complication and Stage 2 or 3 acute kidney injury occurred more frequently in the ViMAC group. Procedural success was highest in the ViV group followed by the ViR and ViMAC groups (73.6% vs. 57.4% vs. 41.4%; $P < 0.001$). In general, there were no significant differences in procedural complications between trans-septal and transapical approaches with the exceptions of higher rates of atrial septal defect closure and alcohol septal ablation and lower rate of life-threatening or fatal bleeding with trans-septal access (see Supplementary material online, *Table S4*). Patients were divided into early experience and late experience groups according to the median number of TMVR procedures at each institution. Compared with the early experience group, the late experience group had lower rates of conversion to surgery, 30-day mortality, life-threatening or fatal

Downloaded from https://academic.oup.com/eurheartj/article-abstract/40/544/5143983 by ST MARIANNA UNIV user on 27 April 2020

Table 2 Procedural data

	Overall ($n = 521$)	VIV ($n = 322$)	VIR ($n = 141$)	VIMAC ($n = 58$)	P-value
Access site					
Trans-septal access	206 (39.5)	125 (38.8)	50 (35.5)	31 (53.4)	0.09
Transapical access	310 (59.5)	193 (59.9)	91 (64.5)	26 (44.8)	
Transatrial access	5 (1.0)	4 (1.2)	0 (0.0)	1 (1.7)	
Device type					
Sapien valves	469 (90.0)	302 (93.8)	120 (85.1)	47 (81.0)	<0.001[a,b]
Sapien	27 (5.8)	20 (6.6)	7 (5.8)	0 (0.0)	0.004[b,c]
Sapien XT	154 (32.8)	108 (35.8)	40 (33.3)	6 (12.8)	
Sapien 3	288 (61.4)	174 (57.6)	73 (60.8)	41 (87.2)	
Lotus	30 (5.8)	12 (3.7)	9 (6.4)	9 (15.5)	<0.001[a,b]
Direct flow	18 (3.5)	4 (1.2)	12 (8.5)	2 (3.4)	
Melody	4 (0.8)	4 (1.2)	0 (0.0)	0 (0.0)	
Device size					
Small	48 (9.2)	28 (8.7)	18 (12.8)	2 (3.4)	0.03[a,c]
Medium	196 (37.6)	115 (35.7)	62 (44.0)	19 (32.8)	
Large	277 (53.2)	179 (55.6)	61 (43.3)	37 (63.8)	
Planned concomitant aortic valve replacement	20 (3.8)	12 (3.7)	1 (0.7)	7 (12.1)	0.001[b,c]
TAVR	16 (3.1)	8 (2.5)	1 (0.7)	7 (12.1)	0.001[b,c]
Surgery	4 (0.8)	4 (1.2)	0 (0.0)	0 (0.0)	0.58
Apical rail	20 (3.8)	10 (3.1)	7 (5.0)	3 (5.2)	0.54
Balloon pre-dilatation	49 (9.4)	35 (10.9)	5 (3.5)	9 (15.5)	0.01[a,c]
Balloon post-dilatation	45 (8.6)	12 (3.7)	22 (15.6)	11 (19.0)	<0.001[a,b]
Contrast dose (mL)	42.7 ± 57.2	36.5 ± 51.5	45.9 ± 66.5	64.8 ± 55.7	0.01[b]
Fluoroscopic time (min)	25.7 ± 24.1	24.0 ± 26.2	28.1 ± 20.1	29.0 ± 20.2	0.30

TAVR, transcatheter aortic valve replacement; VIMAC, valve in mitral annular calcification; VIR, valve in ring; VIV, valve in valve.
[a]$P < 0.05$ for VIV vs. VIR.
[b]$P < 0.05$ for VIV vs. VIMAC.
[c]$P < 0.05$ for VIR vs. VIMAC.

bleeding, and Stage 2 or 3 acute kidney injury, mainly driven by the improved outcomes of VIV with increased experience (see Supplementary material online, *Table S5* and *Figure S2A–C*).

Mid-term mortality

Over a median follow-up period of 160 days (interquartile range 60–420 days), a total of 117 patients died in the overall cohort (53 patients in the VIV group, 34 patients in the VIR group, and 30 patients in the VIMAC group). The 1-year all-cause and cardiovascular mortality were 23.5% and 20.2% in the entire cohort, respectively (*Figure 1*). The 1-year all-cause mortality rate was highest in the VIMAC group followed by VIR and VIV groups (62.8% vs. 30.6% vs. 14.0%; VIR vs. VIV; adjusted HR 1.99, 95% CI 1.27–3.12; $P = 0.003$; VIMAC vs. VIV; adjusted HR 5.29, 95% CI 3.29–8.51; $P < 0.001$) (*Figure 2A* and Supplementary material online, *Figure S3*). Landmark analysis showed higher late mortality (30–360 days) in the VIMAC group (43.2%) compared with the VIR (23.0%) and VIV groups (8.4%) (*Figure 2B*). Patients with post-procedural MR ≥moderate had significantly higher 1-year all-cause mortality compared with those with MR ≤mild (41.5% vs. 21.4%; log rank $P = 0.01$) (*Figure 3*). However, there was no significant difference in 1-year all-cause mortality between trans-septal and transapical approaches (see Supplementary material online, *Figure S4*). After adjustment with multivariable analysis, STS score, chronic pulmonary disease, pre-procedural status of mitral valve (VIV vs. VIR vs. VIMAC), and post-procedural MR ≥moderate were independently associated with all-cause mortality in the entire cohort (*Table 4*). For each TMVR procedure, factors associated with increased mortality were STS score and LVEF for VIV group, post-procedural MR ≥moderate for VIR group, STS score and prior CABG for VIMAC group (see Supplementary material online, *Tables S6–S8*).

Thrombosis and anticoagulation

Information regarding antithrombotic prophylaxis and valve thrombosis was available in 411 patients (78.9%). Among them, 295 patients (71.8%) received anticoagulation therapy and the remaining 116 (28.2%) patients received antiplatelet therapy after TMVR (see Supplementary material online, *Figure S5A*). During the entire follow-up, clinical thrombosis was observed in 10 patients after VIV (nine patients with stented porcine valves and one patient with a pericardial valve) and one patient after VIR but none after VIMAC. The timing of thrombosis varied significantly from within 24 h to 2 years after the index TMVR procedure (see Supplementary material online, *Figure S5B*). At 1-year follow-up, the cumulative incidence of thrombosis was significantly higher in patients without anticoagulation compared with those with anticoagulation (6.6% vs. 1.6%; log-rank $P = 0.019$) (*Figure 4*).

Downloaded from https://academic.oup.com/eurheartj/article-abstract/40/5/441/5143983 by ST MARIANNA UNIV user on 27 April 2020

Table 3 Procedural and 30-day outcomes

	Overall (n = 521)	ViV (n = 322)	ViR (n = 141)	ViMAC (n = 58)	P-value
Procedural outcomes					
Conversion to surgery	12 (2.3)	3 (0.9)	4 (2.8)	5 (8.6)	0.004[d]
Valve embolization	9 (1.7)	3 (0.9)	2 (1.4)	4 (6.9)	0.01[d]
Left ventricular perforation	4 (0.8)	4 (1.2)	0 (0.0)	0 (0.0)	0.58
Need for second valve implantation	28 (5.4)	8 (2.5)	17 (12.1)	3 (5.2)	<0.001[c]
LVOT obstruction	37 (7.1)	7 (2.2)	7 (5.0)	23 (39.7)	<0.001[d,e]
Technical success	454 (87.1)	304 (94.4)	114 (80.9)	36 (62.1)	<0.001[c,d,e]
Re-intervention	72 (14.0)	35 (10.9)	25 (17.7)	13 (22.4)	0.02[c,d]
Paravalvular leak closure	18 (3.5)	7 (2.2)	11 (7.8)	0 (0.0)	0.006[c,e]
Atrial septal defect closure	36 (6.9)	23 (7.1)	7 (5.0)	6 (10.3)	0.38
Alcohol septal ablation	10 (1.9)	2 (0.6)	1 (0.7)	7 (12.1)	<0.001[d,e]
Mitral valve replacement	10 (1.9)	6 (1.9)	3 (2.1)	1 (1.7)	0.98
Surgery	8 (1.5)	4 (1.2)	3 (2.1)	1 (1.7)	0.77
TMVR	2 (0.4)	2 (0.6)	0 (0.0)	0 (0.0)	>0.99
Device success	402 (77.2)	273 (84.8)	98 (69.5)	31 (53.4)	<0.001[c,d,e]
Post-procedural echocardiographic findings					
LVEF (%)	51.4 ± 13.7	53.3 ± 12.5	44.4 ± 14.7	58.0 ± 11.5	<0.001[c,e]
Mean gradient (mmHg)	6.1 ± 2.9	5.9 ± 2.8	6.7 ± 3.1	5.4 ± 3.1	0.019[c,e]
Mean gradient ≥10 mmHg	43 (8.3)	23 (7.1)	16 (11.3)	4 (6.9)	0.29
Mitral valve area (cm^2)	2.2 ± 1.0	2.2 ± 1.2	2.0 ± 0.6	2.6 ± 1.1	0.10
Mitral stenosis[a]	7 (1.3)	3 (0.9)	4 (2.8)	0 (0.0)	0.24
Mitral regurgitation moderate or higher after procedure	52 (10.0)	18 (5.6)	26 (18.4)	8 (13.8)	<0.001[c,e]
Mitral regurgitation moderate or higher at 30 days[b]	31 (6.6)	10 (3.3)	16 (12.6)	5 (13.2)	<0.001[c,d]
30-Day outcomes					
All-cause mortality	54 (10.4)	20 (6.2)	14 (9.9)	20 (34.5)	<0.001[d,e]
Stroke	9 (1.9)	7 (2.3)	0 (0.0)	2 (3.9)	0.10
Bleeding					
Major or extensive	20 (4.2)	14 (4.6)	5 (3.9)	1 (1.8)	0.81
Life-threatening or fatal	18 (3.7)	7 (2.3)	9 (6.7)	2 (4.5)	0.07
Major vascular complication	14 (2.8)	5 (1.6)	5 (3.8)	4 (8.0)	0.019[d]
Acute kidney injury (Stage 2 or 3)	34 (7.0)	14 (4.6)	13 (9.7)	7 (15.3)	0.006[c,d]
Procedural success	343 (65.8)	237 (73.6)	81 (57.4)	24 (41.4)	<0.001[c,d,e]

LVOT, left ventricular outflow tract; TMVR, transcatheter mitral valve replacement; ViMAC, valve in mitral annular calcification; ViR, valve in ring; ViV, valve in valve.
[a]Defined as mean gradient ≥10 mmHg and mitral valve area ≤1.0 cm^2.
[b]Four hundred and sixty-seven patients survived at 30 days were included.
[c]P < 0.05 for ViV vs. ViR.
[d]P < 0.05 for ViV vs. ViMAC.
[e]P < 0.05 for ViR vs. ViMAC.

Discussion

The major findings of the present study are as follows: (i) TMVR provided excellent outcomes for patients with degenerated bioprosthetic valves but TMVR for failed annuloplasty rings and MAC were associated with frequent procedural complications; (ii) patients with failed annuloplasty rings and severe MAC were at increased risk of mortality after TMVR; and (iii) valve thrombosis was more frequently observed after TMVR in patients without anticoagulation compared with those with anticoagulation.

The present study is the largest TMVR registry published to date demonstrating procedural challenges and prognosis across different population. TMVR provided excellent outcomes for patients with degenerated bioprosthetic valves despite high surgical risk. Procedural complications were observed in less than 3% of procedures, consistent with the previous reports.[17] The 30-day mortality after mitral ViV in the present study (6.2%) was acceptable considering the higher in-hospital and 30-day mortality after redo mitral valve surgeries (9.2–12.6%) in previously published studies.[18–20] As the present large study is consistent with recent reports with comparable early and mid-term mortality, TMVR is an attractive option for patients with degenerated bioprosthetic mitral valves.

Transcatheter mitral valve replacement for patients with failed annuloplasty repair and severe MAC poses unique and serious procedural challenges, namely LVOT obstruction and post-procedural MR. Previous studies showed that LVOT obstruction occurred more frequently after ViMAC (7.4% to 17%) and ViR (13.3% to 20%) compared with ViV and was associated with increased 1-year

Downloaded from https://academic.oup.com/eurheartj/article-abstract/40/5/441/5143983 by ST MARTIN/NA, UNIV user on 27 April 2020

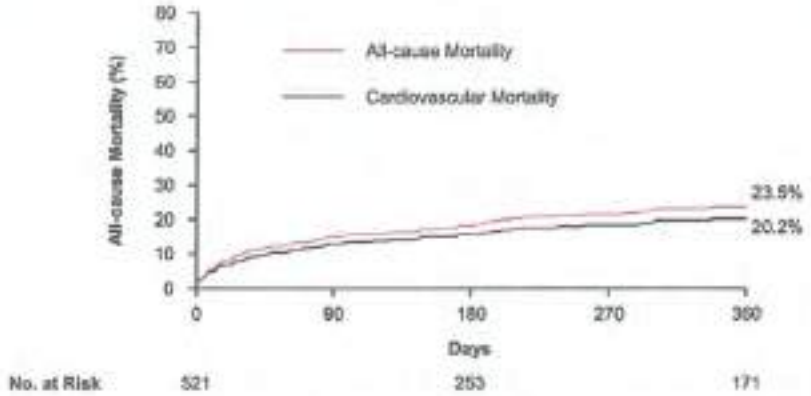

Figure 1 Cumulative incidences of all-cause and cardiovascular mortality in overall cohort. The cumulative incidences of all-cause (red line) and cardiovascular mortality (black line) of the overall cohort are shown.

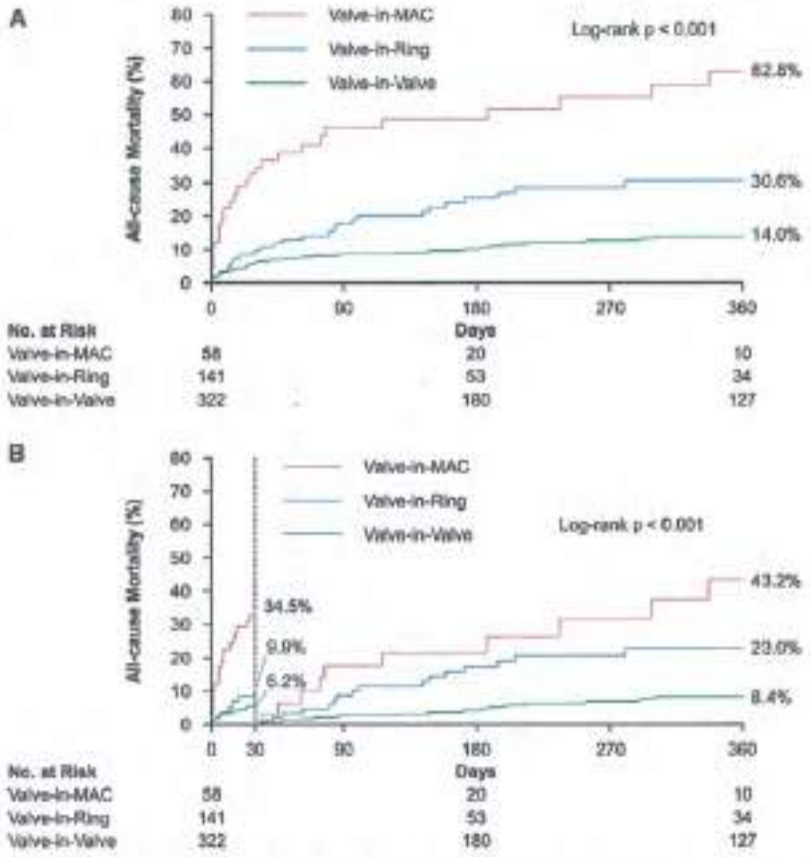

Figure 2 All-cause mortality according to transcatheter mitral valve replacement procedure. (A) The cumulative all-cause mortality rates of patients undergoing mitral valve-in-valve (green line), valve-in-ring (blue line), and valve-in-MAC (red line) are shown. (B) The cumulative all-cause mortality rates with landmark analyses (0–30 days and 30–360 days) showed increased early mortality (0–30 days) but also late mortality (30–360 days) after valve-in-MAC compared with valve-in-ring and valve-in-valve. MAC, mitral annular calcification.

Downloaded from https://academic.oup.com/eurheartj/article-abstract/40/5/441/5143583 by ST MARIANNA UNIV user on 27 April 2020

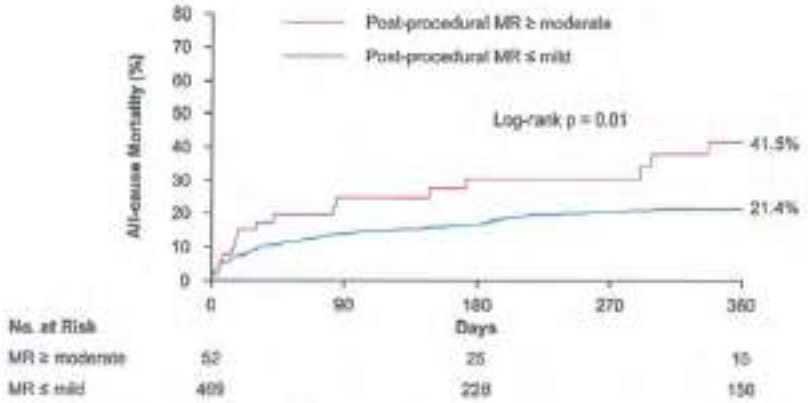

Figure 3 All-cause mortality according to post-procedural mitral regurgitation. The cumulative all-cause mortality rates in patients with moderate or greater post-procedural mitral regurgitation (red line) and those with none or mild post-procedural mitral regurgitation (blue line) are shown. MR, mitral regurgitation.

Table 4 Predictors of all-cause mortality

	Univariate model		Multivariate model	
	HR (95% CI)	*P*-value	HR (95% CI)	*P*-value
Age	1.02 (1.00–1.04)	0.015		
Female	1.09 (0.75–1.58)	0.65		
NYHA functional Class IV	1.29 (0.63–2.67)	0.48		
STS score	1.04 (1.02–1.06)	0.001	1.02 (1.01–1.06)	0.006
Peripheral vascular disease	1.39 (0.83–2.32)	0.21		
Previous cerebrovascular accident	1.07 (0.66–1.76)	0.78		
Chronic pulmonary disease	1.80 (1.25–2.61)	0.002	1.54 (1.06–2.24)	0.025
Predominant mitral regurgitation at baseline	1.26 (0.88–1.81)	0.22		
LVEF per increase of 10%	0.92 (0.80–1.05)	0.21		
Prior CABG	0.99 (0.67–1.45)	0.95		
Prior myocardial infarction	1.02 (0.62–1.69)	0.93		
Transseptal access	1.12 (0.76–1.65)	0.58		
Pre-procedural mitral valve status				
Failed annuloplasty rings vs. degenerated bioprostheses	1.96 (1.27–3.02)	0.003	1.99 (1.22–3.12)	0.003
Severe MAC vs. degenerated bioprostheses	5.85 (3.68–9.29)	<0.001	5.29 (3.29–8.51)	<0.001
Need for second valve implantation	1.21 (0.56–2.59)	0.63		
LVOT obstruction	2.87 (1.66–4.96)	<0.001		
Post-procedural mitral regurgitation moderate or greater	2.00 (1.25–3.21)	0.004	1.72 (1.06–2.81)	0.029
Mean gradient 10 mmHg or more at post-procedure	1.30 (0.71–2.35)	0.40		

CABG, coronary artery bypass graft surgery; CI, confidence interval; HR, hazard ratio; LVEF, left ventricular ejection fraction; LVOT, left ventricular outflow tract; MAC, mitral annular calcification; NYHA, New York Heart Association; STS, society of thoracic surgeons.

mortality.[7,21,22] Therefore, identifying patients at high risk for LVOT obstruction is essential for successful VMAC and VIR procedures. The incidence of LVOT obstruction was surprisingly high in the present study (39.7%), which may be attributable to the following (i) inconsistent assessment of risk for LVOT obstruction with imaging modalities, particularly in the early experiences and (ii) variable definitions of LVOT obstruction between the studies. Left ventricular outflow tract obstruction was defined according to MVARC (increment in mean gradient ≥10 mmHg from baseline) in the present study but defined as LVOT obstruction with hemodynamic compromise in recently reported studies.[7,22] A comprehensive analysis of mitral valve and left ventricular anatomy to predict LVOT

Downloaded from https://academic.oup.com/eurheartj/article-abstract/40/5/441/5143083 by ST MARIANNA UNIV user on 27 April 2020

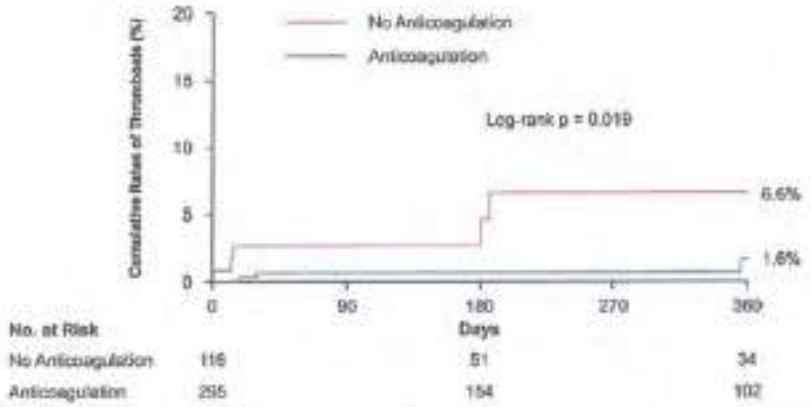

Figure 4 Incidences of valve thrombosis. The cumulative rates of valve thrombosis in patients with or without anticoagulation (blue and red lines, respectively) are shown.

obstruction is essential for optimal TMVR patient selection. Furthermore, prophylactic alcohol septal ablation and laceration of mitral anterior leaflet have recently emerges as option to prevent TMVR associated LVOT obstruction and promise to mitigate this important complications.[23,24]

The impact of significant residual MR on increased mortality and late adverse events has been widely recognized in patients undergoing surgical or transcatheter mitral valve repair.[25,26] The present study identified significant post-procedural MR as an independent predictor of increased mortality after TMVR. The rates of MR ≥moderate after ViR (18.4%) and VIMAC (13.8%) were suboptimal although post-procedural MR ≥Grade 3 (moderate to severe) was modest (4.2% and 1.7%, respectively). The present study demonstrated improved major clinical outcomes with increased experience, but no significant improvements in LVOT obstruction and post-procedural MR were observed in the late experience group. Further clinical experience, better patient selection and advancement in device technology promise to improve TMVR outcomes.

Increased mid-term mortality after ViR in the present study may be affected by frequent procedural complications as well as underlying mitral valve disease. Patients treated with ViR had more frequent prior CABG and myocardial infarction with lower LVEF, suggesting higher proportion of functional MR as the underlying aetiology of mitral valve disease. Since recurrence of MR after mitral valve repair was associated with increased long-term mortality, the potential benefit of ViR for severe MR may be confounded by advanced age, cardiac and non-cardiac comorbidities.[35,37] The 30-day mortality in the present study (9.9%) was comparable to those after ViR from reported studies (6.7–11.4%),[32,38] as well as those after redo mitral valve repair (9.0% and 9.2%).[19,29] Nevertheless, relatively high rates of 1-year mortality after ViR in the present study (30.6%) should be cautiously interpreted. Recent study reported that the 1-year mortality rate after mitral valve reoperation of 23.1%, mainly related to high in-hospital mortality (12.6%).[30] Although direct comparison is difficult, landmark analysis in the present study showed higher late mortality after ViR (23.0%), suggesting the adverse impact of post-procedural MR in this population.

Patients with MAC associated with mitral valve disease experienced surprisingly higher early and mid-term mortality after TMVR (34.5% and 62.8%, respectively). Notably, these mortality rates were comparable to those reported recently by Guerrero et al.[7] (25.0% and 53.7%). As LVOT obstruction and post-procedural MR contribute to the increased mortality, every effort should be made to predict and prevent these serious complications with dedicated imaging analysis. Given high late mortality (43.2%) shown by landmark analysis in patients with MAC, appropriate patient selection is essential to avoid futile TMVR procedures.

Bioprosthetic valve thrombosis is a multifactorial phenomenon affected by anatomic, procedural, and pharmacological factors.[30] The risk of valve thrombosis is higher in the mitral position than the aortic position, highest in the first few months after implantation, and may continue thereafter. In the present study, the majority of thrombosis (90.9%) was observed after mitral ViV. Interestingly, the valve thrombosis was more frequently observed in previous porcine valves (nine patients) compared with pericardial valves (one patient), consistent with previous surgical aortic valve replacement and aortic valve-in-valve publications.[31,32] The lower rate of thrombosis in patients with anticoagulation compared with those without anticoagulation suggests that anticoagulant thromboprophylaxis may be beneficial, particularly for the first few months after TMVR procedures. Considering the wide-ranged timeframe of thrombosis after TMVR, serial echocardiographic follow-up, while balancing individual thromboembolic and haemorrhage risks may guide decisions regarding the extension of anticoagulation until future studies clarify the optimal thromboprophylaxis after TMVR.

Study limitations

This study had the inherent limitations of an observational study without centre-independent adjudication of adverse events. Our findings are subject to potential selection bias and confounding factors including differences in baseline characteristics across the groups. Despite adjustment with available covariates, the residual confounding factors might account for biased outcomes. Several variables that are known to affect the outcomes such as anaemia

Downloaded from https://academic.oup.com/eurheartj/article-abstract/46/5/441/5143583 by ST MARIANNA UNIV user on 27 April 2020

or frailty were not available in the present study. The cumulative rates of cardiovascular mortality and nonfatal outcomes might be overestimated by competing risk of non-cardiovascular and all-cause mortality, respectively. Finally, selections of device type and access site were determined at each institution and may have affected the observed outcomes.

Conclusions

The TMVR provided excellent outcomes for patients with degenerated bioprostheses despite high surgical risk. However, VIR and VIMAC were associated with higher rates of adverse events and mid-term mortality compared with VIV.

Supplementary material

Supplementary material is available at *European Heart Journal* online.

Conflict of interest: The department of Cardiology of the Leiden University Medical Center received unrestricted research grants from Edwards Lifesciences, Biotronik, Medtronic and Boston Scientific. B.K.W. has served as a consultant for Edwards Lifesciences and Boston Scientific. S.B. has serves as a consultant to Medtronic and as a proctor for JenaValve, Highlife, and Boston Scientific. V.D. has received speaking fees from Abbott Vascular. A.D. has served as a proctor and consultant for Abbott Vascular, Edward Lifesciences, and Keystone Heart; physician review Committee for Keystone Heart REFLECT Trial. N.S. received travel compensation from Edwards Lifesciences and St. Jude Medical, as well as speaker honoraria and travel compensation from Boston Scientific. T.S. has received speaker honoraria and travel grants from Edwards and Medtronic, as well as travel grants from Boston Scientific. W.-K.K. has served as proctors for Symmetis and St. Jude Medical. A.U. and J.K. have served as proctors for Abbott, Boston Scientific, Edwards Lifesciences, and Medtronic. G.H.L.T. has served as a proctor for Edwards Lifesciences. C.M.B. is on the Advisory Board of Medtronic and Boston Scientific and on the Speakers' Bureau of Abbott Vascular. J.E.D. has served as a consultant for Edwards and the Medtronic advisory board. A.L. has received a consulting fees from P&F. L.N.-F. has served as a proctor for Abbott Vascular and has received speaking fees from Edwards Lifesciences. J.-B.M. has served as a consultant for Edwards Lifesciences. F.D. has served as a proctor and consultant for Edwards Lifesciences and Neovasc and received a travel grant from Abbott, Boston Scientific, Edwards Lifesciences, and Neovasc, and participated in clinical trials (TIARA II CE Mark trial and TENDYNE CE Mark trial). H.C.W. has received research grants from Edwards Lifesciences and Medtronic. H.S. has received study honoraria, travel expenses, and consulting fees from 4tech Cardio, Abbott Vascular, Ablative Solutions, Ancora Heart, Bavaria Medizin Technologie GmbH, Bioventrix, Boston Scientific, Carag, Celonova, Cibiem, Comed B.V., CVRx, Edwards Lifesciences, Endologix, Hemoteq, Lifetech, Maquet Getinge Group, Medtronic, Mitralign, Nuomao Medtech, Occlutech, pfm Medical, Renal Guard, Rox Medical, Vascular Dynamics, and Vivasure Medical. D.J.B. and D.H.-S. have served as a proctor for Medtronic and Boston Scientific. F.S.B.Jr has served as proctor for Edwards Lifesciences and Medtronic. T.C. has received research support from Edwards Lifesciences. S.R. and B.D.P. have received speaker fees from Edwards Lifescience, Boston Scientific and Symetis. M.A. has received travel compensation from Edwards Lifesciences, served as a proctor for Edwards Lifesciences, and a proctor and consultant for St. Jude Medical and received speaker honoraria from JenaValve. A.M.K. has served as a consultant and proctor for Edwards Lifesciences and received research support from Edwards Lifesciences. F.M. has served as a consultant for Edwards Lifesciences, Medtronic, St. Jude Medical, Abbott Vascular, and Veltech and has received royalties from Edwards Lifesciences. H.L.T. has served as a proctor and consultant for Edwards Lifesciences. S.M.E. has served as a proctor for JenaValve, received speaker Honoria from Edwards Lifesciences, JenaValve, and Symetis, and received travel compensation from Edwards Lifesciences, JenaValve, and Symetis. S.K. has received research grants and consulting fees from Abbott Vascular and St. Jude Medical. T.K. has served as a proctor and speaker for Edwards Lifescience, Abbott and Medtronic. T.P. has received research grants to the institution from Edwards Lifesciences, Boston Scientific, and Biotronik, and has received speaker fees from Boston Scientific and Biotronik. P.S. has served as a consultant for Abbott Vascular, Medtronic, Boston Scientific, and Integer and has received research grants and speakers fee from Abbott Vascular, Medtronic, Boston Scientific, and Integer. V.B. has served as a consultant for Edwards Lifesciences, Medtronic, Abbott Vascular, Boston Scientific, and 4tech. T.M. has served as a consultant for Boston Scientific. C.F. has received speaker honoraria and travel grants from Edwards Lifesciences, Medtronic and Abbott Vascular. G.F.A. has served as a proctor for Edwards Lifesciences and Medtronic, on the speaker Bureau for Medtronic and Abbott Vascular, and as a consultant to St. Jude Medical. A.L. has served as a consultant for Medtronic, Abbott Vascular and Edwards Lifesciences. U.S. has served as a proctor and consultant for Edwards Lifesciences, Jena Valve Technology, Boston Scientific, St. Jude Medical, Medtronic, Biotronik and has received travel support and speakers honoraria from Edwards Lifesciences, Jena Valve Technology, Boston Scientific, St. Jude Medical, Medtronic, Biotronik, Direct Flow Medical. J.G.W. has served as a consultant to and received research funding from Edwards Lifesciences. R.R.M. has received grants from Edwards Lifesciences and personal fees from St. Jude Medical and Medtronic. R.W.S. has received consulting fees and research support from Abbott Vascular and Edwards Lifesciences. All other authors declared no conflict of interest.

References

1. Nkomo VT, Gardin JM, Skelton TN, Gottdiener JS, Scott CG, Enriquez-Sarano M. Burden of valvular heart diseases: a population-based study. Lancet 2006;**368**:1005–1011.
2. O'Gara PT, Grayburn PA, Badhwar V, Afonso LC, Carroll JD, Elmariah S, Kithcart AP, Nishimura RA, Ryan TJ, Schwartz A, Stevenson LW. 2017 ACC Expert Consensus Decision Pathway on the management of mitral regurgitation: a report of the American College of Cardiology Task Force on Expert Consensus Decision Pathways. *J Am Coll Cardiol* 2017;**70**:2421–2449.
3. Goldstone AB, Chiu P, Baiocchi M, Lingala B, Patrick WL, Fischbein MP, Woo YJ. Mechanical or biologic prostheses for aortic-valve and mitral-valve replacement. *N Engl J Med* 2017;**377**:1847–1857.
4. Goldstein D, Moskowitz AJ, Gelijns AC, Ailawadi G, Parides MK, Perrault LP, Hung JW, Voisine P, Dagenais F, Gillinov AM, Thourani V, Argenziano M, Gammie JS, Mack M, Demers P, Adams P, Rose EA, O'Sullivan K, Williams DL, Bagiella E, Michler RE, Weisel RD, Miller MA, Geller NL, Taddei-Peters WC, Smith PK, Moquete E, Overbey JR, Kron IL, O'Gara PT, Acker MA; CTSN. Two-

Downloaded from https://academic.oup.com/eurheartj/article-abstract/40/5/441/5143983 by ST MARIANNA UNIV user on 27 April 2020

year outcomes of surgical treatment of severe ischemic mitral regurgitation. *N Engl J Med* 2016;**374**:344–353.
5. Papadopoulos N, Dietrich M, Christodoulou T, Moritz A, Doss M. Mitraclip survival after decalcification of the mitral annulus. *Ann Thorac Surg* 2009;**87**: 1143–1147.
6. Yoon SH, Whisenant BK, Bleiziffer S, Delgado V, Schofer N, Eschenbach L, Fujita B, Sharma R, Ancona M, Yzeiraj E, Cannata S, Barker C, Davies JE, Frangieh AH, Deuschl F, Podlesnikar T, Asami M, Dhoble A, Chyou A, Masson JB, Wijeysundera HC, Blackman DJ, Rampat R, Taramasso M, Gutierrez-Ibanes E, Chakravarty T, Attizzani GF, Kaneko T, Wong SC, Sievert H, Nietlispach F, Hildick-Smith D, Nombela-Franco L, Conrad L, Hengstenberg C, Reardon MJ, Kasel AM, Redwood S, Colombo A, Kar S, Maisano F, Windecker S, Pilgrim T, Eminiger SM, Prendergast BD, Scholer J, Schaefer U, Bax J, Latib A, Makkar RR. Transcatheter mitral valve replacement for degenerated bioprosthetic valves and failed annuloplasty rings. *J Am Coll Cardiol* 2017;**70**:1121–1131.
7. Guerrero M, Urena M, Himbert D, Wang DD, Eleid M, Kodali S, George I, Chakravarty T, Mathur M, Holzhey D, Pershad A, Fang HK, O'Hair D, Jones N, Mahadevan VS, Dumontell N, Rodes-Cabau J, Piazza N, Ferrari E, Ciaburri D, Nejari M, DeLago A, Sonoja P, Zahr F, Rajagopal V, Whisenant B, Shah PB, Sinning JM, Witkowski A, Eltchaninoff H, Dvir D, Martin B, Attizzani GF, Gaia D, Nunes NSV, Fassa AA, Kerendi F, Pavlides G, Iyer V, Kaddissi G, Witzke C, Wudel J, Michel G, Rayburn B, Wang C, Waloman R, Palacios I, Cribier A, Webb J, Bapat V, Reisman M, Makkar R, Leon M, Rihal C, Vahanian A, O'Neill W, Feldman T. 1-Year outcomes of transcatheter mitral valve replacement in patients with severe mitral annular calcification. *J Am Coll Cardiol* 2018;**71**: 1841–1853.
8. Bapat V, Mydin I, Chudalavada S, Tehrani H, Attia R, Thomas M. A guide to fluoroscopic identification and design of bioprosthetic valves: a reference for valve-in-valve procedure. *Catheter Cardiovasc Interv* 2013;**81**:853–861.
9. Hamid NB, Khalique OK, Monaghan MJ, Kodali SK, Dvir D, Bapat VN, Nazif TM, Vahl T, George I, Leon MB, Hahn RT. Transcatheter valve implantation in failed surgically inserted bioprosthesis: review and practical guide to echocardiographic imaging in valve-in-valve procedures. *JACC Cardiovasc Imaging* 2015;**8**:960–979.
10. Cheung A, Webb JG, Barbanti M, Freeman M, Binder RK, Thompson C, Wood DA, Ye J. 5-Year experience with transcatheter transapical mitral valve-in-valve implantation for bioprosthetic valve dysfunction. *J Am Coll Cardiol* 2013;**61**: 1759–1766.
11. Webb JG, Pasupati S, Humphries K, Thompson C, Altwegg L, Moss R, Sinhal A, Carere RG, Munt B, Ricci D, Ye J, Cheung A, Lichtenstein SV. Percutaneous transarterial aortic valve replacement in selected high-risk patients with aortic stenosis. *Circulation* 2007;**116**:755–763.
12. Ye J, Cheung A, Lichtenstein SV, Altwegg LA, Wong DR, Carere RG, Thompson CR, Moss RR, Munt B, Pasupati S, Boone RH, Masson JB, Al Ali A, Webb JG. Transapical transcatheter aortic valve implantation: 1-year outcome in 26 patients. *J Thorac Cardiovasc Surg* 2009;**137**:167–173.
13. Meredith Am IT, Walters DL, Dumontell N, Worthley SG, Tchetche D, Manoharan G, Bladonan DJ, Rioufol G, Hildick-Smith D, Whitbourn RJ, Lefevre T, Lange R, Muller R, Redwood S, Allocco DJ, Dawkins KD. Transcatheter aortic valve replacement for severe symptomatic aortic stenosis using a repositionable valve system: 30-day primary endpoint results from the REPRISE II study. *J Am Coll Cardiol* 2014;**64**:1339–1348.
14. Zahn EM, Hellenbrand WE, Lock JE, McElhinney DB. Implantation of the melody transcatheter pulmonary valve in patients with a dysfunctional right ventricular outflow tract conduit: early results from the U.S. Clinical trial. *J Am Coll Cardiol* 2009;**54**:1722–1729.
15. Schofer J, Colombo A, Klugmann S, Fajadet J, DeMarco F, Tchetche D, Maisano F, Bruschi G, Latib A, Bijukic K, Weissman N, Low R, Thomas M, Young C, Redwood S, Mullen M, Yap J, Grube E, Nickenig G, Sinning JM, Hauptmann KE, Friedrich I, Lauterbach M, Schmoeckel M, Davidson C, Lefevre T. Prospective multicenter evaluation of the direct flow medical transcatheter aortic valve. *J Am Coll Cardiol* 2014;**63**:763–768.
16. Stone GW, Adams DH, Abraham WT, Kappetein AP, Genereux P, Vranckx P, Mehran R, Kuck KH, Leon MB, Piazza N, Head SJ, Filippatos G, Vahanian AS; Mitral Valve Academic Research Consortium. Clinical trial design principles and endpoint definitions for transcatheter mitral valve repair and replacement: part 2: endpoint definitions: a consensus document from the Mitral Valve Academic Research Consortium. *Eur Heart J* 2015;**36**:1878–1891.
17. Eleid MF, Cabalka AK, Williams MR, Whisenant BK, Alli OO, Fam N, Pollak PM, Barnow E, Malouf JF, Nishimura RA, Joyce LD, Dearani JA, Rihal CS. Percutaneous transvenous transseptal transcatheter valve implantation in failed bioprosthetic mitral valves, ring annuloplasty, and severe mitral annular calcification. *JACC Cardiovasc Interv* 2016;**9**:1161–1174.
18. Mehaffey HJ, Hawkins RB, Schubert S, Fonner C, Yarbono LT, Quader M, Spelr A, Rich J, Kron IL, Allawadi G. Contemporary outcomes in reoperative mitral valve surgery. *Heart* 2018;**104**:652–656.
19. Onorati F, Mariscalco G, Reichart D, Perrotti A, Gatti G, De Feo M, Rubino A, Santarpino G, Biancari F, Detter C, Santini F, Faggian G. Hospital outcome and risk indices of mortality after redo-mitral valve surgery in potential candidates for transcatheter procedures: results from a European Registry. *J Cardiothorac Vasc Anesth* 2018;**32**:646–653.
20. Kiwedar K, McNeely C, Zajarias A, Markwell S, Vassileva CM. Outcomes of early mitral valve recoperation in the medicare population. *Ann Thorac Surg* 2017;**104**: 1516–1521.
21. Eleid MF, Whisenant BK, Cabalka AK, Williams MR, Nejjari M, Atkins D, Fam N, Amoroso N, Foley TA, Pollak PM, Alli OO, Pislaru SV, Said SM, Dearani JA, Rihal CS. Early outcomes of percutaneous transvenous transseptal transcatheter valve implantation in failed bioprosthetic mitral valves, ring annuloplasty, and severe mitral annular calcification. *JACC Cardiovasc Interv* 2017;**10**:1933–1942.
22. Urena M, Brochet E, Laconte M, Kornels C, Carrasco JL, Ghodbane W, Abtan J, Alkhoder S, Rafiqui R, Iung B, Nataf P, Vahanian A, Himbert D. Clinical and haemodynamic outcomes of balloon-expandable transcatheter mitral valve implantation: a 7-year experience. *Eur Heart J* 2018;**39**:2679–2689.
23. Babaliaros VC, Greenbaum AB, Khan JM, Rogers T, Wang DD, Eng MH, O'Neill WW, Paone G, Thourani VH, Lerakis S, Kim DW, Chen MY, Lederman RJ. Intentional percutaneous laceration of the anterior mitral leaflet to prevent outflow obstruction during transcatheter mitral valve replacement: first-in-human experience. *JACC Cardiovasc Interv* 2017;**10**:798–809.
24. Guerrero M, Wang DD, Himbert D, Urena M, Punnam A, Kaddissi G, Iyer V, Salinger M, Chakravarty T, Greenbaum A, Makkar R, Vahanian A, Feldman T, O'Neill W. Short-term results of alcohol septal ablation as a bail-out strategy to treat severe left ventricular outflow tract obstruction after transcatheter mitral valve replacement in patients with severe mitral annular calcification. *Catheter Cardiovasc Interv* 2017;**90**:1220–1226.
25. Suri RM, Clavel MA, Schaff HV, Michelena HI, Huebner M, Nishimura RA, Enriquez-Sarano M. Effect of recurrent mitral regurgitation following degenerative mitral valve repair: long-term analysis of competing outcomes. *J Am Coll Cardiol* 2016;**67**:488–498.
26. Sonoja P, Vemulapalli S, Feldman T, Mack M, Holmes DR Jr, Stebbins A, Kar S, Thourani V, Allawadi G. Outcomes with transcatheter mitral valve repair in the United States: an STS/ACC TVT Registry Report. *J Am Coll Cardiol* 2017;**70**:2315–2327.
27. Michler RE, Smith PK, Parides MK, Allawadi G, Thourani V, Moskowitz AJ, Acker MA, Hung JW, Chang HL, Perrault LP, Gillinov AM, Argenziano M, Bagiella E, Overbey JR, Moquete EG, Gupta LN, Miller MA, Taddei-Peters WC, Jeffries N, Wolad RD, Rose EA, Gammie JS, DeRose JJ, Puskas JD, Dagenais F, Burks SG, El-Hamamsy I, Milano CA, Ailawi P, Voisine P, O'Gara PT, Geltjes AC. Two-year outcomes of surgical treatment of moderate ischemic mitral regurgitation. *N Engl J Med* 2016;**374**:1932–1941.
28. Paradis J-M, Del Trigo M, Puri R, Rodés-Cabau J. Transcatheter valve-in-valve and valve-in-ring for treating aortic and mitral surgical prosthetic dysfunction. *J Am Coll Cardiol* 2015;**66**:2019–2037.
29. Aphram G, De Kerchove L, Mastrobuoni S, Navarra E, Solari S, Tamer S, Baert J, Poncelet A, Rubay J, Astarci P, Noirhomme P, El Khoury G. Re-repair of the failed mitral valve: insights into aetiology and surgical management. *Eur J Cardiothorac Surg* 2018; doi:10.1093/ejcts/ezy111.
30. Dangas GD, Weitz JI, Giustino G, Makkar R, Mehran R. Prosthetic heart valve thrombosis. *J Am Coll Cardiol* 2016;**68**:2670–2689.
31. Brown ML, Park SJ, Sundt TM, Schaff HV. Early thrombosis risk in patients with biologic valves in the aortic position. *J Thorac Cardiovasc Surg* 2012;**144**: 108–111.
32. Jose J, Sulimov DS, El-Mawardy M, Sato T, Allali A, Holy EW, Becker B, Lanck M, Kobernik J, Schwarz B, Richardt G, Abdel-Wahab M. Clinical bioprosthetic heart valve thrombosis after transcatheter aortic valve replacement: incidence, characteristics, and treatment outcomes. *JACC Cardiovasc Interv* 2017;**10**: 686–697.

Downloaded from https://academic.oup.com/eurheartj/article-abstract/40/5/441/5143993 by ST MARIANNA UNIV user on 27 April 2020

J. Clin. Physiol., Vol. 49, No. 1, 2019.

Original Article

Long-term Effects and Prognosis in Heart Failure Patients Receiving Tolvaptan after Discharge

Chikayuki ITO,[*1] Keisuke KIDA,[*1] Norio SUZUKI,[*2] Ryo KAMIJIMA,[*3] Takeru NABETA,[*4] Hideyuki MAEZAWA,[*5] Shiro ISHIHARA,[*6] Toshitaka OKABE,[*7] Tae ISHIKAWA[*8] and Yoshihiro J AKASHI[*1]

ABSTRACT

Background: The short-term clinical effects of Tolvaptan (TLV) in patients hospitalized for heart failure (HF) are well known. Only a few of studies have investigated its long-term efficacy and safety in HF outpatients after discharge, however. The purpose of this study was to investigate the long-term effects, prognosis, and safety of TLV in HF outpatients after discharge.

Methods: A total of 167 HF patients admitted to 8 hospitals in Kanagawa, Japan, between January 2013 and August 2015 were enrolled in the study. All were treated with TLV, even after discharge. The rates of continued administration of TLV, prognosis, and safety at 6 months were retrospectively evaluated.

Results: A total of 121 patients continued to take TLV for 6 months after discharge (Treatment Continued group); 24 did not require TLV therapy due to HF stabilization (Treatment Unnecessary group); and 22 discontinued TLV therapy (Treatment Discontinued group). A comparison of patient backgrounds at discharge among these groups revealed significant differences in history of hospitalization due to HF exacerbation, B-type natriuretic peptide level, and dose of furosemide. A significant number of events were observed in the Treatment Discontinued group ($p < 0.001$), most of which occurred within 30 days after discharge. In this group, 55% of the patients were readmitted within 30 days after discharge.

[*1] Division of Cardiology, Department of Internal Medicine, St. Marianna University School of Medicine
[*2] Division of Cardiology, Department of Internal Medicine, St. Marianna University School of Medicine Yokohama City Seihu Hospital
[*3] Division of Cardiology, Department of Internal Medicine, Kawasaki Municipal Tama Hospital
[*4] Department of Cardiovascular Medicine, Kitasato University School of Medicine
[*5] Division of Cardiology, Department of Internal Medicine, Showa University Fujigaoka Hospital
[*6] Division of Cardiology, Department of Internal Medicine, Nippon Medical School Musashi-Kosugi Hospital
[*7] Division of Cardiology and Cardiac Catheterization Laboratories, Showa University Northern Yokohama Hospital
[*8] Division of Cardiology, Department of Internal Medicine, Shinyurigaoka General Hospital
(Received September 3, 2018)

Presented by Medical*Online

Conclusions: The present results showing that it is possible to identify the effects of TLV in HF outpatients within 30 days after discharge suggest that long-term administration of this drug is relatively safe.

INTRODUCTION

Heart failure (HF) is a disease that gradually progresses with repeated exacerbation and remission. The current trend toward an increase in the number of patients with HF is a matter of concern. Repeated hospitalization has been reported to indicate a poor prognosis,[1] suggesting that preventing readmission is important in improving the outlook in such patients. The readmission rates of HF patients within 30 days after discharge are reported to be 11% to 32% in the U.S. and EU[2-6] and <10% in Japan.[3,6] The education and comprehensive management of HF patients by a dedicated multidisciplinary team has been shown to significantly reduce readmission rates, however.[7,8]

Tolvaptan (TLV), a newly developed diuretic agent, selectively inhibits reabsorption of water. One large-scale clinical study, the Efficacy of Vasopressin Antagonism in hEart failuRE Outcome Study With Tolvaptan (EVEREST), demonstrated that TLV, initiated for acute treatment of patients hospitalized with HF, had no effect on long-term mortality or HF-related morbidity.[9] A meta-analysis revealed no improvement in survival rates or cardiovascular events in HF patients treated with TLV.[10] Meanwhile, TLV was reported to reduce readmission in patients with renal failure[11] and improve long-term outcomes, including in survival and readmission rates, in those with a serum sodium level of <130 mEq/L.[12] One study demonstrated that HF outpatients treated with TLV tended to have a longer duration until re-hospitalization compared to those treated with furosemide.[13] Heart failure can be stabilized in the short-term in some cases. Therefore, it is difficult to determine which patients will require long-term TLV therapy. The purpose of the present study was to investigate the long-term effects, prognosis, and safety of TLV in HF outpatients after discharge.

METHODS

Patients

A total of 167 patients admitted to 8 hospitals in Kanagawa, Japan, between January 2013 and August 2015 were enrolled in this retrospective study. All were diagnosed with HF according to the Framingham criteria (age ≥ 20 years) and treated with TLV, even after discharge. The rates of continued administration of TLV and prognosis at 6 months after discharge were evaluated. Patients who took TLV only occasionally were excluded from the study population. The patients were divided into the following 3 groups: a Treatment Continued group, comprising patients still receiving TLV at 6 months after discharge; a Treatment Unnecessary group, comprising patients in whom TLV therapy was terminated due to HF stabilization; and a Treatment Discontinued group, in whom TLV therapy was terminated due to readmission owing to exacerbation of HF or death.

Data collection

Patient data were obtained from clinical records. They included the date of admission or discharge; the number of HF hospitalizations since the first HF event; the primary cause of HF; the presence or absence of risk factors or complications; prescriptions at discharge; and the use of pacemakers or cardiac resynchronization therapy devices. Systolic and diastolic blood pressure, pulse, heart rate, weight, and hematological findings at discharge and at 3 and 6 months later were analyzed. All patients underwent echocardiography for assessment of cardiac function at discharge and again at 6 months later. Furosemide 40 mg was considered equivalent to azosemide 60 mg or torasemide 8 mg based on the results of an earlier study.[14]

Outcomes

Outcomes were assessed based on all-cause mortality within 30, 90, and 180 days after discharge; and the readmission rates due to HF within 30, 90, and 180 days

Presented by Medical*Online

Table 1 Patient characteristics at discharge.

Male, n (%)	101 (60.5)
Age (years)	73.4 ± 11.8
Body mass index (kg/m^2)	21.4 ± 3.7
Systolic blood pressure (mmHg)	106.5 ± 18.4
Heart rate (bpm)	70.5 ± 11.8
Previous HF admission, n (%)	103 (61.7)
Number of HF admission, n	2.8 ± 2.5
Etiology of HF, n (%)	
Ischemic heart disease	41 (24.6)
Cardiomyopathy	30 (18.0)
Structural heart disease	35 (21.0)
Constrictive pericarditis	7 (4.2)
Postoperative heart disease	25 (14.9)
Other	29 (17.3)
Hypertension, n (%)	91 (54.5)
Diabetes mellitus, n (%)	63 (37.7)
Chronic kidney disease, n (%)	123 (73.7)
Atrial fibrillation, n (%)	45 (26.9)
Pacemaker, n (%)	17 (10.2)
ICD, n (%)	2 (1.2)
CRT, n (%)	20 (12.0)
Hemoglobin (g/dL)	11.0 ± 2.0
Serum albumin (g/dL)	3.5 ± 0.5
Total bilirubin (mg/dL)	0.9 ± 0.5
Serum creatinine (mg/dL)	1.64 ± 1.01
eGFR (mL/min/1.73 m^2)	33.3 ± 18.9
Blood urea nitrogen (mg/dL)	33.6 ± 17.9
Serum sodium (mEq/L)	138.6 ± 4.1
Serum uric acid (mg/dL)	6.9 ± 2.0
BNP (pg/mL) median (IQR)	345.5 (161.8–990.8)
EF (%)	46.4 ± 16.5
EF ≧ 50 (%)	65 (42.5)
50 > EF ≧ 40 (%)	20 (13.1)
EF < 40 (%)	68 (44.4)
TRPG (mmHg)	37.0 ± 17.9
IVC (mm)	20.5 ± 6.2
Medications, n (%)	
ACE-I or ARB	125 (74.9)
β-blocker	108 (64.7)
MRA	109 (65.3)
Loop diuretic	159 (95.2)
Furosemide (mg/day)	40.2 ± 27.7
Tolvaptan (mg/day)	8.8 ± 5.4

HF: heart failure, ICD: implantable cardioverter defibrillator, CRT: cardiac resynchronization therapy, GFR: glomerular filtration rate, BNP: brain natriuretic peptide, EF: ejection fraction, TRPG: tricuspid regurgitation pressure gradient, IVC: inferior vena cava, ACE-I: angiotensin-converting enzyme inhibitor, ARB: angiotensin-II receptor blocker, MRA: mineralocorticoid receptor antagonist.

after discharge.

Follow-up prognosis

All patients were followed up at each hospital. Data from clinical records, including on the presence or absence of all-cause mortality or readmission and the date of event occurrence and its trigger, were assessed in patients regularly visiting the primary care provider. Patients who terminated their visits were excluded from the analysis. Tolvaptan intake, the reason for its discontinuation, and the duration of TLV therapy were also investigated.

Statistical analysis

All measurements are indicated as the mean ± standard deviation. Kaplan-Meier analysis was employed for assessment of treatment methods. The log-rank test was used to analyze survival rates. The Wilcoxon rank-sum test was used to compare categorical variables. A p value of less than 0.05 was considered to indicate statistical significance.

Ethics

The present study was performed in accordance with the ethical principles set forth in the Declaration of Helsinki. The study protocol was reviewed and approved by the Institutional Review Board of St. Marianna University School of Medicine (No. 3280). It was then implemented in compliance with the Personal Information Protection Law. While details of the treatment methods used in clinical practice were investigated, the relevant data were insufficient for any patient to be identified. Thus, written informed consent was not obtained from the study patients. The information concerning the present study protocol was released on the homepage of each hospital concerned to provide an opportunity for the study patients to refuse participation.

RESULTS

Patient characteristics at discharge

The patient characteristics at discharge are summarized in Table 1. Overall, a total of 167 patients treated with TLV at discharge were enrolled. The average patient age was 73.4 ± 11.8 years, and 60.5% of the patients were male. The average number of admissions in each patient due to HF was 2.8 ± 2.5, and 61.7% of them had a history of prior hospitalization due to HF.

Presented by Medical*Online

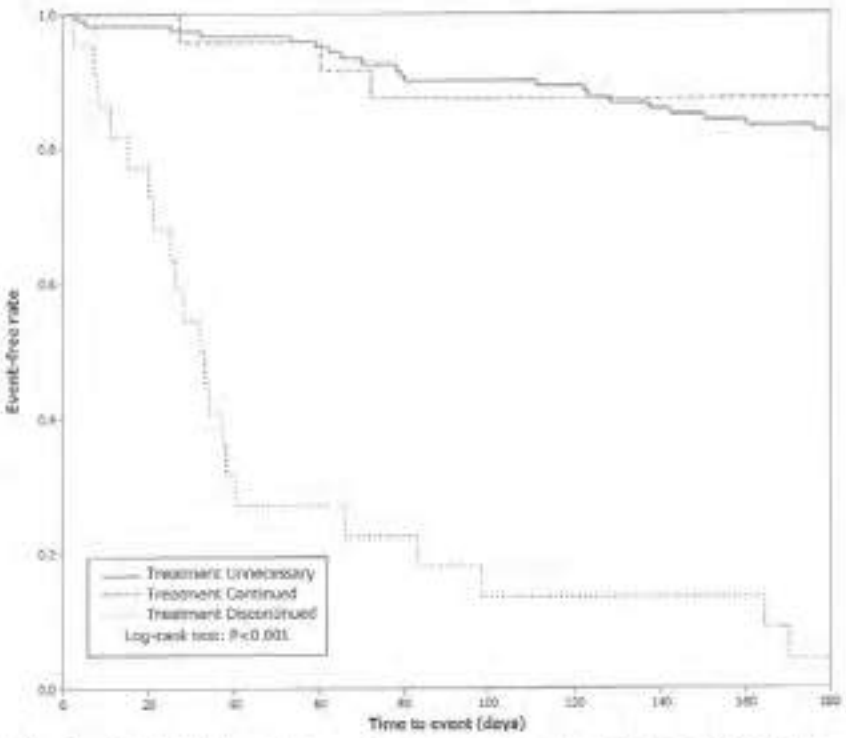

Fig. 1 Kaplan-Meier estimates of event-free rates among 3 groups at discharge.

The etiologies of HF comprised ischemic heart disease (24.6%), structural heart disease (21.0%), and cardiomyopathy (18.0%). Kidney dysfunction was observed in 73.7% of the patients, and the average serum creatinine level was 1.64 ± 1.01 mg/dL. The median B-type natriuretic peptide (BNP) level was 345.5 pg/mL (interquartile range, 161.8, 990.8). The mean left ventricular ejection fraction (EF) was 46.4 ± 16.5%. A preserved EF of > 50% was observed in 42.5% of patients, and a reduced EF of < 40% in 44.4%. At discharge, angiotensin-converting enzyme inhibitors or angiotensin-receptor blockers, β-blockers, and mineralocorticoid-receptor antagonists were prescribed to 74.9%, 64.7%, and 65.3% of the patients, respectively. Loop diuretics were prescribed for 95.2% of the patients, and the average dose of furosemide was 40.2 ± 27.7 mg at discharge. The TLV dose at discharge was 8.8 ± 5.4 mg.

Clinical outcome in patients during 6-month follow-up

Of the total number of 167 patients, 121 outpatients continued to take TLV for 6 months after discharge (Treatment Continued group); TLV therapy was terminated in 24 patients due to HF stabilization (Treatment Unnecessary group); and 22 patients discontinued TLV therapy (Treatment Discontinued group). Twenty-one patients in the Treatment Continued group and 4 patients in the Treatment Unnecessary group were readmitted. In the Treatment Discontinued group, 13 patients were readmitted, 8 patients died, only 1 patient suffered from liver dysfunction, and no patient presented with hypernatremia or dehydration requiring termination of TLV therapy during the study period.

Figure 1 shows the Kaplan-Meier estimates of event-free rates for 6 months after discharge each group. A significant number of events was observed in the Treatment Discontinued group ($p < 0.001$), most of which occurred within 30 days after discharge. In this group, 55% of the patients were readmitted within 30 days after discharge.

Table 2 shows the numbers of patients who were readmitted and/or died at 30, 90, or 180 days after discharge. The readmission rate within 30 days after discharge was 6%. A comparison of patient backgrounds at discharge among the 3 groups revealed significant

Presented by Medical*Online

Table 2 Accumulation of clinical events during Tolvaptan administration after discharge.

	30 days	90 days	180 days
Mortality (%)	3 (2.4)	6 (3.6)	8 (4.8)
Re-admission (%)	10 (6.0)	26 (15.6)	41 (24.6)
Adverse event (%)	1 (0.6)	1 (0.6)	1 (0.6)

Table 3 Comparison of clinical parameters among 3 groups at discharge.

	Treatment Unnecessary n = 24	Treatment Continued n = 121	Treatment Discontinued n = 22	p-value
Previous HF admission, n (%)	8 (33.3%)	75 (62.0%)	20 (90.9%)	0.002
Number of HF admissions, n	2.1 ± 1.6	2.9 ± 2.9	3.1 ± 2.2	0.086
Creatinine (mg/dL)	1.6 ± 0.9	1.6 ± 0.9	2.2 ± 1.6	0.380
eGFR (mL/min)	42.7 ± 22.5	40.9 ± 21.6	35.0 ± 23.8	0.316
Blood urea nitrogen (mg/dL)	27.1 ± 12.5	33.1 ± 16.5	42.7 ± 26.0	0.063
Serum sodium (mEq/L)	138.1 ± 4.1	138.7 ± 4.4	138.6 ± 3.0	0.789
BNP (pg/mL); median/IQR	296; 107–296	350; 168–1000	573; 272–1682	0.011
EF (%)	48.7 ± 18.6	45.5 ± 19.4	42.7 ± 17.8	0.312
Furosemide (mg/day)	28.3 ± 5.6	41.1 ± 2.5	48.2 ± 5.8	0.037
Tolvaptan (mg/day)	8.3 ± 5.7	9.0 ± 5.6	8.5 ± 4.4	0.679

HF: heart failure, GFR: glomerular filtration rate, BNP: brain natriuretic peptide, EF: ejection fraction.

differences in the history of hospitalization due to HF exacerbation, BNP level, and furosemide dose (Table 3). Multivariable Cox regression analysis revealed an association between the incidence of adverse events and the Treatment Discontinued group (Hazard Ratio: 8.12; Confidence Interval: 4.03–16.57) vs Treatment Unnecessary group, $p < 0.001$) after adjusting for the number of HF admissions, BNP level, and dose of furosemide, whereas no such association was observed in the Treatment Continued group (Table 4).

DISCUSSION

The goal of this study was to investigate the long-term effects, prognosis, and safety of TLV in HF outpatients after discharge, as we believe that such data might provide new insights concerning the use of this drug.

Effects of TLV in HF outpatients after discharge

Earlier studies have focused on the efficacy of TLV in cases of severe HF, such as in patients presenting with chronic kidney disease (CKD) who had resistance to furosemide,[17-18] or those with acute HF undergoing short-term hospitalization.[19, 20] Many studies on outpatients treated with TLV have been released from Japan. Some of these studies have reported it to be effective,[15, 21] whereas others have found the opposite.[15, 22] The EVEREST study clearly demonstrated that long-term administration of TLV, unlike that of angiotensin-converting-enzyme inhibitors or beta-blockers, did not improve the prognosis in HF patients.[8] Meanwhile, other studies have reported that TLV is associated with more favorable effects and, possibly, long-term outcomes in patients with decompensated HF or hyponatremia.[15, 21] The present study was not a comparative control study. Therefore, it was not possible to directly determine whether long-term administration of TLV led to an improvement in prognosis. The readmission rate within 30 days after discharge was 6%. One earlier Japanese study reported a readmission rate of 4.6%,[9] while the Diagnosis Procedure Combination database reported a rate of 6.6%.[23] These percentages are similar those observed here. The present patients required TLV therapy at discharge, which suggests that these cases of HF

Presented by Medical*Online

Table 4 Association of Tolvaptan use with composite events.

	Multivariable Cox regression	
	Adjusted hazard ratio (95% confidence interval)	p value
Unnecessary	Reference	
Continued	1.04 (0.65, 1.80)	0.856
Discontinued	8.12 (4.03, 16.57)	<0.001

Model included the number of HF admission, BNP and dose of furosemide.
HF: heart failure, BNP: B-type natriuretic peptide.

were more severe than those targeted in other studies. This suggests that TLV therapy for HF outpatients reduces the rate of readmission. Furthermore, it became clear that the necessity of continuing TLV administration could be evaluated to some extent at 30 days after discharge. Frequent follow-ups may be required for outpatients receiving TLV therapy for 30 days after discharge. Some of the present patients (14%) required no long-term TLV therapy due to stabilization of HF. Uemura et al. also demonstrated that 18% of patients in their study population terminated TLV therapy for this reason.[11] Meanwhile, Kiuchi et al. demonstrated that, of 105 patients who continued to receive TLV after discharge, 57 (54.3%) ceased receiving TLV within 1 year of discharge.[12] The rate seen in that study was higher than that observed here. Unfortunately, detailed reasons for this finding were not provided. In the present study, the rate of re-hospitalization due to exacerbation of HF was significantly higher in patients continuing to receive TLV after discharge than in those who did not. In one earlier study, no differences were observed in the dose of furosemide (< 40 mg), patient background, or severity of HF among 3 groups of patients: those ceasing to receive TLV after discharge (25.8 ± 20.9 mg); those continuing to receive TLV upon discharge, but ceasing to receive TLV within 1 year of discharge (36.1 ± 25.4 mg); and those continuing to receive TLV 1 year after discharge (29.3 ± 20.9 mg).[13] Matsumoto et al. reported no significant differences between patients with or without TLV therapy after discharge. In an additional analysis incorporating TLV dose after discharge, the survival rate was lower in the high-dose TLV group than in the non-TLV group, whereas the low-dose TLV group showed the highest survival rate among the groups. That particular study included patients with CKD G3b. The dose of furosemide was 24 mg (22–27 mg) and no differences were observed in patient background or severity of HF, however.[28]

Uemura et al. reported that cardiac-related death-free and HF-related hospitalization-free survival rates and median dose of loop diuretics was 40 mg at discharge.[11] In the present study, it was determined that 24 patients (14%) did not need TLV after discharge due to stabilization of HF. The average dose of furosemide was 40.2 ± 27.7 mg at discharge. Accordingly, in the two studies described above, a low dose of furosemide was used.[13,22] On the other hand, it should be taken into consideration that administration of TLV could affect the dosage of furosemide.[29]

Safety of TLV in HF outpatients after discharge

Continued administration of TLV may reduce the risk of medium-term worsening of renal function (WRF), possibly leading to an improvement in long-term adverse outcomes in HF patients with CKD.[30] In the present study, only 1 patient discontinued TLV due to suspected drug-induced worsening of liver function. No patient discontinued TLV due to hypernatremia or WRF. The Samsca Post-Marketing Surveillance In Heart faiLurE (SMILE) study found that 90% of patients developed hypernatremia within 7 days after initiation of treatment.[31] In general, when a patient starts receiving TLV during hospitalization, hypernatremia, if detected, is managed before discharge. Increased salinity and water intake after discharge from hospital are one of the causes of re-hospitalization in cases of HF.[30] Elderly patients with HF have difficulties in realizing that they are thirsty.[27]

Presented by Medical*Online

Study limitations

Firstly, this was not a comparative control study. Therefore, it was not possible to directly investigate the effects of long-term administration of TLV as there was no control group with which to make a comparison. The results might also differ depending on what kind of control group was used for a comparison.[11,17,21,22] This indicates the need for further prospective studies.

Secondly, this was a retrospective observational study, and sufficient unification was not obtained in the examination criteria (BNP and NT-proBNP). The NT-proBNP levels were only determined at 1 of the 8 facilities, which only had a small number of patients, Therefore, only BNP was taken into consideration here. Thirdly, although this was a multicenter collaborative research project, the study period was short, and the sample size relatively small, like that of earlier studies. Further prospective multicenter collaborative studies employing larger study populations are thus required. Fourthly, this was a retrospective observational study, so no uniform standard was established for administration of TLV, with it being left to the discretion of the physician-in-charge. This suggests a lack of objective indicators. Several studies have investigated the dosages of TLV[22] and furosemide[23] in outpatients. In the present study, however, this was decided by the attending physician at each facility. Therefore, no detailed evaluation was available.

CONCLUSION

The effects of TLV in HF outpatients were identified within 30 days after discharge. The present findings suggest that long-term administration of TLV is relatively safe after discharge.

The authors would like to thank Professor Jeremy Williams, Tokyo Medical University, for his editing of the English of this paper.

Funding

This research received no grant from any funding agency in the public, commercial, or not-for-profit sectors.

Disclosure

The authors declare no conflict of interest.

REFERENCES

1) Setoguchi S, Stevenson LW, Schneeweiss S: Repeated hospitalizations predict mortality in the community population with heart failure. *Am Heart J* 2007, **154**(2): 260–266
2) Epstein AM, Jha AK, Orav EJ: The relationship between hospital admission rates and rehospitalizations. *N Engl J Med* 2011, **365**(24): 2287–2295
3) Ross JS, Chen J, Lin Z, et al: Recent national trends in readmission rates after heart failure hospitalization. *Circ Heart Fail* 2010, **3**(1): 97–103
4) Fudim M, O'Connor CM, Dunning A, et al: Aetiology, timing and clinical predictors of early vs. late readmission following index hospitalization for acute heart failure: insights from ASCEND-HF. *Eur J Heart Fail* 2018, **20**(2): 304–314
5) Aizawa H, Imai S, Fushimi K: Factors associated with 30-day readmission of patients with heart failure from a Japanese administrative database. *BMC Cardiovasc Disord* 2015, **15**: 134
6) Kimura M, Kohno T, Yoshikawa T: Early versus late readmission during the vulnerable phase following hospitalization for heart failure. *Eur J Heart Fail* 2018, **20**(7): 1165–1166
7) Dunbar-Yaffe R, Stitt A, Lee JJ, Mohamed S, Lee DS: Assessing risk and preventing 30-day readmissions in decompensated heart failure: opportunity to intervene? *Curr Heart Fail Rep* 2015, **12**(5): 309–317
8) Eapen ZJ, Reed SD, Li Y, et al: Do countries or hospitals with longer hospital stays for acute heart failure have lower readmission rates? Findings from ASCEND-HF. *Circ Heart Fail* 2013, **6**(4): 727–732
9) Konstam MA, Gheorghiade M, Burnett JC Jr, et al: Effects of oral tolvaptan in patients hospitalized for worsening heart failure: the EVEREST Outcome Trial. *JAMA* 2007, **297**(12): 1319–1331
10) Xiong B, Huang Y, Tan J, et al: The short-term and long-term effects of tolvaptan in patients with heart failure: a meta-analysis of randomized controlled trials. *Heart Fail Rev* 2015, **20**(6): 633–642
11) Uemura Y, Shibata R, Takemoto K, et al: Clinical benefit of tolvaptan in patients with acute decompensated heart failure and chronic kidney disease. *Heart Vessels* 2016, **31**(10): 1643–1649
12) Hauptman PJ, Burnett J, Gheorghiade M, et al: Clinical course of patients with hyponatremia and decompensated systolic heart failure and the effect of vasopressin receptor antagonism with tolvaptan. *J Card Fail* 2013, **19**(6): 390–397
13) Kiuchi S, Fujii T, Hisatake S, et al: Experience with long-term administration of tolvaptan to patients with acute decompensated heart failure. *Drug Discov Ther* 2017, **11**(3): 133–139

Presented by Medical*Online

14) Masuyama T, Tsujino T, Origasa H, et al: Superiority of long-acting to short-acting loop diuretics in the treatment of congestive heart failure. *Circ J* 2012, **76**(4): 833–842
15) Kida K, Shibagaki Y, Tominaga N, et al: Efficacy of tolvaptan added to furosemide in heart failure patients with advanced kidney dysfunction: a pharmacokinetic and pharmacodynamic study. *Clin Pharmacokinet* 2015, **54**(3): 273–284
16) Tominaga N, Kida K, Matsumoto N, et al: Safety of add-on tolvaptan in patients with furosemide-resistant congestive heart failure complicated by advanced chronic kidney disease: a sub-analysis of a pharmacokinetics/pharmacodynamics study. *Clin Nephrol* 2015, **84**(1): 29–38
17) Inomata T, Ikeda Y, Kida K, et al: Effects of additive tolvaptan vs. increased furosemide on heart failure with diuretic resistance and renal impairment—results from the K-STAR study. *Circ J* 2017, **82**(1): 159–167
18) Tominaga N, Kida K, Inomata T, et al: Effects of tolvaptan addition to furosemide in normo- and hyponatremia patients with heart failure and chronic kidney disease stages G3b-5: a subanalysis of the K-STAR study. *Am J Nephrol* 2017, **46**(5): 417–426
19) Jujo K, Saito K, Ishida I, et al: Randomized pilot trial comparing tolvaptan with furosemide on renal and neurohumoral effects in acute heart failure. *ESC Heart Fail* 2016, **3**(3): 177–188
20) Matsue Y, Suzuki M, Torii S, et al: Prognostic impact of early treatment with tolvaptan in patients with acute heart failure and renal dysfunction. *Int J Cardiol* 2016, **221**: 188–193
21) Uemura Y, Shibata R, Takemoto K, et al: Safety and efficacy of long-term use of tolvaptan in patients with heart failure and chronic kidney disease. *Circ J* 2017, **81**(11): 1736–1738
22) Matsumoto K, Ehara S, Nakamura Y, Otsuka K, Kawase Y: The effects of tolvaptan dose on cardiac mortality in patients with acute decompensated heart failure after hospital discharge. *Heart Vessels* 2018, **33**(10): 1204–1213
23) Nakamura M, Sunagawa O, Kinugawa K: Tolvaptan improves prognosis in responders with acute decompensated heart failure by reducing the dose of loop diuretics. *Int Heart J* 2018, **59**(1): 87–93
24) Nakano Y, Mizuno T, Niwa T, et al: Impact of continuous administration of tolvaptan on preventing medium-term worsening renal function and long-term adverse events in heart failure patients with chronic kidney disease. *Int Heart J* 2018, **59**(1): 105–111
25) Kinugawa K, Sato N, Inomata T, et al: Novel risk score efficiently prevents tolvaptan-induced hypernatremic events in patients with heart failure. *Circ J* 2018, **82**(5): 1344–1350
26) Tsuchihashi M, Tsutsui H, Kodama K, Kasagi F, Takeshita A: Clinical characteristics and prognosis of hospitalized patients with congestive heart failure—a study in Fukuoka, Japan. *Jpn Circ J* 2000, **64**(12): 953–959
27) Kinugawa K, Inomata T, Sato N, et al: Effectiveness and adverse events of tolvaptan in octogenarians with heart failure. Interim analyses of Samsca Post-Marketing Surveillance in Heart faiLurE (SMILE study). *Int Heart J* 2015, **56**(2): 137–143

Presented by Medical*Online

J. Clin. Physiol., Vol. 49, No. 1, 2019.

Original Article

Syncope Unit Plays Important Role in Reducing Syncope Reoccurrence

Yui NAKAYAMA,[*1, *2] Toshiyuki FURUKAWA,[*2] Akira KASAGAWA,[*1] Yasushi TAKAGI,[*2] Marika YAMADA,[*1] Makoto TAKANO,[*1] Ikutaro NAKAJIMA,[*1] Hidekazu MIYAZAKI,[*1] Tomoo HARADA[*1] and Yoshihiro J. AKASHI[*1]

ABSTRACT

Background: Management of syncope in accordance with a guidelines-based algorithm has recently been shown to improve the rate of diagnosis. This algorithm is not yet widely used in Japan, however. This report describes comprehensive risk stratification by means of a guidelines-based algorithm in current clinical practice in Japan, and an attempt to clarify the frequency of cardiac syncope.

Methods: Data on consecutive patients presenting with syncope between April 2012 and March 2014 were retrospectively reviewed and clinical characteristics analyzed. Our syncope management strategy is based on guidelines published by the Japanese Circulation Society and European Society of Cardiology.

Results: A total of 210 patients were included in the analysis. Risk factors for cardiac syncope were defined by the guidelines. Cardiac syncope was diagnosed in 25% of the patients following guidelines-based evaluation. Cardiac syncope was more frequent in patients with at least one risk factor in this Japanese population. The rate of recurrence of syncope in patients in whom management was completed in accordance with the guidelines was lower than that in those it was not.

Conclusion: A syncope unit and management in accordance with current guidelines are useful in improving the rate of diagnosis and preventing recurrence.

Key words: syncope, syncope clinic, electrocardiogram, diagnosis, algorithm

BACKGROUND

Recent reports have indicated that management based on a guidelines-based algorithm has increased the rate of correct diagnoses of syncope,[1] while facilities dedicated to dealing with this condition have also

[*1] Division of Cardiology, Department of Internal Medicine, St. Marianna University School of Medicine
[*2] Syncope Unit, St. Marianna University School of Medicine Toyoko Hospital
(Received July 18, 2018)

Presented by Medical*Online

Table 1 Syncope risk factor rates (n = 210).

Age > 65 yr	100	48%
Electrocardiogram abnormality	108	51%
Structural heart disease	41	20%
Syncope during effort or while in supine position	30	14%

More than 48% of patients were older than 65 years. Of these, 51% had abnormalities on electrocardiogram; 20% had structural heart disease; and 14% had syncope during effort or while in supine position.

Table 2 Percentage of patients with syncope and one or more risk factors (n = 210).

One or more risk factors	138	66%
No risk factors	72	34%

Risk factors included age, electrocardiogram abnormality, presence of structural heart disease or trauma, shortness of breath, anemia or hypotension, prodromal symptoms, and syncope during effort or while in supine position.

proven useful from an economic perspective. Several randomized trials, such as the Syncope Evaluation Emergency Department Study (SEEDS)[2] and Evaluation of Guidelines in Syncope Study (EGSYS),[3] have demonstrated the effectiveness of syncope units. The results of these studies suggest that syncope units provide effective management at low cost. In Italy, there are currently approximately 70 such syncope units, which has contributed to improving the rate of diagnosis and saving medical resources in cases of unexplained or high-risk syncope. The large-scale clinical observational Syncope Unit Project aimed to verify the practicality and effectiveness of syncope units.[4] The results serve as a useful resource for those who wish to replicate this model in other hospitals, as they provide clinicians with a frame of reference for dealing with syncope on a daily basis. There are few such syncope management facilities in Japan, however. The syncope unit at our hospital sees a lot of patients with syncope of unknown cause. Management of syncope here is based on the guidelines of the European Society of Cardiology (ESC)[1] and those of the Japanese Circulation Society (JCS).[5] The purpose of the present study was to investigate the effectiveness of the guidelines-based algorithm used at our syncope unit in Japan.

METHODS

This study was a single-center, retrospective analysis. The study population comprised consecutive patients referred to our syncope unit between April 2012 and March 2014. This syncope unit is located at a university hospital with approximately 1000 beds and a 24-hour tertiary emergency medical care facility. The syncope unit is open once per week. There are approximately 10 outpatients per day, and an average of 0.5 patients are hospitalized. Therefore, patients presenting at the emergency department with syncope may attend our syncope unit on another day, if necessary. If hospital admission is required, then the patients are managed in the cardiology department.

The clinical characteristics (including age, sex, heart disease, and number and kind of examinations), diagnosis, and number of admissions were analyzed. Specific invasive examinations for syncope management, such as the tilt-table test, electrophysiological study (EPS), and use of an implantable loop recorder (ILR) were also analyzed. Recurrence of syncope during the follow-up period in patients in whom management was or was not completed was determined. Recurrence was determined based on medical records at our hospital and/or

Presented by Medical*Online

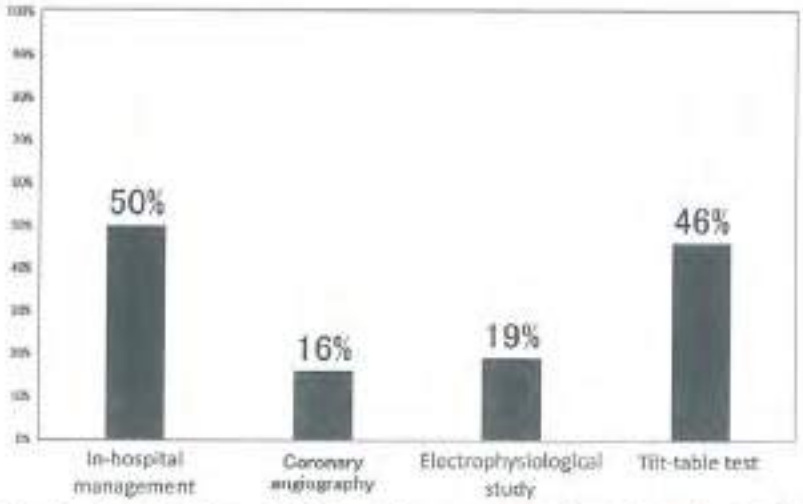

Fig. 1 Examinations administered in syncope patients. A total of 50% of patients required hospitalization; 16% underwent cardiac catheterization; 19% underwent an electrophysiological study; and 46% underwent tilt-table test.

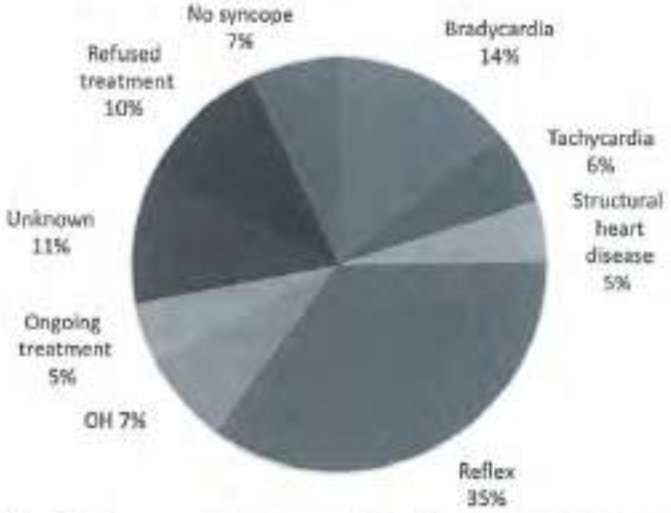

Fig. 2 Diagnoses of syncope patients. Most common diagnosis was reflex syncope (35%), followed by cardiogenic syncope with bradycardia (14%), tachycardia (6%), and structural heart disease (5%). A total of 7% of patients had orthostatic hypotension (OH); 5% were currently undergoing examination; and 11% had unexplained syncope. At halfway through management program, 10% of patients decided to leave hospital.

referrals to our unit. Our syncope management strategy is based on the guidelines published by the JCS[8] and ESC.[9] A questionnaire is also given to each patient to confirm syncope status.

STATISTICAL ANALYSIS

The data are reported as the mean ± standard deviation. Categorical variables and continuous variables

Presented by Medical*Online

were compared between groups using Fisher's exact test and Student's t-test, respectively. Two-tailed values of $p<0.05$ were considered statistically significant. This study was approved by the St. Marianna University School of Medicine Ethics Committee (approval number, 3435). In this observational study, information obtained from standard medical examinations was used to reach a diagnosis.

RESULTS

A total of 210 patients were analyzed. The mean age was 57 ± 22 years, and 56% of them were male. The median number of syncope events was 2 (interquartile range, 1 to 4). Risk factors for cardiac syncope were defined by the guidelines,[1,5] and comprised older age (>65 years), abnormal electrocardiogram results, structural heart disease, and syncope during effort or while in the supine position, which were observed in 48%, 51%, 20%, and 14% of patients, respectively (Table 1). Of these patients, 66% had at least one risk factor (Table 2). The median number of examinations was 6, and 70% of patients underwent brain computed tomography and/or magnetic resonance imaging. An EPS was performed in 19% of patients, coronary angiography (CAG) in 16%, and the tilt-table test in 46% (Fig. 1).

A diagnosis was reached in 74% of the total number of patients. No diagnosis was reached in the remaining 26%. Clinical management before diagnosis was refused in 10%. Unexplained syncope after guideline-based management was observed in 11%, and 5% were currently undergoing management. The most common cause of syncope was reflex syncope (35%). A cardiac origin was observed in 25% of patients (Fig. 2). Among tachyarrhythmias, those of ventricular origin place patients at risk of sudden cardiac death, and this occurred in 3 cases (1.4% of the total number of patients: one case of Brugada syndrome and 2 of QT-prolonged syndrome). A diagnosis was not determined in 21% of patients. Of these, 41% were at very low risk of cardiac syncope, however, and the others dropped out of the management program before a diagnosis was determined. Cardiac syncope was observed more frequently in patients with at least one risk factor (17% vs 6%; $p = 0.03$).

Half of the patients were managed at the hospital. Meanwhile, diagnosis was reached in 76% within 35 ± 53 days as outpatients. The appropriate treatment was administered in accordance with the guidelines after determination of diagnosis. After 8 ± 4 months of follow-up, syncope recurred in 26 patients, with secondary injury occurring in 4. One patient who underwent observation using an ILR after multidisciplinary assessment, including an electrophysiological study, died suddenly. Her ILR showed sudden asystole without any previous signs.

In this population, 10% of the patients did not comply with the management guidelines. Implantation of an ILR (39%) was the most commonly refused treatment, with hospitalization to investigate the origin of the syncope the second most common (20%). Other treatments refused by the patients comprised pacemaker implantation and invasive tests such as CAG and EPS. The recurrence rate in these patients was higher than that in those who were completely compliant with the management guidelines (21% vs 9%; $p<0.01$).

DISCUSSION

The current practice at our syncope unit in Japan is described in this report. Several important results were observed during this study. First, management in accordance with the guidelines[1,5] reduced the rate of recurrence. Second, syncope was successfully diagnosed in approximately 90% of the total number of patients (excluding those who refused management). The diagnostic rate was not inferior to those seen in other studies of syncope units[1-4] or in Japanese studies of syncope.[6,7] Usually, the presence or absence of cardiac syncope is determined by a cardiologist. At our unit, however, risk of syncope is determined using interviews and screening examinations. Other advanced examinations, such as invasive tests, are performed depending on the presence of risk factors. If a patient is at low risk of cardiac syncope, then it is possible to avoid invasive tests. This lowers the number of examinations performed, making management more efficient. Syncope can still occur, however, in patients deemed at no risk. Indeed, the patient who died in this study had been referred to our syn-

Presented by Medical*Online

cope unit, where the diagnosis was recurrence. Thus, a proper cardiovascular examination was only performed some considerable time after the initial appearance of syncope. If the problem had been diagnosed earlier, it would have been possible to use an ILR in accordance with the guidelines, which may have prevented their death.

The present results suggest that there are several problems with the management of syncope in Japan. First, 70% of the patients underwent brain imaging due to a class III indication in accordance with the ESC guidelines.[1] This number is much higher than the 10% reported in a recent study performed in Italy.[9] In the present study, all the patients underwent screening examinations prior to referral to the syncope unit. It is usually assumed that syncope is caused by brain dysfunction, such as transient ischemic attack, or some other cerebrovascular disease. Here, after referral to the syncope unit, examinations were performed to distinguish between syncope and seizure in patients with several seizure symptoms. Second, approximately 10% of patients refused management, although the reasons for this were unclear. We believe that this may have been because they did not understand the risks associated with syncope. Third, the Japanese social security system makes it is easy for patients to visit the emergency department. Therefore, many patients think they can just leave and return if the problem recurs. Fourth, refusal to undergo important clinical examinations is detrimental, especially that of observation with an ILR. This device is not available in many units, and few patients realize how useful it is.[8-10] Recognition of the utility of such devices is increasing, however. Moreover, technological advances have meant that these devices are now smaller than when this study was being performed. This suggests that the number of patients refusing management with an ILR may decrease in the future.

The present results demonstrate that management of syncope in line with the guidelines is effective in preventing recurrence. According to SEEDS, having a syncope facility in the emergency department did not affect the recurrence rate of syncope.[3] Another study reported that the 1-year rate of recurrence was 17% after visiting an emergency department with a syncope facility.[11] The present study only included data on patients attending the syncope unit at least once, however. Some of these patients agreed to undergo complete follow-up, while others refused. These results suggest that guidelines-based management with complete follow-up is necessary for a correct diagnosis and prevention of recurrence. Although this study did not describe the current strategy as regards the clinical management of syncope in Japan, it did describe early-stage results observed at one such syncope unit.

LIMITATIONS

This study had several limitations. The first was that our syncope unit did not always meet the standards set out in the ESC guidelines.[1] Because this unit has not been open for long, there are no specialists among the medical staff or sufficient collaboration with other departments, such as neurology. The second limitation was that this was a single-center, retrospective analysis. This unit is the first to offer such specialized treatment for syncope in Japan, however. Therefore, our experiences may provide a helpful reference for other new syncope units opening in this country. The third limitation was related to the subtypes of reflex syncope. Reflex syncope is usually classified as vasodepressor, cardioinhibitory, or mixed. In this report, these types were not discussed. Reflex syncope is usually classified according to electrocardiography and blood pressure during the tilt-table test or some other ambulatory monitoring test. Here, however, the diagnosis was often reached based on symptoms and/or other factors.

CONCLUSION

This study described current practice at our syncope unit in Japan. Although this unit is only one example of a specialized syncope management facility, the present results indicate that such units are useful in improving the rate of diagnosis and preventing recurrence by providing treatment in accordance with established guidelines.

REFERENCES

1) Task Force for the Diagnosis and Management of Syn-

Presented by Medical*Online

cope; European Society of Cardiology (ESC); European Heart Rhythm Association (EHRA); Heart Failure Association (HFA); Heart Rhythm Society (HRS), Moya A, Sutton R, Ammirati F, Blanc JJ, Brignole M, Dahan JB, Deharo JC, Gajek J, Gjesdal K, Krahn A, Massin M, Pepi M, Pezawas T, Ruiz Granell R, Sarasin F, Ungar A, van Dijk JG, Walma EP, Wieling W: Guidelines for the diagnosis and management of syncope (version 2009). *Eur Heart J* 2009, **30**(21): 2631-2671

2) Shen WK, Decker WW, Smars PA, Goyal DG, Walker AE, Hodge DO, Trusty JM, Brekke KM, Jahangir A, Brady PA, Munger TM, Gersh BJ, Hammill SC, Frye RL: Syncope Evaluation in the Emergency Department Study (SEEDS): a multidisciplinary approach to syncope management. *Circulation* 2004, **110**(24): 3636-3645

3) Del Rosso A, Ungar A, Maggi R, Giada F, Petix NR, De Santo T, Menozzi C, Brignole M: Clinical predictors of cardiac syncope at initial evaluation in patients referred urgently to a general hospital: the EGSYS score. *Heart* 2008, **94**(12): 1620-1626

4) Brignole M, Ungar A, Casagranda I, Gulizia M, Lunati M, Ammirati F, Del Rosso A, Sasdelli M, Santini M, Maggi R, Vitale E, Morrione A, Francese GM, Vecchi MR, Giada F; Syncope Unit Project (SUP) investigators: Prospective multicentre systematic guideline-based management of patients referred to the Syncope Units of general hospitals. *Europace* 2010, **12**(1): 109-118

5) Inoue H, Abe H, Otsuji Y: Guidelines for diagnosis and management of syncope (The Japanese Circulation Society 2012). Available at http://www.j-circ.or.jp/guideline/pdf/JCS2012_inoue_h.pdf (Accessed May 2018)

6) Furukawa T, Hachiya H, Isobe M, Hirao K: Is head injury characteristic of arrhythmic syncope? *J Arrhythmia* 2013, **29**(4): 217-220

7) Omiki T, Ito H, Ochi A, Chiba Y, Kawasaki S, Onishi Y, Munetsugu Y, Kikuchi M, Minoura Y, Watanabe N, Adachi T, Asano T, Tanno K, Kobayashi Y: Single center experience in Japanese patients with syncope. *J Cardiol* 2015, **66**(5): 395-402

8) Task Force members, Brignole M, Vardas P, Hoffman E, Huikuri H, Moya A, Ricci R, Sulke N, Wieling W; EHRA Scientific Documents Committee, Auricchio A, Lip GY, Almendral J, Kirchhof P, Aliot E, Gasparini M, Braunschweig F; Document Reviewers, Lip GY, Almendral J, Kirchhof P, Botto GL; EHRA Scientific Documents Committee; Indications for the use of diagnostic implantable and external ECG loop recorders. *Europace* 2009, **11**(5): 671-687

9) Furukawa T, Maggi R, Bertolone C, Fontana D, Brignole M: Additional diagnostic value of very prolonged observation by implantable loop recorder in patients with unexplained syncope. *J Cardiovasc Electrophysiol* 2012, **23**(1): 67-71

10) Edvardsson N, Frykman V, van Mechelen R, Mitro P, Mohil-Oskarsson A, Pasquie JL, Ramanna H, Schwertfeger F, Ventura R, Voulgaraki D, Garutti C, Stolt P, Linger NJ; PICTURE Study Investigators: Use of an implantable loop recorder to increase the diagnostic yield in unexplained syncope: results from the PICTURE registry. *Europace* 2011, **13**(2): 262-269

11) Ungar A, Del Rosso A, Giada F, Bartoletti A, Furlan R, Quartieri F, Lagi A, Morrione A, Mussi C, Lunati M, De Marchi G, De Santo T, Marchionni N, Brignole M; Evaluation of Guidelines in Syncope Study 2 Group: Early and late outcome of treated patients referred for syncope to emergency department: the EGSYS 2 follow-up study. *Eur Heart J* 2010, **31**(16): 2021-2026

Presented by Medical*Online

JACC: CARDIOVASCULAR INTERVENTIONS
VOL. 12, NO. 8, 2019
© 2019 BY THE AMERICAN COLLEGE OF CARDIOLOGY FOUNDATION
PUBLISHED BY ELSEVIER

Calcified Plaques in Patients With Acute Coronary Syndromes

Tomoyo Sugiyama, MD, PhD,[a] Erika Yamamoto, MD, PhD,[a] Francesco Fracassi, MD,[a] Hang Lee, PhD,[b] Taishi Yonetsu, MD,[c] Tsunekazu Kakuta, MD, PhD,[d] Tsunenari Soeda, MD, PhD,[e] Yoshihiko Saito, MD, PhD,[f] Bryan P. Yan, MBBS,[g] Osamu Kurihara, MD, PhD,[h] Masamichi Takano, MD, PhD,[h] Giampaolo Niccoli, MD, PhD,[i] Filippo Crea, MD,[i] Takumi Higuma, MD, PhD,[j] Shigeki Kimura, MD, PhD,[j] Yoshiyasu Minami, MD, PhD,[k] Junya Ako, MD, PhD,[k] Tom Adriaenssens, MD, PhD,[l] Niklas F. Boeder, MD,[m] Holger M. Nef, MD,[m] James G. Fujimoto, PhD,[n] Valentin Fuster, MD, PhD,[o] Aloke V. Finn, MD,[p] Erling Falk, MD, DMSc,[q] Ik-Kyung Jang, MD, PhD[a,r]

ABSTRACT

OBJECTIVES This study conducted detailed analysis of calcified culprit plaques in patients with acute coronary syndromes (ACS).

BACKGROUND Calcified plaques as an underlying pathology in patients with ACS have not been systematically studied.

METHODS From 1,241 patients presenting with ACS who had undergone pre-intervention optical coherence tomography imaging, 157 (12.7%) patients were found to have a calcified plaque at the culprit lesion. Calcified plaque was defined as a plaque with superficial calcification at the culprit site without evidence of ruptured lipid plaque.

RESULTS Three distinct types were identified: eruptive calcified nodules, superficial calcific sheet, and calcified protrusion (prevalence of 25.5%, 67.4%, and 7.1%, respectively). Eruptive calcified nodules were frequently located in the right coronary arteries (44.4%), whereas superficial calcific sheet was most frequently found in the left anterior descending coronary arteries (68.4%) ($p = 0.012$). Calcification index (mean calcification arc × calcification length) was greatest in eruptive calcified nodules, followed by superficial calcific sheet, and smallest in calcified protrusion (median 3,284.9 [interquartile range (IQR): 2,113.3 to 5,385.3] vs. 1,644.3 [IQR: 1,012.4 to 3,058.7] vs. 472.5 [IQR: 176.7 to 865.2]; $p < 0.001$). The superficial calcific sheet group had the highest peak post-intervention creatine kinase values among the groups (eruptive calcified nodules vs. superficial calcific sheet vs. calcified protrusion: 241 [IQR: 116 to 612] IU/l vs. 834 [IQR: 141 to 3,394] IU/l vs. 745 [IQR: 69 to 1,984] IU/l; $p = 0.032$).

CONCLUSIONS Three distinct types of calcified culprit plaques are identified in patients with ACS. Superficial calcific sheet, which is frequently located in the left anterior descending coronary artery, is the most prevalent type and is also associated with greatest post-intervention myocardial damage. (Identification of Predictors for Coronary Plaque Erosion in Patients With Acute Coronary Syndrome; NCT03479723) (J Am Coll Cardiol Intv 2019;12:531–40)
© 2019 by the American College of Cardiology Foundation.

From the [a]Cardiology Division, Massachusetts General Hospital, Harvard Medical School, Boston, Massachusetts; [b]Biostatistics Center, Massachusetts General Hospital, Harvard Medical School, Boston, Massachusetts; [c]Department of Interventional Cardiology, Tokyo Medical and Dental University, Tokyo, Japan; [d]Department of Cardiovascular Medicine, Tsuchiura Kyodo General Hospital, Tsuchiura, Japan; [e]Department of Cardiovascular Medicine, Nara Medical University, Kashihara, Japan; [f]Department of Medicine and Therapeutics, Chinese University of Hong Kong, Hong Kong, China; [g]Cardiovascular Center, Nippon Medical School Chiba Hokusoh Hospital, Inzai, Japan; [h]Department of Cardiovascular and Thoracic Science, Catholic University of the Sacred Heart, Rome, Italy; [i]Department of Cardiology, Hirosaki University Graduate School of Medicine, Hirosaki, Japan; [j]Department of Cardiology, Kameda Medical Center, Kamogawa, Japan; [k]Department of Cardiovascular Medicine, Ritsumeikan University School of Medicine, Suganthara, Japan; [l]Department of Cardiovascular Medicine, University Hospitals Leuven, Leuven, Belgium; [m]Department of Cardiology, University of Giessen, Giessen, Germany; [n]Research Laboratory of Electronics, Department of Electrical Engineering and Computer Science, Massachusetts Institute of Technology, Cambridge, Massachusetts; [o]Zena and Michael A. Wiener Cardiovascular Institute, Icahn School of Medicine at Mount Sinai, New York, New York; [p]CVPath Institute, Gaithersburg, Maryland; [q]Department of Cardiology, Aarhus University Hospital, Aarhus, Denmark; and the [r]Division of Cardiology, Kyung Hee University Hospital, Seoul, Republic of Korea. Dr. Sugiyama is supported in part by the grant from the Strategic International Research Collaboration Program with Harvard Medical School to Cultivate Professionals with Knowledge and Humanity from the Japan Society for the Promotion of Science, and the subvention from Sumitomo Life Welfare and Culture Foundation.

ISSN 1936-8798/$36.00
https://doi.org/10.1016/j.jcin.2018.12.013

JACC: CARDIOVASCULAR INTERVENTIONS VOL. 11, NO. 6, 2018
MARCH 26, 2018:531–40

ABBREVIATIONS AND ACRONYMS

ACS = acute coronary syndrome(s)

CK = creatine kinase

IVUS = intravascular ultrasound

LAD = left anterior descending coronary artery

OCT = optical coherence tomography

PCI = percutaneous coronary intervention

RCA = right coronary artery

Acute coronary syndromes (ACS) arise from acute occlusive thrombosis of a coronary artery (1). The leading cause of acute occlusive coronary thrombosis is a rupture of a lipid plaque with subsequent release of thrombogenic substrate into the bloodstream, which triggers activation of platelets and a coagulation system (2). Ruptured lipid plaque is characterized by the presence of a large necrotic core with disruption of an overlying thin fibrous cap (1). In contrast, 2% to 7% of fatal acute coronary thrombosis is caused by calcified nodules (1,3). The definition of calcified nodule in pathology is a lesion with acute thrombi showing eruptive calcific nodules through a disrupted fibrous tissue with an underlying fibrocalcific plaque (1,3). However, in vivo data on calcified plaques at the culprit lesion responsible for ACS are limited.

SEE PAGE 541

In this study, we aimed to conduct detailed analysis of calcified plaques in patients with ACS to study the prevalence, optical coherence tomography (OCT) findings, and clinical significance.

METHODS

STUDY POPULATION. This was a multicenter longitudinal international collaborative study of ACS patients enrolled from 11 sites across 6 countries (NCT03479723). Patients presenting with ACS who had undergone OCT imaging of the culprit lesion at index procedure were eligible for the study. Among 1,241 patients, 607 (48.9%) patients had a ruptured lipid plaque and 477 (38.4%) patients had plaque erosion at the culprit lesion (**Figure 1**). Consequently, we identified 157 (12.7%) patients who had a calcified plaque at the culprit lesion. Diagnosis of ACS included ST-segment elevation myocardial infarction and non-ST-segment elevation ACS, as previously described (4). The culprit lesion was identified based on angiographic findings, electrocardiogram changes, or left ventricular wall motion abnormalities. In patients with multiple stenoses, the culprit lesion was identified as the lesion having the most severe stenosis or with evidence of recent plaque disruption such as filling defect suggestive of thrombus on angiogram. Demographic, angiographic, and OCT findings of the culprit lesions, peak post-percutaneous coronary intervention (PCI) creatine kinase (CK) values, and in-hospital outcomes (death and target lesion revascularization) were evaluated. This study was approved by the Institutional Review Board at each participating site and written informed consent was obtained from all patients before enrollment.

CORONARY ANGIOGRAPHY ANALYSIS. Quantitative coronary angiography analysis was performed using CAAS 5.10.1 software (Pie Medical Imaging BV, Maastricht, the Netherlands). The minimal lumen diameter, reference vessel diameter, diameter stenosis, and length of the culprit lesions were measured (5). Coronary flow was assessed according to the Thrombolysis In Myocardial Infarction (TIMI) flow grade (6). Lesion complexity was assessed using the American College of Cardiology/American Heart Association classification (7). Thrombus was defined as an intraluminal filling defect or a haze seen in multiple angiographic projections (8). Calcification was identified as readily apparent radiopacities within the vascular wall at the site of the stenosis (9).

OCT IMAGE ACQUISITION AND ANALYSIS. OCT examination was performed using either a frequency-domain (C7/C8, OCT Intravascular Imaging System, St. Jude Medical, St. Paul, Minnesota) or time-domain (M2/M3 Cardiology Imaging Systems, LightLab Imaging Inc., Westford, Massachusetts) OCT system. All OCT images were submitted to the core laboratory at Massachusetts General Hospital and analyzed by 2 independent investigators (E.Y. and T.S.) who were blinded to clinical, angiographic, and laboratory data, using an offline review workstation (St. Jude Medical). Any discordance was resolved by consensus with a third reviewer. Plaque was identified as a segment with a loss of the normal 3-layered structure of the

Dr. Saito has received personal fees from Mitsubishi Tanabe Pharma Corporation, Otsuka Pharmaceutical, Daiichi Sankyo, Pfizer Japan, Nippon Boehringer Ingelheim, and Novartis Pharma; and has received research support from Mitsubishi Tanabe Pharma Corporation, Otsuka Pharmaceutical, Daiichi Sankyo, Pfizer Japan, Nippon Boehringer Ingelheim, Novartis Pharma, Ono Pharmaceutical, St. Jude Medical Japan, Bayer, Terumo, Kyowa Hakko Kirin, and Dainippon Sumitomo Pharma. Dr. Ako has received speaker honoraria from Abbott Vascular. Dr. Adriaenssens has received educational grants and consulting fees from Abbott Vascular. Dr. Fujimoto has received royalties from intellectual property owned by Massachusetts Institute of Technology. Dr. Finn has received honoraria and research grant support from Abbott Vascular. Dr. Ing has received grant support from Abbott Vascular and Medtronic; and consulting fees from Lycotec. All other authors have reported that they have no relationships relevant to the contents of this paper to disclose.

Manuscript received September 30, 2018; revised manuscript received November 16, 2018, accepted December 12, 2018.

vessel wall (10). Proximal and distal references were identified as the sites with the largest lumen area proximal and distal to the plaque within a 10-mm segment, and mean reference lumen area was calculated (11). Minimal flow area was defined as the smallest flow area within the length of the plaque. Percent area stenosis was calculated as follows: [(mean reference lumen area − minimal flow area) / mean reference lumen area] × 100 (11). Calcification was identified by the presence of well-delineated low-backscattering heterogeneous regions (10). Calcified plaque was identified by the presence of superficial substantive calcification at the culprit site without evidence of ruptured lipid plaque. Calcified plaques were classified into 3 types: 1) eruptive calcified nodules; 2) superficial calcific sheet; and 3) calcified protrusion. Eruptive calcified nodules were defined by expulsion of small calcific nodules into the lumen (**Figures 2A and 2B**). Superficial calcific sheet, also called sheet calcium by pathologists, was defined by: 1) sheet-like superficial calcific plate without erupted nodules or protruding mass into the lumen; 2) minimal or no visible disruption of overlying fibrous tissue; and 3) minimal compromise of the lumen (**Figures 2C and 2D**). Calcified protrusion, also called protruding nodular calcification by pathologists, was defined by protruding calcific mass without eruptive nodules (**Figures 2E and 2F**). Quantitative analysis was performed at 1-mm intervals on cross-sectional OCT images. Calcification arc and calcification thickness were measured in each cross-sectional image. Calcification length was obtained on the longitudinal view. Calcification index was calculated as the product of mean calcification arc and calcification length (12). Thrombus was defined as an irregular mass with minimum diameter >250 μm attached to the luminal surface or floating within the lumen (11). Type of thrombus was determined by the predominance of either red thrombus (high backscattering with high signal attenuation) or white thrombus (homogenous backscattering with low signal attenuation) (10,13).

STATISTICAL ANALYSIS. All analyses were performed using SPSS Statistics 23.0 software (International Business Machines Corporation, Armonk, New York). Categorical data were expressed as absolute frequencies and percentages and compared using the chi-square test or Fisher exact test, as appropriate. Continuous variables were expressed as mean ± SD for normally distributed variables and as median (interquartile range) for non-normally distributed variables, and compared using the Student's *t*-test, 1-way analysis of variance, Mann-Whitney *U* test, or Kruskal-Wallis test, as appropriate. In case of significance, pairwise post hoc tests were performed with the Bonferroni correction. Intraobserver and interobserver differences were quantified using the kappa coefficient of agreement for the plaque classification. A p value <0.05 was considered statistically significant.

FIGURE 1 Prevalence of Subtypes of Calcified Plaques

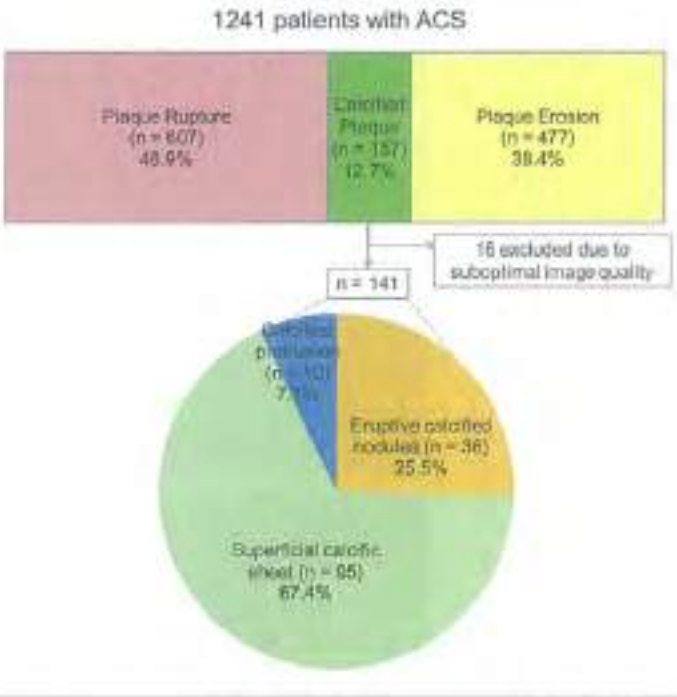

In 1,241 culprit lesions, calcified plaque was the underlying etiology in 12.7% of patients. Among the 3 subtypes of calcified plaque, superficial calcific sheet was the most common type, followed by eruptive calcified nodules and calcified protrusion. ACS = acute coronary syndrome(s).

RESULTS

PATIENT CHARACTERISTICS. Among 157 patients with calcified culprit plaque, 16 cases were excluded due to suboptimal image quality and 141 patients were included in the final analysis. Among them, 36 (25.5%) patients had eruptive calcified nodules, 95 (67.4%) patients had superficial calcific sheet, and 10 (7.1%) patients had calcified protrusion (**Figure 1**). Mean age was 69.1 years and 73.0% of patients were men. There were no significant differences in patient characteristics and laboratory findings among the groups (**Table 1**).

ANGIOGRAPHIC FINDINGS. Eruptive calcified nodules were most frequently located in the right coronary arteries (RCAs), whereas superficial calcific sheet

JACC: CARDIOVASCULAR INTERVENTIONS VOL. 12, NO. 8, 2019
MARCH 25, 2019:531–40

FIGURE 2 Representative Optical Coherence Tomography Images of Calcified Plaques at the Culprit Lesions

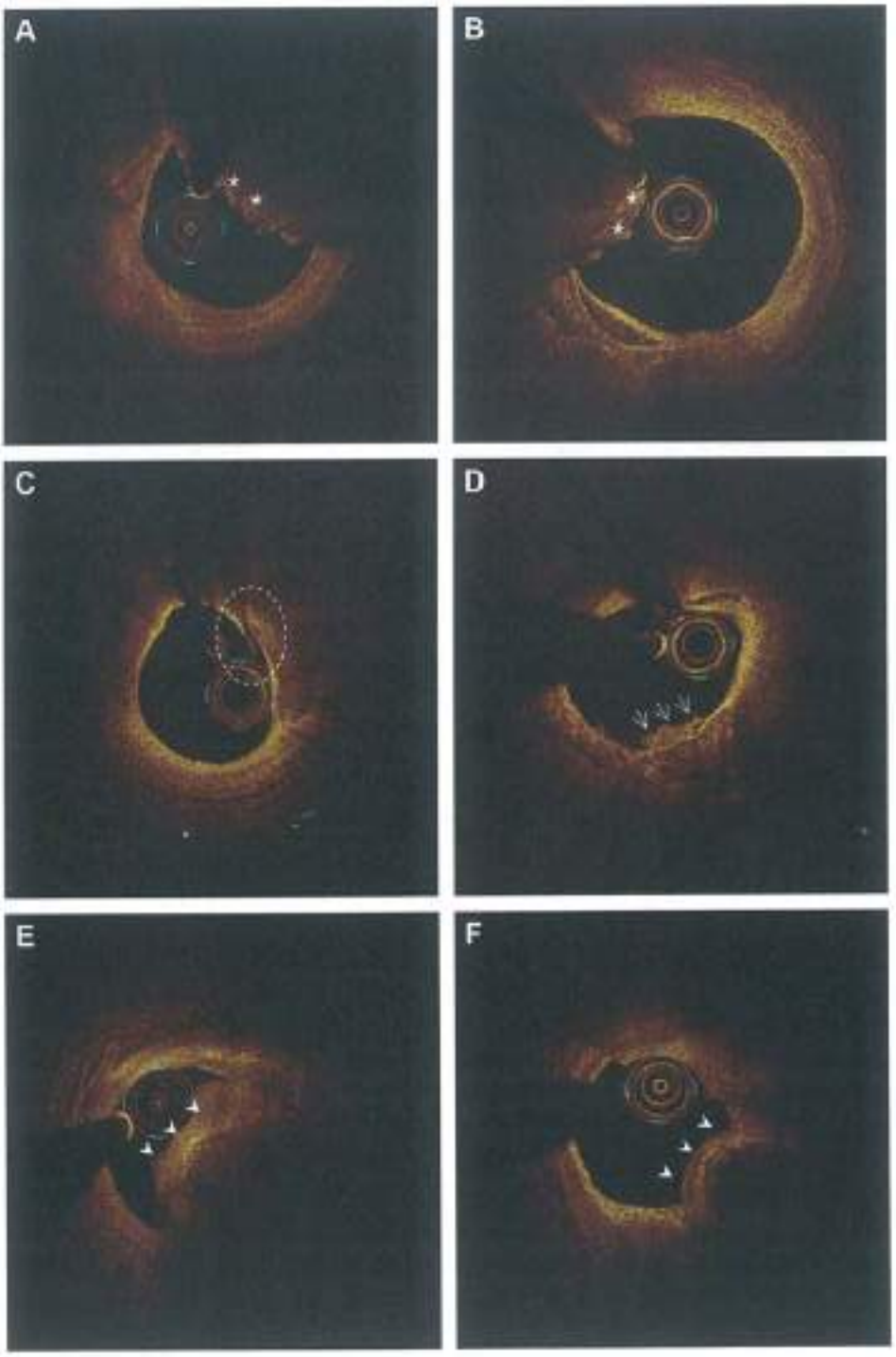

(A, B) Eruptive calcified nodules represent expulsion of a cluster of small calcific nodules into the lumen (*). **(C, D)** Superficial calcific sheet represents sheet-like superficial calcific plate with minimal or no disruption of overlying fibrous tissue, and minimal compromise of the lumen, but without erupted nodules or protruding mass into the lumen. Calcific plate is accompanied by **(C)** disruption of fibrous tissue **(dashed circle)** or discontinuity of fibrous tissue, or by **(D)** intact but thin fibrous tissue **(arrows)**. **(E, F)** Calcified protrusion represents protruding calcific mass without small eruptive calcific nodules **(arrowheads)**.

was most frequently located in the left anterior descending coronary arteries (LADs) (Table 2). The prevalence of complex lesion and multivessel disease were not different among the groups. The superficial calcific sheet group had the worst pre-PCI coronary flow, smallest minimal lumen diameter, and greatest percent diameter stenosis.

OCT FINDINGS. OCT findings are shown in Table 3. Among 95 patients with superficial calcific sheet, 81 patients had minimally disrupted fibrous tissue and 14 patients had intact fibrous tissue. Calcium burden (calcification arc, thickness, length, and index) was greatest in the eruptive calcified nodule group, followed by the superficial calcific sheet group, and smallest in the calcified protrusion group. The superficial calcific sheet group had smallest minimal flow area and reference lumen area. White thrombus was predominant in the superficial calcific sheet group, in contrast to eruptive calcified nodules, which had predominantly red thrombus.

Excellent intraobserver and interobserver agreement was observed in the diagnosis of each subtype of calcified culprit plaque (kappa = 0.868 and 0.854, respectively).

IN-HOSPITAL OUTCOMES. In-hospital outcomes are shown in Table 4. Post-PCI coronary flow was comparable among the groups. The superficial calcific sheet group had highest peak post-PCI CK values. In-hospital cardiac event rate during initial hospitalization was low in all 3 groups.

TABLE 1 Patient Characteristics

	Eruptive Calcified Nodules (n = 36)	Superficial Calcific Sheet (n = 95)	Calcified Protrusion (n = 10)	p Value
Age, yrs	70.2 ± 11.1	69.0 ± 9.9	65.4 ± 6.0	0.414
Sex				0.523
Male	28 (77.8)	69 (72.6)	6 (60.0)	
Female	8 (22.2)	26 (27.4)	4 (40.0)	
Clinical presentation				0.263
STEMI	13 (36.1)	43 (45.3)	2 (20.0)	
NSTE-ACS	23 (63.9)	52 (54.7)	8 (80.0)	
Prior MI	6 (16.7)	11 (11.6)	0 (0.0)	0.428
Prior PCI	4 (11.1)	15 (15.8)	1 (10.0)	0.850
Hypertension	30 (83.3)	74 (77.9)	6 (60.0)	0.290
Dyslipidemia	20 (55.6)	65 (68.4)	7 (70.0)	0.375
Diabetes mellitus	17 (47.2)	36 (37.9)	5 (50.0)	0.537
Renal insufficiency	12 (33.3)	28 (29.5)	5 (50.0)	0.418
Family history of CAD	4 (11.1)	18 (18.9)	3 (30.0)	0.306
Current smoking	9 (25.0)	23 (24.2)	2 (20.0)	1.000
Creatinine, mg/dl	0.82 (0.69–1.26)	0.92 (0.76–1.10)	0.96 (0.89–1.39)	0.376
Low-density lipoprotein cholesterol, mg/dl	107.9 ± 40.3	109.3 ± 40.5	93.6 ± 28.8	0.696
High-density lipoprotein cholesterol, mg/dl	49.3 ± 13.2	48.1 ± 13.9	42.7 ± 3.2	0.596
Triglyceride, mg/dl	104.9 ± 61.3	135.6 ± 99.2	160.6 ± 110.6	0.197
HbA_{1c}, %	8.2 ± 3.7	7.0 ± 2.3	5.9 ± 0.7	0.080
WBC count/μl	7,400 (6,700–8,700)	9,000 (6,930–10,510)	8,200 (5,845–9,450)	0.283
Hemoglobin, g/dl	13.4 ± 2.0	13.4 ± 2.2	11.9 ± 1.6	0.127
Initial CK, IU/l	110 (78–238)	131 (83–443)	96 (30–439)	0.382

Values are mean ± SD, n (%), or median (interquartile range).

CAD = coronary artery disease; CK = creatine kinase; HbA_{1c} = glycosylated hemoglobin; MI = myocardial infarction; NSTE-ACS = non-ST-segment elevation acute coronary syndrome(s); PCI = percutaneous coronary intervention; STEMI = ST-segment elevation myocardial infarction; WBC = white blood cell.

DISCUSSION

This is the first report that demonstrates 3 distinct types of calcified plaques at the culprit lesion in patients presenting with ACS: eruptive calcified nodules, superficial calcific sheet, and calcified protrusion. The additional findings of this study include that: 1) superficial calcific sheet is the most common type; 2) eruptive calcified nodules are frequently located in the RCA, whereas superficial calcific sheet is most frequently found in the LAD; 3) the superficial calcific sheet group has a poor baseline TIMI flow and smallest luminal diameter; 4) the eruptive calcified nodule group has the largest calcium burden; 5) red thrombus is predominant in eruptive calcified nodules and white thrombus in superficial calcific sheet; and 6) post-PCI myocardial damage is greatest in the superficial calcific sheet group.

PREVALENCE OF CALCIFIED CULPRIT PLAQUES IN PATIENTS WITH ACS. Calcification is a signature of advanced atherosclerosis, and the presence and the extent of calcification is strongly associated with poor prognosis (14). Fibrocalcific plaques are mainly accompanied by calcific sheet (>3 mm), whereas fragmented calcification and microcalcification (0.5 to 15 μm) were frequently found in ruptured lipid plaques (15). Several imaging studies including computed tomography (16) and intravascular ultrasound (IVUS) (17) showed that spotty calcification was prevalent in the culprit lesions associated with ACS, although OCT studies reported conflicting results (12,18,19). Taken together, small calcium deposits may play a role in destabilization of lipid plaque, whereas extensive calcification may be a signature of advanced atherosclerosis and more likely to be associated with plaque stabilization. Nevertheless, calcified plaques are occasionally found in the absence of ruptured lipid core at the culprit lesion in patients with ACS. In this subset of patients, calcified plaques are likely to be responsible for ACS, but the pathogenesis and detailed information of calcified culprit plaque leading to ACS has not been fully investigated.

JACC: CARDIOVASCULAR INTERVENTIONS VOL. 12, NO. 6, 2019
MARCH 26, 2019:531–43

TABLE 2 Angiographic Findings

	Eruptive Calcified Nodules (n = 36)	Superficial Calcific Sheet (n = 88)	Calcified Protrusion (n = 10)	p Value
Culprit artery				0.012
Left anterior descending	15 (41.7)	65 (68.4)	4 (40.0)	
Left circumflex	5 (13.9)	12 (12.6)	3 (30.0)	
Right	16 (44.4)	18 (18.9)	3 (30.0)	
Initial TIMI flow grade 0–1	1 (2.8)	22 (23.2)	2 (20.0)	0.009
Thrombus	6 (16.7)	9 (9.5)	2 (20.0)	0.571
Moderate to heavy calcification	20 (55.6)	40 (42.1)	2 (20.0)	0.265
Type B2/C lesion	25 (69.4)	69 (72.6)	9 (90.0)	0.471
Multivessel disease	22 (61.1)	43 (45.2)	5 (50.0)	0.253
Quantitative coronary angiography analysis				
Minimal lumen diameter, mm	1.05 ± 0.82	0.63 ± 0.57	0.92 ± 0.51	0.003
Reference vessel diameter, mm	2.82 ± 0.65	2.77 ± 0.68	3.12 ± 1.22	0.387
Diameter stenosis, %	65.3 ± 21.8	77.3 ± 20.2	68.9 ± 13.9	0.002
Lesion length, mm	16.4 ± 7.0	19.0 ± 9.2	15.4 ± 6.0	0.203

Values are n (%) or mean ± SD.
TIMI = Thrombolysis in Myocardial Infarction.

A recent study reported the clinical characteristics of calcified nodules at the culprit lesion. However, in that study, both ACS and stable angina pectoris cases were combined (20). In our study, we included calcified plaque at the culprit lesion only in patients with ACS to investigate the role of calcified plaque in the development of ACS.

ERUPTIVE CALCIFIED NODULES. Previous pathology studies reported that 2% to 7% of fatal coronary thromboses were caused by calcified nodules (1,3). Several OCT studies also reported calcified nodules in 2% to 8% of patients with ACS (4,20,21). Our result demonstrating that eruptive calcified nodules were identified in 2.9% (n = 36 of 1,241) of the entire ACS cohort was in line with these studies. Calcified nodules are found predominantly in heavily calcified coronary arteries (1,3). Pathology studies surmise that eruption of calcific nodules causes disruption of the endothelium, leading to thrombus formation (1,3). Fracture of calcific sheet, turning into nodules, breaks through the overlying tissue into the lumen. A recent OCT study supports this concept by demonstrating that calcified nodules were most frequently found in the mid segment of the RCA and were associated with larger hinge movement on angiogram (20). RCAs are situated in the atrioventricular groove and known to have an increased risk for stent fracture (22). Continuous cyclic mechanical forces exerted on the segment of hinge movement over a prolonged period may cause weakening of calcified plaque, leading to fracture. Calcified nodules are commonly surrounded by fibrin, potentially arising from surrounding capillaries that are leaky or damaged (3). Eruptive nodules also cause local flow turbulence that activates procoagulant factors triggering thrombosis (23). In our study, eruptive calcified nodules were indeed associated with a higher prevalence of red thrombus.

SUPERFICIAL CALCIFIC SHEETS. In calcified culprit plaques, in the absence of typical calcified nodules, we observed the following 2 distinctly different patterns: superficial calcific sheets and calcified protrusions. In these 2 types, the underlying mechanism of thrombosis may be different from eruptive calcified nodules. The superficial calcific sheet group had the smallest minimal lumen area among the 3 groups. Luminal narrowing creates a local high endothelial shear stress environment that could lead to platelet aggregation and thrombosis (24). Alternatively, high local plaque structural stress at the junction of fibrous tissue with a rigid calcified plate within the intima could cause intimal tearing (25). Furthermore, because calcium contains collagenous matrix, exposure of collagen could also initiate platelet thrombus formation (26). Taken together, narrow lumen with high biomechanical stress as well as minimal disruption of fibrous tissue could initiate thrombosis. These processes may explain the higher frequency of platelet-rich white thrombus in this group. It should be noted, however, that there has been no pathology report that showed superficial calcific sheets as a cause of cardiac death. However, it may be related to selection bias of the pathology studies. An OCT study on superficial calcific sheet in a patient with ACS has been reported (27).

Spotty calcification is occasionally found in ruptured lipid plaques (18). However, the significance of spotty calcification in the pathogenesis of ACS was recently questioned (12). In the present study, patients who had a ruptured lipid plaque at the culprit lesion were not included in the analysis. All cases in the superficial calcific sheet group did not fulfill the previously reported definition of spotty calcification (12,19). A ruptured lipid plaque with spotty calcification is easily distinguished from a superficial calcific sheet, as the latter does not contain superficial lipid.

CALCIFIED PROTRUSIONS. OCT-derived calcified protrusions were least frequent among the 3 types. This type may correspond to protruding "nodular calcification" in pathology studies. Pathologists claim not to confuse nodular calcification with calcified nodules. The terminology "protruding nodular calcification" is sometimes used to refer a benign bystander protruding plaque with calcification. In a previous IVUS study, pathologically validated calcified nodules corresponded well to convex calcification and irregular luminal surface (28). Another study reported that IVUS-derived calcified nodules at the

TABLE 3 Culprit Plaque Characteristics on Optical Coherence Tomography

	Eruptive Calcified Nodules (n = 36)	Superficial Calcific Sheet (n = 95)	Calcified Protrusion (n = 10)	p Value: Eruptive Calcified Nodules vs. Superficial Calcific Sheet	p Value: Eruptive Calcified Nodules vs. Calcified Protrusion	p Value: Superficial Calcific Sheet vs. Calcified Protrusion
Maximal calcification arc, degree	306.3 (208.2–360.0)	231.7 (158.8–324.7)	88.5 (73.4–141.5)	0.029	<0.001	<0.001
Maximal calcification thickness, μm	1,015 (770–1,198)	930 (760–1,090)	710 (575–795)	0.211	0.001	0.005
Calcification length, mm	21.0 (17.0–33.8)	15.0 (10.0–18.0)	7.0 (3.5–12.0)	<0.001	<0.001	0.001
Calcification index	3,284.9 (2,113.3–5,385.3)	1,644.3 (1,012.4–3,068.7)	472.5 (176.7–865.2)	<0.001	<0.001	<0.001
Minimal flow area, mm^2	2.32 ± 1.79	1.46 ± 0.87	1.82 ± 1.41	0.001	0.740	1.000
Reference lumen area, mm^2	8.54 ± 4.08	6.32 ± 2.58	7.58 ± 2.86	<0.001	1.000	0.546
Area stenosis, %	72.0 ± 16.9	75.6 ± 11.8	75.6 ± 12.3	0.521	1.000	1.000
Thrombus				<0.001	0.016	0.261
White	5 (13.9)	63 (66.3)	5 (50.0)			
Red	30 (83.3)	17 (17.9)	4 (40.0)			
No	1 (2.8)	15 (15.8)	1 (10.0)			

Values are median (interquartile range), mean ± SD, or n (%).

nonculprit lesion were benign, with a very low incidence of future cardiac events (29). However, IVUS does not always accurately distinguish noneruptive protruding nodular calcifications from eruptive calcified nodules, or clearly visualize the plaque surface due to its limited resolution. OCT may be the only imaging modality capable of distinguishing protruding multiple small calcific nodules in the eruptive calcified nodule group from protuberant calcific mass without eruptive nodules in the calcified protrusion group. As shown in **Figure 2**, the leading edge of eruptive calcified nodules is often irregular due to a cluster of small calcific nodules, whereas calcified protrusions typically show smooth leading edge. In our results, calcified protrusions had the smallest calcium burden among the 3 groups and showed high signal attenuation on OCT which was similar to that of lipid pools. This finding implies that this group may have not reached the advanced stage of atherosclerosis or calcific sheet formation compared with the other 2 groups. Given that the necrotic core itself as well as the surrounding collagenous matrix becomes calcified in the atherosclerotic process (15), calcified protrusions may be related to a previously ruptured necrotic core. Eccentric protruding mass into the lumen could induce local flow disturbance and high endothelial shear stress, resulting in platelet aggregation and thrombus formation (23,24).

NEW CLASSIFICATION AND CLINICAL IMPLICATIONS. We previously reported an algorithm for in vivo plaque classification including calcified nodules as assessed by OCT in patients with ACS (4). In the referenced study, the number of patients with calcified culprit plaques was small and the understanding of calcified plaque was limited. As we have reviewed a larger number of cases, we came to acknowledge that a subset of patients had severe calcification at the culprit plaques with luminal thrombi without evidence of ruptured lipid plaque or typical eruptive calcified nodules.

TABLE 4 In-Hospital Outcomes

	Eruptive Calcified Nodules (n = 36)	Superficial Calcific Sheet (n = 95)	Calcified Protrusion (n = 10)	p Value: Eruptive Calcified Nodules vs. Superficial Calcific Sheet	p Value: Eruptive Calcified Nodules vs. Calcified Protrusion	p Value: Superficial Calcific Sheet vs. Calcified Protrusion
Final TIMI flow grade 0–2	1 (2.8)	2 (2.1)	1 (10.0)	1.000	0.391	0.262
Peak CK, IU/l	241 (115–612)	834 (141–3,394)	745 (69–1,984)	0.011	0.542	0.289
In-hospital outcome						
Death	0 (0.0)	0 (0.0)	0 (0.0)	1.000	1.000	1.000
Target lesion revascularization	0 (0.0)	1 (1.1)	0 (0.0)	1.000	1.000	1.000

Values are (%) or median (interquartile range).
Abbreviations as in Tables 1 and 3.

JACC: CARDIOVASCULAR INTERVENTIONS VOL. 12, NO. 6, 2019
MARCH 25, 2019:531–40

CENTRAL ILLUSTRATION Optical Coherence Tomography Diagnostic Algorithm for Acute Coronary Syndromes

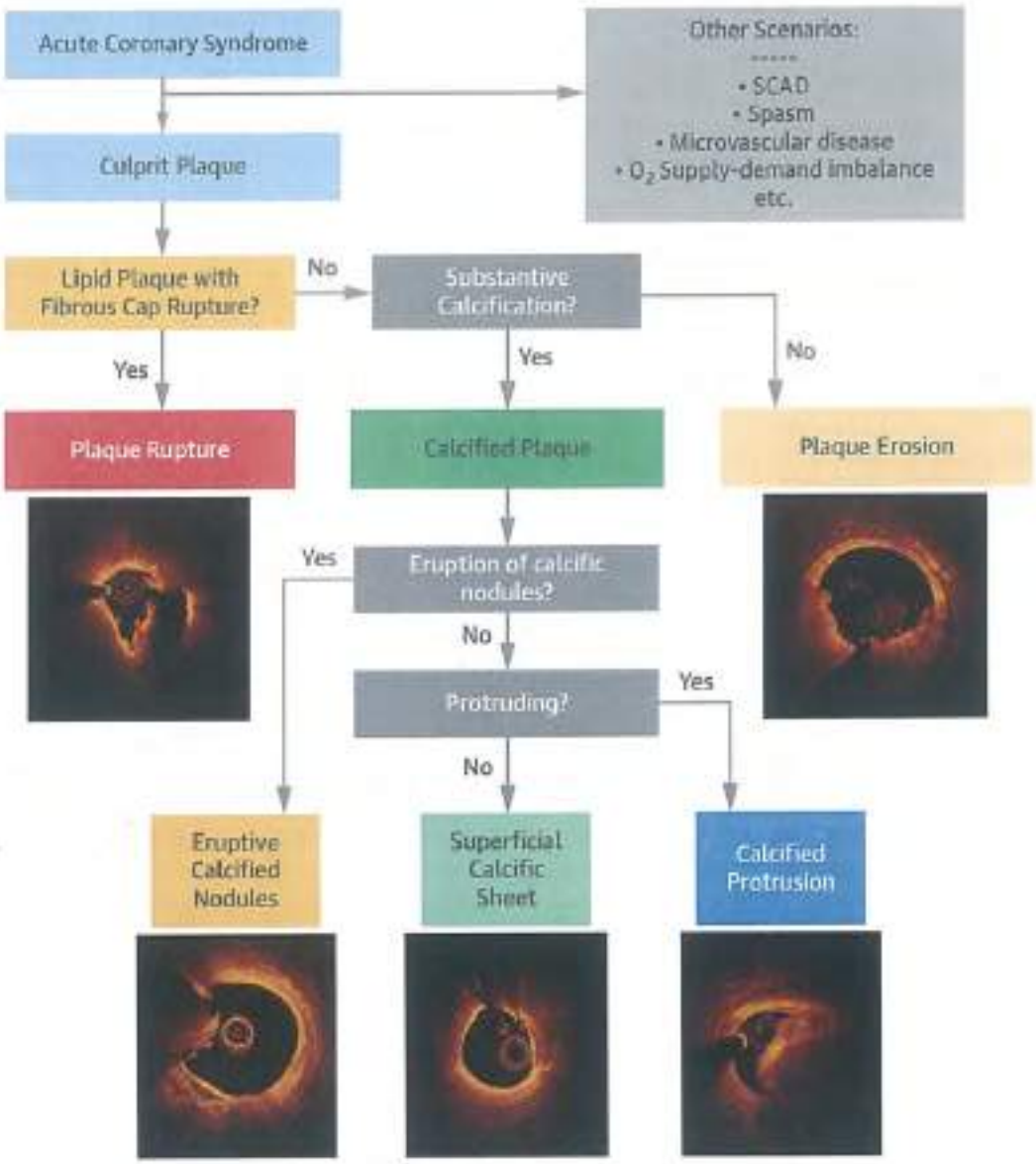

Sugiyama, T. et al. J Am Coll Cardiol Intv. 2019;12(6):531–40.

The presence or absence of rupture of a lipid plaque is the most distinguishing finding. In plaques with the absence of ruptured lipid core, calcified plaques are characterized by the presence of substantive superficial calcification. Depending on the morphology of calcification, calcified culprit plaques are categorized into 3 groups. Plaque erosion is finally identified by the diagnosis of exclusion. SCAD = spontaneous coronary artery dissection.

The present study represents the first and largest series that describes the detailed OCT characteristics of calcified plaques. In this study, we revised the previous algorithm and classified calcified plaques into 3 types based on the pattern of calcification and the presence of disruption of fibrous tissue. We proposed to put these 3 subgroups under "calcified plaque" (Central Illustration). In understanding the underlying mechanism of ACS, the presence or absence of rupture of a lipid plaque is the key finding. In plaques without

evidence of ruptured lipid core, calcified plaques are characterized by the presence of substantive superficial calcification. Our study showed a higher prevalence of calcified culprit plaque (12.7%) compared with the previous studies (2% to 8%) (1,3,4,20,21). Our result was derived from a combination of the previously reported "calcified nodules," superficial calcific sheet, and calcified protrusion.

The association between calcification and prognosis is not fully understood. In our study, the superficial calcific sheet group had higher peak post-PCI CK elevation compared with the eruptive calcified nodule group. These findings imply that we may need to pay more attention to superficial calcific sheet subtype in the setting of PCI that may potentially result in greater myocardial damage. Furthermore, management of calcified plaques in patients with ACS is still challenging. In the superficial calcific sheet group, the presence of smaller minimal lumen area suggests that debulking or plaque modification such as rotational and orbital atherectomy may have a role. In contrast, the eruptive calcified nodule group may require fracture-resistant stents with constant hinge movement. The calcified protrusion group may result in stent malapposition. We believe that our updated OCT diagnosis algorithm and classification will help with understanding of the pathobiology of calcified culprit plaques and selecting efficient treatment strategy in patients with ACS.

STUDY LIMITATIONS. First, this is a retrospective observational study and therefore has intrinsic risk of selection bias. However, the data were prospectively collected at each participating site. All the investigators had extensive experience in OCT and pre-intervention OCT was routinely performed at those institutions in all ACS patients whenever it was feasible. Therefore, ACS cases with pre-intervention OCT were consecutively collected at all participating sites. Nevertheless, selection bias could not be totally excluded, as the study was not prospectively designed. Second, due to its shallow penetration, OCT could not always be useful to detect deep calcification. Because deep calcification may not affect the incidence of luminal thrombosis, we focused on superficial calcification in this study. When the trailing edge of calcium was not clearly visible at the thickest part, we measured the thickness of calcium at the thickest part where the trailing edge was detectable. In the cases with eruptive calcified nodules, maximal calcification arc was measured as a maximal part of circumferential calcification, but not limited to the erupted part. Therefore, calcification arc might have been overestimated in this group, as small calcified nodules erupted into the lumen might have been mixed with thrombus. Third, these OCT findings are not validated by histopathology data. A pathology validation case report demonstrated OCT-derived calcified nodules casting major dorsal shadow in the absence of red thrombus (30). When it was difficult to differentiate calcific nodules from red thrombus, we reviewed adjacent image frames to minimize the chance of misinterpretation. The presence or absence of endothelium and microcalcification cannot be imaged by the current OCT system despite its high resolution. Fourth, massive thrombus may sometimes obscure OCT images. Because the aim of this study was to evaluate the underlying plaque morphology, the use of aspiration thrombectomy before OCT imaging was allowed to obtain optimal OCT images of the culprit lesion. An extreme caution was exercised not to disrupt the underlying structure. Fifth, the culprit lesion in patients with ACS is usually easily identified. However, in patients with non-ST-segment elevation ACS who have multiple stenoses, it can sometimes be challenging to identify the culprit lesion. When it was not obvious, additional findings in OCT images were used to confirm the culprit lesion. Finally, this study, despite the largest series to date, did not evaluate clinical outcomes. Further studies to evaluate the best treatment options and long-term outcomes of each type of calcified culprit plaques are warranted.

CONCLUSIONS

In this study, we report the 3 distinct types of calcified plaques in patients with ACS and proposed a new in vivo OCT diagnosis algorithm, which will help us to better understand the pathobiology and to provide optimal care.

ACKNOWLEDGMENTS The authors thank Lally Chan (The Chinese University of Hong Kong), Sarah Reniers (University Hospitals Leuven), and Masahiro Imura (Nippon Medical School Chiba Hokusoh Hospital) for data collection and management work; and Gregory Gheewalla, BS (Massachusetts General Hospital) for his support. Dr. Jang's research was supported by Mr. and Mrs. Michael and Kathryn Park, and by Mrs. and Mr. Gill and Allan Gray.

ADDRESS FOR CORRESPONDENCE: Dr. Ik-Kyung Jang, Cardiology Division, Massachusetts General Hospital, Harvard Medical School, 55 Fruit Street, GRB 800, Boston, Massachusetts 02114. E-mail: ijang@mgh.harvard.edu. OR Dr. Taishi Yonetsu, Department of Interventional Cardiology, Tokyo Medical and Dental University, 1-5-45, Yushima, Bunkyo Ward, Tokyo 113-8519, Japan. E-mail: t-yonetsu.cvm@tmd.ac.jp.

JACC: CARDIOVASCULAR INTERVENTIONS VOL. 12, NO. 6, 2019
MARCH 25, 2019:531–40

PERSPECTIVES

WHAT IS KNOWN? Pathology studies showed that calcified nodule is responsible for 2% to 7% of sudden cardiac death. In vivo data on calcified plaques at the culprit lesion in patients with ACS are limited.

WHAT IS NEW? Three distinct types of calcified plaques are identified at the culprit lesion in patients with ACS: superficial calcific plate, eruptive calcified nodules, and calcified protrusion. Superficial calcific plate is frequently located in the LAD and is associated with white thrombus. Eruptive calcified nodules are most frequent in the RCA and are associated with red thrombus. A new OCT diagnosis algorithm and classification are proposed.

WHAT IS NEXT? These new findings may help to better understand the pathobiology of calcified culprit plaques, to guide for optimal treatment strategy and to predict outcomes after PCI in patients with ACS.

REFERENCES

1. Virmani R, Burke AP, Farb A, Kolodgie FD. Pathology of the vulnerable plaque. J Am Coll Cardiol 2006;47:C13–18.

2. Bentzon JF, Otsuka F, Virmani R, Falk E. Mechanisms of plaque formation and rupture. Circ Res 2014;114:1852–66.

3. Yahagi K, Kolodgie FD, Otsuka F, et al. Pathophysiology of native coronary, vein graft, and in-stent atherosclerosis. Nat Rev Cardiol 2016;13:79–98.

4. Jia H, Abtahian F, Aguirre AD, et al. In vivo diagnosis of plaque erosion and calcified nodule in patients with acute coronary syndrome by intravascular optical coherence tomography. J Am Coll Cardiol 2013;62:1748–58.

5. Serruys PW, Foley DP, de Feyter PJ. Quantitative Coronary Angiography in Clinical Practice. Dordrecht, the Netherlands: Kluwer Academic, 1994.

6. TIMI Study Group. The Thrombolysis in Myocardial Infarction (TIMI) trial. Phase I findings. N Engl J Med 1985;312:932–6.

7. Ellis SG, Vandormael MG, Cowley MJ, et al. Coronary morphologic and clinical determinants of procedural outcome with angioplasty for multivessel coronary disease. Implications for patient selection. Multivessel Angioplasty Prognosis Study Group. Circulation 1990;82:1193–202.

8. Teirstein PS, Schatz RA, Dellanzo SJ, Jensen EE, Johnson AD. Angioscopic versus angiographic detection of thrombus during coronary interventional procedures. Am J Cardiol 1995;75:1083–7.

9. Mintz GS, Popma JJ, Pichard AD, et al. Patterns of calcification in coronary artery disease. A statistical analysis of intravascular ultrasound and coronary angiography in 1155 lesions. Circulation 1995;91:1959–65.

10. Prati F, Regar E, Mintz GS, et al. Expert review document on methodology, terminology, and clinical applications of optical coherence tomography: physical principles, methodology of image acquisition, and clinical application for assessment of coronary arteries and atherosclerosis. Eur Heart J 2010;31:401–15.

11. Sugiyama T, Yamamoto E, Bryniarski K, et al. Nonculprit plaque characteristics in patients with acute coronary syndrome caused by plaque erosion vs plaque rupture: A 3-vessel optical coherence tomography study. JAMA Cardiol 2018;3:207–14.

12. Ong DS, Lee JS, Soeda T, et al. Coronary calcification and plaque vulnerability: An optical coherence tomographic study. Circ Cardiovasc Imaging 2016;9:e003929.

13. Kume T, Akasaka T, Kawamoto T, et al. Assessment of coronary arterial thrombus by optical coherence tomography. Am J Cardiol 2006;97:1713–7.

14. Detrano R, Guerci AD, Carr JJ, et al. Coronary calcium as a predictor of coronary events in four racial or ethnic groups. N Engl J Med 2008;358:1336–45.

15. Mori H, Torii S, Kutyna M, Sakamoto A, Finn AV, Virmani R. Coronary artery calcification and its progression: what does it really mean? J Am Coll Cardiol Img 2018;11:127–42.

16. Motoyama S, Kondo T, Sarai M, et al. Multislice computed tomographic characteristics of coronary lesions in acute coronary syndromes. J Am Coll Cardiol 2007;50:319–26.

17. Ehara S, Kobayashi Y, Yoshiyama M, et al. Spotty calcification typifies the culprit plaque in patients with acute myocardial infarction: an intravascular ultrasound study. Circulation 2004;110:3424–9.

18. Mizukoshi M, Kubo T, Takarada S, et al. Coronary superficial and spotty calcium deposits in culprit coronary lesions of acute coronary syndrome as determined by optical coherence tomography. Am J Cardiol 2013;112:34–40.

19. Kataoka Y, Puri R, Hammadah M, et al. Spotty calcification and plaque vulnerability in vivo frequency-domain optical coherence tomography analyses. Cardiovasc Diagn Ther 2014;4:460–9.

20. Lee T, Mintz GS, Matsumura M, et al. Prevalence, predictors, and clinical presentation of a calcified nodule as assessed by optical coherence tomography. J Am Coll Cardiol Img 2017;10:883–91.

21. Kajander OA, Pinilla-Echeverri N, Jolly SS, et al. Culprit plaque morphology in STEMI - an optical coherence tomography study: Insights from the TOTAL-OCT substudy. EuroIntervention 2016;12:716–23.

22. Chakravarty T, White AJ, Buch M, et al. Meta-analysis of incidence, clinical characteristics and implications of stent fracture. Am J Cardiol 2010;106:1075–80.

23. Malek AM, Alper SL, Izumo S. Hemodynamic shear stress and its role in atherosclerosis. JAMA 1999;282:2035–42.

24. Nesbitt WS, Westein E, Tovar-Lopez FJ, et al. A shear gradient-dependent platelet aggregation mechanism drives thrombus formation. Nat Med 2009;15:665–73.

25. Richardson PD, Davies MJ, Born GV. Influence of plaque configuration and stress distribution on fissuring of coronary atherosclerotic plaques. Lancet 1989;2:941–4.

26. Fernandez-Ortiz A, Badimon JJ, Falk E, et al. Characterization of the relative thrombogenicity of atherosclerotic plaque components: implications for consequences of plaque rupture. J Am Coll Cardiol 1994;23:1562–9.

27. Alfonso F, Gonzalo N, Nunez-Gil I, Bunsueles C. Coronary thrombosis from large, nonprotruding, superficial calcified coronary plaques. J Am Coll Cardiol 2013;62:2254.

28. Lee JB, Mintz GS, Lisauskas JB, et al. Histopathologic validation of the intravascular ultrasound diagnosis of calcified coronary artery nodules. Am J Cardiol 2011;108:1547–51.

29. Xu Y, Mintz GS, Tam A, et al. Prevalence, distribution, predictors, and outcomes of patients with calcified nodules in native coronary arteries: a 3-vessel intravascular ultrasound analysis from Providing Regional Observations to Study Predictors of Events in the Coronary Tree (PROSPECT). Circulation 2012;126:537–45.

30. Hao H, Fujii K, Shibuya M, et al. Different findings in a calcified nodule between histology and intravascular imaging such as intravascular ultrasound, optical coherence tomography, and coronary angioscopy. J Am Coll Cardiol Intv 2014;7:937–8.

KEY WORDS acute coronary syndrome(s), calcification, plaque, optical coherence tomography

Prognostic Value of Energy Loss Coefficient for Predicting Asymptomatic Aortic Stenosis Outcomes: Direct Comparison With Aortic Valve Area

Hirokazu Yoshida, MT, Yoshihiro Seo, MD, PhD, Tomoko Ishizu, MD, PhD, Masaki Izumo, MD, PhD, Yoshihiro J. Akashi, MD, PhD, Eiji Yamashita, MD, Yutaka Otsuji, MD, PhD, Kazuaki Negishi, MD, PhD, and Masaaki Takeuchi, MD, PhD, *Kitakyushu, Tsukuba, Kawasaki, and Machashi, Japan; and Hobart, Australia*

Background: The pressure recovery–adjusted aortic valve area (AVA), called the energy loss coefficient (ELCo), is theoretically a more accurate parameter for evaluating aortic stenosis (AS) severity. The aim of this study was to compare the prognostic value of ELCo with that of conventional AVA.

Methods: Indexed AVA (iAVA) was measured using Doppler echocardiography in 301 asymptomatic Japanese patients with AS and preserved left ventricular ejection fractions. Sinotubular junction diameter was also measured, and the indexed ELCo (iELCo) was calculated. Patients were followed for major cardiac events, including cardiac death, ventricular fibrillation, myocardial infarction, heart failure requiring admission, and aortic valve replacement.

Results: The mean sinotubular junction diameter was 2.5 ± 0.3 cm, and >90% of patients had sinotubular junction diameters < 3 cm. There was a quadratic correlation between iAVA and iELCo ($r = 0.97$, $P < .001$). During a median of 17.4 months of follow-up, 90 patients had major cardiac events. Statistical analysis failed to show any superiority of iELCo over iAVA for predicting major cardiac events. However, iELCo stratified high-risk patients for cardiac outcome in a subset of patients whose AS grades were classified as severe using iAVA and in those whose AS severity was inconsistent (iAVA < 0.6 cm^2/m^2 but mean pressure gradient < 40 mm Hg).

Conclusions: The calculation of iELCo may not be always required, even in patients with asymptomatic AS with small aortic roots. However, this index should be calculated in patients whose AS grading assessed by iAVA is severe and in those in whom AS severity criteria are inconsistent. (J Am Soc Echocardiogr 2019;32:351-8.)

Keywords: Aortic stenosis, Aortic valve area, Energy loss coefficient, Prognosis

The pressure gradient across the aortic valve and aortic valve area (AVA) using a continuity equation are the primary hemodynamic parameters recommended for the evaluation of aortic stenosis (AS) severity.[1-3] Doppler echocardiography–derived instantaneous pressure gradient overestimates the net pressure gradient imposed on the left ventricle because of the presence of the pressure recovery phenomenon beyond the stenotic aortic valve.[4-6] To overcome this problem, the pressure recovery–adjusted effective AVA, called the energy loss coefficient (ELCo), was established by Garcia *et al.*[7,8] Those authors found that ELCo was superior to AVA for predicting composite end points including all mortality and aortic valve replacement (AVR) in their retrospective analysis.[7] A recent prospective large observational study reported that lower ELCo, independently of mean pressure gradient or peak aortic jet velocity, predicted higher risk for future adverse outcome in the subgroup of patients with small aortic roots,[9] which was in agreement with previous studies.[5,6] Thus, the evaluation of clinical usefulness of ELCo is of paramount importance in physically smaller individuals, such as elderly Japanese patients with AS. A previous study reported that the mean diameter of the sinotubular junction (STJ) in the healthy aged Japanese population is 2.9 cm in men and 2.6 cm in women.[10] These values are quite small compared with those in normal adults (3.4 cm in men and 3.0 cm in women) reported in the cardiac chamber quantification guideline from the American Society of Echocardiography and the European Association of Cardiovascular Imaging.[11]

From the Department of Laboratory and Transfusion Medicine, University of Occupational and Environmental Health Hospital (H.Y., M.T.), and the Second Department of Internal Medicine, University of Occupational and Environmental Health, School of Medicine (Y.O.), Kitakyushu; the Cardiovascular Division, University of Tsukuba, Tsukuba (Y.S., T.I.); the Division of Cardiology, Department of Internal Medicine, St. Marianna University School of Medicine, Kawasaki (M.I., Y.J.A.); the Department of Cardiology, Gunma Prefectural Cardiovascular Center, Maebashi (E.Y.), Japan; and the Menzies Institute for Medical Research, University of Tasmania, Hobart, Australia (K.N.).

Reprint requests: Masaaki Takeuchi, MD, PhD, Department of Laboratory and Transfusion Medicine, University of Occupational and Environmental Health Hospital, 1-1 Iseigaoka, Yahatanishi-ku, Kitakyushu 807-8555, Japan (E-mail: takeuchi@med.uoeh-u.ac.jp).

0894-7317/$36.00

Copyright 2018 by the American Society of Echocardiography.

https://doi.org/10.1016/j.echo.2018.10.018

Abbreviations

AS = Aortic stenosis

AUC = Area under the curve

AVA = Aortic valve area

AVR = Aortic valve replacement

CE = Cardiac event

ELCo = Energy loss coefficient

iAVA = Indexed aortic valve area

IDI = Integrated discrimination improvement

iELCo = Indexed energy loss coefficient

LV = Left ventricular

LVEF = Left ventricular ejection fraction

LVOT = Left ventricular outflow tract

NRI = Net reclassification improvement

ROC = Receiver operating characteristic

STJ = Sinotubular junction

Accordingly, the aim of this study was to compare the prognostic value of ELCo and AVA for predicting outcomes in asymptomatic Japanese patients with AS and preserved left ventricular ejection fractions (LVEFs).

METHODS

Study Population

This study was part of a recently conducted multicenter study (Japanese Multicenter Aortic Stenosis Study, Prospective registry). We prospectively enrolled patients with AS (peak velocity across the aortic valve > 2.5 m/sec) who underwent comprehensive echocardiographic examinations at one of four Japanese cardiovascular centers (University of Occupational and Environmental Health, University of Tsukuba, St. Marianna University, and Gunma Prefectural Cardiovascular Center) from January 2013 to December 2014. Of the 618 echocardiographic examinations of patients with AS performed during the study enrollment period, we excluded 317 for symptoms (n = 243), inadequate data acquisition (n = 15), LVEF < 50% (n = 44), and <1 month of follow-up (n = 15). Thus, a total of 301 asymptomatic patients with AS and preserved LVEFs were included in this study. The study protocol was approved by the ethics committee at each hospital, and the requirement to obtain informed consent was waived because of the retrospective nature of the analysis. The echocardiographic image data set for each patient was sent to the core laboratory, and all analyses were conducted by one investigator.

Two-Dimensional and Doppler Echocardiography

A comprehensive echocardiographic examination was performed using a commercially available ultrasound machine and equipment following the guidelines.[11] Left ventricular (LV) end-diastolic and end-systolic volumes were measured using the biplane Simpson formula in the apical four- and two-chamber views, and LVEF was calculated. Maximum left atrial volume was also measured using the biplane Simpson formula. LV inflow velocity was obtained at the level of the mitral leaflet tips. Mitral annular velocity (e') was measured at the septal corner of the mitral annulus. Pulse-wave LV outflow tract (LVOT) velocity was obtained with the sample volume placed just below the aortic valve, while LVOT diameter was measured at the level of the aortic valve annulus using zoom mode. Peak aortic valve jet velocity was obtained from multiple acoustic windows to yield the highest velocity signal. Stroke volume was calculated as $\pi \times$ (LVOT diameter/2)^2 $\times$ velocity-time integral of pulse-wave LVOT velocity. AVA was defined as stroke volume divided by the velocity-time integral of the peak aortic jet velocity and indexed to body surface area. STJ diameter was measured at the level of the STJ using an inner edge–to–inner edge method. STJ area was defined as $\pi \times$ (STJ diameter/2)^2. ELCo was calculated as AVA $\times$ STJ area/(STJ area − AVA) and indexed to body surface area.[3] Systolic pulmonary arterial pressure was measured (4 $\times$ [peak velocity of the tricuspid regurgitation]^2 + right atrial pressure). Right atrial pressure was estimated on the basis of inferior vena cava diameter and its change during respiration.[12]

AS Severity Grading

A value < 0.6 cm^2/m^2 was used as the cutoff for severe AS by both indexed AVA (iAVA) and indexed ELCo (iELCo). Patients who had values from 0.6 to 0.85 cm^2/m^2 were diagnosed with moderate AS by both methods. Mild AS was defined as >0.85 cm^2/m^2 by both iAVA and iELCo.

Follow-Up

All patients were followed up regularly at an outpatient clinic. Patients, physicians, and family members were contacted by telephone if the patients were treated at other hospitals. Final follow-up data were obtained between January and May 2016. The primary end point was major cardiac events (CEs), which included cardiac death, ventricular fibrillation, nonfatal myocardial infarction, heart failure exacerbation requiring hospitalization, and surgical or transcatheter AVR.

Reliability of Measurements

Intraobserver variability was assessed in 30 randomly selected patients by repetition of the observer's AVA and ELCo measurements 2 weeks apart. Interobserver variability was determined when a second observer performed these measurements in the same 30 patients. The intra- and interobserver variability values were calculated as the absolute differences between the corresponding the two measurements as percentages of the mean and intraclass correlation.

Statistical Analysis

Continuous data are expressed as mean ± SD or median and interquartile range according to the data distribution. The normality of the data distribution was evaluated using the Kolmogorov-Smirnov test. Categorical data are expressed as numbers or percentages. Student's t test, the Mann-Whitney U test, or the Wilcoxon rank sum test was used to compare continuous variables between the two groups. The Fisher exact test or the χ^2 test was used to compare categorical values. A regression analysis was performed of iAVA and iELCo values. A survival analysis was performed using the Kaplan-Meier method, while group differences were determined using the log-rank test. A Cox proportional-hazard regression analysis was used to determine the prognostic value of iAVA and iELCo with hazard ratios and 95% CIs. Number needed to treat was calculated as a marker of effect size.[13] To compare the predictive strengths of iAVA and iELCo, receiver operating characteristic (ROC) curves for major CEs were created. We conducted a pairwise comparison of the area under the curve (AUC) using DeLong's test. A net reclassification improvement (NRI) and integrated discrimination improvement (IDI) analysis to compare the predictive ability of iAVA and iELCo was also performed.[14,15] A two-sided P value < .05

HIGHLIGHTS

- Japanese patients with AS have small aortic roots.
- iELCo was not superior to iAVA for predicting major CEs in the whole population.
- iELCo was useful in patients with iAVA < 0.6 cm^2/m^2.
- iELCo was also useful in patients with discordant AS severity grading.

was considered significant. All statistical analyses were performed using commercial software (JMP version 13.1.0 [SAS Institute, Cary, NC], R version 3.4.3 and EZR version 1.36 [R Foundation for Statistical Computing, Vienna, Austria], and Prism 7 [GraphPad Software, La Jolla, CA]).

RESULTS

Table 1 shows the clinical and echocardiographic characteristics of the study subjects. As expected, the mean STJ diameter was 2.46 ± 0.33 cm, and only 23 patients (8%) had STJ diameters > 3 cm.

Median iAVA and iELCo Values

The median iAVA value was 0.59 cm^2/m^2 (range, 0.48–0.78 cm^2/m^2). The corresponding median iELCo value was 0.74 cm^2/m^2 (range, 0.57–1.04 cm^2/m^2), and the paired comparison revealed that median iELCo was significantly larger than median iAVA ($P < .001$). There was a quadratic correlation between the two indices (Figure 1). Measurement differences between iAVA and iELCo were significantly larger in patients with STJ diameters < 3 cm (median, 0.15 cm^2/m^2; range, 0.09–0.26 cm^2/m^2) than those with STJ diameters ≥ 3 cm (median, 0.09 cm^2/m^2; range, 0.07–0.14 cm^2/m^2) ($P = .006$). The numbers of patients with mild, moderate, and severe AS determined by iAVA were 47, 100, and 154, respectively. The corresponding numbers assessed by iELCo were 117, 91, and 93, respectively. There was a significant difference for severe AS using iAVA and iELCo ($P < .001$). The complete agreement of AS severity between the two methods was 56% (170 of 301 patients). Among the 154 patients who were classified as having severe AS using iAVA, 61 (39.6%) were classified as having moderate AS using iELCo.

Prognosis

During a median of 17.4 months of follow-up, 90 patients had 96 major CEs, including cardiac death in six, ventricular fibrillation in two, myocardial infarction in one, and heart failure required for admission in 17. A total of 70 patients underwent AVR. Reasons for AVR included symptom onset in 28 (40%), patient's or attending physician's willingness in 20 (28%), rapid progression in 10 (14%), very severe AS (peak aortic jet velocity > 5.0 m/sec) in four (6%), concomitant cardiac surgery in four (6%), reduced LVEF in two (2%), and prophylactic surgery before major noncardiac surgery in two (2%). Figure 2 depicts the Kaplan-Meier survival analysis according to AS severity grading assessed by iAVA and iELCo. In contrast to the group of patients with mild or moderate AS, the group with severe AS assessed by both methods showed significantly worse prognosis for future major CEs.

Table 1 represents the clinical and echocardiographic variables of patients with or without major CE. Regarding effect size, peak velocity had the smallest number needed to treat (1.62), followed by mean pressure gradient (1.67), iAVA (1.80), and iELCo (1.91). Tables 2 and 3 show the univariate and multivariate Cox proportional-hazard analyses for predicting major CEs. Univariate analysis revealed that both iAVA and iELCo were significant predictors. Multivariate analysis showed that iAVA was a significant predictor after the adjustment for mean pressure gradient but not a significant predictor after the adjustment for peak velocity (models 1 and 2, respectively); iELCo was also a significant predictor after adjustment for mean pressure gradient but not a significant predictor after adjustment for peak velocity (models 3 and 4, respectively). The ROC analysis revealed that the best cutoff value of iAVA for predicting major CEs was 0.52 cm^2/m^2, with sensitivity of 81.5% and specificity of 71.1%. The corresponding value of iELCo was 0.63 cm^2/m^2, with sensitivity of 80.6% and specificity of 73.3%. Comparison of the paired AUCs showed no significant differences in the AUC for iAVA (0.80) and that for iELCo (0.80) ($P = .785$).

Reclassification analysis showed that NRI was a positive value, but iELCo did not significantly improve outcome compared with iAVA (NRI = 0.151, $P = .230$; IDI = 0.001, $P = .351$).

Subgroup Analysis

Patients with mild to moderate AS assessed by iAVA are inevitably classified into mild and moderate AS when AS severity is determined by iELCo. Thus, we selected patients whose AS grading was severe using iAVA (<0.6 cm^2/m^2, n = 154). Kaplan-Meier analysis revealed that event-free survival was significantly better in patients whose AS grading was converted to "moderate" using iELCo than those whose grading remained "severe" despite the use of iELCo (Figure 3). Clinical and echocardiographic variables between the group of patients with severe AS by iAVA but not by iELCo and the group of patients with severe AS by both iAVA and iELCo are shown in Supplemental Table 1 (available at www.onlinejase.com). The group of patients with severe AS by both iAVA and iELCo had significantly larger LV volumes, lower LVEFs, and higher both peak aortic valve jet velocity and mean pressure gradient than those with severe AS by iAVA but not by iELCo.

A reclassification analysis revealed that iELCo had no significant improvement in classification for predicting outcome (NRI = 0.026, $P = .872$; IDI = 0.005, $P = .399$) compared with iAVA. Tables 4 and 5 show the univariate and multivariate Cox proportional-hazard analyses for predicting major CEs in the subset of patients who had iAVA < 0.6 cm^2/m^2. Although univariate analysis revealed that both iAVA and iELCo were significant predictors of major CEs, multivariate analysis showed that neither iAVA nor iELCo was a significant predictor after adjusting stroke volume index, mean pressure gradient (peak aortic valve jet velocity), and STJ diameter.

We also selected 91 patients whose AS severity showed discordant results (iAVA < 0.6 cm^2/m^2 but mean pressure gradient < 40 mm Hg). Univariate Cox proportional analysis revealed that iELCo ($P = .035$) but not iAVA ($P = .096$) was a significant predictor of major CEs. Comparison of the paired AUCs showed no significant differences in the AUC for iAVA (0.60) and the AUC for iELCo (0.63) ($P = .078$). Although Kaplan-Meier analysis stratified by the cutoff value of 0.6 cm^2/m^2 showed no intergroup survival differences (Figure 4A), Kaplan-Meier analysis stratified by the best cutoff value of iELCo using ROC analysis (0.63 cm^2/m^2) showed significant intergroup survival differences (Figure 4B). The patients who had mean pressure gradients

Table 1 Clinical and echocardiographic variables in the whole cohort and patients with or without major CEs

Variable	Whole cohort (N = 301)	Major CE (n = 90)	No major CE (n = 211)	P (major CE vs no major CE)
Age (y)	76 ± 10	74 ± 8	77 ± 11	.0113
Male/female	145/156	46/44	99/112	.5053
Body surface area (m^2)	1.53 ± 0.19	1.58 ± 0.20	1.51 ± 0.19	.0060
Heart rate (beats/min)	66 ± 11	67 ± 12	65 ± 11	.0853
Systolic blood pressure (mm Hg)	140 ± 29	135 ± 35	142 ± 26	.0760
Diastolic blood pressure (mm Hg)	71 ± 17	70 ± 19	72 ± 16	.3049
Hypertension (yes/no)	224/77	68/22	156/55	.8163
Diabetes (yes/no)	80/221	27/63	53/158	.3960
Hyperlipidemia (yes/no)	127/74	39/51	88/123	.8439
Chronic kidney disease (yes/no)	145/156	45/45	100/111	.7326
Coronary artery disease (yes/no)	54/247	12/78	42/169	.1537
LVEDVI	63.2 ± 15.5	66.7 ± 16.1	61.7 ± 15.0	.0109
LVESVI	25.6 ± 7.9	28.0 ± 8.2	24.6 ± 7.6	.0007
LVEF	60 ± 5	58 ± 5	60 ± 5	.0008
LVSVI	45.2 ± 10.2	44.1 ± 9.2	45.7 ± 10.5	.2108
LAVImax	34.8 (27.2–47.2)	39.6 (31.4–52.4)	32.9 (25.8–46.9)	.0034
E wave	74.8 (60.7–94.1)	80 (63.4–98.9)	71.7 (59.6–89.3)	.0229
A wave	103.9 ± 28.3	105.1 ± 26.9	103.4 ± 28.9	.6384
e'	5.0 (4.0–6.4)	4.9 (4.0–6.2)	5 (4.0–6.5)	.4023
E/e' ratio	15.2 (11.4–20.9)	16.3 (12.6–23.1)	14.2 (10.8–20.3)	.0145
SPAP	33.1 (29.6–37.5)	33.4 (29.9–40.6)	33 (29.2–37)	.2642
Peak velocity (m/sec)	3.51 ± 0.86	4.16 ± 0.81	3.22 ± 0.72	<.0001
Mean pressure gradient (mm Hg)	25.2 (17.7–38.2)	32.3 (22.4–40.1)	21.5 (15.5–28.8)	<.0001
iAVA (cm^2/m^2)	0.59 (0.48–0.78)	0.46 (0.39–0.55)	0.66 (0.55–0.82)	<.0001
iELCo (cm^2/m^2)	0.74 (0.57–1.04)	0.54 (0.46–0.67)	0.84 (0.67–1.11)	<.0001
STJ diameter (cm)	2.46 ± 0.33	2.47 ± 0.30	2.46 ± 0.33	.8074
STJ area (cm^2)	4.83 ± 1.30	4.85 ± 1.23	4.82 ± 1.33	.8902

LAVImax, Maximal left atrial volume index; *LVEDVI*, LV end-diastolic volume index; *LVEF*, LV ejection fraction; *LVESVI*, LV end-systolic volume index; *LVSVI*, LV stroke volume index; *MACE*, major adverse CE; *SPAP*, systolic pulmonary arterial pressure.

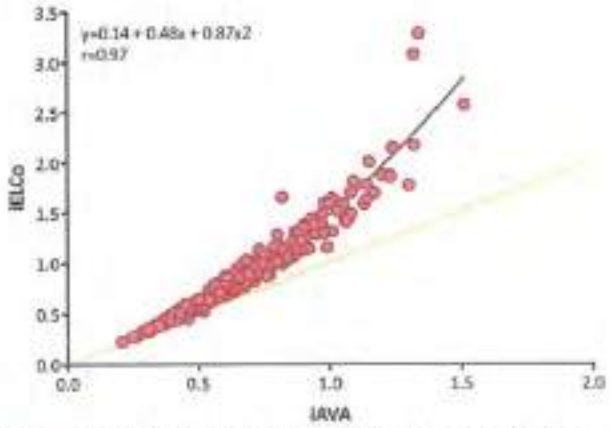

Figure 1 Correlation curve between iELCo and iAVA. A quadratic correlation is seen between the two parameters with the identity line (*in orange*).

< 40 mm Hg with severe AS by iAVA but not by iELCo had lower peak velocities and mean pressure gradients than the group of patients with mean pressure gradients < 40 mm Hg and severe AS by both iAVA and iELCo (Supplemental Table 2, available at www.onlinejase.com). Both NRI analysis and IDI analysis showed that iELCo did not significantly improve outcome compared with iAVA (NRI = 0.402, $P = .055$; IDI = 0.032, $P = .076$).

Among 154 patients whose AS grading was severe using iAVA, 92 patients did not undergo AVR. We divided these 92 patients into two groups, those who remained classified as having severe AS using iELCo ($n = 45$) and those who were reclassified as having moderate AS using iELCo ($n = 47$). Kaplan-Meier analysis revealed that the patients reclassified as having moderate AS had fewer events, but the difference did not reach statistical significance ($P = .077$; Supplemental Figure 1, available at www.onlinejase.com). However, this comparison was underpowered because of the small sample size and low event rate ($n = 15$).

Reliability of Stroke Volume Measurements among the Three Methods

The intraobserver variability values and intraclass correlation coefficients for the measurements of iAVA and iELCo were 7 ± 5% and 11 ± 9% and 0.95 and 0.97, respectively. The corresponding interobserver variability values and ICC were 13 ± 10% and 15 ± 18% and 0.91 and 0.79, respectively.

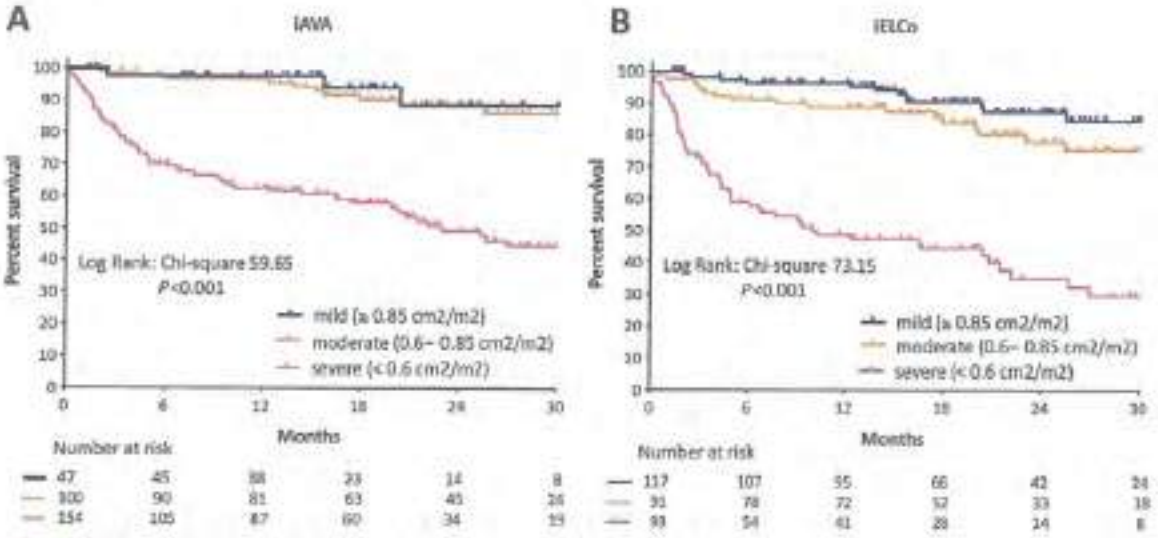

Figure 2 Kaplan-Meier survival analysis according to AS severity grading assessed by iAVA **(A)** and iELCo **(B)**.

Table 2 Univariate Cox proportional-hazard analysis for predicting major CEs in the entire population

Variable	HR (95% CI)	P
SVI	0.99 (0.97–1.01)	.2647
PV	2.92 (2.37–3.61)	<.0001
mPG	1.04 (1.04–1.05)	<.0001
iAVA	0.0035 (0.001–0.015)	<.0001
iELCo	0.024 (0.009–0.067)	<.0001
STJ diameter	1.9 (0.58–2.04)	.7987

HR, Hazard ratio; *mPG*, mean pressure gradient; *PV*, peak velocity; *SVI*, stroke volume index.

DISCUSSION

The major findings of this study can be summarized as follows: (1) STJ diameter in the Japanese AS population was quite small, with a mean value of 2.5 cm, so that >90% of the population met at least one of the recommended criteria for the calculation of ELCo (STJ diameter < 3 cm) reported in the previous literature[4,6]; (2) there were excellent quadratic correlations between iAVA and iELCo because they contain many of the same variables; (3) iELCo failed to show any superiority over iAVA to predict cardiac outcomes in the entire group of patients with asymptomatic AS and preserved LVEFs; (4) however, iELCo stratified the high-risk group of patients for future cardiac outcomes in a subset of patients whose AS grading was classified as severe using iAVA and in those whose AS severity was inconsistent; and (5) ROC analysis revealed that optimal cutoff value of iELCo (0.63 cm^2/m^2) was similar to the current partition value (0.6 cm^2/m^2) used to discriminate severe AS from nonsevere AS.

Previous Studies

Several previous studies demonstrated that Doppler echocardiography–derived instantaneous pressure gradient across the aortic valve in patients with AS significantly overestimates catheter gradients and that Doppler gradients corrected for pressure recovery showed good agreement with catheter gradients.[8,16-19] The impact of pressure recovery as a proportion of the total peak transvalvular gradient was more remarkable in patients whose peak velocities were relatively lower (<2.79 m/sec) or who had small aortic roots.[20] Doppler gradients corrected for pressure recovery were useful for predicting LV mass regression after AVR.[21,22] Few studies addressed the prognostic value of Doppler measurements corrected for pressure recovery. Garcia *et al.*[7] reported that iELCo was superior to iAVA for predicting cardiac outcomes, defined as total mortality and AVR, in 138 patients with moderate to severe AS (mean age, 67 ± 14 years; 80 men).[7] Bahlmann *et al.*[9] described the prognostic value of iELCo in a large number of asymptomatic patients with AS (n = 1,563, severe AS by iELCo in 24%). NRI analysis revealed that the addition of iELCo significantly improves classification for predicting aortic valve–related events but not secondary end points, including total mortality and hospitalization for heart failure. It is worth mentioning that the AUC for iELCo and that for iAVA were equivalent for predicting aortic valve–related events (0.68 vs 0.68) as well as secondary end points (0.59 vs 0.59).

The Present Study

The mean STJ diameter (2.46 ± 0.33 cm) in this study was less than that reported in healthy elderly Japanese subjects (2.9 ± 0.3 cm in male subjects ≥60 years of age and 2.6 ± 0.3 cm in female subjects ≥60 years old)[10] and that in European patients with AS (2.82 ± 0.43 cm)[9] but in agreement with a previous three-dimensional transesophageal echocardiographic study.[23] We previously reported that long- and short-axis diameters of the STJ in patients with tricuspid AS were 2.50 ± 0.30 and 2.43 ± 0.31 cm, respectively,[13] values that were quite similar to that obtained in this study. We also measured STJ diameter in elderly patients without AS in the previous study,[25] and the corresponding values (2.75 ± 0.34 and 2.70 ± 0.33 cm) were similar to those obtained in healthy male subjects and female subjects in the previous study.[10] These results reconfirmed that Japanese subjects are associated with small aortic roots, and this characteristic is more prominent in patients with tricuspid AS because of negative remodeling of the aortic root.[13] Thus, the routine adjustment of Doppler-derived AVA using ELCo is quite important in the Japanese AS population.

Table 3 Multivariate Cox proportional-hazard analysis for predicting major CEs in the entire population

	Model 1		Model 2		Model 3		Model 4	
Variable	HR (95% CI)	P	HR (95% CI)	P	HR (95% CI)	P	HR (95% CI)	P
SVI	0.99 (0.96–1.03)	.7685	1.02 (0.98–1.05)	.3562	0.99 (0.95–1.02)	.3772	1.01 (0.98–1.04)	.7516
PV	2.13 (1.35–3.39)	.0013			2.43 (1.60–3.66)	<.0001		
mPG			1.02 (1.00–1.04)	.0267			1.03 (1.01–1.04)	.0013
iAVA	0.053 (0.002–1.04)	.0532	0.009 (0.00–0.13)	.0005				
iELCo					0.26 (0.05–1.46)	.1275	0.084 (0.017–0.42)	.0026
STJ diameter	2.03 (1.05–3.92)	.0353	1.96 (1.01–3.80)	.0465	1.82 (0.93–3.57)	.0811	1.63 (0.83–3.19)	.1579

In addition to SVI, iAVA, and STJ diameter, model 1 includes PV and model 2 includes mPG. In addition to SVI, iELCo, and STJ diameter, model 3 includes PV and model 4 includes mPG.
HR, Hazard ratio; *mPG*, mean pressure gradient; *PV*, peak velocity; *SVI*, stroke volume index.

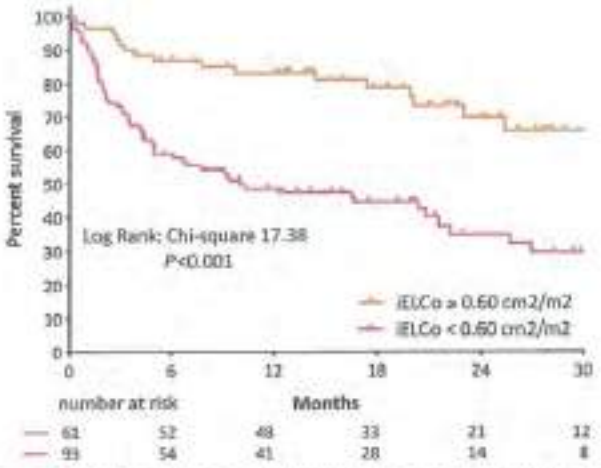

Figure 3 Kaplan-Meier survival curve for patients whose AS grading was severe using iAVA. Patients were divided into two groups according to AS severity grading by iELCo.

Table 4 Univariate Cox proportional-hazard analysis for predicting major CEs in patients with severe AS, defined as iAVA < 0.6 cm^2/m^2

Variable	HR (95% CI)	P
SVI	1.01 (0.99–1.04)	.2599
PV	2.18 (1.68–32.83)	<.0001
mPG	1.03 (1.02–1.04)	<.0001
iAVA	0.0047 (0.0004–0.05)	<.0001
iELCo	0.017 (0.003–0.098)	<.0001
STJ diameter	2.4 (1.01–4.10)	.0461

HR, Hazard ratio; *mPG*, mean pressure gradient; *PV*, peak velocity; *SVI*, stroke volume index.

Our study showed that iELCo had no obvious advantage over iAVA for predicting CEs in a whole group of patients with asymptomatic AS and normal LVEFs in this study, which was not in agreement with the results of a previous study.[9] One potential reason for this discrepancy could be related to the sample size of the study population ($n = 1,563$ in Bahlmann *et al.'s*[9] study and $n = 301$ in our study). However, if we performed a subgroup analysis of patients with severe AS assessed by iAVA, iELCo stratified a high-risk group of patients for future adverse outcomes. The discordant results of AS severity grading are the clinical dilemma for managing AS. We also demonstrated that iELCo had a significant advantage over iAVA in patients with iAVA < 0.60 cm^2/m^2 but mean pressure gradients < 40 mm Hg, which supports the results of previous studies showing that pressure recovery is particularly important in patients with moderate to severe AS or discordant severity grading.[6]

The current grading of AS severity was originally derived from cardiac catheterization data,[7] which involved measuring the pressure gradient between the left ventricle and the ascending aorta distal to the pressure recovery. The optimal cutoff value of iELCo (0.63 cm^2/m^2) to predict major CEs in this study was quite similar to the partition value to diagnose severe AS in the current guidelines.[1,3,20,24] Bahlmann *et al.*[9] reported that the best cutoff values of iELCo and iAVA to predict aortic valve related events were 0.76 and 0.60 cm^2/m^2, respectively, in asymptomatic patients with AS. The discrepant cutoff values between our study and Bahlmann *et al.'s* study could be caused by several proposed reasons. First, the prevalence of severe AS (24% in Bahlmann *et al.'s* study and 31% in our study) and follow-up period (4.3 vs 1.5 years) were different. The longer follow-up period increases the chance that time-dependent adverse outcomes will develop, especially in those with less severe AS at baseline. Second, different baseline characteristics (history of coronary artery disease 10% in Bahlmann *et al.'s* study and 18% in our study), mean age (67 vs 76 years) affects differently for the optimal cutoff value of iELCo. Last, different methods were used for stroke volume calculation. Bahlmann *et al.* did not use a standard Doppler method but alternatively used the Teichholz-corrected cube formula to calculate stroke volume in their study because of the possibility of underestimating LVOT flow velocity recording.

Clinical Implications

Even in patients with asymptomatic AS and small aortic roots (<3 cm), the calculation of iELCo may not always be required for proper management. This is especially true in patients with mild to moderate AS determined by iAVA criteria because they are usually associated with good outcomes. However, the assessment of AS severity using iELCo is particularly important (1) when iAVA is <0.6 cm^2/m^2 and (2) when discrepant AS severity grading (iAVA < 0.6 cm^2/m^2 but mean pressure gradient < 40 mm Hg) is observed. Because pressure recovery depends on STJ diameter and peak aortic valve jet velocity and both parameters are distributed widely, we may not establish the new cutoff values of iAVA but will

Table 5 Multivariate Cox proportional-hazard analysis for predicting major CEs in patients with severe AS, defined as iAVA < 0.6 cm^2/m^2

	Model 1		Model 2		Model 3		Model 4	
Variable	HR (95% CI)	P	HR (95% CI)	P	HR (95% CI)	P	HR (95% CI)	P
SVI	0.97 (0.92–1.02)	.1883	1.00 (0.95–1.04)	.870	0.96 (0.92–1.01)	.1241	0.99 (0.95–1.03)	.6888
PV	2.74 (1.50–5.03)	.0011			2.80 (1.61–5.21)	.0004		
mPG			1.03 (1.00–1.05)	.0287			1.03 (1.00–1.05)	.0110
iAVA	1.39 (0.007–280.5)	.9034	0.008 (0.00–13.4)	.3347				
iELCo					1.88 (0.05–77.3)	.7386	0.25 (0.007–8.7)	.4486
STJ diameter	3.13 (1.51–6.49)	.0022	3.03 (1.45–6.34)	.0032	3.22 (1.52–6.82)	.0022	2.89 (1.33–6.18)	.0072

In addition to SVI, iAVA, and STJ diameter, model 1 includes PV and model 2 includes mPG. In addition to SVI, iELCo, and STJ diameter, model 3 includes PV and model 4 includes mPG.
HR, Hazard ratio; *mPG*, mean pressure gradient; *PV*, peak velocity; *SVI*, stroke volume index.

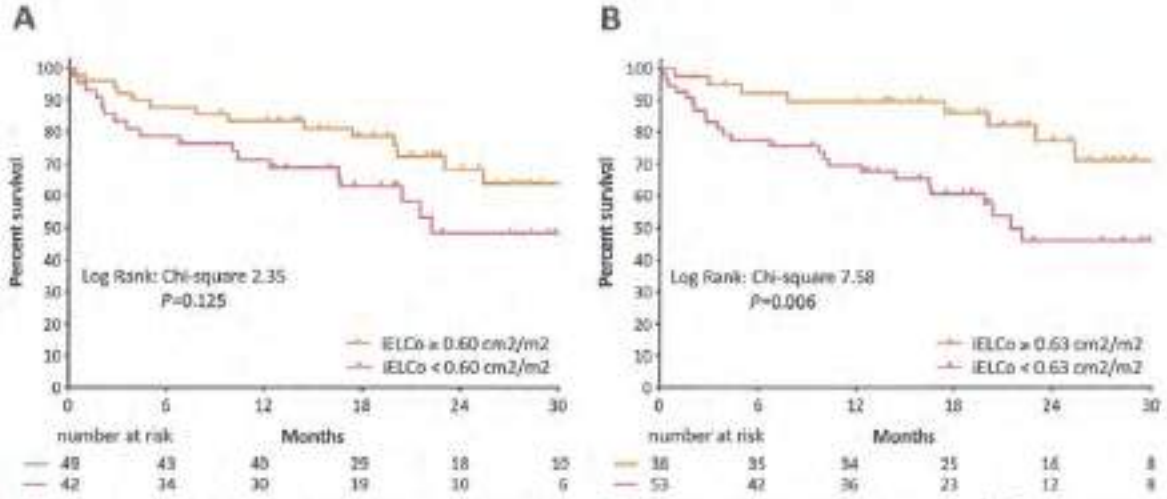

Figure 4 Kaplan-Meier analysis in patients with discordant AS severity criteria (iAVA < 0.6 cm^2/m^2 but mean pressure gradient < 40 mm Hg). Patients were divided into two groups according to the cutoff value of 0.6 cm^2/m^2 for iELCo **(A)** or the best cutoff value of iELCo (0.63 cm^2/m^2) by ROC analysis **(B)**.

use iELCo to stratify severe AS with the cutoff value of 0.6 cm^2/m^2 (or 0.63 cm^2/m^2) in daily clinical practice.

Study Limitations

Several limitations of this study should be addressed. First, the results obtained in this study were solely in Japanese patients with AS with small body size; thus, our results may not be generalized to other ethnicities. Second, AVR accounted for 80% of major CEs in this study. The decision for AVR might depend heavily on the attending physician's evaluation of AS severity, which is largely influenced by peak aortic valve jet velocity or mean pressure gradient. However, this situation equally affected the predictive power of both iAVA and iELCo. And finally, the subgroup analysis may not draw definite conclusions, because their numbers were insufficient for an extensive multivariate analysis, and we did find any statistical significance because of underpower of the smaller sample size as well as number of events. Further large-scale prospective studies will be required to validate our results.

CONCLUSION

We compared the prognostic value of iELCo with that of iAVA in asymptomatic patients with AS and small aortic roots. Overall, iELCo was not superior to iAVA for predicting major CEs. However, the calculation of iELCo appeared most useful in patients whose AS grades were severe using iAVA or those in whom AS severity criteria were inconsistent.

SUPPLEMENTARY DATA

Supplementary data related to this article can be found at https://doi.org/10.1016/j.echo.2018.10.016.

REFERENCES

1. Nishimura RA, Otto CM, Bonow RO, Carabello BA, Erwin JP III, Guyton RA, et al. 2014 AHA/ACC guideline for the management of

patients with valvular heart disease: executive summary: a report of the American College of Cardiology/American Heart Association Task Force on Practice Guidelines. J Am Coll Cardiol 2014;63:2438-88.
2. Baumgartner H, Falk V, Bax JJ, De Bonis M, Hamm C, Holm PJ, et al. 2017 ESC/EACTS guidelines for the management of valvular heart disease. Eur Heart J 2017;38:2739-91.
3. Baumgartner H, Hung J, Bermejo J, Chambers JB, Edvardsen T, Goldstein S, et al. Recommendations on the echocardiographic assessment of aortic valve stenosis: a focused update from the European Association of Cardiovascular Imaging and the American Society of Echocardiography. J Am Soc Echocardiogr 2017;30:372-92.
4. Pibarot P, Dumesnil JG. New concepts in valvular hemodynamics: implications for diagnosis and treatment of aortic stenosis. Can J Cardiol 2007; 23(Suppl B):40B-7B.
5. Pibarot P, Dumesnil JG. Improving assessment of aortic stenosis. J Am Coll Cardiol 2012;60:169-80.
6. Pibarot P, Garcia D, Dumesnil JG. Energy loss index in aortic stenosis: from fluid mechanics concept to clinical application. Circulation 2013;127:1101-4.
7. Garcia D, Pibarot P, Dumesnil JG, Sakr F, Durand LG. Assessment of aortic valve stenosis severity: a new index based on the energy loss concept. Circulation 2000;101:765-71.
8. Garcia D, Dumesnil JG, Durand L-G, Kadem L, Pibarot P. Discrepancies between catheter and Doppler estimates of valve effective orifice area can be predicted from the pressure recovery phenomenon. J Am Coll Cardiol 2003;41:435-42.
9. Bahlmann E, Gerdts E, Cramariuc D, Gohlke-Baerwolf C, Nienaber CA, Wachtell K, et al. Prognostic value of energy loss index in asymptomatic aortic stenosis. Circulation 2013;127:1149-56.
10. Daimon M, Watanabe H, Abe Y, Hirata K, Hozumi T, Ishii K, et al. Normal values of echocardiographic parameters in relation to age in a healthy Japanese population: the JAMP study. Circ J 2008;72:1859-66.
11. Lang RM, Badano LP, Mor-Avi V, Afilalo J, Armstrong A, Ernande L, et al. Recommendations for cardiac chamber quantification by echocardiography in adults: an update from the American Society of Echocardiography and the European Association of Cardiovascular Imaging. J Am Soc Echocardiogr 2015;28:1-39.e14.
12. Rudski LG, Lai WW, Afilalo J, Hua L, Handschumacher MD, Chandrasekaran K, et al. Guidelines for the echocardiographic assessment of the right heart in adults: a report from the American Society of Echocardiography endorsed by the European Association of Echocardiography, a registered branch of the European Society of Cardiology, and the Canadian Society of Echocardiography. J Am Soc Echocardiogr 2010;23:685-713.
13. Furukawa TA, Leucht S. How to obtain NNT from Cohen's d: comparison of two methods. PLoS One 2011;6:e19070-5.
14. Pencina MJ, D'Agostino RB Sr., D'Agostino RB Jr., Vasan RS. Evaluating the added predictive ability of a new marker: from area under the ROC curve to reclassification and beyond. Stat Med 2008;27:157-72.
15. Jewell ES, Maile MD, Engoren M, Elliott M. Net reclassification improvement. Anesth Analg 2016;122:818-24.
16. Baumgartner H, Stefenelli T, Niederberger J, Schima H, Maurer G. "Overestimation" of catheter gradients by Doppler ultrasound in patients with aortic stenosis: a predictable manifestation of pressure recovery. J Am Coll Cardiol 1999;33:1655-61.
17. Barker PC, Ensing G, Ludomirsky A, Bradley DJ, Lloyd TR, Rocchini AP. Comparison of simultaneous invasive and noninvasive measurements of pressure gradients in congenital aortic valve stenosis. J Am Soc Echocardiogr 2002;15:1496-502.
18. Kume T, Okura H, Kawamoto T, Watanabe N, Hayashida A, Neishi Y, et al. Clinical implication of energy loss coefficient in patients with severe aortic stenosis diagnosed by Doppler echocardiography. Circ J 2008;72:1265-9.
19. Spevack DM, Almuti K, Ostfeld R, Bello R, Gordon GM. Routine adjustment of Doppler echocardiographically derived aortic valve area using a previously derived equation to account for the effect of pressure recovery. J Am Soc Echocardiogr 2008;21:34-7.
20. Bahlmann E, Cramariuc D, Gerdts E, Gohlke-Baerwolf C, Nienaber CA, Eriksen E, et al. Impact of pressure recovery on echocardiographic assessment of asymptomatic aortic stenosis: a SEAS substudy. JACC Cardiovasc Imaging 2010;3:555-62.
21. Kume T, Okura H, Kawamoto T, Watanabe N, Neishi Y, Hayashida A, et al. Impact of energy loss coefficient on left ventricular mass regression in patients undergoing aortic valve replacement: preliminary observation. J Am Soc Echocardiogr 2009;22:454-7.
22. Koyama T, Okura H, Kume T, Fukuhara K, Imai K, Hayashida A, et al. Impact of energy loss index on left ventricular mass regression after aortic valve replacement. J Echocardiogr 2014;12:51-8.
23. Wu VC, Kaku K, Takeuchi M, Otani K, Yoshitani H, Tamura M, et al. Aortic root geometry in patients with aortic stenosis assessed by real-time three-dimensional transesophageal echocardiography. J Am Soc Echocardiogr 2014;27:32-41.
24. Rahimtoola SH. Determining that aortic valve stenosis is severe: back-to-the-future: physical examination and aortic valve area index/energy loss index < or =0.6 cm2/m2. JACC Cardiovasc Imaging 2010;3:563-6.

APPENDIX

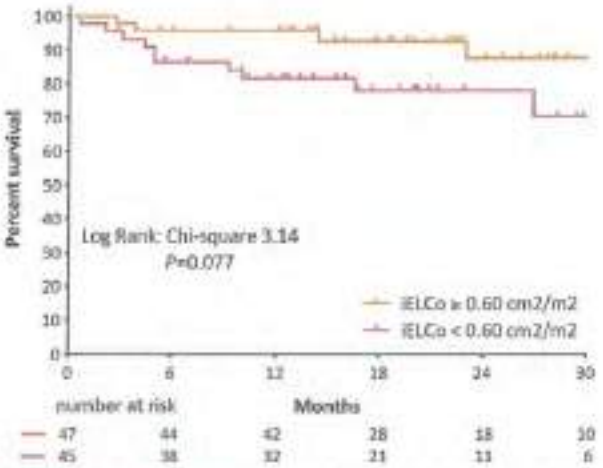

Supplemental Figure 1 Kaplan-Meier analysis in patients whose AS grading was severe by IAVA but who did not undergo AVR. Patients were divided into two groups, those who remained classified as having severe AS using IELCo (n = 45) and those who were reclassified as having moderate AS using IELCo (n = 47).

Supplemental Table 1 Clinical and echocardiographic variables between patients with severe AS by iAVA but not by iELCo and patients with severe AS by both iAVA and iELCo

Variable	Severe AS by iAVA but not by iELCo (n = 61)	Severe AS by both iAVA and iELCo (n = 93)	P
Age (y)	76 ± 12	76 ± 9	.9554
Male/female	24/37	49/44	.1039
Body surface area (m^2)	1.54 ± 0.20	1.54 ± 0.18	.8464
Heart rate (beats/min)	67 ± 12	66 ± 11	.4048
Systolic blood pressure (mm Hg)	140 ± 26	137 ± 27	.5621
Diastolic blood pressure (mm Hg)	73 ± 15	70 ± 16	.1928
Hypertension (yes/no)	38/23	72/21	.0435
Diabetes (yes/no)	17/44	26/67	.9935
Hyperlipidemia (yes/no)	25/36	36/57	.7779
Chronic kidney disease (yes/no)	27/34	49/44	.3060
Coronary artery disease (yes/no)	11/50	14/79	.1537
LVEDVI	59.4 ± 16.1	65.3 ± 16.0	.0272
LVESVI	24.2 ± 8.0	27.6 ± 8.3	.0112
LVEF	60 ± 5	58 ± 5	.0410
LVSVI	43.1 ± 10.9	40.5 ± 7.0	.0684
LAVImax	35.6 (29.0–46.7)	38.8 (29.5–46.7)	.2849
E wave	77.2 (58.8–97.5)	80 (60.3–97.5)	.8028
A wave	111.1 ± 32.3	100.6 ± 25.3	.0302
e′	4.5 (3.9–6.2)	4.9 (4–6.1)	.9535
E/e′ ratio	16.8 (10.5–22.6)	16.4 (11.8–22.7)	.9461
SPAP	35.7 (30.3–40.1)	34.5 (30.3–40.4)	.5530
Peak velocity (m/sec)	3.59 ± 0.68	4.29 ± 0.74	<.0001
Mean pressure gradient (mm Hg)	30.3 ± 12.5	44.3 ± 17.2	<.0001
iAVA (cm^2/m^2)	0.55 ± 0.03	0.41 ± 0.07	<.0001
iELCo (cm^2/m^2)	0.68 ± 0.05	0.48 ± 0.09	<.0001
STJ diameter (cm)	2.41 ± 0.29	2.41 ± 0.32	.8640
STJ area (cm^2)	4.61 ± 1.14	4.66 ± 1.25	.8096

LAVImax, Maximal left atrial volume index; *LVEDVI*, LV end-diastolic volume index; *LVEF*, LV ejection fraction; *LVESVI*, LV end-systolic volume index; *LVSVI*, LV stroke volume index; *MACE*, major adverse CE; *SPAP*, systolic pulmonary arterial pressure.

Supplemental Table 2 Clinical and echocardiographic variables between patients with mean pressure gradient < 40 mm Hg and severe AS by iAVA criteria but not severe AS by iELCo criteria and those with mean pressure gradient < 40 mm Hg and severe AS by both iAVA and iELCo criteria

Variable	Severe AS by iAVA but not by iELCo (n = 49)	Severe AS by both iAVA and iELCo (n = 42)	*P*
Age (y)	77 ± 11	76 ± 9	.8918
Male/female	21/28	22/20	.3641
Body surface area (m^2)	1.54 ± 0.20	1.53 ± 0.17	.6770
Heart rate (beats/min)	68 ± 13	65 ± 11	.1719
Systolic blood pressure (mm Hg)	140 ± 25	141 ± 24	.7369
Diastolic blood pressure (mm Hg)	74 ± 16	71 ± 13	.3224
Hypertension (yes/no)	30/19	31/11	.2908
Diabetes (yes/no)	14/35	16/26	.3356
Hyperlipidemia (yes/no)	18/31	18/24	.5517
Chronic kidney disease (yes/no)	22/27	21/21	.6269
Coronary artery disease (yes/no)	11/38	11/31	.6780
LVEDVI	55.5 ± 11.3	59.9 ± 12.8	.0769
LVESVI	22.8 ± 6.5	24.6 ± 6.7	.2031
LVEF	59 ± 5	59 ± 5	.9678
LVSVI	39.0 ± 6.8	37.1 ± 5.8	.1662
LAVImax	33.1 (28.4–46.2)	35.3 (26.8–50.9)	.5828
E wave	77.2 (58.8–96.7)	81.7 (58.3–104.8)	.5346
A wave	109.0 ± 31.8	96.7 ± 26.1	.0554
e′	4.5 (3.9–6.1)	5.0 (4.1–5.8)	.6846
E/e′ ratio	16.5 (11.1–22.3)	15.9 (12.3–21.8)	.9841
SPAP	36.2 (32.3–40.8)	33.8 (30.1–39.6)	.5530
Peak velocity (m/sec)	3.34 ± 0.47	3.70 ± 0.32	<.0001
Mean pressure gradient (mm Hg)	25.5 ± 7.5	31.1 ± 5.5	<.0001
iAVA (cm^2/m^2)	0.55 ± 0.03	0.44 ± 0.06	<.0001
iELCo (cm^2/m^2)	0.68 ± 0.05	0.51 ± 0.07	<.0001
STJ diameter (cm)	2.40 ± 0.29	2.49 ± 0.38	.2254
STJ area (cm^2)	4.58 ± 1.15	4.96 ± 1.49	.1848

LAVImax, Maximal left atrial volume index; *LVEDVI*, LV end-diastolic volume index; *LVEF*, LV ejection fraction; *LVESVI*, LV end-systolic volume index; *LVSVI*, LV stroke volume index; *MACE*, major adverse CE; *SPAP*, systolic pulmonary arterial pressure.

ARGENTINE JOURNAL OF CARDIOLOGY
OFFICIAL PRESS ORGAN OF THE ARGENTINE SOCIETY OF CARDIOLOGY
ISSN 2314-2286 (English ed. Online)

Vol 86, No 2 (2018)

Table of Contents

Editorials

AKASHI, YOSHIHIRO J.
Modification of Diagnostic Criteria in Takotsubo Syndrome . Pp. 81-83
PDF

HERREROS, JESÚS
Comprehensive Treatment of Obstructive Hypertrophic Cardiomyopathy . Pp. 84-85
PDF

Original Articles

PÁEZ, DIAMELA; BIN, ELINA P.; CASANOVA, VERÓNICA; CICALE, ELIANA; GELPI, RICARDO J.; DONATO, MARTÍN
Role of Adenosine A1 Receptors in Remote Ischemic Preconditioning Protection . Pp. 86-89
PDF ABSTRACT

ARIAS, ANIBAL; LUCAS, LUCIANO O.; ESPINOSA, EZEQUIEL; IEZZI, SEBASTIÁN; ROSSI, EMILIANO; SAN ROMÁN, EDUARDO; PIZARRO, RODOLFO; BELZITI, CÉSAR A.; CAGIDE, ARTURO M.; DOVAL, HERNÁN C.
Clinical Features and Outcomes of Takotsubo Syndrome at a University Hospital . Pp. 90-95
PDF ABSTRACT

VRANCIC, JUAN; COSTABEL, JUAN P.; ESPINOZA, JUAN C.; PICCININI, FERNANDO; CAMPORROTONDO, MARIANO; PEDERNERA, GUSTAVO O.; AVEGLIANO, GUSTAVO; DIEZ, MIRTA; DORSA, ALBERTO; NAVIA, DANIEL
Extended Septal Myectomy in Obstructive Hypertrophic Cardiomyopathy. Clinical Results and Mid-term Echocardiographic Outcome . Pp. 96-102
PDF ABSTRACT

GÓMEZ, ANDREA; HELMAN, LORENA; GIUNTA, GUSTAVO; TOSCANINI, ULISES; CUNIBERTI, LUIS
Genetic Testing of Familial Hypercholesterolemia in a Hospital-Based Population of the City of Buenos Aires . Pp. 103-109
PDF ABSTRACT

LEITE VINCENTI, FERNANDO; SERCPIAN, IGNACIO M.; PORTALUPPI, RAFAEL; COHEN, FERNANDO; ROJAS MATAS, CARLOS A.; FERNÁNDEZ, ALEJANDRO D.; AGATIELLO, CARLA R.; BERROCAL, DANIEL H.
Percutaneous Coronary Intervention in Octogenarian Patients. Long-term Results and Predictors of Poor Outcome . Pp. 110-115
PDF ABSTRACT

FORTUNATO, GERMAN ALBERTO; MARENCHINO, RICARDO G.; CIRIO, SEBASTIÁN; ROSSI, EMILIANO; DOMENECH, ALBERTO; KOTOWICZ, VADIM
Aortic Valve Replacement in Intermediate Risk Patients: Surgical Outcomes . Pp. 116-120
PDF ABSTRACT

Esta revista cuenta con el apoyo editorial del
CAICYT
CONICET

USER
Username
Password
Remember me
Log In

LANGUAGE
English

JOURNAL CONTENT
Search
All
Search

Browse
- By Issue
- By Author
- By Title
- Other Journals

KEYWORDS
Breaking News Aorta Aortic Valve Stenosis Coronary Artery Disease Factores de riesgo Hypertension Infarto de miocardio Miocardiopatía Myocardial Infarction Obesity Prognosis Pronóstico Stents Tomography aneurisma ecocardiografía enfermedad coronaria epidemiología infarto agudo de miocardio infarto de miocardio reperfusión video

Esta revista pertenece al
NB

EDITORIAL

Modification of Diagnostic Criteria in Takotsubo Syndrome

Modificación de los criterios diagnósticos en el síndrome de Takotsubo

YOSHIHIRO J AKASHI

Takotsubo syndrome (TTS) is characterized by transient regional systolic dysfunction in the left ventricle. The dysfunctional areas do not correspond to the coronary artery perfusion territory and are often identified in the circumferential apical, mid-ventricular, or basal ventricle. This syndrome is a relatively novel concept: the first report of TTS was described in 1990 by Sato, et al. in Japan. (1) Following this first case, numerous TTS cases have been globally reported under multiple names, such as stress cardiomyopathy, apical ballooning syndrome, broken heart syndrome and catecholamine induced cardiomyopathy. Since then, although various data obtained from TTS cases have been accumulated, controversies remain about the diagnostic criteria. Arias et al. have reported the clinical features of TTS in their hospital located in Buenos Aires, Argentina. (2) Their report plays an important role in the field of TTS, since most of the registered data is originated from countries in the northern hemisphere.

Arias, et al. described that the clinical features of TTS were similar to those of acute coronary syndrome (ACS), including ECG changes and abnormal serum biomarkers. They also reported that female predominance in TTS was the same as in the study by Lyon, et al., (2, 3) and demonstrated that NT-proBNP concentration was the prognostic indicator in patients with TTS. The current classification for TTS severity suggests that elevated BNP concentration is associated with higher risk and such patients should be treated in the intensive care unit. Arias et al., described in their study a cut-off value of NT-proBNP >12000 ng/L, (2) whereas this was >2000 ng/L in the report of Lyon, et al. (3) This author defined high-risk patients as follows:

1. Patients >75 years
2. Systolic blood pressure <110 mmHg
3. Presence of lung edema
4. Patients with complicated with or lethal arrhytmias
5. Patients with severe systolic dysfunction (left ventricular ejection fraction <35%)
6. Outflow tract pressure gradient >40 mmHg
7. Presence of mitral regurgitation
8. Patients with cardiac thrombus
9. Patients complicated with ventricular septal perforation
10. Patients with left ventricle ventricular rupture
11. Patients with prolonged QT interval
12. Presence of abnormal Q wave
13. Patients with fluctuating ST-segment elevation
14. BNP ≥600 or NT-proBNP ≥2000 ng/L
15. Right ventricular involvement.(3)

When a patient with TTS is classified as having high risk, it is necessary to observe his/her hemodynamics for more than 72 hours in the intensive care unit. Moreover, the patient with significant symptoms should have delayed enhancement cardiac magnetic resonance (CMR) imaging, since an earlier conducted study demonstrated that in approximately 10% of the study patients who received CMR imaging at the time of initial clinical presentation, it provided relevant functional and tissue information that could aid in the establishment of TTS diagnosis. (4) Various other left ventricular wall motion abnormalities in TTS patients have been reported. A study found that nearly 20% of all TTS patients did not have typical apical ballooning of the left ventricle but variants of left ventricular dysfunction. (5) However, in the present study, no alternative forms were presented; hence, the TTS variants were possibly misdiagnosed. We should closely look for various patterns of ventricular contraction in the acute phase of TTS.

The present study demonstrated that patients with TTS who had coronary artery stenosis did not present high in-hospital mortality. In general, TTS is not associated with acute plaque rupture in the coronary arteries. Some studies reviewing cohorts of TTS patients have reported that bystander coronary artery disease accounts for 10% of TTS cases. (6, 7) The pathophysiology of TTS remains unclear. The latest hypotheses have considered it as the integrated cardiovascular response to a sudden surge in endogenous catecholamine concentrations or to exogenously administered catecholamines in acute severe stress. (8) Because of the acute coronary syndrome-like clinical features and the unclear pathophysiology, the diagnosis of TTS is still challenging. The prognosis of TTS

REV ARGENT CARDIOL 2018;86:79-81. http://dx.doi.org/10.7775/rac.v86.i2.13151
SEE RELATED ARTICLE: REV ARGENT CARDIOL 2018;86:88-93. http://dx.doi.org/10.7775/rac.v86.i2.12294

Address for reprints: Yoshihiro J AKASHI, MD., PhD., FESC, FJCC, FJCS. 2-16-1 Sugao, Miyamae-ku, Kawasaki, 216-8511, Japan
Tel: +81-44-977-8111 - Fax: +81-44-9978-7083 - E-mail: yoakashi-circ@umin.ac.jp
Division of Cardiology, Department of Internal Medicine, St. Marianna University School of Medicine, Kawasaki, JAPAN

Table 1. Changes of Diagnostic Criteria for Takotsubo Syndrome

Position Statement from the Taskforce on Takotsubo Syndrome of the Heart Failure Association of the European Society of Cardiology (2015) (3)	1. Transient regional wall motion abnormalities of the left or right ventricular myocardium which are frequently, but not always, preceded by a stressful trigger (emotional or physical) 2. The regional wall motion abnormalities usually* extend beyond a single epicardial vascular distribution, and often result in circumferential dysfunction of the ventricular segments involved. 3. **Absence of culprit atherosclerotic coronary artery disease, including acute plaque rupture, thrombus formation, and coronary dissection or other pathological conditions to explain the pattern of temporary left ventricular dysfunction observed (e.g. hypertrophic cardiomyopathy, viral myocarditis).** 4. New ECG abnormalities (ST-segment elevation, ST-segment depression, left bundle branch block, T-wave inversion, and/or QTc prolongation) during the acute phase (3 months). 5. Significantly elevated serum natriuretic peptide (BNP or NT-proBNP) during the acute phase. 6. Positive but relatively small elevation of cardiac troponin measured with a conventional assay (i.e. disparity between the troponin level and the amount of dysfunctional myocardium present). 7. Recovery of ventricular systolic function on cardiac imaging studies at follow-up (3-6 months).
International Expert Consensus (2016 accepted) (11)	1. Patients show transient left ventricular dysfunction (hypokinesis, akinesis, or dyskinesis) presenting as apical ballooning, or midventricular, basal, or focal wall motion abnormalities. Right ventricular involvement can be present. In addition to these regional wall motion patterns, variations between all types can exist. The regional wall motion abnormality usually extends beyond a single epicardial vascular distribution; however, rare cases can exist where a coronary lesion is present in the outranded myocardial territory of the wall motion abnormality. **Therefore, coronary artery disease is not a contradiction in takotsubo syndrome.** 2. An emotional, physical, or combined trigger can precede the takotsubo syndrome event, but this is not obligatory. 3. The presence of neurologic disorders (e.g. subarachnoid hemorrhage, cerebrovascular ischemic attack, seizures) as well as **pheochromocytoma does not exclude the diagnosis of takotsubo syndrome.** 4. Presence of new electrocardiographic abnormalities (ST-segment elevation, ST-segment depression, T-wave inversion, QTc prolongation); however, rare cases exist without any ECG changes. 5. Cardiac biomarkers (troponin and creatine kinase) are moderately elevated in most cases; significant elevation of brain natriuretic peptide is common. 6. Patients have no evidence of infective myocarditis. 7. Postmenopausal women are predominantly affected.

was initially reported favorable compared with that of ST-segment elevated myocardial infarction, whereas subsequent studies have demonstrated that acute and long-term mortalities are higher than previously recognized. (5, 9) Therefore, an accurate diagnosis is crucial for the patients with TTS.

Regarding diagnosis, the first TTS criteria introduced by the Mayo Clinic were the most commonly employed. (10) The conventional criteria proposed the exclusion of significant coronary artery stenosis; however, recent criteria accepted the presence of coronary artery disease in patients with TTS. Since the presence of obstructive coronary artery disease should not be included in the exclusion criteria, these should be revised. Although conventional diagnostic criteria have excluded pheochromocytoma as a specific cause of TTS, the clinical features of TTS coincide with those of this tumor. The European Society of Cardiology is going to present the novel diagnostic criteria, including pheochromocytoma and subarachnoid hemorrhage as secondary causes of TTS. (11)

CONFLICTS OF INTEREST

None declared.

(See authors' conflicts of interest forms on the website/Supplementary material).

REFERENCES

1. Sato H, Tateishi H, Dote K, Uchida T, Ishihara M. Tako-tsubo-like left ventricular dysfunction due to multivessel coronary spasm. In: Kodama K, Haze K, Hon M, eds. Clinical Aspect of Myocardial Injury: From Ischemia to Heart Failure. Kagakuhyouronsha, Tokyo 1990:56-64.

2. Arias AM, Lucas LO, Espinosa E, Iezzi, S, Rossi E, San Romano E, y cols. Clinical features and outcomes of takotsubo syndrome at a university hospital. Rev Argent Cardiol 2018;86:88-93.

3. Lyon AR, Bossone E, Schneider B, Sechtem U, Citro R, Underwood SR, et al. Current state of knowledge on Takotsubo syndrome: a Position Statement from the Taskforce on Takotsubo Syndrome of

the Heart Failure Association of the European Society of Cardiology. Eur J Heart Fail 2016;18:8-27. http://doi.org/fhm/2s8
4. Eitel I, von Knobelsdorff-Brenkenhoff F, Bernhardt P, Carbone I, Muellerleile K, Aldrovandi A, et al. Clinical characteristics and cardiovascular magnetic resonance findings in stress (takotsubo) cardiomyopathy. JAMA 2011;306:277-86. http://doi.org/c2f5nvk
5. Templin C, Ghadri JR, Diekmann J, Napp LC, Bataiosu DR, Jaguszewski M, et al. Clinical Features and Outcomes of Takotsubo (Stress) Cardiomyopathy. N Engl J Med 2015;373:929-38. http://doi.org/75b
6. Previtali M, Repetto A, Panigada S, Camporotondo R, Tavazzi L. Left ventricular apical ballooning syndrome: prevalence, clinical characteristics and pathogenetic mechanisms in a European population. Int J Cardiol 2009;134:91-6. http://doi.org/fwjkdh
7. Gaibazzi N, Ugo F, Vignali L, Zoni A, Reverberi C, Gherli T. Tako-Tsubo cardiomyopathy with coronary artery stenosis: a case-series challenging the original definition. Int J Cardiol 2009;133:205-12. http://doi.org/dm7wcf
8. Akashi YJ, Nef HM, Lyon AR. Epidemiology and pathophysiology of Takotsubo syndrome. Nat Rev Cardiol 2015;12:387-97. http://doi.org/f7rfzq
9. Stiermaier T, Moeller C, Oehler K, Desch S, Graf T, Eitel C, et al. Long-term excess mortality in takotsubo cardiomyopathy: predictors, causes and clinical consequences. Eur J Heart Fail. 2016;18:650-6. http://doi.org/cph9
10. Prasad A, Lerman A, Rihal CS. Apical ballooning syndrome (Tako-Tsubo or stress cardiomyopathy): a mimic of acute myocardial infarction. Am Heart J 2008;155:408-17. http://doi.org/cdfgr
11. Ghadri JR, Wittstein IS, Prasad AL. International Expert Consensus Document on Takotsubo Syndrome - PART I: Characteristics and Clinical Presentation. Eur Heart J 2018 in-press.

Published, citable research in only 14 days.
Followed by transparent, invited open peer-review.
We think it makes sense too

F1000Research
SUBMIT TODAY

Taylor & Francis Online
Log in | Register

Journal
Expert Review of Cardiovascular Therapy >
Volume 16, 2018 - Issue 4

2100 1
Views Crossref citations to date Altmetric

Review

Cardiovascular magnetic resonance imaging in heart failure

Kihei Yoneyama, Yuki Kitanaka, Osamu Tanaka & Yoshihiro J. Akashi

Pages 237-248 | Received 29 Sep 2017, Accepted 22 Feb 2018, Accepted author version posted online: 26 Feb 2018, Published online: 27 Feb 2018

Download citation https://doi.org/10.1080/14779072.2018.1445525

言語を選択
Translator disclaimer

ABSTRACT

Introduction: Heart failure is a complex clinical syndrome resulting from heart structural remodeling and impaired function in ejecting blood; its incidence is increasing markedly worldwide. The observed variations in the structure and function of the heart are attributable to differences in etiology of heart failure. Cardiac magnetic resonance imaging (CMR) can characterize myocardial tissue, assess myocardial viability, and help diagnose specific cardiomyopathies. The emergence of T1 mapping techniques further improves our knowledge and the clinical assessment

of myocardial disease features. Physicians, therefore, must identify the variations using CMR to improve patient's symptoms, survival, and quality of life.

Area covered: Current reports regarding CMR and the evidence for heart failure diagnosis and therapy as a potential marker of therapeutic response, including low- and high-risk patients, were reviewed. Literature search was performed using PubMed and Google Scholar for literature relevant to CMR, late gadolinium enhancement, T1 mapping, assessment of fibrosis and remodeling, coronary artery, myocardial infarction, heart failure, and its outcomes.

Expert commentary: The authors review current evidence and discuss the potential ability of CMR to guide, diagnose, plan risk strategies, and treat patients with heart failure.

KEYWORDS: Amyloidosis, cardiovascular, heart failure, hypertrophic cardiomyopathy, late gadolinium enhancement, magnetic resonance imaging, myocardial infarction, myocarditis, T1 mapping, T2 mapping, sarcoidosis, scar

Login options

- Log In
- Shibboleth
- OpenAthens

Restore content access

- Restore content access for purchases made as guest

Purchase *

Save for later

Online

Article Purchase
24 hours to view or download: USD 90.00

Add to cart

Issue Purchase
30 days to view or download: USD 478.00 Add to cart

* Local tax will be added as applicable

Additional information

Funding

This paper was funded by the Mitsubishi Tanabe Pharma Corporation, grant ID: MTPS20160519008.

Acknowledgements

This paper was funded by the Mitsubishi Tanabe Pharma Corporation, grant ID: MTPS20160519008.

Declaration of interest

K Yoneyama receives research grant from Mitsubishi Tanabe Pharma Corporation. The authors have no other relevant affiliations or financial involvement with any organization or entity with a financial interest in or financial conflict with the subject matter or materials discussed in the manuscript apart from those disclosed.

Peer reviewers on this manuscript have no relevant financial or other relationships to disclose.

People also read

Review

Evaluation of the right ventricle by echocardiography: particularities and major challenges >

Michael Dandel et al.

Expert Review of Cardiovascular Therapy
Volume 16, 2018 - Issue 4

Published online: 14 Mar 2018

Review

Mechanisms, diagnosis, and treatment of heart failure with preserved ejection fraction and diastolic dysfunction >

Gilman D. Plitt et al.

Expert Review of Cardiovascular Therapy
Volume 16, 2018 - Issue 8

Published online: 16 Jul 2018

Latest two full volumes
FREE to you for 14 days

ESC European Society of Cardiology car

OXFORD ACADEMIC

European Heart Journal
Cardiovascular Imaging

EACVI European Association of Cardiovascular Imaging
European Society of Cardiology

Article Navigation

Echo-fluoro fusion imaging guidance for no contrast transfemoral aortic valve implantation

Alberto Pozzoli ✉, Maurizio Taramasso, Shingo Kuwata, Michel Zuber, Fabian Nietlispach, Francesco Maisano

European Heart Journal - Cardiovascular Imaging, Volume 19, Issue 6, 1 June 2018, Pages 710–711, https://doi.org/10.1093/ehjci/jey048
Published: 22 March 2018

PDF Cite Permissions Share ▾

Over the past decade, transcatheter aortic valve implantation (TAVI) emerged as preferred treatment for high-risk patients with severe aortic stenosis (AS), expanding towards lower risk patients. Chronic kidney disease (CKD) is one of the most frequent comorbidity. Preprocedural screening includes application of contrast media [computed tomography (CT)], followed by repeated contrast during procedure (coronary angiography, aortic root angiography, and peripheral angiography), increasing risk of acute kidney injury (AKI). AKI in presence of CKD increases the incidence of kidney disorders after TAVI up to 30%. Efforts to abolish periprocedural contrast appear therefore beneficial, like the use of EchoNavigator (Philips, the Netherlands). An 80-year-old male patient with low-flow, low-gradient severe AS (mean aortic valve area 0.6 cmq, mean gradient 29 mmHg, LVEF 10%) and pre-dialytic CKD (creatinine 5.5 mg/dL) was scheduled for no contrast TAVI, under general anaesthesia and fusion guidance. The aortic valve (AV) plane was identified with EchoNavigator and three fiducial markers were placed in correspondence of the nadir of the cusps (*Panels A* and *B*), in X-plane view. By superimposing the echo images, the AV and the root become visible on the fluoroscopic screen and the angulation of C-arm was gradually adjusted to co-align the three

IMAGE FOCUS

doi:10.1093/ehjci/jey048
Online publish-ahead-of-print 22 March 2018

Echo-fluoro fusion imaging guidance for no contrast transfemoral aortic valve implantation

Alberto Pozzoli*, Maurizio Taramasso, Shingo Kuwata, Michel Zuber, Fabian Nietlispach, and Francesco Maisano

Heart Center, Zürich University Hospital, University of Zürich, Rämistrasse 100, 8091 Zürich, Switzerland

* Corresponding author. Tel: +41044253298; Fax: +41044254446, E-mail: alberto.pozzoli@usz.ch

Over the past decade, transcatheter aortic valve implantation (TAVI) emerged as preferred treatment for high-risk patients with severe aortic stenosis (AS), expanding towards lower risk patients. Chronic kidney disease (CKD) is one of the most frequent comorbidity. Preprocedural screening includes application of contrast media [computed tomography (CT)], followed by repeated contrast during procedure (coronary angiography, aortic root angiography, and peripheral angiography), increasing risk of acute kidney injury (AKI). AKI in presence of CKD increases the incidence of kidney disorders after TAVI up to 30%. Efforts to abolish periprocedural contrast appear therefore beneficial, like the use of EchoNavigator (Philips, the Netherlands). An 80-year-old male patient with low-flow, low-gradient severe AS (mean aortic valve area 0.6 cm$_2$, mean gradient 29 mmHg, LVEF 10%) and pre-dialytic CKD (creatinine 5.5 mg/dL) was scheduled for no contrast TAVI, under general anaesthesia and fusion guidance. The aortic valve (AV) plane was identified with EchoNavigator and three fiducial markers were placed in correspondence of the nadir of the cusps (*Panels A* and *B*), in X-plane view. By superimposing the echo images, the AV and the root become visible on the fluoroscopic screen and the angulation of C-arm was gradually adjusted to co-align the three markers on correct plane (*Panel C*). The overlayed 3D echo fusion allowed successful implantation of a Sapien 3 26 mm (Edwards

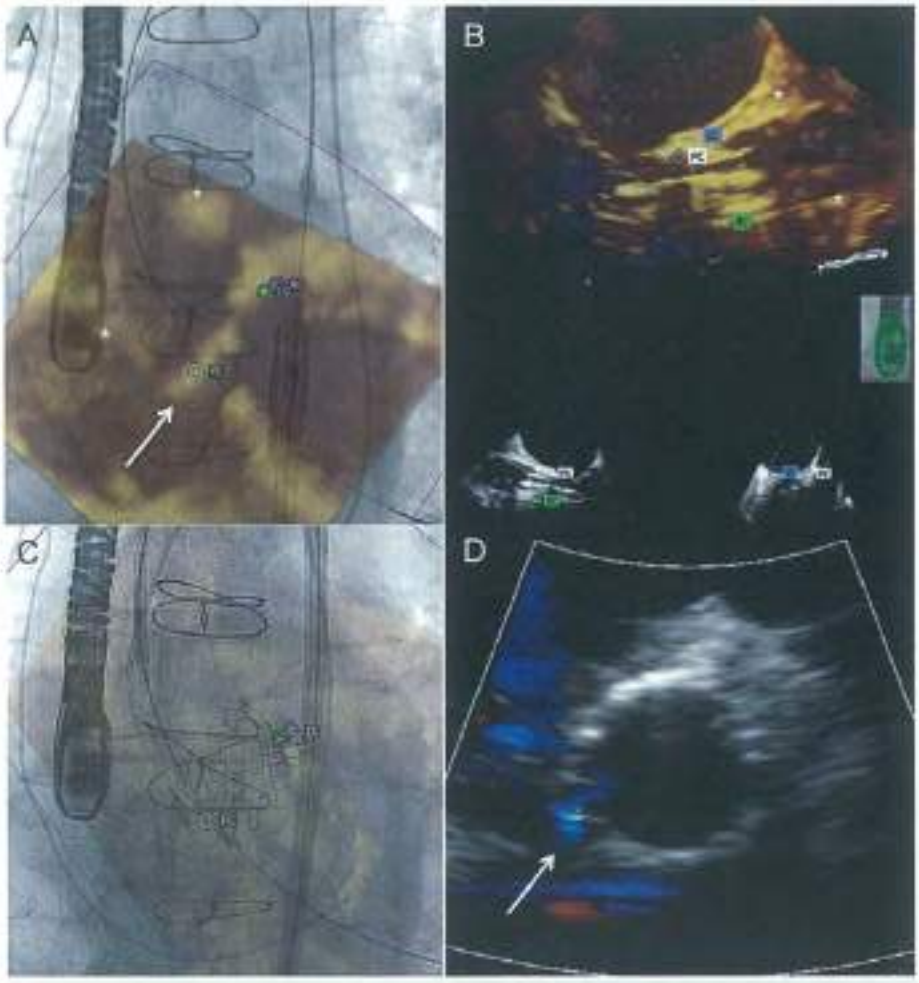

Downloaded from https://academic.oup.com/ehjcimaging/article-abstract/19/6/710/4961567 by EndocrineSociety Admin user on 27 April 2020

Lifesciences, USA), without contrast and preoperative CT (Supplementary data online, *Video 51*). At transthoracic echo at discharge, only a trivial paravalvular leak was detected (*Panel D*). In high-risk patients with CKD, use of EchoNavigator as a measure to minimize the risk of AKI during TAVI appears extremely beneficial. (*Panels A and B*) The three markers, placed at the level of the nadir cusp, are overlayed on fluoroscopy and aligned to reach the coaxial planar projection. Using the echo 3D modality, it is possible to crop thickness of soft tissues, obtaining clearcut imaging of the aortic root (asterisks) and of the valvular plane itself (arrow). (*Panel C*) During TAVI implantation, the translucency of overlayed 3D tissues is reduced through a specific tool, making catheters and device well visible. (*Panel D*) Trivial paravalvular leak at 8 o'clock at discharge transthoracic echo.

Supplementary data are available at *European Heart Journal - Cardiovascular Imaging* online.

Published on behalf of the European Society of Cardiology. All rights reserved. © The Author(s) 2018. For permissions, please email: journals.permissions@oup.com.

Downloaded from https://academic.oup.com/ehjcimaging/article-abstract/19/6/710/4951537 by EndocrineSociety Admin user on 27 April 2020

Published, citable research in only 14 days.
Followed by transparent, invited open peer-review.
We think it makes sense too

F1000Research
SUBMIT TODAY

Taylor & Francis Online

Log in | Register

Journal
Expert Review of Medical Devices ›
Volume 15, 2018 - Issue 6

58 0 0
Views CrossRef citations to date Altmetric

Review

Cardioband system as a treatment for functional mitral regurgitation

Adolfo Ferrero Guadagnoli, Carlotta De Carlo, Francesco Maisano, Edwin Ho, Matteo Saccocci, Oscar Cuevas, ...Show all

Pages 415-421 | Received 10 Feb 2018, Accepted 04 Jun 2018, Accepted author version posted online: 07 Jun 2018, Published online: 19 Jun 2018

Download citation https://doi.org/10.1080/17434440.2018.1485487 Check for updates

言語を選択 ▼
Translator disclaimer

ABSTRACT

Introduction: Are the current data on the Cardioband in the clinical area enough to consider it a tool for mitral regurgitation treatment? Severe secondary mitral valve insufficiency frequently affects high-risk surgical patients. The Cardioband system is a novel percutaneous surgical-like device for direct annuloplasty. It is implanted into the beating heart by transvenous femoral access, with minimal impact on hemodynamic and cardiac function during implantation. So far, it has demonstrated safety and feasibility in high-risk patients with functional mitral regurgitation; it has imparted significant annular reduction and regurgitation improvements. In well-selected patients, it could be an option for mitral valve repair.

Areas covered: This is a bibliographic review based on scientific publications and medical congress reports. It includes the most current information related to Cardioband in mitral regurgitation.

Expert commentary: This novel, less-invasive and effective tool is an option for the open repair or replacement of the mitral valve in high-risk surgical patients. Although the current results of Cardioband are promising, more data and longer follow-up times are necessary to confirm its safety and efficacy and to evaluate the durability of the results.

KEYWORDS: Annuloplasty, cardioband system, mitral regurgitation, mitral repair, percutaneous treatment

Login options

- Log in
- Shibboleth
- OpenAthens

Restore content access

- Restore content access for purchases made as guest

Purchase *

Save for later

Online

Article Purchase
24 hours to view or download: USD 90.00

Add to cart

Issue Purchase
30 days to view or download: USD 446.00

Add to cart

* Local tax will be added as applicable

ESC European Society of Cardiology

car

OXFORD ACADEMIC

European Heart Journal
Cardiovascular Imaging

EACVI European Association of Cardiovascular Imaging
European Society of Cardiology

Article Navigation

3D echo-fluoro fusion imaging to guide Cardioband transcatheter mitral annuloplasty

Alberto Pozzoli ✉, Michel Zuber, Maurizio Taramasso, Shingo Kuwata, Francesco Maisano

European Heart Journal - Cardiovascular Imaging, jey062, https://doi.org/10.1093/ehjci/jey062
Published: 19 April 2018

PDF Cite Permissions Share ▾

The Cardioband mitral system (Edwards Lifesciences, Irvine, USA) is a transcatheter, surgical-like, direct annuloplasty, which is implanted beating heart, on the posterior mitral valve (MV) annulus. A polyester sleeve with radiopaque markers is inserted from commissure to commissure, by multiple anchors. Once accomplished, the Cardioband size can be reduced under transesophageal echo guidance, obtaining the mitral regurgitation (MR) reduction. Fusion imaging technology can be used to facilitate four main procedural steps, taking advantage of EchoNavigator® (Philips, Best, Netherlands) tools. A 73-year-old man presented with post-ischaemic cardiomyopathy and severe functional MR to be treated with Cardioband. EchoNavigator can be helpful to mark the trans-septal puncture site with fiducial markers (in correspondence of the postero-medial commissure, 4 cm high from MV plane), having it displayed on live fluoroscopy. Once crossed in the left atrium, atrial navigation is assisted by echo-fusion overlay, visualizing the chamber itself, and the MV annulus. This helps to reach the adequate trajectory between the tip of implant catheter and the first anchoring point, the anterolateral commissure, using 3D or X-plane (intercommissural and anteroposterior) echo overlay. Then, each anchoring site can be marked on the annulus and keeping them displayed on fluoroscopy. As a basic functionality three orthogonal 2D echo views could be helpful, enhancing localization of the anchoring site. Echo-fluoro fusion can provide more intuitive

IMAGE FOCUS

doi:10.1093/ehjci/jey062
Online publish-ahead-of-print 19 April 2018

3D echo-fluoro fusion imaging to guide Cardioband transcatheter mitral annuloplasty

Alberto Pozzoli*, Michel Zuber, Maurizio Taramasso, Shingo Kuwata, and Francesco Maisano

Heart Valve Clinic, Zürich University Hospital, University of Zürich, Rämistrasse 100, 8091 Zürich, Switzerland

* Corresponding author. Tel: +41-44 255 32 98; Fax: +41-44 255 44 46. E-mail: alberto.pozzoli@usz.ch

The Cardioband mitral system (Edwards Lifesciences, Irvine, USA) is a transcatheter, surgical-like, direct annuloplasty, which is implanted beating heart, on the posterior mitral valve (MV) annulus. A polyester sleeve with radiopaque markers is inserted from commissure to commissure, by multiple anchors. Once accomplished, the Cardioband size can be reduced under transesophageal echo guidance, obtaining the mitral regurgitation (MR) reduction. Fusion imaging technology can be used to facilitate four main procedural steps, taking advantage of EchoNavigator® (Philips, Best, Netherlands) tools. A 73-year-old man presented with post-ischaemic cardiomyopathy and severe functional MR to be treated with Cardioband. EchoNavigator can be helpful to mark the trans-septal puncture site with fiducial markers (in correspondence of the postero-medial commissure, 4 cm high from MV plane), having it displayed on live fluoroscopy. Once crossed in the left atrium, atrial navigation is assisted by echo-fusion overlay, visualizing the chamber itself, and the MV annulus. This helps to reach the adequate trajectory between the tip of implant catheter and the first anchoring point, the anterolateral commissure, using 3D or X-plane (intercommissural and anteroposterior) echo overlay. Then, each anchoring site can be marked on the annulus and keeping them displayed on fluoroscopy. As a basic functionality three orthogonal 2D echo views could be helpful, enhancing localization of the anchoring site. Echo-fluoro fusion can provide more intuitive knowledge to multimodality imaging in the hybrid room, assisting intraprocedural guidance at any level of training and stages of technological development in the mitral space, due to superior orientation in 3D space.

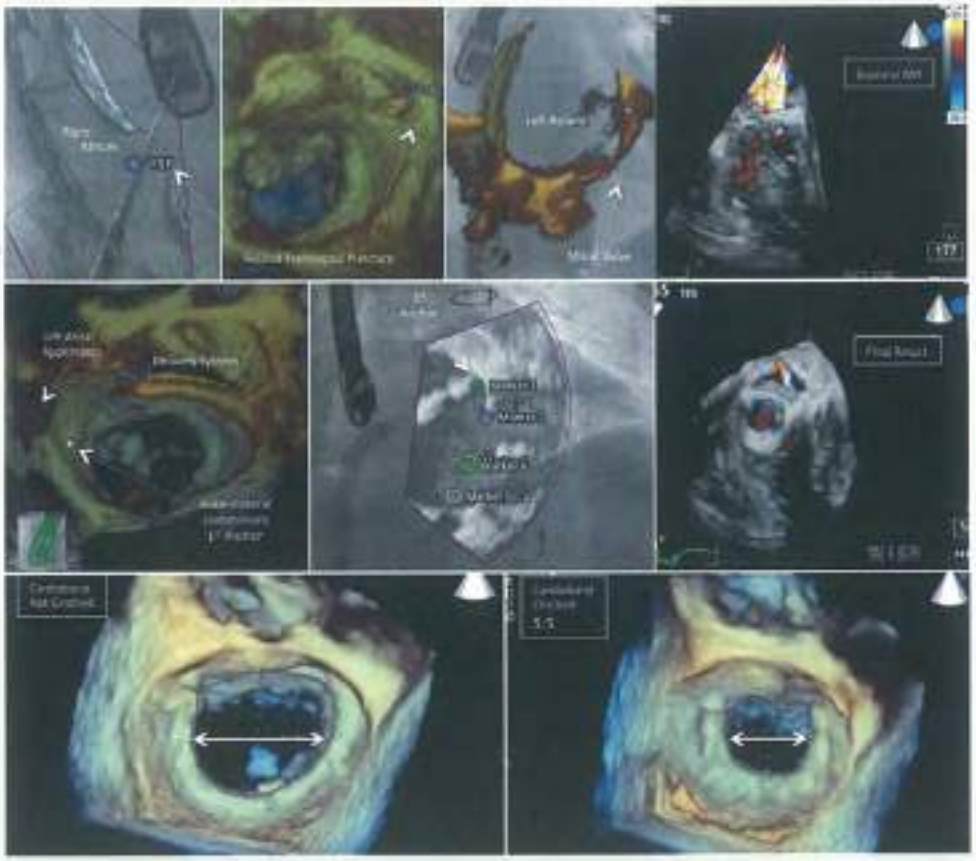

Published on behalf of the European Society of Cardiology. All rights reserved. © The Author(s) 2018. For permissions, please email: journals.permissions@oup.com.

Downloaded from https://academic.oup.com/ehjcimaging/article-abstract/19/7/827/4976239 by smarianmuniv user on 27 April 2020

ESC European Society of Cardiology
European Heart Journal - Cardiovascular Imaging (2018) 19, 715–726
doi:10.1093/ehjci/jey067

REVIEW

Echocardiographic-fluoroscopic fusion imaging for transcatheter mitral valve repair guidance

Francesco F. Faletra[1]*, Alberto Pozzoli[2], Eustachio Agricola[2], Andrea Guidotti[3], Luigi Biasco[1], Laura Anna Leo[1], Maurizio Taramasso[3], Elena Pasotti[1], Shingo Kuwata[3], Marco Moccetti[1], Felix C. Tanner[3], Giovanni Pedrazzini[1], Fabian Nietlispach[3], Tiziano Moccetti[1], Michel Zuber[3], and Francesco Maisano[3]

[1]Department of Cardiology, Fondazione Cardiocentro Ticino, Via Tesserete 48, CH-6900 Lugano, Switzerland; [2]Istituto Scientifico San Raffaele, via Olgettina 60, 20132 Milan, Italy; and [3]University Hospital Zürich, Rämistrasse 100, 8091 Zürich, Switzerland

Received 7 February 2018; editorial decision 2 April 2018; accepted 4 April 2018; online publish-ahead-of-print 27 April 2018

The echocardiographic-fluoroscopic fusion imaging is a new imaging system which has recently become available, with the proposal to facilitate catheters and device navigation during catheter-based structural heart disease interventions. Several reports have described the early developments and the first clinical experiences, but literature focusing on the practical applications of fusion imaging technology to mitral valve transcatheter interventions, and on its potential advantages and current limitations, is still limited. In this review, we, therefore, describe the role of this novel imaging system during Mitraclip, Cardioband, and paravalvular leak closure interventions. The technical principles and the fluoroscopic anatomy of the interatrial septum and mitral valve are also described.

Keywords transoesophageal echocardiography • fluoroscopy • mitral valve repair • fusion images

Introduction

Over the past 10 years, percutaneous mitral valve (MV) therapies have emerged as alternatives to open heart surgery in high-risk patients with mitral regurgitation (MR).[1–4] The principles lying behind two of these percutaneous approaches have been developed from well-established surgical techniques: edge-to-edge MV repair with the Mitraclip system (Abbott Vascular, Santa Rosa, CA, USA) and transfemoral direct annuloplasty with the Cardioband system (Edwards Lifesciences, Irvine, CA, USA). Similarly, transcatheter closure of mitral paravalvular leak (PVL) is nowadays a feasible alternative to surgical repair especially in patients who, for clinical reasons are poor candidates to redo-surgery.[5] Two-dimensional (2D) and three-dimensional (3D) transoesophageal echocardiography (TOE) are crucial tools in the guidance these procedures, and they are considered to have the same relevance as fluoroscopy in term of efficacy and frequency of use.[6–9]

However, the 'dual imaging-based approach' (i.e. fluoroscopy and TOE) suffers from a lack of precise spatial and temporal integration. While catheters and devices are best visualized through fluoroscopy on one screen, MV leaflets and the mitral annulus can be exclusively visualized with 2D/3D TOE on a second screen. Interventional cardiologists are therefore obliged to consult repetitively and sequentially the two screens during each catheter manipulation. Moreover, echocardiography and fluoroscopy have their own tridimensional spatial co-ordinates and display cardiac structures in different orientations, thus requiring an interpretative effort to the operators to integrate ultrasound and fluoroscopic data. Because of the technical complexity of transcatheter MV procedures, a better integration between echocardiographic and fluoroscopic imaging data has become mandatory.

A novel imaging technique (Echo-Navigator, Philips Medical System, Best, the Netherlands) is able to acquire patient-specific imaging data from both fluoroscopic projections and bi-dimensional and 3D TOE volumetric data set. These two real-time imaging techniques are then 3-dimensionally overlapped. Co-registration is a term that describes this spatial and temporal alignment process. The result is a sort of 'hybrid image' which has the unquestionable advantage of providing an easy to interpret and reliable interface to interventional cardiologists, since soft tissues are displayed within the standard fluoroscopic projections. These echocardiographic-fluoroscopic hybrid images (the so-called 'fusion images') have been designed with the purpose to facilitate catheters' and devices' manipulation during catheter-based structural heart disease (SHD) interventions. Several

* Corresponding author. Tel: +41 (91) 805 3179; Fax: +41 (91) 805 3167. E-mail: francesco.faletra@cardiocentro.org

Published on behalf of the European Society of Cardiology. All rights reserved. © The Author(s) 2018. For permissions, please email: journals.permissions@oup.com.

Downloaded from https://academic.oup.com/ehjcimaging/article-abstract/19/7/715/4989316 by smsulaimanuniv user on 27 April 2020

reports have described the early developments and the first clinical experiences[10–15] with this approach, but literature focusing on the practical applications of this fusion imaging technology to MV transcatheter interventions, and on its potential advantages and current limitations, is still limited. In this review, we describe the technical principles regarding this novel imaging modality, the fluoroscopic anatomy of the important structures involved in these procedures, the novel echocardiographic 2D/3D TOE perspectives, and its potential role in each step of the main percutaneous interventions, such as Mitraclip, Cardioband, and PVL closure. The review is based on the experience gained in more than 100 percutaneous MV procedures performed in the departments of Cardiology of Cardiocentro Ticino in Lugano, of the University Heart Center in Zurich and of the Scientific Institute San Raffaele in Milan (Table 1).

Basic principles of fusion imaging

The method is based on the localization of the 3D TOE probe into the fluoroscopic space as described by Gao *et al.*[12] Their hypothesis was that using an efficient and robust image-based TOE probe-tracking algorithm and one or more fluoroscopic images, the position and orientation of the TOE probe could be automatically determined from the fluoroscopic data. The image-based TOE probe-tracking algorithm is based on an ultra-high resolution tomographic data set of a 3D model of a 3D TOE probe (nano-PET TM/CT, Mediso Ltd, Budapest, Hungary), previously calibrated on fluoroscopic images. The algorithm compares the reconstructed projections of the model (digitally reconstructed radiograph [DRR]) with the actual fluoroscopic image. At each comparison, the system calculates the similarity between fluoroscopic images and DRR and iteratively adjusts its estimation of the position and orientation of the TOE probe. The process continues until the best match between the TOE probe model and the actual fluoroscopic image of the TOE probe is identified. Two fluoroscopic projections [usually 30° left anterior oblique (LAO) projection and 30° right anterior oblique (RAO) projection at the time of TOE probe co-registration] minimize potential registration errors which may occur in the 3D space in the direction of the fluoroscopic beam or when the area of interest moves from the near field to the far field. A digitized, green-coloured, 3D model overlaying the fluoroscopic image, confirms that the probe is correctly coordinated with the intervention table and with the angulation of the C-arm.

Table 1 Number of percutaneous MV procedures

Procedures	Fondazione Cardiocentro Lugano	University Heart Center Zurich	Istituto Scientifico S. Raffaele Milan
Mitral clip	32	19	68
Cardioband	2	4	3
Paravalvular leak	3	2	9
Complications	2[a]	0	2[b]

[a]Vascular complications.
[b]Valve damage requiring surgery.

When fluoroscopy is activated, the system immediately overlaps the 2D or 3D echo image with the fluoroscopic silhouette and every time C-arm angulation is changed, the system recognizes and registers it and automatically updates the 2D/3D TOE image orientation on the screen. Additional hardware system permits to reconstruct the probe head model projection and registration to the X-ray plane by transferring the echo machine's live 3D imaging data to the X-ray system and by showing the rendering in the proper orientation and fusion with X-ray. However, since the additional hardware system is coupled with the X-ray system (Philips Allura Xper FD20/10 fluoroscopic system) and to the echo-machine hardware system (Philips CX50 or IE33 or Philips EPIC 7) which is provided by the same vendor (Philips Medical system), implementation of this system in the context of a hybrid room is straightforward. A wireless mouse, controlled either by interventional cardiologist or by the echocardiographer, regulates the different options, and tools of the fusion imaging system. Both 2D and 3D images may be displayed in a large fluoroscopic screen that can be split in separate panels (up to four) as they are visualized in the echo-machine (2D echo planes and 3D echo perspectives) or as they appear when they are aligned to the fluoroscopic projection. A dedicated panel shows the fused images.

The system provides several options to display and to process fused images:

a. Redundant extraneous tissues may be cropped directly on fluoroscopy, thus revealing soft tissue anatomy that is relevant to the procedure.
b. 2D TOE slices derived by 3D data set can be moved from the near to the far field in the direction of the fluoroscopic beam.
c. A specific tool that increases translucency of 3D TOE images relative to fluoroscopy makes catheters and devices well visible through the partially translucent soft tissues.
d. A dedicated software allows to place fiducial reference markers on 2D/3D images. When deemed accurate, reference markers are then accepted and immediately transferred and superimposed to the fluoroscopic image.

Fluoroscopic anatomy of interatrial septum and MV

In patients lying in the supine position [antero-posterior (AP) fluoroscopic projection], the right atrial (RA) cavity is right and anterior, whereas the left atrial (LA) cavity is left and posterior. As a result, the fossa ovalis (FO) is oriented left-to-right with an angle of about 65° with respect to the sagittal plane of the body. Owing to this obliquity, in the AP projection the FO is partially overlapped with the aortic root (Ao), which lies anterior and left to the FO. In the standard 30° RAO view the FO is 'en face' and Ao lies on the left with no overlapping, whilst in the 30° LAO view the FO is projected tangentially, thus precisely dividing the left from the RA cavity, with an almost complete overlap with the Ao (Figure 1).

For this reason, a RAO 20–30° is the ideal projection to confirm that the tip of the needle is positioned in the precise site within the FO, whilst in the LAO 20–30° the curvature of the FO (tenting) pointing towards the LA cavity appears maximal. Although most interventional cardiologists use pre-defined fluoroscopic angulations in order to perform trans-septal puncture (TSP), no specific angle in

Downloaded from https://academic.oup.com/ehjcimaging/article-abstract/19/7/715/4969316 by simaria@rau.ro user on 27 April 2020

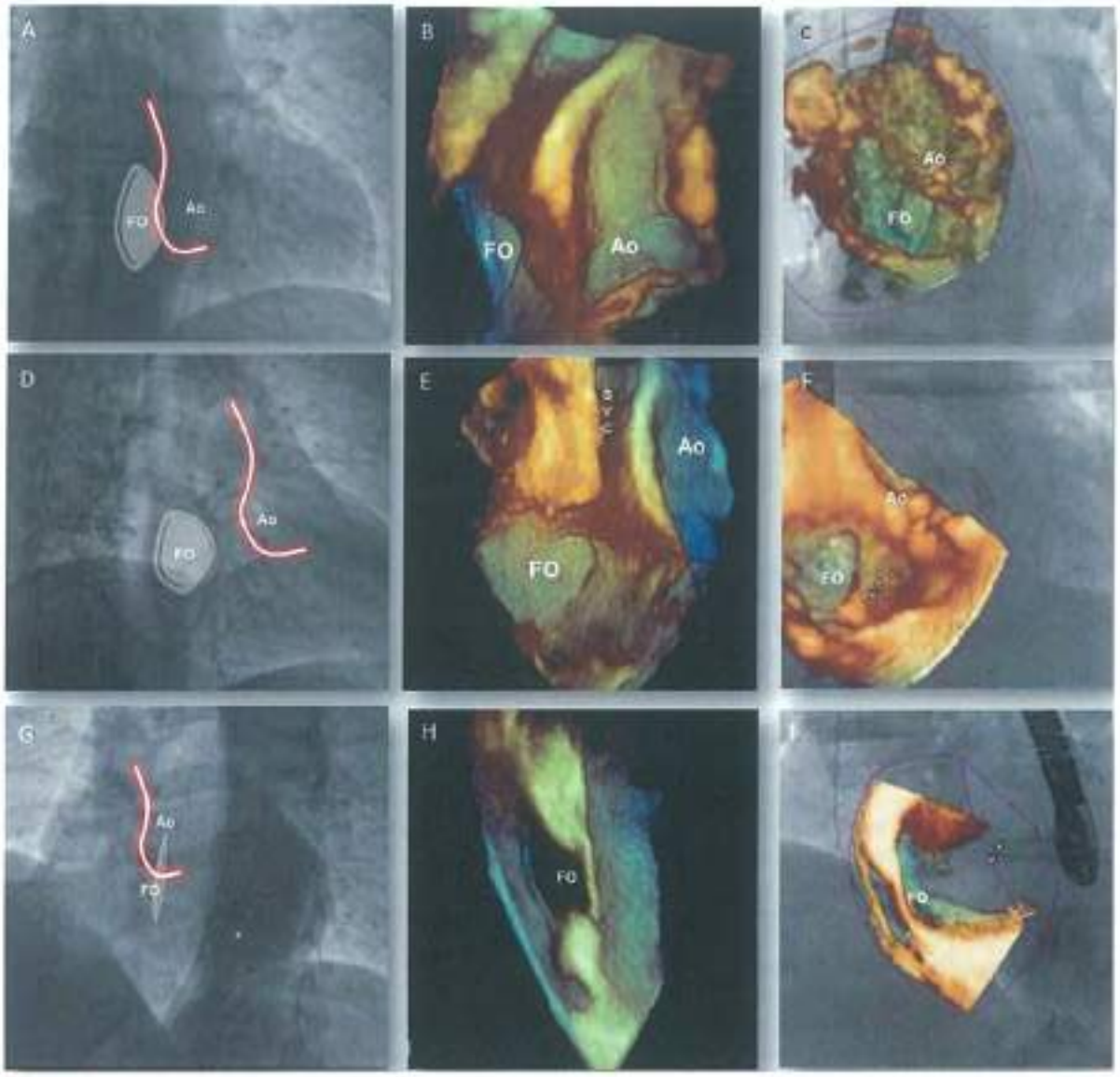

Figure 1 Fluoroscopic, 3D TOE and fusion image: (*A–C*) AP projection, the white/red line marks the right profile of the Ao, partially overlapping the FO; (*D–F*) RAO 30° projection, the FO is displayed 'en face' and the Ao does not overlap the FO; (*G–I*) LAO 30° projection, the Ao nearly completely overlaps the FO, thus both in 3D TOE and in fusion imaging the aorta has been removed for visualizing the FO in cross section. SVC, superior vena cava.

the RAO or LAO projections is anatomically consistent in all patients. Indeed, the position of the FO and its spatial relationship with surrounding structures may significantly change either physiological conditions (due to individual anatomical variations) or in pathological states.[16,17] For example, both dilatation of the LA and of the Ao tend to displace the FO more posteriorly. Moreover, the size of the FO may vary considerably from heart to heart, ranging from a large and round FO, frequently found in LA dilatation, to a very small and oval FO seen in patients with a lipomatous septum. One of the potential advantages of hybrid imaging is that when echocardiographic and angiographic images are overlapped, the FO becomes visible on the fluoroscopic screen and, consequently, C-arm angulation can gradually be adjusted until the FO appears in the correct perspective, allowing a perfect patient-tailored fluoroscopic view.

Understanding position and orientation of mitral leaflets and mitral annulus in different fluoroscopic projections is essential to guide transcatheter MV interventions. Two echocardiographic-fluoroscopic fusion projections are particularly relevant in transcatheter MV repair: the RAO projection 20–30° and the LAO projection 20–30°[16] (*Figure 2*). In the RAO (20–30°) cranial (10–20°) projection leaflets are displayed inside the cardiac silhouette in a cross section which roughly corresponds to the commissural view of 2D TOE. In this view, the maximal mitral annulus diameter is projected. This projection clearly separates segments of leaflets, but as in 2D TOE, it overlaps A1, A2,

Downloaded from https://academic.oup.com/ejcimaging/article-abstract/19/7/715/4989316 by stmarianmsu.rlv user on 27 April 2020

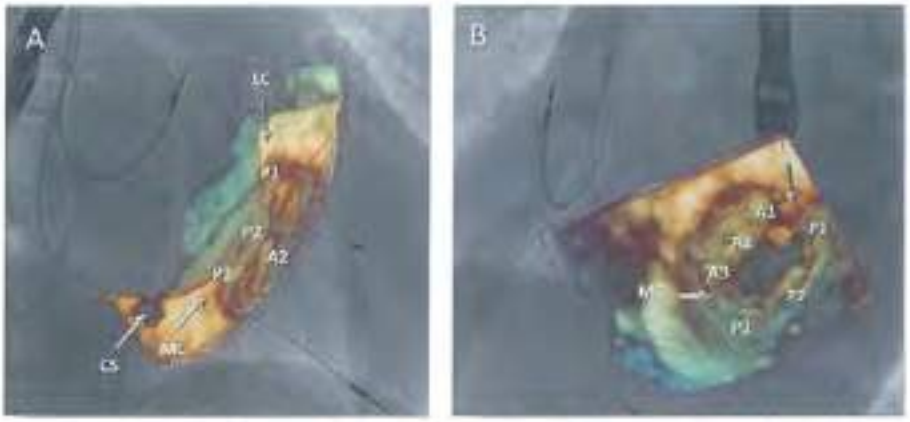

Figure 2 (A) Fused image of mitral valve in RAO projection. This projection separate segments of leaflets, but overlaps A1, A2, and A3 and P1, P2, and P3. The medial commissure (MC) is right-inferior, while the lateral commissure (LC) is left-superior. (B) Fused image of mitral valve in LAO projection. The image of mitral valve is seen from a ventricular perspective. This projection clearly separates segments of anterior from segments of posterior leaflet.

and A3 and P1, P2, and P3. Since the annular plane has an oblique direction from right-inferior to left-superior, this projection appears extremely useful during Mitraclip procedures for the visualization of the supero-inferior clip trajectory which must be perfectly perpendicular to the annular plane. Moreover, 2D TOE colour Doppler nicely shows the site of the regurgitant jet on fluoroscopy, thus greatly facilitating the steering manoeuvre towards the regurgitant orifice (see below). The origin of the regurgitant jet is particularly important after the first (or second) clip deployment in order to decide if the implantation of an additional clip is necessary. The position of trigones and commissures, relevant during the Cardioband procedure, are easily detected with the antero-lateral commissure superior and leftward, and posterior-medial commissure inferior and rightward. To clearly separate anterior from posterior MV leaflets the C-arm is rotated up to RAO 70° and tilted caudally up to 30–40°. In this fluoroscopic projection, the 2D/3D TOE image within the fluoroscopic silhouette is analogous to the 2D TOE long axis view 120° in which the minimum MV annular diameter is projected. This extreme RAO can be useful in the Mitraclip procedure for the grasping of A2–P2. However, the latter is rarely used by interventional cardiologists. In LAO (20–50°) with a slight caudal inclination (20–30°), the fluoroscopic projection is perpendicular to the mitral annulus, thus showing the en face view of the MV from the left ventricle perspective (analogous to 3D TOE ventricular perspectives of MV). In this view, the perimeter of the mitral annulus is entirely projected on the fluoroscopic plane. The fusion image allows to safely navigate into the LA around the perimeter of the valve. The same projection appears also useful after Mitraclip(s) deployment to appreciate the two orifices and the amount of leaflet tissue that has been grasped.

The role of fusion imaging during Mitraclip

Nowadays, percutaneous edge-to-edge MV repair with Mitraclip system is the only commercially available option for transcatheter treatment of both functional and degenerative MR. After its initial introduction in clinical practice, thousands of Mitraclip procedures have been performed worldwide. Although the implant is effectively guided by 2D/3D TOE echocardiography, there are several steps of the procedure where echocardiographic-fluoroscopic fusion imaging proves more useful and reliable than separate imaging. In particular, we found fusion imaging very helpful in (i) guiding the search of TSP site, (ii) navigating in the left atrium (to avoid impinging on the lateral wall or left lateral ridge), (iii) establishing the exact distance between the tip of the guiding catheter and the interatrial septum (for a safer withdrawing of the delivery system when needed), (iv) in assessing superior-inferior clip trajectory and, finally, and (v) in localizing the origin of the regurgitant jet on fluoroscopy (particularly useful after the implant of one or two clips).

Site-specific TSP

In general, the procedure requires a TSP near the superior and posterior margin of FO in order to obtain a good steerability of the delivery system within the LA.[8] This 'site-specific' TSP using 2D TOE requires two planes: a mid-oesophageal aortic valve short-axis view to determine the AP position and a bi-caval view to determine the supero-inferior position. An adjunctive cross section (usually the four chamber view) is necessary to measure the distance between the tip of leaflets and the annular plane. Using fused imaging in RAO projection the FO is projected in 'en face' view making it easier to determine the site-specific point. The addition of fiducial markers on standard fluoroscopic images, may further facilitate the correct positioning of the tip of the needle during the withdrawal and torqueing of the trans-septal needle. When the catheter approaches the desired point, the interventional cardiologist should be asked to rotate the C-arm in the LAO 30° projection. This projection displays the FO in sagittal view, clearly demonstrating the tenting of the FO and, following a further pressure the crossing of the needle which appears in the LA[17] (*Figure 3A–C* and Supplementary data online, *Movie S1*).

Downloaded from https://academic.oup.com/ehjcimaging/article-abstract/19/7/716/4989316 by sfmariansuntiv user on 27 April 2020

LA navigation with bulky and stiff delivery system might constitute a difficult and potentially dangerous manoeuvre. Advancing and withdrawing the guidewire and guiding catheter into the LA or steering the delivery system towards the MV may prove safer, if soft tissues of the atrial wall and FO are visible on fluoroscopy (*Figure 3D–F*).

After localizing the regurgitant jet (target lesion), the delivery system is advanced towards the target lesion and its trajectory should be exactly perpendicular to the valvular plane. Perpendicularity is of utmost importance to prevent oblique implantation of the clip with eventual ineffective grasping and distortion of the coaptation line. By the aid of fusion imaging, using either the 2D biplane or the 3D modality, the correct trajectory and alignment of the delivery system can be easily obtained. During this step, we usually prefer the dual panel display which simultaneously shows the perpendicularity of the clip arms to the coaptation line (*Figure 4A*) and the perpendicularity of the delivery system to the valvular plane (*Figure 4B* and Supplementary data online, *Movie S2*).

Localizing the site(s) of MR with 2D TOE colour Doppler on the fluoroscopic screen rather than using the 2D/3D TOE monitor alone, may greatly facilitate the advancement of the Mitraclip delivery system towards the origin of the jet by just coupling hand's manipulation with fluoroscopic advancement of the system towards a well-visible regurgitant jet. Notably, to further facilitate navigation, the regurgitant jet can be labelled with a fiducial marker positioned on its origin. In the common scenario of multiple clips implantation, the localization of the origin of any significant residual regurgitant jet may result of great usefulness to effectively direct the mitral clip delivery system towards the residual regurgitant orifice (*Figure 5* and Supplementary data online, *Movie S3*).

The role of fusion imaging during Cardioband procedure

Cardioband (Edwards Lifesciences, Irvine, CA, USA) is a percutaneous surgical-like direct annuloplasty device that is implanted in the beating heart on the posterior annulus. A polyester sleeve with radiopaque markers is fixed through multiple anchors inserted into annular tissue from the antero-lateral to the postero-medial commissure. At the end of implantation, the device size is adjusted, by assessing adequate reduction of MR severity under TOE guidance. Preliminary results appear promising.[4] The main steps of the Cardioband procedure are TSP, system insertion and navigation within the LA, implant deployment and implant size adjustment.

A patient-tailored TSP allows a good steerability of the delivery system around the entire perimeter of the annulus. The site-specific

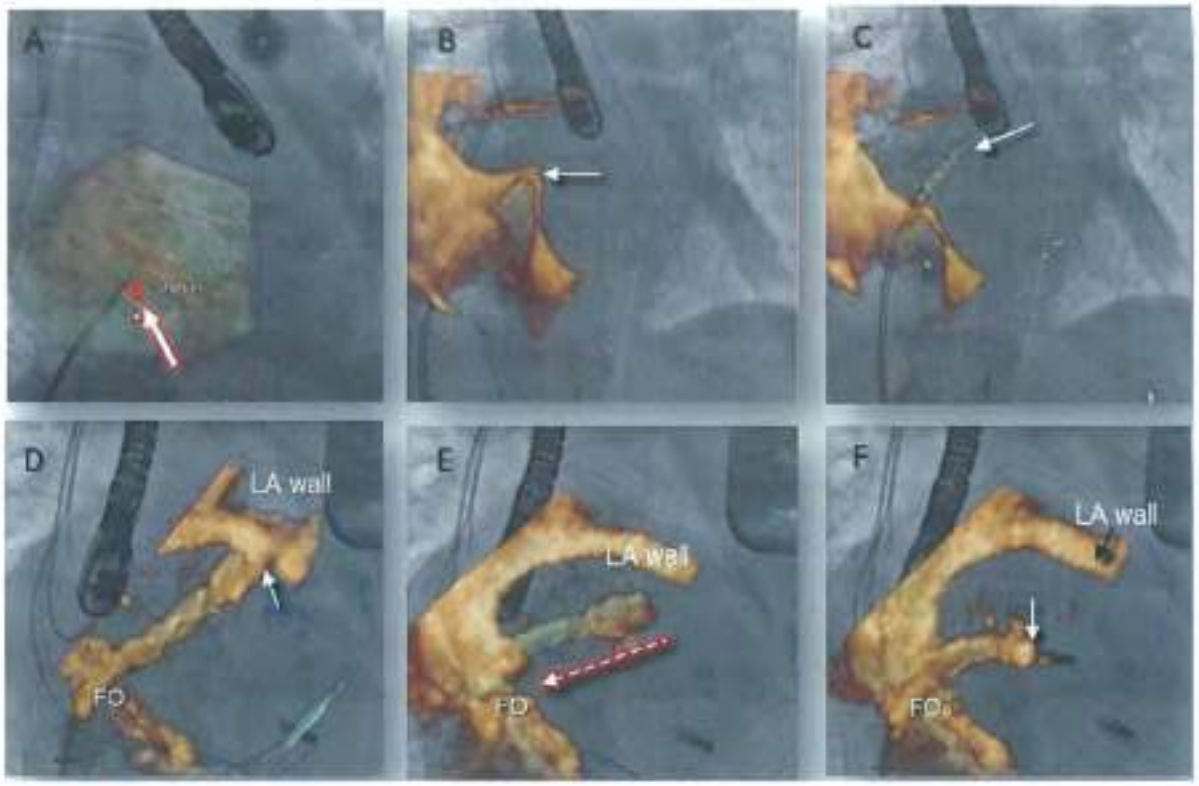

Figure 3 (*A*) Site-specific transseptal puncture. The site of the puncture is best localized in RAO 30° where the FO is seen 'en face'. The fiducial marker (circle and arrow) facilitates the manoeuvre. (*B*) The 'tenting' seen in LAO 30°. (*C*) The guide wire is seen crossing the FO (arrow). (*D–F*) Navigation within the atrium. (*D*) The delivery system is blocked on the lateral wall of the left atrium (LA) (arrow). (*E* and *F*) The system is safely pulled back and steering since the soft tissue of the lateral wall and FO are clearly visible on fluoroscopic image.

Downloaded from https://academic.oup.com/ehjcimaging/article-abstract/16/7/715/549283 by stmarianmaurv user on 27 April 2020

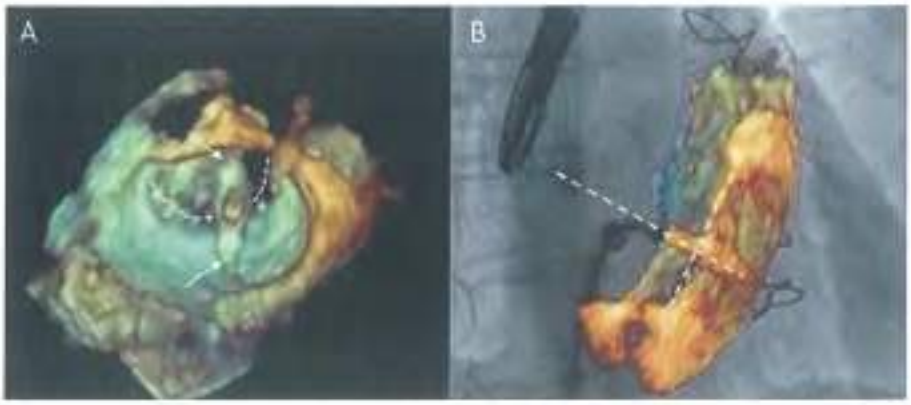

Figure 4. The dual panel display showing (*A*) the correct orientation of the arms of the clip perpendicular (arrows) to the coaptation line (dotted line) and (*B*) the trajectory of the clip delivery system perpendicular to the valvular plane (dotted lines).

TSP is pre-defined through a computed tomography scan performed before the procedure. However, as a general rule, it should take place at the level of the postero-medial commissure with a distance that is equal to or higher than 3.5 cm from the annular plane. As for the Mitraclip procedure, fusion imaging may greatly facilitate TSP. Following TSP, the implant delivery system (IDS) is advanced into the LA. The IDS comprises a steerable guide catheter and an implant catheter (IC) with the Cardioband implant loaded on its distal end. The delivery system is steered until the tip of the IC is placed over the anterior commissure where the first anchors are deployed as close to the aorta as possible (*Figure 6A–C*). The site of the first implant is displayed on 3D TOE imaging on the left of the screen while on fluoroscopy the same point is displayed on the right upper corner.

Fusion imaging offers a more familiar vision where the 'soft' echo image of the lateral commissure is oriented according to the fluoroscopic projection (*Figure 6C* and Supplementary data online, *Movie S4*).

The IC tip is then driven to the next anchoring point along the posterior annulus. These actions are repeated until the IC tip reaches the last anchoring site on the posterior commissure. Navigation within the LA is usually monitored using a 3D overhead perspective of the LA (*Figure 6* and Supplementary data online, *Movies S5* and *S6*). During Cardioband implant, fusion imaging may help to obtain the correct orientation of the catheter with respect to the annular plane and its correct positioning in relation to the leaflets' hinge line, well visible within the fluoroscopic silhouette (*Figure 5C*). Moreover, we noticed that in some steps shadowing artefacts might reduce the quality of echocardiographic imaging. In such a cases, fusion imaging improves the visualization of all the components (catheter, anchors, and annulus). Finally, each anchor site may be labelled with fiducial markers which, once displayed on the fluoroscopic screen, may facilitate device implantation.

The role of fusion imaging during MV PVL closure

Paravalvular leak (PVL) occurs in 5–17% of patients after prosthetic valve replacement.[18–20] For symptomatic patients, repeat surgery has been the traditional treatment, but it is associated with high operative mortality.[18,19] PVL percutaneous repair has therefore, emerged as an alternative therapy especially in high-risk patients.[20–22] However, successful PVL closure relies on a good understanding of PVL anatomy. Number, location, severity, and shape of PVL defects are currently assessed with transthoracic and transoesophageal 2D and 3D echocardiography, which is performed before the procedure. Mitral percutaneous PVL closure can be performed using the anterograde (venous, trans-septal), retrograde (arterial, transfemoral), or transapical access. The access-site selection depends on the location of the PVL, operator experience and preference, and the anatomical peculiarities of the individual patient.

In PVL closure fusion imaging is, to our experience, extremely helpful. *Figure 7* shows two PVLs identified and labelled on 3D TOE image (*Figure 7A*). The fiducial markers appear on the fluoroscopic image (*Figure 7B*) precisely indicating the fluoroscopic position of the leaks. Overlapping the regurgitant jet on the fluoroscopic screen, the operator may select the best fluoroscopic orientation that displays the largest 'vena contracta' which roughly corresponds to the largest diameter of the leak (*Figure 8A* and *B*). Both fiducial markers and the vena contracta greatly facilitate leak crossing (*Figures 7* and *8* and Supplementary data online, *Movies S7* and *S8*). Finally, the reduction (or abolition) of regurgitation after the deployment of the plug is directly detected on fluoroscopy to avoid the use of contrast.

Discussion

The aim of this review is to illustrate the potential advantages of this novel technology specifically tailored to guide MV procedures. Despite previous papers reporting single initial experiences, to the best of our knowledge this is the first review that specifically describes the potential advantages and limitations of this fusion imaging in the context of MV procedures on the basis of more than 100 cases performed in three different institutions.

Echocardiography-fluoroscopy fusion technique has undoubtedly opened a new perspective in the field of percutaneous structural

Downloaded from https://academic.oup.com/ehjcimaging/article-abstract/19/7/715/4968316 by stmarianmsuniv user on 27 April 2020

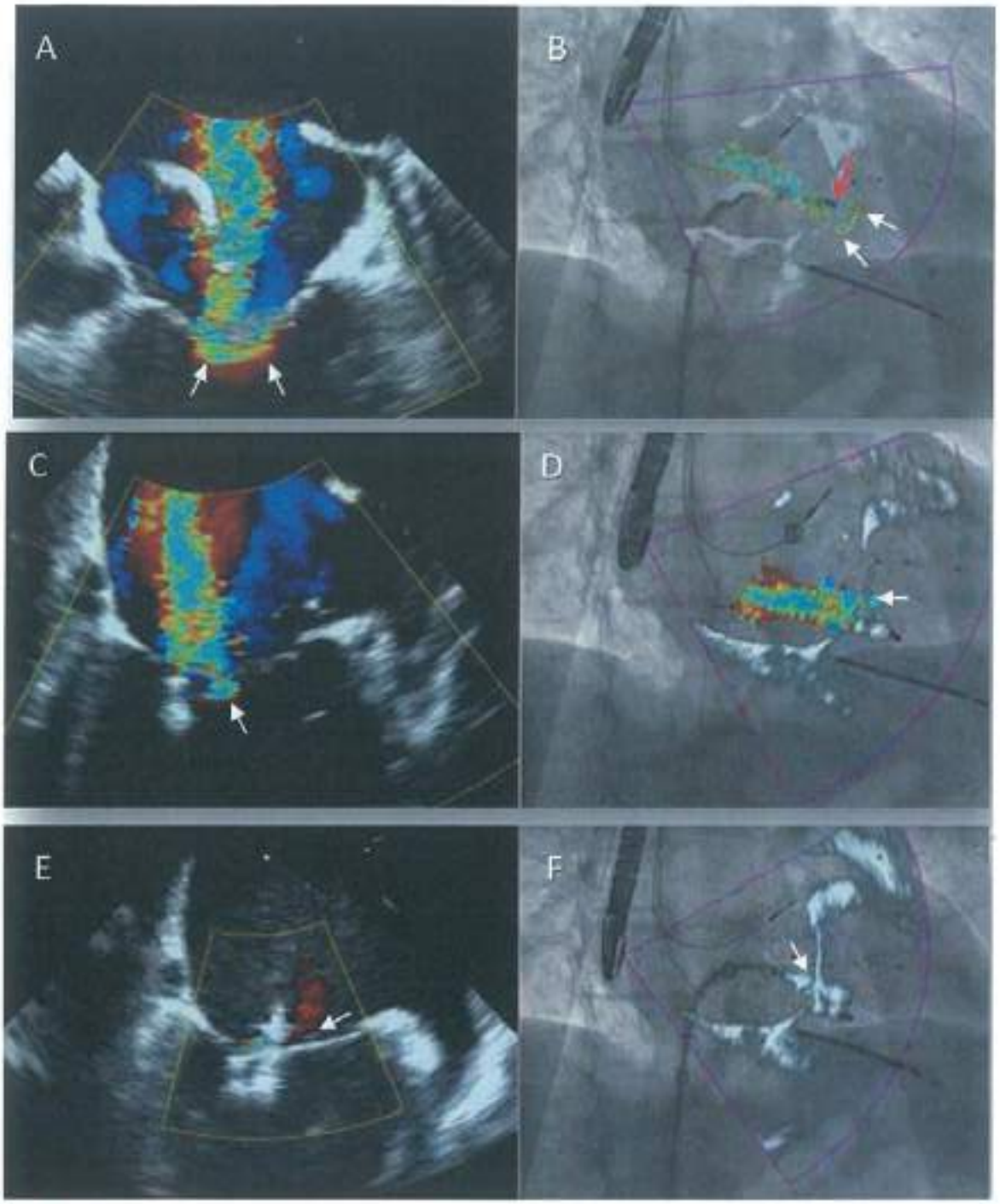

Figure 5 (*A* and *B*) The dual panel display showing a large mitral regurgitation (arrows). In fused image is clearly visible the clip delivery system approaching towards the origin of the jet (red arrow). (*C* and *D*) After a first clip, there is a residual regurgitant jet lateral to the first clip (arrow). (*E* and *F*) A second clip is then implanted on the origin of this residual jet.

interventions and has the potential to influence the catheterization laboratory structure in terms of medical devices' design and the skills required. In fact, while fusion imaging certainly facilitates the communication between the echocardiographist and the interventional cardiologist, proper and effective use of this novel technique requires a learning curve. From the echocardiographist point of view, such learning curve consists of a thorough understanding of the new 2D/3D TOE projections that characterize fusion images (which differ

Downloaded from https://academic.oup.com/ehjcimaging/article-abstract/19/7/715/4989316 by stmariannaunIv user on 27 April 2020

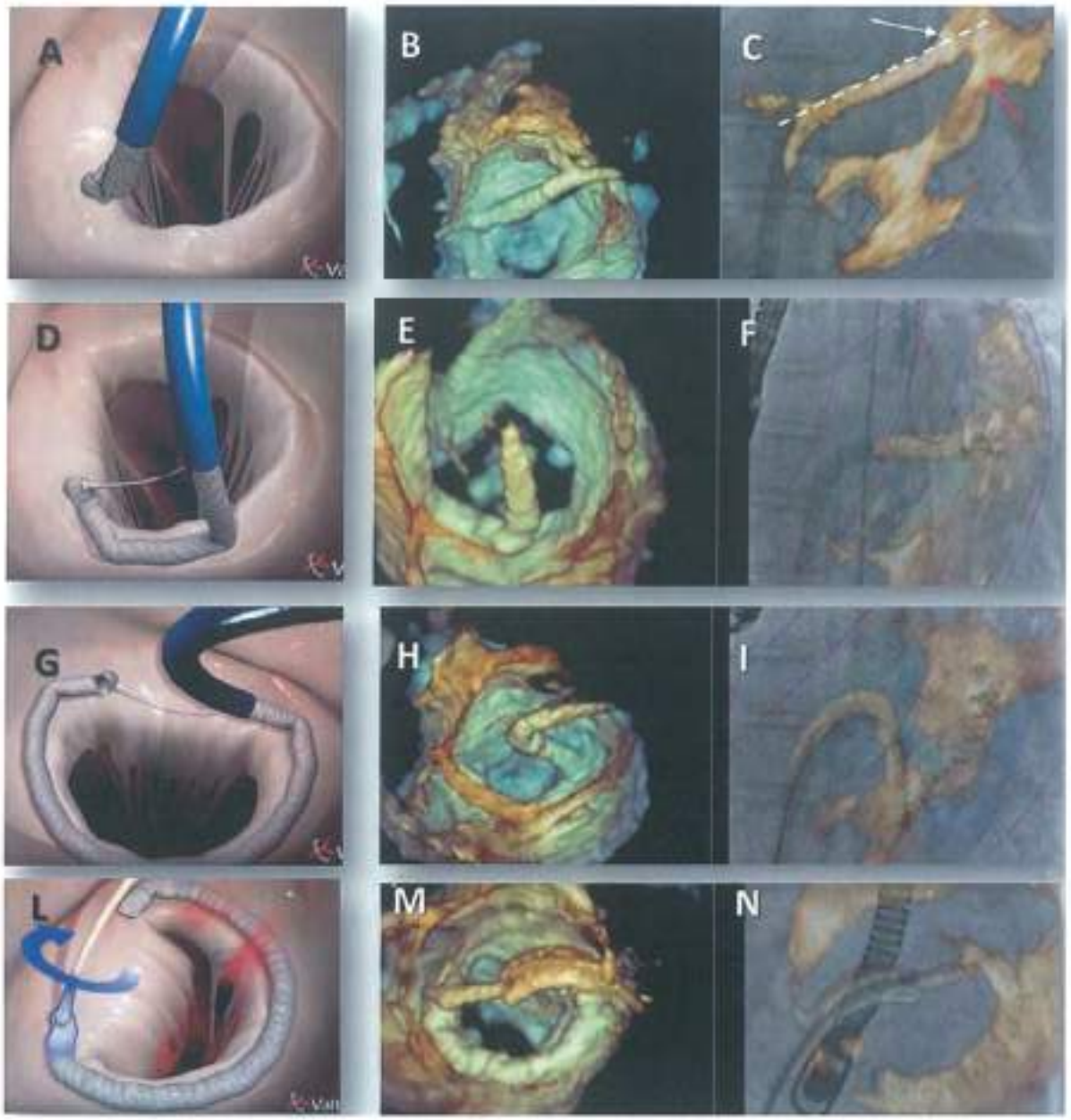

Figure 6 Steps of the procedure visualized by a cartoon (*A, D, G, L*) provided by the vendor, 3D TOE (*B, E, H, M*) from an overhead perspective, and fusion imaging (*C, F, I, N*). (*C*) The orientation of the catheter is marked by the dotted line, the white arrow points at the tip of catheter on the annulus while the red arrow at the hinge line.

from typical 2D/3D TOE images) and of the proper use of the available tools (i.e. adequate cropping to visualize target lesions, knowing when to apply 2D rather than 3D images and vice versa and increasing or reducing transparency of soft tissues according the procedure's ongoing step).

Interventional cardiologists could more easily familiarize with hybrid images, since they are basically fluoroscopic images enriched with soft tissue data. On the other hand, they would have to change their 'eye-hand co-ordination' gained in years in the SHD field using fluoroscopic and TOE imaging separately; for this reason, not all interventional cardiologists are willing to accept this new imaging modality in the absence of scientific evidence. Additionally, this huge amount of visual data may be distractive ('fusion or confusion?'), and it will likely require time and training to be fully appreciated. Thus, it is not surprising that experienced cardiologists consider the clinical usefulness of this new technology questionable. However, in our

Downloaded from https://academic.oup.com/ehjcimaging/article-abstract/19/7/716/4989316 by stmariannauniv user on 27 April 2020

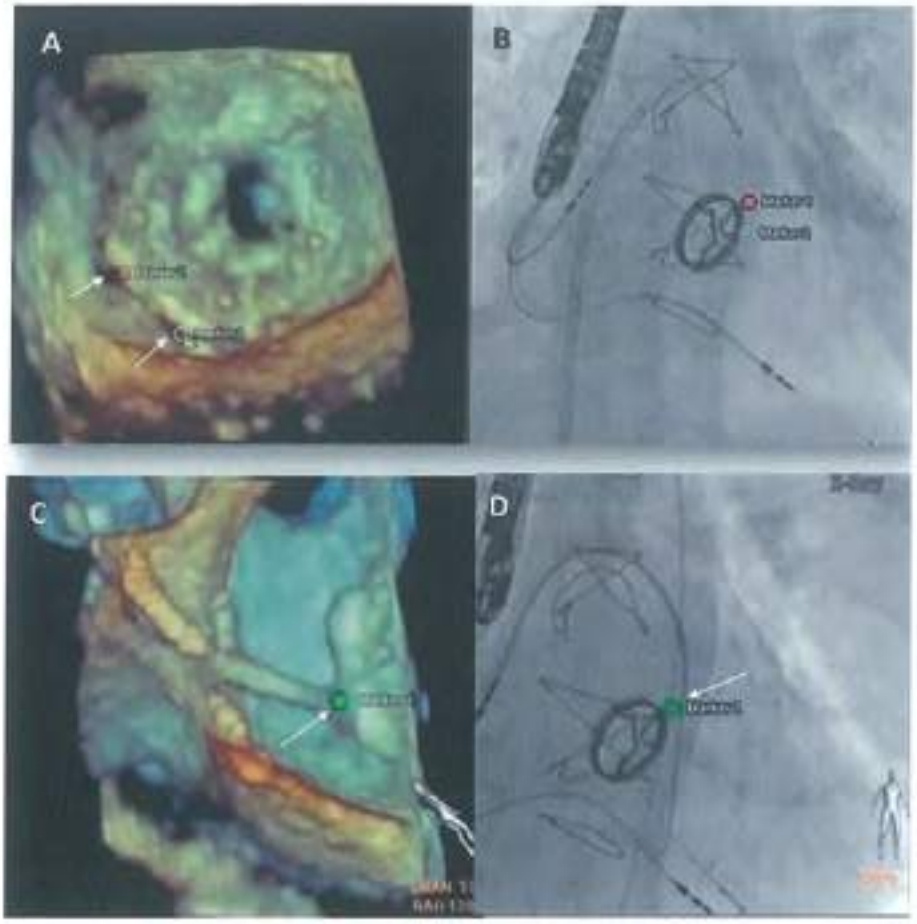

Figure 7 (*A*) 3D TOE image showing two paravalvular leaks (arrows). Locations marked with fiducial markers on the 3D images, immediately appear on the fluoroscopic screen (*B*) allowing an easier identification of the site. (*C*) 3D TOE image showing the catheter crossing one paravalvular leak (arrow) marked by marker. (*D*) Fluoroscopic image of the same step of procedure.

experience less experienced interventional cardiologists and trainees in invasive cardiology might benefit from this more intuitive imaging technique and as a result their learning curve might be shortened.

The exponential clinical advantages that may be gained from this new technology is not yet established. In the absence of comparative data, it is difficult to evaluate the impact of this imaging modality in terms of reduction of procedural times, radiation exposure, incidence and seriousness of complications, and operator confidence improvement, when compared with traditional 2D/3D TOE guidance. On the other hand, obtaining comparative data remains challenging. Multiple determinants such as experience of the operator, difficulties related to the single procedure, quality of echocardiographic imaging might make comparative data rather unreliable. Currently, there is a very limited experience worldwide, and the collection of adequate case series is difficult to obtain. Sündermann *et al.*[15] demonstrated a trend towards a reduction in terms of both radiation dose and procedural times in patients undergoing percutaneous edge-to-edge MV repair in which more than one clip was required. In a subgroup of patients from Zurich University (unpublished data), a comparison between MV procedures performed with and without the aid of fusion imaging, did not reveal differences in terms of procedural length, fluoroscopy time, and radiation dose (*Table 2*). Finally, future advances in spatial and temporal resolution of 3D TOE and new computational techniques in valves' modelling will be essential to develop a more effective guidance of complex SHD interventions.

Limitations

Current existing limitations which may prevent an extensive use of this fusion imaging technique must be mentioned. One is the restricted rotation of the C-arm, which impedes the appropriate overlap of some very useful 3D TOE perspectives with the fluoroscopic background. For example, in the setting of Mitraclip procedure, interventional cardiologists consider the 3D TOE view of the left atrium to be the most appropriate to place the clip's arms as perpendicular as possible to the leaflets' coaptation line. Such perspective

Downloaded from https://academic.oup.com/ehjcimaging/article-abstract/19/7/715/4989318 by stmarianmaunty user on 27 April 2020

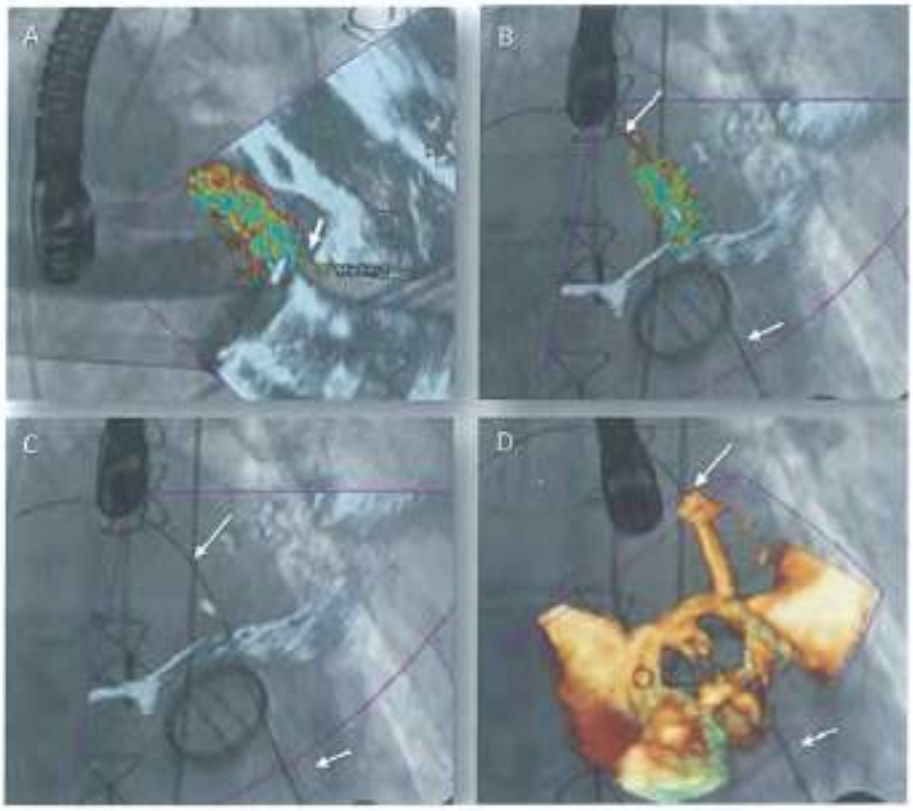

Figure 8 (*A*) 2D colour Doppler fused image showing the regurgitant jet originating from the paravalvular leak (arrow). (*B*) Colour Doppler (as well as fiducial markers) may facilitate the interventionalist in crossing the leak. The arrows point the guide wire across the leak. (*C* and *D*) Same step in 2D and 3D image.

cannot be merged with fluoroscopy. This can be overcome by splitting the screen in two (or more) panels showing the 3D TOE overhead perspective and the fused image, respectively.

A second limitation is the fact that, once positioned, fiducial markers remain fixed on the screen and do not follow soft tissue motion. This limitation is particularly relevant when the fiducial markers are positioned to localize PVLs. Because of heart motion, location indicated by markers may be correct in one frame of the cardiac cycle and incorrect in another. Malalignment between fiducial markers and structure could lead to operator misperception and errors during the procedure.

Another limitation is the inconsistency of co-registration when the probe is placed in the stomach, where the position and orientation of the probe cannot be easily tracked by the image-processing algorithm; as consequence fusion images from the trans-gastric view are difficult to obtain. Since trans-gastric views are currently the most used views to guide percutaneous clipping of the tricuspid valve, this procedure can hardly be guided by fusion imaging.

Last but not least, in our opinion the main limitation is linked to the fact that in the current fusion system both the fluoroscopy apparatus and the echo-machine at present are provided by the same vendor; such a restriction limits the application of this technique in those institutions where the echo-machine and/or the fluoroscopic system are provided by different vendors. Other manufacturers will shortly commercialize their own 'fusion imaging technique' and their more widespread use will allow to clarify its clinical role.

Conclusion

Echocardiograpy-fluoroscopic fusion imaging couples two 'real-time' imaging techniques showing in the same screen a sort of 'hybrid image' where soft tissues appear onto the fluoroscopic cardiac silhouette. This new imaging modality has the potential to become the main imaging technique in catheter-based SHD interventions. However, the absence of data showing a reduction in terms of procedural and fluoroscopic times, radiation exposure and improved outcomes, hampers its clinical applicability. Though new approach to fusion imaging from different manufactures are likely to emerge in the near future, the fact that this imaging modality is currently provided by a single vendor limits its more widespread use, experience and data collection.

Downloaded from https://academic.oup.com/ehjcimaging/article-abstract/19/7/715/4986316 by stmarianna/unity user on 27 April 2020

Table 2 Unpublished data from University Heart Center Zurich on procedural length, fluoroscopic time, and radiation dose with a without fusion

Mitral clip	With fusion	Without fusion	P-value
Degenerative/functional	11/8	11/8	
1, 2, and 3 clips	9/9/1	9/9/1	
Procedural length (min ± ds)			
1 clip	56 ± 20	61 ± 15	0.25 ns
2 clips	65 ± 16	75 ± 21	0.12 ns
3 clips	99 ± 35	108 ± 43	0.51 ns
Fluoroscopy time (min ± ds)			
1 clip	18 ± 7	17 ± 7	0.7 ns
2 clips	22 ± 6	23 ± 10	0.41 ns
3 clips	31 ± 15	33 ± 19	0.93 ns
Radiation dose (Gy/cm^2 ± ds)			
1 clip	25 ± 12	24 ± 15	0.61 ns
2 clip	31 ± 15	32 ± 19	0.73 ns
3 clip	66 ± 21	70 ± 19	0.71 ns
Cardioband	**With fusion**	**Without fusion**	**P-value**
Procedural length (min ± ds)	143 ± 36	125 ± 21	0.41 ns
Fluoroscopy time (min ± ds)	47 ± 12	52 ± 9	0.61 ns
Radiation dose (Gy/cm^2 ± ds)	36 ± 28	40 ± 31	0.85 ns
Paravalvular leak	**With EchoNav (2)**	**Without EchoNav (2)**	**P-value**
	2	2	1 ns
Procedural length (min ± ds)	128 ± 11	115 ± 35	0.65 ns
Fluoroscopy time (min ± ds)	83 ± 27	86 ± 36	0.9 ns

Supplementary data

Supplementary data are available at *European Heart Journal - Cardiovascular Imaging* online.

Funding

F.F.F. reports several talks supported by Philips. F.M. reports personal fees and other from Edwards Lifesciences; personal fees and non-financial support from Abbott Vascular, other from 4Tech Cardio; personal fees from Medtronic, outside the submitted work. M.T. reports personal fees from Abbot Vascular, personal fees from 4Tech Cardio, outside the submitted work.

Conflict of interest: none declared.

References

1. Feldman T, Wasserman HS, Herrmann HC, Gray W, Block PC, Whitlow P, EVEREST II Investigator. Percutaneous mitral valve repair using the edge-to-edge technique: six-month results of the EVEREST Phase I Clinical Trial. *J Am Coll Cardiol* 2005;**46**:2134–40.
2. Philip F, Athappan G, Tuzcu EM, Svensson LG, Kapadia SR. MitraClip for severe symptomatic mitral regurgitation in patients at high surgical risk: a comprehensive systematic review. *Catheter Cardiovasc Interv* 2014;**84**:581–90.
3. Franzen O, Baldus S, Rudolph V, Meyer S, Knap M, Koschyk D et al. Acute outcomes of MitraClip therapy for mitral regurgitation in high-surgical-risk patients: emphasis on adverse valve morphology and severe left ventricular dysfunction. *Eur Heart J* 2010;**31**:1373–81.
4. Maisano F, Taramasso M, Nickenig G, Hammerstingl C, Vahanian A, Messika-Zeitoun D et al. Cardioband, a transcatheter surgical-like direct mitral valve annuloplasty system: early results of the feasibility trial. *Eur Heart J* 2016;**37**:817–25.
5. Taramasso M, Maisano F, Pozzoli A, Alfieri O, Meier B, Nietlispach F. Catheter-based treatment of paravalvular leaks. *EuroIntervention* 2016;**12**:X55–60.
6. Silvestry FE, Rodriguez LL, Herrmann HC, Rohatgi S, Weiss SJ, Stewart WJ et al. Echocardiographic guidance and assessment of percutaneous repair for mitral clip regurgitation with the Evalve MitraClip: lesson learned from EVEREST I. *J Am Soc Echocardiogr* 2007;**20**:1131–40.
7. Altiok E, Becker M, Hamada S, Grabskaya E, Reith S, Marx N et al. Real-time 3D TEE allows optimized guidance of percutaneous edge-to-edge repair of mitral valve. *JACC Cardiovasc Imaging* 2010;**3**:1196–8.
8. Biner S, Park G, Kar S, Rafique AM, Slater J, Shiota T et al. Utility of combined two-dimensional and three-dimensional transesophageal imaging for catheter-based mitral valve clip repair of mitral regurgitation. *J Am Soc Echocardiogr* 2011;**24**:611.
9. Faletra FF, Pedrazzini G, Pasotti E, Muzzarelli S, Dequarti MC, Murzilli R et al. 3D TEE during catheter-based interventions. *JACC Cardiovasc Imaging* 2014;**7**:293–308.
10. Clegg SD, Chen SJ, Nijhof N, Kim MS, Salcedo EE, Qualls RA et al. Integrated 3D echo-x ray to optimize image guidance for structural heart interventions. *JACC Cardiovasc Imaging* 2015;**8**:371–4.
11. Balzer J, Zeus T, Hellhammer K, Veulemans V, Eschenhagen S, Kelmeier E et al. Initial clinical experience using the EchoNavigator®-system during structural heart disease. *World J Cardiol* 2015;**7**:563–70.
12. Gao G, Penney G, Ma Y, Gogin N, Cathier P, Arujuna A et al. Registration of 3D trans-esophageal echocardiography to X-ray fluoroscopy using image-based probe tracking. *Med Image Anal* 2012;**16**:38–4.
13. Faletra FF, Pedrazzini G, Pasotti E, Murzilli R, Leo LA, Moccetti T. Echocardiography-X-ray image fusion. *JACC Cardiovasc Imaging* 2016;**9**:1114–7.
14. Jone P-N, Ross MM, Bracken JA, Mulvahill MJ, Di Maria MV, Fagan TE. Feasibility and safety of using a fused echocardiography/fluoroscopy imaging system in patients with congenital heart disease. *J Am Soc Echocardiogr* 2016;**29**:513–21.
15. Sündermann SH, Biaggi P, Grünenfelder J, Gessat M, Felix C, Bettex D et al. Safety and feasibility of novel technology fusing echocardiography and fluoroscopy images during MitraClip interventions. *EuroIntervention* 2014;**9**:1210–6.
16. Thériault-Lauzier P, Andalib A, Martucci G, Mylotte D, Cecere R, Lange R et al. Fluoroscopic anatomy of left-sided heart structures for transcatheter

Downloaded from https://academic.oup.com/ehjcimaging/article-abstract/19/7/715/4989316 by stmarianmaunv user on 27 April 2020

interventions: insight from multislice computed tomography. *JACC Cardiovasc Interv* 2014;**7**:947–57.
17. Faletra FF, Biasco L, Pedrazzini G, Moccetti M, Pasotti E, Leo LA *et al.* Echocardiographic-fluoroscopic fusion imaging in transseptal puncture: a new technology for an old procedure. *J Am Soc Echocardiogr* 2017;**30**:886–95.
18. Gerosa M, Franzen D, Vogt P, Seifert B, Jenni R, Kunzli A *et al.* Paravalvular leakage after mitral valve replacement: improved long-term survival with aggressive surgery! *Eur J Cardiothorac Surg* 2000;**17**:14–9.
19. Taramasso M, Maisano F, Denti P, Guidotti A, Selicchi A, Pozzoli A *et al.* Surgical treatment of paravalvular leaks long-term results in a single-center experience (up to 14 years). *J Thorac Cardiovasc Surg* 2015;**149**:1270–5.
20. Binder RK, Niethipach F, Holubec T, Maisano F. Percutaneous treatment of severe transvalvular and paravalvular regurgitation in failed surgical aortic valve prosthesis due to recurrent endocarditis. *Eur Heart J* 2016;**37**:3419.
21. Ruiz CE, Jelnin V, Kronzon I, Dudy Y, Del Valle-Fernandez R, Einhorn BN *et al.* Clinical outcome in patients undergoing percutaneous closure of periprosthetic paravalvular leaks. *J Am Coll Cardiol* 2011;**58**:2210–7.
22. Garcia-Bardella Fernández R, Sancho Jaldón M, Calle Pérez G, Gómez Menchero AE, de Zayas Rueda R, Arora Granado R *et al.* Percutaneous treatment of mitral valve periprosthetic leakage: an alternative to high-risk surgery? *Rev Esp Cardiol* 2009;**62**:438–41.

Downloaded from https://academic.oup.com/ehjcimag/ehp/article-abstract/19/7/715/4989318 by stmariamaunv user on 27 April 2020

ISSN-2189-3926

Volume 4 No. 1
August 2018

ANC

Annals of Nuclear Cardiology

Clinical and Technological Aspects of Nuclear Cardiology

EDITOR'S PAGE
Art and Science P1

SPECIAL REVIEW ARTICLE
Adipose Tissue and Atherosclerosis P5

ORIGINAL ARTICLES
Utility of a Phase Analysis with the Heart Function View P11
Detecting of Primary Cardiac Tumors P23
Phase Analysis in 99mTc Pharmacological Stress MPI P34

RAPID COMMUNICATIONS
Updated JMHLW Insurance Coverage P42
^{18}F-FDG PET for Large-vessel Vasculitis P46

REVIEW ARTICLES
Device Infection and NC P52
Ragadenoson in Lung Disease P60
Intro to Kinetic Modeling for MBF P68
Image Fusion for CAD P74
AI and Nuclear Cardiology P79
The t-Test: Pitfalls and Options P83
Clinical Research under the Law P88

REVIEW ARTICLE—FOCUS ISSUE
Disease Discovered in Japan and the Role of Nuclear Cardiology
Diagnostic Criteria and Severity Score for TGCV P94
Diagnostic Criteria of Takotsubo Syndrome P101
Nuclear Imaging for Takotsubo Syndrome P106
Unsolved Problems with Cardiac Sarcoidosis P110

JSNC ANNUAL SCIENTIFIC MEETING
JSNC 2018 Highlights P114

INTERNATIONAL CORNER
^{123}I-MIBG in Latin America P115
Korean Nuclear Cardiology P120
J-ACCESS P123

CARDIOVASCULAR IMAGING FOR NUCLEAR CARDIOLOGISTS
OCT in Coronary Artery Disease P127
Plaque Imaging in CTA P132

ASNC INTERNATIONAL SESSION
Radiation and Competition in Cardiac Imaging P137
NC in Developing World P139
Present Status of Nuclear Cardiology in Japan P142

EDUCATIONAL TRACK
Radioactive Shipments P149
^{18}F-FDG PET for CS P151

AWARDS
JSNC AWARDS
Nuclear Molecular Imaging of the Failing Heart: Evaluation of Cardiac Sympathetic Nerve Activity and Mitochondrial Function in Patients with Cardiomyopathy P155
Clinical Value of Ischemia Evaluation with Nuclear Cardiology to Predict a Risk of Cardiovascular Events: Award from the 18th Meeting of the Japanese Society of Nuclear Cardiology P163

JSNC TECHNICAL AWARD
^{123}I-Metaiodobenzylguanidine SPECT and Myocardial Perfusion Mismatch in Pediatric Patients with Congenital Heart Disease: Comparison with Simultaneous ^{99m}Tc-Sestamibi SPECT Image and Phase Analysis P167

JSNC NEWS UPDATE

Official Journal of
The Japanese Society of Nuclear Cardiology

JSNC

REVIEW ARTICLE—DISEASE DISCOVERED IN JAPAN AND THE ROLE OF NUCLEAR CARDIOLOGY

Takotsubo Syndrome: Changes in Diagnostic Criteria and Role of Nuclear Imaging

Kazuaki Okuyama, MD and Yoshihiro J. Akashi, MD, PhD

Received: May 7, 2018/Revised manuscript received: July 25, 2018/Accepted: July 29, 2018
© The Japanese Society of Nuclear Cardiology 2018

Abstract

Takotsubo syndrome (TTS) was first described in 1990. A wide variety of TTS cases have been reported since then; the international consensus has proposed several diagnostic criteria. The current diagnostic system often relies on identifying combinations of subsets of symptoms, or criteria, to define diagnoses. In the recently proposed TTS diagnostic criteria, obstructive coronary syndrome and pheochromocytoma involvement changes. Here, we review the criteria and the role of nuclear imaging in TTS diagnosis and discuss new directions that can provide better information

Keywords: Acute coronary syndrome, Diagnosis, Nuclear imaging, Takotsubo syndrome
Ann Nucl Cardiol 2018; 4 (1): 101-104

Takotsubo syndrome (TTS) is characterized by transient regional systolic dysfunction in the left ventricle. The dysfunctional area is not corresponding to the coronary artery perfusion territory and often including the circumferential apical, mid-ventricular, and/or basal ventricle. TTS is relatively novel; the first TTS case was reported in 1990 by Sato, et al. in Japan (1). Since then, Many TTS cases have been reported worldwide under the multiple names, such as stress cardiomyopathy, apical ballooning syndrome, broken heart syndrome and catecholamine induced cardiomyopathy. The various data of TTS have been accumulated, although, its diagnosis remains controversial.

The clinical presentation of TTS in electrocardiographic changes and abnormal serum biomarkers is similar to that of acute coronary syndrome (ACS). The pathophysiology of TTS remains unclear. The latest hypothesis consider it as the integrated cardiovascular response to sudden surges in endogenous catecholamine concentrations or to exogenously administered catecholamines often in the context of acute severe stress (2). Accordingly, the diagnosis of TTS is still challenging because of ACS like clinical phenotype and unclear pathogenesis. The prognosis of TTS was initially reported to be favorable compared with that of ST-segment elevated myocardial infarction, whereas subsequent studies have demonstrated that the acute and long-term mortality in TTS are higher than previously recognized (3, 4). Therefore, the accurate diagnosis is crucial for this entity. Here, we review the diagnostic criteria of TTS and discuss the availability of nuclear imaging in its diagnosis.

Changes in diagnostic criteria

The first diagnostic criteria were introduced by Abe et al. in 2003. Several criteria have been published since then; the Mayo Clinic Diagnostic Criteria are the most commonly applied (5). The conventional criteria have proposed the exclusion of significant stenosis of the coronary artery; however, the recent data have demonstrated that coronary artery disease (CAD) is frequently observed in patients with TTS (3). When the patients have CAD, the diagnosis of TTS become notably complicated. Such patients are more likely to be misdiagnosed as having ACS. The presence of obstructive CAD should not be considered as an exclusion criterion (6).

Pheochromocytoma is a rare neuroendocrine tumor derived from the medulla of the adrenal gland or extra-adrenal chromaffin tissue, and it secretes enormous catecholamines. Catecholamine storm triggers electrocardiographic abnormali-

doi: 10.17996/anc.18-00068

Kazuaki Okuyama, Yoshihiro J Akashi
Division of Cardiology, Department of Internal Medicine, St. Marianna University School of Medicine, Kawasaki, Japan
E-mail: yoakashi-circ@umin.ac.jp

Table 1 Changes in diagnostic criteria for takotsubo syndrome

Mayo Clinic (2008) (5)	1. Transient hypokinesis, akinesis, or dyskinesis of the left ventricular mid segments with or without apical involvement; the regional wall motion abnormalities extend beyond a single epicardial vascular distribution; a stressful trigger is often, but not always, present. Electrocardiographic changes in ST segment elevation or T wave inversion. 2. The Absence of obstructive coronary disease or angiographic evidence of acute plaque rupture. 3. New electrocardiographic abnormalities (either ST-segment elevation and/or T-wave inversion) or modest elevation in cardiac troponin. 4. The Absence of Pheochromocytoma and myocarditis.
Position Statement from the HFA of the European Society of Cardiology (2016) (7)	1. Transient regional wall motion abnormalities of left ventricular or right ventricular myocardium that precede frequently, but not always, by a stressful trigger (emotional or physical). 2. The regional wall motion abnormalities usually* extend beyond a single epicardial vascular distribution, and often result in circumferential dysfunction of the ventricular segments involved. 3. The absence of culprit atherosclerotic coronary artery disease including acute plaque rupture, thrombus formation, and coronary dissection or other pathological conditions to explain the pattern of temporary LV dysfunction observed (e.g. hypertrophic cardiomyopathy, viral myocarditis). 4. New and reversible electrocardiographic (ECG) abnormalities (ST-segment elevation, ST depression, LBBB ↑, T-wave inversion, and/or QTc prolongation) during the acute phase (3 months). 5. Significantly elevated serum natriuretic peptide (BNP or NT proBNP) during the acute phase. 6. Positive but relatively small elevation in cardiac troponin measured with a conventional assay (i.e. disparity between the troponin level and the amount of dysfunctional myocardium present). 7. Recovery of ventricular systolic function on cardiac imaging at follow-up (3-6 months).
International Expert Consensus (2018) (6)	1. Patients show transient left ventricular dysfunction (hypokinesia, akinesia, or dyskinesia) presenting as apical ballooning or midventricular-, basal-, or focal wall motion abnormalities. Right ventricular involvement can be present. Besides these regional wall-motion patterns, transitions between all types can exist. The regional wall motion abnormality usually extends beyond a single epicardial vascular distribution; however, rare cases can exist where a coronary lesion is present in the subtended myocardial territory of the wall-motion abnormality. Therefore, coronary artery disease is not a contradiction in takotsubo syndrome. 2. An emotional, physical, or combined trigger can precede the takotsubo syndrome event, but this is not obligatory. 3. The presence of neurologic disorders (e.g. subarachnoid hemorrhage, stroke/transient ischemic attack, seizures) as well and pheochromocytoma do not exclude the diagnosis of takotsubo syndrome. 4. New ECG abnormalities, including ST-segment elevation, ST-segment depression, T wave inversion and QTc prolongation are present; however, rare cases exist without any ECG changes. 5. The levels of cardiac biomarkers, such as troponin and creatine kinase, are moderately elevated in most cases; significantly elevated BNP is common. 6. Patients have no evidence of infectious myocarditis. 7. Postmenopausal women are predominantly affected.

ties, left ventricular systolic dysfunction, and an increase in the biomarkers; thus, it should be considered as the main pathophysiology of TTS. The conventional diagnostic criteria have excluded pheochromocytoma as a specific cause of TTS, whereas the clinical phenotype of TTS is consistent with that of pheochromocytoma. The diagnostic criterion of European Society of Cardiology thus includes pheochromocytoma as a secondary cause of TTS (7).

Based on the above-mentioned situation and current knowledge, the international expert consensus has provided new diagnostic criterion of TTS, International Expert Consensus Document on TTS, which helps to improve identification and classification of TTS (6). In the new criterion, it is noteworthy that coronary artery disease is not a contradiction in TTS and pheochromocytoma do not exclude the diagnosis of TTS (Table 1).

The role of nuclear cardiology

The nuclear imaging assesses coronary perfusion; cardiac metabolic function and sympathetic nervous are closely associated with the onset of TTS. The role of nuclear imaging in TTS diagnosis has not been well established yet. So far, no diagnostic criteria describe the usefulness of nuclear imaging in TTS diagnosis, which is already discussed in some papers (7, 8). Nuclear imaging provides useful information, particularly on CAD and pheochromocytoma combined with TTS.

TTS should be distinguished from ACS; then, nuclear metabolic imaging greatly contribute to the accurate diagnosis. One study concluded that fatty acid metabolism depicted by ^{123}I-BMIPP myocardial scintigraphy was more severely

impaired than myocardial perfusion depicted by ^{201}Tl scintigraphy in acute phase of TTS patients (9). The discrepancy between ^{99m}Tc scintigraphy and ^{123}I-BMIPP scintigraphy is markedly lower in TTS than ST-segment elevated myocardial infarction (10). Under the perfusion tracers, the reduction of apical counts occurs by regional myocardial wall thinning in the apex, which is due to not the artifact but the partial volume effects. Others, it might be due to reduced regional perfusion in the takotsubo infarcted area and increased perfusion in non-takotsubo area or combined all these factors. No study has presented the use of stress-test gated single-photon emission computed tomography in patients with TTS; it provides the evaluation of not only perfusion but also global and regional functions as well as the possible presence of ischemia.

^{123}I-MIBG scintigraphy assesses myocardial sympathetic nerve terminal activity and detects adrenal and ectopic pheochromocytoma. Even in the subacute phase of TTS, decreased delayed H/M ratio and increased washout rate of ^{123}I-MIBG represent the adrenergic hyperactivity in patients with TTS (11). The uptake of ^{123}I-MIBG is impaired for months, and it is corresponding to a regional disturbance of sympathetic neuronal activity (12). The combination of ^{123}I-MIBG scintigraphy and myocardial perfusion scintigraphy is useful to distinguish TTS from ACS in which innervation and myocardial scarring is matched.

Cardiac positron emission tomography (PET) using [^{18}F]2-fluoro-deoxy-glucose (FDG) depicts abnormal glucose metabolism in normal myocardial perfusion in patients with TTS; one of the recent studies demonstrated heterogeneous accumulation of FDG in the patients with TTS (13). One study using $^{13}NH_3/^{82}$Rb PET demonstrated impaired left ventricular perfusion in the acute phase and unchanged midventricular and apical flow in the acute and follow-up phases (14). Global left ventricular hyperemia and impaired coronary flow reserve (CFR) in the takotsubo infarcted area have been presented in their case series (14). In typical TTS, basal hyperperfusion probably caused by regionally increased metabolic requirement in which basal contractility increases to compensate for failing the heart. Also, it should be kept in mind that the findings of perfusion and CFR depend on the timing of acquiring the images after the onset of TTS.

Conclusion

The diagnostic criteria of TTS is updated; CAD and pheochromocytoma are also included into the new criteria. Therefore, it seems that now is favorable time to assess the availability of nuclear imaging for providing more accurate TTS diagnosis.

Acknowledgment

None.

Sources of funding

None.

Conflicts of interest

None

Reprint requests and correspondence

Yoshihiro J. Akashi, MD, PhD

Division of Cardiology, Department of Internal Medicine, St. Marianna University School of Medicine, 2-16-1 Sugao, Miyamae-ku, Kawasaki, 216-8511, Japan

E-mail: yoakashi-circ@marian.ac.jp

References

1. Sato H, Tateishi H, Uchida T. Takotsubo-type cardiomyopathy due to multivessel spasm. In: Kodama K, Haze K, Hon M, eds. Clinical Aspect of Myocardial Injury: From Ischemia to Heart Failure. Tokyo. Kagakihyouronsya Co.; 1990. p56-64.
2. Akashi YJ, Nef HM, Lyon AR. Epidemiology and pathophysiology of Takotsubo syndrome. Nat Rev Cardiol 2015; 12: 387-97.
3. Templin C, Ghadri JR, Diekmann J, et al. Clinical features and outcomes of Takotsubo (Stress) cardiomyopathy. N Engl J Med 2015; 373: 929-38.
4. Stiermaier T, Thiele H, Eitel I. Long-term excess mortality in Takotsubo syndrome: is it justified to charge Takotsubo for the excess long term mortality?: Reply. Eur J Heart Fail 2016; 18: 879.
5. Prasad A, Lerman A, Rihal CS. Apical ballooning syndrome (Tako-Tsubo or stress cardiomyopathy): a mimic of acute myocardial infarction. Am Heart J 2008; 155: 408-17.
6. Ghadri JR, Wittstein IS, Prasad A, et al. International expert consensus document on Takotsubo syndrome (PART I): clinical characteristics, diagnostic criteria, and pathophysiology. Eur Heart J 2018; 39: 2032-46.
7. Lyon AR, Bossone E, Schneider B, et al. Current state of knowledge on Takotsubo syndrome: A Position Statement from the Taskforce on Takotsubo Syndrome of the Heart Failure Association of the European Society of Cardiology. Eur J Heart Fail 2016; 18: 8-27.
8. Ghadri JR, Wittstein IS, Prasad A, et al. International expert consensus document on Takotsubo syndrome (PART II): Diagnostic workup and outcome, and management. Eur Heart J 2018; 39: 2047-2062.
9. Kurisu S, Inoue I, Kawagoe T, et al. Myocardial perfusion and fatty acid metabolism in patients with tako-tsubo-like left ventricular dysfunction. J Am Coll Cardiol 2004; 41: 743-8.
10. Matsuo S, Nakajima K, Kinuya S, et al. Diagnostic utility of ^{123}I-BMIPP imaging in patients with Takotsubo cardiomyopathy. J Cardiol 2014; 64: 49-56.
11. Christensen TE, Bang LE, Holmvang L, et al. ^{123}I-MIBG scintigraphy in the subacute state of takotsubo cardiomyopathy. JACC Cardiovasc Imaging; 2016; 9: 982-90.
12. Akashi YJ, Nakazawa K, Sakakibara M, et al. ^{123}I-MIBG myocardial scintigraphy in patients with "takotsubo" car-

diomyopathy. J Nucl Med 2004; 45: 1121-7.
13. Kobylecka M, Budnik M, Kochanowski J, et al. Takotsubo cardiomyopathy: FDG myocardial uptake pattern in fasting patients. Comparison of PET/CT, SPECT, and ECHO results. J Nucl Cardiol 2017. [Epub ahead of print]
14. Christensen TE, Ahtarovski KA, Bang LE, et al. Basal hyperaemia is the primary abnormality of perfusion in Takotsubo cardiomyopathy: a quantitive cardiac perfusion positron emission tomography study. Eur Heart J Cardiovasc Imaging 2015; 16: 1162-9.

Organização / Organized by

Informações / Information
www.prcardio.org/icm2019

Rua João Negrão, 731, conj. 302
80010-200 – Curitiba / Paraná
Fone/fax: 55 41 3232-8691
e-mail: sociedade@prcardio.org

State of the Art of Transcatheter Mitral Annuloplasty: Present and Future

An appraisal of current and upcoming devices for direct and indirect transcatheter annuloplasty procedures.

BY SHINGO KUWATA, MD, PHD, AND FRANCESCO MAISANO, MD

Mitral annular remodeling with mitral valve (MV) annuloplasty is the most commonly performed technique to surgically treat mitral regurgitation (MR) and is frequently encountered in clinical practice. Surgical MV annuloplasty is the gold standard to treat degenerative MR. This technique works well because an undersized annuloplasty ring increases leaflet coaptation length and reduces structural strain on valvular tissue in functional MR (FMR).[1] During surgical MV repair, annuloplasty is performed either alone or in conjunction with artificial chords, leaflet resection or augmentation, closure of perforations or clefts, and edge-to-edge repair. Transcatheter approaches to annuloplasty would be needed if transcatheter mitral repair is to reach its full potential. Transcatheter MV annuloplasty is the most surgical-like alternative option to treat MR in high-risk patients.

With the availability of transcatheter mitral annuloplasty, CT has become an essential imaging tool in defining patients' anatomy and eligibility for mitral annuloplasty. Because it offers a comprehensive assessment of the real three-dimensional anatomy, CT allows assessment of the MV anatomy as well as the surrounding structures. In certain preprocedural evaluations, there is a need to identify the target zone of the implant; assess the angle between aortic valve and the MV plane; measure the distance between the coronary artery, coronary sinus (CS), and the valve annulus; and evaluate the risk of injury to surrounding structures. It is also occasionally necessary to obtain detailed measurements of the target zone to implant the ideal annuloplasty device.

Different annuloplasty devices complete the wide spectrum of repair technologies, but only limited clinical data are available at this time. Heart teams dedicated to transcatheter mitral therapies should become expert in selecting solo annuloplasty or a combination procedure to improve outcomes and increase the number of patients who are potentially eligible for transcatheter mitral therapies.

INDIRECT TRANSCATHETER ANNULOPLASTY DEVICES

Indirect annuloplasty devices are based on the anatomic proximity of the CS to the posterior mitral annulus. This approach is particularly attractive because the cannulation of the CS is an easy and reproducible venous access technique.[2]

The Carillon mitral contour system (Cardiac Dimensions, Inc.) (Figure 1A) is the only indirect device that has obtained CE Mark approval. There have been several modifications of the device to improve its safety and efficacy, as

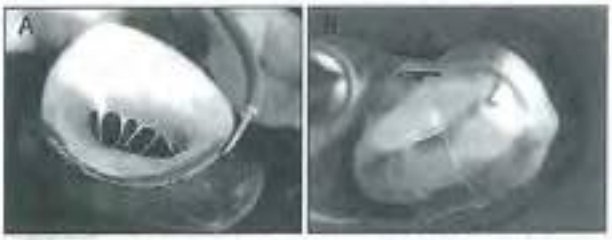

Figure 1. Clinical devices used for indirect transcatheter mitral annuloplasty. Carillon mitral contour system* (A); the Arto system (B). *CE Mark approved.

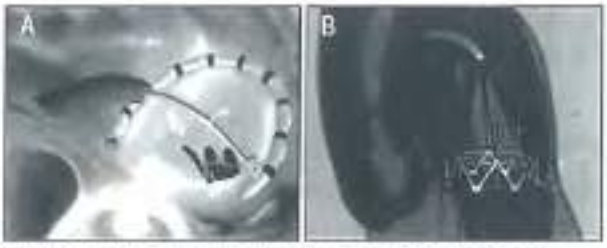

Figure 2. Clinical devices used for antegrade direct annuloplasty. Cardioband mitral system* (A); the Iris device (B). *CE Mark approved.

initial results with this approach have not been satisfactory mainly due to suboptimal efficacy and the risk of delayed complications.[5-6] The Arto system (MVRx, Inc.) (Figure 1B) is another indirect transcatheter system for treating FMR. The mechanism of the device consists of a suture that connects interatrial-septal and CS anchors. This suture is tensioned to shorten the anteroposterior diameter of the mitral annulus, thereby improving mitral leaflet coaptation and reducing FMR.[7]

Anatomic assessment of the CS, coronary artery, and mitral annulus relationship is crucial before considering the use of these devices due to the risks of coronary artery compression and device dislocation.

DIRECT ANNULOPLASTY DEVICES

The Cardioband mitral system (Edwards Lifesciences) (Figure 2A) is the closest transcatheter device to a surgical prosthetic ring. A surgical-like, adjustable Dacron band is deployed on the atrial side of the posterior mitral annulus from lateral trigone to medial trigone by a transseptal approach.[8,9] A clinical study of Cardioband has shown the safety and efficacy of the device during the 6 months following treatment.[10] Cinching of the implanted Cardioband significantly reduced the annular septolateral dimension and MR and also showed significant improvement in functional status after 6 months.

The Iris device (Millipede, Inc.) (Figure 2B) is being developed as a catheter-delivered complete ring device that mimics surgical annuloplasty via a transseptal approach. The ring is anchored to the annulus, resulting in size adjustment of the annulus. Although only small clinical experiences exist as of now, the devices have shown no interference with electrical conduction nor trouble with anchoring, according to previous report.

The Mitralign percutaneous annuloplasty system (Mitralign, Inc.) (Figure 3A) allows for retrograde placement of MV annular pledgeted sutures to achieve annular size reduction. The pledgets are placed and cinched on the mitral annulus, thus reducing annular circumference.[11] Nickenig et al have reported initial 6-month safety and clinical outcome results of 71 patients using the Mitralign system.[12] The procedure significantly reduced anteroposterior and septolateral dimensions and also induced reverse left ventricular remodeling. The Mitralign system has received CE Mark approval to treat FMR but is not available for sale in the United States.

Amend (Valcare Medical) (Figure 3B) is a different transcatheter MV annuloplasty ring with a semirigid, D-shaped ring, which is delivered via transapical approach. It is designed to stabilize the mitral annulus, reduce the septolateral dimension of the native valve, improve leaflets coaptation, and reduce MR.[13]

The AccuCinch system (Ancora Heart, Inc.) (Figure 3C) has a different concept, with spaced anchors in the basal left ventricular subannular space to reduce the basal left ventricle and mitral annular dimensions.[14]

CONCLUSION

Patients with severe MR who are very ill and cannot undergo conventional surgical intervention can successfully be treated with transcatheter intervention. The long-term durability and effectiveness of annuloplasty devices remain unclear, requiring additional study of larger patient cohorts with longer-term follow-up to definitively determine the future of this class of devices.

Surgical experience has shown that recurrence of MR after valve repair is higher in the absence of concomitant annuloplasty.[15] In selected cases, such as in those with a

Figure 3. Clinical devices used for retrograde direct annuloplasty. Mitralign percutaneous annuloplasty system* (A); Amend annuloplasty ring (B); AccuCinch system (C). *CE Mark approved.

Figure 4. Complementary role of transcatheter intervention. DMR, degenerative mitral regurgitation; IMR, ischemic mitral regurgitation.

high risk of recurrence, transcatheter annuloplasty should be considered as a first-line procedure because a major advantage of this approach is maintaining the potential for future open intervention. Specific algorithms with detailed indications will be required to guide the optimal treatment for each patient (Figure 4). Simplified algorithms to define the complementary role of the different solo or combined transcatheter mitral therapies are also needed. The role of the combination of different repair devices (leaflet or chordal plus annular repair) has to be defined in selected patients. In a few years, this safe and low-commitment approach may drive a shift toward earlier intervention for MR in heart failure patients. ■

1. De Bonis M, Maisano F, La Canna G, Alfieri O. Treatment and management of mitral regurgitation. Nat Rev Cardiol. 2011;9:139–146.
2. Tamburino M, Condrevin A, Pozzoli A, et al. Current challenges in interventional mitral valve treatment. J Thorac Dis. 2016;7:1536–1543.
3. Schofer J, Siminiak T, Haude M, et al. Percutaneous mitral annuloplasty for functional mitral regurgitation: results of the Cardiac mitral annuloplasty device European Union study. Circulation. 2009;120:326–333.
4. Siminiak T, Wu JC, Haude M, et al. Treatment of functional mitral regurgitation by percutaneous annuloplasty: results of the TRAM trial. Eur J Heart Fail. 2012;14:987–994.
5. Goldberg SL, Lipiecki J, Sievert H. The Cardiac mitral coronal transcatheter indirect mitral valve annuloplasty system. EuroIntervention. 2015;11(suppl W):W64–66.
6. Lipiecki J, Siminiak T, Sievert H, et al. Coronary sinus-based percutaneous annuloplasty as treatment for functional mitral regurgitation: the TITAN II trial. Open Heart. 2016;3:e000411.
7. Regan JA, Thomas M, Marlow MC, et al. Treatment of heart failure with associated functional mitral regurgitation using the ARTO system: initial results of the first-in-human MAVERIC trial (mitral valve repair clinical trial). JACC Cardiovasc Interv. 2015;8:1065–1104.
8. Maisano F, La Canna G, Latib A, et al. First-in-man transapical implantation of a "surgical-like" mitral valve annuloplasty device for functional mitral regurgitation. JACC Cardiovasc Interv. 2014;7:1326–1328.
9. Maisano F, Taramasso M, Nickenig G, et al. CardioBand, a transcatheter surgical-like direct mitral valve annuloplasty system: early results of the feasibility trial. Eur Heart J. 2016;37:817–825.
10. Nickenig G, Kreuzenmeyer C, Schueler R, et al. Transcatheter mitral annuloplasty in chronic functional mitral regurgitation: 6-month results with the CardioBand percutaneous mitral repair system. JACC Cardiovasc Interv. 2016;9:2019–2027.
11. Siminiak T, Dankowski R, Bayles A, et al. Percutaneous direct mitral annuloplasty using the Mitralign bident system: description of the method and a case report. Kardiol Pol. 2013;71:1287–1290.
12. Nickenig G, Schueler R, Doger A, et al. Treatment of chronic functional mitral valve regurgitation with a percutaneous annuloplasty system. J Am Coll Cardiol. 2016;67:2917–2926.
13. Rainer Y, Rousseau SD, Yellin M, et al. Biocompatibility and systemic safety of a novel implantable annuloplasty ring for the treatment of mitral regurgitation in a mini pig model. Cardiol Pathol. 2016;24:655–662.
14. Gooley RP, Meredith IT. The Accucinch transcatheter direct mitral valve annuloplasty system. EuroIntervention. 2015;11(suppl W):W60–61.
15. De Bonis M, Lapenna E, Maisano F, et al. Long-term results (up to 18 years) of the edge-to-edge mitral valve repair without annuloplasty in degenerative mitral regurgitation: implications for the percutaneous approach. Circulation. 2014;130(suppl 1):S19–24.

Shingo Kuwata, MD, PhD
University Heart Center Zurich
University of Zürich
Zürich, Switzerland
Cardiology Department
St. Marianna University School of Medicine
Kanagawa, Japan
shingo.k.571019@gmail.com
Disclosures: None.

Francesco Maisano, MD
Division of Cardiovascular Surgery
University Hospital Zürich
Zürich, Switzerland
francesco.maisano@usz.ch
Disclosures: Consultant for Abbott Vascular, Edwards Lifesciences, Medtronic; cofounder of 4Tech.

Rev Esp Cardiol. 2018;71(8):655–667

Review article

Past, Present and Future of Coronary Physiology

Takayuki Warisawa,[a,b] Christopher M. Cook,[a] Yoshihiro J. Akashi,[b] and Justin E. Davies[a,*]

[a] International Centre for Circulatory Health, National Heart and Lung Institute, Imperial College London, London, United Kingdom
[b] Division of Cardiology, Department of Internal Medicine, St. Marianna University School of Medicine, Kawasaki, Japan

Article history:
Available online 16 March 2018
Keywords:
Coronary physiology
Fractional flow reserve
Instantaneous wave-free ratio

ABSTRACT

It is well known that the apparent significant coronary stenosis on angiography sometimes does not cause significant ischemia, and vice versa. For this reason, decision-making based on coronary physiology is becoming more and more important. Fractional flow reserve (FFR), which has emerged as a useful tool to determine which lesions need revascularization in the catheterization laboratory, now has a class IA indication in the European Society of Cardiology guidelines. More recently, the instantaneous wave-free ratio, which is considered easier to use than FFR, has been graded as equivalent to FFR. This review discusses the concepts of FFR and instantaneous wave-free ratio, current evidence supporting their use, and future directions in coronary physiology.

© 2018 Sociedad Española de Cardiología. Published by Elsevier España, S.L.U. All rights reserved.

Pasado, presente y futuro de la fisiología coronaria

Palabras clave:
Fisiología coronaria
Reserva fraccional de flujo
Cociente diastólico instantáneo sin ondas

RESUMEN

Es bien sabido que ocasionalmente una lesión coronaria angiográficamente aparentemente significativa podría no causar isquemia y viceversa. Por eso las decisiones terapéuticas basadas en un conocimiento de la fisiología coronaria son cada vez más importantes. El uso de la reserva fraccional de flujo (RFF), una herramienta útil para determinar en el laboratorio de hemodinámica las lesiones que se pueden beneficiar de revascularización, ha conseguido una indicación de clase IA en las guías de la Sociedad Europea de Cardiología. Recientemente, el índice diastólico instantáneo sin ondas, de más facilidad de uso que la RFF, se considera equivalente a ella. En esta revisión se repasan y se profundiza en los conceptos de RFF e índice diastólico instantáneo sin ondas y se revisan las evidencias que justifican su uso, así como sus perspectivas futuras.

© 2018 Sociedad Española de Cardiología. Publicado por Elsevier España, S.L.U. Todos los derechos reservados.

Abbreviations

ACS: acute coronary syndrome
CABG: coronary artery bypass graft
CAD: coronary artery disease
FFR: fractional flow reserve
iFR: instantaneous wave-free ratio
OMT: optimal medical therapy
PCI: percutaneous coronary intervention

INTRODUCTION

Coronary physiology has established its position in the field of catheter intervention. Fractional flow reserve (FFR) has enabled us to manage patients with coronary artery disease (CAD) more accurately and safely than by angiographical visual estimation. Currently, FFR is widely used worldwide (Figure 1). Because abundant evidence including 3 major randomized trials (DEFER, FAME, and FAME 2 trial[1–3]) has been amassed for over 20 years, use of FFR for stable CAD is recommended by the guidelines of the ESC/EACTS (European Society of Cardiology/European Association for Cardio-Thoracic Surgery) and the ACC/AATS/AHA/ASE/ASNC/SCAI/SCCT/STS (American College of Cardiology/American Association for Thoracic Surgery/American Heart Association/American Society of Echocardiography/American Society of Nuclear Cardiology/Society for Cardiovascular Angiography and Interventions/Society of Cardiovascular Computed Tomography/Society of Thoracic Surgeons).[4–6] Recently, the instantaneous wave-free ratio (iFR) has been introduced as an alternative to FFR, which does not require hyperemia.[7] Five years after the initial

* Corresponding author: Imperial College London, Hammersmith Hospital, B Block South, 2nd floor, NHLI – Cardiovascular Science, Du Cane Rd, London W12 0NN, United Kingdom.
E-mail address: justin.davies@imperial.ac.uk (J.E. Davies).

https://doi.org/10.1016/j.rec.2018.02.003
1885-5857/© 2018 Sociedad Española de Cardiología. Published by Elsevier España, S.L.U. All rights reserved.

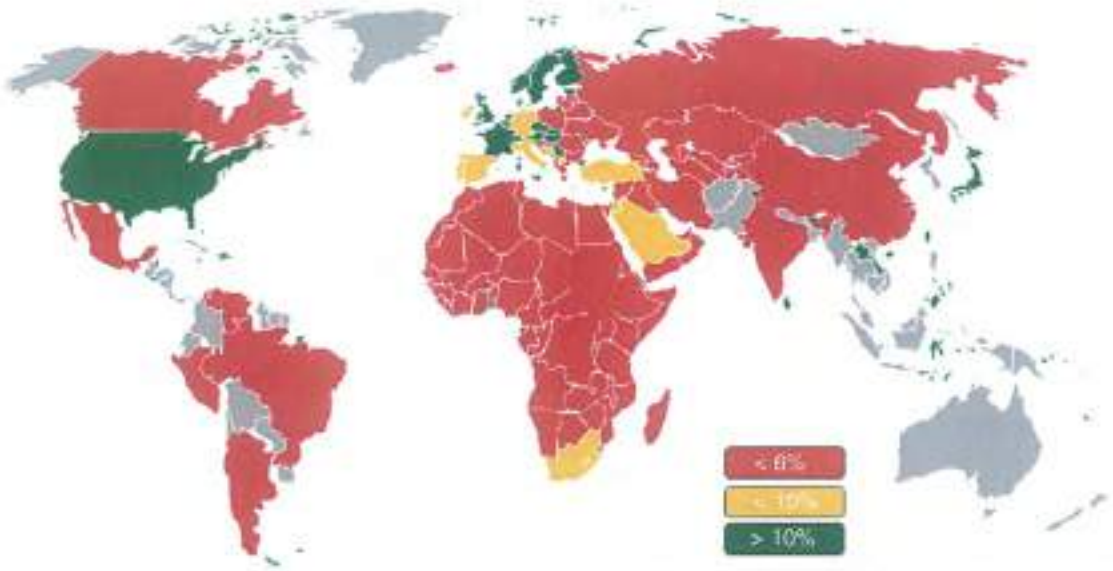

Figure 1. Fractional flow reserve use in different parts of the world in 2016. Fractional flow reserve is currently used worldwide in decision-making. However, the frequency of its use in the catheterization laboratory is not high, despite clinical guideline recommendations. Reproduced with permission from Philips Volcano, market research report by Decision Resources Group.

introduction, 2 large randomized trials, DEFINE-FLAIR and iFR-SWEDEHEART trial, have simultaneously reported the noninferiority of iFR compared with FFR.[8,9] Currently, iFR is considered equivalent as a diagnostic modality for ischemic heart disease in the latest guidelines.[6] In this review article, we summarize the evidence of coronary physiology, especially concerning these 2 modalities, and we also discuss future directions in this field.

HISTORICAL SITUATION

Pre-FFR-Era

Forty years ago, the world's first percutaneous coronary intervention (PCI) was performed by Andreas Grüntzig.[10] In fact, coronary pressure across the stenosis before and after PCI was recorded for the first time at the same time (Figure 2). Grüntzig

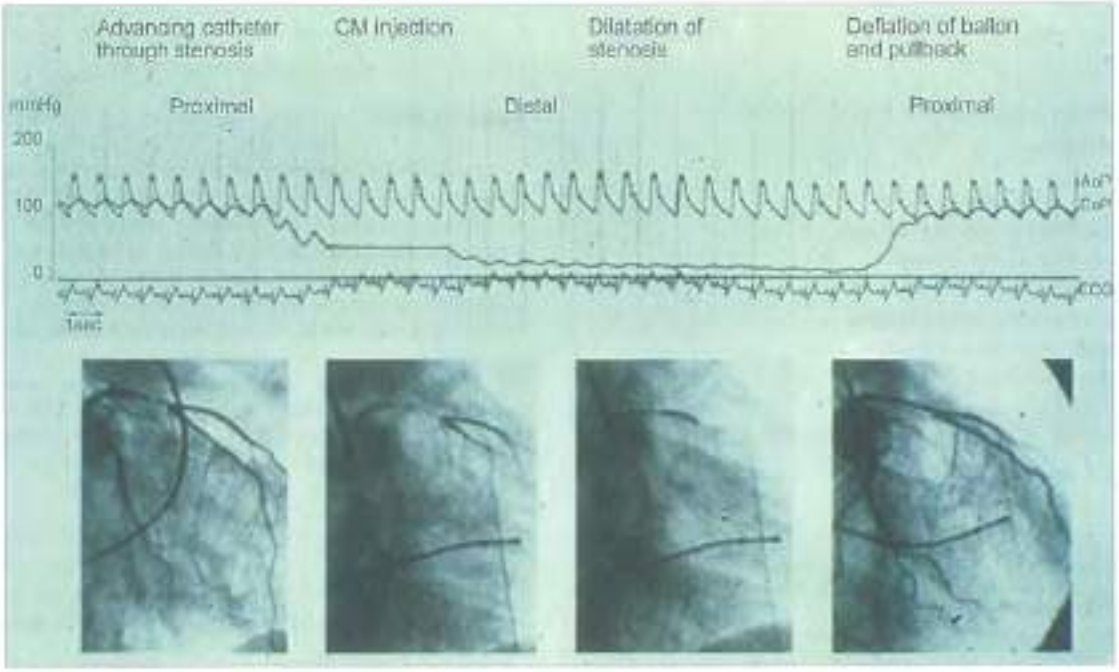

Figure 2. First case of percutaneous coronary intervention. In 1979, coronary pressure across the stenosis before and after balloon angioplasty was recorded in the first case of coronary intervention. AoP, aortic pressure; CM, contrast media; CoP, coronary pressure. Reproduced with permission from Grüntzig et al.[10]

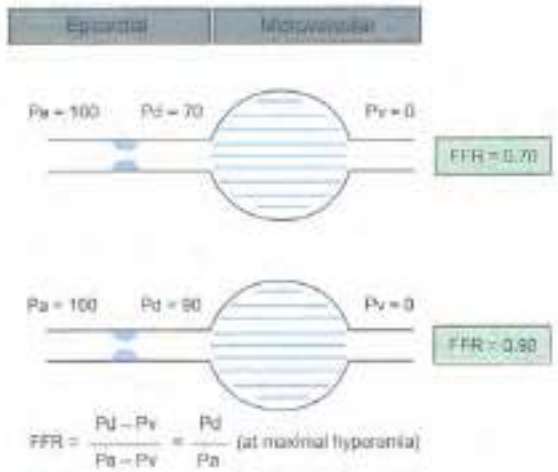

Figure 3. Schema for the concept of FFR. During maximal hyperemia, a direct relationship between coronary pressure and flow could be presumed because the effect from microvascular could be ignored. Despite the same degree of stenoses on visual estimation, the illustrated cases show totally different FFR values. FFR, fractional flow reserve; Pa, aortic pressure; Pd, distal pressure; Pv, central venous pressure.

measured the trans-stenotic pressure gradient through the fluid-filled guiding catheter. Despite early introduction to the field of PCI, practical use of coronary physiology in the catheterization laboratory did not begin until the late 1990s because of technological and theoretical aspects. Because the currently used well-matured pressure wires were not available, coronary pressure was measured for years by the catheter itself, which was found to be not very reliable due to the impaired antegrade flow induced by catheter engagement.[11] The relationship between coronary pressure and coronary flow was actively investigated after the notion of hyperemia was introduced.[12] Finally, technological and theoretical advances allowed the development of the concept of FFR.

The Concept of FFR and Evidence

FFR was first described by Pijls et al. in 1993.[13] The concept of FFR is based on the notion that maximal hyperemia could achieve a linear correlation between coronary flow and coronary pressure because coronary resistance is stable and minimal during maximal arterial dilation. FFR is defined as the ratio of mean distal pressure (Pd) relative to mean aortic pressure (Pa) during maximal hyperemia induced by vasodilating agents. For example, an FFR of 0.70 means that coronary flow is reduced by 30% from normal and an FFR of 0.90 means that coronary flow is reduced by only 10% from normal due to the existence of stenoses (Figure 3). Taking into account stenosis severity, myocardial territory and viability, and collateral perfusion, FFR is able to assess the functional significance of CAD. The cutoff value to detect significant ischemia was suggested to be 0.75 by a relatively small study, which demonstrated high diagnostic performance of FFR, with a sensitivity of 88%, specificity of 100% and accuracy of 93% compared with dobutamine stress echocardiography, stress myocardial perfusion scintigraphy and exercise stress electrocardiography.[14] Subsequently, numerous studies were conducted to compare FFR with noninvasive functional testing and found an acceptable overall correlation[15–28] (Table 1). Nowadays, the best cutoff value to defer PCI in clinical practice is considered to be 0.80 after validation in multiple prospective, randomized trials with this threshold.[2,3]

We summarize the 3 major randomized trials that played a very important role in establishing evidence of FFR:

DEFER Study

The initial randomized DEFER study was conducted to evaluate the safety of deferring PCI guided by FFR.[7] In that study, patients with stable angina and intermediate stenosis but FFR > 0.75 were randomized to deferral (deferral group) or performance (perform group). Subsequent to this original report, long and longer-term follow-up of the DEFER cohort is now available at 5 years[29] and 15 years.[30] Event-free survival did not differ between the deferral and performance groups. The authors concluded that patients with FFR > 0.75 were stable and safe and that stenting did not decrease the risk of cardiac events for CAD without significant ischemia.

FAME Study

The second randomized control trial was larger than DEFER. The FAME study was performed to assess the effectiveness of FFR-guided PCI compared with angio-guided PCI in patients with multivessel CAD.[2] In this trial, 1005 patients with at least 50%

Table 1
Studies of Fractional Flow Reserve Compared With Noninvasive Functional Testing

Publication	Comparison with noninvasive tests	No. of patients	Best cutoff value	Accuracy
Pijls et al.,[15] 1995	X-ECG	60	0.74	97
De Bruyne et al.,[16] 1995	MPS, X-ECG	60	0.66	87
Pijls et al.,[14] 1996	DSE, MPS, X-ECG	45	0.75	93
Bartunek et al.,[17] 1997	DSE	25	0.75	81
Cajmar et al.,[18] 2000	MPS	30	0.75	95
Abe et al.,[19] 2000	MPS	46	0.75	91
Chamuleau et al.,[20] 2001	MPS	127	0.74	77
Yanagisawa et al.,[21] 2002	MPS	165	0.75	76
Seo et al.,[22] 2002	MPS	25	0.75	60
Morishima et al.,[23] 2004	MPS	30	0.75	85
Kobori et al.,[24] 2005	MPS	147	0.75	70
Hacker et al.,[25] 2005	MPS	50	0.75	86
Krüger et al.,[26] 2005	MPS	42	0.75	88
Samady et al.,[27] 2006	DSE, MPS	48	0.78	92
Van de Hoef et al.,[28] 2012	MPS	232	0.76	74

DSE, dobutamine stress echocardiogram; MPS, myocardial perfusion scintigraphy; X-ECG, exercise electrocardiogram.

stenoses of the vessel diameter in at least 2 of the 3 major epicardial coronary arteries were randomly assigned to undergo PCI with drug-eluting stents (DES) guided by FFR measurements or guided by angiography alone. The cutoff value for decision-making was 0.80. The authors concluded that FFR-guided PCI significantly reduced the rate of the composite endpoint of death, nonfatal myocardial infarction, and repeat revascularization at 1 year (13.2% vs 18.3%; relative risk, 0.72; 95% confidence interval, 0.54 to 0.96, respectively; $P = .02$). After this study, the cutoff value of FFR 0.80 has been often used to judge whether to perform or defer PCI in clinical practice, although FFR 0.75 is the definitive cutoff to determine significant ischemia or not, which subsequently generated the problem of the "gray zone FFR".

FAME 2 Study

The third trial was the FAME 2 study to examine whether FFR-guided PCI plus optimal medical therapy (OMT) was superior to OMT alone or not.[2] A 2-year clinical follow-up was planned for 1220 patients. However, the adverse event of urgent revascularization in the OMT alone group occurred more frequently than expected and the study was discontinued (mean follow-up: 7 months). The authors concluded that FFR-guided PCI plus OMT, as compared with OMT alone, decreased the need for urgent revascularization in patients with stable CAD with proven ischemia. Because of the discontinuance of the study, the investigators could not reach any conclusions regarding the hard endpoint of death or myocardial infarction.

CURRENT SITUATION

With over 20 years of investigations and clinical experience, coronary physiology has established its place in the field of catheter intervention. Clinical outcomes during the 15-year follow-up of the DEFER study and the 5-year follow-up of the FAME study have strengthen the idea that FFR-guided decision-making is safe and rational.[29,30] During this period, knowledge and evidence of FFR have encountered more specific problems in the various clinical settings. Some of them will be discussed in the first part of this section.

Usefulness of FFR in Real-world Clinical Practice

Multivessel Disease

As the DES-Era has started and newer-generation DES have become available, PCI is currently widely performed in multivessel disease. However, long-term clinical outcomes of PCI in 3-vessel disease is less satisfactory than expected despite newer DES use when revascularization is guided by angiography.[31,32] On the other hand, in the FAME study, FFR-guided PCI in multivessel disease achieved better clinical outcomes, and additionally, showed that the number of stents used per patient was significantly lower in the FFR-guided group (1.9 ± 1.3 vs 2.7 ± 1.2; $P < .001$).[2]

Although myocardial perfusion scintigraphy is considered the standard modality for detecting ischemia, several studies showed there was discordance in the results compared with FFR in multivessel disease.[33,34] This discordance could be explained by the phenomenon of balanced ischemia, in which the nuclear stress test appears normal as a result of reduced myocardial perfusion in all coronary territories in patients with multivessel disease. Therefore, evaluation with FFR for multivessel disease is considered rational in decision-making for revascularization.

It is well known that physiological evaluation with FFR reduces the number of functionally diseased vessels and could also change patient management[35,36] (Figure 4). Recently, a Japanese multicenter registry showed that reclassification of the treatment strategy was observed in approximately 40% of patients with CAD by FFR measurement[37,38] (Figure 5).

Relationship between FFR and Intracoronary Imaging Modalities

The relationship between FFR and intracoronary imaging modalities has been also evaluated.[39–47] In the early day of this investigation, intravascular ultrasound (IVUS) showed good correlation with FFR.[39] However, recent reports revealed that the accuracy to predict significant FFR by minimum lumen area (MLA) on IVUS was approximately 60% to 70%, which was considered unsatisfactory in clinical practice (Table 2). This discordance could be explained by the fact that evaluations with MLA alone do not consider the target vessel diameter, lesion lengths, and collateral flow.[44,45] Optical coherence tomography has emerged as an invasive intracoronary imaging modality that provides better resolution than IVUS, offering more precise evaluation of the vessel lumen and stent edge.[46] However, its correlation with significant FFR was also limited and the best cutoff values of MLA to predict significant FFR tended to be smaller than those of IVUS[46,47] (Table 2). Thus, IVUS and optical coherence tomography could not be an alternative to FFR and complimentary use of intracoronary imaging modalities and functional assessment should be applied at present.

Jailed Side-branch

PCI of bifurcation lesion is still challenging, whereas FFR has provided useful knowledge in such cases. Koo et al.,[48,50] used FFR

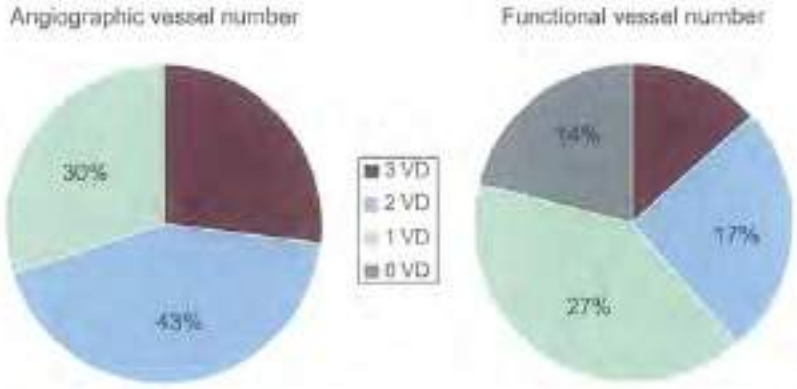

Figure 4. Vessel number evaluated by angiography and fractional flow reserve. The number of functional diseased vessels can change markedly from the initial angiographic assessment. VD, vessel disease. Reproduced with permission from Sant'Anna et al.[35]

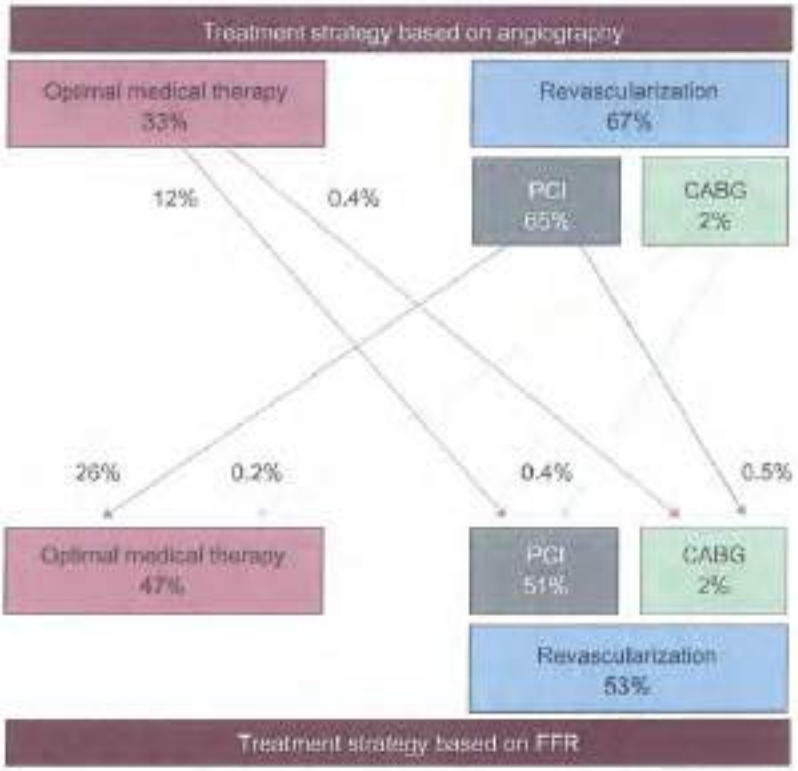

Figure 5. Results from the CVIT-DEFER registry. The treatment strategy can be changed drastically by functional assessment. CABG, coronary artery bypass graft; FFR, fractional flow reserve; PCI, percutaneous coronary intervention. Reproduced with permission from Nakamura et al.[37,38]

to assess the jailed side-branch after crossover stenting in bifurcation lesions. Although angiographic stenosis was apparent in many of the cases, less than one-third of these ostial lesions with a stenosis diameter > 75% were found to have FFR < 0.75. The authors suggested that an additional intervention for the jailed side-branch was not necessary if coronary blood flow was preserved. Nowadays, this knowledge has been expanded to left main bifurcation lesions, which are one of the most challenging themes for PCI, supporting the feasibility of left main crossover stenting.[51]

Hyperemic Agents

Several hyperemic agents are available. Intravenous (IV) injection of adenosine, particularly via a central venous line, is the gold standard, and acts within 1 to 2 minutes, creates a steady level of maximum hyperemia, and is relatively safe as drug-stress.[52,53] During adenosine injection, patients often feel discomfort in the chest or the throat. Intracoronary (IC) injection of adenosine can be applied safely and other hyperemic agents, such as adenosine 5'-triphosphate (IV or IC), papaverine (IC) and nicorandil (IC) are available.[54–56] The difference between each hyperemic agent is summarized in Table 3.

Effects on Medical Economy

It is also known that the introduction of FFR to clinical practice makes economic sense since the FAME study demonstrated that FFR-guided PCI saved $675 per patient in procedure time and saved > $2000 per patient at 1 year while achieving preferable clinical outcomes.[57] Most recently, the cost-effectiveness of FFR-guided PCI was shown by the 3-year follow-up of the FAME 2 trial, which demonstrated that PCI in patients with stable CAD and reduced FFR was advantageous compared with OMT alone because it resulted in improved clinical outcomes and quality of life at no increased cost at the 3-year follow-up.[58]

Table 2
Correlation in Studies Between Fractional Flow Reserve and Imaging Modalities

Publication	Number of lesions	FFR cutoff	Modality	MLA, mm²	Accuracy, %
Takagi et al.,[39] 1999	51	0.75	IVUS	3.0	84
Briguori et al.,[40] 2001	53	0.75	IVUS	4.0	64
Kang et al.,[41] 2011	236	0.80	IVUS	3.4	68
Koo et al.,[42] 2011	267	0.80	IVUS	2.75	67
Ben-Dor et al.,[43] 2012	205	0.80	IVUS	3.09	70
Kang et al.,[44] 2012	784	0.80	IVUS	2.4	69
Waksman et al.,[45] 2013	367	0.80	IVUS	3.07	64
Gonzalo et al.,[46] 2012	61	0.80	OCT	2.36	66
Shiono et al.,[47] 2012	62	0.75	OCT	1.91	85

FFR, fractional flow reserve; IVUS, intravascular ultrasound; MLA, minimum lumen area; OCT, optical coherence tomography.

Table 3
Properties of Several Hyperemic Agents

Hyperemic agents	Injection type	Dose	Time to maximal hyperemia	Duration	Advantages	Adverse effects and other disadvantages
Adenosine/ATP	IV	140–150 μg/kg/min	2–3 min	1–2 min	Safe	Chest discomfort and face flush (30%–70%), blood pressure drop, AV block (very rare), contraindication for asthma
Adenosine/ATP	IC	LCA: ≥ 80 μg RCA: ≥ 40 μg	5–10 sec	5 sec	Quick response	AV block (rare) Does not allow pullback due to short duration*
Papaverine	IC	LCA:12–20 mg RCA: 8–12 mg	15 sec	30–60 sec	Quick response	QT time prolongation, torsade de pointes (0.5%)
Nicorandil	IC	2 mg	15 sec	20–30 sec	Safe and quick response	VF (extremely rare) Expensive*

AV block, atrioventricular block; ATP, adenosine 5′-triphosphate; IC, intracoronary injection; IV, intravenous injection; LCA, left coronary artery; RCA, right coronary artery; VF, ventricular fibrillation.
* Other disadvantages.

Limitations of FFR

Although the use of FFR in clinical practice has many benefits, as shown, there are also some problems.

Low Performance Rate

Despite strong recommendation from clinical guidelines, FFR is not as frequently used as expected (Figure 1). The potential reasons for the low performance rate may include the time needed to take FFR measurements, the additional invasiveness of wiring in coronary angiography, the adverse effects of hyperemic agents, the costs associated with adenosine, patient-related discomfort, contraindications, and lack of reimbursement.[59]

Difference in Drug Response

Although adenosine (IV) is the gold standard for hyperemia, previous studies revealed that there were various types of response to adenosine (IV), which might make it difficult to assess true FFR, separate from minimum Pd/Pa,[60,61] and it is also known that some patients do not respond well to adenosine.

Tandem Lesions

Tandem lesions are defined as 2 separate lesions with > 50% stenosis each in the same coronary artery, separated by an angiographically normal segment. FFR in tandem lesions often misleads the interventional cardiologists because each stenosis will influence hyperemic blood flow and therefore an accurate pressure gradient due to each stenosis cannot be known before one is treated.[62] Although equations for predicting the FFR of each individual lesion separately were suggested,[63] they are not practical because wedge pressure measurement requires balloon inflation at the distal vessel (Figure 6). Practical intervention should be based on a step-by-step strategy: after the stenosis with the largest gradient has been stented, the pullback recording should be repeated to determine whether and where a second stent should be deployed,[64] which seems time-consuming and bothersome for most of the interventional cardiologists.

Discordance between CFR and FFR

Although the diagnostic accuracy of FFR and coronary flow reserve (CFR) for ischemic heart disease is known to be equivalent, the results of FFR and CFR are discordant in 30% to 40% of CAD[65]: a phenomenon that has been proposed to originate from the different distribution of epicardial and microvascular involvement[66] (Figure 7). The adverse outcome of discordance between FFR and CFR was demonstrated compared with cases in which FFR and CFR were normal, which was particularly attributable to those cases with normal FFR and abnormal CFR, whereas discordance with abnormal FFR and normal CFR was predominantly associated with equivalent clinical outcomes compared with concordantly normal FFR and CFR.[67]

Gray Zone FFR

The best approach for the management of lesions with gray zone FFR, defined as an FFR value between 0.75 and 0.80, is unknown since previous studies have shown conflicting outcome data for these patients.[68,69] It would be rational to make decisions based on multilateral clinical judgment for individual patients with gray zone FFR, including other perfusion imaging modalities, considering anatomical features, patient background, and the risk-benefit profile for PCI.

iFR-Era Just Around the Corner

More recently, interest in resting gradients has emerged, given the many limitations of FFR discussed above. Most notably, iFR was introduced as an alternative to FFR in 2012[7] and has shown equivalent diagnostic performance compared with FFR in several studies with invasive and noninvasive modalities in a very short time span.[70–74] Additionally, iFR-guided PCI was noninferior to FFR-guided PCI for adverse cardiovascular events at 1-year follow-up in 2 separate, large randomized multicenter trials,[8,9] which led

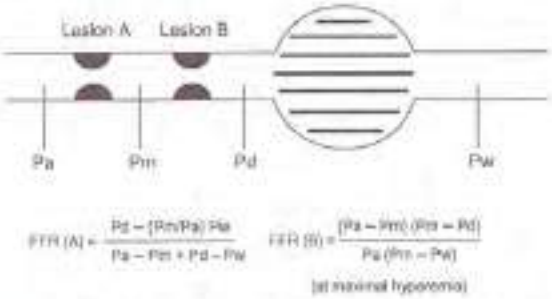

Figure 6. Schema for the concept of FFR in tandem lesions. Equations for predicting FFR of each individual lesion separately is available but complicated. FFR, fractional flow reserve; Pa, aortic pressure; Pd, distal pressure; Pm, coronary pressure between 2 lesions; Pw, coronary wedge pressure.

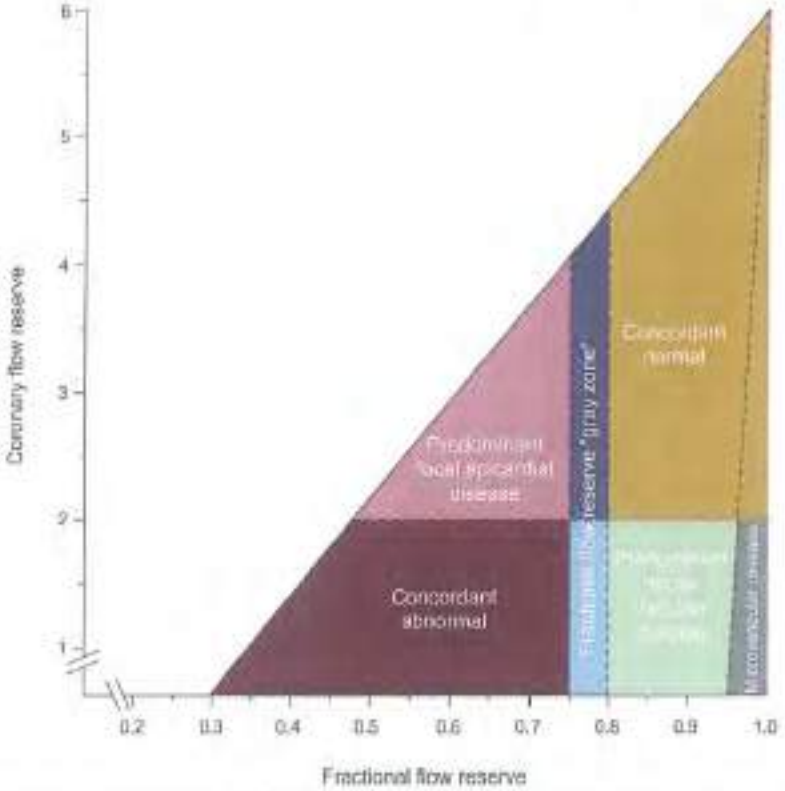

Figure 7. Conceptual plot of the fractional flow reserve-coronary flow reserve relationship. There is discordance between them. Reproduced with permission from Van de Hoef et al.[47]

to iFR being included in the clinical guidelines as equivalent to FFR in the United States.[6]

Concept

The iFR is measured in the mid to late diastolic period of low and constant coronary resistance, called the wave-free period, and the mean pressure during the wave-free period is obtained distal to the lesion and indexed to simultaneous Pa.[7] In this period, pressure and flow velocity are linearly related, allowing for the pressure-only index to evaluate the severity of the coronary lesion. Furthermore, isolation of the pressure measurement to the wave-free period eliminates the interaction between the myocardium and coronary microvasculature in systole and early diastole, during which the compression of the microvasculature increases intracoronary resistance[75,76] (Figure 8).

Validation

Several studies after the introduction of iFR concluded that concordance with FFR was observed in approximately 80%, which also revealed that detection of the wave-free period was necessary in measurement.[77–79] Following these comparisons of iFR with FFR, a series of further comparison studies were conducted between iFR, FFR, and third-party arbiters of ischemia (Table 4). These studies found not only equivalent diagnostic performance of iFR[70–74] but also the possibility of a higher correlation between iFR and microvascular function compared with FFR.[71,72]

Established Clinical Evidence

Most recently, the effectiveness of iFR to guide PCI compared with FFR was reported in DEFINE-FLAIR and iFR-SWEDEHEART, the largest randomized clinical trials in the field of coronary physiology to date.[8,9] Over 4500 patients were randomized in 2 different studies in a 1:1 fashion to either iFR-guided or FFR-guided PCI, with iFR ≤ 0.89 and FFR ≤ 0.80 as cutoffs for revascularization. The primary endpoint, a composite of death from any cause, nonfatal myocardial infarction, or unplanned revascularization at 1 year, occurred in DEFINE-FLAIR and iFR-SWEDEHEART in 6.8% and 6.7% in the iFR groups and in 7.0% and 6.1% in the FFR groups, respectively. The investigators concluded that iFR-guided PCI was noninferior to FFR-guided PCI with respect to the risk of cardiovascular events at 1 year (Figure 9). In addition, in the iFR groups, the number of functionally significant stenoses and rates of revascularization were lower, the duration of the procedural time was shorter, and the percentage of patients who developed adverse symptoms related to the procedure was smaller.

Summary of Current Coronary Physiology

In current clinical practice, FFR is preferred because evidence has been generated for years, whereas iFR tends to be preferred because of additional advantages and emerging new evidence. Clinical guidelines have ranked them as equivalent.[6] The recently published SYNTAX II study data showed that the application of coronary physiology to the PCI technique, regardless of FFR or iFR, could improve clinical outcomes for patients with 3-vessel disease.[80]

FUTURE DIRECTIONS

Coronary Physiology in ACS

One of the current interests in this field is physiological interrogation of nonculprit lesions in acute coronary syndrome

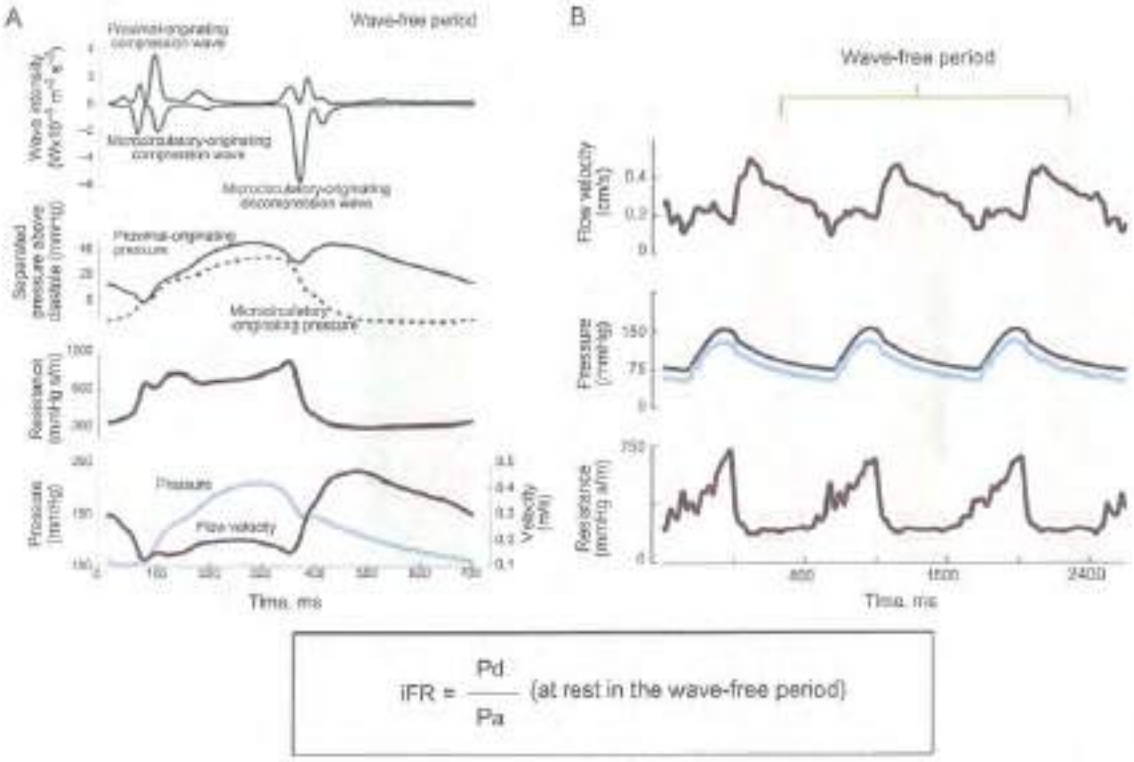

Figure 8. Schema for the concept of wave-free period and iFR. A: The green shading highlights the wave-free period of diastole where the multiple different waves propagating from the proximal and distal ends of the vessel are quiescent. B: Flow velocity (top trace), proximal (light blue), and distal (purple) pressure traces and instantaneous resistance (bottom trace) demonstrate the stability of the wave-free period beat to beat. iFR, instantaneous wave-free ratio; Pa, aortic pressure; Pd, distal pressure. Reproduced with permission from Nijjer et al.[70]

Table 4
Comparison Between Instantaneous Wave-free Ratio and Fractional Flow Reserve in Ischemia Assessment

Publication	Modality	No.	FFR diagnostic accuracy of AUC (%)	iFR diagnostic accuracy of AUC (%)	P
Sen et al.,[70] 2013	HSR	51	92	92	NS
Sen et al.,[71] 2013	HSR	120	82	89	< .01
Petraco et al.,[72] 2014	CFR	216	57	74	< .01
Van de Hoef et al.,[73] 2015	MPS	85	63	62	NS
Hwang et al.,[74] 2017	PET	115	76	74	NS

AUC, area under the curve; CFR, coronary flow reserve; FFR, fractional flow reserve; HSR, hyperemic stenosis resistance; iFR, instantaneous wave-free ratio; MPS, myocardial perfusion scintigraphy; NS, not significant; PET, positron emission tomography.

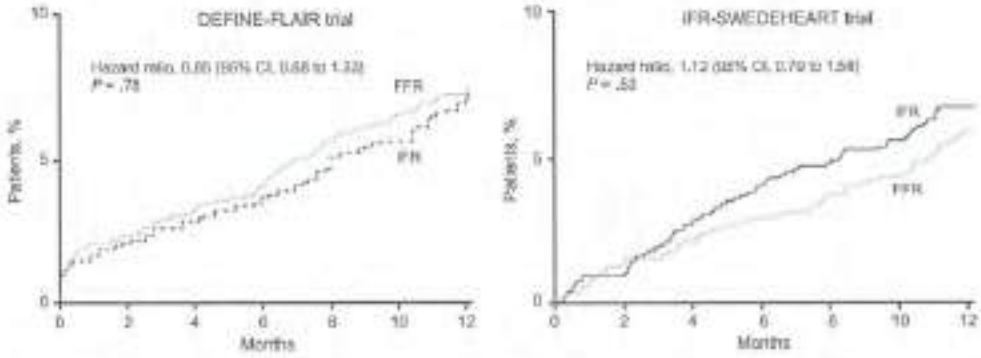

Figure 9. Results of DEFINE-FLAIR and iFR-SWEDEHEART. Kaplan-Meier curves demonstrating noninferiority of iFR vs FFR for major adverse cardiac events at 12 months in both trials. 95%CI, 95% confidence interval; FFR, fractional flow reserve; iFR, instantaneous wave-free ratio. Reproduced with permission from Davies et al.[8] and Götberg et al.[9]

(ACS). Two recent randomized trials have supported revascularization of the noninfarct-related artery with FFR guidance. The DANAMI-3-PRIMULTI trial demonstrated that FFR-guided staged complete revascularization before hospital discharge led to significantly decreased future revascularizations at 1-year follow-up compared with PCI for the infarct-related artery only.[81] Similarly, the Compare-Acute trial investigators examined whether FFR-guided treatment improved outcomes in patients with ST-segment elevation myocardial infarction and multivessel disease to evaluate the benefit of revascularization in the acute setting of noninfarct-related lesions.[82] FFR -guided revascularization at the time of primary PCI resulted in a lower rate of the composite cardiovascular event rate at 1 year, mainly driven by decreased subsequent revascularizations. However, due to the lack of a physiological comparator arm, the full potential of coronary physiology applied to ACS could not be revealed, and should therefore be evaluated in future studies. In addition, it is important to note that invasive physiological assessment of the noninfarct-related artery in ACS is not a benign process. Serious adverse events occurred in 0.2% of the Compare-Acute trial population, including dissection of a coronary artery with subsequent vessel occlusion, myocardial infarction, and death. The risk-benefit balance of additional wiring to nonculprit lesions or inducing hyperemia in ACS is obscure and requires evaluation.

As Guidance for CABG

Evidence for using coronary physiology to guide coronary artery bypass graft (CABG) is lacking. Only one study has shown that the rate of occlusion was significantly higher on angiography at 1 year when the bypass was placed on functionally nonsignificant stenoses, which suggested that coronary physiology could provide better clinical outcomes of CABG as well as in the field of PCI.[83] Prospective, randomized trials focusing on hard clinical endpoints are needed to address the merits of FFR/iFR-guided CABG.

Potential of iFR

Regarding the frequency of use, iFR will become more widely used when longer-term clinical outcomes are reported from the DEFINE-FLAIR and iFR-SWEDEHEART trials.

Because of the application of resting index, a recent report suggested that iFR could resolve one of the limitation of FFR: hemodynamic crosstalk between stenoses in tandem lesions during hyperemic status.[83] Intracoronary pressure mapping, which allows identification of the segments that contribute most to hemodynamic impairment caused by diffuse or tandem lesions and prediction of post-iFR after virtual stenting, was demonstrated in the iFR pullback study[84] (Figure 10). This technology is more

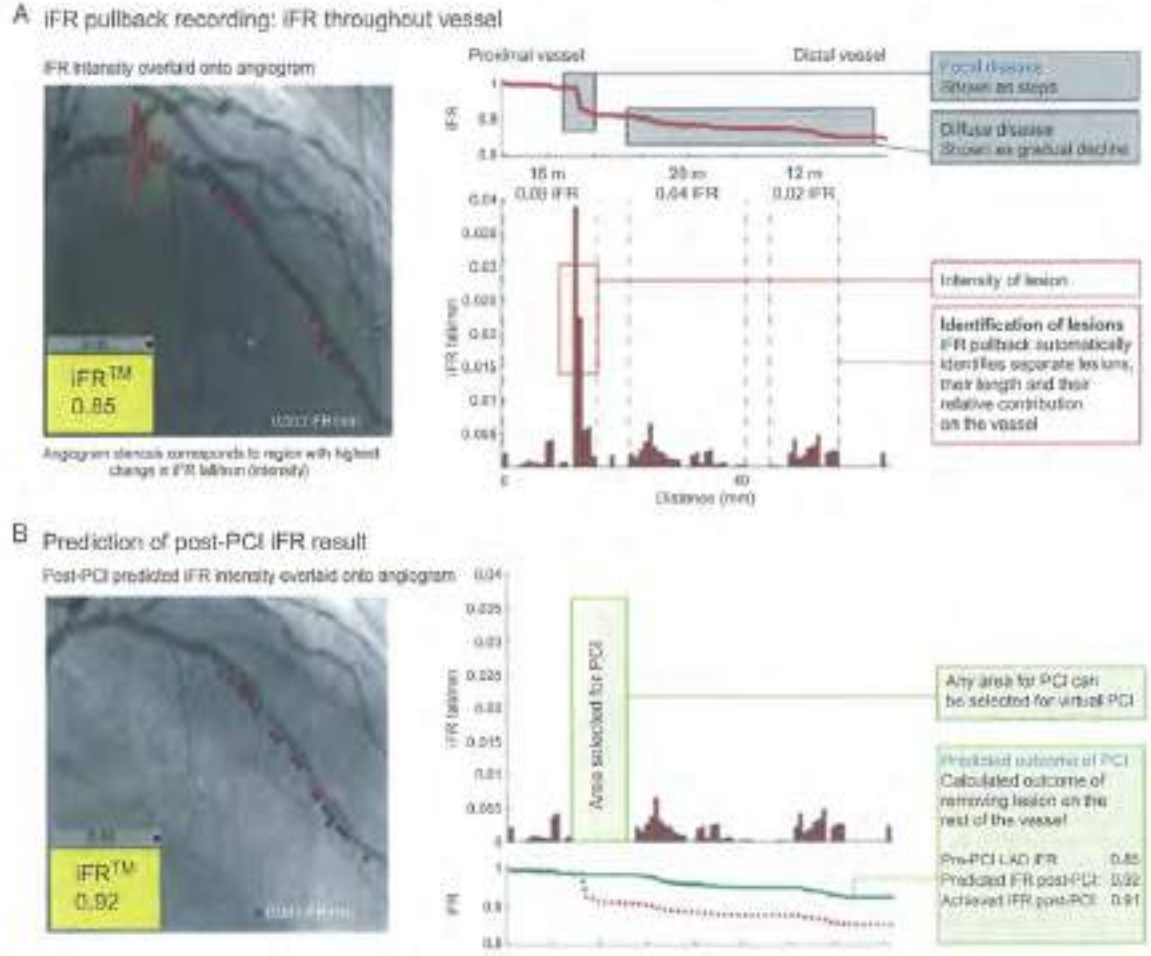

Figure 10. Representative case from the iFR pullback study. A: The coregistration of the iFR pullback trace with coronary angiography identifies pressure loss along the length of the vessel and distinguishes focal from diffuse disease. B: Virtual percutaneous coronary intervention (PCI) calculates the expected post-PCI iFR result for the area selected for PCI. iFR, instantaneous wave-free ratio; LAD, left anterior descending coronary artery. Reproduced with permission from Nijjer et al.[84]

advanced and should be validated in the near future. However, to use this technology maximally, improvement in the property of the pressure wire is mandatory so that the pressure wire can be used as a PCI guidewire in real-world interventions.

Application of Computed Fluid Dynamics

Recently, the notion of computed fluid dynamics has contributed to combining coronary imaging with coronary physiology and has produced several promising modalities. Cardiac computed tomography-based FFR has achieved high diagnostic performance in several prospective multicenter studies compared with computed tomography angiography[65–67] and has suggested advantages in quality of life and economic outcomes compared with conventional clinical practice.[68] The quantitative flow ratio, which is a 3-dimensional quantitative coronary angiography-based FFR, could determine the hemodynamically significant lesion without pressure wire or hyperemia.[69] Optical coherence tomography-derived virtual FFR might elucidate the relationship between coronary morphology and physiology.[70] These technologies are aimed to indicate the simulated value of FFR from coronary imaging only, taking advantages of each modality's features.

CONCLUSIONS

Coronary physiology is becoming increasingly important for current interventional cardiologists with abundant evidence and an evolving future. The evidence amassed to date would have to say "Use FFR/iFR for better PCI". Growing novel technologies in this field are also attracting a great deal of interest.

CONFLICTS OF INTEREST

T. Warisawa and C.M. Cook have received consulting fees from Philips. J.E. Davies has received research grants from Philips and AstraZeneca, consulting fees from Medtronic, Philips, and ReCor Medical, and holds patents pertaining to the iFR technology, which is under license to Philips.

REFERENCES

1. Bech GJW, De Bruyne B, Pijls NHJ, et al. Fractional flow reserve to determine the appropriateness of angioplasty in moderate coronary stenosis: a randomized trial. *Circulation*. 2001;103:2928–2934.
2. Tonino PAL, De Bruyne B, Pijls NHJ, et al. Fractional flow reserve versus angiography for guiding percutaneous coronary intervention. *N Engl J Med*. 2009;360:213–224.
3. De Bruyne B, Pijls NHJ, Kalesan B, et al. Fractional flow reserve-guided PCI versus medical therapy in stable coronary disease. *N Engl J Med*. 2012;367:991–1001.
4. Windecker S, Kolh P, Alfonso F, et al. 2014 ESC/EACTS guidelines on myocardial revascularization:the Task Force on Myocardial Revascularization of the European Society of Cardiology (ESC) and the European Association for Cardio-Thoracic Surgery (EACTS). *Eur Heart J*. 2014;35:2541–2619.
5. Fihn SD, Gardin JM, Abrams J, et al. 2012 ACCF/AHA/ACP/AATS/PCNA/SCAI/STS Guideline for the diagnosis and management of patients with stable ischemic heart disease: a report of the American College of Cardiology Foundation/American Heart Association Task Force on Practice Guidelines, and the American College of Physicians, American Association for Thoracic Surgery, Preventive Cardiovascular Nurses Association, Society for Cardiovascular Angiography and Interventions, and Society of Thoracic Surgeons. *J Am Coll Cardiol*. 2012;60:e44–e164.
6. Patel MR, Calhoon JH, Dehmer GJ, et al. ACC/AATS/AHA/ASE/ASNC/SCAI/SCCT/STS 2017 appropriate use criteria for coronary revascularization in patients with stable ischemic heart disease: a report of the American College of Cardiology Appropriate Use Criteria Task Force, American Association for Thoracic Surgery, American Heart Association, American Society of Echocardiography, American Society of Nuclear Cardiology, Society for Cardiovascular Angiography and Interventions, Society of Cardiovascular Computed Tomography, and Society of Thoracic Surgeons. *J Am Coll Cardiol*. 2017;69:2212–2241.
7. Sen S, Escaned J, Malik IS, et al. Development and validation of a new adenosine-independent index of stenosis severity from coronary wave-intensity analysis: results of the ADVISE (Adenosine Vasodilator Independent Stenosis Evaluation) study. *J Am Coll Cardiol*. 2012;59:1392–1402.
8. Davies JE, Sen S, Dehbi HM, et al. Use of the instantaneous wave-free ratio or fractional flow reserve in PCI. *N Engl J Med*. 2017;376:1824–1834.
9. Götberg M, Christiansen EH, Gudmundsdottir IJ, et al. Instantaneous wave-free ratio Versus fractional flow reserve to guide PCI. *N Engl J Med*. 2017;376:1813–1823.
10. Grüntzig AR, Senning A, Siegenthaler WE. Nonoperative dilatation of coronary-artery stenosis: percutaneous transluminal coronary angioplasty. *N Engl J Med*. 1979;301:61–68.
11. Serruys PW, Wijns W, Reiber JH, et al. Values and limitations of transstenotic pressure gradients measured during percutaneous coronary angioplasty. *Herz*. 1985;10:137–142.
12. Serruys PW, Di Mario C, Meneveau N, et al. Intracoronary pressure and flow velocity with sensor-tip guidewires: a new methodologic approach for assessment of coronary hemodynamics before and after coronary interventions. *Am J Cardiol*. 1993;71:41D–53D.
13. Pijls NH, Van Son JA, Kirkeeide RL, De Bruyne B, Gould KL. Experimental basis of determining maximum coronary, myocardial, and collateral blood flow by pressure measurements for assessing functional stenosis severity before and after percutaneous transluminal coronary angioplasty. *Circulation*. 1993;87:1354–1367.
14. Pijls NHJ, De Bruyne B, Peels K, et al. Measurement of fractional flow reserve to assess the functional severity of coronary-artery stenoses. *N Engl J Med*. 1996;334:1703–1708.
15. Pijls NHJ, Gelder BV, der Voort PV, et al. Fractional flow reserve. A useful index to evaluate the influence of an epicardial coronary stenosis on myocardial blood flow. *Circulation*. 1995;92:3183–3193.
16. De Bruyne B, Bartunek J, Sys SU, Heyndrickx GR. Relation between myocardial fractional flow reserve calculated from coronary pressure measurements and exercise-induced myocardial ischemia. *Circulation*. 1995;92:39–46.
17. Bartunek J, Van Schuerbeeck E, De Bruyne B. Comparison of exercise electrocardiography and dobutamine echocardiography with invasively assessed myocardial fractional flow reserve in evaluation of severity of coronary arterial narrowing. *Am J Cardiol*. 1997;79:478–481.
18. Caymaz O, Fok AS, Tezcan H, et al. Correlation of myocardial fractional flow reserve with thallium-201 SPECT imaging in intermediate-severity coronary artery lesions. *J Invasive Cardiol*. 2000;12:345–350.
19. Abe M, Tomiyama H, Yoshida H, Doba N. Diastolic fractional flow reserve to assess the functional severity of moderate coronary artery stenoses: comparison with fractional flow reserve and coronary flow velocity reserve. *Circulation*. 2000;102:2365–2370.
20. Chamuleau SA, Meuwissen M, Van Eck-Smit BL, et al. Fractional flow reserve, absolute and relative coronary blood flow velocity reserve in relation to the results of technetium-99m sestamibi single-photon emission computed tomography in patients with two-vessel coronary artery disease. *J Am Coll Cardiol*. 2001;37:1316–1322.
21. Yanagisawa H, Chikamori T, Tanaka N, et al. Correlation between thallium-201 myocardial perfusion defects and the functional severity of coronary artery stenosis as assessed by pressure-derived myocardial fractional flow reserve. *Circ J*. 2002;66:1105–1109.
22. Seo JK, Kwan J, Suh JH, et al. Early dipyridamole stress myocardial SPECT to detect residual stenosis of infarct related artery: comparison with coronary angiography and fractional flow reserve. *Korean J Intern Med*. 2002;17:7–13.
23. Morishima T, Chikamori T, Hatano T, Tanaka N, Takazawa K, Yamashina A. Correlation between myocardial uptake of technetium-99m-sestamibi and pressure-derived myocardial fractional flow reserve. *J Cardiol*. 2004;43:155–163.
24. Kobori Y, Tanaka N, Takazawa K, Yamashina A. Usefulness of fractional flow reserve in determining the indication of target lesion revascularization. *Catheter Cardiovasc Interv*. 2005;65:355–360.
25. Hacker M, Rieber J, Schmid R, et al. Comparison of Tc-99m sestamibi SPECT with fractional flow reserve in patients with intermediate coronary artery stenoses. *J Nucl Cardiol*. 2005;12:645–654.
26. Krüger S, Koch KC, Baumann I, et al. Use of fractional flow reserve versus stress perfusion scintigraphy in stent restenosis. *Eur J Intern Med*. 2005;16:429–431.
27. Samady H, Lepper W, Powers ER, et al. Fractional flow reserve of infarct-related arteries identifies reversible defects on noninvasive myocardial perfusion imaging early after myocardial infarction. *J Am Coll Cardiol*. 2006;47:2187–2193.
28. Van de Hoef TP, Nolte F, Damman P, et al. Diagnostic accuracy of combined intracoronary pressure and flow velocity information during baseline conditions: adenosine-free assessment of functional coronary lesion severity. *Circ Cardiovasc Interv*. 2012;5:508–514.
29. Pijls NH, Van Schaardenburgh P, Manoharan G, et al. Percutaneous coronary intervention of functionally nonsignificant stenosis: 5-year follow-up of the DEFER Study. *J Am Coll Cardiol*. 2007;49:2105–2111.
30. Zimmermann FM, Ferrara A, Johnson NP, et al. Deferral vs. performance of percutaneous coronary intervention of functionally non-significant coronary stenosis: 15-year follow-up of the DEFER trial. *Eur Heart J*. 2015;36:3182–3188.
31. Yoshizaki T, Naganuma T, Kobayashi T, et al. Long-term follow-up of first generation versus new-generation drug-eluting stents in three-vessel coronary artery disease. *Cardiovasc Revasc Med*. 2017;18:490–496.
32. Jensen LO, Thayssen P, Christiansen EH, et al. Safety and Efficacy of Everolimus-Versus Sirolimus-Eluting Stents: 5-Year Results From SORT OUT IV. *J Am Coll Cardiol*. 2016;67:751–762.

33. Melikian N, De Bondt P, Tonino P, et al. Fractional flow reserve and myocardial perfusion imaging in patients with angiographic multivessel coronary artery disease. *JACC Cardiovasc Interv*. 2010;3:307–314.
34. Ragosta M, Bishop AH, Lipson LC, et al. Comparison between angiography and fractional flow reserve versus single-photon emission computed tomographic myocardial perfusion imaging for determining lesion significance in patients with multivessel coronary disease. *Am J Cardiol*. 2007;99:896–902.
35. Sant'Anna FM, Silva EE, Batista LA, Ventura FM, Barreto CA, Pijls NH. Influence of routine assessment of fractional flow reserve on decision making during coronary interventions. *Am J Cardiol*. 2007;99:504–508.
36. Curzen N, Rana O, Nicholas Z, et al. Does routine pressure wire assessment influence management strategy at coronary angiography for diagnosis of chest pain? The RIPCORD Study. *Circ Cardiovasc Interv*. 2014;7:248–255.
37. Nakamura M, Yamagishi M, Ueno T, et al. Prevalence of visual-functional mismatch regarding coronary artery stenosis in the CVIT-DEFER registry. *Cardiovasc Interv Ther*. 2014;29:300–308.
38. Nakamura M, Yamagishi M, Ueno T, et al. Modification of treatment strategy after FFR measurement: CVIT-DEFER registry. *Cardiovasc Interv Ther*. 2015;30:12–21.
39. Takagi A, Tsurumi Y, Ishii Y, et al. Clinical potential of intravascular ultrasound for physiological assessment of coronary stenotic relationship between quantitative ultrasound tomography and pressure-derived fractional flow reserve. *Circulation*. 1999;100:250–255.
40. Brugaletta S, Anzuini A, Airoldi F, et al. Intravascular ultrasound criteria for the assessment of the functional significance of intermediate coronary artery stenoses and comparison with fractional flow reserve. *Am J Cardiol*. 2011;67:136–141.
41. Kang SJ, Lee JY, Ahn JM, et al. Validation of intravascular ultrasound-derived parameters with fractional flow reserve for assessment of coronary stenosis severity. *Circ Cardiovasc Interv*. 2011;4:63–71.
42. Koo BK, Yang HM, Doh JH, et al. Optimal intravascular ultrasound criteria and their accuracy for defining the functional significance of intermediate coronary stenoses of different locations. *JACC Cardiovasc Interv*. 2011;4:803–811.
43. Ben-Dor I, Torguson R, Deksissa T, et al. Intravascular ultrasound lumen area parameters for assessment of physiological ischemia by fractional flow reserve in intermediate coronary artery stenosis. *Cardiovasc Revasc Med*. 2012;13:177–182.
44. Kang SJ, Ahn JM, Song H, et al. Usefulness of minimal luminal coronary area determined by intravascular ultrasound to predict functional significance in stable and unstable angina pectoris. *Am J Cardiol*. 2012;108:947–953.
45. Waksman R, Legutko J, Singh J, et al. FIRST: Fractional Flow Reserve and Intravascular Ultrasound Relationship Study. *J Am Coll Cardiol*. 2013;61:917–923.
46. Gonzalo N, Escaned J, Alfonso F, et al. Morphometric assessment of coronary stenosis relevance with optical coherence tomography: a comparison with fractional flow reserve and intravascular ultrasound. *J Am Coll Cardiol*. 2012;59:1080–1089.
47. Shiono Y, Kitabata H, Kubo T, et al. Optical coherence tomography-derived anatomical criteria for functionally significant coronary stenosis assessed by fractional flow reserve. *Circ J*. 2012;76:2218–2225.
48. Ioufi A, Jeremias A, Fearon WF, et al. Expert consensus statement on the use of fractional flow reserve, intravascular ultrasound, and optical coherence tomography: a consensus statement of the Society for Cardiovascular Angiography and Interventions. *Catheter Cardiovasc Interv*. 2014;83:509–518.
49. Koo BK, Kang HJ, Youn TJ, et al. Physiologic assessment of jailed side branch lesions using fractional flow reserve. *J Am Coll Cardiol*. 2005;46:633–637.
50. Koo BK, Park KW, Kang HJ, et al. Physiological evaluation of the provisional side-branch lesions using fractional flow reserve. *Eur Heart J*. 2008;29:726–732.
51. Kang SJ, Ahn JM, Kim WJ, et al. Functional and morphological assessment of side branch after left main coronary artery bifurcation stenting with cross-over technique. *Catheter Cardiovasc Interv*. 2014;83:545–552.
52. Di Segni E, Higano ST, Rihal CS, Holmes Jr DR, Lennon R, Lerman A. Incremental doses of intracoronary adenosine for the assessment of coronary velocity reserve for clinical decision making. *Catheter Cardiovasc Interv*. 2001;54:34–40.
53. Pijls NH. Fractional flow reserve to guide coronary revascularization. *Circ J*. 2013;77:561–569.
54. De Bruyne B, Pijls NH, Barbato E, et al. Intracoronary and intravenous adenosine 5'-triphosphate, adenosine, papaverine, and contrast medium to assess fractional flow reserve in humans. *Circulation*. 2003;107:1877–1883.
55. Wilson RF, White CW. Intracoronary papaverine: An ideal coronary vasodilator for studies of the coronary circulation in conscious humans. *Circulation*. 1986;73:444–451.
56. Jang HJ, Koo BK, Lee HS, et al. Safety and efficacy of a novel hyperaemic agent, intracoronary nicorandil, for invasive physiological assessments in the cardiac catheterization laboratory. *Eur Heart J*. 2013;34:2055–2062.
57. Fearon WF, Bornschein B, Tonino PA, et al. Economic evaluation of fractional flow reserve–guided percutaneous coronary intervention in patients with multivessel disease. *Circulation*. 2010;122:2545–2550.
58. Fearon WF, Nishi T, De Bruyne B, et al. Clinical Outcomes and Cost-Effectiveness of Fractional Flow Reserve-Guided Percutaneous Coronary Intervention in Patients With Stable Coronary Artery es and Cost-Effectiveness of Fractional Flow Reserve-Guided Percutaneous Coronary Intervention in Patients With Stable Coronary Artery Disease: Three-Year Follow-Up of the FAME 2 Trial. *Circulation*. 2017. https://doi.org/10.1161/CIRCULATIONAHA.117.031907
59. Göhberg M, Cook CM, Sen S, Nijjer S, Escaned J, Davies JE. The Evolving Future of Instantaneous Wave-Free Ratio and Fractional Flow Reserve. *J Am Coll Cardiol*. 2017;70:1370–1402.
60. Tarkin JM, Nijjer S, Sen S, et al. Hemodynamic response to intravenous adenosine and its effect on fractional flow reserve assessment: Results of the Adenosine for the Functional Evaluation of Coronary Stenosis Severity (AFFECTS) Study. *Circ Cardiovasc Interv*. 2013;6:654–661.
61. Echavarría-Pinto M, Petraco R, Van de Hoef TP, et al. Fractional flow reserve and minimum Pd/Pa ratio during intravenous adenosine infusion: very similar but not always the same. *EuroIntervention*. 2016;11:1015–1019.
62. Hirota M, Iwasaki K, Yamamoto K, et al. Coronary pressure measurement to identify the lesion requiring percutaneous coronary intervention in equivocal tandem lesions. *Coron Artery Dis*. 2006;17:181–186.
63. De Bruyne B, Pijls NH, Heyndrickx GR, Hodeige D, Kirkeeide R, Gould KL. Pressure-derived fractional flow reserve to assess serial epicardial stenoses: Theoretical basis and animal validation. *Circulation*. 2000;101:1840–1847.
64. Kim HL, Koo BK, Nam CW, et al. Clinical and physiological outcomes of fractional flow reserve-guided percutaneous coronary intervention in patients with serial stenoses within one coronary artery. *JACC Cardiovasc Interv*. 2012;5:1013–1018.
65. Meuwissen M, Chamuleau SA, Siebes M, et al. The prognostic value of combined intracoronary pressure and blood flow velocity measurements after deferral of percutaneous coronary intervention. *Catheter Cardiovasc Interv*. 2008;71:291–297.
66. Johnson NP, Kirkeeide RL, Gould KL. Is discordance of coronary flow reserve and fractional flow reserve due to methodology or clinically relevant coronary pathophysiology? *JACC Cardiovasc Imaging*. 2012;5:193–202.
67. Van de Hoef TP, Van Lavieren MA, Damman P, et al. Physiological basis and long-term clinical outcome of discordance between fractional flow reserve and coronary flow velocity reserve in coronary stenoses of intermediate severity. *Circ Cardiovasc Interv*. 2014;7:301–311.
68. Courtis J, Rodés-Cabau J, Larose E, et al. Comparison of medical treatment and coronary revascularization in patients with moderate coronary lesions and borderline fractional flow reserve measurements. *Catheter Cardiovasc Interv*. 2008;71:541–548.
69. Umdenzeit M, Hallikainen-Kaukonen Y, Yazar A, et al. Clinical outcome following conservative vs revascularization therapy in patients with stable coronary artery disease and borderline fractional flow reserve measurements. *Clin Cardiol*. 2010;33:77–83.
70. Sen S, Asrress KN, Nijjer S, et al. Diagnostic classification of the instantaneous wave-free ratio is equivalent to fractional flow reserve and is not improved with adenosine administration. Results of CLARIFY (Classification Accuracy of Pressure-Only Ratios Against Indices Using Flow Study). *J Am Coll Cardiol*. 2013;61:1409–1420.
71. Sen S, Nijjer S, Petraco R, Malik IS, Francis DP, Davies J. Instantaneous wave-free ratio numerically different, but diagnostically superior to FFR? Is lower always better? *J Am Coll Cardiol*. 2013;62:566.
72. Petraco R, Van de Hoef TP, Nijjer S, et al. Baseline instantaneous wave-free ratio as a pressure-only estimation of underlying coronary flow reserve: results of the JUSTIFY-CFR Study. *Circ Cardiovasc Interv*. 2014;7:452–502.
73. Van de Hoef TP, Meuwissen M, Escaned J, et al. Head-to-head comparison of basal stenosis resistance index, instantaneous wave-free ratio, and fractional flow reserve: diagnostic accuracy for stenosis-specific myocardial ischaemia. *EuroIntervention*. 2015;11:914–925.
74. Hwang D, Jeon KH, Lee JM, et al. Diagnostic performance of resting and hyperemic invasive physiological indices to define myocardial ischemia: validation with 13N-ammonia positron emission tomography. *JACC Cardiovasc Interv*. 2017;10:751–760.
75. Davies JE, Whinnett ZI, Francis DP, et al. Evidence of a dominant backward-propagating "suction" wave responsible for diastolic coronary filling in humans, attenuated in left ventricular hypertrophy. *Circulation*. 2006;113:1768–1778.
76. Nijjer SS, Sen S, Petraco R, Davies JE. Advances in coronary physiology. *Circ J*. 2015;79:1172–1184.
77. Petraco R, Escaned J, Sen S, et al. Classification performance of instantaneous wave-free ratio (iFR) and fractional flow reserve in a clinical population of intermediate coronary stenoses: results of the ADVISE registry. *EuroIntervention*. 2013;9:91–101.
78. Berry C, van 't Veer M, Witt N, et al. VERIFY (VERification of Instantaneous Wave-Free Ratio and Fractional Flow Reserve for the Assessment of Coronary Artery Stenosis Severity in EverydaY Practice): a multicenter study in consecutive patients. *J Am Coll Cardiol*. 2013;61:1421–1427.
79. Jeremias A, Maehara A, Généreux P, et al. Multicenter core laboratory comparison of the instantaneous wave-free ratio and resting Pd/Pa with fractional flow reserve: the RESOLVE study. *J Am Coll Cardiol*. 2014;63:1253–1261.
80. Escaned J, Collet C, Ryan N, et al. Clinical outcomes of state-of-the-art percutaneous coronary revascularization in patients with de novo three vessel disease: 1-year results of the SYNTAX II study. *Eur Heart J*. 2017;38:3124–3134.
81. Engstrøm T, Kelbæk H, Helqvist S, et al. Complete revascularisation versus treatment of the culprit lesion only in patients with ST-segment elevation myocardial infarction and multivessel disease (DANAMI-3–PRIMULTI): an open-label, randomised controlled trial. *Lancet*. 2015;386:665–671.
82. Sinclair PC, Abdel-Wahab M, Neumann FJ, et al. Fractional flow reserve-guided multivessel angioplasty in myocardial infarction. *N Engl J Med*. 2017;376:1234–1244.
83. Botman CJ, Schumberger J, Kuphen S, et al. Does stenosis severity of native vessels influence bypass graft patency?. A prospective fractional flow reserve-guided study. *Ann Thorac Surg*. 2007;83:2093–2097.

84. Nijjer SS, Sen S, Petraco R, et al. Pre-angioplasty instantaneous wave-free ratio pullback provides virtual intervention and predicts hemodynamic outcome for serial lesions and diffuse coronary artery disease. *JACC Cardiovasc Interv*. 2014;7:1386–1396.
85. Koo BK, Erglis A, Doh JH, et al. Diagnosis of ischemia-causing coronary stenoses by noninvasive fractional flow reserve computed from coronary computed tomographic angiograms. Results from the prospective multicenter DISCOVER-FLOW study. *J Am Coll Cardiol*. 2011;58:1989–1997.
86. Min JK, Leipsic J, Pencina MJ, et al. Diagnostic accuracy of fractional flow reserve from anatomic CT angiography. *JAMA*. 2012;308:1237–1245.
87. Norgaard BL, Leipsic J, Gaur S, et al. Diagnostic performance of noninvasive fractional flow reserve derived from coronary computed tomography angiography in suspected coronary artery disease: the NXT trial. *J Am Coll Cardiol*. 2014;63:1145–1155.
88. Hlatky MA, De Bruyne B, Pontone G, et al. Quality-of-Life and Economic Outcomes of Assessing Fractional Flow Reserve With Computed Tomography Angiography: PLATFORM. *J Am Coll Cardiol*. 2015;66:2315–2323.
89. Tu S, Westra J, Yang J, et al. Diagnostic accuracy of fast computational approaches to derive fractional flow reserve from diagnostic coronary angiography: The International Multicenter FAVOR Pilot Study. *JACC Cardiovasc Interv*. 2016;9:2024–2035.
90. Seike F, Uetani T, Nishimura K, et al. Intracoronary Optical Coherence Tomography-Derived Virtual Fractional Flow Reserve for the Assessment of Coronary Artery Disease. *Am J Cardiol*. 2017;120:1772–1779.

EuroIntervention 2018;14:849-851

From saline to serial FFR measurement - the continued rationale for physiological stenosis assessment in stable coronary artery disease

Christopher M. Cook[1]*, MBBS, BSc; Takayuki Warisawa[1], MD; Justin E. Davies[2], MD, PhD

1. Imperial College London, London, United Kingdom; 2. Hammersmith Hospital, London, United Kingdom

In this issue of EuroIntervention are two studies that provide novel findings relevant to the field of coronary physiology. The first of these studies by Fujimori et al explores the potential of the saline-induced Pd/Pa ratio (SPR) to identify ischaemia as quantified by fractional flow reserve (FFR) in patients with stable coronary artery disease (SCD)[1].

Article, see page 898

The second of these studies, by Xaplanteris et al, determines the evolution of FFR values in intermediate-severity stable coronary lesions, as assessed in patients returning to the coronary catheter laboratory for repeat physiological stenosis assessment[2].

Article, see page 907

Although these studies are at different ends of the maturation spectrum (the first introducing a new physiological index and the second providing evolutional data on the well-established FFR), both are united by the common theme of supporting the more widespread use of functional stenosis assessment in patients with SCD.

LOW VISCOSITY, HIGH YIELD? SALINE-INDUCED Pd/Pa RATIO PREDICTS THE FUNCTIONAL SIGNIFICANCE OF CORONARY STENOSIS ASSESSED USING FFR

Despite the strong evidence base to support the use of FFR-guided revascularisation decision making, the adoption of FFR in clinical practice remains stubbornly low[3]. Multiple factors contribute to this. Paramount amongst these is the strength of belief that still persists in the oculostenotic reflex as a reliable marker of ischaemia detection. However, more practical issues around the availability and cost of adenosine and patient side effects associated with pharmacological hyperaemia also contribute.

In the manuscript by Fujimori et al, the authors provide an interesting alternative to both resting and hyperaemic stenosis assessment, namely the SPR. By use of an intracoronary bolus of saline administered at a rate of 2 mL/second for a duration of either five heartbeats (SPR-5) or three heartbeats (SPR-3), the authors were able to demonstrate a transient and rapid decline in distal coronary pressure (Pd) that occurred quicker than would be expected if arising from hyperaemia. Following a plateau period, the Pd was gradually noted to return to baseline. With the aortic pressure (Pa) remaining largely unchanged, the dip in Pd resulted in a lowering of the trans-stenotic pressure ratio (Pd/Pa), providing a potential hyperaemia-independent index of physiological stenosis assessment. In 414 stenoses from 331 patients, the authors demonstrated strong correlations between SPR-5 or SPR-3 and FFR ($R=0.941$, $p<0.001$, and $R=0.933$, $p<0.001$, respectively). Tests of reproducibility were also good – an important consideration for any index wishing to be used in clinical practice. Overall, the authors demonstrated a classification agreement ("diagnostic accuracy") of

Corresponding author: Hammersmith Hospital, B block South, 2nd floor, NHLI – Cardiovascular Science, Du Cane Road, London, W12 0NN, United Kingdom. E-mail: christopher.cook@nhs.net

© Europa Digital & Publishing 2018. All rights reserved.

The opinions expressed in this article are not necessarily those of the Editors of EuroIntervention or of the European Association of Percutaneous Cardiovascular Interventions.

DOI: 10.4244/EIJV14I8A152

SPR-5 with FFR of 86.3%. The take-home clinical message is that SPR has the potential to decrease the need for adenosine in FFR-based catheter laboratories by up to three quarters. Crucially, unlike the logistically similar contrast-FFR (cFFR) approach, the use of saline as an adjunctive agent avoids the potential for increased quantities of contrast media.

The authors are to be congratulated on their excellently conducted comparison between SPR and FFR for functional stenosis assessment. However, the sole use of FFR as the gold standard measure of ischaemia presents a limitation to their study that should be addressed by subsequent investigation. Specifically, further insight into the ischaemia-detecting capabilities of SPR should be elucidated by additional comparison with other markers of ischaemia such as instantaneous wave-free ratio (iFR), coronary flow reserve or non-invasive positron emission tomography (PET). Secondly, when considering the potential clinical applicability of SPR, owing to the transient physiological state induced by saline infusion, SPR is not able to provide a pressure wire pullback assessment. As the complexity of SCD continues to increase, the ability of a physiological index to quantify individual stenosis severity along the length of a diseased coronary artery will probably become critically important in the planning of physiologically optimised revascularisation strategies[4].

However, the main point of interest of this study comes when deciding where SPR sits in the spectrum of coronary pressure-based physiological indices. At one end of this spectrum you have the true resting indices such as whole-cycle Pd/Pa and iFR. In the middle of the spectrum you have the sub-maximal hyperaemic index of contrast FFR (cFFR). At the extreme end of the spectrum you have FFR - whose experimental basis is predicated on the attainment of maximal hyperaemia[5]. As the authors chide to, the proposed low-viscosity mechanism of SPR does not fit neatly into this classification. This fascinating proposal requires more investigation to appreciate fully how SPR works, and exactly what it is measuring.

STABLE IS STABLE – CORONARY LESION PROGRESSION AS ASSESSED BY FFR AND ANGIOGRAPHY

Xaplanteris et al provide novel data on the progression of coronary lesions in patients with SCD, assessed both angiographically and also physiologically with FFR[3]. From a selected population of 331 patients returning to the catheter laboratory for clinically driven repeat FFR measurement, the authors explore the natural history of intermediate lesions using FFR as an endpoint.

Over a median time period of 24 months (17-37 months), the change in percent diameter stenosis was just 2% (-5%-11%) and the rate of change of FFR was just -0.007 (-0.028, 0.10) per year. Considering the variability that exists in any physiological index upon repeated measurements, as well as the variability resulting from different methods of adenosine administration, the results are highly supportive of the stability of coronary lesions in stable coronary artery disease. Although this stability was true at the population level of the study, at the patient level certain individuals did experience large fluctuations in their FFR value upon follow-up assessment. Such findings emphasise the value of repeat physiological assessment as part of a holistic approach to patients with persistent stable angina symptoms.

RUNNING BEFORE WE CAN WALK?

Common to both studies are questions that remain concerning the underlying physiological mechanisms to explain the results reported. Specifically, without combined coronary pressure and flow data, it is not possible to investigate microcirculatory function. Particularly in the case of FFR, whose action is dependent on maximal vasodilatation of the microcirculation, the unmeasured effects of microvascular disease are especially relevant. As interventionalists, we must strive to consider (and investigate) myocardial ischaemia in terms beyond those simply of coronary pressure.

THE CLINICAL TAKE-HOME MESSAGES

So, how do we integrate the novel findings provided by these two studies into the contemporary management of patients with SCD? First, we must acknowledge that, for the busy interventional cardiologist, making sense of the growing number of indices proposed for physiological stenosis assessment is potentially bewildering. However, the clinical take-home message is simple. Whichever three-letter acronym you choose to adopt, whether it be FFR, iFR, CFR, HSR (or potentially SPR), the incorporation of coronary physiology into routine revascularisation decision making provides a superior assessment of myocardial ischaemia to that of the angiogram alone.

Second, we must also acknowledge that the evidence supporting the "stability" of "stable" coronary artery disease is abundant. As Xaplanteris and colleagues have identified, there is very little change in functional stenosis severity over time. When assimilated with the clinical outcome results of FAME 2[6] and the recently published pooled analysis of DEFINE-FLAIR and iFR-SWEDEHEART[7], the safe deferral of coronary revascularisation is perhaps the most important role for coronary physiology, whichever index you choose to use (**Figure 1**).

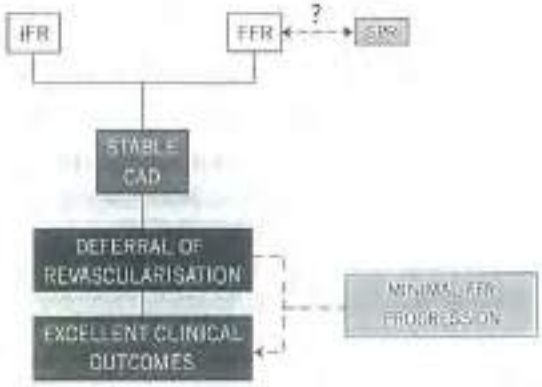

Figure 1. *The safety of deferral of stable coronary lesions using coronary physiology.*

Conflict of interest statement

J. Davies holds patents pertaining to the iFR technology. J. Davies and C. Cook are consultants for Philips Volcano. T. Warisawa has no conflicts of interest to declare.

References

1. Fujimori Y, Baba T, Yamazaki K, Hashimoto S, Yamanaka Y, Ehisuda K, Kurihara K, Koike N, Takeuchi N, Nishiyama S, Terasawa Y, Wakabayashi T, Imai T. Saline-induced Pd/Pa ratio predicts functional significance of coronary stenosis assessed using fractional flow reserve. *EuroIntervention.* 2018;14:898-906.

2. Xaplanteris P, Ntalianis A, De Bruyne B, Strisciuglio T, Pellicano M, Ciccarelli G, Milkas A, Barbato E. Coronary lesion progression as assessed by fractional flow reserve (FFR) and angiography. *EuroIntervention.* 2018;14:907-14.

3. Götberg M, Cook CM, Sen S, Nijjer S, Escaned J, Davies JE. The Evolving Future of Instantaneous Wave-Free Ratio and Fractional Flow Reserve. *J Am Coll Cardiol.* 2017;70:1379-1402.

4. Kikuta Y, Cook CM, Sharp ASP, Sallinas P, Kawase Y, Shiono Y, Giavarini A, Nakayama M, De Rosa S, Sen S, Nijjer SS, Al-Lamee R, Petraco R, Malik IS, Mikhail GW, Kaprielian RR, Wijntjens GWM, Mori S, Hagikura A, Mates M, Mizuno A, Hellig F, Lee K, Janssens L, Horie K, Mohdonzri S, Herrera R, Krackhardt F, Yamawaki M, Davies J. Pre-Angioplasty Instantaneous Wave-Free Ratio Pullback Predicts Hemodynamic Outcome In Humans With Coronary Artery Disease: Primary Results of the International Multicenter iFR GRADIENT Registry. *JACC Cardiovasc Interv.* 2018;11:757-67.

5. Pijls NH, van Son JA, Kirkeeide RL, De Bruyne B, Gould KL. Experimental basis of determining maximum coronary, myocardial, and collateral blood flow by pressure measurements for assessing functional stenosis severity before and after percutaneous transluminal coronary angioplasty. *Circulation.* 1993;87:1354-67.

6. Xaplanteris P, Fournier S, Pijls NHJ, Fearon WF, Barbato E, Tonino PAL, Engstrom T, Kääb S, Dambrink JH, Rioufol G, Toth GG, Piroth Z, Witt N, Fröbert O, Kala P, Linke A, Jagic N, Mates M, Mavromatis K, Samady H, Irimpen A, Oldroyd K, Campo G, Rothenbühler M, Jüni P, De Bruyne B; FAME 2 Investigators. Five-Year Outcomes with PCI Guided by Fractional Flow Reserve. *N Engl J Med.* 2018;379:250-9.

7. Escaned J, Ryan N, Mejía-Renteria H, Cook CM, Dehbi HM, Alegria-Barrero E, Alghamdi A, Al-Lamee R, Altman J, Ambrosia A, Baptista SB, Bertilsson M, Bhindi R, Birgander M, Bojara W, Bruguletta S, Buller C, Calais F, Silva PC, Carlsson J, Christiansen EH, Danielewicz M, Di Mario C, Doh JH, Erglis A, Erlinge D, Gerber RT, Going O, Gudmundsdottir I, Härle T, Hauer D, Hellig F, Indolfi C, Jakobsen L, Janssens L, Jensen J, Jeremias A, Kåregren A, Karlsson AC, Kharbanda RK, Khashaba A, Kikuta Y, Krackhardt F, Koo BK, Koul S, Laine M, Lehman SJ, Lindroos P, Malik IS, Maeng M, Matsuo H, Meuwissen M, Nam CW, Niccoli G, Nijjer SS, Olsson H, Olsson SE, Omerovic E, Parayil G, Petraco R, Piek JJ, Ribichini F, Samady H, Samuels B, Sandhall L, Sapontis J, Sen S, Seto AH, Sezer M, Sharp ASP, Shin ES, Singh J, Takashima H, Talwar S, Tanaka N, Tang K, Van Belle E, van Royen N, Varenhorst C, Vinhas H, Vrints CJ, Walters D, Yokoi H, Fröbert O, Patel MR, Serruys P, Davies JE, Götberg M. Safety of the Deferral of Coronary Revascularization on the Basis of Instantaneous Wave-Free Ratio and Fractional Flow Reserve Measurements in Stable Coronary Artery Disease and Acute Coronary Syndromes. *JACC Cardiovasc Interv.* 2018;11:1437-49.

Cardiovascular Revascularization Medicine 20 (2019) 70–79

Contents lists available at ScienceDirect

Cardiovascular Revascularization Medicine

Review

Takotsubo syndrome: State-of-the-art review by an expert panel – Part 1

Andre Dias [a,b], Ivan J. Núñez Gil [c], Francesco Santoro [d], John E. Madias [e], Francesco Pelliccia [f], Natale Daniele Brunetti [d], Elena Salmoirago-Blotcher [g], Scott W. Sharkey [h], Ingo Eitel [i], Yoshihiro J. Akashi [j], Ibrahim El-Battrawy [k,l], Emiliana Franco [b], Ibrahim Akin [k,l], Milosz Jaguszewski [m], Dana Dawson [n], Vincent M. Figueredo [b], L. Christian Napp [o], Thomas Emil Christensen [p], Kathy Hebert [q], Itsik Ben-Dor [a], Yuichi Ozaki [a], Héctor M. García-Garcia [a], Alexandre H. Kajita [a], Takashi Akasaka [r], Satoshi Kurisu [s], Amir Lerman [t], Ron Waksman [a,*]

[a] Section of Interventional Cardiology, MedStar Washington Hospital Center, Washington, DC, United States of America
[b] Department of Cardiology, Einstein Medical Center, Philadelphia, PA, United States of America
[c] Interventional Cardiology, Cardiovascular Institute, Hospital Clínico San Carlos, Madrid, Spain
[d] Department of Medical & Surgery Sciences, University of Foggia, Foggia, Italy
[e] Icahn School of Medicine at Mount Sinai/Division of Cardiology, Elmhurst Hospital Center, Elmhurst, NY, United States of America
[f] Interventional Cardiology Unit, Sapienza University, Rome, Italy
[g] Centers for Behavioral and Preventive Medicine, The Miriam Hospital, Warren Alpert Medical School of Brown University, Providence, RI, United States of America
[h] Minneapolis Heart Institute Foundation, Minneapolis, MN, United States of America
[i] Cardiology, Angiology, Intensive Care Medicine, University Lübeck, Schleswig-Holstein, Germany
[j] Division of Cardiology, Department of Internal Medicine, St. Marianna University School of Medicine, Kawasaki, Kanagawa, Japan
[k] Department of Internal Medicine, University Heidelberg, Mannheim, Germany
[l] DZHK (German Center for Cardiovascular Research), Partner Site Heidelberg-Mannheim, Germany
[m] Department of Cardiology, Medical University of Gdansk, Poland
[n] School of Medicine and Dentistry, University of Aberdeen, Aberdeen, UK
[o] Department of Cardiology and Angiology, Hannover Medical School, Hannover, Germany
[p] Copenhagen University Hospital, Copenhagen, Denmark
[q] GE Healthcare, Miami, FL, United States of America
[r] Department of Cardiovascular Medicine, Wakayama Medical University, Wakayama, Japan
[s] Department of Cardiovascular Medicine, Hiroshima University, Hiroshima, Japan
[t] Department of Cardiovascular Medicine, Mayo Clinic, Rochester, MN, United States of America

ARTICLE INFO

Article history:
Received 14 November 2018
Accepted 14 November 2018

Keywords:
Takotsubo
Heart failure
Catecholamine

ABSTRACT

Takotsubo syndrome (TTS) is an acute cardiac condition independent of epicardial coronary obstruction that mimics acute coronary syndrome and is characterized by acute heart failure with reversible ventricular motion abnormalities. This consensus paper is the result of a multinational effort aiming to summarize the current state of the art on TTS. Experts in the field provide a thorough and detailed review of this syndrome. Several novel and unique sections are emphasized in this document, including the current state of the art on genetics of takotsubo syndrome, microRNAs (miRs), racial differences, role of cardiac spectroscopy and intracoronary imaging, as well as mechanical circulatory support.

In part 1 of this two-part manuscript, we discuss how TTS came to be known, several patterns and forms it can take in patients, epidemiology and pathophysiology of the syndrome, and clinical presentation.

© 2018 Elsevier Inc. All rights reserved.

Contents

1. Introduction 71
1.1. Historical perspective 71

Abbreviations: ACS, acute coronary syndrome; BNP, B-type natriuretic peptide; CRP, C-reactive protein; LV, left ventricle/ventricular; MACE, major adverse cardiac events; miRs, microRNAs; RV, right ventricle/ventricular; STEMI, ST-elevation myocardial infarction; TIMI, Thrombolysis in Myocardial Infarction; TTS, Takotsubo syndrome.

* Corresponding author at: MedStar Heart and Vascular Institute, MedStar Washington Hospital Center, 110 Irving St., NW, Suite 4B-1, Washington, DC 20010, United States of America.
E-mail address: ron.waksman@medstar.net (R. Waksman).

https://doi.org/10.1016/j.carrev.2018.11.015
1553-8389/0 2018 Elsevier Inc. All rights reserved.

1.2. Nomenclature . . . 71
1.3. Diagnostic criteria . . . 72
2. The different patterns of takotsubo . . . 73
2.1. Anatomical variants . . . 73
2.2. Primary and secondary forms . . . 73
3. Epidemiology . . . 74
3.1. Prevalence . . . 74
3.2. Inpatient morbidity . . . 74
3.3. Inpatient mortality . . . 74
3.4. Gender differences . . . 74
3.5. Age disparity . . . 74
3.6. Racial disparities . . . 74
3.7. Malignancy association . . . 75
3.8. Genetic perspective . . . 75
4. Pathophysiology . . . 75
4.1. Catecholamine surge . . . 75
4.2. Beta receptors mechanism and myocardial ischemia . . . 75
4.3. Depressed cardiac energetic measured with 31 P cardiac spectroscopy . . . 75
4.4. Role of hormonal/reproductive factors . . . 76
4.5. Inflammation and interleukins' role in TTS . . . 76
4.6. Low prevalence of diabetes in TTS patients . . . 77
5. Clinical presentation . . . 77
5.1. Primary and secondary forms . . . 77
5.2. Right ventricle involvement . . . 77
5.3. Inverted forms . . . 77
5.4. Potential triggers . . . 77
5.5. Pharmacologic triggers . . . 77
5.6. Procedure-related triggers . . . 77
Declarations of Interest . . . 77
Funding . . . 78
References . . . 78

1. Introduction

1.1. Historical perspective

Takotsubo syndrome (TTS) was described for the first time decades ago [1]. In 1986, a female case of transient left ventricular apical wall motion abnormalities after her son's suicide was reported from United States [2]. In this case, coronary angiography revealed no significant stenosis. Similar conditions complicated by pheochromocytoma or subarachnoid hemorrhage were already recognized around that time [3,4].

In 1990, Dr. Hikaru Sato first recognized the mysterious condition of reversible left ventricular apical wall motion abnormalities without coronary artery disease, which was often associated with emotional or physical stress, and proposed the term "takotsubo-like left ventricular dysfunction" from Hiroshima City Hospital. This name derives from the shape of systolic left ventriculogram resembling a takotsubo (Fig. 1) [5].

After 2000, Japanese researchers introduced knowledge of this disorder outside Japan with English papers [6,7], and the concept and name "takotsubo cardiomyopathy" became recognized worldwide.

1.2. Nomenclature

TTS is a peculiar condition that clinically mimics an acute coronary syndrome (chest pain, heart failure, ECG changes, biomarkers) with reversible ventricular motion abnormalities [8].

The main feature is the absence of coronary artery findings potentially responsible and, usually, the involvement of myocardium territories dependent on various coronary arteries. Most researchers describe it as a myocardial stunning process, possibly secondary to catecholamine injury [8–10].

Initially TTS was deemed to be a cardiomyopathy, but some scientists criticized the fact that the term implies a primary disease of the myocardium and proposed to define it as an acute and usually reversible heart failure syndrome [10].

However, although the condition does not seem to be a "primary disease" of the cardiac muscle – in most cases, at least – or we have not yet identified a clear genetic basis, the fact that most of the patients do not present heart failure symptoms makes it difficult to accept the latter definition [9–11]. Others, consider that the problem is a transient cardiomyopathy, since a number of recurrences have been reported and some underlying pathophysiologic abnormalities at the myocardium level have been described, explaining why only some people develop the syndrome after intense stressful situations [12].

Moreover, due to its clinical heterogeneity (clinical profile, different triggers, different anatomic forms, left ventricle or right ventricle or RV

Fig. 1. A takotsubo used for trapping octopuses in Japan (Courtesy Dr. Kuroiso S).

variable involvement, different pathophysiology) it could be a cluster of different diseases with similar expression (phenocopies), fulfilling the definition of "syndrome" [9,11–13].

The entity has commonly received several names, with >30 reported [13,14], highlighting among them: takotsubo cardiomyopathy or syndrome, Ampulla syndrome or transient cardiac/apical ballooning because of the LV shape (Japanese octopus pot) in the imaging techniques, transient apical dyskinesia, and broken heart syndrome or stress cardiomyopathy due to its clear link with stressful situations.

The term "stress cardiomyopathy" has the problem that, frequently, we are not able to find a particular stress as trigger and that there are other catecholaminergic situations, such as pheochromocytoma, that are frequently excluded as takotsubo syndromes [13–16].

We support the unifying term suggested for this disease as "takotsubo syndrome," despite not all patients having the typical "takotsubo trap" shape in their ventricles [10].

1.3. Diagnostic criteria

Since the syndrome description in 1986, several sets of diagnostic criteria have been published, usually making the syndrome an "exclusion diagnosis" [17] that entered into National Center for Biotechnology Information (NCBI) databases as a distinct clinical entity in 2008 [17]. Among these criteria stand out the Mayo criteria (2004, modified and simplified in 2008) [18], the Japanese Takotsubo Cardiomyopathy Group (2007) [6], the Johns Hopkins criteria (2012) [19], the Gothenburg Group (2013) [20], the Takotsubo Italian Network (2014) [21], those proposed by Madias [22] and, most recently, the Heart Failure Association of the European Society of Cardiology Takotsubo Syndrome Diagnostic Criteria in 2015 [10], which added the elevation of serum natriuretic peptide as a separate criterion.

Currently, the most widely used criteria are the 2008 modified Mayo criteria (i.e., InterTAK [23], Retako [24]). However, in this set, the presence of pheochromocytoma is considered an exclusion criterion while, in fact, several authors consider those cases to be within the takotsubo spectrum [16,18]. Probably, a simplified set of diagnostic criteria for a syndromic approach followed by a diagnostic workup in order to get a more precise etiological diagnosis would be warranted, as we do with dilated myocardiopathy, for example [12]. Interestingly, more recently, a genetic basis has been suggested to be involved in TTS with several familial cases of and small studies reporting a potential association between TTS and several genes [25–29].

Our proposed working algorithm including a simplified set of criteria, is displayed in Fig. 2.

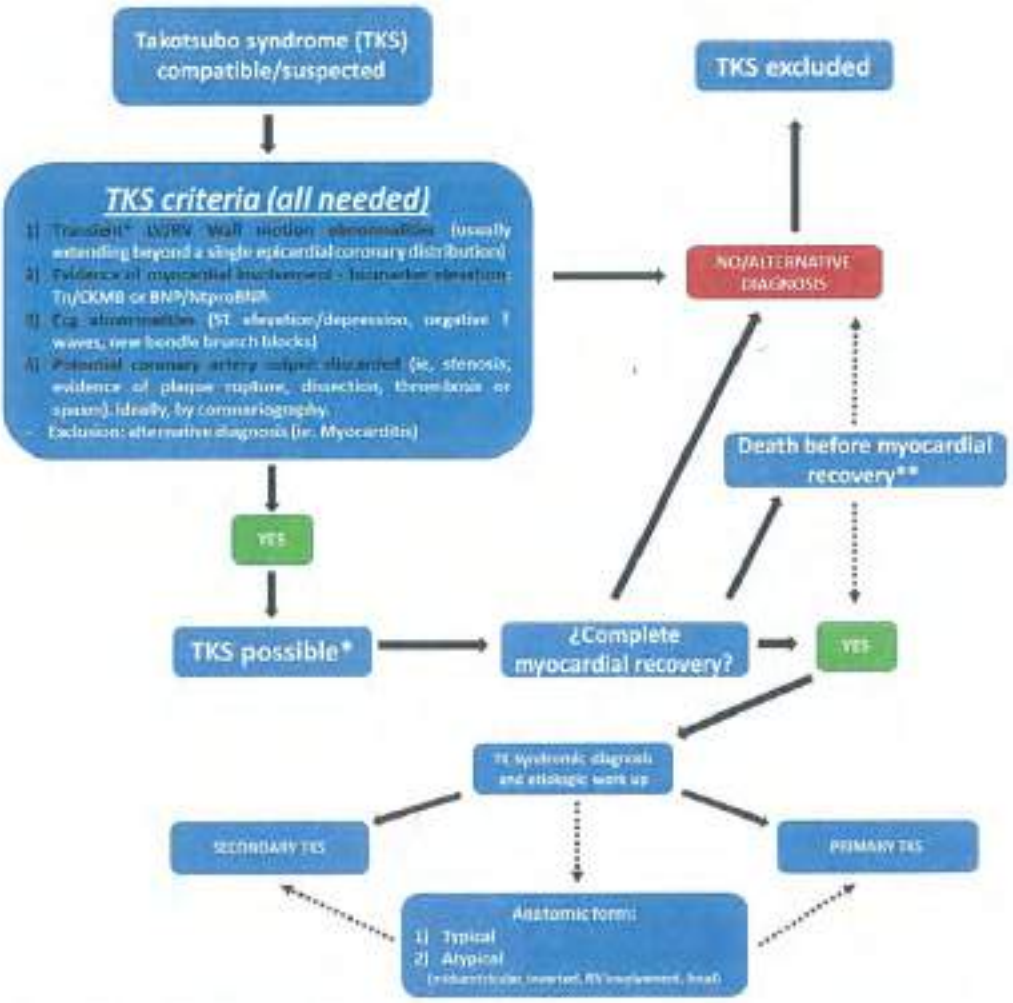

Fig. 2. Working algorithm proposed including a simplified set of diagnostic criteria. *Transient refers to a variable period of time ranging from days to weeks until a complete myocardial recovery is depicted by imaging techniques. **If a patient dies before an established diagnosis, the complete clinical profile (comorbidities, stressful situation) must be assessed.

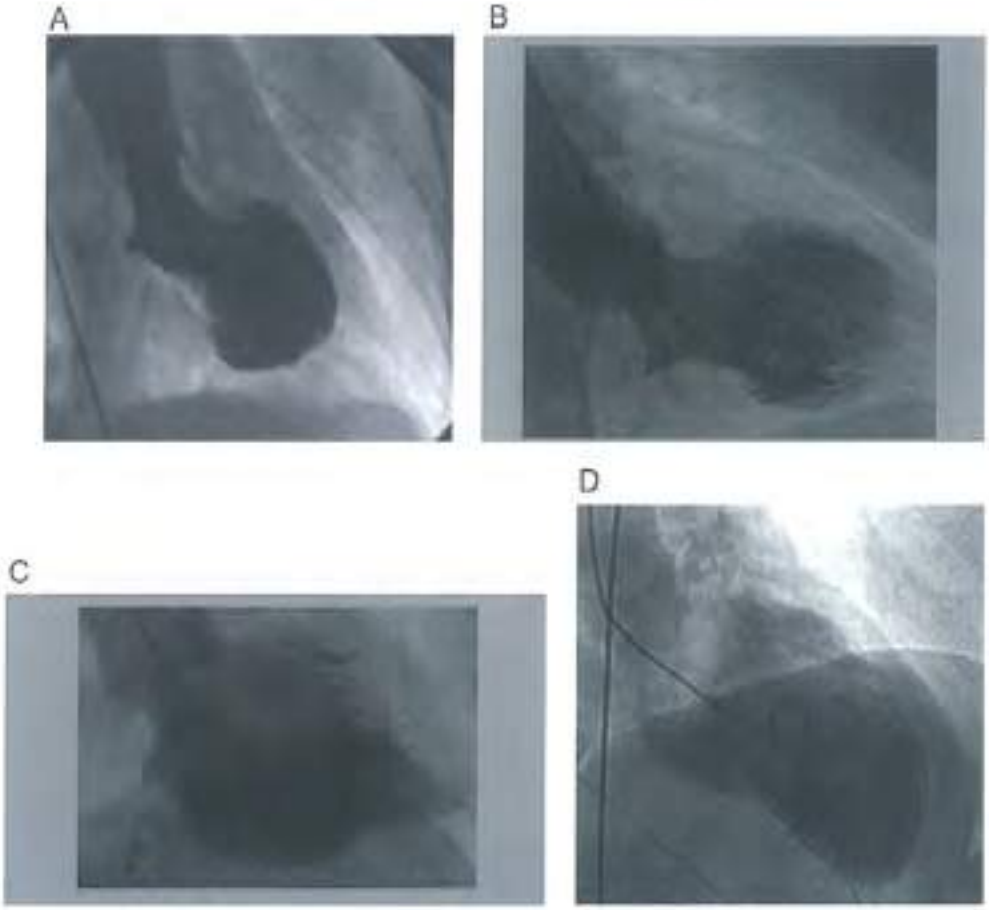

Fig. 3. A – *Apical (classic) pattern* – End-systolic image from left ventriculography. B – *Mid ventricular* – End-systolic image from left ventriculography. C – *Inverted or basal type* – End-systolic image from left ventriculography. D – *Focal type* – end-systolic image from left ventriculography.

2. The different patterns of takotsubo

2.1. Anatomical variants

Since this initial description of apical ballooning, also known as the classical pattern, and characterized by apical akinesis or hypokinesis with preserved and/or hypercontractile basal segments, several different types of left ventricular involvement have been described [23,30,31].

1) **Classical pattern** – Present in up to 80% of patients. (Fig. 3A).
2) **Mid-ventricular pattern** – Characterized by hypokinesis of the mid left ventricle and hypercontractile apical and basal segments. Present in up to 15% of patients. (Fig. 3B).
3) **Inverted (reverse) or basal pattern** – Characterized by basal and mid-ventricular segment hypokinesis or akinesis with preserved contractility or hypercontractility of apical segments. Present in 2–5% of patients (Fig. 3C).
4) **Focal type** – Characterized by hypokinesis or akinesis of an isolated segment; usually an anterolateral segment. Present in up to 1.5% of patients (Fig. 3D).
5) **Atypical patterns including right ventricular involvement** – Includes apical tip sparing variant, biventricular apical dysfunction, isolated RV involvement and global type. Their prevalence is unknown, but likely represents a small minority of TTS cases [23,32,33].

Probably, the most useful classification on this regard comprises 2 main types:

The most common or **typical form** – takotsubo pot-shaped, with apical affectation – and the first type described. Usually occurs in 70–85% cases, being 81.7% in the largest series published, over 1750 patients (InterTAK) [23,24]. The imaging techniques depict a distinctive LV apical and mid-ventricular dis/a/hypokinesia together with basal hypercontractility.

The **atypical forms**, less frequent and heterogeneous, usually sparing the apex cordis [34]. We could include in this type those with mid-ventricular affectation – about 15% – and, less frequently, the basal type (also known as inverted or reverse, "nutmeg" or "artichoke" heart) often related to neurologic comorbidities – e.g., subarachnoid hemorrhage – or pheochromocytoma [32]; global and focal types; and, finally, those with right ventricular affectation (biventricular or rarely isolated right involvement). Also, there was described a case of "double takotsubo," where the typical form was followed by the inverted type [33].

The clinical RV expression is rare [10]. Some authors have reported that RV contractile abnormalities may follow the same LV regional distribution and could influence the prognosis [10]. It is possible that the RV affectation, observed about in 25–30% of the cases in some series, evolved unnoticed in some cases. In fact, a recent small study with 31 patients reported that visually, echocardiography was able to identify only 52% of patients who showed RV wall motion abnormalities on cardiac magnetic resonance [35].

2.2. Primary and secondary forms

The anatomic classification can be complemented by another simple distinction between primary and secondary forms [10,12]. This is

intended to be a more etiologic grouping and thus would probably have management and prognostic value. Although the concept varies slightly among clinicians and researchers, we can assume these two separate groups of takotsubo syndromes [10,12]:

Primary forms – In this group of patients, the most common (about 80% in a 2016 Retako analysis of 328 patients) [12], the acute cardiac symptoms are the primary reason for seeking medical attention. These patients do not have clearly identifiable triggers (28.5% over 1750 cases in InterTAK [36]) or when present, the stressful triggers are emotional/psychic (27.7% in InterTAK) [36].

Secondary forms – Those with physical factors or comorbidities, potentially acting as directly responsible for the cardiac condition (asthma, drugs, surgery, trauma, subarachnoid hemorrhage, hyperthyroidism, pheochromocytoma or paraganglioma, etc.) [10,36–38]. Some consider these cases as takotsubo phenocopies.

3. Epidemiology

3.1. Prevalence

TTS may occur in up to 2% of patients presenting with suspected acute coronary syndrome (ACS) [9,23]. The fact that it commonly presents with signs and symptoms resembling an ACS poses an important diagnosis challenge since the distinction between these two entities is frequently not immediately evident.

Despite initially being considered a relatively benign condition, more current data have shown that TTS may be associated with considerable inpatient morbidity and carry a small but important mortality risk [23]. The prevalence of TTS has been increasing worldwide, especially among Caucasians. This is likely a consequence of an improved awareness of the existence of this syndrome and easier access to early coronary angiography than a true increase in TTS incidence [9,10,23]. Prior studies have consistently shown that TTS affects predominantly postmenopausal women (66–80 years). The most common clinical symptoms are chest pain (67%) and dyspnea (17%). TTS patients also have higher frequencies of psychiatric disorders, such as depression and/or anxiety, in comparison to ACS patients [23,39].

3.2. Inpatient morbidity

According to data from the Nationwide Inpatient Sample (NIS-USA) (2008–2009 and 2009–2010), considered one of largest reported cohorts, a higher mortality was observed in men, likely related to an increased prevalence of acute critical illnesses, ventricular arrhythmia, and sudden cardiac arrest [18,39]. Of note, TTS patients were identified based on the International Classification of Diseases (ICD) discharge codes and not on a systematic and detailed review of each individual clinical case, which could potentially lead to inconsistencies in TTS diagnosis. As per the International Takotsubo Registry (group of 26 centers in Europe and the United States) which included a total of 1750 TTS patients, cardiogenic shock may affect 4.2% and ventricular fibrillation 1.5% of cases [9,23].

Acute respiratory failure, acute neurologic or psychiatric diseases, physical triggers, higher troponin levels, and lower ejection fraction on admission were independent predictors for in-hospital complications [23,39,40].

3.3. Inpatient mortality

In the literature, the reported in-hospital mortality ranges from 1 to 5%, depending on the series. However, according to more recent data from larger registries, TTS may carry 30-day mortality in the range of 4–6%, which is considered comparable to ST-elevation myocardial infarction (STEMI) and non-ST-elevation myocardial infarction (NSTEMI) [23].

3.4. Gender differences

TTS is more frequent in women than men, predominantly affecting postmenopausal females. According to the International Takotsubo Registry, TTS exhibits a female-to-male ratio of approximately 9:1. Overall, male and female TTS patients have similar demographics and clinical characteristics; however, they do have some important differences worth mentioning. Physical triggers are more prevalent in men, whereas emotional triggers are more common in women. Acute neurological disorders, such as intracranial bleeding, are more frequently seen in men [23,41,42].

In-hospital complications, such sepsis, ventricular arrhythmias, the need for invasive or noninvasive ventilation, and the use of catecholamines, are more common among men. Cardiac arrest on presentation, particularly out-of-hospital cardiac arrest, is also reported more frequently in men.

In-hospital mortality and rate of major adverse cardiac events (MACE) have been consistently higher in men than in women [23]. During the first 30 days after admission, men remain at higher risk of MACE and all-cause mortality than women [9,23,40].

Long-term follow-up has also shown that men have an increased rate of all-cause mortality and major adverse cardiac and cerebrovascular events beyond 30 days.

3.5. Age disparity

Women have significantly higher odds of developing TTS, and the vast majority (up to 80%) are older than 50 years of age. In a study of 6837 patients diagnosed with TTS among 33,506,402 hospitalizations in the Nationwide Inpatient Sample database – using discharge records in 2008 using the International Classification of Diseases, Ninth Revision, code 429.83 – older women (>55 years) had 10.7 times higher odds of developing TTS in comparison to men of similar age and 4.8 times higher odds for developing TTS when compared with women <55 years old [18,23,43,44]. In men, there was no significant association of age with development of TTS. At the time of TTS diagnosis, men are usually younger than women [23].

Potential changes in the density and responsiveness of local myocardial adrenergic receptors from base to apex during menopause could account for some of the gender and age differences noted [23]. Overall, elderly patients have a higher prevalence of comorbid cardiovascular conditions and worse in-hospital major adverse cardiovascular outcomes such as acute heart failure, life-threatening arrhythmias, stroke, lower ejection fraction upon admission, and cardiogenic shock [23,40].

3.6. Racial disparities

There is a relative paucity of data regarding the potential impact of race and/or ethnicity in TTS presentation and outcomes. However, after European and North American TTS registries started publishing their data, it became evident that race and ethnicity could play an important role in TTS [44].

Caucasians present more commonly with chest pain and after an emotional trigger in comparison to other racial groups. Asians and African-Americans may have a higher rate of in-patient complications, such as stroke and acute respiratory failure, requiring mechanical ventilation in comparison to Caucasians and Hispanics [23,44].

Distinctive racial electrocardiographic differences have also been reported in these registries, with T-wave inversion and QT prolongation being more prevalent among African-Americans. Higher prevalence of ST-segment elevation has been observed in Asians, whereas ST-segment depression is more frequently seen in non-African-Americans. Prospective clinical trials are needed to confirm these findings [23,44,45].

3.7. Malignancy association

Noteworthy, evidence now exists that patients with TTS have an elevated rate of malignancy that greatly exceeds the expected prevalence of cancer in age-matched populations in the United States and European countries [46–48].

In their pivotal work, Burgdorf et al. reported that patients with TTS more commonly had a previous diagnosis of malignancy or developed malignancies during follow-up as compared with patients with acute myocardial infarction [49]. Similarly, El-Sayed et al. found that patients with TTS have higher odds of malignancy than orthopedic and myocardial infarction patients in a large population of patients hospitalized with TTS in the United States over a 2-year period [50]. The results of the COUNT study, an international collaborative review including a large series of 1109 patients with TTS, found that the frequency of malignancy ranged from 4 to 29% (average: 10%) [51].

More recently, it has been shown that those TTS patients with a diagnosis of malignancy have higher peak BNP, leukocyte levels, CRP and experience a higher mortality rate [52]. These findings provide a reliable confirmation of the hypothesis that malignancy predisposes to TTS [53]. Although the exact mechanisms of action of malignancy remain speculative, a number of clinical and experimental studies have convincingly elucidated the potential links between cancer and emotional stress, inflammation, and neurohormonal activation in TTS [54]. Indeed, cancer is accompanied by increased psychological stress, which in turn increases susceptibility to TTS.

3.8. Genetic perspective

Several familial cases of TTS have been described [25]. The recently identified genetic variants in key cardiac regulator genes imply a genetic predisposition in TTS through increased sensitivity to catecholamine toxicity. Moreover, other reasons that make a genetic predisposition in TTS reasonable are a) There have been several reports of familial cases [25,26]; b) TTS recurs in 5–10% of patients, suggesting a genetically mediated vulnerability; c) Most postmenopausal women experience acute stressful events, but only a small subset develop TTS.

Small studies in individual patients have reported an association between TTS and several genes, including Bcl-2–associated athanogene 3 (BAG3) [26]. However, conflicting results have been published in small studies regarding the presence or absence of functional polymorphisms in relevant candidate genes, such as α1-, β1-, and β2-adrenergic receptors, G-protein coupled receptor kinase (GRK)-5, and estrogen receptors [27].

The first genome-wide association study (GWAS) in TTS patients identified potential genetic risk variants and found promising preliminary results, but the study was too small to draw definite conclusions [28]. Another recent study investigated a genetic predisposition for TTS by using an in vitro induced pluripotent stem cell (iPSC) model of TTS [29]. Several genetic variants in different key regulators of cardiac function could be uncovered, including an overactive β-adrenergic pathway and higher sensitivity of catecholamines in TS iPSC-CMs and TTS engineered heart muscle [29]. Receptor desensitization and different β_1/β_2-AR were identified as potentially important pathophysiological components of TTS. According to current available data, it is likely that a genetic predisposition may interact with environmental factors, polygenic etiology and/or recessive susceptibility alleles; however, small genetic studies have failed to identify significant causative genetic variants [27,55]. A small number of case reports suggest an association between rare genetic syndromes and TTS [55–57].

4. Pathophysiology

4.1. Catecholamine surge

Catecholamine surge constitutes one of the most intriguing features of TTS [31]. Both circulating epinephrine and norepinephrine released from the adrenal medulla and norepinephrine released locally from sympathetic nerves are increased in the acute phase of TTS. This catecholamine surge leads, through multiple mechanisms, to myocardial damage, which is the substrate of transient apical left ventricular ballooning (Fig. 4).

Acute emotional and/or physical stressors, i.e., the well-known triggers of TTS, have been shown to induce brain activation, thus increasing epinephrine and norepinephrine levels [46]. Specifically, the stress-induced increase in norepinephrine secretion stimulates the hypothalamic-pituitary-adrenal axis, causing adrenal medullary cells to synthesize and release predominantly epinephrine. Plasma levels of catecholamines and their metabolites are elevated in the acute phase of TTS in nearly 75% of patients, as originally demonstrated by Akashi et al. [58], and subsequently reported by Wittstein et al. [59].

Along with higher levels of circulating catecholamine, there is also evidence of increased catecholamine at the myocardial level in the acute phase of TTS. Kume et al. have demonstrated increased norepinephrine spillover in the coronary sinus in a small series of patients with TTS, suggesting increased local myocardial release of catecholamine from cardiac nerve endings [60]. Indeed, norepinephrine spillover from the cardiac sympathetic nerves induces calcium overload, thus resulting in contraction band necrosis – one of the pathological hallmarks of TTS [61].

4.2. Beta receptors mechanism and myocardial ischemia

Catecholamine surge acts on beta-adrenergic receptors, which in turn affect chronotropic, inotropic, and lusitropic cardiac functions and trigger the onset of LV dysfunction [46]. Regional differences in density of different types of adrenergic receptors seem to explain the typical pattern of left ventricular dysfunction often seen in TTS. The beta2-adrenergic receptors are more frequently expressed in apical than in basal segments of the left ventricle, whereas a reverse distribution is present for norepinephrine beta1-adrenergic receptors, which are expressed mainly at the base than at the apex of the left ventricle [10].

Both epinephrine and norepinephrine have positive inotropic effects through Gs-coupling protein. The rise in levels of epinephrine trigger beta2-adrenoceptors to switch from Gs to Gi coupling, which is associated with a negative inotropic response of the left ventricular apex [10]. This mechanism protects left ventricular myocardium from the catecholamine storm, thus limiting the degree of myocardial injury in the acute phase of TTS [10].

A further pathogenetic mechanism of TTS is transient myocardial ischemia. Since the 1990s, epicardial coronary artery spasm and/or diffuse coronary vasoconstriction have commonly been reported in most series of patients from Japan. Indeed, development of coronary spasm with acetylcholine testing has been found in patients with TTS [37]. Also, spontaneous coronary artery dissection is reported with increasing frequency in patients with TTS [62].

Recently, microvascular dysfunction has been advocated as a further pathogenetic determinant of myocardial ischemia in TTS based on the evidence that invasive and noninvasive diagnostic tools have documented abnormal coronary microvascular responses in TTS [48]. The demonstration of reduced TIMI (Thrombolysis in Myocardial Infarction) frame count at emergency coronary angiography, the finding of perfusion defect in the left ventricular segments showing reduced contractility with myocardial contrast echocardiography, the evidence of a decrease in tracer uptake during the acute phase of TTS, and a return to normal at follow-up with single-photon emission computed tomography strongly suggest a role for coronary microvascular dysfunction as a trigger of myocardial ischemia in this condition [31].

4.3. Depressed cardiac energetic measured with 31 P cardiac spectroscopy

There is little mechanistic evidence regarding the acute intramyocyte pathophysiology processes that occur and evolve in the

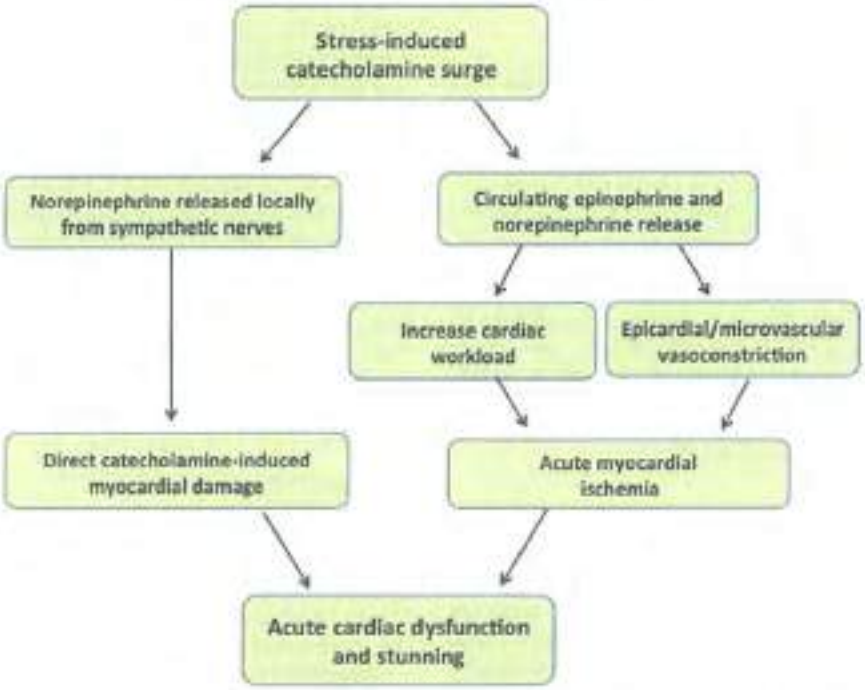

Fig. 4. Pathophysiology of TTS: Acute emotional and/or physical stressors cause an acute catecholamine surge, with an increase in myocardial release of catecholamine as well as a raise in circulating epinephrine and norepinephrine levels. Endogenous catecholamine released into the heart via nerve terminals cause a direct catecholamine-induced myocardial toxicity. The catecholamine surge acts on beta-adrenergic receptors thus affecting chronotropic, inotropic, and lusitropic cardiac functions. Also, catecholamine surge with excessive cardiac sympathetic activity can induce either epicardial coronary artery spasm or diffuse coronary microvascular constriction, thus contributing to the acute myocardial dysfunction and stunning.

human takotsubo heart beyond that of small myocardial biopsies [63], which have been collected predominantly from the right ventricle due to the high risk posed by performing a biopsy from an akinetic or dyskinetic myocardial territory.

Nevertheless, it has been demonstrated that myocardial energetics (the phosphocreatine/gamma-adenosine triphosphate (PCr/γATP) ratio obtained non-invasively by ^{31}P-cardiac magnetic resonance spectroscopy) is severely reduced in acute TTS patients [64].

This occurs alongside a strikingly edematous myocardium [64,65].

While it is well-known that a fundamental characteristic of the human takotsubo heart is a prompt and spontaneous recovery of the left ventricular ejection fraction, the recovery of the cardiac energetics as well as that of the myocardial edema appears to lag behind that of the ejection fraction, since residual levels of edema have been shown to persist at 4 months in the regions that were acutely affected and, in addition, there is only partial recovery of the cardiac energetic status at 4 months post-index event [64].

4.4. Role of hormonal/reproductive factors

Animal studies showing that estrogen supplementation reduces the incidence of TTS in response to emotional stress [66,67] have led researchers to hypothesize that reproductive factors could play a role in the onset of TTS.

To date, however, there is very limited information in humans, and the few clinical studies examining the role of hormonal/reproductive factors in the development of TTS have several limitations (i.e., small sample size, retrospective design).

A small study compared estradiol, progesterone, luteinizing hormone, and follicle-stimulating hormone levels in women with TTS, MI, and healthy women and found – unexpectedly – higher concentrations of estradiol in TTS compared to both controls [68]. Estrogen levels, though, were measured at admission and likely increased in response to stress [68].

A retrospective case-control study found no differences in the prevalence of menopausal status, frequency of oophorectomy, and average years since the onset of menopause across female TTS cases, age- and event date-matched female controls with ST-segment elevation myocardial infarction, and women with neither diagnosis [69].

Another small prospective case-control study compared reproductive characteristics of TTS female cases, MI controls, and healthy women [70]. TTS women more frequently reported a history of irregular menses and menopausal symptoms, higher parity, and using hormone replacement therapy compared to MI and healthy female controls.

In multivariable adjusted models, a history of irregular menses, parity, and use of postmenopausal hormone replacement were significantly associated with the onset of TTS.

The absence of associations between TTS and a history of oophorectomy, and the fact that the use of hormone replacement therapy was not protective, suggest that in contrast with animal studies [66,67], estrogen levels per se may not play a role in the physiopathology of TTS in humans. Instead, this study suggested a possible important association between premenopausal factors (e.g., disruptions in ovulatory cycling, parity) and the onset of TTS at a later age.

4.5. Inflammation and interleukins' role in TTS

An inflammatory reaction is observed during the acute phase of TTS, but its role is still not clearly defined. Catecholamines may cause endothelial damage with consequent release of growth factors (VEFG and EFG) and interleukins [71].

Higher serum levels of interleukins 6 and 10 at TTS admission are associated with risk of in-hospital complications and adverse events at follow-up [72]. When compared with acute myocardial infarction (AMI), TTS is featured by higher prevalence of macrophages (CD68) and anti-inflammatory interleukins during both the acute and recovery phases [63].

4.6. Low prevalence of diabetes in TTS patients

It has been postulated that patients with diabetes mellitus (DM) with complicated ASNS peripheral neuropathy would either be protected from suffering TTS or experience mild forms of the disease. Accordingly, patients with TTS would be expected to have a low prevalence of DM; also, patients with DM who have suffered TTS would be expected to have mild and/or short-duration DM, and certainly without complicating ASNS neuropathy.

To explore this, a meta-analysis of 33,894 patients (88.9% women) with TTS reported between 2001 and February 22, 2014, was carried out, employing 5 subanalyses (all patients, patients reported individually, patients reported collectively in case series, patients <60 years old reported individually, and patients >65 years old reported individually. The prevalence of DM was 16.8%, 10.2%, 17.0%, 11.9%, and 12.5%, correspondingly, and lower than the 26.9% found by the National Health and Nutrition Examination Survey (NHANES) [47].

5. Clinical presentation

5.1. Primary and secondary forms

When we divide TTS patients between primary and secondary forms, we are probably separating different diseases (phenocopies) and thus will obtain different clinical presentations and prognoses. Recent data have shown that "primary" patients suffered more frequent chest pain as the main complaint (89.4% vs. 50.7%, $p < 0.0001$) with vegetative symptoms (57.4% vs. 38.1%; $p = 0.006$). Palpitations, syncope or heart failure/shock on admission were numerically more frequent in secondary forms.

During admission, differences were related to more intensive antithrombotic and anxiolytic drug use in the primary group. Inotropic and mechanical ventilation use was higher in the secondary forms, which also displayed higher biomarker elevation and more in-hospital stay and evolutive complications (death, recurrences) [12].

5.2. Right ventricle involvement

Up to 34% of TTS patients may have some degree of RV involvement, even if not immediately clinically apparent [10]. Biventricular involvement is typically identified on imaging studies such as echocardiography and MRI. In observational retrospective studies, the most frequently affected RV segments were the apico-lateral, antero-lateral and inferior walls [23]. The presence of RV involvement has been associated with a higher prevalence of in-hospital major adverse cardiovascular events, including heart failure, cardiogenic shock, and in-hospital mortality [23,34]. RV involvement is more prevalent in older patients with a lower baseline left ventricular ejection fraction and is associated with higher frequency of significant or bilateral pleural effusions [23,34].

5.3. Inverted forms

Inverted (Reverse) or Basal Pattern: Patients with an inverted or basal pattern are younger and more commonly present with an identifiable emotional or physical triggering event in comparison to TTS patients presenting with the classical pattern [37]. Heart failure symptoms and significant mitral regurgitation are less prevalent in the inverted forms [37] while subarachnoid hemorrhage may be more common [38]. More recent data suggest that some atypical forms, particularly the reverse patterns, may carry worse prognosis [10].

5.4. Potential triggers

Both emotional and physical events are established triggers, although more recently, an increasing association with physical stressors has emerged, as well as the realization that the condition may occur spontaneously, without an identifiable trigger, in a minority of patients. Triggering events, particularly those of a personal nature, may be concealed at the time of presentation [73,74].

In the Minneapolis Heart Institute experience of nearly 400 TTS patients, 10% provided no history of a triggering event, physical stressors were present in 50%, and emotional events in 40% [73]. In comparison, a report from the International Takotsubo Registry [23] noted triggering events as physical in 36%, emotional in 28%, both in 8%, and neither in 29%. The rising importance of physical triggers of TTS likely reflects greater awareness of this condition occurring in a health-care environment in association with an acute illness, medication administration, medical testing, or an invasive procedure.

The diversity of precipitating events associated with TTS ranges from the ordinary to the catastrophic; furthermore, seemingly minor events can act as a trigger [23,73,75].

5.5. Pharmacologic triggers

Drugs with a variety of pharmacologic actions, ranging from chemotherapeutic agents to antidepressants, have been reported as TTS triggers, often when administered in accidental or deliberate overdose [10,23,42]. Illicit drug use (cocaine) and withdrawal from drugs (alcohol, opioids, metoprolol) are also known triggers [36,73].

Catecholamine administration in both therapeutic and excessive doses has been temporally related to TTS onset.

Among the endogenous catecholamines, epinephrine has received the most attention, likely reflecting the widespread use of this drug in health-care settings. In most cases, epinephrine was administered during a minor surgical procedure, although reports of intentional overdose during suicide attempt exist [10,76].

Norepinephrine overdose has also been reported to induce TTS [77]. The synthetic catecholamines dobutamine, isoproterenol, and salbutamol have each been reported to provoke TTS, most commonly when used during stress testing, electrophysiologic testing, or treatment of chronic obstructive lung disease and asthma [10,76].

Notably, intraocular injection of phenylephrine has been reported as a takotsubo trigger [10,76]. These takotsubo-catecholamine administration events provide support for the potential participation of the sympathetic nervous system in the mechanism of TTS.

5.6. Procedure-related triggers

The evidence for TTS complicating medical or surgical procedures is extensive and ranges from minor (colonoscopy) to major (prolonged spinal surgery) [23,40]. Ironically, procedures performed by cardiologists and cardiothoracic surgeons are regularly reported TTS triggers, including dobutamine stress testing, pericardiocentesis, cardioversion of atrial fibrillation, pacemaker insertion, electrophysiologic testing and ablation, and surgical and transcatheter valve replacement [10,16].

It is important, therefore, to consider TTS when encountering patients with hemodynamic or rhythm instability after cardiovascular procedures. Resuscitation from cardiac arrest represents a particularly profound physiologic stress, frequently requiring epinephrine administration and defibrillation, each of which can itself trigger a TTS event [16].

Declarations of interest

Milosz Jaguszewski, MD, FESC, has received lecture honoraria from St. Jude Medical.

Dana Dawson, DM, FRCP, DPhil, FESC, has a research agreement with Philips Healthcare and holds an MTA with AMAG Pharmaceuticals.

L. Christian Napp, MD, received lecture honoraria from Abiomed, Maquet and Cytosorbents, consultant fees from Bayer, and traveling or

congress support from Abbott, Abiomed, Bayer, Biotronik, Boston Scientific, Lilly, Medtronic, Merit Medical, Pfizer, Servier, and Volcano.

Kathy Hebert, MD, MPH, is an employee of GE Healthcare.

Takashi Akasaka, MD, has received lecture fees and research funds from Kowa Pharmaceutical Co. Ltd.

Ron Waksman, MD, received honoraria from Abbott Vascular, Amgen, Boston Scientific, Chiesi, Medtronic and Philips Volcano, and consulting fees from Biosensors, Biotronik, Corindus, Lifetech Medical and Pi-Cardia LTD. He is on the advisory boards of Abbott Vascular, Amgen, Boston Scientific, Medtronic, Philips Volcano and Pi-Cardia LTD, is a consultant for Abbott Vascular, Amgen, Biosensors, Biotronik, Boston Scientific, Corindus, Lifetech Medical, Medtronic, Philips Volcano and Pi-Cardia LTD, received grant support from Abbott Vascular, Biosensors, Biotronik, Boston Scientific, Chiesi and Edwards Lifesciences, and is an investor in MedAlliance.

All other authors have no conflicts of interest to disclose.

Funding

This research did not receive any specific grant from funding agencies in the public, commercial, or not-for-profit sectors.

References

[1] Takinka M, Miura H, Masaoka Y, Nishizaki S, Mikouchi H, Nishizaki Y, et al. Transient appearance of asynergy on the echocardiogram and electrocardiographic changes simulating acute myocardial infarction following non-cardiac surgery. J Cardiogr 1985 Sep;15(3):639–53.
[2] Ryan TJ, Fallon JT. Case records of the Massachusetts General Hospital. Weekly clinicopathological exercises. Case 18–1986. A 44-year-old woman with substernal pain and pulmonary edema after severe emotional stress. N Engl J Med 1986 May 8;314(19):1240–7.
[3] Takada K, Seino Y, Shimai S, Tanaka K, Kato T, Takano T, et al. A case report of pheochromocytoma showing AMI like ECG changes and transient apical defect on 201-Tl myocardial SPECT. Nippon Naika Gakkai Zasshi 1987 Aug;76(8):1256–63.
[4] Pollick C, Cujec B, Parker S, Tator C. Left ventricular wall motion abnormalities in subarachnoid hemorrhage: an echocardiographic study. J Am Coll Cardiol 1988 Sep;12(3):600–5.
[5] Dote K, Sato H, Tateishi H, Uchida T, Ishihara M. Myocardial stunning due to simultaneous multivessel coronary spasm: a review of 5 cases. J Cardiol 1991;21(2):203–14.
[6] Kawai S, Kitabatake A, Tomoike H, Takotsubo Cardiomyopathy Group. Guidelines for diagnosis of takotsubo (ampulla) cardiomyopathy. Circ J 2007 Jun;71(6):980–2.
[7] Ito K, Sugihara H, Kawasaki T, Yuba T, Doue T, Tanabe T, et al. Assessment of ampulla (Takotsubo) cardiomyopathy with coronary angiography, two-dimensional echocardiography and 99mTc-tetrofosmin myocardial single photon emission computed tomography. Ann Nucl Med 2001 Aug;15(4):351–5.
[8] Sharkey SW, Lesser JR, Zenovich AG, Maron MS, Lindberg J, Longe TF, et al. Acute and reversible cardiomyopathy provoked by stress in women from the United States. Circulation 2005 Feb 1;111(4):472–9.
[9] Nunez Gil IJ, Andres M, Almendro Delia M, Sionis A, Martin A, Bastante T, et al. Characterization of Tako-tsubo cardiomyopathy in Spain: results from the RETAKO National Registry. Rev Esp Cardiol (Engl Ed) 2015 Jun;68(6):505–12.
[10] Lyon AR, Bossone E, Schneider B, Sechtem U, Citro R, Underwood SR, et al. Current state of knowledge on Takotsubo syndrome: a Position Statement from the Taskforce on Takotsubo Syndrome of the Heart Failure Association of the European Society of Cardiology. Eur J Heart Fail 2016 Jan;18(1):8–27.
[11] Nunez-Gil IJ, Molina M, Bernardo E, Ibanez B, Ruiz-Mateos B, Garcia-Rubira JC, et al. Tako-tsubo syndrome and heart failure: long-term follow-up. Rev Esp Cardiol (Engl Ed) 2012 Nov;65(11):996–1002.
[12] Nunez-Gil IJ, Almendro-Delia M, Andres M, Sionis A, Martin A, Bastante T, et al. Secondary forms of Takotsubo cardiomyopathy: a whole different prognosis. Eur Heart J Acute Cardiovasc Care 2016 Aug;5(4):308–16.
[13] Mejia-Renteria HD, Nunez-Gil IJ. Takotsubo syndrome: advances in the understanding and management of an enigmatic stress cardiomyopathy. World J Cardiol 2016 Jul 26;8(7):413–24.
[14] Sharkey SW, Lesser JR, Maron MS, Maron BJ. Why not just call it tako-tsubo cardiomyopathy: a discussion of nomenclature. J Am Coll Cardiol 2011 Mar 29;57(14):1496–7.
[15] Movahed MR. Transient cardiac ballooning is not best nomenclature for Takotsubo cardiomyopathy as it does not capture all variants of this syndrome. Stress cardiomyopathy is a much better term for this syndrome. Clin Cardiol 2010 Apr;33(4):241–2 [author reply 242].
[16] Sharkey SW, McAllister N, Dasiewicz D, Lin D, Han K, Maron BJ. Evidence that high catecholamine levels produced by pheochromocytoma may be responsible for Tako-Tsubo cardiomyopathy. Am J Cardiol 2015 Jun 1;115(11):1615–8.
[17] Scantlebury DC, Prasad A. Diagnosis of Takotsubo cardiomyopathy. Circ J 2014;78(9):2129–39.
[18] Prasad A, Lerman A, Rihal CS. Apical ballooning syndrome (Tako-Tsubo or stress cardiomyopathy): a mimic of acute myocardial infarction. Am Heart J 2008 Mar;155(3):408–17.
[19] Wittstein IS. Stress cardiomyopathy: a syndrome of catecholamine-mediated myocardial stunning? Cell Mol Neurobiol 2012 Jul;32(5):847–57.
[20] Redfors B, Shao Y, Omerovic E. Stress-induced cardiomyopathy (Takotsubo)-broken heart and mind? Vasc Health Risk Manag 2013;9:149–54.
[21] Pelotti G, Citro R, Bellandi B, Provenza G, Marzani M, Bossone E, et al. Revised clinical diagnostic criteria for Tako-tsubo syndrome: the Tako-tsubo Italian Network proposal. Int J Cardiol 2014 Mar 1;172(1):282–3.
[22] Madias JE. Why the current diagnostic criteria of Takotsubo syndrome are outmoded: a proposal for new criteria. Int J Cardiol 2014 Jul 1;174(3):468–70.
[23] Templin C, Ghadri JR, Diekmann J, Napp LC, Bataiosu DR, Jaguszewski M, et al. Clinical features and outcomes of Takotsubo (stress) cardiomyopathy. N Engl J Med 2015 Sep 3;373(10):929–38.
[24] Nunez Gil IJ, Andres M, Almendro Delia M, Sionis A, Martin A, Bastante T, et al. Characterization of Tako-tsubo cardiomyopathy in Spain: results from the RETAKO National Registry. Rev Esp Cardiol (Engl Ed) 2015 Jun;68(6):505–12.
[25] Kumar G, Holmes Jr DR, Prasad A. "Familial" apical ballooning syndrome (Takotsubo cardiomyopathy). Int J Cardiol 2010 Oct 29;144(3):444–5.
[26] Citro R, D'Ovenia M, De Marco M, Giudice R, Mirra M, Ravera A, et al. Polymorphisms of the antiapoptotic protein bag3 may play a role in the pathogenesis of tako-tsubo cardiomyopathy. Int J Cardiol 2013 Sep 30;168(2):1663–5.
[27] Spinelli L, Trimarco V, Di Marino S, Marino M, Iaccarino G, Trimarco B, L41Q polymorphism of the G protein coupled receptor kinase 5 is associated with left ventricular apical ballooning syndrome. Eur J Heart Fail 2010 Jan;12(1):13–6.
[28] Eitel I, Moeller C, Munz M, Stiermaier T, Meitinger T, Thiele H, et al. Genome-wide association study in takotsubo syndrome - preliminary results and future directions. Int J Cardiol 2017 Jun 1;236:335–9.
[29] Borcherr T, Hubscher D, Gunsioum CI, Lam TD, Ghadri JR, Schellinger IN, et al. Catecholamine-dependent beta-adrenergic signaling in a pluripotent stem cell model of Takotsubo cardiomyopathy. J Am Coll Cardiol 2017 Aug 22;70(8):975–91.
[30] Dawson DK. Acute stress-induced (takotsubo) cardiomyopathy. Heart 2017 Aug;20.
[31] Pelliccia F, Kaski JC, Crea F, Camici PG. Pathophysiology of Takotsubo syndrome. Circulation 2017 Jun 13;135(24):2426–41.
[32] Gervais MK, Gagnon A, Henri M, Bendavid Y. Pheochromocytoma presenting as inverted Takotsubo cardiomyopathy: a case report and review of the literature. J Cardiovasc Med (Hagerstown) 2015 Jan;16(Suppl. 2):S113–7.
[33] Ehl NF, Zurek M, Rickli H, Mander MT. "Double takotsubo": first description of the sequence of classical followed by inverted type in a young woman. Int J Cardiol 2014 Jun 15;174(2):e36–7.
[34] Ghadri JR, Cammann VL, Napp LC, Jurisic S, Diekmann J, Bataiosu DR, et al. Differences in the clinical profile and outcomes of typical and atypical Takotsubo syndrome: data from the International Takotsubo Registry. JAMA Cardiol 2016 Jun 1;1(3):335–40.
[35] Scally C, Abbam T, Rudd A, Nell CJ, Selvanayagam J, Jagpal B, et al. Right ventricular involvement and recovery after acute stress-induced (Tako-tsubo) cardiomyopathy. Am J Cardiol 2016 Mar 1;117(5):775–80.
[36] Cuddens J, Van Alphen J, Deloof T, Hendrickx J. Dynamic left ventricular outflow tract obstruction caused by afterload reduction induced by intra-aortic balloon counterpulsation. J Cardiothorac Vasc Anesth 2002;16:749–51.
[37] Angelini P. Reverse, or inverted, transient Takotsubo cardiomyopathy: terms and status of an open discussion. Tex Heart Inst J 2013;40(1):60–3.
[38] Elgendy AY, Elgendy IY, Mansour H, Mahmoud AN. Clinical presentations and outcomes of Takotsubo syndrome in the setting of subarachnoid hemorrhage: a systematic review and meta-analysis. Eur Heart J Acute Cardiovasc Care 2016 Nov;16.
[39] Sharkey SW, Maron BJ. Epidemiology and clinical profile of Takotsubo cardiomyopathy. Circ J 2014;78(9):2139–28.
[40] Sharkey SW, Windenburg DC, Lesser JR, Maron MS, Hauser RG, Lesser JN, et al. Natural history and expansive clinical profile of stress (tako-tsubo) cardiomyopathy. J Am Coll Cardiol 2010 Jan 26;55(4):333–41.
[41] Dias A, Franco E, Figueredo VM, Hebert K. Can previous oophorectomy worsen the clinical course of takotsubo cardiomyopathy females? Age and gender-related outcome analysis. Int J Cardiol 2014 Dec 20;177(3):1134–6.
[42] Dias A, Franco E, Figueredo VM, Hebert K, Quaweda HC. Occurrence of Takotsubo cardiomyopathy and use of antidepressants. Int J Cardiol 2014 Jun 15;174(2):433–6.
[43] Schneider B, Athanasiadis A, Stollberger C, Pistner W, Schwab J, Gottwald U, et al. Gender differences in the manifestation of tako-tsubo cardiomyopathy. Int J Cardiol 2013 Jul 1;166(3):584–8.
[44] Dias A, Franco E, Koshkelashvili N, Pressman GS, Hebert K, Figueredo VM. Racial and ethnic differences in Takotsubo cardiomyopathy presentation and outcomes. Int J Cardiol 2015 Sep 1;194:100–3.
[45] Franco E, Dias A, Koshkelashvili N, Pressman GS, Hebert K, Figueredo VM. Distinctive electrocardiographic features in African Americans diagnosed with Takotsubo cardiomyopathy. Ann Noninvasive Electrocardiol 2016 Sep;21(5):486–92.
[46] Wittstein IS, Thiemann DR, Lima JA, Baughman KL, Schulman SP, Gerstenblith G, et al. Neurohumoral features of myocardial stunning due to sudden emotional stress. N Engl J Med 2005 Feb 10;352(6):539–48.
[47] Madias JE. Low prevalence of diabetes mellitus in patients with Takotsubo syndrome: a plausible 'protective' effect with pathophysiologic connotations. Eur Heart J Acute Cardiovasc Care 2016 Apr;5(2):164–70.
[48] Pelliccia F, Greco C, Vitale C, Rosano G, Gaudio C, Kaski JC. Takotsubo syndrome (stress cardiomyopathy): an intriguing clinical condition in search of its identity. Am J Med 2014 Aug;127(8):688–704.
[49] Burgdorf C, von Hof K, Schunkert H, Kurowski V. Regional alterations in myocardial sympathetic innervation in patients with transient left-ventricular apical ballooning (Tako-Tsubo cardiomyopathy). J Nucl Cardiol 2008 Jan–Feb;15(1):65–72.

[50] El-Sayed AM, Bringiga W, Salka S. Demographic and co-morbid predictors of stress (takotsubo) cardiomyopathy. Am J Cardiol 2012 Nov 1;110(9):1368–72.
[51] Pelliccia F, Pasceri G, Greco C, Antoniucci D, Brenner R, Bossone E, et al. Comorbidities frequency in Takotsubo syndrome: an international collaborative systematic review including 1109 patients. Am J Med 2015 Jun;128(6):654.e11–8.
[52] Sattler K, El-Battrawy I, Lang S, Zhou X, Schramm K, Tulumen E, et al. Prevalence of cancer in Takotsubo cardiomyopathy: short and long-term outcome. Int J Cardiol 2017 Jul 1;238:159–65.
[53] Madias JE. What is/are the trigger(s) of takotsubo syndrome in cancer patients receiving chemotherapy? Int J Cardiol 2016 Nov 1;222:253.
[54] Burgdorf C, Nef HM, Haghi D, Kurowski V, Radke PW. Tako-tsubo (stress-induced) cardiomyopathy and cancer. Ann Intern Med 2010 Jun 15;152(12):830–1.
[55] Limongelli G, D'Alessandro R, Masarone D, Maddaloni V, Vriz O, Minisini R, et al. Takotsubo cardiomyopathy: do the genetics matter? Heart Fail Clin 2013 Apr;9(2):207–16 [b].
[56] Eitel I, Friedrich MG. T2-weighted cardiovascular magnetic resonance in acute cardiac disease. J Cardiovasc Magn Reson 2011 Feb 18;13 (13–4200-13-13).
[57] Kushiro T, Saito F, Kusama J, Takahashi H, Imazeki T, Tani S, et al. Takotsubo-shaped cardiomyopathy with type I CD36 deficiency. Heart Vessels 2005 May;20(3):123–5.
[58] Akashi YJ, Nef HM, Lyon AR. Epidemiology and pathophysiology of Takotsubo syndrome. Nat Rev Cardiol 2015 Jul;12(7):387–97.
[59] Wittstein IS, Thiemann DR, Lima JA, Baughman KL, Schulman SP, Gerstenblith G, et al. Neurohumoral features of myocardial stunning due to sudden emotional stress. N Engl J Med 2005 Feb 10;352(6):539–48.
[60] Kume T, Akasaka T, Kawamoto T, Yoshitani H, Watanabe N, Neishi Y, et al. Assessment of coronary microcirculation in patients with takotsubo-like left ventricular dysfunction. Circ J 2005 Aug;69(8):934–9.
[61] Bolso C, Thiene G. The pathophysiology of myocardial reperfusion: a pathologist's perspective. Heart 2006 Nov;92(11):1550–62.
[62] Madias JE. Spontaneous coronary dissection misdiagnosed as, or triggering, or triggered by, Takotsubo syndrome? Catheter Cardiovasc Interv 2017 May 2;92:E206–7.
[63] Nef HM, Mollmann H, Kostin S, Troidl C, Voss S, Weber M, et al. Tako-Tsubo cardiomyopathy: intraindividual structural analysis in the acute phase and after functional recovery. Eur Heart J 2007 Oct;28(20):2456–64.
[64] Dawson DK, Neil CJ, Henning A, Cameron D, Jagpal B, Bruce M, et al. Tako-Tsubo cardiomyopathy: a heart stressed out of energy? JACC Cardiovasc Imaging 2015 Aug;8(8):985–7.
[65] Eitel I, Lucke C, Grothoff M, Suenkel M, Schuler G, Thiele H, et al. Inflammation in Takotsubo cardiomyopathy: insights from cardiovascular magnetic resonance imaging. Eur Radiol 2010 Feb;20(2):422–31.
[66] Ueyama T, Hano T, Kasamatsu K, Yamamoto K, Tsuruo Y, Nishio I. Estrogen attenuates the emotional stress-induced cardiac responses in the animal model of Takotsubo (Ampulla) cardiomyopathy. J Cardiovasc Pharmacol 2003 Dec;42(Suppl. 1):S117–9.
[67] Ueyama T, Ishikura F, Matsuda A, Asanuma T, Ueda K, Ichinose M, et al. Chronic estrogen supplementation following ovariectomy improves the emotional stress-induced cardiovascular responses by indirect action on the nervous system and by direct action on the heart. Circ J 2007 Apr;71(4):565–73.
[68] Brenner R, Wellemann D, Maeder MT, Jung L, Blauaite I, Rickli H, et al. Clinical characteristics, sex hormones, and long-term follow-up in Swiss postmenopausal women presenting with Takotsubo cardiomyopathy. Clin Cardiol 2012 Jun;35(6):340–7.
[69] Scantlebury DC, Prasad A, Rabinstein AA, Best PJ. Prevalence of migraine and Raynaud phenomenon in women with apical ballooning syndrome (Takotsubo or stress cardiomyopathy). Am J Cardiol 2013 May 1;111(9):1284–8.
[70] Salmoirago-Blotcher E, Dunsiger S, Swales HH, Auriemma CP, Ockene I, Rosman L, et al. Reproductive history of women with Takotsubo cardiomyopathy. Am J Cardiol 2016 Dec 15;118(12):1902–8.
[71] Park SY, Kang JH, Jeong KJ, Lee J, Han JW, Choi WS, et al. Norepinephrine induces VEGF expression and angiogenesis by a hypoxia-inducible factor-1alpha protein-dependent mechanism. Int J Cancer 2011 May 15;128(10):2306–16.
[72] Santoro F, Ieva R, Ferrantelli A, Fanelli M, Musaico F, Tarantino N, et al. Hemodynamic effects, safety, and feasibility of intravenous esmolol infusion during takotsubo cardiomyopathy with left ventricular outflow tract obstruction: results from a multicenter registry. Cardiovasc Ther 2016 Jun;34(3):161–6.
[73] Sharkey SW, Maron BJ. Epidemiology and clinical profile of Takotsubo cardiomyopathy. Circ J 2014;78(9):2119–28.
[74] Sharkey SW, Lesser JR, Zenovich AG, Maron MS, Lindberg J, Longe TF, et al. Acute and reversible cardiomyopathy provoked by stress in women from the United States. Circulation 2005 Feb 1;111(4):472–9.
[75] Sharkey SW, Park VR, Lesser JR, Carberich RF, Maron MS, Maron BJ. Clinical profile of patients with high-risk Tako-Tsubo cardiomyopathy. Am J Cardiol 2015 Sep 1;116(5):765–72.
[76] Patel B, Assad D, Wiemann C, Zughaib M. Repeated use of albuterol inhaler as a potential cause of Takotsubo cardiomyopathy. Am J Case Rep 2014 May 10;15:221–5.
[77] Sherif K, Sehli S, Jenkins LA. Takotsubo cardiomyopathy after administration of norepinephrine. Proc (Bayl Univ Med Cent) 2016 Apr;29(2):166–7.

Cardiovascular Revascularization Medicine 20 (2019) 153–166

Contents lists available at ScienceDirect

Cardiovascular Revascularization Medicine

Review

Takotsubo syndrome: State-of-the-art review by an expert panel – Part 2

Andre Dias [a,b], Ivan J. Núñez Gil [c], Francesco Santoro [d], John E. Madias [e,f], Francesco Pelliccia [g], Natale Daniele Brunetti [d], Elena Salmoirago-Blotcher [h], Scott W. Sharkey [i], Ingo Eitel [j], Yoshihiro J. Akashi [k], Ibrahim El-Battrawy [l,m], Emiliana Franco [n], Ibrahim Akin [l,m], Milosz Jaguszewski [o], Dana Dawson [p], Vincent M. Figueredo [b], L. Christian Napp [p], Thomas Emil Christensen [q], Kathy Hebert [r], Itsik Ben-Dor [a], Yuichi Ozaki [a], Héctor M. García-Garcia [a], Alexandre H. Kajita [a], Takashi Akasaka [s], Satoshi Kurisu [t], Amir Lerman [u], Ron Waksman [a,*]

[a] Section of Interventional Cardiology, MedStar Washington Hospital Center, Washington, DC, United States of America
[b] Department of Cardiology, Einstein Medical Center, Philadelphia, PA, United States of America
[c] Interventional Cardiology, Cardiovascular Institute, Hospital Clínico San Carlos, Madrid, Spain
[d] Department of Medical & Surgery Sciences, University of Foggia, Foggia, Italy
[e] Icahn School of Medicine at Mount Sinai, Elmhurst, NY, United States of America
[f] Division of Cardiology, Elmhurst Hospital Center, Elmhurst, NY, United States of America
[g] Interventional Cardiology Unit, Sapienza University, Rome, Italy
[h] Centers for Behavioral and Preventive Medicine, The Miriam Hospital, Warren Alpert Medical School of Brown University, Providence, RI, United States of America
[i] Minneapolis Heart Institute Foundation, Minneapolis, MN, United States of America
[j] Cardiology, Angiology, Intensive Care Medicine, University Lübeck, Schleswig-Holstein, Germany
[k] Division of Cardiology, Department of Internal Medicine, St. Marianna University School of Medicine, Kawasaki, Kanagawa, Japan
[l] Department of Internal Medicine, University Heidelberg, Mannheim, Germany
[m] DZHK (German Center for Cardiovascular Research), Partner Site, Heidelberg-Mannheim, Germany
[n] Department of Cardiology, Medical University of Gdansk, Poland
[o] School of Medicine and Dentistry, University of Aberdeen, Aberdeen, UK
[p] Department of Cardiology and Angiology, Hannover Medical School, Hannover, Germany
[q] Copenhagen University Hospital, Copenhagen, Denmark
[r] GE Healthcare, Miami, FL, United States of America
[s] Department of Cardiovascular Medicine, Wakayama Medical University, Wakayama, Japan
[t] Department of Cardiovascular Medicine, Hiroshima University, Hiroshima, Japan
[u] Department of Cardiovascular Medicine, Mayo Clinic, Rochester, MN, United States of America

ARTICLE INFO

Article history:
Received 14 November 2018
Accepted 14 November 2018

Keywords:
Takotsubo
Heart failure
Catecholamine

ABSTRACT

In part 2 of this two-part manuscript on takotsubo syndrome (TTS), we discuss typical biomarkers (particularly excess catecholamines and what kinds of electrocardiographic information operators should look for) and numerous complications the syndrome can cause. This consensus paper is the result of a multinational effort aiming to summarize the current state of the art on TTS. Several novel and unique sections are emphasized in this document, including the current state of the art on genetics of takotsubo syndrome, microRNAs (miRs), racial differences, role of cardiac spectroscopy and intracoronary imaging, as well as mechanical circulatory support. New structured algorithms are also proposed to aid clinicians in the decision-making process as well as future directions for research given the current lack of evidence-based medical approaches.

© 2018 Elsevier Inc. All rights reserved.

Contents

1. Workup 154
1.1. Biomarkers 154

Abbreviations: ACS, acute coronary syndrome; BNP, B-type natriuretic peptide; CRP, C-reactive protein; LV, left ventricle/ventricular; MACE, major adverse cardiac events; miRs, microRNAs; RV, right ventricle/ventricular; STEMI, ST-elevation myocardial infarction; TIMI, Thrombolysis in Myocardial Infarction; TTS, takotsubo syndrome.

* Corresponding author at: MedStar Heart and Vascular Institute, MedStar Washington Hospital Center, 110 Irving St., NW, Suite 4B-1, Washington, DC 20010, United States of America.
E-mail address: ron.waksman@medstar.net (R. Waksman).

https://doi.org/10.1016/j.carrev.2018.11.016
1553-8389/© 2018 Elsevier Inc. All rights reserved.

Cardiovascular Revascularization Medicine 20 (2019) 153–168

Contents lists available at ScienceDirect

Cardiovascular Revascularization Medicine

Review

Takotsubo syndrome: State-of-the-art review by an expert panel – Part 2

Andre Dias [a,b], Ivan J. Núñez Gil [c], Francesco Santoro [d], John E. Madias [e,f], Francesco Pelliccia [g], Natale Daniele Brunetti [d], Elena Salmoirago-Blotcher [h], Scott W. Sharkey [i], Ingo Eitel [j], Yoshihiro J. Akashi [k], Ibrahim El-Battrawy [l,m], Emiliana Franco [b], Ibrahim Akin [l,m], Milosz Jaguszewski [n], Dana Dawson [o], Vincent M. Figueredo [p], L. Christian Napp [p], Thomas Emil Christensen [q], Kathy Hebert [r], Itsik Ben-Dor [a], Yuichi Ozaki [a], Héctor M. Garcia-Garcia [a], Alexandre H. Kajita [a], Takashi Akasaka [s], Satoshi Kurisu [t], Amir Lerman [u], Ron Waksman [a,*]

[a] Section of Interventional Cardiology, MedStar Washington Hospital Center, Washington, DC, United States of America
[b] Department of Cardiology, Einstein Medical Center, Philadelphia, PA, United States of America
[c] Interventional Cardiology, Cardiovascular Institute, Hospital Clínico San Carlos, Madrid, Spain
[d] Department of Medical & Surgery Sciences, University of Foggia, Foggia, Italy
[e] Icahn School of Medicine at Mount Sinai, Elmhurst, NY, United States of America
[f] Division of Cardiology, Elmhurst Hospital Center, Elmhurst, NY, United States of America
[g] Interventional Cardiology Unit, Sapienza University, Rome, Italy
[h] Centers for Behavioral and Preventive Medicine, The Miriam Hospital, Warren Alpert Medical School of Brown University, Providence, RI, United States of America
[i] Minneapolis Heart Institute Foundation, Minneapolis, MN, United States of America
[j] Cardiology, Angiology, Intensive Care Medicine, University Lübeck, Schleswig-Holstein, Germany
[k] Division of Cardiology, Department of Internal Medicine, St. Marianna University School of Medicine, Kawasaki, Kanagawa, Japan
[l] Department of Internal Medicine, University Heidelberg, Mannheim, Germany
[m] DZHK (German Center for Cardiovascular Research), Partner Site, Heidelberg-Mannheim, Germany
[n] Department of Cardiology, Medical University of Gdansk, Poland
[o] School of Medicine and Dentistry, University of Aberdeen, Aberdeen, UK
[p] Department of Cardiology and Angiology, Hannover Medical School, Hannover, Germany
[q] Copenhagen University Hospital, Copenhagen, Denmark
[r] GE Healthcare, Miami, FL, United States of America
[s] Department of Cardiovascular Medicine, Wakayama Medical University, Wakayama, Japan
[t] Department of Cardiovascular Medicine, Hiroshima University, Hiroshima, Japan
[u] Department of Cardiovascular Medicine, Mayo Clinic, Rochester, MN, United States of America

ARTICLE INFO

Article history:
Received 14 November 2018
Accepted 14 November 2018

Keywords:
Takotsubo
Heart failure
Catecholamine

ABSTRACT

In part 2 of this two-part manuscript on takotsubo syndrome (TTS), we discuss typical biomarkers (particularly excess catecholamines and what kinds of electrocardiographic information operators should look for) and numerous complications the syndrome can cause. This consensus paper is the result of a multinational effort aiming to summarize the current state of the art on TTS. Several novel and unique sections are emphasized in this document, including the current state of the art on genetics of takotsubo syndrome, microRNAs (miRs), racial differences, role of cardiac spectroscopy and intracoronary imaging, as well as mechanical circulatory support.
New structured algorithms are also proposed to aid clinicians in the decision-making process as well as future directions for research given the current lack of evidence-based medical approaches.
© 2018 Elsevier Inc. All rights reserved.

Contents

1. Workup 154
1.1. Biomarkers 154

Abbreviations: ACS, acute coronary syndrome; BNP, B-type natriuretic peptide; CRP, C-reactive protein; LV, left ventricle/ventricular; MACE, major adverse cardiac events; miRs, microRNAs; RV, right ventricle/ventricular; STEMI, ST-elevation myocardial infarction; TIMI, Thrombolysis in Myocardial Infarction; TTS, takotsubo syndrome.

* Corresponding author at: MedStar Heart and Vascular Institute, MedStar Washington Hospital Center, 110 Irving St., NW, Suite 4B-1, Washington, DC 20010, United States of America.
E-mail address: ron.waksman@medstar.net (R. Waksman).

https://doi.org/10.1016/j.carrev.2018.11.016
1553-8389/© 2018 Elsevier Inc. All rights reserved.

1.2. Brain natriuretic peptide (BNP) and N-terminal-pro-BNP (NT-proBNP) . . . 154
1.3. Troponin (Tn), Creatine kinase (CK), CK-MB . . . 154
1.4. Catecholamines and other biomarkers . . . 154
1.5. MicroRNAs (miRs) . . . 155
1.6. Detailed electrocardiographic information . . . 155
1.7. Transient reduction of the amplitude of the QRS complexes . . . 156
1.8. Role of iodine-123 meta-iodo-benzyl-guanidine (mIBG) . . . 156
1.9. Optical coherence tomography . . . 156
1.10. Angiography data . . . 157
1.11. MRI . . . 158
1.12. Echocardiographic findings – systolic and diastolic mechanics cardiomyopathy . . . 159
2. Complications . . . 159
2.1. Acute heart failure syndrome . . . 159
2.2. Arrhythmias in patients with takotsubo syndrome . . . 160
2.3. Thromboembolic events . . . 160
2.4. In-hospital mortality . . . 161
3. Management . . . 161
3.1. Role of Levosimendan and short-acting beta blockers . . . 161
3.2. Mechanical circulatory support . . . 161
3.2.1. TandemHeart . . . 161
3.2.2. ECMO . . . 161
3.2.3. Impella . . . 161
3.3. Dilemma of ACE inhibitors . . . 161
3.4. Role of long-term beta blockers . . . 162
3.5. Is there any role for aspirin alone or dual antiplatelet therapy? . . . 162
3.6. Long-term prognosis: Cardiac and non-cardiac mortality . . . 163
3.7. Role of psychological distress . . . 163
4. Treatment of psychological distress . . . 164
5. Recurrence of TTS . . . 164
6. Conclusion . . . 164
Declarations of interest . . . 164
Funding . . . 164
References . . . 164

1. Workup

1.1. Biomarkers

As patients with TTS and ACS commonly present with similar symptoms, distinguishing one disease from the other remains a challenge in the clinical setting [1].

Although several biomarkers have been proposed for the differential diagnosis of TTS, currently there is no specific and sensitive biomarker for TTS (Table 1).

1.2. Brain natriuretic peptide (BNP) and N-terminal-pro-BNP (NT-proBNP)

TTS is associated with severe LV dysfunction, and subsequently, brain natriuretic peptides, i.e., BNPs, NT-proBNPs, rise within the first few hours after the onset of symptoms, in response to myocardial stretch [1,2]. NT-proBNP levels correlate with plasma catecholamine levels as well as the wall motion score index and LV ejection fraction. As a consequence, BNP levels are higher in patients with typical TTS vs. atypical TTS, i.e., mid-ventricular-, inverted- or focal TTS [2].

Table 1
Biomarkers. Laboratory diagnostic tests to distinguish TTS and ACS/AMI.

Natriuretic peptides	BNP, NT-proBNP
Markers of myocardial necrosis	troponin I, troponin T, hsTn, myoglobin, CK, CK-MB
Catecholamines	metanephrine, normetanephrine
Other biomarkers	copeptin, sST2, sLOX-1, IMA
MicroRNAs	miR-16, miR-26a, miR-1, miR-133a
Relative elevation of different Biomarker assays	NT-proBNP/TnT, BNP/TnT, BNP/CKMB, BNP/TnI, NT-proBNP/myoglobin, hs-TnT/CKMB, copeptin/NT-proBNP

ACS = acute coronary syndrome; AMI = acute myocardial infarction; BNP = Brain natriuretic peptide; NT-proBNP = N-terminal proBNP; sLOX-1 = soluble lectin like oxidized LDL receptor-1; CK-MB = Creatine kinase-MB fraction; sST2 = soluble suppression of tumorigenicity-2.

1.3. Troponin (Tn), Creatine kinase (CK), CK-MB

Although autopsy specimens are not characterized by the histological features of infarction, serum troponin levels are usually positive in the acute course of TTS [3]. Troponin levels are relatively low as compared to the extent of myocardial dysfunction peaking earlier in TTS than ACS (6 h vs. 12 h) [4,5].

Although a vast body of literature describes higher markers of cardiac necrosis in ACS when compared to TTS on admission, the last report from the largest InterTAK Registry did not reveal significant differences in troponin levels. Interestingly, no differences were noted in Tn levels between patients with typical and atypical TTS [2]. Recently, the hs-TnT/CKMB ratio has been presented as a potential novel, readily available parameter to distinguish TTS from MI [6].

1.4. Catecholamines and other biomarkers

Despite the widely recognized pathophysiological role of catecholamine excess in TTS, its diagnostic role remains uncertain. Although initial reports showed markedly higher plasma catecholamine levels at presentation in TTS vs. acute myocardial infarction [7], recent studies have demonstrated similar plasma normetanephrine, metanephrine and cortisol levels as well as normal 24-hour urine catecholamine values in both subsets [8]. On the other hand, soluble lectin-like oxidized LDL receptor-1 (sLOX-1) elevation has been found comparable to troponin rise in ACS and essentially lower in the non-ACS setting

comprising TTS patients [8]. The soluble suppression of tumorigenicity-2 (sST2) can be an additional predictive value for TTS in patients with normal TnI. Thus, a combination of sST2 and cTnI may be useful to predict TTS in patients referred for invasive diagnostics due to the prior diagnosis of ACS. Last but not least, copeptin, a novel sensitive biomarker of endogenous stress response, was markedly elevated in TTS vs. AMI.

1.5. MicroRNAs (miRs)

MicroRNAs (miRs) are a class of highly conserved, small noncoding mRNA transcribed as regions of longer RNA molecules that can be as long as 1000 nt [9].

MiRs are implicated in regulating diverse cellular processes, such as proliferation, differentiation, development, and cell death [9]. MiRs are considered to act as intracellular endogenous RNAs controlling gene expression at a posttranslational level. In some pathological conditions, miRs in the systemic circulation may reflect tissue damage [9]. Interestingly, their tissue- and cell-specific expression profile can directly reflect the status of the disease. Recent studies have revealed the role of miR in a variety of basic biological and pathological processes, and as sensitive biomarkers in some conditions, for instance, cardiac hypertrophy, heart failure, acute hind-limb ischemia, myocardial infarction, and coronary artery disease.

In 2013, Jaguszewski et al. proposed a unique signature of circulating miRs (miR-1, miR-16, miR-26a, and miR-133a) as a biomarker suitable for confirming the diagnosis of an acute TTS, and for distinguishing TTS from acute MI, thus suggesting a different etiology for both conditions [10]. Interestingly, the up-regulation of stress and depression biomarkers (miR-16 and miR-26a) suggests a close connection between TTS and neuropsychiatric disorders. A down-regulation of endothelin-1 (ET-1)-regulating miR-125a-5p and increased ET-1 plasma levels stresses the potential mechanistic hypothesis of microvascular spasm in TTS [10]. The field of circulating miRs is expanding rapidly and holds great promise to become an important diagnostic tool to differentiate TTS from myocardial infarction.

1.6. Detailed electrocardiographic information

The classic evolutionary electrocardiographic changes that have been described in TTS include transient ST segment elevation, most commonly in anterior leads, followed by development of diffuse T-wave inversion involving most leads, as well as prolongation of the corrected QT interval [11].

These ECG changes are similar to those seen in patients with anterior STEMI [12].

The prevalence of ST elevation has been described with a wide variability, with a prevalence from 11% to 100% [11].

Four ECG phases have been described in TTS: Phase 1, initial ST elevation; Phase 2, initial T-wave inversion after ST elevation from days 1 to 3; Phase 3, transient improvement in T-wave inversion in the subacute period; Phase 4, second deeper T-wave inversion persisting for several months (Fig. 1).

T-wave inversion is the most prevalent ECG abnormality after 24 h, reaching a plateau between days 2 and 30; with 17% of patients having residual T-wave inversion up until 1 year.

It has been reported than African-Americans more commonly present with diffuse T-wave inversions and QTc prolongation, which is more consistent with a non-STEMI picture. The most common ECG abnormalities in Hispanics include T-wave inversions, followed by ST elevations and ST depressions [13,14].

Several detailed ECG findings in TTS include more frequent ST elevations in inferior leads, with a percentage ranging from 30 to 50% [15]; ST depression in aVR (also known as ST elevation in -aVR); and a longer maximal QTc interval with normalization by day 14. TTS has been less frequently associated with ST elevation in V1 or with pathologic Q waves, with a prevalence of 10%, with complete resolution by one month.

In TTS patients presenting with ST elevations, the ST elevations are less prominent than in STEMI, and there tends to be absence of reciprocal ST depression [13].

TTS has previously been associated with transient attenuation of the amplitude of QRS complexes when compared to a prior ECG, or low voltage QRS on admission ECG [16].

Some authors have attempted to develop a systematic approach to differentiate TTS from acute coronary syndrome using ECG criteria. Frangieh et al. reported that patients with ST depression in aVR and ST elevation in anteroseptal leads or ST elevation in inferior leads or concomitant T-wave inversion in any lead without ST elevation in V1 was 98–100% specific for TTS, with a sensitivity of 8–14% [17]. When ST depression was present in V2 to V4 or the inferior leads, with associated ST elevation in aVR, there was >95% specificity for acute coronary syndrome.

Mugnai et al. reported that the combination of lack of ST elevation in lead V1, absence of abnormal Q waves, and ST depression in aVR identified TTS with a specificity of 95% and positive predictive value of 85.7% [18].

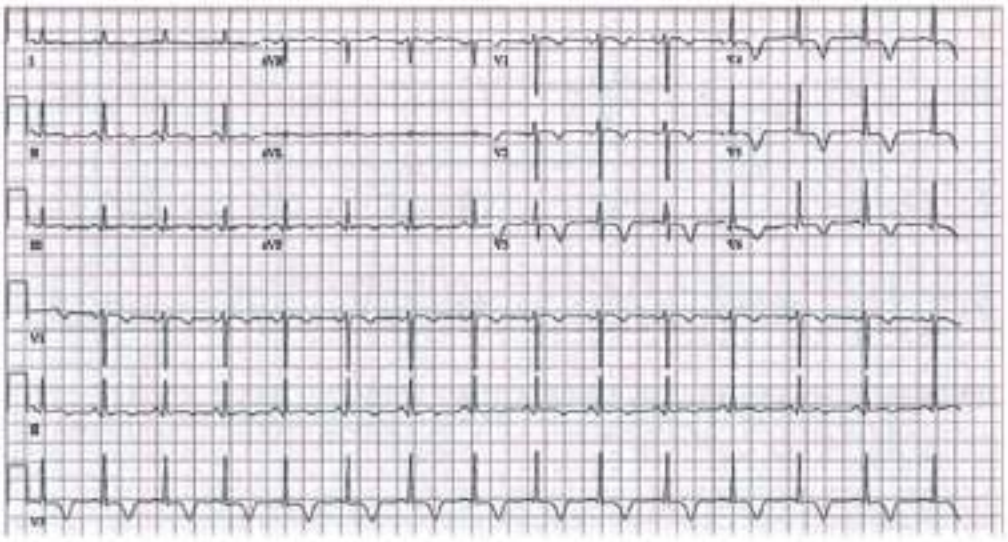

Fig. 1. 12 lead electrocardiogram with deep T wave inversion of a 62-year-old African American woman with TTS.

1.7. Transient reduction of the amplitude of the QRS complexes

The full array of the electrocardiogram (ECG) changes, pertaining particularly to repolarization and associated with all forms of acute coronary syndromes (ACS), have been encountered in patients with all topographic variants of TTS; thus, ST-segment elevations and depressions, and inverted and upright T-waves in various groups of ECG leads have been described [19,20]. In reference to changes in the QRS complexes, q- and Q-waves have been noted in patients with TTS early in the clinical course, abolished in subsequent ECGs. Review of ECGs of published TTS cases has disclosed that often the voltage amplitude of the QRS complexes is low (<5 mm in the limb leads and <10 mm in the precordial leads) (lQRS), or in case reports of patients with ≥2 ECGs, a transient attenuation of the QRS complexes (attQRS) is occasionally appreciated (Fig. 2). Previous work has shown that peripheral edema, particularly anasarca, of various etiologies, is associated with reversible attQRS, attributed to a decrease in the electrical impedance of the edematous body volume conductor [21].

Indeed edematous states affect the heart itself, via the compromise of its venous and lymphatic systems, in association with the edema apparent in the periphery [22]. TTS is characterized by transient appearance of myocardial edema (ME), documented in serial cardiac magnetic resonance imaging [23].

The above was the impetus to systematically explore the published literature of the association of TTS and the ECG attQRS. In a meta-analysis involving a total of 368 patients with TTS, lQRS was found in 91.5% of 200 patients with TTS and one ECG, with a distribution of 49.0, 42.8, 51.0, 52.0, and 46.9% in lead aVR, and inferior, anterior, lateral, and high lateral ECG lead groups, respectively, and attQRS as seen in 93.5% of 168 patients with TTS and ≥2 ECGs, with a distribution of 78.3, 74.5, 60.1, 70.7, and 74.5% in lead aVR, and inferior, anterior, lateral, and high lateral ECG lead groups, respectively [16].

1.8. Role of iodine-123 meta-iodo-benzyl-guanidine (mIBG)

Iodine-123-metaiodobenzylguanidine (^{123}I-mIBG) is a radioactive tracer that is analogue to noradrenaline in regard to presynaptic uptake, storage, and release [24,25] and ^{123}I-mIBG scintigraphy can therefore be used to visualize cardiac sympathetic nerve activity in vivo. It is unlikely that mIBG will have a clinical indication for assessing patients with TTS, but the modality may be used to investigate the underlying pathophysiology of the TTS. Several studies have investigated mIBG imaging in patients with TTS, and the results are uniform. Overall cardiac sympathetic activity appears increased [24,26,27], but ^{123}I-mIBG uptake is reduced in the akinetic regions of the left ventricle when compared to the surrounding contracting myocardium.

Thus, TTS is clearly associated with increased cardiac sympathetic activity, and the typical regional impairment of ^{123}I-mIBG uptake may be caused by excess adrenergic activity that leads to akinesia and sympathetic axon terminal damage in the vulnerable middle to apical myocardium. The main limitation to the published studies is that all patients inherently were examined after the onset of TTS; therefore, it cannot be ruled out that the observed increase in cardiac sympathetic activity observed with ^{123}I-mIBG scintigraphy is an adaptive mechanism rather than the underlying cause of the syndrome.

1.9. Optical coherence tomography

Intravascular imaging using optical coherence tomography (OCT) or intravascular ultrasound (IVUS) may help us either elucidate some of the pathophysiological mechanisms behind TTS or understand the natural history of the disease in terms of recovery (some patients fully recover ejection fraction while others do not). The following findings have been reported in the literature: Virtual histology IVUS evaluation of the left anterior descending coronary artery in patients with transient left

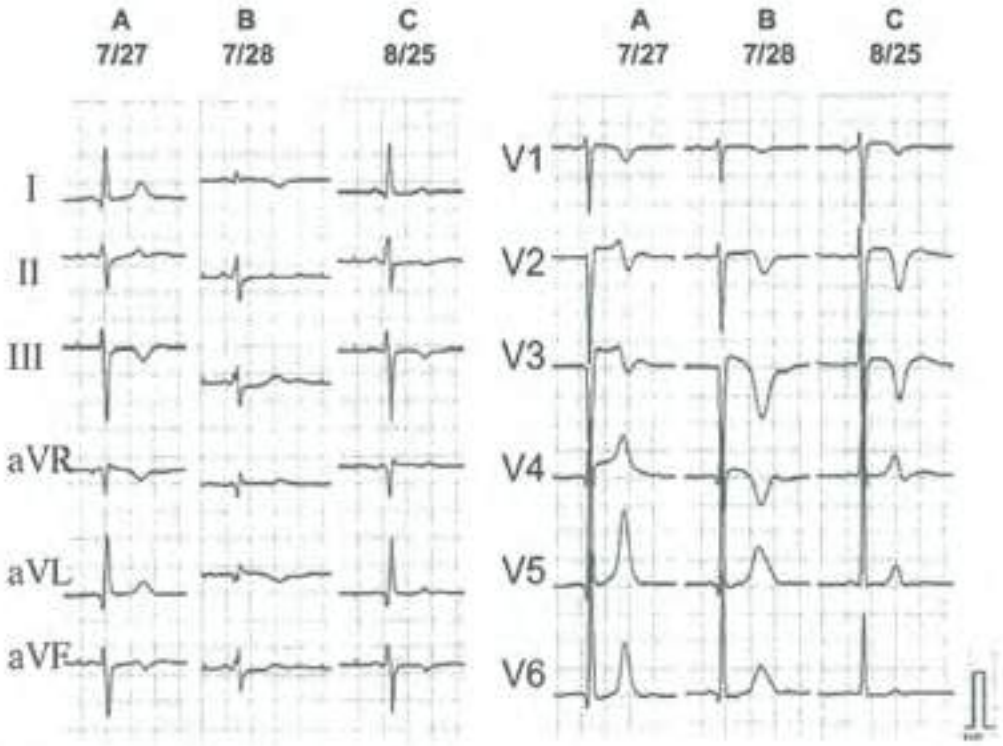

Fig. 2. Transient attenuation of the QRS complexes in a patient with TTS: ECGs on days 1, 2, and at 30-day follow-up of a 59-year-old woman with TTS following an epileptic seizure. Comparison of the ECG B with the ECGs A and C, reveals transient attenuation of the QRS complexes in the 6 limb and V1 and V2 leads.
(Reproduced and adapted from Sakuragi S et al. Heart Vessels 2007; 22:59–63, with the permission of Springer.)

ventricular ballooning syndrome found that there were 7 ruptured plaques, VH-TCFAs were found in 8 patients, 6 patients had a necrotic core >25%. The authors of this paper concluded that vulnerable plaques are observed in patients with TTS and even implied that the syndrome may be related to the natural course of atherosclerotic plaque development [28].

In another similar study, but using only IVUS grayscale in a limited number of patients, the authors did not find any plaque rupture; positive remodeling or intracoronary thrombus were absent in patients suffering from this disease [28].

There have been also reports using OCT (Fig. 3). In 23 consecutive patients, OCT in LAD to LMT was performed. Sixteen patients showed atherosclerotic plaque in the LAD or both LAD and LMT. Predominant fibrocalcific plaque: 52%, lipid rich plaque: 30.4%, TCFA: 26.1% were found, but ruptured plaque and intracoronary thrombi were not observed [29]. Some other isolated case reports using OCT did not find plausible explanations related to TTS [29,30].

There have been reports showing either no atherosclerosis or advanced CAD concomitantly at the time of the event; whether this is anecdotal or related to the disease needs further investigation.

1.10. Angiography data

In TTS, the epicardial coronary arteries are typically normal and unobstructed. The initial set of criteria proposed by researchers from the Mayo Clinic for the diagnosis of TTS required the absence of obstructive CAD. However, these criteria were later modified, and the authors acknowledged that patients with obstructive CAD may also develop TTS [11]. Patients with TTS can have coexisting CAD, as reported by Templin et al. in the largest International Takotsubo Registry, a consortium of 26 centers in Europe and the United States including 1750 patients with TTS. 15.3% of patients with TTS had evidence of significant coexisting coronary artery disease on angiography [31]. This finding shows that the presence of CAD is not an exclusion criterion for the diagnosis of TTS.

Differentiating TTS from acute coronary syndrome in an individual patient can be a difficult task. This is particularly true in cases where the LAD is involved (Fig. 4). In cases with acute plaque rupture, thrombus formation, and coronary dissection, the role of ACS is clear. Recently, Chou et al. reported that 8% of patients with TTS diagnosis had been overlooked for spontaneous coronary artery dissection (SCAD) on careful review of coronary angiography [32].

Plaque rupture with subsequent transient thrombotic coronary occlusion by a fast-dissolving clot is one of the proposed pathogenic mechanisms in TTS. In subsequent studies of TTS patients who underwent IVUS, some degree of CAD was found. Those studies conclude that coronary lesion in the LAD causing an aborted MI was not the primary underlying cause of TTS and that nonobstructive CAD and TTS could coexist without sharing a direct causal association [28].

OCT in these patients has revealed a high prevalence of atherosclerotic plaques, including a considerable number of highly vulnerable

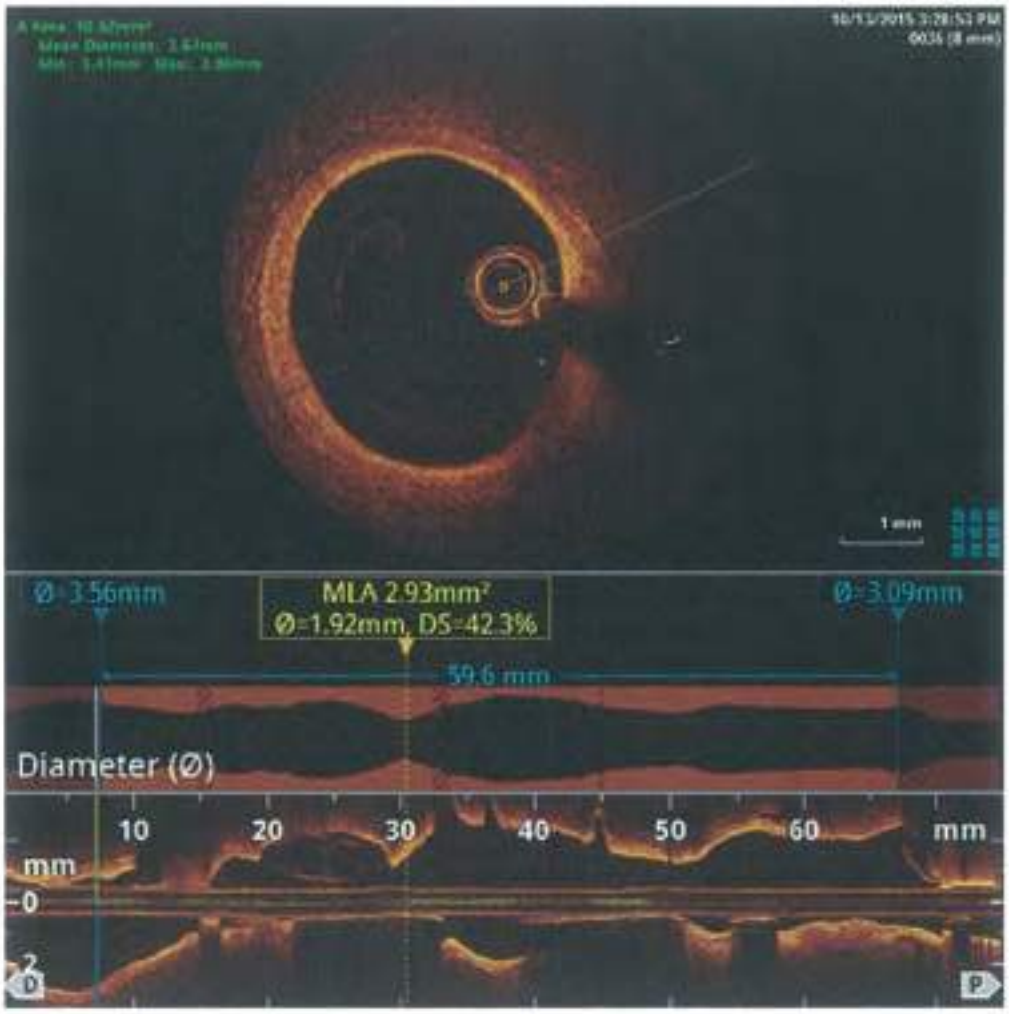

Fig. 3. OCT of TTS patient – coronary artery wall without evidence of significant plaque.

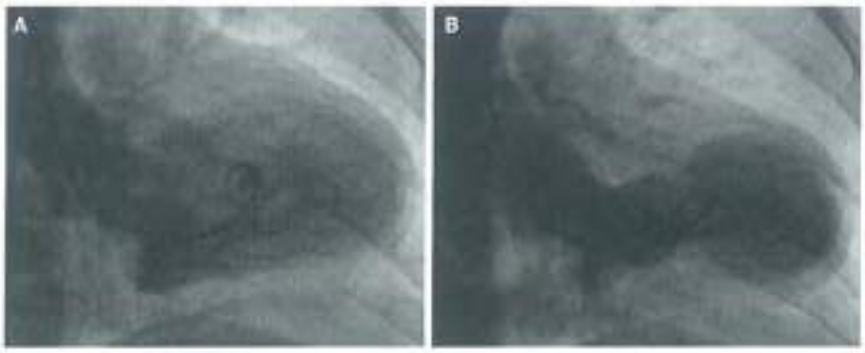

Fig. 4. Typical apical ballooning illustrated in the end-diastolic (A) and end-systolic (B) images from left ventriculography. (Courtesy Dr. Eitel et al. in Eitel I et al. J Am Heart Assoc. (2016).)

thin-cap fibroatheromas. However, ruptured plaques or intracoronary thrombi were not observed and are therefore most likely not the underlying mechanism of TTS [29].

1.11. MRI

Cardiac magnetic resonance (CMR) presents excellent anatomical information, enabling proper diagnosis and follow-up (Fig. 5) [33]. The diagnostic criteria for TTS using CMR have been proposed by Eitel et al. [34]; the absence of late gadolinium enhancement (LGE) in TTS is useful for differentiating TTS from myocardial infarction and other myocarditis. LGE exhibits the differences in the volume of distribution of gadolinium between the normal and diseased myocardium. However, clinicians should keep in mind that minor LGE can be found in patients with TTS. It has been reported that minor LGE is present in approximately 9% of patients with TTS when LGE is defined at a cutoff

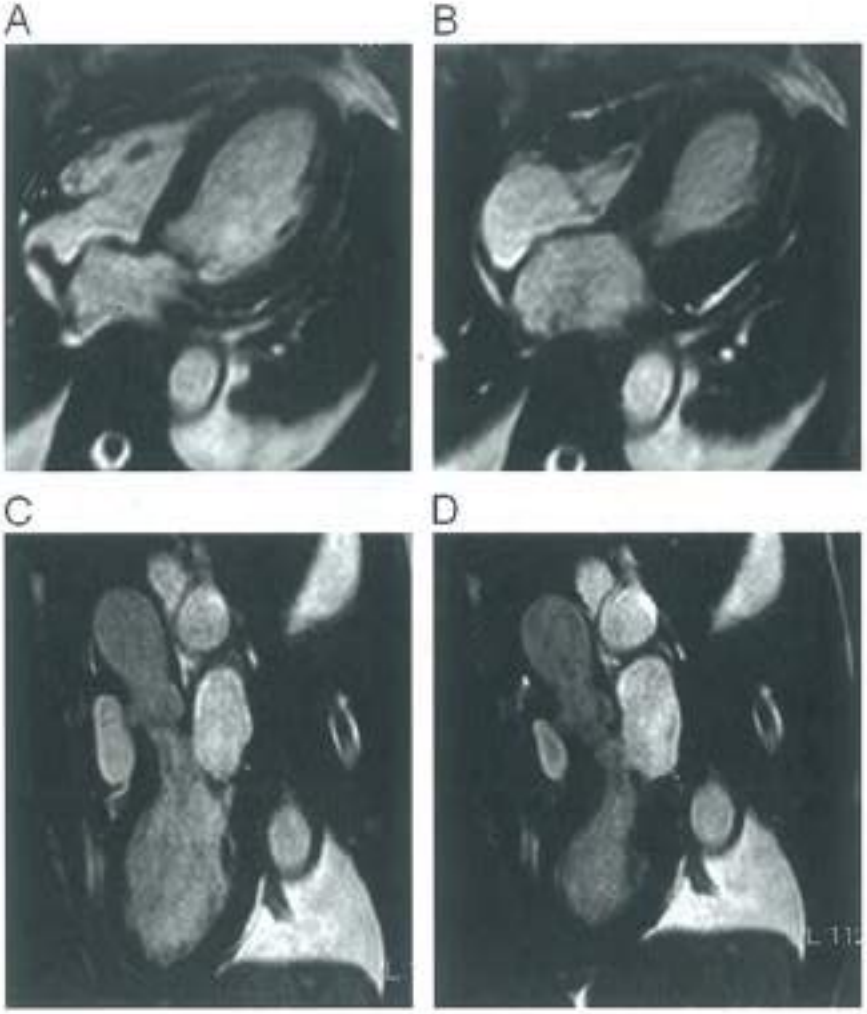

Fig. 5. Typical apical ballooning during the systolic period in the patient with TTS. Cine CMR (4-chamber view A-diastole, B-systole; 2-chamber C-diastole, D-systole).

value of >3 SD above the mean; however, none of those reveals evidence of LGE with a cutoff value of >5 SD above the mean [33].

CMR is useful to provide the accurate diagnosis for TTS and helpful to rule out acute coronary syndrome and myocarditis (Table 2).

Myocardial edema should be assessed before taking LGE images. Corresponding to the wall motion abnormality, high T2 signal intensity is usually observed in patients with TTS, without increasing ventricular mass or accompanying wall motion thickness [35]. The existence of myocardial edema is thought to be the presence of myocardial injury and inflammation. This edema, the finding of T2 high intensity, is gradually resolved after the wall motion is normalized (Fig. 6) [36].

CMR can provide not only the assessment of wall motion variabilities but also the calculation of extracellular volumes using T1 mapping technique [23]. This technique would be beneficial to observe specific phenomenon in TTS because of rapid increasing extracellular matrix in the myocardium. T2 mapping technique would be a promising option to quantity the volume of myocardial edema, although this new method has not been fully established in patients with TTS.

Volumetric CMR is valuable as three-dimensional modality to identify various cardiac function beyond the structure alone. Although the usefulness of the two- or three-dimensional speckle tracking echocardiography is clearly demonstrated [37,38], tracking technique using CMR is still for research use. Apical thrombus is often identified in patients with TTS; thus, CMR, including cine CMR and early gadolinium enhancement sequence, is useful to detect a thrombus.

1.12. Echocardiographic findings – systolic and diastolic mechanics cardiomyopathy

The acute depression in left ventricular ejection fraction brings no surprise that the strain and deformation of the entire left ventricle are profoundly abnormal. Perhaps the most extreme finding is the fact that the early propping twist disappears completely in the acute stage. This early motion occurs during isovolumic contraction and is directed clockwise at the apex and counterclockwise at the base (thus opposite to the normal direction of movement to follow during systole, like an athlete throwing a discus who first turns to the right before spinning leftward to throw). However, significant mechano-temporal alterations characterizing both systole (global longitudinal strain and apical circumferential strain, $p < 0.01$ for both; LV twist, twist rate, and torsion, $p < 0.0001$ for all) and diastole (untwist rate and time to peak untwisting, $p < 0.001$ for both) persist at 4-month follow-up compared with control subjects, despite normalization of LV ejection fraction and volumes. These findings show that there is a both a reduction in the amplitude of twist and untwist of the heart as well as a delay in the timing of these processes during the cardiac cycle [37].

Although the changes are subtle enough to allow a normal or near normal ejection fraction during this convalescent stage, they do affect the overall left ventricular twist, which has the potential to impact the stroke volume of these patients. It remains unknown at this stage whether this recovery is simply more protracted than initially assumed or if it is exhausted and results in a new clinical phenotype that remains to be defined. Nevertheless, the EF normalization remains clinically useful in consolidating the diagnosis at follow-up.

2. Complications

2.1. Acute heart failure syndrome

Acute heart failure syndrome in patients with TTS is unique in that it is completely reversible, usually one to four weeks after the triggering event. Patient symptoms may range from shortness of breath with or without pulmonary edema to cardiogenic shock, with the latter quite rare [39,40].

The prevalence of acute heart failure is reported in case series ranging from 12 to 45% followed by left ventricular outflow obstruction (10–25%), mitral regurgitation (14–25%), and cardiogenic shock (6–20%). This transient heart failure manifests with elevated brain natriuretic peptide (BNP) and elevated left ventricular end diastolic pressure (LVEDP) [41,42].

Upon presentation, patients can be risk-stratified into low- versus high-risk based upon several factors. Low-risk patients' ejection fraction is >45% and usually requires no treatment. High-risk patients, in addition to an ejection fraction <45%, may have right ventricular involvement contributing to low output syndrome and shock [4,43,44].

The mechanisms contributing to acute heart failure syndrome are complex and include both systolic and diastolic dysfunction. Elderly hypertensive patients with pre-existing septal hypertrophy may develop a dynamic left ventricular outflow tract obstruction (LVOTO) and further worsening of symptoms. Systolic anterior motion of the mitral valve increases mitral regurgitation as well as worsening of the LVOTO. In up to one-third of cases, right ventricular involvement has been reported, contributing to a marked decrease in left ventricular pre-load, low cardiac output syndrome, and possible shock. In addition to increasing tricuspid regurgitation, right ventricular involvement is associated with an increase in-patient mortality [31].

With chest pain as the most common symptom in TTS, the excellent temporal and special resolution found with newer coronary computed tomography angiography (CCTA) may provide evidence of lack of obstructive CAD, thus confirming the diagnosis. CMR provides addition diagnostic and prognostic information, including extent of right ventricular involvement, mitral regurgitation, LVOTO, SAM, and left ventricular thrombus.

Table 2
Differences in CMR features of TTS acute myocardial infarction and acute myocarditis (quoted with permission).

	Takotsubo syndrome	Myocardial infarction	Myocarditis
Site of wall motion abnormality	Concentric mid- and apical LV wall	Follows expected epicardial coronary artery distribution	Usually global unless regional edema/LGE is severe
Myocardial edema	Typically transmural in a concentric mid and apical LV wall distribution	Subendocardial or transmural at sites of wall motion abnormalities	Subepicardial, mid-myocardial or transmural
Left ventricular impairment	Yes: typically impaired ejection fraction with elevated indexed end systolic volume	Yes: typically impaired ejection fraction with elevated indexed end systolic volume	Yes, but may show only mild/borderline low normal ejection fraction
Right ventricular impairment	>33% of patients	May be seen, particularly if right coronary artery territory involved	Rarely impacts on right ventricular function
LGE	Maybe (10–40%)	Yes	Often
Site of LGE	Concentric transmural mid and apical LV wall	Typically subendocardial or transmural in recognized epicardial coronary artery distribution	Mid-myocardial or subepicardial in a focal non-coronary artery distribution
Type of LGE	Low-intensity LGE	Bright LGE	Low-intensity or Bright LGE
Microvascular obstruction	No	Maybe	No
Resolution at 3 months	Yes	No	Potentially but may show residual myocardial fibrosis and impairment

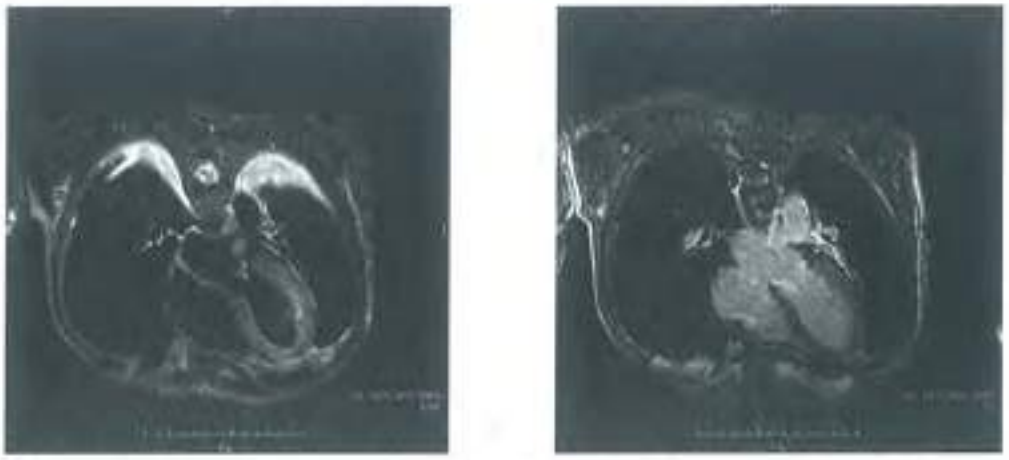

Fig. 6. Left side: myocardial edema. T2-weighted 4-chamber view showing slight transmural signal hyperintensity in the mid apical segments of left ventricle. Right side, the absence of late gadolinium enhancement in the patient with TTS was documented by CMR 4-chamber view.

On admission, 86.5% of patients had a reduced EF. The National Inpatient Sample (NIS) from 2007 to 2012 collected data on 22,005 patients with a primary diagnosis of TTS and 31,942 patients with a secondary diagnosis of TTS, making this the largest TTS registry of hospitalized patients in the United States. In this cohort, 64% reported hypertension, 4% presented with either cardiogenic shock or cardiac arrest, and 2.8% were treated with an intra-aortic balloon pump (IABP) [1,4,40,45]. There is a lack of prospective randomized clinical trials to clarify treatment protocols and guide therapy.

2.2. Arrhythmias in patients with takotsubo syndrome

Patients with TTS often have sinus tachycardia, although sinus bradycardia or other bradyarrhythmias are occasionally noted, suggesting an underlying vagal effect. Also, multiple atrial and ventricular premature beats, sinus node dysfunction (SND), asystole, paroxysmal supraventricular tachycardia (PSVT), atrial fibrillation (AF), nonsustained and sustained ventricular tachycardia (VT) (both monomorphic and polymorphic torsades de pointes (TdP)), ventricular fibrillation (VF), ventricular asystole, pulseless electrical activity, sudden cardiac death (SCD), and right and left bundle branch blocks are noted. AF was diagnosed in 4.7% of patients with TTS [46], but occasionally it was not clear whether this represented a new AF. SND and atrioventricular nodal dysfunction were reported in 1.3% and 2.9% of cases [46], but often details are lacking. The combined incidence of sustained VT and VF was 3.4%, with potentially threatening ventricular arrhythmias (VA) and SCD occurring in 1.1% and 0.9%, respectively [46]. In a large database of patients with TTS, arrhythmias were noted in 26%, with AF/atrial flutter seen in 8.8%, PSVT in 0.8%, and life-threatening VA in 4.2% of cases. The issue occasionally arises whether VT/VF is a complication of, or the trigger for, TTS [47]. Arrhythmias in patients with TTS tend to adversely influence the hospital course and outcome, and use of β-blockers for tachyarrhythmias to counter the excessive sympathetic discharge may play a preventive/ameliorating/therapeutic role, although proof is lacking.

AF in patients with TTS is associated with older age, fewer emotional triggers, higher incidence of cardiogenic shock, lower left ventricular ejection fraction (LVEF), prolonged hospital stay, and higher long-term mortality [48]. AF is an independent determinant of outcome, even after adjustment for clinical variables, left ventricular function, and cardiogenic shock, and thus it should be employed upon its emergence for risk stratification of patients with TTS [48].

Long-term anticoagulation following a transient episode of AF in the course of TTS should be considered, as is done currently for AF in association with other cardiac illnesses.

Both transient and persisting CHB [49,50] have been reported in association with TTS. Permanent pacemakers (PPM) have been implanted in patients with persisting CHB, with or without prior electrophysiologic evaluation [50]. Temporary pacing is often necessary in the acute/subacute phase of the illness to manage the CHB and the associated bradycardia, which in the presence of a prolonged QTc predisposes patients to TdP [51]. Temporary pacing should have preference over the employment of isoproterenol infusion for CHB, other atrioventricular conduction abnormalities, or SND. Occasionally, CHB is transient and does not need temporary or PPM. Notably, implantation of a PPM has led to TTS, triggered by the associated stress.

Compared to arrhythmias encountered in the setting of AMI, VA, including VT, VF, and SCD, are less frequent in TTS, even in patients with prolonged QTc [46,52]. Regardless, continuous telemetry monitoring of patients with TTS for at least 3 days, or longer when QTc is >500 ms, is recommended [53]. To prevent TdP in patients with TTS and prolonged QTc, a form of acquired long QT syndrome, one should avoid QTc prolonging drugs, evaluate for hypokalemia and hypomagnesemia, manage bradycardia, and consider predisposing congenital/genetic long QT syndromes [53]. Magnesium is recommended for the prevention/treatment of TdP, and β-blockers should be avoided, or discontinued, until the prolongation of the QTc is resolved. Implantation of cardioverter-defibrillators (ICD) should follow consideration of persistence of QTc prolongation and bradycardia, and clinical presentation with SCD. Indeed, occasionally, TTS follows resuscitated SCD, with documentation of sustained VT, VF, or TdP, suggesting that the VA had triggered the TTS [54] rather than being its complication, and in such patients, ICD implantation is mandatory. Whether patients who had VT, VF, and TdP, in the course of TTS, should receive an ICD needs to be handled on a case-by-case basis [52,53].

2.3. Thromboembolic events

The incidence and clinical significance of thromboembolic events in TTS has not yet been sufficiently established. Data documenting these events are scarce; however, a recent in-depth analysis of existing references reveals the common occurrence of intra-ventricular thrombus among these patients, thus signifying a potential relevance [55,56].

The incidence of ventricular thrombus formation and stroke varies between 2.5%–8% and 1%–5%, respectively [31,56].

Right ventricular involvement, apical TTS form, and elevated troponin I levels might be positive predictors of thromboembolic events in TTS [55].

There are many inherent difficulties in diagnosing intraventricular thrombus formation and its peripheral embolization in TTS. Two-

JACC: CARDIOVASCULAR INTERVENTIONS
© 2019 BY THE AMERICAN COLLEGE OF CARDIOLOGY FOUNDATION
PUBLISHED BY ELSEVIER

VOL. 12, NO. 2, 2019

EDITORIAL COMMENT

From Color to Hemodynamic Assessment

Is it Time to Change the Paradigm in Judging MitraClip Outcomes?*

Maurizio Taramasso, MD, PhD,[a] Mara Gavazzoni, MD,[a] Shingo Kuwata, MD, PhD,[a] Pascal Meier, MD,[b] Francesco Maisano, MD[a]

In this issue of *JACC: Cardiovascular Interventions*, Ikenaga et al. (1) showed for the first time in a structured way and in a substantial number of patients that the changes in pulmonary vein (PV) flow pattern following MitraClip (Abbott Vascular, Santa Clara, California) implantation have an important and independent association with clinical outcomes. The study has limitations, being single-center, retrospective, observational, and includes patients with mixed etiologies of mitral regurgitation (MR) (both degenerative and functional) without any differentiation. Yet, the clinical message is extremely relevant for the interventional community: evaluation of the immediate result after MitraClip implantation should be performed in a more integrated way, taking into account both residual MR (color jet) and its hemodynamic effect.

SEE PAGE 140

INVASIVE HEMODYNAMIC ASSESSMENT

Invasive hemodynamic measurements should be mandatory results assessment, shifting the paradigm of evaluation of MitraClip results from an echocardiography-based color Doppler evaluation to a hemodynamic-based approach. Live monitoring of hemodynamic changes during MitraClip procedures is routinely used in our daily clinical practice, because it has been observed to have an important impact on outcomes, independently from residual color jet, and it represents a valuable tool to guide decision making. In our practice, after transseptal puncture, 2 parallel wires are inserted in the left superior pulmonary vein through the transseptal sheath. While one wire is conventionally used to introduce the MitraClip Steerable Guide Catheter, the adjacent wire is used to deliver a 5-F pigtail catheter into the pulmonary vein. This parallel wire is used to continuously monitor left atrial (LA) pressure during all the phases of the implantation. A second 5-F pigtail catheter is inserted in the left ventricle (LV), retrograde through the aortic valve, in order to monitor LV pressures. The 2 pressure lines are constantly observed during the procedure and used to guide decision making.

The ideal situation should be as the color jet is reduced, the V-wave and mean LA pressure are reduced as well, with an increase in the systolic blood pressure and no residual gradient. It is not infrequent to observe a discrepancy between the color Doppler result and hemodynamic changes, with many patients having a residual color jet, but dramatic reduction of V-wave and mean LA pressure or having no residual MR and no gradient at echocardiographic assessment, but a significant invasive gradient. It has been observed in our experience that the most important predictor of outcome after MitraClip implantation is reduction of the mean LA pressure, independent from a residual color jet. Therefore, we have already switched in our practice from color-based to hemodynamic-based assessment of the outcomes (**Figure 1**). Reduction of mean LA pressure and absence of an invasive gradient should be the main determinants to drive the procedure and to guide the operator in case of discrepancies.

NONINVASIVE HEMODYNAMIC ASSESSMENT

Echocardiographic assessment of residual MR after MitraClip implantation presents several challenges

*Editorials published in *JACC: Cardiovascular Interventions* reflect the views of the authors and do not necessarily represent the views of *JACC: Cardiovascular Interventions* or the American College of Cardiology.

From the [a]Cardiovascular Surgery Department, University Hospital of Zurich, University of Zurich, Zurich, Switzerland; and the [b]Cardiology Department, Kantonsspital Graubünden, Chur, Switzerland. Dr. Taramasso has been a consultant for Abbott, Boston Scientific, atech, and CardiaMetic. All other authors have reported that they have no relationships relevant to the contents of this paper to disclose.

ISSN 1936-8798/$36.00

https://doi.org/10.1016/j.jcin.2018.11.035

JACC: CARDIOVASCULAR INTERVENTIONS VOL. 12, NO. 2, 2019
JANUARY 28, 2019:151–4

FIGURE 1 Hemodynamic Changes After MitraClip

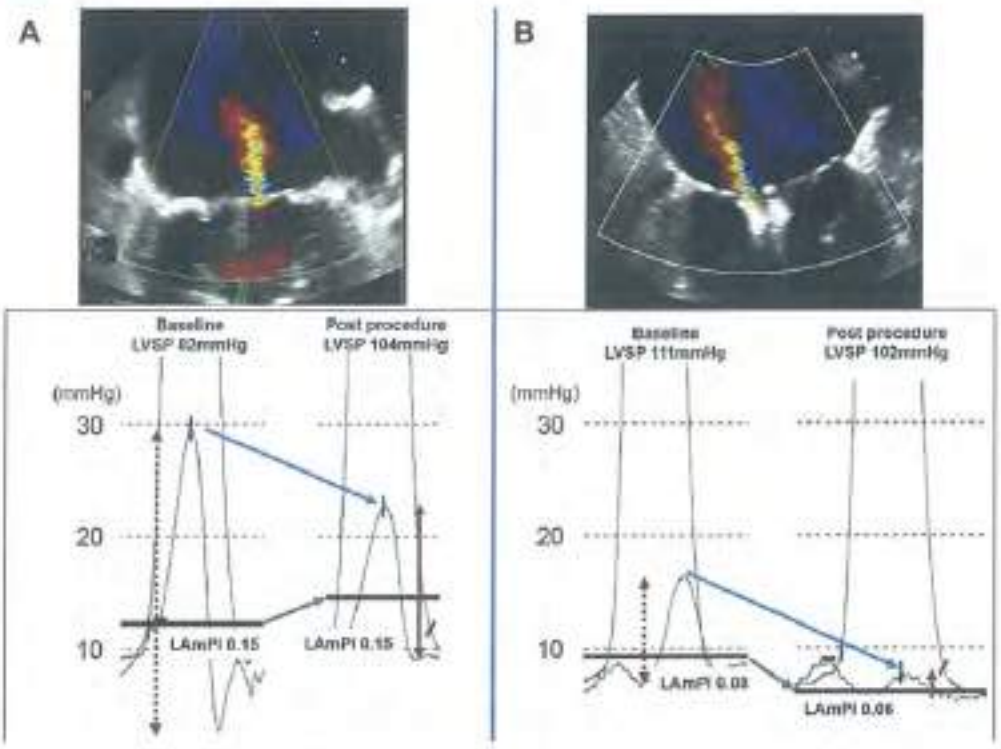

The figure shows the echocardiographic results of 2 different patients (**A and B**) following MitraClip implantation. According to the echocardiographic evaluation based on residual color jet, they both have a residual mild mitral regurgitation. However, the 2 hemodynamic traces are different. Patient A, despite an increase in left ventricular systolic pressure (LVSP) (from 82 mm Hg to 104 mm Hg) and a reduction of the LA V-wave (**blue arrow**), had no reduction of mean LA pressure (**green arrow**). Conversely, Patient B had reduction of both V-wave peak (**blue arrow**) and mean LA pressure (**green arrow**). Despite similar echocardiographic outcomes, clinical outcomes were totally different: Patient A experienced recurrent heart failure hospitalization within 1 year after MitraClip implantation and remained symptomatic (NYHA functional class III); Patient B had improvement in clinical situation (NYHA functional class II and no events during follow-up. The 2 different courses could have been predicted by the different hemodynamic profiles immediately after MitraClip implantation. LA = left atrial; LAmPl = left atrial mean pressure; NYHA = New York Heart Association.

and can be inaccurate due to the double orifice configuration of the valve and/or the presence of multiple regurgitant jets, suggesting the need for adjunctive tools (2-5). Evaluation of pulmonary venous flow is an easy and reproducible technique, which is widely used to aid in the assessment of quantification of the severity of MR and should be routinely used after MitraClip implantation.

As a matter of fact, the most important determinants of outcomes after MitraClip implantation are residual MR and increased transvalvular gradient (6,7). Because residual relevant MR is associated with increased risk of mortality after MitraClip implantation, the decision making and the procedural strategy during the intervention assume a crucial importance. The operators have to face several difficult situations or "gray zones" from a decisional standpoint, and intraprocedural decisions can have a strong impact on procedural outcomes, long-term results, and prognosis. Many questions commonly present. What should be done in the case of a residual jet? In case of a second or third clip implantation, would the adjunctive benefit of more MR reduction be nullified by the incremental increase in the gradient? What should be done in the case of MR reduction, but a significant increase in transmitral gradient? The answers to each are not always clear, suggesting that a more integrated approach, in conjunction with conventional methods (color jet and echocardiographic gradient solely), is needed to guide such decisions.

In the case of a residual color jet after the implantation of a first clip, the operator has to decide whether to proceed with a second clip implantation, and this decision is mainly driven by the severity of

the residual jet and by the risk of increase of the gradient by adding a further clip. Often the situation is clear, and the decision is relatively easy. In the presence of severe residual MR and large mitral valve area, with low transmitral gradient, the decision to proceed with an additional clip is obvious. Similar is the situation of effective reduction of the color jet, where in absence of valvular gradient, the decision would be to accept that result. The use of an adjunctive technique such as systolic/diastolic velocity time integral (Svti/Dvti) ratio is extremely useful to guide decisions in gray situations, which are not so infrequent. A typical example would be the case of a residual jet with an increase of the gradient after the implantation of a further clip. In such a case, the evaluation of the pulmonary flow would assume a crucial importance: in the presence of an improvement of the pulmonary flow, the result should be accepted despite the presence of a residual color jet; in case of no changes in the pulmonary flow, a further clip would be considered.

The decision whether to reposition or remove a clip, or to proceed with further clip implantation should never be solely based on the assessment of the color jet, but should rather be based on an integrated judgment of further echocardiographic and hemodynamic tools, shifting the conventional paradigm toward a functional and physiological rather than anatomic approach. The same concept should be applied to other structural mitral interventions, including annuloplasty and valve replacement.

CHALLENGES

The concept of including different etiologies can support the value of PV Doppler evaluation in all clinical settings. Despite this, evaluating PV Doppler changes can have different clinical implications in degenerative (DMR) versus functional (FMR) mitral regurgitation.

In the setting of pure DMR, atrial function and volume are the most important factors affecting PV flow in the short term, so in this setting, short-term changes in PV Doppler after the procedure can strongly reflect the impact of MitraClip implantation on MR. The positive predictive value of significant change in PV Doppler is very strong. Therefore, given the more frequent eccentric jet of DMR, the negative predictive value could be poor, and only color flow imaging can help to understand hemodynamic involvement.

In the case of FMR, long-standing high LV end-diastolic pressures and longer neurohormonal activation mainly leads to structural alteration of LA function. In such cases of poor LV function and increased LA stiffness, color Doppler evaluation of residual MR could have several pitfalls (underestimation of residual MR). Significant changes in PV Doppler immediately after the procedure, irrespective of color Doppler, identifies patients in which good remodeling after MV repair is expected, being the ones with still preserved LA/LV interaction.

So, Svti/Dvti is not only a predictor of outcome, but also a marker of more advanced heart failure disease, that is characterized mostly by less compliance of the atrial and ventricular cavities. As proof of concept, in the present study at baseline, patients with lower Svti/Dvti had more advanced heart failure, with more frequent FMR, higher levels of brain natriuretic peptide, reduced LV function, and greater dilation of cardiac chambers.

So, the questions that remain to be clarified are as follows: "Should we obtain the same results on MR when the PV flow pattern is not changing during the procedure? Could we be satisfied with lesser results based on color flow when the PV flow is clearly getting better? When we treat with FMR, is the most important clinical point to find the hemodynamic stage at which escalation of the procedure is no more useful. The right target for each patient may be reached by using a combination of the 2 methods: less color flow MR reduction and no changes in PV flow. Future studies are expected to compare residual MR as color Doppler and PV Doppler for DMR and FMR to confirm this observation.

ADDRESS FOR CORRESPONDENCE: Dr. Maurizio Taramasso, Cardiovascular Surgical Department, University Hospital of Zurich, Rämistrasse 100, 8091 Zurich, Switzerland. E-mail: Maurizio.Taramasso@usz.ch.

REFERENCES

1. Benaiga H, Yoshida J, Hayashi A, et al. Usefulness of intraprocedural pulmonary venous flow for predicting recurrent mitral regurgitation and clinical outcomes after percutaneous mitral valve repair with the MitraClip. J Am Coll Cardiol Intv 2019;12:140–50.

2. Corrigan FE 3rd, Chen JH, Maini A, et al. Pulmonary venous waveforms predict rehospitalization and mortality after percutaneous mitral valve repair. J Am Coll Cardiol Img 2018 Sep 6 [E-pub ahead of print].

3. Deff A, Prieschott C, Eckert F, et al. 3D vena contracta area after MitraClip(c) procedure: precise quantification of residual mitral regurgitation and identification of prognostic information. Cardiovasc Ultrasound 2018;16:1.

JACC: CARDIOVASCULAR INTERVENTIONS VOL. 12, NO. 2, 2019
JANUARY 28, 2019:151–4

4. Hamilton-Craig C, Scrugneli W, Gaikwad N, et al. Quantitation of mitral regurgitation after percutaneous MitraClip repair: comparison of Doppler echocardiography and cardiac magnetic resonance imaging. Ann Cardiovasc Surg 2015;4:341–51.

5. Palmiero G, Ascione L, Brigonti C, et al. The mitral-to-aortic flow-velocity integral ratio in the real world: echocardiographic evaluation of functional mitral regurgitation before and after percutaneous repair. J Interv Cardiol 2017;30:368–73.

6. Neuss M, Schau T, Isotani A, Pitz M, Schopp M, Butter C. Elevated mitral valve pressure gradient after MitraClip implantation deteriorates long-term outcome in patients with severe mitral regurgitation and severe heart failure. J Am Coll Cardiol Intv 2017;10:931–9.

7. Scotje P, Vemulapalli S, Feldman T, et al. Outcomes with transcatheter mitral valve repair in the United States: an STS/ACC TVT registry report. J Am Coll Cardiol 2017;70:2315–27.

KEY WORDS hemodynamic, mitral regurgitation, transcatheter mitral repair

Cardiovascular Revascularization Medicine 20 (2019) 153–166

Contents lists available at ScienceDirect

Cardiovascular Revascularization Medicine

Review

Takotsubo syndrome: State-of-the-art review by an expert panel – Part 2

Andre Dias [a,b], Ivan J. Núñez Gil [c], Francesco Santoro [d], John E. Madias [e,f], Francesco Pelliccia [g], Natale Daniele Brunetti [d], Elena Salmoirago-Blotcher [h], Scott W. Sharkey [i], Ingo Eitel [j], Yoshihiro J. Akashi [k], Ibrahim El-Battrawy [l,m], Emiliana Franco [b], Ibrahim Akin [l,m], Milosz Jaguszewski [n], Dana Dawson [o], Vincent M. Figueredo [b], L. Christian Napp [p], Thomas Emil Christensen [q], Kathy Hebert [r], Itsik Ben-Dor [a], Yuichi Ozaki [a], Héctor M. García-Garcia [a], Alexandre H. Kajita [a], Takashi Akasaka [s], Satoshi Kurisu [t], Amir Lerman [u], Ron Waksman [a,v]

[a] Section of Interventional Cardiology, MedStar Washington Hospital Center, Washington, DC, United States of America
[b] Department of Cardiology, Einstein Medical Center, Philadelphia, PA, United States of America
[c] Interventional Cardiology, Cardiovascular Institute, Hospital Clínico San Carlos, Madrid, Spain
[d] Department of Medical & Surgery Sciences, University of Foggia, Foggia, Italy
[e] Icahn School of Medicine at Mount Sinai, Elmhurst, NY, United States of America
[f] Division of Cardiology, Elmhurst Hospital Center, Elmhurst, NY, United States of America
[g] Interventional Cardiology Unit, Sapienza University, Rome, Italy
[h] Centers for Behavioral and Preventive Medicine, The Miriam Hospital, Warren Alpert Medical School of Brown University, Providence, RI, United States of America
[i] Minneapolis Heart Institute Foundation, Minneapolis, MN, United States of America
[j] Cardiology, Angiology, Intensive Care Medicine, University Lübeck, Schleswig-Holstein, Germany
[k] Division of Cardiology, Department of Internal Medicine, St. Marianna University School of Medicine, Kawasaki, Kanagawa, Japan
[l] Department of Internal Medicine, University Heidelberg, Mannheim, Germany
[m] DZHK (German Center for Cardiovascular Research), Partner Site, Heidelberg-Mannheim, Germany
[n] Department of Cardiology, Medical University of Gdansk, Poland
[o] School of Medicine and Dentistry, University of Aberdeen, Aberdeen, UK
[p] Department of Cardiology and Angiology, Hannover Medical School, Hannover, Germany
[q] Copenhagen University Hospital, Copenhagen, Denmark
[r] GE Healthcare, Miami, FL, United States of America
[s] Department of Cardiovascular Medicine, Wakayama Medical University, Wakayama, Japan
[t] Department of Cardiovascular Medicine, Hiroshima University, Hiroshima, Japan
[u] Department of Cardiovascular Medicine, Mayo Clinic, Rochester, MN, United States of America

ARTICLE INFO

Article history:
Received 14 November 2018
Accepted 14 November 2018

Keywords:
Takotsubo
Heart failure
Catecholamine

ABSTRACT

In part 2 of this two-part manuscript on takotsubo syndrome (TTS), we discuss typical biomarkers (particularly excess catecholamines and what kinds of electrocardiographic information operators should look for) and numerous complications the syndrome can cause. This consensus paper is the result of a multinational effort aiming to summarize the current state of the art on TTS. Several novel and unique sections are emphasized in this document, including the current state of the art on genetics of takotsubo syndrome, microRNAs (miRs), racial differences, role of cardiac spectroscopy and intracoronary imaging, as well as mechanical circulatory support.
New structured algorithms are also proposed to aid clinicians in the decision-making process as well as future directions for research given the current lack of evidence-based medical approaches.
© 2018 Elsevier Inc. All rights reserved.

Contents

1. Workup 154
1.1. Biomarkers 154

Abbreviations: ACS, acute coronary syndrome; BNP, B-type natriuretic peptide; CRP, C-reactive protein; LV, left ventricle/ventricular; MACE, major adverse cardiac events; miRs, microRNAs; RV, right ventricle/ventricular; STEMI, ST-elevation myocardial infarction; TIMI, Thrombolysis in Myocardial Infarction; TTS, takotsubo syndrome.

* Corresponding author at: MedStar Heart and Vascular Institute, MedStar Washington Hospital Center, 110 Irving St., NW, Suite 48-1, Washington, DC 20010, United States of America.
E-mail address: ron.waksman@medstar.net (R. Waksman).

https://doi.org/10.1016/j.carrev.2018.11.016
1553-8389/© 2018 Elsevier Inc. All rights reserved.

1.2. Brain natriuretic peptide (BNP) and N-terminal-pro-BNP (NT-proBNP) . . . 154
1.3. Troponin (Tn), Creatine kinase (CK), CK-MB . . . 154
1.4. Catecholamines and other biomarkers . . . 154
1.5. MicroRNAs (miRs) . . . 155
1.6. Detailed electrocardiographic information . . . 155
1.7. Transient reduction of the amplitude of the QRS complexes . . . 156
1.8. Role of iodine-123 meta-iodo-benzyl-guanidine (mIBG) . . . 156
1.9. Optical coherence tomography . . . 156
1.10. Angiography data . . . 157
1.11. MRI . . . 158
1.12. Echocardiographic findings – systolic and diastolic mechanics cardiomyopathy . . . 159
2. Complications . . . 159
2.1. Acute heart failure syndrome . . . 159
2.2. Arrhythmias in patients with takotsubo syndrome . . . 160
2.3. Thromboembolic events . . . 160
2.4. In-hospital mortality . . . 161
3. Management . . . 161
3.1. Role of Levosimendan and short-acting beta blockers . . . 161
3.2. Mechanical circulatory support . . . 161
3.2.1. TandemHeart . . . 161
3.2.2. ECMO . . . 161
3.2.3. Impella . . . 161
3.3. Dilemma of ACE inhibitors . . . 161
3.4. Role of long-term beta blockers . . . 162
3.5. Is there any role for aspirin alone or dual antiplatelet therapy? . . . 162
3.6. Long-term prognosis: Cardiac and non-cardiac mortality . . . 163
3.7. Role of psychological distress . . . 163
4. Treatment of psychological distress . . . 164
5. Recurrence of TTS . . . 164
6. Conclusion . . . 164
Declarations of interest . . . 164
Funding . . . 164
References . . . 164

1. Workup

1.1. Biomarkers

As patients with TTS and ACS commonly present with similar symptoms, distinguishing one disease from the other remains a challenge in the clinical setting [1].

Although several biomarkers have been proposed for the differential diagnosis of TTS, currently there is no specific and sensitive biomarker for TTS (Table 1).

1.2. Brain natriuretic peptide (BNP) and N-terminal-pro-BNP (NT-proBNP)

TTS is associated with severe LV dysfunction, and subsequently, brain natriuretic peptides, i.e., BNPs, NT-proBNPs, rise within the first few hours after the onset of symptoms, in response to myocardial stretch [1,2]. NT-proBNP levels correlate with plasma catecholamine levels as well as the wall motion score index and LV ejection fraction. As a consequence, BNP levels are higher in patients with typical TTS vs. atypical TTS, i.e., mid-ventricular-, inverted- or focal TTS [2].

Table 1
Biomarkers. Laboratory diagnostic tests to distinguish TTS and ACS/AMI.

Natriuretic peptides	BNP, NT-proBNP
Markers of myocardial necrosis	troponin I, troponin T, hsTn, myoglobin, CK, CK-MB
Catecholamines	metanephrine, normetanephrine
Other biomarkers	copeptin, sST2, sLOX-1, IMA
MicroRNAs	miR-16, miR-26a, miR-1, miR-133a
Relative elevation of different Biomarker assays	NT-proBNP/TnT, BNP/TnT, BNP/CKMB, BNP/Tn, NT-proBNP/myoglobin, hs-TnT/CKMB, copeptin/NT-proBNP

ACS = acute coronary syndrome; AMI = acute myocardial infarction; BNP = Brain natriuretic peptide; NT-proBNP = N-terminal proBNP; sLOX-1 = soluble lectin like oxidized LDL receptor-1; CK-MB = Creatine kinase-MB fraction; sST2 = soluble suppression of tumorigenicity-2.

1.3. Troponin (Tn), Creatine kinase (CK), CK-MB

Although autopsy specimens are not characterized by the histological features of infarction, serum troponin levels are usually positive in the acute course of TTS [3]. Troponin levels are relatively low as compared to the extent of myocardial dysfunction peaking earlier in TTS than ACS (6 h vs. 12 h) [4,5].

Although a vast body of literature describes higher markers of cardiac necrosis in ACS when compared to TTS on admission, the last report from the largest InterTAK Registry did not reveal significant differences in troponin levels. Interestingly, no differences were noted in Tn levels between patients with typical and atypical TTS [2]. Recently, the hs-TnT/CKMB ratio has been presented as a potential novel, readily available parameter to distinguish TTS from MI [6].

1.4. Catecholamines and other biomarkers

Despite the widely recognized pathophysiological role of catecholamine excess in TTS, its diagnostic role remains uncertain. Although initial reports showed markedly higher plasma catecholamine levels at presentation in TTS vs. acute myocardial infarction [7], recent studies have demonstrated similar plasma normetanephrine, metanephrine and cortisol levels as well as normal 24-hour urine catecholamine values in both subsets [8]. On the other hand, soluble lectin-like oxidized LDL receptor-1 (sLOX-1) elevation has been found comparable to troponin rise in ACS and essentially lower in the non-ACS setting

comprising TTS patients [8]. The soluble suppression of tumorigenicity-2 (sST2) can be an additional predictive value for TTS in patients with normal TnI. Thus, a combination of sST2 and cTnI may be useful to predict TTS in patients referred for invasive diagnostics due to the prior diagnosis of ACS. Last but not least, copeptin, a novel sensitive biomarker of endogenous stress response, was markedly elevated in TTS vs. AMI.

1.5. MicroRNAs (miRs)

MicroRNAs (miRs) are a class of highly conserved, small noncoding mRNA transcribed as regions of longer RNA molecules that can be as long as 1000 nt [9].

MiRs are implicated in regulating diverse cellular processes, such as proliferation, differentiation, development, and cell death [9]. MiRs are considered to act as intracellular endogenous RNAs controlling gene expression at a posttranslational level. In some pathological conditions, miRs in the systemic circulation may reflect tissue damage [9]. Interestingly, their tissue- and cell-specific expression profile can directly reflect the status of the disease. Recent studies have revealed the role of miR in a variety of basic biological and pathological processes, and as sensitive biomarkers in some conditions, for instance, cardiac hypertrophy, heart failure, acute hind-limb ischemia, myocardial infarction, and coronary artery disease.

In 2013, Jaguszewski et al. proposed a unique signature of circulating miRs (miR-1, miR-16, miR-26a, and miR-133a) as a biomarker suitable for confirming the diagnosis of an acute TTS, and for distinguishing TTS from acute MI, thus suggesting a different etiology for both conditions [10]. Interestingly, the up-regulation of stress and depression biomarkers (miR-16 and miR-26a) suggests a close connection between TTS and neuropsychiatric disorders. A down-regulation of endothelin-1 (ET-1)-regulating miR-125a-5p and increased ET-1 plasma levels stresses the potential mechanistic hypothesis of microvascular spasm in TTS [10]. The field of circulating miRs is expanding rapidly and holds great promise to become an important diagnostic tool to differentiate TTS from myocardial infarction.

1.6. Detailed electrocardiographic information

The classic evolutionary electrocardiographic changes that have been described in TTS include transient ST segment elevation, most commonly in anterior leads, followed by development of diffuse T-wave inversion involving most leads, as well as prolongation of the corrected QT interval [11].

These ECG changes are similar to those seen in patients with anterior STEMI [12].

The prevalence of ST elevation has been described with a wide variability, with a prevalence from 11% to 100% [11].

Four ECG phases have been described in TTS: Phase 1, initial ST elevation; Phase 2, initial T-wave inversion after ST elevation from days 1 to 3; Phase 3, transient improvement in T-wave inversion in the subacute period; Phase 4, second deeper T-wave inversion persisting for several months (Fig. 1).

T-wave inversion is the most prevalent ECG abnormality after 24 h, reaching a plateau between days 2 and 30; with 17% of patients having residual T-wave inversion up until 1 year.

It has been reported than African-Americans more commonly present with diffuse T-wave inversions and QTc prolongation, which is more consistent with a non-STEMI picture. The most common ECG abnormalities in Hispanics include T-wave inversions, followed by ST elevations and ST depressions [13,14].

Several detailed ECG findings in TTS include more frequent ST elevations in inferior leads, with a percentage ranging from 30 to 50% [15]; ST depression in aVR (also known as ST elevation in -aVR); and a longer maximal QTc interval with normalization by day 14. TTS has been less frequently associated with ST elevation in V1 or with pathologic Q waves, with a prevalence of 10%, with complete resolution by one month.

In TTS patients presenting with ST elevations, the ST elevations are less prominent than in STEMI, and there tends to be absence of reciprocal ST depression [13].

TTS has previously been associated with transient attenuation of the amplitude of QRS complexes when compared to a prior ECG, or low voltage QRS on admission ECG [16].

Some authors have attempted to develop a systematic approach to differentiate TTS from acute coronary syndrome using ECG criteria. Frangieh et al. reported that patients with ST depression in aVR and ST elevation in anteroseptal leads or ST elevation in inferior leads or concomitant T-wave inversion in any lead without ST elevation in V1 was 98–100% specific for TTS, with a sensitivity of 8–14% [17]. When ST depression was present in V2 to V4 or the inferior leads, with associated ST elevation in aVR, there was >95% specificity for acute coronary syndrome.

Mognai et al. reported that the combination of lack of ST elevation in lead V1, absence of abnormal Q waves, and ST depression in aVR identified TTS with a specificity of 95% and positive predictive value of 85.7% [18].

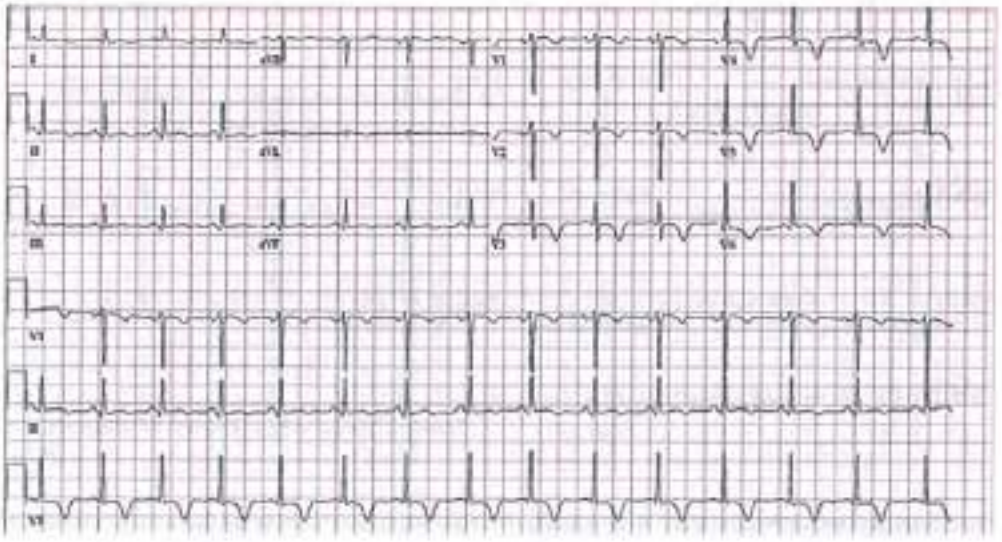

Fig. 1. 12 lead electrocardiogram with deep T wave inversion of a 62-year-old African American woman with TTS.

1.7. Transient reduction of the amplitude of the QRS complexes

The full array of the electrocardiogram (ECG) changes, pertaining particularly to repolarization and associated with all forms of acute coronary syndromes (ACS), have been encountered in patients with all topographic variants of TTS; thus, ST-segment elevations and depressions, and inverted and upright T-waves in various groups of ECG leads have been described [19,20]. In reference to changes in the QRS complexes, q- and Q-waves have been noted in patients with TTS early in the clinical course, abolished in subsequent ECGs. Review of ECGs of published TTS cases has disclosed that often the voltage amplitude of the QRS complexes is low (<5 mm in the limb leads and <10 mm in the precordial leads) (lQRS), or in case reports of patients with ≥2 ECGs, a transient attenuation of the QRS complexes (attQRS) is occasionally appreciated (Fig. 2). Previous work has shown that peripheral edema, particularly anasarca, of various etiologies, is associated with reversible attQRS, attributed to a decrease in the electrical impedance of the edematous body volume conductor [21].

Indeed edematous states affect the heart itself, via the compromise of its venous and lymphatic systems, in association with the edema apparent in the periphery [22]. TTS is characterized by transient appearance of myocardial edema (ME), documented in serial cardiac magnetic resonance imaging [23].

The above was the impetus to systematically explore the published literature of the association of TTS and the ECG attQRS. In a meta-analysis involving a total of 368 patients with TTS, lQRS was found in 91.5% of 200 patients with TTS and one ECG, with a distribution of 49.0, 42.8, 51.0, 52.0, and 46.9% in lead aVR, and inferior, anterior, lateral, and high lateral ECG lead groups, respectively, and attQRS as seen in 93.5% of 168 patients with TTS and ≥2 ECGs, with a distribution of 78.3, 74.5, 60.1, 70.7, and 74.5% in lead aVR, and inferior, anterior, lateral, and high lateral ECG lead groups, respectively [16].

1.8. Role of iodine-123 meta-iodo-benzyl-guanidine (mIBG)

Iodine-123–metaiodobenzylguanidine (^{123}I-mIBG) is a radioactive tracer that is analogue to noradrenaline in regard to presynaptic uptake, storage, and release [24,25] and ^{123}I-mIBG scintigraphy can therefore be used to visualize cardiac sympathetic nerve activity in vivo. It is unlikely that mIBG will have a clinical indication for assessing patients with TTS, but the modality may be used to investigate the underlying pathophysiology of the TTS. Several studies have investigated mIBG imaging in patients with TTS, and the results are uniform. Overall cardiac sympathetic activity appears increased [24,26,27], but ^{123}I-mIBG uptake is reduced in the akinetic regions of the left ventricle when compared to the surrounding contracting myocardium.

Thus, TTS is clearly associated with increased cardiac sympathetic activity, and the typical regional impairment of ^{123}I-mIBG uptake may be caused by excess adrenergic activity that leads to akinesia and sympathetic axon terminal damage in the vulnerable middle to apical myocardium. The main limitation to the published studies is that all patients inherently were examined after the onset of TTS; therefore, it cannot be ruled out that the observed increase in cardiac sympathetic activity observed with ^{123}I-mIBG scintigraphy is an adaptive mechanism rather than the underlying cause of the syndrome.

1.9. Optical coherence tomography

Intravascular imaging using optical coherence tomography (OCT) or intravascular ultrasound (IVUS) may help us either elucidate some of the pathophysiological mechanisms behind TTS or understand the natural history of the disease in terms of recovery (some patients fully recover ejection fraction while others do not). The following findings have been reported in the literature: Virtual histology IVUS evaluation of the left anterior descending coronary artery in patients with transient left

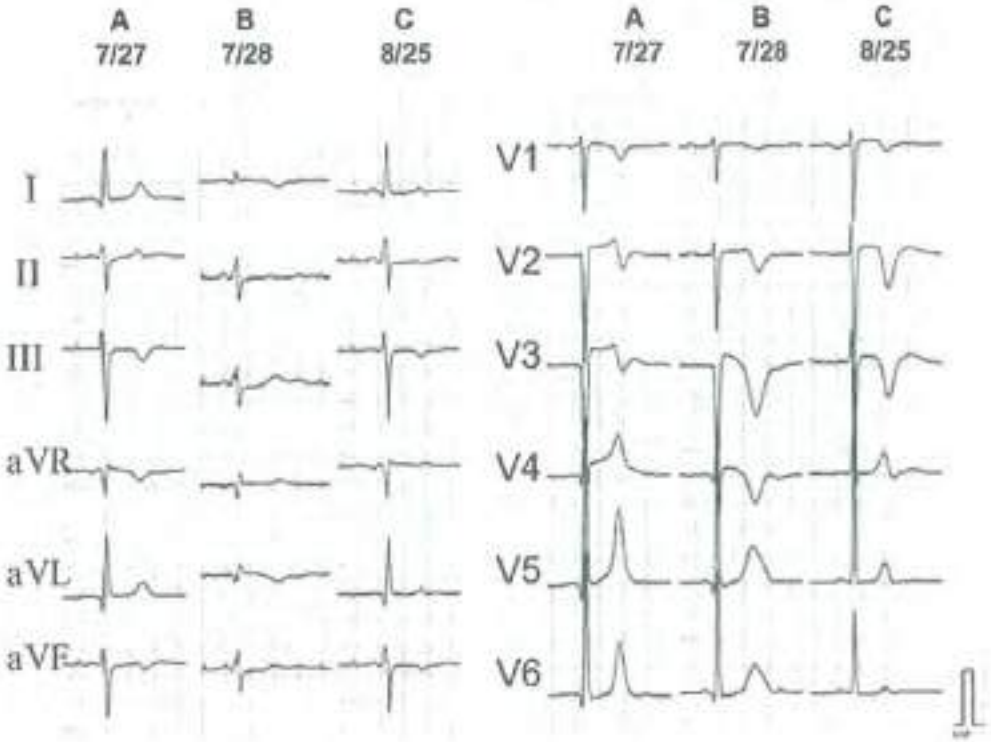

Fig. 2. Transient attenuation of the QRS complexes in a patient with TTS: ECGs on days 1, 2, and at 30-day follow-up of a 59-year-old woman with TTS following an epileptic seizure. Comparison of the ECG B with the ECGs A and C, reveals transient attenuation of the QRS complexes in the 6 limb and V1 and V2 leads.
(Reproduced and adapted from Sakuraji S et al. Heart Vessels 2007; 22:59–63, with the permission of Springer.)

ventricular ballooning syndrome found that there were 7 ruptured plaques, VH-TCFAs were found in 8 patients, 6 patients had a necrotic core >25%. The authors of this paper concluded that vulnerable plaques are observed in patients with TTS and even implied that the syndrome may be related to the natural course of atherosclerotic plaque development [28].

In another similar study, but using only IVUS grayscale in a limited number of patients, the authors did not find any plaque rupture; positive remodeling or intracoronary thrombus were absent in patients suffering from this disease [28].

There have been also reports using OCT (Fig. 3). In 23 consecutive patients, OCT in LAD to LMT was performed. Sixteen patients showed atherosclerotic plaque in the LAD or both LAD and LMT. Predominant fibrocalcific plaque: 52%, lipid rich plaque: 30.4%, TCFA: 26.1% were found, but ruptured plaque and intracoronary thrombi were not observed [29]. Some other isolated case reports using OCT did not find plausible explanations related to TTS [29,30].

There have been reports showing either no atherosclerosis or advanced CAD concomitantly at the time of the event; whether this is anecdotal or related to the disease needs further investigation.

1.10. Angiography data

In TTS, the epicardial coronary arteries are typically normal and unobstructed. The initial set of criteria proposed by researchers from the Mayo Clinic for the diagnosis of TTS required the absence of obstructive CAD. However, these criteria were later modified, and the authors acknowledged that patients with obstructive CAD may also develop TTS [11]. Patients with TTS can have coexisting CAD, as reported by Templin et al. in the largest International Takotsubo Registry, a consortium of 26 centers in Europe and the United States including 1750 patients with TTS, 15.3% of patients with TTS had evidence of significant coexisting coronary artery disease on angiography [31]. This finding shows that the presence of CAD is not an exclusion criterion for the diagnosis of TTS.

Differentiating TTS from acute coronary syndrome in an individual patient can be a difficult task. This is particularly true in cases where the LAD is involved (Fig. 4). In cases with acute plaque rupture, thrombus formation, and coronary dissection, the role of ACS is clear. Recently, Chou et al. reported that 8% of patients with TTS diagnosis had been overlooked for spontaneous coronary artery dissection (SCAD) on careful review of coronary angiography [32].

Plaque rupture with subsequent transient thrombotic coronary occlusion by a fast-dissolving clot is one of the proposed pathogenic mechanisms in TTS. In subsequent studies of TTS patients who underwent IVUS, some degree of CAD was found. Those studies conclude that coronary lesion in the LAD causing an aborted MI was not the primary underlying cause of TTS and that nonobstructive CAD and TTS could coexist without sharing a direct causal association [28].

OCT in these patients has revealed a high prevalence of atherosclerotic plaques, including a considerable number of highly vulnerable

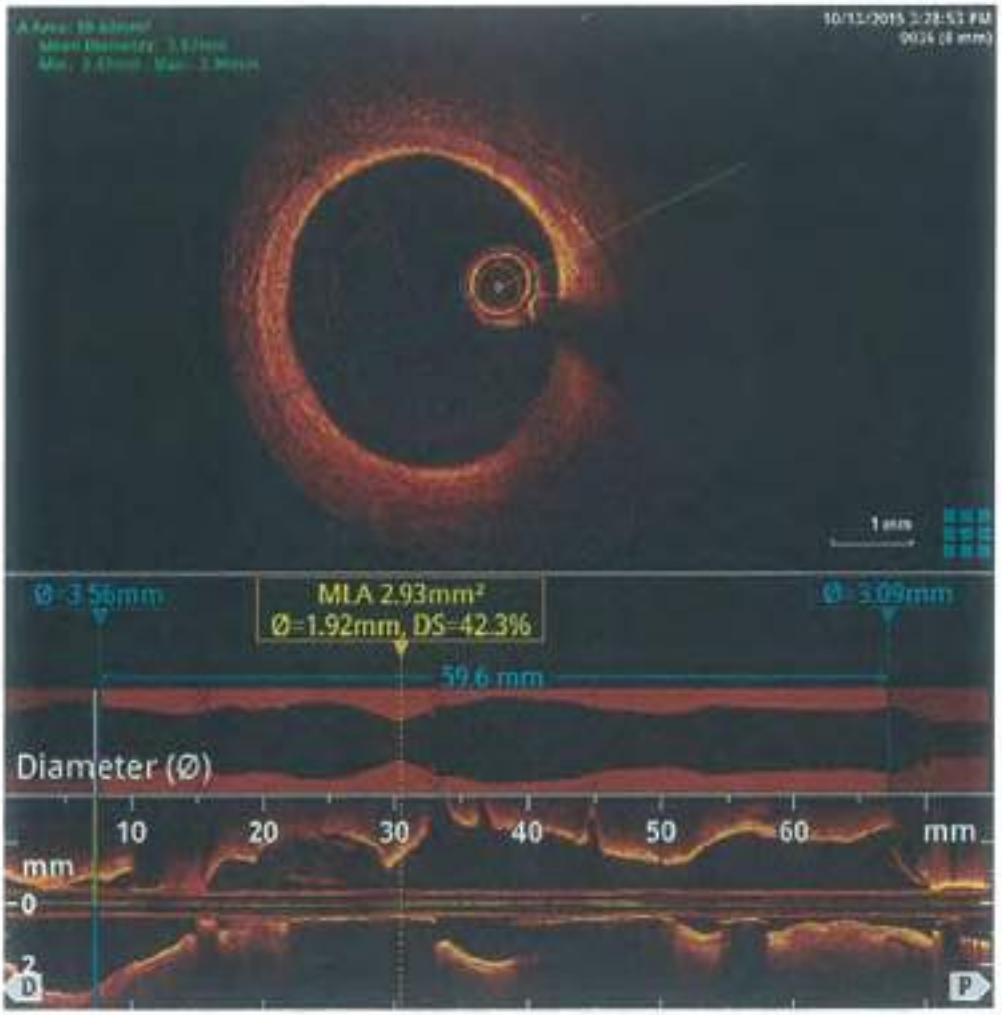

Fig. 3. OCT of TTS patient – coronary artery wall without evidence of significant plaque.

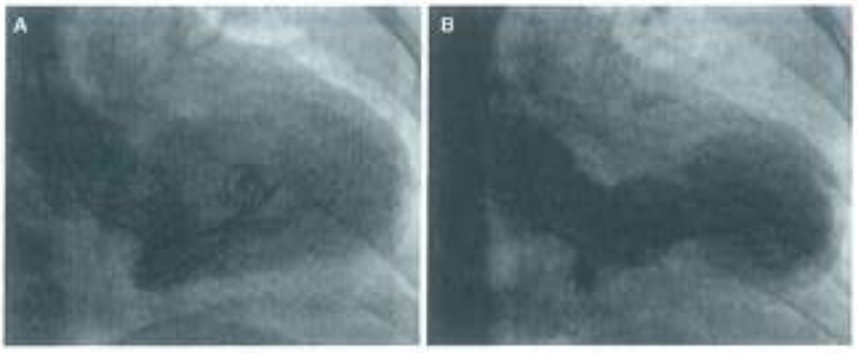

Fig. 4. Typical apical ballooning illustrated in the end-diastolic (A) and end-systolic (B) images from left ventriculography. (Courtesy Dr. Eitel et al. in Eitel I et al. J Am Heart Assoc. (2016).)

thin-cap fibroatheromas. However, ruptured plaques or intracoronary thrombi were not observed and are therefore most likely not the underlying mechanism of TTS [29].

7.11. MRI

Cardiac magnetic resonance (CMR) presents excellent anatomical information, enabling proper diagnosis and follow-up (Fig. 5) [33]. The diagnostic criteria for TTS using CMR have been proposed by Eitel et al. [34]: the absence of late gadolinium enhancement (LGE) in TTS is useful for differentiating TTS from myocardial infarction and other myocarditis. LGE exhibits the differences in the volume of distribution of gadolinium between the normal and diseased myocardium. However, clinicians should keep in mind that minor LGE can be found in patients with TTS. It has been reported that minor LGE is present in approximately 9% of patients with TTS when LGE is defined at a cutoff

Fig. 5. Typical apical ballooning during the systolic period in the patient with TTS. Cine CMR (4-chamber view A-diastole, B-systole; 2-chamber C-diastole, D-systole).

value of >3 SD above the mean; however, none of those reveals evidence of LGE with a cutoff value of >5 SD above the mean [33].

CMR is useful to provide the accurate diagnosis for TTS and helpful to rule out acute coronary syndrome and myocarditis (Table 2).

Myocardial edema should be assessed before taking LGE images. Corresponding to the wall motion abnormality, high T2 signal intensity is usually observed in patients with TTS, without increasing ventricular mass or accompanying wall motion thickness [35]. The existence of myocardial edema is thought to be the presence of myocardial injury and inflammation. This edema, the finding of T2 high intensity, is gradually resolved after the wall motion is normalized (Fig. 6) [36].

CMR can provide not only the assessment of wall motion variabilities but also the calculation of extracellular volumes using T1 mapping technique [23]. This technique would be beneficial to observe specific phenomenon in TTS because of rapid increasing extracellular matrix in the myocardium. T2 mapping technique would be a promising option to quantity the volume of myocardial edema, although this new method has not been fully established in patients with TTS.

Volumetric CMR is valuable as three-dimensional modality to identify various cardiac function beyond the structure alone. Although the usefulness of the two- or three-dimensional speckle tracking echocardiography is clearly demonstrated [37,38], tracking technique using CMR is still for research use. Apical thrombus is often identified in patients with TTS; thus, CMR, including cine CMR and early gadolinium enhancement sequence, is useful to detect a thrombus.

1.12. Echocardiographic findings – systolic and diastolic mechanics cardiomyopathy

The acute depression in left ventricular ejection fraction brings no surprise that the strain and deformation of the entire left ventricle are profoundly abnormal. Perhaps the most extreme finding is the fact that the early propping twist disappears completely in the acute stage. This early motion occurs during isovolumic contraction and is directed clockwise at the apex and counterclockwise at the base (thus opposite to the normal direction of movement to follow during systole, like an athlete throwing a discus who first turns to the right before spinning leftward to throw). However, significant mechano-temporal alterations characterizing both systole (global longitudinal strain and apical circumferential strain, $p < 0.01$ for both; LV twist, twist rate, and torsion, $p < 0.0001$ for all) and diastole (untwist rate and time to peak untwisting, $p < 0.001$ for both) persist at 4-month follow-up compared with control subjects, despite normalization of LV ejection fraction and volumes. These findings show that there is a both a reduction in the amplitude of twist and untwist of the heart as well as a delay in the timing of these processes during the cardiac cycle [37].

Although the changes are subtle enough to allow a normal or near normal ejection fraction during this convalescent stage, they do affect the overall left ventricular twist, which has the potential to impact the stroke volume of these patients. It remains unknown at this stage whether this recovery is simply more protracted than initially assumed or if it is exhausted and results in a new clinical phenotype that remains to be defined. Nevertheless, the EF normalization remains clinically useful in consolidating the diagnosis at follow-up.

2. Complications

2.1. Acute heart failure syndrome

Acute heart failure syndrome in patients with TTS is unique in that it is completely reversible, usually one to four weeks after the triggering event. Patient symptoms may range from shortness of breath with or without pulmonary edema to cardiogenic shock, with the latter quite rare [39,40].

The prevalence of acute heart failure is reported in case series ranging from 12 to 45% followed by left ventricular outflow obstruction (10–25%), mitral regurgitation (14–25%), and cardiogenic shock (6–20%). This transient heart failure manifests with elevated brain natriuretic peptide (BNP) and elevated left ventricular end diastolic pressure (LVEDP) [41,42].

Upon presentation, patients can be risk-stratified into low- versus high-risk based upon several factors. Low-risk patients' ejection fraction is >45% and usually requires no treatment. High-risk patients, in addition to an ejection fraction <45%, may have right ventricular involvement contributing to low output syndrome and shock [4,43,44].

The mechanisms contributing to acute heart failure syndrome are complex and include both systolic and diastolic dysfunction. Elderly hypertensive patients with pre-existing septal hypertrophy may develop a dynamic left ventricular outflow tract obstruction (LVOTO) and further worsening of symptoms. Systolic anterior motion of the mitral valve increases mitral regurgitation as well as worsening of the LVOTO. In up to one-third of cases, right ventricular involvement has been reported, contributing to a marked decrease in left ventricular pre-load, low cardiac output syndrome, and possible shock. In addition to increasing tricuspid regurgitation, right ventricular involvement is associated with an increase in-patient mortality [31].

With chest pain as the most common symptom in TTS, the excellent temporal and special resolution found with newer coronary computed tomography angiography (CCTA) may provide evidence of lack of obstructive CAD, thus confirming the diagnosis. CMR provides addition diagnostic and prognostic information, including extent of right ventricular involvement, mitral regurgitation, LVOTO, SAM, and left ventricular thrombus.

Table 2
Differences in CMR features of TTS acute myocardial infarction and acute myocarditis (quoted with permission).

	Takotsubo syndrome	Myocardial infarction	Myocarditis
Site of wall motion abnormality	Concentric mid- and apical LV wall	Follows expected epicardial coronary artery distribution	Usually global unless regional edema/LGE is severe
Myocardial edema	Typically transmural in a concentric mid and apical LV wall distribution	Subendocardial or transmural at sites of wall motion abnormalities	Subepicardial, mid-myocardial or transmural
Left ventricular impairment	Yes: typically impaired ejection fraction with elevated indexed end systolic volume	Yes: typically impaired ejection fraction with elevated indexed end systolic volume	Yes, but may show only mild/borderline low normal ejection fraction
Right ventricular impairment	>33% of patients	May be seen, particularly if right coronary artery territory involved	Rarely impacts on right ventricular function
LGE	Maybe (10–40%)	Yes	Often
Site of LGE	Concentric transmural mid and apical LV wall	Typically subendocardial or transmural in recognized epicardial coronary artery distribution	Mid-myocardial or subepicardial in a focal non-coronary artery distribution
Type of LGE	Low-intensity LGE	Bright LGE	Low-intensity or Bright LGE
Microvascular obstruction	No	Maybe	No
Resolution at 3 months	Yes	No	Potentially but may show residual myocardial fibrosis and impairment

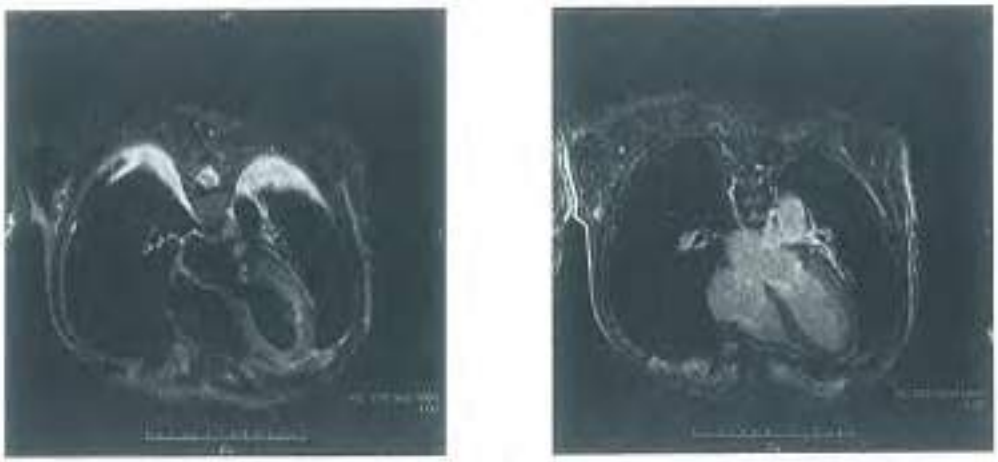

Fig. 6. Left side: myocardial edema. T2-weighted 4-chamber view showing slight transmural signal hyperintensity in the mid apical segments of left ventricle. Right side, the absence of late gadolinium enhancement in the patient with TTS was documented by CMR 4-chamber view.

On admission, 86.5% of patients had a reduced EF. The National Inpatient Sample (NIS) from 2007 to 2012 collected data on 22,005 patients with a primary diagnosis of TTS and 31,942 patients with a secondary diagnosis of TTS, making this the largest TTS registry of hospitalized patients in the United States. In this cohort, 64% reported hypertension, 4% presented with either cardiogenic shock or cardiac arrest, and 2.8% were treated with an intra-aortic balloon pump (IABP) [1,4,40,45]. There is a lack of prospective randomized clinical trials to clarify treatment protocols and guide therapy.

2.2. Arrhythmias in patients with takotsubo syndrome

Patients with TTS often have sinus tachycardia, although sinus bradycardia or other bradyarrhythmias are occasionally noted, suggesting an underlying vagal effect. Also, multiple atrial and ventricular premature beats, sinus node dysfunction (SND), asystole, paroxysmal supraventricular tachycardia (PSVT), atrial fibrillation (AF), nonsustained and sustained ventricular tachycardia (VT) (both monomorphic and polymorphic torsades de pointes ('TdP')), ventricular fibrillation (VF), ventricular asystole, pulseless electrical activity, sudden cardiac death (SCD), and right and left bundle branch blocks are noted. AF was diagnosed in 4.7% of patients with TTS [46], but occasionally it was not clear whether this represented a new AF. SND and atrioventricular nodal dysfunction were reported in 1.3% and 2.9% of cases [46], but often details are lacking. The combined incidence of sustained VT and VF was 3.4%, with potentially threatening ventricular arrhythmias (VA) and SCD occurring in 1.1% and 0.9%, respectively [46]. In a large database of patients with TTS, arrhythmias were noted in 28%, with AF/atrial flutter seen in 8.8%, PSVT in 0.8%, and life-threatening VA in 4.2% of cases. The issue occasionally arises whether VT/VF is a complication of, or the trigger for, TTS [47]. Arrhythmias in patients with TTS tend to adversely influence the hospital course and outcome, and use of β-blockers for tachyarrhythmias to counter the excessive sympathetic discharge may play a preventive/ameliorating/therapeutic role, although proof is lacking.

AF in patients with TTS is associated with older age, fewer emotional triggers, higher incidence of cardiogenic shock, lower left ventricular ejection fraction (LVEF), prolonged hospital stay, and higher long-term mortality [48]. AF is an independent determinant of outcome, even after adjustment for clinical variables, left ventricular function, and cardiogenic shock, and thus it should be employed upon its emergence for risk stratification of patients with TTS [48].

Long-term anticoagulation following a transient episode of AF in the course of TTS should be considered, as is done currently for AF in association with other cardiac illnesses.

Both transient and persisting CHB [40,50] have been reported in association with TTS. Permanent pacemakers (PPM) have been implanted in patients with persisting CHB, with or without prior electrophysiologic evaluation [50]. Temporary pacing is often necessary in the acute/subacute phase of the illness to manage the CHB and the associated bradycardia, which in the presence of a prolonged QTc predisposes patients to TdP [51]. Temporary pacing should have preference over the employment of isoproterenol infusion for CHB, other atrioventricular conduction abnormalities, or SND. Occasionally, CHB is transient and does not need temporary or PPM. Notably, implantation of a PPM has led to TTS, triggered by the associated stress.

Compared to arrhythmias encountered in the setting of AMI, VA, including VT, VF, and SCD, are less frequent in TTS, even in patients with prolonged QTc [46,52]. Regardless, continuous telemetry monitoring of patients with TTS for at least 3 days, or longer when QTc is >500 ms, is recommended [53]. To prevent TdP in patients with TTS and prolonged QTc, a form of acquired long QT syndrome, one should avoid QTc prolonging drugs, evaluate for hypokalemia and hypomagnesemia, manage bradycardia, and consider predisposing congenital/genetic long QT syndromes [53]. Magnesium is recommended for the prevention/treatment of TdP, and β-blockers should be avoided, or discontinued, until the prolongation of the QTc is resolved. Implantation of cardioverter-defibrillators (ICD) should follow consideration of persistence of QTc prolongation and bradycardia, and clinical presentation with SCD. Indeed, occasionally, TTS follows resuscitated SCD, with documentation of sustained VT, VF, or TdP, suggesting that the VA had triggered the TTS [54] rather than being its complication, and in such patients, ICD implantation is mandatory. Whether patients who had VT, VF, and TdP, in the course of TTS, should receive an ICD needs to be handled on a case-by-case basis [52,53].

2.3. Thromboembolic events

The incidence and clinical significance of thromboembolic events in TTS has not yet been sufficiently established. Data documenting these events are scarce; however, a recent in-depth analysis of existing references reveals the common occurrence of intra-ventricular thrombus among these patients, thus signifying a potential relevance [55,56].

The incidence of ventricular thrombus formation and stroke varies between 2.5%–8% and 1%–5%, respectively [31,56].

Right ventricular involvement, apical TTS form, and elevated troponin I levels might be positive predictors of thromboembolic events in TTS [55].

There are many inherent difficulties in diagnosing intraventricular thrombus formation and its peripheral embolization in TTS. Two-

dimensional echocardiogram and transesophageal echocardiogram remain the gold standard.

2.4. In-hospital mortality

In-hospital mortality is 3–5%, greater in males, and remarkably similar to that of patients with acute myocardial infarction due to obstructive CAD [44]. Cardiac-related in-hospital death is usually attributable to intractable cardiogenic shock or cardiac arrest [40,57].

In those with cardiac arrest, anoxic brain injury is an important influence on outcome. Rarely, takotsubo-related death is consequent to left ventricular free wall rupture or ventricular septal perforation [58].

Predictors of in-hospital mortality include hemodynamic instability (cardiogenic shock, use of catecholamine drugs), age >70 years, physical illness trigger, male gender, and cardiac arrest [31]. More than 80% of in-hospital deaths occur in those with a co-existing critical illness, most commonly subarachnoid hemorrhage, acute respiratory failure, sepsis, and ischemic stroke [31].

Examination of large data sets, segregating patients into those with TTS as either a primary or secondary event (in the context of an accompanying major illness), has revealed short-term mortality to be 2–3 times greater in the secondary event category, likely reflecting the importance of co-morbid conditions in determining ultimate outcome [31,59]. Importantly, even those with profoundly reduced LV ejection fraction and cardiogenic shock may experience complete normalization of LV contractile function [60].

3. Management

3.1. Role of Levosimendan and short-acting beta blockers

Levosimendan may be occasionally preferred in patients with acute heart failure over other inotropes because of lower oxygen consumption and acute myocardial depression. Its use, however, is limited to those patients with impaired systolic function, without left ventricular outflow tract obstruction and with systolic arterial pressure ≥90 mm Hg. Clinical data showed safety and feasibility of this treatment in patients with TTS [61]; Levosimendan infusion should be performed preferably for 24 h at an infusion rate of 0.1 μg/kg/min without loading dose. Invasive hemodynamic and ECG monitoring should be performed during infusion and at least for the following 48 h due to a minimal risk of hypotension and/or arrhythmias [62].

In the presence of elevated intraventricular gradients and hemodynamic impairment, patients with TTS and left ventricular outflow obstruction may benefit from the infusion of beta-blockers (BB). Although selective and non-selective BB have been proven to reduce intraventricular gradient [61], experimental data showed an increasing density of β2 adrenergic receptors from the base to the apex and a potential higher concentration of β1-adrenergic receptors in basal left ventricular segments [4,63]; therefore, β1 cardio-selective BB could be preferred. Short-acting BB like esmolol, a beta-1 cardio-selective with a short half-life (9 min) is a potential therapeutic option that could be stopped quickly in case of hemodynamic worsening [63]; the treatment usually requires invasive hemodynamic monitoring.

3.2. Mechanical circulatory support

Approximately 9–15% of patients with TTS develop cardiogenic shock [31,45], and 4–9% have cardiac arrest or need cardiopulmonary resuscitation (CPR), respectively [31,45]. Catecholamines are generally avoided in patients with TTS, given their role in TTS pathogenesis and the risk of inducing or aggravating LVOTO [60]. Mechanical circulatory support (MCS) should be evaluated early in patients with TTS and cardiogenic shock (Fig. 7) [4], although there is no reason for MCS in TTS patients without shock.

Currently there are four different percutaneous MCS systems: Intra-aortic balloon pump (IABP), TandemHeart, extracorporeal membrane oxygenation (ECMO), and microaxial pumps (i.e., Impella™, Abiomed). As TTS is a transient acute heart failure syndrome per definition [11], MCS is used in a bridge-to-recovery strategy. TTS hemodynamics are characterized by already severely increased filling pressures in the absence of shock [31], probably due to stunning-related impairment of myocardial relaxation and compliance.

IABP reduces afterload in systole and increases coronary blood flow during diastole. IABP is potentially harmful in patients with TTS, as deflation of the intra-aortic balloon during systole may increase the transaortic gradient [1] and thereby induce or aggravate LVOTO. If used, it is mandatory to perform emergent bedside echocardiogram to assess for the presence of LVOTO prior to IABP implantation.

IABP has been used in TTS with shock [64] and after CPR [65]. Upgrade to ECMO has been reported due to LVOTO [66] or lack of efficacy [67,68].

3.2.1. TandemHeart

TandemHeart drains blood from the left atrium and returns it to the iliac artery toward the aorta, like an ECMO with a left atrial cannula. TandemHeart is not as widely used as ECMO and Impella and requires transseptal cannulation. Nonetheless, left atrial unloading appears attractive for facilitating myocardial recovery. There is one published report on the successful use of TandemHeart in a patient with TTS [69].

3.2.2. ECMO

Venoarterial ECMO drains blood from the right atrium and reinfuses oxygenated and decarboxylated blood to the femoral artery [70]. This massive right-to-left shunt reduces preload and enhances end-organ perfusion at the cost of increased afterload. The latter may impede myocardial recovery and aggravate mitral regurgitation and pulmonary edema during LVOTO. ECMO is well-established for interhospital transfer and broadly available. There are several reports on ECMO in TTS, primarily for TTS with shock [71]. ECMO is effective for bridging right ventricular failure during TTS. ECMO delivers circulatory and respiratory support, and accordingly, ECMO has been used in patients with TTS and CPR, either after ROSC [72] or in refractory arrest [73]. ECMO has been used successfully without anticoagulation for a short period of time, such as in patients with TTS after polytrauma [74].

3.2.3. Impella

Impella drains blood from the left ventricle and expels it in the aortic root, thus providing antegrade transaortic blood flow. It drains blood during systole and diastole, thereby effectively unloading the left ventricle and contributing to myocardial recovery. Both the 2.5 variant [75] and the CP variant [76] have been used for bridge-to-recovery in TTS. Mechanistically, Impella appears to be the most meaningful support form in most TTS cases, and effectively bridges LVOTO and reduces associated mitral regurgitation. Notwithstanding the very positive experience in infarction-related shock and positive initial experience in TTS, controlled studies on Impella support in TTS are urgently needed.

3.3. Dilemma of ACE inhibitors

ACE-inhibitors (ACEi) are the first-line treatment in subjects with left ventricular systolic dysfunction; however, their role in patients with transient left ventricular obstruction as observed in TTS is not clear. In one of the largest populations of patients with TTS, subjects in treatment with ACEi or angiotensin-receptor blockers (ARBs) showed at 1-year follow-up a 1-year mortality rate nearly one-fourth of those not treated with such classes of drugs [31].

The study, however, was observational, and a meta-analysis of observational studies previously failed to reach statistical significance when the hypothesis was that ACEi could reduce the recurrence of TTS (odds ratio 0.42, 95% confidence interval 0.08–2.36). A meta-

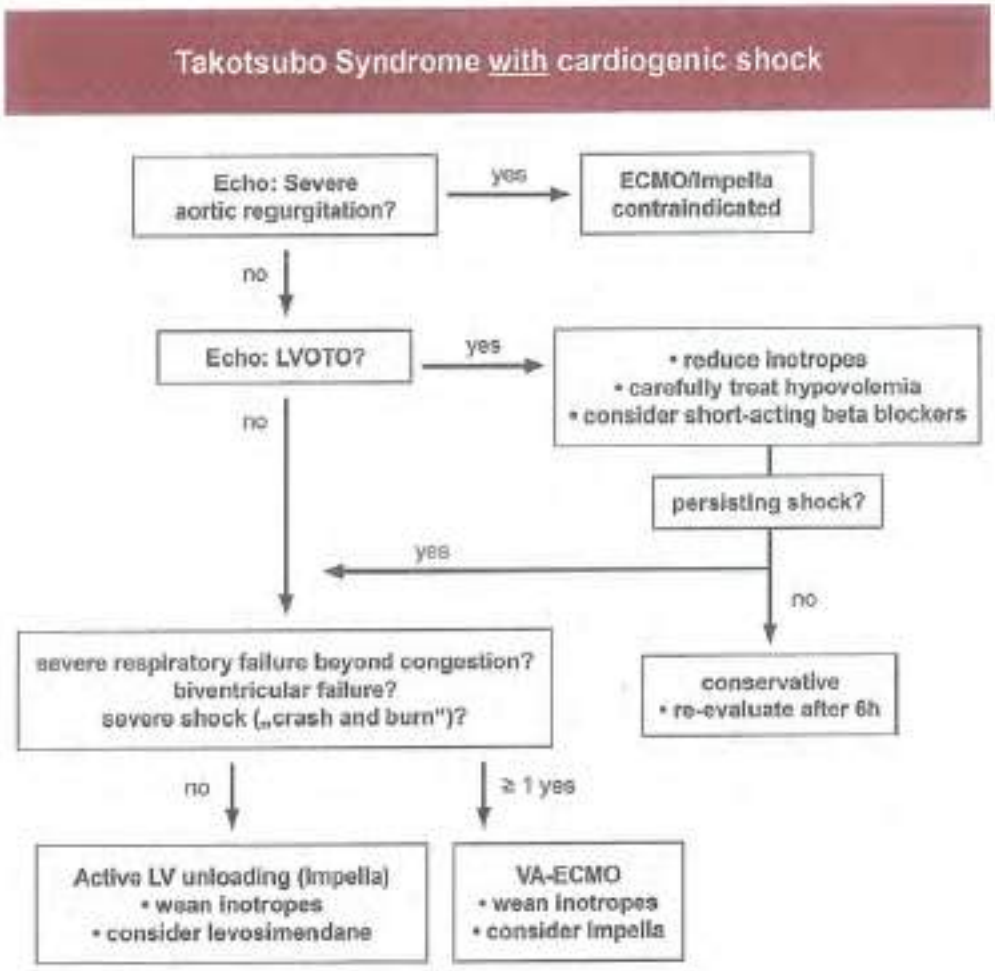

Fig. 7. Proposed criteria for mechanical circulatory support in TTS with shock.

regression by Singh et al. analyzed the effect of drug treatment on recurrence of TTS; the study, after a comprehensive search of four major databases for original research studies, recruiting ≥5 participants with ≥3 months of follow-up published in English language that reported data on recurrence in patients with TTS, included 31 cohorts (1664 patients) with a mean follow-up of 24.5 months [59,77]. The authors found that recurrence rates were independent of ambulatory utilization of BB, but inversely correlated with ACEi/ARB prescription [77,78]. The same data were subsequently reanalyzed, now weighted for populations' size, in a meta-regression analysis. Brunetti et al. have shown that recurrence of TTS is less frequent among TTS patients who have higher rates of treatment with ACEi/ARB [77,78].

However, these data should be interpreted with caution since this does not necessarily imply that ACEi may prevent recurrence of TTS. It is conceptually possible that some TTS patients or cohorts may have received more frequent and careful outpatient medical care were more compliant with guideline-directed medical therapy and therefore had lower rates of TTS recurrence.

Interestingly, statistical analysis of previously published data seems to suggest the hypothesis that rates of recurrence are lower in populations treated with combination of ACEi-BBs [77,78].

3.4. Role of long-term beta blockers

Chronic administration of BB for the prevention of TTS recurrence has been commonly used based on the speculation that, by opposing the actions of catecholamines, BB could prevent or attenuate clinical severity of a TTS recurrence. However, no study has proven any clear benefit at long-term follow-up so far. Templin et al., in a registry of 1750 patients, showed comparable death rates at 1 year whether or not patients with TTS are treated with BBs [1]; a meta-analysis including 8 studies and 511 patients found no difference in terms of recurrence rate between patients given BBs and those who were not [74]. Even the severity of TTS is not affected by pretreatment with low doses of BB [79]. Randomized controlled trials are surely warranted in order to clarify the real efficacy of BB at long term (Fig. 8).

3.5. Is there any role for aspirin alone or dual antiplatelet therapy?

TTS patients are frequently started on single or dual antiplatelet therapy on the basis of suspected acute coronary syndrome. However, to date, there are no randomized clinical trials on antithrombotic medication and respective duration.

Catecholamines can stimulate platelet activation, leading to transient thrombosis and microvascular endothelial dysfunction. As previously reported, TTS patients may have disproportionally high levels of catecholamines during a psychologically or emotionally stressful event; therefore, in theory, single or dual antiplatelet therapy could potentially decrease the risk of future cardiac events [4,31]. Recently published data show that single antiplatelet therapy with aspirin or dual with aspirin plus clopidogrel may reduce major adverse cardiovascular events during hospitalization [80]. In the International Takotsubo Registry, 67% of TTS patients were discharged on aspirin, and antithrombotic therapy, including aspirin, P2Y12 antagonists or oral anticoagulation,

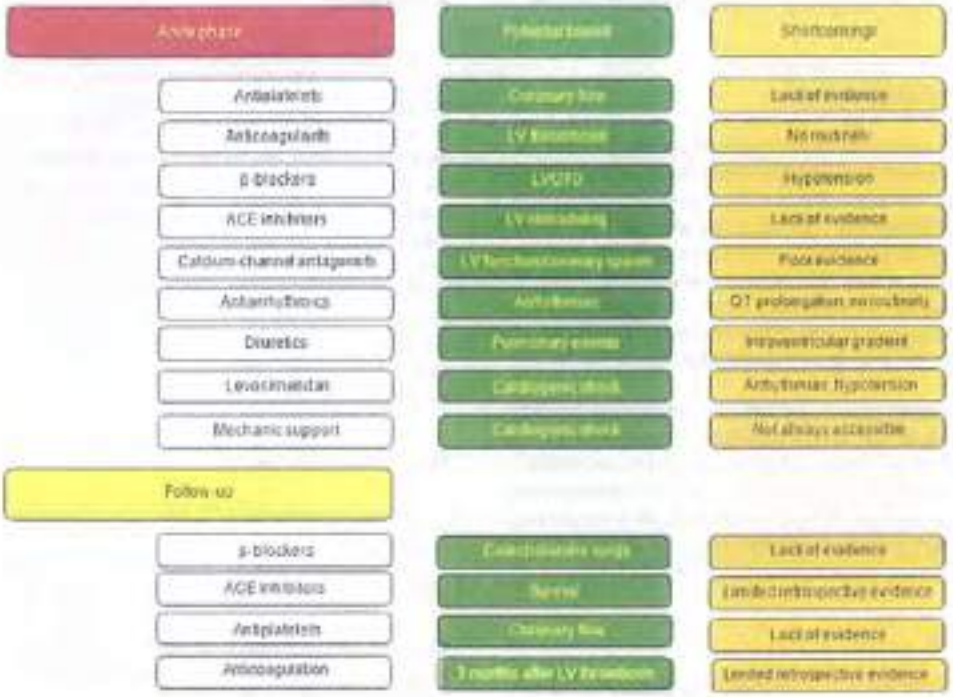

Fig. 8. Potential benefit and field of application of main therapeutic options in TTS during the acute phase and at follow-up.
(Modified from Brunetti ND, Santoro F et al. Therapy of TTS: present shortcomings and future perspectives. Future Cardiol. 2016;12 (5):563–72.)

was recommended in >80% of the patients [31]. TTS patients appear to have low bleeding rates; therefore, some authors advocate that they may benefit from short-term antiplatelet therapy, particularly those with significant LV dysfunction and until wall motion abnormalities improve [80].

In a recent subanalysis of the Intertako Registry, recurrence of TTS and MACE were not influenced by use of aspirin [1,66]. Similarly, aspirin did not reduce the risk of TTS recurrence or MACE among those discharged without BB and ACE-inhibitors [81].

3.6. Long-term prognosis: Cardiac and non-cardiac mortality

Recently published data suggest that TTS is not associated with a favorable prognosis [1]. The correlation of TTS with a bevy of complications as compared to ACS highlights a similar outcome in each scenario.

The large InterTAK-Registry reported a 5.6% mortality per patient year [1].

The recurrence rate of TTS has been reported to be up to 12% in a mean follow-up of four years [77], which might be affected by a variable pattern. It has been reported that male gender, reduced ejection fraction, old age and high Killip score are associated with a poor long-term prognosis [43,82–84]. The discussion pertaining to the prognostic impact of diabetes mellitus is still unclear. While some reports suggested an adverse outcome among diabetic TTS patients, which could potentially be attributed to long-term diabetes-associated complications, other studies have postulated a possible protective effect and lower event rates in TTS patients with diabetes mellitus [84].

Recent reports have suggested a high rate of non-cardiovascular long-term mortality in TTS, which could possibly be linked to malignancies [43].

3.7. Role of psychological distress

Psychological distress (anxiety and depression) clearly plays an important role both in the onset of TTS and in the aftermath of an acute episode. Retrospective, registry-based studies consistently report a higher prevalence of psychological distress in TTS patients compared to controls. The prevalence of anxiety and mood disorders in TTS patients was 13% and 9%, respectively, in a systematic review of registry-based studies from North America, Europe, Asia, and Australia (n = 1109) [85]. In the International Takotsubo Registry (n = 1750, 90% women), women with TTS had a greater prevalence of anxiety (10% vs. 1%) and depression (20% vs. 8%) compared to age- and sex-matched historical MI controls [31]. A large observational study involving >20,000 patients from the National Inpatient Samples found a higher prevalence of anxiety disorders in TTS (9%) compared to both MI patients (3.4%) and controls hospitalized with joint injuries (3.7%), while the prevalence of depression was 15%, 7%, and 12%, respectively [86]. Taken together, these findings suggest that anxiety and possibly depression are likely predisposing factors for the onset of TTS, particularly for the primary form of this condition. Anxiety and depression could predispose to the onset of TTS risk by affecting the magnitude of the catecholamine discharge following exposure to a stressor. In fact, both anxiety and depression have been associated with excessive reactivity to emotional stress and decreased catecholamine re-uptake.

In contrast, information on psychological distress after an acute episode and the role of distress in increasing the risk of TTS recurrence is scarce. A prospective study conducted in women with a first episode of TTS found that TTS women had significantly higher psychological distress (Hospital Anxiety and Depression scores), perceived stress, and post-traumatic stress disorder symptoms (scores on the Impact of Events Scale-Revised) compared to MI or healthy controls 4 weeks after discharge [84,87–89]. PTSD symptoms remained significantly higher in TTS women even after adjustment for confounding variables ($p < 0.05$ vs. MI and < 0.01 vs. healthy controls). The only other study that examined the psychological sequelae of TTS reported an increase in depressive symptoms in TTS compared to a group of MI patients 1 year after the acute event. The presence of PTSD symptoms in the aftermath of an acute episode suggests that women with a first episode of

TTS may be at risk for poor psychological adjustment and, possibly, future recurrences.

4. Treatment of psychological distress

To our knowledge, no studies have yet examined whether the use of anxiolytics or antidepressants could prevent the onset of a first TTS episode or their role in the treatment of distress after an acute episode. The prescription of medications to treat depression or anxiety (i.e., serotonin/norepinephrine uptake inhibitors, tricyclic antidepressants, SSRIs) appears contraindicated based on data suggesting that the use of these and other drugs that decrease catecholamine reuptake can actually increase the risk of occurrence of TTS [88–90], possibly by increasing the release of catecholamines during an acute episode.

While psychotherapy, counseling, and stress reduction approaches are reasonable and viable options for these patients, the systematic prescription of antidepressants and anxiolytics cannot be recommended, also in consideration of the lack of data on the benefit of antidepressants and anxiolytics in the prevention of a first TTS episode or future recurrences. Such treatments should be decided on an individual basis, with careful consideration of the risks and benefits involved.

5. Recurrence of TTS

Experience with TTS recurrence is inherently limited by the infrequency of the condition itself and incomplete long-term follow-up. Initial studies, with 2–4 years follow-up, noted a recurrence rate of 1–2% per year [39]. More recently, a meta-analysis of 31 takotsubo cohorts (1664 patients, mean follow-up 2 years) yielded an annual recurrence rate of 1.5%, cumulative incidence of 5% at 6 years, and average age at recurrence of 66 years [59,82]. These are likely underestimates given the difficulty in systematically tracking this diverse population over a number of years [59]. Recurrence is associated with the magnitude of LV systolic dysfunction, measured by ejection fraction, at initial event [59,82]. At recurrence, the triggering event, i.e., physical or emotional, may differ from the index event [40,83,91].

Recurrence onset may be as early as 3 weeks, or as late as several years, after the initial event. Inexplicably, in recurrent TTS, the LV ballooning pattern may differ, for example with apical ballooning during the initial event and mid-ventricular ballooning during the second event. Multiple takotsubo events (six) in the same individual have been encountered [40,82].

Current information suggests regional LV contraction and global ejection fraction recover promptly and completely during recurrence, similar to that of the index event [40,59,82,84,87]. Nonetheless, other measures of cardiac function remain abnormal for an extended time post-event, including LV global longitudinal strain, LV diastolic function, left atrial emptying volume, and NT-proBNP level [36,40]. Histologic studies have shown microscopic foci of contraction bands [4,66]. Low-intensity late gadolinium enhancement on CMR has been demonstrated in about 10% of cases, corresponding to an increase in myocardial type 1 collagen staining [92].

Recurrent TTS events could lead to a cumulative, delayed cardiac injury process, although no reports of late deterioration of LV systolic function or heart failure have yet emerged [92].

Both initial and recurrent TTS events have been reported in patients receiving beta-blocker therapy, usually administered for co-existing systemic hypertension [31,40,82]. Contemporary analyses have revealed 20–25% of TTS patients were receiving beta-blocker drugs at the time of their initial event, and 40% at the time of a second episode. Consistent with this observation, a meta-analysis found no benefit of drug therapy for prevention of TTS recurrence [74]. At this time, there is no evidence that pharmacologic therapy is effective for prevention of TTS recurrence.

6. Conclusion

This paper is the result of a multinational crowdsourcing effort aiming to provide the current state of the art on takotsubo syndrome. Several experts in the field contributed to it.

Important spikes of TTS cases have been consistently reported over the past few years. It is still unclear if the growing numbers reflect an increasing awareness of this acute heart failure syndrome by clinicians or if it is in fact a true rise in its incidence. Nonetheless, multiple aspects of this syndrome are still unknown or not completely understood. Moreover, our current knowledge is mostly based on case reports and relatively small cohorts. Since individual health facilities may see a small number of TTS cases per annum, it is crucial to establish national and international TTS registries. These networks will enable us to better understand this specific syndrome and improve the accuracy of identifying the disease and its prognosis.

Declarations of interest

Milosz Jaguszewski, MD, FESC, has received lecture honoraria from St. Jude Medical.

Dana Dawson, DM, FRCP, DPhil, FESC, has a research agreement with Philips Healthcare and holds an MTA with AMAG Pharmaceuticals.

L. Christian Napp, MD, received lecture honoraria from Abiomed, Maquet and Cytosorbents, consultant fees from Bayer, and traveling or congress support from Abbott, Abiomed, Bayer, Biotronik, Boston Scientific, Lilly, Medtronic, Merit Medical, Pfizer, Servier, and Volcano.

Kathy Hebert, MD, MPH, is an employee of GE Healthcare.

Takashi Akasaka, MD, has received lecture fees and research funds from Kowa Pharmaceutical Co. Ltd.

Ron Waksman, MD, received honoraria from Abbott Vascular, Amgen, Boston Scientific, Chiesi, Medtronic and Philips Volcano, and consulting fees from Biosensors, Biotronik, Corindus, Lifetech Medical and Pi-Cardia LTD. He is on the advisory boards of Abbott Vascular, Amgen, Boston Scientific, Medtronic, Philips Volcano and Pi-Cardia LTD, is a consultant for Abbott Vascular, Amgen, Biosensors, Biotronik, Boston Scientific, Corindus, Lifetech Medical, Medtronic, Philips Volcano and Pi-Cardia LTD, received grant support from Abbott Vascular, Biosensors, Biotronik, Boston Scientific, Chiesi and Edwards Lifesciences, and is an investor in MedAlliance.

All other authors have no conflicts of interest to disclose.

Funding

This research did not receive any specific grant from funding agencies in the public, commercial, or not-for-profit sectors.

References

[1] Coddens J, Van Alphen J, Deloof T, Hendricks J. Dynamic left ventricular outflow tract obstruction caused by afterload reduction induced by intra-aortic balloon counterpulsation. J Cardiothorac Vasc Anesth 2002;16:749–51.
[2] Ghadri JR, Cammann VL, Napp LC, Jurisic S, Diekmann J, Bataiou DR, et al. Differences in the clinical profile and outcomes of typical and atypical takotsubo syndrome: data from the International Takotsubo Registry. JAMA Cardiol 2016 Jun 1;1(3):335–40.
[3] Jaguszewski M, Pijalkowski M, Nowak R, Czapiewski P, Ghadri JR, Templin C, et al. Ventricular rupture in Takotsubo cardiomyopathy. Eur Heart J 2013 Apr;33(8):1027.
[4] Lyon AR, Bossone E, Schneider B, Sechtem U, Citro R, Underwood SR, et al. Current state of knowledge on Takotsubo syndrome: a position statement from the Taskforce on Takotsubo Syndrome of the Heart Failure Association of the European Society of Cardiology. Eur J Heart Fail 2016 Jan;18(1):8–27.
[5] Patel G, Assad D, Wiemann C, Zughaib M. Repeated use of albuterol inhaler as a potential cause of Takotsubo cardiomyopathy. Am J Case Rep 2014 May 19;15:221–5.
[6] Pirlet C, Pierard L, Legrand V, Gach O. Ratio of high-sensitivity troponin to creatine kinase-MB in takotsubo syndrome. Int J Cardiol 2017 Sep 15;243:300–5.
[7] Madhavan M, Borlaug BA, Lerman A, Rihal CS, Prasad A. Stress hormone and circulating biomarker profile of apical ballooning syndrome (Takotsubo cardiomyopathy): insights into the clinical significance of B-type natriuretic peptide and troponin levels. Heart 2009 Sep;95(17):1436–41.

[8] Kobayashi N, Hata N, Kume N, Shinada T, Tomita K, Shirakabe A, et al. Soluble lectin-like oxidized LDL receptor-1 and high-sensitivity troponin T as diagnostic biomarkers for acute coronary syndrome. Improved values with combination usage in emergency rooms. Circ J 2011;75(12):2862–71.
[9] Jeyaseelan K, Lim KY, Armugam A. MicroRNA expression in the blood and brain of rats subjected to transient focal ischemia by middle cerebral artery occlusion. Stroke 2008 Mar;39(3):959–66.
[10] Jagusiewski M, Chipova J, Ghadri JR, Napp LC, Widera C, Franke J, et al. A signature of circulating microRNAs differentiates takotsubo cardiomyopathy from acute myocardial infarction. Eur Heart J 2014 Apr;35(15):999–1006.
[11] Prasad A, Lerman A, Rihal CS. Apical ballooning syndrome (Tako-Tsubo or stress cardiomyopathy): a mimic of acute myocardial infarction. Am Heart J 2008 Mar;155(3):408–17.
[12] Bybee KA, Kara T, Prasad A, Lerman A, Barsness GW, Wright RS, et al. Systematic review: transient left ventricular apical ballooning: a syndrome that mimics ST-segment elevation myocardial infarction. Ann Intern Med 2004 Dec 7;141(11):858–65.
[13] Ogura R, Hiasa Y, Takahashi T, Yamaguchi K, Fujiwara K, Ohara Y, et al. Specific findings of the standard 12-lead ECG in patients with 'Takotsubo' cardiomyopathy: comparison with the findings of acute anterior myocardial infarction. Circ J 2003 Aug;67(8):687–90.
[14] Franco E, Dias A, Kushbelashvili N, Pressman GS, Hebert K, Figueredo VM. Distinctive electrocardiographic features in African Americans diagnosed with Takotsubo cardiomyopathy. Ann Noninvasive Electrocardiol 2016 Sep;21(5):486–92.
[15] Perazzolo Marra M, Zorzi A, Corbetti F, De Lazzari M, Migliore F, Tona F, et al. Apicobasal gradient of left ventricular myocardial edema underlies transient T-wave inversion and QT interval prolongation (Wellens' ECG pattern) in Tako-Tsubo cardiomyopathy. Heart Rhythm 2013 Jan;10(1):70–7.
[16] Madias JE. Transient attenuation of the amplitude of the QRS complexes in the diagnosis of Takotsubo syndrome. Eur Heart J Acute Cardiovasc Care 2014 Mar;3(1):28–36.
[17] Frangieh AH, Obeid S, Ghadri JR, Imori Y, D'Ascenzo F, Kovac M, et al. ECG criteria to differentiate between Takotsubo (stress) cardiomyopathy and myocardial infarction. J Am Heart Assoc 2016 Jun 13;5(6). https://doi.org/10.1161/JAHA.116.003418.
[18] Mognai G, Pasquale G, Benfari G, Bertagnolli L, Mugnai F, Vassanelli F, et al. Acute electrocardiographic differences between Takotsubo cardiomyopathy and anterior ST elevation myocardial infarction. J Electrocardiol 2015 Jan-Feb;48(1):78–85.
[19] Y-Hassan S. The causal link between the blood borne catecholamines and takotsubo syndrome: too many flaws. Int J Cardiol 2015 Jun 15;189:194–5.
[20] Kurisu S, Kato Y, Mitsuba N, Ishibashi K, Dohi Y, Nishioka K, et al. Comparison of electrocardiographic findings between the midventricular ballooning form and apical ballooning form of takotsubo cardiomyopathy. Clin Cardiol 2011 Sep;34(9):555–9.
[21] Madias JE, Bazaz R, Agarwal H, Win M, Medepalli L. Anasarca-mediated attenuation of the amplitude of electrocardiogram complexes: a description of a heretofore unrecognized phenomenon. J Am Coll Cardiol 2001 Sep;38(3):756–64.
[22] Madias JE. QRS voltage changes in heart failure: a 3-compartment mechanistic model and its implications. Indian Pacing Electrophysiol J 2010 Oct 31;10(10):464–73.
[23] Akashi YJ, Nef HM, Lyon AR. Epidemiology and pathophysiology of Takotsubo syndrome. Nat Rev Cardiol 2015 Jul;12(7):387–97.
[24] Christensen TE, Bang LE, Holmvang L, Skovgaard DC, Ottesen DB, Soholm H, et al. (123)I-MIBG scintigraphy in the subacute state of Takotsubo cardiomyopathy. JACC Cardiovasc Imaging 2016 Aug;9(8):982–90.
[25] Christensen TE, Kjaer A, Hasbak P. The clinical value of cardiac sympathetic imaging in heart failure. Clin Physiol Funct Imaging 2014 May;34(3):178–82.
[26] Bergdorf C, von Hof K, Schunkert H, Karowski V. Regional alterations in myocardial sympathetic innervation in patients with transient left-ventricular apical ballooning (Tako-Tsubo cardiomyopathy). J Nucl Cardiol 2008 Jan-Feb;15(1):65–72.
[27] Akashi YJ, Nakazawa K, Sakakibara M, Miyake F, Musha H, Sasaka K. 123I-MIBG myocardial scintigraphy in patients with "takotsubo" cardiomyopathy. J Nucl Med 2004 Jul;45(7):1121–7.
[28] Haghi D, Roehm S, Hamm K, Harder N, Suselbeck T, Borggrefe M, et al. Takotsubo cardiomyopathy is not due to plaque rupture: an intravascular ultrasound study. Clin Cardiol 2010 May;33(5):307–10.
[29] Eitel I, Stiermaier T, Graf T, Moller C, Rommel KP, Eitel C, et al. Optical coherence tomography to evaluate plaque burden and morphology in patients with Takotsubo syndrome. J Am Heart Assoc 2016 Dec 22;5(12). https://doi.org/10.1161/JAHA.116.
[30] Alfonso F, Nunez-Gil IJ, Hernandez R. Optical coherence tomography findings in Tako-Tsubo cardiomyopathy. Circulation 2012 Sep 25;126(13):1663–4.
[31] Templin C, Ghadri JR, Diekmann J, Napp LC, Bataiosu DR, Jaguszewski M, et al. Clinical features and outcomes of Takotsubo (stress) cardiomyopathy. N Engl J Med 2015 Sep 3;373(10):929–38.
[32] Chou AY, Setlak T, Ayinong E, Sheth T, Starovoytov A, Humphries KH, et al. Spontaneous coronary artery dissection misdiagnosed as Takotsubo cardiomyopathy: a case series. Can J Cardiol 2015 Aug;31(8):1073.e5–8.
[33] Eitel I, Friedrich MG. T2-weighted cardiovascular magnetic resonance in acute cardiac disease. J Cardiovasc Magn Reson 2011 Feb 18;13 [13-428X-13-13].
[34] Ueyama T, Ishikura F, Matsuda A, Asazuma T, Ueda K, Ichikawa M, et al. Chronic estrogen supplementation following ovariectomy improves the emotional stress-induced cardiovascular responses by indirect action on the nervous system and by direct action on the heart. Circ J 2007 Apr;71(4):565–73.
[35] Eitel I, Friedrich MG. T2-weighted cardiovascular magnetic resonance in acute cardiac disease. J Cardiovasc Magn Reson 2011 Feb 18;13 [13-428X-13-13].
[36] Nell C, Nguyen TH, Kucia A, Crouch B, Svendsen A, Chirkov Y, et al. Slowly resolving global myocardial inflammation/oedema in Tako-Tsubo cardiomyopathy: evidence from T2-weighted cardiac MRI. Heart 2012 Sep;98(17):1278–84.
[37] Schwarz K, Akerom T, Srinivasan J, Neil CJ, Scally C, Rudd A, et al. Alterations in cardiac deformation, timing of contraction and relaxation, and early myocardial fibrosis accompany the apparent recovery of acute stress-induced (Takotsubo) cardiomyopathy: an end to the concept of transience. J Am Soc Echocardiogr 2017 Aug;30(8):745–55.
[38] Kobayashi Y, Okura H, Kobayashi Y, Fukuda S, Hirohata A, Yoshida K. Left ventricular myocardial function assessed by three-dimensional speckle tracking echocardiography in Takotsubo cardiomyopathy. Echocardiography 2017 Apr;34(4):523–9.
[39] Sharkey SW, Windenburg DC, Lesser JR, Maron MS, Hauser RG, Lesser JN, et al. Natural history and expansive clinical profile of stress (tako-tsubo) cardiomyopathy. J Am Coll Cardiol 2010 Jan 26;55(4):333–41.
[40] Sharkey SW, Maron BJ. Epidemiology and clinical profile of Takotsubo cardiomyopathy. Circ J 2014;78(9):2119–28.
[41] Elgendy AY, Elgendy IY, Mansour H, Mahmoud AN. Clinical presentations and outcomes of Takotsubo syndrome in the setting of subarachnoid hemorrhage: a systematic review and meta-analysis. Eur Heart J Acute Cardiovasc Care 2016 Nov;16.
[42] Dias A, Franco E, Figueredo VM, Hebert K. Can previous oophorectomy worsen the clinical course of takotsubo cardiomyopathy females? Age- and gender-related outcome analysis. Int J Cardiol 2014 Dec 20;177(3):1134–6.
[43] Sattler K, El-Battrawy I, Lang S, Zhao X, Schramm K, Tulmann E, et al. Prevalence of cancer in Takotsubo cardiomyopathy: short and long-term outcome. Int J Cardiol 2017 Jul 1;238:159–65.
[44] Redfors B, Vedad R, Angeras O, Ramunddal T, Petursson P, Haraldsson I, et al. Mortality in takotsubo syndrome is similar to mortality in myocardial infarction - a report from the SWEDEHEART registry. Int J Cardiol 2015 Apr 15;185:192–9.
[45] Sharkey SW, Park VR, Lesser JR, Garberich RF, Maron MS, Maron BJ. Clinical profile of patients with high-risk Tako-Tsubo cardiomyopathy. Am J Cardiol 2015 Sep 1;110(5):765–72.
[46] Syed FF, Ashrafian S, Francis J. Arrhythmia occurrence with takotsubo cardiomyopathy: a literature review. Europace 2011 Jun;13(6):780–6.
[47] Case records of the Massachusetts General Hospital Weekly clinicopathological exercises Case 18–1986 A 64-year-old woman with substernal pain and pulmonary edema after severe emotional stress. N Engl J Med 1986 May 8;314(19):1240–7.
[48] Stiermaier T, Santoro F, Eitel C, Graf T, Moller C, Tarantino N, et al. Prevalence and prognostic relevance of atrial fibrillation in patients with Takotsubo syndrome. Int J Cardiol 2017 Oct 15;245:156–61.
[49] Inoue M, Kanaya H, Matsubara T, Uno Y, Yasuda T, Miwa K. Complete atrioventricular block associated with takotsubo cardiomyopathy. Circ J 2009 Mar;73(3):589–92.
[50] Oshima T, Butomi M, Ishiwata J, Shinohara H, Ouchi K, Kozaki T, et al. Takotsubo cardiomyopathy associated with complete atrioventricular block and Torsades de pointes. Int J Cardiol 2015 Feb 15;181:357–9.
[51] Oshima T, Butomi M, Ishiwata J, Shinohara H, Ouchi K, Kozaki T, et al. Takotsubo cardiomyopathy associated with complete atrioventricular block and Torsades de pointes. Int J Cardiol 2015 Feb 15;181:357–9.
[52] Brown KH, Trohman RG, Madias C. Arrhythmias in takotsubo cardiomyopathy. Card Electrophysiol Clin 2015 Jun;7(2):331–40.
[53] Madias C, Fitzgibbons TP, Alsheikh-Ali AA, Bouchard JL, Kalsmith B, Garlitski AC, et al. Acquired long QT syndrome from stress cardiomyopathy is associated with ventricular arrhythmias and torsades de pointes. Heart Rhythm 2011 Apr;8(4):555–61.
[54] Madias JE. Cardiac arrest-triggered takotsubo syndrome vs. takotsubo syndrome complicated by cardiac arrest. Int J Cardiol 2016 Dec 15;225:142–3.
[55] El-Battrawy I, Behnes M, Hillenbrand D, Haghi D, Hoffmann U, Papavassiliu T, et al. Prevalence, clinical characteristics, and predictors of patients with thromboembolic events in Takotsubo cardiomyopathy. Clin Med Insights Cardiol 2016 Jul 12;10:117–22.
[56] El-Battrawy I, Borggrefe M, Akin I. Takotsubo syndrome and embolic events. Heart Fail Clin 2016 Oct;12(4):543–50.
[57] Sharkey SW, Maron BJ. Epidemiology and clinical profile of Takotsubo cardiomyopathy. Circ J 2014;78(9):2119–28.
[58] Akashi YJ, Tejima T, Sakurada H, Matsuda H, Suzuki K, Kawasaki K, et al. Left ventricular rupture associated with Takotsubo cardiomyopathy. Mayo Clin Proc 2004 Jun;79(6):821–4.
[59] Singh K, Carson K, Shah R, Sawhney G, Singh B, Parsaik A, et al. Meta-analysis of clinical correlates of acute mortality in takotsubo cardiomyopathy. Am J Cardiol 2014 Apr 15;113(8):1420–8.
[60] Citro R, Rigo F, D'Andrea A, Ciampi Q, Parodi G, Provenza G, et al. Echocardiographic correlates of acute heart failure, cardiogenic shock, and in-hospital mortality in tako-tsubo cardiomyopathy. JACC Cardiovasc Imaging 2014 Feb;7(2):119–29.
[61] Santoro F, Ieva R, Ferranti A, Ieno V, Carpagnano G, Lodispoto M, et al. Safety and feasibility of levosimendan administration in takotsubo cardiomyopathy: a case series. Cardiovasc Ther 2013 Dec;31(6):e133–7.
[62] Brunetti ND, Santoro F, De Gennaro L, Correale M, Kontaxis H, Gaglione A, et al. Therapy of stress (takotsubo) cardiomyopathy: present shortcomings and future perspectives. Future Cardiol 2016 Sep;12(5):563–72.
[63] Santoro F, Ieva R, Ferranti A, Fanelli M, Musaico P, Tarantino N, et al. Hemodynamic effects, safety, and feasibility of intravenous esmolol infusion during Takotsubo cardiomyopathy with left ventricular outflow tract obstruction: results from a multicenter registry. Cardiovasc Ther 2016 Jun;34(3):151–6.
[64] Rahal JP, Malek AM, Hellman CB. Intra-aortic balloon pump counterpulsation in aneurysmal subarachnoid hemorrhage. World Neurosurg 2013;80:e203–7.
[65] Bleser T, Werth C, Gorge G. Reverse takotsubo cardiomyopathy-a life-threatening disease. Successful resuscitation of a 31-year-old woman with cardiologic shock after a visit to the dentist. Med Klin Intensivmed Notfmed 2013 Nov;108(8):575–8.
[66] Nunez Gil IJ, Andres M, Almendro Delia M, Sionis A, Martin A, Bastante T, et al. Characterization of Tako-tsubo cardiomyopathy in Spain: results from the RETAKO National Registry. Rev Esp Cardiol 2015 Jun;68(6):505–12.

[67] Bonacchi M, Maiani M, Harmelin G, Sani G. Intractable cardiogenic shock in stress cardiomyopathy with left ventricular outflow tract obstruction: is extra-corporeal life support the best treatment? Eur J Heart Fail 2009 Jul;11(7):721–7.
[68] Ghanim D, Adler Z, Qarawani D, Kuniec F, Amir O, Carasso S. Takotsubo cardiomyopathy caused by epinephrine-treated bee sting anaphylaxis: a case report. J Med Case Reports 2015;9:247.
[69] Hassid B, Armoon S, Arnouw WS, Palaniswamy C, Cohen M, Gass A. Hemodynamic support with TandemHeart in takotsubo cardiomyopathy – a case report. Arch Med Sci 2010 Dec;6(6):971–5.
[70] Napp LC, Kuhn C, Hoeper MM, Vogel-Claussen J, Haverich A, Schafer A, et al. Cannulation strategies for percutaneous extracorporeal membrane oxygenation in adults. Clin Res Cardiol 2016 Apr;105(4):283–96.
[71] Renault P, Nee L, Signouret T, Jaussaud N, Kerbaul F. Reverse Takotsubo cardiomyopathy after iatrogenic epinephrine injection requiring percutaneous extracorporeal membrane oxygenation. Can J Anaesth 2014;61:1093–7.
[72] van Zwet CJ, Riot A, Haeusler A, Graves K, Zollinger A, Blumenthal S. Extracorporeal membrane oxygenation for treatment of acute inverted takotsubo-like cardiomyopathy from hemorrhagic pheochromocytoma in late pregnancy. A A Case Rep 2016;7:196–9.
[73] Flam B, Broome M, Frenckner B, Brunstrom R, Bell M. Pheochromocytoma-induced inverted takotsubo-like cardiomyopathy leading to cardiogenic shock successfully treated with extracorporeal membrane oxygenation. J Intensive Care Med 2015 Sep;30(6):365–72.
[74] Bonacchi M, Vannini A, Harmelin G, et al. Inverted-Takotsubo cardiomyopathy: severe refractory heart failure in poly-trauma patients saved by emergency extracorporeal life support. Interact Cardiovasc Thorac Surg 2015;20:365–71.
[75] Rashed A, Wan S, Saad M, Schreiber T. Use of the Impella 2.5 left ventricular assist device in a patient with cardiogenic shock secondary to takotsubo cardiomyopathy. BMJ Case Rep 2015:2015.
[76] Sundaravel S, Alrifai A, Kabach M, Ghumman W. POLFOX induced Takotsubo cardiomyopathy treated with Impella assist device. Case Rep Cardiol 2017;2017:8507096.
[77] Brunetti ND, Santoro F, De Gennaro L, Correale M, Gaglione A, Di Biase M. Drug treatment rates with beta-blockers and ACE-inhibitors/angiotensin receptor blockers and recurrences in takotsubo cardiomyopathy: a meta-regression analysis. Int J Cardiol 2016 Jul 1;214:340–2.
[78] Brunetti ND, Santoro F, De Gennaro L, Correale M, Gaglione A, Di Biase M, et al. Combined therapy with beta-blockers and ACE-inhibitors/angiotensin receptor blockers and recurrence of Takotsubo (stress) cardiomyopathy: a meta-regression study. Int J Cardiol 2017 Mar 1;230:281–3.
[79] Santoro F, Ieva R, Musaico F, Ferraretti A, Triggiani G, Tarantino N, et al. Lack of efficacy of drug therapy in preventing takotsubo cardiomyopathy recurrence: a meta-analysis. Clin Cardiol 2014 Jul;37(7):434–9.
[80] Dias A, Franco E, Janzer S, Kochkelashvili N, Bhalla V, Rubio M, et al. Incidence and predictors of stroke during the index event in an ethnically diverse Takotsubo cardiomyopathy population. Pancr Neurol 2016 Jul-Sep;31(3):157–62.
[81] Bertaina M, D'Ascenzo F, Iannaccone M, Frangieh A, Galta F, Templin C. Is aspirin needed after Takotsubo syndrome?: a propensity score sub-analysis of inter-tak registry. August 2017;38(suppl_1).
[82] Singh K. Tako-Tsubo syndrome: issue of incomplete recovery and recurrence. Eur J Heart Fail 2016 Dec;18(12):1408–10.
[83] Bleiber AA, Prasad A, Lerman RJ, Wright RS, Lerman A, Rihal CS. Four-year recurrence rate and prognosis of the apical ballooning syndrome. J Am Coll Cardiol 2007 Jul 31;50(5):448–52.
[84] Stiermaier T, Moeller C, Oehler K, Desch S, Graf T, Eitel C, et al. Long-term excess mortality in takotsubo cardiomyopathy: predictors, causes and clinical consequences. Eur J Heart Fail 2016 Jun;18(6):650–6.
[85] Pelliccia F, Parodi G, Greco C, Antoniucci D, Brenner R, Bossone E, et al. Comorbidities frequency in Takotsubo syndrome: an international collaborative systematic review including 1109 patients. Am J Med 2015 Jun;128(6):654e11–9.
[86] El-Sayed AM, Brizjikji W, Salha S. Demographic and co-morbid predictors of stress (takotsubo) cardiomyopathy. Am J Cardiol 2012 Nov 1;110(9):1368–72.
[87] El-Battrawy I, Borggrefe M, Akin I. Predictors of mortality in Takotsubo cardiomyopathy. Eur J Heart Fail 2017 Jan;19(1):158.
[88] Salmoirago-Blotcher E, Rosman L, Wittstein IS, Dunziger S, Swales HH, Auriemma CP, et al. Psychiatric history, post-discharge distress, and personality characteristics among incident female cases of takotsubo cardiomyopathy: a case-control study. Heart Lung 2016 Nov - Dec;45(6):503–9.
[89] Nell CJ, Cheng CR, Nguyen TH, Horowitz JD. Occurrence of Tako-Tsubo cardiomyopathy in association with ingestion of serotonin/noradrenaline reuptake inhibitors. Heart Lung Circ 2012 Apr;21(4):203–5.
[90] Singh K, Carson K, Usmani Z, Sawhney G, Shah R, Horowitz J. Systematic review and meta-analysis of incidence and correlates of recurrence of takotsubo cardiomyopathy. Int J Cardiol 2014 Jul 1;174(3):696–701.
[91] Sherif K, Sehli S, Jenkins LA. Takotsubo cardiomyopathy after administration of norepinephrine. Proc (Bayl Univ Med Cent) 2016 Apr;29(2):166–7.
[92] Eitel I, von Knobelsdorff-Brenkenhoff F, Bernhardt P, Carbone I, Muellerleile K, Aldrovandi A, et al. Clinical characteristics and cardiovascular magnetic resonance findings in stress (takotsubo) cardiomyopathy. JAMA 2011 Jul 20;306(3):277–86.

Endothelialization of an Amplatzer Septal Occluder Device 6 Months Post Implantation: Is This Enough Time? An *In Vivo* Angioscopic Assessment

Yasuhiro Tanabe, MD, PhD; Yukio Sato, MD, PhD; Masaki Izumo, MD, PhD; Yuki Ishibashi, MD, PhD; Takumi Higuma, MD, PhD; Tomoo Harada, MD, PhD; Yoshihiro J. Akashi, MD, PhD

J INVASIVE CARDIOL 2019;31(2):E44.
KEY WORDS: Amplatzer septal occluder, angioscopy, antithrombotic therapy, atrial septal defect, neointimal coverage

The current guidelines recommend a minimum of 6 months of antithrombotic and antibiotic prophylaxis following septal occluding device placement for transcatheter closure of atrial septal defect (ASD). Full neoendothelialization is thought to be completed within 6 months of device implantation; however, there is no method available that can assess the level of neoendothelialization *in vivo*. An autopsy study detected minimal epithelialization on the surface of the metallic mesh 5 months post implantation, while a case of bacterial endocarditis detected 30 months post implantation concluded that the poor tissue endothelialization might have been a cause of the infection.

The Amplatzer atrial septal occluder (ASO; St. Jude Medical) is a commonly used device for percutaneous transcatheter closure of ASDs worldwide; however, to our knowledge, there is currently no *in vivo* angioscopic investigation that can accurately assess the degree of endothelialization. Therefore, we set out to evaluate the neointimal coverage of ASO using angioscopy (Visible; Fiber Tech Co, Ltd) from a right atrial access (Figure 1A) in a 78-year-old woman with a 22 mm ASO implanted 6 months prior.

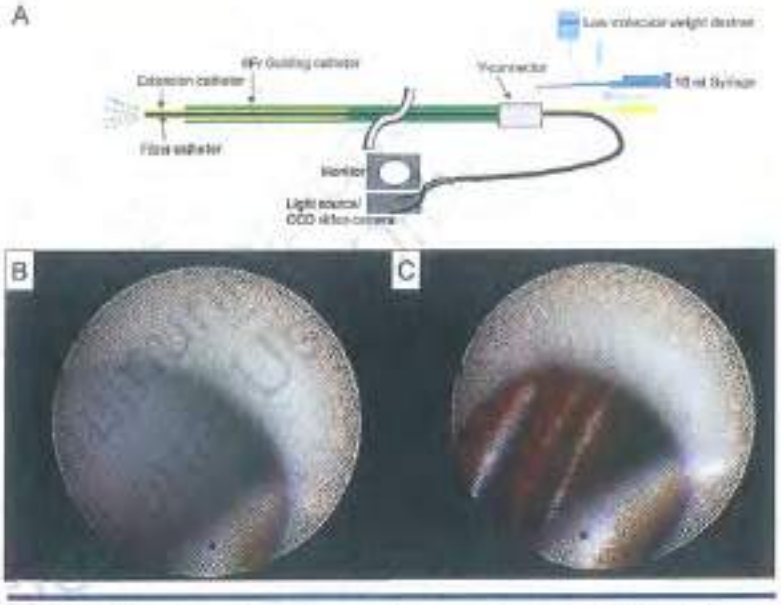

FIGURE 1. (A) Angioscopic system evaluating surface of the atrial septal occluder (ASO): low-molecular-weight dextran is infused from the guiding catheter and the tip of the GuideLiner extension catheter during observation. (B) Neointima covering most of the 22 mm ASO 6 months post implantation. (C) Around the central part of the device, the struts were exposed with marked thrombus formation. Guidewire marked by asterisks (*) in panels B and C.

Angioscopy revealed that many parts of the device were well covered with white endothelium (Figure 1B; Video 1); however, the metallic wires were exposed, with marked thrombus formation around the center of the device (Figure 1C; Video 2), indicating incomplete endothelialization despite the 6-month postimplantation period.

This first report evaluating endothelialization *in vivo* demonstrates that 6 months of postimplantation prophylactic therapy may not provide sufficient time for adequate endothelialization. Further investigations are warranted to determine the optimal duration of these treatments after ASD closure.

Acknowledgment. The authors would like to thank Dr Daisuke Fukamachi of the Division of Cardiology, Department of Medicine, Nihon University School of Medicine, for his excellent technical assistance.

From the Division of Cardiology, Department of Internal Medicine, St. Marianna University School of Medicine, Kanagawa, Japan.
Disclosure: The authors have completed and returned the ICMJE Form for Disclosure of Potential Conflicts of Interest. Dr Tanabe, Dr Izumo, and Dr Akashi report grants-in-aid for scientific research from the Japan Society for the Promotion of Science. The remaining authors report no conflicts of interest regarding the content herein.
The authors report that patient consent was provided for publication of the images used herein.
Manuscript accepted September 6, 2018.
Address for correspondence: Yasuhiro Tanabe, MD, PhD, Division of Cardiology, Department of Internal Medicine, St. Marianna University School of Medicine, 2-16-1, Sugao, Miyamae-ku, Kawasaki-City, Kanagawa 216-8511, Japan. Email: y-tanabe@mu.biglobe.ne.jp

Cardiovascular Intervention and Therapeutics
https://doi.org/10.1007/s12928-018-0532-y

ORIGINAL ARTICLE

Stent implantation for May–Thurner syndrome with acute deep venous thrombosis: acute and long-term results from the ATOMIC (AcTive stenting for May–Thurner Iliac Compression syndrome) registry

Atsushi Funatsu[1] · Hitoshi Anzai[2] · Kota Komiyama[3] · Kuniomi Oi[4] · Hiroshi Araki[5] · Yasuhiro Tanabe[6] · Masashi Nakao[7] · Makoto Utsunomiya[8] · Atsushi Mizuno[9] · Michiaki Higashitani[10] · Shigeru Nakamura[1]

Received: 6 April 2018 / Accepted: 31 May 2018
© Japanese Association of Cardiovascular Intervention and Therapeutics 2018

Abstract

The outcomes of stent implantation in managing May–Thurner syndrome (MTS) are not well understood. To clarify the acute and long-term outcomes of stent implantation in patients with MTS having acute deep venous thrombosis (DVT), we retrospectively investigated consecutive 59 patients from 10 hospitals in Japan who were treated with stents for left iliac vein stenosis with acute DVT. Stents were considered successful if the stent was patent at discharge, which in turn was defined as patient success. The primary endpoint for the study was stent patency, and the secondary endpoint was recurrence of DVT and development of post-thrombotic syndrome (PTS) during follow-up. The patient success was achieved in 56 patients (95%). Clinical follow-up was conducted for 50 patients (89%) for a median duration of 40 months (range 8–165 months). Among them, 44 patients (79%) were followed up using imaging modalities. During this period, stent occlusion was revealed in four patients (9%), and one patient was successfully treated using balloon angioplasty. Primary and secondary patency rates were 84% at 19 months and 93% at 20 months, respectively. Recurrence of DVT was documented in 3 (8%) patients. PTS was evaluated from 36 patients. Three patients (8%) had PTS; however, none of the patients had severe PTS. This multicenter retrospective study of the use of stents for treating patients with MTS having acute DVT demonstrated good acute and long-term outcomes and long-term stent patency.

Keywords May–Thurner syndrome · Deep venous thrombosis · Venous intervention

✉ Atsushi Funatsu
keve.funatsu@katsura.com

[1] Kyoto Katsura Hospital, 17 Yamada hirao-cho, Nishikyo-ku, Kyoto 615-8256, Japan

[2] Ota Memorial Hospital, Gunma, Japan

[3] Metropolitan Hiroo Hospital, Tokyo, Japan

[4] Hiroshima City Hiroshima Citizen's Hospital, Hiroshima, Japan

[5] Showa University Northern Yokohama Hospital, Kanagawa, Japan

[6] St. Marianna University School of Medicine, Kanagawa, Japan

[7] Tokyo Women's Medical University Hospital, Tokyo, Japan

[8] Tokyo Rosai Hospital, Tokyo, Japan

[9] St. Luke's International Hospital, Tokyo, Japan

[10] Tokyo Medical University Ibaraki Medical Center, Ibaraki, Japan

Introduction

In 1991, Okrent et al. reported the first case of stent implantation following catheter-directed thrombolysis (CDT) for May–Thurner syndrome (MTS) complicated with acute deep venous thrombosis (DVT) [1]. Since then, this treatment has emerged as an effective option to quickly relieve leg symptoms and reduce the risk of developing post-thrombotic syndrome (PTS) [2–6]. Although many studies demonstrating favorable clinical outcomes associated with stent implantation have been published, there are few clinical studies about stent implantation for MTS in Japan.

The aim of this study is to investigate the efficacy and safety of stent implantation for treating MTS with acute DVT in Japanese patients.

Published online: 08 June 2018

Methods

Study design and patient population

This is a multicenter, retrospective study conducted in association with 10 hospitals in Japan. All patients with had acute symptomatic DVT involving the left common iliac vein (LCIV) and underwent stent implantation in one of these hospitals were enrolled. There were no exclusion criteria except for patient's refusal.

Diagnosis of MTS

Severe LCIV compression by iliac artery was diagnosed as MTS using computed tomography (CT) or intravascular ultrasound (IVUS) images before stent implantation. Stent selection and implantation procedures were determined by the physicians.

Interventional procedures and anticoagulation therapy

An inferior vena cava (IVC) filter was utilized during thrombolysis. CDT was performed pre- or post-stent implantation using urokinase (UK) administration via a multi-side hole infusion catheter until thrombus was resolved and blood flow into the iliac vein was normal. After CDT, oral anti-coagulants were administered for at least 6 months. Procedural success was defined as successful stent implantation with residual diameter stenosis (DS) < 50% and without delayed venous flow at the stented site. Stents were considered successful if the stent was patent at discharge, which in turn was defined as patient success. IVC filter was retrieved when the risk of pulmonary embolism (PE) was diminished. Figure 1 shows a representative case of CDT and stent implantation for MTS with acute DVT.

Study end points

The primary end point was stent patency during follow-up. Stent patency was assessed by ultrasound (US), CT, or venography. The choice of imaging modality was entrusted to each physician. Stent patency was defined as DS < 50% for each modality. Primary patency was defined as uninterrupted vessel patency with no procedure performed on the treated segment, and secondary patency was defined as whenever maintenance of patency required a secondary intervention at the target lesion [7].

The secondary end point was the recurrence of acute DVT and the occurrence of PTS during follow-up. Patient follow-up visits were conducted at outpatient clinics. PTS was assessed using the Villalta score calculated at the last visit to the cardiovascular physicians. According to five patient-rated venous symptoms and six clinician-rated signs, each item is rated as 0 (none), 1 (mild), 2 (moderate), 3 (severe), and summed to produce a total score. Total score < 5 was identified as no PTS, 5–9 as mild, 10–14 as moderate, and ≧ 15 or skin ulcer was identified as severe PTS [8].

Target lesion revascularization was defined as repeat intervention for stent restenosis or occlusion. Bleeding complications were classified using the bleeding academic

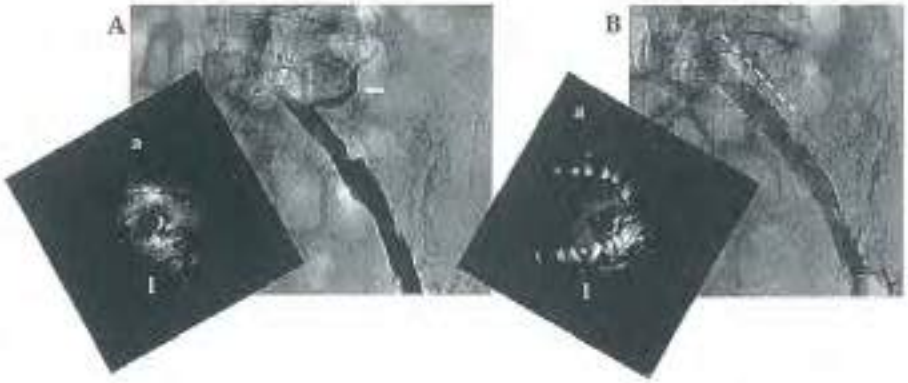

Fig. 1 Representative case of CDT and stent implantation for MTS with acute DVT. The patient was an 80-year-old female with swelling in the left leg for 3 days. Venography revealed venous thrombosis at the iliofemoral vein that extended below the knee. A 30-cm infusion catheter was inserted via the left popliteal vein and placed at the left iliac vein out flow tract. CDT was performed using UK doses of 60,000 IU administered four times per day. After 6 days, venography showed severe stenosis at the left iliac vein, although iliofemoral thrombus was resolved. IVUS revealed left iliac vein which was severely compressed by the right common iliac artery (a) and lumber vertebra (l) (A: white arrow indicates collateral channel). A SMART stent (10×40 mm) was implanted at the compression site. Stenosis was resolved as confirmed by IVUS and angiography (B: white dotted line indicates stented site). Two weeks after the procedure, the patient's leg swelling was seen to be resolved. Angiography showed that the thrombus was completely lysed with good venous flow into the stent

research consortium (BARC) criteria [9]. Major bleeding events were defined as type 3 or more.

Statistical analysis

Continuous variables are expressed as mean ± SD with either range or median. Values were reported as the numbers with a relative percentage. For continuous data, the groups were compared using the student's *t* test. Categorical variables were compared using the Chi-squared test. *P* values < 0.05 were considered statistically significant. StatView 5.0 (SAS Institute Inc, Cary, NC) was used for all statistical calculations.

Results

1. Patient lesion and procedural characteristics

From December 2000 to August 2014, consecutive 59 patients who received stent for MTS with acute DVT were enrolled. In this cohort, implantation has been performed since 2000, with more than half of implantations performed after 2011, reflecting the increasing rates of implantations (Fig. 2). Baseline patient and lesion characteristics are shown in Table 1. Sixty-six percent of the patients were females and the mean age of the patients was 68 years. In this study, immobilization state was the major risk factors for DVT, which was noted in 18 patients (31%). All patients had left iliac DVT, and in 41 patients (70%), DVT was extended to the popliteal vein. At baseline, 10 patients (17%) presented with symptomatic PE complication. Eight patients (14%) had recurrent thrombosis in the left iliac vein despite anticoagulation therapy at the first DVT event.

Table 1 Baseline patient and lesion characteristics

	N = 59
Female	39 (66%)
Age, years	68 ± 14 (range 29–88)
Onset to admission (days)	6.6 ± 9.1 (median 4; range 1–62)
Risk factor	
Immobilization	18 (31%)
Current smoking	8 (14%)
Cancer	6 (10%)
Steroid use	4 (7%)
Coagulation abnormality	3 (5%)
DVT distribution	
Involved IVCs	6 (10%)
Left iliac vein	59 (100%)
Involved femoral vein	50 (85%)
Involved popliteal vein	41 (70%)
Right side DVT	0
Symptomatic PE	10 (17%)
Recurrence of left iliac DVT	8 (14%)

DVT deep venous thrombosis, *PE* pulmonary embolism

Table 2 shows the characteristics of the stent implantation procedures. Temporary or retrievable IVC filters were used in 58 patients (98%). CDT was performed in 50 patients (85%). Remaining nine patients were treated by systemic UK administration. The mean duration of thrombolysis was 5 days, and the mean total amount of UK was 2,090,000 international units (IU). For the stenting procedure, ipsilateral common femoral vein was accessed in 58% of the

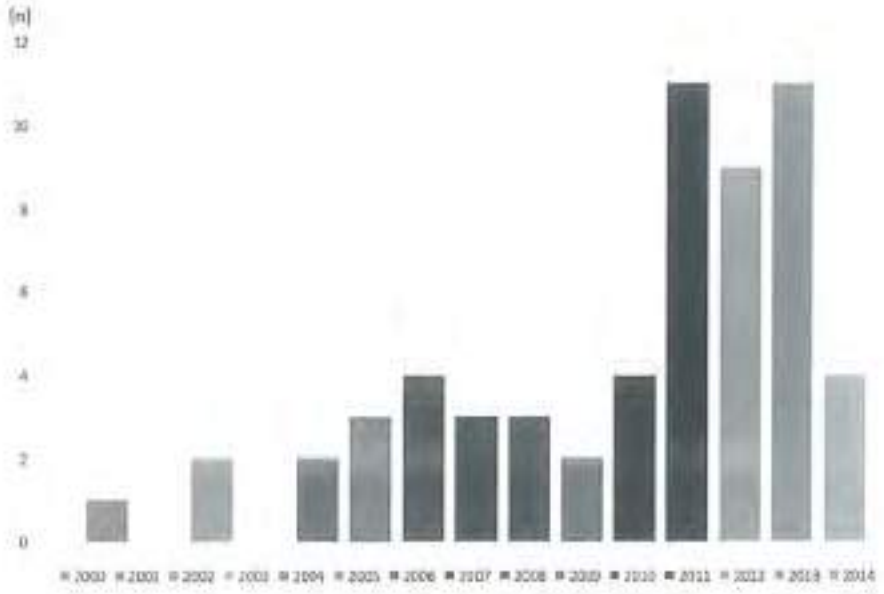

Fig. 2 Transition graph of the number of enrolled patients treated each year

Table 2 Procedural characteristics

	$N=59$
IVC filter	58 (98%)
Aspiration	24 (41%)
CDT	50 (85%)
Duration of thrombolysis	5.1±3.7 days
Total amount of urokinase	$209\times10^4\pm135\times10^4$ IU
Approach site	
Left CFV/left Pop.V/left SV	34 (58%)/23 (39%)/2 (3%)
IVUS use	39 (66%)
Total stent number	71 stents
Self-expandable stent	51 (72%)
LUMINEXX	26
SMART	10
EPIC	8
WALL	7
Balloon expandable	20 (28%)
PALMAZ	16
Express LD	4
Stent size	9.9±1.8 mm (range 6–14 mm)
Total length	69±34 mm (range 16.8–157 mm)
Post balloon	9.0±1.5 mm (range 6–14 mm)

IVC inferior vena cava, *CDT* catheter directed thrombolysis, *CFV* common femoral vein, *Pop.V* popliteal vein, *SV* saphenous vein, *IVUS* intravascular ultrasound

patients and ipsilateral popliteal vein was accessed in 39% patients. Twenty of the earlier cases were implanted with balloon expandable stent; recently, self-expandable stent was used in almost all the cases. The mean stent diameter was 9.9 mm, the total stent length was 69 mm, and the final balloon size was 9.0 mm.

2. Acute results and in-hospital outcomes (Table 3)

Stent implantation was successful in all cases (100%). There were no deaths or symptomatic PEs during hospitalization. IVC filters could be removed in 50 (85%) patients after median 9 days (range 1–118 days) of stent implantation. As an anticoagulation therapy, 53 patients received warfarin and five patients received factor Xa inhibitor after CDT and stent implantation. Fifteen patients received antiplatelet agents, including aspirin and clopidogrel. Bleeding complications during hospitalization were documented in 6 (10%) patients. Four of them suffered intra-muscular hemorrhage, including iliopsoas hemorrhage. Two bleeding complication events occurred during CDT procedures and the remaining four bleeding complication events occurred while anticoagulation therapy was being administered.

Subacute stent occlusion was identified in six patients. Possible causes of stent occlusion include the following: in two patients, anticoagulation therapy was discontinued

Table 3 Acute results and in-hospital outcomes

	$N=59$
Procedural success	59 (100%)
Removal IVC filter	50/58 (85%)
Mean duration of hospitalization	21±14 days (median 17)
All death	0
Symptomatic PE	0
Subacute stent occlusion	6 (10%)
Successful revascularization	3/6
Patent success	56 (95%)
Bleeding complication (BARC ≧ type 3)	6 (10%)
Medication at discharge	
Warfarin	53 (90%)
DOAC	5 (9%)
Antiplatelet drugs only	1 (1%)

Patient success indicates that stent is patent at discharge

BARC Bleeding Academic Research Consortium, *DOAC* direct oral anticoagulant, other abbreviations as in Tables 1 and 2

because of bleeding complications; in two patients, there was insufficient flow into the stented site from the femoral vein; in one patient, there was insufficient lesion coverage by the first stent; and in one patient, there was embolization by a distal floating thrombus into the stented segment. Among these subacute stent thrombosis cases, 3 cases were successfully reopened by repeat intervention during hospitalization. Thus, the patient success was achieved in 56 patients (95%) (Fig. 3).

3. Long-term clinical outcomes

Among the 56 successful cases, 50 cases were clinically followed up (follow-up rate was 89%) (Fig. 3). Table 4 shows the long-term results. During a median duration of 40 months of follow-up, six patients died. Recurrence of acute DVT was documented in three patients. One patient had iliofemoral thrombosis because of stent occlusion. Two patients suffered SFV thrombosis after discontinuation of warfarization; these two patients had autoimmune disease as a risk of DVT. Patency of the stents in the patients with SFV was confirmed by US and CT. Bleeding complication ≧ BARC type 3 occurred in only one patient, and was caused by a gastric ulcer after 28 months of warfarization.

4. Stent patency rates during follow-up (Table 4)

Forty-four lesions were examined by angiography, CT, or US during follow-up (follow-up rate, 79%; median duration, 21 months; range 1–117 months). Three stents that had been occluded once during hospitalization were

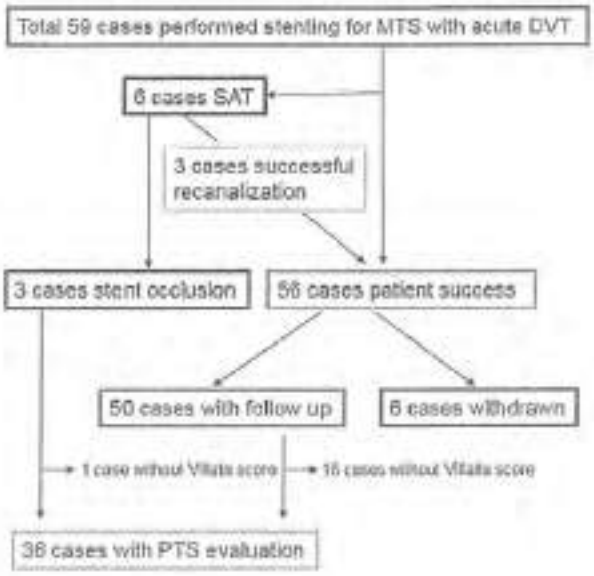

Fig. 3 Patient flow chart. *MTS* May–Thurner syndrome, *DVT* deep venous thrombosis, *PTS* post-thrombotic syndrome

Table 4 Long-term clinical and imaging results

	$N=50$
Follow-up duration	Median 40 (range 8–165) months
All death	6 (12%)
Malignancy	3 (6%)
Sudden death	2 (4%)
Respiratory disease	1 (2%)
DVT recurrent	3 (8%)
Bleeding event (BARC ≧ type 3)	1 (2%)
Evaluation of stent patency	$N=44$ (79%)
Follow-up duration	Median 21 (range 1–117) months
Stent occlusion (acute phase)	3 (7%)
Stent occlusion (chronic phase)	4 (9%)
Successful repeat intervention	4 (9%)
Primary patency	37 (84% at 19 months)
Secondary patency	41 (93% at 20 months)

Abbreviations as in Tables 1 and 3. Acute phase indicates during hospitalization, and chronic phase indicates after discharge

successfully reconstructed in the acute phase and remained open during follow-up. Four stents were found to be occluded after 6, 13, 19, and 21 months, respectively, even though all patients were on anticoagulation therapy. Figure 4 shows stent patency across all patients during the follow-up period. One case was reopened for repeat intervention. Primary patency and secondary patency rates were 84% at 19 months and 93% at 20 months, respectively.

5. Post-thrombotic syndrome evaluation

PTS was analyzed using the Villalta scores obtained from 36 patients (Fig. 3). Thirty-four of these patients are from the group of patient success cases with adequate follow-up data ($N=50$) and two patients are from the group of unsuccessful patients with adequate follow-up data ($N=3$) obtained at median 43 months (range 13–165). The mean Villalta score was 1.3 ± 1.8. Thirty-three patients in the study showed no signs of PTS. Three patients (8%) presented with mild PTS. There were no patients with moderate and severe PTS. We classified the 36 patients into the following three groups: group A, patients with confirmed patent stents (27 patients); group B, patients with patient success but no follow-up imaging diagnosis (6 patients); and group C, patients with stent occlusion (3 patients). The Villalta scores in group C were significantly higher than that in group A (3.7 ± 2.1 and 1.0 ± 1.6, respectively; $P=0.012$) (Fig. 5). When the prevalence of PTS (defined as Villalta score ≧ 5) was compared between the three groups, no statistical difference was observed between them (4, 17, and 33% in groups A, B, and C, respectively).

Discussion

Previous studies on CDT and stenting for MTS showed < 90% initial success rate and approximately 80% primary patency rate during 12–63 months of follow-up [2–4, 6]. Matsuda et al. reported an initial success rate of 92% and a 90% patency rate after 80 months in 13 patients who received stent implantations for MTS with acute DVT [10]. We also reported that the restenosis rate after iliac vein stenting was 6% at median 19 months in 20 patients [11]. These results demonstrate the effectiveness of CDT and stent implantation for MTS with acute DVT. However, interventional treatment for venous disease has not been established. The number of patients with DVT was smaller than that of patients with other cardiovascular diseases, such as acute myocardial infarction or peripheral artery disease; thus, we examined a small cohort in single center, which could be a limitation of this study, and our clinical results should be validated in a larger cohort. Hence, we conducted this multicenter study to confirm the efficacy of stents in treating MTS with acute DVT. To our knowledge, this study contains the largest number of Japanese patients who underwent stent implantation for MTS with acute DVT.

The main purpose of DVT treatment is to obtain immediate relief from symptoms and to prevent recurrence of thrombosis. However, if iliac venous compression at LCIV exists, the patient has a high risk of rethrombosis. Mickley et al. reported that 73% of the patients with untreated venous stenosis after CDT had iliac vein rethrombosis despite

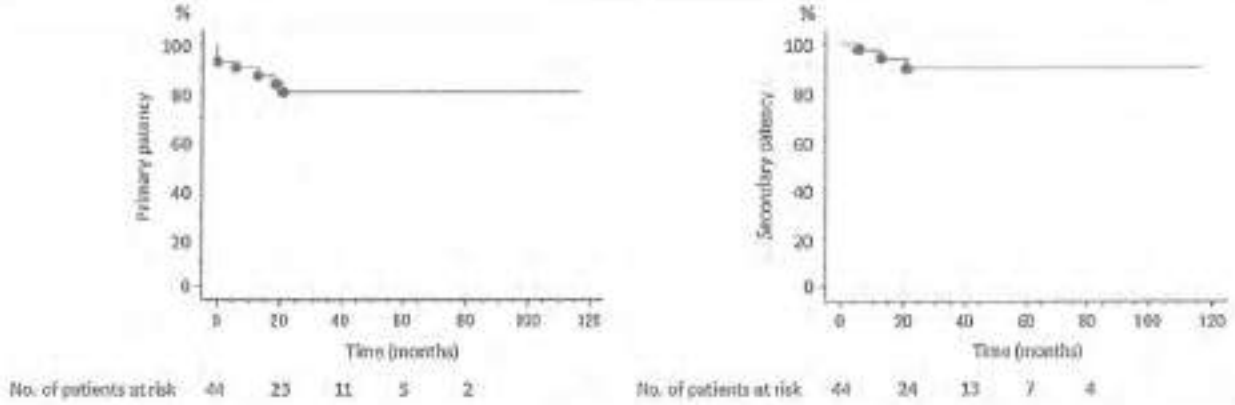

Fig. 4 Kaplan–Meier curve of primary (left) and secondary (right) patency of the implanted stent during follow-up. Patients at risk are reported at the bottom

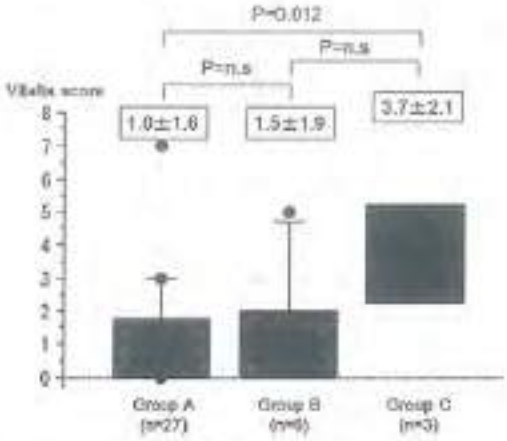

Fig. 5 Comparison of the Villalta scores between the three groups. Group A included patients with confirmed patent stents (27 patients). Group B included patients with patent success at discharge but no follow-up imaging diagnosis (6 patients). Group C included patients with stent occlusion (3 patients)

adequate anticoagulation therapy [2]. In the study cohort, eight patients (14%) had recurrent thrombosis after successful recanalization using CDT and subsequent anticoagulation at the first DVT event. Therefore, it is important to keep the left iliac vein open at the compression site.

Previous studies have reported that CDT is more effective in reducing thrombus and bleeding complications than systematic thrombolysis [12, 13]. However, these findings may not be applicable to Japanese patients because UK doses used in the previous studies were significantly higher than the doses used in daily practice in Japan. A UK dose of approximately three million IU per day was used in the previous studies for CDT treatment. In this study, CDT was performed using approximately 0.4 million IU of UK per day. Even though the exact dose of UK required for CDT treatment of Japanese patients with DVT was not clear [14], we believe approximately 0.4 million IU per day is an appropriate dose.

We generally performed CDT before stent implantation to clarify residual stenosis and maintain adequate inflow into the iliac vein. However, six of fifty cases received CDT after stent implantation due to the presence of residual thrombus. Although the iliac vein was successfully aspirated before stent implantation in these six cases, longer stents were required than those used in other cases (87 ± 24 vs. 67 ± 35 mm, respectively) to ensure residual thrombus is covered by the stent. Therefore, placing stents at compressed sites after reducing thrombus by CDT is recommended.

Retrievable IVC filters are occasionally indicated to prevent PE during CDT for iliocaval DVT [15]. However, PE is not rare. In a large scale observational study where IVC filters were used in 35% of patients, Bashir et al. reported that the incidence of PE during CDT for lower extremity proximal deep vein thrombosis was 17.9% [16]. In this study, we used IVC filters in 98% of cases and there were no complications due to PE during hospitalization. We believe that retrievable IVC filters should be used until completion of the catheter intervention and then should be retrieved once the risk of PE has been minimized.

Bleeding complications must be monitored not only during CDT, but also during the anticoagulation phase. Four of the six cases with BARC type 3 bleeding complications in the hospital occurred several days after the CDT procedure. Furthermore, stent thrombosis occurred in two of these patients because of discontinuation of anticoagulation therapy. Recanalization of the stent could not be achieved in these patients.

In this study, PTS developed in only 8% of the 36 patients with Villalta scores obtained after 43 months of follow-up. PTS occurred at a lower frequency in the present study than that observed in other large randomized trials that examined the efficacy of pharmacomechanical thrombolysis for acute DVT. In the ATTRACT Trial, the 47% of the patients developed PTS during 6 and 24 months follow-up in pharmacomechanical thrombolysis group [17]. Similarly, in the CaVent trial, 43% of patients undergoing pharmacomechanical thrombolysis developed PTS after 5 years of follow-up [18]. However, these two trials included patients not only with MTS but also with DVT caused by other reasons. Stent implantation was performed in 28 and 17% of patients in each of the studies, respectively.

This multicenter, retrospective study examined the acute and long-term efficacy of stenting for Japanese patients with MTS having acute DVT. High success rates in the acute phase and high patency rates for the stent in the long-term phase were observed. The Villalta scores were observed to be significantly lower in patients with patent stents than in those without patent stents.

Study limitations

This was a retrospective study of patients who underwent CDT and stent implantation in 10 different hospitals. Therefore, diagnosis of MTS, indications and strategies for CDT, and implantation of stents were performed differently each of these hospitals. Moreover, no comparison of outcomes between MTS patients with and without stent implantation was studied. Further investigation should be conducted to assess whether CDT and stent implantation can improve the outcome of MTS patients with acute DVT.

Conclusion

This multicenter retrospective study of stenting to treat MTS with acute DVT in Japanese patients strongly suggests that stents are safe and effective, demonstrating good long-term stent patency and clinical results.

Compliance with ethical standards

Ethical approval All procedures performed in studies involving human participants were in accordance with the ethical standards of the institutional and/or national research committee and with the 1964 Helsinki Declaration and its later amendments or comparable ethical standards. For this type of study formal consent is not required. The study protocol was reviewed and approved by the institutional review boards and ethics committee of each participating hospital, and posted for eligible patients.

Conflict of interest The authors declare that they have no conflict of interest.

References

1. Okrent D, Mesterszmith R, Buckman J. Transcatheter fibrinolytic therapy and angioplasty for left iliofemoral venous thrombosis. JVIR. 1991;2:195–200.
2. Mickley V, Schwagierek R, Rilinger N, Gorich J, Sunder-Plassmann L. Left iliac venous thrombosis caused by venous spur: treatment with thrombectomy and stent implantation. J Vasc Surg. 1998;28:492–7.
3. O'Sullivan GJ, Semba CP, Bittner CA, Kee CA, Razavi MK, Sze DY, et al. Endovascular management of iliac vein compression (May–Thurner) syndrome. JVIR. 2000;11:823–36.
4. Hurst DR, Forauer AR, Bloom JR, Greenfield LJ, Wakefield TW, Williams DM. Diagnosis and endovascular treatment of iliocaval compression syndrome. J Vasc Surg. 2001;34:106–13.
5. Raju S, Neglen P. High prevalence of nonthrombotic iliac vein lesions in chronic venous disease: a permissive role in pathogenesis. J Vasc Surg. 2006;44:136–44.
6. Hurtung O, Beaniloud F, Barthelemy P, Dubuc M, Boufi M, Alimi YS. Late results of surgical venous thrombectomy with iliocaval stenting. J Vasc Surg. 2008;47:381–7.
7. Mahnken AH, Thomson K, Haan M, O'Sullivan GJ. CIRSE Standards of Practice Guidelines on iliocaval stenting. Cardiovasc Interv Radiol. 2014;37:889–97.
8. Prandoni P, Villalta S, Bagatella P, Rossi L, Marchiori A, Piccioli A, et al. The clinical course of deep-vein thrombosis. Prospective long-term follow-up of 528 symptomatic patients. Haematologica. 1997;82(4):423–8.
9. Mehran R, Rao SV, Bhatt DL, Gibson M, Caixeta A, Eikelboom J, et al. Standardized bleeding definitions for cardiovascular clinical trials. A consensus report from the Bleeding Academic Research Consortium. Circulation. 2011;123:2736–47.
10. Matsuda A, Yamada N, Ogihara Y, Tsuji A, Ota S, Ishikura K, et al. Early and long-term outcomes of venous stent implantation for iliac venous stenosis after catheter-directed thrombosis for acute deep vein thrombosis. Circ J. 2014;78:1234–9.
11. Funatsu A, Nakamura S. Stent implantation for iliac compression syndrome with acute deep venous thrombosis. Jpn Phlebol. 2012;23:283–93.
12. Mewissen MW, Seabrook GR, Meissner MH, Cynamon J, Labropoulos N, Haughton SH. Catheter-directed thrombolysis for lower extremity deep venous thrombosis: report of a national multicenter registry. Radiology. 1999;211:39–49.
13. Srinivas BC, Patra S, Nagesh CM, Reddy B, Manjunath CN. Catheter-directed thrombolysis along with mechanical thrombaspiration versus anticoagulation alone in the management of lower limb deep venous thrombosis—a comparative study. Int J Angiol. 2014;23:247–54.
14. Mizuno A, Anzai H, Utsunomiya M, Yajima J, Ohta H, Ando H, et al Real clinical practice of catheter therapy for deep venous thrombosis: periprocedural and 6-months outcomes from the EDO registry. Cardiovasc Interv Ther. 2015;30:251–9
15. Weinberg I, Kaufman J, Jaff MR. Inferior vena cava filters. J Am Coll Cardiol Interv. 2013;6:539–47.
16. Bashir R, Zack CJ, Zhao H, Comerota AJ, Bove AA. Comparative outcomes of catheter-directed thrombolysis plus anticoagulation vs

anticoagulation alone to treat lower-extremity proximal deep vein thrombosis. JAMA Intern Med. 2014;174:1494–501.
17. Vedantham S, Goldhaber SZ, Julian JA, Kahn SR, Jaff MR, Cohen DJ, et al. for the ATTRACT Trial Investigators. Pharmacomechanical catheter-directed thrombolysis for deep-vein thrombosis. N Engl J Med. 2017;377:2240–52.
18. Haig Y, Enden T, Grøtta O, Kløw NE, Slagsvold CE, Ghanima W, et al. on behalf of the CaVenT Study Group. Post-thrombotic syndrome after catheter-directed thrombolysis for deep vein thrombosis (CaVenT): 5-year follow-up results of an open-label, randomized controlled trial. Lancet Haematol. 2016;3:64–71.

ORIGINAL RESEARCH

Prevalence of Unexplained Left Ventricular Hypertrophy by Cardiac Magnetic Resonance Imaging in MESA

Daniele Massera, MD, MSc; Robyn L. McClelland, PhD; Bharath Ambale-Venkatesh, PhD; Antoinette S. Gomes, MD; W. Gregory Hundley, MD; Nadine Kawel-Boehm, MD; Kihei Yoneyama, MD, PhD; David S. Owens, MD, MS; Mario J. Garcia, MD; Mark V. Sherrid, MD; Jorge R. Kizer, MD, MSc; Joao A. C. Lima, MD, MBA; David A. Bluemke, MD, PhD

Background—Hypertrophic cardiomyopathy is defined as unexplained left ventricular (LV) hypertrophy (wall thickness ≥15 mm) and is prevalent in 0.2% of adults (1:500) in population-based studies using echocardiography. Cardiac magnetic resonance imaging (MRI) allows for more accurate wall thickness measurement across the entire ventricle than echocardiography. The prevalence of unexplained LV hypertrophy by cardiac MRI is unknown. MESA (Multi-Ethnic Study of Atherosclerosis) recruited individuals without overt cardiovascular disease 45 to 84 years of age.

Methods and Results—We studied 4972 individuals who underwent measurement of regional LV wall thickness by cardiac MRI as part of the MESA baseline exam. American Heart Association criteria were used to define LV segments. We excluded participants with hypertension, LV dilation (≥95% predicted end-diastolic volume) or dysfunction (ejection fraction ≤50%), moderate-to-severe left-sided valve lesions by cardiac MRI, severe aortic valve calcification by cardiac computed tomography (aortic valve Agatston calcium score >1200 in women or >2000 in men), obesity (body mass index >35 kg/m^2), diabetes mellitus, and current smoking. Sixty-seven participants (aged 64±10 years, 9% female) had unexplained LV hypertrophy (wall thickness ≥15 mm in at least 2 adjacent LV segments), representing 1.4% (1 in 74) participants, 2.6% of men and 0.2% of women. Prevalence was similar across categories of race/ethnicity. Hypertrophy was focal in 17 (25.4%), intermediate in 44 (65.7%), and diffuse in 5 (7.5%) participants.

Conclusions—The prevalence of unexplained LV hypertrophy in a population-based cohort using cardiac MRI was 1.4%. This may have implications for the diagnosis of patients with hypertrophic cardiomyopathy and will require further study. (***J Am Heart Assoc.* 2019;8:e012250. DOI: 10.1161/JAHA.119.012250.**)

Key Words: hypertrophic cardiomyopathy • magnetic resonance imaging • population-based study

Unexplained left ventricular (LV) hypertrophy is defined as wall thickness ≥15 mm in the absence of conditions that predispose to hypertrophy.[1,2] Based on echocardiograms of 4111 participants in the CARDIA (Coronary Artery Risk Development in Young Adults) study performed in 1990–1991, the prevalence of hypertrophic cardiomyopathy (HCM) is ≈0.2% (1 in 500) adults.[3] This study included participants 23 to 35 years of age who were either African American or white. Other population-based echocardiographic studies corroborated these findings.[4,5]

In HCM, any segment of the left ventricle may be affected alone or in combination.[6] In contrast to cardiac magnetic resonance imaging (MRI), not all myocardial segments may be easily visible by echocardiography. Given the limitations of echocardiography, MRI has emerged as a powerful complementary imaging modality in the contemporary management of HCM.[7] Moreover, clinically relevant discrepancies in LV thickness measurements between echocardiography and cardiac MRI have been described.[8] Given these differences between echocardiography and MRI, our goal was to investigate the prevalence of unexplained LV hypertrophy by MRI in a population-based cohort.

From the New York University School of Medicine, New York, NY (D.M., M.V.S.); University of Washington, Seattle, WA (R.L.M., D.S.O.); Johns Hopkins School of Medicine, Baltimore, MD (B.A.-V., J.A.C.L.); University of California, Los Angeles, CA (A.S.G.); Virginia Commonwealth University Health Sciences, Richmond, VA (W.G.H.); Kantonsspital Graubünden, Chur, Switzerland (N.K.-B.); St. Marianna University School of Medicine, Kawasaki, Japan (K.Y.); Montefiore Medical Center, Bronx, NY (M.J.G.); San Francisco Veterans Affairs Health Care System and University of California San Francisco, San Francisco, CA (J.R.K.); University of Wisconsin School of Medicine and Public Health, Madison, WI (D.A.B.).

An accompanying Figure S1 is available at https://www.ahajournals.org/doi/suppl/10.1161/JAHA.119.012250

Correspondence to: Daniele Massera, MD, MSc, Leon H. Charney Division of Cardiology, New York University School of Medicine, 530 First Ave, Skirball 9N, New York, NY 10016. E-mail: daniele.massera@nyulangone.org

Received February 6, 2019; accepted March 13, 2019.

© 2019 The Authors. Published on behalf of the American Heart Association, Inc., by Wiley. This is an open access article under the terms of the Creative Commons Attribution-NonCommercial-NoDerivs License, which permits use and distribution in any medium, provided the original work is properly cited, the use is non-commercial and no modifications or adaptations are made.

Downloaded from http://ahajournals.org by on May 13, 2019

Clinical Perspective

What Is New?

- This is the first study to evaluate the prevalence of unexplained left ventricular hypertrophy in a population-based cohort utilizing cardiac magnetic resonance imaging.
- A total of 1.4% participants had unexplained left ventricular hypertrophy, 2.6% of men and 0.2% of women, which represents a higher prevalence than in previous echocardiographic studies.

What Are the Clinical Implications?

- It is unclear whether participants with unexplained hypertrophy have true hypertrophic (or infiltrative) cardiomyopathy or whether the diagnostic criteria for hypertrophic cardiomyopathy are overly sensitive when applied to cardiac magnetic resonance imaging.
- This may have implications for the diagnosis of patients with hypertrophic cardiomyopathy and will require further study.

Methods

Study Population

MESA (Multi-Ethnic Study of Atherosclerosis), a multicenter, prospective cohort study designed to investigate subclinical cardiovascular disease, has been previously described.[9] Briefly, 6814 community-dwelling women and men who ranged in age from 45 to 84 years, were free of cardiovascular disease and self-identified as either white, African American, Hispanic, or Chinese American, were enrolled from 6 communities in the United States (Baltimore County, MA; Chicago, IL; Forsyth County, NC; Los Angeles County, CA; Northern Manhattan and Bronx, NY; St. Paul, MN) between 2000 and 2002. A total of 5098 underwent cardiac MRI and 5004 had technically adequate data. Informed consent was obtained at enrollment, and the study was approved by the institutional review boards at all participating centers. Data from the MESA study are available to other researchers via the National Heart, Lung, and Blood Institute's Biologic Specimen and Data Repository. Further information on the methods used in this manuscript may be obtained from the first author.

Cardiac MRI

Cardiac MRI was performed with 1.5-T magnets at all participating centers, with electrocardiographic gating, blood pressure monitoring, and a 4-element phased-array surface coil placed anteriorly and posteriorly, as previously described.[10,11] Briefly, a stack of short-axis images covering the entire left ventricle was acquired using a flow-compensated fast gradient echo sequence, with time to repetition/time to echo 8 to 10 ms/3 to 5 ms, flip angle 20°, 6-mm slice thickness, 4-mm gap, in-plane resolution 1.4 to 1.6 mm (frequency direction)×2.2 to 2.5 mm (phase direction). Contouring of the endocardial and epicardial LV borders was performed using a semiautomated method (Q-MASS 4.2, Medis, Leiden, The Netherlands) with manual correction for outliers. The left ventricle was divided on the basis of the midpoint of the LV septum, with superior levels defined as basal and more inferior locations as apical. Six segments per level were derived in the basal and midventricular levels and 4 segments at the apex.[12,13] Thickness of each segment was calculated by Q-MASS software. LV volumes were adjusted for body size based on the following formula: %predicted LV volume=100×LV volume/(b×height^1.25×weight^0.43), where b=10.0 (women) or 10.5 (men) and volume is in milliliters, based on a previously derived allometric model.[11,14] LV dilation was defined as ≥95% predicted LV volume. The difference between the epicardial and endocardial areas in all levels was multiplied by the slice thickness and section gap, and then further multiplied by the myocardial specific gravity (1.04 g/mL) in order to determine the ventricular mass. Papillary muscle mass was included in the LV cavity and excluded from the LV mass. The technical error of measurement percent of the mean was 6% and 4% for LV mass and end-diastolic volume, respectively, and the intraclass correlation coefficients were 0.98 and 0.98, respectively.[10] Moderate-to-severe valve lesions were recorded prospectively by the interpreting physician. Information on infiltrative cardiomyopathies was not available.

Cardiac Computed Tomography

Participants underwent noncontrast cardiac computed tomography scans for evaluation of coronary and extracoronary calcification by the Agatston method, as previously described.[15] Aortic valve calcification was defined as calcification focus with Agatston score >0 Agatston units in the aortic valve leaflets (not in the aortic annulus or a coronary artery).[16] Severe aortic valve calcification was defined as >2000 Agatston units (men) and >1200 Agatston units (women) based on prior research correlating these parameters with echocardiographic severity.[17] All scans were centrally read at the Harbor-UCLA Research and Education Institute, Los Angeles, California.

Electrocardiography

Standard 12-lead ECGs were recorded digitally at 10 mm/mV calibration and a speed of 25 mm/s using MAC 1200 ECG machines (Marquette Electronics, Milwaukee, WI) in all clinical

Downloaded from http://ahajournals.org by on May 13, 2019

centers. All ECGs were centrally read and visually checked for quality; ECG interpretation was performed automatically with the GE Marquette 12-SL program 2001 version (GE Marquette, Milwaukee, WI). Finally, trained staff manually confirmed computer-detected ECG abnormalities. The Cornell voltage criteria (R in lead aVL+S in lead V3 >2.8 mV (for men) and >2.0 mV (for women) were used to identify LV hypertrophy by ECG.

Covariates

Baseline demographic, clinical, and anthropometric information was obtained by trained research personnel, including self-reported ethnicity, history of cardiovascular disease and risk factors, smoking status, physical activity, and medication inventory. Blood samples were obtained after a 12-hour fast and analyzed by a central laboratory. Brachial blood pressure was measured 3 times at rest in a sitting position using a Dinamap model Pro 100 automatic oscillometric sphygmomanometer (Critikon, GE Healthcare, Waukesha, WI), and the second and third measurements were averaged. Hypertension was defined as systolic blood pressure ≥140 mm Hg, diastolic blood pressure ≥90 mm Hg or treatment with antihypertensive medication in the presence of a self-reported history of hypertension. Diabetes mellitus was defined as fasting glucose ≥126 mg/dL or use of antidiabetic medication. Impaired fasting glucose was defined as fasting glucose between 100 and 125 mg/dL. Current smoking was defined as having smoked a cigarette in the preceding 30 days.

Left Ventricular Hypertrophy by MRI

LV hypertrophy was primarily defined as LV wall thickness ≥15 mm in at least 2 adjacent segments of the standardized American Heart Association 16-segment model.[13] Adjacency was defined as neighboring segments either on the same level (basal, midventricular, or apical) or across levels. We used the following exclusion criteria to define the group of participants with unexplained LV hypertrophy: hypertension, LV dilation (≥95% predicted end-diastolic volume) or dysfunction (ejection fraction ≤50%), moderate-to-severe left-sided valve lesions by cardiac MRI or severe aortic valve calcification by cardiac computed tomography, diabetes mellitus, current smoking, and body mass index >35 kg/m^2. Participants were classified as having secondary LV hypertrophy if they met at least one of the aforementioned criteria.

In addition to our main analysis, we applied less stringent sequential wall thickness criteria as sensitivity analyses: (1) LV wall thickness ≥15 mm in at least 1 segment, (2) borderline LV hypertrophy (defined as LV wall thickness ≥13 mm) in at least 2 adjacent segments, and (3) borderline LV hypertrophy in at least 1 segment (Figure 1).

Participants with unexplained LV hypertrophy were categorized as having focal (2 segments), intermediate (3–7 segments), or diffuse (≥8 segments) hypertrophy. Furthermore, participants were categorized into the following morphologic phenotypes: asymmetric septal (ratio of any basal septal or midventricular septal segment to the average of lateral segments ≥1.5:1), apical (any apical segment ≥15 mm), midventricular (any midventricular segment ≥15 mm), basal (any basal segment ≥15 mm), and concentric (all segments ≥15 mm). Because the definition of LV hypertrophy requires 2 adjacent hypertrophied segments, which can occur across walls and levels, participants can be classified as having multiple morphological phenotypes.

Statistical Methods

Participants in the study sample were categorized by presence of unexplained, secondary or no LV hypertrophy. Continuous variables are presented as mean± SD and were compared with the unpaired Student *t* or ANOVA test, as appropriate. Categorical variables are presented as counts and proportions and were analyzed with the chi-squared or Fisher's exact tests. For the comparison of phenotypes between categories of race/ethnicity, *P* values were calculated conditional on having unexplained LV hypertrophy using a Fisher's exact test. All analyses were performed using Stata 15.0 for Windows (StataCorp LP, College Station, TX). Figures were created with Prism 7.0e for Mac OS X (GraphPad Software, La Jolla, CA). A 2-tailed $P<0.05$ was used to define statistical significance.

Results

Of 5004 MESA study participants with technically adequate data, 4972 had available wall thickness measurements from at least 12 segments and were included in the study sample. Mean (SD) age was 61.5 (10.1) years, and 52.3% were women (Table 1). A total of 333 (6.7%) participants had at least 2 adjacent hypertrophied LV segments (wall thickness ≥15 mm), and 266 participants were excluded for secondary causes (Figure 1). Sixty-seven participants were classified as having unexplained LV hypertrophy, 61 men and 6 women. This represents a prevalence of 1.4% (1 in 74 participants), 2.6% of men, and 0.2% of women. Utilizing less stringent inclusion criteria of at least 1 LV segment with ≥15 mm wall thickness, 160 (3.2%) participants were classified as having unexplained LV hypertrophy (1 in 31); when applying criteria for borderline LV hypertrophy (≥13 mm), 226 (4.6%) participants were classified as having unexplained hypertrophy based on 2 adjacent LV segments, and 570 (11.5%) in at least 1 segment (Figure 1).

Downloaded from http://ahajournals.org by on May 13, 2019

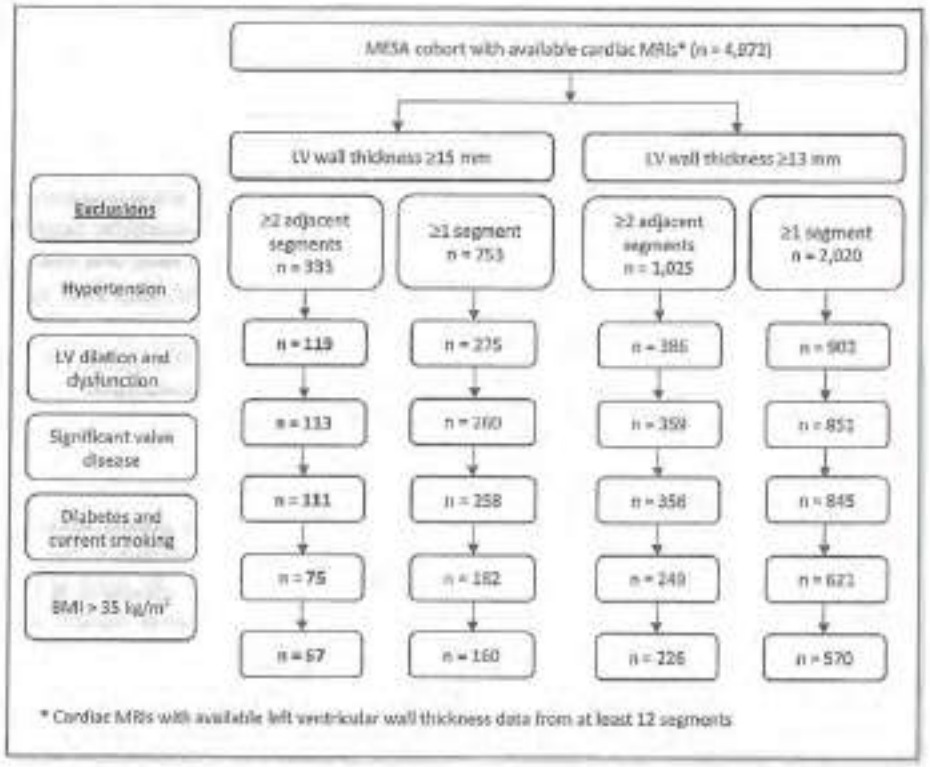

Figure 1. Flow diagram of screening strategy for participants with unexplained left ventricular hypertrophy. BMI indicates body mass index; LV, left ventricular, MESA, Multi-Ethnic Study of Atherosclerosis; MRI, magnetic resonance imaging.

Downloaded from http://ahajournals.org by on May 13, 2019

Regional Distribution and Maximum Wall Thickness

Among those with unexplained hypertrophy, the most frequently hypertrophied segments in each level were the basal anterior septal (46%), midventricular anterior lateral (40%), and apical lateral (33%) segments (Figure 2). The thickest individual segments in each level were the basal inferior lateral (20 mm), the midventricular anterior lateral (21 mm), and the apical lateral segment (20 mm) (wall thickness in whole study group and by sex in Figure 3; by race/ethnicity in Figure S1).

Extent of Hypertrophy

Hypertrophy was focal in 17 (25.4%), intermediate in 44 (65.7%), and diffuse in 5 (7.5%) participants (Table 2). Most Chinese American participants had focal hypertrophy (n=5 [83.3%]), while African American participants had the highest proportion of intermediate (n=16 [69.6%]) and diffuse (n=4 [17.4%]) hypertrophy. Mean (SD) total LV mass index was 88.2 (9.5) g/m^2 in the focal group, 101.0 (14.9) g/m^2 in the intermediate group, and 103.7 (11.7) g/m^2 in the diffuse group. The number of hypertrophied LV segments and LV mass index were correlated (r=0.38, P=0.002).

Morphologic Phenotype

Asymmetric septal hypertrophy was present in n=21 (31.3%) participants, while the lateral wall (n=50 [74.6%]) and basal segments (n=47 [70.2%]) were the most commonly involved walls and segments, respectively. Isolated basal septal hypertrophy was present in 4 participants (all men). There was no statistically significant difference in race/ethnicity among distribution of hypertrophy across morphologic phenotypes (Table 2).

Associated Factors

The prevalence of unexplained hypertrophy increased by decade of age: 14 (0.9%) in the 45- to 54-year-old group, 18 (1.3%) in the 55- to 64-year-old group, 23 (1.6%) in the 65- to 74-year-old group, and 12 (1.9%) in the 75- to 84-year-old group. Participants with unexplained LV hypertrophy were more likely to be male, white, and taller than those with secondary LV hypertrophy but had similar weight. They also had lower LV mass, LV end-diastolic volumes and stroke volumes. Compared with participants without LV hypertrophy, those with unexplained or secondary LV hypertrophy were more likely to be male and have a higher body mass index.

Table 1. Characteristics by Categories of Unexplained, Secondary, and No Hypertrophy

Characteristics	Unexplained Hypertrophy (n=67)	Secondary Hypertrophy (n=264)	No Hypertrophy (n=4539)	P Value
Age, y	64.3±10.1	65.2±9.3	61.3±10.1	<0.001
Female, n (%)	6 (9.0%)	50 (18.8%)	2545 (54.9%)	<0.001
Race/ethnicity, n (%)				<0.001
White	25 (37.3)	82 (30.8)	1834 (39.5)	
Chinese American	6 (9.0)	10 (3.8)	633 (13.6)	
African American	23 (34.3)	125 (47.0)	1132 (24.4)	
Hispanic	13 (19.4)	49 (18.4)	1040 (22.4)	
Height, cm	175.2±7.3	171.9±8.5	166.0±9.9	<0.001
Weight, kg	95.7±13.3	89.3±15.0	76.2±15.9	<0.001
BMI, kg/m^2	28.2±3.7	30.2±4.8	27.6±4.9	<0.001
Smoking status				<0.001
Never	28 (41.8%)	101 (38.3%)	2427 (52.5%)	
Former	39 (58.2%)	102 (38.6%)	1633 (35.3%)	
Current	0 (0.0%)	61 (23.1%)	567 (12.3%)	
Systolic blood pressure, mm Hg	118.4±11.6	142.9±23.8	124.6±20.8	<0.001
Diastolic blood pressure, mm Hg	72.5±8.0	79.0±11.6	71.4±10.1	<0.001
Hypertension, n (%)	0	214 (80.5)	1892 (40.8)	<0.001
Antihypertensive medication, n (%)	7 (10.4)	177 (66.5)	1570 (33.9)	<0.001
Total cholesterol, mg/dL	189.9±30.4	189.8±35.6	194.6±35.4	0.057
LDL cholesterol, mg/dL	118.2±29.4	116.3±32.1	117.2±31.3	0.79
HDL cholesterol, mg/dL	46.3±13.7	46.9±12.7	51.5±15.1	<0.001
Lipid-lowering medication, n (%)	4 (6.0)	53 (20.0)	736 (15.9)	0.016
Diabetes mellitus status, n (%)				<0.001
Impaired fasting glucose	17 (25.4)	54 (20.3)	570 (12.3)	
Diabetes mellitus	0 (0.0)	72 (27.1)	503 (10.9)	
LV ejection fraction (%)	66.1±6.6	65.5±9.8	69.2±7.2	<0.001
LV mass/BSA, g/m^2	97.8±14.5	103.6±20.6	76.3±14.4	<0.001
LV end-systolic volume/BSA, mL/m^2	21.3±6.7	23.3±11.2	21.3±7.9	<0.001
LV end-diastolic volume/BSA, mL/m^2	62.2±13.7	65.8±17.3	68.4±13.2	<0.001
LV stroke volume/BSA, mL/m^2	40.9±9.4	42.4±10.3	47.1±8.7	<0.001
LV hypertrophy by ECG (Cornell), n (%)	2 (3.0)	23 (8.6)	158 (3.4)	<0.001
Any major ECG abnormalities, n (%)	10 (15.2)	71 (26.7)	406 (8.8)	<0.001
Any minor ECG abnormalities, n (%)	41 (62.1)	181 (68.0)	2025 (44.0)	<0.001

BMI indicates body mass index; BSA, body surface area; HDL, high-density lipoprotein; LDL, low-density lipoprotein; LV, left ventricular.

Downloaded from http://ahajournals.org by on May 13, 2019

ECG Abnormalities

Major ECG abnormalities were identified in 10 (15.2%) participants with unexplained hypertrophy and included complete left or right bundle branch block in 7, Q-wave abnormalities with or without ST-segment abnormalities in 3, and isolated ST-segment or T-wave abnormalities in 3 participants. Minor ECG abnormalities were identified in 41 (62.1%) participants with unexplained hypertrophy and included minor isolated Q, ST, or T changes; tall R waves; ST-segment elevations; incomplete left or right bundle branch block; left axis deviation; first-degree atrioventricular block; and frequent premature beats. Major and minor ECG abnormalities in participants with unexplained hypertrophy were as common as in participants with secondary hypertrophy but more common than in participants without hypertrophy (Table 1).

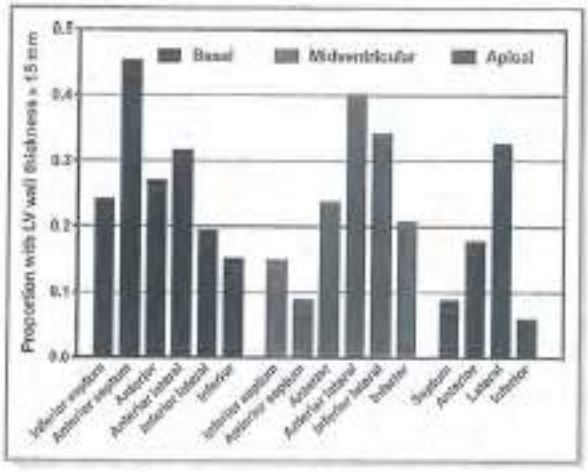

Figure 2. Proportion with LV thickness ≥15 mm by level and segment among a group of participants with unexplained LV hypertrophy. LV indicates left ventricular.

Discussion

In this study, we investigated the prevalence of unexplained LV hypertrophy by cardiac MRI in a population-based cohort. While in echocardiographic studies the prevalence of unexplained hypertrophy among young adults was ≈0.2% (1 in 500 people),[3] we found a prevalence of 1.4% (1 in 74 people), 2.6% of men and 0.2% of women, among middle-aged and older adults who were free of clinical cardiovascular disease after exclusion of conditions associated with secondary hypertrophy. Whether these individuals have HCM or infiltrative cardiomyopathy or belong to the spectrum of normal wall thickness is unknown.

Phenotypic expression of HCM is variable, with incomplete and age-dependent penetrance. Echocardiography is the most accessible imaging modality in the management of HCM. However, cardiac MRI enables more accurate and precise imaging of cardiac morphology and is commonly used as a "tiebreaker" in equivocal cases or in individuals with suboptimal echocardiographic image quality. Cardiac MRI covers the entire ventricle with high spatial resolution and allows wall thickness measurements of all LV segments with high fidelity attributable to the sharp contrast between blood and endocardial borders. Therefore, an updated estimate of the prevalence of unexplained LV hypertrophy has become necessary. Although we report an estimated prevalence of 1.4% based on 2 adjacent segments with increased wall thickness (≥15 mm), it may be as high as 3.3% based on just 1 hypertrophied segment, and higher still if a lower cutoff (≥13 mm) is used. Using the requirement for 2 adjacent hypertrophied segments may mitigate possible measurement errors introduced in the reporting process but may sacrifice

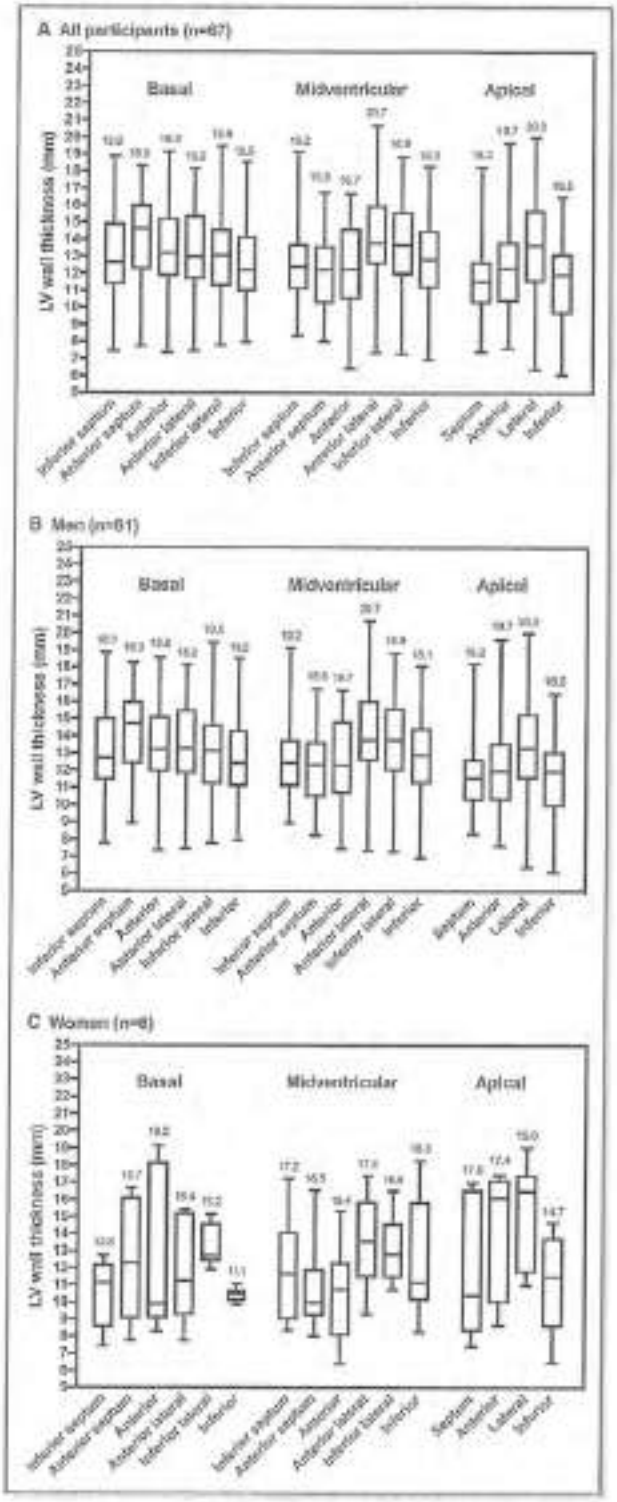

Figure 3. Distribution of left ventricular wall thickness by segment among all (A), male (B), and female (C) participants with unexplained LV hypertrophy. Maximum wall thickness in millimeters is noted for each segment. LV indicates left ventricular.

Downloaded from http://ahajournals.org by on May 13, 2019

Table 2. Distribution of Participants With Unexplained Hypertrophy by Race/Ethnicity

	Total	White	Chinese	African American	Hispanic	*P* Value
Unexplained hypertrophy, n (% total cohort)	67 (1.4)	25 (1.3)	6 (0.9)	23 (1.8)	13 (1.2)	0.38
Extent*, n (% participants with unexplained hypertrophy)						0.02
Focal (2 segments)	17 (25.4)	6 (24)	5 (83.3)	3 (13.0)	3 (23.1)	
Intermediate (3–7 segments)	44 (65.7)	17 (68.0)	1 (16.7)	16 (69.6)	10 (76.9)	
Diffuse (≥8 segments)	5 (7.5)	1 (4.0)	0	4 (17.4)	0	
Location†, n (% participants with unexplained hypertrophy)						
Septum	35 (52.2)	13 (52.0)	2 (33.0)	13 (56.5)	7 (53.9)	0.83
Lateral wall	50 (74.6)	19 (76.0)	5 (83.3)	16 (69.6)	10 (76.9)	0.93
Anterior wall	36 (53.7)	14 (56.0)	2 (33.0)	12 (52.2)	8 (61.5)	0.76
Inferior wall	19 (28.4)	10 (40.0)	0	7 (30.4)	2 (15.4)	0.19
Phenotype†, n (% participants with unexplained hypertrophy)						
Asymmetric septal	21 (31.3)	7 (28.0)	2 (33.0)	7 (30.4)	5 (38.5)	0.86
Isolated basal septal	4 (6.0)	1 (4.0)	1 (16.7)	2 (8.7)	0	0.36
Apical	26 (38.8)	9 (36.0)	2 (33.0)	11 (47.8)	4 (30.8)	0.77
Midventricular	44 (65.7)	17 (68.0)	3 (50.0)	15 (65.2)	9 (69.2)	0.89
Basal	47 (70.2)	18 (72.0)	3 (50.0)	18 (78.3)	8 (61.5)	0.20

*One participant was not classifiable because of missing data.
†Participants can be counted multiple times because the definition of unexplained hypertrophy requires 2 adjacent hypertrophied segments in 1 or across levels.

sensitivity. Nevertheless, our prevalence is considerably higher than prior estimates.

There are 2 main possible explanations for these findings. First, the true prevalence of HCM may be higher than previously thought. Image quality and sensitivity for regional wall thickness measurements by cardiac MRI are better compared with echocardiography.[8,18] In clinical practice, basal septal and inferolateral wall thickness measurements are part of standardized echocardiographic protocols, while other segments may not be consistently measured. Cardiac MRI can identify hypertrophied segments that are undetected by echocardiography, especially in the anterior and lateral walls. Furthermore, discordances in wall thickness measurements between the 2 modalities are common: discrepancies of ≥10% were present in half of the study participants in one study; both over- and underestimation by echocardiography were common.[8] In a study examining ECG abnormalities in 155 athletes, echocardiography identified 31 cases of HCM, while cardiac MRI added another 20 cases that were not found by echocardiography.[19] Limitations of echocardiography that are not present in cardiac MRI include acoustic shadowing, poor endocardial definition, and predefined imaging views leading to gaps in myocardial visualization.[20]

In addition, age may explain the higher prevalence of unexplained hypertrophy. The MESA cohort was older (45–84 years at enrollment) compared with CARDIA (23–35 years). In individuals with sarcomeric mutations associated with HCM, the prevalence of hypertrophy increases with age,[21] while in the general population wall thickness is not associated with age.[22] Furthermore, the prevalence of known pathogenic sarcomeric mutations is 0.6% in population-based studies[23,24] but may be higher considering that not all disease-associated genes have yet been identified. Therefore, the true prevalence of HCM is potentially higher than previously thought.

The second possible explanation for our findings is the erroneous labeling of participants without pathology as having hypertrophy. Given the aforementioned advantages of MRI, diagnostic criteria for HCM may be overly sensitive and may inadvertently capture individuals with normal wall thickness. Guidelines for HCM define unexplained hypertrophy by the universal application of a 15-mm cutoff in at least 1 segment despite substantial variability in normal wall thickness of different segments. Normal values for regional wall thickness in all segments have previously been published in a subset of MESA participants using the steady-state free precession sequence.[22] In this study, maximum wall thickness was highest in the basal, followed by the midventricular and apical segments, with differences of up to 4 mm between segments. Moreover, mean regional wall thickness was greater in men compared with women (1 mm difference), another factor that is unaccounted for in the current diagnostic criteria for HCM. Finally, although we excluded participants with body mass index >35 kg/m^2 to eliminate outliers in weight, there is no

Downloaded from http://ahajournals.org by on May 13, 2015

established methodology to adjust wall thickness measurements for body size. The diagnostic criteria for HCM when applied to cardiac MRI may require refinement to reflect differences in normal wall thickness by segment, sex, and body size.

Study Limitations

We acknowledge several limitations to our study. First, although we attempted to exclude all possible causes of secondary LV hypertrophy, the reported prevalence may be overestimated because of incomplete exclusion of secondary causes. Most importantly, we were unable to exclude participants with masked hypertension if they had normal blood pressure at the time of their in-person examination, were not taking antihypertensive medication, and did not have a diagnosis of hypertension. Notably, 7 participants were taking antihypertensive agents presumably for other reasons because they did not report a diagnosis of hypertension. Similarly, because echocardiography was not performed in this cohort, cases of severe valve lesions may have been missed, although we attempted to capture those with severe aortic stenosis by surrogate measures of cardiac computed tomography calcium scoring. Of note, chronic kidney disease stage 4 or greater (estimated glomerular filtration rate <30 mL/min per kg^2) was not present in the group with unexplained hypertrophy.

Second, of the 6814 total MESA participants, 5004 underwent cardiac MRI, of which 4972 (73%) had technically adequate data. Those who did not complete the cardiac MRI were most commonly ineligible because of metal implants, claustrophobia, or refusal, and were slightly older, more hypertensive, and had a higher body mass index.[25] However, given the small differences, we believe that the prevalence of unexplained hypertrophy would not be meaningfully different among those who did not undergo cardiac MRI. Third, we were unable to provide information on symptoms or LV outflow tract gradients because this was not routinely reported in MESA. Fourth, gadolinium contrast and T1 mapping were not used in the baseline MESA exam, which may have provided valuable added information to better characterize our study group. In addition, rare cases of infiltrative diseases such as amyloid or Anderson-Fabry cardiomyopathy may thus have been missed. Fifth, short-axis wall thickness measurements of the basal and midventricular segments were only minimally larger compared with long-axis measurements (6% and 10%, respectively), in contrast to measurements of apical segments, which were substantially larger (20%).[22] Given that we used short axis measurements in our study, apical hypertrophy may have been overestimated.

Sixth, the fast gradient echo sequence used in this study has largely been replaced by the steady-state free precession sequence in clinical practice, and there are known differences in LV mass measurements between sequences. However, wall thickness measurements in MESA on the latter were available in only a small subset of participants. In MESA, LV mass was found to be 4.8% higher on the fast gradient echo sequence compared with steady-state free precession.[26] Therefore, there may be a discrepancy in wall thickness as well. Because mass is proportional to volume, the discrepancy in 1-dimensional wall thickness measurements is expected to be smaller yet.

Seventh, as the number of hypothesis tests presented in the tables is large, the possibility of false-positive results exists. These associations will have to be confirmed in future studies. Finally, we were unable to include multivariable adjusted analyses given the arbitrary definition of unexplained hypertrophy that was driven by exclusion of participants. While the perfect cohort to answer the question of "true" hypertrophic cardiomyopathy prevalence would include echocardiography in parallel with cardiac MRI, MESA currently provides the closest possible opportunity available to attempt an estimation.

Conclusion

In a multiethnic population-based cohort without clinical cardiovascular disease, the prevalence of unexplained LV hypertrophy by cardiac MRI is 1.4%, defined as wall thickness ≥15 mm in at least 2 adjacent LV segments. This estimate is higher than previously described by echocardiography, likely reflecting the better image quality and superior endocardial/epicardial border definition afforded by cardiac MRI and the older age of our sample. Additional studies are required to define the clinical implications of this higher MRI-determined prevalence.

Acknowledgments

The authors thank the other investigators, the staff, and the participants of the MESA study for their valuable contributions. A full list of participating MESA investigators and institutions can be found at http://www.mesa-nhlbi.org.

Sources of Funding

This research was supported by contracts HHSN268201500003I, N01-HC-95159, N01-HC-95160, N01-HC-95161, N01-HC-95162, N01-HC-95163, N01-HC-95164, N01-HC-95165, N01-HC-95166, N01-HC-95167, N01-HC-95168, and N01-HC-95169 from the National Heart, Lung, and Blood Institute, and by grants UL1-TR-000040, UL1-TR-001079, and UL1-TR-001420 from the National Center for Advancing Translational Sciences (NCATS). Massera was supported by The

Downloaded from http://ahajournals.org by on May 13, 2019

Glorney-Raisbeck Fellowship Program, Corlette Glorney Foundation, and The New York Academy of Medicine. Kizer was supported by K24 HI135413 from the National Heart, Lung, and Blood Institute.

Disclosures

Kizer reports stock ownership in Amgen, Gilead Sciences, Johnson & Johnson, and Pfizer. The remaining authors have no disclosures to report.

References

1. Gersh BJ, Maron BJ, Bonow RO, Dearani JA, Fifer MA, Link MS, Naidu SS, Nishimura RA, Ommen SR, Rakowski H, Seidman CE, Towbin JA, Udelson JE, Yancy CW; American College of Cardiology Foundation/American Heart Association Task Force on Practice Guidelines, American Association for Thoracic Surgery, American Society of Echocardiography, American Society of Nuclear Cardiology, Heart Failure Society of America, Heart Rhythm Society, Society for Cardiovascular Angiography and Interventions, Society of Thoracic Surgeons. 2011 ACCF/AHA guideline for the diagnosis and treatment of hypertrophic cardiomyopathy: a report of the American College of Cardiology Foundation/American Heart Association Task Force on Practice Guidelines. *Circulation*. 2011;124:e783–e831.
2. Elliott PM, Anastasakis A, Borger MA, Borggrefe M, Cecchi F, Charron P, Hagege AA, Lafont A, Limongelli G, Mahrholdt H, McKenna WJ, Mogensen J, Nihoyannopoulos P, Nistri S, Pieper PG, Pieske B, Rapezzi C, Rutten FH, Tillmanns C, Watkins H. 2014 ESC guidelines on diagnosis and management of hypertrophic cardiomyopathy: the task force for the diagnosis and management of hypertrophic cardiomyopathy of the European Society of Cardiology (ESC). *Eur Heart J*. 2014;35:2733–2779.
3. Maron BJ, Gardin JM, Flack JM, Gidding SS, Kurosaki TT, Bild DE. Prevalence of hypertrophic cardiomyopathy in a general population of young adults. Echocardiographic analysis of 4111 subjects in the CARDIA Study. Coronary Artery Risk Development in (YOUNG) Adults. *Circulation*. 1995;92:785–789.
4. Maro EE, Janabi M, Kaushik R. Clinical and echocardiographic study of hypertrophic cardiomyopathy in Tanzania. *Trop Doct*. 2006;36:225–227.
5. Codd MB, Sugrue DD, Gersh BJ, Melton LJ III. Epidemiology of idiopathic dilated and hypertrophic cardiomyopathy. A population-based study in Olmsted County, Minnesota, 1975–1984. *Circulation*. 1989;80:564–572.
6. Klues HG, Schiffers A, Maron BJ. Phenotypic spectrum and patterns of left ventricular hypertrophy in hypertrophic cardiomyopathy: morphologic observations and significance as assessed by two-dimensional echocardiography in 600 patients. *J Am Coll Cardiol*. 1995;26:1699–1708.
7. Olivotto I, Maron MS, Autore C, Lesser JR, Rega L, Casolo G, De Santis M, Quarta G, Nistri S, Cecchi F, Salton CL, Udelson JE, Manning WJ, Maron BJ. Assessment and significance of left ventricular mass by cardiovascular magnetic resonance in hypertrophic cardiomyopathy. *J Am Coll Cardiol*. 2008;52:559–566.
8. Hindieh W, Weissler-Snir A, Hammer H, Adler A, Rakowski H, Chan RH. Discrepant measurements of maximal left ventricular wall thickness between cardiac magnetic resonance imaging and echocardiography in patients with hypertrophic cardiomyopathy. *Circ Cardiovasc Imaging*. 2017;10:e006309.
9. Bild DE, Bluemke DA, Burke GL, Detrano R, Diez Roux AV, Folsom AR, Greenland P, Jacob DR Jr, Kronmal R, Liu K, Nelson JC, O'Leary D, Saad MF, Shea S, Szklo M, Tracy RP. Multi-Ethnic Study of Atherosclerosis: objectives and design. *Am J Epidemiol*. 2002;156:871–881.
10. Natori S, Lai S, Finn JP, Gomes AS, Hundley WG, Jerosch-Herold M, Pearson G, Sinha S, Arai A, Lima JA, Bluemke DA. Cardiovascular function in Multi-Ethnic Study of Atherosclerosis: normal values by age, sex, and ethnicity. *AJR Am J Roentgenol*. 2006;186:S357–S365.
11. Bluemke DA, Kronmal RA, Lima JA, Liu K, Olson J, Burke GL, Folsom AR. The relationship of left ventricular mass and geometry to incident cardiovascular events: the MESA (Multi-Ethnic Study of Atherosclerosis) study. *J Am Coll Cardiol*. 2008;52:2148–2155.
12. Yan RT, Bluemke D, Gomes A, Burke G, Shea S, Liu K, Bahrami H, Sinha S, Wu C, Fernandes V, McClelland R, Lima JA. Regional left ventricular myocardial dysfunction as a predictor of incident cardiovascular events: MESA (Multi-Ethnic Study of Atherosclerosis). *J Am Coll Cardiol*. 2011;57:1735–1744.
13. Cerqueira MD, Weissman NJ, Dilsizian V, Jacobs AK, Kaul S, Laskey WK, Pennell DJ, Rumberger JA, Ryan T, Verani MS; American Heart Association Writing Group on Myocardial Segmentation and Registration for Cardiac Imaging. Standardized myocardial segmentation and nomenclature for tomographic imaging of the heart. A statement for healthcare professionals from the Cardiac Imaging Committee of the Council on Clinical Cardiology of the American Heart Association. *Circulation*. 2002;105:539–542.
14. Brumback LC, Kronmal R, Heckbert SR, Ni H, Hundley WG, Lima JA, Bluemke DA. Body size adjustments for left ventricular mass by cardiovascular magnetic resonance and their impact on left ventricular hypertrophy classification. *Int J Cardiovasc Imaging*. 2010;26:459–468.
15. Carr JJ, Nelson JC, Wong ND, McNitt-Gray M, Arad Y, Jacobs DR Jr, Sidney S, Bild DE, Williams OD, Detrano RC. Calcified coronary artery plaque measurement with cardiac CT in population-based studies: standardized protocol of Multi-Ethnic Study of Atherosclerosis (MESA) and Coronary Artery Risk Development in Young Adults (CARDIA) study. *Radiology*. 2005;234:35–43.
16. Budoff MJ, Takasu J, Katz R, Mao S, Shavelle DM, O'Brien KD, Blumenthal RS, Carr JJ, Kronmal R. Reproducibility of CT measurements of aortic valve calcification, mitral annulus calcification, and aortic wall calcification in the Multi-Ethnic Study of Atherosclerosis. *Acad Radiol*. 2006;13:166–172.
17. Clavel MA, Messika-Zeitoun D, Pibarot P, Aggarwal SR, Malouf J, Araoz PA, Michelena HI, Cueff C, Larose E, Capoulade R, Vahanian A, Enriquez-Sarano M. The complex nature of discordant severe calcified aortic valve disease grading: new insights from combined Doppler echocardiographic and computed tomographic study. *J Am Coll Cardiol*. 2013;62:2329–2338.
18. Valente AM, Lakdawala NK, Powell AJ, Evans SP, Cirino AL, Orav EJ, MacRae CA, Colan SD, Ho CY. Comparison of echocardiographic and cardiac magnetic resonance imaging in hypertrophic cardiomyopathy sarcomere mutation carriers without left ventricular hypertrophy. *Circ Cardiovasc Genet*. 2013;6:230–237.
19. Schnell F, Riding N, O'Hanlon R, Axel Lentz P, Donal E, Kervio G, Matelot D, Leurent G, Doutreleau S, Chevalier L, Guerard S, Wilson MG, Caire F. Recognition and significance of pathological T-wave inversions in athletes. *Circulation*. 2015;131:165–173.
20. Hindieh W, Chan R, Rakowski H. Complementary role of echocardiography and cardiac magnetic resonance in hypertrophic cardiomyopathy. *Curr Cardiol Rep*. 2017;19:81.
21. Charron P, Dubourg O, Desnos M, Isnard R, Hagege A, Millaire A, Cartier L, Bonne G, Tesson F, Richard P, Bouhour JB, Schwartz K, Komajda M. Diagnostic value of electrocardiography and echocardiography for familial hypertrophic cardiomyopathy in a genotyped adult population. *Circulation*. 1997;96:214–219.
22. Kawel N, Turkbey EB, Carr JJ, Eng J, Gomes AS, Hundley WG, Johnson C, Masri SC, Prince MR, van der Geest RJ, Lima JA, Bluemke DA. Normal left ventricular myocardial thickness for middle-aged and older subjects with steady-state free precession cardiac magnetic resonance: the Multi-Ethnic Study of Atherosclerosis. *Circ Cardiovasc Imaging*. 2012;5:500–508.
23. Bick AG, Flannick J, Ito K, Cheng S, Vasan RS, Parfenov MG, Herman DS, DePalma SR, Gupta N, Gabriel SB, Funke BH, Rehm HL, Benjamin EJ, Anagnostou P, Taylor HA Jr, Fox ER, Newton-Cheh C, Kathiresan S, O'Donnell CJ, Wilson JG, Altshuler DM, Hirschhorn JN, Seidman JG, Seidman C. Burden of rare sarcomere gene variants in the Framingham and Jackson Heart Study cohorts. *Am J Hum Genet*. 2012;91:513–519.
24. Natarajan P, Gold MR, Bick AG, McLaughlin H, Kraft P, Rehm HL, Palacio GM, Wilson JG, Correa A, Seidman JG, Seidman CE, Kathiresan S, Green RC. Aggregate penetrance of genomic variants for actionable disorders in European and African Americans. *Sci Transl Med*. 2016;8:364ra151.
25. Heckbert SR, Post W, Pearson GD, Arnett DK, Gomes AS, Jerosch-Herold M, Hundley WG, Lima JA, Bluemke DA. Traditional cardiovascular risk factors in relation to left ventricular mass, volume, and systolic function by cardiac magnetic resonance imaging: the Multiethnic Study of Atherosclerosis. *J Am Coll Cardiol*. 2006;48:2285–2292.
26. Maliyeri AA, Johnson WC, Macedo R, Bathon J, Lima JA, Bluemke DA. Cardiac cine MRI: quantification of the relationship between fast gradient echo and steady-state free precession for determination of myocardial mass and volumes. *J Magn Reson Imaging*. 2008;28:60–66.

ORIGINAL RESEARCH

Downloaded from http://ahajournals.org by on May 13, 2019

SUPPLEMENTAL MATERIAL

Downloaded from http://ahajournals.org by on May 13, 2019

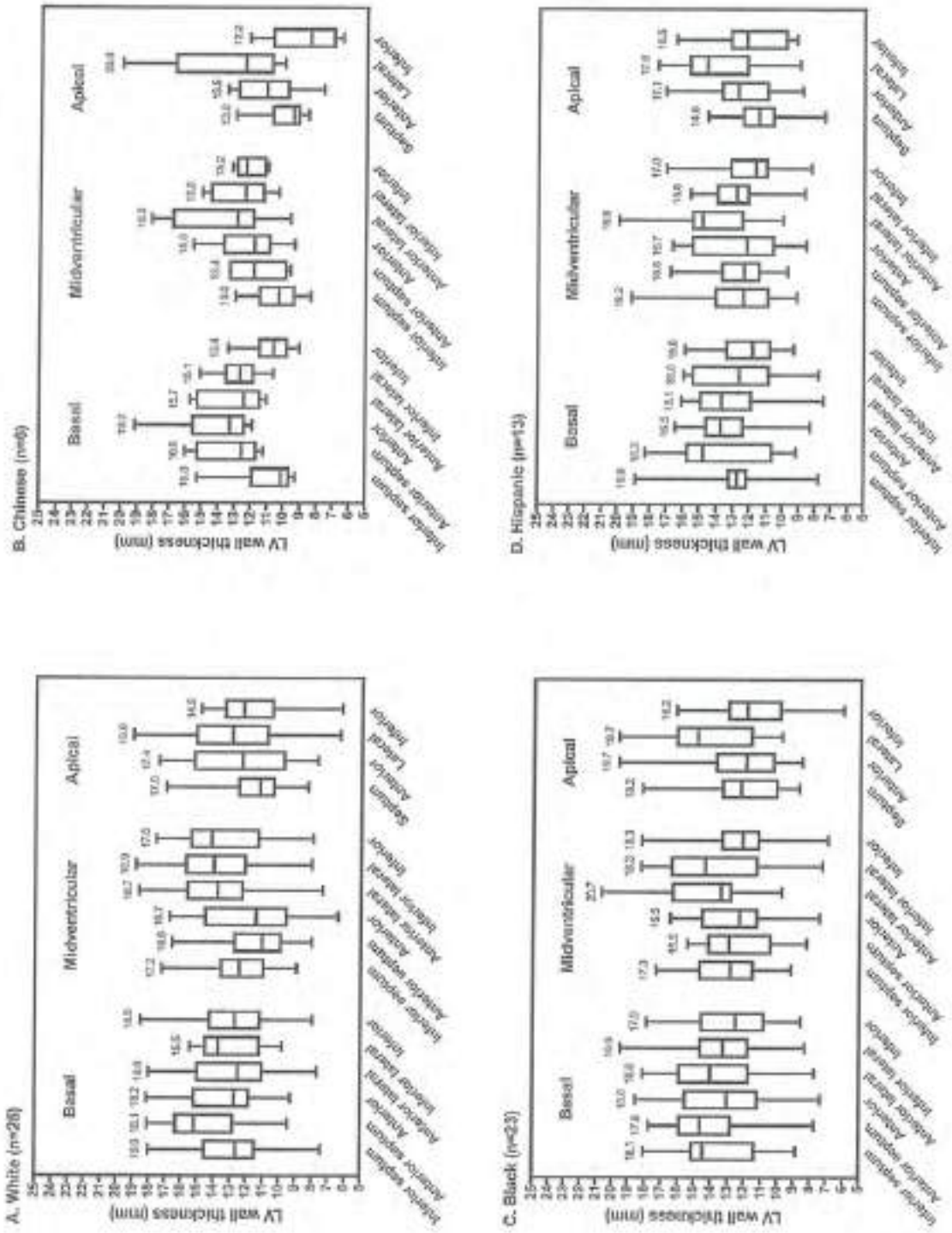

Figure S1. Distribution of LV wall thickness by segment by race/ethnicity, among white (A), Chinese (B), African-American (C) and Hispanic (D) MESA participants with unexplained LV hypertrophy. Maximum wall thickness in mm is noted for each segment.

Downloaded from http://shajournals.org by on May 13, 2019

Circulation: Cardiovascular Interventions

ORIGINAL ARTICLE

Physiological Pattern of Disease Assessed by Pressure-Wire Pullback Has an Influence on Fractional Flow Reserve/Instantaneous Wave-Free Ratio Discordance

Insights From the Multicenter AJIP Registry

Takayuki Warisawa, MD et al

BACKGROUND: Fractional flow reserve (FFR) and instantaneous wave-free ratio (iFR) disagree on the hemodynamic significance of a coronary lesion in ≈20% of cases. It is unknown whether the physiological pattern of disease is an influencing factor for this. This study assessed whether the physiological pattern of coronary artery disease influences discordance between FFR and iFR measurement.

METHODS AND RESULTS: Three-hundred and sixty intermediate coronary lesions (345 patients; mean age, 64.4±10.3 years; 76% men) with combined FFR, iFR, and iFR pressure-wire pullback were included for analysis from an international multicenter registry. Cut points for hemodynamic significance were FFR ≤0.80 and iFR ≤0.89, respectively. Lesions were classified into FFR+/iFR+ (n=154; 42.7%), FFR−/iFR+ (n=38; 10.6%), FFR+/iFR− (n=41; 11.4%), and FFR−/iFR− (n=127; 35.3%) groups. The physiological pattern of disease was classified according to the iFR pullback recordings as predominantly physiologically focal (n=171; 47.5%) or predominantly physiologically diffuse (n=189; 52.5%). Median FFR and iFR were 0.80 (interquartile range, 0.75–0.85) and 0.89 (interquartile range, 0.86–0.92), respectively. FFR disagreed with iFR in 22% (79 of 360). The physiological pattern of disease was the only influencing factor relating to FFR/iFR discordance: predominantly physiologically focal was significantly associated with FFR+/iFR− (58.5% [24 of 41]), and predominantly physiologically diffuse was significantly associated with FFR−/iFR+ (81.6% [31 of 38]; $P<0.001$ for pattern of disease between FFR+/iFR− and FFR−/iFR+ groups).

CONCLUSIONS: The physiological pattern of coronary artery disease was an important influencing factor for FFR/iFR discordance.

VISUAL OVERVIEW: A visual overview is available for this article.

The full author list is available on page 8.

Key Words: coronary artery disease ■ fractional flow reserve, myocardial ■ hemodynamics ■ humans ■ registries

© 2019 The Authors. Circulation: Cardiovascular Interventions is published on behalf of the American Heart Association, Inc., by Wolters Kluwer Health, Inc. This is an open access article under the terms of the Creative Commons Attribution License, which permits use, distribution, and reproduction in any medium, provided that the original work is properly cited.

https://www.ahajournals.org/journal/circinterventions

Downloaded from http://ahajournals.org by on May 15, 2019

WHAT IS KNOWN

- Proximal lesion location, diabetes mellitus, female sex, and differences in hyperemic coronary flow have all been suggested as factors contributing to fractional flow reserve (FFR)/instantaneous wave-free ratio (iFR) discordance.

WHAT THE STUDY ADDS

- The present study further demonstrated that the physiological pattern of coronary artery disease, as assessed by iFR pressure-wire pullback, also appeared a critical determinant of FFR/iFR discordance. Specifically, FFR+/iFR− discordance was more associated with physiologically focal disease, whereas FFR−/iFR+ discordance was more associated with physiologically diffuse disease. The performance of pressure-wire pullback as part of routine physiological stenosis assessment may provide useful additive information in cases of FFR/iFR discordance.

Coronary physiology permits vessel-specific identification of ischemia, and its use is recommended to guide revascularization decision-making in intermediate-severity coronary stenosis.[1] The 2 most commonly used pressure-based indices in clinical practice are the fractional flow reserve (FFR) and the instantaneous wave-free ratio (iFR). FFR is measured during maximal hyperemia induced by vasodilating agents,[2] whereas iFR is measured under resting conditions, without pharmacological hyperemia.[3]

It is well known that FFR and iFR disagree on the hemodynamic significance of a coronary lesion in ≈20% of cases.[4] Previous studies showed influencing factors for FFR/iFR discordance included the lesion location,[5,6] particular patient characteristics,[7] and difference in hyperemic coronary flow.[8] However, it is unknown whether the physiological pattern of coronary artery disease also influences FFR/iFR discordance.

In this study, we sought to determine whether the physiological pattern of coronary artery disease as assessed by iFR pullback was an influencing factor for FFR/iFR discordance.

METHODS

The data, analytic methods, and study materials will not be made available to other researchers for purposes of reproducing the results or replicating the procedure.

Study Population

AJIP is an international multicenter registry that includes patients with intermediate coronary lesions and measurement of iFR pullback performed for clinical indications. This ongoing registry includes retrospective cases from the first-in-man iFR pullback case in March 9, 2015, and also will cover prospective cases by December 2018. From this registry, all consecutive cases (March 2015 to April 2018) with a combined measurement of FFR were included for this analysis (Figure I in the Data Supplement). Exclusion criteria were lesion severity >90% by visual estimation, acute coronary syndrome, previous coronary artery bypass grafting to the target vessel, vessels with angiographically identifiable myocardial bridging or collaterals, cardiac hypertrophy, and severe valvular pathology. All patients provided written informed consent. This study was approved by the local ethical committees at each participating center and was conducted according to the principles of the Declaration of Helsinki.

Baseline Characteristics Data

Baseline characteristics data of the patients included age, sex, hypertension (defined as systolic blood pressure ≥140 mm Hg, diastolic blood pressure ≥90 mm Hg, or the use of antihypertensive medication), dyslipidemia (defined as low-density lipoprotein cholesterol ≥140 mg/dL or the use of antilipidemic medication), diabetes mellitus (defined as hemoglobin A1c ≥6.5% or the use of antidiabetic medication), renal insufficiency (defined as estimated glomerular filtration rate <60 mL/min per 1.73 m^2), and severe left ventricular systolic dysfunction (defined as left ventricular ejection fraction <30%).

Coronary Catheterization and Measurement of Physiological Indices

Coronary angiography was performed using standard techniques according to routine clinical practice in the participating centers. The decision to perform FFR and iFR assessment was clinically oriented and thus left to operator's discretion. Intracoronary nitrates (100–300 mg) were administered in all cases.

After normalization of the pressure wire (PrimeWire Prestige/Verrata; Philips, Amsterdam, the Netherlands) at the ostium of each vessel, the wire was advanced to the target vessel. FFR was calculated as the ratio of mean distal coronary pressure to mean aortic pressure across the whole cardiac cycle during maximal hyperemia. Hyperemia was induced by intravenous adenosine infusion (140–150 μg/kg per min; 334 of 360), intracoronary adenosine injection (40–150 μg; 24 of 360), or intracoronary nicorandil injection (2 mg; 2 of 360) as recommended.[9] iFR was calculated as the ratio of mean distal coronary pressure to mean aortic pressure during the wave-free period of diastole.

Routine cutoff values of hemodynamic significance (FFR ≤0.80 and iFR ≤0.89) were used to classify stenoses into 4 groups: FFR+/iFR+ (FFR ≤0.80 and iFR ≤0.89), FFR−/iFR+ (FFR >0.80 and iFR ≤0.89), FFR+/iFR− (FFR ≤0.80 and iFR >0.89), and FFR−/iFR− (FFR >0.80 and iFR >0.89).

iFR Pressure-Wire Pullback Measurement and Physiological Classification

iFR pullback recordings were performed manually at a pullback speed of ≈0.5 to 1.0 mm/s. After the pressure sensor reached the ostium of left main or right coronary artery as appropriate, the presence of pressure-wire drift was checked. If significant drift was identified, defined as ±0.02 units,[10] measurements were repeated. Cases were excluded from the

Downloaded from http://circinterventions.ahajournals.org/ on May 15, 2019

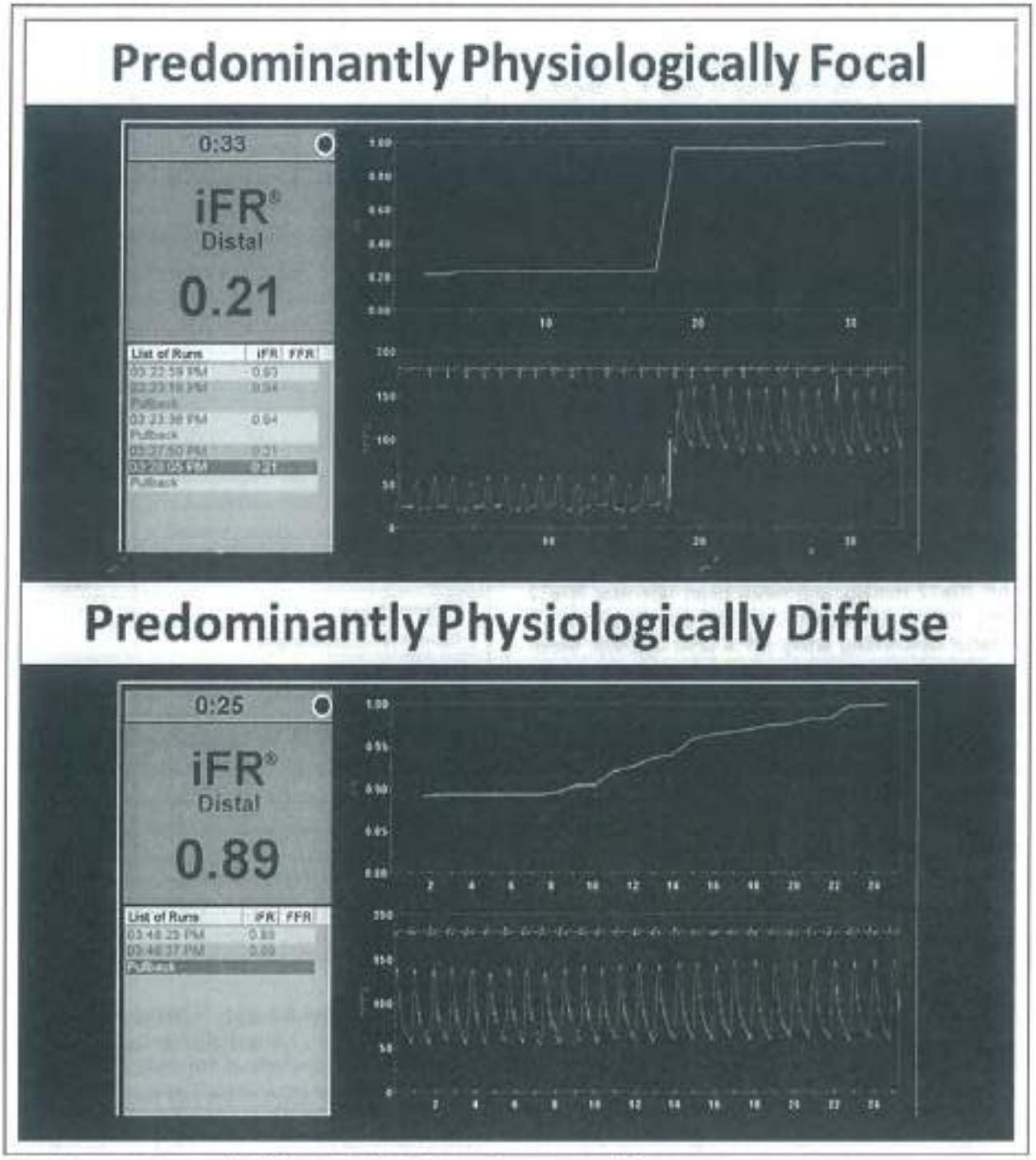

Figure 1. Representative examples of different physiological patterns of coronary artery disease.
Predominantly physiologically focal disease (**top**) and predominantly physiologically diffuse disease (**bottom**). iFR indicates instantaneous wave-free ratio.

Downloaded from http://ahajournals.org by on May 15, 2019

analysis if pressure-wire pullback was not performed from an adequately distal point of the vessel or if fluoroscopy was not provided to confirm the distal wire position.

All pullback traces were jointly evaluated by 3 expert interventional cardiologists (R.P., S.S., and R.A.L.) who were blinded to the clinical presentation, patient characteristics, and coronary angiography. For each case, the consensus opinion for the physiological pattern of disease was generated by the unanimous agreement of the 3 experts. The physiological pattern of disease was classified as predominantly physiologically focal or predominantly physiologically diffuse by the consensus opinion. Representative examples of these classifications are shown in Figure 1.

Statistical Analysis

Categorical data were expressed as numbers and percentages, whereas continuous variables were expressed as mean

and (±) SD or as median accompanied by interquartile range as appropriate. Tests of normality were first performed using the Shapiro-Wilk test. Continuous variables were compared with Student *t* or Mann-Whitney *U* tests, and categorical variables with χ^2 or Fisher exact tests, as appropriate. All probability values were 2 sided, and $P<0.05$ was considered statistically significant. All the statistical analysis was performed using R, version 3.2.1 (R Foundation for Statistical Computing, Vienna, Austria).

RESULTS

Study Population

A total of 360 coronary vessels (345 patients) were included for analysis from 6 centers (Imperial College London Hammersmith Hospital, St. Marianna University School of Medicine Yokohama City Seibu Hospital, Toda Central General Hospital, Kanazawa Cardiovascular Hospital, Okaya City Hospital, and Hospital Clínico San Carlos). The mean age was 64.4±10.3 years (76% men). The mean respective systolic and diastolic blood pressures on admission were 136±23 and 70±12 mm Hg, and mean heart rate was 70±12 bpm. The most frequently assessed vessel was the left anterior descending artery (81% [290 of 360]). Mean percentage diameter stenosis and lesion length were 51.6±13.5% and 20.9±14.8 mm, respectively. Full description of baseline, vessel, and stenosis characteristics are provided in Table 1. Median FFR and iFR values were 0.80 (interquartile range, 0.75–0.85) and 0.89 (interquartile range, 0.86–0.92), respectively. The relationship between FFR and iFR values is displayed in Figure 2 (R=0.73; $P<0.001$).

Classification by FFR/iFR Values and iFR Pressure-Wire Pullback

FFR agreed with iFR in 78.1% (281 of 360) of cases, consisting of FFR+/iFR+ (n=154; 42.7%) and FFR−/iFR− (n=127; 35.3%). FFR disagreed with iFR in 21.9% (79 of 360) of cases, consisting of FFR−/iFR+ (n=38; 10.6%) and FFR+/iFR− (n=41; 11.4%). The iFR pullback curve, the physiological pattern of disease, was classified as 47.5% (171 of 360) predominantly physiologically focal and 52.5% (189 of 360) predominantly physiologically diffuse (Table 2).

Comparison Among Groups Classified by FFR and iFR

Clinical and lesion characteristics between concordant (FFR+/iFR+ and FFR−/iFR−) and discordant (FFR−/iFR+ and FFR+/iFR−) groups are displayed in Table I in the Data Supplement. There were no differences in patient and lesion characteristics between 2 groups. The prevalence of proximal lesions, defined as Syntax segments 1, 5, 6, and 11,[11] was also similar (52.3% [147 of 281] versus 50.6% [40 of 79]; $P=0.79$). More specifically, stenosis location in the left main or ostial left anterior descending artery showed some tendency for FFR/iFR discordance; however, this did not meet statistical significance within the current dataset (9.6% [27 of 281] versus 17.7% [14 of 79]; $P=0.071$).

In the FFR/iFR discordant (FFR−/iFR+ and FFR+/iFR−) groups, mean FFR and iFR values were 0.80±0.05 and 0.89±0.03, respectively. Baseline, vessel, and anatomic stenosis characteristics were all comparable between 2 discordant groups ($P>0.05$ for all; Table 3). Only the physiological pattern of disease as determined by the iFR pullback was significantly different between FFR−/iFR+ and FFR+/iFR− groups. In comparison to the FFR+/iFR− group, the FFR−/iFR+ group demonstrated a significantly higher

Table 1. Patient and Vessel Characteristics

Patients	345
Age, y	64.4±10.3
Men	261 (76)
Height, cm	168±9.2
Weight, kg	78.5±15.3
Hypertension	240 (70)
Dyslipidemia	220 (64)
Diabetes mellitus	108 (31)
Renal insufficiency	57 (17)
Current smoker	77 (21)
Family history of CAD	61 (18)
Previous MI	83 (24)
Severe LVSD	14 (4.1)
Vessels	360
Coronary artery	
LAD	290 (81)
LCx	33 (9.2)
RCA	33 (9.2)
LM	23 (6.4)
Diagonal branch	4 (1.1)
Quantitative coronary angiography	
Diameter stenosis, %	51.6±13.5
Minimum lumen diameter, mm	1.42±0.49
Reference diameter, mm	2.94±0.63
Lesion length, mm	20.9±14.8
Physiological indices	
FFR	0.80 (0.75–0.85)
iFR	0.89 (0.86–0.92)

Values are n (mean±SD), n (%), or median (interquartile range). All the LM cases involved LAD lesions. CAD indicates coronary artery disease; FFR, fractional flow reserve; FR, instantaneous wave-free ratio; LAD, left anterior descending artery; LCx, left circumflex artery; LM, left main; LVSD, left ventricular systolic dysfunction; MI, myocardial infarction; and RCA, right coronary artery.

Downloaded from http://circinterventions.ahajournals.org by on May 15, 2019

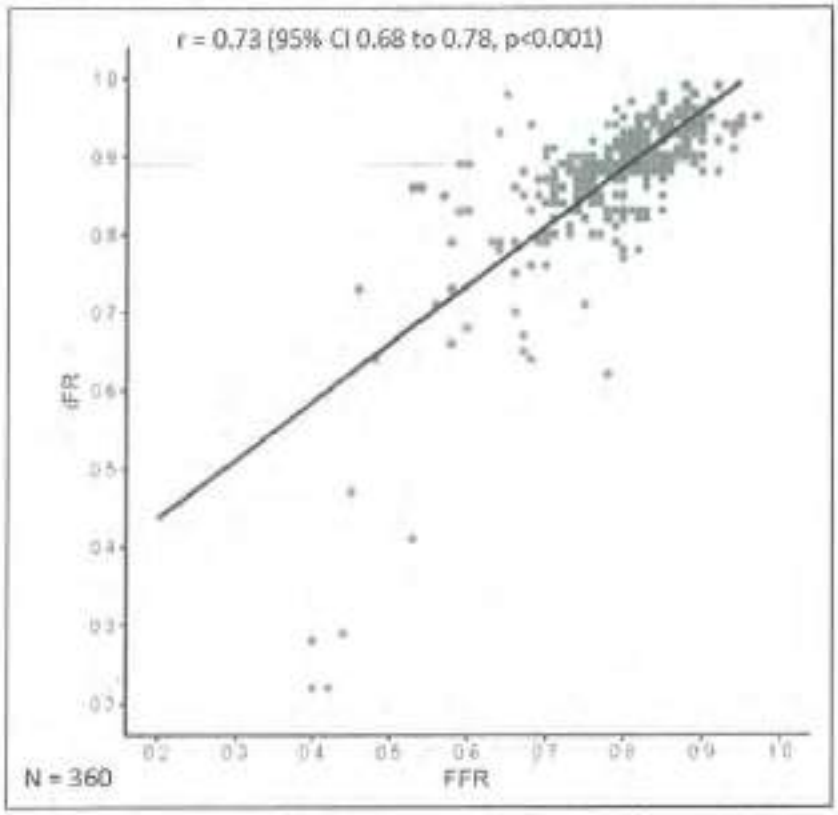

Figure 2. Scatter plot showing the relationship between fractional flow reserve (FFR) and instantaneous wave-free ratio (iFR) values.
The black line represents the line of best fit. The gray lines represent the respective cutoff values for FFR (≤0.80) and iFR (≤0.89). Concordant cases are colored blue; discordant cases are colored orange.

prevalence of predominantly physiologically diffuse (82% [31 of 38] versus 42% [17 of 41]; *P*<0.001; Figure 3). Of note, within the discordant groups, there were no patients in whom coronary physiology was measured in multiple vessels. Accordingly, both patient and vessel number were the same (n=79) in the discordant groups.

DISCUSSION

This study sought to determine whether the physiological pattern of coronary artery disease was an influencing factor for FFR/iFR discordance. The main findings of this study were as follows. First, unlike patient, vessel, or stenosis characteristics, the physiological pattern of disease was identified as a significant influencing factor for FFR/iFR discordance. Second, FFR+/iFR− discordance was significantly more associated with a physiologically focal pattern of disease. Last, FFR−/iFR+ discordance was significantly more associated with a physiologically diffuse pattern of disease.

FFR/iFR Discordance—Influencing Clinical Features

It is well recognized that FFR and iFR disagree in the hemodynamic significance of a coronary lesion in ≈20% of cases.[4] To date, several studies have investigated the clinically important topic of FFR/iFR discordance. Previous works have demonstrated that the discordance was observed more frequently in lesions in the proximal segment[5] or left main and proximal left anterior descending artery lesion location[6] compared with other lesion locations. Patient characteristics too have also been demonstrated to influence FFR/iFR discordance, with female sex and comorbidity with diabetes mellitus[7] identified as significant influencing factors. The findings of the current study provided some consistency with these previous observations. Namely, most proximal stenosis location (left main/ostial left anterior descending artery) and patient comorbidity with diabetes mellitus demonstrated a tendency for determining FFR/iFR discordance (*P*=0.071 and *P*=0.094, respectively). In addition to corroborating these known factors, the current study identified that the physiological

Table 2. Classification by FFR/iFR and iFR Pressure-Wire Pullback

Physiological Classification (n=360)	
Physiological indices	
FFR+/iFR+	154 (43)
FFR−/iFR+	38 (11)
FFR+/iFR−	41 (11)
FFR−/iFR−	127 (35)
Physiological pattern of disease	
Predominantly physiologically focal	171 (48)
Predominantly physiologically diffuse	189 (53)

Values are n (%). FFR indicates fractional flow reserve; and iFR, instantaneous wave-free ratio.

Downloaded from http://circinterventions.ahajournals.org by on May 15, 2019

Table 3. Comparison of 2 Discordant Groups

	FFR−/iFR+ Group (n=38)	FFR+/iFR− Group (n=41)	*P* Value
Patient characteristics			
Age, y	65.1±11.5	62.7±11.1	0.34
Men	28 (74)	32 (78)	0.85
Height, cm	166±9.2	168±8.7	0.48
Weight, kg	77.9±18.0	78.8±16.7	0.82
Hypertension	30 (79)	30 (73)	0.74
Dyslipidemia	24 (63)	26 (63)	1.00
Diabetes mellitus	16 (42)	10 (24)	0.094
Renal insufficiency	6 (16)	10 (24)	0.50
Current smoker	6 (16)	8 (20)	0.67
Family history of CAD	7 (18)	9 (22)	0.91
Previous myocardial infarction	7 (18)	10 (24)	0.71
Severe LVSD	2 (5.3)	3 (7)	1.00
Target vessel and lesion location			
LAD	31 (82)	34 (83)	1.00
LCx	3 (7.9)	4 (9.8)	1.00
RCA	3 (7.9)	3 (7.3)	1.00
LM	3 (7.9)	5 (12)	0.80
Diagonal branch	1 (2.6)	0 (0)	0.97
Proximal lesions (LAD, LCx, RCA, and LM)	22 (58)	18 (44)	0.22
LM or ostial LAD lesion	6 (16)	8 (20)	0.89
Quantitative coronary angiography			
Diameter stenosis, %	44.9±13.0	45.4±12.0	0.87
Minimum lumen diameter, mm	1.64±0.51	1.66±0.40	0.88
Reference diameter, mm	2.97±0.57	3.09±0.70	0.44
Lesion length, mm	18.2±12.8	18.0±12.9	0.93
Physiological indices			
FFR	0.84±0.03	0.77±0.04	
iFR	0.87±0.03	0.92±0.02	
Physiological pattern of disease			
Predominantly physiologically focal	7 (18)	24 (59)	<0.001
Predominantly physiologically diffuse	31 (82)	17 (41)	<0.001

Values are mean±SD or n (%). CAD indicates coronary artery disease; FFR, fractional flow reserve; iFR, instantaneous wave-free ratio; LAD, left anterior descending artery; LCx, left circumflex artery; LM, left main; LVSD, left ventricular systolic dysfunction; and RCA, right coronary artery.

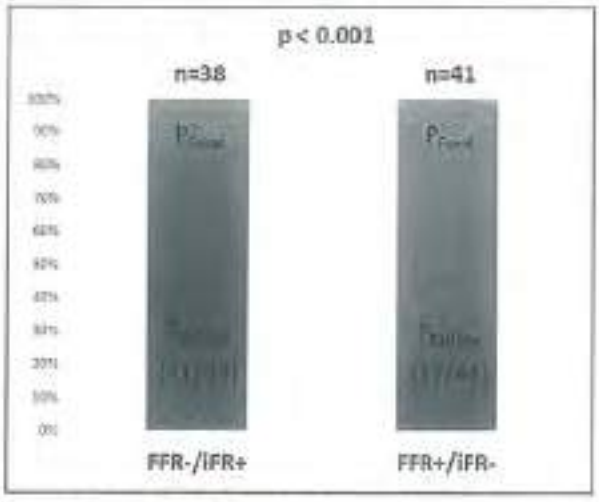

Figure 3. The association between physiological pattern of disease and fractional flow reserve (FFR)/instantaneous wave-free ratio (iFR) discordance.
FFR−/iFR+ was significantly more associated with physiologically diffuse pattern of disease, whereas FFR+/iFR− was significantly more associated with physiologically focal pattern of disease. $P_{diffuse}$ indicates predominantly physiologically diffuse; and P_{focal}, predominantly physiologically focal.

pattern of disease determined by pressure-wire pullback further influenced the discordance.

FFR/iFR Discordance and the Physiological Pattern of Disease—Helping to Refine the Underlying Physiological Mechanism

The physiological mechanism underlying FFR/iFR discordance has recently been proposed as being due to differential coronary flow responses to pharmacological hyperemia.[3] Specifically, FFR+/iFR− discordance was characterized by high hyperemic coronary flow velocity and FFR−/iFR+ discordance by low hyperemic coronary flow velocity. The findings of the present study may help provide a more refined mechanistic explanation for FFR/iFR discordance.

In the fluid dynamic equation that determines the degree of pressure loss across a stenosis because of variations in coronary flow velocity, linear and quadratic components are highly dependent on the geometry of the lesion itself. Although combined measurements of coronary pressure and flow were not performed in the current study, our findings suggested that in physiologically diffuse disease, frictional losses along the length of the vessel would be the predominant mode of a pressure energy loss, evident at rest (iFR+) and with only minimal increase during hyperemia (FFR−). Conversely, in physiologically focal disease, separation losses in the near vicinity of the stenosis itself would be the predominant mode of a pressure energy loss, minimally present at rest (iFR−) and evident only during hyperemia (FFR+).

Clinical Implications

Discordance between FFR and iFR has been demonstrated to be multifactorial in origin, consisting of patient, anatomic, and physiological diversities.[5–8] Such factors should be considered when interpreting the results of FFR/iFR discordant cases. However, given that the majority of discordance occurs close to the respective FFR and iFR cut points as in the literature,[5–8] the clinical importance of FFR/iFR discordance itself should

Downloaded from http://circinterv.ahajournals.org by on May 15, 2019

be interpreted with a degree of caution. In our datasets, the respective mean FFR and iFR values were also 0.80±0.05 and 0.89±0.03 in the discordant groups. Within this borderline diagnostic ranges, clinical outcome data are conflicting and only available from relatively small nonrandomized studies and are a subject of debate.[12-14] More specifically, 1 study demonstrated the safety of deferral of percutaneous coronary intervention (PCI) in patients with gray-zone FFR (between 0.75 and 0.80) and suggested the prognostic threshold for FFR was in fact much lower (FFR, 0.67).[12] A more recent study has also shown no significant difference in major adverse clinical events between PCI and medical therapy in the FFR gray-zone,[13] whereas others have shown that PCI compared with medical therapy was associated with better clinical outcomes in patients with gray-zone FFR.[14]

Although there are no clinical outcome–related data to define the optimal treatment strategy when FFR/iFR discordance occurs, the predominance of physiologically focal or diffuse disease might be used to determine the treatment strategy if revascularization is contemplated. For example, in FFR+/iFR− discordance with an associated physiologically focal disease pattern, focal PCI may provide a preferred treatment strategy. However, if physiological values are borderline, it should be reconsidered whether the lesion causes sufficient ischemia to require stenting in patients with likely preserved coronary flow. Similarly, in FFR−/iFR+ discordance with an associated physiologically diffuse pattern, consideration should be given to the efficacy of PCI over long segments of disease. Even though resting physiology may support the indication of revascularization, clinicians should consider the balanced risks and benefits for revascularization with long stenting, which may not achieve an optimum post-PCI physiological result or good long-term outcomes.[15]

In summary, the routine performance of coronary pressure-wire pullback could better help clinicians determine the revascularization strategy in patients with intermediate-severity coronary artery disease, above and beyond simply the FFR or iFR value.

Study Limitations

This study is not without limitation. First, owing to the retrospective registry-based design of this study, potential for selection bias of patients undergoing iFR pullback for clinical indications must be considered, and we could not provide information on baseline ratio of distal coronary pressure to aortic pressure during whole cardiac cycle. However, the value of such a registry-based approach reflects both real-world practice and clinically encountered disease populations. In addition, median FFR and iFR values in the present study were 0.80 and 0.89, respectively, whereas those in previous reports ranged 0.81 to 0.87 for FFR and 0.90 to 0.94 for iFR.[5-8] Therefore, the populations in this study were comparable to those previously published in the literature.

Second, our findings should only be considered applicable to patients with isolated stable coronary artery disease. It has been demonstrated that acute coronary syndrome, cardiac hypertrophy, and severe aortic stenosis could attenuate the hyperemic response of the microcirculation to adenosine.[16] Accordingly, it is likely the prevalence (and possibly mechanism) of FFR/iFR discordance may be different in these selected populations.

Third, in the present study, combined measurements of coronary flow velocity were not performed. Such measurements would be required to fully determine our proposed association between hyperemic coronary flow characteristics and physiological disease pattern, which remains speculative.

Finally, there is no clear criteria to define the physiological pattern of disease as assessed by coronary pressure-wire pullback. Although several studies proposed focal (abrupt) pattern and diffuse (gradual) pattern on FFR pullback, all definitions were different depending on investigators.[17,18] Recent report demonstrated a simple predictive equation could accurately evaluate the component contributions of individual stenoses in serial lesions using FFR pullback, which might be helpful for determining the physiological pattern of disease in the future.[19] As a result, currently, classification of the physiological pattern of disease is operator dependent and thus prone to both intra and interoperator variability. Mindful of this, within the present study, each iFR pullback trace was judged by the consensus opinion of 3 expert interventional cardiologists who reviewed the pullback data together. However, such an approach does not fully replicate clinical practice where data are often interpreted only by the performing physician. Further studies are being conducted to investigate the intraobserver and interobserver differences in the interpretation of pressure-wire pullback that may alter clinical decision-making.

Conclusions

The physiological pattern of disease is an important influencing contributing factor for the discordance between FFR and iFR. Specifically, FFR+/iFR− discordance is more frequently associated with a focal disease pattern, and FFR−/iFR+ discordance is more frequently associated with a diffuse disease pattern.

ARTICLE INFORMATION

Received October 9, 2018; accepted February 8, 2019.

The Data Supplement is available at https://www.ahajournals.org/doi/suppl/10.1161/CIRCINTERVENTIONS.118.007494.

Downloaded from http://ahajournals.org by on May 15, 2019

Authors

Tekayuki Warisawa, MD; Christopher M. Cook, MD; James P. Howard, MD; Yousif Ahmad, MD; Shunichi Doi, MD; Masafumi Nakayama, MD; Sonoka Goto, MD; Yohei Yakusa, MD; Kenichi Kanise, MD; Matthew J. Shun-Shin, MD; Ricardo Petraco, MD, PhD; Sayan Sen, MD, PhD; Sukhjinder Nijjer, MD, PhD; Rasha Al Lamee, MD, PhD; Yuki Ishibashi, MD, PhD; Hisao Matsuda, MD, PhD; Javier Escaned, MD, PhD; Carlo di Mario, MD, PhD; Darrel P. Francis, MD, PhD; Yoshihiro J. Akashi, MD, PhD; Justin E. Davies, MD, PhD

Correspondence

Justin E. Davies, MD, PhD, National Heart and Lung Institute–Cardiovascular Science, B Block 5, 2nd floor, Du Cane Rd, London W12 0NN, United Kingdom. Email drjustindavies@gmail.com

Affiliations

International Center for Circulatory Health, National Heart and Lung Institute, Imperial College London, Hammersmith Hospital, United Kingdom (T.W., C.M.C., J.P.H., Y.A., M.J.S.-S., R.P., S.S., S.N., R.A.L., D.P.F., J.E.D.). Division of Cardiology, Department of Internal Medicine, St. Marianna University School of Medicine, Kawasaki, Japan (T.W., Y.J., Y.J.A.). Department of Cardiovascular Medicine, St. Marianna University School of Medicine, Yokohama City Seibu Hospital, Japan (S.D., H.M.). Cardiovascular Center, Toda Central General Hospital, Japan (M.N., S.G.). Tokyo Women's Medical University–Waseda University Joint Institution for Advanced Biomedical Sciences, Japan (M.N.). Cardiovascular Institute, Hospital Clinico San Carlos, Madrid, Spain (S.G., J.E.). Department of Cardiology, Kanazawa Cardiovascular Hospital, Japan (Y.Y.). Department of Cardiovascular Medicine, Okaya City Hospital, Japan (K.K.). Structural Interventional Cardiology, Careggi University Hospital, Florence, Italy (C.d.M.).

Acknowledgments

We appreciate all the staff of catheter laboratory at collaborating centers for their effort and understanding to clinical research work.

Disclosures

Drs Warisawa and Davies report consultancy work for Philips. Dr Davies is an inventor of instantaneous wave-free ratio technology and holds intellectual property, which is under license. Drs Cook, Al Lamee, Sen, Petraco, and Nijjer have received speaker's honoraria from Philips. The other authors report no conflicts.

REFERENCES

1. Neumann FJ, Sousa-Uva M, Ahlsson A, Alfonso F, Banning AP, Benedetto U, Byrne RA, Collet JP, Falk V, Head SJ, Jüni P, Kastrati A, Koller A, Kristensen SD, Niebauer J, Richter DJ, Seferovic PM, Sibbing D, Stefanini GG, Windecker S, Yadav R, Zembala MO; ESC Scientific Document Group. 2018 ESC/EACTS Guidelines on myocardial revascularization. *Eur Heart J*. 2019;40:87–165. doi: 10.1093/eurheartj/ehy394.
2. Pijls NH, van Son JA, Kirkeeide RL, De Bruyne B, Gould KL. Experimental basis of determining maximum coronary, myocardial, and collateral blood flow by pressure measurements for assessing functional stenosis severity before and after percutaneous transluminal coronary angioplasty. *Circulation*. 1993;87:1354–1367.
3. Sen S, Escaned J, Malik IS, Mikhail GW, Foale RA, Mila R, Tarkin J, Petraco R, Broyd C, Jabbour R, Sethi A, Baker CS, Bellamy M, Al-Bustami M, Hackett D, Khan M, Lefroy D, Parker KH, Hughes AD, Francis DP, Di Mario C, Mayet J, Davies JE. Development and validation of a new adenosine-independent index of stenosis severity from coronary wave-intensity analysis: results of the ADVISE (Adenosine Vasodilator Independent Stenosis Evaluation) study. *J Am Coll Cardiol*. 2012;59:1390–1400. doi: 10.1016/j.jacc.2011.11.003
4. Jeremias A, Maehara A, Généreux P, Asrress KN, Berry C, De Bruyne B, Davies JE, Escaned J, Fearon WF, Gould KL, Johnson NP, Kirtane AJ, Koo BK, Marques KM, Nijjer S, Oldroyd KG, Petraco R, Piek JJ, Pijls NH, Redwood S, Siebes M, Spaan JAE, van 't Veer M, Mintz GS, Stone GW. Multicenter core laboratory comparison of the instantaneous wave-free ratio and resting Pd/Pa with fractional flow reserve: the RESOLVE study. *J Am Coll Cardiol*. 2014;63:1253–1261. doi: 10.1016/j.jacc.2013.09.060
5. Hennigan B, Oldroyd KG, Berry C, Johnson N, McClure J, McCartney P, McEntegart MB, Eteiba H, Petrie MC, Rocchiccioli P, Good R, Lindsay MM, Hood S, Watkins S. Discordance between resting and hyperemic indices of coronary stenosis severity: the VERIFY 2 study. *Circ Cardiovasc Interv*. 2016;9:e004016. doi: 10.1161/CIRCINTERVENTIONS.116.004016
6. Kobayashi Y, Johnson NP, Berry C, De Bruyne B, Gould KL, Jeremias A, Oldroyd KG, Pijls NHJ, Fearon WF; CONTRAST Study Investigators. The influence of lesion location on the diagnostic accuracy of adenosine-free coronary pressure wire measurements. *JACC Cardiovasc Interv*. 2016;9:2390–2399. doi: 10.1016/j.jcin.2016.08.041
7. Lee JM, Shin ES, Nam CW, Doh JH, Hwang D, Park J, Kim KJ, Zhang J, Koo BK. Discrepancy between fractional flow reserve and instantaneous wave-free ratio: clinical and angiographic characteristics. *Int J Cardiol*. 2017;245:63–68. doi: 10.1016/j.ijcard.2017.07.099
8. Cook CM, Jeremias A, Petraco R, Sen S, Nijjer S, Shun-Shin MJ, Ahmad Y, de Waard G, van de Hoef T, Echavarria-Pinto M, van Lavieren M, Al Lamee R, Kikuta Y, Shiono Y, Buch A, Meuwissen M, Danad I, Knaapen P, Meehara A, Koo BK, Mintz GS, Escaned J, Stone GW, Francis DP, Mayet J, Piek JJ, van Royen N, Davies JE. Fractional flow reserve/instantaneous wave-free ratio discordance in angiographically intermediate coronary stenoses: an analysis using doppler-derived coronary flow measurements. *JACC Cardiovasc Interv*. 2017;10:2514–2524. doi: 10.1016/j.jcin.2017.09.031
9. Warisawa T, Cook CM, Akashi YJ, Davies JE. Past, present and future of coronary physiology. *Rev Esp Cardiol (Engl Ed)*. 2018;71:656–667. doi: 10.1016/j.rec.2018.02.003
10. Cook CM, Ahmad Y, Shun-Shin MJ, Nijjer S, Petraco R, Al-Lamee R, Mayet J, Francis DP, Sen S, Davies JE. Quantification of the effect of pressure wire drift on the diagnostic performance of fractional flow reserve, instantaneous wave-free ratio, and whole-cycle Pd/Pa. *Circ Cardiovasc Interv*. 2016;9:e002988. doi: 10.1161/CIRCINTERVENTIONS.115.002988
11. Serruys PW, Onuma Y, Garg S, Sarno G, van den Brand M, Kappetein AP, Van Dyck N, Mack M, Holmes D, Feldman T, Morice MC, Colombo A, Bass E, Leadley K, Dawkins KD, van Es GA, Morel MA, Mohr FW. Assessment of the SYNTAX score in the syntax study. *EuroIntervention*. 2009;5:50–58.
12. Johnson NP, Toth GG, Lai D, Zhu H, Açar G, Agostoni P, Appelman Y, Arslan F, Barbato E, Chen SL, Di Serafino L, Domínguez-Franco AJ, Dupouy P, Esen AM, Esen OB, Hamilos M, Iwasaki K, Jensen LO, Jiménez-Navarro MF, Katritsis DG, Kocaman SA, Koo BK, López-Palop R, Lorin JD, Miller LH, Muller O, Nam CW, Oud N, Piaymirat E, Rieber J, Rioufol G, Rodés-Cabau J, Sedlis SP, Takashi Y, Tonino PA, Van Belle E, Varna E, Werner GS, Fearon WF, Pijls NH, De Bruyne B, Gould KL. Prognostic value of fractional flow reserve: linking physiologic severity to clinical outcomes. *J Am Coll Cardiol*. 2014;64:1641–1654. doi: 10.1016/j.jacc.2014.07.973
13. Kang DY, Ahn JM, Lee CH, Lee PH, Park DW, Kang SJ, Lee SW, Kim YH, Lee CW, Park SW, Park SJ. Deferred vs. performed revascularization for coronary stenosis with grey-zone fractional flow reserve values: data from the IRIS-FFR registry. *Eur Heart J*. 2018;39:1610–1619. doi: 10.1093/eurheartj/ehy079
14. Kubo T, Takahata M, Terada K, Mori K, Arito Y, Ino Y, Matsuo Y, Kitabata H, Shiono Y, Shimamura K, Kameyama T, Emori H, Katayama Y, Tanimoto T, Akasaka T. Retrospective comparison of long-term clinical outcomes between percutaneous coronary intervention and medical therapy in stable coronary artery disease with gray zone fractional flow reserve - COMFORTABLE retrospective study. *Circ J*. 2018;82:3044–3051. doi: 10.1253/circj.CJ-18-0672
15. Baranauskas A, Peace A, Kibarskis A, Shannon J, Abraitis V, Bajoras V, Bilkis V, Aidietis A, Laucevicius A, Dwikinickus G. FFR result post PCI is suboptimal in long diffuse coronary artery disease. *EuroIntervention*. 2016;12:1473–1480. doi: 10.4244/EIJ-D-15-00514
16. Benenati S, De Maria GL, Scarsini R, Porto I, Banning AP. Invasive "In the cath-lab" assessment of myocardial ischemia in patients with coronary artery disease: when does the gold standard not apply? *Cardiovasc Revasc Med*. 2018;19(3 pt B):362–372. doi: 10.1016/j.carrev.2018.01.005
17. Shiono Y, Kubo T, Honda K, Katayama Y, Aoki H, Satogami K, Kashiyama K, Tsuya A, Nishiguchi T, Kuroi A, Orii M, Kameyama T, Yamano T, Yamaguchi T, Matsuo Y, Ino Y, Tanaka A, Hozumi T, Nishimura Y, Okamura Y, Akasaka T. Impact of functional focal versus diffuse coronary artery disease on bypass graft patency. *Int J Cardiol*. 2016;222:16–21. doi: 10.1016/j.ijcard.2016.07.052
18. Ando H, Takashima H, Suzuki A, Sakurai S, Kumagai S, Kurita A, Waseda K, Amano T. Impact of lesion characteristics on the prediction of optimal poststent fractional flow reserve. *Am Heart J*. 2016;182:115–124. doi: 10.1016/j.ahj.2016.09.015
19. Modi BN, Ryan M, Chatterjee A, Ensslaone K, Ellis H, Gaddum N, Lee J, Clapp B, Chowienczyk P, Perera D. Optimal application of fractional flow reserve to assess serial coronary artery disease: a 3D-printed experimental study with clinical validation. *J Am Heart Assoc*. 2018;7:e010279. doi: 10.1161/JAHA.118.010279

Downloaded from http://ahajournals.org by on May 15, 2019

Heart and Vessels (2019) 34:957–964
https://doi.org/10.1007/s00380-018-01326-5

ORIGINAL ARTICLE

Effect of carvedilol on heart rate response to cardiopulmonary exercise up to the anaerobic threshold in patients with subacute myocardial infarction

Shinji Nemoto[1,2] · Yusuke Kasahara[1] · Kazuhiro P. Izawa[3] · Satoshi Watanabe[4] · Kazuya Yoshizawa[1] · Naoya Takeichi[4] · Kentaro Kamiya[2] · Norio Suzuki[5] · Kazuto Omiya[6] · Atsuhiko Matsunaga[2] · Yoshihiro J. Akashi[6]

Received: 19 July 2018 / Accepted: 21 December 2018 / Published online: 2 January 2019
© Springer Japan KK, part of Springer Nature 2019

Abstract
Resting heart rate (HR) plus 20 or 30 beats per minute (bpm), i.e., a simplified substitute for HR at the anaerobic threshold (AT), is used as a tool for exercise prescription without cardiopulmonary exercise testing data. While resting HR plus 20 bpm is recommended for patients undergoing beta-blocker therapy, the effects of specific beta blockers on HR response to exercise up to the AT (ΔAT HR) in patients with subacute myocardial infarction (MI) are unclear. This study examined whether carvedilol treatment affects ΔAT HR in subacute MI patients. MI patients were divided into two age- and sex-matched groups [carvedilol (+), $n=66$; carvedilol (−), $n=66$]. All patients underwent cardiopulmonary exercise testing at 1 month after MI onset. ΔAT HR was calculated by subtracting resting HR from HR at AT. ΔAT HR did not differ significantly between the carvedilol (+) and carvedilol (−) groups (35.64 ± 9.65 vs. 34.67 ± 11.68, $P=0.604$). Multiple regression analysis revealed that old age and heart failure after MI were significant predictors of lower ΔAT HR ($P=0.039$ and $P=0.013$, respectively), but not carvedilol treatment. Our results indicate that carvedilol treatment does not affect ΔAT HR in subacute MI patients. Therefore, exercise prescription based on HR plus 30 bpm may be feasible in this patient population, regardless of carvedilol use, without gas-exchange analysis data.

Keywords Myocardial infarction · Beta blocker · Anaerobic threshold · Heart rate response · Cardiac rehabilitation

✉ Yoshihiro J. Akashi
yoakashi-circ@umin.ac.jp

1 Department of Rehabilitation Medicine, St. Marianna University School of Medicine Yokohama City Seibu Hospital, Yokohama, Japan

2 Department of Rehabilitation Sciences, Kitasato University Graduate School of Medical Sciences, Sagamihara, Japan

3 Department of Public Health, Kobe University Graduate School of Health Sciences, Kobe, Japan

4 Department of Rehabilitation Medicine, St. Marianna University School of Medicine Hospital, Kawasaki, Japan

5 Division of Cardiology, Department of Internal Medicine, St. Marianna University School of Medicine Yokohama City Seibu Hospital, Yokohama, Japan

6 Division of Cardiology, Department of Internal Medicine, St. Marianna University School of Medicine, 2-16-1 Sugao, Miyamae-ku, Kawasaki, Kanagawa 216-8511, Japan

Introduction

Exercise training reduces cardiovascular mortality after acute myocardial infarction (MI) [1]. Many guidelines recommend exercise for MI patients as part of prevention of cardiovascular death [2, 3]. When prescribing exercise intensity in patients with subacute MI, heart rate (HR) at anaerobic threshold (AT) is frequently measured by cardiopulmonary exercise testing (CPX) to ensure effectiveness and safety of training [2, 4, 5]. However, it is not feasible to perform CPX for all patients due to the high cost of equipment and need for manpower. Thus, exercise prescription based on resting HR plus 20 or 30 beats per minute (bpm), i.e., a simplified substitute for HR at AT [6, 7], is used as a way to determine exercise intensity without gas-exchange analysis data. This method is based on the physiologic HR response to exercise up to the AT.

The use of beta blockers is recommended to prevent cardiovascular death in MI patients [2], and consequently, many patients with subacute MI are administered beta

blockers, including carvedilol, which is frequently prescribed worldwide due to its effectiveness [2, 8]. A recent study reported that beta blocker treatment decreased HR at rest and during exercise in patients with coronary artery disease [9]. Thus, experts recommend that a lower value (i.e., resting HR plus 20 bpm) should be used if patients are treated with beta blockers [6]. However, the previous study did not sufficiently evaluate HR response to cardiopulmonary exercise up to the AT in subacute MI patients treated with a specific kind of beta blocker. Therefore, the effect of single beta blocker treatment on HR response to exercise up to the AT in this patient population remains unclear. Accordingly, the present study aimed to examine whether carvedilol affects HR response to cardiopulmonary exercise up to the AT in patients with subacute MI, as this information may help physicians to prescribe appropriate exercise for subacute MI patients treated with beta blockers.

Methods

The study protocol conformed to the ethical guidelines of the Declaration of Helsinki and was approved by the Ethics Committee of St. Marianna University School of Medicine (Chairperson of the ethics committee, Masashi Taki; Protocol number, No. 2258; date of approval by the ethics committee, November 30, 2012). Informed consent was obtained from each patient before conducting the CPX.

Study design and patients

Of the 641 consecutive acute MI patients who had undergone cardiac rehabilitation at St. Marianna University School of Medicine Yokohama City Seibu Hospital from August 1998 to November 2017, 289 patients who were able to undergo symptom-limited CPX at 1 month after the onset of MI were enrolled in this retrospective cross-sectional study. Exclusion criteria were the presence of atrial fibrillation, complex arrhythmia, a pacemaker, and recent myocardial infarction, a history of cardiac surgery, and the use of beta blockers other than carvedilol or any other drugs with negative or positive chronotropic effects (e.g., verapamil, diltiazem hydrochloride). Of the 289 subacute MI patients, 229 met the study criteria. Patients were divided into the following two groups according to carvedilol treatment, matched by age (± 5 years) and sex: the carvedilol (+) group (66 patients) and the carvedilol (−) group (66 patients). Ultimately, these 132 patients were included in this study. All patients were clinically stable and examined while on stable doses of medication.

Clinical characteristics

Age, sex, body mass index, site of infarction, residual coronary artery stenosis, past medical history, complications, medications, time between MI onset and exercise testing, and year of hospitalization were evaluated using medical records. Maximum serum creatine kinase-myocardial band (max CK-MB) was measured using blood samples obtained during hospitalization. Left ventricular ejection fraction (LVEF) was echocardiographically determined using a modified Simpson's method and served as the index of left ventricular systolic function at hospital discharge.

Symptom-limited cardiopulmonary exercise testing

All patients underwent symptom-limited CPX on a treadmill (MAT-2700, Fukuda Denshi Co., Tokyo, Japan). After 3 min of rest in the seated position, patients performed exercise with an increasing load (speed or grade; every 60 s) [10] following 3 min of warm-up (speed, 1.0 mph; grade, 0%). A 12-lead electrocardiogram (ECG) was continuously monitored, and HR was measured from the R–R interval of the ECG (ML-9000, Fukuda Denshi Co., Tokyo, Japan) during the test. Systolic blood pressure (SBP) and diastolic blood pressure (DBP) were measured by the cuff method with an automatic blood pressure monitor (STBP-780, Colin Co., Aichi, Japan) at 1-min intervals. Oxygen uptake ($\dot{V}O_2$), carbon dioxide production ($\dot{V}CO_2$), minute ventilation ($\dot{V}E$), tidal volume (TV), end tidal O_2 (ETO_2), and end tidal CO_2 ($ETCO_2$) were measured with an aeromonitor (AE-310s, Minato Ikagaku Co., Tokyo, Japan) throughout the test. Expired gas was sampled using a breath-by-breath method. The endpoint of testing was determined as previously described [11]. Specifically, the appearance of a plateau in $\dot{V}O_2$ despite an increasing exercise intensity indicated the exercise endpoint.

Ventilatory equivalents were calculated for O_2 ($\dot{V}E/\dot{V}O_2$), CO_2 ($\dot{V}E/\dot{V}CO_2$), and the gas exchange ratio (GER) ($\dot{V}CO_2/\dot{V}O_2$) on a personal computer (Model PC-9801, NEC Co., Tokyo, Japan). AT was determined by the V-slope method [12].

HR at rest (HR_{rest}), HR at AT (HR_{AT}), and HR at peak $\dot{V}O_2$ (HR_{peak}) were determined from the recorded HR during the course of CPX. Increases from HR_{rest} to HR_{peak} (Δpeak HR), from HR_{rest} to HR_{AT} (ΔAT HR), and from HR_{AT} to HR_{peak} (ΔAT-peak HR) were calculated for all patients.

Statistical analysis

Results are expressed as mean ± SE. The Kolmogorov–Smirnov test was performed to assess the normality

of distribution. Differences in clinical characteristics among patients were analyzed using the unpaired t test, Mann–Whitney U test, and χ^2 test. Differences in the results of CPX between carvedilol (+) and carvedilol (−) groups were analyzed using the unpaired t test and Mann–Whitney U test. Analysis of covariance (ANCOVA) was used if GER at peak was determined to be a covariate according to the results of CPX. Clinically important factors and carvedilol treatment were entered into a multiple regression model for the prediction of ΔAT HR by the forced-entry method. In the carvedilol (+) group, Spearman's rank correlation coefficient was used to examine correlations between ΔAT HR and carvedilol doses. The χ^2 test was used to compare the number of patients with (HR_{rest} + 30 bpm − HR_{AT}) ≥ 10% HR_{AT} in each group, given that a difference of ≥ 10% HR_{AT} is considered clinically relevant [13]. $P < 0.05$ was considered statistically significant. All statistical analyzes were performed with JMP® pro 13 (SAS Institute Inc., Cary, NC, USA). A priori power analysis was performed for multiple regression analysis using G*Power 3 program (Heinrich-Heine-Universität, Düsseldorf, Germany). The sample size was calculated to be 123 in the regression model for ΔAT HR (effect size = 0.15, α error probability = 0.05, power (1 − β error probability) = 0.8, number of predictors = 11) and, thus, the sample size of the present study was considered sufficient for conducting multiple regression analysis. Effect sizes were also calculated using G*Power 3 program.

Results

The clinical characteristics of patients are shown in Table 1. No significant differences were observed in clinical characteristics between the carvedilol (+) and carvedilol (−) groups, except that the proportion of patients hospitalized after 2006 was significantly higher in the carvedilol (+) group than in the carvedilol (−) group ($P < 0.001$).

The results of CPX are shown in Tables 2 and 3. None of the patients showed ischemic ST changes or experienced chest pain or serious arrhythmia during CPX. The variables obtained during cardiopulmonary exercise up to the AT are shown in Table 2. The values of HR_{rest} were significantly lower in the carvedilol (+) group compared to the carvedilol (−) group ($P = 0.047$; effect size, $d = 0.350$). The values of DBP_{rest} were significantly higher in the carvedilol (+) group compared to the carvedilol (−) group ($P = 0.011$; effect size, $d = 0.452$). Moreover, in the carvedilol (+) group, the values of HR_{AT} tended to be lower compared to the carvedilol (−) group ($P = 0.153$; effect size, $d = 0.250$). In contrast, the values of ΔAT HR did not differ significantly between the two groups ($P = 0.604$; effect size, $d = 0.091$).

The variables obtained during cardiopulmonary exercise up to peak $\dot{V}O_2$ are shown in Table 3. These results were analyzed by ANCOVA with GER at peak as the covariate, since the values of GER at peak were significantly lower in the carvedilol (+) group compared to the carvedilol (−) group (1.17 ± 0.09 vs. 1.13 ± 0.10; $P = 0.022$). In the carvedilol (+) group, HR_{peak} and ΔAT-peak HR were significantly lower compared to the carvedilol (−) group ($P = 0.009$ and $P = 0.010$, respectively). In contrast, Δpeak HR did not differ significantly between the two groups ($P = 0.440$).

The results of multiple regression analysis on the prediction of ΔAT HR are shown in Table 4. Old age (≥ 65 years) and heart failure after MI, but not carvedilol treatment, were significant predictors of ΔAT HR ($P = 0.039$ and $P = 0.013$, respectively).

Mean carvedilol dose was 5.76 ± 3.16 mg/day in the carvedilol (+) group (Table 1). No significant correlation was observed between ΔAT HR and carvedilol dose ($P = 0.903$) (Fig. 1).

No significant difference was observed in the number of patients with (HR_{rest} + 30 bpm − HR_{AT}) ≥10% HR_{AT} between the carvedilol (+) and carvedilol (−) groups ($P = 0.300$) (Table 5). A total of nine patients had values ≥ 10% HR_{AT}, and of these, three were treated with carvedilol (4.6% of all patients treated with carvedilol), five were older patients (7.8% of all older patients), and four had heart failure after MI (31% of all patients with heart failure after MI).

Discussion

In the present study, the values of ΔAT HR did not differ significantly between the carvedilol (+) and carvedilol (−) groups and the effect size (d) was very small. In addition, carvedilol treatment was not a significant predictor of ΔAT HR, even after adjusting for multiple factors. These results suggest that carvedilol treatment does not affect HR response to cardiopulmonary exercise up to the AT in subacute MI patients.

Differences in patient clinical characteristics between the two groups

Year of hospitalization significantly differed between the two groups. Almost all patients in the carvedilol (+) group were hospitalized after 2006. This likely reflects the fact that, in Japan, the administration of beta-blockers was first recommended by Guidelines for Secondary Prevention of MI in 2006 [14]. In fact, almost all patients in the carvedilol (−) group were hospitalized prior to 2006.

Effect of carvedilol on HR response during CPX in subacute MI patients

HR responses during exercise are greatly affected by autonomic nerve activity. A previous study suggested that a

Table 1 Patient clinical characteristics

	Carvedilol (+) group (n = 66)	Carvedilol (−) group (n = 66)	*P* value
Age (years)	64.35 ± 9.95	64.71 ± 9.30	0.829
Sex, men/women	58/8	58/8	1.000
Body mass index (kg/m^2)	23.30 ± 2.84	22.86 ± 2.65	0.369
MI			0.285
Inferior	24 (36.4)	33 (50.0)	
Anterior	36 (54.5)	28 (42.4)	
Lateral	6 (9.1)	5 (7.6)	
Residual coronary artery stenosis	24 (36.4)	28 (42.4)	0.476
Medical history			
Old MI	5 (7.6)	5 (7.6)	1.000
Hypertension	42 (63.6)	37 (56.1)	0.375
Dyslipidemia	35 (53.6)	41 (62.1)	0.291
Chronic kidney disease	6 (9.1)	7 (10.6)	0.770
Diabetes mellitus	20 (30.3)	22 (33.3)	0.709
Orthopedic disorder	1 (1.5)	2 (3.0)	0.559
Respiratory disease	0 (0)	1 (1.5)	0.315
Hyperuricemia	6 (9.1)	7 (10.6)	0.770
Peripheral arterial disease	0 (0)	2 (3.0)	0.154
Dementia	0 (0)	1 (1.5)	0.316
Heart failure after MI	6 (9.1)	7 (10.6)	0.770
Medication			
Renin–angiotensin system inhibitor	60 (90.9)	55 (83.3)	0.194
Calcium antagonist (dihydropyridine)	10 (15.2)	6 (9.1)	0.286
Cardiac stimulant	0 (0)	0 (0)	–
Anticlotting drug	2 (3.0)	2 (3.0)	1.000
Antiplatelet drug	66 (100)	66 (100)	1.000
Max CK-MB (≥ 300 ng/ml)	27 (40.9)	19 (28.8)	0.144
LVEF (< 50%)	44 (66.7)	52 (78.8)	0.118
Time between MI and exercise testing (days)	32.68 ± 12.35	31.62 ± 12.82	0.629
Carvedilol dose (mg/day)	5.76 ± 3.16		–
Hospitalization, before/after 2006	14/52	54/9	< 0.001

Patient clinical characteristics were compared between the carvedilol (+) and carvedilol (−) groups. Values are expressed as mean ± SD, No. (%), or No. /No

MI myocardial infarction, *LVEF* left ventricular ejection fraction, *Max CK-MB* maximum value of serum creatine kinase-myocardial band

decrease in parasympathetic nervous system activity mainly affects HR responses when exercise intensity is low to moderate and that an increase in sympathetic nervous system activity mainly affects HR responses when exercise intensity is moderate to high [15]. Parasympathetic nervous system activity is similarly affected during exercise in subacute MI patient [16]. On the other hand, beta blockers decrease sympathetic nervous system activity by inhibiting the interaction between noradrenaline and beta receptors. Beta blockers have been reported to mainly decrease HR responses when exercise intensity is moderate to high [17]. In the present study, although ΔAT HR did not differ significantly between the two groups, ΔAT-peak HR was significantly lower in the carvedilol (+) group than in the carvedilol (−) group. In addition, ΔAT HR represented a higher proportion of the HR response during exercise than ΔAT-peak HR. Therefore, Δpeak HR did not differ significantly between the two groups.

We conducted multiple regression analysis for predicting ΔAT HR. The analysis revealed that carvedilol treatment was not a significant predictor of ΔAT HR. In other words, carvedilol did not affect HR response to CPX up to the AT, after controlling for other main clinical factors. Old age and heart failure after MI were significant predictors of ΔAT HR. Previous studies suggested that old age decreases HR responses during exercise [18]. Moreover, chronotropic incompetence during maximal exercise is

Table 2 Variables of gas analysis during cardiopulmonary exercise up to the anaerobic threshold

	Carvedilol (+) group ($n=66$)	Carvedilol (−) group ($n=66$)	*P* value	Effect size *d*
Average time of exercise (min)	7.16 ± 1.54	7.22 ± 1.46	0.830	0.037
AT (ml/kg/min)	16.09 ± 3.38	16.18 ± 3.20	0.873	0.027
GER at AT	0.88 ± 0.05	0.87 ± 0.05	0.732	0.028
HR_{rest} (bpm)	71.86 ± 10.38	75.77 ± 11.93	0.047	0.350
HR_{AT} (bpm)	107.50 ± 10.67	110.44 ± 12.74	0.153	0.250
ΔAT HR (bpm)	35.64 ± 9.65	34.67 ± 11.68	0.604	0.091
SBP_{rest} (mmHg)	128.50 ± 15.20	135.96 ± 20.01	0.412	0.143
SBP_{AT} (mmHg)	161.03 ± 24.14	155.61 ± 29.29	0.248	0.202
DBP_{rest} (mmHg)	78.06 ± 11.34	72.97 ± 11.21	0.011	0.452
DBP_{AT} (mmHg)	79.20 ± 15.97	76.46 ± 12.83	0.986	0.189

Variables of gas analysis during cardiopulmonary exercise up to the anaerobic threshold were compared between the carvedilol (+) and carvedilol (−) groups using the unpaired *t* test and Mann–Whitney *U* test. Values are expressed as mean ± SD

AT anaerobic threshold, *GER* gas exchange ratio, *HR* heart rate, HR_{rest} HR at rest, HR_{AT} HR at AT, *ΔAT HR* (HR_{AT}) − (HR_{rest}), *SBP* systolic blood pressure, SBP_{rest} SBP at rest, SBP_{AT} SBP at AT, DBP_{rest} DBP at rest, *DBP* diastolic blood pressure, DBP_{AT} DBP at AT

caused by heart failure [19]. Thus, old age and heart failure after MI might predict ΔAT HR.

Effect of carvedilol on resting HR and HR at AT in subacute MI patients

Resting HR is affected by both parasympathetic nervous system activity and sympathetic nervous system activity. In particular, resting sympathetic nervous system activity is increased in subacute MI patients [20]. On the other hand, beta blockers decrease sympathetic nervous system activity. In the present study, HR_{rest} was significantly lower in the carvedilol (+) group than in the carvedilol (−) group. Moreover, in the carvedilol (+) group, HR_{AT} tended to be lower compared to the carvedilol (−) group, because ΔAT HR did not differ significantly between the two groups. These findings were consistent with previously reported results [9].

Table 3 Variables of gas analysis during cardiopulmonary exercise up to peak oxygen uptake (results of analysis of covariance with GER at peak oxygen uptake as the covariate)

	Carvedilol (+) group ($n=66$)	Carvedilol (−) group ($n=66$)	*P* value	*F* value
HR_{peak} (bpm)	139.62 ± 13.37	144.94 ± 15.50	0.009	5.862
SBP_{peak} (mmHg)	186.70 ± 29.02	186.79 ± 30.33	0.966	0.046
DBP_{peak} (mmHg)	87.05 ± 21.11	84.24 ± 16.84	0.279	1.204
Δpeak HR (bpm)	67.76 ± 12.98	69.17 ± 15.81	0.440	0.794
ΔAT-peak HR (bpm)	32.12 ± 9.64	34.50 ± 11.36	0.010	18.80
Peak $\dot{V}O_2$ (ml/kg/min)	23.09 ± 5.44	23.57 ± 4.64	0.615	0.169

Variables of gas analysis during cardiopulmonary exercise up to peak oxygen uptake were compared between the carvedilol (+) and carvedilol (−) groups using the analysis of covariance (ANCOVA) with GER at peak oxygen uptake as the covariate. Values are expressed as mean ± SD

peak$\dot{V}O_2$ peak oxygen uptake, *GER* gas exchange ratio, *AT* anaerobic threshold, *HR* heart rate, HR_{AT} HR at AT, HR_{peak} HR at peak $\dot{V}O_2$, HR_{rest} HR at rest, *ΔAT HR* (HR_{AT}) − (HR_{rest}), *Δpeak HR* (HR_{peak}) − (HR_{rest}), *ΔAT-peak HR* (HR_{peak}) − (HR_{AT})

Clinical application of the present study findings

In clinical practice, target HR for exercise prescription is often calculated as resting HR plus 20 or 30 bpm. This rate is used as a simplified substitute for HR at AT, as CPX is not feasible for all patients. Experts recommend a lower value (i.e., resting HR plus 20 bpm) for patients treated with beta blockers [6]. In the present study, carvedilol treatment did not affect HR response to exercise up to the AT in subacute MI patients. Moreover, no significant difference was observed in the number of patients with (HR_{rest} + 30 bpm − HR_{AT}) ≥ 10% HR_{AT} between the carvedilol (+) and carvedilol (−) groups. Furthermore, only 6.8% of all patients had values ≥ 10% HR_{AT}. This rate (i.e., 6.8%) is considered clinically valid compared with a previous study, in which the Karvonen formula was used to determine the target HR range (peak HR was obtained by stress test). In that study, 5.3% of subacute MI patients treated with beta-blockers had (target HR−HR_{AT}) ≥ 10% of HR_{AT} [21]. Thus, when prescribing exercise regimens for subacute MI patients, it may be feasible to use resting HR plus 30 bpm, regardless of carvedilol use. A previous study suggested that exercise tolerance is more readily improved by exercise training using an optimum target HR rather than a lower target HR [22]. It was also suggested that if exercise intensity determined by HR is lower by only 10 bpm as compared to recommended target HR, improvement in exercise tolerance is expected to be lower [22]. Therefore, the findings of this study may help

Table 4 Results of multiple regression analysis for the prediction of ΔAT HR

Independent variables	Dependent variable: ΔAT HR			
	$B \pm SE$	β	95% CI	P value
Age (≥ 65 years)	−2.063 ± 0.989	−0.194	−4.020 to −0.105	0.039
Female	2.753 ± 1.426	0.169	−0.070 to 5.576	0.056
Body mass index	0.436 ± 0.371	0.112	−0.298 to 1.169	0.242
Max CK−MB (≥ 300 ng/ml)	0.925 ± 1.020	0.083	−1.095 − 2.945	0.366
Inferior infarct[a]	−0.276 ± 1.492	−0.025	−3.231 to 2.679	0.854
Lateral infarct[a]	−0.581 ± 1.519	0.051	−3.588 to 2.426	0.702
Residual coronary artery stenosis	−0.498 ± 0.973	−0.046	−2.425 to 1.429	0.610
Heart failure after MI	−4.239 ± 1.676	−0.237	−7.559 − 0.920	0.013
Diabetes mellitus	−0.833 ± 1.004	−0.073	−2.821 to 1.154	0.408
LVEF (<50%)	−0.761 ± 1.183	−0.064	−3.103 to 1.582	0.366
Treatment with carvedilol	0.377 ± 0.937	0.035	−1.478 to 2.232	0.688
Constant	19.24 ± 9.550	0.000	0.324 to 38.144	0.046
			Coefficient of determination $R^2 = 0.158$, $F = 1.862$, $P = 0.046$	

The results of multiple regression analysis for the prediction of ΔAT HR by the forced-entry method are shown

ΔAT HR (HR_{AT}) − (HR_{rest}), *B* ± *SE* partial regression coefficient ± standard error, *β* standardized partial regression coefficient, *CI* confidence interval, *Max CK-MB* maximum value of serum creatine kinase-myocardial band, *MI* myocardial infarction

[a]Compared with anterior infarct

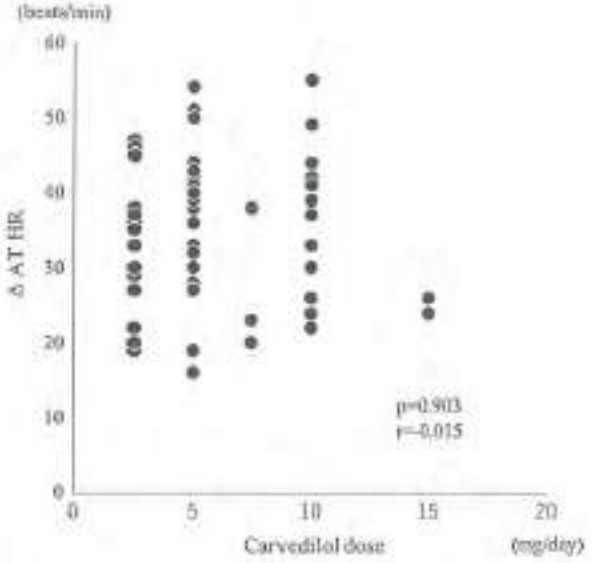

Fig. 1 Correlation between ΔAT HR and carvedilol dose. No significant correlation was observed between ΔAT HR and carvedilol dose in the carvedilol (+) group. *HR* heart rate, *AT* anaerobic threshold, HR_{AT} HR at AT, HR_{rest} HR at rest, *ΔAT HR* (HR_{AT}) − (HR_{rest})

physicians to prescribe appropriate exercise for subacute MI patients treated with beta blockers.

On the other hand, 31% of patients with heart failure after MI had (HR_{rest} + 30 bpm − HR_{AT}) ≥ 10% HR_{AT}, suggesting that prescribing exercise intensity requires caution in this patient population, regardless of carvedilol use.

Table 5 Number of patients with (HR_{rest} + 30 bpm − HR_{AT}) < 10% or ≥ 10% HR_{AT}

	Carvedilol (+) group ($n = 66$)	Carvedilol (−) group ($n = 66$)	P value
(HR_{rest} + 30 bpm − HR_{AT}) < 10% HR_{AT}	63 (95.5)	60 (90.9)	0.300
(HR_{rest} + 30 bpm − HR_{AT}) ≥ 10% HR_{AT}	3 (4.5)	6 (9.1)	

Values are expressed as No. (%)

HR heart rate, *bpm* beat per minutes, HR_{rest} HR at rest, *AT* anaerobic threshold, HR_{AT} HR at AT

Carvedilol dosage

In the present study, mean carvedilol dose was 5.76 ± 3.16 mg/day in the carvedilol (+) group. Previously, a prospective, multi-center, open-label, randomized controlled study including 67 centers in Japan reported a mean carvedilol dose of 5.8 ± 3.9 mg among MI patients at 3 months from onset [23]. Moreover, despite that carvedilol was started from low doses and up-titrated to a target dose of 20 mg daily, only 3.8% of patients were administered 20 mg carvedilol (i.e., the maximum approved dose) at 12 month

from onset. Thus, the mean carvedilol dose in this study is likely considered clinically appropriate.

The negative chronotropic effect of carvedilol depends on its concentration in blood. However, in addition to dose [24–26], several clinical factors can affect the blood concentration of carvedilol, such as body weight, renal function, and liver function. In clinical practice, physicians determine appropriate doses for each MI patient based on these factors. In the present study, no significant correlation was observed between ΔAT HR and carvedilol dose in the carvedilol (+) group, as we could not examine effect of such factors on the blood concentration of carvedilol in our study population.

Limitations

The present study has several limitations worth noting. First, we did not demonstrate the effect of other beta blockers on HR response to CPX up to the AT in subacute MI patients. Previous studies suggested that carvedilol had the lowest negative chronotropic effect compared to other beta blockers [27, 28]. Thus, a future study will be needed to examine the effect of other beta blockers in this patient population. It should also be noted that the influence of potential factors (e.g., body weight, renal function, liver function, genetic polymorphism) on the blood concentration of carvedilol was not examined in the present study. Second, all patients underwent symptom-limited CPX using a treadmill in this study; therefore, the effect of carvedilol on HR responses during other symptom-limited CPX (e.g., on a bicycle ergometer) remains to be clarified. Third, patients in this study received low to moderate doses of carvedilol according to clinical decisions. Thus, whether carvedilol affects HR response to CPX up to the AT in patients receiving high doses remains unclear. Finally, this study has a selection bias in that patients who were unable to undergo symptom-limited CPX on a treadmill due to frailty were excluded from the study and that our patients were matched according to age (± 5 years) and sex by the authors. A future prospective study will be needed to verify the results of the present study.

Conclusions

Our data suggest that carvedilol treatment does not affect HR response to CPX up to the AT in subacute MI patients. Therefore, exercise prescription based on resting HR plus 30 bpm may be feasible in subacute MI patients, regardless of carvedilol use, if gas-exchange analysis data cannot be obtained.

Acknowledgements The authors thank the staff members of the Department of Rehabilitation Medicine and the Department of Cardiology at St. Marianna University School of Medicine Yokohama City Seibo Hospital for their assistance in data collection.

Funding This study received no specific grant from any funding agency in the public, commercial, or not-for-profit sectors.

Compliance with ethical standards

Conflict of interest The authors certify that there is no conflict of interest with any financial organization regarding the material discussed in the manuscript.

References

1. Taylor RS, Brown A, Ebrahim S, Jolliffe J, Noorani H, Rees K, Skidmore B, Stone JA, Thompson DR, Oldridge N (2004) Exercise-based rehabilitation for patients with coronary heart disease: systematic review and meta-analysis of randomized controlled trials. Am J Med 116:682–692
2. JCS Joint Working Group (2013) Guidelines for Secondary Prevention of Myocardial Infarction (JCS 2011). Circ J 77:231–248
3. Perk J, De Backer G, Gohlke H, Graham I, Reiner Z, Verschuren M, Albus C, Benlian P, Boysen G, Cifkova R, Deaton C, Ebrahim S, Fisher M, Germano G, Hobbs R, Hoes A, Karadeniz S, Mezzani A, Prescott E, Ryden L, Scherer M, Syvanne M Scholte op Reimer WJ, Vrints C, Wood D, Zamorano JL, Zannad F, European Association for Cardiovascular P, Rehabilitation,Guidelines ESCCfP (2012) European Guidelines on cardiovascular disease prevention in clinical practice (version 2012). The Fifth Joint Task Force of the European Society of Cardiology and Other Societies on Cardiovascular Disease Prevention in Clinical Practice (constituted by representatives of nine societies and by invited experts). Eur Heart J 33:1635–1701
4. Adachi H, Koike A, Obayashi T, Umezawa S, Aonuma K, Inada M, Kurenaga M, Niwa A, Marumo F, Hiroe M (1996) Does appropriate endurance exercise training improve cardiac function in patients with prior myocardial infarction? Eur Heart J 17:1511–1521
5. Wasserman K, Beaver WL, Whipp BJ (1990) Gas exchange theory and the lactic acidosis (anaerobic) threshold. Circulation 81:II14-II30
6. JCS Joint Working Group (2014) Guidelines for rehabilitation in patients with cardiovascular disease (JCS 2012). Circ J 78:2022–2093
7. Ketreyfan SJ (2017) Exercise prescription for patients with cardiac, peripheral, cerebrovascular, and pulmonary disease. In: Pescatello LS, Arena R, Riebe D, Thompson PD (eds) ACSM's guidelines for exercise testing and prescription. Lippincott Williams & Wilkins, Philadelphia, pp 226–245
8. Dargie HJ (2001) Effect of carvedilol on outcome after myocardial infarction in patients with left-ventricular dysfunction: the CAPRICORN randomised trial. Lancet 357:1385–1390
9. Diaz-Buschmann I, Jauregui-Garrido R, Calero MJ, Aquino RS (2014) Programming exercise intensity in patients on beta-blocker treatment: the importance of choosing an appropriate method. Eur J Prev Cardiol 21:1474–1480
10. Yamamoto A, Tanabe K, Yokoyama Y, Itoh H, Murayama M (1998) Influence of aerobic exercise training on brain natriuretic peptide secretion in patients in the chronic phase of myocardial infarction. Jpn Circ J 62:658–664
11. Hanson P (2012) Clinical exercise testing. In: Thompson WR, Gordon NF, Pescatello LS (eds) American College of Sports

Medicine, Resource Manual for Guidelines for Exercise Testing and Prescription. Lea & Febiger, Philadelphia, pp 205–222
12. Beaver WL, Wasserman K, Whipp BJ (1986) A new method for detecting anaerobic threshold by gas exchange. J Appl Physiol (1985) 60:2020–2027
13. Strzelczyk TA, Quigg RJ, Pfeifer PB, Parker MA, Greenland P (2001) Accuracy of estimating exercise prescription intensity in patients with left ventricular systolic dysfunction. J Cardiopulm Rehabil 21:158–163
14. Guidelines for the diagnosis and treatment of cardiovascular diseases (2004-2005 joint working groups report). Guidelines for secondary prevention of myocardial infarction (JCS 2006). https://www.j-circ.or.jp/guideline/pdf/JCS2006_ishikawa_h.pdf. (in Japanese). Accessed 22 Nov 2018.
15. White DW, Raven PB (2014) Autonomic neural control of heart rate during dynamic exercise: revisited. J Physiol 592:2491–2500
16. Kasahara Y, Izawa K, Omiya K, Osada N, Watanabe S, Saitoh M, Matsunaga A, Masuda T (2006) Influence of autonomic nervous dysfunction characterizing effect of diabetes mellitus on heart rate response and exercise capacity in patients undergoing cardiac rehabilitation for acute myocardial infarction. Circ J 70:1017–1025
17. Peel C, Mossberg KA (1995) Effects of cardiovascular medications on exercise responses. Phys Ther 75:387–396
18. Ozemek C, Whaley MH, Finch WH, Kaminsky LA (2016) High cardiorespiratory fitness levels slow the decline in peak heart rate with age. Med Sci Sports Exerc 48:73–81
19. Phan TT, Shivu GN, Abozguia K, Davies C, Nassimizadeh M, Jimenez D, Weaver R, Ahmed I, Frenneaux M (2010) Impaired heart rate recovery and chronotropic incompetence in patients with heart failure with preserved ejection fraction. Circ Heart Fail 3:29–34
20. Hogarth AJ, Mackintosh AF, Mary DA (2006) The sympathetic drive after acute myocardial infarction in hypertensive patients. Am J Hypertens 19:1070–1076
21. Tabet JY, Meurin P, Driss AB, Thabut G, Weber H, Renaud N, Odjinkem N, Solal CA (2006) Determination of exercise training heart rate in patients on beta-blockers after myocardial infarction. Eur J Cardiovasc Prev Rehabil 13:538–543
22. Reed JL, Blais AZ, Kraft ML, Pipe AL, Reid RD (2017) Performance of fixed heart rate increment targets of 20 vs 30 beats per minute for exercise rehabilitation prescription in outpatients with heart failure. Can J Cardiol 33:777–784
23. Watanabe H, Ozaki N, Morimoto T, Shiomi H, Bingyuan B, Suwa S, Nakagawa Y, Izumi C, Kadota K, Ikeguchi S, Hihi K, Furukawa Y, Kaji S, Suzuki T, Akao M, Inada T, Hayashi Y, Nanasato M, Okutsu M, Kametani R, Sone T, Sugimura Y, Kawai K, Abe M, Kitaoka H, Nakamura S, Kimura T (2018) Long-term use of carvedilol in patients with ST-segment elevation myocardial infarction treated with primary percutaneous coronary intervention. PLoS ONE 13:e0199347
24. Saito M, Kawana J, Otsuo T, Hanada K, Kaneko M, Mihara K, Shiomi M, Nagayama M, Sumiyoshi T, Ogata H (2010) Population pharmacokinetics of R- and S-carvedilol in Japanese patients with chronic heart failure. Biol Pharm Bull. 33:1378–1384
25. Hakusui H, Fujimaki M (1988) Pharmacokinetics of carvedilol in hypertensive patients with renal failure. Drugs 36:144–147
26. Neugebauer G, Gabor M, Reiff K (1988) Pharmacokinetics and bio-availability of carvedilol in patients with liver cirrhosis. Drugs 36:148–154
27. Hori M, Nagai R, Izumi T, Matsuzaki M (2014) Efficacy and safety of bisoprolol fumarate compared with carvedilol in Japanese patients with chronic heart failure: results of the randomized, controlled, double-blind, Multistep Administration of bisoprolol IN Chronic Heart Failure II (MAIN-CHF II) study. Heart Vessels 29:238–247
28. Vittorio TJ, Zolty R, Kasper ME, Khandwalla RM, Hirsh DS, Tseng CH, Jorde UP, Ahuja K (2008) Differential effects of carvedilol and metoprolol succinate on plasma norepinephrine release and peak exercise heart rate in subjects with chronic heart failure. J Cardiovasc Pharmacol Ther 13:51–57

Publisher's Note Publisher's Note Springer Nature remains neutral with regard to jurisdictional claims in published maps and institutional affiliations.

Interactive CardioVascular and Thoracic Surgery (2019) 1–8
doi:10.1093/icvts/ivy341

ORIGINAL ARTICLE

Cite this article as: Andreas M, Russo M, Kuwata S, Cesarovic N, Wang C, Guidotti A et al. Transcatheter aortic valve-in-ring implantation: feasibility in an acute, preclinical, pilot trial. Interact CardioVasc Thorac Surg 2019; doi:10.1093/icvts/ivy341.

INTERACTIVE CARDIOVASCULAR AND THORACIC SURGERY

Transcatheter aortic valve-in-ring implantation: feasibility in an acute, preclinical, pilot trial

Martin Andreas[a,b,†], Marco Russo[a,b,c,†], Shingo Kuwata[a], Nikola Cesarovic[c], Changtian Wang[a], Andrea Guidotti[a], Miriam Lipiski[c], J. Scott Rankin[d], Evelyn Regar[a], Maurizio Taramasso[a], Francesco Maisano[a] and Alberto Weber[a]

[a] Department of Cardiac Surgery, University Heart Center, Universitätsspital Zurich, University of Zurich, Zurich, Switzerland
[b] Department of Cardiac Surgery, Medical University of Vienna, Vienna, Austria
[c] Division of Surgical Research, University Hospital Zurich, University of Zurich, Zurich, Switzerland
[d] Division of Cardiothoracic Surgery, West Virginia University, Morgantown, WV, USA

* Corresponding author. Department of Cardiac Surgery, Medical University of Vienna, Währinger Gürtel 18-20, 1090 Vienna, Austria. Tel: +39-328-3528248; e-mail: mar.russo1987@gmail.com (M. Russo).

Received 11 September 2018; received in revised form 24 October 2018; accepted 15 November 2018

Key question

Is the implantation of a self-expandable transcatheter aortic valve into a rigid aortic annuloplasty ring (HAART ring) feasible?

Key finding(s)

Implantation success was achieved in 86% of cases. Optimal haemodynamics occurred when the proposed sizing chart was respected.

Take-home message

The Medtronic EvolutR optimally adapts itself inside a rigid elliptical ring. A depth of implantation of 5 mm is crucial. Postdilation is feasible.

Abstract

OBJECTIVES: The HAART ring device has been introduced as a novel strategy to facilitate aortic valve repair. This rigid, elliptical device aims to restore normal leaflet configuration and to provide annular stabilization in the setting of aortic regurgitation. The goal of this preclinical study is to evaluate the *in vivo* feasibility of 'aortic valve-in-ring' transcatheter aortic valve replacement (TAVR).

METHODS: Six animals (landrace pigs, 87.6 [standard deviation (SD) 4.5] kg) underwent HAART ring implantation (5 cases #19 mm and 1 case #21 mm) via full sternotomy with cardiopulmonary bypass. Seven transfemoral TAVR implantations were performed with the Medtronic EvolutR prosthesis to assess the sizing and outcome (5 cases #23 mm, 1 case #26 mm and 1 case #29 mm).

†The first two authors contributed equally to this work.

© The Author(s) 2019. Published by Oxford University Press on behalf of the European Association for Cardio-Thoracic Surgery. All rights reserved.

Downloaded from https://academic.oup.com/icvts/advance-article-abstract/doi/10.1093/icvts/ivy341/5289780 by EndocrineSociety Admin user on 03 April 2019

RESULTS: TAVR implantation was successful in 6 of 7 attempts. Post-dilatation was performed in 1 case without damage of the ring or the valve. One embolization occurred due to oversizing (EvolutR valve 29 mm in HAART ring 19 mm). No clinically relevant postimplantation gradient [7.6 (SD 4.0) mmHg] or regurgitation was detected by invasive and echocardiographic measurements. Postoperative computed tomography scans revealed good device configuration.

CONCLUSIONS: Transcatheter aortic valve-in-ring implantation of a self-expandable TAVR into a rigid aortic annuloplasty ring after aortic valve repair appears feasible. Proper sizing and correct depth of implantation are crucial.

Keywords: Aortic valve repair • Transcatheter aortic valve implantation • Valve-in-ring

INTRODUCTION

The armamentarium of therapeutic approaches for aortic valve disease is growing fast, and the standard for surgical valve replacement with mechanical or biological valves has rapidly changed over the last decade [1]. Transcatheter aortic valve replacement (TAVR) has been proposed as an alternative option, and valuable results in intermediate-risk and high-risk patient populations have been reported [2, 3]. Although these therapeutic approaches are mainly applied in the elderly, the optimal strategy for young patients is still a matter of debate.

Aortic valve repair represents an elegant strategy to treat patients experiencing aortic valve regurgitation, avoiding anticoagulation and taking advantage of native leaflet tissue that provides durability, resistance to infection, remodelling and physiological movement [4–7]. However, as in every repair technique, the risk of short- or long-term failure and the possibility of reoperation during follow-up must be considered. Several techniques are available to provide a sustained aortic valve repair, but the rate of reoperation is also related to the primary mechanisms of aortic regurgitation (AR) and the complexity of leaflet repair [8]. Annulus stabilization represents a key protective factor against the recurrence of regurgitation comparable to the mitral position and tricuspid position [9, 10].

The HAART 300™ aortic annuloplasty ring (BioStable Science and Engineering, Austin, TX, USA) was recently introduced to achieve annular stabilization in patients with tricuspid aortic valve anatomy (CE mark 0086). It was developed from mathematical analyses of normal human computed tomography (CT) angiograms and presents a 2:3 elliptical shape with 3 equidistant subcommissural posts, flaring 10° outwards. Mazzitelli et al. [11, 12] reported promising results with no valve-related events or mortality recorded at 2-year follow-up despite a rate of reoperation of approximately 10%, which was primarily due to technical aspects in the early learning curve. An alternative suturing technique was applied in subsequent cases [11], which reduced early failure rates to approximately 2% (unpublished data). Long-term durability may be influenced by calcification, leaflet prolapse or other mechanisms.

Recently, several percutaneous strategies have been described for the treatment of patients with dysfunctional biological prostheses, recurrence of mitral regurgitation after surgical ring annuloplasty or recurrence of aortic valve regurgitation after valve sparing operations. Valve-in-valve (VIV) and mitral valve-in-ring (VIR) procedures represent nowadays a valid option to minimize the risk of a surgical reoperation [13–16].

Therefore, TAVR may also be an option in patients who underwent aortic valve repair with the HAART 300 device and subsequently require reintervention. The elliptic shape, the subannular position and the rigid architecture require technical considerations and new challenges for an eventual 'aortic VIR' procedure, not yet assessed in the literature.

This preclinical animal trial is designed to evaluate the feasibility and the technical aspects of transfemoral (TF) TAVR as a 'valve-in-ring' procedure after aortic valve repair with the HAART ring device.

MATERIALS AND METHODS

Study design and end points

This acute animal model has been conducted in the animal hybrid room of the Zurich University. Six female landrace pigs (87.6 [standard deviation (SD) 4.5] kg) underwent surgical HAART ring implantation and subsequently TF TAVR with the Medtronic EvolutR prosthesis (Medtronic, Minneapolis, MN, USA) within the same session. After the first, successful procedure, the EvolutR valve was surgically removed, and the second TAVR was implanted in 1 case. Therefore, a total of 7 TF TAVRs were performed.

Primary end points (feasibility) were defined as procedural success (delivery of the prosthesis in the correct position) and risk of periprocedural adverse events [embolization, coronary obstruction and complete atrioventricular (AV) block]. Secondary end points were defined as the rate of residual paravalvular leaks (PVLs), residual transvalvular gradients and valve configuration analysis according to multimodality imaging techniques and post-mortem examination.

Animal preparation and ethical considerations

The animal study was conducted in compliance with the European Union's guideline (86/609/EEC) and the Swiss Federal animal protection law and ordinance (license ZH 219/2016).

After the loss of postural reflexes following premedication with ketamine (20 mg/kg), azaperone (1.5 mg/kg) and atropine (0.75 mg), anaesthesia was induced by a bolus injection of propofol (1–2 mg/kg body weight), and the animals were intubated. Anaesthesia was then maintained with 2–3% isoflurane and propofol (2–5 mg/kg/h). Amiodarone (2–3 mg/kg bolus iv) was administered to stabilize the heart rhythm. Pain management included fentanyl infusion (0.02 mg/kg/h) for the duration of the procedure. On the completion of the study procedure, all animals were euthanized by the administration of an overdose of pentobarbital while still under general anaesthesia according to the animal study protocol.

Downloaded from https://academic.oup.com/icvts/advance-article-abstract/doi/10.1093/icvts/ivy341/5289780 by EndocrinesSociety Admin user on 03 April 2019

Video 1: Surgical implantation of the HAART ring 19-mm device (case II).

Implantation of the aortic annuloplasty ring

Median sternotomy was performed in all cases. Cardiopulmonary bypass (CPB) was established with direct arterial cannulation of the brachiocephalic common trunk and venous cannulation of the right atrium. The trunk was cannulated instead of the aorta to facilitate TF TAVR with the cannulas in place. Antegrade crystalloid cardioplegia was directly administered in the aortic root. Venting was achieved with cannulation of the pulmonary artery.

The HAART ring implantation was performed according to the manufacturer's instructions (Video 1) [12]. Three 4-0 polypropylene sutures were placed to fix the ring posts to the 3 subcommissural triangles, and 1–2 looping stitches fixed the ring in each sinus region, just below the native aortic annulus. Aortic closure was performed with 2 layers of 4-0 polypropylene continuous sutures.

Transcatheter aortic valve-in-ring implantation

TAVR was performed in all cases with TF access through a 20-Fr sheath in the right common femoral artery. A pigtail catheter was inserted via the left femoral artery to the non-coronary sinus and used as a landmark. However, the radiopaque titanium HAART ring structure represented an excellent additional referral point. A stiff Terumo wire 0.035" (Terumo Medical, Hatagaya, Shibuya-ku, Tokyo), manually shaped like a Safari wire (Boston Scientific, Marlborough, MA), was advanced through the aortic valve with a pigtail catheter and used for the TAVR implantation. Valve deployment during the first 2 cases was performed on CPB to optimize haemodynamic stability. Four implants were attempted after the complete weaning from CPB and without pacing (Video 2), whereas 1 case required fast pacing at 120 bpm. Post-dilatation with a 20-mm balloon (True Dilatation; BARD Peripheral Vascular, Inc., Tempe, AZ, USA) was performed in 1 case. The targeted depth of implantation was 5 mm below the annular ring (Figs 1 and 2). All procedures were performed with fluoroscopic guidance perpendicular to the aortic ring.

Data collection and statistical analysis

Diagnostic aortography for the evaluation of residual AR and invasive evaluation of the peak-to-peak gradient through the aortic valve was performed after HAART ring implantation and after the VIR procedure. The HAART ring and EvolutR function were

Video 2: Deployment of a transfemoral Medtronic EVOLUT R 23-mm prosthesis inside the HAART ring 19-mm device (case IV).

evaluated by a transoesophageal and epicardial echocardiogram, performed in all animals with procedural success. The ECG-gated CT with 3-dimensional reconstruction was performed for the evaluation of the anatomical configuration of the EvolutR valve, its relationship to the HAART ring device, the depth of implantation as well as coronary arteries patency.

Animals were sacrificed, and the hearts were explanted to inspect the anatomical configuration. Only descriptive data are presented, and no further statistical analyses were performed due to the limited number of animals. Continuous variables are expressed as mean and SD, and discrete variables are expressed as numbers and percentages.

RESULTS

Six female landrace pigs [87.6 (SD 4.5) kg] underwent the surgical HAART ring implantation (5 cases #19 mm and 1 case #21 mm) without intraoperative complications and with a mean implant time of 39 (SD 18) min and a mean X-clamp time of 42 (SD 18) min. Surgical inspection showed a normal aortic valve prior to implantation, and postimplant aortography showed no residual AR. The mean postoperative transvalvular gradient was 12 (SD 7) mmHg.

A total of 7 TF TAVRs with the Medtronic EvolutR prosthesis (Medtronic, Minneapolis, MN, USA) were performed in the same session (5 cases #23 mm, 1 case #26 mm and 1 case #29 mm): in 1 animal, after the first successful procedure, the properly seated EvolutR valve was surgically removed, and a second transcatheter heart valve (THV) was implanted.

The valve could be placed in the annulus in 6 of 7 attempts (86%). Implantation failure occurred in an animal, which was unstable due to ventilation problems after weaning from CPB. Because of a more acute implantation approach, the stiff guide wire accidentally went between the aortic wall and the ring structure at the level of the right/non-coronary commissure. This was

ORIGINAL ARTICLE
Downloaded from http://icvts.oxfordjournals.org/icvts/advance-article-abstract/doi/10.1093/icvts/ivy341/5289780 by EndocrineSociety Admin user on 03 April 2019

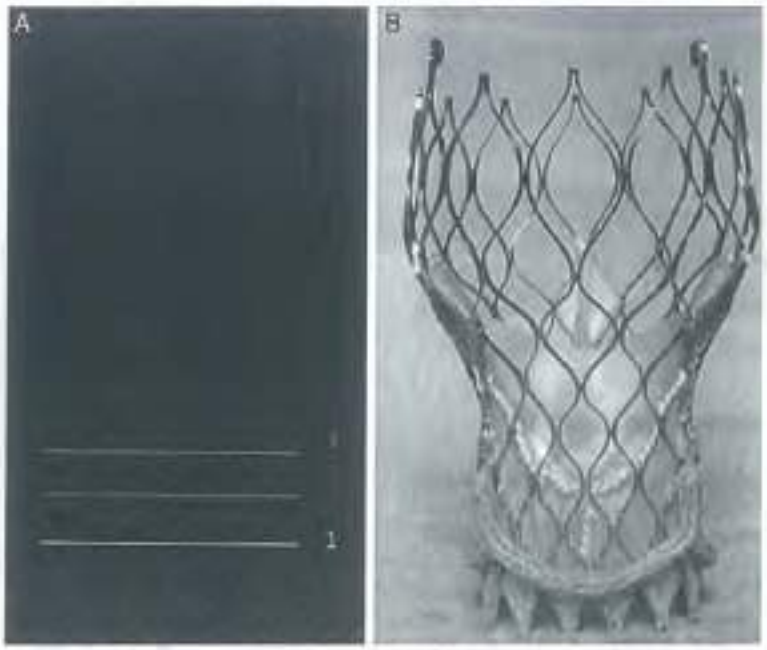

Figure 1: An *ex vivo* model of the valve-in-ring. (**A**) Fluoroscopy image with different nodes of the EvolutR valve. Target of implantation just below the first node (1) located 6 mm from the distal part of the stent. The third node (3) represents the leaflet position. (**B**) The valve-in-ring configuration with the EvolutR valve 23 mm and the HAART ring 21 mm.

not noticed immediately, and an attempt to cross the ring with the 23-mm TAVR system caused complete AV block that spontaneously resolved after the retraction of the wire. The experiment was stopped due to haemodynamic instability. The post-mortem analysis revealed complete ring detachment.

After successful implantation, the mean depth of implantation was of 5.3 (SD 1.9) mm. No other cases of complete AV block or severe PVL were detected. The postoperative mean gradients through aortic prosthesis were 7.6 (4.0) mmHg. No alterations in the mitral valve function were detected.

The HAART ring device #19 mm was implanted in 5 animals, and a #23-mm Medtronic EvolutR TF valve was successfully implanted in 3 of these animals: haemodynamic and echo assessment showed low mean gradients after VIR implantation (Table 1). In this subgroup, a case of mild-to-moderate PVL was successfully managed by post-dilatation with a 20-mm valvuloplasty balloon inflated to 3 atm. Coronary arteries were studied using angiography and were patent after the procedure.

To evaluate the effect of gross oversizing, a #29-mm Medtronic EvolutR prosthesis was implanted in a #19-mm HAART ring. The procedure was successfully performed with a depth of implantation of 3 mm. After sheet retraction, the THV migrated in a 'super-high' position. The valve showed a good function, and the animal could be weaned off from bypass. During haemostasis, the animal experienced sudden cardiac arrest due to ventricular fibrillation. Aortography showed acute embolization of the valve with coronary artery obstruction. This event reduced the calculated procedural success to 71%.

The HAART ring #21 mm was implanted in 1 animal, and a #26-mm Medtronic EvolutR prosthesis was successfully deployed 5 mm below the aortic ring in physiological conditions (Fig. 2) with no AR and a mean gradient of 3 mmHg. The animal was stable without any inotropic support. We performed one more implant to evaluate the effect of different sizing. CPB was reinstituted, the ascending aorta was cross-clamped very distally and the EvolutR valve was removed by irrigation with cold water. After weaning off from the bypass, the haemodynamic evaluation revealed normal aortic valve function. A #23-mm Medtronic EvolutR prosthesis was successfully implanted with a residual mild PVL.

Computed tomography and postexplant analysis

Post-implantation ECG-gated CT was performed in 2 cases (HAART ring #19 mm and EvolutR valve #23 mm). In both cases, the prosthesis showed no area of malpositioning or incomplete expansion with an optimal sealing, both in the sub- and supra-annular position (Fig. 3A–D). Three-dimensional post-processing revealed that the inflow part was well adapted to the non-circular shape of the ring. Interestingly, the circular shape of the waist and outflow portions were not altered by the presence of the HAART ring device (Fig. 3E–H). The coronary arteries were patent in both cases, and the depth of implantation estimated with fluoroscopy was confirmed in the CT scan.

Post-mortem inspection of the heart confirmed the deployment and positioning of the prosthesis with no area of leakage or stent distortion when appropriate sizing was applied (Fig. 4A–C) (Table 2). The subvalvular component of the EvolutR valve was capable to adapt itself to the elliptic shape of the ring device without creating any alteration in the supra-annular parts (Fig. 4D). Because of the subannular position of the HAART ring, the TAVR prosthesis was close to the anterior mitral leaflet (Fig. 4E).

Downloaded from https://academic.oup.com/icvts/advance-article-abstract/doi/10.1093/icvts/iny341/5289780 by EndocrineSociety Admin user on 03 April 2018

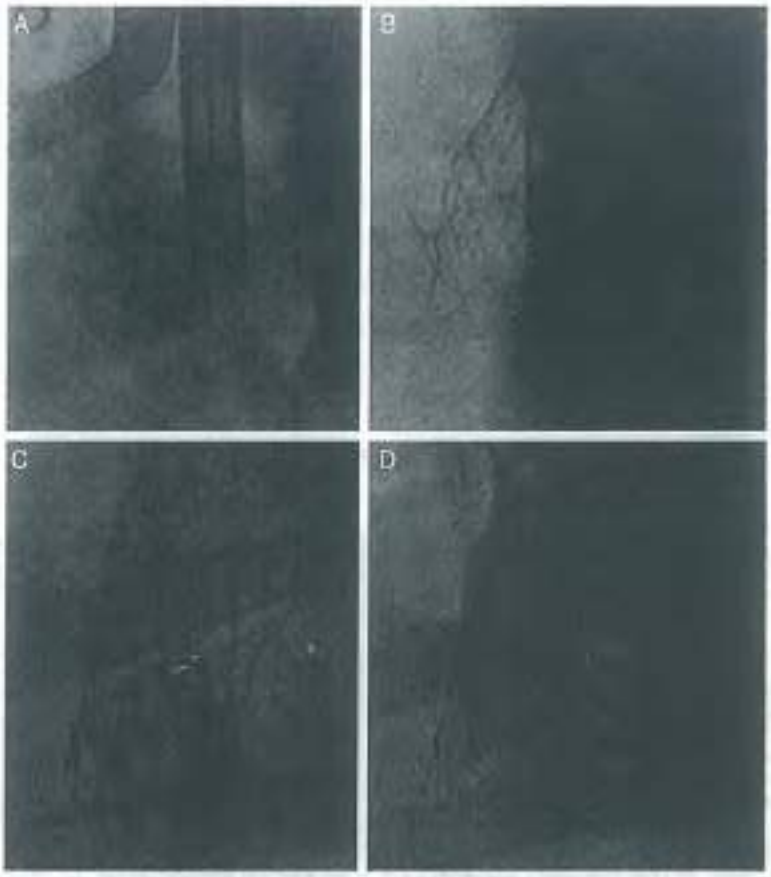

Figure 2: Valve-in-ring implantation. (A) The guidewire is positioned into the left ventricle after the crossing of the repaired aortic valve; (B, C) valve deployment; and (D) aortography performed after the valve-in-ring procedure shows no signs of aortic regurgitation.

DISCUSSION

The present pilot trial analysed the results of a novel transcatheter VIR procedure applying the Medtronic EvolutR prosthesis in the HAART 300 device. Seven TF TAVRs were performed, which were successful in 5 cases (71%). No complete AV block or severe PVL occurred after successful implantation, whereas a single case of moderate PVL was managed with balloon post-dilatation. One case of acute embolization was associated with gross oversizing for study purposes. The postoperative imaging analysis with transoesophageal and epicardial echocardiogram showed optimal function of the THV inside the rigid ring with low gradients of 7.6 (SD 4.0) mmHg, whereas ECG-gated CT reported the optimal expansion of the EvolutR valve inside the rigid aortic ring.

Aortic valve repair is increasingly applied in cardiac surgery, and technical developments such as the HAART 300 device as well as improved repair techniques and appropriate patient selection enable more reliable results [17]. However, aortic valve repair may fail and require reoperation, which has an increased procedural risk [18]. Transcatheter VIV and mitral or tricuspid VIR procedures have been recently introduced and have rapidly become a valid option [19–22]. The combination of the HAART 300 device and the Medtronic EvolutR system may be a promising approach to avoid surgical reoperation after the failed valve repair.

The size and the anatomical characteristics of the previously implanted device represent a potential limiting factor for the implantation of a THV inside a surgical ring [23]. Optimal positioning of a correctly sized valve is crucial to avoid embolization, paravalvular regurgitation or suboptimal valve function [24].

The HAART 300 ring has an elliptical shape, is made of titanium and cannot be reshaped to a circular ring [11]. The CoreValve EvolutR is a self-expandable system that offers the advantage of a supra-annular leaflet mounting. The stent structure of the EvolutR valve is organized in 3 different parts: inflow, waist and outflow. The inflow part is covered with porcine pericardium and stays in the left ventricular outflow tract. The specific configuration enables the EvolutR valve to adapt its structure to the left ventricular outflow tract without altering the position of the porcine pericardial leaflets that are located in the supra-annular position. This feature is designed to optimize the orifice area and flow while preserving circularity and coaptation in an asymmetrical left ventricular outflow tract. This device's characteristic was crucial in our series to adapt to the elliptic and rigid prosthetic ring without any modification of pericardial leaflet anatomy and function. Multimodality imaging on post-mortem inspection confirmed this result (Fig. 4).

A depth of implantation of 5 mm beyond the HAART ring level was targeted as described for procedures in native valves. The

ONLINE CARDIAC
Downloaded from https://academic.oup.com/icvts/advance-article-abstract/doi/10.1093/icvts/ivy241/5286780 by Endocrine Society Admin user on 03 April 2019

Table 1: Intra- and periprocedural results

	I	II	III	IV	V	VI	VII	N (%)/mean (SD)
HAART ring size	19	19	19	19	19	21	21	
EvolutR size (mm)	23	23	29	23	23	26	23	
Deployment	CPB	Fast pacing	CPB	Failure	SR	SR	SR	6 (86)[a]
AV block	No	No	No	Yes	No	No	No	1 (14)
PVL	No	Mild[b]	No		No	No	Mild	0 (0)[c]
Embolization	No	No	Yes		No	No	No	1 (14)
Coronary obstruction	No	No	Yes		No	No	No	1 (14)
Mean gradient (mmHg)	9	6			5	3	14	7.6 (4.0)
Depth of implantation (mm)	5	9	3		5	5	5	5.3 (1.9)
Post-dilatation	No	Yes	No		No	No	No	1 (14)

[a]Success of deployment.
[b]After post-dilatation.
[c]Number of severe aortic regurgitation.
AV: atrioventricular; CPB: cardiopulmonary bypass; PVL: paravalvular leakage; SD: standard deviation; SR: sinus rhythm.

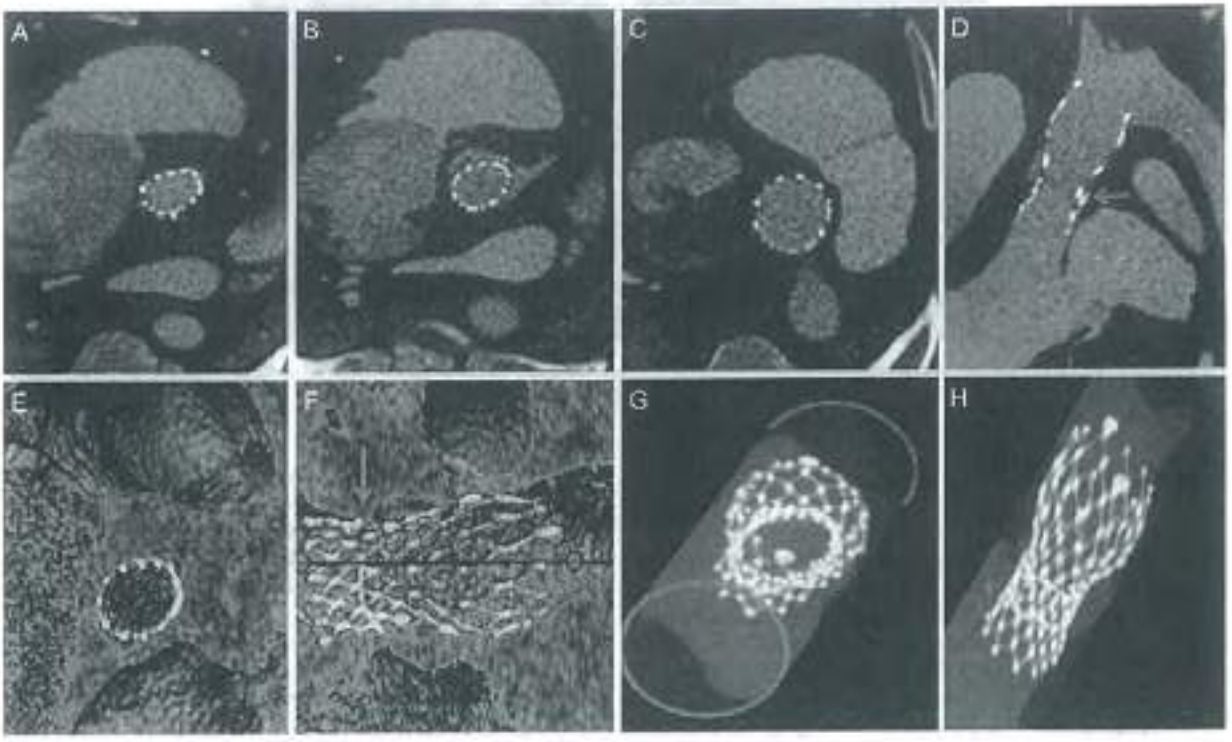

Figure 3: Computed tomography analysis. **(A–C)** Transversal section at different levels showing optimal configuration of the EvolutR valve after implantation and patency of the left main coronary artery; **(D)** sagittal view; and **(E–H)** post-processing images with 3-dimensional characteristics of the EvolutR valve in the ring (green arrow in **D** and **F** and green asterisk in **H** indicate the HAART ring).

optimal height was achieved in 4 cases, which showed good results if sized according to the sizing chart proposed (Table 2). In 1 case, the valve deployment was too deep, which probably induced PVL. It is important to keep in mind that the sealing point of the native leaflets is higher than the subannular ring, which is used as reference in this experiment.

We decided to implant different sizes in the 19-mm and 21-mm HAART rings to test the effect of sizing on valve deployment and stability (Table 2). The #23-mm EvolutR valve in the HAART ring 19 and the #26-mm EvolutR valve in the HAART ring 21 showed perfect alignment. Although the #29-mm EvolutR valve may have the theoretical advantage of higher radial forces, leading to a stronger apposition, its shape led to acute migration and further embolization, whereas the #23 mm, even if well implanted in ring 21 mm, revealed residual regurgitation due to improper apposition. A bench test is currently under preparation to confirm the sizing chart proposed herein.

There are several key findings in this study. Aortic VIR implantation is technically feasible with good alignment using a TF approach. Valve fixation within a rigid aortic annuloplasty ring was dependent on the correct depth of implantation and proper sizing. The risk of paravalvular regurgitation after deep

Downloaded from http://academic.oup.com/icvts/advance-article-abstract/doi/10.1093/icvts/ivy341/5269780 by EndocrineSociety Admin user on 03 April 2019

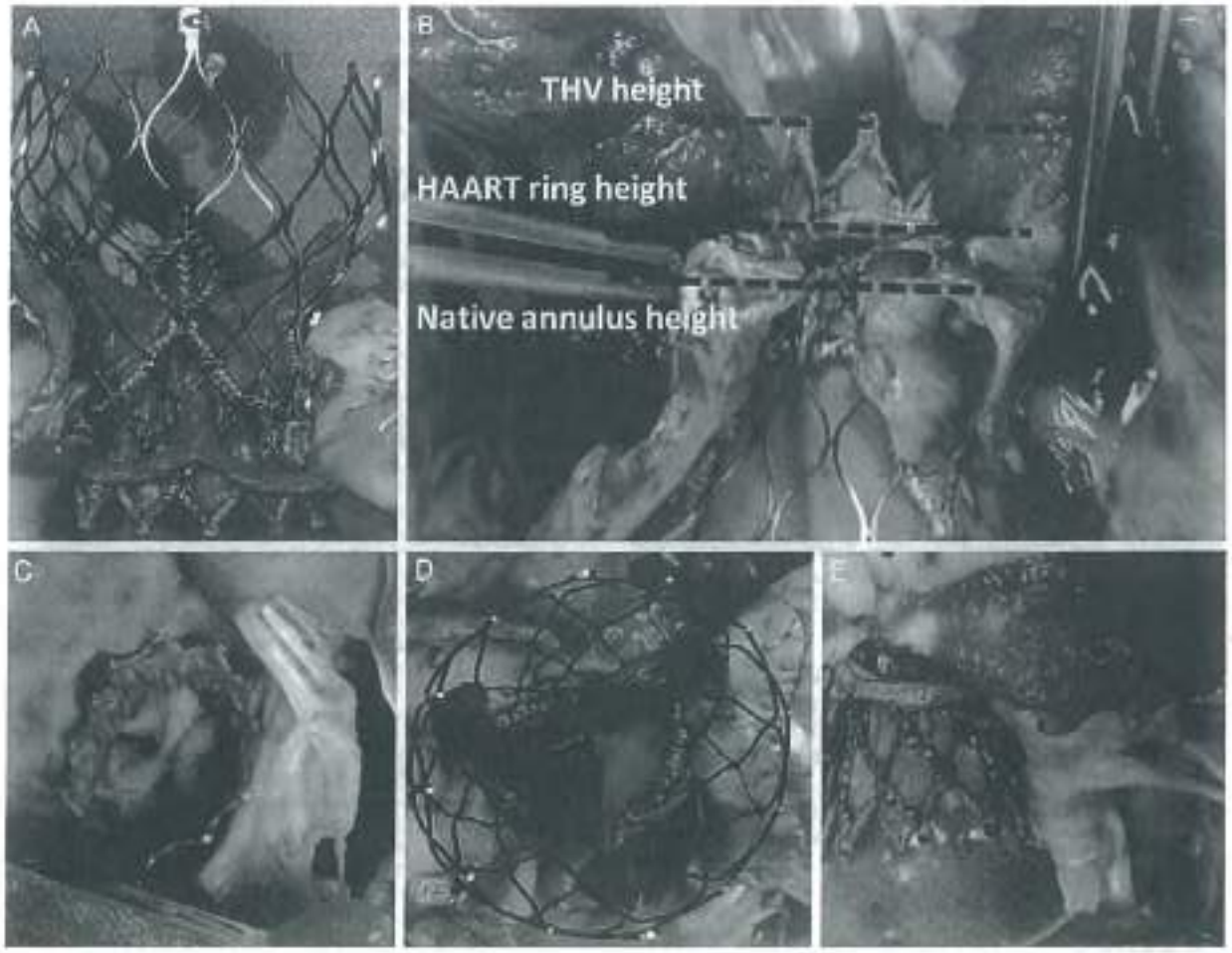

Figure 4: Explanted heart images. (**A**) Aortic valve-in-ring configuration (the HAART ring 19 mm and the EvolutR valve 23 mm); (**B**) the view after the removal of mitroaortic continuity showing the depth of implantation and the relationship among the native aortic annulus, the ring and the THV; (**C**) THV view from the ventricular side; (**D**) view from the aorta; and (**E**) relationship with the mitral valve. THV: transcatheter heart valve.

implantation could be managed by balloon valvuloplasty. Interestingly, the dilatation did not damage nor deform the strong titanium core of the device.

A potential mode of failure in this procedure is, however, wire malpositioning between the ventricular wall and the ring. This can only happen in acute cases, as the ring becomes rapidly endothelialized in long-term models.

As already described for VIV and mitral VIR, this new procedure could represent a novel treatment option for recurrent aortic valve disease after the HAART ring implantation [25–27].

These positive results should be confirmed by larger experimental series. However, they may also lead to a higher acceptance of the HAART device and a broader application of the aortic valve repair in patients with AR.

Limitations

This pilot trial represents a limited number of animals. The initial results should be extended in a larger series. Furthermore, only #19-mm and #21-mm HAART ring devices have been implanted.

Table 2: Sizing match proposed for the aortic valve-in-ring procedure with Medtronic EvolutR and the HAART ring

HAART ring (mm)	EvolutR 23	EvolutR 26	EvolutR 29
19	✓	✗	✗
21	✗	✓	✗
23*	✗	✗	✓
25*	✗	✗	✓

*Not yet assessed during an *in vivo* experiment.

A larger spectrum of sizes is currently evaluated in an *in vitro* trial. Sizing issues need to be further investigated. Haemodynamic measurement in this acute trial may not reflect long-term haemodynamic probabilities. For this study, only the EvolutR THV has been tested, and specific characteristics of different devices could represent a matter of future debate, although a balloon-expandable system cannot be implanted without the risk of intravalvular leakage or PVL in this setting. Furthermore, the mode of failure of native leaflets could play a role in THV deployment and

ADVANCE ARTICLE
Downloaded from https://academic.oup.com/icvts/advance-article-abstract/doi/10.1093/icvts/ivy341/5289780 by Endocrine Society Admin user on 03 April 2019

periprocedural adverse events occurrence as described for VIV procedures [18]. In addition, we herein report a proposal for a sizing chart that comes from empirical observation and guided our experiment, but further analysis should be performed to confirm these initial results.

CONCLUSION

We describe a novel aortic VIR procedure, which was technically feasible and reproducible for the treatment of recurrent aortic valve disease after aortic rigid ring implantation with a HAART device. Optimal sizing and proper depth of implantation play a major role for procedural success. Further experiences are required to confirm these preliminary data and improve optimal sizing.

Funding

This work was supported by the BioStable Science and Engineering (Austin, TX, USA). The EvolutR prostheses were contributed by Medtronic, Minneapolis, MN, USA.

Conflict of interest: Alberto Weber is the consultant surgeon for Biostable. Francesco Maisano is a consultant and has received research grant from Abbott, Valtech Cardio, Medtronic and St. Jude. Martin Andreas has received a research grant, is a proctor (Edwards) and a member in the advisory board (Medtronic). Scott Rankin is the Chief Medical Officer for Biostable Science and Engineering Inc. The other authors have no conflict of interest.

REFERENCES

[1] David TE. Surgical treatment of aortic valve disease. Nat Rev Cardiol 2013;10:375–86.
[2] Leon MB, Smith CR, Mack MJ, Makkar RR, Svensson LG, Kodali SK et al. Transcatheter or surgical aortic-valve replacement in intermediate-risk patients. N Engl J Med 2016;374:1609–20.
[3] Ussia GP, Barbanti M, Petronio AS, Tarantini G, Ettori F, Colombo A et al. Transcatheter aortic valve implantation: 3-year outcomes of self-expanding CoreValve prosthesis. Eur Heart J 2012;33:969–76.
[4] Richardt D, Bucsky B, Charitos EI, Sievers HH, Scharfschwerdt M. A novel rigid annuloplasty ring for aortic valve reconstruction: an in vitro investigation. Ann Thorac Surg 2014;97:811–5.
[5] de Meester C, Pasquet A, Gerber BL, Vancraeynest D, Noirhomme P, El Khoury G et al. Valve repair improves the outcome of surgery for chronic severe aortic regurgitation: a propensity score analysis. J Thorac Cardiovasc Surg 2014;148:1913–20.
[6] Boodhwani M, El Khoury G. Aortic valve repair: indications and outcomes. Curr Cardiol Rep 2014;16:490.
[7] Price J, De Kerchove L, Glineur D, Vanoverschelde JL, Noirhomme P, El Khoury G. Risk of valve-related events after aortic valve repair. Ann Thorac Surg 2013;95:606–12; discussion 13.
[8] El Khoury G, de Kerchove L. Principles of aortic valve repair. J Thorac Cardiovasc Surg 2013;145:S26–9.
[9] Boodhwani M, de Kerchove L, Glineur D, Poncelet A, Rubay J, Astarci P et al. Repair-oriented classification of aortic insufficiency: impact on surgical techniques and clinical outcomes. J Thorac Cardiovasc Surg 2009; 137:286–94.
[10] Aicher D, Schneider U, Schmied W, Kunihara T, Tochii M, Schäfers HJ. Early results with annular support in reconstruction of the bicuspid aortic valve. J Thorac Cardiovasc Surg 2013;145:530–4.
[11] Mazzitelli D, Pfeiffer S, Rankin JS, Fischlein T, Choi YH, Wahlers T et al. A regulated trial of bicuspid aortic valve repair supported by geometric ring annuloplasty. Ann Thorac Surg 2015;99:2010–6.
[12] Mazzitelli D, Fischlein T, Rankin JS, Choi YH, Stamm C, Pfeiffer S et al. Geometric ring annuloplasty as an adjunct to aortic valve repair: clinical investigation of the HAART 300 device. Eur J Cardiothorac Surg 2016;49: 987–93.
[13] Webb JG, Wood DA, Ye J, Gurvitch R, Masson JB, Rodés-Cabau J et al. Transcatheter valve-in-valve implantation for failed bioprosthetic heart valves. Circulation 2010;12:1848–57.
[14] Khawaja MZ, Haworth P, Ghunan A, Lee L, de Belder A, Hutchinson N et al. Transcatheter aortic valve implantation for stenosed and regurgitant aortic valve bioprostheses: CoreValve for failed bioprosthetic aortic valve replacements. J Am Coll Cardiol 2010;55:97–101.
[15] Descoutures F, Himbert D, Maisano F, Casselman F, de Weger A, Rodea O et al. Transcatheter valve-in-ring implantation after failure of surgical mitral repair. Eur J Cardiothorac Surg 2013;44:e8–15.
[16] Tay EL, Kong WK, Yip JW, Low TT, Han JK. Successful transcatheter aortic valve replacement for severe aortic valve regurgitation following a David I valve-sparing procedure. JACC Cardiovasc Interv 2017;10:e101–3.
[17] Aicher D, Fries R, Rodionycheva S, Schmidt K, Langer F, Schäfers HJ. Aortic valve repair leads to a low incidence of valve-related complications. Eur J Cardiothorac Surg 2010;37:127–32.
[18] Roques F, Nashef SA, Michel P, Gauducheau E, de Vincentiis C, Baudet E et al. Risk factors and outcome in European cardiac surgery: analysis of the EuroSCORE multinational database of 19030 patients. Eur J Cardiothorac Surg 1999;15:816–22; discussion 22–3.
[19] Dvir D, Webb JG, Bleiziffer S, Pasic M, Waksman R, Kodali S et al. Transcatheter aortic valve implantation in failed bioprosthetic surgical valves. JAMA 2014;312:162–70.
[20] Bapat V, Attres KN. Transcatheter valve-in-valve implantation for failing prosthetic valves. EuroIntervention 2014;10:900–2.
[21] Bedogni F, Laudisa ML, Pizzocri S, Laudisa ML, Pizzocri S, Tamburino C et al. Transcatheter valve-in-valve implantation using Corevalve Revalving System for failed surgical aortic bioprostheses. JACC Cardiovasc Interv 2011;4:1228–34.
[22] Andreas M, Coti I, Laufer G, Kastner J. Valve-in-valve transcatheter aortic valve implantation into a novel, sutureless bioprosthesis: technical considerations. EuroIntervention 2017;13:1902–3.
[23] Wenaweser P, Boeddeleld L, Gerckens U, Grube E. Percutaneous aortic valve replacement for severe aortic regurgitation in degenerated bioprosthesis: the first valve in valve procedure using the Corevalve Revalving system. Catheter Cardiovasc Interv 2007;70:760–4.
[24] Bapat VN, Attia RQ, Condemi F, Visagan R, Guthrie M, Sunni S et al. Fluoroscopic guide to an ideal implant position for Sapien XT and CoreValve during a valve-in-valve procedure. JACC Cardiovasc Interv 2013;6:1186–94.
[25] Kempfert JB, Lumenstein J, Chu MW, Pritzwald-Stegmann P, Kohlike T, Falk V et al. Minimally invasive off-pump valve-in-a-ring implantation: the atrial transcatheter approach for re-operative mitral valve replacement after failed repair. Eur J Cardiothorac Surg 2009;35:965–9; discussion 9.
[26] Maisano F, Reser D, Pavcevic J, Niedlspach F, Gämperli O, Schmid M et al. Successful first-in-man Melody transcatheter valve implant in a dehisced mitral annuloplasty ring transapical valve-in-ring implant. EuroIntervention 2014;10:961–7.
[27] Bapat V. Valve-in-valve apps: why and how they were developed and how to use them. EuroIntervention 2014;10(Suppl U):U44–51.

Downloaded from https://academic.oup.com/icvts/advance-article-abstract/doi/10.1093/icvts/iny341/5089780 by EndocrineSociety Admin user on 03 April 2019

This Issue | Views 1,328 | Citations 1 | Altmetric 44

PDF Full Text Share

Brief Report

May 1, 2019

Association Between Physiological Stenosis Severity and Angina-Limited Exercise Time in Patients With Stable Coronary Artery Disease

Christopher M. Cook, MBBS, BSc[1]; Yousif Ahmad, BMBS[1]; James P. Howard, MB BChir[1]; Matthew J. Shun-Shin, BM BCh[1]; Amarjit Sethi, MBBS, PhD[1]; Gerald J. Clesham, MB BChir, PhD[2,3]; Kare H. Tang, MBBS[2]; Sukhjinder S. Nijjer, MB ChB, PhD[1]; Paul A. Kelly, MB ChB, MD[2]; John R. Davies, MBBS, PdD[2,3]; Iqbal S. Malik, MBBChir, MA, PhD[1]; Raffi Kaprielian, MBBS, MD[1]; Ghada Mikhail, MBBS, MD[1]; Ricardo Petraco, MD[1]; Takayuki Warisawa, MD[1]; Firas Al-Janabi, MBBS[2,3]; Grigoris V. Karamasis, MD[2,3]; Shah Mohdnazri, MD[2,3]; Reto Gamma, MD[2]; Guus A. de Waard, MD[1]; Rasha Al-Lamee, MBBS, PhD[1]; Thomas R. Keeble, MBBS, MD[2,3]; Jamil Mayet, MB ChB, MD, MBA[1]; Sayan Sen, MBBS, PhD[1]; Darrel P. Francis, MB BChir, MA, MD[1]; Justin E. Davies, MD, PhD[1]

Author Affiliations

[1]Imperial College London, London, United Kingdom

[2]Essex Cardiothoracic Centre, Basildon, United Kingdom

[3]Anglia Ruskin School of Medicine, Chelmsford, Essex, United Kingdom

JAMA Cardiol. 2019;4(6):569-574. doi:10.1001/jamacardio.2019.1139

Key Points

Question Are measurements of physiological stenosis severity associated with angina-limited exercise time in patients with stable angina and coronary stenosis?

Findings In this cohort study, anatomical stenosis characteristics were not significantly associated with angina-limited exercise time. Conversely, fractional flow reserve, instantaneous wave-free ratio, hyperemic stenosis resistance, and coronary flow reserve were all associated with angina-limited exercise time.

Our website uses cookies to enhance your experience. By continuing to use our site, you are agreeing to our Cookie Policy | Continue

Meaning In a selected group of patients with severe, single-vessel stable angina, fractional flow reserve, instantaneous wave-free ratio, hyperemic stenosis resistance, and coronary flow reserve were all modestly correlated with angina-limited exercise time to varying degrees; notwithstanding the limited sample size, no clear association was demonstrated between anatomical stenosis severity and angina-limited exercise time.

Abstract

Importance Physiological stenosis assessment is recommended to guide percutaneous coronary intervention (PCI) in patients with stable angina.

Objective To determine the association between all commonly used indices of physiological stenosis severity and angina-limited exercise time in patients with stable angina.

Design, Setting, and Participants This cohort study included data (without follow-up) collected over 1 year from 2 cardiac hospitals. Selected patients with stable angina and physiologically severe single-vessel coronary artery disease presenting for clinically driven elective PCI were included.

Exposures Fractional flow reserve (FFR), instantaneous wave-free ratio (iFR), hyperemic stenosis resistance (HSR), and coronary flow reserve (CFR) were measured invasively. Immediately after this, patients maximally exercised on a catheter-table-mounted supine ergometer until they developed rate-limiting angina. Subsequent PCI was performed in most patients, followed by repeat maximal supine exercise testing.

Main Outcomes and Measures Associations between FFR, iFR, HSR, CFR, and angina-limited exercise time were assessed using linear regression and Pearson correlation coefficients. Additionally, the associations between the post-PCI increment in exercise time and baseline FFR, iFR, HSR, and CFR were assessed.

Results Twenty-three patients (21 [91.3%] of whom were male; mean [SD] age, 60.6 [8.1] years) completed the pre-PCI component of the study protocol. Mean (SD) stenosis diameter was 74.6% (10.4%). Median (interquartile range [IQR]) values were 0.54 (0.44-0.72) for FFR, 0.53 (0.38-0.83) for iFR, 1.67 (0.84-3.16) for HSR, and 1.35 (1.11-1.63) for CFR. Mean (SD) angina-limited exercise time was 144 (77) seconds. Anatomical stenosis characteristics were not significantly associated with angina-limited exercise time. Conversely, FFR (R^2 = 0.27; P = .01), iFR (R^2 = 0.46; P < .001), HSR (R^2 = 0.39; P < .01), and CFR (R^2 = 0.16; P < .05) were all associated with angina-limited exercise time. Twenty-one patients (19 [90.5%] of whom were male; mean [SD] age, 60.1 [8.2] years) completed the full protocol of PCI, post-

Our website uses cookies to enhance your experience. By continuing to use our site, or clicking "Continue," you are agreeing to our Cookie Policy | Continue

PCI physiological assessment, and post-PCI maximal exercise. After PCI, the median (IQR) FFR rose to 0.91 (0.85-0.96), median (IQR) iFR to 0.98 (0.94-0.99), and median (IQR) CFR to 2.73 (2.50-3.12), while the median (IQR) HSR fell to 0.16 (0.06-0.37) ($P<.001$ for all). The post-PCI increment in exercise time was most significantly associated with baseline iFR ($R^2=0.26$; $P=.02$).

Conclusions and Relevance In a selected group of patients with severe, single-vessel stable angina, FFR, iFR, HSR, and CFR were all modestly correlated with angina-limited exercise time to varying degrees. Notwithstanding the limited sample size, no clear association was demonstrated between anatomical stenosis severity and angina-limited exercise time.

Full Text

Advertisement

Read More About

Cardiology | Lifestyle Behaviors | Physical Activity | Ischemic Heart Disease

New! *JAMA Network Open* is now accepting submissions. Learn more.

Trending

Research

Instantaneous Wave-Free Ratio or Fractional Flow Reserve–Guided Strategy in Patients With Diabetes

July 17, 2019

Research

Baseline Characteristics of Participants in the ISCHEMIA Study

March 1, 2019

Research

Coronary Hyperemic and Resting Hemodynamic Indices in Nonculprit Vessels in STEMI

July 3, 2019

Our website uses cookies to enhance your experience. By continuing to use our site, or clicking "Continue," you are agreeing to our Cookie Policy | Continue

Journal of Cardiology 73 (2019) 536–543

Contents lists available at ScienceDirect

Journal of Cardiology

journal homepage: www.elsevier.com/locate/jjcc

Original article

Symptomatic paradoxical low gradient severe aortic stenosis: A possible link to heart failure with preserved ejection fraction

Hidehiro Namisaki (RDCS)[a], Yasufumi Nagata (MD, PhD)[b], Yoshihiro Seo (MD, PhD, FJCC)[c], Tomoko Ishizu (MD, PhD, FJCC)[c], Masaki Izumo (MD, PhD)[d], Yoshihiro J. Akashi (MD, PhD, FJCC)[d], Eiji Yamashita (MD)[e], Yutaka Otsuji (MD, PhD, FJCC)[b], Masaaki Takeuchi (MD, PhD, FJCC)[a,*]

[a] Department of Laboratory and Transfusion Medicine, University of Occupational and Environmental Health Hospital, Kitakyushu, Japan
[b] Second Department of Internal Medicine, University of Occupational and Environmental Health, School of Medicine, Kitakyushu, Japan
[c] Department of Cardiology, University of Tsukuba, Tsukuba, Japan
[d] Division of Cardiology, Department of Internal Medicine, St. Marianna University School of Medicine, Kawasaki, Japan
[e] Department of Cardiology, Gunma Prefectural Cardiovascular Center, Maebashi, Japan

ARTICLE INFO

Article history:
Received 12 October 2018
Received in revised form 14 December 2018
Accepted 18 December 2018
Available online 5 January 2019

Keywords:
Low pressure gradient
Aortic stenosis
Symptom
Heart failure with preserved ejection fraction

ABSTRACT

Background: There is an ongoing debate regarding optimal management of patients with paradoxical low gradient severe aortic stenosis (PLG-SAS). We hypothesized that the presence of symptoms is closely associated with future adverse outcome. We aimed to determine the relation between symptoms and outcome in patients with PLG-SAS.

Methods: We prospectively enrolled 222 patients with PLG-SAS. Left ventricular (LV) volumes, mass, and strain were measured by three-dimensional echocardiography. The primary end-point was cardiac events including cardiac death, ventricular fibrillation, and heart failure leading to hospitalization.

Results: There were 65 cases of symptomatic PLG-SAS and 157 cases of asymptomatic PLG-SAS. Patients with symptomatic PLG-SAS received beta-blockers, angiotensin blockers, and diuretics more frequently and showed higher levels of B-type natriuretic peptide than patients with asymptomatic PLG-SAS. Although LV chamber parameters were not different, patients with symptomatic PLG-SAS had significantly higher E-wave velocity and E/A ratio than patients with asymptomatic PLG-SAS. During the median follow-up of 18 months, 20 patients reached the primary end-point. Patients with symptomatic PLG-SAS had significantly worse prognosis than patients with asymptomatic PLG-SAS. A similar trend was observed while comparing with the propensity-score-matched cohort after adjusting for age, sex, stroke volume index, and severity of AS.

Conclusions: Symptomatic PLG-SAS is associated with poorer prognosis even after adjusting for flow status and severity of AS. Therefore, presence of symptoms is not always related to the severity of AS itself but might be related to the underlying comorbidities. Our results suggest a possible link between PLG-SAS and heart failure with preserved ejection fraction in some symptomatic patients.

© 2019 Published by Elsevier Ltd on behalf of Japanese College of Cardiology.

Introduction

There is an ongoing debate regarding pathophysiology, optimal management, and prognosis of low gradient severe aortic stenosis with preserved left ventricular ejection fraction (LVEF), so-called paradoxical low gradient severe aortic stenosis (PLG-SAS) [1–9]. Current European Society of Cardiology guidelines recommended that "aortic valve replacement (AVR) should be considered in symptomatic patients with low flow, PLG-SAS only after careful confirmation of SAS" [10]. Although several imaging parameters could identify a high-risk group of patients with symptomatic PLG-SAS [11–13], discrepant results from each parameter could not help in making an appropriate decision.

Since PLG-SAS often shares similar clinical features with those of heart failure with preserved ejection fraction (HFpEF) [14,15],

* Corresponding author at: Department of Laboratory and Transfusion Medicine, University of Occupational and Environmental Health Hospital, 1-1 Iseigaoka, Yahatanishi-ku, Kitakyushu 807-8556, Japan.
E-mail address: takeuchi@med.uoeh-u.ac.jp (M. Takeuchi).

https://doi.org/10.1016/j.jjcc.2018.12.017
0914-5087/© 2019 Published by Elsevier Ltd on behalf of Japanese College of Cardiology.

and reliable diagnosis of HFpEF is not always easy, whether existing symptoms in patients with PLG-SAS are solely related to the AS itself or are mainly linked with HFpEF is unclear. Previous studies have paid less attention to the symptomatic status during the prognosis of patients with PLG-SAS [5]. Therefore, it is important to compare the clinical characteristics and their prognosis of symptomatic and asymptomatic patients with PLG-SAS. A recent meta-analysis revealed that AVR is associated with favorable outcome in patients with PLG-SAS [16]. However, less information exists whether pressure gradient (PG) status remains constant or converts from low PG (LPG) to high PG (HPG) at the time of aortic valve surgery.

Accordingly, we aimed: (1) to compare clinical and echocardiography parameters between symptomatic and asymptomatic patients with PLG-SAS; (2) to determine their prognosis; and (3) to investigate the PG status at the time of aortic valve surgery and the impact of AVR on prognosis.

Materials and methods

Study patients

This study was a part of the prospective multicenter observational study in patients with aortic stenosis (AS) [Japanese Multicenter Aortic Stenosis Study, Prospective (JUST-P) registry]. From January 2013 to December 2014, we acquired transthoracic 3D echocardiography (3DE) datasets of patients with AS who underwent clinically indicated echocardiographic examinations in four Japanese cardiovascular centers. Of 618 AS patients enrolled during the study period, we excluded 396 patients due to poor echo image quality ($n = 36$), reduced LVEF ($n = 104$), mild to moderate AS ($n = 118$), HPG-SAS ($n = 137$), and whose follow-up data were not available ($n = 1$). The remaining 222 patients with PLG-SAS were considered as a final group of study subjects. LPG was defined as mean PG of <40 mmHg across the aortic valve on Doppler echocardiography. Stroke volume (SV) was calculated using 3DE. Flow status was divided into two groups [normal flow: stroke volume index (SVI) $\geq$ 35 mL/m^2, and low flow: SVI < 35 mL/m^2]. Indexed aortic valve area (IAVA) was defined as SV measured by 3DE divided by the velocity time integral of peak aortic valve jet velocity indexed by body surface area. SAS was defined as IAVA of <0.6 cm^2/m^2. The study protocol was approved by the Ethics Committee of each hospital, and informed consent was obtained from all patients.

Clinical characteristics

At the time of echocardiographic examination, a cardiologist directly asked the patients regarding symptomatic status with chest pain, syncope, and dyspnea. Blood test reports within <3 months of indexed echocardiography were collected from the electronic medical records.

Echocardiography

Comprehensive transthoracic 2D echocardiography (2DE) and Doppler echocardiography were performed according to the American Society of Echocardiography guideline [17]. Aortic valve jet velocity was recorded in multiple transducer positions in order to obtain the highest jet velocity signal. Envelope of peak velocity was manually traced, yielding peak velocity, mean PG, and velocity time integral. LV inflow velocity was obtained at the tip of the mitral leaflets, and mitral annular velocity was recorded at the septal corner of the mitral annulus. E/e' was calculated. Maximum left atrial volume was measured by biplane Simpson's method. Systolic pulmonary arterial pressure was estimated by the formula: [4 × (peak velocity of tricuspid regurgitation)^2 + right atrial pressure]. Right atrial pressure was estimated based on the inferior vena cava diameter and its change during respiration [18].

Full-volume 3DE datasets were acquired using an apical approach with fully sampled matrix array transducers (iE33 with X5-1/3-1, Philips Healthcare, Andover, MA, USA; Vivid 7/E9 with 4 V, GE Healthcare, Horten, Norway). All echocardiography data were sent to the core laboratories (University of Occupational and Environmental Health for 3DE assessment, St Marianna University for 2DE and Doppler assessment) for the analysis. An independent examiner in each institution who did not know the patient's symptomatic status and outcome performed echocardiography analysis.

3DE measurements

3DE analysis was performed by speckle tracking software (4D LV analysis version 3.1.2, TomTec Imaging Systems, Unterschleissheim, Germany) by an experienced investigator. The methods have been described in detail in a previous report [12]. Briefly, endocardial border was semi-automatically delineated after 2-point clicks of a specific anatomical landmark. Manual adjustment of the endocardial border was performed, when required. The software performed a 3DE speckle tracking analysis throughout 1 cardiac cycle, and generated time domain LV volume curves, from which LV volumes, SV, and LVEF were calculated. The software also provided global longitudinal, circumferential, and radial strain (GLS, GCS, and GRS, respectively) values. GLS and GCS were presented as absolute values.

Follow ups

Patients were followed up regularly in an outpatient clinic. If patients were treated in other hospitals, we contacted patients, physicians, and next of kin. Final follow-up data were obtained from January 2016 to June 2016. The primary endpoint was cardiac events, including cardiac death, ventricular fibrillation/tachycardia, and development of heart failure requiring hospitalization. To determine natural history of PLG-SAS, patients who had surgical or trans-catheter AVR (SAVR/TAVR) were censored at the time of surgery.

The secondary endpoint was a composite of cardiac events and AVR. While comparing the cardiac events that occurred in the patients who received conservative treatment with those that occurred in patients who underwent AVR, follow-up duration was calculated from the time of surgery to the date when the cardiac event occurred or from the date of final follow up in patients who underwent AVR. In patients who underwent conservative treatment, follow-up duration was determined from the index echocardiography to the date of occurrence of cardiac events or the final follow-up date.

Observer variabilities

Intra-observer variability was assessed by having the observer repeat the measurement of 3DE SV and LVEF at 2 weeks apart in 20 randomly selected patients. Inter-observer variability was determined by employing a second observer to perform these measurements in the same 20 patients. The intra- and interobserver variability values were calculated as the absolute differences between the two corresponding measurements in percentages of their mean and intraclass correlation (ICC).

Statistical analysis

Continuous data were presented as mean ± SD or median and 25th to 75th percentile. Categorical data were expressed as

numbers or percentages. A *t*-test or Wilcoxon sum rank test was used to compare continuous variables between the two groups. Categorical variables were compared by Chi-square test. Survival analysis was conducted by Kaplan–Meier method, and group differences were determined by log-rank test. The prognostic value of echocardiography parameters was determined by univariable Cox proportional hazard analysis. To compare the predictive strengths of echocardiographic parameters and symptomatic status, which was usually graded as New York Heart Association (NYHA) class, receiver operating characteristic (ROC) curves for cardiac events were created. We conducted a pairwise comparison of the areas under the curve (AUC) using DeLong's test. A net reclassification improvement (NRI) analysis with and without NYHA class was also performed [19,20]. Furthermore, the robustness of symptomatic status was tested using progressive models. Echocardiographic parameters showing $p < 0.1$ of univariable analysis were used for the analysis. A logistic regression model was used to develop propensity score for the prediction of symptomatic status. To adjust the severity of AS, we included age, sex, heart rate, systolic blood pressure, mean PG, SVI, and IAVA. To generate propensity-score matched cohort, asymptomatic patients were matched with symptomatic patients by using the one-to-one matching technique. A two-sided *p*-value < 0.05 was considered statistically significant. All statistical analyses were performed by using a commercial software (JMP 13.1.0, SAS Institute Inc., Cary, NC, USA; SPSS 24, Chicago, IL, USA; and R 3.4.3, The R Foundation for Statistical Computing, Vienna, Austria).

Results

Clinical characteristics

Among 222 patients with PLG-SAS, 65 patients manifested possible AS-related symptoms (29%), including chest pain in 22, syncope in 9, and dyspnea in 42 patients. Table 1 depicts clinical characteristics of patients with symptomatic and asymptomatic PLG-SAS. Patients with symptomatic PLG-SAS received beta-blockers, angiotensin-converting enzyme inhibitors/angiotensin receptor blockers, and diuretics more frequently than patients with asymptomatic PLG-SAS. BNP level was significantly higher in the symptomatic group ($n = 47$) than in the asymptomatic group ($n = 87$, $p = 0.014$). Patients with chest pain had a higher prevalence of coronary artery disease (9/22, 41%) than those without chest pain (38/200, 19%, $p = 0.026$).

Echocardiography parameters between the two groups

Table 2 represents echocardiography parameters between the two groups. There were no significant differences in the LV volumes, LVEF, and LV mass index between both symptomatic PLG-SAS and asymptomatic PLG-SAS groups. Prevalence of low flow was also not different between the two groups. Regarding the parameters of LV diastolic function, patients with symptomatic PLG-SAS presented with significantly higher E-wave velocity, and E/A ratio than patients with asymptomatic PLG-SAS. Peak velocity, mean PG, IAVA, and systolic pulmonary arterial pressure were not different between the two groups.

Primary end points

During the median follow-up of 18 months, 20 patients reached the primary end-point, including cardiac deaths in 6; heart failure requiring hospitalization in 13; and ventricular fibrillation in 1 patient. Fig. 1A shows cardiac-event-free survival curve. Patients with symptomatic PLG-SAS had significantly worse prognosis than patients with asymptomatic PLG-SAS ($p = 0.003$). An estimated 2-year cardiac-event-free rate was 77 ± 7% in patients with symptomatic PLG-SAS, and 92 ± 3% in patients with asymptomatic

Table 1
Clinical characteristics in study population.

Variables	All (n = 222)	Symptomatic PLG-SAS (n = 65)	Asymptomatic PLG-SAS (n = 157)	p-value
Age (year)	78 ± 9	78 ± 8	78 ± 9	0.93
Sex (male/female)	92/130	24/41	68/89	0.38
BSA (m^{-2})	1.53 ± 0.18	1.52 ± 0.17	1.53 ± 0.19	0.84
BMI	23.2 ± 3.5	23.6 ± 3.6	23.1 ± 3.5	0.37
Heart rate (bpm)	67 ± 11	69 ± 11	66 ± 11	0.074
Systolic blood pressure (mmHg)	141 ± 26	146 ± 28	140 ± 24	0.23
Diastolic blood pressure (mmHg)	73 ± 14	74 ± 14	72 ± 14	0.27
Hypertension (%)	168 (76)	53 (81)	115 (73)	0.18
Diabetes	70 (32)	25 (38)	45 (29)	0.16
Hypercholesterolemia	96 (43)	32 (49)	64 (41)	0.25
Chronic kidney disease	105 (47)	31 (48)	74 (47)	0.94
Coronary artery disease	47 (21)	18 (27)	29 (18)	0.13
Current smoking	27 (12)	6 (9)	21 (13)	0.31
COPD	23 (10)	10 (15)	13 (8)	0.13
CVA	28 (13)	13 (20)	15 (10)	0.040
Atrial fibrillation	32 (14)	11 (17)	21 (13)	0.50
Active malignancy	32 (14)	5 (8)	27 (17)	0.053
Frailty	37 (17)	15 (23)	22 (14)	0.13
Beta blocker	58 (26)	24 (37)	34 (22)	0.021
ACEI/ARB	114 (51)	41 (63)	73 (47)	0.024
Ca antagonists	107 (48)	32 (49)	75 (48)	0.84
Diuretics	46 (21)	20 (31)	26 (17)	0.031
Statin	75 (34)	25 (38)	50 (32)	0.35
SAVR/TAVR	59 (27)	23 (35)	36 (23)	0.060
Hemoglobin (g/dL)	12.1 ± 1.8	12.0 ± 1.7	12.2 ± 1.9	0.59
Creatinine (mg/mL)	0.81 (0.63–1.05)	0.88 (0.67–1.06)	0.8 (0.62–1.05)	0.53
eGFR (mL/min/1.73 m^2)	58 ± 24	56 ± 22	59 ± 24	0.39
hsCRP (mg/dL)	0.11 (0.04–0.47)	0.22 (0.05–0.50)	0.1 (0.04–0.46)	0.34
BNP (μg/mL)	101 (49–202)	114 (67–264)	91 (42–151)	0.014

ACEI/ARB, angiotensin converting enzyme inhibitor/angiotensin receptor blocker; BMI, body mass index; BNP, brain natriuretic peptide; BSA, body surface area; COPD, chronic obstructive pulmonary disease; CVA, cerebrovascular accident; eGFR, estimated glomerular filtration rate; hsCRP, high sensitivity C-reactive protein; PLG-SAS, paradoxical low gradient severe aortic stenosis; SAVR/TAVR, surgical aortic valve replacement/transcatheter aortic valve replacement.

Table 2
Echocardiography parameters in the study population.

Variables	All (n = 222)	Symptomatic PLG-SAS (n = 65)	Asymptomatic PLG-SAS (n = 157)	p-Value
LVEDVI (mL/m²)	57.5 ± 12.3	58.2 ± 14.5	57.3 ± 11.3	0.60
LVESVI (mL/m²)	21.6 ± 6.8	24.2 ± 7.8	23.3 ± 6.4	0.39
LVSVI (mL/m²)	34.0 ± 6.8	34.0 ± 7.7	34.0 ± 6.4	0.99
Low flow (%)	123 (55%)	39 (60%)	84 (54%)	0.37
LVEF (%)	59.4 ± 5.3	58.8 ± 5.1	59.6 ± 5.4	0.32
LV mass index (g/m²)	73 ± 17	72 ± 20	73 ± 15	0.75
Maximum LAVI (mL/m²)	39.2 ± 17.7	41.9 ± 21.7	38.1 ± 15.7	0.35
E wave velocity (cm/s)	81 ± 27	88 ± 33	78 ± 23	0.015
A wave velocity (cm/s)	103 ± 28	101 ± 30	104 ± 28	0.39
E/A ratio	0.82 ± 0.42	0.92 ± 0.53	0.78 ± 0.35	0.041
e' (cm/s)	5.1 ± 1.9	5.1 ± 1.8	5.2 ± 1.9	0.69
E/e'	17.3 ± 7.4	18.2 ± 7.7	16.9 ± 7.3	0.23
Systolic PAP (mmHg)	33.4 ± 8.6	34.1 ± 9.8	33.0 ± 8.2	0.48
Peak velocity (m/s)	3.4 ± 0.5	3.5 ± 0.5	3.4 ± 0.5	0.12
Mean pressure gradient (mmHg)	26 ± 8	27 ± 7	26 ± 8	0.34
Index aortic valve area (cm²/m²)	0.46 ± 0.09	0.45 ± 0.09	0.46 ± 0.08	0.38
Zva (mmHg/mL/m²)	5.07 ± 1.18	5.27 ± 1.32	4.99 ± 1.07	0.31
Global longitudinal strain (%)	15.6 ± 2.4	15.1 ± 2.4	15.8 ± 2.4	0.060
Global circumferential strain (%)	30.4 ± 4.1	30.4 ± 3.9	30.4 ± 4.2	0.99
Global radial strain (%)	37.8 ± 4.5	37.4 ± 4.4	37.9 ± 4.6	0.41
MR				
No-trivial/mild/moderate/severe	177/44/1/0	48/17/0/0	129/27/1/0	0.30
AR				
No-trivial/mild/moderate/severe	138/83/1/0	36/29/0/0	102/54/1/0	0.09

AR, aortic regurgitation; e', early diastolic mitral annular velocity; LAVI, left atrial volume index; LV, left ventricular; LVEDVI, LV end-diastolic volume index; LVESVI, LV end-systolic volume index; LVEF, left ventricular ejection fraction; LVSVI, left ventricular stroke volume index; MR, mitral regurgitation; PAP, pulmonary arterial pressure; PLG-SAS, paradoxical low gradient severe aortic stenosis; Zva, valvulo-arterial impedance.

PLG-SAS. Table 3 presents results of univariable analysis of clinical, echocardiographic, and blood examination parameters in predicting the occurrence of cardiac events. Presence of symptoms and NYHA class were significant predictors of future cardiac events. Among echocardiographic parameters, LV mass index, E-wave velocity, *E/e'*, and GLS were significant predictors of future cardiac events. Hemoglobin, eGFR, high sensitivity CRP, and BNP were also significant predictors of future cardiac events.

Online Fig. 1 shows comparison of ROC curves between echocardiographic parameters and the corresponding parameters plus NYHA class. Addition of NYHA class increased AUC, but no statistically significant differences in AUC were noted. However, a reclassification analysis showed that addition of NYHA class significantly improved the classification for predicting outcome compared with each echocardiography parameter except *E/e'* (Online Table 1).

We further analyzed the robustness of NYHA class using progressive models. NYHA class significantly improved models based on LV mass index, E wave velocity, *E/e'*, iAVA, and GLS (Table 4).

Among 64 paired propensity-score-matched cohort, patients with symptomatic PLG-SAS had still significantly worse prognosis than patients with asymptomatic PLG-SAS (p = 0.022) (Fig. 2A).

Secondary end points

During the follow-up period, AVR was performed in 59 patients (49 SAVR and 10 TAVR; 23 symptomatic and 36 asymptomatic patients). The number of isolated AVR, AVR + coronary bypass surgery, and AVR + the other valve surgery was 48, 8, and 3, respectively. Patients with symptomatic PLG-SAS showed a higher incidence of AVR than patients with asymptomatic PLG-SAS (31 ±

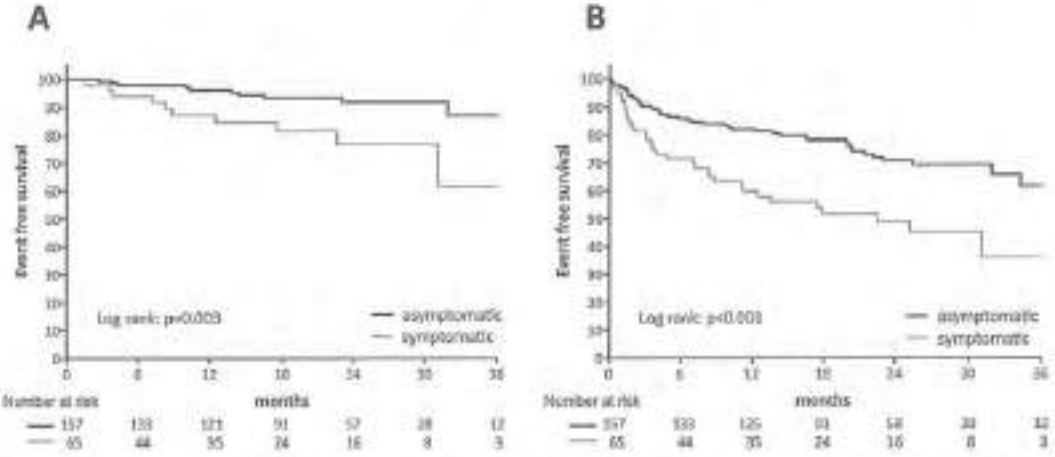

Fig. 1. Kaplan–Meier analysis for cardiac events (A) and a composite of cardiac events and SAVR/TAVR (B) between asymptomatic patients with PLG-SAS and symptomatic patients with PLG-SAS. PLG-SAS, paradoxical low gradient severe aortic stenosis; SAVR, surgical aortic valve replacement; TAVR, transcatheter aortic valve replacement.

Table 3
Clinical and echocardiography parameters in patients with cardiac events and those without events and univariable Cox proportional analysis.

Variables	CE (+) (n=20)	CE (−) (n=202)	p-Value	Univariate analysis		
				HR	95% CI	p-Value
Age (years)	78 ± 7	78 ± 9	0.75	1.01	0.96–1.07	0.65
Female	9 (45%)	121 (60%)	0.20	0.58	0.24–1.41	0.23
BSA (m^{-2})	1.54 ± 0.18	1.53 ± 0.18	0.68	1.58	0.14–17.7	0.71
BMI	23.2 ± 3.5	23.2 ± 3.6	0.98	1.01	0.88–1.14	0.94
Symptom (yes)	10 (50%)	55 (27%)	0.041	3.43	1.42–8.27	0.006
NYHA class I/II/III/IV	16/6/2/2	159/40/2/1	0.004	3.03[a]	1.09–8.44	0.034
				24.9[b]	5.3–119	<0.001
				36.7[c]	7.4–182	<0.001
Hypertension (%)	14 (70%)	154 (76%)	0.54	0.75	0.28–1.85	0.55
Diabetes (%)	9 (45%)	61 (30%)	0.19	1.86	0.77–4.50	0.17
Hypercholesterolemia (%)	8 (40%)	88 (44%)	0.76	0.85	0.35–2.09	0.73
Chronic kidney disease (%)	14 (78%)	91 (45%)	0.032	2.49	0.96–6.49	0.061
Coronary artery disease (%)	6 (30%)	41 (20%)	0.33	1.59	0.61–4.14	0.34
Smoking (%)	4 (20%)	23 (11%)	0.33	2.37	0.73–7.61	0.15
COPD (%)	5 (25%)	18 (9%)	0.047	3.54	1.28–10.00	0.015
CVA (%)	7 (35%)	21 (10%)	0.006	4.19	1.67–10.5	0.002
Atrial fibrillation (%)	5 (25%)	27 (13%)	0.19	2.30	0.83–6.39	0.11
Active malignancy (%)	4 (20%)	28 (14%)	0.47	1.60	0.53–4.82	0.41
Frailty (%)	7 (35%)	30 (15%)	0.036	3.23	1.28–8.15	0.013
Heart rate (bpm)	89 ± 11	66 ± 11	0.30	1.03	0.99–1.07	0.18
Systolic blood pressure (mmHg)	131 ± 29	142 ± 25	0.014	0.98	0.97–1.00	0.063
Diastolic blood pressure (mmHg)	69 ± 12	73 ± 14	0.20	0.99	0.96–1.01	0.25
LVEDVI (mL/m^2)	57.9 ± 14.4	57.6 ± 12.1	0.84	1.00	0.97–1.04	0.87
LVSVI (mL/m^2)	33.1 ± 8.7	34.0 ± 6.6	0.54	0.99	0.92–1.06	0.69
LVEF (%)	58.0 ± 5.1	59.6 ± 5.3	0.22	0.93	0.86–1.02	0.12
LV mass index (g/m^2)	79 ± 18	72 ± 16	0.033	1.03	1.00–1.05	0.040
Maximum LAVI (mL/m^2)	43.1 ± 22.8	38.8 ± 17.1	0.29	1.02	0.99–1.04	0.17
E wave velocity (cm/s)	102 ± 39	79 ± 24	<0.001	1.03	1.01–1.04	<0.001
A wave velocity (cm/s)	111 ± 37	103 ± 28	0.26	1.01	0.99–1.03	0.18
E/A ratio	0.92 ± 0.49	0.81 ± 0.41	0.29	1.46	0.61–3.47	0.39
e′ (cm/s)	5.3 ± 2.2	5.1 ± 1.8	0.68	1.04	0.83–1.30	0.75
E/e′	21.0 ± 10.8	16.9 ± 6.9	0.023	1.07	1.02–1.13	0.012
Systolic PAP (mmHg)	36.6 ± 9.8	33.0 ± 8.5	0.16	1.04	0.99–1.09	0.15
Peak velocity (m/s)	3.3 ± 0.5	3.4 ± 0.5	0.49	2.11	0.79–5.66	0.14
Mean pressure gradient (mmHg)	27 ± 8	26 ± 7	0.45	1.05	0.99–1.12	0.11
Index aortic valve area (cm^2/m^2)	0.43 ± 0.10	0.46 ± 0.08	0.16	0.01	0–1.37	0.066
Zva ($mmHg/mL/m^2$)	4.98 ± 1.07	5.08 ± 1.17	0.71	0.94	0.62–1.41	0.76
Global longitudinal strain (%)	14.1 ± 2.5	15.8 ± 2.4	0.003	0.69	0.56–0.84	<0.001
Global circumferential strain (%)	30.6 ± 3.6	30.4 ± 4.2	0.86	1.00	0.90–1.11	0.98
Global radial strain (%)	36.2 ± 4.5	37.9 ± 4.5	0.096	0.91	0.82–1.00	0.052
Hb (g/dL)	10.7 ± 1.6	12.3 ± 1.8	<0.001	0.65	0.51–0.82	<0.001
Creatinine (mg/dL)	1.15 (0.83–1.88)	0.8 (0.62–1.03)	0.002	1.18	0.99–1.41	0.056
eGFR ($ml/min/1.73\ m^2$)	41 ± 21	60 ± 23	<0.001	0.97	0.95–0.99	<0.001
hsCRP (mg/dL)	0.68 (0.37–2.36)	0.1 (0.03–0.35)	<0.001	1.23	1.09–1.40	0.001
Log BNP (μg/mL)	5.4 (4.2–6.2)	4.0 (3.8–5.1)	0.008	2.53	1.65–3.88	<0.001

95% CI, 95% (confidence interval; BMI, body mass index; BSA, body surface area; CE, cardiac event; COPD, chronic obstructive pulmonary disease; CVA, cerebrovascular accident; eGFR, estimated glomerular filtration rate; e′, early diastolic mitral annular velocity; Hb, hemoglobin; HR, hazard ratio; hsCRP, high sensitivity C-reactive protein; Log BNP, log-transformed brain natriuretic peptide; LAVI, left atrial volume index; LV, left ventricular; LVEDVI, left ventricular end-diastolic volume index; LVEF, left ventricular ejection fraction; LVSVI, left ventricular stroke volume index; NYHA, New York Heart Association; PAP, pulmonary arterial pressure; Zva, valvulo-arterial impedance.
[a] NYHA I vs. II.
[b] NYHA I vs. III.
[c] NYHA I vs. IV.

Table 4
Bivariable models for predicting cardiac events.

Model	Variables	Incremental value		
		χ^2	Comparison model	p
1	LV mass index	4.2	–	
2	LV mass index + NYHA class	66.2	1	<0.001
3	E	14.8	–	
4	E + NYHA class	63.8	3	0.019
5	E/e′	6.5	–	
6	E/e′ + NYHA class	63.8	5	0.002
7	LAVA	3.4	–	
8	LAVA + NYHA class	63.7	7	<0.001
9	GLS	13.3	–	
10	GLS + NYHA class	75.3	9	<0.001

E, E wave velocity; LAVA, indexed aortic valve area; GLS, global longitudinal strain; LV, left ventricular; NYHA, New York Heart Association.

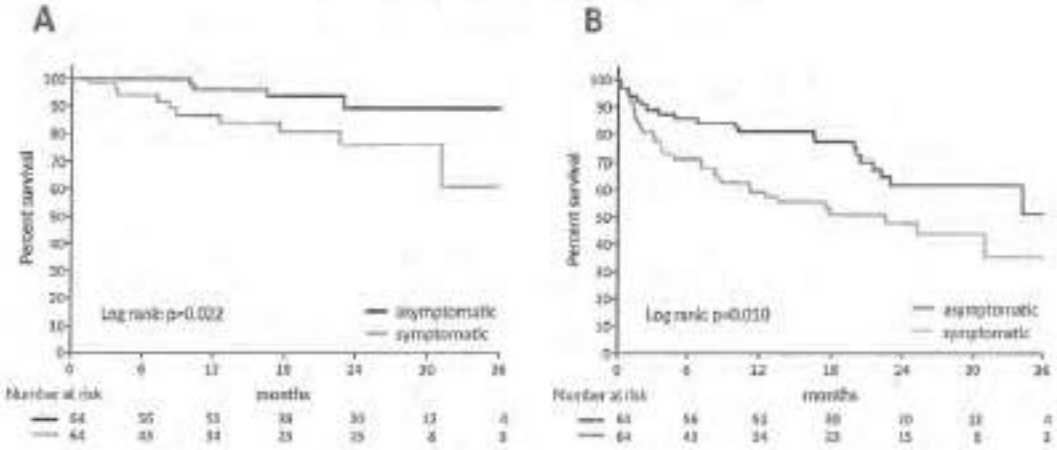

Fig. 2. Kaplan–Meier analysis for cardiac events (A) and a composite of cardiac events and SAVR/TAVR (B) between propensity score matched asymptomatic patients with PLG-SAS (n = 64) and symptomatic patients with PLG-SAS (n = 64). PLG-SAS, paradoxical low gradient severe aortic stenosis; SAVR, surgical aortic valve replacement; TAVR, transcatheter aortic valve replacement.

6% vs. 16 ± 3% at 1 year; 36 ± 6% vs. 24 ± 4% at 2 years; $p = 0.013$). Baseline echocardiography revealed that peak velocity (3.7 ± 0.3 m/s vs. 3.3 ± 0.5 m/s, $p < 0.001$) and mean PG (32 ± 5 mmHg vs. 24 ± 7 mmHg, $p < 0.001$) were significantly higher in patients who underwent AVR than in those without AVR. Kaplan–Meier analysis revealed that patients with symptomatic PLG-SAS had significantly lower event-free rate than patients with asymptomatic PLG-SAS (Fig. 1B). The same trend was also observed in the propensity-score-matched cohort (Fig. 2B).

We performed subgroup analysis of prognosis in the patients with low flow PLG-SAS ($n = 123$) and normal flow PLG-SAS ($n = 99$). Prevalence of symptoms was not different between the two groups (32% vs. 26%, $p = 0.374$). Cardiac event rate was similar between the two groups (11% vs. 10%, $p = 0.909$). However, secondary end-point rate was significantly lower in patients with low flow PLG-SAS (28%) than in patients with normal flow PLG-SAS (42%, $p = 0.021$). Thus, presence of symptoms was significantly associated with the future outcome, except for the occurrence of cardiac events, in patients with low-flow PLG-SAS (Online Fig. 2).

Among 23 patients with symptomatic PLG-SAS who underwent AVR, the median time-interval between the index echocardiography and the surgical treatment was 3.1 months. Seventeen patients (74%) underwent another echocardiographic examination before the surgery. Mean PG significantly increased from 32 ± 5 mmHg at baseline echocardiography to 42 ± 10 mmHg at echocardiography before the AVR, and 53% of patients (9/17) showed the conversion in their PG status from LPG to HPG (Fig. 3A).

Of 36 patients with asymptomatic PLG-SAS who underwent AVR, the median time-period from the index echocardiography to the surgery was 5.4 months. Reasons for opting for AVR were symptom-onset in 13 patients, attending physician's recommendation or patients' willingness in 12 patients, rapid disease progression in 5 patients, as concomitant cardiac surgery in 5 patients, and reduced LVEF in 1 patient. Twenty-nine patients (81%) underwent another echocardiographic examination before the surgery. Mean PG significantly increased from 32 ± 5 mmHg at baseline to 43 ± 7 mmHg at echocardiography before the AVR ($p < 0.001$), and 76% of patients (22/29) converted from LPG to HPG (Fig. 3B).

In patients who underwent AVR, there were 3 postoperative cardiac events, including 1 case of cardiac death early after the surgery, and 2 cases of heart failure late after the surgery. Online Fig. 3A shows cardiac-event-free rate between patients with symptomatic PLG-SAS who underwent AVR and those who were

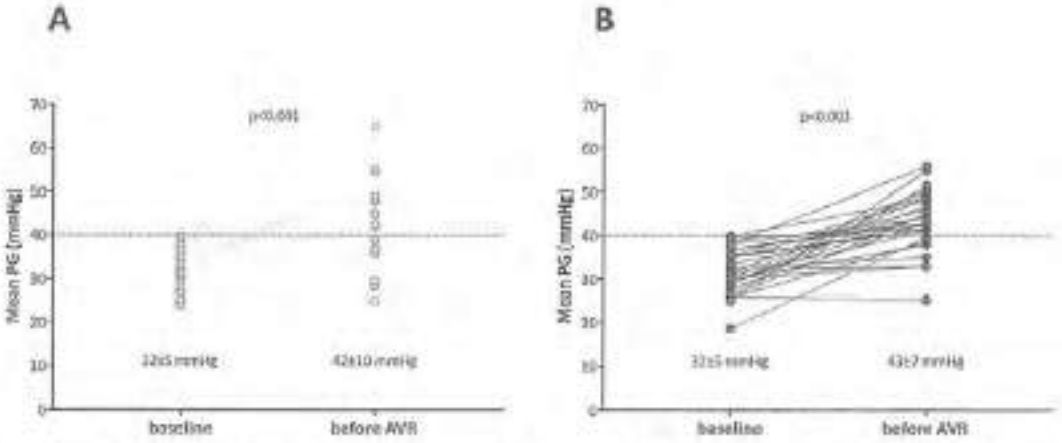

Fig. 3. Serial change in mean PG from baseline to before aortic valve replacement in symptomatic PLG-SAS (A) and asymptomatic PLG-SAS (B). AVR, aortic valve replacement; PG, pressure gradient.

managed conservatively. Event rates were higher in symptomatic patients who received conservative treatment than in those who underwent AVR but the difference did not reach statistical significance ($p = 0.087$). No significant differences were noted in the event rate between asymptomatic patients who received conservative treatment and those who underwent AVR (Online Fig. 3B).

Reliability of 3DE measurements

The intra-observer variability and ICC for the measurements of 3DE SV and LVEF were 5.9 ± 7.6% and 4.0 ± 3.1% and 0.94 and 0.91, respectively. The corresponding inter-observer variability and ICC values were 7.1 ± 9.4% and 6.7 ± 5.7%, 0.87 and 0.80, respectively.

Discussion

The main findings of this study are summarized as follows: (1) approximately 30% of patients with PLG-SAS were symptomatic; (2) symptomatic patients had a higher prevalence of the usage of beta-blockers, angiotensin blockers, and diuretics, and higher levels of BNP as compared to asymptomatic patients; (3) some diastolic function parameters showed more advanced stage of diastolic dysfunction in symptomatic patients; (4) prognosis was significantly worse in patients with symptomatic PLG-SAS than in patients with asymptomatic PLG-SAS, even after adjusting anthropometric factors, flow status, and the severity of AS; (5) PG increased significantly from that noted during the index echocardiographic examination to that noted during the echocardiography before the AVR.

Symptom and clinical characteristics of patients with LPG-SAS

Although history taking of AS-related symptoms is the initial step for proper management of patients with SAS, appropriate symptom evaluation is often difficult, because the existing comorbidities can limit physical activity in the elderly patients making them asymptomatic [21]. Even though patients are symptomatic, we are not sure whether the symptom is solely related to SAS itself. This is particularly important for the situations for which definite treatment guideline is not established, such as symptomatic PLG-SAS. Since results of previous studies revealed a higher prevalence of symptomatic PLG-SAS patients to be associated with worse prognosis [1,2,5–9], it is relevant to divide patients with PLG-SAS according to the symptoms in order to determine its functional properties and prognosis.

Symptomatic PLG-SAS was observed in 30% of patients in this study. Its prevalence was lower than that in some studies [1,2,6,7], but similar to that in other studies [5,8,9]. Patients with symptomatic PLG-SAS received beta-blockers, angiotensin blockers, and diuretics more frequently, and presented with higher BNP levels, all of which represent a possible association between PLG-SAS and HFpEF [15]. Although LV volumes and mass, and severity of AS were similar between both groups, E-wave velocity and E/A ratio were significantly higher in patients with symptomatic PLG-SAS, reflecting that patients with symptomatic PLS-SAS had a more advanced stage of diastolic dysfunction.

Symptom and prognosis in patients with PLG-SAS

Patients with symptomatic PLG-SAS had significantly worse prognosis than patients with asymptomatic PLG-SAS, which was in agreement with the previous studies [5,9]. In addition to the symptomatic status, several echocardiographic parameters remained as significant prognosticators in univariable analysis. A reclassification analysis revealed that NYHA class significantly improved reclassification over each echocardiographic parameter except E/e' (Online Table 1). We also found that NYHA class had a significant incremental value for future outcomes over several echocardiographic parameters using progressive model (Table 4). These results reinforced the close association between symptomatic status and prognosis in PLS-SAS. Echocardiographic parameters showing significant predictors in this study are also known as important predictors in patients with HFpEF. Even after propensity score matching, symptomatic PLG-SAS was still associated with a significantly worse outcome than asymptomatic PLG-SAS. These results suggest that the presence of symptoms is not closely associated with the severity of AS itself but can be related with the underlying comorbidities [15,22]. Some blood examination parameters, which had also been verified as significant predictors of SAS [4,23–26], were selected as significant univariable predictors of future cardiac events. All these blood examination parameters can be abnormal even in patients with HFpEF, since a high prevalence of comorbidities such as hypertension, diabetes, anemia, and chronic kidney disease can induce a systemic inflammatory state, resulting in myocardial hypertrophy and fibrosis. Both may contribute to high diastolic LV stiffness, resulting in elevated levels of BNP [27].

AVR in PLG-SAS

The finding that the AVR rate in patients with symptomatic PLG-SAS was 31% in the 1st year, and 36% in the 2nd year reflects that many attending physicians involved in this study may treat symptomatic patients with PLG-SAS as having symptomatic but moderate AS. Although AVR tended to be beneficial over conservative management for preventing cardiac events in patients with symptomatic PLG-SAS, no benefit was observed in patients with asymptomatic PLG-SAS. The prognostic impact of AVR in PLG-SAS is the subject of an ongoing debate. Our results underscored that PG status frequently changed at the time of AVR. PG across the aortic valve changes according to the progressive nature of AS [28] and LV function. In agreement with previous studies, our results demonstrate that PG increased according to the elapsed time, resulting in the conversion of the PG status from low gradient to high gradient in most patients with PLG-SAS [3,5]. This is another reason for the discrepant results of the impact of AVR on prognosis in patients with PLG-SAS.

Clinical implications

The presence of symptoms is important to stratify the high-risk patients with future adverse outcome in PLG-SAS. Asymptomatic patients with PLG-SAS can be managed medically with regular clinical and echocardiographic follow up, until symptoms develop, or pressure status converts to HPG-SAS. Symptomatic PLG-SAS has been a clinical dilemma, because it is often difficult to verify whether symptoms are related to AS itself or the existing comorbidities. In addition to risk-factor modification and searching for other potential pathology [22], AVR should be individualized after taking into consideration a number of abnormal findings that are closely related to poor prognosis, operative risk, cost, and expertise of the surgery.

Study limitations

Several limitations should be addressed in this study. First, AVR was performed at the discretion of the attending physician and as per the patient's approval, which might recall some bias. However, our results reflect the real world situation regarding how to manage patients with PLG-SAS. Second, not all patients with AVR underwent another echocardiographic examination before the

AVR. This might have affected the conversion rate from LPG to HPG. Third, PLG-SAS includes both normal-flow and low-flow patient populations. Although prognostic outcome in normal flow PLG-SAS has been reported to be better than that in other types of SAS [29], recent studies revealed that half of these patients manifest SAS; therefore, they may benefit from AVR when symptoms are presented [30,31]. Our results showed that cardiac event rate was similar between the two groups, and cardiac event plus AVR rate was higher in normal-flow PLG-SAS group. Finally, the number of cardiac events was small, and, thus, it precluded to perform extensive multivariable analysis. However, due to the progressive nature of the disease, AS-phenotype and LV geometry may change during longer follow-up period, and this change may affect the prognosis.

Conclusions

Since symptomatic PLG-SAS is associated with poorer prognosis even after adjusting for flow status and severity of AS, symptoms are not always caused by the severity of AS itself but might be associated with the underlying comorbidities. These results suggest a possible link between PLG-SAS and HFpEF in some patients.

Conflicts of interest

All authors have nothing to disclose.

Acknowledgments

We acknowledge Drs Kyoko Otani, Dan Koto, and Tomofumi Nakatsukasa for preparing data.

Appendix A. Supplementary data

Supplementary data associated with this article can be found, in the online version, at doi:10.1016/j.jjcc.2018.12.017.

References

[1] Clavel M-A, Dumesnil JG, Capoulade R, Mathieu P, Sénéchal M, Pibarot P. Outcome of patients with aortic stenosis, small valve area, and low-flow, low-gradient despite preserved left ventricular ejection fraction. J Am Coll Cardiol 2012;60:1259–67.
[2] Eleid MF, Sorajja P, Jander N, Malouf JF, Scott CG, Pellikka PA. Flow-gradient patterns in severe aortic stenosis with preserved ejection fraction: clinical characteristics and predictors of survival. Circulation 2013;128:1781–9.
[3] Jander N, Minners J, Holme I, Gerdts E, Boman K, Brudi P, et al. Outcome of patients with low-gradient "severe" aortic stenosis and preserved ejection fraction. Circulation 2011;123:887–95.
[4] Tancredi R, Magne J, Donal E, Davin L, O'Connor K, Rosca M, et al. Clinical outcome in asymptomatic severe aortic stenosis. J Am Coll Cardiol 2012;59:235–43.
[5] Maes F, Boulif J, Pierard S, de Meester C, Melchior J, Garbar B, et al. Natural history of paradoxical low-gradient severe aortic stenosis. Circ Cardiovasc Imaging 2014;7:714–22.
[6] Mehrotra P, Jansen K, Flynn AW, Tan TC, Elmariah S, Picard MH, et al. Differential left ventricular remodelling and longitudinal function distinguishes low flow from normal-flow preserved ejection fraction low gradient severe aortic stenosis. Eur Heart J 2013;34:1906–14.
[7] Orkin A, Hachamovitch R, Kapadia SR, Tuzcu EM, Marwick TH. Impact of aortic valve replacement on outcome of symptomatic patients with severe aortic stenosis with low gradient and preserved left ventricular ejection fraction. Circulation 2013;128:022–31.
[8] Tribouilloy C, Rusinaru D, Mahéchard S, Castel A-L, Debry N, Mainet J, et al. Low-gradient, low-flow severe aortic stenosis with preserved left ventricular ejection fraction: characteristics, outcome, and implications for surgery. J Am Coll Cardiol 2015;65:55–66.
[9] Yamashita E, Takeuchi M, Seo Y, Izumo M, Ishizu T, Sato K, et al. Prognostic value of paradoxical low-gradient severe aortic stenosis in Japan: Japanese Multicenter Aortic Stenosis Study Retrospective (JUST-R) Registry. J Cardiol 2015;65:360–8.
[10] Joint Task Force on the Management of Valvular Heart Disease of the European Society of Cardiology (ESC), European Association for Cardio-Thoracic surgery (EACTS), Vahanian A, Alfieri O, Andreotti F, Antunes MJ, et al. Guidelines on the management of valvular heart disease (version 2012). Eur Heart J 2012;33:2451–96.
[11] Clavel MA, Ennezat PV, Marechaux S, Dumesnil JG, Capoulade R, Hachicha Z, et al. Stress echocardiography to assess stenosis severity and predict outcome in patients with paradoxical low-flow, low-gradient aortic stenosis and preserved LVEF. J Am Coll Cardiol Imaging 2013;6:175–83.
[12] Nagata Y, Takeuchi M, Wu VC-C, Izumo M, Suzuki K, Sato K, et al. Prognostic value of LV deformation parameters using 2D and 3D speckle-tracking echocardiography in asymptomatic patients with severe aortic stenosis and preserved LV ejection fraction. J Am Coll Cardiol Imaging 2015;8:235–45.
[13] Sato K, Seo Y, Ishizu T, Takeuchi M, Izumo M. Prognostic value of global longitudinal strain in paradoxical low-flow, low-gradient severe aortic stenosis with preserved ejection fraction. Circ J 2014;78:2750–9.
[14] Arber S, Chan W, Beckhart B, Aguilar D, Ramasubbu K, Zachariah AA, et al. Impact of noncardiac comorbidities on morbidity and mortality in a predominantly male population with heart failure and preserved versus reduced ejection fraction. J Am Coll Cardiol 2012;59:998–1005.
[15] Chin CWL, Ding ZP, Lam CSP, Ling LH. Paradoxical low-gradient aortic stenosis: the HFpEF of aortic stenosis. J Am Coll Cardiol 2016;67:2447–8.
[16] Dayan V, Vignolo G, Magne J, Clavel M-A, Mohty D, Pibarot P. Outcome and impact of aortic valve replacement in patients with preserved LVEF and low-gradient aortic stenosis. J Am Coll Cardiol 2015;66:2594–603.
[17] Lang RM, Badano LP, Mor-Avi V, Afilalo J, Armstrong A, Ernande L, et al. Recommendations for cardiac chamber quantification by echocardiography in adults: an update from the American Society of Echocardiography and the European Association of Cardiovascular Imaging. J Am Soc Echocardiogr 2015;28:1–39.
[18] Rudski LG, Lai WW, Afilalo J, Hua L, Handschumacher MD, Chandrasekaran K, et al. Guidelines for the echocardiographic assessment of the right heart in adults: a report from the American Society of Echocardiography. J Am Soc Echocardiogr 2010;23:685–713.
[19] Jewell ES, Maile MD, Engoren M, Ellison M. Net reclassification improvement. Anesth Analg 2016;122:818–24.
[20] Pencina MJ, D'Agostino Sr RB, D'Agostino Jr RB, Vasan RS. Evaluating the added predictive ability of a new marker: from area under the ROC curve to reclassification and beyond. Stat Med 2007;27:157–72.
[21] Izumo M, Takeuchi M, Seo Y, Yamashita E, Suzuki K, Ishizu T, et al. Prognostic implications in patients with symptomatic aortic stenosis and preserved ejection fraction: Japanese multicenter aortic stenosis, retrospective (JUST-R) registry. J Cardiol 2017;69:110–8.
[22] Sperry BW, Jones BM, Vranian MN, Hanna M, Jaber WA. Recognizing transthyretin cardiac amyloidosis in patients with aortic stenosis: impact on prognosis. J Am Coll Cardiol Imaging 2016;9:904–6.
[23] Bruch C, Kaulbg D, Reinecke H, Rothenberger M, Schmid MM, Breithardt G, et al. Prevalence and prognostic impact of comorbidities in patients with severe aortic valve stenosis. Clin Res Cardiol 2006;96:23–8.
[24] Casado J, Montero M, Formiga F, Carrera M, Urrutia A, Arévalo JC, et al. Clinical characteristics and prognostic influence of renal dysfunction in heart failure patients with preserved ejection fraction. Eur J Intern Med 2013;24:677–83.
[25] Gómez M, Ríz M, Cladellas M, Molina L, Comín-Colet J, Enjuanes C, et al. Effect of correction of anemia on echocardiographic and clinical parameters in patients with aortic stenosis involving a tricuspid aortic valve and normal left ventricular ejection fraction. Am J Cardiol 2015;116:270–4.
[26] Imai K, Okura H, Kume T, Yamada R, Miyamoto Y, Kawamoto T, et al. C-reactive protein predicts severity, progression, and prognosis of asymptomatic aortic valve stenosis. Am Heart J 2008;156:713–8.
[27] Paulus WJ, Tschope C. A novel paradigm for heart failure with preserved ejection fraction. J Am Coll Cardiol 2013;62:263–71.
[28] Akahori H, Tsujino T, Masuyama T, Ishihara M. Mechanisms of aortic stenosis. J Cardiol 2018;71:215–20.
[29] Ravishi C, Balasundaram K, Argulian E. Integration of flow-gradient patterns into clinical decision making for patients with suspected severe aortic stenosis and preserved LVEF: a systematic review of evidence and meta-analysis. JACC Cardiovasc Imaging 2016;9:1255–63.
[30] Clavel M-A, Messika-Zeitoun D, Pibarot P, Aggarwal SR, Malouf J, Araoz PA, et al. The complex nature of discordant severe calcified aortic valve disease grading: new insights from combined Doppler echocardiographic and computed tomographic study. J Am Coll Cardiol 2013;62:2329–38.
[31] Dulgheru R, Pibarot P, Sengupta PP, Rosenhek R, Magne J, Donal E, et al. Multimodality imaging strategies for the assessment of aortic stenosis. Circ Cardiovasc Imaging 2016;9:e004352.

JACC: CARDIOVASCULAR INTERVENTIONS
Vol. 12, No. 14, 2019
© 2019 THE AUTHORS. PUBLISHED BY ELSEVIER ON BEHALF OF THE AMERICAN COLLEGE OF CARDIOLOGY FOUNDATION. THIS IS AN OPEN ACCESS ARTICLE UNDER THE CC BY LICENSE (http://creativecommons.org/licenses/by/4.0/).

Algorithmic Versus Expert Human Interpretation of Instantaneous Wave-Free Ratio Coronary Pressure-Wire Pull Back Data

Christopher M. Cook, MBBS, BSc,[a,b] Takayuki Warisawa, MD,[a,b,c] James P. Howard, MB BCh,[a] Thomas R. Keeble, MRBS, MD,[c,d] Juan F. Iglesias, MD,[e] Erick Schampaert, MD,[f] Ravinay Bhindi, MBBS, PhD,[g] Alphonse Ambrosia, DO,[h] Hitoshi Matsuo, MD, PhD,[i] Hidetaka Nishina, MD, PhD,[j] Yuetsu Kikuta, MD,[i] Yasutsugu Shiono, MD, PhD,[i] Masafumi Nakayama, MD,[m] Shunichi Doi, MD,[k] Manabu Takai, MD, PhD,[n] Sonoka Goto, MD,[o,p] Yohei Yamada, MD,[p] Kenichi Karube, MD,[q] Yoshihiro J. Akashi, MD, PhD,[r] Gerald J. Clesham, MB BCh,[c,d] Paul A. Kelly, MB ChB, MD,[c] John R. Davies, MBBS, PhD,[c,d] Grigoris V. Karamasis, MD,[c,d] Yoshiaki Kawase, MD,[i] Nicholas M. Robinson, MD,[c] Andrew S.P. Sharp, MD,[i] Javier Escaned, MD, PhD,[e] Justin E. Davies, MD, PhD[a]

ABSTRACT

OBJECTIVES The aim of this study was to investigate whether algorithmic interpretation (AI) of instantaneous wave-free ratio (iFR) pressure-wire pull back data would be noninferior to expert human interpretation.

BACKGROUND Interpretation of iFR pressure-wire pull back data can be complex and is subjective.

METHODS Fifteen human experts interpreted 1,008 iFR pull back traces (691 unique, 317 duplicate). For each trace, experts determined the hemodynamic appropriateness for percutaneous coronary intervention (PCI) and, in such cases, the optimal physiological strategy for PCI. The heart team (HT) interpretation was determined by consensus of the individual expert opinions. The same 1,008 pull back traces were also interpreted algorithmically. The coprimary hypotheses of this study were that AI would be noninferior to the interpretation of the median expert human in determining: 1) the hemodynamic appropriateness for PCI; and 2) the physiological strategy for PCI.

RESULTS Regarding the hemodynamic appropriateness for PCI, the median expert human demonstrated 89.3% agreement with the HT in comparison with 89.4% for AI ($p < 0.01$ for noninferiority). Across the 372 cases judged as hemodynamically appropriate for PCI according to the HT, the median expert human demonstrated 88.8% agreement with the HT in comparison with 89.7% for AI ($p < 0.0001$ for noninferiority). On reproducibility testing, the HT opinion itself changed 1 in 10 times for both the appropriateness for PCI and the physiological PCI strategy. In contrast, AI showed no change.

CONCLUSIONS AI of iFR pressure-wire pull back data was noninferior to expert human interpretation in determining both the hemodynamic appropriateness for PCI and the optimal physiological strategy for PCI.
(J Am Coll Cardiol Intv 2019;12:1315–24) © 2019 The Authors. Published by Elsevier on behalf of the American College of Cardiology Foundation. This is an open access article under the CC BY license (http://creativecommons.org/licenses/by/4.0/).

From the [a]Hammersmith Hospital, Imperial College NHS Trust, London, United Kingdom; [b]St. Marianna University School of Medicine, Kawasaki, Japan; [c]Essex Cardiothoracic Centre, Basildon, United Kingdom; [d]Anglia Ruskin School of Medicine, Chelmsford, Essex, United Kingdom; [e]Geneva University Hospital, Geneva, Switzerland; [f]Hôpital Saint-Cœur de Montréal, Université de Montréal, Montréal, Canada; [g]Royal North Shore, Sydney, Australia; [h]Banner Heart Hospital, Mesa, Arizona; [i]Gifu Heart Center, Gifu, Japan; [j]Tsukuba Medical Center Hospital, Tsukuba, Japan; [k]Fukuyama Cardiovascular Hospital, Fukuyama, Japan; [l]Wakayama Medical University, Wakayama, Japan; [m]Toda Central General Hospital, Toda, Japan; [n]St. Marianna University school of Medicine Yokohama City Seiko Hospital, Yokohama, Japan; [o]Hospital Clínico San Carlos, Madrid, Spain; [p]Kanazawa Cardiovascular Hospital, Kanazawa, Japan; [q]Okaya City Hospital, Okaya, Japan; and the [r]Royal Devon and Exeter Hospital, Exeter, United Kingdom. *Drs. Cook and Warisawa contributed equally to this work. This work was supported by the Imperial College Healthcare NHS Trust Biomedical Research Centre. Dr. Davies holds patents pertaining to the iFR technology; is a consultant for Philips Volcano; and has received research grants from Philips Volcano. Dr. Cook has received speaking honoraria from Philips

ISSN 1936-8798
https://doi.org/10.1016/j.jcin.2019.05.005

JACC: CARDIOVASCULAR INTERVENTIONS VOL. 12, NO. 14, 2019
JULY 22, 2019:1315–24

ABBREVIATIONS AND ACRONYMS

AI = algorithmic interpretation

HT = heart team

iFR = instantaneous wave-free ratio

IQR = interquartile range

PCI = percutaneous coronary intervention

Revascularization in stable coronary artery disease should be performed only for ischemia-producing coronary lesions (1-4). Physiological measurements obtained using a coronary pressure-wire permit the identification of myocardial ischemia on a per vessel basis (5). Consequently, coronary physiology is recommended in international treatment guidelines (6-8) to guide revascularization decision making.

In addition to vessel-level ischemia detection, under resting conditions, a coronary pressure wire can also be used to produce an instantaneous wave-free ratio (iFR) pressure-wire pull back trace: a longitudinal assessment of coronary pressure loss along the length of a coronary artery. Such a trace permits the identification of lesion-level ischemia, as well as the ability to predict the physiological outcome following a proposed percutaneous coronary intervention (PCI) revascularization strategy (9). However, in the absence of clinical outcome data, a definitive interpretation of iFR coronary pressure-wire pull back data is lacking. Individual interpretation of coronary pressure-wire pull back data is complex, subjective, and dependent on the physiological expertise of the operator.

Algorithmic interpretation (AI) of coronary pressure-wire pull back data may help circumvent these limitations. Within this study, we aimed to determine if AI of iFR coronary pressure-wire pull back data could provide a standardized alternative to expert-level human interpretation. The coprimary hypotheses of this study were that AI would be noninferior to the interpretation of the median expert human in determining: 1) the hemodynamic appropriateness for PCI; and 2) the physiological PCI strategy, compared with the expert heart team (HT) opinion.

SEE PAGE 1325

METHODS

STUDY POPULATION. Six cardiac centers (St. Marianna University School of Medicine Yokohama City Seibu Hospital, Toda Central General Hospital, Okaya City Hospital, Kanazawa Cardiovascular Hospital, Hospital Clínico San Carlos, and Hammersmith Hospital) contributed retrospectively acquired iFR coronary pressure-wire pull back traces to a stable coronary artery disease all-comers clinical registry. No angiographic, clinical circumstances, or inclusion or exclusion criteria were used in the selection process. All cases were acquired by operators using manual pull back. Each pull back tracing was anonymized to prevent the identification of patient-specific data. Because no exclusion criteria were applied, traces were included regardless of whether there was evidence of pressure-wire drift or measurement artifact. The investigator core laboratory determined the technical quality of each pull back tracing. Measurement artifact was determined by the presence of artifact in either the iFR pull back curve or electrocardiographic trace. The expert graders were blinded to the core laboratory's classification of technical quality. This study received ethical approval from the local ethics committee at each participating center.

EXPERT HUMAN INTERPRETATION. The study design is displayed in Figure 1. Fifteen interventional cardiologists with significant experience in the acquisition and interpretation of coronary physiology data evaluated 1,008 coronary pressure-wire pull back traces. Of these 1,008 coronary pressure-wire pull back traces, 691 were unique traces. The remaining 317 traces (31.4%) were duplicates, presented as new to each expert, to allow the assessment of intraobserver variability.

Using a dedicated online web portal system (Thalamus AI, Birmingham, United Kingdom), experts interpreted each trace independently, in a randomized order, without access to the coronary angiogram or additional clinical information. For each trace, experts were asked to determine the hemodynamic appropriateness for PCI. No specific criteria were provided to the experts to guide their decisions of hemodynamic appropriateness for PCI. In cases deemed hemodynamically appropriate for PCI, experts were further asked to determine their physiological strategy for PCI. This involved annotation on the pressure-wire pull back trace of the location(s) of physiologically significant lesion(s) the operator believed should be revascularized by PCI (Online Figure 1). This 2-step approach was used to replicate

Volcano. Dr. Warisawa has received consulting fees from Philips Volcano. Dr. Howard has received a grant (203183/Z/16/Z) from Wellcome Trust. Dr. Shiono has received speaking and manuscript honoraria from Philips Volcano. Dr. Schampaert has received speaking honoraria from Philips Volcano. All other authors have reported that they have no relationships relevant to the contents of this paper to disclose.

Manuscript received April 8, 2019; revised manuscript received May 15, 2019, accepted May 21, 2019.

the cognitive steps involved in iFR-guided, ischemia-driven revascularization decision making. Specifically, the first step encapsulated the decision of whether revascularization should be performed on the basis of the iFR value, and in such cases, the second step encapsulated the decision of what the interventional strategy should be to obtain an optimal physiological outcome.

DETERMINING THE HT INTERPRETATION. In the absence of clinical outcome data to provide a definitive interpretation of coronary pressure-wire pull back data, consensus expert opinion was used to determine the HT interpretation. Following grading, the annotated pressure-wire pull back traces were exported from the web portal and analyzed. For each of the 1,008 pull back cases, the HT PCI strategy was created by annotating only portions of the coronary pressure-wire pull back trace in areas in which the majority of the human experts (8 of 15) had indicated those areas for PCI (Figure 2).

AI. The same 1,008 coronary pressure-wire pull back traces were then analyzed by a computer using computer algorithms to identify lesions on the pull back trace suitable for PCI. This AI considered information including the distal iFR value, the presence of physiologically significant pressure-wire drift, a Savitzky-Golay-filtered derivative (10) of the pull back trace, and the change in iFR value over any identified discrete lesions. Additional details regarding the development of the algorithm are provided in Online Appendix 1. The output from the algorithm was then compared with that of the HT interpretation and those of the individual experts. The algorithm was able to process 1.33 iFR pull-back traces per second.

STUDY HYPOTHESES. AI, individual expert human interpretation, and median expert human interpretation (i.e., the single human grader in the middle of the distribution of grader accuracies) were assessed against the HT interpretation. The coprimary hypotheses were: 1) noninferiority of algorithmic versus the median expert human interpretation for determining the hemodynamic appropriateness for PCI (the noninferiority margin was 5%); and 2) noninferiority of algorithmic versus the median expert human interpretation for determining the PCI strategy, compared with the expert HT opinion (the noninferiority margin was 5%).

STATISTICAL ANALYSIS. Categorical variables are expressed as numbers and percentages. Continuous variables are expressed as mean ± SD or median (interquartile range [IQR]), as appropriate. For the revascularization decision-making endpoint, the

FIGURE 1 Study Design

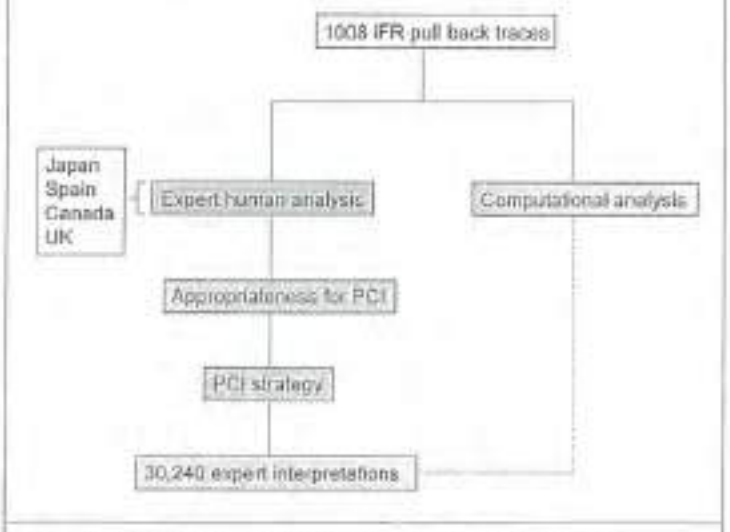

iFR = instantaneous wave-free ratio; PCI = percutaneous coronary intervention.

McNemar exact test was used with noninferiority analysis obtained through balanced reclassification of cases. For the PCI strategy endpoint, the accuracy (percentage of the pull back classified in agreement with the HT as PCI or non-PCI) for each case for both the computer algorithm and median expert human were compared. Additional details regarding the statistical analysis, noninferiority margin rationale, and sample size calculations are provided in Online Appendix 2. All analyses were performed using R version 3.2.1 (R Foundation for Statistical Computing, Vienna, Austria).

RESULTS

STUDY POPULATION. The baseline demographic characteristics of the patients are shown in Table 1. The mean age of the patients was 65.4 years, and 74% were men. The physiological characteristics of the vessels are shown in Table 2. The median iFR value was 0.87 (IQR: 0.81 to 0.91). The distribution of iFR values is shown in Online Figure 3.

Prior to correcting for pressure-wire drift, across the 691 unique pressure-wire pull back traces, 470 traces (68.0%) demonstrated distal iFRs ≤0.89, with 221 traces (32.0%) demonstrating distal iFRs >0.89. AI detected physiologically significant pressure-wire drift in 217 traces (31.4%), 70 (32.3%) with positive drift with proximal iFRs >1.02 and 147 (67.7%) with negative drift with proximal iFRs <0.98. After correcting for pressure-wire drift, 64 cases (9.3%) changed

JACC: CARDIOVASCULAR INTERVENTIONS VOL. 12, NO. 14, 2019
JULY 22, 2019:1315–24

FIGURE 2 Determining the Consensus Opinion

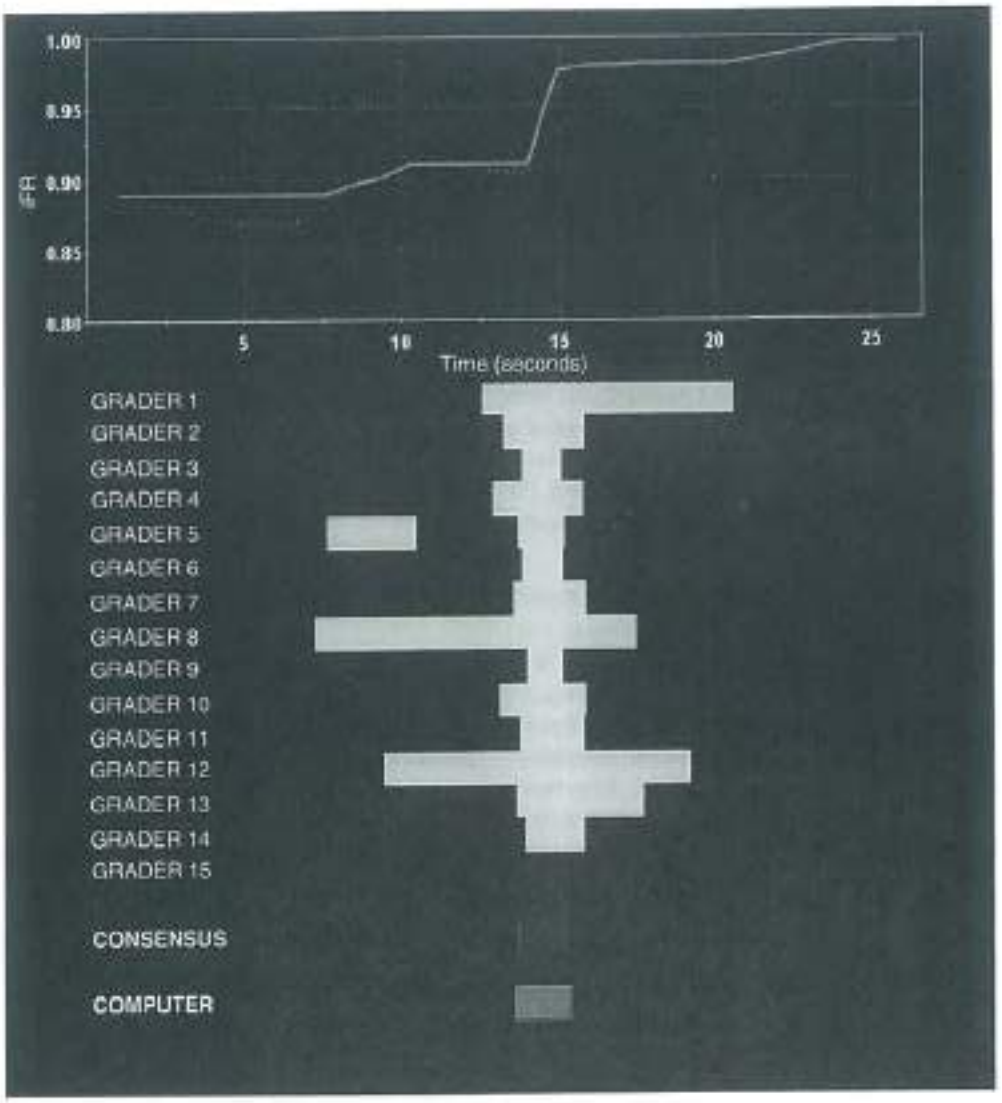

Shown is the coronary pressure-wire pull back trace (**blue line, top**), the segment(s) of the pull back trace annotated for percutaneous coronary intervention (PCI) by the individual expert humans (**yellow blocks**, 1 row for each expert, **bottom**), the consensus expert human interpretation (**green block, bottom**), and the algorithmic interpretation (**orange block, bottom**). The PCI strategy consensus expert interpretation was created from segment(s) of the pull back trace that at least 50% of the individual expert humans had annotated for PCI. iFR = instantaneous wave-free ratio.

hemodynamic classification, with 45 cases (6.5%) becoming hemodynamically nonsignificant and 19 cases (2.7%) becoming hemodynamically significant.

HEMODYNAMIC APPROPRIATENESS FOR PCI. Across all 691 unique cases, the median expert human agreed with the HT in 617 of 691 cases (89.3%; Cohen's kappa = 0.78). AI agreed with the HT in 618 of 691 cases (89.4%; Cohen's kappa = 0.79) and was noninferior to the median expert human ($p = 0.0073$; Cohen's kappa = 0.70) (Figure 3A).

Across the 372 cases that the HT determined were hemodynamically appropriate for PCI, 14 cases (3.8%) had hemodynamically nonsignificant physiology due to physiologically significant pressure-wire drift not corrected for by the consensus (Figure 4A). In

TABLE 1 Baseline Characteristics of the Patients (n = 640)

Age, yrs	65.4 ± 10.8
Male	473 (73.9)
Hypertension	442 (69.1)
Dyslipidemia	387 (60.5)
Diabetes mellitus	236 (36.9)
Chronic kidney disease	98 (15.3)
Current or ex-smoker	253 (39.5)
Family history of CAD	98 (15.3)
Previous myocardial infarction	148 (23.1)
Impaired LV function (EF <30%)	33 (5.2)

Values are mean ± SD or n (%).
CAD = coronary artery disease; EF = ejection fraction; LV = left ventricular.

contrast, using AI, there were no cases in which PCI was determined appropriate for hemodynamically nonsignificant physiology, as pressure-wire drift was always identified by the computer.

There were 319 cases that were determined as not hemodynamically appropriate for PCI according to the HT. Of these, 86 cases (27.0%) had hemodynamically significant physiology (Figure 4B) that was not identified by the HT. In contrast, there were 296 cases that were determined as not appropriate for PCI according to AI. Of these, 49 cases (16.6%) had hemodynamically significant but diffuse nonfocal physiology (Figure 4C).

PHYSIOLOGICAL PCI STRATEGY. The HT determined 372 of the 691 unique cases (53.8%) as hemodynamically appropriate for PCI. Across these cases, the median expert human demonstrated 88.8% agreement with the HT regarding the physiological PCI strategy. AI demonstrated 89.7% agreement (IQR: 85.6% to 97.2%) on the same cases and was noninferior to the median expert human ($p < 0.0001$) (Figure 3B).

TABLE 2 Physiological Characteristics of the Vessels (n = 691)

Distal iFR value	
Median	0.87
Interquartile range	0.81–0.91
Proximal iFR value	
Median	0.99
Interquartile range	0.93–1.01
Vessel evaluated	
Total	691 (100%)
Left anterior descending coronary artery	549 (79.5%)
Left circumflex coronary artery	72 (10.4%)
Right coronary artery	56 (8.1%)
Other	14 (2.0%)
Hemodynamic significance	
Distal iFR ≤0.89	470 (68.0%)
Distal iFR >0.89	221 (32.0%)
Significant pressure-wire drift	
Total	217 (31.4%)
Proximal iFR <0.98	147 (21.3%)
Proximal iFR >1.02	70 (10.1%)

iFR = instantaneous wave-free ratio.

INTRAOBSERVER VARIABILITY. Of the 1,008 traces reported by the expert humans, 317 traces were duplicates. Across the expert humans, the reproducibility of determining the hemodynamic appropriateness for PCI varied between 81.6% and 93.7%. The reproducibility of the median expert human was 90.8%, meaning that expert human decision making changed in ~1 in 10 cases when reviewing the same coronary pressure-wire pull back data. In contrast, AI was identical on repeated testing of the appropriateness for PCI.

Of the 317 duplicate traces, 174 cases were determined to be hemodynamically appropriate for PCI according to the HT. Across the expert humans, the reproducibility of determining the physiological PCI strategy varied between 82.9% and 92.4%. The reproducibility of the median expert human was 90.4%. In contrast, AI was identical on repeated testing of PCI strategy.

PERFORMANCE IN THE BORDERLINE iFR ZONE. Borderline iFR values (0.88 to 0.92) were present in 228 of the 691 unique cases. For the hemodynamic appropriateness for PCI in the borderline iFR zone, the median expert human agreed with the HT in 193 of 228 cases (84.6%). The algorithm was numerically but statistically nonsignificantly superior to this, with accuracy of 85.5%. For PCI strategy in the borderline iFR zone, the median expert human demonstrated 89.3% agreement with the HT (IQR: 83.3% to 97.5%). AI demonstrated 91.4% agreement (IQR: 89.3% to 97.7%) on the same cases and was noninferior to the median expert human ($p < 0.0001$).

PERFORMANCE IN PHYSIOLOGICALLY TANDEM LESIONS. Analysis of the physiological PCI strategy endpoint in tandem lesions yielded 185 cases for analysis. The median human accuracy was 87.6% (IQR: 81.6% to 96.4%). The algorithm was numerically but statistically nonsignificantly superior to this, with accuracy of 87.8% (IQR: 83.1% to 94.0%).

DISAGREEMENT BETWEEN AI AND HT INTERPRETATION. Across the 691 unique cases, there were 73 cases (10.6%) in which AI and HT interpretation disagreed on the hemodynamic appropriateness for PCI. Of these, 48 cases (65.8%) were when the HT interpretation was to defer, whereas the algorithm indicated hemodynamic appropriateness for PCI. In 15 of these

JACC: CARDIOVASCULAR INTERVENTIONS VOL. 12, NO. 14, 2019
JULY 22, 2019:1315–24

FIGURE 3 Percentage Agreement With Consensus Opinion

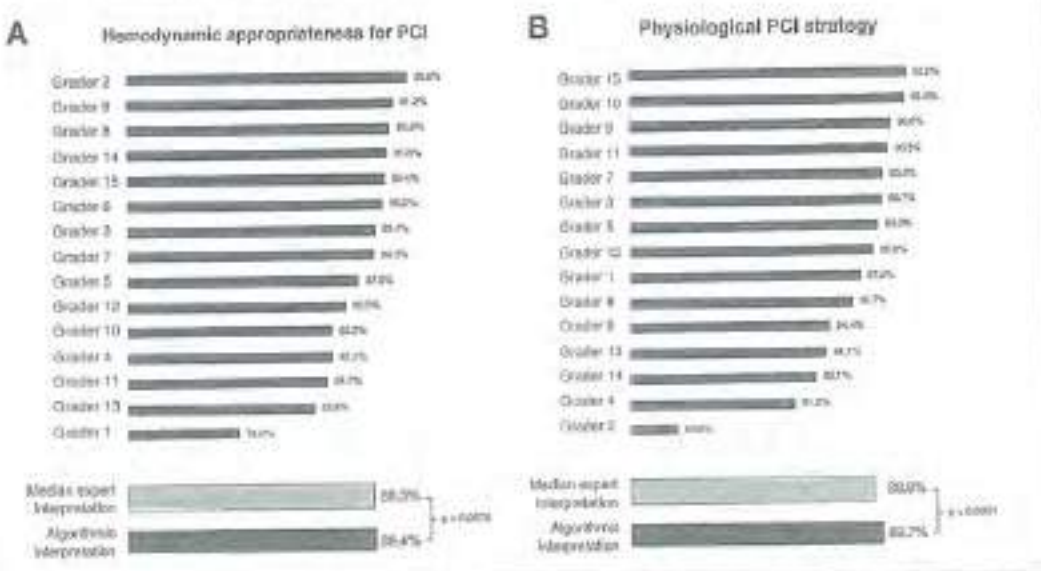

Shown is the percentage agreement between individual expert humans (**blue bars**), the median expert human (**orange bar**), and algorithmic interpretation (**green bar**) compared with the consensus expert human interpretation for (**A**) the appropriateness for percutaneous coronary intervention (PCI) and (**B**) the PCI strategy.

cases (31.3%), this recommendation was explained by the presence of significant pressure-wire drift that was unrecognized by the HT. In the remaining 33 cases (68.7%) in which the HT interpretation was to defer but the algorithm chose to perform PCI, there was always at least 1 human who agreed with the algorithm.

Conversely, there were 25 cases (34.2%) in which the HT interpretation was to perform PCI, whereas the algorithm indicated deferral. In 13 of these cases (52.0%), this recommendation was explained by the presence of pressure-wire drift that was unrecognized by the HT. In the remaining 12 cases (48.0%) in which the HT interpretation was to perform PCI but the algorithm chose to defer, there was always at least 1 human who agreed with the algorithm. Details regarding disagreement between AI and HT interpretations within the borderline iFR zone (0.88 to 0.92) are provided in Online Appendix 3.

SUMMARY OF IMPLICATIONS. Tabulated summaries of the overall implications of algorithmic versus HT interpretation of iFR pressure-wire pull back data are presented in Online Tables 1 and 2. In summary, across all 691 iFR pull back traces, compared with the HT consensus, AI recommended a greater rate of revascularization (53.8% vs. 57.2%; $p < 0.01$) and a greater number of stented segments per pull back trace (1.28 vs. 1.48; $p < 0.0001$).

DISCUSSION

In this study we demonstrated that AI of iFR pressure-wire pull back data was noninferior to the interpretation of the median expert human in determining both the hemodynamic appropriateness for PCI and the physiological PCI strategy when judged against an expert HT opinion. AI correctly interpreted physiologically significant coronary pressure gradients and modified treatment accordingly in the presence of pressure-wire drift (**Central Illustration**).

HT DECISION MAKING. Group decision making has become commonplace in cardiology, with the role of the HT well established in the management of complex clinical decision making (11-13). Additionally, group decision making can be valuable in areas of medicine in which the optimal treatment approach remains uncertain because of a lack of clinical outcome data. In that regard, the interpretation of coronary pressure-wire pull back data is often complex, and a treatment plan must usually be decided upon instantaneously. However, practically speaking, HT opinion for this task is rarely available. As such,

FIGURE 4 Appropriateness for Percutaneous Coronary Intervention

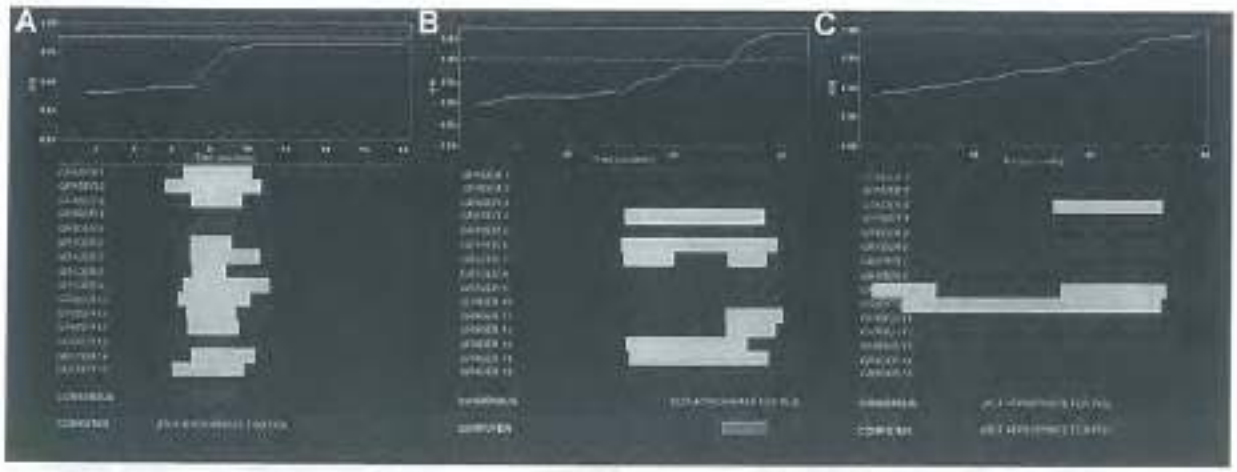

(A) Disagreement between the consensus expert human interpretation (appropriate for percutaneous coronary intervention [PCI]) and algorithmic interpretation (inappropriate for PCI) because of the presence of physiologically significant negative pressure-wire drift. (B) Disagreement between the consensus expert human interpretation (inappropriate for PCI) and algorithmic interpretation (appropriate for PCI) because of the presence of physiologically significant positive pressure-wire drift. (C) Agreement between the consensus expert human interpretation (inappropriate for PCI) and algorithmic interpretation (inappropriate for PCI) because of the presence of a physiologically diffuse pattern of coronary artery disease, despite hemodynamic significance. iFR = instantaneous wave-free ratio.

having a computer-aided tool instantaneously capable of providing high agreement with expert HT opinion could provide a useful adjunct to clinical decision making, lessening the burden of ad hoc decision making placed upon individual physicians.

DISAGREEMENT BETWEEN AI AND HT INTERPRETATION. In the absence of clinical outcome data, there currently exists no definitive gold standard for interpreting iFR pressure-wire pull back data. Accordingly, in this study, we have assessed AI by judging it against the expert HT opinion. However, this approach may actually bias the results in favor of an expert human over the algorithmic approach, as each individual human's decision will have contributed toward determining the HT opinion for that case. Furthermore, in a number of cases in which the AI and the HT interpretation differed (thereby reducing the accuracy of the AI), the HT consensus interpretation itself could be considered to be flawed. This occurred primarily because of the inability of the HT to recognize hemodynamically significant pressure-wire drift.

UNIFORM IMPLEMENTATION OF TREATMENT GUIDELINES. Advantages of an algorithmic approach are that it provides uniform implementation of treatment guidelines independent of environmental and sensory limitations that may present pitfalls for coronary physiology-guided revascularization decision making. Common examples of this include the failure of the human operator to notice and correct for physiologically significant pressure-wire drift or interpret data in the presence of measurement artifact. The failure to acknowledge pressure-wire drift in particular can lead to large changes in the hemodynamic significance of stenoses in borderline zone iFR values (14). In this study, we have shown that an algorithmic approach can ensure that no hemodynamically nonsignificant lesions receive PCI, while also reducing the number of hemodynamically significant lesions that are deferred from PCI.

Additionally, there was variation in how individual expert humans performed in determining the hemodynamic appropriateness of PCI compared with determining the physiological PCI strategy. The human expert with the highest agreement with consensus for the hemodynamic appropriateness of PCI subsequently demonstrated the lowest agreement with consensus for the PCI strategy (Figure 3). This indicates that at the 2 levels of expertise required for the interpretation of coronary pressure-wire pull back data, these levels of expertise can be different.

Last, an algorithmic approach allows modifications to be made in light of new evidence and updated guideline recommendations. Using such a system could help improve the overall appropriateness of

JACC: CARDIOVASCULAR INTERVENTIONS VOL. 12, NO. 14, 2019
JULY 22, 2019:1315–24

CENTRAL ILLUSTRATION Algorithmic Versus Expert Human Interpretation of Instantaneous Wave-Free Ratio Coronary Pressure-Wire Pull Back Data

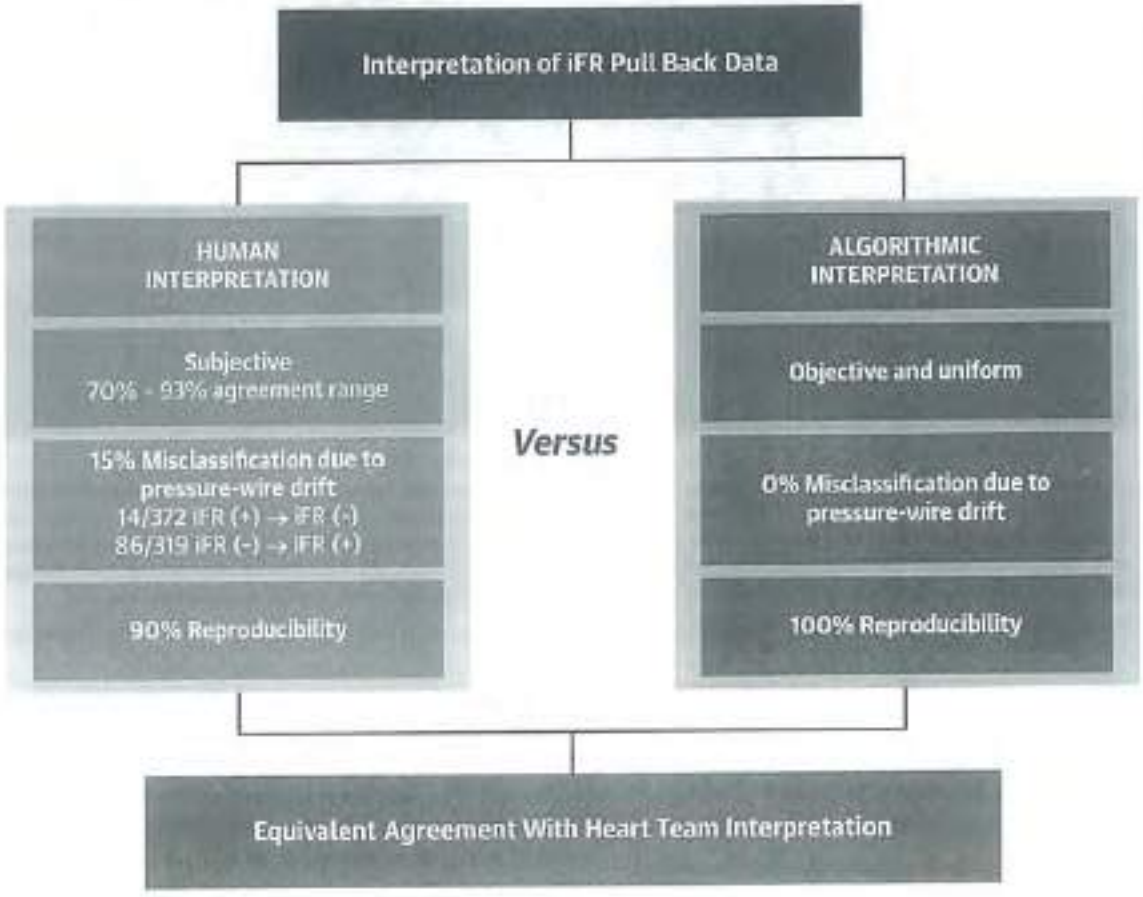

Cook, C.M. et al. J Am Coll Cardiol Intv. 2019;12(14):1315–24.

revascularization decision making (7) and ensure that the latest guidelines and evidence propagates immediately to all physicians and patients.

STUDY LIMITATIONS. In this study, experts were asked to determine their optimal physiological PCI strategy solely on the basis of the interpretation of coronary pressure-wire pull back data. Accordingly, we did not capture additional data that may have influenced these decision (e.g., the physiological length of disease or diffuseness of disease). Furthermore, it is likely that such decisions may be modified when pull back data are subsequently integrated with the coronary angiogram and individual patient characteristics. Because these factors were not available, we are unable to determine how they may have modulated the interpretation of physiological data with regard to revascularization decision making.

The majority of pressure-wire pull back traces in our all-comers clinical dataset were from left anterior descending vessels. This high prevalence of left anterior descending vessels (79.5%) is similar to that observed in other nonselected real-world physiological datasets (15). Furthermore, neither the human graders nor the algorithm was ever aware which vessel the iFR measurements were performed in.

Although in this study we applied our AI to iFR pull back data alone, should the post-PCI predictive accuracy of the resting indexes such as the diastolic pressure ratio be demonstrated, our algorithmic approach could be applied. This would help ensure broader application of computer-assisted

interpretation of physiological data, independent of the provider of coronary catheter laboratory equipment.

Not captured within our study methodology are the additional barriers that exist to iFR pull back data interpretation in real-world physical environments. Such barriers include, for example, limitations of the human visual system to discern small hemodynamic gradients on a physiology screen that may be positioned at a distance away from the operator. Additionally, the very nature of performing an invasive physiological assessment necessitates multitasking of the operator, whose ability to focus solely on interpretation of hemodynamic data is limited. However, within our study, these types of barriers were not replicated, and thus their influence on human decision making remains unmeasured. Although speculative, it is possible that true real-world interpretation of coronary pressure-wire data may be more variable and heterogenous than that recorded within our study.

Last, because of the retrospective nature of our dataset, the actual clinical decisions made at the time of iFR pull back measurement were neither recorded nor informed by knowledge of the AI.

CONCLUSIONS

AI of iFR pressure-wire pull back data provided a standardized interpretation that was automatically corrected for the presence of pressure-wire drift. When judged against an expert HT opinion, AI was noninferior to that of the median expert human in determining both the hemodynamic appropriateness for PCI and the PCI strategy.

ACKNOWLEDGMENTS The authors thank Jeremy Walker and Thalamus AI for software support.

ADDRESS FOR CORRESPONDENCE: Dr. Justin E. Davies, The Hammersmith Hospital, Du Cane Road, London W12 0NN, United Kingdom. E-mail: justindavies@heart123.com.

PERSPECTIVES

WHAT IS KNOWN? In the absence of clinical outcomes data, a definitive interpretation of iFR pull back data is lacking. Individual interpretation of coronary pressure-wire pull back data can be complex, subjective, and dependent on the physiological expertise of the operator.

WHAT IS NEW? AI data provided a standardized and instantaneous interpretation of iFR pressure-wire pull back that was automatically corrected for the presence of pressure-wire drift. When judged against an expert HT opinion, AI was noninferior to that of an expert human.

WHAT IS NEXT? This study investigated the AI of only 1 aspect of coronary revascularization decision making (i.e., iFR pressure-wire pull back data). Future innovations should be tailored toward developing systems that can analyze and interpret the multiple additional factors that influence human clinical decision making (e.g., angiographic characteristics, patient-specific factors).

REFERENCES

1. Hachamovitch R, Berman DS, Shaw LJ, et al. Incremental prognostic value of myocardial perfusion single photon emission computed tomography for the prediction of cardiac death: differential stratification for risk of cardiac death and myocardial infarction. Circulation 1998;97:535–43.

2. Hachamovitch R, Berman DS, Kiat H, et al. Exercise myocardial perfusion SPECT in patients without known coronary artery disease: incremental prognostic value and use in risk stratification. Circulation 1996;93:905–14.

3. Iskander S, Iskandrian AE. Risk assessment using single-photon emission computed tomographic technetium-99m sestamibi imaging. J Am Coll Cardiol 1998;32:57–62.

4. Lauermann ML, Pollock BH, Rozanski A, et al. Extent and severity of myocardial hypoperfusion as predictors of prognosis in patients with suspected coronary artery disease. J Am Coll Cardiol 1996;7:464–71.

5. Bruyne B, Baumbach J, Sys SU, Hendrikse GR. Relation between myocardial fractional flow reserve calculated from coronary pressure measurements and exercise-induced myocardial ischemia. Circulation 1996;93:29–46.

6. Fihn SD, Gardin JM, Abrams J, et al. 2012 ACCF/AHA/ACP/AATS/PCNA/SCAI/STS guideline for the diagnosis and management of patients with stable ischemic heart disease: a report of the American College of Cardiology Foundation/American Heart Association Task Force on Practice Guidelines, and the American College of Physicians, American Association for Thoracic Surgery, Preventive Cardiovascular Nurses Association, Society for Cardiovascular Angiography and Interventions, and Society of Thoracic Surgeons. J Am Coll Cardiol. 2012;60:e44–164.

7. Patel MR, Calhoon JH, Dehmer GJ, et al. ACC/AATS/AHA/ASE/ASNC/SCAI/SCCT/STS 2017 appropriate use criteria for coronary revascularization in patients with stable ischemic heart disease. J Am Coll Cardiol 2017;69:2212–41.

8. Neumann F-J, Sousa-Uva M, Ahlsson A, et al. 2018 ESC/EACTS guidelines on myocardial revascularization. Eur Heart J 2019;40:87–165.

9. Maeda Y, Cook CM, Sharp ASP, et al. Pre-angiography instantaneous wave-free ratio pullback predicts hemodynamic outcome in humans with coronary artery disease: primary results of the international multicenter iFR GRADIENT registry. J Am Coll Cardiol Intv 2018;11:757–67.

10. Dairy PA. General least-squares smoothing and differentiation by the convolution (Savitzky-Golay) method. Anal Chem 1990;62:520–5.

11. Baumgartner H, Falk V, Bax JJ, et al. 2017 ESC/EACTS guidelines for the management of valvular heart disease. Eur Heart J 2017;38:2739–91.

JACC: CARDIOVASCULAR INTERVENTIONS VOL. 12, NO. 14, 2019
JULY 22, 2019:1315–24

12. Serruys PW, Morice M-C, Kappetein AP, et al. Percutaneous coronary intervention versus coronary-artery bypass grafting for severe coronary artery disease. N Engl J Med 2009;360:961–72.

13. Escaned J, Collet C, Ryan N, et al. Clinical outcomes of state-of-the-art percutaneous coronary revascularization in patients with de novo three vessel disease: 1-year results of the SYNTAX II study. Eur Heart J 2017;38:3124–34.

14. Cook CM, Ahmad Y, Shun-Shin MJ, et al. Quantification of the effect of pressure wire drift on the diagnostic performance of fractional flow reserve, instantaneous wave-free ratio, and whole-cycle Pd/Pa. Circ Cardiovasc Interv 2016;9:e002988.

15. Petraco R, Escaned J, Sen S, et al. Classification performance of instantaneous wave-free ratio (iFR) and fractional flow reserve in a clinical population of intermediate coronary stenoses: results of the ADVISE registry. EuroIntervention 2013;9:91–101.

KEY WORDS artificial intelligence, coronary physiology, iFR, instantaneous wave-free ratio, percutaneous coronary intervention

APPENDIX For supplemental methods, tables and figures, please see the online version of this paper.

Circulation Reports
Circ Rep 2019; 1: 313–319
doi:10.1253/circrep.CR-19-0041

ORIGINAL ARTICLE
Cardiovascular Intervention

Sex-Related Differences in In-Hospital Mortality in Japanese ST-Elevation Acute Myocardial Infarction Patients Presenting to Hospital in the 24 Hours After Symptom Onset

— Results From K-ACTIVE —

Sakura Nagumo, MD, PhD; Hiroyoshi Mori, MD, PhD; Atsuo Maeda, MD, PhD; Yoshihiro J. Akashi, MD, PhD; Junya Ako, MD, PhD; Yuji Ikari, MD, PhD; Toshiaki Ebina, MD, PhD; Naoki Sato, MD, PhD; Kouichi Tamura, MD, PhD; Atsuo Namiki, MD, PhD; Kazuki Fukui, MD, PhD; Ichiro Michishita, MD, PhD; Kazuo Kimura, MD, PhD; Hiroshi Suzuki, MD, PhD

Background: Despite the drastic advances in clinical care for patients with acute ST-elevation myocardial infarction (STEMI), female STEMI patients have higher in-hospital mortality rates than male patients. This study assessed the influence of sex on in-hospital mortality in STEMI patients in Kanagawa Prefecture, Japan.

Methods and Results: From October 2015 to June 2018, 2,491 consecutive STEMI patients (23.8% female) who presented to hospital in the 24h after symptom onset were analyzed. The female patients were 9 years older and less frequently had diabetes, smoking and prior MI than male patients. Pre-hospital managements, including prehospital 12-lead electrocardiography, and symptom-to-door time were similar between the sexes. A door-to-device time ≤90min was achieved in 61.3% of female cases and in 65.0% of male cases (P=0.13). Reperfusion therapy was provided to 94.6% of female and 97.6% of male patients (P<0.001). In-hospital mortality rate was not significantly different between female and male patients (6.6% vs. 7.8%, P=0.37). On multivariate logistic regression analysis, female sex itself was not associated with in-hospital mortality (OR, 1.52; 95% CI: 0.67–3.47, P=0.32).

Conclusions: There was no sex discrepancy in the in-hospital mortality of STEMI patients in this study. Guideline-based treatment, such as advanced pre-hospital management and a high use of reperfusion therapy might have attenuated the sex-related differences in the in-hospital mortality.

Key Words: Female; In-hospital mortality; ST-elevation acute myocardial infarction

ST-elevation myocardial infarction (STEMI) is a common disease that is associated with high rates of in-hospital mortality worldwide.[1] Traditionally, female patients have higher rates of in-hospital mortality than male patients.[1-4] Several studies have even suggested that female sex itself was an independent predictor of in-hospital mortality after STEMI in Europe.[2,3] In a meta-analysis adjusted for relative risk, the in-hospital mortality of female STEMI patients remained significantly greater.[4-6] This trend seems to be similar in Japan, which is at the forefront of super-aging societies. Toyota et al studied 1,197 female and 3,182 male patients in Kyoto from 2005 to 2007 and reported that the in-hospital mortality rate of female patients was higher (female 8.7% vs. male 4.9%).[7]

Received May 13, 2019; revised manuscript received June 14, 2019; accepted June 17, 2019; J-STAGE Advance Publication released online July 9, 2019 Time for primary review: 1 day

Division of Cardiology, Department of Internal Medicine, Showa University Fujigaoka Hospital, Yokohama (S.N., H.M., H.S.); Department of Emergency and Disaster Medicine, Showa University Hospital, Tokyo (A.M.); Division of Cardiology, Department of Internal Medicine, St. Marianna University School of Medicine, Kawasaki (Y.J.A.); Department of Cardiovascular Medicine, Kitasato University School of Medicine, Sagamihara (J.A.); Department of Cardiology, Tokai University School of Medicine, Isehara (Y.I.); Department of Laboratory Medicine and Clinical Investigation (T.E.), Division of Cardiology (K.K.), Yokohama City University Medical Center, Yokohama; Division of Cardiology, Nippon Medical University Musashi Kosugi Hospital, Kawasaki (N.S.); Department of Medical Science and Cardiorenal Medicine, Yokohama City University Graduate School of Medicine, Yokohama (K.T.); Department of Cardiology, Kanto Rosai Hospital, Kawasaki (A.N.); Department of Cardiovascular Medicine, Kanagawa Cardiovascular and Respiratory Center, Yokohama (K.F.); and Division of Cardiology, Yokohama Sakae Kyosai Hospital, Yokohama (I.M.), Japan

Y.J.A., J.A., and Y.I. are members of *Circulation Reports'* Editorial Team.

Mailing address: Hiroshi Suzuki, MD, PhD, Division of Cardiology, Department of Internal Medicine, Showa University Fujigaoka Hospital, 1-30 Fujigaoka, Aoba-ku, Yokohama 227-8501, Japan. E-mail: hrsuzuki@med.showa-u.ac.jp

ISSN-2434-0790 All rights are reserved to the Japanese Circulation Society. For permissions, please e-mail: cr@j-circ.or.jp

Table 1. Baseline Characteristics

	Female	Male	P-value
No. patients	595	1,835	
Age (years)	74.6±11.6	65.8±12.7	<0.001
Hypertension	394 (57.8)	1,204 (64.9)	0.27
Diabetes mellitus	174 (29.8)	636 (34.4)	0.04
Dyslipidemia	318 (54.7)	1,018 (55.2)	0.82
Smoking	145 (26.8)	1,353 (77.8)	<0.001
Current smoking	84 (15.6)	768 (44.1)	<0.001
Prior MI	33 (5.7)	170 (9.3)	0.006
eGFR (mL/min/1.73m²)	61.9±25.9	64.2±23.6	0.04
eGFR <30mL/min/1.73m² (%)	56 (9.6)	133 (7.1)	0.06

Data given as mean±SD or n (%). eGFR, estimated glomerular filtration rate; MI, myocardial infarction.

Furthermore, Cui et al showed that this trend has been consistent over 3 decades (1985–2014) in Miyagi Prefecture, which is located in north-eastern Japan.[1] Despite the many reports that have emphasized the importance of guideline-based treatment, however, the rate of reperfusion therapy had not reached 90% in these studies.[1,7] Furthermore, regional differences might exist, even within Japan. Thus, we assessed the sex-related differences in the in-hospital mortality in Japanese STEMI patients.

Methods

Kanagawa-ACuTe cardIoVascular rEgistry (K-ACTIVE) is an observational prospective multicenter registry of acute myocardial infarction (MI) cases. It has enrolled patients from 52 primary coronary intervention (PCI)-capable hospitals in Kanagawa, the second largest prefecture in Japan, since October 2015. Patients who present to participating hospitals with STEMI or non-STEMI (NSTEMI) ≤24 h after the onset of symptoms are registered. The diagnoses of STEMI and NSTEMI are based on the Third Universal Definition of Myocardial Infarction Consensus Document, which was published in 2012.[8] The participating hospitals are cardiovascular specialist training facilities certified by the Japanese Circulation Society, and include large and small hospitals located in rural and urban areas. Each hospital is required to submit data from consecutive patients to the online database. This study was performed in accordance with the Declaration of Helsinki, and was reviewed and approved by the local Institutional Review Board. The research content was posted, and patients who refused to participate in the registry were excluded. K-ACTIVE was registered in the University Hospital Medical Information Network (UMIN) in October 2015 (UMIN000019156).

Baseline patient characteristics included the following factors: age, sex, hypertension, diabetes mellitus (DM), dyslipidemia, smoking, prior MI, and estimated glomerular filtration rate (eGFR). eGFR was calculated using the equation described in a previous study.[9] The following clinical data were obtained on admission: systolic blood pressure, heart rate, Killip classification, out-of-hospital cardiac arrest (OHCA), chest pain symptom, symptom-to-door time, pre-hospital 12-lead electrocardiogram (ECG), and transportation (ambulance, walk in, transfer from another hospital, in-hospital onset). The procedure characteristics included reperfusion therapy (emergency PCI, thrombolytic therapy, coronary artery bypass), door-to-device time, culprit artery (left main trunk, left anterior descending, left circumflex branch, right coronary artery), multi-vessel disease, artery approach route (radial, brachial, femoral), peak serum creatine phosphokinase (CK), use of intra-aortic balloon pumping (IABP) and percutaneous cardiopulmonary support (PCPS), and Thrombolysis In Myocardial Infarction (TIMI) flow grade at initial and final coronary angiography. The primary endpoint was in-hospital mortality. The definitions of hypertension, DM, and dyslipidemia were based on those of the J-PCI Registry.[10] The symptom-to-door time and door-to-device time were calculated as the hospital arrival time minus the symptom onset time; and the first device insertion time to the target lesion minus the hospital arrival time, respectively. The reperfusion procedure was left to the individual interventionist. Patients who were discharged to other medical hospitals were treated as the survivor group, given that some cardiac rehabilitation facilities were included among those hospitals. These data, including the in-hospital mortality rate, were compared between female and male patients.

Statistical Analysis

Continuous variables are summarized as mean±SD or median (IQR) as appropriate. The normality of distribution was assessed using Shapiro-Wilk test or Kolmogorov-Smirnov Lilliefors test. Categorical variables are presented as numbers and percentages. Differences in the baseline characteristics between the sexes were evaluated using Student's t-test or the Mann-Whitney U-test for continuous variables and the chi-squared test or Fisher's exact probability test for categorical variables. A univariate logistic regression model was used to calculate the unadjusted odds of adverse events. To determine the independent predictors of in-hospital mortality, we performed a multivariate logistic regression analysis. Female sex was kept in the multivariate model. Possible confounders were chosen based on clinical knowledge to investigate their potential association with the outcome. When the factors correlated with each other, 1 was deleted. In addition, to reduce the effect of selection bias, we performed rigorous adjustment for patient baseline characteristics with propensity score matching using 1:1 optimal matching without replacement. In-hospital mortality was then compared in this propensity-matched cohort. OR and 95% CI were calculated. $P<0.05$ was considered to indicate statistical significance. All statistical analyses were performed using JMP Pro 11 (SAS Institute, Cary, NC, USA) and EZR (Saitama Medical Center, Jichi Medical

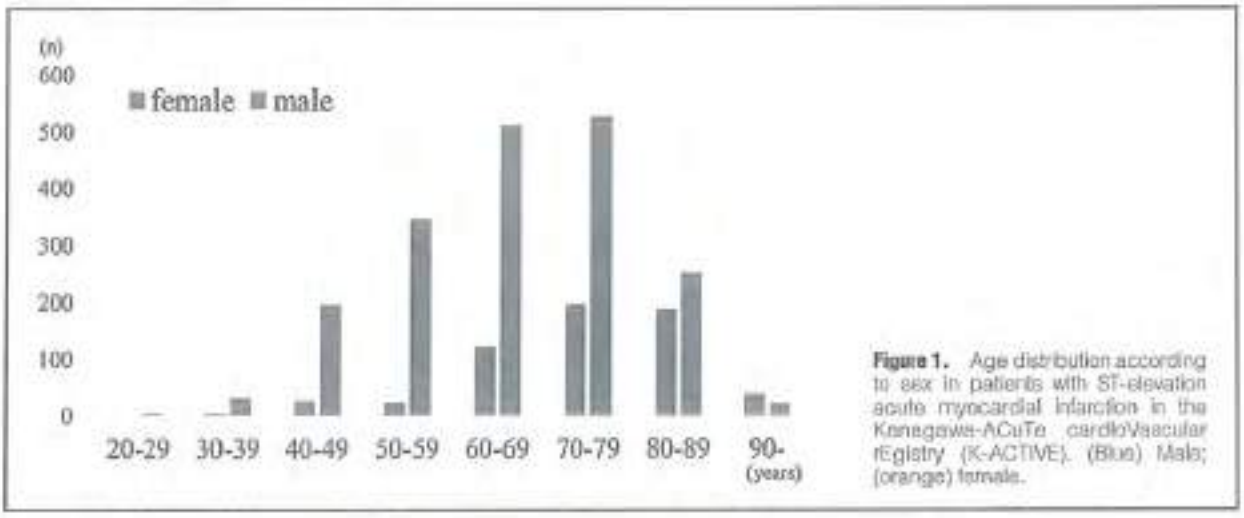

Figure 1. Age distribution according to sex in patients with ST-elevation acute myocardial infarction in the Kanagawa-ACuTe cardioVascular rEgistry (K-ACTIVE). (Blue) Male; (orange) female.

Table 2. Characteristics at Admission

	Female	Male	P-value
No. patients	595	1,896	
SBP (mmHg)	137.2±34.4	139.3±32.3	0.19
Heart rate (beats/min)	77.6±23.9	79.2±21.5	0.13
Killip class			
1	394 (71.8)	1,323 (77.0)	0.05
2	66 (12.0)	149 (8.7)	
3	23 (4.2)	72 (4.2)	
4	65 (11.8)	173 (10.1)	
Killip class ≥2	88 (16.1)	245 (14.3)	0.30
OHCA	24 (4.2)	121 (6.8)	0.03
Chest pain	452 (76.1)	1,558 (82.7)	<0.001
Symptom-to-door time (min)	104 (59.75–255)	97 (54–230)	0.08
Prehospital 12-lead ECG	265 (45.9)	807 (44.4)	0.31
Transportation			
Ambulance	369 (62.3)	1,210 (64.1)	0.004
Walk in	65 (11.0)	287 (15.2)	
Transfer from another hospital	143 (24.2)	360 (19.0)	
In-hospital onset	15 (2.5)	32 (1.7)	

Data given as mean±SD, n (%) or median (IQR). ECG, electrocardiogram; OHCA, out-of-hospital cardiac arrest; SBP, systolic blood pressure.

University, Saitama, Japan), a graphical user interface for R (R Foundation for Statistical Computing, Vienna, Austria).

Results

From October 2015 to June 2018, 2,755 patients with STEMI were registered in the K-ACTIVE database. From these cases, we excluded cases of missing in-hospital mortality data (n=264). The final subject group consisted of 2,491 patients admitted with STEMI. The average age of the overall group was 67.9 years, and 23.9% (n=595) were female. The baseline clinical characteristics are listed in **Table 1**. The average age of the female patients was approximately 9 years older than that of the male patients (74.6 years vs. 65.8 years, P<0.001). Accordingly, the percentage of octogenarians was greater in the female group than in the male group (38.0% vs. 14.5%, P<0.001). **Figure 1** shows the distribution of age by decade. The most common age group was 70–79 years in both women and men. There were no sex differences in the prevalence of hypertension or dyslipidemia. The female patients had a lower prevalence of DM, smoking (both current and past), and prior MI, but a greater prevalence of lower eGFR.

Table 2 lists clinical presentation at admission. There were no significant differences in blood pressure or heart rate between the sexes, and the proportion of patients with Killip class 3/4 was similar. Male patients presented with OHCA and symptoms of chest pain more frequently than female patients. There were no significant differences in the symptom-to-door time or the proportion of patients who underwent 12-lead ECG in the prehospital setting. The procedural characteristics are listed in **Table 3**. Female patients underwent emergency PCI and any reperfusion therapy significantly less frequently than male patients (90.9% vs. 95.5%,

Table 3. Procedure Characteristics

	Female	Male	P-value
No. patients	595	1,895	
Reperfusion therapy†	561 (94.6)	1,849 (97.6)	<0.001
Emergency PCI	541 (90.9)	1,810 (95.5)	<0.001
Thrombolytic therapy	8 (1.3)	24 (1.3)	0.84
CABG	9 (1.5)	25 (1.3)	0.69
Door-to-device time (min)	78 (56–109)	77 (60–113)	0.04
Door-to-device time ≤90min	315 (61.3)	1,136 (65.0)	0.13
Culprit artery			
LMT	14 (2.6)	55 (3.1)	0.58
LAD	250 (46.1)	909 (50.7)	
LCX	49 (9.1)	165 (9.2)	
RCA	217 (40.2)	664 (37.0)	
Multi-vessel disease	244 (45.4)	867 (48.1)	0.28
Arterial approach			
Radial	261 (48.3)	1,016 (57.4)	<0.001
Brachial	14 (2.6)	29 (1.6)	
Femoral	265 (49.1)	725 (41.0)	
Peak CK (IU/L)	1,488.5 (578.75–2,958.75)	2,288 (976–4,259)	<0.001
Peak CK (IU/L) >3,000IU/L	144 (24.4)	722 (38.3)	<0.001
IABP	80 (13.6)	343 (18.2)	0.009
PCPS	10 (1.7)	72 (3.8)	0.01
IABP or PCPS	80 (13.6)	353 (18.8)	0.004
Initial TIMI flow grade			
0	327 (62.3)	1,185 (67.6)	0.09
1	68 (13.0)	183 (10.4)	
2	104 (19.8)	291 (16.6)	
3	26 (4.9)	94 (5.4)	
Final TIMI flow grade			
0	11 (2.1)	13 (0.7)	0.04
1	5 (0.9)	16 (0.9)	
2	31 (5.9)	126 (7.2)	
3	480 (91.1)	1,595 (91.1)	
Final TIMI flow 2/3	511 (97.0)	1,721 (98.3)	0.04
In-hospital mortality	147 (7.8)	39 (6.6)	0.37
Cardiac death	110 (5.8)	33 (5.6)	0.92

Data given as mean±SD, n (%) or median (IQR). †Some patients received multiple treatments. CABG, coronary artery bypass graft; CK, creatine phosphokinase; IABP, intra-aortic balloon pumping; LAD, left anterior descending; LCX, left circumflex branch; LMT, left main trunk; PCI, percutaneous coronary intervention; PCPS, percutaneous cardiopulmonary support; RCA, right coronary artery; TIMI, Thrombolysis in Myocardial Infarction.

P<0.001; and 94.6% vs. 97.6%, P<0.001, respectively). Door-to-device time ≤90min, which is the cut-off time recommended by the American College of Cardiology Foundation/American Heart Association Task Force,[11] were similar between the sexes (female 61.3% vs. male 65.0%, P=0.13). Accordingly, the achievement rate of symptom-to-device time ≤12h was also similar (female 90.0% vs. male 91.3%, P=0.41). The culprit artery and the incidence of multi-vessel disease did not differ to a statistically significant extent. Regarding the arterial approach, the femoral artery was more frequently selected for female patients while the radial artery was for male patients. Men had a significantly higher peak CK and required IABP and PCPS more frequently than women (female 13.6% vs. male 18.2%, P=0.009; and female 1.7% vs. male 3.8%, P=0.01, respectively). Although the initial TIMI flow grade at coronary angiography did not differ to a statistically significant extent, a final TIMI flow grade of 2/3 was achieved in a greater percentage of men than women (female 97.0% vs. male 98.3%, P=0.04).

The in-hospital mortality was similar between the sexes (female 6.6% vs. male 7.8%, P=0.37; **Figure 2A**). The incidence of cardiac death did not differ to a statistically significant extent (female 5.6% vs. male 5.8%, P=0.92). **Figure 2B** shows the distribution of in-hospital mortality between the sexes, which was stratified according to age (by decade). Men had a significantly higher in-hospital mortality in the 60–69-year group (female 1.7% vs. male 6.8%, P=0.03) and 70–79-year group (female 4.1% vs. male 8.9%, P=0.03). In these groups, the rate of IABP and/or PCPS usage was significantly higher in male patients than in female patients (60–69 years: female 11.0% vs. male 19.5%, P=0.03; 70–79 years: female 10.3% vs. male 18.7%, P=0.006, respectively). After excluding OHCA patients from analysis, the in-hospital mortality rate was still similar between the sexes

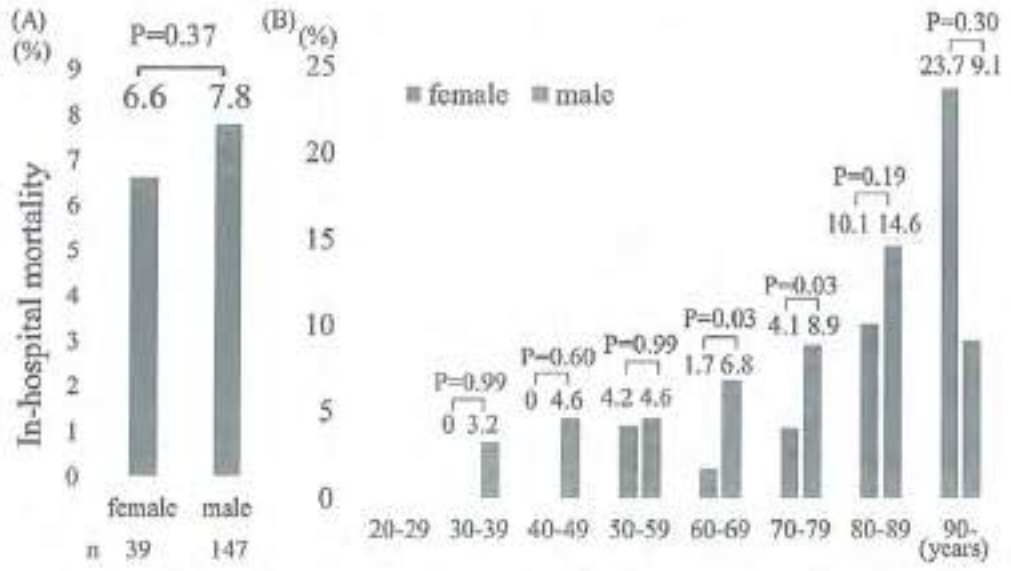

Figure 2. In-hospital mortality according to sex in patients with ST-elevation acute myocardial infarction in the Kanagawa-ACuTe cardioVascular rEgistry (K-ACTIVE): (**A**) overall and (**B**) by age. (Blue) Male; (orange) female.

Table 4. Indicators of In-Hospital Mortality

	Univariate			Multivariate		
	OR	95% CI	P-value	OR	95% CI	P-value
Age	1.04	1.02–1.06	<0.001	1.05	1.02–1.09	0.005
Female	0.83	0.58–1.20	0.35	1.52	0.67–3.47	0.32
Hypertension	0.70	0.52–0.97	0.03	0.96	0.46–1.97	0.90
Diabetes mellitus	1.60	1.14–2.14	0.006	1.30	0.61–2.80	0.49
Dyslipidemia	0.50	0.36–0.69	<0.001	0.68	0.34–1.37	0.28
Current smoker	0.84	0.59–1.19	0.32	0.76	0.33–1.79	0.54
Prior MI	1.54	0.91–2.52	0.08	1.04	0.32–3.44	0.95
eGFR <30 mL/min/1.73m²	4.83	3.31–7.03	<0.001	2.37	0.83–6.81	0.11
Blood pressure	0.97	0.97–0.98	<0.001	0.99	0.98–1.00	0.20
Killip class ≥3	14.7	10.3–20.8	<0.001	1.83	0.82–4.09	0.14
OHCA	12.4	8.47–18.1	<0.001	3.94	1.17–13.3	0.03
Symptom-to-device time	0.99	0.99–1.00	0.04	1.00	0.99–1.00	0.60
Prehospital 12-lead ECG	0.52	0.36–0.74	<0.001	0.69	0.34–1.41	0.31
Reperfusion therapy	0.16	0.09–0.27	<0.001			
LMT region	7.02	4.53–10.9	<0.001	4.70	1.79–12.3	0.002
Multi-vessel disease	1.64	1.18–2.28	0.003	0.88	0.43–1.77	0.71
Peak CK >3,000 IU/L	2.79	2.05–3.82	<0.001	3.32	1.56–7.04	0.002
Final TIMI flow grade	0.44	0.35–0.56	<0.001	0.88	0.43–1.80	0.73
IABP	9.00	6.56–12.4	<0.001			
PCPS	37.9	23.1–62.4	<0.001			
IABP/PCPS	11.0	7.96–15.2	<0.001	6.05	2.76–13.3	<0.001

Abbreviations as in Tables 1–3.

(female 5.9% vs. male 5.0%, P=0.44). In patients <90 years of age, all of the male groups had higher rates of in-hospital mortality than the female groups of the corresponding age group. In patients ≥90 years of age, female patients had a higher in-hospital mortality rate, but the difference was not statistically significant.

On multivariate logistic regression analysis of factors associated with in-hospital mortality, female sex itself was not associated with in-hospital mortality (OR, 1.52; 95% CI: 0.67–3.47, P=0.32; **Table 4**). Higher age, OHCA, left main trunk region, peak CK >3,000 IU/L, and IABP and/or PCPS use were associated with a higher incidence of

in-hospital mortality. In the propensity matched analysis, 323 female patients were matched to an equal number of men (**Supplementary Table**). The OR for in-hospital death in women was not significantly high (OR, 1.78; 95% CI: 0.74–4.31, P=0.20).

Discussion

This study was unique for a number of reasons. Despite the fact that the Kanagawa STEMI registry included substantial numbers of octogenarians (female 38.0% vs. male 14.5%), the rate of any reperfusion therapy use was as high as 94.6% in women and 97.6% in men. In this setting, unlike other studies,[7,12] the in-hospital mortality rate of STEMI patients did not differ between the sexes (female 6.6% vs. male 7.8%, P=0.37). The in-hospital mortality rates of STEMI patients consistently showed no difference, even on multivariate logistic regression and propensity score-matched analyses.

In terms of sex difference, there are some known female-specific features. Female sex was associated with a delay in presentation to hospital (symptom-to-door time) and in in-hospital management (door-to-device time) in some STEMI studies.[7,13,14] The reasons for this delayed presentation are as follows: (1) female patients are likely to have atypical symptoms, such as neck, back, shoulder, and jaw pain or sweating, nausea, vomiting and shortness of breath;[15,16] and (2) the severity of pain in female patients may be mild because of their older age and the presence of DM.[14,16] Indeed, in this study, female STEMI patients less frequently had typical chest pain in comparison with male patients. There were, however, no significant differences between the sexes in symptom-to-door time or in the rate of door-to-device time ≤90 min. Another important point is that the median symptom-to-door time (104 min for women, 97 min for men) was much shorter than in previous studies.[7,13,15] For example, Miyachi et al reported that in Tokyo (the largest city in Japan) the median symptom-to-door time for STEMI patients was 165 min for female and male patients.[17] Also Toyota et al reported that the median time from symptom onset to admission was 240 min in female patients and 180 min in male patients, although the values in the clinical setting might be different, because that study was performed before a universal definition of AMI had been established.[7]

Pre-hospital management is an important factor for the clinical outcomes because it substantially affects symptom-to-door time. All ambulances in Yokohama City (the largest area in Kanagawa) – and only in Yokohama City – carry 12-lead ECG. In the present study, pre-hospital 12-lead ECG was performed in a similar number of men and women, thereby facilitating the diagnosis of STEMI equally between the sexes. These regional features might have helped to shorten symptom-to-door time and door-to-device time, leading to the attenuation of sex-related in-hospital mortality.

The rate of reperfusion therapy in female patients was lower than in male patients in previous studies.[1,12,18] Jneid et al suggested that female patients with STEMI had less opportunity to receive any reperfusion therapy in comparison with male patients (56.3% vs. 73.0%).[12] This trend did not differ in the last 3 decades even in Japan.[18] In the present study, however, the sex-related difference is decreasing: 90.9% of female STEMI patients received emergency PCI and 94.6% of them received any reperfusion therapy, regardless of their higher age. Although thrombolytic therapy without PCI tended to be chosen for female patients in the past,[12,19] there was no sex-related difference in the present study (female 1.3% vs. male 1.3%, P=0.84). This suggests that female patients were given appropriate treatment more frequently than they were in the past. These improvements in the treatment of female patients might have reduced the sex-related difference in the in-hospital mortality.

Several previous studies have reported that female patients had higher age and more comorbidities (e.g., hypertension, DM, renal failure, and advanced Killip class) compared with male patients.[7,15,20–24] In the present study, the female patients were 9 years older and had a higher prevalence of renal failure, which is in line with previous reports, but other factors that are associated with worse clinical outcomes did not differ between the sexes. Although the eGFR in female patients was lower than that in male patients, there was no significant difference in the incidence of eGFR <30 mL/min/1.73 m^2 between the sexes.

OHCA was more frequently observed in men than in women, which might have been associated with a higher need for IABP and/or PCPS. In the 60–69- and 70–79-year-old groups, in which the rate of in-hospital mortality was higher in men than in women, the rates of IABP and/or PCPS usage were significantly higher in male patients. This higher severity of STEMI might have led to worse clinical outcomes in men of these ages. There was a possibility that OHCA was a cause of the increased death rate in male patients but, even after excluding OHCA patients, the in-hospital mortality rate was similar between the sexes. In addition, on propensity-matched analysis there was no significant difference in the in-hospital mortality rates between the sexes after matching the percentage of patients with OHCA.

Conclusions

On analysis of this Kanagawa STEMI registry, in-hospital mortality did not differ between the sexes. This could be explained by the higher rate of reperfusion therapy and advanced pre-hospital management. These findings might facilitate diagnosis and evidence-based treatment for STEMI in female patients.

Acknowledgments

This work was supported by JSPS KAKENHI Grant Number JP15K09101. We thank Dr. Hiroki Nishiwaki and Assistant Professor Takenori Yamauchi for their valuable suggestions on the manuscript.

Disclosure

The authors declare no conflicts of interest.

References

1. Cui Y, Hao K, Takahashi J, Miyata S, Shindo T, Nishimiya K, et al. Age-specific trends in the incidence and in-hospital mortality of acute myocardial infarction over 30 years in Japan: Report from the Miyagi AMI Registry Study. *Circ J* 2017; **81**: 520–528.
2. Velders MA, Boden H, van Boven AJ, van der Hoeven BL, Hoestenmans AACM, Cannegieter SC, et al. Influence of gender on ischemic times and outcomes after ST-elevation myocardial infarction. *Am J Cardiol* 2013; **111**: 312–318.
3. Benamer H, Tafflet M, Bataille S, Escolano S, Livarek B, Fourchard V, et al. Female gender is an independent predictor of in-hospital mortality after STEMI in the era of primary PCI: Insights from the greater Paris area PCI Registry. *EuroIntervention* 2011; **6**: 1073–1079.
4. Pancholy SB, Shantha GPS, Patel T, Cheskin LJ. Sex differences in short-term and long-term all-cause mortality among patients

with ST-segment elevation myocardial infarction treated by primary percutaneous intervention: A meta-analysis. *JAMA Intern Med* 2014; **174:** 1822–1830.
5. Bavishi C, Bangalore S, Patel D, Chatterjee S, Trivedi V, Tamis-Holland JE. Short and long-term mortality in women and men undergoing primary angioplasty: A comprehensive meta-analysis. *Int J Cardiol* 2015; **198:** 123–130.
6. Cozzolo F, D'Ascenzo F, Humphries KH, Webb JG, Scacciatella P, Grasso C, et al. A meta-analysis of sex-related differences in outcomes after primary percutaneous intervention for ST-segment elevation myocardial infarction. *J Interv Cardiol* 2015; **28:** 132–140.
7. Toyota T, Furukawa Y, Ehara N, Funakoshi S, Morimoto T, Kaji S, et al. Sex-based differences in clinical practice and outcomes for Japanese patients with acute myocardial infarction undergoing primary percutaneous coronary intervention. *Circ J* 2013; **77:** 1508–1517.
8. Thygesen K, Alpert JS, Jaffe AS, Simoons ML, Chaitman BR, White HD, et al. Third universal definition of myocardial infarction. *J Am Coll Cardiol* 2012; **60:** 1581–1598.
9. Matsuo S, Imai E, Horio M, Yasuda Y, Tomita K, Nitta K, et al. Revised equations for estimated GFR from serum creatinine in Japan. *Am J Kidney Dis* 2009; **53:** 982–992.
10. Sakakura K, Inohara T, Kohsaka S, Amano T, Uemura S, Ishii H, et al. Incidence and determinants of complications in rotational atherectomy: Insights from the National Clinical Data (J-PCI Registry). *Circ Cardiovasc Interv* 2016; **9:** 1–6.
11. O'Gara PT, Kushner FG, Ascheim DD, Casey DE, Chung MK, de Lemos JA, et al. 2013 ACCF/AHA guideline for the management of ST-elevation myocardial infarction: Executive summary: A report of the American College of Cardiology Foundation/American Heart Association Task Force on Practice Guidelines: Developed in collaboration with the American College of Emergency Physicians and Society for Cardiovascular Angiography and Interventions. *Catheter Cardiovasc Interv* 2013; **82:** E1–E27.
12. Jneid H, Fonarow GC, Cannon CP, Hernandez AF, Palacios IF, Maree AO, et al. Sex differences in medical care and early death after acute myocardial infarction. *Circulation* 2008; **118:** 2803–2810.
13. Dreyer RP, Beltrame JF, Tavella R, Air T, Hoffmann B, Pati PK, et al. Evaluation of gender differences in door-to-balloon time in ST-elevation myocardial infarction. *Heart Lung Circ* 2013; **22:** 861–869.
14. Sullivan AL, Beshansky JR, Ruthazer R, Murman DH, Mader TJ, Selker HP. Factors associated with longer time to treatment for patients with suspected acute coronary syndromes: A cohort study. *Circ Cardiovasc Qual Outcomes* 2014; **7:** 86–94.
15. Kosuge M, Kimura K, Ishikawa T, Ebina T, Hibi K, Tsukahara K, et al. Differences between men and women in terms of clinical features of ST-segment elevation acute myocardial infarction. *Circ J* 2006; **70:** 222–226.
16. Culić V, Eterović D, Miric D, Sibé N. Symptom presentation of acute myocardial infarction: Influence of sex, age, and risk factors. *Am Heart J* 2002; **144:** 1012–1017.
17. Miyachi H, Takagi A, Miyauchi K, Yamasaki M, Tanaka H, Yoshikawa M, et al. Current characteristics and management of ST elevation and non-ST elevation myocardial infarction in the Tokyo metropolitan area: From the Tokyo CCU network registered cohort. *Heart Vessels* 2016; **31:** 1740–1751.
18. Takii T, Yamada S, Takahashi J, Ito K, Shiba N, Shirato K, et al. Trends in acute myocardial infarction incidence and mortality over 30 years in Japan: Report from the MIYAGI-AMI Registry Study. *Circ J* 2010; **74:** 93–100.
19. Alabas OA, Gale CP, Hall M, Rutherford MJ, Szummer K, Lawesson SS, et al. Sex differences in treatments, relative survival, and excess mortality following acute myocardial infarction: National cohort study using the SWEDEHEART registry. *J Am Heart Assoc* 2017; **6:** e007123.
20. Jackson EA, Moscucci M, Smith DE, Share D, Dixon S, Greenbaum A, et al. The association of sex with outcomes among patients undergoing primary percutaneous coronary intervention for ST elevation myocardial infarction in the contemporary era: Insights from the Blue Cross Blue Shield of Michigan Cardiovascular Consortium (BMC2). *Am Heart J* 2011; **161:** 106–112.e1.
21. Eitel I, Desch S, de Waha S, Fuernau G, Gutberlet M, Schuler G, et al. Sex differences in myocardial salvage and clinical outcome in patients with acute reperfused ST-elevation myocardial infarction. *Circ Cardiovasc Imaging* 2012; **5:** 119–126.
22. Biava LM, Scacciatella P, Calcagnile C, Dalmasso P, Cozzolo F, Fanelli AL, et al. Sex-related differences in patients with ST-elevation myocardial infarction undergoing primary PCI: A long-term mortality study. *Cardiovasc Revascularization Med* 2015; **16:** 135–140.
23. Canto JG, Rogers WJ, Goldberg RJ, Peterson ED, Wenger NK, Vaccarino V, et al. Association of age and sex with myocardial infarction symptom presentation and in-hospital mortality. *JAMA* 2012; **307:** 813–822.
24. van der Meer MG, Nathoe HM, van der Graaf Y, Doevendans PA, Appelman Y. Worse outcome in women with STEMI: A systematic review of prognostic studies. *Eur J Clin Invest* 2015; **45:** 226–235.

Supplementary Files

Please find supplementary file(s):
http://dx.doi.org/10.1253/circrep.CR-19-0041

Taylor & Francis Online

Log in | Register

Journal
Clinical and Experimental Hypertension >
Volume 41, 2019 - Issue 8

24 0 20
Views CrossRef citations to date Altmetric

Articles

Maximum home systolic blood pressure is a marker of carotid atherosclerosis

Toshiki Kaihara, Satoshi Hoshide, Naoko Tomitani, Hiroshi Kanegae, Kazuomi Kario & J-HOP Study Group

Pages 774-778 | Received 12 Jun 2018, Accepted 06 Nov 2018, Published online: 11 Jan 2019

Download citation https://doi.org/10.1080/10641963.2018.1557678 Check for updates

言語を選択 | ▼
Translator disclaimer

ABSTRACT

Background: Maximum home systolic blood pressure (maximum SBP) has been reported as a parameter of blood pressure (BP) variability. We tested the hypothesis that maximum SBP is one of the risk factors of hypertensive target organ damage (TOD).

Methods: We conducted a cross-sectional study of 1,575 subjects with 1 cardiovascular risk factor. The subjects measured their home BP for 14 consecutive days. Mean and maximum SBPs were used as independent variables. As dependent variables, we used left ventricular mass index (LVMI), brachial-ankle pulse wave velocity (baPWV), maximum carotid intima-media thickness (CIMT), and urine albumin creatinine ratio (UACR).

Results: In a multiple regression analysis, the subjects' mean and maximum SBPs were significantly associated with the above TOD markers. Compared to mean SBP, maximum SBP demonstrated a significantly stronger association with CIMT ($p<0.001$).

Conclusion: Based on its clinical significance herein, measurement of maximum home SBP is warranted in addition to measurement of mean home SBP.

KEYWORDS: Blood pressure variability, maximum systolic blood pressure, carotid atherosclerosis, carotid intima-media thickness

frontiers in Physiology

ORIGINAL RESEARCH
published: 22 August 2019
doi: 10.3389/fphys.2019.01090

Reintroducing Heart Sounds for Early Detection of Acute Myocardial Ischemia in a Porcine Model – Correlation of Acoustic Cardiography With Gold Standard of Pressure-Volume Analysis

Marco Luciani[1*], *Matteo Saccocci*[1], *Shingo Kuwata*[1], *Nikola Cesarovic*[2], *Miriam Lipiski*[2], *Patricia Arand*[3], *Peter Bauer*[4], *Andrea Guidotti*[1], *Evelyn Regar*[1], *Paul Erne*[4], *Michel Zuber*[5] *and Francesco Maisano*[1]

[1] Department of Cardiovascular Surgery, University Hospital Zurich, Zurich, Switzerland, [2] Division of Surgical Research, University Hospital Zurich, Zurich, Switzerland, [3] VisCardia, Inc., Portland, OR, United States, [4] Faculty of Biomedical Sciences, Università della Svizzera Italiana, Lugano, Switzerland, [5] Department of Cardiology, University Hospital Zurich, Zurich, Switzerland

Background: Acoustic cardiography is a hybrid technique that couples heart sounds recording with ECG providing insights into electrical-mechanical activity of the heart in an unsupervised, non-invasive and inexpensive manner. During myocardial ischemia hemodynamic abnormalities appear in the first minutes and we hypothesize a putative diagnostic role of acoustic cardiography for prompt detection of cardiac dysfunction for future patient management improvement.

Methods and Results: Ten female Swiss large white pigs underwent permanent distal coronary occlusion as a model of acute myocardial ischemia. Acoustic cardiography analyses were performed prior, during and after coronary occlusion. Pressure-volume analysis was conducted in parallel as an invasive method of hemodynamic assessment for comparison. Similar systolic and diastolic intervals obtained with the two techniques were significantly correlated [Q to min dP/dt vs. Q to second heart sound ($r^2 = 0.9583$, $p < 0.0001$), PV diastolic filling time vs. AC perfusion time ($r^2 = 0.9686$, $p < 0.0001$)]. Indexes of systolic and diastolic impairment correlated with quantifiable features of heart sounds [Tau vs. fourth heart sound Display Value ($r^2 = 0.2721$, $p < 0.0001$) cardiac output vs. third heart sound Display Value ($r^2 = 0.0791$ $p = 0.0023$)]. Additionally, acoustic cardiography diastolic time (AUC 0.675, $p = 0.008$), perfusion time (AUC 0.649, $p = 0.024$) and third heart sound Display Value (AUC 0.654, $p = 0.019$) emerged as possible indicators of coronary occlusion. Finally, these three parameters, when joined with heart rate into a composite joint-index, represent the best model in our experience for ischemia detection (AUC 0.770, $p < 0.001$).

OPEN ACCESS

Edited by:
Gaetano Santulli,
Columbia University, United States

Reviewed by:
Vladimir Lj Jakovljevic,
University of Kragujevac, Serbia
Adam Stańczyk,
Military Institute of Medicine (Poland), Poland
Gerard Amorós-Figueras,
IR-Sant Pau, Spain

***Correspondence:**
Marco Luciani
marco.luciani@mail.com

Specialty section:
This article was submitted to Clinical and Translational Physiology, a section of the journal Frontiers in Physiology

Received: 05 February 2019
Accepted: 07 August 2019
Published: 22 August 2019

Citation:
Luciani M, Saccocci M, Kuwata S, Cesarovic N, Lipiski M, Arand P, Bauer P, Guidotti A, Regar E, Erne P, Zuber M and Maisano F (2019) Reintroducing Heart Sounds for Early Detection of Acute Myocardial Ischemia in a Porcine Model – Correlation of Acoustic Cardiography With Gold Standard of Pressure-Volume Analysis. Front. Physiol. 10:1090. doi: 10.3389/fphys.2019.01090

Conclusion: In the rapidly evolving setting of acute myocardial ischemia, acoustic cardiography provided meaningful insights of mechanical dysfunction in a prompt and non-invasive manner. These findings should propel interest in resurrecting this technique for future translational studies as well as reconsidering its reintroduction in the clinical setting.

Keywords: acute coronary syndrome, acute myocardial ischemia, heart sound, hemodynamics, animal model

INTRODUCTION

Cardiac auscultation has been a pivotal part of patients' examination since the stethoscope invention in 1816 by the French physician René Laennec. Despite technical refinements, knowledge advancements and limited costs, auscultation has lost momentum over time in favor of less operator-dependent techniques. In fact, findings obtained from acoustic examination can be affected by operator's expertise, limited sensitivity of the human ear and lack of reproducibility.

Nevertheless, by coupling heart sound recordings together with ECG tracings, investigators can acquire important insights regarding the electrical-mechanical activity of the heart in an unsupervised, non-invasive and inexpensive manner. Such a hybrid technique, acoustic cardiography (AC) (Erne, 2008), has been proven as a reliable method for patient stratification and prognosis in diverse pathological conditions [pulmonary arterial hypertension (Chan et al., 2013), atrial fibrillation (Dillier et al., 2010), coronary artery disease (Zuber and Erne, 2010; Thomas et al., 2017), acute myocardial ischemia (AMI) (Lee et al., 2009), premature ventricular contractions (Walia et al., 2019), heart failure with either preserved or reduced ejection fraction (Wang et al., 2013, 2016)].

In the specific setting of acute coronary syndrome, AC might play a role in patient management by detecting cardiac dysfunction (Marcus et al., 2005) in a prompt and accurate manner. For this reason we employed a porcine model of permanent acute coronary occlusion, and evaluated a possible correlation between parameters obtained by AC and the ones obtained with a reliable yet invasive technique, pressure-volume (PV) assessment. The present study aims to identify mechanical alterations of physiological significance such as indexes of contractile and relaxation function as well as systolic and diastolic time intervals (STIs and DTIs, respectively) occurring during AMI and detected with two different techniques (AC and PV measurements) in both stable and rapidly evolving conditions (prior and upon coronary occlusion) (Lewis et al., 1977).

MATERIALS AND METHODS

Study Population

Ethical Committee

The animal housing and experimental protocols were approved by the Cantonal Veterinary Department, Zurich, Switzerland, under license no. ZH 219/2016, and were in accordance with Swiss Animal Protection Law. Housing and experimental procedures also conformed to the European Directive 2010/63/EU of the European Parliament and of the Council on the Protection of Animals used for scientific purposes and to the Guide for the Care and Use of Laboratory Animals (Institute of Laboratory Animal Resources, National Research Council, National Academy of Sciences, 2011).

Animal Care

Ten female Swiss large white pigs (50 ± 2 kg) were included in this study. All animals were pre-medicated with an intramuscular injection of 15 mg/kg BW Ketamine (Ketasol-100; Dr. E. Graeub AG, Berne Switzerland), 2 mg/kg BW Azaperone (Stresnil, Provet AG, Lyssach Switzerland) and 0.5 mg/kg BW Atropine sulfate 0.1%. All animals were intubated and ventilated with an inspired oxygen fraction (FiO_2) of 0.5, tidal volume of 6–8 mL/kg, a frequency of 20 breaths per min, and a positive end-expiratory pressure (PEEP) of 5 cm H_2O. Anesthesia was maintained with 0.6–1% isoflurane and deepened in accordance with the study protocol with a continuous infusion of propofol (2–5 mg/kg/h) (Propofol Lipuro 1% Braun Medical AG, Sempach, Switzerland).

Experimental Procedures

Porcine Model of Coronary Occlusion

Continuous myocardial ischemia was induced by complete occlusion of the left circumflex artery distal to second marginal branch employing an adequately sized PCI balloon [Falcon CTO, PTCA Balloon, Invatec S.p.A. Roncadelle (BS), Italy]. Both AC and PV assessment were simultaneously conducted in supine position before, during and after coronary occlusion. **Figure 1** provides an overview of our experimental setup and working model.

Cardiac Ultrasound Assessment

Echocardiography was performed with a Philips IE 33 machine (Philips Ultrasound, Andover, MA, United States) and its 3D-transesophageal probe. All data were stored digitally and evaluated by one person (MZ). After optimal placement of the transesophageal probe in a four chamber view, the probe was not moved throughout the study. Firstly, a 3D dataset for volume and ejection fraction analysis was registered. Secondly, transmitral flow was aquired with Pulsed Wave (PW) Doppler [Evmax (cm/s), Tdec time (ms), E-VTI (cm), Avmax (cm/s), A-VTI (cm)] and tissue velocities of medial mitral anulus with PW-Doppler [Eamax (cm/s), Ea-VTI (cm), Aamax (cm/s), Aa-VTI (cm), systolic vmax (cm/s), systolic-VTI (cm)] after optimization to a most perpendicular view as possible. E/A and E/E' ratios were obtained by dividing Evmax by Avmax and Eamax, respectively.

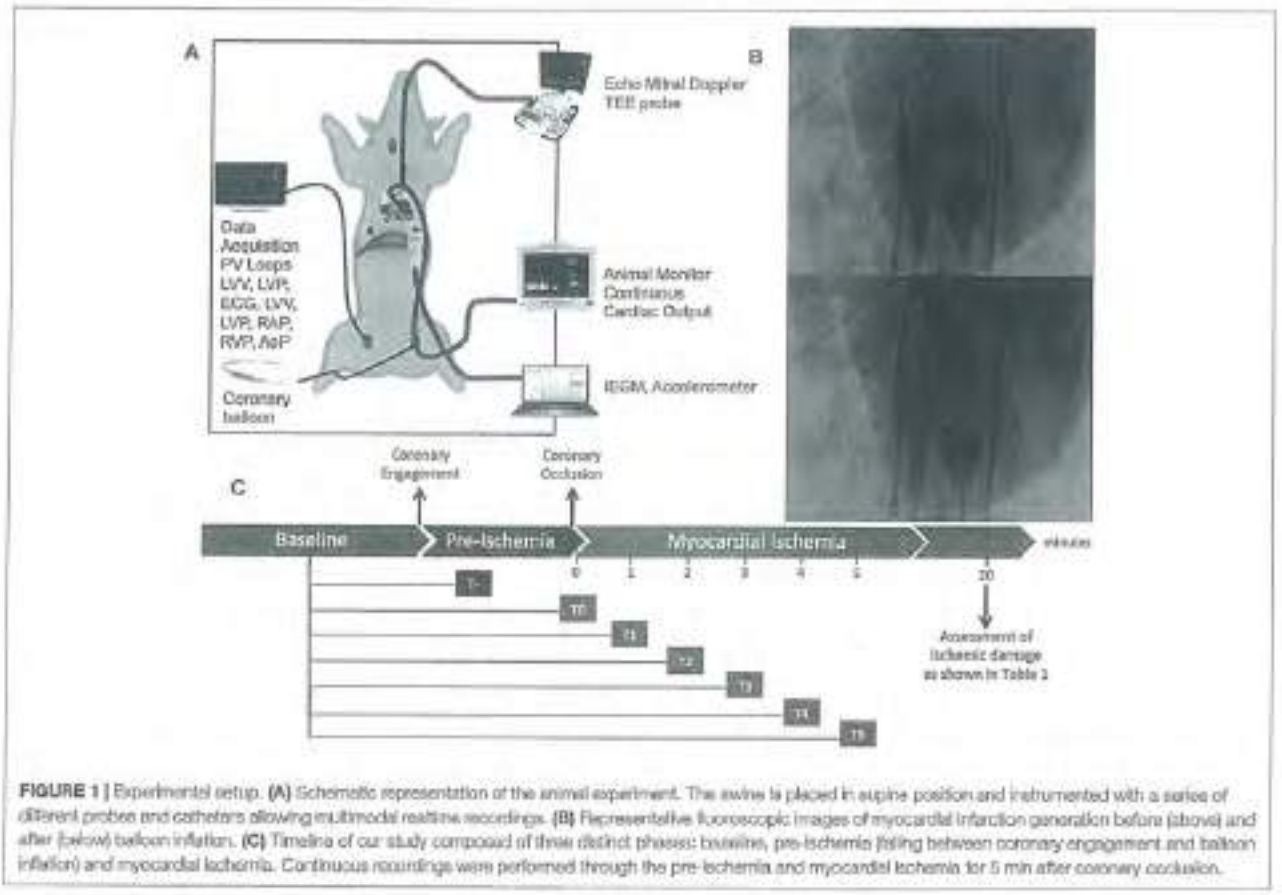

FIGURE 1 | Experimental setup. **(A)** Schematic representation of the animal experiment. The swine is placed in supine position and instrumented with a series of different probes and catheters allowing multimodal realtime recordings. **(B)** Representative fluoroscopic images of myocardial infarction generation before (above) and after (below) balloon inflation. **(C)** Timeline of our study composed of three distinct phases: baseline, pre-ischemia (lasting between coronary engagement and balloon inflation) and myocardial ischemia. Continuous recordings were performed through the pre-ischemia and myocardial ischemia for 5 min after coronary occlusion.

Acoustic Cardiography Assessment

Acoustic cardiography was performed with AUDICOR (Inovise Medical, Inc., Portland, OR, United States) allowing simultaneous dual acquisition of heart sounds and ECG signals. The sensor was placed approximately between V2 and V4 lead location. Raw data were recorded and transferred to Inovise Medical Inc., and subsequently analyzed by the computerized algorithm for the measurement of ECG, heart sounds and systolic and diastolic interval times.

The following parameters were conceived and employed for our study. Intensities and persistence of heart sounds S1 (mitral valve closure), S2 (aortic valve closure), S3 (diastolic sound of limited ventricular longitudinal expansion), and S4 (diastolic sound of stiffness) were recorded and a derivative parameter called Display Value (DV) was generated. The AUDICOR automated heart sound algorithm is a hidden Markov model with inputs derived from a 6-level stationary wavelet transformation of the acoustic signal and from select fiducial times of the simultaneous ECG signal. The output includes a segmentation of the acoustic signal into individual heart sounds, as well as measurements derived from that segmentation. The S3 and S4 DV parameters are a combination of intensity and persistence of the acoustic signal within the segments appropriate in timing for those heart sounds. S3 and S4 DV is expressed on a 0 to 10 scale where if the DV is ≥5.0 a third or fourth heart sound is considered present. STIs were as follows: the Q-S1 interval is the time from the onset of the Q-wave on the ECG to the mitral valve closure (peak of the first heart sound or S1), also known as electromechanical activation time (EMAT). Left ventricular systolic time (LVST) is defined between (S1) and aortic valve closure (peak "aortic component" of the second heart sound or S2). Electromechanical systolic time (AC EMST) is defined by the time-window between the Q-wave onset and the aortic valve closure (S2). Concerning DTIs, the following parameters were employed: diastolic time (DT) as the time between aortic valve closure (S2) and the next mitral valve closure (S1), perfusion time (PT) as the interval between S2 and the next Q-wave onset.

Pressure-Volume Assessment

Simultaneous pressure-volume (PV) measurements were performed with a conductance catheter (CD Leycom, Zoetermeer, Netherlands). The conductance method calculates continuous volume tracings by measuring parallel electric conductance between adjacent electrodes. Correct positioning was verified by fluoroscopy and by inspecting segmental signals. Volume calibration was obtained by transoesophageal 3D echocardiography and/or by injection of NaCl hypertonic boluses. Data analysis was performed with dedicated data acquisition and analysis software (Conduct NT, CD Leycom). Along with real-time pressure, volumes, and a series of

normally employed derivative parameters regarding myocardial contractility (ejection fraction, stroke work, cardiac output, minimal and maximal dP/dt, isovolumic relaxation constant Tau) additional intervals were conceived for our comparison. STIs were defined as follows: one interval starting from the onset of the Q wave until max dP/dt (Q to max dP/dt) also known as Pre-Ejection Period (PEP), and a longer one lasting until min dP/dt (Q to min dP/dt) (PV EMST). Additionally, the time window between maximal and minimal dP/dt values was also calculated. A DTI called diastolic filling time (DFT) was defined as the interval between dP/dt min and diastole's end according to the Conduct NT manual.

Data Analysis

Correlation Analysis

As shown in **Figure 2** parameters obtained by PV loop analysis are overlapping with a number of corresponding parameters derived from AC; this figure provides a summary overview of correlated and overlapping parameters from the two techniques. In **Figures 3, 4** each datapoint shown in the scatterplots represents a 30 s-averaged assessment both at baseline, pre-ischemia (time window between coronary engagement and occlusion) and each minute after coronary occlusion up to 5 min.

Heatmap Generation

Heatmaps were generated by comparing a constant baseline timepoint after the animal was fully instrumented and before engaging the coronary arteries with a pre-ischemic timepoint and every minute upon complete balloon inflation for 5 min as reported in **Figure 1C**. Fold change with respect to the aforementioned timepoint and obtained *p*-value obtained from paired *t*-test and Wilcoxon signed rank test were reported in two distinct heatmaps. Significant parameter changes at specific timepoints are indicated with an asterisk symbol in order to increase readability.

Area Under the Receiver Operating Characteristic Curve

In order to identify parameters that could be of diagnostic usefullness in detecting ischemic insult, we employed areas under the receiver operating characteristic (ROC) curve (AUC) for each single AC parameter during our experiment and allocated timepoints into two groups (ischemic and non-ischemic) based on the status of coronary patency. Data obtained prior to coronary engagement were considered as non-ischemic; on the other hand, data gathered after complete coronary occlusion were allocated into the ischemic group. With the intention of identifying a superior parameter in terms of predictive power we tested different models containing various combinations of the four significant single parameters. AUC was assessed for each model and the first three outperforming the single most significant one were reported. For this specific analysis, data obtained within the interval of coronary engagement and occlusion (pre-ischemia) were not employed in order to reduce a heterogenous confounding factor.

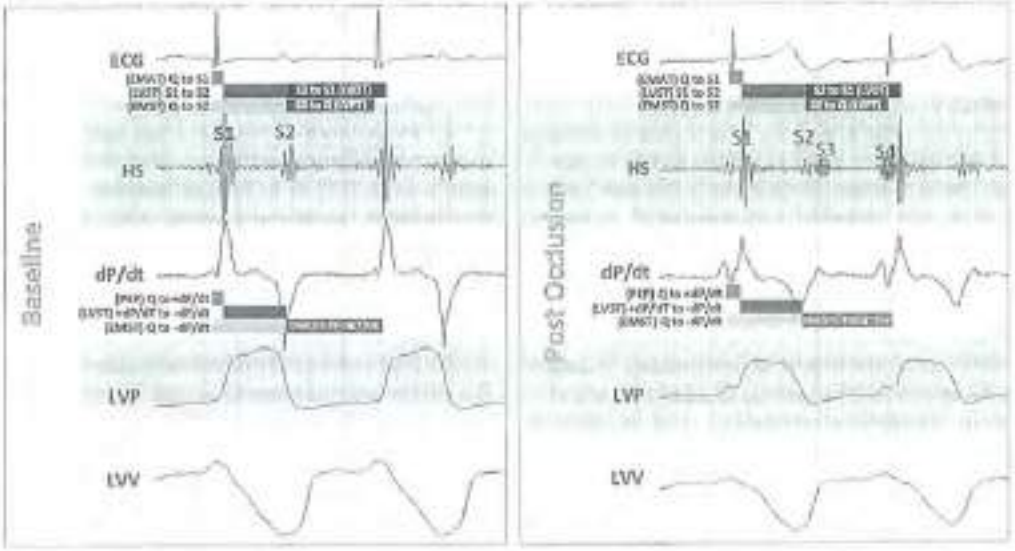

FIGURE 2 | Concerned acoustic and pressure-volume derived parameters during baseline and after coronary occlusion. Acoustic systolic times were defined as follows: Q to S1 (electromechanical activation time or EMAT), S1 to S2 (left ventricular systolic time or LVST), and Q to S2 (electromechanical systolic time or EMST). Acoustic diastolic times were S2 to S1 (left ventricular diastolic time or LVDT), S2 to Q (left ventricular partusion time or LVPT). Pressure-volume derived systolic times were: Q to +dP/dt (pre-ejection period), +dP/dt to −dP/dt (left ventricular systolic time) and Q to −dP/dt (electromechanical systolic time). The systolic time obtained by pressure-volume was delimited within −dP/dt to diastole's and according to the company booklet. Upon occlusion a series of changes in shown tracings can be noticed: S1 and S2 intervalles decrease, S3 and S4 start appearing, both maximal dP/dt and minimal dP/dt absolute values decrease indicating systolic and diastolic impairment, respectively. In addition, smaller excursions of left ventricular pressures and volumes (LVP and LVV) of tracings translate into lower systolic pressure generation and increased end-systolic volumes.

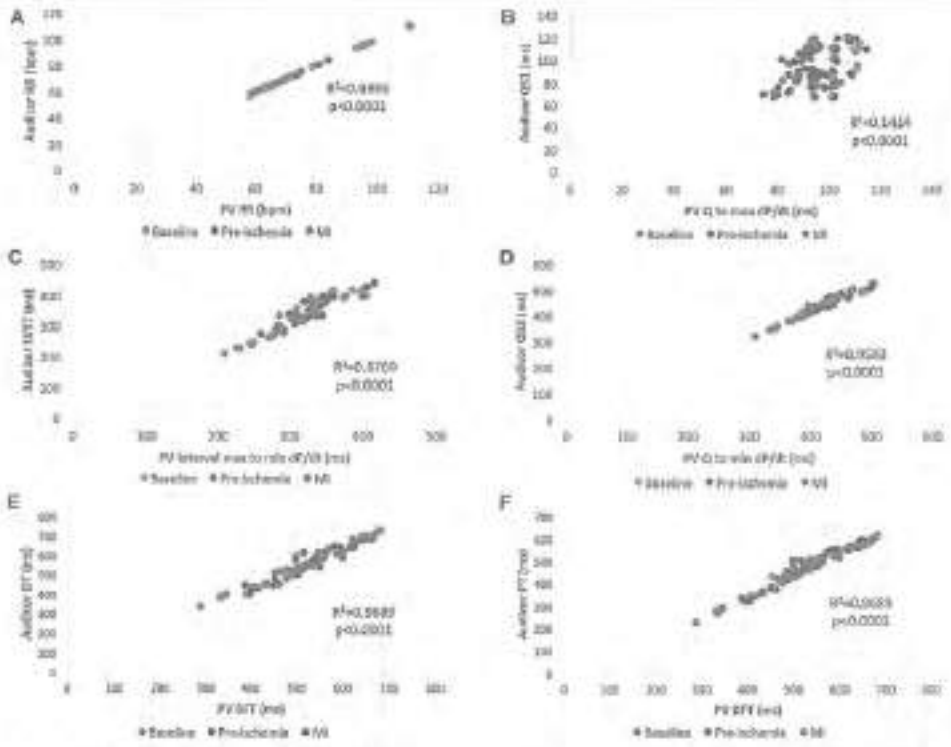

FIGURE 3 | Scatter plots of overlapping interval times obtained by acoustic cardiography and pressure-volume analysis. **(A)** PV Heart Rate vs. AC Heart Rate; **(B)** Q to max dP/dt vs. QS1; **(C)** max to min dP/dt vs. S1 to S2 (LVST); **(D)** Q to min dP/dt vs. QS2; **(E)** Diastolic Filling Time vs. S2 to S1 (LVDT); **(F)** Diastolic Filling Time vs. S2 to Q (LVPT). Color key: blue (baseline), pre-ischemia (purple), red (myocardial ischemia). Each dot represents a 30-s assessment. Pressure-Volume data are reported on the *x*-axis, data obtained from acoustic cardiography are on the *y*-axis.

Statistical Analysis

Continuous variables were initially tested (Shapiro-Wilk) for normal distribution. Data are presented as mean ± standard deviation or median (IQR) when appropriate. Parametric and non-parametric tests for paired comparisons between two datasets included paired *t*-test and Wilcoxon signed rank test, respectively. Areas under the receiver operating characteristic (ROC) curve (AUC) were used to quantify the predictive accuracy of AC parameters for coronary occlusion detection. Using logistic regression, the four most significant AC parameters were modeled for ischemic detection improvement.

A two-tailed p-value < 0.05 was considered significant. Statistical analyses were performed on GraphPad Prism 8 (GraphPad Software, San Diego, CA, United States) and STATA14 (StataCorp LP, College Station, TX, United States).

Data and Materials Disclosure

The data that support the findings of this study are available from the authors.

RESULTS

During our 5 min study time-window, 3 out of 10 animals suffered from ventricular arrhythmias which required prompt defibrillation and therefore seven pigs completed the protocol. In all three cases, resuscitation maneuvers were successful and subsequent echocardiographic assessment was performed in all ten animals. Recordings were of good quality in the entire cohort. Coronary occlusion was effective in inducing significant morpho-functional alterations consistent with myocardial ischemic damage as shown in **Table 1**. Our porcine model was primarily characterized by systolic dysfunction [Left Ventricular Ejection Fraction (LVEF) decreased from 52.6 to 44.6%, $p < 0.001$, Left Ventricular End-Systolic Pressure (LVESP) from 73.8 to 64.9 mmHg, $p < 0.001$, Left Ventricular End-Systolic Volume (LVESV) from 45.6 mL at baseline to 56.6 mL after balloon occlusion, $p = 0.005$]. Upon experiment termination, venous blood was drawn for Troponin-T assessment in all animals and a median value of 48.5 ng/mL (41.25–211.5) was detected. Taken together these alterations prove the reliability of our working animal model and subsequently of our dataset.

Figure 3 shows a series of scatterplots assessing the relationship between "overlapping" time parameters obtained with AC and PV. Recorded Heart Rate (HR) (**Figure 3A**) was similar in both detection methods ($r^2 = 0.9995$, $p < 0.0001$). As for STIs, an overall positive correlation between parameters was found. For instance, the correlation between Electromechanical activation time (EMAT or QS1) and Q to max dP/dt (**Figure 3B**) was significant ($r^2 = 0.1414$, $p < 0.0001$), nevertheless longer STIs

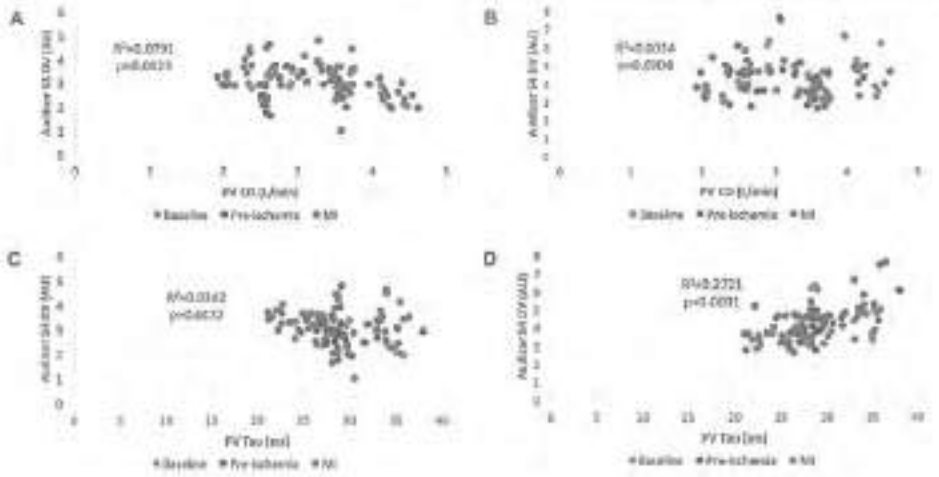

FIGURE 4 | Scatter plots of systolic and diastolic performance obtained by acoustic cardiography and pressure-volume analysis. **(A)** Cardiac Output vs. S3 Display Value; **(B)** Cardiac Output vs. S4 Display Value; **(C)** Isovolumic Relaxation Constant (Tau) vs. S3 Display Value; **(D)** Isovolumic Relaxation Constant (Tau) vs. S4 Display Value. Color key: blue (baseline), pre-ischemia (purple), red (myocardial ischemia). Each dot represents a 30-s assessment. Pressure-Volume data are reported on the *x*-axis, whereas data obtained from acoustic cardiography are on the *y*-axis.

TABLE 1 | Cardiac ultrasound and PV assessment parameters prior and after coronary occlusion in 10 female pigs.

Parameters	Baseline (n = 10)	Post-occlusion (n = 10)	*p*-value
Pressure volume analysis			
Heart rate (bpm)	82 (69.25 – 84)	84.5 (81.25 – 88.5)	0.179
Stroke volume (mL)	49.81 ± 9.00	45.62 ± 10.46	0.074
Cardiac output (L/min)	3.15 ± 0.66	3.03 ± 0.71	0.530
Ejection fraction (%)	52.82 ± 2.09	44.57 ± 4.27	<0.001
Stroke work (mmHg × mL)	2872 ± 471	2194 ± 474	0.001
Tau (ms)	28.59 ± 3.24	27.96 ± 2.60	0.889
Max dP/dt (mmHg/s)	771.19 ± 199.02	698.43 ± 134.04	0.087
Min dP/dt (mmHg/s)	−816.32 ± 170.80	−614.87 ± 169.71	0.002
End-diastolic pressure (mmHg)	13.41 ± 2.43	13.69 ± 3.16	0.725
End-systolic pressure (mmHg)	73.78 ± 9.55	64.86 ± 8.24	<0.001
End-diastolic volume (mL)	92.88 ± 16.36	100.70 ± 16.85	0.098
End-systolic volume (mL)	45.62 ± 7.78	56.62 ± 8.34	0.005
Trans-esophageal cardiac ultrasound analysis			
Emax (cm/s)	48.11 ± 10.26	52.23 ± 11.92	0.419
E deceleration time (ms)	89.80 ± 27.30	73.70 ± 17.06	0.166
Amax (cm/s)	60.63 ± 12.19	46.02 ± 13.33	0.317
E VTI (cm)	5.07 ± 1.29	4.87 ± 1.36	0.536
A VTI (cm)	2.43 ± 0.95	2.48 ± 0.95	0.934
Ea max (cm/s)	7.55 ± 2.24	7.42 ± 2.76	0.854
Aa max (cm/s)	10.81 ± 3.71	10.06 ± 2.86	0.337
Ea max (cm/s)	5.30 ± 0.91	5.46 ± 1.13	0.579
Ea VTI (cm)	0.61 ± 0.16	0.55 ± 0.23	0.368
Aa VTI (cm)	0.54 ± 0.12	0.52 ± 0.14	0.341
Ea VTI (cm)	1.18 ± 0.22	1.03 ± 0.21	0.027
E/A ratio	1.01 ± 0.22	1.20 ± 0.41	0.256
E/E'	7.67 ± 2.49	7.71 ± 2.62	0.122

Results are reported as mean ± standard deviation or median (interquartile range) when appropriate. Paired t-test and Wilcoxon signed rank test were employed for normal and non-normal distributed datasets. Data obtained for post-occlusion were on average gathered after 20 min upon coronary occlusion.

such as left ventricular systolic time (LVST) was better correlated with its PV associated parameter (max to min dP/dt) ($r^2 = 0.876$, $p < 0.0001$) (**Figure 3C**). This was valid for an additional and even longer STI EMST: QS2 strongly correlated with Q to min dP/dt ($r^2 = 0.9583$, $p < 0.0001$) (**Figure 3D**).

As DTIs are concerned, AC and PV defined similar overlapping intervals: PV diastolic filling time was significantly correlated with AC perfusion time (PT or S2-Q) ($r^2 = 0.9689$, $p < 0.0001$) (**Figure 3F**) as well as with AC diastolic time (DT or S2-S1) ($r^2 = 0.9689$, $p < 0.0001$) (**Figure 3E**).

Figure 4 shows scatterplots correlating quantifiable heart sound features (DV as explained above) with indexes of systolic and diastolic function. Cardiac output was significantly correlated with Audicor S3 DV (**Figure 4A**) ($r^2 = 0.0791$, $p = 0.0023$) which was not valid for Audicor S4 DV (**Figure 4B**) ($r^2 = 0.0014$, $p = 0.6904$). As for diastolic function assessment, Tau weakly correlated with Audicor S3 DV (**Figure 4C**) ($r^2 = 0.0342$, $p = 0.0472$), however, a more significant correlation was found with Audicor S4 DV (**Figure 4D**) ($r^2 = 0.2721$, $p < 0.0001$).

Heatmaps provide valuable information regarding the fold change of various parameters and their respective statistical significance during the first 5 min of coronary occlusion in comparison to baseline measurements as reported in **Figure 5**.

Among them, PV identified these parameters as significantly changed within the 5-min observation time: left ventricular ejection fraction (LVEF) (up to −12.1%), stroke work (SW) (up to −22.7%), min dP/dt (up to −18.5%), max dP/dt/end diastolic volume (up to −9.7%), left ventricular end systolic pressure (LVESP) (up to −15.1%), left ventricular end systolic volume (LVESV) (up to +19.0%), pre-recruitable stroke work (PRSW) (up to−23.7%), Q to max dP/dt (up to −10.2%). Of note, SW, min dP/dt and ESP were significantly and constantly decreased compared to baseline reference at every timepoint during the 5 min observation window.

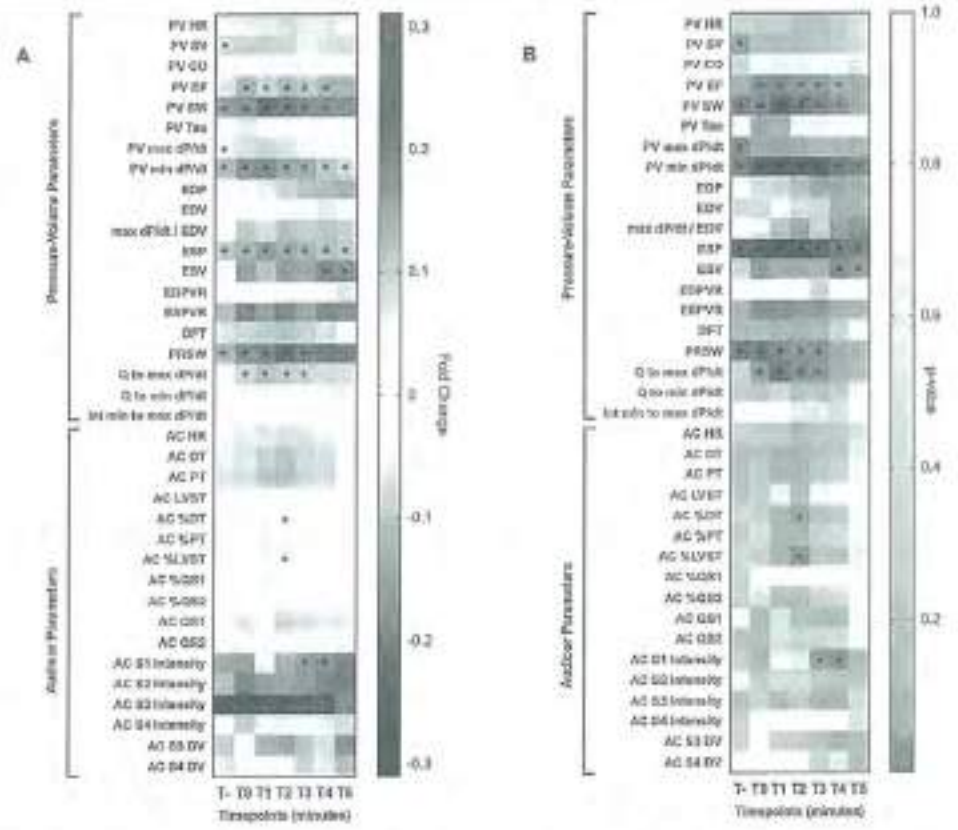

FIGURE 5 | Heatmaps. **(A)** Reported fold changes obtained by comparing baseline measurement with their respective at each minute for 5 min upon coronary occlusion. **(B)** Reported two tailed *t*-test *p*-values obtained by with the same exact approach employed for the other heatmap. HR, heart rate; SV, stroke volume; CO, cardiac output; EF, ejection fraction; EDP, end diastolic pressure; EDV, end diastolic volume; ESP, end systolic pressure; ESV, end systolic volume; EDPVR, end diastolic pressure-volume relationship; ESPVR, end systolic pressure-volume relationship; DFT, diastolic filling time; PRSW, pre-recruitable stroke work; DT, diastolic time; PT, perfusion time; LVST, left ventricular systolic time; DV, display value. Significant changes are marked with an asterisk sign (*).

On the other hand, AC identified the following parameters as significantly changed in comparison to baseline: diastolic time percentage (DT%) (up to −3.7%), left ventricular systolic time percentage (up to + 6.3%) and first heart sound intensity (up to −20.8%). Single dataset trends over our observation window for AC parameters are presented for clarity in **Figure 6**.

As anticipated, **Figure 7A** shows the four significant AC parameters in terms of predictive power in detecting an ischemic condition: Heart Rate (AUC 0.720, CI95% 0.592–0.849, $p < 0.001$), Diastolic Time (AUC 0.675, CI95% 0.556–0.795, $p = 0.008$), S3 DV (AUC 0.654, CI95% 0.544–0.763, $p = 0.019$), Perfusion Time (AUC 0.649, CI95% 0.528–0.770, $p = 0.024$). With the intention of identifying a more powerful joint-index that could outperform any of the above mentioned single parameters we employed models upon linear regression with different combinations of the four AC parameters shown in **Figure 7A**. **Figure 7B** shows the three most significant joint-indexes: HR + DT + PT + S3DV (AUC 0.770, CI95% 0.663–0.877, $p < 0.001$), HR + S3DV (AUC 0.768, CI95% 0.658–0.878, $p < 0.001$), HR + PT + S3DV (AUC 0.767, CI95% 0.658–0.878, $p < 0.001$).

DISCUSSION

Reintroducing an Old Technique

Cardiac auscultation has known a crescendo-decrescendo use trend in the medical community. Despite acknowledging the usefulness of information obtained by auscultatory examination, other diagnostic methods are usually preferred. Nevertheless the digitalization, in addition to the ECG coupling has propelled new interest in acoustics in light of the minimal invasiveness of such technique. Being already proven as an effective diagnostic and prognostic method, we envisioned a diagnostic role of AC in the setting of myocardial ischemia, a well-known condition characterized by mechanical dysfunction that could be detectable in the first minutes of coronary occlusion. In the past, different investigations have led to divergent results in light of heterogeneous infarct sizes, adrenergic tone, time of infarct onset and adopted methods of detection (Hamosh et al., 1972; Weissler, 1987).

In order to overcome a number of these biases, we employed a porcine model of AMI by occluding the coronary artery at similar levels of the coronary tree thus reducing confounding factors in

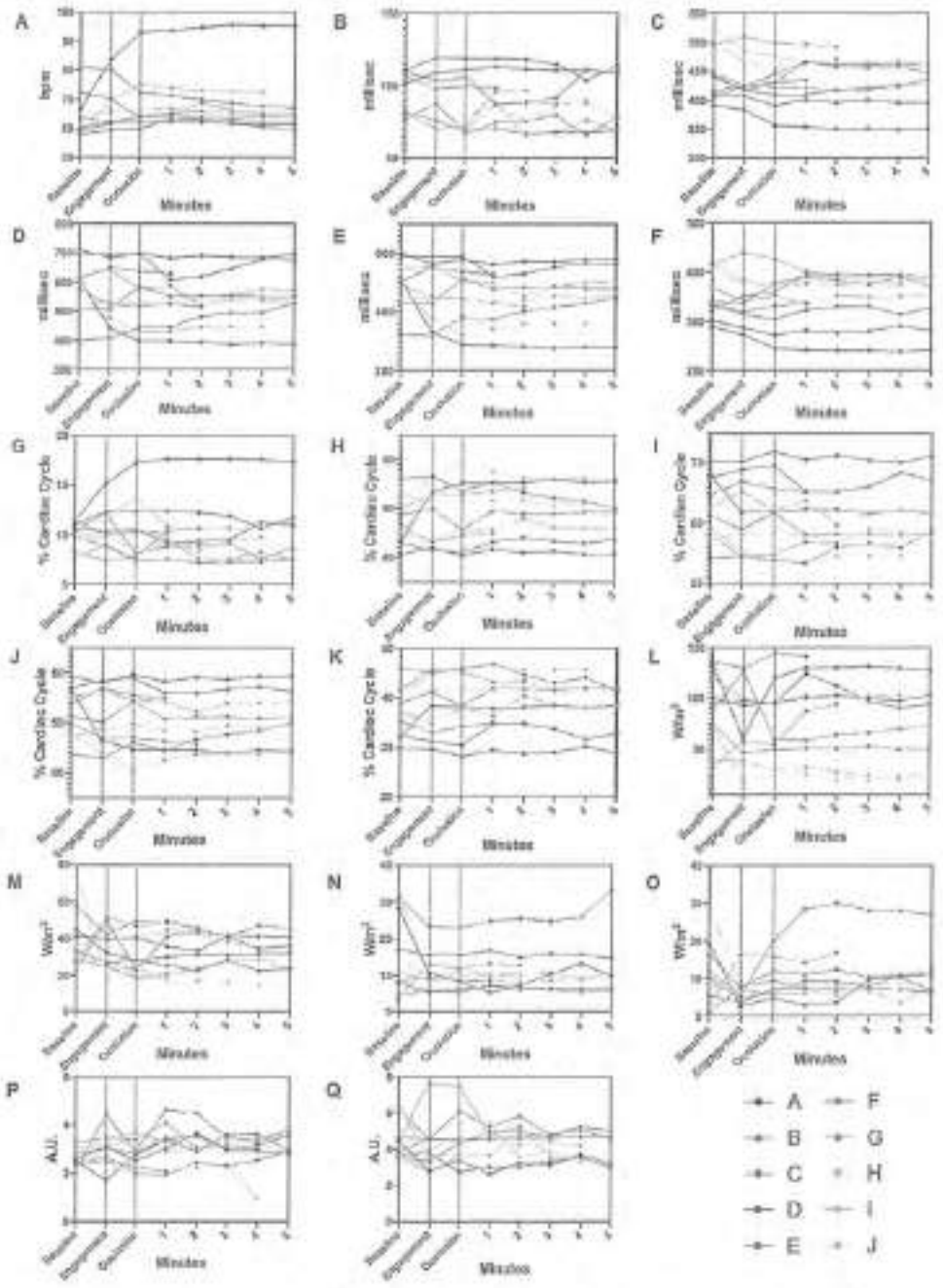

FIGURE 6 | Single Datapoint Charts AC parameters shown for each animal from baseline, pre-ischemia, and ischemia phases. Dashed lines delimit the three different experimental steps. **(A)** heart rate, **(B)** QS1, **(C)** QS2, **(D)** Diastolic time, **(E)** Perfusion time, **(F)** Left ventricular systolic time, **(G)** QS1 shown in percentage of a complete cardiac cycle, **(H)** QS2 shown in percentage of a complete cardiac cycle, **(I)** Diastolic time shown in percentage of a complete cardiac cycle, **(J)** Perfusion time shown in percentage of a complete cardiac cycle, **(K)** Left ventricular systolic time shown in percentage of a complete cardiac cycle, **(L)** S1 Intensity, **(M)** S2 Intensity, **(N)** S3 Intensity, **(O)** S4 Intensity, **(P)** S3 display value, **(Q)** S4 display value. Color-coded legends are provided for single animal identification.

a stable and rapidly evolving condition by dissecting the role of acoustic changes and derivative parameters in AMI.

Table 1 offers a rapid overview of myocardial dysfunction observed in our porcine model. These significant changes are observed on average 20 min after coronary occlusion and they are not expected to change to this magnitude in the very first minutes during ischemia. However, our multimodal realtime recording allows the detection of several parameters that can

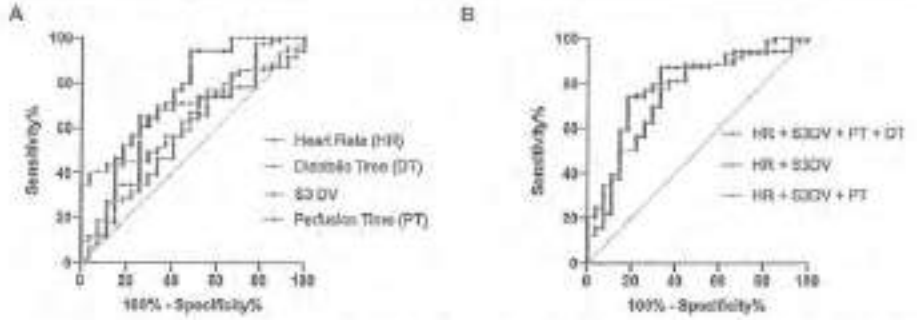

Parameters	AUC	95% CI	p-value
Heart Rate	0.720	0.592 – 0.848	<0.001
Diastolic Time	0.675	0.556 – 0.795	0.008
S3 DV	0.694	0.544 – 0.768	0.019
Perfusion Time	0.640	0.528 – 0.775	0.024

Models	AUC	95% CI	p-value
HR+S3DV+DT+PT	0.770	0.663 – 0.877	<0.001
HR+S3DV	0.768	0.656 – 0.876	<0.001
HR+S3DV+PT	0.767	0.658 – 0.876	<0.001

FIGURE 7 | Area under the receiver operating characteristic curves AC parameters were tested for ischemia detection. AUC, 95% confidence interval and *p*-values are included. **(A)** The significant single AC parameters (HR, PT, DT, S3DV) are here reported. **(B)** Combinatory models derived from logistic regression outperforming single parameters are reported.

rapidly change upon ischemia and might represent candidates of damage sensing.

Systolic Time Intervals

Contractile dysfunction can be detected by abnormalities in force generation, wall shortening, ejected blood volume and temporal relationships of contraction phases (Boudoulas, 1990).

As shown in the heatmaps in **Figure 5**, indexes of dysfunction were already detectable in the first minute after occlusion and permanently present with invasive techniques (SW, LVESP, min dP/dt, PRSW). In regard to STIs, their correlations were significant between the techniques employed in our study, particularly for longer duration intervals (**Figures 3C,D**).

As extensively described by Lewis, STIs bear limited diagnostic significance in AMI compared to chronic conditions particularly if no pre-existing comorbidities are present, as in the case of our study (Lewis et al., 1977). In the setting of myocardial infarction, the shortening of QS1 is paradoxically coupled with an increase of QS percentage (QS1%). Despite being non-significant, both trends are not mutually exclusive, in fact they are in accordance with the rationales to which the absolute shortening (QS1) is driven by an adrenergic burst and the relative prolongation (QS1%) is due to diminished rate of increase in LV pressure in isovolumic contraction (Boudoulas, 1990). Unfortunately, max dP/dt abruptly decreases in the first seconds of ischemia (10% relative reduction) but it is not coupled with a relevant QS1% magnitude increase (4% relative increase) supporting the notion that STIs, especially EMAT (QS1), should be solely employed for prognosis in convalescence phase (Diamant and Killip, 1970) rather than diagnosis in the acute setting of myocardial infarction (Hamosh et al., 1972; Hodges et al., 1972). On the other hand, PV assessment rapidly identified significant shortening of the compared STI (Q to max dP/dt) proving a superior sensitivity over AC for these specific intervals (**Figure 3B**) The main difference observed in this suboptimal comparison relies on the fact that the interval Q to max dP/dt, also known as Pre-Ejection Period (PEP), is a much longer interval, which encompasses EMAT, and it is markedly affected by systolic dysfunction, whilst EMAT is a shorter interval that is majorly prolonged in case of conduction defect.

Diastolic Time Intervals

With regard to DTIs, our study provides evidence of significant correlations between PV and AC analysis in identifying overlapping intervals. Of note is the significant reduction observed in diastolic time (expressed as percentage within the entire cardiac cycle) upon coronary occlusion even with a non-invasive method, therefore configuring itself as a possible criterion for ischemic damage. Despite being significant for a single timepoint, statistical significance was reached with a relatively small sample as our cohort and more importantly this finding is not unexpected. In fact, clinical investigations conducted by Ferro et al. (1991, 1995) have proven the relevance of diastolic time in assessing degree of coronary occlusion and stress-induced ischemic threshold. In support of such findings, AUC of ROC identified both diastolic and perfusion times (reported as unit of time) as possible parameters with clinical significance in detecting ischemic acute event.

Whether reported as unit of time or as a ratio, diastolic duration, appears as pivotal indicator of ischemic damage independently of the primary limiting factor: coronary lumen patency or vasodilator capacity in coronary artery disease or syndrome X patients, respectively.

Heart Sounds

The prominent feature of AC is certainly the quantification of heart sound properties, particularly diastolic ones, which are of difficult interpretation even for experienced clinicians (Marcus et al., 2006; Vukanovic-Criley et al., 2006).

The S3 and S4 heart sounds are diastolic filling cardiac sounds generated for a series of pathological causes. They are validated as relatively specific and non-invasive indicators of

heart failure (Shah et al., 1968) and found to appear during acute ischemia (Harris et al., 2006). The former is caused by a limited longitudinal expansion of the ventricular wall during early diastolic filling yielding to a rapid deceleration of ejected blood (Ozawa et al., 1983a,b) and it correlates with parameters of impaired diastolic function in particular left ventricular filling pressures (Kono et al., 1993; Tribouilloy et al., 2001; Horwich et al., 2003). Not surprisingly, in our study, S3 DV rapidly increases (+ 19% at minute 5) along with augmented filling pressures (LVEDP + 14% at minute 5) consistent with the body of literature produced on this subject in the last decades. Out of a series of indexes of systolic function S3 DV better and inversely correlated with Cardiac Output (**Figure 4A**). In addition, S3 DV itself was proven as a statistically significant parameter ($p = 0.019$, **Figure 7**) for ischemic damage detection.

On the other hand S4, is a better indicator of diastolic stiffness and our dataset confirms such axiom as S4 DV positively and significantly correlated with the isovolumic relaxation constant (Tau) (**Figure 4D**). These findings are in line with the current knowledge in physiology proving a degree of specificity of these two heart sounds in detecting two contemporary yet distinct defects occurring during AMI.

Study Limitations

The current study has a number of contemplated limitations: here we presented a pre-clinical study with a relatively small cohort composed of healthy animals under general anesthesia. Despite the abovementioned limitations, our experience sheds light on putative immediate mechanical alterations that would be otherwise unfeasible to replicate in a real-world clinical scenario and it might represent a reference point for future studies involving AC with more complex and heterogenous conditions.

CONCLUSION

In conclusion, the present study provides novel and preliminary evidence of the usefulness, reliability and responsiveness of AC in detecting mechanical defects (particularly S3 heart sound and DTIs) appearing in the very first minutes during coronary occlusion. This responsive detection might have a possible application in peculiar patient subpopulations who would benefit from a chronic, non-invasive monitoring approach. Lastly, the digitalization of this hybrid technique will allow the quantification of acoustic parameters which could be of great diagnostic importance (Schwartz and Little, 1961) in an unbiased manner and, more importantly, independently of operator's expertise (Mangione and Nieman, 1997) and propel new interest toward this non-invasive method.

ETHICS STATEMENT

The animal housing and experimental protocols were approved by the Cantonal Veterinary Department, Zurich, Switzerland, under license no. ZH 219/2016, and were in accordance with Swiss Animal Protection Law. Housing and experimental procedures also conformed to the European Directive 2010/63/EU of the European Parliament and of the Council on the Protection of Animals used for scientific purposes and to the Guide for the Care and Use of Laboratory Animals (Institute of Laboratory Animal Resources, National Research Council, National Academy of Sciences, 2011).

AUTHOR CONTRIBUTIONS

NC, PB, AG, ER, PE, MZ, and FM conceived and designed the study. MaL, MS, SK, PA, PB, and MZ analyzed the data. MaL and PA performed the statistical analysis. MaL wrote the first draft of the manuscript. NC, MiL, PA, and MZ wrote the sections of the manuscript. All authors contributed to the manuscript revision, and read and approved the submitted version.

FUNDING

This work was co-sponsored by the Schweizerische Herz- und Kreislauf- Stiftung (SHK) and VisCardia, Inc.

REFERENCES

Boudoulas, H. (1990). Systolic time intervals. *Eur. Heart J.* 11(Suppl. I), 93–104.

Chan, W., Woldeyohannes, M., Colman, R., Anand, P., Michaels, A. D., Parker, J. D., et al. (2013). Haemodynamic and structural correlates of the first and second heart sounds in pulmonary arterial hypertension: an acoustic cardiography cohort study. *BMJ Open* 3:e002660. doi: 10.1136/bmjopen-2013-002660

Diamant, B., and Killip, T. (1970). Indirect assessment of left ventricular performance in acute myocardial infarction. Circulation 42, 579–593. doi: 10.1161/01.cir.42.4.579

Dillier, R., Kohn, R., Erne, S., Zuber, M., Arand, P., and Erne, P. (2010). Noninvasive detection of left-ventricular systolic dysfunction by acoustic cardiography in atrial fibrillation. *Cardiol. Res. Pract.* 2011:173102. doi: 10.4061/2011/173102

Erne, P. (2008). Beyond auscultation–acoustic cardiography in the diagnosis and assessment of cardiac disease. *Swiss. Med. Wkly.* 138, 439–452.

Ferro, G., Dallio, C., Spinelli, L., Lucci, G. A., Marra, F., and Indolfi, C. (1995). Relation between diastolic perfusion time and coronary artery stenosis during stress-induced myocardial ischemia. *Circulation* 92, 342–347. doi: 10.1161/01.cir.92.3.342

Ferro, G., Spinelli, L., Dallio, C., Spadafora, M., Guarracciu, F., and Condorelli, M. (1991). Diastolic perfusion time at ischemic threshold in patients with stress-induced ischemia. *Circulation* 84, 49–56. doi: 10.1161/01.cir.84.1.49

Hanoch, P., Cohn, J. N., Engelman, E., and Broder, M. F. E. (1972). Systolic time intervals and left ventricular function in acute myocardial infarction. *Circulation* 45, 375–381. doi: 10.1161/01.cir.45.2.375

Harris, I. S., Lee, E., Yeghiazarians, Y., Drew, B. J., and Michaels, A. D. (2006). Phonocardiographic timing of third and fourth heart sounds during acute myocardial infarction. *J. Electrocardiol.* 39, 305–309. doi: 10.1016/j.jelectrocard.2005.12.004

Hodges, M., Halpern, B. L., Preisinger, G. C., and Dagenais, G. R. (1972). Left ventricular projection period and ejection time in patients with acute myocardial infarction. Circulation 45, 933–942. doi: 10.1161/01.cir.45.5.933

Horwich, T. B., Patel, J., Macellan, W. R., and Fonarow, G. C. (2003). Cardiac troponin I is associated with impaired hemodynamics, progressive left ventricular dysfunction, and increased mortality rates in advanced heart failure. *Circulation* 108, 833–838. doi: 10.1161/01.cir.0000084543.79087.34

Koro, T., Ibrman, H., Alam, M., Stein, P. D., and Sabbah, H. N. (1993). Hemodynamic correlates of the third heart sound during the evolution of chronic heart failure. *J. Am. Coll. Cardiol.* 21, 419–423. doi: 10.1016/0735-1097(93)90684-s

Lee, E., Drew, B. J., Sylvester, R. H., and Michaels, A. D. (2009). Diastolic heart sounds as an adjunctive diagnostic tool with ST criteria for acute myocardial ischemia. *Acute Card. Care* 11, 229–235. doi: 10.1080/17482940903203071

Lewis, R. P., Rittogers, S. F., Froester, W. F., and Boudoulas, H. (1977). A critical review of the systolic time intervals. *Circulation* 56, 146–158.

Mangione, S., and Nieman, L. Z. (1997). Cardiac auscultatory skills of internal medicine and family practice trainees. A comparison of diagnostic proficiency. *JAMA* 278, 717–722. doi: 10.1001/jama.278.9.717

Marcus, G. M., Gerber, I. L., McKeown, B. H., Vessey, J. C., Jordan, M. V., Huddleston, M., et al. (2005). Association between phonocardiographic third and fourth heart sounds and objective measures of left ventricular function. *JAMA* 295, 2238–2244.

Marcus, G. M., Vessey, J., Jordan, M. V., Huddleston, M., McKeown, B., Gerber, I. L., et al. (2006). Relationship between accurate auscultation of a clinically useful third heart sound and level of experience. *Arch. Intern. Med.* 166, 617–622.

Ozawa, Y., Smith, D., and Craige, E. (1983a). Origin of the third heart sound. I. Studies in dogs. *Circulation* 67, 393–398. doi: 10.1161/01.cir.67.2.393

Ozawa, Y., Smith, D., and Craige, E. (1983b). Origin of the third heart sound. II. Studies in human subjects. *Circulation* 67, 399–404. doi: 10.1161/01.cir.67.2.399

Schwartz, M. L., and Little, R. C. (1961). Physiologic basis for the heart sounds and their clinical significance. *N. Engl. J. Med.* 264, 280–285. doi: 10.1056/nejm196102092640606

Shah, P. M., Gramiak, R., Kramer, D. H., and Yu, P. N. (1968). Determinants of atrial (S4) and ventricular (S3) gallop sounds in primary myocardial disease. *N. Engl. J. Med.* 278, 753–758. doi: 10.1056/nejm196804042781402

Thomas, J. L., Winther, S., Wilson, R. F., and Bottcher, M. (2017). A novel approach to diagnosing coronary artery disease: acoustic detection of coronary turbulence. *Int. J. Cardiovasc. Imaging* 33, 129–136. doi: 10.1007/s10554-016-0970-5

Triboulloy, C. M., Enriquez-Sarano, M., Mahoy, D., Hoen, R. A., Bailey, K. R., Seward, J. B., et al. (2001). Pathophysiologic determinants of third heart sounds: a prospective clinical and Doppler echocardiographic study. *Am. J. Med.* 111, 96–102. doi: 10.1016/s0002-9343(01)00769-6

Vukanovic-Criley, J. M., Criley, S., Warde, C. M., Boker, J. R., Guevara-Matheus, L., Churchill, W. H., et al. (2006). Competency in cardiac examination skills in medical students, trainees, physicians, and faculty: a multicenter study. *Arch. Intern. Med.* 166, 610–616.

Wang, B., Chang, S. L., Lin, Y. J., Lo, L. W., Hu, Y. F., Chao, T. F., et al. (2019). Early detection of electromechanical dysfunction in patients with idiopathic premature ventricular contractions. *Pacing Clin. Electrophysiol.* 42, 637–645. doi: 10.1111/pace.13650

Wang, S., Lam, Y. Y., Liu, M., Fang, F., Wang, L., Shang, Q., et al. (2013). Acoustic cardiography helps to identify heart failure and its phenotypes. *Int. J. Cardiol.* 167, 681–686. doi: 10.1016/j.ijcard.2012.03.067

Wang, S., Liu, M., Fang, F., Shang, Q., Sun, J. P., Sanderson, J. E., et al. (2016). Prognostic value of acoustic cardiography in patients with chronic heart failure. *Int. J. Cardiol.* 219, 121–126. doi: 10.1016/j.ijcard.2016.06.004

Weissler, A. M. (1987). The systolic time intervals and risk stratification after acute myocardial infarction. *J. Am. Coll. Cardiol.* 9, 161–163. doi: 10.1016/s0735-1097(87)80095-5

Zuber, M., and Erne, P. (2010). Acoustic cardiography to improve detection of coronary artery disease with stress testing. *World J. Cardiol.* 2, 118–124. doi: 10.4330/wjc.v2i5.118

Conflict of Interest Statement: PA and PB work for VisCardia, Inc., United States.

The remaining authors declare that the research was conducted in the absence of any commercial or financial relationships that could be construed as a potential conflict of interest.

Copyright © 2019 Luciani, Saccucci, Kuwata, Cosirovic, Lipski, Arand, Bauer, Goldstein, Regis, Erne, Zuber and Maisano. This is an open-access article distributed under the terms of the Creative Commons Attribution License (CC BY). The use, distribution or reproduction in other forums is permitted, provided the original author(s) and the copyright owner(s) are credited and that the original publication in this journal is cited, in accordance with accepted academic practice. No use, distribution or reproduction is permitted which does not comply with these terms.

International Journal of
Environmental Research and Public Health

MDPI

Article

Effects of αβ-Blocker Versus β1-Blocker Treatment on Heart Rate Response During Incremental Cardiopulmonary Exercise in Japanese Male Patients with Subacute Myocardial Infarction

Shinji Nemoto [1,2,*], Yusuke Kasahara [1], Kazuhiro P. Izawa [3], Satoshi Watanabe [4], Kazuya Yoshizawa [5], Naoya Takeichi [4], Kentaro Kamiya [2], Norio Suzuki [6], Kazuto Omiya [7], Atsuhiko Matsunaga [2] and Yoshihiro J. Akashi [8]

1. Department of Rehabilitation Medicine, St. Marianna University School of Medicine Yokohama City Seibu Hospital, Yokohama 241-0811 Japan
2. Department of Rehabilitation Sciences, Kitasato University Graduate School of Medical Sciences, Sagamihara 252-0373, Japan
3. Department of Public Health, Kobe University Graduate School of Health Sciences, Kobe 654-0142, Japan
4. Department of Rehabilitation Medicine, St. Marianna University School of Medicine Hospital, Kawasaki 216-8511, Japan
5. Department of Rehabilitation Medicine, Kawasaki Municipal Tama Hospital, Kawasaki 214-8525, Japan
6. Division of Cardiology, Department of Internal Medicine, St. Marianna University School of Medicine Yokohama City Seibu Hospital, Yokohama 241-0811, Japan
7. Department of Internal Medicine, Shimazu Medical Clinic, Yokohama 226-0026, Japan
8. Division of Cardiology, Department of Internal Medicine, St. Marianna University School of Medicine Hospital, Kawasaki 216-8511, Japan

* Correspondence: shinji4df@marianna-u.ac.jp; Tel.: +81-45-366-1111

Received: 24 June 2019; Accepted: 7 August 2019; Published: 8 August 2019

check for updates

Abstract: A simplified substitute for heart rate (HR) at the anaerobic threshold (AT), i.e., resting HR plus 30 beats per minute or a percentage of predicted maximum HR, is used as a way to determine exercise intensity without cardiopulmonary exercise testing (CPX) data. However, difficulties arise when using this method in subacute myocardial infarction (MI) patients undergoing beta-blocker therapy. This study compared the effects of αβ-blocker and β1-blocker treatment to clarify how different beta blockers affect HR response during incremental exercise. MI patients were divided into αβ-blocker ($n = 67$), β1-blocker ($n = 17$), and no-β-blocker ($n = 47$) groups. All patients underwent CPX one month after MI onset. The metabolic chronotropic relationship (MCR) was calculated as an indicator of HR response from the ratio of estimated HR to measured HR at AT (MCR-AT) and peak exercise (MCR-peak). MCR-AT and MCR-peak were significantly higher in the αβ-blocker group than in the β1-blocker group ($p < 0.001$, respectively). Multiple regression analysis revealed that β1-blocker but not αβ-blocker treatment significantly predicted lower MCR-AT and MCR-peak ($\beta = -0.432$, $p < 0.001$; $\beta = -0.473$, $p < 0.001$, respectively). Based on these results, when using the simplified method, exercise intensity should be prescribed according to the type of beta blocker used.

Keywords: myocardial infarction; beta-blocker; metabolic chronotropic relationship; chronotropic index; heart rate response; cardiac rehabilitation

1. Introduction

Many guidelines recommend exercise training for patients with myocardial infarction (MI) [1,2] because exercise training has been associated with reduced cardiovascular mortality after acute MI [3].

When prescribing exercise for subacute MI patients, it is important to determine the optimum exercise intensity to ensure safe and effective training. The recommended technique for determining the target heart rate (HR) is by measuring HR at the anaerobic threshold (AT) via cardiopulmonary exercise testing (CPX). Exercise prescription using HR at AT is effective and safe for MI patients [4,5]. Although prescribing exercise intensity based on the AT measured by CPX is desirable, it is not easy to perform CPX for all patients due to staffing requirements and the high cost of equipment. It is recommended to first perform an exercise stress test to determine the target HR range by the Karvonen formula, if gas-exchange analysis data cannot be obtained [2]. Meanwhile, a simplified substitute for HR at AT, i.e., resting HR plus 30 beats per minute (bpm) or a percentage of predicted maximum HR (% predicted max HR), is used as a way to determine exercise intensity without gas-exchange analysis data or exercise stress test data [2,6]. This simplified method, however, is considered difficult to use if patients are undergoing beta-blocker treatment, since beta blockers reportedly affect calculations by reducing HR responses during incremental exercise [7,8]. Although the negative chronotropic effect of beta blockers is considered to differ depending on beta-blocker type (e.g., αβ-blocker or β1-blocker), previous studies have not fully evaluated the effects of beta-blocker type on HR response during incremental exercise in subacute MI patients. The effect of beta-blocker type on this simplified method of exercise prescription, therefore, remains unclear. The present study aimed to compare the effects of αβ-blockers and β1-blockers on HR response during incremental exercise in subacute MI patients, because both αβ-blockers and β1-blockers are frequently prescribed for MI patients due to their effectiveness [9–11]. Clarifying differences in the effects of αβ-blockers and β1-blockers on HR response would help physicians to prescribe appropriate exercise intensities for subacute MI patients who are undergoing beta-blocker treatment.

2. Materials and Methods

2.1. Study Design and Patients

A total of 665 consecutive acute MI patients underwent cardiac rehabilitation at St. Marianna University School of Medicine, Yokohama City Seibu Hospital, between June 1998 and March 2018. Of these, 297 were able to undergo symptom-limited CPX one month after the onset of MI, and 131 who did not meet the following exclusion criteria were enrolled in this retrospective cross-sectional study: the presence of atrial fibrillation, complex arrhythmia, or pacemaker; recent myocardial infarction; history of cardiac surgery; female sex; maximum respiratory exchange ratio (RER) during CPX < 1.10; and use of drugs other than beta blockers with positive or negative chronotropic effects (e.g., verapamil, diltiazem hydrochloride). Patients were divided into the following three groups according to the type of beta blocker used: the αβ-blocker group (67 patients), the β1-blocker group (17 patients), and the no-β-blocker group (47 patients). All patients were clinically stable and were examined while being treated with stable doses of medication.

The study protocol conformed to the ethical guidelines of the Declaration of Helsinki and was approved by the Ethics Committee of St. Marianna University School of Medicine (Chairperson of the Ethics Committee, Masashi Taki; Protocol No. 2258; date of approval by the Ethics Committee, November 30, 2012). Informed consent was obtained from all patients before conducting CPX.

2.2. Clinical Characteristics

Age, body mass index (BMI), site of infarction, residual coronary artery stenosis, past medical history, complications, medications, beta-blocker dose, time between MI onset and exercise testing, and year of hospitalization were evaluated through a review of patient medical records. The ratio of administered beta-blocker dose to maximum beta-blocker dose (% maximum beta-blocker dose) was calculated by dividing the administered beta-blocker dose by the maximum beta-blocker dose for Japanese patients (e.g., carvedilol 20 mg/day, bisoprolol 5 mg/day, and atenolol 50 mg/day). Maximum serum creatine kinase-myocardial band (max CK-MB) was measured using blood samples obtained

during hospitalization. Left ventricular ejection fraction (LVEF) was echocardiographically determined by a modified Simpson's method and used as the index of left ventricular systolic function at the time of hospital discharge.

2.3. Symptom-Limited CPX

All patients underwent symptom-limited CPX using a treadmill (MAT-2700, Fukuda Denshi Co., Tokyo, Japan). After three minutes of resting in a seated position, patients performed exercises with an increasing load (speed or grade) every 60 s after three minutes of warm-up activity (1 mph speed, 0% grade [12]. A 12-lead electrocardiogram was continuously monitored, and HR was measured from the R-R interval of the electrocardiogram (ML-9000, Fukuda Denshi Co., Tokyo, Japan) during the test. Systolic blood pressure (SBP) and diastolic blood pressure (DBP) were measured using a blood pressure cuff and an automatic blood pressure monitor (STBP-780, Colin Co., Aichi, Japan) at one-minute intervals. Oxygen uptake (VO_2), carbon dioxide production, minute ventilation, tidal volume, end-tidal O_2, and end-tidal CO_2 were measured throughout the test using an aeromonitor (AE-310s, Minato Ikagaku Co., Tokyo, Japan). Expired gas was sampled using a breath-by-breath method. The endpoint of testing was determined as previously described [13]. Specifically, the appearance of a plateau in VO_2 despite an increasing exercise intensity indicated the exercise endpoint.

Ventilatory equivalents were calculated for O_2, CO_2, and RER using a personal computer (Model PC-9801, NEC Co., Tokyo, Japan). AT was determined by the V-slope method [14].

HR at rest (HR_{rest}), HR at AT (HR_{AT}), and HR at peak VO_2 (HR_{peak}) were determined from the recorded HR during the course of CPX. Increases from HR_{rest} to HR_{peak} (Δpeak HR), from HR_{rest} to HR_{AT} (ΔAT HR), and from HR_{AT} to HR_{peak} (ΔAT-peak HR) were calculated for all patients.

2.4. Calculation of the Chronotropic Index

The metabolic chronotropic relationship (MCR), also referred to as the chronotropic index, was calculated as an indicator of HR response during incremental exercise at each stage (i.e., AT and peak VO_2) based on the relationship between HR and VO_2 during exercise [15–17]. The MCR, proposed by Wilkoff, allows for comparison between patients irrespective of age, physical fitness, functional capacity, exercise testing mode, or protocol. Estimated HR was calculated at AT and peak VO_2 using the following formula:

$$\text{Estimated } HR_{stage} = (220 - \text{age} - HR_{rest}) \times [(METs_{stage} - 1) / (METs_{peak} - 1)] + HR_{rest}, \quad (1)$$

where metabolic equivalents (METs) were defined as VO_2 (ml/kg/min) divided by 3.5. The chronotropic index at AT (MCR-AT) was calculated as the ratio of estimated HR_{AT} to measured HR_{AT}, and at peak VO_2 (MCR-peak) was calculated as the ratio of estimated HR_{peak} to measured HR_{peak}, as follows:

$$\text{MCR-AT} = HR_{AT} / \text{estimated } HR_{AT}, \quad (2)$$

$$\text{MCR-peak} = HR_{peak} / \text{estimated } HR_{peak}, \quad (3)$$

MCR-AT and MCR-peak were used as indicators of HR response to incremental exercise up to the AT and peak exercise, respectively. A chronotropic index < 0.8 was previously determined to indicate chronotropic incompetence [15,16].

2.5. Statistical Analysis

Results are expressed as mean ± standard error (SE). The Kolmogorov–Smirnov test was performed to assess the normality of distribution. Differences in clinical characteristics, CPX results, and MCR findings among the three groups were analyzed using one-way analysis of variance (ANOVA), χ^2 test, and Tukey's honestly significant difference test. Tukey's honestly significant difference test

was used if the results of one-way ANOVA were statistically significant. Pearson's correlation coefficient and Spearman's rank correlation coefficient were used in a regression analysis to determine correlations between MCR-AT, MCR-peak, and clinical characteristics (age and BMI were excluded from correlations as the formula of MCR included these factors), and correlations in which $p < 0.2$ were considered statistically significant. Correlations, clinically important factors on the nominal scale, αβ-blocker treatment, and β1-blocker treatment were entered into a multiple regression model for predictions of MCR-AT or MCR-peak using the forced-entry method. For patients undergoing beta-blocker treatment, Spearman's rank correlation coefficient was used to examine correlations between MCR-AT, MCR-peak, and % maximum beta-blocker dose. $p < 0.05$ was considered statistically significant. All statistical analyses were performed with JMP® Pro 13 (SAS Institute Inc., Cary, NC, USA). A priori power analysis was performed for multiple regression analysis using G*Power 3 (Heinrich-Heine-Universität, Düsseldorf, Germany). The sample size was calculated to be 123 in the regression model for MCR-peak (effect size = 0.15; α error probability = 0.05; power (1−β error probability) = 0.8; number of predictors = 11). Accordingly, the sample size of the present study was considered sufficient for conducting multiple regression analysis. Effect sizes were also calculated using G*Power 3.

3. Results

Table 1 shows the clinical characteristics of patients included in this study. Significant differences between αβ-blocker, β1-blocker, and no-β-blocker groups were observed in renin-angiotensin system inhibitor treatment and hospitalization before 2006 ($p = 0.024$ and $p < 0.001$, respectively). The value of % maximum beta-blocker dose was significantly lower in the αβ-blocker group compared to the β1-blocker group ($p < 0.001$). No significant differences were observed in other clinical characteristics between the three groups.

Table 1. Patient clinical characteristics.

Clinical Characteristics	αβ-Blocker Group (n = 67)	β1-Blocker Group (n = 17)	No-β-Blocker Group (n = 47)	p-Value
Age (years)	64.98 ± 10.48	61.59 ± 8.91	61.62 ± 10.83	0.184
Body mass index (kg/m²)	23.44 ± 2.78	23.58 ± 3.27	23.12 ± 3.10	0.804
MI				0.621
Inferior	23 (37.5)	7 (41.2)	24 (51.1)	
Anterior	34 (50.8)	9 (52.9)	19 (40.4)	
Lateral	8 (11.9)	1 (5.9)	4 (8.5)	
Residual coronary artery stenosis	30 (44.9)	11 (64.7)	19 (40.4)	0.221
Medical history				
Prior MI	4 (5.8)	2 (11.8)	4 (8.5)	0.696
Hypertension	48 (71.6)	13 (76.5)	31 (66.0)	0.673
Dyslipidemia	39 (58.2)	12 (70.6)	30 (63.8)	0.605
Chronic kidney disease	7 (10.5)	2 (11.8)	6 (12.8)	0.929
Diabetes mellitus	19 (28.4)	4 (23.5)	19 (40.4)	0.287
Orthopedic disorder	2 (3.0)	1 (6.3)	0 (0)	0.309
Cerebrovascular disease	1 (1.5)	0 (0)	3 (6.4)	0.241
Respiratory disease	2 (3.0)	0 (0)	1 (2.1)	0.760
Hyperuricemia	7 (10.5)	3 (17.7)	8 (17.0)	0.533
Peripheral arterial disease	1 (1.5)	1 (5.9)	1 (2.1)	0.503
Dementia	0 (0)	0 (0)	1 (2.1)	0.406
Heart failure after MI	6 (9.0)	1 (5.9)	5 (10.6)	0.841
Medication				
Diuretic	9 (13.4)	2 (11.8)	4 (8.5)	0.718
Renin-angiotensin system inhibitor	63 (94.0)	12 (70.6)	41 (87.2)	0.024
Calcium antagonist	12 (17.9)	1 (5.9)	3 (6.4)	0.125
Aldosterone antagonist	5 (7.5)	3 (17.6)	2 (4.3)	0.104
Anticlotting drug	2 (3.0)	1 (5.9)	1 (2.1)	0.742
Antiplatelet drug	67 (100)	17 (100)	47 (100)	1.00
αβ-blocker, Carvedilol	67 (100)	-	-	-
β1-blocker, Bisoprolol/Atenolol	-	11 (64.7)/6 (35.3)	-	-

Table 1. *Cont.*

Clinical Characteristics	αβ-Blocker Group (n = 67)	β1-Blocker Group (n = 17)	No-β-Blocker Group (n = 47)	p-Value
Beta-blocker dose				
Carvedilol (mg/day)	5.48 ± 2.39	-	-	-
Bisoprolol/Atenolol (mg/day)	-	2.50 ± 1.40/33.33 ± 12.91	-	-
% maximum dose of beta-blocker (%)	27.41 ± 14.94	44.12 ± 24.65	-	<0.001
Max CK-MB (ng/ml)	306.70 ± 128.05	232.01 ± 214.07	275.43 ± 225.89	0.477
Log max CK-MB	5.40 ± 0.90	5.03 ± 1.08	5.18 ± 0.10	0.262
LVEF (%)	52.91 ± 8.81	57.94 ± 13.60	54.24 ± 12.28	0.230
Time between MI and CPX (days)	32.09 ± 11.50	27.76 ± 8.72	31.19 ± 12.35	0.387
Hospitalization before 2006	7 (10.4%)	10 (58.8%)	40 (85.1%)	<0.001

Table 1 shows comparison results for patient clinical characteristics in the αβ-blocker group, the β1-blocker group, and the no-β-blocker group. Values are expressed as mean ± standard deviation (SD), number (%), or number / number. CPX, cardiopulmonary exercise testing; LVEF, left ventricular ejection fraction; Max CK-MB, maximum value of serum creatine kinase-myocardial band; MI, myocardial infarction.

Table 2 summarizes the data obtained during CPX. None of the patients showed ischemic ST changes or experienced chest pain or serious arrhythmias during CPX. The AT and peak VO_2 did not differ significantly between the three groups ($p = 0.297$ and $p = 0.276$, respectively). HR_{AT}, HR_{peak}, ΔAT HR, and Δpeak HR were significantly higher in the αβ-blocker group compared to the β1-blocker group ($p = 0.004$, $p = 0.002$, $p = 0.004$, and $p = 0.003$, respectively). HR_{rest}, HR_{AT}, and HR_{peak} were significantly lower in the αβ-blocker group compared to the no-β-blocker group ($p < 0.001$, $p = 0.014$, and $p = 0.002$, respectively). HR_{rest}, HR_{AT}, HR_{peak}, Δpeak HR, and ΔAT-peak HR were significantly lower in the β1-blocker group compared to the no-β-blocker group ($p < 0.001$, $p < 0.001$, $p < 0.001$, $p = 0.001$, and $p = 0.011$, respectively). MCR-AT and MCR-peak were both significantly higher in the αβ-blocker group compared to the β1-blocker group ($p < 0.001$, effect size (d) = 1.143; $p < 0.001$, d = 1.215, respectively). However, compared to the no-β-blocker group, MCR-peak was significantly lower in the αβ-blocker group ($p = 0.038$, d = 0.448), although no significant difference was observed in MCR-AT between the two groups ($p = 0.406$, d = 0.279). Both MCR-AT and MCR-peak were significantly lower in the β1-blocker group compared to the no-β-blocker group ($p < 0.001$, d = 1.429; $p < 0.001$, d = 1.346, respectively).

Table 2. Cardiopulmonary exercise testing data with gas analysis.

Cardiopulmonary Exercise Testing Data	β-Blocker Group (n = 67)	β1-Blocker Group (n = 17)	No-β-Blocker Group (n = 47)	F-Value	p-Value
Average time of exercise (min)	7.03 ± 1.57	7.27 ± 1.63	7.53 ± 1.61	1.372	0.402
AT (ml/kg/min)	15.92 ± 3.24	14.72 ± 2.24	15.91 ± 2.73	1.226	0.297
Peak VO_2 (ml/kg/min)	23.27 ± 5.32	21.47 ± 3.72	23.66 ± 4.42	1.302	0.276
RER_{AT}	0.89 ± 0.05	0.89 ± 0.05	0.89 ± 0.07	0.033	0.968
RER_{peak}	1.20 ± 0.07	1.20 ± 0.07	1.18 ± 0.06	2.086	0.128
HR_{rest} (bpm)	71.49 ± 9.86 ‡†	66.65 ± 11.14 ‡†	79.02 ± 11.39	11.147	<0.001
HR_{AT} (bpm)	105.76 ± 11.19 ‡‡	95.47 ± 10.20 ‡†	111.19 ± 12.24 §§	11.940	<0.001
HR_{peak} (bpm)	138.76 ± 14.59 ‡‡	123.77 ± 18.80 ‡†	148.38 ± 16.21 §§	15.865	<0.001
SBP_{rest} (mmHg)	127.43 ± 16.14 †	129.77 ± 18.91	119.64 ± 17.23	3.734	0.027
SBP_{AT} (mmHg)	158.49 ± 21.23	151.77 ± 27.66	149.30 ± 29.78	1.904	0.153
SBP_{peak} (mmHg)	185.93 ± 28.23	180.00 ± 29.19	183.40 ± 32.46	0.295	0.745
DBP_{rest} (mmHg)	77.03 ± 12.16	84.29 ± 10.73 ††	74.02 ± 10.39	5.099	0.007
DBP_{AT} (mmHg)	76.00 ± 17.21	80.24 ± 10.13	76.81 ± 11.83	0.575	0.564
DBP_{peak} (mmHg)	84.51 ± 18.20	85.65 ± 15.96	82.77 ± 12.83	0.2576	0.773
ΔAT HR (bpm)	34.27 ± 8.79 ‡	28.82 ± 8.10	32.17 ± 7.76	3.098	0.049
Δpeak HR (bpm)	67.27 ± 13.43 ‡	57.12 ± 13.97 §	69.36 ± 16.44	4.464	0.013
ΔAT-peak HR (bpm)	32.76 ± 9.99	28.29 ± 11.46 §	37.41 ± 12.11	4.965	0.008

Table 2. Cont.

Cardiopulmonary Exercise Testing Data	β-Blocker Group (n = 67)	β1-Blocker Group (n = 17)	No-β-Blocker Group (n = 47)	F-Value	p-Value
MCR-AT	0.83 ± 0.07 ‡‡	0.77 ± 0.07 ††	0.87 ± 0.07	13.122	<0.001
MCR-peak	0.90 ± 0.08 ‡‡	0.78 ± 0.11 ††	0.94 ± 0.09 §	19.205	<0.001

Comparison results of variables during cardiopulmonary exercise testing with gas analysis in the αβ-blocker group, the β1-blocker group, and the no-β-blocker group were analyzed using one-way analysis of variance and Tukey's honestly significant difference test. Values are expressed as mean ± standard deviation (SD). AT, anaerobic threshold; DBP, diastolic blood pressure; DBP_{AT}, DBP at AT; DBP_{peak}, DBP at peak oxygen uptake; DBP_{rest}, DBP at rest; RER, Respiratory exchange ratio; RER_{AT}, RER at AT; RER_{peak}, RER at peak oxygen uptake; HR, heart rate; HR_{AT}, HR at AT; HR_{peak}, HR at peak oxygen uptake; HR_{rest}, HR at rest; MCR, metabolic chronotropic relationship; MCR-AT, estimated heart rate at AT / measured heart rate at AT; MCR-peak, estimated heart rate at peak / measured heart rate at peak; Peak VO_2, peak oxygen uptake; SBP, systolic blood pressure; SBP_{AT}, SBP at AT; SBP_{peak}, SBP at peak VO_2; SBP_{rest}, SBP at rest; ΔAT HR, $(HR_{AT}) - (HR_{rest})$; Δpeak HR, $(HR_{peak}) - (HR_{rest})$; ΔAT-peak HR, $(HR_{peak}) - (HR_{AT})$; †, $p < 0.05$ vs. no-β-blocker group; ††, $p < 0.01$ vs. no-β-blocker group; ‡, $p < 0.05$ vs. β1-blocker group; ‡‡, $p < 0.01$ vs. β1-blocker group; §, $p < 0.05$ vs. αβ-blocker group; §§, $p < 0.01$ vs. αβ-blocker group.

The results of the regression analysis revealed no correlation between MCR-AT and Log max CK-MB, LVEF, and time between MI onset and exercise testing. MCR-peak was positively correlated with Log max CK-MB ($p = 0.188$), and negatively correlated with LVEF ($p = 0.053$). Multiple regression analysis revealed that β1-blocker but not αβ-blocker treatment significantly predicted lower MCR-AT and MCR-peak ($\beta = -0.432$, $p < 0.001$; $\beta = -0.473$, $p < 0.001$, respectively) (Tables 3 and 4).

Table 3. Results of multiple regression analysis for the prediction of MCR-AT.

Independent Variables	Dependent Variable: MCR-AT			
	B ± SE	β	95% CI of B	p-Value
Inferior infarct *	−0.002 ± 0.012	−0.025	−0.025 to 0.021	0.865
Anterior infarct *	−0.001 ± 0.011	−0.001	−0.023 to 0.022	0.946
Residual coronary artery stenosis	−0.009 ± 0.007	−0.117	−0.022 to 0.004	0.170
Heart failure after MI	−0.007 ± 0.011	−0.053	−0.029 to 0.015	0.518
Diabetes mellitus	0.001 ± 0.007	0.016	−0.012 to 0.015	0.836
Renin-angiotensin system inhibitor	−0.004 ± 0.010	−0.031	−0.025 to 0.017	0.719
αβ-blocker treatment **	−0.008 ± 0.010	−0.108	−0.028 to 0.011	0.394
β1-blocker treatment **	−0.050 ± 0.011	−0.432	−0.071 to −0.028	<0.001
Hospitalization before 2006	0.000 ± 0.001	0.003	−0.018 to 0.018	0.979
Constant	0.807 ± 0.016	0.000	0.776 to 0.839	<0.001
	Coefficient of determination $R^2 = 0.187$, $F = 3.092$, $p = 0.002$			

Multiple regression analysis for the prediction of MCR-AT was performed using the forced-entry method. MCR, metabolic chronotropic relationship; AT, anaerobic threshold; MCR-AT, measured heart rate at AT / estimated heart rate at AT; B ± SE, partial regression coefficient ± standard error; β, standardized partial regression coefficient; CI, confidence interval; MI, myocardial infarction. * Compared with lateral infarct. ** Compared with not undergoing beta-blocker treatment.

Table 4. Results of multiple regression analysis for the prediction of MCR-peak.

Independent Variables	Dependent Variable: MCR-Peak			
	B ± SE	β	95% CI of B	p-Value
Inferior infarct *	−0.002 ± 0.015	−0.017	−0.031 to 0.027	0.907
Anterior infarct *	−0.001 ± 0.001	−0.007	−0.029 to 0.028	0.962
Residual coronary artery stenosis	−0.012 ± 0.008	−0.114	−0.028 to 0.005	0.166
Heart failure after MI	0.002 ± 0.015	0.012	−0.026 to 0.031	0.883
Diabetes mellitus	0.004 ± 0.009	0.038	−0.013 to 0.021	0.642
Log max CK-MB	0.018 ± 0.024	0.067	−0.029 to 0.064	0.449
LVEF	−0.027 ± 0.025	−0.100	−0.077 to 0.021	0.266
Renin-angiotensin system inhibitor	0.003 ± 0.013	0.021	−0.023 to 0.030	0.800

Table 4. *Cont.*

Independent Variables	Dependent Variable: MCR-Peak			
	B ± SE	β	95% CI of B	*p*-Value
αβ-blocker treatment **	−0.019 ± 0.012	−0.185	−0.043 to 0.006	0.134
β1-blocker treatment **	−0.071 ± 0.014	−0.473	−0.099 to −0.044	<0.001
Hospitalization before 2006	−0.004 ± 0.012	−0.043	−0.019 to 0.027	0.786
Constant	0.844 ± 0.020	0.000	0.840 to 0.884	<0.001
	Coefficient of determination $R^2 = 0.263$, $F = 3.865$, $p < 0.001$			

Multiple regression analysis for the prediction of MCR-peak was performed using the forced-entry method. MCR, metabolic chronotropic relationship; MCR-peak, measured heart rate at peak/estimated heart rate at peak; B ± SE, partial regression coefficient ± standard error; β, standardized partial regression coefficient; CI, confidence interval; LVEF, left ventricular ejection fraction; Max CK-MB, maximum value of serum creatine kinase-myocardial band; MI, myocardial infarction. * Compared with lateral infarct. ** Compared with not receiving beta-blocker treatment.

Figure 1a and 1b show the correlation results between MCR-AT, MCR-peak, and % maximum beta-blocker dose. In patients undergoing beta-blocker treatment, no significant correlations were observed between MCR-AT, MCR-peak, and % maximum beta-blocker dose ($p = 0.419$, $r = -0.089$; and $p = 0.760$, $r = -0.034$, respectively).

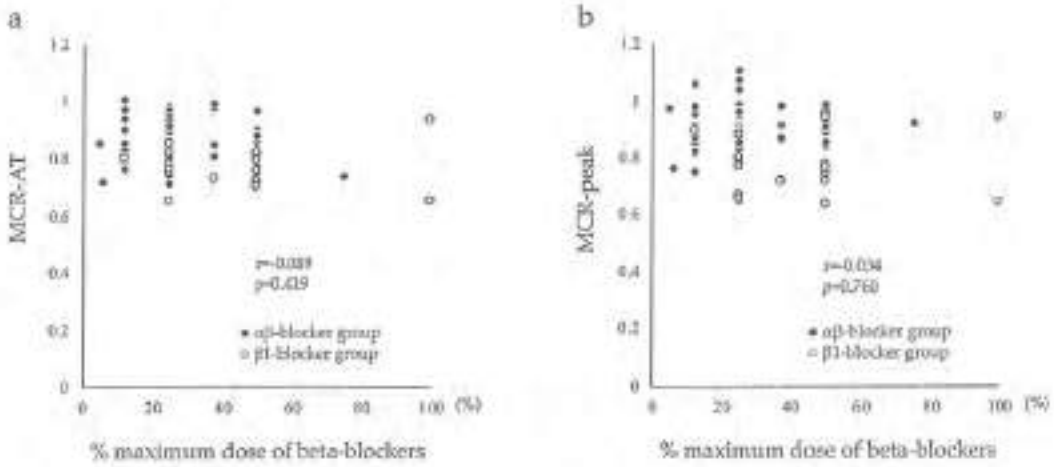

Figure 1. Correlations between MCR-AT, MCR-peak, and % maximum dose of beta blockers. Figure 1a shows correlation results between MCR-AT and % maximum beta-blocker dose. In patients undergoing beta-blocker treatment, no significant correlations were observed between MCR-AT and % maximum beta-blocker dose. Figure 1b shows correlation results between MCR-peak and % maximum beta-blocker dose. In patients undergoing beta-blocker treatment, no significant correlations were observed between MCR-peak and % maximum beta-blocker dose. MCR, metabolic chronotropic relationship; MCR-AT, ratio of estimated heart rate at the AT to measured heart rate at the AT; MCR-peak, ratio of estimated heart rate at peak oxygen uptake to measured heart rate at peak oxygen uptake; % maximum beta-blocker dose, ratio of administered beta-blocker dose to maximum beta-blocker dose.

4. Discussion

The present study compared the effects of β1-blocker versus αβ-blocker treatment on HR response during incremental CPX in subacute MI patients, using MCR as an indicator of HR response. Both MCR-AT and MCR-peak were significantly lower in the β1-blocker group than in the αβ-blocker group. Multiple regression analysis revealed that β1-blocker but not αβ-blocker treatment significantly predicted lower MCR-AT and MCR-peak. These results suggest that the negative chronotropic effect of beta blockers during incremental CPX may be stronger with β1-blockers than with αβ-blockers in subacute MI patients.

4.1. Selecting Beta-Blocker Type for Subacute MI Patients

Existing guidelines recommend administration of beta blockers to MI patients in order to reduce post-MI mortality [2,18]. However, there are no criteria for selecting a specific type of beta blocker for MI patients. A previous study reported no differences in the risk of all-cause death or MI between MI patients treated with αβ-blockers versus β1-blockers [10]. In the present study, the type of beta blocker used (i.e., αβ-blocker or β1-blocker) was determined based on clinical decisions made by physicians. Despite guideline recommendations, some patients were not treated with beta blockers. This is likely because, in Japan, the administration of beta blockers was first recommended by the Guidelines for Secondary Prevention of Myocardial Infarction in 2006 [19]. In fact, most patients who did not undergo beta-blocker treatment were hospitalized prior to 2006.

4.2. Differences in HR Response During CPX Among Subacute MI Patients Undergoing αβ-Blocker Versus β1-Blocker Treatment

HR responses during incremental exercise are greatly affected by cardiac autonomic nerve activity. When exercise intensity is low to moderate, HR response is considered to be mainly affected by decreased parasympathetic nervous system activity; when exercise intensity is moderate to high, HR response is considered to be mainly affected by increased sympathetic nervous system activity [20]. Increases in HR from rest to maximal exercise result from a transition in workload from a 4:1 parasympathetic/sympathetic balance to a 1:4 parasympathetic / sympathetic balance [20]. Among MI patients, the autonomic nerve balance is considered to trend more toward increasing sympathetic nervous system activity due to unbalanced cardiac autonomic modulation (i.e., increased sympathetic outflow and reduced parasympathetic activity) [21]. Beta blockers decrease sympathetic nervous system activity by inhibiting the interactions between noradrenaline and beta receptors. β1-blockers selectively inhibit the interaction between noradrenaline and β1 receptors in the heart, while αβ-blockers non-selectively inhibit the interactions between noradrenaline and β1 receptors. The effect of αβ-blockers to decrease cardiac sympathetic nervous system activity is thus considered to be lower than that of β1-blockers. In the present study, MCR-AT and MCR-peak were significantly lower in the αβ-blocker group than in the β1-blocker group. A chronotropic index < 0.8 has been previously determined to indicate chronotropic incompetence [15,16]. In the present study, the values of MCR-AT and MCR-peak were 0.85 ± 0.07 and 0.90 ± 0.08, respectively, in the αβ-blocker group, and 0.77 ± 0.07 and 0.78 ± 0.11, respectively, in the β1-blocker group. These results show that the β1-blocker group had a low chronotropic index, while the αβ-blocker group did not, suggesting that the effect of β1-blockers decreasing HR response during incremental CPX may be stronger than with αβ-blockers.

4.3. Effects of αβ-Blocker Versus β1-Blocker Treatment on HR Response During CPX in Subacute MI Patients After Adjusting for Multiple Factors

Previous studies suggested that several factors other than beta-blocker treatment could affect HR response during exercise, including age, body weight, functional capacity, cardiac function, high max CK-MB, diabetes mellitus, and heart failure after MI [22–26]. The present study used MCR as an indicator of HR response, because MCR allows for the assessment of HR response without the effects of age, physical fitness, or functional capacity [15,16]. In order to adjust for other several factors, multiple regression analysis was performed to predict MCR. The analysis revealed that β1-blocker but not αβ-blocker treatment significantly predicted lower MCR-AT and MCR-peak.

4.4. Beta-Blocker Doses

In the present study, the mean dose of carvedilol was 5.48 ± 2.99 mg/day in the αβ-blocker group, and mean doses of bisoprolol and atenolol were 2.50 ± 1.40 and 33.33 ± 12.91 mg/day, respectively, in the β1-blocker group. A previous study reported that Japanese MI patients were treated with a mean carvedilol dose of 3.48 ± 1.61 mg/day before hospital discharge and 7.71 ± 4.58 mg/day at 12

months after MI onset, or a mean bisoprolol dose of 1.26 ± 0.57 mg/day before hospital discharge and 2.47 ± 1.20 mg/day at 12 months after MI onset [11]. Another study in Japan reported that atenolol was started at a low dose and titrated up to the target dose of 25–50 mg/day at one month after MI onset [27]. In the present study population (i.e., MI patients at one month after MI onset), although the mean doses of carvedilol and atenolol were considered clinically appropriate, the mean dose of bisoprolol was slightly higher than that noted in previous study populations. To examine the effect of beta-blocker doses on HR response, we also examined the correlations between MCR-AT, MCR-peak, and % maximum beta-blocker dose. No significant correlations were observed between MCR-AT, MCR-peak, and % maximum beta-blocker dose. The negative chronotropic effect of beta blockers depends on the concentration of these medications in the blood. In addition to dose, several clinical factors can affect the blood concentration of beta blockers, such as body weight, renal function, liver function, and genetic polymorphism [28–30]. In clinical practice, physicians determine appropriate doses for each MI patient based on these factors. In other words, optimum beta-blocker doses for blood concentration are different for each patient. Thus, no significant correlations were observed between MCR-AT, MCR-peak, and % maximum beta-blocker dose in the present study. However, from the results of the present study, we could not conclude that there is no relationship between the dose of a β-blocker and HR response. Because it is difficult to assess whether each patient was on a low, moderate, or high dose relative to the individual response to treatment, the effect of beta-blockers on each patient was not assessed in the present study.

4.5. Clinical Application of Study Findings

In clinical practice, a simplified method of determining exercise intensity without gas-exchange analysis data or exercise stress test data is to use a substitute for HR at AT, i.e., resting HR plus 30 bpm or % predicted max HR. [2,6]. This simplified method is considered difficult to use in patients undergoing beta-blocker treatment, based on reports from previous studies that beta blockers affect calculations by reducing HR responses during incremental exercise [7,8]. Although the negative chronotropic effect of beta blockers is considered to differ depending on beta-blocker type (e.g., αβ-blocker or β1-blocker), previous studies have not fully evaluated the effects of beta-blocker type on HR response during incremental exercise in subacute MI patients. The effect of beta-blocker type on this simplified method of exercise prescription, therefore, remains unclear. Our previous study [31] examined the effect of αβ-blocker treatment on HR response during incremental exercise in subacute MI patients, because αβ-blockers are frequently prescribed for MI patients due to their effectiveness [9]. αβ-blocker treatment was found to have no effect on HR response to exercise up to the AT in subacute MI patients [31], suggesting that exercise intensity can be prescribed using the simplified method (i.e., resting HR plus 30 bpm) in subacute MI patients regardless of αβ-blocker use. Although β1-blockers are also frequently used in MI patients [10,11], the effect of β1-blockers on HR response during incremental exercise in subacute MI patients remains unclear. The present study compared the effects of β1-blocker versus αβ-blocker treatment on HR response during incremental exercise in subacute MI patients, and found that both MCR-AT and MCR-peak values were significantly lower in the β1-blocker group than in the αβ-blocker group. These results suggest that, when prescribing exercise intensity for subacute MI patients in clinical practice based on calculations of resting HR plus 30 bpm or % predicted max HR, we may need to use a lower target HR/predicted max HR value for those who are undergoing β1-blocker treatment, compared to those who are undergoing αβ-blocker treatment. In order to determine an appropriate target HR value for subacute MI patients undergoing β1-blocker treatment, further evaluation of training effectiveness and safety is needed. A previous study presented a prediction formula for maximum HR among patients with coronary heart disease receiving beta-blocker treatment (i.e., predicted maximum HR = 164 − 0.7 × age) [6]. However, this prediction formula was not specific for each type of beta blocker. Prediction formulas for maximum HR in MI patients treated with each type of beta blocker need to be established in future studies.

4.6. Limitations

The present study has several limitations. First, the influence of potential factors (e.g., body weight, renal function, liver function, genetic polymorphism) on the blood concentration of beta blockers was not examined in the present study. Second, all patients underwent symptom-limited CPX using a treadmill. The effects of beta-blocker type on HR response during other symptom-limited CPX (e.g., on a bicycle ergometer) have not yet been clarified. Third, this study was analyzed retrospectively. Hence, the effect of several biases such as an imbalance in the number of patients and a difference in the treatment of MI between the groups cannot be completely excluded in this study. A future randomized controlled trial will be needed to verify the results of the present study. Finally, this study is affected by selection bias as patients who were unable to undergo symptom-limited CPX on a treadmill due to frailty were excluded from the study. As a result, the population in this study comprised lean and young patients. A future study will be needed to verify the results of the present study in a broader age range of patients.

5. Conclusions

Our data suggest that the effects of β1-blockers to decrease HR response during incremental CPX may be stronger than that of αβ-blockers in subacute MI patients. Therefore, exercise intensity based on a simplified substitute for HR at AT (i.e., resting HR plus 30 bpm or % predicted max HR) without gas-exchange analysis data or exercise stress test data should be prescribed according to the type of beta blocker used in subacute MI patients.

Author Contributions: Conceptualization, S.N. and Y.K.; data curation, S.N., Y.K., K.Y., N.T., S.W., N.S., K.O., and Y.J.A.; formal analysis, S.N.; investigation, S.N.; methodology, S.N. and Y.K.; project administration, S.N. and Y.K.; Software, S.N.; Supervision, Y.K., K.P.I., K.K., A.M. and Y.J.A.; Validation, Y.K.; visualization, S.N. and Y.K.; writing—original draft, S.N.; writing—review and editing, S.N., Y.K., K.P.I., K.K., A.M., and Y.J.A. All authors approved the manuscript for submission.

Funding: This research received no external funding.

Acknowledgments: The authors thank the staff members of the Department of Rehabilitation Medicine and the Department of Cardiology at St. Marianna University School of Medicine, Yokohama City Seibu Hospital, for their assistance in data collection.

Conflicts of Interest: The authors declare no conflict of interest.

References

1. Piepoli, M.F.; Hoes, A.W.; Agewall, S.; Albus, C.; Brotons, C.; Catapano, A.L.; Cooney, M.T.; Corra, U.; Cosyns, B.; Deaton, C.; et al. 2016 European Guidelines on cardiovascular disease prevention in clinical practice: The Sixth Joint Task Force of the European Society of Cardiology and Other Societies on Cardiovascular Disease Prevention in Clinical Practice (constituted by representatives of 10 societies and by invited experts)Developed with the special contribution of the European Association for Cardiovascular Prevention & Rehabilitation (EACPR). *Eur. Heart J.* **2016**, *37*, 2315–2381. [PubMed]
2. JCS Joint Working Group. Guidelines for rehabilitation in patients with cardiovascular disease (JCS 2012). *Circ. J.* **2014**, *78*, 2022–2093. [CrossRef]
3. Anderson, L.; Oldridge, N.; Thompson, D.R.; Zwisler, A.D.; Rees, K.; Martin, N.; Taylor, R.S. Exercise-Based Cardiac Rehabilitation for Coronary Heart Disease: Cochrane Systematic Review and Meta-Analysis. *J. Am. Coll. Cardiol.* **2016**, *67*, 1–12. [CrossRef] [PubMed]
4. Wasserman, K.; Beaver, W.L.; Whipp, B.J. Gas exchange theory and the lactic acidosis (anaerobic) threshold. *Circulation* **1990**, *81*, II14–II30. [PubMed]
5. Adachi, H.; Koike, A.; Obayashi, T.; Umezawa, S.; Aonuma, K.; Inada, M.; Korenaga, M.; Niwa, A.; Marumo, F.; Hiroe, M. Does appropriate endurance exercise training improve cardiac function in patients with prior myocardial infarction? *Eur. Heart J.* **1996**, *17*, 1511–1521. [CrossRef] [PubMed]

6. Brawner, C.A.; Ehrman, J.K.; Schairer, J.R.; Cao, J.J.; Keteyian, S.J. Predicting maximum heart rate among patients with coronary heart disease receiving beta-adrenergic blockade therapy. *Am. Heart J.* **2004**, *148*, 910–914. [CrossRef] [PubMed]
7. Diaz-Buschmann, I.; Jaureguizar, K.V.; Calero, M.J.; Aquino, R.S. Programming exercise intensity in patients on beta-blocker treatment: The importance of choosing an appropriate method. *Eur. J. Prev. Cardiol.* **2014**, *21*, 1474–1480. [CrossRef]
8. Tabet, J.Y.; Meurin, P.; Ben Driss, A.; Thabut, G.; Weber, H.; Renaud, N.; Odjinkem, N.; Solal, A.C. Determination of exercise training heart rate in patients on beta-blockers after myocardial infarction. *Eur. J. Cardiovasc. Prev. Rehabil.* **2006**, *13*, 538–543. [CrossRef]
9. Dargie, H.J. Effect of carvedilol on outcome after myocardial infarction in patients with left-ventricular dysfunction: The CAPRICORN randomised trial. *Lancet* **2001**, *357*, 1385–1390.
10. Seo, G.W.; Kim, D.K.; Kim, K.H.; Seol, S.H.; Jin, H.Y.; Yang, T.H.; Ahn, Y.; Jeong, M.H.; Song, P.S.; Kim, D.I.; et al. Impact of Carvedilol versus beta1-selective beta blockers (bisoprolol, metoprolol, and nebivolol) in patients with acute myocardial infarction undergoing percutaneous coronary intervention. *Am. J. Cardiol.* **2015**, *116*, 1502–1508. [CrossRef]
11. Konishi, M.; Haraguchi, G.; Yoshikawa, S.; Kimura, S.; Inagaki, H.; Isobe, M. Additive Effects of β-Blockers on Renin-Angiotensin System Inhibitors for Patients After Acute Myocardial Infarction Treated with Primary Coronary Revascularization. *Circ. J.* **2011**, *75*, 1982–1991. [CrossRef] [PubMed]
12. Yamamoto, A.; Tanabe, K.; Yokoyama, Y.; Itoh, H.; Murayama, M. Influence of aerobic exercise training on brain natriuretic peptide secretion in patients in the chronic phase of myocardial infarction. *Jpn. Circ. J.* **1998**, *62*, 658–664. [CrossRef] [PubMed]
13. Hanson, P. Clinical exercise testing. In *American College of Sports Medicine, Resource Manual for Guidelines for Exercise Testing and Prescription*; Thompson, W.R., Gordon, N.F., Pescatello, L.S., Eds.; Lea & Febiger: Philadelphia, PA, USA, 2012; pp. 205–222.
14. Beaver, W.L.; Wasserman, K.; Whipp, B.J. A new method for detecting anaerobic threshold by gas exchange. *J. Appl. Physiol. (1985)* **1986**, *60*, 2020–2027. [CrossRef] [PubMed]
15. Wilkoff, B.L.; Miller, R.E. Exercise testing for chronotropic assessment. *Cardiol. Clin.* **1992**, *10*, 705–717. [CrossRef]
16. Takano, N.; Takano, H.; Fukuda, T.; Kikuchi, H.; Oguri, G.; Fukumura, K.; Iwasawa, K.; Nakajima, T. Relationship between chronotropic incompetence and beta-blockers based on changes in chronotropic response during cardiopulmonary exercise testing. *Int. J. Cardiol. Heart Vasc.* **2015**, *6*, 12–18. [PubMed]
17. Brubaker, P.H.; Kitzman, D.W. Chronotropic incompetence: Causes, consequences, and management. *Circulation* **2011**, *123*, 1010–1020. [CrossRef]
18. Ibanez, B.; James, S.; Agewall, S.; Antunes, M.J.; Bucciarelli-Ducci, C.; Bueno, H.; Caforio, A.L.P.; Crea, F.; Goudevenos, J.A.; Halvorsen, S.; et al. 2017 ESC Guidelines for the management of acute myocardial infarction in patients presenting with ST-segment elevation. *Eur. Heart J.* **2018**, *39*, 119–177. [CrossRef]
19. Japanese Circulation Society web. Guidelines for Secondary Prevention of Myocardial Infarction (JCS 2006). Available online: http://www.circ.or.jp/guideline/pdf/JCS2006_ishikawa_h.pdf (accessed on 21 June 2019).
20. White, D.W.; Raven, P.B. Autonomic neural control of heart rate during dynamic exercise: Revisited. *J. Physiol.* **2014**, *592*, 2491–2500. [CrossRef]
21. Bigger, J.T.; Fleiss, J.L.; Rolnitzky, L.M.; Steinman, R.C.; Schneider, W.J. Time course of recovery of heart period variability after myocardial infarction. *J. Am. Coll. Cardiol.* **1993**, *18*, 1643–1649. [CrossRef]
22. Dominguez, E.; Palau, P.; Nunez, E.; Ramon, J.M.; Lopez, L.; Melero, J.; Bellver, A.; Santas, E.; Chorro, F.J.; Nunez, J. Heart rate response and functional capacity in patients with chronic heart failure with preserved ejection fraction. *ESC Heart Fail.* **2018**, *5*, 579–585. [CrossRef]
23. Robergs, R.; Landwehr, R. The surprising history of the "HRmax = 220-age" equation. *J. Exerc. Physiol. Online* **2002**, *5*, 1–10.
24. Kasahara, Y.; Izawa, K.; Omiya, K.; Osada, N.; Watanabe, S.; Saitoh, M.; Matsunaga, A.; Masuda, T. Influence of autonomic nervous dysfunction characterizing effect of diabetes mellitus on heart rate response and exercise capacity in patients undergoing cardiac rehabilitation for acute myocardial infarction. *Circ. J.* **2006**, *70*, 1017–1025. [CrossRef] [PubMed]

25. Anjos-Andrade, E.D.; Sousa, A.C.; Barreto-Filho, J.A.; Alves, E.O.; Nascimento-Junior, A.C.; De Santana, N.O.; De Vasconcelos, F.L.; Garcez, F.B.; De Araujo, V.P.; De Araujo, A.C.; et al. Chronotropic incompetence and coronary artery disease. *Acta Cardiol.* **2010**, *65*, 631–638. [CrossRef] [PubMed]
26. Buchholz, B.; Donato, M.; Perez, V.; Deutsch, A.C.R.; Hocht, C.; Del Mauro, J.S.; Rodriguez, M.; Gelpi, R.J. Changes in the loading conditions induced by vagal stimulation modify the myocardial infarct size through sympathetic-parasympathetic interactions. *Pflugers Arch.* **2015**, *467*, 1509–1522. [CrossRef] [PubMed]
27. Nakagomi, A.; Kodani, E.; Takano, H.; Uchida, T.; Sato, N.; Ibuki, C.; Kusama, Y.; Seino, Y.; Munakata, K.; Mizuno, K.; et al. Secondary preventive effects of a calcium antagonist for ischemic heart attack: Randomized parallel comparison with beta-blockers. *Circ. J.* **2011**, *75*, 1696–1705. [CrossRef] [PubMed]
28. Saito, M.; Kawana, J.; Obro, T.; Harada, K.; Kaneko, M.; Mihara, K.; Shioni, M.; Nagayama, M.; Sumiyoshi, T.; Ogata, H. Population pharmacokinetics of R- and S-carvedilol in Japanese patients with chronic heart failure. *Biol. Pharm. Bull.* **2010**, *33*, 1378–1384. [CrossRef] [PubMed]
29. Hakusui, H.; Fujimaki, M. Pharmacokinetics of carvedilol in hypertensive patients with renal failure. *Drugs* **1988**, *36*, 144–147. [CrossRef]
30. Neugebauer, G.; Gabor, M.; Reiff, K. Pharmacokinetics and bio-availability of carvedilol in patients with liver cirrhosis. *Drugs* **1988**, *36*, 148–154. [CrossRef]
31. Nemoto, S.; Kasahara, Y.; Izawa, K.P.; Watanabe, S.; Yoshizawa, K.; Takeichi, N.; Kamiya, K.; Suzuki, N.; Omiya, K.; Matsunaga, A.; et al. Effect of carvedilol on heart rate response to cardiopulmonary exercise up to the anaerobic threshold in patients with subacute myocardial infarction. *Heart Vessel.* **2019**, *34*, 957–964. [CrossRef] [PubMed]

© 2019 by the authors. Licensee MDPI, Basel, Switzerland. This article is an open access article distributed under the terms and conditions of the Creative Commons Attribution (CC BY) license (http://creativecommons.org/licenses/by/4.0/).

Circulation Journal
Circ J 2019; 83: 2002–2009
doi:10.1253/circj.CJ-19-0512

ORIGINAL ARTICLE
Arrhythmia/Electrophysiology

Novel Device-Based Algorithm Provides Optimal Hemodynamics During Exercise in Patients With Cardiac Resynchronization Therapy

Akira Kasagawa, MD; Ikutaro Nakajima, MD, PhD; Masaki Izumo, MD, PhD; Yui Nakayama, MD, PhD; Marika Yamada, MD, PhD; Makoto Takano, MD, PhD; Hisao Matsuda, MD, PhD; Toshiyuki Furukawa, MD, PhD; Hidekazu Miyazaki, MD, PhD; Tomoo Harada, MD, PhD; Yoshihiro J Akashi, MD, PhD

Background: An adaptive cardiac resynchronization therapy (aCRT) algorithm has been described for synchronized left ventricular (LV) pacing and continuous optimization of cardiac resynchronization therapy (CRT). However, there are few algorithmic data on the effect of changes during exercise.

Methods and Results: We enrolled 27 patients with availability of the aCRT algorithm. Eligible patients were manually programmed to optimal atrioventricular (AV) and interventricular (VV) delays by using echocardiograms at rest or during 2 stages of supine bicycle exercise. We compared the maximum cardiac output between manual echo-optimization and aCRT-on during each phase. After initiating exercise, the optimal AV delay progressively shortened ($P<0.05$) with incremental exercise levels. The manual-optimized settings and aCRT resulted in similar cardiac performance, as demonstrated by a high concordance correlation coefficient between the LV outflow tract velocity time integral (LVOT-VTI) during each exercise stage (Ex.1: $r=0.94$ $P<0.0006$, Ex.2: $r=0.88$ $P<0.001$, respectively). Synchronized LV-only pacing in patients with normal AV conduction could provide a higher LVOT-VTI as compared with manual-optimized conventional biventricular pacing at peak exercise ($P<0.05$).

Conclusions: The aCRT algorithm was physiologically sound during exercise by patients.

Key Words: Algorithms; Cardiac resynchronization therapy; Exercise tests; Heart failure; Optimization

Cardiac resynchronization therapy (CRT) is an efficient therapeutic strategy for heart failure (HF) patients with reduced left ventricular (LV) ejection fraction (EF) and cardiac dyssynchrony who are unresponsive even with adequate medication. CRT improves symptoms, reduces hospitalizations for HF, and increases survival in such patients, but approximately one-third of patients may not obtain any improvement in their clinical status even after initiating biventricular (BiV) pacing.[1-3] There can be many post-implant factors that contribute to a suboptimal response, among which suboptimal atrioventricular (AV) timing could be a common reason.[4] Although optimization of the AV and interventricular (VV) delay during BiV pacing could be 1 solution to maximize the acute hemodynamic effect of CRT,[5,6] a single AV and VV optimization at rest could be considered to have only limited meaning for improving the clinical prognosis.[7] One explanation could be that the physiological conduction may vary dramatically depending on the patient's exercise level,[8,9] and therefore, the optimal AV and VV timings are frequently changing. Recently, several studies used echocardiography to examine the effect of exercise on the optimal AV delay in CRT patients and their results suggest that AV optimization during exercise improves the cardiac performance in CRT patients.[8,10,11] Based on these findings, an algorithm that can provide ambulatory CRT optimization and more physiologic pacing has been developed.

The effectiveness of the AdaptivCRT algorithm (aCRT, Medtronic, Mounds View, MN, USA) has been published.[12] The algorithm automatically adjusts the pacing mode or AV/VV pacing intervals every minute based on the intrinsic AV conduction. When normal AV conduction occurs, synchronized LV-only pacing is provided and withholds right ventricular (RV) pacing. During periods of prolonged

Received June 12, 2019; revised manuscript received July 9, 2019; accepted July 16, 2019; J-STAGE Advance Publication released online August 27, 2019 Time for primary review: 9 days

Division of Cardiology, St. Marianna University School of Medicine, Kawasaki (A.K., I.N., M.I., M.Y., M.T., H. Miyazaki, T.H., Y.J.A.); Division of Cardiology, St Marianna University School of Medicine, Yokohama City Seibu Hospital, Yokohama (Y.N., H. Matsuda); and Division of Cardiology, St. Marianna University School of Medicine, Toyoko Hospital, Kawasaki (T.F.), Japan

Mailing address: Ikutaro Nakajima, MD, PhD, Division of Cardiology, St. Marianna University School of Medicine, 2-16-1 Sugao, Miyamae-ku, Kawasaki 216-8511, Japan. E-mail: ikutaro0817@icloud.com

ISSN-1346-9843 All rights are reserved to the Japanese Circulation Society. For permissions, please e-mail: cj@j-circ.or.jp

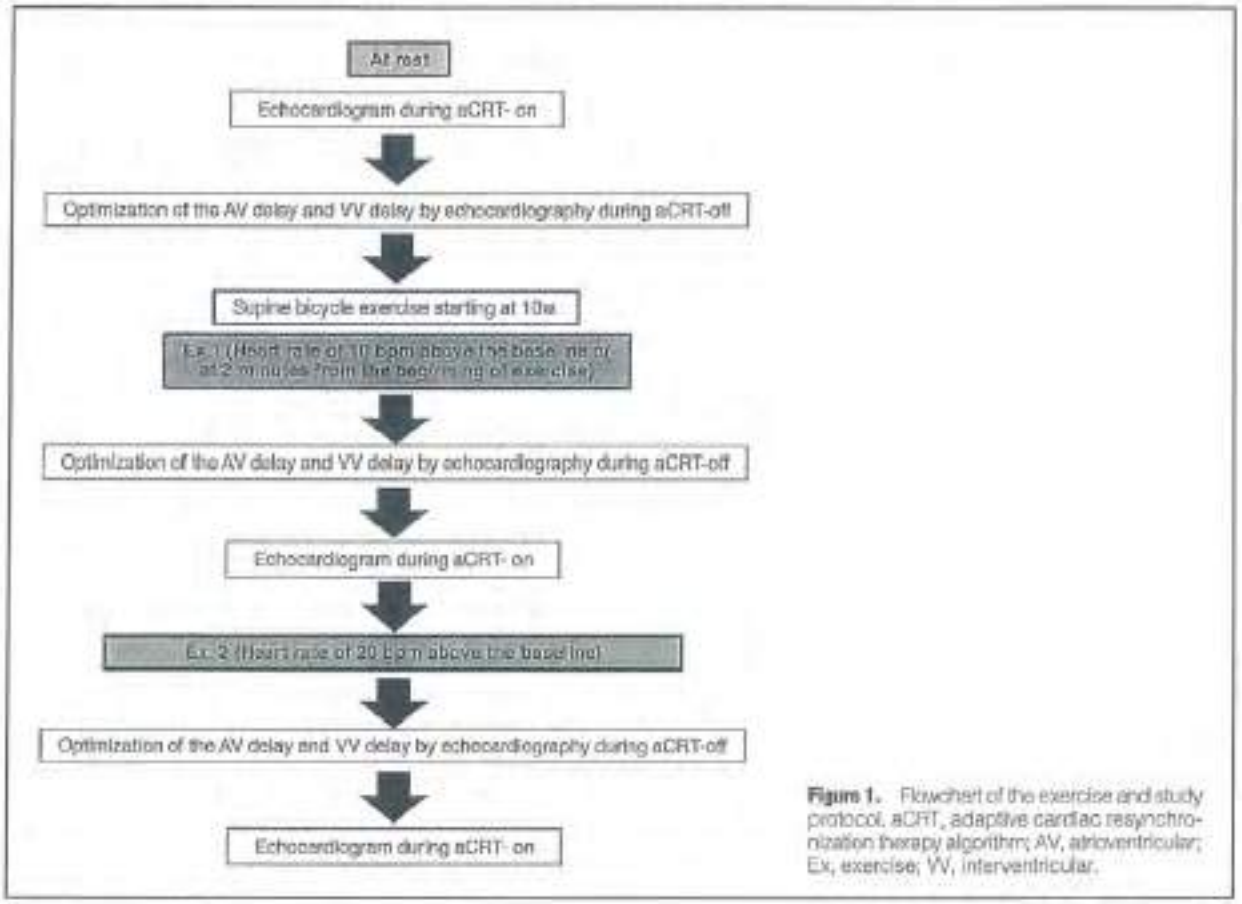

Figure 1. Flowchart of the exercise and study protocol. aCRT, adaptive cardiac resynchronization therapy algorithm; AV, atrioventricular; Ex, exercise; VV, interventricular.

AV conduction, the algorithm continuously optimizes the AV and VV intervals. The aCRT algorithm has been demonstrated to decrease the risk of HF hospitalization as compared with echocardiography-optimized BiV pacing, and especially when the percent synchronized LV-only pacing exceeds more than 50%, a significant reduction in death or HF hospitalizations has been shown.[13] Furthermore, the aCRT is also reported to reduce the risk of developing atrial fibrillation.[14] To date, few studies have been conducted regarding the effect of its validity during exercise-induced changes. Thus, the goal of this study using exercise stress echocardiography was to identify whether this algorithm could provide hemodynamically reasonable and beneficial effects when compared with conventional echocardiographic AV and VV optimization during exercise.

Methods

Study Population

Patients with HF previously implanted with a CRT device were recruited. The eligibility for CRT was based on international guidelines, including advanced HF (NYHA functional class II, III, or IV), depressed LV function (LVEF ≤35%), and a wide QRS complex (>120 ms) on ECG.[15,16] Inclusion criteria were as follows: able to complete a supine bicycle exercise stress protocol, in sinus rhythm at baseline, and received a CRT device equipped with the aCRT algorithm. Exclusion criteria were patients with atrial fibrillation, prior valvular surgery, significant sinus node dysfunction, and absence or lack of intrinsic AV conduction or pacing dependence. The study protocol was approved by the institutional research ethics committee and all patients provided written informed consent.

The aCRT Algorithm

The aCRT algorithm is designed to automatically adjust the pacing mode by evaluating the intrinsic AV conduction every minute. During a normal AV conduction interval (intrinsic AV ≤200 ms during sinus rhythm, or AV ≤250 ms during atrial pacing) and a heart rate that did not exceed 100 beats/min, the synchronized LV-only pacing provides an atrial to RV sense interval of ≥40 ms (adaptive LV). Contrarily, during a prolonged AV conduction interval, the BiV pacing adjusts the AV and VV timing based on the intervals of the atrial to RV sense, atrial to P-wave end, and RV sense to QRS end (adaptive BiV).[12,14] Once the algorithm is activated, the algorithm-determined pacing mode or AV/VV delays are delivered immediately.

Echocardiographic Imaging and CRT Optimization

The echocardiographic images were recorded with a Vivid E9 ultrasound system (VingMed Ultrasound, General Electric, Milwaukee, WI, USA) equipped with a 3.5-MHz imaging probe and offline cine-loop analysis software. The images were acquired in a semi-supine position at rest and supine during exercise.

Pulsed-wave Doppler images of the transmitral flow velocity were recorded by placing the sample volume at the

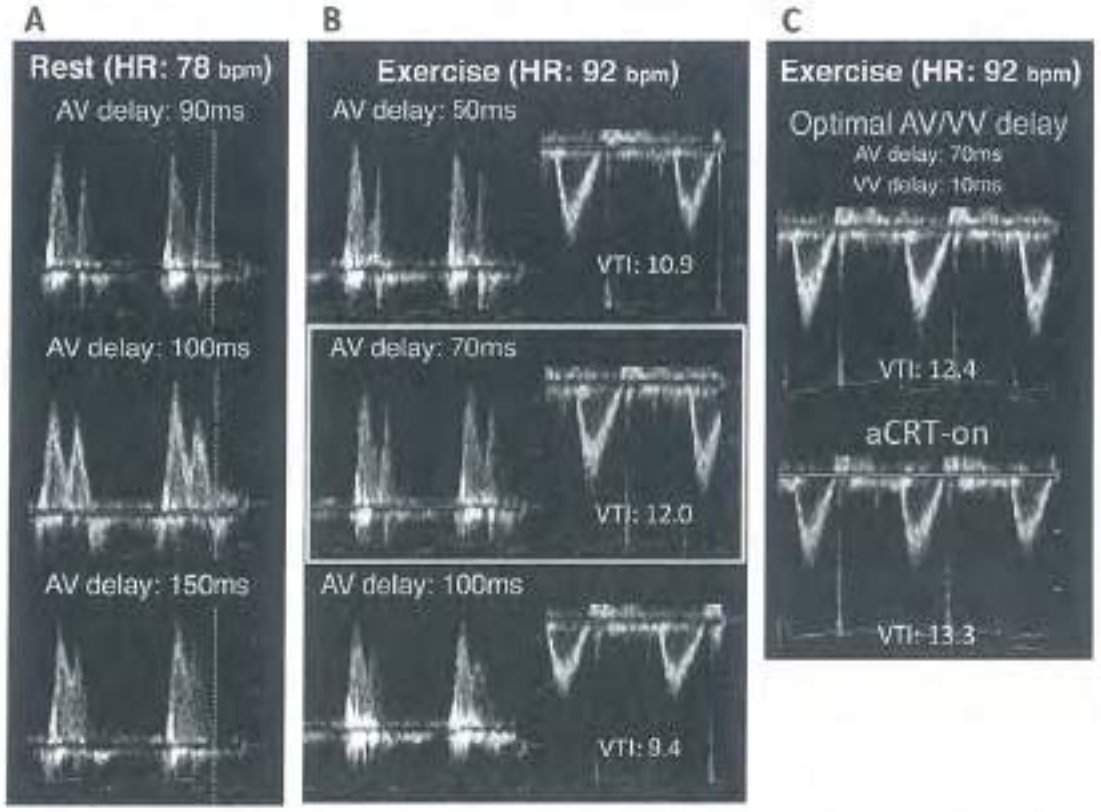

Figure 2. Echocardiographic images of a representative patient. (**A**) Transmitral Doppler flow at baseline with a shorter AV delay (90ms) shows partial truncation of the A-wave, and LV filling time of 291 ms (**Upper panel**). With a longer AV delay (150ms), the E-wave end and A-wave head partially overlap and the LV filling time is 247ms (**Lower panel**). The maximal E-wave and A-wave separation without truncation of the A wave is shown in this setting when the AV delay is 100ms, and the LV filling time is the longest (322ms). This AV delay time was defined as the optimal value (**Middle panel**). (**B**) After initiating exercise, the optimal AV delay shortened to 70ms, and as compared to that with shorter and longer AV delay patterns, the corresponding LVOT-VTI was largest in this setting (yellow frame). Of note, during exercise, the optimal AV delay at baseline was no longer optimal and the LVOT-VTI increased after AV optimization (**Lower panel**). (**C**) The LVOT-VTI with an optimal AV and VV delay during exercise and with aCRT-on. The aCRT algorithm provided a higher LVOT-VTI as compared with the manual echo-optimized setting. HR, heart rate; LV, left ventricle/ventricular; LVOT-VTI, left ventricular outflow tract velocity time integral. Other abbreviations as in Figure 1.

tips of the mitral valve leaflets and using a sweep speed of 100mm/s. Pulsed-wave Doppler sampling of the LV outflow tract (LVOT) was recorded by placing the sample volume 1cm below the aortic valve in the apical 5-chamber view or 3-chamber view, and the LVOT velocity time integral (LVOT-VTI) was measured at a sweep speed of 100mm/s. The iterative method was used for AV optimization.[17] The optimal AV delay was defined as the maximal E-wave and A-wave separation without truncation of the A wave. Subsequently, VV optimization was performed. The optimal VV delay was defined as the delay that produced the maximum LVOT-VTI. The echocardiographic images were recorded over 3 consecutive cardiac cycles and the measurement values were averaged. All echocardiographic data were analyzed by 2 experienced sonographers with disagreements settled by consensus, and they were blinded to the algorithm being on or off.

Exercise and the Study Protocol

Prior to acquiring the echocardiographic images, a device interrogation was performed and the intra-device ECG/marker signals were continuously viewed and recorded throughout the study. Blood pressure and 12-lead ECG were recorded at 1-min intervals. The 12-lead ECGs were assessed for an appropriate BiV or synchronized LV capture throughout the test. In all eligible patients the devices were programmed to the atrial tracking mode (DDD), the aCRT algorithm (aCRT-on) was activated before the study, and a full baseline echocardiographic examination was performed. Next, the aCRT algorithm was de-activated (aCRT-off) and resting AV/VV echo-optimization was applied according to the previously mentioned method. The heart rate at the end of this phase was defined as the baseline heart rate and an exercise test was initiated while remaining in the aCRT-off mode.

The patients underwent supine bicycle exercise at a fixed workload (10W) and the resistance of the bicycle was continually adjusted; the patients were coached to remain alert to the pedaling speed as necessary in order to obtain the target heart rate. After achieving a first target heart rate of 10beats/min above baseline or at 2min from the beginning of the exercise (Ex.1), echocardiographic AV

optimization was performed by the same method as performed at rest. After optimizing the AV delay, the VV intervals were programmed starting with an interval of 0ms, which was increased iteratively by 10ms (=LV pacing preceding the RV pacing by 10ms) intervals up to 50ms and the LVOT-VTI at each setting was recorded. Next, the aCRT algorithm was activated (aCRT-on) and pulsed-wave Doppler images of the transmitral flow velocity and LVOT-VTI were recorded. After completing the first exercise stage and once more turning off the aCRT algorithm (aCRT-off), the patients began the second stage of the exercise protocol with a target heart rate of 20 beats/min above baseline (Ex.2) by adjusting the workload until the patient developed symptoms. Similar to the first exercise stage, after achieving the target heart rate, the reprogramed AV echocardiographic optimizations and subsequent LVOT-VTI evaluation for each VV delay interval were performed. Finally, the aCRT algorithm was again activated (aCRT-on) in the patient and consequently the transmitral flow velocity and LVOT-VTI were recorded (**Figure 1**). A representative case is illustrated in **Figure 2**. The phase at the maximum exercise workload was described as peak exercise in this study.

During the study protocol, as the pacing mode was changed from aCRT-on to aCRT-off, a ≥30-s waiting period was provided to allow for the change in function to stabilize. The real-time VV delay echo-optimization was often inaccurate because of the difficulty in obtaining precise LVOT-VTI measurements during exercise. Thus, we analyzed the optimal VV delay by reviewing the recorded echocardiographic images after completing the study. Of note, the aCRT algorithm is designed to provide synchronized LV-only pacing only when the heart rate is <100 beats/min, and therefore our exercise protocol was intended to keep the patients' heart rate under 100 beats/min. To verify reproducibility, 7 CRT patients in whom the exercise stress echo-optimization had been repeated with the same protocol were preliminarily examined by 2 different independent observers. The inter- and intraobserver variabilities, expressed as the intraclass correlation coefficient regarding the post-optimized LVOT-VTIs, was more than 0.80 throughout the phase.

Statistical Analysis

The continuous data are expressed as mean±SD for a normal distribution, or the median (25th and 75th percentiles) for a skewed distribution. Dichotomous data are presented as numbers and percentages. A comparison of the continuous data was performed with Student's t-test for paired and unpaired data. Nonparametric data were compared using the Wilcoxon rank sum test.

Correlations between continuous variables were calculated with a Pearson correlation coefficient. A Spearman rank correlation coefficient was used to calculate the continuous variables that were not normally distributed. Hazard ratios (HRs) with 95% confidence intervals (CIs) and 2-sided P values were reported. A 2-tailed P value of <0.05 was considered statistically significant. All statistical analyses were performed with JMP 12 software (SAS Institute, Inc., Cary, NC, USA).

Results

Study Population

As our cohort of CRT patients, a total of 27 patients were enrolled. Their baseline characteristics are summarized in **Table 1**. Most were men with moderate HF, a prolonged QRS with left bundle branch block (LBBB), equivalent representation of ischemic and non-ischemic, and a severely reduced LVEF. The majority of the patients were prescribed negative chronotropic agents such as β-blockers or amiodarone. At the 6-month follow-up, the mean NYHA functional class improved from 3.0±0.3 to 2.0±0.7 (P<0.001) and the LVEF from 25.6±8.4 to 32.9±14.1 (P<0.003). All eligible patients had their atrial leads placed in the right atrial appendage and the RV lead in the RV apex. The LV lead was placed in an anterolateral (n=8), lateral (n=11) or posterior (n=8) cardiac vein.

Table 1. Baseline Characteristics

	All patients (n=27)
Baseline characteristics	
Age (years)	69±11
Male, n (%)	22 (81)
Ischemic heart disease, n (%)	13 (48)
Hypertension, n (%)	16 (56)
Diabetes, n (%)	7 (26)
CKD, n (%)	14 (52)
Treatments	
β-blocker, n (%)	26 (96)
ACE inhibitor, n (%)	20 (74)
Diuretics, n (%)	17 (63)
Amiodarone n (%)	7 (26)
Pre-CRT	
NYHA functional class (III/IV) (%)	7/83/4
QRS duration (ms)	164±26
LBBB, n (%)	22 (81)
LVEF (%)	26±8
LVEDV (mL)	186±89
LVESV (mL)	136±79
Post-CRT	
ΔNYHA class	−1.0±0.9
LVEF (%)	33±14
LVEDV (mL)	175±59
LVESV (mL)	122±51

Data are n (%) or mean±SD. ACE, angiotensin-converting enzyme; CKD, chronic kidney disease; CRT, cardiac resynchronization therapy; LBBB, left bundle branch block; LVEDV, left ventricular end-diastolic volume; LVEF, left ventricular ejection fraction; LVESV, left ventricular end-systolic volume; NYHA, New York Heart Association.

Exercise Tolerance and the Pacing Mode

All patients were able to successfully complete the protocol of the first exercise stage (Ex.1), but 3 patients could not achieve the target heart rate in the second exercise stage (Ex.2) because of reported symptoms of fatigue and inability to increase their heart rate. The resting heart rate was 74.3±9.0 beats/min, which increased to 80.8±9.4 beats/min during Ex.1 and 89.6±8.3 beats/min during Ex.2. Before initiating the exercise, 18 (66%) patients were programmed to the adaptive BiV mode and 9 (33%) subjects to the adaptive LV mode. Interestingly, during exercise, 2 patients converted to an adaptive LV from an adaptive BiV, and conversely 3 patients converted to an adaptive BiV from

Table 2. Pacing Mode of the aCRT Algorithm During Each Phase

Pacing mode	Rest (n, %)	Ex. 1 (n, %)		Ex. 2 (n, %)	
Adaptive BiV	18 (66)	19 (70)		17 (71)	
		BiV at rest to BiV	16 (59)	BiV at rest to BiV	15 (63)
		LV at rest to BiV	3 (11)	LV at rest to BiV	2 (8)
Adaptive LV	9 (33)	8 (30)		7 (29)	
		BiV at rest to LV	2 (7)	BiV at rest to LV	1 (4)
		LV at rest to LV	6 (22)	LV at rest to LV	6 (25)

aCRT, adaptive cardiac resynchronization therapy algorithm; BiV, biventricular pacing; LV, synchronized left ventricular pacing.

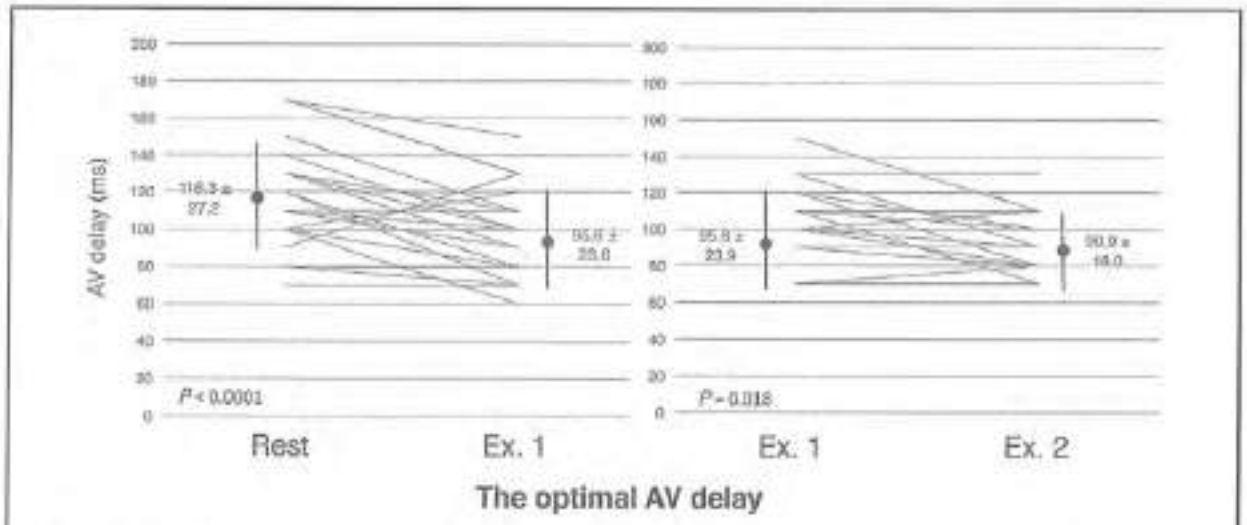

Figure 3. Changes in the optimal atrioventricular (AV) delay assessed at baseline and during each exercise phase. Ex., exercise protocol.

an adaptive LV. The pacing mode of the aCRT algorithm during each exercise phase is shown in **Table 2**.

Optimal AV/VV Delay and the LV Filling Time at Rest and During Exercise

At baseline, the mean optimal AV delay was 116.3±27.2 ms. During exercise, the optimal AV delay was significantly reduced to 95.8±23.9 ms during Ex.1 (mean difference 20.7 ms; 95% CI 29.6–11.9 ms; P<0.0001), and progressively shortened to 90.9±18.0 ms during Ex.2 (mean difference from Ex.1: 8.2 ms; 95% CI 15.8–0.6 ms; P=0.018) (**Figure 3**). There was no significant difference in the LV filling time at rest (pre-optimization 442±88 ms; post-optimization 438±19 ms; P=0.6). After initiating the exercise, the LV filling time significantly decreased from 438±19 ms to 365±25 ms (P<0.01); however, a corresponding increase was observed in the mean LV filling time from 365±75 ms to 386±84 ms following the AV optimization at peak exercise (P<0.01).

The median VV delay at rest was 0 ms (0–20 ms) and exercise induced a change in the VV delay programming in 13 (48%) patients. The rest-to-peak exercise variations in the optimal VV delay ranged from 0 to 50 ms, with a median value of 20 ms. There were no concordant correlations between the heart rates and optimal VV delays (r=−0.04, P=0.9). Importantly, 2 patients developed ineffective LV pacing at a VV delay of 0 ms and successfully converted to an effective LV pacing at a VV delay of up to 20 ms during exercise.

Correlation Between Manual Echo-Optimization and aCRT

In the overall patients, the baseline mean LVOT-VTI for the manual echo-optimized settings and aCRT was 12.5±3.0 cm and 12.5±3.1 cm, respectively (P=0.8). During Ex.1, the LVOT-VTI for the manual echo-optimized settings and aCRT was 14.2±3.5 cm and 14.2±4.0 cm, respectively (P=0.9), and 13.8±3.0 cm and 14.5±3.3 cm (P=0.005) during Ex.2. There were no significant differences in the heart rate between that at the time of the maximal LVOT-VTI with a manual echo-optimized setting and that of the aCRT both during Ex.1 (80.8±9.9 beats/min and 81.2±9.2 beats/min, respectively; P=0.9) and Ex. 2 (89.6±8.5 beats/min and 89.6±7.6 beats/min, respectively; P=0.95). Surprisingly, the manual echo-optimized setting and aCRT resulted in a similar cardiac performance, as demonstrated by a high concordance correlation coefficient between the LVOT-VTI at each exercise stage (baseline: r=0.95 P<0.001, Ex.1: r=0.94 P<0.0008, Ex.2: r=0.88, P<0.001, respectively) (**Figure 4A**). Similarly, only among the patients with an adaptive BiV pacing mode, there was a high concordance correlation coefficient between the manual echo-optimized setting and aCRT for each exercise

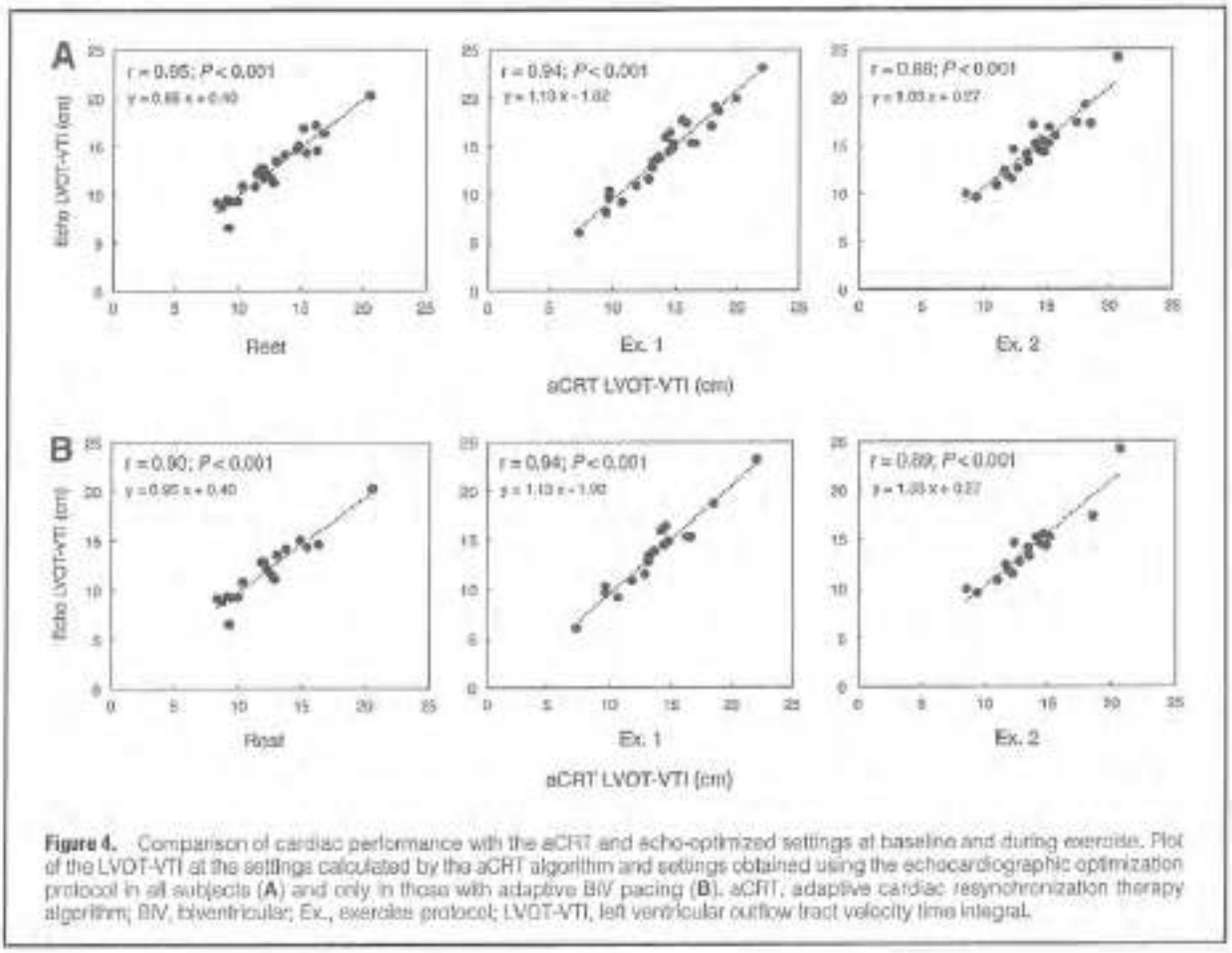

Figure 4. Comparison of cardiac performance with the aCRT and echo-optimized settings at baseline and during exercise. Plot of the LVOT-VTI at the settings calculated by the aCRT algorithm and settings obtained using the echocardiographic optimization protocol in all subjects (**A**) and only in those with adaptive BiV pacing (**B**). aCRT, adaptive cardiac resynchronization therapy algorithm; BiV, biventricular; Ex., exercise protocol; LVOT-VTI, left ventricular outflow tract velocity time integral.

stage regarding the LVOT-VTI (baseline: r=0.90 P<0.001, Ex.1: r=0.94 P<0.001, Ex.2: r=0.89, P<0.001, respectively) (**Figure 4B**).

When compared with the manual echo-optimized conventional BiV pacing, synchronized LV-only pacing (adaptive LV) had a tendency for a higher LVOT-VTI at rest (median 13.2cm, range 12.2–16.9cm vs. median 11.7cm, range 10.8–13.4cm, P=0.08). Interestingly, the adaptive LV at peak exercise provided a higher value compared with manual echo-optimized BiV pacing at peak exercise (17.6cm, range 15.4–19.7cm vs. 14.7cm, range 9.8–15.9cm, P=0.016) (**Figure 5**).

Discussion

The main findings of our study on the validity of the aCRT algorithm during exercise can be summarized as follows: (1) the optimal AV delay progressively shortened with incremental exercise levels; (2) AV optimization during exercise could increase LV filling time; (3) the optimal VV delay varied from rest to exercise without a concordant correlation; (4) a significant correlation was shown between the aCRT and echo-optimization regarding stroke volume, both at rest and during exercise; and (5) synchronized LV-only pacing in CRT patients with normal AV conduction could provide a higher stroke volume during exercise as compared with manual-optimized conventional BiV pacing. In the present study, we showed the hemodynamic validity of the aCRT algorithm during exercise.

Effects of Optimization Performed During Exercise

Normal physiological adaptation to exercise leads to an increase in the heart rate, shortening of the AV node conduction time, and increased myocardial contractility, and therefore, generally results in a shorter AV interval at higher heart rates. Increasing the heart rate plays a major role in producing a cardiac output increase with exercise and the maximum cardiac output depends on the maximum heart rate. However, AV synchrony contributes to the cumulative effects for heart rates up to approximately 80 beats/min and increases the myocardial contractility dose above 80 beats/min in normal hearts.[15] Accordingly, the significance of AV synchrony for maximizing cardiac performance is well described and is more pronounced in patients with systolic HF.[5,8,10,11] To date, several studies have shown that AV and VV optimization improves LV systolic performance even during exercise.[8,10,11] We demonstrated that the optimal AV delay progressively shortened during exercise, and similar findings have been reported by Sun et al,[8] who showed an almost 40% reduction in the programmed AV delay during exercise. They also suggested that the magnitude of the change in the AV delay with increasing heart rates in CRT patients appeared to be significantly greater than the physiological exercise-induced

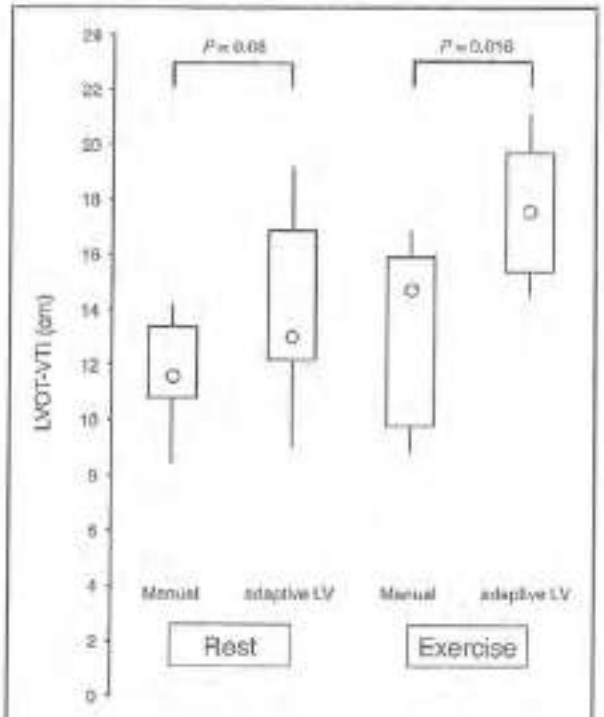

Figure 5. Comparison of stroke volume during synchronized LV pacing (adaptive LV) and at the echo-optimized settings at baseline and during exercise. Boxplot (25–75th percentile) and median values (open circles) showing the distribution of the LVOT-VTI during synchronized LV pacing and echo-optimized conventional BiV pacing, both at rest and during exercise. The adaptive LV shows a higher value compared with manual echo-optimized BiV pacing at peak exercise. BiV, biventricular; LVOT-VTI, left ventricular outflow tract velocity time integral.

change in the PR intervals observed in healthy subjects. Similarly, Shanmugam et al[10] also reported that over 90% of patients with CRT showed a significant reduction (mean 50 ms) in the optimal AV delay during exercise and they demonstrated a corresponding increase in the LV filling time following AV optimization during exercise as well. Moreover, they successfully showed a 10% improvement in exercise capacity with a programmable rate-adaptive AV delay. Our findings concur with those reports and led us to believe that it may be beneficial to program the device to automatically adjust the AV delay according to the activity level.

Furthermore, we demonstrated significant variation in the optimal VV delay between rest and exercise. Unlike the AV delay, the optimal VV delay cannot be considered as correlated to the heart rate and a large variation can be seen between individual subjects. Notably, some patients developed ineffective LV pacing during exercise and this phenomenon may be found in the general population of patients with CRT. Valzania et al[9] showed that the optimal VV delay varied considerably from rest to exercise and a re-assessment during exercise yielded an additional hemodynamic benefit. They also demonstrated the validity of their algorithm, which was based on the intracardiac electrogram method (QuickOpt™), as having a strong agreement with the echo-optimization during exercise regarding the LVOT-VTI. However, the Frequent Optimization Study Using the QuickOpt Method study (FREEDOM) did not show its superiority to conventional methods of optimization when the clinical composite score was compared.[19] Moreover, the SMART-AV study that compared device-based, echo-based, and empirical programing of the AV delay did not show any significant changes in the LV volume and LVEF.[7] Much evidence has suggested that the optimal AV and VV delay varies between rest and exercise, but it could still be challenging to discover an algorithm that can provide an adaptive AV/VV delay for general patients with CRT.

The aCRT algorithm can provide better clinical outcomes, or at least those as effective as comprehensive echo-optimized BiV pacing, through synchronized LV pacing and continuous optimization.[12,13] Importantly, this novel algorithm is based on clinical research conducted essentially during the resting phase,[20-23] and thus it has been unclear whether these results can be applied during exercise. As mentioned before, the major role of AV synchrony in contributing to the hemodynamics is during exercise with a heart rate of less than 100 beats/min,[18] and the aCRT algorithm can only provide synchronized LV-only pacing when the heart rate is under 100 beats/min. Thus, our study protocol was designed to target a heart rate under 100 beats/min. In the present study, we provide new information regarding the validity of this algorithm even during low-intensity exercise. Through all the phases, a high correlation was shown between aCRT and echo-optimization regarding the stroke volume among patients with prolonged AV conduction. Furthermore, when normal AV conduction was observed, synchronized LV-only pacing could also provide a better stroke volume compared with echo-optimized BiV pacing during exercise. Synchronized LV-only pacing may prevent RV pacing-induced dyssynchrony and allow for simultaneous RV and LV electrical activation. A previous study on CRT in patients with LBBB and preserved RV conduction showed that the RV dP/dtmax was greater when CRT produced synchronized LV-only pacing.[24] Avoidance of RV pacing can provide superior RV function in patients with sufficiently preserved conduction to the RV. The results of our study indicated that aCRT offered a similar or greater stroke volume compared with real-time echo-optimization both at rest and during low-intensity exercise, which could be a possible explanation for the better clinical outcomes in some clinical trials of this novel algorithm.

Study Limitations

A potential weakness of this study was that it was conducted at a single center with a relatively small patient cohort and only included sinus rhythm patients with availability of the aCRT algorithm, which could expose the study to a myriad of biases, particularly selection bias and statistical power limitations. A higher prevalence of patients with prolonged AV conduction and moderate to severe HF could be considered as a limitation. Moreover, it is important to emphasize that the stroke volume is affected by multiple factors such as the cardiac pre- or afterload or exercise-induced mitral regurgitation, which make it difficult to clearly distinguish whether or not this additional hemodynamic contribution was only based on pacing settings. Also, it was unclear how the duration of exercise, passage of time, and order of the measurements from aCRT-off to aCRT-on affected the results. Finally, the study design

did not intend to determine whether other hemodynamic benefits, excepted for stroke volume, would be observed when using the aCRT algorithm, as well as whether the same was true with much harder exercise or during tachycardia. Therefore, the current data need to be confirmed in a larger number of participants with a wider HF status and AV conduction range, and further studies are needed to evaluate the validity of the aCRT algorithm for other hemodynamic factors or during harder exercise.

Conclusions

Among the study patients with CRT, the optimal AV delay progressively shortened with incremental exercise levels. The aCRT algorithm is a novel device-based algorithm that has a significant correlation to echo-optimization regarding the stroke volume both at rest and during exercise. Once the patients developed a normal AV conduction following exercise, the aCRT algorithm provided an additional hemodynamic benefit through synchronized LV-only pacing.

Conflicts of Interest

Dr. Nakajima received a scholarship from the Japanese Heart Rhythm Society and received speaking honoraria from Medtronic Japan Co., Ltd.

References

1. Abraham WT, Fisher WG, Smith AL, Delurgio DB, Leon AR, Loh E, et al. Cardiac resynchronization in chronic heart failure. *N Engl J Med* 2002; **346:** 1845–1853.
2. Cleland JG, Daubert JC, Erdmann E, Freemantle N, Gras D, Kappenberger L, et al; Cardiac Resynchronization-Heart Failure (CARE-HF) Study Investigators. The effect of cardiac resynchronization on morbidity and mortality in heart failure. *N Engl J Med* 2005; **352:** 1539–1549.
3. Moss AJ, Hall WJ, Cannom DS, Klein H, Brown MW, Daubert JP, et al. Cardiac-resynchronization therapy for the prevention of heart-failure events. *N Engl J Med* 2009; **361:** 1329–1338.
4. Mullens W, Grimm RA, Verga T, Dresing T, Starling RC, Wilkoff BL, et al. Insight from a cardiac resynchronization optimization clinic as part of a heart failure disease management program. *J Am Coll Cardiol* 2009; **53:** 765–773.
5. Auricchio A, Stellbrink C, Block M, Sack S, Vogt J, Bakker P, et al. Effect of pacing chamber and atrioventricular delay on acute systolic function of paced patients with congestive heart failure. The Pacing Therapies for Congestive Heart Failure Study Group. The Guidant Congestive Heart Failure Research Group. *Circulation* 1999; **99:** 2993–3001.
6. Sawhney NS, Waggoner AD, Garhwal S, Chawla MK, Osborn J, Fadlis MN. Randomized prospective trial of atrioventricular delay programming for cardiac resynchronization therapy. *Heart Rhythm* 2004; **1:** 562–565.
7. Ellenbogen KA, Gold MR, Meyer TE, Fernndez Lozano I, Mittal S, Waggoner AD, et al. Primary results from the SmartDelay determined AV optimization: A comparison to other AV delay methods used in cardiac resynchronization therapy (SMART-AV) trial: A randomized trial comparing empirical, echocardiography-guided, and algorithmic atrioventricular delay programming in cardiac resynchronization therapy. *Circulation* 2010; **122:** 2660–2668.
8. Sun JP, Lee AP, Grimm RA, Hung MJ, Yang XS, Delurgio D, et al. Optimisation of atrioventricular delay during exercise improves cardiac output in patients stabilised with cardiac resynchronisation therapy. *Heart* 2012; **98:** 54–59.
9. Valzania C, Eriksson MJ, Boriani G, Gadler F. Cardiac resynchronization therapy during rest and exercise: Comparison of two optimization methods. *Europace* 2008; **10:** 1161–1169.
10. Shanmugam N, Prada-Delgado O, Campos AG, Campos AG, Grimster A, Valencia O, et al. Rate-adaptive AV delay and exercise performance following cardiac resynchronization therapy. *Heart Rhythm* 2012; **9:** 1815–1821.
11. Grimm RA, Sun JP, Agler D, Fitzgerald B, Wilkoff B, Hilpisch K, et al. Shorter AV delay provide improved echocardiographic hemodynamics during exercise in patients receiving cardiac resynchronization therapy. *Pacing Clin Electrophysiol* 2009; **32:** 457–465.
12. Martin DO, Lemke B, Birnie D, Krum H, Lee KL, Aonuma K, et al. Investigation of a novel algorithm for synchronized left-ventricular pacing and ambulatory optimization of cardiac resynchronization therapy: Results of the adaptive CRT trial. *Heart Rhythm* 2012; **9:** 1807–1814.
13. Birnie D, Lemke B, Aonuma K, Kurm H, Lee KL, Gasparini M, et al. Clinical outcomes with synchronized left ventricular pacing: Analysis of the adaptive CRT trial. *Heart Rhythm* 2013; **10:** 1368–1374.
14. Birnie D, Hudnall H, Lemke B, Aonuma K, Lee KL, Gasparini M, et al. Continuous optimization of cardiac resynchronization therapy reduces atrial fibrillation in heart failure patients: Results of the Adaptive Cardiac Resynchronization Therapy Trial. *Heart Rhythm* 2017; **14:** 1820–1825.
15. Epstein AE, DiMarco JP, Ellenbogen KA, Estes NA 3rd, Freedman RA, Gettes LS, et al. ACCF/AHA/HRS 2008 guidelines for device-based therapy of cardiac rhythm abnormalities-executive summary; a report of the American College of Cardiology/American Heart Association Task Force on Practice Guidelines. *J Am Coll Cardiol* 2008; **51:** 2085–2105.
16. Epstein AE, DiMarco JP, Ellenbogen KA, Estes NA 3rd, Freedman RA, Gettes LS, et al. 2012 ACCF/AHA/HRS focused update incorporated into the ACCF/AHA/HRS 2008 guidelines for device-based therapy of cardiac rhythm abnormalities: A report of the American College of Cardiology Foundation/American Heart Association Task Force on Practice Guidelines and the Heart Rhythm Society. *J Am Coll Cardiol* 2013; **61:** e6–e75.
17. Kerlan JE, Sawhney NS, Waggoner AD, Chawla MK, Garhwal S, Osborn JL, et al. Prospective comparison of echocardiographic atrioventricular delay optimization methods for cardiac resynchronization therapy. *Heart Rhythm* 2006; **3:** 148–154.
18. Benditt DG, Milstein S, Bastikofer J, Gornick CC, Mianuli M, Fetter J. Sensor-triggered, rate-variable cardiac pacing: Current technologies and clinical implications. *Ann Intern Med* 1987; **107:** 714–724.
19. Abraham WT, Gras D, Yu CM, Guzzo L, Gupta MS; FREEDOM Steering Committee. Rationale and design of a randomized clinical trial to assess the safety and efficacy of frequent optimization of cardiac resynchronization therapy: The Frequent Optimization Study Using the QuickOpt Method (FREEDOM) trial. *Am Heart J* 2010; **159:** 944–948.
20. van Gelder BM, Bracke FA, Meijer A, Pijls NH. The hemodynamic effect of intrinsic conduction during left ventricular pacing as compared to biventricular pacing. *J Am Coll Cardiol* 2005; **46:** 2305–2310.
21. Lee KL, Burnes JE, Mullen TJ, Hettrick DA, Tse HF, Lau CP. Avoidance of right ventricular pacing in cardiac resynchronization therapy improves right ventricular hemodynamics in heart failure patients. *J Cardiovasc Electrophysiol* 2007; **18:** 497–504.
22. Jones RC, Svilanich T, Rubin A, Levin V, Phang R, Murillo J, et al. Optimal atrioventricular delay in CRT patients can be approximated using surface electrocardiography and device electrogram. *J Cardiovasc Electrophysiol* 2010; **21:** 1226–1232.
23. Khaykin Y, Exner D, Birnie D, Sapp J, Aggarwal S, Sambelashvili A. Adjusting the timing of left-ventricular pacing using electrocardiogram and device electrograms. *Europace* 2011; **13:** 1464–1470.
24. Lee KL, Burnes JE, Mullen TJ, Hettrick DA, Tse HF, Lau CP. Avoidance of right ventricular pacing in cardiac resynchronization therapy improves right ventricular hemodynamics in heart failure patients. *J Cardiovasc Electrophysiol* 2007; **18:** 497–504.

Journal of Echocardiography (2019) 17:147–156
https://doi.org/10.1007/s12574-018-0404-6

ORIGINAL INVESTIGATION

Prognostic value of exercise stress echocardiography in patients with secondary mitral regurgitation: a long-term follow-up study

Tomomi Suzuki[1] · Masaki Izumo[1] · Kengo Suzuki[1] · Dan Koto[1] · Maya Tsukahara[1] · Kanako Teramoto[1] · Yukio Sato[1] · Mika Watanabe[1] · Kei Mizukoshi[1] · Ryo Kamijima[1] · Manabu Takai[1] · Seisyou Kou[1] · Tomoo Harada[1] · Sachihiko Nobuoka[2] · Yoshihiro J. Akashi[1]

Received: 7 September 2018 / Revised: 9 October 2018 / Accepted: 22 October 2018 / Published online: 29 October 2018
© Japanese Society of Echocardiography 2018

Abstract

Background Secondary mitral regurgitation (MR) remains a challenging problem in the diagnosis and treatment of patients with heart failure. Although it is well known that secondary MR is dynamic, the impact of the severity of MR during exercise on long-term outcome has not been fully evaluated. The aim of the present study was to investigate the prognostic value of exercise stress echocardiography (ESE) in patients with secondary MR.

Methods This prospective study included 118 consecutive patients with secondary MR and left ventricular dysfunction (mean ejection fraction at rest: 38 ± 14%) who underwent semi-supine ESE. Their major cardiovascular events (MACE) including cardiac death were followed up for a median of 41.7 (range: 6–128) months.

Results MR significantly increased from rest to exercise (effective regurgitant orifice: 0.18 ± 0.09 vs. 0.25 ± 0.12 cm^2, $P < 0.001$). The prevalence of severe MR was higher during exercise than those at rest (37% vs. 56%, $P < 0.001$). During follow-up, MACE occurred in 49 patients (41.5%) including 12 cardiac deaths. Cox proportional-hazard multivariate analysis revealed that older age and MR severity during exercise were significantly associated with increased risk of MACE (hazard ratio: 1.04 and 8.4, respectively, both $P < 0.05$).

Conclusions ESE provides prognostic information in patients with secondary MR that is useful for predicting long-term outcome.

Keywords Secondary mitral regurgitation · Echocardiography · Exercise stress echocardiography · Heart failure

Introduction

From a public health perspective, valvular heart disease, which has a poor prognosis, affects entire communities in developed countries [1]. Secondary mitral regurgitation (MR) occurs in 11% to 59% [2, 3] of patients after a myocardial infarction and is present in ~50% of patients with dilated cardiomyopathy [4–6]. Despite this high prevalence, secondary MR remains as a challenging issure in the diagnostic workup and treatment of patients with heart failure. It is well known that secondary MR is dynamic, [7–14] however, current therapy is primarily focused on resting conditions and the impact of MR severity during exercise on long-term outcome has not been fully evaluated. Therefore, we aimed to investigate the prognostic value of exercise stress echocardiography (ESE) in patients with secondary MR.

✉ Masaki Izumo
heartizumo@yahoo.co.jp

[1] Division of Cardiology, Department of Internal Medicine, St. Marianna University School of Medicine, 2-16-1 Sugao, Miyamae-ku, Kawasaki 216-8511, Japan

[2] Department of Clinical Laboratory, St. Marianna University School of Medicine, Kawasaki, Japan

Methods

Study population

This prospective single-center study included 138 consecutive patients with secondary MR and reduced left ventricular ejection fraction (LVEF < 50%) who underwent ESE using semi-supine bicycle ergometer between April 2006 and August 2017 at St. Marianna University School of Medicine Hospital. Of these, ten patients who underwent mitral valve

surgery, eight patients who were lost to follow-up, and two patients with poor image quality for quantifying MR were excluded. Finally, 118 patients (mean age: 64 ± 14 years, 24% female) were enrolled. All patients were in a stable condition at the time of enrollment and none of them met the following exclusion criteria, (1) more than mild aortic regurgitation, mild or greater aortic stenosis or severe tricuspid regurgitation, (2) history of myocardial infarction < 6 months prior, (3) evidence of inducible ischemia; and (4) extensive myocardial ischemia requiring coronary angiography and revascularization. This study was approved by the institutional review board at St. Marianna University School of Medicine (No. 1288). All patients provided written informed consent before study enrollment.

Exercise echocardiography

After a comprehensive Doppler echocardiography at rest, a symptom-limited bicycle exercise test was performed in the semi-supine position on a dedicated tilting exercise table. Patients started with an initial workload of 10 W maintained for 3 min; the workload was increased every 3 min by 10 W. Blood pressure and heart rate were recorded every 1 min. Two-dimensional and Doppler echocardiography was available throughout the exercise test.

Echocardiographic measurements

Echocardiographic examinations were performed with commercially available ultrasound system (Vivid E9; GE Vingmed Milwaukee, WI, USA or iE33, Philips, Andover, MA, USA). All echocardiographic and Doppler data were obtained at rest and at peak exercise in digital format and stored on a workstation for offline analysis (EchoPAC, version 12; GE Vingmed Milwaukee, WI, USA). All measurements were averaged over three cardiac cycles. MR was quantified according to the proximal isovelocity surface area (PISA) method at rest and during exercise; effective regurgitant orifice (ERO) and regurgitant volume (RV), which indicates the severity of secondary MR. The PISA radius was measured from at least three frames with optimal flow convergence. The most appropriate negative aliasing velocity to obtain PISA was selected offline on the workstation. The PISA radius was measured in mid-systole. RV and ERO were calculated with standard formulas [15]. According to the guidelines, severe secondary MR was defined as an ERO of 0.20 cm^2 [16]. We also quantified MR evaluated by volumetric method only at rest. The diameter of the left ventricular (LV) outflow tract (inner edge) was measured only at rest in the parasternal long-axis view. The mitral and aortic stroke volumes were calculated as the pulsed-wave Doppler time–velocity integral × the area of the annulus of the mitral and aortic valves, respectively. RV (quantitative Doppler echocardiography) was calculated as the difference between the mitral and aortic stroke volumes. ERO was measured as RV/VTI of the regurgitant jet [16]. The biplane Simpson method was used to measure LV end-diastolic volume (LVEDV) and end-systolic volume (LVESV), stroke volume, EF, and left atrial (LA) maximal volume. Mitral E- and A-wave velocities were measured with pulsed-wave Doppler, and e' wave velocity was obtained by tissue Doppler imaging in the septal position of the mitral annulus. These measurements were repeated at exercise before or just after the eventual fusion of E and A. Systolic pulmonary artery pressure (SPAP) was derived from the regurgitant jet of tricuspid regurgitation using systolic transtricuspid pressure gradient calculated by the modified Bernoulli equation ($P4v^2$, where v is maximal tricuspid regurgitant jet velocity in m/s) and the addition of right atrial pressure. Mean right atrial pressure was estimated based on the most recent ASE recommendation [17]. Right atrial pressure was assumed to be constant from rest to exercise. Mitral valve tenting height and tenting area were measured by the apical long-axis view at mid-systole. Mitral valve tenting height was defined as the distance from the mitral annular plane to mitral leaflet coaptation point. The mitral valve tenting area was measured by the area enclosed between the annular plane and mitral leaflets.

Study endpoints

The primary study endpoint was cardiac death during follow-up and the secondary endpoint was major adverse cardiovascular events (MACE) defined as cardiac death, and hospitalization for heart failure.

Statistical analysis

The results are expressed as mean ± standard deviation (SD) or percentage unless otherwise specified. Data for the MACE and no-MACE groups were compared by Student's *t* test, Chi-squared test, or Fisher exact test as appropriate. Pearson's correlation coefficient was used to evaluate the correlation between two parameters. Probabilities of event-free survival among the severe and non-severe groups were obtained using Kaplan–Meier analysis and compared using the two-sided log-rank test. The effect of clinical, resting and exercise echocardiographic parameters was assessed using the Cox proportional-hazard model in univariate and multivariate analyses. Variables with a univariate value of $P < 0.1$ were incorporated into the multivariate models. ERO was entered into the multivariate model without RV as MR severity because of collinearity. Sequential Cox models were performed to determine the incremental prognostic benefit of exercise echocardiographic parameters over clinical and resting echocardiographic data. A statistically significant

increase in the global log-likelihood χ^2 of the model defined the incremental prognostic value. P values < 0.05 were considered as statistically significant. Both the interobserver and intraobserver variabilities for ERO and RV were obtained according to the blind analysis of twenty-eight random images by two independent observers at two different time points. The results were analyzed by both an intraclass correlation coefficient for absolute agreement (ICCa) and the Bland–Altman method. Statistical analyses were performed with SPSS 22.0 software (SPSS, Inc., Chicago, IL, USA).

Results

Clinical and echocardiographic features

Table 1 shows the clinical characteristics of the study population (mean age: 64 ± 14 years, 24% female). None of the patients, at the time of the study, had suspected significant coronary artery disease requiring myocardial revascularization. Among the 118 patients, 49 patients (41.5%) developed MACE during follow-up (12 cardiac death and 37 heart failure hospitalization). We found no differences in clinical characteristics between the MACE and no-MACE groups except for systolic blood pressure at peak exercise.

In the entire cohort, MR significantly increased from rest to exercise (0.18 ± 0.09 vs. 0.25 ± 0.12 cm², $P < 0.001$, Fig. 1). The prevalence of severe secondary MR was significantly higher at peak exercise than at rest (37% vs. 56%, $P < 0.001$). Table 2 shows resting and exercise echocardiographic findings. Although the MACE group had significantly greater LV volumes and lower LVEF than the no-MACE group (all $P < 0.05$), there were no significant differences in E wave velocity, E/e', and SPAP between the two groups at rest. During exercise, LV volumes, E/e' and SPAP were significantly greater in the MACE group than in the no-MACE group. Despite similar resting MR severity and tethering parameters of the mitral valve between the two groups, the MACE group had greater tenting height and area, ERO, and RV during exercise than the no-MACE group.

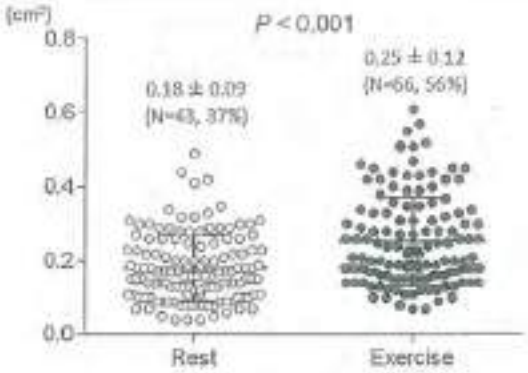

Fig. 1 Effective regurgitant orifice at rest and peak exercise in the whole cohort. Mitral regurgitation (MR) significantly increased from rest to exercise. The number and percent indicate the number and percentage of patients with severe secondary MR

Table 1 Baseline characteristics

	All (n = 118)	No MACE (n = 69)	MACE (n = 49)	P value
Age, (years)	64 ± 14	64 ± 15	63 ± 14	0.522
Female, n (%)	28 (24)	18 (26)	11 (22)	0.691
Blood pressure and heart rate at rest				
Systolic BP, (mmHg)	112 ± 24	113 ± 20	111 ± 24	0.624
Diastolic BP, (mmHg)	72 ± 14	73 ± 14	70 ± 15	0.565
Heart rate, (beats/min)	68 ± 12	67 ± 10	68 ± 12	0.686
Blood pressure and heart rate at peak exercise				
Systolic BP, (mmHg)	156 ± 35	162 ± 36	141 ± 30	0.029
Diastolic BP, (mmHg)	79 ± 14	80 ± 15	77 ± 14	0.591
Heart rate, (beats/min)	113 ± 24	115 ± 25	110 ± 21	0.733
Etiology				
Ischemic cardiomyopathy, n (%)	45 (38)	27 (39)	18 (37)	0.822
Medications				
ACEI/ARB, n(%)	105 (89)	60 (87)	45 (91)	0.802
β-blocker, n (%)	95 (81)	57 (83)	38 (78)	0.331
Diuretics, n (%)	101 (86)	60 (86)	41 (84)	0.841

MACE major cardiovascular event, *BP* blood pressure, *ACEI* angiotensin converting enzyme inhibitor, *ARB* angiotensin II receptor blocker

Table 2 Echocardiographic findings at rest and peak exercise

	All (n=118)	No MACE (n=69)	MACE (n=49)	*P* value
Rest				
LVEDV, (ml)	168±64	161±64	176±57	0.017
LVESV, (ml)	111±59	101±55	120±62	0.013
LVEF, (%)	34.0±13.8	37.2±17.4	31.8±12.6	0.043
S', (cm/s)	5.1±1.6	5.4±1.7	4.9±1.3	0.073
LAVi, (ml)	47.5±29.5	51.0±30.8	44.1±28.0	0.600
E wave velocity, (cm/s)	80.0±30.1	77.5±28.4	89.2±32.7	0.547
E', (cm/s)	6.3±2.7	5.9±2.4	6.4±3.4	0.937
E/E'	14.5±6.8	13.5±6.7	15.1±6.1	0.188
SPAP, (mmHg)	34.0±10.0	34.1±10.2	34.9±10.4	0.138
Tenting height, (mm)	7.0±2.0	6.8±2.0	7.2±2.1	0.277
Tenting area, (cm^2)	1.4±0.5	1.3±0.5	1.5±0.5	0.280
ERO (PISA), (cm^2)	0.18±0.09	0.19±0.09	0.17±0.09	0.843
RV (PISA), (ml)	26.9±15.1	28.8±14.0	24.8±15.5	0.991
ERO (volumetric), (cm^2)	0.19±0.11	0.20±0.12	0.18±0.10	0.723
RV (volumetric), (ml)	29.8±16.7	30.8±17.8	27.9±15.3	0.841
Exercise				
LVEDV, (ml)	176±64	171±64	188±66	0.028
LVESV, (ml)	113±59	106±57	124±58	0.019
LVEF, (%)	35.5±14.6	38.5±12.7	34.0±12.2	0.004
S', (cm/s)	5.5±2.2	5.8±1.9	5.0±2.0	0.176
E wave velocity, (cm/s)	129±32	131±34	127±28	0.302
E', (cm/s)	7.4±3.5	7.7±3.8	6.4±2.4	0.420
E/E'	18.6±8.6	17.5±9.5	20.1±7.8	0.046
SPAP, (mmHg)	53.3±14.4	51.0±13.4	57.0±15.6	0.015
Tenting height, (mm)	8.0±2.5	7.5±2.3	9.0±2.9	0.013
Tenting area, (cm^2)	1.6±0.5	1.5±0.5	1.9±0.6	0.006
ERO, (cm^2)	0.25±0.12	0.23±0.10	0.30±0.14	<0.001
RV, (ml)	34.0±19.2	32.2±14.1	44.1±21.4	<0.001

MACE major cardiovascular events, *LVEDV* left ventricular end-diastolic volume, *LVESV* left ventricular end-systolic volume, *LVEF* left ventricular ejection fraction, *LAVi* left atrial volume index, *SPAP* systolic pulmonary artery pressure, *ERO* effective regurgitant orifice area, *RV* regurgitant volume

Clinical outcomes

During a median follow-up of 41.7 (range: 6–128) months, 12 patients (10.1%) developed the primary endpoint (cardiac death), and 49 patients (41.5%) reached the secondary endpoint (MACE; 12 cardiac death and 37 heart failure hospitalization). The Cox-hazard multivariate analysis showed that older age (HR: 1.036, $P=0.032$) and ERO during exercise (HR: 8.402, $P=0.012$) were independently associated with an increased risk of MACE (Table 3). In the entire cohort, the cardiac death-free survival rates were 97±4%, 90±7%, 82±12%, and 72±14% and MACE-free survival rates were 90±8%, 78±12%, 62±15%, and 39±17% at 1, 3, 5, and 7 years, respectively. Figure 2 illustrates the cardiac death and MACE-free survival rates of the study population stratified according to the severity of secondary MR at rest (A and C) and exercise (B and D). Patients with severe secondary MR during exercise had significantly lower rates of cardiac death and MACE-free survival than those without severe secondary MR; we could not stratify the cardiac death-free survival rate according to the resting severity of secondary MR. Receiver-operating characteristic curve analysis revealed that exercise ERO was more accurate in predicting MACE during follow-up than resting ERO (area under the curve: 0.692 vs. 0.504). Figure 3 shows the incremental benefit of exercise echocardiographic parameters in the prediction of MACE. The addition of exercise echocardiographic parameters significantly improved the prognostic power of a model containing clinical and resting echocardiographic variables (model 1: age, resting LVEF and LVESV, $\chi^2=15.9$; model 2: plus resting ERO, $\chi^2=16.9$, $P=0.324$; model 3: plus exercise LVESV, $\chi^2=19.8$, $P=0.038$; model 4: plus exercise ERO, $\chi^2=29.6$, $P=0.020$). Figure 4 shows

Table 3 Univariate and multivariate analyses for predicting major cardiovascular event

	Univariate analysis			Multivariate analysis		
	HR	95% CI	*P* value	HR	95% CI	*P* value
Age	1.024	1.002–1.048	0.032	1.036	1.002–1.064	0.032
Female sex	0.983	0.651–1.713	0.953			
Ischemic cardiomyopathy	0.824	0.436–1.472	0.618			
Resting parameters						
LVESV	1.005	1.001–1.021	0.010	1.003	0.987–1.021	0.583
LVEF	0.988	0.950–1.010	0.080	1.032	0.872–1.094	0.412
E/e'	1.030	0.986–1.102	0.214			
SPAP	1.028	0.994–1.080	0.094	1.040	0.948–1.108	0.120
ERO	3.12	0.512–26.20	0.130			
Exercise parameters						
LVESV	1.010	1.001–1.016	0.014	1.004	0.984–1.022	0.662
LVEF	0.950	0.946–0.998	0.016	0.942	0.822–1.014	0.242
E/e'	1.052	1.015–1.084	0.002	0.992	0.944–1.042	0.524
SPAP	1.032	1.006–1.048	0.014	1.020	0.961–1.030	0.210
ERO	16.20	6.82–33.42	<0.001	8.402	1.980–41.70	0.012

Abbreviations are shown in Table 2

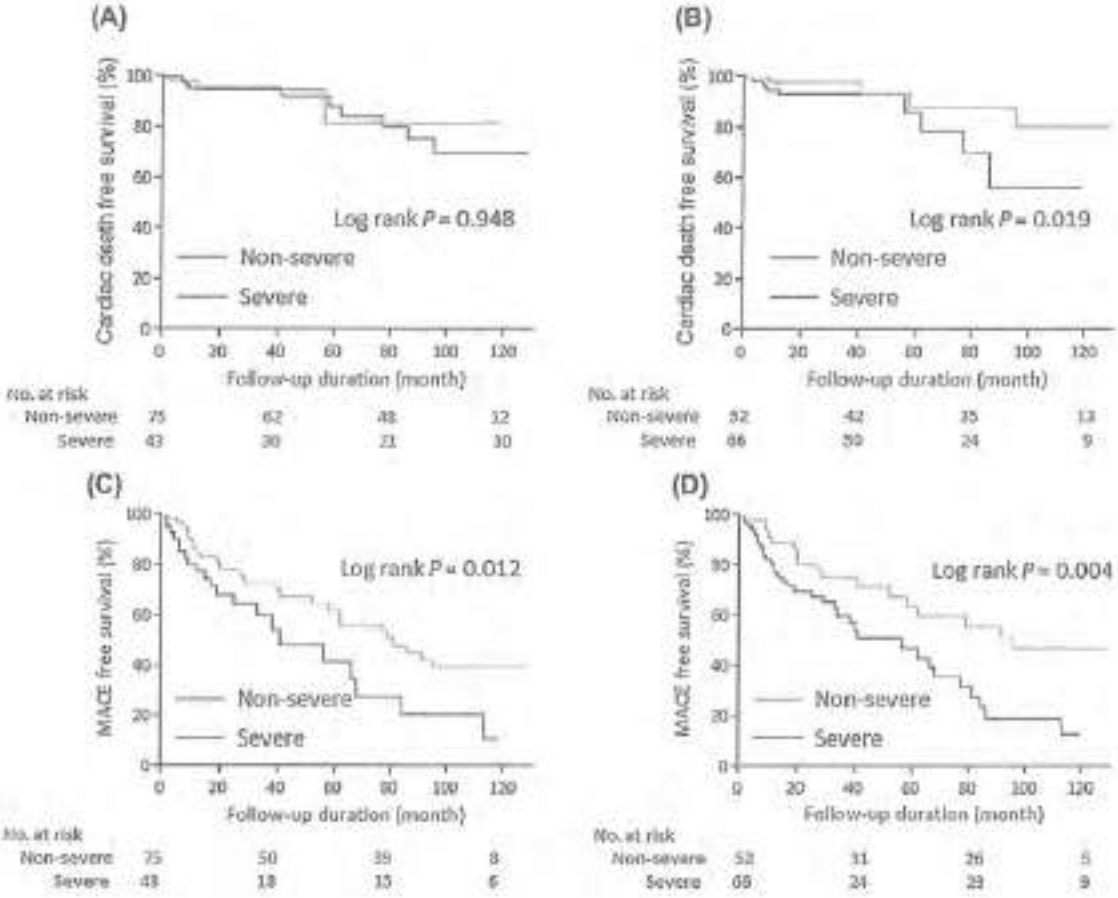

Fig. 2 Kaplan–Meyer analysis of cardiac death (**a**, **b**) and major cardio-cerebrovascular events (**c**, **d**) free survival in patients with and without severe secondary mitral regurgitation at rest (**a**, **c**) and during exercise (**b**, **d**)

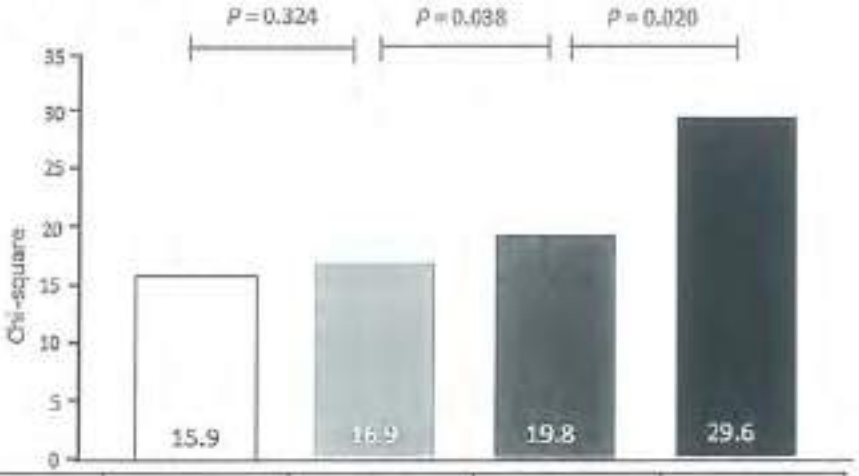

Fig. 3 Incremental value of exercise stress echocardiographic parameters to clinical and resting echocardiographic data. The figure illustrates the global χ^2 of sequential Cox models incorporating clinical (age), resting left ventricular (LV) end-systolic volume (ESV) and ejection fraction (EF), effective regurgitant orifice area (ERO), exercise LVESV and exercise ERO

	Age + resting LVEF and LVESV	+ resting ERO	+ exercise ESV	+ exercise ERO
Age	1.043 (1.012-1.091) P=0.004	1.045 (1.013-1.072) P=0.003	1.046 (1.012-1.082) P=0.004	1.036 (1.002-1.068) P=0.024
LVEF rest	1.005 (0.951-1.061) P=0.923	1.003 (0.954-1.071) P=0.916	1.005 (0.960-1.052) P=0.844	1.011 (0.965-1.059) P=0.611
LVESV rest	1.010 (1.000-1.021) P=0.062	1.009 (0.998-1.020) P=0.081	1.008 (0.990-1.020) P=0.394	1.006 (0.992-1.020) P=0.418
ERO rest		5.218 (0.164-15.23) P=0.331	5.260 (0.181-15.50) P=0.330	3.330 (0.024-5.980) P=0.336
LVESV exercise			1.015 (1.002-1.026) P=0.020	1.022 (0.980-1.044) P=0.082
ERO exercise				9.920 (6.280-16.20) P=0.001

the representative cases of the MACE (A) and no-MACE (B) groups.

Reproducibility

The intraobserver variabilities assessed using the ICCa were 0.93 (95% CI, 0.89–0.95, $n=28$) for ERO, and 0.94 (95% CI, 0.89–0.97, $n=28$) for RV. The interobserver variabilities were 0.90 (95% CI, 0.78–0.95) for ERO, and 0.88 (95% CI, 0.76–0.94) for RV. The Bland–Altman method showed that interobserver and intraobserver variabilities were 0.04 ± 0.05 and 0.02 ± 0.04 cm^2 for ERO, 1.9 ± 7.0 and 2.7 ± 4.2 ml for RV, respectively.

Discussion

Although it is well known that secondary MR is dynamic, and depends on the loading conditions, current diagnostic workup and therapeutic strategies are mainly based on resting conditions. The main findings of this study were that (1) the prevalence of severe secondary MR was significantly higher during exercise than at rest, (2) patients with MACE had significantly greater MR severity during exercise despite similar MR severity at rest, (3) MR severity during exercise was significantly associated with MACE, and (4) ESE provided incremental prognostic value in patients with secondary MR.

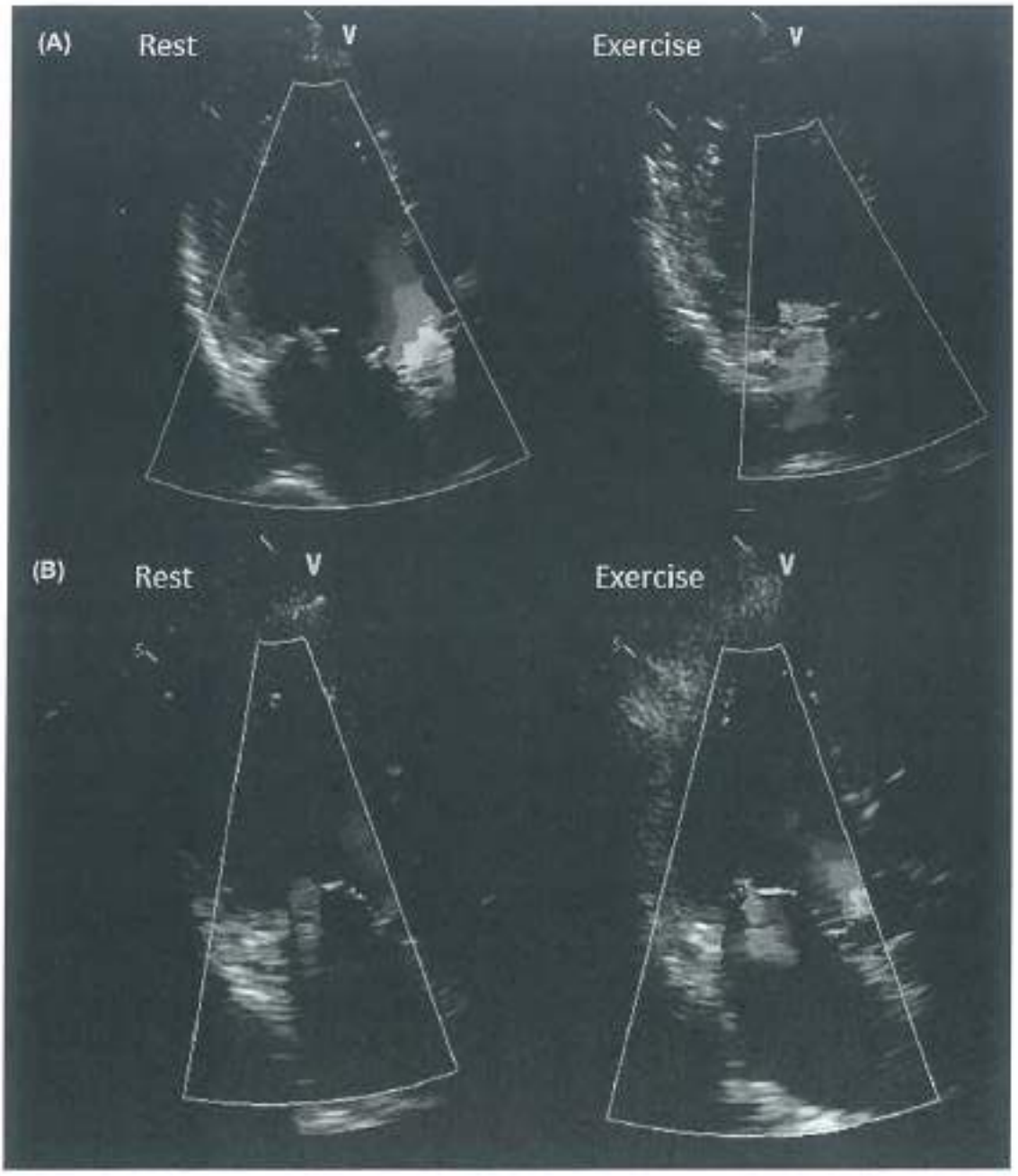

Fig. 4 Two representative MACE (**a**) and no MACE (**b**) cases. **a** 73 patients with non-ischemic cardiomyopathy. Exercise echocardiography showed severe secondary mitral regurgitation (MR) at peak exercise (right panel) despite of mid MR at rest (left panel). **b** 76 patients with ischemic cardiomyopathy. Exercise echocardiography showed that secondary MR was not increased during exercise

Mechanisms of exercise-increased secondary MR

In healthy individuals, the cardiovascular system adapts to meet increased oxygen demands of peripheral muscles. [18] During dynamic exercise, multiple muscle groups contract to achieve joint movement; this activity is associated with vasodilation in the intramuscular vasculature, reduction in systemic vascular resistance, and increased venous return due to the skeletal muscle pump. [19] Also, dynamic exercise is associated with no (or transient) increase in LVEDV and a concomitant decrease in LVESV. This results in a substantially increased stroke volume, LVEF and cardiac output. [20] In patients with ischemic or non-ischemic cardiomyopathy, LV response to dynamic exercise may differ from that of the healthy individuals. [21] Both the volume and pressure loading result in exercise-induced LV dilatation, whereas LVEF remains unchanged. Significant increases in systemic venous resistance are generally not observed during

dynamic exercise; however, failure of adequate arterial dilatation during exercise occurs. [22] In addition, exercise may result in dyssynchronous contraction of the left ventricle. [12, 13] Previous studies demonstrated increases in secondary MR in > 50% of patients with ischemic and non-ischemic cardiomyopathy. [7–14] Neither LV volumes nor LVEF at rest are a reliable predictor of exercise-increased secondary MR. In fact, with respect to exercise-induced LV dilatation, changes in shape (local remodeling) of LV may play more critical role than changes in the actual volume. [7, 13] An increase in left ventricular sphericity, which correlates with greater papillary muscle distance, may have a pronounced effect on mitral geometry even without a significant change in volume. In contrast, an increase in left ventricular volume caused by apical dilatation of the cavity (which does not involve the papillary muscles) will have no effect on mitral valve geometry. Therefore, it is not surprising that, when looking at variables at rest that can predict worsening of MR during exercise, left ventricular sphericity and papillary muscle dyssynchrony are more useful, as is mitral valve tenting, which reveals an already strained balance between closing and tethering forces. [13, 23] In addition, progressive annular dilation during exercise may be a contributor to exercise-induced MR in a majority of cases and is most predictive in non-ischemic cardiomyopathy. [11].

Prognostic importance of secondary MR during exercise

The present study is the first to examine the incremental prognostic value of ESE for secondary MR evaluated using very long-term follow-up. Our results indicate that patients with severe (ERO ≥ 0.20 cm^2) secondary MR during exercise have a worse outcome including both cardiac death and MACE. An earlier study reported that all-cause mortality in patients with heart failure and secondary MR follows a graded correlation with respect to MR severity, with ERO > 0.20 cm^2 already implying poor outcome. [24] This value contrasts to the 0.40 cm^2 cut-off traditionally used in primary MR. Although the occurrence of secondary MR is also a marker of underlying heart disease, the lower ERO threshold in secondary MR could also be rooted in the typically dynamic nature of secondary MR, which is frequently underestimated at rest. Our observations emphasize the importance of ESE in the setting of secondary MR. We could stratify patients into the MACE-free survival but not cardiac death-free survival according to resting severity during long-term follow-up. In our study, 27 patients (22%) with non-severe secondary MR at rest progressed to severe secondary MR during exercise and one-third of these patients developed cardiac death during follow-up. In contrast, none of the 22 patients (nine with severe MR at rest) with a decrease in MR during exercise developed cardiac death during long-term follow-up. Piérard and Lancellotti [25] demonstrated that exercise-induced MR deterioration, by augmenting backward flow and pulmonary vascular congestion, may contribute to the development of acute pulmonary edema. They also noted that a significant increase in ERO during exercise (defined as an increase > 0.13 cm^2) is observed in 30% of patients with HF and associated with increased mortality and readmissions. [7, 26] The link between severe MR during exercise and cardiac events could involve several mechanisms. [27] Intermittent increases in MR severity during daily life activities can acutely increase left atrial and pulmonary vascular pressures contributing to worsening of dyspnea and flash pulmonary edema. [10, 28] Acute increase in pulmonary systolic artery pressure as estimated by the exercise-induced changes in transtricuspid pressure gradient was also an independent predictor of cardiac events. [29] In our study, exercise ERO correlated well with systolic pulmonary artery pressure during exercise ($R = 0.435$, $P < 0.001$). Other factors can play a role, such as pulmonary vascular compliance. Repetitive transient increase in MR may also worsen LV volume overload and contribute to myocardial disease progression [30]. Chronic volume overload is also associated with a high incidence of ventricular tachyarrhythmias [31, 32]. Impaired LV contractile reserve, a marker of more severe disease, leads to inadequate cardiac adaptation to exercise. Dynamic MR is also a determinant of rapid increase in QRS duration at short-term follow-up; this may subsequently induce permanent electromechanical dyssynchronization [32]. LV asynchrony further deteriorates LV systolic function which in turn reduces mitral valve closing force and accelerates the progression to refractory heart failure [33, 34]. Dynamic MR is also associated with poor exercise capacity [35, 36]. Exercise capacity is one of the important factors in patients with heart failure.

Study limitations

This investigation has several limitations. First, despite of its large number of subjects with secondary MR, this study was a single-center analysis. A large population, multicenter study is, thus, warranted. Second, this study included both ischemic and non-ischemic cardiomyopathy even the increase in LVEDV during exercise is reported to be greater in ischemic cardiomyopathy compared to idiopathic dilated cardiomyopathy [21], which may be directly related to the extent of myocardial scar [37], a finding of particular importance for the exercise dynamics of secondary MR. However, previous dynamic exercise studies demonstrate increases in secondary MR in > 50% of patients with HF, both with ischemic and non-ischemic etiology [7–14]. None of the patient included in the present study had evidence of exercise-induced myocardial ischemia, and the prevalence of severe secondary MR during exercise was not different

between the ischemic and non-ischemic cardiomyopathy group (55.1 vs 51.1%, $P = 0.533$); the prognostic effect of exercise-induced secondary MR was also similar. Third, the cardiac death-free survival rate in this population was lower than that in previous studies. [7, 24, 25] We hypothesized that this discrepancy was caused by variations in patients' characteristics. We excluded patients with NYHA IV who could not perform an exercise test in the semi-supine position, the prevalence of resting PH was relatively low, and medical treatment for heart failure was adequately standardized in this study (i.e., over 80% of the study patients received βblockers and ACEi/ARBs). Finally, Doppler methods used to quantify MR have some pitfalls [38]. In the present study, a limitation of the PISA method is the measurement of the PISA radius at only one velocity and time point. Nevertheless, an earlier study validated the use of PISA and volumetric methods at rest and during exercise. [28].

Conclusions

Exercise-induced severe secondary MR provides incremental prognostic information that is useful for predicting long-term outcome. This study showed that the evaluation of secondary MR is important not only at rest but also during exercise.

Compliance with ethical standards

Conflict of interest Tomomi Suzuki, Masaki Izumo, Kengo Suzuki, Dan Koto, Maya Tsukahara, Kayako Teramoto, Yukio Sato, Mika Watanabe, Kei Mizukoshi, Ryo Kamijima, Manabu Takai, Seisyou Kou, Tomoo Harada, Sachihiko Nobooka, and Yoshihiro J Akashi declare that they have no conflicts of interest.

Human rights statements and informed consent All procedure followed were in accordance with the ethical standards of the responsible committee on human experimentation (institutional and national) and with the Helsinki Declaration of 1964 and later revisions. The participants were well informed prior to the test; written informed consent was obtained before enrollment.

References

1. Nkomo VT, Gardin JM, Skelton TN, et al. Burden of valvular heart diseases: a population-based study. Lancet. 2006;368:1005–11.
2. Lamas GA, Mitchell GF, Flaker GC, et al. Clinical significance of mitral regurgitation after acute myocardial infarction: survival and ventricular enlargement investigators. Circulation. 1997;96:827–33.
3. Borsi F, Enriquez-Sarano M, Jacobsen SJ, et al. Mitral regurgitation after myocardial infarction: a review. Am J Med. 2006;119:103–12.
4. Trichon BH, Felker GM, Shaw LK, et al. Relation of frequency and severity of mitral regurgitation to survival among patients with left ventricular systolic dysfunction and heart failure. Am J Cardiol. 2003;91:538–43.
5. Levine RA, Schwammenthal E. Ischemic mitral regurgitation on the threshold of a solution: from paradoxes to unifying concepts. Circulation. 2005;112:745–58.
6. Koelling TM, Aaronson KD, Cody RJ, et al. Prognostic significance of mitral regurgitation and tricuspid regurgitation in patients with left ventricular systolic dysfunction. Am Heart J. 2002;144:524–9.
7. Lancellotti P, Lebrun F, Piérard LA. Determinants of exercise-induced changes in mitral regurgitation in patients with coronary artery disease and left ventricular dysfunction. J Am Coll Cardiol. 2003;42:1921–8.
8. Giga V, Ostojic M, Vujisic-Tesic B, et al. Exercise-induced changes in mitral regurgitation in patients with prior myocardial infarction and left ventricular dysfunction: relation to mitral deformation and left ventricular function and shape. Eur Heart J. 2005;26:1860–5.
9. Lancellotti P, Stainier PY, Lebois F, et al. Effect of dynamic left ventricular dyssynchrony on dynamic mitral regurgitation in patients with heart failure due to coronary artery disease. Am J Cardiol. 2005;96:1304–7.
10. Lapu-Bula R, Robert A, Van Craeyaest D, et al. Contribution of exercise-induced mitral regurgitation to exercise stroke volume and exercise capacity in patients with left ventricular systolic dysfunction. Circulation. 2002;106:1342–8.
11. Ennezat PV, Maréchaux S, Le Tourneau T, et al. Myocardial asynchronism is a determinant of changes in functional mitral regurgitation severity during dynamic exercise in patients with chronic heart failure due to severe left ventricular systolic dysfunction. Eur Heart J. 2006;27:679–83.
12. D'Andrea A, Caso P, Cuomo S, et al. Effect of dynamic myocardial dyssynchrony on mitral regurgitation during supine bicycle exercise stress echocardiography in patients with idiopathic dilated cardiomyopathy and "narrow" QRS. Eur Heart J. 2007;28:1004–11.
13. Izumo M, Lancellotti P, Suzuki K, et al. Three-dimensional echocardiographic assessments of exerciseinduced changes in left ventricular shape and dyssynchrony in patients with dynamic functional mitral regurgitation. Eur J Echocardiogr. 2009;10:961–7.
14. Yamano T, Nakatani S, Kanzaki H, et al. Exercise-induced changes of functional mitral regurgitation in asymptomatic or mildly symptomatic patients with idiopathic dilated cardiomyopathy. Am J Cardiol. 2008;102:481–5.
15. Zoghbi WA, Adams D, Bonow RO, et al. Recommendations for noninvasive evaluation of native valvular regurgitation: a report from the american society of echocardiography developed in collaboration with the society for cardiovascular magnetic resonance. J Am Soc Echocardiogr. 2017;30:303–71.
16. Baumgartner H, Falk V, Bax JJ, et al. 2017 ESC/EACTS guidelines for the management of valvular heart disease. Eur Heart J. 2017;38:2739–91.
17. Rudski LG, Lai WW, Afilalo J, et al. Guidelines for the echocardiographic assessment of the right heart in adults: a report from the American Society of Echocardiography endorsed by the European Association of Echocardiography, a registered branch of the European Society of Cardiology, and the Canadian Society of Echocardiography. J Am Soc Echocardiogr. 2010;23:685–713.
18. Laughlin MH. Cardiovascular response to exercise. Am J Physiol. 1999;277:S244–59.
19. Manou-Stathopoulou V, Goodwin CD, Patterson T, et al. The effects of cold and exercise on the cardiovascular system. Heart. 2015;101:808–20.
20. Libby P, Bonow RO, Mann DL, et al. Braunwald's heart disease: a textbook of cardiovascular medicine. Philadelphia: WB Saunders Co.; 2007. p. p579.

21. Shen WF, Roubin GS, Hirasawa K, et al. Left ventricular volume and ejection fraction response to exercise in chronic congestive heart failure; difference between dilated cardiomyopathy and previous myocardial infarction. Am J Cardiol. 1985;55:1027–31.
22. Sullivan MJ, Knight JD, Higginbotham MB, et al. Relation between central and peripheral hemodynamics during exercise in patients with chronic heart failure: muscle blood flow is reduced with maintenance of arterial perfusion pressure. Circulation. 1989;80:769–81.
23. Bertrand PB, Schwammenthal E, Levine RA, et al. Exercise dynamics in secondary mitral regurgitation: pathophysiology and therapeutic implications. Circulation. 2017;135:297–314.
24. Grigioni F, Enriquez-Sarano M, Zehr KJ, et al. Ischemic mitral regurgitation: long-term outcome and prognostic implications with quantitative Doppler assessment. Circulation. 2001;103:1759–64.
25. Piérard LA, Lancellotti P. The role of ischemic mitral regurgitation in the pathogenesis of acute pulmonary edema. N Engl J Med. 2004;351:1627–34.
26. Lancellotti P, Gérard PL, Piérard LA. Long-term outcome of patients with heart failure and dynamic functional mitral regurgitation. Eur Heart J. 2005;26:1528–32.
27. Izumo M, Akashi Y. Exercise echocardiography for structural heart disease. J Echocardiogr. 2016;14:21–9.
28. Lebrun F, Lancellotti P, Pierard LA. Quantitation of functional mitral regurgitation during bicycle exercise in patients with heart failure. J Am Coll Cardiol. 2001;38:1685–92.
29. Lancellotti P, Magne J, Dulgheru R, et al. Clinical significance of exercise pulmonary hypertension in secondary mitral regurgitation. Am J Cardiol. 2015;115:1454–61.
30. Dal-Bianco JP, Beaudoin J, Handschumacher MD, et al. Basic mechanisms of mitral regurgitation. Can J Cardiol. 2014;30:971–81.
31. Stein KM, Borer JS, Hochreiter C, et al. Prognostic value and physiological correlates of heart rate variability in chronic severe mitral regurgitation. Circulation. 1993;88:127–35.
32. Martinez-Rubio A, Schwammenthal Y, Schwammenthal E, et al. Patients with valvular heart disease presenting with sustained ventricular tachyarrhythmias or syncope: results of programmed ventricular stimulation and long-term follow-up. Circulation. 1997;96:500–8.
33. Hung J, Otsuji Y, Handschumacher MD, et al. Mechanism of dynamic regurgitant orifice area variation in functional mitral regurgitation: physiologic insights from the proximal flow convergence technique. J Am Coll Cardiol. 1999;33:538–45.
34. Breithardt OA, Sinha AM, Schwammenthal E, et al. Acute effects of cardiac resynchronization therapy on functional mitral regurgitation in advanced systolic heart failure. J Am Coll Cardiol. 2003;41:765–70.
35. Takano H, Adachi H, Ohshima S, et al. Functional mitral regurgitation during exercise in patients with heart failure. Circ J. 2006;70:1563–7.
36. Izumo M, Suzuki K, Moonen M, et al. Changes in mitral regurgitation and left ventricular geometry during exercise affect exercise capacity in patients with systolic heart failure. Eur J Echocardiogr. 2011;12:54–60.
37. Mann DL, Scharf J, Ahnve S, et al. Left ventricular volume during supine exercise: importance of myocardial scar in patients with coronary heart disease. J Am Coll Cardiol. 1987;9:26–34.
38. Enriquez-Sarano M, Seward JB, Bailey KR, et al. Effective regurgitant orifice area: a noninvasive Doppler development of an old hemodynamic concept. J Am Coll Cardiol. 1994;23:443–51.

PubMed

Format: Abstract

Full text links

SpringerLink 聖マリアンナ医科大学

Cardiovasc Interv Ther. 2019 Oct;34(4):373-374. doi: 10.1007/s12928-018-[illegible]

RotaWire fracturing due to spinning under the maximum rotational speed.

Warisawa T[1,2], Cook CM[3], Doi S[4], Kasahara M[5], Takai M[5], Akashi YJ[4].

Author information

1 International Center for Circulatory Health, National Heart and Lung Institute, Imperial College London, Hammersmith Hospital, London, UK. rsxnj580@yahoo.co.jp.

2 Division of Cardiology, Department of Internal Medicine, St. Marianna University School of Medicine, 2-16-1 Sugao, Miyamae-Ku, Kawasaki, Kanagawa Prefecture, 216-8511, Japan. rsxnj580@yahoo.co.jp.

3 International Center for Circulatory Health, National Heart and Lung Institute, Imperial College London, Hammersmith Hospital, London, UK.

4 Division of Cardiology, Department of Internal Medicine, St. Marianna University School of Medicine, 2-16-1 Sugao, Miyamae-Ku, Kawasaki, Kanagawa Prefecture, 216-8511, Japan.

5 Department of Cardiology, St. Marianna University School of Medicine Yokohama City Seibu Hospital, Yokohama, Japan.

KEYWORDS: Complication; Guidewire fracture; Rotational atherectomy

PMID: 30426306 DOI: 10.1007/s12928-018-0558-1

LinkOut - more resources

Springer

RotaWire fracturing due to spinning under the maximum rotational speed

Cardiovascular Intervention and Therapeutics

October 2019, Volume 34, Issue 4, pp 373–374

| Cite as

Images in Cardiovascular Intervention

First Online: 13 November 2018

46

Downloads

Keywords

Rotational atherectomy Complication Guidewire fracture

This is a preview of subscription content, log in to check access.

Notes

Funding

None.

Compliance with ethical standards

Conflict of interest

The authors declare that they have no competing interest.

Heart and Vessels (2019) 34:1665–1673
https://doi.org/10.1007/s00380-019-01397-y

ORIGINAL ARTICLE

Physical performance as a predictor of midterm outcome after mitral valve surgery

Kohei Ashikaga[1,2] · Mike Saji[1] · Shuichiro Takanashi[3] · Masatoshi Nagayama[1] · Yoshihiro J. Akashi[2] · Mitsuaki Isobe[1]

Received: 12 October 2018 / Accepted: 5 April 2019 / Published online: 10 April 2019
© Springer Japan KK, part of Springer Nature 2019

Abstract

The usefulness of performing physical function assessments for evaluating clinical outcomes after all cardiac surgeries has been reported. However, no studies have evaluated the relationship between physical function and prognosis in patients undergoing cardiac open surgery with mitral valve regurgitation (MR). This study investigated whether physical assessment, such as the short physical performance battery (SPPB), could predict unplanned readmission events in patients undergoing mitral valve surgery due to MR. SPPB could predict unplanned admission events in patients undergoing mitral valve surgery due to MR. This retrospective study included 168 patients who underwent mitral valve surgery. SPPB was performed 1.6 ± 1.1 days before surgery. The primary endpoint was unplanned readmission. The mean follow-up period was 762 ± 480 days, mean age was 73.8 ± 6.3 years, and 43% of the patients were women. Of the study patients, 46 required unplanned readmissions; 29 of these patients required readmissions within 1 year. Multivariate Cox regression analysis demonstrated that SPPB was independently associated with the primary endpoint. Receiver-operating characteristic analysis showed that SPPB had an area under the curve of 0.71, with an optimal cutoff of 11. The study patients were stratified into SPPB 12 or SPPB ≤ 11 groups. Kaplan–Meier analysis showed that the event-free rate was significantly lower in the SPPB ≤ 11 group (hazard ratio 3.8, 95% confidence interval 2.1–7.0; $p < 0.001$). SPPB was a useful tool for predicting unplanned readmission in patients undergoing mitral valve surgery due to MR.

Keywords Physical performance · Mitral valve regurgitation · Midterm outcome · Mitral valve surgery

Introduction

Recently, in this aging society, the number of older Japanese patients undergoing cardiac surgery has increased owing to medical technological breakthroughs and high incidence of valvular heart disease in aged persons. Preoperative risk evaluation has played a crucial role in this occurrence [1, 2]. Predicting postoperative risk based on preoperative evaluations is indispensable for appropriate operation adaptation and perioperative care. Preoperative frailty assessment, which mainly evaluates physical status in cardiac surgery patients, is useful for predicting short- and midterm cardiac events and mortality [3, 4]. Furthermore, physical assessment has been reported to predict unplanned readmission [5]. A short physical performance battery (SPPB), which encompasses slowness, weakness, and balance, initially emerged as an objective tool for measuring the lower extremity physical performance status and, currently, is regarded as one of the promising physical frailty markers [6]. Earlier published studies demonstrated associations between a low SPPB score and poor outcomes such as prolonged hospital stay, readmission, disability, and mortality in patients with decompensated heart failure [7–9]. In 2016, Pavasini et al. [10] reported that if an SPPB score ≤ 6 points had twofold increase risk of all-cause mortality, and even if it was ≤ 9 points, the risk of death was 1.5 times. These studies also indicated the usefulness of gait speed in the evaluation of slowness. To date, several studies have reported the usefulness of SPPB as a predictor of poor clinical outcomes in patients undergoing cardiac surgery [11, 12], but the

✉ Mike Saji
mikesaji8@gmail.com

[1] Department of Cardiology, Sakakibara Heart Institute, 3-16-1 Asahicho, Fuchu 183-0003, Tokyo, Japan

[2] Division of Cardiology, Department of Internal Medicine, St. Marianna University School of Medicine, Kanagawa, Japan

[3] Department of Cardiovascular Surgery, Sakakibara Heart Institute, Tokyo, Japan

usefulness of SPPB in mitral valve surgery has not been reported. The clinical features of physical function in mitral open heart surgery patients have not been fully elucidated. Therefore, this study aimed to investigate whether physical assessment, such as SPPB, could predict unplanned readmission in patients undergoing mitral valve surgery due to mitral regurgitation (MR).

Materials and methods

Study population

Between April 2013 and July 2016, 208 patients with severe MR (aged 65 years and older) underwent surgery at the Sakakibara Heart Institute. The exclusion criteria included patients with other concomitant valve replacement or aortic surgery ($n = 12$), active endocarditis ($n = 2$), and patients who were not physically evaluated using SPPB ($n = 26$). After the application of the exclusion criteria, 168 patients were selected. The Society of Thoracic Surgeons (STS) risk score for predicting the risk of mortality was calculated for each patient. All patients were evaluated using SPPB before cardiac surgery. The discharge time was based on whether the general condition improved, regardless of preoperative SPPB value. This study was performed in accordance with the ethical principles set forth in the Declaration of Helsinki and was approved by the Human Investigation Committee of Sakakibara Heart Institute (Study Protocol No. 1604). All information was retrospectively obtained from patients' medical records and via telephone interview; that is, all patients were followed with accountability.

Parameters

All data were collected using a predefined form, including demographic data and past medical history, cardiovascular risk, preoperative hemodynamic status, surgical characteristics, perioperative data, combined surgery, and postoperative complication. Among them, the definitions are same as the STS score calculation [1].

Physical assessment

SPPB was derived from a composite of 4-m walking velocity, time to rise from a seated position five times, and standing balance [9]. Walking velocity was measured via a 4-m walk performed at the patient's "usual" pace; the patients were allowed to use canes or walkers [13]. Regarding the time to rise from a seated position, the patients sat in a straight-back chair with arms folded across their chests and stood up five times consecutively as quickly as possible. The time to complete five chair rises was measured. For standing balance, the patients were asked to hold three increasingly difficult standing positions for 10 s each: the side-by-side stand, semi-tandem stand (standing with the feet parallel and the heel of one foot touching the base of the first toe of the opposite foot), and full-tandem stand (standing with one foot directly in front of the other). The patients who received 0 points for each task were unable to complete the test, whereas those who obtained 1–4 points were assigned the subsequent tasks, according to the established methods. The points were summed to obtain SPPB, which ranged from 0 to 12, with higher points reflecting better physical function.

Endpoint

The endpoint was unplanned readmission, which was defined as a subsequent or unscheduled readmission to the hospital. Readmission was defined as admission to a hospital ward or an intensive care unit following discharge after the index hospitalization for mitral surgery. The primary diagnosis on the discharge report was used to determine the main cause of readmission. Planned readmission was defined as either readmission for a few specific conditions or elective procedure categories or readmission for which the principal diagnosis was not an acute condition or a complication of care. Readmission not meeting either criterion was categorized as unplanned. Causes of readmission were grouped as being of cardiac or non-cardiac origin. Cardiac causes included heart failure, arrhythmia, endocarditis, and abdominal aortic aneurysm rupture. Non-cardiac causes included infection (respiratory, urinary tract, gastrointestinal, and others), trauma, ischemic stroke, ileus, acute renal failure, and other condition (hyperventilation) [5, 14].

Statistical analysis

Continuous variables are expressed as mean ± standard deviation and categorical variables as number and percentage. Normality of distribution for continuous variables was evaluated using the Shapiro–Wilk test. A two-sided p value of < 0.05 was considered statistically significant. Variables with $p < 0.20$ in the univariate analysis were included into the multivariate Cox regression modeling to investigate their influence on the primary endpoint. Receiver-operating characteristic (ROC) analysis was performed using unplanned readmission at 1 year, and the area under the curve (AUC) was compared using the Delong method. Survival variables were compared using the log-rank test, and Kaplan–Meier survival curves were constructed. All analyses were performed using JMP pro version 13 (SAS Institute, Cary, NC, USA) and R version 2.13 (R Foundation for Statistical Computing).

Results

Overall outcomes after mitral valve surgery

The mean follow-up period was 762 ± 348 days. SPPB evaluation as physical assessment was performed 1.6 ± 1.1 days before operation. The average SPPB was 11.3 ± 1.5 points. Figure 1 shows the SPPB point distribution divided by sex. Only 12 people obtained < 10 points with SPPB, four of them were unable to perform chair stand test, and they had 0 points for that test. Of the study patients, 46 required unplanned readmissions; 29 of these patients required these readmissions within 1 year. Five patients were in rehabilitation or a skilled nursing facility, four of whom had unplanned readmissions. Nine patients had cardiovascular-related death, and two patients had non-cardiovascular-related death. Patients' demographic and clinical characteristics at baseline are shown in Table 1. The mean patient age was 73.8 ± 6.3 years and 43% were women. Patients with unplanned readmission (event group) were older and had a higher New York Heart Association (NYHA) classification, higher STS score, lower SPPB points, and lower hemoglobin and albumin levels than those without the primary endpoint (no-event group). No differences in body mass index were observed between the two groups. The causes of unplanned readmission are shown in Table 2; 21 patients had a cardiac cause, 10 had infection, seven had fracture, and eight had other triggers. Non-cardiac causes occurred more frequently after 1 month. The procedure outcome is shown in Table 3. The mortality at 30 days after mitral valve surgery was 0%. The mean hospital stay after mitral valve surgery was 12.9 ± 10.9 days. The patients in the event group demonstrated a lower atrial fibrillation correction and higher percentage of mitral valve replacement and readmission rate within 30 days. As a reason for the high ratio of mitral valve replacement, this study targeted elderly people aged 65 years and older.

Univariate and multivariate analyses

The results of the univariate analysis for baseline variables (Table 4) indicated that the primary endpoint was significantly associated with age, NYHA classification, diabetes mellitus, hypertension, dyslipidemia, hemoglobin level, albumin level, estimated glomerular filtration rate, ejection fraction, left atrium diameter, mitral valve stenosis, urgent surgery, prior cardiac surgery, mitral valve replacement, STS score and SPPB. These parameters were analyzed in the multivariate Cox regression model (Table 4), resulting in independent associations between the primary endpoint and each of the dyslipidemia, hemoglobin level, and SPPB.

Kaplan–Meier analysis

The ROC analysis for the primary endpoint at 1 year after discharge showed that SPPB had an AUC of 0.71, with an optimal cutoff of 11. The study patients were stratified into two groups according to a cutoff of 11 for SPPB based on the highest AUC. The Kaplan–Meier analysis indicated that the 3-year event-free rate was 0.75 ± 0.06 in patients with SPPB 12 points and 0.43 ± 0.08 in patients with

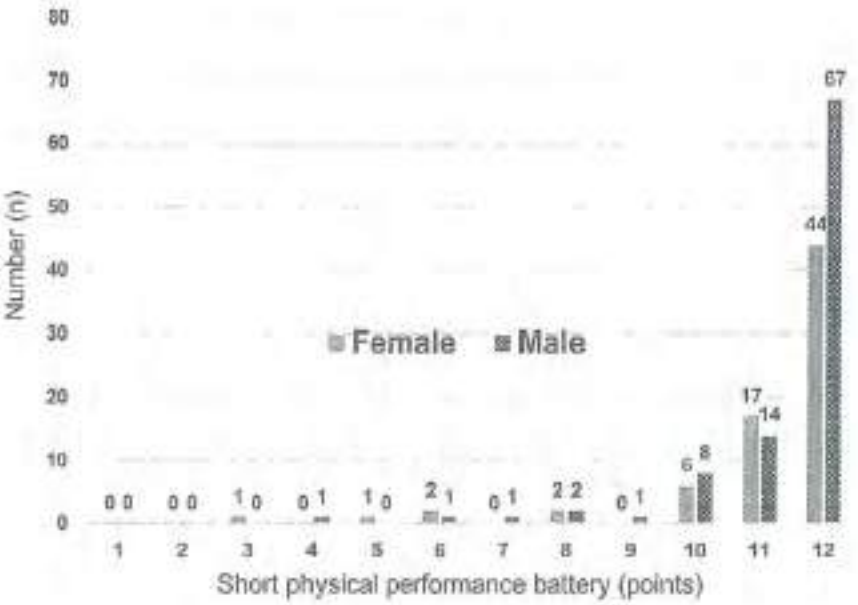

Fig. 1 Distribution of short physical performance battery score stratified by sex. The short physical performance battery score distribution according to the sex of patients undergoing mitral valve surgery

Table 1 Baseline characteristics

Characteristic	Overall ($n=168$)	Unplanned readmission ($n=46$)	Event free ($n=122$)	p value
Age, years	73.8±6.3	75.5±5.8	72.9±5.9	0.01
Men, %	95 (56.5)	27 (58.7)	68 (55.7)	0.70
Body mass index, kg/m^2	21.3±2.6	21.0±3.1	21.5±2.4	0.33
Hypertension, %	95 (56.5)	31 (67.4)	64 (52.5)	0.20
Dyslipidemia, %	41 (24.4)	9 (19.6)	32 (26.2)	0.15
Diabetes mellitus, %	9 (5.4)	4 (8.7)	5 (4.1)	0.24
Peripheral artery disease, %	7 (4.2)	1 (2.2)	6 (4.9)	0.43
COPD, %	9 (5.4)	3 (6.3)	2 (3.6)	0.68
Coronary artery disease, %	33 (19.6)	10 (21.7)	23 (18.9)	0.77
Liver disease, %	9 (5.4)	2 (4.3)	7 (5.7)	0.73
Cancer, %	18 (10.7)	6 (13.0)	12 (9.8)	0.93
Connective tissue disease, %	5 (3.0)	0 (0.0)	5 (4.1)	0.15
Previous myocardial infarction, %	5 (3.0)	2 (4.3)	3 (2.5)	0.52
Previous stroke/TIA, %	17 (10.1)	7 (15.2)	10 (8.2)	0.44
NYHA classification, %				0.02
I	44 (26.2)	6 (13.0)	38 (31.1)	
II	105 (62.5)	32 (65.6)	73 (59.8)	
III	19 (11.3)	8 (17.4)	11 (9.0)	
Euro SCORE II, %	3.9±4.4	5.2±6.4	3.2±3.2	0.01
STS score (mortality), %	3.3±3.2	4.5±3.8	2.8±2.8	<0.01
Short physical performance battery	11.3±1.5	10.4±2.2	11.6±0.9	<0.01
Previous cardiac surgery, %	16 (9.5)	9 (19.6)	7 (5.7)	0.01
Urgent surgery, %	15 (8.9)	7 (15.2)	8 (6.6)	0.14
Atrial fibrillation, %	94 (56.0)	26 (56.5)	68 (55.7)	0.46
Hemoglobin, g/dL	12.3±1.4	11.6±1.4	12.6±1.4	<0.01
Albumin, g/dL	4.1±0.4	4.0±0.3	4.1±0.3	0.04
eGFR, mL/min/1.73 m^2	67.5±20.1	63.2±19.9	69.3±20.1	0.09
LV diastolic diameter, mm	53.0±6.6	52.1±7.5	54.5±5.8	0.36
LV systolic diameter, mm	34.7±6.4	34.5±7.3	34.6±5.8	0.96
LV ejection fraction, %	62.1±7.6	61.6±7.9	62.6±7.0	0.43
Left atrial diameter, mm	50.9±11.3	51.5±11.0	50.7±11.3	0.68
Pulmonary artery pressure, mmHg	42.1±13.5	43.4±17.4	41.5±14.6	0.49
Moderate or severe MS, %	7 (3.6)	3 (6.3)	4 (3.3)	0.94

Values are mean ± SD [median] or n (%)

COPD chronic obstructive pulmonary disease, *TIA* transient ischemic attack, *NYHA* New York Heart Association, *eGFR* estimate glomerular filtration rate, *LV* left ventricle, *MS* mitral valve stenosis

SPPB ≤ 11 points. The event-free rate was significantly lower in patients with SPPB ≤ 11 points ($p<0.001$; Fig. 2).

ROC analysis

ROC analysis was performed for unplanned readmission. AUC of STS mortality score was 0.67. When SPPB was added to the STS mortality score, AUC showed a significantly increased discriminatory performance for predicting unplanned readmission (0.81; $p=0.02$, Fig. 3, Table 5).

Discussion

This study investigated whether SPPB could predict adverse clinical events such as unplanned readmission in the midterm period following mitral valve surgery due to MR. We found that SPPB was independently associated with unplanned readmission in the multivariate analysis. In this study, physical function was relatively maintained in most patients and SPPB points were generally high. In contrast, unplanned readmission was independently higher

Table 2 Causes of unplanned readmission

Causes	First 30 days	More than 1 month	Overall
All-cause unplanned readmission	10	36	46
Cardiac causes	6	15	21
Heart failure	4/6 (67)	13/15 (87)	17/21 (81)
Arrhythmia	2/6 (33)	0	2/19 (10)
Tachycardia	1	0	1
Bradycardia	1	0	1
Endocarditis	0	1/15 (7)	1/21 (5)
Abdominal aortic aneurysm rupture	0	1/15 (7)	1/21 (5)
Non-cardiac causes	4	21	25
Infection	3/4 (75)	7/21 (33)	10/25 (40)
Gastrointestinal infection	0	5	5
Surgical site infection	2	0	2
Pneumonia	1	1	2
Upper respiratory infection	0	1	1
Traumatology	0	7/21 (33)	7/25 (28)
Fracture	0	7	7
Cerebrovascular event	0	4/21 (19)	4/25 (16)
Ileus	0	2/21 (10)	2/25 (8)
Renal failure	1/4 (25)	0	1/25 (4)
Other (hyperventilation)	0	1/21 (5)	1/25 (4)

Values are n (%)

Table 3 Procedure outcomes

Outcome	Overall ($n=168$)	Unplanned readmission ($n=46$)	Event free ($n=122$)	p value
Operative time, min	256.8 ± 93.6	263.5 ± 115.6	250.1 ± 79.7	0.40
Cardiopulmonary bypass time, min	157.2 ± 65.1	155.6 ± 81.7	155.6 ± 62.3	0.99
Cross-clamp time, minutes	114.6 ± 50.9	115.7 ± 63.8	113.3 ± 49.0	0.80
Concomitant procedure, %				
Tricuspid valve repair	86 (51.2)	23 (50.0)	63 (51.6)	0.45
Coronary artery bypass graft	29 (17.3)	9 (19.6)	20 (16.4)	0.87
Left atrial appendage closure	45 (26.8)	14 (30.4)	31 (25.4)	0.43
Atrial fibrillation correction	38 (22.6)	6 (13.0)	32 (26.2)	0.03
Valve repair, %	114 (67.9)	26 (56.5)	88 (72.1)	0.03
Valve replacement, %	54 (32.1)	20 (43.5)	34 (27.9)	
Mechanical valve	18 (9.9)	6 (13.0)	12 (9.8)	
Postoperative length stay, days	12.9 ± 10.9	14.1 ± 13.5	12.1 ± 9.3	0.27
Readmission within 30 days, %	16 (9.5)	10 (21.7)	6 (4.9)	0.01
Mortality at 30 days, %	0 (0.0)	0 (0.0)	0 (0.0)	
Perioperative complication, %	15 (8.9)	7 (14.6)	8 (6.6)	0.10
Reoperation, %	9 (5.4)	2 (4.2)	7 (5.7)	
Ventilation > 24 h, %	4 (2.4)	3 (6.3)	1 (0.8)	
Deep sternal wound infection, %	4 (2.4)	4 (8.7)	0 (0.0)	
Myocardial infarction, %	0 (0.0)	0 (0.0)	0 (0.0)	
Renal failure, %*	2 (1.2)	1 (2.1)	1 (0.8)	
Disabling stroke, %	1 (0.6)	0 (0.0)	1 (0.8)	

Values are mean ± SD [median] or n (%)

*Renal failure: (1) increase of serum creatinine to > 2.0 and 2× most recent preoperative creatinine level, (2) a new requirement for dialysis postoperatively

Table 4 Predictors of unplanned readmission in univariate and multivariate cox regression analyses

Parameters	HR	95% CI	*p* value	Adjusted HR	95% CI	*p* value
Age (every 5-year increase)	1.36	1.05–1.77	0.021	0.98	0.69–1.39	0.916
Women	0.96	0.53–1.73	0.884			
BMI (every 3-kg/m^2 decrease)	1.12	0.78–1.61	0.537			
NYHA	1.82	1.13–2.88	0.014	1.09	0.53–2.25	0.812
Diabetes mellitus	2.14	0.64–5.35	0.191	0.21	0.27–5.39	0.800
Hypertension	1.58	0.89–2.93	0.122	0.68	0.80–3.54	0.173
Dyslipidemia	0.48	0.18–1.06	0.070	0.21	0.07–0.65	0.006
COPD	1.52	0.37–4.16	0.512			
Atrial fibrillation	0.91	0.50–1.64	0.746			
Previous myocardial infarction	2.26	0.37–7.44	0.319			
Previous cerebral infarction	1.35	0.51–2.96	0.506			
Hemoglobin level (≤ 12 g/dL)	2.51	1.39–4.64	0.002	2.87	1.36–6.15	0.006
Albumin (every 0.5-g/dL decrease)	1.52	0.99–2.34	0.057	1.23	0.75–2.01	0.411
eGFR (every 15-mL/min/1.73 m^2 decrease)	1.24	0.97–1.59	0.085	1.24	0.92–1.68	0.163
LVEF (under 50%)	3.71	1.39–8.36	0.012	2.20	0.68–7.14	0.191
Left atrium diameter (every 5-mm increase)	1.13	0.95–1.35	0.170	0.96	0.76–1.21	0.706
PA pressure (every 15-mmHg increase)	1.09	0.89–1.30	0.401			
Moderate or severe MS	4.62	1.45–12.67	0.039	1.62	0.20–13.40	0.653
Urgent surgery	2.32	0.94–4.92	0.065	0.34	0.08–1.39	0.134
Prior cardiac surgery	2.17	0.94–4.44	0.068	0.74	0.23–2.35	0.604
Mitral valve replacement	2.21	1.21–4.00	0.011	1.11	0.46–2.67	0.808
Coronary artery bypass grafting	1.13	0.49–2.31	0.750			
STS score (every 5% increase)	1.66	1.15–2.26	0.010	1.42	0.82–2.45	0.215
SPPB (every 1-point decrease)	1.40	1.23–1.56	<0.001	1.34	1.09–1.65	0.006

CI confidence interval, *HR* hazard ratio, *BMI* body mass index, *NYHA* New York heart association, *COPD* chronic obstructive pulmonary disease, *eGFR* estimated glomerular filtration rate, *LVEF* left ventricular ejection fraction, *PA* pulmonary artery, *MS* mitral valve stenosis, *STS* society of thoracic surgeons, *SPPB* short physical performance battery

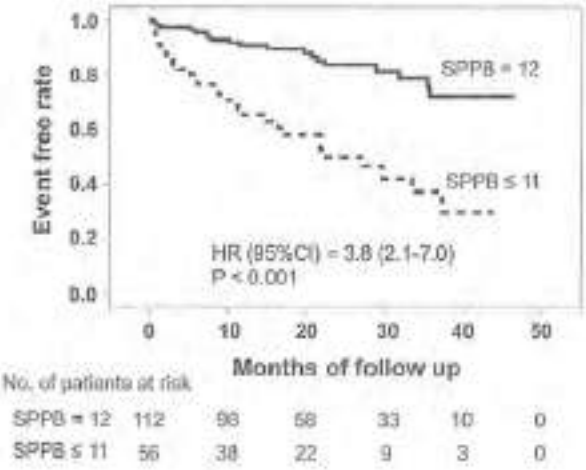

Fig. 2 Kaplan–Meier analysis estimating event-free rate. The Kaplan–Meier analysis, using a short physical performance battery (SPPB), shows the cumulative event-free rates in patients who underwent mitral valve surgery. The patients with a lower SPPB had a higher incidence of unplanned readmission ($p < 0.001$). (*HR* hazard ratio, *CI* confidence interval)

in patients with SPPB ≤ 11 points, and we recognized the importance of the physical function assessment. In addition, SPPB was noted to have improved prognostic power with the addition of the STS score, which is the risk score of open heart surgery.

Usefulness of SPPB for the evaluation of physical function

We found that SPPB was independently associated with the unplanned readmission in the multivariate analysis. SPPB is often used as an indicator of physical function in frailty. Frailty is a concept considered to include physical problems, mental or psychological problems, and social problems; however, social problems are difficult to evaluate. Thus, most frailty indicators often use combinations of cognitive functions and evaluation of depression for physical assessment. Although SPPB, compared to other evaluation tools, focuses on physical frailty, its usefulness has been reported to be comparable to that of other methods

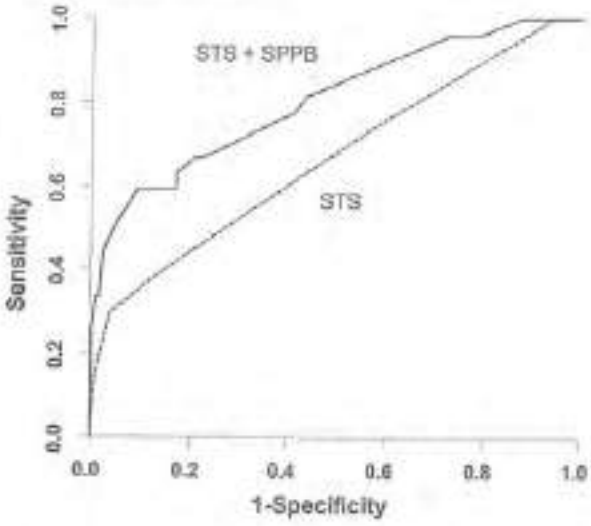

Fig. 3 Receiver-operating characteristic analysis. Receiver-operating characteristic (ROC) analysis for unplanned readmission. The short physical performance battery (SPPB) was added to the Society of Thoracic Surgeons (STS) mortality score model. The ROC curve demonstrates that the STS mortality score plus SPPB had a significantly increased discriminatory performance for predicting unplanned readmission

Table 5 Incremental AUC of SPPB for unplanned readmission

	AUC	95% CI	ΔAUC	*p* value
STS	0.67	0.55–0.79		
STS + SPPB	0.81	0.71–0.91	0.14	0.02

AUC area under the curve, *CI* confidence interval, *SPPB* short physical performance battery, *STS* society of thoracic surgeons

[11, 12]. In 2018, Saji et al. [5] reported the possibility that SPPB can be a good evaluation method compared with gait speed, etc., in the unplanned readmission prediction following transcatheter aortic valve implantation. It is suggested that the decline in physical function relates not only to the risk of unplanned readmission but also to further poor outcomes. One study has demonstrated that patients with poor physical performance tend to have a higher number of comorbidities [11]; poor physical function level is associated with marked endocrine dysfunction, inflammation, and oxidative stress [15–17]. Furthermore, low physical function level appears to be associated with a higher risk of several conditions that accelerate the transition to death, including malnutrition, dementia, and cardiovascular disease [17, 18]. Thus, poor physical performance might indirectly increase the risk of mortality through the development of such severe comorbidities.

Decrease of physical function and prognosis

In this study, physical function was relatively maintained in most patients and 92.9% of the patients had SPPB ≥ 10 points. Generally, the definition of frailty is SPPB < 5 points, while an SPPB of 6–9 points is defined as pre-frailty [6, 9, 10, 19]. Previous reports have suggested that both frailty and pre-frailty have a poor prognosis [6, 7, 11]. In this study, in the ROC analysis predicting the primary endpoint in the 1-year follow-up period, when SPPB ≤ 11 points was taken as the cutoff value, the highest AUC value was 0.71. In patients with SPPB ≤ 11 points, event occurrence increased significantly in the follow-up period compared to patients with 12 points. The results of this study suggest that even in a patient who is not diagnosed with frailty or pre-frailty, a slight decline in physical function may affect the patient's prognosis.

Although the STS score was not a significant prognostic factor in this multivariate analysis, the endpoint of this study was not death but unplanned readmission. Generally, the STS score is used for preoperative risk assessment. However, the STS score does not incorporate physical function assessment. Therefore, when the prediction of unplanned readmission was evaluated by combining the STS score with SPPB, the AUC had a significantly higher predictive ability than that of STS alone. This result reveals the importance of evaluating physical function in addition to the evaluation of STS score, which is a preoperative risk assessment tool.

Evaluation of preoperative function by SPPB and future task

This study is the first to show that physical functioning before mitral valve surgery due to MR affects postoperative outcomes. In the past, especially as part of the frailty evaluation, evaluating physical function before open heart surgery was considered important [3, 4, 11, 12]. Since catheter treatment was started for MR, preoperative assessment including physical functions becomes more important in determining treatment methods.

Patients with impaired physical function may benefit from preoperative, postoperative, or perioperative rehabilitation interventions. These interventions include early mobilization and planned admissions for professional physical rehabilitation, comprehensive geriatric assessment and management, and intensive monitoring [20–22]. We believe that it is most practical to enforce early rehabilitation after surgery and outpatient rehabilitation after discharge from the hospital. Regarding preoperative assessment, the usefulness of physical function assessment has been suggested; thus, it appears necessary to consider in the future not only prognostic prediction via preoperative evaluation but also

the contribution to prognosis in perioperative management including rehabilitation.

Limitations

Several limitation of this study should be acknowledged. First, this single-center study was limited by its retrospective nature and the relatively small number of patients; thus, the generalizability of our findings may be limited. However, the preliminary results of this study suggest that these findings might be adapted to a broader mitral valve surgery population. Second, in this study, the distribution of SPPB was narrow, so we could not evaluate the presence of dose–response relationship. Third, we had not been able to evaluate the physical function of the group of patients who could not perform SPPB, which may have the most decreased physical function. Finally, the changes in SPPB were not obtained; thus, further studies appear necessary in this regard.

Conclusions

Patients who undergo mitral valve surgery and who have decreased physical function were at a higher risk of adverse outcomes; therefore, physical evaluations, such as SPPB, should play a crucial role in selecting surgical or transcatheter mitral valve surgery. Further investigation is required to establish an appropriate assessment in such patients.

Acknowledgements The authors would like to thank Mr. Kentaro Hori, PT, and all members of the rehabilitation room at the Sakakibara Heart Institute.

Funding None.

Compliance with ethical standards

Conflict of Interest The authors declare that there is no conflict of interest.

References

1. O'Brien SM, Shahian DM, Filardo G, Ferraris VA, Haan CK, Rich JB, Normand SL, DeLong ER, Shewan CM, Dokholyan RS, Peterson ED, Edwards FH, Anderson RP, Society of Thoracic Surgeons Quality Measurement Task Force (2009) The Society of Thoracic Surgeons 2008 cardiac surgery risk models: part 2-isolated valve surgery. Ann Thorac Surg 88(1 Suppl):S23–42
2. Roques F, Michel P, Goldstone AR, Nashef SA (2003) The Logistic EuroSCORE. Eur Heart J 24:881–882
3. Lee DH, Buth KJ, Martin BJ, Yip AM, Hirsch GM (2010) Frail patients are at increased risk for mortality and prolonged institutional care after cardiac surgery. Circulation 121:973–978
4. Sepehri A, Beggs T, Hassan A, Rigatto C, Shaw-Daigle C, Tangri N, Arora RC (2014) The impact of frailty on outcomes after cardiac surgery: a systematic review. J Thorac Cardiovasc Surg 148:3110–3117
5. Saji M, Higuchi R, Tohara T, Iguchi N, Takanashi S, Takayama M, Isobe M (2018) Impact of frailty markers for unplanned hospital readmission following transcatheter aortic valve implantation. Circ J 82:2191–2198
6. Guralnik JM, Ferrucci L, Simonsick EM, Salive ME, Wallace RB (1995) Lower-extremity function in persons over the age of 70 years as a predictor of subsequent disability. N Engl J Med 332:556–561
7. Volpato S, Cavalieri M, Guerra G, Sioulis F, Ranzini M, Maraldi C, Fellin R, Guralnik JM (2008) Performance-based functional assessment in older hospitalized patients: feasibility and clinical correlates. J Gerontol A Biol Sci Med Sci 63:1393–1398
8. Chiarantini D, Volpato S, Sioulis F, Bartalucci F, Del Bianco L, Mangani I, Pepe G, Turantini F, Benni A, Marchionni N, Di Bari M (2010) Lower extremity performance measures predict long-term prognosis in older patients hospitalized for heart failure. J Card Fail 16:390–395
9. Volpato S, Cavalieri M, Sioulis F, Guerra G, Maraldi C, Zuliani G, Fellin R, Guralnik JM (2011) Predictive value of the short physical performance battery following hospitalization in older patients. J Gerontol A Biol Sci Med Sci 66:89–96
10. Pavasini R, Guralnanik J, Brown CJ, Bari M, Cesari M, Landi F, Vaes B, Legrand D, Verghese J, Wang C, Stenholm S, Ferrucci L, Lai CJ, Bartes AA, Espaulella J, Ferrer M, Lim YJ, Eastrud EK, Cawthon P, Tarusheva A, Frolova E, Rolland Y, Lauwers V, Corsonello A, Kirk DG, Ferrari I R, Volpato S, Campo G, (2016) Short physical performance battery and all-cause mortality: systematic review and meta-analysis. BMC Med 14:215
11. Lytwyn J, Stamners AN, Kehler DS, Jung P, Alexander B, Hiebert BM, Duhoiel C, Kimber D, Hamm N, Clarke M, Fraser C, Pedrein B, Duhamel TA, Tangri N, Arora RC (2017) The impact of frailty on functional survival in patients 1 year after cardiac surgery. J Thorac Cardiovasc Surg 154:1990–1999
12. Afilalo J, Lauck S, Kim DH, Lefèvre T, Piazza N, Lachapelle K, Marquis G, Lamy A, Labinaz M, Peterson MD, Arora RC, Noiseux N, Rassi A, Palacios IF, Généreux P, Lindman BR, Asgar AW, Kim CA, Tenkus A, Morais JA, Langlois Y, Rudski LG, Morin JF, Popma JJ, Webb JG, Perrault LP (2017) Frailty in older adults undergoing aortic valve replacement: the FRAILTY-AVR study. J Am Coll Cardiol 70:689–700
13. McDermott MM, Greenland P, Liu K, Guralnik JM, Criqui MH, Dolan NC, Chan C, Celic L, Pearce WH, Schneider JR, Sharma L, Clark E, Gibson D, Martin GJ (2001) Leg symptoms in peripheral arterial disease: associated clinical characteristics and functional impairment. JAMA 286:1599–1606
14. Nombela-Franco L, del Trigo M, Morrison-Polo G, Veiga G, Jimenez-Quevedo P, Abdul-Jawad Altisent O, Campelo-Parada F, Biagioni C, Puri R, DeLarochellière R, Dumont E, Doyle D, Paradis JM, Quirós A, Alnveria C, Gonzalo N, Nuñez-Gil I, Salinas P, Mohammadi S, Escaned J, Fernández-Ortiz A, Macaya C, Rodés-Cabau J (2015) Incidence, causes, and predictors of early (≤ 30 days) and late unplanned hospital readmissions after transcatheter aortic valve replacement. JACC Cardiovasc Interv 8:1748–1757
15. Clegg A, Young J, Iliffe S, Rikkert MO, Rockwood K (2013) Frailty in elderly people. Lancet 381:752–762
16. Fontana L, Addante F, Copetti M, Paroni G, Fontana A, Sancarlo D, Pellegrini F, Ferrucci L, Pilotto A (2013) Identification of a metabolic signature for multidimensional impairment and mortality risk in hospitalized older patients. Aging Cell 12:459–466
17. Sergi G, Veronese N, Fontana L, De Rui M, Bolzetta F, Zambon S, Corti MC, Baggio G, Toffanello ED, Crepaldi G, Perissinotto

E, Manzato E (2015) Pre-frailty and risk of cardiovascular disease in elderly men and women: the Pro.V.A. study. J Am Coll Cardiol 65:976–983

18. Veronese N, Stubbs B, Fontana L, Trevisan C, Bolzetta F, Rui M, Sartori L, Maggi S, Perissinotto E, Corti MC, Crepaldi G, Manzato E, Sergi G (2017) A Comparison of objective physical performance tests and future mortality in the elderly people. J Gerontol A Biol Sci Med Sci 72:362–368
19. Afilalo J, Alexander KP, Mack MJ, Maurer MS, Green P, Allen LA, Popma JJ, Ferrucci L, Forman DE (2014) Frailty assessment in the cardiovascular care of older adults. J Am Coll Cardiol 63:747–762
20. Needham DM (2008) Mobilizing patients in the intensive care unit: improving neuromuscular weakness and physical function. JAMA 300:1685–1690
21. Binder EF, Yarasheski KE, Steger-May K, Sinacore DR, Brown M, Schechtman KB, Holloszy JO (2005) Effects of progressive resistance training on body composition in frail older adults: results of a randomized, controlled trial. J Gerontol A Biol Sci Med Sci 60:1425–1431
22. Kircher TT, Wormstall H, Müller PH, Ershoff DH, Wolde-Tsadik G, Rubenstein LZ, Ambrosini VL, Fishman LK, Beck JC (2007) A randomized trial of a geriatric evaluation and management consultation services in frail hospitalized patients. Age Ageing 36:36–42

Publisher's Note Springer Nature remains neutral with regard to jurisdictional claims in published maps and institutional affiliations.

Circulation Journal
Circ J 2019; 83: 2418–2427
doi:10.1253/circj.CJ-19-0602

ORIGINAL ARTICLE
Arrhythmia/Electrophysiology

Current Status and Clinical Outcomes of Oral Anticoagulant Discontinuation After Ablation for Atrial Fibrillation in Japan

— Findings From the AF Frontier Ablation Registry —

Yasuo Okumura, MD; Koichi Nagashima, MD; Masaru Arai, MD; Ryuta Watanabe, MD; Katsuaki Yokoyama, MD; Naoya Matsumoto, MD; Takayuki Otsuka, MD; Shinya Suzuki, MD; Akio Hirata, MD; Masato Murakami, MD; Mitsuru Takami, MD; Masaomi Kimura, MD; Hidehira Fukaya, MD; Shiro Nakahara, MD; Takeshi Kato, MD; Wataru Shimizu, MD; Yu-ki Iwasaki, MD; Hiroshi Hayashi, MD; Tomoo Harada, MD; Ikutaro Nakajima, MD; Ken Okumura, MD; Junjiroh Koyama, MD; Michifumi Tokuda, MD; Teiichi Yamane, MD; Yukihiko Momiyama, MD; Kojiro Tanimoto, MD; Kyoko Soejima, MD; Noriko Nonoguchi, MD; Koichiro Ejima, MD; Nobuhisa Hagiwara, MD; Masahide Harada, MD; Kazumasa Sonoda, MD; Masaru Inoue, MD; Koji Kumagai, MD; Hidemori Hayashi, MD; Kazuhiro Satomi, MD; Yoshinao Yazaki, MD; Yuji Watari, MD on behalf of the AF Ablation Frontier Registry

Background: The safety of discontinuing oral anticoagulant (OAC) after ablation for atrial fibrillation (AF) in Japanese patients has not been clarified.

Methods and Results: A study based on the Atrial Fibrillation registry to Follow the long-teRm Outcomes and use of aNTIcoagulants afIER Ablation (AF Frontier Ablation Registry) was conducted. Data were collected from 3,451 consecutive patients (74.1% men; age, 63.3±10.3 years) who had undergone AF ablation at any of 24 cardiovascular centers in Japan between August 2011 and July 2017. During a 20.7-month follow-up period, OAC therapy was discontinued in 1,836 (53.2%) patients; 51 patients (1.5%) suffered a stroke/transient ischemic attack (TIA), 71 (2.1%) suffered major bleeding, and 36 (1.0%) died. Patients in whom OAC therapy was discontinued were significantly younger than those in whom OACs were continued, and their CHA_2DS_2-VASc scores were significantly lower. The incidences of stroke/TIA, major bleeding, and death were significantly lower among these patients. Upon multivariate adjustment, stroke events were independently associated with relatively high baseline CHA_2DS_2-VASc scores but not with OAC status.

Conclusions: Although the incidences of stroke/TIA, major bleeding, and death were relatively low among patients for whom OAC therapy was discontinued, stroke/TIA occurrence was strongly associated with a high baseline stroke risk rather than with OAC status. Thus, discontinuation of OAC therapy requires careful consideration, especially in patients with a high baseline stroke risk.

Key Words: Ablation; Anticoagulant drugs; Atrial fibrillation; Mortality; Stroke

Atrial fibrillation (AF) affects quality of life and increases the risks of stroke, heart failure, and death.[1] Pulmonary vein isolation (PVI) is reported to be more effective than antiarrhythmic drug (AAD) therapy for relief of symptoms and freedom from AF recurrence,[2,3] and thus might yield improved clinical outcomes in terms of ischemic stroke, heart failure, and death. For patients in whom PVI is truly curative, it should be possible to discontinue oral anticoagulants (OACs) without fear that an AF-related clinical event will occur. Despite

Received July 3, 2019; revised manuscript received September 12, 2019; accepted September 17, 2019; J-STAGE Advance Publication released online October 16, 2019 Time for primary review: 22 days

Division of Cardiology, Nihon University Itabashi Hospital, Tokyo (Y.O., K.N., M.A., R.W.); Department of Cardiology, Nihon University Hospital, Tokyo (K.Y., N.M.); Department of Cardiology, The Cardiovascular Institute, Tokyo (T.O., S.S.); Cardiovascular Division, Osaka Police Hospital, Osaka (A.H.); Division of Cardiology, Shonan-Kamakura General Hospital, Kanagawa (M.M.); Saiseikai Nakatsu Hospital, Osaka (M. Takami); Division of Cardiology, Pulmonary Medicine and Nephrology, Hirosaki University School of Medicine, Aomori (M.K.); Kitasato University Hospital, Kanagawa (H.F.); Dokkyo Medical University Saitama Medical Center, Saitama (S.N.); Kanazawa University Hospital, Ishikawa (T.K.); Nippon Medical Hospital, Tokyo (W.S., Y.I., Hiroshi H.); St. Marianna University School of Medicine Hospital, Kanagawa (T.H., I.N.); Saiseikai Kumamoto Hospital, Kumamoto (K.O., I.K.); Tokyo Jikei University School of Medicine Hospital, Tokyo (M. Tokuda, T.Y.); National
(Footnote continued the next page.)

advancements in ablation technologies and strategies, however, the reported 1-year paroxysmal and non-paroxysmal AF recurrence rates are approximately 20% and >30%, respectively, and the rates increase gradually over the long term.[4,5] Therefore, it remains unclear whether anticoagulant therapy can be safely terminated after PVI. Several current guidelines[6-8] suggest that OAC discontinuation is limited to patients with a low CHADS2 score, and this has been confirmed by several clinical reports.[9-12] Although most of the reported clinical data has been collected in Western countries, the findings may be applicable to Japanese patients, because the incidence of adverse clinical events among Japanese patients with AF appears to be lower than that among Western patients.[13-17] Therefore, we conducted a registry-based observational study to investigate the rate at which anticoagulation therapy is terminated after AF ablation among patients in Japan and the relationship between discontinuation and the long-term incidences of stroke, major bleeding, cardiovascular events, and death.

Methods

Study Population

The study began with a review of the records of 3,530 consecutive patients who had undergone catheter ablation for AF at any of 24 cardiovascular centers in Japan between August 2011 and July 2017. All patients were listed in the Atrial Fibrillation registry to Follow the long-teRm Outcomes and use of aNTIcoagulants aftER Ablation (AF Frontier Ablation Registry) (UMIN Clinical Trials Registry: UMIN000026849). The intended follow-up for each patient was a minimum of 12 months. Of the total patients, 79 were lost to follow-up, leaving 3,451 patients for inclusion in the study. Patients consented to the use of their anonymized clinical data for research purposes by the opt-out method, and the study protocol was approved by the institutional review boards of the 24 hospitals where patients were treated.

Data Collection

Patients' characteristics and pre-ablation (baseline) and follow-up data were obtained through a review of their hospital charts. The anonymized patient data were collected in the Excel form by physicians or the clinical research coordinator at each institution, and included patients' characteristics such as sex, age, body mass index (BMI), type of AF; number of ablation sessions (1, 2, 3 or >3 sessions); any comorbidity (hypertension, diabetes, history of a stroke/transient ischemic attack [TIA]); use of an OAC, including the type (warfarin vs. direct OAC [DOAC]), use of an antiplatelet drug; and laboratory test results (hemoglobin concentration and creatinine clearance [CrCl]); transthoracic echocardiography-derived left atrial diameter (LAd) and left ventricular ejection fraction (LVEF), and the ablation method (radiofrequency [RF], cryoballoon or hot balloon). Follow-up variables included OAC discontinuation, AF recurrence after a blanking period of 3 months, occurrence of any adverse clinical event during the follow-up period, and whether AAD use had been discontinued by the end of the follow-up period.

Ablation Protocol

All AADs were discontinued 1 week before ablation. Generally, OACs were continued, but this varied from institution to institution, and the procedure itself was performed according to each institution's particular protocol but generally as previously described.[18,19] Extensive encircling PVI was guided by a circular mapping catheter or multiple-electrode catheter and a 3D mapping system. The ablation catheter was an irrigated-tip contact force (CF) sensing catheter or irrigated-tip standard non-CF sensing catheter, depending on the hospital's preference or type of catheter available at the time of the procedure. In some patients, adenosine triphosphate was injected intravenously after PVI to provoke dormant PV conduction (performed at the physician's discretion). If acute PV reconnection or dormant PV conduction was evident, touch-up ablation was performed.

Cryoballoon ablation was performed with an Arctic Front Advance cryoballoon (Medtronic, Minneapolis, MN, USA), as described previously.[19] Each PV was encircled once (but twice if necessary). Any touch-up ablation required for dormant conduction or residual PV potentials was performed with a standard irrigated-tip catheter.

Regardless of the ablation method, if sinus rhythm was not restored after PVI, additional linear LA ablation (e.g., mitral isthmus line or LA roof line ablation) was performed, and the residual potentials, including complex fractionated atrial ECGs in the LA, were ablated, as appropriate. Electrical cardioversion was performed when sustained AF/atrial tachycardia was recorded after additional LA ablation. Tricuspid valve isthmus ablation and superior vena cava isolation were also performed when necessary.

Post-Ablation Follow-up

All patients underwent routine follow-up examinations at their hospital's outpatient clinic. AAD and OAC therapies were generally continued during the 3-month post-ablation blanking period. Thereafter, for patients in whom the arrhythmia did not recur, OAC and AAD therapies were discontinued. The post-ablation medications depended on the physician's discretion, generally based on the patient's characteristics or preferences. 24-hour Holter recordings were obtained 3–6 months after ablation. An ECG event recorder was used for any patient who reported cardiac symptoms. Any documented AF episode >30 s in duration on the standard ECG recording, event-activated ECG recording, or 24-hour Holter recording was considered a recurrence.

Study Endpoints

The primary study endpoint was discontinuation of OAC therapy after ablation. There were 2 secondary endpoints: occurrence of a stroke (ischemic stroke or hemorrhagic

Hospital Organization Tokyo Medical Center, Tokyo (Y.M., K.T.); Kyorin University Hospital, Tokyo (K. Suejima, N.N.); Tokyo Women's Medical University Hospital, Tokyo (K.E., N.H.); Fujita University Health Hospital, Aichi (M.H.); Tokyo Rinkai Hospital, Tokyo (K. Sonoda); Ishikawa Prefectural Central Hospital, Ishikawa (M.I.); Gunma Cardiovascular Center, Gunma (K.K.); Juntendo University, Tokyo (Hidemori H.); Tokyo Medical University Hospital, Tokyo (K. Satomi, Y.Y.); and Teikyo University, Tokyo (Y.W.), Japan

Mailing address: Yasuo Okumura, MD, Division of Cardiology, Department of Medicine, Nihon University School of Medicine, Ohyaguchi-kamicho, Itabashi-ku, Tokyo 173-8610, Japan. E-mail: okumura.yasuo@nihon-u.ac.jp

ISSN-1346-9843 All rights are reserved to the Japanese Circulation Society. For permissions, please e-mail: cj@j-circ.or.jp

Table 1. Clinical Characteristics of the Total Patients and per Study Group

	Total (n=3,451)	OAC discontinuation group (n=1,836)	OAC continuation group (n=1,615)	P value*
Age (years)	63.3±10.3	61.3±10.3	65.4±9.9	<0.001
<65	1,869 (52.9)	1,130 (61.5)	696 (43.1)	
≥65, <75	1,200 (34.8)	567 (30.9)	633 (39.2)	<0.001
≥75	425 (12.3)	139 (7.6)	286 (17.7)	
Female sex	893 (25.9)	429 (23.4)	464 (28.7)	<0.001
Body mass index (kg/m²)	24.0±3.6	23.8±3.6	24.2±3.7	<0.001
Type of AF				
Paroxysmal	2,157 (62.5)	1,231 (67.1)	1,926 (57.3)	
Persistent	1,036 (30.0)	504 (27.5)	535 (32.9)	<0.001
Long-standing persistent	258 (7.5)	101 (5.5)	157 (9.7)	
Ablation sessions ≥2	413 (12.0)	176 (9.6)	237 (14.7)	<0.001
Comorbidities				
Hypertension	1,891 (54.8)	878 (47.8)	1,013 (60.7)	<0.001
Diabetes	561 (16.3)	227 (12.4)	334 (20.7)	<0.001
History of stroke/TIA	275 (8.0)	70 (3.8)	205 (12.7)	<0.001
Heart failure	601 (17.4)	294 (16.0)	307 (19.0)	0.021
Vascular disease	302 (8.8)	106 (5.8)	196 (12.1)	<0.001
CHADS₂ score	1.2±1.1	0.9±0.9	1.5±1.2	<0.001
0	1,022 (29.6)	684 (37.3) [66.9]	338 (20.9) [33.1]	<0.001
1	1,370 (39.7)	761 (41.5) [55.5]	609 (37.7) [44.5]	
2	683 (19.8)	292 (15.9) [42.8]	391 (24.2) [57.2]	
≥3	376 (10.9)	99 (5.4) [26.3]	277 (17.2) [73.7]	
CHA₂DS₂-VASc score	2.1±1.5	1.6±1.3	2.5±1.6	<0.001
0	537 (15.6)	372 (20.3) [69.3]	165 (10.2) [30.7]	
1	871 (25.2)	563 (30.7) [64.6]	308 (19.1) [35.4]	
2	878 (25.4)	485 (26.4) [55.2]	393 (24.3) [44.8]	<0.001
3	611 (17.7)	253 (13.8) [41.4]	358 (22.2) [58.6]	
≥4	554 (16.1)	163 (8.9) [29.4]	391 (24.2) [70.6]	
Echocardiographic variables				
LVEF (%)	63.6±9.6	64.3±8.7	62.9±10.5	<0.001
Left atrial diameter (mm)	40.0±6.6	38.9±6.3	41.6±6.6	<0.001
Post-ablation therapy				
Oral anticoagulation				
Warfarin	711 (20.6)	338 (18.4)	373 (23.1)	
Dabigatran	654 (19.0)	353 (19.2)	301 (18.6)	
Rivaroxaban	828 (24.0)	438 (23.9)	390 (24.2)	<0.001
Apixaban	884 (25.6)	503 (27.4)	381 (23.6)	
Edoxaban	332 (9.6)	171 (9.3)	161 (10.0)	
Not reported	42 (1.2)	33 (1.8)	9 (0.6)	
Antiplatelet therapy	240 (7.0)	83 (4.5)	157 (9.7)	<0.001
Antiarrhythmic drug use at final follow-up	1,113 (32.3)	330 (18.0)	783 (48.5)	<0.001
Hb (mg/dL)	14.2±1.5	14.3±1.5	14.0±1.6	<0.001
CrCl (mL/min)	73.4±25.7	76.4±25.0	70.1±26.0	<0.001
AF recurrence	1,046 (30.3)	333 (18.1)	713 (44.2)	<0.001

Values are shown as mean±SD or n (%). [%] indicates the % of the OAC discontinuation rate or continuation rate per each stroke risk score. *Student's t-test, Wilcoxon rank sum test, or chi-square test, as appropriate, for the OAC discontinuation group vs. OAC continuation group. AF, atrial fibrillation; CHADS₂, congestive heart failure=1, hypertension=1, age ≥75 years=1, diabetes=1, and stroke/TIA=2; CHA₂DS₂-VASc, congestive heart failure=1, hypertension=1, age ≥75 years=2, diabetes=1, stroke/TIA=2, vascular disease=1, age 65–74 years=1, and female sex=1; CrCl, creatinine clearance; Hb, hemoglobin; LVEF, left ventricular ejection fraction; OAC, oral anticoagulant; TIA, transient ischemic attack.

stroke) or a TIA (efficacy endpoint) and occurrence of major bleeding (defined as a reduction in the hemoglobin concentration of at least 2 g/dL, transfusion of at least 2 units of blood or symptomatic bleeding in a critical area or organ) (safety endpoint). Cardiovascular events, including hospitalization for heart failure, myocardial infarction/unstable angina or other cardiovascular events, and death from any cause (cardiovascular death, stroke-related death, and non-cardiovascular death) were assessed.

Statistical Analysis

Categorical variables are presented as the number and

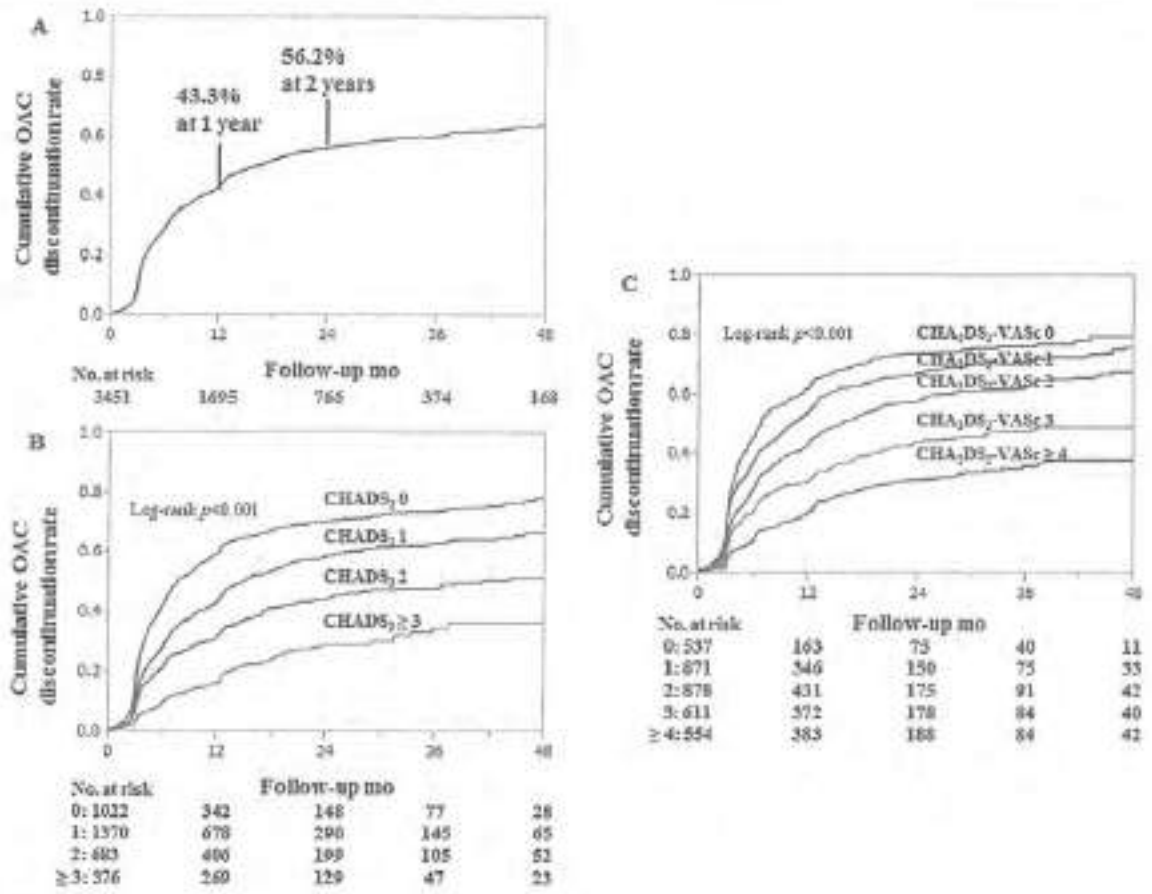

Figure 1. Kaplan-Meier curves for oral anticoagulant (OAC) discontinuation rates in the total patients (**A**), for each CHADS2 score (**B**) and each CHA2DS2-VASc score (**C**).

percentage of patients, and differences in these variables between patients in whom OAC therapy was discontinued (OAC discontinuation group) and in whom OAC therapy was not discontinued (OAC continuation group) were analyzed by chi-square or Fisher's exact test. Continuous variables are presented as mean±SD or median (and interquartile range) values, and between-group differences in these variables were analyzed by Student's t-test or Wilcoxon rank sum test. Cumulative OAC discontinuation and clinical adverse event rates were estimated by the Kaplan-Meier method, and differences were analyzed by log-rank test. Cox proportional hazards modeling was performed to identify the significant determinants for the incidence of stroke/TIA and major bleeding. Actors shown to be significant by univariate analysis were entered into the multivariate Cox model. Receiver-operating characteristic curves were drawn to identify the best cutoff value for each variable and the prognostic performances variables were compared on the basis of the area under the curve (AUC) by the DeLong test. Statistical analyses were performed with JMP 12 (SAS Institute Inc., Cary, NC, USA) or MedCalc Software Version 16.4.1 (Mariakerke, Belgium), and P<0.05 was considered statistically significant for all analyses.

Results

Clinical Characteristics

Clinical characteristics ae shown for the total study patients and per study group in **Table 1**. The total male:female ratio was 2,558:893 and mean age 63.3±10.3 years. The AF was paroxysmal (lasting <7 days) in 2,157 (62.5%) patients, persistent (lasting ≥7 days to 12 months) in 1,036 (30.0%), and long-lasting persistent (lasting ≥12 months) in 258 (7.5%). Mean $CHADS_2$ and CHA_2DS_2-VASc scores were 1.2±1.1 and 2.1±1.5, respectively. Standard RF ablation was performed in 1,523 (44.1%) patients, CF-based RF ablation in 1,678 (48.6%), cryoballoon ablation in 248 (7.1%), and hot balloon ablation in 2 (0.1%). Patients' mean LAd was 40.0±6.6 mm and LVEF was 63.6±9.6%. Of the total 3,451 patients, 3,038 (88.0%) underwent a single AF ablation procedure, and the remaining 413 (12.0%) underwent ≥1 additional ablation procedures. During the post-ablation blanking period, warfarin was used by 711 (20.6%) patients, and DOACs were used by 2,698 (78.0%) patients, but the OAC type in 42 patients (1.2%) was not reported.

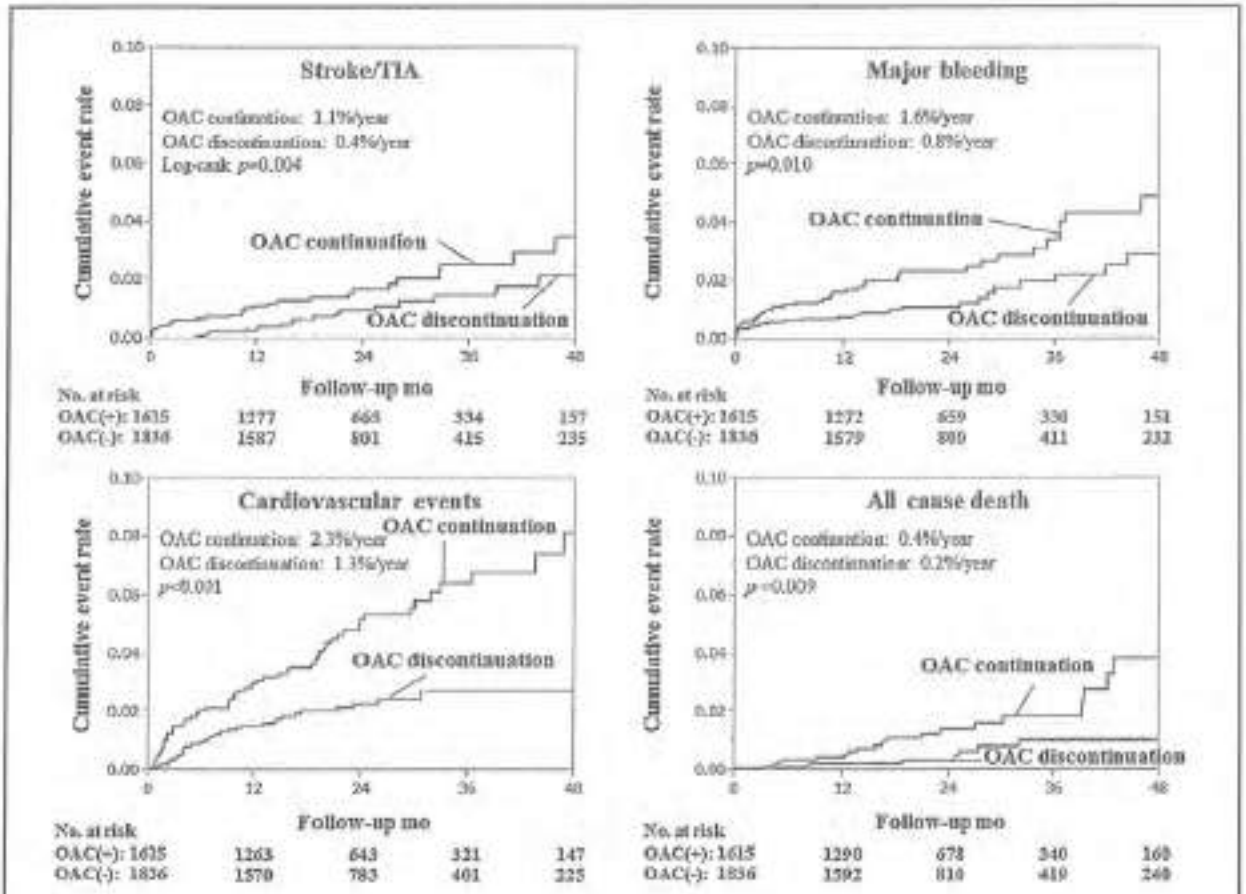

Figure 2. Kaplan-Meier curves for stroke/transient ischemic attack (TIA), major bleeding, cardiovascular events, and all-cause death after ablation for atrial fibrillation in patients in whom oral anticoagulant (OAC) therapy was discontinued (OAC discontinuation) and those in whom it was continued (OAC continuation).

Outcomes and OAC Discontinuation/Continuation During Follow-up

During the final follow-up (median 20.7 [12.7–33.2] months), 2,405 (69.7%) of the 3,451 patients were arrhythmia-free, with 565 (23.5%) of these patients still taking an AAD. Kaplan-Meier freedom rate from AF recurrence among patients who underwent 1 ablation procedure was 78.4% at 1 year and 69.8% at 2 years, whereas that among patients who underwent ≥2 ablation procedures was 76.0% at 1 year and 65.0% at 2 years. OACs were discontinued in 1,836 (53.2%) patients (discontinuation group) at 5.4 (3.1–11.0) months after ablation. The OAC discontinuation rate increased predominantly in 43.3% at 1 year but thereafter increased modestly to 56.2% at 2 years (**Figure 1A**). The OAC discontinuation rate decreased gradually without a tipping point as the $CHADS_2$ and CHA_2DS_2-VASc scores increased (**Figure 1B,C**; **Table 1**). As shown in **Table 1**, male sex was more prevalent in the OAC discontinuation group than in the OAC continuation group, patients in the OAC discontinuation group were significantly younger than those in the OAC continuation group, and BMI was significantly lower in this group. Antiplatelet drugs use was less prevalent, and the baseline hemoglobin concentration and CrCl were higher in this group. Also higher in this group were the prevalence of paroxysmal AF, the percentage of patients who required only 1 ablation session, the percentage of patients without a comorbidity, and the percentage of patients in whom AF did not recur during the follow-up period (P<0.05 for all). $CHADS_2$ and CHA_2DS_2-VASc scores were lower, LVEF was greater, and LAd smaller in this group than in the OAC continuation group. DOAC use was greater in this group, as was non-use of AAD by the time of the final follow-up examination (P<0.05 for all).

By the time of the final follow-up examination, stroke/TIA had occurred in 51 (1.5%) of the total patients, major bleeding had occurred in 71 (2.1%), there was a cardiovascular event in 106 (3.1%), and 36 (1.0%) patients had died. Cardiovascular events consisted of 23 (0.7%) cases of myocardial infarction/unstable angina, 44 (1.3%) hospitalizations for heart failure, and 39 (1.1%) other cardiovascular events. Deaths comprised 5 (0.1%) cardiovascular deaths, 4 (0.1%) stroke-related deaths, and 27 (0.8%) non-cardiovascular deaths. The overall incidence of clinical adverse events, including stroke/TIA, major bleeding, cardiovascular events, and death was significantly lower in the OAC discontinuation group than in the OAC continuation group (P<0.05 for all) (**Figure 2**). In the OAC discontinu-

Table 2. Univariate and Multivariate Cox Hazard Models for Predicting Stroke/TIA and Major Bleeding Events

	Stroke/TIA				Major bleeding			
	Univariate analysis		Multivariate analysis		Univariate analysis		Multivariate analysis	
	HR (95% CI)	P value	HR (95% CI)	P value	HR (95% CI)	P value	HR (95% CI)	P value
Age (+1 year)	1.08 (1.03–1.10)	0.003	1.03 (0.99–1.07)	0.16	1.10 (1.06–1.13)	<0.001	1.06 (1.02–1.11)	0.020
Female	0.94 (0.48–1.72)	0.85			1.59 (0.96–2.58)	0.07		
BMI (+1 kg/m²)	1.00 (0.92–1.00)	0.92			0.91 (0.84–0.97)	0.007	0.95 (0.89–1.03)	0.26
AF type								
Paroxysmal	Ref.		Ref.		Ref.			
Persistent	1.07 (0.54–2.00)	0.84	0.81 (0.45–1.73)	0.76	1.06 (0.62–1.73)	0.85		
Long-standing persistent	3.38 (1.55–6.76)	0.003	3.07 (1.31–6.63)	0.012	0.92 (0.25–2.03)	0.70		
Ablation sessions ≥2	1.54 (0.63–3.24)	0.32			0.40 (0.10–1.07)	0.07		
Comorbidities								
Hypertension	2.01 (1.11–3.85)	0.020			1.14 (0.71–1.86)	0.56		
Diabetes	1.73 (0.89–3.16)	0.11			2.09 (1.21–2.92)	0.009		
Heart failure	2.17 (1.15–3.90)	0.019			1.74 (0.99–2.95)	0.05		
Stroke/TIA	2.09 (0.91–4.22)	0.08			1.07 (0.42–2.28)	0.87		
Vascular disease	2.46 (1.20–4.64)	0.016			2.43 (1.30–4.25)	0.007		
CHA₂DS₂-VASc	1.44 (1.24–1.68)	<0.001	1.31 (1.06–1.60)	0.015	1.43 (1.25–1.63)	<0.001	1.09 (0.84–1.25)	0.78
Echocardiography variables								
LVEF (+1%)	0.99 (0.96–1.02)	0.40			1.01 (0.98–1.04)	0.48		
LAd (+1 mm)	1.05 (1.02–1.10)	0.006	1.04 (0.99–1.08)	0.12	1.01 (0.98–1.05)	0.42		
Post-ablation therapy								
Warfarin (vs. DOAC)	1.40 (0.76–2.51)	0.28			1.47 (0.87–2.42)	0.15		
Antiplatelet therapy	1.15 (0.40–2.63)	0.78			2.91 (1.55–5.06)	0.002	1.79 (0.91–3.31)	0.09
AAD use	1.25 (0.69–2.19)	0.45			1.38 (0.98–1.86)	0.07		
Hb (mg/dL)	0.85 (0.71–1.01)	0.07			0.73 (0.63–0.85)	<0.001	0.88 (0.75–1.04)	0.15
CrCl (mL/min)	0.99 (0.98–1.00)	0.11			0.97 (0.96–0.98)	<0.001	1.00 (0.99–1.01)	0.57
AF recurrence	1.34 (0.76–2.34)	0.31			1.56 (0.96–2.51)	0.07		
OAC discontinuation	0.44 (0.24–0.78)	0.004	0.74 (0.38–1.35)	0.32	0.53 (0.33–0.86)	0.010	0.75 (0.45–1.23)	0.26

AAD use, antiarrhythmic drug use at final follow-up; BMI, body mass index; CI, confidence interval; DOAC, direct oral anticoagulant; HR, hazard ratio; LAd, left atrial diameter; other abbreviations as in Table 1.

ation group 18 patients suffered a stroke/TIA, and these patients were significantly older than those in the same group who did not suffer a stroke/TIA (n=1,818) (69.7±10.9 years vs. 61.3±10.3 years, P<0.001). In addition, their CHADS₂ (1.8±1.2 vs. 0.9±0.9, P<0.001) and CHA₂DS₂-VASc scores were higher (3.0±1.5 vs. 1.6±1.3, P<0.001). In the OAC discontinuation group, AF recurrence was more prevalent among these patients also (38.8% [7/18] vs. 17.9% [326/1,818], P=0.031). Similarly, patients in this group who suffered major bleeding (n=29) were significantly older than those who did not (n=1,807) (71.8±7.3 years vs. 61.2±10.3 years, P<0.001), and their CHADS₂ (1.7±1.4 vs. 0.9±0.9, P<0.001) and CHA₂DS₂-VASc scores were higher (2.9±1.8 vs. 1.6±1.3, P<0.001). AF recurrence tended to be more prevalent among these patients than among those who did not suffer major bleeding (31.0% [9/29] vs. 17.9% [324/1,807], P=0.09).

The major determinants of stroke/TIA and major bleeding are shown in **Table 2**. Age, CHA₂DS₂-VASc score, and LAd were positively related to the incidence of stroke/TIA (hazard ratio [HR] for per year increase in age: 1.06; HR per 1-point increase in CHA₂DS₂-VASc: 1.44; and HR per millimeter increase in LAd: 1.06). Long-lasting-AF (vs. paroxysmal AF), hypertension, heart failure, vascular disease, and OAC continuation were shown to be significantly associated with the incidence of stroke/TIA but not with AF recurrence after ablation. On multivariate Cox hazard analysis, long-lasting-AF (HR: 3.07 [95% confidence interval (CI): 1.31–6.63] vs. paroxysmal AF) and CHA₂DS₂-VASc score (HR: 1.31 [95% CI: 1.06–1.60]) remained significant predictors for the incidence of stroke/TIA. Age and CHA₂DS₂-VASc score were positively related to the incidence of a major bleeding event (HR per year increase in age: 1.10; HR per 1-point increase in CHA₂DS₂-VASc: 1.43). BMI, hemoglobin concentration, and CrCl were inversely related to the occurrence of a major bleeding event. Use of antiplatelet drugs and OAC continuation were significantly associated with the occurrence of a major bleeding event. Multivariate Cox hazard model revealed age (HR: 1.06 [95% CI: 1.02–1.11] per year increase) as a significant predictor of a major bleeding event.

Prognostic Performance of Age, CHADS₂ and CHA₂DS₂-VASc Scores for Stroke/TIA and Major Bleeding Events

The prognostic performance of age and traditional risk scores for stroke/TIA and major bleeding events was investigated (**Figure 3**). Performance of the CHA₂DS₂-VASc score for predicting stroke/TIA was best (AUC, 0.70; best cutoff value, ≥3), followed by the CHADS₂ score (AUC, 0.69, P=0.45 by DeLong test vs. CHA₂DS₂-VASc score; best cutoff value, ≥2) and age (AUC, 0.65, P=0.07 vs. CHA₂DS₂-VASc score; best cutoff value, ≥63 years), and the performance of age for the prediction of major bleeding was best (AUC, 0.73; best cutoff value ≥70 years), fol-

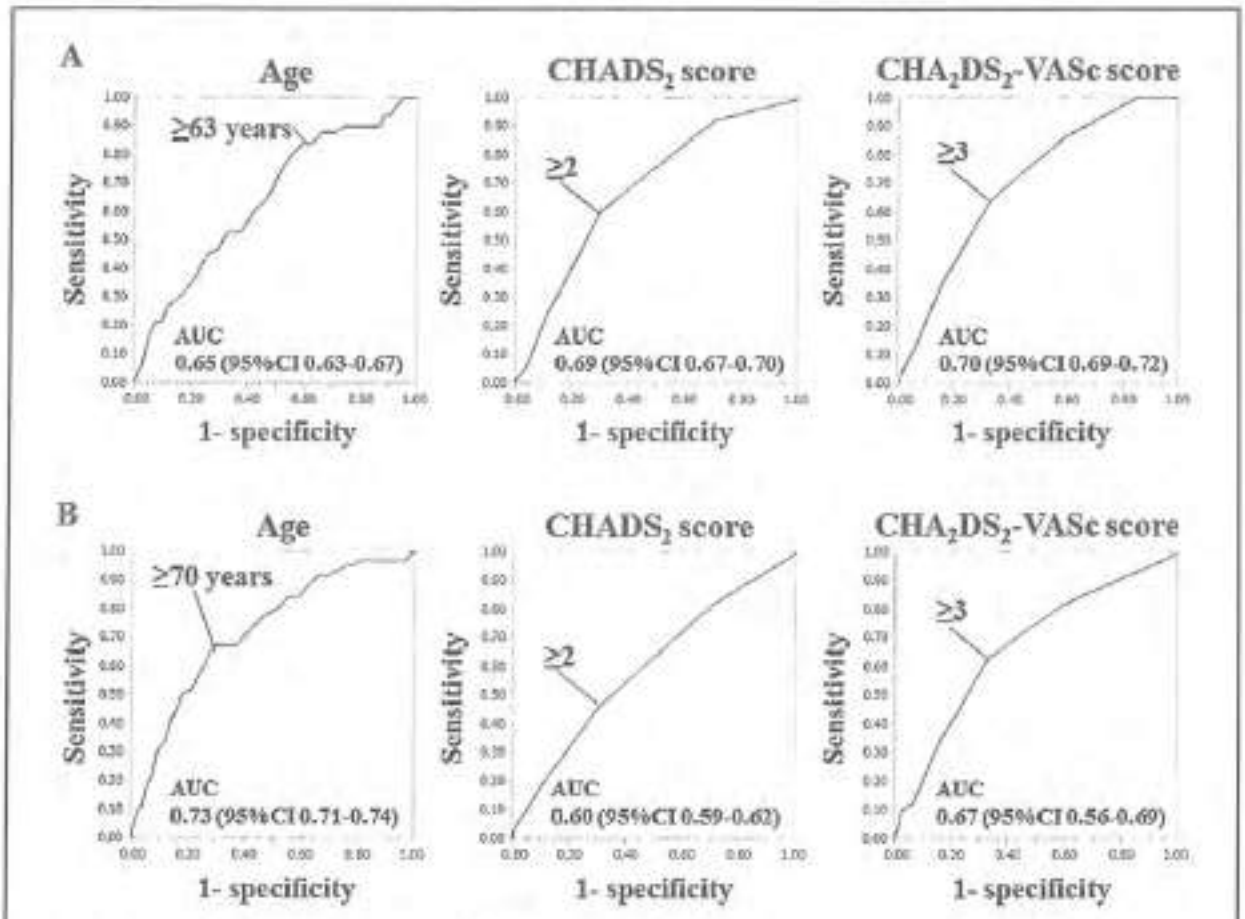

Figure 3. Prognostic performance of traditional predictors of (**A**) stroke risk and (**B**) major bleeding after ablation for atrial fibrillation. AUC, area under the curve; CI, confidence interval.

lowed by CHA_2DS_2-VASc score (AUC, 0.67, P<0.001 vs. age; best cutoff value, ≥3) and $CHADS_2$ score (AUC, 0.60, P<0.001 vs. age; best cutoff value, ≥2). Kaplan-Meier curves for the occurrence of adverse clinical events among patients with a CHA_2DS_2-VASc score ≥3 are shown in **Figure 4**. Among patients with a CHA_2DS_2-VASc score ≥3 the cumulative incidence of stroke/TIA, major bleeding, cardiovascular events, and all-cause death was greater than that among patients with a CHA_2DS_2-VASc score <3.

Discussion

Our main findings were as follows. First, OAC use was discontinued at 5.1 (3.1–11.0) months after ablation in 53.2% of the 3,451 AF Frontier Ablation Registry patients included in our study. OAC discontinuation was associated with a younger age, male sex, paroxysmal AF, a single AF session, absence of comorbidities, a smaller LAd, AAD discontinuation by the time of the final follow-up examination, and absence of AF recurrence after ablation. Second, stroke/TIA and major bleeding events occurred in patients with high stroke risk scores, and such events were associated with patients' baseline clinical characteristics (i.e., CHA_2DS_2-VASc scores and age), rather than with discontinuation vs. continuation of OAC therapy. Third, the CHA_2DS_2-VASc score tended to be superior to age for prediction of post-ablation stroke/TIA, and age was found to be superior to the $CHADS_2$ and CHA_2DS_2-VASc scores for prediction of a major bleeding event.

Post-Ablation OAC Discontinuation and Clinical Outcomes

OACs were discontinued within 21 months after ablation in slightly more than 50% of patients included in our study. Discontinuation of OACs beyond 3 months after ablation is reported in 20–80% of patients,[9-13,20,21] and observational studies have reported that discontinuation of OACs is dependent on multiple factors, such as ablation success and initial stroke risk, but mainly on the treating physician's inclination or patient's preference. In our study, age, male sex, and smaller LAd were associated with OAC discontinuation. A single AF session, absence of comorbidities, and absence of AF recurrence were also associated with OAC discontinuation. Despite the widely varying OAC discontinuation rates documented in previous observational studies, most authors have concluded that OACs can be discontinued in patients judged to be at low risk for a stroke after successful AF ablation,[9-13,20,21] and the increased incidence of major bleeding events associated with continuous OAC use outweighs its benefit in terms of stroke prevention. According to current guidelines,[6-8] OAC therapy should be

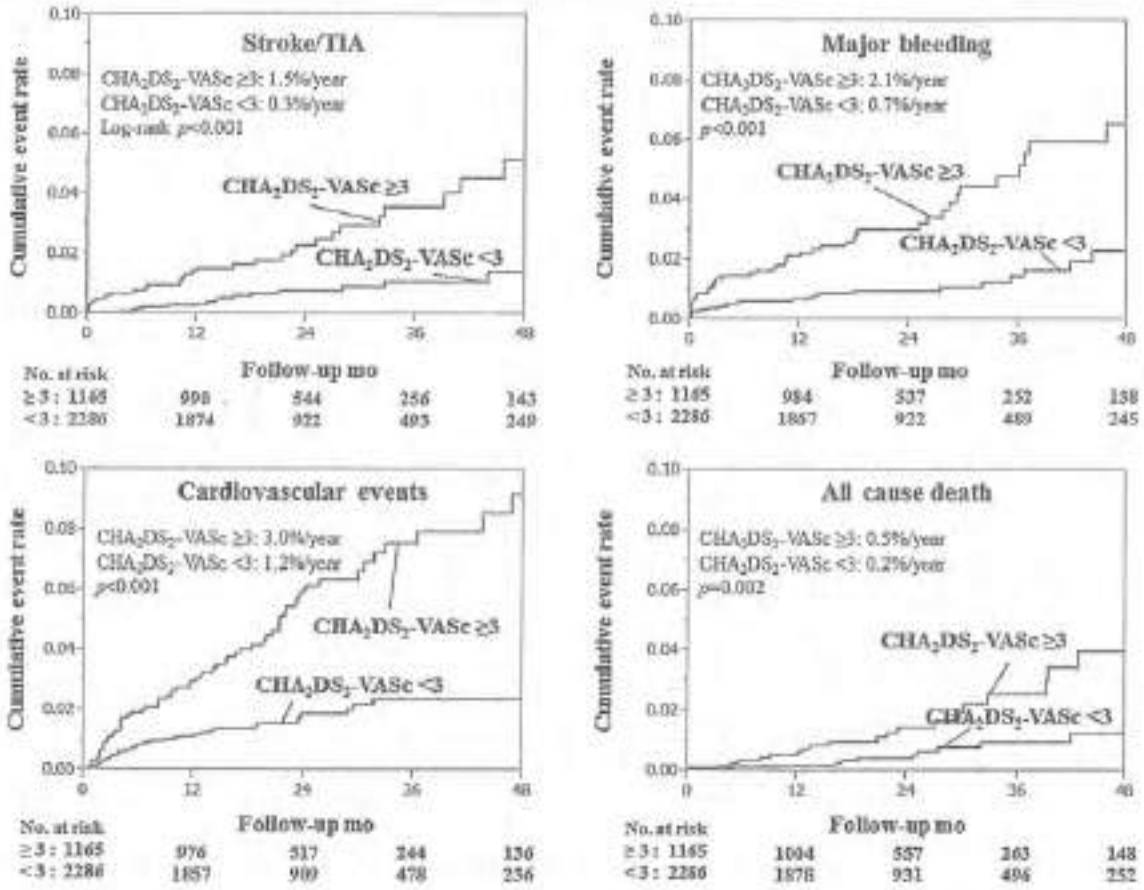

Figure 4. Kaplan-Meier curves for stroke/transient ischemic attack (TIA), major bleeding, cardiovascular events, and all-cause death after ablation for atrial fibrillation in patients with CHA_2DS_2-VASc scores of <3 and ≥3.

continued when, even after AF, the CHA_2DS_2-VASc score is ≥2. Interestingly, we found a score of 2 to be the best cutoff CHA_2DS_2-VASc score for OAC discontinuation but the AUC of 0.65 was low (data not shown in the Results). The OAC discontinuation rate gradually decreased as this score increased and there was no tipping point (**Figure 1**). Moreover, more than one-quarter of high-risk patients with $CHADS_2$ score ≥3 or CHA_2DS_2-VASc score ≥4 discontinued OAC during the follow-up (**Table 1**). These findings suggested that in real-world settings, physicians might not always consider the guidelines. Therefore, clarifying whether the physicians' inclinations regarding OAC discontinuation are appropriate is clinically important, and no pertinent data are available in Japan.

Our Japanese registry-based study showed significantly lower incidences of stroke/TIA, major bleeding, cardiovascular events, and death among patients for whom OAC use was discontinued after AF ablation than among those for whom OAC use was continued. The incidence of stroke/TIA was 0.4%/year among patients for whom OAC use was discontinued, but 1.1%/year among patients for whom OAC use was continued. We assume this is because OAC use was discontinued in patients with low stroke risk scores following successful ablation. Our data suggested that a decision to discontinue OAC therapy based mainly on a patient's characteristics is clinically reasonable. Despite the low incidence of stroke/TIA events among the present patients in whom OAC therapy was discontinued, physicians should be cautious when considering OAC discontinuation, because 35% (18/51) of patients who suffered a stroke/TIA and 40.8% (29/71) of those who suffered major bleeding were part of the OAC discontinuation group. Importantly, those patients were significantly older and their stroke risk scores were higher than those of patients in the same group who did not suffer a stroke/TIA or major bleeding. Furthermore, a CHA_2DS_2-VASc score ≥3, rather than OAC continuation vs. discontinuation, was identified as an independent predictor for each of these clinical events.

There is little data supporting post-AF ablation OAC discontinuation, especially in patients at high risk of stroke/TIA. Numerous investigators have also reported a strong association between advanced age, prior stroke/TIA, high $CHADS_2$, CHA_2DS_2-VASc, and HAS-BLED scores, and stroke/TIA and major bleeding.[8-12,20,21] Although some recent studies have shown a significant association between AF recurrence and stroke/TIA events,[22] our study did not. We cannot say with certainty that AF did not recur asymp-

tomatically in some of the patients who suffered a stroke/TIA. The incidence of asymptomatic AF recurrence increases after ablation, especially among patients at high risk for a stroke/TIA.[23] Therefore, OAC discontinuation in high-stroke risk patients should be carefully considered (or may be unsafe) even if sinus rhythm is thought to be maintained after ablation, because the stroke risk may be high once AF recurs asymptomatically.

Comparison of several Japanese AF registries (majority of patients did not undergo ablation) with a similar age and stroke risk score as this study population (62.3±10.3 years, $CHADS_2$ 1.2±1.1 and CHA_2DS_2-VASc 2.1±1.5) provided further insight into understanding the effect of OAC discontinuation after ablation on the clinical outcomes. Among 3,588 patients (68.1±13.5 years) without OAC therapy in the pooled analysis from 3 large Japanese registries,[24] the incidence of strokes was 0.69 and 0.98 events per 100 person-years for those aged <65 years and 65–75 years, respectively. Those events rates seemed higher than that of our OAC discontinuation group (0.4%/year), and therefore, ablation might have beneficial effects on stroke/TIA events in this group even if OACs are discontinued after ablation. In contrast, the incidences of stroke/systemic embolism (SE) and major bleeding events in a warfarin therapy cohort (2,822 patients aged <70 years in the J-Rhythm Registry[25]) were lower (~0.4%/year and 0.7%/year, respectively) than that in our OAC continuation group (1.1%/year and 1.6%/year, respectively) despite similar ages and stroke risk (61.0±7.0 years and $CHADS_2$ score 1.2±1.0) as our population. In another OAC therapy cohort (1,895 patients aged <75 years in the SAKURA AF registry:[26] 65.9±6.9 years, $CHAD_2$ score 1.3±1.0, CHA_2DS_2-VASc score 2.3±1.3, and 52.0% DOAC users and 48.0% warfarin users), the incidences of stroke/SE and major bleeding events were 1.2 and 1.1 events person-years, respectively, which were similar to those in our OAC continuation group. Those data suggested that in such high-risk patients, the stroke risk might persist even if OACs are continued after ablation. Therefore, our results and those of the other studies are a strong indication that the decision to continue long-term post-ablation OAC therapy in Japanese patients should depend on the patient's age and stroke risk profile derived from the CHA_2DS_2-VASc score and not on the perceived success or failure of ablation, as indicated in the recent guidelines.[27]

Clinical Implications

Our most important finding was that the CHA_2DS_2-VASc score or $CHADS_2$ score was a better predictor of stroke/TIA than age, but age was the best predictor of major bleeding. The best cutoff CHA_2DS_2-VASc score for stroke/TIA events was 3, and the best cutoff age for major bleeding events was 70 years. The incidences not only of stroke/TIA and major bleeding but also of cardiovascular events and death were relatively high among patients with a CHA_2DS_2-VASc score ≥3. Our data implied that, for patients aged ≥71 years and for those with a CHA_2DS_2-VASc score ≥3, OAC continuation after ablation may be safe for stroke prevention. Improving lifestyle factors and, if needed, taking medications appropriately, including antithrombotic agents, antihypertensive drugs or statins, are important for reducing the bleeding risk and adverse events, regardless of ablation success. Nevertheless, the AUCs of each factor for predicting stroke/TIA and bleeding events were relatively low, so the clinical judgement for OAC discontinuation after ablation should be done according to the CHA_2DS_2-VASc score and age while considering other factors including the AF type, history of major bleeding, comorbidities, and severity of atrial remodeling, etc.

Study Limitations

Because this study was retrospective and observational, only associations could be established; causal relationships could not. Such a study is subject to patient selection bias, and the diagnostic and therapy/intervention methods were not controlled for. For example, the decision to discontinue or maintain AAD/OAC therapy depended on the physicians' preference based on the patient's characteristics or preferences. Several patients were lost to follow-up during the follow-up period, and therefore, the clinical event rates might have been underestimated. It is also possible that the AF recurrence rate was underestimated. We might have missed patients with asymptomatic recurrence, even though our method of detecting recurrence was that used routinely in Japan. Finally, the follow-up period was relatively short for clarifying stroke/SE and other clinical events. AF recurrence after ablation increases gradually as time passes, and thus, clarifying the association between late recurrence and stroke events will require further prospective long-term studies. Nevertheless, the study included a relatively large number of patients from multiple centers in Japan, and thus we believe that, despite the study limitations, our findings will help physicians judge whether OAC therapy can be discontinued after ablation in Japanese AF patients.

Conclusions

In approximately half of our registry patients who underwent AF ablation, OACs were discontinued, and some patients experienced AF recurrence, but neither factor was associated with the occurrence of stroke/TIA or major bleeding after AF ablation. Rather, age and initial stroke risk were related to the stroke/TIA and major bleeding events, suggesting that although OACs should be continued in high-risk patients, OACs can be discontinued in low-risk patients, especially those in a low age category.

Acknowledgments

The authors thank all of the centers that participated in this study and all of the patients who gave consent to participate. We thank Ms. Wendy Alexander-Adams and Mr. John Martin for their encouragement and assistance with the reporting of our findings in English.

Funding

This study was supported by a research grant from Bristol-Meyers Squibb.

Disclosures

The following authors have potential conflicts of interest: Y.O. received research funding from Bayer Healthcare, Daiichi-Sankyo, Bristol-Meyers Squibb, Nippon Boehringer Ingelheim, Pfizer Japan, TORAY, and Boston Scientific Japan and has accepted remuneration from Bayer Healthcare, Daiichi-Sankyo, and Bristol-Meyers Squibb. N.M. received research funding from Daiichi-Sankyo. S.S. received research funding from Daiichi-Sankyo and Mitsubishi-Tanabe. A.H. accepted remuneration from Nippon Boehringer Ingelheim, Bayer Healthcare, Bristol-Myers Squibb, Daiichi-Sankyo. M.K. accepted remuneration from Johnson & Johnson K.K., Medtronic Japan, Bayer Healthcare. H.F. received lecture fees from Nippon Boehringer Ingelheim and Daiichi-Sankyo. S.N. received lecture fees from Bayer Healthcare, Daiichi-Sankyo, Bristol-Meyers Squibb, Pfizer Japan, and Nippon Boehringer Ingelheim. T.K. received a research grant from Daiichi-Sankyo, and lecture fees from Bristol-Myers Squibb,

Daiichi-Sankyo and Nippon Boehringer Ingelheim, and honoraria for writing promotional material for Bristol-Myers Squibb. W.S. received research funding from Bristol-Myers Squibb, Daiichi-Sankyo, and Nippon Boehringer Ingelheim, and patent royalties/licensing fees from Daiichi-Sankyo, Pfizer Japan, Bristol-Myers Squibb, Bayer Healthcare, and Nippon Boehringer Ingelheim. T.H. serves as a consultant to Medtronic Japan and has received lecture fees from Daiichi-Sankyo. I.N. received a scholarship from the Japanese Heart Rhythm Society and speaking honoraria from Medtronic Japan. K.O. received remuneration from Nippon Boehringer Ingelheim, Daiichi-Sankyo, Johnson & Johnson, and Medtronic Japan. M. Tokuda serves as a consultant to Medtronic Japan. T.Y. received lecture fees from Daiichi-Sankyo and Abbott Medical Japan. K.T. received lecture fees from Daiichi-Sankyo, Nippon Boehringer Ingelheim, Bristol-Myers Squibb, Pfizer Japan, Bayer Healthcare. K. Soejima received research funding from Daiichi-Sankyo and Nippon Boehringer Ingelheim, and accepted remuneration from Medtronic Japan, Johnson & Johnson, and Abbott Medical Japan. N.H. accepted remuneration from Nippon Boehringer Ingelheim, Bristol-Myers Squibb, Bayer Healthcare, and research funding from Bayer Healthcare, Nippon Boehringer Ingelheim, Daiichi-Sankyo. M.H. received lecture fee from Nippon Boehringer Ingelheim and Bristol-Myers Squibb. K. Satomi and Y.A. received research funding from BIOTRONIK Japan. Other authors have no conflicts of interest.

References

1. Odutayo A, Wong CX, Hsiao AJ, Hopewell S, Altman DG, Emdin CA. Atrial fibrillation and risks of cardiovascular disease, renal disease, and death: Systematic review and meta-analysis. *BMJ* 2016; **354:** i4482.
2. Piccini JP, Lopes RD, Kong MH, Hasselblad V, Jackson K, Al-Khatib SM. Pulmonary vein isolation for the maintenance of sinus rhythm in patients with atrial fibrillation: A meta-analysis of randomized, controlled trials. *Circ Arrhythm Electrophysiol* 2009; **2:** 626–633.
3. Cosedis Nielsen J, Johannessen A, Raatikainen P, Hindricks G, Walfridsson H, Kongstad O, et al. Radiofrequency ablation as initial therapy in paroxysmal atrial fibrillation. *N Engl J Med* 2012; **367:** 1587–1595.
4. Kuck KH, Brugada J, Fürnkranz A, Metzner A, Ouyang F, Chun KR, et al; FIRE AND ICE Investigators. Cryoballoon or radiofrequency ablation for paroxysmal atrial fibrillation. *N Engl J Med* 2016; **374:** 2235–2245.
5. Verma A, Jiang CY, Betts TR, Chen J, Deisenhofer I, Mantovan R, et al; STAR AF II Investigators. Approaches to catheter ablation for persistent atrial fibrillation. *N Engl J Med* 2015; **372:** 1812–1822.
6. Sticherling C, Marin F, Baron O, Boriani G, Calkins H, Dan GA, et al. Antithrombotic management in patients undergoing electrophysiological procedures: A European Heart Rhythm Association (EHRA) position document endorsed by the ESC Working Group Thrombosis, Heart Rhythm Society (HRS), and Asia Pacific Heart Rhythm Society (APHRS). *Europace* 2015; **17:** 1197–1214.
7. January CT, Wann LS, Alpert JS, Calkins H, Cigarroa JE, Cleveland JC Jr, et al; American College of Cardiology/American Heart Association Task Force on Practice Guidelines. 2014 AHA/ACC/HRS guideline for the management of patients with atrial fibrillation: A report of the American College of Cardiology/American Heart Association Task Force on Practice Guidelines and the Heart Rhythm Society. *J Am Coll Cardiol* 2014; **64:** e1–e76.
8. Camm AJ, Lip GY, De Caterina R, Savelieva I, Atar D, Hohnloser SH, et al; ESC Committee for Practice Guidelines-CPG; Document Reviewers. 2012 focused update of the ESC Guidelines for the management of atrial fibrillation: An update of the 2010 ESC Guidelines for the management of atrial fibrillation – developed with the special contribution of the European Heart Rhythm Association. *Europace* 2012; **14:** 1385–1413.
9. Oral H, Chugh A, Ozaydin M, Good E, Fortino J, Sankaran S, et al. Risk of thromboembolic events after percutaneous left atrial radiofrequency ablation of atrial fibrillation. *Circulation* 2006; **114:** 759–765.
10. Gulot A, Jongnarangsin K, Chugh A, Suwanagool A, Latchamsetty R, Myles JD, et al. Anticoagulant therapy and risk of cerebrovascular events after catheter ablation of atrial fibrillation in the elderly. *J Cardiovasc Electrophysiol* 2012; **23:** 36–43.
11. Gaita F, Sardi D, Battaglia A, Gallo C, Toso E, Michielon A, et al. Incidence of cerebral thromboembolic events during long-term follow-up in patients treated with transcatheter ablation for atrial fibrillation. *Europace* 2014; **16:** 980–986.
12. Nührich JM, Kuck KH, Andresen D, Steven D, Spitzer SG, Hoffmann E, et al. Oral anticoagulation is frequently discontinued after ablation of paroxysmal atrial fibrillation despite previous stroke: Data from the German Ablation Registry. *Clin Res Cardiol* 2015; **104:** 463–470.
13. Bunch TJ, Crandall BG, Weiss JP, May HT, Bair TL, Osborn JS, et al. Warfarin is not needed in low-risk patients following atrial fibrillation ablation procedures. *J Cardiovasc Electrophysiol* 2009; **20:** 988–993.
14. Friberg L, Tabrizi F, Englund A. Catheter ablation for atrial fibrillation is associated with lower incidence of stroke and death: Data from Swedish health registries. *Eur Heart J* 2016; **37:** 2478–2487.
15. Kodani E, Atarashi H, Inoue H, Okumura K, Yamashita T, Origasa H; J-RHYTHM Registry Investigators. Beneficial effect of non-vitamin K antagonist oral anticoagulants in patients with non valvular atrial fibrillation: Results of the J-RHYTHM Registry 2. *Circ J* 2016; **80:** 843–851.
16. Yamashita Y, Uozumi R, Hamatani Y, Esato M, Chun YH, Tsuji H, et al. Current status and outcomes of direct oral anticoagulant use in real-world atrial fibrillation patients: Fushimi AF Registry. *Circ J* 2017; **81:** 1278–1285.
17. Okumura Y, Yokoyama K, Matsumoto N, Tachibana E, Kuronuma K, Oiwa K, et al; SAKURA AF Registry Investigators. Three-year clinical outcomes associated with warfarin vs. direct oral anticoagulant use among Japanese patients with atrial fibrillation: Findings from the SAKURA AF Registry. *Circ J* 2018; **82:** 2500–2509.
18. Mosno K, Okumura Y, Saito Y, Aizawa Y, Nagashima K, Arai M, et al. Effect of epicardial fat and metabolic syndrome on reverse atrial remodeling after ablation for atrial fibrillation. *J Arrhythm* 2018; **34:** 607–616.
19. Watanabe R, Okumura Y, Nagashima K, Iso K, Takahashi K, Arai M, et al. Influence of balloon temperature and time to pulmonary vein isolation on acute pulmonary vein reconnection and clinical outcomes after cryoballoon ablation of atrial fibrillation. *J Arrhythm* 2018; **34:** 511–519.
20. Yagishita A, Takahashi Y, Takahashi A, Fujii A, Kusa S, Fujino T, et al. Incidence of late thromboembolic events after catheter ablation of atrial fibrillation. *Circ J* 2011; **75:** 2343–2349.
21. Själander S, Holmqvist F, Smith JG, Platonov PG, Kesek M, Svensson PJ, et al. Assessment of use vs. discontinuation of oral anticoagulation after pulmonary vein isolation in patients with atrial fibrillation. *JAMA Cardiol* 2017; **2:** 146–152.
22. Karasoy D, Gislason GH, Hansen J, Johannessen A, Kober L, Hvidtfeldt M, et al. Oral anticoagulation therapy after radiofrequency ablation of atrial fibrillation and the risk of thromboembolism and serious bleeding: Long term follow-up in nationwide cohort of Denmark. *Eur Heart J* 2015; **36:** 307–314a.
23. Hindricks G, Piorkowski C, Tanner H, Kobza R, Gerds-Li JH, Carbucicchio C, et al. Perception of atrial fibrillation before and after radiofrequency catheter ablation: Relevance of asymptomatic arrhythmia recurrence. *Circulation* 2005; **112:** 307–313.
24. Suzuki S, Yamashita T, Okumura K, Atarashi H, Akao M, Ogawa H, et al. Incidence of ischemic stroke in Japanese patients with atrial fibrillation not receiving anticoagulation therapy: Pooled analysis of the Shinken Database, J-RHYTHM Registry, and Fushimi AF Registry. *Circ J* 2015; **79:** 432–438.
25. Kodani E, Atarashi H, Inoue H, Okumura K, Yamashita T, Origasa H; J-RHYTHM Registry Investigators. Use of warfarin in elderly patients with non-valvular atrial fibrillation: Subanalysis of the J-RHYTHM Registry. *Circ J* 2015; **79:** 2345–2352.
26. Nishida T, Okumura Y, Yokoyama K, Matsumoto N, Tachibana E, Kuronuma K, et al; SAKURA AF Registry Investigators. Oral anticoagulant use and clinical outcomes in elderly Japanese patients: Findings from the SAKURA AF Registry. *Heart Vessels* 2019; **34:** 2021–2030.
27. Calkins H, Hindricks G, Cappato R, Kim YH, Saad EB, Aguinaga L, et al. 2017 HRS/EHRA/ECAS/APHRS/SOLAECE expert consensus statement on catheter and surgical ablation of atrial fibrillation. *Heart Rhythm* 2017; **14:** e275–e444.

Circulation Journal
Circ J 2019; 83: 2394–2398
doi:10.1253/circj.CJ-19-0670

JCS STATEMENT

Standard Cardiac Rehabilitation Program for Heart Failure

Hideo Izawa, MD, PhD; Toshiko Yoshida, PhD; Toshimi Ikegame, BSc;
Kazuhiro P. Izawa, PhD; Yoshihiro Ito, MD, PhD; Hideo Okamura, MD, PhD;
Naohiko Osada, MD, PhD; Shintaro Kinugawa, MD, PhD; Takuro Kubozono, MD, PhD;
Yuji Kono, PhD; Kiyonori Kobayashi, BSc; Kazuhiko Nishigaki, MD, PhD;
Taiki Higo, MD; Akihiro Hirashiki, MD, PhD; Yasushi Miyazawa, PhD;
Yuji Morio, PhD; Masanobu Yanase, MD; Sumio Yamada, PhD;
Hisao Ikeda, MD, PhD; Shin-ichi Momomura, MD, PhD; Yasuki Kihara, MD, PhD;
Kazuhiro Yamamoto, MD, PhD; Yoichi Goto, MD, PhD;
Shigeru Makita, MD, PhD; the Japanese Association of Cardiac Rehabilitation
Standard Cardiac Rehabilitation Program Planning Committee

With the rapid aging of the population in Japan, approximately 1 million people are affected by heart failure (HF).[1] Renin-angiotensin-aldosterone (RAA) system inhibitors and β-blockers, which have come to be widely used for treating HF, drastically improving the patient's long-term prognosis.[2] Several patients experience exacerbation of HF despite the use of such effective pharmacotherapies.[3] In the future, it is expected that the number of patients with HF will increase,[4] as will the associated medical expenses. Therefore, improving the long-term prognosis and reducing the number of hospital admissions for exacerbation of HF are presently urgent issues that need to be addressed as goals for the field of HF treatment.

In the 1970s, cardiac rehabilitation came into practice with the aim of addressing early ambulation, and social rehabilitation in patients following acute myocardial infarction (AMI). Thereafter, satisfactory evidence was established indicating that rehabilitation performed comprehensively with exercise training, patient education, and counseling for patients following AMI improves exercise tolerability and is useful for secondary prevention.[5,6] Such programs also proved effective for patients treated for coronary artery disease in general,[7] including coronary intervention,[8,9] and coronary bypass surgery.[10] Cardiac rehabilitation for HF effectively progresses exercise tolerability, reduces the rate of rehospitalization, and improves long-term prognosis by suppressing neurohumoral factors and inflammatory cytokines, and improving vascular endothelium function and musculoskeletal metabolism through exercise training.[11–16] Cardiac rehabilitation with such multifaceted effects is becoming increasingly perceived as advanced medical care. At the same time, its usefulness as a disease management program implemented by a multidisciplinary team has been recognized.[17,18] In Japan, however, efforts are poured into treatment for acute HF to stabilize hemodynamics. Yet, once hemodynamics are stable, the implementation of systematic patient education, lifestyle guidance, and exercise training as part of a necessary disease management program remains inadequate.

Received July 24, 2019; accepted September 2, 2019; J-STAGE Advance Publication released online November 9, 2019

Department of Cardiology (H. Izawa), Department of Rehabilitation (Y. Kono), Fujita Health University Bantane Hospital, Nagoya; Graduate School of Nursing Science, St. Luke's International University, Tokyo (T.Y.); Department of Nursing Administration, Sakakibara Heart Institute, Japan Research Promotion Society for Cardiovascular Disease, Tokyo (T.I.); Faculty of Health Sciences, School of Medicine, Kobe University, Kobe (K.P.I.); Cocokara Heart Clinic, Nagoya (Y.I.); Department of Cardiovascular Medicine (H.O.), Department of Transplantation (M.Y.), National Cerebral and Cardiovascular Center, Suita; Department of Cardiology, St. Marianna University School of Medicine Tayoko Hospital, Kawasaki (N.O.); Department of Cardiovascular Medicine, Faculty of Medicine and Graduate School of Medicine, Hokkaido University, Sapporo (S.K.); Department of Cardiovascular Medicine and Hypertension, Graduate School of Medical and Dental Sciences, Kagoshima University, Kagoshima (T.K.); Department of Rehabilitation, Nagoya University Hospital, Nagoya (K.K.); First Department of Internal Medicine, Gifu Municipal Hospital, Gifu (K.N.); Department of Cardiovascular Medicine, Kyushu University, Fukuoka (T.H.); Department of Cardiology, National Center for Geriatrics and Gerontology, Obu (A.H.); Department of Dietetics, Tokyo Medical University Hospital, Tokyo (Y. Miyazawa); Department of Rehabilitation Medicine, Showa University of Medical Sciences, Yokohama (Y. Morio); School of Health Sciences, Nagoya University Graduate School of Medicine, Nagoya (S.Y.); Faculty of Fukuoka Medical Technology, Teikyo University, Fukuoka (H. Ikeda); Saitama Medical Center, Jichi Medical University, Saitama (S.M); Department of Cardiovascular Medicine, Graduate School of Biomedical and Health Sciences, Hiroshima University, Hiroshima (Y. Kihara); Department of Molecular Medicine and Therapeutics, Faculty of Medicine, Tottori University, Yonago (K.Y.); Department of Cardiovascular Medicine, Yoka Municipal Hospital, Yabu (Y.G.); and Department of Cardiac Rehabilitation, Saitama Medical University International Medical Center, Hidaka (S.M.), Japan

Created by the Japanese Association of Cardiac Rehabilitation with the approval of the Japanese Circulation Society and the Japanese Heart Failure Society

Mailing address: Hideo Izawa, MD, PhD, Department of Cardiology, Fujita Health University Bantane Hospital, 3-6-10 Otobashi, Nakagawa-ku, Nagoya 454-8509, Japan. E-mail: izawa@fujita-hu.ac.jp

ISSN-1346-9843 All rights are reserved to the Japanese Circulation Society. For permissions, please e-mail: cj@j-circ.or.jp

Furthermore, after hospital discharge, numerous patients are referred back to their general practitioner. Therefore, after discharge, few patients continue cardiac rehabilitation, including exercise training commenced during their hospital stay, and the rate of outpatient cardiac rehabilitation implementation is very low.[19] To function as a HF management program, the popularization of an outpatient cardiac rehabilitation program after hospital discharge is a major challenge. "Guidelines for Rehabilitation in Patients with Cardiovascular Disease (JCS2012)"[20] have been established in Japan. Although this guideline presents the essential policy and implementation summary, there is no mention of specific procedures in actual clinical settings. The Japanese Association of Cardiac Rehabilitation (JACR) has indicated that a standard program needs to be prepared for utilization in clinical settings to promote appropriate cardiac rehabilitation implementation. Therefore, the JACR released a "Standard rehabilitation program from acute-to-recovery phase myocardial infarction" in 2014.

"Standard Heart Failure Program"

Target Outcomes

With the aim of implementing and popularizing appropriate cardiac rehabilitation for HF, we (Japanese Association of Cardiac Rehabilitation with the approval of the Japanese Circulation Society and the Japanese Heart Failure Society) created a standard, comprehensive cardiac rehabilitation program primarily for patients with HF who are able to tolerate exercise training and were previously independent with their activities of daily living (ADLs) prior to hospital admission. The target outcomes of this "Standard Heart Failure Program" are: (1) improve prognosis, (2) prevent rehospitalization, and (3) prevent physical dysfunction. To attain these outcomes, this cardiac rehabilitation program for HF needs to be accessible to all. The standard program includes essential elements, which we would like to see adopted by all institutions implementing the cardiac rehabilitation program, and desirable elements, which require the development and establishment of human resources, education, devices, and facilities at each institution to achieve the target outcomes of the standard program.

Features

This "Standard Heart Failure Program" begins with an acute-phase ambulation program, and introduces exercise training after stabilization of hemodynamics, until cardiac rehabilitation is implemented after hospital discharge while the patient is receiving outpatient treatment. The general rules are designed for implementation within regional core hospitals that provide acute-phase care; however, even at medical institutions that primarily provide chronic-phase care, these guidelines can be used as a reference when performing cardiac rehabilitation.

The content of the Standard Program is based on the "Guidelines for Rehabilitation in Patients with Cardiovascular Disease (JCS2012)",[20] which was created through collaboration of various groups, including the Japanese Circulation Society. Although evidence exists of the benefits of cardiac rehabilitation for patients with HF, there is little detailed evidence, and a substantial portion of what is available is based on the experiences and opinions of experts who have carried out rehabilitation in practical settings.

Each program activity has *essential* and *desirable* elements. This involves creating an exercise program based on the patient's condition after stabilization of hemodynamics, and includes elements that address lifestyle and medication adherence, evaluation and management of comorbidities, disease management such as psychological counseling, medical cooperation and confirmation of medical welfare services following discharge, outpatient disease management to prevent re-admission, and specific evaluations, interventions, and goals. Lastly, the program describes frail patients, and patients with dual-chamber pacing [cardiac resynchronization therapy (CRT)], an implantable cardioverter defibrillator (ICD), or ventricular assist device (VAD), which are used by an increasing number of patients.

The Standard Program Planning Committee consists of members from various disciplines who are highly experienced in cardiac rehabilitation based on JACR recommendations. This committee designed the program to include practical content that can be readily applied in clinical practice settings in Japan. Here, we describe a standard program, guided by JACR recommendations. Following incorporation of a wide spectrum of opinions, we hope to continually revise and improve the program, moving forward.

As a disease management program, comprehensive cardiac rehabilitation is needed during hospital stay, and should also be continued after patients are discharged from the hospital and return to society. Although a consensus has been reached that intervention by a multidisciplinary team is needed for the treatment and management of patients with HF to prevent rehospitalization caused by the exacerbation of HF and to improve long-term prognosis, we hope that comprehensive cardiac rehabilitation will be implemented throughout Japan, based on the standard program within each institution.

Components of the Standard Cardiac Rehabilitation Program (see Supplementary File)

I. Acute phase

Ambulation period

1. Acute phase ambulation program ..... See Below

Preparation period for the exercise training

2. Evaluation of patient backgrounds and acute exacerbation factors 4
3. Evaluation of cardiac function and hemodynamics 7
4. Evaluation of indications and contraindications for exercise training 9
5. Creation of an exercise program for introduction of exercise training 11

II. Early recovery phase

Inpatient rehabilitation period

1. Creation of an exercise program 13
2. Regular evaluation and revision of the exercise program 16
3. Nutrition and fluid management 18
4. Medication management 20
5. Evaluation and management of systemic comorbidities (hypertension, renal dysfunction, diabetes, anemia, sleep-disordered breathing) 21
6. Management of psychological and social factors 23

Discharge preparation period

7. Evaluation of cardiac function and hemodynamics prior to discharge 26
8. Creation of a post-discharge exercise program 28

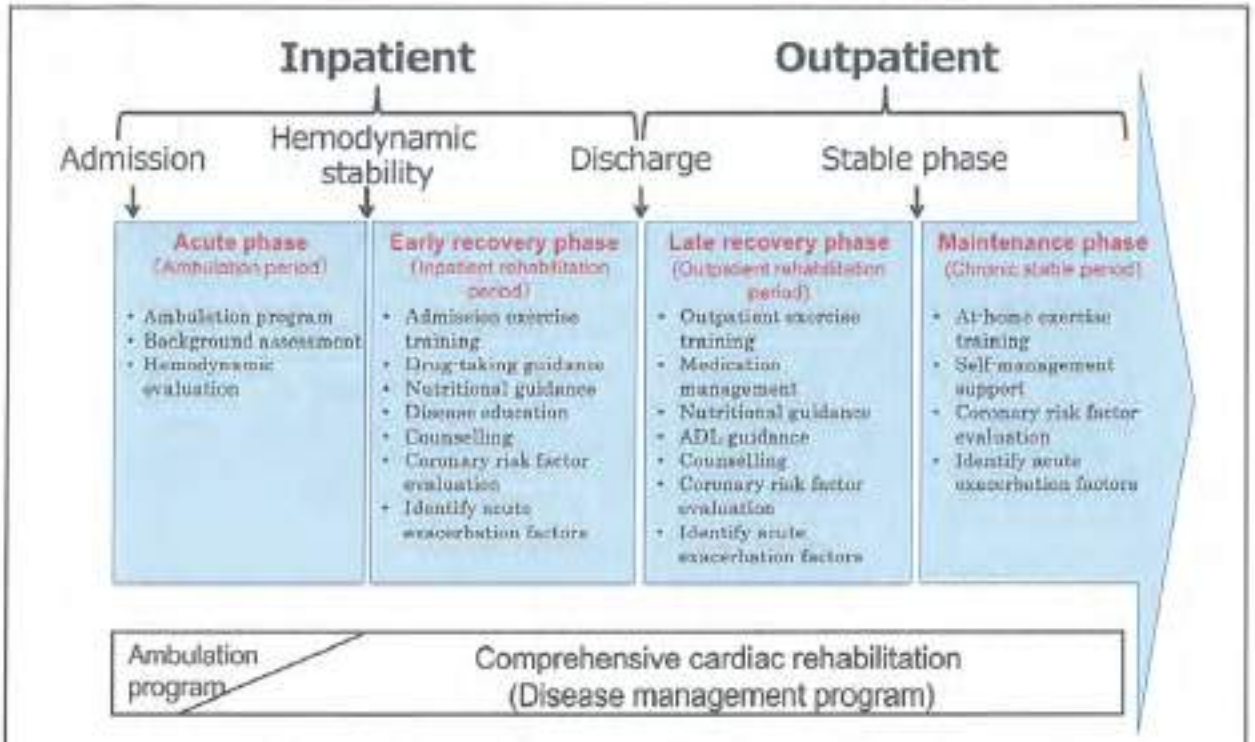

Figure 1. Schematic of planning a heart failure exercise program. ADL, activities of daily living.

9. Guidance for activities of daily living following discharge 30

III. Late recovery phase (Outpatient rehabilitation period)
1. Regular evaluation and revision of the exercise program 31
2. Disease management focusing on acute exacerbation factors 33

IV. Cooperation with local medical institutions and facilities
1. Hospital-clinic coordination and local cooperation 35

V. Patients who require particular attention
1. Frail patients 37
2. Patients receiving cardiac resynchronization therapy (CRT)/ implantable cardioverter defibrillators (ICD) 39
3. Patients receiving a left ventricular assist device (LVAD) 41

VI. Basic requirements for program implementation
1. Program management system 44
2. System to manage emergencies and unusual situations 46

How to Use This Standard Program

The "Standard Cardiac Rehabilitation Program for Heart Failure" is indicated for patients with HF who were independently and adequately performing ADLs prior to hospital admission, and for whom exercise training is not contraindicated.

This program is written according to a time line in which cardiac rehabilitation is commenced following hospital admission for HF, starting from the acute-phase ambulation program, to the early recovery phase, late recovery phase, and maintenance phase (**Figure 1**).

Chapter I describes the acute HF path implemented as the ambulation program of the acute phase after admission. During the acute phase after admission, the ambulation program proceeds in parallel with acute-phase treatment, leading to introduction of exercise training.

When commencing exercise training in the stable disease period, the following items should be checked prior to introducing exercise training: the patient's background, evaluation of the patient's condition (especially acute exacerbation factors that could result in hospitalization), and contraindications for exercise training. During this period, if the patient is able to walk at least 300 m during a 6-min walking test, an exercise program is created and exercise training is commenced. Points to be adopted when introducing exercise training are also noted.

Chapter II discusses the creation of an exercise program based on the results of cardiopulmonary exercise testing (CPX), with periodic evaluations and revisions. This chapter also describes a disease management program implemented during hospitalization, in parallel with exercise training, including ADLs, medication adherence, evaluation and management of comorbidities, and psychological counseling.

Prior to continuing exercise training on an outpatient basis after discharge, cardiac function and hemodynamics should be evaluated immediately prior to discharge. Then, the exercise program can be completed upon evaluation of exercise tolerance, considering ADL needs following discharge.

	Stage 1	Stage 2	Stage 3	Stage 4	Stage 5	Stage 6
Permissible degree of rest	Bed rest	Sitting upright	Free within room	Walk to toilet	Free within ward (up to 80 m)	Free within ward
Rehabilitation venue	On bed	Bedside	Bedside	Ward	Ward (rehabilitation room)	Ward (rehabilitation room)
Target sitting period (total hours per day)	Reclined seating	1 hour	2 hours	3 hours	3 hours	3 hours
Stage up loading test	Sitting upright	Walking test (free speed) 10 m	Walking test (free speed) 40 m	Walking test (free speed) 80 m	Walking test (free speed) 80 m × 2-3 times	6-min walking test

Figure 2. Acute phase ambulation program.

Chapter III discusses re-evaluation and revision of the exercise program during hospital visits conducted during the rehabilitation period. An additional focus is disease management, particularly the management of factors related to the exacerbation of HF, in order to prevent rehospitalization.

Chapter IV discusses multidisciplinary activities and confirmation of medical welfare services following discharge, including items that are necessary when cooperating with local health promotion facilities.

Chapter V discusses the program for frail elderly patients and patients with dual-chamber pacing CRT, an ICD, or VAD, used in increasing numbers of patients.

Chapter VI discusses the provision of a management system, and a system to deal with emergencies/abnormalities as basic programmatic requirements.

All program evaluations, interventions, and target goals are divided between *essential elements* and *desirable elements*, based on the criteria given below. Essential elements are the minimum-necessary requirements for cardiac rehabilitation program implementation. Desirable elements are items that we would ultimately like to be conducted by all institutions that implement cardiac rehabilitation.

We would like members of the cardiac rehabilitation team, regardless of their respective disciplines, to check the items written here, and share their status with their team. We hope to create a system of information-sharing during team meetings in order to determine who is responsible for the various items.

Explanation of the Elements

Essential elements
Minimum required content of the cardiac rehabilitation program
Desirable elements
Content aimed towards developing and ultimately establishing human resources, education, devices, and facilities at each participating institution

I. Acute Phase (Ambulation Period)

In the acute phase after admission (ambulation period), the ambulation program proceeds in parallel with acute-phase treatment, leading to the introduction of exercise training. The ambulation program is an essential element for all medical institutions that provide acute-phase care for patients with HF, and there are no desirable elements in this chapter. A typical example of the acute-phase ambulation program is given below. The program is a sample, and s created in accordance with the circumstances of each institution, such as the walking distance.

1. Acute-Phase Ambulation Program (Figure 2)

During the acute phase, immediately after hospital admission for acute HF, the focus of treatment is hemodynamic stabilization. Prolonged bed rest can reduce muscle strength and exercise tolerance; therefore, the ambulation program given below is commenced at bedside during the acute phase, ideally leading to early implementation of exercise training.

To proceed to the next stage, the patient's hemodynamics must be stable, as demonstrated by the stage completion loading test. For example, when proceeding from stage 1 to stage 2, the degree of rest changes from bed rest to sitting upright; however, hypertension, heart rate, partial arterial pressure of oxygen, and ECG monitors must be checked while the patient is sitting upright to confirm hemodynamic stability before the patient moves on to stage 2.

In stage 2, sitting upright is permitted, and the target sitting period is 1 hour. Thereafter, and before moving up to the next stage, each stage completion loading test must be performed. Importantly, hemodynamic stability must be repeatedly confirmed. Clinicians should also confirm that severe arrhythmia does not arise from loading, and as the patient moves up to the next stage, his or her ambulation improves, and the target sitting time increases. From stage 2 onwards, patients will complete a walking test at their own pace with no specified distance or speed, to determine whether they are able to walk the target distance of each stage. In the 6-min walking test, if the patient can walk

approximately 300 m, he or she completes stage 6, and proceeds onto the introduction of exercise training, as described in chapters one I to five V.

*Patients who progress smoothly through the ambulation program above, with sufficient exercise tolerance, such as younger patients and patients with milder disease, are able to skip stages while paying due care to hemodynamic stability. These patients can also perform CPX without completing the 6-min walk of stage 6.

*Patients with severe disease who cannot progress through the ambulation program and who cannot be weaned off catecholamines: investigate intensification of pharmacotherapy, and the indication of concurrent "Waon" therapy[29] or nonpharmaceutical treatments (CRT, mitral annuloplasty, and auxiliary artificial heart) in order to help them progress even slightly more. In general, exercise training is contraindicated in patients with NYHA class IV HF; however, in patients with stable hemodynamics receiving catecholamine treatment, disuse syndrome can be prevented by carefully performing bedside muscle strength training.

*When frail patients are unable to progress through the ambulation program, they can be transported to the rehabilitation room upon completion of the intravenous drip management, to perform muscle strength training, and train for independence in ADLs. Please refer to Chapter V for details.

Hereafter, please see **Supplementary File** because of the limitation of number of letters.

References

1. Ohsawa Y, Ramadan MM, Ohno Y, Mitsuma W, Tanaka K, Ito M, et al. Impending epidemic: Future projection of heart failure in Japan to the year 2055. *Circ J* 2008; **72:** 489–491.
2. Jong P, Yusuf S, Rousseau MF, Ahn SA, Bangdiwala SI. Effect of enalapril on 12-year survival and life expectancy in patients with left ventricular systolic dysfunction: A follow-up study. *Lancet* 2003; **361:** 1843–1848.
3. Mozaffarian D, Benjamin EJ, Go AS, Arnett DK, Blaha MJ, Cushman M, et al. Executive summary: Heart disease and stroke statistics-2016 update: A report from the American Heart Association. *Circulation* 2016; **133:** 447–454.
4. Shimokawa H, Miura M, Nochioka K, Sakata Y. Heart failure as a general pandemic in Asia. *Eur J Heart Fail* 2015; **17:** 884–892.
5. May GS, Eberlein KA, Furberg CD, Passamani ER, DeMets DL. Secondary prevention after myocardial infarction: A review of long-term trials. *Prog Cardiovasc Dis* 1982; **24:** 331–352.
6. Witt BJ, Jacobsen SJ, Weston SA, Killian JM, Meverden RA, Allison TG, et al. Cardiac rehabilitation after myocardial infarction in the community. *J Am Coll Cardiol* 2004; **44:** 988–996.
7. Wenger NK. Current status of cardiac rehabilitation. *J Am Coll Cardiol* 2008; **51:** 1619–1631.
8. Kubo H, Yano K, Hirai H, Yabuki S, Machii K. Preventive effect of exercise training on recurrent stenosis after percutaneous transluminal coronary angioplasty (PTCA). *Jpn Circ J* 1992; **56:** 413–421.
9. Belardinelli R, Paolini I, Cianci G, Piva R, Georgiou D, Purcaro A. Exercise training intervention after coronary angioplasty: The ETICA Trial. *J Am Coll Cardiol* 2001; **37:** 1891–1900.
10. Dubach P, Litscher K, Kulin M, Laske P, Buser P, Miller P, et al. Cardiac rehabilitation in Switzerland: Efficacy of the residential approach following bypass surgery. *Chest* 1993; **103:** 611–615.
11. Demopoulos L, Bijou R, Fergus I, Jones M, Strom J, LeJemtel TH. Exercise training in patients with severe congestive heart failure: Enhancing peak aerobic capacity while minimizing the increase in ventricular wall stress. *J Am Coll Cardiol* 1997; **29:** 597–603.
12. Hambrecht R, Fiehn E, Weigl C, Gielen S, Hamann C, Kaiser R, et al. Regular physical exercise corrects endothelial dysfunction and improves exercise capacity in patients with chronic heart failure. *Circulation* 1998; **98:** 2709–2715.
13. Belardinelli R, Georgiou D, Giovanni C, Gielen S, Hamann C, Kaiser R, et al. Randomized controlled trial of long term moderate training in chronic heart failure. *Circulation* 1999; **99:** 1173–1182.
14. ExTraMATCH Collaborative. Exercise training meta-analysis of trials in patients with chronic heart failure (ExTraMATCH). *BMJ* 2004; **328:** 189–192.
15. Linke A, Adams V, Schuler PC, Erbs S, Gielen S, Fiehn E, et al. Antioxidative effects of exercise training in patients with chronic heart failure: Increase in radical scavenger enzyme activity in skeletal muscle. *Circulation* 2005; **111:** 1763–1770.
16. O'Connor CM, Whellan DJ, Lee KL, Keteyian SJ, Cooper LS, Ellis SJ, et al. Efficacy and safety of exercise training in patients with chronic heart failure: HF-ACTION randomized controlled trial. *JAMA* 2009; **301:** 1439–1450.
17. McAlister FA, Stewart S, Ferrua S, McMurray JJ. Multidisciplinary strategies for the management of heart failure patients at high risk for admission: A systematic review of randomized trials. *J Am Coll Cardiol* 2004; **44:** 810–819.
18. Davidson PM, Cockburn J, Newton PJ, Webster JK, Beilharz V, Howes L, et al. Can a heart failure-specific cardiac rehabilitation program decrease hospitalizations and improve outcomes in high-risk patients? *Eur J Cardiovasc Prev Rehabil* 2010; **17:** 393–402.
19. Arakawa T, Kumasaka L, Nakanishi M, Negayama M, Adachi H, Ikeda K, et al. Regional clinical alliance path and cardiac rehabilitation after hospital discharge for acute myocardial infarction patients in Japan: A nationwide survey. *Circ J* 2016; **80:** 1750–1755.
20. JCS Joint Working Group. Guidelines for rehabilitation in patients with cardiovascular disease (JCS 2012): Digest version. *Circ J* 2014; **78:** 2022–2093.
21. Tei C, Imamura T, Kinugawa K, Inoue T, Matsuyama T, Inoue H, et al; WAON-CHF Study Investigators. Waon therapy for managing chronic heart failure: Results from a multicenter prospective randomized WAON-CHF Study. *Circ J* 2016; **80:** 827–834.

Supplementary Files

Please find supplementary file(s):
http://dx.doi.org/10.1253/circj.CJ-19-0670

JACC: CARDIOVASCULAR INTERVENTIONS
Vol. 12, No. 23, 2019
© 2019 BY THE AMERICAN COLLEGE OF CARDIOLOGY FOUNDATION
PUBLISHED BY ELSEVIER

Valve-in-Valve Implantation Using the ACURATE Neo in Degenerated Aortic Bioprostheses

An International Multicenter Analysis

Andreas Holzamer, MD,[a] Won-Keun Kim, MD,[b] Andreas Rück, MD,[c] Jamarthanan Sathananthan, MBChB, MPH,[d] Lukas Keller, MD,[e] Joseph Cosma, MD,[f] Timm Bauer, MD,[g] Holger Nef, MD,[g] Ignacio J. Amat-Santos, MD,[h] Miriam Brinkert, MD,[i] Oliver Husser, MD,[j] Costanza Pellegrini, MD,[j] Joachim Schofer, MD,[k] Roberto Nerla, MD,[l] Matteo Montorfano, MD,[m] Francesco Giannini, MD,[m] Pieter Stella, MD, PhD,[n] Shingo Kuwata, MD,[n] Michael Hilker, MD,[a] Fausto Castriota, MD,[l] Gian Paolo Ussia, MD,[f] John G. Webb, MD,[d] Fabian Nietlispach, MD, PhD,[e] Stefan Toggweiler, MD[f]

ABSTRACT

OBJECTIVES This study reports an international experience using the transfemoral ACURATE neo transcatheter heart valve (Boston Scientific, Marlborough, Massachusetts) for the treatment of degenerated surgical aortic bioprostheses.

BACKGROUND Transcatheter valve-in-valve procedures have emerged as an alternative to redo surgery. Supra-annular prostheses might be particularly useful in this indication.

METHODS This is an international multicenter analysis including 85 patients from 14 centers in Europe and Canada undergoing an ACURATE neo valve-in-valve procedure from March 2015 to February 2019.

RESULTS Internal diameter of the degenerated bioprosthesis was 20.3 ± 2.1 mm. Prosthesis size 5 was used in 70 (82%) procedures. The median depth of implantation was 3 mm and the upper crown of the ACURATE neo was positioned above the stent posts of the degenerated bioprosthesis in 54 (64%) and inside in 31 (36%). Mean transvalvular gradient before discharge was significantly lower if the upper crown was above the degenerated bioprosthesis (13.7 ± 5.9 mm Hg vs. 19.5 ± 10.0 mm Hg; p = 0.001). However, a high position of the ACURATE neo resulted in embolization in 1 patient, conversion to open-heart surgery in 1, and need for reintervention due to transcatheter heart valve failure within the first 18 months of follow-up in 4.

CONCLUSIONS This early experience shows that a high implantation of the ACURATE neo with the upper crown above the stent posts of the degenerated bioprosthesis resulted in lower mean transvalvular gradients but a higher rate of malpositioning and early valve degeneration. (J Am Coll Cardiol Intv 2019;12:2309–16) © 2019 by the American College of Cardiology Foundation.

From the [a]Department of Cardiothoracic Surgery, University of Regensburg Medical Center, Regensburg, Germany; [b]Department of Cardiology and Cardiac Surgery, Kerckhoff Heart and Lung Center, Bad Nauheim, Germany; [c]Department of Medicine, Unit of Cardiology, Karolinska University Hospital, Stockholm, Sweden; [d]Centre for Heart Valve Innovation, St. Paul's and Vancouver General Hospitals, University of British Columbia, Vancouver, Canada; [e]Department of Cardiology, University Hospital Zürich, Zurich, Switzerland; [f]Department of Cardiology, University Campus Bio-Medico, University of Rome Tor Vergata, Rome, Italy; [g]Department of Cardiology, University Hospital Giessen, Giessen, Germany; [h]Centro de Investigación Biomédica en Red Enfermedades Cardiovasculares, Department of Cardiology, Hospital Universitario de Valladolid, Valladolid, Spain; [i]Division of Cardiology, Heart Center Lucerne, Luzerner Kantonsspital, Lucerne, Switzerland; [j]Klinik für Herz- und Kreislauferkrankungen, Deutsches Herzzentrum München, Munich, Germany; [k]Albertinen Herzzentrum und Medizinisches Versorgungszentrum Prof. Dr. Mathey, Hamburg, Germany; [l]Cardiovascular Department, Humanitas Gavazzeni, Bergamo, Italy; [m]Interventional Cardiology Unit, San Raffaele Institute, Milan, Italy; and the [n]Department of Cardiology, University Medical Center Utrecht, Utrecht, the Netherlands. Drs. Holzamer and Hilker have served as proctor for and received research grant support from Boston Scientific. Dr. Kim has served as a proctor for Boston Scientific, Abbott, and Edwards Lifesciences; and has received speaker fees from Edwards Lifesciences, Abbott, Medtronic, and Symetis/Boston Scientific. Dr. Rück has received lecture fees from Boston Scientific and Edwards Lifesciences; and has received research grant support from Boston Scientific. Dr. Sathananthan has served as a consultant for Edwards Lifesciences. Drs. Amat-Santos, Husser, and Stella have served as a proctor for Boston Scientific.

ISSN 1936-8798/$36.00
https://doi.org/10.1016/j.jcin.2019.07.043

JACC: CARDIOVASCULAR INTERVENTIONS VOL. 12, NO. 22, 2019
NOVEMBER 25, 2019:2309–18

ABBREVIATIONS AND ACRONYMS

AVA = aortic valve area

ID = inner diameter

PPM = prosthesis-patient mismatch

THV = transcatheter heart valve

ViV = valve-in-valve

The last decade saw a major shift from mechanical toward bioprosthetic heart valves (1). Decision making has to weigh the risk of anticoagulation-related bleeding and thromboembolism of mechanical prosthesis against the limited durability of bioprostheses with the associated increased risk of perioperative complications and mortality of redo procedures (2,3).

New fuel to the debate has been introduced through the availability of transcatheter valve-in-valve (ViV) implantation, a technique that has emerged as an alternative to surgery in high- and extreme-risk patients according to the current American and European guidelines (2,3). A recent report of the global ViV VIVID (Valve-in-Valve International Data Registry) registry highlights the need for future studies to prove that modifying ViV procedures with certain valve choices and high valve implantation are effective in reducing gradients (4). Supra-annular prostheses may be particularly advantageous for this indication (5).

The self-expanding ACURATE neo (Boston Scientific, Marlborough, Massachusetts) is such a supra-annular prosthesis. It has been associated with low residual gradients in native valves (6,7), but clinical data on its use in the ViV indication are scarce and limited to case reports (8).

In the present analysis, we report an international experience using the ACURATE neo transcatheter heart valve (THV) for the treatment of degenerated surgical aortic bioprostheses, which is—to the best of our knowledge—the largest series presented for this valve type to date.

SEE PAGE 2317

METHODS

STUDY DESIGN AND POPULATION. This is an international multicenter, retrospective analysis to evaluate the safety and performance of the ACURATE neo THV in degenerated surgical bioprostheses. The analysis was conducted between March 2015 and February 2019 at 14 centers in Germany, Switzerland, Italy, Spain, Sweden, the Netherlands, and Canada and included all patients undergoing an ACURATE neo ViV procedure at these sites. Surgical valves are listed in Online Table 1. All patients were discussed by an interdisciplinary Heart Team and deemed to be high risk for repeat open-heart surgery.

For this study, baseline and procedural values were evaluated, post-procedural echocardiographic assessments (before discharge) were evaluated, and 30-day complication rates assessed. All but 1 patient with periprocedural mortality underwent echocardiographic follow-up before discharge. In addition, the last available echocardiography was collected. All patients gave written consent for the transcatheter procedure.

STUDY DEVICE. The ACURATE neo prosthesis and implantation procedure have been described in detail previously (9). The THV size was selected according to physician's discretion. In general, the valve size was chosen according to the inner diameter (ID) of the bioprosthesis (a small [S] valve for a minimal diameter <23 mm, a medium (M) valve for an ID between 23 and 25 mm, and a large [L] valve for an ID >25 mm). For analysis in this study, the inner diameter of the prosthesis was derived from the ViV app and computed tomography-based measurements. As this series included many surgical prostheses with an ID ≤18 mm, a substantial degree of oversizing was present in many patients. No patient underwent bioprosthetic valve fracture in this study.

DEFINITIONS OF ENDPOINTS. Clinical endpoints were defined according to the updated definitions of the Valve Academic Research Consortium (10). The aortic valve area (AVA) index was calculated as: aortic valve area/body surface area. An AVA index <0.65 cm^2/m^2 was considered as severe prosthesis-patient mismatch (PPM) and values between 0.65 and 0.85 cm^2/m^2 were considered moderate PPM. For patients with a body mass index ≥30 kg/m^2, an AVA index between 0.55 and 0.70 cm^2/m^2 was considered moderate PPM, and <0.55 cm^2/m^2 was considered severe PPM (11). In addition, a combined endpoint was analyzed defined as the occurrence of at least 1 of the following: mean transvalvular gradient before discharge ≥20 mm Hg,

Dr. Pellegrini has received minor travel grants from Boston Scientific and Edwards Lifesciences. Dr. Castrichini has served as a proctor and consultant for Boston Scientific and has served as a consultant for Medtronic, Abbott, and Terumo. Dr. Webb is a consultant to, and has received research funding from, Edwards Lifesciences, Abbott, and ViVitro Labs; and is a proctor for Boston Scientific. Dr. Niellapach has served as a consultant for Edwards Lifesciences, Abbott Vascular, and Medtronic. Dr. Toggweiler has served as a proctor and consultant for Boston Scientific and New Valve Technology; and has received an institutional research grant from Boston Scientific. All other authors have reported that they have no relationships relevant to the contents of this paper to disclose.

Manuscript received April 21, 2019; revised manuscript received June 26, 2019, accepted July 23, 2019.

malposition of the first THV requiring a second THV, conversion to open-heart surgery, and death or stroke at 30 days. Depth of implantation was measured on fluoroscopic images as the distance between the inflow portion of the ACURATE neo (the lower crown) and the surgical ring. In the same images, it was determined if the upper crown was above or inside the stent posts or leaflets (in patients with stentless bioprostheses) of the degenerated surgical bioprosthesis.

STATISTICAL ANALYSIS. If not indicated otherwise, data are presented as mean ± SD for continuous variables and as number and frequency for categorical variables. Continuous parametric variables were compared using the paired and unpaired Student's *t*-test and the Wilcoxon rank sum test. One-year survival rate was estimated using the Kaplan-Meier method. Statistical analyses were conducted with STATA version 13 (StataCorp, College Station, Texas) and tested using 2-sided tests at a significance level of 0.05.

RESULTS

A cohort of 85 patients (mean age 77 ± 8 years, 46% women) was included in this analysis. Median time from surgical aortic valve replacement to the ViV procedure was 9.2 years (range 1.1 to 18.1 years). As many as 35 of 85 (41%) had a bioprosthesis ID ≤20 mm. Table 1 lists baseline characteristics of the cohort and of the subgroups with the upper crown above and inside the posts of the bioprosthesis.

PROCEDURAL CHARACTERISTICS AND 30-DAY OUTCOMES. Procedural characteristics are summarized in Table 2. The procedure was conducted via transfemoral access using the ACURATE neo prosthesis and using predominantly valve size S (n = 70, 82% of cases). Median depth of implantation was 3 (interquartile range: 1 to 6) mm and the upper crown of the bioprosthesis was positioned above the stent posts and the leaflets of the surgical prosthesis in 64% (n = 54) (Figure 1), and inside in the remaining 36% (n = 31). One patient with baseline coronary artery disease received an ACURATE neo size S with the upper crown above the stenotic Trifecta 21 mm bioprosthesis (internal diameter 18 mm) (St. Jude Medical, St. Paul, Minnesota) and experienced a coronary obstruction that required conversion to surgery. Despite coronary artery bypass grafting, the patient deteriorated and passed away 1 day after the procedure. In 2 patients in which a high implantation was attempted, the prosthesis embolized in the ascending aorta. Both were treated with implantation of a second THV. At 30 days, 4 (5%) patients had died, 1 (1%) stroke had occurred, and 1 (1%) patient had received a permanent pacemaker.

TABLE 1 Baseline Characteristics

	All Patients (N = 85)	Upper Crown Above (n = 54)	Upper Crown Inside (n = 31)	p Value
Age, yrs	77 ± 8	78 ± 6	76 ± 11	0.185
Female	39 (46)	26 (48)	13 (42)	0.580
Hypertension	74 (87)	49 (91)	25 (81)	0.182
Diabetes	26 (30)	17 (31)	8 (26)	0.580
Coronary artery disease	43 (51)	28 (52)	15 (48)	0.758
Prior myocardial infarction	9 (11)	6 (11)	3 (10)	0.814
Chronic kidney disease	49 (58)	31 (57)	18 (58)	0.953
Prior permanent pacemaker	16 (19)	7 (13)	9 (29)	0.068
STS PROM, %	6.8 ± 6.0	7.2 ± 6.9	6.2 ± 4.5	0.457
EuroSCORE II, %	11.4 ± 7.9	11.3 ± 8.2	9.9 ± 7.1	0.174
Nominal inner diameter of bioprosthesis, mm	20.3 ± 2.2	20.5 ± 2.0	19.9 ± 2.3	0.187
Mode of degeneration				
Stenosis	48 (56)	32 (59)	16 (51)	0.468
Regurgitation or mixed	37 (44)	22 (41)	15 (48)	
LVEF, %	54 ± 11	55 ± 10	53 ± 13	0.444
Mean gradient, mm Hg	40 ± 18	38 ± 16	44 ± 21	0.093
Aortic valve area, cm^2	0.80 ± 0.32	0.83 ± 0.34	0.75 ± 0.29	0.332

Values are mean ± SD or n (%).

EuroSCORE = European System for Cardiac Operative Risk Evaluation; LVEF = left ventricular ejection fraction; STS PROM = Society of Thoracic Surgeons Predicted Risk of Mortality.

ECHOCARDIOGRAPHIC OUTCOMES. Echocardiographic results before discharge are listed in Table 2. The mean post-procedural gradient was significantly lower if the upper crown of the ACURATE neo was above the degenerated bioprosthesis (13.3 ± 5.7 mm Hg vs. 19.3 ± 10.3 mm Hg; p = 0.003). The Central Illustration illustrates mean post-procedural gradient according to the ID and the position of the upper crown in relation to the posts of the degenerated surgical bioprosthesis. Linear regression analysis of multivariable predictors of the post-procedural mean transvalvular gradient is shown in Online Table 2. The combined endpoint (elevated mean gradient, malposition of the THV, conversion to open-heart surgery, and death or stroke at 30 days) occurred in 16 of 54 (30%) with the upper crown of the ACURATE neo above and in 13 of 31 (42%) with the upper crown of the ACURATE neo inside the bioprosthesis (p = 0.249). Residual aortic regurgitation was none in 70 (84%) patients, mild in 12 (15%), and moderate in 1 (1%).

MIDTERM OUTCOMES. Median follow-up was 12 months (range of up to 48 months). A total of 4 (5%) patients presented with THV failure. All these

TABLE 2 Procedural Characteristics and Outcomes

	All Patients (N = 85)	Upper Crown Above (n = 54)	Upper Crown Inside (n = 31)	p Value
ACURATE neo size				
S (23 mm)	70 (82)	41 (76)	29 (94)	0.317
M (25 mm)	14 (16)	12 (22)	2 (6)	
L (27 mm)	1 (1)	1 (2)	0 (0)	
Pre-dilatation	26 (31)	17 (31)	9 (29)	0.814
Implantation depth, mm	3.8 ± 3.6	1.8 ± 2.1	7.3 ± 3.3	<0.001
Post-dilatation	33 (39)	24 (44)	9 (29)	0.160
Procedural time, min	55 ± 32	55 ± 24	56 ± 19	0.796
Fluoroscopy time, min	15 ± 9	14 ± 8	17 ± 10	0.204
Acute coronary obstruction	1 (1)	1 (2)	0 (0)	0.446
Need for a second THV	2 (2)	2 (4)	0 (0)	0.278
Conversion to open-heart surgery	1 (1)	1 (2)	0 (0)	0.446
Echocardiography before discharge				
≥mild PVL	7/71 (10)	4/42 (10)	3/29 (10)	0.410
Mean gradient, mm Hg	16 ± 8 (82)	14 ± 6 (51)	19 ± 10 (31)	0.001
AVA, cm^2	1.46 ± 0.37 (82)	1.53 ± 0.37 (51)	1.36 ± 0.34 (31)	0.045
AVA index, cm^2/m^2	0.80 ± 0.22 (82)	0.83 ± 0.22 (51)	0.75 ± 0.21 (31)	0.152
Moderate or severe PPM	35/82 (43)	19/51 (37)	16/31 (52)	0.202
LVEF, %	54 ± 11	55 ± 10	53 ± 13	0.444
30-day outcomes				
Major vascular complication	4 (5)	4 (8)	0 (0)	0.273
Major or life-threatening bleeding	4 (5)	4 (8)	0 (0)	0.273
Stage 2 or 3 acute kidney injury	2 (2)	1 (2)	1 (3)	0.324
New permanent pacemaker	1 (1)	1 (2)	0 (0)	0.442
New left bundle branch block	2 (2)	1 (2)	1 (3)	0.698
New onset atrial fibrillation	2 (2)	1 (2)	1 (3)	0.698
Any stroke	1 (1)	1 (2)	0 (0)	0.442
All-cause mortality	4 (5)	4 (7)	0 (0)	0.121

Values are n (%), mean ± SD, n/N (%), or mean ± SD (N).

AVA = aortic valve area; PPM = prosthesis-patient mismatch; PVL = paravalvular leak; THV = transcatheter heart valve; other abbreviations as in Table 1.

patients had a high implant with the upper crown above the posts and the leaflets of the surgical prosthesis. One patient presented with endocarditis 4 months after the procedure and was successfully treated surgically. Two patients presented with severe transvalvular regurgitation 4 and 8 months after the procedure due to perforation of one of the leaflets of the ACURATE neo, and both were treated surgically. Of note, both these patients had a post-dilatation during the VIV procedure to optimize gradients. One of these 2 patients had a large perforation, most likely due to a large protruding calcification in the patients ascending aorta at the sinotubular junction, resulting in direct contact between the leaflet and the calcification. The other of these 2 patients had direct contact between the stent post of the surgical bioprosthesis, most likely causing accelerated degeneration due to wear and tear of the leaflet. One patient presented with severe restenosis 18 months after the procedure and was treated by implantation of an Allegra THV (New Valve Technology, Muri, Switzerland, and Hechingen, Germany). More details about these 4 patients are provided in the Online Table 3. Kaplan-Meier estimate of survival at 1 year was 92% (95% confidence interval: 83% to 96%). Midterm echocardiological outcome is summarized in Online Table 4.

DISCUSSION

The main findings of this analysis are: 1) implantation of the ACURATE neo in degenerated bioprostheses is feasible; 2) the ACURATE neo has predominantly been used in very small valve sizes; 3) implantation with the upper crown above the posts of the degenerated bioprosthesis resulted in significantly better hemodynamic outcomes; and 4) implantation with the upper crown inside the posts of the degenerated bioprosthesis resulted in a total of 3 patients with THV embolization or conversion to open-heart surgery. According to these results, both implant techniques appear to have some advantages and disadvantages. Clearly, the and the ACURATE neo has not been designed for high implantation (a target depth of implantation of 0 to 4 mm below the ring of the surgical bioprosthesis), as the target implantation depth for the ACURATE neo is usually 7 mm in native valves. This may explain the cases of THV malpositioning and embolization. Furthermore, there were 4 cases of transcatheter aortic valve degeneration within the first 18 months of follow-up, all in patients with a high implantation of the ACURATE neo. One possible explanation for this may be that the leaflets of the ACURATE neo are less well protected by the stent frame compared with other THVs. According to these findings, patients should be followed closely after undergoing implantation of the ACURATE neo in degenerated bioprostheses.

IMPLANTATION IN SMALL DEGENERATED BIOPROSTHESES. In this series, the ACURATE neo was implanted in small bioprosthesis with an ID ≤20 mm in about 40% of the patients. This is not surprising, as previous studies have shown that supra-annular THVs result in lower gradients compared with intra-annular THVs (5). Likewise, in

FIGURE 1 Transcatheter Valve-in-Valve Implantation of an ACURATE Neo in a Degenerated Carpentier-Edwards Bioprosthesis

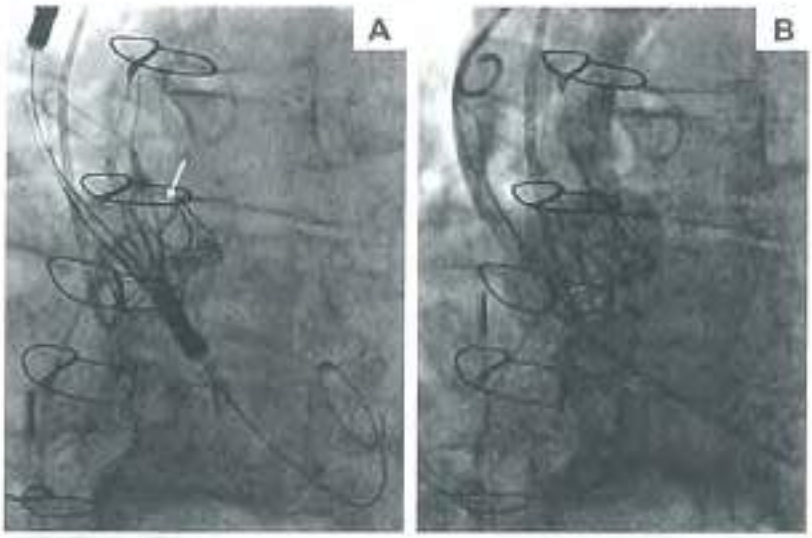

This patient presented with severe stenosis 4 years after aortic valve replacement with a Carpentier-Edwards 25-mm bioprosthesis (Edwards Lifesciences, Irvine, California). An ACURATE neo (Boston Scientific, Marlborough, Massachusetts) size M (25 mm) was successfully (**A**) positioned and (**B**) implanted with the upper crown above the stent posts (**arrow**) of the bioprosthesis. Mean gradient dropped from 42 to 5 mm Hg.

the VIVID registry, use of a balloon expanding (intra-annular) SAPIEN prosthesis (Edwards Lifesciences, Irvine, California) was an independent risk factor for lower indexed effective orifice area and therefore PPM (4). Despite the use in small bioprostheses with small IDs, our hemodynamic outcomes were encouraging, with a mean gradient of 16 ± 8 mm Hg and 16% severe PPM, which compares well to other ViV series that report gradients between 14 and 18.5 mm Hg and severe PPM from 19.5% to 58.4% (4,12–16).

CLINICAL OUTCOMES. Despite being an early series, 30-day mortality (4.7%, n = 4) and stroke rates (1.2%, n = 1) were comparable to other series with 30-day mortality rates of 0.6% to 7.6% and stroke rates of 1.9% to 3.8% (4,12,14–16). Furthermore, the 1-year mortality was comparable to recent series of ACURATE neo implantation in patients with native aortic stenosis (6).

ViV PROCEDURES WITH THE ACURATE NEO: SPECIFIC CONSIDERATIONS. For the ACURATE neo, the optimal implantation depth was unclear at the beginning. Initially, many physicians implanted the prosthesis at a depth of 5 to 7 mm, similar to the target implantation depth in native stenotic valves. However, the ACURATE neo has an upper crown that is 5-mm wider than the waist of the frame, and we noticed a significantly higher mean transvalvular gradient in patients in whom the position of the upper crown was inside the posts of the degenerated surgical prosthesis. The most likely explanation is that, in this scenario, the upper crown interferes with the stent posts and leaflets of the degenerated surgical valve, resulting in incomplete expansion and elevated gradients (Figure 2). Recently, a bench study using the ACURATE neo in different sizes of Mitroflow bioprosthetic valves (Sorin Group, Arvada, Colorado) has shown that avoidance of deep implantation reduced the risk of leaflet pinwheeling and interaction of THV leaflets with the surgical valve (17). Furthermore, gradients were significantly lower if the ACURATE neo was implanted in a high position. In comparison, the optimal implantation depth was evaluated as 0 to 5 mm for the CoreValve (Medtronic, Minneapolis, Minnesota) and 0 to 2 mm for the SAPIEN XT (16). Preclinical assessment of the CoreValve, SAPIEN, and Portico (St. Jude Medical) THVs as well as clinical series showed that higher implantation was associated with not only lower gradients and more regular opening with less plication, but also an increased risk of migration, embolization, and coronary obstruction (5,18,19).

MIDTERM OUTCOMES AND THV FAILURE. In this study, a total of 4 (5%) patients had THV failure

JACC: CARDIOVASCULAR INTERVENTIONS VOL. 12, NO. 22, 2019
NOVEMBER 25, 2019:2309–16

CENTRAL ILLUSTRATION Post-Procedural Mean Echocardiographic Gradient According to the Prosthesis Size and the Position of the Upper Crown

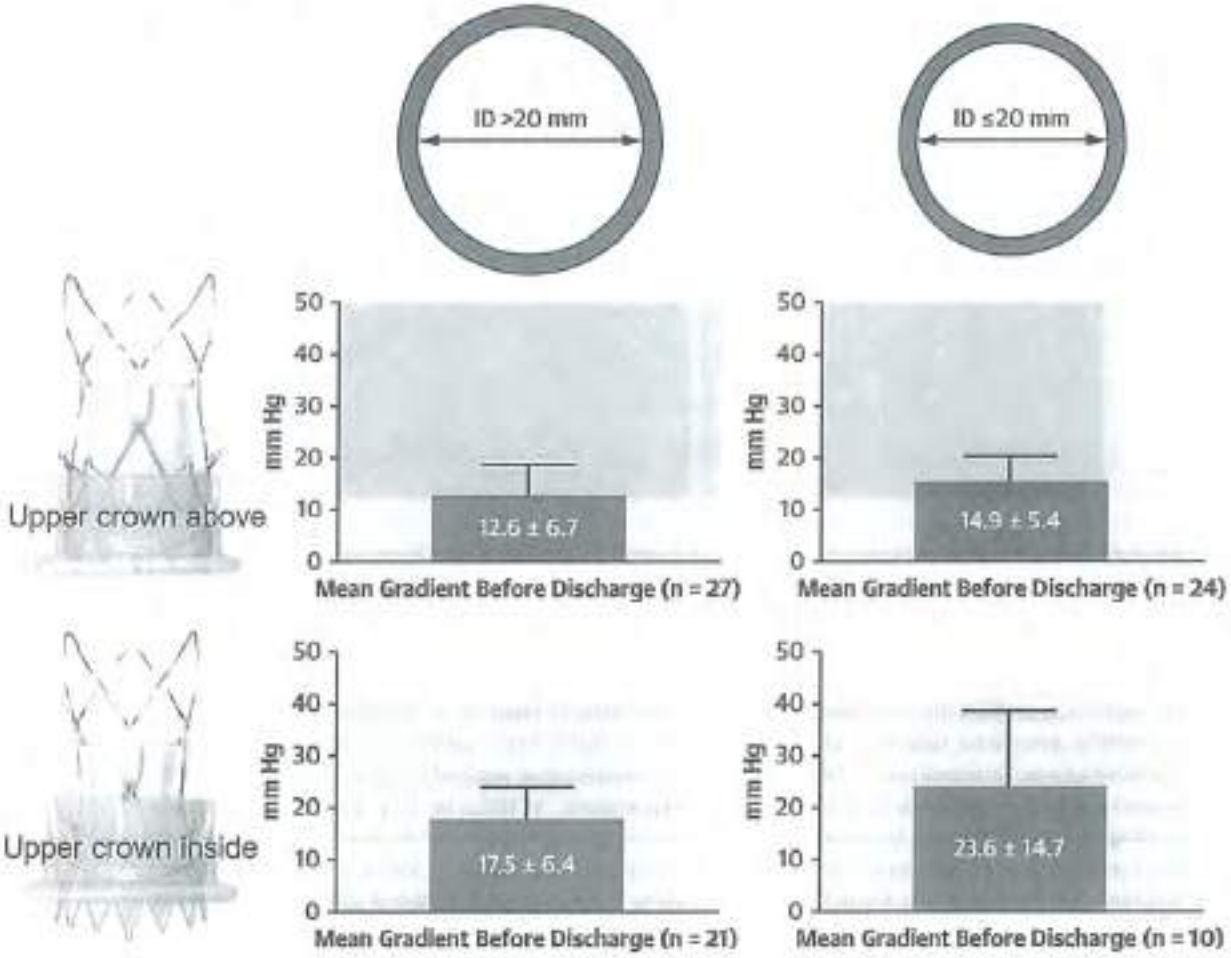

Holzamer, A. et al. J Am Coll Cardiol Intv. 2019;12(22):2309–16.

Mean gradients were significantly lower if the ACURATE neo (Boston Scientific, Marlborough, Massachusetts) was implanted high with the upper crown above the stent posts and leaflets of the degenerated bioprosthesis. Gradients were lowest in larger prostheses >20 mm and a high implantation and highest in smaller prostheses and a low implantation. In the figure, the mean gradient ± SD is shown. ID = inner diameter.

within the first 18 months. The leaflets of the ACURATE neo are not protected by a stent or frame and may be more prone to interaction with stent posts or the leaflets of the degenerated bioprosthesis, as illustrated in **Figure 2**. This risk may be increased after balloon post-dilatation and may be highest after fracturing of the ring of the bioprosthesis. Indeed, both patients presenting with transvalvular regurgitation due to tear of the leaflet of the ACURATE neo had direct contact between the leaflets of the ACURATE neo and calcification of the aortic wall or a stent post of the degenerated surgical prosthesis. Patients should be followed closely to detect early signs of deterioration.

STUDY LIMITATIONS. The baseline population is heterogenous with different valve types that could act as confounding factors for elevated gradients. Furthermore, the population includes the learning curve on how to best implant the device and—in the absence of a standardized protocol—different implantation techniques were applied. Median

FIGURE 2 Ex Vivo Implantation of an ACURATE Neo in a 19-mm Mitroflow With the Upper Crown Above and Inside the Stent Posts and Leaflets of the Degenerated Bioprosthesis

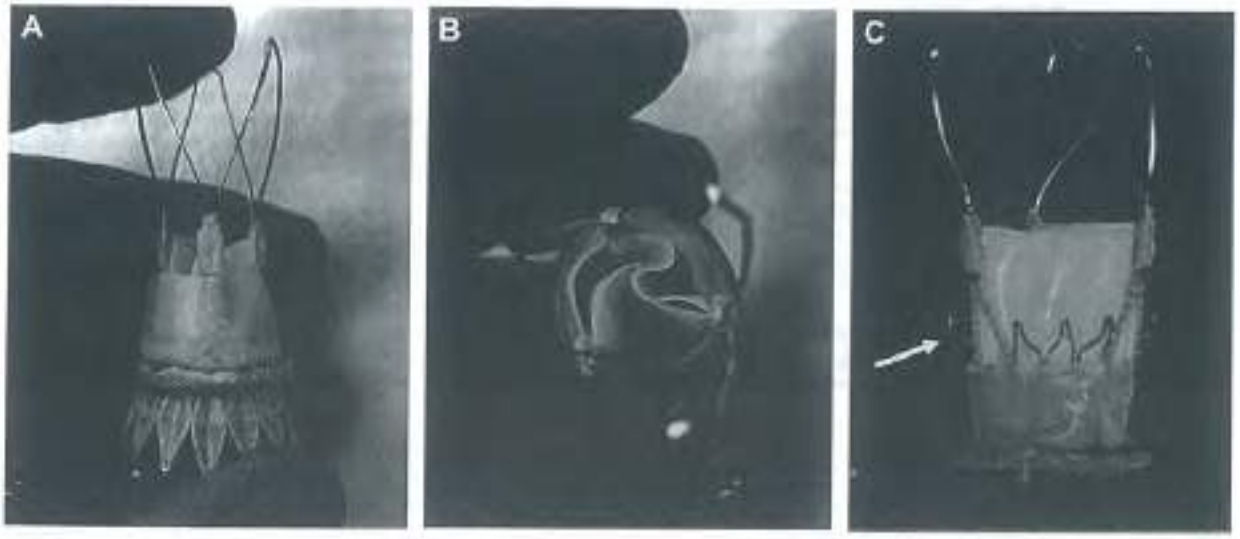

Photography of an ACURATE neo (Boston Scientific, Marlborough, Massachusetts) in a 19 mm Mitroflow (Sorin Group, Arvada, Colorado), a prosthesis with an extremely small internal diameter of 15.5 mm. **(A, B)** A very low implantation of the ACURATE neo with severe underexpansion at the level of the leaflets of the ACURATE neo and the interaction between the degenerated bioprosthetic stent posts and the leaflets of the ACURATE neo. **(C)** High implantation with the upper crown above the stent posts **(arrow)**.

follow-up was only 12 months precluding an assessment of potential long-term effects.

CONCLUSIONS

This early experience shows that a high implantation of the ACURATE neo with the upper crown above the stent posts of the degenerated bioprosthesis resulted in lower mean transvalvular gradients but a higher rate of malpositioning and early valve degeneration.

ACKNOWLEDGMENT The authors thank Beatrix Doerr for her medical writing assistance, reimbursed by Boston Scientific.

ADDRESS FOR CORRESPONDENCE: Dr. Stefan Toggweiler, Division of Cardiology, Heart Center Lucerne, Luzerner Kantonsspital, Spitalstrasse, 6000 Lucerne, Switzerland. E-mail: stefan.toggweiler@luks.ch.

PERSPECTIVES

WHAT IS KNOWN? VIV procedures have emerged as acceptable alternative to surgery in high-risk patients according to current guidelines; however, data on the implantation of the self-expanding ACURATE neo valves are scarce.

WHAT IS NEW? This is the largest series of ACURATE neo in degenerated bioprostheses to date. The analysis shows that the implantation can be performed with good performance outcomes and that implantation with the upper crown above the degenerated prosthesis results in lower gradients. Two leaflet tears occurred, raising concern related to long-term durability.

WHAT IS NEXT? Long-term follow-up and results of current in vitro studies will further elucidate the use of implanting the ACURATE neo THV in degenerated bioprostheses.

REFERENCES

1. Barnett SD, Ad N. Surgery for aortic and mitral valve disease in the United States: a trend of change in surgical practice between 1998 and 2005. J Thorac Cardiovasc Surg 2009;137:1422–8.

2. Nishimura RA, Otto CM, Bonow RO, et al. 2017 AHA/ACC Focused Update of the 2014 AHA/ACC Guideline for the Management of Patients With Valvular Heart Disease: a report of the American College of Cardiology/American Heart Association Task Force on Clinical Practice Guidelines. J Am Coll Cardiol 2017;70:252–89.

3. Baumgartner H, Falk V, Bax JJ, et al. 2017 ESC/EACTS Guidelines for the management of valvular heart disease. Eur Heart J 2017;38:2739–91.

4. Bleiziffer S, Eichinger W, Simonato M, et al. Incidence, predictors and clinical outcomes of residual stenosis after aortic valve-in-valve. Heart 2018;104:828–34.

5. Dasi LP, Hatoum H, Kheradvar A, et al. On the mechanics of transcatheter aortic valve replacement. Ann Biomed Eng 2017;45:310–31.

6. Kim WK, Hengstenberg C, Hilker M, et al. The SAVI-TF registry: 1-year outcomes of the European post-market registry using the ACURATE neo transcatheter heart valve under real-world conditions in 1,000 patients. J Am Coll Cardiol Intv 2018;11:1368–74.

7. Toggweiler S, Nissen H, Mogensen B, et al. Very low pacemaker rate following ACURATE neo transcatheter heart valve implantation. EuroIntervention 2017;13:1273–163.

8. Soon KH, Kiaduira NHM, Vonkeil M, Kraejevski AO, Stella PR. First Dutch experience of the accurate neo self-expanding supra-annular valve for valve-in-valve transcatheter aortic valve implantation. Neth Heart J 2018;26:219–33.

9. Kim WK, Mollmann H, Liebetrau C, et al. The ACURATE neo transcatheter heart valve: a comprehensive analysis of predictors of procedural outcome. J Am Coll Cardiol Intv 2018;11:1721–8.

10. Kappetein AP, Head SJ, Generaux P, et al. Updated standardized endpoint definitions for transcatheter aortic valve implantation: the valve academic research consortium-2 consensus document. J Am Coll Cardiol 2012;60:1438–54.

11. Lancellotti P, Pibarot P, Chambers J, et al. Recommendations for the imaging assessment of prosthetic heart valves: a report from the European Association of Cardiovascular Imaging endorsed by the Chinese Society of Echocardiography, the Inter-American Society of Echocardiography, and the Brazilian Department of Cardiovascular Imaging. Eur Heart J Cardiovasc Imaging 2016;17:589–90.

12. Dvir D, Webb JG, Bleiziffer S, et al. Transcatheter aortic valve implantation in failed bioprosthetic surgical valves. JAMA 2014;312:162–70.

13. Webb JG, Mack MJ, White JM, et al. Transcatheter aortic valve implantation within degenerated aortic surgical bioprostheses: PARTNER 2 valve-in-valve registry. J Am Coll Cardiol 2017;69:2253–62.

14. Abdelaziz S, Chenna AN, Simonato M, et al. Matched comparison of self-expanding transcatheter heart valves for the treatment of failed aortic surgical bioprosthesis: insights from the Valve-in-Valve International Data Registry (VIVID). Circ Cardiovasc Interv 2017;10:e004293.

15. Seiffert M, Treede H, Schofer J, et al. Matched comparison of next- and early-generation balloon-expandable transcatheter heart valve implantations in failed surgical aortic bioprostheses. EuroIntervention 2018;14:e397–404.

16. Simonato M, Webb J, Kornowski R, et al. Transcatheter replacement of failed bioprosthetic valves: large multicenter assessment of the effect of implantation depth on hemodynamics after aortic valve-in-valve. Circ Cardiovasc Interv 2016;9:e003651.

17. Sathananthan J, Sellers SL, Fraser R, et al. Impact of implant depth on hydrodynamic function with the ACURATE neo transcatheter heart valve following valve-in-valve transcatheter aortic valve replacement in Mitroflow bioprosthetic valves: an ex-vivo bench study. EuroIntervention 2019;15:79–87.

18. Zenses AS, Elvin MA, Stanova V, et al. Effect of size and position of self-expanding transcatheter valve on haemodynamics following valve-in-valve procedure in small surgical bioprostheses: an in vitro study. EuroIntervention 2019;14:e282–5.

19. Dvir D. Treatment of small surgical valves: clinical considerations for achieving optimal results in valve-in-valve procedures. J Am Coll Cardiol Intv 2015;8:2034–6.

KEY WORDS degenerated bioprosthesis, transcatheter aortic valve implantation, transcatheter aortic valve replacement, transfemoral, valve-in-valve

APPENDIX For supplemental tables, please see the online version of this paper.

ORIGINAL RESEARCH

Clinical and Laboratory Predictors for Plaque Erosion in Patients With Acute Coronary Syndromes

Erika Yamamoto, MD, PhD; Taishi Yonetsu, MD; Tsunekazu Kakuta, MD, PhD; Tsunenori Soeda, MD, PhD; Yoshihiko Saito, MD, PhD; Bryan P. Yan, MD; Osamu Kurihara, MD, PhD; Masamichi Takano, MD, PhD; Giampaolo Niccoli, MD, PhD; Takumi Higuma, MD, PhD; Shigeki Kimura, MD, PhD; Yoshiyasu Minami, MD, PhD; Junya Ako, MD, PhD; Tom Adriaenssens, MD, PhD; Niklas F. Boeder, MD; Holger M. Nef, MD; Francesco Fracassi, MD; Tomoyo Sugiyama, MD, PhD; Hang Lee, PhD; Filippo Crea, MD; Takeshi Kimura, MD, PhD; James G. Fujimoto, PhD; Valentin Fuster, MD, PhD; Ik-Kyung Jang, MD, PhD

Background—Plaque erosion is responsible for 25% to 40% of patients with acute coronary syndromes (ACS). Recent studies suggest that anti-thrombotic therapy without stenting may be an option for this subset of patients. Currently, however, an invasive procedure is required to make a diagnosis of plaque erosion. The aim of this study was to identify clinical or laboratory predictors of plaque erosion in patients with ACS to enable a diagnosis of erosion without additional invasive procedures.

Methods and Results—Patients with ACS who underwent optical coherence tomography imaging were selected from 11 institutions in 6 countries. The patients were classified into plaque rupture, plaque erosion, or calcified plaque, and predictors were identified using multivariable logistic modelling. Among 1241 patients with ACS, 477 (38.4%) patients were found to have plaque erosion. Plaque erosion was more frequent in non–ST-segment elevation-ACS than in ST-segment–elevation myocardial infarction (47.9% versus 29.8%, $P<0.0002$). Multivariable logistic regression models showed 5 independent parameters associated with plaque erosion: age <68 years, anterior ischemia, no diabetes mellitus, hemoglobin >15.0 g/dL, and normal renal function. When all 5 parameters are present in a patient with non–ST-segment elevation-ACS, the probability of plaque erosion increased to 73.1%.

Conclusions—Clinical and laboratory parameters associated with plaque erosion are explored in this retrospective registry study. These parameters may be useful to identify the subset of ACS patients with plaque erosion and guide them to conservative management without invasive procedures. The results of this exploratory analysis need to be confirmed in large scale prospective clinical studies.

Clinical Trial Registration—URL: http://www.clinicaltrials.gov. Unique identifier: NCT03479723. (*J Am Heart Assoc.* 2019;8: e012322. DOI: 10.1161/JAHA.119.012322.)

Key Words: acute coronary syndrome • optical coherence tomography • plaque erosion

Plaque erosion is reported to be responsible for about 25% to 40% of patients with acute coronary syndromes (ACS).[1–3] Current guidelines recommend early invasive strategy for all ACS patients except for the low-risk subgroups[4,5] and coronary stents are implanted in the majority of the cases. Recent studies reported that ACS

From the Cardiology Division (E.Y., F.F., T. Sugiyama, I.-K.J.) and Biostatistics Center (H.L.), Massachusetts General Hospital, Harvard Medical School, Boston, MA; Department of Cardiovascular Medicine, Kyoto University Graduate School of Medicine, Kyoto, Japan (E.Y., T. Kimura); Department of Interventional Cardiology, Tokyo Medical and Dental University, Tokyo, Japan (T.Y.); Department of Cardiovascular Medicine, Tsuchiura Kyodo General Hospital, Tsuchiura, Ibaraki, Japan (T. Kakuta); Department of Cardiovascular Medicine, Kashihara, Nara Medical University, Nara, Japan (T. Soeda, Y.S.); Department of Medicine and Therapeutics, Faculty of Medicine, The Chinese University of Hong Kong, Hong Kong (B.P.Y.); Cardiovascular Center, Nippon Medical School Chiba Hokusoh Hospital, Inzai, Chiba, Japan (O.K., M.T.); Department of Cardiovascular and Thoracic Science, Catholic University of the Sacred Heart, Fondazione Policlinico Agostino Gemelli – IRCCS, Rome, Italy (G.N., F.C.); Department of Cardiology, Hirosaki University Graduate School of Medicine, Hirosaki, Aomori, Japan (T.H.); Division of Cardiology, Kameda Medical Center, Kamogawa, Chiba, Japan (S.K.); Department of Cardiovascular Medicine, Kitasato University School of Medicine, Sagamihara, Kanagawa, Japan (Y.M., J.A.); Department of Cardiovascular Medicine, University Hospitals Leuven, Leuven, Belgium (T.A.); Department of Cardiology, University of Giessen, Germany (N.F.B., H.M.N.); Research Laboratory of Electronics, Department of Electrical Engineering and Computer Science, Massachusetts Institute of Technology, Cambridge, MA (J.G.F.); Zena and Michael A. Wiener Cardiovascular Institute, Icahn School of Medicine at Mount Sinai, New York, NY (V.F.); Division of Cardiology, Kyung Hee University Hospital, Seoul, Republic of Korea (I.-K.J.).

Accompanying Data S1, Tables S1 through S5, and Figure S1 are available at https://www.ahajournals.org/doi/suppl/10.1161/JAHA.119.012322

Correspondence to: Ik-Kyung Jang, MD, PhD, FACC, Cardiology Division, Massachusetts General Hospital, Harvard Medical School, GRB 800, 55 Fruit Street, Boston, MA 02114. E-mail: ijang@mgh.harvard.edu and Taishi Yonetsu, MD, Department of Cardiovascular Medicine, Tokyo Medical and Dental University, 1-5-45 Yushima, Bunkyo-ku, Tokyo 113-8519, Japan. E-mail: t-yonetsu.cvm@tmd.ac.jp

Received March 5, 2019; accepted September 17, 2019.

© 2019 The Authors. Published on behalf of the American Heart Association, Inc., by Wiley. This is an open access article under the terms of the Creative Commons Attribution-NonCommercial License, which permits use, distribution and reproduction in any medium, provided the original work is properly cited and is not used for commercial purposes.

Downloaded from http://ahajournals.org by on October 24, 2019

Clinical Perspective

What Is New?

- Five parameters associated with plaque erosion have been identified: age <68 years, anterior ischemia, no diabetes mellitus, hemoglobin >15.0 g/dL, and normal renal function.
- These parameters indicate that plaque erosion may have different pathophysiology: "non-traditional" factors including abnormal local fluid dynamics, rather than the traditional vascular inflammation, may play an important role.

What Are the Clinical Implications?

- If these parameters are proven to be predictive of erosion in prospective studies, a subset of acute coronary syndromes patients with high probability of plaque erosion may be easily identified.
- This subset of patients may be managed conservatively with anti-thrombotic therapy without invasive procedures.

patients with plaque erosion might be treated conservatively without stenting.[5–8] In these studies, a diagnosis of plaque erosion was made by intracoronary optical coherence tomography (OCT). If the patients with plaque erosion are identified by demographic information or by simple laboratory tests, invasive procedures and procedure-related complications may be avoided, and healthcare costs may be significantly reduced. However, demographic characteristics specific for the patients with plaque erosion are unknown. Although several groups published reports on plaque erosion,[9–11] the study population in each report was too small or unbalanced to identify comprehensive characteristics associated with plaque erosion. The aim of the current study was to identify the predictors for plaque erosion in patients with ACS.

Methods

The data that support the findings of this study are available from the corresponding author upon reasonable request.

Study Design and Participants

A new multi-center longitudinal international registry was created for this study from 11 institutions in 6 countries (Table S1) (Identification of Predictors for Coronary Plaque Erosion in Patients with Acute Coronary Syndrome study, http://www.clinicaltrials.gov: NCT03479723). Consecutive patients with ACS who had OCT imaging of the culprit lesion were eligible for the study. We included only patients who had undergone an OCT procedure, therefore this study was not "all-comer" registry. ACS includes ST-segment-elevation myocardial infarction (STEMI) and non-ST-segment-elevation ACS (NSTE-ACS) which included non-ST-segment-elevation myocardial infarction (NSTEMI) and unstable angina pectoris. The data set consists of previously published[1,2,9,10] (n=695) and unpublished (n=1004) patients. Among 1699 patients, 458 patients were excluded and 1241 patients were included in the final cross-sectional analysis (Figure S1). The protocol was approved by the institutional review board at each site and written informed consent was obtained from all patients before enrollment. The definitions are described in Data S1. Demographic data, medical history, laboratory data at admission, percutaneous coronary intervention procedure data, post-percutaneous coronary intervention biomarkers, and in-hospital death were collected. OCT imaging and angiographic imaging at index procedure were also collected. All images were de-identified, digitally stored, and sent to Massachusetts General Hospital (Boston, MA, USA), where analysis was performed.

OCT Image Acquisition

A frequency-domain OCT system (C7/C8 ILUMIEN OCT Intravascular Imaging Systems, St. Jude Medical, St. Paul, Minnesota) or a time-domain OCT system (M2/M3 Cardiology Imaging System, St. Jude Medical, Westford, Massachusetts) was used in this study. The detailed technique of intracoronary OCT imaging was described in the previous report.[12]

OCT Analysis

The methods of OCT analysis are summarized in Data S1. Underlying plaque type in the culprit lesion was categorized into 3 groups using the previously established OCT criteria; plaque rupture, plaque erosion, calcified plaque (Figure 1A through 1C). Plaque rupture was defined by the presence of fibrous cap discontinuity with a communication between the lumen and the inner core of plaque or with a cavity formation within the plaque (Figure 1A).[13,14] Plaque erosion was identified by the presence of the attached thrombus overlying an intact and visualized plaque, luminal surface irregularity at the culprit lesion in the absence of thrombus, or attenuation of the underlying plaque by thrombus without superficial lipid or calcification immediately proximal or distal to the site of thrombus (Figure 1B).[1,2,11] Calcified plaque was defined by the presence of superficial substantive calcium at the culprit site without evidence of ruptured lipid plaque (Figure 1C).[1,2] Culprit lesions that did not satisfy these criteria were classified as others. Tissue characterization of underlying plaque was performed using the previously established criteria.[15,16] Plaques were classified into 2 categories: (1) Fibrous plaque (homogeneous and high-backscattering

Downloaded from http://ahajournals.org by on October 24, 2019

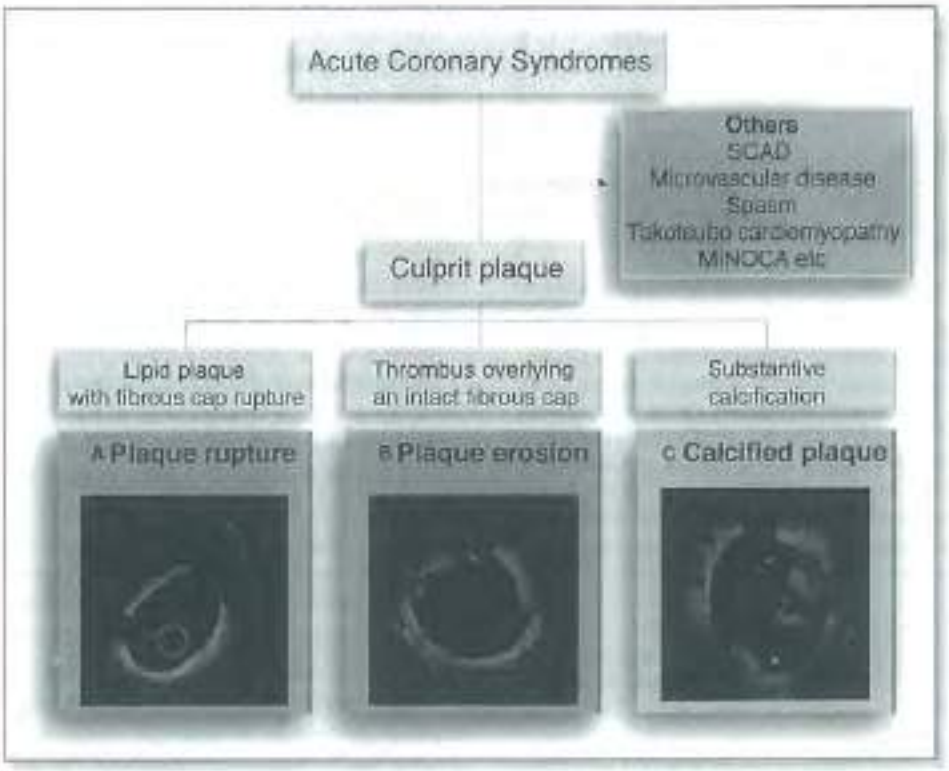

Figure 1. Optical coherence tomography images of 3 plaque pathologies. A, Plaque rupture was defined by the presence of fibrous cap discontinuity with a communication between the lumen and the inner core of a plaque or with a cavity formation within the plaque. B, Plaque erosion was defined as a culprit plaque with an intact fibrous cap with or without attached thrombus. C, Calcified plaque was defined by the presence of superficial substantive calcium at the culprit site without evidence of ruptured lipid plaque. Others include spontaneous coronary artery dissection, microvascular disease, spasm, Takotsubo cardiomyopathy, myocardial infarction with non-obstructive coronary arteries, etc. MINOCA indicates myocardial infarction with non-obstructive coronary arteries; SCAD, spontaneous coronary artery dissection.

Downloaded from http://ahajournals.org by on October 24, 2019

region) or (2) Lipid plaque (low signal region with a diffuse border). Lipid-rich plaque was defined as a plaque with lipid arc >90°. For each lipid plaque, the thinnest fibrous cap thickness and the maximal lipid arc were measured. A thin-cap fibroatheroma was defined as plaque with a lipid arc >90° and the thinnest part of the fibrous cap <65 μm. Macrophage accumulations were defined as signal-rich, distinct, or confluent punctuate regions with heterogeneous backward shadows. Calcification was recorded as well-delineated, low backscattering heterogeneous regions. Minimal flow area was also measured for each lesion.

Angiographic Analysis

Coronary angiograms were analyzed with the Cardiovascular Angiography Analysis System (Pie Medical Imaging B.V., Maastricht, The Netherlands). The reference diameter, minimum lumen diameter, diameter stenosis, area stenosis, and lesion length were measured. Thrombolysis in Myocardial Infarction flow grade was also evaluated for the culprit vessel.

Statistical Analysis

Categorical outcomes were presented as counts and proportions (%). Continuous outcomes were expressed as mean±SD. For overall between-group comparisons, 1-way analysis of variance or Kruskal–Wallis test was applied for continuous outcomes and Chi-square or Fisher exact test for categorical outcomes was applied. Then post-hoc comparisons with controlling type-1 error by using Bonferroni correction were performed if the overall test was significant with $P<0.05$. To identify the parameters associated with plaque erosion, univariable and multivariable logistic regression models were applied using variables that can be readily obtained in the emergency department (age, sex, medical history, medication at admission, location of ischemia, simple laboratory test (white blood cell count, hemoglobin, creatine

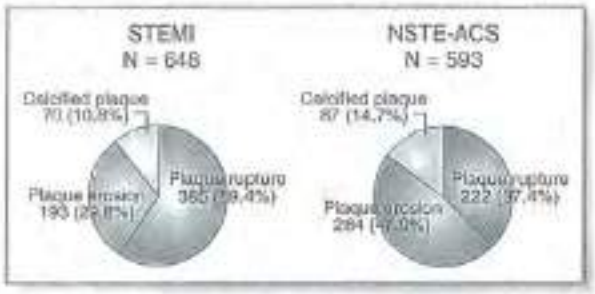

Figure 2. Prevalence of plaque rupture, erosion, and calcified plaque in ST-segment–elevation myocardial infarction and non–ST-segment–elevation acute coronary syndrome. Among 1241 patients, 648 presented with ST-segment–elevation myocardial infarction and 593 with non–ST-segment–elevation acute coronary syndrome. The prevalence of plaque rupture, plaque erosion, and calcified plaque was 59.4%, 29.8%, and 10.8% in ST-segment–elevation myocardial infarction; 37.4%, 47.9%, and 14.7% in non–ST-segment–elevation acute coronary syndrome. The prevalence of plaque erosion was significantly higher in non–ST-segment–elevation acute coronary syndrome than in ST-segment–elevation myocardial infarction patients (47.9% vs 29.8%, $P<0.0002$). NSTE-ACS indicates non–ST-segment–elevation acute coronary syndrome; STEMI, ST-segment–elevation myocardial infarction.

phosphokinase) and renal function (normal renal function was defined as no history of chronic kidney disease and estimated glomerular filtration rate (eGFR) >60 mL/min at admission). Age and hemoglobin cut-off were determined using Youden index. Variables with a $P<0.10$ in the univariate test were entered into the multivariable modeling. All statistical analyses were performed using JMP PRO 13.0 (SAS Institute Inc, Cary, NC).

Results

Among 1241 patients, 607 patients (48.9%) were classified as plaque rupture, 477 patients (38.4%) as plaque erosion, and 157 patients (12.7%) as calcified plaque. In 648 STEMI patients, 385 (59.4%) patients had plaque rupture and 193 (29.8%) patients had plaque erosion. In 593 NSTE-ACS patients, 222 (37.4%) patients had plaque rupture and 284 (47.9%) patients had plaque erosion. Inter-observer and intra-observer variability were assessed by the evaluation of all images by 2 independent observers and by the same observer at 2 separate time points, respectively. The intra-observer Kappa coefficients for plaque rupture, plaque erosion, and calcified plaque were 0.902, 0.922, 0.934, respectively. The inter-observer Kappa coefficients for plaque rupture, plaque erosion, and calcified plaque were 0.878, 0.895, 0.935, respectively. Plaque erosion was significantly more frequent in NSTE-ACS than in STEMI (47.9% versus 29.8%, $P<0.0002$) (Figure 2).

Patients Characteristics

Baseline characteristics of each group are summarized in Table 1 and Table S2. Compared with the non-erosion group, the plaque erosion group was younger and more frequently presented with NSTE-ACS. Hypertension, diabetes mellitus, and chronic kidney disease were significantly less frequent in the plaque erosion group. The plaque erosion group also had higher levels of hemoglobin, lower levels of inflammatory markers (high-sensitivity C-reactive protein and white blood cell count), and a better lipid profile. The calcified plaque group was older and had a higher prevalence of hypertension, diabetes mellitus, and chronic kidney disease, compared with the other groups. The patients in the calcified plaque group were on more medications on admission. Plaque erosion was located more frequently in the left anterior descending artery than in the right coronary artery (56.6% versus 28.5%), whereas plaque rupture was located equally in the left anterior descending and the right coronary artery (45.8% versus 40.5%). Angiographic and OCT analysis consistently showed plaque erosion patients had less complex and less vulnerable lesions, compared with patients with non-erosion.

Procedural detail, clinical course, and in-hospital outcome are shown in Table S3. Thrombectomy and stenting were more frequently performed in the plaque rupture group than in the plaque erosion group. There was no significant difference in in-hospital outcome between the plaque erosion and the non-erosion group except lower level of post-procedure peak creatine phosphokinase in the erosion group (1264±1901 versus 1973±2332, $P<0.001$).

STEMI and NSTE-ACS in Plaque Erosion

When the erosion patients were divided based on clinical presentation, those with STEMI were more frequently smokers, had higher levels of serum low-density lipoproteins, and were on fewer medications (aspirin, P2Y12 inhibitors, statin, angiotensin-converting enzyme inhibitor/ARB, β-blocker) on admission than those with NSTE-ACS (Table S4).

Predictors of Plaque Erosion

Age cut-off <68 years, hemoglobin cut-off <15.0 g/dL were determined to maximize the area under the receiver operating characteristic (ROC) curve. As shown in Table 2, age <68 years (odds ratio [OR]: 1.56, 95% CI; 1.16–2.09, $P=0.003$), anterior ischemia (OR: 1.41, 95% CI: 1.06–1.86, $P=0.02$), no diabetes mellitus (OR: 1.47, 95% CI: 1.08–2.01, $P=0.01$), hemoglobin >15.0 g/dL (OR: 1.48, 95% CI: 1.09–2.01, $P=0.01$), and normal renal function (OR: 1.97, 95% CI: 1.32–2.95, $P=0.0009$) were found to be the independent

Downloaded from http://ahajournals.org by on October 24, 2019

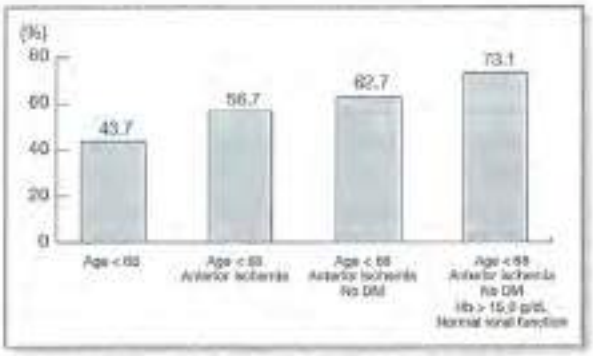

Figure 3. Probability of plaque erosion. When all 5 parameters are present in a patient with non–ST-segment–elevation acute coronary syndrome, the probability of plaque erosion increased to 73.1%. When a patient with non–ST-segment–elevation acute coronary syndrome has all 5 parameters, the odd ratio increases to 3.40. DM indicates diabetes mellitus.

the erosion patients. OCT analysis also demonstrated significantly lower levels of plaque vulnerability (lipid-rich plaque, thin-cap fibroatheroma, and macrophage). Taken together, all these data suggest that plaque erosion has a distinctly different pathobiology compared with plaque rupture. Previous pathology studies reported that the characteristics of plaque erosion, which include thrombus over less atherosclerotic and less vulnerable lesions without disruption of plaque structure and absence of endothelial cell layer.[3,17,18] However, the underlying mechanism of local thrombosis remains unclear. A "2-hit scheme" was proposed for the pathogenesis of plaque erosion.[19,20] The "first-hit" is chronic endothelial activation, propensity to slough, and impaired ability to repair the damaged endothelium. Disturbed flow was suspected to be the etiology, leading to activation of endothelial Toll-like receptor 2. The "second-hit" is recruitment of neutrophils via Toll-like receptor 2 and subsequent formation of neutrophil extracellular traps, as well as local production of chemo-attractants, thrombin, and fibrin, which further entrap platelets and lead to thrombus formation. This process is independent from pan-vascular chronic inflammation that lead to atherosclerosis, therefore plaque erosion can occur in younger patients with less atherosclerosis.

Local Fluid Dynamics in Plaque Erosion

Interestingly, high hemoglobin level was found to be a strong factor associated with plaque erosion. The changes of hemoglobin level over time were not collected. Therefore, a causal relationship cannot be established. However, several studies reported hemoconcentration was the risk factor for myocardial infarction.[21] Hemoconcentration can increase blood viscosity, resulting in elevation of local endothelial shear stress. High shear condition activates both platelets and coagulation factors.[22,23] It was recently reported that high endothelial shear stress was associated with the thrombus in plaque erosion patients.[24] Therefore, high hemoglobin levels attributable to several systemic condition may contribute to formation of occlusive thrombus in plaque erosion. In addition, plaque erosion was more frequently observed in the left anterior descending artery with anterior ischemia than in the right coronary artery or circumflex. The left anterior descending artery has more side branches than other vessels. The presence of side branches affects the conditions of local flow dynamics and distribution of endothelial shear stress,[25] which may play a key role in pathogenesis of erosion.

STEMI and NSTE-ACS in Plaque Erosion

In the current study, 41% of plaque erosion patients presented with STEMI and the remaining 59% of patients presented with NSTE-ACS. Because of relatively preserved vascular structure, plaque erosion may be prone to develop non-occlusive thrombus or occlusive thrombus that may be easily embolized distally. Several differences were noted between these 2 groups: the erosion patients with STEMI were more frequently smokers, had higher levels of serum low-density lipoproteins, and took fewer medications on admission than those with NSTE-ACS (Table S4). The medications might have protected these patients from persistent occlusive thrombus formation. In addition, the smoking rate was significantly higher in plaque erosion patients with STEMI. Several previous studies reported that plaque erosion is associated with smoking.[11,17,18] Smoking promotes activation of both platelets and clotting factors.[26,27] In addition, smoking causes endothelial damage[28] as well as activation of Rho-kinase,[29] which leads to vascular hyperconstriction or vasospasm.

Clinical Significance of Predictors of Plaque Erosion

This study included only patients who had OCT imaging, therefore the result might not represent a general ACS population. Taken together, however, the current study suggests that, contrary to atherosclerotic lesions with underlying chronic inflammatory processes, plaque erosion might be the result of a combination of several "non-traditional" factors including endothelial, vasomotion, fluid dynamic, and systemic effects (Figure 4). Thus, the optimal management for plaque erosion might be different from the traditional treatment of plaque rupture. In the EROSION (Effective Anti-Thrombotic Therapy Without Stenting: Intravascular Optical Coherence Tomography-Based Management in

Downloaded from http://ahajournals.org by on October 24, 2019

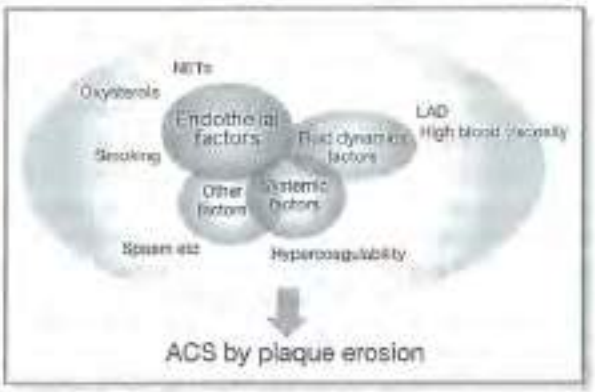

Figure 4. Pathogenesis of plaque erosion. Plaque erosion might be the result of a combination of several "non-traditional" factors; endothelial factors, vasomotion factors, fluid dynamics factors, and systemic factors. ACS indicates acute coronary syndromes; LAD, left anterior descending artery; NETs, neutrophil extracellular traps.

Plaque Erosion) study, we demonstrated the feasibility and safety of anti-thrombotic therapy without stenting in patients with ACS caused by plaque erosion.[6] We also reported a further decrease in thrombus volume between 1 month and 1 year, and a majority of patients with plaque erosion who were managed with aspirin and ticagrelor without stenting remained free of major adverse cardiac events up to 1 year.[30] These results suggest that a tailored approach based on the underlying pathobiology of ACS may be warranted. Ultimately, whereas emergency invasive procedure with primary percutaneous coronary intervention is the standard of care for the patients with STEMI, those with NSTE-ACS can often be stabilized with anti-thrombotic therapy. Identification of a subset of NSTE-ACS patients with high probability of plaque erosion may facilitate an early triage of the patients and provide an opportunity for tailored therapy.

A different approach will be needed not only for the management after ACS, but also for prevention. In the EROSION study, all patients were treated with dual anti-platelet therapy for 1 year.[30,31] Anti-thrombotic therapy should be the mainstay for plaque erosion patients without stenting. However, optimal duration/choice of medications remains unknown. The restoration of endothelial function should also be considered. Cessation of smoking could be particularly important.

Study Limitations

This study has several limitations. First, only patients who had undergone an OCT procedure were included, and the decision to perform OCT was left at the discretion of each operator. Therefore, true denominator is unknown and the inherent selection bias cannot be excluded. However, investigators in participating institutions have extensive experience with OCT and OCT is routinely being performed in almost all comers. Second, since this was not a prospective study, there is the possibility of unmeasured confounders. Third, although data were collected from 11 institutions including 3 in Europe and 1 in the United States, the majority of patients were Asians. Fourth, no biomarkers were measured. If biomarkers specific for plaque erosion are discovered, it may significantly increase the accuracy of non-invasive diagnosis of plaque erosion. Fifth, it can indeed be difficult to make a diagnosis of plaque erosion in the presence of large thrombus burden. Aspiration thrombectomy was allowed, but the cases with balloon angioplasty were excluded to avoid iatrogenic damage to the vessel wall including plaque rupture. The majority of plaque ruptures are associated with superficial lipid and an emptied cavity. Those cases with large residual thrombus after thrombectomy or the cases with unclear diagnosis were excluded.

Conclusions

Plaque erosion was more frequent in NSTE-ACS than in STEMI. Five parameters associated with plaque erosion have been identified; younger age, anterior ischemia, no diabetes mellitus, normal renal function, and higher hemoglobin levels. These parameters might be useful for identification of patients with plaque erosion for possible tailored therapy based on underlying pathobiology of ACS. The results of this exploratory analysis need to be confirmed in large scale prospective clinical studies.

Acknowledgments

We are grateful to Greg Gheewalla (Massachusetts General Hospital), Lally Lay Yee Chan, PhD (The Chinese University of Hong Kong), Sarah Reniers (University Hospitals Leuven), Masahiro Imura (Nippon Medical School Chiba Hokusoh Hospital) for data collection and management work at each site. Dr. Jang's research was supported by Mr. Michael and Mrs. Kathryn Park and by Mrs. Gill and Mr. Allan Gray.

Disclosures

Dr. Jang has received an educational grant from Abbott Vascular and Medicure. Dr. Adriaenssens has received grants and consulting fees from Abbott Vascular. The remaining authors have no disclosures to report.

References

1. Jia H, Abtahian F, Aguirre AD, Lee S, Chia S, Lowe H, Kato K, Yonetsu T, Vergallo R, Hu S, Tian J, Lee H, Park S-J, Jang YS, Raffel OC, Mizuno K, Uemura S, Ishii T, Yokota T, Choi S-Y, Dauerman HL, Prasad A, Toma C, McNulty I, Zhang S, Yu B, Fuster V, Narula J, Virmani R, Jang I-K. In vivo diagnosis of plaque erosion and calcified nodule in patients with acute coronary syndrome by intravascular optical coherence tomography. *J Am Coll Cardiol*. 2013;62:1748–1758.

Downloaded from http://ahajournals.org by on October 24, 2019

2. Higuma T, Soeda T, Abe N, Yamada M, Yokoyama H, Shibuzaki S, Vergallo R, Minami Y, Ong DS, Lee H, Okumura K, Jang IK. A combined optical coherence tomography and intravascular ultrasound study on plaque rupture, plaque erosion, and calcified nodule in patients with ST-segment elevation myocardial infarction. *JACC Cardiovasc Interv*. 2015;8:1166–1176.
3. Falk E, Nakano M, Bentzon JF, Finn AV, Virmani R. Update on acute coronary syndromes: the pathologists' view. *Eur Heart J*. 2013;34:719–728.
4. Roffi M, Patrono C, Collet JP, Mueller C, Valgimigli M, Andreotti F, Bax JJ, Borger MA, Brotons C, Chew DP, Gencer B, Hasenfuss G, Kjeldsen K, Lancellotti P, Landmesser U, Mehilli J, Mukherjee D, Storey RF, Windecker S; ESC Scientific Document Group. 2015 ESC guidelines for the management of acute coronary syndromes in patients presenting without persistent ST-segment elevation: Task Force for the management of acute coronary syndromes in patients presenting without persistent ST-segment elevation of the European Society of Cardiology (ESC). *Eur Heart J*. 2016;37:267–315.
5. Amsterdam EA, Wenger NK, Brindis RG, Casey DE, Ganiats TG, Holmes DR, Jaffe AS, Jneid H, Kelly RF, Kontos MC, Levine GN, Liebson PR, Mukherjee D, Peterson ED, Sabatine MS, Smalling RW, Zieman SJ; ACC/AHA Task Force Members. 2014 AHA/ACC guideline for the management of patients with non-ST-elevation acute coronary syndromes: a report of the American College of Cardiology/American Heart Association Task Force on Practice Guidelines. *Circulation*. 2014;130:e344–e426.
6. Jia H, Dai J, Hou J, Xing L, Ma L, Liu H, Xu M, Yao Y, Hu S, Yamamoto E, Lee H, Zhang S, Yu B, Jang IK. Effective anti-thrombotic therapy without stenting: intravascular optical coherence tomography-based management in plaque erosion (the EROSION study). *Eur Heart J*. 2017;38:792–800.
7. Prati F, Uemura S, Souteyrand G, Virmani R, Motreff P, Di Vito L, Biondi-Zoccai G, Halperin J, Fuster V, Onaki Y, Narula J. OCT-based diagnosis and management of STEMI associated with intact fibrous cap. *JACC Cardiovasc Imaging*. 2013;6:283–287.
8. Souteyrand G, Viallard L, Combaret N, Pereira B, Clerfond G, Malicka G, Barber-Chamoux N, Prati F, Motreff P. Innovative invasive management without stent implantation guided by optical coherence tomography in acute coronary syndrome. *Arch Cardiovasc Dis*. 2018;111:666–677.
9. Niccoli G, Montone RA, Di Vito L, Gramegna M, Refaat H, Scalone G, Leone AM, Trani C, Burzotta F, Porto I, Aurigemma C, Prati F, Crea F. Plaque rupture and intact fibrous cap assessed by optical coherence tomography portend different outcomes in patients with acute coronary syndrome. *Eur Heart J*. 2015;36:1377–1384.
10. Yonetsu T, Lee T, Murai T, Suzuki M, Matsumura A, Hishikawa Y, Kakuta T. Plaque morphologies and the clinical prognosis of acute coronary syndrome caused by lesions with intact fibrous cap diagnosed by optical coherence tomography. *Int J Cardiol*. 2016;203:768–774.
11. Dai J, Xing L, Jia H, Zhu Y, Zhang S, Hu S, Lin L, Ma L, Liu H, Xu M, Ren X, Yu H, Li L, Zou Y, Zhang S, Mintz GS, Hou J, Yu B. In vivo predictors of plaque erosion in patients with ST-segment elevation myocardial infarction: a clinical, angiographical, and intravascular optical coherence tomography study. *Eur Heart J*. 2018;39:2077–2085.
12. Kato K, Yonetsu T, Kim SJ, Xing L, Lee H, McNulty I, Yeh RW, Sakhuja R, Zhang S, Uemura S, Yu B, Mizuno K, Jang IK. Nonculprit plaques in patients with acute coronary syndromes have more vulnerable features compared with those with non-acute coronary syndromes: a 3-vessel optical coherence tomography study. *Circ Cardiovasc Imaging*. 2012;5:433–440.
13. Kubo T, Imanishi T, Takarada S, Kuroi A, Ueno S, Yonetsu T, Tanimoto T, Matsuo Y, Masho T, Kitabata H, Tsuda K, Tomobuchi Y, Akasaka T. Assessment of culprit lesion morphology in acute myocardial infarction: ability of optical coherence tomography compared with intravascular ultrasound and coronary angioscopy. *J Am Coll Cardiol*. 2007;50:933–939.
14. Jang IK, Tearney GJ, MacNeill B, Takano M, Moselewski F, Iftima N, Shishkov M, Houser S, Aretz HT, Halpern EF, Bouma BE. In vivo characterization of coronary atherosclerotic plaque by use of optical coherence tomography. *Circulation*. 2005;111:1551–1555.
15. Yabushita H, Bouma BE, Houser SL, Aretz HT, Jang IK, Schlendorf KH, Kauffman CR, Shishkov M, Kang D-H, Halpern EF, Tearney GJ. Characterization of human atherosclerosis by optical coherence tomography. *Circulation*. 2002;106:1640–1645.
16. Tearney GJ, Regar E, Akasaka T, Adriaenssens T, Barlis P, Bezerra HG, Bouma B, Bruining N, Cho J, Chowdhary S, Costa MA, de Silva R, Dijkstra J, Di Mario C, Dudeck D, Falk E, Feldman MD, Fitzgerald P, Garcia H, Gonzalo N, Granada JF, Guagliumi G, Holm NR, Honda Y, Ikeno F, Kawasaki M, Kochman J, Koltowski L, Kubo T, Kume T, Kyono H, Lam CCS, Lamouche G, Lee DP, Leon MB, Maehara A, Manfrini O, Mintz GS, Mizuno K, Morel M, Nadkarni S, Okura H, Otake H, Pietrasik A, Prati F, Räber L, Radu MD, Rieber J, Riga M, Rollins A, Rosenberg M, Sirbu V, Serruys PWJC, Shimada K, Shinke T, Shite J, Siegel E, Sonada S, Suter M, Takarada S, Tanaka A, Terashima M, Troels T, Uemura S, Ughi GJ, van Beusekom HMM, van der Steen AFW, van Es G-A, van Soest G, Virmani R, Waxman S, Weissman NJ, Weisz G. Consensus standards for acquisition, measurement, and reporting of intravascular optical coherence tomography studies. *J Am Coll Cardiol*. 2012;59:1058–1072.
17. White SJ, Newby AC, Johnson TW. Endothelial erosion of plaques as a substrate for coronary thrombosis. *Thromb Haemost*. 2016;115:509–519.
18. Virmani R, Kolodgie FD, Burke AP, Farb A, Schwartz SM. Lessons from sudden coronary death: a comprehensive morphological classification scheme for atherosclerotic lesions. *Arterioscler Thromb Vasc Biol*. 2000;20:1262–1275.
19. Quillard T, Araújo HA, Franck G, Shvartz E, Sukhova G, Libby P. TLR2 and neutrophils potentiate endothelial stress, apoptosis and detachment: implications for superficial erosion. *Eur Heart J*. 2015;36:1394–1404.
20. Franck G, Mawson T, Sausen G, Salinas M, Masson GS, Cole A, Beltrami-Moreira M, Chatzizisis Y, Quillard T, Tesmenitsky Y, Shvartz E, Sukhova GK, Swirski FK, Nahrendorf M, Aikawa E, Crucu KJ, Libby P. Flow perturbation mediates neutrophil recruitment and potentiates endothelial injury via TLR2 in mice: implications for superficial erosion. *Circ Res*. 2017;121:31–42.
21. Cecchi E, Giglioli A, Gori AM, Valente S, Giglioli C, Lazzeri C, Sofi F, Gensini GF, Abbate R, Mannini L. Comparison of hemorheological variables in ST-elevation myocardial infarction versus those in non-ST-elevation myocardial infarction or unstable angina pectoris. *Am J Cardiol*. 2008;102:125–128.
22. Bark DL, Ku DN. Platelet transport rates and binding kinetics at high shear over a thrombus. *Biophys J*. 2013;105:502–511.
23. Siedlecki CA, Lestini BJ, Kottke-Marchant KK, Eppell SJ, Wilson DL, Marchant RE. Shear-dependent changes in the three-dimensional structure of human von Willebrand factor. *Blood*. 1996;88:2939–2950.
24. Yamamoto E, Thondapu V, Poon E, Sugiyama T, Fracassi F, Dijkstra J, Lee H, Ooi A, Barlis P, Jang IK. Endothelial shear stress and plaque erosion: a computational fluid dynamics and optical coherence tomography study. *JACC Cardiovasc Imaging*. 2019;12:374–375. DOI: 10.1016/j.jcmg.2018.07.024.
25. Barlis P, Poon EKW, Thondapu V, Grundeken MJ, Tu S, Hayat U, Ooi A, Moore S, Tanakozioglu E, Wykrzykowska JJ, Serruys PW. Reversal of flow between serial bifurcation lesions: insights from computational fluid dynamic analysis in a population-based phantom model. *EuroIntervention*. 2019;11:e1–e3.
26. Capoccetta P, Russo C, Di Maria A, Marjanis JB, Barton S, Guarini F, Basile E, Proiti M, Bertino G, Cecconi RR, Pulosa R. Circulating endothelial-coagulative activation markers after smoking cessation: a 12-month observational study. *Eur J Clin Invest*. 2011;41:616–626.
27. Nowak J, Murray JJ, Oates JA, FitzGerald GA. Biochemical evidence of a chronic abnormality in platelet and vascular function in healthy individuals who smoke cigarettes. *Circulation*. 1987;76:6–14.
28. Morrow JD, Frei B, Longmire AW, Gaziano JM, Lynch SM, Shyr Y, Strauss WE, Oates JA, Roberts LJ. Smoking as a cause of oxidative damage. *N Engl J Med*. 1995;332:1198–1203.
29. Hidaka T, Hata T, Soga J, Fujii Y, Idei N, Fujimura N, Kihara Y, Noma K, Liao JK, Higashi Y. Increased leukocyte rho kinase (ROCK) activity and endothelial dysfunction in cigarette smokers. *Hypertens Res*. 2010;33:354–359.
30. Xing L, Yamamoto E, Sugiyama T, Jia H, Ma L, Hu S, Wang C, Zhu Y, Li L, Xu M, Liu H, Bryniarski K, Hou J, Zhang S, Lee H, Yu B, Jang IK. EROSION Study (Effective Anti-Thrombotic Therapy Without Stenting: Intravascular Optical Coherence Tomography-Based Management in Plaque Erosion): a 1-year follow-up report. *Circ Cardiovasc Interv*. 2017;10:e005860.
31. Sugiyama T, Xing L, Yamamoto E, Fracassi F, Lee H, Yu B, Jang IK. Thrombus resolution with bivalirudin in the conservative management of patients presenting with plaque erosion. *Coron Artery Dis*. 2018;29:301–308.

Downloaded from http://ahajournals.org by on October 24, 2019

Supplemental Material

Downloaded from http://ahajournals.org by on October 24, 2019

BMJ Open

Association between the number of board-certified cardiologists and the risk of in-hospital mortality: a nationwide study involving the Japanese registry of all cardiac and vascular diseases

Kihei Yoneyama ,[1] Koshiro Kanaoka,[2] Satoshi Okayama,[2] Kunihiro Nishimura,[3] Michikazu Nakai,[4] Kunihiro Matsushita,[5] Yoshihiro Miyamoto,[4] Keisuke Kida,[6] Yuki Ishibashi,[1] Masaki Izumo,[1] Makoto Watanabe,[2] Tsunenari Soeda,[2] Hiroyuki Okura,[2] Tomoo Harada,[1] Satoshi Yasuda,[7] Toyoaki Murohara,[8] Hisao Ogawa,[7] Yoshihiko Saito,[2] Yoshihiro J Akashi [1]

To cite: Yoneyama K, Kanaoka K, Okayama S, *et al*. Association between the number of board-certified cardiologists and the risk of in-hospital mortality: a nationwide study involving the Japanese registry of all cardiac and vascular diseases. *BMJ Open* 2019;**9**:e024657. doi:10.1136/bmjopen-2018-024657

► Prepublication history and additional material for this paper are available online. To view these files, please visit the journal online (http://dx.doi.org/10.1136/bmjopen-2018-024657).

Received 16 June 2018
Revised 08 June 2019
Accepted 01 August 2019

Check for updates

© Author(s) (or their employer(s)) 2019. Re-use permitted under CC BY-NC. No commercial re-use. See rights and permissions. Published by BMJ.

For numbered affiliations see end of article.

Correspondence to
Dr Yoshihiro J Akashi;
yoakashi-cro@umin.ac.jp

ABSTRACT

Objectives Although there are 14 097 board-certified cardiologists in Japan, it is unknown whether the number of institutional board-certified cardiologists is related to the prognosis of cardiovascular disease patients.

Design Cross-sectional analysis.

Setting Data were collected from the nationwide database of acute care hospitals in Japan (2371 hospitals) between 2012 and 2013.

Participants A total of 1 422 703 consecutive patients were initially included in this study, but 518 610 patients were excluded due to age <18 years, missing data or prior hospitalisations; therefore, 896 171 patients comprised the final sample population.

Main outcome measures The primary outcome was in-hospital mortality due to any cause. For the per-hospital analysis, Poisson regression models were used to estimate the association of board-certified cardiologists with in-hospital mortality, adjusted for hospital facilitation. For the per-patient analysis, hierarchical logistic regression models were used to estimate the ORs of the number of institutional board-certified cardiologists, adjusted for patient demographics, diagnoses, therapies and hospital facilities.

Results The regression model of the per-hospital analysis indicated that the number of board-certified cardiologists was associated with a lower rate ratio of in-hospital mortality (rate ratio, 0.988; 95% CI 0.983 to 0.993; p<0.01). The per-patient analysis indicated that the median age was 73 years and the in-hospital mortality rate was 11.7%. The regression model indicated that the presence of more board-certified cardiologists was associated with a lower risk of in-hospital mortality (OR, 0.980; 95% CI 0.975 to 0.986; p<0.01) after adjustments for hospital facilities, patient characteristics and treatments.

Conclusions Among cardiovascular disease patients admitted to acute care hospitals in Japan, the presence of more board-certified cardiologists was associated with a lower risk of in-hospital mortality. These results have implications for national and institutional strategies for determining the required number of board-certified cardiologists.

Strengths and limitations of this study

- ► We performed the largest nationwide study examining the association between in-hospital mortality and number of board-certified cardiologists in Japan.
- ► Using data from nationwide databases, we found that having more board-certified cardiologists at a hospital was associated with a lower risk of in-hospital mortality, independent of the facility and patient characteristics.
- ► Acute care hospitals with cardiology beds were only included in the present study; therefore, the results may not reflect other institutions.

INTRODUCTION

Cardiovascular diseases are among the leading global and regional causes of death worldwide. Deaths from cardiovascular disease have increased globally by 41% between 1990 and 2013, accounting for an estimated 17.3 million of the 54 million total deaths in 2013.[1 2] However, research of cardiovascular diseases by physicians, researchers and regional heart associations has resulted in an abundance of evidence-based medical therapies such as aspirin, beta-blockers, coronary and valve interventions, device therapies and emerging imaging techniques.[3-8] The expanded use of these therapies is increasing the quality of cardiac medical care and, hopefully, decreasing mortality rates. Physicians with more experience are generally

BMJ Open: first published as 10.1136/bmjopen-2018-024657 on 15 December 2019. Downloaded from http://bmjopen.bmj.com/ on December 15, 2019 at St Marianna-Ika Daigaku. Protected by copyright.

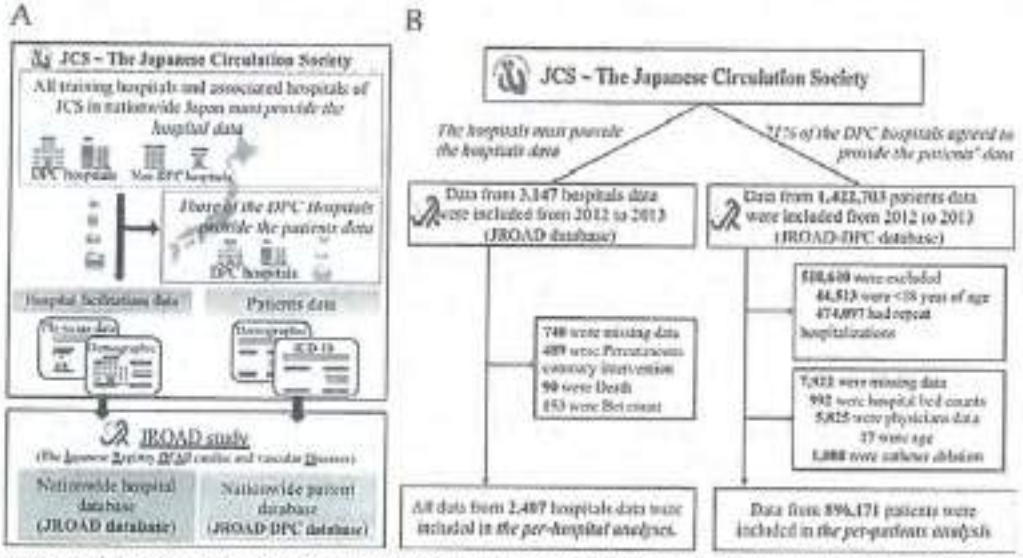

Figure 1 Flowchart of the present study. (A) The JROAD study consisted of a large dataset obtained through the Japanese administrative case-mix DPC system in which individual patient records are continuously collected systematically nationwide using a uniform reporting format. Physicians are required to provide complete diagnostic code data until the time of patient discharge. Nearly all DPC hospitals with cardiovascular beds meet the Japanese Circulation Society (JCS) requirements. All training and associated hospitals of the JCS must provide institutional data (ie, hospital bed count, number of board-certified cardiologists and so on). DPC hospitals also provide patient data (ie, age, sex, ICD-10 codes and so on). (B) A flowchart describing the two datasets used for the per-hospital and per-patient analyses to evaluate the association between board-certified cardiologists and in-hospital mortality. DPC, diagnostic procedure combination; ICD-10, International Classification of Diseases and Injuries,10th revision; JROAD, Japanese registry of all cardiac and vascular diseases.

considered to have accumulated knowledge and skills during practice; therefore, they can provide high-quality patient care.

Board-certified cardiologists are required to complete intense training programmes and successfully complete examinations. Additionally, the certification is usually effective for only a limited time (eg, 5 years in Japan); therefore, cardiologists need to remain current with the latest clinical advances and successfully complete recertification requirements. Although there are 14097 board-certified cardiologists in Japan, there is little information regarding whether the number of institutional board-certified cardiologists is related to better prognoses for patients with cardiovascular diseases in clinical practice. Addressing this question with a randomised, controlled trial (eg, a clustered randomised trial contrasting the care of patients with cardiovascular disease by board-certified cardiologists compared with physicians not certified in cardiology) is not feasible and might be unethical.[9] Therefore, we conducted an observational study using a large, nationwide dataset, the Japanese registry of all cardiac and vascular diseases (JROAD), to determine whether the number of institutional board-certified cardiologists is related to better prognoses for patients with cardiovascular diseases. The JROAD is a nationwide database that includes hospital and patient characteristics, principal diagnoses, comorbidities at admission, complications after admission, procedures during hospitalisation and discharge status.

MATERIALS AND METHODS

Patients and public involvement

The JROAD database is a nationwide prospective registry that was designed to assess the clinical activity of each Japanese institution providing cardiovascular care and to provide adequate feedback to teaching hospitals to improve patient care. A detailed description of the database design and methods has been previously published.[10] Briefly, the Japanese Circulation Society (JCS) developed the JROAD database, which includes each hospital's demographics since 2004, and the JROAD diagnosis procedure combination (JROAD-DPC) nationwide database, which includes data from the Japanese DPC/Per Diem Payment System (DPC/PDPS) since 2014. The DPC database is a mixed-case classification system linked with a lump-sum payment system that was launched in 2002 by the Ministry of Health, Labour, and Welfare of Japan.[11] Compared with other registry databases, the Japanese DPC database enables researchers to conduct nationwide studies of descriptive and/or analytical epidemiology in real-world clinical settings. The DPC database includes data regarding the following elements: demographics for each patient (eg, age and sex); principal diagnoses (coded according to the International Classification of Diseases and Injuries, 10th revision (ICD-10)); comorbidities at admission (ICD-10 code); complications after admission (ICD-10 code); procedures, including surgery, medications and devices used during hospitalisation; length of stay; discharge status; and medical expenses.[10-13]

BMJ Open: first published as 10.1136/bmjopen-2018-024657 on 15 December 2019. Downloaded from http://bmjopen.bmj.com/ on December 15, 2019 at St Marianna-Ika Daigaku. Protected by copyright.

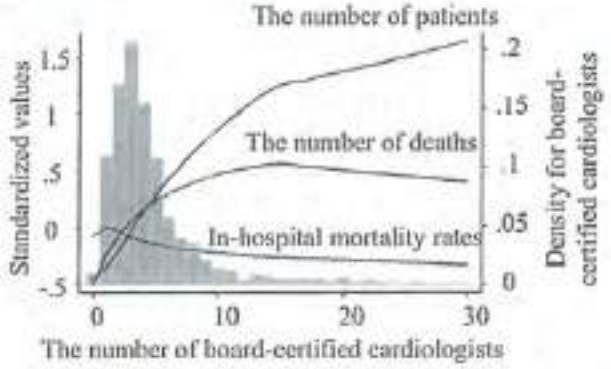

Figure 2 The association between board-certified cardiologists and in-hospital mortality rates for cardiovascular diseases according to the per-hospital analyses. A plot of locally weighted smoothing curves (LOWESS) using unadjusted standardised values of the numbers of patients (blue line), deaths (red line) and in-hospital mortality rates (green line), including a histogram of the distributions of board-certified cardiologists (yellow bars). Unadjusted standardised values were calculated by dividing the differences between the observed values and the sample means by the corresponding SD. Hospitals with more board-certified cardiologists also had more patients, more deaths and lower in-hospital mortality rates than those with fewer board-certified cardiologists. In-hospital morality rates were calculated by dividing the total number of deaths by the total number of patients.

Institutions using the DPC system encompass a wide variety of centres, including academic, urban and rural hospitals.[10 14] All data included in this study were from hospitalised patients with clinically apparent cardiovascular diseases. This research was approved by the institutional review boards at all participating institutions. Each hospital anonymised the patients' identities using code change equations for the original JROAD-DPC data. Individual data (including age, sex and bed count) were sent to the Ministry of Health, Labour, and Welfare, which notified the patients through websites or posters at each hospital that their information was being collected for this study.

Study design and sampling

We conducted a cross-sectional study using both the JROAD and JROAD-DPC data obtained between 1 April 2012 and 31 March 2013. A total of 2407 hospitals were included in the JROAD database; of those, 1247 (52%) hospitals adapted the DPC system and agreed to participate in the JROAD-DPC database (figure 1). Characteristics of JROAD-DPC data from participating and non-participating hospitals and ICD-10 diagnosis codes were previously summarised[10] and are presented in online supplementary eTable1. A total of 1 422 703 consecutive patients were initially included in this study; however, 518 610 patients were excluded due to missing data, age younger than 18 years, prior hospitalisations, or their choice to opt-out of the study. Patients with no missing variables were included in the analyses (n=896 171).

Board-certified cardiologists were defined as board-certified members of the JCS (http://www.j-circ.or.jp/english/about/outline.html). Board-certified cardiologists must be regular members of the JCS for a minimum of 6 years, must be board-certified members of the Japanese Society of Internal Medicine, Japan Surgical Society, Japan Pediatric Society, Japanese Association of Thoracic Surgery or the American Society of Internal Medicine, must have completed 3 years of training at a certified institution and must have successfully completed the examination offered by the JCS. Each hospital annually confirmed the certifications of their board-certified cardiologists, including physician names, but they only provided the total number of board-certified cardiologists per hospital to the JROAD database. Therefore, we were unable to create a merged dataset to identify which physician was responsible for treating which patients. The number of non-board-certified cardiologists per year was defined as the total number of cardiologists within a given hospital minus the number of board-certified cardiologists within the hospital. The ratio of beds to board-certified cardiologists was calculated as the bed count per hospital divided by the number of board-certified cardiologists of that same hospital. A higher index represents a larger number of beds per board-certified cardiologist.

Outcomes

The primary outcome was the occurrence of in-hospital mortality from any cause. The JROAD-DPC data provided a relatively complete perspective regarding mortality during hospitalisation.

Statistical analysis

The numbers of board-certified cardiologists and the ratios of beds to board-certified cardiologist were divided into quartiles. The per-hospital analysis determined the association between the number of board-certified cardiologists and the in-hospital mortality risk of patients hospitalised for cardiovascular diseases in the cardiology department. Multilevel mixed-effects Poisson regression models were used to consider the random effects of hospital variation in the JROAD database. The rate ratio of the board-certified cardiologists was adjusted for hospital demographics, including the number of non-board-certified cardiologists, hospital beds, presence of cardiac surgery services, paediatrics and eight regional divisions (eg, the Kanto district), and for the number of cardiac therapies (percutaneous coronary intervention, coronary artery bypass grafting, congenital surgery, catheter ablation, implantable cardioverter defibrillator and cardiac resynchronisation) per year.

For the per-patient analysis, we excluded all patients who were younger than 18 years and those who had prior hospitalisations according to the DPC reports. If patients were hospitalised more than once during the study period, then we used only the data associated with the last admission; we also counted the number of prior hospitalisations. The characteristics of patients who died

BMJ Open: first published as 10.1136/bmjopen-2018-024657 on 15 December 2019. Downloaded from http://bmjopen.bmj.com/ on December 15, 2019 at St Marianna-Ika Daigaku. Protected by copyright.

in the hospital were compared with the characteristics of the patients who survived using both a non-parametric test for continuous variables and a χ^2 test for categorical variables.

To assess the association of board-certified cardiologists with in-hospital mortality, we used hierarchical logistic regression models to estimate the ORs for in-hospital mortality. Each of the hierarchical logistic regression model variables included a hierarchy level (hospital) that considered the random effects of hospital variations. All estimates were adjusted for hospital demographics, patient demographics (age, sex, Charlson comorbidity index, and the presence of angina pectoris, myocardial infarction, atrial fibrillation, heart failure, aorta disease, cardiac arrest, pulmonary thromboembolism, primary pulmonary hypertension, tetralogy of Fallot and incidental non-cardiac diseases such as stroke, pneumonia, acute renal failure and gastrointestinal bleeding during and after hospitalisation), number of prior hospitalisations and number of cardiac therapies per year. The adjusted probabilities of in-hospital mortality were calculated using the 'marginsplot' for multiple hierarchical logistic regression models using STATA. All analyses were performed using STATA statistical software V.14.

Table 1 Association of board-certified cardiologists and in-hospital mortality rates according to the per-hospital analysis

	Poisson regression	
Hospital (n=2371)	Adjusted rate ratio (95% CI)†	Coefficient (SE)
Board-certified cardiologists		
Continuous value	0.971 (0.969 to 0.973)*	−0.030 (0.001)*
Categorical value		
Q1 (<2)	Reference	
Q2 (3)	0.773 (0.756 to 0.790)*	−0.258 (0.011)*
Q3 (4)	0.800 (0.7820 to 0.819)*	−0.223 (0.012)*
Q4 (5–6)	0.732 (0.715 to 0.749)*	−0.312 (0.012)*
Q5 (>7)	0.562 (0.548 to 0.575)*	−0.577 (0.012)*
Ratio of hospital beds to board-certified cardiologists		
Continuous value‡	1.020 (1.019 to 1.021)*	0.020 (0.001)*
Categorical value		
Q1 (<40)	Reference	
Q2 (40–58)	1.389 (1.359 to 1.420)*	0.328 (0.011)*
Q3 (59–77)	1.407 (1.376 to 1.439)*	0.341 (0.011)*
Q4 (78–104)	1.563 (1.529 to 1.598)*	0.447 (0.011)*
Q5 (>105)	1.600 (1.760 to 1.841)*	0.588 (0.011)*

*P<0.01.
†The rate ratio was adjusted for the number of non-board-certified cardiologists, hospital beds, the presence of cardiac surgery and paediatric services, and eight regional divisions in Japan.
‡ORs of 10 hospital beds to board-certified cardiologists.
Q, quartile.

RESULTS

Hospital characteristics for the per-hospital analysis

Data from a total of 2407 hospitals were included in the per-hospital analysis. There were 11 687 board-certified cardiologists at acute hospitals in Japan between 2012 and 2015. Hospital characteristics are shown in online supplementary eTable2. The overall median bed count was 350, the number of institutional board-certified cardiologists was 4, the ratio of beds to board-certified cardiologists was 68 and median in-hospital mortality was 0.03% per hospital. Additionally, 80% of the hospitals had coronary care units and 56% had cardiac surgery services. Moreover, online supplementary eTable3 shows the hospital characteristics. Hospitals that provided data to the JROAD-DPC more often had larger bed counts, had more board-certificate cardiologists, performed invasive coronary angiography and performed device therapy than hospitals that did not provide data to the JROAD-DPC.

Association of board-certified cardiologists with in-hospital mortality according to the per-hospital analysis

Hospitals with a larger number of board-certified cardiologists were likely to have a larger number of patients and a larger number of deaths than those with fewer

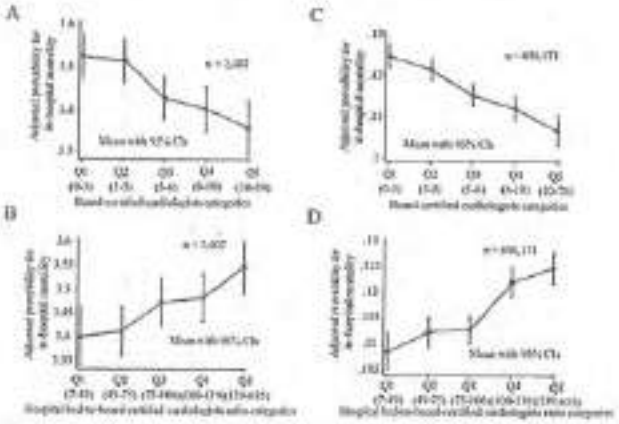

Figure 3 In-hospital mortality rates in relation to board-certified cardiologists for cardiovascular disease. (A) The linear association of the mean adjusted probability for in-hospital mortality across the quartiles of the number of board-certified cardiologists. (B) The linear association of the mean adjusted probability for in-hospital mortality across the quartiles of the ratios of beds to board-certified cardiologists. Adjusted probabilities were calculated using the 'margins' command and the multilevel mixed-effects Poisson regression analyses (table 1). (C) The linear association of the mean adjusted probability for in-hospital mortality across the quartiles of the number of board-certified cardiologists. (D) The linear association of the mean adjusted probability for in-hospital mortality across the quartiles of the ratios of beds to board-certified cardiologists. The bars indicate 95% CIs. The adjusted probability was calculated using the margins command in STATA and was adjusted as indicated in table 3. (A,B) represent the per-hospital analysis, and (C,D) represent the per-patient analysis.

BMJ Open: first published as 10.1136/bmjopen-2018-024657 on 15 December 2019. Downloaded from http://bmjopen.bmj.com/ on December 15, 2019 at St Marianne-Ika Daigaku. Protected by copyright.

Table 2 Characteristics of the patients according to in-hospital death and patient survival

	All	In-hospital death	Patient survival	
	n=896 171	n=104 469	n=791 702	P value
Demographics				
Age, years	73 (64–81)	80 (71–87)	72 (64–80)	<0.01
Male (%)	554 798 (62)	58 054 (56)	496 744 (63)	<0.01
Female (%)	341 373 (38)	46 415 (44)	294 958 (37)	
Cardiovascular disease				
Angina (%)	237 273 (26)	954 (0.9)	236 319 (30)	<0.01
Acute myocardial infarction (%)	47 739 (5)	9931 (10)	37 808 (5)	<0.01
Heart failure (%)	148 323 (17)	23 973 (23)	124 350 (16)	<0.01
Aortic disease (%)	72 678 (8)	9041 (9)	63 637 (8)	<0.01
Pulmonary embolism (%)	6149 (0.7)	725 (0.7)	5424 (0.7)	0.744
Atrial fibrillation or flutter (%)	47 020 (5)	626 (0.6)	46 394 (6)	<0.01
Cardiac arrest (%)	52 794 (6)	49 407 (47)	3387 (0.4)	<0.01
Coexisting condition				
Cerebrovascular disease (%)	64 420 (7)	9340 (9)	791 702 (7)	<0.01
Chronic pulmonary disease (%)	31 859 (3.6)	3428 (3.3)	28 431 (3.6)	<0.01
Chronic kidney disease (%)	69 458 (7.8)	9747 (9.3)	59 722 (7.5)	<0.01
Cancer (%)	45 487 (5.1)	8243 (7.9)	37 244 (4.7)	<0.01
Metastatic cancer (%)	5792 (0.7)	2207 (2.1)	3585 (0.5)	<0.01
Dementia (%)	16 294 (1.8)	2672 (2.6)	13 623 (1.7)	<0.01
Charlson comorbidity index	1 (0–2)	1 (0–2)	1 (0–2)	<0.01
Facility condition				
Hospital beds	470 (330–643)	502 (350–660)	466 (330–641)	<0.01
Hospitals with <300 beds (%)	148 709 (16.6)	14 082 (13.5)	134 627 (17.0)	<0.01
Hospitals with 300–449 beds (%)	261 701 (29.2)	28 786 (27.6)	232 916 (29.4)	
Hospitals with 450–749 beds (%)	348 036 (38.8)	43 238 (41.4)	304 798 (38.5)	
Hospitals with >750 beds (%)	137 725 (15.4)	18 364 (17.6)	119 361 (15.1)	
Cardiac surgery services (%)	701 592 (78)	78 860 (75)	622 732 (79)	<0.01
Board-certified cardiologists	5 (4–9)	5 (3–6)	5 (4–9)	<0.01
Ratios of hospital beds to board-certified cardiologists	57 (36–80)	64 (43–85.5)	56 (35–79)	<0.01

Values are either medians with IQRs (Q1 to Q3) or percentages (when indicated). Baseline characteristics were compared using the Wilcoxon rank-sum test for continuous variables and the χ^2 test for categorical variables.

board-certified cardiologists; however, they were also likely to have lower mortality rates (figure 2). The multilevel mixed-effects Poisson regression model indicated that the number of institutional board-certified cardiologists was associated with a lower rate ratio of in-hospital mortality (rate ratio, 0.988; (95% CI 0.983 to 0.993) per 1 increment of the number of institutional board-certified cardiologists; p<0.01) after adjustments for the number of non-board-certified cardiologists, hospital beds, presence of cardiac surgery and paediatric services, eight regional divisions and number of therapies (table 1 and figure 3A,B). Similarly, the ratio of beds to board-certified cardiologists was associated with an increased risk of in-hospital mortality (rate ratio, 1.006 (95% CI 1.003 to 1.009) per 1 increment of the 10 beds to board-certified cardiologists ratio; p<0.01) after the adjustments.

Patient characteristics used for the per-patient analysis

The final study sample included 896 171 patients with cardiovascular diseases who were admitted to DPC hospitals. The clinical presentation of the patients and the facility characteristics are shown in table 2. Overall, the median age was 73 years, and the male:female ratio was 62:38. The most common cardiovascular diseases of patients admitted to hospitals were angina (26%), heart failure (17%), aortic disease (8%) and myocardial infarction (5%). Patients who died in the hospital were

BMJ Open: first published as 10.1136/bmjopen-2018-024657 on 15 December 2019. Downloaded from http://bmjopen.bmj.com/ on December 15, 2019 at St Marianna-Ika Daigaku. Protected by copyright.

Table 3 Association between the number of board-certified cardiologists and in-hospital mortality rates according to the per-patient analysis

In-hospital mortality	Multilevel mixed-effects logistic regression and adjusted OR (95% CI)		
(No of events: 104 409/896 171)	Adjusted for facility‡	Adjusted for clinical characteristics§	Adjusted for treatments¶
Board-certified cardiologists			
Continuous value	0.976 (0.97 to 0.982)*	0.979 (0.973 to 0.985)*	0.98 (0.975 to 0.986)*
Categorical value			
Q1 (0–3; n=179 234)	Reference	Reference	Reference
Q2 (3–5; n=179 234)	0.981 (0.948 to 1.015)*	0.949 (0.912 to 0.988)*	0.948 (0.911 to 0.987)*
Q3 (5–6; n=179 234)	0.902 (0.856 to 0.950)*	0.841 (0.793 to 0.891)*	0.850 (0.802 to 0.900)*
Q4 (6–10; n=179 234)	0.848 (0.792 to 0.907)*	0.783 (0.729 to 0.841)*	0.789 (0.734 to 0.848)*
Q5 (10–78; n=179 235)	0.834 (0.764 to 0.910)*	0.715 (0.652 to 0.784)*	0.720 (0.656 to 0.790)*
Ratio of hospital beds to board-certified cardiologists			
Continuous value**	1.012 (1.008 to 1.015)*	1.012 (1.008 to 1.015)*	1.012 (1.008 to 1.015)*
Categorical value			
Q1 (7–49; n=185 371)	Reference	Reference	Reference
Q2 (49.75; n=178 944)	0.987 (0.920 to 1.059)	1.064 (1.004 to 1.17)†	1.078 (0.999 to 1.163)
Q3 (75–100; n=180 097)	1.096 (1.012 to 1.187)†	1.095 (1.010 to 1.187)†	1.084 (1.00 to 1.176)†
Q4 (100–139; n=171 897)	1.264 (1.160 to 1.376)*	1.278 (1.177 to 1.386)*	1.279 (1.178 to 1.389)*
Q5 (139–635; n=178 952)	1.306 (1.191 to 1.433)*	1.352 (1.242 to 1.472)*	1.339 (1.23 to 1.458)*

*P<0.01.
†P<0.05.
‡Model included the number of non-board-certified cardiologists, hospital beds, coronary care units, cardiac surgery services and eight regional divisions.
§Model included age, sex, Charlson comorbidity index, and rates of angina pectoris, myocardial infarction, atrial fibrillation, heart failure, aorta disease, cardiac arrest, pulmonary thromboembolism, primary pulmonary hypertension, and tetralogy of Fallot, and rates of non-cardiac disease (stroke, pneumonia, acute renal failure and gastrointestinal bleeding) after hospitalisations and the number of prior hospitalisations, in addition to the facility model.
¶Model included percutaneous coronary interventions, coronary artery bypass grafts, catheter ablations, implantable cardioverter-defibrillators and cardiac resynchronisation therapy in addition to the clinical characteristics model.
**OR of ratios of 10 hospital beds to board-certified cardiologists.
Q, quartile.

older and exhibited a higher prevalence of myocardial infarction, heart failure and cardiac arrest (all p<0.01). Additionally, higher in-hospital mortality was associated with hospitals with higher mean bed counts (502 (350–660) vs 466 (330–641); p<0.01) and with hospitals with fewer board-certified cardiologists (5 (3–8) vs 5 (4–9); p<0.01). Higher in-hospital mortality rates were also associated with hospitals with larger ratios of beds to board-certified cardiologists (64 (45–85.5) vs 56 (35–79); p<0.01).

Association of board-certified cardiologists with in-hospital mortality according to the per-patient analysis

The per-patient analysis indicated a total in-hospital mortality rate of 11.7%. The multilevel mixed-effects logistic regression model showed that the number of institutional board-certified cardiologists was related to lower in-hospital mortality (OR, 0.980; 95% CI 0.975 to 0.986; p<0.01) after adjusting for facilities, patient characteristics and treatments (table 3, online supplementary eTable 4 and figure 3C,D). The ratio of beds to board-certified cardiologists was associated with a higher risk for in-hospital mortality (OR, 1.012 (95% CI 1.008 to 1.015) per 1 increment of ratios of 10 beds to board-certified cardiologists; p<0.01) after adjusting for facilities, patient characteristics and treatments.

An analysis of the number of institutional board-certified cardiologists and in-hospital mortality according to variables is shown in figure 4. Hierarchical logistic regression models demonstrated significant interactions between the number of institutional board-certified cardiologists and patient age (p<0.01), number of hospital beds (p<0.01), angina (p<0.01), myocardial infarction (p=0.012), aortic diseases (p=0.01) and cardiac arrest (p<0.01). The association of the number of institutional board-certified cardiologists with the lower risk of in-hospital mortality was more evident for patients admitted to hospitals with fewer than 300 beds than for those hospitalised at larger institutions (hospitals with >750 beds and hospitals with 450–749 beds vs hospitals with <300 beds; p≤0.01).

BMJ Open: first published as 10.1136/bmjopen-2018-024657 on 15 December 2019. Downloaded from http://bmjopen.bmj.com/ on December 15, 2019 at St Marianna-ika Daigaku. Protected by copyright.

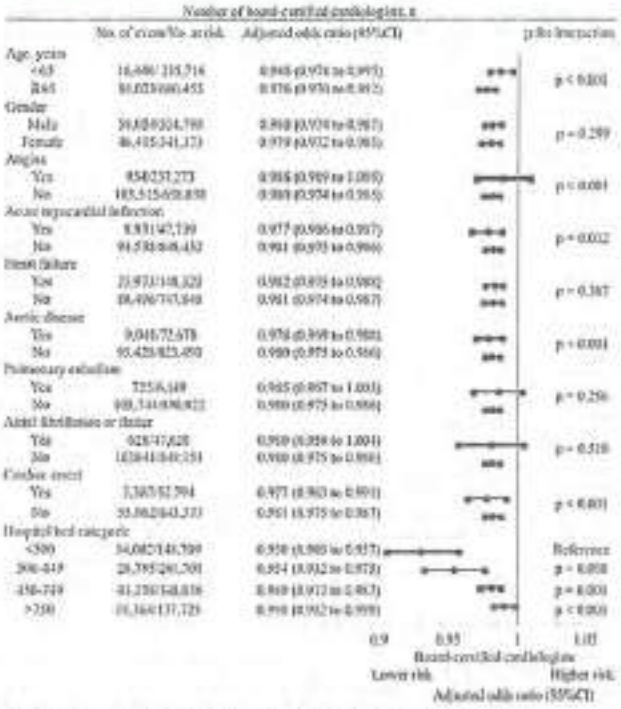

Figure 4 Adjusted ORs and 95% CIs for in-hospital mortality in relation to board-certified cardiologists for cardiovascular disease The interaction of hierarchical logistic regression test results indicated that there the number of board-certified cardiologists had a significant impact on patient characteristics and hospital volume. An OR <1.0 represents a decrease in the risk of in-hospital mortality according to the number of board-certified cardiologists. The OR is indicated by the dot, and the lines represent the 95% CIs. ORs were adjusted for facilities, patient characteristics and treatments, as indicated in table 3.

DISCUSSION

Principal findings

Using data from two large nationwide databases, we found that a large number of board-certified cardiologists at a hospital were associated with a lower risk of in-hospital mortality, independent of facilities and patient characteristics. The lower risk of mortality was consistently observed for each cardiovascular disease and more evident for smaller hospitals. The balance between the bed count and board-certified cardiologists (eg, a high-volume hospital with the relative shortage of board-certified cardiologists) should be considered to improve the care of cardiovascular disease patients (figure 5).

Study strengths and limitations

Data of 2371 hospitals and 896 171 patients from the JROAD and JROAD-DPC databases were analysed during this study, thus making it one of the largest cross-sectional and retrospective studies of nationwide cardiac health outcomes. One limitation of our study was that we only included DPC hospitals with cardiovascular beds that met the JCS requirements. Another limitation was the small number of patients with specific diseases. Although the variable analyses may

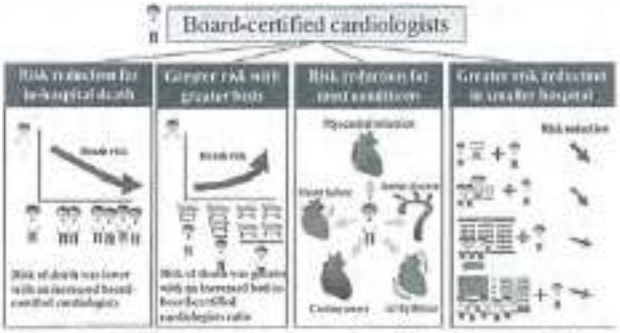

Figure 5 The main findings from this study. A larger number of board-certified cardiologists at a hospital was associated with a lower risk of in-hospital mortality. A higher ratio of beds to board-certified cardiologists at a hospital was associated with a greater risk of death. Board-certified cardiologists were more likely to provide benefits to patients by preventing deaths due to cardiovascular diseases. The risk of in-hospital mortality was attenuated by increasing the hospital volume. These observations suggest that board-certified cardiologists may improve patient outcomes, and that the balance between bed numbers and board-certified cardiologists should be considered to improve patient care.

have lacked the statistical power to demonstrate clinically meaningful differences in mortality among patients with angina and atrial fibrillation (lower mortality rates) and with pulmonary embolism (fewer cases), our findings indicated that an overall increase in board-certified cardiologists may prevent in-hospital mortality for patients with cardiovascular diseases.

Comparison of our results and those of other studies

Previous research has shown that more experience accounts for better outcomes, as reported by studies examining acute myocardial infarction,[15–17] percutaneous coronary intervention,[18] implantable cardioverter-defibrillators[19 20] and heart failure.[21–23] Unlike most previous studies, our study confirmed that a lower risk of mortality and a larger number of board-certified cardiologists was consistently seen for most cardiovascular diseases. Data from the ICD registry indicated that in the USA, implantable cardioverter-defibrillator implantations performed by a non-electrophysiologist were associated with a higher risk of procedural complications and a lower likelihood of receiving cardiac resynchronisation therapy when compared with patients whose implantable cardioverter-defibrillators were implanted by an electrophysiologist.[10] Our findings are consistent with these observations. Board-certified cardiologists may be more likely to utilise guidelines, clinical teams, disease management, discharge programmes and patient education seminars when implementing treatment, all of which improve patient outcomes.[18 24–28]

Meaning of the study: possible explanations of the results

Although our observational study did not determine causality, there were a few plausible mechanisms underlying the observed lower mortality risk related to the number of board-certified cardiologists. For example, the shortage of

BMJ Open: first published as 10.1136/bmjopen-2018-024657 on 15 December 2019. Downloaded from http://bmjopen.bmj.com/ on December 15, 2019 at St Mariana-Ika Daigaku. Protected by copyright.

board-certified cardiologists could delay optimal therapies or prevent eligible patients from receiving potentially life-saving therapies. Additionally, our study found that despite the presence of board-certified cardiologists lowering the risk of patient mortality, we observed heterogeneity among hospitals with differing bed counts, with smaller hospitals having lower mortality rates. This may suggest that patients in smaller hospitals are generally less severely ill than those in larger hospitals; therefore, smaller-volume hospitals may have better patient outcomes. Reports have suggested a recent acceleration in the development of specialty hospitals with a focus on narrow procedural areas, and proponents see these specialty hospitals as an opportunity to improve patient care.[29-31] In contrast, data from a study of Medicare administrative claims in the USA have been inconsistent for high-volume hospitals and lower mortality rates, which could be due to the mismanagement of medicinal conditions by multiple healthcare professionals, including physicians, nurses and other clinical staff.[32] However, that study also found that the relationship was attenuated for larger hospital volumes, and that the highest-volume hospitals were no longer significantly associated with higher mortality rates. This could suggest that the highest-volume hospitals had more experienced cardiologists. According to our study, hospitals with more beds exhibited higher rates of mortality, as did hospitals with higher ratios of beds to board-certified cardiologists.

Meaning of the study: implications for clinical care

Our findings have clear implications. First, our findings indicate evidence that board-certified cardiologists are beneficial to clinical cardiac care by reducing the risk of patient death. Therefore, we suggest that current board-certified cardiologists should successfully maintain competence, develop new skills and gain knowledge in their current field. Second, policymakers should focus on integrating the strategies that have been identified to improve patient care in hospitals with a shortage of board-certified cardiologists. Third, because all-cause mortality can be used to benchmark quality and compare hospital performance, our findings regarding the balance between bed counts and board-certified cardiologists should be considered to improve patient care.

Unanswered questions and future research

Additional findings of lower ORs for elderly patients (65 years or older) and for patients with myocardial infarction, aortic disease and cardiac arrest compared with patients without these conditions could provide further information regarding these specific patient populations.

CONCLUSIONS

According to nationwide hospital databases, a larger number of institutional board-certified cardiologists was associated with a lower risk of in-hospital mortality, independent of potential patient confounders. This relationship was particularly evident at smaller hospitals. Our results have implications for national and institutional strategies because they can help determine the required number of board-certified cardiologists per hospital to reduce mortality rates.

Author affiliations
[1]Division of Cardiology, Department of Internal Medicine, St. Marianna University School of Medicine, Kawasaki, Japan
[2]Department of Cardiovascular Medicine, Nara Medical University, Kashihara, Nara, Japan
[3]Preventive Medicine and Epidemiology Informatics, Center for Cerebral and Cardiovascular Disease Information, National Cerebral and Cardiovascular Center, Suita, Japan
[4]Department of Statistics and Data Analysis, Center for Cerebral and Cardiovascular Disease Information, National Cerebral and Cardiovascular Center, Suita, Osaka, Japan
[5]Department of Epidemiology, Johns Hopkins Bloomberg School of Public Health, Baltimore, Maryland, USA
[6]Department of Pharmacology, St. Marianna University School of Medicine, Kawasaki, Kanagawa, Japan
[7]Department of Cardiovascular Medicine, National Cerebral and Cardiovascular Center, Suita, Osaka, Japan
[8]Department of Cardiology, Nagoya University Graduate School of Medicine Faculty of Medicine, Nagoya, Japan

Acknowledgements The authors thank Yoko Sunaga and the other investigators, staff, and participants in the JROAD study for their valuable contributions. A full list of institutions can be found at http://jroadinfo.ncvc.go.jp.

Contributors The corresponding author attests that all listed authors meet the authorship criteria and that no others meeting the criteria have been omitted. KY, KKa, SO, KM, YM, KN, YI, MI, MW, TS, HOk, TH, TM, YS and YJA developed the study concept and study design. KY, KKa, SO, KN and MN performed the data analysis and interpretation under the supervision of KM, YM, KN, MI, MW, TS, TH, HOg, SY, TM and YS. KY, KM, MI, KKa, SY, YS and YJA drafted the manuscript and all the coauthors provided critical revisions. All the authors approved the final version of the manuscript for submission.

Funding KY has reported receiving personal fees from Sanofi Co. Ltd. SY reported personal fees received from Takeda Pharmaceutical Co. Ltd., Daiichi Sankyo Co. Ltd. and Abbott Co. Ltd. YS reported personal fees received from Mitsubishi Tanabe Pharma Corporation, Otsuka Pharmaceutical Co. Ltd., Daiichi Sankyo Co. Ltd., Novartis Pharma K.K., Pfizer Japan Inc., Nippon Boehringer Ingelheim Co. Ltd., Ono Pharmaceutical Co. Ltd., St. Jude Medical Japan Co., Ltd., Bayer Holding Ltd., Terumo Corporation, Kyowa Hakko Kirin Co. Ltd., Dainippon Sumitomo Pharma Co. Ltd., Astellas Pharma Inc., Takeda Pharmaceutical Co. Ltd., Teijin Pharma Ltd., Shionogi & Co. Ltd., Kowa Pharmaceutical Co. Ltd., Astellas Pharmaceuticals Japan Ltd. and the endowment department of MSD K.K.

Competing interests None declared.

Patient consent for publication Not required.

Ethics approval The present research was designed by the authors and approved by St. Marianna University of Medicine.

Provenance and peer review Not commissioned; externally peer reviewed.

Data availability statement No data are available.

Open access This is an open access article distributed in accordance with the Creative Commons Attribution Non Commercial (CC BY-NC 4.0) license, which permits others to distribute, remix, adapt, build upon this work non-commercially, and license their derivative works on different terms, provided the original work is properly cited, appropriate credit is given, any changes made indicated, and the use is non-commercial. See: http://creativecommons.org/licenses/by-nc/4.0/.

ORCID iDs
Kihei Yoneyama http://orcid.org/0000-0002-3562-6399
Yoshihiro J Akashi http://orcid.org/0000-0001-7670-7326

BMJ Open: first published as 10.1136/bmjopen-2018-024657 on 15 December 2018. Downloaded from http://bmjopen.bmj.com/ on December 15, 2019 at St Marianna-Ika Daigaku. Protected by copyright.

REFERENCES

1. Global Burden of Metabolic Risk Factors for Chronic Diseases Collaboration. Cardiovascular disease, chronic kidney disease, and diabetes mortality burden of cardiometabolic risk factors from 1980 to 2010: a comparative risk assessment. *Lancet Diabetes Endocrinol* 2014;2:634–47.
2. Benjamin EJ, Blaha MJ, Chiuve SE, *et al*. Heart disease and stroke Statistics-2017 update: a report from the American heart association. *Circulation* 2017;135:e146–603.
3. Ogawa H, Nakayama M, Morimoto T, *et al*. Low-dose aspirin for primary prevention of atherosclerotic events in patients with type 2 diabetes: a randomized controlled trial. *JAMA* 2008;300:2134–41.
4. Packer M, Bristow MR, Cohn JN, *et al*. The effect of carvedilol on morbidity and mortality in patients with chronic heart failure. U.S. carvedilol heart failure Study Group. *N Engl J Med* 1996;334:1349–55.
5. Serruys PW, Morice M-C, Kappetein AP, *et al*. Percutaneous coronary intervention versus coronary-artery bypass grafting for severe coronary artery disease. *N Engl J Med* 2009;360:961–72.
6. Holmes DR, Brennan JM, Rumsfeld JS, *et al*. Clinical outcomes at 1 year following transcatheter aortic valve replacement. *JAMA* 2015;313:1019–28.
7. Young JB, Abraham WT, Smith AL, *et al*. Combined cardiac resynchronization and implantable cardioversion defibrillator in advanced chronic heart failure: the miracle ICD trial. *JAMA* 2003;289:2685–94.
8. Min JK, Leipsic J, Pencina MJ, *et al*. Diagnostic accuracy of fractional flow reserve from anatomic CT angiography. *JAMA* 2012;308:1237–45.
9. Smith GCS, Pell JP. Parachute use to prevent death and major trauma related to gravitational challenge: systematic review of randomised controlled trials. *BMJ* 2003;327:1459–61.
10. Yasuda S, Nakao K, Nishimura K, *et al*. The current status of cardiovascular medicine in Japan- Analysis of a large number of health records from a nationwide claim-based database, JROAD-DPC. *Circ J* 2016;80:2327–35.
11. Yasunaga H, Ide H, Imamura T, *et al*. Impact of the Japanese diagnosis procedure combination-based payment system on cardiovascular medicine-related costs. *Int Heart J* 2005;46:855–66.
12. Nakamura K. Diagnosis procedure combination database would develop nationwide clinical research in Japan. *Circ J* 2016;80:2289–90.
13. Yasunaga H, Matsui H, Horiguchi H, *et al*. [Application of the diagnosis procedure combination (DPC) data to clinical studies]. *J Uoeh* 2014;36:191–7.
14. Iihara K, Nishimura K, Kada A, *et al*. The impact of comprehensive stroke care capacity on the hospital volume of stroke interventions: a nationwide study in Japan: J-ASPECT study. *J Stroke Cerebrovasc Dis* 2014;23:1091–18.
15. Chen J, Rathore SS, Wang Y, *et al*. Physician board certification and the care and outcomes of elderly patients with acute myocardial infarction. *J Gen Intern Med* 2006;21:238–44.
16. Park S, Sasaki N, Morichima T, *et al*. The number of cardiologists, case volume, and in-hospital mortality in acute myocardial infarction patients. *Int J Cardiol* 2013;168:4470–1.
17. Cassle PN, Jones JL, Wolf FE, *et al*. Patients treated by cardiologists have a lower in-hospital mortality for acute myocardial infarction. *J Am Coll Cardiol* 1998;32:885–9.
18. Spaulding C, Morice M-C, Lancelin B, *et al*. Is the volume-outcome relation still an issue in the era of PCI with systematic stenting? results of the greater Paris area PCI registry. *Eur Heart J* 2006;27:1054–60.
19. Curtis JP, Luebbert JJ, Wang Y, *et al*. Association of physician certification and outcomes among patients receiving an implantable cardioverter-defibrillator. *JAMA* 2009;301:1661–70.
20. Aversano T, Lemmon CC, Liu L, *et al*. Outcomes of PCI at hospitals with or without on-site cardiac surgery. *N Engl J Med* 2012;366:1792–802.
21. Kulkarni VT, Ross JS, Wang Y, *et al*. Regional density of cardiologists and rates of mortality for acute myocardial infarction and heart failure. *Circ Cardiovasc Qual Outcomes* 2013;6:352–9.
22. Jong P, Gong Y, Liu PP, *et al*. Care and outcomes of patients newly hospitalized for heart failure in the community treated by cardiologists compared with other specialists. *Circulation* 2003;108:184–91.
23. Philbin EF, Jenkins PL. Differences between patients with heart failure treated by cardiologists, internists, family physicians, and other physicians: analysis of a large, statewide database. *Am Heart J* 2000;139:491–6.
24. Bucholz EM, Butala NM, Normand S-LT, *et al*. Association of guideline-based admission treatments and life expectancy after myocardial infarction in elderly medicare beneficiaries. *J Am Coll Cardiol* 2016;67:2378–91.
25. Edep ME, Shah NB, Tatao IM, *et al*. Differences between primary care physicians and cardiologists in management of congestive heart failure: relation to practice guidelines. *J Am Coll Cardiol* 1997;30:518–26.
26. Koelling TM, Johnson ML, Cody RJ, *et al*. Discharge education improves clinical outcomes in patients with chronic heart failure. *Circulation* 2005;111:179–85.
27. Meltzer D, Manning WG, Morrison J, *et al*. Effects of physician experience on costs and outcomes on an academic general medicine service: results of a trial of hospitalists. *Ann Intern Med* 2002;137:868–74.
28. Bello D, Shah NB, Edep ME, *et al*. Self-reported differences between cardiologists and heart failure specialists in the management of chronic heart failure. *Am Heart J* 1999;138:100–7.
29. Bucholz EM, Butala NM, Ma S, *et al*. Life expectancy after myocardial infarction, according to hospital performance. *N Engl J Med* 2016;375:1332–42.
30. Cram P, Rosenthal GE, Vaughan-Sarrazin MS. Cardiac revascularization in specialty and general hospitals. *N Engl J Med* 2006;352:1454–62.
31. Budhiraja AO, Patel NJ, Grover P, *et al*. Impact of annual operator and institutional volume on percutaneous coronary intervention outcomes: a 5-year United States experience (2005-2009). *Circulation* 2014;130:1382–408.
32. Ross JS, Normand S-LT, Wang Y, *et al*. Hospital volume and 30-day mortality for three common medical conditions. *N Engl J Med* 2010;362:1110–8.

BMJ Open: first published as 10.1136/bmjopen-2018-024857 on 15 December 2019. Downloaded from http://bmjopen.bmj.com/ on December 15, 2019 at St Marianna-Ika Daigaku. Protected by copyright.

Circulation: Cardiovascular Interventions

ORIGINAL ARTICLE

Determining the Predominant Lesion in Patients With Severe Aortic Stenosis and Coronary Stenoses

A Multicenter Study Using Intracoronary Pressure and Flow

Yousif Ahmad, MRCP; Jeroen Vendrik, MD; Ashkan Eftekhari, PhD; James P. Howard, MRCP; Christopher Cook, MRCP; Christopher Rajkumar, MRCP; Iqbal Malik, PhD; Ghada Mikhail, FRCP; Neil Ruparelia, PhD; Nearchos Hadjiloizou, PhD; Sukhjinder Nijjer, PhD; Rasha Al-Lamee, PhD; Ricardo Petraco, PhD; Takayuki Warisawa, MD; Gilbert W.M. Wijntjens, MD; Karel T. Koch, PhD; Tim van de Hoef, PhD; Guus de Waard, MD; Mauro Echavarria-Pinto, PhD; Angela Frame, MSc; Nilesh Sutaria, MD; Gajen Kanaganayagam, PhD; Ben Ariff, PhD; Jon Anderson, FRCS; Andrew Chukwuemeka, MD; Michael Fertleman, MBBChir; Sasha Koul, PhD; Juan F. Iglesias, MD; Darrel Francis, MD; Jamil Mayet, MD; Patrick Serruys, PhD; Justin Davies, PhD; Javier Escaned, PhD; Niels van Royen, PhD; Matthias Götberg, PhD; Christian Juhl Terkelsen, MD; Evald Høj Christiansen, PhD; Jan J. Piek, PhD; Jan Baan Jr, PhD; Sayan Sen, PhD

BACKGROUND: Patients with severe aortic stenosis (AS) often have coronary artery disease. Both the aortic valve and the coronary disease influence the blood flow to the myocardium and its ability to respond to stress; leading to exertional symptoms. In this study, we aim to quantify the effect of severe AS on the coronary microcirculation and determine if this is influenced by any concomitant coronary disease. We then compare this to the effect of coronary stenoses on the coronary microcirculation.

METHODS: Group 1: 55 patients with severe AS and intermediate coronary stenoses treated with transcatheter aortic valve implantation (TAVI) were included. Group 2: 85 patients with intermediate coronary stenoses and no AS treated with percutaneous coronary intervention were included. Coronary pressure and flow were measured at rest and during hyperemia in both groups, before and after TAVI (group 1) and before and after percutaneous coronary intervention (group 2).

RESULTS: Microvascular resistance over the wave-free period of diastole increased significantly post-TAVI (pre-TAVI, 2.71±1.4 mm Hg·cm·s^{-1} versus post-TAVI 3.04±1.6 mm Hg·cm·s^{-1} [P=0.03]). Microvascular reserve over the wave-free period of diastole significantly improved post-TAVI (pre-TAVI 1.88±1.0 versus post-TAVI 2.09±0.8 [P=0.003]); this was independent of the severity of the underlying coronary stenosis. The change in microvascular resistance post-TAVI was equivalent to that produced by stenting a coronary lesion with an instantaneous wave-free ratio of ≤0.74.

CONCLUSIONS: TAVI improves microcirculatory function regardless of the severity of underlying coronary disease. TAVI for severe AS produces a coronary hemodynamic improvement equivalent to the hemodynamic benefit of stenting coronary stenoses with instantaneous wave-free ratio values <0.74. Future trials of physiology-guided revascularization in severe AS may consider using this value to guide treatment of concomitant coronary artery disease.

VISUAL OVERVIEW: A visual overview is available for this article.

Key Words: aortic valve stenosis ■ diastole ■ hyperemia ■ microcirculation ■ myocardium

Downloaded from http://ahajournals.org by on December 1, 2019

Correspondence to: Sayan Sen, PhD, National Heart and Lung Institute, 2nd Floor B Block, Hammersmith Hospital, Imperial College London, London W12 0HS. Email sayan.sen@imperial.ac.uk

For Sources of Funding and Disclosures, see page 9.

© 2019 The Authors. *Circulation: Cardiovascular Interventions* is published on behalf of the American Heart Association, Inc., by Wolters Kluwer Health, Inc. This is an open access article under the terms of the Creative Commons Attribution License, which permits use, distribution, and reproduction in any medium, provided that the original work is properly cited.

Circulation: Cardiovascular Interventions is available at www.ahajournals.org/journal/circinterventions

WHAT IS KNOWN

- Patients with severe aortic stenosis undergoing transcatheter aortic valve implantation often have concomitant coronary artery disease. If they present with chest pain or dyspnea, it can be unclear if the coronary stenosis or the aortic valve stenosis is responsible for an individual patient's symptoms.
- It has been demonstrated that hyperemic indices are significantly affected by severe aortic stenosis, with hyperemic flow increasing significantly after transcatheter aortic valve implantation. Resting hemodynamics are less susceptible to this, specifically in the wave-free period of diastole, where it has previously been shown that flow during this period is unchanged post-transcatheter aortic valve implantation.

WHAT THE STUDY ADDS

- Transcatheter aortic valve implantation improves microcirculatory function regardless of the severity of underlying coronary disease.
- This improvement in microcirculatory function is only matched by stenting coronary lesions with an instantaneous wave-free ratio <0.74.
- The predominant lesion affecting microvascular resistance in patients with severe aortic stenosis and coronary stenoses seems to be the aortic stenosis unless the instantaneous wave-free ratio value is ≤0.74.

Nonstandard Abbreviations and Acronyms

AS	aortic stenosis
CAD	coronary artery disease
FFR	fractional flow reserve
IFR	instantaneous wave–free ratio
PCI	percutaneous coronary intervention
TAVI	transcatheter aortic valve implantation

Patients with severe aortic stenosis (AS) often have coronary artery disease (CAD).[1] If they present with chest pain or dyspnea, it can be unclear if the coronary stenosis or the aortic valve stenosis is responsible for an individual patient's symptoms.

The cause of chest pain or shortness of breath in these patients is a result of an inability of the microcirculation to increase blood flow in response to increased demand. While the effects of both the coronary lesion[2] and the aortic valvular stenosis[3] on the microcirculation have been individually studied, it is not known how the 2 interact when they are present in the same patient, and which is the predominant lesion.

It has been demonstrated that hyperemic indices are significantly affected by severe AS,[4] with hyperemic flow increasing significantly after transcatheter aortic valve implantation (TAVI). Resting hemodynamics are less susceptible to this, specifically in the wave-free period of diastole, where it has previously been shown that flow during this period is unchanged post-TAVI.

This study uses the resting hemodynamics of the wave-free period to determine the relative effects of TAVI and percutaneous coronary intervention (PCI) on myocardial perfusion. Microvascular resistance over the wave-free period has been demonstrated to reflect coronary stenosis severity[5]; with low resistance suggesting a more severe stenosis and higher resistance suggesting a less severe stenosis. It has also been shown that microvascular resistance over the wave-free period is affected by severe AS. In patients with both severe AS and CAD, the relative contribution of each to microvascular resistance is unknown.

In this study, we aim to determine when a patient has severe AS and coronary disease which is the predominant lesion affecting myocardial blood flow. We aim to do this by (1) quantifying the effect of severe AS on the function of the coronary microcirculation and determine if this is influenced by concomitant coronary disease; (2) quantifying the effect of a coronary stenosis on the function of the coronary microcirculation; and (3) determining the severity of coronary stenosis that, when stented, provides equivalent improvement in microcirculatory function as TAVI.

METHODS

The methods and materials that support the findings of this study are available from the corresponding author on reasonable request.

Patient Population

Part 1: 55 patients with severe AS undergoing TAVI with moderate coronary lesions were recruited from 4 European centres (The Hammersmith Hospital, Imperial College Healthcare NHS Trust, London, United Kingdom; Amsterdam Medical Center, Amsterdam, the Netherlands; Skane University Hospital, Lund, Sweden; and Aarhus University Hospital, Aarhus, Denmark). The study was approved by an institutional review committee at each site. All patients had prospectively collected combined coronary pressure and flow measurements, with paired measurements pre- and post-TAVI. All patients were scheduled for TAVI on clinical grounds in accordance with clinical guidelines,[6] after a decision at a Heart Team meeting, and gave written informed consent for the study protocol. Exclusion criteria were known nonviable myocardium in the area of the corresponding coronary artery being studied, contra-indication to the administration of adenosine, inability to consent or weight over 200 kg. All patients had concomitant AS and CAD, and physiological assessments were performed in each patient. There was no PCI performed in this group, after Heart Team decision that it was not required before TAVI and enrollment in the study.

Part 2: 65 patients with intermediate coronary lesions undergoing PCI were included from 4 European centres as part of the

Downloaded from http://circinterv.ahajournals.org by on December 1, 2019

IDEAL collaboration[2] (Amsterdam Medical Center, Amsterdam, the Netherlands; The Hammersmith Hospital, Imperial College Healthcare NHS Trust, London, United Kingdom; Hospital Clinico San Carlos, Madrid, Spain; and VU University Medical Center, Amsterdam, the Netherlands). The study was approved by an institutional review committee at each site. All patients had combined coronary pressure and flow measurements, with paired measurements pre- and post-PCI. All patients recruited were scheduled for elective coronary angiography with physiological stenosis assessment by fractional flow reserve and gave written informed consent for acquisition of additional physiological data for study purposes. Exclusion criteria were acute myocardial infarction within 48 hours; contraindication to the administration of adenosine; severe valvular heart disease; weight >200 kg; previous coronary artery bypass surgery; vessels with angiographically identifiable myocardial bridging or collateral arteries; and vessels supplying an infarcted territory. All patients in this group underwent PCI as had been determined by the treating clinical team.

Cardiac Catheterization Protocol

In all patients, cardiac catheterization and coronary angiography was performed via either the transradial or transfemoral route at the operator's discretion. A guiding catheter was used to intubate the target artery. Therapeutic dose heparin was administered. A dual pressure and Doppler sensor-equipped 0.014" guidewire was used for all physiological assessments (ComboWire, Volcano Corp, San Diego, CA). The pressure signals were normalized in the aorta before advancing the wire a minimum of 3-vessel diameters distal to the coronary stenosis. Doppler signals were optimized and stabilized to ensure good tracking profiles. All flow measurements were made by experienced operators; the reproducibility of flow measurements in such hands has been previously demonstrated.[7] At this stage, resting pressure and flow measurements were recorded. Hyperemia was then induced using adenosine, either as an intracoronary bolus of 150 μg or an intravenous infusion of 140 μg/kg per minute. Physiological measurements under hyperemic conditions were then recorded. At the end of each recording, the pressure sensor was returned to the catheter tip to ensure that there was no pressure drift. When drift was identified (≥0.02), all measurements were repeated. For TAVI patients, left ventricular pressures were recorded using a pigtail catheter placed in the LV cavity. All patients then either underwent PCI (for patients without AS) or TAVI (for patients with AS). Subsequent to either intervention, the entire protocol was repeated with the wire sited in the same location as the preintervention measurements.

PCI Procedures

Drug-eluting stents were used as standard of care. Optimization using intracoronary imaging and postdilatation were performed at the operator's discretion.

TAVI Procedures

All patients were treated under local anesthesia and conscious sedation. The valves used were either the Edward's Sapien XT/S3 valves (Edwards Lifesciences LCC, Irvine, CA), the Medtronic CoreValve/Evolut-R valves (Medtronic, Inc, Minneapolis, MN), or Lotus valve (Boston Scientific, Natick, MA). Valve choice was at the Heart Team and operator's discretion.

Analysis of Hemodynamic Data

ECG, pressure, and flow velocity signals were processed with the dedicated device console (ComboMap; Volcano Corp, San Diego, CA). Analog output feeds were taken from the pressure-velocity console and ECG, fed into a National Instruments DAQ-Card AI-16E-4, and acquired at 1 kHz with Labview. Data were analyzed offline with a custom software package designed with Matlab (Mathworks, Natick, MA), which permitted phasic analysis including that of the wave-free period. The wave-free period was identified using wave-intensity analysis[7] and used to perform phasic analysis. Coronary pressure, flow, and resistance were measured during resting conditions and during hyperemia.

Microvascular reserve was derived as a metric of improvement in coronary hemodynamics after intervention. This was defined as a ratio of hyperemic microvascular resistance to resting microvascular resistance.

Definitions of other hemodynamic variables were as follows:

$$\text{Instantaneous wave-free ratio (iFR)} = \frac{Pd_{wfp}}{Pa_{wfp}}$$

$$\text{Hyperemic microvascular resistance (HMR)} = \frac{Pd_h}{v_h}$$

$$\text{Basal microvascular resistance (BMR)} = \frac{Pd_b}{v_b}$$

$$\text{Vasodilator reserve (VDR)} = \frac{BMR}{HMR}$$

$$\text{Wave-free period resistance (Wfp-res)} = \frac{Pd_{wfp}}{v_{wfp}}$$

Where Pa=mean aortic pressure; Pd=mean intracoronary pressure distal to a stenosis; Wfp=the wave-free period of diastole; v_h=mean flow velocity distal to a stenosis during hyperemia; v_b=mean flow velocity distal to a stenosis at baseline.

Statistical Methods

Continuous variables are presented as mean and SD unless otherwise stated. Comparisons before and after intervention were performed with a paired *t* test for continuous variables. Paired ordinal categorical data such as LV function were analyzed using the Wilcoxon signed-rank test. The threshold for statistical significance was set at 0.05. Pearson correlation coefficient was used to assess correlations. All analyses were performed using R version 3.2.1 (R Foundation for Statistical Computing, Vienna, Austria).

RESULTS

Patient Population

TAVI Group

Fifty-five patients (81.7 [±5.9] years; 49.1% male) were included. Baseline clinical characteristics are shown in Table 1. The baseline echocardiographic characteristics are summarized in Table 2.

Downloaded from http://ahajournals.org by on December 1, 2019

Table 1. Baseline Clinical Characteristics of TAVI Group

	n (%)
Age, y	81.7 (±5.9)
Male	27 (49.1)
Body mass index, kg/m²	27.36 (±5.0)
Diabetes mellitus	16 (29.1)
Hypertension	37 (67.3)
Hyperlipidemia	22 (40.0)
Former smoker	20 (36.4)
Previous myocardial infarction	4 (7.3)
Previous percutaneous coronary intervention	8 (14.5)
Previous coronary artery bypass grafting	3 (5.5)

TAVI indicates transcatheter aortic valve implantation.

PCI Group

Eighty-five patients were included (61.3 [±9.4] years; 74.1% male). Baseline clinical characteristics are shown in Table 3.

Quantitative Coronary Angiography

TAVI Group

Quantitative coronary angiography for the patients undergoing TAVI is summarized in Table 4.

PCI Group

Quantitative coronary angiography for the patients undergoing PCI is summarized in Table 5.

Coronary Physiological Parameters Before and After TAVI

Commonly reported coronary physiological parameters before and after TAVI are summarized in Table 6. There was a significant reduction in fractional flow reserve immediately ($P<0.001$) post-TAVI, and a significant increase in coronary flow reserve immediately post-TAVI ($P=0.03$). Instantaneous wave-free ratio (iFR) was unchanged immediately post-TAVI ($P=0.80$).

Microvascular Resistance Over the Wave-Free Period of Diastole Before and After TAVI

Changes in resistance after TAVI are summarized in Figure 1. Resting resistance over the wave-free period of diastole increased significantly post-TAVI (pre-TAVI 2.71±1.4 mmHg·cm·s^{-1} versus post-TAVI 3.04±1.6 mmHg·cm·s^{-1} [$P=0.03$]). Hyperemic resistance over the wave-free period of diastole did not change post-TAVI (pre-TAVI 1.58±0.8 mmHg·cm·s^{-1} versus post-TAVI 1.49±0.7 mmHg·cm·s^{-1} [$P=0.36$]). Microvascular reserve over the wave-free period of diastole significantly improved post-TAVI (pre-TAVI 1.88±1.0 versus post-TAVI 2.09±0.8 [$P=0.003$]).

Table 2. Baseline Echocardiographic Characteristics of TAVI Group

	Pre-TAVI	Post-TAVI	P Value
Peak velocity, cm/s	416.73 (±98.44)	218.36 (±47.60)	<0.001
Peak gradient, mmHg	70.99 (±28.31)	14.41 (±7.6)	<0.001
Mean gradient, mmHg	41.78 (±17.84)	10.17 (±5.0)	<0.001
Aortic valve area, cm²	0.69 (±0.23)	1.48 (±0.3)	<0.001
LV systolic function			0.484
Normal	44 (80.0)	44 (80.0)	
Mildly impaired	6 (10.9)	6 (10.9)	
Moderately impaired	2 (3.6)	4 (7.3)	
Severely impaired	3 (5.5)	1 (1.8)	
Left ventricular end-diastolic pressure, mmHg	17.43 (±7.4)	16.40 (±6.4)	0.09
Paravalvular leak			
None		28 (50.9)	
Mild		23 (41.8)	
Moderate		4 (7.3)	
Severe		0 (0)	

Continuous variables are analyzed using paired t-tests. The categorical variable of LV systolic function was analyzed using the Wilcoxon signed-rank test. LV indicates left ventricular; and TAVI, transcatheter aortic valve implantation.

Improvement in Wave-Free Period Resistance Achieved by TAVI and PCI According to Baseline iFR

Overall, microvascular resistance over the wave-free period improved significantly post-PCI. This improvement was dependent on the baseline iFR value (Figure 2). The more severe the coronary stenosis, the greater the improvement in microvascular resistance. Therefore, microvascular resistance over the wave-free period is a marker of coronary stenosis severity.

Overall, microvascular resistance over the wave-free period improved significantly post-TAVI (Figure 3). This improvement was independent of the baseline iFR value: the improvement in microvascular resistance over the wave-free period post-TAVI is consistent across the spectrum of coronary stenosis severity.

Table 3. Baseline Clinical Characteristics of PCI Group

	n (%)
Age, y	61.3 (±9.4)
Male	63 (74.1)
Diabetes mellitus	22 (25.9)
Hypertension	43 (50.6)
Hyperlipidemia	64 (75.3)
Former smoker	38 (44.7)
Previous myocardial infarction	11 (12.9)

PCI indicates percutaneous coronary intervention.

Downloaded from http://ahajournals.org by on December 1, 2019

Table 4. Quantitative Coronary Angiographic Data for TAVI Patients

Target vessel	
LAD	31 (55.5%)
Cx	10 (18.5%)
RCA	14 (26.0%)
Stenosis location	
Proximal	26 (46.3%)
Mid	26 (46.1%)
Distal	3 (5.6%)
Diameter stenosis by QCA, %	56.11 (±11.1)
Area stenosis by QCA, %	70.42 (±9.7)
Stenosis length, mm	17.64 (±9.0)
Minimum luminal diameter, mm	1.22 (±0.4)
Minimum luminal area, mm²	1.32 (±0.8)

Cx indicates circumflex; LAD, left anterior descending; QCA, quantitative coronary angiography; RCA, right coronary artery; and TAVI, transcatheter aortic valve implantation.

Table 5. Quantitative Coronary Angiographic Data for PCI Patients

Target vessel	
LAD	50 (58.8%)
Cx	17 (20.0%)
RCA	18 (21.2%)
Stenosis location	
Proximal	43 (50.6%)
Mid	39 (45.9%)
Distal	3 (3.5%)
Diameter stenosis by QCA, %	62.59 (±13.4)
Area stenosis by QCA, %	65.00 (±9.8)
Stenosis length, mm	20.86 (±11.3)
Minimum luminal diameter, mm	0.92 (±0.4)
Minimum luminal area, mm²	0.78 (±0.6)

Cx indicates circumflex; LAD, left anterior descending; PCI, percutaneous coronary intervention; QCA, quantitative coronary angiography; and RCA, right coronary artery.

Comparison of the Change in Microvascular Resistance Observed After TAVI and PCI

The average improvement in microvascular resistance over the wave-free period post-TAVI was 19.2±0.5%. Interpolating this data to the improvement of microvascular resistance over the wave-free period post-PCI suggests that at the iFR value 0.74, there is equipoise in the improvement achieved with PCI and TAVI (see Figure 4). That is, stenting lesions with iFR values of 0.74 also provides a 19% improvement in resistance (the same as TAVI). Therefore, the improvement in resistance achieved by PCI seems only able to surpass TAVI when the baseline iFR is <0.74.

DISCUSSION

In this study, we have shown that (1) in patients with severe AS and intermediate coronary lesions, treatment of the valve results in a significant increase in microvascular resistance; (2) this increase is independent of the severity of the underlying coronary lesion; and (3) TAVI for severe AS produces a hemodynamic improvement equivalent to the hemodynamic benefit of stenting coronary stenoses with iFR values <0.74.

Microvascular Reserve and Coronary Stenoses

Microvascular reserve reflects the ability of the microcirculation to increase the blood supply to the heart in response to increased demand or workload. In patients with coronary disease, this ability to respond to increased work load is related to (1) the severity of the stenosis within the epicardial artery[2] and (2) autoregulation of coronary blood flow[8] and its effect on microvascular resistance. In patients with severe coronary disease, microvascular resistance is relatively lower than in patients with no coronary stenosis (Figure 5).

AS and Coronary Stenosis

In this study, we demonstrate that AS also influences coronary microvascular tone and its ability to respond to stress. In patients with AS, microvascular resistance at rest is significantly lower than that of post-TAVI patients. This suggests that the coronary microcirculation treats AS similarly to a coronary stenosis. As the aortic valve becomes more and more

Table 6. Values of Common Coronary Physiological Indices Pre- and Post-TAVI

	Pre-TAVI	Post-TAVI	P Value
Fractional flow reserve	0.86 (±0.08)	0.83 (±0.09)	<0.001
Instantaneous wave-free ratio	0.87 (±0.10)	0.87 (±0.09)	0.60
Coronary flow reserve	1.56 (±0.50)	1.74 (±0.50)	0.08
Whole cycle resting flow (Pa/Pa-flow)	22.54 (±8.86)	23.02 (±10.45)	0.71
Whole cycle hyperemic flow (FFR-flow)	33.44 (±12.66)	38.51 (±16.31)	0.005
Wave-free period resting flow (iFR-flow)	28.28 (±12.77)	27.64 (±16.10)	0.63

Comparisons analyzed using paired *t* tests. FFR indicates fractional flow reserve; iFR, instantaneous wave-free ratio; and TAVI, transcatheter aortic valve implantation.

Downloaded from http://stetjournals.org by on December 1, 2019

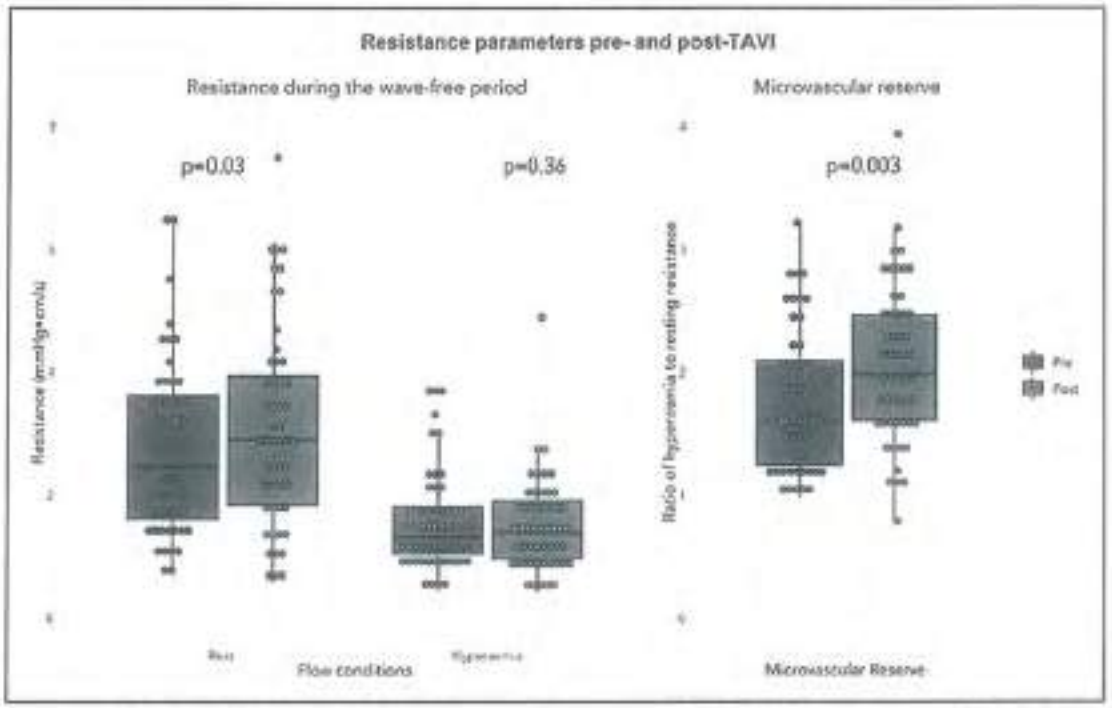

Figure 1. **Figure outlining the changes in resting resistance, hyperemic resistance, and microvascular reserve pre- and post-transcatheter aortic valve implantation (TAVI).**

constricted, the microcirculation dilates to maintain coronary flow and microvascular reserve is depleted (Figure 5).

Therefore, in patients with severe AS and coronary disease, the microcirculation is adapting to 2 variables that affect blood flow: the stenosed aortic valve and the stenosis in the coronary artery. Resting microvascular resistance and therefore microvascular reserve in these patients is therefore limited by both.

Because the microcirculation treats the 2 stenoses similarly, determining the predominant lesion is akin to attempting to determine which stenosis is predominant in a vessel with tandem lesions. It has been demonstrated that this is not possible with hyperemia due to both stenoses influencing the blood flow across the other.[9] However, it has been demonstrated to be possible to isolate the significance of a specific lesion with iFR.[10]

This finding for tandem lesions can be extrapolated to the TAVI population. In these patients, the tandem lesions are the coronary stenosis and the aortic valvular stenosis. Placing a pressure wire in the vessel distal to the coronary stenosis in a patient with severe AS is therefore analogous to placing a pressure wire between 2 serial lesions

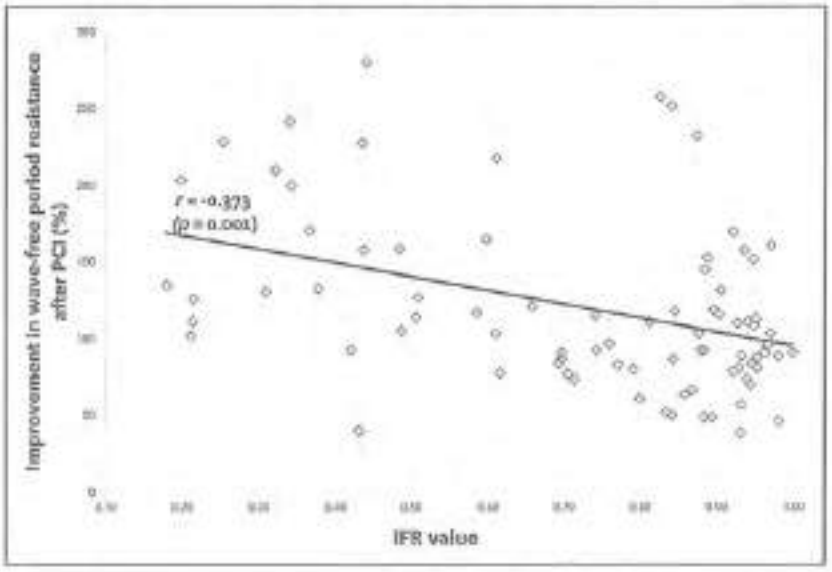

Figure 2. **Correlation between underlying coronary stenosis severity (baseline instantaneous wave-free ratio [iFR] value) and improvement in resistance after percutaneous coronary intervention (PCI) with a strongly statistically significant association.**

Downloaded from http://ahajournals.org by on December 1, 2019

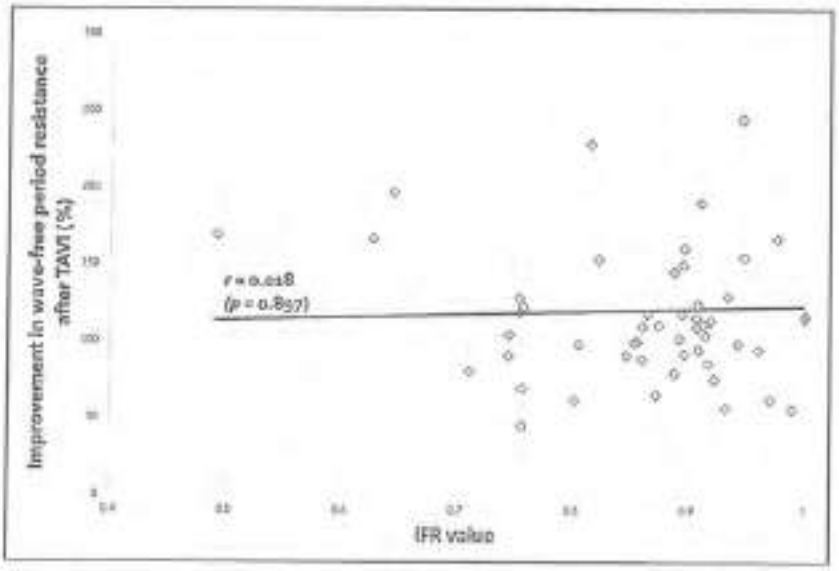

Figure 3. Correlation between underlying coronary stenosis severity (baseline instantaneous wave–free ratio [iFR] value) and improvement in resistance after transcatheter aortic valve implantation (TAVI) with no significant association seen.

in a coronary artery. We have previously demonstrated that hyperemic flow changes significantly post-TAVI suggesting that hyperemic indices cannot be used to isolate coronary stenosis severity in the context of severe AS. However, we have demonstrated that iFR can accurately isolate the coronary stenosis severity independent to the aortic valve in this setting[4]; the iFR pre-TAVI is equivalent to the iFR post-TAVI. Previous studies in the field have also demonstrated identical values of iFR before and after TAVI.[11] The same study also suggested a 15% classification change of coronary stenosis significance by iFR after TAVI, but this is confounded by the use of a conventional 0.89 cut point and also the distribution of iFR values close to this cut point.[12] As in our present study, the iFR and fractional flow reserve values were similar pre-TAVI reflecting the inability of adenosine to augment flow in patients with severe AS.

Post-TAVI, resting microvascular resistance increases because one lesion affecting coronary flow has been treated. It does not normalize, however, as there is a residual coronary stenosis that needs to be accommodated. The change in microvascular resistance post-TAVI is independent of the underlying coronary stenosis.

Furthermore, in this study, we compare the increase in resting microvascular resistance post-TAVI to the effect of treating a coronary stenosis in a cohort of patients with a coronary stenosis but no AS. When we do this, it can be seen that stenting coronary stenoses with iFR values <0.74 are able to produce increases in microvascular resistance equivalent to that observed by treating the AS. This is likely to be a conservative estimate because treating a coronary lesion in a patient post-TAVI may not lead to equivalent microvascular change; due to factors such as advanced age, left ventricular hypertrophy, and elevated left-ventricular end-diastolic pressure.[13,14] As a result, in patients with severe AS, the coronary stenosis may have to be even more severe to achieve similar increases in microvascular resistance as those seen by treating the AS. This would suggest that in patients with AS and coronary disease the predominant lesion is the aortic valve unless the coronary stenosis has an iFR value <0.74.

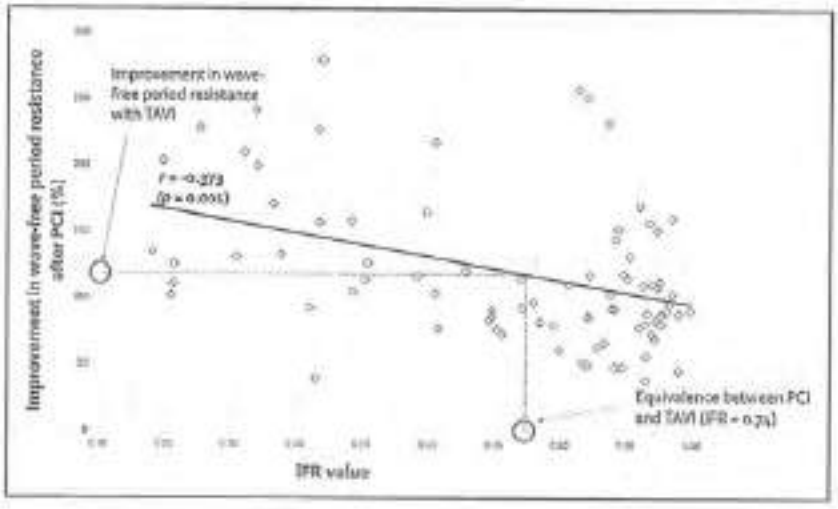

Figure 4. Correlation between underlying coronary stenosis severity (baseline instantaneous wave–free ratio [iFR] value) and improvement in resistance after percutaneous coronary intervention (PCI).
When the improvement in resistance achieved with transcatheter aortic valve implantation (TAVI) is interpolated, equipoise between PCI and TAVI is seen at iFR values of 0.74.

Downloaded from http://ahajournals.org by on December 1, 2019

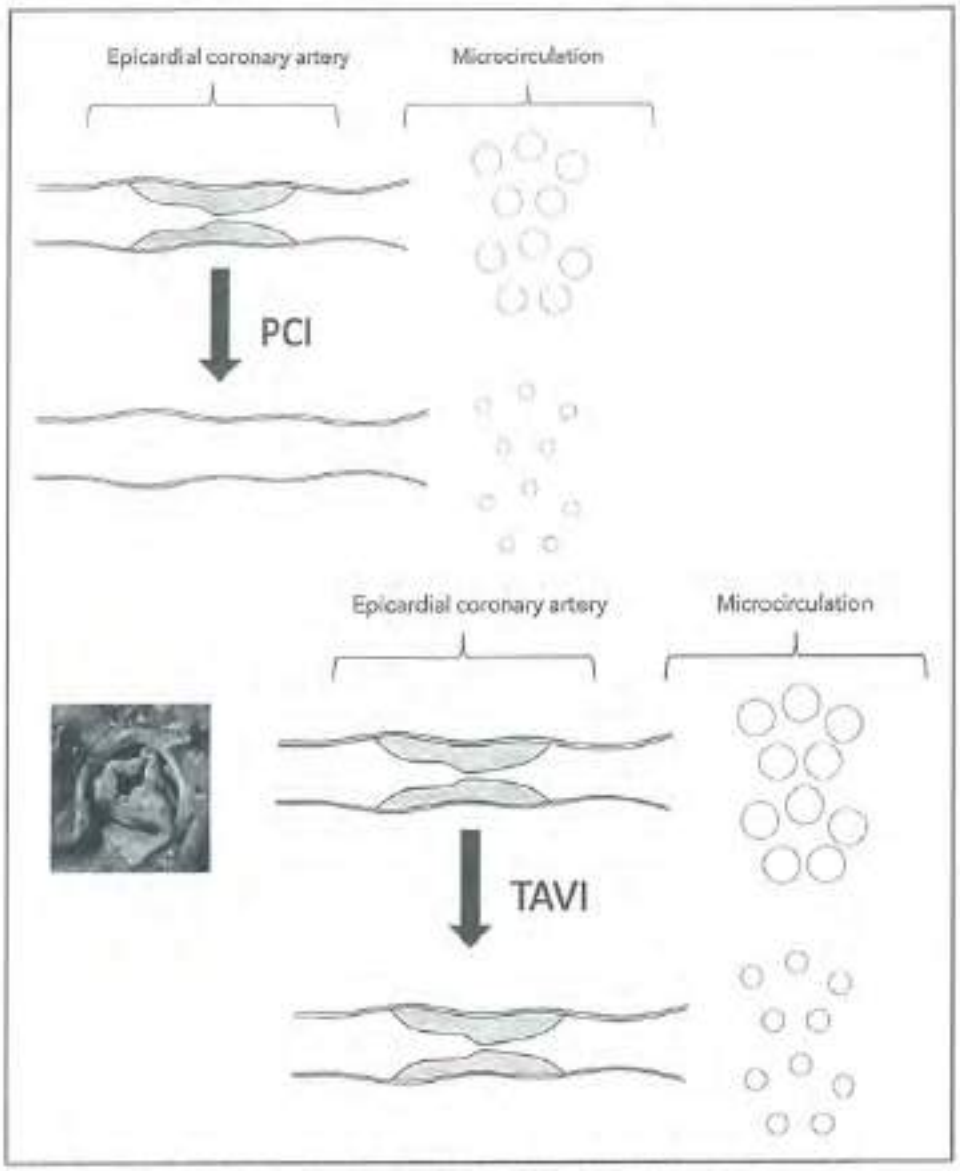

Figure 5. Figure outlining coronary autoregulation in patients with coronary stenoses and aortic stenosis.
In the top, a patient with a severe coronary stenosis; here, the microcirculation is relatively dilated at rest to maintain coronary flow. In these patients, when the need arises to increase coronary flow further, the capacity of the microcirculation to dilate further to increase flow is limited; therefore, the difference between resting and hyperemic flow (microvascular reserve) is small. In patients with no coronary stenosis, or after percutaneous coronary intervention (PCI), the opposite is true. In these patients, the microcirculation is relatively constricted. Therefore, when the need arises to increase coronary flow further, the capacity of the microcirculation to dilate further to increase flow is large; and the difference between resting and hyperemic flow (microvascular reserve) is also large, resulting in greater microvascular reserve. In the bottom, a patient with coronary stenosis and aortic stenosis. As the aortic valve stenoses, so the microcirculation dilates to maintain coronary flow and microvascular reserve is depleted. Therefore, in patients with severe aortic stenosis and coronary disease, the microcirculation is adapting to 2 variables that affect blood flow: the stenosed aortic valve and the stenosis in the coronary artery. Post-transcatheter aortic valve implantation (TAVI), resting microvascular resistance increases because one lesion affecting coronary flow has been treated. It does not normalize, however, as there is a residual coronary stenosis that needs to be accommodated.

Downloaded from http://dhajournals.org by on December 1, 2019

Clinical Implications

It is not uncommon for patients with severe AS referred for TAVI to have concomitant CAD.[15] Both conditions can present with angina or dyspnea on exertion. It can therefore be challenging for clinicians to determine which lesion is predominantly responsible for an individual patient's presentation. There is currently no clear evidence that PCI before TAVI improves clinical outcomes[16] but the importance of accurately assessing the functional significance of coronary disease in these patients is becoming increasingly important as TAVI is being offered to younger, lower-risk patients.

Our study suggests that in such patients, coronary physiology can help to clarify the situation. In patients

with severe AS and coronary lesions, if the iFR value is >0.74, then it is likely that TAVI will lead to a greater improvement in coronary hemodynamics than PCI—and may therefore be the preferred initial strategy. Conversely, if the iFR value is <0.74, then the coronary stenosis may provide a greater contribution to the patient's hemodynamic status. In such a situation, the treating clinician may give greater consideration to treating the coronary lesion in addition to the valve.

This iFR value of 0.74 is not designed to be interpreted as a hard cut point to guide PCI or defer TAVI. Rather, it is more intended to provide a framework for clinicians when treating this challenging patient cohort; when it is unclear whether the aortic valve stenosis or coronary stenosis is the major factor in the patient's presentation. Ultimately, in the absence of robust randomized data in this field, the decision of whether to perform PCI in patients with severe AS scheduled for TAVI must be undertaken on a case by case basis and after the deliberation of the Heart Team. This study suggests iFR may add to these deliberations, along with other factors such as the location of the coronary stenosis, the amount of subtended myocardium, suitability for dual antiplatelet therapy,[17] the ability to access the coronary ostia post-TAVI and the patient's symptoms.

Our findings should be considered hypothesis-generating, and the true clinical value of intracoronary physiology in patients with severe AS will only be appreciated when tested in prospective fashion in a clinical trial.

Limitations

The analysis performed in this study compared the hemodynamic benefit of TAVI with the hemodynamic benefit of PCI. The patients undergoing PCI did not have severe AS, and there were other baseline differences in the groups. These differences are likely to underestimate the true effect of TAVI on coronary flow.[18–20]

Our post-TAVI measurements were all made within the same cath-lab procedure, immediately after the aortic valve had been replaced. This helped to minimize the effect of any potential confounding factors and to truly isolate the effect of the TAVI on coronary hemodynamics. It is possible that there would be further longer-term hemodynamic benefits of TAVI, which would be seen with regression of left ventricular mass and remodeling of the ventricle. We cannot comment on this from our study, but it is the subject of ongoing research. Regardless, the decision to intervene on a coronary stenosis in the context of AS is clinically most relevant before valve treatment, suggesting that the acute effect of TAVI on the microcirculation is most relevant for this analysis and in clinical practice.

We have demonstrated that, in the presence of both AS and CAD, TAVI improves microcirculatory perfusion. However, we cannot tell if (1) concomitant treatment of coronary artery stenosis with percutaneous intervention would have afforded additional benefits; (2) or, if in fact treating CAD would have reduced the benefits of TAVI on microcirculation, as it is conceivable that the negative effects of severe AS could be more prominent in the presence of concomitant CAD.

A larger proportion of patients in the PCI group had more severe coronary lesions with lower iFR values than in the TAVI group. Nevertheless, our patients were representative of a clinical population with severe AS and CAD who were referred for TAVI.

Conclusions

TAVI improves microcirculatory function regardless of the severity of underlying coronary disease. TAVI for severe AS produces a coronary hemodynamic improvement equivalent to the hemodynamic benefit of stenting coronary stenoses with iFR values <0.74. Future trials of physiology-guided revascularization in severe AS may consider using this value to guide treatment of concomitant CAD.

ARTICLE INFORMATION

Received June 12, 2019; accepted September 16, 2019.

Affiliations

National Heart and Lung Institute, Hammersmith Hospital, Imperial College London, United Kingdom (YA., J.P.H., C.C., C.R., R.A.-L., R.P., T.W., D.F., J.M., P.S., S.S.). Amsterdam UMC, University of Amsterdam, Heart Center, Department of Clinical and Experimental Cardiology, the Netherlands (J.V., K.T.K., Ted.H., J.J.P., J.B.). Aarhus University Hospital Skejby, Denmark (A.E., C.J.T., E.H.C.). Department of Cardiology, Hammersmith Hospital, Imperial College Healthcare NHS Trust, London, United Kingdom (I.M., G.M., N.R., N.H., S.N., A.F., N.S., G.K., B.A., J.A., A.C., M.F., J.C.). Department of Cardiology, VU University Medical Center, Amsterdam, the Netherlands (S.d.W., N.v.R.). Hospital Clínico San Carlos, Madrid, Spain (M.E.-P., J.E.). Department of Cardiology, Clinical Sciences, Lund University, Skåne University Hospital, Sweden (S.K., M.G.). Cardiology Department, Lausanne University Hospital, Switzerland (J.F.).

Sources of Funding

We are grateful for infrastructural support from the NIHR Biomedical Research Centre based at Imperial College Healthcare NHS Trust and Imperial College London. The views expressed are those of the authors and not necessarily those of the NIHR or the Department of Health and Social Care. C. Cook (MR/M018369/1) and Dr Sen (G1000857) are supported by the Medical Research Council. J.P. Howard is supported by the Wellcome Trust (PS160_WHCP). Dr Petraco (FS/11/46/28961), Dr Davies (FS/05/006), and Dr Francis (FS 04/079) are supported by the British Heart Foundation.

Disclosures

Drs Golberg, Cook and Petraco have conducted teaching sessions supported by Volcano Corporation. Dr Sen has attended and conducted teaching sessions supported by Volcano Corporation, St. Jude Medical, Medtronic, Pfizer, and AstraZeneca; has received research grant support from Philips, AstraZeneca, Medtronic, and Pfizer; and has received speaking honoraria from Pfizer and Volcano-Philips. Drs. Mayet and Davies hold patents pertaining to the instantaneous wave-free ratio technology, which is under license to Volcano Corporation. Dr Davies has served as a consultant for and has received significant research funding from Volcano Corporation. Professor Serruys has received grants and personal fees from Philips Medtronic and ReCor Medical. The other authors report no conflicts.

Downloaded from http://hiqjournals.org/ by on December 1, 2019

REFERENCES

1. Goel SS, Ige M, Tuzcu EM, Ellis SG, Stewart WJ, Svensson LG, Lytle BW, Kapadia SR. Severe aortic stenosis and coronary artery disease—implications for management in the transcatheter aortic valve replacement era: a comprehensive review. *J Am Coll Cardiol*. 2015;65:1–10. doi: 10.1016/j.jacc.2013.01.096
2. Nijjer SS, de Waard GA, Sen S, van de Hoef TP, Petraco R, Echavarria-Pinto M, van Lavieren MA, Meuwissen M, Danad I, Knaapen P, et al. Coronary pressure and flow relationships in humans: phasic analysis of normal and pathological vessels and the implications for stenosis assessment: a report from the Iberian-Dutch-English (IDEAL) collaborators. *Eur Heart J*. 2016;37:2069–2080. doi: 10.1093/eurheartj/ehv626
3. Wiegerinck EM, van de Hoef TP, Rolandi MC, Yong Z, van Kesteren F, Koch KT, Vis MM, de Mol BA, Piek JJ, Baan J Jr. Impact of aortic valve stenosis on coronary hemodynamics and the instantaneous effect of transcatheter aortic valve implantation. *Circ Cardiovasc Interv*. 2015;8:e002443. doi: 10.1161/CIRCINTERVENTIONS.114.002443
4. Ahmad Y, Götberg M, Cook C, Howard JP, Malik I, Mikhail G, Frame A, Petraco R, Rajkumar C, Demir O, et al. Coronary hemodynamics in patients with severe aortic stenosis and coronary artery disease undergoing transcatheter aortic valve replacement: implications for clinical indices of coronary stenosis severity. *JACC Cardiovasc Interv*. 2018;11:2019–2031. doi: 10.1016/j.jcin.2018.07.019
5. Sen S, Asrress KN, Nijjer S, Petraco R, Malik IS, Foale RA, Mikhail GW, Foin N, Broyd C, Hadjiloizou N, et al. Diagnostic classification of the instantaneous wave-free ratio is equivalent to fractional flow reserve and is not improved with adenosine administration. Results of CLARIFY (Classification Accuracy of Pressure-Only Ratios Against Indices Using Flow Study). *J Am Coll Cardiol*. 2013;61:1409–1420. doi: 10.1016/j.jacc.2013.01.034
6. Baumgartner H, Falk V, Bax JJ, De Bonis M, Hamm C, Holm PJ, Iung B, Lancellotti P, Lansac E, Rodriguez Muñoz D, et al; ESC Scientific Document Group. 2017 ESC/EACTS Guidelines for the management of valvular heart disease. *Eur Heart J*. 2017;38:2739–2791. doi: 10.1093/eurheartj/ehx391
7. Davies JE, Whinnett ZI, Francis DP, Manisty CH, Aguado-Sierra J, Willson K, Foale RA, Malik IS, Hughes AD, Parker KH, et al. Evidence of a dominant backward-propagating "suction" wave responsible for diastolic coronary filling in humans, attenuated in left ventricular hypertrophy. *Circulation*. 2006;113:1768–1778. doi: 10.1161/CIRCULATIONAHA.105.603050
8. de Waard GA, Cook CM, van Royen N, Davies JE. Coronary autoregulation and assessment of stenosis severity without pharmacological vasodilation. *Eur Heart J*. 2018;39:4062–4071. doi: 10.1093/eurheartj/ehx689
9. Gould KL, Kirkeeide R, Johnson NP. Coronary branch steal: experimental validation and clinical implications of interacting stenoses in branching coronary arteries. *Circ Cardiovasc Imaging*. 2010;3:701–709. doi: 10.1161/CIRCIMAGING.110.937656
10. Nijjer SS, Sen S, Petraco R, Escaned J, Echavarria-Pinto M, Broyd C, Al-Lamee R, Foin N, Foale RA, Malik IS, et al. Pre-angioplasty instantaneous wave-free ratio pullback provides virtual intervention and predicts hemodynamic outcome for serial lesions and diffuse coronary artery disease. *JACC Cardiovasc Interv*. 2014;7:1386–1396. doi: 10.1016/j.jcin.2014.06.015
11. Scarsini R, Pesarini G, Zivelonghi C, Piccoli A, Ferrero V, Lunardi M, Gottin L, Zanetti C, Faggian G, Ribichini F. Physiologic evaluation of coronary lesions using instantaneous wave-free ratio (iFR) in patients with severe aortic stenosis undergoing transcatheter aortic valve implantation. *EuroIntervention*. 2018;13:1512–1519. doi: 10.4244/EIJ-D-17-00549
12. Sen S, Ahmad Y, Davies J. Assessing coronary disease in patients with severe aortic stenosis: the need for a 'valid' gold standard for validation studies? *EuroIntervention*. 2018;13:1499–1502. doi: 10.4244/EIJV13I13A240
13. van de Hoef TP, Nolte F, Rolandi MC, Piek JJ, van den Wijngaard JPHM, Spaan JAE, Siebes M. Coronary pressure-flow relations as basis for the understanding of coronary physiology. *J Mol Cell Cardiol*. 2012;52:786–793. doi: 10.1016/j.yjmcc.2011.07.025
14. Broyd CJ, Sen S, Mikhail GW, Francis DP, Mayet J, Davies JE. Myocardial ischemia in aortic stenosis: insights from arterial pulse-wave dynamics after percutaneous aortic valve replacement. *Trends Cardiovasc Med*. 2013;23:185–191. doi: 10.1016/j.tcm.2012.12.001
15. Iung B. Interface between valve disease and ischaemic heart disease. *Heart*. 2000;84:347–352. doi: 10.1136/heart.84.3.347
16. Kolkailah AA, Kwok CS, George S, Capodanno D, Ludman PF, Townend JN, Doshi SN, Khogali SS, Bénézeux P, Hermann HC, et al. Transcatheter aortic valve implantation with or without percutaneous coronary artery revascularization strategy: a systematic review and meta-analysis. *J Am Heart Assoc*. 2017;6:e005960. doi: 10.1161/JAHA.117.005960
17. Ahmad Y, Demir O, Rajkumar C, Howard JP, Shun-Shin M, Cook C, Petraco R, Jabbour R, Arnold A, Frame A, et al. Optimal antiplatelet strategy after transcatheter aortic valve implantation: a meta-analysis. *Open Heart*. 2018;5:e000748. doi: 10.1136/openhrt-2017-000748
18. Layland J, Wilson AM, Whitbourn RJ, Burns AT, Somaratne J, Leitl G, Macisaac AI. Impact of right atrial pressure on decision-making using fractional flow reserve (FFR) in elective percutaneous intervention. *Int J Cardiol*. 2013;167:951–953. doi: 10.1016/j.ijcard.2012.03.087
19. Dixon JA, Spinale FG. Myocardial remodeling: cellular and extracellular events and targets. *Annu Rev Physiol*. 2011;73:47–68. doi: 10.1146/annurev-physiol-012110-142230
20. Heusch G. Alpha-adrenergic coronary vasoconstriction in humans. *J Am Coll Cardiol*. 2010;55:1278; author reply 1278–1278; author reply 1279. doi: 10.1016/j.jacc.2009.09.067

Downloaded from http://ahajournals.org by on December 1, 2019

Heart and Vessels (2019) 34:1909–1916
https://doi.org/10.1007/s00380-019-01439-5

ORIGINAL ARTICLE

Prognostic impact of body mass index and culprit lesion calcification in patients with acute myocardial infarction

Hiroaki Yokoyama[1] · Takumi Higuma[2] · Tomohide Endo[1] · Fumie Nishizaki[1] · Kenji Hanada[1] · Takashi Yokota[1] · Masahiro Yamada[1] · Ken Okumura[3] · Hirofumi Tomita[1,2]

Received: 27 December 2018 / Accepted: 24 May 2019 / Published online: 29 May 2019
© Springer Japan KK, part of Springer Nature 2019

Abstract

Patients with acute myocardial infarction (AMI) with low body mass index (BMI) have worse outcomes than obese patients, and this phenomenon is recognized as "obesity paradox." Coronary calcification is associated with cardiac events. However, the association between BMI and calcification and their involvement in the mortality of AMI patients remain unknown. This study consecutively enrolled 517 patients with AMI who underwent emergent coronary intervention within 24 h after onset. Patients were divided into four groups according to the baseline BMI interquartile ranges: Q1 (BMI < 21.9 kg/m^2), Q2 (21.9 ≤ BMI < 24.0 kg/m^2), Q3 (24.0 ≤ BMI < 26.0 kg/m^2), and Q4 (BMI ≥ 26.0 kg/m^2). Calcification in the culprit lesion was also evaluated. The Q1 group was older and had a lower frequency of coronary risk factors. Moderate/severe calcification was most frequently observed in Q1, followed by Q2, Q3, and Q4. The Q1 group had the highest all-cause mortality, and patients with moderate/severe calcification had a higher all-cause mortality than that in patients without calcification. The highest all-cause mortality was observed in Q1 with calcification, and the lowest was in Q4 without calcification. Q1 and the presence of moderate/severe calcification were independently associated with all-cause mortality. Although low-BMI patients with AMI had a lower frequency of coronary risk factors, they had a worse all-cause mortality than that in high-BMI patients. Our findings suggest that lesion calcification and its possible association with low BMI are involved in the higher mortality rate in these patients.

Keywords Acute myocardial infarction · Body mass index · Coronary calcification

Introduction

Obesity is closely associated with the incidence of cardiovascular diseases and mortality [1–5]. However, some controversial studies have demonstrated that obese patients with concomitant cardiovascular disease have better outcomes than those in normal- or low-body-weight patients. This phenomenon has been recognized as the "obesity paradox" [6–8]. Regarding patients with acute myocardial infarction (AMI), several studies have demonstrated that patients with a lower body mass index (BMI) have worse in-hospital and long-term mortality rates than those of normal- or high-BMI patients [9–15]. However, the underlying mechanisms remain unclear.

Previous studies have suggested that calcified target coronary lesions are associated with higher risks of all-cause mortality and target lesion revascularization in patients treated with percutaneous coronary intervention (PCI) or coronary artery bypass grafting (CABG). A pooled analysis of the HORIZON-AMI and ACUITY trials revealed that patients with moderate/severe target lesion calcification were older and had a higher incidence of 1-year mortality after PCI [16]. In a cohort of patients who underwent CABG, subjects with severe lesion calcification were older, had a

Electronic supplementary material The online version of this article (doi:https://doi.org/10.1007/s00380-019-01439-5) contains supplementary material, which is available to authorized users.

✉ Hirofumi Tomita
tomitah@hirosaki-u.ac.jp

[1] Department of Cardiology, Hirosaki University Graduate School of Medicine, Zaifu-cho 5, Hirosaki 036-8562, Japan

[2] Department of Advanced Cardiovascular Therapeutics, Hirosaki University Graduate School of Medicine, Hirosaki, Japan

[3] Division of Cardiology, Saiseikai Kumamoto Hospital, Kumamoto, Japan

lower BMI, and were associated with increased mortality in comparison to those without lesion calcification [17]. These studies indicate that there are possible associations between aging or low BMI and coronary calcification.

However, the association between BMI and coronary artery calcification and their involvement in the outcomes of patients with AMI remain unknown. The aim of the present study was to evaluate the association between BMI and coronary artery calcification and their involvement in the incidence of all-cause mortality in patients with AMI treated with emergent PCI.

Materials and methods

Study patients

This study enrolled consecutive patients with AMI who presented to Hirosaki University Hospital between December 2008 and March 2013 and underwent emergent PCI within 24 h after symptom onset. Exclusion criteria were cardiac arrest on arrival ($n=2$) and AMI resulting from stent thrombosis ($n=13$). Finally, 517 patients [405 males (78%); mean age, 65 ± 13 years] were enrolled. The diagnosis of AMI was established using the universal definition of myocardial infarction based on clinical symptoms, changes in electrocardiographic readings, and the elevation of cardiac biomarkers [18]. BMI was calculated as body weight (kg) divided by the square of height (m^2) at the time of AMI presentation. Patients were divided into four groups according to the baseline BMI interquartile ranges: Q1 group (BMI < 21.9 kg/m^2, $n=123$), Q2 group ($21.9 \leq$ BMI < 24.0 kg/m^2, $n=126$), Q3 group ($24.0 \leq$ BMI < 26.0 kg/m^2, $n=134$), and Q4 group (BMI $\geq$ 26.0 kg/m^2, $n=134$). This study was conducted according to the principles of the Declaration of Helsinki and approved by the ethics committee of our institution.

Severity of calcification in the culprit lesion

The severity of calcification in the culprit lesion was evaluated using coronary angiography according to the criteria from a previous report [16], and this grading was performed by two physicians blinded to the outcomes of all patients in this study. Patients were divided into three groups according to the severity of calcification in the culprit lesion as follows: no/mild, moderate, and severe calcification groups. Moderate calcification was defined as radiopaque densities that were noted only during the cardiac cycle and that typically involved only one side of the vascular wall. Severe calcification was defined as radiopaque densities that were noted without cardiac motion prior to contrast injection and that generally involved both sides of the arterial wall. The interobserver variability kappa values for the degree of culprit lesion calcification were also evaluated.

Endpoints

The primary endpoint of this study was all-cause mortality. Follow-up was initiated on the day of admission. The patients were followed up for a median of 2.7 years with optimal medical treatment.

Statistical analysis

All continuous variables were expressed as mean ± standard deviation or median (interquartile range), and categorical variables were expressed as numbers and percentages. Continuous variables were compared using one-way analysis of variance, and the statistical significance of differences was calculated using the Tukey–Kramer test. The Mann–Whitney U test was used for nonparametric variables. The chi-square analysis was used to compare categorical variables. Furthermore, we examined the frequency of calcification in the culprit lesion evaluated by coronary angiography stratified by BMI categories using Cochran–Armitage trend test. Mortality was estimated using the Kaplan–Meier method and compared using the log-rank test. Multivariate analysis for the predictors of all-cause mortality was performed using Cox proportional hazards regression. The variables used for analysis included age, male gender, coronary risk factors [including hypertension, dyslipidemia, diabetes mellitus (DM), and smoking habits], CKD (chronic kidney disease), multi-vessel or left main trunk (LMT) disease, Killip classification IV at presentation, left ventricular ejection fraction in an acute phase, BMI categories (four groups), and the presence of moderate/severe coronary calcification. Hazard ratios (HRs) and 95% confidence intervals (CIs) were calculated. Receiver operating characteristic (ROC) curve analysis for predicting all-cause mortality was also performed. Statistical analyses were performed using JMP 13 software (SAS, Cary, NC, USA). A p value of <0.05 was considered statistically significant.

Results

Patient characteristics

The baseline patient characteristics stratified by BMI categories are listed in Table 1. The mean age significantly decreased with increasing BMI. The patients in the Q1 group had a lower prevalence of coronary risk factors, including hypertension, dyslipidemia, and DM. The prevalence of smoking habits did not differ among the four groups. Patients in the Q1 group had a higher prevalence of cardiogenic shock

Table 1 Patient profiles stratified by BMI categories

	Q1 group ($n=123$)	Q2 group ($n=126$)	Q3 group ($n=134$)	Q4 group ($n=134$)	p value
Age, years	72 ± 11	66 ± 11	65 ± 12	60 ± 14	< 0.01
Male gender, n (%)	87 (71)	101 (80)	110 (82)	107 (80)	0.13
BMI, kg/m^2	19.5 ± 1.7	22.9 ± 0.6	24.9 ± 0.5	29.0 ± 3.6	< 0.01
Coronary risk factors					
Hypertension, n (%)	78 (63)	88 (70)	93 (69)	109 (81)	< 0.05
Dyslipidemia, n (%)	75 (61)	97 (77)	100 (75)	110 (82)	< 0.01
Diabetes mellitus, n (%)	36 (29)	57 (45)	61 (46)	72 (54)	< 0.01
Smoking, n (%)	80 (65)	79 (63)	80 (60)	85 (63)	0.83
Previous MI, n (%)	9 (7)	16 (13)	16 (12)	12 (9)	0.45
Previous CABG, n (%)	0 (0)	1 (1)	0 (0)	0 (0)	0.38
Multi-vessel or LMT, n (%)	80 (65)	71 (56)	70 (52)	68 (51)	0.096
CKD	62 (50)	48 (38)	39 (29)	31 (23)	< 0.01
Hemodialysis, n (%)	8 (7)	2 (2)	4 (3)	1 (1)	< 0.05
Killip classification, n (%)					< 0.05
I	88 (72)	104 (83)	115 (86)	111 (83)	
II	14 (11)	12 (10)	11 (8)	10 (7)	
III	6 (5)	7 (6)	5 (4)	7 (5)	
IV	15 (12)	3 (2)	3 (2)	6 (4)	
Forrester classification, n (%)	($n=107$)	($n=101$)	($n=120$)	($n=116$)	0.29
I	46 (43)	51 (51)	64 (53)	53 (46)	
II	14 (13)	7 (7)	10 (8)	16 (14)	
III	23 (22)	21 (21)	32 (27)	25 (22)	
IV	24 (22)	22 (22)	14 (12)	22 (19)	
Culprit lesion, n (%)					0.22
LMT	7 (6)	3 (2)	1 (1)	3 (2)	
RCA	51 (41)	42 (33)	43 (32)	47 (35)	
LAD	45 (37)	62 (49)	70 (52)	64 (48)	
LCx	20 (16)	19 (15)	20 (15)	20 (15)	
Blood chemistry at admission					
Total cholesterol (mg/dL)	190 ± 41	193 ± 43	202 ± 45	205 ± 46	< 0.05
Triglyceride (mg/dL)	106 ± 86	143 ± 116	135 ± 96	153 ± 101	< 0.01
LDL cholesterol (mg/dL)	119 ± 36	119 ± 39	128 ± 40	129 ± 38	< 0.05
HDL cholesterol (mg/dL)	51 ± 14	46 ± 13	47 ± 11	44 ± 10	< 0.01
Admission glucose (mg/dL)	167 ± 72	166 ± 72	161 ± 68	174 ± 74	0.49
HbA1c (%)	5.7 ± 1.2	5.9 ± 1.1	6.0 ± 1.1	6.4 ± 1.5	< 0.01
BNP (pg/mL)	84 (34–229)	40 (19–172)	45 (16–105)	47 (18–116)	< 0.01
eGFR (mL/min/1.73 m^2)	59 (41–77)	69 (51–84)	71 (56–83)	76 (60–89)	< 0.01
Time to admission (hours)	3.6 (2.2–6.0)	3.4 (2.3–6.4)	3.5 (2.3–6.2)	3.3 (2.1–7.3)	0.89
LVEF at acute phase (%)	45 ± 12	44 ± 11	47 ± 10	45 ± 10	0.28

Values are expressed as mean ± standard deviation, median (interquartile range), or n (%)

BMI indicates body mass index, *CABG* coronary artery bypass grafting, *CKD* chronic kidney disease, *CPK* creatinine phosphokinase, *eGFR* estimate glomerular filtration rate, *LMT* left main trunk, *MI* myocardial infarction, *RCA* right coronary artery, *LAD* left ascending artery, *LCx* left circumflex, *LDL* low-density lipoprotein, *HDL* high-density lipoprotein, *HbA1c* hemoglobin A1c, *BNP* brain natriuretic peptide, *LVEF* left ventricular ejection fraction

Q1 group: BMI < 21.9 kg/m^2, Q2 group: 21.9 ≤ BMI < 24.0 kg/m^2; Q3 group: 24.0 ≤ BMI < 26.0 kg/m^2; Q4 group: BMI ≥ 26.0 kg/m^2

(Killip classification IV) on admission than that of patients in other groups. Although the prevalence of multi-vessel or LMT disease tended to be higher in patients in the Q1 group, there was no significant difference in this prevalence among patients in other groups ($p = 0.096$). Patients in the Q1 group had lower levels of total cholesterol, low-density

lipoprotein cholesterol, and triglycerides and higher levels of high-density lipoprotein cholesterol compared with those in patients in the Q4 group. The levels of hemoglobin A1c increased with the BMI. Brain natriuretic peptide levels on admission were significantly higher in patients in the Q1 group than in those in other groups. Estimate glomerular filtration rate (eGFR) was better in the Q4 group, followed by the Q3, Q2, and Q1 groups [76 (60–89), 71 (56–83), 69 (51–84), and 59 (41–77) mL/min/1.73 m^2, respectively; $p < 0.01$]. Moreover, there were more patients with hemodialysis in the Q1 group compared with those in other groups ($p < 0.01$). The time from symptom onset to admission did not differ among the four groups.

Severity of calcification in the culprit lesion

Moderate/severe coronary calcification was observed in 41% of all study patients. The interobserver variability yielded acceptable concordance for no/mild (kappa = 0.90), moderate (kappa = 0.83), and severe (kappa = 0.95) calcifications. As shown in Fig. 1, moderate/severe calcification in the culprit lesion was most frequently observed in the Q1 group, followed by the Q2, Q3, and Q4 groups (72%, 55%, 28%, and 14%, respectively; $p < 0.01$). There was a significant increase in the severity of calcification in the culprit lesion with decrease in BMI level ($p < 0.01$). Patients with moderate/severe coronary calcification were more likely to have a proximal culprit lesion (i.e., in coronary segment 1, 6, or 11, classified according to the definition of the American Heart Association), including LMT, than patients with no/mild calcification (54% versus 33%, respectively; $p < 0.01$) (Table 2). Next, we evaluated the association between renal function and the severity of calcification in the culprit lesion. Patients with CKD ($n = 180$) had more moderate/severe calcification in the culprit compared with those without CKD (58% in patients with CKD vs 33% without CKD, $p < 0.01$).

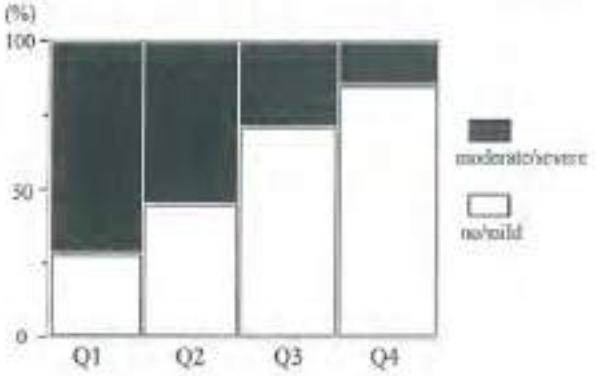

Fig. 1 Prevalence of calcification in the culprit lesion evaluated by coronary angiography stratified by BMI categories

Long-term mortality

The rate of incidence of long-term all-cause mortality is shown in Fig. 2. The Q1 group had the worst all-cause mortality rate, followed by the Q2, Q3, and Q4 groups ($p < 0.01$ by log-rank test) (Fig. 2A). The number of all-cause deaths in the Q1, Q2, Q3, and Q4 groups was 32/123 (26%), 22/126 (18%), 9/134 (7%), and 6/134 (4%), respectively (Table 3). Furthermore, we performed a landmark analysis at 1 month after emergent PCI, because Killip classification IV has a great impact on the short-term mortality in patients with AMI. A landmark analysis revealed that the Q1 group had the worst all-cause mortality rate, followed by the Q2, Q3, and Q4 groups ($p < 0.01$ by log-rank test) (Supplementary Figure). Moreover, patients with moderate/severe coronary calcification had a higher all-cause mortality rate in comparison to those with no/mild calcification ($p < 0.01$ by log-rank test) (Fig. 2B). The number of all-cause deaths in the no/mild and moderate/severe calcification groups was 18/303 (6%) and 51/214 (24%), respectively (Table 3).

We further evaluated impact of the renal function on the all-cause mortality. All-cause mortality was higher in patients with CKD compared with those without CKD (47% in patients with CKD vs 6% without CKD, $p < 0.01$ by log-rank test).

Table 2 Location of the culprit lesion

	No/mild calcification ($n = 303$)	Moderate/severe calcification ($n = 214$)	p value
Proximal culprit lesion, n (%)	101 (33)	115 (54)	< 0.01
LMT	4 (1)	10 (5)	
RCA segment 1	28 (9)	24 (11)	
LAD segment 6	60 (20)	73 (34)	
LCx segment 11	9 (3)	8 (4)	

Values are expressed as n (%)

LMT left main trunk, *RCA* right coronary artery, *LAD* left ascending artery, *LCx* left circumflex

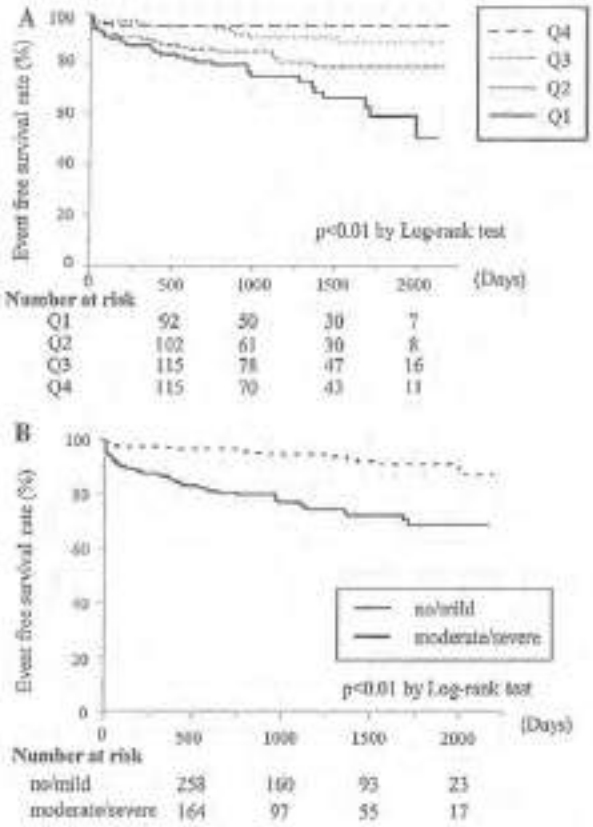

Fig. 2 Kaplan–Meier survival curves in AMI patients. **a** All-cause mortality stratified by BMI categories. **b** All-cause mortality stratified by the severity of calcification in the culprit lesion

Table 3 Mortality stratified by BMI categories and severity of calcification in the culprit lesion

	All-cause death	Cardiovascular death	Non-cardiovascular death
BMI subgroup			
Q1 ($n=123$)	32 (26)	13 (11)	19 (15)
No/mild ($n=35$)	3 (9)	2 (6)	1 (3)
Moderate/severe ($n=88$)	29 (33)	11 (13)	18 (20)
Q2 ($n=126$)	22 (18)	16 (13)	6 (5)
No/mild ($n=57$)	5 (9)	2 (4)	3 (5)
Moderate/severe ($n=69$)	17 (25)	14 (20)	3 (4)
Q3 ($n=134$)	9 (7)	5 (4)	4 (3)
No/mild ($n=96$)	5 (5)	1 (1)	4 (4)
Moderate/severe ($n=38$)	4 (11)	4 (11)	0 (0)
Q4 ($n=134$)	6 (4)	5 (4)	1 (1)
No/mild ($n=115$)	5 (4)	4 (3)	1 (1)
Moderate/severe ($n=19$)	1 (5)	1 (5)	0 (0)
Calcification			
No/mild ($n=303$)	18 (6)	9 (3)	9 (3)
Moderate/severe ($n=214$)	51 (24)	30 (14)	21 (10)

Values are expressed as n (%). Q1 group: BMI < 21.9 kg/m^2; Q2 group: 21.9 ≤ BMI < 24.0 kg/m^2; Q3 group: 24.0 ≤ BMI < 26.0 kg/m^2; Q4 group: BMI ≥ 26.0 kg/m^2

Cardiovascular and non-cardiovascular mortalities

Cardiovascular and non-cardiovascular mortalities were separately analyzed (Table 3). The number of cardiovascular deaths in the Q1, Q2, Q3, and Q4 groups was 13/123 (11%), 16/126 (13%), 5/134 (4%), and 5/134 (4%), respectively, and the number of non-cardiovascular deaths in these groups was 19/123 (15%), 6/126 (5%), 4/134 (3%), and 1/134 (1%), respectively. The number of cardiovascular deaths in the no/mild and moderate/severe calcification groups was 9/303 (3%) and 30/214 (14%), respectively, and the number of non-cardiovascular deaths in these groups was 9/303 (3%) and 21/214 (10%), respectively.

Predictors of all-cause mortality

Owing to a significant association between the presence of coronary calcification and BMI, these valuables were separately analyzed. The results of multivariate Cox proportional hazard analyses for elucidating the predictors of all-cause mortality are shown in Table 4. Even after adjusting for covariates, Q1 and Q2 were associated with all-cause mortality (HR for Q1 3.11, 95% CI 1.34–8.49 and HR for Q2 3.23, 95% CI 1.32–9.13, both $p < 0.01$) (Table 4A). Furthermore, the presence of moderate/severe coronary calcification was associated with all-cause mortality (HR: 1.77, 95% CI: 1.00–3.25, $p < 0.05$) (Table 4B). In both analyses, CKD had the highest HR for all-cause mortality. Moreover, we performed multivariate analysis for the predictor of cardiovascular mortality. When BMI was added in the analysis, age, CKD, Killip classification IV, and LVEF were the independent predictors for cardiovascular mortality, but BMI was not. When the presence of coronary calcification was added in the analysis, age, CKD, DM, Killip classification IV, LVEF, and coronary calcification were the independent predictors for cardiovascular mortality.

To further investigate these associations, the patients were divided into eight groups according to the baseline BMI interquartile ranges and the presence of moderate/severe coronary calcification. Detailed results of mortality are shown in Table 3. The HRs (95% CI) for all-cause mortality in the Q1, Q2, Q3, and Q4 groups with no/mild or moderate/severe calcification were evaluated using the Q4 group with no/mild calcification as a reference. The highest incidence of all-cause mortality was observed in

Table 4 Adjusted hazard ratios for all-cause mortality

	Adjusted HR (95% CI)	p value
A		
BMI		
Q4	Reference	
Q3	1.31 (0.47–3.94)	0.61
Q2	3.23 (1.32–9.13)	<0.01
Q1	3.11 (1.34–8.49)	<0.01
Age	1.05 (1.02–1.09)	<0.01
Male gender	1.92 (0.90–4.24)	0.09
Hypertension	0.95 (0.55–1.71)	0.85
Dyslipidemia	0.58 (0.34–0.98)	<0.05
Diabetes mellitus	1.51 (0.88–2.58)	0.13
Smoking	1.17 (0.64–2.23)	0.62
CKD	3.78 (2.06–7.33)	<0.01
Multi-vessel or LMT disease	2.14 (1.11–4.56)	<0.05
Killip classification IV	2.79 (1.41–5.20)	<0.01
LVEF at acute phase	0.95 (0.93–0.97)	<0.01
B		
Calcification in culprit lesion		
No/mild	Reference	
Moderate/severe	1.77 (1.00–3.25)	<0.05
Age	1.05 (1.02–1.08)	<0.01
Male gender	1.85 (0.88–4.05)	0.11
Hypertension	0.97 (0.56–1.74)	0.91
Dyslipidemia	0.55 (0.32–0.93)	<0.05
Diabetes mellitus	1.49 (0.89–2.48)	0.13
Smoking	1.28 (0.71–2.42)	0.42
CKD	4.46 (2.45–8.57)	<0.01
Multi-vessel or LMT disease	1.73 (0.90–3.69)	0.11
Killip classification IV	2.93 (1.49–5.39)	<0.01
LVEF at acute phase	0.95 (0.93–0.97)	<0.01

Q1 group: BMI < 21.9 kg/m^2; Q2 group: 21.9 ≤ BMI < 24.0 kg/m^2; Q3 group: 24.0 ≤ BMI < 26.0 kg/m^2; Q4 group: BMI ≥ 26.0 kg/m^2

BMI body mass index, *CKD* chronic kidney disease, *LVEF* left ventricular ejection fraction, *LMT* left main trunk, *HR* hazard ratio, *CI* confidence interval

the Q1 group with moderate/severe calcification, followed by the Q2 group with moderate/severe calcification, both of which were statistically significant (Fig. 3).

ROC curve for predicting all-cause mortality

The optimal cutoff value of BMI for long-term all-cause mortality derived from the ROC curve was 23.6 kg/m^2 (C-statistic = 0.73, $p < 0.01$). The use of this cutoff value indicated a sensitivity, specificity, positive predictive value, and negative predictive value of 78%, 60%, 23%, and 95%, respectively.

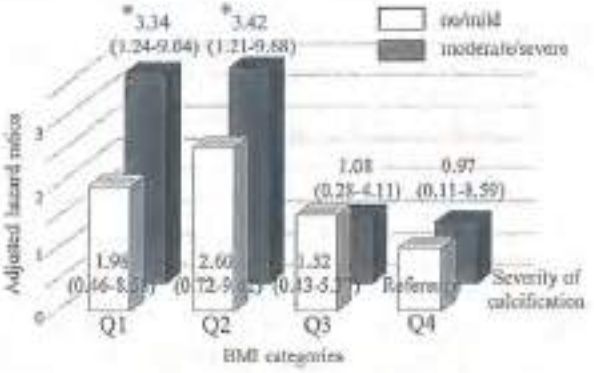

Fig. 3 Adjusted hazard ratios of all-cause mortality stratified by BMI categories and the severity of calcification in the culprit lesion using the Q4 group with no/mild calcification as a reference. Data are shown as hazard ratios and 95% confidence intervals. *$p < 0.05$

Discussion

In the present study, we demonstrated that (1) patients with AMI with a low BMI had a higher mortality rate in comparison to those with a high BMI; (2) patients with AMI with moderate/severe calcification in the culprit lesion had a higher mortality rate in comparison to those with no/mild calcification; (3) moderate/severe calcification in the culprit lesion was most frequently observed in low-BMI patients; (4) the highest mortality was observed in low-BMI patients with moderate/severe calcification in the culprit lesion, and the lowest mortality was observed in high-BMI patients with no/mild calcification; and (5) both BMI and moderate/severe calcification in the culprit lesion were independent predictors of long-term all-cause mortality. Although low-BMI patients with AMI had a lower incidence of coronary risk factors, they had a higher incidence of moderate/severe calcification in the culprit lesion and the highest long-term all-cause mortality. These findings indicate that low BMI and moderate/severe coronary calcification in patients with AMI are likely to be associated with higher mortality.

Associations among BMI, coronary calcification, and mortality

Obesity reduces insulin sensitivity, enhances free fatty acid turnover, increases basal sympathetic tone, induces a hypercoagulable state, and promotes systemic inflammation, all of which contribute to the development and progression of cardiovascular diseases [5]. In the present study, we observed that high-BMI patients with AMI had a higher prevalence of coronary risk factors (i.e., hypertension, dyslipidemia, and DM), which is consistent with the results of other studies [2–4, 15, 19, 20]. Despite such adverse clinical profiles, high-BMI patients with

AMI had a lower long-term all-cause mortality in comparison to low-BMI patients with AMI. These findings are recognized as the "obesity paradox," and our findings support previous reports [6–15]. Moreover, in this study, patients in the Q1 group had a higher prevalence of cardiogenic shock (Killip classification IV) on admission than patients in other groups. Although there was no difference in the culprit lesions among the 4 groups, the prevalence of multi-vessel or LMT disease tended to be higher in patients in the Q1 group ($p = 0.096$). Patients with multi-vessel or LMT disease were known to have worse outcomes compared with those without. Therefore, we think that the higher prevalence of multi-vessel or LMT disease in patients in the Q1 group may contribute to the higher prevalence of cardiogenic shock on admission compared with those in other groups.

Several studies have reported an association between coronary calcification and clinical outcomes in patients undergoing PCI and have revealed that coronary calcification is a predictor of target vessel failure and major adverse events [21–23]. Similarly, patients undergoing CABG who had severe calcification in the lesion exhibited increased mortality [17, 24]. Genereux et al. reported that PCI in patients with AMI with moderately or severely calcified lesions was associated with higher 1-year rates of major adverse cardiac events, including all-cause mortality, myocardial infarction, and target lesion revascularization [16]. These studies support our results that low-BMI patients with AMI had a higher prevalence of moderate/severe calcification in the culprit lesion and higher mortality. Calcified coronary lesions represent an advanced stage in the atherosclerotic process, wherein a soft plaque is converted to a fibrocalcific plaque. It has been reported that coronary calcification is associated with systemic atherosclerosis [25], which might affect mortality. Moreover, our subjects with moderate/severe coronary calcification were more likely to have proximal culprit lesions than those with no/mild calcification, and this association may be related to the increased mortality. Therefore, our finding that patients with AMI with moderate/severe coronary calcification had a higher mortality may be reasonable. However, it remains unclear whether there is a direct association between low BMI and coronary calcification. We compared BMI among the 3 groups divided by the severity of coronary calcification in the culprit lesion. BMI was the highest in the patients with no/mild coronary calcification in the culprit, followed by those with moderate calcification and those with severe calcification (25.5 ± 3.6, 22.8 ± 2.8, and 21.7 ± 3.4 kg/m^2, respectively; $p < 0.01$). These finding suggests a possible association between low BMI and coronary calcification. However, our results were derived from a single-center retrospective analysis, and to the best of our knowledge, there has been no study to clarify the relationship between low BMI and coronary calcification in patients with AMI. Further studies are required to elucidate its underlying mechanisms.

Cardiovascular and non-cardiovascular mortalities

Brian et al. reported that low BMI is a marker of systemic illness in patients treated with PCI, and these patients had a higher prevalence of tumors, leukemia, and lymphoma [3]. Furthermore, other studies have reported that low-BMI patients with cardiovascular disease had higher rates of cachexia-related comorbidities, including cancer, dementia, and hypoalbuminemia [6, 10]. Our study demonstrating that the incidence of non-cardiovascular mortality was the highest in low-BMI patients also supports their results. Moreover, we observed that low- or normal-BMI patients had a higher incidence of cardiovascular death in comparison to high-BMI patients. Thus, both cardiovascular and non-cardiovascular deaths are responsible for higher mortality rates in low-BMI patients with AMI.

Limitations

There are several limitations in the present study. First, our results were derived from a single-center retrospective analysis. Therefore, the generalization of our results would be limited. However, we studied consecutive patients admitted during the study period, which may minimize the biases involved in a retrospective study. Second, the changes in BMI occurring during the follow-up period, which might have impacted long-term mortality, were not assessed [26]. Finally, we evaluated the severity of calcification only in the culprit lesion and did not assess the presence of calcification in segments with non-culprit lesions, which might have affected the outcomes.

Conclusions

Although low-BMI patients with AMI had a lower frequency of coronary risk factors, they had a higher incidence of moderate/severe calcification in the culprit lesion and the highest long-term all-cause mortality in comparison to high-BMI patients. We suggest that calcification in the culprit lesion and its possible association with low BMI are involved in the higher mortality of these patients.

Compliance with ethical standards

Conflict of interest None.

References

1. Stevens J, Cai J, Pamuk ER, Williamson DF, Thun MJ, Wood JL (1998) The effect of age on the association between body-mass index and mortality. N Engl J Med 338:1–7
2. Calle EE, Thun MJ, Petrelli JM, Rodriguez C, Heath CW Jr (1999) Body-mass index and mortality in a prospective cohort of US adults. N Engl J Med 341:1097–1105
3. Powell BD, Lennon RJ, Lerman A, Bell MR, Berger PB, Higano ST, Holmes DR Jr, Rihal CS (2003) Association of body mass index with outcome after percutaneous coronary intervention. Am J Cardiol 91:472–476
4. Allison DB, Fontaine KR, Manson JE, Stevens J, VanItallie TB (1999) Annual deaths attributable to obesity in the United States. JAMA 282:1530–1538
5. Fi-Sanyer FX (2002) The obesity epidemic: pathophysiology and consequences of obesity. Obes Res 10:97s–104s
6. Romero-Corral A, Montori VM, Somers VK, Korinek J, Thomas RJ, Allison TG, Mookadam F, Lopez-Jimenez F (2006) Association of bodyweight with total mortality and with cardiovascular events in coronary artery disease: a systematic review of cohort studies. Lancet 368:666–678
7. Ades PA, Savage PD (2010) The obesity paradox: perception vs knowledge. Mayo Clin Proc 85:112–114
8. Nikolsky E, Stone GW, Grines CL, Cox DA, Garcia E, Tcheng JE, Griffin JJ, Guagliumi G, Stuckey T, Turco M, Negoita M, Lansky AJ, Mehran R (2006) Impact of body mass index on outcomes after primary angioplasty in acute myocardial infarction. Am Heart J 151:168–175
9. Arcoson D, Nassar M, Goldberg T, Kapeliovich M, Hammerman H, Azzam ZS (2010) The impact of body mass index on clinical outcomes after acute myocardial infarction. Int J Cardiol 145:476–480
10. Bucholz EM, Beckman AL, Krumholz HA, Krumholz HM (2016) Excess weight and life expectancy after acute myocardial infarction: the obesity paradox re-examined. Am Heart J 172:173–181
11. Buettner HJ, Mueller C, Gick M, Ferenc M, Allgeier J, Comberg T, Werner KD, Schindler C, Neumann FJ (2007) The impact of obesity on mortality in UA/non-ST-segment elevation myocardial infarction. Eur Heart J 28:1694–1701
12. Krageland C, Hassager C, Hildebrandt P, Torp-Pedersen C, Køber L (2005) Impact of obesity on long-term prognosis following acute myocardial infarction. Int J Cardiol 98:123–131
13. O'Brien EC, Fosbol EL, Peng SA, Alexander KP, Roe MT, Peterson ED (2014) Association of body mass index and long-term outcomes in older patients with non-ST-segment-elevation myocardial infarction: results from the CRUSADE Registry. Circ Cardiovasc Qual Outcomes 7:102–109
14. Wienbergen H, Gitt AK, Juenger C, Schiele R, Heer T, Towae F, Gohlke H, Seages J, MITRA PLUS study group (2008) Impact of the body mass index on occurrence and outcome of acute ST-elevation myocardial infarction. Clin Res Cardiol 97:83–88
15. Kosuge M, Kimura K, Kojima KS, Sakamoto T, Ishihara M, Asada Y, Tei C, Miyazaki S, Sonoda M, Tsuchihashi K, Yamagishi M, Shirai M, Hiraoka H, Honda T, Ogata Y, Ogawa H, Japanese Acute Coronary Syndrome Study (JACSS) Investigators (2008) Impact of body mass index on in-hospital outcomes after percutaneous coronary intervention for ST segment elevation acute myocardial infarction. Circ J 72:521–525
16. Generoux P, Madhavan MV, Mintz GS, Maehara A, Palmerini T, Lasalle L, Xu K, McAndrew T, Kirtane A, Lansky AJ, Breiner SJ, Mehran R, Stone GW (2014) Ischemic outcomes after coronary intervention of calcified vessels in acute coronary syndromes. Pooled analysis from the HORIZONS-AMI (harmonizing outcomes with revascularization and stents in acute myocardial infarction) and ACUITY (acute catheterization and urgent intervention triage strategy) TRIALS. J Am Coll Cardiol 63:1845–1854
17. Bourantas CV, Zhang YJ, Garg S, Mack M, Dawkins KD, Kappetein AP, Mohr FW, Colombo A, Holmes DR, Stähle E, Feldman T, Morice MC, de Vries T, Morel MA, Serruys PW (2015) Prognostic implications of severe coronary calcification in patients undergoing coronary artery bypass surgery: an analysis of the SYNTAX study. Catheter Cardiovasc Interv 85:199–206
18. Thygesen K, Alpert JS, Jaffe AS, Simoons ML, Chaitman BR, White HD (2012) Third universal definition of myocardial infarction. Glob Heart 7:275–295
19. Mehta L, Devlin W, McCullough PA, O'Neill WW, Skelding KA, Stone GW, Boura JA, Grines CL (2007) Impact of body mass index on outcomes after percutaneous coronary intervention in patients with acute myocardial infarction. Am J Cardiol 99:906–910
20. Das SR, Alexander KP, Chen AY, Powell-Wiley TM, Diercks DB, Peterson ED, Roe MT, de Lemos JA (2011) Impact of body weight and extreme obesity on the presentation, treatment, and in-hospital outcomes of 50,149 patients with ST-Segment elevation myocardial infarction results from the NCDR (National Cardiovascular Data Registry). J Am Coll Cardiol 58:2642–2650
21. Onuma Y, Tanimoto S, Ruygrok P, Neumann J, Piek JJ, Seth A, Schofer JJ, Richardt G, Wiemer M, Carrié D, Thuesen L, Dorange C, Miquel-Hebert K, Veldhof S, Serruys PW (2010) Efficacy of everolimus eluting stent implantation in patients with calcified coronary culprit lesions: two-year angiographic and three-year clinical results from the SPIRIT II study. Catheter Cardiovasc Interv 76:634–642
22. Fujimoto H, Nakamura M, Yokoi H (2012) Impact of calcification on the long-term outcomes of sirolimus-eluting stent implantation: subanalysis of the Cypher Post-Marketing Surveillance Registry. Circ J 76:57–64
23. Kawaguchi R, Tsurugaya H, Hoshizaki H, Toyama T, Oshima S, Taniguchi K (2008) Impact of lesion calcification on clinical and angiographic outcome after sirolimus-eluting stent implantation in real-world patients. Cardiovas Revasc Med 9:2–8
24. Estelt K, Generoux P, Mintz GS, Reiss GR, Kirtane AJ, Madhavan MV, Fahy M, Williams MR, Breiner SJ, Mehran R, Stone GW (2013) Impact of the severity of coronary artery calcification on clinical events in patients undergoing coronary artery bypass grafting (from the Acute Catheterization and Urgent Intervention Triage Strategy Trial). Am J Cardiol 112:1730–1737
25. Kim BJ, Lee SH, Kim CK, Ryu WS, Kwon HM, Choi SY, Yoon BW (2011) Advanced coronary artery calcification and cerebral small vessel diseases in the healthy elderly. Circ J 75:451–456
26. Eilat-Adar S, Eldar M, Goldbourt U (2006) Association of intentional changes in body weight with coronary heart disease event rates in overweight subjects who have an additional coronary risk factor. Am J Epidemiol 161:352–358

Publisher's Note Springer Nature remains neutral with regard to jurisdictional claims in published maps and institutional affiliations.

Detection of high-frequency artifact as a function of pulse generator algorithms and outer-insulation material

Ryohsuke Narui, MD, PhD, Tomofumi Nakamura, MD, PhD, Ikutaro Nakajima, MD, PhD, Caleb A. Norton, MD, Eun-jeong Kim, MD, Benjamin B. Holmes, MD, William G. Stevenson, MD, FHRS, Roy M. John, MBBS, PhD, FHRS, Christopher R. Ellis, MD, FHRS, George H. Crossley III, MD, FHRS, Jay A. Montgomery, MD

From the Arrhythmia Section, Cardiovascular Division, Department of Medicine, Vanderbilt University Medical Center, Nashville, Tennessee.

BACKGROUND A high rate of malfunction, predominantly intermittent high-frequency artifacts (HFAs), has been recently reported in Abbott Medical Tendril pacing leads.

OBJECTIVE To investigate the factors associated with the occurrence of HFAs on Tendril leads using a commonly used comparator lead for a control.

METHODS We reviewed institutional data for Medtronic CapSureFix 5076 and Abbott Medical Tendril pace-sense leads retrospectively. Recordings deemed to be due to electromagnetic interference and far-field oversensing were not included in the classification of HFAs.

RESULTS A total of 7673 leads were analyzed: 1628 Optim-insulated Tendril leads, 825 non-Optim Tendril leads, and 5220 CapSureFix 5076. HFAs were seen in 212 leads and were more frequently observed in Tendril compared to CapSureFix leads during a mean follow-up of 4.1 ± 3.6 years. Lower age at implant, defibrillator systems, atrial position, and connection to an Abbott Medical generator were associated with increased HFA. In multivariable analysis, only connection to Abbott Medical generators (odds ratio 7.686, $P < .001$) and age (odds ratio 0.988 per year, $P = .016$) were independently associated with HFAs on pace-sense leads. In an Abbott-generator-only analysis, Optim-insulated Tendril leads were more likely to display HFAs than non-Optim Tendril leads but not Medtronic CapSureFix 5076 leads.

CONCLUSION Abbott Medical pulse generators independently predict HFA in Tendril and CapSureFix 5076 leads, likely the result of displaying short or low-amplitude noise episodes that other devices do not record. When restricted to Abbott generators only, Optim-insulated Tendril leads show an increased incidence of HFAs when compared to non-Optim Tendril leads but not CapSureFix 5076 leads.

KEYWORDS Autosensitivity; Generator algorithm; High-frequency artifact; Noise; Pacing lead

(Heart Rhythm 2019;16:1855–1861) Published by Elsevier Inc. on behalf of Heart Rhythm Society.

Each year, more than 1 million cardiovascular implantable electronic devices (CIEDs) are implanted worldwide.[1] As the population ages and indications for pacemaker and defibrillator implantation increase, the total number of implanted components steadily rises, and the possibility for unintentional harm from suboptimal CIED components increases. A high rate of malfunction, predominantly oversensing of intermittent high-frequency artifacts (HFAs) in St. Jude/Abbott Medical Tendril 1688, 1888, and 2088 pacing leads (St. Jude Medical is now part of Abbott Laboratories, Chicago, IL), has been recently reported.[2] With any higher-than-expected signal of CIED malfunction, questions arise as to whether the product in question should continue to be implanted and whether a product recall should be considered. However, within the same study, there seemed to be a relatively low incidence of objective lead failure and impedance abnormalities in leads with noise. We hypothesized that differences in pulse generator algorithms could lead to a lesser

Disclosures: Ryohsuke Narui, Tomofumi Nakamura, and Ikutaro Nakajima have received a scholarship from the Japanese Heart Rhythm society. William Stevenson has received speaking honoraria from Abbott Medical, Boston Scientific, and Medtronic. Roy John has received lecture honoraria from Medtronic and Abbott Medical. Christopher Ellis has received research funding from Medtronic, AtriCure, Thoratec, and Boston Scientific; and consulting fees from Medtronic, Sentre Heart, Spectranetics, Biosense Webster, Boston Scientific, and Atricure. George Crossley has served as a consultant for Medtronic and Boston Scientific and as a speaker for Medtronic. All other authors have reported that they have no relationships relevant to the contents of this paper to disclose. **Address reprint request and correspondence:** Jay A. Montgomery, MD, Vanderbilt Heart and Vascular Institute, 1215 21st Ave South, MCE 5th Floor South Tower, Nashville, TN 37232. E-mail address: jay.a.montgomery@vanderbilt.edu.

1547-5271/$-see front matter Published by Elsevier Inc. on behalf of Heart Rhythm Society. https://doi.org/10.1016/j.hrthm.2019.05.020

or greater likelihood of recording HFAs across generator manufacturers, which could at least partially account for the high rate of HFAs seen in Tendril leads.

Methods

We retrospectively reviewed data for all patients implanted or followed at our institution with Medtronic (Minneapolis, MN) CapSureFix 5076 or Abbott Tendril (models 1688TC, 1888TC, 20888TC) pacemaker leads between January 2000 and September 2018 via a cardiac device electronic monitoring system (PaceArt, Medtronic). After lead implantation, all patients underwent periodic outpatient follow-up and/or remote device interrogations. All Tendril and CapSureFix 5076 leads were screened using the following search terms: noise, oversensing, artifact, insulation, and lead fracture. HFAs were defined as nonphysiologic artifacts on pacemaker leads detected at least twice in separate episodes and confirmed by the attending electrophysiologist. Transient arrhythmias or episodes only documented on a marker channel were not included as HFAs. Leads displaying clear electromagnetic interference (such as 60 Hz electrical artifact, sine wave pattern, perfectly regular, nonphysiologic pattern, and nonrecurring simultaneous signals on multiple leads) and far-field oversensing of T waves, R waves, or P waves were excluded from the criteria of HFA. Abnormal impedance was defined as below 200 ohms or above 2000 ohms. Leads that underwent a lead revision owing to rapidly rising or falling impedance were also included in the "abnormal impedance" group. Pacing/sensing failure was defined as a nonfunctional lead owing to loss of capture despite maximal output pacing and/or failure to reliably sense. The manufacturer of the generator for a given lead with HFAs was defined as the generator connected when HFAs were first detected, and the generator manufacturer connected to leads without HFA was defined as the most recent generator. Nominal sensing was bipolar. If leads were found to have had unipolar sensing at the time of HFA detection, these leads were excluded from the analysis. Patients with artifacts detected on device interrogation underwent isometric exercises per institutional protocol consisting of pectoral muscle contraction, reaching across the chest, and direct pocket manipulation. The study protocol was approved by the institutional review board at Vanderbilt University Medical Center.

Statistical analyses

Continuous variables are expressed as the mean ± standard deviation. Data were analyzed by a 1-way analysis of variance or Kruskal-Wallis test, with Tukey or Steel-Dwass post hoc test, as appropriate. Categorical variables, expressed as numbers or percentages, were analyzed using the χ^2 test or Fisher exact test. A Kaplan-Meier analysis with the log-rank test was used to determine the probability of freedom from HFA. To analyze independent predictive factors of HFA, univariate factors with $P < .1$ were analyzed using the Cox proportional hazard regression model (multivariate analysis). All tests were 2-tailed, and a P value of $<.05$ was considered to be significant. All statistical analyses were performed with EZR (Saitama Medical Center, Jichi Medical University, Saitama, Japan), which is a graphical user interface for R (The R Foundation for Statistical Computing, Vienna, Austria). More precisely, it is a modified version of R commander designed to add statistical functions frequently used in biostatistics.[3]

Results

A total of 7691 leads were identified in 5186 patients. HFAs were observed in 230 (3.0%) leads, of which 18 were excluded from analysis owing to being programmed to unipolar sensing at the time HFAs were detected (11 ventricular and 7 atrial). A total of 7673 leads, including 1628 Optim-insulated Tendril leads (models 1888 and 2088), 825 non-Optim Tendril leads (model 1688), and 5220 CapSureFix 5076 leads, were analyzed. The baseline lead characteristics are shown in Table 1. The mean age at implant was 68 ± 15 years, 4337 leads (56.5%) were implanted in male patients, 4728 (61.5%) leads were implanted in the atrium, and 1886 (24.6%) were connected to a defibrillator system. Mismatch between lead brand and generator brand was seen in 791 (10.3%) leads. The numbers of leads connected to Abbott Medical generators, Medtronic generators, and other generators were 2323 (30.3%), 4790 (62.4%), and 560 (7.3%), respectively. The mean follow-up period for all leads was 4.1 ± 3.6 years. Non-Optim Tendril leads were more frequently implanted in male patients. Optim-insulated Tendril leads were more likely to be implanted in the atrium and more likely to be connected to a defibrillator system. Approximately 90% of all leads were connected to a same-manufacturer generator, though Tendril leads were slightly less likely to be connected to a mismatched generator. Non-Optim Tendril leads had longer follow-up.

In univariate analysis, HFAs were more common in both Optim-insulated and non-Optim Tendril leads than in CapSureFix 5076 leads (Table 2 and Figure 1A). Leads displaying HFA were more frequently connected to Abbott Medical pulse generators than those without (odds ratio [OR] 10.230, $P < .001$, Table 2). In addition, the mean age at implant was significantly lower, atrial lead position more common, and connection to a defibrillator more likely in leads with HFA compared to those without.

In the multivariate analysis, only age at implant and connection to Abbott Medical generators were independent predictors of HFA (OR 0.988 per year, 95% confidence interval [CI] 0.979–0.997, $P < .001$, and OR 7.686, 95% CI 4.096–14.420, $P < .001$). Optim insulation, atrial lead position, and connection to a defibrillator system showed a nonsignificant trend toward higher incidence of HFAs. While virtually all leads connected to a defibrillator were implanted in the atrium, atrial lead position and connection to a defibrillator system were both included in the multivariate model, as the collinearity between the 2 groups was acceptably low (variance inflation factor = 1.219).

Table 1 Baseline characteristics

	All leads (n = 7673)	Tendril with Optim (n = 1628)	Tendril without Optim (n = 825)	CapSureFix (n = 5220)	P
Age at implant (y)	68 ± 15	67 ± 14	68 ± 15	68 ± 15	.112
Sex (male)	4337 (56.5)	887 (54.5)	498 (60.4)	2952 (56.6)	.021
Atrial lead	4728 (61.6)	1084 (66.6)	515 (62.4)	3129 (59.9)	<.001
Defibrillator system (ICD and CRT-D)	1886 (24.6)	489 (30.3)	227 (27.5)	1170 (22.4)	<.001
Mismatched generator*	791 (10.3)	137 (8.4)	81 (9.8)	573 (11.0)	.011
Abbott generator	2323 (30.3)	1491 (91.6)	744 (90.2)	88 (1.7)	<.001
Medtronic generator	4790 (62.4)	72 (4.4)	71 (8.6)	4647 (89.0)	<.001
Other generator	560 (7.3)	65 (3.9)	10 (1.2)	485 (9.3)	<.001
Follow-up period (y)	4.1 ± 3.6	3.9 ± 2.8	4.7 ± 3.9	4.0 ± 3.7	<.001

Data are presented as mean ± standard deviation or frequency (percentage).
CRT-D = cardiac resynchronization therapy-defibrillator; ICD = implantable cardioverter defibrillator.
*Mismatched generator indicates different manufacturer for generator and lead.

In order to assess for a difference between Tendril leads, the univariate and multivariate analysis was repeated with Optim-insulated leads set as the comparator (adjusting for generator type, which would likely be different across different lead vintages). In this analysis, non-Optim Tendril leads had significantly less HFA detected than Optim-insulated Tendril leads (OR 0.493, 95% CI 0.338–0.720, $P < .001$, Supplementary Table 1). Similarly, in an analysis of only leads connected to Abbott generators, the incidence of HFA was greater in Optim-insulated than in non-Optim Tendril leads. However, there was no significant difference in the HFA rate between Optim-insulated Tendril leads and Medtronic CapSureFix 5076 leads (Table 3 and Figure 1B).

Of 2323 leads connected to Abbott Medical generators, HFAs were detected in 172 leads (7.4%). In contrast, HFAs were detected in 40 of 5350 leads connected to non-Abbott generators (0.7%). While HFAs alone and HFAs with pacing/sensing failure and normal impedance were more frequently observed in leads paired with Abbott Medical generators, artifact in association with abnormal impedance was seen at similar rates in both groups (Supplementary Table 2). No CapSureFix leads were found to have low impedance in association with HFAs (Supplementary Table 3). Of 212 leads with HFA, lead inactivation (including extraction or abandonment), reprogramming, and observation were undertaken in 72, 44, and 75 leads, respectively. Management of HFA was similar for leads connected to Abbott and non-Abbott generators (Supplementary Table 4).

Of extracted leads with HFA, returned product analyses were available in 50 leads (Table 4). No abnormalities or only periprocedural damage was found in 32% of leads, including the only 2 CapSureFix leads connected to Abbott Medical generators for which analysis was available. Clavicular crush seemed to be more common in non-Optim Tendril leads, though Medtronic does not seem to report this abnormality specifically, and many CapSureFix lead fractures seemed to likely fit this description. Lead-to-device abrasion was not reported with CapSureFix leads. HFAs were reproduced in real time with isometric exercises in the clinic in 19.0%, 14.6%, and 24.4% of Optim-insulated Tendril, non-Optim Tendril, and CapSureFix 5076 leads.

HFAs were seen more commonly on the atrial channel than on the ventricular channel in Abbott generators (9.0% vs 4.6%, $P < .001$), but not in non-Abbott generators (0.8% vs 0.7%, $P = .629$). HFAs on right ventricular leads resulted in syncope in 5 patients owing to loss of ventricular pacing and inappropriate shocks in 1 patient who had a Tendril lead connected to a defibrillator as the pace-sense component. All of these leads underwent lead revision. In leads with HFA, the artifact disappeared after generator change in 4 of 14 leads that underwent a generator change or upgrade, 1 of which was changed from an Abbott

Table 2 Factors associated with high-frequency artifact

	Univariate analysis			Multivariable analysis		
	Odds ratio	95% CI	P	Odds ratio	95% CI	P
Age at implant (per year)	0.989	0.981–0.997	.009	0.988	0.979–0.997	<.001
Sex (male)	1.118	0.850–1.470	.424			
Lead type						
CapSureFix	1.000	-	-	1.000	-	-
Tendril without Optim (1688)	4.739	3.094–7.258	<.001	0.864	0.432–1.727	.679
Tendril with Optim (1888/2088)	10.440	7.341–14.850	<.001	1.863	0.970–3.581	.062
Atrial lead	1.729	1.267–2.360	<.001	1.377	0.975–1.945	.070
Defibrillator system	1.787	1.357–2.354	<.001	1.323	0.959–1.823	.088
Mismatched generator	0.629	0.372–1.063	.083	1.029	0.571–1.853	.924
Abbott generator	10.230	7.217–14.500	<.001	7.686	4.096–14.420	<.001

CI = confidence interval; CRT-D = cardiac resynchronization therapy-defibrillator; ICD = implantable cardioverter defibrillator.

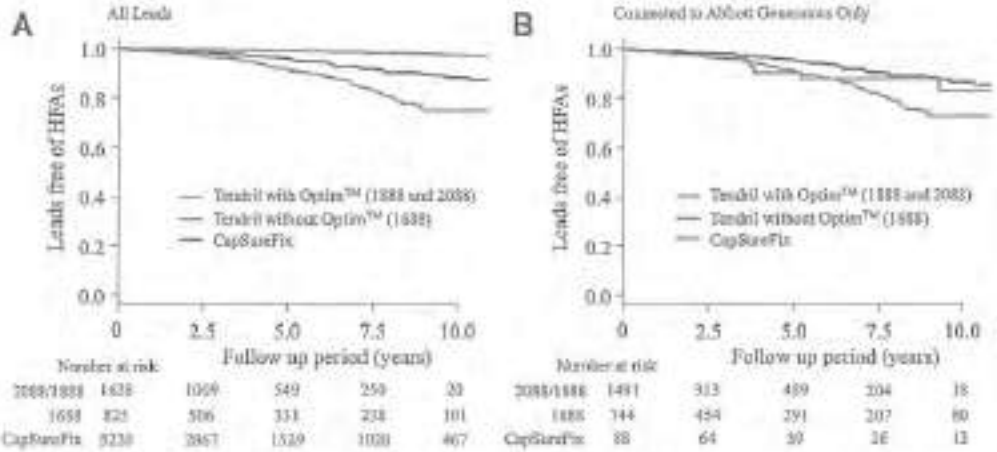

Figure 1 Kaplan-Meier curves for the incidence of high-frequency artifacts (HFAs) in Tendril leads with and without Optim insulation and CapSureFix 5076 leads. **A:** Across all leads, HFAs are more frequently observed in Optim-insulated Tendril and non-Optim Tendril leads than in CapSureFix 5076 leads. **B:** When the analysis was restricted to only leads connected to Abbott Medical pulse generators, no significant difference in HFAs between CapSureFix leads and either group of Tendril leads was seen, though Optim-insulated Tendril leads were more likely to have HFAs than non-Optim Tendril leads.

implantable cardioverter-defibrillator (ICD) to Boston Scientific cardiac resynchronization defibrillator. The other leads were changed to the same manufacturer generators. Rates of HFAs were significantly higher in Abbott ICDs as compared to pacemakers (11.4% vs 5.8%, $P < .001$). In Abbott pacemakers, the Accent series had a higher HFA rate than the Assurity/Endurity/Allure series (8.9% vs 3.0%, $P < .001$, Supplementary Figure 1).

HFAs detected with Abbott generators were most often 1–4 seconds in length with an amplitude similar to or lower than that of the P wave or R wave. The frequency was typically very high, with deflections occurring at <100-ms intervals, though not all deflections were detected (Supplementary Figure 2). HFAs detected with non-Abbott generators were often higher amplitude and were typically longer in duration.

Discussion

In this retrospective observational study, we reviewed 7691 Abbott and Medtronic pacing leads and found that Abbott Medical pacemaker and defibrillator pulse generators, but not Abbott pacing leads, are associated with an increased incidence of recorded HFAs in a multivariate analysis (Table 2, OR 7.686, $P < .001$). Upon direct comparison of Tendril leads, Optim insulation predicted significantly higher rates of HFA when compared to silicone-insulated model 1688 leads (Supplementary Table 1). This effect was unchanged when the analysis was restricted to Abbott generators alone (Figure 1 and Table 3). The increased incidence of HFAs on Abbott generators seems most likely due to episodes of true electrical noise, which other devices may not report owing to their brevity or low amplitude.

Mechanism of HFAs

HFAs can have many causes, including lead fracture with make-break connections; external electromagnetic interference; a lead-header interface issue such as a loose set screw; far-field oversensing of T waves, R waves, or P waves; and diaphragmatic or pectoral myopotentials.[4–6] A previous study reported that the overall incidence of ventricular oversensing in ICDs was 7.3%, and 38% of oversensing was caused by lead failure or myopotentials.[7]

The important work by El-Chami and colleagues[2] initially identified an increased incidence of lead malfunction (predominantly noise with normal impedance) in the Tendril lead family. They concluded that a vulnerability of Optim insulation (a proprietary copolymer of silicone and polyurethane) in some Tendril leads (models 1888 and 2088) may partially explain the high rate of malfunction. A greater incidence of HFAs in Tendril leads with Optim insulation than in those without was confirmed in our study as well (5-year HFA rate 8.8% vs 4.7%, $P < .001$), and this association remained after adjusting for the generator model (Supplementary Table 1). There are 2 primary differences in outer insulation, which could potentially explain this difference. In addition to being composed of a different material, Optim outer insulation on the 6Fr 1888 and 2088

Table 3 Pairwise comparison of 5- and 10-year high-frequency artifact rates among leads connected to Abbott Medical pulse generators

Lead	5-year HFA rate (%)	95% CI	10-year HFA rate (%)	95% CI	P 1688	P CapSureFix
Tendril with Optim (1888 and 2088)	8.8	7.1–11.0	27.7	22.2–34.1	<.001	.387
Tendril without Optim (1688)	4.7	3.0–7.2	13.4	9.5–18.7		.344
CapSureFix (n = 88)	9.6	4.4–20.5	17.0	8.0–44.1		

CI = confidence interval; HFA = high-frequency artifact.

Table 4 Returned product analysis of extracted leads with high-frequency artifact

Analysis result	All leads (n = 50)	Tendril with Optim (n = 27)	Tendril without Optim (n = 11)	CapSureFix* (n = 12)
Normal	10 (20)	6 (22.2)	0 (0)	0 (0)
Procedural damage[1]	6 (12)	6 (22.2)	0 (0)	4 (33.3)
Clavicular crush	5 (10)	1 (3.7)	4 (36.4)	0 (0)
Fracture	9 (18)	0 (0)	1 (9.1)	8 (66.7)
Lead abrasion	17 (34)	12 (44.4)[1]	5 (45.5)	0 (0)
Suture damage	3 (6)	2 (7.4)	1 (9.1)	0 (0)

Data are presented as frequency (percentage).

*Medtronic analysis typically does not subcategorize "clavicular crush" from "fracture."

[1]"Procedural damage" includes leads found to only have procedural damage likely related to extraction. Of Optim leads with only procedural damage, 2 of 6 did not have the entire lead available for analysis (15.5 cm and 38 cm analyzed, respectively).

[2]Eleven of 12 Optim-coated leads with lead abrasion had abrasion in the pocket (presumed lead-to-can abrasion). The other had lead-lead abrasion at the level of the right atrium or superior vena cava. All Abbott leads that were found to be normal or only had procedural damage were connected to Abbott Medical generators. Two Medtronic leads were connected to Abbott Medical generators, and both were found to have only procedural damage.

models is thinner than the silicone outer insulation used on the 1688 lead (0.005 inches vs 0.012 inches). While the difference in HFA could be due to a greater incidence of breach in Optim-insulated leads, it also seems feasible that any given insulation breach may be more likely to lead to detectable artifact with a thinner insulation "spacing" between the conductor and tissue.

Although the study by El-Chami and colleagues[7] noted that mismatched lead-generator combinations did not predict lead malfunction, they did not comment on the association between each generator manufacturer and lead "malfunction" despite having a large population of mismatched devices. In that study, it seems that Optim-insulated leads showed a 7.8% rate of malfunction when paired with Abbott generators (n = 4707) compared to 5.0% when paired with a non-Abbott generator (n = 3290).[7] Given the very large number of leads in both groups, this association is likely statistically significant, though we do not have the primary data available for analysis.

Atrial detections

After establishing that Abbott generators record more HFA, the next logical question is, are Abbott generators seeing things that are not there or reporting things that are common but usually go unnoticed? To answer this question, one must understand the criteria that must be met for a given device to record and display electrograms. An in-depth description of differences in atrial detection algorithms is included in a Supplementary Appendix. In brief, Abbott generators record electrograms continuously and document atrial mode switch or noise episodes typically within 1–2 seconds (Figure 2A, Supplementary Figure 2).[8] In contrast, Medtronic generators do not nominally store electrograms continuously and must reach atrial tachycardia / atrial fibrillation detection criteria and then sustain an atrial rate above atrial tachycardia / atrial fibrillation detection for 32 ventricular cycles before any event will be stored (Figure 2B, Supplementary Figure 3).[9–11] There are also differences in electrogram sensing algorithms between manufacturers. Abbott devices have a more sensitive autosensitivity algorithm, starting at 50% rather than 75% of the last detected P/R wave amplitude. The autosensitivity algorithm is used for ventricular sensing in Abbott ICDs and is nominally turned on for atrial sensing in these devices. It is nominally turned off in pacemakers for both chambers (not available in Zephyr and earlier pacemakers).[8] We saw a significantly higher rate of HFAs in Abbott ICDs, which have autosensitivity nominally turned on (Supplementary Figure 1).[8]

Ventricular detections

Algorithms for detecting ventricular high rate episodes and ventricular lead artifact, are, by necessity, more uniform. Short-duration ventricular tachycardia and ventricular fibrillation is stored by all pacemakers with similar criteria, though again, Medtronic pacemakers do not nominally begin capturing electrograms until detection criteria have been met. In addition, CIEDs are typically engineered to detect and label electrical noise on ventricular leads in an effort to prevent loss of ventricular pacing and to identify fracture of defibrillator leads. We saw a higher rate of HFAs in Accent pacemakers than in other Abbott pacemakers (Supplementary Figure 1). The Accent series was the first to have autosensitivity algorithms present but did not include a noise confirmation window for ventricular noise reversion that is present on later models, though this could be confounded by longer implant time when comparing to later models.[12]

Implications of HFAs

In order to determine whether intermittent short-duration noise uncovered by Abbott algorithms is clinically important, we need to understand the proportion of leads that ultimately failed in some other way than intermittent noise. This could be defined in many ways, including lead replacement/extraction, loss of pacing, or loss of sensing. However, given the retrospective nature of our study, the limited data available, and the many variables that go into the decision to extract or replace a lead, we decided to assess the proportion of leads with HFAs that also displayed an out-of-range impedance, which would seem to be an objective though incomplete measure of true lead failure or impending failure in this dataset. While HFAs were more frequently observed in leads connected to an Abbott generator compared to non-Abbott generator, the rate of abnormal impedance was similar (0.37% vs 0.47%,

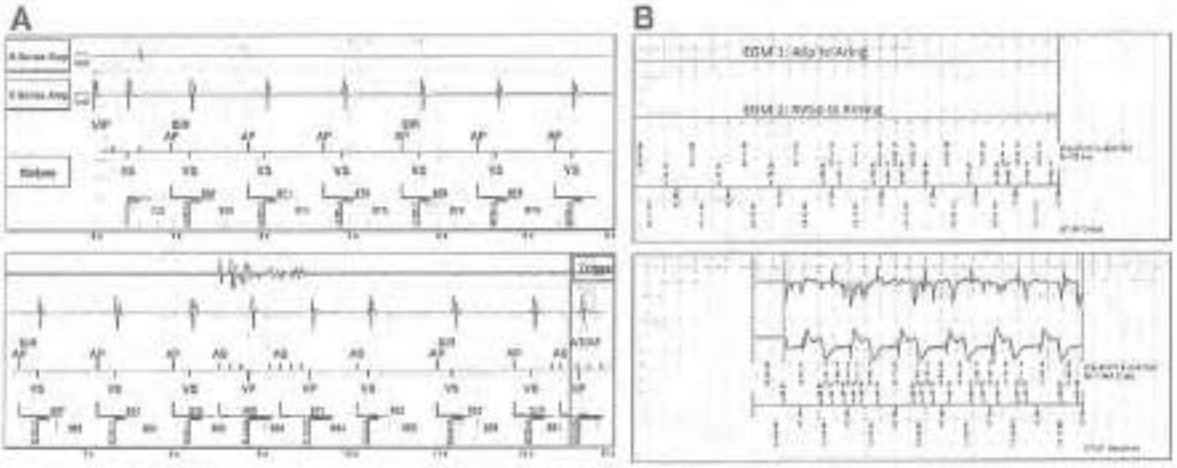

Figure 2 A: Abbott Medical pulse generators such as this Assura DR 2537-40Q record and display electrograms for atrial tachycardia / atrial fibrillation (AT/AF) as soon as the filtered atrial rate interval exceeds 180 beats per minute. This can occur with even brief episodes of high-frequency artifact. B: Medtronic defibrillators such as this Consulta D224TRK and "ICD-platform" pacemakers do not record and display electrograms for AT/AF until 32 ventricular cycles have occurred after meeting AT/AF detection criteria. In this case, atrial lead noise must sustain for 23 seconds before electrograms are stored. AF = atrial fibrillation; AP = atrial pace; AR = atrial refractory sense; AS = atrial sense; AT = atrial tachycardia; BV = biventricular pace; EGM = electrogram; FS = fibrillation sense; ICD = implantable cardioverter defibrillator; RV = right ventricular; SIR = sensor-indicated rate; TS = tachycardia sense; VIP = ventricular intrinsic preference; VP = ventricular pace.

$P = .658$, Supplementary Table 1). Notably, low impedance was a phenomenon primarily seen on Optim-insulated Tendril leads, potentially suggesting a higher rate of outer-insulation breach in this group. Only 6.4% of leads displaying HFA on an Abbott generator developed an abnormal impedance, as opposed to 35.7% of those connected to other generators. This suggests that Abbott generators detect HFA on many leads without an overt fracture or breach.

Treatment for HFAs

Beyond abnormal impedance, another primary reason to be concerned with lead noise is loss of pacing and loss of atrioventricular synchrony. Infrequent loss of atrioventricular synchrony is typically a minor concern. However, loss of ventricular pacing in a pacing-dependent patient can certainly be dangerous. A high density of HFA on ventricular leads resulted in syncope in 5 and inappropriate shocks in 1 patient in this study. It is not clear from our data whether Abbott devices are more or less likely to successfully respond to lead HFA (ie, mode switching, noise reversion pacing), but our data strongly suggest that the Abbott algorithms are more likely to result in the storage and presentation of short-duration or low-amplitude HFAs. It is notable that in our study, approximately one third of leads with HFAs were revised or deactivated (Supplementary Table 3). This is approximately double the rate of revision/deactivation in the study by El-Chami and colleagues,[2] likely owing to local practice patterns. In light of our findings, optimal management for most pace-sense leads with short-duration noise seen on Abbott generators would seem to be reprogramming or monitoring initially.

Age as a risk factor

Younger age is a known risk factor for lead fracture, thought to be due to increased shoulder mobility and overall activity level.[13] This association was seen in our cohort as well, though given that the majority of our patients had HFA without evidence of true fracture, it could also be the case that higher-amplitude intermittent myopotentials are more likely to be sensed in a younger population.

All of this together suggests that Abbott generators are likely reporting true electrical noise that other devices also "see" but may not report owing to its brevity or amplitude. The most likely explanation for this seems to be detection of pectoral myopotentials on bipolar leads owing to breakdown of outer insulation. If these defects are small (allowing fluid but not tissue to directly contact the outer conductor), it is certainly plausible that episodes could be short duration, low amplitude, and intermittent. Second, diaphragmatic myopotentials could be detected on ventricular leads, though ventricular leads constitute a minority of the HFAs detected. Lastly, it is possible, but seems less likely, that more pathologic lead breakdown or lead-header issues (ie, loose set screw) could be present but only cause very short episodes of oversensing and subsequently are more likely to be detected on Abbott CIEDs, though normal impedance and generally low amplitude of the detected signals argues against this. In fact, many of the leads (32%) sent for returned product analysis had no evident abnormalities (Table 4). It is not clear what the mechanism for HFAs is likely to be in this scenario, though it seems plausible that preexisting outer insulation defects could have been present that were indistinguishable from periprocedural trauma or were so small as to evade detection at the time of returned product analysis. It seems unlikely that HFAs were caused by muscle artifact transiting across an intact outer insulation, given that the incidence of HFAs starts out very low and

increases linearly over time (as would be expected with progressive breakdown).

Limitations

Our study has several limitations. We identified leads with HFAs via a cardiac device electronic monitoring system using search terms. If there were any leads with HFAs that were not described using the search terms, they would likely have been excluded. However, all leads were screened with the same protocol. Because our study was retrospective, it cannot definitively adjust for the effect of unmeasured confounders. It is also not known what the natural history of the revised/deactivated leads would have been. Our follow-up is limited, and it is unclear whether longer follow-up would have demonstrated other features of frank lead failure. Lastly, the analysis of only leads connected to Abbott generators is limited by the relatively small numbers of Medtronic leads.

Conclusion

Abbott pacemaker and defibrillator generators are significantly and strongly associated with increased detection of HFAs, likely owing to the detection of brief or low-amplitude noise that may not be recorded by other manufacturers. Optim-insulated Tendril leads have a greater incidence of HFAs compared to non-Optim Tendril leads.

Acknowledgments

We would like to thank William Caudill and Matthew Desmond with Abbott Medical, James T. Reedy Jr and Rachel Tidwell with Medtronic, and Clinton Langston and Elizabeth Weigand with Boston Scientific for their assistance with the technical and manufacturer-specific aspects of the current study. We would like to thank M. Benjamin Shoemaker, MD, MSCI for statistical assistance.

Appendix

Supplementary data

Supplementary data associated with this article can be found in the online version at https://doi.org/10.1016/j.hrthm.2019.05.020.

References

1. Kusumoto FM, Schoenfeld MH, Wilkoff BL, et al. 2017 HRS expert consensus statement on cardiovascular implantable electronic device lead management and extraction. Heart Rhythm 2017;14:e503–e551.
2. El-Chami MF, Roe B, Shah AD, et al. Long-term performance of a pacing lead family: A single-center experience. Heart Rhythm 2019;16:572–578.
3. Kanda Y. Investigation of the freely-available easy-to-use software "EZR" (Easy R) for medical statistics. Bone Marrow Transplant 2013;48:452–458.
4. Swerdlow CD, Friedman PA. Advanced ICD troubleshooting: Part I. Pacing Clin Electrophysiol 2005;28:1322–1346.
5. Yazaki K, Ajiro Y, Hasegawa S, et al. Myopotential increasing noticed by Lead Integrity Alert in a patient with implantable cardioverter defibrillator with a dedicated bipolar epicardial sensing lead. Clin Case Rep 2016;4:1091–1095.
6. Sweeney MO, Ellison KE, Shea JB, Newell JB. Provoked and spontaneous high-frequency, low-amplitude, oversensing noise artefacts in patients with implantable cardioverter defibrillators. J Cardiovasc Electrophysiol 2001;12:402–410.
7. Bunwolf T, Guenther M, Hess N, et al. Ventricular oversensing in 518 patients with implanted cardiac defibrillators: incidence, complications, and solutions. Europace 2007;9:1041–1043.
8. Bradycardia and Tachycardia Devices Merlin Patient Care System Help Manual, US. Abbott Medical. Effective Begin Date April 23 2018 [internet]. Available at: https://manuals.sjm.com/Search-Form/?ve=North-America&co=US&lc=EN&qry=CD3365-40C&lqy=10. Accessed February 11, 2019.
9. Advisa DR A5DR01 Clinical Manual Medtronic, 2010 [internet]. Available at: https://cdn6.ifu/ASATEL/04436-13-0556?Mouse/0B2F00D4-E032-4744-B320-FA236FB3120.PDF. Accessed February 11, 2019.
10. Evera XT DR DDBB1D1 Device Manual Medtronic, 2014 [internet]. Available at: http://manuals.medtronic.com/content/dam/manuals/cmm/CONTRIB_170277.pdf. Accessed February 11, 2019.
11. ADAPTA/ VERSA/ SENSIA/ RELIA Reference Manual Medtronic, 2016 [Internet]. Available at: http://manuals.medtronic.com/content/dam/manuals/cmm/CONTRIB_214793.pdf. Accessed February 11, 2019.
12. Technical Insight: Noise Detection in Assurity, Endurity, and Allure Pacemakers. St. Jude Medical; September, 2014. Available by request from Abbott Medical Technical Services.
13. Binia DH, Parkash R, Exner DV, et al. Clinical predictors of Fidelis lead failure: report from the Canadian Heart Rhythm Society Device Committee. Circulation 2012;125:1217–1225.

Circulation Reports
Circ Rep 2020; 2: 44–50
doi:10.1253/circrep.CR-19-0065

ORIGINAL ARTICLE
Health Services and Outcomes Research

Impact of Board-Certified Cardiologist Characteristics on Risk of In-Hospital Mortality

Mika Watanabe, MD; Kihei Yoneyama, MD, PhD; Michikazu Nakai, PhD; Koshiro Kanaoka, MD, PhD; Satoshi Okayama, MD, PhD; Kunihiro Nishimura, MD, PhD; Yoshihiro Miyamoto, MD, PhD; Masaki Izumo, MD, PhD; Yuki Ishibashi, MD, PhD; Takumi Higuma, MD, PhD; Tomoo Harada, MD, PhD; Satoshi Yasuda, MD, PhD; Toyoaki Murohara, MD, PhD; Yoshihiko Saito, MD, PhD; Yoshihiro J. Akashi, MD, PhD

Background: This study examined the influence of board-certified cardiologist characteristics on the in-hospital mortality of patients with cardiovascular disease.

Methods and Results: Data were collected between 2012 and 2014 from a nationwide database of acute care hospitals in Japan. Overall, there were 1,422,703 patients, of whom 883,746 were analyzed. The primary outcome was all-cause in-hospital mortality. The association between board-certified cardiologist characteristics and in-hospital mortality was estimated using multilevel mixed-effect logistic regression modeling. Median age of cardiologists in a hospital was not related to in-hospital mortality (OR, 1.003; 95% CI: 0.998–1.008, P=0.316), but a greater cardiologist age range was associated with a lower risk of in-hospital mortality (OR, 0.992; 95% CI: 0.988–0.995 per 1-unit increment in age range, P<0.001). Meanwhile, the average years of experience of the board-certified cardiologists in a hospital was not associated with a lower risk of in-hospital mortality (OR, 1.002; 95% CI: 0.996–1.007, P=0.525), but a greater range of years of experience was (OR, 0.988; 95% CI: 0.983–0.993 per 1-unit increment in range of years of experience, P<0.001).

Conclusions: Median board-certified cardiologist age/experience at an institution is not related to in-hospital mortality, but a greater range in age/experience is associated with a lower risk of mortality.

Key Words: Board-certified cardiologist; Cardiovascular disease; In-hospital mortality

Recent advancements in the treatment of cardiovascular disease (CVD) have resulted in substantial decreases in related mortality rates.[1,2] CVD, however, still causes 17.9 million deaths every year, corresponding to 31% of all deaths worldwide. Further, according to World Health Organization projections, the worldwide CVD-related burden will reach 47 million disability adjusted life years (years lost due to disability, ill-health, or death) by 2020.[2]

The expanded use of medical therapies is increasing the quality of cardiac medical care, and hopefully decreasing mortality rates.[3-6] Board-certified physicians are skilled, knowledgeable experts in their specialty, and practice a higher standard of medicine in their fields. Patients who are hospitalized as a result of CVD have been found to receive better care from cardiologists than from physicians who specialize in other disciplines,[7-9] but no study has yet investigated the influence that board-certified physicians have on patient prognosis.

In this study, using the Japanese Registry of all Cardiac and Vascular Diseases (JROAD), we examined the relationship between the characteristics (e.g., age and years of experience) of hospital board-certified cardiologists and the hospitals' respective patient outcomes. JROAD is a nationwide database that stores data concerning hospital and patient characteristics, principal diagnoses, comorbidities at admission, complications after admission, procedures during hospitalization, and discharge status.

Received August 2, 2019; revised manuscript received October 24, 2019; accepted October 31, 2019; J-STAGE Advance Publication released online December 13, 2019 Time for primary review: 1 day
Division of Cardiology, Department of Internal Medicine, St. Marianna University School of Medicine, Kawasaki (M.W., K.Y., M.I., Y.I., T. Higuma, T. Harada, Y.J.A.); National Cerebral and Cardiovascular Center, Suita (M.N., K.N., Y.M., S.Y.); Department of Cardiovascular Medicine, Nara Medical University, Kashihara (K.K., S.O., Y.S.); and Department of Cardiology, Nagoya University Graduate School of Medicine, Nagoya (T.M.), Japan
Y.M., S.Y., T.M., and Y.J.A. are members of *Circulation Reports*' Editorial Team.
ORCIDID: 0000-0001-7670-7326
Mailing address: Yoshihiko Akashi, MD, PhD, Division of Cardiology, Department of internal Medicine, St. Marianna University School of Medicine, 2-16-1 Sugao, Miyamaeku, Kawasaki 216-8511, Japan. E-mail: yjakashi-circ@umin.ac.jp
ISSN-2434-0790 All rights are reserved to the Japanese Circulation Society. For permissions, please e-mail: cr@j-circ.or.jp

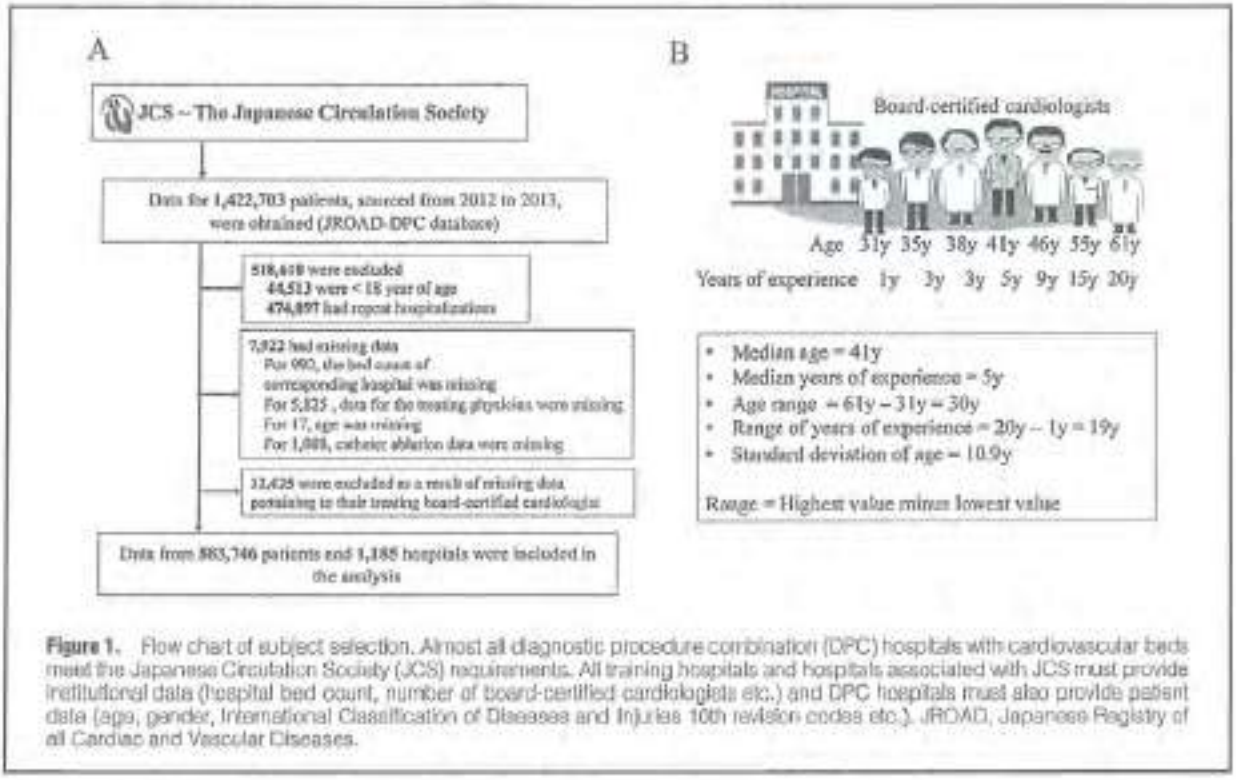

Figure 1. Flow chart of subject selection. Almost all diagnostic procedure combination (DPC) hospitals with cardiovascular beds meet the Japanese Circulation Society (JCS) requirements. All training hospitals and hospitals associated with JCS must provide institutional data (hospital bed count, number of board-certified cardiologists etc.) and DPC hospitals must also provide patient data (age, gender, International Classification of Diseases and Injuries 10th revision codes etc.). JROAD, Japanese Registry of all Cardiac and Vascular Diseases.

Methods

Patient and Public Involvement

The JROAD database is a nationwide prospective registry that was designed to assess the clinical activity of every Japanese institution that provides cardiovascular care, and to provide adequate feedback to teaching hospitals regarding improving patient care. A detailed description of the database's design and methods has previously been published.[9-11] Briefly, however, the JROAD database, which has stored demographic information for every hospital since 2004, and the JROAD-DPC nationwide database, which has stored data pertaining to the Japanese Diagnosis Procedure Combination/Per Diem Payment System (DPC/PDPS) since 2012, were developed by the Japanese Circulation Society (JCS). The DPC database is a mixed-case classification system linked with a lump-sum payment system, and was launched in 2002 by the Ministry of Health, Labour and Welfare of Japan.[12] Compared with other registry databases, the DPC database enables researchers to conduct nationwide studies of both descriptive and/or analytical epidemiology in real-world clinical settings. The DPC database includes data on the following elements: patient demographics (e.g., age and gender); principal diagnosis (coded according to the International Classification of Diseases and Injuries, 10th revision; ICD-10); comorbidities at admission (ICD-10 coded); complications after admission (ICD-10-coded); procedures, including surgery, medication, and devices used during hospitalization; length of stay; discharge status; and medical expenses.[10,12-14] A wide variety of centers, including academic, urban, and rural hospitals, use the DPC system.[10,15]

Considering the aforementioned characteristics of the JROAD-DPC database, we considered it to be an ideal source for the present research topic: namely, the effects of the characteristics of board-certified cardiologists on patient outcome.

All data obtained for this study from the JROAD database concerned hospitalized patients with clinically apparent CVD. This research was approved by the institutional review board of St. Marianna University School of Medicine (registration no. 3419). Further, all patient data were anonymized, given that each hospital used code-change equations to encrypt patient IDs in the database. Individual data (including age, gender, and hospital bed count) were sent to the JROAD data center using an electronic data capture system or recordable compact disc.

Study Design and Sampling

We conducted a cross-sectional study using both the JROAD and JROAD-DPC databases, recording entries made in the databases between 1 April 2012 and 31 March 2014. A total of 2,407 hospitals are included in the JROAD database and, of these, 1,247 (52%) have adopted the DPC system and have agreed to participate in the JROAD-DPC database project (**Figure 1**). The characteristics of hospitals that did provide JROAD-DPC data and those that did not, along with the ICD-10 diagnosis codes, have been summarized in a previous study.[10] A total of 1,422,703 consecutive patients were initially included in this study, but 538,957 patients were later excluded because of missing data, being <18 years of age with no pediatrician data, or having a history of prior hospitalization. Patients who had no missing variables were included in the analyses (n=883,746).

Data for board-certified cardiologists were collected from JCS. According to the JCS website (http://www.j-circ.or.jp/information/senmoni/index.htm), board-certified

Table 1. Patient, Facility, and Cardiologist Characteristics

	Nationwide database
Patient demographics (n=883,746)	
Age (years)	73 (64–81)
Male gender	547,558 (62)
Cardiovascular disease	
Angina	232,404 (26)
Acute MI	46,922 (5)
Heart failure	145,431 (16)
Aortic disease	72,056 (8)
Pulmonary embolism	6,075 (0.7)
Atrial fibrillation or flutter	46,645 (5)
Cardiac arrest	52,155 (6)
Coexisting condition	
Charlson comorbidity index	1 (0–2)
Outcome	
In-hospital death rate	102,667 (13.2)
Facility demographics (n=1,185)	
No. hospital beds	476 (334–646)
Cardiac surgery facility	710,631 (80)
No. board-certified cardiologists	5 (4–9)
No. hospitals with:	
<300 beds	143,621 (16)
300–449 beds	254,721 (29)
450–749 beds	347,678 (39)
>749 beds	137,725 (16)
Board-certified cardiologist demographics (n=14,276)	
Age (years)	47 (41–55)
Male	12,747 (89)
Years of experience (years)	9 (4–17)
Age range per hospital (years)	33 (32–65)†
Range of years of experience per hospital (years)	23 (0–23)†

Data given as n (%), median (IQR) or †median (range). MI, myocardial infarction.

cardiologists must (1) be regular members of the JCS for a minimum of 6 years; (2) be board-certified members of the Japanese Society of Internal Medicine, the Japan Surgical Society, the Japan Pediatric Society, the Japanese Association of Thoracic Surgery, or the American Society of Internal Medicine; (3) have completed 3 years of training at a certified institution; and (4) have passed the board certification examination offered by the JCS. Years of experience was calculated as the difference between the year we sourced the data (2012 or 2013) and the year the individual in question became a board-certified cardiologist.

Each hospital annually confirms the certifications of their board-certified cardiologists, but only records in the JROAD database the total number of board-certified cardiologists employed by the hospital (i.e., no identifying information is provided); this means that we were unable to create a merged dataset through which we could identify which physician was responsible for treating which patients.

For each hospital, the number of non-board-certified cardiologists per year was defined as the total number of cardiologists at a given hospital minus the number of board-certified cardiologists at the hospital. Finally, the ratio of beds to board-certified cardiologists was calculated by dividing the number of beds per hospital by the number of board-certified cardiologists for that same hospital. A higher index represents a greater number of beds per board-certified cardiologist.

Outcome

The primary outcome was the occurrence of in-hospital mortality for any cause (i.e., not necessarily cardiac related). This was possible because JROAD-DPC data can provide a relatively complete perspective of mortality during hospitalization.

Statistical Analysis

For each hospital, board-certified cardiologist age, years of experience, and the range of each of these characteristics were divided into quartiles. If patients were hospitalized more than once during the study period, we used only the data associated with the last admission, while recording the total number of prior hospitalizations. To assess the association between the characteristics of the board-certified cardiologists and in-hospital mortality, we used multilevel mixed-effects logistic regression models to estimate the odds ratios (OR) for in-hospital mortality. Each of the multilevel mixed-effects logistic regression model variables included a hierarchy level (hospital) that considered the random effects of hospital variation. All estimates were adjusted for hospital demographics (number of board-certified cardiologists, board-certified cardiologist gender, number of non-board-certified cardiologists, number of hospital beds, number of coronary care units, cardiac surgery facility, 8 regional divisions of Japan), patient demographics (patient age, gender, Charlson comorbidity index, and incidence rates of angina pectoris, myocardial infarction, atrial fibrillation, heart failure, aortic disease, cardiac arrest, pulmonary thromboembolism, primary pulmonary hypertension, tetralogy of Fallot, incident pneumonia during hospitalizations, and number of prior hospitalizations), and patient therapy (percutaneous coronary intervention, coronary artery bypass grafting, catheter ablation, implantable cardioverter defibrillator, and cardiac resynchronization therapy). The adjusted probabilities of in-hospital mortality were calculated in STATA using marginsplot, after the multilevel mixed-effects logistic regression analysis. All analyses were performed using STATA version 14 (Stata Corp, College Station, TX, USA).

Results

Patient, Facility, and Cardiologist Characteristics

The final study sample consisted of 883,746 patients with CVD who were admitted to DPC-participating hospitals. Both clinical presentation and facility characteristics are listed in **Table 1**. Overall, average patient age was 73 years, and 62% were male. The most common CVD were angina (26%), heart failure (16%), aortic disease (8%), and myocardial infarction (5%). Meanwhile, the median bed count of the institutions was 476, and the mean number of board-certified cardiologists per institution was 5. The average age of the board-certified cardiologists was 47 years, and 89% were male; meanwhile, average years of experience was 9. The average age range of the board-certified cardiologists per institution was 33 years (range, 32–65 years), while the average range of years of experience was 23 years (range, 0–23 years).

Table 2. Cardiologist Board Certification and In-Hospital Death

In-hospital death (No. events: 102,667/883,746)	Adjusted OR (95% CI)†		
	Adjusted for facility‡	Adjusted for clinical characteristics§	Adjusted for treatment‖
Board-certified cardiologists			
Age (years)	1.003 (0.998–1.008)‖	1.006 (1.001–1.010)*	1.006 (1.001–1.011)*
Age range (years)	0.993 (0.990–0.996)***	0.991 (0.988–0.994)***	0.992 (0.989–0.995)***
SD of age (years)	0.991 (0.982–1.000)	0.989 (0.98–0.997)*	0.990 (0.982–0.999)*
Years of experience as board-certified cardiologists			
Years of experience (years)	0.996 (0.99–1.002)	1.002 (0.996–1.007)	1.002 (0.995–1.007)
Range of years of experience (years)	0.983 (0.979–0.987)***	0.986 (0.982–0.990)***	0.986 (0.983–0.990)***
SD of years of experience	0.976 (0.965–0.986)***	0.982 (0.972–0.991)***	0.982 (0.973–0.992)***

*P<0.05, ***P<0.001, ‖P=0.316. †Multilevel mixed-effects logistic regression. ‡Model included no. board-certified cardiologists, board-certified cardiologist gender, no. non-board-certified cardiologists, no. hospital beds, no. coronary care units, cardiac surgery facility, 8-region division. §Model included, in addition to the facility model, patient age, gender, Charlson comorbidity index, and incidence of angina pectoris, myocardial infarction, atrial fibrillation, heart failure, aortic disease, cardiac arrest, pulmonary thromboembolism, primary pulmonary hypertension, tetralogy of Fallot, and incident pneumonia during hospitalizations. It also included no. prior hospitalizations. ‖Model included, in addition to the clinical characteristics model, percutaneous coronary intervention, coronary artery bypass grafting, catheter ablation, implantable cardioverter defibrillators, and cardiac resynchronization therapy.

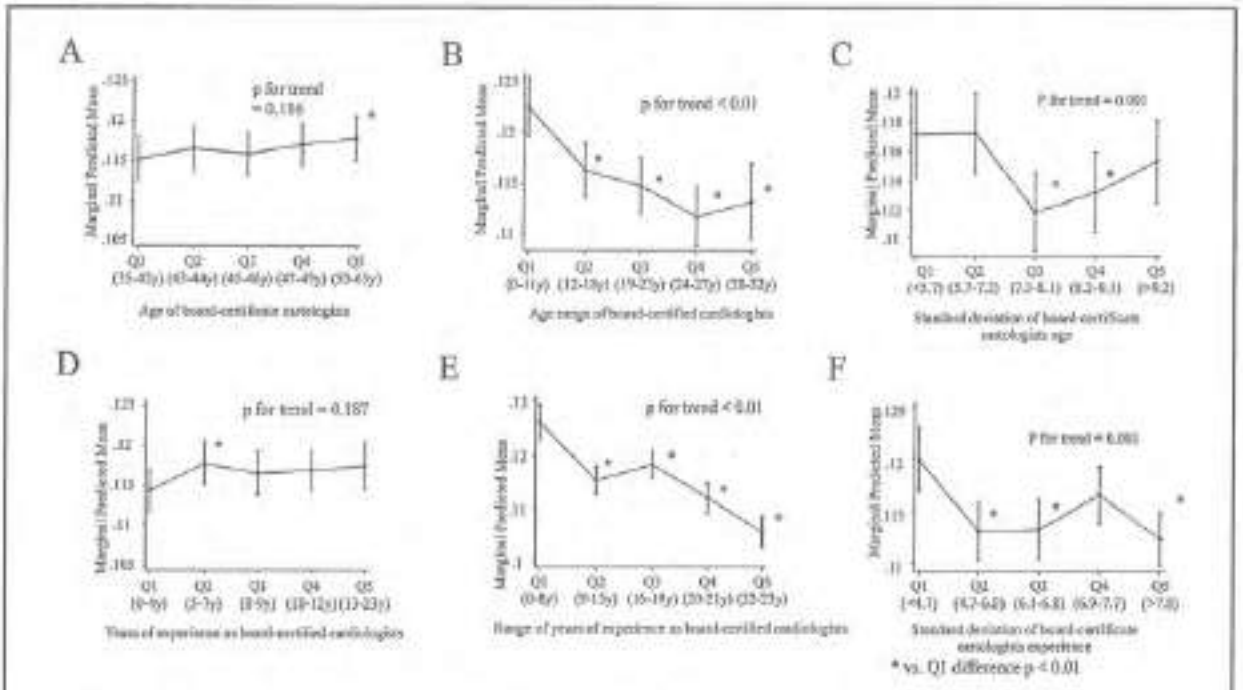

Figure 2. In-hospital mortality rates for cardiovascular disease vs. quintiles of (**A**) age, (**B**) age range, (**C**) age SD, (**D**) years of experience, (**E**) range of years of experience and (**F**) SD of range of years of experience of board-certified cardiologists, on a per-institution basis. Bars, 95% CI. Adjusted probability was calculated using the marginsplot command in STATA, and was adjusted as indicated in Table 2.

Cardiologist Board Certification and In-Hospital Mortality

The overall in-hospital mortality rate was 13.2%. On multilevel mixed-effects logistic regression modeling (**Table 2**), the median age of the board-certified cardiologists per institution was not related to in-hospital mortality (OR, 1.003; 95% CI: 0.998–1.008; P=0.316), after adjusting for facility. A greater board-certified cardiologist age range at an institution, however, and a greater SD of age were found to be associated with a lower risk of in-hospital mortality (age range: OR, 0.992; 95% CI: 0.988–0.995 per 1-unit increment in age range, P<0.001; age SD: OR, 0.990; 95% CI: 0.982–0.999 per 1-unit increment in age range, P<0.05), after adjusting for facility, patient clinical characteristics, and treatment. On a per-institution basis, board-certified cardiologist average years of experience were not associated with a lower risk of in-hospital mortality (OR, 1.002; 95% CI: 0.996–1.007; P=0.525). A greater range of board-certified cardiologist years of experience at an institution, however, and a greater SD were found to be associated with a lower risk of respective in-hospital mortality (age range:

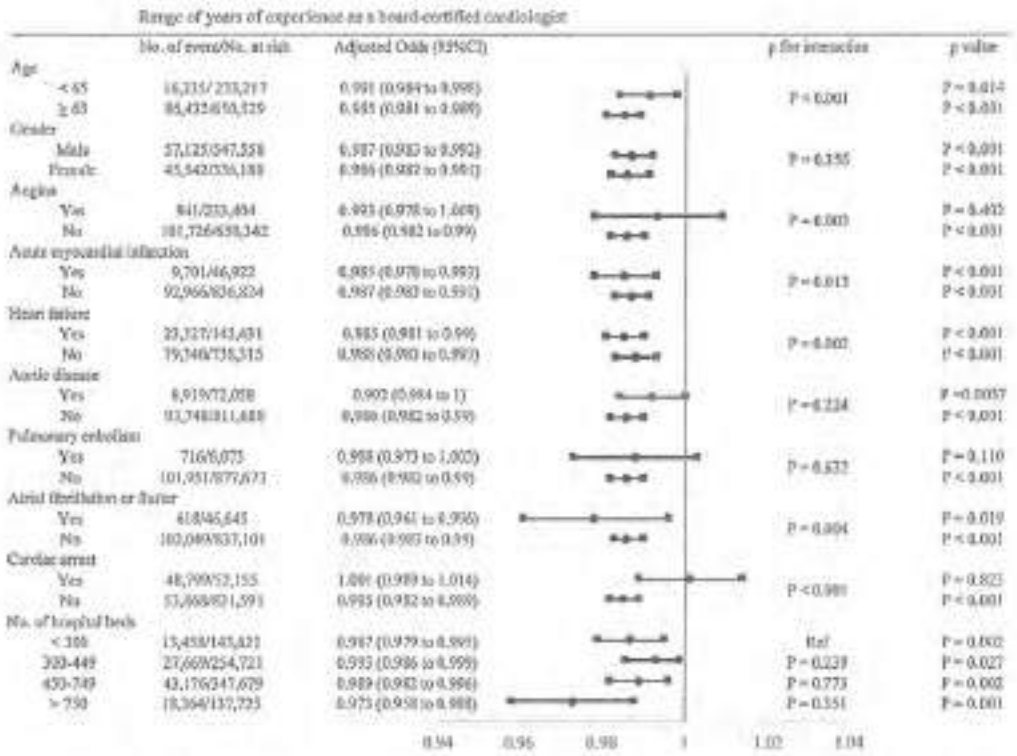

Figure 3. Adjusted OR and 95% CI for in-hospital mortality from cardiovascular disease according to board-certified cardiologist years of experience. OR <1.0 represents a decreased risk of in-hospital mortality as board-certified cardiologist years of experience increase. OR, dot; 95% CI, lines. OR were adjusted for both facility and patient characteristics and treatment, as indicated in Table 2.

OR, 0.986; 95% CI: 0.983–0.990, per 1-unit increment of years of experience, P<0.001; age SD: OR, 0.982; 95% CI: 0.973–0.992, per 1-unit increment in age range, P<0.001), after adjusting for facility, patient clinical characteristics, and treatment.

The association between board-certified cardiologists and in-hospital mortality is shown in **Figure 2**. A non-linear association was observed across the quartile of board-certified cardiologist age (P for trend=0.186; **Figure 2A**) for in-hospital mortality, SD of age (P for trend=0.091, **Figure 2C**), and quartile of board-certified cardiologist years of experience (P for trend=0.187; **Figure 2D**). A linear association was observed, however, across the quartile of board-certified cardiologist age range (P for trend<0.01; **Figure 2B**) for in-hospital mortality, and quartile of board-certified cardiologist range of years of experience (P for trend<0.01, **Figure 2E**), and SD of experience (P for trend=0.003; **Figure 2F**).

Subgroup Analysis According to Heart Disease

Analysis of the association between board-certified cardiologist years of experience and in-hospital mortality according to disease is shown in **Figure 3**. On multilevel mixed-effects logistic regression modeling, significant interactions were seen between board-certified cardiologist years of experience in an institution and respective patient age (P<0.001), angina (P=0.0030; myocardial infarction (P=0.013), heart failure (P=0.002), atrial fibrillation (P=0.004), and cardiac arrest (P<0.001). There was no interaction effect, however, between board-certified cardiologist years of experience (on a per-institution basis), hospital volume, and in-hospital mortality.

Discussion

Data om 1,185 hospitals and 896,171 patients, sourced from the JROAD and JROAD-DPC databases, were analyzed in this study, making it one of the largest, cross-sectional, retrospective studies conducted to date on nationwide, in-hospital health outcomes. We found that the median age/experience of the board-certified cardiologists in an institution is not related to respective in-hospital mortality, but that a greater range of board-certified cardiologist age/experience at an institution is associated with a lower risk of respective in-hospital mortality (**Figure 4**). This suggests that variation in board-certified cardiologist age/experience may have a meaningful impact on patient outcome.

Furthermore, in the present study median board-certified cardiologist age/experience at an institution was not related to respective in-hospital mortality. Patients treated by older physicians have been found to have higher mortality rates than patients treated by younger physicians.[16,17] It has also been reported that invasive treatments performed by specialists result in lower mortality rates than do similar treatments performed by non-specialists.[18,19] The present results are not consistent with those of previous studies.

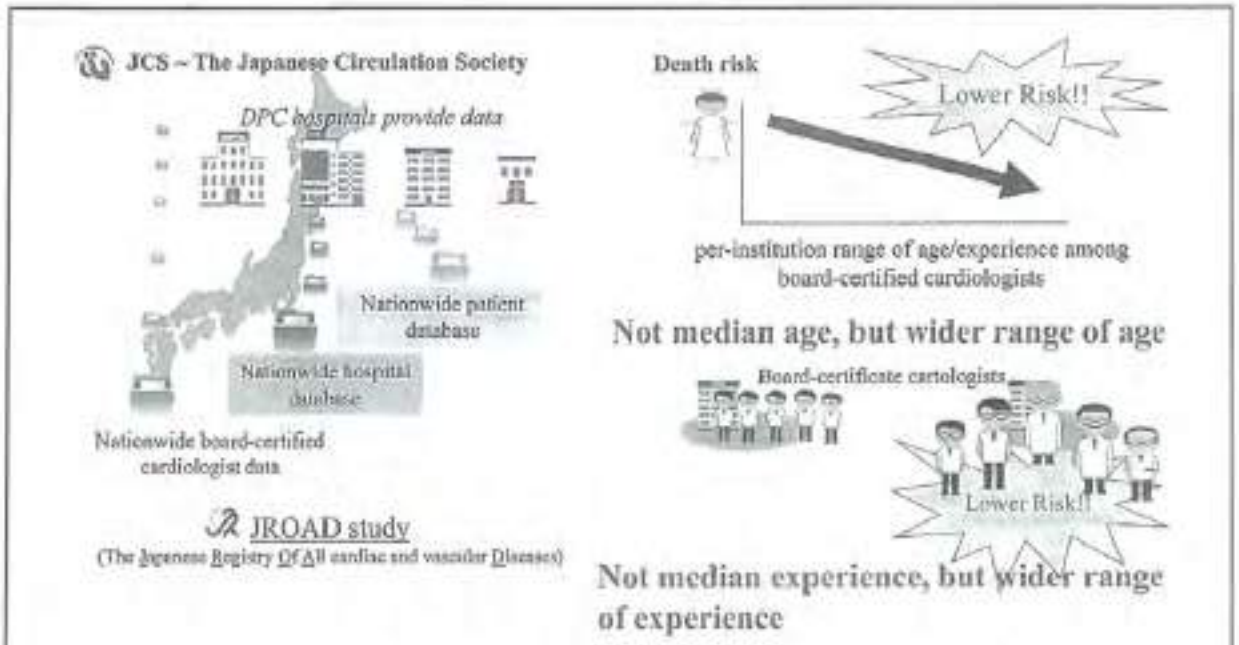

Figure 4. Summary of the present results. Data from the nationwide database of acute care hospitals in Japan, comprising 2,371 hospitals, were collected between 2012 and 2013. DPC, diagnostic procedure combination.

Compared with the previous reports, JROAD included only teaching hospitals and, in the present study, we included only board-certified physicians who have passed a specific exam of medical knowledge, clinical knowledge, and diagnosis skills. Burke et al reported that teaching hospitals were associated with lower mortality compared with non-teaching hospitals.[18] Teaching hospitals are more likely to be higher volume centers and to provide more technologically intensive care requiring specialized knowledge, than non-teaching hospitals.[18] Although physician age/experience may be an important factor for reducing the risk of patient death, other factors independent of physician age, such as special knowledge, skills, hospital volume, and attending professional training, have been confirmed to reduce the risk of patient death.[19,18,21,22] Therefore, physicians working at major teaching hospitals are more likely to continue advancing their knowledge and utilize the most up-to-date standard practices for patient care.

The second finding in the present study was that institutions with a greater range of board-certified cardiologist age/experience have a lower risk of in-hospital mortality. Compared with younger physicians, physicians who have been practicing for a higher number of years and who are older possess less factual knowledge and are less likely to adhere to appropriate standards of care.[17,23,24] In contrast, surgery mortality rates have been found to be lower for older surgeons than for younger surgeons.[25] Although the present findings did not support those of previous studies, it may be hypothesized that if younger physicians have more up-to-date knowledge, and older physicians have more experience, then a combination of the two, as reflected in a wider range of age/experience per hospital, could lower the risk of in-hospital death. In contrast to previous studies, the present study provides new evidence that hospitals with a wide range of board-certified cardiologist age/experience can provide good medical care in cardiology.

Also, according to the present subgroup analysis, board-certified cardiologist range of age/experience at an institution is associated with lower mortality rates for several diseases, excluding angina, pulmonary embolism (PE), and cardiac arrest. The regression models, after adjustment for patient characteristics, however, indicated that the latter 3 were indeed associated with a lower risk of in-hospital mortality. Given that the number of angina and PE cases was very small, these did not influence the result. Meanwhile, mortality rates concerning cardiac arrest have been found to be associated with, aside from hospital characteristics, shockable rhythm, patient age, time to cardiopulmonary resuscitation, and out-of-home events.[26-29] Thus, in institutions with high mortality rates, the influence of cardiac arrest may not be statistically significant.

Study Limitations

This study had several limitations. First, we included only DPC hospitals with cardiovascular beds that met JCS requirements; JROAD, however, is the largest cross-sectional study of nationwide cardiac health outcomes in Japan. Second, evaluating only the association of board-certified cardiologists with any cause of death was not possible, because JROAD does not have data on cause of death. Third, the prevalence of in-hospital death of patients with angina, PE, and atrial fibrillation was low. Fourth, although the analysis of median age/years of experience was limited due to the relatively small number of board-certified cardiologists per hospital, this is the largest study yet to evaluate the association of board-certified cardiologists with in-hospital death, thus allowing for a unique investigation of the risk of death at a national level.

Implications for Clinical Care

According to the present study, institutions with a greater range of board-certified cardiologist age/experience have a lower risk of in-hospital mortality. This suggests that the presence of a wide range of board-certified cardiologist age groups at a hospital is a benefit to clinical cardiac care (by preventing patient deaths), and that such diversity results in the cardiologists successfully maintaining competence and learning new skills and knowledge.

Conclusions

Median board-certified cardiologist age/experience at an institution is not related to in-hospital mortality, but greater board-certified cardiologist age/experience range is associated with a lower risk of in-hospital mortality.

Acknowledgments

The authors would like to thank Yoko Suzuta, the other investigators, the hospital staff, and the participants of the JROAD study for their valuable contributions. A full list of participating institutions can be found at http://jroadinfo.ncvc.go.jp

Author Contributions

M.W. and K.Y. contributed equally to this work. The corresponding author attests that all listed authors meet authorship criteria and that no others meeting the criteria have been omitted.

Disclosures

K.Y. has received personal fees from Sanofi. Y.S. has received personal fees from Mitsubishi Tanabe Pharma Corporation, Otsuka Pharmaceutical, Novartis Pharma, Amgen Astellas BioPharma, Terumo Corporation, Astellas Pharma, Takeda Pharmaceutical, Teijin Pharma, Bayer Holding, Daiichi Sankyo, and MSD. K.N. has received personal fees from Mitsubishi Tanabe Pharma, Fillips Japan Corporation, and Tokyo Energy Holdings. Y.M., S.Y., T.M., and Y.J.A. are members of *Circulation Reports*' Editorial Team. The other authors declare no conflicts of interest.

References

1. Ford ES, Ajani UA, Croft JB, Critchley JA, Labarthe DR, Kottke TE, et al. Explaining the decrease in U.S. deaths from coronary disease, 1980–2000. *N Engl J Med* 2007; **356:** 2388–2398.
2. Lozano R, Naghavi M, Foreman K, Lim S, Shibuya K, Aboyans V, et al. Global and regional mortality from 235 causes of death for 20 age groups in 1990 and 2010: A systematic analysis for the Global Burden of Disease Study 2010. *Lancet* 2012; **380:** 2095–2128.
3. Packer M, Bristow MR, Cohn JN, Colucci WS, Fowler MB, Gilbert EM, et al. The effect of carvedilol on morbidity and mortality in patients with chronic heart failure: U.S. Carvedilol Heart Failure Study Group. *N Engl J Med* 1996; **334:** 1349–1355.
4. Ide T, Ohtani K, Higo T, Tanaka M, Kawasaki Y, Tsutsui H. Ivabradine for the treatment of cardiovascular diseases. *Circ J* 2019; **83:** 252–260.
5. Cho KI, Sakuma I, Sohn IS, Hayashi T, Shimada K, Koh KK. Best treatment strategies with statins to maximize the cardiometabolic benefits. *Circ J* 2018; **82:** 937–943.
6. Marume K, Takashio S, Nagai T, Tsujita K, Saito Y, Yoshikawa T, et al. Effect of statins on mortality in heart failure with preserved ejection fraction without coronary artery disease: Report from the JASPER study. *Circ J* 2019; **83:** 357–367.
7. Bellotti P, Badano LP, Acquarone N, Gelfio R, Lo Pinto G, Maggioni AP, et al. Specialty-related differences in the epidemiology, clinical profile, management and outcome of patients hospitalized for heart failure; the OSCUR study: Outcome dello Scompenso Cardiaco in relazione all'Utilizzo delle Risorse. *Eur Heart J* 2001; **22:** 596–604.
8. Philbin EF, Weil HF, Erb TA, Jenkins PL. Cardiology or primary care for heart failure in the community setting: Process of care and clinical outcomes. *Chest* 1999; **116:** 346–354.
9. Kanaoka K, Obayashi S, Yonezawa K, Nakai M, Nishimura K, Kawata H, et al. Number of board-certified cardiologists and acute myocardial infarction-related mortality in Japan: JROAD and JROAD-DPC registry analysis. *Circ J* 2018; **82:** 2845–2851.
10. Yasuda S, Nakao K, Nishimura K, Miyamoto Y, Suzuta Y, Shishido T, et al. The current status of cardiovascular medicine in Japan: Analysis of a large number of health records from a nationwide claim-based database, JROAD-DPC. *Circ J* 2016; **80:** 2327–2335.
11. Yasuda S, Miyamoto Y, Ogawa H. Current status of cardiovascular medicine in the aging society of Japan. *Circulation* 2018; **138:** 965–967.
12. Yasunaga H, Ide H, Imamura T, Ohe K. Impact of the Japanese diagnosis procedure combination-based payment system on cardiovascular medicine-related costs. *Int Heart J* 2005; **46:** 855–866.
13. Nakamura K. Diagnosis procedure combination database would develop nationwide clinical research in Japan. *Circ J* 2018; **80:** 2289–2290.
14. Yasunaga H, Matsui H, Horiguchi H, Fushimi K, Matsuda S. Application of the diagnosis procedure combination (DPC) data to clinical studies. *J UOEH* 2014; **36:** 191–197 (in Japanese).
15. Iihara K, Nishimura K, Kada A, Nakagawara J, Toyoda K, Ogasawara K, et al. The impact of comprehensive stroke care capacity on the hospital volume of stroke interventions: A nationwide study in Japan: J-ASPECT study. *J Stroke Cerebrovasc Dis* 2014; **23:** 1001–1018.
16. Choudhry NK, Fletcher RH, Soumerai SB. Systematic review: The relationship between clinical experience and quality of health care. *Ann Intern Med* 2005; **142:** 260–273.
17. Tsugawa Y, Newhouse JP, Zaslavsky AM, Blumenthal DM, Jena AB. Physician age and outcomes in elderly patients in hospital in the US: Observational study. *BMJ* 2017; **357:** j1797.
18. Badheka AO, Patel NJ, Grover P, Singh V, Patel N, Arora S, et al. Impact of annual operator and institutional volume on percutaneous coronary intervention outcomes: A 5-year United States experience (2005–2009). *Circulation* 2014; **130:** 1392–1406.
19. Curtis JP, Luebbert JJ, Wang Y, Rathore SS, Chen J, Heidenreich PA, et al. Association of physician certification and outcomes among patients receiving an implantable cardioverter-defibrillator. *JAMA* 2009; **301:** 1661–1670.
20. Burke LG, Frakt AB, Khullar D, Orav EJ, Jha AK. Association between teaching status and mortality in US hospitals. *JAMA* 2017; **317:** 2105–2113.
21. Bertomeu V, Cequier A, Bernal JL, Alfonso F, Anguita MP, Muñiz J, et al. In-hospital mortality due to acute myocardial infarction: Relevance of type of hospital and care provided. RECALCAR study. *Rev Esp Cardiol (Engl Ed)* 2013; **66:** 935–942.
22. Jong P, Gong Y, Liu PP, Austin PC, Lee DS, Tu JV. Care and outcomes of patients newly hospitalized for heart failure in the community treated by cardiologists compared with other specialists. *Circulation* 2003; **108:** 184–191.
23. Salem-Schatz SR, Avorn J, Soumerai SB. Influence of clinical knowledge, organizational context, and practice style on transfusion decision making: Implications for practice change strategies. *JAMA* 1990; **264:** 476–483.
24. Golden NH, Seigel WM, Fisher M, Schneider M, Quijano E, Suss A, et al. Emergency contraception: Pediatricians' knowledge, attitudes, and opinions. *Pediatrics* 2001; **107:** 287–292.
25. Tsugawa Y, Jena AB, Orav EJ, Blumenthal DM, Tsai TC, Mehrotra WT, et al. Age and sex of surgeons and mortality of older surgical patients: Observational study. *BMJ* 2018; **361:** k1343.
26. Callaway CW, Schmicker R, Kampmeyer M, Powell J, Rea TD, Daya MR, et al. Receiving hospital characteristics associated with survival after out-of-hospital cardiac arrest. *Resuscitation* 2010; **81:** 524–529.
27. Ballesteros-Pena S, Abecia-Inchaurregui LC, Echevarria-Orella E. Factors associated with mortality in out-of-hospital cardiac arrests attended in basic life support units in the Basque Country (Spain). *Rev Esp Cardiol (Engl Ed)* 2013; **66:** 269–274.
28. Nakashima T, Noguchi T, Tahara Y, Nishimura K, Ogata S, Yasuda S, et al. Patients with refractory out-of-cardiac arrest and sustained ventricular fibrillation as candidates for extracorporeal cardiopulmonary resuscitation: Prospective multi-center observational study. *Circ J* 2019; **83:** 1011–1018.
29. Kiyohara K, Sado J, Kitamura T, Ayusawa M, Nitta M, Iwami T, et al. Epidemiology of pediatric out-of-hospital cardiac arrest at school: An investigation of a nationwide registry in Japan. *Circ J* 2018; **82:** 1026–1032.

ESC European Society of Cardiology

European Heart Journal - Cardiovascular Imaging (2020) 21, 222–230
doi:10.1093/ehjci/jez076

Anomalous origin of the coronary artery coursing between the great vessels presenting with a cardiovascular event (J-CONOMALY Registry)

Koichi Nagashima[1*], Takafumi Hiro[1], Daisuke Fukamachi[1], Yasuo Okumura[1], Ichiro Watanabe[1], Atsushi Hirayama[1], Masashi Tanaka[2], Tomofumi Tanaka[3], Itaru Takamisawa[3], Isao Taguchi[4], Akira Sato[5], Kazutaka Aonuma[5], Seiji Fukamizu[6], Akihiro Nakada[6], Atsuyuki Watanabe[7], Naofumi Amioka[7], Yasuyuki Suzuki[8], Naoya Matsumoto[8], Junichi Koizumi[9], Kazuya Kumagai[9], Masanao Naya[10], Yoshiharu Higuchi[11], Yoshiro Naito[12], Tohru Masuyama[12], Mitsuharu Kawamura[13], Ryusuke Tsunoda[14], Susumu Suzuki[15], Hideki Ishii[15], Toyoaki Murohara[15], Takeshi Shimizu[16], Yasuchika Takeishi[16], Kazuki Shiina[17], Jun Yamashita[17], Tomohiko Imamura[18], Naokata Sumitomo[18], Teruo Noguchi[19], Toshihide Aso[20], Kojiro Furukawa[21], Yasuteru Yamauchi[22], Kaoru Okishige[22], Kenji Sakata[23], Masakazu Yamagishi[23], Shigeo Shimizu[24], Masakazu Ohno[24], Teruyasu Sugano[25], Koichiro Matsumura[26], Kensuke Matsumoto[27], Kazuyuki Ozaki[28], Shunji Hayashidani[29], Hiroshi Meno[29], Atsushi Iwata[30], Takumi Higuma[31], Hirofumi Tomita[31], Hideaki Yoshino[32], Seiichi Taniai[32], Koki Shishido[33], Masato Murakami[33], Koji Negishi[34], Masaki Nii[35], Daisuke Wakatsuki[36], Hiroshi Suzuki[36], Yuji Motoike[37], Yukio Ozaki[37], Jun Nakazato[38], Hidemori Hayashi[39], Satoshi Higuchi[40], and Morio Shoda[40]

[1]Division of Cardiology, Department of Medicine, Nihon University School of Medicine, 30-1 Oyaguchi-kamicho, Itabashi-ku, Tokyo 173-8610, Japan; [2]Department of Cardiovascular Surgery, Nihon University School of Medicine, 30-1 Oyaguchi Kamicho, Itabashi-ku, Tokyo 173-8610, Japan; [3]Department of Cardiology, Saiseikai Heart Institute, 3-16-1 Aoshi-cho, Fuchu-shi, Tokyo 183-0003, Japan; [4]Department of Cardiology, Dokkyo Medical University Saitama Medical Center, 2-1-50 Minamikoshigaya, Koshigaya, Saitama 343-8555, Japan; [5]Department of Cardiology, Faculty of Medicine, University of Tsukuba, 1-1-1 Tennodai, Tsukuba, Ibaraki 305-8575, Japan; [6]Department of Cardiology, Tokyo Metropolitan Hiroo Hospital, 2-34-10 Ebisu, Shibuya-ku, Tokyo 150-0013, Japan; [7]Department of Cardiovascular Medicine, Graduate School of Medicine, Dentistry, and Pharmaceutical Sciences, Okayama University, 2-5-1 Shikata-cho, Kita-ku, Okayama-shi, Okayama 700-8558, Japan; [8]Department of Cardiology, Nihon University Hospital, 1-6 Kanda-Surugadai, Chiyoda-ku, Tokyo 101-8309, Japan; [9]Department of Cardiovascular Surgery, Memorial Heart Center, Iwate Medical University, 9-1, Uchimaru, Morioka city, Iwate 020-8505, Japan; [10]Department of Cardiovascular Medicine, Graduate School of Medicine, Hokkaido University, Kita 15, Nishi 7, Kita-ku, Sapporo 060-8638, Japan; [11]Cardiovascular Division, Osaka Police Hospital, 10-31 Kitayama-cho, Tennouji-ku, Osaka 543-0035, Japan; [12]Cardiovascular Division, Department of Internal Medicine, Hyogo College of Medicine, 1-1 Mukogawa-cho, Nishinomiya, Hyogo 663-8501, Japan; [13]Division of Cardiology, School of Medicine, Showa University, 1-5-8, Hatanodai Shinagawa, Tokyo 142-8555, Japan; [14]Department of Cardiology, Japanese Red Cross Kumamoto Hospital, 2-1-1 Nagamine Minami, Higashi-ku, Kumamoto 861-8520, Japan; [15]Department of Cardiology, Nagoya University Graduate School of Medicine, 65 Tsurumai-cho, Showa-ku, Nagoya 466-8550, Japan; [16]Department of Cardiovascular Medicine, Fukushima Medical University, 1 Hikarigo-oka, Fukushima City 960-1295, Japan; [17]Department of Cardiology, Tokyo Medical University, 6-1-1 Shinjuku, Shinjuku-ku, Tokyo 160-8402, Japan; [18]Department of Pediatric Cardiology, Saitama Medical University International Medical Center, 1397-1, Yamane, Hidaka-City, Saitama 350-1298, Japan; [19]Department of Cardiovascular Medicine, National Cerebral and Cardiovascular Center, 5-7-1 Fujishiro-dai, Suita, Osaka 565-8565, Japan; [20]Department of Cardiovascular Surgery, Kanagawa Children's Medical Center, 2-138-4 Mutsukawa, Minami-ku, Yokohama, Kanagawa 232-8555, Japan; [21]Department of Cardiovascular Surgery, National Hospital Organization Kyushu Medical Center, 1-8-1 Jigohama, Chuo-ku, Fukuoka 810-8563, Japan; [22]Heart Center, Yokohama-City Bay Red Cross Hospital, 3-12-1, Shinyamashita, Naka-ku, Yokohama-shi, Kanagawa 231-8801, Japan; [23]Department of Cardiovascular and Internal Medicine, Graduate School of Medicine, Kanazawa University, 13-1, Takara-machi, Kanazawa, Ishikawa 920-8640, Japan; [24]Department of Cardiology, National Hospital Organization, National Disaster Medical Center, 3256 Midoricho, Tachikawa, Tokyo 190-0014, Japan; [25]Department of Medical Science and Cardiovascular Medicine, Graduate School of Medicine, Yokohama City University, 3-9 Fukuura, Kanazawa-ku, Yokohama 236-0004, Japan; [26]Department of Cardiology, Kansai Medical University Medical Center, 10-15 Fumizono-cho, Moriguchi 570-8507, Japan; [27]Department of Cardiology, The

*Corresponding author. Tel: +81-3-3972-8111; Fax: +81-3-3972-1096. E-mail: cocalvochan@gmail.com
Published on behalf of the European Society of Cardiology. All rights reserved. © The Author(s) 2019. For permissions, please email: journals.permissions@oup.com.

Downloaded from https://academic.oup.com/ehjcimaging/article-abstract/21/2/222/5479976 by emaranmsu.my user on 09 March 2020

Sakakibara Heart Institute of Okayama, 2-5-1, Nishi-cho, Kita-ku, Okayama 700-0804, Japan; [18]Department of Cardiovascular Biology and Medicine, Graduate School of Medical and Dental Sciences, Niigata University, 2-5274 Gakkocho-dori, Niigata 951-8514, Japan; [19]Division of Cardiology, Fukuoka Red Cross Hospital, 3-1-1 Otoku Hirouchi, Fukuoka-shi, Fukuoka 815-8555, Japan; [20]Department of Cardiology, Fukuoka University School of Medicine, 7-45-1 Nanakuma, Jonan-ku, Fukuoka 814-0180, Japan; [21]Department of Cardiology, Hirosaki University Graduate School of Medicine, 5 Zaifu-cho, Hirosaki, Aomori, 036-8562, Japan; [22]Division of Cardiology, Department of Internal Medicine II, Kyorin University School of Medicine, 6-20-2 Shinkawa, Mitaka-shi, Tokyo 181-8611, Japan; [23]Department of Cardiology, Shonan Kamakura General Hospital, 1370-1 Okamoto, Kamakura 247-8533, Japan; [24]Department of Cardiology, Yokohama Municipal Citizens' Hospital, 56 Okusawa-cho, Hodogaya-ku, Yokohama City, Kanagawa 240-8555, Japan; [25]Shizuoka Children's Hospital, 860 Urushiyama, Aoi-ku, Shizuoka 420-8660, Japan; [26]Division of Cardiology, Department of Internal Medicine, Showa University Fujigaoka Hospital, 1-30 Fujigaoka, Aoba-ku, Yokohama-shi, Kanagawa 227-8501, Japan; [27]Department of Cardiology, Fujita Health University, 1-98 Dengakugakubo, Kutsukake-cho, Toyoake, Aichi 470-1192, Japan; [28]Department of Cardiovascular Medicine, Okinawa Prefectural Chubu Hospital, 281 Miyazato, Urumi-city, Okinawa 904-2293, Japan; [29]Department of Cardiovascular Medicine, Juntendo University Graduate School of Medicine, 2-1-1, Hongo, Bunkyo-ku, Tokyo 113-8421, Japan; and [30]Department of Cardiology, Tokyo Women's Medical University, 8-1 Kawada-cho, Shinjuku-ku, Tokyo 162-8666, Japan

Received 19 January 2019; editorial decision 26 March 2019; accepted 28 March 2019; online publish-ahead-of-print 25 April 2019

Aims Anomalous origin of the coronary artery (AOCA) with an inter-arterial course (IAC) between the great vessels poses a risk for a life-threatening cardiovascular event. We assessed, in a registry-based study, the clinical features, treatment strategies, and prognoses of life-threatening cardiovascular events ensuant to AOCA.

Methods and results Included were 65 AOCA patients (48 men/17 women, aged 41 ± 23 years) from 40 clinical centres who had experienced sudden cardiac arrest (SCA) ($n = 30$), acute myocardial infarction (AMI) ($n = 5$), angina ($n = 23$), or syncope ($n = 7$). The anomalous vessel was the right coronary artery in 72% of patients and left coronary artery in 28%; the ostium was slit-like in 42%. Coronary luminal narrowing ≥75% was absent in patients with SCA or syncope (86% and 57%, respectively), but occlusion or narrowing was seen in those with AMI (100%) or angina (52%). Age ≤40 years, male sex, sporting activity, absence of prodromal symptoms, acutely angled (<30°) take-off from the aorta, and absence of luminal narrowing of the IAC segment were associated with SCA in this patient group. Coronary vasospasm was inducible in 12 of 17 patients without coronary narrowing. Management included surgical revascularization ($n = 26$) percutaneous coronary intervention ($n = 9$), and medical treatment ($n = 26$). Four SCA patients died while hospitalized; no others died during the median 5.0 (range, 1.8–7.0)-year follow-up period.

Conclusions In patients with AOCA, age ≤40 years, male sex, sporting activity, and an acute take-off angle appear to be risk factors for SCA. Appropriate management can be beneficial. Confirmation in a large-scale study is warranted.

Keywords anomalous origin of the coronary artery • coronary vasospasm • sudden cardiac arrest

Introduction

Anomalous origin of the coronary artery (AOCA) is a rare congenital irregularity, with an incidence of 0.3–1%.[1–3] Although AOCA is typically asymptomatic and incidentally identified, AOCAs with an inter-arterial course (IAC) between the ascending aorta and the main pulmonary artery pose a risk for a life-threatening cardiovascular event, such as sudden cardiac death (SCD) or myocardial infarction (MI).[3–5] Recognition of the potential for such an event emerged from observational studies of AOCA identified in asymptomatic patients[3,6] and from autopsies performed after SCD.[3,5] Coronary angiography (CAG),[7] computed tomography (CT),[8] and magnetic resonance imaging (MRI)[9] are reported to be useful for detection of AOCA, despite the drawbacks in terms of radiation exposure, limited spatial resolution, and limited whole-heart coverage. However, little is known about the clinical features and optimal management of patients with AOCA who have actually experienced a life-threatening cardiovascular event, aborted SCD in particular. In addition, there is a generally accepted association between AOCA and coronary vasospasm, but the evidence is limited to a few case reports.[10,11] We, therefore, created a registry, the J-CONOMALY Registry, so that the clinical features, treatment strategies, and prognosis of AOCA in patients who experience a life-threatening cardiovascular event can be assessed. The ultimate goals are clinical risk stratification for predicting sudden cardiac arrest (SCA) in patients with AOCA and identification of optimal secondary prevention strategies for these patients.

Methods

Registry and study design

The registry was set up to investigate clinical and anatomical features, management, and prognosis of AOCA. Information gathering was retrospective. Patients included in the registry were patients with AOCA who presented to 1 of 40 clinical centres in Japan between 2002 and 2018. Inclusion in the registry was contingent on the following criteria: (i) AOCA with an IAC between the great vessels was detected by CAG and/or CT; (ii) the patient suffered an ischaemic cardiovascular event that required hospitalization and treatment; and (iii) the cardiovascular event was caused by ischaemia related specifically to the IAC of the anomalous coronary artery, depicted by CAG and/or CT or determined by the patient's physician on the basis of the diagnostic work-up, which excluded other possible mechanisms. Data collection and analysis were approved by the Institutional Review Board of Nihon University Itabashi Hospital and each participating centre, and patient consent was obtained by an opt-out method. The study reported herein was registered with the University Hospital Medical Information Network (study ID: UMIN000030629).

Downloaded from https://academic.oup.com/ehjimaging/article-abstract/21/2/223/5479076 by ainsiamnmuniv user on 09 March 2020

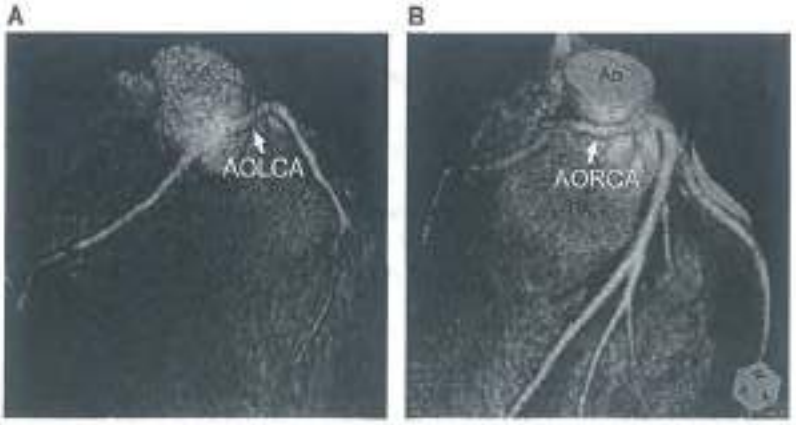

Figure 1 Representative examples of three-dimensional volume-rendered CT images of AOLCA (A) and AORCA (B) with an IAC between the ascending aorta (Ao) and the main pulmonary artery (PA).

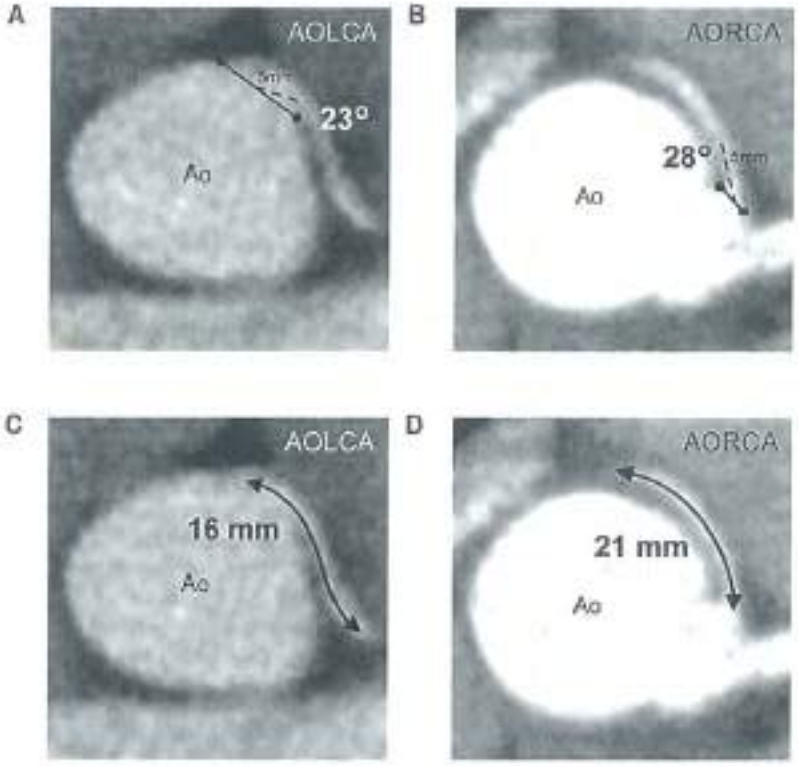

Figure 2 CT measurements of the take-off angle from the ascending aorta (Ao) in (A) AOLCA and (B) AORCA cases shown in Figure 1, and of the length of the IAC in the same (C) AOLCA and (D) AORCA cases. (A–B) The solid line indicates the so-called ostium line, and the dashed line indicates the line drawn from the mid-point of the ostium line to a point 5 mm along the centre of the AOCA. The angle between the two lines at the mid-point is measured and taken as the take-off angle.

Downloaded from https://academic.oup.com/ehjcimaging/article-abstract/21/2/222/5470076 by almanaraunlv user on 09 March 2020

Table 1 Patient characteristics upon presentation

	Total ($n = 65$)	SCA ($n = 30$)	Non-SCA				*P*-value
			Total ($n = 35$)	AMI ($n = 5$)	Angina ($n = 23$)	Syncope ($n = 7$)	
Age (years)	41 ± 23	29 ± 20	52 ± 21	53 ± 26	57 ± 16	34 ± 25	<0.0001
Male sex	48 (74)	26 (87)	22 (63)	3 (60)	14 (61)	5 (71)	0.05
BMI (kg/m^2)	22 ± 5	20 ± 4	24 ± 5	25 ± 8	24 ± 3	25 ± 7	0.0003
Presence of a coronary risk factor	32 (49)	8 (27)	24 (69)	3 (60)	19 (83)	2 (29)	0.0008
Current smoking	17 (26)	5 (17)	12 (34)	1 (20)	11 (48)	0 (0)	0.11
Hypertension	19 (29)	2 (7)	17 (49)	2 (40)	13 (56)	2 (29)	0.0003
Hyperlipidaemia	17 (26)	2 (7)	15 (43)	1 (20)	12 (52)	2 (29)	0.001
Diabetes mellitus	6 (9)	1 (3)	5 (14)	1 (20)	4 (17)	0 (0)	0.21
Hyperuricaemia	2 (3)	1 (3)	1 (3)	0 (0)	1 (4)	0 (0)	1.00
Structural heart disease	5 (8)	1 (3)	4 (11)	1 (20)	1 (4)	2 (29)	0.36
Hypertrophic cardiomyopathy	3 (5)	1 (3)	2 (6)	0 (0)	0 (0)	2 (29)	–
Aortic valve stenosis	1 (2)	0 (0)	1 (3)	0 (0)	1 (4)	0 (0)	–
Mitral regurgitation	1 (2)	0 (0)	1 (3)	1 (20)	0 (0)	0 (0)	–
Atrial fibrillation	6 (9)	4 (13)	2 (6)	1 (20)	1 (4)	1 (14)	0.40
Trigger							
Sporting activity	29 (45)	21 (70)	8 (23)	1 (20)	2 (9)	5 (71)	0.0001
Light exertion	24 (37)	5 (17)	19 (54)	2 (40)	15 (65)	2 (29)	0.002
Rest	12 (18)	4 (13)	8 (23)	2 (40)	6 (26)	0 (0)	0.36
Prodromal symptoms before the acute event	28 (43)	7 (23)	21 (60)	2 (40)	14 (61)	5 (71)	0.003
LVEF (%)	62 ± 10	62 ± 11	62 ± 10	43 ± 15	65 ± 6	61 ± 5	0.72

Values are shown as mean ± SD or n (%). *P*-values are for SCA vs. non-SCA.
AMI, acute myocardial infarction; AOCA, anomalous origin of the coronary artery; BMI, body mass index; LVEF, left ventricular ejection fraction; SCA, sudden cardiac arrest.

Diagnosis of a cardiovascular event and data collection

Diagnosis of ischaemic cardiovascular events and data pertaining to diagnostic work-up, treatment details, and outcomes are provided in the Supplementary file.

CT measurements

Four-, 16-, 64-, 128-, or 320-row cardiac multi-detector contrast-enhanced CT was performed according to established guidelines,[12] and the images were interpreted by trained cardiologists at each centre. Representative images of anomalous origin of the left coronary artery (AOLCA) and anomalous origin of the right coronary artery (AORCA) are shown in *Figure 1A* and *B*. The following anatomical features were determined:

(1) Take-off level of the AOCA, categorized as at/above or below the aortic valve commissure or contralateral coronary artery.
(2) Take-off angle of the AOCA from the aorta (*Figure 2A* and *B*). On the axial acquisition image, where the maximum AOCA ostium diameter could be seen, an ostium line, defined as an imaginary line representing the ostial diameter, was drawn. From the mid-point of this line, a second line, 5-mm long, was drawn along the centre of the AOCA. The take-off angle of the AOCA was measured as the angle between these two lines at the mid-point of the ostium line.[6]
(3) IAC length, i.e. the length of the coronary artery as it coursed between the ascending aorta and main pulmonary artery (*Figure 2C* and *D*).
(4) Presence of a slit-like ostium, defined as ≥50% luminal narrowing of the ostium.

Statistical analysis

Continuous variables are expressed as mean ± SD, and categorical variables are expressed as the number and percentage of patients. Differences in continuous variables were analysed by Student *t*-test or Mann–Whitney *U* test, as appropriate, and differences in dichotomous variables were analysed by χ^2 test unless the expected values in cells were <5, in which case Fisher's exact test was used. Simple linear and simple logistic regression analyses were performed to identify risk factors for SCA. Receiver operating characteristic curves were plotted to determine the cut-off age or acute take-off angle predictive of a risk for SCA. All statistical analyses were performed with JMP 11 software (SAS Institute, Cary, NC, USA), and $P < 0.05$ was considered statistically significant.

Results

Patient characteristics

Sixty-five patients (48 men, 41 ± 23 years of age) with an AOCA were included in the registry. No patient had any other vascular anomaly. Clinical characteristics of these patients and the manifestations of AOCA are shown in *Table 1*. The following ischaemic cardiovascular events occurred: SCA in 30 patients (ventricular fibrillation = 26, pulseless electrical activity = 1, asystole = 1, and

Downloaded from https://academic.oup.com/ehjcimaging/article-abstract/21/2/222/5479876 by stmarianmaumv user on 09 March 2020

Table 2 AOCA features and diagnoses

	Total (n = 65)	SCA (n = 30)	Non-SCA				P-value
			Total (n = 35)	AMI (n = 5)	Angina (n = 23)	Syncope (n = 7)	
CT and CAG findings							
Right anomalous coronary artery	47 (72)	20 (67)	27 (77)	2 (40)	21 (91)	4 (57)	0.35
Left anomalous coronary artery	18 (28)	10 (33)	8 (23)	3 (60)	2 (9)	3 (43)	0.35
Left main trunk	16 (25)	10 (33)	6 (17)	3 (60)	0 (0)	3 (43)	–
Left anterior descendant	2 (3)	0 (0)	2 (6)	0 (0)	2 (8)	0 (0)	–
Left circumflex	0 (0)	0 (0)	0 (0)	0 (0)	0 (0)	0 (0)	–
Take-off level							
At or above commissure	4 (6)	2 (7)	2 (6)	0 (0)	2 (9)	0 (0)	1.00
Below the aortic valve commissure	59 (91)	27 (90)	32 (91)	5 (100)	20 (87)	7 (100)	1.00
Contralateral coronary artery	2 (3)	1 (3)	1 (3)	0 (0)	1 (4)	0 (0)	1.00
Take-off angle from ascending aorta (°)	25 ± 12	21 ± 7	30 ± 15	34 ± 2	31 ± 17	24 ± 8	0.008
Slit-like ostium	27 (42)	12 (41)	15 (43)	2 (40)	9 (39)	4 (57)	0.91
Length courses between great vessels (mm)	18 ± 7	16 ± 8	19 ± 6	26 ± 5	20 ± 6	15 ± 3	0.15
CAG of IAC							
Occlusion (≥99%)	7 (11)	2 (7)	5 (14)	5 (100)	0 (0)	0 (0)	0.44
Luminal narrowing (≥75%)	18 (28)	2 (7)	15 (43)	0 (0)	12 (52)	3 (43)	0.001
Atherosclerotic stenosis	4 (6)	0 (0)	4 (11)	0 (0)	4 (17)	0 (0)	0.12
No luminal narrowing (<75%)	40 (62)	26 (87)	15 (43)	0 (0)	11 (48)	4 (57)	0.0003
Coronary vasospasm	12/17 (71)	7/12 (58)	5/5 (100)		5/5 (100)		0.24
Evidence of ischaemia at the AOCA region	24/45 (53)	12/23 (52)	12/22 (55)	1/2 (50)	9/15 (60)	2/5 (40)	0.87
Treadmill stress test	14/38 (37)	9/21 (43)	5/17 (29)	0/1 (0)	4/11 (36)	1/5 (20)	0.39
Myocardial perfusion scintigraphy	14/32 (44)	6/17 (35)	8/15 (53)	1/1 (100)	6/12 (50)	1/2 (50)	0.30

Values are shown as mean ± SD or n (%). P-values are for SCA vs. non-SCA.
AMI, acute myocardial infarction; AOCA, anomalous origin of the coronary artery; CT, computed tomography; SCA, sudden cardiac arrest.

cardiogenic shock = 2), acute myocardial infarction (AMI) in 5, angina in 23, and syncope in 7. In comparing the circumstances in which the various cardiac events occurred, we found that the patients who suffered SCA were significantly younger than those who suffered from another type of event (non-SCA). We also found that SCA occurred with significant frequency during sporting activity such as playing soccer or basketball or running a marathon. However, only 23% of patients who experienced SCA also experienced prodromal symptoms before the event, whereas 60% of patients who did not experience SCA experienced prodromal symptoms (*Table 1*). In contrast, angina frequently occurred during light exertion in patients with a coronary risk factor. In two elderly patients, one in whom AMI occurred at 63 years of age and one who experienced angina at age 77, the event was attributed to pulmonary artery dilation resulting from pulmonary thromboembolism[13] and to lung lobectomy,[14] respectively.

AOCA features and diagnosis

The AOCA features and diagnoses are shown in *Table 2*. AORCA was seen in 72% of patients, AOLCA was seen in 28%, and a slit-like ostium was seen in 42%. The take-off angle from the aorta was more acute (21° ± 7° vs. 30° ± 15°, $P = 0.008$) in the SCA patients than in others, but no between-group differences were seen in other anatomical features of the anomalous vessel, including whether it was an AORCA or AOLCA, the location and shape of the ostium, and length of the IAC. Coronary luminal narrowing ≥75% was not found in 87% of patients who experienced SCA, whereas non-atherosclerotic coronary occlusion, such as by a thromboembolus (n = 4, 80%) or obstruction of the IAC segment (n = 1, 20%), was found in patients who had suffered AMI. Coronary luminal narrowing ≥75% was quite prevalent among patients with angina (n = 12, 52%) and was due to compression by the great vessels in eight AORCA patients and by atherosclerotic plaque at the IAC segment (detected by intravascular ultrasound following CT and CAG) in four AORCA patients. Non-invasive stress testing revealed ischaemia in the AOCA region in 24 of 45 (53%) patients, including 12 of 23 (52%) SCA patients, 1 of 2 (50%) AMI patients, 9 of 15 (60%) angina patients, and 2 of 5 (40%) syncope patients.

Seventeen patients without coronary luminal narrowing, including 12 SCA patients and 5 angina patients, underwent intracoronary acetylcholine (n = 13) or ergonovine (n = 4) provocation testing for coronary vasospasm. In seven of these patients, the agent was injected only into the contralateral coronary artery because stable catheter engagement was not achieved in the anomalous coronary artery. Coronary vasospasm was inducible in 12 (71%) patients, including 7 (58%) SCA patients and all five angina patients.

Downloaded from https://academic.oup.com/ehj/article-abstract/21/2/222/594978 by shmaranauthy user on 06 March 2020

Table 3 Treatment strategies and outcomes

	Total (n = 62)	SCA (n = 27)	Non-SCA				P-value
			Total (n = 35)	AMI (n = 5)	Angina (n = 23)	Syncope (n = 7)	
Treatment strategy							
Surgery	26 (42)	16 (59)	10 (29)	1 (20)	4 (17)	5 (71)	0.02
CABG	10 (16)	5 (19)	5 (14)	0 (0)	3 (13)	2 (29)	
Internal thoracic artery	8 (80)	5 (100)	3 (60)		1 (33)	2 (100)	
Saphenous vein	3 (30)	0 (0)	3 (60)		3 (100)	0 (0)	
AOCA ligation	3 (30)	2 (40)	1 (20)		0 (0)	1 (50)	
Ostial reimplantation	6 (10)	3 (11)	3 (9)	0 (0)	1 (4)	2 (29)	
Unroofing	10 (16)	8 (30)	2 (6)	1 (20)	0 (0)	1 (14)	
PCI	9 (15)	0 (0)	9 (26)	4 (80)	5 (22)	0 (0)	0.004
Stenting	6 (10)	0 (0)	6 (17)	1 (20)	5 (22)		
Drug eluting stent	1 (17)	0 (0)	5 (83)	1 (100)	4 (80)		
Bare-metal stent	5 (83)	0 (0)	1 (17)	0 (0)	1 (20)		
POBA	3 (5)	0 (0)	3 (8)	3 (60)	0 (0)		
Medication	50 (81)	19 (70)	31 (89)	5 (100)	22 (96)	4 (57)	0.11
Single antiplatelet therapy	22 (35)	10 (37)	12 (34)	3 (60)	6 (26)	3 (43)	0.82
Dual antiplatelet therapy	8 (13)	1 (4)	7 (20)	1 (20)	6 (26)	0 (0)	0.12
Oral anticoagulant therapy	6 (10)	2 (7)	4 (11)	1 (20)	1 (4)	2 (29)	0.69
β-blocker	28 (45)	10 (37)	19 (54)	3 (60)	13 (57)	3 (43)	0.18
Calcium-channel blocker	22 (35)	7 (26)	15 (43)	0 (0)	14 (61)	1 (14)	0.17
ICD	10 (16)	8 (30)	2 (6)	0 (0)	0 (0)	2 (29)	0.02
Outcome							
In-hospital death (Total, n = 65; SCA, n = 30)	4 (6)	4 (13)	0 (0)	0 (0)	0 (0)	0 (0)	0.04
Duration of hospitalization (days)	30 (7, 36)	30 (18, 42)	10 (4, 20)	34 (14, 87)	5 (4, 12)	16 (11, 25)	0.001
Heart transplantation	1 (2)	0 (0)	1 (3)	1 (20)	0 (0)	0 (0)	1.00
All-cause death during follow-up	0/60 (0)	0/26 (0)	0/34 (0)	0/5 (0)	0/23 (0)	0/7 (0)	NA
Revascularization	1/18 (6)	1/12 (8)	0/5 (0)		0/5 (0)		1.00

The three SCA patients who died after unsuccessful resuscitation are not included. Values are shown as mean ± SD, median (25th, 75th percentile) or n (%). P-values are for SCA vs. non-SCA.
AMI, acute myocardial infarction; CABG, coronary artery bypass grafting; ICD, implantable cardioverter-defibrillator; PCI, percutaneous coronary intervention; POBA, plain old balloon angioplasty; SCA, sudden cardiac arrest.

Treatment strategies according to manifestation

Treatment strategies and outcomes are summarized in Table 3 and Supplementary data online, *Figures S1 and S2*.

Surgical repair was performed in all AOLCA patients who had experienced SCA (n = 10) or syncope (n = 3). Surgical revascularization was also performed in 6 (35%) AORCA patients who had experienced SCA and 2 (50%) AORCA patients who had experienced syncope. Eleven (38%) SCA patients and 2 (29%) syncope patients were simply given an appropriate medication, including a beta-blocker (eight SCA patients and one syncope patient) and/or calcium-channel blocker for coronary vasospasm (five SCA patients and one syncope patient).

Thrombus aspiration was performed in four of the five AMI patients, and this was followed by balloon angioplasty (n = 3) or stenting (n = 1) for AOLCA compression by the great vessels. Surgical unroofing was performed in the patient with a proximal intramural course (IMC) within the aortic wall (n = 1).

Percutaneous coronary stenting was performed in four of the angina patients with an atherosclerotic AORCA and in one angina patient with an AORCA compressed by the great vessels. Surgical revascularization was performed in four angina patients with compression, and the other 14 angina patients were treated medically with a calcium-channel blocker for vasospasm and/or a beta-blocker.

An implantable cardioverter-defibrillator (ICD) was placed in 10 patients without surgical revascularization; 8 with SCA and 2 with syncope. Seven patients who underwent stenting (one with AMI and six with angina) were given dual antiplatelet therapy. For coronary artery bypass grafting (CABG), the internal thoracic artery was used in 80% of the grafts and the saphenous vein in 30%. Ligation at the proximal portion of the anomalous coronary artery was performed in all patients who had no significant stenosis of the coronary ostium (n = 3, 30% of CABG patients).

The majority (n = 14, 88%) of the patients with an anomalous left main trunk were managed by surgical revascularization except for two patients (12%) who underwent emergent percutaneous coronary intervention (PCI) due to AMI. In contrast, both patients with an

Downloaded from https://academic.oup.com/eljcm/article/21/2/222/5479876 by Armenian Univ user on 09 March 2020

Table 4 Association between various risk factors and SCA

	Odds ratio (CI)	*P*-value
Age (years)	0.95 (0.93–0.98)	<0.0001
Male sex	3.84 (1.17–15.2)	0.03
Sports activity	7.88 (2.70–25.3)	0.0001
Absence of prodromal symptoms	4.93 (1.67–14.6)	0.004
AOLCA	1.69 (0.57–5.17)	0.35
Take-off angle from ascending aorta (°)	0.91 (0.83–0.97)	0.003
Slit-like ostium	0.94 (0.34–2.56)	0.91
Absence of luminal narrowing (≥75%) of the IAC segment	8.67 (2.49–30.2)	0.0007
Length of interarterial course (mm)	0.94 (0.86–1.02)	0.14

AOLCA, anomalous origin of the left coronary artery; CI, confidence interval; IAC, interarterial course.

anomalous left anterior descending artery and the majority (58%) of AORCA patients were managed by medication. The reasons for medication use in these patients were evidence of coronary vasospasm (35%), no evidence of ischaemia in the AOCA territory (31%), no compression or obstruction of the AOCA vessel (19%), patients' refusal of surgical revascularization (8%), and physicians' discretion (8%).

Outcomes

Sixty of the 65 patients were discharged from the hospital within 20 (7, 36) days. Four patients died while hospitalized, three who presented with SCA and for whom resuscitation was not successful (two with ventricular fibrillation and one with asystole) and one who presented with cardiogenic shock (Supplementary data online, Figure S2). Fifty-nine of the 61 surviving patients were followed up for a median period of 5.0 (1.8–7.0) years; one patient was waiting for surgical revascularization, and one patient was lost to follow-up. One of the patients who suffered AMI underwent heart transplantation because left ventricular dysfunction developed. Of the 18 patients who underwent CAG reassessment (three patients who had undergone reimplantation, two who had undergone CABG, three who had undergone unroofing, three who had undergone stenting, and seven treated medically), one CABG patient without proximal ligation of the AOCA required balloon angioplasty for graft failure (left intrathoracic artery to the left anterior descending artery and right intrathoracic artery to the left circumflex artery). No stent fracture was seen in the three patients with stenting. Coronary vasospasm remained inducible in three of five patients despite coronary reimplantation ($n = 1$) and/or calcium-channel blocker treatment ($n = 2$). No arrhythmia was detected in any patient who received an ICD.

AOCA features associated with SCA

Association between various risk factors and SCA are shown in Table 4. Age ≤40 years in the absence of coronary risk factors, male sex, participation in a sporting activity, absence of prodromal symptoms, acutely angled take-off (≤30°) from the aorta, and absence of luminal narrowing in IAC segment of the anomalous artery were shown to be associated with SCA in our AOCA patients. Receiver operating characteristic curve analysis revealed that age and take-off angle were of good prognostic performance, with areas under the curve of 0.78 ($P = 0.0003$) and 0.69 ($P = 0.02$), respectively. The age best predicting SCA was ≤40 years, with a sensitivity of 73% and specificity of 74%, and the take-off angle best predicting SCA was ≤30°, with a sensitivity of 96% and specificity of 38%.

Discussion

Main findings

This is the first study to assess the features, risks, management, and outcomes of AOCA patients who present with a life-threatening cardiovascular event such as SCA. The main findings were as follows: (*i*) the manifestation of and mechanism contributing to the ischaemic cardiac event varied from patient to patient; (*ii*) age ≤40 years, male sex, participation in a sporting activity, absence of prodromal symptoms, acutely angled take-off (≤30°) from the aorta, and absence of luminal narrowing of the IAC segment were shown to be associated with SCA in our AOCA registry patients; (*iii*) multiple coronary vasospasm was frequently inducible in patients presenting with SCA or angina; and (*iv*) no patient died during the median 5.0-year follow-up period after surgical revascularization, PCI, or medical treatment.

Mechanisms of ischaemic cardiovascular events

Based on several studies of AOCA as a frequent cause of SCD in young athletes, the main mechanism responsible for ischaemic cardiovascular events is thought to be incremental mechanical compression of the IAC by the great vessels or kinking of the sharp angulation at the AOCA ostium during exercise.[1,5,15] Our features for SCA supported both of these hypothesized mechanisms. Consistent with previous reports, increased cardiac output during exercise may easily expand the great vessels, obstructing the flow of blood within the anomalous coronary artery. Interestingly, an acute take-off angle ≤30° was also a risk factor for SCA, but we found no relation between the IAC length and SCA. These findings may support the latter hypothesis rather than compression of the entire vessel along its IAC. On the basis of our findings, CT/MRI-based pre-participation screening might be necessary for young athletes and young people who train at the same level of intensity as professional athletes.[1,8,1,16]

In contrast, the middle-aged and elderly registry patients suffered non-atherosclerotic cardiovascular events, regardless of exercise. In two of our patients, pulmonary artery dilation caused by pulmonary hypertension might have precipitated obstruction of the anomalous coronary artery.[13,14] A concomitant atherosclerotic stenosis at the portion between the great vessels also accounted for the cardiovascular event in each of these patients.

Coronary spasm is another mechanism responsible for cardiovascular events in patients with AOCA. Evaluation of some individual cases has indicated that the vasospasm might be due to accelerated atherosclerosis or endothelial dysfunction due to the mechanical stress that results from compression by the surrounding great vessels.[10,11] However, in all 17 of our patients with vasospasm of the anomalous coronary artery, vasospasm of the contralateral coronary

Downloaded from https://academic.oup.com/eyjcmr/article-abstract/2/1/223/5478975 by smartlibrary user on 09 March 2020

artery (multiple spasm) was also inducible. Furthermore, in one of our patients in whom the origin of the coronary artery was corrected and in a previously reported case,[11] coronary spasm remained inducible even 2 years after successful surgery. Therefore, some intrinsic mechanism within the anomalous coronary wall other than atherosclerosis or localized endothelial dysfunction might be related to the vasospasm occurring in such patients. From this standpoint, the diagnosis and management of coronary vasospasm seems to be of crucial importance, even after successful surgical repair.

Management

Surgical revascularization was more commonly performed among our young registry patients with an anomalous left main trunk than among our older registry patients and AORCA patients, probably due to the fear of recurrent SCA or bleeding caused by long-term antiplatelet therapy. According to the American College of Cardiology/American Heart Association guidelines[4] and to several reports,[6,17–20] surgical revascularization as primary prevention of a cardiovascular event is indicated in all cases of AOLCA, but in cases of AORCA, surgical revascularization is indicated only for patients with documented coronary ischaemia due to an IAC (class I and level B evidence).[4] The same guidelines also support a conservative approach in cases of AORCA without evidence of ischaemia. The majority of AORCA patients in our registry appeared to be managed with medication according to the guidelines even if they had experienced SCA. Our registry, however, showed that AORCA was common among the patients in whom SCA occurred (67%). Furthermore, in 7 of 16 (44%) AORCA patients who experienced SCA, non-invasive stress tests failed to reveal ischaemia in the RCA territory, which is consistent with previous autopsy and individual case findings.[5,10] Close follow-up might thus be warranted for cases of AORCA. The fact that the stress test was negative in patients with angina does not necessarily mean that there was no ischaemia. After surgical revascularization, no patient experienced recurrence of SCA in our registry. Based on this favourable outcome, an ICD might not be always necessary for patients who have undergone surgical correction.

A variety of surgical treatments have been proposed for AOCA. Each surgical strategy, however, has its pros and cons, although unroofing and reimplantation have yielded good outcomes.[17,18] The unroofing procedure might be a reasonable and safe approach for revascularization in cases of AOCA with an IMC, despite the risk of aortic insufficiency[17] or recurrent SCA.[20] Reimplantation is a promising but technically demanding procedure because of the extensive dissection and mobilization of vessels required. CABG is applicable to all AOCA cases, but it is increasingly viewed as a less favourable approach because of the potential risk of early graft failure due to dynamic competitive flow from the native artery, a viewpoint that our data support.[1] Atherosclerosis as the mechanism underlying the cardiovascular event was most common in middle-aged to elderly patients. CABG or PCI may be an option for patients with concomitant atherosclerotic stenosis of the RCA.[19,21] However, stent durability is of major concern because the stent would be exposed continuously to compression by the great vessels. Overall, long-term clinical outcomes and graft/stent patency associated with the procedure should be confirmed.

Outcomes of medical treatment of the registry patients were favourable, even in patients who had suffered SCA. Thus, it appears that appropriate medications can be a reasonable option, particularly for patients shown to be at low risk after appropriate evaluation of risk factors, including coronary spasm. Further study, particularly prospective study, is warranted to confirm whether the efficacy and safety of medical treatment alone are comparable to the efficacy and safety of surgery or PCI in patients with AOCA.

Limitations

Our conclusions should be interpreted in light of our study limitations. The study was limited by its retrospective execution and the relatively small number of patients included. However, our registry is the first to include AOCA patients who have 'already experienced' a cardiovascular event, particularly SCA, and prospective study would require a long time to accumulate sufficient numbers of SCA patients. In addition, patients with asymptomatic AOCA who did not experience a cardiovascular event were not included in our study, and this could have influenced our SCA risk analysis. It is not really feasible, however, to assess AOCA features meticulously in all asymptomatic patients. Another limitation was that coronary vasospasm provocation testing was done at the discretion of individual patients' physicians, which might have increased the pre-test probability and resulted in the high incidence of induced vasospasm. Further, it is possible that mechanisms responsible for the SCA were not identified, despite the fact that various tests were performed that ruled out common triggers of SCA. Overall, identification of the optimal management strategies warrants a larger study, ideally a prospective study, that includes an appropriately long follow-up period.

Conclusions

AOCA poses a risk for a life-threatening cardiovascular event. Age ≤40 years, male sex, participation in a sporting activity, absence of prodromal symptoms, acutely angled (≤30°) take-off from the aorta, and absence of luminal narrowing of the IAC segment were found, in our registry-based study, to be associated with SCA in patients with AOCA. However, the prognosis appears to be favourable for patients in whom the AOCA is appropriately managed. We believe a large-scale study is warranted to confirm our findings.

Supplementary data

Supplementary data are available at *European Heart Journal - Cardiovascular Imaging* online.

Acknowledgements

The authors thank Mr. Ryutaro Aoki (Bayer Yakuhin, Ltd., Japan) for gathering case reports and abstracts pertaining to AOCA cases in Japan that have been presented at the Sudden Cardiac Death Conference, which is held annually by Bayer Yakuhin, Ltd.

Funding

The study was supported by departmental resources only.

Conflict of interest: none declared.

Downloaded from http://academic.oup.com/ehjcimg/article-abstract/21/2/222/5479176 by stmarksnaturly user on 08 March 2020

References

1. Cheezum MK, Liberthson RR, Shah NR, Villines TC, O'Gara PT, Landzberg MJ et al. Anomalous aortic origin of a coronary artery from the inappropriate sinus of valsalva. *J Am Coll Cardiol* 2017;**69**:1592–608.
2. Kimbiris D, Iskandrian AS, Segal BL, Bemis CE. Anomalous aortic origin of coronary arteries. *Circulation* 1978;**58**:606–15.
3. Angelini P, Velasco JA, Flamm S. Coronary anomalies: incidence, pathophysiology, and clinical relevance. *Circulation* 2002;**105**:2449–54.
4. Warnes CA, Williams RG, Bashore TM, Child JS, Connolly HM, Dearani JA et al. ACC/AHA 2008 Guidelines for the Management of Adults with Congenital Heart Disease: a report of the American College of Cardiology/American Heart Association Task Force on Practice Guidelines (writing committee to develop guidelines on the management of adults with congenital heart disease). *Circulation* 2008;**118**:e714–833.
5. Basso C, Maron BJ, Corrado D, Thiene G. Clinical profile of congenital coronary artery anomalies with origin from the wrong aortic sinus leading to sudden death in young competitive athletes. *J Am Coll Cardiol* 2000;**35**:1493–501.
6. Cheezum MK, Ghoshhajra B, Bittencourt MS, Hulten EA, Bhatt A, Moussavi N et al. Anomalous origin of the coronary artery arising from the opposite sinus: prevalence and outcomes in patients undergoing coronary CTA. *Eur Heart J Cardiovasc Imaging* 2017;**18**:314–35.
7. Adjedj J, Ferrara A, Pontana M, Van Meghem C, Wijns W. Coronary artery anomaly and evaluation by PPR computed tomography. *Eur Heart J Cardiovasc Imaging* 2016;**17**:168.
8. Hirono K, Hata Y, Miyao N, Nakaoka H, Sato K, Ibuki K et al. Anomalous origin of the right coronary artery evaluated with multidetector computed tomography and its clinical relevance. *J Cardiol* 2016;**68**:196–201.
9. Clemente A, Del Borrello M, Greco P, Mannella P, Di Gregorio F, Romano S et al. Anomalous origin of the coronary arteries in children: diagnostic role of three-dimensional coronary MR angiography. *Clin Imaging* 2010;**34**:337–43.
10. Nakazato J, Hirata K, Wake M. Coronary spasm as the cause of myocardial ischemia in a patient with anomalous origin of the left anterior descending artery from the proximal right coronary artery. *BMJ Case Rep* 2014;**2014**. pii:bcr2014204408.
11. Nathan M, Singh M, Lakdawala N, Bacha EA. Anomalous left coronary artery from aorta with Pitanguy's angina: a postoperative dilemma successfully managed. *Pediatr Cardiol* 2007;**28**:400–3.
12. Abbara S, Arbab-Zadeh A, Callister TQ, Desai MY, Mamuya W, Thomson L et al. SCCT guidelines for performance of coronary computed tomographic angiography: a report of the Society of Cardiovascular Computed Tomography Guidelines Committee. *J Cardiovasc Comput Tomogr* 2009;**3**:190–204.
13. Shishida K, Moriyama N, Shimizu T, Saito S. Anomalous acute left main myocardial infarction due to compression between pulmonary artery and aorta by acute pulmonary thromboembolism. *JACC Cardiovasc Interv* 2016;**9**:e217–8.
14. Naruse Y, Sato A, Kaneko Y, Hoshi T, Imai A, Takanaga C et al. Anomalous origin of the right coronary artery from the left sinus of valsalva in an elderly man: life-threatening worsening of angina after left lung lobectomy. *Circulation* 2012;**125**:e1021–4.
15. Jacobs ML. Anomalous aortic origin of a coronary artery: the gaps and the guidelines. *J Thorac Cardiovasc Surg* 2017;**153**:1463–5.
16. Van Hare GF, Ackerman MJ, Evangelista JK, Kovacs RJ, Myerburg RJ, Shafer KM et al. Eligibility and disqualification recommendations for competitive athletes with cardiovascular abnormalities: task force 4: congenital heart disease: a scientific statement from the American Heart Association and American College of Cardiology. *J Am Coll Cardiol* 2015;**66**:2372–84.
17. Krasuski RA, Magyar D, Hart S, Kalahasti V, Lorber R, Hobbs R et al. Long-term outcome and impact of surgery on adults with coronary arteries originating from the opposite coronary ostia. *Circulation* 2011;**123**:154–62.
18. Mery CM, De Leon LE, Molossi S, Sexson-Tejtel SK, Agrawal H, Krishnamurthy R et al. Outcomes of surgical intervention for anomalous aortic origin of a coronary artery: a large contemporary prospective cohort study. *J Thorac Cardiovasc Surg* 2018;**155**:105–19.e4.
19. Cho SH, Jeon HC, Yoo KJ, Yoon YN. Anomalous origin of right coronary artery from left coronary sinus: surgical management and clinical result. *Thorac Cardiovasc Surg* 2015;**63**:360–6.
20. Sachdeva S, Frommelt MA, Mitchell MF, Tweddell JS, Frommelt PC. Surgical unroofing of intramural anomalous aortic origin of a coronary artery in pediatric patients: single-center perspective. *J Thorac Cardiovasc Surg* 2018;**155**:1760–8.
21. Bagur R, Gleeton O, Baraille Y, Blodeau S, Rodes CJ, Bertrand OF. Right coronary artery from the left sinus of valsalva: multislice CT and transradial PCI. *World J Cardiol* 2011;**3**:51–6.

Downloaded from https://academic.oup.com/ehjcimaging/article-abstract/21/2/222/5479970 by stmemorialuniv user on 09 March 2020

Change in NT-proBNP (N-Terminal Pro-B-Type Natriuretic Peptide) Level and Risk of Dementia in Multi-Ethnic Study of Atherosclerosis (MESA)

Mohammad R. Ostovaneh,* Kasra Moazzami,* Kihei Yoneyama, Bharath A. Venkatesh, Susan R. Heckbert, Colin O. Wu, Steven Shea, Wendy S. Post, Annette L. Fitzpatrick, Gregory L. Burke, Hossein Bahrami, Otto A. Sanchez, Lori B. Daniels, Erin D. Michos, David A. Bluemke, João A.C. Lima

Abstract—Cross-sectionally measured NT-proBNP (N-terminal pro-B-type natriuretic peptide) is related to incident dementia. However, data linking changes in NT-proBNP to risk of future dementia are lacking. We aimed to examine the association of change in NT-proBNP over 3.2 years with incident dementia. We included 4563 participants in MESA (Multi-Ethnic Study of Atherosclerosis) prospective cohort who were free of cardiovascular disease at enrollment, had NT-proBNP level measured at MESA exams 1 (baseline, 2000–2002) and 3 (2004–2005), and had no diagnosis of dementia before exam 3. The association of change in NT-proBNP level between MESA exams 1 through 3 and all-cause hospitalized dementia (by *International Classification of Diseases, Ninth Revision*, codes) after MESA exam 3 (2004–2005) through 2015 was assessed using competing-risks Cox proportional hazard regression analysis. During 45 522 person-years of follow-up, 223 dementia cases were documented. Increase in log-NT-proBNP from MESA exams 1 through 3 was positively associated with incidence of dementia (multivariable hazard ratio, 1.28 [95% CI, 1.001–1.64]; P=0.049). An increase of at least 25% in NT-proBNP level from MESA exam 1 through 3 was associated with a 55% (P=0.02) increase in the risk of dementia in multivariable analysis. Addition of temporal NT-proBNP change to a model including risk factors and baseline NT-proBNP improved the prediction of dementia (Harrell C statistic from 0.85 to 0.87, P=0.049). Increase in NT-proBNP is independently associated with future all-cause hospitalized dementia and offers a moderately better predictive performance for risk of dementia compared with risk factors and baseline NT-proBNP.

Clinical Trial Registration—URL: https://www.clinicaltrials.gov. Unique identifier: NCT00005487. (*Hypertension*. 2020;75:316-323. DOI: 10.1161/HYPERTENSIONAHA.119.13952.) • Online Data Supplement

Key Words: cardiovascular diseases ■ cognition disorders ■ cohort studies ■ dementia ■ risk factors

Downloaded from http://ahajournals.org by on January 16, 2020

Dementia is a major public health problem worldwide and a leading cause of mortality and disability; it is often rated worse than death by patients.[1,2] Early alterations in brain structure have been shown to precede clinical dementia by 5 to 10 years, but a significant proportion of individuals at risk of dementia are not identified until very late in life and when they clinically become symptomatic.[3,4]

Brain alterations leading to dementia are the byproduct of genetic susceptibility combined with multiple risk factor exposures (including cardiovascular disease [CVD] risk factors) involving several organ systems in the human body.[5,6] Several studies have shown associations between dementia and prior CVDs, in particular, atrial fibrillation and heart failure[7,8]; but the mechanisms for these associations remain incompletely understood.

NT-proBNP (N-terminal pro-B-type natriuretic peptide) is released in response to myocardial wall stress[9] and has been linked to a wide range of adverse cardiovascular outcomes,[10–14] as well as subclinical myocardial dysfunction.[15] NT-proBNP has also been associated with subclinical brain damage, cognitive dysfunction, and incident dementia[17–20]; it likely reflects intermediate processes linking CVD to cerebral damage and dysfunction, thus having potential as a surrogate marker for early dementia detection and risk stratification.[18–20]

Received August 29, 2019; first decision September 12, 2019; revision accepted November 18, 2019.

From the Division of Cardiology, Johns Hopkins University, Baltimore, MD (M.R.O., K.M., K.Y., B.A.V., W.S.P., E.D.M., J.A.C.L.); Department of Medicine, Penn State College of Medicine, Hershey, PA (M.R.O.); Department of Cardiology, Emory University, Atlanta, GA (K.M.); St. Marianna University School of Medicine, Kawasaki, Japan (K.Y.); Departments of Epidemiology (S.R.H.), Family Medicine (A.L.F.), and Epidemiology and Global Health (A.L.F.), University of Washington, Seattle; Office of Biostatistics Research, National Heart, Lung, and Blood Institute, Bethesda, MD (C.O.W.); Departments of Medicine (S.S.) and Epidemiology (S.S.), Columbia University, New York, NY; Division of Public Health Sciences, Wake Forest University, Winston-Salem, NC (G.L.B.); Division of Cardiovascular Medicine, University of Southern California, Los Angles, CA (H.B.); Central Medical Clinic, Saint Paul, MN (O.A.S.); Department of Medicine, Division of Cardiovascular Medicine, University of California, San Diego (L.B.D.); and Department of Radiology, University of Wisconsin School of Medicine and Public Health, Madison (D.A.B.).

*These authors contributed equally to this work.

The online-only Data Supplement is available with this article at https://www.ahajournals.org/doi/suppl/10.1161/HYPERTENSIONAHA.119.13952.

Correspondence to João A.C. Lima, Johns Hopkins Hospital, 600 N Wolfe St, Blalock 524, Baltimore, MD 21287. Email jlima@jhmi.edu

© 2019 American Heart Association, Inc.

Levels of NT-proBNP change substantially over time in response to physiological and pathological alterations.[22-24] We hypothesized that tracking changes in NT-proBNP level over time may have significant implication for risk stratification and prediction of adverse outcomes over and above the cross-sectional NT-proBNP measurement. Previous studies have linked long-term changes in NT-proBNP level with adverse cardiovascular outcomes in patients with congestive heart failure,[24,25] coronary artery disease,[26] as well as those free of CVD.[27] However, the implications of changes in NT-proBNP to risk of future dementia have not been explored.

In the present study, we aimed to investigate the relationship between change in NT-proBNP over time with future all-cause hospitalized dementia and measures of cognitive function in a large multiethnic population of men and women without clinical CVD at enrollment in the MESA (Multi-Ethnic Study of Atherosclerosis).

Participants and Methods

The data and study materials will not be made available to other researchers for purposes of reproducing the results or replicating the procedure. However, the analytic methods are described in detail in this article.

The design of MESA has been described previously.[28] Briefly, a total of 6814 men and women aged 45 to 84 years were enrolled between July 2000 and August 2002 from 6 US communities representing 4 racial/ethnic groups (white, black, Hispanic, and Chinese-American). Individuals with any prior clinical diagnosis of CVD at enrollment were excluded. The study protocol was approved by the institutional review board of each MESA field center, and all participants gave informed consent.

Plasma NT-proBNP Measurements

NT-proBNP was measured in 5597 MESA participants at enrollment (MESA exam 1) between 2000 and 2002. Of these, 4586 participants underwent repeat NT-proBNP measurements in the follow-up MESA exam 3, performed between 2004 and 2005.

Blood samples were stored at −70°C and were thawed before testing (maximum of 3 freeze-thaw cycles). NT-proBNP was measured using the Elecsys 2010 system (Roche Diagnostics, Indianapolis, IN). All analyses were performed at a core laboratory (Veteran's Affairs San Diego Healthcare System, La Jolla, CA). Previous studies have indicated that measurements of NT-proBNP using this assay are not significantly altered after 5 freeze-thaw cycles.[31] Intra- and interassay coefficients of variation at various concentrations of NT-proBNP were 1.3% and 4.8%, respectively.[32] The analytical measurement range for NT-proBNP was 5 to 35 000 pg/mL.

Follow-Up and End Points

In MESA, telephone interviews are conducted every 9 to 12 months with each participant to identify interim hospitalizations, outpatient cardiovascular and other diagnoses, and death. Medical records were obtained for those reporting a hospitalization. Probable dementia including Alzheimer disease, vascular dementia, and Pick disease was classified from the coded hospitalization discharge diagnoses using the *International Classification of Diseases* (*ICD*) Medical Diagnosis Codes, *Ninth Revision*. The following diagnosis codes were used to identify dementia: *ICD, Ninth Revision*: 290, 294, 331.0, 331.1, 331.2, 331.82, 331.83, 331.9, 438.0, and 780.93; *ICD, Tenth Revision*: F00, F01, F03, F04, G30, G31 (excluding G31.2), I69.91, and R41. In addition, a physician blinded to the *ICD, Ninth Revision*, codes ascertained potential cases of dementia by reviewing the medical records of each participant, looking for statements that indicated or contradicted the diagnosis of dementia. The use of hospitalization discharge *ICD* codes for the diagnosis of dementia has been validated and used in prior publications from MESA.[33-35] In this study, we only included dementia events that occurred after MESA exam 3 through 2015.

The diagnoses of interim stroke, heart failure, and coronary heart disease were adjudicated by 2 independent physicians of the MESA adjudication committee. Full details of the MESA follow-up methods, investigators, and institutions are available at the MESA website (http://www.mesa-nhlbi.org). Measures of cognitive function were obtained during MESA exam 5 performed between 2010 and 2012 and included the Cognitive Abilities Screening Instrument score, as well as forward and backward Digit Span.[36]

Statistical Analysis

Data were presented as mean±SD, median (interquartile range), or number (%), as appropriate. Baseline characteristics were compared between subjects with and without dementia using χ^2 tests for categorical variables and 2-sided *t* tests or the Wilcoxon signed-rank test for continuous variables. Variables with non-normal distribution were transformed to logarithmic (NT-proBNP and coronary artery calcium score) or cubic-transformed values (Cognitive Abilities Screening Instrument score) for regression analysis.

We used multivariable competing-risks Cox proportional hazard regression models to investigate the association of temporal change in NT-proBNP levels between MESA exams 1 and 3 and risk of future all-cause hospitalized dementia after MESA exam 3.[16] Change in NT-proBNP levels was included in regression analysis both as continuous but also as a dichotomous variable based on >25% increase in NT-proBNP level since baseline (MESA exam 1). The 25% threshold for change in NT-proBNP levels was chosen based on previous reports on intraindividual variability of NT-proBNP indicating that >25% change is deemed clinically significant and unlikely due to measurement error.[37,38] We also performed a secondary analysis to assess the risk of future dementia in 4 groups of participants based on 75th percentile of baseline NT-proBNP level and ≥25% increase in NT-proBNP level over time. Death before the diagnosis of dementia was considered as a competing event because it hindered the detection of dementia. We used Harrell C statistic to assess the models' performance for predicting dementia and to test whether addition of NT-proBNP and its temporal change improved the discriminative performance of models comprising traditional risk factors. The multivariable models included the following:

Model 1 was adjusted for demographics including age, sex, and race/ethnicity.

Model 2 included variables in model 1 in addition to ApoE lipoprotein isoforms and traditional CVD risk factors and socioeconomic status at MESA exam 3, including systolic blood pressure, use of antihypertensives, resting heart rate, high-density lipoprotein, total cholesterol, antihyperlipidemics, body mass index, glomerular filtration rate, diabetes mellitus, income, education level, health insurance status, cigarette smoking, and study field center at MESA exam 3. This model was also adjusted for coronary artery calcium score measured in the entire cohort at MESA exam 1 but not at MESA exam 3.

Model 3 was adjusted for all variables in model 2 and also interim cardiovascular events before incidence of dementia, including coronary events, heart failure, and clinical stroke as time-varying covariates.

Model 4 was adjusted for all variables in model 3 and left ventricular end diastolic volume, left ventricular ejection fraction, and left ventricular mass by magnetic resonance imaging obtained at baseline (MESA exam 1) but not at MESA exam 3.

Associations of NT-proBNP levels obtained at MESA exams 1 and 3, as well as its change, with measures of cognitive function at MESA exam 5 were tested using multivariable linear regression analysis adjusted for demographics and traditional risk factors obtained at MESA exams 1 or 3, as well as interim CVD events.

We also used regression analysis to identify the correlates of change in NT-proBNP levels from MESA exam 1. Multivariable models for these analyses were constructed using the variables associated with change in NT-proBNP levels reaching $P<0.2$.

Two-tailed $P<0.05$ was used for significance testing. All statistical analyses were performed using Stata 14.0 (StataCorp LP, College Station, TX).

Downloaded from http://ahcocardia.org by on January 19, 2020

Results

Of the 4586 MESA participants with NT-proBNP measurements at both MESA exams 1 and 3, a total of 4563 individuals without dementia before MESA exam 3 were included in the analysis (Figure S1 in the online-only Data Supplement). During 45 522 person-years of follow-up, 223 all-cause hospitalized dementia cases were ascertained. The mean age of the cohort at MESA exam 3 was 65.0±10.01 years, and 2219 (48.6%) were men. Baseline characteristics of the participants at MESA exam 3 are described in Table 1. The median NT-proBNP concentrations at MESA exams 1 and 3 were 52.3 (interquartile range, 23.6–107.0) and 65.7 pg/mL (interquartile range, 32.6–132.1), respectively. NT-proBNP levels increased by a median of 11.7 pg/mL (interquartile range, −93 to 43.9) over a mean of 3.2±0.3 years. Participants with all-cause hospitalized dementia were older and more frequently white, having lower income and lower education level. They were less likely to be without health insurance and had higher systolic and lower diastolic blood pressure, higher use of antihypertensive medications, worse kidney function, slightly lower body mass index, lower total cholesterol, and higher use of lipid lowering therapy. Furthermore, participants who developed dementia had higher levels of NT-proBNP (in pg/mL) at MESA exams 1 and 3, as well as higher temporal increase in NT-proBNP levels between the 2 exams (Table 1).

NT-proBNP Levels and Dementia

Log-NT-proBNP level at either MESA exams 1 (hazard ratio [HR], 1.9; $P<0.001$) or 3 (HR, 1.95; $P<0.001$) was significantly associated with future risk of all-cause hospitalized dementia (Table S1). These associations remained significant after adjustment for demographics, socioeconomic status, CVD risk factors, ApoE lipoprotein isoforms, and interim CVD events (HR, 1.23 [95% CI, 1.03–1.45] and 1.25 [95% CI, 1.03–1.53] at MESA exams 1 and 3, respectively; Table S1).

Increase in log-NT-proBNP levels from MESA 1 through MESA 3 exams was associated with significant increase in the risk of future all-cause hospitalized dementia (HR, 1.21 [95% CI, 1.04–1.42]; Table 2). This association remained significant after adjustment for demographics (HR, 1.24 [95% CI, 1.03–1.49]; model 1), traditional risk factors (HR, 1.25 [95% CI, 1.02–1.52]; model 2), interim CVD events (HR, 1.25 [95% CI, 1.03–1.53]; model 3), and magnetic resonance imaging–derived left ventricular end diastolic volume, left ventricular ejection fraction, and left ventricular mass (HR, 1.28 [95% CI, 1.001–1.64]; model 4; Table 2). Participants with >25% increase in NT-proBNP level had 38% to 55% higher risk of dementia in multivariable analysis (Table 2; Figure). On the contrary, any decrease in NT-proBNP levels from MESA 1 to MESA 3 exams was associated with 26% to 30% reduced risk of future dementia (Table 2). In a separate analysis (Figure S2), subjects with lower baseline NT-proBNP and smaller increase in its level over time had the lowest risk for future all-cause hospitalized dementia versus those with both high baseline NT-proBNP and >25% increase in its level, in whom the risk of future dementia was the greatest. Participants with either greater baseline NT-proBNP level or >25% increase in its level over time (but not both of these criteria) had moderate risk of future all-cause hospitalized dementia. Interestingly, the risk of future all-cause hospitalized dementia in subjects with only >25% increase over time (and low baseline NT-proBNP) was greater than those with only high baseline NT-proBNP level (and <25% increase in NT-proBNP level).

Risk Discrimination

The Harrell *C* statistic for a multivariable model of demographics, traditional risk factors, and interim CVD events for prediction of future all-cause hospitalized dementia was 0.85 ([95% CI, 0.83–0.88] Table 3). Addition of NT-proBNP at MESA exam 1 did not improve the discriminative power of the multivariable model (Table 3). Importantly, however, the inclusion of change in NT-proBNP significantly increased the Harrell *C* statistics to 0.87 ([95% CI, 0.84–0.89]; $P=0.049$; Table 3) for dementia prediction over and above baseline NT-proBNP levels.

NT-proBNP and Cognitive Function

As shown in Table 4, log-NT-proBNP level at MESA exam 1 but not at MESA exam 3 was associated with a lower cubic-transformed Cognitive Abilities Screening Instrument score ($\beta=-7808.98$; $P=0.02$) and backward digit span ($\beta=-0.12$; $P=0.003$) at MESA exam 5. There was no significant association between change in log-NT-proBNP level (exams 1–3) and exam 5 cognitive function indices.

Correlates of Changes in Log(NT-proBNP)

Table S2 illustrates the MESA exam 1 correlates of change in log-NT-proBNP levels. Older age and nonblack race/ethnicity were associated with greater increase in NT-proBNP levels. Moreover, lower glomerular filtration rate ($\beta=-0.003$; $P<0.001$), hypertension medication use ($\beta=0.06$; $P=0.02$), diabetes mellitus ($\beta=0.14$; $P<0.001$), current smoking ($\beta=0.09$; $P=0.01$), and high coronary artery calcium score ($\beta=0.01$; $P=0.01$) were correlated with increase in log-NT-proBNP levels. Log-NT-proBNP level at exam 1 was inversely associated with its increase over time (−0.36; $P<0.001$).

Discussion

In this study, we showed that (1) A 3-year increase in NT-proBNP level is associated with increased risk of future all-cause hospitalized dementia over and above cross-sectionally measured NT-proBNP level at baseline. This association was independent of demographics, CVD risk factors, interim CVD events, and volume and remodeling indices measured by magnetic resonance imaging. On the contrary, any decrease in NT-proBNP level over time was associated with reduced risk of dementia; (2) increase in NT-proBNP levels between the baseline and MESA 3 follow-up exams moderately improved discriminative performance of demographics, CVD risk factors, and baseline NT-proBNP levels for predicting future all-cause hospitalized dementia; (3) baseline NT-proBNP level but not its change over time was associated with impaired cognitive function later in life; (4) impaired kidney function, hypertension, diabetes mellitus, smoking, and coronary artery calcification were among the modifiable or treatable correlates of NT-proBNP increase and thus represent potential targets for dementia prevention. Greater NT-proBNP at MESA 1

Downloaded from http://ahajournals.org by on January 19, 2020

Table 1. Clinical Characteristics of Study Participants at MESA Exam 3 in Those Who Did and Did Not Develop Dementia During Follow-Up

Characteristics	No Dementia (n=4340)	Dementia (n=223)	*P* Value
Demographics			
Age, y; mean±SD	64.3±9.7	76.3±7.6	<0.001*
Men, n (%)	2097 (48.3)	122 (54.7)	0.06
Race/ethnicity, n (%)			<0.001*
White	1780 (41.0)	119 (53.4)	
Chinese	580 (13.4)	13 (5.8)	
Black	1013 (23.3)	48 (21.5)	
Hispanic	967 (22.3)	43 (19.3)	
Income, USD			<0.001*
<20 000	931 (22.2)	78 (39.0)	
20 000–49 999	1452 (34.0)	67 (33.5)	
≥50 000	1811 (43.2)	55 (27.5)	
Education, n (%)			0.04*
High school or less	1442 (33.3)	92 (41.3)	
College or undergraduate degree	2058 (47.5)	97 (43.5)	
Graduate degree	832 (19.21)	34 (15.2)	
Health insurance, n (%)			<0.001*
Yes	4056 (93.6)	220 (99.1)	
No	277 (6.4)	2 (0.9)	
Site, n (%)			0.03*
Wake Forest University	605 (13.9)	39 (17.5)	
Columbia University	598 (13.8)	34 (15.2)	
Johns Hopkins University	646 (14.9)	31 (13.9)	
University of Minnesota	702 (16.2)	49 (22.0)	
Northwestern University	809 (18.6)	36 (16.1)	
University of California, Los Angles	980 (22.6)	34 (15.2)	
Cardiovascular risk factors			
Systolic blood pressure, mm Hg; mean±SD	122.6±20.2	131.2±23.1	<0.001*
Diastolic blood pressure, mm Hg; mean±SD	69.7±9.9	68.3±10.3	0.03*
Estimated glomerular filtration rate, mL/min; mean±SD	79.3±17.6	71.6±19.2	<0.001*
Hypertension medication use, n (%)	1898 (44.4)	141 (65.0)	<0.001*
Heart rate, mean±SD	64.9±10.2	65.6±12.4	0.31
Body mass index, kg/m²; mean±SD	28.3±5.5	27.4±4.8	0.02*
HDL cholesterol, mg/dL; mean±SD	51.5±15.06	51.9±14.8	0.75
Total cholesterol, mg/dL; mean±SD	188.2±36.5	182.9±35.2	0.04*

(Continued)

Table 1. Continued

Characteristics	No Dementia (n=4340)	Dementia (n=223)	*P* Value
Antihyperlipidemic use, n (%)	1181 (27.6)	74 (34.1)	0.02*
Diabetes mellitus, n (%)	642 (14.8)	33 (14.8)	0.99
Smoking status, n (%)			0.18
Never	1973 (45.8)	90 (40.7)	
Former	1904 (44.2)	112 (50.7)	
Current	433 (10.0)	19 (8.6)	
ApoE isoforms, n (%)			0.59*
ε2/ε2	34 (0.8)	1 (0.5)	
ε2/ε3	492 (11.7)	25 (11.6)	
ε2/ε4	95 (2.3)	5 (2.3)	
ε3/ε3	2557 (60.9)	120 (55.8)	
ε3/ε4	928 (22.1)	58 (27.0)	
ε4/ε4	94 (2.2)	6 (2.8)	
NT-proBNP at MESA 1, pg/mL; median (IQR)	51.0 (22.9 to 102)	117.3 (52.0 to 213)	<0.001*
NT-proBNP at MESA 3, pg/mL; median (IQR)	63.7 (31.3 to 125.3)	146.7 (69.0 to 317.4)	<0.001*
Change in NT-proBNP, pg/mL; median (IQR)	11.0 (−9.3 to 41.3)	31.2 (−6.8 to 102.1)	<0.001*

HDL indicates high-density lipoprotein; IQR, interquartile range; MESA, Multi-Ethnic Study of Atherosclerosis; and NT-proBNP, N-terminal pro-B-type natriuretic peptide.

*p<0.05.

exam was associated with smaller increase in its level through MESA exam 3. This is likely attributable to sicker individuals with already high NT-proBNP at MESA 1 exam and little room for increase in NT-proBNP level. The other possible explanation is that patients with lower NT-proBNP at baseline are more likely to be obese and have dyslipidemia and insulin resistance[21] and thus are at higher risk of developing diabetes mellitus and CVD, as well as higher likelihood for greater change in NT-proBNP levels during follow-up.

A few prior studies have demonstrated that NT-proBNP is independently associated with cognitive dysfunction and incident dementia.[18–21] In 2 large population-based studies, one in 6040 participants from the Rotterdam study, and the other in 7114 subjects from the National FINRISK study, high NT-proBNP was associated with 27% and 32% increase in the risk of dementia, respectively.[19,20] Our results are in line with those 2 studies indicating the association of cross-sectionally measured NT-proBNP with future all-cause hospitalized dementia. However, this study, for the first time, demonstrates the prognostic role of increase in NT-proBNP over time as a predictor of future dementia. In recent years, the prognostic importance of changes in NT-proBNP has been investigated in different clinical settings. In MESA, an increase in NT-proBNP levels has been associated with higher risk of incident coronary heart disease, stroke, and death.[28,29] A reduction in NT-proBNP level over time was shown to correlate with better outcomes among patients with congestive heart

Downloaded from http://ahajournals.org by on January 19, 2020

Table 2. HR of Association Between Change in Log-NT-proBNP Level (pg/mL) and Risk of Future All-Cause Hospitalized Dementia

	HR (95% CI)	P Value
Change in log-NT-proBNP		
Unadjusted	1.21 (1.04–1.42)	0.013*
Model 1	1.24 (1.03–1.48)	0.024*
Model 2	1.25 (1.02–1.52)	0.029*
Model 3	1.25 (1.03–1.53)	0.026*
Model 4	1.28 (1.001–1.64)	0.049*
Increase of ≥25% in NT-proBNP		
Unadjusted	1.45 (1.11–1.89)	0.007*
Model 1	1.38 (1.05–1.81)	0.019*
Model 2	1.48 (1.1–2.0)	0.011*
Model 3	1.49 (1.1–2.01)	0.010*
Model 4	1.55 (1.10–2.25)	0.023*
Any decrease in NT-proBNP		
Unadjusted	0.73 (0.54–0.97)	0.032*
Model 1	0.74 (0.56–0.98)	0.041*
Model 2	0.70 (0.50–0.97)	0.03*
Model 3	0.70 (0.50–0.97)	0.03*
Model 4	0.71 (0.47–1.1)	0.101

Model 1 was adjusted for age, sex, race/ethnicity, and log-NT-proBNP at MESA exam 1. Model 2 included all variables in model 1 in addition to ApoE lipoprotein isoforms and traditional CVD risk factors and socioeconomic status at MESA exam 3, including systolic blood pressure, use of antihypertensives, resting heart rate, high-density lipoprotein, total cholesterol, antihyperlipidemics, body mass index, glomerular filtration rate, diabetes mellitus, income, education level, health insurance status, cigarette smoking, and study field center at MESA exam 3 and coronary artery calcium score at MESA exam 1. Model 3 was adjusted for all variables in model 2 and interim cardiovascular events, including coronary events, heart failure, and clinical stroke as time-varying covariates. Model 4 was adjusted for all variables in model 3 and left ventricular end diastolic volume, left ventricular ejection fraction, and left ventricular mass at MESA exam 1. CVD indicates cardiovascular disease; HR, hazard ratio; MESA, Multi-Ethnic Study of Atherosclerosis; and NT-proBNP, N-terminal pro B-type natriuretic peptide.

*p<0.05.

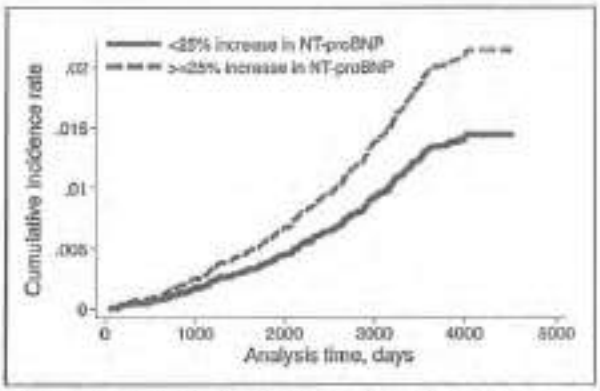

Figure. Cumulative incidence rate for future all-cause hospitalized dementia in participants with and without ≥25% change in NT-proBNP (N-terminal pro-B-type natriuretic peptide) since MESA (Multi-Ethnic Study of Atherosclerosis) exam 1 adjusted for baseline demographics (age, sex, and race/ethnicity), ApoE lipoprotein isoforms and traditional cardiovascular disease risk factors and socioeconomic status at MESA exam 3, including systolic blood pressure, use of antihypertensives, resting heart rate, high-density lipoprotein, total cholesterol, antihyperlipidemics, body mass index, glomerular filtration rate, diabetes mellitus, income, education level, health insurance status, cigarette smoking, and study field center at MESA exam 3 and coronary artery calcium score at MESA exam 1 and interim cardiovascular events, including coronary events, heart failure, and clinical stroke as time-varying covariates.

failure with both reduced[27] and preserved ejection fraction.[28] The present study extends our body of knowledge by further emphasizing the prognostic significance of serial NT-proBNP measurements in relation not only to established CVD but also to cerebral morbidity and outcomes. Our findings may have significant implication for early detection and secondary prevention of dementia and suggest that disrupting the pathological process leading to continuous rise in NT-proBNP may help prevent dementia in older adults.

There are several hypotheses to explain the link between NT-proBNP and its change with dementia. The first and more intuitive possibility is that individuals with elevated NT-proBNP levels are more likely to have both clinically expressed and silent cerebrovascular events; however, change in NT-proBNP remained associated with dementia even after adjusting for CVD risk factors and interim CVD, including clinically manifested cerebrovascular events (stroke).[30] Second, we propose that the longitudinal increase in NT-proBNP as an index of enhanced myocardial stress reflects mechanisms leading to progressive subclinical cardiac dysfunction that could entail concomitant myocardial and cerebral microvascular disease,[40,41] adverse response to neuroendocrine hormonal overstimulation,[42] and hypoxia leading to progressive cardiomyocyte and neuronal death.[16,43–46] In this regard, overt heart failure, unassociated with clinical cerebrovascular events, has been shown to relate to increased incident dementia.[7] Previous studies have shown an association between NT-proBNP and hypoperfusion of the myocardium and chronic state of hypoxia,[43] loss of cardiomyocytes, and interstitial fibrosis.[16] NT-proBNP has been also associated with retinal microvascular damage.[41] A similar process may

Table 3. Risk Prediction Metrics for the Baseline and Change in Log-NT-proBNP (pg/mL) for Predicting Future All-Cause Hospitalized Dementia

Model	Harrell C Statistic (95% CI)	P Value
Multivariable model	0.85 (0.83–0.88)	Ref
Multivariable model+baseline log-NT-proBNP	0.85 (0.83–0.88)	0.26
Multivariable model+baseline and change in log-NT-proBNP	0.87 (0.84–0.89)	0.049*

Multivariable model adjusted for baseline demographics (age, sex, race/ethnicity), ApoE lipoprotein isoforms, and traditional CVD risk factors and socioeconomic status at MESA exam 3, including systolic blood pressure, use of antihypertensives, resting heart rate, high-density lipoprotein, total cholesterol, antihyperlipidemics, body mass index, glomerular filtration rate, diabetes mellitus, income, education level, health insurance status, cigarette smoking, and study field center at MESA exam 3 and coronary artery calcium score at MESA exam 1 and interim cardiovascular events, including coronary events, heart failure, and clinical stroke as time-varying covariates. CVD indicates cardiovascular disease; MESA, Multi-Ethnic Study of Atherosclerosis; NT-proBNP, N-terminal pro B-type natriuretic peptide; and Ref, reference.

*p<0.05.

Downloaded from http://ahajournals.org by on January 19, 2020

Table 4. Association of Log-NT-proBNP at MESA Exams 1 and 3 and Its Change With Measures of Cognitive Function at MESA Exam 5, β (P Value)

NT-proBNP	MESA Exam 1	MESA Exam 3	Change in Log-NT-proBNP
Cubic-transformed CASI	−7808.58 (0.006)*	−4475.65 (0.15)	3317.71 (0.33)
Digit span, forward	−0.06 (0.2)	−0.07 (0.16)	−0.008 (0.88)
Digit span, backward	−0.12 (0.003)*	−0.06 (0.18)	−0.06 (0.18)

Mean CASI and cubic-transformed CASI for the cohort is 87.1 (11.2) and 689374.6 (189370.9). Regression coefficients adjusted for baseline demographics (age, sex, race/ethnicity), ApoE lipoprotein isoforms, and traditional CVD risk factors and socioeconomic status at MESA exam 3, including systolic blood pressure, use of antihypertensives, resting heart rate, high-density lipoprotein, total cholesterol, antihyperlipidemics, body mass index, glomerular filtration rate, diabetes mellitus, income, education level, health insurance status, cigarette smoking, and study field center at MESA exam 3 and coronary artery calcium score at MESA exam 1 and interim cardiovascular events, including coronary events, heart failure, and clinical stroke as time-varying covariates. CASI indicates Cognitive Abilities Screening Instrument; CVD, cardiovascular disease; MESA, Multi-Ethnic Study of Atherosclerosis; and NT-proBNP, N-terminal pro B-type natriuretic peptide.

*p<0.05.

explain the association of NT-proBNP and dementia, given that hypoperfusion and microvascular endothelial dysfunction have been linked to structural and functional changes in the brain, as well as incident dementia.[43–45] The fact that increasing NT-proBNP levels remained significantly associated with incident dementia despite adjustment for CVD risk factors may indicate that brain alterations in patients with subclinical CVD accompanied by high NT-proBNP begin early in the course of progressive cardiac dysfunction. This suggests that early and aggressive control of risk factors associated with increased NT-proBNP levels (such as hypertension, diabetes mellitus, smoking, kidney dysfunction, and atherosclerosis as documented in this and other studies) could significantly alter progressive cerebral dysfunction and dementia in older adults.

In the present study, the measures of cognitive dysfunction at MESA exam 5 were only associated with NT-proBNP levels measured at the baseline MESA exam (exam 1) but not with either its change over time or NT-proBNP levels measured at the 3-year follow-up examination (exam 3). One possible explanation for this finding is a selection bias arising from people who died before the 10-year follow-up exam (MESA exam 5) or did not return to clinic for MESA exam 5 because of dementia, subclinical cognitive dysfunction, or other comorbidities. Further studies are required to assess the relationship of longitudinal changes in cognitive function and changes in NT-proBNP level over time.

The major strengths of our study were the serial measurements of NT-proBNP during a 3-year interval in a large community-based cohort with detailed clinical phenotyping and long follow-up time. The major limitation of our study was the ascertainment of incident dementia cases from hospitalization records using *ICD, Ninth Revision*, codes. This method of diagnosing dementia cases likely underestimates the incidence of disease, since it only identifies participants who were hospitalized, and in whom dementia was included in their discharge diagnoses. However, this method of identifying dementia events has been recently validated in MESA and has shown to have adequate positive predictive value for diagnosing clinically established dementia.[33] Also, the biological variability of NT-proBNP because of seasonal changes or circadian rhythm was not taken into account in our analysis; however, we expect that these factors have randomly affected the patients with or without dementia and, therefore, may have only diluted the effect size but could not change the direction of the observed associations.

In conclusion, in a multiethnic, large cohort, we demonstrate that an increase in NT-proBNP level over time is significantly associated with risk of future all-cause hospitalized dementia above and beyond clinical risk factors and cross-sectionally measured NT-proBNP level. Disruption of the processes leading to increased NT-proBNP by controlling treatable or modifiable cardiovascular risk factors may help prevent dementia in older adults.

Perspectives

This is the first study to demonstrate that increase in NT-proBNP is independently associated with future all-cause hospitalized dementia and offers a moderately better predictive performance for risk of dementia compared with risk factors and baseline NT-proBNP. The greatest risk of dementia was observed in subjects with high baseline NT-proBNP and increase in its level over time. The mechanisms for association of increase in NT-proBNP and dementia are not completely understood, and further studies are required to elaborate the mechanisms for this association. However, findings of this study may help prevention of dementia by controlling the risk factors that are responsible for increase in NT-proBNP.

Acknowledgments

We thank the other investigators, the staff, and the participants of MESA (Multi-Ethnic Study of Atherosclerosis) for their valuable contributions. A full list of participating MESA investigators and institutions can be found at http://www.mesa-nhlbi.org.

Sources of Funding

The views expressed in this article are those of the authors and do not necessarily represent the views of the National Heart, Lung, and Blood Institute; the National Institutes of Health; or the US Department of Health and Human Services. This research was supported by contracts N01-HC-95159, N01-HC-95160, N01-HC-95161, N01-HC-95162, N01-HC-95163, N01-HC-95164, N01-HC-95165, N01-HC-95166, N01-HC-95167, N01-HC-95168, and N01-HC-95169 from the National Heart, Lung, and Blood Institute and by grants UL1-TR-000040 and UL1-TR-001079 from the National Center for Research Resources.

Disclosures

None.

Downloaded from http://ahajournals.org by on January 19, 2020

References

1. Todd S, Barr S, Roberts M, Passmore AP. Survival in dementia and predictors of mortality: a review. *Int J Geriatr Psychiatry*. 2013;28:1109–1124. doi: 10.1002/gps.3946
2. Patrick DL, Pearlman RA, Starks HE, Cain KC, Cole WG, Uhlmann RF. Validation of preferences for life-sustaining treatment: implications for advance care planning. *Ann Intern Med*. 1997;127:509–517. doi: 10.7326/0003-4819-127-7-199710010-00002
3. Kaye JA, Swihart T, Howieson D, Dame A, Moore MM, Karnos T, Camicioli R, Ball M, Oken B, Sexton G. Volume loss of the hippocampus and temporal lobe in healthy elderly persons destined to develop dementia. *Neurology*. 1997;48:1297–1304. doi: 10.1212/wnl.48.5.1297
4. Fox NC, Crum WR, Scahill RI, Stevens JM, Janssen JC, Rossor MN. Imaging of onset and progression of Alzheimer's disease with voxel-compression mapping of serial magnetic resonance images. *Lancet*. 2001;358:201–205. doi: 10.1016/S0140-6736(01)05408-3
5. De Luca V, Spalletta G, Sorm RP, Graff A, Bastos-Rodrigues L, Camargos Bicalho MA. Definition of late onset Alzheimer's disease and anticipation effect of genome-wide significant risk variants: pilot study of the APOE e4 Allele. *Neuropsychobiology*. 2019;77:8–12. doi: 10.1159/000490719
6. Forette F, Seux ML, Staessen JA, Thijs L, Birkenhäger WH, Babarskiene MR, Babeanu S, Bossini A, Gil-Extremera B, Girerd X, et al. Prevention of dementia in randomised double-blind placebo-controlled Systolic Hypertension in Europe (Syst-Eur) trial. *Lancet*. 1998;352:1347–1351. doi: 10.1016/s0140-6736(98)03085-4
7. Qiu C, Winblad B, Marengoni A, Klarin I, Fastbom J, Fratiglioni L. Heart failure and risk of dementia and Alzheimer disease: a population-based cohort study. *Arch Intern Med*. 2006;166:1003–1008. doi: 10.1001/archinte.166.9.1003
8. Kwok CS, Loke YK, Hale R, Potter JF, Myint PK. Atrial fibrillation and incidence of dementia: a systematic review and meta-analysis. *Neurology*. 2011;76:914–922. doi: 10.1212/WNL.0b013e318208e38
9. Daniels LB, Maisel AS. Natriuretic peptides. *J Am Coll Cardiol*. 2007;50:2357–2368. doi: 10.1016/j.jacc.2007.09.021
10. Omland T, Dorn-Wauchope A, McKelvie R, Santaguida PL, Hill S, Bolton C, Booth R, Brown JA, Ali U, Bustamam A, et al. BNP and NT-proBNP as prognostic markers in persons with chronic stable heart failure. *Heart Fail Rev*. 2014;19:471–505. doi: 10.1007/s10741-014-9439-6
11. Bibbins-Domingo K, Gupta R, Na B, Wu AH, Schiller NB, Whooley MA. N-terminal fragment of the prohormone brain-type natriuretic peptide (NT-proBNP), cardiovascular events, and mortality in patients with stable coronary heart disease. *JAMA*. 2007;297:169–176. doi: 10.1001/jama.297.2.169
12. Wang TJ, Larson MG, Levy D, Benjamin EJ, Leip EP, Omland T, Wolf PA, Vasan RS. Plasma natriuretic peptide levels and the risk of cardiovascular events and death. *N Engl J Med*. 2004;350:655–663. doi: 10.1056/NEJMoa031994
13. Wang AY, Lam CW, Yu CM, Wang M, Chan IH, Zhang Y, Lui SF, Sanderson JE. N-terminal pro-brain natriuretic peptide: an independent risk predictor of cardiovascular congestion, mortality, and adverse cardiovascular outcomes in chronic peritoneal dialysis patients. *J Am Soc Nephrol*. 2007;18:321–330. doi: 10.1681/ASN.2005121299
14. Olsen MH, Hansen TW, Christensen MK, Gustafsson F, Rasmussen S, Wachtell K, Ibsen H, Torp-Pedersen C, Hildebrandt PR. N-terminal pro-brain natriuretic peptide, but not high sensitivity C-reactive protein, improves cardiovascular risk prediction in the general population. *Eur Heart J*. 2007;28:1374–1381. doi: 10.1093/eurheartj/ehl448
15. Rutten JH, Mattace-Raso FU, Steyerberg EW, Lindemans J, Hofman A, Wieberdink RG, Breteler MM, Witteman JC, van den Meiracker AH. Amino-terminal pro-B-type natriuretic peptide improves cardiovascular and cerebrovascular risk prediction in the population: the Rotterdam study. *Hypertension*. 2010;55:785–791. doi: 10.1161/HYPERTENSIONAHA.109.143313
16. Liu CY, Herkbert SR, Lai S, Ambale-Venkatesh B, Ostovaneh MR, McClelland RL, Lima JA, Bluemke DA. Association of elevated NT-proBNP with myocardial fibrosis in the Multi-Ethnic Study of Atherosclerosis (MESA). *J Am Coll Cardiol*. 2017;70:3102–3109. doi: 10.1016/j.jacc.2017.10.044
17. Zonneveld HI, Ikram MA, Hofman A, Niessen WJ, van der Lugt A, Krestin GP, Franco OH, Vernooij MW. N-terminal pro-B-type natriuretic peptide and subclinical brain damage in the general population. *Radiology*. 2017;283:205–214. doi: 10.1148/radiol.2016160548
18. Kerola T, Nieminen T, Hartikainen S, Sulkava R, Vuoksimaa O, Kettunen R. B-type natriuretic peptide as a predictor of declining cognitive function and dementia—a cohort study of an elderly general population with a 5-year follow-up. *Ann Med*. 2010;42:207–215. doi: 10.3109/07853891003652542
19. Tynkkynen J, Laatikainen T, Salomaa V, Havulinna AS, Blankenberg S, Zeller T, Hannesmann J, Niemi M, Jousilahti P. NT-proBNP and the risk of dementia: a prospective cohort study with 14 years of follow-up. *J Alzheimers Dis*. 2015;44:1007–1013. doi: 10.3233/JAD-141809
20. Mirza SS, de Bruijn RF, Koudstaal PJ, van den Meiracker AH, Franco OH, Hofman A, Tiemeier H, Ikram MA. The N-terminal pro B-type natriuretic peptide, and risk of dementia and cognitive decline: a 10-year follow-up study in the general population. *J Neurol Neurosurg Psychiatry*. 2016;87:356–362. doi: 10.1136/jnnp-2014-309968
21. Daniels LB, Laughlin GA, Kritz-Silverstein D, Clopton P, Chen WC, Maisel AS, Barrett-Connor E. Elevated natriuretic peptide levels and cognitive function in community-dwelling older adults. *Am J Med*. 2011;124:670.e1–670.e8. doi: 10.1016/j.amjmed.2011.02.027
22. Sanchez OA, Duprez DA, Bahrami H, Daniels LB, Folsom AR, Lima JA, Maisel A, Peralta CA, Jacobs DR Jr. The associations between metabolic variables and NT-proBNP are blunted at pathological ranges: the Multi-Ethnic Study of Atherosclerosis. *Metabolism*. 2014;63:475–483. doi: 10.1016/j.metabol.2013.11.017
23. Eggers KM, Venge P, Lind L. Prognostic usefulness of the change in N-terminal pro B-type natriuretic peptide levels to predict mortality in a single community cohort aged ≥ 70 years. *Am J Cardiol*. 2013;111:131–136. doi: 10.1016/j.amjcard.2012.08.058
24. Wu AH. Serial testing of B-type natriuretic peptide and NTpro-BNP for monitoring therapy of heart failure: the role of biologic variation in the interpretation of results. *Am Heart J*. 2006;152:828–834. doi: 10.1016/j.ahj.2006.08.021
25. Ying W, Zhao D, Ouyang P, Subramanya V, Vaidya D, Ndumele CE, Sharma K, Shah SJ, Herkbert SR, Lima JA, et al. Sex hormones and change in N-terminal pro-B-type natriuretic peptide levels: the Multi-Ethnic Study of Atherosclerosis. *J Clin Endocrinol Metab*. 2018;103:4304–4314. doi: 10.1210/jc.2018-01437
26. Jhund PS, Anand IS, Komajda M, Claggett BL, McKelvie RS, Zile MR, Carson PE, McMurray JJ. Changes in N-terminal pro-B-type natriuretic peptide levels and outcomes in heart failure with preserved ejection fraction: an analysis of the I-Preserve study. *Eur J Heart Fail*. 2015;17:809–817. doi: 10.1002/ejhf.274
27. Zile MR, Claggett BL, Prescott MF, McMurray JJ, Packer M, Rouleau JL, Swedberg K, Desai AS, Gong J, Shi VC, et al. Prognostic implications of changes in N-terminal pro-B-type natriuretic peptide in patients with heart failure. *J Am Coll Cardiol*. 2016;68:2425–2436. doi: 10.1016/j.jacc.2016.09.931
28. Mishra RK, Judson G, Christenson RH, DeFilippi C, Wu AHB, Whooley MA. The association of five-year changes in the levels of n-terminal fragment of the prohormone brain-type natriuretic peptide (NT-proBNP) with subsequent heart failure and death in patients with stable coronary artery disease: the heart and soul study. *Cardiology*. 2017;137:201–206. doi: 10.1159/000466682
29. Daniels LB, Clopton P, deFilippi CR, Sanchez OA, Bahrami H, Lima JA, Tracy RP, Siscovick D, Bertoni AG, Greenland P, et al. Serial measurement of N-terminal pro-B-type natriuretic peptide and cardiac troponin T for cardiovascular disease risk assessment in the Multi-Ethnic Study of Atherosclerosis (MESA). *Am Heart J*. 2015;170:1170–1183. doi: 10.1016/j.ahj.2015.09.010
30. Bild DE, Bluemke DA, Burke GL, Detrano R, Diez Roux AV, Folsom AR, Greenland P, Jacob DR Jr, Kronmal R, Liu K, et al. Multi-Ethnic Study of Atherosclerosis: objectives and design. *Am J Epidemiol*. 2002;156:871–881. doi: 10.1093/aje/kwf113
31. Ordonez-Llanos J, Collinson PO, Christenson RH. Amino-terminal pro-B-type natriuretic peptide: analytic considerations. *Am J Cardiol*. 2008;101:9–15. doi: 10.1016/j.amjcard.2007.11.013
32. Karl J, Borgya A, Gallhofer A, Huber E, Krueger K, Rollinger W, Schenk J. Development of a novel, N-terminal-proBNP (NT-proBNP) assay with a low detection limit. *Scand J Clin Lab Invest Suppl*. 1999;230:177–181.
33. Fujiyoshi A, Jacobs DR Jr, Alonso A, Lachsinger JA, Rapp SR, Duprez DA. Validity of death certificate and hospital discharge ICD codes for dementia diagnosis: the Multi-Ethnic Study of Atherosclerosis. *Alzheimer Dis Assoc Disord*. 2017;31:168–172. doi: 10.1097/WAD.0000000000000164
34. Fujiyoshi A, Jacobs DR Jr, Fitzpatrick AL, Alonso A, Duprez DA, Sharrett AR, Seeman T, Blaha MJ, Lachsinger JA, Rapp SR. Coronary artery calcium and risk of dementia in MESA (Multi-Ethnic Study of Atherosclerosis). *Circ Cardiovasc Imaging*. 2017;10:e005349. doi: 10.1161/CIRCIMAGING.116.005349

Downloaded from http://ahajournals.org by on January 19, 2020

35. Mosteiro K, Ostovanch MR, Ambale Venkatesh B, Habibi M, Yoneyama K, Wu C, Liu K, Piuzzeta T, Fitzpatrick A, Shea S, et al. Left ventricular hypertrophy and remodeling and risk of cognitive impairment and dementia: MESA (Multi-Ethnic Study of Atherosclerosis). *Hypertension*. 2018;71:429–436. doi: 10.1161/HYPERTENSIONAHA.117.10289
36. Fine JP. Regression modeling of competing crude failure probabilities. *Biostatistics*. 2001;2:85–97. doi: 10.1093/biostatistics/2.1.85
37. deFilippi CR, Christenson RH, Gottdiener JS, Kop WJ, Seliger SL. Dynamic cardiovascular risk assessment in elderly people. The role of repeated N-terminal pro-B-type natriuretic peptide testing. *J Am Coll Cardiol*. 2010;55:441–450. doi: 10.1016/j.jacc.2009.07.069
38. Schou M, Gustafsson F, Nielsen FH, Madsen LH, Kjaer A, Hildebrandt PR. Unexplained week-to-week variation in BNP and NT-proBNP is low in chronic heart failure patients during steady state. *Eur J Heart Fail*. 2007;9:68–74. doi: 10.1016/j.ejheart.2006.05.001
39. Sanchez OA, Jacobs JD, Bahrami H, Peralta CA, Daniels LB, Lima JA, Maisel A, Duprez DAJfeh. Increasing aminoterminal-pro-B-type natriuretic peptide precedes the development of arterial hypertension: the Multiethnic Study of Atherosclerosis. *J Hypertens*. 2015;33:968–974. doi: 10.1097/HJH.0000000000000500
40. Mitchell A, Miniaiek JR, Folsom AR, Duprez D, Alonso A, Jerosch-Herold M, Sanchez OA, Watson KE, Sallam T, Konety SH. Usefulness of N-terminal pro-brain natriuretic peptide and myocardial perfusion in asymptomatic adults (from the Multi-Ethnic Study of Atherosclerosis). *Am J Cardiol*. 2015;115:1341–1345. doi: 10.1016/j.amjcard.2015.02.040
41. Mattu U, Ikram MA, Hofman A, Jong PTVM, Klaver CCW, Ikram MK. N-Terminal pro-B-type natriuretic peptide is related to retinal microvascular damage: The Rotterdam Study. *Arterioscler Thromb Vasc Biol*. 2016;36:1698–1702. doi: 10.1161/ATVBAHA.116.307545
42. Sharp TE III, Polhemus DJ, Li Z, Spaeth P, Jenkins JS, Reilly JP, White CJ, Kapusta DR, Lefer DJ, Goodchild TT. Renal denervation prevents heart failure progression via inhibition of the renin-angiotensin system. *J Am Coll Cardiol*. 2018;72:2609–2621. doi: 10.1016/j.jacc.2018.08.2166
43. del Zoppo GJ, Mabuchi T. Cerebral microvessel responses to focal ischemia. 2003;23:879–894. doi: 10.1097/01.WCB.0000078322.96027.78
44. Abete P, Della-Morte D, Gargiulo G, Basile C, Langellotto A, Galizia G, Testa G, Canonico V, Bonaduce D, Cacciatore F. Cognitive impairment and cardiovascular diseases in the elderly. A heart–brain continuum hypothesis. *Ageing Res Rev*. 2014;18:41–52. doi: 10.1016/j.arr.2014.07.003
45. Holm H, Nilsson ED, Ricci F, Melander O, Hansson O, Buchan E, Magnusson M, Fedorowski A. Biomarkers of microvascular endothelial dysfunction predict incident dementia: a population-based prospective study. *J Intern Med*. 2017;282:94–101. doi: 10.1111/joim.12621

Novelty and Significance

What Is New?

- NT-proBNP (N-terminal pro-B-type natriuretic peptide)—a serum biomarker—is historically related to heart failure.
- But it is unknown whether increase in NT-proBNP over time can predict dementia in future.

What Is Relevant?

- This study showed that increase in NT-proBNP is associated with future dementia earlier than diagnosis of clinical dementia or heart failure.
- Multiple risk factors including hypertension are responsible for increase in NT-proBNP and subsequently dementia.

Summary

Increase in NT-proBNP is independently associated with future dementia. Controlling risk factors may help prevention of dementia.

Downloaded from http://ahajournals.org by on January 19, 2020

ESC European Society of Cardiology

European Journal of Heart Failure (2019)
doi:10.1002/ejhf.1417

EDITORIAL COMMENT

Long-term prognosis in patients with Takotsubo syndrome

Yoshihiro J. Akashi*

Division of Cardiology, Department of Internal Medicine, St. Marianna University School of Medicine, Kawasaki, Japan

This article refers to 'Long-term outcome in patients with Takotsubo syndrome presenting with severely reduced left ventricular ejection fraction' by R. Citro et al., published in this issue on pages xxx.

In this issue of the journal, Citro and colleagues sought to assess the long-term prognosis of Takotsubo syndrome (TTS) patients with reduced left ventricular ejection fraction (LVEF).[1] LVEF < 35% on admission was a prognostic indicator not only in the acute phase but also in the long-term follow-up period in TTS patients. Although various studies have already presented enough clinical data in TTS, this study provides directly associated hints and tips in TTS prognosis.

Takotsubo syndrome was previously thought to be a benign condition, not requiring any specific treatments; however, nowadays the prognosis of TTS is regarded not as optimistic as before due to several complications and life-threatening conditions. El-Battrawy et al.[2] demonstrated that LVEF < 35% was an independent predictor of short- and long-term mortality in TTS patients. Citro et al.[3] reported the results of 326 patients with TTS from the Italian multicenter registry data that included approximately three times as much as the previous published data. Recently, the RETAKO registry promoted by a Spanish researcher group reported that cardiogenic shock was associated with short- and long-term prognosis in patients with TTS.[3] Decreased systolic blood pressure on admission is thought to be a prognostic indicator in TTS patients[4]; thus, these findings support risk stratification, which has previously been proposed and described in a European Society of Cardiology (ESC) position statement.[5]

In this study, many TTS patients with LVEF < 35% were elderly; old age was the independent prognostic predictor even in multivariate analysis. The authors reported that reduced beta$_1$-adrenergic receptor density was the cause of this phenomenon. However, attention should be paid to the increased incidence of mitral regurgitation (MR) in the aged TTS patients. MR in TTS patients is frequently triggered by systolic anterior motion of the mitral anterior leaflet and the tethering by papillary muscle displacement along with regional or global ventricular dysfunction.[6] In this study, no significant differences were found in left ventricular outflow tract obstruction (LVOTO) in TTS patients regardless of left ventricular systolic function. We need to precisely evaluate the presence of LVOTO in the elderly, that is because we encounter patients with sigmoid septum and concentric hypertrophy of the left ventricle. Not only functional alternation but also left ventricular anatomical change in the elderly might affect the unfavourable outcome in TTS in the acute phase. The most common clinical complication in TTS patients is heart failure with or without pulmonary oedema. The authors have previously clarified that E/e' ratio is an independent predictor of heart failure and in-hospital mortality in multivariate analyses.[7]

Citro et al.[1] also demonstrated that TTS patients with LVEF < 35% taking beta-blockers showed a lower incidence of major adverse cardiac events compared to those not taking beta-blockers. Several studies, though not prospective or randomized, demonstrated that beta-blocker administration did not contribute to better outcome[8] or recurrence prevention[9] in this study, a similar trend can be seen in TTS patients with LVEF > 35%. Given that the ESC position statement[5] and an international expert consensus[10] have advised beta-blocker intake in TTS patients with low risks, the results of this study support this recommended treatment regardless of LVEF. When we treat TTS patients with LVOTO, beta-blocker administration should first be considered. Intra-aortic balloon pumping is contraindicated in TTS patients with LVOTO in order not to reduce their afterload. The administration of beta-blockers should be also cautious in TTS patients presenting with bradycardia.

Takotsubo syndrome is known to be characterized by a wide variety of wall motion abnormalities. Approximately 80% of TTS patients have a typical and classical apical ballooning type.[11] The remaining 20% of patients show a mid-ventricular, basal and focal pattern.[11] In the BOREAS-TCM registry, data accumulated in Japan demonstrated no significant differences in prognosis between TTS patients with and without apical ballooning.[12] Ghadri et al.[13] evaluated prognosis in TTS patients according to their wall motion

The opinions expressed in this article are not necessarily those of the Editors of the *European Journal of Heart Failure* or of the European Society of Cardiology. doi: 10.1002/ejhf.1373

*Corresponding author. Department of Internal Medicine, St. Marianna University School of Medicine, 2-16-1 Sugao, Kawasaki 216-8511, Japan. Tel: +81 44 977-8111, E-mail: yoakashi-cim@umin.ac.jp

© 2019 The Authors
European Journal of Heart Failure © 2019 European Society of Cardiology

abnormalities. Patients with the atypical type had better prognosis than those with the typical type in the first year after TTS onset; however, mortality rates were comparable afterwards.

Current InterTAK registry data have clarified the long-term prognosis in TTS patients.[14] TTS patients had a comparable long-term mortality risk with those with acute coronary syndrome. Additionally, patients with classical TTS due to emotional stress had a favourable short- and long-term prognosis. These results were the same as what I presumed. Considering from the standpoint of prognosis, personalized treatment strategy and follow-up are mandatory in TTS. In the All New Zealand Acute Coronary Syndrome Quality Improvement Program,[15] in-hospital mortality of TTS patients was equivalent to that of patients with acute coronary syndrome, whereas TTS patients had better long-term survival than acute coronary syndrome patients after discharge. Even in the southern hemisphere, the trend in prognosis was quite similar to that in the northern hemisphere.[15] Accordingly, long-term prognosis in TTS patients becomes favourable when adequate and accurate treatment is provided in the acute phase. It is necessary to reconsider the prognosis of TTS patients.

Conflict of interest: none declared.

References

1. Citro R, Radano I, Parodi G, Di Vece D, Zito C, Novo G, Provenza G, Bellino M, Prota C, Silverio A, Antonini-Canterin F, Tigo F, Vriz O, Galasso G, Bossone E, Salerno-Uriarte J, Piscione F. Long-term outcome in patients with Takotsubo syndrome presenting with severely reduced left ventricular ejection fraction. *Eur J Heart Fail* 2019, in press. https://doi.org/10.1002/ejhf.1373.
2. El-Battrawy I, Ansari U, Lang S, Behnes M, Schramm K, Fastner C, Zhou X, Kuschyk J, Tokarska E, Roger S, Borggrefe M, Akin I. Impact and management of left ventricular function on the prognosis of Takotsubo syndrome. *Eur J Clin Invest* 2017;**47**:477–485.
3. Almendro-Delia M, Nunez-Gil IJ, Lobo M, Andrea R, Vedia O, Sionis A, Martin-Garcia A, Cruz Aguilera M, Pereyra E, Martin de Miguel I, Linares Vicente JA, Corbi-Pascual M, Bosch X, Fabregat Andreu O, Sanchez Grande Fiesta A, Perez-Castellanos A, Pak JL, De Mora Martin M, Escudier Villa JM, Martin Asenjo R, Guillen Merzo M, Rueda Sobella F, Acena A, Garcia Arana JM, Garcia-Rubira JC; RETAKO Investigators. Short- and long-term prognostic relevance of cardiogenic shock in Takotsubo syndrome: results from the RETAKO registry. *JACC Heart Fail* 2018;**6**:928–936.
4. Bohm M, Cammann VL, Ghadri JR, Ukena C, Gili S, Di Vece D, Kato K, Ding KJ, Szawan KA, Micek J, Jurisic S, D'Ascenzo F, Frangieh AH, Rechsteiner D, Seifert B, Ruschitzka F, Luscher T, Templin C, InterTAK Collaborators. Interaction of systolic blood pressure and resting heart rate with clinical outcomes in takotsubo syndrome: insights from the International Takotsubo Registry. *Eur J Heart Fail* 2018;**20**:1021–1030.
5. Lyon AR, Bossone E, Schneider B, Sechtem U, Citro R, Underwood SR, Sheppard MN, Figtree GA, Parodi G, Akashi YJ, Ruschitzka F, Filippatos G, Mebazaa A, Omerovic E. Current state of knowledge on Takotsubo syndrome: a position statement from the Taskforce on Takotsubo Syndrome of the Heart Failure Association of the European Society of Cardiology. *Eur J Heart Fail* 2016;**18**:8–27.
6. Izumo M, Nakowski S, Shiota M, Dao J, Dohad S, Kawahara E, Fukuoka Y, Siegel RJ, Shiota T. Mechanisms of acute mitral regurgitation in patients with takotsubo cardiomyopathy: an echocardiographic study. *Circ Cardiovasc Imaging* 2011;**4**:392–398.
7. Citro R, Rigo F, D'Andrea A, Ciampi Q, Parodi G, Provenza G, Piccolo R, Mirra M, Zito C, Giudice R, Patella MM, Antonini-Canterin F, Bossone E, Piscione F, Salerno-Uriarte J; Takotsubo Italian Network Investigators. Echocardiographic correlates of acute heart failure, cardiogenic shock, and in-hospital mortality in tako-tsubo cardiomyopathy. *JACC Cardiovasc Imaging* 2014;**7**:119–129.
8. Inoue T, Matsui H, Tanaka H, Fushimi K, Yasunaga H. Early beta-blocker use and in-hospital mortality in patients with Takotsubo cardiomyopathy. *Heart* 2016;**102**:1029–1035.
9. Singh K, Carson K, Usmani Z, Sawhney G, Shah R, Horowitz J. Systematic review and meta-analysis of incidence and correlates of recurrence of takotsubo cardiomyopathy. *Int J Cardiol* 2014;**174**:696–701.
10. Ghadri JR, Wittstein IS, Prasad A, Sharkey S, Dote K, Akashi YJ, Cammann VL, Crea F, Galiuto L, Desmet W, Yoshida T, Manfredini R, Eitel I, Kosaka M, Naf HM, Deshmukh A, Lerman A, Bossone E, Citro R, Ueyama T, Corrado D, Kurisu S, Ruschitzka F, Winchester D, Lyon AR, Omerovic E, Bax JJ, Meimoun P, Tarantini G, Rihal C, Y-Hassan S, Migliore F, Horowitz JD, Shimokawa H, Luscher TF, Templin C. International expert consensus document on Takotsubo syndrome (Part II): diagnostic workup, outcome, and management. *Eur Heart J* 2018;**39**:2047–2062.
11. Templin C, Ghadri JR, Diekmann J, Napp LC, Bataiosu DR, Jaguszewski M, Cammann VL, Sarcon A, Geyer V, Neumann CA, Seifert B, Hellemann J, Schwyzer M, Eisenhardt K, Jenewein J, Franke J, Katus HA, Burgdorf C, Schunkert H, Moeller C, Thiele H, Bauersachs J, Tschope C, Schultheiss HP, Laney CA, Rajan L, Michels G, Pfister R, Ukena C, Bohm M, Erbel R, Cuneo A, Kuck KH, Jacobshagen C, Hasenfuss G, Karakas M, Koenig W, Rottbauer W, Said SM, Braun-Dullaeus RC, Cuculi F, Banning A, Fischer TA, Vasankari T, Airaksinen KE, Fijalkowski M, Rynkiewicz A, Pawlak M, Opolski G, Dworakowski R, MacCarthy P, Kaiser C, Osswald S, Galiuto L, Crea F, Dichl W, Franz WM, Empen K, Felix SB, Delmas C, Lairez O, Erne P, Bax JJ, Ford I, Ruschitzka F, Prasad A, Luscher TF. Clinical features and outcomes of takotsubo (stress) cardiomyopathy. *N Engl J Med* 2015;**373**:929–938.
12. Nishida J, Kouzu H, Hashimoto A, Fujita T, Kawamukai M, Mochizuki A, Murayama A, Kokubo N, Shimoshige S, Yuda S, Hase M, Tsuchihashi K, Miura T. "Ballooning" patterns in takotsubo cardiomyopathy reflect different clinical backgrounds and outcomes: a BOREAS-TCM study. *Heart Vessels* 2015;**30**:789–797.
13. Ghadri JR, Cammann VL, Napp LC, Jurisic S, Diekmann J, Bataiosu DR, Seifert B, Jaguszewski M, Sarcon A, Neumann CA, Geyer V, Prasad A, Bax JJ, Ruschitzka F, Luscher TF, Templin C; International Takotsubo (InterTAK) Registry. Differences in the clinical profile and outcomes of typical and atypical Takotsubo syndrome: data from the International Takotsubo Registry. *JAMA Cardiol* 2016;**1**:335–340.
14. Ghadri JR, Kato K, Cammann VL, Gili S, Jurisic S, Di Vece D, Candreva A, Ding KJ, Micek J, Szawan KA, Bacchi B, Bianchi R, Levinson RA, Wischnewsky M, Seifert B, Schlossbauer SA, Citro R, Bossone E, Munzel T, Knorr M, Heiner S, D'Ascenzo F, Franke J, Sarcon A, Napp LC, Jaguszewski M, Noutsias M, Katus HA, Burgdorf C, Schunkert H, Thiele H, Bauersachs J, Tschope C, Fleske BM, Rajan L, Michels G, Pfister R, Cuneo A, Jacobshagen C, Hasenfuss G, Karakas M, Koenig W, Rottbauer W, Said SM, Braun-Dullaeus RC, Banning A, Cuculi F, Kobza R, Fischer TA, Vasankari T, Airaksinen KEJ, Opolski G, Dworakowski R, MacCarthy P, Kaiser C, Osswald S, Galiuto L, Crea F, Dichl W, Empen K, Felix SB, Delmas C, Lairez O, El-Battrawy I, Akin I, Borggrefe M, Horowitz J, Kosal M, Tousek P, Widimsky P, Gilyarova E, Shilova A, Gilyarov M, Winchester DE, Ukena C, Bax JJ, Prasad A, Bohm M, Luscher TF, Ruschitzka F, Templin C. Long-term prognosis of patients with Takotsubo syndrome. *J Am Coll Cardiol* 2018;**72**:874–882.
15. Looi JL, Lee M, Webster MW, To AC, Kerr AJ. Postdischarge outcome after Takotsubo syndrome compared with patients post-ACS and those without prior CVD: ANZACS-QI 19. *Open Heart* 2018;**5**:e000918.

© 2019 The Authors
European Journal of Heart Failure © 2019 European Society of Cardiology

JACC: CARDIOVASCULAR INTERVENTIONS
VOL. 12, NO. 20, 2019
© 2019 BY THE AMERICAN COLLEGE OF CARDIOLOGY FOUNDATION
PUBLISHED BY ELSEVIER

EDITORIAL COMMENT

iFR or FFR

Is That the Real Question?*

Takayuki Warisawa, MD,[a,b,†] Justin E. Davies, MD, PhD[b,†]

Both fractional flow reserve (FFR) and instantaneous wave-free ratio (iFR) are used in routine clinical practice, following the results of large-scale clinical outcomes trials (DEFER [Fractional Flow Reserve to Determine the Appropriateness of Angioplasty in Moderate Coronary Stenosis], FAME [Fractional Flow Reserve versus Angiography for Guiding Percutaneous Coronary Intervention], FAME II [The Fractional Flow Reserve versus Angiography for Multivessel Evaluation 2], DEFINE-FLAIR [Functional Lesion Assessment of Intermediate Stenosis to Guide Revascularisation], and iFR SWEDEHEART [The Instantaneous Wave-free Ratio versus Fractional Flow Reserve in Patients with Stable Angina Pectoris or Acute Coronary Syndrome]) (1–5). These studies showed the safety of deferral of percutaneous coronary intervention on the basis of coronary physiology, the benefits of FFR-guided revascularization over angiography-guided revascularization, and clinical equivalence between iFR and FFR. These results were achieved despite classification mismatch between FFR and iFR in approximately 20% of cases (6).

Over the past few years, the interventional community has moved from a position of "right" or "wrong" when comparing discordant results between physiological indexes to a more scientific approach by instead looking for justifications to explain the reported results. In this issue of *JACC: Cardiovascular Interventions*, Lee et al. (7) further explore potential differences between the iFR and FFR indexes and explore whether it is possible to produce even more insights by combining indexes to explain clinical outcome results. It is striking that after largely "abandoning" flow indexes in search of simpler and more robust pressure measurements more than 20 years ago, much of the mechanistic understanding behind the results of the present study by Lee et al. (7) lies in differences in blood flow among different grades of stenoses and interrogation with either resting or hyperemic indexes (8). This combination of pressure and flow was perhaps was most elegantly presented in a recent analysis of IDEAL (Iberian-Dutch-English) collaborators registry by Cook et al. (9) (Figure 1). It is also important to remember that discordance by indexes is not necessarily always due to underlying differences in flow (10).

SEE PAGE 2018

Kobayashi et al. (11), in a core laboratory assessment of the CONTRAST (Can Contrast Injection Better Approximate FFR Compared to Pure Resting Physiology?) study, showed that despite measurements being made by some of the leading experts in the field, about 30% of pressure wire traces could not be included in the study analysis (11). This was due to artifacts and failure to correctly identify drift and pressure dampening. It is striking to see that the rate of exclusion of data due to artifacts at 30% exceeded the discordance between iFR and FFR (which is approximately 20%). The CEREBRIA-2 (Artificial Intelligence for Aortic Pressure Waveform Analysis during Coronary Angiography) study (12) showed that by using artificial intelligence, it was possible to distinguish damped from normal beats and thereby alert physicians to pressure dampening in real time during measurement.

Although vessel-level ischemia has previously been the stalwart of physiological assessment for clinical decision making, there is increasingly a move toward a more systematic approach to ischemia

*Editorials published in *JACC: Cardiovascular Interventions* reflect the views of the authors and do not necessarily represent the views of *JACC: Cardiovascular Interventions* or the American College of Cardiology.

From the [a]Hammersmith Hospital, Imperial College London, London, United Kingdom; and the [b]St. Marianna University School of Medicine, Kawasaki, Japan. [†]Drs. Warisawa and Davies contributed equally to this work. Dr. Warisawa has received consulting fees from Abbott Vascular and Philips. Dr. Davies holds patents pertaining to iFR technology; and is a consultant for Philips; and has received research grants and holds intellectual property pertaining to Philips.

ISSN 1936-8798/$36.00
https://doi.org/10.1016/j.jcin.2019.07.051

assessment by looking at lesion-level ischemia with pressure-wire pull back and coregistration (13). Using nonhyperemic iFR, these techniques have been shown to have significant benefit over hyperemic FFR, specifically when assessing serial focal stenoses (14). Using such techniques, it is possible to characterize diffuse and focal disease and quantify the effect they will have on the coronary physiological assessment of the interrogated vessel. This means, in practice, that it is possible to plan percutaneous coronary intervention by making a pressure-wire pull back. This is particularly important, as was recently demonstrated in a 500-patient pilot study, DEFINE-PCI (Blinded Physiological Assessment of Residual Ischemia after Successful Angiographic PCI) (15). This showed that in 24% of cases, patients were left with physiologically significant stenoses after angiography-guided percutaneous coronary intervention. Most importantly, in these cases, more than 80% of stenoses were focal in nature. This raises very important questions about physiological assessment and whether it is now still best to use fixed cut points measured at the vessel level or whether it would be better to target lesions with focal stenoses, aiming to maximize the physiological gain. These results have profound implications on this study by Lee et al. (7). The way in which the coronary microcirculation behaves during autoregulation in baseline and hyperemic conditions is critically dependent on the vessel substrate (10,16). Specifically, diffuse disease tends to lead to longer periods of autoregulatory dilatation, whereas focal disease tends to cause autoregulatory dilation during periods of exercise only. These differences lead to diverging results between iFR and FFR assessment, which may be linked to differences in clinical outcomes. However, they are likely surrogates for underlying conditions of focal or diffuse disease and the state of the coronary microcirculation.

Over the past few years, there has been a huge surge in interest in the field of coronary physiology as we move to the post-FFR era. Now, there is a range of new indexes increasingly measured under resting conditions (iFR) in addition to a range of angiographic and noninvasive physiological tools, such as angiographic FFR and computed tomographic FFR. However, we still lack tools that can easily and reliably measure ischemia (rather than surrogates of ischemia) and tools that are able to simply assess the coronary microcirculation. These tools, together with more clinical trial outcomes data, will help further shape revascularization decision making in the next decade as we learn how to best treat diffuse and focal disease and how to differentially manage patients presenting with myocardial edema following acute coronary syndromes and ST-segment elevation myocardial infarction. This study by Lee et al. (7) is a great reminder that although we have gained much knowledge in the field of coronary physiology over the past 30 years, there is still much more work to do.

FIGURE 1 Relationship Between Pressure Indexes and Coronary Flow Reserve

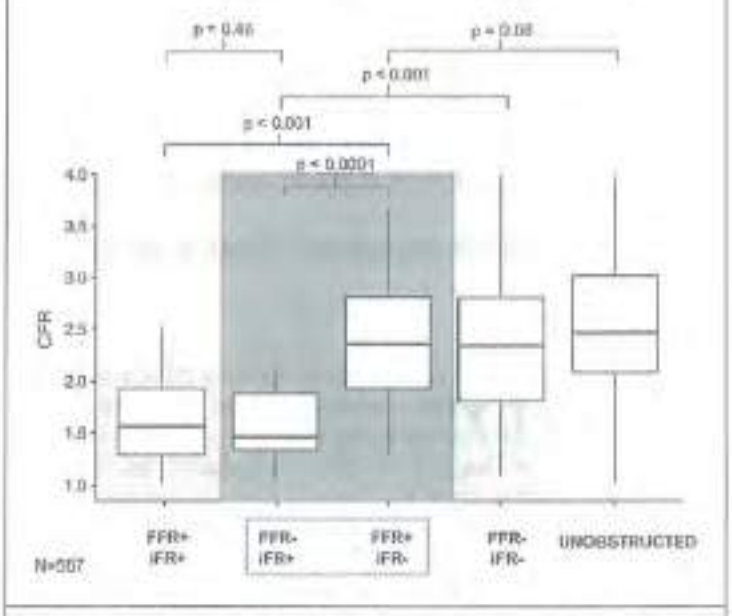

As for a mechanism for discordance between fractional flow reserve (FFR) and instantaneous wave-free ratio (iFR), it has been demonstrated that the iFR−/FFR+ discordance group was characterized by preserved coronary flow reserve (CFR), as high as those of the iFR−/FFR− and control groups. In contrast, the iFR+/FFR− discordant group was characterized by reduced CFR, as low as that of the iFR+/FFR+ group. Reproduced with permission from Cook et al. (9).

ADDRESS FOR CORRESPONDENCE: Dr. Justin E. Davies, The Hammersmith Hospital, Du Cane Road, London W12 0NN, United Kingdom. E-mail: justindavies@heart123.com.

REFERENCES

1. Bech GJW, De Bruyne B, Pijls NHJ, et al. Fractional flow reserve to determine the appropriateness of angioplasty in moderate coronary stenosis: a randomized trial. Circulation 2001;103:2928–34.

2. Tonino PAL, De Bruyne B, Pijls NHJ, et al. Fractional flow reserve versus angiography for guiding percutaneous coronary intervention. N Engl J Med 2009;360:213–24.

3. De Bruyne B, Pijls NHJ, Kalesan B, et al. Fractional flow reserve-guided PCI versus medical therapy in stable coronary disease. N Engl J Med 2012;367:991–1001.

JACC: CARDIOVASCULAR INTERVENTIONS VOL. 12, NO. 20, 2019
OCTOBER 28, 2019:2032–4

4. Davies JE, Sen S, Dehbi HM, et al. Use of the instantaneous wave-free ratio or fractional flow reserve in PCI. N Engl J Med 2017;376:1824–34.

5. Göthberg M, Christiansen EH, Gudmundsdóttir IJ, et al. Instantaneous wave-free ratio versus fractional flow reserve to guide PCI. N Engl J Med 2017;376:1813–23.

6. Jeremias A, Maehara A, Genereux P, et al. Multicentre core laboratory comparison of the instantaneous wave-free ratio and resting Pd/Pa with fractional flow reserve: the RESOLVE study. J Am Coll Cardiol 2014;63:1253–61.

7. Lee SH, Choi KH, Lee JM, et al. Physiologic characteristics and clinical outcomes of patients with discordance between FFR and iFR. J Am Coll Cardiol Intv 2019;12:2018–31.

8. Gould KL, Lipscomb K, Calvert C. Compensatory changes of the distal coronary vascular bed during progressive coronary constriction. Circulation 1975;51:1085–94.

9. Cook CM, Jeremias A, Petraco R, et al. Fractional flow reserve/instantaneous wave-free ratio discordance in angiographically intermediate coronary stenoses: an analysis using doppler-derived coronary flow measurements. J Am Coll Cardiol Intv 2017;10:2034–34.

10. Warisawa T, Cook CM, Howard JP, et al. Physiological pattern of disease assessed by pressure-wire pullback has an influence on fractional flow reserve/instantaneous wave-free ratio discordance. Circ Cardiovasc Interv 2019;12:e007494.

11. Kobayashi Y, Johnson NP, Berry C, et al. for the CONTRAST Study Investigators. The influence of lesion location on the diagnostic accuracy of adenosine-free coronary pressure wire measurements. J Am Coll Cardiol Intv 2016;9:2390–5.

12. Howard JP, Cook CM, van de Hoef TP, et al. Artificial intelligence for aortic pressure waveform analysis during coronary angiography: machine learning for patient safety. J Am Coll Cardiol Intv 2019;12:2093–101.

13. Kikuta Y, Cook CM, Sharp ASP, et al. Pre-angioplasty instantaneous wave-free ratio pullback predicts hemodynamic outcome in patients with coronary artery disease: primary results of the international multicenter IFR GRADIENT registry. J Am Coll Cardiol Intv 2018;11:757–67.

14. Warisawa T. The identification of physiological predominance in serial coronary lesions using pressure-wire pullback: differences between iFR, FFR and hyperemic-iFR. Presented at: EuroPCR 2019; May 28, 2019; Paris, France.

15. Jeremias A. Blinded physiological assessment of residual ischemia after successful angiographic PCI. Presented at: ACC 19; March 17, 2019; New Orleans, LA.

16. de Waard GA, Cook CM, van Royen N, Davies JE. Coronary autoregulation and assessment of stenosis severity without pharmacological vasodilation. Eur Heart J 2018;39:1062–71.

KEY WORDS coronary circulation, discordance, fractional flow reserve, instantaneous wave-free ratio, vasodilatory capacity

ARTICLE IN PRESS

European Journal of Pharmacology xxx (xxxx) xxx–xxx

Contents lists available at ScienceDirect

European Journal of Pharmacology

journal homepage: www.elsevier.com/locate/ejphar

Full length article

Renoprotective effect of the xanthine oxidoreductase inhibitor Topiroxostat under decreased angiotensin II type 1_a receptor expression

Keiichi Ohata[a,d], Atsuko Kamijo-Ikemori[a,b,*], Takeshi Sugaya[a,c], Chihiro Hibi[c], Takashi Nakamura[c], Takayo Murase[d], Tsuyoshi Oikawa[e], Seiko Hoshino[b], Kimie Katayama[a], Junko Asano[a], Kenjiro Kimura[f], Yugo Shibagaki[a]

[a] Division of Nephrology and Hypertension, Department of Internal Medicine, St. Marianna University School of Medicine, Kanagawa, Japan
[b] Department of Anatomy, St. Marianna University School of Medicine, Kanagawa, Japan
[c] Biopharmaceutical Study Group, Pharmaceutical Research Laboratories, Sanwa Kagaku Kenkyusho Company, Limited, Mie, Japan
[d] Radioisotope and Chemical Analysis Center, Laboratory Management Department, Sanwa Kagaku Kenkyusho Company, Limited, Mie, Japan
[e] CMIC Holdings Company, Limited, Tokyo, Japan
[f] JCHO Tokyo Takanawa Hospital, Tokyo, Japan

ARTICLE INFO

Keywords:
Topiroxostat
Xanthine oxidoreductase
Xanthine oxidoreductase inhibitor
Renin–angiotensin system
L-FABP
Adenine
Tubulointerstitial damage
Blood pressure

ABSTRACT

The aim of this study was to confirm the renoprotective effect of xanthine oxidoreductase (XOR) inhibitor, topiroxostat, compared with another XOR inhibitor, febuxostat, under decreased angiotensin II type 1_a ($AT1_a$) receptor expression in the model of renal injury caused by adenine. To evaluate the degree of tubular damage using urinary liver-type fatty acid-binding protein (L-FABP) under decreased $AT1_a$ expression, we used $AT1_a$ receptor knockdown hetero and human L-FABP chromosomal transgenic (Tg) mice ($AT1_a^{+/-}$L-FABP$^{+/-}$). Male $AT1_a^{+/-}$L-FABP$^{+/-}$ mice were divided into two groups: the adenine diet group (n = 40) was given a diet containing only 0.2% w/w adenine, and the normal diet group (n = 5) was given a normal diet. When renal dysfunction was confirmed in the adenine diet group 4 weeks after starting the diet, the adenine diet group was further divided into five groups. The adenine diet group (n = 8) was continuously given only the adenine diet. Each group receiving high-dose (3 mg/kg) or low-dose (1 mg/kg) topiroxostat (Topiroxostat-H group, n = 8, Topiroxostat-L group, n = 8) or febuxostat (Febuxostat-H group, n = 8, Febuxostat-L group, n = 8) was given the adenine diet including the drug for another 4 weeks. The levels of renal XOR, renal dysfunction, urinary L-FABP, tubulointerstitial damage, hypoxia, and oxidative stress were decreased or attenuated after treatment with topiroxostat or febuxostat compared with the adenine diet group. Furthermore, antioxidant capacity was maintained owing to these treatments.

In conclusion, topiroxostat and febuxostat attenuated renal damage under decreased $AT1_a$ expression in the adenine-induced renal injury model.

1. Introduction

Inhibitors of uric acid production and uricosuric agents are well-known drugs for the treatment of hyperuricemia and gout. Xanthine oxidoreductase (XOR) inhibitors inhibit uric acid production by suppressing the activity of XOR in the final stage of uric acid formation. Hyperuricemia causes chronic kidney disease (CKD) (Chang et al., 2010; Chonchol et al., 2007; Ohno et al., 2001; Yamanaka et al., 2011) and is an aggravating factor in chronic renal failure (Isaka et al., 2016; Waisman et al., 1975). Some clinical studies suggest that XOR inhibitors suppress renal dysfunction in patients with hyperuricemia and CKD (Hosoya et al., 2014a, b). On the other hand, in an experimental study using rodents that have uricase that degrades uric acid to allantoin and rarely show renal damage due to hyperuricemia, a renoprotective action of XOR inhibitors was reported (Lee et al., 2014; Nakamura et al., 2016a, b; Sánchez-Lozada et al., 2008). We also reported previously that topiroxostatiroxostat (Topiroxostat), one of the selective XOR inhibitors, had a renoprotective action against adenine-induced renal damage via decrease in oxidative stress produced by renal XO converted from XOR (Kamijo-Ikemori et al., 2016). XOR inhibitors may function as renoprotective agents as well as antioxidants in addition to their beneficial effect on hyperuricemia.

Topiroxostat interacts with amino acid residues of the solvent channel of XOR and also binds covalently to molybdenum via oxygen in

* Correspondence to: Department of Anatomy, St. Marianna University School of Medicine, 2-16-1 Sugao, Miyamae-Ku, Kawasaki 216-8511, Japan.
E-mail address: akam@marianna-u.ac.jp (A. Kamijo-Ikemori).

http://dx.doi.org/10.1016/j.ejphar.2017.09.005
Received 18 April 2017; Received in revised form 2 September 2017; Accepted 4 September 2017
0014-2999/ © 2017 Elsevier B.V. All rights reserved.

Please cite this article as: Ohata, K., European Journal of Pharmacology (2017), http://dx.doi.org/10.1016/j.ejphar.2017.09.005

the hydroxylation intermediate reaction (Okamoto et al., 2003, 2004). A multicenter, double-blind, comparative study showed that topiroxostat had the potency to decrease the urinary albumin/creatinine ratio, even in hyperuricemic patients with stage 3 CKD, with concomitantly therapy with renin-angiotensin system (RAS) inhibitors, which was considered the first-line treatment for CKD to suppress the progression of the disease (Hosoya et al., 2014b; Jomori et al., 2015). There is a possibility that XOR inhibitors and RAS inhibitors synergistically retard the progression of renal disease.

The present study was performed to determine whether Topiroxostat had a renoprotective effect even during suppression of the RAS in an adenine-induced renal injury model, in which activation of both XOR and the RAS was related to the onset and progression of renal injury (Iijima et al., 2014; Kamijo-Ikemori et al., 2016). Because RAS activation generates angiotensin II (Ang II), which causes tubulointerstitial damage through Ang II type 1_a ($AT1_a$) receptor in rodents, the kidneys of $AT1_a$ receptor knockdown hetero mice are considered to be resistant to renal damage. Furthermore, the evaluation of renal tubulointerstitial damage was performed using one of the urinary tubular markers, urinary liver type fatty acid binding protein (L-FABP), which accurately reflects the degree of oxidative stress, peritubular blood flow, and tubulointerstitial damage (Ichikawa et al., 2015; Kamijo-Ikemori et al., 2016; Matsui et al., 2011, 2012, 2016; Yamamoto et al., 2007). Renal L-FABP is not expressed in the kidney of mice (Kamijo et al., 2004b; Simon et al., 1993). Therefore, we used $AT1_a$ receptor knockdown hetero and human L-FABP chromosomal transgenic (Tg) mice ($AT1_a^{+/-}$L-FABP$^{+/-}$), as established previously (Ichikawa et al., 2014).

2. Materials and methods

2.1. Animals

Animal studies were performed at CMIC Pharma Science Co., Ltd (Hokuto, Yamanashi, Japan). The examination facility was approved by the Institutional Animal Care and Use Committee (no.2015-155), which is certified by the Association for the Assessment and Accreditation of Laboratory Animal Care International (AAALAC, no. 001182) in order to obtain high-quality data. C57BL/6 background $AT1_a$ receptor knockdown homo mice ($AT1_a^{-/-}$) (Sugaya et al., 1995) and C57BL/6 background human L-FABP Tg mice (human L-FABP$^{+/-}$) (World Intellectual Property Organization patent WO0073791) (Kamijo et al., 2004b) were generated as described previously. To obtain $AT1_a^{+/-}$L-FABP$^{+/-}$ mice, $AT1_a^{-/-}$ mice without the human L-FABP transgene ($AT1_a^{-/-}$ L-FABP$^{-/-}$) were crossed with human L-FABP$^{+/-}$ mice ($AT1_a^{+/+}$ L-FABP$^{+/-}$) (Ichikawa et al., 2014). Eight-week-old male $AT1_a^{+/-}$L-FABP$^{+/-}$ mice (n = 45, body weight 25.5–27.6 g) were evaluated for the experiment.

2.2. Model of adenine-induced renal damage

Male $AT1_a^{+/-}$L-FABP$^{+/-}$ mice (n = 40) were fed a diet containing 0.2% w/w adenine ad libitum (Ali et al., 2013; Kamijo-Ikemori et al., 2016). They were divided into five groups: the adenine diet group (n = 8) was given the diet containing only adenine for 8 weeks. The Topiroxostat and Febuxostat groups were given the diet containing only adenine for 4 weeks, and thereafter, were given the diet containing each XOR inhibitor in addition to adenine for another 4 weeks. Four weeks after initiation of this adenine diet, the renal dysfunction of these mice was confirmed. The daily dosage of XOR inhibitors was 1 mg/kg as a low dose (Topiroxostat-L, n = 8; Febuxostat-L, n = 8) or 3 mg/kg as a high dose (Topiroxostat-H, n = 8; Febuxostat-H, n = 8) in each group. The normal diet group (n = 5) was given the diet not containing adenine throughout the test period. Topiroxostat was obtained from Sanwa Kagaku Kenkyusho, and Febuxostat was synthesized in the laboratory of Sanwa Kagaku Kenkyusho.

Body weight and consumption of the adenine diet were measured every week. Urine and serum were collected once every 2 weeks. All of the mice were housed individually in metabolic cages with free access to tap water. Mouse kidneys were collected at week 8 for light microscopy analysis, real-time quantitative polymerase chain reaction analysis, western blot analysis and measurement of XOR. A part of the kidney was fixed with methyl Carnoy solution for light microscopy analysis and the rest was quick-frozen with liquid nitrogen for other analyses.

2.3. Blood pressure

Blood pressure was measured with a tail-cuff apparatus (Softron BP-98A; Softron, Tokyo, Japan) at weeks 0 and 8. Systolic blood pressure (SBP) values were derived from an average of three measurements per animal at each time point.

2.4. Serum and urinary biochemistry

Blood urea nitrogen (BUN) was measured by the urease-LEDH method (Iatro LQ UN Rate (A) II, LSI Medience Corporation, Tokyo, Japan). Serum and urinary creatinine were measured by the Jaffe method (LabAssay™ Creatinine, WAKO Pure Chemical Industries, Osaka, Japan). Urinary albumin was determined with the Mouse Albumin ELISA kit (Bethyl Laboratories, Montgomery, TX). Urinary human L-FABP was measured by a two-step sandwich ELISA procedure (human L-FABP ELISA kit, CMIC Co., Tokyo, Japan) (Kamijo et al., 2004a).

2.5. Renal histological and morphometric analysis

The kidneys were dehydrated and embedded in paraffin. Serial sections (2-μm thick) were obtained for conventional histological assessments, such as periodic acid–Schiff (PAS) staining, as described previously (Kamijo-Ikemori et al., 2016). Tubulointerstitial injury in the PAS-stained sections was categorized as tubular dilation with epithelial atrophy or tubular atrophy. All fields from the entire cortical areas were selected, and the areas of tubulointerstitial injury were measured with an image analyzer, version 6.4 (Auto/Manual Measurement Software, WinRoof, Mitani Co., Tokyo, Japan). The amount of remaining renal tubules was evaluated as the ratio relative to the entire cortical area.

2.6. Immunohistological analysis

Tissues fixed in methyl Carnoy solution were embedded in paraffin. An indirect immunoperoxidase method was used to identify the antigens, as described previously (Ichikawa et al., 2012, 2014; Kamijo-Ikemori et al., 2016). Aquaporin-1 as a proximal tubular marker was identified with the use of rabbit polyclonal antibodies (1:400, Santa Cruz Biotechnology, Dallas, TX). Types I and type III collagen were identified with the use of rabbit polyclonal antibodies (1:200, Cedarlane Laboratories Ltd, Burlington, Ontario, Canada). Macrophages were identified with the use of the rat monoclonal antibody F4/80 (1:200, BMA Biomedicals, Augst, Switzerland). Visualization was performed by incubation with polymeric horseradish peroxidase–conjugated secondary antibodies (ready-to-use, ImmPRESS™ Polymer Detection kit, Vector Laboratories, Burlingame, CA). Peroxidase activity was revealed by the diaminobenzidine reaction (Liquid DAB+, DAKO Japan, Tokyo, Japan), and the sections were counterstained with hematoxylin. All fields from the entire cortical interstitium were selected, and the areas positive for aquaporin-1 and types I and III collagen were identified. The positive areas were expressed as ratios of the positively stained areas relative to the entire cortical area under × 100 magnification, measured with an image analyzer (WinRoof, MITANI Corporation, Fukui, Japan). Similarly, the degree of macrophage infiltration was measured as the positively stained areas of F4/80 and

was expressed as the ratio of the F4/80-positive areas relative to the entire cortical area.

2.7. Real-time quantitative polymerase chain reaction analysis

Total RNA was extracted from each frozen kidney and reverse transcribed, as described previously (Ichikawa et al., 2014, 2015; Kamijo-Ikemori et al., 2016). The TaqMan real-time polymerase chain reaction (PCR) was performed with an Applied Biosystems Step One Plus™ Real-Time PCR System (Applied Biosystems). Real-time PCR was used to quantify the mRNA of hypoxia-inducible factor-1alpha (HIF-1α) for evaluation of the degree of renal hypoxia and the mRNA of catalase for the evaluation of resistance against oxidative stress. The expression levels of these mRNAs were normalized to glyceraldehyde 3-phosphate dehydrogenase (GAPDH) expression levels. Part numbers of Taqman probes were as follows: HIF-1α, Mm00468869; catalase, Mm00437992; and GAPDH, Mm99999915 (Applied Biosystems).

2.8. Western blot analysis

Proteins were extracted from each frozen kidney, and protein concentrations were measured as previously described (Kamijo-Ikemori et al., 2016; Yokoyama et al., 2009). These extracts were separated by sodium dodecyl sulfate-polyacrylamide gel electrophoresis (SDS-PAGE) using NuPAGE 4–12% Bis-Tris gel and the XCell SureLock Mini-Cell system (Thermo Fisher Scientific, Rockford, IL). After proteins were transferred from the gel to a polyvinylidene difluoride membrane using the iBlot Dry Blotting System (iBlot™ Gel Transfer Device, Thermo Fisher Scientific), the membranes were blocked in Blocking One (Nacalai tesque, Kyoto, Japan). Primary antibodies against HIF-1α (mouse monoclonal antibody, 1:2000, Abcam, Cambridge, MA), catalase (rabbit polyclonal antibody, 1:5000, Calbiochem, San Diego, CA), and hexanoyl-Lys (HEL) (mouse monoclonal antibody, 1:2000, JaICA, Shizuoka, Japan) diluted in Can Get Signal Solution I (TOYOBO CO, Osaka, Japan) were incubated overnight at 4 °C. After washing, the primary antibodies were detected with horseradish peroxidase–conjugated anti-mouse or anti-rabbit antibody (Cell signaling technology, Danvers, MA) diluted 1:2000 in phosphate-buffered saline/Tween20 for 1 h at room temperature. Subsequently, the chemiluminescent signal labeled with ECL Prime Western Blotting Detection Reagent (GE Healthcare, Little Chalfont, UK) was detected with a CCD camera system (Ez-Capture II, ATTO Co., Tokyo, Japan). The 1:2000 diluted rabbit monoclonal antibody to GAPDH (Cell Signaling technology) was also used for detection of GAPDH on the same membrane with HIF-1α and HEL-modified protein analysis after treatment with stripping buffer (Wako, Osaka, Japan), and the expression levels of HIF-1α protein and HEL-modified protein were normalized to GAPDH. The expression of these proteins was measured with a CS analyzer, version 3.0 (ATTO Co.).

2.9. Measurement of XOR by LC-FTMS

The kidney homogenates were centrifuged for 60 min at 105,000 × g, 4 °C (Murase et al., 2016). The cytosols were added to reaction mixtures containing [15N2]-xanthine (0.8 mM), NAD+ (1 mM), and oxonate (0.013 mM). Tris-HCl buffer (20 mM, pH 8.5) was added to adjust the total volume to 150 μL for each reaction mixture. These mixtures were incubated at 37 °C for 30 min, and then 50 μL of 200 μmol/l [13C2, 15N2]-UA was added as an internal standard. Subsequently, the mixture was heated for 5 min at 95 °C to stopiroxostat the reaction. The resulting suspensions were centrifuged for 10 min at 15,000 × g and 4 °C. The supernatants were filtered through ultrafiltration membranes (Amicon® Ultra-0.5 centrifugal filter devices, 3 K, Millipore) and the production levels of [15N2]-UA were measured by LC/MS (LTQ-Orbitrap, Thermo Fisher Scientific, Waltham, MA). Each activity was expressed as [15N2]-UA nmol/min/mg protein.

2.10. Measurement of urinary angiotensinogen and angiotensin II

Urinary angiotensinogen and angiotensin II were measured with a mouse total angiotensinogen assay kit (IBL, Gunma, Japan) and an angiotensin II assay kit (Peninsula Laboratories International, San Carlos, CA, USA); these levels were reported as ratios relative to the urinary creatinine level.

2.11. Statistical analysis

All values were expressed as means ± S.E.M. $P < 0.05$ or < 0.01 was considered to indicate statistical significance. Paired results of temporal course were analyzed by one-way analysis of variance with repeated measures, and six groups were analyzed by one-way analysis of variance, followed by the Mann–Whitney *U* test using JMP11.2.1 (SAS Institute, Cary, NC, USA).

3. Results

3.1. Body weight and consumption of feed

At week 0, body weights were similar in the six groups. The body weight of mice in the normal diet group was moderately increased, whereas that of mice in the adenine diet group significantly decreased throughout the experimental period compared with the normal diet group (Fig. 1A). At 4 weeks, there was no difference in the body weight of mice in the adenine diet, Topiroxostat, and Febuxostat groups. The body weight of mice in the Topiroxostat-L group at weeks 7 and 8, in the Topiroxostat-H group at weeks 6, 7, and 8, in the Febuxostat-L group at week 8, and in the Febuxostat-H group at weeks 6, 7, and 8 were significantly higher than those of mice in the adenine diet group at the same time points (Fig. 1A). One mouse in the Febuxostat-L group was euthanized at week 5 because it was in a moribund condition. The amount of adenine feed consumed, except for the normal diet group, was similar in the five groups (Fig. 1B).

3.2. Serum and urinary biochemistry

In the normal diet group, the levels of BUN and serum creatinine

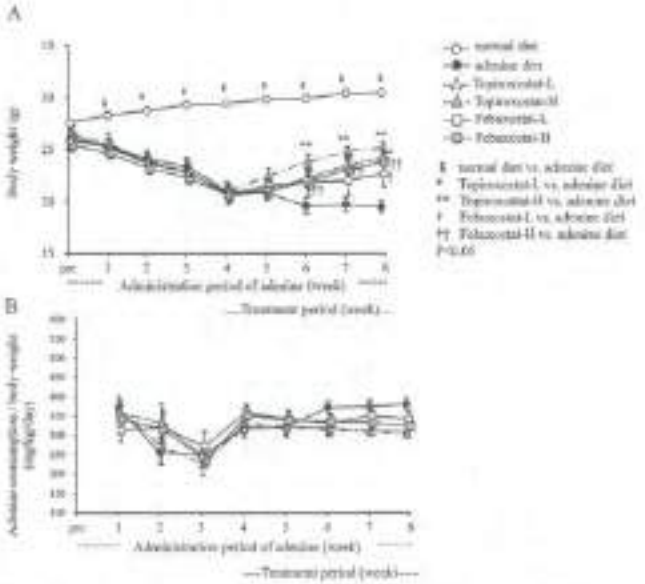

Fig. 1. Changes in body weight (A) and consumption of adenine diet (B) throughout the test period. *Topiroxostat-L (n = 8), **Topiroxostat-H (n = 8), †Febuxostat-L (n = 8), ††Febuxostat-H (n = 8), §normal-diet (n = 5) group vs. adenine diet group (n = 8); each symbol indicates $P < 0.05$ at same week. Values are represented as means ± S.E.M.

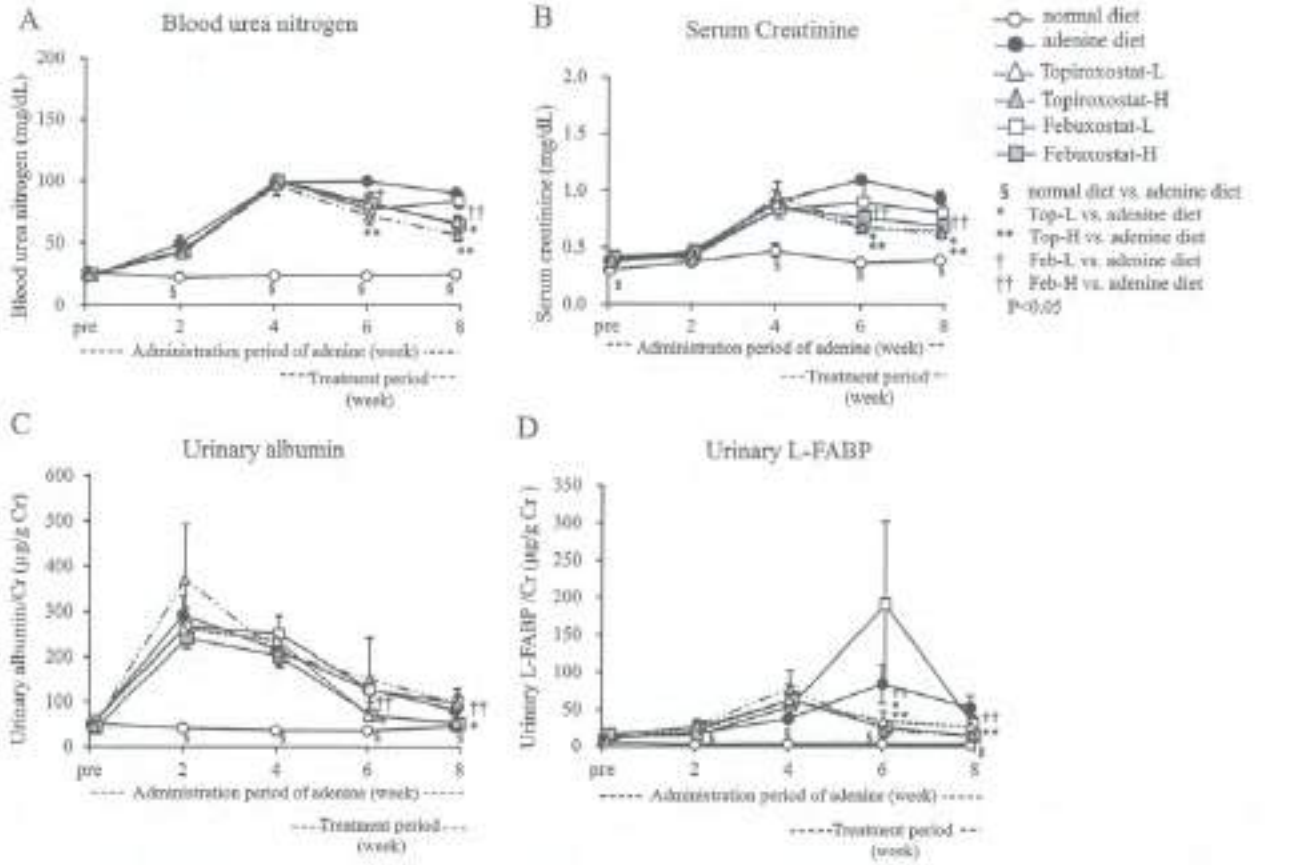

Fig. 2. Changes in blood urea nitrogen (BUN) (A), serum creatinine (B), urinary albumin (C), urinary human L-FABP levels (D). *Topiroxostat-L (n = 8), **Topiroxostat-H (n = 8), †Febuxostat-L (n = 8), ††Febuxostat-H (n = 8), §normal-diet (n = 5) group vs. adenine diet group (n = 8); each symbol indicates P < 0.05 at same week. Values are represented as mean ± S.E.M.

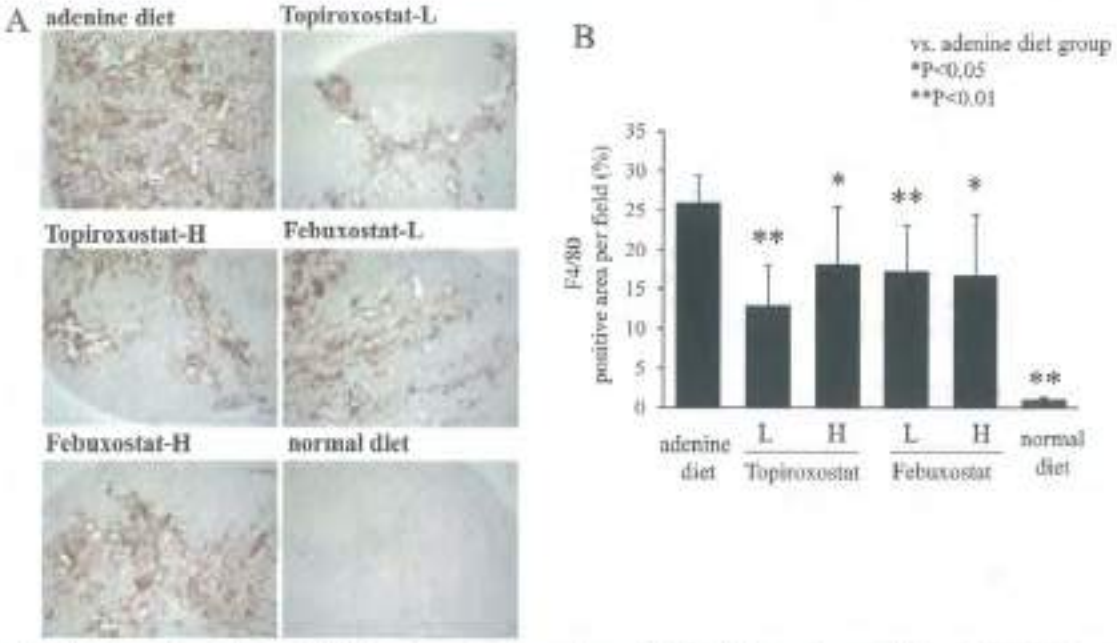

Fig. 3. Histological findings of macrophage infiltration in the kidney. Representative images of immunohistological staining using an antibody against F4/80 (A). Quantification of the positive staining areas of F4/80 (B). Original magnification, × 100. Adenine diet group, n = 8; Topiroxostat-L group, n = 8; Topiroxostat-H group, n = 8; Febuxostat-L group, n = 8; Febuxostat-H group, n = 8; normal-diet group, n = 5. *P < 0.05, ** P < 0.01 vs. the adenine diet group at week 8. Values are represented as mean ± S.E.M.

were low and did not change throughout the test period. The levels of BUN and serum creatinine significantly increased during weeks 2–8 in the adenine diet group. At 4 weeks, there were no differences in BUN and serum creatinine levels in the adenine diet, Topiroxostat, and Febuxostat groups. BUN levels at week 8 in the Topiroxostat-L group, weeks 6 and 8 in the Topiroxostat-H group, week 6 in the Febuxostat-L group, and week 8 in the Febuxostat-H group were significantly lower than those in the adenine diet group at the same time points (Fig. 2A). The levels of serum creatinine at weeks 6 and 8 in the Topiroxostat-L, Topiroxostat-H, and Febuxostat-H groups were significantly lower than the levels in the adenine diet group at the same time points (Fig. 2B).

The level of urinary albumin in the adenine diet group was significantly higher at week 2 than in the normal diet group and decreased from week 4 to week 8, with significantly higher levels than in the normal diet group (Fig. 2C). At 4 weeks, there was no difference in urinary albumin levels in the adenine-diet, Topiroxostat, and Febuxostat groups. The levels in the Topiroxostat-L and Febuxostat-H groups were significantly lower than those in the adenine diet group at weeks 6 and 8 (Fig. 2C).

The levels of urinary human L-FABP in the adenine diet group were significantly increased at weeks 2, 4, 6, and 8 compared with those in the normal diet group. At 4 weeks, there were no differences in urinary human L-FABP levels in the adenine diet, Topiroxostat, and Febuxostat groups. The urinary human L-FABP levels at week 6 in the Topiroxostat-L group and at weeks 6 and 8 in the Topiroxostat-H group were significantly lower than the levels in the adenine diet group at the same time points ($P < 0.05$) (Fig. 2D). The urinary L-FABP levels at weeks 6 and 8 in the Febuxostat-H group were significantly lower in the adenine diet group, but the levels in the Febuxostat-L group were not significant lower than in the adenine diet group.

3.3. Evaluation of macrophage infiltration

For evaluation of macrophage infiltration in the kidney, F4/80-positive cells were immunohistochemically detected and analyzed (Fig. 3A). The percentages of F4/80- positive areas in the adenine diet group were significantly higher than those in the normal diet group ($P < 0.01$) (Fig. 3B). The percentages of F4/80-positive areas in all the Topiroxostat- and Febuxostat-treated groups were significantly lower than those in the adenine diet group (Topiroxostat-L and Febuxostat-L, $P < 0.01$; Topiroxostat-H and Febuxostat-H, $P < 0.05$) (Fig. 3B).

3.4. Renal histological and morphometric analysis

In the adenine diet group, the PAS-stained sections revealed severe tubulointerstitial damage, including dilatation of tubules and degeneration of proximal tubular epithelial cells (Fig. 4A). The percentages of remaining tubule area in the kidneys of mice in the adenine diet group were significantly lower than those in the normal diet group ($P < 0.01$) (Fig. 4B). The percentages of remaining tubule area in the kidneys of mice in the Topiroxostat-L, Topiroxostat-H, and Febuxostat-H groups were significantly higher than those in the adenine diet group ($P < 0.01$) (Fig. 4B). However, the percentages of remaining tubule area in the kidneys of mice in the Febuxostat-L group were similar to those in the adenine diet group (Fig. 4B).

3.5. Immunohistological analysis of aquaporin-1 and types I and III collagen

For evaluation of the remaining proximal tubules, aquaporin-1 was immunohistochemically detected and analyzed, in addition to PAS staining (Fig. 4C). The percentages of aquaporin-1-positive areas in the adenine diet group were significantly lower than those in the normal diet group ($P < 0.01$) (Fig. 4C and D). The positive areas in the Topiroxostat-L, Topiroxostat-H, and Febuxostat-H groups were significantly greater than those in the adenine diet group ($P < 0.01$). In the Febuxostat-L group, although the positive areas were significantly greater than those in the adenine diet group ($P < 0.05$) (Fig. 4D), the percentages of the remaining proximal tubules tended to be lower than those in the other three groups given XOR inhibitors (Fig. 4D).

Expression of both type I (Fig. 5A) and type III (Fig. 5C) collagen was immunohistochemically detected for evaluation of tubulointerstitial fibrosis. The deposition of both type I and type III collagen in the adenine diet group was significantly higher than in the normal diet group ($P < 0.01$) (Fig. 5B and D). The deposition of both type I collagen (Topiroxostat-L, Topiroxostat-H, and Febuxostat-L, $P < 0.01$; Febuxostat-H, $P < 0.05$) (Fig. 5B) and type III collagen (Topiroxostat-H and Febuxostat-L, $P < 0.01$; Topiroxostat-L and Febuxostat-H, $P < 0.05$) (Fig. 5D) in each Topiroxostat- and Febuxostat- treated group was significantly suppressed compared with the adenine diet group, and a clear difference between the therapeutic effects of Topiroxostat and Febuxostat was not detected.

3.6. Evaluation of renal hypoxia and oxidative stress

The expression levels of HIF-1α mRNA in the kidney were measured for evaluation of renal hypoxia. The HIF-1α mRNA levels in the kidney were significantly higher in the adenine diet group than in the normal diet group ($P < 0.01$) and were significantly suppressed in the Topiroxostat-H ($P < 0.05$), Febuxostat-L ($P < 0.05$), and Febuxostat-H ($P < 0.01$) groups (Fig. 6A). The HIF-1α mRNA levels in the Topiroxostat-L group tended to be lower than in the adenine diet group (Fig. 6A). The protein expression levels of HIF-1α in the kidney were significantly higher in the adenine diet group than in the normal diet group ($P < 0.01$) and were lower in the Topiroxostat-L ($P < 0.05$), Topiroxostat-H ($P < 0.01$), Febuxostat-L ($P < 0.05$) and Febuxostat-H ($P < 0.01$) groups than in the adenine diet group (Fig. 6B).

The expression levels of HEL-modified protein in kidney were significantly higher in the adenine diet group than in the normal diet group ($P < 0.01$) and were significantly lower in the Topiroxostat-L ($P < 0.01$), Topiroxostat-H ($P < 0.05$), Febuxostat-L ($P < 0.01$), and Febuxostat-H ($P < 0.01$) group than in the adenine diet group (Fig. 7).

The expression levels of catalase mRNA in the kidney were measured for evaluation of antioxidant ability. The catalase mRNA levels in the kidney were significantly lower in the adenine diet group than those in the normal diet group ($P < 0.05$) (Fig. 8A). The catalase mRNA levels in the Topiroxostat-H group were significantly higher than those in the adenine diet group ($P < 0.01$) (Fig. 8A). The protein expression levels of catalase in the kidney were significantly lower in the adenine diet group than those in the normal diet group ($P < 0.01$) and were higher in the Topiroxostat-H ($P < 0.05$) and Febuxostat-H ($P < 0.05$) groups than those in the adenine diet group (Fig. 8B).

3.7. Evaluation of renal XOR activity

For evaluation of the suppressive effect of Topiroxostat or Febuxostat treatment on renal XOR, the activity of XOR in the kidney was evaluated. XOR activity in the kidney was significantly increased by ingestion of the adenine diet compared with the normal diet, and XOR activity was significantly suppressed by each dose of Topiroxostat or Febuxostat treatment compared with the adenine diet group (Fig. 9). The suppressive effects of XOR activity in the Topiroxostat-L, Topiroxostat-H, and Febuxostat-H groups were comparable, whereas the suppressive effect in the Febuxostat-L group tended to be lower than that in other groups treated with XOR inhibitors (Fig. 9).

3.8. Evaluation of blood pressure, urinary angiotensinogen, and urinary angiotensin II

SBP levels before ingestion of the adenine diet were similar in all groups. SBP at week 8 was significantly increased in the adenine diet group compared with the normal diet group ($P < 0.01$) (Fig. 10A). SBP

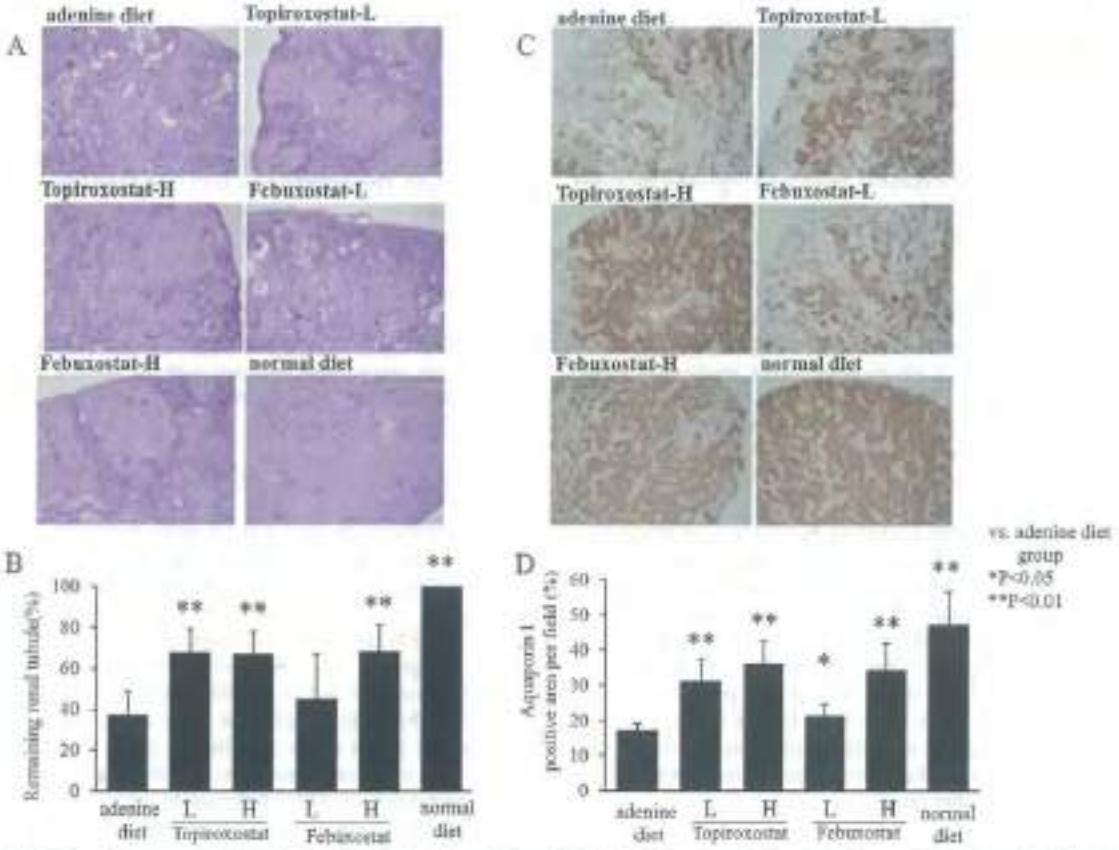

Fig. 4. Histological findings. Representative images of histological staining with periodic acid-Schiff (PAS) showing tubulointerstitial damage (A), and immunohistological staining using an antibody against aquaporin-1 (C). Quantification of tubulointerstitial damage in tissues stained with PAS (B), and the positive staining areas of aquaporin-1 (D) at week 8. Original magnification, × 100. Adenine diet group, n = 8; Topiroxostat-L group, n = 8; Topiroxostat-H group, n = 8; Febuxostat-L group, n = 8; Febuxostat-H group, n = 8; normal-diet group, n = 5. *P < 0.05, ** P < 0.01 vs. the adenine diet group at week 8. Values are represented as means ± S.E.M.

was significantly suppressed by each Topiroxostat and Febuxostat treatment ($P < 0.01$) (Fig. 10A).

Both urinary angiotensinogen (Fig. 10B) and urinary angiotensin II (Fig. 10C) levels were significantly increased by ingestion of the adenine diet compared with the normal diet ($P < 0.01$). These levels were significantly lower in the Topiroxostat-L, Topiroxostat-H, and Febuxostat-H groups than in the adenine diet group. The levels of urinary angiotensinogen tended to be lower in the Febuxostat-L group than in the adenine diet group (Fig. 10B), and the level of urinary angiotensin II was not lower in the Febuxostat-L group than in the adenine diet group (Fig. 10C).

4. Discussion

This study showed the renoprotective effect of topiroxostat and febuxostat due to their antioxidant effect under decreased $AT1_a$ expression in a model of adenine-induced nephropathy. This result indicates that combination treatment with an XOR inhibitor and an RAS inhibitor might be a useful strategy for prevention of the progression of CKD.

Tubulointerstitial damage is strongly associated with progression of CKD and renal prognosis. Therefore, treatment for prevention of tubulointerstitial damage is needed to prevent progression to chronic renal failure (Hodgkins et al., 2012). The adenine-induced nephropathy model is known as a renal failure model due to severe tubulointerstitial damage (Ali et al., 2013; Kamijo-Ikemori et al., 2016; Nasr et al., 2010). Adenine, one of the purines, is catalyzed by XOR, which leads to the production of 2,8-dihydroxyadenine (DHA) in the liver with low solubility. DHA crystals directly affect the renal tubules, and tubular occlusion by DHA crystals provides pressure load to the peritubular capillary in addition to tubular cells, with subsequent renal hypoxia (Fong et al., 2016; Kamijo-Ikemori et al., 2016). Hypoxia accelerates degradation of cellular ATP and increases the production of hypoxanthine, which activates renal XOR with subsequently production of oxidative stress (Saugstad et al., 1988). Renal hypoxia is a common aggravating factor for progression of tubulointerstitial damage in various renal diseases (Fine et al., 2000; Nangaku et al., 2006). Under such a pathophysiological condition, topiroxostat and febuxostat suppressed the progression of tubulointerstitial damage via decrease in renal oxidative stress by suppression of renal XOR activity and via maintenance of antioxidant capacity. These results indicate that both topiroxostat and febuxostat might play a crucial role in prevention of tubulointerstitial damage in CKD.

AT1 receptor blocker was reported to have a renoprotective effect in adenine-induced nephropathy (Iijima et al., 2014). While our previous study showed an approximately threefold increase in serum creatinine from the start of the adenine diet to 4 weeks in the adenine-induced model using $AT1_a^{+/+}$L-FABP$^{+/-}$ mice (Kamijo-Ikemori et al., 2016), the present study showed an approximately twofold increase in serum creatinine using $AT1_a^{+/}$L-FABP$^{+/-}$ mice; renal dysfunction is considered to be more severe in the former mice than in the latter mice. Oxidative stress stimulated activation of the intrarenal RAS (Osaki et al., 2013; Yu et al., 2010) and subsequently induced activation of the $AT1_a$ receptor, which produced oxidative stress again for a vicious circle, resulting in tubulointerstitial damage (Tanifuji et al., 2005). Decreased $AT1_a$ receptor expression may inhibit the adverse effect brought by intrarenal RAS activation, which is induced by oxidative stress produced via renal XOR activity, and may suppress the progression of renal dysfunction in this model. Because the present study

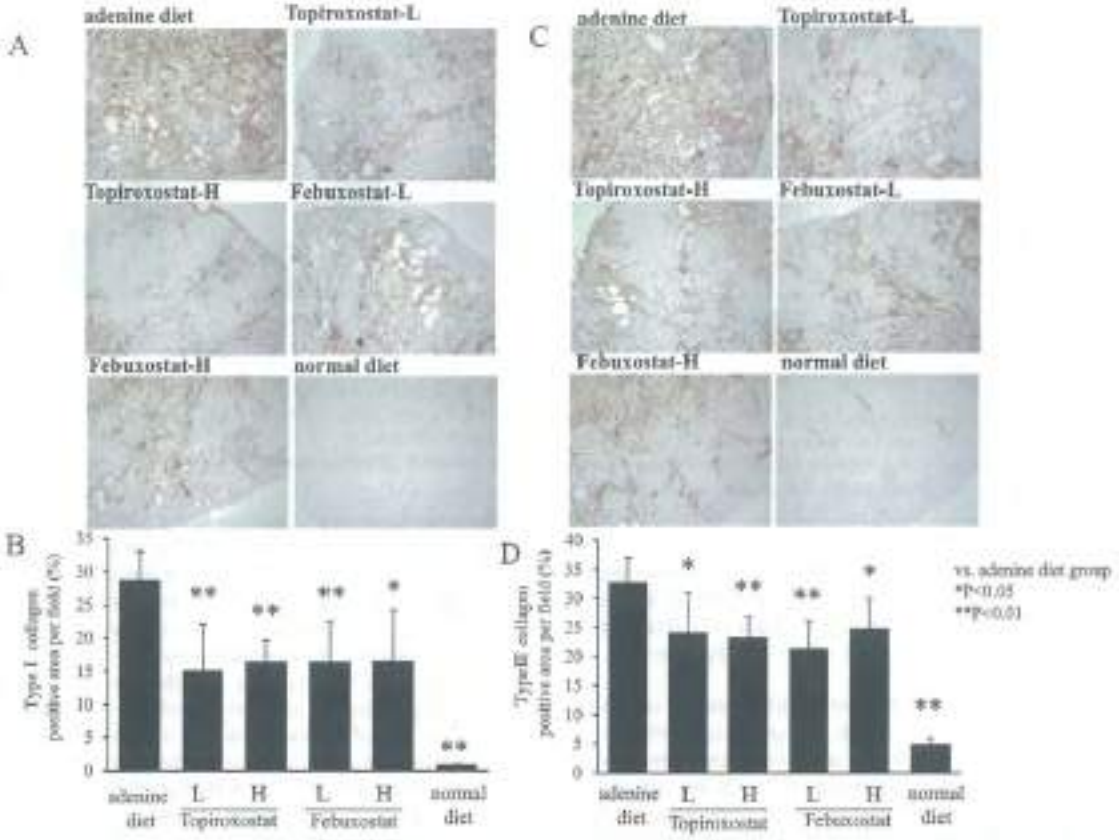

Fig. 5. Histological findings. Representative images of immunohistological staining using an antibody against type I collagen (A) and type III collagen (C). Quantification of the positive staining areas of type I collagen (B) and type III collagen (D) at week 8. Original magnification, × 100. Adenine diet group, n = 8; Topiroxostat-L group, n = 8; Topiroxostat-H group, n = 8; Febuxostat-L group, n = 8; Febuxostat-H group, n = 8; normal-diet group, n = 5. *P < 0.05, ** P < 0.01 vs. the adenine diet group at week 8. Values are represented as means ± S.E.M.

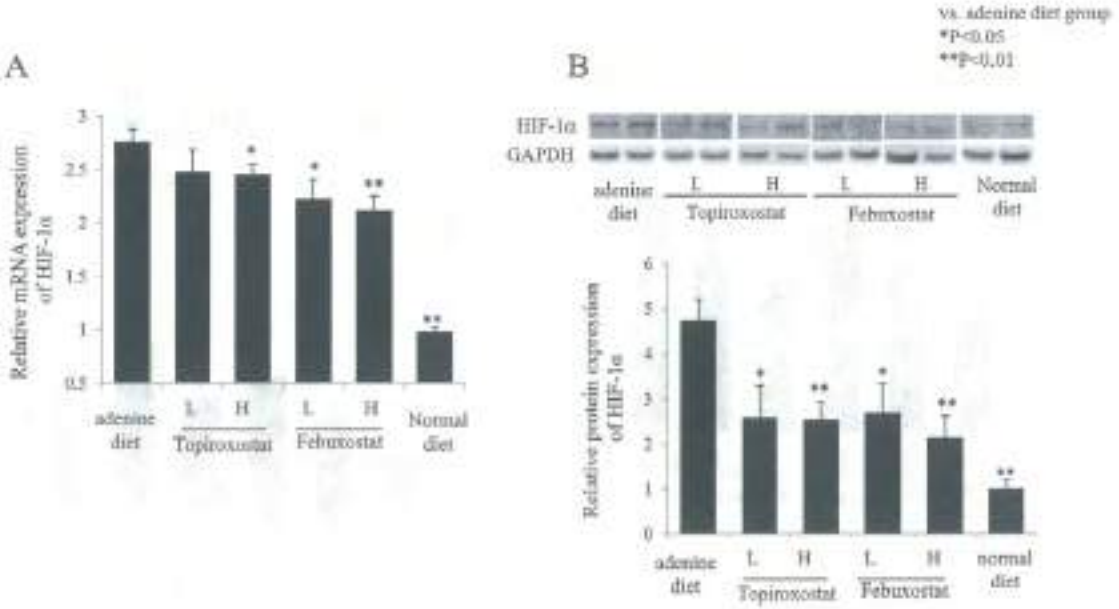

Fig. 6. Evaluation of renal hypoxia in the kidney. Gene expression (A) and protein expression (B) of HIF-1α at week 8. Adenine diet group, n = 8; Topiroxostat-L group, n = 8; Topiroxostat-H group, n = 8; Febuxostat-L group, n = 8; Febuxostat-H group, n = 8; normal-diet group, n = 5. *P < 0.05, ** P < 0.01 vs. the adenine diet group at week 8. Values are represented as means ± S.E.M.

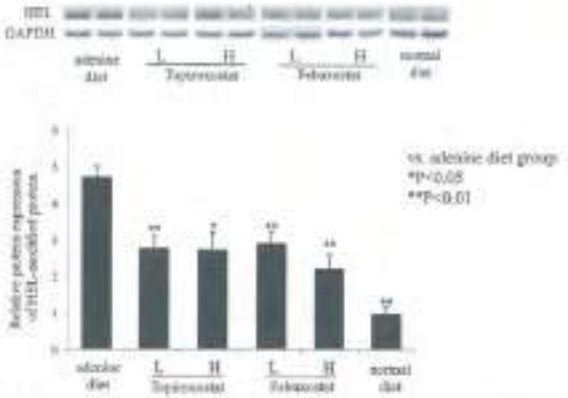

Fig. 7. Evaluation of oxidative stress in the kidney. Protein expression of HEL-modified protein at week 8. Adenine diet group, n = 8; Topiroxostat-L group, n = 8; Topiroxostat-H group, n = 8; Febuxostat-L group, n = 8; Febuxostat-H group, n = 8; normal-diet group, n = 5. *P < 0.05, ** P < 0.01 vs. the adenine diet group at week 8. Values are represented as mean ± S.E.M.

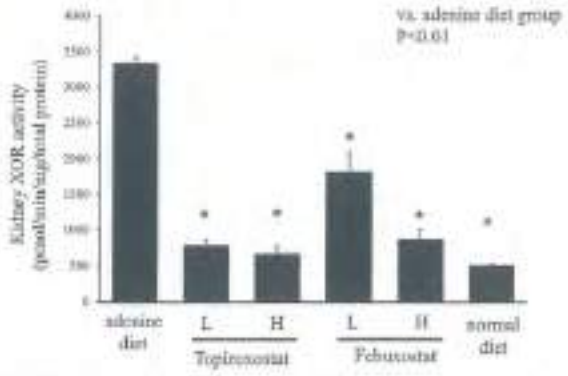

Fig. 9. Renal xanthine oxidoreductase (XOR) activity in the kidney. Adenine diet group, n = 8; Topiroxostat-L group, n = 8; Topiroxostat-H group, n = 8; Febuxostat-L group, n = 8; Febuxostat-H group, n = 8; normal-diet group, n = 5. *P < 0.01 vs. the adenine diet group at week 8. Values are represented as mean ± S.E.M.

showed that topiroxostat and febuxostat also suppressed renal injury under decreased $AT1_a$ receptor expression, the combination treatment of topiroxostat or febuxostat with an RAS inhibitor may retard renal dysfunction in patients with CKD more effectively than the RAS inhibitor alone.

This study found a significant increase in SBP at week 8 compared with week 0 in the nontreatment adenine diet group and a significant suppression of the increase in SBP at week 8 in all treatment groups under decreased $AT1_a$ receptor expression. Although urinary angiotensinogen and angiotensin II levels were significantly higher in the nontreatment adenine diet group than in the normal diet group, and their levels were significantly lower in the Topiroxostat-L, Topiroxostat-H, and Febuxostat-H groups than in the nontreatment adenine group, their levels in the Febuxostat-L group were not lower than in the nontreatment adenine group. On the other hand, SBP levels at week 8 in the Febuxostat-L group were similar to those in the other treatment groups. These results indicate that although topiroxostat and febuxostat might furthermore suppress RAS activity under partial deficiency of the $AT1_a$ receptor, there was a possibility that the decrease in SBP in the treatment groups was independent of further suppression of RAS activity in this model. Tubulointerstitial damage, especially injury to the proximal tubules, induces glomerulotubular disconnection, which ultimately leads to formation of atubularglomeruli (Chevalier et al., 2008). Benigni et al. (2001) reported that the percentage of atubular glomeruli was significantly positively correlated with SBP. From the result that severe loss of proximal tubules, as determined by aquaporin-1-positive cells, was observed in the nontreatment adenine diet group and that topiroxostat and febuxostat attenuated this damage, the decrease in SBP by topiroxostat and febuxostat might be due to preservation of glomerulotubular connections following improvement in proximal tubular damage.

In the present study, renoprotection by topiroxostat and febuxostat was evaluated by various measures including serum and urinary markers and histological analysis. Although changes in urinary albumin did not parallel the progression of renal damage in the nontreatment adenine diet group, the other parameters reflected its progression. The

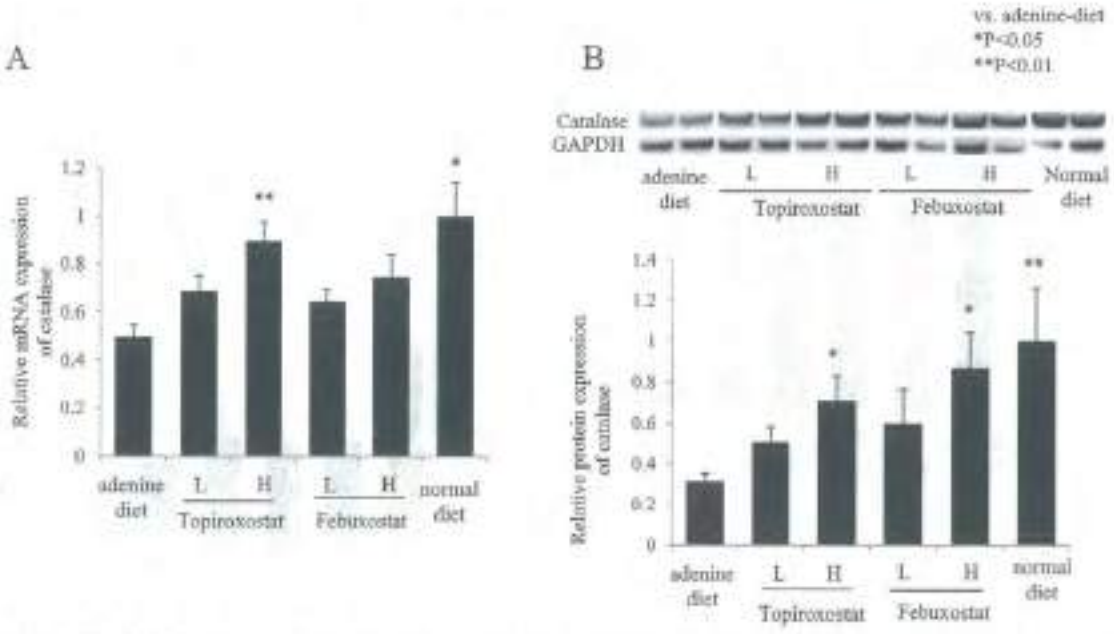

Fig. 8. Expression of catalase in the kidney. Gene expression (A) and protein expression (B) of catalase at week 8. Adenine diet group, n = 8; Topiroxostat-L group, n = 8; Topiroxostat-H group, n = 8; Febuxostat-L group, n = 8; Febuxostat-H group, n = 8; normal-diet group, n = 5. *P < 0.05, ** P < 0.01 vs. the adenine diet group at week 8. Values are represented as mean ± S.E.M.

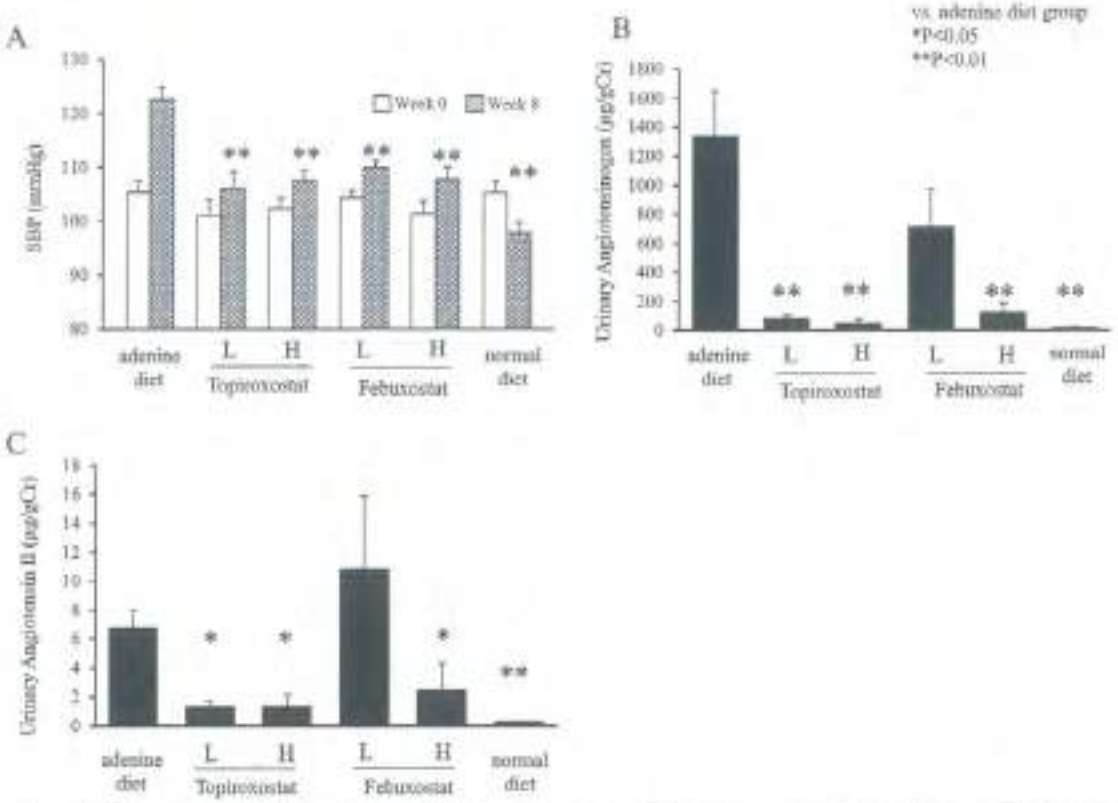

Fig. 10. Change in systemic blood pressure (SBP) levels at week 0 and 8 (A), urinary angiotensinogen (B) and urinary angiotensin II levels (C) at week 8. Adenine diet group, n = 6; Topiroxostat-L group, n = 8; Topiroxostat-H group, n = 8; Febuxostat-L group, n = 8; Febuxostat-H group, n = 8; normal-diet group, n = 5. *P < 0.05, ** P < 0.01 vs. the adenine diet group. Values are represented as mean ± S.E.M.

degree of renal dysfunction evaluated by BUN and creatinine was significantly attenuated at week 8 in the Topiroxostat-L, Topiroxostat-H, and Febuxostat-H groups, and the urinary L-FABP levels at week 8 in the Topiroxostat-H and Febuxostat-H groups were significantly lower than in the nontreatment group. With regard to the histological evaluation, the degree of remaining renal tubules evaluated by PAS staining sections in the Topiroxostat-L, Topiroxostat-H, and Febuxostat-H groups was significantly greater than that in the nontreatment adenine group, but not in the Febuxostat-L group. Considering these results obtained from various parameters, there is a possibility that administration of Topiroxostat-H and Febuxostat-H had especially useful effects as renoprotective treatment under decreased $AT1_a$ receptor expression in adenine-induced nephropathy, although there were no differences in the degree of renal oxidative stress and renal hypoxia in all treatment groups. Because the 3 mg/kg dose of topiroxostat used in the Topiroxostat-H group is similar to the 1 mg/kg dose of febuxostat in the Febuxostat-L group, topiroxostat may have superior potency to febuxostat for the prevention of progression of CKD.

In conclusion, this study showed that topiroxostat and febuxostat had a renoprotective role due to their antioxidant effect under decreased $AT1_a$ receptor expression in adenine-induced nephropathy. These results indicate the effectiveness of a combination treatment with an XOR inhibitor and an RAS inhibitor for prevention of the progression of renal damage. Recently, limited efficacy of RAS suppression on inhibition of renal dysfunction was reported in some clinical studies (Agodoa et al., 2001; Appel et al., 2008). Although further clinical studies are needed to show the effectiveness of combination therapy for prevention of renal dysfunction compared with the RAS inhibitor alone, there is a possibility that XOR inhibitors may be among the therapeutic agents to add to the RAS inhibitor in the management of CKD treatment.

Sources of funding

This work was supported by the consigned research fund from Sanwa Kagaku Kenkyusho Co., Ltd., Tokyo, Japan.

Disclosures

T. Sugaya is the director and senior scientist, K. Ohata and T. Oikawa is the scientist of CMIC HOLDINGS Co., Ltd., the company that produced the kits for L-FABP analysis. C. Hibi, T. Nakamura and T. Murase are the employees of Sanwa Kagaku Kenkyusho Co., Ltd., the company that produced the topiroxostatiroxostat. None of the other authors have conflicts of interest or financial disclosures of any relevance to the present study.

Contribution

KO, AK-I, TS, TO and CH, study design; KO, AK-I, TN, TM, TO, SH, JA and KK, data collection; KO, AK-I and TN, data analysis; KO, AK-I, TS, CH, TN, TO, KH, KK and YS, data interpretation; KO, AK-I, TO, TN literature search and generation of figures; KO and AK-I, writing of the manuscript. All authors gave their final approval of the submitted version.

Acknowledgments

We would like to thank Kazuho Inoue for technical assistance.

References

Agodoa, L.Y., Appel, L., Bakris, G.L., Beck, G., Bourgoignie, J., Briggs, J.P., Charleston, J., Cheek, D., Cleveland, W., Douglas, J.G., Douglas, M., Dowie, D., Faulkner, M.,

Gabriel, A., Gassman, J., Greene, T., Hall, Y., Hebert, L., Hiremath, L., Jamerson, K., Johnson, C.J., Kopple, J., Kusek, J., Lash, J., Lea, J., Lewis, J.B., Lipkowitz, M., Massry, S., Middleton, J., Miller 3rd, E.R., Norris, K., O'Connor, D., Ojo, A., Phillips, R.A., Pogue, V., Rahman, M., Randall, O.S., Rastogi, S., Schulman, G., Smith, W., Thornley-Brown, D., Tisher, C.C., Toto, R.D., Wright Jr., J.T., Xu, S., African American Study of Kidney Disease and Hypertension (AASK) Study Group, 2001. Effect of ramipril vs amlodipine on renal outcomes in hypertensive nephrosclerosis: a randomized controlled trial. JAMA 285, 2719–2728.

Ali, B.H., Al-Salam, S., Al Za'abi, M., Waly, M.I., Rankanur, A., Beegam, S., Al-Lawati, I., Adham, S.A., Nemmar, A., 2013. New model for adenine-induced chronic renal failure in mice, and the effect of gum acacia treatment thereon: comparison with rats. J. Pharmacol. Toxicol. Methods 68, 384–393.

Appel, L.J., Wright Jr., J.T., Greene, T., Kusek, J.W., Lewis, J.B., Wang, X., Lipkowitz, M.S., Norris, K.C., Bakris, G.L., Rahman, M., Contreras, G., Rostand, S.G., Kopple, J.D., Gabbai, F.B., Schulman, G.I., Gassman, J.J., Charleston, J., Agodoa, L.Y., African american study of kidney disease and hypertension collaborative research group, 2008. Long-term effects of renin-angiotensin-system-blocking therapy and a low blood pressure goal on progression of hypertensive chronic kidney disease in african americans. Arch. Intern. Med. 168, 832–839.

Benigni, A., Cioffaretti, E., Rottanzi, A., Cresa, D., Remuzzi, G., 2001. Angiotensin-converting enzyme inhibition prevents glomerular-tubule disconnection and atrophy in passive heymann nephritis, an effect not observed with a calcium antagonist. Am. J. Pathol. 159, 1743–1750.

Chang, H.Y., Tung, C.W., Lee, P.H., Lei, C.C., Hsu, Y.C., Chang, H.H., Yang, H.F., Lai, L.C., Jong, M.C., Chen, C.Y., Fang, K.Y., Chao, Y.S., Shih, Y.H., Lin, C.L., 2010. Hyperuricemia as an independent risk factor of chronic kidney disease in middle-aged and elderly population. Am. J. Med. Sci. 339, 509–515.

Chevalier, R.L., Forbes, M.S., 2008. Generation and evolution of tubular glomeruli in the progression of renal disorders. J. Am. Soc. Nephrol. 19, 197–206.

Chonchol, M., Shlipak, M.G., Katz, R., Sarnak, M.J., Newman, A.B., Siscovick, D.S., Kestenbaum, B., Carney, J.K., Fried, L.F., 2007. Relationship of uric acid with progression of kidney disease. Am. J. Kidney Dis. 50, 239–247.

Fine, L.G., Bandyopadhay, D., Norman, J.T., 2000. Is there a common mechanism for the progression of different types of renal diseases other than proteinuria? Towards the unifying theme of chronic hypoxia. Kidney Int. (Suppl. 75), S22–S26.

Fang, D., Ullah, M.M., Lal, J.G., Abdelkader, A., Ou, C.R., Hillard, L.M., Ricardo, S.D., Kelly, D.J., Evans, R.G., 2016. Renal cellular hypoxia in adenine-induced chronic kidney disease. Clin. Exp. Pharmacol. Physiol. 43, 896–905.

Hodgkins, K.S., Schnaper, H.W., 2012. Tubulointerstitial injury and the progression of chronic kidney disease. Pediatr. Nephrol. 27, 901–909.

Hosoya, T., Kimura, K., Itoh, S., Inaba, M., Uchida, S., Tomino, Y., Makino, H., Maruyo, S., Yamamoto, T., Ohno, I., Shibagaki, Y., Ikeuchi, S., Inui, N., Kawahara, M., Hayakawa, H., 2014a. The effect of febuxostatcontrol topiroxostatprevent a further reduction in renal function of patients with hyperuricemia who have never had gout and are complicated by chronic kidney disease stage 3: study protocol for a multicenter randomized controlled study. Trials 15, 28–34.

Hosoya, T., Ohno, I., Nomura, S., Hiratome, I., Uchida, K., Fujinori, S., Yamamoto, T., Nara, S., 2014b. Effects of topiroxostatfebuxostat on the serum urate levels and urinary albumin excretion in hyperuricemic stage 3 chronic kidney disease patients with or without gout. Clin. Exp. Nephrol. 18, 875–884.

Ichikawa, D., Kamijo-Ikemori, A., Sugaya, T., Shibagaki, Y., Yamada, T., Hoshino, S., Katayama, K., Igarashi-Migitaka, J., Hirata, K., Kimura, K., 2015. Human liver-type fatty acid-binding protein protects against tubulointerstitial injury in aldosterone-induced renal injury. Am. J. Physiol. Ren. Physiol. 308, 114–121.

Ichikawa, D., Kamijo-Ikemori, A., Sugaya, T., Shibagaki, Y., Yamada, T., Katayama, K., Hoshino, S., Igarashi-Migitaka, J., Hirata, K., Kimura, K., 2014. Renoprotective effect of renal liver-type fatty acid binding protein and angiotensin II type 1a receptor loss in renal injury caused by RAS activation. Am. J. Physiol. Ren. Physiol. 306, 655–663.

Ichikawa, D., Kamijo-Ikemori, A., Sugaya, T., Yamada, T., Hoshino, S., Igarashi-Migitaka, J., Hirata, K., Kimura, K., 2012. Renal liver-type fatty acid binding protein attenuates angiotensin II-induced renal injury. Hypertension 60, 973–980.

Ijima, K., Ito, Y., Sen, S.K., Akishita, M., Ouchi, Y., 2014. Pravastatin and olmesartan synergistically ameliorate renal failure-induced vascular calcification. J. Atheroscler. Thromb. 21, 917–929.

Inoue, Y., Takahashi, Y., Takahashi, A., Saitoh, T., Yoshimori, T., 2016. Hyperuricemia-induced inflammasome and kidney diseases. Nephrol. Dial. Transplant. 31, 890–896.

Jamerson, T., Saitoh, K., Hosoya, T., 2015. Effect of topiroxostatfebuxostat on the serum urate levels and urinary albumin excretion in concomitant therapy or in primary disease of chronic kidney disease. Jpn. Pharmacol. Ther. 43, 39–50.

Kamijo-Ikemori, A., Sugaya, T., Hibi, C., Nakamura, T., Murase, T., Ohkawa, T., Hoshino, S., Hasegawa, M., Hirata, K., Kimura, K., Shibagaki, Y., 2016. Nonprotective effect of the xanthine oxidoreductase inhibitor topiroxostatfebuxostat on adenine-induced renal injury. Am. J. Physiol. Ren. Physiol. 310, 1366–1376.

Kamijo, A., Kimura, K., Sugaya, T., Yamanouchi, M., Hikita, A., Hirata, N., Hirata, Y., Goto, A., Omata, M., 2004a. Urinary fatty acid-binding protein as a new clinical marker of the progression of chronic renal disease. J. Lab. Clin. Med. 143, 23–30.

Kamijo, A., Sugaya, T., Hikita, A., Okada, M., Okumura, F., Yamanouchi, M., Hosada, A., Okabe, M., Fujita, T., Hirata, Y., Omata, M., Kaneko, R., Fujii, H., Fukamizu, A., Kimura, K., 2004b. Urinary excretion of fatty acid-binding protein reflects stress overload on the proximal tubules. Am. J. Pathol. 165, 1243–1255.

Lee, H.J., Jeong, K.H., Kim, Y.G., Moon, J.Y., Lee, S.H., Ihm, C.G., Hong, J.Y., Lee, T.W., 2014. Febuxostatfebuxostat ameliorates diabetic renal injury in a streptozotocin-induced diabetic rat model. Am. J. Nephrol. 40, 56–63.

Matsui, K., Kamijo-Ikemori, A., Inai, N., Sugaya, T., Yasuda, T., Tatsunami, S., Toyama, T., Shimizu, M., Furuichi, K., Wada, T., Shibagaki, Y., Kimura, K., 2016. Clinical significance of urinary liver-type fatty acid binding protein as a predictor of ESRD and CVD in patients with CKD. Clin. Exp. Nephrol. 20, 195–203.

Matsui, K., Kamijo-Ikemori, A., Sugaya, T., Yasuda, T., Kimura, K., 2012. Usefulness of urinary biomarkers to early detection of acute kidney injury after cardiac surgery in adults. Circ. J. 76, 213–220.

Matsui, K., Kamijo-Ikemori, A., Sugaya, T., Yasuda, T., Kimura, K., 2011. Renal liver-type fatty acid binding protein (L-FABP) attenuates acute kidney injury in aristolochic acid nephrotoxicity. Am. J. Pathol. 178, 1021–1032.

Murase, T., Nampei, M., Oka, M., Ashizawa, N., Matsumoto, K., Miyachi, A., Nakamura, T., 2016. Xanthine oxidoreductase activity assay in tissue using stable isotope-labelled substrate and liquid chromatography high-resolution mass spectrometry. J. Chromatogr. B Anal. Technol. Biomed. Life Sci. 1008, 189–197.

Nakamura, T., Murase, T., Nampei, M., Morimoto, N., Ashizawa, N., Iwanaga, T., Sakamoto, R., 2016a. Effects of topiroxostatfebuxostat and febuxostatfebuxostat on urinary albumin excretion and plasma xanthine oxidoreductase activity in db/db mice. Eur. J. Pharmacol. 785, 224–231.

Nakamura, T., Nagao, G., Nampei, M., Murase, T., Morimoto, N., Ashizawa, N., Iwanaga, T., Sakamoto, R., 2016b. Topiroxostatfebuxostat showed renoprotection via various mechanisms including suppression of xanthine oxidoreductase-induced oxidative stress and inflammation in db/db mice. J. Clin. Exp. Nephrol. 1, 1–9.

Nangaku, M., 2006. Chronic hypoxia and tubulointerstitial injury: a final common pathway to end-stage renal failure. J. Am. Soc. Nephrol. 17, 17–25.

Nair, S.H., Sethi, S., Cornell, L.D., Milliner, D.S., Boelkins, M., Broviac, J., Fidler, M.E., 2010. Crystalline nephropathy due to 2,8-dihydroxyadeninuria: an under-recognized cause of irreversible renal failure. Nephrol. Dial. Transplant. 25, 1909–1915.

Ohno, I., Hosoya, T., Gomi, H., Ichida, K., Okabe, H., Hikita, M., 2001. Serum uric acid and renal prognosis in patients with IgA nephropathy. Nephron 87, 333–339.

Okamoto, K., Eger, B.T., Nishino, T., Kondo, S., Pai, E.F., Nishino, T., 2003. An extremely potent inhibitor of xanthine oxidoreductase. Crystal structure of the enzyme-inhibitor complex and mechanism of inhibition. J. Biol. Chem. 278, 1848–1855.

Okamoto, K., Matsumoto, K., Hille, R., Eger, B.T., Pai, E.F., Nishino, T., 2004. The crystal structure of xanthine oxidoreductase during catalysis: implications for reaction mechanism and enzyme inhibition. Proc. Natl. Acad. Sci. USA 101, 7931–7936.

Osaki, K., Suzuki, Y., Sugaya, T., Tanifuji, C., Nishiyama, A., Horikoshi, S., Tomino, Y., 2013. Amelioration of angiotensin II-induced salt-sensitive hypertension by liver-type fatty acid-binding protein in proximal tubules. Hypertension 62, 712–718.

Sánchez-Lozada, L.G., Tapia, E., Soto, V., Avila-Casado, C., Franco, M., Wesseling, J.L., Zhao, L., Johnson, R.J., 2008. Effect of febuxostatcontrol on the progression of renal disease in 5/6 nephrectomy rats with and without hyperuricemia. Nephron Physiol. 108, 69–78.

Sergiev, O.D., 1988. Hypoxanthine as an indicator of hypoxia: its role in health and disease through free radical production. Pediatr. Res. 23, 143–150.

Simon, F.C., Roth, K.A., Gordon, J.I., 1993. Use of transgenic mice to map cis-acting elements in the liver fatty acid-binding protein gene (Fabpl) that regulate its cell lineage-specific, differentiation-dependent, and spatial patterns of expression in the gut epithelium and in the liver acinus. J. Biol. Chem. 268, 18345–18358.

Sugaya, T., Nishimatsu, S., Tanimoto, K., Takimoto, E., Yamagishi, T., Imamura, K., Goto, S., Inazawa, K., Hisada, Y., Ozaka, A., Uchida, H., Sugiura, M., Fukuta, K., Fukamizu, A., Murakami, K., 1995. Angiotensin II type 1a receptor-deficient mice with hypotension and hyperreninemia. J. Biol. Chem. 270, 18719–18722.

Tanifuji, C., Suzuki, Y., Goor, W.M., Horikoshi, S., Sugaya, T., Ruiz-Ortega, M., Egido, J., Tomino, Y., 2005. Reactive oxygen species-mediated signaling pathways in angiotensin II-induced MCP-1 expression of proximal tubular cells. Antioxid. Redox Signal. 7, 1261–1268.

Weinman, J., Morel, L.M., Rhoades, R., Blumenberg, J.B., 1975. Acute hyperuricemic nephropathy in rats. An electron microscopic study. Am. J. Pathol. 81, 367–378.

Yamamoto, T., Noiri, E., Ono, T., Doi, K., Negishi, K., Kamijo, A., Kimura, K., Fujita, T., Kinukawa, T., Taniguchi, H., Nakamura, K., Goto, M., Shinozaki, N., Ohshima, S., Sugaya, T., 2007. Renal l-type fatty acid-binding protein in acute ischemic injury. J. Am. Soc. Nephrol. 18, 2894–2902.

Yamanaka, H., Japanese society of gout and nucleic acid metabolism, 2011. Japanese guideline for the management of hyperuricemia and gout: second edition. Nucleosides Nucleotides Nucleic Acids 30, 1018–1029.

Yokoyama, T., Kamijo-Ikemori, A., Sugaya, T., Hoshino, S., Yasuda, T., Kimura, K., 2009. Urinary excretion of liver type fatty acid binding protein accurately reflects the degree of tubulointerstitial damage. Am. J. Pathol. 174, 2096–2106.

Yu, M.A., Sánchez-Lozada, L.G., Johnson, R.J., Kang, D.H., 2010. Oxidative stress with an activation of the renin-angiotensin system in human vascular endothelial cells as a novel mechanism of uric acid-induced endothelial dysfunction. J. Hypertens. 28, 1234–1242.

Hypertension Research (2018) 41, 8–17
Official journal of the Japanese Society of Hypertension
www.nature.com/hr

OPEN

ORIGINAL ARTICLE

Role of bardoxolone methyl, a nuclear factor erythroid 2-related factor 2 activator, in aldosterone- and salt-induced renal injury

Mikako Hisamichi[1], Atsuko Kamijo-Ikemori[1,2], Takeshi Sugaya[1], Seiko Hoshino[2], Kenjiro Kimura[3] and Yugo Shibagaki[1]

The aim of this study was to investigate the renoprotective effect of bardoxolone methyl (BM), a nuclear factor erythroid 2-related factor 2 (Nrf2) activator with an antioxidant effect, in a salt-sensitive hypertension model induced by aldosterone (Ald) and salt. Tubulointerstitial damage with urinary liver-type fatty acid-binding protein (L-FABP) was evaluated using human L-FABP chromosomal transgenic (L-FABP$^{+/-}$) male mice. The mice in the Ald group ($n = 7$) received systemic Ald infusions via an osmotic minipump and were given 1% NaCl water for 35 days. Those in the Ald-BM group ($n = 8$) were administered BM intraperitoneally in addition to an injection of Ald and salt. The dose of BM was gradually increased every 7 days up to 10 mg kg^{-1} per day, which was maintained for 14 days. The administration of BM significantly increased renal expression of the Nrf2 target antioxidant gene. Tubulointerstitial damage was significantly ameliorated in the Ald-BM group compared to the Ald group. The increase in reactive oxygen species (ROS) and upregulation of angiotensinogen expression in the kidneys of the Ald group was significantly prevented in the Ald-BM group. The upregulation of human L-FABP expression induced in the kidneys and increase in urinary L-FABP in the Ald group were significantly suppressed by BM administration. In conclusion, BM ameliorated tubulointerstitial damage in the Ald- and salt-induced hypertension model through suppression of both ROS production and intrarenal renin–angiotensin system activation. Urinary L-FABP may be a useful marker reflecting the therapeutic efficacy of BM.

Hypertension Research (2018) **41**, 8–17; doi:10.1038/hr.2017.83; published online 5 October 2017

Keywords: aldosterone (Ald); bardoxolone methyl (BM); liver-type fatty acid-binding protein (L-FABP); nuclear factor erythroid 2-related factor 2 (Nrf2); oxidative stress

INTRODUCTION

Salt-sensitive hypertension induces redundant activation of the renin–angiotensin–aldosterone (Ald) system.[1] Accumulating evidence shows that Ald, an end product of that system, plays a key role in the progression of chronic kidney disease (CKD) due to salt-sensitive hypertension,[2–4] and that mineralocorticoid receptor (MR) blockers, which inhibit the injurious effect of Ald on the kidney, contribute to a reduction in albuminuria and proteinuria in CKD patients.[5,6] MR blockers are therefore considered to play a crucial role in preventing the progression of CKD with hypertension. However, treatment with MR blockers can induce hyperkalemia, which is a concern in patients with renal dysfunction and requires caution in prescribing MR blockers for advanced CKD patients.

Ald is associated with cellular oxidative stress,[7,8] inducing both glomerular and tubulointerstitial injury in the salt-sensitive hypertension model.[9–12] As tubulointerstitial damage is strongly associated with the prognosis of CKD,[13,14] a new strategy with antioxidant activity is needed for preventing the progression of such damage due to hypertension.

Liver-type fatty acid-binding protein (L-FABP), a small protein with a molecular weight of 14 kDa, is expressed in proximal tubules of the human kidneys and has an antioxidant activity through the inactivation of free radicals by its methionine and cysteine amino acids.[15] As L-FABP is not expressed in mouse kidneys,[16] we have generated chromosomal transgenic mice in which human L-FABP was expressed in the proximal tubules by microinjecting human L-FABP genomic DNA, including its promoter region.[17] Our previous study using these mice showed that upregulated expression of human L-FABP in the proximal tubules suppressed the progression of tubulointerstitial injury through reducing oxidative stress in an Ald- and salt-induced hypertension model,[18] although this did not result in complete renoprotection. On the other hand, levels of urinary human L-FABP, one of the tubular markers, reflected the amelioration of tubulointerstitial damage by treatment with MR blockers in the model[18]

[1]Department of Anatomy, Kanagawa, Japan; [2]Department of Anatomy, St. Marianna University School of Medicine, Kanagawa, Japan and [3]JCHO Tokyo Takanawa Hospital, Tokyo, Japan
Correspondence: Dr A Kamijo-Ikemori, Department of Anatomy, 2-16-1 Sugao, Miyamae-Ku, Kawasaki 216-8511, Japan.
E-mail: a2kami@marianna-u.ac.jp
Received 30 March 2017; revised 6 July 2017; accepted 31 July 2017; published online 5 October 2017

and urinary L-FABP may be a useful marker for the evaluation of tubulointerstitial damage in the Ald- and salt-induced hypertension model.

The activation of nuclear factor erythroid 2-related factor 2 (Nrf2) has antioxidant and anti-inflammatory effects. Protective effects of Nrf2 activators have been reported for organs such as the lung, liver, gastrointestinal tract and nervous system.[19] Their renoprotective effects have been verified using Nrf2-deficient mice in, for instance, diabetic nephropathy,[20] lupus-like autoimmune nephritis[21] and ischemic reperfusion injury.[22] Bardoxolone methyl (BM), one such Nrf2 activator, has been reported in clinical practice to have a beneficial effect on the renal function of patients with type 2 diabetic nephropathy.[23] In hypertension models, Nrf2 activators were reported to be related to improvement of vascular function via antioxidant property.[24] Its effects might therefore be expected to extend to tubulointerstitial injury due to salt-sensitive hypertension.

The aim of this study was to investigate the renoprotective effect of BM through its antioxidative mechanism in an Ald- and salt-induced hypertension model under the presence of human L-FABP expression in the proximal tubules. In addition, we evaluated how the dynamics of human L-FABP in the kidneys changed with the administration of BM and the utility of urinary human L-FABP as an indicator of the renoprotective effect of BM.

METHODS

Animals

The studies were conducted in accordance with the St Marianna University School of Medicine's Institutional Guide for Animal Experiments and the Guide for the Care and Use of Laboratory Animals. Human L-FABP chromosomal transgenic mice of C57/BL6 background (L-FABP$^{+/-}$) (World Intellectual Property Organization patent WO0073791) were generated by microinjection of the genomic DNA of human L-FABP including its promoter region as described previously.[17] Therefore, it seems possible that the transcription of the human L-FABP gene in the kidneys of the L-FABP$^{+/-}$ mice may be regulated by the same mode in that of human. The experiment used 8 to 10-week-old male L-FABP$^{+/-}$ mice ($n = 25$). Surgical procedure was performed under appropriate anesthesia and animal suffering was avoided at each stage of the experiments.

Experimental design

The L-FABP$^{+/-}$ mice were divided into four groups. The Ald group ($n = 7$) received a systemic Ald infusion (0.125 μg kg^{-1} min^{-1}, A9477; Sigma-Aldrich, St Louis, MO, USA) using an osmotic minipump (Alzet 1004 for 28 days and 1007D for 7 days; Durect, Cupertino, CA, USA) and was given 1% NaCl water for 35 days. The Ald was dissolved in polyethylene glycol (PEG 300; Sigma-Aldrich Japan, Tokyo, Japan) and was infused via an implanted osmotic minipump into the subcutaneous space, while the mice were anesthetized with isoflurane. As the phase II clinical trial to determine the effect of BM (RTA402) on glomerular filtration rate in patients with type 2 diabetes and CKD (TURAKI study) has been performed in Japan, the Ald-BM group ($n = 8$) received BM (RTA 402) (AdooQ Bioscience, Irvine, CA, USA) intraperitoneally in addition to an injection of both Ald and salt. As mice in our preliminary study died when the daily dose of BM was 10 mg kg^{-1} right from the start of the study, in the present study we increased the daily dose from 1.25 to 10 mg kg^{-1} in steps every 7 days as follows: 1.25 mg kg^{-1} for 7 days, 2.5 mg kg^{-1} for 7 days, 5 mg kg^{-1} for 7 days and 10 mg kg^{-1} for 14 days. The control group ($n = 5$) was given only a vehicle and the control-BM group ($n = 5$) was given the vehicle plus the BM in the same doses as the BM group.

On day 35, blood was drawn from the inferior vena cava of all mice and the kidneys were removed while the mice were under intraperitoneal anesthesia with pentobarbital at 75 mg kg^{-1} body weight. Part of the kidney was snap-frozen in liquid nitrogen for protein and mRNA analyses, and unfixed frozen cross-sections were stained. The remainder was fixed in methyl Carnoy's solution or 10% buffered formalin (Wako Pure Chemical Industries, Osaka, Japan).

Blood pressure

Blood pressure was measured in conscious, restrained mice by using a tail-cuff apparatus (Softron BP-98A; Softron, Tokyo, Japan).[25] Systolic blood pressure (SBP) values were derived from the mean of three measurements per animal on days 0, 14 and 35.

Serum and urinary biochemistry

For urine collection on day 35, all of the mice were housed overnight individually in metallic cages with free access to 1% NaCl water or water. The sediment was removed from the urine samples by centrifugation at 15,000 r.p.m. for 5 min. Serum and urinary creatinine levels were measured by an enzymatic method (Nescoat VI. II CRE; Alfresa Pharma, Osaka, Japan).[25] Serum and urinary sodium were measured using an electrode method provided by the clinical laboratory testing services of SRL. Urinary parameters were reported as ratios relative to the urinary creatinine levels. Albuminuria was determined using the Albowell assay (Exocell, Philadelphia, PA, USA). Urinary L-FABP was measured by a two-step sandwich enzyme-linked immunosorbent assay (L-FABP ELISA kit; CMIC, Tokyo, Japan).[17]

Renal histological and morphometric analyses

For light microscopic analysis, the kidneys were dehydrated and embedded in paraffin. Serial sections 2 μm-thick were obtained for conventional histological assessment, such as periodic acid–Schiff staining and Masson's trichrome staining, and for immunohistochemistry. In the tissue sections stained with periodic acid–Schiff staining, tubular injury was categorized as tubular dilation with epithelial atrophy, brush border loss and the presence of cast. Tissue fibrosis was defined as accumulation of extracellular matrix shown in blue in Masson's trichrome staining assessed under ×100 magnification. Ten non-overlapping fields from the cortical and outer medullary areas were selected under ×100 magnification and the regions with tubular injury or fibrosis, as well as the entire cortical and outer medullary areas, were measured with WinROOF image analysis software version 6.1 (Mitani Co., Tokyo, Japan). The degrees of tubular injury and fibrosis in each region were expressed as the ratio of the area of injury or fibrosis relative to the entire area. These histological evaluations were performed in a blinded manner by one observer.

Immunohistological analysis

Tissues fixed in methyl Carnoy's solution were embedded in paraffin. An indirect immunoperoxidase method was used to identify the antigens, as described previously.[26,27] Type I and type III collagens were identified using rabbit polyclonal antibodies (Cedarlane Laboratories Ltd, Burlington, ON, Canada). Macrophages were identified using a rat monoclonal antibody against F4/80 (BMA Biomedicals, Augst, Switzerland). The primary antibodies were diluted with DAKO Antibody Diluent with Background Reducing Components (S3022, Dako Japan, Tokyo, Japan). Ten non-overlapping fields from the cortical and outer medullary areas were selected under ×100 magnification and areas positively stained for type I and type III collagens were measured with WinROOF and expressed as ratios relative to the total cortical and outer medullary areas. Similarly, the degree of macrophage infiltration in the cortical and outer medullary areas was expressed as a ratio of the area positively stained for F4/80 relative to the entire area.

Tissues fixed in formalin solution were also embedded in paraffin and Nrf2 was identified using a rabbit monoclonal antibody against Nrf2 (sc-13032X; Santa Cruz Biotechnology, Santa Cruz, CA, USA), according to the method previously described.[28] The primary antibody was diluted with DAKO Antibody Diluent with Background Reducing Components (S3022, Dako Japan). For the staining with anti-Nrf2 antibody, antigen retrieval was performed using a microwave oven to heat the slide for 15 min in PH 6.0 citric acid buffer. The degree of Nrf2 expression in the cortical and outer medullary areas was expressed as the ratio of the area positively stained for Nrf2 relative to the entire area, as for the other staining described earlier.

In situ detection of ROS production

To assess the kidneys' production of reactive oxygen species (ROS) in situ, we stained unfixed frozen cross sections from the kidneys with 5 μM dihydroethidium (DHE, Thermo Fisher Scientific, Inc., Waltham, MA, USA) for 30 min in a dark, humidified chamber at 37 °C. ROS generation was labeled with red fluorescence and visualized by fluorescence microscopy.[14,29,30] The DHE fluorescence intensities (exposure time: 200 ms) of kidney cross-sections were examined in ten nonoverlapping fields from the cortical areas and were expressed as the ratio of the positively stained area of DHE relative to the entire cortical area under ×200 magnification measured with WinROOF.

Real-time quantitative PCR analysis

Total RNA was extracted from frozen kidneys and reverse transcribed as described previously.[26,27] Real-time quantitative PCR analysis was performed using a TaqMan StepOnePlus system (Thermo Fisher Scientific) to measure the mRNA levels of Nrf2, NAD(P)H quinone oxidoreductase-1, glutathione S-transferase μ1, glutathione S-transferase α4, monocyte chemoattractant protein-1 (MCP-1), regulated on activation, normal T cell expressed and secreted (RANTES), α-1 collagen type I and type III, human L-FABP and glyceraldehyde-3-phosphate dehydrogenase. The expression levels of these transcripts in each sample were normalized to the glyceraldehyde-3-phosphate dehydrogenase expression levels.

Measurement of MCP-1 and human L-FABP by enzyme-linked immunosorbent assay

Proteins were extracted from frozen kidneys and protein concentration was measured as described previously.[25] The inflammatory cytokine MCP-1 and human L-FABP were measured using enzyme-linked immunosorbent assay (R&D Systems, Minneapolis, MN, USA for MCP-1; CMIC for human L-FABP).[22] The concentrations of MCP-1 and human L-FABP were corrected for total protein concentration.

Statistical analysis

Values are expressed as means ± s.e. Statistical significance was set at $P<0.05$. The Wilcoxon signed-rank test for paired data was used for comparisons. The four groups were analyzed by Kruskal-Wallis one-way analysis of variance followed by Mann-Whitney *U*-tests. To assess the correlation of two parameters, Spearman's rank correlation coefficient was used to evaluate nonparametric data. Analyses were performed using JMP 11.2.1 (SAS Institute, Cary, NC, USA).

RESULTS

Systolic blood pressure

SBP was similar among the four groups on day 0; by days 14 and 35, it had increased significantly in the Ald and Ald-BM groups (both $P<0.05$). In the Ald group, SBPs were significantly higher than in the control and control-BM groups on days 14 and 35 ($P<0.05$) (Figure 1). In the Ald-BM group, SBPs were significantly higher than in the control and control-BM groups on day 14 ($P<0.05$) (Figure 1). SBPs of the Ald-BM group were similar to those of the Ald group on days 14 and 35 (Figure 1).

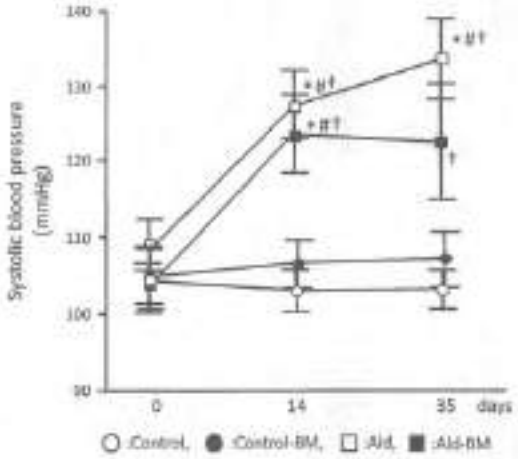

Figure 1 Time-related changes in SBP on days 0, 14 and 35. *$P<0.05$ vs the control group on the same day; #$P<0.05$ vs the control-BM group on the same day; †$P<0.05$ vs the same group on day 0. Abbreviations: Ald, aldosterone; BM, bardoxolone methyl.

Body weight and renal weight

Body weight was similar between the four groups on day 0. By day 35, body weights had significantly increased in the control and Ald groups (Table 1). Renal weights on day 35 were significantly higher in the Ald and Ald-BM groups than in the control and control-BM groups (Table 1).

Serum and urinary biochemistry

The levels of serum creatinine were similar between the four groups on day 35 (Table 1). Serum sodium level was significantly higher in the Ald-BM group than in the other groups ($P<0.05$) (Table 1). Although urinary sodium levels were significantly higher in the Ald and Ald-BM groups than in the control and control-BM groups ($P<0.05$) (Table 1), these levels were significantly higher in the Ald-BM group than in the Ald group ($P<0.05$).

By day 35, the levels of urinary albumin were significantly higher in the Ald and Ald-BM groups than in the control and control-BM groups (Figure 2). The levels in the Ald-BM group were significantly lower than those in the Ald group ($P<0.05$).

Table 1 Time-related changes in body weight, findings of renal weight, serum sodium concentration and urinary excretion of sodium on day 35.

	Body weight			*Serum*		
	Day 0 g	*Day 35 g*	*Renal weight, g*	*Creatinine, mg dl⁻¹*	*Sodium, mEq l⁻¹*	*Urinary sodium, mEq per mg Cr*
Control	25.7 ± 0.4	27.5 ± 0.3†	0.17 ± 0.01	0.30 ± 0.13	149.4 ± 1.6	0.33 ± 0.03
Control-BM	25.8 ± 0.6	25.8 ± 0.8	0.18 ± 0.01	0.19 ± 0.04	151.6 ± 1.4	0.38 ± 0.06
Ald	25.8 ± 0.3	29.0 ± 0.7†	0.24 ± 0.01*,#	0.22 ± 0.03	154.4 ± 1.7	2.84 ± 0.46*,#
Ald-BM	24.8 ± 0.4	26.3 ± 1.2	0.25 ± 0.01*,#	0.20 ± 0.07	161.9 ± 2.1*,#,§	1.37 ± 0.29*,#,§

Abbreviations: Ald, aldosterone; BM, bardoxolone methyl; Cr, creatinine.
Values are means ± s.e.
*$P<0.05$ vs the control group on the same day; #$P<0.05$ vs the control-BM group on the same day; †$P<0.05$ vs the same group on day 0; §$P<0.05$ vs the Ald-BM group on the same day.

Gene expressions of Nrf2 and Nrf2 target antioxidant genes, and the immunohistological analysis for Nrf2

The mRNA levels of Nrf2 were significantly lower in the control-BM and Ald-BM groups than in the control and Ald groups (Figure 3a). The levels in the Ald and control groups were similar.

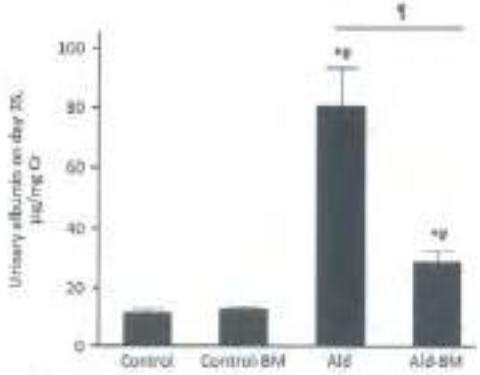

Figure 2 Urinary albumin excretion on day 35. Values are mean ± s.e. *$P<0.05$ vs the control group; #$P<0.05$ vs the control-BM group; ¶$P<0.05$ vs the Ald group. Abbreviations: Ald, aldosterone; BM, Bardoxolone methyl.

The mRNA expressions of the Nrf2 target antioxidant genes (NAD(P)H quinone oxidoreductase-1, glutathione *S*-transferase μ1 and glutathione *S*-transferase α4) were significantly higher in the control-BM and Ald-BM groups than in the control and Ald groups (Figures 3b–d). The levels in the Ald-BM and control-BM groups were similar.

The expression of Nrf2 was observed in the nucleus and cytoplasm of the tubular cells (Figure 3e). The degree of Nrf2 positive area tended to be higher in the Ald-BM group than in the Ald group ($P=0.15$, Figure 3f) and in the control-BM group than in the control group ($P=0.06$).

Renal expression of MCP-1 and immunohistological analysis for macrophage infiltration

The gene (Figure 4a) and protein (Figure 4b) expression levels of MCP-1 in the kidneys were significantly higher in the Ald and Ald-BM groups than in the control and control-BM groups. The renal expressions of MCP-1 were significantly lower in the Ald group than in the Ald-BM group (Figures 4a and b).

The levels of macrophage infiltration were significantly higher in the Ald group than in the control and control-BM groups, and significantly higher in the Ald-BM group than in the control-BM group (Figures 4c and d). The levels in the Ald-BM group were significantly lower compared with those in the Ald group (Figures 4c and d).

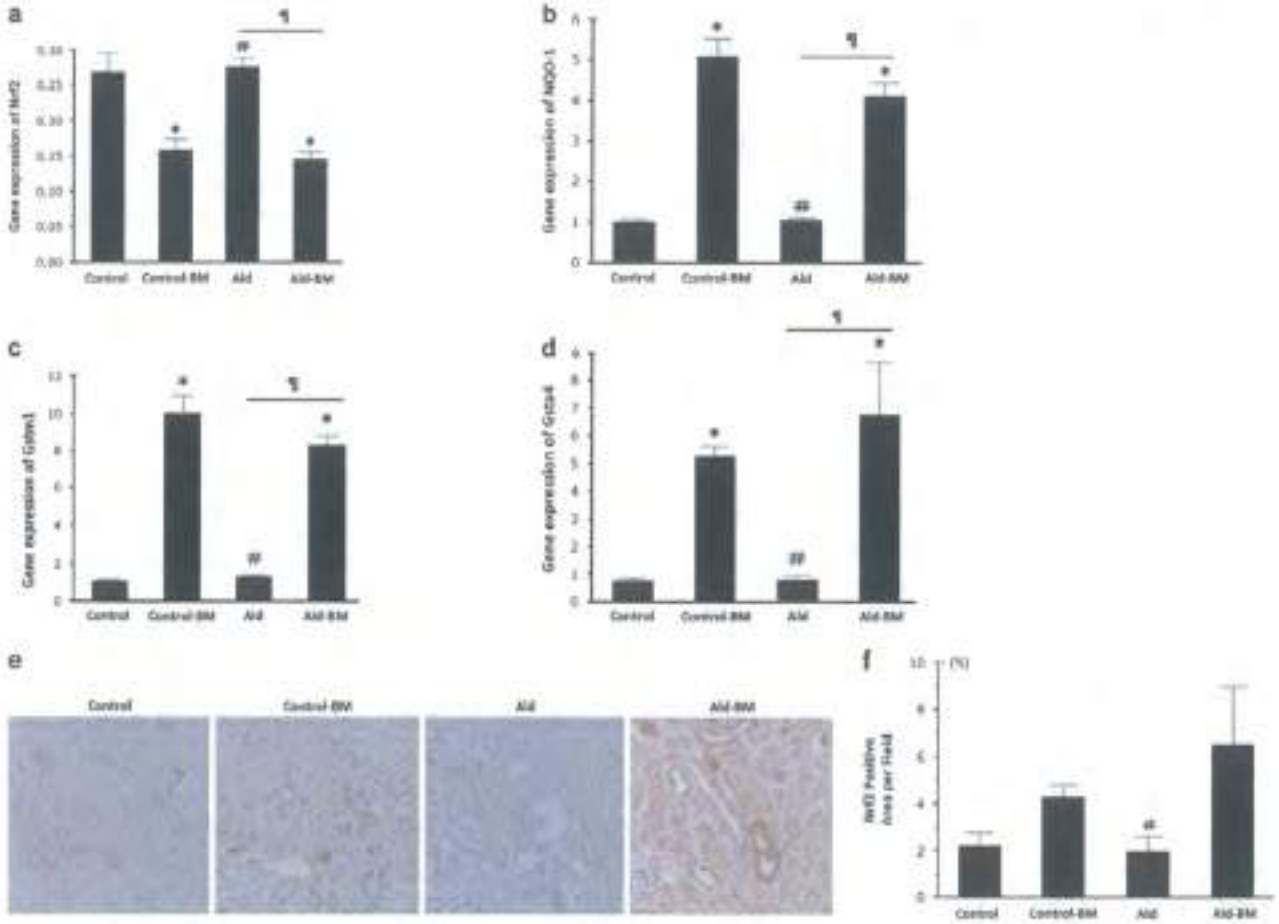

Figure 3 mRNA transcript expression of Nrf2 (a) and the Nrf2 target antioxidant genes *NQO-1* (b), *Gstm1* (c) and *Gsta4* (d). Immunohistological staining for Nrf2 (e) and positively stained areas were assessed quantitatively (f). Original magnification, ×100. *$P<0.05$ vs the control group; #$P<0.05$ vs the control-BM group; ¶$P<0.05$ vs the Ald group. Abbreviations: Ald, aldosterone; BM, bardoxolone methyl; Gsta4, glutathione *S*-transferase α4; Gstm1, glutathione *S*-transferase μ1; Nrf2, nuclear factor erythroid 2-related factor 2; NQO-1, NAD(P)H quinone oxidoreductase-1.

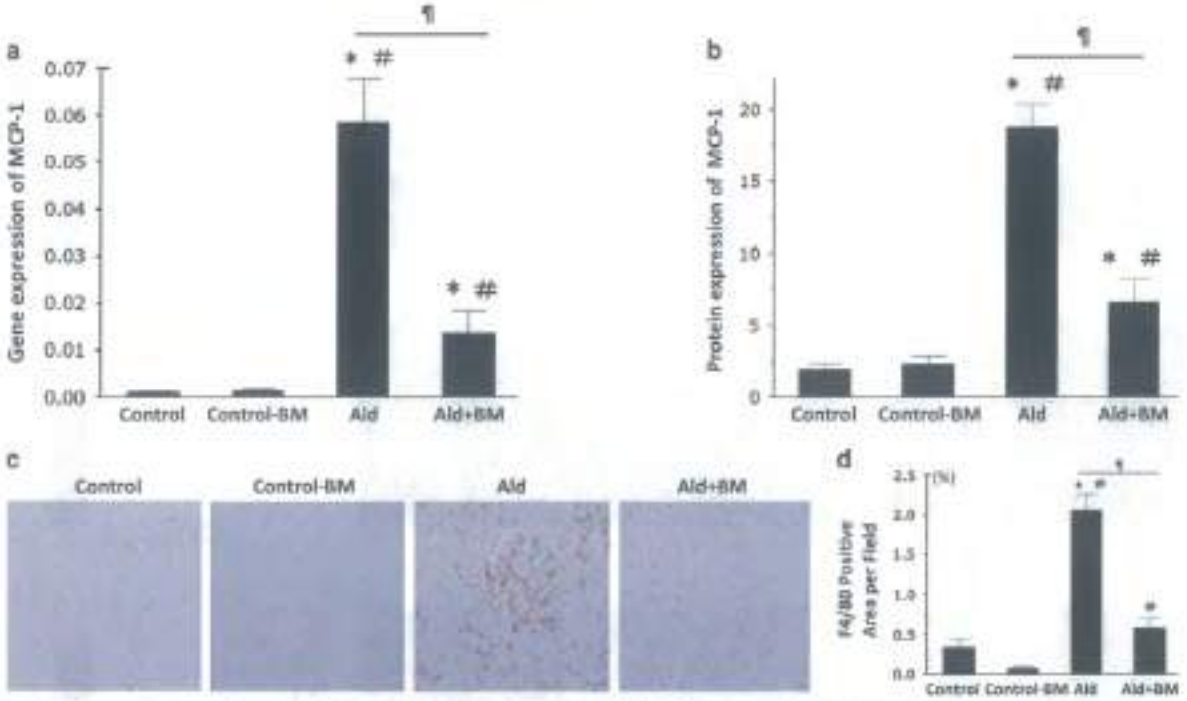

Figure 4 mRNA transcript expression of MCP-1 (a) and the protein expression of MCP-1 (b). Immunohistological staining for macrophages using an antibody against F4/80 (c) and the positively stained areas were assessed quantitatively (d). Original magnification, ×100. *$P<0.05$ vs the control group; #$P<0.05$ vs the control-BM group; ¶$P<0.05$ vs the Ald group. Abbreviations: Ald, aldosterone; BM, bardoxolone methyl; MCP-1, monocyte chemoattractant protein-1.

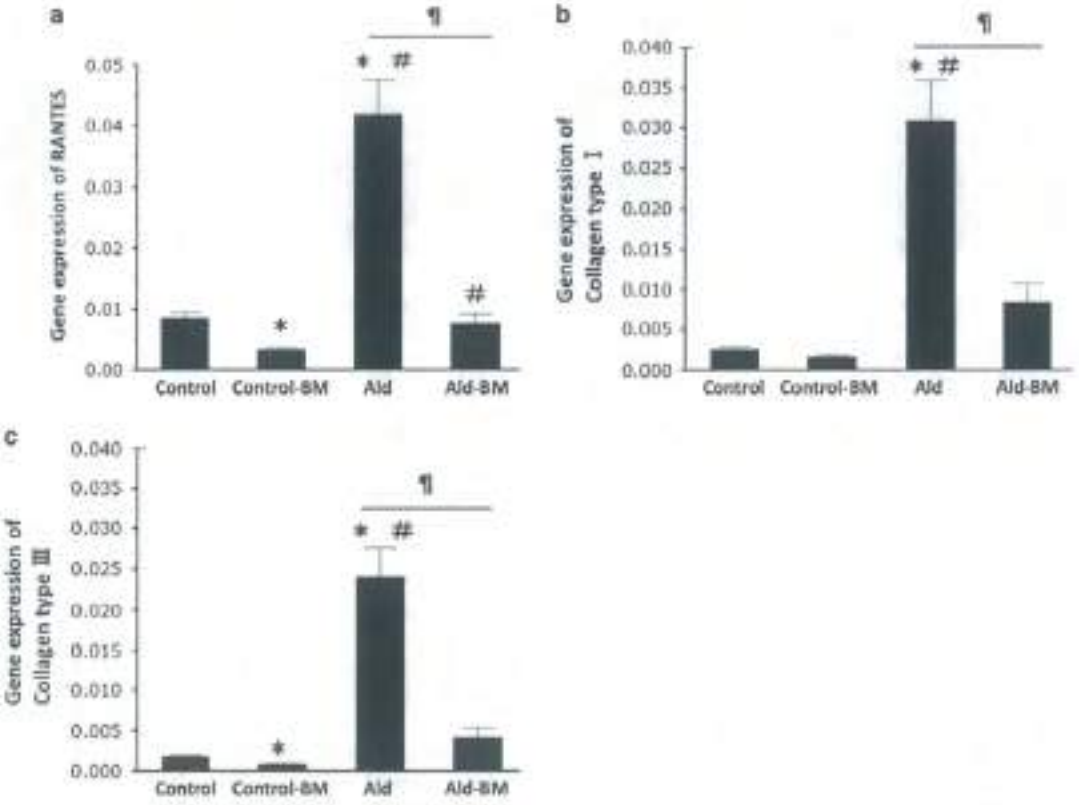

Figure 5 mRNA transcript expression of RANTES (a), α-1 collagen type α (b) and α-1 collagen type β (c). *$P<0.05$ vs the control group; #$P<0.05$ vs the control-BM group; ¶$P<0.05$ vs the Ald group. Abbreviations: Ald, aldosterone; BM, bardoxolone methyl; RANTES, regulated on activation, normal T cell expressed and secreted.

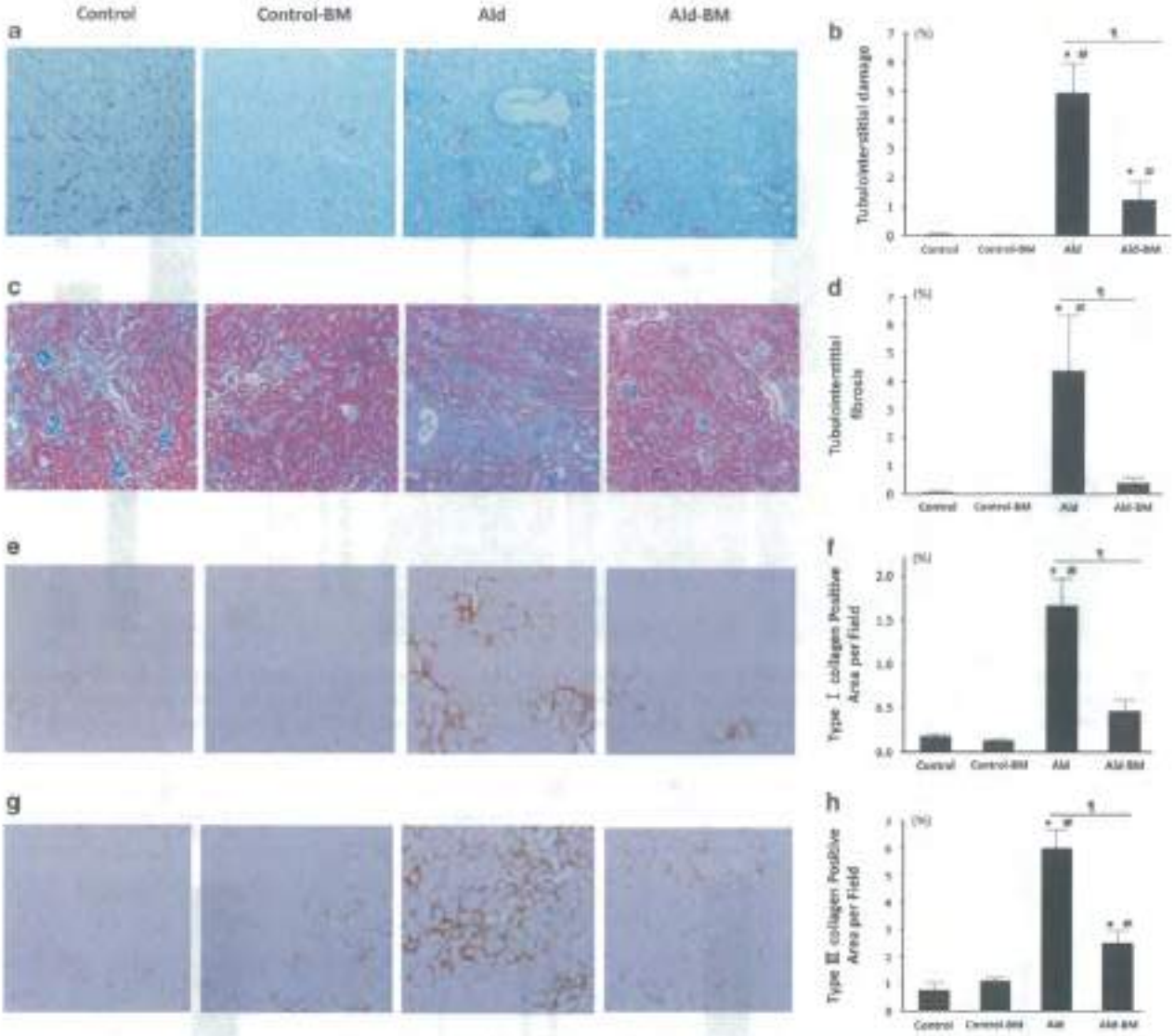

Figure 6 Histological analyses for tubular damage stained with periodic acid–Schiff (PAS) (a). Tubular damage was assessed quantitatively in PAS-stained sections (b). Tubulointerstitial fibrosis was stained with Masson Trichrome stain (c) and assessed quantitatively (d). Immunohistological staining for type α collagen (e) and type β collagen (g); the positively stained areas were assessed quantitatively (f and h). Original magnification, ×100. Values are mean ± s.e. *$P<0.05$ vs the control group; #$P<0.05$ vs the control-BM group; ¶$P<0.05$ vs the Ald group. Abbreviations: Ald, aldosterone; BM, bardoxolone methyl.

Gene expressions of RANTES and type I and III collagens in the kidney

The mRNA level of RANTES was measured to evaluate the inflammatory response. The level was significantly higher in the Ald group than in the control and control-BM groups (Figure 5a), and in the Ald-BM than in the control-BM group. The increase in RANTES level in the Ald group was significantly ameliorated in the Ald-BM group. The gene expression of RANTES was significantly lower in the control-BM group than in the control group.

The levels of α-1 collagen type I and type III were measured to evaluate interstitium fibrosis. In the Ald group, the mRNA expressions of α-1 collagen type I (Figure 5b) and type III (Figure 5c) were significantly higher than in the control and control-BM groups. Their expressions were significantly lower in the Ald-BM group than in the Ald group and the mRNA level of α-1 collagen type III was significantly lower in the control-BM group than in the control group.

Renal histological and morphometric analyses

Although tubular damage as assessed by periodic acid–Schiff staining staining was significantly more severe in the Ald and Ald-BM groups than in the control and control-BM groups, it was significantly attenuated in the Ald-BM group compared with the Ald group ($P<0.05$, Figures 6a and b). The tubulointerstitial fibrosis as assessed by Masson's trichrome staining was significantly more severe in the Ald group than in the control and control-BM groups, and was significantly attenuated in the Ald-BM group ($P<0.05$, Figures 6c and d).

Immunohistological analysis for type I and III collagens

Areas of type I and III collagen deposition were observed in the interstitium (Figures 6e and g). The areas positively stained for type I (Figure 6f) and type III (Figure 6h) collagens were significantly higher ($P<0.05$) in the Ald group than in the control and control-BM

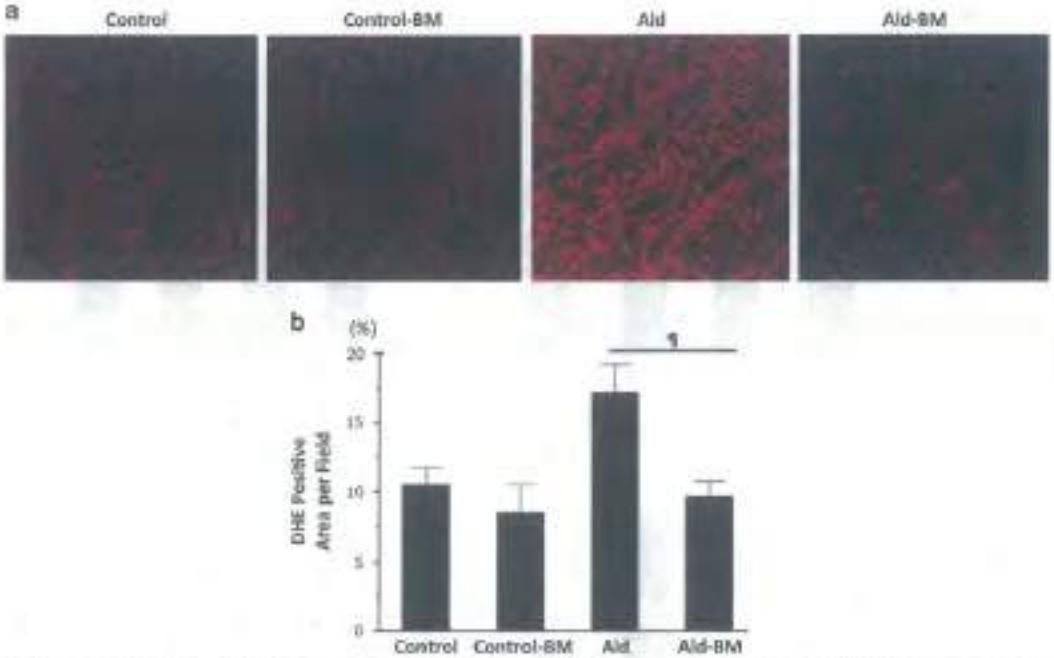

Figure 7 Immunofluorescent staining for DHE (a). The positively stained areas of DHE were assessed quantitatively (b). Values are mean ± s.e. *$P<0.05$ vs the control group; #$P<0.05$ vs the control-BM group; ¶$P<0.05$ vs the Ald group. Abbreviations: Ald, aldosterone; BM, bardoxolone methyl; DHE, dihydroethidium.

groups. Their deposition areas were significantly lower in the Ald-BM group compared with the Ald group, although the type III collagen deposition area was significantly higher in the Ald-BM group than in the control and control-BM groups.

Evaluation of oxidative stress

DHE staining was applied to the kidney sections to evaluate ROS production. DHE fluorescence tended to be greater in the Ald group than in the control group and was significantly lower in the Ald-BM group ($P<0.05$, Figures 7a and b).

Gene and protein expressions in the kidneys and urinary excretion of human L-FABP

The mRNA levels of human L-FABP in the kidneys were significantly higher in the Ald group than in the control and control-BM groups and significantly lower in the Ald-BM group than in the Ald group. Furthermore, the levels in the Ald-BM group were significantly lower than in the control and control-BM groups (Figure 8a). The protein expressions of human L-FABP in the kidneys were significantly higher in the Ald group than in the control group, and significantly lower in the Ald-BM group (Figure 8b). Urinary human L-FABP levels on day 35 were significantly higher in the Ald group than in the control and control-BM groups and significantly higher in the Ald-BM group than in the control group (Figure 8c). The levels were significantly lower in the Ald-BM group than in the Ald group ($P<0.05$).

Correlation between urinary L-FABP and the degree of tubulointerstitial damage on day 35

Urinary L-FABP levels significantly correlated with the degree of tubulointerstitial damage as assessed by periodic acid–Schiff staining staining, infiltration of macrophage as evaluated using an antibody against F4/80 and tubulointerstitial fibrosis as indicated using antibodies against both type I and type III collagens (Figure 9).

DISCUSSION

This study revealed that administration of the Nrf2 activator BM attenuated the renal oxidative stress, excessive activation of the intrarenal RAS, inflammation and tubulointerstitial damage induced by both Ald and salt. Furthermore, the dynamics of human L-FABP changed with the administration of BM, with urinary human L-FABP levels reflecting the other changes caused by the BM.

Administering BM reduced the renal gene expression of Nrf2 in the present study. The BM bound to cysteine residues of Keap1 and leaded to conformational changes in Keap1 disrupting the interaction between Nrf2 and Keap1, resulting in inhibiting the degradation of the Nrf2 by polyubiquitination.[31,32] We considered that because the renal Nrf2 protein expression was maintained at a higher level by BM, the mRNA expression of Nrf2 was suppressed. Therefore, the BM enhanced the renal expressions of the Nrf2 target antioxidant genes, which led to the suppression of ROS production as evaluated by DHE fluorescence and subsequently to significant attenuation of the tubulointerstitial damage induced by both Ald and salt (Figure 10).

We have previously reported a study of human L-FABP chromosomal transgenic mice in an Ald- and salt-induced hypertension model, which showed human L-FABP was upregulated in the proximal tubules and attenuated tubulointerstitial damage via antioxidative action, as compared to the wild-type mice without L-FABP expression in their proximal tubules.[18] Although the duration of Ald-injection was longer in the present study (5 weeks) than in the previous study (4 weeks),[18] the present study also demonstrated the upregulation of renal human L-FABP with Ald and salt, and that administration of BM suppressed this upregulation in the FABP$^{+/-}$ mice. These results suggest that BM exhibited antioxidative action in human proximal tubules with L-FABP expression and may retard the progression of tubulointerstitial damage in clinical practice.

The present study demonstrated that systemic Nrf2 activation due to a chemical inducer of Nrf2 ameliorated tubulointerstitial damage in

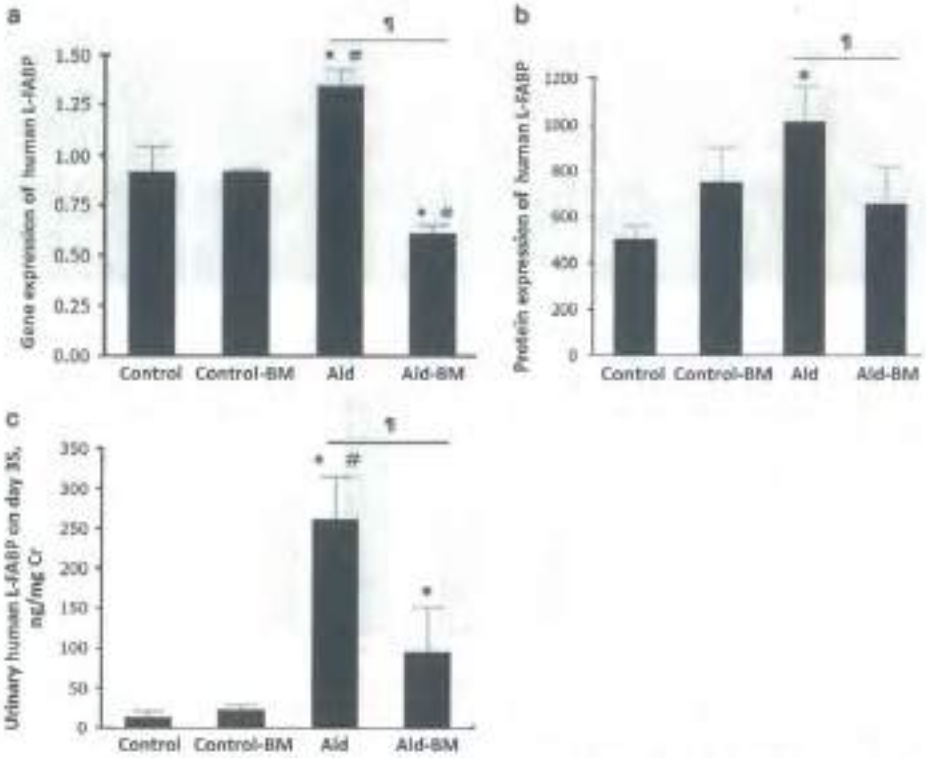

Figure 8 mRNA transcript expression (a) and protein expression (b) of human L-FABP. Urinary excretion of human L-FABP on day 35 (c). Values are mean ± s.e. *$P<0.05$ vs the control group; #$P<0.05$ vs the control-BM group; ¶$P<0.05$ vs the Ald group. Abbreviations: Ald, aldosterone; BM, bardoxolone methyl; L-FABP, liver-type fatty acid-binding protein.

the Ald- and salt-induced hypertension model. The kidney is composed of various types of cells and pharmacological Nrf2 activation has been reported to work on glomerular mesangial cells[23] in addition to the tubules. Although significant glomerular damage was not induced in the Ald- and salt-induced hypertension mouse model[18] and this study did not show an increase in the Nrf2 protein expression in the glomeruli (data not shown), it is possible that the increase in Nrf2 target antioxidant in these cells due to the BM influenced the improvement to the tubulointerstitial damage observed in the Ald-BM mice. To clarify this point requires a genetic approach with cell-specific Nrf2 deletion mice.

In the present study, SBP on day 35 tended to be lower in the Ald-BM mice than in the Ald mice, suggesting the possibility that BM influenced SBP. Some studies have reported that Nrf2 activators attenuate blood pressure elevation in hypertension models[34,35] via regulation of myogenic tone due to increased expression of Nrf2-regulated antioxidant genes in vascular smooth muscle.[24] As vascular Nrf2-antioxidant system may exert vasoprotective effects in hypertension-associated vascular changes induced by increased vascular oxidative stress, the effects of the BM may be related to the decrease in SBP by BM in the Ald- and salt-induced model. Although decrease in blood pressure is reported not to lead to attenuation of renal injury and reduction of oxidative stress in the Ald- and salt- induced renal injury model,[18,36] such vasoprotective actions of BM may be useful for the improvement of vascular function in hypertension.

In contrast to the renoprotective effect of BM, a pathogenic role of Nrf2 in inflammasome activation has been reported.[37,38] Freigang *et al.*[37] reported that an Nrf2 activator was a positive regulator of the inflammasome and enhanced interleukin-1-mediated vascular inflammation. Zhao *et al.*[38] also reported that Nrf2 mediated inflammasome activation, leading to an increase in inflammatory response. Administration of an initial daily dose of BM of 10 mg kg^{-1} induced high mouse mortality in our preliminary study. A clinical study of treatment with BM for stage 4 CKD patients with diabetes mellitus showed that it significantly increased the risk of heart failure and of a composite cardiovascular outcome (nonfatal myocardial infarction, nonfatal stroke, hospitalization for heart failure or death from cardiovascular causes).[39] Zoja *et al.*[40] demonstrated the divergent result of Nrf2 activator RTA405, a synthetic triterpenoid analog of BM, against renoprotective effect using Zucker diabetic fatty rats.[40] Furthermore, they also showed acute liver toxicity of RTA405 in the diabetic rats. As the roles of Nrf2 and Nrf2 activators differ between various pathophysiological conditions, further studies are needed to examine the utility of BM for each disease and severity of disease to establish when it can be applied in clinical practice.

Urinary human L-FABP is a tubular marker that accurately reflects the degree of tubulointerstitial damage and has the potential to predict prognosis in CKD.[17,41] In a clinical study of BM, urinary albumin did not change in line with the treatment effect of BM;[22] it was speculated that BM reduced the expression of megalin in the proximal tubules, and that this was related to reabsorbing the albumin filtered through glomeruli.[42] In the present study, urinary L-FABP levels significantly correlated with the degree of tubulointerstitial damage. Although urinary albumin levels decreased in response to the administration of BM and this study did not demonstrate the superiority of urinary human L-FABP over urinary albumin for evaluating the renoprotective effect of BM, urinary L-FABP may be useful for determining the effect of BM in clinical practice.

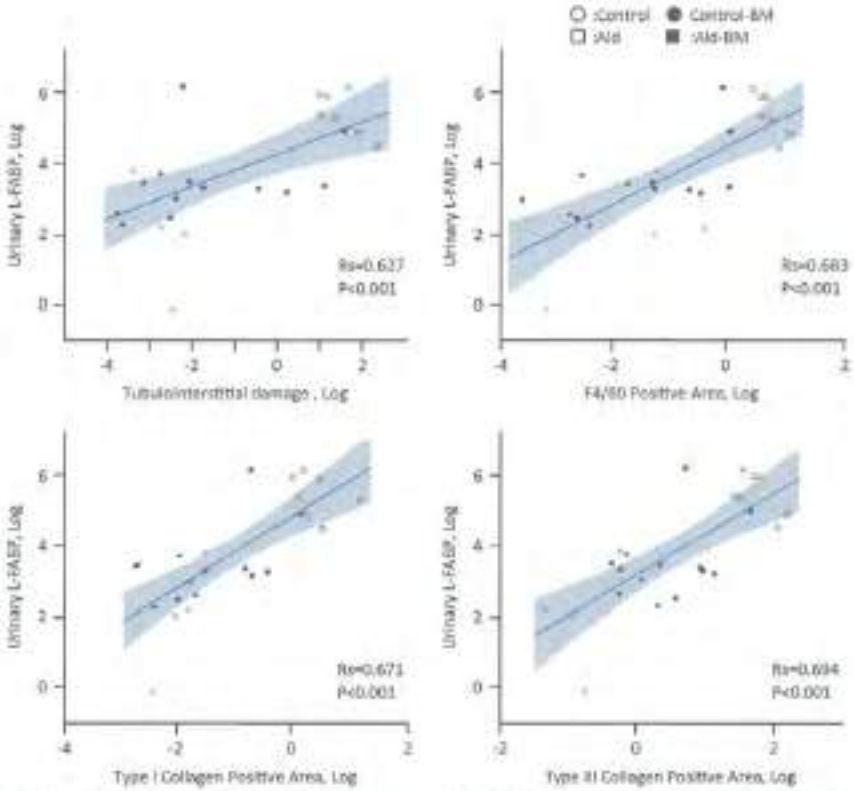

Figure 9 Correlations between urinary L-FABP and each histological marker on day 35. White circle (○) shows control group, black circle (●) shows control-BM group, white square (□) shows Ald group and black square (■) shows Ald-BM group. Abbreviations: Ald, aldosterone; BM, bardoxolone methyl; L-FABP, liver-type fatty acid-binding protein.

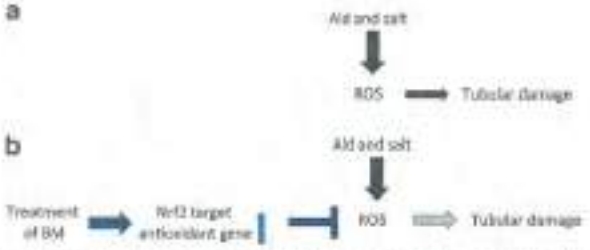

Figure 10 Mechanism for renal tubular damage in the Ald- and salt-induced hypertension model. Reactive oxygen species (ROS) produced by the Ald and salt in the proximal tubules leads to the progression of tubular damage (a). Treatment with BM upregulates the renal expression of the Nrf2 target antioxidant genes and suppresses ROS production, resulting in the attenuation of the tubular damage induced by the Ald and salt (b). Abbreviations: Ald, aldosterone; BM, bardoxolone methyl; Nrf2, nuclear factor erythroid 2-related factor 2.

There is a critical limitation in this study. As urinary sodium levels were significantly lower in the Ald-BM group than in the Ald group, there is a possibility that 1% NaCl water intake in the Ald-BM group significantly decreased compared with that in the Ald group, which may be related to renoprotection in the Ald-BM group. Zoja *et al.*[40] also reported that BM analog RTA405 caused decreases in food intake and diuresis in rats with diabetic nephropathy. However, because severe tubulointerstitial damage causes a decrease in the reabsorption of urinary sodium, suppression of tubulointerstitial damage in the Ald-BM group may lead to the decrease in urinary excretion of sodium. In fact, serum sodium concentration in the Ald-BM group was higher than that in the Ald group. Further studies are needed to clarify this point.

In conclusion, this study showed that treatment with BM suppressed the progression of tubulointerstitial damage in Ald- and salt-induced hypertension under the expression of human L-FABP in the proximal tubules. Recent clinical studies in hypertensive CKD have reported RAS inhibitors to have only a limited effect on the suppression of renal dysfunction[43] and BM may be expected to be part of a new strategy for preventing tubulointerstitial damage due to salt-sensitive hypertension. Furthermore, urinary L-FABP is a useful tubular marker that reflects the renoprotective effect of BM.

CONFLICT OF INTEREST

TS is the director and senior scientist of CMIC HOLDINGS Co., Ltd., the company that produced the kits for L-FABP analysis. All other authors declare no conflicts of interest.

ACKNOWLEDGEMENTS

We thank Ms. Kimie Katayama, Ms. Jyunko Asano and Mr. Kazuho Inoue for technical assistance. This research did not receive any specific grant from funding agencies in the public, commercial or not-for-profit sectors.

1 Fujita T. Mineralocorticoid receptors, salt-sensitive hypertension, and metabolic syndrome. *Hypertension* 2010; **55**: 813–818.
2 Blasi ER, Rocha R, Rudolph AE, Blomme EA, Polly ML, McMahon EG. Aldosterone/salt induces renal inflammation and fibrosis in hypertensive rats. *Kidney Int* 2003; **63**: 1791–1800.

3 Kawanazaki W, Nagase M, Yoshida S, Takeuchi M, Ishizawa K, Ayoboe K, Ueda K, Fujita T. Angiotensin II- and salt-induced kidney injury through Rac1-mediated mineralocorticoid receptor activation. *J Am Soc Nephrol* 2012; **23**: 997–1007.
4 Nagase M, Shibata S, Yoshida S, Nagase T, Gotoda T, Fujita T. Podocyte injury underlies the glomerulopathy of Dahl salt-hypertensive rats and is reversed by aldosterone blocker. *Hypertension* 2006; **47**: 1084–1093.
5 Ando K, Ohtsu H, Uchida S, Kanamu S, Arakawa Y, Fujita T, Group ES: Anti-albuminuric effect of the aldosterone blocker eplerenone in non-diabetic hypertensive patients with albuminuria a double-blind, randomized, placebo-controlled trial. *Lancet Diabetes Endocrinol* 2014; **2**: 944–953.
6 Navaneethan SD, Nigwekar SU, Sehgal AR, Strippoli GF. Aldosterone antagonists for preventing the progression of chronic kidney disease: a systematic review and meta-analysis. *Clin J Am Soc Nephrol* 2009; **4**: 542–551.
7 Iida J, Okura T, Jotsiku M, Nagao T, Enomoto D, Kurata M, Deslia VR, Miyoshi K, Matsui Y, Ueda T, Danhardt DT, Kitlling SR, Higaki J. Osteopontin deficiency protects against aldosterone-induced inflammation, oxidative stress, and interstitial fibrosis in the kidney. *Am J Physiol Renal Physiol* 2011; **301**: F833–F844.
8 Nagase M, Fujita T. Role of Rac1-mineralocorticoid-receptor signalling in renal and cardiac disease. *Nat Rev Nephrol* 2013; **9**: 86–98.
9 Kiyomoto H, Rafiq K, Mostofa M, Nishiyama A. Possible underlying mechanisms responsible for aldosterone and mineralocorticoid receptor-dependent renal injury. *J Pharm Sci* 2008; **108**: 399–405.
10 Nishiyama A, Yao L, Nagai Y, Miyata K, Yoshizumi M, Kagami S, Kondo S, Kiyomoto H, Shokoji T, Kimura S, Kohno M, Abe Y. Possible contributions of reactive oxygen species and mitogen-activated protein kinase to renal injury in aldosterone/salt-induced hypertensive rats. *Hypertension* 2004; **43**: 841–848.
11 Shibata S, Nagase M, Yoshida S, Kawachi H, Fujita T. Podocyte as the target for aldosterone: roles of oxidative stress and Sgk1. *Hypertension* 2007; **49**: 355–364.
12 Sun GP, Kohno M, Guo P, Nagai Y, Miyata K, Fan YY, Kimura S, Kiyomoto H, Ohmori K, Li DT, Abe Y, Nishiyama A. Involvements of Rho-kinase and TGF-beta pathways in aldosterone-induced renal injury. *J Am Soc Nephrol* 2006; **17**: 2193–2201.
13 Prunotto M, Budd DC, Gabbiani G, Meier M, Formentini I, Hartmann G, Porpopiello S, Moll S. Epithelial-mesenchymal crosstalk alteration in kidney fibrosis. *J Pathol* 2012; **228**: 131–147.
14 Remuzzi G, Bertani T. Pathophysiology of progressive nephropathies. *N Engl J Med* 1998; **339**: 1448–1456.
15 Yan J, Gong Y, She YM, Wang G, Roberts MS, Burczynski FJ. Molecular mechanism of recombinant liver fatty acid binding protein's antioxidant activity. *J Lipid Res* 2009; **50**: 2445–2454.
16 Simon TC, Roth KA, Gordon JI. Use of transgenic mice to map cis-acting elements in the liver fatty acid-binding protein gene (Fabp1) that regulate its cell lineage-specific, differentiation-dependent, and spatial patterns of expression in the gut epithelium and in the liver acinus. *J Biol Chem* 1993; **268**: 18345–18358.
17 Kamijo A, Sugaya T, Hikawa A, Okada M, Okumura F, Yamanouchi M, Hondo A, Okabe M, Fujino T, Hirata Y, Omata M, Kaneko R, Fujii H, Fukamizu A, Kimura K. Urinary excretion of fatty acid-binding protein reflects stress overload on the proximal tubules. *Am J Pathol* 2004; **165**: 1243–1255.
18 Ichikawa D, Kamijo-Ikemori A, Sugaya T, Shibagaki Y, Yasuda T, Hoshino S, Katayama K, Igarashi-Migitaka J, Hirata K, Kimura K. Human liver-type fatty acid-binding protein protects against tubulointerstitial injury in aldosterone-induced renal injury. *Am J Physiol Renal Physiol* 2015; **308**: F114–F121.
19 Lee JM, Li J, Johnson DA, Stein TD, Kraft AD, Calkins MJ, Jakel RJ, Johnson JA. Nrf2, a multi-organ protector? *FASEB J* 2005; **19**: 1061–1066.
20 Yoh K, Hirayama A, Ishizaki K, Yamada A, Takeuchi M, Yamagishi S, Morito N, Nakano T, Ojima M, Shimohata H, Itoh K, Takahashi S, Yamamoto M. Hyperglycemia induces oxidative and nitrosative stress and increases renal functional impairment in Nrf2-deficient mice. *Genes Cells* 2008; **13**: 1159–1170.
21 Yoh K, Itoh K, Enomoto A, Hirayama A, Yamaguchi N, Kobayashi M, Morito N, Koyama A, Yamamoto M, Takahashi S. Nrf2-deficient female mice develop lupus-like autoimmune nephritis. *Kidney Int* 2001; **60**: 1343–1353.
22 Nezu M, Souma T, Yu L, Suzuki T, Saigusa D, Ito S, Suzuki N, Yamamoto M. Transcription factor Nrf2 hyperactivation in early-phase renal ischemia-reperfusion injury prevents tubular damage progression. *Kidney Int* 2017; **91**: 387–401.
23 Pergola PE, Raskin P, Toto RD, Meyer CJ, Huff JW, Grossman EB, Krauth M, Ruiz S, Audhya P, Christ-Schmidt H, Wittes J, Warnock DG(Investigators BS. Bardoxolone methyl and kidney function in CKD with type 2 diabetes. *N Engl J Med* 2011; **365**: 327–336.
24 Lopes RA, Neves KB, Tostes RC, Montezano AC, Touyz RM. Downregulation of nuclear factor erythroid 2-related factor and associated antioxidant genes contributes to redox-sensitive vascular dysfunction in hypertension. *Hypertension* 2015; **66**: 1240–1250.
25 Ichikawa D, Kamijo-Ikemori A, Sugaya T, Yasuda T, Hoshino S, Igarashi-Migitaka J, Hirata K, Kimura K. Renal liver-type fatty acid binding protein attenuates angiotensin II-induced renal injury. *Hypertension* 2012; **60**: 973–980.
26 Matsui K, Kamijo-Ikemori A, Sugaya T, Yasuda T, Kimura K. Renal liver-type fatty acid binding protein (L-FABP) attenuates acute kidney injury in aristolochic acid nephrotoxicity. *Am J Pathol* 2011; **178**: 1021–1032.
27 Yokoyama T, Kamijo-Ikemori A, Sugaya T, Hoshino S, Yasuda T, Kimura K. Urinary excretion of liver type fatty acid binding protein accurately reflects the degree of tubulointerstitial damage. *Am J Pathol* 2009; **174**: 2096–2106.
28 Inoue D, Suzuki T, Mitsuishi Y, Miki Y, Suzuki S, Sugawara S, Watanabe M, Sakurada A, Endo C, Uruno A, Sasano H, Nakagawa T, Satoh K, Tanaka N, Kubo H, Motohashi H, Yamamoto M. Accumulation of p62/SQSTM1 is associated with poor prognosis in patients with lung adenocarcinoma. *Cancer Sci* 2012; **103**: 760–766.
29 Ichikawa D, Kamijo-Ikemori A, Sugaya T, Shibagaki Y, Yasuda T, Katayama K, Hoshino S, Igarashi-Migitaka J, Hirata K, Kimura K. Renoprotective effect of renal liver-type fatty acid binding protein and angiotensin II type 1a receptor loss in renal injury caused by RAS activation. *Am J Physiol Renal Physiol* 2014; **306**: F655–F663.
30 Lopez-Parra V, Mallavia B, Lopez-Franco O, Ortiz-Munoz G, Ogaiza A, Recio C, Blanco J, Nimmerjahn F, Egido J, Gomez-Guerrero C. Fcgamma receptor deficiency attenuates diabetic nephropathy. *J Am Soc Nephrol* 2012; **23**: 1518–1527.
31 Spom MB, Liby KT, Yore MM, Fu L, Lopchuk JM, Gribble GW. New synthetic triterpenoids: potent agents for prevention and treatment of tissue injury caused by inflammatory and oxidative stress. *J Nat Prod* 2011; **74**: 537–545.
32 Yates MS, Tauchi M, Katsuoka F, Flanders KC, Liby KT, Honda T, Gribble GW, Johnson DA, Johnson JA, Burton NC, Guilarte TR, Yamamoto M, Sporn MB, Kensler TW. Pharmacodynamic characterization of chemopreventive triterpenoids as exceptionally potent inducers of Nrf2-regulated genes. *Mol Cancer Ther* 2007; **6**: 154–162.
33 Ding Y, Stidham RD, Bumenker R, Trevino I, Winters A, Spruce M, Ding M, Ferguson DA, Meyer CJ, Wigley WC, Ma R. The synthetic triterpenoid, RTA 405, increases the glomerular filtration rate and reduces angiotensin II-induced contraction of glomerular mesangial cells. *Kidney Int* 2013; **83**: 845–854.
34 Senanayake GV, Banigesh A, Wu L, Lee P, Juurlink BH. The dietary phase 2 protein inducer sulforaphane can normalize the kidney epigenome and improve blood pressure in hypertensive rats. *Amoumal J Hypertens* 2012; **25**: 229–235.
35 Wu L, Noyan Ashraf MH, Facci M, Wang R, Paterson PG, Ferrie A, Juurlink BH. Dietary approach to attenuate oxidative stress, hypertension, and inflammation in the cardiovascular system. *Proc Natl Acad Sci U84* 2004; **101**: 7094–7099.
36 Sawada H, Naito Y, Oboshi M, Iwasaku T, Okuhara Y, Morisawa D, Eguchi A, Hirotani S, Masuyama T. Iron restriction inhibits renal injury in aldosterone/salt-induced hypertensive mice. *Hypertens Res* 2015; **38**: 317–322.
37 Freigang S, Ampenberger F, Spohn G, Heer S, Shamshiev AT, Kisielow J, Hersberger M, Yamamoto M, Bachmann MF, Kopf M. Nrf2 is essential for cholesterol crystal-induced inflammasome activation and exacerbation of atherosclerosis. *Eur J Immunol* 2011; **41**: 2040–2051.
38 Zhao C, Gillette DD, Li X, Zhong Z, Wen H. Nuclear factor E2-related factor-2 (Nrf2) is required for NLRP3 and AIM2 inflammasome activation. *J Biol Chem* 2014; **289**: 17020–17029.
39 deZeeuw D, Akizawa T, Audhya P, Bakris GL, Chin M, Christ-Schmidt H, Goldsberry A, Houser M, Krauth M, Lambers Heerspink HJ, McMurray JJ, Meyer CJ, Parving HH, Remuzzi G, Toto RD, Vaziri ND, Wanner C, Wittes J, Wrolstad D, Chertow GM, Investigators BT. Bardoxolone methyl in type 2 diabetes and stage 4 chronic kidney disease. *N Engl J Med* 2013; **369**: 2492–2503.
40 Zoja C, Corna D, Nava V, Locchetti M, Abbate M, Gaspari F, Carrera F, Sangalli F, Remuzzi G, Benigni A. Analogs of bardoxolone methyl worsen diabetic nephropathy in rats with additional adverse effects. *Am J Physiol Renal Physiol* 2013; **304**: F808–F819.
41 Kamijo A, Kimura K, Sugaya T, Yamanouchi M, Hikawa A, Hirano N, Hirata Y, Goto A, Omata M. Urinary fatty acid-binding protein as a new clinical marker of the progression of chronic renal disease. *J Lab Clin Med* 2004; **143**: 23–30.
42 Reisman SA, Chertow GM, Hebbar S, Vaziri ND, Ward KW, Meyer CJ. Bardoxolone methyl decreases megalin and activates nrf2 in the kidney. *J Am Soc Nephrol* 2012; **23**: 1663–1673.
43 Appel LJ, Wright JT Jr, Greene T, Kusek JW, Lewis JB, Wang X, Lipkowitz MS, Norris KC, Bakris GL, Rahman M, Costerse G, Rostand SG, Kopple JD, Gabbai FB, Schulman G, Gassman JJ, Charleston J, Agodoa LY, African American Study of Kidney D, Hypertension Collaborative Research G. Long-term effects of renin-angiotensin system-blocking therapy and a low blood pressure goal on progression of hypertensive chronic kidney disease in African Americans. *Arch Intern Med* 2008; **168**: 832–839.

This work is licensed under a Creative Commons Attribution-NonCommercial-NoDerivs 4.0 International License. The images or other third party material in this article are included in the article's Creative Commons license, unless indicated otherwise in the credit line; if the material is not included under the Creative Commons license, users will need to obtain permission from the license holder to reproduce the material. To view a copy of this license, visit http://creativecommons.org/licenses/by-nc-nd/4.0/

© The Author(s) 2018

Kidney & Blood Pressure Research

Kidney Blood Press Res 2018;43:1716-1729
DOI: 10.1159/000495389
Published online: 23 November 2018
Accepted: 14 November 2018

© 2018 The Author(s)
Published by S. Karger AG, Basel
www.karger.com/kbr

Karger Open access

This article is licensed under the Creative Commons Attribution-NonCommercial-NoDerivatives 4.0 International License (CC BY-NC-ND) (http://www.karger.com/Services/OpenAccessLicense). Usage and distribution for commercial purposes as well as any distribution of modified material requires written permission.

Original Paper

Urinary Level of Liver-Type Fatty Acid Binding Protein Reflects the Degree of Tubulointerstitial Damage in Polycystic Kidney Disease

Shiika Watanabe[a] Daisuke Ichikawa[a] Takeshi Sugaya[a] Keiichi Ohata[a]
Kazuho Inoue[b] Seiko Hoshino[b] Kenjiro Kimura[c] Yugo Shibagaki[a]
Atsuko Kamijo-Ikemori[a,b]

[a]Division of Nephrology and Hypertension, Department of Internal Medicine, St. Marianna University School of Medicine, Kanagawa, [b]Department of Anatomy, St. Marianna University School of Medicine, Kanagawa, [c]JCHO Tokyo Takanawa Hospital, Tokyo, Japan

Key Words
Polycystic kidney disease • Urinary marker • Liver-type fatty acid binding protein • Tubulointerstitial damage

Abstract
Background/Aims: Polycystic kidney disease (PKD) is a common, progressive, and heritable type of kidney disease. Although certain imaging modalities are useful for the diagnosis and staging of PKD, they cannot adequately monitor the severity of interstitial inflammation and fibrosis. Therefore, the present study evaluated the urinary level of liver-type fatty acid binding protein (L-FABP) as a marker of interstitial inflammation and fibrosis in PKD. ***Methods:*** Male PCK/CrljCrl-Pkhd1pck/Crl (PCK) rats (n = 34) were used as an animal model of the PKD. Age- and sex-matched Sprague–Dawley rats (SD) (n = 34) were used as controls. Urine samples were obtained from the rats at 8, 12, 16, 20, and 24 weeks of age, and the sera and kidney tissues were obtained at 8, 16, 20, and 24 weeks of age. ***Results:*** All PCK rats developed cysts, and the degrees of tubular epithelial cell proliferation and interstitial inflammation increased linearly with age in these model rats relative to the controls. Interstitial fibrosis tended to increase in the PCK rats from 8 to 20 weeks of age, and revealed a peak level at 20 weeks. The urinary L-FABP levels increased linearly with age in the PCK rats, and the levels at 12, 16, 20, and 24 weeks were significantly higher than those in the controls. The urinary levels of L-FABP in the PCK rats correlated significantly with the severity of tubulointerstitial damage; specifically, we observed a significant correlation of the urinary levels at 16 weeks of age with the total kidney volume at 20 weeks. In contrast, both PCK and SD rats exhibited similar serum levels of

Atsuko Kamijo-Ikemori, M.D., Ph.D. Division of Nephrology and Hypertension, Department of Internal Medicine and Department of Anatomy, St. Marianna University School of Medicine 2-16-1 Sugao, Miyamae-ku, Kawasaki 216-8511 (Japan), Tel. +81-44-977-8111 ext. 3630, Fax. +81-44-977-7083, E-Mail a2kamijo@marianna-u.ac.jp

L-FABP. ***Conclusion:*** Urinary L-FABP reflects the progression of tubulointerstitial damage, and therefore, may be a useful marker for monitoring the progression of PKD.

© 2018 The Author(s)
Published by S. Karger AG, Basel

Introduction

Polycystic kidney disease (PKD) is a common and progressive hereditary renal disease encountered frequently in clinical nephrology practice. Two forms of PKD—autosomal dominant polycystic kidney disease (ADPKD) and autosomal recessive polycystic kidney disease (ARPKD) —have been identified, and although these forms differ in terms of gene mutation, they share a common renal pathogenesis involving the formation of renal fluid-filled cysts linked to an abnormality in the primary cilia originating in the medullar collecting ducts [1, 2]. In both forms of PKD, renal failure is a consequence of the massive enlargement of these cysts [3-5].

Imaging modalities, such as ultrasonography, computed tomography, or magnetic resonance imaging (MRI), can detect the cyst number and volume as well as the kidney volume, and are thus useful for diagnosing and staging PKD [6]; however, it is not only costly and potentially harmful by radiation but also difficult to reproduce the parameters measured using these modalities because these values depend on the type of modalities or experience of the clinical technician [7]. Therefore, these values should be measured carefully to account for changes in the modalities used at a particular facility or when comparing the values in a multicenter clinical trial. Furthermore, the roles of renal interstitial inflammation and fibrosis as exacerbating factors of renal dysfunction in PKD have recently received attention, leading to the consideration of both phenomena as crucial targets for PKD therapy [7-9]; however, the imaging modalities cannot detect these interstitial changes. Therefore, a noninvasive and high reproducible alternative is needed.

The urinary level of liver-type fatty acid binding protein (L-FABP) was identified as an excellent tubular marker of chronic kidney disease (CKD) and acute kidney injury (AKI) in a clinical setting, and was subsequently approved as a tubular biomarker by the Ministry of Health, Labor and Welfare in Japan [10-12]. Furthermore, higher urinary L-FABP levels were reported in the patients with ADPKD, compared to healthy subjects [13]; however, the relationship between the urinary L-FABP levels and the renal pathology associated with PKD, or between the change in urinary L-FABP levels and PKD progression, has not previously been investigated. The present study aimed to elucidate these points in an experimental rat model of PKD.

Materials and Methods

Animals

All animal studies were conducted in accordance with the St. Marianna University School of Medicine Institutional Guide for Animal Experiments and the Guide for the Care and Use of Laboratory Animals. In this study, we used male PCK/CrlJCrl-Pkhd1pck/Crl (PCK, n = 34) rats derived from a Sprague–Dawley (SD, n = 34) colony as a model of PKD. Four-week-old male PCK rats and SD rats (controls) were purchased from Charles River Japan and were allowed free access to laboratory chow and water.

For the experiments, 8-, 12-, 16-, 20-, and 24-week-old rats were individually housed overnight in metabolic cages with free access to tap water. Urine was collected for the measurement of urinary markers, and body weight was also measured. Additionally, serum samples and kidney tissues were obtained at 8-, 16-, 20-, and 24-week-old rats. The extracted kidneys were weighted and cut into pieces for various analyzes.

Blood pressure measurement

Systolic blood pressure (SBP) was measured using a tail-cuff apparatus (Softron BP-98A; Softron, Tokyo, Japan) at every 4 weeks from 8 to 24 weeks of age. The averages of three measurements per animal per time point were recorded.

Serum and urinary biochemistry

Serum and urinary creatinine levels were measured using a Quantichrom™ creatinine Assay Kit (BioAssay Systems, Hayward, CA, USA). Albuminuria was determined using a NEPHRAT III ELISA kit (Exocell, Philadelphia, PA, USA). Serum and urinary levels of rat L-FABP were measured using a Rat L-FABP ELISA kit (CMIC, Tokyo, Japan). All urinary parameters were reported as ratios relative to the urinary creatinine levels. Serum urea nitrogen (UN) levels were measured via urease-LED-ultraviolet absorption spectrophotometry, and the serum aspartate amino transferase (AST) and alanine amino transferase (ALT) levels were measured using the Japan Society of Clinical Chemistry transferable method provided as a clinical laboratory testing service by SRL (Tokyo, Japan).

To evaluate the renal function, creatinine clearance was measured using the following formula:

Creatinine clearance, ml/min =
[(concentration of urinary creatinine, mg/dL) × (urinary volume, ml)]
/ [(serum creatinine, mg/dL) × (time when rats were placed in the metabolic cage, min)]

Immunohistochemical Analysis

The midsection of each excised kidney was cut in the minor axial direction, fixed in 10% buffered formalin, and was embedded in paraffin. Serial sections (3-μm thickness) were then prepared for immunohistochemical analysis. An indirect immunoperoxidase method was used to detect the target antigens. Proliferating tubular epithelial cells were detected using a mouse monoclonal antibody specific for proliferating cell nuclear antigen (PCNA, 1:200; DAKO Japan, Tokyo, Japan) after the slides were microwave heated for 15 min in citric acid buffer (pH 6.0) for antigen retrieval. Additionally, myofibroblasts and tubular cells exhibiting the epithelial–mesenchymal shift were identified using a mouse monoclonal antibody specific for α-smooth muscle actin (α-SMA, 1:800; Sigma-Aldrich, St. Louis, MO, USA).

For the immunohistochemical assessment of macrophages and type I collagen, tissue specimens fixed in methyl Carnoy's solution (60% methanol, 30% chloroform and 10% glacial acetic acid) and embedded in paraffin were immunostained using a mouse monoclonal antibody specific for ED-1 (1:100; Abcam, Tokyo, Japan) to detect the rat macrophages and a goat polyclonal antibody against type I collagen (1:200; Southern Biotech, Birmingham, AL, USA). Labeled proteins were visualized using polymeric horseradish peroxidase-conjugated secondary antibodies (ready-to-use, ImmPRESS™ polymer detection kit; Vector Laboratories, Burlingame, CA, USA). Peroxidase activity was revealed via the diaminobenzidine reaction (Liquid DAB+; DAKO Japan), and sections were counterstained with hematoxylin.

Images from 10 nonoverlapping fields throughout the cortical and outer medullary region were captured at 100× magnification. The degrees of macrophage and interstitial myofibroblast infiltration in the cortical and outer medullary interstitia were automatically measured using an image analyzer (Auto/Manual Measurement Software version 6.4, WinRoof, Mitani Co., Tokyo, Japan). Briefly, the areas positively stained for PCNA, α-SMA, and ED-1 were separately measured and expressed as ratios relative to the area of the entire cortical and outer medullary region. The same method was used to measure the expression of type I collagen.

Real-time quantitative polymerase chain reaction

Total RNA was extracted from the kidney tissues using a RNeasy Midi kit (Qiagen, Valencia, CA, USA) according to the manufacturer's instructions, and a 0.5-μg aliquot was reverse-transcribed. TaqMan real-time polymerase chain reaction (PCR) with an Applied Biosystems StepOnePlusTM real-time PCR System (Applied Biosystems, Waltham, MA) was used to measure the mRNA levels of monocyte chemoattractant protein (MCP-1), transforming growth factor (TGF-β), α1-type I collagen, and glyceraldehyde-3-phosphate dehydrogenase (GAPDH). MCP-1 mRNA was measured to evaluate the inflammatory response, whereas TGF-β and α1-type I collagen mRNAs were measured to assess renal fibrosis. The expression levels of all mRNAs were normalized to the levels of GAPDH in all samples.

Total kidney volume (TKV)

TKV is widely considered as a surrogate marker of PKD severity. To evaluate the potential use of urinary parameters as a predictor of an increased TKV, the basic ellipsoid equation, which correlates strongly with the kidney volume measured by MRI, was used to estimate the TKV in 20- (n=12) and 24-week-old (n=12) rats as described below [14]:

TKV = (maximal longitudinal length × maximal width × maximal depth × π/6) of the left kidney + (maximal longitudinal length × maximal width × maximal depth × π/6) of the right kidney

The degrees of severe interstitial inflammation and fibrosis and increases in TKV were similar between the 20- and 24-week-old PCK rats in the present study, suggesting that interstitial damage might peak at 20-week-old rats in this model. Accordingly, the severity of kidney disease findings in the 20-week-old rats was considered almost comparable to that of the end-stage kidney disease in humans, although significant renal failure was not observed in the rats. Therefore, we evaluated correlations of the urinary parameter levels at 8, 12 and 16 weeks of age with TKV at 20 and 24 weeks of age in the PCK rats.

Statistical analysis

All values are expressed as means ± standard errors. A p value <0.05 was considered to indicate statistical significance. Multiple groups were compared using a one-way analysis of variance, followed by the Mann–Whitney U-test. Spearman's rank correlation coefficient was used to evaluate the nonparametric data and assess the correlations of the two parameters. All statistical analyzes were performed using the JMP® version 13.0.0 software (SAS Institute, Cary, NC, USA).

Results

Body weight and SBP

The body weights and SBP values were measured at every 4 weeks in rats aged between 8 and 24 weeks (Table 1). Among the PCK rats, 16-week-old rats revealed a significantly increased body weight, compared to the 8- and 12-week-old rats, whereas significant increases in the body weight were observed in the 20- and 24-week-old rats relative to earlier time points (Table 1). In contrast, the body weights of the SD rats increased gradually and significantly through the observation period (Table 1). Despite this difference, the body weights of PCK rats and SD rats did not differ significantly at any point during the observation period (Table 1). Similarly, although the SBP levels in the PCK rats were significantly higher at 16 weeks of age relative to 8 and 24 weeks, no significant differences were observed in this parameter between PCK and SD rats throughout the observation period (Table 1).

Kidney weight and renal function

In the SD rats, the kidney weights at 16, 20, and 24 weeks of age were significantly higher than those measured at 8 weeks of age. In contrast, the kidney weights of the PCK rats tended to increase throughout the observation period (Table 2), with significant increases at 16, 20, and 24 weeks relative to 8 weeks and at 20 and 24 weeks relative to 16 weeks (Table 2). Additionally, the kidney weights of the PCK rats were significantly higher than those in the age-matched SD rats at all time points (Table 2).

Table 1. Body weight and systolic blood pressure (SBP). Values are the mean ± standard errors. [a]P<0.05 vs PCK rats at 8 weeks of age; [b]P<0.05 vs PCK rats at 12 weeks of age; [c]P<0.05 vs PCK rats at 16 weeks of age; [d]P<0.05 vs SD rats at 8 weeks of age; [e]P<0.05 vs SD rats at 12 weeks of age; [f]P<0.05 vs SD rats at 16 weeks of age; [h]<0.05 vs SD rats at 20 weeks of age

Variable	Species	8 weeks of age	12 weeks of age	16 weeks of age	20 weeks of age	24 weeks of age
SBP, mmHg	PCK	121 ± 3.6	130 ± 2.2	139 ± 3.2[a]	130 ± 3.7	122 ± 2.6[b]
	SD	124 ± 2.9	125 ± 3.5	132 ± 3.2	124 ± 3.5	118 ± 5.2
Body weight,	PCK	325 ± 9.5	400 ± 6.1	487 ± 7.5[a,b]	543 ± 5.6[a,b]	563 ± 7.2[a,b]
	SD	300 ± 3.5	415 ± 11.0[d]	476 ± 12.1[b]	535 ± 10.5[d,f]	593 ± 17.6[c,h,e]

Table 2. Kidney weight and renal function. Values are the mean ± standard errors. CCr, creatinine clearance. [a]P<0.05 vs SD rats at the same age; [b]P<0.05 vs PCK rats at 8 weeks of age; [c]P<0.05 vs PCK rats at 16 weeks of age; [d]P<0.05 vs PCK rats at 20 weeks of age; [e]P<0.05 vs SD rats at 8 weeks of age; [f]P<0.05 vs SD rats at 16 weeks of age

Variable / Biomarker	Species	8 weeks of age	16 weeks of age	20 weeks of age	24 weeks of age
Kidney weight, g	PCK	1.8 ± 0.04[a]	2.7 ± 0.10[ab]	3.6 ± 0.37[abc]	4.3 ± 0.41[abc]
	SD	1.2 ± 0.06	1.5 ± 0.04[e]	1.5 ± 0.04[e]	1.5 ± 0.06[e]
Creatinine, mg/dL	PCK	0.41 ± 0.04	0.48 ± 0.04	0.46 ± 0.03	0.55 ± 0.02[bd]
	SD	0.40 ± 0.03	0.46 ± 0.04	0.47 ± 0.02	0.52 ± 0.02
Urea nitrogen, mg/dL	PCK	17.7 ± 0.62	19.7 ± 0.36[c]	27.4 ± 4.20[bd]	30.6 ± 2.68[abd]
	SD	18.4 ± 0.73	19.2 ± 0.85	20.6 ± 0.75[e]	22.1 ± 0.93[ef]
CCr, ml/min	PCK	1.7 ± 0.18	2.1 ± 0.15	2.5 ± 0.20	2.3 ± 0.07
	SD	1.7 ± 0.22	3.0 ± 0.61	3.0 ± 0.14	2.4 ± 0.32

Table 3. Serum biochemistry. Values are the mean ± standard errors. [a]P<0.05 vs SD rats at the same age; [b]P<0.05 vs PCK rats at 8 weeks of age; [d]P<0.05 vs PCK rats at 20 weeks of age; [e]P<0.05 vs PCK rats at 24weeks of age; [f]P<0.05 vs SD rats at 8 weeks of age; [g]P<0.05 vs SD rats at 16 weeks of age

Biomarker	Species	8 weeks of age	16 weeks of age	20 weeks of age	24 weeks of age
L-FABP, ng/mL	PCK	91.3 ± 20.3	67.3 ± 7.9	48.7 ± 12.5	67.4 ± 21.2
	SD	72.7 ± 21.9	61.0 ± 18.4	39.7 ± 17.0	101.3 ± 22.5
AST, U/L	PCK	171.6 ± 19.3	220.1 ± 30.7[ad]	103.0 ± 9.0	183.0 ± 22.1[d]
	SD	98.6 ± 8.7	100.6 ± 7.0	123.0 ± 10.5	144.8 ± 23.1
ALT, U/L	PCK	70.7 ± 4.7	96.3 ± 5.9[abd]	54.4 ± 1.9[ad]	72.7 ± 5.0[d]
	SD	51.3 ± 2.1	56.6 ± 4.5	38.0 ± 1.7[f]	56.2 ± 14.6

Considering the renal function, the PCK rats exhibited significant increases in the serum creatinine levels at 24 weeks, compared to those at 8 and 20 weeks (Table 2). No significant differences in this parameter were observed between the PCK and SD rats at any time point (Table 2). Furthermore, the PCK rats exhibited significant increases in the serum UN levels at each 16, 20, and 24 weeks relative to 8 weeks and at 20 and 24 weeks relative to 16 weeks (Table 2). In SD rats, the serum UN levels increased significantly at 20 and 24 weeks relative to 8 weeks and at 24 weeks relative to 16 weeks (Table 2). Notably, the serum UN levels were higher in the PCK rats than in the SD rats at 24 weeks of age (Table 2); however, no changes in the levels of creatinine clearance were observed in either the PCK or SD rats throughout the observation period (Table 2).

Serum biochemistry

In both the PCK and SD rats, the serum L-FABP levels did not change significantly throughout the observation period (Table 3), with no significant differences between the groups (Table 3); however, in the PCK groups, the serum AST levels were significantly higher at 8 and 16 weeks than at 20 weeks and at 24 weeks than at 20 weeks. By contrast, the serum AST levels in the SD rats did not change significantly throughout the observation period (Table 3). The serum AST levels in the PCK rats were significantly higher than those in the SD rats at 16 weeks of age (Table 3).

The serum ALT levels in the PCK rats were significantly higher at 16 weeks than at 8, 20 and 24 weeks and at 24 weeks than at 20 weeks (Table 3). Furthermore, the serum ALT levels in the PCK rats were significantly higher than those in the SD rats at both 16 and 20 weeks of age (Table 3).

Immunohistological analysis of the kidneys

To evaluate the tubular epithelial cell proliferation, we conducted an immunohistochemical analysis of the PCNA expression (Fig. 1). In the PCK rats, PCNA expression was detected in the tubular epithelial cell nuclei (Fig. 1A, B, C and D), and the degrees of PCNA positivity tended to increase with age. Specifically, the PCNA-positive areas at 16, 20, and 24 weeks were significantly greater than those at 8 weeks, and the areas at 24 weeks were significantly

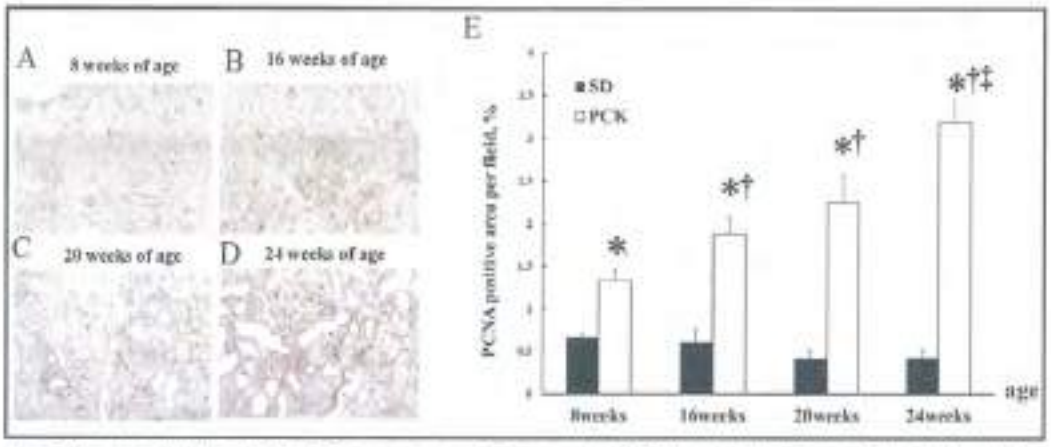

Fig. 1. Immunohistological staining using an antibody against PCNA in the PCK rats (A, B, C, D) and the PCNA-positive areas per field were assessed quantitatively (E). Original magnification, x100. *P<0.05 vs SD rats at the same age; †P<0.05 vs PCK rats at 8 weeks of age; ‡P<0.05 vs PCK rats at 16weeks of age.

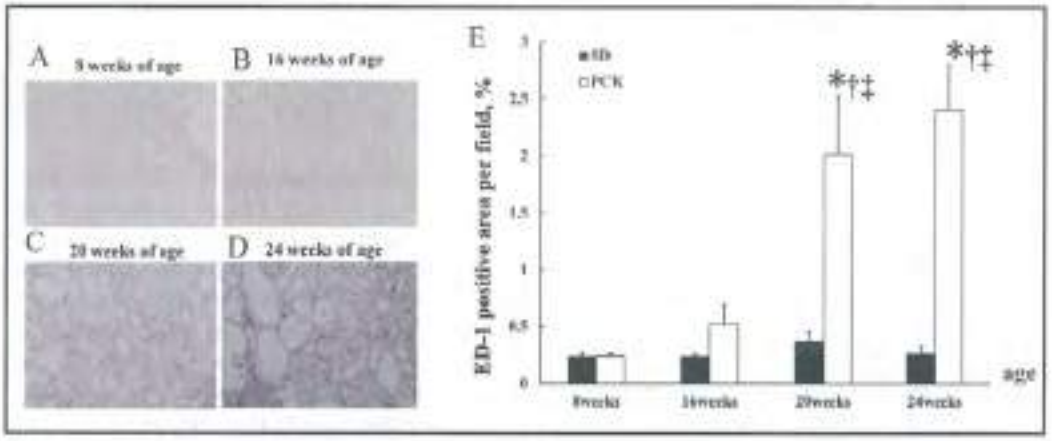

Fig. 2. Immunohistological staining using an antibody against ED-1 in the PCK rats (A, B, C, D) and the ED-1 positive areas per field (E). Original magnification, x100. *P<0.05 vs SD rats at the same age; †P<0.05 vs PCK rats at 8 weeks of age; ‡P<0.05 vs PCK rats at 16 weeks of age.

greater than those at 16 weeks (Fig. 1E). Furthermore, significantly greater PCNA expression was observed in the PCK rats relative to the age-matched SD rats throughout the observation period (Fig. 1E).

To evaluate the degree of renal interstitial inflammation, we immunohistochemically detected the macrophage marker ED1 (Fig. 2). In the PCK rats, macrophages were detected in the interstitium (Fig. 2A, B, C, and D), and the degree of infiltration tended to increase with age. The degrees of infiltration were significantly greater in the PCK rats than in the SD rats at both 20 and 24 weeks of age and, than in the PCK rats at both 8 and 16 weeks (Fig. 2E).

Additionally, an immunohistochemical analysis of α-SMA and type I collagen expression was performed to evaluate the degree of tubulointerstitial fibrosis. In the PCK rats, α-SMA-positive areas were observed in the tubules and interstitium. The extent of these areas tended to increase with age (Fig. 3A, B, C, and D), and was significantly greater in the PCK rats at all time points relative to the age-matched SD rats (Fig. 3E). Furthermore, the extent of α-SMA-positive areas in the 20- and 24-week-old PCK rats was significantly greater than that in the 8-week-old rats and in the 24-week-old rats relative to the 16-week-old rats (Fig. 3E).

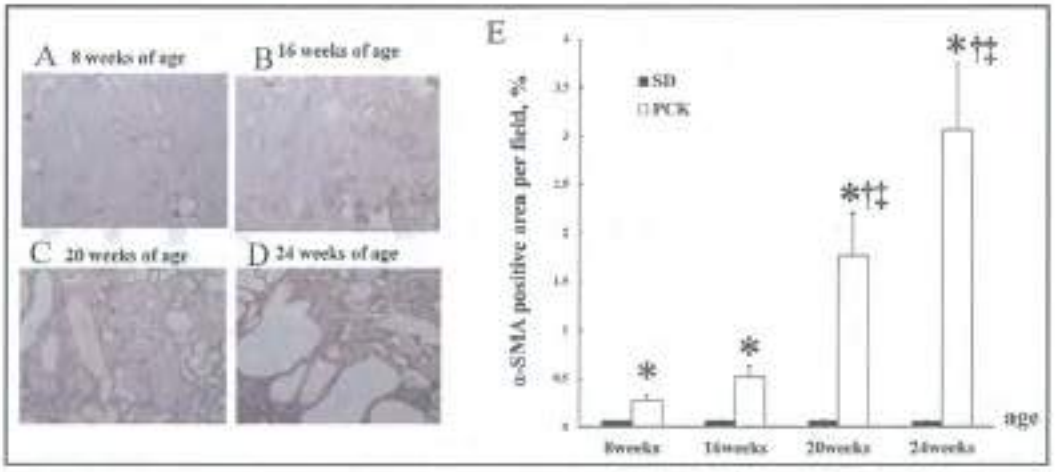

Fig. 3. Immunohistological staining using an antibody against α-SMA in the PCK rats (A, B, C, D) and the α-SMA positive areas per field (E). Original magnification, x100. *P<0.05 vs SD rats at the same age; †P<0.05 PCK rats at 8 weeks of age; ‡P<0.05 vs PCK rats at 16weeks of age.

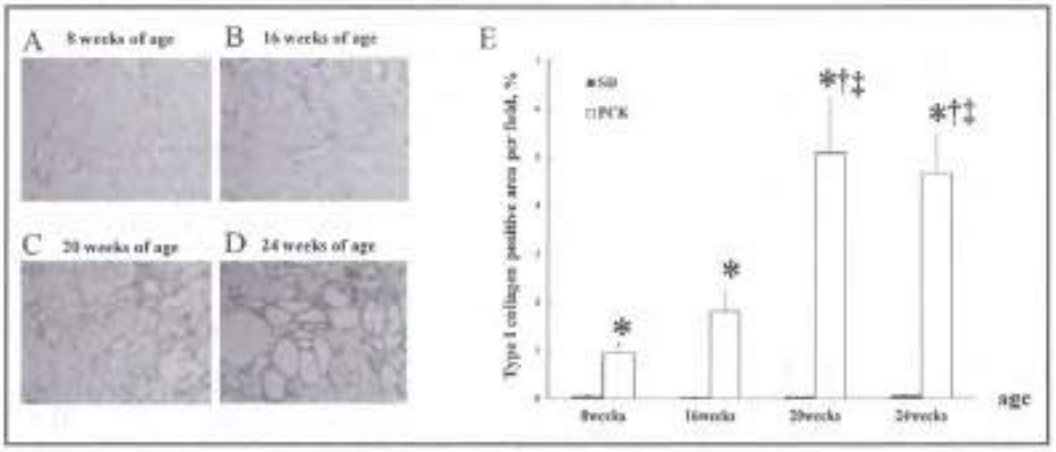

Fig. 4. Immunohistological staining using an antibody against type I collagen in the PCK rats (A, B, C, D) and the type I collagen positive areas per field (E). Original magnification, x100. *P<0.05 vs SD rats at the same age; †P<0.05 vs PCK rats at 8 weeks of age; ‡P<0.05 vs PCK rats at 16 weeks of age.

Further analysis revealed type I collagen expression in the interstitium (Fig. 4A, B, C, and D). In the PCK rats, the degree of type I collagen expression tended to increase with age up to 20 weeks and remained significantly higher than the degree of expression in the SD rats throughout the observation period (Fig. 4E). Furthermore, the degrees of type I collagen expression in the 20- and 24-week-old PCK rats were significantly greater than those in the 8- and 16-week-old rats (Fig. 4E).

Gene expression analysis in the kidneys

In the PCK rats, MCP-1 mRNA levels tended to increase with age, and the expression of this gene was significantly higher than in the age-matched SD rats throughout the observation period (Fig. 5A). Furthermore, the MCP-1 mRNA levels were significantly higher at 20 and 24 weeks relative to 8 weeks and at 24 weeks relative to 16 weeks. Similarly, the TGF-β mRNA levels increased with age in the PCK rats, and the levels at 16, 20, and 24 weeks were significantly higher than those in the age-matched SD rats (Fig. 5B). In the PCK rats, the

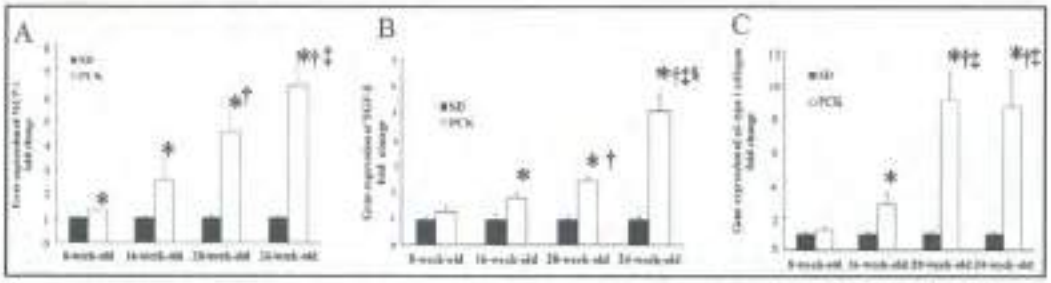

Fig. 5. mRNA transcript expressions of MCP-1 (A), TGF-β (B), and α1-type I collagen (C). *P<0.05 vs SD rats at the same age; †P<0.05 vs PCK rats at 8 weeks of age; ‡P<0.05 vs PCK rats at 16 weeks of age; §P<0.05 vs PCK rats at 20 weeks of age.

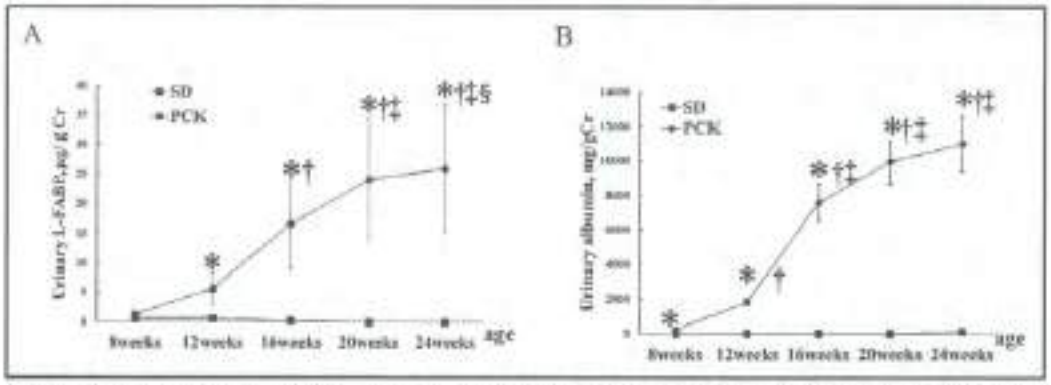

Fig. 6. Change in urinary L-FABP (A), and urinary albumin (B). *P<0.05 vs the SD rats at the same age; †P<0.05 vs PCK rats at 8 weeks of age; ‡P<0.05 vs PCK rats at 12 weeks of age.;§P<0.05 vs PCK rats at 16 weeks of age.

TGF-β mRNA levels were significantly higher at 20 and 24 weeks relative to 8 weeks and at 24 weeks relative to 16 and 20 weeks.

The expression of α1-typel collagen mRNA in the PCK rats tended to increase with age up to 20 weeks and remained high at 24 weeks and were significantly higher at 16, 20, and 24 weeks relative to those in the age-matched SD rats (Fig. 5C). Furthermore, the mRNA levels in the PCK rats were significantly higher at 20 and 24 weeks, compared to 8 and 16 weeks (Fig. 5C).

Change in the urinary biomarkers

Both the urinary L-FABP and urinary albumin levels were measured at every 4weeks from 8 to 24 weeks of age (Fig. 6). Notably, the urinary L-FABP levels tended to increase with age in the PCK rats and were significantly higher than those in the age-matched SD rats between 12 and 24 weeks of age (Fig. 6A). In the PCK rats, these levels were significantly higher at 16, 20, and 24 weeks relative to 8 weeks, at 20 and 24 weeks relative to 12 weeks, and at 24 weeks relative to 16 weeks (Fig. 6A).

In the PCK rats, urinary albumin levels similarly tended to increase with age and were significantly higher than those in the age-matched SD rats between 8 and 24 weeks of age (Fig. 6B). Furthermore, the levels in the PCK rats were significantly higher at 12, 16, 20, and 24 weeks relative to 8 weeks and at 16, 20, and 24 weeks relative to 12 weeks (Fig. 6B).

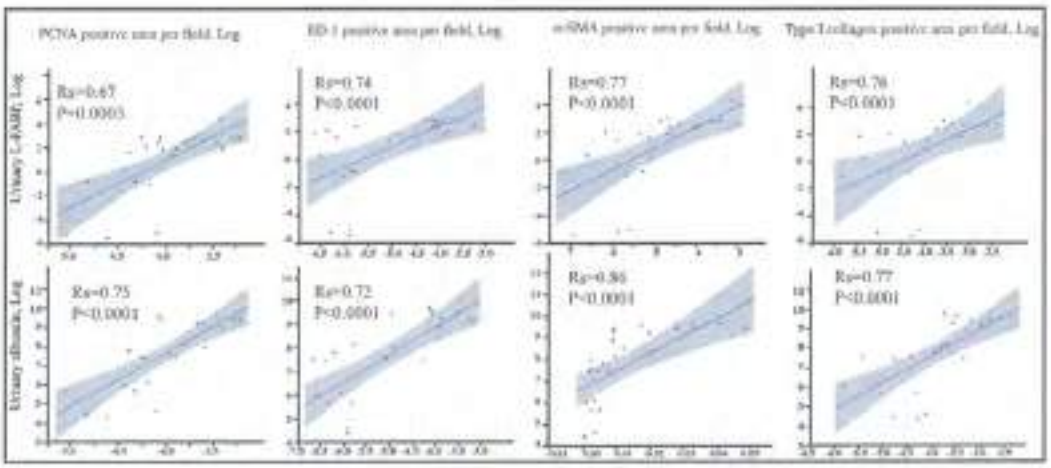

Fig. 7. Correlations between each urinary marker and each histological evaluation.

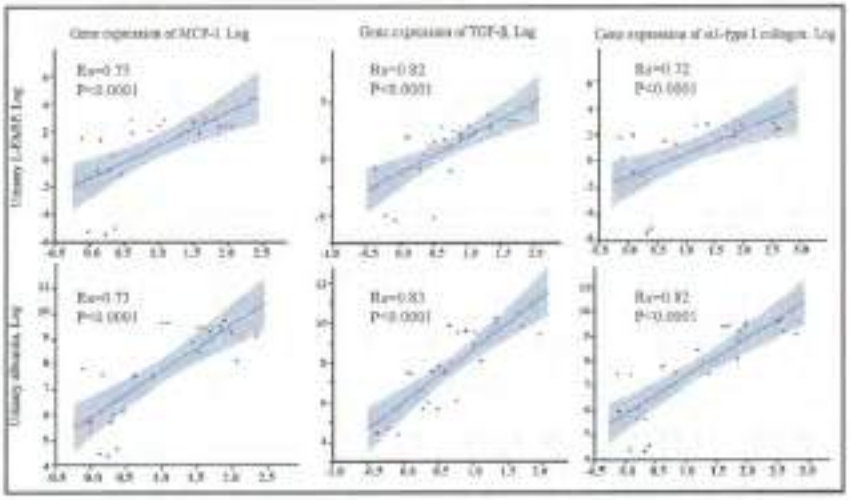

Fig. 8. Correlations between each urinary marker and each gene expression.

Correlation between the urinary marker levels and histological changes

The urinary levels of both L-FABP and albumin were found to correlate significantly with the degree of tubular epithelial cell proliferation (i.e., PCNA-positive area), macrophage infiltration (i.e., ED-1-positive area), and tubulointerstitial fibrosis (i.e., α-SMA-positive area and type I collagen deposition; $p < 0.0005$, Fig. 7).

Correlation between the urinary marker levels and gene expression

The urinary levels of both L-FABP and albumin were found to correlate significantly with the mRNA expression of MCP-1 (inflammatory cytokine), TGF-β (profibrotic cytokine), and α1-type I collagen (universal fibrotic marker; $p < 0.0001$, Fig. 8).

Correlation between the urinary parameters in the 8-, 12-, and 16-week-old PCK rats and TKV in the 20- and 24-week-old rats

Two rats each in the 20- and 24-week-old groups of PCK rats died during the observation period. Therefore, this evaluation included the 11 remaining PCK rats in each group. Notably, the 20- and 24-week-old PCK rats revealed a significantly greater TKV, compared to the age-matched SD rats; however, the TKVs of the 20- and 24-week-old PCK rats were similar (Fig. 9A).

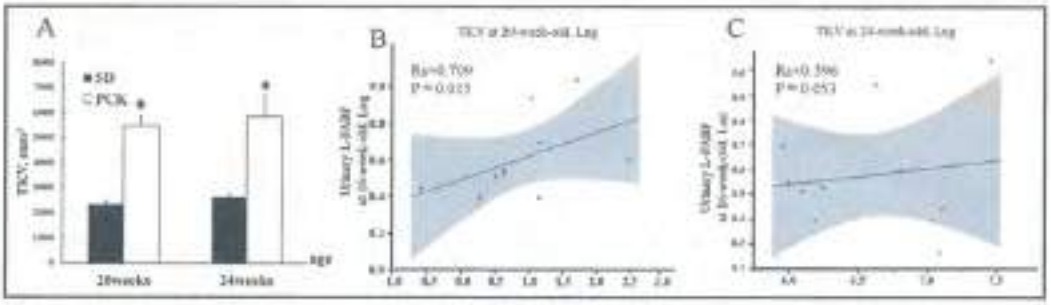

Fig. 9. TKV at both 20 and 24 weeks of age (A). Correlations between urinary L-FABP at 16 weeks of age and TKV at each 20 (B) and 24 weeks of age (C).

Furthermore, the urinary L-FABP levels of the 16-week-old PCK rats were found to correlate significantly with the TKV at 20 weeks of age ($Rs = 0.709$, $p < 0.0001$, Fig. 9B) and tended to correlate with the TKV at 24 weeks of age ($Rs = 0.596$, $p = 0.053$, Fig. 9C); however, the urinary L-FABP at 8 and 12 weeks and urinary albumin levels at 8, 12, and 16 weeks did not correlate significantly with the TKV at 20 and 24 weeks in the PCK rats (data not shown).

Discussion

In the present PCK rat model study, we observed increasing urinary levels of L-FABP and albumin with age and found that these markers correlated significantly with the degrees of tubular epithelial cell proliferation, interstitial inflammation, and fibrosis. Furthermore, the urinary L-FABP level may be a marker of PKD progression, as this parameter at 16 weeks was found to correlate significantly with the TKV at 20 weeks and tended to correlate with the TKV at 24 weeks. These results suggest that both the urinary L-FABP and urinary albumin levels might be clinically useful for monitoring the PKD progression. Despite the growing evidence of a relationship between the urinary L-FABP levels and tubulointerstitial damage or renal prognosis in both CKD and AKI [15-17], the correlations of this parameter with PKD have not yet been investigated. Therefore, the present study is the first to report the potential utility of urinary L-FABP as a monitoring marker of PKD progression.

In the PCK rats, cyst formation is induced via a splicing mutation of the human orthologous polycystic kidney and hepatic disease 1 (PKHD1) gene, which encodes the polycystin proteins [18]. Consequently, the PCK rats suffer from congenital hepatic fibrosis [19]. Therefore, these rats are presumed to mimic human ARPKD. In contrast, Lager et al. reported that the slow progression of renal cyst growth in a PCK rat model of a hepatic disorder resembled the human ADPKD, a disease first diagnosed in children or adolescents that is characterized by the prolonged (i.e., several decades) and persistent expansion of renal cysts [20]. We further note that the changes in renal pathology, such as interstitial inflammation and fibrosis, as well as tubular epithelial cell proliferation leading to cyst enlargement, are related to renal dysfunction during PKD progression and occur similarly in ARPKD and ADPKD, despite their different genetic etiologies [21]. Therefore, we assume that our PCK rat model is instrumental to evaluations of the relationship between the renal pathological changes occurring during PKD progression and the urinary marker levels.

TKV can be measured via imaging and used as a surrogate marker of PKD. In particular, the TKV determined using high-resolution MRI was confirmed to correlate strongly with a reduced estimated glomerular filtration rate and PKD progression [5]. In general, however, MRI is costly and only available at the medical university or advanced treatment hospitals. Furthermore, the requirement for sedation makes it difficult to perform MRI in children [22]. Therefore, a simple, urine-based clinical marker of PKD is needed. Considering our observation of a significant association between the urinary L-FABP level at 16 weeks and

the TKV at 20 weeks (estimated using the basic ellipsoid equation rather than MRI), urinary L-FABP may be useful as a marker for the routine clinical monitoring of PKD.

Tubulointerstitial damage, which is induced by inflammatory cytokines and growth factors and characterized by interstitial inflammation and subsequent fibrosis, is more associated with CKD progression than the degree of glomerular damage [23, 24]. Similarly, tubulointerstitial pathology is useful for monitoring the slow progression of ADPKD and some cases of ARPKD because the inflammatory cytokines and growth factors produced by the cyst epithelial cells induce macrophage infiltration and provoke interstitial fibrosis. These processes, collectively, with the exacerbation of cyst enlargement, eventually lead to renal function impairment [8, 9,21]. In the present study, MCP-1 expression was upregulated in the 8-week-old PCK rats consequent to tubular epithelial cell proliferation, and subsequently induced macrophage infiltration began at16 weeks, although this change was not significant. Although early (8-week) increases were observed in both the α-SMA positive area and type I collagen deposition, significant increases in both TGF-β and type I collagen mRNA were not observed until 16 weeks. Collectively, the changes in the interstitial pathophysiology and PKD progression observed were similar to the features of the noncystic CKD. A previous study found a significant correlation of urinary L-FABP with the degree of tubulointerstitial damage in noncystic CKD [25]. Therefore, urinary L-FABP might reflect the degree of PKD-associated interstitial damage.

The present study further revealed a significant and early increase in the urinary albumin levels in the PCK rats, compared to the SD rats. A previous morphometric study of glomerular damage found that segmental glomerular basement membrane thickening and foot process effacement was observed via transmission electron microscopy in the 10-week-old PCK rats [20]. Furthermore, the urinary albumin level, which increases as a consequent to dysfunctional reabsorption in the proximal tubules, may be useful as a tubular marker [15, 16, 26]. This marker might be particularly sensitive because it reflects both glomerular and tubulointerstitial pathological changes that occur during the early disease phase in the PCK rats.

In our previous report, we confirmed an increase in the serum level of L-FABP in human patients with hepatic disease [27]; however, we did not find a correlation between the serum and urinary levels of L-FABP in CKD. Another research group reported a significant correlation of the urinary level of L-FABP with changes in the serum levels of various liver enzymes in critically ill patients admitted to an intensive care unit [28]. Furthermore, a previous report identified a progressive hepatic disorder in the PCK rats [19]. In our study, significantly higher changes in the serum liver enzyme levels, especially ALT, were observed in the PCK rats relative to the SD rats at two points; however, we did not observe a significant increase in the serum levels of L-FABP in the PCK rats relative to the SD rats. Therefore, the observed increase in the urinary L-FABP levels was not attributed to an increase in the serum L-FABP level.

Certain strategies for preventing PKD progression are presently at the research stage or in clinical practice; however, the present study did not examine the effects of these interventions on the urinary marker levels in the PCK rats. Although the vasopressin V2-receptor antagonist, Tolvaptan, was reported to slow the increase in TKV and the decline in renal function in patients with ADPKD [3, 4], it did not trigger a decrease in the urinary albumin level [4]. In contrast, an angiotensin II receptor blocker known to inhibit renal dysfunction [29] was reported to reduce the urinary L-FABP levels in patients with ADPKD [13]. These findings suggest that the urinary level of the tubular specific marker L-FABP may determine the effect of Tolvaptan treatment on the effects of PKD.

This study had some limitations, notably, pertaining the inability of animal models to completely mimic human pathophysiology. First, the degree of cyst growth differs between PCK rats and humans with PKDs. Although the cysts in human patients spread from the surface of the kidney and compress the surrounding organs, most cysts formed in the PCK rats remained within the enlarged kidneys [20, 30, 31]. Second, the degree of renal

dysfunction in the PCK rats was relatively slight, compared to the degree of tubulointerstitial damage. Third, the SBP did not increase significantly in the PCK rats relative to the SD rats; in contrast, hypertension is a frequent characteristic of slow progressive human PKD.

Conclusion

The urinary levels of L-FABP and albumin appear to reflect the degree of tubulointerstitial damage and may be useful for monitoring PKD in clinical practice. Furthermore, clinical studies are necessary to validate the clinical superiority of urinary markers relative to imaging modalities for monitoring the progression of PKD or therapeutic responses to the interventions.

Acknowledgements

This work was partly supported by the Scholarship Fund for Young Researchers, funded by the Promotion and Mutual Aid Corporation for Private Schools of Japan.

We thank Ms. Kimie Katayama and Junko Asano for providing technical assistance.

The authors contributed as following: SW, DI, and AK-I: study design; SW, AK-I, KO, KI, and SH: data collection; SW and AK-I: data analysis; SW, DI, AK-I, TS, KK, and YS: data interpretation; SW, DI, and AK-I: literature search and figure generation; and SW and AK-I, writing of the manuscript. All authors provided final approval of the submitted version.

Disclosure Statement

T. Sugaya is the Director and Senior Scientist and K. Ohata is a Scientist of CMIC HOLDINGS Co., Ltd., which produced the kits used for L-FABP analysis. None of the other authors had conflicts of interest or financial disclosures relevant to the present study.

References

1 Verani RR, Silva FG: Histogenesis of the renal cysts in adult (autosomal dominant) polycystic kidney disease: a histochemical study. Mod Pathol 1988;1:457–463.

2 Inage Z, Kikkawa Y, Minato M, Owada M, Kitagawa T, Ohno K, Kondo K, Ueda Y, Iidaka K: Autosomal recessive polycystic kidney in rats. Nephron 1991;59:637–640.

3 Higashihara E, Torres VE, Chapman AB, Grantham JJ, Bae K, Watnick TJ, Horie S, Nutahara K: Tolvaptan in autosomal dominant polycystic kidney disease: three years' experience. Clin J Am Soc Nephrol 2011;6:2499–2507.

4 Torres V, Chapman A, Devuyst O, Gansevoort R, Grantham J, Higashihara E, Perrone RD, Krasa HB, Ouyang J, Czerwiec FS: Tolvaptan in Patients with Autosomal Dominant Polycystic Kidney Disease. N Engl J Med 2012;367:2407–2418.

5 Higashihara E, Nutahara K, Okegawa T, Shishido T, Tanbo M, Kobayasi K, Nitadori T: Kidney volume and function in autosomal dominant polycystic kidney disease. Clin Exp Nephrol 2014;18:157–165.

6 Grantham JJ, Torres VE: The importance of total kidney volume in evaluating progression of polycystic kidney disease. Nat Rev Nephrol 2016;12:667–677.

7 Huang B, Paka P, Mccormack S, Zhou P, Paka L, Yamin M, Goldberg ID, Narayan P: A Biomarker Cluster for Polycystic Kidney Disease: Correlation with Cystic Index. Recent Pat Biomark 2015;5:35–43.

8 Ta MHT, Harris DCH, Rangan GK: Role of interstitial inflammation in the pathogenesis of polycystic kidney disease. Nephrology 2013;18:317–330.

9 Chen L, Zhou X, Fan LX, Yao Y, Swenson-fields KI, Gadjeva M, Wallace DP, Peters DJM, Yu A, Grantham JJ, Li X: Macrophage migration inhibitory factor promotes cyst growth in polycystic kidney disease. J Clin Invest 2015;125:2399–2412.

10 Matsui K, Kamijo-Ikemori A, Imai N, Sugaya T, Yasuda T, Tatsunami S, Toyama T, Shimizu M: Clinical significance of urinary liver-type fatty acid-binding protein as a predictor of ESRD and CVD in patients with CKD. Clin Exp Nephrol 2016;20:195–203.

11 Kamijo-Ikemori A, Sugaya T, Ichikawa D, Hoshino S, Matsui K, Yokoyama T, Yasuda T, Hiruta K, Kimura K: Urinary liver type fatty acid binding protein in diabetic nephropathy. Clin Chim Acta 2013;424:104–108.

12 Matsui K, Kamijo-Ikemori A, Sugaya T, Yasuda T, Kimura K: Usefulness of Urinary Biomarkers in Early Detection of Acute Kidney Injury After Cardiac Surgery in Adults. Circ J 2012;76:213–220.

13 Nakamura T, Sugaya T, Kawagoe Y, Ueda Y, Osada S, Koide H: Candesartan reduces urinary fatty acid-binding protein excretion in patients with autosomal dominant polycystic kidney disease. Am J Med Sci 2005;330:161–165.

14 Higashihara E, Nutahara K, Okegawa T, Tanbo M, Hara H, Miyazaki I, Kobayasi K, Nitadori T: Kidney volume estimations with ellipsoid equations by magnetic resonance imaging in autosomal dominant polycystic kidney disease. Nephron 2015;12:253–262.

15 Hisamichi M, Kamijo-Ikemori A, Sugaya T, Ichikawa D, Hoshino S, Hirata K, Kimura K, Shibagaki Y: Increase in u rinary markers during the acute phase reflects the degree of chronic tubulointerstitial injury after ischemia-reperfusion renal injury. Biomarkers 2017;22:5–13.

16 Ichikawa D, Kamijo-Ikemori A, Sugaya T, Ohata K, Hisamichi M, Hoshino S, Kimura K, Shibagaki Y: Utility of urinary tubular markers for monitoring chronic tubulointerstitial injury after ischemia–reperfusion. Nephrology 2018;23:308–316.

17 Kamijo-Ikemori A, Sugaya T, Matsui K, Yokoyama T, Kimura K: Roles of human liver type fatty acid binding protein in kidney disease clarified using hL-FABP chromosomal transgenic mice. Nephrology 2011;16:539–544.

18 Ward CJ, Hogan MC, Rossetti S, Walker D, Sneddon T, Wang X, Kubly V, Cunningham JM, Bacallao R, Ishibashi M, Milliner DS, Torres VE, Harris PC: The gene mutated in autosomal recessive polycystic kidney disease encodes a large, receptor-like protein. Nat Genet 2002;30:259–269.

19 Sanzen T, Harada K, Yasoshima M, Kawamura Y, Ishibashi M, Nakanuma Y: Polycystic kidney rat is a novel animal model of Caroli's disease associated with congenital hepatic fibrosis. Am J Pathol 2001;158:1605–1612.

20 Lager DJ, Qian Q, Bengal RJ, Ishibashi M, Torres VE: The pck rat: A new model that resembles human autosomal dominant polycystic kidney and liver disease. Kidney Int 2001;59:126–136.

21 Grantham JJ, Mulamalla S, Swenson-Fields KI: Why kidneys fail in autosomal dominant polycystic kidney disease. Nat Rev Nephrol 2011;7:556–566.

22 Liebau MC, Serra AL: Looking at the (w)hole: Magnet resonance imaging in polycystic kidney disease. Pediatr Nephrol 2013;28:1771–1783.

23 Remuzzi G, Bertani T: Pathophysiology of progressive nephropathies. Epstein FH, editor. N Engl J Med 1998;339:1448–1456.

24 Prunotto M, Budd DC, Gabbiani G, Meier M, Formenton I, Hartmann G, Pomposiello S, Moll S: Epithelial-mesenchymal crosstalk alteration in kidney fibrosis. J Pathol 2012;228:131–147.

25 Kamijo A, Sugaya T, Hikawa A, Okada M, Okumura F, Yamanouchi M, Honda A, Okabe M, Fujino T, Hirata Y, Omata M, Kaneko R, Fujii H, Fukamizu A, Kimura K: Urinary excretion of fatty acid-binding protein reflects stress overload on the proximal tubules. Am J Pathol 2004;165:1243–1255.

26 Weyer K, Andersen PK, Schmidt K, Mollet G, Antignac C, Birn H, Nielsen R, Christensen EI: Abolishment of proximal tubule albumin endocytosis does not affect plasma albumin during nephrotic syndrome in mice. Kidney Int 2018;93:375–389.

27 Kamijo A, Sugaya T, Hikawa A, Yamanouchi M, Hirata Y, Ishimitsu T, Numabe A, Takagi M, Hayakawa H, Tabei F, Sugimoto T, Mise N, Omata M, Kimura K: Urinary liver-type fatty acid binding protein as a useful biomarker in chronic kidney disease. Mol Cell Biochem 2006;284:175–182.

28 Asada T, Isshiki R, Hayase N, Sumida M, Inokuchi R, Noiri E, Nangaku M, Yahagi N, Doi K: Impact of clinical context on acute kidney injury biomarker performances: Differences between neutrophil gelatinase-associated lipocalin and L-type fatty acid-binding protein. Sci Rep 2016;6:1–9.

29 Nutahara K, Higashihara E, Horie S, Kamura K, Tsuchiya K, Mochizuki T, Hosoya T, Nakayama T, Yamamoto N, Higaki Y, Shimizu T: Calcium channel blocker versus angiotensin II receptor blocker in autosomal dominant polycystic kidney disease. Nephron Clin Pract 2005;99:c18-23.

30 Katsuyama M, Masuyama T, Komura I, Hibino T, Takahashi H: Characterization of a novel polycystic kidney rat model with accompanying polycystic liver. Exp Anim 2000;49:51-55.

31 Kapoor S, Rodriguez D, Mitchell K, Wüthrich RP: High resolution ultrasonography for assessment of renal cysts in the PCK rat model of autosomal recessive polycystic kidney disease. Kidney Blood Press Res 2016;41:186-196.

NEPHROLOGY

Nephrology 23 (2018) 308–316

Original Article

Utility of urinary tubular markers for monitoring chronic tubulointerstitial injury after ischemia–reperfusion

DAISUKE ICHIKAWA,[1] ATSUKO KAMIJO-IKEMORI,[1,2] TAKESHI SUGAYA,[1] KEIICHI OHATA,[1] MIKAKO HISAMICHI,[1] SEIKO HOSHINO,[2] KENJIRO KIMURA[3] and YUGO SHIBAGAKI[1]

[1]Division of Nephrology and Hypertension, Department of Internal Medicine, and [2]Department of Anatomy, St. Marianna University School of Medicine, Kanagawa and [3]JCHO Tokyo Takanawa Hospital, Tokyo, Japan

KEY WORDS:
albumin, ischaemia–reperfusion, kidney injury molecule-1, L-type fatty acid binding protein, urinary marker

Correspondence:
Dr Atsuko Kamijo-Ikemori, Department of Anatomy, St. Marianna University School of Medicine, 2-16-1 Sugao, Miyamae-Ku, Kawasaki 216-8511, Japan. Email: a2kamijo@marianna-u.ac.jp

Accepted for publication 4 January 2017.
Accepted manuscript online 7 January 2017.

doi: 10.1111/nep.12998

SUMMARY AT A GLANCE

L-FABP is a promising biomarker of several kidney diseases. However, experimental modelling has been problematic due to its lack of expression in the mouse kidney. In this study, Ichikawa et al. use a transgenic model of L-FABP expression to compare L-FABP and other biomarkers in murine ischaemia–reperfusion injury.

ABSTRACT:

Aim: **The aim of this study was to elucidate whether urinary tubular markers during the chronic phase of acute kidney injury (AKI) are associated with chronic tubulointerstitial damage.**

Methods: **Male human L-type fatty acid binding protein (*L-FABP*) chromosomal transgenic (Tg) mice underwent ischaemic reperfusion (I/R) injury via renal pedicle clamping for either 10 min or 20 min. Contralateral nephrectomy was performed at the time of tissue reperfusion. The kidneys were analyzed 20 days after the last I/R.**

Results: **Serum creatinine levels 20 days post-I/R were significantly higher in the 20 min I/R than in the 10 min I/R and control groups and were similar between the 10 min I/R and control groups. The degree of tubulointerstitial damage 20 days post-I/R was significantly more severe in the 20 min I/R than in the 10 min I/R and control groups, as well as in the 10 min I/R than in the control group. Urinary levels of human L-FABP, albumin, and kidney injury molecule-1 (KIM-1) 20 days post-I/R were significantly higher in the 20 min I/R than in the control group, whereas urinary L-FABP was significantly higher in the 10 min I/R than in the control group. Conversely, urinary neutrophil gelatinase-associated lipocalin levels did not significantly differ between the three groups. Finally, the urinary levels of human L-FABP, albumin, and KIM-1 levels 20 days post-I/R were significantly correlated with the degree of renal damage.**

Conclusions: **Urinary levels of human L-FABP, albumin and, KIM-1 may be useful for monitoring AKI-to-CKD transition in clinical practice.**

The global incidence of acute kidney injury (AKI) is steadily increasing in parallel with the growing aging population and several comorbidities, including diabetes, hypertension, cardiovascular disease, cirrhosis, cancer and complex surgery.[1–3] Renal dysfunction in AKI was previously assumed to be transient and reversible. However, epidemiological studies and one meta-analysis showed that AKI led to subsequent chronic kidney disease (CKD); AKI is now widely considered to be a risk factor for CKD.[3–6] Therefore, follow-up with nephrologists of patients with experience of AKI is critical to prevent chronic renal dysfunction and transition to CKD.[4]

Regardless of the aetiology, tubulointerstitium is a common target of injury during AKI,[7] and multiple factors are involved in AKI-to-CKD progression. Sustained tubulointerstitial damage due to interstitial immune cell infiltration[8] or tubular hypoxia induced by reduced peritubular capillary density,[9,10] and subsequent interstitial fibrosis after AKI leads to glomerulotubular disruption and ultimate formation of atubular glomeruli,[11] which develops into chronic renal dysfunction.[12] Thus, urinary tubular markers during the chronic phase after AKI may reflect the degree of chronic tubulointerstitial damage after AKI and may be useful for monitoring AKI-to-CKD progression.

The urinary levels of several molecules including liver-type fatty acid binding protein (L-FABP),[13,14] kidney injury molecule-1 (KIM-1)[15] and neutrophil gelatinase-associated lipocalin (NGAL)[16] were demonstrated to be excellent tubular markers for CKD and AKI in clinical practice. Furthermore, urinary albumin, glomerular marker, has been recently

© 2017 Asian Pacific Society of Nephrology

considered as a potential tubular marker.[17,18] The present study aimed to elucidate whether changes in urinary tubular markers during the chronic phase after AKI were associated with chronic tubulointerstitial damage in AKI-to-CKD transition in an *in vivo* model.

METHODS

Animals

All animal studies were conducted in accordance with the St. Marianna University School of Medicine Institutional Guide for Animal Experiments and the Guide for the Care and Use of Laboratory Animals. In this study, we used human *L-FABP* chromosomal transgenic (Tg) mice generated by microinjection of human *L-FABP* genomic DNA including its promoter region into fertilized eggs of BALB/c and CBA mice (World Intellectual Property Organization patent no. WO 0073791).[19] These human L-FABP-Tg mice express human L-FABP in proximal tubules and are an excellent model to evaluate urinary human L-FABP as a potential marker, given that L-FABP is not expressed in mouse kidneys. Ten- to 12-week-old male human L-FABP Tg mice of C57/BL6 background (body weight: 25-28 g) were used for all experiments in this study.

Ischaemia–reperfusion model

Renal ischaemia was induced by left renal pedicle clamping after left dorsal laparotomy, followed by reperfusion, as a model for ischaemia–reperfusion (I/R) injury. To examine the relationship between urinary markers and severity of AKI, we induced short- and long-term ischaemia to model mild and moderate AKI, respectively. First, in a preliminary study, we determined that approximately 90% of male mice that were clamped for either 25 or 30 min died at the end of 7 days. Therefore, animals in the short-term ischaemia group were clamped for 10 min (10 min I/R), whereas those in the long-term ischaemia group were clamped for 20 min (20 min I/R). Briefly, while under inhalation anaesthesia with 2% isoflurane, mice underwent left renal pedicle clamping using a blood vessel clamp for microsurgery (20–32.5 g pressure clamp, S22B; Keisei Medical Industry, Niigata, Japan) for the designated duration, and tissue reperfusion was confirmed before surgery completion. Contralateral nephrectomy was performed at the same time. Sham-operated group was anesthetized, underwent left dorsal laparotomy without ischaemic injury for 20 min, and subjected to right nephrectomy thereafter; this group served as control for I/R mice sacrificed at Day 20. In all groups, 100 μL of blood was collected from orbital venous plexus of mice under inhalation anesthesia with 2% isoflurane at 1 and 20 days after surgery, and kidneys were removed under anaesthesia 20 days after surgery(20 min sham, $n = 8$; 10 min I/R, $n = 8$; 20 min I/R, $n = 8$). Urine was collected for up to 24 h after I/R and 10 and 20 days after surgery in the mice designated to be sacrificed on Day 20, which were individually housed overnight in metabolic cages with free access to tap water.

Serum and urinary biochemistry

Serum and urinary creatinine were measured using a Quantichrom™ creatinine Assay Kit (BioAssay Systems, Hayward, CA, USA). Albuminuria was determined using the Albuwell assay (Exocell, Philadelphia, PA, USA). Urinary levels of L-FABP, NGAL and KIM-1 were measured using enzyme-linked immunosorbent assay (ELISA) kits (human L-FABP, CMIC, Tokyo, Japan; mouse NGAL, Bioporto Diagnostics, Gentofte, Denmark; mouse KIM-1 ELISA kit, R&D Systems, Minneapolis, MN, USA). Urinary parameters were reported as ratios relative to urinary creatinine levels.

Renal histological and immunohistological analysis

Tissues fixed in methyl Carnoy's solution (60% methanol, 30% chloroform, and 10% glacial acetic acid) were embedded in paraffin. Serial sections (2-μm thickness) were prepared for conventional histological assessment of Masson's trichrome staining, and for immunohistochemistry, and an indirect immunoperoxidase method was used to detect target antigens, as described previously.[17,20]

Tissue fibrosis was defined as accumulation of extracellular matrix shown in blue in Masson's trichrome staining assessed at under ×100 magnification. Ten nonoverlapping fields from cortical and outer medullary areas were selected. The areas of tubulointerstitial fibrosis in cortical and outer medullary areas were measured with an image analyzer (Auto/Manual Measurement Software version 6.4, WinRoof, Mitani Co., Tokyo, Japan), and the degree of tubulointerstitial fibrosis in each mouse was expressed as a ratio relative to the total cortical and outer medullary area.

Macrophages and proximal tubules were identified using a rat monoclonal antibody (F4/80, 1:200; BMA Biomedicals, Augst, Switzerland) and a rabbit polyclonal antibody against aquaporin-1 (1:400; Santa Cruz Biotechnology, TX, USA), respectively. Additionally, both type I and type III collagens were identified using rabbit polyclonal antibodies (1:200; Cedarlane Laboratories, Ontario, Canada) specific for each target.

Additionally, for immunohistological assessment of myofibroblasts, tissue specimens fixed in 10% buffered formalin and embedded in paraffin were immunostained using a mouse monoclonal antibody against α-smooth muscle actin (α-SMA, 1:800; Sigma-Aldrich, St. Louis, MO, USA).

Visualization was achieved by incubation with polymeric horseradish peroxidase-conjugated secondary antibodies (ready-to-use, ImmPRESS polymer detection kit; Vector

© 2017 Asian Pacific Society of Nephrology

Laboratories, Burlingame, CA, USA). Peroxidase activity was revealed by the diaminobenzidine reaction (Liquid DAB+; DAKO Japan, Tokyo, Japan), and sections were counterstained with haematoxylin.

Images from 10 non-overlapping fields from the entire cortical and outer medullary region were captured at 100× magnification. The degrees of macrophage infiltration and interstitial myofibroblasts in the cortical and outer medulla interstitium were automatically measured with an image analyzer of WinRoof. Briefly, areas positively stained for F4/80 and α-SMA were separately measured and expressed as ratios relative to the area of the entire cortical and outer medullary region. The same method was used to measure the expression of aquaporin-1, and both type I and type III collagens.

We used tissues fixed in 10% buffered formalin for immunohistochemistry with a monoclonal antibody against human L-FABP. Human L-FABP immunostaining in the kidneys of mice was performed with a mouse monoclonal antibody generated previously against human L-FABP (1:1000, CMIC Co, Ltd).

Measurement of monocyte chemoattractant protein-1 and human L-FABP

Proteins were extracted from frozen kidneys, and protein concentrations were measured as described previously.[20] Inflammatory cytokine monocyte chemoattractant protein-1 (MCP-1) was measured by ELISA (MCP-1; R&D Systems), and renal protein expression of human L-FABP was measured by ELISA (CMIC Co, Ltd). Their values were normalized to total protein concentration.

Real-time quantitative polymerase chain reaction

Total RNA was extracted from frozen kidneys and reverse transcribed as described previously.[20] TaqMan real-time polymerase chain reaction (PCR) was used to measure mRNA levels of *MCP-1*, transforming growth factor-β *(TGF-β)*, α-1 type I collagen, α-1 type III collagen, and glyceraldehyde-3-phosphate dehydrogenase *(GAPDH)* with Applied Biosystems StepOnePlus real-time PCR System (Applied Biosystems, Waltham, MA, USA). *MCP-1* mRNA was measured to evaluate inflammatory response, whereas mRNAs of *TGF-β*, and α-1 type I and α-1 type III collagens were measured to assess renal fibrosis. Expression levels of all mRNAs were normalized to *GAPDH* expression levels in all samples.

Statistical analysis

All values were expressed as mean ± standard error (SE). All $P < 0.05$ indicated statistical significance. Comparison of multiple groups was performed using one-way analysis of variance (ANOVA), followed by the Mann–Whitney *U*-test. To assess correlations of two parameters, Spearman's rank correlation coefficient was used to evaluate nonparametric data. All statistical analyses were performed with JMP version 12.2.0 (SAS Institute, Cary, NC, USA).

RESULTS

Evaluation of serum creatinine

We first determined serum creatinine levels in both acute and chronic phases of AKI. Serum creatinine levels were significantly higher in the 20 min I/R group than in both the 10 min I/R and sham-operated groups ($P < 0.05$) both 1 day post-I/R during the acute phase of AKI (Fig. 1A) and 20 days post-I/R during the chronic phase (Fig. 1B).

MCP-1 expression and macrophages in filtration

MCP-1 mRNA (Fig. 2A) and protein (Fig. 2B) levels in the 20 min I/R group were significantly higher than those in the 10 min I/R and sham-operated groups 20 days after I/R. Additionally, while macrophage infiltration was observed in the renal interstitium of both the 10 min and 20 min I/R groups, and the extent of infiltration in the 20 min I/R group was significantly more than that in both the 10 min I/R and sham-operated groups ($P < 0.05$, Figs. 2C, D).

Histological evaluation of tubulointerstitial damage

Masson's trichrome staining revealed the presence of tubulointerstitial fibrosis (blue staining; Fig. 3A) in the I/R tissue. The degree of tubulointerstitial fibrosis in both the 10 min and 20 min I/R groups were significantly higher than that in the sham-operated group (Fig. 3B). Furthermore, the tubulointerstitial fibrosis was significantly worse in the 20 min I/R group than in the 10 min I/R group ($P < 0.05$; Fig. 3B).

To determine if proximal tubules were either resistant to I/R-induced renal injury or regenerated after such injury, we performed immunohistochemical analysis to detect aquaporin-1 expression (Fig. 3C). As quantified in Figure 3D, the areas of aquaporin-1-positive proximal tubules in both the 10 min and 20 min I/R groups were significantly smaller than that in the sham-operated group, indicating worse tubulointerstitial damage. Additionally, the area of aquaporin-1-positive cells in the 20 min I/R group was significantly lower than that in the 10 min I/R group ($P < 0.05$; Fig. 3D).

In order to examine the degree of tubulointerstitial fibrosis, the expressions of α-SMA, and both type I and type III collagens were determined using immunohistochemical analysis. Whereas α-SMA-positive areas were observed in parts of tubules and interstitium (Fig. 3E), depositions of type I collagen (Fig. 3G) and type III collagen (Fig. 3I)

© 2017 Asian Pacific Society of Nephrology

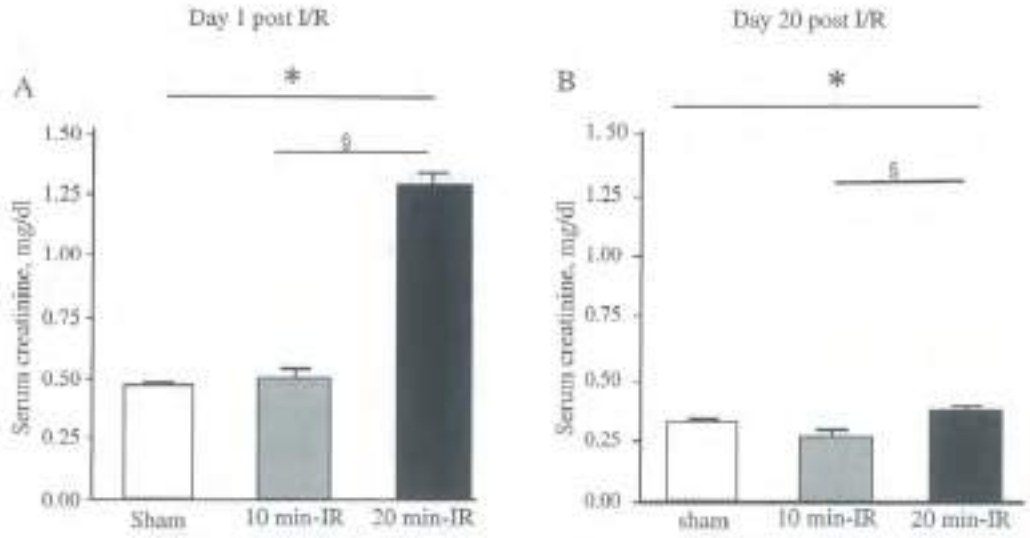

Fig. 1 Serum creatinine levels 1 day post-I/R (A) and 20 days post-I/R (B). *$P < 0.05$ vs the sham-operated group at the same day; §$P < 0.05$ vs the 10 min I/R at the same day.

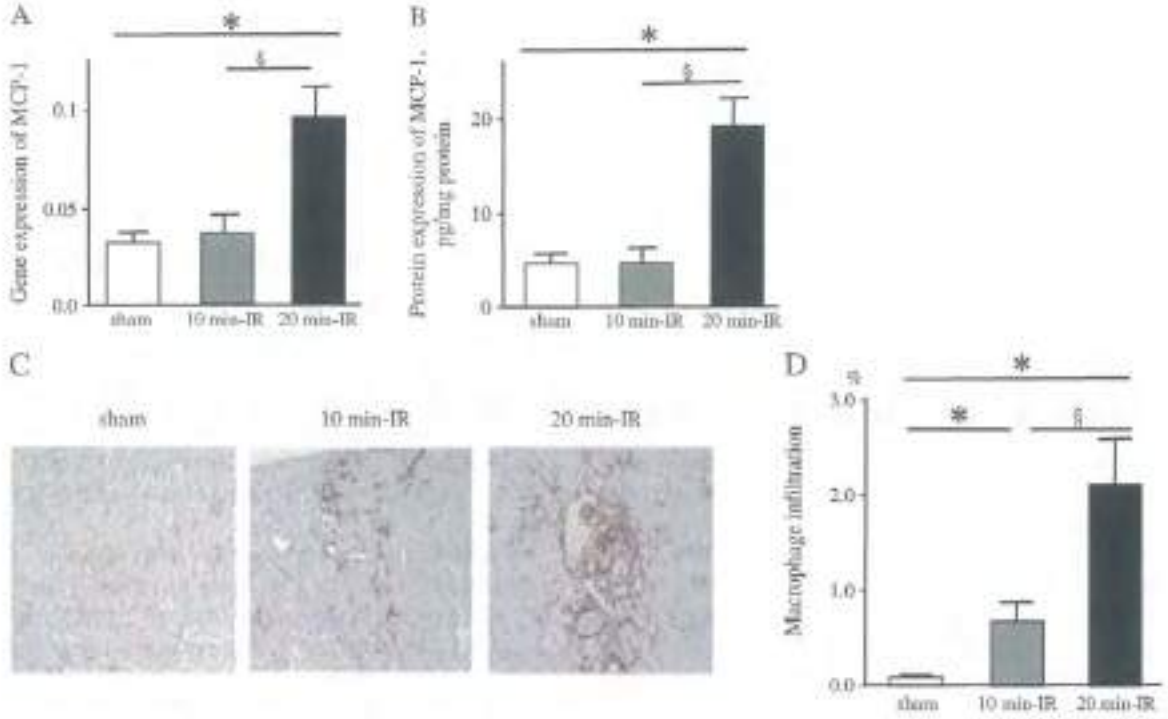

Fig. 2 Gene (A) and protein (B) expressions of MCP-1 in the kidney and representative images of immunohistological staining using an antibody against F4/80 (C). Original magnification, ×100. The areas in C were assessed quantitatively as described in the Materials and Methods section (D). *$P < 0.05$ vs the sham-operated group at the same day; §$P < 0.05$ vs the 10 min I/R at the same day.

were observed in the interstitium. Quantification revealed that the extent of α-SMA-positive areas (Figs. 3E, F) and the deposition levels of type I (Figs. 3G, H) and type III collagens (Figs. 3I, J) were significantly greater in the kidneys of the 10 min and the 20 min I/R groups than in specimens from sham-operated mice. Furthermore, tubulointerstitial fibrosis was significantly worse in the 20 min I/R group than in the 10 min I/R group ($P < 0.05$; Fig. 3F, H, J).

Gene expression analysis for renal interstitial fibrosis

We next evaluated the expression of genes involved in renal interstitial fibrosis. As presented in Figure 4, mRNA levels of

© 2017 Asian Pacific Society of Nephrology

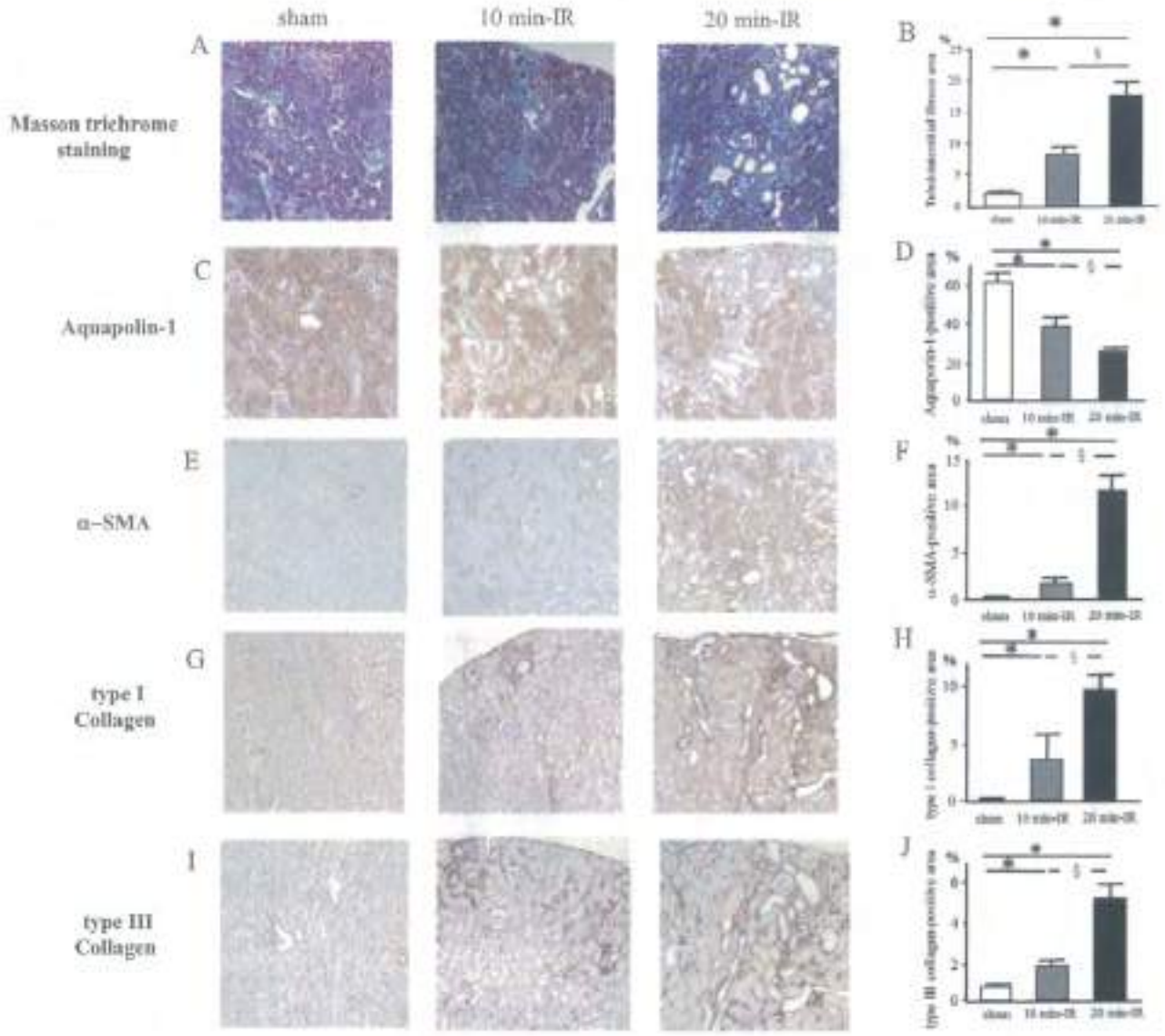

Fig. 3 Histological findings. Representative images of histological staining with Masson's trichrome (A) and immunohistological staining using an antibody against aquaporin-1 (C), α-SMA (E), type I collagen (G) and an antibody against type III collagen (I). Original magnification, ×100. B, D, F, H and J: The areas in A, C, E, G and I were assessed quantitatively as described in the Materials and Methods section. *$P < 0.05$ vs the sham-operated group at the same day; §$P < 0.05$ vs the 10 min IR at the same day.

TGF-β (Fig. 4A), a profibrotic marker, and of α_1-type I (Fig. 4B) and α_1-type III collagens (Fig. 4C), which are universal indicators of fibrosis, were significantly higher in the 20 min I/R group than in the 10 min I/R and sham-operated groups ($P < 0.05$).

Changes in urinary L-FABP levels, immunohistological analysis, and renal protein expression of human L-FABP

Urinary L-FABP levels (Fig. 5A) on Day 0 were comparable between all surgical groups. Importantly, urinary L-FABP levels were significantly higher on Day 1 post-I/R than on Day 0 and were decreased on Day 20 post-I/R in both the 10 min and the 20 min I/R groups. On Days 10 and 20 post-I/R, urinary L-FABP levels were significantly higher in both the 10 min and 20 min I/R groups than in the sham-operated group. On Day 1, urinary L-FABP levels in the 20 min I/R group were significantly higher than those in the 10 min I/R group. Furthermore, urinary L-FABP levels on Day 10 post-I/R in both the 10 min and 20 min I/R groups were significantly higher than those in the same groups on Day 0. While urinary L-FABP levels in the 10 min I/R group on Day 20 post-I/R were not significantly higher than those on Day 0, urinary L-FABP levels in the 20 min I/R group on Day 20 post-I/R were significantly higher than those on Day 0 post-I/R ($P < 0.05$).

© 2017 Asian Pacific Society of Nephrology

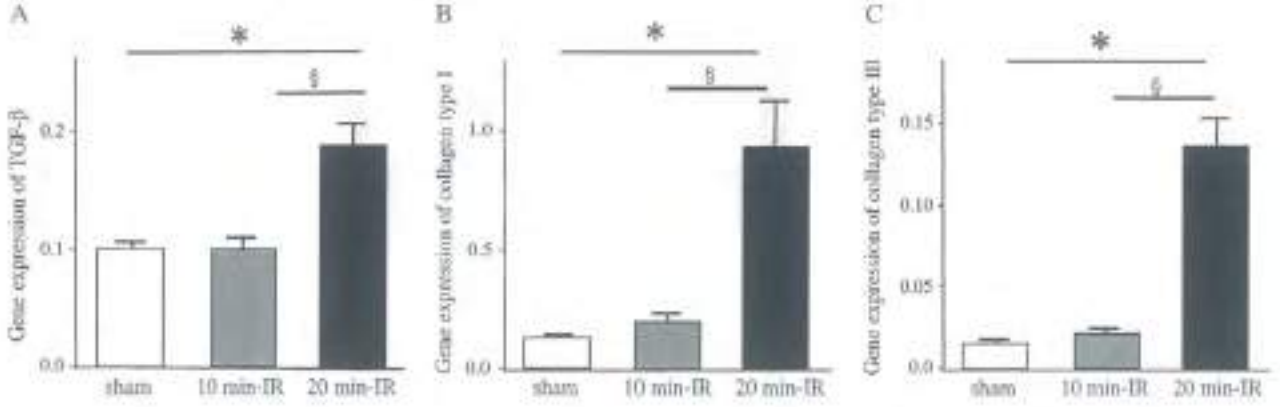

Fig. 4 Gene expressions of TGF-β (A), type I collagen (B) and type III collagen (C) mRNA transcripts in the kidney. *P < 0.05 vs the sham-operated group at the same day.

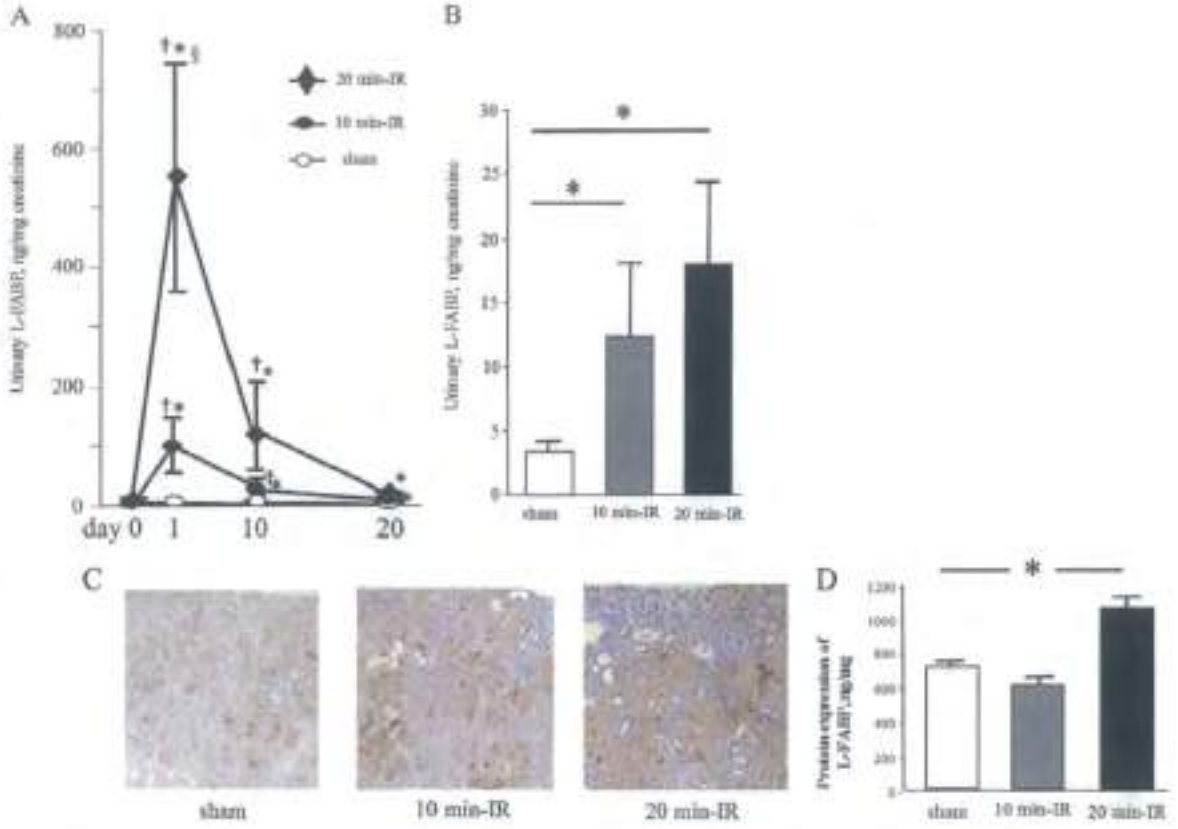

Fig. 5 Time-related changes in urinary human L-FABP levels (A), urinary excretion of L-FABP levels 20 days post-I/R (B), immunohistochemical staining of human L-FABP in the kidney (C), and renal protein expression of human L-FABP (D). *P < 0.05 vs the sham-operated group at the same day; †P < 0.05 vs the same group on Day 0; §P < 0.05 vs the 10 min I/R group at the same day. Original magnification, ×100.

In the immunohistochemical staining, human L-FABP were expressed in the proximal tubules in each 20 min I/R, 10 min I/R, and sham-operated groups (Fig. 5C). In the 20 min I/R group, most of positive tubules were stained intensely.

The protein expression levels of human L-FABP were significantly higher in the 20 min I/R group compared to the 10 min I/R and sham-operated groups (Fig. 5D).

Urinary biochemistry

Twenty days post-I/R, urinary levels of both albumin (Fig. 6A) and KIM-1 (Fig. 6B) were significantly higher in the 20 min I/R group than in the 10 min I/R and sham-operated groups; however, there were no differences in urinary NGAL levels between the three groups (Fig. 6C).

© 2017 Asian Pacific Society of Nephrology

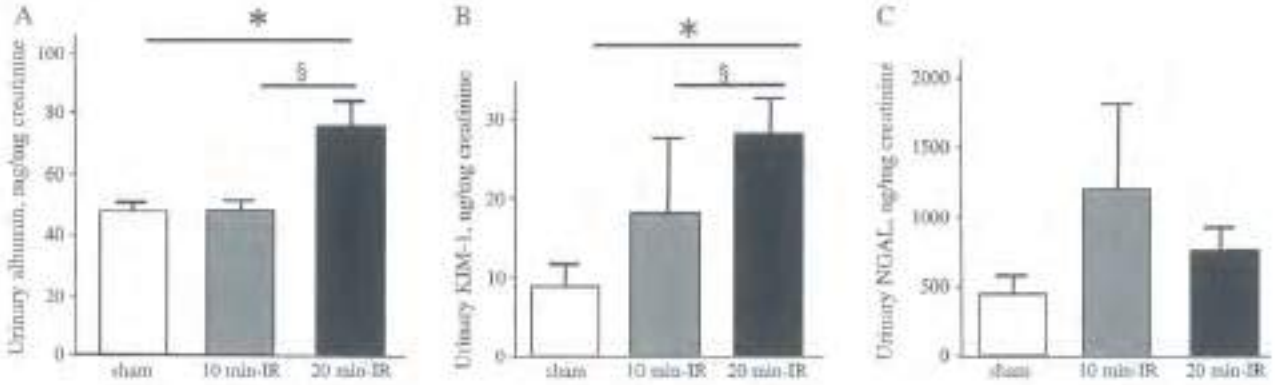

Fig. 6 Urinary excretion of albumin (A), KIM-1 (B) and NGAL (C) 20 days post-I/R. *$P < 0.05$ vs the sham-operated group at the same day; §$P < 0.05$ vs the 10 min I/R at the same day.

Correlation between urinary parameters and the degree of tubulointerstitial damage 20 days post-I/R

Urinary levels of L-FABP, albumin and KIM-1 20 days post-I/R were significantly correlated with the extent of chronic tubulointerstitial injury as indicated by the decrease in aquaporin-1-positive area, α-SMA-positive area and both type I and type III collagens deposition ($P < 0.05$, Table 1 and Fig. 7); however, there was no correlation of urinary NGAL or serum creatinine with the degree of renal injury (Table 1).

DISCUSSION

In the present study using a model of I/R injury with two levels of severity, we found that urinary levels of human L-FABP, albumin and KIM-1 during the chronic phase after AKI were persistently elevated and significantly correlated with markers of chronic tubulointerstitial damage after AKI. These results suggested that urinary tubular markers might be useful for monitoring ongoing kidney injury after AKI in clinical practice.

Although molecular mechanisms underlying AKI-to-CKD progression were not evaluated in the present study, the presence of multifactorial mechanism is expected. Interstitial fibrosis was reported to initiate around injured proximal tubules, and proximal tubular injury has been the focus of intense investigation as the trigger of this transition. Takaori *et al.* reported that selectively damaged proximal tubules secreted factors that induced the transition of fibroblasts to myofibroblasts, subsequently leading to nephron loss and renal fibrosis.[21] Furthermore, I/R injury was reported to provoke acute abnormalities in renal peritubular capillaries and to lead to rarefaction of peritubular capillaries because of poor regenerative capacity of renal microvascular system.[22] Such a capillary rarefaction in the kidney induced tubular hypoxia and contributed to tubular damage.[10,23] Proximal tubules are especially vulnerable to tubular hypoxic injury because of the lower capacity for anaerobic glycolytic ATP production.[24] We also showed that the loss of proximal tubules, as determined by aquaporin-1-positive cells, was augmented in mice with more severe AKI. Therefore, urinary markers of proximal tubular injury might be capable of reflecting the degree of renal tubulointerstitial damage during the chronic phase after AKI.

I/R injury can also occur during AKI after cardiopulmonary bypass (CPB). A recent study conducting long-term assessment of urinary markers in paediatric patients who underwent CPB ($n = 372$) revealed that the levels of urinary L-FABP and KIM-1 but not that of urinary NGAL remained elevated 7 years after one episode of AKI after cardiac surgery, and that the levels of these markers were significantly higher than those in age-matched healthy children and AKI-negative patients.[25] Although renal histological findings in patients with a history of AKI were not evaluated in that study, the presence of chronic tubulointerstitial damage after CPB-associated AKI is speculated from the results of the present study.

Even in animals with mild ischaemia (10 min I/R), which did not show elevations in serum creatinine levels at either 1 or 20 days post-I/R, urinary L-FABP sharply increased on Day 1 post-I/R and remained significantly elevated even 20 days after

Table 1 Correlations between urinary levels of markers and renal histological change

Parameters	Aquaporin-1	α-SMA	Type I collagen	Type III collagen
Urinary L-FABP	Rs = −0.828 $P < 0.000$	Rs = 0.584 $P < 0.005$	Rs = 0.661 $P < 0.000$	Rs = 0.666 $P < 0.000$
Urinary albumin	Rs = −0.684 $P < 0.000$	Rs = 0.675 $P < 0.001$	Rs = 0.533 $P < 0.05$	Rs = 0.560 $P < 0.01$
Urinary KIM-1	Rs = −0.657 $P < 0.01$	Rs = 0.738 $P < 0.001$	Rs = 0.660 $P < 0.01$	Rs = 0.727 $P < 0.000$
Urinary NGAL	Rs = −0.102 $P = 0.651$	Rs = 0.383 $P = 0.0785$	Rs = 0.289 $P = 0.193$	Rs = 0.344 $P = 0.117$
Serum creatinine	Rs = −0.345 $P = 0.116$	Rs = 0.360 $P = 0.100$	Rs = 0.070 $P = 0.759$	Rs = 0.314 $P = 0.155$

Values are the mean ± standard errors. L-FABP, liver-type fatty acid-binding protein; KIM-1, kidney injury molecule-1; NGAL, neutrophil gelatinase-associated lipocalin.

© 2017 Asian Pacific Society of Nephrology

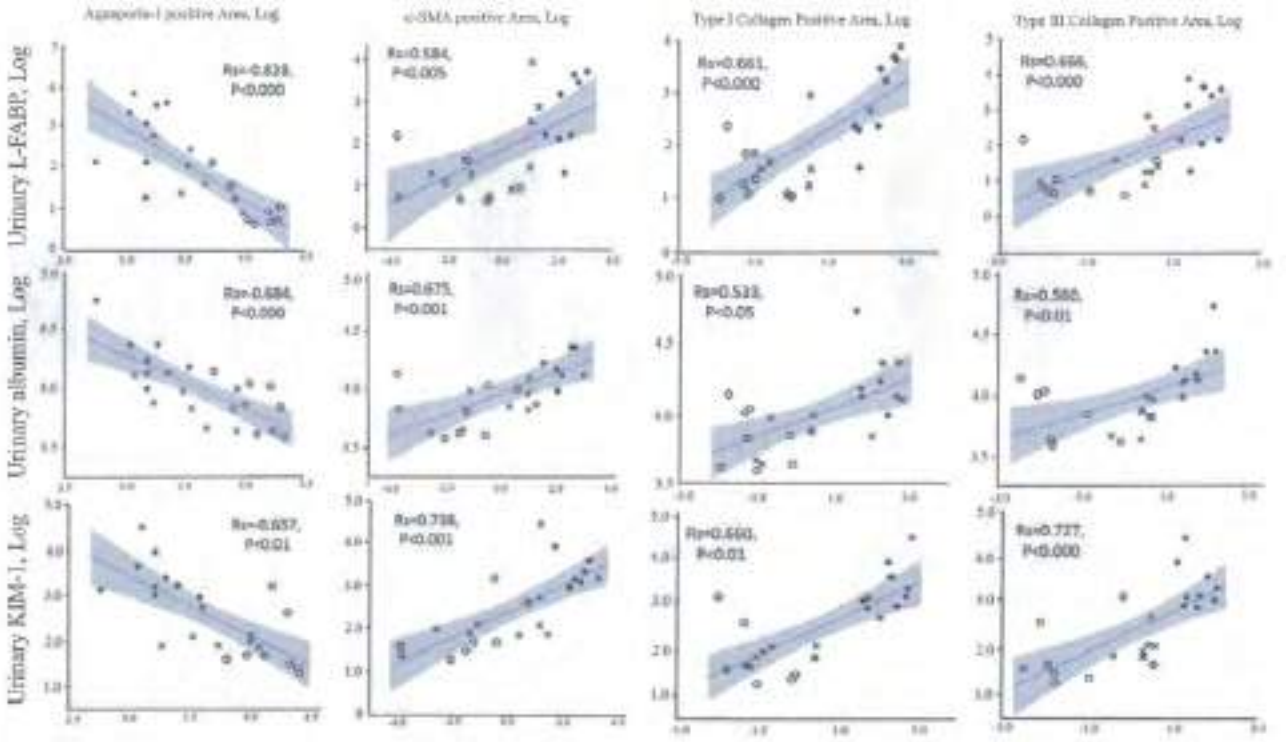

Fig. 7 Correlations between each urinary L-FABP, urinary albumin and urinary KIM-1 level and each histological marker 20 days post-I/R. Black diamond (◆) showed 20 min I/R, x-mark (x) showed 10 min I/R and white square (□) showed sham-operated group.

I/R, compared to sham-operated mice; importantly, chronic renal fibrosis was observed in these animals. Forbes et al. also reported the significance of chronic renal fibrosis without renal dysfunction after acute I/R injury.[26] Cooper *et al.* showed that urinary L-FABP levels remained above normal limits 7 years after one episode of AKI in the absence of abnormal serum creatinine levels.[25] Due to the functional reserve of the kidneys that compensates for the reduced function of the nephron, serum creatinine may not adequately reflect the actual anatomic and functional limitation of the kidney, and may partially explain the discrepancy between the changes in serum creatinine and tubular markers. The significance of urinary tubular markers was illustrated by the evaluation of surviving nephrons after AKI in the present study.

We previously showed that urinary levels of L-FABP, albumin, KIM-1 and NGAL during the acute phase of AKI due to I/R injury were significantly correlated with the degree of chronic renal fibrosis.[17] In addition to their significance in reflecting the extent on tubulointerstitial damage in the chronic phase after AKI as demonstrated in the present study, evaluation of their markers during the acute phase after I/R injury might be useful for identification of patients who are at higher risk for progression to CKD in clinical practice. This approach should be useful in initiating appropriate and effective therapeutic approaches for AKI and decreasing CKD incidence.

In a previous study, we evaluated the potential of urinary markers during the acute phase after injury to predict AKI-to-CKD transition using female human L-FABP Tg mice.[17] Intriguingly, the levels of urinary markers 20 or 40 days post-I/R in these female mice were not different from those measured in sham-operated mice. Therefore, we aimed to develop a model with more severe AKI using male mice of the same genetic background in the present study, given that male mice are more vulnerable to renal injury-inducing stimuli.[27,28] In fact, approximately 90% of male animals that were clamped for 30 min, which induced only mild AKI in female mice in our previous study,[17] died within 7 days. These results demonstrated that the duration of I/R was shorter in male mice than in female mice; thus, the follow-up period in the present study was 20 days.

L-FABP binds strongly to long-chain fatty acid oxidation products[29] or works as a scavenger of reactive oxygen species.[30] Therefore, it is considered renoprotective in various renal disease models.[31] Increased L-FABP protein expression levels in the proximal tubules of the 20 min I/R group lets us expect that L-FABP may attenuate chronic tubulointerstitial damage after I/R. However, serum creatinine levels and the degree of chronic tubulointerstitial damage after 20 min I/R injury were similar between WT mice and human L-FABP Tg mice (data not shown). The severity of injury seen here may however overwhelm any renoprotective actions.

In conclusion, urinary levels of human L-FABP, albumin, and KIM-1 during the chronic phase after AKI reflected the degree of chronic tubulointerstitial damage, and may be useful for monitoring CKD after AKI in clinical practice. Furthermore, before initiating procedures or treatments with a high risk of

© 2017 Asian Pacific Society of Nephrology

inducing AKI, these markers might be used to evaluate the degree of chronic tubulointerstitial damage for prevention of iatrogenic AKI.

FUNDING SOURCE

This work was supported by a grant for medical research subsidized by St. Marianna University School of Medicine Research Grant, Japan.

ACKNOWLEDGMENTS

We thank Ms. Kimie Katayama and Jyunko Asano for technical assistance.

DISCLOSURES

T. Sugaya is the Director and Senior scientist and K. Ohata is the scientist of CMIC HOLDINGS Co., Ltd., the company that produced the kits for L-FABP analysis.

None of the other authors have conflicts of interest or financial disclosures of any relevance to the present study.

CONTRIBUTION

DI and AK-I, study design; DI, AK-I, KO, MH and SH, data collection; DI and AK-I, data analysis; DI, AK-I, TS, KK and YS, data interpretation; DI, AK-I and TS, literature search and generation of figures; DI and AK-I, writing of the manuscript. All authors gave their final approval of the submitted version.

REFERENCES

1. Hoste EA, Bagshaw SM, Bellomo R *et al.* Epidemiology of acute kidney injury in critically ill patients: the multinational AKI-EPI study. *Intensive Care Med.* 2015; 41: 1411–1423.
2. Lameire NH, Bagga A, Cruz D *et al.* Acute kidney injury: an increasing global concern. *Lancet* 2013; 382: 170–179.
3. Siew ED, Davenport A. The growth of acute kidney injury: a rising tide or just closer attention to detail? *Kidney Int.* 2015; 87: 46–61.
4. Chawla LS, Kimmel PL. Acute kidney injury and chronic kidney disease: an integrated clinical syndrome. *Kidney Int.* 2012; 82: 516–524.
5. Coca SG, Singanamala S, Parikh CR. Chronic kidney disease after acute kidney injury: a systematic review and meta-analysis. *Kidney Int.* 2012; 81: 442–448.
6. Ishani A, Xue JL, Himmelfarb J *et al.* Acute kidney injury increases risk of ESRD among elderly. *J. Am. Soc. Nephrol.* 2009; 20: 223–228.
7. Venkatachalam MA, Weinberg JM, Kriz W, Bidani AK. Failed Tubule Recovery, AKI-CKD Transition, and Kidney Disease Progression. *J. Am. Soc. Nephrol.* 2015; 26: 1765–1776.
8. Ascon M, Ascon DB, Liu M *et al.* Renal ischemia–reperfusion leads to long term infiltration of activated and effector-memory T lymphocytes. *Kidney Int.* 2009; 75: 526–535.
9. Austin JK, Huber LC, Dunn DW, Shore CP, Johnson CS, Perkins SM. Children with new onset seizures: A prospective study of parent variables, child behavior problems, and seizure occurrence. *Epilepsy Behav.* 2015; 53: 73–77.
10. Tanaka S, Tanaka T, Nangaku M. Hypoxia as a key player in the AKI-to-CKD transition. *Am. J. Physiol. Renal Physiol.* 2014; 307: F1187–F1195.
11. Chevalier RL. The proximal tubule is the primary target of injury and progression of kidney disease: role of the glomerulotubular junction. *Am. J. Physiol. Renal Physiol.* 2016; 311: F145–F161.
12. Nath KA. Tubulointerstitial changes as a major determinant in the progression of renal damage. *Am. J. Kidney Dis.* 1992; 20: 1–17.
13. Kamijo A, Kimura K, Sugaya T *et al.* Urinary fatty acid-binding protein as a new clinical marker of the progression of chronic renal disease. *J. Lab. Clin. Med.* 2004; 143: 23–30.
14. Kamijo-Ikemori A, Sugaya T, Yasuda T *et al.* Clinical significance of urinary liver-type fatty acid-binding protein in diabetic nephropathy of type 2 diabetic patients. *Diabetes Care* 2011; 34: 691–696.
15. Xu PC, Zhang JJ, Chen M *et al.* Urinary kidney injury molecule-1 in patients with IgA nephropathy is closely associated with disease severity. *Nephrol. Dialys. Transplantat.* 2011; 26: 3229–3236.
16. Lin HY, Hwang DY, Lee SC *et al.* Urinary neutrophil gelatinase-associated lipocalin and clinical outcomes in chronic kidney disease patients. *Clin. Chem. Lab. Med.* 2015; 53: 73–83.
17. Hisanishi M, Kamijo-Ikemori A, Sugaya T *et al.* Increase in urinary markers during the acute phase reflects the degree of chronic tubulointerstitial injury after ischemia–reperfusion renal injury. *Biomarkers* 2016 [Epub ahead of print].
18. Zappitelli M, Coca SG, Garg AX *et al.* The association of albumin/creatinine ratio with postoperative AKI in children undergoing cardiac surgery. *Clin. J. Am. Soc. Nephrol.* 2012; 7: 1761–1769.
19. Kamijo A, Sugaya T, Hikawa A *et al.* Urinary excretion of fatty acid-binding protein reflects stress overload on the proximal tubules. *Am. J. Pathol.* 2004; 165: 1243–1255.
20. Kamijo-Ikemori A, Sugaya T, Hibi C *et al.* Renoprotective effect of the xanthine oxidoreductase inhibitor topiroxostat on adenine-induced renal injury. *Am. J. Physiol. Renal Physiol.* 2016; 310: F1366–F1376.
21. Takaori K, Nakamura J, Yamamoto S *et al.* Severity and Frequency of Proximal Tubule Injury Determines Renal Prognosis. *J. Am. Soc. Nephrol.* 2016; 27: 2393–2406.
22. Basile DP, Donohoe D, Roethe K, Osborn JL. Renal ischemic injury results in permanent damage to peritubular capillaries and influences long-term function. *Am. J. Physiol. Renal Physiol.* 2001; 281: F887–F899.
23. Basile DP. Rarefaction of peritubular capillaries following ischemic acute renal failure: a potential factor predisposing to progressive nephropathy. *Curr. Opin. Nephrol. Hypertens.* 2004; 13: 1–7.
24. Gobe GC, Johnson DW. Distal tubular epithelial cells of the kidney: Potential support for proximal tubular cell survival after renal injury. *Int. J. Biochem. Cell Biol.* 2007; 39: 1553–1561.
25. Cooper DS, Claes D, Goldstein SL *et al.* Follow-Up Renal Assessment of Injury Long-Term After Acute Kidney Injury (FRAIL-AKI). *Clin. J. Am. Soc. Nephrol.* 2016; 11: 21–29.
26. Forbes JM, Hewitson TD, Becker GJ, Jones CL. Ischemic acute renal failure: long-term histology of cell and matrix changes in the rat. *Kidney Int.* 2000; 57: 2375–2385.
27. Neugarten J, Acharya A, Silbiger SR. Effect of gender on the progression of nondiabetic renal disease: a meta-analysis. *J. Am. Soc. Nephrol.* 2000; 11: 319–329.
28. Neugarten J, Golestaneh L. Gender and the prevalence and progression of renal disease. *Adv. Chronic Kidney Dis.* 2013; 20: 390–395.
29. Ek-Von Mentzer BA, Zhang P, Hamilton JA. Binding of 13-HODE and 15-HETE to phospholipid bilayers, albumin, and intracellular fatty acid binding proteins. Implications for transmembrane and intracellular transport and for protection from lipid peroxidation. *J. Biol. Chem.* 2001; 276: 15575–15580.
30. Ichikawa D, Kamijo-Ikemori A, Sugaya T *et al.* Human liver-type fatty acid-binding protein protects against tubulointerstitial injury in aldosterone-induced renal injury. *Am. J. Physiol. Renal Physiol.* 2015; 308: F114–F121.
31. Kamijo-Ikemori A, Sugaya T, Matsui K, Yokoyama T, Kimura K. Roles of human liver type fatty acid binding protein in kidney disease clarified using hL-FABP chromosomal transgenic mice. *Nephrol.* 2011; 16: 539–544.

© 2017 Asian Pacific Society of Nephrology

Hypertension Research (2019) 42:1518–1527
https://doi.org/10.1038/s41440-019-0273-z

ARTICLE

Renoprotective effects of voluntary running exercise training on aldosterone-induced renal injury in human L-FABP chromosomal transgenic mice

Keisei Kosaki[1,2,3] · Takeshi Sugaya[1] · Keiichi Ohata[1] · Jun Tanabe[1] · Seiko Hoshino[4] · Kazuho Inoue[4] · Kenjiro Kimura[5] · Seiji Maeda[2] · Yugo Shibagaki[1] · Atsuko Kamijo-Ikemori[1,4]

Received: 21 September 2018 / Revised: 8 April 2019 / Accepted: 30 April 2019 / Published online: 6 June 2019
© The Japanese Society of Hypertension 2019

Abstract

Tubulointerstitial damage is a crucial therapeutic target in preventing chronic kidney disease (CKD) progression. Inappropriately activated renin–angiotensin–aldosterone system (RAAS) in the tubulointerstitial area is strongly associated with tubulointerstitial damage progression. Therefore, this study aimed to determine whether there is a beneficial effect of voluntary running exercise training on aldosterone-induced renal injury. Human L-type fatty acid-binding protein (L-FABP) chromosomal transgenic (L-FABP$^{+/-}$) male mice were used to evaluate the effect of exercise by using urinary L-FABP, a tubular marker. The mice were assigned to either the exercise group that performed voluntary running exercise training using a running wheel or the control group. Subsequently, two groups were injected with aldosterone (0.125 μg kg^{-1} min^{-1}) and administered 1% NaCl water, and two groups were administered aldosterone only in solvent 4 weeks after initiating the exercise. Aldosterone was injected for another 4 weeks, and NaCl water was administered from 5 weeks after starting the exercise until 8 weeks. Although both aldosterone and NaCl water significantly decreased the running distance, tubulointerstitial damage involving interstitial infiltration of macrophages and fibrosis and the elevation of urinary human L-FABP induced by aldosterone injection was prevented by voluntary running exercise training. Urinary human L-FABP levels were significantly correlated with the degree of tubulointerstitial damage. In conclusion, voluntary running exercise training delayed tubulointerstitial damage progression in the aldosterone-induced renal injury model and therefore may be a promising nonpharmacological strategy in CKD.

Keywords Tubulointerstitial damage · Urinary L-type fatty acid-binding protein · Renin–angiotensin–aldosterone system · Exercise training

Introduction

Compared with the degree of glomerular damage, tubulointerstitial damage is widely known to be strongly associated with chronic kidney disease (CKD) progression [1, 2]. Inappropriate activation of the renin–angiotensin–aldosterone system (RAAS) in the tubulointerstitial area is a crucial aggravating factor for CKD progression [3], and RAAS inhibition should be the first-line therapy to prevent aggravation of CKD in clinical practice. However, various side effects induced by RAAS inhibition, such as hypotension, hyperkalemia, and decreased glomerular filtration, make complete RAAS inhibition impossible in patients with CKD. Therefore, another strategy is needed to improve tubulointerstitial damage due to excessive RAAS activation.

Supplementary information The online version of this article (https://doi.org/10.1038/s41440-019-0273-z) contains supplementary material, which is available to authorized users.

✉ Atsuko Kamijo-Ikemori
a2kamijo@marianna-u.ac.jp

[1] Division of Nephrology and Hypertension, Department of Internal Medicine, St. Marianna University School of Medicine, Kanagawa, Japan

[2] Faculty of Health and Sport Sciences, University of Tsukuba, Ibaraki, Japan

[3] Japan Society for the Promotion of Science, Tokyo, Japan

[4] Department of Anatomy, St. Marianna University School of Medicine, Kanagawa, Japan

[5] JCHO Tokyo Takanawa Hospital, Tokyo, Japan

Recently, studies have focused on several beneficial effects of exercise training to prevent CKD progression [4, 5]. A prospective study with a large cohort revealed that high-intensity physical activity might decrease the risk of the onset of diabetic nephropathy in patients with type 1 diabetes [6]. Similar to the mechanisms of the effects of exercise training against CKD, some experimental studies showed that exercise induces a protective endothelial function via an anti-inflammatory effect [7, 8] with the potential for improving renal microcirculation due to increased production of a vasodilator, nitric oxide (NO), which is synthesized by activation of endothelial NO synthase (eNOS) [9–11] and an anti-oxidative effect [7, 12, 13]. Various factors, such as inflammation, abnormalities of renal hemodynamics, and oxidative stress, are linked to tubulointerstitial damage progression under the excessive activation of RAAS [14–16], and thus, exercise training may be a nonpharmacologically useful strategy against tubulointerstitial damage in CKD.

In the current study, the usefulness of voluntary running exercise training on tubulointerstitial damage due to RAAS activation was examined using an aldosterone-induced model of renal injury, which is established by continuous injection of aldosterone (Aldo), the end-product of RAAS, and high salt intake. In the model, human L-type fatty acid-binding protein (L-FABP), which is expressed in human proximal tubules, was revealed to have a renoprotective role against tubulointerstitial damage [17]. Furthermore, we previously reported that levels of urinary human L-FABP, a tubular marker reflecting the degree of renal microcirculation [18, 19], in addition to the degree of oxidative stress and severity of tubulointerstitial damage [20–22], were significantly correlated with exercise capacity [23] and decreased by exercise training in humans [24]. Therefore, to investigate whether voluntary running exercise training combined with the expression of human L-FABP prevents the progression of tubulointerstitial damage and whether renal histological findings and urinary L-FABP are changed by exercise training, we used human L-FABP chromosomal transgenic mice because L-FABP is not expressed in mouse kidneys [25].

Materials and methods

Animals

Human L-FABP chromosomal transgenic (L-FABP-Tg) mice on a C57/BL6 background were used to evaluate the degree of tubulointerstitial damage by using urinary L-FABP, a tubular marker, in this study. The human L-FABP-Tg mice were generated by microinjection of the genomic DNA of human L-FABP, including its promoter region, as previously described (patent WO0073791; World Intellectual Property Organization, Switzerland) [26]. The present study was performed in accordance with the St. Marianna University School of Medicine Institutional Guide for Animal Experiments and the Guide for the Care and Use of Laboratory Animals (National Institutes of Health, USA).

Experimental design

The current study consisted of an 8-week observation period. At first, the human L-FABP-Tg mice (8-week-old to 10-week-old male mice, $n = 34$) were divided into four groups as follows: Control ($n = 12$), Exercise ($n = 4$), Aldosterone (Aldo) ($n = 9$), and Exercise–Aldosterone (Ex-Aldo) groups ($n = 9$). The mice in the Exercise and Ex-Aldo groups performed voluntary running exercise training for 8 weeks. The mice in the Aldo and Ex-Aldo groups were injected with aldosterone 4 weeks after starting the exercise until 8 weeks, and 1% NaCl water was administered 5 weeks after starting the exercise (1 week after starting aldosterone injection) until 8 weeks. During the experimental periods, all mice were housed overnight individually in metabolic cages to collect the urine at weeks 0, 4, and 8 and had free access to tap water. Body weight and blood pressure were evaluated biweekly. The kidneys, skeletal muscles (gastrocnemius), and serum were collected at week 8 for various analyses.

Aldosterone-induced renal injury

Aldosterone-induced renal injury has been established by both systemic infusion of aldosterone ($0.125\,\mu g^{-1}\,kg^{-1}\,min^{-1}$, A9477; Sigma-Aldrich, MO, USA) and drinking of 1% NaCl water. The aldosterone was dissolved in polyethylene glycol (PEG 300; Sigma-Aldrich, MO, USA) and infused via an osmotic minipump (Alzet 1004; Durect, CA, USA) implanted into the subcutaneous space of mice anesthetized with isoflurane as previously described [27]. In contrast, both the Control and Exercise groups were infused with vehicle only using the osmotic minipump.

Voluntary running exercise training

Voluntary running exercise training was conducted using a running wheel (ENV-044; Med Associates, VT, USA) for 8 weeks. The number of rotations and running distance were automatically recorded using a Bluetooth device (SOF-860; Med Associates).

Blood pressure

Blood pressure was measured biweekly by using a tail-cuff apparatus (Softron BP-98A; Softron, Tokyo, Japan).

Systolic blood pressure values were derived from the mean of three measurements per animal at each time point.

Serum and urinary biochemistry

Serum potassium and sodium levels were measured using an electrode method provided by the clinical laboratory testing services of SRL (Tokyo, Japan). Serum cystatin C levels were evaluated using a sandwich enzyme-linked immunosorbent assay (ELISA) method (Cystatin C Mouse ELISA kit; BioVendor Laboratory Medicine, Modrice, Czech Republic). Serum and urinary creatinine levels were measured using the Jaffe method (Creatinine Assay Kit; BioAssay Systems, CA, USA). Urinary albumin levels were determined using a Mouse Albumin ELISA kit (Albuwell M; Exocell, Inc., PA, USA). Urinary human L-FABP levels were measured using a two-step sandwich ELISA procedure (human L-FABP ELISA kit, CMIC, Tokyo, Japan) as previously described [21]. All urinary parameters are reported as ratios relative to urinary creatinine levels.

Renal histologic and morphometric analysis

For renal histologic and morphometric analysis, the kidneys were fixed in methyl Carnoy's solution or 10% buffered formalin, dehydrated, and embedded in paraffin. Some sections (3-μm thick) were obtained for renal histological assessments, such as periodic acid–Schiff staining and immunohistochemistry. Tubulointerstitial damage in periodic acid–Schiff-stained sections was categorized as tubular dilation with epithelial and tubular atrophy. Under magnification (×100), 7–10 nonoverlapping fields from the entire cortical and outer medulla areas were selected. Tubulointerstitial damage areas were measured manually using an image analyzer (version 6.4, Auto/Manual Measurement Software, WinRoof, Mitani, Tokyo, Japan). The degree of tubulointerstitial damage was evaluated as ratios relative to the entire cortical and outer medulla areas [27].

Immunohistologic analysis

Using the sections preprocessed as described above, an indirect immunoperoxidase method was used to identify the antigens, as previously described [20]. Macrophage infiltration was identified using rat monoclonal antibody F4/80 (1:200, BMA Biomedicals, Augst, Switzerland). Collagen types I and III were identified using rabbit polyclonal antibodies (1:200, Southern Biotech, AL, USA). For immunohistological assessment of myofibroblasts, tissue specimens fixed in 10% buffered formalin and embedded in paraffin were immunostained using a mouse monoclonal antibody to α-smooth muscle actin (α-SMA) (1:800, Sigma-Aldrich, MO, USA).

Visualization was performed by incubation with polymeric horseradish peroxidase-conjugated secondary antibodies (ready-to-use, ImmPRESS Polymer Detection kit, Vector Laboratories, CA, USA). Peroxidase activity was revealed by a diaminobenzidine reaction (Liquid DAB+, DAKO Japan, Tokyo, Japan), and sections were counterstained with hematoxylin. We selected 7–10 nonoverlapping fields from the entire cortical and outer medulla areas. The degree of macrophage infiltration and interstitial myofibroblasts in the cortical and outer medulla interstitium were automatically measured by separating positively stained areas of F4/80 and α-SMA and are expressed as ratios of F4/80-positive and α-SMA-positive areas relative to the entire cortical and outer medulla areas under 100× magnification, as measured with the image analyzer (WinRoof). Similarly, the positive areas for collagen types I and III were automatically measured by separating positively stained areas for collagen types I and III and are expressed as ratios of collagen type I-positive and III-positive areas relative to the entire cortical and outer medulla areas.

Statistical analysis

All data are shown as the means ± SE. The differences between the four groups at week 8 were analyzed using one-way analysis of variance with the Tukey–Kramer test, as the sample numbers were different among the groups. The relationships between urinary human L-FABP levels and the degree of tubulointerstitial damage and systolic blood pressure were analyzed using Spearman's rank correlation coefficients (r_s). Statistical significance was set a priori at $P < 0.05$ for all comparisons. Statistical analyses were performed using SPSS software (version 21).

Results

Running distance

Figure 1a shows time-related changes in the mean running distance in the Exercise and Ex-Aldo groups. The mean running distance of both groups gradually increased from week 1 to week 4. The mean running distance of both groups gradually decreased after the osmotic minipump was injected (at week 4). Furthermore, the average running distance in the Ex-Aldo group notably decreased after drinking 1% NaCl water, and significant differences were found between the groups in weeks 6, 7, and 8.

Systolic blood pressure

Time-related changes in systolic blood pressure are presented in Fig. 1b. From week 0 to week 4, the systolic blood

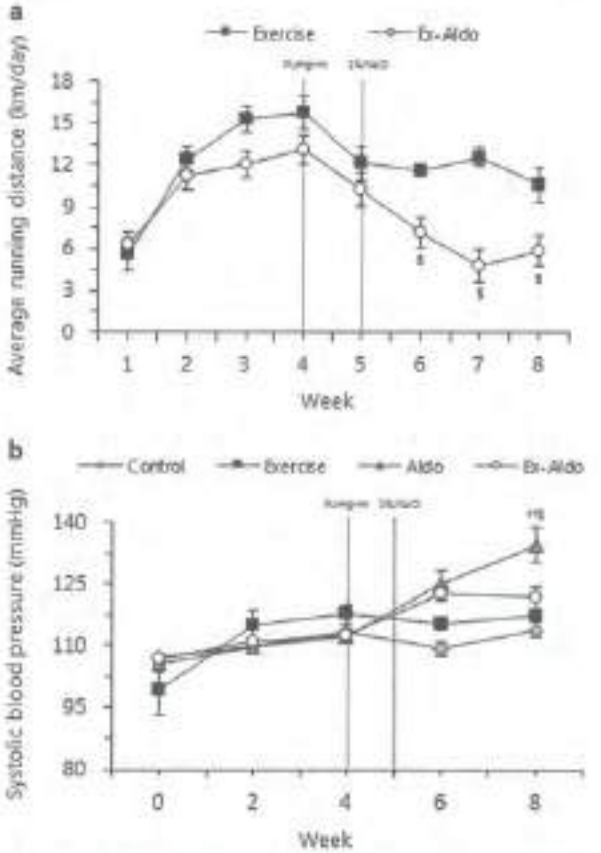

Fig. 1 Time-related changes in the mean running distance (a) and systolic blood pressure (b). Control, $n = 12$; Exercise, $n = 4$; Aldosterone (Aldo), $n = 9$; Exercise–Aldosterone (Ex-Aldo), $n = 9$. Values are represented as the mean ± SE. $^{\#}P < 0.001$ vs. control group, $^{\S}P < 0.05$ vs. Ex-Aldo group, $^{\dagger}P < 0.05$ vs. exercise group

pressure levels were similar in all four groups. The systolic blood pressure levels increased in the Aldo and Ex-Aldo groups after systemic aldosterone infusion and drinking 1% NaCl water. The systolic blood pressure levels were significantly higher in the Aldo group than in the other three groups at week 8.

Animal characteristic findings

Table 1 outlines the animal characteristic findings, including body weight, renal and muscle weight, serum biochemistry findings, urine volume, and total and mean running distance at week 8. The body weight in the exercise and Ex-Aldo groups was significantly lower than that in the control group (both $P < 0.05$), and the body weight in the Ex-Aldo group was significantly lower than that in the Aldo group ($P < 0.05$). The renal weights in the Aldo and Ex-Aldo groups were significantly higher than those in the control group ($P < 0.001$). In contrast, the muscle weight was similar in all four groups.

The serum creatinine levels in the Aldo group were significantly higher than those in the control group ($P < 0.05$). Although the serum creatinine levels were significantly lower in the Ex-Aldo group than in the Aldo group ($P < 0.05$), serum cystatin C levels in the Ex-Aldo group were similar to those in the Aldo group and were significantly lower than those in the control group ($P < 0.05$). The serum sodium levels in the Aldo and Ex-Aldo mice were significantly higher than those in the control mice (both $P < 0.001$). The serum potassium levels in the Aldo group were significantly lower than those in the control group ($P < 0.05$).

The urine volume tended to be higher in the Aldo group and was significantly higher in the Ex-Aldo group compared with the control group ($P < 0.05$). The total and mean running distance tended to be lower in the Ex-Aldo group compared with the exercise group.

Urinary biochemistry findings

Figure 2 shows the urinary biochemistry findings at week 8. Urinary human L-FABP levels in the Aldo and Ex-Aldo mice at week 8 were significantly higher than those in the control mice ($P < 0.001$, $P < 0.05$, respectively; Fig. 2a). Furthermore, the urinary human L-FABP levels in the Ex-Aldo group were significantly lower than those in the Aldo group ($P < 0.05$; Fig. 2a). The urinary albumin levels in the Aldo and Ex-Aldo mice at week 8 were also significantly higher than those in the control mice (both $P < 0.001$; Fig. 2b), and the levels in the Ex-Aldo group were significantly lower than those in the Aldo group ($P < 0.05$; Fig. 2b). In contrast, both urinary sodium levels (Fig. 2c) and urinary potassium levels (Fig. 2d) in the Aldo and Ex-Aldo mice at week 8 were significantly higher than those in the control mice (both $P < 0.05$).

Renal histologic and morphometric analysis

Periodic acid–Schiff-stained sections revealed tubulointerstitial damage, including dilatation of tubules and degeneration of proximal tubular epithelial cells in both the Aldo and Ex-Aldo groups. However, the degree of tubulointerstitial damage in the Ex-Aldo mice was significantly lower than that in the Aldo mice ($P < 0.05$; Fig. 3a, b).

Evaluation of macrophage infiltration

The degree of tubulointerstitial inflammation was evaluated by macrophage infiltration via immunohistochemical analysis using the rat monoclonal antibody F4/80 (Fig. 4a, b). Macrophage infiltration into the kidney in both Aldo and Ex-Aldo mice was significantly higher than that in the control mice (both $P < 0.001$); however, the degree of

Table 1 Animal characteristic findings

Variable	Control ($n = 12$)	Exercise ($n = 4$)	Aldosterone ($n = 9$)	Exercise-aldosterone ($n = 9$)
Body weight (g)	30.4 ± 0.5	27.8 ± 0.8*	30.2 ± 0.4	27.7 ± 0.4*#
Renal weight (g/body weight)	0.57 ± 0.02	0.60 ± 0.02	0.92 ± 0.03**	0.95 ± 0.04**
Muscle weight (g/body weight)	0.50 ± 0.01	0.52 ± 0.02	0.47 ± 0.01	0.48 ± 0.01
Serum creatinine levels (ng/mL)	0.59 ± 0.02	0.53 ± 0.04	0.70 ± 0.03*	0.58 ± 0.03#
Serum cystatin C levels (ng/mL)[a]	1.18 ± 0.05	0.96 ± 0.08	1.04 ± 0.03	1.01 ± 0.03*
Serum sodium levels (meq/L)	150 ± 1	153 ± 2	161 ± 1**	161 ± 2**
Serum potassium levels (meq/L)	5.2 ± 0.2	5.2 ± 0.5	3.9 ± 0.2*	4.6 ± 0.3
Urine volume (mL)	1.1 ± 0.1	1.7 ± 0.3	4.6 ± 1.3	6.5 ± 2.5*
Total running distance (km)	–	670 ± 39	–	482 ± 54
Average running distance (km/day)	–	12.0 ± 0.7	–	8.6 ± 1.0

Data are mean ± SE

**$P < 0.001$, *$P < 0.05$ vs. control. #$P < 0.05$ vs. Aldo

[a]Data available in as follows: control, $n = 12$; exercise, $n = 2$; aldosterone, $n = 9$; exercise-aldosterone, $n = 9$

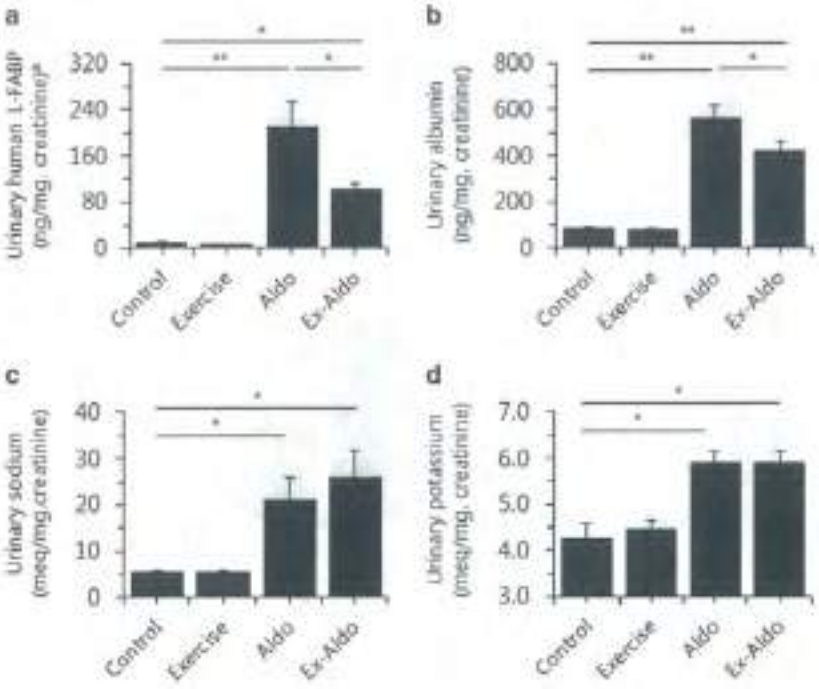

Fig. 2 Urinary biochemistry findings at week 8 (**a**, **b**, **c**, **d**). Control, $n = 12$; Exercise, $n = 4$; Aldosterone (Aldo), $n = 9$; exercise-aldosterone (Ex-Aldo), $n = 9$. #Data available as follows: Control, $n = 9$; Exercise, $n = 4$; Aldo, $n = 7$; Ex-Aldo, $n = 9$. *P*-values were evaluated using one-way ANOVA with a post hoc Tukey–Kramer test. Values are presented as the mean ± SE. **$P < 0.001$, *$P < 0.05$. L-FABP, L-type fatty acid-binding protein

tubulointerstitial inflammation in the Ex-Aldo mice was significantly lower than that in the Aldo mice ($P < 0.05$).

Evaluation of tubulointerstitial fibrosis

The degree of tubulointerstitial fibrosis was assessed by α-SMA and types I and III collagen expression using immunohistochemical analysis. The α-SMA-positive cells (Fig. 4c, d) and deposition levels of types I (Fig. 4e, f) and III (Fig. 4g, h) collagen in the kidneys in both Aldo and Ex-Aldo mice were significantly higher than those in the control mice ($P < 0.001$). However, the degree of tubulointerstitial fibrosis (α-SMA-positive cells and deposition levels of types I and III collagen) in the Ex-Aldo mice was significantly lower than that in the Aldo mice ($P < 0.001$, $P < 0.05$, and $P < 0.05$, respectively).

Relationship between urinary human L-FABP levels and the degree of tubulointerstitial damage, inflammation, and fibrosis

Urinary human L-FABP levels at week 8 were significantly correlated with tubulointerstitial damage in periodic acid–Schiff-stained sections ($r_s = 0.785$, $P < 0.001$; Fig. 5a), the degree of tubulointerstitial inflammation by immunohistological staining using an antibody against F4/80 ($r_s = 0.783$, $P < 0.001$; Fig. 5b), and the degree of tubulointerstitial fibrosis evaluated by α-SMA ($r_s = 0.818$, $P < 0.001$;

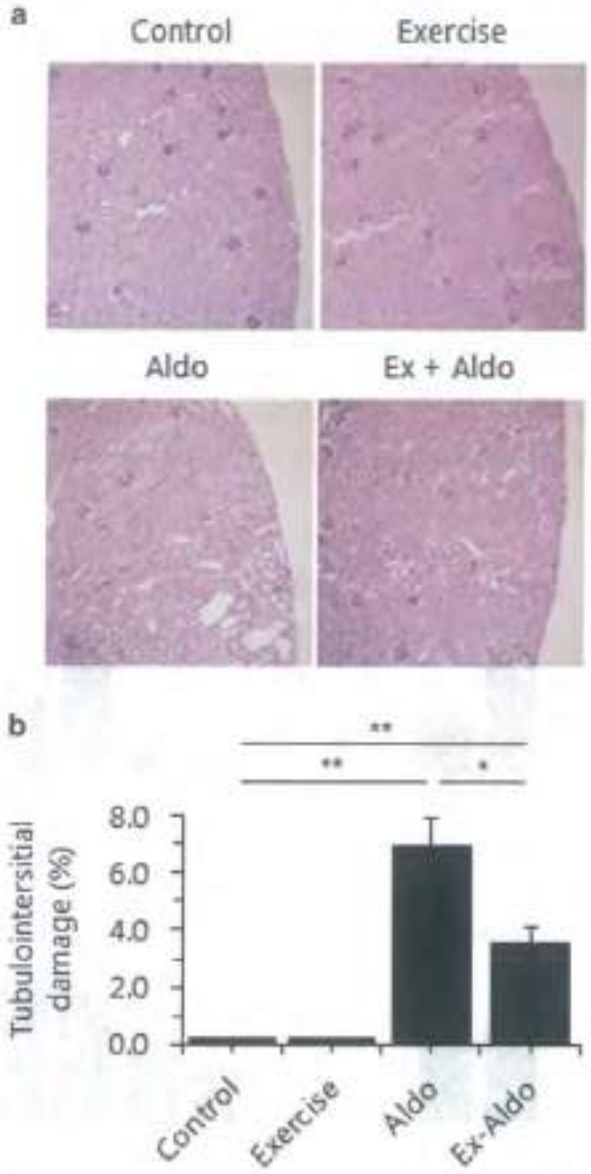

Fig. 3 Histological staining with periodic acid–Schiff showing tubulointerstitial damage (a, b). Control, $n = 12$; exercise, $n = 4$; Aldosterone (Aldo), $n = 9$; exercise-aldosterone (Ex-Aldo), $n = 9$. P-values were evaluated using one-way ANOVA with a post hoc Tukey–Kramer test. Values are presented as the mean ± SE. $^{**}P < 0.001$, $^{*}P < 0.05$

Fig. 5c), type I ($r_s = 0.759$, $P < 0.001$; Fig. 5d) and III collagen ($r_s = 0.723$, $P < 0.001$; Fig. 5e) expression using immunohistochemical analysis.

Discussion

In the current study, we showed the effects of voluntary running exercise training as well as the expression of human L-FABP on histological tubulointerstitial damage in an aldosterone-induced renal injury model using human L-FABP-Tg mice. Furthermore, the elevation of urinary L-FABP levels was suppressed by exercise in the model. These results suggest the possibility of exercise as another strategy to improve tubulointerstitial damage due to excessive activation of RAAS in clinical practice.

Both angiotensin II and aldosterone produced by RAAS activation play a central role in the progression of tubulointerstitial damage [28, 29]. Agarwal et al. reported that forced exercise training using a motor-driven treadmill for 16 weeks attenuated both glomerular and tubulointerstitial damage in spontaneously hypertensive rats [7], in which renal damage was attenuated by angiotensin II receptor blockers without a reduction in blood pressure [30]. Furthermore, the renoprotective effects of the combination of exercise training and antihypertensive therapy have been reported in several other CKD rat models [31, 32]. In addition to these studies, our study showed that voluntary running exercise training prevented tubulointerstitial damage progression in an aldosterone-induced renal injury mouse model, in which renal damage was attenuated by the mineralocorticoid receptor blocker [17]. Taken together, the previous and current results suggest the importance of exercise as a nonpharmacological strategy in CKD for several reasons, including RAAS activation.

The mechanisms underlying the renoprotective effects of exercise training are still not fully clarified, although several factors might be involved. Several previous studies have demonstrated that anti-inflammatory [7, 8] and anti-oxidative action [7, 12, 13], which is known to prevent CKD progression due to RAAS activation, participated in the beneficial effects of exercise training. We analyzed the differences in gene expression between the kidneys of the mice with voluntary running exercise training for 8 weeks and those of the mice without the exercise by microarray (Cell Innovator, Fukuoka, Kyushu, Japan) and found a significant decrease in the expression of the plasminogen activator inhibitor (PAI-1) gene, one of the well-known mediators in the pathogenesis of renal fibrosis, in the kidneys of the mice with exercise compared with those without exercise (data not shown). PAI-1 expression was reported to decrease with the improvement in tubulointerstitial damage in the aldosterone-induced renal injury model [33]. Therefore, we examined renal PAI-1 gene expression using real-time PCR analysis in our models. The PAI-1 gene expression that was upregulated in both Aldo and Ex-Aldo mice tended to be lower in the Ex-Aldo mice than in the Aldo mice ($P = 0.128$; Supplementary Fig. 1A). Furthermore, the PAI-1 gene expression levels at week 8 tended to be negatively correlated with running distance ($r_s = -0.396$, $P = 0.180$). There is a possibility that exercise may prevent the increase in renal PAI-1 expression, leading to

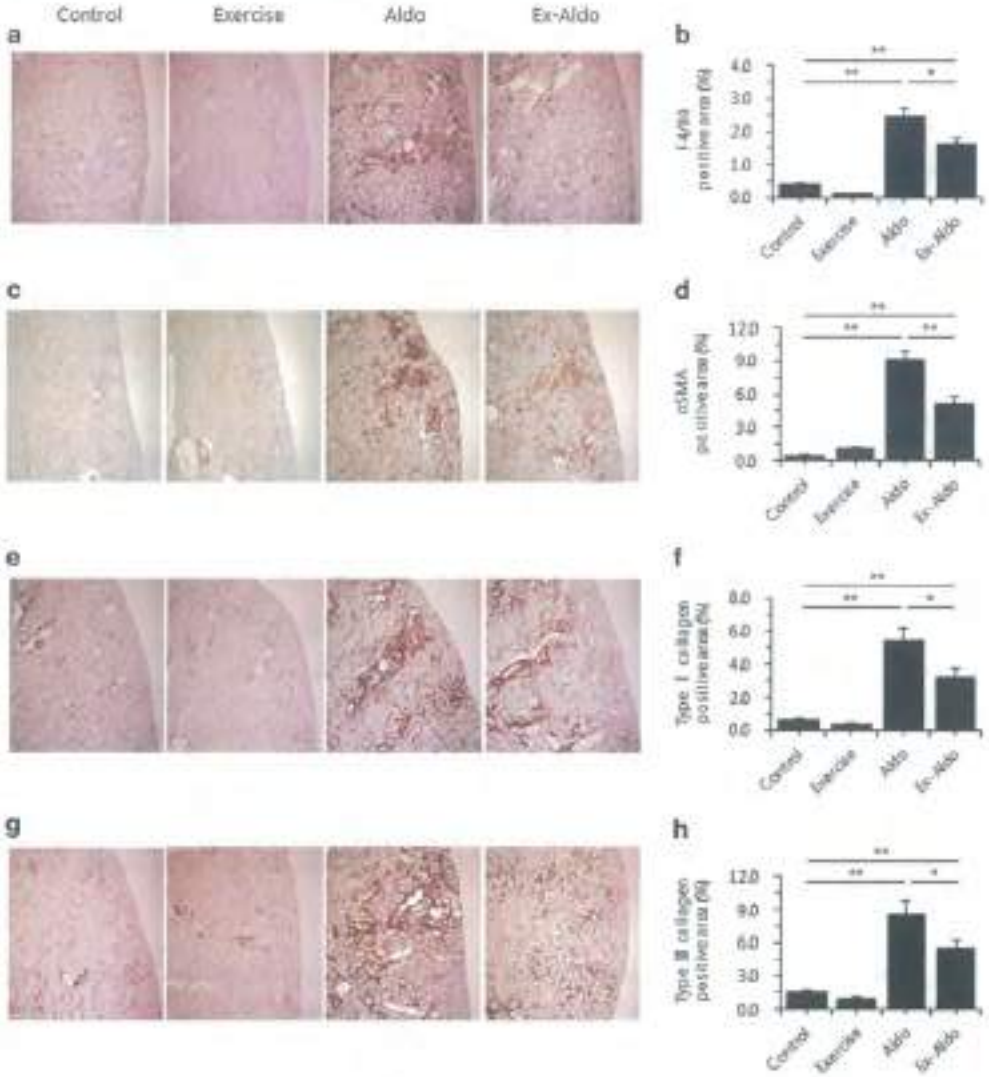

Fig. 4 Immunohistological staining using an antibody against F4/80 (**a**, **b**), α-smooth muscle actin (α-SMA) (**c**, **d**), type I collagen (**e**, **f**), and type III collagen (**g**, **h**). Control, $n = 12$; exercise, $n = 4$; aldosterone (Aldo), $n = 9$; exercise-aldosterone (Ex-Aldo), $n = 9$. *P*-values were evaluated using one-way ANOVA with a post hoc Tukey–Kramer test. Values are presented as the mean ± SE. $^{**}P < 0.001$, $^{*}P < 0.05$

amelioration of tubulointerstitial damage in the Aldo model. Regarding the reduction in oxidative stress by exercise, because oxidative stress is produced by NADPH oxidase, we examined the gene expression of p47-phox (NCF1), a cytosolic subunit of the multiprotein complex forming NADPH oxidase, and obtained the same results as those of PAI-1 expression ($P = 0.436$; Supplementary Fig. 1B). A decrease in oxidative stress by voluntary running exercise training might lead to attenuation of tubulointerstitial damage. Alternatively, the eNOS-NO pathway accelerates local inflammation by increasing vascular permeability to allow access to inflammatory cells, such as macrophages. Furthermore, Aldo induces the upregulation of eNOS expression in endothelial cells [34, 35]. Our results showed that eNOS gene expression in both the Aldo and Ex-Aldo mice was significantly higher than that in the control mice ($P < 0.001$) and that the eNOS expression in the Ex-Aldo mice tended to be lower than that in the Aldo mice ($P = 0.490$; data not shown). These results showed that the eNOS-NO pathway might not contribute to the renoprotective effect caused by exercise in the Aldo model.

Momentum (i.e., running distance) gradually decreased after injection with aldosterone and NaCl water in the Ex-Aldo group. This result coincides with the results of the human observational study indicating that physical activity decreases with kidney disease progression [36]. Hence, securing sufficient momentum in both humans and mice will be difficult based on the degree of kidney disease.

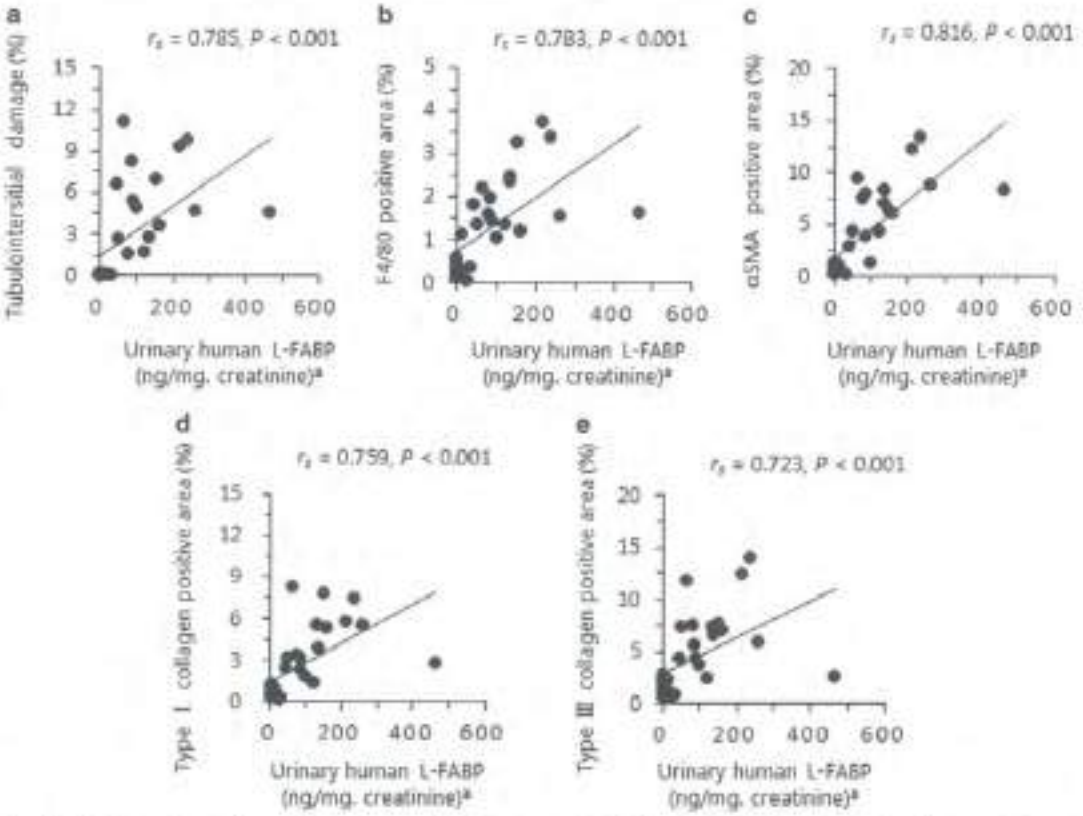

Fig. 5 Relationship between urinary human L-type fatty acid-binding protein (L-FABP) levels and tubulointerstitial damage by periodic acid–Schiff staining (a), F4/80-positive area (b), α-smooth muscle actin (αSMA)-positive area (c), type I collagen-positive area (d), type III collagen-positive area (e). [a]Data available for 29 animals

Even with less momentum, however, tubulointerstitial damage was significantly reduced in the Ex-Aldo group compared with the Aldo group. Therefore, continuing exercise might be important when considering a preventive strategy for CKD progression.

The current study has several critical limitations. First, the human L-FABP-Tg mice used in this study have been reported to have enhanced anti-oxidative effects and reduced tubulointerstitial damage progression compared with the wild-type mice without L-FABP expression in their proximal tubules [17]. Thus, several of the beneficial effects demonstrated in this study might have been affected by human L-FABP expression as well as voluntary running exercise training. Accordingly, an investigation using wild-type mice is required to reveal the renoprotective effects of exercise training on the aldosterone-induced renal injury model. However, because L-FABP is expressed in human kidneys, it is important to study the renoprotective role of exercise in addition to the L-FABP expression in the present renal injury model before trying a clinical application of exercise therapy in CKD patients. Second, although we examined the possible factors (e.g., monocyte chemotactic protein-1, etc.) related to the mechanism underlying the beneficial effects of exercise training on the kidneys, the crucial mechanistic factors were not completely clarified in this study. However, we think that the results of several previous studies and our present study suggest the possibility that a number of pathways and small changes in many factors, rather than one specific pathway, were involved in the mechanism underlying the renoprotective effect caused by exercise. Furthermore, several beneficial effects of exercise training on the kidneys might be associated with not only the intrarenal but also the extrarenal factors (e.g., myokines). Indeed, a recent previous study reported the possibility that some myokines were involved in renal injury prevention [37]. Finally, we cannot suggest the most effective exercise training (intensity, duration, and frequency) for kidney health because the current study investigated only the effects of "8 weeks" of "voluntary" exercise training. Therefore, further studies are needed to investigate the more detailed underlying mechanisms and the optimization of exercise training to recommend optimal exercise to patients with CKD. Alternatively, the present study showed that urinary L-FABP levels decreased with the improvement in tubulointerstitial damage induced by exercise and that the levels were significantly correlated with the

degree of tubulointerstitial damage, interstitial inflammation, and renal fibrosis, which supported the results reported in previous studies. Furthermore, urinary human L-FABP is a biomarker promulgated by the Ministry of Health, Labor, and Welfare in Japan. Therefore, urinary L-FABP may be useful not only for the evaluation of the renoprotective effect of exercise but also for deciding suitable effective exercise training in clinical practice.

In conclusion, the current study showed that voluntary running exercise training suppressed tubulointerstitial damage progression and elevation of urinary human L-FABP in an aldosterone-induced renal injury model. Although further study is needed to reveal the optimal exercise training program to prevent CKD, performing exercise habitually might be beneficial for kidney health and may be a promising nonpharmacological strategy for CKD patients.

Acknowledgements We thank Ms. Kimie Katayama and Ms. Junko Asano for technical assistance.

Funding This study was supported by a grant-in-Aid for the Japan Society for the Promotion of Science Fellows KAKENHI Grant Number 17J01405, Mitsui Sumitomo Insurance Welfare Foundation, and Akaeda Medical Research Foundation.

Compliance with ethical standards

Conflict of interest TS is the director and a senior scientist, and KO is a scientist at CMIC HOLDINGS Co., Ltd., which produced the kits for L-FABP analysis. The remaining authors declare that they have no conflict of interest.

Publisher's note: Springer Nature remains neutral with regard to jurisdictional claims in published maps and institutional affiliations.

References

1. Prunotto M, Budd DC, Gabbiani G, Meier M, Formenton I, Hartmann G, et al. Epithelial-mesenchymal crosstalk alteration in kidney fibrosis. J Pathol. 2012;228:131–47.
2. Remuzzi G, Bertani T. Pathophysiology of progressive nephropathies. N Engl J Med. 1998;339:1448–56.
3. Levey AS, de Jong PE, Coresh J, El Nahas M, Astor BC, Matsushita K, et al. The definition, classification, and prognosis of chronic kidney disease: a KDIGO Controversies Conference report. Kidney Int. 2011;80:17–28.
4. Hama T, Oikawa K, Ushijima A, Morita N, Matsukage T, Ikari YJ, et al. Effect of cardiac rehabilitation on the renal function in chronic kidney disease—analysis using serum cystatin-C based glomerular filtration rate. Int J Cardiol Heart Vasc. 2018;19:27–33.
5. Greenwood SA, Koufaki P, Mercer TH, MacLaughlin HL, Rush R, Lindup H, et al. Effect of exercise training on estimated GFR, vascular health, and cardiorespiratory fitness in patients with CKD: a pilot randomized controlled trial. Am J Kidney Dis. 2015;65:425–34.
6. Waden J, Tikkanen HK, Forsblom C, Harjutsalo V, Thorn LM, Saraheimo M, et al. Leisure-time physical activity and development and progression of diabetic nephropathy in type 1 diabetes: the FinnDiane Study. Diabetologia. 2015;58:929–36.
7. Agarwal D, Elks CM, Reed SD, Mariappan N, Majid DS, Francis J. Chronic exercise preserves renal structure and hemodynamics in spontaneously hypertensive rats. Antioxid Redox Signal. 2012;16:139–52.
8. Fukao K, Shimada K, Naito H, Sumiyoshi K, Inoue N, Iesaki T, et al. Voluntary exercise ameliorates the progression of atherosclerotic lesion formation via anti-inflammatory effects in apolipoprotein E-deficient mice. J Atheroscler Thromb. 2010;17:1226–36.
9. Ito D, Cao P, Kakihana T, Sato E, Suda C, Muroya Y, et al. Chronic running exercise alleviates early progression of nephropathy with Upregulation of nitric oxide synthases and suppression of glycation in Zucker diabetic rats. PLoS ONE. 2015;10:e0138037.
10. Ito D, Ito O, Mori N, Cao P, Suda C, Muroya Y, et al. Exercise training upregulates nitric oxide synthases in the kidney of rats with chronic heart failure. Clin Exp Pharm Physiol. 2013;40:617–25.
11. Ito D, Ito O, Cao P, Mori N, Suda C, Muroya Y, et al. Effects of exercise training on nitric oxide synthase in the kidney of spontaneously hypertensive rats. Clin Exp Pharm Physiol. 2013;40:74–82.
12. George L, Lokhandwala MF, Asghar M. Exercise activates redox-sensitive transcription factors and restores renal D1 receptor function in old rats. Am J Physiol Ren Physiol. 2009;297:F1174–1180.
13. Asghar M, George L, Lokhandwala MF. Exercise decreases oxidative stress and inflammation and restores renal dopamine D1 receptor function in old rats. Am J Physiol Ren Physiol. 2007;293:F914–919.
14. Irita J, Okura T, Jotoku M, Nagao T, Enomoto D, Kurata M, et al. Osteopontin deficiency protects against aldosterone-induced inflammation, oxidative stress, and interstitial fibrosis in the kidney. Am J Physiol Ren Physiol. 2011;301:F833–844.
15. Greene EL, Kren S, Hostetter TH. Role of aldosterone in the remnant kidney model in the rat. J Clin Invest. 1996;98:1063–8.
16. Blasi ER, Rocha R, Rudolph AE, Blomme EA, Polly ML, McMahon EG. Aldosterone/salt induces renal inflammation and fibrosis in hypertensive rats. Kidney Int. 2003;63:1791–1800.
17. Ichikawa D, Kamijo-Ikemori A, Sugaya T, Shibagaki Y, Yasuda T, Hoshino S, et al. Human liver-type fatty acid-binding protein protects against tubulointerstitial injury in aldosterone-induced renal injury. Am J Physiol Ren Physiol. 2015;308:F114–121.
18. Imai N, Yasuda T, Kamijo-Ikemori A, Shibagaki Y, Kimura K. Distinct roles of urinary liver-type fatty acid-binding protein in non-diabetic patients with anemia. PLoS ONE. 2015;10:e0126990.
19. Yamamoto T, Noiri E, Ono Y, Doi K, Negishi K, Kamijo A, et al. Renal L-type fatty acid–binding protein in acute ischemic injury. J Am Soc Nephrol. 2007;18:2894–902.
20. Ichikawa D, Kamijo-Ikemori A, Sugaya T, Ohata K, Hisamichi M, Hoshino S, et al. Utility of urinary tubular markers for monitoring chronic tubulointerstitial injury after ischemia-reperfusion. Nephrology. 2018;23:308–16.
21. Ohata K, Kamijo-Ikemori A, Sugaya T, Hibi C, Nakamura T, Murase T, et al. Renoprotective effect of the xanthine oxidoreductase inhibitor Topiroxostat under decreased angiotensin II type 1a receptor expression. Eur J Pharm. 2017;815:88–97.
22. Yokoyama T, Kamijo-Ikemori A, Sugaya T, Hoshino S, Yasuda T, Kimura K. Urinary excretion of liver type fatty acid binding protein accurately reflects the degree of tubulointerstitial damage. Am J Pathol. 2009;174:2096–106.
23. Kosaki K, Kamijo-Ikemori A, Sugaya T, Tanahashi K, Kumagai H, Sawano Y, et al. Relationship between exercise capacity and urinary liver-type fatty acid-binding protein in middle-aged and older individuals. Clin Exp Nephrol. 2017;21:810–7.

24. Kosaki K, Kamijo-Ikemori A, Sugaya T, Tanahashi K, Sawano Y, Akazawa N, et al. Effect of habitual exercise on urinary liver-type fatty acid-binding protein levels in middle-aged and older adults. Scand J Med Sci Sports. 2018;28:152–60.
25. Simon TC, Roth KA, Gordon JI. Use of transgenic mice to map cis-acting elements in the liver fatty acid-binding protein gene (Fabpl) that regulate its cell lineage-specific, differentiation-dependent, and spatial patterns of expression in the gut epithelium and in the liver acinus. J Biol Chem. 1993;268:18345–58.
26. Kamijo A, Sugaya T, Hikawa A, Okada M, Okumura F, Yamanouchi M, et al. Urinary excretion of fatty acid-binding protein reflects stress overload on the proximal tubules. Am J Pathol. 2004;165:1243–55.
27. Hasamichi M, Kamijo-Ikemori A, Sugaya T, Hoshino S, Kimura K, Shibagaki Y. Role of bardoxolone methyl, a nuclear factor erythroid 2-related factor 2 activator, in aldosterone- and salt-induced renal injury. Hypertens Res. 2018;41:8–17.
28. Kadoya H, Satoh M, Sasaki T, Taniguchi S, Tokuhashi M, Kashihara N. Excess aldosterone is a critical danger signal for inflammasome activation in the development of renal fibrosis in mice. FASEB J. 2015;29:3899–910.
29. Kobori H, Nangaku M, Navar LG, Nishiyama A. The intrarenal renin-angiotensin system: from physiology to the pathobiology of hypertension and kidney disease. Pharm Rev. 2007;59:251–87.
30. Susic D, Frohlich ED, Kobori H, Shao W, Seth D, Navar LG. Salt-induced renal injury in SHRs is mediated by AT1 receptor activation. J Hypertens. 2011;29:716–23.
31. Tufescu A, Kanazawa M, Ishida A, Lu H, Sasaki Y, Ootaka T, et al. Combination of exercise and losartan enhances renoprotective and peripheral effects in spontaneously type 2 diabetes mellitus rats with nephropathy. J Hypertens. 2008;26:312–21.
32. Kanazawa M, Kuwamura T, Li L, Sasaki Y, Matsumoto K, Kataoka H, et al. Combination of exercise and enalapril enhances renoprotective and peripheral effects in rats with renal ablation. Am J Hypertens. 2006;19:80–86.
33. Wang B, Ding W, Zhang M, Li H, Gu Y. Rapamycin attenuates aldosterone-induced tubulointerstitial inflammation and fibrosis. Cell Physiol Biochem. 2015;35:116–25.
34. Lyngso KS, Assersen K, Dalgaard EG, Skott O, Jensen BL, Hansen PB. Does aldosterone play a significant role for regulation of vascular tone? J Cardiovasc Pharm. 2016;68:1–10.
35. Nagata D, Takahashi M, Sawai K, Tagami T, Usui T, Shimatsu A, et al. Molecular mechanism of the inhibitory effect of aldosterone on endothelial NO synthase activity. Hypertension. 2006;48:165–71.
36. Zelle DM, Klaassen G, van Adrichem E, Bakker SJ, Corpeleijn E, Navis G. Physical inactivity: a risk factor and target for intervention in renal care. Nat Rev Nephrol. 2017;13:152–68.
37. Hanatani S, Izumiya Y, Araki S, Rokutanda T, Kimura Y, Walsh K, et al. Akt1-mediated fast/glycolytic skeletal muscle growth attenuates renal damage in experimental kidney disease. J Am Soc Nephrol. 2014;25:2800–11.

Hindawi
Journal of Diabetes Research
Volume 2020, Article ID 7614035, 14 pages
https://doi.org/10.1155/2020/7614035

Research Article

Relationship between Urinary Liver-Type Fatty Acid-Binding Protein (L-FABP) and Sarcopenia in Spontaneously Diabetic Torii Fatty Rats

Jun Tanabe,[1] Yuji Ogura,[2] Keisei Kosaki,[1,3,4] Yoshio Nagai,[5] Takeshi Sugaya,[1] Keiichi Ohata,[1] Shiika Watanabe,[1] Daisuke Ichikawa,[1] Kazuho Inoue,[6] Seiko Hoshino,[6] Kenjiro Kimura,[7] Seiji Maeda,[3] Yugo Shibagaki,[1] and Atsuko Kamijo-Ikemori[1,6]

[1]*Division of Nephrology and Hypertension, Department of Internal Medicine, St. Marianna University School of Medicine, Kanagawa, Japan*
[2]*Department of Physiology, St. Marianna University School of Medicine, Kanagawa, Japan*
[3]*Faculty of Health and Sport Sciences, University of Tsukuba, Ibaraki, Japan*
[4]*Japan Society for the Promotion of Science, Tokyo, Japan*
[5]*Division of Metabolism and Endocrinology, Department of Internal Medicine, St. Marianna University School of Medicine, Kanagawa, Japan*
[6]*Department of Anatomy, St. Marianna University School of Medicine, Kanagawa, Japan*
[7]*JCHO Tokyo Takanawa Hospital, Tokyo, Japan*

Correspondence should be addressed to Atsuko Kamijo-Ikemori; a2kamijo@marianna-u.ac.jp

Received 6 September 2019; Revised 16 November 2019; Accepted 26 November 2019; Published 13 January 2020

Academic Editor: Steven F. Abcouwer

Copyright © 2020 Jun Tanabe et al. This is an open access article distributed under the Creative Commons Attribution License, which permits unrestricted use, distribution, and reproduction in any medium, provided the original work is properly cited.

Background. Type 2 diabetes (T2D) is a known risk factor for diabetic kidney disease (DKD) and sarcopenia in older patients. Because there may be an interaction between DKD and sarcopenia, the aim of the present study is to investigate the relationship between urinary levels of liver-type fatty acid-binding protein (L-FABP) and sarcopenia using a novel rat model of T2D. *Methods.* Male spontaneously diabetic Torii (SDT) fatty rats ($n = 5$) at 16 weeks of age were used as an animal model of T2D. Age- and sex-matched Sprague-Dawley (SD) rats ($n = 7$) were used as controls. Urine samples were obtained from the rats, and muscle strength was evaluated with the use of the forelimb grip test at 16, 20, and 24 weeks of age. Serum, kidney, soleus, and extensor digitorum longus (EDL) muscle samples were collected at 24 weeks of age. Urinary L-FABP levels were measured using dedicated enzyme-linked immunosorbent assays. *Results.* Increased urinary L-FABP levels, focal glomerular sclerosis, moderate interstitial inflammation and fibrosis, and accumulation of renal oxidative proteins were significantly observed in the SDT fatty rats, compared to the SD rats. Muscle weight, muscle strength, cross-sectional areas of both type I and type IIb muscle fibers, and increasing rate of muscle strength were significantly decreased in the SDT fatty rats compared to the SD rats at 24 weeks. Urinary L-FABP levels at 20 and 24 weeks were significantly negatively correlated with muscle strength. Urinary L-FABP levels at 16 weeks were significantly negatively correlated with the increasing rate of muscle strength. *Conclusions.* Urinary L-FABP reflects the degree of muscle strength and weight, as well as cross-sectional areas of muscle fibers. Although further clinical study is needed, urinary L-FABP may be useful to monitor the progression of sarcopenia and DKD in T2D patients.

1. Introduction

Chronic kidney disease (CKD) is a common disease in aging societies worldwide. Many studies have focused on the involvement of CKD in the onset of sarcopenia which is characterized by decreased skeletal muscle mass and strength and has been the focus of many studies in order to sustain satisfactory quality of life and prevent fatal

diseases in the super-aging populations of advanced countries [1–5].

Type 2 diabetes (T2D) with insulin resistance is a common risk factor for diabetic kidney disease (DKD) and sarcopenia [1, 2]. Furthermore, there may be an association between the development of DKD and sarcopenia. Therefore, comprehensive medical management of T2D to prevent both DKD and sarcopenia is needed in clinical practice. However, at present, there are no universally accepted markers to monitor the degree of sarcopenia in DKD patients.

There is a possibility that exercise not only is indispensable for the prevention of sarcopenia but may also be useful to inhibit the progression of DKD. Although the effects of aerobic training on renal morphometric abnormalities in a Zucker fatty rat model of impaired glucose tolerance remains controversial [3], a recent study with the Zucker diabetic fatty rat reported that chronic exercise more certainly prevented interstitial profibrotic change rather than glomerular sclerosis via decreased oxidative stress and improved renal microcirculation by upregulation of endothelial nitric oxide synthase expression [4]. Another study demonstrated the renal antifibrosis effects of exercise by promoting skeletal muscle growth in a model of advanced renal interstitial fibrosis [5]. A recent study by our group revealed that tubulointerstitial damage due to inappropriate activation of the renin-angiotensin-aldosterone system was attenuated by voluntary running exercise [6]. Based on these results, we hypothesize that there may be some sort of relationship between tubulointerstitial damage and sarcopenia.

Urinary liver-type fatty acid-binding protein (L-FABP) accurately reflects the degree of tubulointerstitial damage [7, 8] and has been accepted as a tubular marker by the Ministry of Health, Labour and Welfare in Japan [9]. Moreover, a study by our group found that urinary L-FABP levels were inversely associated with exercise capacity or physical activity and that aerobic exercise training decreased urinary L-FABP levels in healthy middle-aged and older adults [10, 11]. Therefore, urinary L-FABP may be useful to monitor the progression of sarcopenia.

Among the limited models of both DKD and sarcopenia, the spontaneously diabetic Torii (SDT) fatty rat is a unique experimental novel model of T2D with kidney disease and sarcopenia [12–14] that mimics the pathophysiology of human T2D. Therefore, the aim of the present study was to elucidate the relationship between urinary L-FABP and sarcopenia using the SDT fatty rat.

2. Materials and Methods

2.1. Animals. All animal studies were conducted in strict accordance with the St. Marianna University School of Medicine Institutional Guide for Animal Experiments and the Guide for the Care and Use of Laboratory Animals. All surgery was performed under 3% isoflurane anesthesia, and all efforts were made to minimize suffering.

In this study, male SDT fatty (SDT.Cg-*Lepr*^{fa}/Jtt|cl) rats, derived from a Sprague-Dawley (SD) colony, were used as a model of T2D. Five-week-old male SDT fatty rats ($n = 5$) and SD rats ($n = 7$) of the same age (controls) were purchased from CLEA Japan, Inc. (Tokyo, Japan) and housed under standard conditions with free access to laboratory chow (CRF-2, Charles River Laboratories Japan, Inc., Yokohama, Japan) and water. Body weight, chow consumption, and muscle strength were measured every 4 weeks from 16 to 24 weeks of age, which is equivalent to a late middle-aged human patient. Urine was collected from the rats using metabolic cages. Muscle strength was measured using the forelimb grip test with a grip strength meter (MK-380CM/FM; Muromachi Kikai, Co., Ltd., Tokyo, Japan). The average of three measurements of muscle strength per animal per time point was recorded for comparative analysis.

For the experiments, 16-, 20-, and 24-week-old rats were individually housed overnight in metabolic cages with free access to tap water. Urine was collected for the measurement of urinary markers. Additionally, serum samples, leg muscle tissues, and kidney tissues were collected from rats that were sacrificed at the age of 24 weeks. The extracted kidneys were weighted and cut into pieces for various analyses. The extracted muscles specimens were sectioned into the soleus muscle as a slow muscle and the extensor digitorum longus (EDL) muscle as a fast muscle. After weighing, each muscle was frozen individually in liquid nitrogen and stored at -80°C for further analyses.

2.2. Blood Pressure Measurement. Systolic blood pressure (SBP) was measured using a tail-cuff apparatus (Softron BP-98A; Softron, Co., Ltd., Tokyo, Japan) every 4 weeks from 16 to 24 weeks of age. The average of three measurements of SBP per animal per time point was recorded for analysis.

2.3. Serum and Urinary Biochemistry. Serum and urine creatinine levels were measured using a QuantiChrom™ Creatinine Assay Kit (BioAssay Systems LLC, Hayward, CA, USA). Serum cystatin C levels were measured using a rat cystatin C enzyme-linked immunosorbent assay (ELISA) kit (BioVendor Instruments a.s., Brno, Czech Republic). Serum insulin (FUJIFILM Wako Shibayagi Corporation, Shibukawa, Japan) and insulin-like growth factor-1 (IGF-1; R&D Systems, Inc., Minneapolis, MN, USA) levels were measured using dedicated ELISAs. Serum urea nitrogen levels were measured via urease ultraviolet absorption spectrophotometry, serum total cholesterol levels were measured using the cholesterol oxidase enzymatic method, and serum triglyceride levels were measured using an enzymatic method conducted by SRL Clinical Laboratory Testing Services (Tokyo, Japan). Urinary glucose levels were determined semiquantitatively using urinary dipsticks (Wako Pure Chemical Industries, Ltd., Osaka, Japan). Urinary glucose was graded as follows: 0, negative; 1+, >100 mg/dl; 2+, >250 mg/dl; 3+, >500 mg/dl; and 4+, >2000 mg/dl.

Urinary levels of L-FABP and albumin were measured using rat L-FABP (CMIC Co., Ltd., Tokyo, Japan) and rat albumin (Exocell, Inc., Philadelphia, PA, USA) ELISA kits, respectively. Urinary levels of rat L-FABP and albumin were reported as ratios relative to urinary creatinine levels.

2.4. Renal Histological and Morphometric Analysis. The midsection of each excised kidney was dissected along the

minor axis. The two pieces were fixed in 10% buffered formalin or methyl Carnoy's solution (60% methanol, 30% chloroform, and 10% glacial acetic acid) and embedded in paraffin. Serial sections (3 μm thickness) were prepared for renal immunohistochemical assessment and periodic acid-Schiff (PAS) staining.

Glomerulosclerosis in PAS-stained sections was evaluated by grading the extent of sclerosis in each glomerulus as follows: 0, no sclerosis; 1, sclerosis in 1%–25% of the glomerulus; 2, sclerosis in 26%–50% of the glomerulus; 3, sclerosis in 51%–75% of the glomerulus; and 4, sclerosis in 76%–100% of the glomerulus. At 100x magnification, the glomerulosclerosis score for each animal was calculated as follows: (1 × the number of grade 1 glomeruli, %) + (2 × the number of grade 2 glomeruli, %) + (3 × the number of grade 3 glomeruli, %) + (4 × the number of grade 4 glomeruli, %). Fifty glomeruli were examined for each animal [15].

2.5. Renal Immunohistochemical Analysis. Target antigens in the preprocessed sections were stained using the indirect immunoperoxidase method, as described previously [7]. Briefly, formalin-fixed, paraffin-embedded tissue specimens were used to stain for myofibroblasts and tubular cells exhibiting epithelial-mesenchymal transition using a mouse monoclonal antibody specific for α-smooth muscle actin (α-SMA; dilution, 1:800; Sigma-Aldrich Corporation, St. Louis, MO, USA). The tissue specimens fixed in methyl Carnoy's solution were assessed immunohistochemically for macrophages using a mouse monoclonal antibody (ED-1) specific for CD68 (1:100; Abcam, Tokyo, Japan) and goat polyclonal antibodies specific for type I and III collagen (1:200; Southern Biotech, Birmingham, AL, USA). Labeled proteins were visualized using polymeric horseradish peroxidase-conjugated secondary antibodies (ImmPRESS™ Polymer Detection Kit; Vector Laboratories, Burlingame, CA, USA). Peroxidase activity was detected via the diaminobenzidine reaction (Liquid DAB+; DAKO Japan, Inc., Tokyo, Japan), and sections were counterstained with hematoxylin. For quantification, images from 10 nonoverlapping fields throughout the cortical and outer medullary regions were captured at 100x magnification. The extent of macrophage and myofibroblast infiltration of the cortical and outer medullary interstitia was automatically measured using an image analyzer (WinRoof version 6.4; Mitani Corporation, Tokyo Japan). Briefly, the areas positively stained for CD68 and α-SMA were independently measured and expressed as ratios relative to the areas of the entire cortical and outer medullary regions. The same method was used to measure the expression levels of type I and III collagen.

2.6. Immunohistochemical Analysis of Muscle Tissues. The frozen excised soleus and EDL muscle tissues were cut centrally along the width and embedded in Tissue-Tek® O.C.T.™ Compound (Sakura Finetek Japan Co., Ltd., Tokyo, Japan). Continuous frozen sections sliced to a thickness of 10 μm were prepared using a cryostat (HM 550; Thermo Fisher Scientific, Rockford, IL, USA). Double-color immunofluorescent staining was performed in order to evaluate the diameter of each type I and IIb fiber.

The dried sections were washed three times with phosphate-buffered saline (PBS) for 5 min each time and soaked in methanol solution containing 0.3% hydrogen peroxide for 20 min. After washing three times with PBS for 5 min again, the sections were incubated with the following primary antibodies at 4°C overnight: anti-type I myosin heavy chain (MyHC) isoform IgG2b (MyHCI; 1:200; BA-F8; Developmental Studies Hybridoma Bank (DSHB), the University of Iowa, Iowa City, IA, USA), anti-type IIb MyHC isoform immunoglobulin (Ig)G1 (MyHCIIb; 1:100; F18; DSHB), and anti-laminin IgG2a (1:200; 2E8; DSHB). After washing three times with PBS, the sections were incubated with the following fluorescent-labeled secondary antibodies at room temperature for 1 h: Alexa Flour 488-labeled goat anti-mouse IgG2b (1:500; Invitrogen Corporation, Carlsbad, CA, USA), DyLight 405-labeled goat anti-mouse IgG1 (1:500; Invitrogen Corporation), and Alexa Flour 488-labeled goat anti-mouse IgG2a (1:500; Invitrogen Corporation).

For quantification, tissue images of the soleus and EDL muscles were obtained using ZEN 2 pro imaging software (Carl Zeiss Microscopy Co., Ltd., Tokyo, Japan). The cross-sectional areas of the specimens were evaluated using 300 fibers in two visual fields at 100x magnification per animal using an image analyzer (WinRoof).

2.7. Western Blot Analysis. Proteins were extracted from the collected muscle tissues and concentrations were measured as described previously [16]. Next, 30 μg of extracts were separated by sodium dodecyl sulfate-polyacrylamide gel electrophoresis using NuPAGE 4%–12% Bis-Tris gels and the XCell SureLock Mini-Cell system (Thermo Fisher Scientific). The separated proteins were transferred to polyvinylidene difluoride membranes using the iBlot™ dry blotting system (Thermo Fisher Scientific). The membranes were blocked with Blocking One solution (Nacalai Tesque, Inc., Kyoto, Japan) and then incubated overnight at 4°C with primary antibodies diluted in Can Get Signal Solution 1 (TOYOBO, Osaka, Japan) against Akt (rabbit monoclonal; #9272; 1:1000; Cell Signaling Technology, Inc., Danvers, MA, USA), phospho-Akt (Ser473) (rabbit monoclonal; #9271; 1:1000; Cell Signaling Technology, Inc.), mammalian target of rapamycin (mTOR; rabbit monoclonal; #2983; 1:1000; Cell Signaling Technology, Inc.), phospho-mTOR (Ser2448) (rabbit monoclonal; #5536; 1:1000; Cell Signaling Technology, Inc.), ribosomal protein S6 kinase beta-1 (S6K; rabbit monoclonal; #2708; 1:1000; Cell Signaling Technology, Inc.), phospho-S6K (rabbit monoclonal; #9234; 1:1000; Cell Signaling Technology, Inc.), 5′AMP-activated protein kinase (AMPK; rabbit monoclonal; #2603; 1:1000; Cell Signaling Technology, Inc.), phospho-AMPK (Thr172; rabbit monoclonal; #2535; 1:1000; Cell Signaling Technology, Inc.), Forkhead box protein O1 (FoxO1; rabbit monoclonal; #9454; 1:1000; Cell Signaling Technology, Inc.), phospho-FoxO1 (Ser256) (rabbit monoclonal; #9461; 1:1000; Cell Signaling Technology, Inc.), Atrogin-1 (rabbit polyclonal; 1:1000; ECM Biosciences, Versailles, KY, USA), and muscle RING-finger protein-1 (MuRF-1; rabbit polyclonal; 1:1000; ECM Biosciences). After washing, the membranes were incubated

with a horseradish peroxidase-conjugated anti-rabbit antibody (Santa Cruz Biotechnology, Inc., Dallas, TX, USA) diluted at 1:2000 in Blocking One solution for 1 h at room temperature. Subsequently, chemiluminescence was detected using an ECL Prime western blotting detection reagent (GE Healthcare, Little Chalfont, UK), and images were obtained with a charge-coupled device camera system (ImageQuant LAS4000; GE Healthcare Japan, Tokyo, Japan).

The ratios of phosphorylated to total proteins were quantitated by densitometry analysis of immunoblots using ImageJ software (https://imagej.nih.gov/ij/). The same membranes that were incubated with antibodies against FoxO1 and phospho-FoxO1A were also incubated with rabbit monoclonal anti-α-tubulin antibody (1:4000; Abcam). After treatment with a stripping buffer (Wako), FoxO1 protein expression was normalized to that of α-tubulin.

2.8. Evaluation of Oxidative Stress in Muscle and Kidney Tissues. After determining protein concentrations, to evaluate oxidative stress in the muscle and kidney tissues, protein carbonyls, which are the most common products of protein oxidation, were quantified using an OxiSelect™ Protein Carbonyl ELISA Kit (Cell Biolabs, Inc., San Diego, CA, USA) with 100 μg of protein extracted from both tissue types.

2.9. Statistical Analysis. All values are expressed as the mean ± standard error of the mean (SEM). A probability (p) value of <0.05 was considered statistically significant. Following the Kruskal-Wallis test, differences among each SD and SDT rat were identified using the Steel-Dwass test. The Mann-Whitney U test was used for comparisons between two groups. Spearman's rank correlation coefficient was used to evaluate nonparametric data and assess correlations between two parameters. Changes in muscle strength of each rat throughout the experimental period were defined as the slope of the regression line of a line-graph plot of muscle strength against experimental duration (weeks). All statistical analyses were performed using JMP® software, version 13.0.0 (SAS Institute, Cary, NC, USA).

3. Results

3.1. Changes in Body Weight, Blood Glucose Level, SBP, and Food Intake. The body weight, blood glucose level, SBP, and food intake of all rats in both groups were measured every 4 weeks between the ages of 16 and 24 weeks. As shown in Table 1, while the mean body weight in the SD group was significantly greater at 24 weeks than 16 weeks, that of the SDT group increased, but not significantly. There were no significant differences in the body weights between the two groups throughout the experimental period. Blood glucose levels were significantly higher in the SDT group than the SD group throughout the experimental period. Although there was no change over time in the SD group, SBP levels in the SDT group moderately increased throughout the experimental period. Food intake increased significantly at 20 and 24 weeks compared to 16 weeks in the SD group. Additionally, food intake at 16 and 20 weeks was significantly greater in the SDT group than the SD group.

3.2. Comparison of Kidney Function and Serum Parameters at 24 Weeks of Age. As shown in Table 2, at 24 weeks, serum creatinine and urea nitrogen levels were significantly increased in the SDT group compared to the SD group, while there was no significant difference in serum cystatin C levels. Serum insulin levels were comparable between the two groups, while serum IGF-1 levels were significantly lower in the SDT group. Both serum total cholesterol and triglyceride levels were significantly greater in the SDT group than the SD group.

3.3. Changes in Urinary Glucose, L-FABP, and Albumin Levels. The urinary glucose scores of the SDT and SD groups at 16, 20, and 24 weeks remained unchanged at 4 and 0, respectively. In the SD group, urinary L-FABP (Figure 1(a)) and urinary albumin (Figure 1(b)) levels remained unchanged throughout the experimental period. Conversely, urinary L-FABP at 24 weeks (Figure 1(a)) and urinary albumin at both 20 and 24 weeks (Figure 1(b)) were significantly increased in the SDT group compared to 16 weeks. Also, urinary L-FABP (Figure 1(a)) and urinary albumin (Figure 1(b)) levels were significantly higher in the SDT group than the SD group throughout the experimental period.

3.4. Immunohistological Analysis of Kidney Tissues. To evaluate the degree of renal interstitial inflammation, immunohistochemical analysis of the macrophage marker CD68 was conducted. Macrophages were detected in the interstitium of the SDT fatty rats (Figure 2(a)), and the degree of macrophage infiltration was significantly greater in the SDT group than the SD group (Figure 2(b)).

Additionally, immunohistochemical analyses of α-SMA and type I and III collagen were performed to evaluate the extent of tubulointerstitial fibrosis. Areas positive for α-SMA were observed in the tubules and interstitium of the SDT group (Figure 2(c)) to a significantly greater extent compared to the SD group (Figure 2(d)). Further analysis revealed that the expression levels of type I (Figures 2(e) and 2(f)) and III (Figures 2(g) and 2(h)) collagen were significantly greater in the SDT group than the SD group.

3.5. Evaluation of Glomerular Sclerosis. The mean glomerular sclerosis score was significantly greater for the PAS-stained kidney tissues of the SDT group than the SD group throughout the experimental period (Figures 2(i) and 2(j)).

3.6. Changes in Muscle Strength. Muscle strength significantly increased in the SD and SDT groups at 24 weeks compared to 16 and 20 weeks but was significantly lower in the SDT group compared to the SD group at 20 and 24 weeks (Figure 3(a)). The rate of increased muscle strength was significantly lower in the SDT group than the SD group (Figure 3(b)).

3.7. Comparison of Muscle Weight and Immunohistological Analysis of Muscle Tissues. The muscle weights of the soleus and EDL muscles were significantly lower in the SDT group than the SD group (Figures 3(c) and 3(d)). Since the soleus is mainly composed of slow-twitch muscle fibers [17], a cross-sectional area of type I muscle fibers was evaluated (Figure 3(e)). The EDL muscle has a high proportion of

Table 1: Time-related changes in body weight, blood glucose, systolic blood pressure, and food intake per weight.

Variable	Species	16weeks of age	20 weeks of age	24 weeks of age
Body weight (g)	SD	549.5 (12.8)	616.3 (20.8)	643.3† (19.4)
	SDT	546.7 (25.5)	574.9 (31.0)	580.0 (39.7)
Blood glucose (mg/dl)	SD	67.3 (6.1)	61.6 (3.6)	63.3 (3.3)
	SDT	199.6** (61.7)	184.0** (70.3)	215.6** (78.0)
Systolic blood pressure (mmHg)	SD	112.0 (5.1)	127.6 (5.8)	127.9 (3.7)
	SDT	120.6 (4.8)	131.0 (4.0)	140.6 (5.6)
Food intake per weight (g/kg)	SD	22.6 (4.7)	46.3† (2.1)	47.1† (1.4)
	SDT	74.4** (7.1)	67.0* (8.2)	47.1 (10.9)

Data are presented as the mean (standard error). *$p < 0.05$ and **$p < 0.01$ vs. the SD rats at the same week; †$p < 0.05$ and ‡$p < 0.01$ vs. the same group at 16 weeks of age.

Table 2: Serum parameters at 24 weeks of age.

Variable	SD rat	SDT fatty rat
Serum creatinine (mg/dl)	0.45 (0.02)	0.55 (0.02)**
Cystatin C (ng/ml)	3.68 (0.16)	4.01 (0.17)
Urea nitrogen (mg/dl)	18.79 (0.35)	29.42 (2.71)**
Insulin (μU/ml)	0.91 (0.29)	0.89 (0.21)
IGF-1 (pg/ml)	1199 (40.5)	826 (73.00)**
Total cholesterol (mg/dl)	75.25 (3.92)	161.50 (6.94)**
Triglyceride (mg/dl)	68.86 (4.09)	470.0 (119.00)**

Data are presented as the mean (standard error). **$p < 0.01$ vs. the SD rats.

fast-twitch muscle fibers [17]; thus, a cross-sectional area of type IIb muscle fibers was evaluated (Figure 3(f)). Type I muscle fiber was stained green (Figure 3(e)) and type IIb muscle fiber was stained red (Figure 3(f)). The cross-sectional areas of muscle fiber types I (Figure 3(g)) and IIb (Figure 3(h)) were significantly decreased in the SDT group compared to the SD group.

3.8. Evaluation of Muscle Protein Synthesis or Degradation. Maintenance of muscle mass is regulated by the balance between protein synthesis and degradation. Hence, the activation of insulin/IGF-1-Akt and mTOR-S6K signaling as markers of protein synthesis and the activation of insulin/IGF-1-Akt-FoxO signaling, phosphorylation of AMPK, and expression of E3 ubiquitin ligases as markers of protein degradation were evaluated.

The phosphorylation levels of Akt (Figure 4(a)), mTOR (Figure 4(b)), and S6K (Figure 4(c)) were significantly lower, while that of AMPK (Figure 5(a)) was significantly higher in the soleus muscle of the SDT group compared to the SD group. Regarding the EDL muscle, although the phosphorylation levels of both Akt (Figure 4(a)) and AMPK (Figure 5(a)) were not significantly different between the SDT and SD groups, those of mTOR (Figure 4(b)) and S6K (Figure 4(c)) were significantly lower in the SDT group.

FoxO1 protein expression was significantly higher (Figure 5(b)), while that of phospho-FoxO1 was significantly lower, in both the soleus and EDL muscles of the SDT group compared to the SD group (Figure 5(c)).

Regarding the protein expression profiles of E3 ubiquitin ligases (Figures 5(d) and 5(e)), Atrogin-1 (Figure 5(e)) expression levels were significantly higher in the EDL muscle of the SDT group than the SD group, but not MuRF-1 (Figure 5(d)). There was no significant change in Atrogin-1 and MuRF-1 expression levels in the soleus muscle between the SDT and SD groups (Figures 5(d) and 5(e)).

3.9. Correlations between Each Urinary Marker and Muscle Strength. Urinary L-FABP levels were inversely correlated with muscle strength ($\rho = -0.34$, $p < 0.05$), but not urinary albumin, throughout the experimental period ($\rho = -0.23$, $p = 0.188$). At 16 weeks, urinary L-FABP and albumin levels were not significantly correlated with muscle strength (Figure 6(a)). At 20 and 24 weeks, while urinary L-FABP levels were inversely correlated with muscle strength (Figures 6(b) and 6(c)), urinary albumin levels were inversely correlated with muscle strength only at 24 weeks (Figure 6(c)).

Urinary L-FABP ($\rho = -0.76$, $p < 0.005$, Figure 7(a)) and albumin ($\rho = -0.68$, $p < 0.05$, Figure 7(b)) levels at 16 weeks were inversely correlated with an increasing rate of muscle strength. In the SDT group at 16 weeks, urinary L-FABP levels were inversely correlated with an increasing rate of muscle strength ($\rho = -1.00$, $p < 0.001$, Figure 7(c)), but not urinary albumin levels ($\rho = 0.10$, $p = 0.87$, Figure 7(d)). Regarding urinary L-FABP, the significance was maintained even after removing an extreme deviation from the mean, as shown in Figures 7(a) and 7(c).

3.10. Correlation between Urinary L-FABP and Muscle Weight, and Cross-Sectional Areas of Both Type I and IIb Muscle Fibers. Urinary L-FABP levels at 24 weeks were inversely correlated with the weight of the soleus ($\rho = -0.92$, $p < 0.0001$, Figure 8(a)) and EDL ($\rho = -0.82$, $p < 0.005$, Figure 8(b)) muscles, as well as cross-sectional areas of both type I ($\rho = -0.76$, $p < 0.01$, Figure 8(c)) and IIb ($\rho = -0.66$, $p < 0.05$, Figure 8(d)) muscle fibers.

3.11. Correlation between Urinary L-FABP and Urinary Albumin, and Glomerular Sclerosis Score. Urinary L-FABP levels were significantly correlated with both urinary albumin ($\rho = 0.83$, $p < 0.0001$, Figure 9(a)) and glomerular sclerosis scores ($\rho = 0.68$, $p < 0.05$, Figure 9(b)).

3.12. Correlation between Renal Morphological Change and Muscle Strength and Weight. The degrees of macrophage infiltration and α-SMA expression at 24 weeks were inversely

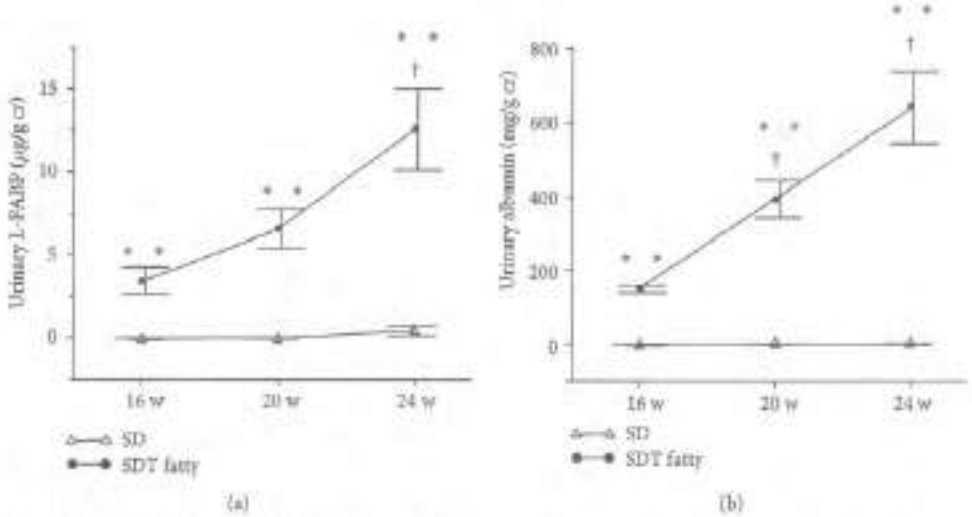

Figure 1: Changes in urinary parameters of SD and SDT fatty rats. Urinary L-FABP levels at 16, 20, and 24 weeks of age (a) and urinary albumin levels at 16, 20, and 24 weeks of age (b). Values are presented as the mean ± standard error of the mean (SEM). $^{**}p < 0.01$ vs. SD rats at the same age; $^{\dagger}p < 0.05$ vs. SDT fatty rats at 16 weeks of age.

correlated with the strength and weight of the soleus and EDL muscles (Table 3). Type I and III collagen expressions were inversely correlated with the weights of the soleus and EDL muscles, but not strength (Table 3). Glomerular sclerosis score was inversely correlated with the strength and weight of EDL muscles, but not the weight of the soleus (Table 3).

3.13. Evaluation of Oxidative Stress in Kidney and Muscle Tissues. While protein carbonyl levels in kidney tissues were significantly higher in the SDT group (Figure 10(a)), those in the soleus muscle, but not the EDL muscle, were significantly lower compared to those in the SD group (Figures 10(b) and 10(c)).

4. Discussion

The results of the present study revealed that urinary L-FABP secretion reflected decreases in muscle strength, muscle weight, and cross-sectional areas of muscle fibers, and the high levels of urinary L-FABP at 16 weeks were associated with a lower increasing rate of muscle strength in mature SDT fatty rats with hyperglycemia, hyperlipidemia, low levels of serum IGF-1, and kidney disease. The current study indicated that urinary L-FABP might be useful to monitor the progression of sarcopenia in addition to DKD in T2D patients.

There is growing evidence of a correlation between sarcopenia and kidney disease, including DKD [18]. The results of the present study indicated a correlation between urinary markers and sarcopenia in mature rats with T2D and DKD. Our previous studies found that lower physical activity or weaker muscle strength was related to increased urinary L-FABP levels, but not urinary albumin [10], and that intervention with aerobic exercise training facilitated a reduction in increased urinary L-FABP in healthy middle-aged and older adults [11]. Furthermore, decreased muscle strength was independently associated with increased intrarenal vascular resistance [19], suggesting that sarcopenia might lead to impairments to the intrarenal vasculature. Considering that increased urinary L-FABP is induced by decreased renal microvascular blood flow [20] and that renal hypoxia was observed in the SDT fatty rats with DKD (unpublished data), urinary L-FABP might be useful for the detection of abnormalities in renal hemodynamics aggravated by sarcopenia in addition to glomerular sclerosis leading to renal hypoxia derived from reduction of postglomerular blood flow. On the contrary, accumulation of uremic toxins, metabolic acidosis, and anemia due to deterioration of renal function is reported to lead to sarcopenia [18]. Although renal dysfunction was mild in the SDT fatty rats in the present study, muscle mass loss was reported to appear in the early phase of CKD [21]. Therefore, in the present study, DKD might have influenced the progression of sarcopenia.

The progression of sarcopenia in T2D patients has been associated with lower renal function and higher urinary albumin levels [22]. As a marker of the severity of kidney disease, urinary albumin may reflect the degree of muscle weakness in patients with kidney disease. In the present study, urinary albumin at 16 weeks was significantly related to continued muscle growth in all rats used in the study, although the significant correlation disappeared in only SDT fatty rats. Hence, further studies are needed to determine whether urinary albumin, like urinary L-FABP, is a risk factor for the onset of sarcopenia.

In the skeletal muscle, there are four major kinds of muscle fiber: type I, type IIa, type IIx, and type IIb. The predominance of one over the other is dependent on the contractile rate and metabolic characteristics. While type I

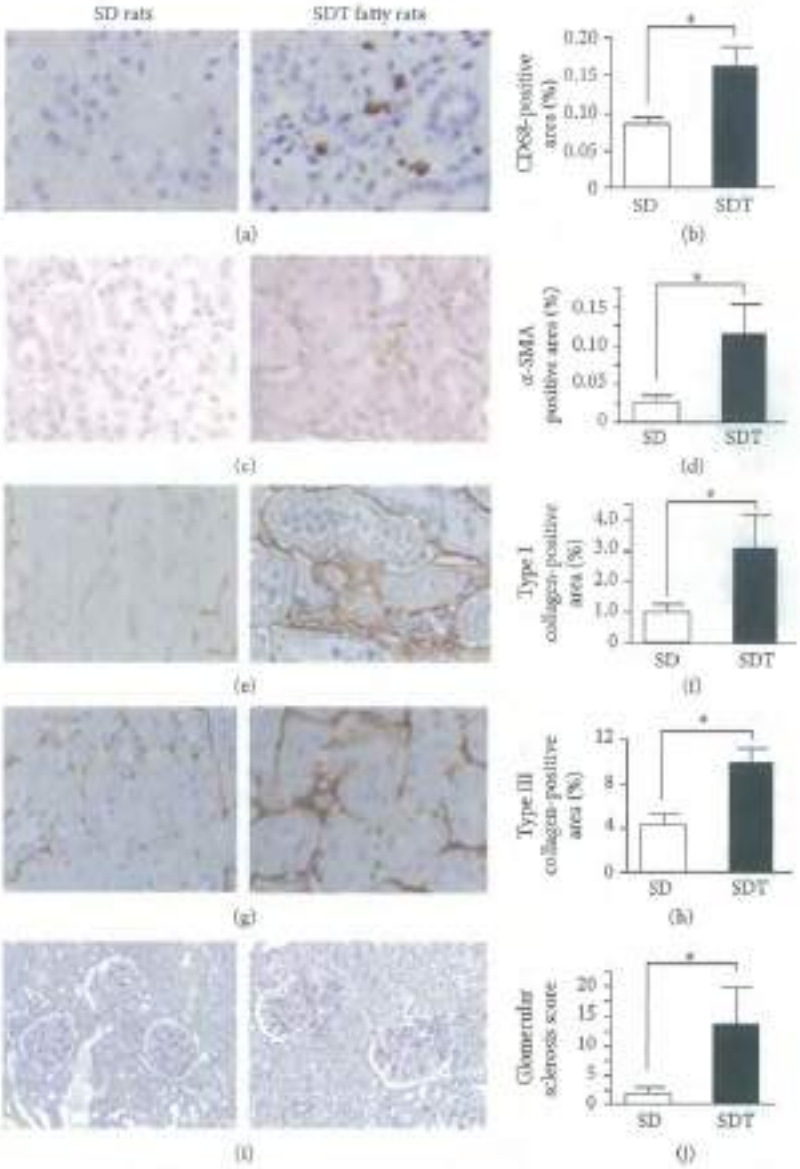

Figure 2: Histological evaluation of the kidney in SD and SDT fatty rats. Immunohistological staining of kidney tissues using antibodies against CD68 (a, b), α-SMA (c, d), type I collagen (e, f), and type III collagen (g, h). Histological PAS staining showing focal glomerular sclerosis (i) and semiquantitative assessment of focal glomerular sclerosis (j). Original magnification: ×100. Values are presented as the mean ± SEM. $^{*}p < 0.05$ vs. SD rats.

fibers, which are slow-twitch and oxidative fibers, are influenced by insulin resistance in T2D [23], type IIb fibers, which are fast-twitch and glycolytic fibers, are influenced by aging [24]. Although serum insulin levels were similar in the SDT and SD groups, blood glucose levels were significantly higher in the SDT group, suggesting the presence of insulin resistance. Regarding the influence of muscle fiber on kidney disease, CKD induced insulin resistance [25], leading to a decrease in the proportion of type I fibers, as previously shown in the gastrocnemius muscle of a CKD model [26, 27]. In the present study, type I fibers in the soleus muscle and type IIb fibers in the EDL muscle were assessed separately, which revealed decreases in both muscle weight and cross-sectional areas of type I and IIb fibers in the present study. Based on these results, insulin resistance, aging, and DKD might be related to the progression of sarcopenia in SDT fatty rats.

Insulin or the IGF-1 signaling pathway plays a critical role in the regulation of muscle mass by controlling the balance between protein synthesis and degradation in muscle [28]. As a critical downstream effector of the insulin/IGF-1 pathway, phosphorylation of Akt leads to activation of protein synthesis via phosphorylation of both mTOR and S6K or inhibition of protein degradation via FoxO1

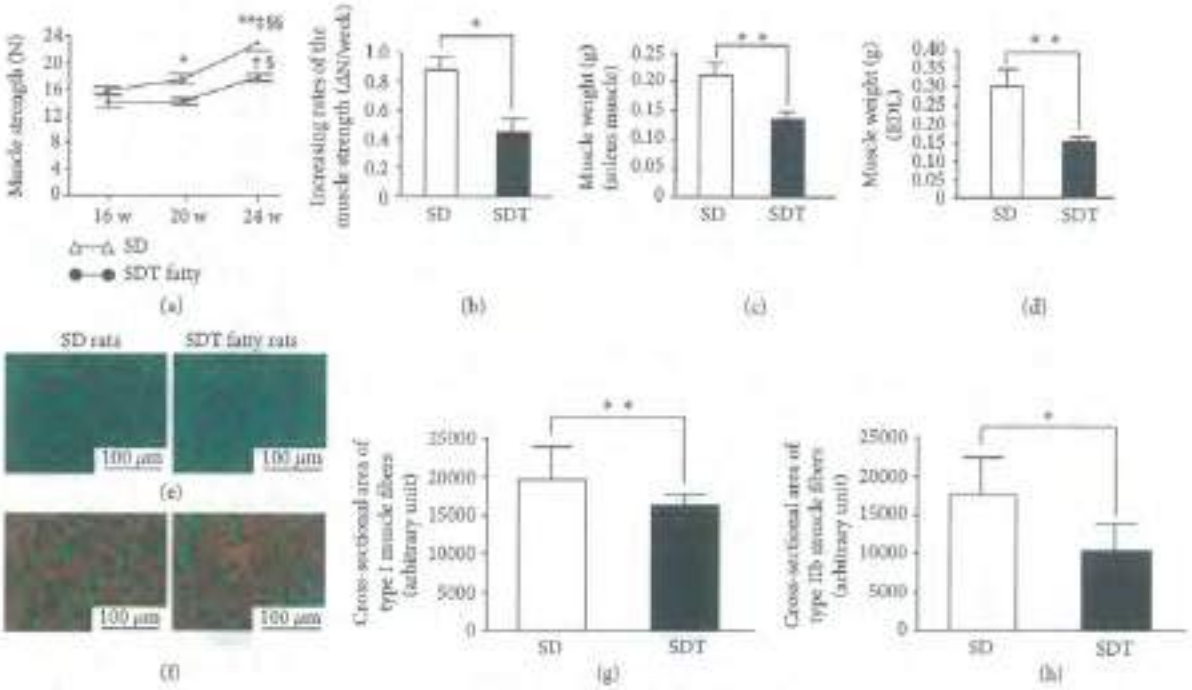

Figure 3: Evaluation of muscle strength, muscle weight, and muscle histological analysis. Change in muscle strength in SD and SDT fatty rats (a) and increasing rates of muscle strength (b). Weight of lower limb muscles in SD and SDT fatty rats. Soleus muscle (c) and EDL muscle (d) at 24 weeks of age. Multiple fluorescent staining of soleus muscle fibers (e) and semiquantitative assessment of type I fibers in the soleus muscle (g). Multiple fluorescent staining of EDL muscle fibers (f) and semiquantitative assessment of type IIb fibers in EDL muscle (h). Type I fibers are stained green using antibodies against MyHCI and type IIb fibers are stained red using antibodies against MyHCIIb. The frame of the fibers stained green show laminin. Original magnification: ×100. Values are presented as the mean ± SEM. $^{*}p < 0.05$ and $^{**}p < 0.01$ vs. SD rats at the same age; $^{\dagger}p < 0.05$ and $^{\dagger\dagger}p < 0.01$ vs. the same group at 16 weeks of age; $^{\S}p < 0.05$ and $^{\S\S}p < 0.01$ vs. the same group at 20 weeks of age.

phosphorylation, which results in downregulated expression levels of the E3 ligases Atrogin-1 and MuRF-1 [28]. Furthermore, AMPK, which is known to be a cellular fuel sensor activated by ATP depletion, is related to suppression of protein synthesis via decreased phosphorylation of mTOR [29] and activation of the FoxO-dependent protein degradation pathway [30]. In the present study, phosphorylation of Akt decreased and that of AMPK increased in the soleus muscle, but not in the EDL muscle, in the SDT fatty rats. Phosphorylation of mTOR, S6K, and FoxO1 was reduced in both the soleus and EDL muscles. Although increased Atrogin-1 expression was observed in the EDL muscle, there was no significant difference in MuRF-1 expression in the soleus and EDL muscles between the SDT and SD groups. Regarding the molecular mechanism underlying the progression of sarcopenia in the SDT group, disruption to insulin/IGF-1-Akt signaling due to insulin resistance and low serum IGF-1 levels was considered to provoke abnormalities in muscle strength and mass in the SDT group (Figure 11). Furthermore, while decreased muscle protein synthesis was considered to contribute to weakness of both the soleus and EDL muscles in the SDT group, the involvement of muscle protein degradation signaling in muscle depression in the SDT group may be low (Figure 11). Although the results of this study support those of a previous study [14], further studies are needed to investigate the association of FoxO-associated downstream pathways with muscle depression in SDT fatty rats.

Oxidative stress is reported to promote muscle atrophy and weakness [31–33] in addition to CKD. However, decreased oxidative stress, as evaluated by carbonylation of muscle proteins, was observed in the soleus muscle of SDT fatty rats, despite increased oxidative stress in the kidney tissues. Antioxidants are reported to diminish the positive effects of exercise training via decreased generation of reactive oxidative species by exercise [34]. Misu et al. reported that selenoprotein P in the liver, which has antioxidative activities, was increased in T2D patients and contributed to the elimination of the beneficial effects of exercise on muscle [35]. Although the mechanism underlying the decreased oxidative stress in the soleus muscle of SDT fatty rats remains unknown, a certain degree of oxidative stress may be needed to maintain muscle mass and force mainly by type I oxidative fibers. Oxidative stress is not a common aggravating factor related to the progression of sarcopenia and DKD.

The results of the present study may be limited by several factors. First, we found no independent association between DKD and muscle atrophy in the SDT fatty rats. This point

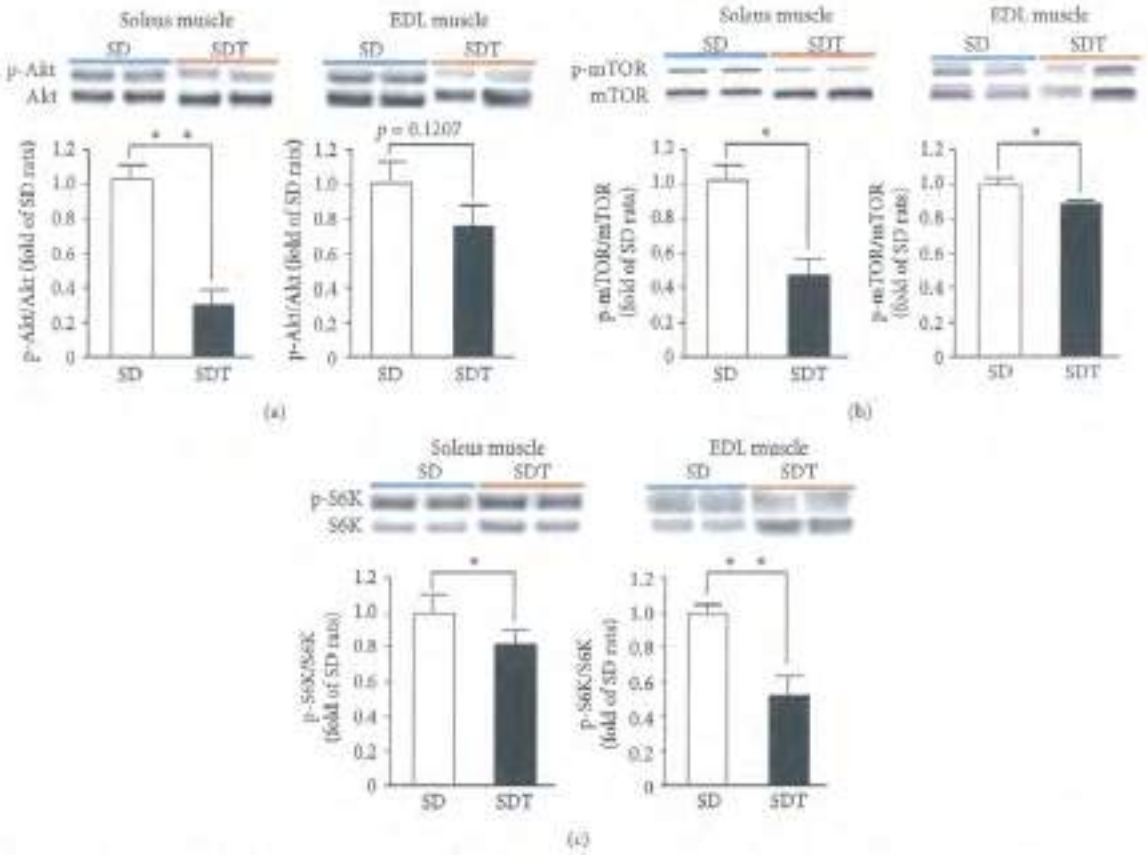

Figure 4: Muscle protein synthesis in SD and SDT fatty rats, as determined by western blot analysis. Phosphorylated Akt (a), mTOR (b), and S6K (c) in the soleus and EDL muscles. $^{*}p < 0.05$ and $^{**}p < 0.01$ vs. SD rats.

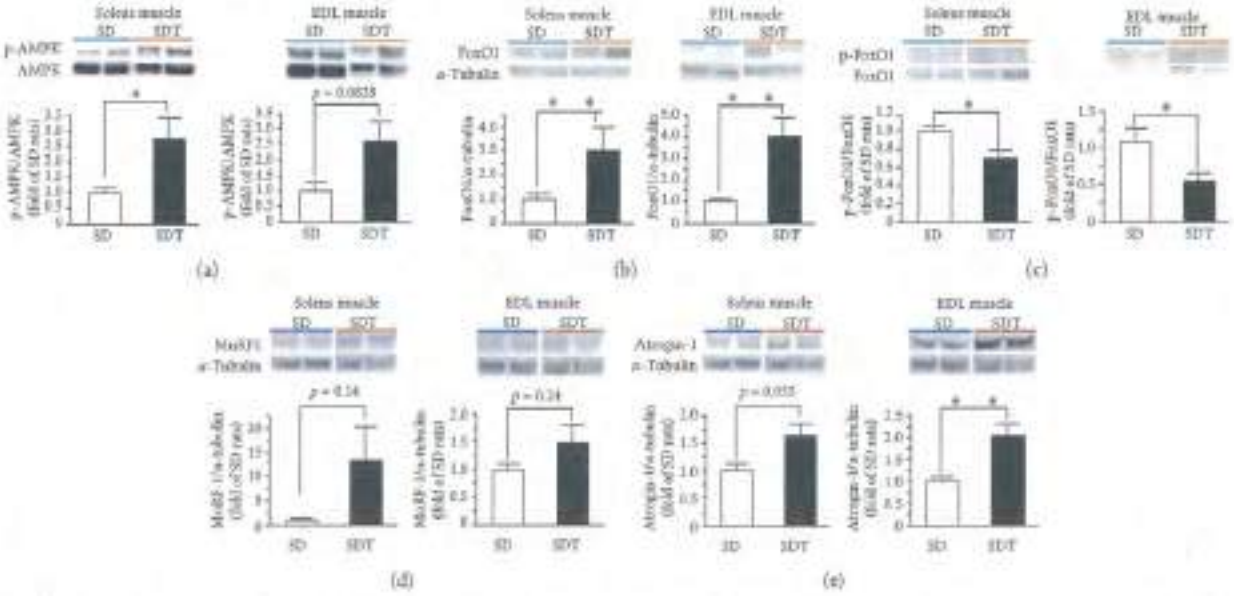

Figure 5: Muscle protein degradation in SD and SDT fatty rats, as determined by western blot analysis. Phosphorylated AMPK in the soleus and EDL muscles (a). Protein expression of FoxO1 in the soleus and EDL muscles (b). Phosphorylated FoxO1 in the soleus and EDL muscles (c). Protein expression of the E3 ubiquitin ligases MuRF-1 (d) and Atrogin-1 (e) in SD and SDT fatty rats, as determined by western blot analysis. $^{*}p < 0.05$ and $^{**}p < 0.01$ vs. SD rats.

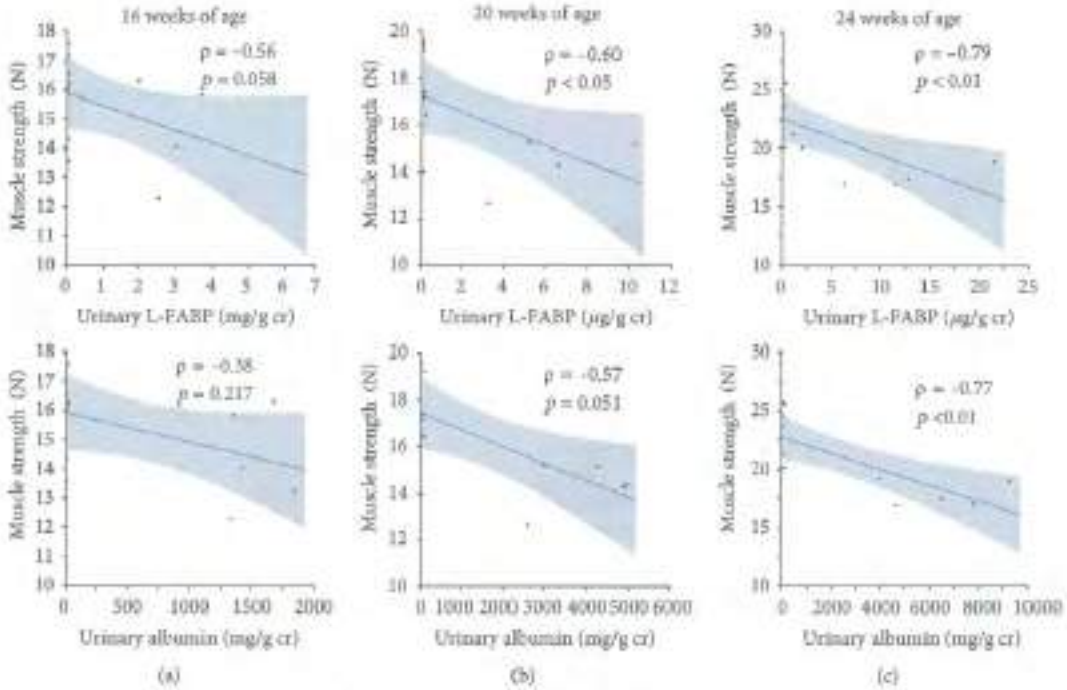

Figure 6: Correlations between each urinary marker and muscle strength at 16 (a), 20 (b), and 24 weeks of age (c).

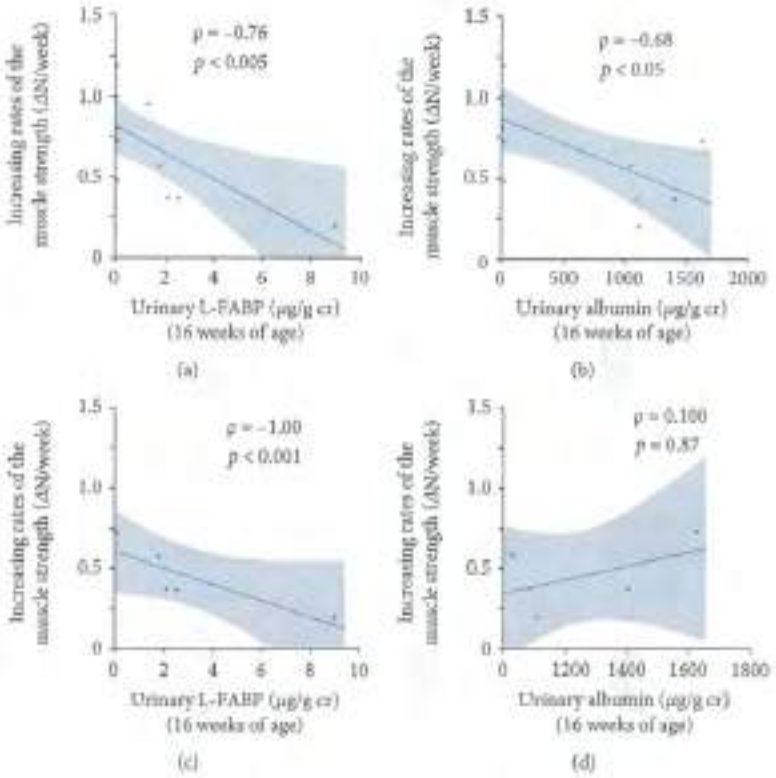

Figure 7: Correlations between each urinary marker at 16 weeks of age and increasing rate of muscle strength from 16 to 24 weeks of age in SD and SDT fatty rats (a, b). Correlations between each urinary marker and increasing rate of muscle strength from 16 to 24 weeks of age in SDT fatty rats (c, d).

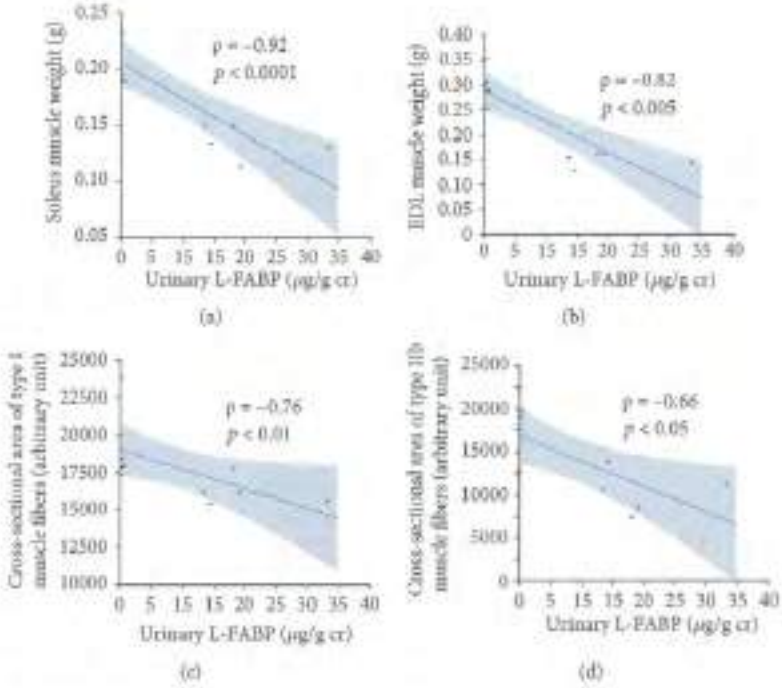

Figure 8: Correlations of urinary L-FABP with the weights of the soleus (a) and EDL muscles (b) and cross-sectional areas of type I (c) and IIb (d) muscle fibers.

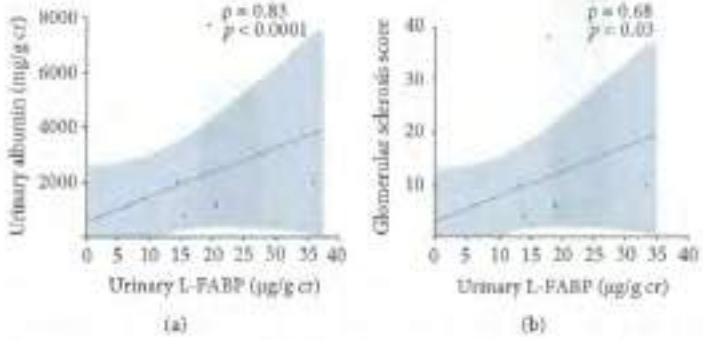

Figure 9: Correlations of urinary L-FABP with urinary albumin (a) and glomerular sclerosis (b).

needs to be clarified in further studies aimed to determine whether muscle atrophy is prevented along with treatment of DKD. Second, while muscle strength decreases along with age and develops to sarcopenia in humans, muscle strength slightly increased during the experimental period and retention of muscle growth was observed in the SDT fatty rats from 16 to 24 weeks of age. Therefore, sarcopenia in humans was not completely reproduced in the present study; thus, further clinical studies of T2D patients are needed in order to reveal the clinical usefulness of urinary L-FABP as a marker of the progression of sarcopenia. Third, we did not determine the most suitable marker for sarcopenia because sample size was limited in the basic research. Future clinical research is needed to reveal the point. Finally, we did not investigate changes in urinary L-FABP levels in response to interventions that ameliorate renal hypoxia. Finally, we did not investigate changes in urinary L-FABP levels in response to interventions that prevent muscle atrophy. Because we recently demonstrated that habitual exercise led to a reduction in urinary L-FABP levels in healthy middle-aged and older adults [11], urinary L-FABP may respond to the relief of secondary sarcopenia due to diabetes and kidney disease.

5. Conclusion

In conclusion, urinary L-FABP reflects the degrees of muscle strength, muscle weight, and cross-sectional areas of muscle fibers. Although the detailed mechanisms of the interaction between sarcopenia and DKD was not revealed in this study, urinary L-FABP may be useful to monitor the progression of sarcopenia in addition to DKD in T2D patients. Nonetheless, future clinical studies of T2D patients are needed.

Table 3: Relationships between renal morphological change and muscle strength, and weights of the soleus and extensor digitorum longus (EDL) muscles in 24-week-old SD and SDT fatty rats.

Renal interstitial change	Muscle strength and weight	Correlation coefficient (ρ)
Macrophage infiltration	Muscle strength	-0.76**
	Weight of soleus muscle	-0.67*
	Weight of EDL muscle	-0.64*
α-SMA expression	Muscle strength	-0.69*
	Weight of soleus muscle	-0.67*
	Weight of EDL muscle	-0.61*
Collagen type I expression	Muscle strength	-0.57
	Weight of soleus muscle	-0.67*
	Weight of EDL muscle	-0.62*
Collagen type III expression	Muscle strength	-0.58
	Weight of soleus muscle	-0.83*
	Weight of EDL muscle	-0.70**
Glomerular sclerosis score	Muscle strength	-0.79**
	Weight of soleus muscle	-0.49
	Weight of EDL muscle	-0.71*

*$p < 0.05$ and **$p < 0.01$.

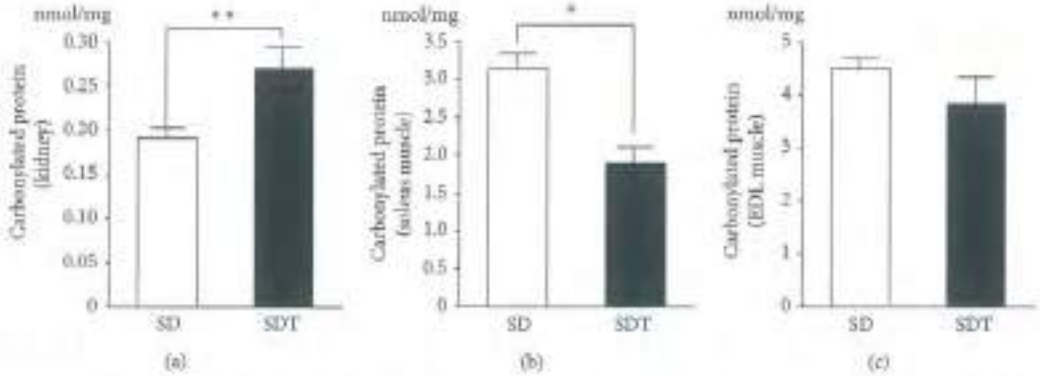

Figure 10: Expression profiles of carbonylated proteins in kidney (a), soleus (b), and EDL muscle (c) tissues. Values are presented as the mean ± SEM. *$p < 0.05$ and **$p < 0.01$ vs. SD rats.

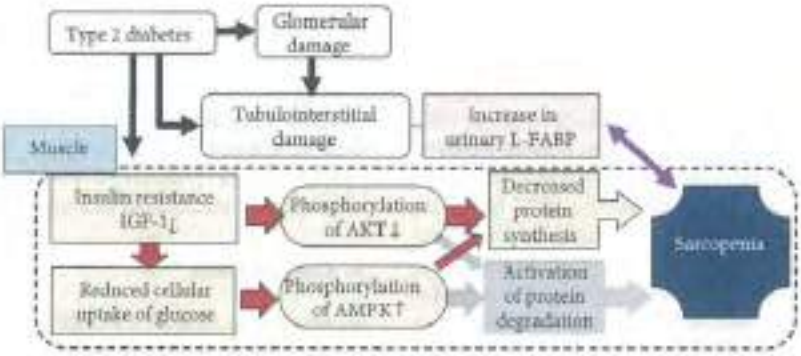

Figure 11: Molecular mechanism underlying the progression of sarcopenia in type 2 diabetes. Disruption to insulin/IGF-1-Akt signaling due to insulin resistance and low serum IGF-1 levels was considered to reduce muscle protein synthesis and to provoke abnormalities in muscle strength and mass in the SDT fatty rats. Furthermore, phosphorylation of AMPK due to reduced cellular uptake of glucose led to suppression of muscle protein synthesis. On the other hand, the involvement of muscle protein degradation signaling in muscle depression in the SDT group may be low.

Data Availability

The data used to support the findings of this study are included within the article.

Conflicts of Interest

T.S. is the director and a senior scientist at CMIC Holdings Co., Ltd., and K.O. is a scientist at CMIC Holdings Co., Ltd., which produced the kits for L-FABP analysis. All other authors declare no conflicts of interest.

Authors' Contributions

Study design was handled by JT, YO, TS, KO, and AK-I; data collection by JT, YO, KK, KO, SW, KI, SH, and AK-I; data analysis by JT and AK-I; data interpretation by JT, YO, YN, DI, TS, KO, KK, YS, and AK-I; literature search and figure generation by JT and AK-I; and writing of the manuscript by JT, YO, and AK-I. All authors approved the final version of the manuscript for publication.

Acknowledgments

We thank Ms. Naomi Saito (Department of Anatomy, St. Marianna University School of Medicine), Ms. Kimie Katayama (Division of Nephrology and Hypertension, Department of Internal Medicine, St. Marianna University School of Medicine), and Ms. Junko Asano (Department of Internal Medicine, St. Marianna University School of Medicine) for technical assistance.

References

[1] M. Roden, "Future of muscle research in diabetes: a look into the crystal ball," *Diabetologia*, vol. 58, no. 8, pp. 1693–1698, 2015.

[2] R. R. Kalyani, M. Corriere, and L. Ferrucci, "Age-related and disease-related muscle loss: the effect of diabetes, obesity, and other diseases," *The Lancet Diabetes and Endocrinology*, vol. 2, no. 10, pp. 819–829, 2014.

[3] J. M. Chiasera, K. M. Ward-Cook, S. A. McCune, and G. M. Wardlaw, "Effect of aerobic training on diabetic nephropathy in a rat model of type 2 diabetes mellitus," *Annals of Clinical and Laboratory Science*, vol. 30, no. 4, pp. 346–353, 2000.

[4] D. Ito, P. Cao, T. Kakihana et al., "Chronic running exercise alleviates early progression of nephropathy with upregulation of nitric oxide synthases and suppression of glycation in Zucker diabetic rats," *PLoS One*, vol. 10, no. 9, article e0138037, 2015.

[5] S. Hanatani, Y. Izumiya, S. Araki et al., "Akt1-mediated fast/glycolytic skeletal muscle growth attenuates renal damage in experimental kidney disease," *Journal of the American Society of Nephrology*, vol. 25, no. 12, pp. 2800–2811, 2014.

[6] K. Kosaki, T. Sugaya, K. Ohata et al., "Renoprotective effects of voluntary running exercise training on aldosterone-induced renal injury in human L-FABP chromosomal transgenic mice," *Hypertension Research*, vol. 42, no. 10, pp. 1518–1527, 2019.

[7] S. Watanabe, D. Ichikawa, T. Sugaya et al., "Urinary level of liver-type fatty acid binding protein reflects the degree of tubulointerstitial damage in polycystic kidney disease," *Kidney & Blood Pressure Research*, vol. 43, no. 6, pp. 1716–1729, 2018.

[8] T. Yokoyama, A. Kamijo-Ikemori, T. Sugaya, S. Hoshino, T. Yasuda, and K. Kimura, "Urinary excretion of liver type fatty acid binding protein accurately reflects the degree of tubulointerstitial damage," *The American Journal of Pathology*, vol. 174, no. 6, pp. 2096–2106, 2009.

[9] K. Matsui, A. Kamijo-Ikemori, N. Imai et al., "Clinical significance of urinary liver-type fatty acid-binding protein as a predictor of ESRD and CVD in patients with CKD," *Clinical and Experimental Nephrology*, vol. 20, no. 2, pp. 195–203, 2016.

[10] K. Kosaki, A. Kamijo-Ikemori, T. Sugaya et al., "Relationship between exercise capacity and urinary liver-type fatty acid-binding protein in middle-aged and older individuals," *Clinical and Experimental Nephrology*, vol. 21, no. 5, pp. 810–817, 2017.

[11] K. Kosaki, A. Kamijo-Ikemori, T. Sugaya et al., "Effect of habitual exercise on urinary liver-type fatty acid-binding protein levels in middle-aged and older adults," *Scandinavian Journal of Medicine & Science in Sports*, vol. 28, no. 1, pp. 152–160, 2018.

[12] T. Masuyama, Y. Katsuda, and M. Shinohara, "A novel model of obesity-related diabetes: introgression of the Lepr(fa) allele of the Zucker fatty rat into nonobese spontaneously diabetic Torii (SDT) rats," *Experimental Animals*, vol. 54, no. 1, pp. 13–20, 2005.

[13] K. Matsui, T. Ohta, T. Oda et al., "Diabetes-associated complications in spontaneously diabetic Torii fatty rats," *Experimental Animals*, vol. 57, no. 2, pp. 111–121, 2008.

[14] Y. Kemmochi, T. Ohta, Y. Motohashi et al., "Pathophysiological analyses of skeletal muscle in obese type 2 diabetes SDT fatty rats," *Journal of Toxicologic Pathology*, vol. 31, no. 2, pp. 113–123, 2018.

[15] D. Ichikawa, A. Kamijo-Ikemori, T. Sugaya et al., "Renal liver-type fatty acid binding protein attenuates angiotensin II-induced renal injury," *Hypertension*, vol. 60, no. 4, pp. 973–980, 2012.

[16] K. Ohata, A. Kamijo-Ikemori, T. Sugaya et al., "Renoprotective effect of the xanthine oxidoreductase inhibitor topiroxostat under decreased angiotensin II type 1_a receptor expression," *European Journal of Pharmacology*, vol. 815, pp. 88–97, 2017.

[17] D. Deveci, J. M. Marshall, and S. Egginton, "Relationship between capillary angiogenesis, fiber type, and fiber size in chronic systemic hypoxia," *American Journal of Physiology. Heart and Circulatory Physiology*, vol. 281, no. 1, pp. H241–H252, 2001.

[18] D. M. Zelle, G. Klaassen, E. van Adrichem, S. J. L. Bakker, E. Corpeleijn, and G. Navis, "Physical inactivity: a risk factor and target for intervention in renal care," *Nature Reviews. Nephrology*, vol. 13, no. 3, pp. 152–168, 2017.

[19] K. Kosaki, A. Kamijo-Ikemori, T. Sugaya et al., "Association between muscular strength and intrarenal vascular resistance in middle-aged and older individuals," *Experimental Gerontology*, vol. 91, pp. 72–78, 2017.

[20] T. Yamamoto, E. Noiri, Y. Ono et al., "Renal L-type fatty acid-binding protein in acute ischemic injury," *Journal of the American Society of Nephrology*, vol. 18, no. 11, pp. 2894–2902, 2007.

[21] E. Tynkevich, M. Flamant, J. P. Haymann et al., "Decrease in urinary creatinine excretion in early stage chronic kidney disease," *PLoS One*, vol. 9, no. 11, article e111949, 2014.

[22] R. Yang, Y. Zhang, X. Shen, and S. Yan, "Sarcopenia associated with renal function in the patients with type 2 diabetes," *Diabetes Research and Clinical Practice*, vol. 118, pp. 121–129, 2016.

[23] M. S. Hickey, J. O. Carey, J. L. Azevedo et al., "Skeletal muscle fiber composition is related to adiposity and in vitro glucose transport rate in humans," *American Journal of Physiology-Endocrinology and Metabolism*, vol. 268, no. 3, pp. E453–E457, 1995.

[24] E. Marzetti, H. A. Lees, S. E. Wohlgemuth, and C. Leeuwenburgh, "Sarcopenia of aging: underlying cellular mechanisms and protection by calorie restriction," *BioFactors*, vol. 35, no. 1, pp. 28–35, 2009.

[25] I. H. de Boer, L. Zelnick, M. Afkarian et al., "Impaired glucose and insulin homeostasis in moderate-severe CKD," *Journal of the American Society of Nephrology*, vol. 27, no. 9, pp. 2861–2871, 2016.

[26] M. Tamaki, A. Hagiwara, K. Miyashita et al., "Improvement of physical decline through combined effects of muscle enhancement and mitochondrial activation by a gastric hormone ghrelin in male 5/6Nx CKD model mice," *Endocrinology*, vol. 156, no. 10, pp. 3638–3648, 2015.

[27] M. Tamaki, K. Miyashita, S. Wakino, M. Mitsuishi, K. Hayashi, and H. Itoh, "Chronic kidney disease reduces muscle mitochondria and exercise endurance and its exacerbation by dietary protein through inactivation of pyruvate dehydrogenase," *Kidney International*, vol. 85, no. 6, pp. 1330–1339, 2014.

[28] S. Schiaffino and C. Mammucari, "Regulation of skeletal muscle growth by the IGF1-Akt/PKB pathway: insights from genetic models," *Skeletal Muscle*, vol. 1, no. 1, p. 4, 2011.

[29] T. Egawa, A. Goto, Y. Ohno et al., "Involvement of AMPK in regulating slow-twitch muscle atrophy during hindlimb unloading in mice," *American Journal of Physiology-Endocrinology and Metabolism*, vol. 309, no. 7, pp. E651–E662, 2015.

[30] D. R. Bolster, S. J. Crozier, S. R. Kimball, and L. S. Jefferson, "AMP-activated protein kinase suppresses protein synthesis in rat skeletal muscle through down-regulated mammalian target of rapamycin (mTOR) signaling," *The Journal of Biological Chemistry*, vol. 277, no. 27, pp. 23977–23980, 2002.

[31] F. Derbre, B. Ferrando, M. C. Gomez-Cabrera et al., "Inhibition of xanthine oxidase by allopurinol prevents skeletal muscle atrophy: role of p38 MAPKinase and E3 ubiquitin ligases," *PLoS One*, vol. 7, no. 10, article e46668, 2012.

[32] H. Kondo, J. Kodama, T. Kishibe, and Y. Itokawa, "Oxidative stress during recovery from muscle atrophy," *FEBS Letters*, vol. 326, no. 1-3, pp. 189–191, 1993.

[33] J. M. Lawler, W. Song, and S. R. Demaree, "Hindlimb unloading increases oxidative stress and disrupts antioxidant capacity in skeletal muscle," *Free Radical Biology & Medicine*, vol. 35, no. 1, pp. 9–16, 2003.

[34] M. Ristow, K. Zarse, A. Oberbach et al., "Antioxidants prevent health-promoting effects of physical exercise in humans," *Proceedings of the National Academy of Sciences*, vol. 106, no. 21, pp. 8665–8670, 2009.

[35] H. Misu, H. Takayama, Y. Saito et al., "Deficiency of the hepatokine selenoprotein P increases responsiveness to exercise in mice through upregulation of reactive oxygen species and AMP-activated protein kinase in muscle," *Nature Medicine*, vol. 23, no. 4, pp. 508–516, 2017.

Kidney & Blood Pressure Research

Kidney Blood Press Res 2019;44:1476–1492
DOI: 10.1159/000503926
Received: July 16, 2019
Accepted: October 4, 2019
Published online: November 15, 2019

© 2019 The Author(s)
Published by S. Karger AG, Basel
www.karger.com/kbr

Karger Open access

This article is licensed under the Creative Commons Attribution-NonCommercial-NoDerivatives 4.0 International License (CC BY-NC-ND) (http://www.karger.com/Services/OpenAccessLicense). Usage and distribution for commercial purposes as well as any distribution of modified material requires written permission.

Research Article

The Possibility of Urinary Liver-Type Fatty Acid-Binding Protein as a Biomarker of Renal Hypoxia in Spontaneously Diabetic Torii Fatty Rats

Jun Tanabe[a] Yuji Ogura[b] Mikie Nakabayashi[c] Yoshio Nagai[d] Shiika Watanabe[a] Takeshi Sugaya[a] Keiichi Ohata[a] Daisuke Ichikawa[a] Kazuho Inoue[e] Seiko Hoshino[e] Kenjiro Kimura[f] Yugo Shibagaki[a] Yumie Ono[c] Atsuko Kamijo-Ikemori[a, e]

[a]Division of Nephrology and Hypertension, Department of Internal Medicine, St. Marianna University School of Medicine, Kanagawa, Japan; [b]Department of Physiology, St. Marianna University School of Medicine, Kanagawa, Japan; [c]Department of Electronics and Bioinformatics, School of Science and Technology, Meiji University, Kanagawa, Japan; [d]Division of Metabolism and Endocrinology, Department of Internal Medicine, St. Marianna University School of Medicine, Kanagawa, Japan; [e]Department of Anatomy, St. Marianna University School of Medicine, Kanagawa, Japan; [f]JCHO Tokyo Takanawa Hospital, Tokyo, Japan

Keywords
Diabetes · Diabetic kidney disease · Hypoxia · Kidney · Liver-type fatty acid-binding protein · Tubulointerstitial damage

Abstract
Background: Renal hypoxia is an aggravating factor for tubulointerstitial damage, which is strongly associated with renal prognosis in diabetic kidney disease (DKD). Therefore, urinary markers that can detect renal hypoxia are useful for monitoring DKD. ***Objective:*** To determine the correlation between urinary liver-type fatty acid-binding protein (L-FABP) and renal hypoxia using a novel animal model of type 2 diabetes. ***Methods:*** Male spontaneously diabetic Torii (SDT) fatty rats (n = 6) were used as an animal model of type 2 diabetes. Age- and sex-matched Sprague-Dawley (SD) rats (n = 8) were used as controls. Body weight, systolic blood pressure, and blood glucose levels were measured at 8, 12, 16, and 24 weeks of age. Urine samples and serum and kidney tissues were collected at 24 weeks of age. Microvascular blood flow index (BFI) was measured using diffuse correlation spectroscopy before sampling both the serum and kidneys for the evaluation of renal microcirculation at the corticomedullary junction. ***Results:*** Obesity, hyperglycemia, and hypertension were observed in the SDT fatty

Atsuko Kamijo-Ikemori, MD, PhD
Division of Nephrology and Hypertension, Department of Internal Medicine and Department of Anatomy, St. Marianna University School of Medicine
2-16-1 Sugao, Miyamae-Ku, Kawasaki 216-8511 (Japan)
E-Mail a2kamijo@marianna-u.ac.jp

KARGER

rats. Focal glomerular sclerosis, moderate interstitial inflammation, and fibrosis were significantly more frequent in SDT fatty rats than in SD rats. While the frequency of peritubular endothelial cells and phosphoendothelial nitric oxide synthase levels were similar in both types of rats, the degree of renal hypoxia-inducible factor-1α (HIF-1α) expression was significantly higher (and with no change in renal vascular endothelial growth factor expression levels) in the SDT fatty rats. Urinary L-FABP levels were significantly higher and renal microvascular BFI was significantly lower in the SDT fatty rats than in the SD rats. Urinary L-FABP levels exhibited a significant positive correlation with renal HIF-1α expression and a significant negative correlation with renal microvascular BFI. ***Conclusions:*** Urinary L-FABP levels reflect the degree of renal hypoxia in DKD in a type 2 diabetic animal model. Urinary L-FABP may thus prove useful as a renal hypoxia marker for monitoring DKD in patients with type 2 diabetes in clinical practice.

© 2019 The Author(s)
Published by S. Karger AG, Basel

Introduction

Despite the development of numerous therapeutics for diabetes, diabetic kidney disease (DKD) remains a major cause of end-stage renal failure globally [1, 2] and is associated with an increase in medical care expenses [3]. Owing to the limited number of therapeutic strategies presently available, monitoring for DKD is critical for prompt multidisciplinary management, and novel biomarkers that can provide detailed kidney status of patients with DKD are sorely required.

Tubulointerstitial damage is strongly associated with renal prognosis in DKD [4–6], and renal hypoxia is an aggravating factor for the progression of this damage [7–9]. Tubular biomarkers that reflect the degree of renal hypoxia as well as tubulointerstitial damage would therefore be useful for monitoring DKD.

Urinary liver-type fatty acid-binding protein (L-FABP) is a tubular marker that accurately reflects the severity of tubulointerstitial damage in chronic kidney disease including DKD [10–12] and acute kidney disease [13, 14]. L-FABP has been promulgated as a tubular biomarker by the Ministry of Health, Labour and Welfare in Japan [15]. An increase in urinary L-FABP has been reported to be an independent risk factor for DKD progression in type 1 and 2 diabetes [16–18]. Although urinary L-FABP levels were reported to be associated with renal microcirculation in donors during surgery for renal transplantation [19], no correlation with renal hypoxia in DKD has been elucidated to date. Therefore, we assessed the correlation between urinary L-FABP levels and renal hypoxia in a rat model of type 2 diabetes using spontaneously diabetic Torii (SDT) fatty (SDT.Cg-*Lepr*^{fa}/Jtt]cl) rats, a novel model that mimics the human pathophysiology of type 2 diabetes that is accompanied by obesity, hyperlipidemia, and hypertension [20]. The renal hypoxia was evaluated by renal hypoxia-inducible factor-1α (HIF-1α) expression, and the microvascular blood flow index (BFI) was measured using diffuse correlation spectroscopy (DCS).

Materials and Methods

Animals

All animal studies were conducted in accordance with the St. Marianna University School of Medicine Institutional Guide for Animal Experiments and the Guide for the Care and Use of Laboratory Animals. Male SDT fatty rats derived from a Sprague-Dawley (SD) colony were used as a model of type 2 diabetes. Four-week-old male SDT fatty rats ($n = 7$) and age-matched

control SD rats (n = 8) were purchased from CLEA Japan (Tokyo, Japan) and allowed free access to laboratory chow (CRF-2; Charles River Laboratories Japan, Yokohama, Japan) and water. One STD fatty rat died at 23 weeks of age, but the remaining 6 underwent extensive analyses. To confirm the diabetic status, blood glucose levels were measured 4 h after the removal of the chow with the Free Style Freedom Lite (Niporo, Osaka, Japan) in blood collected from the tail vein.

For all experiments, 24-week-old rats were individually housed overnight in metabolic cages with free access to tap water. Urine was collected for the measurement of urinary markers. Additionally, under inhalation anesthesia using 2% isoflurane, serum samples and kidney tissues were collected. The extracted kidneys were weighed, sectioned, and stored either at −80 °C or in liquid nitrogen for downstream analyses.

Body Weight and Blood Pressure Measurement

Body weight and systolic blood pressure (SBP) were measured every 4 weeks from 8 to 24 weeks of age. SBP was measured using a tail-cuff apparatus (Softron BP-98A; Softron, Tokyo, Japan), and averages of 3 SBP measurements per animal per time point were recorded [11].

Determination of Microvascular BFI Using DCS

Microvascular BFI was measured using DCS, which detects tissue blood flow velocity using intensity fluctuations of a reflected near-infrared light due to the movement of red blood cells in the microvasculature [21–23]. The measurements were performed immediately before sampling both the serum and kidneys at 24 weeks of age. Briefly, under inhalation anesthesia using 2% isoflurane, the rats underwent left abdominal laparotomy. Photon-emitter and detector probes were placed at 4-mm intervals directly on the left renal surface to detect the emitted near-infrared light from the renal parenchyma for 2 min. The DCS system enables BFI measurements of the region in approximately half the depth (2 mm) of the distance between the 2 probes below the renal surface [24]; this allows the detection of microvascular blood flow in the corticomedullary area. The near-infrared light sent from the photon-emitter probe is irradiated from the renal surface to the blood flowing in the peritubular capillaries of the renal cortex. The light is diffused by the red blood cells, and this reflected light is recorded by the detector probe. Microvascular BFI is defined as the blood velocity calculated from an autocorrelation-related change in the reflected light [21] and we used it to determine the degree of change in microvascular blood flow.

Serum and Urinary Biochemistry

Serum and urine creatinine levels were measured using a Quantichrom™ creatinine assay kit (BioAssay Systems, Hayward, CA, USA). Serum cystatin C levels were measured using a rat cystatin C enzyme-linked immunosorbent assay (ELISA) kit (BioVendor, Brno, Czech Republic). Serum urea nitrogen levels were measured via urease-LED-ultraviolet absorption spectrophotometry, serum total cholesterol levels using the cholesterol oxidase enzymatic method, and serum triglyceride levels using an enzymatic method provided by the SRL clinical laboratory testing services (Tokyo, Japan). Urinary glucose levels were determined semiquantitatively using urinary dipsticks (WAKO Pure Chemical Industries, Osaka, Japan). Grading for urinary glucose was as follows: 0, negative; 1+, >100 mg/dL; 2+, >250 mg/dL; 3+, >500 mg/dL; and 4+, >2,000 mg/dL. Levels of urinary L-FABP and albumin were measured using rat L-FABP (CMIC, Tokyo, Japan) and rat albumin (Fujifilm WAKO Shibayagi, Gunma, Japan) ELISA kits, respectively. They were reported as ratios relative to the urinary creatinine levels.

Renal Histological and Morphometric Analyses

The midsection of each excised kidney was dissected in the minor axial direction. The 2 pieces were fixed in 10% buffered formalin or methyl Carnoy's solution (60% methanol, 30% chloroform, and 10% glacial acetic acid) and embedded in paraffin. Serial sections (3 μm thick) were prepared for renal histological assessment including periodic acid-Schiff (PAS) staining and immunohistochemistry (IHC).

Glomerulosclerosis in PAS-stained sections was evaluated by grading the extent of sclerosis in each glomerulus as follows: 0, no sclerosis; 1, sclerosis in 1–25% of the glomerulus; 2, sclerosis in 26–50% of the glomerulus; 3, sclerosis in 51–75% of the glomerulus; and 4, sclerosis in 76–100% of the glomerulus. At ×100 magnification, the glomerulosclerosis score for each animal was calculated as follows: ([1 × the number of grade 1 glomeruli, %] + [2 × the number of grade 2 glomeruli, %] + [3 × the number of grade 3 glomeruli, %] + [4 × the number of grade 4 glomeruli, %]). We examined 50 glomeruli for each animal [25].

IHC Analyses of the Renal Tissues

Target antigens in the preprocessed sections were stained using the indirect immunoperoxidase method, as described previously [11]. Briefly, the formalin-fixed/paraffin-embedded tissue specimens were used to stain for myofibroblasts and tubular cells exhibiting the epithelial-mesenchymal transition by using a mouse monoclonal antibody specific for α-smooth muscle actin (α-SMA, 1:800; Sigma-Aldrich, St. Louis, MO, USA). The tissue specimens fixed in methyl Carnoy's solution were assessed immunohistochemically for macrophages using a mouse monoclonal antibody (ED-1) specific for CD68 (1:100; Abcam, Tokyo, Japan), for type I and type III collagens using goat polyclonal antibodies specific for type I (1:200; Southern Biotech, Birmingham, AL, USA) and type III (1:200; Southern Biotech) collagen, and for endothelial cells using a mouse monoclonal antibody specific for rat endothelial cell antigen-1 (RECA-1) (1:100; Abcam). Labeled proteins were visualized using polymeric horseradish peroxidase (HRP)-conjugated secondary antibodies (ImmPRESS™ polymer detection kit; Vector Laboratories, Burlingame, CA, USA). Peroxidase activity was detected via the diaminobenzidine reaction (Liquid DAB+; DAKO Japan, Tokyo, Japan), and sections were counterstained with hematoxylin.

For quantification, images from 10 nonoverlapping fields throughout the cortical and outer medullary regions were captured at ×100 magnification. The extent of macrophage and interstitial myofibroblast infiltration in the cortical and outer medullary interstitia were automatically measured using an image analyzer (WinRoof v6.4, Mitani, Tokyo, Japan). Briefly, the areas positively stained for α-SMA, CD68, and RECA-1 were independently measured and expressed as ratios relative to the areas of the entire cortical and outer medullary regions. The same method was used to measure the expression levels of both type I and type III collagen. Furthermore, to evaluate the expansion of mesangial matrix, type IV collagen was labeled using a rabbit polyclonal antibody (1:500; Cedarlane Laboratories, ON, Canada) in sections that were fixed in formalin [26]. Thirty glomeruli in the cortical area were analyzed. Briefly, areas positively stained for type IV collagen in each glomerulus as well as the size of each glomerulus were measured with WinRoof image analyzer, and then expressed as ratios relative to the total glomerular areas.

Real-Time Quantitative Reverse Transcription Polymerase Chain Reaction

Total RNA was extracted from the kidney tissues using a RNeasy midi kit (Qiagen, Valencia, CA, USA) according to the manufacturer's instructions, and a 0.5-μg aliquot was reverse-transcribed. TaqMan real-time polymerase chain reaction (PCR) with StepOnePlus™ real-time PCR system (Applied Biosystems, Waltham, MA, USA) was used to measure the mRNA levels of monocyte chemoattractant protein (*Mcp-1*), transforming growth

factor-β (*Tgf-β*), *CD31*, *Hif-1α*, vascular endothelial growth factor (*Vegf*), and 18S ribosomal RNA (*18s*). The expression levels of all mRNAs were normalized to the levels of *18s* in all samples.

Renal Protein Expression of Vascular Endothelial Growth Factor

Renal vascular endothelial growth factor (VEGF) protein expression levels were determined using an ELISA kit from R&D Systems (Minneapolis, MN, USA) with protein extracted from frozen kidney tissues, after determining protein concentrations as described previously [27].

Western Blotting

Proteins were extracted from frozen kidney tissues, and protein concentrations were measured as described previously [28]. Next, 60 μg of extracts were separated by SDS-PAGE using NuPAGE 4–12% Bis-Tris gels and the XCell SureLock Mini-Cell system (Thermo Fisher Scientific, Rockford, IL, USA). The separated proteins were transferred to PVD membranes using the iBlot™ dry blotting system (Thermo Fisher Scientific), and the membranes were blocked in Blocking One solution (Nacalai Tesque, Kyoto, Japan). Primary antibodies against HIF-1α (rabbit monoclonal, #14179, 1:1,000; Cell Signaling Technology, Danvers, MA, USA), endothelial nitric oxide synthase (eNOS, rabbit polyclonal, #9572, 1:1,000; Cell Signaling Technology), and phospho-eNOS (rabbit polyclonal, #9571, 1:1,000; Cell Signaling Technology) diluted in Can Get Signal Solution I (TOYOBO, Osaka, Japan) were incubated overnight at 4 °C. After washing, the membranes were incubated with an HRP-conjugated anti-rabbit antibody (Santa Cruz Biotechnology, Dallas, TX, USA) diluted at 1:2,000 for phospho-eNOS and eNOS or 1:4,000 for HIF-1α in Blocking One solution for 1 h at room temperature. Subsequently, chemiluminescence was detected using ECL Prime Western blotting detection reagent (GE Healthcare, Little Chalfont, UK) with a CCD camera system (Ez-Capture II, ATTO, Tokyo, Japan). A rabbit monoclonal antibody to α-tubulin (1:4,000; Abcam) was also used to detect α-tubulin on the same membranes that were incubated with HIF-1α, eNOS, and phospho-eNOS, after treatment with a stripping buffer (WAKO); the expression levels of the 3 proteins were normalized to that of α-tubulin. The expression levels of all proteins were quantified using ImageJ software (National Institutes of Health, Frederick, MD, USA).

Statistical Analysis

All values were expressed as means ± standard error of the mean (SEM). A p value <0.05 was considered to indicate statistical significance. Differences between SD and SDT rats were analyzed by the Steel test. The 2 groups were compared using the Mann-Whitney U test. Spearman's rank correlation coefficient was used to evaluate nonparametric data and assess correlations between 2 parameters. All statistical analyses were performed using JMP® software v13.0.0 (SAS Institute, Cary, NC, USA).

Results

Changes in Body Weight, Blood Glucose, and SBP

In both groups, the body weight, blood glucose, and SBP values were measured every 4 weeks in rats aged between 8 and 24 weeks (Table 1). Body weight was significantly higher in the 12-, 16-, 20-, and 24-week-old rats than in the 8-week-old rats in both groups. Additionally, the body weights of the 8-, 12-, and 16-week-old SDT fatty rats were significantly higher than those of the age-matched SD rats. Similarly, the blood glucose levels of the SDT fatty rats were significantly higher than those of the SD rats throughout the observation

Kidney Blood Press Res 2019;44:1475–1482
DOI: 10.1159/000503926
© 2019 The Author(s). Published by S. Karger AG, Basel
www.karger.com/kbr

Table 1. Time-related changes in body weight, blood glucose, and SBP

	Group	At 8 weeks of age	At 12 weeks of age	At 16 weeks of age	At 20 weeks of age	At 24 weeks of age
Body weight, g	SD	300.70 (6.21)	443.83† (6.36)	538.08† (6.94)	595.89† (8.56)	592.25† (9.44)
	SDT	393.13** (5.19)	506.32**,‡ (9.06)	567.20*,‡ (12.09)	572.77† (11.67)	536.08† (12.32)
Blood glucose, mg/dL	SD	71.63 (5.67)	60.25 (2.82)	63.50 (4.36)	59.50 (2.57)	90.38 (3.79)
	SDT	162.00** (11.61)	322.33**,† (14.38)	331.50**,† (28.26)	406.50**,‡ (27.53)	325.67**,† (9.37)
SBP, mm Hg	SD	113.00 (6.29)	116.13 (4.12)	132.13 (4.84)	111.88 (4.25)	120.38 (5.26)
	SDT	126.67 (2.35)	151.33**,† (2.50)	143.00 (3.26)	135.50** (5.51)	135.50 (3.17)

Data are presented as the mean (SEM). SBP, systolic blood pressure. * $p < 0.05$ and ** $p < 0.01$ versus the SD rats in the same week; † $p < 0.05$ and ‡ $p < 0.01$ versus the same group at 8 weeks of age.

Table 2. Renal function and serum total cholesterol at 24 weeks of age

	SD rats	SDT fatty rats
Serum creatinine, mg/dL	0.45 (0.02)	0.55 (0.02)**
Cystatin C, ng/mL	3.68 (0.16)	4.01 (0.17)
Urea nitrogen, mg/dL	18.79 (0.35)	29.42 (2.71)**
Total cholesterol, mg/dL	75.25 (3.92)	161.50 (6.94)**

Data are presented as the mean (SEM). ** $p < 0.01$ versus the SD rats.

KARGER

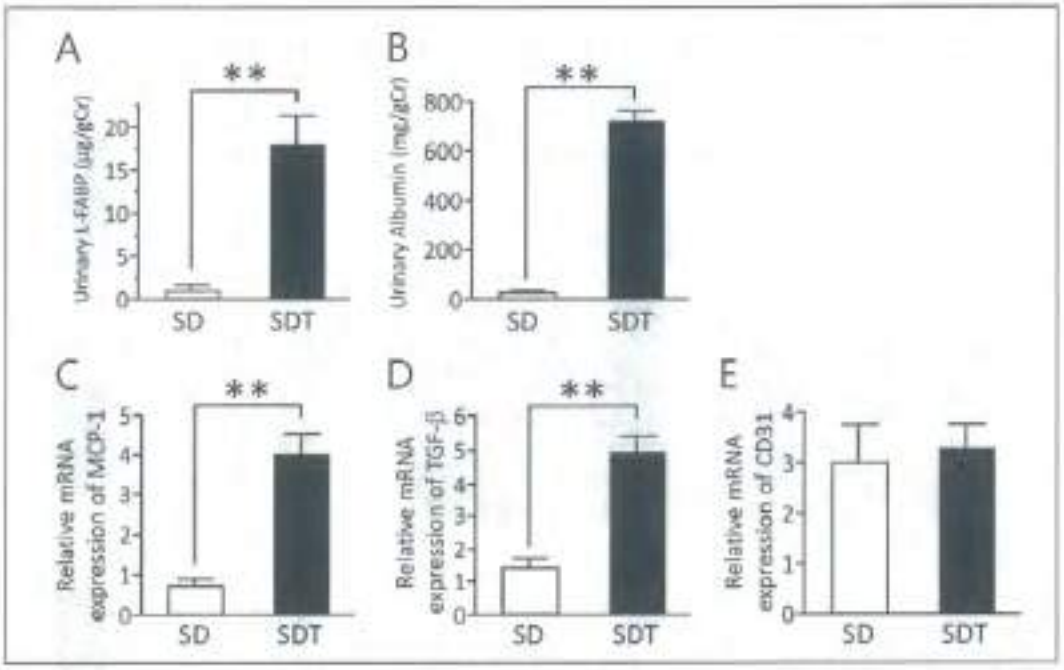

Fig. 1. Comparison of urinary parameters and renal mRNA transcript levels in Sprague-Dawley (SD) and spontaneously diabetic Torii (SDT) fatty rats at 24 weeks of age. **A** Urinary liver-type fatty acid-binding protein (L-FABP) levels at 24 weeks of age. **B** Urinary albumin at 24 weeks of age. mRNA transcript levels of monocyte chemoattractant protein (*Mcp-1*) (**C**), transforming growth factor (*Tgf-β*) (**D**), and *CD31* (**E**) in the kidney. Values are presented as means ± standard error of the mean (SEM). ** $p < 0.01$.

period. Although the SBP levels did not change over time in the SD rats, they were significantly higher at 12 weeks than at 8 weeks in the SDT fatty rats. Furthermore, they were significantly higher in the SDT fatty rats than in the SD rats at both 12 and 20 weeks.

Comparison of Kidney Function and Total Cholesterol

The SDT fatty rats exhibited significant increases in the levels of serum creatinine and urea nitrogen compared to the SD rats at 24 weeks of age (Table 2), but there was no significant difference in the serum cystatin C levels between the 2 groups. Conversely, the serum total cholesterol level in the SDT fatty rats was significantly higher than in the SD rats at 24 weeks of age.

Comparison of Urinary Glucose, L-FABP, and Albumin Levels

The mean scores for urinary glucose were 4 and 0 in the SDT fatty rats and SD rats, respectively, at 24 weeks of age. The levels of both urinary L-FABP and albumin were significantly higher in the SDT fatty rats than in the SD rats at 24 weeks of age (Fig. 1A, B).

Increased Inflammatory Response and Profibrotic Activity in the SDT Fatty Rat Model of DKD

The mRNA levels of *Mcp-1*, *Tgf-β*, and *CD31* were measured to evaluate the inflammatory response, profibrotic activity, and presence of endothelial cells, respectively. The *Mcp-1* (Fig. 1C) and *Tgf-β* (Fig. 1D) levels were significantly higher in the SDT fatty rats than in the SD rats, whereas the level of *CD31* was comparable between the SDT fatty rats and SD rats (Fig. 1E).

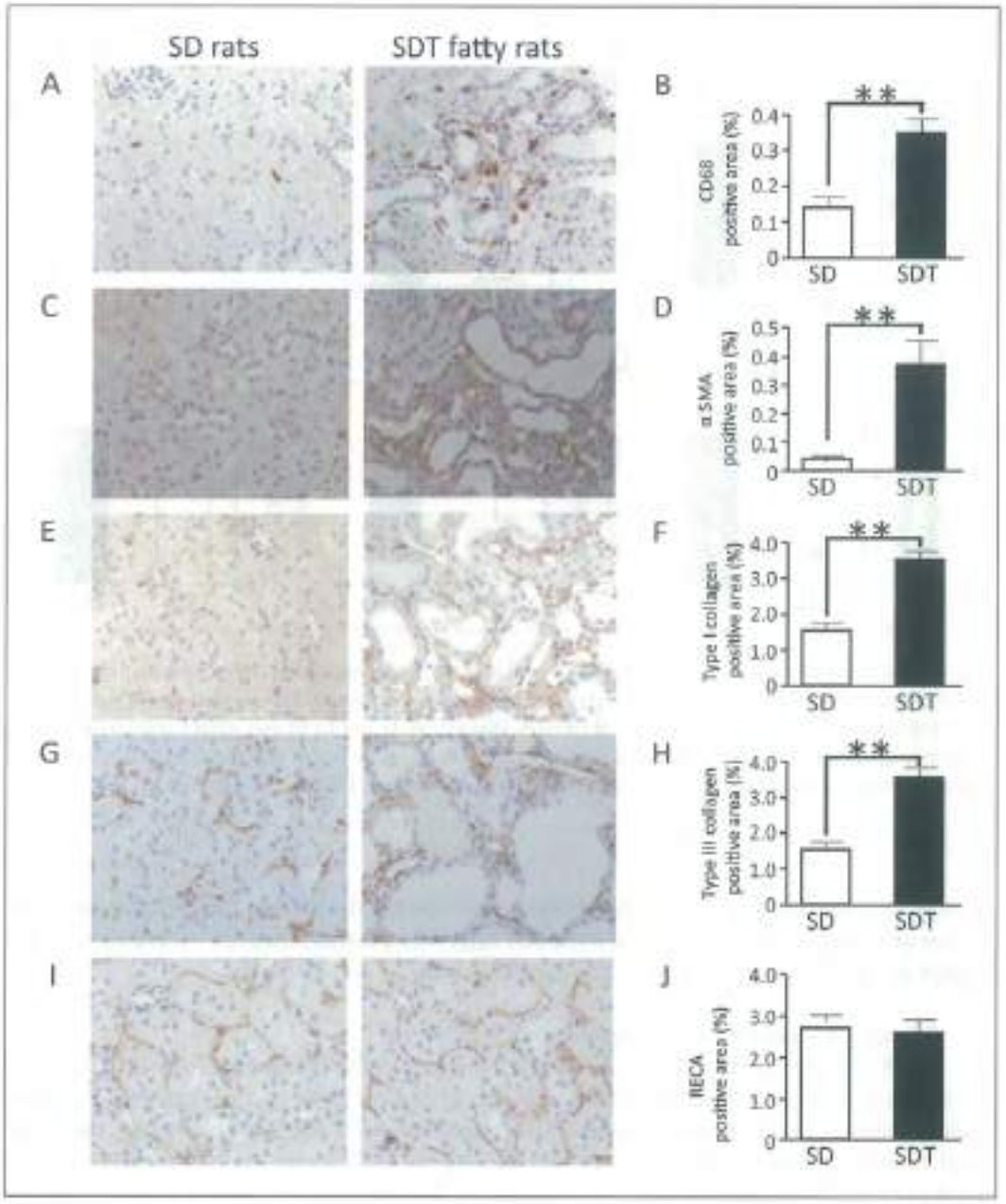

Fig. 2. Immunohistological staining using antibodies against CD68 (**A**, **B**), α-smooth muscle actin (α-SMA) (**C**, **D**), type I collagen (**E**, **F**), type III collagen (**G**, **H**), and rat endothelial cell antigen-1 (RECA-1) (**I**, **J**). ×100. Values are presented as means ± SEM. ** $p < 0.01$.

IHC Analysis of the Kidneys

To evaluate the degree of renal interstitial inflammation, we utilized the macrophage marker CD68 in IHC analysis. The macrophages were detected in the interstitium of the SDT fatty rats (Fig. 2A), and the degree of macrophage infiltration was significantly greater than in the SD rats (Fig. 2B).

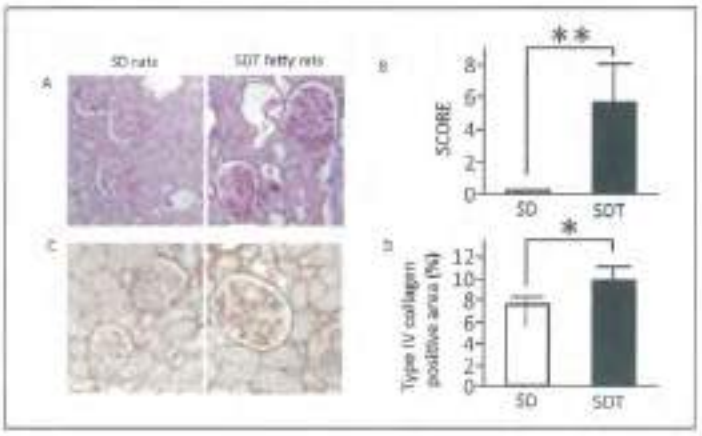

Fig. 3. Histological staining with periodic acid-Schiff showing focal glomerular sclerosis (**A**) and semiquantitative assessment of focal glomerular sclerosis (**B**). IHC staining using an antibody against type IV collagen in the glomerulus (**C**, **D**). ×100. Values are presented as means ± SEM. * $p < 0.01$.

IHC analyses were also performed to evaluate tubulointerstitial fibrosis based on the expression levels of α-SMA and type I and type III collagens. In the SDT fatty rats, α-SMA-positive areas were observed in the tubules and the interstitium (Fig. 2C); the extent of α-SMA positivity was significantly greater in the SDT fatty rats than in the SD rats (Fig. 2D). Further analysis of the expression levels for type I (Fig. 2E) and type III (Fig. 2G) collagen in the interstitium revealed that the extent of positivity for both type I (Fig. 2F) and type III (Fig. 2H) collagen was significantly greater in the SDT fatty rats than in the SD rats.

Assessment of the number of endothelial cells in the peritubular capillaries by IHC analysis for RECA-1 revealed that the extent of RECA-1 positivity was comparable between the SDT fatty rats and the SD rats (Fig. 2I, J).

Evaluation of Glomerular Sclerosis

Focal glomerular sclerosis was observed in the PAS-stained kidney tissues of the SDT fatty rats (Fig. 3A), and the score for glomerular sclerosis was significantly greater than in the SD rats (Fig. 3B). Additionally, type IV collagen was immunolocalized to the mesangial areas in the glomeruli (Fig. 3C). Furthermore, the glomerular area that was positively stained for type IV collagen was significantly increased in the SDT fatty rats compared to the SD rats (Fig. 3D).

Correlation between Urinary L-FABP Level and Histological Changes

The urinary L-FABP levels correlated significantly with both the degree of macrophage infiltration determined by the CD68-positive areas (Fig. 4A), and tubulointerstitial fibrosis determined by the areas positive for α-SMA (Fig. 4B) and type I (Fig. 4C) and type III (Fig. 4D) collagen.

Analysis of HIF-1α Expression and Correlation of HIF-1α Protein Expression with Urinary L-FABP Levels and Histological Changes

The measurement of HIF-1α expression levels in the kidneys to assess renal hypoxia revealed that both the mRNA (Fig. 5A) and protein (Fig. 5B) levels were significantly higher in the SDT fatty rats than in the SD rats.

The protein expression levels of HIF-1α correlated significantly with the urinary L-FABP levels (Fig. 6A), macrophage infiltration determined by the CD68-positive areas (Fig. 6B), and tubulointerstitial fibrosis determined by the areas positive for α-SMA (Fig. 6C) and type I

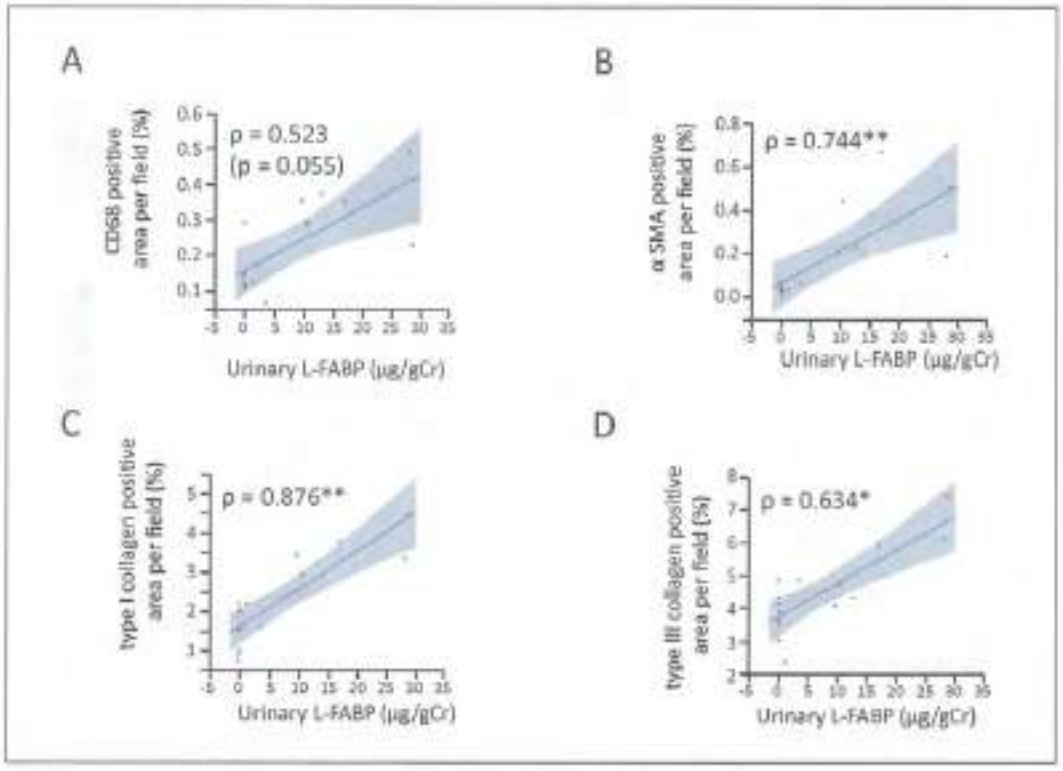

Fig. 4. Correlation between urinary L-FABP and the indicated renal tubulointerstitial damage markers. * $p < 0.05$, ** $p < 0.01$.

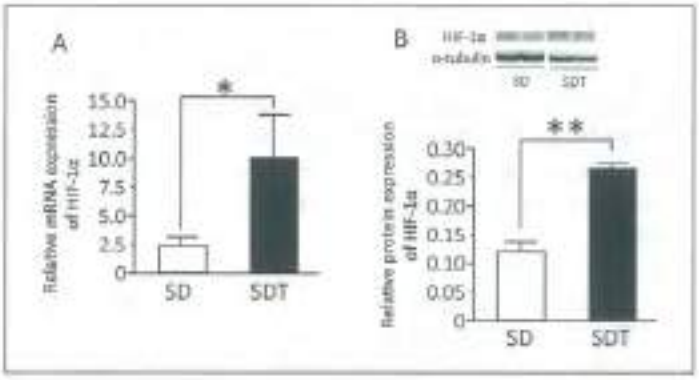

Fig. 5. Evaluation of renal hypoxia in the kidney. Gene expression (**A**) and protein expression (**B**) of hypoxia-inducible factor 1α (HIF-1α). Values are presented as means ± SEM. * $p < 0.05$, ** $p < 0.01$.

collagen (Fig. 6D). However, no similar correlation was observed between the protein expression levels of HIF-1α and type III collagen (Fig. 6E).

Evaluation of Renal Blood Flow Using DCS and Correlation of Renal BFI with Urinary L-FABP Levels, Histological Changes, and Renal HIF-1α Protein Expression

The analysis of the kidneys with DCS revealed that the microvascular BFI in the SDT fatty rats was significantly lower than in the SD rats (Fig. 7).

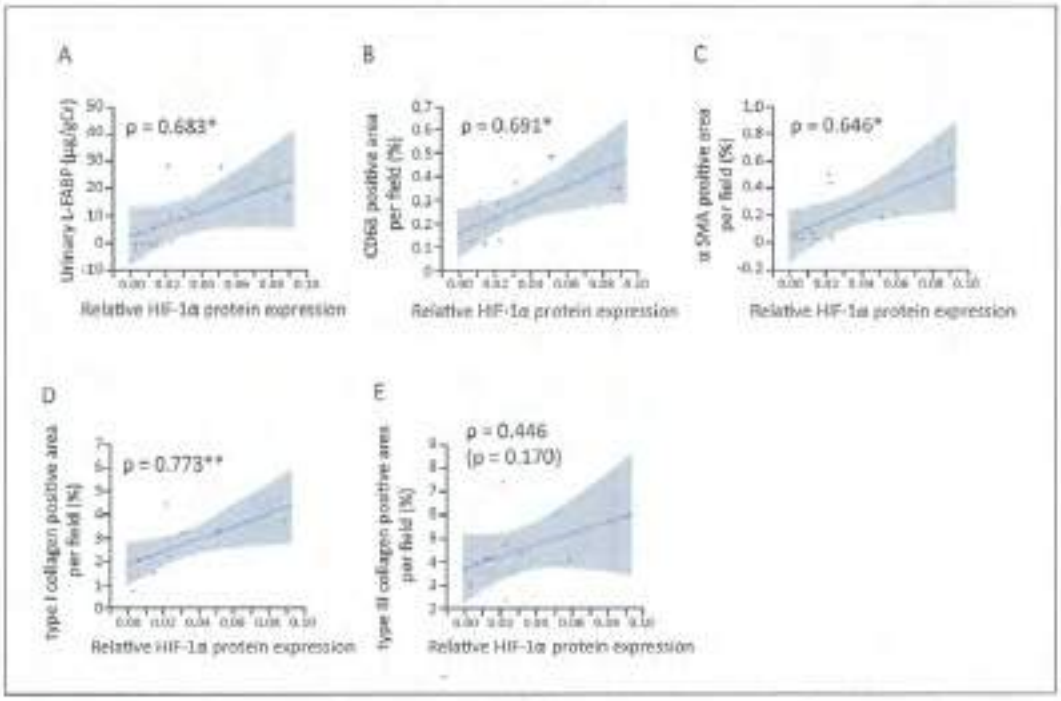

Fig. 6. Correlation between protein expression levels of HIF-1α and urinary L-FABP (**A**) and the indicated renal tubulointerstitial damage markers (**B–E**). * $p < 0.05$, ** $p < 0.01$.

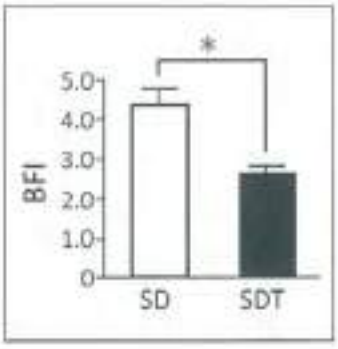

Fig. 7. Comparison of blood flow index (BFI) between the SD and SDT fatty rats. Values are presented as means ± SEM. * $p < 0.05$.

The renal BFI correlated significantly with the urinary L-FABP levels (Fig. 8A), tubulointerstitial fibrosis determined by the area positive for type I collagen (Fig. 8D), and renal protein expression levels of HIF-1α (Fig. 8F). However, no such correlations were observed between the renal BFI and α-SMA (Fig. 8C), or between the renal BFI and type III collagen (Fig. 8E). Conversely, the BFI tended to correlate with the macrophage infiltration determined by the CD68-positive areas (Fig. 8B).

Analyses for eNOS Expression and Phosphorylation

The endothelial function in the kidneys was determined by measuring the protein expression and phosphorylation levels of eNOS. The results indicated that the protein

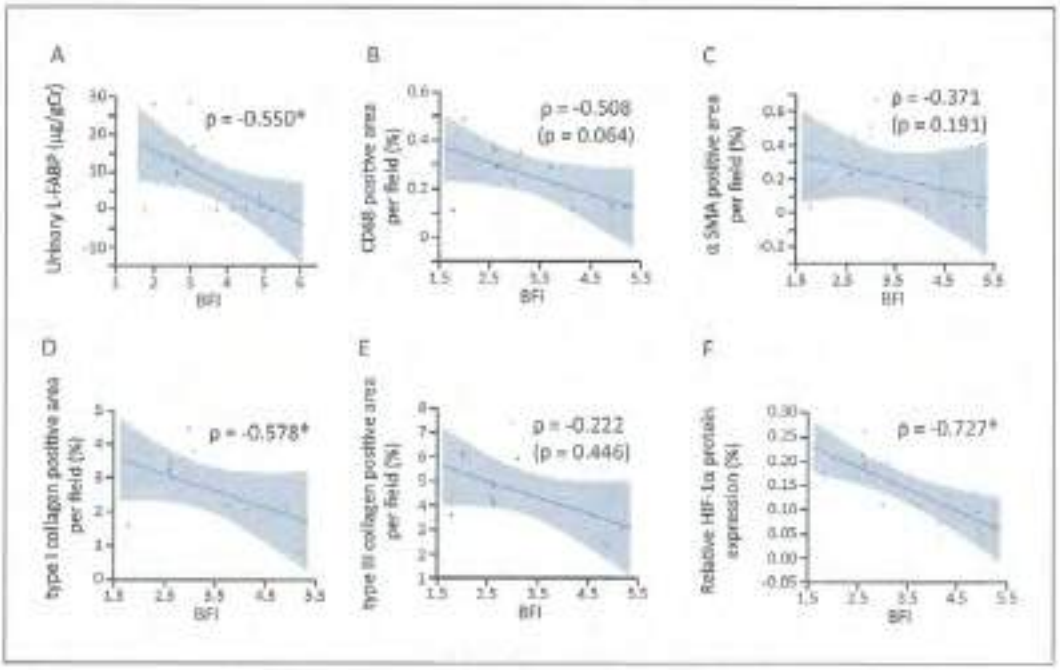

Fig. 8. Correlation between BFI and urinary L-FABP (**A**), the indicated renal tubulointerstitial damage markers (**B–E**), and renal protein expression levels of HIF-1α (**F**). * $p < 0.05$.

expression levels of eNOS were significantly higher in the kidneys of the SDT fatty rats than in the SD rats (Fig. 9A, B), and that the phosphorylation (Fig. 9A, C) levels of eNOS were comparable between the SDT fatty rats and SD rats. Phosphorylated protein amount of eNOS was therefore considered to be higher in the kidneys of the SDT fatty rats than in the SD rats.

Analysis of VEGF Expression

The angiogenic activity in response to renal hypoxia was assessed by the measurement of VEGF expression levels in the kidneys, which revealed that both the mRNA (Fig. 9D) and protein (Fig. 9E) levels of VEGF were comparable between the SDT fatty rats and SD rats.

Discussion

Utilizing SDT fatty rats as a novel animal model of type 2 diabetes with obesity, we revealed that, compared to the control SD rats, the renal HIF-1α levels were elevated and renal BFI was reduced in the SDT fatty rats, accompanied by renal tissue damage including glomerulosclerosis, interstitial inflammation, and fibrosis. The study also revealed a comparable frequency of endothelial cells in the peritubular capillaries, eNOS phosphorylation, and VEGF expression between the SDT fatty rats and the SD rats. These results suggest that the kidneys in the SDT fatty rats were under hypoxic conditions. In addition, the urinary L-FABP levels, which were significantly higher in the SDT fatty rats than in the SD rats, were positively correlated with the degree of renal HIF-1α expression and negatively correlated with the renal BFI, suggesting that urinary L-FABP might reflect the degree of renal hypoxia in DKD. Along with previous evidence, the observed correlation of the renal expression of HIF-1α and renal BFI with interstitial inflammation and interstitial fibrosis (Fig. 6, 8) provides support

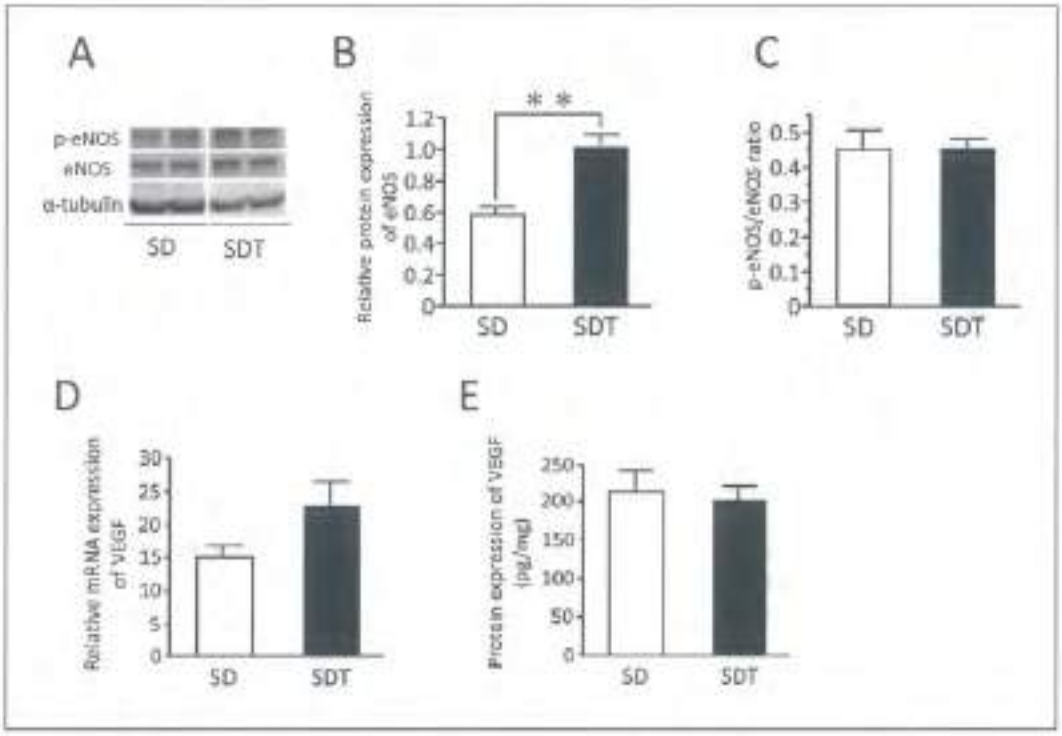

Fig. 9. Evaluations of endothelial nitric oxide synthase (eNOS) protein expression, phosphorylation of eNOS, and vascular endothelial growth factor (VEGF) gene and protein expressions in the kidney. Representative immunoblots (**A**), and quantitative evaluation of the protein expression (**B**) and phosphorylation (**C**) of eNOS. Gene (**D**) and protein expression (**E**) levels of VEGF. Values are presented as means ± SEM. ** $p < 0.01$.

for the notion that renal hypoxia is a crucial aggravating factor for tubulointerstitial damage in DKD [7, 8]. These results further suggest that, by detecting renal hypoxia, urinary L-FABP might be useful for monitoring DKD in clinical practice. Although urinary L-FABP was reported to be associated with renal microvascular blood flow in renal transplantation [19], our study is the first to report its potential as a renal hypoxic marker in DKD in type 2 diabetes.

SDT fatty rats, utilized in numerous diabetic animal models, exhibit various metabolic complications frequently observed in patients with type 2 diabetes, such as obesity, hyperlipidemia, and hypertension [20]. In patients with type 2 diabetes, various metabolic abnormalities have an impact on the kidneys, in addition to hyperglycemia, and numerous factors contribute to the onset and/or progression of kidney disease. The renal pathophysiology in SDT fatty rats may mimic the DKD observed in type 2 diabetic patients with numerous metabolic complications. Both macroalbuminuria and mild renal dysfunction were observed in the 24-week-old SDT fatty rats. Our results may thus reflect the relationship between renal hypoxia and urinary L-FABP levels in DKD with macroalbuminuria observed in humans.

Two mechanisms underlie the induction of renal hypoxia in type 2 diabetes: elevated renal oxygen consumption and changes in renal hemodynamics. One study reported a >40% increase in oxygen consumption in the renal tubules of diabetic rats compared to nondiabetic rats [29]. The increase in renal oxygen consumption is attributed to increased renal tubular reabsorption of massive levels of glucose filtered in the glomeruli as a result of hyperglycemia, increased electrolyte levels after glomerular hyperfiltration [7, 30], and increased oxidative stress in diabetes [31]. Conversely, renal hemodynamics are altered by both

glomerular and tubular damage in addition to a decrease in whole renal blood flow due to arteriosclerosis. Glomerular damage, which is induced by hyperglycemia, obesity, hypertension, and arteriolosclerosis, leads to a decrease in postglomerular blood flow, resulting in tubular hypoxia. Furthermore, a direct insult to the tubular cells by hyperglycemia leads to the production of inflammatory cytokines which provoke peritubular capillary damage [32, 33], resulting in the induction of tubular hypoxia [34]. In this study, there was an increase in urinary glucose excretion in the SDT fatty rats. Furthermore, while we failed to observe a decrease in endothelial cell numbers or eNOS activation, we found an increase in renal HIF-1α expression, a reduction in renal BFI, and mild glomerulosclerosis in the SDT fatty rats. Therefore, we attribute the renal hypoxia observed in 24-week-old SDT fatty rats to elevated renal oxygen consumption that was due to the increased renal tubular absorption of glucose as well as a reduction in glomerular and postglomerular blood flow as a result of glomerulosclerosis.

Adaptation of the kidneys to renal hypoxia occurs via an increase in HIF-1α expression, which leads to the upregulation of VEGF that accelerates angiogenesis [35–37]. Our results did not reveal an increase in the renal expression of VEGF in the SDT fatty rats compared to the SD rats, but the renal HIF-1α expression was significantly increased in the SDT fatty rats.

It has been reported that hyperglycemia suppresses angiogenesis despite the increased gene expression of VEGF receptors in cocultures of human proximal tubular cells and endothelial cells [36]. Furthermore, hyperglycemia during hypoxia was found to inhibit the upregulation of VEGF expression due to oxidative stress in rat proximal tubular cells [38]. Our results lend further support to these previous in vitro findings.

We used DCS to measure renal microvascular blood flow. The currently adopted interval between photon-emitter and detector probes is 4 mm, with which the microvascular blood flow of the corticomedullary junction approximately 2 mm below the renal surface can be detected. The corticomedullary junction is reported to consume approximately half the oxygen of the whole kidney due to the wide distribution of the electrolytic pumps using ATP [39]; this area is therefore particularly vulnerable to hypoxia. Conversely, the corticomedullary junction is susceptible to hypoxia in kidney disease because the blood flow in this area is solely dependent on the postglomerular flow of the juxtamedullary glomeruli. Specifically, hypertension, a major and frequent complication of type 2 diabetes [40], initially induces vascular damage in the juxtamedullary glomeruli, and this leads to hypoxia in the corticomedullary and medullary regions by impairing renal circulation [41]. Therefore, the DCS method for measuring microvascular blood flow in the corticomedullary region utilized here was suitable for detecting renal hypoxia.

The results of this study may have been limited by several factors. First, the presence of anemia was not evaluated. There is a possibility that renal anemia occurs in SDT fatty rats with mild renal function. As the DCS method detects the movement of red blood cells, changes in the number of these cells might affect BFI measurement. The potential confounding effect of anemia should be elucidated in future studies. Second, the correlation between renal hypoxia and DKD progression was not investigated. The progression of DKD was mild, even in the SDT fatty rats with macroalbuminuria [42, 43]; therefore, older SDT fatty rats, such as 60-week-old animals, should be evaluated for the correlation of renal hypoxia with the progression to advanced DKD [44]. One of the SDT fatty rats died at 23 weeks of age and the presumed cause was malnutrition due to the long-term impairment of glucose utilization, although necropsy was not performed. So no long-term assessment was conducted. Third, because of the small sample size in the basic research, we did not determine the most suitable marker to accurately reflect the degree of renal hypoxia. More clinical research is needed to reveal the point. Finally, we did not investigate changes in urinary L-FABP levels in response to interventions that ameliorate renal hypoxia. A recent study demonstrated that habitual

exercise leads to a reduction in urinary L-FABP levels via a decrease in renovascular resistance and an improvement of renal microcirculation in healthy middle-aged and older adults [45]. Another clinical study reported that urinary L-FABP decreased along with the improvement of renal disease due to various treatments [46]. Urinary L-FABP may thus respond to the elimination of renal hypoxia.

In conclusion, we revealed that urinary L-FABP levels reflect the degree of renal hypoxia, as evaluated by renal HIF-1α expression and BFI measured with DCS in DKD using a type 2 diabetic animal model. Although further investigation is necessary, these findings suggest that urinary L-FABP might be useful as a renal hypoxic marker to monitor DKD in patients with type 2 diabetes in clinical practice because renal hypoxia is an aggravating factor for the progression of DKD.

Acknowledgments

We thank Ms. Kimie Katayama and Ms. Junko Asano for the technical assistance.

Disclosure Statement

T.S. is the director and a senior scientist at CMIC Holdings Co., Ltd., and K.O. is a scientist at CMIC Holdings Co., Ltd., which produced the kits for L-FABP analysis. All other authors declare no conflicts of interest.

Funding Sources

This research did not receive any specific grant from funding agencies in the public, commercial, or not-for-profit sectors.

Author Contributions

J.T., T.S., K.O., and A.K.-I.: study design. J.T., Y.O., M.N., K.O., K.K., S.W., K.I., S.H., Y.O., and A.K.-I.: data collection. J.T. and A.K.-I.: data analysis, literature search, and the generation of the figures. J.T., Y.N., D.I., T.S., K.O., K.K., Y.S., and A.K.-I.: data interpretation. J.T., Y.S., and A.K.-I.: writing of the manuscript. All authors provided final approval of the submitted version.

References

1 Afkarian M, Zelnick LR, Hall YN, Heagerty PJ, Tuttle K, Weiss NS, et al. Clinical manifestations of kidney disease among US adults with diabetes, 1988-2014. JAMA. 2016 Aug;316(6):602–10.
2 Doshi SM, Friedman AN. Diagnosis and Management of Type 2 Diabetic Kidney Disease. Clin J Am Soc Nephrol. 2017 Aug;12(8):1366–73.
3 Tuttle KR, Bakris GL, Bilous RW, Chiang JL, de Boer IH, Goldstein-Fuchs J, et al. Diabetic kidney disease: a report from an ADA Consensus Conference. Am J Kidney Dis. 2014 Oct;64(4):510–33.
4 Mise K, Hoshino J, Ueno T, Hazue R, Hasegawa J, Sekine A, et al. Prognostic Value of Tubulointerstitial Lesions, Urinary N-acetyl-β-d-glucosaminidase, and urinary β2-microglobulin in patients with type 2 diabetes and biopsy-proven diabetic nephropathy. Clin J Am Soc Nephrol. 2016 Apr;11(4):593–601.
5 Mise K, Hoshino J, Ueno T, Hazue R, Sumida K, Hiramatsu R, et al. Clinical and pathological predictors of estimated GFR decline in patients with type 2 diabetes and overt proteinuric diabetic nephropathy. Diabetes Metab Res Rev. 2015 Sep;31(6):572–81.

6 Shimizu M, Furuichi K, Toyama T, Kitajima S, Hara A, Kitagawa K, et al.; Kanazawa Study Group for Renal Diseases and Hypertension. Long-term outcomes of Japanese type 2 diabetic patients with biopsy-proven diabetic nephropathy. Diabetes Care. 2013 Nov;36(11):3655–62.
7 Friederich-Persson M, Thörn E, Hansell P, Nangaku M, Levin M, Palm F. Kidney hypoxia, attributable to increased oxygen consumption, induces nephropathy independently of hyperglycemia and oxidative stress. Hypertension. 2013 Nov;62(5):914–9.
8 Hansell P, Welch WJ, Blantz RC, Palm F. Determinants of kidney oxygen consumption and their relationship to tissue oxygen tension in diabetes and hypertension. Clin Exp Pharmacol Physiol. 2013 Feb;40(2):123–37.
9 Nangaku M. Chronic hypoxia and tubulointerstitial injury: a final common pathway to end-stage renal failure. J Am Soc Nephrol. 2006 Jan;17(1):17–25.
10 Susaki H, Kamijo-Ikemori A, Sugaya T, Yamashita K, Yokoyama T, Koike J, et al. Urinary fatty acids and liver-type fatty acid binding protein in diabetic nephropathy. Nephron Clin Pract. 2009;112(3):c148–56.
11 Watanabe S, Ichikawa D, Sugaya T, Ohata K, Inoue K, Hoshino S, et al. Urinary Level of Liver-Type Fatty Acid Binding Protein Reflects the Degree of Tubulointerstitial Damage in Polycystic Kidney Disease. Kidney Blood Press Res. 2018;43(6):1716–29.
12 Yokoyama T, Kamijo-Ikemori A, Sugaya T, Hoshino S, Yasuda T, Kimura K. Urinary excretion of liver type fatty acid binding protein accurately reflects the degree of tubulointerstitial damage. Am J Pathol. 2009 Jun;174(6):2096–106.
13 Hisamichi M, Kamijo-Ikemori A, Sugaya T, Ichikawa D, Hoshino S, Hirata K, et al. Increase in urinary markers during the acute phase reflects the degree of chronic tubulointerstitial injury after ischemia-reperfusion renal injury. Biomarkers. 2017 Feb;22(1):5–13.
14 Ichikawa D, Kamijo-Ikemori A, Sugaya T, Ohata K, Hisamichi M, Hoshino S, et al. Utility of urinary tubular markers for monitoring chronic tubulointerstitial injury after ischemia-reperfusion. Nephrology (Carlton). 2018 Apr;23(4):308–16.
15 Matsui K, Kamijo-Ikemori A, Imai N, Sugaya T, Yasuda T, Tatsunami S, et al. Clinical significance of urinary liver-type fatty acid-binding protein as a predictor of ESRD and CVD in patients with CKD. Clin Exp Nephrol. 2016 Apr;20(2):195–203.
16 Kamijo-Ikemori A, Sugaya T, Yasuda T, Kawata T, Ota A, Tatsunami S, et al. Clinical significance of urinary liver-type fatty acid-binding protein in diabetic nephropathy of type 2 diabetic patients. Diabetes Care. 2011 Mar;34(3):691–6.
17 Panduru NM, Forsblom C, Saraheimo M, Thorn L, Bierhaus A, Humpert PM, et al.; FinnDiane Study Group. Urinary liver-type fatty acid-binding protein and progression of diabetic nephropathy in type 1 diabetes. Diabetes Care. 2013 Jul;36(7):2077–83.
18 Colhoun HM, Marcovecchio ML. Biomarkers of diabetic kidney disease. Diabetologia. 2018 May;61(5):996–1011.
19 Yamamoto T, Noiri E, Ono Y, Doi K, Negishi K, Kamijo A, et al. Renal L-type fatty acid—binding protein in acute ischemic injury. J Am Soc Nephrol. 2007 Nov;18(11):2894–902.
20 Matsui K, Ohta T, Oda T, Sasase T, Ueda N, Miyajima K, et al. Diabetes-associated complications in spontaneously diabetic Torii fatty rats. Exp Anim. 2008 Apr;57(2):111–21.
21 Durduran T, Choe R, Baker WB, Yodh AG. Diffuse Optics for Tissue Monitoring and Tomography. Rep Prog Phys. 2010 Jul;73(7):73.
22 Ichinose M, Nakabayashi M, Ono Y. Sympathoexcitation constrains vasodilation in the human skeletal muscle microvasculature during postocclusive reactive hyperemia. Am J Physiol Heart Circ Physiol. 2018 Aug;315(2):H242–53.
23 Ichinose M, Nakabayashi M, Ono Y. Difference in the integrated effects of sympathetic vasoconstriction and local vasodilation in human skeletal muscle and skin microvasculature. Physiol Rep. 2019 Apr;7(7):e14070.
24 Yu G, Durduran T, Lech G, Zhou C, Chance B, Mohler ER 3rd, et al. Time-dependent blood flow and oxygenation in human skeletal muscles measured with noninvasive near-infrared diffuse optical spectroscopies. J Biomed Opt. 2005 Mar-Apr;10(2):024027.
25 Ichikawa D, Kamijo-Ikemori A, Sugaya T, Yasuda T, Hoshino S, Igarashi-Migitaka J, et al. Renal liver-type fatty acid binding protein attenuates angiotensin II-induced renal injury. Hypertension. 2012 Oct;60(4):973–80.
26 Hisamichi M, Kamijo-Ikemori A, Sugaya T, Ichikawa D, Natsuki T, Hoshino S, et al. Role of angiotensin II type 1a receptor in renal injury induced by deoxycorticosterone acetate-salt hypertension. FASEB J. 2017 Jan;31(1):72–84.
27 Hisamichi M, Kamijo-Ikemori A, Sugaya T, Hoshino S, Kimura K, Shibagaki Y. Role of bardoxolone methyl, a nuclear factor erythroid 2-related factor 2 activator, in aldosterone- and salt-induced renal injury. Hypertens Res. 2018 Jan;41(1):8–17.
28 Ohata K, Kamijo-Ikemori A, Sugaya T, Hibi C, Nakamura T, Murase T, et al. Renoprotective effect of the xanthine oxidoreductase inhibitor Topiroxostat under decreased angiotensin II type 1a receptor expression. Eur J Pharmacol. 2017 Nov;815:88–97.
29 Ries M, Basseau F, Tyndal B, Jones R, Deminière C, Catargi B, et al. Renal diffusion and BOLD MRI in experimental diabetic nephropathy. Blood oxygen level-dependent. J Magn Reson Imaging. 2003 Jan;17(1):104–13.
30 Baines A, Ho P. Glucose stimulates O2 consumption, NOS, and Na/H exchange in diabetic rat proximal tubules. Am J Physiol Renal Physiol. 2002 Aug;283(2):F286–93.

31 Palm F, Cederberg J, Hansell P, Liss P, Carlsson PO. Reactive oxygen species cause diabetes-induced decrease in renal oxygen tension. Diabetologia. 2003 Aug;46(8):1153–60.
32 Navarro-González JF, Mora-Fernández C, Muros de Fuentes M, García-Pérez J. Inflammatory molecules and pathways in the pathogenesis of diabetic nephropathy. Nat Rev Nephrol. 2011 Jun;7(6):327–40.
33 Mudaliar H, Pollock C, Komala MG, Chadban S, Wu H, Panchapakesan U. The role of Toll-like receptor proteins (TLR) 2 and 4 in mediating inflammation in proximal tubules. Am J Physiol Renal Physiol. 2013 Jul;305(2):F143–54.
34 Gilbert RE. Proximal Tubulopathy: Prime Mover and Key Therapeutic Target in Diabetic Kidney Disease. Diabetes. 2017 Apr;66(4):791–800.
35 Shweiki D, Itin A, Soffer D, Keshet E. Vascular endothelial growth factor induced by hypoxia may mediate hypoxia-initiated angiogenesis. Nature. 1992 Oct;359(6398):843–5.
36 Kim BS, Chen J, Weinstein T, Noiri E, Goligorsky MS. VEGF expression in hypoxia and hyperglycemia: reciprocal effect on branching angiogenesis in epithelial-endothelial co-cultures. J Am Soc Nephrol. 2002 Aug;13(8):2027–36.
37 Shu S, Wang Y, Zheng M, Liu Z, Cai J, Tang C, et al. Hypoxia and Hypoxia-Inducible Factors in Kidney Injury and Repair. Cells. 2019 Feb;8(3):8.
38 Katavetin P, Miyata T, Inagi R, Tanaka T, Sassa R, Ingelfinger JR, et al. High glucose blunts vascular endothelial growth factor response to hypoxia via the oxidative stress-regulated hypoxia-inducible factor/hypoxia-responsible element pathway. J Am Soc Nephrol. 2006 May;17(5):1405–13.
39 Ochi M, Yoshioka H, Sawada T, Kusunoki T, Hattori T. New adipocyte formation in mice during refeeding after long-term deprivation. Am J Physiol. 1991 Mar;260(3 Pt 2):R468–74.
40 Tatsumi Y, Ohkubo T. Hypertension with diabetes mellitus: significance from an epidemiological perspective for Japanese. Hypertens Res. 2017 Sep;40(9):795–806.
41 Ito S, Nagasawa T, Abe M, Mori T. Strain vessel hypothesis: a viewpoint for linkage of albuminuria and cerebro-cardiovascular risk. Hypertens Res. 2009 Feb;32(2):115–21.
42 Katsuda Y, Kemmochi Y, Maki M, Sano R, Ishii Y, Miyajima K, et al. Physiological changes induced by salt intake in female Spontaneously Diabetic Torii-Lepr(fa) (SDT fatty) rat, a novel obese type 2 diabetic model. Anim Sci J. 2014 May;85(5):588–94.
43 Katsuda Y, Kemmochi Y, Maki M, Sano R, Toriniwa Y, Ishii Y, et al. Effects of unilateral nephrectomy on renal function in male Spontaneously Diabetic Torii fatty rats: a novel obese type 2 diabetic model. J Diabetes Res. 2014;2014:363126.
44 Kemmochi Y, Fukui K, Maki M, Kimura S, Ishii Y, Sasase T, et al. Metabolic Disorders and Diabetic Complications in Spontaneously Diabetic Torii Lepr (fa) Rat: A New Obese Type 2 Diabetic Model. J Diabetes Res. 2013;2013:948257.
45 Kosaki K, Kamijo-Ikemori A, Sugaya T, Tanahashi K, Sawano Y, Akazawa N, et al. Effect of habitual exercise on urinary liver-type fatty acid-binding protein levels in middle-aged and older adults. Scand J Med Sci Sports. 2018 Jan;28(1):152–60.
46 Kamijo-Ikemori A, Sugaya T, Ichikawa D, Hoshino S, Matsui K, Yokoyama T, et al. Urinary liver type fatty acid binding protein in diabetic nephropathy. Clin Chim Acta. 2013 Sep;424:104–8.

Received: 26 July 2018 | Revised: 29 January 2019 | Accepted: 13 February 2019

DOI: 10.1111/1756-185X.13540

ORIGINAL ARTICLE

WILEY International Journal of Rheumatic Diseases

Association of cardiac magnetic resonance-detected myocardial abnormalities with disease characteristics and brain natriuretic peptide levels in systemic sclerosis without cardiac symptoms

Kaita Sugiyama[1] | Hitomi Kobayashi[1] | Yasuyuki Kobayashi[2] | Isamu Yokoe[3] | Masami Takei[1] | Noboru Kitamura[1]

[1]Division of Hematology and Rheumatology, Nihon University School of Medicine, Tokyo, Japan

[2]Department of Advanced Biomedical Imaging Informatics, St. Marianna University School of Medicine, Kawasaki, Japan

[3]Division of Internal Medicine, Kyoundo Hospital, Tokyo, Japan

Correspondence
Noboru Kitamura, Division of Hematology and Rheumatology, Department of Medicine, Nihon University School of Medicine, Tokyo, Japan.
Email: kitamura.noboru@nihon-u.ac.jp

Abstract

Aim: This study aimed to evaluate the association between myocardial abnormalities and left ventricular (LV) geometry as assessed using cardiac magnetic resonance imaging (CMRI) in systemic sclerosis (SSc) patients without cardiac symptoms.

Methods: SSc patients without cardiac symptoms or cardiovascular risk factors underwent contrast CMRI. CMRI were assessed for structural and functional LV parameters and myocardial fibrosis based on myocardial late gadolinium enhancement (LGE). The correlation between brain natriuretic peptide (BNP) levels and LGE status was evaluated.

Results: Among 49 patients, 27 (55%) showed LGE positivity. The most common identified LGE pattern was a linear pattern. LGE was not consistent with coronary artery distribution. There was no difference in ejection fraction between those with and without LGE. LV morphological changes were observed in 29% of SSc patients. An abnormal LV structure was detected in 44% and 14% of patients in the LGE+ and LGE− groups, respectively. The BNP levels were higher by 57% in the LGE+ group than in the LGE−group. Receiver operating characteristic analysis showed that BNP levels reliably detected myocardial abnormalities (area under the curve, 0.72; 95% confidence interval 0.58–0.88).

Conclusions: Myocardial abnormalities were common in SSc patients without cardiac symptoms. We suggest that LV morphological changes may have resulted from myocardial abnormalities. BNP may be useful as a screening tool for the detection of myocardial abnormalities in SSc patients.

KEYWORDS

brain natriuretic peptide, cardiac magnetic resonance imaging, late gadolinium enhancement, myocardial abnormalities, systemic sclerosis

1 | INTRODUCTION

Systemic sclerosis (SSc) is an autoimmune disease characterized by increased collagen synthesis. Its clinical symptoms are caused by fibrosis of various organs, including the skin, lungs and heart. The 10-year survival rate following its initial diagnosis is 65% in Western countries, and death is more commonly secondary to cardiac disorders, interstitial pneumonia, pulmonary hypertension, heart failure,

 © 2019 Asia Pacific League of Associations for Rheumatology and John Wiley & Sons Australia, Ltd

and arrhythmia.[1-4] Autopsy studies identified myocardial abnormalities in 12%–80% of patients with SSc.[5] Myocardial abnormalities account for 36% of deaths among patients with SSc[6] and strongly influence the prognosis of SSc; therefore, assessing asymptomatic myocardial abnormalities at an early stage is considered important.[7-9]

Although myocardial biopsy is the most accurate method for the assessment of myocardial abnormalities, it is invasive. Various noninvasive modalities for the early assessment of myocardial abnormalities, such as cardiac magnetic resonance imaging (CMRI), echocardiography, and cardiac single-photon emission computed tomography, have been proposed. Pathologically, the cardiac lesion of SSc is myocardial fibrosis,[10] and the performance of CMRI, which is excellent for evaluating fibrosis compared with other modalities, is extremely useful.

Our previous study showed that asymptomatic myocardial abnormalities could be complications of SSc.[11] Similarly, previous studies reported that asymptomatic myocardial abnormalities (myocardial fibrosis) could be detected using late gadolinium enhancement (LGE) by CMRI in patients with SSc.[12-14] Although left ventricular (LV) morphological changes may be expected in the LGE+ group, few studies have investigated their association with LGE.

Enhanced gene expression secondary to cardiac wall stress, especially LV wall stress, results in the production and secretion of brain natriuretic peptide (BNP).[15-19] Morphological changes may contribute to increased wall stress, possibly leading to elevated BNP levels. BNP levels may be proportional to the severity of morphological changes.

We assessed the relationship between myocardial abnormalities and morphological changes in SSc patients without cardiac symptoms by CMRI. Furthermore, we analyzed the prevalence of myocardial abnormalities in patients with SSc and its association with disease characteristics and BNP levels. We also sought to correlate BNP levels with LGE positivity and morphological changes. We hypothesized that myocardial abnormalities are associated with LV morphological changes and BNP levels.

2 | METHODS

2.1 | Study population

This retrospective study included patients with SSc who attended the outpatient rheumatology clinic of Itabashi Chuo Medical Center (Tokyo, Japan) between December 2012 and April 2015. Patients were diagnosed with SSc using the American Rheumatism Association classification criteria[20] and underwent CMRI to evaluate cardiac involvement associated with SSc. Only female patients were included in this study to prevent gender from being a potential confounding factor. The modified Rodnan total skin thickness score[21] was used as an index of skin hardening severity in SSc. Patients with the following conditions were excluded: history or clinical findings suggestive of systemic or pulmonary hypertension, coronary artery disease, valvular heart disease, atrial fibrillation, diabetes mellitus (glycosylated hemoglobin levels >6.1%), hypertension (systolic blood pressure >140 mm Hg and/or diastolic blood pressure >90 mm Hg), dyslipidemia (serum levels of low-density lipoprotein cholesterol >140 mg/dL, high-density lipoprotein cholesterol <40 mg/dL, or triglycerides >150 mg/dL), past and current history of smoking, estimated glomerular filtration rate <60 mL/min/1.73 m^2, and asthma.

Our study was approved by the local ethics committee of Itabashi Chuo Medical Center and Nihon University Itabashi Hospital, Japan (research number: RK-160913-15; approval date: September 21, 2016). Informed consent was obtained from all patients in accordance with the 1975 Declaration of Helsinki (revised in 1983).

2.2 | Acquisition and analysis of cardiac magnetic resonance imaging

All patients underwent cine MRI and gadolinium-enhanced MRI with a 1.5 or 3.0 T MRI scanner (Achieva and Intera Philips Medical Systems BV, Best, the Netherlands). Gadolinium–diethylenetriamine pentaacetic acid (Magnevist, Schering AG, Berlin, Germany), a gadolinium-based contrast agent, was injected at 0.1 mmol/kg body weight, and four contiguous short-axis orientations were acquired for every two heartbeats. Imaging was performed using a 3-dimensional turbo field echo sequence. The following variables were measured: global LV function (LV ejection fraction [EF], end-systolic volume, end-diastolic volume [EDV], stroke volume, cardiac output) and LV hypertrophy (absolute LV mass [LVM], LV mass index [LVMI; mass/body surface area]). Areas showing LGE corresponded to myocardial fibrosis as confirmed on histopathology.[22] Images were analyzed independently by two radiologists who were blinded to clinical information.

We classified contrast patterns of LGE in accordance with Kobayashi et al's report.[23] The upper limits of normal values for LVMI (66.6 g/m^2) and LVM/EDV (1.02 g/mL) were determined by these values in healthy volunteers and calculating the mean ± 2 standard deviations of each measure. LV geometry was classified as follows: (a) concentric remodeling, LVMI <66.6 g/m^2 and LVM/EDV >1.02 g/mL; (b) concentric hypertrophy, LVMI >66.6 g/m^2 and LVM/EDV >1.02 g/mL; (c) eccentric hypertrophy, LVMI >66.6 g/m^2 and LVM/EDV <1.02 g/mL; and (d) normal geometry, LVMI <66.6 g/m^2 and LVM/EDV <1.02 g/mL.

2.3 | Laboratory assessment

Collected serum and plasma samples were separated by centrifugation and stored at −70°C. All assays were performed in our institution and governed by in-house internal quality controls. All subjects underwent routine laboratory investigations and basic screening for risk factors of atherosclerotic disease, including serum levels of cholesterol, triglycerides, high-density lipoprotein, low-density lipoprotein, fasting blood glucose, rheumatoid factor, and anti-Scl-70 antibodies. BNP levels (normal range, ≤18.4 pg/mL) were measured simultaneously using fluorescence enzyme immunoassay.

2.4 | Statistical analyses

Group comparisons were conducted using Wilcoxon rank-sum test, Steel–Dwass test, and Fisher's exact test, as appropriate. Univariate

and multivariate linear regression analyses were performed to assess the association between LGE and disease characteristics. A multivariate logistic regression model was employed to evaluate the association between LGE and BNP levels. Receiver operating characteristic (ROC) curves were constructed to identify the cutoff value for BNP levels that may identify LGE. All statistical analyses were performed using JMP 9 software (SAS Institute Inc, Cary, NC). In all tests, a 2-tailed α value of 0.05 was considered statistically significant.

3 | RESULTS

3.1 | Baseline patient characteristics

Among 49 female patients (median age, 58 [range, 50-61] years) included, 25 had diffuse-type SSc, whereas 24 had limited-type SSc. Furthermore, 13 (27%) patients had digital ulcers, 25 (51%) patients were positive for anti-Scl-70 antibodies, and 17 (35%) patients had interstitial pneumonia (Table 1).

TABLE 1 Characteristics of patients with SSc

Demographics	
Age, (y), median (IQR)	58 (50-61)
Female, n (%)	49 (100)
Cardiovascular risk factors	
Diabetes mellitus, n (%)	0 (0)
Systolic blood pressure, mm Hg, median (IQR)	125.5 (112-130)
Diastolic blood pressure, mm Hg, median (IQR)	69.5 (67-78)
Total cholesterol, mg/dL, median (IQR)	178 (167-189.8)
LDL cholesterol, mg/dL, median (IQR)[a]	105.5 (88.3-119)
HDL cholesterol, mg/dL, median (IQR)	54.5 (49-63.3)
Triglycerides, mg/dL, median (IQR)	120.5 (104-134)
Smoking status	
Current smoker, n (%)	0 (0)
	SSc (n = 49)
Cutaneous subtype, diffuse: limited, n (%)	25 (51): 24 (49)
Digital ulcer, n (%)	13 (27)
Anti-Scl-70 antibodies, n (%)	25 (51)
Anti-centromere antibodies, n (%)	11 (22)
Interstitial pneumonia, n (%)	17 (35)
Reflux esophagitis, n (%)	18 (37)
Normal ECG: Q wave (−), arrhythmia (−), block (−), n (%)	49 (100)

ECG, electrocardiography; HDL, high-density lipoprotein; IQR, interquartile range; LDL, low-density lipoprotein; SSc, systemic sclerosis. Data are shown as median (range) unless otherwise indicated. Values are presented as n (%).
[a]Indirect method was used.

3.2 | Myocardial enhancement by cardiac magnetic resonance imaging

Among 27 (55%) LGE-positive patients, 16 (59%) had a linear LGE pattern without coronary artery distribution. A nodular enhancement pattern was observed in 7 (26%) patients (data not shown). In this study, we showed typical images of LGE in linear and nodular enhancement patterns (Figure 1A,B).

3.3 | Association of myocardial abnormalities with systemic sclerosis features

There was a significant association between LGE and anti-Scl-70 antibody positivity ($P = 0.01$). BNP levels were significantly higher in the LGE+ group than in the LGE− group ($P < 0.001$). However, no significant association was observed between LGE positivity and age, body mass index, disease duration, 10-year Framingham risk score, total skin thickness score, diffuse-type SSc, or presence of digital ulcers (Table 2). Additionally, there was no association between anti-centromere antibodies and risk factors for atherosclerosis (data not shown).

3.4 | Comparison of left ventricular structure between LGE+ and LGE− groups

The results for cardiac geometry were as follows: 35 patients with normal geometry, four patients with concentric remodeling, four patients with concentric hypertrophy, and six patients with eccentric hypertrophy. There was no significant association between LVMI

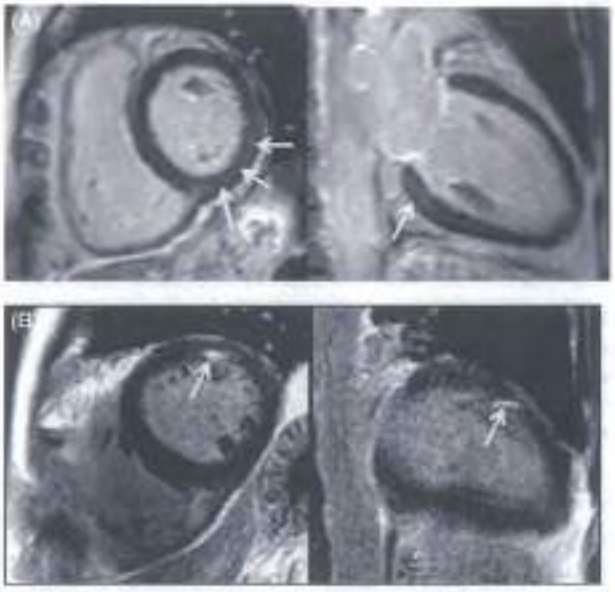

FIGURE 1 Actual photographs of late gadolinium enhancement (LGE). A, LGE showed linear enhancement in the basal layer of the inferior wall. B, LGE showed nodular enhancement in the middle layer of the lateral wall

TABLE 2 Association of LGE+ with SSc characteristics

Characteristics	LGE+ n = 27	LGE− n = 22	P-value
Age, (y), median (IQR)[a]	58 (48-61)	57.5 (50.8-58.5)	0.98
BMI, kg/m², median (IQR)[a]	20.1 (19.2-22.2)	19.8 (19-21.6)	0.48
Disease duration,[b] (y), median (IQR)[a]	3 (2-5)	3.5 (2-6)	0.83
10-y Framingham risk score, median (IQR)[a]	2 (2-3)	2 (2-3)	0.53
BNP, pg/mL, median (IQR)[a]	23.1 (19.9-28.3)	13.2 (10.5-20.3)	<0.001
Total skin thickness score, median (IQR)[a]	13 (9-18)	12.5 (7.8-16.5)	0.37
Diffuse, n (%)[c]	16 (64)	9 (36)	0.20
Digital ulcer, n (%)[c]	8 (62)	5 (38)	0.58
Anti-Scl-70 antibodies, n (%)[c]	18 (72)	7 (28)	0.01

BMI, body mass index; BNP, brain natriuretic peptide; IQR, interquartile range; LGE, late gadolinium enhancement; SSc, systemic sclerosis.
[a]Wilcoxon rank-sum test.
[b]Disease duration refers to the period from onset.
[c]Fisher's exact test.

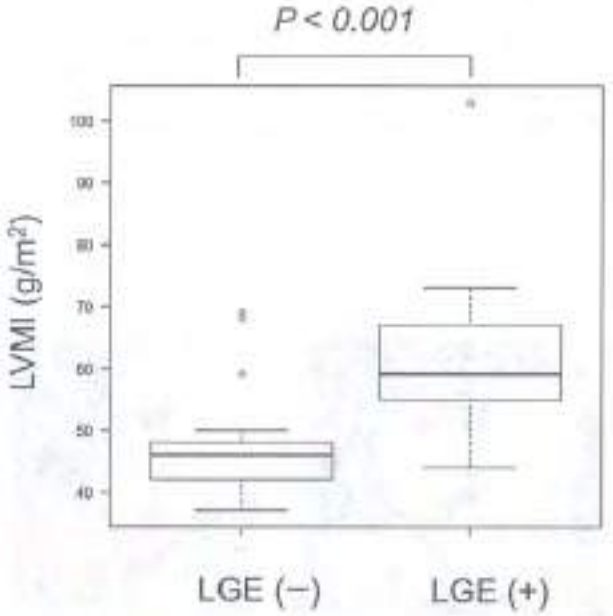

FIGURE 2 Left ventricular mass index (LVMI) of the late gadolinium enhancement (LGE) + and − groups. LVMI was significantly higher in the LGE+ group than in the LGE− group ($P < 0.001$). Group comparisons were performed using Wilcoxon rank-sum test

and each factor, as shown in Table 1 (data not shown). Additionally, no significant difference in LV function was observed between the LGE+ and LGE− groups. LVMI and LVM/EDV were significantly higher in the LGE+ group than in the LGE−group ($P < 0.001$; Figure 2). Overall, 44% of patients in the LGE+ group had abnormal LV structure (concentric hypertrophy, 11%; eccentric hypertrophy, 19%; and concentric remodeling, 15%), whereas only 14% of patients in the LGE− group had abnormal LV structure. Anti-Scl-70 antibody positivity had no significant association with LVMI and LVM/EDV (data not shown).

3.5 | Association of myocardial abnormalities with brain natriuretic peptide levels

Brain natriuretic peptide levels were higher by 57% in the LGE+group than in the LGE−group ($P < 0.01$; data not shown) and also significantly correlated with LVMI ($r = 0.75$, $P < 0.001$; Figure 3A).

3.6 | Multivariate analysis

After adjustment for age, disease duration, and anti-Scl-70 antibody positivity, a significant association was found between LGE and LVMI ($R^2 = 0.31$; Table 3).

3.7 | Receiver operating characteristic analysis for late gadolinium enhancement detection

The ROC curve for BNP levels to detect overall LGE is shown in Figure 3B. A BNP level cutoff value of ≥16.7 pg/mL had a sensitivity of 81% and specificity of 60% (Figure 3B) as well as a positive predictive value of 81% and negative predictive value of 64% for LGE by cardiac MRI (data not shown).

4 | DISCUSSION

The present study yielded the following findings: First, asymptomatic myocardial abnormalities were detected in 55% of patients with SSc, with morphological changes observed in 29%. Second, LV morphological changes were mostly observed in the LGE+ group.

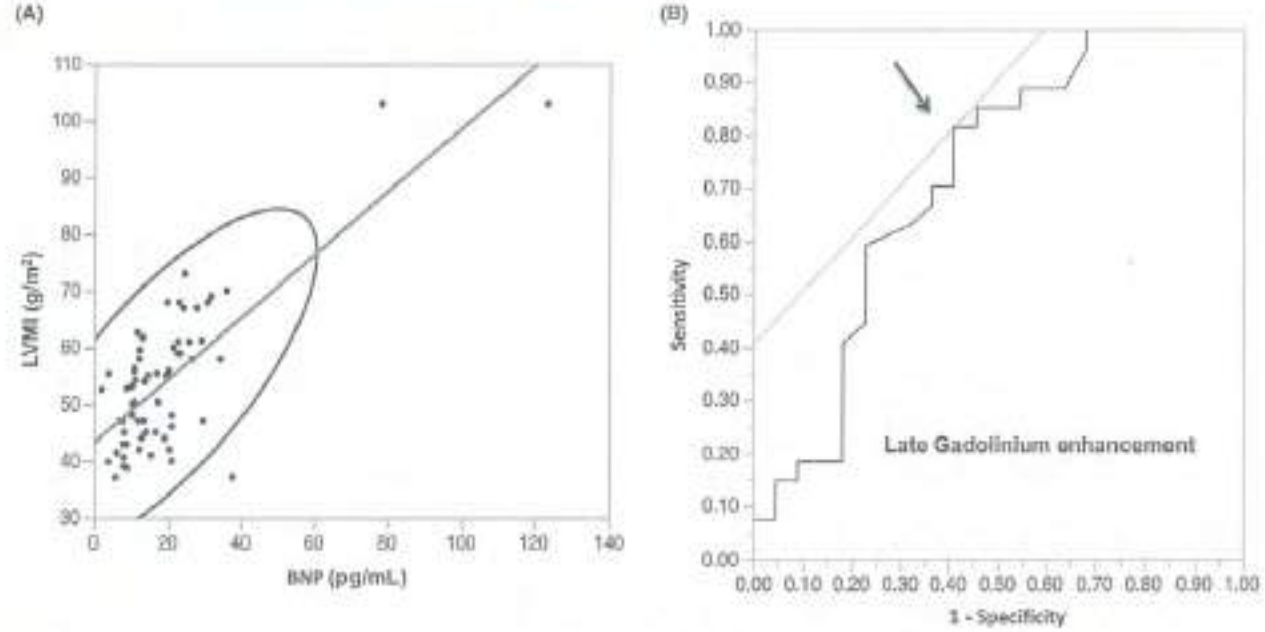

FIGURE 3 A, Correlation between brain natriuretic peptide (BNP) levels and left ventricular mass index (LVMI). BNP levels were significantly correlated with LVMI in the SSc group ($P < 0.001$). Group comparisons were performed using Wilcoxon rank-sum test. B, Correlation between BNP levels and late gadolinium enhancement (LGE). A receiver operating characteristic (ROC) curve for BNP levels for the detection of overall cardiac involvement is shown ($P = 0.01$). Using a cutoff value of 16.7 pg/mL to examine patients with SSc and normal CMR imaging findings, the sensitivity and specificity of BNP levels to detect LGE were >81% and >60%, respectively. The area under the curve (AUC) was 0.72

TABLE 3 Adjusted association of LGE with LVMI by multivariate logistic regression

	Model 1		Model 2		Model 3		Model 4	
Variables	β	P value	β	P value	β	P value	β	P value
LVMI	−0.167	<0.001	−0.166	<0.001	−0.185	<0.001	−0.166	<0.001
Anti-Scl-70 antibodies			0.712	0.06	0.648	0.1	0.87	0.04
Age					0.05	0.29		
Disease duration							0.12	0.34
R^2	0.31		0.37		0.38		0.38	

LGE, late gadolinium enhancement; LVMI, left ventricular mass index.
β coefficients represent the average change in the outcome per 1-unit increase in the characteristic.
R^2 is the percentage of total variation in the outcome explained by the aggregate of predictors in the model.
Adjustment for age, disease duration, and anti-Scl-70 antibodies did not modify the association of LGE with LVMI.

Third, serum BNP levels were significantly higher in the LGE+ group than in the LGE− group. Furthermore, patients who were positive for anti-Scl-70 antibodies were likely to develop asymptomatic myocardial abnormalities.

In our study, we found a higher incidence rate of asymptomatic myocardial abnormalities among patients with SSc, which was consistent with the results of previous studies.[24-26] In support of our study, using coronary angiotomography, Rodriguez-Reyna et al[27] showed that cardiac involvement in patients with SSc was unrelated to coronary artery disease. To our knowledge, only a single study has identified the relation between LGE and LV wall thickening by assessing morphological changes in patients with SSc by CMRI,[28] and no previous studies have classified cardiac morphological changes based on geometric patterns. Several studies have reported that cardiac morphological changes may result in heart failure.[29-34] Although normal EF was shown on cine MRI, cardiac morphological changes developed asymptomatically. Therefore, assessment of morphological changes may be employed to predict cardiac involvement in patients with SSc. As most patients in the LGE+ group showed cardiac morphological changes, it can be suggested that these changes have resulted from myocardial fibrosis accompanying SSc. However, few reports have indicated the association between LGE and morphological changes in patients with SSc; thus, further studies are warranted to examine this issue.

Several studies have already analyzed the role of BNP in patients with SSc complicated with pulmonary arterial hypertension (PAH).[35-37] In these studies, higher BNP levels appear to be associated with the presence of PAH. However, little is known about the association between serum BNP levels and myocardial abnormality status. Our study indicated that elevated BNP levels in the LGE+ group were associated with myocardial fibrosis. Patients with PAH were excluded from this analysis. We suggest that data on BNP levels may be associated with myocardial abnormalities secondary to LV changes alone. BNP levels ≥16.7 pg/mL were reasonably accurate in identifying the existence of myocardial fibrosis. Although BNP levels ≥18.4 pg/mL are known to indicate heart failure, patients with SSc may have myocardial abnormalities even at lower BNP levels. Therefore, it can be considered that, in the absence of PAH, asymptomatic cardiac involvement cannot be ruled out regardless of normal BNP levels.

In our study, elevated serum BNP levels positively correlated with cardiac morphological changes. These results suggest that serum BNP levels may elevate secondary to LV wall stress depending on underlying morphological changes. In addition, considering that the positive predictive value was 81%, our results suggest that the LGE+ group of patients with SSc may be predicted by measuring serum BNP levels. Although CMRI can facilitate the establishment of an early diagnosis of myocardial abnormalities, BNP level monitoring is a simple procedure that can be frequently repeated for follow-up.

Although BNP cannot replace CMRI in the evaluation of asymptomatic myocardial abnormalities in patients with SSc and cannot guide further treatment, we suggest that BNP might become a useful biomarker for asymptomatic myocardial abnormalities in patients with SSc. Further studies on this matter are required in the future.

Our study also identified the association between anti-Scl-70 antibodies and myocardial fibrosis, which had not been previously reported. Studies with a larger sample size are required to support our study finding.

The present study has limitations. First, this study was retrospective in nature; further follow-up is required to elucidate long-term prognosis. Second, cardiac lesions may be detected in patients with SSc with a history of classical atherosclerotic diseases such as hypertension, and the absence of these patients in our study could also be a limitation. Third, we did not have any pathological confirmation of myocardial fibrosis. Fourth, we did not quantitatively evaluate LGE. It is currently supposed that quantitative evaluation of lesions can be performed by combining methods such as T1 mapping and extracellular volume fraction measurement with LGE. Quantification is believed to allow for more detailed identification of early myocardial fibrosis not detected by myocardial biomarkers such as BNP.[38-40] Furthermore, ischemia, which can be a cause of myocardial lesions, might have been missed because cardiac catheterization was not performed. However, as LGE did not correspond to coronary distribution, it is reasonable to rule out ischemia as a cause of enhancement.

In conclusion, our study showed a high prevalence of myocardial abnormalities in patients with SSc, including myocardial fibrosis and LV morphological changes. Additionally, elevated levels of serum BNP and anti-Scl-70 antibodies may identify asymptomatic myocardial abnormalities. These factors, which can easily be determined, might be important as early diagnostic indicators. However, further prospective studies with large sample sizes are required.

ACKNOWLEDGEMENTS

We would like to express our sincere gratitude to all members and staff of Division of Hematology and Rheumatology, Nihon University School of Medicine.

CONFLICT OF INTEREST

All authors attest that they have no financial conflicts of interest pertaining to this investigation.

ORCID

Noboru Kitamura https://orcid.org/0000-0002-7817-6941

REFERENCES

1. Tyndall AJ, Bannert B, Vonk M, et al. Causes and risk factors for death in systemic sclerosis: a study from the EULAR Scleroderma Trials and Research (EUSTAR) database. *Ann Rheum Dis*. 2010;69:1809-1815.
2. Rubio-Rivas M, Royo C, Simeón CP, Corbella X, Fonollosa V. Mortality and survival in systemic sclerosis: systematic review and meta-analysis. *Semin Arthritis Rheum*. 2014;44:208-219.
3. Simeón-Aznar Cp, Fonollosa-Pla V, Tolosa-Vilella C, et al. Registry of the Spanish network for systemic sclerosis: survival, prognostic factors, and causes of death. *Medicine (Baltimore)*. 2015;94:e1728.
4. Poormoghim H, Andalib E, Jalali A, Ghaderi A, Ghorbannia A, Mojtabavi N. Survival and causes of death in systemic sclerosis patients: a single center registry report from Iran. *Rheumatol Int*. 2016;36:925-934.
5. Buldev BH, Ridolfi RL, Salyer WR, Hutchins GM. Myocardial lesions of progressive systemic sclerosis. A cause of cardic dysfunction. *Circulation*. 1976;53:483-490.
6. Ferri C, Valentini G, Cozzi F, et al. Systemic sclerosis: demographic, clinical, and serologic features and survival in 1,012 Italian patients. *Medicine (Baltimore)*. 2002;81:139-153.
7. Allanore Y, Kahan A. Heart involvement in systemic sclerosis. *Presse Med*. 2006;35:1938-1942.
8. González-Cambeiro MC, Abu-Assi E, Abumuaileq RR, et al. Systemic sclerosis: a rare cause of heart failure? *Rev Port Cardiol*. 2015;34:617.e1-5.
9. Fernández-Codina A, Simeón-Aznar CP, Pinal-Fernandez I, et al. Cardiac involvement in systemic sclerosis: differences between clinical subsets and influence on survival. *Rheumatol Int*. 2017;37:75-84.
10. D'Angelo WA, Fries JF, Masi AT, et al. Pathologic observation in systemic sclerosis (scleroderma): a study of 58 autopsy cases and 58 matched controls. *Am J Med*. 1965;46:428-440.
11. Naßenstein K, Breuckmann F, Huger M, et al. Detection of myocardial fibrosis in systemic sclerosis by contrast-enhanced magnetic resonance imaging. *Rofo*. 2008;180:1054-1060.
12. Kobayashi H, Yokoe I, Hirano M, et al. Cardiac magnetic resonance imaging with pharmacological stress perfusion and delayed

enhancement in asymptomatic patients with systemic sclerosis. *J Rheumatol*. 2009;36:106-112.
13. Di Cesare E, Battisti S, Di Sibio A, et al. Early assessment of subclinical cardiac involvement in systemic sclerosis (SSc) using delayed enhancementcardiac magnetic resonance (CE-MRI). *Eur J Radiol*. 2013;82:268-273.
14. Kobayashi Y, Kobayashi H, T Giles J, et al. Detection of left ventricular regional dysfunction and myocardial abnormalities using complementary cardiac magnetic resonance imaging in patients with systemic sclerosis without cardiac symptoms: a pilot study. *Intern Med*. 2016;55:237-243.
15. Yandle TG, Richards AM. B-type natriuretic peptide circulating forms: analytical and bioactivity issues. *Clin Chim Acta*. 2015;448:195-205.
16. Kremastinos DT, Hamodraka E, Parissis J, et al. Predictive value of B-type natriuretic peptides in detecting latent left ventricular diastolic dysfunction in beta-thalassemia major. *Am Heart J*. 2010;159:68-74.
17. Yoo BS. Clinical significance of B-type natriuretic peptide in heart failure. *J Lifestyle Med*. 2014;4:34-38.
18. Gopal DJ, Iqbal MN, Maisel A. Updating the role of natriuretic peptide levels in cardiovascular disease. *Postgrad Med*. 2011;123:102-113.
19. Espiner EA. Physiology of natriuretic peptides. *J Intern Med*. 1994;235:527-541.
20. van den Hoogen F, Khanna D, Fransen J, et al. 2013 classification criteria for systemic sclerosis: an American college of rheumatology/European league against rheumatism collaborative initiative. *Ann Rheum Dis*. 2013;72:1747-1755.
21. Clements PJ, Lachenbruch PA, Seibold JR, et al. Skin thickness score in systemic sclerosis: an assessment of interobserver variability in 3 independent studies. *J Rheumatol*. 1993;20:1892-1896.
22. Kim RJ, Elliott MD, Judd RM. Assessment of myocardial viability by contrast enhancement. In: Higgins CB, Roos A, ed. *MRI and CT of the Cardiovascular System*, 2nd edn. Philadelphia, PA: Lippincott Williams & Wilkins;2006:233-62.
23. Kobayashi Y, Giles JT, Hirano M, et al. Assessment of myocardial abnormalities in rheumatoid arthritis using a comprehensive cardiac magnetic resonance approach: a pilot study. *Arthritis Res Ther*. 2010;12:R171.
24. Mavrogeni SI, Bratis K, Karabela G, et al. Cardiovascular magnetic resonance imaging clarifies cardiac pathophysiology in early, asymptomatic diffuse systemic sclerosis. *Inflamm Allergy Drug Targets*. 2015;14:29-36.
25. Barison A, Gargani L, De Marchi D, et al. Early myocardial and skeletal muscle interstitial remodelling in systemic sclerosis: insights from extracellular volume quantification using cardiovascular magnetic resonance. *Eur Heart J Cardiovasc Imaging*. 2015;16:74-80.
26. Ntusi N, Piechnik SK, Francis JM, et al. Subclinical myocardial inflammation and diffuse fibrosis are common in systemic sclerosis-a clinical study using myocardial T1-mapping and extracellular volume quantification. *J Cardiovasc Magn Reson*. 2014;16:21.
27. Rodriguez-Reyna Ts, Morelos-Guzman M, Hernandez-Reyes P, et al. Assessment of myocardial fibrosis and microvascular damage in systemic sclerosis by magnetic resonance imaging and coronary angiotomography. *Rheumatology (Oxford)*. 2015;54:647-654.
28. Hachulla A-L, Launay D, Gaxotte V, et al. Cardiac magnetic resonance imaging in systemic sclerosis: a cross-sectional observational study of 52 patients. *Ann Rheum Dis*. 2009;68:1878-1884.
29. Bakir M, Wei J, Nelson MD, et al. Cardiac magnetic resonance imaging for myocardial perfusion and diastolic function-reference control values for women. *Cardiovasc Diagn Ther*. 2016;6:78-86.
30. Gaudron P, Eilles C, Kugler I, Ertl G. Progressive left ventricular dysfunction and remodeling after myocardial infarction. Potential mechanisms and early predictors. *Circulation*. 1993;87:755-763.
31. Pfeffer MA, Braunwald E. Ventricular remodeling after myocardial infarction. Experimental observations and clinical implications. *Circulation*. 1990;81:1161-1172.
32. Konstam MA, Kramer DG, Patel AR, Maron MS, Udelson JE. Left ventricular remodeling in heart failure: current concepts in clinical significance and assessment. *JACC Cardiovasc Imaging*. 2011;4:98-108.
33. Bluemke DA, Kronmal RA, Lima J, et al. The relationship of left ventricular mass and geometry to incident cardiovascular events: the MESA (Multi-Ethnic Study of Atherosclerosis) study. *J Am Coll Cardiol*. 2008;52:2148-2155.
34. Yeboah J, Bluemke DA, Hundley WG, Rodriguez CJ, Lima J, Herrington DM. Left ventricular dilation and incident congestive heart failure in asymptomatic adults without cardiovascular disease: multi-ethnic study of atherosclerosis (MESA). *J Card Fail*. 2014;20:905-911.
35. Allanore Y, Meune C. N-terminal pro brain natriuretic peptide: the new cornerstone of cardiovascular assessment in systemic sclerosis. *Clin Exp Rheumatol*. 2009;27:59-63.
36. Ciurzyński M, Bienias P, Lichodziejewska B, et al. Non-invasive diagnostic and functional evaluation of cardiac involvement in patients with systemic sclerosis. *Clin Rheumatol*. 2008;27:991-997.
37. Dimitroulas T, Giannakoulas G, Karvounis H, et al. Neurohormonal activation in patients with systemic sclerosis-related pulmonary arterial hypertension. *Int J Cardiol*. 2007;121:135-137.
38. Mavrogeni SI, Sfikakis PP, Koutsogeorgopoulou L, et al. Cardiac tissue characterization and imaging in autoimmune rheumatic diseases. *JACC Cardiovasc Imaging*. 2017;10:1387-1396.
39. Ambale-Venkatesh B, Lima JA. Cardiac MRI: a central prognostic tool in myocardial fibrosis. *Nat Rev Cardiol*. 2015;12:18-29.
40. Buckert D, Cieslik M, Tibi R, Rademacher M, Rottbauer W, Bernhardt P. Cardiac magnetic resonance imaging derived quantification of myocardial ischemia and scar improves risk stratification and patient management in stable coronary artery disease. *Cardiol J*. 2017;24:293-304.

How to cite this article: Sugiyama K, Kobayashi H, Kobayashi Y, Yokoe I, Takei M, Kitamura N. Association of cardiac magnetic resonance-detected myocardial abnormalities with disease characteristics and brain natriuretic peptide levels in systemic sclerosis without cardiac symptoms. *Int J Rheum Dis*. 2019;22:1016–1022. https://doi.org/10.1111/1756-185X.13540

Japanese Journal of Radiology (2019) 37:9–14
https://doi.org/10.1007/s11604-018-0793-5

INVITED REVIEW

How will "democratization of artificial intelligence" change the future of radiologists?

Yasuyuki Kobayashi[1] · Maki Ishibashi[1] · Hitomi Kobayashi[2]

Received: 7 November 2018 / Accepted: 12 November 2018 / Published online: 21 December 2018
© Japan Radiological Society 2018

Abstract
The "democratization of AI" is progressing, and it is becoming an era when anyone can utilize AI. What kind of radiologists are new generation radiologists suitable for the AI era? The first is maintaining a broad perspective regarding healthcare in its entirety. Next, it is necessary to study the basic knowledge and latest information concerning AI and possess the latest knowledge concerning modalities such as CT/MRI and imaging information systems. Finally, it is important for radiologists to not forget the viewpoint of patient-centered healthcare. It is an urgent task to nurture human resources by realizing such a healthcare AI education program to educate radiologists at an early stage. If we can evolve to become radiologists suitable for the AI era, AI will likely be our ally more than ever and healthcare will progress dramatically. As we approach the "democratization of AI," it is becoming an era in which all radiologists must learn AI as they learn statistics.

Keywords Democratization · Artificial Intelligence · Medicine · Radiology · Radiologist

Introduction

"This might be rather rude, but since I heard that radiologists and pathologists will be replaced by artificial intelligence (AI) in the future, I will not become a radiologist." This was a response I received when I spoke about the appeal of diagnostic imaging to medical students this January and recommended radiology as a specialty. It reminded me of the shocking words I heard from Dr. Geoffrey E. Hinton in 2016: "I think if you work as a radiologist you are like the coyote that's already over the edge of the cliff, but hasn't realize there's no ground underneath. It is just completely obvious that within five years, deep learning is going to do better than radiologist, because it is going to be able to obtain a lot more experience. It might be 10 years, but we got plenty of radiologists already. We should stop training radiologists." It is said that AI will take many jobs from humans. Is AI an enemy or ally of radiologists? There is an expression, "democratization of AI," which encompasses the idea that in a society, "everyone can utilize AI technology." As the era of AI approaches, what should radiologists do to make AI their ally?

Recent progress in AI and ICT

The speed at which AI and information and communication technology (ICT) have progressed in recent years is astonishing. New technologies that seemed far off in the future are rapidly becoming reality (Fig. 1). Wearable devices, such as heart rate monitors, pedometers, activity monitors, sphygmomanometers, and ECG monitors, are sold for home use at affordable prices. Voice-activated AI that is "always connected" and robot phones are also commercially available for the general public. If you watch YouTube videos of robots, such as Robot Kitchen from Moley [1] and Atlas from Boston Dynamics [2], you can see that both robots are already available for application

✉ Yasuyuki Kobayashi
yasukoba2@gmail.com; yasukoba@marianna-u.ac.jp

Maki Ishibashi
maki.ishibashi@marianna-u.ac.jp

Hitomi Kobayashi
kobayashi.hitomi48@nihon-u.ac.jp

[1] Department of Medical Information and Communication Technology Research, Graduate School of Medicine, St. Marianna University School of Medicine, 2-16-1, Sugao, Miyamae-ku, Kawasaki, Kanagawa 216-8511, Japan

[2] Division of Hematology and Rheumatology, Department of Medicine, Nihon University School of Medicine, 30-1 Oyaguchi Itabashi-Ward, Tokyo 173-8610, Japan

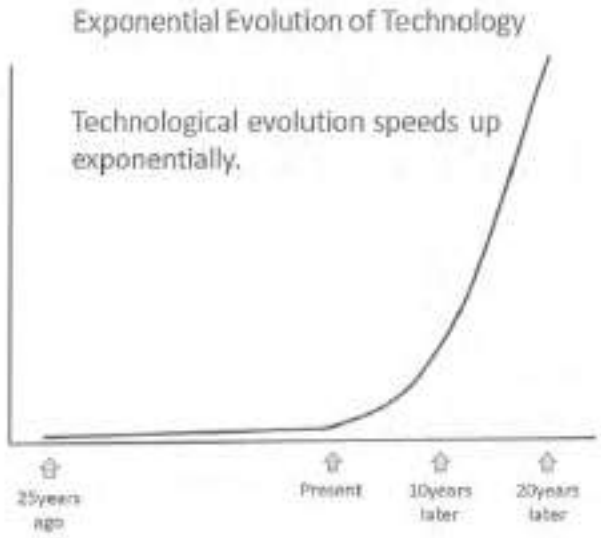

Fig. 1 Exponential evolution of technology

in the general public. Various cutting-edge technologies, such as AI (machine learning/deep learning), big data, Internet of Things/Everything/Human, Virtual/Augmented/Mixed Reality, robotics, wearable devices, and 5G, are widely used daily and will be integrated into the medical field (Fig. 2).

Utilization of AI in medical care

I believe that you are all aware that the number of academic papers on AI is rapidly increasing in the field of medicine [3]. A 2017 paper published in Nature reported that GoogLeNet, which is provided by Google to the public, was shockingly able to diagnose melanoma from photographs of skin lesions at the same level of diagnostic performance as dermatologists, indicating the possibility of an inexpensive smartphone application [4]. Furthermore, a paper published this year reported that AI had in fact performed better than dermatologists [5]. There have also been reports on AI performing better than pathologists in the diagnosis of lymph node metastasis of breast cancer [6] and in the prediction of cardiovascular risk factors using fundus photography [7].

Regardless of our involvement, it is inevitable that AI will be used in daily tasks. It is said that "In the future, AI will definitely play a part in diagnostic and therapeutic policy decisions, and as medicine dramatically progresses, physicians will gain time and mental leeway, which will allow physicians to go back to the original purpose of 'healing people'." Regarding AI as a device to support the diagnoses of physicians due to the risk of AI making a misdiagnosis in diagnosis, the government announced the other day its policy to stipulate the principle that "physicians will be responsible for final diagnosis and treatment policy decisions and responsibilities" in the Medical Practitioners' Act. This is good news; nevertheless, we cannot let our guard down. In April of this year, the U.S. FDA granted the first approval to sell AI medical devices that are able to diagnose retinal

Fig. 2 Medical ICT (information and communication technology) utilization

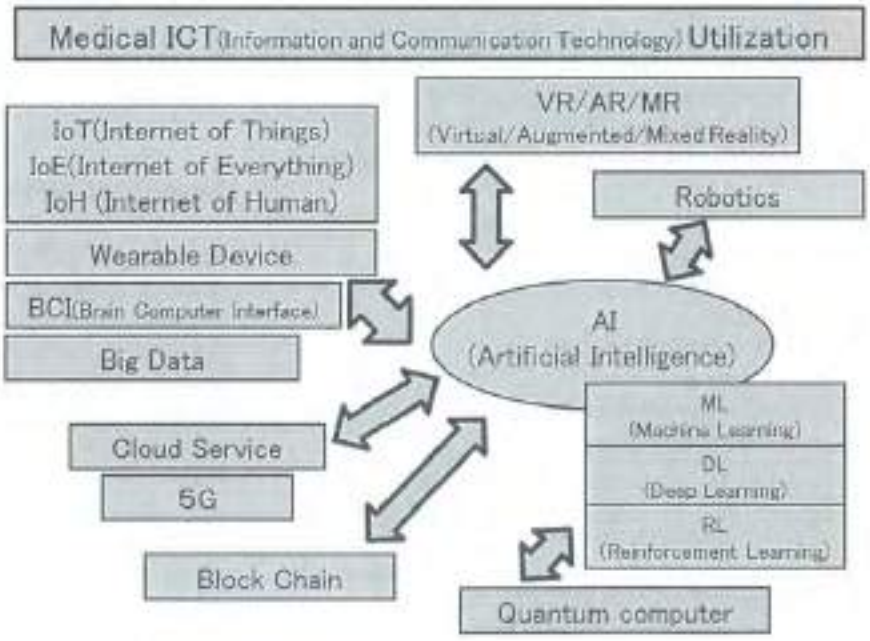

Table 1 Role of AI in diagnostic imaging

Image quality improvement
Image generation
Automatic detection
Segmentation
Classification
Regression (measurement/ qtantification)
Appropriate workflow
Automatic creation of reports

lesions without a physician [8]. We must actively become involved and control the directionality of AI development, such that it suits daily tasks performed in Japan.

The use of AI in diagnostic imaging is classified as follows: (1) improvement of image quality; (2) image generation; (3) automatic detection; (4) segmentation; (5) classification; (6) regression analysis (measurement and quantification); (7) optimization of work flow; and (8) automatic preparation of reports (Table 1). There are academic papers on AI that are being published one after another on topics such as the detection of pneumonia from simple chest images [9, 10], detection and improved work flow of cerebral hemorrhaging and infarction from head CTs [11, 12], detection of cerebral aneurysm from head MRIs [13], assessment of skeletal maturity on pediatric hand radiographs [14], differentiation of brain and liver tumor [15, 16], determination of necessity for contrast imaging with bone and soft tissue MRIs [17], classification of fibrosis in liver CTs [18], image reconstruction [19], the ability of deep learning to classify head MRI sequences [20], and MR-based synthetic CT generation [21]. AI, deep learning with a convolutional neural network, is gaining attention recently for its high performance in image recognition [22]. Imaging diagnosis is becoming increasingly complicated [23]; therefore, it is indispensable for radiologists to use positively AI in clinical practice.

Democratization of AI

The "democratization of AI" is progressing, and it is becoming an era when anyone can utilize AI. There is a case in which individual farmers developed a cucumber sorting machines that utilized AI with the library that companies provide free of charge at a cost of 20,000 yen [24]. In fact, many papers introduced in the previous section used the library (learning framework) free of charge provided by various companies or cloud platform at low costs, which is a method anyone can use (Table 2). This is an era wherein one does not have to be an AI expert to develop applications that utilize medical AI technology. In recent years, there

Table 2 "Democratization of AI" machine learning platform

Cloud platform	Library (learning framework):
Microsoft Azure	Caffe (yahoo)/Caffe2(Facebook)
IBM Bluemix Cloud: Watson AI	Chainer (Preferred Networks)
Google Cloud Platform (GCP)	TensorFlow (Google)
Amazon Web Services (AWS)	Keras (Google; Francois Chollet)
LINE Clova	Theano (Montreal University)
IDCF Cloud (inc: yahoo)	MXNet (Amazon)
NIFTY Cloud	Cognitive Toolkit (Microsoft)
NTT Communications Cloud	Torch / Pytorch
Sakura Cloud	PaddlePaddle(Baidu)
Apple CoreML	DL4J (Skymind)
Oracle Adaptive Intelligence	Scikit-learn (David Cournapeau), PyML(Asa Ben-Hur),PyBrain
NVIDIA GPU Cloud	
Sony Neural Network Libraries	
Fujitsu Zinrai	

have been reports on physicians developing diagnostic imaging applications and medical devices that utilize AI as a new business. This is all thanks to the "democratization of AI." Even in the medical industry, it is expected that large companies will make practical use of profitable medical AI devices; however, in the field of medicine, there are various issues over a wide range of areas, some of which are problems that could likely be solved by radiologists and physicians using AI.

Medical AI in Japan

Although the number of radiologists per population is extremely low in Japan, the number of CT and MRI devices per radiologist is the highest in the world [25], suggesting that Japan requires the utilization of AI the most.

The level of enthusiasm for AI shown during the 2017 Radiological Society of North America conference was shocking. One could not enter the venue unless they arrived at least 30 min prior to the start of a lecture if the session had "AI" in the title. In contrast, the level of enthusiasm for AI in Japan is not particularly high, with opinions such as "I am too busy with my daily tasks to learn AI. That is something for the future. Even if I learned AI, it would not be useful …".

Professor Yutaka Matsuo of the University of Tokyo has warned that Japan is an underdeveloped country when it comes to AI, and "it is unlikely that we can win in the international platform; in fact, we have almost lost." In recent years, young Japanese radiologists are losing interest in modalities such as CT and MRI due to the increasing number of daily tasks in their practice. If they are similarly unable to develop interest in AI, there may not be any need

for such radiologists in the future. Radiologists work day after day with the latest technologies, such as modalities like CT and MRI, and are most familiar with the latest technologies, such as AI.

Challenges with AI in medicine in Japan

In utilizing AI in medicine, in addition to the above-mentioned responsibilities, there are the following challenges.

1. Insufficient usable medical data.

   Over several years, since it was said that "data are the crude oil of the twenty-first century (Martin Jetter/World Summit 2014 ICT), data (crude oil) have been changing into a valuable resource (oil) due to advancements in various technologies. Unfortunately, particularly in the medical field in Japan, medical data remain as crude oil due to the protection of personal information. There is a business opportunity in "refining" medical data into usable oil as soon as possible, so that researchers and companies can utilize the same.

   Presently, the government is promoting a national database for AI utilization, but it will take time. The NIH prepared simple chest images from over 100,000 cases and CT scan data from 10,600 cases as an open database. In Japan, it is urgent that a similar database be created with instructors.
2. The process of making a conclusion is unclear in deep learning (DL).

   To solve the unique nature of medical AI, wherein the diagnostic process must be explained, the development of a mechanical learning method that is most suited to medicine is necessary. In recent years, a hybrid-type algorithm was developed, wherein other machine-learning methods were added to DL, and there are new applications that are able to determine these processes. Furthermore, technology is being developed to solve the "black box problem" of AI.
3. Insufficient number of IT technicians.

   In Japan, the lack of IT technicians is a serious problem, and the number will start to decrease further starting in 2020. Thus, it is necessary to promptly establish an AI education program in the medical industry.
4. Technology updates are extremely fast.

   It is difficult to determine at what technological stage AI will become usable in a clinical setting, and continued learning after the purchase could lower precision. This makes AI management difficult.
5. Insufficient social understanding.

   It will be extremely difficult to use AI if it cannot be used in medical sites until a perfect support system is developed. Good systems cannot be built without actually using them on site. Control of personal information is extremely strict.
6. The cloud is difficult to use due to protection of personal information.

   It is impossible for just one company to create a next-generation environment for AI use; thus, a multi-vendor system is essential. Many international companies are developing applications that only operate on the cloud. Furthermore, individual hospitals are able to use high-performance and expensive super computers. For these reasons, the cloud is essential in AI use.
7. There is no standard model.

   A national-level database is necessary. At the present time, the J-MID (Japan Medical Image Database) Project, which is an AMED (Japan Agency for Medical Research and Development) project, is in progress.

To realize next-generation medical care utilizing AI, radiologists have to solve the above-mentioned problems. We believe Japanease radiologists can solve them.

Radiologists in the era of AI

At the Radiological Society of North America conference last year, Prof. Curits Langlotz answered the question "Will AI ever replace radiologists?" by stating the following: "I say the answer is no—but radiologists who use AI will replace radiologists who don't." He further stated that "Radiology was a high-tech field from its beginning, and we have always been a high-tech specialty. We have partnered with technology innovators and learned clinically how to adopt new technologies." "We're going to learn how to deploy it clinically, when it's worth using and when it shouldn't be used.".

Let us now consider what the experts of diagnostic imaging must do to "provide service to each department through diagnostic imaging": (1) provide accurate diagnostic imaging to all departments; (2) provide diagnostic imaging that uses the latest technology to all departments; and (3) build an appropriate image information system (PACS/RIS) and provide image information promptly and accurately to all departments. In the future, in addition to the above-mentioned services, establishing how AI is used in a clinical setting will be the responsibility of radiologists.

As photon-counting CT progresses, the modality itself will continue to evolve and new diagnostic imaging methods will appear. Only radiologists are capable of thinking of the appropriate clinical use, associated with AI. More than ever, the acquisition of knowledge (education) on the latest modality will be important for radiologists.

It is also important to develop AI devices and put them into practical use. For that purpose, co-creation by university

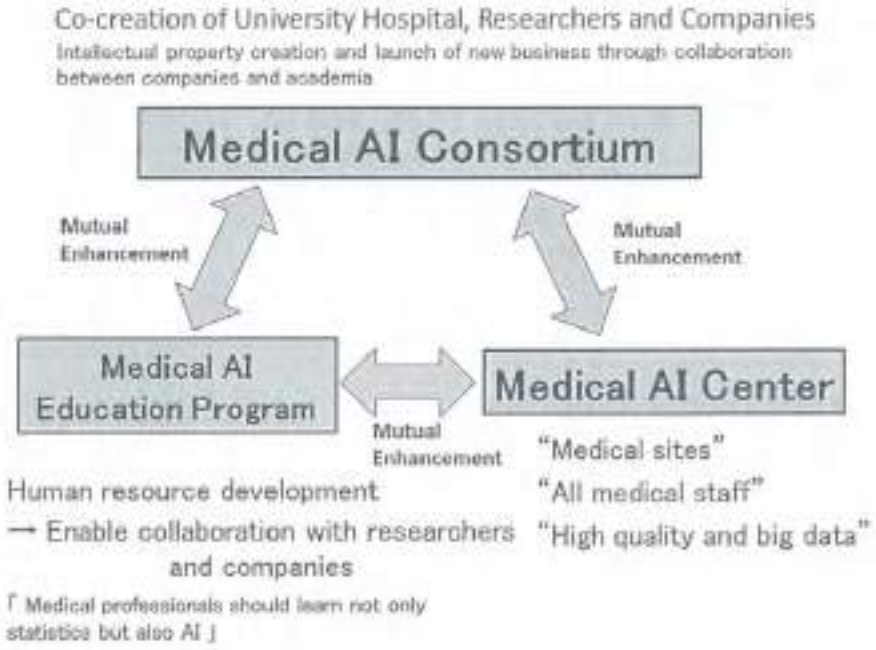

Fig. 3 Ideal platform for medical AI utilization

Table 3 Medical AI Education Program

Introduction
AI
Latest ICT such as IoT, Robotics, VR/AR/MR, Block Chain, 5G, Cloud, etc.
Knowledge on AI/ICT:
Basic knowledge
AI Environment improvement and programming (practical training)
e-Learning
Latest information
Medical policy and medical economics
Legal protection and intellectual property application
MOT(management of technology)
Business strategy and lecture on entrepreneurship (workshop)
Funding: Cloud funding, etc.
Understand the special problems of AI in medicine
Solving real tasks in medical field (workshop) by collaboration
Education and Approach to Middle Management Level

hospitals, enterprises, and AI researchers is important in the future, and it is necessary for the radiologists to lead the way to establish creative cooperative relationships (Fig. 3).

Considering the future of radiologists, we can visualize a data scientist who utilizes AI for analysis of not only imaging information but also clinical information and data to make a diagnosis. However, in this era where various technologies progress exponentially, it is almost impossible to predict a specific future. It is the responsibility of young radiologists to create next-generation medical care, where radiologists and AI coexist 10 or more years from now, as it is an era, where "all radiologists must learn AI just, as they learn statistics.".

Who are the new generation of radiologists suited to this era of AI? First, they must have a broad perspective on overall medical care. Next, they must acquire basic information with regard to AI as well as the latest knowledge on modalities such as CT, MRI, and image information systems. Finally, as Dr. Obermeyer [26] said, "As in other industries, this challenge will create winners and losers in medicine. But we are optimistic that patients will emerge as the biggest winners as machine-learning transforms clinical medicine." It will become increasingly more important for us as radiologists to not forget patient-centered medical care. It is an urgent matter to promptly actualize a medical AI education program that educates such radiologists and nurtures human resources (Table 3).

Conclusions

My response to the question "Is AI an enemy or ally of radiologists?" is "It could be either." "If radiologists remain as they are, AI could become an enemy. However, if radiologists evolve to a new generation of radiologists suited to the era of AI, AI could become an unprecedented ally and dramatically progress medical care." With the "democratization of AI," it has now become an era where "all radiologists must learn AI just as they learned statistics.".

Compliance with ethical standards

Conflict of interest YK has received a research grant from Canon Medical Systems. MI and HK has no conflict of interest.

References

1. https://www.youtube.com/watch?v=BSBTCOEdLkA
2. https://www.youtube.com/watch?v=6vYA8L_r850
3. Litjens G, Kooi T, Bejnordi BE, Setio AAA, Ciompi F, Ghafoorian M, et al. A survey on deep learning in medical image analysis. Med Image Anal. 2017;42:60–88.
4. Esteva A, Kuprel B, Novoa RA, Ko J, Swetter SM, Blau HM, et al. Dermatologist-level classification of skin cancer with deep neural networks. Nature 2017;542:115–118.
5. Haenssle HA, Fink C, Schneiderbauer R, Toberer F, Buhl T, Blum A, et al. Man against machine: diagnostic performance of a deep learning convolutional neural network for dermoscopic melanoma recognition in comparison to 58 dermatologists. Ann Oncol. 2018;29:1836–42.
6. Ehteshami Bejnordi B, Veta M, Johannes van Diest P, van Ginneken B, Karssemeijer N, Litjens G, et al. Diagnostic assessment of deep learning algorithms for detection of lymph node metastases in women with breast cancer. JAMA. 2017;318:2199–210.
7. Poplin R, Varadarajan AV, Blumer K, Liu Y, McConnell MV, Corrado SG, et al. Prediction of cardiovascular risk factors from retinal fundus photographs via deep learning. Nature Biomedical Engineering. 2018;2:158–64.
8. https://www.fda.gov/newsevents/newsroom/pressannouncements/ucm604357.htm
9. Lakhani P, Sundaram B. Deep Learning at Chest Radiography: Automated Classification of Pulmonary Tuberculosis by Using Convolutional Neural Networks. Radiology. 2017;284:574–82.
10. Rajpurkar P, Irvin J, Zhu K, Yang B, Mehta H, Duan T, et al. CheXNet: radiologist-level pneumonia detection on chest X-rays with deep learning. 2017.arXiv:1711.05225.
11. Prevedello LM, Erdal BS, Ryu JL, Little KJ, Demirer M, Qian S, et al. Automated critical test findings identification and online notification system using artificial intelligence in imaging. Radiology. 2017;285:923–31.
12. Titano JJ, Badgeley M, Schefflein J, Pain M, Su A, Cai M, et al. Automated deep-neural-network surveillance of cranial images for acute neurologic events. Nat Med. 2018;24:1337–41.
13. Nakao T, Hanaoka S, Nomura Y, Sato I, Nemoto M, Miki S, et al. Deep neural network-based computer-assisted detection of cerebral aneurysms in MR angiography. J Magn Reson Imaging. 2018;47:948–53.
14. Larson DB, Chen MC, Lungren MP, Halabi SS, Stence NV, Langlotz CP. Performance of a deep-learning neural network model in assessing skeletal maturity on pediatric hand radiographs. Radiology. 2018;287:313–22.
15. Kunimatsu A, Kunimatsu N, Yasaka K, Akai H, Kamiya K, Watadani T, et al. Machine learning-based texture analysis of contrast-enhanced MR Imaging to differentiate between glioblastoma and primary central nervous system lymphoma. Magn Reson Med Sci. 2018. https://doi.org/10.2463/mrms.mp.2017-0178.
16. Yasaka K, Akai H, Abe O, Kiryu S. Deep learning with convolutional neural network for differentiation of liver masses at dynamic contrast-enhanced CT: a preliminary study. Radiology. 2018;286:887–96.
17. Trivedi H, Mesterhazy J, Laguna B, Vu T, Sohn JH. Automatic determination of the need for intravenous contrast in musculoskeletal MRI examinations using IBM Watson's natural language processing algorithm. J Digit Imaging. 2018;31:245–51.
18. Yasaka K, Akai H, Kunimatsu A, Abe O, Kiryu S. Deep learning for staging liver fibrosis on CT: a pilot study. Eur Radiol. 2018. https://doi.org/10.1007/s00330-018-5499-7.
19. Zhu B, Liu JZ, Cauley SF, Rosen BR, Rosen MS. Image reconstruction by domain-transform manifold learning. Nature. 555(7697):487–492. https://doi.org/10.1038/nature25988
20. Noguchi T, Higa D, Asada T, Kawata Y, Machitori A, Shida Y, et al. Artificial intelligence using neural network architecture for radiology (AINNAR): classification of MR imaging sequences. Jpn J Radiol. 2018. https://doi.org/10.1007/s11604-018-0779-3.
21. Han X. MR-based synthetic CT generation using a deep convolutional neural network method. Med Phys. 2017;44:1408–19.
22. Yasaka K, Akai H, Kunimatsu A, Kiryu S, Abe O. Deep learning with convolutional neural network in radiology. Jpn J Radiol. 2018;36:257–72.
23. García-Figueiras R, Baleato-González S, Padhani AR, Luna-Alcalá A, Marhuenda A, Vilanova JC, et al. Advanced imaging techniques in evaluation of colorectal cancer. Radiographics. 2018;38:740–65.
24. https://business.nikkeibp.co.jp/atcl/opinion/15/221103/051100577
25. Nakajima Y, Yamada K, Imamura K, Kobayashi K. Radiologist supply and workload: international comparison. Working Group of Japanese College of Radiology. Radiat Med. 2008;26:455–65.
26. Obermeyer Z, Emanuel EJ. Predicting the future - big data, machine learning, and clinical medicine. N Engl J Med. 2016;375:1216–9.

The Journal of Rheumatology

The Journal of Rheumatology Volume 45, no. 12

Heart Rate–corrected QT Interval Duration in Rheumatoid Arthritis and Its Reduction with Treatment with the Interleukin 6 Inhibitor Tocilizumab

Hitomi Kobayashi, Yasuyuki Kobayashi, Isamu Yokoe, Noboru Kitamura, Atsuma Nishiwaki, Masami Takei and Jon T. Giles

J Rheumatol 2018;45;1620-1627
http://www.jrheum.org/content/45/12/1620

1. Sign up for TOCs and other alerts
http://www.jrheum.org/alerts

2. Information on Subscriptions
http://jrheum.com/faq

3. Information on permissions/orders of reprints
http://jrheum.com/reprints_permissions

The Journal of Rheumatology is a monthly international serial edited by Earl D. Silverman featuring research articles on clinical subjects from scientists working in rheumatology and related fields.

Downloaded from www.jrheum.org on April 24, 2020 - Published by The Journal of Rheumatology

Heart Rate–corrected QT Interval Duration in Rheumatoid Arthritis and Its Reduction with Treatment with the Interleukin 6 Inhibitor Tocilizumab

Hitomi Kobayashi, Yasuyuki Kobayashi, Isamu Yokoe, Noboru Kitamura, Atsuma Nishiwaki, Masami Takei, and Jon T. Giles

ABSTRACT. ***Objective.*** Individuals with rheumatoid arthritis (RA) are at a heightened risk of sudden cardiac death, an outcome increased in those with prolongation of the corrected electrocardiographic QT interval (QTc). We compared QTc between patients with RA and demographically matched controls and studied the change in QTc after treatment with the interleukin 6 inhibitor tocilizumab (TCZ).

Methods. Standard 12-lead electrocardiograms were obtained and QTc was measured in patients with RA at baseline and after 24 weeks of TCZ treatment, then compared with non-RA controls who were frequency-matched on age and sex. Indicators of the baseline QTc and predictors of change in QTc were studied using multivariable linear regression.

Results. A total of 94 RA and 42 non-RA controls were studied. The average baseline QTc was 10 ms longer in the RA group vs controls (422 vs 412 ms, respectively; $p < 0.001$) and decreased to an average of 406 ms with treatment ($p < 0.001$). Baseline QTc was significantly and independently higher among those with anticyclic citrullinated peptide antibodies seropositivity, higher swollen joint counts, and higher levels of C-reactive protein (CRP) and matrix metalloproteinase 3. Each log unit decrease in CRP with treatment was associated with an average reduction in QTc of 2.9 ms ($p = 0.002$) after adjusting for age and baseline QTc. Clinical response measures were not associated with the change in QTc.

Conclusion. The marked normalization of QTc observed with TCZ treatment, and its close parallel with CRP reduction, support the premise that systemic inflammation contributes to cardiac repolarization abnormalities in RA that may be amenable to treatment. (First Release September 1 2018; J Rheumatol 2018;45:1620–7; doi:10.3899/jrheum.180065)

Key Indexing Terms:
RHEUMATOID ARTHRITIS CARDIOVASCULAR DISEASE
CARDIAC ELECTROPHYSIOLOGY CYTOKINE INHIBITION INFLAMMATION

Individuals with rheumatoid arthritis (RA) have a 2-fold higher risk of sudden cardiac death compared with age- and sex-matched controls[1]. Among the general (i.e., non-RA) population, several large studies have established that the risk of sudden cardiac death is increased in individuals with prolongation of the corrected QT (QTc) interval, as measured with electrocardiography (ECG)[2,3]. Chauhan, *et al* reported a significantly elevated risk of developing QTc prolongation among patients with RA[4], and as reported by Panaoulas, *et al*, each 50 ms longer QTc was associated with a more than 2-fold higher hazard of all-cause mortality over an average followup time of 6 years[5].

In many of these studies, circulating C-reactive protein (CRP)[4,6] and/or circulating inflammatory cytokines[7] were correlated with longer QTc intervals. These findings raise the possibility that RA treatments that reduce circulating levels of these offending cytokines may reduce the incidence of cardiac repolarization abnormalities that contribute to sudden cardiac death. However, whether QTc prolongation is reduced with treatment has not yet been well established. In a study of 17 patients with RA, Lazzerini, *et al* reported QTc normalization after treatment with the interleukin 6 (IL-6) inhibitor tocilizumab (TCZ), an effect that was correlated with the degree of reduction in CRP[8]. However, that study did not include comparison with a non-RA control group, and

From the Division of Hematology and Rheumatology, Nihon University School of Medicine, Tokyo; Department of Advanced Biomedical Imaging Informatics, St. Marianna University School of Medicine, Kawasaki, Japan; Division of Rheumatology, Columbia University, College of Physicians and Surgeons, New York, New York, USA.

H. Kobayashi, MD, PhD, Division of Hematology and Rheumatology, Nihon University School of Medicine; Y. Kobayashi, MD, PhD, Department of Advanced Biomedical Imaging Informatics, St. Marianna University School of Medicine; I. Yokoe, MD, Division of Hematology and Rheumatology, Nihon University School of Medicine; N. Kitamura, MD, Division of Hematology and Rheumatology, Nihon University School of Medicine; A. Nishiwaki, MD, Division of Hematology and Rheumatology, Nihon University School of Medicine; M. Takei, MD, PhD, Division of Hematology and Rheumatology, Nihon University School of Medicine; J.T. Giles, MD, MPH, Division of Rheumatology, Columbia University, College of Physicians and Surgeons.

Address correspondence to Dr. J.T. Giles, Division of Rheumatology, Columbia University, College of Physicians and Surgeons, 630 West 168th St., P&S Building, 3rd Floor, Suite 3450, New York, New York 10032, USA. E-mail: jtg2122@cumc.columbia.edu

Accepted for publication May 28, 2018.

Personal non-commercial use only. The Journal of Rheumatology Copyright © 2018. All rights reserved.

Downloaded from www.jrheum.org on April 24, 2020 - Published by The Journal of Rheumatology

with the small sample size, only simple correlations of characteristics with QTc were possible. We sought to examine the QTc interval in a larger group of patients with RA compared with a demographically matched group of non-RA controls. Additionally, we sought to study the independent inflammatory and noninflammatory indicators of QTc in patients with RA and characterize the predictors of change in QTc associated with 24 weeks of treatment with TCZ. We hypothesized that clinical response to TCZ would be associated with a reduction in QTc in patients with RA, potentially returning to levels comparable to those of individuals without RA.

MATERIALS AND METHODS

Study population. Patients with RA were recruited from the Itabashi Chuo Medical Center from March 2012 to May 2016. Patients met the 2010 American College of Rheumatology/European League Against Rheumatism (EULAR) criteria for RA[9], had moderate to severe RA disease activity based on the 28-joint count Disease Activity Score (DAS28) cutpoints[10], and complied with the Guideline for Biological Products of the Japanese College of Rheumatology. Healthy volunteers were recruited as a control group to be frequency-matched to the age and sex distribution of the RA group. Both patients and controls were excluded if they reported prior cardiovascular (CV) events or procedures, whether self-reported or physician-diagnosed, including myocardial infarction, angioplasty, chronic heart failure, or arrhythmia. ECG exclusions included tachycardia (i.e., heart rate > 100 bpm), left bundle branch block, and ST elevations or depressions. The study was approved by the local ethics committee (Nihon University Itabashi Hospital RK-170912-12), and informed consent was obtained from each patient in accordance with the Helsinki Declaration of 1975 (revised in 1983).

Assessment and treatment protocol. Patients received TCZ either once a month (8 mg/kg intravenously) or 162 mg subcutaneously biweekly for 24 weeks. Electrocardiogram, clinical assessments, and laboratory monitoring were performed at baseline and Week 24. All patients were clinically evaluated by the same observer for disease activity measures. Low disease activity (LDA) was achieved if the DAS28 using CRP (DAS28-CRP) was < 3.2 units, and remission was achieved if the DAS28-CRP was < 2.6 units[11]. A EULAR good response was achieved if the DAS28-CRP achieved was < 3.2 units and the change from baseline was ≥ 1.2 units[11].

ECG assessment. Resting 12-lead ECG (25 mm/s paper speed and 10 mm/mV amplitude) were recorded using a 3-channel direct writing machine at baseline and Week 24. The QT interval was corrected with the Bazett formula. A QTc ≥ 440 ms was considered prolonged, because this threshold has been demonstrated in several large studies to be associated with an increased risk of sudden cardiac death[12,13]. Accordingly, in this study the QTc interval of 440 ms was considered prolonged.

Clinical and laboratory assessments. Fasting samples of serum and plasma were collected at baseline and at Week 24, separated by centrifugation, and stored at −70°C. All assays were performed at our institution using our internal quality control procedures. At the time of the study visit, all subjects underwent routine laboratory investigations, and basic screening for traditional atherosclerotic disease risk factors, including history of cigarette smoking, serum cholesterol, triglycerides, high-density lipoprotein, low-density lipoprotein, fasting blood glucose concentration, rheumatoid factor, and anticyclic citrullinated peptide antibodies (anti-CCP). Collected samples were assessed blinded to group status or clinical characteristics. Matrix metalloproteinase (MMP-3) level was measured by the blood sample reacting with mouse antihuman MMP-3 monoclonal antibody in a turbidimetric immunoassay with sensitized latex-enhanced particles. CRP was measured by latex agglutination turbidimetric immunoassay.

Statistical analysis. Differences in participant characteristics according to disease status were compared using t tests for normally distributed continuous variables, the Kruskal-Wallis test for non-normally distributed continuous variables, and the chi-square goodness-of-fit test or Fisher's exact test, as appropriate, for categorical variables. Linear regression was used to model predictors of baseline and change in QTc interval. Predictors were first modeled separately, and those with an association p value < 0.20 were carried into an extended multivariable (MV) model. Noncontributory covariates were excluded using Akaike Information Criterion for nested models. The adjusted R^2 was used to assess the proportion of the variability in the outcome explained by the modeled covariates. The Shapiro-Wilk test was used to assess that normality assumptions for linear regression were met, which was the case for all the final MV models. Variance inflation factors were calculated to assess for collinearity among modeled covariates, and none was detected in all models. Statistical interaction of change in CRP with baseline QTc was tested in linear regression by introducing a QTc × change in CRP interaction term into the model. All statistical calculations were performed using Intercooled Stata 14 (StataCorp). A 2-tailed α of 0.05 was used throughout.

RESULTS

Baseline (pretreatment) characteristics of the 94 patients with RA and 42 non-RA controls are summarized in Table 1. The groups did not significantly differ on age or sex. Three-quarters of the patients had no CV disease (CVD) risk factors. Among those with CVD risk factors, the majority had hypertension (n = 14). Hyperlipidemia was present in 6 patients with RA, and only 1 had diabetes. RA disease activity was moderate to high, on average, and was reflected in above-normal markers of systemic inflammation in most. The majority of patients with RA (81%) were treated with disease-modifying antirheumatic drugs (DMARD), most prominently with methotrexate (MTX) at a median dose of 8 mg per week. Other DMARD (bucillamine, tacrolimus, and sulfasalazine) were uncommon (15%) and were used alone or in combination with MTX. Almost half were treated with prednisolone at baseline.

After 24 weeks of treatment, statistically significant improvements were observed in all disease activity measures, circulating inflammatory markers, and Health Assessment Questionnaire scores. Eighty-five percent achieved DAS LDA, 80% were in DAS remission, and 71% had no more than 1 swollen joint.

Elevated baseline QTc intervals decreased with TCZ treatment. The average baseline QTc was 10 ms longer in the RA group compared with controls (422 vs 412 ms, respectively; p < 0.001; Figure 1A). After treatment, the average QTc decreased to 406 ms in the RA group and was now significantly lower than the level of the control group. There were 12 RA patients with a baseline QTc ≥ 440 ms compared with none of the controls (p = 0.018, data not shown). After treatment, only 1 patient still had a QTc ≥ 440 ms. Treatment-associated reduction in QTc to levels at or below those of non-RA controls was observed in both men and women with RA (Figure 1B).

Baseline QTc interval was associated with anti-CCP seropositivity and multiple indicators of disease activity. Univariate

Personal non-commercial use only. The Journal of Rheumatology Copyright © 2018. All rights reserved.

Downloaded from www.jrheum.org on April 24, 2020 - Published by The Journal of Rheumatology

Table 1. Baseline and followup characteristics. Data are median (interquartile range) unless otherwise indicated.

Characteristics	RA, n = 94	Controls, n = 42	p
Age, yrs, mean ± SD	56 ± 11	57 ± 11	0.71
Male, n (%)	18 (19)	10 (24)	0.54
Systolic blood pressure, mm Hg, mean ± SD	121 ± 11	120 ± 7	0.54
Diastolic blood pressure, mm Hg, mean ± SD	70 ± 9	70 ± 6	0.63
HbA1c, %, mean ± SD	5.5 ± 0.3	5.5 ± 0.3	0.31
Total cholesterol, mg/dl	187 ± 26	187 ± 15	0.95
LDL-C, mg/dl, mean ± SD	102 ± 22	101 ± 13	0.83
HDL-C, mg/dl, mean ± SD	63 ± 15	65 ± 10	0.34
Triglycerides, mg/dl	116 (92–133)	101 (90–120)	0.11
RA duration, mos	15 (7–72)		
RF > 40 units, n (%)	59 (63)		
anti-CCP > 20 units, n (%)	67 (71)		
DAS28, units, mean ± SD	4.9 ± 1.2		
SJC	4 (2–6)		
TJC	4 (2–6)		
SDAI, units	22.0 (14.3–30.0)		
CRP, mg/dl	2.0 (0.8–3.4)		
ESR, mm/h	34 (20–52)		
MMP-3, ng/ml	150 (107–277)		
VAS, mm	50 (30–75)		
mVAS, mm	58 (40–70)		
HAQ, units	0.25 (0.12–0.94)		
Any DMARD, n (%)	76 (81)		
MTX, n (%)	66 (70)		
MTX dose, mg	8 (8–10)		
Other DMARD, n (%)	14 (15)		
Prednisolone, n (%)	45 (48)		
Prednisolone dose (users), mg/day	5 (4–5)		
Change in DAS28, units, mean ± SD	−2.93 ± 1.31*		
EULAR good response, n (%)	74 (79)*		
Low disease activity, n (%)	80 (85)*		
Remission, n (%)	75 (80)*		
SJC ≤ 1 joint, n (%)	67 (71)*		
% change, mean ± SD	−59 ± 20*		
Change in CRP, mg/dl	−2.0 (−3.4 to −0.8)*		
Change in ESR, mm/h	−24 (−47 to −14)*		
Change in MMP-3, ng/ml	−85 (−197 to −27)*		
Change in VAS, mm	−30 (−50 to −10)*		
Change in HAQ, units	−0.12 (−0.44 to 0)*		
Change in prednisolone dose, mg/day	−2 (−4 to −1)		
Stopped prednisolone, n (%)	13 (14)		

* P value < 0.05 for change between baseline and Week 24. RA: rheumatoid arthritis; HDL-C: high-density lipoprotein cholesterol; LDL-C: low-density lipoprotein cholesterol; RF: rheumatoid factor; anti-CCP: anticyclic citrullinated peptide; DAS28: 28-joint count Disease Activity Score; SDAI: Simplified Disease Activity Index; CRP: C-reactive protein; ESR: erythrocyte sedimentation rate; MMP: matrix metalloproteinase; VAS: visual analog scale; mVAS: modified VAS; DMARD: disease-modifying antirheumatic drug; HAQ: Health Assessment Questionnaire; MTX: methotrexate; EULAR: European League Against Rheumatism; SJC: swollen joint count; TJC: tender joint count.

and multivariable associations of RA patient characteristics with baseline QTc interval are summarized in Table 2. In the final model, those seropositive for anti-CCP had an adjusted QTc interval that was 8.3 ms longer than those who were seronegative ($p = 0.021$). On average, each additional swollen joint was associated with a 1-ms longer adjusted QTc ($p = 0.038$). Each log unit higher CRP was associated with a 3.7 ms longer adjusted QTc, on average, while each log unit higher MMP-3 was associated with a 5.2-ms longer adjusted QTc. Together, these 4 variables accounted for 26% of the explainable variability in baseline QTc interval (i.e., $R^2 = 0.255$; $p < 0.001$). Neither demographics, the presence of CVD risk factors, nor baseline use of DMARD or prednisolone were significantly associated with baseline QTc.

Patients above the median for swollen joint count (SJC; 4 joints), CRP (2.0 mg/dl), and MMP-3 (150 units) were classified as having the feature present. Those seropositive for anti-CCP and SJC, CRP, and MMP-3 all above the

Personal non-commercial use only. The Journal of Rheumatology Copyright © 2018. All rights reserved.

Downloaded from www.jrheum.org on April 24, 2020 - Published by The Journal of Rheumatology

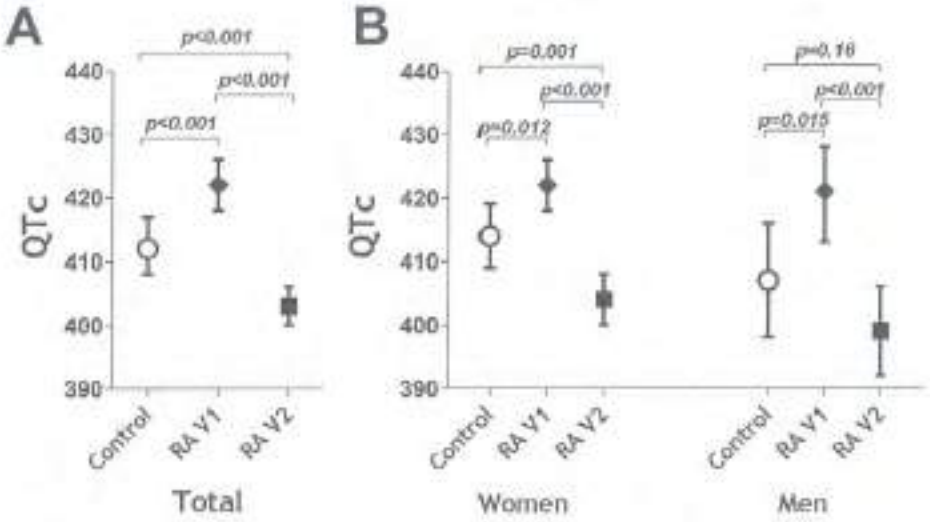

Figure 1. Comparison of QTc interval pre- and post-tocilizumab between RA patients and non-RA controls (baseline). Means and 95% CI are depicted. QTc: corrected electrocardiographic QT interval; RA: rheumatoid arthritis.

Table 2. Associations of patient characteristics with baseline QTc interval.

Variables	Univariate Models		Extended MV Model		Reduced MV Model	
	β	p	β	p	β	p
Age, per year	−0.12	0.48				
Male	−1.62	0.73				
Any CVD risk factors	−3.71	0.38				
RA duration, per month	−0.0021	0.93				
RF > 40 units	5.75	0.13	1.16	0.74		
Anti-CCP > 20 units	11.51	0.004	7.94	0.038	8.31	0.021
DAS28, per unit	3.82	0.012				
SJC, per joint	1.48	0.005	0.91	0.18	1.01	0.038
TJC, per joint	0.67	0.090	0.091	0.85		
Log SDAI, per unit	1.89	0.60				
Log CRP, per mg/dl	5.30	0.001	3.74	0.016	3.69	0.016
√ESR, per mm/h	1.48	0.095				
Log MMP-3, per ng/ml	8.24	< 0.001	5.12	0.018	5.16	0.015
VAS, per mm	0.13	0.074				
mVAS, per mm	−0.012	0.89				
HAQ, per unit	6.65	0.047	2.87	0.42		
Any DMARD	−3.05	0.51				
MTX	1.24	0.76				
MTX dose, mg	0.42	0.32				
Other DMARD	−0.39	0.94				
Prednisolone	1.28	0.73				
Prednisolone dose, per mg/day	0.81	0.21				
Adjusted R^2			0.239	< 0.001	0.255	< 0.001

β coefficients represent the average difference in baseline QTc interval per 1 unit higher of the indicated independent variable from linear regression modeling. The first column of univariate models represents individual models in which the indicated independent variable is the only covariate in the model. The MV models are single models containing each of the listed covariates. R^2 represents the proportion of the variability of the baseline QTc interval explained by the covariates in the model. MV: multivariable; RA: rheumatoid arthritis; CVD: cardiovascular disease; RF: rheumatoid factor; anti-CCP: anticyclic citrullinated peptide; DAS28: 28-joint count Disease Activity Score; SJC: swollen joint count; TJC: tender joint count; SDAI: Simplified Disease Activity Index; CRP: C-reactive protein; ESR: erythrocyte sedimentation rate; MMP: matrix metalloproteinase; VAS: visual analog scale; mVAS: modified VAS; DMARD: disease-modifying antirheumatic drug; QTc: corrected electrocardiographic QT interval; HAQ: Health Assessment Questionnaire; MTX: methotrexate.

Personal non-commercial use only. The Journal of Rheumatology Copyright © 2016. All rights reserved.

Downloaded from www.jrheum.org on April 24, 2020 - Published by The Journal of Rheumatology

median had a mean baseline QTc of 436 ms compared with 412 ms for those without anti-CCP and SJC, CRP, and MMP-3 all below median levels (p = 0.003; Figure 2). Having any 1, 2, or 3 of these features was associated with progressively longer baseline QTc. Seven of the 22 RA patients with all 4 of the identified indicators of baseline QTc had a baseline QTc > 440 ms (32%) compared with none of those with none of the indicators (p = 0.029, data not shown).

RA patients with the greatest reduction in CRP had the greatest reduction in QTc after TCZ treatment. Although a number of baseline characteristics were univariately associated with the change in QTc (Table 3, univariate models), only the change in CRP and the baseline QTc were significantly associated with the change in QTc when modeled together (Table 3, reduced multivariable model). Together, these 2 characteristics along with age accounted for 44% of the explainable variability in the change in QTc (i.e., $R^2 = 0.438$; $p < 0.001$). Interestingly, clinical responders did not have a greater change in QTc compared with non-responders independent of the change in CRP or baseline QTc, even when more stringent definitions of response were applied (i.e., DAS remission or having a maximum of 1 swollen joint).

Patients with RA who were in the highest tertile of CRP reduction (a reduction of ≥ 4.0 mg/dl) had a 26-ms decrease in QTc, on average, compared with a 14-ms reduction among those in the tertile with the smallest reduction in CRP (+0.09 to −1.0 mg/dl; Figure 3A), a difference that was significant (p = 0.003). Those in the highest tertile of baseline QTc had a nearly 3-fold larger reduction in QTc after treatment compared with those in the lowest tertile of baseline QTc (Figure 3B). Interestingly, among those with a baseline QTc ≥ 440 ms, each 1.0 mg/dl reduction in CRP was associated, on average, with a reduction in QTc of 11.2 ms (p = 0.002) compared with an average reduction in QTc of 3.4 ms for each mg/dl reduction in CRP among those with a baseline QTC < 440 ms (p = 0.001; p value for interaction = 0.039; Figure 3C).

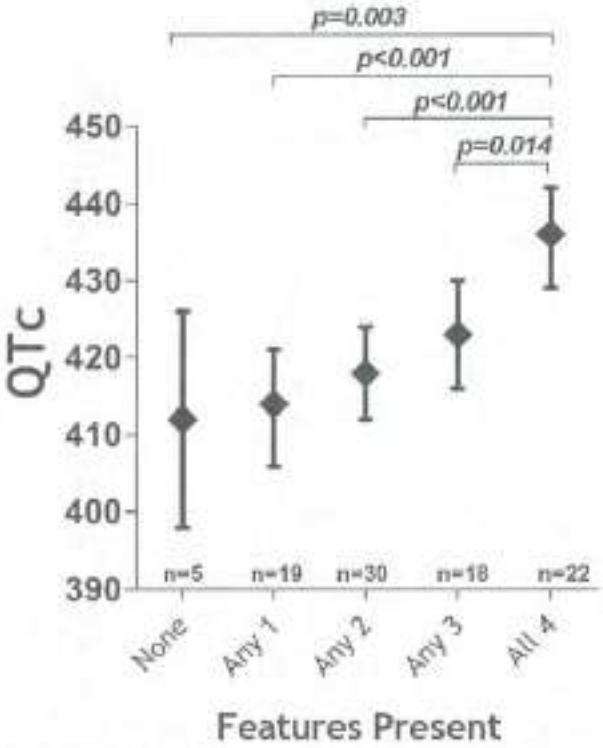

Figure 2. Adjusted baseline QTc according to the number of features present. Means and 95% CI are depicted. The features are the count of those identified from the reduced multivariable model depicted in Table 2. Presence for each feature was designated for anti-CCP > 20 units, swollen joint count above the median of 4 joints, C-reactive protein greater than the median of 2.0 mg/dl, and MMP-3 greater than the median of 150 units. Anti-CCP: anticyclic citrullinated peptide; MMP-3: matrix metalloproteinase 3; QTc: corrected electrocardiographic QT interval.

DISCUSSION

In this, to our knowledge, the largest study to date examining the effect of anticytokine therapy on QTc in RA, we observed a significantly higher QTc among a group of RA patients with a low prevalence of CV risk factors compared with a demographically matched group of non-RA controls. After 24 weeks of treatment with TCZ, QTc was reduced to levels that were significantly lower than those of the control group. The baseline QTc interval was strongly and independently associated with anti-CCP seropositivity, articular swelling, and several circulating inflammatory intermediates (CRP and MMP-3). However, only the change in CRP was a predictor of the change in QTc occurring with TCZ treatment. No other RA features were associated with the change in QTc independent of the change in CRP, including whether the patient had a clinical response to the drug. Interestingly, the association of the change in CRP with the change in QTc was markedly stronger among those with a prolonged baseline QTc.

Prolongation of the QTc interval is an established predictor of arrhythmia and sudden cardiac death in the general population, with moderate (QTc of 420–440 ms) and extensive QTc prolongation (> 440 ms) predictive of all-cause mortality[13]. Sudden cardiac death is also recognized as an important cause of death in patients with RA[1]; however, the pathophysiological mechanisms remain unclear. A strong link to systemic inflammation is suggested by several prior studies. Lazzerini, *et al* demonstrated a significant positive correlation between CRP and QTc duration in a cohort of 101 patients with chronic inflammatory arthritis[6], and this association has been extended to circulating IL-6 levels[14] and other inflammatory cytokines in RA[7]. How elevated circulating inflammatory cytokines prolong QTc is unclear, because they may affect the myocardium directly, or indirectly by increasing central nervous system sympathetic drive on the heart[1].

Personal non-commercial use only. The Journal of Rheumatology Copyright © 2018. All rights reserved.

Downloaded from www.jrheum.org on April 24, 2020 - Published by The Journal of Rheumatology

Table 3. Univariate and multivariable determinants of change in QTc.

Variables	Univariate Models		Extended MV Model		Reduced MV Model	
	β	p	β	p	β	p
Age, per year	0.25	0.16	0.18	0.22	0.20	0.15
Male	−3.08	0.53				
Any CVD risk factors	2.96	0.51				
RA duration, per month	0.026	0.28				
RF > 40 units	−2.88	0.47				
CCP > 20 units	−8.25	0.05	−0.47	0.89		
DAS28, per unit	−3.75	0.02				
SJC, per joint	−1.43	0.011	0.10	0.87		
TJC, per joint	−0.9	0.03	−0.48	0.28		
Log SDAI, per unit	−6.4	0.064				
Log CRP, per mg/dl	−6.35	< 0.001	0.25	0.92		
√ESR, per mm/h	−1.70	0.068				
Log MMP-3, per ng/ml	−8.34	< 0.001	−1.51	0.47		
VAS, per mm	−0.069	0.36				
mVAS, per mm	0.026	0.77				
HAQ, per unit	−6.55	0.055				
Any DMARD	1.98	0.69				
MTX	−2.07	0.62				
MTX dose, mg	−0.43	0.33				
Other DMARD	3.35	0.54				
Prednisolone	−2.26	0.56				
Prednisolone dose, per mg	−0.98	0.16	0.47	0.52		
Change in DAS28, per unit	2.00	0.17				
EULAR good response	1.7	0.72				
Low disease activity	2.95	0.58				
Remission	3.09	0.52				
SJC ≤ 1 joint	−1.02	0.81				
% change	−0.022	0.82				
Change in SDAI, per unit	0.10	0.36				
Change in CRP, per mg/dl	4.95	< 0.001	2.81	0.096	2.92	0.002
Change in ESR, per mm/h	0.15	0.075				
Change in MMP-3, per ng/ml	0.013	0.010	−0.0016	0.77		
Change in VAS, per mm	0.077	0.24				
Change in HAQ, per unit	4.32	0.31				
Stopped prednisolone	−8.05	0.15	−3.52	0.51		
Baseline QTc, per ms	−0.65	< 0.001	−0.51	< 0.001	−0.55	< 0.001
Baseline QTc > 440 ms	−25.6	< 0.001				
Adjusted R^2			0.421	< 0.001	0.438	< 0.001

β coefficients represent the average difference in the change in QTc interval per 1 unit higher of the indicated independent variable from linear regression modeling. The first column of univariate models represent individual models in which the indicated independent variable is the only covariate in the model. The MV models are single models containing each of the listed covariates. R^2 represents the proportion of the variability of the change in QTc interval explained by the covariates in the model. MV: multivariable; RA: rheumatoid arthritis; CVD: cardiovascular disease; RF: rheumatoid factor; anti-CCP: anticyclic citrullinated peptide; DAS28: 28-joint count Disease Activity Score; SJC: swollen joint count; TJC: tender joint count; SDAI: Simplified Disease Activity Index; CRP: C-reactive protein; ESR: erythrocyte sedimentation rate; MMP: matrix metalloproteinase; VAS: visual analog scale; mVAS: modified VAS; DMARD: disease-modifying antirheumatic drug; QTc: corrected electrocardiographic QT interval; HAQ: Health Assessment Questionnaire; MTX: methotrexate; EULAR: European League Against Rheumatism.

Our study confirms these prior findings of a longer QTc associated with higher levels of circulating inflammatory markers, specifically CRP and MMP-3. We also found independent additive effects of SJC and seropositivity for anti-CCP on baseline QTc. Swollen joints are likely representative of additional unmeasured cytokines and inflammatory mediators, and indicative of additional inflammatory burden not determined by CRP or MMP-3. We also observed that anti-CCP–seropositive patients had longer QTc intervals. This could also represent a higher inflammatory burden in these patients, or there may be a direct link between antibodies against citrullinated proteins (ACPA) and the myocardium. In a prior publication[15], we reported markedly higher staining for citrullinated proteins in the myocardial interstitium of patients with RA compared with non-RA controls and controls with systemic sclerosis and myocarditis. How ACPA may interact with the myocardium to prolong the QTc interval is unknown. However, the presence of anti-CCP did not impair the ability of TCZ to reduce QTc in our study after accounting for the change in CRP.

Personal non-commercial use only. The Journal of Rheumatology Copyright © 2018. All rights reserved.

Downloaded from www.jrheum.org on April 24, 2020 - Published by The Journal of Rheumatology

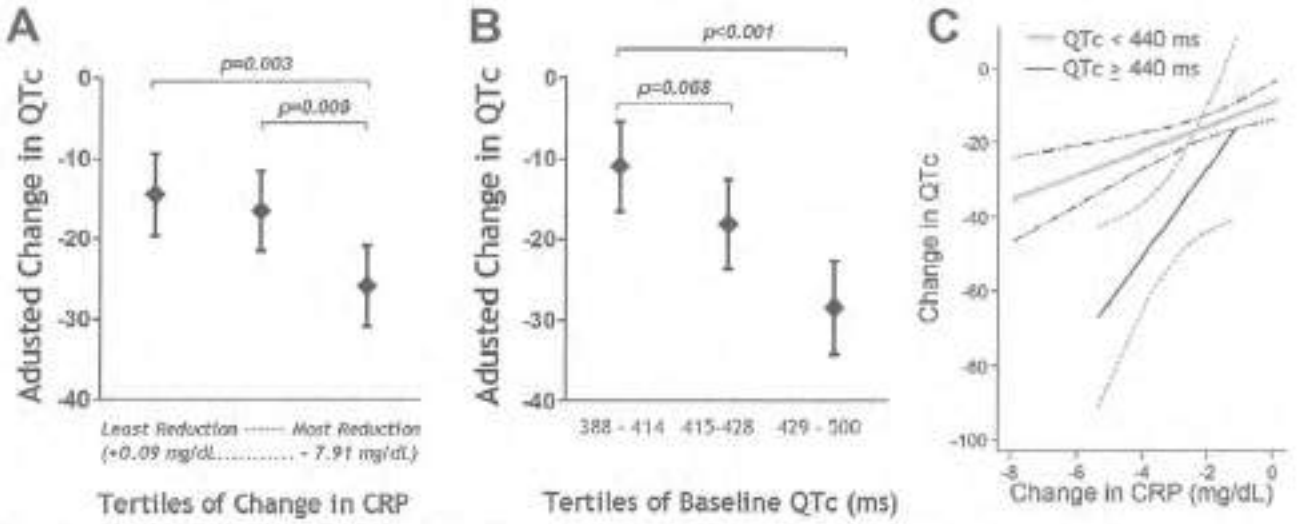

Figure 3. Adjusted change in QTc interval after tocilizumab treatment according to change in CRP and baseline QTc interval. Means and 95% CI are depicted in panels A and B. Panel C depicts a more profound reduction in QTc according to the change in CRP among those with a higher baseline QTc interval (p value for interaction = 0.039). QTc: corrected electrocardiographic QT interval; CRP: C-reactive protein.

Our study also lends additional credence to the concept of IL-6 as a driver of QTc prolongation in RA, because targeted inhibition of IL-6 was associated with a marked reduction in QTc to levels that were even lower than those in the non-RA healthy population controls. This could be through direct inhibition of IL-6, or indirectly through the ability of IL-6 inhibition to reduce other cytokines and inflammatory mediators in RA. Our study expands on the findings of a pilot study[8] in which a decrease in QTc was observed in 17 patients with RA after 12 weeks of TCZ treatment and was sustained to 24 weeks. Interestingly, this effect was independent of clinical response to TCZ, suggesting that the effect of TCZ on QTc is unrelated to its immunomodulating effect on synovitis. The ability of TCZ to reduce QTc to a level well below that found in healthy controls was somewhat unexpected. However, because the mechanism linking circulating IL-6 to QTc prolongation is likely not restricted to RA, it is possible, albeit speculative, that IL-6 inhibition in the general population may also have the effect of QTc reduction to the level we observed in the TCZ-treated patients with RA[16].

The mechanism by which IL-6 inhibition reduced QTc is unclear. Previously, we reported that TCZ treatment significantly decreased left ventricular hypertrophy and normalized the aberrant left ventricular morphology that was associated with disease activity[17]. It is reasonable to posit that remodeling the myocardium to a more normalized structure may lead to QTc normalization. Additionally, an increasing body of evidence implicates macrophage-derived inflammatory cytokines, including tumor necrosis factor, IL-1, and IL-6, in electrophysiologic changes in cardiomyocytes, resulting in electrical remodeling of the heart that may predispose to prolonged QTc and ventricular arrhythmia (reviewed in Lazzerini, *et al*[18]). These include impaired potassium channel function[19,20,21,22] and enhanced calcium channel function[23,24] in cardiomyocytes, leading to prolongation of the cardiomyocyte action potential duration. Whether reduction of macrophage-derived cytokines with IL-6 inhibition is capable of reversing this electrical remodeling in RA warrants further study. Because the effect of TCZ on QTc was observed as early as 12 weeks in the pilot study by Lazzerini, *et al*[8], it seems likely that the effect is mediated through electrical remodeling rather than structural remodeling, at least initially.

Our study has notable strengths and limitations. Among the strengths, the robust decline in QTc associated with decreasing CRP is a strong indicator of causality. However, without a comparison to untreated controls or a group treated with an immunomodulator targeting a different cytokine, we cannot assert that the observed normalization of QTc was not a natural phenomenon or that it is specific to IL-6 inhibition. In addition, IL-6 is the major cytokine determinant of hepatic CRP production. Thus, CRP may not be reflective of overall systemic inflammation in the setting of targeted IL-6 inhibition. While we focused on ECG as a marker of CVD, the ECG lacks specificity to detect early/preclinical myocardial lesions. We did not have additional imaging or advanced electrophysiological assessments to examine the mechanisms whereby IL-6 inhibition normalizes TCZ; however, based on our findings, such studies are certainly warranted and could prove useful not only to the study of arrhythmia in RA, but also for the general population. Finally, medications known to prolong QTc were not part of our data collection. However, for these to have impugned the differences detected they would have to have been markedly unbalanced between the RA and control groups and changed after TCZ treatment among enough patients with RA to normalize

Personal non-commercial use only. The Journal of Rheumatology Copyright © 2018. All rights reserved.

Downloaded from www.jrheum.org on April 24, 2020 - Published by The Journal of Rheumatology

the QTc of the entire group. Such a scenario is unlikely to account for the magnitude of the differences and changes detected.

The marked normalization of QTc observed with TCZ treatment, and its close parallel with CRP reduction, support the premise that systemic inflammation contributes to cardiac repolarization abnormalities in RA that may be amenable to treatment, and suggest an antiarrhythmic effect of IL-6 inhibition that may be beneficial for patients with RA. Our data provide further evidence of the close link between RA autoimmunity, inflammation, and cardiac repolarization that may contribute to the known higher CVD risk in this population. Further investigation is warranted to evaluate the effect of TCZ on arrhythmia and sudden cardiac death in RA.

ACKNOWLEDGMENT

The authors thank all the clinical engineers, and the hematology and rheumatology staff at Nihon University School of Medicine Hospital for their assistance.

REFERENCES

1. Maradit-Kremers H, Crowson CS, Nicola PJ, Ballman KV, Roger VL, Jacobsen SJ, et al. Increased unrecognized coronary heart disease and sudden deaths in rheumatoid arthritis: a population-based cohort study. Arthritis Rheum 2005;52:402-11.
2. Huikuri HV, Castellanos A, Myerburg RJ. Sudden death due to cardiac arrhythmias. N Engl J Med 2001;345:1473-82.
3. Montanez A, Ruskin JN, Hebert PR, Lamas GA, Hennekens CH. Prolonged QTc interval and risks of total and cardiovascular mortality and sudden death in the general population: a review and qualitative overview of the prospective cohort studies. Arch Intern Med 2004;164:943-8.
4. Chauhan K, Ackerman MJ, Crowson CS, Matteson EL, Gabriel SE. Population-based study of QT interval prolongation in patients with rheumatoid arthritis. Clin Exp Rheumatol 2015;33:84-9.
5. Panoulas VF, Toms TE, Douglas KM, Sandoo A, Metsios GS, Stavropoulos-Kalinoglou A, et al. Prolonged QTc interval predicts all-cause mortality in patients with rheumatoid arthritis: an association driven by high inflammatory burden. Rheumatology 2014;53:131-7.
6. Lazzerini PE, Acampa M, Capecchi PL, Hammoud M, Maffei S, Bisogno S, et al. Association between high sensitivity C-reactive protein, heart rate variability and corrected QT interval in patients with chronic inflammatory arthritis. Eur J Int Med 2013;24:368-74.
7. Adlan AM, Panoulas VF, Smith JP, Fisher JP, Kitas GD. Association between corrected QT interval and inflammatory cytokines in rheumatoid arthritis. J Rheumatol 2015;42:421-8.
8. Lazzerini PE, Acampa M, Capecchi PL, Fineschi I, Selvi E, Moscadelli V, et al. Antiarrhythmic potential of anticytokine therapy in rheumatoid arthritis: tocilizumab reduces corrected QT interval by controlling systemic inflammation. Arthritis Care Res 2015;67:332-9.
9. Aletaha D, Neogi T, Silman AJ, Funovits J, Felson DT, Bingham CO 3rd, et al. 2010 rheumatoid arthritis classification criteria: an American College of Rheumatology/European League Against Rheumatism collaborative initiative. Arthritis Rheum 2010; 62:2569-81.
10. Prevoo ML, van 't Hof MA, Kuper HH, van Leeuwen MA, van de Putte LB, van Riel PL. Modified disease activity scores that include twenty-eight-joint counts. Development and validation in a prospective longitudinal study of patients with rheumatoid arthritis. Arthritis Rheum 1995;38:44-8.
11. Fransen J, van Riel PL. The Disease Activity Score and the EULAR response criteria. Rheum Dis Clin North Am 2009;35:745-57.
12. Algra A, Tijssen JG, Roelandt JR, Pool J, Lubsen J. QTc prolongation measured by standard 12-lead electrocardiography is an independent risk factor for sudden death due to cardiac arrest. Circulation 1991;83:1888-94.
13. Straus SM, Kors JA, De Bruin ML, van der Hooft CS, Hofman A, Heeringa J, et al. Prolonged QTc interval and risk of sudden cardiac death in a population of older adults. J Am Coll Cardiol 2006;47:362-7.
14. Lazzerini PE, Capecchi PL, Bertolozzi I, Moruzzi G, Lorenzini S, Simpatico A, et al. Marked QTc prolongation and torsades de pointes in patients with chronic inflammatory arthritis. Front Cardiovasc Med 2016;3:31.
15. Giles JT, Fert-Bober J, Park JK, Bingham CO 3rd, Andrade F, Fox-Talbot K, et al. Myocardial citrullination in rheumatoid arthritis: a correlative histopathologic study. Arthritis Res Ther 2012;14:R39.
16. Lazzerini PE, Laghi-Pasini F, Bertolozzi I, Morozzi G, Lorenzini S, Simpatico A, et al. Systemic inflammation as a novel QT-prolonging risk factor in patients with torsades de pointes. Heart 2017;103:1821-9.
17. Kobayashi H, Kobayashi Y, Giles JT, Yoneyama K, Nakajima Y, Takei M. Tocilizumab treatment increases left ventricular ejection fraction and decreases left ventricular mass index in patients with rheumatoid arthritis without cardiac symptoms: assessed using 3.0 tesla cardiac magnetic resonance imaging. J Rheumatol 2014;41:1916-21.
18. Lazzerini PE, Capecchi PL, Laghi-Pasini F. Systemic inflammation and arrhythmic risk: lessons from rheumatoid arthritis. Eur Heart J 2017;38:1717-27.
19. Fernandez-Velasco M, Ruiz-Hurtado G, Hurtado O, Moro MA, Delgado C. TNF-alpha downregulates transient outward potassium current in rat ventricular myocytes through iNOS overexpression and oxidant species generation. Am J Physiol Heart Circ Physiol 2007;293:H238-45.
20. Petkova-Kirova PS, Gursoy E, Mehdi H, McTiernan CF, London B, Salama G. Electrical remodeling of cardiac myocytes from mice with heart failure due to the overexpression of tumor necrosis factor-alpha. Am J Physiol Heart Circ Physiol 2006;290:H2098-107.
21. Wang J, Wang H, Zhang Y, Gao H, Nattel S, Wang Z. Impairment of HERG K(+) channel function by tumor necrosis factor-alpha: role of reactive oxygen species as a mediator. J Biol Chem 2004;279:13289-92.
22. Monnerat G, Alarcón ML, Vasconcellos LR, Hochman-Mendez C, Brasil G, Bassani RA, et al. Macrophage-dependent IL-1β production induces cardiac arrhythmias in diabetic mice. Nature Com 2016;7:13344.
23. Hagiwara Y, Miyoshi S, Fukuda K, Nishiyama N, Ikegami Y, Tanimoto K, et al. SHP2-mediated signaling cascade through gp130 is essential for LIF-dependent I CaL, [Ca2+]i transient, and APD increase in cardiomyocytes. J Mol Cell Cardiol 2007;43:710-6.
24. Li YH, Rozanski GJ. Effects of human recombinant interleukin-1 on electrical properties of guinea pig ventricular cells. Cardiovasc Res 1993;27:525-30.

Personal non-commercial use only. The Journal of Rheumatology Copyright © 2018. All rights reserved.

Downloaded from www.jrheum.org on April 24, 2020 - Published by The Journal of Rheumatology

Journal of Echocardiography (2018) 16:162–172
https://doi.org/10.1007/s12574-018-0383-7

ORIGINAL INVESTIGATION

Geometry of the left ventricular outflow tract assessed by 3D TEE in patients with aortic stenosis: impact of upper septal hypertrophy on measurements of Doppler-derived left ventricular stroke volume

Dan Koto[1] · Masaki Izumo[1] · Takafumi Machida[2] · Kengo Suzuki[1] · Kihei Yoneyama[1] · Tomomi Suzuki[1] · Ryo Kamijima[1] · Yasuyuki Kobayashi[3] · Tomoo Harada[1] · Yoshihiro J. Akashi[1]

Received: 25 December 2017 / Revised: 14 May 2018 / Accepted: 19 May 2018 / Published online: 24 May 2018
© Japanese Society of Echocardiography 2018

Abstract

Background It is unclear how upper septal hypertrophy (USH) affects Doppler-derived left ventricular stroke volume (SV) in patients with AS. The aims of this study were to: (1) validate the accuracy of 3D transesophageal echocardiography (TEE) measurements of the left ventricular outflow tract (LVOT), (2) evaluate the differences in LVOT geometry between AS patients with and without USH, and (3) assess the impact of USH on measurement of SV.

Methods In protocol 1, both 3D TEE and multi-detector computed tomography were performed in 20 patients with AS [aortic valve area (AVA) ≤ 1.5 cm^2]. Multiplanar reconstruction was used to measure the LVOT short and long diameters in four parts from the tip of the septum to the annulus. In protocol 2, the same 3D TEE measurements were performed in AS patients (AVA ≤ 1.5 cm^2, $n=129$) and controls ($n=30$). We also performed 2D and 3D transthoracic echocardiography in all patients.

Results In protocol 1, excellent correlations of LVOT parameters were found between the two modalities. In protocol 2, the USH group had smaller LVOT short and long diameters than the non-USH group. Although no differences in mean pressure gradient, or SV calculated with the 3D method existed between the two groups, the USH group had greater SV calculated with the Doppler method (73 ± 15 vs. 66 ± 15 ml) and aortic valve area (0.89 ± 0.26 vs. 0.73 ± 0.24 cm^2) than the non-USH group.

Conclusions 3D TEE can provide a precise assessment of the LVOT in AS. USH affects the LVOT geometry in patients with AS, which might lead to inaccurate assessments of disease severity.

Keywords Aortic valve stenosis · Echocardiography · Three-dimensional echocardiography · Transesophageal echocardiography

Introduction

From a public health perspective, valvular heart disease, which has a poor prognosis, affects entire communities, and presents an important public health problem in developed countries [1]. Aortic stenosis (AS) is the most common form of valvular heart disease in developed countries and its prevalence is increasing along with the aging population [1–4]. AS is detected in 2–7% of adults aged 65 years and older and characterized by degenerative calcification and congenital valvular defects [1–4]. The accurate assessment of disease severity is critical for the appropriate treatment of patients with AS. Conventional two-dimensional (2D) transthoracic echocardiography (TTE) is the standard approach for evaluating aortic valve area (AVA) calculated by the continuity equation method. AVA derived from continuity equation method relies on geometric assumptions of the left ventricular (LV) outflow tract (LVOT) area, which can amplify errors, particularly in the presence of upper septal hypertrophy (USH). USH, which increases the LVOT velocity, is relatively common in the elderly. However, it is not clear how USH can affect continuity-equation-derived AVA from TTE results in patients with AS. The recently

✉ Masaki Izumo
heartizumo@yahoo.co.jp

[1] Division of Cardiology, Department of Internal Medicine, St. Marianna University School of Medicine, 2-16-1 Sugao, Miyamae-ku, Kawasaki 216-8511, Japan

[2] Department of Pharmacology, St. Marianna University School of Medicine, Kawasaki, Japan

[3] Department of Radiology, St. Marianna University School of Medicine, Kawasaki, Japan

developed three-dimensional (3D) transesophageal echocardiography (TEE) has been a preferred method for the evaluation of aortic root geometry because of its greater accuracy than two-dimensional (2D) TTE and 2D TEE. Earlier studies evaluated the geometry of the aortic root from the aortic annulus to the sinotubular junction; however, the LVOT geometry was not fully elucidated [5–10]. We hypothesized that AS patients with USH have a greater stroke volume (SV) due to increased LVOT velocity despite less LVOT velocity of 1.5 m/s than the AS patients without USH and that this leads to the overestimation of AVA calculated using the continuity equation.

The aims of this study were to: (1) validate the accuracy of 3D TEE measurements of LVOT against multi-detector computed tomography (MDCT) measurements as a reference, (2) evaluate the geometric differences in LVOT geometry between AS patients with and without USH, and (3) assess the impact of USH on the measurement of SV.

Methods

Study population

In protocol 1, 20 patients with AS (AVA ≤ 1.5 cm^2) who underwent both MDCT and 3D TEE within 1 month were retrospectively enrolled. Patients allergic to iodine contrast agents and those at high risk for contrast nephropathy were excluded from the analysis. In protocol 2, a total of 152 patients with more-than-moderate AS measured using continuity equation method (AVA < 1.5 cm^2), who underwent TEE between November 2011 and April 2014 and 30 controls were prospectively enrolled. Patients with poor quality images ($n = 5$, 3.3%), atrial fibrillation ($n = 16$, 10.5%), moderate or severe mitral regurgitation ($n = 0$, 0%), and high LVOT velocity (> 1.5 m/s; $n = 2$, 1.3%) were excluded from the study population. Finally, 129 AS patients and 30 controls were enrolled. The inclusion criteria for the controls in this study were: (1) no significant valvular heart disease, (2) preserved LVEF (≥ 60%), (3) no left ventricular wall motion abnormalities, and (4) no dilated left ventricle. This group was identified from the patients undergoing clinically indicated TEE for investigating a cardioembolic source of stroke. This study was approved by the institutional review board at St. Marianna University School of Medicine. All patients gave their written informed consent before study enrollment.

MDCT

Twenty patients underwent retrospective electrocardiographically gated conventional scans with tube current dose modulation using an MDCT scanner (Aquilion ONE ViSION Edition, Toshiba Medical Systems, Odawara, Japan). This system was equipped with 320-row detector arrays. Computed tomography was performed with a slice thickness of 0.5 mm, tube voltage of 120 kV, and maximum tube current of 580 mA with a gantry rotation time of 275 ms. The voltage was occasionally reduced to 100 kV in patients with thin chests. All patients with heart rates > 65 beats per minute received 10 mg propranolol hydrochloride or 0.125 mg/kg landiolol hydrochloride.

2D and 3D TEE

TEE was performed using an iE33 ultrasound imaging system (Philips Medical Systems, Andover, MA) equipped with a fully sampled matrix array TEE transducer that can display both 2D and live 3D images. After the application of topical anesthetics in the pharynx and intravenous sedation (propofol), the probe was advanced into the esophagus. The aortic valve was visualized from the mid-esophageal position in the zoomed 2D long-axis view (approximately 135°). The 3D full-volume mode of the entire left ventricle, including the aortic root, was then acquired in four consecutive cardiac cycles (frame rate, 23 ± 5 frame/s; range 16–34 frame/s) and stored digitally. The acquisition was triggered with an electrocardiogram R-wave.

MDCT measurements of LVOT

The standard orthogonal axial and sagittal views were used for the initial orientation of the LVOT. The LVOT short and long diameters and areas were analyzed in the coronal, sagittal, and double-oblique transverse views (Fig. 1a). Image reconstruction was performed in 5% intervals from R-wave to R-wave; all 20 phases were loaded into an external workstation. For the LVOT measurements, mid-systolic data sets (20 or 30% of the RR interval) were used. The LVOT from the tip of the septum to the aortic annulus was equally sliced into four parts and each parameter was measured (LVOT 1 = tip of the septum, LVOT 4 = the aortic annulus). These measurements were performed using commercial software (zioTerm2009; Ziosoft Inc, Tokyo, Japan).

3D TEE measurements of LVOT

From the full-volume mode 3D data sets, the two orthogonal long-axis views of LVOT were extracted. A third plane, which was perpendicular to the two long-axis planes, was shifted to adjust the orthogonal 2D cutting plane of the LVOT with quantitative software (QLAB cardiac 3DQ, Philips Medical Systems, Andover, MA, USA). After selecting the mid-systolic frame in which maximal LVOT was visualized, the multiplanar reconstruction planes were aligned at each level of the LVOT to measure the LVOT short and

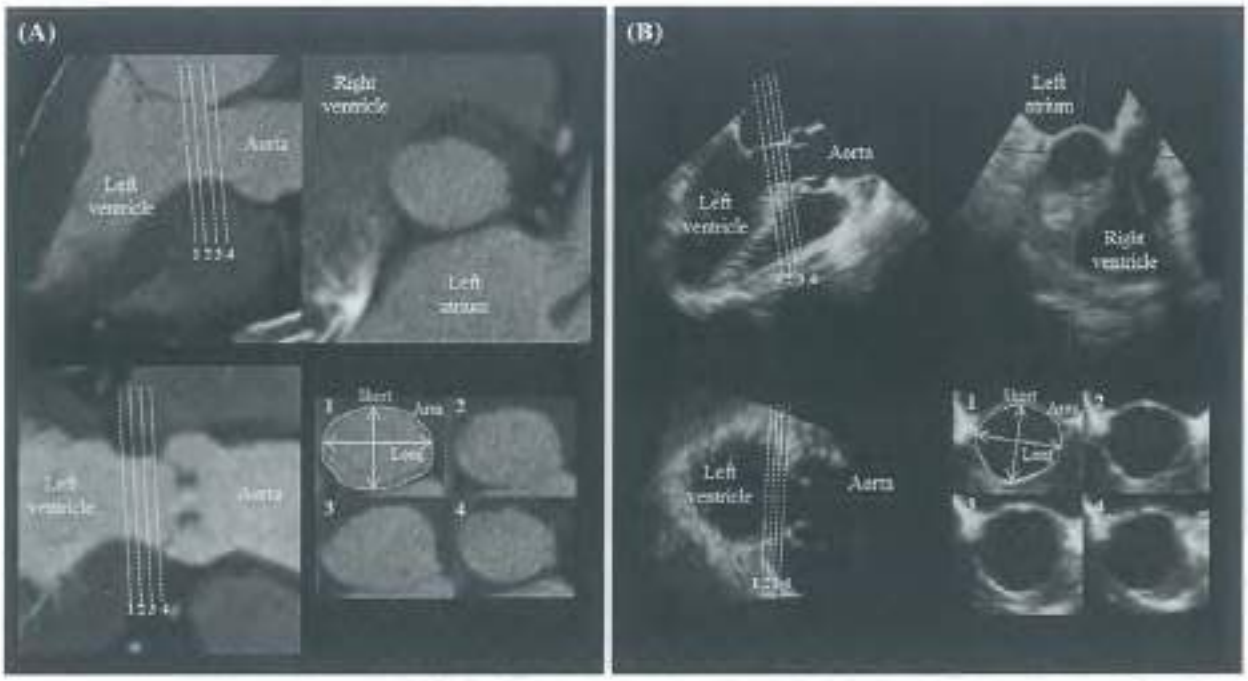

Fig. 1 Left ventricular outflow tract (LVOT) assessed using (a) multi-detector computed tomography (MDCT) and b three-dimensional (3D) transesophageal echocardiography (TEE)

long axis diameters and areas (LVOT 1 = tip of the septum, LVOT 4 = the aortic annulus, Fig. 1b). The LVOT sphericity index (shot/long diameter) was also assessed.

2D TTE

Comprehensive TTE, including 2D and Doppler echocardiography, was performed using commercially available ultrasound equipment according to the American Society of Echocardiography guidelines within 1 week before and after TEE [11]. The aortic valve jet velocity was recorded from the multiple acoustic windows to obtain the highest velocity signal. The AVA was calculated using the time–velocity integral of the aortic valve (AV) and LVOT spectral curves in the standard continuity equation. SV was determined using the velocity–time integral (VTI) from pulsed wave Doppler echocardiography at the LVOT × LV outflow area, which was determined using the following formula: $3.14 \times (\text{LVOT diameter}/2)^2$. The LVOT diameters were measured carefully using the zoom mode of the parasternal long-axis view in mid-systole from the black-and-white interface at the level of the aortic annulus [12]. LVOT velocity was recorded with pulsed Doppler using an apical approach in the 5-chamber view or in the apical long-axis view. The pulsed Doppler sample volume was positioned just proximal to the aortic valve with a length of 3–5 mm. The relative wall thickness was estimated as 2 × (diastolic LV posterior wall thickness)/LV end-diastolic diameter [13]. The LV mass was calculated using linear measurement. The maximum left atrial volume was measured according to the biplane Simpson's method and indexed to the body surface area. The peak early and late diastolic velocities of LV inflow (E and A velocity), deceleration time of early diastolic velocity, and peak early diastolic velocity on the septal corner of the mitral annulus (E') were measured in the apical four-chamber view. The ratio of the upper septal wall thickness to the mid-septum wall thickness in diastole was measured to determine the degree of USH. USH was defined according to the following criteria: (1) upper septum knuckle evaluated by visual assessment, (2) upper interventricular septum thickness ≥ 1.4 cm, and (3) ratio of upper septal wall thickness to mid-septal wall thickness ≥ 1.3 (Fig. 2) [14, 15].

3D TTE

3D TTE was also performed using an iE33 scanner (Philips Medical Systems) equipped with fully sampled matrix-array transducer (X3-1) for 3D data acquisition in AS patients and controls. Full-volume data sets were acquired from the apical transducer position during held respiration. To ensure the inclusion of the entire LV volumes within the pyramidal scan volume with a relatively higher volume rate, data sets throughout one cardiac cycle were acquired using the wide-angle mode, wherein four wedge-shaped sub-volumes were

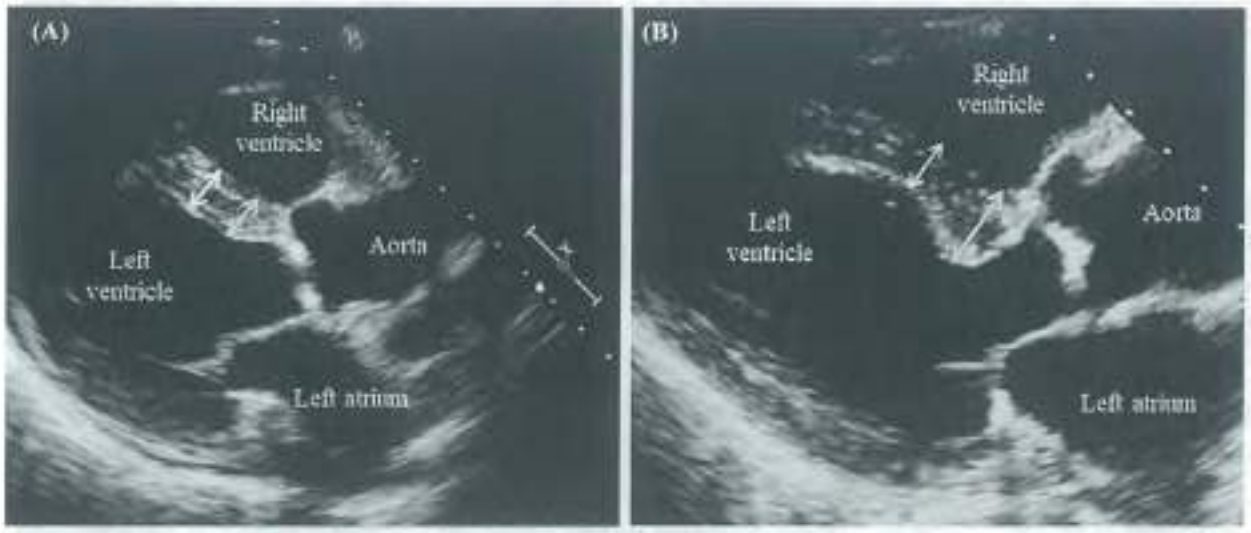

Fig. 2 Example cases of non-upper septal hypertrophy (a) and upper septal hypertrophy (b) in aortic stenosis. Case A met none of the following USH criteria: (1) upper septum knuckle evaluated with visual assessment, (2) upper interventricular septum thickness of ≥ 1.4 cm (1.1 cm), and (3) ratio of upper septal wall thickness to mid-septal wall thickness of ≥ 1.3 (1.0). Case B met all the following USH criteria: (1) upper septum knuckle evaluated with visual assessment, (2) upper interventricular septum thickness of ≥ 1.4 cm (1.5 cm), and 3) ratio of upper septal wall thickness to mid-septal wall thickness of ≥ 1.3 (1.4). White arrow: mid-septal wall thickness. Yellow arrow: upper septal wall thickness

acquired with electrocardiographic gating during a single 5–7-s breath hold. A 3D volumetric assessment of LV was performed according to the biplane Simpson's method using data extracted from 3D data sets with commercially available quantitative software (3DQ, QLAB, version 9.0, Philips Medical Systems, Andover, MA).

Statistical analysis

The results are expressed as mean ± standard deviation (SD) or percentage unless otherwise specified. Data for the USH and non-USH groups were compared using Student's *t* test, Chi-squared test, or Fisher's exact test as appropriate. Differences were considered significant if $P < 0.05$. Pearson's correlation coefficient was used to evaluate the correlation between two parameters. Bland–Altman plots were used to evaluate differences in LVOT areas using 3D TEE and MDCT. The mean differences and limits of agreement were reported. Bland–Altman plots were also used to evaluate differences in SV between Doppler and 3D methods. Both the interobserver and intraobserver variabilities for LVOT areas measured with 3D TEE and MDCT were obtained according to blinded analysis of 10 random images by two independent observers at two different time points. The results were analyzed using both an intraclass correlation coefficient for absolute agreement (ICCa) and the Bland–Altman method. Statistical analyses were performed with SPSS 22.0 software (SPSS, Inc, Chicago, IL, USA).

Results

Protocol 1

The LVOT parameters were successfully measured on MDCT and 3D TEE in all patients. Baseline and echocardiographic findings in this protocol are summarized in Table 1. Figure 3 shows the linear correlation and Bland–Altman plot between MDCT and 3D TEE measurements in each LVOT area. All LVOT areas measured using 3D TEE were slightly, but significantly smaller than those measured using MDCT; however, a favorable correlation was found between the two imaging modalities (Fig. 3, $r = 0.846$–0.941).

Protocol 2

Comparisons in LVOT geometry between the three groups

The baseline characteristics are summarized in Table 2. Of the study patients, 64 were men (49.6%). The mean age of patients was 75 ± 9 years (range, 55–89 years), and 41 of them had USH (31.8%). No differences in the demographic findings without the prevalence of coronary artery disease were found between the USH and non-USH groups. Moreover, no differences in the prevalence of left ventricular asynergy or scar in antero-septal area were found between the two groups (6.8 vs. 4.9%, $P = 0.523$). The LVOT geometries in the three groups are shown in Table 3. No differences in LVOT short and long

Table 1 Baseline and echocardiographic characteristics in protocol 1 ($n=20$)

Variable	($N=20$)
Clinical characteristics	
Age (years)	80±8
Male (%)	51
Height (cm)	154±10
Body weight (kg)	54±10
BSA (m^2)	1.51±0.18
Systolic BP (mmHg)	120±31
Diastolic BP (mmHg)	70±19
HR (bpm)	72±15
Echocardiographic findings	
AVA (cm^2)	0.68±0.26
Indexed AVA (cm^2/m^2)	0.45±0.16
Peak velocity (m/s)	4.0±1.2
Mean PG (mm Hg)	44±32
Severe (AVA ≤ 1.0 cm^2) n (%)	18 (90%)
SV_{Dopp} (ml)	67±20
SVI_{Dopp} (ml/m^2)	44±13
LVMI (g/m^2)	117±33
LVDd (mm)	47±7
LVDs (mm)	30±7
EDV (ml)	96±34
ESV (ml)	43±31
LVEF (%)	62±15
RVSP (mm Hg)	37±16
E/A	0.94±0.96
E/E'	17.0±9.6

BP blood pressure; *HR* heart rate; *AVA* aortic valve area; *PG* pressure gradient; *SV* stroke volume; *SVI* stroke volume index; *LVMI* left ventricular mass index; *LVDd* left ventricular end-diastolic diameter; *LVDs* left ventricular end-systolic diameter; *EDV* end-systolic volume; *ESV* end-systolic volume; *RVSP* right ventricular systolic pressure

diameters, area or shape were found between the non-USH group and controls. Although the USH group had smaller short and long diameters, smaller LVOT area, and lower sphericity index than the non-USH group at LVOT 1, the tip of the septum, and LVOT 2, no significant differences in LVOT area and the sphericity index at LVOT-3 and -4 or the aortic annulus were observed between the two groups. The valve annulus of peripheral side (LVOT-3 or -4) was larger than that of the left ventricle central side (LVOT-1 or -2) in the controls and non-USH group, whereas the left ventricle side was smaller than the valve annulus in the USH group. The representative cases are shown in Fig. 4.

Impact of USH on measurement of left ventricular SV and AVA

The results of standard 2D TTE are shown in Table 2. No significant difference in the measured SV was found between Doppler echocardiography and 3D TTE in the controls (58±9 vs. 55±16 ml, $P=0.314$) and the non-USH group (56±15 vs. 56±16 ml, $P=0.264$; Fig. 5). However, the USH group revealed a significantly greater SV calculated with the Doppler method than that obtained with the 3D TTE method (Fig. 5). Moreover, no differences in peak velocity or mean pressure gradient between the USH and the non-USH groups were found; however, the USH group had greater AVA than the non-USH group (0.89±0.26 vs. 0.73±0.24 cm^2, $P=0.002$).

Reproducibility

The intraobserver variabilities assessed using the ICCs were 0.89–0.93 for LVOT areas measured with 3D TEE and 0.90–0.94 for LVOT areas measured with MDCT. The interobserver variabilities were 0.87–0.92 for LVOT areas measured with 3D TEE and 0.88–0.93 for LVOT areas measured with MDCT. The Bland–Altman method showed that interobserver and intraobserver variabilities were 0.32±0.10 and 0.34±0.11 cm^2 for the LVOT areas measured with 3D TEE, and 0.30±0.11 and 0.32±0.10 cm^2 for the LVOT areas measured with MDCT, respectively.

Discussion

The main findings of this study were as follows: (1) the LVOT parameters obtained by 3D TEE were well-correlated with those by MDCT, (2) more than 30% AS patients had USH, (3) USH affected not distal, but proximal LVOT geometry, and (4) the Doppler method overestimated SV in AS patients with USH, which might lead to an underestimation of the AS severity.

Comparison of LVOT morphology between the USH and non-USH groups

The evaluation of aortic root geometry is increasingly important for decision-making in patients with AS and usually performed using MDCT [6–10, 16]. The earlier studies defined the aortic root from the aortic annulus to the sinotubular junction, not including LVOT [5–10]. 3D imaging techniques have provided the unique anatomic views of cardiac structures and improved the definitions of spatial relation in complex abnormalities. To the best of our knowledge, this study first reports the use of 3D TEE to compare the LVOT geometry in AS patients with and without

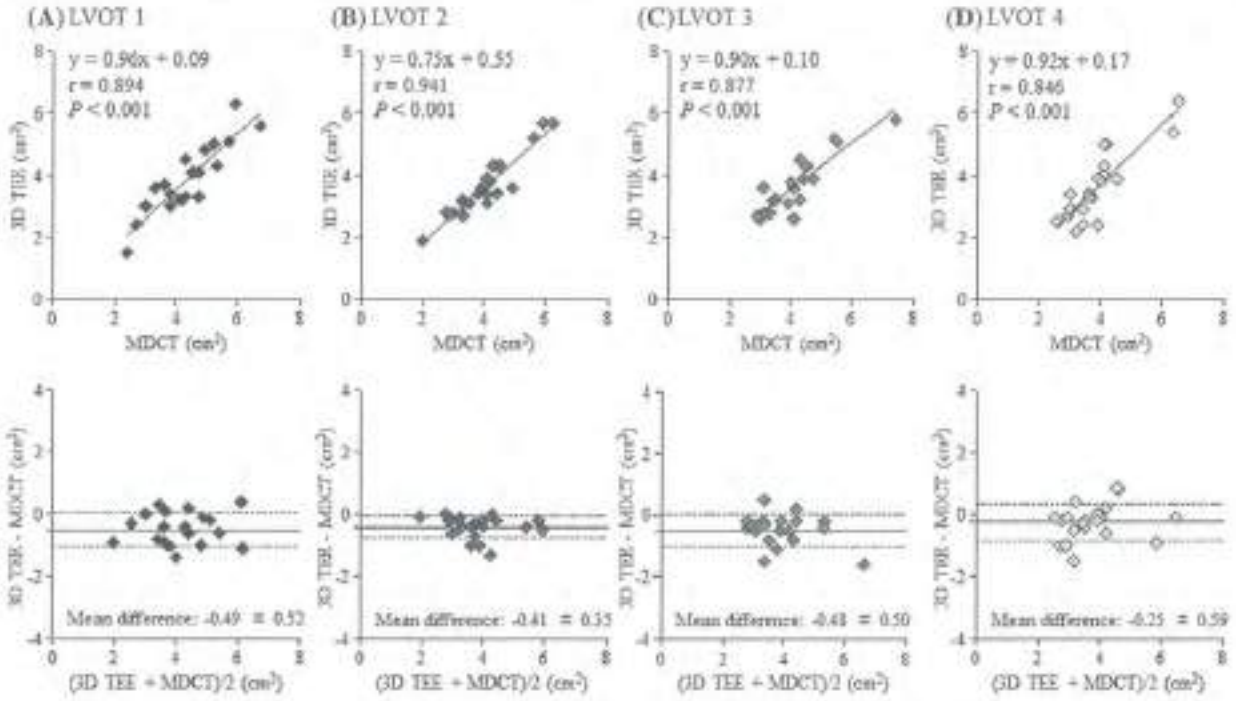

Fig. 3 Linear correlations (upper panel) and Bland–Altman analysis (lower panel) of LVOT parameters on MDCT and 3D TEE. **a** LVOT 1, **b** LVOT 2, **c** LVOT 3, and **d** LVOT 4

USH as well as controls. The LVOT areas measured with 3D TEE were slightly, but significantly smaller than those with MDCT; the results of our study consisted with those of earlier studies [6–10, 16]. This underestimation might be related with lower temporal resolution of 3D TEE images. The presence of calcification might also affect smaller 3D TEE planimetric measurements. The USH group revealed shorter LVOT short diameters and smaller areas at the tip of the septum than the non-USH group, resulting in a more elliptical LVOT shape. Our study result was consistent with the result of an earlier study demonstrating an association between the sigmoid-shaped septum versus the left ventricle and the ascending aorta, which might lead to shorter anterior–posterior diameters (short-diameter) and more elliptical shape of the LVOT [15].

Associations between LVOT geometry and Doppler-derived SV

The primary parameters proposed for the clinical evaluation of AS severity are: (1) peak velocity, (2) mean pressure gradient, and (3) AVA calculated with the continuity equation. Some recent studies have reported decreased peak velocity and mean pressure gradient regardless of ejection fraction [17–19]; thus, AVA calculated by the continuity equation is vital in the assessment of disease severity. The calculation of the valve area by the continuity equation requires three measurements as follows: (1) AS jet velocity evaluated with continuous wave Doppler, (2) LVOT diameters for the calculation of a circular cross-sectional area, and (3) LVOT velocity recorded with pulsed Doppler echocardiography. Its pitfalls are well-known due to inherent assumptions and simplifications. Some studies demonstrated that the calculations of continuity equation-derived AVA using 2D TTE underestimated AVA because of the elliptical shape of LVOT with its shorter anteroposterior diameters [20, 21]. Garcia, et al. conducted a subsequent assessment study using multimodal imaging and reported that the underestimation of LVOT area with TTE was compensated by the overestimation of LVOT VTI, thereby resulting in a good concordance between TTE and cardiac magnetic resonance for the estimation of AVA [22]. In our study, no difference in SV was found between the Doppler and 3D TTE methods in the non-USH group; however, the USH group had greater SV calculated by Doppler echocardiography than 3D TTE because of the greater VTI in this group. This difference is assumed not due to an oval-shaped LVOT, but faster blood flow in the USH group. Figure 6 shows the prevalence of a low-flow status (SV index, ≤ 35 ml/m^2) in the non-USH and USH groups. No significant differences in the prevalence of the low-flow status between the two methods were found in the non-USH group (19.5 vs. 23.7%, $P = 0.624$); however,

Table 2 Baseline characteristics

	Controls ($N=30$)	Non-USH ($N=88$)	USH ($N=41$)	P value non-USH versus USH	P value non-USH versus controls	P value USH versus controls
Clinical characteristics						
Age (years)	61±13	74±10	76±9	0.214	<0.001	<0.001
Male n (%)	22 (54)	47 (53)	17 (42)	0.174	0.519	0.321
BSA (m^2)	1.65±0.18	1.53±0.17	1.54±0.19	0.889	0.022	0.016
Systolic BP (mmHg)	128±26	129±26	136±24	0.927	0.928	0.137
Diastolic BP (mmHg)	75±15	74±15	73±15	0.911	0.133	0.414
Heart rate (bpm)	70±14	73±20	70±12	0.912	0.718	0.882
Hemoglobin (g/dl)	13.6±6.6	13.7±6.5	14.8±4.3	0.567	0.933	0.213
Medical history n (%)						
Hypertension	–	52 (59)	30 (73)	0.128	–	–
Dyslipidemia	–	23 (34)	15 (37)	0.913	–	–
Diabetes mellitus	–	25 (28)	12 (29)	0.788	–	–
Coronary artery disease	–	29 (33)	6 (15)	0.009	–	–
Chronic kidney disease	–	27 (31)	15 (37)	0.824	–	–
2D transthoracic echocardiographic findings						
AVA (cm^2)	–	0.73±0.24	0.89±0.26	0.002	–	–
Indexed AVA (cm^2/m^2)	–	0.46±0.21	0.58±0.15	0.003	–	–
Peak velocity (m/s)	–	4.0±1.1	4.1±0.9	0.172	–	–
Mean PG (mm Hg)	–	39±25	33±18	0.115	–	–
Severe (AVA ≤ 1.0 cm^2) n (%)	–	76 (86)	34 (83)	0.821	–	–
LVOT VTI (cm)	18±6	20±3	23±4	0.001	0.003	<0.001
LVOT peak velocity (cm/s)	82±24	86±16	101±43	0.028	0.072	0.014
SV_{Dopp} (ml)	58±9	56±15	73±15	0.027	0.103	0.012
SVI_{Dopp} (ml/m^2)	35±10	36±15	47±12	0.016	0.007	0.001
$SV_{Simpson}$ (ml)	57±15	61±14	57±11	0.239	0.284	0.434
LVMI (g/m^2)	72±21	115±31	113±29	0.933	<0.001	<0.001
Aortic annulus diameter (cm)	2.0±0.3	2.0±0.2	2.0±0.2	0.462	0.762	0.323
LVDd (mm)	45±4	47±6	46±5	0.190	0.053	0.434
LVDs (mm)	29±4	31±7	28±5	0.014	0.052	0.822
EDV (mL)	90±20	100±30	87±22	0.047	0.053	0.821
ESV (mL)	33±11	39±21	30±11	0.022	0.034	0.391
LVEF (%)	63±6	61±8	68±8	0.043	0.651	0.201
RVSP (mm Hg)	25±4	31±10	31±11	0.726	0.001	0.002
E/A	0.97±0.42	0.94±0.64	0.78±0.33	0.216	0.283	0.101
E/E'	7.3±2.0	17±9	15±7	0.014	<0.001	0.004
3D transthoracic echocardiography						
EDV (ml)	91±22	100±31	93±30	0.028	0.041	0.202
ESV (ml)	36±10	44±14	32±16	0.001	0.001	0.123
SV (ml)	55±16	56±16	60±18	0.340	0.433	0.223
SVI (ml/m^2)	33±11	37±12	39±10	0.328	0.243	0.101
EF (%)	60±5	56±9	65±9	0.018	0.092	0.081

USH upper septal hypertrophy; *LVOT* left ventricular outflow tract; *VTI* velocity–time integral; the other abbreviations are shown in Table 1

the USH group had a lower prevalence rate of low-flow status calculated using the Doppler method than 3D TTE method (7.3 vs. 18.4%, $P<0.001$). In addition, measurement errors of SV directly affected AVA estimation calculated using a continuity equation as the gold standard method. Therefore, the continuity equation based on the 2D Doppler method may underestimate AS severity, especially in AS patients with USH. Figure 7 presents the association between VTI and SVs calculated with Doppler echocardiography and 3D TTE. A positive correlation was recognized

Table 3 LVOT geometry in each group

	Controls ($N=30$)	Non-USH ($N=88$)	USH ($N=41$)	P value (non-USH vs. USH)
LVOT 1 short (cm)	2.08 ± 0.37	2.02 ± 0.30	1.66 ± 0.35[a]	< 0.001
Long (cm)	2.76 ± 0.54	2.73 ± 0.50	2.45 ± 0.37	0.013
area (cm^2)	4.64 ± 1.65	4.32 ± 1.36	3.25 ± 1.05[a]	< 0.001
Sphericity index	0.76 ± 0.09	0.74 ± 0.11	0.68 ± 0.12[a]	< 0.001
LVOT 2 short (cm)	1.98 ± 0.30	1.96 ± 0.28	1.67 ± 0.29[a]	< 0.001
Long (cm)	2.51 ± 0.48	2.52 ± 0.45	2.35 ± 0.34	0.245
Area (cm^2)	3.97 ± 1.28	3.89 ± 1.2	3.16 ± 0.87[a]	< 0.001
Sphericity index	0.79 ± 0.1	0.79 ± 0.12	0.71 ± 0.11[a]	0.002
LVOT 3 short (cm)	1.98 ± 0.26	1.93 ± 0.27	1.81 ± 0.28	0.081
Long (cm)	2.27 ± 0.38	2.37 ± 0.37	2.29 ± 0.40	0.438
Area (cm^2)	3.59 ± 0.99	3.59 ± 1.0	3.29 ± 0.90	0.239
Sphericity index	0.88 ± 0.12	0.82 ± 0.13	0.80 ± 0.12[b]	0.524
LVOT 4 short (cm)	1.97 ± 0.23	1.92 ± 0.27	1.90 ± 0.27	0.889
Long (cm)	2.22 ± 0.36	2.25 ± 0.41	2.26 ± 0.38	0.924
Area (cm^2)	3.49 ± 0.88	3.41 ± 1.1	3.41 ± 0.97	0.842
Sphericity index	0.89 ± 0.1	0.86 ± 0.13	0.86 ± 0.13	0.924

Abbreviations are shown in Table 2

[a] $P < 0.01$ versus controls

[b] $P < 0.05$ versus controls

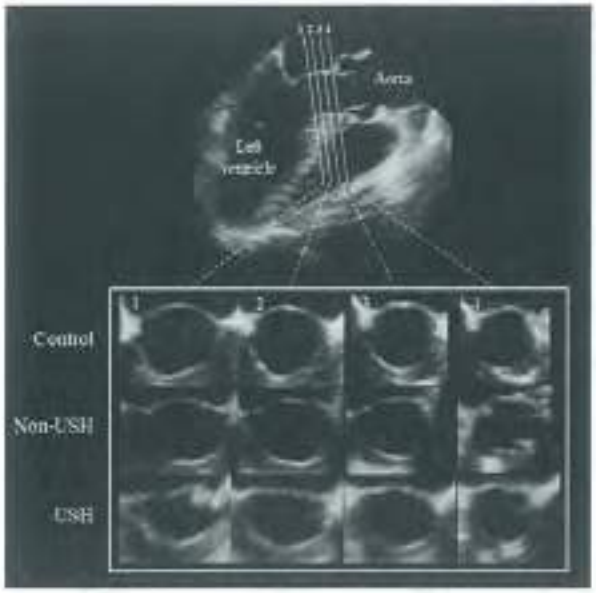

Fig. 4 Examples of LVOT in each group

between VTI and difference in SVs (Dopppler-3D). At the approximately 20 cm VTI, the SV calculated with Doppler echocardiography was consistent with that calculated with 3D TTE; in such cases, many patients in the USH group had VTI > 25 cm. Figure 8 shows the representative LVOT VTI in patients with USH and non-USH. The results of our study supported that of Garcia et al. because the mean VTI was 21 cm in their study. However, the USH group had higher VTI than the non-USH group, which might lead to the overestimation of SV [22]. Currently, flow-pressure status is considered crucial in the prognostic assessment [17–19, 23, 24] and it remains uncertain why normal-flow and low-gradient can be observed. A recent meta-analysis conducted by Dayan V et al. has reported that AS patients with normal-flow and low-gradient despite preserved ejection fraction have similar outcomes to those with normal-flow and high-gradient [25]. Their study discussed that the measurement error of SV might be the reason why AS patients with normal-flow low-gradient had similar outcomes to those with normal-flow high-gradient. This study suggested that the SV derived from the Doppler method should be overestimated rather than showing the real transvalvular flow in the USH group, which might be associated with errors in the measurement of SV. Of the patients in the USH group, 15% patients might be underestimated as having low-flow (SV index ≤ 35 ml/m^2, Fig. 7). In such cases, 3D assessment of SV might be crucial for evaluating disease severity in patients with AS [26–28].

Study limitations

Our study has several limitations. First, the study population consisted entirely of Japanese patients, and the relevance of this study to patients of other ethnicities needs to be confirmed with future research. Second, the MDCT and TEE evaluations were not performed on the same day. Third,

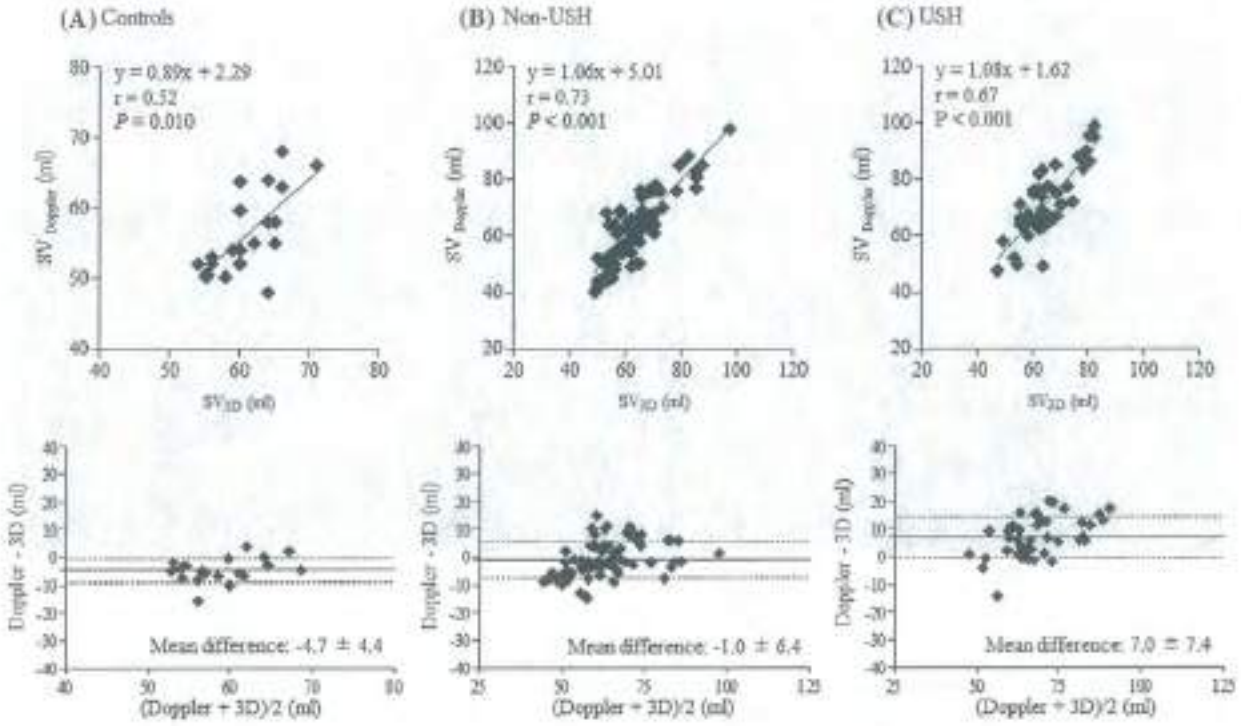

Fig. 5 Linear correlations (upper panel) and Bland–Altman scatter plot (lower panel) determining the agreement in the measurement of left ventricular stroke volume (SV) calculated by Doppler echocardiography and 3D TTE as a gold standard. SV was underestimated by Doppler echocardiography compared with 3D TTE in the controls (**a**) and the non-USH group (**b**); however, SV was overestimated by Doppler echocardiography compared with 3D TTE in the USH group (**c**)

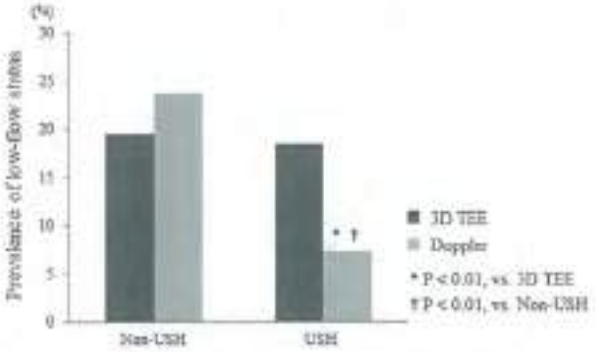

Fig. 6 Prevalence of low-flow status (SV index ≤ 35 ml/m²) in the non-USH group (left) and the USH group (right). No significant differences in the prevalence of low-flow status between the two methods were observed in the non-USH group (19.5 vs. 23.7%, $P = 0.624$); however, the USH group had the lower prevalence rate of low-flow status calculated using the Doppler method than 3D TTE method (7.3 vs. 18.4%, $P < 0.001$)

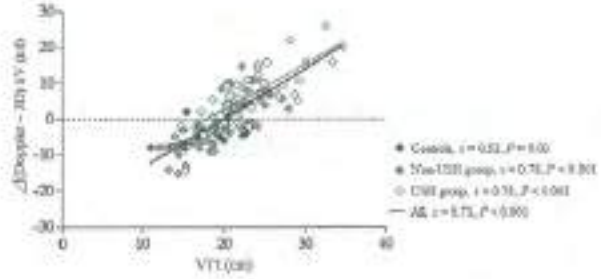

Fig. 7 Linear correlation between velocity–time integral and Δ(Doppler—3D) SV

the anesthetics used during TEE and the β-blockers used during MDCT might have affected the loading conditions. Forth, because of the differences in heart rate and frame rate between the MDCT and 3D TEE studies, the measurements were not performed at exactly the same point during the cardiac cycle. Fifth, this study employed 3D TTE which was thought to be superior to two-dimensional echocardiography and regarded as a gold standard to compare SV evaluated by Doppler echocardiography between the USH and non-USH groups, we did not have invasive measurements. Sixth, the control group in protocol 2 was not a strict representation of controls because the patients had some comorbidities affecting the LVOT geometry. However, the control group in earlier MDCT and TEE studies on aortic root geometry including the LVOT also had the same prevalence of those

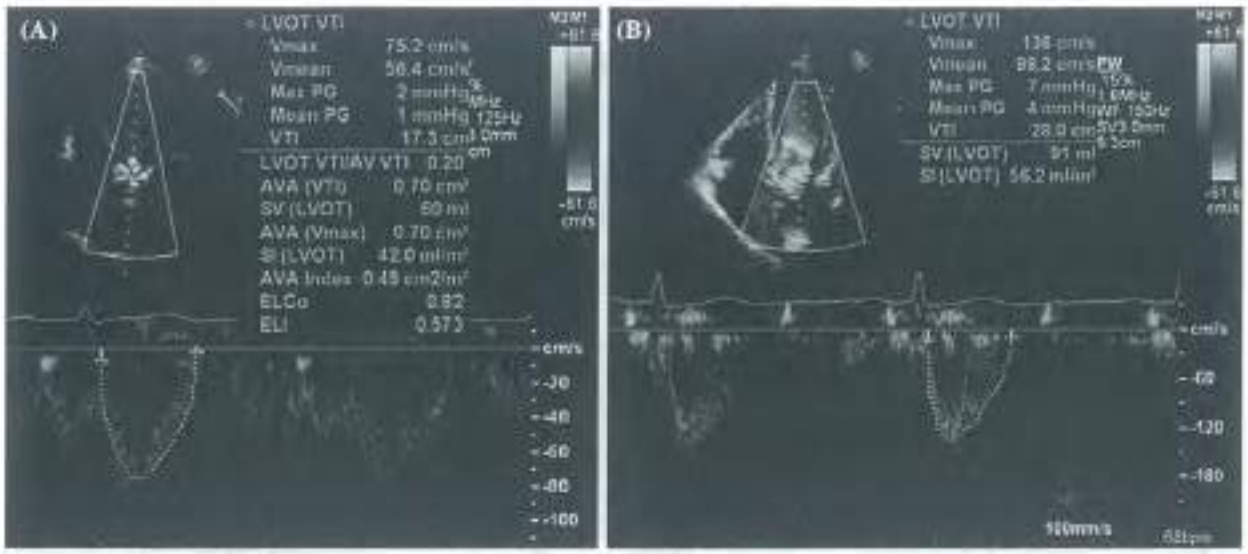

Fig. 8 Examples of LVOT VTI in each group (a non-USH, b USH)

comorbidities [7–10]. Finally, this study included only AS patients; however, we found USH in not only AS patients, but also in the other population. Further investigation with a larger population is warranted

Conclusions

3D TEE can provide a precise assessment of LVOT geometry in patients with AS. USH affects the LVOT geometry, which might lead to inaccurate assessments of AS severity.

Compliance with Ethical Standards

Conflict of Interest Dan Koto, Masaki Izumo, Takafumi Machida, Kihei Yoneyama, Tomomi Suzuki, Ryo Kumijima, Yasuyuki Kobayashi, Tomoo Harada, and Yoshihiro J. Akashi declare that they have no conflicts of interest.

Human rights statements and informed consent All procedure followed were in accordance with the ethical standards of the responsible committee on human experimentation (institutional and national) and with the Helsinki Declaration of 1964 and later revisions. The participants were well-informed prior to the test; written informed consent was obtained before enrollment.

References

1. Nkomo VT, Gardin JM, Skelton TN, et al. Burden of valvular heart diseases: a population-based study. Lancet. 2006;368:1005–11.
2. Carabello BA, Paulus WJ. Aortic stenosis. Lancet. 2009;373:956–66.
3. Carabello BA. Clinical practice. Aortic stenosis. N Engl J Med. 2002;346:677–82.
4. Saikrishnan N, Kumar G, Sawaya FJ, et al. Accurate assessment of aortic stenosis: a review of diagnostic modalities and hemodynamics. Circulation. 2014;129:244–53.
5. Delgado V, Ng AC, Schuijf JD, et al. Automated assessment of the aortic root dimensions with multidetector row computed tomography. Ann Thorac Surg. 2011;91:716–23.
6. Tops LF, Wood DA, Delgado V, et al. Noninvasive evaluation of the aortic root with multislice computed tomography implications for transcatheter aortic valve replacement. J Am Coll Cardiol Img. 2008;1:321–30.
7. Akhtar M, Tuzcu EM, Kapadia SR, et al. Aortic root morphology in patients undergoing percutaneous aortic valve replacement: evidence of aortic root remodeling. J Thorac Cardiovasc Surg. 2009;137:950–6.
8. Stolzmann P, Knight J, Desbiolles L, et al. Remodelling of the aortic root in severe tricuspid aortic stenosis: implications for transcatheter aortic valve implantation. Eur Radiol. 2009;19:1316–23.
9. Otani K, Takeuchi M, Kaku K, et al. Assessment of the aortic root using real-time 3D transesophageal echocardiography. Circ J. 2010;74:2649–57.
10. Wu VC, Kaku K, Takeuchi M, et al. Aortic root geometry in patients with aortic stenosis assessed by real-time three-dimensional transesophageal echocardiography. J Am Soc Echocardiogr. 2014;27:32–41.
11. Lang RM, Bierig M, Devereux RB, et al. Chamber Quantification Writing Group; American Society of Echocardiography's Guidelines and Standards Committee; European Association of Echocardiography. Recommendations for chamber quantification: a report from the American Society of Echocardiography's Guidelines and Standards Committee and the Chamber Quantification Writing Group, developed in conjunction with the European Association of Echocardiography, a branch of the European Society of Cardiology. J Am Soc Echocardiogr. 2005;18:1440–63.
12. Pibarot P, Clavel MA. Left ventricular outflow tract geometry and dynamics in aortic stenosis: Implications for the echocardiographic assessment of aortic valve area. J Am Soc Echocardiogr. 2015;28:1267–9.

13. Goor D, Lillehei W, Edwards JE. The "sigmoid septum" variation in the contour of the left ventricular outlet. AJR Am J Roentgenol. 1969;107:366–76.
14. Diaz T, Pencina MJ, Benjamin EJ, et al. Prevalence, clinical correlates, and prognosis of discrete upper septal thickening on echocardiography: the Framingham Heart Study. Echocardiography. 2009;26:247–53.
15. Funabashi N, Umazume T, Takaoka H, et al. Sigmoid shaped interventricular septum exhibit normal myocardial characteristics and has a relationship with aging, ascending aortic sclerosis and its tilt to left ventricle. Int J Cardiol. 2013;168:4484–8.
16. Jilaihawi H, Kashif M, Fontana G, et al. Cross-sectional computed tomographic assessment improves accuracy of aortic annular sizing for transcatheter aortic valve replacement and reduces the incidence of paravalvular aortic regurgitation. J Am Coll Cardiol. 2012;59:1275–86.
17. Hachicha Z, Dumesnil JG, Bogaty P, et al. Paradoxical low-flow, low-gradient severe aortic stenosis despite preserved ejection fraction is associated with higher afterload and reduced survival. Circulation. 2007;115:2856–64.
18. Lancellotti P, Magne J, Donal E, et al. Clinical outcome in asymptomatic severe aortic stenosis: insights from the new proposed aortic stenosis grading classification. J Am Coll Cardiol. 2012;59:235–43.
19. Ozkan A, Hachamovitch R, Kapadia SR, et al. Impact of aortic valve replacement on outcome of symptomatic patients with severe aortic stenosis with low gradient and preserved left ventricular ejection fraction. Circulation. 2013;128:622–31.
20. Doddamani S, Grushko MJ, Makaryus AN, et al. Demonstration of left ventricular outflow tract eccentricity by 64-slice multidetector CT. Int J Cardiovasc Imaging. 2009;25:175–81.
21. Saitoh T, Shiota M, Izumo M, et al. Comparison of left ventricular outflow geometry and aortic valve area in patients with aortic stenosis by 2-dimensional versus 3-dimensional echocardiography. Am J Cardiol. 2012;109:1626–31.
22. Garcia J, Kadem L, Larose E, et al. Comparison between cardiovascular magnetic resonance and transthoracic Doppler echocardiography for the estimation of effective orifice area in aortic stenosis. J Cardiovasc Magn Reson. 2011;13:25.
23. Le Ven F, Freeman M, Webb J, et al. Impact of low flow on the outcome of high-risk patients undergoing transcatheter aortic valve replacement. J Am Coll Cardiol. 2013;62:782–8.
24. Clavel MA, Berthelot-Richer M, Le Ven F, et al. Impact of classic and paradoxical low flow on survival after aortic valve replacement for severe aortic stenosis. J Am Coll Cardiol. 2015;65:645–53.
25. Dayan V, Vignolo G, Magne J, et al. Outcome and impact of aortic valve replacement in patients with preserved LVEF and low-gradient aortic stenosis. J Am Coll Cardiol. 2015;66:2594–603.
26. Poh KK, Levine RA, Solis J, et al. Assessing aortic valve area in aortic stenosis by continuity equation: a novel approach using real-time three-dimensional echocardiography. Eur Heart J. 2008;29:2526–35.
27. Mehrotra P, Flynn AW, Jansen K, et al. Differential left ventricular outflow tract remodeling and dynamics in aortic stenosis. J Am Soc Echocardiogr. 2015;28:1259–66.
28. Sato K, Seo Y, Ishizu T, et al. Reliability of aortic stenosis severity classified by 3-dimensional echocardiography in the prediction of cardiovascular events. Am J Cardiol. 2016;118:410–7.